

PTEP

Progress of Theoretical and Experimental Physics

Review of Particle Physics

P.A. Zyla *et al.* (Particle Data Group), *Prog. Theor. Exp. Phys.* 2020, 083C01 (2020)

PDG
particle data group

Downloaded from <https://academic.oup.com/ptep/article/2020/8/083C01/5891211> by guest on 20 August 2020



The Physical Society of Japan

OXFORD
UNIVERSITY PRESS

REVIEW OF PARTICLE PHYSICS*

Particle Data Group

Abstract

The *Review* summarizes much of particle physics and cosmology. Using data from previous editions, plus 3,324 new measurements from 878 papers, we list, evaluate, and average measured properties of gauge bosons and the recently discovered Higgs boson, leptons, quarks, mesons, and baryons. We summarize searches for hypothetical particles such as supersymmetric particles, heavy bosons, axions, dark photons, etc. Particle properties and search limits are listed in Summary Tables. We give numerous tables, figures, formulae, and reviews of topics such as Higgs Boson Physics, Supersymmetry, Grand Unified Theories, Neutrino Mixing, Dark Energy, Dark Matter, Cosmology, Particle Detectors, Colliders, Probability and Statistics. Among the 120 reviews are many that are new or heavily revised, including a new review on High Energy Soft QCD and Diffraction and one on the Determination of CKM Angles from B Hadrons.

The *Review* is divided into two volumes. Volume 1 includes the Summary Tables and 98 review articles. Volume 2 consists of the Particle Listings and contains also 22 reviews that address specific aspects of the data presented in the Listings.

The complete *Review* (both volumes) is published online on the website of the Particle Data Group (pdg.lbl.gov) and in a journal. Volume 1 is available in print as the *PDG Book. A Particle Physics Booklet* with the Summary Tables and essential tables, figures, and equations from selected review articles is available in print and as a web version optimized for use on phones as well as an Android app.

The 2020 edition of the *Review of Particle Physics* should be cited as:
P.A. Zyla *et al.* (Particle Data Group), *Prog. Theor. Exp. Phys.* **2020**, 083C01 (2020)

DOI: 10.1093/ptep/ptaa104

For the online version see pdg.lbl.gov:



©2020 Regents of the University of California

*The publication of the *Review of Particle Physics* is supported by the Director, Office of Science, Office of High Energy Physics of the U.S. Department of Energy under Contract No. DE-AC02-05CH11231; by the European Laboratory for Particle Physics (CERN); by an implementing arrangement between the governments of Japan (MEXT: Ministry of Education, Culture, Sports, Science and Technology) and the United States (DOE) on cooperative research and development; by the Italian National Institute of Nuclear Physics (INFN); and by the Physical Society of Japan (JPS). Individual collaborators receive support for their PDG activities from their respective funding agencies.

Particle Data Group

P.A. Zyla,¹ R.M. Barnett,¹ J. Beringer,¹ O. Dahl,¹ D.A. Dwyer,¹ D.E. Groom,¹ C.-J. Lin,¹ K.S. Lugovsky,^{1,2} E. Pianori,¹ D.J. Robinson,¹ C.G. Wohl,¹ W.-M. Yao,¹ K. Agashe,³ G. Aielli,⁴ B.C. Allanach,⁵ C. Amsler,⁶ M. Antonelli,⁷ E.C. Aschenauer,⁸ D.M. Asner,⁸ H. Baer,⁹ Sw. Banerjee,¹⁰ L. Baudis,¹¹ C.W. Bauer,¹ J.J. Beatty,¹² V.I. Belousov,² S. Bethke,¹³ A. Bettini*,¹⁴ O. Biebel,¹⁵ K.M. Black,¹⁶ E. Blucher,¹⁷ O. Buchmüller,¹⁸ V. Burkert,¹⁹ M.A. Bychkov,²⁰ R.N. Cahn,¹ M. Carena,^{21,17,22} A. Ceccucci,²³ A. Cerri,²⁴ D. Chakraborty,²⁵ R. Sekhar Chivukula,²⁶ G. Cowan,²⁷ G. D'Ambrosio,²⁸ T. Damour,²⁹ D. de Florian,³⁰ A. de Gouvêa,³¹ T. DeGrand,³² P. de Jong,³³ G. Dissertori,³⁴ B.A. Dobrescu,²¹ M. D'Onofrio,³⁵ M. Doser,²³ M. Drees,³⁶ H.K. Dreiner,³⁶ P. Eerola,³⁷ U. Egede,³⁸ S. Eidelman,^{39,40} J. Ellis,^{41,23} J. Erler,^{42,43} V.V. Ezhela,² W. Fetscher,³⁴ B.D. Fields,^{44,45} B. Foster,^{46,47,48} A. Freitas,⁴⁹ H. Gallagher,⁵⁰ L. Garren,²¹ H.-J. Gerber†,³⁴ G. Gerbier,⁵¹ T. Gershon,⁵² Y. Gershtein,⁵³ T. Gherghetta,⁵⁴ A.A. Godizov,² M.C. Gonzalez-Garcia,^{55,56,57} M. Goodman,⁵⁸ C. Grab,³⁴ A.V. Gritsan,⁵⁹ C. Grojean,^{60,61} M. Grünewald,⁶² A. Gurtu,^{63,23} T. Gutsche,⁶⁴ H.E. Haber,⁶⁵ C. Hanhart,⁶⁶ S. Hashimoto,⁶⁷ Y. Hayato,⁶⁸ A. Hebecker,⁶⁹ S. Heinemeyer,^{70,71,72} B. Heltsley,⁷³ J. J. Hernández-Rey‡,⁷⁴ K. Hikasa,⁷⁵ J. Hisano,⁷⁶ A. Höcker,²³ J. Holder,^{77,78} A. Holtkamp,²³ J. Huston,⁷⁹ T. Hyodo,⁸⁰ K.F. Johnson,⁸¹ M. Kado,^{82,83,84} M. Karliner,⁸⁵ U.F. Katz,⁸⁶ M. Kenzie,⁵² V.A. Khoze,^{87,88} S.R. Klein,^{89,90} E. Klempt,⁹¹ R.V. Kowalewski,⁹² F. Krauss,⁸⁷ M. Kreps,⁵² B. Krusche,⁹³ Y. Kwon,⁹⁴ O. Lahav,⁹⁵ J. Laiho,⁹⁶ L.P. Lellouch,⁹⁷ J. Lesgourgues,⁹⁸ A. R. Liddle,^{99,100} Z. Ligeti,¹ C. Lippmann,¹⁰¹ T.M. Liss,¹⁰² L. Littenberg,⁸ C. Lourenço,²³ S.B. Lugovsky,² A. Lusiani,^{103,104} Y. Makida,⁶⁷ F. Maltoni,^{105,106} T. Mannel,¹⁰⁷ A.V. Manohar,²⁶ W.J. Marciano,⁸ A. Masoni,¹⁰⁸ J. Matthews,¹⁰⁹ U.-G. Meißner,^{91,66} M. Mikhasenko,²³ D.J. Miller,¹¹⁰ D. Milstead,¹¹¹ R.E. Mitchell,¹¹² K. Mönig,¹¹³ P. Molaro,¹¹⁴ F. Moortgat,^{23,115} M. Moskovic,²³ K. Nakamura,^{116,67} M. Narain,¹¹⁷ P. Nason,^{118,119} S. Navas‡,¹²⁰ M. Neubert,¹²¹ P. Nevski§,⁸ Y. Nir,¹²² K.A. Olive,⁵⁴ C. Patrignani,¹²³ J.A. Peacock,¹²⁴ S.T. Petcov,^{125,116,126} V.A. Petrov,² A. Pich,⁷⁴ A. Piepke,¹²⁷ A. Pomarol,^{128,129} S. Profumo,⁶⁵ A. Quadt,¹³⁰ K. Rabbertz,¹³¹ J. Rademacker,¹³² G. Raffelt,¹³³ H. Ramani,¹ M. Ramsey-Musolf,^{134,135,136} B.N. Ratcliff,¹³⁷ P. Richardson,⁸⁷ A. Ringwald,⁴⁷ S. Roesler,²³ S. Rolli,¹³⁸ A. Romaniouk,¹³⁹ L.J. Rosenberg,¹⁴⁰ J.L. Rosner,¹⁷ G. Rybka,¹⁴⁰ M. Ryskin,⁸⁸ R.A. Ryutin,² Y. Sakai,⁶⁷ G.P. Salam,^{23,141,142} S. Sarkar,¹⁴² F. Sauli§,²³ O. Schneider,¹⁴³ K. Scholberg,¹⁴⁴ A.J. Schwartz,¹⁴⁵ J. Schwiening,¹⁰¹ D. Scott,¹⁴⁶ V. Sharma,²⁶ S.R. Sharpe,¹⁴⁰ T. Shutt,¹³⁷ M. Silari,²³ T. Sjöstrand,¹⁴⁷ P. Skands,³⁸ T. Skwarnicki,⁹⁶ G.F. Smoot,^{148,149,90,1} A. Soffer,⁸⁵ M.S. Sozzi,¹⁵⁰ S. Spanier,¹⁵¹ C. Spiering,¹¹³ A. Stahl,¹⁵² S.L. Stone,⁹⁶ Y. Sumino,⁷⁵ T. Sumiyoshi,¹⁵³ M.J. Syphers,^{25,21} F. Takahashi,⁷⁵ M. Tanabashi,^{154,76} J. Tanaka,¹⁵⁵ M. Taševský,¹⁵⁶ K. Terashi,¹⁵⁵ J. Terning,¹⁵⁷ U. Thoma,⁹¹ R.S. Thorne,⁹⁵ L. Tiator,¹⁵⁸ M. Titov,⁵¹ N.P. Tkachenko,² D.R. Tovey,¹⁵⁹ K. Trabelsi,⁸⁴ P. Urquijo,¹⁶⁰ G. Valencia,³⁸ R. Van de Water,²¹ N. Varelas,¹⁶¹ G. Venanzoni,¹⁰⁴ L. Verde,^{57,56} M.G. Vincter,¹⁶² P. Vogel,¹⁶³ W. Vogelsang,⁶⁴ A. Vogt,¹⁶⁴ V. Vorobyev,^{39,40} S.P. Wakely,^{17,22} W. Walkowiak,¹⁰⁷ C.W. Walter,¹⁴⁴ D. Wands,¹⁶⁵ M.O. Wascko,¹⁸ D.H. Weinberg,¹⁶⁶ E.J. Weinberg,¹⁶⁷ M. White,^{90,1} L.R. Wiencke,¹⁶⁸ S. Willocq,¹³⁶ C.L. Woody,⁸ R.L. Workman,¹⁶⁹ M. Yokoyama,^{170,116} R. Yoshida,¹⁹ G. Zanderighi,¹³ G.P. Zeller,²¹ O.V. Zenin,^{2,171} R.-Y. Zhu,¹⁷² S.-L. Zhu,¹⁷³ F. Zimmermann²³

Technical Associates: J. Anderson,¹ T. Basaglia,²³ V.S. Lugovsky,² P. Schaffner,¹ W. Zheng,¹⁷⁴

1. *Physics Division, Lawrence Berkeley National Laboratory, Berkeley, CA, USA*
2. *Institute for High Energy Physics, COMPAS Group, Protvino, Russia*
3. *University of Maryland, Department of Physics, College Park, MD, USA*
4. *Università degli Studi di Roma "Tor Vergata", Rome, Italy*
5. *Department of Applied Mathematics and Theoretical Physics, University of Cambridge, Cambridge, UK*
6. *Stefan Meyer Institute for Subatomic Physics, Austrian Academy of Sciences, Vienna, Austria*
7. *Lab. Nazionali di Frascati dell'INFN, Frascati, Italy*
8. *Brookhaven National Laboratory, Nuclear and Particle Physics Directorate, Upton, NY, USA*
9. *University of Oklahoma, Department of Physics and Astronomy, Norman, OK, USA*
10. *University of Louisville, Louisville, KY, USA*
11. *Universität Zürich, Physik-Institut, Zürich, Switzerland*
12. *Ohio State University, Department of Physics, Columbus, OH, USA*
13. *Max-Planck-Institute of Physics, Munich, Germany*
14. *INFN and Dipartimento di Fisica e Astronomia, Università di Padova, Padova, Italy*
15. *Ludwig-Maximilians-Universität, Fakultät für Physik, München, Germany*
16. *University of Wisconsin, Department of Physics, Madison, WI, USA*
17. *University of Chicago, Enrico Fermi Institute and Department of Physics, Chicago, IL, USA*

* Coordination activities supported directly by INFN.

† Deceased.

‡ Support from Programa Estatal de Generación de Conocimiento MCIU, Spain and ERDF of the European Union (PGC2018-096663-B-C41 and C44).

§ Retired.

18. *Imperial College, High Energy Physics Group, Blackett Laboratory, London, UK*
19. *Jefferson Lab, Newport News, VA, USA*
20. *University of Virginia, Department of Physics, Charlottesville, VA, USA*
21. *Fermi National Accelerator Laboratory, Batavia, IL, USA*
22. *University of Chicago, Kavli Institute for Cosmological Physics, Chicago, IL, USA*
23. *CERN, European Organization for Nuclear Research, Genève, Switzerland*
24. *Department of Physics and Astronomy, University of Sussex, Brighton, UK*
25. *Department of Physics, Northern Illinois University, DeKalb, IL, USA*
26. *Department of Physics, University of California at San Diego, La Jolla, CA, USA*
27. *Department of Physics, Royal Holloway, University of London, London, UK*
28. *INFN Sezione di Napoli, Napoli, Italy*
29. *Institut des Hautes Etudes Scientifiques, Bures-sur-Yvette, France*
30. *UNSAM - Universidad Nacional de San Martín, International Center for Advanced Studies (ICAS) and Instituto de Ciencias Físicas (ICIFI), Buenos Aires, Argentina*
31. *Northwestern University, Department of Physics and Astronomy, Evanston, IL, USA*
32. *University of Colorado at Boulder, Department of Physics, Boulder, CO, USA*
33. *Nikhef and University of Amsterdam, Amsterdam, The Netherlands*
34. *ETH Zurich, Institute for Particle Physics and Astrophysics, Zurich, Switzerland*
35. *University of Liverpool, Department of Physics, Liverpool, UK*
36. *Universität Bonn, Physikalisches Institut, Bonn, Germany*
37. *University of Helsinki, Department of Physics, Helsinki, Finland*
38. *Monash University, School of Physics and Astronomy, Melbourne, Australia*
39. *Budker Institute of Nuclear Physics SB RAS, Novosibirsk, Russia*
40. *Novosibirsk State University, Novosibirsk, Russia*
41. *King's College London, Department of Physics, London, UK*
42. *Universidad Nacional Autónoma de México, Departamento de Física Teórica, Instituto de Física, México, Mexico*
43. *Helmholtz Institute Mainz, Johannes Gutenberg-University, Mainz, Germany*
44. *University of Illinois, Department of Astronomy, Urbana, IL, USA*
45. *University of Illinois, Department of Physics, Urbana, IL, USA*
46. *University of Hamburg, Hamburg, Germany*
47. *Deutsches Elektronen-Synchrotron DESY, Hamburg, Germany*
48. *University of Oxford, Denys Wilkinson Building, Department of Physics, Oxford, UK*
49. *University of Pittsburgh, Department of Physics and Astronomy, Pittsburgh, PA, USA*
50. *Tufts University, Department of Physics and Astronomy, Medford, MA, USA*
51. *CEA Saclay, DSM/IRFU/SPP, Gif-sur-Yvette, France*
52. *University of Warwick, Department of Physics, Coventry, UK*
53. *Department of Physics and Astronomy, Rutgers University, NJ, USA*
54. *University of Minnesota, School of Physics and Astronomy, Minneapolis, MN, USA*
55. *CN Yang Institute for Theoretical Physics, Stony Brook University, Stony Brook, NY, USA*
56. *Institució Catalana de Recerca i Estudis Avancats, Barcelona, Spain*
57. *Instituto de ciencias del Cosmos (ICC), University of Barcelona, Barcelona, Spain*
58. *Argonne National Laboratory, Argonne, IL, USA*
59. *Johns Hopkins University, Baltimore, MD, USA*
60. *Theoriegruppe, Deutsches Elektronen-Synchrotron DESY, Hamburg, Germany*
61. *Institut für Physik, Humboldt-Universität zu Berlin, Berlin, Germany*
62. *University College Dublin, School of Physics, Dublin, Ireland*
63. *Physics Department, Kyung Hee University, Seoul 02447, Republic of Korea*
64. *Universität Tübingen, Institut für Theoretische Physik, Tübingen, Germany*
65. *Santa Cruz Institute for Particle Physics, University of California, Santa Cruz, CA, USA*
66. *Institut für Kernphysik and Institute for Advanced Simulation, Forschungszentrum Jülich, Jülich, Germany*
67. *KEK, High Energy Accelerator Research Organization, Tsukuba, Japan*
68. *Kamioka Observatory, ICRP, The University of Tokyo, Tokyo, Japan*
69. *Heidelberg University, Institute for Theoretical Physics, Heidelberg, Germany*
70. *Instituto de Física Teórica (UAM/CSIC), Universidad Autónoma de Madrid, Madrid, Spain*

71. *Campus of International Excellence UAM+CSIC, Universidad Autónoma de Madrid, Madrid, Spain*
72. *Instituto de Física de Cantabria, CSIC-UC, Santander, Spain*
73. *Cornell University, Laboratory of Elementary-Particle Physics, Ithaca, NY, USA*
74. *IFIC — Instituto de Física Corpuscular, Universitat de València — C.S.I.C., Valencia, Spain*
75. *Tohoku University, Department of Physics, Sendai, Japan*
76. *Nagoya University, Kobayashi-Maskawa Institute, Nagoya, Japan*
77. *University of Delaware, Department of Physics and Astronomy, Newark, DE, USA*
78. *University of Delaware, Bartol Research Institute, Newark, DE, USA*
79. *Michigan State University, Dept. of Physics and Astronomy, East Lansing, MI, USA*
80. *Department of Physics, Tokyo Metropolitan University, Tokyo, Japan*
81. *Florida State University, Department of Physics, Tallahassee, FL, USA*
82. *Dipartimento di Fisica, Sapienza Università di Roma, Rome, Italy*
83. *INFN Sezione di Roma, Rome, Italy*
84. *IJCLab, CNRS/IN2P3, Université Paris-Saclay, Orsay, France*
85. *Department of Particle Physics, Tel-Aviv University, Tel Aviv, Israel*
86. *Friedrich-Alexander University of Erlangen-Nürnberg, Erlangen Centre for Astroparticle Physics, Erlangen, Germany*
87. *University of Durham, Institute for Particle Physics Phenomenology, Department of Physics, Durham, UK*
88. *Petersburg Nuclear Physics Institute, Petersburg, Russia*
89. *Nuclear Science Division, Lawrence Berkeley National Laboratory, Berkeley, CA, USA*
90. *University of California, Department of Physics, Berkeley, CA, USA*
91. *Universität Bonn, Helmholtz-Institut für Strahlen- und Kernphysik, Bonn, Germany*
92. *University of Victoria, Victoria, BC, Canada*
93. *University of Basel, Institute of Physics, Basel, Switzerland*
94. *Yonsei University, Department of Physics, Seoul, Republic of Korea*
95. *University College London, Department of Physics and Astronomy, London, UK*
96. *Syracuse University, Department of Physics, Syracuse, NY, USA*
97. *Aix-Marseille Univ, Université de Toulon, CNRS, CPT, Marseille, France*
98. *Institute of Theoretical Particle Physics and Cosmology (TTK), RWTH, Aachen, Germany*
99. *Perimeter Institute for Theoretical Physics, Waterloo, Canada*
100. *Instituto de Astrofísica e Ciências do Espaço, Universidade de Lisboa, Lisbon, Portugal*
101. *GSI, Helmholtzzentrum für Schwerionenforschung, Darmstadt, Germany*
102. *Division of Science, City College of New York, New York, NY, USA*
103. *Scuola Normale Superiore, Pisa, Italy*
104. *INFN Sezione di Pisa, Pisa, Italy*
105. *Université catholique de Louvain, Centre for Cosmology, Particle Physics and Phenomenology (CP³), Louvain-la-Neuve, Belgium*
106. *Università di Bologna and INFN, Dipartimento di Fisica e Astronomia, Bologna, Italy*
107. *Universität Siegen, Department für Physik, Siegen, Germany*
108. *INFN Sezione di Cagliari, Monserrato, Italy*
109. *Louisiana State University, Department of Physics and Astronomy, Baton Rouge, LA, USA*
110. *University of Glasgow, School of Physics and Astronomy, Glasgow, UK*
111. *Stockholms Universitet, AlbaNova University Centre, Fysikum, Stockholm, Sweden*
112. *Indiana University, Department of Physics, Bloomington, IN, USA*
113. *DESY, Zeuthen, Germany*
114. *INAF-OATS, Trieste, Italy*
115. *University of Ghent, Dept. of Physics and Astronomy, Ghent, Belgium*
116. *University of Tokyo, Kavli IPMU (WPI), The University of Tokyo Institutes for Advanced Study, Kashiwa, Japan*
117. *Brown University, Department of Physics, Providence, RI, USA*
118. *INFN Sezione di Milano-Bicocca, Piazza della Scienza, Milano, Italy*
119. *Dip. di Fisica "G. Occhialini", Università di Milano-Bicocca, Milano, Italy*
120. *Universidad de Granada, Dpto. de Física Teórica y del Cosmos & C.A.F.P.E., Granada, Spain*
121. *Johannes Gutenberg University, PRISMA Cluster of Excellence and Mainz Institute for Theoretical Physics, Mainz, Germany*
122. *Department of Particle Physics and Astrophysics, Weizmann Institute of Science, Rehovot, Israel*

123. *Università di Bologna and INFN, Dip. Scienze per la Qualità della Vita, Rimini, Italy*
124. *University of Edinburgh, Royal Observatory, Institute for Astronomy, Edinburgh, UK*
125. *SISSA/INFN, Trieste, Italy*
126. *INRNE, Bulgarian Academy of Sciences, Sofia, Bulgaria*
127. *University of Alabama, Department of Physics and Astronomy, Tuscaloosa, AL, USA*
128. *Universitat Autònoma de Barcelona, Departament de Física, Barcelona, Spain*
129. *IFAE, Universitat Autònoma de Barcelona, Barcelona, Spain*
130. *Georg-August-Universität Göttingen, II. Physikalisches Institut, Göttingen, Germany*
131. *Karlsruhe Institute of Technology, Karlsruhe, Germany*
132. *University of Bristol, HH Wills Physics Laboratory, Bristol, UK*
133. *Max-Planck-Institut für Physik (Werner-Heisenberg-Institut), München, Germany*
134. *Tsung-Dao Lee Institute, Shanghai Jiao Tong University, Shanghai, China*
135. *Shanghai Jiao Tong University, Shanghai, China*
136. *University of Massachusetts, Department of Physics, Amherst, MA, USA*
137. *SLAC National Accelerator Laboratory, Menlo Park, CA, USA*
138. *DOE, Washington, DC, USA*
139. *National Research Nuclear University "MEPhI", Moscow, Russia*
140. *University of Washington, Department of Physics, Seattle, WA, USA*
141. *LPTHE, UPMC Université de Paris 6, Paris, France*
142. *University of Oxford, Rudolf Peierls Centre for Theoretical Physics, Oxford, UK*
143. *Institute of Physics, Ecole Polytechnique Fédérale de Lausanne (EPFL), Lausanne, Switzerland*
144. *Duke University, Physics Department, Durham, NC, USA*
145. *University of Cincinnati, Department of Physics, Cincinnati, OH, USA*
146. *University of British Columbia, Department of Physics and Astronomy, Vancouver, BC, Canada*
147. *Lund University, Department of Astronomy and Theoretical Physics, Lund, Sweden*
148. *The Hong Kong University of Science and Technology, Kowloon, Hong Kong*
149. *Paris Centre for Cosmological Physics, APC (CNRS), Université de Paris, Paris, France*
150. *Pisa University, Pisa, Italy*
151. *University of Tennessee, Department of Physics and Astronomy, Knoxville, TN, USA*
152. *III. Physikalisches Institut, Physikzentrum, RWTH Aachen University, Aachen, Germany*
153. *Tokyo Metropolitan University, High Energy Physics Laboratory, Tokyo, Japan*
154. *Department of Physics, Nagoya University, Nagoya, Japan*
155. *International Center for Elementary Particle Physics (ICEPP), University of Tokyo, Tokyo, Japan*
156. *Institute of Physics, Czech Academy of Sciences, Prague, Czech Republic*
157. *Department of Physics, University of California, Davis, CA, USA*
158. *Institut für Kernphysik, Johannes Gutenberg University, Mainz, Germany*
159. *University of Sheffield, Department of Physics and Astronomy, Sheffield, UK*
160. *University of Melbourne, School of Physics, Victoria, Australia*
161. *University of Illinois at Chicago, Chicago, IL, USA*
162. *Carleton University, Department of Physics, Ottawa, ON, Canada*
163. *California Institute of Technology, Kellogg Radiation Laboratory, Pasadena, CA, USA*
164. *The University of Liverpool, Division of Theoretical Physics, Department of Mathematical Sciences, Liverpool, UK*
165. *University of Portsmouth, Institute of Cosmology and Gravitation, Portsmouth, UK*
166. *Ohio State University, Department of Astronomy and CCAPP, Columbus, OH, USA*
167. *Columbia University, Department of Physics, New York, NY, USA*
168. *Dept. of Physics, Colorado School of Mines, Golden, CO, USA*
169. *George Washington University Virginia Campus, Department of Physics, Ashburn, VA, USA*
170. *University of Tokyo, Department of Physics, Tokyo, Japan*
171. *Moscow Institute of Physics and Technology, Dolgoprudny, Russia*
172. *California Institute of Technology, High Energy Physics, Pasadena, CA, USA*
173. *School of Physics, Peking University, Beijing, China*
174. *Institute of High Energy Physics, Beijing, China*

HIGHLIGHTS OF THE 2020 EDITION OF THE REVIEW OF PARTICLE PHYSICS

All PDG data and review articles are available online at pdg.lbl.gov.

878 new papers with 3,324 new measurements

120 reviews (most are revised)

- 411 new papers from *LHC* experiments (ATLAS, CMS and LHCb).
 - Extensive up-to-date *Higgs boson* coverage from 117 new papers with 201 measurements, including latest results on mass, couplings, decay width and branching ratios, plus searches for other neutral and charged Higgs bosons.
 - *Supersymmetry*: 83 new papers with major exclusions.
 - *Top quark*: 36 new papers provide latest results on mass, coupling, and constraints on various models of physics beyond the Standard Model involving top-quark production and decay.
 - Latest from *B-meson physics*: 85 papers and 356 measurements, including observations of new excited Λ_b baryons and new pentaquark states.
 - 5 new sections including limits of cross sections in *WIMP and Dark Matter Searches* for masses in the GeV range (65 new entries, including also older results).
 - *Heavy Neutral Lepton* Listings reorganized and extended.
 - New *proton charge radius* measurements appear to resolve charge radius puzzle.
- New reviews on:
 - *High Energy Soft QCD and Diffraction*.
 - *Determination of CKM Angles from B Hadrons*.
 - Significant update/revision to reviews on:
 - Major revision of *Physical Constants* following the 2019 redefinition of units in the International System of Units.
 - *Electroweak Model* and *CKM* reviews provide latest fits of Standard Model parameters.
 - *Structure Functions* review includes new discussion on transverse momentum dependent distributions (TMDs).
 - *Top Quark* review summarizes latest results and constraints on new physics from top quark.
 - D^0 - \bar{D}^0 *Mixing* summarizes latest results and discusses implications of first observation of CP violation in D^0 decays.
 - Completely rewritten review on *Neutrino Masses, Mixing and Oscillations* discusses latest results from solar, atmospheric, reactor and accelerator-based neutrino experiments and provides global fit values for mixing parameters and mass spectrum.
 - *Pentaquarks* review updated based on new LHCb measurement of hidden-charm pentaquarks.
 - *Monte Carlo Neutrino Generators* includes new extensive discussion on nuclear scattering.
 - Completely rewritten review on *Dark Matter*.
 - *Experimental Tests of Gravitational Theory* revised and extended to include gravitational waves.

VOLUME 1: SUMMARY TABLES AND REVIEWS

Highlights	6	Experimental Methods and Colliders	
Introduction	11	31. Accelerator physics of colliders (rev.)	521
History plots	19	32. High-energy collider parameters (rev.)	529
Online particle physics information (rev.)	20	33. Neutrino beam lines at high-energy proton synchrotrons (rev.)	534
SUMMARY TABLES		34. Passage of particles through matter (rev.)	535
Gauge and Higgs bosons	31	35. Particle detectors at accelerators (rev.)	551
Leptons	34	36. Particle detectors for non-accelerator phys. (rev.)	589
Quarks	37	37. Radioactivity and radiation protection (rev.)	612
Mesons	38	38. Commonly used radioactive sources (rev.)	618
Meson quick reference table	91	Mathematical Tools	
Baryon quick reference table	92	39. Probability (rev.)	621
Baryons	93	40. Statistics (rev.)	626
Searches not in Other Sections	111	41. Monte Carlo techniques (rev.)	642
Tests of conservation laws	113	42. Monte Carlo event generators	646
REVIEWS, TABLES, AND PLOTS		43. Monte Carlo neutrino event generators (rev.)	657
Constants, Units, Atomic and Nuclear Properties		44. Monte Carlo particle numbering scheme (rev.)	661
1. Physical constants (rev.)	137	45. Clebsch-Gordan coefficients, spherical harmonics, and d functions	665
2. Astrophysical constants (rev.)	138	46. SU(3) isoscalar factors and representation matrices	666
3. International system of units (SI)	140	47. SU(n) multiplets and Young diagrams	667
4. Periodic table of the elements (rev.)	141	Kinematics, Cross-Section Formulae, and Plots	
5. Electronic structure of the elements	142	48. Kinematics (rev.)	671
6. Atomic and nuclear properties of materials	144	49. Resonances (rev.)	675
7. Electromagnetic relations	146	50. Cross-section formulae for specific processes (rev.)	682
8. Naming scheme for hadrons (rev.)	148	51. Neutrino cross section measurements (rev.)	691
Standard Model and Related Topics		52. Plots of cross sections and related quantities (rev.)	696
9. Quantum chromodynamics (rev.)	153	Particle Properties	
10. Electroweak model and constraints on new physics (rev.)	180	<u>Gauge Bosons</u>	
11. Higgs boson physics, status of (rev.)	203	53. Mass and width of the W boson (rev.)	715
12. CKM quark-mixing matrix (rev.)	261	54. Z boson	717
13. CP violation in the quark sector (rev.)	271	<u>Charged Leptons</u>	
14. Neutrino masses, mixing, and oscillations (new)	285	55. Muon anomalous magnetic moment (rev.)	722
15. Quark model (rev.)	312	56. Muon decay parameters (rev.)	725
16. Heavy-quark & soft-collinear effective theory (rev.)	325	57. τ branching fractions (rev.)	728
17. Lattice quantum chromodynamics (rev.)	333	58. τ -lepton decay parameters	731
18. Structure functions (rev.)	347	<u>Quarks</u>	
19. Fragmentation functions in e^+e^- , ep and pp collisions (rev.)	368	59. Quark masses (rev.)	733
20. High Energy Soft QCD and Diffraction (new)	385	60. Top quark (rev.)	741
Astrophysics and Cosmology			
21. Experimental tests of gravitational theory (rev.)	409		
22. Big-Bang cosmology (rev.)	422		
23. Inflation (rev.)	435		
24. Big-Bang nucleosynthesis (rev.)	451		
25. Cosmological parameters (rev.)	458		
26. Neutrinos in cosmology (rev.)	467		
27. Dark matter (new)	474		
28. Dark energy (rev.)	490		
29. Cosmic microwave background (rev.)	499		
30. Cosmic rays (rev.)	510		

(Continued on next page.)

<u>Mesons</u>			
61. Form factors for radiative pion & kaon decays (rev.)	762		
62. Scalar mesons below 2 GeV (rev.)	764		
63. Pseudoscalar and pseudovector mesons in the 1400 MeV region (rev.)	771		
64. Rare kaon decays (rev.)	774		
65. CPT invariance tests in neutral kaon decay (rev.)	779		
66. V_{ud} , V_{us} , Cabibbo angle, and CKM unitarity (rev.)	781		
67. CP -violation in K_L decays	784		
68. Review of multibody charm analyses (rev.)	788		
69. D^0 - \bar{D}^0 mixing (rev.)	792		
70. D_s^+ branching fractions (rev.)	801		
71. Leptonic decays of charged pseudoscalar mesons (rev.)	803		
72. Production and decay of b -flavored hadrons (rev.)	814		
73. Polarization in B decays (rev.)	824		
74. B^0 - \bar{B}^0 mixing (rev.)	828		
75. Semileptonic B decays, V_{cb} and V_{ub} (rev.)	835		
76. CKM angles from B hadrons, determination of (new)	849		
77. Spectroscopy of mesons containing two heavy quarks (rev.)	854		
78. Non- $q\bar{q}$ mesons (rev.)	861		
<u>Baryons</u>			
79. Baryon decay parameters	868		
80. N and Δ resonances (rev.)	869		
81. Baryon magnetic moments	874		
82. Λ and Σ resonances (rev.)	875		
83. Pole structure of the $\Lambda(1405)$ region (rev.)	878		
84. Charmed baryons (rev.)	879		
85. Pentaquarks (rev.)	881		
Hypothetical Particles and Concepts			
86. Extra dimensions (rev.)	889		
87. W' -boson searches (rev.)	897		
88. Z' -boson searches (rev.)	900		
89. Supersymmetry: theory (rev.)	905		
90. Supersymmetry: experiment (rev.)	923		
91. Axions and other similar particles (rev.)	939		
92. Quark and lepton compositeness, searches for (rev.)	953		
93. Dynamical electroweak symmetry breaking: implications of the $H(0)$ (rev.)	958		
94. Grand unified theories (rev.)	971		
95. Leptoquarks (rev.)	986		
96. Magnetic monopoles (rev.)	989		
		VOLUME 2: PARTICLE LISTINGS	
		(available online only)	
		Illustrative key and abbreviations	
		Illustrative key	999
		Abbreviations	1000
		Gauge and Higgs bosons	
		(γ , gluon, graviton, W , Z , Higgs, Axions)	1013
		Leptons	
		(e , μ , τ , Heavy-charged lepton searches, Neutrino properties, Number of neutrino types, Double- β decay, Neutrino mixing, Heavy-neutral lepton searches)	1101
		Quarks	
		(u , d , s , c , b , t , b' , t' (4^{th} gen.), Free quarks)	1173
		Mesons	
		Light unflavored (π , ρ , a , b) (η , ω , f , ϕ , h)	1209
		Other light unflavored	1332
		Strange (K , K^*)	1337
		Charmed (D , D^*)	1391
		Charmed, strange (D_s , D_s^* , D_{sJ})	1448
		Bottom (B , V_{cb}/V_{ub} , B^* , B_J^*)	1465
		Bottom, strange (B_s , B_s^* , B_{sJ}^*)	1640
		Bottom, charmed (B_c)	1664
		$c\bar{c}$ (η_c , $J/\psi(1S)$, χ_c , h_c , ψ)	1668
		$b\bar{b}$ (η_b , Υ , χ_b , h_b)	1782
		Baryons	
		N	1825
		Δ	1878
		Λ	1902
		Σ	1927
		Ξ	1959
		Ω	1971
		Charmed (Λ_c , Σ_c , Ξ_c , Ω_c)	1974
		Doubly charmed (Ξ_{cc})	1996
		Bottom (Λ_b , Σ_b , Ξ_b , Ω_b , b -baryon admixture)	1997
		Exotic baryons (P_c pentaquarks)	2014
		Searches not in Other Sections	
		Magnetic monopole searches	2017
		Supersymmetric particle searches	2019
		Technicolor	2062
		Searches for quark and lepton compositeness	2063
		Extra dimensions	2067
		WIMP and dark matter searches	2073
		Other particle searches	2085

INTRODUCTION

1. Overview	11
2. Particle Listings responsibilities	11
3. Consultants	12
4. Naming scheme for hadrons	15
5. Procedures	15
5.1 Selection and treatment of data	15
5.2 Averages and fits	15
5.2.1 Treatment of errors	15
5.2.2 Unconstrained averaging	16
5.2.3 Constrained fits	16
5.3 Rounding	17
5.4 Discussion	17
History plots	19

ONLINE PARTICLE PHYSICS INFORMATION

1. Introduction	20
2. Particle Data Group (PDG) resources	20
3. Particle physics information platforms	20
4. Literature databases	20
5. Particle physics journals and conference proceedings series	21
6. Conference databases	21
7. Research institutions	21
8. People	21
9. Experiments	21
10. Jobs	21
11. Software repositories	22
12. Data repositories	22
13. Data preservation	24
14. Particle physics education and outreach sites	24

Introduction

1 Overview

The *Review of Particle Physics* is a comprehensive review of the field of Particle Physics and of related areas in Cosmology. It is divided into two volumes. Volume 1 includes the “Summary Tables” and “Reviews, Tables, and Plots”. Volume 2 consists of the “Particle Listings”.

The *Review* is updated each year and made available on the PDG website (pdg.lbl.gov). In even-numbered years, the *Review* is also published in a journal and printed as the *PDG Book* together with an abridged *Particle Physics Booklet* containing Summary Tables and essential tables, figures, and equations from selected review articles. This edition is an updating through January 2020.

The Summary Tables give our best values and limits for particle properties such as masses, widths or lifetimes, and branching fractions, as well as an extensive summary of searches for hypothetical particles and a summary of experimental tests of conservation laws.

The 96 review articles in Reviews, Tables and Plots cover a wide variety of theoretical and experimental topics. Together with the Summary Tables they provide a quick reference for the practicing particle physicist. Two more review articles, Online Particle Physics Information and Tests of Conservation Laws, can be found in the Introduction and Summary Tables, respectively.

The Particle Listings are a compilation/evaluation of data on particle properties. They contain all the data used to get the values given in the Summary Tables. They also give information on unconfirmed particles and particle searches. In this edition, the Particle Listings include 3,324 new measurements from 878 papers, in addition to the 41,371 measurements from 11,322 papers that first appeared in previous editions [1]. 22 review articles are part of the Particle Listings and address specific aspects of the data presented in the Listings. Because of the large quantity of data, the Particle Listings are not an archive of all published data on particle properties. We refer interested readers to earlier editions for data now considered to be obsolete.

We organize the particles into six categories:

- Gauge and Higgs bosons
- Leptons
- Quarks
- Mesons
- Baryons
- Searches not in other sections

The last category only includes searches for particles that do not belong to the previous groups. For example, it includes searches for supersymmetric particles, compositeness and extra dimensions, while searches for heavy charged leptons and massive neutrinos are with the leptons.

In Sec. 2 of this Introduction, we list the main areas of responsibility of the authors of the Particle Listings. Our many consultants, without whom we would not have been able to produce this *Review*, are acknowledged in Sec. 3. In Sec. 4, we mention briefly the naming scheme for hadrons, which was extended in the previous edition [1]. In Sec. 5, we discuss our procedures for choosing among measurements of particle properties and for obtaining best values of the properties from the measurements.

The accuracy and usefulness of this *Review* depend in large part on interaction between its users and the authors. We appreciate comments, criticisms, and suggestions for improvements of any kind. Please send them to the appropriate author, according to the list of responsibilities in Sec. 2 below, or to pdg@lbl.gov.

In addition to the online publication at pdg.lbl.gov, the *Review* is available in different formats:

- The printed *PDG Book* includes volume 1 only, *i.e.* it contains the Summary Tables and most review articles. Since the 2016 edition [2] the detailed tables from the Particle Listings are no longer printed.
- The *Particle Physics Booklet* includes the Summary Tables plus essential tables, figures, and equations from selected review articles. Starting with the Booklets of the 2018 edition,

we have excluded most text and explanations in order to revert back to a more pocket-sized format. The Booklet is available in print and as a web version optimized for use on phones as well as an Android app (see pdg.lbl.gov/booklet).

- *pdgLive* (pdgLive.lbl.gov) is a web application giving more interactive access to PDG data than the static web pages and PDF files that are also available.
- Files that can be downloaded from the PDG website include a table of masses, widths, and PDG Monte Carlo particle ID numbers; PDF files of volume 1 (PDG Book), volume 2 (Particle Listings) and Booklet; individual review articles; all figures; and an archive file containing the complete PDG website (except for pdgLive).

Copies of the *PDG Book* or the *Particle Physics Booklet* can be ordered from our website or directly at pdg.lbl.gov/order. For special requests only, please email pdg@lbl.gov in North and South America, Australia, and the Far East, and pdg-products@cern.ch in all other areas.

This *Review* is considered to be a single comprehensive review of particle physics and related areas. Therefore we prefer that it be cited as a whole, rather than citing *e.g.* an individual review article that is part of this *Review*. For the 2020 edition, the proper citation is:

P.A. Zyla *et al.* (Particle Data Group), Prog. Theor. Exp. Phys. **2020**, 083C01 (2020).

If you wish to refer to a specific part of the *Review*, for example to the Higgs boson review article, the following form should be used:

Status of Higgs Boson Physics in P.A. Zyla *et al.* (Particle Data Group), Prog. Theor. Exp. Phys. **2020**, 083C01 (2020).

2 Particle Listings responsibilities

* Asterisk indicates the people to contact with questions or comments about Particle Listings sections.

• Gauge and Higgs bosons

γ	A. Bettini, D.E. Groom*
Gluons	R.M. Barnett,* A.V. Manohar
Graviton	A. Bettini,* D.E. Groom
W, Z	M. Grünewald,* A. Gurtu*
Higgs bosons	S. Heinemeyer,* K. Hikasa, J. Tanaka
Heavy bosons	R.M. Barnett,* K.A. Olive, M. Tanabashi
Axions	K.A. Olive, G. Raffelt,* F. Takahashi

• Leptons

Neutrinos	M. Goodman, C.-J. Lin,* K. Nakamura, K.A. Olive, A. Piepke, P. Vogel
e, μ	A. Bettini,* C. Grab
τ	A. Lusiani, K. Mönig*

• Quarks

Quarks	R.M. Barnett,* A.V. Manohar
Top quark	R.M. Barnett,* Y. Sumino
b', t'	R.M. Barnett,* Y. Sumino
Free quark	A. Bettini,* C.-J. Lin

• Mesons

π, η	A. Bettini,* C. Grab
Unstable mesons	C. Amsler, M. Doser,* S. Eidelman,* T. Gutsche, C. Hanhart, J.J. Hernández-Rey, C. Lourenco, A. Masoni, M. Mikhasenko, R.E. Mitchell, S. Navas, C. Patrignani, S. Spanier, G. Venanzoni, V. Vorobyev
K (stable)	G. D'Ambrosio, C.-J. Lin*
D (stable, no mix.)	J. Rademacker, D. Robinson*
D^0 mixing	D.M. Asner, W.-M. Yao*
B (stable)	A. Cerri,* P. Eerola, M. Kreps, Y. Kwon, W.-M. Yao*

- Baryons
 - Stable baryons C. Grab, D. Robinson*
 - Unstable baryons V. Burkert, E. Klempt, U. Thoma, L. Tiator, R.L. Workman*
 - Charmed baryons J. Rademacker, D. Robinson*
 - Bottom baryons A. Cerri,* P. Eerola, M. Kreps, Y. Kwon, W.-M. Yao*
- Miscellaneous searches
 - Monopole A. Bettini,* D. Milstead
 - Supersymmetry M. D’Onofrio, H.K. Dreiner,* A. de Gouvêa, F. Moortgat K.A. Olive
 - Technicolor K. Agashe,* K.A. Olive, M. Tanabashi
 - Compositeness M. Tanabashi, J. Terning*
 - Extra Dimensions T. Gherghetta, K.A. Olive, D. Robinson*
 - WIMP, DM, Other H. Baer, A. Bettini,* W.-M. Yao*

3 Consultants

The Particle Data Group benefits greatly from the assistance of hundreds of physicists who are asked to referee review articles and verify every piece of data entered into this *Review*. Of special value is the advice of the PDG Advisory Committee, which meets biennially and thoroughly reviews all aspects of our operation. The members of the 2020 committee are:

- S. Demers (Yale)
- D. d’Enterria (CERN)
- J. Frieman (FNAL)
- L. Hall (UC Berkeley/LBNL)
- T. Nakada (EPFL)
- M. Yokoyama (Tokyo)
- Q. Zhao (IHEP Beijing)

We have especially relied on the expertise of the following people for advice on particular topics:

- I. Abt (MPI Munich)
- M. Achasov (Budker Inst., Novosibirsk)
- M. Albrow (FNAL)
- A. Antognini (ETH Zurich)
- F. Anulli (INFN, Rome)
- E. Aprile (Columbia U.)
- G. Arduini (CERN)
- E. Armengaud (CEA Saclay, DSM/IRFU/SPP)
- M. Artuso (Syracuse U.)
- P. Azzurri (INFN, Pisa)
- H. Bachacou (IRFU, Saclay)
- K. Backes (Yale U.)
- A. Barabash (ITEP)
- E. Barberis (FNAL)
- M. Bardeen (FNAL)
- W. Barter (Imperial Coll. London)
- M. Battaglieri (U. di Genova)
- G. Bell (Siegen U.)
- V. Belyaev (ITEP)
- S. Benson (CERN)
- Z. Berezhiani (INFN, LNGS)
- F. Bernlochner (Karlsruhe U.)
- E. Berti (Johns Hopkins U.)
- V. Bertone (NIKHEF)
- M. Bettler (CERN)
- M. Beznogov (Astro. Inst. UNAM)
- M. Borsato (CERN)
- J. Bramante (Queen’s U.)
- J.E. Brau (Oregon U.)
- T. Bringmann (Oslo U.)
- J. Brod (Cincinnati U.)
- G. Brooijmans (Columbia U.)
- R. Bruce (CERN)
- T. Brune (TU)
- O. Bruning (CERN)
- D.A. Bryman (TRIUMF)
- J. Butterworth (UCL)
- F. Calore (LAPTH)
- F. Canelli (Zurich U.)
- A. Canto (CERN)
- J. Cao (IHEP Beijing)
- L. Cardani (INFN, Rome)
- V. Cavaliere (BNL)
- G. Cavallero (CERN)
- M. Cepeda (CIEMAT)
- F. Cerutti (LBNL)
- M. Charles (CNRS)
- M. Chen (Queen’s U.)
- K. Cheung (Tsinghua U.)
- G. Chiarelli (INFN, Pisa)
- V. Chobanova (CERN)
- J. Chou (Rutgers U.)
- S. Choudhury (Indian Inst. Tech., Mumbai)
- R. Ciesielski (Rockefeller U.)
- G. Colangelo (Bern U.)
- J.I. Collar (Chicago U.)
- G. Compère (ULB, Brussels)
- M. Crisler (FNAL)
- A. Czarnecki (Alberta U.)
- G. D’Ambrosio (INFN, Napoli)
- A. Danilov (INR, Moscow)
- M. Daum (PSI)
- I. David (Glasgow U.)
- C. Davies (Glasgow U.)
- B. Dawson (Adelaide U.)
- J. De Blas (INFN, Padua)
- P. Decowski (NIKHEF)
- G. de Lellis (INFN, Napoli)
- M. Della Morte (SDU)
- S. Demidov (INR, Moscow)
- D. Denisov (FNAL)
- D. d’Enterria (CERN)
- A.V. Derbin (Petersburg Nuclear Phys. Inst.)
- S. Derenzo (LBNL)
- S. Desai (Boston U.)
- U. De Sanctis (Rome U. Tor Vergata)
- S. Descotes-Genon (Paris-Sud U.)
- B. Dey (CERN)
- M. Diamond (Toronto U.)
- A. Di Domenica (INFN, Rome)
- F. Dordei (CERN)
- K. Dundas (Columbia U.)
- S.R. Elliott (LANL)
- K. Ellis (Durham U.)
- C. Englert (Glasgow U.)
- D. Epifanov (Budker Inst., Novosibirsk)
- M. Escudero (King’s Coll. London)
- S. Esen (CERN)
- R. Essig (YITP, Stony Brook)
- P. Everaerts (MIT)

- V. Ezhov (NRC Kurchatov Inst. PNPI)
- S. Fang (IHEP Beijing)
- P. Fayet (LPTENS)
- M. Fedderke (Stanford U.)
- A. Ferrari (CERN)
- W. Fischer (BNL)
- J. Formaggio (MIT)
- J. Fortin (UC San Diego)
- T. Fujita (Kyoto U.)
- T. Gaisser (Delaware U., Bartol Inst.)
- P. Gambino (INFN, Torino)
- A. Gangapshev (INR, Moscow)
- J. Gao (IHEP Beijing)
- R. Garisto (APS)
- A. Gasparian (Jefferson Lab)
- C. Gatti (INFN, LNF)
- A. Geiser (DESY, Hamburg)
- M. Genest (CNRS)
- M. Gersabeck (Manchester U.)
- L. Gironi (INFN, Milano-Bicocca)
- C. Glasman (U. Autònoma de Madrid)
- S.N. Gninenko (Russian Academy of Sciences)
- T. Golling (Geneva U.)
- B. Golob (Jozef Stefan Inst.)
- J. Gomez Cadenas (DIPIC)
- j. goodman (Maryland U.)
- P. Grabmayr (Tübingen U.)
- P. Grafstroem (INFN, Bologna)
- L. Grandi (Chicago U.)
- E. Grauges (ICC, U. of Barcelona)
- R. Gray (U. Washington)
- G. Greene (Tennessee U.)
- Y. Grossman (Cornell U.)
- Y. Guo (KPH, JGU Mainz)
- C. Gwilliam (Liverpool U.)
- C. Ha (Northwestern U.)
- F. Halzen (Wisconsin U.)
- S. Harnew (Oxford U.)
- F.A. Harris (Hawaii U.)
- A. Hasenfratz (Colorado U., Boulder)
- K.M. Heeger (Yale U.)
- A. Hinzmann (Hamburg U.)
- A. Hoang (HEPHY, Vienna)
- Y. Hochberg (Racah Inst. Hebrew U.)
- T. Huege (KIT)
- A. Ianni (INFN, LNGS)
- N. Ilic (NIKHEF)
- I.G. Irastorza (U. de Zaragoza)
- A. Jafari (DESY, Zeuten)
- N. Jafari (DESY, Zeuten)
- P. Janot (CERN)
- L. Jeanty (Oregon U.)
- X. Ji (SJTU)
- C. Joram (CERN)
- J. Jowett (CERN)
- A. Jung (Purdue U.)
- K. Kaadze (CERN)
- H. Kamano (Osaka U.)
- J. Kamenik (Jozef Stefan Inst.)
- J. Kaminski (Bonn U.)
- D. Karlen (Victoria U.)
- S. Karshenboim (Pulkovo Obs., St.Petersburg)
- E.T. Kearns (Boston U.)
- V. Kekelidze (JINR, Dubna)
- J. Kile (CFTP)
- S. Kim (Seoul National U.)
- K. Kirch (ETH Zurich)
- M. Kitaguchi (Nagoya U.)
- R. Klanner (DESY, Hamburg)
- S. Klaver (CERN)
- S. Knirck (Werner-Heisenberg-Inst.)
- R. Kogler (Hamburg U.)
- A. Kopylov (INR, Moscow)
- E. Kovetz (Ben-Gurion U.)
- A. Krasznahorkay (Hungarian Academy of Sciences)
- P. Krokovny (Budker Inst., Novosibirsk)
- A. Kronfeld (FNAL)
- B. Kubis (Bonn U.)
- A. Kupsc (Uppsala U.)
- M. Kuzniak (Carleton U.)
- G. Landsberg (Brown U.)
- C. Lange (CERN)
- G. Latyshev (COMPAS Group, IHEP)
- H. Lee (ANL)
- H. Lee (BNL)
- L.B. Leinson (Russian Academy of Sciences)
- G.P. Lepage (Cornell U.)
- O. Leroy (CPPM Marseille)
- J. Libby (Indian Inst. Tech., Madras)
- Z. Ligeti (LBNL)
- E. Lisi (INFN, Bari)
- Y. Liu (Lanzhou U.)
- S. Lloyd (Phys. Dep. Durham U.)
- H. Long (Inst. of Physics, Vietnamese Academy of Science & Technology)
- P.T. Lukens (FNAL)
- O. Lupton (Warwick U.)
- X. Lyu (UCAS, Beijing)
- H. Ma (IHEP Beijing)
- P. Maksimovic (Johns Hopkins U.)
- B. Malaescu (CNRS)
- S. Malde (Oxford U.)
- Y. Mambrini (Paris-Sud U.)
- G. Mandaglio (Messina U.)
- D.M. Manley (Kent U.)
- M. Margoni (INFN, Padova)
- Z. Marshall (LBNL)
- S.P. Martin (Northern Illinois U.)
- G. Martinelli (INFN, Rome)
- M. Martinelli (CERN)
- A. Masiero (INFN, Padua)
- R. Massarczyk (LANL)
- K. Matchev (Florida U.)
- A. Mathad (ETH Zurich)
- V. Matiunin (CERN)
- N. Mavromatos (King's Coll. London)
- M. Mazziotta (INFN, Bari)
- P. Mcdonald (LBNL)
- S. Meinel (Arizona U.)
- W. Melnitchouk (Jefferson Lab)
- F. Meloni (CERN)
- E. Meoni (CERN)

- P. Merkel (FNAL)
- P.D. Meyers (Princeton U.)
- T. Mibe (KEK)
- I. Mikulec (Austrian Academy of Sciences)
- V. Mitsou (IFIC, Valencia)
- R.N. Mohapatra (Maryland U.)
- S. Moosavi (Ryerson U.)
- M. Morello (SNS, Pisa)
- O. Moreno (SLAC)
- S. Moretti (Southampton U.)
- S. Moriyama (ICRR)
- M. Mulder (CERN)
- S. Murgia (UC Irvine)
- W. Murray (Warwick U.)
- B. Nachman (LBNL)
- R. Nahnauer (DESY, Hamburg)
- T. Nakadaira (KEK)
- T. Nakaya (Kyoto U.)
- S. Narison (Montpellier U.)
- A. Nelles (DESY, Zeuten)
- P. Newman (IFAE)
- V. Obraztsov (IHEP, Protvino)
- H.B. O'Connell (Chicago U.)
- K. Oide (KEK)
- Y. Onishi (KEK)
- G. Orebi Gann (LBNL)
- A. Orso Maria Iorio (INFN, Napoli)
- P. Osland (Bergen U.)
- S. Ostapchenko (Frankfurt U.)
- C. Palomba (INFN, Rome)
- T. Papadopoulou (Athens U.)
- E. Passemar (Indiana U.)
- S. Paul (TU)
- C. Paus (MIT)
- F. Petricca (MPI Munich)
- G. Petrucciani (CERN)
- G. Piacquadio (NYU)
- L. Piilonen (Virginia Tech)
- P. Piminov (Budker Inst., Novosibirsk)
- I. Polyakov (Syracuse U.)
- A. Poon (NSD LBNL)
- N. Porayako (MPIK)
- W. QIAN (IHEP Beijing)
- S. Rakshit (Indian Inst. of Technology)
- K. Ramanathan (Chicago U.)
- A. Rana (Delhi U.)
- A. Rebhan (TU Vienna)
- M. Redi (CERN)
- C.F. Redmer (IKP)
- J. Richard (IP2I, Lyon)
- W. Richard (Dep. of Phys. Texas Tech U.)
- J. Rico (ICREA, Barcelona; SISSA/INFN, Trieste)
- A. Ritz (Victoria U.)
- A. Rodas (UCM, Madrid)
- G. Ross (Oxford U.)
- M. Rotondo (INFN, Frascati)
- G. Ruggiero (Lancaster U.)
- C.T. Sachrajda (Southampton U.)
- R. Salerno (CNRS)
- M. Santimaria (INFN, LNF)
- V. Sanz (Sussex U.)
- N. Saoulidou (Athens U.)
- A.V. Sarantsev (Bonn U.)
- E. Sarkisyan-Grinbaum (Texas U.)
- A. Saunders (LANL)
- M. Schmaltz (Boston U.)
- B. Schmidt (CERN)
- F. Schroeder (Delaware U.)
- C. Schwanda (HEPHY, Vienna)
- R. Schwienhorst (Michigan State U.)
- B. Schwingenheur (MPIK)
- D. Scott (U. of British Columbia)
- R. Seidl (BNL)
- I. Seong (UC Irvine)
- S. Seon-Hee (IBS, Daejeon)
- A.P. Serebrov (Petersburg Nuclear Phys. Inst.)
- S. Serednyakov (Budker Inst., Novosibirsk)
- E. Shabalina (Georg August U. Goettingen)
- L. Shchutska (ETH Zurich)
- V. Shiltsev (FNAL)
- Y. Shirman (UC Irvine)
- D. Shwartz (Budker Inst., Novosibirsk)
- P. Sikivie (Florida U.)
- L. Silvestrini (INFN, Rome)
- S. Simula (INFN, Rome)
- A. Soffer (Tel Aviv U.)
- F. Spano (RHUL)
- H. Spiesberger (JGU, Mainz)
- M. Spira (PSI)
- Y. Stadnik (New South Wales U.)
- O. Stelzer-Chilton (TRIUMF)
- I.W. Stewart (MIT)
- A. Szczepaniak (Indiana U.)
- F. Tackmann (DESY, Zeuten)
- K. Tackmann (DESY, Hamburg)
- T.M. Tait (UC Irvine)
- A. Tapper (Imperial Coll. London)
- C. Ternes (IFIC, Valencia)
- R. Tesarek (FNAL)
- A. Thomas (KPH, JGU Mainz)
- J. Thomas (NSD LBNL)
- J. Timmermans (NIKHEF)
- K. Todyshev (Budker Inst., Novosibirsk)
- S. Trifinopoulos (Zurich U.)
- J. Uzan (CNRS)
- P.L. Vahle (William and Mary Coll.)
- K.A. van Bibber (UC Berkeley)
- R.G. Van De Water (LANL)
- C. van Eldik (Erlangen U.)
- R. Van Kooten (Indiana U.)
- A. Vartak (UC San Diego)
- C. Vincenzo (LANL)
- B. von Krosigk (DESY, Hamburg)
- A. Vossen (Duke U.)
- W. Wagner (Wuppertal U.)
- J. Walder (Lancaster U.)
- D. Wang (School of Physics, Peking U.)
- Y. Wang (JGU, Mainz)
- G. Watt (Durham U.)
- B. Webber (Cambridge U.)
- R. Wendell (Kyoto U.)
- N. Wex (MPIFR, Bonn)

- M. Whitehead (RWTH Aachen)
- M. Williams (Manchester U.)
- J.S. Wilson (FNAL)
- M. Wing (UCL)
- H.T. Wong (Academia Sinica, Inst. of Physics)
- G. Wormser (U. Paris-Saclay)
- Z. Xia (PMO, Nanjing)
- C. Yaguna (UPTC)
- T. Yamanaka (Osaka U.)
- T. Yamazaki (Tokyo U.)
- W. Yan (USTC China)
- W. Yan (Beihang U.)
- L. Yang (UC San Diego)
- S. Youn (IBS, Daejeon)
- A. Young (NCSU)
- C. Yuan (IHEP Beijing)
- C. Yue (Liaoning Normal U.)
- Q. Yue (Tsinghua U.)
- V. Zacek (U. de Montreal)
- A. Zakharov (ITEP)
- L. Zani (INFN, Pisa)
- D. Zerwas (LAL Orsay)
- C. Zhang (IHEP Beijing)
- Y. Zhang (Phys. Dep. Oxford U.)
- B. Zheng (South China U.)
- A. Zhevlakov (Tamsk State U.)
- K. Zhu (IHEP Beijing)
- J. Zupan (Cincinnati U.)
- R.M. Zwaska (FNAL)

4 Naming scheme for hadrons

We introduced in the 1986 edition [3] a new naming scheme for the hadrons. Changes from older terminology affected mainly the heavier mesons made of u , d , and s quarks. Otherwise, the only important change to known hadrons was that the F^\pm became the D_s^\pm . None of the lightest pseudoscalar or vector mesons changed names, nor did the $c\bar{c}$ or $b\bar{b}$ mesons (we do, however, now use χ_c for the $c\bar{c}$ χ states), nor did any of the established baryons. The Summary Tables give both the new and old names whenever a change has occurred.

In the previous edition [1] the naming scheme was extended to address the naming of charmonium and bottomonium states that are commonly referred to as X, Y or Z states in the literature. The current scheme is described in “Naming Scheme for Hadrons” (p. 1) of this *Review*. A table details the correspondence between the names newly adopted by the PDG and those that have appeared in the literature.

We give here our conventions on type-setting style. Particle symbols are italic (or slanted) characters: e^- , p , Λ , π^0 , K_L , D_s^+ , b . Charge is indicated by a superscript: B^- , Δ^{++} . Charge is not normally indicated for p , n , or the quarks, and is optional for neutral isosinglets: η or η^0 . Antiparticles and particles are distinguished by charge for charged leptons and mesons: τ^+ , K^- . Otherwise, distinct antiparticles are indicated by a bar (overline): $\bar{\nu}_\mu$, \bar{t} , \bar{p} , \bar{K}^0 , and $\bar{\Sigma}^+$ (the antiparticle of the Σ^-).

5 Procedures

5.1 Selection and treatment of data

The Particle Listings contain all relevant data known to us that are published in journals. With very few exceptions, we do not include results from preprints or conference reports. Nor do we include data that are of historical importance only (the Listings are not an archival record). We search every volume of 20 journals through our cutoff date for relevant data. We also include later published papers that are sent to us by the authors (or others).

In the Particle Listings, we clearly separate measurements that are used to calculate or estimate values given in the Summary Tables from measurements that are not used. We give explanatory

comments in many such cases. Among the reasons a measurement might be excluded are the following:

- It is superseded by or included in later results.
- No error is given.
- It involves assumptions we question.
- It has a poor signal-to-noise ratio, low statistical significance, or is otherwise of poorer quality than other data available.
- It is clearly inconsistent with other results that appear to be more reliable. Usually we then state the criterion, which sometimes is quite subjective, for selecting “more reliable” data for averaging. See Sec. 5.4.
- It is not independent of other results.
- It is not the best limit (see below).
- It is quoted from a preprint or a conference report.

In some cases, *none* of the measurements is entirely reliable and no average is calculated. For example, the masses of many of the baryon resonances, obtained from partial-wave analyses, are quoted as estimated ranges thought to probably include the true values, rather than as averages with errors. This is discussed in the Baryon Particle Listings.

For upper limits, we normally quote in the Summary Tables the strongest limit. We do not average or combine upper limits except in a very few cases where they may be re-expressed as measured numbers with Gaussian errors.

As is customary, we assume that particle and antiparticle share the same spin, mass, and mean life. The Tests of Conservation Laws table, following the Summary Tables, lists tests of CPT as well as other conservation laws.

We use the following indicators in the Particle Listings to tell how we get values from the tabulated measurements:

- OUR AVERAGE —From a weighted average of selected data.
- OUR FIT —From a constrained or overdetermined multiparameter fit of selected data.
- OUR EVALUATION —Not from a direct measurement, but evaluated from measurements of related quantities.
- OUR ESTIMATE —Based on the observed range of the data. Not from a formal statistical procedure.
- OUR LIMIT —For special cases where the limit is evaluated by us from measured ratios or other data. Not from a direct measurement.

An experimentalist who sees indications of a particle will of course want to know what has been seen in that region in the past. Hence we include in the Particle Listings all reported states that, in our opinion, have sufficient statistical merit and that have not been disproved by more reliable data. However, we promote to the Summary Tables only those states that we feel are well established. This judgment is, of course, somewhat subjective and no precise criteria can be given. For more detailed discussions, see the minireviews in the Particle Listings.

5.2 Averages and fits

We divide this discussion on obtaining averages and errors into three sections: (1) treatment of errors; (2) unconstrained averaging; (3) constrained fits.

5.2.1 Treatment of errors

In what follows, the “error” δx means that the range $x \pm \delta x$ is intended to be a 68.3% confidence interval about the central value x . We treat this error as if it were Gaussian. Thus when the error *is* Gaussian, δx is the usual one standard deviation (1σ). Many experimenters now give statistical and systematic errors separately, in which case we usually quote both errors, with the statistical error first. For averages and fits, we then add the two errors in quadrature and use this combined error for δx .

When experimenters quote asymmetric errors $(\delta x)^+$ and $(\delta x)^-$ for a measurement x , the error that we use for that measurement in making an average or a fit with other measurements is a continuous function of these three quantities. When the resultant average or fit \bar{x} is less than $x - (\delta x)^-$, we use $(\delta x)^-$; when it is

greater than $x + (\delta x)^+$, we use $(\delta x)^+$. In between, the error we use is a linear function of x . Since the errors we use are functions of the result, we iterate to get the final result. Asymmetric output errors are determined from the input errors assuming a linear relation between the input and output quantities.

In fitting or averaging, we usually do not include correlations between different measurements, but we try to select data in such a way as to reduce correlations. Correlated errors are, however, treated explicitly when there are a number of results of the form $A_i \pm \sigma_i \pm \Delta$ that have identical systematic errors Δ . In this case, one can first average the $A_i \pm \sigma_i$ and then combine the resulting statistical error with Δ . One obtains, however, the same result by averaging $A_i \pm (\sigma_i^2 + \Delta_i^2)^{1/2}$, where $\Delta_i = \sigma_i \Delta [\sum (1/\sigma_j^2)]^{1/2}$. This procedure has the advantage that, with the modified systematic errors Δ_i , each measurement may be treated as independent and averaged in the usual way with other data. Therefore, when appropriate, we adopt this procedure. We tabulate Δ and invoke an automated procedure that computes Δ_i before averaging and we include a note saying that there are common systematic errors.

Another common case of correlated errors occurs when experimenters measure two quantities and then quote the two and their difference, e.g., m_1 , m_2 , and $\Delta = m_2 - m_1$. We cannot enter all of m_1 , m_2 and Δ into a constrained fit because they are not independent. In some cases, it is a good approximation to ignore the quantity with the largest error and put the other two into the fit. However, in some cases correlations are such that the errors on m_1 , m_2 and Δ are comparable and none of the three values can be ignored. In this case, we put all three values into the fit and invoke an automated procedure to increase the errors prior to fitting such that the three quantities can be treated as independent measurements in the constrained fit. We include a note saying that this has been done.

5.2.2 Unconstrained averaging

To average data, we use a standard weighted least-squares procedure and in some cases, discussed below, increase the errors with a “scale factor.” We begin by assuming that measurements of a given quantity are uncorrelated, and calculate a weighted average and error as

$$\bar{x} \pm \delta\bar{x} = \frac{\sum_i w_i x_i}{\sum_i w_i} \pm \left(\sum_i w_i\right)^{-1/2}, \quad (1)$$

where

$$w_i = 1/(\delta x_i)^2.$$

Here x_i and δx_i are the value and error reported by the i th experiment, and the sums run over the N experiments. We then calculate $\chi^2 = \sum w_i (\bar{x} - x_i)^2$ and compare it with $N - 1$, which is the expectation value of χ^2 if the measurements are from a Gaussian distribution.

If $\chi^2/(N - 1)$ is less than or equal to 1, and there are no known problems with the data, we accept the results.

If $\chi^2/(N - 1)$ is very large, we may choose not to use the average at all. Alternatively, we may quote the calculated average, but then make an educated guess of the error, a conservative estimate designed to take into account known problems with the data.

Finally, if $\chi^2/(N - 1)$ is greater than 1, but not greatly so, we still average the data, but then also do the following:

(a) We increase our quoted error, $\delta\bar{x}$ in Eq. (1), by a scale factor S defined as

$$S = \left[\chi^2/(N - 1)\right]^{1/2}. \quad (2)$$

Our reasoning is as follows. The large value of the χ^2 is likely to be due to underestimation of errors in at least one of the experiments. Not knowing which of the errors are underestimated, we assume they are all underestimated by the same factor S . If we scale up all the input errors by this factor, the χ^2 becomes $N - 1$, and of course the output error $\delta\bar{x}$ scales up by the same factor. See Ref. [4].

When combining data with widely varying errors, we modify this procedure slightly. We evaluate S using only the experiments with smaller errors. Our cutoff or ceiling on δx_i is arbitrarily chosen to be

$$\delta_0 = 3N^{1/2} \delta\bar{x},$$

where $\delta\bar{x}$ is the unscaled error of the mean of all the experiments. Our reasoning is that although the low-precision experiments have little influence on the values \bar{x} and $\delta\bar{x}$, they can make significant contributions to the χ^2 , and the contribution of the high-precision experiments thus tends to be obscured. Note that if each experiment has the same error δx_i , then $\delta\bar{x}$ is $\delta x_i/N^{1/2}$, so each δx_i is well below the cutoff. (More often, however, we simply exclude measurements with relatively large errors from averages and fits: new, precise data chase out old, imprecise data.)

Our scaling procedure has the property that if there are two values with comparable errors separated by much more than their stated errors (with or without a number of other values of lower accuracy), the scaled-up error $\delta\bar{x}$ is approximately half the interval between the two discrepant values.

We emphasize that our scaling procedure for errors in no way affects central values. And if you wish to recover the unscaled error $\delta\bar{x}$, simply divide the quoted error by S .

(b) If the number M of experiments with an error smaller than δ_0 is at least three, and if $\chi^2/(M - 1)$ is greater than 1.25, we show in the Particle Listings an ideogram of the data. Figure 1 is an example. Sometimes one or two data points lie apart from the main body; other times the data split into two or more groups. We extract no numbers from these ideograms; they are simply visual aids, which the reader may use as he or she sees fit.

Each measurement in an ideogram is represented by a Gaussian with a central value x_i , error δx_i , and area proportional to $1/\delta x_i$. The choice of $1/\delta x_i$ for the area is somewhat arbitrary. With this choice, the center of gravity of the ideogram corresponds to an average that uses weights $1/\delta x_i$ rather than the $(1/\delta x_i)^2$ actually used in the averages. This may be appropriate when some of the experiments have seriously underestimated systematic errors. However, since for this choice of area the height of the Gaussian for each measurement is proportional to $(1/\delta x_i)^2$, the peak position of the ideogram will often favor the high-precision measurements at least as much as does the least-squares average. See our 1986 edition [3] for a detailed discussion of the use of ideograms.

5.2.3 Constrained fits

In some cases, such as branching ratios or masses and mass differences, a constrained fit may be needed to obtain the best values of a set of parameters. For example, most branching ratios and rate measurements are analyzed by making a simultaneous least-squares fit to all the data and extracting the partial decay fractions P_i , the partial widths Γ_i , the full width Γ (or mean life), and the associated error matrix.

Assume, for example, that a state has m partial decay fractions P_i , where $\sum P_i = 1$. These have been measured in N_r different ratios R_r , where, e.g., $R_1 = P_1/P_2$, $R_2 = P_1/P_3$, etc. [We can handle any ratio R of the form $\sum \alpha_i P_i / \sum \beta_i P_i$, where α_i and β_i are constants, usually 1 or 0. The forms $R = P_i/P_j$ and $R = (P_i P_j)^{1/2}$ are also allowed.] Further assume that each ratio R has been measured by N_k experiments (we designate each experiment with a subscript k , e.g., R_{rk}). We then find the best values of the fractions P_i by minimizing the χ^2 as a function of the $m - 1$ independent parameters:

$$\chi^2 = \sum_{r=1}^{N_r} \sum_{k=1}^{N_k} \left(\frac{R_{rk} - R_r}{\delta R_{rk}} \right)^2, \quad (3)$$

where the R_{rk} are the measured values and R_r are the fitted values of the branching ratios.

In addition to the fitted values \bar{P}_i , we calculate an error matrix $(\delta\bar{P}_i \delta\bar{P}_j)$. We tabulate the diagonal elements of $\delta\bar{P}_i = \langle \delta\bar{P}_i \delta\bar{P}_i \rangle^{1/2}$ (except that some errors are scaled as discussed below). In the Particle Listings, we give the complete correlation matrix; we also calculate the fitted value of each ratio, for comparison with the input data, and list it above the relevant input, along with a simple unconstrained average of the same input.

Three comments on the example above:

(1) There was no connection assumed between measurements of the full width and the branching ratios. But often we also have information on partial widths Γ_i as well as the total width Γ . In this case we must introduce Γ as a parameter in the fit, along

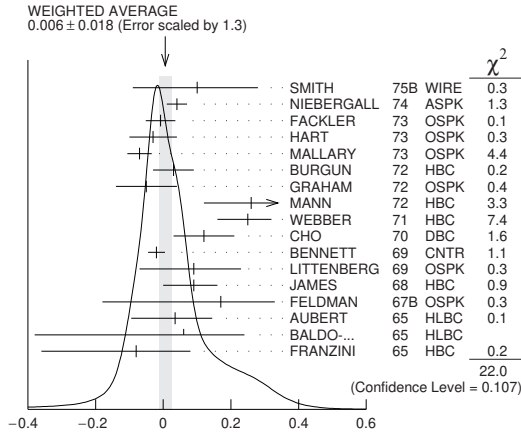


Figure 1: A typical ideogram. The arrow at the top shows the position of the weighted average, while the width of the shaded pattern shows the error in the average after scaling by the factor S . The column on the right gives the χ^2 contribution of each of the experiments. Note that the next-to-last experiment, denoted by the incomplete error flag (\perp), is not used in the calculation of S (see the text).

with the P_i , and we give correlation matrices for the widths in the Particle Listings.

(2) We try to pick those ratios and widths that are as independent and as close to the original data as possible. When one experiment measures all the branching fractions and constrains their sum to be one, we leave one of them (usually the least well-determined one) out of the fit to make the set of input data more nearly independent. We now do allow for correlations between input data.

(3) We calculate scale factors for both the R_r and P_i when the measurements for any R give a larger-than-expected contribution to the χ^2 . According to Eq. (3), the double sum for χ^2 is first summed over experiments $k = 1$ to N_k , leaving a single sum over ratios $\chi^2 = \sum \chi_r^2$. One is tempted to define a scale factor for the ratio r as $S_r^2 = \chi_r^2 / \langle \chi_r^2 \rangle$. However, since $\langle \chi_r^2 \rangle$ is not a fixed quantity (it is somewhere between N_k and N_{k-1}), we do not know how to evaluate this expression. Instead we define

$$S_r^2 = \frac{1}{N_k} \sum_{k=1}^{N_k} \frac{(R_{rk} - \bar{R}_r)^2}{\langle (R_{rk} - \bar{R}_r)^2 \rangle}. \quad (4)$$

With this definition the expected value of S_r^2 is one. We can show that

$$\langle (R_{rk} - \bar{R}_r)^2 \rangle = \langle (\delta R_{rk})^2 \rangle - (\delta \bar{R}_r)^2, \quad (5)$$

where $\delta \bar{R}_r$ is the fitted error for ratio r .

The fit is redone using errors for the branching ratios that are scaled by the larger of S_r and unity, from which new and often larger errors $\delta \bar{P}'_i$ are obtained. The scale factors we finally list in such cases are defined by $S_i = \delta \bar{P}'_i / \delta \bar{P}_i$. However, in line with our policy of not letting S affect the central values, we give the values of \bar{P}_i obtained from the original (unscaled) fit.

There is one special case in which the errors that are obtained by the preceding procedure may be changed. When a fitted branching ratio (or rate) \bar{P}_i turns out to be less than three standard deviations ($\delta \bar{P}'_i$) from zero, a new smaller error ($\delta \bar{P}''_i$)⁻ is calculated on the low side by requiring the area under the Gaussian between $\bar{P}_i - (\delta \bar{P}''_i)$ ⁻ and \bar{P}_i to be 68.3% of the area between zero and \bar{P}_i . A similar correction is made for branching fractions that are within three standard deviations of one. This keeps the quoted errors from overlapping the boundary of the physical region.

5.3 Rounding

While the results shown in the Particle Listings are usually exactly those published by the experiments, the numbers that

appear in the Summary Tables (means, averages and limits) are subject to a set of rounding rules.

The basic rule states that if the three highest order digits of the error lie between 100 and 354, we round to two significant digits. If they lie between 355 and 949, we round to one significant digit. Finally, if they lie between 950 and 999, we round up to 1000 and keep two significant digits. In all cases, the central value is given with a precision that matches that of the error. So, for example, the result (coming from an average) 0.827 ± 0.119 would appear as 0.83 ± 0.12 , while 0.827 ± 0.367 would turn into 0.8 ± 0.4 .

Rounding is not performed if a result in a Summary Table comes from a single measurement, without any averaging. In that case, the number of digits published in the original paper is kept, unless we feel it inappropriate. Note that, even for a single measurement, when we combine statistical and systematic errors in quadrature, rounding rules apply to the result of the combination. It should be noted also that most of the limits in the Summary Tables come from a single source (the best limit) and, therefore, are not subject to rounding.

Finally, we should point out that in several instances, when a group of results come from a single fit to a set of data, we have chosen to keep two significant digits for all the results. This happens, for instance, for several properties of the W and Z bosons and the τ lepton.

5.4 Discussion

The problem of averaging data containing discrepant values is nicely discussed by Taylor in Ref. [5]. He considers a number of algorithms that attempt to incorporate inconsistent data into a meaningful average. However, it is difficult to develop a procedure that handles simultaneously in a reasonable way two basic types of situations: (a) data that lie apart from the main body of the data are incorrect (contain unreported errors); and (b) the opposite—it is the main body of data that is incorrect. Unfortunately, as Taylor shows, case (b) is not infrequent. He concludes that the choice of procedure is less significant than the initial choice of data to include or exclude.

We place much emphasis on this choice of data. Often we solicit the help of outside experts (consultants). Sometimes, however, it is simply impossible to determine which of a set of discrepant measurements are correct. Our scale-factor technique is an attempt to address this ignorance by increasing the error. In effect, we are saying that present experiments do not allow a precise determination of this quantity because of unresolvable discrepancies, and one must await further measurements. The reader is warned of this situation by the size of the scale factor, and if he or she desires can go back to the literature (via the Particle Listings) and redo the average with a different choice of data.

Our situation is less severe than most of the cases Taylor considers, such as estimates of the fundamental constants like \hbar , *etc.* Most of the errors in his case are dominated by systematic effects. For our data, statistical errors are often at least as large as systematic errors, and statistical errors are usually easier to estimate. A notable exception occurs in partial-wave analyses, where different techniques applied to the same data yield different results. In this case, as stated earlier, we often do not make an average but just quote a range of values.

A brief history of early Particle Data Group averages is given in Ref. [4]. On the following page, our History Plots show the time evolution of some of our values of a few particle properties. Sometimes large changes occur. These usually reflect the introduction of significant new data or the discarding of older data. Older data are discarded in favor of newer data when it is felt that the newer data have smaller systematic errors, or have more checks on systematic errors, or simply have much smaller errors. Sometimes, the scale factor becomes large near the time at which a large jump takes place, reflecting the uncertainty introduced by the new and inconsistent data. By and large, however, a full scan of our history plots shows a dull progression toward greater precision at central values quite consistent with the first data points shown.

We conclude that the reliability of the combination of experimental data and our averaging procedures is usually good, but it

is important to be aware that fluctuations outside of the quoted errors can and do occur.

ACKNOWLEDGMENTS

The publication of the *Review of Particle Physics* is supported by the Director, Office of Science, Office of High Energy Physics of the U.S. Department of Energy under Contract No. DE-AC02-05CH11231; by the European Laboratory for Particle Physics (CERN); by an implementing arrangement between the governments of Japan (MEXT: Ministry of Education, Culture, Sports, Science and Technology) and the United States (DOE) on cooperative research and development; by the Italian National Institute of Nuclear Physics (INFN); and by the Physical Society of Japan (JPS). Individual collaborators receive support for their PDG activities from their respective funding agencies.

We thank all those who have assisted in the many phases of preparing this *Review*. We particularly thank the many who have responded to our requests for verification of data entered in the Listings, and those who have made suggestions or pointed out errors.

We are grateful to the staff at CERN, IHEP Beijing, KEK, and LBNL who take care of the mailing and distribution of our

products.

This work used resources of the National Energy Research Scientific Computing Center, a DOE Office of Science User Facility supported by the Office of Science of the U.S. Department of Energy under Contract No. DE-AC02-05CH11231.

References

- [1] The previous edition was: M. Tanabashi *et al.* (Particle Data Group), *Phys. Rev.* **D98**, 030001 (2018).
- [2] C. Patrignani *et al.* (Particle Data Group), *Chin. Phys.* **C40**, 10, 100001 (2016).
- [3] M. Aguilar-Benitez *et al.* (Particle Data Group), *Phys. Lett.* **170B**, 1 (1986).
- [4] A. H. Rosenfeld, *Ann. Rev. Nucl. Part. Sci.* **25**, 555 (1975).
- [5] B.N. Taylor, “Numerical Comparisons of Several Algorithms for Treating Inconsistent Data in a Least-Squares Adjustment of the Fundamental Constants,” U.S. National Bureau of Standards NBSIR 81-2426 (1982).

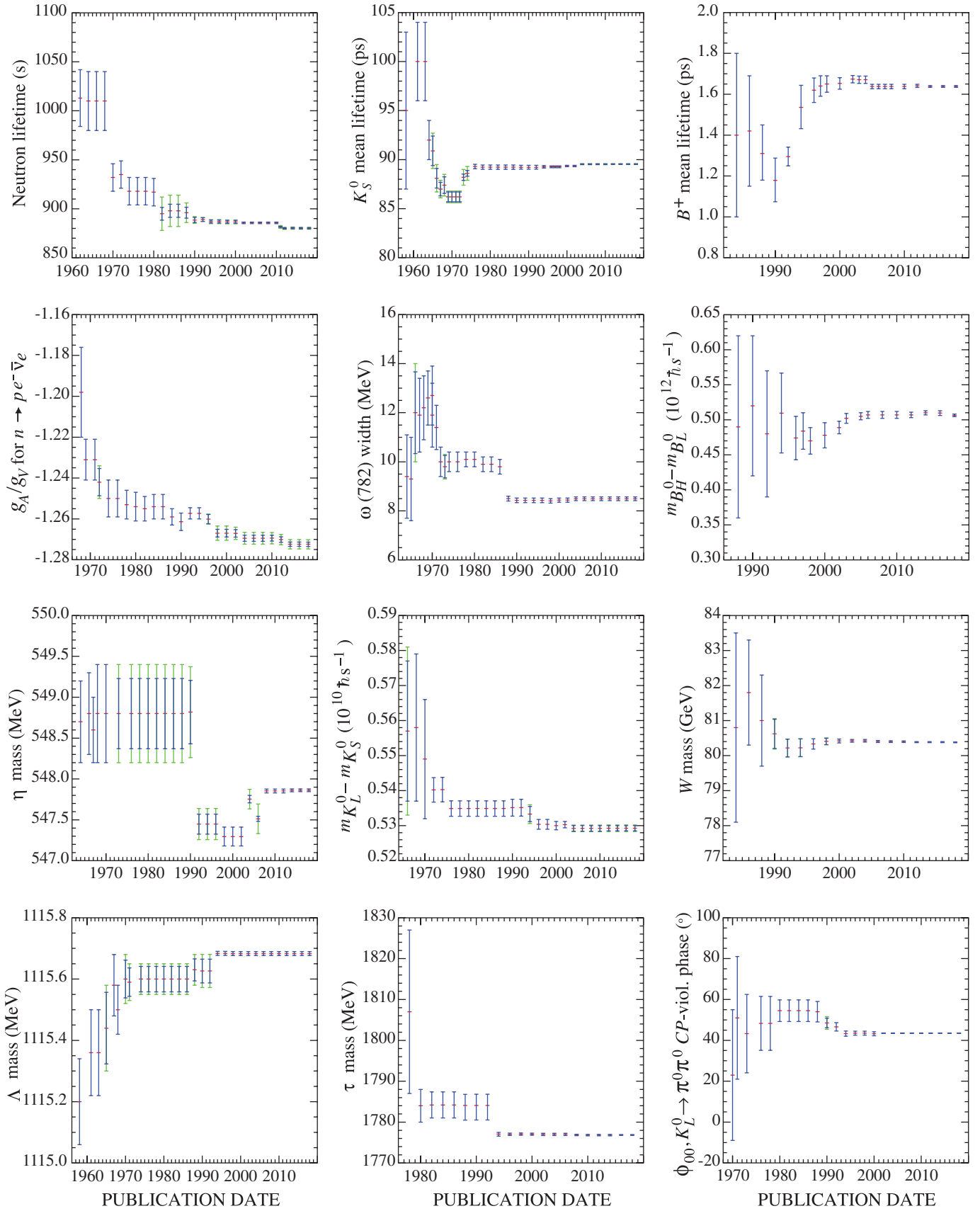


Figure 1: A historical perspective of values of a few particle properties tabulated in this *Review* as a function of date of publication of the *Review*. A full error bar indicates the quoted error; a thick-lined portion indicates the same but without the “scale factor.”

Online Particle Physics Information

1	Introduction	20
2	Particle Data Group (PDG) resources	20
3	Particle Physics Information Platforms	20
4	Literature Databases	20
5	Particle Physics Journals and Conference Proceedings Series	21
6	Conference Databases	21
7	Research Institutions	21
8	People	21
9	Experiments	21
10	Jobs	21
11	Software Packages and Repositories	22
11.1	Particle Physics Software	22
11.2	Astrophysics Software	22
11.3	Web Apps	23
11.4	Mobile Apps	23
12	Data repositories	23
12.1	Particle Physics	23
12.2	Astrophysics	23
12.3	General Physics	23
13	Data preservation activities	24
13.1	Particle Physics	24
13.2	Astrophysics	24
14	Particle Physics Education and Outreach Sites	24
14.1	Science Educators' Networks	24
14.2	Physics Courses	24
14.3	Masterclasses	24
14.4	General Sites	25
14.5	General Physics Activities	25
14.6	Particle Physics Activities	25
14.7	Lab Education Offices	26
14.8	Educational Programs of Experiments	27
14.9	News	27
14.10	Art in Physics	28
14.11	Blogs and Twitter	28

Revised August 2019 by M. Moskvic (CERN).

1 Introduction

The collection of online information resources in particle physics and related areas presented in this chapter is of necessity incomplete. An expanded and regularly updated online version can be found at:

http://library.cern/particle_physics_information
Suggestions for additions and updates are very welcome.¹

2 Particle Data Group (PDG) resources

- **Review of Particle Physics (RPP):** A comprehensive report on the fields of particle physics and related areas of cosmology and astrophysics, including both review articles and a compilation/evaluation of data on particle properties. The review section includes articles, tables and plots on a wide variety of theoretical and experimental topics of interest to particle physicists and astrophysicists. The particle properties section provides tables of published measurements as well as the Particle Data Group's best values and limits for particle properties such as masses, widths, lifetimes, and branching fractions, as well as an extensive summary of searches for hypothetical particles. RPP is published as a large book every two years, with partial updates made available once each year on the web.

All the contents of the book version of RPP are available online:

<http://pdg.lbl.gov>

The printed book can be ordered:

[http:](http://pdg.lbl.gov/2019/html/receive_our_products.html)

[//pdg.lbl.gov/2019/html/receive_our_products.html](http://pdg.lbl.gov/2019/html/receive_our_products.html)

Of historical interest is the complete RPP collection which can be found online:

<http://pdg.lbl.gov/rpp-archive/>

¹Please send comments and corrections to micha.moshe.moskvic@cern.ch

http://library.cern/PDG_publications/review_particle_physics

- **Particle Physics booklet:** An abridged version of the Review of Particle Physics, available as a pocket-sized 250-page booklet. It is one of the most useful summaries of physics data. The booklet contains an abbreviated set of reviews and the summary tables from the most recent edition of the Review of Particle Physics.

The PDF file of the booklet can be downloaded:

<http://pdg.lbl.gov/current/booklet.pdf>

The printed booklet can be ordered:

[http:](http://pdg.lbl.gov/2019/html/receive_our_products.html)

[//pdg.lbl.gov/2019/html/receive_our_products.html](http://pdg.lbl.gov/2019/html/receive_our_products.html)

- **PDGLive:** A web application for browsing the contents of the PDG database that contains the information published in the Review of Particle Physics. It allows one to navigate to a particle of interest, see a summary of the information available, and then proceed to the detailed information published in the Review of Particle Physics. Data entries are directly linked to the corresponding bibliographic information in INSPIRE.

<http://pdglive.lbl.gov>

- **Computer-readable files:** Data files that can be downloaded from the PDG include tables of particle masses and widths, PDG Monte Carlo particle numbers, and cross-section data. The files are updated with each new edition of the Review of Particle Physics.

http://pdg.lbl.gov/current/html/computer_read.html

3 Particle Physics Information Platforms

- **INSPIRE:** INSPIRE serves as a one-stop information platform for the particle physics community, comprising 8 interlinked databases on literature, conferences, institutions, journals, researchers, experiments, jobs and data. Run in collaboration by CERN, DESY, Fermilab, IHEP, IN2P3, and SLAC, it has been serving the scientific community for almost 50 years. Previously known as SPIRES, it was the first website outside Europe and the first database on the web. Close interaction with the user community and with arXiv, ADS, HEPData, ORCID, PDG and publishers is the backbone of INSPIRE's evolution.

<http://inspirehep.net/>

In 2019, INSPIRE launched INSPIRE beta, featuring all-new literature search, author profiles and job postings. INSPIRE beta is running in parallel with the current platform and it will fully replace it in the future. The INSPIRE beta site is available at:

<http://beta.inspirehep.net>

– Blog: <http://blog.inspirehep.net/>

– Twitter: @inspirehep

4 Literature Databases

- **ADS:** The SAO/NASA Astrophysics Data System is a Digital Library portal offering access to 13 million bibliographic records in Astronomy and Physics. The ADS search engine also indexes the full-text for approximately four million publications in this collection and tracks citations, which now amount to over 80 million links. The system also provides access and links to a wealth of external resources, including electronic articles hosted by publishers and arXiv, data catalogs and a variety of data products hosted by the astronomy archives worldwide. The ADS can be accessed at:

<http://ads.harvard.edu/>

- **arXiv.org:** A repository of full-text articles in physics, astronomy, mathematics, computer science, statistics, nonlinear sciences, quantitative finance, quantitative biology, electrical engineering and systems science, and economics. Papers are submitted by registered authors to arXiv, often as preprints in advance of submission to a journal for publication; includes postprints, working papers, and other relevant material. Established in 1991, the repository is interlinked

with ADS and INSPIRE, among others. Readers can browse subject categories or search by author, title, abstract, date, and other fields. Receive daily update alerts for subfields by email or RSS.

<https://arXiv.org>

- Blog: <https://blogs.cornell.edu/arXiv>
- Twitter: @arxiv

- **CDS:** The CERN Document Server contains records of about 700,000 CERN and non-CERN articles, preprints, theses. It includes records for internal and technical notes, official CERN committee documents, and multimedia objects. CDS is planning to focus on its role as an institutional repository covering all CERN material from the early 50s and reflecting the holdings of the CERN library. Non-CERN particle and accelerator physics content is in the process of being exported to INSPIRE.

<http://cds.cern.ch>

- **INSPIRE HEP:** The HEP collection, the flagship of the INSPIRE suite, serves more than 1.3 million bibliographic records with a growing number of full-text articles attached and metadata including author affiliations, abstracts, references, experiments, keywords as well as links to arXiv, ADS, PDG, HEPData, publisher platforms and other servers. It provides fast metadata and full-text searches, plots extracted from full text, author disambiguation, author profile pages and citation analysis and is expanding its content to, e.g., experimental notes.

<http://inspirehep.net>

- **JACoW:** The Joint Accelerator Conference Website publishes the proceedings of several accelerator conferences held around the world. A custom interface allows searching based on keywords, titles, authors, and in the full text.

<http://www.jacow.org/>

- **KEK Library Preprints and Reports Database:** This database contains bibliographic records of preprints and technical reports held in the KEK library, with links to the full-text images of more than 100,000 papers scanned from their worldwide preprint collection. Particularly useful for older scanned preprints. Links to it are included in INSPIRE HEP.

https://www.i-repository.net/il/meta_pub/engG0000128Lib

- **MathSciNet:** This database of almost 3 million items provides reviews, abstracts and bibliographic information for much of the mathematical sciences literature. Over 100,000 new items, most of them classified according to the Mathematics Subject Classification, and more than 80,000 reviews of the current published literature are added each year. Author identification allows users to search for publications by author and citation data allows users to track the history and influence of research publications.

<http://www.ams.org/mathscinet>

- **OSTI.GOV:** A portal to free, publicly available DOE-sponsored R&D results including technical reports, bibliographic citations, journal articles, conference papers, books, multimedia and data information. It consolidates OSTI's home page and the now-retired primary search tool SciTech Connect. It contains over 3 million records, including citations to 1.5 million journal articles, 1 million of which have digital object identifiers (DOIs) linking to full-text articles on publishers' websites.

<http://www.osti.gov>

5 Particle Physics Journals and Conference Proceedings Series

- **CERN Journal List:** This list of journals and conference series publishing particle physics content provides information on Open Access, copyright policies and terms of use.

<http://library.cern/oa/where-publish>

- **INSPIRE Journals:** The database contains over 3,600 journals publishing HEP-related articles.

<http://inspirehep.net/collection/journals>

6 Conference Databases

- **INSPIRE Conferences:** The database of more than 23,000 past, present, and future conferences, schools, and meetings relevant to high-energy physics and related fields is searchable by title, acronym, series, date and location. Included are information about published proceedings, links to conference contributions in the INSPIRE HEP database, and links to the conference website when available. New conferences can be submitted from the entry page.

<http://inspirehep.net/conferences>

7 Research Institutions

- **INSPIRE Institutions:** INSPIRE Institutions contains over 11,500 institutes, laboratories, and universities, where research on particle physics and astrophysics is led. Every record includes, whenever possible, as detailed information, such as address, web links, experiments, and links to INSPIRE papers authored by people affiliated to that institution. One can search for a particular institution by name, acronym, and location.

<http://inspirehep.net/institutions>

8 People

- **INSPIRE HEPNames:** Searchable worldwide database of over 125,000 active, departed, retired, and deceased people associated with particle physics and related fields. The affiliation history of these researchers, their e-mail addresses, ORCIDs, web pages, experiments they participated in, PhD advisor, information on their graduate students and links to their papers in the INSPIRE HEP, arXiv and ADS databases are provided, as well as a user interface to update this information.

<http://inspirehep.net/hepnames>

- **ORCID:** Registry providing persistent digital identifiers allowing to unambiguously identify researchers. Through integration in key research workflows such as manuscript and grant submission, it supports automated linkages between scientists and their professional activities ensuring that their work is recognized.

<https://orcid.org>

9 Experiments

- **INSPIRE Experiments:** Contains more than 3,500 past, present, and future experiments in particle physics. Lists both accelerator and non-accelerator experiments. Includes official experiment name and number, location, and collaboration lists. Simple searches by participant, title, experiment number, institution, date approved, accelerator, or detector, return a description of the experiment, including a complete list of authors, title, overview of the experiment's goals and methods, and a link to the experiment's web page if available. Recently, it has expanded its scope to include particle accelerators besides experiments and to link them together.

<http://inspirehep.net/Experiments>

- **Cosmic ray/Gamma ray/Neutrino and similar experiments:** This extensive collection of experiment websites is organized by focus of study and by location. Additional sections link to educational materials, organizations, and other useful resources. The site is maintained at the Max Planck Institute for Nuclear Physics, Heidelberg.

<http://www.mpi-hd.mpg.de/hfm/CosmicRay/CosmicRaySites.html>

10 Jobs

- **AAS Job Register:** The American Astronomical Society publishes once a month graduate, postgraduate, faculty and other positions mainly in astronomy and astrophysics.

<http://jobregister.aas.org/>

- **Academic Jobs Online:** A full-service online recruiting site for academic institutions worldwide in all disciplines and areas.

<https://academicjobsonline.org/ajo>

- **APS Careers:** A gateway for physicists, students, and physics enthusiasts to information about physics jobs and careers. It contains Physics job listings, career advice, upcoming workshops and meetings, and career and job-related resources provided by the American Physical Society.
<http://www.aps.org/careers/employment>
- **brightrecruits.com:** A recruitment service run by IOP Publishing that connects employers from different industry sectors with jobseekers who have a background in physics and engineering.
<http://brightrecruits.com/>
- **IOP Careers:** Career information and resources primarily aimed at university students are provided by the UK Institute of Physics.
<http://www.iop.org/careers/>
- **INSPIRE HEPJobs:** Lists academic and research jobs in high energy physics, nuclear physics, accelerator physics and astrophysics with the option to post a job or to receive email notices of new job listings. About 500 jobs are currently listed.
<http://inspirehep.net/jobs>
- **Physics Today Jobs:** Online recruitment advertising website for Physics Today magazine, published by the American Institute of Physics. Physics Today Jobs is the managing partner of the AIP Career Network, an online job board network for the physical science, engineering, and computing disciplines. Over 6,000 resumes are currently available, and nearly 5,000 jobs were posted in 2018.
<http://www.physicstoday.org/jobs>

11 Software Packages and Repositories

Most relevant software is hosted by general-purpose repositories like GitHub, GitLab or BitBucket, but here are a few specific repositories focused on astrophysics or HEP. ## Repositories

- **ASCL:** The Astrophysics Source Code Library (ASCL) is a free online registry for source codes of interest to astronomers and astrophysicists. It lists codes that have been used in research that has appeared in, or been submitted to, peer-reviewed publications.
<http://ascl.net>
- **GenSer:** The Generator Services project collaborates with Monte Carlo (MC) generator authors and with LHC experiments in order to prepare validated LCG compliant code for both theoretical and experimental communities at the LHC, sharing the user support duties, providing assistance for the development of the new object-oriented generators, and guaranteeing the maintenance of the older packages on the LCG supported platforms. The project consists of the generators repository, validation, HepMC record and MCDB event databases.
<http://ep-dep-sft.web.cern.ch/project/generator-service-project-genser>
- **Hepforge:** A development environment for high-energy physics software projects, in particular housing many event-generator related projects, that offers a ready-made, easy-to-use set of web-based tools, including shell account with up-to-date development tools, web page hosting, subversion, git and Mercurial code management systems, mailing lists, bug tracker and wiki system.
<http://www.hepforge.org/>

11.1 Particle Physics Software

- **FastJet:** This is a software package for jet finding in pp and e^+e^- collisions. It includes fast native implementations of many sequential recombination clustering algorithms, plugins for access to a range of cone jet finders and tools for advanced jet manipulation.
<http://fastjet.fr/>
- **GAMBIT:** A global fitting code for generic Beyond the Standard Model theories, designed to allow fast and easy definition of new models, observables, likelihoods, scanners and

backend physics codes.

- **Geant4:** This is a toolkit for the simulation of the passage of particles through matter. Its areas of application include high energy, nuclear and accelerator physics, as well as studies in medical and space science.
<http://geant4.web.cern.ch/geant4/>
 - **LHAPDF:** HEP community standard library for parton distribution function interpolation, including official collection of PDF data sets.
<http://lhpdf.hepforge.org/>
 - **QUADA:** Library for performing calculations in lattice QCD on GPUs using NVIDIA's CUDA platform. The current release includes optimized solvers for Wilson, Clover-improved Wilson, Twisted mass, Staggered, Improved staggered, Domain wall and Mobius fermion actions.
<http://lattice.github.io/quada/>
 - **Rivet:** The Rivet toolkit, a system for validation of Monte Carlo event generators, provides a large set of experimental analyses useful for MC generator development, validation, and tuning.
<http://rivet.hepforge.org/>
 - **ROOT:** This framework for data processing in high-energy physics, born at CERN, offers applications to store, access, process, analyze and represent data or perform simulations.
<http://root.cern.ch>
 - **Scikit-HEP:** This is a community-driven and community-oriented project with the aim of providing Particle Physics at large with an ecosystem for data analysis in Python. The project started in Autumn 2016 and is under active development. It focuses on providing core and common tools for the community but also on improving the interoperability between HEP tools and the scientific ecosystem in Python as well as the discoverability of utility packages and projects.
<http://scikit-hep.org>
 - **tmLQCD:** This freely available software suite provides a set of tools to be used in lattice QCD simulations, mainly a HMC implementation for Wilson and Wilson twisted mass fermions and inverter for different versions of the Dirac operator.
<https://github.com/etmc/tmLQCD>
 - **USQCD:** The software suite enables lattice QCD computations to be performed with high performance across a variety of architectures. The page contains links to the project web pages of the individual software modules, as well as to complete lattice QCD application packages which use them.
<http://usqcd-software.github.io>
 - **Software lists:** A list of Monte Carlo generators may be found at:
<http://cmsdoc.cern.ch/cms/PRS/gentools/www/geners/collection/>
- The homepage of the SUSY Les Houches Accord contains links to codes relevant for supersymmetry calculations and phenomenology.
<http://skands.physics.monash.edu/slha/>
- A variety of codes and algorithmic tools for analysing supersymmetric phenomenology is described in
<http://arxiv.org/abs/0805.2088>
- G. Cowan's list provides links to HEP software, general statistics and data analysis links.
<http://www.pp.rhul.ac.uk/~cowan/sda/statlinks.html>
- An extended list of more specialized HEP-related software can be found in the online version of this review:
http://library.cern/particle_physics_information#sof

11.2 Astrophysics Software

- **Astropy:** The Astropy Project is a community effort to develop a single core package for Astronomy in Python and foster interoperability between Python astronomy packages.
<http://www.astropy.org>
- **Starlink:** Starlink was a UK Project supporting astronomi-

cal data processing. It was shut down in 2005 but its open-source software continued to be developed at the Joint Astronomy Centre until March 2015. It is currently maintained by the East Asian Observatory. The open-source software products are a collection of applications and libraries, usually focused on a specific aspect of data reduction or analysis.

<http://starlink.eao.hawaii.edu/starlink>

- Links to a large number of astronomy software archives are listed at:

<http://heasarc.nasa.gov/docs/heasarc/astro-update/>

11.3 Web Apps

- **APFEL Web:** This online parton density function plotter allows to compare predictions for different PDF fits.
<https://apfel.mi.infn.it/>
- **ColliderReach:** A tool to give a simple estimate of the relation between the mass reaches of different proton-proton collider configurations.
<http://collider-reach.web.cern.ch/>
- **TMDplotter:** Allows to plot TMDs and PDFs as a function of different variables.
<http://tmdplotter.desy.de/>

11.4 Mobile Apps

- **arXiv eXplorer:** Android app for browsing and searching arXiv.org, and for reading, saving and sharing articles.
<https://play.google.com/store/apps/details?id=com.gbeatty.arxiv>
- **Collider:** This mobile app allows users to see data from the ATLAS experiment at the LHC.
<http://collider.physics.ox.ac.uk/>
- **LHSee:** This smartphone app allows users to see collisions from the Large Hadron Collider.
<http://www2.physics.ox.ac.uk/about-us/outreach/public/lhsee>
- **The Particles:** App for Apple iPad, Windows 8 and Microsoft Surface. Allows users to browse a wealth of real “event” images and videos, read popular “biographies” of each of the particles and explore the A-Z of particle physics with its details and definitions of key concepts, laboratories and physicists. Developed by Science Photo Library in partnership with Prof. Frank Close.
<http://www.sciencephoto.com/apps/particles.html>

12 Data repositories

Data is increasingly deposited in general-purpose repositories like Zenodo (<https://zenodo.org/>), figshare (<https://figshare.com/>) or the Open Science Framework (<https://osf.io/>), but here are a few specific repositories focused on physics.

12.1 Particle Physics

- **HEPData:** The HEPData project, funded by the STFC (UK) and based at Durham University, has been built up over the past four decades as a unique repository for scattering data from experimental particle physics papers. It currently comprises the data points from plots and tables related to several thousand publications including those from the LHC. The data from HEPData can also be accessed through INSPIRE. A new enhanced service was recently developed in collaboration with CERN.
<https://hepdata.net>
- **CERN Open Data:** The CERN Open Data portal provides data from real collision events, as well as simulated and simplified datasets, produced by the experiments at the LHC, virtual machines to reproduce the analysis environment, and software to process the data. It serves over 2 PB of data in total and encourages their use for both educational and research purposes.
<http://opendata.cern.ch>
- **HepSim:** A repository with Monte Carlo simulations for particle-collision experiments. It contains predictions from

parton shower models and includes Monte Carlo events after fast and full detector simulations and event reconstruction.

<http://atlaswww.hep.anl.gov/hepsim/>

- **ILDG:** The International Lattice Data Grid is an international organization which provides standards, services, methods and tools that facilitate the sharing and interchange of lattice QCD gauge configurations among scientific collaborations by uniting their regional data grids. It offers semantic access with local tools to worldwide distributed data.
<http://www.usqcd.org/ildg/>
- **MCDB - Monte Carlo Database:** This central database of MC events aims to facilitate communication between Monte-Carlo experts and users of event samples in LHC collaborations. Having these events stored in a public place along with the corresponding documentation allows for direct cross checks of the performances on reference samples.
<http://mcdb.cern.ch/>
- **MCPLOTS:** MCPLOTS is a repository of Monte Carlo plots comparing High Energy Physics event generators to a wide variety of available experimental data. The website is supported by the LHC Physics Centre at CERN.
<http://mcplots.cern.ch/>

12.2 Astrophysics

- **CfA Dataverse:** This astronomy data repository at Harvard is open to all scientific data from astronomical institutions worldwide.
<https://dataverse.harvard.edu/dataverse/cfa>
- **NASA’s HEASARC:** The High Energy Astrophysics Science Archive Research Center (HEASARC) is the primary archive for NASA’s (and other space agencies’) missions dealing with electromagnetic radiation from extremely energetic phenomena ranging from black holes to the Big Bang.
<http://heasarc.gsfc.nasa.gov/>
- **NASA archives:** The NASA archives provide access to raw and processed datasets from numerous NASA missions. Mikulski Archive for Space Telescopes (MAST): Hubble telescope, other missions (UV, optical):
<http://archive.stsci.edu/>
NASA/IPAC Infrared Science Archive: Spitzer, Herschel, Planck telescope, other missions:
<http://irsa.ipac.caltech.edu/>
- **NASA/IPAC Extragalactic Database (NED):** An astronomical database that collates and cross-correlates information on extragalactic objects. It contains their positions, basic data, and names as well as bibliographic references to published papers, and notes from catalogs and other publications. NED supports searches for objects and references, and offers browsing capabilities for abstracts of articles of extragalactic interest.
<http://ned.ipac.caltech.edu/>
- **SIMBAD:** The SIMBAD astronomical database provides basic data, cross-identifications, bibliography and measurements for astronomical objects outside the solar system. It can be queried by object name, coordinates and various criteria. Lists of objects and scripts can be submitted.
<http://simbad.u-strasbg.fr/simbad/>
- **VizieR:** VizieR provides access to the most complete library of published astronomical catalogues and data tables, available online organized in a self-documented database. Query tools allow users to select relevant data tables and extract and format records matching given criteria. Currently, more than 19,000 catalogues are available.
<http://vizier.u-strasbg.fr/>

12.3 General Physics

- **NIST Physical Measurement Laboratory:** The National Institute of Standards and Technology provides access to physical reference data (physical constants, atomic spectroscopy data, x-ray and gamma-ray data, radiation dosimetry data, nuclear physics data and more) and measurements

and calibrations data (dimensional and electromagnetic measurements).

<https://www.nist.gov/pml/>

- **Springer Materials - The Landolt-Börnstein Database:** Landolt-Börnstein is a data collection covering all areas of physical sciences and engineering, such as particle physics, electronic structure and transport, magnetism, superconductivity. International experts scan the primary literature in more than 8,000 peer-reviewed journals and evaluate and select the most valid information to be included in the database. It includes more than 130,000 online documents, 1.2 million references, and covers 250,000 chemical substances. SpringerMaterials Interactive allows to visualise and analyse data. The search functionality is freely accessible and the search results are displayed in their context, whereas the full text is secured to subscribers.

<http://materials.springer.com>

13 Data preservation activities

13.1 Particle Physics

- **CERN Analysis Preservation:** CERN Analysis Preservation is a platform for preserving knowledge and assets of individual physics analyses in LHC collaborations. Its aim is to capture and document all the elements needed to understand and rerun an analysis even several years later: data, software, environment, workflow, context, and documentation. This platform is currently in a pilot stage. It is accessible by LHC experimental groups (standard collaboration access restrictions are applied).

<https://analysispreservation.cern.ch>

- **DASPOS:** A collective effort to explore the realisation of a viable data, software and algorithm preservation architecture in High Energy Physics

<https://daspos.crc.nd.edu>

- **DPHEP:** DPHEP coordinates the efforts to define and implement Data Preservation and Long Term Analysis in HEP. DPHEP, which was initiated as a study group in 2008-2009, includes all major HEP experiments and labs. In 2014, it has become a Collaboration through the signature of a Collaboration Agreement by a number of large funding agencies. The group is endorsed by the International Committee for Future Accelerators (ICFA).

DPHEP regularly organizes workshops, creates status reports, and maintains links with similar activities in other disciplines. Details of the organizational structure, the objectives, workshops and publications can be found on the website.

<http://dphep.org>

- **REANA:** REANA (REusable ANALyses) is a system for instantiating research data analyses on the cloud using container-based solutions. It complements CERN Analysis Preservation permitting the reuse and revalidation of preserved analyses. It is being developed in close collaboration with DASPOS and RECAST.

<http://reanahub.io/>

- **RECAST:** Building on analysis preservation and re-use infrastructure of the LHC experiments, RECAST acts as a science gateway allowing theorists to suggest new reinterpretations of archived analyses of the LHC dataset. Experiments review suggestions and, if approved, simulate the proposed models and re-run the archived analysis to determine their viability. Such reinterpretation results are then appended to the records of the original publication in the relevant digital archives.

<https://recast.cern.ch>

13.2 Astrophysics

More formal and advanced data preservation activity is ongoing in the field of Experimental Astrophysics, including:

- Fermi Data
<https://fermi.gsfc.nasa.gov/ssc/data>

- IVOA (International Virtual Observatory Alliance)
<http://www.ivoa.net/astronomers/applications.html>
- GWOSC (Gravitational Wave Open Science Center)
<https://www.gw-openscience.org/about/>
- PLA (Planck Legacy Archive)
<http://pla.esac.esa.int/pla/>
- SDSS (Sloan Digital Sky Survey)
<http://sdss.org>

14 Particle Physics Education and Outreach Sites

A useful list of resources can also be found at

<http://www.stfc.ac.uk/research/particle-physics-and-particle-astronautics/particle-physics-resources/>

14.1 Science Educators' Networks

- **IPPOG:** The International Particle Physics Outreach Group is a network of scientists, science educators and communication specialists working across the globe in informal science education and outreach for particle physics. The IPPOG collaboration comprises 30 members: 24 countries, 5 experiments and CERN as an international laboratory.

<http://ippog.web.cern.ch>

- **Interactions.org:** Designed to serve as a central resource for communicators of particle physics. The daily updated website provides links to current particle physics news from the world's press, high-resolution photos and graphics from the particle physics laboratories of the world; links to education and outreach programs; information about science policy and funding; a glossary; and links to many educational sites.

<http://www.interactions.org>

- **QuarkNet:** The QuarkNet Collaboration is a national program that partners high school science teachers with particle physicists working in experiments at CERN or Fermilab. The network consists of over 50 centers at research groups in universities and labs across the United States. About 100,000 students from 500+ U.S. high schools learn fundamental physics as they participate in inquiry-oriented investigations and analyze authentic data online. QuarkNet is supported in part by the National Science Foundation and Fermilab.

<https://quarknet.org/>

- **Netzwerk Teilchenwelt:** Behind the project are about 200 researchers from 30 institutes and universities doing research in particle physics, astroparticle physics and hadron and nuclear physics in Germany. Exciting young scientists throughout Germany for particle physics and accompanying them from school to top-level particle physics research—that's what they have set their sights on.

<https://www.teilchenwelt.de>

14.2 Physics Courses

- **MIT OpenCourseWare - Physics:** These MIT course materials reflect almost all the undergraduate and graduate subjects taught at MIT. In addition to physics courses, supplementary educational resources are also available.

<http://ocw.mit.edu/courses/physics/>

- **OnlineCourses.com:** A collection of online tests, video lectures, and related course materials from mostly prestigious universities around the world.

<http://www.onlinecourses.com/physics/>

14.3 Masterclasses

- **Cosmic Ray Studies:** There are more than 12 projects around the world that address young people and teachers giving them an opportunity to explore cosmic particles, collecting, uploading and analyzing data and sharing results. Two annual events include International Cosmic Day and International Muon Week.

<https://icd.desy.de>

<https://quarknet.org/content/international-muon-week>

- **Hands-On Universe:** This program enables students to investigate the Universe while applying tools and concepts from science, math and technology.

<http://handsonuniverse.org/>

- **HYPATIA:** HYPATIA (Hybrid Pupil's Analysis Tool for Interactions in ATLAS) is a tool for high school students to inspect the graphic visualization of particle collision products in the ATLAS detector at CERN.

<http://hypatia.phys.uoa.gr/>

- **International Masterclasses:** Each year about 13,000 high school students in 55 countries come to one of about 225 nearby universities or research centres for a day to unravel the mysteries of particle physics. Lectures from active scientists give insight in topics and methods of basic research enabling the students to perform measurements on real data from one of seven experiments. At the end of the day, like an international research collaboration, participants join a video conference for discussion and combination of results. The program is coordinated from Institut für Kern- und Teilchenphysik at TU Dresden and the Notre Dame University QuarkNet Center within the framework of the International Particle Physics Outreach Group (IPPOG). CERN, Fermilab and TRIUMF support videoconferences.

<https://physicsmasterclasses.org>

World Wide Data Day is an annual event.

<https://quarknet.org/content/world-wide-data-day>

- **LHC physics Masterclasses:** Lectures from active scientists give insight into methods of basic research, enabling the students to perform measurements on real data from LHC experiments. Like in a real research collaboration, the participants then discuss their results and compare with expectations.

<http://cms.web.cern.ch/content/cms-physics-masterclass>

<http://lhcb-public.web.cern.ch/lhcb-public/en/LHCb-outreach/masterclasses/en>

<http://alice.physicsmasterclasses.org/MasterClassWebpage.html>

<http://atlas-minerva.web.cern.ch/atlas-minerva>

- **IceCube Masterclass:** The program is inspired by the International Masterclasses program started by IPPOG and is coordinated by the Wisconsin IceCube Particle Astrophysics Center with support from QuarkNet.

<https://masterclass.icecube.wisc.edu/>

14.4 General Sites

- **Contemporary Physics Education Project (CPEP):** Provides charts, brochures, Web links, and classroom activities. Online interactive courses include: Fundamental Particles and Interactions; Plasma Physics and Fusion; History and Fate of the Universe; and Nuclear Science.

<http://www.cpepweb.org/>

- **PhysicsCentral:** This site maintained by the American Physical Society provides information about current research and people in physics, experiments that can be performed at home or at school and the possibility to get physics questions answered by physicists.

<http://www.physicscentral.com>

14.5 General Physics Activities

- **HyperPhysics:** An exploration environment for concepts in physics employing concept maps and other linking strategies and providing opportunities for numerical exploration.

<http://hyperphysics.phy-astr.gsu.edu/hbase/hph.html>

- **PhET Interactive Simulations:** Founded in 2002 by Nobel Laureate Carl Wieman, the PhET Interactive Simulations project at the University of Colorado Boulder creates free interactive math and science simulations. PhET sims are based on extensive education research and engage students through an intuitive, game-like environment where students learn through exploration and discovery.

<https://phet.colorado.edu/en/simulations/category/physics>

14.6 Particle Physics Activities Citizen Science

- **Higgs Hunters:** A web-based citizen science project to help search for unknown exotic particles in the LHC data.

<http://HiggsHunters.org>

- **LHC @ home:** Volunteer computing platform to help physicists compare theory with experiment, in the search for new fundamental particles and answers to questions about the Universe.

<http://lhcatome.web.cern.ch>

Classroom Activities Collections

- **Contemporary Physics Education Project - Fundamental particle and interactions:**

<http://www.cpepphysics.org/particles.html>

- **Fermilab Physical Science/Physics Resources:**

<https://ed.fnal.gov/home/educators1000-physics.shtml>

- **IceCube Activities:**

<https://icecube.wisc.edu/outreach/activities>

- **IPPOG Resources:**

<http://ippog.org/resources>

- **Jefferson Lab Teacher Resources:**

<https://education.jlab.org/indexpages/teachers.html>

- **LIGO Classroom Activities:**

<https://www.ligo.caltech.edu/page/classroom-activities>

- **MINERvA Neutrinos in the Classroom:**

<https://neutrino-classroom.org>

- **Perimeter Institute Educational Resources:**

<https://resources.perimeterinstitute.ca>

- **Quarked Lesson Plans:**

<http://www.quarked.org/parents/lessonplans.html>

- **QuarkNet Data Activities Portfolio:**

<https://quarknet.org/data-portfolio>

- **Sanford Lab curriculum materials:**

<https://sanfordlab.org/educators/curriculum-modules>

Interactive Sites

- **CAMELIA:** CAMELIA (Cross-platform Atlas Multimedia Educational Lab for Interactive Analysis) is a discovery tool for the general public, based on computer gaming technology.

<https://www.atlasexperiment.org/camelia.html>

- **CERNland:** With a range of games, multimedia applications and films CERNland is a virtual theme park developed to bring the excitement of CERN's research to a young audience aged between 7 and 12. CERNland is designed to show children what is being done at CERN and inspire them with some physics.

<http://www.cernland.net/>

- **In particular:** Podcast and more about physics and the process of discovering physics at the ATLAS experiment.

<https://inparticular.web.cern.ch/>

- **Lancaster Particle Physics:** Suitable for 16+ students, this site offers a number of simulations and explanations of particle physics, including a section on the LHC.

<http://www.lppp.lancs.ac.uk/>

- **Quarked!** - Adventures in the Subatomic Universe: This project, targeted to kids aged 7-12 (and their families), brings subatomic physics to life through a multimedia project including an interactive website, a facilitated program for museums and schools, and an educational outreach program.

<http://www.quarked.org/>

Planetarium Show

- **Phantom of the Universe:** A planetarium show about dark matter that covers astrophysics, an underground experiment, and the LHC. It is distributed to planetariums for free.

<http://phantomoftheuniverse.com/>

Video/Film

- **Angels and Demons:** With the aim of looking at the myth versus reality of antimatter and science at CERN this site describes the science behind the story including a set of videos.
<http://angelsanddemons.web.cern.ch/>
- **CollidingParticles:** A series of films following a team of physicists involved in research at the LHC.
<http://www.collidingparticles.com/>
- **Rewarding Learning videos about CERN:** The three videos based on interviews with scientists and engineers at CERN introduce pupils to CERN and the type of research and work undertaken there and are accompanied by teachers' notes.
<http://www.nicurriculum.org.uk/STEMWorks/resources/cern/index.asp>
- **Videos by Don Lincoln:** Short YouTube videos on basic particle physics and cosmology.
<https://www.youtube.com/playlist?list=PLCfRa7MXBEsoJuAM8s6D8oKDPyBepBosS>

Websites * Cambridge Relativity and Cosmology: Materials for the greater public to learn about the Origins of the Universe, including information on black holes, string theory, M-theory, the cosmic microwave background and the structure of the Universe.

<http://www.damtp.cam.ac.uk/research/gr/public/index.html>

* **Imagine the Universe:** This site is for students age 14 and up and for anyone interested in learning about the Universe.

<http://imagine.gsfc.nasa.gov/home.html>

* **Particle Adventure:** An interactive tour of quarks, neutrinos, antimatter, extra dimensions, dark matter, accelerators and particle detectors from the Particle Data Group of Lawrence Berkeley National Laboratory. Simple elegant graphics and translations into 16 languages.

<http://particleadventure.org/>

14.7 Lab Education Offices

- **Argonne National Laboratory (ANL) Educational Programs:** Connecting today's world-class research to tomorrow's STEM problem solvers.
<http://www.anl.gov/education/>
- **Brookhaven National Laboratory (BNL) Educational Programs:** The Office of Educational Programs mission is to design, develop, implement, and facilitate workforce development and education initiatives that support the scientific mission at Brookhaven National Laboratory and the Department of Energy.
<http://www.bnl.gov/education/>
- **CERN's education programmes:** CERN's education and outreach programmes cover all ages from high-school students to university students. Specifically, CERN offers the tailor-made High-School Students Internship Programme several times per year and the Beamline for Schools Competition, challenging high-school students from around the world to propose an experiment to carry out at a real research laboratory. The Laboratory also runs residential programmes for high-school teachers from around the world and a summer programme for undergraduate students.
<https://home.cern/about/what-we-do/our-educational-programmes>
- **DESY Education:** DESY Hamburg offers a regular series of public lectures and the DESY Science Café for young and old alike.
https://fortbildung.desy.de/index_eng.html

- **DESY Zeuthen Outreach:** Posters, photos, lectures, videos and blogs. Projects for teachers and students include School Labs, Cosmic@Web, Teilchenwelt and International Cosmic Day.

<https://astro.desy.de/outreach>

- **Fermilab Office of Education and Public Outreach:** Provides education resources and information about activities for 's, physicists, students and visitors to the Lab. In addition to information about 25 programs, the website provides online data-based investigations for high school students, online versions of exhibits in the Lederman Science Center, links to particle physics discovery resources, web-based instructional resources, tips for education and outreach, and links to the Lederman Science Center and the Teacher Resource Center.

<http://ed.fnal.gov/>

- **Perimeter Institute Outreach:** Perimeter Institute shares ideas with students, teachers, and like-minded people through programs and resources that communicate the power, joy, and mystery of science. Perimeter's award-winning Outreach team brings science to life and raises scientific literacy through classroom resources, public lectures, teacher workshops, an educator network, and a summer school where students interact with Perimeter researchers.

<https://www.perimeterinstitute.ca/outreach>

- **Science Education at Jefferson Lab:** Jefferson Lab's long-term commitment to science education continues to focus on increasing the number of teachers with a substantial background in math and science, strengthening the motivation and preparation of all students, especially minorities and females, and addressing the serious under representation of minorities and females in science, math, engineering and technology careers.

<http://education.jlab.org/>

- **Joint Institute for Nuclear Research Education (JINR):** The JINR educational portal has resources, programs for teachers and school students and lab tours.

<http://www.jinr.ru/schoolstudents-teachers-en/>

- **Laboratori Nazionali di Frascati Educational (INFN):** INFN educational programs are addressed to students, teachers and general audiences of every age, from Italy and abroad. Insights and education about the INFN-LNF research are offered thanks to the organization of guided tours and open days, stages for students, refresher courses for teachers, seminars and divulgation events. The aim is to create a constant exchange between the research world and society, thanks to direct contact and via the internet and other social media.

<http://edu.lnf.infn.it/about/?lang=en>

- **Laboratori Nazionali del Gran Sasso Outreach Activities:** The Lab offers pupils the opportunity to approach the fascinating world of Physics and Science in general through stages, summer schools and training camps. It makes young researchers' skills and competences available to people both in public events, such as the Open Day and the European Researchers' Night, and in guided tours to visit the underground experimental halls.

<https://www.lngs.infn.it/en/outreach-activities>

- **Lawrence Berkeley National Laboratory (LBNL) Workforce Development and Education:** Working with our partners both within and outside Berkeley Lab, LBNL promotes equal access to scientific and technical careers for students from all backgrounds, supports STEM teachers, and build scientific literacy through innovative education programs. The lab also supports educational outreach efforts from Berkeley Lab's divisions by providing program development assistance, materials, funding, volunteers, project management, marketing, and administrative support.

<https://education.lbl.gov/>

- **Sanford Underground Research Facility Education and Outreach:** Leveraging research being conducted underground at Sanford Lab, staff provide training, teaching

tools and materials for teachers so they can inspire and challenge students.

<https://sanfordlab.org/educators>

- **SNOLAB Outreach:** The goal at SNOLAB is to develop new educational material that fosters an appreciation of the field of astroparticle physics. The education team endeavours to facilitate an exchange of knowledge with the public and scientists from around the world to better understand our solar system. The desired outcome of the educational work is to have a network of healthy and resilient community partners with informed and active citizens better equipped to understand the goals here at SNOLAB now and in the future.

<https://www.snolab.ca/outreach>

- **TRIUMF High School Programs:** TRIUMF offers outreach programs for high-school students, teachers, and the general public with a mission of promoting science and research in the public arena. TRIUMF's outreach activities are also designed to tell Canadian students, teachers, and the public about the excitement of curiosity-driven research and about how a laboratory like TRIUMF adds value to Canada in new technologies, medical applications, and highly qualified people.

<https://www.triumf.ca/for-public/high-school-programs>

- **LBL Workforce Development and Education:** This group carries out Berkeley Lab's mission to inspire and prepare the next generation of scientists, engineers, and technicians.

<https://education.lbl.gov/>

14.8 Educational Programs of Experiments

- **ATLAS Education:** The ATLAS Experiment has a wide range of educational resources available for students and teachers. Categories include primary and secondary school students, university students, teachers, citizen science, and multimedia and resources.

<https://atlas.cern/resources/education>

- **CMS Education and Outreach Resources:** Access to 110 resources from Activities and Artworks to Visualizations.

<https://cds.cern.ch/collection/CMS%20Education%20and%20Outreach%20Resources?ln=en>

- **HiSPARC at UCU:** HiSPARC is an outreach, educational and research experiment on cosmic rays detection, which was initiated in the Netherlands in 2004. It brings together secondary school students and teachers, undergraduate students and university researchers in the quest to understand the origin of the most energetic particles in our universe. HSPARC has stations in the Netherlands, the United Kingdom, Denmark and Namibia.

<https://www.uu.nl/en/organisation/university-college-utrecht/hisparc-at-ucu>

- **IceCube Education and Outreach:** IceCube is committed to bringing science to a wider audience. Learning opportunities for high school students, research experiences for teachers and undergraduates, learning activities for the classroom or at home, and webcasts.

<https://icecube.wisc.edu/outreach>

- **KASCADE and KASCADE-Grande KDC:** The aim of the project KDC (KASCADE Cosmic Ray Data Centre) is the installation and establishment of a public data centre for high-energy astroparticle physics based on the data of the KASCADE experiment.

<https://kdc.icp.kit.edu>

- **LIGO Education Resources:** Something fun and educational for K-12 educators, parents and interested students.

<https://www.ligo.caltech.edu/page/educational-resources>

- **MINERvA Neutrinos in the Classroom:** Information and educational materials provide high school physics students with an in-depth hands-on interactive experience with real high-energy particle physics. The materials should be

suitable for a 1-2 weeks module on particle physics as it's done by professional scientists.

<https://neutrino-classroom.org>

- **VIRGO Educational Resources:** Useful resources (websites, texts, videos) for teachers and students related to gravitational waves and the interferometers like Virgo.

<http://public.virgo-gw.eu/educational-resources/>

- **Pierre Auger Observatory's Educational Pages:** The site offers information about cosmic rays and their detection, and provides material for students and teachers.

<https://www.auger.org/index.php/edu-outreach>

14.9 News

- **Asimmetrie:** Bimonthly magazine about particle physics published by INFN, the Istituto Nazionale di Fisica Nucleare (in Italian).

<http://www.asimmetrie.it/>

- **CERN Courier:**

– Website: <https://cerncourier.com>

– Twitter: @cerncourier

- **DESY inForm:**

– Website: http://www.desy.de/news/desy_inform/index_eng.html

– Twitter: @desy

- **Fermilab News:**

– Website: <https://news.fnal.gov>

– Twitter: @Fermilab

- **LC Newsline:** The newsletter of the Linear Collider community.

<http://newsline.linearcollider.org/>

– Twitter: @LCnewsline

- **IOP News:**

<http://www.iop.org/news/>

- **JINR News:**

http://www1.jinr.ru/News/Jinrnews_index.html

- **News at Interactions.org:** The Interactions site provides news and press releases on particle physics.

<http://www.interactions.org/news-center>

– Twitter: @particlnews

- **Perimeter Institute News:**

– Website: <https://www.perimeterinstitute.ca/news>

– Twitter: @perimeter

- **Sanford News and Events:**

– Website: <https://sanfordlab.org/news-and-events>

– Twitter: @SanforLab

- **SLAC Signals:** This email newsletter reports about cutting-edge science, major SLAC milestones and other lab information. It has replaced SLAC Today in November 2013. Its signup page can be found at

<http://eepurl.com/IqP11>

- **SNOLAB News and Headline:**

<https://www.snolab.ca/news>

- **Symmetry:** This magazine about particle physics and its connections to other aspects of life and science, from interdisciplinary collaborations to policy to culture is published 6 times per year by Fermilab and SLAC.

<http://www.symmetrymagazine.org/>

– Twitter: @symmetrymag

- **TRIUMF on NewsWise:**

<https://www.newswise.com/institutions/newsroom/19528>

14.10 *Art in Physics*

- **Arts@CERN - When Art Meets Science:** Arts at CERN is the leading art and science programme promoting the dialog between artists and particle physicists. Programmes include Art Commissions and Exhibitions, Collide, Accelerate and Guest Artists.

<https://arts.cern>

The Collide@CERN residency programme aims to develop expert knowledge in the arts through the connection with fundamental science. Since 2011 the COLLIDE award calls to artists to win a fully funded residency for up to 3 months.

<https://arts.cern/programme/collide>

Accelerate@CERN is a country specific one-month research award for artists who have never spent time at a science lab before.

<https://arts.cern/programme/accelerate>

- **Art of Physics Competition:** The Canadian Association of Physicists organizes this competition, the first was launched in 1992, with the aim of stimulating interest, especially among non-scientists, in some of the captivating imagery associated with physics. The challenge is to capture photographically a beautiful or unusual physics phenomenon and explain it in less than 200 words in terms that everyone can understand.

<https://www.cap.ca/programs/art-physics/>

- **Fermilab Art Gallery:** The convergence of art and science occurs daily in the Fermilab Art Gallery open to the public. To initiate and stimulate communication and interactions among scientists, artists and the public, the laboratory hosts an artist-in-residence program. The artist-in-residence interacts with scientists to learn about their research and how it connects to society. They use this information to create a body of work, leading to presentations in the community and possibly an exhibition of the artwork at Fermilab.

<http://events.fnal.gov/art-gallery/>

- **TRIUMF Science through Art:** TRIUMF's Science through Art initiatives explore the space where art and science collide. These programs bring artists and TRIUMF researchers, engineers, technicians, tradespeople, and students together to explore new ways of thinking about science, discovery, creativity, and our universe.

<https://www.triumf.ca/science-through-art>

14.11 *Blogs and Twitter*

Lists of active blogs and tweets can be found on INSPIRE:

- **Scientist blogs:**
<http://tinyurl.com/nmku27s>
- **Scientists with twitter accounts:**
<http://tinyurl.com/nrg5k63>
- **Experiments with twitter accounts:**
<http://tinyurl.com/q86kma8>
- **Institutions with twitter accounts:**
<http://tinyurl.com/mzcm3nw>

List of physicists on Twitter at TrueSciPhi:

<http://truesciphi.org/phy.html>

Some selected particle physics related blogs:

- **ATLAS blog:**
<https://atlas.cern/updates/blog>
- **Life and Physics:** Jon Butterworth's blog in the Guardian.
<http://www.guardian.co.uk/science/life-and-physics>
- **Of Particular Significance:** Conversations about science, with a current focus on particle physics, with theoretical physicist Matt Strassler.
<http://profmattstrassler.com/>
- **Particle People:** This interactions.org page highlights a new blogger involved in particle physics research each month.
<http://www.interactions.org/particle-people>
- **Preposterous Universe:** Theoretical physicist Sean Carroll's blog.
<https://www.preposterousuniverse.com/blog/>
- **Quantum diaries:** Thoughts on work and life from particle physicists from around the world, from 2005 to 2016.
<http://www.quantumdiaries.org/>
- **Quantum diaries survivor:** Experimental particle physicist Tommaso Dorigo's blog.
https://www.science20.com/quantum_diaries_survivor
- **Science blogs:** Launched in January 2006, ScienceBlogs features bloggers from a wide array of scientific disciplines, including physics.
<http://scienceblogs.com/channel/physical-science/>
- **AstroBetter:** Blog with tips and tricks for professional astronomers.
<https://www.astrobetter.com/>

SUMMARY TABLES OF PARTICLE PHYSICS

Gauge and Higgs bosons	31
Leptons	34
Quarks	37
Mesons	38
Baryons	93
Searches not in Other Sections*	111
Tests of conservation laws	113
Meson Quick Reference Table	91
Baryon Quick Reference Table	92

* There are also search limits in the Summary Tables for the Gauge and Higgs Bosons, the Leptons, the Quarks, and the Mesons.



SUMMARY TABLES OF PARTICLE PROPERTIES

Extracted from the Particle Listings of the
Review of Particle Physics

P.A. Zyla *et al.* (Particle Data Group),
Prog. Theor. Exp. Phys. **2020**, 083C01 (2020)

Available at <http://pdg.lbl.gov>

Particle Data Group

P.A. Zyla, R.M. Barnett, J. Beringer, O. Dahl, D.A. Dwyer, D.E. Groom, C.-J. Lin, K.S. Lugovsky, E. Pianori, D.J. Robinson, C.G. Wohl, W.-M. Yao, K. Agashe, G. Aielli, B.C. Allanach, C. Amsler, M. Antonelli, E.C. Aschenauer, D.M. Asner, H. Baer, Sw. Banerjee, L. Baudis, C.W. Bauer, J.J. Beatty, V.I. Belousov, S. Bethke, A. Bettini, O. Biebel, K.M. Black, E. Blucher, O. Buchmuller, V. Burkert, M.A. Bychkov, R.N. Cahn, M. Carena, A. Ceccucci, A. Cerri, D. Chakraborty, R. Sekhar Chivukula, G. Cowan, G. D'Ambrosio, T. Damour, D. de Florian, A. de Gouvêa, T. DeGrand, P. de Jong, G. Dissertori, B.A. Dobrescu, M. D'Onofrio, M. Doser, M. Drees, H.K. Dreiner, P. Eerola, U. Egede, S. Eidelman, J. Ellis, J. Erler, V.V. Ezhela, W. Fetscher, B.D. Fields, B. Foster, A. Freitas, H. Gallagher, L. Garren, H.-J. Gerber, G. Gerbier, T. Gershon, Y. Gershtein, T. Gherghetta, A.A. Godizov, M.C. Gonzalez-Garcia, M. Goodman, C. Grab, A.V. Gritsan, C. Grojean, M. Grünewald, A. Gurtu, T. Gutsche, H.E. Haber, C. Hanhart, S. Hashimoto, Y. Hayato, A. Hebecker, S. Heinemeyer, B. Heltsley, J. J. Hernández-Rey, K. Hikasa, J. Hisano, A. Höcker, J. Holder, A. Holtkamp, J. Huston, T. Hyodo, K.F. Johnson, M. Kado, M. Karliner, U.F. Katz, M. Kenzie, V.A. Khoze, S.R. Klein, E. Klempt, R.V. Kowalewski, F. Krauss, M. Kreps, B. Krusche, Y. Kwon, O. Lahav, J. Laiho, L.P. Lellouch, J. Lesgourgues, A. R. Liddle, Z. Ligeti, C. Lippmann, T.M. Liss, L. Littenberg, C. Lourenço, S.B. Lugovsky, A. Lusiani, Y. Makida, F. Maltoni, T. Mannel, A.V. Manohar, W.J. Marciano, A. Masoni, J. Matthews, U.-G. Meißner, M. Mikhasenko, D.J. Miller, D. Milstead, R.E. Mitchell, K. Mönig, P. Molaro, F. Moortgat, M. Moskvic, K. Nakamura, M. Narain, P. Nason, S. Navas, M. Neubert, P. Nevski, Y. Nir, K.A. Olive, C. Patrignani, J.A. Peacock, S.T. Petcov, V.A. Petrov, A. Pich, A. Piepke, A. Pomarol, S. Profumo, A. Quadt, K. Rabbertz, J. Rademacker, G. Raffelt, H. Ramani, M. Ramsey-Musolf, B.N. Ratcliff, P. Richardson, A. Ringwald, S. Roesler, S. Rolli, A. Romaniouk, L.J. Rosenberg, J.L. Rosner, G. Rybka, M. Ryskin, R.A. Ryutin, Y. Sakai, G.P. Salam, S. Sarkar, F. Sauli, O. Schneider, K. Scholberg, A.J. Schwartz, J. Schwiening, D. Scott, V. Sharma, S.R. Sharpe, T. Shutt, M. Silari, T. Sjöstrand, P. Skands, T. Skwarnicki, G.F. Smoot, A. Soffer, M.S. Sozzi, S. Spanier, C. Spiering, A. Stahl, S.L. Stone, Y. Sumino, T. Sumiyoshi, M.J. Syphers, F. Takahashi, M. Tanabashi, J. Tanaka, M. Taševský, K. Terashi, J. Terning, U. Thoma, R.S. Thorne, L. Tiator, M. Titov, N.P. Tkachenko, D.R. Tovey, K. Trabelsi, P. Urquijo, G. Valencia, R. Van de Water, N. Varelas, G. Venanzoni, L. Verde, M.G. Vincter, P. Vogel, W. Vogelsang, A. Vogt, V. Vorobyev, S.P. Wakely, W. Walkowiak, C.W. Walter, D. Wands, M.O. Wascko, D.H. Weinberg, E.J. Weinberg, M. White, L.R. Wiencke, S. Willocq, C.L. Woody, R.L. Workman, M. Yokoyama, R. Yoshida, G. Zanderighi, G.P. Zeller, O.V. Zenin, R.-Y. Zhu, S.-L. Zhu, F. Zimmermann

Technical Associates:

J. Anderson, T. Basaglia, V.S. Lugovsky, P. Schaffner, W. Zheng

©2020 Regents of the University of California
(Approximate closing date for data: January 15, 2020)

GAUGE AND HIGGS BOSONS

 γ (photon)

$$I(J^{PC}) = 0.1(1^{--})$$

Mass $m < 1 \times 10^{-18}$ eV
Charge $q < 1 \times 10^{-46}$ e (mixed charge)
Charge $q < 1 \times 10^{-35}$ e (single charge)
Mean life $\tau = \text{Stable}$

 g
or gluon

$$I(J^P) = 0(1^-)$$

Mass $m = 0$ [a]
SU(3) color octet

graviton

$$J = 2$$

Mass $m < 6 \times 10^{-32}$ eV

 W

$$J = 1$$

Charge = ± 1 e
Mass $m = 80.379 \pm 0.012$ GeV
 W/Z mass ratio = 0.88147 ± 0.00013
 $m_Z - m_W = 10.809 \pm 0.012$ GeV
 $m_{W^+} - m_{W^-} = -0.029 \pm 0.028$ GeV
Full width $\Gamma = 2.085 \pm 0.042$ GeV
 $\langle N_{\pi^\pm} \rangle = 15.70 \pm 0.35$
 $\langle N_{K^\pm} \rangle = 2.20 \pm 0.19$
 $\langle N_p \rangle = 0.92 \pm 0.14$
 $\langle N_{\text{charged}} \rangle = 19.39 \pm 0.08$

W^- modes are charge conjugates of the modes below.

W^+ DECAY MODES	Fraction (Γ_i/Γ)	Confidence level	ρ (MeV/c)
$\ell^+ \nu$	[b] $(10.86 \pm 0.09) \%$		–
$e^+ \nu$	$(10.71 \pm 0.16) \%$		40189
$\mu^+ \nu$	$(10.63 \pm 0.15) \%$		40189
$\tau^+ \nu$	$(11.38 \pm 0.21) \%$		40170
hadrons	$(67.41 \pm 0.27) \%$		–
$\pi^+ \gamma$	< 7	$\times 10^{-6}$	95% 40189
$D_S^+ \gamma$	< 1.3	$\times 10^{-3}$	95% 40165
cX	$(33.3 \pm 2.6) \%$		–
$c\bar{s}$	$(31 \pm_{-11}^{+13}) \%$		–
invisible	[c] $(1.4 \pm 2.9) \%$		–
$\pi^+ \pi^+ \pi^-$	< 1.01	$\times 10^{-6}$	95% 40189

 Z

$$J = 1$$

Charge = 0
Mass $m = 91.1876 \pm 0.0021$ GeV [d]
Full width $\Gamma = 2.4952 \pm 0.0023$ GeV
 $\Gamma(\ell^+ \ell^-) = 83.984 \pm 0.086$ MeV [h]
 $\Gamma(\text{invisible}) = 499.0 \pm 1.5$ MeV [e]
 $\Gamma(\text{hadrons}) = 1744.4 \pm 2.0$ MeV
 $\Gamma(\mu^+ \mu^-)/\Gamma(e^+ e^-) = 1.0001 \pm 0.0024$
 $\Gamma(\tau^+ \tau^-)/\Gamma(e^+ e^-) = 1.0020 \pm 0.0032$ [f]

Average charged multiplicity

$$\langle N_{\text{charged}} \rangle = 20.76 \pm 0.16 \quad (S = 2.1)$$

Couplings to quarks and leptons

$$g_V^\ell = -0.03783 \pm 0.00041$$

$$g_V^u = 0.266 \pm 0.034$$

$$g_V^d = -0.38 \pm_{-0.05}^{+0.04}$$

$$g_A^\ell = -0.50123 \pm 0.00026$$

$$g_A^u = 0.519 \pm_{-0.033}^{+0.028}$$

$$g_A^d = -0.527 \pm_{-0.028}^{+0.040}$$

$$g^{\nu\ell} = 0.5008 \pm 0.0008$$

$$g^{\nu e} = 0.53 \pm 0.09$$

$$g^{\nu\mu} = 0.502 \pm 0.017$$

Gauge & Higgs Boson Summary Table

Asymmetry parameters [8]

$$\begin{aligned}
 A_e &= 0.1515 \pm 0.0019 \\
 A_\mu &= 0.142 \pm 0.015 \\
 A_\tau &= 0.143 \pm 0.004 \\
 A_s &= 0.90 \pm 0.09 \\
 A_c &= 0.670 \pm 0.027 \\
 A_b &= 0.923 \pm 0.020
 \end{aligned}$$

Charge asymmetry (%) at Z pole

$$\begin{aligned}
 A_{FB}^{(0\ell)} &= 1.71 \pm 0.10 \\
 A_{FB}^{(0u)} &= 4 \pm 7 \\
 A_{FB}^{(0s)} &= 9.8 \pm 1.1 \\
 A_{FB}^{(0c)} &= 7.07 \pm 0.35 \\
 A_{FB}^{(0b)} &= 9.92 \pm 0.16
 \end{aligned}$$

Z DECAY MODES	Fraction (Γ_i/Γ)	Scale factor/ Confidence level	p (MeV/c)
e^+e^-	[h] (3.3632±0.0042) %		45594
$\mu^+\mu^-$	[h] (3.3662±0.0066) %		45594
$\tau^+\tau^-$	[h] (3.3696±0.0083) %		45559
$\ell^+\ell^-$	[b,h] (3.3658±0.0023) %		—
$\ell^+\ell^-\ell^+\ell^-$	[j] (4.63 ±0.21) × 10 ⁻⁶		45594
invisible	[h] (20.000 ±0.055) %		—
hadrons	[h] (69.911 ±0.056) %		—
($u\bar{u}+c\bar{c}$)/2	(11.6 ±0.6) %		—
($d\bar{d}+s\bar{s}+b\bar{b}$)/3	(15.6 ±0.4) %		—
$c\bar{c}$	(12.03 ±0.21) %		—
$b\bar{b}$	(15.12 ±0.05) %		—
$b\bar{b}b\bar{b}$	(3.6 ±1.3) × 10 ⁻⁴		—
$g g g$	< 1.1 %	CL=95%	—
$\pi^0\gamma$	< 2.01 × 10 ⁻⁵	CL=95%	45594
$\eta\gamma$	< 5.1 × 10 ⁻⁵	CL=95%	45592
$\rho^0\gamma$	< 2.5 × 10 ⁻⁵	CL=95%	45591
$\omega\gamma$	< 6.5 × 10 ⁻⁴	CL=95%	45590
$\eta'(958)\gamma$	< 4.2 × 10 ⁻⁵	CL=95%	45589
$\phi\gamma$	< 9 × 10 ⁻⁷	CL=95%	45588
$\gamma\gamma$	< 1.46 × 10 ⁻⁵	CL=95%	45594
$\pi^0\pi^0$	< 1.52 × 10 ⁻⁵	CL=95%	45594
$\gamma\gamma\gamma$	< 2.2 × 10 ⁻⁶	CL=95%	45594
$\pi^\pm W^\mp$	[j] < 7 × 10 ⁻⁵	CL=95%	10167
$\rho^\pm W^\mp$	[j] < 8.3 × 10 ⁻⁵	CL=95%	10142
$J/\psi(1S)X$	(3.51 ^{+0.23} _{-0.25}) × 10 ⁻³	S=1.1	—
$J/\psi(1S)\gamma$	< 1.4 × 10 ⁻⁶	CL=95%	45541
$\psi(2S)X$	(1.60 ±0.29) × 10 ⁻³		—
$\psi(2S)\gamma$	< 4.5 × 10 ⁻⁶	CL=95%	45519
$J/\psi(1S)J/\psi(1S)$	< 2.2 × 10 ⁻⁶	CL=95%	45489
$\chi_{c1}(1P)X$	(2.9 ±0.7) × 10 ⁻³		—
$\chi_{c2}(1P)X$	< 3.2 × 10 ⁻³	CL=90%	—
$\Upsilon(1S)X + \Upsilon(2S)X$ + $\Upsilon(3S)X$	(1.0 ±0.5) × 10 ⁻⁴		—
$\Upsilon(1S)X$	< 3.4 × 10 ⁻⁶	CL=95%	—
$\Upsilon(1S)\gamma$	< 2.8 × 10 ⁻⁶	CL=95%	45103
$\Upsilon(2S)X$	< 6.5 × 10 ⁻⁶	CL=95%	—
$\Upsilon(2S)\gamma$	< 1.7 × 10 ⁻⁶	CL=95%	45043
$\Upsilon(3S)X$	< 5.4 × 10 ⁻⁶	CL=95%	—
$\Upsilon(3S)\gamma$	< 4.8 × 10 ⁻⁶	CL=95%	45006
$\Upsilon(1, 2, 3S) \Upsilon(1, 2, 3S)$	< 1.5 × 10 ⁻⁶	CL=95%	—
(D^0/\bar{D}^0)X	(20.7 ±2.0) %		—
$D^\pm X$	(12.2 ±1.7) %		—
$D^*(2010)^\pm X$	[j] (11.4 ±1.3) %		—
$D_{s1}(2536)^\pm X$	(3.6 ±0.8) × 10 ⁻³		—
$D_{sJ}(2573)^\pm X$	(5.8 ±2.2) × 10 ⁻³		—
$D^*(2629)^\pm X$	searched for		—
B^+X	[k] (6.08 ±0.13) %		—
$B_s^0 X$	[k] (1.59 ±0.13) %		—
$B_c^\pm X$	searched for		—
$A_c^\pm X$	(1.54 ±0.33) %		—
$\Xi_c^0 X$	seen		—
$\Xi_c^\pm X$	seen		—
b-baryon X	[k] (1.38 ±0.22) %		—
anomalous γ + hadrons	[j] < 3.2 × 10 ⁻³	CL=95%	—
$e^+e^-\gamma$	[l] < 5.2 × 10 ⁻⁴	CL=95%	45594
$\mu^+\mu^-\gamma$	[l] < 5.6 × 10 ⁻⁴	CL=95%	45594

$\tau^+\tau^-\gamma$	[l] < 7.3	× 10 ⁻⁴	CL=95%	45559
$\ell^+\ell^-\gamma\gamma$	[n] < 6.8	× 10 ⁻⁶	CL=95%	—
$q\bar{q}\gamma\gamma$	[n] < 5.5	× 10 ⁻⁶	CL=95%	—
$\nu\bar{\nu}\gamma\gamma$	[n] < 3.1	× 10 ⁻⁶	CL=95%	45594
$e^\pm\mu^\mp$	LF [j] < 7.5	× 10 ⁻⁷	CL=95%	45594
$e^\pm\tau^\mp$	LF [j] < 9.8	× 10 ⁻⁶	CL=95%	45576
$\mu^\pm\tau^\mp$	LF [j] < 1.2	× 10 ⁻⁵	CL=95%	45576
pe	L,B < 1.8	× 10 ⁻⁶	CL=95%	45589
$p\mu$	L,B < 1.8	× 10 ⁻⁶	CL=95%	45589

H⁰

J = 0

Mass $m = 125.10 \pm 0.14$ GeVFull width $\Gamma < 0.013$ GeV, CL = 95% (assumes equal on-shell and off-shell effective couplings)**H⁰ Signal Strengths in Different Channels**

Combined Final States = 1.13 ± 0.06

 $WW^* = 1.19 \pm 0.12$ $ZZ^* = 1.20^{+0.12}_{-0.11}$ $\gamma\gamma = 1.11^{+0.10}_{-0.09}$ $c\bar{c}$ Final State < 110, CL = 95% $b\bar{b} = 1.04 \pm 0.13$ $\mu^+\mu^- = 0.6 \pm 0.8$ $\tau^+\tau^- = 1.15^{+0.16}_{-0.15}$ $Z\gamma < 6.6$, CL = 95%

top Yukawa coupling < 1.7, CL = 95%

 $t\bar{t}H^0$ Production = 1.28 ± 0.20 H^0 Production Cross Section in pp Collisions at $\sqrt{s} = 13$ TeV = 59 ± 5 pb**H⁰ DECAY MODES**

H ⁰ DECAY MODES	Fraction (Γ_i/Γ)	Confidence level	p (MeV/c)
e^+e^-	< 3.6 × 10 ⁻⁴	95%	62550
$J/\psi\gamma$	< 3.5 × 10 ⁻⁴	95%	62511
$J/\psi J/\psi$	< 1.8 × 10 ⁻³	95%	62473
$\psi(2S)\gamma$	< 2.0 × 10 ⁻³	95%	62495
$\Upsilon(1S)\gamma$	< 4.9 × 10 ⁻⁴	95%	62192
$\Upsilon(2S)\gamma$	< 5.9 × 10 ⁻⁴	95%	62148
$\Upsilon(3S)\gamma$	< 5.7 × 10 ⁻⁴	95%	62121
$\Upsilon(nS) \Upsilon(mS)$	< 1.4 × 10 ⁻³	95%	—
$\rho(770)\gamma$	< 8.8 × 10 ⁻⁴	95%	62547
$\phi(1020)\gamma$	< 4.8 × 10 ⁻⁴	95%	62546
$e\mu$	LF < 6.1 × 10 ⁻⁵	95%	62550
$e\tau$	LF < 4.7 × 10 ⁻³	95%	62537
$\mu\tau$	LF < 2.5 × 10 ⁻³	95%	62537
γ invisible	< 4.6 %	95%	—

Neutral Higgs Bosons, Searches for**Mass limits for heavy neutral Higgs bosons (H_2^0, A^0) in the MSSM** $m > 389$ GeV, CL = 95% ($\tan\beta = 10$) $m > 863$ GeV, CL = 95% ($\tan\beta = 20$) $m > 1157$ GeV, CL = 95% ($\tan\beta = 30$) $m > 1341$ GeV, CL = 95% ($\tan\beta = 40$) $m > 1496$ GeV, CL = 95% ($\tan\beta = 50$) $m > 1613$ GeV, CL = 95% ($\tan\beta = 60$)**Charged Higgs Bosons (H^\pm and $H^{\pm\pm}$), Searches for****Mass limits for $m_{H^\pm} < m(\text{top})$** $m > 155$ GeV, CL = 95%**Mass limits for $m_{H^\pm} > m(\text{top})$** $m > 181$ GeV, CL = 95% ($\tan\beta = 10$) $m > 249$ GeV, CL = 95% ($\tan\beta = 20$) $m > 390$ GeV, CL = 95% ($\tan\beta = 30$) $m > 894$ GeV, CL = 95% ($\tan\beta = 40$) $m > 1017$ GeV, CL = 95% ($\tan\beta = 50$) $m > 1103$ GeV, CL = 95% ($\tan\beta = 60$)

**New Heavy Bosons
(W' , Z' , leptoquarks, etc.),
Searches for**

Additional W Bosons

- W' with standard couplings
Mass $m > 5200$ GeV, CL = 95% (pp direct search)
 W_R (Right-handed W Boson)
Mass $m > 715$ GeV, CL = 90% (electroweak fit)

Additional Z Bosons

- Z'_{SM} with standard couplings
Mass $m > 4.500 \times 10^3$ GeV, CL = 95% (pp direct search)
 Z_{LR} of $SU(2)_L \times SU(2)_R \times U(1)$ (with $g_L = g_R$)
Mass $m > 630$ GeV, CL = 95% ($p\bar{p}$ direct search)
Mass $m > 1162$ GeV, CL = 95% (electroweak fit)
 Z_χ of $SO(10) \rightarrow SU(5) \times U(1)_\chi$ (with $g_\chi = e/\cos\theta_W$)
Mass $m > 4.100 \times 10^3$ GeV, CL = 95% (pp direct search)
 Z_ψ of $E_6 \rightarrow SO(10) \times U(1)_\psi$ (with $g_\psi = e/\cos\theta_W$)
Mass $m > 3900$ GeV, CL = 95% (pp direct search)
 Z_η of $E_6 \rightarrow SU(3) \times SU(2) \times U(1) \times U(1)_\eta$ (with $g_\eta = e/\cos\theta_W$)
Mass $m > 3.900 \times 10^3$ GeV, CL = 95% (pp direct search)

Scalar Leptoquarks

- $m > 1050$ GeV, CL = 95% (1st gen., pair prod., $B(\tau t)=1$)
 $m > 1755$ GeV, CL = 95% (1st gen., single prod., $B(\tau b)=1$)
 $m > 1420$ GeV, CL = 95% (2nd gen., pair prod., $B(\mu t)=1$)
 $m > 660$ GeV, CL = 95% (2nd gen., single prod., $B(\mu q)=1$)
 $m > 900$ GeV, CL = 95% (3rd gen., pair prod., $B(e q)=1$)
 $m > 740$ GeV, CL = 95% (3rd gen., single prod., $B(e q)=1$)
(See the Particle Listings for assumptions on leptoquark quantum numbers and branching fractions.)

Diquarks

- Mass $m > 6000$ GeV, CL = 95% (E_6 diquark)

Axiguon

- Mass $m > 6100$ GeV, CL = 95%

**Axions (A^0) and Other
Very Light Bosons, Searches for**

See the review on "Axions and other similar particles."

The best limit for the half-life of neutrinoless double beta decay with Majoron emission is $> 7.2 \times 10^{24}$ years (CL = 90%).

NOTES

In this Summary Table:

When a quantity has "($S = \dots$)" to its right, the error on the quantity has been enlarged by the "scale factor" S , defined as $S = \sqrt{\chi^2/(N-1)}$, where N is the number of measurements used in calculating the quantity. We do this when $S > 1$, which often indicates that the measurements are inconsistent. When $S > 1.25$, we also show in the Particle Listings an ideogram of the measurements. For more about S , see the Introduction.

A decay momentum p is given for each decay mode. For a 2-body decay, p is the momentum of each decay product in the rest frame of the decaying particle. For a 3-or-more-body decay, p is the largest momentum any of the products can have in this frame.

- [a] Theoretical value. A mass as large as a few MeV may not be precluded.
[b] ℓ indicates each type of lepton (e , μ , and τ), not sum over them.
[c] This represents the width for the decay of the W boson into a charged particle with momentum below detectability, $p < 200$ MeV.
[d] The Z -boson mass listed here corresponds to a Breit-Wigner resonance parameter. It lies approximately 34 MeV above the real part of the position of the pole (in the energy-squared plane) in the Z -boson propagator.
[e] This partial width takes into account Z decays into $\nu\bar{\nu}$ and any other possible undetected modes.
[f] This ratio has not been corrected for the τ mass.
[g] Here $A \equiv 2g_V g_A / (g_V^2 + g_A^2)$.
[h] This parameter is not directly used in the overall fit but is derived using the fit results; see the note "The Z boson" and ref. LEP-SLC 06 (Physics Reports (Physics Letters C) **427** 257 (2006)).
[i] Here ℓ indicates e or μ .
[j] The value is for the sum of the charge states or particle/antiparticle states indicated.
[k] This value is updated using the product of (i) the $Z \rightarrow b\bar{b}$ fraction from this listing and (ii) the b -hadron fraction in an unbiased sample of weakly decaying b -hadrons produced in Z -decays provided by the Heavy Flavor Averaging Group (HFLAV, <http://www.slac.stanford.edu/xorg/hflav/osc/PDG.2009/#FRACZ>).
[l] See the Z Particle Listings for the γ energy range used in this measurement.
[n] For $m_{\gamma\gamma} = (60 \pm 5)$ GeV.

Lepton Summary Table

LEPTONS

e

$$J = \frac{1}{2}$$

Mass $m = (548.5799070 \pm 0.000000016) \times 10^{-6} \text{ u}$
 Mass $m = 0.5109989461 \pm 0.0000000031 \text{ MeV}$
 $|m_{e^+} - m_{e^-}|/m < 8 \times 10^{-9}$, CL = 90%
 $|q_{e^+} + q_{e^-}|/e < 4 \times 10^{-8}$
 Magnetic moment anomaly
 $(g-2)/2 = (1159.65218091 \pm 0.00000026) \times 10^{-6}$
 $(g_{e^+} - g_{e^-}) / g_{\text{average}} = (-0.5 \pm 2.1) \times 10^{-12}$
 Electric dipole moment $d < 0.11 \times 10^{-28} \text{ ecm}$, CL = 90%
 Mean life $\tau > 6.6 \times 10^{28} \text{ yr}$, CL = 90% [a]

 μ

$$J = \frac{1}{2}$$

Mass $m = 0.1134289257 \pm 0.0000000025 \text{ u}$
 Mass $m = 105.6583745 \pm 0.0000024 \text{ MeV}$
 Mean life $\tau = (2.1969811 \pm 0.0000022) \times 10^{-6} \text{ s}$
 $\tau_{\mu^+}/\tau_{\mu^-} = 1.00002 \pm 0.00008$
 $c\tau = 658.6384 \text{ m}$
 Magnetic moment anomaly $(g-2)/2 = (11659209 \pm 6) \times 10^{-10}$
 $(g_{\mu^+} - g_{\mu^-}) / g_{\text{average}} = (-0.11 \pm 0.12) \times 10^{-8}$
 Electric dipole moment $|d| < 1.8 \times 10^{-19} \text{ ecm}$, CL = 95%

Decay parameters [b]

$\rho = 0.74979 \pm 0.00026$
 $\eta = 0.057 \pm 0.034$
 $\delta = 0.75047 \pm 0.00034$
 $\xi P_{\mu} = 1.0009^{+0.0016}_{-0.0007} [c]$
 $\xi P_{\mu} \delta / \rho = 1.0018^{+0.0016}_{-0.0007} [c]$
 $\xi' = 1.00 \pm 0.04$
 $\xi'' = 0.98 \pm 0.04$
 $\alpha/A = (0 \pm 4) \times 10^{-3}$
 $\alpha'/A = (-10 \pm 20) \times 10^{-3}$
 $\beta/A = (4 \pm 6) \times 10^{-3}$
 $\beta'/A = (2 \pm 7) \times 10^{-3}$
 $\overline{\eta} = 0.02 \pm 0.08$

μ^+ modes are charge conjugates of the modes below.

μ^- DECAY MODES	Fraction (Γ_i/Γ)	Confidence level	ρ (MeV/c)
$e^- \overline{\nu}_e \nu_{\mu}$	$\approx 100\%$		53
$e^- \overline{\nu}_e \nu_{\mu} \gamma$	[d] $(6.0 \pm 0.5) \times 10^{-8}$		53
$e^- \overline{\nu}_e \nu_{\mu} e^+ e^-$	[e] $(3.4 \pm 0.4) \times 10^{-5}$		53
Lepton Family number (LF) violating modes			
$e^- \nu_e \overline{\nu}_{\mu}$	LF [f] < 1.2	%	90% 53
$e^- \gamma$	LF < 4.2	$\times 10^{-13}$	90% 53
$e^- e^+ e^-$	LF < 1.0	$\times 10^{-12}$	90% 53
$e^- 2\gamma$	LF < 7.2	$\times 10^{-11}$	90% 53

 τ

$$J = \frac{1}{2}$$

Mass $m = 1776.86 \pm 0.12 \text{ MeV}$
 $(m_{\tau^+} - m_{\tau^-})/m_{\text{average}} < 2.8 \times 10^{-4}$, CL = 90%
 Mean life $\tau = (290.3 \pm 0.5) \times 10^{-15} \text{ s}$
 $c\tau = 87.03 \mu\text{m}$
 Magnetic moment anomaly > -0.052 and < 0.013 , CL = 95%
 $\text{Re}(d_{\tau}) = -0.220$ to $0.45 \times 10^{-16} \text{ ecm}$, CL = 95%
 $\text{Im}(d_{\tau}) = -0.250$ to $0.0080 \times 10^{-16} \text{ ecm}$, CL = 95%

Weak dipole moment

$\text{Re}(d_{\tau}^W) < 0.50 \times 10^{-17} \text{ ecm}$, CL = 95%
 $\text{Im}(d_{\tau}^W) < 1.1 \times 10^{-17} \text{ ecm}$, CL = 95%

Weak anomalous magnetic dipole moment

$\text{Re}(\alpha_{\tau}^W) < 1.1 \times 10^{-3}$, CL = 95%
 $\text{Im}(\alpha_{\tau}^W) < 2.7 \times 10^{-3}$, CL = 95%
 $\tau^{\pm} \rightarrow \pi^{\pm} K_S^0 \nu_{\tau}$ (RATE DIFFERENCE) / (RATE SUM) = $(-0.36 \pm 0.25)\%$

Decay parameters

See the τ Particle Listings for a note concerning τ -decay parameters.

$\rho(e \text{ or } \mu) = 0.745 \pm 0.008$
 $\rho(e) = 0.747 \pm 0.010$
 $\rho(\mu) = 0.763 \pm 0.020$
 $\xi(e \text{ or } \mu) = 0.985 \pm 0.030$
 $\xi(e) = 0.994 \pm 0.040$
 $\xi(\mu) = 1.030 \pm 0.059$
 $\eta(e \text{ or } \mu) = 0.013 \pm 0.020$
 $\eta(\mu) = 0.094 \pm 0.073$
 $(\delta\xi)(e \text{ or } \mu) = 0.746 \pm 0.021$
 $(\delta\xi)(e) = 0.734 \pm 0.028$
 $(\delta\xi)(\mu) = 0.778 \pm 0.037$
 $\xi(\pi) = 0.993 \pm 0.022$
 $\xi(\rho) = 0.994 \pm 0.008$
 $\xi(a_1) = 1.001 \pm 0.027$
 $\xi(\text{all hadronic modes}) = 0.995 \pm 0.007$
 $\overline{\eta}(\mu)$ PARAMETER = -1.3 ± 1.7
 $\xi_{\kappa}(e)$ PARAMETER = -0.4 ± 1.2
 $\xi_{\kappa}(\mu)$ PARAMETER = 0.8 ± 0.6

τ^+ modes are charge conjugates of the modes below. " h^{\pm} " stands for π^{\pm} or K^{\pm} . " e^{\pm} " stands for e or μ . "Neutrals" stands for γ 's and/or π^0 's.

τ^- DECAY MODES	Fraction (Γ_i/Γ)	Scale factor / Confidence level	ρ (MeV/c)
Modes with one charged particle			
particle $^- \geq 0$ neutrals $\geq 0K^0 \nu_{\tau}$ ("1-prong")	$(85.24 \pm 0.06) \%$		-
particle $^- \geq 0$ neutrals $\geq 0K_L^0 \nu_{\tau}$	$(84.58 \pm 0.06) \%$		-
$\mu^- \overline{\nu}_{\mu} \nu_{\tau}$	[g] $(17.39 \pm 0.04) \%$		885
$\mu^- \overline{\nu}_{\mu} \nu_{\tau} \gamma$	[e] $(3.67 \pm 0.08) \times 10^{-3}$		885
$e^- \overline{\nu}_e \nu_{\tau}$	[g] $(17.82 \pm 0.04) \%$		888
$e^- \overline{\nu}_e \nu_{\tau} \gamma$	[e] $(1.83 \pm 0.05) \%$		888
$h^- \geq 0K_L^0 \nu_{\tau}$	$(12.03 \pm 0.05) \%$		883
$h^- \nu_{\tau}$	$(11.51 \pm 0.05) \%$		883
$\pi^- \nu_{\tau}$	[g] $(10.82 \pm 0.05) \%$		883
$K^- \nu_{\tau}$	[g] $(6.96 \pm 0.10) \times 10^{-3}$		820
$h^- \geq 1$ neutrals ν_{τ}	$(37.01 \pm 0.09) \%$		-
$h^- \geq 1\pi^0 \nu_{\tau}$ (ex. K^0)	$(36.51 \pm 0.09) \%$		-
$h^- \pi^0 \nu_{\tau}$	$(25.93 \pm 0.09) \%$		878
$\pi^- \pi^0 \nu_{\tau}$	[g] $(25.49 \pm 0.09) \%$		878
$\pi^- \pi^0$ non- $\rho(770) \nu_{\tau}$	$(3.0 \pm 3.2) \times 10^{-3}$		878
$K^- \pi^0 \nu_{\tau}$	[g] $(4.33 \pm 0.15) \times 10^{-3}$		814
$h^- \geq 2\pi^0 \nu_{\tau}$	$(10.81 \pm 0.09) \%$		-
$h^- 2\pi^0 \nu_{\tau}$	$(9.48 \pm 0.10) \%$		862
$h^- 2\pi^0 \nu_{\tau}$ (ex. K^0)	$(9.32 \pm 0.10) \%$		862
$\pi^- 2\pi^0 \nu_{\tau}$ (ex. K^0)	[g] $(9.26 \pm 0.10) \%$		862
$\pi^- 2\pi^0 \nu_{\tau}$ (ex. K^0), scalar	< 9	$\times 10^{-3}$ CL=95%	862
$\pi^- 2\pi^0 \nu_{\tau}$ (ex. K^0), vector	< 7	$\times 10^{-3}$ CL=95%	862
$K^- 2\pi^0 \nu_{\tau}$ (ex. K^0)	[g] $(6.5 \pm 2.2) \times 10^{-4}$		796
$h^- \geq 3\pi^0 \nu_{\tau}$	$(1.34 \pm 0.07) \%$		-
$h^- \geq 3\pi^0 \nu_{\tau}$ (ex. K^0)	$(1.25 \pm 0.07) \%$		-
$h^- 3\pi^0 \nu_{\tau}$	$(1.18 \pm 0.07) \%$		836
$\pi^- 3\pi^0 \nu_{\tau}$ (ex. K^0)	[g] $(1.04 \pm 0.07) \%$		836
$K^- 3\pi^0 \nu_{\tau}$ (ex. K^0)	[g] $(4.8 \pm 2.1) \times 10^{-4}$		765
η			
$h^- 4\pi^0 \nu_{\tau}$ (ex. K^0)	$(1.6 \pm 0.4) \times 10^{-3}$		800
$h^- 4\pi^0 \nu_{\tau}$ (ex. K^0, η)	[g] $(1.1 \pm 0.4) \times 10^{-3}$		800
$a_1(1260) \nu_{\tau} \rightarrow \pi^- \gamma \nu_{\tau}$	$(3.8 \pm 1.5) \times 10^{-4}$		-
$K^- \geq 0\pi^0 \geq 0K^0 \geq 0\gamma \nu_{\tau}$	$(1.552 \pm 0.029) \%$		820
$K^- \geq 1(\pi^0 \text{ or } K^0 \text{ or } \gamma) \nu_{\tau}$	$(8.59 \pm 0.28) \times 10^{-3}$		-
Modes with K^0 's			
$K_S^0(\text{particles})^- \nu_{\tau}$	$(9.43 \pm 0.28) \times 10^{-3}$		-
$h^- K^0 \nu_{\tau}$	$(9.87 \pm 0.14) \times 10^{-3}$		812
$\pi^- K^0 \nu_{\tau}$	[g] $(8.38 \pm 0.14) \times 10^{-3}$		812
$\pi^- \overline{K}^0 \nu_{\tau}$	$(5.4 \pm 2.1) \times 10^{-4}$		812
$(\text{non-}K^*(892)^- \nu_{\tau})$			
$K^- K^0 \nu_{\tau}$	[g] $(1.486 \pm 0.034) \times 10^{-3}$		737
$K^- K^0 \geq 0\pi^0 \nu_{\tau}$	$(2.99 \pm 0.07) \times 10^{-3}$		737
$h^- \overline{K}^0 \pi^0 \nu_{\tau}$	$(5.32 \pm 0.13) \times 10^{-3}$		794
$\pi^- \overline{K}^0 \pi^0 \nu_{\tau}$	[g] $(3.82 \pm 0.13) \times 10^{-3}$		794
$\overline{K}^0 \rho^- \nu_{\tau}$	$(2.2 \pm 0.5) \times 10^{-3}$		612

Lepton Summary Table

$K^- K^0 \pi^0 \nu_\tau$	[g]	$(1.50 \pm 0.07) \times 10^{-3}$	685	$K^- K^+ K^- \pi^0 \nu_\tau$	< 4.8	$\times 10^{-6}$ CL=90%	345
$\pi^- \bar{K}^0 \geq 1 \pi^0 \nu_\tau$		$(4.08 \pm 0.25) \times 10^{-3}$	-	$\pi^- K^+ \pi^- \geq 0$ neut. ν_τ	< 2.5	$\times 10^{-3}$ CL=95%	794
$\pi^- \bar{K}^0 \pi^0 \pi^0 \nu_\tau$ (ex. K^0)	[g]	$(2.6 \pm 2.3) \times 10^{-4}$	763	$e^- e^- e^+ \bar{\nu}_e \nu_\tau$	$(2.8 \pm 1.5) \times 10^{-5}$		888
$K^- K^0 \pi^0 \pi^0 \nu_\tau$		< 1.6	$\times 10^{-4}$ CL=95%	$\mu^- e^- e^+ \bar{\nu}_\mu \nu_\tau$	< 3.2	$\times 10^{-5}$ CL=90%	885
$\pi^- K^0 \bar{K}^0 \nu_\tau$		$(1.55 \pm 0.24) \times 10^{-3}$	682	$\pi^- \mu^- \mu^+ \nu_\tau$	< 1.14	$\times 10^{-5}$ CL=90%	870
$\pi^- K_S^0 K_S^0 \nu_\tau$	[g]	$(2.35 \pm 0.06) \times 10^{-4}$	682	Modes with five charged particles			
$\pi^- K_S^0 K_L^0 \nu_\tau$	[g]	$(1.08 \pm 0.24) \times 10^{-3}$	682	$3h^- 2h^+ \geq 0$ neutrals ν_τ	$(9.9 \pm 0.4) \times 10^{-4}$		794
$\pi^- K_L^0 K_L^0 \nu_\tau$		$(2.35 \pm 0.06) \times 10^{-4}$	682	(ex. $K_S^0 \rightarrow \pi^- \pi^+$)			
$\pi^- K^0 \bar{K}^0 \pi^0 \nu_\tau$		$(3.6 \pm 1.2) \times 10^{-4}$	614	("5-prong")			
$\pi^- K_S^0 K_S^0 \pi^0 \nu_\tau$	[g]	$(1.82 \pm 0.21) \times 10^{-5}$	614	$3h^- 2h^+ \nu_\tau$ (ex. K^0)	$(8.29 \pm 0.31) \times 10^{-4}$		794
$K^{*-} K^0 \pi^0 \nu_\tau \rightarrow$		$(1.08 \pm 0.21) \times 10^{-5}$	-	$3\pi^- 2\pi^+ \nu_\tau$ (ex. K^0, ω)	$(8.27 \pm 0.31) \times 10^{-4}$		794
$\pi^- K_S^0 K_S^0 \pi^0 \nu_\tau$				$3\pi^- 2\pi^+ \nu_\tau$ (ex. K^0, ω , $f_1(1285)$)	[g] $(7.75 \pm 0.30) \times 10^{-4}$		-
$f_1(1285) \pi^- \nu_\tau \rightarrow$		$(6.8 \pm 1.5) \times 10^{-6}$	-	$K^- 2\pi^- 2\pi^+ \nu_\tau$ (ex. K^0)	[g] $(6 \pm 12) \times 10^{-7}$		716
$\pi^- K_S^0 K_S^0 \pi^0 \nu_\tau$				$K^+ 3\pi^- \pi^+ \nu_\tau$	< 5.0	$\times 10^{-6}$ CL=90%	716
$f_1(1420) \pi^- \nu_\tau \rightarrow$		$(2.4 \pm 0.8) \times 10^{-6}$	-	$K^+ K^- 2\pi^- \pi^+ \nu_\tau$	< 4.5	$\times 10^{-7}$ CL=90%	528
$\pi^- K_S^0 K_S^0 \pi^0 \nu_\tau$				$3h^- 2h^+ \pi^0 \nu_\tau$ (ex. K^0)	$(1.65 \pm 0.11) \times 10^{-4}$		746
$\pi^- K_S^0 K_L^0 \pi^0 \nu_\tau$	[g]	$(3.2 \pm 1.2) \times 10^{-4}$	614	$3\pi^- 2\pi^+ \pi^0 \nu_\tau$ (ex. K^0)	$(1.63 \pm 0.11) \times 10^{-4}$		746
$\pi^- K_L^0 K_L^0 \pi^0 \nu_\tau$		$(1.82 \pm 0.21) \times 10^{-5}$	614	$3\pi^- 2\pi^+ \pi^0 \nu_\tau$ (ex. K^0, η , $f_1(1285)$)	$(1.11 \pm 0.10) \times 10^{-4}$		-
$K^- K_S^0 K_S^0 \nu_\tau$	< 6.3	$\times 10^{-7}$ CL=90%	466	$3\pi^- 2\pi^+ \pi^0 \nu_\tau$ (ex. K^0, η , ω , $f_1(1285)$)	[g] $(3.8 \pm 0.9) \times 10^{-5}$		-
$K^- K_S^0 K_L^0 \nu_\tau$	< 4.0	$\times 10^{-7}$ CL=90%	337	$K^- 2\pi^- 2\pi^+ \pi^0 \nu_\tau$ (ex. K^0)	[g] $(1.1 \pm 0.6) \times 10^{-6}$		657
$K^0 h^+ h^- h^- \geq 0$ neutrals ν_τ	< 1.7	$\times 10^{-3}$ CL=95%	760	$K^+ 3\pi^- \pi^+ \pi^0 \nu_\tau$	< 8	$\times 10^{-7}$ CL=90%	657
$K^0 h^+ h^- h^- \nu_\tau$	[g]	$(2.5 \pm 2.0) \times 10^{-4}$	760	$3h^- 2h^+ 2\pi^0 \nu_\tau$	< 3.4	$\times 10^{-6}$ CL=90%	687
Modes with three charged particles							
$h^- h^- h^+ \geq 0$ neutrals $\geq 0 K_L^0 \nu_\tau$		$(15.20 \pm 0.06) \%$	861	Miscellaneous other allowed modes			
$h^- h^- h^+ \geq 0$ neutrals ν_τ		$(14.55 \pm 0.06) \%$	861	$(5\pi)^- \nu_\tau$	$(7.8 \pm 0.5) \times 10^{-3}$		800
(ex. $K_S^0 \rightarrow \pi^+ \pi^-$)				$4h^- 3h^+ \geq 0$ neutrals ν_τ	< 3.0	$\times 10^{-7}$ CL=90%	682
("3-prong")				("7-prong")			
$h^- h^- h^+ \nu_\tau$		$(9.80 \pm 0.05) \%$	861	$4h^- 3h^+ \nu_\tau$	< 4.3	$\times 10^{-7}$ CL=90%	682
$h^- h^- h^+ \nu_\tau$ (ex. K^0)		$(9.46 \pm 0.05) \%$	861	$4h^- 3h^+ \pi^0 \nu_\tau$	< 2.5	$\times 10^{-7}$ CL=90%	612
$h^- h^- h^+ \nu_\tau$ (ex. K^0, ω)		$(9.43 \pm 0.05) \%$	861	$X^- (S=-1) \nu_\tau$	$(2.92 \pm 0.04) \%$		-
$\pi^- \pi^+ \pi^- \nu_\tau$		$(9.31 \pm 0.05) \%$	861	$K^*(892)^- \geq 0$ neutrals \geq	$(1.42 \pm 0.18) \%$	S=1.4	665
$\pi^- \pi^+ \pi^- \nu_\tau$ (ex. K^0)		$(9.02 \pm 0.05) \%$	861	$0 K^0 \nu_\tau$			
$\pi^- \pi^+ \pi^- \nu_\tau$ (ex. K^0),	< 2.4	%	CL=95%	$K^*(892)^- \nu_\tau$	$(1.20 \pm 0.07) \%$	S=1.8	665
non-axial vector				$K^*(892)^- \nu_\tau \rightarrow \pi^- \bar{K}^0 \nu_\tau$	$(7.82 \pm 0.26) \times 10^{-3}$		-
$\pi^- \pi^+ \pi^- \nu_\tau$ (ex. K^0, ω)	[g]	$(8.99 \pm 0.05) \%$	861	$K^*(892)^0 K^- \geq 0$ neutrals ν_τ	$(3.2 \pm 1.4) \times 10^{-3}$		542
$h^- h^- h^+ \geq 1$ neutrals ν_τ		$(5.29 \pm 0.05) \%$	-	$K^*(892)^0 K^- \nu_\tau$	$(2.1 \pm 0.4) \times 10^{-3}$		542
$h^- h^- h^+ \geq 1\pi^0 \nu_\tau$ (ex. K^0)		$(5.09 \pm 0.05) \%$	-	$\bar{K}^*(892)^0 \pi^- \geq 0$ neutrals ν_τ	$(3.8 \pm 1.7) \times 10^{-3}$		655
$h^- h^- h^+ \pi^0 \nu_\tau$		$(4.76 \pm 0.05) \%$	834	$\bar{K}^*(892)^0 \pi^- \nu_\tau$	$(2.2 \pm 0.5) \times 10^{-3}$		655
$h^- h^- h^+ \pi^0 \nu_\tau$ (ex. K^0)		$(4.57 \pm 0.05) \%$	834	$(\bar{K}^*(892) \pi)^- \nu_\tau \rightarrow$	$(1.0 \pm 0.4) \times 10^{-3}$		-
$h^- h^- h^+ \pi^0 \nu_\tau$ (ex. K^0, ω)		$(2.79 \pm 0.07) \%$	834	$\pi^- \bar{K}^0 \pi^0 \nu_\tau$			
$\pi^- \pi^+ \pi^- \pi^0 \nu_\tau$		$(4.62 \pm 0.05) \%$	834	$K_1(1270)^- \nu_\tau$	$(4.7 \pm 1.1) \times 10^{-3}$		447
$\pi^- \pi^+ \pi^- \pi^0 \nu_\tau$ (ex. K^0)		$(4.49 \pm 0.05) \%$	834	$K_1(1400)^- \nu_\tau$	$(1.7 \pm 2.6) \times 10^{-3}$	S=1.7	335
$\pi^- \pi^+ \pi^- \pi^0 \nu_\tau$ (ex. K^0, ω)	[g]	$(2.74 \pm 0.07) \%$	834	$K^*(1410)^- \nu_\tau$	$(1.5 \pm 1.4) \times 10^{-3}$		326
$h^- h^- h^+ \geq 2\pi^0 \nu_\tau$ (ex. K^0)		$(5.17 \pm 0.31) \times 10^{-3}$	-	$K_0^*(1430)^- \nu_\tau$	< 5	$\times 10^{-4}$ CL=95%	317
$h^- h^- h^+ 2\pi^0 \nu_\tau$		$(5.05 \pm 0.31) \times 10^{-3}$	797	$K_2^*(1430)^- \nu_\tau$	< 3	$\times 10^{-3}$ CL=95%	315
$h^- h^- h^+ 2\pi^0 \nu_\tau$ (ex. K^0)		$(4.95 \pm 0.31) \times 10^{-3}$	797	$\eta \pi^- \nu_\tau$	< 9.9	$\times 10^{-5}$ CL=95%	797
$h^- h^- h^+ 2\pi^0 \nu_\tau$ (ex. K^0, ω, η)	[g]	$(10 \pm 4) \times 10^{-4}$	797	$\eta \pi^- \pi^0 \nu_\tau$	[g] $(1.39 \pm 0.07) \times 10^{-3}$		778
$h^- h^- h^+ 3\pi^0 \nu_\tau$		$(2.13 \pm 0.30) \times 10^{-4}$	749	$\eta \pi^- \pi^0 \pi^0 \nu_\tau$	[g] $(2.0 \pm 0.4) \times 10^{-4}$		746
$2\pi^- \pi^+ 3\pi^0 \nu_\tau$ (ex. K^0)		$(1.95 \pm 0.30) \times 10^{-4}$	749	$\eta K^- \nu_\tau$	[g] $(1.55 \pm 0.08) \times 10^{-4}$		719
$2\pi^- \pi^+ 3\pi^0 \nu_\tau$ (ex. K^0, η , $f_1(1285)$)		$(1.7 \pm 0.4) \times 10^{-4}$	-	$\eta K^*(892)^- \nu_\tau$	$(1.38 \pm 0.15) \times 10^{-4}$		511
$2\pi^- \pi^+ 3\pi^0 \nu_\tau$ (ex. K^0, η , ω , $f_1(1285)$)	[g]	$(1.4 \pm 2.7) \times 10^{-5}$	-	$\eta K^- \pi^0 \nu_\tau$	[g] $(4.8 \pm 1.2) \times 10^{-5}$		665
$K^- h^+ h^- \geq 0$ neutrals ν_τ		$(6.29 \pm 0.14) \times 10^{-3}$	794	$\eta K^- \pi^0$ (non- $K^*(892)) \nu_\tau$	< 3.5	$\times 10^{-5}$ CL=90%	-
$K^- h^+ \pi^- \nu_\tau$ (ex. K^0)		$(4.37 \pm 0.07) \times 10^{-3}$	794	$\eta \bar{K}^0 \pi^- \nu_\tau$	[g] $(9.4 \pm 1.5) \times 10^{-5}$		661
$K^- h^+ \pi^- \pi^0 \nu_\tau$ (ex. K^0)		$(8.6 \pm 1.2) \times 10^{-4}$	763	$\eta \bar{K}^0 \pi^- \pi^0 \nu_\tau$	< 5.0	$\times 10^{-5}$ CL=90%	590
$K^- \pi^+ \pi^- \geq 0$ neutrals ν_τ		$(4.77 \pm 0.14) \times 10^{-3}$	794	$\eta K^- K^0 \nu_\tau$	< 9.0	$\times 10^{-6}$ CL=90%	430
$K^- \pi^+ \pi^- \geq 0\pi^0 \nu_\tau$ (ex. K^0)		$(3.73 \pm 0.13) \times 10^{-3}$	794	$\eta \pi^+ \pi^- \pi^- \geq 0$ neutrals ν_τ	< 3	$\times 10^{-3}$ CL=90%	744
$K^- \pi^+ \pi^- \nu_\tau$ (ex. K^0)		$(3.45 \pm 0.07) \times 10^{-3}$	794	$\eta \pi^- \pi^+ \pi^- \nu_\tau$ (ex. K^0)	[g] $(2.20 \pm 0.13) \times 10^{-4}$		744
$K^- \pi^+ \pi^- \nu_\tau$ (ex. K^0)		$(2.93 \pm 0.07) \times 10^{-3}$	794	$\eta \pi^- \pi^+ \pi^- \nu_\tau$ (ex. $K^0, f_1(1285)$)	$(9.9 \pm 1.6) \times 10^{-5}$		-
$K^- \pi^+ \pi^- \nu_\tau$ (ex. K^0, ω)	[g]	$(2.93 \pm 0.07) \times 10^{-3}$	794	$\eta a_1(1260)^- \nu_\tau \rightarrow \eta \pi^- \rho^0 \nu_\tau$	< 3.9	$\times 10^{-4}$ CL=90%	-
$K^- \rho^0 \nu_\tau \rightarrow$		$(1.4 \pm 0.5) \times 10^{-3}$	-	$\eta \eta \pi^- \nu_\tau$	< 7.4	$\times 10^{-6}$ CL=90%	637
$K^- \pi^+ \pi^- \pi^- \nu_\tau$		$(1.31 \pm 0.12) \times 10^{-3}$	763	$\eta \eta \pi^- \pi^0 \nu_\tau$	< 2.0	$\times 10^{-4}$ CL=95%	559
$K^- \pi^+ \pi^- \pi^0 \nu_\tau$ (ex. K^0)		$(7.9 \pm 1.2) \times 10^{-4}$	763	$\eta \eta K^- \nu_\tau$	< 3.0	$\times 10^{-6}$ CL=90%	382
$K^- \pi^+ \pi^- \pi^0 \nu_\tau$ (ex. K^0, η)		$(7.6 \pm 1.2) \times 10^{-4}$	763	$\eta'(958) \pi^- \nu_\tau$	< 4.0	$\times 10^{-6}$ CL=90%	620
$K^- \pi^+ \pi^- \pi^0 \nu_\tau$ (ex. K^0, ω)		$(3.7 \pm 0.9) \times 10^{-4}$	763	$\eta'(958) \pi^- \pi^0 \nu_\tau$	< 1.2	$\times 10^{-5}$ CL=90%	591
$K^- \pi^+ \pi^- \pi^0 \nu_\tau$ (ex. K^0, ω, η)	[g]	$(3.9 \pm 1.4) \times 10^{-4}$	763	$\eta'(958) K^- \nu_\tau$	< 2.4	$\times 10^{-6}$ CL=90%	495
$K^- \pi^+ K^- \geq 0$ neut. ν_τ	< 9	$\times 10^{-4}$ CL=95%	685	$\phi \pi^- \nu_\tau$	$(3.4 \pm 0.6) \times 10^{-5}$		585
$K^- K^+ \pi^- \geq 0$ neut. ν_τ		$(1.496 \pm 0.033) \times 10^{-3}$	685	$\phi K^- \nu_\tau$	[g] $(4.4 \pm 1.6) \times 10^{-5}$		445
$K^- K^+ \pi^- \nu_\tau$	[g]	$(1.435 \pm 0.027) \times 10^{-3}$	685	$f_1(1285) \pi^- \nu_\tau$	$(3.9 \pm 0.5) \times 10^{-4}$	S=1.9	408
$K^- K^+ \pi^- \pi^0 \nu_\tau$	[g]	$(6.1 \pm 1.8) \times 10^{-5}$	618	$f_1(1285) \pi^- \nu_\tau \rightarrow$	$(1.18 \pm 0.07) \times 10^{-4}$	S=1.3	-
$K^- K^+ K^- \nu_\tau$		$(2.2 \pm 0.8) \times 10^{-5}$	472	$\eta \pi^- \pi^+ \pi^- \nu_\tau$			
$K^- K^+ K^- \nu_\tau$ (ex. ϕ)	< 2.5	$\times 10^{-6}$ CL=90%	-	$f_1(1285) \pi^- \nu_\tau \rightarrow$			
				$3\pi^- 2\pi^+ \nu_\tau$	[g] $(5.2 \pm 0.4) \times 10^{-5}$		-
				$\pi(1300)^- \nu_\tau \rightarrow (\rho \pi)^- \nu_\tau \rightarrow$	< 1.0	$\times 10^{-4}$ CL=90%	-
				$(3\pi)^- \nu_\tau$			

Lepton Summary Table

$\pi(1300)^- \nu_\tau \rightarrow ((\pi\pi)_{S\text{-wave}} \pi)^- \nu_\tau \rightarrow (3\pi)^- \nu_\tau$	< 1.9	$\times 10^{-4}$ CL=90%	-
$h^- \omega \geq 0$ neutrals ν_τ	(2.40 ± 0.08) %		708
$h^- \omega \nu_\tau$	(1.99 ± 0.06) %		708
$\pi^- \omega \nu_\tau$	[g] (1.95 ± 0.06) %		708
$K^- \omega \nu_\tau$	[g] (4.1 ± 0.9) $\times 10^{-4}$		610
$h^- \omega \pi^0 \nu_\tau$	[g] (4.1 ± 0.4) $\times 10^{-3}$		684
$h^- \omega 2\pi^0 \nu_\tau$	(1.4 ± 0.5) $\times 10^{-4}$		644
$\pi^- \omega 2\pi^0 \nu_\tau$	[g] (7.2 ± 1.6) $\times 10^{-5}$		644
$h^- 2\omega \nu_\tau$	< 5.4	$\times 10^{-7}$ CL=90%	250
$2h^- h^+ \omega \nu_\tau$	(1.20 ± 0.22) $\times 10^{-4}$		641
$2\pi^- \pi^+ \omega \nu_\tau$ (ex. K^0)	[g] (8.4 ± 0.6) $\times 10^{-5}$		641

Lepton Family number (LF), Lepton number (L), or Baryon number (B) violating modes

L means lepton number violation (e.g. $\tau^- \rightarrow e^+ \pi^- \pi^-$). Following common usage, LF means lepton family violation and not lepton number violation (e.g. $\tau^- \rightarrow e^- \pi^+ \pi^-$). B means baryon number violation.

$e^- \gamma$	LF	< 3.3	$\times 10^{-8}$ CL=90%	888
$\mu^- \gamma$	LF	< 4.4	$\times 10^{-8}$ CL=90%	885
$e^- \pi^0$	LF	< 8.0	$\times 10^{-8}$ CL=90%	883
$\mu^- \pi^0$	LF	< 1.1	$\times 10^{-7}$ CL=90%	880
$e^- K_S^0$	LF	< 2.6	$\times 10^{-8}$ CL=90%	819
$\mu^- K_S^0$	LF	< 2.3	$\times 10^{-8}$ CL=90%	815
$e^- \eta$	LF	< 9.2	$\times 10^{-8}$ CL=90%	804
$\mu^- \eta$	LF	< 6.5	$\times 10^{-8}$ CL=90%	800
$e^- \rho^0$	LF	< 1.8	$\times 10^{-8}$ CL=90%	719
$\mu^- \rho^0$	LF	< 1.2	$\times 10^{-8}$ CL=90%	715
$e^- \omega$	LF	< 4.8	$\times 10^{-8}$ CL=90%	716
$\mu^- \omega$	LF	< 4.7	$\times 10^{-8}$ CL=90%	711
$e^- K^*(892)^0$	LF	< 3.2	$\times 10^{-8}$ CL=90%	665
$\mu^- K^*(892)^0$	LF	< 5.9	$\times 10^{-8}$ CL=90%	659
$e^- \bar{K}^*(892)^0$	LF	< 3.4	$\times 10^{-8}$ CL=90%	665
$\mu^- \bar{K}^*(892)^0$	LF	< 7.0	$\times 10^{-8}$ CL=90%	659
$e^- \eta'(958)$	LF	< 1.6	$\times 10^{-7}$ CL=90%	630
$\mu^- \eta'(958)$	LF	< 1.3	$\times 10^{-7}$ CL=90%	625
$e^- f_0(980) \rightarrow e^- \pi^+ \pi^-$	LF	< 3.2	$\times 10^{-8}$ CL=90%	-
$\mu^- f_0(980) \rightarrow \mu^- \pi^+ \pi^-$	LF	< 3.4	$\times 10^{-8}$ CL=90%	-
$e^- \phi$	LF	< 3.1	$\times 10^{-8}$ CL=90%	596
$\mu^- \phi$	LF	< 8.4	$\times 10^{-8}$ CL=90%	590
$e^- e^+ e^-$	LF	< 2.7	$\times 10^{-8}$ CL=90%	888
$e^- \mu^+ \mu^-$	LF	< 2.7	$\times 10^{-8}$ CL=90%	882
$e^+ \mu^- \mu^-$	LF	< 1.7	$\times 10^{-8}$ CL=90%	882
$\mu^- e^+ e^-$	LF	< 1.8	$\times 10^{-8}$ CL=90%	885
$\mu^+ e^- e^-$	LF	< 1.5	$\times 10^{-8}$ CL=90%	885
$\mu^- \mu^+ \mu^-$	LF	< 2.1	$\times 10^{-8}$ CL=90%	873
$e^- \pi^+ \pi^-$	LF	< 2.3	$\times 10^{-8}$ CL=90%	877
$e^+ \pi^- \pi^-$	L	< 2.0	$\times 10^{-8}$ CL=90%	877
$\mu^- \pi^+ \pi^-$	LF	< 2.1	$\times 10^{-8}$ CL=90%	866
$\mu^+ \pi^- \pi^-$	L	< 3.9	$\times 10^{-8}$ CL=90%	866
$e^- \pi^+ K^-$	LF	< 3.7	$\times 10^{-8}$ CL=90%	813
$e^- \pi^- K^+$	LF	< 3.1	$\times 10^{-8}$ CL=90%	813
$e^+ \pi^- K^-$	L	< 3.2	$\times 10^{-8}$ CL=90%	813
$e^- K_S^0 K_S^0$	LF	< 7.1	$\times 10^{-8}$ CL=90%	736
$e^- K^+ K^-$	LF	< 3.4	$\times 10^{-8}$ CL=90%	738
$e^+ K^- K^-$	L	< 3.3	$\times 10^{-8}$ CL=90%	738
$\mu^- \pi^+ K^-$	LF	< 8.6	$\times 10^{-8}$ CL=90%	800
$\mu^- \pi^- K^+$	LF	< 4.5	$\times 10^{-8}$ CL=90%	800
$\mu^+ \pi^- K^-$	L	< 4.8	$\times 10^{-8}$ CL=90%	800
$\mu^- K_S^0 K_S^0$	LF	< 8.0	$\times 10^{-8}$ CL=90%	696
$\mu^- K^+ K^-$	LF	< 4.4	$\times 10^{-8}$ CL=90%	699
$\mu^+ K^- K^-$	L	< 4.7	$\times 10^{-8}$ CL=90%	699
$e^- \pi^0 \pi^0$	LF	< 6.5	$\times 10^{-6}$ CL=90%	878
$\mu^- \pi^0 \pi^0$	LF	< 1.4	$\times 10^{-5}$ CL=90%	867
$e^- \eta \eta$	LF	< 3.5	$\times 10^{-5}$ CL=90%	699
$\mu^- \eta \eta$	LF	< 6.0	$\times 10^{-5}$ CL=90%	653
$e^- \pi^0 \eta$	LF	< 2.4	$\times 10^{-5}$ CL=90%	798
$\mu^- \pi^0 \eta$	LF	< 2.2	$\times 10^{-5}$ CL=90%	784
$p \mu^- \mu^-$	L,B	< 4.4	$\times 10^{-7}$ CL=90%	618
$\bar{p} \mu^+ \mu^-$	L,B	< 3.3	$\times 10^{-7}$ CL=90%	618
$\bar{p} \gamma$	L,B	< 3.5	$\times 10^{-6}$ CL=90%	641
$\bar{p} \pi^0$	L,B	< 1.5	$\times 10^{-5}$ CL=90%	632
$\bar{p} 2\pi^0$	L,B	< 3.3	$\times 10^{-5}$ CL=90%	604
$\bar{p} \eta$	L,B	< 8.9	$\times 10^{-6}$ CL=90%	475
$\bar{p} \pi^0 \eta$	L,B	< 2.7	$\times 10^{-5}$ CL=90%	360
$\Lambda \pi^-$	L,B	< 7.2	$\times 10^{-8}$ CL=90%	525

$\bar{\Lambda} \pi^-$	L,B	< 1.4	$\times 10^{-7}$ CL=90%	525
e^- light boson	LF	< 2.7	$\times 10^{-3}$ CL=95%	-
μ^- light boson	LF	< 5	$\times 10^{-3}$ CL=95%	-

Heavy Charged Lepton Searches

 L^\pm – charged lepton

Mass $m > 100.8$ GeV, CL = 95% [h] Decay to νW .

 L^\pm – stable charged heavy lepton

Mass $m > 102.6$ GeV, CL = 95%

Neutrino Properties

See the note on “Neutrino properties listings” in the Particle Listings.

Mass $m < 1.1$ eV, CL = 90% (tritium decay)

Mean life/mass, $\tau/m > 300$ s/eV, CL = 90% (reactor)

Mean life/mass, $\tau/m > 7 \times 10^9$ s/eV (solar)

Mean life/mass, $\tau/m > 15.4$ s/eV, CL = 90% (accelerator)

Magnetic moment $\mu < 0.28 \times 10^{-10} \mu_B$, CL = 90% (solar + radiochemical)

Number of Neutrino Types

Number $N = 2.996 \pm 0.007$ (Standard Model fits to LEP-SLC data)

Number $N = 2.92 \pm 0.05$ ($S = 1.2$) (Direct measurement of invisible Z width)

Neutrino Mixing

The following values are obtained through data analyses based on the 3-neutrino mixing scheme described in the review “Neutrino Masses, Mixing, and Oscillations.”

$$\sin^2(\theta_{12}) = 0.307 \pm 0.013$$

$$\Delta m_{21}^2 = (7.53 \pm 0.18) \times 10^{-5} \text{ eV}^2$$

$$\sin^2(\theta_{23}) = 0.547 \pm 0.021 \text{ (Inverted order)}$$

$$\sin^2(\theta_{23}) = 0.545 \pm 0.021 \text{ (Normal order)}$$

$$\Delta m_{32}^2 = (-2.546^{+0.034}_{-0.040}) \times 10^{-3} \text{ eV}^2 \text{ (Inverted order)}$$

$$\Delta m_{32}^2 = (2.453 \pm 0.034) \times 10^{-3} \text{ eV}^2 \text{ (Normal order)}$$

$$\sin^2(\theta_{13}) = (2.18 \pm 0.07) \times 10^{-2}$$

$$\delta, \text{ CP violating phase} = 1.36 \pm 0.17 \pi \text{ rad}$$

$$\langle \Delta m_{21}^2 - \Delta \bar{m}_{21}^2 \rangle < 1.1 \times 10^{-4} \text{ eV}^2, \text{ CL} = 99.7\%$$

$$\langle \Delta m_{32}^2 - \Delta \bar{m}_{32}^2 \rangle = (-0.12 \pm 0.25) \times 10^{-3} \text{ eV}^2$$

NOTES

In this Summary Table:

When a quantity has “(S = . . .)” to its right, the error on the quantity has been enlarged by the “scale factor” S, defined as $S = \sqrt{\chi^2/(N-1)}$, where N is the number of measurements used in calculating the quantity. We do this when $S > 1$, which often indicates that the measurements are inconsistent. When $S > 1.25$, we also show in the Particle Listings an ideogram of the measurements. For more about S, see the Introduction.

A decay momentum p is given for each decay mode. For a 2-body decay, p is the momentum of each decay product in the rest frame of the decaying particle. For a 3-or-more-body decay, p is the largest momentum any of the products can have in this frame.

[a] This is the best limit for the mode $e^- \rightarrow \nu \gamma$. The best limit for Nuclear de-excitation experiments is 6.4×10^{24} yr.

[b] See the review on “Muon Decay Parameters” for definitions and details.

[c] P_μ is the longitudinal polarization of the muon from pion decay. For V–A coupling, $P_\mu = 1$ and $\rho = \delta = 3/4$.

[d] This only includes events with energy of $e > 45$ MeV and energy of $\gamma > 40$ MeV. Since the $e^- \bar{\nu}_e \nu_\mu$ and $e^- \bar{\nu}_e \nu_\mu \gamma$ modes cannot be clearly separated, we regard the latter mode as a subset of the former.

[e] See the relevant Particle Listings for the energy limits used in this measurement.

[f] A test of additive vs. multiplicative lepton family number conservation.

[g] Basis mode for the τ .

[h] L^\pm mass limit depends on decay assumptions; see the Full Listings.

Quark Summary Table

QUARKS

The u -, d -, and s -quark masses are estimates of so-called “current-quark masses,” in a mass-independent subtraction scheme such as $\overline{\text{MS}}$ at a scale $\mu \approx 2$ GeV. The c - and b -quark masses are the “running” masses in the $\overline{\text{MS}}$ scheme. This can be different from the heavy quark masses obtained in potential models.

u

$$I(J^P) = \frac{1}{2}(\frac{1}{2}^+)$$

$$m_u = 2.16^{+0.49}_{-0.26} \text{ MeV} \quad \text{Charge} = \frac{2}{3} e \quad I_z = +\frac{1}{2}$$

$$m_u/m_d = 0.47^{+0.06}_{-0.07}$$

d

$$I(J^P) = \frac{1}{2}(\frac{1}{2}^+)$$

$$m_d = 4.67^{+0.48}_{-0.17} \text{ MeV} \quad \text{Charge} = -\frac{1}{3} e \quad I_z = -\frac{1}{2}$$

$$m_s/m_d = 17\text{--}22$$

$$\overline{m} = (m_u + m_d)/2 = 3.45^{+0.55}_{-0.15} \text{ MeV}$$

s

$$I(J^P) = 0(\frac{1}{2}^+)$$

$$m_s = 93^{+11}_{-5} \text{ MeV} \quad \text{Charge} = -\frac{1}{3} e \quad \text{Strangeness} = -1$$

$$m_s / ((m_u + m_d)/2) = 27.3^{+0.7}_{-1.3}$$

c

$$I(J^P) = 0(\frac{1}{2}^+)$$

$$m_c = 1.27 \pm 0.02 \text{ GeV} \quad \text{Charge} = \frac{2}{3} e \quad \text{Charm} = +1$$

$$m_c/m_s = 11.72 \pm 0.25$$

$$m_b/m_c = 4.577 \pm 0.008$$

$$m_b - m_c = 3.45 \pm 0.05 \text{ GeV}$$

b

$$I(J^P) = 0(\frac{1}{2}^+)$$

$$m_b = 4.18^{+0.03}_{-0.02} \text{ GeV} \quad \text{Charge} = -\frac{1}{3} e \quad \text{Bottom} = -1$$

t

$$I(J^P) = 0(\frac{1}{2}^+)$$

$$\text{Charge} = \frac{2}{3} e \quad \text{Top} = +1$$

$$\text{Mass (direct measurements)} \quad m = 172.76 \pm 0.30 \text{ GeV} \quad [a,b] \quad (S = 1.2)$$

$$\text{Mass (from cross-section measurements)} \quad m = 162.5^{+2.1}_{-1.5} \text{ GeV} \quad [a]$$

$$\text{Mass (Pole from cross-section measurements)} \quad m = 172.4 \pm 0.7 \text{ GeV}$$

$$m_t - m_{\bar{t}} = -0.16 \pm 0.19 \text{ GeV}$$

$$\text{Full width } \Gamma = 1.42^{+0.19}_{-0.15} \text{ GeV} \quad (S = 1.4)$$

$$\Gamma(Wb)/\Gamma(Wq(q = b, s, d)) = 0.957 \pm 0.034 \quad (S = 1.5)$$

t-quark EW Couplings

$$F_0 = 0.687 \pm 0.018$$

$$F_- = 0.320 \pm 0.013$$

$$F_+ = 0.002 \pm 0.011$$

$$F_{V+A} < 0.29, \text{ CL} = 95\%$$

DECAY MODES	Fraction (Γ_i/Γ)	Confidence level	$\frac{p}{(\text{MeV}/c)}$
$Wq(q = b, s, d)$			—
Wb			—
$e\nu_e b$	$(11.10 \pm 0.30) \%$		—
$\mu\nu_\mu b$	$(11.40 \pm 0.20) \%$		—
$\tau\nu_\tau b$	$(11.1 \pm 0.9) \%$		—
$q\bar{q}b$	$(66.5 \pm 1.4) \%$		—
$\gamma q(q = u, c)$	$[c] < 1.8$	$\times 10^{-4}$	95%
$\Delta T = 1$ weak neutral current ($T1$) modes			
$Zq(q = u, c)$	$T1$	$[d] < 5$	$\times 10^{-4}$ 95% —
Hu	$T1$	< 1.2	$\times 10^{-3}$ 95% —
Hc	$T1$	< 1.1	$\times 10^{-3}$ 95% —
$\ell^+ \bar{q}q'(q = d, s, b; q' = u, c)$	$T1$	< 1.6	$\times 10^{-3}$ 95% —

 b' (4th Generation) Quark, Searches for

$$\text{Mass } m > 190 \text{ GeV, CL} = 95\% \quad (p\bar{p}, \text{ quasi-stable } b')$$

$$\text{Mass } m > 1130 \text{ GeV, CL} = 95\% \quad (\text{B}(b' \rightarrow Zb) = 1)$$

$$\text{Mass } m > 1350 \text{ GeV, CL} = 95\% \quad (\text{B}(b' \rightarrow Wt) = 1)$$

$$\text{Mass } m > 46.0 \text{ GeV, CL} = 95\% \quad (e^+ e^-, \text{ all decays})$$

 t' (4th Generation) Quark, Searches for

$$m(t'(2/3)) > 1280 \text{ GeV, CL} = 95\% \quad (\text{B}(t' \rightarrow Zt) = 1)$$

$$m(t'(2/3)) > 1295 \text{ GeV, CL} = 95\% \quad (\text{B}(t' \rightarrow Wb) = 1)$$

$$m(t'(2/3)) > 1310 \text{ GeV, CL} = 95\% \quad (\text{singlet } t')$$

$$m(t'(5/3)) > 1350 \text{ GeV, CL} = 95\%$$

Free Quark Searches

All searches since 1977 have had negative results.

NOTES

- [a] A discussion of the definition of the top quark mass in these measurements can be found in the review “The Top Quark.”
- [b] Based on published top mass measurements using data from Tevatron Run-I and Run-II and LHC at $\sqrt{s} = 7$ TeV. Including the most recent unpublished results from Tevatron Run-II, the Tevatron Electroweak Working Group reports a top mass of 173.2 ± 0.9 GeV. See the note “The Top Quark” in the Quark Particle Listings of this Review.
- [c] This limit is for $\Gamma(t \rightarrow \gamma q)/\Gamma(t \rightarrow Wb)$.
- [d] This limit is for $\Gamma(t \rightarrow Zq)/\Gamma(t \rightarrow Wb)$.

Meson Summary Table

LIGHT UNFLAVORED MESONS (S = C = B = 0)

For $I = 1$ (π, b, ρ, a): $u\bar{d}, (u\bar{u}-d\bar{d})/\sqrt{2}, d\bar{u}$;
for $I = 0$ ($\eta, \eta', h, h', \omega, \phi, f, f'$): $c_1(u\bar{u} + d\bar{d}) + c_2(s\bar{s})$

π^\pm

$$I^G(J^{PC}) = 1^-(0^-)$$

Mass $m = 139.57039 \pm 0.00018$ MeV ($S = 1.8$)
Mean life $\tau = (2.6033 \pm 0.0005) \times 10^{-8}$ s ($S = 1.2$)
 $c\tau = 7.8045$ m

$\pi^\pm \rightarrow \ell^\pm \nu \gamma$ form factors [a]

$F_V = 0.0254 \pm 0.0017$
 $F_A = 0.0119 \pm 0.0001$
 F_V slope parameter $a = 0.10 \pm 0.06$
 $R = 0.059^{+0.009}_{-0.008}$

π^\mp modes are charge conjugates of the modes below.

For decay limits to particles which are not established, see the section on Searches for Axions and Other Very Light Bosons.

π^\pm DECAY MODES	Fraction (Γ_i/Γ)	Confidence level	p (MeV/c)
$\mu^+ \nu_\mu$	[b] (99.98770 \pm 0.00004) %		30
$\mu^+ \nu_\mu \gamma$	[c] (2.00 \pm 0.25) $\times 10^{-4}$		30
$e^+ \nu_e$	[b] (1.230 \pm 0.004) $\times 10^{-4}$		70
$e^+ \nu_e \gamma$	[c] (7.39 \pm 0.05) $\times 10^{-7}$		70
$e^+ \nu_e \pi^0$	(1.036 \pm 0.006) $\times 10^{-8}$		4
$e^+ \nu_e e^+ e^-$	(3.2 \pm 0.5) $\times 10^{-9}$		70
$e^+ \nu_e \nu \bar{\nu}$	< 5 $\times 10^{-6}$	90%	70

Lepton Family number (LF) or Lepton number (L) violating modes			
$\mu^+ \bar{\nu}_e$	L [d] < 1.5	$\times 10^{-3}$	90% 30
$\mu^+ \nu_e$	LF [d] < 8.0	$\times 10^{-3}$	90% 30
$\mu^- e^+ e^+ \nu$	LF < 1.6	$\times 10^{-6}$	90% 30

π^0

$$I^G(J^{PC}) = 1^-(0^{++})$$

Mass $m = 134.9768 \pm 0.0005$ MeV ($S = 1.1$)
 $m_{\pi^\pm} - m_{\pi^0} = 4.5936 \pm 0.0005$ MeV
Mean life $\tau = (8.52 \pm 0.18) \times 10^{-17}$ s ($S = 1.2$)
 $c\tau = 25.5$ nm

For decay limits to particles which are not established, see the appropriate Search sections (A^0 (axion) and Other Light Boson (X^0) Searches, etc.).

π^0 DECAY MODES	Fraction (Γ_i/Γ)	Scale factor/ Confidence level	p (MeV/c)
2γ	(98.823 \pm 0.034) %	S=1.5	67
$e^+ e^- \gamma$	(1.174 \pm 0.035) %	S=1.5	67
γ positronium	(1.82 \pm 0.29) $\times 10^{-9}$		67
$e^+ e^+ e^- e^-$	(3.34 \pm 0.16) $\times 10^{-5}$		67
$e^+ e^-$	(6.46 \pm 0.33) $\times 10^{-8}$		67
4γ	< 2 $\times 10^{-8}$	CL=90%	67
$\nu \bar{\nu}$	[e] < 2.7 $\times 10^{-7}$	CL=90%	67
$\nu_e \bar{\nu}_e$	< 1.7 $\times 10^{-6}$	CL=90%	67
$\nu_\mu \bar{\nu}_\mu$	< 1.6 $\times 10^{-6}$	CL=90%	67
$\nu_\tau \bar{\nu}_\tau$	< 2.1 $\times 10^{-6}$	CL=90%	67
$\gamma \nu \bar{\nu}$	< 1.9 $\times 10^{-7}$	CL=90%	67

Charge conjugation (C) or Lepton Family number (LF) violating modes			
3γ	C < 3.1	$\times 10^{-8}$	CL=90% 67
$\mu^+ e^-$	LF < 3.8	$\times 10^{-10}$	CL=90% 26
$\mu^- e^+$	LF < 3.4	$\times 10^{-9}$	CL=90% 26
$\mu^+ e^- + \mu^- e^+$	LF < 3.6	$\times 10^{-10}$	CL=90% 26

η

$$I^G(J^{PC}) = 0^+(0^{-+})$$

Mass $m = 547.862 \pm 0.017$ MeV
Full width $\Gamma = 1.31 \pm 0.05$ keV

C-nonconserving decay parameters

$\pi^+ \pi^- \pi^0$ left-right asymmetry = $(0.09^{+0.11}_{-0.12}) \times 10^{-2}$
 $\pi^+ \pi^- \pi^0$ sextant asymmetry = $(0.12^{+0.10}_{-0.11}) \times 10^{-2}$
 $\pi^+ \pi^- \pi^0$ quadrant asymmetry = $(-0.09 \pm 0.09) \times 10^{-2}$
 $\pi^+ \pi^- \gamma$ left-right asymmetry = $(0.9 \pm 0.4) \times 10^{-2}$
 $\pi^+ \pi^- \gamma$ β (D-wave) = -0.02 ± 0.07 ($S = 1.3$)

CP-nonconserving decay parameters

$\pi^+ \pi^- e^+ e^-$ decay-plane asymmetry $A_\phi = (-0.6 \pm 3.1) \times 10^{-2}$

Other decay parameters

$\pi^0 \pi^0 \pi^0$ Dalitz plot $\alpha = -0.0288 \pm 0.0012$ ($S = 1.1$)
Parameter Λ in $\eta \rightarrow \ell^+ \ell^- \gamma$ decay = 0.716 ± 0.011 GeV/ c^2

η DECAY MODES	Fraction (Γ_i/Γ)	Scale factor/ Confidence level	p (MeV/c)
Neutral modes			
neutral modes	(72.12 \pm 0.34) %	S=1.2	-
2γ	(39.41 \pm 0.20) %	S=1.1	274
$3\pi^0$	(32.68 \pm 0.23) %	S=1.1	179
$\pi^0 2\gamma$	(2.56 \pm 0.22) $\times 10^{-4}$		257
$2\pi^0 2\gamma$	< 1.2 $\times 10^{-3}$	CL=90%	238
4γ	< 2.8 $\times 10^{-4}$	CL=90%	274
invisible	< 1.0 $\times 10^{-4}$	CL=90%	-
Charged modes			
charged modes	(27.89 \pm 0.29) %	S=1.2	-
$\pi^+ \pi^- \pi^0$	(22.92 \pm 0.28) %	S=1.2	174
$\pi^+ \pi^- \gamma$	(4.22 \pm 0.08) %	S=1.1	236
$e^+ e^- \gamma$	(6.9 \pm 0.4) $\times 10^{-3}$	S=1.3	274
$\mu^+ \mu^- \gamma$	(3.1 \pm 0.4) $\times 10^{-4}$		253
$e^+ e^-$	< 7 $\times 10^{-7}$	CL=90%	274
$\mu^+ \mu^-$	(5.8 \pm 0.8) $\times 10^{-6}$		253
$2e^+ 2e^-$	(2.40 \pm 0.22) $\times 10^{-5}$		274
$\pi^+ \pi^- e^+ e^- (\gamma)$	(2.68 \pm 0.11) $\times 10^{-4}$		235
$e^+ e^- \mu^+ \mu^-$	< 1.6 $\times 10^{-4}$	CL=90%	253
$2\mu^+ 2\mu^-$	< 3.6 $\times 10^{-4}$	CL=90%	161
$\mu^+ \mu^- \pi^+ \pi^-$	< 3.6 $\times 10^{-4}$	CL=90%	113
$\pi^+ e^- \bar{\nu}_e + c.c.$	< 1.7 $\times 10^{-4}$	CL=90%	256
$\pi^+ \pi^- 2\gamma$	< 2.1 $\times 10^{-3}$		236
$\pi^+ \pi^- \pi^0 \gamma$	< 5 $\times 10^{-4}$	CL=90%	174
$\pi^0 \mu^+ \mu^- \gamma$	< 3 $\times 10^{-6}$	CL=90%	210

Charge conjugation (C), Parity (P), Charge conjugation \times Parity (CP), or Lepton Family number (LF) violating modes

$\pi^0 \gamma$	C [f] < 9	$\times 10^{-5}$	CL=90% 257
$\pi^+ \pi^-$	P,CP < 1.3	$\times 10^{-5}$	CL=90% 236
$2\pi^0$	P,CP < 3.5	$\times 10^{-4}$	CL=90% 238
$2\pi^0 \gamma$	C < 5	$\times 10^{-4}$	CL=90% 238
$3\pi^0 \gamma$	C < 6	$\times 10^{-5}$	CL=90% 179
3γ	C < 1.6	$\times 10^{-5}$	CL=90% 274
$4\pi^0$	P,CP < 6.9	$\times 10^{-7}$	CL=90% 40
$\pi^0 e^+ e^-$	C [g] < 8	$\times 10^{-6}$	CL=90% 257
$\pi^0 \mu^+ \mu^-$	C [g] < 5	$\times 10^{-6}$	CL=90% 210
$\mu^+ e^- + \mu^- e^+$	LF < 6	$\times 10^{-6}$	CL=90% 264

$f_0(500)$

$$I^G(J^{PC}) = 0^+(0^{++})$$

also known as σ ; was $f_0(600)$

See the review on "Scalar Mesons below 2 GeV."

Mass (T-Matrix Pole \sqrt{s}) = $(400-550) - i(200-350)$ MeV
Mass (Breit-Wigner) = $(400-550)$ MeV
Full width (Breit-Wigner) = $(400-700)$ MeV

$f_0(500)$ DECAY MODES	Fraction (Γ_i/Γ)	p (MeV/c)
$\pi \pi$	seen	-
$\gamma \gamma$	seen	-

$\rho(770)$

$$I^G(J^{PC}) = 1^+(1^{--})$$

See the note in $\rho(770)$ Particle Listings.

Mass $m = 775.26 \pm 0.25$ MeV
Full width $\Gamma = 149.1 \pm 0.8$ MeV
 $\Gamma_{ee} = 7.04 \pm 0.06$ keV

Meson Summary Table

$\rho(770)$ DECAY MODES	Fraction (Γ_i/Γ)	Scale factor/ Confidence level	p (MeV/c)
$\pi^+\pi^-$	~ 100 %		363
$\rho(770)^\pm$ decays			
$\pi^\pm\gamma$	(4.5 ± 0.5) $\times 10^{-4}$	S=2.2	375
$\pi^\pm\eta$	< 6 $\times 10^{-3}$	CL=84%	152
$\pi^\pm\pi^+\pi^-\pi^0$	< 2.0 $\times 10^{-3}$	CL=84%	254
$\rho(770)^0$ decays			
$\pi^+\pi^-\gamma$	(9.9 ± 1.6) $\times 10^{-3}$		362
$\pi^0\gamma$	(4.7 ± 0.6) $\times 10^{-4}$	S=1.4	376
$\eta\gamma$	(3.00 ± 0.21) $\times 10^{-4}$		194
$\pi^0\pi^0\gamma$	(4.5 ± 0.8) $\times 10^{-5}$		363
$\mu^+\mu^-$	[h] (4.55 ± 0.28) $\times 10^{-5}$		373
e^+e^-	[h] (4.72 ± 0.05) $\times 10^{-5}$		388
$\pi^+\pi^-\pi^0$	($1.01 \pm_{-0.36}^{0.54} \pm 0.34$) $\times 10^{-4}$		323
$\pi^+\pi^-\pi^+\pi^-$	(1.8 ± 0.9) $\times 10^{-5}$		251
$\pi^+\pi^-\pi^0\pi^0$	(1.6 ± 0.8) $\times 10^{-5}$		257
$\pi^0e^+e^-$	< 1.2 $\times 10^{-5}$	CL=90%	376

 $\omega(782)$

$$I^G(J^{PC}) = 0^-(1^{--})$$

Mass $m = 782.65 \pm 0.12$ MeV (S = 1.9)
 Full width $\Gamma = 8.49 \pm 0.08$ MeV
 $\Gamma_{ee} = 0.60 \pm 0.02$ keV

$\omega(782)$ DECAY MODES	Fraction (Γ_i/Γ)	Scale factor/ Confidence level	p (MeV/c)
$\pi^+\pi^-\pi^0$	(89.3 ± 0.6) %		327
$\pi^0\gamma$	(8.40 ± 0.22) %	S=1.8	380
$\pi^+\pi^-$	(1.53 ± 0.06) %		366
neutrals (excluding $\pi^0\gamma$)	($7 \pm_{-4}^{+7}$) $\times 10^{-3}$	S=1.1	-
$\eta\gamma$	(4.5 ± 0.4) $\times 10^{-4}$	S=1.1	200
$\pi^0e^+e^-$	(7.7 ± 0.6) $\times 10^{-4}$		380
$\pi^0\mu^+\mu^-$	(1.34 ± 0.18) $\times 10^{-4}$	S=1.5	349
e^+e^-	(7.36 ± 0.15) $\times 10^{-5}$	S=1.5	391
$\pi^+\pi^-\pi^0\pi^0$	< 2 $\times 10^{-4}$	CL=90%	262
$\pi^+\pi^-\gamma$	< 3.6 $\times 10^{-3}$	CL=95%	366
$\pi^+\pi^-\pi^+\pi^-$	< 1 $\times 10^{-3}$	CL=90%	256
$\pi^0\pi^0\gamma$	(6.7 ± 1.1) $\times 10^{-5}$		367
$\eta\pi^0\gamma$	< 3.3 $\times 10^{-5}$	CL=90%	162
$\mu^+\mu^-$	(7.4 ± 1.8) $\times 10^{-5}$		377
3γ	< 1.9 $\times 10^{-4}$	CL=95%	391

Charge conjugation (C) violating modes

$\eta\pi^0$	C < 2.2 $\times 10^{-4}$	CL=90%	162
$2\pi^0$	C < 2.2 $\times 10^{-4}$	CL=90%	367
$3\pi^0$	C < 2.3 $\times 10^{-4}$	CL=90%	330
invisible	< 7 $\times 10^{-5}$	CL=90%	-

 $\eta'(958)$

$$I^G(J^{PC}) = 0^+(0^{-+})$$

Mass $m = 957.78 \pm 0.06$ MeV
 Full width $\Gamma = 0.188 \pm 0.006$ MeV

$\eta'(958)$ DECAY MODES	Fraction (Γ_i/Γ)	Confidence level	p (MeV/c)
$\pi^+\pi^-\eta$	(42.5 ± 0.5) %		232
$\rho^0\gamma$ (including non-resonant $\pi^+\pi^-\gamma$)	(29.5 ± 0.4) %		165
$\pi^0\pi^0\eta$	(22.4 ± 0.5) %		239
$\omega\gamma$	(2.52 ± 0.07) %		159
ωe^+e^-	(2.0 ± 0.4) $\times 10^{-4}$		159
$\gamma\gamma$	(2.307 ± 0.033) %		479
$3\pi^0$	(2.50 ± 0.17) $\times 10^{-3}$		430
$\mu^+\mu^-\gamma$	(1.13 ± 0.28) $\times 10^{-4}$		467
$\pi^+\pi^-\mu^+\mu^-$	< 2.9 $\times 10^{-5}$	90%	401
$\pi^+\pi^-\pi^0$	(3.61 ± 0.17) $\times 10^{-3}$		428
$(\pi^+\pi^-\pi^0)$ S-wave	(3.8 ± 0.5) $\times 10^{-3}$		428
$\pi^\mp\rho^\pm$	(7.4 ± 2.3) $\times 10^{-4}$		106
$\pi^0\rho^0$	< 4 %	90%	111
$2(\pi^+\pi^-)$	(8.4 ± 0.9) $\times 10^{-5}$		372
$\pi^+\pi^-2\pi^0$	(1.8 ± 0.4) $\times 10^{-4}$		376
$2(\pi^+\pi^-)$ neutrals	< 1 %	95%	-

$2(\pi^+\pi^-)\pi^0$	< 1.8 $\times 10^{-3}$	90%	298
$2(\pi^+\pi^-)2\pi^0$	< 1 %	95%	197
$3(\pi^+\pi^-)$	< 3.1 $\times 10^{-5}$	90%	189
$K^\pm\pi^\mp$	< 4 $\times 10^{-5}$	90%	334
$\pi^+\pi^-e^+e^-$	($2.4 \pm_{-1.0}^{+1.3}$) $\times 10^{-3}$		458
$\pi^+e^-\nu_e$ + c.c.	< 2.1 $\times 10^{-4}$	90%	469
γe^+e^-	(4.91 ± 0.27) $\times 10^{-4}$		479
$\pi^0\gamma\gamma$	(3.20 ± 0.24) $\times 10^{-3}$		469
$\pi^0\gamma\gamma$ (non resonant)	(6.2 ± 0.9) $\times 10^{-4}$		-
$\eta\gamma\gamma$	< 1.33 $\times 10^{-4}$	90%	322
$4\pi^0$	< 3.2 $\times 10^{-4}$	90%	380
e^+e^-	< 5.6 $\times 10^{-9}$	90%	479
invisible	< 6 $\times 10^{-4}$	90%	-

**Charge conjugation (C), Parity (P),
Lepton family number (LF) violating modes**

$\pi^+\pi^-$	P, CP < 1.8 $\times 10^{-5}$	90%	458
$\pi^0\pi^0$	P, CP < 4 $\times 10^{-4}$	90%	459
$\pi^0e^+e^-$	C [g] < 1.4 $\times 10^{-3}$	90%	469
ηe^+e^-	C [g] < 2.4 $\times 10^{-3}$	90%	322
3γ	C < 1.0 $\times 10^{-4}$	90%	479
$\mu^+\mu^-\pi^0$	C [g] < 6.0 $\times 10^{-5}$	90%	445
$\mu^+\mu^-\eta$	C [g] < 1.5 $\times 10^{-5}$	90%	273
$e\mu$	LF < 4.7 $\times 10^{-4}$	90%	473

 $f_0(980)$

$$I^G(J^{PC}) = 0^+(0^{++})$$

See the review on "Scalar Mesons below 2 GeV."

Mass $m = 990 \pm 20$ MeVFull width $\Gamma = 10$ to 100 MeV

$f_0(980)$ DECAY MODES	Fraction (Γ_i/Γ)	p (MeV/c)
$\pi\pi$	seen	476
$K\bar{K}$	seen	36
$\gamma\gamma$	seen	495

 $a_0(980)$

$$I^G(J^{PC}) = 1^-(0^{++})$$

See the review on "Scalar Mesons below 2 GeV."

Mass $m = 980 \pm 20$ MeVFull width $\Gamma = 50$ to 100 MeV

$a_0(980)$ DECAY MODES	Fraction (Γ_i/Γ)	p (MeV/c)
$\eta\pi$	seen	319
$K\bar{K}$	seen	†
$\rho\pi$	not seen	137
$\gamma\gamma$	seen	490

 $\phi(1020)$

$$I^G(J^{PC}) = 0^-(1^{--})$$

Mass $m = 1019.461 \pm 0.016$ MeVFull width $\Gamma = 4.249 \pm 0.013$ MeV (S = 1.1)

$\phi(1020)$ DECAY MODES	Fraction (Γ_i/Γ)	Scale factor/ Confidence level	p (MeV/c)
K^+K^-	(49.2 ± 0.5) %	S=1.3	127
$K_L^0K_S^0$	(34.0 ± 0.4) %	S=1.3	110
$\rho\pi + \pi^+\pi^-\pi^0$	(15.24 ± 0.33) %	S=1.2	-
$\eta\gamma$	(1.303 ± 0.025) %	S=1.2	363
$\pi^0\gamma$	(1.30 ± 0.05) $\times 10^{-3}$		501
l^+l^-	-		510
e^+e^-	(2.973 ± 0.034) $\times 10^{-4}$	S=1.3	510
$\mu^+\mu^-$	(2.86 ± 0.19) $\times 10^{-4}$		499
ηe^+e^-	(1.08 ± 0.04) $\times 10^{-4}$		363
$\pi^+\pi^-$	(7.3 ± 1.3) $\times 10^{-5}$		490
$\omega\pi^0$	(4.7 ± 0.5) $\times 10^{-5}$		172
$\omega\gamma$	< 5 %	CL=84%	209
$\rho\gamma$	< 1.2 $\times 10^{-5}$	CL=90%	215
$\pi^+\pi^-\gamma$	(4.1 ± 1.3) $\times 10^{-5}$		490
$f_0(980)\gamma$	(3.22 ± 0.19) $\times 10^{-4}$	S=1.1	29
$\pi^0\pi^0\gamma$	(1.12 ± 0.06) $\times 10^{-4}$		492
$\pi^+\pi^-\pi^+\pi^-$	($3.9 \pm_{-2.2}^{+2.8}$) $\times 10^{-6}$		410

Meson Summary Table

$\pi^+\pi^+\pi^-\pi^-\pi^0$	< 4.6	$\times 10^{-6}$	CL=90%	342
$\pi^0 e^+ e^-$	(1.33 \pm 0.07 $$)	$\times 10^{-5}$		501
$\pi^0 \eta \gamma$	(7.27 \pm 0.30)	$\times 10^{-5}$	S=1.5	346
$a_0(980) \gamma$	(7.6 \pm 0.6)	$\times 10^{-5}$		39
$K^0 \bar{K}^0 \gamma$	< 1.9	$\times 10^{-8}$	CL=90%	110
$\eta'(958) \gamma$	(6.22 \pm 0.21)	$\times 10^{-5}$		60
$\eta \pi^0 \pi^0 \gamma$	< 2	$\times 10^{-5}$	CL=90%	293
$\mu^+ \mu^- \gamma$	(1.4 \pm 0.5)	$\times 10^{-5}$		499
$\rho \gamma \gamma$	< 1.2	$\times 10^{-4}$	CL=90%	215
$\eta \pi^+ \pi^-$	< 1.8	$\times 10^{-5}$	CL=90%	288
$\eta \mu^+ \mu^-$	< 9.4	$\times 10^{-6}$	CL=90%	321
$\eta U \rightarrow \eta e^+ e^-$	< 1	$\times 10^{-6}$	CL=90%	-
invisible	< 1.7	$\times 10^{-4}$	CL=90%	-

Lepton Family number (LF) violating modes

$e^\pm \mu^\mp$	LF	< 2	$\times 10^{-6}$	CL=90%	504
-----------------	----	-----	------------------	--------	-----

 $h_1(1170)$

$$I^G(J^{PC}) = 0^-(1^+ -)$$

Mass $m = 1166 \pm 6$ MeV
Full width $\Gamma = 375 \pm 35$ MeV

$h_1(1170)$ DECAY MODES	Fraction (Γ_i/Γ)	ρ (MeV/c)
$\rho \pi$	seen	305

 $b_1(1235)$

$$I^G(J^{PC}) = 1^+(1^+ -)$$

Mass $m = 1229.5 \pm 3.2$ MeV (S = 1.6)
Full width $\Gamma = 142 \pm 9$ MeV (S = 1.2)

$b_1(1235)$ DECAY MODES	Fraction (Γ_i/Γ)	Confidence level	ρ (MeV/c)
$\omega \pi$	seen		348
	[D/S amplitude ratio = 0.277 \pm 0.027]		
$\pi^\pm \gamma$	(1.6 \pm 0.4)	$\times 10^{-3}$	607
$\eta \rho$	seen		†
$\pi^+ \pi^+ \pi^- \pi^0$	< 50	%	84%
$K^*(892)^\pm K^\mp$	seen		†
$(K\bar{K})^\pm \pi^0$	< 8	%	90%
$K_S^0 K_L^0 \pi^\pm$	< 6	%	90%
$K_S^0 K_S^0 \pi^\pm$	< 2	%	90%
$\phi \pi$	< 1.5	%	84%

 $a_1(1260)$ [1]

$$I^G(J^{PC}) = 1^-(1^+ +)$$

Mass $m = 1230 \pm 40$ MeV [1]
Full width $\Gamma = 250$ to 600 MeV

$a_1(1260)$ DECAY MODES	Fraction (Γ_i/Γ)	ρ (MeV/c)
3π	seen	577
$(\rho\pi)_{S\text{-wave}}, \rho \rightarrow \pi\pi$	seen	353
$(\rho\pi)_{D\text{-wave}}, \rho \rightarrow \pi\pi$	seen	353
$(\rho(1450)\pi)_{S\text{-wave}}, \rho \rightarrow \pi\pi$	seen	†
$(\rho(1450)\pi)_{D\text{-wave}}, \rho \rightarrow \pi\pi$	seen	†
$f_0(500)\pi, f_0 \rightarrow \pi\pi$	seen	-
$f_0(980)\pi, f_0 \rightarrow \pi\pi$	not seen	179
$f_0(1370)\pi, f_0 \rightarrow \pi\pi$	seen	†
$f_2(1270)\pi, f_2 \rightarrow \pi\pi$	seen	†
$\pi^+ \pi^- \pi^0$	seen	576
$\pi^0 \pi^0 \pi^0$	not seen	577
$KK\pi$	seen	250
$K^*(892)K$	seen	†
$\pi \gamma$	seen	608

 $f_2(1270)$

$$I^G(J^{PC}) = 0^+(2^+ +)$$

Mass $m = 1275.5 \pm 0.8$ MeV
Full width $\Gamma = 186.7^{+2.2}_{-2.5}$ MeV (S = 1.4)

$f_2(1270)$ DECAY MODES	Fraction (Γ_i/Γ)	Scale factor/ Confidence level	ρ (MeV/c)
$\pi \pi$	(84.2 \pm 2.9 $$) %	S=1.1	623
$\pi^+ \pi^- 2\pi^0$	(7.7 \pm 1.1 $$) %	S=1.2	563

 $K\bar{K}$

$K\bar{K}$	(4.6 \pm 0.5 $$) %	S=2.7	404
$2\pi^+ 2\pi^-$	(2.8 \pm 0.4) %	S=1.2	560
$\eta \eta$	(4.0 \pm 0.8) $\times 10^{-3}$	S=2.1	326
$4\pi^0$	(3.0 \pm 1.0) $\times 10^{-3}$		565
$\gamma \gamma$	(1.42 \pm 0.24) $\times 10^{-5}$	S=1.4	638
$\eta \pi \pi$	< 8	$\times 10^{-3}$	CL=95%
$K^0 K^- \pi^+ + \text{c.c.}$	< 3.4	$\times 10^{-3}$	CL=95%
$e^+ e^-$	< 6	$\times 10^{-10}$	CL=90%

 $f_1(1285)$

$$I^G(J^{PC}) = 0^+(1^+ +)$$

Mass $m = 1281.9 \pm 0.5$ MeV (S = 1.8)
Full width $\Gamma = 22.7 \pm 1.1$ MeV (S = 1.5)

 $f_1(1285)$ DECAY MODES

$f_1(1285)$ DECAY MODES	Fraction (Γ_i/Γ)	Scale factor/ Confidence level	ρ (MeV/c)
4π	(32.7 \pm 1.9) %	S=1.2	568
$\pi^0 \pi^0 \pi^+ \pi^-$	(21.8 \pm 1.3) %	S=1.2	566
$2\pi^+ 2\pi^-$	(10.9 \pm 0.6) %	S=1.2	563
$\rho^0 \pi^+ \pi^-$	(10.9 \pm 0.6) %	S=1.2	336
	seen		†
$4\pi^0$	< 7	$\times 10^{-4}$	CL=90%
$\eta \pi^+ \pi^-$	(35 \pm 15) %		479
$\eta \pi \pi$	(52.2 \pm 2.0) %	S=1.2	482
$a_0(980) \pi$ [ignoring $a_0(980) \rightarrow K\bar{K}$]	(38 \pm 4) %		238
$\eta \pi \pi$ [excluding $a_0(980) \pi$]	(14 \pm 4) %		482
$K\bar{K} \pi$	(9.0 \pm 0.4) %	S=1.1	308
$K\bar{K}^*(892)$	not seen		†
$\pi^+ \pi^- \pi^0$	(3.0 \pm 0.9) $\times 10^{-3}$		603
$\rho^\pm \pi^\mp$	< 3.1	$\times 10^{-3}$	CL=95%
$\gamma \rho^0$	(6.1 \pm 1.0) %	S=1.7	406
$\phi \gamma$	(7.4 \pm 2.6) $\times 10^{-4}$		236
$e^+ e^-$	< 9.4	$\times 10^{-9}$	CL=90%

 $\eta(1295)$

$$I^G(J^{PC}) = 0^+(0^- +)$$

See the review on "Pseudoscalar and pseudovector mesons in the 1400 MeV region."

Mass $m = 1294 \pm 4$ MeV (S = 1.6)
Full width $\Gamma = 55 \pm 5$ MeV

 $\eta(1295)$ DECAY MODES

$\eta(1295)$ DECAY MODES	Fraction (Γ_i/Γ)	ρ (MeV/c)
$\eta \pi^+ \pi^-$	seen	487
$a_0(980) \pi$	seen	248
$\eta \pi^0 \pi^0$	seen	490
$\eta(\pi\pi)_{S\text{-wave}}$	seen	-

 $\pi(1300)$

$$I^G(J^{PC}) = 1^-(0^- +)$$

Mass $m = 1300 \pm 100$ MeV [1]
Full width $\Gamma = 200$ to 600 MeV

 $\pi(1300)$ DECAY MODES

$\pi(1300)$ DECAY MODES	Fraction (Γ_i/Γ)	ρ (MeV/c)
$\rho \pi$	seen	404
$\pi(\pi\pi)_{S\text{-wave}}$	seen	-

 $a_2(1320)$

$$I^G(J^{PC}) = 1^-(2^+ +)$$

Mass $m = 1316.9 \pm 0.9$ MeV (S = 1.9)
Full width $\Gamma = 107 \pm 5$ MeV [1]

 $a_2(1320)$ DECAY MODES

$a_2(1320)$ DECAY MODES	Fraction (Γ_i/Γ)	Scale factor/ Confidence level	ρ (MeV/c)
3π	(70.1 \pm 2.7) %	S=1.2	623
$\eta \pi$	(14.5 \pm 1.2) %		535
$\omega \pi \pi$	(10.6 \pm 3.2) %	S=1.3	364
$K\bar{K}$	(4.9 \pm 0.8) %		436
$\eta'(958) \pi$	(5.5 \pm 0.9) $\times 10^{-3}$		287
$\pi^\pm \gamma$	(2.91 \pm 0.27) $\times 10^{-3}$		651
$\gamma \gamma$	(9.4 \pm 0.7) $\times 10^{-6}$		658
$e^+ e^-$	< 5	$\times 10^{-9}$	CL=90%

Meson Summary Table

 $f_0(1370)$

$$I^G(J^{PC}) = 0^+(0^{++})$$

See the review on "Scalar Mesons below 2 GeV."

Mass $m = 1200$ to 1500 MeV
Full width $\Gamma = 200$ to 500 MeV

$f_0(1370)$ DECAY MODES	Fraction (Γ_i/Γ)	ρ (MeV/c)
$\pi\pi$	seen	672
4π	seen	617
$4\pi^0$	seen	617
$2\pi^+2\pi^-$	seen	612
$\pi^+\pi^-2\pi^0$	seen	615
$\rho\rho$	seen	†
$2(\pi\pi)_{S\text{-wave}}$	seen	–
$\pi(1300)\pi$	seen	†
$a_1(1260)\pi$	seen	35
$\eta\eta$	seen	411
$K\bar{K}$	seen	475
$K\bar{K}n\pi$	not seen	†
6π	not seen	508
$\omega\omega$	not seen	†
$\gamma\gamma$	seen	685
e^+e^-	not seen	685

 $\pi_1(1400)$ [k]

$$I^G(J^{PC}) = 1^-(1^{-+})$$

See the review on "Non- $q\bar{q}$ Mesons."Mass $m = 1354 \pm 25$ MeV ($S = 1.8$)
Full width $\Gamma = 330 \pm 35$ MeV

$\pi_1(1400)$ DECAY MODES	Fraction (Γ_i/Γ)	ρ (MeV/c)
$\eta\pi^0$	seen	557
$\eta\pi^-$	seen	556
$\rho(770)\pi$	not seen	442

 $\eta(1405)$

$$I^G(J^{PC}) = 0^+(0^{-+})$$

See the review on "Pseudoscalar and Pseudovector Mesons in the 1400 MeV Region."

Mass $m = 1408.8 \pm 2.0$ MeV ($S = 2.2$)
Full width $\Gamma = 50.1 \pm 2.6$ MeV ($S = 1.7$)

$\eta(1405)$ DECAY MODES	Fraction (Γ_i/Γ)	Confidence level	ρ (MeV/c)
$K\bar{K}\pi$	seen		424
$\eta\pi\pi$	seen		562
$a_0(980)\pi$	seen		345
$\eta(\pi\pi)_{S\text{-wave}}$	seen		–
$f_0(980)\pi^0 \rightarrow \pi^+\pi^-\pi^0$	not seen		–
$f_0(980)\eta$	seen		†
4π	seen		639
$\rho\rho$	<58 %	99.85%	†
$\rho^0\gamma$	seen		491
$K^*(892)K$	seen		123

 $h_1(1415)$

$$I^G(J^{PC}) = 0^-(1^{+-})$$

was $h_1(1380)$ Mass $m = 1416 \pm 8$ MeV ($S = 1.5$)
Full width $\Gamma = 90 \pm 15$ MeV **$f_1(1420)$**

$$I^G(J^{PC}) = 0^+(1^{++})$$

See the review on "Pseudoscalar and Pseudovector Mesons in the 1400 MeV Region."

Mass $m = 1426.3 \pm 0.9$ MeV ($S = 1.1$)
Full width $\Gamma = 54.5 \pm 2.6$ MeV

$f_1(1420)$ DECAY MODES	Fraction (Γ_i/Γ)	ρ (MeV/c)
$K\bar{K}\pi$	seen	438
$K\bar{K}^*(892) + c.c.$	seen	163

 $\eta\pi\pi$
 $\phi\gamma$ possibly seen
seen573
349 **$\omega(1420)$ [l]**

$$I^G(J^{PC}) = 0^-(1^{--})$$

Mass $m = 1410 \pm 60$ MeV [l]
Full width $\Gamma = 290 \pm 190$ MeV [l]

$\omega(1420)$ DECAY MODES	Fraction (Γ_i/Γ)	ρ (MeV/c)
$\rho\pi$	seen	480
$\omega\pi\pi$	seen	437
$b_1(1235)\pi$	seen	112
e^+e^-	seen	705

 $a_0(1450)$

$$I^G(J^{PC}) = 1^-(0^{++})$$

See the review on "Scalar Mesons below 2 GeV."

Mass $m = 1474 \pm 19$ MeV
Full width $\Gamma = 265 \pm 13$ MeV

$a_0(1450)$ DECAY MODES	Fraction (Γ_i/Γ)	ρ (MeV/c)
$\pi\eta$	0.093 ± 0.020	627
$\pi\eta'(958)$	0.033 ± 0.017	410
$K\bar{K}$	0.082 ± 0.028	547
$\omega\pi\pi$	DEFINED AS 1	484
$a_0(980)\pi\pi$	seen	342
$\gamma\gamma$	seen	737

 $\rho(1450)$

$$I^G(J^{PC}) = 1^+(1^{--})$$

See the note in $\rho(1450)$ Particle Listings.Mass $m = 1465 \pm 25$ MeV [l]
Full width $\Gamma = 400 \pm 60$ MeV [l]

$\rho(1450)$ DECAY MODES	Fraction (Γ_i/Γ)	ρ (MeV/c)
$\pi\pi$	seen	720
$\pi^+\pi^-$	seen	719
4π	seen	669
e^+e^-	seen	732
$\eta\rho$	seen	311
$a_2(1320)\pi$	not seen	58
$K\bar{K}$	seen	541
K^+K^-	seen	541
$K\bar{K}^*(892) + c.c.$	possibly seen	229
$\eta\gamma$	seen	630
$f_0(500)\gamma$	not seen	–
$f_0(980)\gamma$	not seen	398
$f_0(1370)\gamma$	not seen	92
$f_2(1270)\gamma$	not seen	177

 $\eta(1475)$

$$I^G(J^{PC}) = 0^+(0^{-+})$$

See the review on "Pseudoscalar and Pseudovector Mesons in the 1400 MeV Region."

Mass $m = 1475 \pm 4$ MeV ($S = 1.4$)
Full width $\Gamma = 90 \pm 9$ MeV ($S = 1.6$)

$\eta(1475)$ DECAY MODES	Fraction (Γ_i/Γ)	ρ (MeV/c)
$K\bar{K}\pi$	seen	477
$K\bar{K}^*(892) + c.c.$	seen	244
$a_0(980)\pi$	seen	396
$\gamma\gamma$	seen	738
$K_S^0 K_S^0 \eta$	possibly seen	†
$\gamma\phi(1020)$	possibly seen	385

 $f_0(1500)$

$$I^G(J^{PC}) = 0^+(0^{++})$$

See the reviews on "Scalar Mesons below 2 GeV" and on "Non- $q\bar{q}$ Mesons".Mass $m = 1506 \pm 6$ MeV ($S = 1.4$)
Full width $\Gamma = 112 \pm 9$ MeV

Meson Summary Table

$f_0(1500)$ DECAY MODES	Fraction (Γ_i/Γ)	Scale factor	ρ (MeV/c)
$\pi\pi$	(34.5±2.2) %	1.2	741
$\pi^+\pi^-$	seen		740
$2\pi^0$	seen		741
4π	(48.9±3.3) %	1.2	692
$4\pi^0$	seen		692
$2\pi^+2\pi^-$	seen		687
$2(\pi\pi)_{S\text{-wave}}$	seen		–
$\rho\rho$	seen		†
$\pi(1300)\pi$	seen		145
$a_1(1260)\pi$	seen		219
$\eta\eta$	(6.0±0.9) %	1.1	517
$\eta\eta'(958)$	(2.2±0.8) %	1.4	20
$K\bar{K}$	(8.5±1.0) %	1.1	569
$\gamma\gamma$	not seen		753

$$f_2'(1525) \quad I^G(J^{PC}) = 0^+(2^{++})$$

Mass $m = 1517.4 \pm 2.5$ MeV ($S = 2.8$)
 Full width $\Gamma = 86 \pm 5$ MeV ($S = 2.2$)

$f_2'(1525)$ DECAY MODES	Fraction (Γ_i/Γ)	Scale factor	ρ (MeV/c)
$K\bar{K}$	(87.6±2.2) %	1.1	576
$\eta\eta$	(11.6±2.2) %	1.1	525
$\pi\pi$	(8.3±1.6) $\times 10^{-3}$		747
$\gamma\gamma$	(9.5±1.1) $\times 10^{-7}$	1.1	759

$$\pi_1(1600) \quad I^G(J^{PC}) = 1^-(1^{+-})$$

See the review on "Non- $q\bar{q}$ Mesons" and a note in PDG 06, Journal of Physics **G33** 1 (2006).

Mass $m = 1660^{+15}_{-11}$ MeV ($S = 1.2$)
 Full width $\Gamma = 257 \pm 60$ MeV ($S = 1.9$)

$\pi_1(1600)$ DECAY MODES	Fraction (Γ_i/Γ)	ρ (MeV/c)
$\pi\pi\pi$	seen	802
$\rho^0\pi^-$	seen	640
$f_2(1270)\pi^-$	not seen	316
$b_1(1235)\pi$	seen	355
$\eta'(958)\pi^-$	seen	542
$f_1(1285)\pi$	seen	312

$$a_1(1640) \quad I^G(J^{PC}) = 1^-(1^{++})$$

Mass $m = 1655 \pm 16$ MeV ($S = 1.2$)
 Full width $\Gamma = 254 \pm 40$ MeV ($S = 1.8$)

$a_1(1640)$ DECAY MODES	Fraction (Γ_i/Γ)	ρ (MeV/c)
$\pi\pi\pi$	seen	800
$f_2(1270)\pi$	seen	314
$\sigma\pi$	seen	–
$\rho\pi_{S\text{-wave}}$	seen	638
$\rho\pi_{D\text{-wave}}$	seen	638
$\omega\pi\pi$	seen	607
$f_1(1285)\pi$	seen	309
$a_1(1260)\eta$	not seen	†

$$\eta_2(1645) \quad I^G(J^{PC}) = 0^+(2^{-+})$$

Mass $m = 1617 \pm 5$ MeV
 Full width $\Gamma = 181 \pm 11$ MeV

$\eta_2(1645)$ DECAY MODES	Fraction (Γ_i/Γ)	ρ (MeV/c)
$a_2(1320)\pi$	seen	243
$K\bar{K}\pi$	seen	580
$K^*\bar{K}$	seen	404
$\eta\pi^+\pi^-$	seen	685
$a_0(980)\pi$	seen	499
$f_2(1270)\eta$	not seen	†

$$\omega(1650) [n] \quad I^G(J^{PC}) = 0^-(1^{--})$$

Mass $m = 1670 \pm 30$ MeV [J]
 Full width $\Gamma = 315 \pm 35$ MeV [J]

$\omega(1650)$ DECAY MODES	Fraction (Γ_i/Γ)	ρ (MeV/c)
$\rho\pi$	seen	647
$\omega\pi\pi$	seen	617
$\omega\eta$	seen	500
e^+e^-	seen	835
$\pi^0\gamma$	not seen	830

$$\omega_3(1670) \quad I^G(J^{PC}) = 0^-(3^{--})$$

Mass $m = 1667 \pm 4$ MeV
 Full width $\Gamma = 168 \pm 10$ MeV

$\omega_3(1670)$ DECAY MODES	Fraction (Γ_i/Γ)	ρ (MeV/c)
$\rho\pi$	seen	645
$\omega\pi\pi$	seen	615
$b_1(1235)\pi$	possibly seen	361

$$\pi_2(1670) \quad I^G(J^{PC}) = 1^-(2^{-+})$$

Mass $m = 1670.6^{+2.9}_{-1.2}$ MeV ($S = 1.3$)
 Full width $\Gamma = 258^{+8}_{-9}$ MeV ($S = 1.2$)

$\pi_2(1670)$ DECAY MODES	Fraction (Γ_i/Γ)	Confidence level	ρ (MeV/c)
3π	(95.8±1.4) %		808
$f_2(1270)\pi$	(56.3±3.2) %		327
$\rho\pi$	(31 ± 4) %		647
$\sigma\pi$	(10 ± 4) %		–
$\pi(\pi\pi)_{S\text{-wave}}$	(8.7±3.4) %		–
$\pi^\pm\pi^+\pi^-$	(53 ± 4) %		806
$K\bar{K}^*(892) + c.c.$	(4.2±1.4) %		453
$\omega\rho$	(2.7±1.1) %		302
$\pi^\pm\gamma$	(7.0±1.2) $\times 10^{-4}$		829
$\gamma\gamma$	< 2.8 $\times 10^{-7}$	90%	835
$\eta\pi$	< 5 %		739
$\pi^\pm 2\pi^+ 2\pi^-$	< 5 %		735
$\rho(1450)\pi$	< 3.6 $\times 10^{-3}$	97.7%	145
$b_1(1235)\pi$	< 1.9 $\times 10^{-3}$	97.7%	364
$f_1(1285)\pi$	possibly seen		322
$a_2(1320)\pi$	not seen		292

$$\phi(1680) \quad I^G(J^{PC}) = 0^-(1^{--})$$

Mass $m = 1680 \pm 20$ MeV [J]
 Full width $\Gamma = 150 \pm 50$ MeV [J]

$\phi(1680)$ DECAY MODES	Fraction (Γ_i/Γ)	ρ (MeV/c)
$K\bar{K}^*(892) + c.c.$	seen	462
$K_S^0 K\pi$	seen	621
$K\bar{K}$	seen	680
e^+e^-	seen	840
$\omega\pi\pi$	not seen	623
$K^+K^-\pi^+\pi^-$	seen	544
$\eta\phi$	seen	290
$\eta\gamma$	seen	751

$$\rho_3(1690) \quad I^G(J^{PC}) = 1^+(3^{--})$$

Mass $m = 1688.8 \pm 2.1$ MeV
 Full width $\Gamma = 161 \pm 10$ MeV ($S = 1.5$)

$\rho_3(1690)$ DECAY MODES	Fraction (Γ_i/Γ)	Scale factor	ρ (MeV/c)
4π	(71.1 ± 1.9) %		790
$\pi^\pm\pi^+\pi^-\pi^0$	(67 ± 22) %		787
$\omega\pi$	(16 ± 6) %		655
$\pi\pi$	(23.6 ± 1.3) %		834
$K\bar{K}\pi$	(3.8 ± 1.2) %		629
$K\bar{K}$	(1.58 ± 0.26) %	1.2	685
$\eta\pi^+\pi^-$	seen		727

Meson Summary Table

$\rho(770)\eta$	seen	520
$\pi\pi\rho$	seen	633
$a_2(1320)\pi$	seen	308
$\rho\rho$	seen	335

 $\rho(1700)$

$$I^G(J^{PC}) = 1^+(1^- -)$$

See the note in $\rho(1700)$ Particle Listings.

Mass $m = 1720 \pm 20$ MeV [1] ($\eta\rho^0$ and $\pi^+\pi^-$ modes)
 Full width $\Gamma = 250 \pm 100$ MeV [1] ($\eta\rho^0$ and $\pi^+\pi^-$ modes)

$\rho(1700)$ DECAY MODES	Fraction (Γ_i/Γ)	ρ (MeV/c)
$2(\pi^+\pi^-)$	seen	803
$\rho\pi\pi$	seen	653
$\rho^0\pi^+\pi^-$	seen	651
$\rho^\pm\pi^\mp\pi^0$	seen	652
$a_1(1260)\pi$	seen	404
$h_1(1170)\pi$	seen	450
$\pi(1300)\pi$	seen	349
$\rho\rho$	seen	372
$\pi^+\pi^-$	seen	849
$\pi\pi$	seen	849
$K\bar{K}^*(892) + c.c.$	seen	496
$\eta\rho$	seen	545
$a_2(1320)\pi$	not seen	335
$K\bar{K}$	seen	704
e^+e^-	seen	860
$\pi^0\omega$	seen	674
$\pi^0\gamma$	not seen	855

 $a_2(1700)$

$$I^G(J^{PC}) = 1^-(2^+ +)$$

Mass $m = 1705 \pm 40$ MeV
 Full width $\Gamma = 258 \pm 40$ MeV

$a_2(1700)$ DECAY MODES	Fraction (Γ_i/Γ)	ρ (MeV/c)
$\eta\pi$	$(3.7 \pm 1.0) \%$	758
$\gamma\gamma$	$(1.16 \pm 0.27) \times 10^{-6}$	852
$\rho\pi$	seen	668
$f_2(1270)\pi$	seen	356
$K\bar{K}$	$(1.9 \pm 1.2) \%$	695
$\omega\pi^-\pi^0$	seen	638
$\omega\rho$	seen	346

 $f_0(1710)$

$$I^G(J^{PC}) = 0^+(0^+ +)$$

See the review on "Non- $q\bar{q}$ Mesons."

Mass $m = 1704 \pm 12$ MeV
 Full width $\Gamma = 123 \pm 18$ MeV

$f_0(1710)$ DECAY MODES	Fraction (Γ_i/Γ)	ρ (MeV/c)
$K\bar{K}$	seen	694
$\eta\eta$	seen	652
$\pi\pi$	seen	841
$\gamma\gamma$	seen	852
$\omega\omega$	seen	337

 $\pi(1800)$

$$I^G(J^{PC}) = 1^-(0^- +)$$

Mass $m = 1810^{+9}_{-11}$ MeV ($S = 2.2$)
 Full width $\Gamma = 215^{+7}_{-8}$ MeV

$\pi(1800)$ DECAY MODES	Fraction (Γ_i/Γ)	ρ (MeV/c)
$\pi^+\pi^-\pi^-$	seen	878
$f_0(500)\pi^-$	seen	-
$f_0(980)\pi^-$	seen	624
$f_0(1370)\pi^-$	seen	366
$f_0(1500)\pi^-$	not seen	247
$\rho\pi^-$	not seen	731

$\eta\eta\pi^-$	seen	660
$a_0(980)\eta$	seen	471
$a_2(1320)\eta$	not seen	†
$f_2(1270)\pi^-$	not seen	441
$f_0(1370)\pi^-$	not seen	366
$f_0(1500)\pi^-$	seen	247
$\eta\eta'(958)\pi^-$	seen	373
$K_0^*(1430)K^-$	seen	†
$K^*(892)K^-$	not seen	568

 $\phi_3(1850)$

$$I^G(J^{PC}) = 0^-(3^- -)$$

Mass $m = 1854 \pm 7$ MeV
 Full width $\Gamma = 87^{+28}_{-23}$ MeV ($S = 1.2$)

$\phi_3(1850)$ DECAY MODES	Fraction (Γ_i/Γ)	ρ (MeV/c)
$K\bar{K}$	seen	785
$K\bar{K}^*(892) + c.c.$	seen	602

 $\eta_2(1870)$

$$I^G(J^{PC}) = 0^+(2^- +)$$

Mass $m = 1842 \pm 8$ MeV
 Full width $\Gamma = 225 \pm 14$ MeV

$\eta_2(1870)$ DECAY MODES	Fraction (Γ_i/Γ)	ρ (MeV/c)
$\gamma\gamma$	seen	921

 $\pi_2(1880)$

$$I^G(J^{PC}) = 1^-(2^- +)$$

Mass $m = 1874^{+26}_{-5}$ MeV ($S = 1.6$)
 Full width $\Gamma = 237^{+33}_{-30}$ MeV ($S = 1.2$)

$f_2(1950)$ DECAY MODES	Fraction (Γ_i/Γ)	ρ (MeV/c)
$K^*(892)\bar{K}^*(892)$	seen	377
$\pi^+\pi^-$	seen	958
$\pi^0\pi^0$	seen	959
4π	seen	921
$\eta\eta$	seen	798
$K\bar{K}$	seen	833
$\gamma\gamma$	seen	968
$\rho\bar{\rho}$	seen	238

 $a_4(1970)$

$$I^G(J^{PC}) = 1^-(4^+ +)$$

was $a_4(2040)$

Mass $m = 1967 \pm 16$ MeV ($S = 2.1$)
 Full width $\Gamma = 324^{+15}_{-18}$ MeV

$a_4(1970)$ DECAY MODES	Fraction (Γ_i/Γ)	ρ (MeV/c)
$K\bar{K}$	seen	851
$\pi^+\pi^-\pi^0$	seen	959
$\rho\pi$	seen	825
$f_2(1270)\pi$	seen	559
$\omega\pi^-\pi^0$	seen	801
$\omega\rho$	seen	601
$\eta\pi$	seen	902
$\eta'(958)\pi$	seen	743

 $f_2(2010)$

$$I^G(J^{PC}) = 0^+(2^+ +)$$

Mass $m = 2011^{+60}_{-80}$ MeV
 Full width $\Gamma = 202 \pm 60$ MeV

$f_2(2010)$ DECAY MODES	Fraction (Γ_i/Γ)	ρ (MeV/c)
$\phi\phi$	seen	†
$K\bar{K}$	seen	876

Meson Summary Table

$f_4(2050)$	$J^G(JPC) = 0^+(4^{++})$	ρ (MeV/c)
Mass $m = 2018 \pm 11$ MeV ($S = 2.1$)		
Full width $\Gamma = 237 \pm 18$ MeV ($S = 1.9$)		
$f_4(2050)$ DECAY MODES	Fraction (Γ_i/Γ)	ρ (MeV/c)
$\omega\omega$	seen	637
$\pi\pi$	(17.0 ± 1.5) %	1000
$K\bar{K}$	(6.8 ^{+3.4} _{-1.8}) × 10 ⁻³	880
$\eta\eta$	(2.1 ± 0.8) × 10 ⁻³	848
$4\pi^0$	< 1.2 %	964
$a_2(1320)\pi$	seen	568

$\phi(2170)$	$J^G(JPC) = 0^-(1^{--})$	ρ (MeV/c)
Mass $m = 2160 \pm 80$ MeV [1]		
Full width $\Gamma = 125 \pm 65$ MeV [1]		
$\phi(2170)$ DECAY MODES	Fraction (Γ_i/Γ)	ρ (MeV/c)
e^+e^-	seen	1080
$\phi f_0(980)$	seen	396
$K^+K^- f_0(980) \rightarrow$ $K^+K^-\pi^+\pi^-$	seen	-
$K^+K^- f_0(980) \rightarrow K^+K^-\pi^0\pi^0$	seen	-
$K^{*0}K^\pm\pi^\mp$	not seen	759
$K^*(892)^0\bar{K}^*(892)^0$	not seen	609

$f_2(2300)$	$J^G(JPC) = 0^+(2^{++})$	ρ (MeV/c)
Mass $m = 2297 \pm 28$ MeV		
Full width $\Gamma = 149 \pm 40$ MeV		
$f_2(2300)$ DECAY MODES	Fraction (Γ_i/Γ)	ρ (MeV/c)
$\phi\phi$	seen	529
$K\bar{K}$	seen	1037
$\gamma\gamma$	seen	1149

$f_2(2340)$	$J^G(JPC) = 0^+(2^{++})$	ρ (MeV/c)
Mass $m = 2345^{+50}_{-40}$ MeV		
Full width $\Gamma = 322^{+70}_{-60}$ MeV		
$f_2(2340)$ DECAY MODES	Fraction (Γ_i/Γ)	ρ (MeV/c)
$\phi\phi$	seen	580
$\eta\eta$	seen	1037

STRANGE MESONS ($S = \pm 1, C = B = 0$)

$K^+ = u\bar{s}, K^0 = d\bar{s}, \bar{K}^0 = \bar{d}s, K^- = \bar{u}s,$ similarly for K^{*s}

K^\pm	$J^G(JPC) = \frac{1}{2}(0^-)$	ρ (MeV/c)
Mass $m = 493.677 \pm 0.016$ MeV [0] ($S = 2.8$)		
Mean life $\tau = (1.2380 \pm 0.0020) \times 10^{-8}$ s ($S = 1.8$)		
$c\tau = 3.711$ m		

CPT violation parameters ($\Delta =$ rate difference/sum)

$$\Delta(K^\pm \rightarrow \mu^\pm \nu_\mu) = (-0.27 \pm 0.21)\%$$

$$\Delta(K^\pm \rightarrow \pi^\pm \pi^0) = (0.4 \pm 0.6)\% [b]$$

CP violation parameters ($\Delta =$ rate difference/sum)

$$\Delta(K^\pm \rightarrow \pi^\pm e^+ e^-) = (-2.2 \pm 1.6) \times 10^{-2}$$

$$\Delta(K^\pm \rightarrow \pi^\pm \mu^+ \mu^-) = 0.010 \pm 0.023$$

$$\Delta(K^\pm \rightarrow \pi^\pm \pi^0 \gamma) = (0.0 \pm 1.2) \times 10^{-3}$$

$$\Delta(K^\pm \rightarrow \pi^\pm \pi^+ \pi^-) = (0.04 \pm 0.06)\%$$

$$\Delta(K^\pm \rightarrow \pi^\pm \pi^0 \pi^0) = (-0.02 \pm 0.28)\%$$

T violation parameters

$$K^+ \rightarrow \pi^0 \mu^+ \nu_\mu \quad P_T = (-1.7 \pm 2.5) \times 10^{-3}$$

$$K^+ \rightarrow \mu^+ \nu_\mu \gamma \quad P_T = (-0.6 \pm 1.9) \times 10^{-2}$$

$$K^+ \rightarrow \pi^0 \mu^+ \nu_\mu \quad \text{Im}(\xi) = -0.006 \pm 0.008$$

Slope parameter $g^{[q]}$

(See Particle Listings for quadratic coefficients and alternative parametrization related to $\pi\pi$ scattering)

$$K^\pm \rightarrow \pi^\pm \pi^+ \pi^- \quad g = -0.21134 \pm 0.00017$$

$$K^\pm \rightarrow \pi^\pm \pi^0 \pi^0 \quad g = 0.626 \pm 0.007$$

$$g = (g_+ - g_-) / (g_+ + g_-) = (-1.5 \pm 2.2) \times 10^{-4}$$

$$g = (g_+ - g_-) / (g_+ + g_-) = (1.8 \pm 1.8) \times 10^{-4}$$

K^\pm decay form factors [a,r]

Assuming μ -e universality

$$\lambda_+(K_{\mu 3}^+) = \lambda_+(K_{e 3}^+) = (2.959 \pm 0.025) \times 10^{-2}$$

$$\lambda_0(K_{\mu 3}^+) = (1.76 \pm 0.25) \times 10^{-2} \quad (S = 2.7)$$

Not assuming μ -e universality

$$\lambda_+(K_{e 3}^+) = (2.956 \pm 0.025) \times 10^{-2}$$

$$\lambda_+(K_{\mu 3}^+) = (3.09 \pm 0.25) \times 10^{-2} \quad (S = 1.5)$$

$$\lambda_0(K_{\mu 3}^+) = (1.73 \pm 0.27) \times 10^{-2} \quad (S = 2.6)$$

$K_{e 3}$ form factor quadratic fit

$$\lambda'_+(K_{e 3}^\pm) \text{ linear coeff.} = (2.59 \pm 0.04) \times 10^{-2}$$

$$\lambda''_+(K_{e 3}^\pm) \text{ quadratic coeff.} = (0.186 \pm 0.021) \times 10^{-2}$$

$$\lambda'_+(K_{\mu 3}^\pm) \text{ FORM FACTOR FROM QUADRATIC FIT}$$

$$= (24 \pm 4) \times 10^{-3}$$

$$\lambda''_+(K_{\mu 3}^\pm) \text{ FORM FACTOR} = (1.8 \pm 1.5) \times 10^{-3}$$

$$M_V \text{ (VECTOR POLE MASS FOR } K_{e 3}^\pm \text{ DECAY)} = 890.3 \pm 2.8 \text{ MeV}$$

$$M_V \text{ (VECTOR POLE MASS FOR } K_{\mu 3}^\pm \text{ DECAY)} = 878 \pm 12 \text{ MeV}$$

$$M_S \text{ (SCALAR POLE MASS FOR } K_{\mu 3}^\pm \text{ DECAY)} = 1215 \pm 50 \text{ MeV}$$

$$\Lambda_+ \text{ (DISPERSIVE VECTOR FORM FACTOR IN } K_{e 3}^\pm \text{ DECAY)} = (2.460 \pm 0.017) \times 10^{-2}$$

$$\Lambda_+ \text{ (DISPERSIVE VECTOR FORM FACTOR IN } K_{\mu 3}^\pm \text{ DECAY)} = (25.4 \pm 0.9) \times 10^{-3}$$

$$\ln(C) \text{ (DISPERSIVE SCALAR FORM FACTOR IN } K_{\mu 3}^\pm \text{ decays)} = (182 \pm 16) \times 10^{-3}$$

$$K_{e 3}^+ \quad |f_S/f_+| = (-0.08^{+0.34}_{-0.40}) \times 10^{-2}$$

$$K_{e 3}^+ \quad |f_T/f_+| = (-1.2^{+1.3}_{-1.1}) \times 10^{-2}$$

$$K_{\mu 3}^+ \quad |f_S/f_+| = (0.2 \pm 0.6) \times 10^{-2}$$

$$K_{\mu 3}^+ \quad |f_T/f_+| = (-0.1 \pm 0.7) \times 10^{-2}$$

$$K^+ \rightarrow e^+ \nu_e \gamma \quad |F_A + F_V| = 0.133 \pm 0.008 \quad (S = 1.3)$$

$$K^+ \rightarrow \mu^+ \nu_\mu \gamma \quad |F_A + F_V| = 0.165 \pm 0.013$$

$$K^+ \rightarrow e^+ \nu_e \gamma \quad |F_A - F_V| < 0.49, \text{ CL} = 90\%$$

$$K^+ \rightarrow \mu^+ \nu_\mu \gamma \quad |F_A - F_V| = -0.153 \pm 0.033 \quad (S = 1.1)$$

Charge radius

$$\langle r \rangle = 0.560 \pm 0.031 \text{ fm}$$

Forward-backward asymmetry

$$A_{FB}(K_{\pi\mu}^\pm) = \frac{\Gamma(\cos(\theta_{K\mu}) > 0) - \Gamma(\cos(\theta_{K\mu}) < 0)}{\Gamma(\cos(\theta_{K\mu}) > 0) + \Gamma(\cos(\theta_{K\mu}) < 0)} < 2.3 \times 10^{-2}, \text{ CL} = 90\%$$

K^- modes are charge conjugates of the modes below.

K^+ DECAY MODES	Fraction (Γ_i/Γ)	Scale factor / Confidence level (MeV/c)	ρ
Leptonic and semileptonic modes			
$e^+ \nu_e$	(1.582 ± 0.007) × 10 ⁻⁵		247
$\mu^+ \nu_\mu$	(63.56 ± 0.11) %	S=1.2	236
$\pi^0 e^+ \nu_e$	(5.07 ± 0.04) %	S=2.1	228
Called $K_{e 3}^+$.			

Meson Summary Table

$\pi^0 \mu^+ \nu_\mu$	(3.352 ± 0.033) %	S=1.9	215
Called $K_{\mu 3}^+$.			
$\pi^0 \pi^0 e^+ \nu_e$	(2.55 ± 0.04) × 10 ⁻⁵	S=1.1	206
$\pi^+ \pi^- e^+ \nu_e$	(4.247 ± 0.024) × 10 ⁻⁵		203
$\pi^+ \pi^- \mu^+ \nu_\mu$	(1.4 ± 0.9) × 10 ⁻⁵		151
$\pi^0 \pi^0 \pi^0 e^+ \nu_e$	< 3.5 × 10 ⁻⁶	CL=90%	135

Hadronic modes

$\pi^+ \pi^0$	(20.67 ± 0.08) %	S=1.2	205
$\pi^+ \pi^0 \pi^0$	(1.760 ± 0.023) %	S=1.1	133
$\pi^+ \pi^+ \pi^-$	(5.583 ± 0.024) %		125

Leptonic and semileptonic modes with photons

$\mu^+ \nu_\mu \gamma$	[s,t] (6.2 ± 0.8) × 10 ⁻³		236
$\mu^+ \nu_\mu \gamma (SD^+)$	[a,u] (1.33 ± 0.22) × 10 ⁻⁵		-
$\mu^+ \nu_\mu \gamma (SD^+ INT)$	[a,u] < 2.7 × 10 ⁻⁵	CL=90%	-
$\mu^+ \nu_\mu \gamma (SD^- + SD^- INT)$	[a,u] < 2.6 × 10 ⁻⁴	CL=90%	-
$e^+ \nu_e \gamma$	(9.4 ± 0.4) × 10 ⁻⁶		247
$\pi^0 e^+ \nu_e \gamma$	[s,t] (2.56 ± 0.16) × 10 ⁻⁴		228
$\pi^0 e^+ \nu_e \gamma (SD)$	[a,u] < 5.3 × 10 ⁻⁵	CL=90%	228
$\pi^0 \mu^+ \nu_\mu \gamma$	[s,t] (1.25 ± 0.25) × 10 ⁻⁵		215
$\pi^0 \pi^0 e^+ \nu_e \gamma$	< 5 × 10 ⁻⁶	CL=90%	206

Hadronic modes with photons or $\ell\bar{\ell}$ pairs

$\pi^+ \pi^0 \gamma (INT)$	(- 4.2 ± 0.9) × 10 ⁻⁶		-
$\pi^+ \pi^0 \gamma (DE)$	[s,v] (6.0 ± 0.4) × 10 ⁻⁶		205
$\pi^+ \pi^0 e^+ e^-$	(4.24 ± 0.14) × 10 ⁻⁶		205
$\pi^+ \pi^0 \pi^0 \gamma$	[s,t] (7.6 ± 3.0) × 10 ⁻⁶		133
$\pi^+ \pi^+ \pi^- \gamma$	[s,t] (7.1 ± 0.5) × 10 ⁻⁶		125
$\pi^+ \gamma \gamma$	[s] (1.01 ± 0.06) × 10 ⁻⁶		227
$\pi^+ 3\gamma$	[s] < 1.0 × 10 ⁻⁴	CL=90%	227
$\pi^+ e^+ e^- \gamma$	(1.19 ± 0.13) × 10 ⁻⁸		227

Leptonic modes with $\ell\bar{\ell}$ pairs

$e^+ \nu_e \nu\bar{\nu}$	< 6 × 10 ⁻⁵	CL=90%	247
$\mu^+ \nu_\mu \nu\bar{\nu}$	< 2.4 × 10 ⁻⁶	CL=90%	236
$e^+ \nu_e e^+ e^-$	(2.48 ± 0.20) × 10 ⁻⁸		247
$\mu^+ \nu_\mu e^+ e^-$	(7.06 ± 0.31) × 10 ⁻⁸		236
$e^+ \nu_e \mu^+ \mu^-$	(1.7 ± 0.5) × 10 ⁻⁸		223
$\mu^+ \nu_\mu \mu^+ \mu^-$	< 4.1 × 10 ⁻⁷	CL=90%	185

Lepton family number (LF), Lepton number (L), $\Delta S = \Delta Q$ (SQ) violating modes, or $\Delta S = 1$ weak neutral current (S1) modes

$\pi^+ \pi^+ e^- \bar{\nu}_e$	SQ < 1.3 × 10 ⁻⁸	CL=90%	203
$\pi^+ \pi^+ \mu^- \bar{\nu}_\mu$	SQ < 3.0 × 10 ⁻⁶	CL=95%	151
$\pi^+ e^+ e^-$	S1 (3.00 ± 0.09) × 10 ⁻⁷		227
$\pi^+ \mu^+ \mu^-$	S1 (9.4 ± 0.6) × 10 ⁻⁸	S=2.6	172
$\pi^+ \nu\bar{\nu}$	S1 (1.7 ± 1.1) × 10 ⁻¹⁰		227
$\pi^+ \pi^0 \nu\bar{\nu}$	S1 < 4.3 × 10 ⁻⁵	CL=90%	205
$\mu^- \nu e^+ e^+$	LF < 2.1 × 10 ⁻⁸	CL=90%	236
$\mu^+ \nu_e$	LF [d] < 4 × 10 ⁻³	CL=90%	236
$\pi^+ \mu^+ e^-$	LF < 1.3 × 10 ⁻¹¹	CL=90%	214
$\pi^+ \mu^- e^+$	LF < 5.2 × 10 ⁻¹⁰	CL=90%	214
$\pi^- \mu^+ e^+$	L < 5.0 × 10 ⁻¹⁰	CL=90%	214
$\pi^- e^+ e^+$	L < 2.2 × 10 ⁻¹⁰	CL=90%	227
$\pi^- \mu^+ \mu^+$	L < 4.2 × 10 ⁻¹¹	CL=90%	172
$\mu^+ \bar{\nu}_e$	L [d] < 3.3 × 10 ⁻³	CL=90%	236
$\pi^0 e^+ \bar{\nu}_e$	L < 3 × 10 ⁻³	CL=90%	228
$\pi^+ \gamma$	[x] < 2.3 × 10 ⁻⁹	CL=90%	227

 K^0

$$I(J^P) = \frac{1}{2}(0^-)$$

50% K_S , 50% K_L Mass $m = 497.611 \pm 0.013$ MeV (S = 1.2) $m_{K^0} - m_{K^\pm} = 3.934 \pm 0.020$ MeV (S = 1.6)

Mean square charge radius

$$\langle r^2 \rangle = -0.077 \pm 0.010 \text{ fm}^2$$

T-violation parameters in $K^0-\bar{K}^0$ mixing [r]Asymmetry A_T in $K^0-\bar{K}^0$ mixing = $(6.6 \pm 1.6) \times 10^{-3}$

CP-violation parameters

$$\text{Re}(\epsilon) = (1.596 \pm 0.013) \times 10^{-3}$$

CPT-violation parameters [r]

$$\text{Re } \delta = (2.5 \pm 2.3) \times 10^{-4}$$

$$\text{Im } \delta = (-1.5 \pm 1.6) \times 10^{-5}$$

$$\text{Re}(y), K_{e3} \text{ parameter} = (0.4 \pm 2.5) \times 10^{-3}$$

$$\text{Re}(x_-), K_{e3} \text{ parameter} = (-2.9 \pm 2.0) \times 10^{-3}$$

$$|m_{K^0} - m_{\bar{K}^0}| / m_{\text{average}} < 6 \times 10^{-19}, \text{CL} = 90\% [\nu]$$

$$(\Gamma_{K^0} - \Gamma_{\bar{K}^0}) / m_{\text{average}} = (8 \pm 8) \times 10^{-18}$$

Tests of $\Delta S = \Delta Q$

$$\text{Re}(x_+), K_{e3} \text{ parameter} = (-0.9 \pm 3.0) \times 10^{-3}$$

 K_S^0

$$I(J^P) = \frac{1}{2}(0^-)$$

Mean life $\tau = (0.8954 \pm 0.0004) \times 10^{-10}$ s (S = 1.1) Assuming CPTMean life $\tau = (0.89564 \pm 0.00033) \times 10^{-10}$ s Not assuming CPT

$$c\tau = 2.6844 \text{ cm} \text{ Assuming CPT}$$

CP-violation parameters [z]

$$\text{Im}(\eta_{+-0}) = -0.002 \pm 0.009$$

$$\text{Im}(\eta_{000}) = -0.001 \pm 0.016$$

$$|\eta_{000}| = |A(K_S^0 \rightarrow 3\pi^0)/A(K_L^0 \rightarrow 3\pi^0)| < 0.0088, \text{CL} = 90\%$$

$$\text{CP asymmetry } A \text{ in } \pi^+ \pi^- e^+ e^- = (-0.4 \pm 0.8)\%$$

 K_S^0 DECAY MODES

	Fraction (Γ_i/Γ)	Scale factor / Confidence level	p (MeV/c)
Hadronic modes			
$\pi^0 \pi^0$	(30.69 ± 0.05) %		209
$\pi^+ \pi^-$	(69.20 ± 0.05) %		206
$\pi^+ \pi^- \pi^0$	(3.5 ± 1.1 / -0.9) × 10 ⁻⁷		133
Modes with photons or $\ell\bar{\ell}$ pairs			
$\pi^+ \pi^- \gamma$	[t,aa] (1.79 ± 0.05) × 10 ⁻³		206
$\pi^+ \pi^- e^+ e^-$	(4.79 ± 0.15) × 10 ⁻⁵		206
$\pi^0 \gamma \gamma$	[aa] (4.9 ± 1.8) × 10 ⁻⁸		230
$\gamma \gamma$	(2.63 ± 0.17) × 10 ⁻⁶	S=3.0	249
Semileptonic modes			
$\pi^\pm e^\mp \nu_e$	[bb] (7.04 ± 0.08) × 10 ⁻⁴		229
CP violating (CP) and $\Delta S = 1$ weak neutral current (S1) modes			
$3\pi^0$	CP < 2.6 × 10 ⁻⁸	CL=90%	139
$\mu^+ \mu^-$	S1 < 8 × 10 ⁻¹⁰	CL=90%	225
$e^+ e^-$	S1 < 9 × 10 ⁻⁹	CL=90%	249
$\pi^0 e^+ e^-$	S1 [aa] (3.0 ± 1.5 / -1.2) × 10 ⁻⁹		230
$\pi^0 \mu^+ \mu^-$	S1 (2.9 ± 1.5 / -1.2) × 10 ⁻⁹		177

 K_L^0

$$I(J^P) = \frac{1}{2}(0^-)$$

$$m_{K_L} - m_{K_S}$$

$$= (0.5293 \pm 0.0009) \times 10^{10} \hbar \text{ s}^{-1} \text{ (S = 1.3) Assuming CPT}$$

$$= (3.484 \pm 0.006) \times 10^{-12} \text{ MeV Assuming CPT}$$

$$= (0.5289 \pm 0.0010) \times 10^{10} \hbar \text{ s}^{-1} \text{ Not assuming CPT}$$

$$\text{Mean life } \tau = (5.116 \pm 0.021) \times 10^{-8} \text{ s (S = 1.1)}$$

$$c\tau = 15.34 \text{ m}$$

Slope parameters [q]

(See Particle Listings for other linear and quadratic coefficients)

$$K_L^0 \rightarrow \pi^+ \pi^- \pi^0: g = 0.678 \pm 0.008 \text{ (S = 1.5)}$$

$$K_L^0 \rightarrow \pi^+ \pi^- \pi^0: h = 0.076 \pm 0.006$$

$$K_L^0 \rightarrow \pi^+ \pi^- \pi^0: k = 0.0099 \pm 0.0015$$

$$K_L^0 \rightarrow \pi^0 \pi^0 \pi^0: h = (0.6 \pm 1.2) \times 10^{-3}$$

 K_L decay form factors [r]Linear parametrization assuming μ -e universality

$$\lambda_+(K_{\mu 3}^0) = \lambda_+(K_{e 3}^0) = (2.82 \pm 0.04) \times 10^{-2} \text{ (S = 1.1)}$$

$$\lambda_0(K_{\mu 3}^0) = (1.38 \pm 0.18) \times 10^{-2} \text{ (S = 2.2)}$$

Meson Summary Table

Quadratic parametrization assuming μ - e universality

$$\lambda'_+(K_{\mu 3}^0) = \lambda'_+(K_{e 3}^0) = (2.40 \pm 0.12) \times 10^{-2} \quad (S = 1.2)$$

$$\lambda''_+(K_{\mu 3}^0) = \lambda''_+(K_{e 3}^0) = (0.20 \pm 0.05) \times 10^{-2} \quad (S = 1.2)$$

$$\lambda_0(K_{\mu 3}^0) = (1.16 \pm 0.09) \times 10^{-2} \quad (S = 1.2)$$

Pole parametrization assuming μ - e universality

$$M_V^\mu(K_{\mu 3}^0) = M_V^e(K_{e 3}^0) = 878 \pm 6 \text{ MeV} \quad (S = 1.1)$$

$$M_S^\mu(K_{\mu 3}^0) = 1252 \pm 90 \text{ MeV} \quad (S = 2.6)$$

Dispersive parametrization assuming μ - e universality

$$\Lambda_+ = (2.51 \pm 0.06) \times 10^{-2} \quad (S = 1.5)$$

$$\ln(C) = (1.75 \pm 0.18) \times 10^{-1} \quad (S = 2.0)$$

$$K_{e 3}^0 \quad |f_S/f_+| = (1.5 \pm 1.4) \times 10^{-2}$$

$$K_{e 3}^0 \quad |f_T/f_+| = (5 \pm 4) \times 10^{-2}$$

$$K_{\mu 3}^0 \quad |f_T/f_+| = (12 \pm 12) \times 10^{-2}$$

$$K_L \rightarrow \ell^+ \ell^- \gamma, K_L \rightarrow \ell^+ \ell^- \ell'^+ \ell'^-: \alpha_{K^*} = -0.205 \pm 0.022 \quad (S = 1.8)$$

$$K_L^0 \rightarrow \ell^+ \ell^- \gamma, K_L^0 \rightarrow \ell^+ \ell^- \ell'^+ \ell'^-: \alpha_{DIP} = -1.69 \pm 0.08 \quad (S = 1.7)$$

$$K_L \rightarrow \pi^+ \pi^- e^+ e^-: a_1/a_2 = -0.737 \pm 0.014 \text{ GeV}^2$$

$$K_L \rightarrow \pi^0 2\gamma: a_V = -0.43 \pm 0.06 \quad (S = 1.5)$$

CP-violation parameters [z]

$$A_L = (0.332 \pm 0.006)\%$$

$$|\eta_{00}| = (2.220 \pm 0.011) \times 10^{-3} \quad (S = 1.8)$$

$$|\eta_{+-}| = (2.232 \pm 0.011) \times 10^{-3} \quad (S = 1.8)$$

$$|\epsilon| = (2.228 \pm 0.011) \times 10^{-3} \quad (S = 1.8)$$

$$|\eta_{00}/\eta_{+-}| = 0.9950 \pm 0.0007^{[cc]} \quad (S = 1.6)$$

$$\text{Re}(\epsilon'/\epsilon) = (1.66 \pm 0.23) \times 10^{-3}^{[cc]} \quad (S = 1.6)$$

Assuming CPT

$$\phi_{+-} = (43.51 \pm 0.05)^\circ \quad (S = 1.2)$$

$$\phi_{00} = (43.52 \pm 0.05)^\circ \quad (S = 1.3)$$

$$\phi_\epsilon = \phi_{SW} = (43.52 \pm 0.05)^\circ \quad (S = 1.2)$$

$$\text{Im}(\epsilon'/\epsilon) = -(\phi_{00} - \phi_{+-})/3 = (-0.002 \pm 0.005)^\circ \quad (S = 1.7)$$

Not assuming CPT

$$\phi_{+-} = (43.4 \pm 0.5)^\circ \quad (S = 1.2)$$

$$\phi_{00} = (43.7 \pm 0.6)^\circ \quad (S = 1.2)$$

$$\phi_\epsilon = (43.5 \pm 0.5)^\circ \quad (S = 1.3)$$

$$CP \text{ asymmetry } A \text{ in } K_L^0 \rightarrow \pi^+ \pi^- e^+ e^- = (13.7 \pm 1.5)\%$$

$$\beta_{CP} \text{ from } K_L^0 \rightarrow e^+ e^- e^+ e^- = -0.19 \pm 0.07$$

$$\gamma_{CP} \text{ from } K_L^0 \rightarrow e^+ e^- e^+ e^- = 0.01 \pm 0.11 \quad (S = 1.6)$$

$$j \text{ for } K_L^0 \rightarrow \pi^+ \pi^- \pi^0 = 0.0012 \pm 0.0008$$

$$f \text{ for } K_L^0 \rightarrow \pi^+ \pi^- \pi^0 = 0.004 \pm 0.006$$

$$|\eta_{+-\gamma}| = (2.35 \pm 0.07) \times 10^{-3}$$

$$\phi_{+-\gamma} = (44 \pm 4)^\circ$$

$$|\epsilon'_{+-\gamma}|/\epsilon < 0.3, \text{ CL} = 90\%$$

$$|\bar{g}_{E1}| \text{ for } K_L^0 \rightarrow \pi^+ \pi^- \gamma < 0.21, \text{ CL} = 90\%$$

T-violation parameters

$$\text{Im}(\xi) \text{ in } K_{\mu 3}^0 = -0.007 \pm 0.026$$

CPT invariance tests

$$\phi_{00} - \phi_{+-} = (0.34 \pm 0.32)^\circ$$

$$\text{Re}(\frac{2}{3}\eta_{+-} + \frac{1}{3}\eta_{00}) - \frac{A}{2} = (-3 \pm 35) \times 10^{-6}$$

$\Delta S = -\Delta Q$ in K_{23}^0 decay

$$\text{Re } x = -0.002 \pm 0.006$$

$$\text{Im } x = 0.0012 \pm 0.0021$$

K_L^0 DECAY MODES

	Fraction (Γ_i/Γ)	Scale factor/ Confidence level (MeV/c)	p
Semileptonic modes			
$\pi^\pm e^\mp \nu_e$ Called $K_{e 3}^0$.	[bb] (40.55 \pm 0.11) %	S=1.7	229
$\pi^\pm \mu^\mp \nu_\mu$ Called $K_{\mu 3}^0$.	[bb] (27.04 \pm 0.07) %	S=1.1	216
$(\pi \mu \text{ atom}) \nu$	(1.05 \pm 0.11) $\times 10^{-7}$		188
$\pi^0 \pi^\pm e^\mp \nu$	[bb] (5.20 \pm 0.11) $\times 10^{-5}$		207
$\pi^\pm e^\mp \nu e^+ e^-$	[bb] (1.26 \pm 0.04) $\times 10^{-5}$		229
Hadronic modes, including Charge conjugation \times Parity Violating (CPV) modes			
$3\pi^0$	(19.52 \pm 0.12) %	S=1.6	139
$\pi^+ \pi^- \pi^0$	(12.54 \pm 0.05) %		133
$\pi^+ \pi^-$	CPV [dd] (1.967 \pm 0.010) $\times 10^{-3}$	S=1.5	206
$\pi^0 \pi^0$	CPV (8.64 \pm 0.06) $\times 10^{-4}$	S=1.8	209
Semileptonic modes with photons			
$\pi^\pm e^\mp \nu_e \gamma$	[t,bb,ee] (3.79 \pm 0.06) $\times 10^{-3}$		229
$\pi^\pm \mu^\mp \nu_\mu \gamma$	(5.65 \pm 0.23) $\times 10^{-4}$		216
Hadronic modes with photons or $\ell\bar{\ell}$ pairs			
$\pi^0 \pi^0 \gamma$	< 2.43 $\times 10^{-7}$	CL=90%	209
$\pi^+ \pi^- \gamma$	[t,ee] (4.15 \pm 0.15) $\times 10^{-5}$	S=2.8	206
$\pi^+ \pi^- \gamma (\text{DE})$	(2.84 \pm 0.11) $\times 10^{-5}$	S=2.0	206
$\pi^0 2\gamma$	[ee] (1.273 \pm 0.033) $\times 10^{-6}$		230
$\pi^0 \gamma e^+ e^-$	(1.62 \pm 0.17) $\times 10^{-8}$		230
Other modes with photons or $\ell\bar{\ell}$ pairs			
2γ	(5.47 \pm 0.04) $\times 10^{-4}$	S=1.1	249
3γ	< 7.4 $\times 10^{-8}$	CL=90%	249
$e^+ e^- \gamma$	(9.4 \pm 0.4) $\times 10^{-6}$	S=2.0	249
$\mu^+ \mu^- \gamma$	(3.59 \pm 0.11) $\times 10^{-7}$	S=1.3	225
$e^+ e^- \gamma \gamma$	[ee] (5.95 \pm 0.33) $\times 10^{-7}$		249
$\mu^+ \mu^- \gamma \gamma$	[ee] (1.0 \pm 0.8 \pm 0.6) $\times 10^{-8}$		225
Charge conjugation \times Parity (CP) or Lepton Family number (LF) violating modes, or $\Delta S = 1$ weak neutral current (S1) modes			
$\mu^+ \mu^-$	S1 (6.84 \pm 0.11) $\times 10^{-9}$		225
$e^+ e^-$	S1 (9 \pm 6 \pm 4) $\times 10^{-12}$		249
$\pi^+ \pi^- e^+ e^-$	S1 [ee] (3.11 \pm 0.19) $\times 10^{-7}$		206
$\pi^0 \pi^0 e^+ e^-$	S1 < 6.6 $\times 10^{-9}$	CL=90%	209
$\pi^0 \pi^0 \mu^+ \mu^-$	S1 < 9.2 $\times 10^{-11}$	CL=90%	57
$\mu^+ \mu^- e^+ e^-$	S1 (2.69 \pm 0.27) $\times 10^{-9}$		225
$e^+ e^- e^+ e^-$	S1 (3.56 \pm 0.21) $\times 10^{-8}$		249
$\pi^0 \mu^+ \mu^-$	CP,S1 [ff] < 3.8 $\times 10^{-10}$	CL=90%	177
$\pi^0 e^+ e^-$	CP,S1 [ff] < 2.8 $\times 10^{-10}$	CL=90%	230
$\pi^0 \nu \bar{\nu}$	CP,S1 [gg] < 3.0 $\times 10^{-9}$	CL=90%	230
$\pi^0 \pi^0 \nu \bar{\nu}$	S1 < 8.1 $\times 10^{-7}$	CL=90%	209
$e^\pm \mu^\mp$	LF [bb] < 4.7 $\times 10^{-12}$	CL=90%	238
$e^\pm e^\pm \mu^\mp \mu^\mp$	LF [bb] < 4.12 $\times 10^{-11}$	CL=90%	225
$\pi^0 \mu^\pm e^\mp$	LF [bb] < 7.6 $\times 10^{-11}$	CL=90%	217
$\pi^0 \pi^0 \mu^\pm e^\mp$	LF < 1.7 $\times 10^{-10}$	CL=90%	159

$K_0^*(700)$

$$I(J^P) = \frac{1}{2}(0^+)$$

also known as κ ; was $K_0^*(800)$

$$\text{Mass (T-Matrix Pole } \sqrt{s}) = (630-730) - i(260-340) \text{ MeV}$$

$$\text{Mass (Breit-Wigner)} = 824 \pm 30 \text{ MeV}$$

$$\text{Full width (Breit-Wigner)} = 478 \pm 50 \text{ MeV}$$

$K_0^*(700)$ DECAY MODES

	Fraction (Γ_i/Γ)	p (MeV/c)
$K\pi$	100 %	240

$K^*(892)$

$$I(J^P) = \frac{1}{2}(1^-)$$

$$K^*(892)^\pm \text{ hadroproduced mass } m = 891.66 \pm 0.26 \text{ MeV}$$

$$K^*(892)^\pm \text{ in } \tau \text{ decays mass } m = 895.5 \pm 0.8 \text{ MeV}$$

$$K^*(892)^0 \text{ mass } m = 895.55 \pm 0.20 \text{ MeV} \quad (S = 1.7)$$

$$K^*(892)^\pm \text{ hadroproduced full width } \Gamma = 50.8 \pm 0.9 \text{ MeV}$$

$$K^*(892)^\pm \text{ in } \tau \text{ decays full width } \Gamma = 46.2 \pm 1.3 \text{ MeV}$$

$$K^*(892)^0 \text{ full width } \Gamma = 47.3 \pm 0.5 \text{ MeV} \quad (S = 1.9)$$

Meson Summary Table

K*(892) DECAY MODES	Fraction (Γ_i/Γ)	Confidence level	ρ (MeV/c)
$K\pi$	~ 100	%	289
$K^0\gamma$	$(2.46 \pm 0.21) \times 10^{-3}$		307
$K^\pm\gamma$	$(9.9 \pm 0.9) \times 10^{-4}$		309
$K\pi\pi$	< 7	$\times 10^{-4}$	95% 223

K₁(1270)

$$I(J^P) = \frac{1}{2}(1^+)$$

Mass $m = 1253 \pm 7$ MeV [J] (S = 2.2)
 Full width $\Gamma = 90 \pm 20$ MeV [J]

K₁(1270) DECAY MODES	Fraction (Γ_i/Γ)	ρ (MeV/c)
$K\rho$	(42 ± 6) %	†
$K_0^*(1430)\pi$	(28 ± 4) %	†
$K^*(892)\pi$	(16 ± 5) %	286
$K\omega$	(11.0 ± 2.0) %	†
$Kf_0(1370)$	(3.0 ± 2.0) %	†
γK^0	seen	528

K₁(1400)

$$I(J^P) = \frac{1}{2}(1^+)$$

Mass $m = 1403 \pm 7$ MeV
 Full width $\Gamma = 174 \pm 13$ MeV (S = 1.6)

K₁(1400) DECAY MODES	Fraction (Γ_i/Γ)	ρ (MeV/c)
$K^*(892)\pi$	(94 ± 6) %	402
$K\rho$	(3.0 ± 3.0) %	293
$Kf_0(1370)$	(2.0 ± 2.0) %	†
$K\omega$	(1.0 ± 1.0) %	284
$K_0^*(1430)\pi$	not seen	†
γK^0	seen	613

K*(1410)

$$I(J^P) = \frac{1}{2}(1^-)$$

Mass $m = 1414 \pm 15$ MeV (S = 1.3)
 Full width $\Gamma = 232 \pm 21$ MeV (S = 1.1)

K*(1410) DECAY MODES	Fraction (Γ_i/Γ)	Confidence level	ρ (MeV/c)
$K^*(892)\pi$	> 40 %	95%	410
$K\pi$	(6.6 ± 1.3) %		612
$K\rho$	< 7 %	95%	305
γK^0	< 2.3 $\times 10^{-4}$	90%	619

K₀^{*}(1430) [hh]

$$I(J^P) = \frac{1}{2}(0^+)$$

Mass $m = 1425 \pm 50$ MeV
 Full width $\Gamma = 270 \pm 80$ MeV

K₀[*](1430) DECAY MODES	Fraction (Γ_i/Γ)	ρ (MeV/c)
$K\pi$	(93 ± 10) %	619
$K\eta$	$(8.6 \pm \frac{2.7}{3.4})$ %	486
$K\eta'(958)$	seen	†

K₂^{*}(1430)

$$I(J^P) = \frac{1}{2}(2^+)$$

$K_2^*(1430)^\pm$ mass $m = 1427.3 \pm 1.5$ MeV (S = 1.3)
 $K_2^*(1430)^0$ mass $m = 1432.4 \pm 1.3$ MeV
 $K_2^*(1430)^\pm$ full width $\Gamma = 100.0 \pm 2.1$ MeV
 $K_2^*(1430)^0$ full width $\Gamma = 109 \pm 5$ MeV (S = 1.9)

K₂[*](1430) DECAY MODES	Fraction (Γ_i/Γ)	Scale factor/ Confidence level	ρ (MeV/c)
$K\pi$	(49.9 ± 1.2) %		620
$K^*(892)\pi$	(24.7 ± 1.5) %		420
$K^*(892)\pi\pi$	(13.4 ± 2.2) %		373
$K\rho$	(8.7 ± 0.8) %	S=1.2	320
$K\omega$	(2.9 ± 0.8) %		313
$K^\pm\gamma$	$(2.4 \pm 0.5) \times 10^{-3}$	S=1.1	628

$K\eta$	$(1.5 \pm \frac{3.4}{-1.0}) \times 10^{-3}$	S=1.3	488
$K\omega\pi$	< 7.2 $\times 10^{-4}$	CL=95%	106
$K^0\gamma$	< 9 $\times 10^{-4}$	CL=90%	627

K*(1680)

$$I(J^P) = \frac{1}{2}(1^-)$$

Mass $m = 1718 \pm 18$ MeV
 Full width $\Gamma = 322 \pm 110$ MeV (S = 4.2)

K*(1680) DECAY MODES	Fraction (Γ_i/Γ)	ρ (MeV/c)
$K\pi$	(38.7 ± 2.5) %	782
$K\rho$	$(31.4 \pm \frac{5.0}{-2.1})$ %	571
$K^*(892)\pi$	$(29.9 \pm \frac{2.2}{-5.0})$ %	618
$K\phi$	seen	387

K₂(1770) [ij]

$$I(J^P) = \frac{1}{2}(2^-)$$

Mass $m = 1773 \pm 8$ MeV
 Full width $\Gamma = 186 \pm 14$ MeV

K₂(1770) DECAY MODES	Fraction (Γ_i/Γ)	ρ (MeV/c)
$K\pi\pi$		794
$K_2^*(1430)\pi$	seen	287
$K^*(892)\pi$	seen	654
$Kf_2(1270)$	seen	53
$K\phi$	seen	441
$K\omega$	seen	607

K₃^{*}(1780)

$$I(J^P) = \frac{1}{2}(3^-)$$

Mass $m = 1776 \pm 7$ MeV (S = 1.1)
 Full width $\Gamma = 159 \pm 21$ MeV (S = 1.3)

K₃[*](1780) DECAY MODES	Fraction (Γ_i/Γ)	Confidence level	ρ (MeV/c)
$K\rho$	(31 ± 9) %		613
$K^*(892)\pi$	(20 ± 5) %		656
$K\pi$	(18.8 ± 1.0) %		813
$K\eta$	(30 ± 13) %		719
$K_2^*(1430)\pi$	< 16 %	95%	290

K₂(1820) [ij]

$$I(J^P) = \frac{1}{2}(2^-)$$

Mass $m = 1819 \pm 12$ MeV
 Full width $\Gamma = 264 \pm 34$ MeV

K₂(1820) DECAY MODES	Fraction (Γ_i/Γ)	ρ (MeV/c)
$K_2^*(1430)\pi$	seen	328
$K^*(892)\pi$	seen	683
$Kf_2(1270)$	seen	191
$K\omega$	seen	640
$K\phi$	seen	483

K₄^{*}(2045)

$$I(J^P) = \frac{1}{2}(4^+)$$

Mass $m = 2048 \pm \frac{8}{9}$ MeV (S = 1.1)
 Full width $\Gamma = 199 \pm \frac{27}{-19}$ MeV

K₄[*](2045) DECAY MODES	Fraction (Γ_i/Γ)	ρ (MeV/c)
$K\pi$	(9.9 ± 1.2) %	960
$K^*(892)\pi\pi$	(9 ± 5) %	804
$K^*(892)\pi\pi\pi$	(7 ± 5) %	770
$\rho K\pi$	(5.7 ± 3.2) %	744
$\omega K\pi$	(5.0 ± 3.0) %	740
$\phi K\pi$	(2.8 ± 1.4) %	597
$\phi K^*(892)$	(1.4 ± 0.7) %	368

Meson Summary Table

CHARMED MESONS ($C = \pm 1$)

$$D^+ = c\bar{d}, D^0 = c\bar{u}, \bar{D}^0 = \bar{c}u, D^- = \bar{c}d, \text{ similarly for } D^{*s}$$

 D^\pm

$$J(P) = \frac{1}{2}(0^-)$$

Mass $m = 1869.65 \pm 0.05$ MeV
 Mean life $\tau = (1040 \pm 7) \times 10^{-15}$ s
 $c\tau = 311.8$ μm

c-quark decays

$$\Gamma(c \rightarrow \ell^+ \text{ anything}) / \Gamma(c \rightarrow \text{ anything}) = 0.096 \pm 0.004 \text{ [kk]}$$

$$\Gamma(c \rightarrow D^*(2010)^+ \text{ anything}) / \Gamma(c \rightarrow \text{ anything}) = 0.255 \pm 0.017$$

CP-violation decay-rate asymmetries

$$A_{CP}(\mu^\pm \nu) = (8 \pm 8)\%$$

$$A_{CP}(K_S^0 e^\pm \nu) = (-0.6 \pm 1.6)\%$$

$$A_{CP}(K_S^0 \pi^\pm) = (-0.41 \pm 0.09)\%$$

$$A_{CP}(K_L^0 K^\pm) \text{ in } D^\pm \rightarrow K_L^0 K^\pm = (-4.2 \pm 3.4) \times 10^{-2}$$

$$A_{CP}(K^\mp 2\pi^\pm) = (-0.18 \pm 0.16)\%$$

$$A_{CP}(K^\mp \pi^\pm \pi^\pm \pi^0) = (-0.3 \pm 0.7)\%$$

$$A_{CP}(K_S^0 \pi^\pm \pi^0) = (-0.1 \pm 0.7)\%$$

$$A_{CP}(K_S^0 \pi^\pm \pi^+ \pi^-) = (0.0 \pm 1.2)\%$$

$$A_{CP}(\pi^\pm \pi^0) = (2.4 \pm 1.2)\%$$

$$A_{CP}(\pi^\pm \eta) = (1.0 \pm 1.5)\% \quad (S = 1.4)$$

$$A_{CP}(\pi^\pm \eta'(958)) = (-0.6 \pm 0.7)\%$$

$$A_{CP}(\bar{K}^0 / K^0 K^\pm) = (0.11 \pm 0.17)\%$$

$$A_{CP}(K_S^0 K^\pm) = (-0.01 \pm 0.07)\%$$

$$A_{CP}(K_S^0 K^\pm \pi^0) \text{ in } D^\pm \rightarrow K_S^0 K^\pm \pi^0 = (1 \pm 4) \times 10^{-2}$$

$$A_{CP}(K_L^0 K^\pm \pi^0) \text{ in } D^\pm \rightarrow K_L^0 K^\pm \pi^0 = (-1 \pm 4) \times 10^{-2}$$

$$A_{CP}(K^+ K^- \pi^\pm) = (0.37 \pm 0.29)\%$$

$$A_{CP}(K^\pm K^*0) = (-0.3 \pm 0.4)\%$$

$$A_{CP}(\phi \pi^\pm) = (0.01 \pm 0.09)\% \quad (S = 1.8)$$

$$A_{CP}(K^\pm K_0^*(1430)^0) = (8_{-7}^{+6})\%$$

$$A_{CP}(K^\pm K_2^*(1430)^0) = (43_{-26}^{+20})\%$$

$$A_{CP}(K^\pm K_0^*(700)) = (-12_{-13}^{+18})\%$$

$$A_{CP}(a_0(1450)^0 \pi^\pm) = (-19_{-16}^{+14})\%$$

$$A_{CP}(\phi(1680) \pi^\pm) = (-9 \pm 26)\%$$

$$A_{CP}(\pi^+ \pi^- \pi^\pm) = (-2 \pm 4)\%$$

$$A_{CP}(K_S^0 K^\pm \pi^+ \pi^-) = (-4 \pm 7)\%$$

$$A_{CP}(K^\pm \pi^0) = (-4 \pm 11)\%$$

 χ^2 tests of CP-violation (CPV)

Local CPV in $D^\pm \rightarrow \pi^+ \pi^- \pi^\pm = 78.1\%$
 Local CPV in $D^\pm \rightarrow K^+ K^- \pi^\pm = 31\%$

CP violating asymmetries of P-odd (T-odd) moments

$$A_T(K_S^0 K^\pm \pi^+ \pi^-) = (-12 \pm 11) \times 10^{-3} \text{ [ll]}$$

 D^+ form factors

$$f_+(0) |V_{cs}| \text{ in } \bar{K}^0 \ell^+ \nu_\ell = 0.719 \pm 0.011 \quad (S = 1.6)$$

$$r_1 \equiv a_1/a_0 \text{ in } \bar{K}^0 \ell^+ \nu_\ell = -2.13 \pm 0.14$$

$$r_2 \equiv a_2/a_0 \text{ in } \bar{K}^0 \ell^+ \nu_\ell = -3 \pm 12 \quad (S = 1.5)$$

$$f_+(0) |V_{cd}| \text{ in } \pi^0 \ell^+ \nu_\ell = 0.1407 \pm 0.0025$$

$$r_1 \equiv a_1/a_0 \text{ in } \pi^0 \ell^+ \nu_\ell = -2.00 \pm 0.13$$

$$r_2 \equiv a_2/a_0 \text{ in } \pi^0 \ell^+ \nu_\ell = -4 \pm 5$$

$$f_+(0) |V_{cd}| \text{ in } D^+ \rightarrow \eta e^+ \nu_e = (8.3 \pm 0.5) \times 10^{-2}$$

$$r_1 \equiv a_1/a_0 \text{ in } D^+ \rightarrow \eta e^+ \nu_e = -5.3 \pm 2.7 \quad (S = 1.9)$$

$$r_\nu \equiv V(0)/A_1(0) \text{ in } D^+ \rightarrow \omega e^+ \nu_e = 1.24 \pm 0.11$$

$$r_2 \equiv A_2(0)/A_1(0) \text{ in } D^+ \rightarrow \omega e^+ \nu_e = 1.06 \pm 0.16$$

$$r_\nu \equiv V(0)/A_1(0) \text{ in } D^+, D^0 \rightarrow \rho e^+ \nu_e = 1.64 \pm 0.10 \quad (S = 1.2)$$

$$r_2 \equiv A_2(0)/A_1(0) \text{ in } D^+, D^0 \rightarrow \rho e^+ \nu_e = 0.84 \pm 0.06$$

$$r_\nu \equiv V(0)/A_1(0) \text{ in } \bar{K}^*(892)^0 \ell^+ \nu_\ell = 1.49 \pm 0.05 \quad (S = 2.1)$$

$$r_2 \equiv A_2(0)/A_1(0) \text{ in } \bar{K}^*(892)^0 \ell^+ \nu_\ell = 0.802 \pm 0.021$$

$$r_3 \equiv A_3(0)/A_1(0) \text{ in } \bar{K}^*(892)^0 \ell^+ \nu_\ell = 0.0 \pm 0.4$$

$$\Gamma_L/\Gamma_T \text{ in } \bar{K}^*(892)^0 \ell^+ \nu_\ell = 1.13 \pm 0.08$$

$$\Gamma_+/ \Gamma_- \text{ in } K^*(892)^0 \ell^+ \nu_\ell = 0.22 \pm 0.06 \quad (S = 1.6)$$

Most decay modes (other than the semileptonic modes) that involve a neutral K meson are now given as K_S^0 modes, not as \bar{K}^0 modes. Nearly always it is a K_S^0 that is measured, and interference between Cabibbo-allowed and doubly Cabibbo-suppressed modes can invalidate the assumption that $2\Gamma(K_S^0) = \Gamma(\bar{K}^0)$.

D^+ DECAY MODES	Fraction (Γ_i/Γ)	Scale factor/ Confidence level	p (MeV/c)
Inclusive modes			
e^+ semileptonic	$(16.07 \pm 0.30) \%$		—
μ^+ anything	$(17.6 \pm 3.2) \%$		—
K^- anything	$(25.7 \pm 1.4) \%$		—
\bar{K}^0 anything + K^0 anything	$(61 \pm 5) \%$		—
K^+ anything	$(5.9 \pm 0.8) \%$		—
$K^*(892)^- \text{ anything}$	$(6 \pm 5) \%$		—
$\bar{K}^*(892)^0 \text{ anything}$	$(23 \pm 5) \%$		—
$K^*(892)^0 \text{ anything}$	$< 6.6 \%$	CL=90%	—
η anything	$(6.3 \pm 0.7) \%$		—
η' anything	$(1.04 \pm 0.18) \%$		—
ϕ anything	$(1.12 \pm 0.04) \%$		—
Leptonic and semileptonic modes			
$e^+ \nu_e$	< 8.8	$\times 10^{-6}$ CL=90%	935
$\gamma e^+ \nu_e$	< 3.0	$\times 10^{-5}$ CL=90%	935
$\mu^+ \nu_\mu$	$(3.74 \pm 0.17) \times 10^{-4}$		932
$\tau^+ \nu_\tau$	$(1.20 \pm 0.27) \times 10^{-3}$		90
$\bar{K}^0 e^+ \nu_e$	$(8.73 \pm 0.10) \%$		869
$\bar{K}^0 \mu^+ \nu_\mu$	$(8.76 \pm 0.19) \%$		865
$K^- \pi^+ e^+ \nu_e$	$(4.02 \pm 0.18) \%$	S=3.2	864
$\bar{K}^*(892)^0 e^+ \nu_e, \bar{K}^*(892)^0 \rightarrow K^- \pi^+$	$(3.77 \pm 0.17) \%$		722
$(K^- \pi^+) [0.8-1.0] \text{ GeV } e^+ \nu_e$	$(3.39 \pm 0.09) \%$		864
$(K^- \pi^+)_{S\text{-wave}} e^+ \nu_e$	$(2.28 \pm 0.11) \times 10^{-3}$		—
$\bar{K}^*(1410)^0 e^+ \nu_e$	< 6	$\times 10^{-3}$ CL=90%	—
$\bar{K}^*(1410)^0 \rightarrow K^- \pi^+$			
$\bar{K}_2^*(1430)^0 e^+ \nu_e$	< 5	$\times 10^{-4}$ CL=90%	—
$\bar{K}_2^*(1430)^0 \rightarrow K^- \pi^+$			
$K^- \pi^+ e^+ \nu_e$ nonresonant	< 7	$\times 10^{-3}$ CL=90%	864
$\bar{K}^*(892)^0 e^+ \nu_e$	$(5.40 \pm 0.10) \%$	S=1.1	722
$K^- \pi^+ \mu^+ \nu_\mu$	$(3.65 \pm 0.34) \%$		851
$\bar{K}^*(892)^0 \mu^+ \nu_\mu$	$(3.52 \pm 0.10) \%$		717
$\bar{K}^*(892)^0 \rightarrow K^- \pi^+$			
$K^- \pi^+ \mu^+ \nu_\mu$ nonresonant	$(1.9 \pm 0.5) \times 10^{-3}$		851
$\bar{K}^*(892)^0 \mu^+ \nu_\mu$	$(5.27 \pm 0.15) \%$		717
$K^- \pi^+ \pi^0 \mu^+ \nu_\mu$	< 1.5	$\times 10^{-3}$ CL=90%	825
$\bar{K}_1^*(1270)^0 e^+ \nu_e, \bar{K}_1^0 \rightarrow K^- \pi^+ \pi^0$	$(1.06 \pm 0.15) \times 10^{-3}$		—
$\bar{K}_0^*(1430)^0 \mu^+ \nu_\mu$	< 2.3	$\times 10^{-4}$ CL=90%	380
$\bar{K}^*(1680)^0 \mu^+ \nu_\mu$	< 1.5	$\times 10^{-3}$ CL=90%	105
$\pi^0 e^+ \nu_e$	$(3.72 \pm 0.17) \times 10^{-3}$	S=2.0	930
$\pi^0 \mu^+ \nu_\mu$	$(3.50 \pm 0.15) \times 10^{-3}$		927
$\eta e^+ \nu_e$	$(1.11 \pm 0.07) \times 10^{-3}$		855
$\pi^- \pi^+ e^+ \nu_e$	$(2.45 \pm 0.10) \times 10^{-3}$		924
$f_0(500)^0 e^+ \nu_e, f_0(500)^0 \rightarrow \pi^+ \pi^-$	$(6.3 \pm 0.5) \times 10^{-4}$		—
$\rho^0 e^+ \nu_e$	$(2.18 \pm 0.17) \times 10^{-3}$		774
$\rho^0 \mu^+ \nu_\mu$	$(2.4 \pm 0.4) \times 10^{-3}$		770
$\omega e^+ \nu_e$	$(1.69 \pm 0.11) \times 10^{-3}$		771
$\eta'(958) e^+ \nu_e$	$(2.0 \pm 0.4) \times 10^{-4}$		690
$a(980)^0 e^+ \nu_e, a(980)^0 \rightarrow \eta \pi^0$	$(1.7 \pm 0.8) \times 10^{-4}$		—
$\phi e^+ \nu_e$	< 1.3	$\times 10^{-5}$ CL=90%	657
$D^0 e^+ \nu_e$	< 1.0	$\times 10^{-4}$ CL=90%	5
Hadronic modes with a \bar{K} or $\bar{K}K\bar{K}$			
$K_S^0 \pi^+$	$(1.562 \pm 0.031) \%$	S=1.7	863
$K_L^0 \pi^+$	$(1.46 \pm 0.05) \%$		863
$K^- 2\pi^+$	$[nn] (9.38 \pm 0.16) \%$	S=1.6	846
$(K^- \pi^+)_{S\text{-wave}} \pi^+$	$(7.52 \pm 0.17) \%$		846
$\bar{K}_S^*(1430)^0 \pi^+, \bar{K}_S^*(1430)^0 \rightarrow K^- \pi^+$	$[oo] (1.25 \pm 0.06) \%$		382
$\bar{K}^*(892)^0 \pi^+$	$(1.04 \pm 0.12) \%$		714
$\bar{K}^*(892)^0 \rightarrow K^- \pi^+$			
$\bar{K}^*(1410)^0 \pi^+, \bar{K}^*0 \rightarrow$	not seen		381
$K^- \pi^+ \pi^+$			
$\bar{K}_2^*(1430)^0 \pi^+, \bar{K}_2^*(1430)^0 \rightarrow K^- \pi^+$	$[oo] (2.3 \pm 0.7) \times 10^{-4}$		371

Meson Summary Table

$\bar{K}^*(1680)^0 \pi^+$, $\bar{K}^*(1680)^0 \rightarrow K^- \pi^+$	[oo]	$(2.2 \pm 1.1) \times 10^{-4}$	58	$K^+ \bar{K}_0^*(1430)^0$, $\bar{K}_0^*(1430)^0 \rightarrow K^- \pi^+$	$(1.82 \pm 0.35) \times 10^{-3}$	-
$K_S^0 \pi^+ \pi^0$	[nn]	$(7.36 \pm 0.21) \%$	845	$K^+ \bar{K}_2^*(1430)^0$, $\bar{K}_2^* \rightarrow$ $K^- \pi^+$	$(1.6 \pm \frac{1.2}{0.8}) \times 10^{-4}$	-
$K_S^0 \rho^+$		$(6.14 \pm \frac{0.60}{0.35}) \%$	677	$K^+ \bar{K}_0^*(700)$, $\bar{K}_0^* \rightarrow$ $K^- \pi^+$	$(6.8 \pm \frac{3.5}{2.1}) \times 10^{-4}$	-
$K_S^0 \rho(1450)^+$, $\rho^+ \rightarrow \pi^+ \pi^0$		$(1.5 \pm \frac{1.2}{1.4}) \times 10^{-3}$	-	$a_0(1450)^0 \pi^+$, $a_0^0 \rightarrow$ $K^+ K^-$	$(4.5 \pm \frac{7.0}{1.8}) \times 10^{-4}$	-
$\bar{K}^*(892)^0 \pi^+$, $\bar{K}^*(892)^0 \rightarrow K_S^0 \pi^0$		$(2.64 \pm 0.32) \times 10^{-3}$	714	$\phi(1680) \pi^+$, $\phi \rightarrow$ $K^+ K^-$	$(4.9 \pm \frac{4.0}{1.9}) \times 10^{-5}$	-
$\bar{K}_0^*(1430)^0 \pi^+$, $\bar{K}_0^{*0} \rightarrow$ $K_S^0 \pi^0$		$(2.7 \pm 0.9) \times 10^{-3}$	-	$K_S^0 K_S^0 \pi^+$	$(2.70 \pm 0.13) \times 10^{-3}$	741
$\bar{K}_0^*(1680)^0 \pi^+$, $\bar{K}_0^{*0} \rightarrow$ $K_S^0 \pi^0$		$(10 \pm \frac{7}{-10}) \times 10^{-4}$	-	$K_S^+ K_S^0 \pi^+ \pi^-$	$(1.74 \pm 0.18) \times 10^{-3}$	678
$\bar{\pi}^0 \pi^+$, $\bar{\pi}^0 \rightarrow K_S^0 \pi^0$		$(6 \pm \frac{5}{-4}) \times 10^{-3}$	-	$K_S^0 K^- 2\pi^+$	$(2.38 \pm 0.17) \times 10^{-3}$	678
$K_S^0 \pi^+ \pi^0$ nonresonant		$(3 \pm 4) \times 10^{-3}$	845	$K^+ K^- 2\pi^+ \pi^-$	$(2.3 \pm 1.2) \times 10^{-4}$	601
$K_S^0 \pi^+ \pi^0$ nonresonant and $\bar{\pi}^0 \pi^+$		$(1.37 \pm \frac{0.21}{0.40}) \%$	-	A few poorly measured branching fractions:		
$(K_S^0 \pi^0)_{S\text{-wave}} \pi^+$		$(1.27 \pm \frac{0.27}{0.33}) \%$	845	$\phi \pi^+ \pi^0$	$(2.3 \pm 1.0) \%$	619
$K_S^0 \pi^+ \eta'(958)$		$(1.90 \pm 0.21) \times 10^{-3}$	481	$\phi \rho^+$	$< 1.5 \%$ CL=90%	260
$K^- 2\pi^+ \pi^0$	[pp]	$(6.25 \pm 0.18) \%$	816	$K^+ K^- \pi^+ \pi^0$ non- ϕ	$(1.5 \pm \frac{0.7}{0.6}) \%$	682
$K_S^0 2\pi^+ \pi^-$	[pp]	$(3.10 \pm 0.09) \%$	814	$K^*(892)^+ K_S^0$	$(1.7 \pm 0.8) \%$	612
$K^- 3\pi^+ \pi^-$	[nn]	$(5.7 \pm 0.5) \times 10^{-3}$	772	Doubly Cabibbo-suppressed modes		
$\bar{K}^*(892)^0 2\pi^+ \pi^-$, $\bar{K}^*(892)^0 \rightarrow K^- \pi^+$		$(1.2 \pm 0.4) \times 10^{-3}$	645	$K^+ \pi^0$	$(2.08 \pm 0.21) \times 10^{-4}$	S=1.4 864
$\bar{K}^*(892)^0 \rho^0 \pi^+$, $\bar{K}^*(892)^0 \rightarrow K^- \pi^+$		$(2.3 \pm 0.4) \times 10^{-3}$	239	$K^+ \eta$	$(1.25 \pm 0.16) \times 10^{-4}$	S=1.1 776
$\bar{K}^*(892)^0 a_1(1260)^+$	[qq]	$(9.3 \pm 1.9) \times 10^{-3}$	†	$K^+ \eta'(958)$	$(1.85 \pm 0.20) \times 10^{-4}$	571
$K^- \rho^0 2\pi^+$		$(1.72 \pm 0.28) \times 10^{-3}$	524	$K^+ \pi^+ \pi^-$	$(4.91 \pm 0.09) \times 10^{-4}$	846
$K^- 3\pi^+ \pi^-$ nonresonant		$(4.0 \pm 2.9) \times 10^{-4}$	772	$K^+ \rho^0$	$(1.9 \pm 0.5) \times 10^{-4}$	679
$K^+ 2K_S^0$		$(2.54 \pm 0.13) \times 10^{-3}$	545	$K^*(892)^0 \pi^+$, $K^*(892)^0 \rightarrow$ $K^+ \pi^-$	$(2.3 \pm 0.4) \times 10^{-4}$	714
$K^+ K^- K_S^0 \pi^+$		$(2.4 \pm 0.5) \times 10^{-4}$	436	$K^+ f_0(980)$, $f_0(980) \rightarrow$ $\pi^+ \pi^-$	$(4.4 \pm 2.6) \times 10^{-5}$	-
Pionic modes				$K_2^*(1430)^0 \pi^+$, $K_2^*(1430)^0 \rightarrow$ $K^+ \pi^-$	$(3.9 \pm 2.7) \times 10^{-5}$	-
$\pi^+ \pi^0$		$(1.247 \pm 0.033) \times 10^{-3}$	925	$K^+ \pi^+ \pi^-$ nonresonant	not seen	846
$2\pi^+ \pi^-$		$(3.27 \pm 0.18) \times 10^{-3}$	909	$2K^+ K^-$	$(6.14 \pm 0.11) \times 10^{-5}$	550
$\rho^0 \pi^+$		$(8.3 \pm 1.5) \times 10^{-4}$	767	$\phi(1020)^0 K^+$	$< 2.1 \times 10^{-5}$ CL=90%	-
$\pi^+ (\pi^+ \pi^-)_{S\text{-wave}}$		$(1.83 \pm 0.16) \times 10^{-3}$	909	$K^+ \phi(1020)$, $\phi \rightarrow$ $K^+ K^-$	$(4.4 \pm 0.6) \times 10^{-6}$	-
$\sigma \pi^+$, $\sigma \rightarrow \pi^+ \pi^-$		$(1.38 \pm 0.12) \times 10^{-3}$	-	$K^+ (K^+ K^-)_{S\text{-wave}}$	$(5.77 \pm 0.12) \times 10^{-5}$	550
$f_0(980) \pi^+$, $f_0(980) \rightarrow \pi^+ \pi^-$		$(1.56 \pm 0.33) \times 10^{-4}$	669	$\Delta C = 1$ weak neutral current (CI) modes, or Lepton Family number (LF) or Lepton number (L) violating modes		
$f_0(1370) \pi^+$, $f_0(1370) \rightarrow \pi^+ \pi^-$		$(8 \pm 4) \times 10^{-5}$	-	$\pi^+ e^+ e^-$	CI $< 1.1 \times 10^{-6}$ CL=90%	930
$f_2(1270) \pi^+$, $f_2(1270) \rightarrow \pi^+ \pi^-$		$(5.0 \pm 0.9) \times 10^{-4}$	485	$\pi^+ \pi^0 e^+ e^-$	$< 1.4 \times 10^{-5}$ CL=90%	925
$\rho(1450)^0 \pi^+$, $\rho(1450)^0 \rightarrow \pi^+ \pi^-$		$< 8 \times 10^{-5}$ CL=95%	338	$\pi^+ \phi$, $\phi \rightarrow e^+ e^-$	[rr] $(1.7 \pm \frac{1.4}{0.9}) \times 10^{-6}$	-
$f_0(1500) \pi^+$, $f_0(1500) \rightarrow \pi^+ \pi^-$		$(1.1 \pm 0.4) \times 10^{-4}$	-	$\pi^+ \mu^+ \mu^-$	CI $< 7.3 \times 10^{-8}$ CL=90%	918
$f_0(1710) \pi^+$, $f_0(1710) \rightarrow \pi^+ \pi^-$		$< 5 \times 10^{-5}$ CL=95%	-	$\pi^+ \phi$, $\phi \rightarrow \mu^+ \mu^-$	[rr] $(1.8 \pm 0.8) \times 10^{-6}$	-
$f_0(1790) \pi^+$, $f_0(1790) \rightarrow \pi^+ \pi^-$		$< 7 \times 10^{-5}$ CL=95%	-	$\rho^+ \mu^+ \mu^-$	CI $< 5.6 \times 10^{-4}$ CL=90%	757
$(\pi^+ \pi^+)_{S\text{-wave}} \pi^-$		$< 1.2 \times 10^{-4}$ CL=95%	909	$K^+ e^+ e^-$	[ss] $< 1.0 \times 10^{-6}$ CL=90%	870
$2\pi^+ \pi^-$ nonresonant		$< 1.1 \times 10^{-4}$ CL=95%	909	$K^+ \pi^0 e^+ e^-$	$< 1.5 \times 10^{-5}$ CL=90%	864
$\pi^+ 2\pi^0$		$(4.7 \pm 0.4) \times 10^{-3}$	910	$K_S^0 \pi^+ e^+ e^-$	$< 2.6 \times 10^{-5}$ CL=90%	-
$2\pi^+ \pi^- \pi^0$		$(1.16 \pm 0.08) \%$	883	$K_S^0 K^+ e^+ e^-$	$< 1.1 \times 10^{-5}$ CL=90%	-
$3\pi^+ 2\pi^-$		$(1.66 \pm 0.16) \times 10^{-3}$	845	$K^+ \mu^+ \mu^-$	[ss] $< 4.3 \times 10^{-6}$ CL=90%	856
$\eta \pi^+$		$(3.77 \pm 0.09) \times 10^{-3}$	848	$\pi^+ e^+ \mu^-$	LF $< 2.9 \times 10^{-6}$ CL=90%	927
$\eta \pi^+ \pi^0$		$(1.38 \pm 0.35) \times 10^{-3}$	831	$\pi^+ e^- \mu^+$	LF $< 3.6 \times 10^{-6}$ CL=90%	927
$\omega \pi^+$		$(2.8 \pm 0.6) \times 10^{-4}$	764	$K^+ e^+ \mu^-$	LF $< 1.2 \times 10^{-6}$ CL=90%	866
$\eta'(958) \pi^+$		$(4.97 \pm 0.19) \times 10^{-3}$	681	$K^+ e^- \mu^+$	LF $< 2.8 \times 10^{-6}$ CL=90%	866
$\eta'(958) \pi^+ \pi^0$		$(1.6 \pm 0.5) \times 10^{-3}$	654	$\pi^- 2e^+$	L $< 1.1 \times 10^{-6}$ CL=90%	930
Hadronic modes with a $K\bar{K}$ pair				$\pi^- 2\mu^+$	L $< 2.2 \times 10^{-8}$ CL=90%	918
$K^+ K_S^0$		$(3.04 \pm 0.09) \times 10^{-3}$	S=2.2 793	$\pi^- e^+ \mu^+$	L $< 2.0 \times 10^{-6}$ CL=90%	927
$K_L^0 K^+$		$(3.21 \pm 0.16) \times 10^{-3}$	793	$\rho^- 2\mu^+$	L $< 5.6 \times 10^{-4}$ CL=90%	757
$K_S^0 K^+ \pi^0$		$(5.07 \pm 0.30) \times 10^{-3}$	744	$K^- 2e^+$	L $< 9 \times 10^{-7}$ CL=90%	870
$K_L^0 K^+ \pi^0$		$(5.24 \pm 0.31) \times 10^{-3}$	744	$K_S^0 \pi^- 2e^+$	$< 3.3 \times 10^{-6}$ CL=90%	863
$K^+ K^- \pi^+$	[nn]	$(9.68 \pm 0.18) \times 10^{-3}$	744	$K^- \pi^0 2e^+$	$< 8.5 \times 10^{-6}$ CL=90%	864
$\phi \pi^+$		$(5.70 \pm 0.14) \times 10^{-3}$	647	$K^- 2\mu^+$	L $< 1.0 \times 10^{-5}$ CL=90%	856
$\phi \pi^+$, $\phi \rightarrow K^+ K^-$		$(2.69 \pm \frac{0.07}{0.08}) \times 10^{-3}$	647	$K^- e^+ \mu^+$	L $< 1.9 \times 10^{-6}$ CL=90%	866
$K^+ \bar{K}^*(892)^0$, $\bar{K}^*(892)^0 \rightarrow K^- \pi^+$		$(2.49 \pm \frac{0.08}{0.13}) \times 10^{-3}$	613	$K^*(892)^- 2\mu^+$	L $< 8.5 \times 10^{-4}$ CL=90%	703

D⁰

$$I(J^P) = \frac{1}{2}(0^-)$$

Mass $m = 1864.83 \pm 0.05$ MeV

$m_{D^\pm} - m_{D^0} = 4.822 \pm 0.015$ MeV

Mean life $\tau = (410.1 \pm 1.5) \times 10^{-15}$ s

$c\tau = 122.9 \mu\text{m}$

Meson Summary Table

Mixing and related parameters

$$\begin{aligned}
 |m_{D_1^0} - m_{D_2^0}| &= (0.95_{-0.44}^{+0.41}) \times 10^{10} \text{ h s}^{-1} \\
 (\Gamma_{D_1^0} - \Gamma_{D_2^0})/\Gamma &= 2\gamma = (1.29_{-0.18}^{+0.14}) \times 10^{-2} \\
 |q/p| &= 0.92_{-0.09}^{+0.12} \\
 A_\Gamma &= (-0.125 \pm 0.526) \times 10^{-3} \\
 \phi_{K_S^0 \pi \pi} &= -0.09_{-0.13}^{+0.10} \\
 K^+ \pi^- \text{ relative strong phase: } \cos \delta &= 0.97 \pm 0.11 \\
 K^- \pi^+ \pi^0 \text{ coherence factor } R_{K \pi \pi^0} &= 0.82 \pm 0.06 \\
 K^- \pi^+ \pi^0 \text{ average relative strong phase } \delta^{K \pi \pi^0} &= (199 \pm 14)^\circ \\
 K^- \pi^- 2\pi^+ \text{ coherence factor } R_{K 3\pi} &= 0.53_{-0.21}^{+0.18} \\
 K^- \pi^- 2\pi^+ \text{ average relative strong phase } \delta^{K 3\pi} &= (125_{-14}^{+22})^\circ \\
 D^0 \rightarrow K^- \pi^- 2\pi^+, R_{K 3\pi} (\gamma \cos \delta^{K 3\pi} - x \sin \delta^{K 3\pi}) &= (-3.0 \pm 0.7) \times 10^{-3} \text{ TeV}^{-1} \\
 K_S^0 K^+ \pi^- \text{ coherence factor } R_{K_S^0 K \pi} &= 0.70 \pm 0.08 \\
 K_S^0 K^+ \pi^- \text{ average relative strong phase } \delta^{K_S^0 K \pi} &= (0 \pm 16)^\circ \\
 K^* K \text{ coherence factor } R_{K^* K} &= 0.94 \pm 0.12 \\
 K^* K \text{ average relative strong phase } \delta^{K^* K} &= (-17 \pm 18)^\circ
 \end{aligned}$$

CP-violation decay-rate asymmetries (labeled by the D^0 decay)

$$\begin{aligned}
 A_{CP}(K^+ K^-) &= (-0.07 \pm 0.11)\% \\
 A_{CP}(2K_S^0) &= (0.4 \pm 1.4)\% \\
 A_{CP}(\pi^+ \pi^-) &= (0.13 \pm 0.14)\% \\
 A_{CP}(\pi^0 \pi^0) &= (0.0 \pm 0.6)\% \\
 A_{CP}(\rho \gamma) &= (6 \pm 15) \times 10^{-2} \\
 A_{CP}(\phi \gamma) &= (-9 \pm 7) \times 10^{-2} \\
 A_{CP}(\overline{K}^*(892)^0 \gamma) &= (-0.3 \pm 2.0) \times 10^{-2} \\
 A_{CP}(\pi^+ \pi^- \pi^0) &= (0.3 \pm 0.4)\% \\
 A_{CP}(\rho(770)^+ \pi^- \rightarrow \pi^+ \pi^- \pi^0) &= (1.2 \pm 0.9)\% \text{ [tt]} \\
 A_{CP}(\rho(770)^0 \pi^0 \rightarrow \pi^+ \pi^- \pi^0) &= (-3.1 \pm 3.0)\% \text{ [tt]} \\
 A_{CP}(\rho(770)^- \pi^+ \rightarrow \pi^+ \pi^- \pi^0) &= (-1.0 \pm 1.7)\% \text{ [tt]} \\
 A_{CP}(\rho(1450)^+ \pi^- \rightarrow \pi^+ \pi^- \pi^0) &= (0 \pm 70)\% \text{ [tt]} \\
 A_{CP}(\rho(1450)^0 \pi^0 \rightarrow \pi^+ \pi^- \pi^0) &= (-20 \pm 40)\% \text{ [tt]} \\
 A_{CP}(\rho(1450)^- \pi^+ \rightarrow \pi^+ \pi^- \pi^0) &= (6 \pm 9)\% \text{ [tt]} \\
 A_{CP}(\rho(1700)^+ \pi^- \rightarrow \pi^+ \pi^- \pi^0) &= (-5 \pm 14)\% \text{ [tt]} \\
 A_{CP}(\rho(1700)^0 \pi^0 \rightarrow \pi^+ \pi^- \pi^0) &= (13 \pm 9)\% \text{ [tt]} \\
 A_{CP}(\rho(1700)^- \pi^+ \rightarrow \pi^+ \pi^- \pi^0) &= (8 \pm 11)\% \text{ [tt]} \\
 A_{CP}(f_0(980) \pi^0 \rightarrow \pi^+ \pi^- \pi^0) &= (0 \pm 35)\% \text{ [tt]} \\
 A_{CP}(f_0(1370) \pi^0 \rightarrow \pi^+ \pi^- \pi^0) &= (25 \pm 18)\% \text{ [tt]} \\
 A_{CP}(f_0(1500) \pi^0 \rightarrow \pi^+ \pi^- \pi^0) &= (0 \pm 18)\% \text{ [tt]} \\
 A_{CP}(f_0(1710) \pi^0 \rightarrow \pi^+ \pi^- \pi^0) &= (0 \pm 24)\% \text{ [tt]} \\
 A_{CP}(f_2(1270) \pi^0 \rightarrow \pi^+ \pi^- \pi^0) &= (-4 \pm 6)\% \text{ [tt]} \\
 A_{CP}(\sigma(400) \pi^0 \rightarrow \pi^+ \pi^- \pi^0) &= (6 \pm 8)\% \text{ [tt]} \\
 A_{CP}(\text{nonresonant } \pi^+ \pi^- \pi^0) &= (-13 \pm 23)\% \text{ [tt]} \\
 A_{CP}(a_1(1260)^+ \pi^- \rightarrow 2\pi^+ 2\pi^-) &= (5 \pm 6)\% \\
 A_{CP}(a_1(1260)^- \pi^+ \rightarrow 2\pi^+ 2\pi^-) &= (14 \pm 18)\% \\
 A_{CP}(\pi(1300)^+ \pi^- \rightarrow 2\pi^+ 2\pi^-) &= (-2 \pm 15)\% \\
 A_{CP}(\pi(1300)^- \pi^+ \rightarrow 2\pi^+ 2\pi^-) &= (-6 \pm 30)\% \\
 A_{CP}(a_1(1640)^+ \pi^- \rightarrow 2\pi^+ 2\pi^-) &= (9 \pm 26)\% \\
 A_{CP}(\pi_2(1670)^+ \pi^- \rightarrow 2\pi^+ 2\pi^-) &= (7 \pm 18)\% \\
 A_{CP}(s f_0(1370) \rightarrow 2\pi^+ 2\pi^-) &= (-15 \pm 19)\% \\
 A_{CP}(s \rho(770)^0 \rightarrow 2\pi^+ 2\pi^-) &= (3 \pm 27)\% \\
 A_{CP}(2\rho(770)^0 \rightarrow 2\pi^+ 2\pi^-) &= (-6 \pm 6)\% \\
 A_{CP}(2f_2(1270) \rightarrow 2\pi^+ 2\pi^-) &= (-28 \pm 24)\% \\
 A_{CP}(K^+ K^- \pi^0) &= (-1.0 \pm 1.7)\% \\
 A_{CP}(K^*(892)^+ K^- \rightarrow K^+ K^- \pi^0) &= (-0.9 \pm 1.3)\% \text{ [tt]} \\
 A_{CP}(K^*(1410)^+ K^- \rightarrow K^+ K^- \pi^0) &= (-21 \pm 24)\% \text{ [tt]} \\
 A_{CP}((K^+ \pi^0)_{S\text{-wave}} K^- \rightarrow K^+ K^- \pi^0) &= (7 \pm 15)\% \text{ [tt]} \\
 A_{CP}(\phi(1020) \pi^0 \rightarrow K^+ K^- \pi^0) &= (1.1 \pm 2.2)\% \text{ [tt]} \\
 A_{CP}(f_0(980) \pi^0 \rightarrow K^+ K^- \pi^0) &= (-3 \pm 19)\% \text{ [tt]} \\
 A_{CP}(a_0(980)^0 \pi^0 \rightarrow K^+ K^- \pi^0) &= (-5 \pm 16)\% \text{ [tt]} \\
 A_{CP}(f_2'(1525) \pi^0 \rightarrow K^+ K^- \pi^0) &= (0 \pm 160)\% \text{ [tt]} \\
 A_{CP}(K^*(892)^- K^+ \rightarrow K^+ K^- \pi^0) &= (-5 \pm 4)\% \text{ [tt]} \\
 A_{CP}(K^*(1410)^- K^+ \rightarrow K^+ K^- \pi^0) &= (-17 \pm 29)\% \text{ [tt]} \\
 A_{CP}((K^- \pi^0)_{S\text{-wave}} K^+ \rightarrow K^+ K^- \pi^0) &= (-10 \pm 40)\% \text{ [tt]} \\
 A_{CP}(K_S^0 \pi^0) &= (-0.20 \pm 0.17)\% \\
 A_{CP}(K_S^0 \eta) &= (0.5 \pm 0.5)\% \\
 A_{CP}(K_S^0 \eta') &= (1.0 \pm 0.7)\% \\
 A_{CP}(K_S^0 \phi) &= (-3 \pm 9)\% \\
 A_{CP}(K^- \pi^+) &= (0.2 \pm 0.5)\% \\
 A_{CP}(K^+ \pi^-) &= (-0.9 \pm 1.4)\%
 \end{aligned}$$

$$\begin{aligned}
 A_{CP}(D_{CP(\pm 1)} \rightarrow K^\mp \pi^\pm) &= (12.7 \pm 1.5)\% \\
 A_{CP}(K^- \pi^+ \pi^0) &= (0.1 \pm 0.5)\% \\
 A_{CP}(K^+ \pi^- \pi^0) &= (0 \pm 5)\% \\
 A_{CP}(K_S^0 \pi^+ \pi^-) &= (-0.1 \pm 0.8)\% \\
 A_{CP}(K^*(892)^- \pi^+ \rightarrow K_S^0 \pi^+ \pi^-) &= (0.4 \pm 0.5)\% \\
 A_{CP}(K^*(892)^+ \pi^- \rightarrow K_S^0 \pi^+ \pi^-) &= (1 \pm 6)\% \\
 A_{CP}(\overline{K}^0 \rho^0 \rightarrow K_S^0 \pi^+ \pi^-) &= (-0.1 \pm 0.5)\% \\
 A_{CP}(\overline{K}^0 \omega \rightarrow K_S^0 \pi^+ \pi^-) &= (-13 \pm 7)\% \\
 A_{CP}(\overline{K}^0 f_0(980) \rightarrow K_S^0 \pi^+ \pi^-) &= (-0.4 \pm 2.7)\% \\
 A_{CP}(\overline{K}^0 f_2(1270) \rightarrow K_S^0 \pi^+ \pi^-) &= (-4 \pm 5)\% \\
 A_{CP}(\overline{K}^0 f_0(1370) \rightarrow K_S^0 \pi^+ \pi^-) &= (-1 \pm 9)\% \\
 A_{CP}(\overline{K}^0 \rho^0(1450) \rightarrow K_S^0 \pi^+ \pi^-) &= (-4 \pm 10)\% \\
 A_{CP}(\overline{K}^0 f_0(600) \rightarrow K_S^0 \pi^+ \pi^-) &= (-3 \pm 5)\% \\
 A_{CP}(K^*(1410)^- \pi^+ \rightarrow K_S^0 \pi^+ \pi^-) &= (-2 \pm 9)\% \\
 A_{CP}(K_0^*(1430)^+ \pi^- \rightarrow K_S^0 \pi^+ \pi^-) &= (4 \pm 4)\% \\
 A_{CP}(K_0^*(1430)^+ \pi^- \rightarrow K_S^0 \pi^+ \pi^-) &= (12 \pm 15)\% \\
 A_{CP}(K_2^*(1430)^- \pi^+ \rightarrow K_S^0 \pi^+ \pi^-) &= (3 \pm 6)\% \\
 A_{CP}(K_2^*(1430)^+ \pi^- \rightarrow K_S^0 \pi^+ \pi^-) &= (-10 \pm 32)\% \\
 A_{CP}(K^- \pi^+ \pi^+ \pi^-) &= (0.2 \pm 0.5)\% \\
 A_{CP}(K^+ \pi^- \pi^+ \pi^-) &= (-2 \pm 4)\% \\
 A_{CP}(K^+ K^- \pi^+ \pi^-) &= (1.3 \pm 1.7)\% \\
 A_{CP}(K_1^*(1270)^+ K^- \rightarrow K^+ K^- \pi^+ \pi^-) &= (-2.3 \pm 1.7)\% \\
 A_{CP}(K_1^*(1270)^+ K^- \rightarrow K^+ K^- \pi^+ \pi^-) &= (-1 \pm 10)\% \\
 A_{CP}(K_1^*(1270)^- K^+ \rightarrow \overline{K}^{*0} \pi^- K^+) &= (-10 \pm 32)\% \\
 A_{CP}(K_1^*(1270)^- K^+ \rightarrow K^+ K^- \pi^+ \pi^-) &= (1.7 \pm 3.5)\% \\
 A_{CP}(K_1^*(1270)^+ K^- \rightarrow \rho^0 K^+ K^-) &= (-7 \pm 17)\% \\
 A_{CP}(K_1^*(1270)^- K^+ \rightarrow \rho^0 K^- K^+) &= (10 \pm 13)\% \\
 A_{CP}(K_1(1400)^+ K^- \rightarrow K^+ K^- \pi^+ \pi^-) &= (-4.4 \pm 2.1)\% \\
 A_{CP}(K^*(1410)^+ K^- \rightarrow K^{*0} \pi^+ K^-) &= (-20 \pm 17)\% \\
 A_{CP}(K^*(1410)^- K^+ \rightarrow \overline{K}^{*0} \pi^- K^+) &= (-1 \pm 14)\% \\
 A_{CP}(K^*(1680)^+ K^- \rightarrow K^+ K^- \pi^+ \pi^-) &= (-17 \pm 29)\% \\
 A_{CP}(K^{*0} \overline{K}^{*0}) \text{ in } D^0, \overline{D}^0 \rightarrow K^{*0} \overline{K}^{*0} &= (-5 \pm 14)\% \\
 A_{CP}(K^{*0} \overline{K}^{*0} S\text{-wave}) &= (-3.9 \pm 2.2)\% \\
 A_{CP}(\phi \rho^0) \text{ in } D^0, \overline{D}^0 \rightarrow \phi \rho^0 &= (1 \pm 9)\% \\
 A_{CP}(\phi \rho^0 S\text{-wave}) &= (-3 \pm 5)\% \\
 A_{CP}(\phi \rho^0 D\text{-wave}) &= (-37 \pm 19)\% \\
 A_{CP}(\phi(\pi^+ \pi^-)_{S\text{-wave}}) &= (6 \pm 6)\% \\
 A_{CP}(K^*(892)^0 (K^- \pi^+)_{S\text{-wave}}) &= (-10 \pm 40)\% \\
 A_{CP}(K^+ K^- \pi^+ \pi^- \text{ non-resonant}) &= (8 \pm 20)\% \\
 A_{CP}((K^- \pi^+)_{P\text{-wave}} (K^+ \pi^-)_{S\text{-wave}}) &= (3 \pm 11)\% \\
 A_{CP}(K^+ K^- \mu^+ \mu^-) \text{ in } D^0, \overline{D}^0 \rightarrow K^+ K^- \mu^+ \mu^- &= (0 \pm 11)\% \\
 A_{CP}(\pi^+ \pi^- \mu^+ \mu^-) \text{ in } D^0, \overline{D}^0 \rightarrow \pi^+ \pi^- \mu^+ \mu^- &= (5 \pm 4)\%
 \end{aligned}$$

CP-even fractions (labeled by the D^0 decay)

$$\begin{aligned}
 \text{CP-even fraction in } D^0 \rightarrow \pi^+ \pi^- \pi^0 \text{ decays} &= (97.3 \pm 1.7)\% \\
 \text{CP-even fraction in } D^0 \rightarrow K^+ K^- \pi^0 \text{ decays} &= (73 \pm 6)\% \\
 \text{CP-even fraction in } D^0 \rightarrow \pi^+ \pi^- \pi^+ \pi^- \text{ decays} &= (76.9 \pm 2.3)\% \\
 \text{CP-even fraction in } D^0 \rightarrow K_S^0 \pi^+ \pi^- \pi^0 \text{ decays} &= (23.8 \pm 1.7)\% \\
 \text{CP-even fraction in } D^0 \rightarrow K^+ K^- \pi^+ \pi^- \text{ decays} &= (75 \pm 4)\%
 \end{aligned}$$

CP-violation asymmetry difference

$$\Delta A_{CP} = A_{CP}(K^+ K^-) - A_{CP}(\pi^+ \pi^-) = (-0.154 \pm 0.029)\%$$

χ^2 tests of CP-violation (CPV) p-values

$$\begin{aligned}
 \text{Local CPV in } D^0, \overline{D}^0 \rightarrow \pi^+ \pi^- \pi^0 &= 4.9\% \\
 \text{Local CPV in } D^0, \overline{D}^0 \rightarrow \pi^+ \pi^- \pi^+ \pi^- &= (0.6 \pm 0.2)\% \\
 \text{Local CPV in } D^0, \overline{D}^0 \rightarrow K_S^0 \pi^+ \pi^- &= 96\% \\
 \text{Local CPV in } D^0, \overline{D}^0 \rightarrow K^+ K^- \pi^0 &= 16.6\% \\
 \text{Local CPV in } D^0, \overline{D}^0 \rightarrow K^+ K^- \pi^+ \pi^- &= 9.1\%
 \end{aligned}$$

T-violation decay-rate asymmetry

$$\begin{aligned}
 A_T(K^+ K^- \pi^+ \pi^-) &= (2.9 \pm 2.2) \times 10^{-3} \text{ [I]} \\
 A_{T\text{viol}}(K_S \pi^+ \pi^- \pi^0) \text{ in } D^0, \overline{D}^0 \rightarrow K_S \pi^+ \pi^- \pi^0 &= (-0.3_{-1.6}^{+1.4}) \times 10^{-3}
 \end{aligned}$$

CPT-violation decay-rate asymmetry

$$A_{CP T}(K^\mp \pi^\pm) = 0.008 \pm 0.008$$

Form factors

$$\begin{aligned}
 r_V &\equiv V(0)/A_1(0) \text{ in } D^0 \rightarrow K^*(892)^- \ell^+ \nu_\ell = 1.46 \pm 0.07 \\
 r_2 &\equiv A_2(0)/A_1(0) \text{ in } D^0 \rightarrow K^*(892)^- \ell^+ \nu_\ell = 0.68 \pm 0.06 \\
 f_+(0) &\text{ in } D^0 \rightarrow K^- \ell^+ \nu_\ell = 0.736 \pm 0.004 \\
 f_+(0) |V_{cs}| &\text{ in } D^0 \rightarrow K^- \ell^+ \nu_\ell = 0.7166 \pm 0.0030 \\
 r_1 &\equiv a_1/a_0 \text{ in } D^0 \rightarrow K^- \ell^+ \nu_\ell = -2.40 \pm 0.16 \\
 r_2 &\equiv a_2/a_0 \text{ in } D^0 \rightarrow K^- \ell^+ \nu_\ell = 5 \pm 4 \\
 f_+(0) &\text{ in } D^0 \rightarrow \pi^- \ell^+ \nu_\ell = 0.637 \pm 0.009 \\
 f_+(0) |V_{cd}| &\text{ in } D^0 \rightarrow \pi^- \ell^+ \nu_\ell = 0.1436 \pm 0.0026 \quad (S = 1.5) \\
 r_1 &\equiv a_1/a_0 \text{ in } D^0 \rightarrow \pi^- \ell^+ \nu_\ell = -1.97 \pm 0.28 \quad (S = 1.4) \\
 r_2 &\equiv a_1/a_0 \text{ in } D^0 \rightarrow \pi^- \ell^+ \nu_\ell = -0.2 \pm 2.2 \quad (S = 1.7)
 \end{aligned}$$

Meson Summary Table

Most decay modes (other than the semileptonic modes) that involve a neutral K meson are now given as K_S^0 modes, not as \bar{K}^0 modes. Nearly allowed it is a K_S^0 that is measured, and interference between Cabibbo-allowed and doubly Cabibbo-suppressed modes can invalidate the assumption that $2\Gamma(K_S^0) = \Gamma(\bar{K}^0)$.

D^0 DECAY MODES	Fraction (Γ_i/Γ)	Scale factor/ Confidence level (MeV/c)	p		
Topological modes					
0-prongs	$[uu]$ (15 \pm 6) %	–			
2-prongs	(71 \pm 6) %	–			
4-prongs	$[vv]$ (14.6 \pm 0.5) %	–			
6-prongs	$[xx]$ (6.5 \pm 1.3) $\times 10^{-4}$	–			
Inclusive modes					
e^+ anything	$[yy]$ (6.49 \pm 0.11) %	–			
μ^+ anything	(6.8 \pm 0.6) %	–			
K^- anything	(54.7 \pm 2.8) %	S=1.3	–		
\bar{K}^0 anything + K^0 anything	(47 \pm 4) %	–			
K^+ anything	(3.4 \pm 0.4) %	–			
$K^*(892)^-$ anything	(15 \pm 9) %	–			
$\bar{K}^*(892)^0$ anything	(9 \pm 4) %	–			
$K^*(892)^+$ anything	< 3.6 %	CL=90%	–		
$K^*(892)^0$ anything	(2.8 \pm 1.3) %	–			
η anything	(9.5 \pm 0.9) %	–			
η' anything	(2.48 \pm 0.27) %	–			
ϕ anything	(1.08 \pm 0.04) %	–			
invisibles	< 9.4 $\times 10^{-5}$	CL=90%	–		
Semileptonic modes					
$K^- e^+ \nu_e$	(3.542 \pm 0.035) %	S=1.3	867		
$K^- \mu^+ \nu_\mu$	(3.41 \pm 0.04) %		864		
$K^*(892)^- e^+ \nu_e$	(2.15 \pm 0.16) %		719		
$K^*(892)^- \mu^+ \nu_\mu$	(1.89 \pm 0.24) %		714		
$K^- \pi^0 e^+ \nu_e$	(1.6 \pm 1.3) %		861		
$\bar{K}^0 \pi^- e^+ \nu_e$	(1.44 \pm 0.04) %		860		
$(\bar{K}^0 \pi^-) S\text{-wave } e^+ \nu_e$	(7.9 \pm 1.7) $\times 10^{-4}$		860		
$K^- \pi^+ \pi^- e^+ \nu_e$	(2.8 \pm 1.4) $\times 10^{-4}$		843		
$K_1(1270)^- e^+ \nu_e$	(7.6 \pm 4.0) $\times 10^{-4}$		511		
$K^- \pi^+ \pi^- \mu^+ \nu_\mu$	< 1.3 $\times 10^{-3}$	CL=90%	821		
$(\bar{K}^*(892)^0 \pi^-)^- \mu^+ \nu_\mu$	< 1.5 $\times 10^{-3}$	CL=90%	692		
$\pi^- e^+ \nu_e$	(2.91 \pm 0.04) $\times 10^{-3}$		927		
$\pi^- \mu^+ \nu_\mu$	(2.67 \pm 0.12) $\times 10^{-3}$	S=1.3	924		
$\pi^- \pi^0 e^+ \nu_e$	(1.45 \pm 0.07) $\times 10^{-3}$		922		
$\rho^- e^+ \nu_e$	(1.50 \pm 0.12) $\times 10^{-3}$	S=1.9	771		
$a(980)^- e^+ \nu_e, a^- \rightarrow \eta \pi^-$	(1.33 \pm 0.34) $\times 10^{-4}$		–		
Hadronic modes with one \bar{K}					
$K^- \pi^+$	(3.950 \pm 0.031) %	S=1.2	861		
$K_S^0 \pi^0$	(1.240 \pm 0.022) %		860		
$K^0 \pi^0$	(10.0 \pm 0.7) $\times 10^{-3}$		860		
$K_S^0 \pi^+ \pi^-$	$[nn]$ (2.80 \pm 0.18) %	S=1.1	842		
$K_S^0 \rho^0$	(6.3 \pm 0.6) $\times 10^{-3}$		674		
$K_S^0 \omega, \omega \rightarrow \pi^+ \pi^-$	(2.0 \pm 0.6) $\times 10^{-4}$		670		
$K_S^0 (\pi^+ \pi^-) S\text{-wave}$	(3.3 \pm 0.8) $\times 10^{-3}$		842		
$K_S^0 f_0(980), f_0 \rightarrow \pi^+ \pi^-$	(1.20 \pm 0.40) $\times 10^{-3}$		549		
$K_S^0 f_0(1370), f_0 \rightarrow \pi^+ \pi^-$	(2.8 \pm 0.9) $\times 10^{-3}$		†		
$K_S^0 f_2(1270), f_2 \rightarrow \pi^+ \pi^-$	(9 \pm 10) $\times 10^{-5}$		262		
$K^*(892)^- \pi^+, K^* \rightarrow$	(1.64 \pm 0.14) %		711		
$K_S^0 \pi^-$	(0.17) %				
$K_0^*(1430)^- \pi^+, K_0^* \rightarrow$	(2.67 \pm 0.40) $\times 10^{-3}$		378		
$K_S^0 \pi^-$	(0.33) $\times 10^{-3}$				
$K_2^*(1430)^- \pi^+, K_2^* \rightarrow$	(3.4 \pm 1.9) $\times 10^{-4}$		367		
$K_S^0 \pi^-$	(1.0) $\times 10^{-4}$				
$K^*(1680)^- \pi^+, K^* \rightarrow$	(4.4 \pm 3.5) $\times 10^{-4}$		46		
$K_S^0 \pi^-$	(0.17) $\times 10^{-4}$				
$K^*(892)^+ \pi^-, K^* \rightarrow$	$[zz]$ (1.13 \pm 0.60) $\times 10^{-4}$		711		
$K_S^0 \pi^+$	(0.34) $\times 10^{-4}$				
$K_0^*(1430)^+ \pi^-, K_0^* \rightarrow$	$[zz]$ < 1.4 $\times 10^{-5}$	CL=95%	–		
$K_S^0 \pi^+$	(0.34) $\times 10^{-5}$				
$K_2^*(1430)^+ \pi^-, K_2^* \rightarrow$	$[zz]$ < 3.4 $\times 10^{-5}$	CL=95%	–		
$K_S^0 \pi^+$	(0.20) $\times 10^{-5}$				
$K_S^0 \pi^+ \pi^-$ nonresonant	(2.5 \pm 1.6) $\times 10^{-4}$		842		
$K^- \pi^+ \pi^0$	$[nn]$ (14.4 \pm 0.5) %	S=2.0	844		
$K^- \rho^+$	(11.3 \pm 0.7) %		675		
$K^- \rho(1700)^+, \rho^+ \rightarrow \pi^+ \pi^0$	(8.2 \pm 1.8) $\times 10^{-3}$		†		
$K^*(892)^- \pi^+, K^*(892)^- \rightarrow$	(2.31 \pm 0.40) %		711		
$K^- \pi^0$	(0.20) %				
$\bar{K}^*(892)^0 \pi^0, \bar{K}^*(892)^0 \rightarrow$	(1.95 \pm 0.24) %		711		
$K^- \pi^+$	(0.24) %				
$K_0^*(1430)^- \pi^+, K_0^* \rightarrow$	(4.8 \pm 2.2) $\times 10^{-3}$		378		
$K^- \pi^0$	(2.2) $\times 10^{-3}$				
$\bar{K}_0^*(1430)^0 \pi^0, \bar{K}_0^* \rightarrow$	(5.9 \pm 5.0) $\times 10^{-3}$		379		
$K^- \pi^+$	(5.0) $\times 10^{-3}$				
$K^*(1680)^- \pi^+, K^* \rightarrow$	(1.9 \pm 0.7) $\times 10^{-3}$		46		
$K^- \pi^0$	(0.7) $\times 10^{-3}$				
$K^- \pi^+ \pi^0$ nonresonant	(1.15 \pm 0.60) %		844		
$K_S^0 2\pi^0$	(9.1 \pm 1.1) $\times 10^{-3}$	S=2.2	843		
$K_S^0 (2\pi^0) S\text{-wave}$	(2.6 \pm 0.7) $\times 10^{-3}$		–		
$\bar{K}^*(892)^0 \pi^0, \bar{K}^{*0} \rightarrow K_S^0 \pi^0$	(8.1 \pm 0.7) $\times 10^{-3}$		711		
$\bar{K}^*(1430)^0 \pi^0, \bar{K}^{*0} \rightarrow$	(4 \pm 23) $\times 10^{-5}$		–		
$K_S^0 \pi^0$	(23) $\times 10^{-5}$				
$\bar{K}^*(1680)^0 \pi^0, \bar{K}^{*0} \rightarrow$	(1.0 \pm 0.4) $\times 10^{-3}$		–		
$K_S^0 \pi^0$	(0.4) $\times 10^{-3}$				
$K_S^0 f_2(1270), f_2 \rightarrow 2\pi^0$	(2.3 \pm 1.1) $\times 10^{-4}$		–		
$2K_S^0, \text{one } K_S^0 \rightarrow 2\pi^0$	(3.2 \pm 1.1) $\times 10^{-4}$		–		
$K^- 2\pi^+ \pi^-$	$[nn]$ (8.23 \pm 0.14) %	S=1.1	813		
$K^- \pi^+ \rho^0 \text{ total}$	(6.87 \pm 0.31) %		609		
$K^- \pi^+ \rho^0 3\text{-body}$	(6.1 \pm 1.6) $\times 10^{-3}$		609		
$\bar{K}^*(892)^0 \rho^0, \bar{K}^{*0} \rightarrow$	(1.01 \pm 0.05) %		416		
$\bar{K}^*(892)^0 \rho^0 \text{ transverse,}$	(1.2 \pm 0.4) %		417		
$\bar{K}^{*0} \rightarrow K^- \pi^+$	(0.4) %				
$K^- a_1(1260)^+, a_1^+ \rightarrow$	(4.33 \pm 0.32) %		327		
$\rho^0 \pi^+$	(0.32) %				
$K_1(1270)^- \pi^+, K_1^- \rightarrow$	(3.9 \pm 0.4) $\times 10^{-3}$		–		
$K^- \pi^+ \pi^- \text{ total}$	(6.6 \pm 2.3) $\times 10^{-4}$		484		
$K_1(1270)^- \pi^+, K_1^- \rightarrow$	(2.3) $\times 10^{-4}$				
$\bar{K}^*(892)^0 \pi^-, \bar{K}^{*0} \rightarrow$	(2.3) $\times 10^{-4}$				
$K^- 2\pi^+ \pi^-$ nonresonant	(1.81 \pm 0.07) %		813		
$[aaa]$ $K_S^0 \pi^+ \pi^- \pi^0$	(5.2 \pm 0.6) %		813		
$K_S^0 \eta, \eta \rightarrow \pi^+ \pi^- \pi^0$	(1.17 \pm 0.03) $\times 10^{-3}$		772		
$K_S^0 \omega, \omega \rightarrow \pi^+ \pi^- \pi^0$	(9.9 \pm 0.6) $\times 10^{-3}$		670		
$K^- \pi^+ 2\pi^0$	(8.86 \pm 0.23) %		815		
$K^- 2\pi^+ \pi^- \pi^0$	(4.3 \pm 0.4) %		771		
$\bar{K}^*(892)^0 \pi^+ \pi^- \pi^0, \bar{K}^{*0} \rightarrow$	(1.3 \pm 0.6) %		643		
$K^- \pi^+$	(0.6) %				
$K^- \pi^+ \omega, \omega \rightarrow \pi^+ \pi^- \pi^0$	(2.8 \pm 0.5) %		605		
$\bar{K}^*(892)^0 \omega, \bar{K}^{*0} \rightarrow$	(6.5 \pm 3.0) $\times 10^{-3}$		410		
$K^- \pi^+$	(3.0) $\times 10^{-3}$				
$\pi^+ \pi^- \pi^0$	(5.7 \pm 1.1) $\times 10^{-3}$		721		
$K_S^0 \eta \pi^0$	(1.1) $\times 10^{-3}$				
$K_S^0 a_0(980), a_0 \rightarrow \eta \pi^0$	(6.8 \pm 2.1) $\times 10^{-3}$		–		
$\bar{K}^*(892)^0 \eta, \bar{K}^{*0} \rightarrow K_S^0 \pi^0$	(1.7 \pm 0.5) $\times 10^{-3}$		–		
$K_S^0 2\pi^+ 2\pi^-$	(2.66 \pm 0.30) $\times 10^{-3}$		768		
$K_S^0 \rho^0 \pi^+ \pi^-, \text{no } K^*(892)^-$	(1.1 \pm 0.7) $\times 10^{-3}$		–		
$K^*(892)^- 2\pi^+ \pi^-,$	(5 \pm 7) $\times 10^{-4}$		642		
$K^*(892)^- \rightarrow K_S^0 \pi^-,$	(7) $\times 10^{-4}$				
$\text{no } \rho^0$	(0.7) $\times 10^{-4}$				
$K^*(892)^- \rho^0 \pi^+,$	(1.6 \pm 0.6) $\times 10^{-3}$		230		
$K^*(892)^- \rightarrow K_S^0 \pi^-$	(0.6) $\times 10^{-3}$				
$K_S^0 2\pi^+ 2\pi^-$ nonresonant	< 1.2 $\times 10^{-3}$	CL=90%	768		
$K^- 3\pi^+ 2\pi^-$	(2.2 \pm 0.6) $\times 10^{-4}$		713		
Fractions of some of the following modes with resonances have already appeared above as submodes of particular charged-particle modes. These nine modes below are all corrected for unseen decays of the resonances.					
$K_S^0 \eta$	(5.09 \pm 0.13) $\times 10^{-3}$		772		
$K_S^0 \omega$	(1.11 \pm 0.06) %		670		
$K_S^0 \eta'(958)$	(9.49 \pm 0.32) $\times 10^{-3}$		565		
$\bar{K}^*(892)^0 \pi^+ \pi^- \pi^0$	(1.9 \pm 0.9) %		643		
$K^- \pi^+ \omega$	(3.1 \pm 0.6) %		605		

Meson Summary Table

$\bar{K}^*(892)^0 \omega$	(1.1 ± 0.5) %	410	Resonant $(\pi^+ \pi^-) \pi^+ \pi^-$	(1.51 ± 0.12) × 10 ⁻³	-
$K^- \pi^+ \eta'(958)$	(6.43 ± 0.34) × 10 ⁻³	479	3-body total		
$K_S^0 \eta'(958) \pi^0$	(2.52 ± 0.27) × 10 ⁻³	479	$\sigma \pi^+ \pi^-$	(6.2 ± 0.9) × 10 ⁻⁴	-
$\bar{K}^*(892)^0 \eta'(958)$	< 1.0 × 10 ⁻³	CL=90% 119	$\sigma \rho(770)^0$	(5.0 ± 2.5) × 10 ⁻⁴	-
Hadronic modes with three K's			$f_0(980) \pi^+ \pi^-, f_0 \rightarrow$	(1.8 ± 0.5) × 10 ⁻⁴	-
$K_S^0 K^+ K^-$	(4.42 ± 0.32) × 10 ⁻³	544	$\pi^+ \pi^-$		
$K_S^0 a_0(980)^0, a_0^0 \rightarrow K^+ K^-$	(2.9 ± 0.4) × 10 ⁻³	-	$f_2(1270) \pi^+ \pi^-, f_2 \rightarrow$	(3.7 ± 0.6) × 10 ⁻⁴	-
$K^- a_0(980)^+, a_0^+ \rightarrow$	(5.9 ± 1.8) × 10 ⁻⁴	-	$\pi^+ \pi^-$		
$K^+ K_S^0$			$2f_2(1270), f_2 \rightarrow \pi^+ \pi^-$	(1.6 ± 1.8) × 10 ⁻⁴	-
$K^+ a_0(980)^-, a_0^- \rightarrow$	< 1.1 × 10 ⁻⁴	CL=95% -	$f_0(1370) \sigma, f_0 \rightarrow$	(1.6 ± 0.5) × 10 ⁻³	-
$K^- K_S^0$			$\pi^+ \pi^- 2\pi^0$	(1.02 ± 0.09) %	882
$K_S^0 f_0(980), f_0 \rightarrow K^+ K^-$	< 9 × 10 ⁻⁵	CL=95% -	$\eta \pi^0$	[bbb] (6.3 ± 0.6) × 10 ⁻⁴	S=1.1 846
$K_S^0 \phi, \phi \rightarrow K^+ K^-$	(2.03 ± 0.15) × 10 ⁻³	520	$\omega \pi^0$	[bbb] (1.17 ± 0.35) × 10 ⁻⁴	761
$K_S^0 f_0(1370), f_0 \rightarrow K^+ K^-$	(1.7 ± 1.1) × 10 ⁻⁴	-	$\omega \eta$	(1.98 ± 0.18) × 10 ⁻³	S=1.1 648
$3K_S^0$	(7.5 ± 0.7) × 10 ⁻⁴	S=1.4 539	$2\pi^+ 2\pi^- \pi^0$	(4.2 ± 0.5) × 10 ⁻³	844
$K^+ 2K^- \pi^+$	(2.25 ± 0.32) × 10 ⁻⁴	434	$\eta \pi^+ \pi^-$	[bbb] (1.09 ± 0.16) × 10 ⁻³	827
$K^+ K^- \bar{K}^*(892)^0, \bar{K}^{*0} \rightarrow$	(4.5 ± 1.8) × 10 ⁻⁵	†	$\omega \pi^+ \pi^-$	[bbb] (1.6 ± 0.5) × 10 ⁻³	738
$K^- \pi^+$			$\eta 2\pi^0$	(3.8 ± 1.3) × 10 ⁻⁴	829
$K^- \pi^+ \phi, \phi \rightarrow K^+ K^-$	(4.1 ± 1.7) × 10 ⁻⁵	422	$3\pi^+ 3\pi^-$	(4.3 ± 1.2) × 10 ⁻⁴	795
$\phi \bar{K}^*(892)^0, \phi \rightarrow K^+ K^-,$	(1.08 ± 0.21) × 10 ⁻⁴	†	$\eta'(958) \pi^0$	(9.2 ± 1.0) × 10 ⁻⁴	678
$\bar{K}^{*0} \rightarrow K^- \pi^+$			$\eta'(958) \pi^+ \pi^-$	(4.5 ± 1.7) × 10 ⁻⁴	650
$K^+ 2K^- \pi^+$ nonresonant	(3.4 ± 1.5) × 10 ⁻⁵	434	2η	(2.11 ± 0.19) × 10 ⁻³	S=2.2 754
$2K_S^0 K^\pm \pi^\mp$	(5.9 ± 1.3) × 10 ⁻⁴	427	$2\eta \pi^0$	(7.3 ± 2.2) × 10 ⁻⁴	699
Pionic modes			3η	< 1.3 × 10 ⁻⁴	CL=90% 421
$\pi^+ \pi^-$	(1.455 ± 0.024) × 10 ⁻³	S=1.3 922	$\eta \eta'(958)$	(1.01 ± 0.19) × 10 ⁻³	537
$2\pi^0$	(8.26 ± 0.25) × 10 ⁻⁴	923	Hadronic modes with a K \bar{K} pair		
$\pi^+ \pi^- \pi^0$	(1.49 ± 0.06) %	S=2.1 907	$K^+ K^-$	(4.08 ± 0.06) × 10 ⁻³	S=1.6 791
$\rho^+ \pi^-$	(1.01 ± 0.04) %	764	$2K_S^0$	(1.41 ± 0.05) × 10 ⁻⁴	S=1.1 789
$\rho^0 \pi^0$	(3.86 ± 0.23) × 10 ⁻³	764	$K_S^0 K^- \pi^+$	(3.3 ± 0.5) × 10 ⁻³	S=1.1 739
$\rho^- \pi^+$	(5.15 ± 0.25) × 10 ⁻³	764	$\bar{K}^*(892)^0 K_S^0, \bar{K}^{*0} \rightarrow$	(8.2 ± 1.6) × 10 ⁻⁵	608
$\rho(1450)^+ \pi^-, \rho^+ \rightarrow \pi^+ \pi^0$	(1.6 ± 2.1) × 10 ⁻⁵	-	$K^- \pi^+$		
$\rho(1450)^0 \pi^0, \rho^0 \rightarrow \pi^+ \pi^-$	(4.5 ± 2.0) × 10 ⁻⁵	-	$K^*(892)^+ K^-, K^{*+} \rightarrow$	(1.89 ± 0.30) × 10 ⁻³	-
$\rho(1450)^- \pi^+, \rho^- \rightarrow \pi^- \pi^0$	(2.7 ± 0.4) × 10 ⁻⁴	-	$K_S^0 \pi^-$		
$\rho(1700)^+ \pi^-, \rho^+ \rightarrow \pi^+ \pi^0$	(6.1 ± 1.5) × 10 ⁻⁴	-	$\bar{K}^*(1410)^0 K_S^0, \bar{K}^{*0} \rightarrow$	(1.3 ± 1.9) × 10 ⁻⁴	-
$\rho(1700)^0 \pi^0, \rho^0 \rightarrow \pi^+ \pi^-$	(7.4 ± 1.8) × 10 ⁻⁴	-	$K^- \pi^+$		
$\rho(1700)^- \pi^+, \rho^- \rightarrow \pi^- \pi^0$	(4.8 ± 1.1) × 10 ⁻⁴	-	$K^*(1410)^+ K^-, K^{*+} \rightarrow$	(3.2 ± 1.9) × 10 ⁻⁴	-
$f_0(980) \pi^0, f_0 \rightarrow \pi^+ \pi^-$	(3.7 ± 0.9) × 10 ⁻⁵	-	$K_S^0 \pi^+$		
$f_0(500) \pi^0, f_0 \rightarrow \pi^+ \pi^-$	(1.22 ± 0.22) × 10 ⁻⁴	-	$(K^- \pi^+)_{S\text{-wave}} K_S^0$	(6.0 ± 2.9) × 10 ⁻⁴	739
$f_0(1370) \pi^0, f_0 \rightarrow \pi^+ \pi^-$	(5.5 ± 2.1) × 10 ⁻⁵	-	$(K_S^0 \pi^+)_{S\text{-wave}} K^-$	(3.9 ± 1.0) × 10 ⁻⁴	739
$f_0(1500) \pi^0, f_0 \rightarrow \pi^+ \pi^-$	(5.8 ± 1.6) × 10 ⁻⁵	-	$a_0(980)^- \pi^+, a_0^+ \rightarrow K_S^0 K^-$	(1.3 ± 1.4) × 10 ⁻⁴	-
$f_0(1710) \pi^0, f_0 \rightarrow \pi^+ \pi^-$	(4.6 ± 1.6) × 10 ⁻⁵	-	$a_0(1450)^- \pi^+, a_0^- \rightarrow$	(2.5 ± 2.0) × 10 ⁻⁵	-
$f_2(1270) \pi^0, f_2 \rightarrow \pi^+ \pi^-$	(1.97 ± 0.21) × 10 ⁻⁴	-	$K_S^0 K^-$		
$\pi^+ \pi^- \pi^0$ nonresonant	(1.3 ± 0.4) × 10 ⁻⁴	907	$a_2(1320)^- \pi^+, a_2^- \rightarrow$	(5 ± 5) × 10 ⁻⁶	-
$3\pi^0$	(2.0 ± 0.5) × 10 ⁻⁴	908	$K_S^0 K^-$		
$2\pi^+ 2\pi^-$	(7.56 ± 0.20) × 10 ⁻³	880	$\rho(1450)^- \pi^+, \rho^- \rightarrow K_S^0 K^-$	(4.6 ± 2.5) × 10 ⁻⁵	-
$a_1(1260)^+ \pi^-, a_1^+ \rightarrow$	(4.54 ± 0.31) × 10 ⁻³	-	$K_S^0 K^+ \pi^-$	(2.17 ± 0.34) × 10 ⁻³	S=1.1 739
$2\pi^+ \pi^-$ total			$K^*(892)^0 K_S^0, K^{*0} \rightarrow$	(1.12 ± 0.21) × 10 ⁻⁴	608
$a_1(1260)^+ \pi^-, a_1^+ \rightarrow$	(3.14 ± 0.21) × 10 ⁻³	-	$K^+ \pi^-$		
$\rho^0 \pi^+$ S-wave			$K^*(892)^- K^+, K^{*-} \rightarrow$	(6.2 ± 1.0) × 10 ⁻⁴	-
$a_1(1260)^+ \pi^-, a_1^+ \rightarrow$	(1.9 ± 0.5) × 10 ⁻⁴	-	$K_S^0 \pi^-$		
$\rho^0 \pi^+$ D-wave			$K^*(1410)^0 K_S^0, K^{*0} \rightarrow$	(5 ± 8) × 10 ⁻⁵	-
$a_1(1260)^+ \pi^-, a_1^+ \rightarrow$	(6.4 ± 0.7) × 10 ⁻⁴	-	$K^+ \pi^+$		
$\sigma \pi^+$			$K^*(1410)^- K^+, K^{*-} \rightarrow$	(2.6 ± 2.0) × 10 ⁻⁴	-
$a_1(1260)^- \pi^+, a_1^- \rightarrow$	(2.3 ± 0.9) × 10 ⁻⁴	-	$K_S^0 \pi^-$		
$\rho^0 \pi^-$ S-wave			$(K^+ \pi^-)_{S\text{-wave}} K_S^0$	(3.7 ± 1.9) × 10 ⁻⁴	739
$a_1(1260)^- \pi^+, a_1^- \rightarrow \sigma \pi^-$	(6.1 ± 3.4) × 10 ⁻⁵	-	$(K_S^0 \pi^-)_{S\text{-wave}} K^+$	(1.4 ± 0.6) × 10 ⁻⁴	739
$\pi(1300)^+ \pi^-, \pi(1300)^+ \rightarrow$	(5.1 ± 2.7) × 10 ⁻⁴	-	$a_0(980)^+ \pi^-, a_0^+ \rightarrow K_S^0 K^+$	(6 ± 4) × 10 ⁻⁴	-
$\sigma \pi^+$			$a_0(1450)^+ \pi^-, a_0^+ \rightarrow$	(3.2 ± 2.5) × 10 ⁻⁵	-
$\pi(1300)^- \pi^+, \pi(1300)^- \rightarrow$	(2.3 ± 2.2) × 10 ⁻⁴	-	$K_S^0 K^+$		
$\sigma \pi^-$			$\rho(1700)^+ \pi^-, \rho^+ \rightarrow K_S^0 K^+$	(1.1 ± 0.6) × 10 ⁻⁵	-
$a_1(1640)^+ \pi^-, a_1^+ \rightarrow$	(3.2 ± 1.6) × 10 ⁻⁴	-	$K^+ K^- \pi^0$	(3.42 ± 0.14) × 10 ⁻³	743
$\rho^0 \pi^+$ D-wave			$K^*(892)^+ K^-, K^*(892)^+ \rightarrow$	(1.52 ± 0.07) × 10 ⁻³	-
$a_1(1640)^+ \pi^-, a_1^+ \rightarrow \sigma \pi^+$	(1.8 ± 1.4) × 10 ⁻⁴	-	$K^+ \pi^0$		
$\pi_2(1670)^+ \pi^-, \pi_2^+ \rightarrow$	(2.0 ± 0.9) × 10 ⁻⁴	-	$K^*(892)^- K^+, K^*(892)^- \rightarrow$	(5.4 ± 0.4) × 10 ⁻⁴	-
$f_2(1270)^0 \pi^+, f_2^0 \rightarrow$			$K^- \pi^0$		
$\pi^+ \pi^-$			$(K^+ \pi^0)_{S\text{-wave}} K^-$	(2.43 ± 0.18) × 10 ⁻³	743
$\pi_2(1670)^+ \pi^-, \pi_2^+ \rightarrow \sigma \pi^+$	(2.6 ± 1.0) × 10 ⁻⁴	-	$(K^- \pi^0)_{S\text{-wave}} K^+$	(1.3 ± 0.5) × 10 ⁻⁴	743
$2\rho^0$ total	(1.85 ± 0.13) × 10 ⁻³	518	$f_0(980) \pi^0, f_0 \rightarrow K^+ K^-$	(3.6 ± 0.6) × 10 ⁻⁴	-
$2\rho^0$, parallel helicities	(8.3 ± 3.2) × 10 ⁻⁵	-	$\phi \pi^0, \phi \rightarrow K^+ K^-$	(6.6 ± 0.4) × 10 ⁻⁴	-
$2\rho^0$, perpendicular helicities	(4.8 ± 0.6) × 10 ⁻⁴	-	$2K_S^0 \pi^0$	< 5.9 × 10 ⁻⁴	740
$2\rho^0$, longitudinal helicities	(1.27 ± 0.10) × 10 ⁻³	-	$K^+ K^- \pi^+ \pi^-$	(2.47 ± 0.11) × 10 ⁻³	677
$2\rho(770)^0$, S-wave	(1.8 ± 1.3) × 10 ⁻⁴	-	$\phi(\pi^+ \pi^-)_{S\text{-wave}}, \phi \rightarrow$	(10 ± 5) × 10 ⁻⁵	614
$2\rho(770)^0$, P-wave	(5.3 ± 1.3) × 10 ⁻⁴	-	$K^+ K^-$		
$2\rho(770)^0$, D-wave	(6.2 ± 3.0) × 10 ⁻⁴	-	$(\phi \rho^0)_{S\text{-wave}}, \phi \rightarrow K^+ K^-$	(6.9 ± 0.6) × 10 ⁻⁴	250
			$(\phi \rho^0)_{P\text{-wave}}, \phi \rightarrow K^+ K^-$	(4.0 ± 1.9) × 10 ⁻⁵	-

Meson Summary Table

$(\phi\rho^0)_{D\text{-wave}}, \phi \rightarrow K^+K^-$	$(4.2 \pm 1.4) \times 10^{-5}$	-	$\pi^+\pi^-\mu^+\mu^-$	CI	$(9.6 \pm 1.2) \times 10^{-7}$	894	
$(K^*(892)^0\bar{K}^*(892)^0)_{S\text{-wave}}, K^{*0} \rightarrow K^\pm\pi^\mp$	$(2.24 \pm 0.13) \times 10^{-4}$	-	$\pi^+\pi^-\mu^+\mu^-$ (non-res)		$< 5.5 \times 10^{-7}$	CL=90% -	
$(K^*(892)^0\bar{K}^*(892)^0)_{P\text{-wave}}, K^* \rightarrow K^\pm\pi^\mp$	$(1.20 \pm 0.08) \times 10^{-4}$	-	$\rho^0\mu^+\mu^-$	CI	$< 2.2 \times 10^{-5}$	CL=90% 754	
$(K^*(892)^0\bar{K}^*(892)^0)_{D\text{-wave}}, K^* \rightarrow K^\pm\pi^\mp$	$(4.7 \pm 0.4) \times 10^{-5}$	-	ωe^+e^-	CI	$< 6 \times 10^{-6}$	CL=90% 768	
$K^*(892)^0(K^-\pi^+)_{S\text{-wave}}, 3\text{-body}, K^{*0} \rightarrow K^+\pi^-$	$(1.4 \pm 0.6) \times 10^{-4}$	-	$\omega\mu^+\mu^-$	CI	$< 8.3 \times 10^{-4}$	CL=90% 751	
$K_1(1270)^+K^-, K_1^+ \rightarrow K^0\pi^+$	$(1.4 \pm 0.9) \times 10^{-4}$	-	$K^-K^+e^+e^-$	CI	$< 1.1 \times 10^{-5}$	CL=90% 791	
$K_1(1270)^+K^-, K_1^+ \rightarrow K^*(1430)^0\pi^+, K^{*0} \rightarrow K^+\pi^-$	$(1.5 \pm 0.5) \times 10^{-4}$	-	ϕe^+e^-	CI	$< 5.2 \times 10^{-5}$	CL=90% 654	
$K_1(1270)^+K^-, K_1^+ \rightarrow K^*(1430)^0\pi^+, K^{*0} \rightarrow K^+\pi^-$	$(2.2 \pm 0.6) \times 10^{-4}$	-	$K^-K^+\mu^+\mu^-$	CI	$(1.54 \pm 0.32) \times 10^{-7}$	710	
$K_1(1270)^+K^-, K_1^+ \rightarrow K^*(1430)^0\pi^+, K^{*0} \rightarrow K^+\pi^-$	$(1.5 \pm 1.2) \times 10^{-5}$	-	$K^-K^+\mu^+\mu^-$ (non-res)		$< 3.3 \times 10^{-5}$	CL=90% -	
$K_1(1270)^-K^+, K_1^- \rightarrow \rho^0K^-$	$(4.6 \pm 0.4) \times 10^{-4}$	-	$\phi\mu^+\mu^-$	CI	$< 3.1 \times 10^{-5}$	CL=90% 631	
$K_1(1400)^+K^-, K_1^+ \rightarrow K^*(892)^0\pi^+, K^{*0} \rightarrow K^+\pi^-$	$(2.7 \pm 0.6) \times 10^{-4}$	-	$\bar{K}^0 e^+e^-$	[ss]	$< 2.4 \times 10^{-5}$	CL=90% 866	
$K^*(1410)^-K^+, K^{*-} \rightarrow K^+\pi^-$	$(7.0 \pm 1.1) \times 10^{-5}$	-	$\bar{K}^0\mu^+\mu^-$	[ss]	$< 2.6 \times 10^{-4}$	CL=90% 852	
$K_1(1680)^+K^-, K_1^+ \rightarrow K^0\pi^-$	$(8.9 \pm 3.2) \times 10^{-5}$	-	$K^-\pi^+e^+e^-, 675 < m_{ee} < 875 \text{ MeV}$		$(4.0 \pm 0.5) \times 10^{-6}$	-	
$2K_S^0\pi^+\pi^-$	$(1.22 \pm 0.23) \times 10^{-3}$	673	$m_{ee} < 1.035 \text{ GeV}$		$< 5 \times 10^{-7}$	CL=90% -	
$K^+K^-\pi^+\pi^-$ non-resonant	$(2.7 \pm 0.6) \times 10^{-4}$	-	$\bar{K}^*(892)^0 e^+e^-$	[ss]	$< 4.7 \times 10^{-5}$	CL=90% 719	
$K_S^0 K^- 2\pi^+ \pi^-$	$< 1.4 \times 10^{-4}$	CL=90% 595	$K^-\pi^+\mu^+\mu^-$	CI	$< 3.59 \times 10^{-4}$	CL=90% 829	
$K^+K^-\pi^+\pi^-$	$(3.1 \pm 2.0) \times 10^{-3}$	600	$K^-\pi^+\mu^+\mu^-, 675 < m_{\mu\mu} < 875 \text{ MeV}$		$(4.2 \pm 0.4) \times 10^{-6}$	-	
Other $K\bar{K}X$ modes. They include all decay modes of the $\phi, \eta,$ and ω .							
$\phi\pi^0$	$(1.17 \pm 0.04) \times 10^{-3}$	645	$\bar{K}^*(892)^0\mu^+\mu^-$	[ss]	$< 2.4 \times 10^{-5}$	CL=90% 700	
$\phi\eta$	$(1.8 \pm 0.5) \times 10^{-4}$	489	$\pi^+\pi^-\pi^0\mu^+\mu^-$	CI	$< 8.1 \times 10^{-4}$	CL=90% 863	
$\phi\omega$	$< 2.1 \times 10^{-3}$	CL=90% 238	$\mu^\pm e^\mp$	LF [bb]	$< 1.3 \times 10^{-8}$	CL=90% 929	
Radiative modes							
$\rho^0\gamma$	$(1.82 \pm 0.32) \times 10^{-5}$	771	$\pi^0 e^\pm\mu^\mp$	LF [bb]	$< 8.6 \times 10^{-5}$	CL=90% 924	
$\omega\gamma$	$< 2.4 \times 10^{-4}$	CL=90% 768	$\eta e^\pm\mu^\mp$	LF [bb]	$< 1.0 \times 10^{-4}$	CL=90% 848	
$\phi\gamma$	$(2.81 \pm 0.19) \times 10^{-5}$	654	$\pi^+\pi^-e^\pm\mu^\mp$	LF [bb]	$< 1.5 \times 10^{-5}$	CL=90% 911	
$\bar{K}^*(892)^0\gamma$	$(4.2 \pm 0.7) \times 10^{-4}$	719	$\rho^0 e^\pm\mu^\mp$	LF [bb]	$< 4.9 \times 10^{-5}$	CL=90% 767	
Doubly Cabibbo suppressed (DC) modes or $\Delta C = 2$ forbidden via mixing (C2M) modes							
$K^+\ell^-\bar{\nu}_\ell$ via \bar{D}^0	$< 2.2 \times 10^{-5}$	CL=90% -	$\omega e^\pm\mu^\mp$	LF [bb]	$< 1.2 \times 10^{-4}$	CL=90% 764	
K^+ or $K^*(892)^+$ $e^-\bar{\nu}_e$ via \bar{D}^0	$< 6 \times 10^{-5}$	CL=90% -	$K^-K^+e^\pm\mu^\mp$	LF [bb]	$< 1.8 \times 10^{-4}$	CL=90% 754	
$K^+\pi^-$ DC	$(1.50 \pm 0.07) \times 10^{-4}$	S=3.0 861	$\phi e^\pm\mu^\mp$	LF [bb]	$< 3.4 \times 10^{-5}$	CL=90% 648	
$K^+\pi^-$ via DCS	$(1.364 \pm 0.026) \times 10^{-4}$	-	$\bar{K}^0 e^\pm\mu^\mp$	LF [bb]	$< 1.0 \times 10^{-4}$	CL=90% 863	
$K^+\pi^-$ via \bar{D}^0	$< 1.6 \times 10^{-5}$	CL=95% 861	$K^-\pi^+e^\pm\mu^\mp$	LF [bb]	$< 5.53 \times 10^{-4}$	CL=90% 848	
$K_S^0\pi^+\pi^-$ in $D^0 \rightarrow \bar{D}^0$	$< 1.8 \times 10^{-4}$	CL=95% -	$\bar{K}^*(892)^0 e^\pm\mu^\mp$	LF [bb]	$< 8.3 \times 10^{-5}$	CL=90% 714	
$K^*(892)^+\pi^-, K^{*+} \rightarrow K_S^0\pi^+$	$(1.13 \pm_{0.34}^{0.60}) \times 10^{-4}$	711	$2\pi^-2e^+$ + c.c.	L	$< 1.12 \times 10^{-4}$	CL=90% 922	
$K_S^0(1430)^+\pi^-, K_0^{*+} \rightarrow K_S^0\pi^+$	$< 1.4 \times 10^{-5}$	-	$2\pi^-2\mu^+$ + c.c.	L	$< 2.9 \times 10^{-5}$	CL=90% 894	
$K_2^*(1430)^+\pi^-, K_2^{*+} \rightarrow K_S^0\pi^+$	$< 3.4 \times 10^{-5}$	-	$K^-\pi^-2e^+$	L	$< 2.8 \times 10^{-6}$	CL=90% 861	
$K^+\pi^-\pi^0$ DC	$(3.06 \pm 0.15) \times 10^{-4}$	844	$K^-\pi^-2\mu^+$ + c.c.	L	$< 3.9 \times 10^{-4}$	CL=90% 829	
$K^+\pi^-\pi^0$ via \bar{D}^0	$(7.6 \pm_{0.6}^{0.5}) \times 10^{-4}$	-	$2K^-2e^+$ + c.c.	L	$< 1.52 \times 10^{-4}$	CL=90% 791	
$K^+\pi^+2\pi^-$ via DCS	$(2.49 \pm 0.07) \times 10^{-4}$	-	$2K^-2\mu^+$ + c.c.	L	$< 9.4 \times 10^{-5}$	CL=90% 710	
$K^+\pi^+2\pi^-$ DC	$(2.65 \pm 0.06) \times 10^{-4}$	813	$\pi^-\pi^-e^+\mu^+$ + c.c.	L	$< 7.9 \times 10^{-5}$	CL=90% 911	
$K^+\pi^+2\pi^-$ via \bar{D}^0	$(7.9 \pm 3.0) \times 10^{-6}$	812	$K^-\pi^-e^+\mu^+$ + c.c.	L	$< 2.18 \times 10^{-4}$	CL=90% 848	
μ^- anything via \bar{D}^0	$< 4 \times 10^{-4}$	CL=90% -	$2K^-e^+\mu^+$ + c.c.	L	$< 5.7 \times 10^{-5}$	CL=90% 754	
$\Delta C = 1$ weak neutral current (CI) modes, Lepton Family number (LF) violating modes, Lepton (L) or Baryon (B) number violating modes							
$\gamma\gamma$	CI	$< 8.5 \times 10^{-7}$	$p e^-$	L,B [ccc]	$< 1.0 \times 10^{-5}$	CL=90% 696	
e^+e^-	CI	$< 7.9 \times 10^{-8}$	$\bar{p} e^+$	L,B [ddd]	$< 1.1 \times 10^{-5}$	CL=90% 696	
$\mu^+\mu^-$	CI	$< 6.2 \times 10^{-9}$					
$\pi^0 e^+e^-$	CI	$< 4 \times 10^{-6}$					
$\pi^0\mu^+\mu^-$	CI	$< 1.8 \times 10^{-4}$					
ηe^+e^-	CI	$< 3 \times 10^{-6}$					
$\eta\mu^+\mu^-$	CI	$< 5.3 \times 10^{-4}$					
$\pi^+\pi^-e^+e^-$	CI	$< 7 \times 10^{-6}$					
$\rho^0 e^+e^-$	CI	$< 1.0 \times 10^{-4}$					

 $D^*(2007)^0$

$$I(J^P) = \frac{1}{2}(1^-)$$

I, J, P need confirmation.

$$\text{Mass } m = 2006.85 \pm 0.05 \text{ MeV} \quad (S = 1.1)$$

$$m_{D^{*0}} - m_{D^0} = 142.014 \pm 0.030 \text{ MeV} \quad (S = 1.5)$$

$$\text{Full width } \Gamma < 2.1 \text{ MeV, CL} = 90\%$$

$\bar{D}^*(2007)^0$ modes are charge conjugates of modes below.

 $D^*(2007)^0$ DECAY MODES

$D^*(2007)^0$ DECAY MODES	Fraction (Γ_i/Γ)	p (MeV/c)
$D^0\pi^0$	$(64.7 \pm 0.9)\%$	43
$D^0\gamma$	$(35.3 \pm 0.9)\%$	137

 $D^*(2010)^\pm$

$$I(J^P) = \frac{1}{2}(1^-)$$

I, J, P need confirmation.

$$\text{Mass } m = 2010.26 \pm 0.05 \text{ MeV}$$

$$m_{D^*(2010)^+} - m_{D^+} = 140.603 \pm 0.015 \text{ MeV}$$

$$m_{D^*(2010)^+} - m_{D^0} = 145.4257 \pm 0.0017 \text{ MeV}$$

$$\text{Full width } \Gamma = 83.4 \pm 1.8 \text{ keV}$$

$D^*(2010)^-$ modes are charge conjugates of the modes below.

 $D^*(2010)^\pm$ DECAY MODES

$D^*(2010)^\pm$ DECAY MODES	Fraction (Γ_i/Γ)	p (MeV/c)
$D^0\pi^+$	$(67.7 \pm 0.5)\%$	39
$D^+\pi^0$	$(30.7 \pm 0.5)\%$	38
$D^+\gamma$	$(1.6 \pm 0.4)\%$	136

Meson Summary Table

 $D_0^*(2300)^0$

$$I(J^P) = \frac{1}{2}(0^+)$$

was $D_0^*(2400)^0$

Mass $m = 2300 \pm 19$ MeV
 Full width $\Gamma = 274 \pm 40$ MeV

$D_0^*(2300)^0$ DECAY MODES	Fraction (Γ_i/Γ)	ρ (MeV/c)
$D^+ \pi^-$	seen	369

 $D_1(2420)^0$

$$I(J^P) = \frac{1}{2}(1^+)$$

Mass $m = 2420.8 \pm 0.5$ MeV ($S = 1.3$)
 $m_{D_1^0} - m_{D^{*+}} = 410.6 \pm 0.5$ MeV ($S = 1.3$)
 Full width $\Gamma = 31.7 \pm 2.5$ MeV ($S = 3.5$)

 $\bar{D}_1(2420)^0$ modes are charge conjugates of modes below.

$D_1(2420)^0$ DECAY MODES	Fraction (Γ_i/Γ)	ρ (MeV/c)
$D^*(2010)^+ \pi^-$	seen	353
$D^0 \pi^+ \pi^-$	seen	425
$D^+ \pi^-$	not seen	472
$D^{*0} \pi^+ \pi^-$	not seen	279

 $D_2^*(2460)^0$

$$I(J^P) = \frac{1}{2}(2^+)$$

 $J^P = 2^+$ assignment strongly favored.

Mass $m = 2460.7 \pm 0.4$ MeV ($S = 3.1$)
 $m_{D_2^{*0}} - m_{D^{*+}} = 591.0 \pm 0.4$ MeV ($S = 2.9$)
 $m_{D_2^0} - m_{D^{*+}} = 450.4 \pm 0.4$ MeV ($S = 2.9$)
 Full width $\Gamma = 47.5 \pm 1.1$ MeV ($S = 1.8$)

 $\bar{D}_2^*(2460)^0$ modes are charge conjugates of modes below.

$D_2^*(2460)^0$ DECAY MODES	Fraction (Γ_i/Γ)	ρ (MeV/c)
$D^+ \pi^-$	seen	505
$D^*(2010)^+ \pi^-$	seen	389
$D^0 \pi^+ \pi^-$	not seen	462
$D^{*0} \pi^+ \pi^-$	not seen	324

 $D_2^*(2460)^\pm$

$$I(J^P) = \frac{1}{2}(2^+)$$

 $J^P = 2^+$ assignment strongly favored.

Mass $m = 2465.4 \pm 1.3$ MeV ($S = 3.1$)
 $m_{D_2^*(2460)^\pm} - m_{D_2^*(2460)^0} = 2.4 \pm 1.7$ MeV
 Full width $\Gamma = 46.7 \pm 1.2$ MeV

 $D_2^*(2460)^\mp$ modes are charge conjugates of modes below.

$D_2^*(2460)^\pm$ DECAY MODES	Fraction (Γ_i/Γ)	ρ (MeV/c)
$D^0 \pi^+$	seen	513
$D^{*0} \pi^+$	seen	396
$D^+ \pi^+ \pi^-$	not seen	462
$D^{*+} \pi^+ \pi^-$	not seen	326

**CHARMED, STRANGE MESONS
($C = S = \pm 1$)** $D_s^+ = c\bar{s}$, $D_s^- = \bar{c}s$, similarly for D_s^{*} 's **D_s^\pm**

$$I(J^P) = 0(0^-)$$

Mass $m = 1968.34 \pm 0.07$ MeV
 $m_{D_s^\pm} - m_{D^\pm} = 98.69 \pm 0.05$ MeV
 Mean life $\tau = (504 \pm 4) \times 10^{-15}$ s ($S = 1.2$)
 $c\tau = 151.2$ μm

CP-violating decay-rate asymmetries

$$\begin{aligned}
 A_{CP}(\mu^\pm \nu) &= (5 \pm 6)\% \\
 A_{CP}(K^\pm K_S^0) &= (0.09 \pm 0.26)\% \\
 A_{CP}(K^\pm K_L^0) \text{ in } D_s^\pm \rightarrow K^\pm K_L^0 &= (-1.1 \pm 2.7) \times 10^{-2} \\
 A_{CP}(K^+ K^- \pi^\pm) &= (-0.5 \pm 0.9)\% \\
 A_{CP}(\phi \pi^\pm) &= (-0.38 \pm 0.27)\% \\
 A_{CP}(K^\pm K_S^0 \pi^0) &= (-2 \pm 6)\% \\
 A_{CP}(2K_S^0 \pi^\pm) &= (3 \pm 5)\% \\
 A_{CP}(K^+ K^- \pi^\pm \pi^0) &= (0.0 \pm 3.0)\% \\
 A_{CP}(K^\pm K_S^0 \pi^+ \pi^-) &= (-6 \pm 5)\% \\
 A_{CP}(K_S^0 K^\mp 2\pi^\pm) &= (4.1 \pm 2.8)\% \\
 A_{CP}(\pi^+ \pi^- \pi^\pm) &= (-0.7 \pm 3.1)\% \\
 A_{CP}(\pi^\pm \eta) &= (1.1 \pm 3.1)\% \\
 A_{CP}(\pi^\pm \eta') &= (-0.9 \pm 0.5)\% \\
 A_{CP}(\eta \pi^\pm \pi^0) &= (-1 \pm 4)\% \\
 A_{CP}(\eta' \pi^\pm \pi^0) &= (0 \pm 8)\% \\
 A_{CP}(K^\pm \pi^0) &= (-27 \pm 24)\% \\
 A_{CP}(\bar{K}^0 / K^0 \pi^\pm) &= (0.4 \pm 0.5)\% \\
 A_{CP}(K_S^0 \pi^\pm) &= (0.20 \pm 0.18)\% \\
 A_{CP}(K^\pm \pi^+ \pi^-) &= (4 \pm 5)\% \\
 A_{CP}(K^\pm \eta) &= (9 \pm 15)\% \\
 A_{CP}(K^\pm \eta'(958)) &= (6 \pm 19)\%
 \end{aligned}$$

CP violating asymmetries of P-odd (T-odd) moments

$$A_T(K_S^0 K^\pm \pi^+ \pi^-) = (-14 \pm 8) \times 10^{-3} [11]$$

 $D_s^+ \rightarrow \phi \ell^+ \nu_\ell$ form factors

$$\begin{aligned}
 r_2 &= 0.84 \pm 0.11 \quad (S = 2.4) \\
 r_V &= 1.80 \pm 0.08 \\
 \Gamma_L/\Gamma_T &= 0.72 \pm 0.18 \\
 f_+(0) |V_{cs}| \text{ in } D_s^+ \rightarrow \eta e^+ \nu_e &= 0.446 \pm 0.007 \\
 f_+(0) |V_{cs}| \text{ in } D_s^+ \rightarrow \eta' e^+ \nu_e &= 0.48 \pm 0.05
 \end{aligned}$$

CP violating asymmetries of P-odd (T-odd) moments

$$\begin{aligned}
 f_+(0) |V_{cd}| \text{ in } D_s^+ \rightarrow K^0 e^+ \nu_e &= 0.162 \pm 0.019 \\
 r_V \equiv V(0)/A_1(0) \text{ in } D_s^+ \rightarrow K^*(892)^0 e^+ \nu_e &= 1.7 \pm 0.4 \\
 r_2 \equiv A_2(0)/A_1(0) \text{ in } D_s^+ \rightarrow K^*(892)^0 e^+ \nu_e &= 0.77 \pm 0.29 \\
 f_{D_s^+}^+ |V_{cs}| \text{ in } D_s^+ \rightarrow \mu^+ \nu_\mu &= 246 \pm 5 \text{ MeV}
 \end{aligned}$$

Unless otherwise noted, the branching fractions for modes with a resonance in the final state include all the decay modes of the resonance. D_s^- modes are charge conjugates of the modes below.

D_s^\pm DECAY MODES	Fraction (Γ_i/Γ)	Scale factor/ Confidence level	ρ (MeV/c)
Inclusive modes			
e^+ semileptonic	[eee] (6.5 \pm 0.4) %		—
π^+ anything	(119.3 \pm 1.4) %		—
π^- anything	(43.2 \pm 0.9) %		—
π^0 anything	(123 \pm 7) %		—
K^- anything	(18.7 \pm 0.5) %		—
K^+ anything	(28.9 \pm 0.7) %		—
K_S^0 anything	(19.0 \pm 1.1) %		—
η anything	[fff] (29.9 \pm 2.8) %		—
ω anything	(6.1 \pm 1.4) %		—
η' anything	[ggg] (10.3 \pm 1.4) %	S=1.1	—
$f_0(980)$ anything, $f_0 \rightarrow \pi^+ \pi^-$	< 1.3 %	CL=90%	—
ϕ anything	(15.7 \pm 1.0) %		—
$K^+ K^-$ anything	(15.8 \pm 0.7) %		—
$K_S^0 K^+$ anything	(5.8 \pm 0.5) %		—
$K_S^0 K^-$ anything	(1.9 \pm 0.4) %		—
$2K_S^0$ anything	(1.70 \pm 0.32) %		—
$2K^+$ anything	< 2.6 $\times 10^{-3}$	CL=90%	—
$2K^-$ anything	< 6 $\times 10^{-4}$	CL=90%	—

Leptonic and semileptonic modes

$e^+ \nu_e$	< 8.3 $\times 10^{-5}$	CL=90%	984
$\mu^+ \nu_\mu$	(5.49 \pm 0.16) $\times 10^{-3}$		981
$\tau^+ \nu_\tau$	(5.48 \pm 0.23) %		182
$\gamma e^+ \nu_e$	< 1.3 $\times 10^{-4}$	CL=90%	984
$K^+ K^- e^+ \nu_e$	—		851
$\phi e^+ \nu_e$	[hhh] (2.39 \pm 0.16) %	S=1.3	720
$\phi \mu^+ \nu_\mu$	(1.9 \pm 0.5) %		715

Meson Summary Table

$\eta e^+ \nu_e + \eta'(958) e^+ \nu_e$	[hhh]	(3.03±0.24) %	-	
$\eta e^+ \nu_e$	[hhh]	(2.32±0.08) %	908	
$\eta'(958) e^+ \nu_e$	[hhh]	(8.0 ±0.7) × 10 ⁻³	751	
$\eta \mu^+ \nu_\mu$		(2.4 ±0.5) %	905	
$\eta'(958) \mu^+ \nu_\mu$		(1.1 ±0.5) %	747	
$\omega e^+ \nu_e$	[iii]	< 2.0 × 10 ⁻³	829	CL=90%
$K^0 e^+ \nu_e$		(3.4 ±0.4) × 10 ⁻³	921	
$K^*(892)^0 e^+ \nu_e$	[hhh]	(2.15±0.28) × 10 ⁻³	S=1.1 782	
Hadronic modes with a $K\bar{K}$ pair				
$K^+ K_S^0$		(1.46±0.04) %	S=1.1 850	
$K^+ K^0$		(1.49±0.06) %	850	
$K^+ \bar{K}^0$		(2.95±0.14) %	850	
$K^+ K^- \pi^+$	[nn]	(5.39±0.15) %	S=1.2 805	
$\phi \pi^+$	[hhh, jii]	(4.5 ±0.4) %	712	
$\phi \pi^+, \phi \rightarrow K^+ K^-$	[jii]	(2.24±0.08) %	712	
$K^+ \bar{K}^*(892)^0, \bar{K}^{*0} \rightarrow$		(2.58±0.08) %	416	
$K^- \pi^+$				
$f_0(980) \pi^+, f_0 \rightarrow K^+ K^-$		(1.14±0.31) %	732	
$f_0(1370) \pi^+, f_0 \rightarrow K^+ K^-$		(7 ±5) × 10 ⁻⁴	-	
$f_0(1710) \pi^+, f_0 \rightarrow K^+ K^-$		(6.6 ±2.8) × 10 ⁻⁴	198	
$K^+ \bar{K}_0^*(1430)^0, \bar{K}_0^{*0} \rightarrow$		(1.8 ±0.4) × 10 ⁻³	218	
$K^+ K_S^0 \pi^0$		(1.52±0.22) %	805	
$2K_S^0 \pi^+$		(7.7 ±0.6) × 10 ⁻³	802	
$K^0 \bar{K}^0 \pi^+$		-	802	
$K^*(892)^+ \bar{K}^0$	[hhh]	(5.4 ±1.2) %	683	
$K^+ K^- \pi^+ \pi^0$		(6.2 ±0.6) %	S=1.1 748	
$\phi \rho^+$	[hhh]	(8.4 ^{+1.9} _{-2.3}) %	401	
$K_S^0 K^- 2\pi^+$		(1.65±0.10) %	744	
$K^*(892)^+ \bar{K}^*(892)^0$	[hhh]	(7.2 ±2.6) %	417	
$K^+ K_S^0 \pi^+ \pi^-$		(9.9 ±0.8) × 10 ⁻³	744	
$K^+ K^- 2\pi^+ \pi^-$		(8.6 ±1.5) × 10 ⁻³	673	
$\phi 2\pi^+ \pi^-$	[hhh]	(1.21±0.16) %	640	
$\phi \rho^0 \pi^+, \phi \rightarrow K^+ K^-$		(6.5 ±1.3) × 10 ⁻³	181	
$\phi a_1(1260)^+, \phi \rightarrow$		(7.4 ±1.2) × 10 ⁻³	†	
$K^+ K^-, a_1^+ \rightarrow$				
$\rho^0 \pi^+$				
$\phi 2\pi^+ \pi^- \text{ non-}\rho, \phi \rightarrow$		(1.8 ±0.7) × 10 ⁻³	-	
$K^+ K^-$				
$K^+ K^- \rho^0 \pi^+ \text{ non-}\phi$	< 2.6	× 10 ⁻⁴	CL=90%	249
$K^+ K^- 2\pi^+ \pi^- \text{ nonresonant}$	(9 ±7)	× 10 ⁻⁴	673	
$2K_S^0 2\pi^+ \pi^-$	(8.4 ±3.5)	× 10 ⁻⁴	669	
Hadronic modes without K's				
$\pi^+ \pi^0$	< 3.4	× 10 ⁻⁴	CL=90%	975
$2\pi^+ \pi^-$	(1.08±0.04) %	S=1.1	959	
$\rho^0 \pi^+$	(1.9 ±1.2) × 10 ⁻⁴	825		
$\pi^+ (\pi^+ \pi^-)_{S\text{-wave}}$	[kkk]	(9.0 ±0.4) × 10 ⁻³	959	
$f_2(1270) \pi^+, f_2 \rightarrow \pi^+ \pi^-$		(1.09±0.20) × 10 ⁻³	559	
$\rho(1450)^0 \pi^+, \rho^0 \rightarrow \pi^+ \pi^-$		(3.0 ±1.9) × 10 ⁻⁴	421	
$\pi^+ 2\pi^0$		(6.5 ±1.3) × 10 ⁻³	961	
$2\pi^+ \pi^- \pi^0$		-	935	
$\eta \pi^+$	[hhh]	(1.68±0.10) %	S=1.2 902	
$\omega \pi^+$	[hhh]	(1.92±0.30) × 10 ⁻³	822	
$3\pi^+ 2\pi^-$		(7.9 ±0.8) × 10 ⁻³	899	
$2\pi^+ \pi^- 2\pi^0$		-	902	
$\eta \rho^+$	[hhh]	(8.9 ±0.8) %	724	
$\eta \pi^+ \pi^0$		(9.5 ±0.5) %	885	
$\eta (\pi^+ \pi^0)_{P\text{-wave}}$		(5.1 ±3.1) × 10 ⁻³	885	
$a_0(980)^+ \pi^0, a_0(980)^+ \rightarrow \eta \pi^+$		(2.2 ±0.4) %	-	
$\omega \pi^+ \pi^0$	[hhh]	(2.8 ±0.7) %	802	
$3\pi^+ 2\pi^- \pi^0$		(4.9 ±3.2) %	856	
$\omega 2\pi^+ \pi^-$	[hhh]	(1.6 ±0.5) %	766	
$\eta'(958) \pi^+$	[ggg, hhh]	(3.94±0.25) %	743	
$3\pi^+ 2\pi^- 2\pi^0$		-	803	
$\omega \eta \pi^+$	[hhh]	< 2.13 %	CL=90%	654
$\eta'(958) \rho^+$	[ggg, hhh]	(5.8 ±1.5) %	465	
$\eta'(958) \pi^+ \pi^0$		(5.6 ±0.8) %	720	
$\eta'(958) \pi^+ \pi^0 \text{ nonresonant}$	< 5.1	%	CL=90%	720
Modes with one or three K's				
$K^+ \pi^0$	(6.1 ±2.1)	× 10 ⁻⁴	917	
$K_S^0 \pi^+$	(1.19±0.05) × 10 ⁻³	916		
$K^+ \eta$	[hhh]	(1.72±0.34) × 10 ⁻³	835	
$K^+ \omega$	[hhh]	(8.7 ±2.5) × 10 ⁻⁴	741	
$K^+ \eta'(958)$	[hhh]	(1.7 ±0.5) × 10 ⁻³	646	

$K^+ \pi^+ \pi^-$	(6.5 ±0.4) × 10 ⁻³	900		
$K^+ \rho^0$	(2.5 ±0.4) × 10 ⁻³	745		
$K^+ \rho(1450)^0, \rho^0 \rightarrow \pi^+ \pi^-$	(6.9 ±2.4) × 10 ⁻⁴	-		
$K^*(892)^0 \pi^+, K^{*0} \rightarrow$	(1.41±0.24) × 10 ⁻³	775		
$K^+ \pi^-$				
$K^*(1410)^0 \pi^+, K^{*0} \rightarrow$	(1.23±0.28) × 10 ⁻³	-		
$K^+ \pi^-$				
$K^*(1430)^0 \pi^+, K^{*0} \rightarrow$	(5.0 ±3.5) × 10 ⁻⁴	-		
$K^+ \pi^-$				
$K^+ \pi^+ \pi^- \text{ nonresonant}$	(1.03±0.34) × 10 ⁻³	900		
$K^0 \pi^+ \pi^0$	(1.00±0.18) %	899		
$K_S^0 2\pi^+ \pi^-$	(3.0 ±1.1) × 10 ⁻³	870		
$K^+ \omega \pi^0$	[hhh] < 8.2	× 10 ⁻³	CL=90%	
$K^+ \omega \pi^+ \pi^-$	[hhh] < 5.4	× 10 ⁻³	CL=90%	
$K^+ \omega \eta$	[hhh] < 7.9	× 10 ⁻³	CL=90%	
$2K^+ K^-$	(2.16±0.20) × 10 ⁻⁴	628		
$\phi K^+, \phi \rightarrow K^+ K^-$	(8.8 ±2.0) × 10 ⁻⁵	-		
Doubly Cabibbo-suppressed modes				
$2K^+ \pi^-$	(1.28±0.04) × 10 ⁻⁴	805		
$K^+ K^*(892)^0, K^{*0} \rightarrow$	(6.0 ±3.4) × 10 ⁻⁵	-		
$K^+ \pi^-$				
Baryon-antibaryon mode				
$p\bar{n}$	(1.22±0.11) × 10 ⁻³	295		
$p\bar{p} e^+ \nu_e$	< 2.0	× 10 ⁻⁴	CL=90%	
$\Delta C = 1$ weak neutral current (C1) modes, Lepton family number (LF), or Lepton number (L) violating modes				
$\pi^+ e^+ e^-$	[ss] < 1.3	× 10 ⁻⁵	CL=90%	
$\pi^+ \phi, \phi \rightarrow e^+ e^-$	[rr] (6 ⁺⁸ ₋₄)	× 10 ⁻⁶	-	
$\pi^+ \mu^+ \mu^-$	[ss] < 4.1	× 10 ⁻⁷	CL=90%	
$K^+ e^+ e^-$	C1 < 3.7	× 10 ⁻⁶	CL=90%	
$K^+ \mu^+ \mu^-$	C1 < 2.1	× 10 ⁻⁵	CL=90%	
$K^*(892)^+ \mu^+ \mu^-$	C1 < 1.4	× 10 ⁻³	CL=90%	
$\pi^+ e^+ \mu^-$	LF < 1.2	× 10 ⁻⁵	CL=90%	
$\pi^+ e^- \mu^+$	LF < 2.0	× 10 ⁻⁵	CL=90%	
$K^+ e^+ \mu^-$	LF < 1.4	× 10 ⁻⁵	CL=90%	
$K^+ e^- \mu^+$	LF < 9.7	× 10 ⁻⁶	CL=90%	
$\pi^- 2e^+$	L < 4.1	× 10 ⁻⁶	CL=90%	
$\pi^- 2\mu^+$	L < 1.2	× 10 ⁻⁷	CL=90%	
$\pi^- e^+ \mu^+$	L < 8.4	× 10 ⁻⁶	CL=90%	
$K^- 2e^+$	L < 5.2	× 10 ⁻⁶	CL=90%	
$K^- 2\mu^+$	L < 1.3	× 10 ⁻⁵	CL=90%	
$K^- e^+ \mu^+$	L < 6.1	× 10 ⁻⁶	CL=90%	
$K^*(892)^- 2\mu^+$	L < 1.4	× 10 ⁻³	CL=90%	

 $D_s^{*\pm}$

$$I(J^P) = 0(??)$$

 J^P is natural, width and decay modes consistent with 1^- .

Mass $m = 2112.2 \pm 0.4$ MeV

$m_{D_s^{*\pm}} - m_{D_s^\pm} = 143.8 \pm 0.4$ MeV

Full width $\Gamma < 1.9$ MeV, CL = 90%

 D_s^{*-} modes are charge conjugates of the modes below. **D_s^{*+} DECAY MODES**

Decay Mode	Fraction (Γ_i/Γ)	ρ (MeV/c)
$D_s^{*+} \gamma$	(93.5±0.7) %	139
$D_s^{*+} \pi^0$	(5.8±0.7) %	48
$D_s^{*+} e^+ e^-$	(6.7±1.6) × 10 ⁻³	139

 $D_{s0}^{*+}(2317)^\pm$

$$I(J^P) = 0(0^+)$$

 J, P need confirmation. J^P is natural, low mass consistent with 0^+ .

Mass $m = 2317.8 \pm 0.5$ MeV

$m_{D_{s0}^{*+}(2317)^\pm} - m_{D_s^\pm} = 349.4 \pm 0.5$ MeV

Full width $\Gamma < 3.8$ MeV, CL = 95%

 $D_{s0}^{*+}(2317)^-$ modes are charge conjugates of modes below. **$D_{s0}^{*+}(2317)^\pm$ DECAY MODES**

Decay Mode	Fraction (Γ_i/Γ)	Confidence level	ρ (MeV/c)
$D_{s0}^{*+} \pi^0$	(100 ₋₂₀ ±0) %		298
$D_{s0}^{*+} \gamma$	< 5 %	90%	323
$D_{s0}^{*+}(2112)^+ \gamma$	< 6 %	90%	-

Meson Summary Table

$D_s^+ \gamma \gamma$	< 18	%	95%	323
$D_s^*(2112)^+ \pi^0$	< 11	%	90%	–
$D_s^+ \pi^+ \pi^-$	< 4	$\times 10^{-3}$	90%	194
$D_s^+ \pi^0 \pi^0$	not seen			205

$D_{s1}(2460)^\pm$

$$I(J^P) = 0(1^+)$$

Mass $m = 2459.5 \pm 0.6$ MeV ($S = 1.1$)
 $m_{D_{s1}(2460)^\pm} - m_{D_s^\pm} = 347.3 \pm 0.7$ MeV ($S = 1.2$)
 $m_{D_{s1}(2460)^\pm} - m_{D_s^\pm} = 491.2 \pm 0.6$ MeV ($S = 1.1$)
 Full width $\Gamma < 3.5$ MeV, CL = 95%

$D_{s1}(2460)^-$ modes are charge conjugates of the modes below.

$D_{s1}(2460)^+$ DECAY MODES	Fraction (Γ_i/Γ)	Scale factor/ Confidence level	ρ (MeV/c)
$D_s^{*+} \pi^0$	(48 ± 11) %		297
$D_s^+ \gamma$	(18 ± 4) %		442
$D_s^+ \pi^+ \pi^-$	(4.3 ± 1.3) %	S=1.1	363
$D_s^{*+} \gamma$	< 8 %	CL=90%	323
$D_{s0}^*(2317)^+ \gamma$	(3.7 $^{+5.0}_{-2.4}$) %		138

$D_{s1}(2536)^\pm$

$$I(J^P) = 0(1^+)$$

J, P need confirmation.

Mass $m = 2535.11 \pm 0.06$ MeV
 Full width $\Gamma = 0.92 \pm 0.05$ MeV

$D_{s1}(2536)^-$ modes are charge conjugates of the modes below.

$D_{s1}(2536)^+$ DECAY MODES	Fraction (Γ_i/Γ)	Confidence level	ρ (MeV/c)
$D^*(2010)^+ K^0$	0.85 ± 0.12		149
$(D^*(2010)^+ K^0)_{S\text{-wave}}$	0.61 ± 0.09		149
$D^+ \pi^- K^+$	0.028 ± 0.005		176
$D^*(2007)^0 K^+$	DEFINED AS 1		167
$D^+ K^0$	< 0.34	90%	381
$D^0 K^+$	< 0.12	90%	391
$D_s^{*+} \gamma$	possibly seen		388
$D_s^+ \pi^+ \pi^-$	seen		437

$D_{s2}^*(2573)$

$$I(J^P) = 0(2^+)$$

J^P is natural, width and decay modes consistent with 2^+ .

Mass $m = 2569.1 \pm 0.8$ MeV ($S = 2.4$)
 Full width $\Gamma = 16.9 \pm 0.7$ MeV

$D_{s2}^*(2573)^-$ modes are charge conjugates of the modes below.

$D_{s2}^*(2573)^+$ DECAY MODES	Fraction (Γ_i/Γ)	ρ (MeV/c)
$D^0 K^+$	seen	431
$D^*(2007)^0 K^+$	not seen	238

$D_{s1}^*(2700)^\pm$

$$I(J^P) = 0(1^-)$$

Mass $m = 2708.3^{+4.0}_{-3.4}$ MeV
 Full width $\Gamma = 120 \pm 11$ MeV

BOTTOM MESONS ($B = \pm 1$)

$B^+ = u\bar{b}, B^0 = d\bar{b}, \bar{B}^0 = \bar{d}b, B^- = \bar{u}b$, similarly for B^{*s}

B-particle organization

Many measurements of B decays involve admixtures of B hadrons. Previously we arbitrarily included such admixtures

in the B^\pm section, but because of their importance we have created two new sections: “ B^\pm/B^0 Admixture” for $\Upsilon(4S)$ results and “ $B^\pm/B^0/B_s^0/b$ -baryon Admixture” for results at higher energies. Most inclusive decay branching fractions and χ_b at high energy are found in the Admixture sections. $B^0-\bar{B}^0$ mixing data are found in the B^0 section, while $B_s^0-\bar{B}_s^0$ mixing data and $B-\bar{B}$ mixing data for a B^0/B_s^0 admixture are found in the B_s^0 section. CP -violation data are found in the B^\pm, B^0 , and B^\pm/B^0 Admixture sections. b -baryons are found near the end of the Baryon section.

The organization of the B sections is now as follows, where bullets indicate particle sections and brackets indicate reviews.

- B^\pm
mass, mean life, CP violation, branching fractions
- B^0
mass, mean life, $B^0-\bar{B}^0$ mixing, CP violation, branching fractions
- B^\pm/B^0 Admixtures
 CP violation, branching fractions
- $B^\pm/B^0/B_s^0/b$ -baryon Admixtures
mean life, production fractions, branching fractions
- B^*
mass
- $B_1(5721)^+$
mass
- $B_1(5721)^0$
mass
- $B_2^*(5747)^+$
mass
- $B_2^*(5747)^0$
mass
- $B_s^*(5970)^+$
mass
- $B_s^*(5970)^0$
mass
- B_s^0
mass, mean life, $B_s^0-\bar{B}_s^0$ mixing, CP violation, branching fractions
- B_s^*
mass
- $B_{s1}(5830)^0$
mass
- $B_{s2}^*(5840)^0$
mass
- B_c^\pm
mass, mean life, branching fractions

At the end of Baryon Listings:

- Λ_b
mass, mean life, branching fractions
- $\Lambda_b(5912)^0$
mass, mean life
- $\Lambda_b(5920)^0$
mass, mean life
- Σ_b
mass
- Σ_b^*
mass
- Ξ_b^0, Ξ_b^-
mass, mean life, branching fractions
- $\Xi_b'(5935)^-$
mass

- $\Xi_b(5945)^0$
mass
- $\Xi_b^*(5955)^-$
mass
- Ω_b^-
mass, branching fractions
- b -baryon Admixture
mean life, branching fractions

B[±]

$$I(J^P) = \frac{1}{2}(0^-)$$

I, J, P need confirmation. Quantum numbers shown are quark-model predictions.

Mass $m_{B^\pm} = 5279.34 \pm 0.12$ MeV
 Mean life $\tau_{B^\pm} = (1.638 \pm 0.004) \times 10^{-12}$ s
 $c\tau = 491.1 \mu\text{m}$

CP violation

$A_{CP}(B^+ \rightarrow J/\psi(1S)K^+) = (1.8 \pm 3.0) \times 10^{-3}$ (S = 1.5)	$A_{CP}(B^+ \rightarrow [K^+ K^-]_D K^+ \pi^- \pi^+) = -0.04 \pm 0.06$
$A_{CP}(B^+ \rightarrow J/\psi(1S)\pi^+) = (1.8 \pm 1.2) \times 10^{-2}$ (S = 1.3)	$A_{CP}(B^+ \rightarrow [\pi^+ \pi^-]_D K^+ \pi^- \pi^+) = -0.05 \pm 0.10$
$A_{CP}(B^+ \rightarrow J/\psi \rho^+) = -0.05 \pm 0.05$	$A_{CP}(B^+ \rightarrow [K^- \pi^+]_D K^+ \pi^- \pi^+) = 0.013 \pm 0.023$
$A_{CP}(B^+ \rightarrow J/\psi K^*(892)^+) = -0.048 \pm 0.033$	$A_{CP}(B^+ \rightarrow [K^+ K^-]_D \pi^+ \pi^- \pi^+) = -0.019 \pm 0.015$
$A_{CP}(B^+ \rightarrow \eta_c K^+) = 0.01 \pm 0.07$ (S = 2.2)	$A_{CP}(B^+ \rightarrow [\pi^+ \pi^-]_D \pi^+ \pi^- \pi^+) = -0.013 \pm 0.019$
$A_{CP}(B^+ \rightarrow \psi(2S)\pi^+) = 0.03 \pm 0.06$	$A_{CP}(B^+ \rightarrow [K^- \pi^+]_D \pi^+ \pi^- \pi^+) = -0.002 \pm 0.011$
$A_{CP}(B^+ \rightarrow \psi(2S)K^+) = 0.012 \pm 0.020$ (S = 1.5)	$A_{CP}(B^+ \rightarrow \bar{D}^{*0} \pi^+) = 0.0010 \pm 0.0028$
$A_{CP}(B^+ \rightarrow \psi(2S)K^*(892)^+) = 0.08 \pm 0.21$	$A_{CP}(B^+ \rightarrow (D_{CP(+1)}^*)^0 \pi^+) = 0.016 \pm 0.010$ (S = 1.2)
$A_{CP}(B^+ \rightarrow \chi_{c1}(1P)\pi^+) = 0.07 \pm 0.18$	$A_{CP}(B^+ \rightarrow (D_{CP(-1)}^*)^0 \pi^+) = -0.09 \pm 0.05$
$A_{CP}(B^+ \rightarrow \chi_{c0} K^+) = -0.20 \pm 0.18$ (S = 1.5)	$A_{CP}(B^+ \rightarrow D^{*0} K^+) = -0.001 \pm 0.011$ (S = 1.1)
$A_{CP}(B^+ \rightarrow \chi_{c1} K^+) = -0.009 \pm 0.033$	$A_{CP}(B^+ \rightarrow D_{CP(+1)}^{*0} K^+) = -0.11 \pm 0.08$ (S = 2.7)
$A_{CP}(B^+ \rightarrow \chi_{c1} K^*(892)^+) = 0.5 \pm 0.5$	$A_{CP}(B^+ \rightarrow D_{CP(-1)}^{*0} K^+) = 0.07 \pm 0.10$
$A_{CP}(B^+ \rightarrow D^0 \ell^+ \nu_\ell) = (-0.14 \pm 0.20) \times 10^{-2}$	$A_{CP}(B^+ \rightarrow D_{CP(+1)} K^*(892)^+) = 0.08 \pm 0.06$
$A_{CP}(B^+ \rightarrow \bar{D}^0 \pi^+) = -0.007 \pm 0.007$	$A_{CP}(B^+ \rightarrow D_{CP(-1)} K^*(892)^+) = -0.23 \pm 0.22$
$A_{CP}(B^+ \rightarrow D_{CP(+1)} \pi^+) = -0.0080 \pm 0.0026$	$A_{CP}(B^+ \rightarrow D_S^+ \phi) = 0.0 \pm 0.4$
$A_{CP}(B^+ \rightarrow D_{CP(-1)} \pi^+) = 0.017 \pm 0.026$	$A_{CP}(B^+ \rightarrow D_S^+ \bar{D}^0) = (-0.4 \pm 0.7)\%$
$A_{CP}([K^\mp \pi^\pm \pi^\pm \pi^-]_D \pi^+) = 0.02 \pm 0.05$	$A_{CP}(B^+ \rightarrow D_S^{*+} \bar{D}^{*0}) = -0.15 \pm 0.11$
$A_{CP}(B^+ \rightarrow [\pi^+ \pi^+ \pi^- \pi^-]_D K^+) = 0.10 \pm 0.04$	$A_{CP}(B^+ \rightarrow D_S^{*+} \bar{D}^0) = -0.06 \pm 0.13$
$A_{CP}(B^+ \rightarrow [\pi^+ \pi^- \pi^+ \pi^-]_D K^*(892)^+) = 0.02 \pm 0.11$	$A_{CP}(B^+ \rightarrow D^+ \bar{D}^{*0}) = 0.13 \pm 0.18$
$A_{CP}(B^+ \rightarrow \bar{D}^0 K^+) = -0.017 \pm 0.005$	$A_{CP}(B^+ \rightarrow D^+ \bar{D}^0) = 0.016 \pm 0.025$
$A_{CP}([K^\mp \pi^\pm \pi^\pm \pi^-]_D K^+) = -0.31 \pm 0.11$	$A_{CP}(B^+ \rightarrow K_S^0 \pi^+) = -0.017 \pm 0.016$
$A_{CP}(B^+ \rightarrow [\pi^+ \pi^+ \pi^- \pi^-]_D \pi^+) = (-4 \pm 8) \times 10^{-3}$	$A_{CP}(B^+ \rightarrow K^+ \pi^0) = 0.037 \pm 0.021$
$A_{CP}(B^+ \rightarrow [K^- \pi^+]_D K^+) = -0.58 \pm 0.21$	$A_{CP}(B^+ \rightarrow \eta' K^+) = 0.004 \pm 0.011$
$A_{CP}(B^+ \rightarrow [K^- \pi^+ \pi^0]_D K^+) = 0.07 \pm 0.30$ (S = 1.5)	$A_{CP}(B^+ \rightarrow \eta' K^*(892)^+) = -0.26 \pm 0.27$
$A_{CP}(B^+ \rightarrow [K^+ K^- \pi^0]_D K^+) = 0.30 \pm 0.20$	$A_{CP}(B^+ \rightarrow \eta' K_S^0(1430)^+) = 0.06 \pm 0.20$
$A_{CP}(B^+ \rightarrow [\pi^+ \pi^- \pi^0]_D K^+) = 0.05 \pm 0.09$	$A_{CP}(B^+ \rightarrow \eta' K_S^0(1430)^+) = 0.15 \pm 0.13$
$A_{CP}(B^+ \rightarrow \bar{D}^0 K^*(892)^+) = -0.007 \pm 0.019$	$A_{CP}(B^+ \rightarrow \eta K^+) = -0.37 \pm 0.08$
$A_{CP}(B^+ \rightarrow [K^- \pi^+]_D K^*(892)^+) = -0.75 \pm 0.16$	$A_{CP}(B^+ \rightarrow \eta K^*(892)^+) = 0.02 \pm 0.06$
$A_{CP}(B^+ \rightarrow [K^- \pi^+ \pi^- \pi^+]_D K^*(892)^+) = -0.45 \pm 0.25$	$A_{CP}(B^+ \rightarrow \eta K_S^0(1430)^+) = 0.05 \pm 0.13$
$A_{CP}(B^+ \rightarrow [K^- \pi^+]_D \pi^+) = 0.00 \pm 0.09$	$A_{CP}(B^+ \rightarrow \eta K_S^0(1430)^+) = -0.45 \pm 0.30$
$A_{CP}(B^+ \rightarrow [K^- \pi^+ \pi^0]_D \pi^+) = 0.35 \pm 0.16$	$A_{CP}(B^+ \rightarrow \omega K^+) = -0.02 \pm 0.04$
$A_{CP}(B^+ \rightarrow [K^+ K^- \pi^0]_D \pi^+) = -0.03 \pm 0.04$	$A_{CP}(B^+ \rightarrow \omega K^{*+}) = 0.29 \pm 0.35$
$A_{CP}(B^+ \rightarrow [\pi^+ \pi^- \pi^0]_D \pi^+) = -0.016 \pm 0.020$	$A_{CP}(B^+ \rightarrow \omega(K\pi)_0^{*+}) = -0.10 \pm 0.09$
$A_{CP}(B^+ \rightarrow [K^- \pi^+]_{(D\pi)} \pi^+) = -0.09 \pm 0.27$	$A_{CP}(B^+ \rightarrow \omega K_S^0(1430)^+) = 0.14 \pm 0.15$
$A_{CP}(B^+ \rightarrow [K^- \pi^+]_{(D\gamma)} \pi^+) = -0.7 \pm 0.6$	$A_{CP}(B^+ \rightarrow K^{*0} \pi^+) = -0.04 \pm 0.09$ (S = 2.1)
$A_{CP}(B^+ \rightarrow [K^- \pi^+]_{(D\pi)} K^+) = 0.8 \pm 0.4$	$A_{CP}(B^+ \rightarrow K^*(892)^+ \pi^0) = -0.39 \pm 0.21$ (S = 1.6)
$A_{CP}(B^+ \rightarrow [K^- \pi^+]_{(D\gamma)} K^+) = 0.4 \pm 1.0$	$A_{CP}(B^+ \rightarrow K^+ \pi^- \pi^+) = 0.027 \pm 0.008$
$A_{CP}(B^+ \rightarrow [\pi^+ \pi^- \pi^0]_D K^+) = -0.02 \pm 0.15$	$A_{CP}(B^+ \rightarrow K^+ K^- K^+ \text{nonresonant}) = 0.06 \pm 0.05$
$A_{CP}(B^+ \rightarrow [K_S^0 K^+ \pi^-]_D K^+) = 0.04 \pm 0.09$	$A_{CP}(B^+ \rightarrow f(980)^0 K^+) = -0.08 \pm 0.09$
$A_{CP}(B^+ \rightarrow [K_S^0 K^- \pi^+]_D K^+) = 0.23 \pm 0.13$	$A_{CP}(B^+ \rightarrow f_2(1270) K^+) = -0.68^{+0.19}_{-0.17}$
$A_{CP}(B^+ \rightarrow [K_S^0 K^- \pi^+]_D \pi^+) = -0.052 \pm 0.034$	$A_{CP}(B^+ \rightarrow f_0(1500) K^+) = 0.28 \pm 0.30$
$A_{CP}(B^+ \rightarrow [K_S^0 K^+ \pi^-]_D \pi^+) = -0.025 \pm 0.026$	$A_{CP}(B^+ \rightarrow f_2'(1525)^0 K^+) = -0.08^{+0.05}_{-0.04}$
$A_{CP}(B^+ \rightarrow [K^*(892)^- K^+]_D K^+) = 0.03 \pm 0.11$	$A_{CP}(B^+ \rightarrow \rho^0 K^+) = 0.37 \pm 0.10$
$A_{CP}(B^+ \rightarrow [K^*(892)^+ K^-]_D K^+) = 0.34 \pm 0.21$	$A_{CP}(B^+ \rightarrow K^0 \pi^+ \pi^0) = 0.07 \pm 0.06$
$A_{CP}(B^+ \rightarrow [K^*(892)^+ K^-]_D \pi^+) = -0.05 \pm 0.05$	$A_{CP}(B^+ \rightarrow K_S^0(1430)^0 \pi^+) = 0.061 \pm 0.032$
$A_{CP}(B^+ \rightarrow [K^*(892)^- K^+]_D \pi^+) = -0.012 \pm 0.030$	$A_{CP}(B^+ \rightarrow K_S^0(1430)^+ \pi^0) = 0.26^{+0.18}_{-0.14}$
$A_{CP}(B^+ \rightarrow D_{CP(+1)} K^+) = 0.120 \pm 0.014$ (S = 1.4)	$A_{CP}(B^+ \rightarrow K_S^0(1430)^0 \pi^+) = 0.05^{+0.29}_{-0.24}$
$A_{ADS}(B^+ \rightarrow D K^+) = -0.40 \pm 0.06$	$A_{CP}(B^+ \rightarrow K^+ \pi^0 \pi^0) = -0.06 \pm 0.07$
$A_{ADS}(B^+ \rightarrow D \pi^+) = 0.100 \pm 0.032$	$A_{CP}(B^+ \rightarrow K^0 \rho^+) = -0.03 \pm 0.15$
$A_{ADS}(B^+ \rightarrow [K^- \pi^+]_D K^+ \pi^- \pi^+) = -0.33 \pm 0.35$	$A_{CP}(B^+ \rightarrow K^{*+} \pi^+ \pi^-) = 0.07 \pm 0.08$
$A_{ADS}(B^+ \rightarrow [K^- \pi^+]_D \pi^+ \pi^- \pi^+) = -0.01 \pm 0.09$	$A_{CP}(B^+ \rightarrow \rho^0 K^*(892)^+) = 0.31 \pm 0.13$
$A_{CP}(B^+ \rightarrow D_{CP(-1)} K^+) = -0.10 \pm 0.07$	$A_{CP}(B^+ \rightarrow K^*(892)^+ f_0(980)) = -0.15 \pm 0.12$
	$A_{CP}(B^+ \rightarrow a_1^+ K^0) = 0.12 \pm 0.11$
	$A_{CP}(B^+ \rightarrow b_1^+ K^0) = -0.03 \pm 0.15$
	$A_{CP}(B^+ \rightarrow K^*(892)^0 \rho^+) = -0.01 \pm 0.16$
	$A_{CP}(B^+ \rightarrow b_1^0 K^+) = -0.46 \pm 0.20$
	$A_{CP}(B^+ \rightarrow K^0 K^+) = 0.04 \pm 0.14$
	$A_{CP}(B^+ \rightarrow K_S^0 K^+) = -0.21 \pm 0.14$
	$A_{CP}(B^+ \rightarrow K^+ K_S^0 K_S^0) = 0.025 \pm 0.031$
	$A_{CP}(B^+ \rightarrow K^+ K^- \pi^+) = -0.122 \pm 0.021$
	$A_{CP}(B^+ \rightarrow K^+ K^- \pi^+ \text{nonresonant}) = -0.11 \pm 0.06$
	$A_{CP}(B^+ \rightarrow K^+ \bar{K}^*(892)^0) = 0.12 \pm 0.10$
	$A_{CP}(B^+ \rightarrow K^+ \bar{K}_0^*(1430)^0) = 0.10 \pm 0.17$
	$A_{CP}(B^+ \rightarrow \phi \pi^+) = 0.1 \pm 0.5$
	$A_{CP}(B^+ \rightarrow \pi^+(K^+ K^-)_{S\text{-wave}}) = -0.66 \pm 0.04$
	$A_{CP}(B^+ \rightarrow K^+ K^- K^+) = -0.033 \pm 0.008$
	$A_{CP}(B^+ \rightarrow \phi K^+) = 0.024 \pm 0.028$ (S = 2.3)
	$A_{CP}(B^+ \rightarrow X_0(1550) K^+) = -0.04 \pm 0.07$
	$A_{CP}(B^+ \rightarrow K^{*+} K^+ K^-) = 0.11 \pm 0.09$
	$A_{CP}(B^+ \rightarrow \phi K^*(892)^+) = -0.01 \pm 0.08$
	$A_{CP}(B^+ \rightarrow \phi(K\pi)_0^{*+}) = 0.04 \pm 0.16$

Meson Summary Table

$A_{CP}(B^+ \rightarrow \phi K_1(1270)^+) = 0.15 \pm 0.20$
$A_{CP}(B^+ \rightarrow \phi K_2^*(1430)^+) = -0.23 \pm 0.20$
$A_{CP}(B^+ \rightarrow K^+ \phi) = -0.10 \pm 0.08$
$A_{CP}(B^+ \rightarrow K^+[\phi\phi]_{\eta_c}) = 0.09 \pm 0.10$
$A_{CP}(B^+ \rightarrow K^*(892)^+ \gamma) = 0.014 \pm 0.018$
$A_{CP}(B^+ \rightarrow X_{S_1} \gamma) = 0.028 \pm 0.019$
$A_{CP}(B^+ \rightarrow \eta K^+ \gamma) = -0.12 \pm 0.07$
$A_{CP}(B^+ \rightarrow \phi K^+ \gamma) = -0.13 \pm 0.11 \quad (S = 1.1)$
$A_{CP}(B^+ \rightarrow \rho^+ \gamma) = -0.11 \pm 0.33$
$A_{CP}(B^+ \rightarrow \pi^+ \pi^0) = 0.03 \pm 0.04$
$A_{CP}(B^+ \rightarrow \pi^+ \pi^- \pi^+) = 0.057 \pm 0.013$
$A_{CP}(B^+ \rightarrow \rho^0 \pi^+) = 0.009 \pm 0.019$
$A_{CP}(B^+ \rightarrow f_2(1270) \pi^+) = 0.40 \pm 0.06$
$A_{CP}(B^+ \rightarrow \rho^0(1450) \pi^+) = -0.11 \pm 0.05$
$A_{CP}(B^+ \rightarrow \rho_3(1690) \pi^+) = -0.80 \pm 0.28$
$A_{CP}(B^+ \rightarrow \mathbf{f}_6(1370) \pi^+) = 0.72 \pm 0.22$
$A_{CP}(B^+ \rightarrow \pi^+ \pi^- \pi^+ \text{ nonresonant}) = -0.14^{+0.23}_{-0.16}$
$A_{CP}(B^+ \rightarrow \rho^+ \pi^0) = 0.02 \pm 0.11$
$A_{CP}(B^+ \rightarrow \rho^+ \rho^0) = -0.05 \pm 0.05$
$A_{CP}(B^+ \rightarrow \omega \pi^+) = -0.04 \pm 0.05$
$A_{CP}(B^+ \rightarrow \omega \rho^+) = -0.20 \pm 0.09$
$A_{CP}(B^+ \rightarrow \eta \pi^+) = -0.14 \pm 0.07 \quad (S = 1.4)$
$A_{CP}(B^+ \rightarrow \eta \rho^+) = 0.11 \pm 0.11$
$A_{CP}(B^+ \rightarrow \eta' \pi^+) = 0.06 \pm 0.16$
$A_{CP}(B^+ \rightarrow \eta' \rho^+) = 0.26 \pm 0.17$
$A_{CP}(B^+ \rightarrow b_1^0 \pi^+) = 0.05 \pm 0.16$
$A_{CP}(B^+ \rightarrow \rho \bar{\rho} \pi^+) = 0.00 \pm 0.04$
$A_{CP}(B^+ \rightarrow \rho \bar{\rho} K^+) = 0.00 \pm 0.04 \quad (S = 2.2)$
$A_{CP}(B^+ \rightarrow \rho \bar{\rho} K^*(892)^+) = 0.21 \pm 0.16 \quad (S = 1.4)$
$A_{CP}(B^+ \rightarrow \rho \bar{\Lambda} \gamma) = 0.17 \pm 0.17$
$A_{CP}(B^+ \rightarrow \rho \bar{\Lambda} \pi^0) = 0.01 \pm 0.17$
$A_{CP}(B^+ \rightarrow K^+ \ell^+ \ell^-) = -0.02 \pm 0.08$
$A_{CP}(B^+ \rightarrow K^+ e^+ e^-) = 0.14 \pm 0.14$
$A_{CP}(B^+ \rightarrow K^+ \mu^+ \mu^-) = 0.011 \pm 0.017$
$A_{CP}(B^+ \rightarrow \pi^+ \mu^+ \mu^-) = -0.11 \pm 0.12$
$A_{CP}(B^+ \rightarrow K^* e^+ e^-) = -0.09 \pm 0.14$
$A_{CP}(B^+ \rightarrow K^* \mu^+ \mu^-) = -0.12 \pm 0.24$
$\gamma = (71.1^{+4.6}_{-5.3})^\circ$
$\Gamma_B(B^+ \rightarrow D^0 K^+) = 0.0993 \pm 0.0046$
$\delta_B(B^+ \rightarrow D^0 K^+) = (129.6^{+5.0}_{-6.0})^\circ$
$\Gamma_B(B^+ \rightarrow D^0 K^{*+}) = 0.076 \pm 0.020$
$\delta_B(B^+ \rightarrow D^0 K^{*+}) = (98^{+18}_{-37})^\circ$
$\Gamma_B(B^+ \rightarrow D^{*0} K^+) = 0.140 \pm 0.019$
$\delta_B(B^+ \rightarrow D^{*0} K^+) = (319.2^{+7.7}_{-8.7})^\circ$

B^- modes are charge conjugates of the modes below. Modes which do not identify the charge state of the B are listed in the B^\pm/B^0 ADMIXTURE section.

The branching fractions listed below assume 50% $B^0 \bar{B}^0$ and 50% $B^+ B^-$ production at the $\Upsilon(4S)$. We have attempted to bring older measurements up to date by rescaling their assumed $\Upsilon(4S)$ production ratio to 50:50 and their assumed D, D_s, D^* , and ψ branching ratios to current values whenever this would affect our averages and best limits significantly.

Indentation is used to indicate a subchannel of a previous reaction. All resonant subchannels have been corrected for resonance branching fractions to the final state so the sum of the subchannel branching fractions can exceed that of the final state.

For inclusive branching fractions, e.g., $B \rightarrow D^\pm X$, the values usually are multiplicities, not branching fractions. They can be greater than one.

B^+ DECAY MODES	Fraction (Γ_i/Γ)	Scale factor/ ρ	
		Confidence level (MeV/c)	
Semileptonic and leptonic modes			
$\ell^+ \nu_\ell X$	[III] (10.99 \pm 0.28) %	-	
$e^+ \nu_e X_c$	(10.8 \pm 0.4) %	-	
$D \ell^+ \nu_\ell X$	(9.7 \pm 0.7) %	-	
$\bar{D}^0 \ell^+ \nu_\ell$	[III] (2.35 \pm 0.09) %	2310	
$\bar{D}^0 \tau^+ \nu_\tau$	(7.7 \pm 2.5) $\times 10^{-3}$	1911	
$\bar{D}^*(2007)^0 \ell^+ \nu_\ell$	[III] (5.66 \pm 0.22) %	2258	
$\bar{D}^*(2007)^0 \tau^+ \nu_\tau$	(1.88 \pm 0.20) %	1839	
$D^- \pi^+ \ell^+ \nu_\ell$	(4.4 \pm 0.4) $\times 10^{-3}$	2306	

$\bar{D}_0^*(2420)^0 \ell^+ \nu_\ell, \bar{D}_0^{*0} \rightarrow$	(2.5 \pm 0.5) $\times 10^{-3}$	-
$\bar{D}_2^*(2460)^0 \ell^+ \nu_\ell, \bar{D}_2^{*0} \rightarrow$	(1.53 \pm 0.16) $\times 10^{-3}$	2065
$D^{(*)-} n \pi \ell^+ \nu_\ell (n \geq 1)$	(1.88 \pm 0.25) %	-
$D^{*-} \pi^+ \ell^+ \nu_\ell$	(6.0 \pm 0.4) $\times 10^{-3}$	2254
$\bar{D}_1(2420)^0 \ell^+ \nu_\ell, \bar{D}_1^0 \rightarrow$	(3.03 \pm 0.20) $\times 10^{-3}$	2084
$\bar{D}_1^*(2430)^0 \ell^+ \nu_\ell, \bar{D}_1^{*0} \rightarrow$	(2.7 \pm 0.6) $\times 10^{-3}$	-
$\bar{D}_2^*(2460)^0 \ell^+ \nu_\ell,$	(1.01 \pm 0.24) $\times 10^{-3}$	S=2.0 2065
$\bar{D}_2^{*0} \rightarrow D^{*-} \pi^+$		
$\bar{D}^0 \pi^+ \pi^- \ell^+ \nu_\ell$	(1.7 \pm 0.4) $\times 10^{-3}$	2301
$\bar{D}^{*0} \pi^+ \pi^- \ell^+ \nu_\ell$	(8 \pm 5) $\times 10^{-4}$	2248
$D^{(*)-} K^+ \ell^+ \nu_\ell$	(6.1 \pm 1.0) $\times 10^{-4}$	-
$D_s^- K^+ \ell^+ \nu_\ell$	(3.0 \pm 1.4) $\times 10^{-4}$	2242
$D_s^{*-} K^+ \ell^+ \nu_\ell$	(2.9 \pm 1.9) $\times 10^{-4}$	2185
$\pi^0 \ell^+ \nu_\ell$	(7.80 \pm 0.27) $\times 10^{-5}$	2638
$\eta \ell^+ \nu_\ell$	(3.9 \pm 0.5) $\times 10^{-5}$	2611
$\eta' \ell^+ \nu_\ell$	(2.3 \pm 0.8) $\times 10^{-5}$	2553
$\omega \ell^+ \nu_\ell$	[III] (1.19 \pm 0.09) $\times 10^{-4}$	2582
$\rho^0 \ell^+ \nu_\ell$	[III] (1.58 \pm 0.11) $\times 10^{-4}$	2583
$\rho \bar{\rho} \ell^+ \nu_\ell$	(5.8 \pm 2.6) $\times 10^{-6}$	2467
$\rho \bar{\rho} \mu^+ \nu_\mu$	< 8.5 $\times 10^{-6}$	CL=90% 2446
$\rho \bar{\rho} e^+ \nu_e$	(8.2 \pm 4.0) $\times 10^{-6}$	2467
$e^+ \nu_e$	< 9.8 $\times 10^{-7}$	CL=90% 2640
$\mu^+ \nu_\mu$	2.90 $\times 10^{-07}$ to 1.07 $\times 10^{-06}$	CL=90% 2639
$\tau^+ \nu_\tau$	(1.09 \pm 0.24) $\times 10^{-4}$	S=1.2 2341
$\ell^+ \nu_\ell \gamma$	< 3.0 $\times 10^{-6}$	CL=90% 2640
$e^+ \nu_e \gamma$	< 4.3 $\times 10^{-6}$	CL=90% 2640
$\mu^+ \nu_\mu \gamma$	< 3.4 $\times 10^{-6}$	CL=90% 2639
$\mu^+ \mu^- \mu^+ \nu_\mu$	< 1.6 $\times 10^{-8}$	CL=95% 2634

Inclusive modes

$D^0 X$	(8.6 \pm 0.7) %	-
$\bar{D}^0 X$	(79 \pm 4) %	-
$D^+ X$	(2.5 \pm 0.5) %	-
$D^- X$	(9.9 \pm 1.2) %	-
$D_s^+ X$	(7.9 \pm 1.4) %	-
$D_s^- X$	(1.10 \pm 0.40) %	-
$\Lambda_c^+ X$	(2.1 \pm 0.9) %	-
$\bar{\Lambda}_c^- X$	(2.8 \pm 1.1) %	-
$\bar{c} X$	(97 \pm 4) %	-
$c X$	(23.4 \pm 2.2) %	-
$c/\bar{c} X$	(120 \pm 6) %	-

 D, D^* , or D_s modes

$\bar{D}^0 \pi^+$	(4.68 \pm 0.13) $\times 10^{-3}$	2308
$D_{CP(+1)} \pi^+$	[nnn] (2.05 \pm 0.18) $\times 10^{-3}$	-
$D_{CP(-1)} \pi^+$	[nnn] (2.0 \pm 0.4) $\times 10^{-3}$	-
$\bar{D}^0 \rho^+$	(1.34 \pm 0.18) %	2237
$\bar{D}^0 K^+$	(3.63 \pm 0.12) $\times 10^{-4}$	2281
$D_{CP(+1)} K^+$	[nnn] (1.80 \pm 0.07) $\times 10^{-4}$	-
$D_{CP(-1)} K^+$	[nnn] (1.96 \pm 0.18) $\times 10^{-4}$	-
$D^0 K^+$	(3.57 \pm 0.35) $\times 10^{-6}$	2281
$[K^- \pi^+]_D K^+$	[ooo] < 2.8 $\times 10^{-7}$	CL=90% -
$[K^+ \pi^-]_D K^+$	[ooo] < 1.5 $\times 10^{-5}$	CL=90% -
$[K^- \pi^+ \pi^0]_D K^+$	seen	-
$[K^+ \pi^- \pi^0]_D K^+$	seen	-
$[K^- \pi^+ \pi^+ \pi^-]_D K^+$	seen	-
$[K^+ \pi^- \pi^+ \pi^-]_D K^+$	seen	-
$[K^- \pi^+]_D \pi^+$	[ooo] (6.3 \pm 1.1) $\times 10^{-7}$	-
$[K^+ \pi^-]_D \pi^+$	(1.78 \pm 0.32) $\times 10^{-4}$	-
$[K^- \pi^+ \pi^0]_D \pi^+$	seen	-
$[K^+ \pi^- \pi^0]_D \pi^+$	seen	-
$[K^- \pi^+ \pi^+ \pi^-]_D \pi^+$	seen	-
$[K^+ \pi^- \pi^+ \pi^-]_D \pi^+$	seen	-
$[\pi^+ \pi^- \pi^0]_D K^-$	(4.6 \pm 0.9) $\times 10^{-6}$	-
$[K_S^0 K^+ \pi^-]_D K^+$	seen	-
$[K_S^0 K^- \pi^+]_D K^+$	seen	-
$[K^*(892)^+ K^-]_D K^+$	seen	-
$[K_S^0 K^- \pi^+]_D \pi^+$	seen	-

Meson Summary Table

$[K^*(892)^+ K^-]_D \pi^+$	seen	-	$\bar{D}'_1(2427)^0 \pi^+$	$(5.0 \pm 1.2) \times 10^{-4}$	-
$[K^*_S K^+ \pi^-]_D \pi^+$	seen	-	$\times B(\bar{D}'_1(2427)^0 \rightarrow D^{*-} \pi^+)$		
$[K^*(892)^- K^+]_D \pi^+$	seen	-	$\bar{D}_1(2420)^0 \pi^+ \times B(\bar{D}_1^0 \rightarrow D^{*0} \pi^+ \pi^-)$	< 6	$\times 10^{-6}$ CL=90% 2082
$\bar{D}^0 K^*(892)^+$	$(5.3 \pm 0.4) \times 10^{-4}$	2213	$\bar{D}_1^*(2420)^0 \rho^+$	< 1.4	$\times 10^{-3}$ CL=90% 1996
$D_{CP(-1)} K^*(892)^+$	[nnn] $(2.7 \pm 0.8) \times 10^{-4}$	-	$\bar{D}_2^*(2460)^0 \pi^+$	< 1.3	$\times 10^{-3}$ CL=90% 2063
$D_{CP(+1)} K^*(892)^+$	[nnn] $(6.2 \pm 0.7) \times 10^{-4}$	-	$\bar{D}_2^*(2460)^0 \pi^+ \times B(\bar{D}_2^{*0} \rightarrow D^{*0} \pi^+ \pi^-)$	< 2.2	$\times 10^{-5}$ CL=90% 2063
$D^0 K^*(892)^+$	$(3.1 \pm 1.6) \times 10^{-6}$	2213	$\bar{D}_1^*(2680)^0 \pi^+, \bar{D}_1^*(2680)^0 \rightarrow D^- \pi^+$	$(1.00 \pm 0.22) \times 10^{-5}$	-
$\bar{D}^0 K^+ \pi^+ \pi^-$	$(5.2 \pm 2.1) \times 10^{-4}$	2237	$\bar{D}_3^*(2760)^0 \pi^+, \bar{D}_3^*(2760)^0 \pi^+ \rightarrow D^- \pi^+$	$(2.0 \pm 1.4) \times 10^{-6}$	-
$\bar{D}^0 K^+ \bar{K}^0$	$(5.5 \pm 1.6) \times 10^{-4}$	2189	$\bar{D}_2^*(3000)^0 \pi^+ \rightarrow D^- \pi^+$	< 4.7	$\times 10^{-3}$ CL=90% 1977
$\bar{D}^0 K^+ \bar{K}^*(892)^0$	$(7.5 \pm 1.7) \times 10^{-4}$	2072	$\bar{D}_2^*(2460)^0 \rho^+$	$(9.0 \pm 0.9) \times 10^{-3}$	1815
$\bar{D}^0 \pi^+ \pi^+ \pi^-$	$(5.6 \pm 2.1) \times 10^{-3}$	S=3.6 2289	$\bar{D}^0 D_s^+$	$(8.0 \pm 1.6 / 1.3) \times 10^{-4}$	1605
$\bar{D}^0 \pi^+ \pi^+ \pi^-$ nonresonant	$(5 \pm 4) \times 10^{-3}$	2289	$D_{s0}^*(2317)^+ \bar{D}^0, D_{s0}^{*+} \rightarrow D_s^+ \pi^0$	< 7.6	$\times 10^{-4}$ CL=90% 1605
$\bar{D}^0 \pi^+ \rho^0$	$(4.2 \pm 3.0) \times 10^{-3}$	2208	$B(D_{s0}(2317)^+ \rightarrow D_s^+ \gamma)$	$(9 \pm 7) \times 10^{-4}$	1511
$\bar{D}^0 \rho_1(1260)^+$	$(4 \pm 4) \times 10^{-3}$	2123	$D_{s0}(2317)^+ \bar{D}^* (2007)^0 \times B(D_{s0}(2317)^+ \rightarrow D_s^+ \pi^0)$	$(3.1 \pm 1.0 / 0.9) \times 10^{-3}$	-
$\bar{D}^0 \omega \pi^+$	$(4.1 \pm 0.9) \times 10^{-3}$	2206	$D_{sJ}(2457)^+ \bar{D}^0$	$(4.6 \pm 1.3 / 1.1) \times 10^{-4}$	-
$D^*(2010)^- \pi^+ \pi^+$	$(1.35 \pm 0.22) \times 10^{-3}$	2247	$B(D_{sJ}(2457)^+ \rightarrow D_s^+ \gamma)$	< 2.2	$\times 10^{-4}$ CL=90% -
$D^*(2010)^- K^+ \pi^+$	$(8.2 \pm 1.4) \times 10^{-5}$	2206	$D_{sJ}(2457)^+ \bar{D}^0 \times B(D_{sJ}(2457)^+ \rightarrow D_s^+ \pi^0)$	< 2.7	$\times 10^{-4}$ CL=90% -
$\bar{D}_1(2420)^0 \pi^+, \bar{D}_1^0 \rightarrow D^*(2010)^- \pi^+$	$(5.2 \pm 2.2) \times 10^{-4}$	2081	$D_{sJ}(2457)^+ \bar{D}^0 \times B(D_{sJ}(2457)^+ \rightarrow D_s^+ \pi^0)$	< 9.8	$\times 10^{-4}$ CL=90% -
$D^- \pi^+ \pi^+$	$(1.07 \pm 0.05) \times 10^{-3}$	2299	$D_{sJ}(2457)^+ \bar{D}^0 \times B(D_{sJ}(2457)^+ \rightarrow D_s^+ \gamma)$	$(1.20 \pm 0.30) \%$	-
$D^- K^+ \pi^+$	$(7.7 \pm 0.5) \times 10^{-5}$	2260	$D_{sJ}(2457)^+ \bar{D}^* (2007)^0 \times B(D_{sJ}(2457)^+ \rightarrow D_s^+ \gamma)$	$(1.4 \pm 0.7 / 0.6) \times 10^{-3}$	-
$D_0^*(2300)^0 K^+, D_0^{*0} \rightarrow D^- \pi^+$	$(6.1 \pm 2.4) \times 10^{-6}$	-	$D_{sJ}(2457)^+ \bar{D}^0 \times B(D_{s1}(2536)^+ \rightarrow D^*(2007)^0 K^+ + D^*(2010)^+ K^0)$	$(2.2 \pm 0.7) \times 10^{-4}$	1447
$D_2^*(2460)^0 K^+, D_2^{*0} \rightarrow D^- \pi^+$	$(2.32 \pm 0.23) \times 10^{-5}$	-	$\bar{D}^0 D_{s1}(2536)^+ \times B(D_{s1}(2536)^+ \rightarrow D^*(2007)^0 K^+)$	$(5.5 \pm 1.6) \times 10^{-4}$	1339
$D_1^*(2760)^0 K^+, D_1^{*0} \rightarrow D^- \pi^+$	$(3.6 \pm 1.2) \times 10^{-6}$	-	$\bar{D}^0 D_{s1}(2536)^+ \times B(D_{s1}(2536)^+ \rightarrow D^*(2007)^0 K^+)$	$(2.3 \pm 1.1) \times 10^{-4}$	1447
$D^+ K^0$	< 2.9	CL=90% 2278	$\bar{D}^0 D_{s1}(2536)^+ \times B(D_{s1}(2536)^+ \rightarrow D^* K^0)$	$(5.6 \pm 1.8) \times 10^{-4}$	S=1.7 -
$D^+ K^+ \pi^-$	$(5.6 \pm 1.1) \times 10^{-6}$	2260	$\bar{D}^0 D_{sJ}(2700)^+ \times B(D_{sJ}(2700)^+ \rightarrow D^0 K^+)$	$(3.9 \pm 2.6) \times 10^{-4}$	1339
$D_2^*(2460)^0 K^+, D_2^{*0} \rightarrow D^+ \pi^-$	< 6.3	CL=90% -	$\bar{D}^{*0} D_{s1}(2536)^+, D_{s1}^+ \rightarrow D^{*+} K^0$	$(8 \pm 15) \times 10^{-6}$	-
$D^+ K^{*0}$	< 4.9	CL=90% 2211	$\bar{D}^{*0} D_{sJ}(2573)^+, D_{sJ}^+ \rightarrow D^{*0} K^+$	< 2	$\times 10^{-4}$ CL=90% 1306
$D^+ \bar{K}^{*0}$	< 1.4	CL=90% 2211	$\bar{D}^{*0} D_{sJ}(2573)^+, D_{sJ}^+ \rightarrow D^{*0} K^+$	< 5	$\times 10^{-4}$ CL=90% 1306
$\bar{D}^*(2007)^0 \pi^+$	$(4.90 \pm 0.17) \times 10^{-3}$	2256	$\bar{D}^0 D_s^{*+}$	$(7.6 \pm 1.6) \times 10^{-3}$	1734
$\bar{D}_{CP(+1)}^{*0} \pi^+$	[ppp] $(2.7 \pm 0.6) \times 10^{-3}$	-	$\bar{D}^*(2007)^0 D_s^+$	$(8.2 \pm 1.7) \times 10^{-3}$	1737
$\bar{D}_{CP(-1)}^{*0} \pi^+$	[ppp] $(2.4 \pm 0.9) \times 10^{-3}$	-	$\bar{D}^*(2007)^0 D_s^+$	$(1.71 \pm 0.24) \%$	1651
$\bar{D}^*(2007)^0 \omega \pi^+$	$(4.5 \pm 1.2) \times 10^{-3}$	2149	$D^{(*)+} \bar{D}^{*0}$	$(2.7 \pm 1.2) \%$	-
$\bar{D}^*(2007)^0 \rho^+$	$(9.8 \pm 1.7) \times 10^{-3}$	2181	$\bar{D}^*(2007)^0 D^*(2010)^+$	$(8.1 \pm 1.7) \times 10^{-4}$	1713
$\bar{D}^*(2007)^0 K^+$	$(3.97 \pm 0.31 / 0.28) \times 10^{-4}$	2227	$\bar{D}^0 D^*(2010)^+ + \bar{D}^*(2007)^0 D^+$	< 1.30	CL=90% 1792
$\bar{D}_{CP(+1)}^{*0} K^+$	[ppp] $(2.60 \pm 0.33) \times 10^{-4}$	-	$\bar{D}^0 D^*(2010)^+$	$(3.9 \pm 0.5) \times 10^{-4}$	1792
$\bar{D}_{CP(-1)}^{*0} K^+$	[ppp] $(2.19 \pm 0.30) \times 10^{-4}$	-	$\bar{D}^0 D^+$	$(3.8 \pm 0.4) \times 10^{-4}$	1866
$D^*(2007)^0 K^+$	$(7.8 \pm 2.2) \times 10^{-6}$	2227	$\bar{D}^0 D^+ K^0$	$(1.55 \pm 0.21) \times 10^{-3}$	1571
$\bar{D}^*(2007)^0 K^*(892)^+$	$(8.1 \pm 1.4) \times 10^{-4}$	2156	$D^+ \bar{D}^*(2007)^0$	$(6.3 \pm 1.7) \times 10^{-4}$	1791
$\bar{D}^*(2007)^0 K^+ \bar{K}^0$	< 1.06	CL=90% 2132	$\bar{D}^*(2007)^0 D^+ K^0$	$(2.1 \pm 0.5) \times 10^{-3}$	1475
$\bar{D}^*(2007)^0 K^+ \bar{K}^*(892)^0$	$(1.5 \pm 0.4) \times 10^{-3}$	2009	$\bar{D}^0 D^*(2010)^+ K^0$	$(3.8 \pm 0.4) \times 10^{-3}$	1476
$\bar{D}^*(2007)^0 \pi^+ \pi^+ \pi^-$	$(1.03 \pm 0.12) \%$	2236	$\bar{D}^*(2007)^0 D^*(2010)^+ K^0$	$(9.2 \pm 1.2) \times 10^{-3}$	1362
$\bar{D}^*(2007)^0 a_1(1260)^+$	$(1.9 \pm 0.5) \%$	2063	$\bar{D}^0 D^0 K^+$	$(1.45 \pm 0.33) \times 10^{-3}$	S=2.6 1577
$\bar{D}^*(2007)^0 \pi^- \pi^+ \pi^+ \pi^0$	$(1.8 \pm 0.4) \%$	2219			
$\bar{D}^{*0} 3\pi^+ 2\pi^-$	$(5.7 \pm 1.2) \times 10^{-3}$	2196			
$D^*(2010)^+ \pi^0$	< 3.6	$\times 10^{-6}$ 2255			
$D^*(2010)^+ K^0$	< 9.0	$\times 10^{-6}$ CL=90% 2225			
$D^*(2010)^- \pi^+ \pi^+ \pi^0$	$(1.5 \pm 0.7) \%$	2235			
$D^*(2010)^- \pi^+ \pi^+ \pi^+ \pi^-$	$(2.6 \pm 0.4) \times 10^{-3}$	2217			
$\bar{D}^{*0} \pi^+$	[qqq] $(5.7 \pm 1.2) \times 10^{-3}$	-			
$\bar{D}_1^*(2420)^0 \pi^+$	$(1.5 \pm 0.6) \times 10^{-3}$	S=1.3 2082			
$\bar{D}_1(2420)^0 \pi^+ \times B(\bar{D}_1^0 \rightarrow \bar{D}^0 \pi^+ \pi^-)$	$(2.5 \pm 1.6 / 1.4) \times 10^{-4}$	S=3.9 2082			
$\bar{D}_1(2420)^0 \pi^+ \times B(\bar{D}_1^0 \rightarrow \bar{D}^0 \pi^+ \pi^-)$	$(2.2 \pm 1.0) \times 10^{-4}$	2082			
$\bar{D}_2^*(2462)^0 \pi^+$	$(3.56 \pm 0.24) \times 10^{-4}$	-			
$\times B(\bar{D}_2^*(2462)^0 \rightarrow D^- \pi^+)$					
$\bar{D}_2^*(2462)^0 \pi^+ \times B(\bar{D}_2^{*0} \rightarrow \bar{D}^0 \pi^+ \pi^+)$	$(2.2 \pm 1.0) \times 10^{-4}$	-			
$\bar{D}_2^*(2462)^0 \pi^+ \times B(\bar{D}_2^{*0} \rightarrow \bar{D}^0 \pi^- \pi^+)$	< 1.7	$\times 10^{-4}$ CL=90% -			
$\bar{D}_2^*(2462)^0 \pi^+ \times B(\bar{D}_2^{*0} \rightarrow \bar{D}^0 \pi^- \pi^+)$	$(2.2 \pm 1.1) \times 10^{-4}$	-			
$D^*(2010)^- \pi^+$	$(6.4 \pm 1.4) \times 10^{-4}$	2136			
$\times B(\bar{D}_0^*(2400)^0 \rightarrow D^- \pi^+)$					
$\bar{D}_1(2421)^0 \pi^+$	$(6.8 \pm 1.5) \times 10^{-4}$	-			
$\times B(\bar{D}_1(2421)^0 \rightarrow D^{*-} \pi^+)$					
$\bar{D}_2^*(2462)^0 \pi^+$	$(1.8 \pm 0.5) \times 10^{-4}$	-			
$\times B(\bar{D}_2^*(2462)^0 \rightarrow D^{*-} \pi^+)$					

Meson Summary Table

$\bar{D}^*(2007)^0 D^0 K^+$	$(2.26 \pm 0.23) \times 10^{-3}$	1481	$X(3915) K^+$	< 2.8	$\times 10^{-4}$	CL=90%	1103		
$\bar{D}^0 D^*(2007)^0 K^+$	$(6.3 \pm 0.5) \times 10^{-3}$	1481	$X(3915)^0 K^+, X^0 \rightarrow \eta_c \eta$	< 4.7	$\times 10^{-5}$	CL=90%	-		
$\bar{D}^*(2007)^0 D^*(2007)^0 K^+$	$(1.12 \pm 0.13) \%$	1368	$X(3915)^0 K^+, X^0 \rightarrow \eta_c \pi^0$	< 1.7	$\times 10^{-5}$	CL=90%	-		
$D^- D^+ K^+$	$(2.2 \pm 0.7) \times 10^{-4}$	1571	$X(4014)^0 K^+, X^0 \rightarrow \eta_c \eta$	< 3.9	$\times 10^{-5}$	CL=90%	-		
$D^- D^*(2010)^+ K^+$	$(6.3 \pm 1.1) \times 10^{-4}$	1475	$X(4014)^0 K^+, X^0 \rightarrow \eta_c \pi^0$	< 1.2	$\times 10^{-5}$	CL=90%	-		
$D^*(2010)^- D^+ K^+$	$(6.0 \pm 1.3) \times 10^{-4}$	1475	$Z_c(3900)^0 K^+, Z_c^0 \rightarrow$	< 4.7	$\times 10^{-5}$	CL=90%	-		
$D^*(2010)^- D^*(2010)^+ K^+$	$(1.32 \pm 0.18) \times 10^{-3}$	1363	$\eta_c \pi^+ \pi^-$						
$(\bar{D} + \bar{D}^*)(D + D^*) K$	$(4.05 \pm 0.30) \%$	-	$X(4020)^0 K^+, X^0 \rightarrow$	< 1.6	$\times 10^{-5}$	CL=90%	-		
$D_s^+ \pi^0$	$(1.6 \pm 0.5) \times 10^{-5}$	2270	$\eta_c \pi^+ \pi^-$						
$D_s^{*+} \pi^0$	< 2.6	$\times 10^{-4}$	CL=90%	2215	$\chi_{c1}(3872) K^*(892)^+, \chi_{c1} \rightarrow$	< 4.8	$\times 10^{-6}$	CL=90%	939
$D_s^+ \eta$	< 4	$\times 10^{-4}$	CL=90%	2235	$J/\psi \gamma$				
$D_s^{*+} \eta$	< 6	$\times 10^{-4}$	CL=90%	2178	$\chi_{c1}(3872) K^*(892)^+, \chi_{c1} \rightarrow$	< 2.8	$\times 10^{-5}$	CL=90%	939
$D_s^+ \rho^0$	< 3.0	$\times 10^{-4}$	CL=90%	2197	$\psi(2S) \gamma$				
$D_s^{*+} \rho^0$	< 4	$\times 10^{-4}$	CL=90%	2138	$\chi_{c1}(3872)^+ K^0, \chi_{c1}^+ \rightarrow$	[<i>rrr</i>] < 6.1	$\times 10^{-6}$	CL=90%	-
$D_s^+ \omega$	< 4	$\times 10^{-4}$	CL=90%	2195	$J/\psi(1S) \pi^+ \pi^0$				
$D_s^{*+} \omega$	< 6	$\times 10^{-4}$	CL=90%	2136	$\chi_{c1}(3872) K^0 \pi^+, \chi_{c1} \rightarrow$	$(1.06 \pm 0.31) \times 10^{-5}$			-
$D_s^+ a_1(1260)^0$	< 1.8	$\times 10^{-3}$	CL=90%	2079	$J/\psi(1S) \pi^+ \pi^-$				
$D_s^{*+} a_1(1260)^0$	< 1.3	$\times 10^{-3}$	CL=90%	2015	$Z_c(4430)^+ K^0, Z_c^+ \rightarrow J/\psi \pi^+$	< 1.5	$\times 10^{-5}$	CL=95%	-
$D_s^+ K^+ K^-$	$(7.2 \pm 1.1) \times 10^{-6}$	2149	$Z_c(4430)^+ K^0, Z_c^+ \rightarrow$	< 4.7	$\times 10^{-5}$	CL=95%	-		
$D_s^+ \phi$	< 4.2	$\times 10^{-7}$	CL=90%	2141	$\psi(2S) \pi^+$				
$D_s^{*+} \phi$	< 1.2	$\times 10^{-5}$	CL=90%	2079	$\psi(4260)^0 K^+, \psi^0 \rightarrow$	< 1.56	$\times 10^{-5}$	CL=95%	-
$D_s^+ \bar{K}^0$	< 8	$\times 10^{-4}$	CL=90%	2242	$J/\psi \pi^+ \pi^-$				
$D_s^{*+} \bar{K}^0$	< 9	$\times 10^{-4}$	CL=90%	2185	$X(3915) K^+, X \rightarrow J/\psi \gamma$	< 1.4	$\times 10^{-5}$	CL=90%	-
$D_s^+ \bar{K}^*(892)^0$	< 4.4	$\times 10^{-6}$	CL=90%	2172	$X(3915) K^+, X \rightarrow$	< 3.8	$\times 10^{-5}$	CL=90%	-
$D_s^{*+} \bar{K}^*(892)^0$	< 3.5	$\times 10^{-6}$	CL=90%	2172	$\chi_{c1}(1P) \pi^0$				
$D_s^{*+} \bar{K}^*(892)^0$	< 3.5	$\times 10^{-4}$	CL=90%	2112	$X(3930)^0 K^+, X^0 \rightarrow J/\psi \gamma$	< 2.5	$\times 10^{-6}$	CL=90%	-
$D_s^- \pi^+ K^+$	$(1.80 \pm 0.22) \times 10^{-4}$	2222	$J/\psi(1S) K^+$	$(1.006 \pm 0.027) \times 10^{-3}$	1684				
$D_s^{*-} \pi^+ K^+$	$(1.45 \pm 0.24) \times 10^{-4}$	2164	$J/\psi(1S) K^0 \pi^+$	$(1.14 \pm 0.11) \times 10^{-3}$	1651				
$D_s^{*-} \pi^+ K^*(892)^+$	< 5	$\times 10^{-3}$	CL=90%	2138	$J/\psi(1S) K^+ \pi^+ \pi^-$	$(8.1 \pm 1.3) \times 10^{-4}$	S=2.5	1612	
$D_s^{*-} \pi^+ K^*(892)^+$	< 7	$\times 10^{-3}$	CL=90%	2076	$J/\psi(1S) K^+ K^- K^+$	$(3.37 \pm 0.29) \times 10^{-5}$		1252	
$D_s^- K^+ K^+$	$(9.7 \pm 2.1) \times 10^{-6}$	2149	$X(3915) K^+, X \rightarrow \rho \bar{\rho}$	< 7.1	$\times 10^{-8}$	CL=95%	-		
$D_s^{*-} K^+ K^+$	< 1.5	$\times 10^{-5}$	CL=90%	2088	$J/\psi(1S) K^*(892)^+$	$(1.43 \pm 0.08) \times 10^{-3}$		1571	
					$J/\psi(1S) K(1270)^+$	$(1.8 \pm 0.5) \times 10^{-3}$		1402	
					$J/\psi(1S) K(1400)^+$	< 5	$\times 10^{-4}$	CL=90%	1308
					$J/\psi(1S) \eta K^+$	$(1.24 \pm 0.14) \times 10^{-4}$		1510	
					$\chi_{c1-odd}(3872) K^+,$	< 3.8	$\times 10^{-6}$	CL=90%	-
					$\chi_{c1-odd} \rightarrow J/\psi \eta$				
					$\psi(4160) K^+, \psi \rightarrow J/\psi \eta$	< 7.4	$\times 10^{-6}$	CL=90%	-
					$J/\psi(1S) \eta K^+$	< 8.8	$\times 10^{-5}$	CL=90%	1273
					$J/\psi(1S) \phi K^+$	$(5.0 \pm 0.4) \times 10^{-5}$		1227	
					$J/\psi(1S) K_1(1650), K_1 \rightarrow$	$(6 \pm 10/6) \times 10^{-6}$		-	
					ϕK^+				
					$J/\psi(1S) K^*(1680)^+, K^* \rightarrow$	$(3.4 \pm 1.9/2.2) \times 10^{-6}$		-	
					ϕK^+				
					$J/\psi(1S) K_2^*(1980), K_2^* \rightarrow$	$(1.5 \pm 0.9/0.5) \times 10^{-6}$		-	
					ϕK^+				
					$J/\psi(1S) K(1830)^+,$	$(1.3 \pm 1.3/1.1) \times 10^{-6}$		-	
					$K(1830)^+ \rightarrow \phi K^+$				
					$\chi_{c1}(4140) K^+, \chi_{c1} \rightarrow$	$(10 \pm 4) \times 10^{-6}$		-	
					$J/\psi(1S) \phi$				
					$\chi_{c1}(4274) K^+, \chi_{c1} \rightarrow$	$(3.6 \pm 2.2/1.8) \times 10^{-6}$		-	
					$J/\psi(1S) \phi$				
					$\chi_{c0}(4500) K^+, \chi_c^0 \rightarrow$	$(3.3 \pm 2.1/1.7) \times 10^{-6}$		-	
					$J/\psi(1S) \phi$				
					$\chi_{c0}(4700) K^+, \chi_{c0} \rightarrow$	$(6 \pm 5/4) \times 10^{-6}$		-	
					$J/\psi(1S) \phi$				
					$J/\psi(1S) \omega K^+$	$(3.20 \pm 0.60/0.32) \times 10^{-4}$		1388	
					$\chi_{c1}(3872) K^+, \chi_{c1} \rightarrow$	$(6.0 \pm 2.2) \times 10^{-6}$		1141	
					$J/\psi \omega$				
					$X(3915) K^+, X \rightarrow J/\psi \omega$	$(3.0 \pm 0.9/0.7) \times 10^{-5}$		1103	
					$J/\psi(1S) \pi^+$	$(3.87 \pm 0.11) \times 10^{-5}$		1728	
					$J/\psi(1S) \pi^+ \pi^+ \pi^+ \pi^- \pi^-$	$(1.16 \pm 0.13) \times 10^{-5}$		1635	
					$\psi(2S) \pi^+ \pi^+ \pi^-$	$(1.9 \pm 0.4) \times 10^{-5}$		1304	
					$J/\psi(1S) \rho^+$	$(4.1 \pm 0.5) \times 10^{-5}$	S=1.4	1611	
					$J/\psi(1S) \pi^+ \pi^0$ nonresonant	< 7.3	$\times 10^{-6}$	CL=90%	1717
					$J/\psi(1S) a_1(1260)^+$	< 1.2	$\times 10^{-3}$	CL=90%	1415
					$J/\psi(1S) \rho \bar{\rho} \pi^+$	< 5.0	$\times 10^{-7}$	CL=90%	643
					$J/\psi(1S) p \bar{p}$	$(1.46 \pm 0.12) \times 10^{-5}$		567	
					$J/\psi(1S) \Sigma^0 p$	< 1.1	$\times 10^{-5}$	CL=90%	-
					$J/\psi(1S) D^+$	< 1.2	$\times 10^{-4}$	CL=90%	871
					$J/\psi(1S) \bar{D}^0 \pi^+$	< 2.5	$\times 10^{-5}$	CL=90%	665
					$\psi(2S) \pi^+$	$(2.44 \pm 0.30) \times 10^{-5}$		1347	
					$\psi(2S) K^+$	$(6.19 \pm 0.22) \times 10^{-4}$		1284	
					$\psi(2S) K^*(892)^+$	$(6.7 \pm 1.4) \times 10^{-4}$	S=1.3	1116	

Meson Summary Table

$\psi(2S)K^+\pi^+\pi^-$	$(4.3 \pm 0.5) \times 10^{-4}$	1179	$f_0(1370)^0 K^+ \times$	< 1.07	$\times 10^{-5}$	CL=90%	-
$\psi(2S)\phi(1020)K^+$	$(4.0 \pm 0.7) \times 10^{-6}$	417	$B(f_0(1370)^0 \rightarrow \pi^+\pi^-)$				
$\psi(3770)K^+$	$(4.9 \pm 1.3) \times 10^{-4}$	1218	$\rho^0(1450)K^+ \times$	< 1.17	$\times 10^{-5}$	CL=90%	-
$\psi(3770)K^+, \psi \rightarrow D^0\bar{D}^0$	$(1.5 \pm 0.5) \times 10^{-4}$	S=1.4 1218	$B(\rho^0(1450) \rightarrow \pi^+\pi^-)$				
$\psi(3770)K^+, \psi \rightarrow D^+D^-$	$(9.4 \pm 3.5) \times 10^{-5}$	1218	$f_2'(1525)K^+ \times$	< 3.4	$\times 10^{-6}$	CL=90%	2394
$\psi(3770)K^+, \psi \rightarrow \rho\bar{\rho}$	< 2	$\times 10^{-7}$	$B(f_2'(1525) \rightarrow \pi^+\pi^-)$				
$\psi(4040)K^+$	< 1.3	$\times 10^{-4}$	$K^+\rho^0$	$(3.7 \pm 0.5) \times 10^{-6}$			2559
$\psi(4160)K^+$	$(5.1 \pm 2.7) \times 10^{-4}$	868	$K_S^0(1430)^0\pi^+$	$(3.9 \pm 0.6) \times 10^{-5}$		S=1.4	2445
$\psi(4160)K^+, \psi \rightarrow \bar{D}^0D^0$	$(8 \pm 5) \times 10^{-5}$	-	$K_0^*(1430)^+\pi^0$	$(1.19 \pm 0.20) \times 10^{-5}$			-
$\chi_{c0}\pi^+, \chi_{c0} \rightarrow \pi^+\pi^-$	< 1	$\times 10^{-7}$	$K_2^*(1430)^0\pi^+$	$(5.6 \pm 2.2) \times 10^{-6}$			2445
$\chi_{c0}K^+$	$(1.50 \pm 0.15) \times 10^{-4}$	1478	$K^*(1410)^0\pi^+$	< 4.5	$\times 10^{-5}$	CL=90%	2448
$\chi_{c0}K^*(892)^+$	< 2.1	$\times 10^{-4}$	$K^*(1680)^0\pi^+$	< 1.2	$\times 10^{-5}$	CL=90%	2358
$\chi_{c1}(1P)\pi^+$	$(2.2 \pm 0.5) \times 10^{-5}$	1468	$K^+\pi^0\pi^0$	$(1.62 \pm 0.19) \times 10^{-5}$			2610
$\chi_{c1}(1P)K^+$	$(4.85 \pm 0.33) \times 10^{-4}$	S=1.5 1412	$f_0(980)K^+ \times B(f_0 \rightarrow \pi^0\pi^0)$	$(2.8 \pm 0.8) \times 10^{-6}$			2522
$\chi_{c1}(1P)K^*(892)^+$	$(3.0 \pm 0.6) \times 10^{-4}$	S=1.1 1265	$K^-\pi^+\pi^+$	< 4.6	$\times 10^{-8}$	CL=90%	2609
$\chi_{c1}(1P)K^0\pi^+$	$(5.8 \pm 0.4) \times 10^{-4}$	1370	$K^-\pi^+\pi^+$ nonresonant	< 5.6	$\times 10^{-5}$	CL=90%	2609
$\chi_{c1}(1P)K^+\pi^0$	$(3.29 \pm 0.35) \times 10^{-4}$	1373	$K_1(1270)^0\pi^+$	< 4.0	$\times 10^{-5}$	CL=90%	2489
$\chi_{c1}(1P)K^+\pi^+\pi^-$	$(3.74 \pm 0.30) \times 10^{-4}$	1319	$K_1(1400)^0\pi^+$	< 3.9	$\times 10^{-5}$	CL=90%	2451
$\chi_{c1}(2P)K^+, \chi_{c1}(2P) \rightarrow$	< 1.1	$\times 10^{-5}$	$K^0\pi^+\pi^0$	< 6.6	$\times 10^{-5}$	CL=90%	2609
$\pi^+\pi^-\chi_{c1}(1P)$			$K^0\rho^+$	$(7.3 \pm 1.0) \times 10^{-6}$			2558
$\chi_{c2}K^+$	$(1.1 \pm 0.4) \times 10^{-5}$	1379	$K^*(892)^+\pi^+\pi^-$	$(7.5 \pm 1.0) \times 10^{-5}$			2557
$\chi_{c2}K^+, \chi_{c2} \rightarrow \rho\bar{\rho}\pi^+\pi^-$	< 1.9	$\times 10^{-7}$	$K^*(892)^+\rho^0$	$(4.6 \pm 1.1) \times 10^{-6}$			2504
$\chi_{c2}K^*(892)^+$	< 1.2	$\times 10^{-4}$	$K^*(892)^+f_0(980)$	$(4.2 \pm 0.7) \times 10^{-6}$			2466
$\chi_{c2}K^0\pi^+$	$(1.16 \pm 0.25) \times 10^{-4}$	1336	$a_1^+K^0$	$(3.5 \pm 0.7) \times 10^{-5}$			-
$\chi_{c2}K^+\pi^0$	< 6.2	$\times 10^{-5}$	$b_1^+K^0 \times B(b_1^+ \rightarrow \omega\pi^+)$	$(9.6 \pm 1.9) \times 10^{-6}$			-
$\chi_{c2}K^+\pi^+\pi^-$	$(1.34 \pm 0.19) \times 10^{-4}$	1284	$K^*(892)^0\rho^+$	$(9.2 \pm 1.5) \times 10^{-6}$			2504
$\chi_{c2}(3930)\pi^+, \chi_{c2} \rightarrow \pi^+\pi^-$	< 1	$\times 10^{-7}$	$K_1(1400)^+\rho^0$	< 7.8	$\times 10^{-4}$	CL=90%	2388
$h_c(1P)K^+$	$(3.7 \pm 1.2) \times 10^{-5}$	1401	$K_2^*(1430)^+\rho^0$	< 1.5	$\times 10^{-3}$	CL=90%	2381
$h_c(1P)K^+, h_c \rightarrow \rho\bar{\rho}$	< 6.4	$\times 10^{-8}$	$b_1^0K^+ \times B(b_1^0 \rightarrow \omega\pi^0)$	$(9.1 \pm 2.0) \times 10^{-6}$			-
			$b_1^+K^* \times B(b_1^+ \rightarrow \omega\pi^+)$	< 5.9	$\times 10^{-6}$	CL=90%	-
			$b_1^0K^* \times B(b_1^0 \rightarrow \omega\pi^0)$	< 6.7	$\times 10^{-6}$	CL=90%	-
K or K* modes			$K^+\bar{K}^0$	$(1.31 \pm 0.17) \times 10^{-6}$		S=1.2	2593
$K^0\pi^+$	$(2.37 \pm 0.08) \times 10^{-5}$	2614	$\bar{K}^0K^+\pi^0$	< 2.4	$\times 10^{-5}$	CL=90%	2578
$K^+\pi^0$	$(1.29 \pm 0.05) \times 10^{-5}$	2615	$K^+K_S^0K_S^0$	$(1.05 \pm 0.04) \times 10^{-5}$			2521
$\eta'K^+$	$(7.04 \pm 0.25) \times 10^{-5}$	2528	$f_0(980)K^+, f_0 \rightarrow K_S^0K_S^0$	$(1.47 \pm 0.33) \times 10^{-5}$			-
$\eta'K^*(892)^+$	$(4.8 \pm 1.8) \times 10^{-6}$	2472	$f_0(1710)K^+, f_0 \rightarrow K_S^0K_S^0$	$(4.8 \pm 4.0) \times 10^{-7}$			-
$\eta'K_S^0(1430)^+$	$(5.2 \pm 2.1) \times 10^{-6}$	-	$K^+K_S^0K_S^0$ nonresonant	$(2.0 \pm 0.4) \times 10^{-5}$			2521
$\eta'K_2^*(1430)^+$	$(2.8 \pm 0.5) \times 10^{-5}$	2346	$K_S^0K_S^0\pi^+$	< 5.1	$\times 10^{-7}$	CL=90%	2577
ηK^+	$(2.4 \pm 0.4) \times 10^{-6}$	S=1.7 2588	$K^+K^-\pi^+$	$(5.2 \pm 0.4) \times 10^{-6}$			2578
$\eta K^*(892)^+$	$(1.93 \pm 0.16) \times 10^{-5}$	2534	$K^+K^-\pi^+$ nonresonant	$(1.68 \pm 0.26) \times 10^{-6}$			2578
$\eta K_S^0(1430)^+$	$(1.8 \pm 0.4) \times 10^{-5}$	-	$K^+\bar{K}^*(892)^0$	$(5.9 \pm 0.8) \times 10^{-7}$			2540
$\eta K_2^*(1430)^+$	$(9.1 \pm 3.0) \times 10^{-6}$	2414	$K^+\bar{K}_0^0(1430)^0$	$(3.8 \pm 1.3) \times 10^{-7}$			2421
$\eta(1295)K^+ \times B(\eta(1295) \rightarrow$	$(2.9 \pm 0.8) \times 10^{-6}$	2455	$\pi^+(K^+K^-) s\text{-wave}$	$(8.5 \pm 0.9) \times 10^{-7}$			2578
$\eta\pi\pi)$			$K^+K^+\pi^-$	< 1.1	$\times 10^{-8}$	CL=90%	2578
$\eta(1405)K^+ \times B(\eta(1405) \rightarrow$	< 1.3	$\times 10^{-6}$	$K^+K^+\pi^-$ nonresonant	< 8.79	$\times 10^{-5}$	CL=90%	2578
$\eta\pi\pi)$			$f_2'(1525)K^+$	$(1.8 \pm 0.5) \times 10^{-6}$		S=1.1	2394
$\eta(1405)K^+ \times B(\eta(1405) \rightarrow$	< 1.2	$\times 10^{-6}$	$K^*+\pi^+K^-$	< 1.18	$\times 10^{-5}$	CL=90%	2524
$K^*K)$			$K^*(892)^+K^*(892)^0$	$(9.1 \pm 2.9) \times 10^{-7}$			2485
$\eta(1475)K^+ \times B(\eta(1475) \rightarrow$	$(1.38 \pm 0.21) \times 10^{-5}$	2407	$K^*+K^+\pi^-$	< 6.1	$\times 10^{-6}$	CL=90%	2524
$K^*K)$			$K^+K^-K^+$	$(3.40 \pm 0.14) \times 10^{-5}$		S=1.4	2523
$f_1(1285)K^+$	< 2.0	$\times 10^{-6}$	$K^+\phi$	$(8.8 \pm 0.7) \times 10^{-6}$		S=1.1	2516
$f_1(1420)K^+ \times B(f_1(1420) \rightarrow$	< 2.9	$\times 10^{-6}$	$f_0(980)K^+ \times B(f_0(980) \rightarrow$	$(9.4 \pm 3.2) \times 10^{-6}$			2522
$\eta\pi\pi)$			$K^+K^-)$				
$f_1(1420)K^+ \times B(f_1(1420) \rightarrow$	< 4.1	$\times 10^{-6}$	$a_2(1320)K^+ \times$	< 1.1	$\times 10^{-6}$	CL=90%	2449
$K^*K)$			$B(a_2(1320) \rightarrow K^+K^-)$				
$\phi(1680)K^+ \times B(\phi(1680) \rightarrow$	< 3.4	$\times 10^{-6}$	$X_0(1550)K^+ \times$	$(4.3 \pm 0.7) \times 10^{-6}$			-
$K^*K)$			$B(X_0(1550) \rightarrow K^+K^-)$				
$f_0(1500)K^+$	$(3.7 \pm 2.2) \times 10^{-6}$	2398	$\phi(1680)K^+ \times B(\phi(1680) \rightarrow$	< 8	$\times 10^{-7}$	CL=90%	2344
ωK^+	$(6.5 \pm 0.4) \times 10^{-6}$	2558	$K^+K^-)$				
$\omega K^*(892)^+$	< 7.4	$\times 10^{-6}$	$f_0(1710)K^+ \times B(f_0(1710) \rightarrow$	$(1.1 \pm 0.6) \times 10^{-6}$			2336
$\omega(K\pi)_0^{*+}$	$(2.8 \pm 0.4) \times 10^{-5}$	-	$K^+K^-)$				
$\omega K_0^*(1430)^+$	$(2.4 \pm 0.5) \times 10^{-5}$	-	$K^+K^-\pi^+$ nonresonant	$(2.38 \pm 0.28) \times 10^{-5}$			2523
$\omega K_2^*(1430)^+$	$(2.1 \pm 0.4) \times 10^{-5}$	2379	$K^*(892)^+K^+K^-$	$(3.6 \pm 0.5) \times 10^{-5}$			2466
$a_0(980)^+K^0 \times B(a_0(980)^+ \rightarrow$	< 3.9	$\times 10^{-6}$	$K^*(892)^+\phi$	$(10.0 \pm 2.0) \times 10^{-6}$		S=1.7	2460
$\eta\pi^+)$			$\phi(K\pi)_0^{*+}$	$(8.3 \pm 1.6) \times 10^{-6}$			-
$a_0(980)^0K^+ \times B(a_0(980)^0 \rightarrow$	< 2.5	$\times 10^{-6}$	$\phi K_1(1270)^+$	$(6.1 \pm 1.9) \times 10^{-6}$			2380
$\eta\pi^0)$			$\phi K_1(1400)^+$	< 3.2	$\times 10^{-6}$	CL=90%	2339
$K^*(892)^0\pi^+$	$(1.01 \pm 0.08) \times 10^{-5}$	2562	$\phi K^*(1410)^+$	< 4.3	$\times 10^{-6}$	CL=90%	-
$K^*(892)^+\pi^0$	$(6.8 \pm 0.9) \times 10^{-6}$	2563	$\phi K_0^*(1430)^+$	$(7.0 \pm 1.6) \times 10^{-6}$			-
$K^+\pi^-\pi^+$	$(5.10 \pm 0.29) \times 10^{-5}$	2609	$\phi K_2^*(1430)^+$	$(8.4 \pm 2.1) \times 10^{-6}$			2332
$K^+\pi^-\pi^+$ nonresonant	$(1.63 \pm 0.21) \times 10^{-5}$	2609	$\phi K_2^*(1770)^+$	< 1.50	$\times 10^{-5}$	CL=90%	-
$\omega(782)K^+$	$(6 \pm 9) \times 10^{-6}$	2558					
$K^+f_0(980) \times B(f_0(980) \rightarrow$	$(9.4 \pm 1.0) \times 10^{-6}$	2522					
$\pi^+\pi^-)$							
$f_2(1270)^0K^+$	$(1.07 \pm 0.27) \times 10^{-6}$	-					

Meson Summary Table

$\phi K_2^*(1820)^+$	$< 1.63 \times 10^{-5}$	CL=90%	-
$a_1^+ K^{*0}$	$< 3.6 \times 10^{-6}$	CL=90%	-
$K^+ \phi$	$(5.0 \pm 1.2) \times 10^{-6}$	S=2.3	2306
$\eta' \eta' K^+$	$< 2.5 \times 10^{-5}$	CL=90%	2338
$\omega \phi K^+$	$< 1.9 \times 10^{-6}$	CL=90%	2374
$X(1812) K^+ \times B(X \rightarrow \omega \phi)$	$< 3.2 \times 10^{-7}$	CL=90%	-
$K^*(892)^+ \gamma$	$(3.92 \pm 0.22) \times 10^{-5}$	S=1.7	2564
$K_1(1270)^+ \gamma$	$(4.4 \pm 0.7) \times 10^{-5}$		2491
$\eta K^+ \gamma$	$(7.9 \pm 0.9) \times 10^{-6}$		2588
$\eta' K^+ \gamma$	$(2.9 \pm 1.0) \times 10^{-6}$		2528
$\phi K^+ \gamma$	$(2.7 \pm 0.4) \times 10^{-6}$	S=1.2	2516
$K^+ \pi^- \pi^+ \gamma$	$(2.58 \pm 0.15) \times 10^{-5}$	S=1.3	2609
$K^*(892)^0 \pi^+ \gamma$	$(2.33 \pm 0.12) \times 10^{-5}$		2562
$K^+ \rho^0 \gamma$	$(8.2 \pm 0.9) \times 10^{-6}$		2559
$(K^+ \pi^-)_{NR} \pi^+ \gamma$	$(9.9 \pm 1.7) \times 10^{-6}$		2609
$K^0 \pi^+ \pi^0 \gamma$	$(4.6 \pm 0.5) \times 10^{-5}$		2609
$K_1(1400)^+ \gamma$	$(10 \pm 5) \times 10^{-6}$		2453
$K^*(1410)^+ \gamma$	$(2.7 \pm 0.8) \times 10^{-5}$		-
$K_0^*(1430)^0 \pi^+ \gamma$	$(1.32 \pm 0.26) \times 10^{-6}$		2445
$K_2^*(1430)^+ \gamma$	$(1.4 \pm 0.4) \times 10^{-5}$		2447
$K^*(1680)^+ \gamma$	$(6.7 \pm 1.7) \times 10^{-5}$		2360
$K_3^*(1780)^+ \gamma$	$< 3.9 \times 10^{-5}$	CL=90%	2341
$K_4^*(2045)^+ \gamma$	$< 9.9 \times 10^{-3}$	CL=90%	2242

Light unflavored meson modes

$\rho^+ \gamma$	$(9.8 \pm 2.5) \times 10^{-7}$		2583
$\pi^+ \pi^0$	$(5.5 \pm 0.4) \times 10^{-6}$	S=1.2	2636
$\pi^+ \pi^+ \pi^-$	$(1.52 \pm 0.14) \times 10^{-5}$		2630
$\rho^0 \pi^+$	$(8.3 \pm 1.2) \times 10^{-6}$		2581
$\pi^+ f_0(980), f_0 \rightarrow \pi^+ \pi^-$	$< 1.5 \times 10^{-6}$	CL=90%	2545
$\pi^+ f_2(1270)$	$(2.2 \pm 0.7) \times 10^{-6}$		2484
$\rho(1450)^0 \pi^+, \rho^0 \rightarrow \pi^+ \pi^-$	$(1.4 \pm 0.6) \times 10^{-6}$		2434
$\rho(1450)^0 \pi^+, \rho^0 \rightarrow K^+ K^-$	$(1.60 \pm 0.14) \times 10^{-6}$		-
$f_0(1370) \pi^+, f_0 \rightarrow \pi^+ \pi^-$	$< 4.0 \times 10^{-6}$	CL=90%	2460
$f_0(500) \pi^+, f_0 \rightarrow \pi^+ \pi^-$	$< 4.1 \times 10^{-6}$	CL=90%	-
$\pi^+ \pi^- \pi^+$ nonresonant	$(5.3 \pm 1.5) \times 10^{-6}$		2630
$\pi^+ \pi^0 \pi^0$	$< 8.9 \times 10^{-4}$	CL=90%	2631
$\rho^+ \pi^0$	$(1.09 \pm 0.14) \times 10^{-5}$		2581
$\pi^+ \pi^- \pi^+ \pi^0$	$< 4.0 \times 10^{-3}$	CL=90%	2622
$\rho^+ \rho^0$	$(2.40 \pm 0.19) \times 10^{-5}$		2523
$\rho^+ f_0(980), f_0 \rightarrow \pi^+ \pi^-$	$< 2.0 \times 10^{-6}$	CL=90%	2486
$a_1(1260)^+ \pi^0$	$(2.6 \pm 0.7) \times 10^{-5}$		2494
$a_1(1260)^0 \pi^+$	$(2.0 \pm 0.6) \times 10^{-5}$		2494
$\omega \pi^+$	$(6.9 \pm 0.5) \times 10^{-6}$		2580
$\omega \rho^+$	$(1.59 \pm 0.21) \times 10^{-5}$		2522
$\eta \pi^+$	$(4.02 \pm 0.27) \times 10^{-6}$		2609
$\eta \rho^+$	$(7.0 \pm 2.9) \times 10^{-6}$	S=2.8	2553
$\eta' \pi^+$	$(2.7 \pm 0.9) \times 10^{-6}$	S=1.9	2551
$\eta' \rho^+$	$(9.7 \pm 2.2) \times 10^{-6}$		2492
$\phi \pi^+$	$(3.2 \pm 1.5) \times 10^{-8}$		2539
$\phi \rho^+$	$< 3.0 \times 10^{-6}$	CL=90%	2480
$a_0(980)^0 \pi^+, a_0^0 \rightarrow \eta \pi^0$	$< 5.8 \times 10^{-6}$	CL=90%	-
$a_0(980)^+ \pi^0, a_0^+ \rightarrow \eta \pi^+$	$< 1.4 \times 10^{-6}$	CL=90%	-
$\pi^+ \pi^+ \pi^+ \pi^- \pi^-$	$< 8.6 \times 10^{-4}$	CL=90%	2608
$\rho^0 a_1(1260)^+$	$< 6.2 \times 10^{-4}$	CL=90%	2433
$\rho^0 a_2(1320)^+$	$< 7.2 \times 10^{-4}$	CL=90%	2411
$b_1^0 \pi^+, b_1^0 \rightarrow \omega \pi^0$	$(6.7 \pm 2.0) \times 10^{-6}$		-
$b_1^+ \pi^0, b_1^+ \rightarrow \omega \pi^+$	$< 3.3 \times 10^{-6}$	CL=90%	-
$\pi^+ \pi^+ \pi^+ \pi^- \pi^-$	$< 6.3 \times 10^{-3}$	CL=90%	2592
$b_1^+ \rho^0, b_1^+ \rightarrow \omega \pi^+$	$< 5.2 \times 10^{-6}$	CL=90%	-
$a_1(1260)^+ a_1(1260)^0$	< 1.3	CL=90%	2336
$b_1^0 \rho^+, b_1^0 \rightarrow \omega \pi^0$	$< 3.3 \times 10^{-6}$	CL=90%	-

Charged particle (h^\pm) modes

$h^\pm = K^\pm$ or π^\pm			
$h^+ \pi^0$	$(1.6 \pm 0.7) \times 10^{-5}$		2636
ωh^+	$(1.38 \pm 0.27) \times 10^{-5}$		2580
$h^+ X^0$ (Familon)	$< 4.9 \times 10^{-5}$	CL=90%	-
$K^+ X^0, X^0 \rightarrow \mu^+ \mu^-$	$< 1 \times 10^{-7}$	CL=95%	-

Baryon modes

$p \bar{p} \pi^+$	$(1.62 \pm 0.20) \times 10^{-6}$		2439
$p \bar{p} \pi^+$ nonresonant	$< 5.3 \times 10^{-5}$	CL=90%	2439
$p \bar{p} K^+$	$(5.9 \pm 0.5) \times 10^{-6}$	S=1.5	2348
$\Theta(1710)^{++} \bar{p}, \Theta^{++} \rightarrow p K^+$	[sss] $< 9.1 \times 10^{-8}$	CL=90%	-
$f_J(2220) K^+, f_J \rightarrow p \bar{p}$	[sss] $< 4.1 \times 10^{-7}$	CL=90%	2135
$\rho \bar{\Lambda}(1520)$	$(3.1 \pm 0.6) \times 10^{-7}$		2322
$\rho \bar{p} K^+$ nonresonant	$< 8.9 \times 10^{-5}$	CL=90%	2348
$\rho \bar{p} K^*(892)^+$	$(3.6 \pm 0.8) \times 10^{-6}$		2215
$f_J(2220) K^{*+}, f_J \rightarrow p \bar{p}$	$< 7.7 \times 10^{-7}$	CL=90%	2059
$\rho \bar{\Lambda}$	$(2.4 \pm 1.0) \times 10^{-7}$		2430
$\rho \bar{\Lambda} \gamma$	$(2.4 \pm 0.5) \times 10^{-6}$		2430
$\rho \bar{\Lambda} \pi^0$	$(3.0 \pm 0.7) \times 10^{-6}$		2402
$\rho \bar{\Sigma}(1385)^0$	$< 4.7 \times 10^{-7}$	CL=90%	2362
$\Delta^+ \bar{\Lambda}$	$< 8.2 \times 10^{-7}$	CL=90%	-
$\rho \bar{\Sigma} \gamma$	$< 4.6 \times 10^{-6}$	CL=90%	2413
$\rho \bar{\Lambda} \pi^+ \pi^-$	$(1.13 \pm 0.13) \times 10^{-5}$		2367
$\rho \bar{\Lambda} \pi^+ \pi^-$ nonresonant	$(5.9 \pm 1.1) \times 10^{-6}$		2367
$\rho \bar{\Lambda} \rho^0, \rho^0 \rightarrow \pi^+ \pi^-$	$(4.8 \pm 0.9) \times 10^{-6}$		2214
$\rho \bar{\Lambda} f_2(1270), f_2 \rightarrow \pi^+ \pi^-$	$(2.0 \pm 0.8) \times 10^{-6}$		2026
$\rho \bar{\Lambda} K^+ K^-$	$(4.1 \pm 0.7) \times 10^{-6}$		2132
$\rho \bar{\Lambda} \phi$	$(8.0 \pm 2.2) \times 10^{-7}$		2119
$\bar{p} \Lambda K^+ K^-$	$(3.7 \pm 0.6) \times 10^{-6}$		2132
$\bar{\Lambda} \bar{\Lambda} \pi^+$	$< 9.4 \times 10^{-7}$	CL=90%	2358
$\bar{\Lambda} \bar{\Lambda} K^+$	$(3.4 \pm 0.6) \times 10^{-6}$		2251
$\bar{\Lambda} \bar{\Lambda} K^{*+}$	$(2.2 \pm 1.2) \times 10^{-6}$		2098
$\bar{\Lambda}(1520) \bar{\Lambda} K^+$	$(2.2 \pm 0.7) \times 10^{-6}$		2126
$\bar{\Lambda} \bar{\Lambda}(1520) K^+$	$< 2.08 \times 10^{-6}$		2126
$\bar{\Delta}^0 \rho$	$< 1.38 \times 10^{-6}$	CL=90%	2403
$\Delta^{++} \bar{p}$	$< 1.4 \times 10^{-7}$	CL=90%	2403
$D^+ p \bar{p}$	$< 1.5 \times 10^{-5}$	CL=90%	1860
$D^*(2010)^+ p \bar{p}$	$< 1.5 \times 10^{-5}$	CL=90%	1786
$\bar{D}^0 p \bar{p} \pi^+$	$(3.72 \pm 0.27) \times 10^{-4}$		1789
$\bar{D}^{*0} p \bar{p} \pi^+$	$(3.73 \pm 0.32) \times 10^{-4}$		1709
$D^- p \bar{p} \pi^+ \pi^-$	$(1.66 \pm 0.30) \times 10^{-4}$		1705
$D^{*-} p \bar{p} \pi^+ \pi^-$	$(1.86 \pm 0.25) \times 10^{-4}$		1621
$\rho \bar{\Lambda}^0 \bar{D}^0$	$(1.43 \pm 0.32) \times 10^{-5}$		-
$\rho \bar{\Lambda}^0 \bar{D}^*(2007)^0$	$< 5 \times 10^{-5}$	CL=90%	-
$\bar{\Lambda}_c^- p \pi^+$	$(2.3 \pm 0.4) \times 10^{-4}$	S=2.2	1980
$\bar{\Lambda}_c^- \Delta(1232)^{++}$	$< 1.9 \times 10^{-5}$	CL=90%	1928
$\bar{\Lambda}_c^- \Delta_X(1600)^{++}$	$(4.7 \pm 1.0) \times 10^{-5}$		-
$\bar{\Lambda}_c^- \Delta_X(2420)^{++}$	$(3.7 \pm 0.8) \times 10^{-5}$		-
$(\bar{\Lambda}_c^- p)_s \pi^+$	[ttt] $(3.1 \pm 0.7) \times 10^{-5}$		-
$\bar{\Sigma}_c^-(2520)^0 p$	$< 3 \times 10^{-6}$	CL=90%	1904
$\bar{\Sigma}_c^-(2800)^0 p$	$(2.6 \pm 0.9) \times 10^{-5}$		-
$\bar{\Lambda}_c^- p \pi^+ \pi^0$	$(1.8 \pm 0.6) \times 10^{-3}$		1935
$\bar{\Lambda}_c^- p \pi^+ \pi^+ \pi^-$	$(2.2 \pm 0.7) \times 10^{-3}$		1880
$\bar{\Lambda}_c^- p \pi^+ \pi^+ \pi^- \pi^0$	< 1.34	CL=90%	1823
$\Lambda_c^+ \bar{\Lambda}_c^- K^+$	$(4.9 \pm 0.7) \times 10^{-4}$		739
$\Xi_c^-(2930) \Lambda_c^+, \Xi_c^- \rightarrow K^+ \Lambda_c^-$	$(1.7 \pm 0.5) \times 10^{-4}$		-
$\bar{\Sigma}_c^-(2455)^0 p$	$(2.9 \pm 0.7) \times 10^{-5}$		1938
$\bar{\Sigma}_c^-(2455)^0 p \pi^0$	$(3.5 \pm 1.1) \times 10^{-4}$		1896
$\bar{\Sigma}_c^-(2455)^0 p \pi^- \pi^+$	$(3.5 \pm 1.1) \times 10^{-4}$		1845
$\bar{\Sigma}_c^-(2455)^0 p \pi^+ \pi^+$	$(2.37 \pm 0.20) \times 10^{-4}$		1845
$\bar{\Lambda}_c^-(2593)^- / \bar{\Lambda}_c^-(2625)^- p \pi^+$	$< 1.9 \times 10^{-4}$	CL=90%	-
$\Xi_c^0 \Lambda_c^+$	$(9.5 \pm 2.3) \times 10^{-4}$		1144
$\Xi_c^0 \Lambda_c^+, \Xi_c^0 \rightarrow \Xi^+ \pi^-$	$(1.76 \pm 0.29) \times 10^{-5}$		1144
$\Xi_c^0 \Lambda_c^+, \Xi_c^0 \rightarrow \Lambda K^+ \pi^-$	$(1.14 \pm 0.26) \times 10^{-5}$		1144
$\Xi_c^0 \Lambda_c^+, \Xi_c^0 \rightarrow p K^- K^- \pi^+$	$(5.5 \pm 1.9) \times 10^{-6}$		-
$\Lambda_c^+ \Xi_c^0$	$< 6.5 \times 10^{-4}$	CL=90%	1023
$\Lambda_c^+ \Xi_c^-(2645)^0$	$< 7.9 \times 10^{-4}$	CL=90%	-
$\Lambda_c^+ \Xi_c^-(2790)^0$	$(1.1 \pm 0.4) \times 10^{-3}$		-

Lepton Family number (LF) or Lepton number (L) or Baryon number (B) violating modes, or/and $\Delta B = 1$ weak neutral current (BI) modes

$\pi^+ \ell^+ \ell^-$	BI	$< 4.9 \times 10^{-8}$	CL=90%	2638
$\pi^+ e^+ e^-$	BI	$< 8.0 \times 10^{-8}$	CL=90%	2638
$\pi^+ \mu^+ \mu^-$	BI	$(1.75 \pm 0.22) \times 10^{-8}$		2634
$\pi^+ \nu \bar{\nu}$	BI	$< 1.4 \times 10^{-5}$	CL=90%	2638
$K^+ \ell^+ \ell^-$	BI	[III] $(4.51 \pm 0.23) \times 10^{-7}$	S=1.1	2617
$K^+ e^+ e^-$	BI	$(5.5 \pm 0.7) \times 10^{-7}$		2617
$K^+ \mu^+ \mu^-$	BI	$(4.41 \pm 0.22) \times 10^{-7}$	S=1.2	2612

Meson Summary Table

$S_{D^{*+}D^-} (B^0 \rightarrow D^{*+}D^-) = -0.59 \pm 0.14$ (S = 1.8)	$S_{\pi\pi} (B^0 \rightarrow \pi^+\pi^-) = -0.65 \pm 0.04$
$C_+ (B^0 \rightarrow D^{*+}D^-) = 0.00 \pm 0.10$ (S = 1.6)	$C_{\rho^0\pi^0} (B^0 \rightarrow \rho^0\pi^0) = -0.33 \pm 0.22$
$S_+ (B^0 \rightarrow D^{*+}D^-) = -0.73 \pm 0.09$	$C_{\rho\pi} (B^0 \rightarrow \rho^+\pi^-) = -0.03 \pm 0.07$ (S = 1.2)
$C_- (B^0 \rightarrow D^{*+}D^-) = 0.19 \pm 0.31$	$S_{\rho\pi} (B^0 \rightarrow \rho^+\pi^-) = 0.05 \pm 0.07$
$S_- (B^0 \rightarrow D^{*+}D^-) = 0.1 \pm 1.6$ (S = 3.5)	$\Delta C_{\rho\pi} (B^0 \rightarrow \rho^+\pi^-) = 0.27 \pm 0.06$
$C (B^0 \rightarrow D^*(2010)^+D^*(2010)^-K_S^0) = 0.01 \pm 0.29$	$\Delta S_{\rho\pi} (B^0 \rightarrow \rho^+\pi^-) = 0.01 \pm 0.08$
$S (B^0 \rightarrow D^*(2010)^+D^*(2010)^-K_S^0) = 0.1 \pm 0.4$	$C_{\rho^0\pi^0} (B^0 \rightarrow \rho^0\pi^0) = 0.27 \pm 0.24$
$C_{D^+D^-} (B^0 \rightarrow D^+D^-) = -0.22 \pm 0.24$ (S = 2.5)	$S_{\rho^0\pi^0} (B^0 \rightarrow \rho^0\pi^0) = -0.23 \pm 0.34$
$S_{D^+D^-} (B^0 \rightarrow D^+D^-) = -0.76^{+0.15}_{-0.13}$ (S = 1.2)	$C_{a_1\pi} (B^0 \rightarrow a_1(1260)^+\pi^-) = -0.05 \pm 0.11$
$C_{J/\psi(1S)\pi^0} (B^0 \rightarrow J/\psi(1S)\pi^0) = 0.03 \pm 0.17$ (S = 1.5)	$S_{a_1\pi} (B^0 \rightarrow a_1(1260)^+\pi^-) = -0.2 \pm 0.4$ (S = 3.2)
$S_{J/\psi(1S)\pi^0} (B^0 \rightarrow J/\psi(1S)\pi^0) = -0.88 \pm 0.32$ (S = 2.2)	$\Delta C_{a_1\pi} (B^0 \rightarrow a_1(1260)^+\pi^-) = 0.43 \pm 0.14$ (S = 1.3)
$C (B^0 \rightarrow J/\psi(1S)\rho^0) = -0.06 \pm 0.06$	$\Delta S_{a_1\pi} (B^0 \rightarrow a_1(1260)^+\pi^-) = -0.11 \pm 0.12$
$S (B^0 \rightarrow J/\psi(1S)\rho^0) = -0.66^{+0.16}_{-0.12}$	$C (B^0 \rightarrow b_1^-K^+) = -0.22 \pm 0.24$
$C_{D_{CP}^{(*)}h^0} (B^0 \rightarrow D_{CP}^{(*)}h^0) = -0.02 \pm 0.08$	$\Delta C (B^0 \rightarrow b_1^-K^+) = -1.04 \pm 0.24$
$S_{D_{CP}^{(*)}h^0} (B^0 \rightarrow D_{CP}^{(*)}h^0) = -0.66 \pm 0.12$	$C_{\rho^0\rho^0} (B^0 \rightarrow \rho^0\rho^0) = 0.2 \pm 0.9$
$C_{K^0\pi^0} (B^0 \rightarrow K^0\pi^0) = 0.00 \pm 0.13$ (S = 1.4)	$S_{\rho^0\rho^0} (B^0 \rightarrow \rho^0\rho^0) = 0.3 \pm 0.7$
$S_{K^0\pi^0} (B^0 \rightarrow K^0\pi^0) = 0.58 \pm 0.17$	$C_{\rho\rho} (B^0 \rightarrow \rho^+\rho^-) = 0.00 \pm 0.09$
$C_{\eta'(958)K_S^0} (B^0 \rightarrow \eta'(958)K_S^0) = -0.04 \pm 0.20$ (S = 2.5)	$S_{\rho\rho} (B^0 \rightarrow \rho^+\rho^-) = -0.14 \pm 0.13$
$S_{\eta'(958)K_S^0} (B^0 \rightarrow \eta'(958)K_S^0) = 0.43 \pm 0.17$ (S = 1.5)	$ \lambda (B^0 \rightarrow J/\psi K^*(892)^0) < 0.25$, CL = 95%
$C_{\eta'K^0} (B^0 \rightarrow \eta'K^0) = -0.06 \pm 0.04$	$\cos 2\beta (B^0 \rightarrow J/\psi K^*(892)^0) = 1.7^{+0.7}_{-0.9}$ (S = 1.6)
$S_{\eta'K^0} (B^0 \rightarrow \eta'K^0) = 0.63 \pm 0.06$	$\cos 2\beta (B^0 \rightarrow [K_S^0\pi^+\pi^-]_{D^{(*)}h^0}) = 0.91 \pm 0.25$
$C_{\omega K_S^0} (B^0 \rightarrow \omega K_S^0) = 0.0 \pm 0.4$ (S = 3.0)	$(S_+ + S_-)/2 (B^0 \rightarrow D^{*-}\pi^+) = -0.039 \pm 0.011$
$S_{\omega K_S^0} (B^0 \rightarrow \omega K_S^0) = 0.70 \pm 0.21$	$(S_- - S_+)/2 (B^0 \rightarrow D^{*-}\pi^+) = -0.009 \pm 0.015$
$C (B^0 \rightarrow K_S^0\pi^0\pi^0) = -0.21 \pm 0.20$	$(S_+ + S_-)/2 (B^0 \rightarrow D^-\pi^+) = -0.046 \pm 0.023$
$S (B^0 \rightarrow K_S^0\pi^0\pi^0) = 0.89^{+0.27}_{-0.30}$	$(S_- - S_+)/2 (B^0 \rightarrow D^-\pi^+) = -0.022 \pm 0.021$
$C_{\rho^0 K_S^0} (B^0 \rightarrow \rho^0 K_S^0) = -0.04 \pm 0.20$	$S_+ (B^0 \rightarrow D^-\pi^+) = 0.058 \pm 0.023$
$S_{\rho^0 K_S^0} (B^0 \rightarrow \rho^0 K_S^0) = 0.50^{+0.17}_{-0.21}$	$S_- (B^0 \rightarrow D^+\pi^-) = 0.038 \pm 0.021$
$C_{f_0 K_S^0} (B^0 \rightarrow f_0(980)K_S^0) = 0.29 \pm 0.20$	$(S_+ + S_-)/2 (B^0 \rightarrow D^-\rho^+) = -0.024 \pm 0.032$
$S_{f_0 K_S^0} (B^0 \rightarrow f_0(980)K_S^0) = -0.50 \pm 0.16$	$(S_- - S_+)/2 (B^0 \rightarrow D^-\rho^+) = -0.10 \pm 0.06$
$S_{f_2 K_S^0} (B^0 \rightarrow f_2(1270)K_S^0) = -0.5 \pm 0.5$	$C_{\eta_c K_S^0} (B^0 \rightarrow \eta_c K_S^0) = 0.08 \pm 0.13$
$C_{f_2 K_S^0} (B^0 \rightarrow f_2(1270)K_S^0) = 0.3 \pm 0.4$	$S_{\eta_c K_S^0} (B^0 \rightarrow \eta_c K_S^0) = 0.93 \pm 0.17$
$S_{f_x K_S^0} (B^0 \rightarrow f_x(1300)K_S^0) = -0.2 \pm 0.5$	$C_{c\bar{c}K^{(*)0}} (B^0 \rightarrow c\bar{c}K^{(*)0}) = (0.5 \pm 1.7) \times 10^{-2}$
$C_{f_x K_S^0} (B^0 \rightarrow f_x(1300)K_S^0) = 0.13 \pm 0.35$	$\sin(2\beta) = 0.695 \pm 0.019$
$S_{K^0\pi^+\pi^-} (B^0 \rightarrow K^0\pi^+\pi^- \text{ nonresonant}) = -0.01 \pm 0.33$	$C_{J/\psi(nS)K^0} (B^0 \rightarrow J/\psi(nS)K^0) = (0.5 \pm 2.0) \times 10^{-2}$
$C_{K^0\pi^+\pi^-} (B^0 \rightarrow K^0\pi^+\pi^- \text{ nonresonant}) = 0.01 \pm 0.26$	$S_{J/\psi(nS)K^0} (B^0 \rightarrow J/\psi(nS)K^0) = 0.701 \pm 0.017$
$C_{K_S^0 K_S^0} (B^0 \rightarrow K_S^0 K_S^0) = 0.0 \pm 0.4$ (S = 1.4)	$C_{J/\psi K^{*0}} (B^0 \rightarrow J/\psi K^{*0}) = 0.03 \pm 0.10$
$S_{K_S^0 K_S^0} (B^0 \rightarrow K_S^0 K_S^0) = -0.8 \pm 0.5$	$S_{J/\psi K^{*0}} (B^0 \rightarrow J/\psi K^{*0}) = 0.60 \pm 0.25$
$C_{K^+K^-K_S^0} (B^0 \rightarrow K^+K^-K_S^0 \text{ nonresonant}) = 0.06 \pm 0.08$	$C_{\chi_{c0} K_S^0} (B^0 \rightarrow \chi_{c0} K_S^0) = -0.3^{+0.5}_{-0.4}$
$S_{K^+K^-K_S^0} (B^0 \rightarrow K^+K^-K_S^0 \text{ nonresonant}) = -0.66 \pm 0.11$	$S_{\chi_{c0} K_S^0} (B^0 \rightarrow \chi_{c0} K_S^0) = -0.7 \pm 0.5$
$C_{K^+K^-K_S^0} (B^0 \rightarrow K^+K^-K_S^0 \text{ inclusive}) = 0.01 \pm 0.09$	$C_{\chi_{c1} K_S^0} (B^0 \rightarrow \chi_{c1} K_S^0) = 0.06 \pm 0.07$
$S_{K^+K^-K_S^0} (B^0 \rightarrow K^+K^-K_S^0 \text{ inclusive}) = -0.65 \pm 0.12$	$S_{\chi_{c1} K_S^0} (B^0 \rightarrow \chi_{c1} K_S^0) = 0.63 \pm 0.10$
$C_{\phi K_S^0} (B^0 \rightarrow \phi K_S^0) = 0.01 \pm 0.14$	$\sin(2\beta_{\text{eff}})(B^0 \rightarrow \phi K^0) = 0.22 \pm 0.30$
$S_{\phi K_S^0} (B^0 \rightarrow \phi K_S^0) = 0.59 \pm 0.14$	$\sin(2\beta_{\text{eff}})(B^0 \rightarrow \phi K_0^*(1430)^0) = 0.97^{+0.03}_{-0.52}$
$C_{K_S K_S K_S} (B^0 \rightarrow K_S K_S K_S) = -0.23 \pm 0.14$	$\sin(2\beta_{\text{eff}})(B^0 \rightarrow [K_S^0\pi^+\pi^-]_{D^{(*)}h^0}) = 0.80 \pm 0.16$
$S_{K_S K_S K_S} (B^0 \rightarrow K_S K_S K_S) = -0.5 \pm 0.6$ (S = 3.0)	$\beta_{\text{eff}} (B^0 \rightarrow [K_S^0\pi^+\pi^-]_{D^{(*)}h^0}) = (22 \pm 5)^\circ$
$C_{K_S^0\pi^0\gamma} (B^0 \rightarrow K_S^0\pi^0\gamma) = 0.36 \pm 0.33$	$2\beta_{\text{eff}} (B^0 \rightarrow J/\psi\rho^0) = (42^{+10}_{-11})^\circ$
$S_{K_S^0\pi^0\gamma} (B^0 \rightarrow K_S^0\pi^0\gamma) = -0.8 \pm 0.6$	$ \lambda (B^0 \rightarrow [K_S^0\pi^+\pi^-]_{D^{(*)}h^0}) = 1.01 \pm 0.08$
$C_{K_S^0\pi^+\pi^-\gamma} (B^0 \rightarrow K_S^0\pi^+\pi^-\gamma) = -0.39 \pm 0.20$	$ \sin(2\beta + \gamma) > 0.40$, CL = 90%
$S_{K_S^0\pi^+\pi^-\gamma} (B^0 \rightarrow K_S^0\pi^+\pi^-\gamma) = 0.14 \pm 0.25$	$2\beta + \gamma = (83 \pm 60)^\circ$
$C_{K^{*0}\gamma} (B^0 \rightarrow K^*(892)^0\gamma) = -0.04 \pm 0.16$ (S = 1.2)	$\alpha = (84.9^{+5.1}_{-4.5})^\circ$
$S_{K^{*0}\gamma} (B^0 \rightarrow K^*(892)^0\gamma) = -0.15 \pm 0.22$	$x_+ (B^0 \rightarrow DK^{*0}) = 0.04 \pm 0.17$
$C_{\eta K^0\gamma} (B^0 \rightarrow \eta K^0\gamma) = 0.1 \pm 0.4$ (S = 1.4)	$x_- (B^0 \rightarrow DK^{*0}) = -0.16 \pm 0.14$
$S_{\eta K^0\gamma} (B^0 \rightarrow \eta K^0\gamma) = -0.5 \pm 0.5$ (S = 1.2)	$y_+ (B^0 \rightarrow DK^{*0}) = -0.68 \pm 0.22$
$C_{K^0\phi\gamma} (B^0 \rightarrow K^0\phi\gamma) = -0.3 \pm 0.6$	$y_- (B^0 \rightarrow DK^{*0}) = 0.20 \pm 0.25$ (S = 1.2)
$S_{K^0\phi\gamma} (B^0 \rightarrow K^0\phi\gamma) = 0.7^{+0.7}_{-1.1}$	$r_{B^0} (B^0 \rightarrow DK^{*0}) = 0.220^{+0.041}_{-0.047}$
$C (B^0 \rightarrow K_S^0\rho^0\gamma) = -0.05 \pm 0.19$	$\delta_{B^0} (B^0 \rightarrow DK^{*0}) = (194^{+30}_{-22})^\circ$
$S (B^0 \rightarrow K_S^0\rho^0\gamma) = -0.04 \pm 0.23$	
$C (B^0 \rightarrow \rho^0\gamma) = 0.4 \pm 0.5$	
$S (B^0 \rightarrow \rho^0\gamma) = -0.8 \pm 0.7$	
$C_{\pi\pi} (B^0 \rightarrow \pi^+\pi^-) = -0.32 \pm 0.04$	

\bar{B}^0 modes are charge conjugates of the modes below. Reactions indicate the weak decay vertex and do not include mixing. Modes which do not identify the charge state of the B are listed in the B^\pm/B^0 ADMIXTURE section.

The branching fractions listed below assume 50% $B^0\bar{B}^0$ and 50% B^+B^- production at the $\Upsilon(4S)$. We have attempted to bring older measurements up to date by rescaling their assumed $\Upsilon(4S)$ production ratio to 50:50 and their assumed D, D_s, D^* , and ψ branching ratios to current values whenever this would affect our averages and best limits significantly.

Meson Summary Table

Indentation is used to indicate a subchannel of a previous reaction. All resonant subchannels have been corrected for resonance branching fractions to the final state so the sum of the subchannel branching fractions can exceed that of the final state.

For inclusive branching fractions, e.g., $B \rightarrow D^{\pm} X$, the values usually are multiplicities, not branching fractions. They can be greater than one.

B^0 DECAY MODES	Fraction (Γ_i/Γ)	Scale factor / Confidence level	ρ (MeV/c)
$\ell^+ \nu_\ell X$	[[III]]	(10.33 ± 0.28) %	-
$e^+ \nu_e X_c$		(10.1 ± 0.4) %	-
$D \ell^+ \nu_\ell X$		(9.4 ± 0.9) %	-
$D^- \ell^+ \nu_\ell$	[[III]]	(2.31 ± 0.10) %	2309
$D^- \tau^+ \nu_\tau$		(1.08 ± 0.23) %	1909
$D^*(2010)^- \ell^+ \nu_\ell$	[[III]]	(5.05 ± 0.14) %	2257
$D^*(2010)^- \tau^+ \nu_\tau$		(1.57 ± 0.09) %	S=1.1 1838
$\bar{D}^0 \pi^- \ell^+ \nu_\ell$		(4.1 ± 0.5) × 10 ⁻³	2308
$D_0^*(2300)^- \ell^+ \nu_\ell, D_0^{*-} \rightarrow$		(3.0 ± 1.2) × 10 ⁻³	S=1.8 -
$\bar{D}_1^0 \pi^-$			
$D_2^*(2460)^- \ell^+ \nu_\ell, D_2^{*-} \rightarrow$		(1.21 ± 0.33) × 10 ⁻³	S=1.8 2065
$\bar{D}_1^0 \pi^-$			
$\bar{D}^{(*)} n \pi \ell^+ \nu_\ell$ (n ≥ 1)		(2.3 ± 0.5) %	-
$\bar{D}^{*0} \pi^- \ell^+ \nu_\ell$		(5.8 ± 0.8) × 10 ⁻³	S=1.4 2256
$D_1(2420)^- \ell^+ \nu_\ell, D_1^- \rightarrow$		(2.80 ± 0.28) × 10 ⁻³	-
$\bar{D}^{*0} \pi^-$			
$D_1'(2430)^- \ell^+ \nu_\ell, D_1'^- \rightarrow$		(3.1 ± 0.9) × 10 ⁻³	-
$\bar{D}^{*0} \pi^-$			
$D_2^*(2460)^- \ell^+ \nu_\ell, D_2^{*-} \rightarrow$		(6.8 ± 1.2) × 10 ⁻⁴	2065
$\bar{D}^{*0} \pi^-$			
$D^- \pi^+ \pi^- \ell^+ \nu_\ell$		(1.3 ± 0.5) × 10 ⁻³	2299
$D^{*-} \pi^+ \pi^- \ell^+ \nu_\ell$		(1.4 ± 0.5) × 10 ⁻³	2247
$\rho^- \ell^+ \nu_\ell$	[[III]]	(2.94 ± 0.21) × 10 ⁻⁴	2583
$\pi^- \ell^+ \nu_\ell$	[[III]]	(1.50 ± 0.06) × 10 ⁻⁴	2638
$\pi^- \tau^+ \nu_\tau$	< 2.5	× 10 ⁻⁴	CL=90% 2339
Inclusive modes			
$K^{\pm} X$	(78 ± 8) %	-	-
$D^0 X$	(8.1 ± 1.5) %	-	-
$\bar{D}^0 X$	(47.4 ± 2.8) %	-	-
$D^+ X$	< 3.9	%	CL=90% -
$D^- X$	(36.9 ± 3.3) %	-	-
$D_s^+ X$	(10.3 ± 2.1) %	-	-
$D_s^- X$	< 2.6	%	CL=90% -
$\Lambda_c^+ X$	< 3.1	%	CL=90% -
$\bar{\Lambda}_c^- X$	(5.0 ± 2.1) %	-	-
ΞX	(95 ± 5) %	-	-
$c X$	(24.6 ± 3.1) %	-	-
$\bar{c} / c X$	(119 ± 6) %	-	-
D, D*, or D_s modes			
$D^- \pi^+$	(2.52 ± 0.13) × 10 ⁻³	S=1.1	2306
$D^- \rho^+$	(7.6 ± 1.2) × 10 ⁻³		2235
$D^- K^0 \pi^+$	(4.9 ± 0.9) × 10 ⁻⁴		2259
$D^- K^*(892)^+$	(4.5 ± 0.7) × 10 ⁻⁴		2211
$D^- \omega \pi^+$	(2.8 ± 0.6) × 10 ⁻³		2204
$D^- K^+$	(1.86 ± 0.20) × 10 ⁻⁴		2279
$D^- K^+ \pi^+ \pi^-$	(3.5 ± 0.8) × 10 ⁻⁴		2236
$D^- K^+ \bar{K}^0$	< 3.1	× 10 ⁻⁴	CL=90% 2188
$D^- K^+ \bar{K}^*(892)^0$	(8.8 ± 1.9) × 10 ⁻⁴		2070
$\bar{D}^0 \pi^+ \pi^-$	(8.8 ± 0.5) × 10 ⁻⁴		2301
$\bar{D}^*(2010)^- \pi^+$	(2.74 ± 0.13) × 10 ⁻³		2255
$\bar{D}^0 K^+ K^-$	(5.9 ± 0.5) × 10 ⁻⁵		2191
$D^- \pi^+ \pi^+ \pi^-$	(6.0 ± 0.7) × 10 ⁻³	S=1.1	2287
$(D^- \pi^+ \pi^+ \pi^-)$ nonresonant	(3.9 ± 1.9) × 10 ⁻³		2287
$D^- \pi^+ \rho^0$	(1.1 ± 1.0) × 10 ⁻³		2206
$D^- a_1(1260)^+$	(6.0 ± 3.3) × 10 ⁻³		2121
$D^*(2010)^- \pi^+ \pi^0$	(1.5 ± 0.5) %		2248
$D^*(2010)^- \rho^+$	(6.8 ± 0.9) × 10 ⁻³		2180
$D^*(2010)^- K^+$	(2.12 ± 0.15) × 10 ⁻⁴		2226
$D^*(2010)^- K^0 \pi^+$	(3.0 ± 0.8) × 10 ⁻⁴		2205
$D^*(2010)^- K^*(892)^+$	(3.3 ± 0.6) × 10 ⁻⁴		2155
$D^*(2010)^- K^+ \bar{K}^0$	< 4.7	× 10 ⁻⁴	CL=90% 2131
$D^*(2010)^- K^+ \bar{K}^*(892)^0$	(1.29 ± 0.33) × 10 ⁻³		2007
$D^*(2010)^- \pi^+ \pi^+ \pi^-$	(7.21 ± 0.29) × 10 ⁻³		2235
$(D^*(2010)^- \pi^+ \pi^+ \pi^-)$ nonresonant	(0.0 ± 2.5) × 10 ⁻³		2235
$D^*(2010)^- \pi^+ \rho^0$	(5.7 ± 3.2) × 10 ⁻³		2150

$D^*(2010)^- a_1(1260)^+$	(1.30 ± 0.27) %		2061
$\bar{D}_1(2420)^0 \pi^- \pi^+, \bar{D}_1^0 \rightarrow$	(1.47 ± 0.35) × 10 ⁻⁴		-
$D^{*-} \pi^+$			
$D^*(2010)^- K^+ \pi^- \pi^+$	(4.7 ± 0.4) × 10 ⁻⁴		2181
$D^*(2010)^- \pi^+ \pi^+ \pi^- \pi^0$	(1.76 ± 0.27) %		2218
$D^{*-} 3\pi^+ 2\pi^-$	(4.7 ± 0.9) × 10 ⁻³		2195
$D^*(2010)^- \omega \pi^+$	(2.46 ± 0.18) × 10 ⁻³	S=1.2	2148
$\bar{D}_1(2430)^0 \omega, \bar{D}_1^0 \rightarrow$	(2.7 ± 0.8) × 10 ⁻⁴		1992
$D^{*-} \pi^+$			
$D^{*-} \rho(1450)^+, \rho^+ \rightarrow \omega \pi^+$	(1.07 ± 0.40) × 10 ⁻³		-
$\bar{D}_1(2420)^0 \omega, \bar{D}_1^0 \rightarrow$	(7.0 ± 2.2) × 10 ⁻⁵		1995
$D^{*-} \pi^+$			
$\bar{D}_2^*(2460)^0 \omega, \bar{D}_2^0 \rightarrow$	(4.0 ± 1.4) × 10 ⁻⁵		1975
$D^{*-} \pi^+$			
$D^{*-} b_1(1235)^+, b_1^+ \rightarrow$	< 7	× 10 ⁻⁵	CL=90% -
$\bar{D}^{*-} \pi^+$			
$\bar{D}^{*-} \pi^+ [\bar{q}qq]$	(1.9 ± 0.9) × 10 ⁻³		-
$D_1(2420)^- \pi^+, D_1^- \rightarrow$	(9.9 ± 2.0) × 10 ⁻⁵		-
$D_1(2420)^- \pi^+ \pi^-$			
$D_1(2420)^- \pi^+, D_1^- \rightarrow$	< 3.3	× 10 ⁻⁵	CL=90% -
$D^{*-} \pi^+ \pi^-$			
$\bar{D}_2^*(2460)^- \pi^+, (D_2^*)^- \rightarrow$	(2.38 ± 0.16) × 10 ⁻⁴		2062
$D^0 \pi^-$			
$\bar{D}_0^*(2400)^- \pi^+, (D_0^*)^- \rightarrow$	(7.6 ± 0.8) × 10 ⁻⁵		2090
$D^0 \pi^-$			
$D_2^*(2460)^- \pi^+, (D_2^*)^- \rightarrow$	< 2.4	× 10 ⁻⁵	CL=90% -
$D^{*-} \pi^+ \pi^-$			
$\bar{D}_2^*(2460)^- \rho^+$	< 4.9	× 10 ⁻³	CL=90% 1974
$D^0 \bar{D}^0$	(1.4 ± 0.7) × 10 ⁻⁵		1868
$D^* \bar{D}^0$	< 2.9	× 10 ⁻⁴	CL=90% 1794
$D^- D^+$	(2.11 ± 0.18) × 10 ⁻⁴		1864
$D^\pm D^{*\mp}$ (CP-averaged)	(6.1 ± 0.6) × 10 ⁻⁴		-
$D^- D_s^+$	(7.2 ± 0.8) × 10 ⁻³		1812
$D^*(2010)^- D_s^+$	(8.0 ± 1.1) × 10 ⁻³		1735
$D^- D_s^{*+}$	(7.4 ± 1.6) × 10 ⁻³		1732
$D^*(2010)^- D_s^{*+}$	(1.77 ± 0.14) %		1649
$D_{s0}(2317)^- K^+, D_{s0}^- \rightarrow$	(4.2 ± 1.4) × 10 ⁻⁵		2097
$D_s^- \pi^0$			
$D_{s0}(2317)^- \pi^+, D_{s0}^- \rightarrow$	< 2.5	× 10 ⁻⁵	CL=90% 2128
$D_s^- \pi^0$			
$D_{sJ}(2457)^- K^+, D_{sJ}^- \rightarrow$	< 9.4	× 10 ⁻⁶	CL=90% -
$D_s^- \pi^0$			
$D_{sJ}(2457)^- \pi^+, D_{sJ}^- \rightarrow$	< 4.0	× 10 ⁻⁶	CL=90% -
$D_s^- \pi^0$			
$D_s^- D_s^+$	< 3.6	× 10 ⁻⁵	CL=90% 1759
$D_s^- D_s^+$	< 1.3	× 10 ⁻⁴	CL=90% 1674
$D_s^- D_s^+$	< 2.4	× 10 ⁻⁴	CL=90% 1583
$D_s^* D_s^+$			
$D_{s0}^*(2317)^+ D^-, D_{s0}^{*+} \rightarrow$	(1.06 ± 0.16) × 10 ⁻³	S=1.1	1602
$D_s^+ \pi^0$			
$D_{s0}(2317)^+ D^-, D_{s0}^+ \rightarrow$	< 9.5	× 10 ⁻⁴	CL=90% -
$D_s^{*+} \gamma$			
$D_{s0}(2317)^+ D^*(2010)^-, D_{s0}^+ \rightarrow D_s^+ \pi^0$	(1.5 ± 0.6) × 10 ⁻³		1509
$D_{sJ}(2457)^+ D^-, D_{sJ}^+ \rightarrow$	(3.5 ± 1.1) × 10 ⁻³		-
$D_{sJ}(2457)^+ D^-, D_{sJ}^+ \rightarrow$	(6.5 ± 1.7) × 10 ⁻⁴		-
$D_s^+ \gamma$			
$D_{sJ}(2457)^+ D^-, D_{sJ}^+ \rightarrow$	< 6.0	× 10 ⁻⁴	CL=90% -
$D_s^{*+} \gamma$			
$D_{sJ}(2457)^+ D^-, D_{sJ}^+ \rightarrow$	< 2.0	× 10 ⁻⁴	CL=90% -
$D_s^+ \pi^+ \pi^-$			
$D_{sJ}(2457)^+ D^-, D_{sJ}^+ \rightarrow$	< 3.6	× 10 ⁻⁴	CL=90% -
$D_s^+ \pi^0$			
$D^*(2010)^- D_{sJ}(2457)^+$	(9.3 ± 2.2) × 10 ⁻³		-
$D_{sJ}(2457)^+ D^*(2010)^-, D_{sJ}^+ \rightarrow$	(2.3 ± 0.9) × 10 ⁻³		-
$D_s^+ \gamma$			
$D^- D_{s1}(2536)^+, D_{s1}^- \rightarrow$	(2.8 ± 0.7) × 10 ⁻⁴		1444
$D^* \rho K^+ + D^{*+} K^0$			
$D^- D_{s1}(2536)^+, D_{s1}^- \rightarrow$	(1.7 ± 0.6) × 10 ⁻⁴		1444
$D^* \rho K^+$			
$D^- D_{s1}(2536)^+, D_{s1}^- \rightarrow$	(2.6 ± 1.1) × 10 ⁻⁴		1444
$D^* K^0$			

Meson Summary Table

$D^*(2010)^- D_{s1}(2536)^+$	$(5.0 \pm 1.4) \times 10^{-4}$	1336	$D^*(2010)^- D^0 K^+$	$(2.47 \pm 0.21) \times 10^{-3}$	1479
$D_{s1}^+ \rightarrow D^{*0} K^+ + D^{*+} K^0$			$D^*(2010)^- D^*(2007)^0 K^+$	$(1.06 \pm 0.09) \%$	1366
$D^*(2010)^- D_{s1}(2536)^+$	$(3.3 \pm 1.1) \times 10^{-4}$	1336	$D^- D^+ K^0$	$(7.5 \pm 1.7) \times 10^{-4}$	1568
$D_{s1}^+ \rightarrow D^{*0} K^+$			$D^*(2010)^- D^+ K^0 +$	$(6.4 \pm 0.5) \times 10^{-3}$	1473
$D^{*-} D_{s1}(2536)^+$	$(5.0 \pm 1.7) \times 10^{-4}$	1336	$D^- D^*(2010)^+ K^0$		
$D^{*+} K^0$			$D^*(2010)^- D^*(2010)^+ K^0$	$(8.1 \pm 0.7) \times 10^{-3}$	1360
$D^- D_{sJ}(2573)^+, D_{sJ}^+ \rightarrow$	$(3.4 \pm 1.8) \times 10^{-5}$	1414	$D^{*-} D_{s1}(2536)^+, D_{s1}^+ \rightarrow$	$(8.0 \pm 2.4) \times 10^{-4}$	1336
$D^0 K^+$			$D^{*+} K^0$		
$D^*(2010)^- D_{sJ}(2573)^+$	$< 2 \times 10^{-4}$	CL=90% 1304	$\overline{D}^0 D^0 K^0$	$(2.7 \pm 1.1) \times 10^{-4}$	1574
$D_{sJ}^+ \rightarrow D^0 K^+$			$\overline{D}^0 D^*(2007)^0 K^0 +$	$(1.1 \pm 0.5) \times 10^{-3}$	1478
$D^- D_{sJ}(2700)^+, D_{sJ}^+ \rightarrow$	$(7.1 \pm 1.2) \times 10^{-4}$	-	$\overline{D}^*(2007)^0 D^0 K^0$		
$D^0 K^+$			$\overline{D}^*(2007)^0 D^*(2007)^0 K^0$	$(2.4 \pm 0.9) \times 10^{-3}$	1365
$D^+ \pi^-$	$(7.4 \pm 1.3) \times 10^{-7}$	2306	$(\overline{D} + \overline{D}^*)(D + D^*) K$	$(3.68 \pm 0.26) \%$	-
$D_s^+ \pi^-$	$(2.16 \pm 0.26) \times 10^{-5}$	2270			
$D_s^+ \pi^-$	$(2.1 \pm 0.4) \times 10^{-5}$	S=1.4 2215	Charmonium modes		
$D_s^+ \rho^-$	$< 2.4 \times 10^{-5}$	CL=90% 2197	$\eta_c K^0$	$(8.0 \pm 1.1) \times 10^{-4}$	1751
$D_s^+ \rho^-$	$(4.1 \pm 1.3) \times 10^{-5}$	2138	$\eta_c(1S) K^+ \pi^-$	$(6.0 \pm 0.7) \times 10^{-4}$	1722
$D_s^+ a_0^-$	$< 1.9 \times 10^{-5}$	CL=90% -	$\eta_c(1S) K^+ \pi^-$ (NR)	$(6.2 \pm 1.3) \times 10^{-5}$	-
$D_s^+ a_0^-$	$< 3.6 \times 10^{-5}$	CL=90% -	$X(4100)^- K^+, X^- \rightarrow$	$(2.0 \pm 1.0) \times 10^{-5}$	-
$D_s^+ a_1(1260)^-$	$< 2.1 \times 10^{-3}$	CL=90% 2080	$\eta_c \pi^-$		
$D_s^+ a_1(1260)^-$	$< 1.7 \times 10^{-3}$	CL=90% 2015	$\eta_c(1S) K^*(1410)^0$	$(1.9 \pm 1.5) \times 10^{-4}$	1395
$D_s^+ a_2^-$	$< 1.9 \times 10^{-4}$	CL=90% -	$\eta_c(1S) K_0^*(1430)^0$	$(1.6 \pm 0.4) \times 10^{-4}$	1387
$D_s^+ a_2^-$	$< 2.0 \times 10^{-4}$	CL=90% -	$\eta_c(1S) K_2^*(1430)^0$	$(4.9 \pm \frac{2.2}{2.7}) \times 10^{-5}$	1386
$D_s^- K^+$	$(2.7 \pm 0.5) \times 10^{-5}$	S=2.7 2242	$\eta_c(1S) K^*(1680)^0$	$(3 \pm 4) \times 10^{-5}$	1166
$D_s^{*-} K^+$	$(2.19 \pm 0.30) \times 10^{-5}$	2185	$\eta_c(1S) K_0^*(1950)^0$	$(4.4 \pm \frac{2.9}{4.0}) \times 10^{-5}$	-
$D_s^- K^*(892)^+$	$(3.5 \pm 1.0) \times 10^{-5}$	2172	$\eta_c K^*(892)^0$	$(5.2 \pm \frac{0.7}{0.8}) \times 10^{-4}$	S=1.5 1646
$D_s^{*-} K^*(892)^+$	$(3.2 \pm \frac{1.5}{1.3}) \times 10^{-5}$	2112	$\eta_c(2S) K_S^0, \eta_c \rightarrow \rho \bar{\rho} \pi^+ \pi^-$	$(4.2 \pm \frac{1.4}{1.2}) \times 10^{-7}$	-
$D_s^- \pi^+ K^0$	$(9.7 \pm 1.4) \times 10^{-5}$	2222	$\eta_c(2S) K^* 0$	$< 3.9 \times 10^{-4}$	CL=90% 1159
$D_s^{*-} \pi^+ K^0$	$< 1.10 \times 10^{-4}$	CL=90% 2164	$h_c(1P) K_S^0$	$< 1.4 \times 10^{-5}$	1401
$D_s^- K^+ \pi^+ \pi^-$	$(1.7 \pm 0.5) \times 10^{-4}$	2198	$h_c(1P) K^* 0$	$< 4 \times 10^{-4}$	CL=90% 1253
$D_s^- \pi^+ K^*(892)^0$	$< 3.0 \times 10^{-3}$	CL=90% 2138	$J/\psi(1S) K^0$	$(8.68 \pm 0.30) \times 10^{-4}$	1683
$D_s^{*-} \pi^+ K^*(892)^0$	$< 1.6 \times 10^{-3}$	CL=90% 2076	$J/\psi(1S) K^+ \pi^-$	$(1.15 \pm 0.05) \times 10^{-3}$	1652
$\overline{D}^0 K^0$	$(5.2 \pm 0.7) \times 10^{-5}$	2280	$J/\psi(1S) K^*(892)^0$	$(1.27 \pm 0.05) \times 10^{-3}$	1571
$\overline{D}^0 K^+ \pi^-$	$(8.8 \pm 1.7) \times 10^{-5}$	2261	$J/\psi(1S) \eta K_S^0$	$(5.4 \pm 0.9) \times 10^{-5}$	1508
$\overline{D}^0 K^*(892)^0$	$(4.5 \pm 0.6) \times 10^{-5}$	2213	$J/\psi(1S) \eta' K_S^0$	$< 2.5 \times 10^{-5}$	CL=90% 1271
$\overline{D}^0 K_0^*(1430)^0$	$< 6.7 \times 10^{-5}$	CL=90% 2062	$J/\psi(1S) \phi K^0$	$(4.9 \pm 1.0) \times 10^{-5}$	S=1.3 1224
$\overline{D}^0 K_0^*(1430)^0$	$(7 \pm 7) \times 10^{-6}$	2058	$J/\psi(1S) \omega K^0$	$(2.3 \pm 0.4) \times 10^{-4}$	1386
$\overline{D}^0 K_2^*(1430)^0$	$(2.1 \pm 0.9) \times 10^{-5}$	2057	$\chi_{c1}(3872) K^0, \chi_{c1} \rightarrow$	$(6.0 \pm 3.2) \times 10^{-6}$	1140
$D_0^*(2300)^- K^+, D_0^{*-} \rightarrow$	$(1.9 \pm 0.9) \times 10^{-5}$	-	$J/\psi \omega$		
$\overline{D}^0 \pi^-$			$X(3915), X \rightarrow J/\psi \omega$	$(2.1 \pm 0.9) \times 10^{-5}$	1102
$D_2^*(2460)^- K^+, D_2^{*-} \rightarrow$	$(2.03 \pm 0.35) \times 10^{-5}$	2029	$J/\psi(1S) K(1270)^0$	$(1.3 \pm 0.5) \times 10^{-3}$	1402
$\overline{D}^0 \pi^-$			$J/\psi(1S) \pi^0$	$(1.66 \pm 0.10) \times 10^{-5}$	1728
$D_3^*(2760)^- K^+, D_3^{*-} \rightarrow$	$< 1.0 \times 10^{-6}$	CL=90% -	$J/\psi(1S) \eta$	$(1.08 \pm 0.23) \times 10^{-5}$	S=1.5 1673
$\overline{D}^0 \pi^-$			$J/\psi(1S) \pi^+ \pi^-$	$(3.94 \pm 0.17) \times 10^{-5}$	1716
$\overline{D}^0 K^+ \pi^-$ nonresonant	$< 3.7 \times 10^{-5}$	CL=90% 2261	$J/\psi(1S) \pi^+ \pi^-$ nonresonant	$< 1.2 \times 10^{-5}$	CL=90% 1716
$[K^+ K^-]_D K^*(892)^0$	$(4.2 \pm 0.7) \times 10^{-5}$	-	$J/\psi(1S) f_0(500), f_0 \rightarrow \pi \pi$	$(8.8 \pm \frac{1.2}{1.6}) \times 10^{-6}$	-
$[\pi^+ \pi^-]_D K^*(892)^0$	$(6.0 \pm 1.1) \times 10^{-5}$	-	$J/\psi(1S) f_2$	$(3.3 \pm 0.5) \times 10^{-6}$	S=1.5 -
$[\pi^+ \pi^- \pi^+ \pi^-]_D K^* 0$	$(4.6 \pm 0.9) \times 10^{-5}$	-	$J/\psi(1S) \rho^0$	$(2.55 \pm \frac{0.18}{0.16}) \times 10^{-5}$	1612
$\overline{D}^0 \pi^0$	$(2.63 \pm 0.14) \times 10^{-4}$	2308	$J/\psi(1S) f_0(980), f_0 \rightarrow$	$< 1.1 \times 10^{-6}$	CL=90% -
$\overline{D}^0 \rho^0$	$(3.21 \pm 0.21) \times 10^{-4}$	2237	$\pi^+ \pi^-$		
$\overline{D}^0 f_2$	$(1.56 \pm 0.21) \times 10^{-4}$	-	$J/\psi(1S) \rho(1450)^0, \rho^0 \rightarrow$	$(2.9 \pm \frac{1.6}{0.7}) \times 10^{-6}$	-
$\overline{D}^0 \eta$	$(2.36 \pm 0.32) \times 10^{-4}$	S=2.5 2274	$\pi \pi$		
$\overline{D}^0 \eta'$	$(1.38 \pm 0.16) \times 10^{-4}$	S=1.3 2198	$J/\psi \rho(1700)^0, \rho^0 \rightarrow \pi^+ \pi^-$	$(2.0 \pm 1.3) \times 10^{-6}$	-
$\overline{D}^0 \omega$	$(2.54 \pm 0.16) \times 10^{-4}$	2235	$J/\psi(1S) \omega$	$(1.8 \pm \frac{0.7}{0.5}) \times 10^{-5}$	1609
$D^0 \phi$	$< 2.3 \times 10^{-6}$	CL=95% 2183	$J/\psi(1S) K^+ K^-$	$(2.50 \pm 0.35) \times 10^{-6}$	1534
$D^0 K^+ \pi^-$	$(5.3 \pm 3.2) \times 10^{-6}$	2261	$J/\psi(1S) a_0(980), a_0 \rightarrow$	$(4.7 \pm 3.4) \times 10^{-7}$	-
$D^0 K^*(892)^0$	$(2.2 \pm \frac{0.9}{1.0}) \times 10^{-6}$	2213	$K^+ K^-$		
$\overline{D}^{*0} \gamma$	$< 2.5 \times 10^{-5}$	CL=90% 2258	$J/\psi(1S) \phi$	$< 1.9 \times 10^{-7}$	CL=90% 1520
$\overline{D}^*(2007)^0 \pi^0$	$(2.2 \pm 0.6) \times 10^{-4}$	S=2.6 2256	$J/\psi(1S) \eta'(958)$	$(7.6 \pm 2.4) \times 10^{-6}$	1546
$\overline{D}^*(2007)^0 \rho^0$	$< 5.1 \times 10^{-4}$	CL=90% 2182	$J/\psi(1S) K^0 \pi^+ \pi^-$	$(4.3 \pm 0.4) \times 10^{-4}$	1611
$\overline{D}^*(2007)^0 \eta$	$(2.3 \pm 0.6) \times 10^{-4}$	S=2.8 2220	$J/\psi(1S) K^0 K^- \pi^+ +$ c.c.	$< 2.1 \times 10^{-5}$	CL=90% 1467
$\overline{D}^*(2007)^0 \eta'$	$(1.40 \pm 0.22) \times 10^{-4}$	2141	$J/\psi(1S) K^0 K^+ K^-$	$(2.5 \pm 0.7) \times 10^{-5}$	S=1.8 1249
$\overline{D}^*(2007)^0 \pi^+ \pi^-$	$(6.2 \pm 2.2) \times 10^{-4}$	2249	$J/\psi(1S) K^0 \rho^0$	$(5.4 \pm 3.0) \times 10^{-4}$	1390
$\overline{D}^*(2007)^0 K^0$	$(3.6 \pm 1.2) \times 10^{-5}$	2227	$J/\psi(1S) K^*(892)^+ \pi^-$	$(8 \pm 4) \times 10^{-4}$	1515
$\overline{D}^*(2007)^0 K^*(892)^0$	$< 6.9 \times 10^{-5}$	CL=90% 2157	$J/\psi(1S) \pi^+ \pi^- \pi^+ \pi^-$	$(1.42 \pm 0.12) \times 10^{-5}$	1670
$D^*(2007)^0 K^*(892)^0$	$< 4.0 \times 10^{-5}$	CL=90% 2157	$J/\psi(1S) f_1(1285)$	$(8.4 \pm 2.1) \times 10^{-6}$	1385
$D^*(2007)^0 \pi^+ \pi^+ \pi^- \pi^-$	$(2.7 \pm 0.5) \times 10^{-3}$	2219	$J/\psi(1S) K^*(892)^0 \pi^+ \pi^-$	$(6.6 \pm 2.2) \times 10^{-4}$	1447
$D^*(2010)^+ D^*(2010)^-$	$(8.0 \pm 0.6) \times 10^{-4}$	1711	$\chi_{c1}(3872)^- K^+$	$< 5 \times 10^{-4}$	CL=90% -
$\overline{D}^*(2007)^0 \omega$	$(3.6 \pm 1.1) \times 10^{-4}$	S=3.1 2180	$\chi_{c1}(3872)^- K^+,$	$[rrr] < 4.2 \times 10^{-6}$	CL=90% -
$D^*(2010)^+ D^-$	$(6.1 \pm 1.5) \times 10^{-4}$	S=1.6 1790	$\chi_{c1}(3872)^- \rightarrow$		
$D^*(2007)^0 \overline{D}^*(2007)^0$	$< 9 \times 10^{-5}$	CL=90% 1715	$J/\psi(1S) \pi^- \pi^0$		
$D^- D^0 K^+$	$(1.07 \pm 0.11) \times 10^{-3}$	1574	$\chi_{c1}(3872) K^0, \chi_{c1} \rightarrow$	$(4.3 \pm 1.3) \times 10^{-6}$	1140
$D^- D^*(2007)^0 K^+$	$(3.5 \pm 0.4) \times 10^{-3}$	1478	$J/\psi \pi^+ \pi^-$		
			$\chi_{c1}(3872) K^0, \chi_{c1} \rightarrow J/\psi \gamma$	$< 2.4 \times 10^{-6}$	CL=90% 1140

Meson Summary Table

$\chi_{c1}(3872)K^*(892)^0, \chi_{c1} \rightarrow$ $J/\psi\gamma$	< 2.8	$\times 10^{-6}$	CL=90%	940	$\omega(K\pi)_0^{*0}$	$(1.84 \pm 0.25) \times 10^{-5}$	-
$\chi_{c1}(3872)K^0, \chi_{c1} \rightarrow \psi(2S)\gamma$	< 6.62	$\times 10^{-6}$	CL=90%	1140	$\omega K_0^*(1430)^0$	$(1.60 \pm 0.34) \times 10^{-5}$	2380
$\chi_{c1}(3872)K^*(892)^0, \chi_{c1} \rightarrow$ $\psi(2S)\gamma$	< 4.4	$\times 10^{-6}$	CL=90%	940	$\omega K_2^*(1430)^0$	$(1.01 \pm 0.23) \times 10^{-5}$	2380
$\chi_{c1}(3872)K^0, \chi_{c1} \rightarrow$ $D^0\bar{D}^0\pi^0$	$(1.7 \pm 0.8) \times 10^{-4}$			1140	$\omega K^+\pi^-$ nonresonant	$(5.1 \pm 1.0) \times 10^{-6}$	2542
$\chi_{c1}(3872)K^0, \chi_{c1} \rightarrow \bar{D}^{*0}D^0$	$(1.2 \pm 0.4) \times 10^{-4}$			1140	$K^+\pi^-\pi^0$	$(3.78 \pm 0.32) \times 10^{-5}$	2609
$\chi_{c1}(3872)K^+\pi^-, \chi_{c1} \rightarrow$ $J/\psi\pi^+\pi^-$	$(7.9 \pm 1.4) \times 10^{-6}$			-	$K^+\rho^-$	$(7.0 \pm 0.9) \times 10^{-6}$	2559
$\chi_{c1}(3872)K^*(892)^0, \chi_{c1} \rightarrow$ $J/\psi\pi^+\pi^-$	$(4.0 \pm 1.5) \times 10^{-6}$			-	$K^+\rho(1450)^-$	$(2.4 \pm 1.2) \times 10^{-6}$	-
$\chi_{c1}(3872)\gamma, \chi_{c1} \rightarrow$ $J/\psi\pi^+\pi^-$	< 5.1	$\times 10^{-7}$	CL=90%	-	$K^+\rho(1700)^-$	$(6 \pm 7) \times 10^{-7}$	-
$Z_c(4430)^\pm K^\mp, Z_c^\pm \rightarrow$ $\psi(2S)\pi^\pm$	(6.0 ± 3.0) (2.4)	$\times 10^{-5}$		583	$(K^+\pi^-\pi^0)$ nonresonant	$(2.8 \pm 0.6) \times 10^{-6}$	2609
$Z_c(4430)^\pm K^\mp, Z_c^\pm \rightarrow$ $J/\psi\pi^\pm$	(5.4 ± 4.0) (1.2)	$\times 10^{-6}$		583	$(K\pi)_0^{*+}\pi^-, (K\pi)_0^{*+} \rightarrow$	$(3.4 \pm 0.5) \times 10^{-5}$	-
$Z_c(3900)^\pm K^\mp, Z_c^\pm \rightarrow$ $J/\psi\pi^\pm$	< 9	$\times 10^{-7}$		-	$(K\pi)_0^{*0}\pi^0, (K\pi)_0^{*0} \rightarrow$	$(8.6 \pm 1.7) \times 10^{-6}$	-
$Z_c(4200)^\pm K^\mp, X^\pm \rightarrow$ $J/\psi\pi^\pm$	(2.2 ± 1.3) (0.8)	$\times 10^{-5}$		-	$K^+\pi^-$	< 4.0	$\times 10^{-6}$ CL=90%
$J/\psi(1S)p\bar{p}$	$(4.5 \pm 0.6) \times 10^{-7}$			862	$K_2^*(1430)^0\pi^0$	< 7.5	$\times 10^{-6}$ CL=90%
$J/\psi(1S)\gamma$	< 1.5	$\times 10^{-6}$	CL=90%	1732	$K_x^0\pi^0$	$(6.1 \pm 1.6) \times 10^{-6}$	-
$J/\psi(1S)\bar{D}^0$	< 1.3	$\times 10^{-5}$	CL=90%	877	$K^0\pi^+\pi^-$	$(4.97 \pm 0.18) \times 10^{-5}$	2609
$\psi(2S)\pi^0$	$(1.17 \pm 0.19) \times 10^{-5}$			1348	$K^0\pi^+\pi^-$ nonresonant	(1.39 ± 0.26) (0.18)	$\times 10^{-5}$ S=1.6
$\psi(2S)K^0$	$(5.8 \pm 0.5) \times 10^{-4}$			1283	$K^0\rho^0$	$(3.4 \pm 1.1) \times 10^{-6}$	S=2.3
$\psi(3770)K^0, \psi \rightarrow \bar{D}^0D^0$	< 1.23	$\times 10^{-4}$	CL=90%	1217	$K^*(892)^+\pi^-$	$(7.5 \pm 0.4) \times 10^{-6}$	2563
$\psi(3770)K^0, \psi \rightarrow D^-D^+$	< 1.88	$\times 10^{-4}$	CL=90%	1217	$K_0^*(1430)^+\pi^-$	$(3.3 \pm 0.7) \times 10^{-5}$	S=2.0
$\psi(2S)\pi^+\pi^-$	$(2.21 \pm 0.35) \times 10^{-5}$			1331	$K_x^{*+}\pi^-$	$(5.1 \pm 1.6) \times 10^{-6}$	-
$\psi(2S)K^+\pi^-$	$(5.8 \pm 0.4) \times 10^{-4}$			1239	$K^*(1410)^+\pi^-, K^{*+} \rightarrow$	< 3.8	$\times 10^{-6}$ CL=90%
$\psi(2S)K^*(892)^0$	$(5.9 \pm 0.4) \times 10^{-4}$			1116	$(K\pi)_0^{*+}\pi^-, (K\pi)_0^{*+} \rightarrow$	$(1.62 \pm 0.13) \times 10^{-5}$	-
$\chi_{c0}K^0$	(1.11 ± 0.24) (0.21)	$\times 10^{-6}$		1477	$K^0\pi^+$	$(8.1 \pm 0.8) \times 10^{-6}$	S=1.3
$\chi_{c0}K^*(892)^0$	$(1.7 \pm 0.4) \times 10^{-4}$			1342	$f_0(980)K^0, f_0 \rightarrow \pi^+\pi^-$	(1.6 ± 2.5) (1.6)	$\times 10^{-7}$
$\chi_{c1}\pi^0$	$(1.12 \pm 0.28) \times 10^{-5}$			1468	$K^0f_0(500)$	$(1.3 \pm 0.8) \times 10^{-6}$	2397
$\chi_{c1}K^0$	$(3.95 \pm 0.27) \times 10^{-4}$			1411	$K^0f_0(1500)$	(2.7 ± 1.3) (1.2)	$\times 10^{-6}$
$\chi_{c1}\pi^-K^+$	$(4.97 \pm 0.30) \times 10^{-4}$			1371	$f_2(1270)K^0$	$(1.8 \pm 0.7) \times 10^{-6}$	-
$\chi_{c1}K^*(892)^0$	$(2.38 \pm 0.19) \times 10^{-4}$		S=1.2	1265	$f_x(1300)K^0, f_x \rightarrow \pi^+\pi^-$	$(3.3 \pm 0.6) \times 10^{-6}$	2563
$X(4051)^-K^+, X^- \rightarrow$ $\chi_{c1}\pi^-$	(3.0 ± 4.0) (1.8)	$\times 10^{-5}$		-	$K^*(892)^0\pi^0$	$(3.65 \pm 0.34) \times 10^{-6}$	2445
$X(4248)^-K^+, X^- \rightarrow$ $\chi_{c1}\pi^-$	(4.0 ± 20.0) (1.0)	$\times 10^{-5}$		-	$K^*(1680)^+\pi^-$	$(1.41 \pm 0.10) \times 10^{-5}$	2358
$\chi_{c1}\pi^+\pi^-K^0$	$(3.2 \pm 0.5) \times 10^{-4}$			1318	$K^+\pi^-\pi^+\pi^-$	< 2.8	$\times 10^{-4}$ CL=90%
$\chi_{c1}\pi^-\pi^0K^+$	$(3.5 \pm 0.6) \times 10^{-4}$			1321	$\rho^0K^+\pi^-$	$(2.3 \pm 0.7) \times 10^{-6}$	2543
$\chi_{c2}K^0$	< 1.5	$\times 10^{-5}$	CL=90%	1379	$f_0(980)K^+\pi^-, f_0 \rightarrow \pi\pi$	(1.4 ± 0.5) (0.6)	$\times 10^{-6}$
$\chi_{c2}K^*(892)^0$	$(4.9 \pm 1.2) \times 10^{-5}$		S=1.1	1228	$K^+\pi^-\pi^+\pi^-$ nonresonant	< 2.1	$\times 10^{-6}$ CL=90%
$\chi_{c2}\pi^-K^+$	$(7.2 \pm 1.0) \times 10^{-5}$			1338	$K^*(892)^0\pi^+\pi^-$	$(5.5 \pm 0.5) \times 10^{-5}$	2557
$\chi_{c2}\pi^+\pi^-K^0$	< 1.70	$\times 10^{-4}$	CL=90%	1282	$K^*(892)^0\rho^0$	$(3.9 \pm 1.3) \times 10^{-6}$	S=1.9
$\chi_{c2}\pi^-\pi^0K^+$	< 7.4	$\times 10^{-5}$	CL=90%	1286	$K^*(892)^0f_0(980), f_0 \rightarrow \pi\pi$	(3.9 ± 2.1) (1.8)	$\times 10^{-6}$ S=3.9
$\psi(4660)K^0, \psi \rightarrow \Lambda_c^+\Lambda_c^-$	< 2.3	$\times 10^{-4}$	CL=90%	-	$K_1(1270)^+\pi^-$	< 3.0	$\times 10^{-5}$ CL=90%
$\psi(4260)^0K^0, \psi^0 \rightarrow$ $J/\psi\pi^+\pi^-$	< 1.7	$\times 10^{-5}$	CL=90%	-	$K_1(1400)^+\pi^-$	< 2.7	$\times 10^{-5}$ CL=90%
K or K* modes					$a_1(1260)^-K^+$	$(1.6 \pm 0.4) \times 10^{-5}$	2471
$K^+\pi^-$	$(1.96 \pm 0.05) \times 10^{-5}$			2615	$K^*(892)^+\rho^-$	$(1.03 \pm 0.26) \times 10^{-5}$	2504
$K^0\pi^0$	$(9.9 \pm 0.5) \times 10^{-6}$			2615	$K_0^*(1430)^+\rho^-$	$(2.8 \pm 1.2) \times 10^{-5}$	-
$\eta'K^0$	$(6.6 \pm 0.4) \times 10^{-5}$		S=1.4	2528	$K_1(1400)^0\rho^0$	< 3.0	$\times 10^{-3}$ CL=90%
$\eta'K^*(892)^0$	$(2.8 \pm 0.6) \times 10^{-6}$			2472	$K_0^*(1430)^0\rho^0$	$(2.7 \pm 0.6) \times 10^{-5}$	2381
$\eta'K_0^*(1430)^0$	$(6.3 \pm 1.6) \times 10^{-6}$			2346	$K_0^*(1430)^0f_0(980), f_0 \rightarrow \pi\pi$	$(2.7 \pm 0.9) \times 10^{-6}$	-
$\eta'K_2^*(1430)^0$	$(1.37 \pm 0.32) \times 10^{-5}$			2346	$K_2^*(1430)^0f_0(980), f_0 \rightarrow \pi\pi$	$(8.6 \pm 2.0) \times 10^{-6}$	-
ηK^0	(1.23 ± 0.27) (0.24)	$\times 10^{-6}$		2587	K^+K^-	$(7.8 \pm 1.5) \times 10^{-8}$	2593
$\eta K^*(892)^0$	$(1.59 \pm 0.10) \times 10^{-5}$			2534	$K^0\bar{K}^0$	$(1.21 \pm 0.16) \times 10^{-6}$	2593
$\eta K_0^*(1430)^0$	$(1.10 \pm 0.22) \times 10^{-5}$			2415	$K^0K^-\pi^+$	$(6.7 \pm 0.5) \times 10^{-6}$	2578
$\eta K_2^*(1430)^0$	$(9.6 \pm 2.1) \times 10^{-6}$			2414	$K^*(892)^\pm K^\mp$	< 4	$\times 10^{-7}$ CL=90%
ωK^0	$(4.8 \pm 0.4) \times 10^{-6}$			2557	$\bar{K}^{*0}K^0 + K^{*0}\bar{K}^0$	< 9.6	$\times 10^{-7}$ CL=90%
$a_0(980)^0K^0, a_0^0 \rightarrow \eta\pi^0$	< 7.8	$\times 10^{-6}$	CL=90%	-	$K^+K^-\pi^0$	$(2.2 \pm 0.6) \times 10^{-6}$	2579
$b_1^0K^0, b_1^0 \rightarrow \omega\pi^0$	< 7.8	$\times 10^{-6}$	CL=90%	-	$K_S^0K_S^0\pi^0$	< 9	$\times 10^{-7}$ CL=90%
$a_0(980)^\pm K^\mp, a_0^\pm \rightarrow \eta\pi^\pm$	< 1.9	$\times 10^{-6}$	CL=90%	-	$K_S^0K_S^0\eta$	< 1.0	$\times 10^{-6}$ CL=90%
$b_1^-K^+, b_1^- \rightarrow \omega\pi^-$	$(7.4 \pm 1.4) \times 10^{-6}$			-	$K_S^0K_S^0\eta'$	< 2.0	$\times 10^{-6}$ CL=90%
$b_1^0K^{*0}, b_1^0 \rightarrow \omega\pi^0$	< 8.0	$\times 10^{-6}$	CL=90%	-	$K^0K^+K^-$	$(2.68 \pm 0.11) \times 10^{-5}$	2522
$b_1^-K^{*+}, b_1^- \rightarrow \omega\pi^-$	< 5.0	$\times 10^{-6}$	CL=90%	-	$K^0\phi$	$(7.3 \pm 0.7) \times 10^{-6}$	2516
$a_0(1450)^\pm K^\mp, a_0^\pm \rightarrow \eta\pi^\pm$	< 3.1	$\times 10^{-6}$	CL=90%	-	$f_0(980)K^0, f_0 \rightarrow K^+K^-$	(7.0 ± 3.5) (3.0)	$\times 10^{-6}$
$K_S^0X^0$ (Familon)	< 5.3	$\times 10^{-5}$	CL=90%	-	$f_0(1500)K^0$	(1.3 ± 0.7) (0.5)	$\times 10^{-5}$
$\omega K^*(892)^0$	$(2.0 \pm 0.5) \times 10^{-6}$			2503	$f_2'(1525)^0K^0$	(3 ± 5) (4)	$\times 10^{-7}$
					$f_0(1710)K^0, f_0 \rightarrow K^+K^-$	$(4.4 \pm 0.9) \times 10^{-6}$	-
					$K^0K^+K^-$ nonresonant	$(3.3 \pm 1.0) \times 10^{-5}$	2522
					$K_S^0K_S^0K_S^0$	$(6.0 \pm 0.5) \times 10^{-6}$	S=1.1
					$f_0(980)K^0, f_0 \rightarrow K_S^0K_S^0$	$(2.7 \pm 1.8) \times 10^{-6}$	-
					$f_0(1710)K^0, f_0 \rightarrow K_S^0K_S^0$	(5.0 ± 5.0) (2.6)	$\times 10^{-7}$
					$f_2(2010)K^0, f_2 \rightarrow K_S^0K_S^0$	$(5 \pm 6) \times 10^{-7}$	-
					$K_S^0K_S^0K_S^0$ nonresonant	$(1.33 \pm 0.31) \times 10^{-5}$	2521

$\bar{\Lambda}_c^- \rho \pi^+ \pi^- \pi^0$	< 5.07	$\times 10^{-3}$	CL=90%	1883
$\bar{\Lambda}_c^- \rho \pi^+ \pi^- \pi^+ \pi^-$	< 2.74	$\times 10^{-3}$	CL=90%	1821
$\bar{\Lambda}_c^- \rho \pi^+ \pi^-$ (nonresonant)	(5.5 ± 1.0)	$\times 10^{-4}$	S=1.3	1934
$\bar{\Sigma}_c(2520)^- \rho \pi^+$	(1.02 ± 0.18)	$\times 10^{-4}$		1860
$\bar{\Sigma}_c(2520)^0 \rho \pi^-$	< 3.1	$\times 10^{-5}$	CL=90%	1860
$\bar{\Sigma}_c(2455)^0 \rho \pi^-$	(1.08 ± 0.16)	$\times 10^{-4}$		1895
$\bar{\Sigma}_c(2455)^0 N^0, N^0 \rightarrow \rho \pi^-$	(6.4 ± 1.7)	$\times 10^{-5}$		-
$\bar{\Sigma}_c(2455)^- \rho \pi^+$	(1.83 ± 0.24)	$\times 10^{-4}$		1895
$\Lambda_c^- \rho K^+ \pi^-$	(3.4 ± 0.7)	$\times 10^{-5}$		1786
$\bar{\Sigma}_c(2455)^- \rho K^+, \bar{\Sigma}_c^- \rightarrow \bar{\Lambda}_c^- \pi^-$	(8.8 ± 2.5)	$\times 10^{-6}$		1754
$\Lambda_c^- \rho K^*(892)^0$	< 2.42	$\times 10^{-5}$	CL=90%	1647
$\Lambda_c^- \rho K^+ K^-$	(2.0 ± 0.4)	$\times 10^{-5}$		1588
$\Lambda_c^- \rho \phi$	< 1.0	$\times 10^{-5}$	CL=90%	1567
$\Lambda_c^- \rho \bar{p} p$	< 2.8	$\times 10^{-6}$		677
$\bar{\Lambda}_c^- \Lambda K^+$	(4.8 ± 1.1)	$\times 10^{-5}$		1767
$\bar{\Lambda}_c^- \Lambda^+$	< 1.6	$\times 10^{-5}$	CL=95%	1319
$\bar{\Lambda}_c(2593)^- / \bar{\Lambda}_c(2625)^- p$	< 1.1	$\times 10^{-4}$	CL=90%	-
$\bar{\Xi}_c^+ \Lambda_c^+$	(1.2 ± 0.8)	$\times 10^{-3}$		1147
$\bar{\Xi}_c^+ \Lambda_c^+, \bar{\Xi}_c^- \rightarrow \bar{\Xi}^+ \pi^- \pi^-$	(2.4 ± 1.1)	$\times 10^{-5}$	S=1.8	1147
$\bar{\Xi}_c^+ \Lambda_c^+, \bar{\Xi}_c^- \rightarrow \bar{p} K^+ \pi^-$	(5.3 ± 1.7)	$\times 10^{-6}$		-
$\bar{\Xi}_c^+ \Lambda_c^+ K^0$	(4.0 ± 0.9)	$\times 10^{-4}$		732
$\bar{\Xi}_c(2930)^- \Lambda_c^+, \bar{\Xi}_c^- \rightarrow \Lambda_c^- K^0$	(2.4 ± 0.6)	$\times 10^{-4}$		-

Lepton Family number (LF) or Lepton number (L) or Baryon number (B) violating modes, or/and $\Delta B = 1$ weak neutral current (BI) modes

$\gamma \gamma$	BI	< 3.2	$\times 10^{-7}$	CL=90%	2640
$e^+ e^-$	BI	< 8.3	$\times 10^{-8}$	CL=90%	2640
$e^+ e^- \gamma$	BI	< 1.2	$\times 10^{-7}$	CL=90%	2640
$\mu^+ \mu^-$	BI	(1.1 ± 1.4)	$\times 10^{-10}$	S=1.6	2638
$\mu^+ \mu^- \gamma$	BI	< 1.6	$\times 10^{-7}$	CL=90%	2638
$\mu^+ \mu^- \mu^+ \mu^-$	BI	< 6.9	$\times 10^{-10}$	CL=95%	2629
$S P, S \rightarrow \mu^+ \mu^-, P \rightarrow \mu^+ \mu^-$	BI [aaaa]	< 6.0	$\times 10^{-10}$	CL=95%	-
$\tau^+ \tau^-$	BI	< 2.1	$\times 10^{-3}$	CL=95%	1952
$\pi^0 \ell^+ \ell^-$	BI	< 5.3	$\times 10^{-8}$	CL=90%	2638
$\pi^0 e^+ e^-$	BI	< 8.4	$\times 10^{-8}$	CL=90%	2638
$\pi^0 \mu^+ \mu^-$	BI	< 6.9	$\times 10^{-8}$	CL=90%	2634
$\eta \ell^+ \ell^-$	BI	< 6.4	$\times 10^{-8}$	CL=90%	2611
$\eta e^+ e^-$	BI	< 1.08	$\times 10^{-7}$	CL=90%	2611
$\eta \mu^+ \mu^-$	BI	< 1.12	$\times 10^{-7}$	CL=90%	2607
$\pi^0 \nu \bar{\nu}$	BI	< 9	$\times 10^{-6}$	CL=90%	2638
$K^0 \ell^+ \ell^-$	BI [III]	(3.1 ± 0.8)	$\times 10^{-7}$		2616
$K^0 e^+ e^-$	BI	(1.6 ± 1.0)	$\times 10^{-7}$		2616
$K^0 \mu^+ \mu^-$	BI	(3.39 ± 0.34)	$\times 10^{-7}$		2612
$K^0 \nu \bar{\nu}$	BI	< 2.6	$\times 10^{-5}$	CL=90%	2616
$\rho^0 \nu \bar{\nu}$	BI	< 4.0	$\times 10^{-5}$	CL=90%	2583
$K^*(892)^0 \ell^+ \ell^-$	BI [III]	(9.9 ± 1.2)	$\times 10^{-7}$		2565
$K^*(892)^0 e^+ e^-$	BI	(1.03 ± 0.19)	$\times 10^{-6}$		2565
$K^*(892)^0 \mu^+ \mu^-$	BI	(9.4 ± 0.5)	$\times 10^{-7}$		2560
$\pi^+ \pi^- \mu^+ \mu^-$	BI	(2.1 ± 0.5)	$\times 10^{-8}$		2626
$K^*(892)^0 \nu \bar{\nu}$	BI	< 1.8	$\times 10^{-5}$	CL=90%	2565
invisible	BI	< 2.4	$\times 10^{-5}$	CL=90%	-
$\nu \bar{\nu} \gamma$	BI	< 1.7	$\times 10^{-5}$	CL=90%	2640
$\phi \nu \bar{\nu}$	BI	< 1.27	$\times 10^{-4}$	CL=90%	2541
$e^\pm \mu^\mp$	LF [bb]	< 1.0	$\times 10^{-9}$	CL=90%	2639
$\pi^0 e^\pm \mu^\mp$	LF	< 1.4	$\times 10^{-7}$	CL=90%	2637
$K^0 e^\pm \mu^\mp$	LF	< 2.7	$\times 10^{-7}$	CL=90%	2615
$K^*(892)^0 e^+ \mu^-$	LF	< 1.6	$\times 10^{-7}$	CL=90%	2563
$K^*(892)^0 e^- \mu^+$	LF	< 1.2	$\times 10^{-7}$	CL=90%	2563
$K^*(892)^0 e^\pm \mu^\mp$	LF	< 1.8	$\times 10^{-7}$	CL=90%	2563
$e^\pm \tau^\mp$	LF [bb]	< 2.8	$\times 10^{-5}$	CL=90%	2341
$\mu^\pm \tau^\mp$	LF [bb]	< 1.4	$\times 10^{-5}$	CL=95%	2339
$\Lambda_c^+ \mu^-$	L,B	< 1.4	$\times 10^{-6}$	CL=90%	2143
$\Lambda_c^+ e^-$	L,B	< 4	$\times 10^{-6}$	CL=90%	2145

B^\pm/B^0 ADMIXTURE

CP violation

$A_{CP}(B \rightarrow K^*(892)\gamma)$	= -0.003 ± 0.011
$A_{CP}(B \rightarrow s\gamma)$	= 0.015 ± 0.011
$A_{CP}(B \rightarrow (s+d)\gamma)$	= 0.010 ± 0.031
$A_{CP}(B \rightarrow X_s \ell^+ \ell^-)$	= 0.04 ± 0.11
$A_{CP}(B \rightarrow X_s \ell^+ \ell^-)$	(1.0 < q ² < 6.0 GeV ² /c ⁴) = -0.06 ± 0.22
$A_{CP}(B \rightarrow X_s \ell^+ \ell^-)$	(10.1 < q ² < 12.9 or q ² > 14.2 GeV ² /c ⁴) = 0.19 ± 0.18
$A_{CP}(B \rightarrow K^* e^+ e^-)$	= -0.18 ± 0.15
$A_{CP}(B \rightarrow K^* \mu^+ \mu^-)$	= -0.03 ± 0.13
$A_{CP}(B \rightarrow K^* \ell^+ \ell^-)$	= -0.04 ± 0.07
$A_{CP}(B \rightarrow \eta \text{ anything})$	= -0.13 ± 0.05
$\Delta A_{CP}(X_s \gamma) = A_{CP}(B^\pm \rightarrow X_s \gamma) - A_{CP}(B^0 \rightarrow X_s \gamma)$	= 0.041 ± 0.023
$\bar{A}_{CP}(B \rightarrow X_s \gamma) = (A_{CP}(B^+ \rightarrow X_s \gamma) + A_{CP}(B^0 \rightarrow X_s \gamma))/2$	= 0.009 ± 0.012
$\Delta A_{CP}(B \rightarrow K^* \gamma) = A_{CP}(B^+ \rightarrow K^{*+} \gamma) - A_{CP}(B^0 \rightarrow K^{*0} \gamma)$	= 0.024 ± 0.028
$\bar{A}_{CP}(B \rightarrow K^* \gamma) = (A_{CP}(B^+ \rightarrow K^{*+} \gamma) + A_{CP}(B^0 \rightarrow K^{*0} \gamma))/2$	= -0.001 ± 0.014

The branching fraction measurements are for an admixture of B mesons at the $\Upsilon(4S)$. The values quoted assume that $B(\Upsilon(4S) \rightarrow B\bar{B}) = 100\%$.

For inclusive branching fractions, e.g., $B \rightarrow D^\pm \text{ anything}$, the treatment of multiple D 's in the final state must be defined. One possibility would be to count the number of events with one-or-more D 's and divide by the total number of B 's. Another possibility would be to count the total number of D 's and divide by the total number of B 's, which is the definition of average multiplicity. The two definitions are identical if only one D is allowed in the final state. Even though the "one-or-more" definition seems sensible, for practical reasons inclusive branching fractions are almost always measured using the multiplicity definition. For heavy final state particles, authors call their results inclusive branching fractions while for light particles some authors call their results multiplicities. In the B sections, we list all results as inclusive branching fractions, adopting a multiplicity definition. This means that inclusive branching fractions can exceed 100% and that inclusive partial widths can exceed total widths, just as inclusive cross sections can exceed total cross section.

\bar{B} modes are charge conjugates of the modes below. Reactions indicate the weak decay vertex and do not include mixing.

B DECAY MODES	Fraction (Γ_i/Γ)	Scale factor / Confidence level (MeV/c)	p
Semileptonic and leptonic modes			
$\ell^+ \nu_\ell \text{ anything}$	[III, bbaa]	(10.86 ± 0.16) %	-
$D^- \ell^+ \nu_\ell \text{ anything}$	[III]	(2.6 ± 0.5) %	-
$\bar{D}^0 \ell^+ \nu_\ell \text{ anything}$	[III]	(7.3 ± 1.5) %	-
$\bar{D} \ell^+ \nu_\ell$		(2.42 ± 0.12) %	2310
$D^{*-} \ell^+ \nu_\ell \text{ anything}$	[ccaa]	(6.7 ± 1.3) $\times 10^{-3}$	-
$D^* \ell^+ \nu_\ell$	[ddaa]	(4.95 ± 0.11) %	2257
$\bar{D}^{*+} \ell^+ \nu_\ell$	[III, eaaa]	(2.7 ± 0.7) %	-
$\bar{D}_1(2420) \ell^+ \nu_\ell \text{ anything}$		(3.8 ± 1.3) $\times 10^{-3}$	S=2.4
$D \pi \ell^+ \nu_\ell \text{ anything} + D^* \pi \ell^+ \nu_\ell \text{ anything}$		(2.6 ± 0.5) %	S=1.5
$D \pi \ell^+ \nu_\ell \text{ anything}$		(1.5 ± 0.6) %	-
$D^* \pi \ell^+ \nu_\ell \text{ anything}$		(1.9 ± 0.4) %	-
$\bar{D}_2^*(2460) \ell^+ \nu_\ell \text{ anything}$		(4.4 ± 1.6) $\times 10^{-3}$	-
$D^{*-} \pi^+ \ell^+ \nu_\ell \text{ anything}$		(1.00 ± 0.34) %	-
$\bar{D} \pi^+ \pi^- \ell^+ \nu_\ell$		(1.62 ± 0.32) $\times 10^{-3}$	2301
$\bar{D}^* \pi^+ \pi^- \ell^+ \nu_\ell$		(9.4 ± 3.2) $\times 10^{-4}$	2247
$D_s^- \ell^+ \nu_\ell \text{ anything}$	[III]	< 7	$\times 10^{-3}$ CL=90%
$D_s^- \ell^+ \nu_\ell K^+ \text{ anything}$	[III]	< 5	$\times 10^{-3}$ CL=90%
$D_s^- \ell^+ \nu_\ell K^0 \text{ anything}$	[III]	< 7	$\times 10^{-3}$ CL=90%
$X_c \ell^+ \nu_\ell$		(10.65 ± 0.16) %	-
$X_{cb} \ell^+ \nu_\ell$		(2.13 ± 0.30) $\times 10^{-3}$	-
$K^+ \ell^+ \nu_\ell \text{ anything}$	[III]	(6.3 ± 0.6) %	-
$K^- \ell^+ \nu_\ell \text{ anything}$	[III]	(10 ± 4) $\times 10^{-3}$	-
$K^0 / \bar{K}^0 \ell^+ \nu_\ell \text{ anything}$	[III]	(4.6 ± 0.5) %	-
$\bar{D} \tau^+ \nu_\tau$		(9.9 ± 1.2) $\times 10^{-3}$	1911
$D^* \tau^+ \nu_\tau$		(1.50 ± 0.08) %	1838

Meson Summary Table

D, D*, or D_s modes				Baryon modes			
D^\pm anything	(23.1 ± 1.2) %	-	-	ρ^0 anything	(21 ± 5) %	-	-
D^0/\bar{D}^0 anything	(61.5 ± 2.9) %	S=1.3	-	ω anything	< 81 %	CL=90%	-
$D^*(2010)^\pm$ anything	(22.5 ± 1.5) %	-	-	ϕ anything	(3.43 ± 0.12) %	-	-
$D^*(2007)^0$ anything	(26.0 ± 2.7) %	-	-	$\phi K^*(892)$	< 2.2 × 10 ⁻⁵	CL=90%	2460
D_s^\pm anything	[bb] (8.3 ± 0.8) %	-	-	π^+ gluon (charmless)	(3.7 ± 0.8) × 10 ⁻⁴	-	-
$D_s^{*\pm}$ anything	(6.3 ± 1.0) %	-	-	Baryon modes			
$D_s^{*\pm} \bar{D}^*(*)$	(3.4 ± 0.6) %	-	-	$\Lambda_c^+ / \bar{\Lambda}_c^-$ anything	(3.6 ± 0.4) %	-	-
$\bar{D} D_{s0}(2317)$	seen	1605	-	Λ_c^+ anything	< 1.3 %	CL=90%	-
$\bar{D} D_{sJ}(2457)$	seen	-	-	$\bar{\Lambda}_c^-$ anything	< 7 %	CL=90%	-
$D^*(*) \bar{D}^*(*) K^0 + D^*(*) \bar{D}^*(*) K^\pm$	[bb, ffaa] (7.1 ± 2.7 / -1.7) %	-	-	$\bar{\Lambda}_c^- \ell^+$ anything	< 9 × 10 ⁻⁴	CL=90%	-
$b \rightarrow c \bar{c} s$	(22 ± 4) %	-	-	$\bar{\Lambda}_c^- e^+$ anything	< 1.8 × 10 ⁻³	CL=90%	-
$D_s^*(*) \bar{D}^*(*)$	[bb, ffaa] (3.9 ± 0.4) %	-	-	$\bar{\Lambda}_c^- \mu^+$ anything	< - 1.4 × 10 ⁻³	CL=90%	-
$D^* D^*(2010)^\pm$	[bb] < 5.9 × 10 ⁻³	CL=90%	1711	$\bar{\Lambda}_c^- p$ anything	(2.04 ± 0.33) %	-	-
$D^*(2010)^\pm + D^* D^\pm$	[bb] < 5.5 × 10 ⁻³	CL=90%	-	$\bar{\Lambda}_c^- p e^+ \nu_e$	< 8 × 10 ⁻⁴	CL=90%	2021
DD^\pm	[bb] < 3.1 × 10 ⁻³	CL=90%	1866	Σ_c^{*-} anything	(3.3 ± 1.7) × 10 ⁻³	-	-
$D_s^*(*)^\pm \bar{D}^*(*) X (n\pi^\pm)$	[bb, ffaa] (9 ± 5 / -4) %	-	-	Σ_c^0 anything	< 8 × 10 ⁻³	CL=90%	-
$D^*(2010)\gamma$	< 1.1 × 10 ⁻³	CL=90%	2257	Σ_c^0 anything	(3.7 ± 1.7) × 10 ⁻³	-	-
$D_s^+ \pi^-, D_s^{*+} \pi^-, D_s^+ \rho^-, D_s^{*+} \rho^-, D_s^+ \pi^0, D_s^{*+} \pi^0, D_s^+ \eta, D_s^{*+} \eta, D_s^+ \rho^0, D_s^{*+} \rho^0, D_s^+ \omega, D_s^{*+} \omega$	[bb] < 4 × 10 ⁻⁴	CL=90%	-	$\Sigma_c^0 N (N = p \text{ or } n)$	< 1.2 × 10 ⁻³	CL=90%	1938
$D_{s1}(2536)^+$ anything	< 9.5 × 10 ⁻³	CL=90%	-	Ξ_c^0 anything, $\Xi_c^0 \rightarrow \Xi^- \pi^+$	(1.93 ± 0.30) × 10 ⁻⁴	S=1.1	-
Charmonium modes				$\Xi_c^+ \rightarrow \Xi^- \pi^+ \pi^+$	(4.5 ± 1.3 / -1.2) × 10 ⁻⁴	-	-
$J/\psi(1S)$ anything	(1.094 ± 0.032) %	S=1.1	-	p/\bar{p} anything	[bb] (8.0 ± 0.4) %	-	-
$J/\psi(1S)$ (direct) anything	(7.8 ± 0.4) × 10 ⁻³	S=1.1	-	p/\bar{p} (direct) anything	[bb] (5.5 ± 0.5) %	-	-
$\psi(2S)$ anything	(3.07 ± 0.21) × 10 ⁻³	-	-	$\bar{p} e^+ \nu_e$ anything	< 5.9 × 10 ⁻⁴	CL=90%	-
$\chi_{c1}(1P)$ anything	(3.55 ± 0.27) × 10 ⁻³	S=1.3	-	$\Lambda/\bar{\Lambda}$ anything	[bb] (4.0 ± 0.5) %	-	-
$\chi_{c1}(1P)$ (direct) anything	(3.08 ± 0.19) × 10 ⁻³	-	-	Λ anything	seen	-	-
$\chi_{c2}(1P)$ anything	(10.0 ± 1.7) × 10 ⁻⁴	S=1.6	-	$\bar{\Lambda}$ anything	seen	-	-
$\chi_{c2}(1P)$ (direct) anything	(7.5 ± 1.1) × 10 ⁻⁴	-	-	$\Xi^- / \bar{\Xi}^+$ anything	[bb] (2.7 ± 0.6) × 10 ⁻³	-	-
$\eta_c(1S)$ anything	< 9 × 10 ⁻³	CL=90%	-	baryons anything	(6.8 ± 0.6) %	-	-
$K\chi_{c1}(3872), \chi_{c1} \rightarrow D^0 \bar{D}^0 \pi^0$	(1.2 ± 0.4) × 10 ⁻⁴	-	1141	$\rho/\bar{\rho}$ anything	(2.47 ± 0.23) %	-	-
$K\chi_{c1}(3872), \chi_{c1} \rightarrow D^{*0} \bar{D}^0$	(8.0 ± 2.2) × 10 ⁻⁵	-	1141	$\Lambda\bar{\Lambda}/\bar{\Lambda}\Lambda$ anything	[bb] (2.5 ± 0.4) %	-	-
$KX(3940), X \rightarrow D^{*0} D^0$	< 6.7 × 10 ⁻⁵	CL=90%	1084	Lepton Family number (LF) violating modes or $\Delta B = 1$ weak neutral current (B_1) modes			
$KX(3915), X \rightarrow \omega J/\psi$	[ggaa] (7.1 ± 3.4) × 10 ⁻⁵	-	1103	$s e^+ e^-$	B_1 (6.7 ± 1.7) × 10 ⁻⁶	S=2.0	-
K or K* modes				$s\mu^+ \mu^-$	B_1 (4.3 ± 1.0) × 10 ⁻⁶	-	-
K^\pm anything	[bb] (78.9 ± 2.5) %	-	-	$s\ell^+ \ell^-$	B_1 [III] (5.8 ± 1.3) × 10 ⁻⁶	S=1.8	-
K^+ anything	(66 ± 5) %	-	-	$\pi \ell^+ \ell^-$	B_1 < 5.9 × 10 ⁻⁸	CL=90%	2638
K^- anything	(13 ± 4) %	-	-	$\pi e^+ e^-$	B_1 < 1.10 × 10 ⁻⁷	CL=90%	2638
K^0/\bar{K}^0 anything	[bb] (64 ± 4) %	-	-	$\pi \mu^+ \mu^-$	B_1 < 5.0 × 10 ⁻⁸	CL=90%	2634
$K^*(892)^\pm$ anything	(18 ± 6) %	-	-	$K e^+ e^-$	B_1 (4.4 ± 0.6) × 10 ⁻⁷	-	2617
$K^*(892)^0/\bar{K}^*(892)^0$ anything	[bb] (14.6 ± 2.6) %	-	-	$K^*(892) e^+ e^-$	B_1 (1.19 ± 0.20) × 10 ⁻⁶	S=1.2	2565
$K^*(892)\gamma$	(4.2 ± 0.6) × 10 ⁻⁵	2565	-	$K\mu^+ \mu^-$	B_1 (4.4 ± 0.4) × 10 ⁻⁷	-	2612
$\eta K\gamma$	(8.5 ± 1.8 / -1.6) × 10 ⁻⁶	2588	-	$K^*(892) \mu^+ \mu^-$	B_1 (1.06 ± 0.09) × 10 ⁻⁶	-	2560
$K_1(1400)\gamma$	< 1.27 × 10 ⁻⁴	CL=90%	2454	$K\ell^+ \ell^-$	B_1 (4.8 ± 0.4) × 10 ⁻⁷	-	2617
$K_2^*(1430)\gamma$	(1.7 ± 0.6 / -0.5) × 10 ⁻⁵	2447	-	$K^*(892) \ell^+ \ell^-$	B_1 (1.05 ± 0.10) × 10 ⁻⁶	-	2565
$K_2(1770)\gamma$	< 1.2 × 10 ⁻³	CL=90%	2342	$K\nu\bar{\nu}$	B_1 < 1.6 × 10 ⁻⁵	CL=90%	2617
$K_3^*(1780)\gamma$	< 3.7 × 10 ⁻⁵	CL=90%	2341	$K^* \nu\bar{\nu}$	B_1 < 2.7 × 10 ⁻⁵	CL=90%	-
$K_4^*(2045)\gamma$	< 1.0 × 10 ⁻³	CL=90%	2243	$\pi\nu\bar{\nu}$	B_1 < 8 × 10 ⁻⁶	CL=90%	2638
$K\eta'(958)$	(8.3 ± 1.1) × 10 ⁻⁵	2528	-	$\rho\nu\bar{\nu}$	B_1 < 2.8 × 10 ⁻⁵	CL=90%	2583
$K^*(892)\eta'(958)$	(4.1 ± 1.1) × 10 ⁻⁶	2472	-	$s e^\pm \mu^\mp$	LF [bb] < 2.2 × 10 ⁻⁵	CL=90%	-
$K\eta$	< 5.2 × 10 ⁻⁶	CL=90%	2588	$\pi e^\pm \mu^\mp$	LF < 9.2 × 10 ⁻⁸	CL=90%	2637
$K^*(892)\eta$	(1.8 ± 0.5) × 10 ⁻⁵	2534	-	$\rho e^\pm \mu^\mp$	LF < 3.2 × 10 ⁻⁶	CL=90%	2582
$K\phi$	(2.3 ± 0.9) × 10 ⁻⁶	2306	-	$K e^\pm \mu^\mp$	LF < 3.8 × 10 ⁻⁸	CL=90%	2616
$\bar{b} \rightarrow \bar{s} \gamma$	(3.49 ± 0.19) × 10 ⁻⁴	-	-	$K^*(892) e^\pm \mu^\mp$	LF < 5.1 × 10 ⁻⁷	CL=90%	2563
$\bar{b} \rightarrow \bar{d} \gamma$	(9.2 ± 3.0) × 10 ⁻⁶	-	-	$B^\pm/B^0/B_s^0/b$-baryon ADMIXTURE			
$\bar{b} \rightarrow \bar{s}$ gluon	< 6.8 %	CL=90%	-	These measurements are for an admixture of bottom particles at high energy (LHC, LEP, Tevatron, $Sp\bar{P}S$).			
η anything	(2.6 ± 0.5 / -0.8) × 10 ⁻⁴	-	-	Mean life $\tau = (1.5668 \pm 0.0028) \times 10^{-12}$ s			
η' anything	(4.2 ± 0.9) × 10 ⁻⁴	-	-	Mean life $\tau = (1.72 \pm 0.10) \times 10^{-12}$ s Charged b -hadron admixture			
K^+ gluon (charmless)	< 1.87 × 10 ⁻⁴	CL=90%	-	Mean life $\tau = (1.58 \pm 0.14) \times 10^{-12}$ s Neutral b -hadron admixture			
K^0 gluon (charmless)	(1.9 ± 0.7) × 10 ⁻⁴	-	-	$\tau^{\text{charged } b\text{-hadron}}/\tau^{\text{neutral } b\text{-hadron}} = 1.09 \pm 0.13$			
Light unflavored meson modes				$ \Delta\tau_b /\tau_{b,\bar{b}} = -0.001 \pm 0.014$			
$\rho\gamma$	(1.39 ± 0.25) × 10 ⁻⁶	S=1.2	2583	The branching fraction measurements are for an admixture of B mesons and baryons at energies above the $\mathcal{T}(4S)$. Only the highest energy results (LHC, LEP, Tevatron, $Sp\bar{P}S$) are used in the branching fraction averages. In the following, we assume that the production fractions are the same at the LHC, LEP, and at the Tevatron.			
$\rho/\omega\gamma$	(1.30 ± 0.23) × 10 ⁻⁶	S=1.2	-	For inclusive branching fractions, e.g., $B \rightarrow D^\pm$ anything, the values usually are multiplicities, not branching fractions. They can be greater than one.			
π^\pm anything	[bb, hhaa] (358 ± 7) %	-	-				
π^0 anything	(235 ± 11) %	-	-				
η anything	(17.6 ± 1.6) %	-	-				

Meson Summary Table

The modes below are listed for a \bar{b} initial state. b modes are their charge conjugates. Reactions indicate the weak decay vertex and do not include mixing.

\bar{b} DECAY MODES	Fraction (Γ_i/Γ)	Scale factor/ Confidence level	p (MeV/c)
-----------------------	--------------------------------	-----------------------------------	----------------

PRODUCTION FRACTIONS

The production fractions for weakly decaying b -hadrons at high energy have been calculated from the best values of mean lives, mixing parameters, and branching fractions in this edition by the Heavy Flavor Averaging Group (HFLAV) as described in the note “ B^0 - \bar{B}^0 Mixing” in the B^0 Particle Listings. We no longer provide world averages of the b -hadron production fractions, where results from LEP, Tevatron and LHC are averaged together; indeed the available data (from CDF and LHCb) shows that the fractions depend on the kinematics (in particular the p_T) of the produced b hadron. Hence we would like to list the fractions in Z decays instead, which are well-defined physics observables. The production fractions in $p\bar{p}$ collisions at the Tevatron are also listed at the end of the section. Values assume

$$\begin{aligned} \text{B}(\bar{b} \rightarrow B^+) &= \text{B}(\bar{b} \rightarrow B^0) \\ \text{B}(\bar{b} \rightarrow B^+) + \text{B}(\bar{b} \rightarrow B^0) + \text{B}(\bar{b} \rightarrow B_s^0) + \text{B}(b \rightarrow b\text{-baryon}) &= 100\%. \end{aligned}$$

The correlation coefficients between production fractions are also reported:

$$\begin{aligned} \text{cor}(B_s^0, b\text{-baryon}) &= 0.064 \\ \text{cor}(B_s^0, B^\pm = B^0) &= -0.633 \\ \text{cor}(b\text{-baryon}, B^\pm = B^0) &= -0.813. \end{aligned}$$

The notation for production fractions varies in the literature (f_d , d_{B^0} , $f(b \rightarrow \bar{B}^0)$, $\text{Br}(b \rightarrow \bar{B}^0)$). We use our own branching fraction notation here, $\text{B}(\bar{b} \rightarrow B^0)$.

Note these production fractions are b -hadronization fractions, not the conventional branching fractions of b -quark to a B -hadron, which may have considerable dependence on the initial and final state kinematic and production environment.

B^+	(40.8 ± 0.7) %	—
B^0	(40.8 ± 0.7) %	—
B_s^0	(10.0 ± 0.8) %	—
b -baryon	(8.4 ± 1.1) %	—

DECAY MODES

Semileptonic and leptonic modes

ν anything	(23.1 ± 1.5) %	—
$\ell^+ \nu_\ell$ anything	[III] (10.69 ± 0.22) %	—
$e^+ \nu_e$ anything	(10.86 ± 0.35) %	—
$\mu^+ \nu_\mu$ anything	(10.95 ± 0.29) %	—
$D^- \ell^+ \nu_\ell$ anything	[III] (2.2 ± 0.4) %	S=1.9
$D^- \pi^+ \ell^+ \nu_\ell$ anything	(4.9 ± 1.9) × 10 ⁻³	—
$D^- \pi^- \ell^+ \nu_\ell$ anything	(2.6 ± 1.6) × 10 ⁻³	—
$\bar{D}^0 \ell^+ \nu_\ell$ anything	[III] (6.79 ± 0.34) %	—
$\bar{D}^0 \pi^- \ell^+ \nu_\ell$ anything	(1.07 ± 0.27) %	—
$\bar{D}^0 \pi^+ \ell^+ \nu_\ell$ anything	(2.3 ± 1.6) × 10 ⁻³	—
$D^{*-} \ell^+ \nu_\ell$ anything	[III] (2.75 ± 0.19) %	—
$D^{*-} \pi^- \ell^+ \nu_\ell$ anything	(6 ± 7) × 10 ⁻⁴	—
$D^{*-} \pi^+ \ell^+ \nu_\ell$ anything	(4.8 ± 1.0) × 10 ⁻³	—
$\bar{D}_j^0 \ell^+ \nu_\ell$ anything × B($\bar{D}_j^0 \rightarrow D^{*+} \pi^-$)	[III, iiaa] (2.6 ± 0.9) × 10 ⁻³	—
$D_j^- \ell^+ \nu_\ell$ anything × B($D_j^- \rightarrow D^0 \pi^-$)	[III, iiaa] (7.0 ± 2.3) × 10 ⁻³	—
$\bar{D}_2^*(2460)^0 \ell^+ \nu_\ell$ anything × B($\bar{D}_2^*(2460)^0 \rightarrow$ $D^{*-} \pi^+$)	< 1.4 × 10 ⁻³ CL=90%	—
$D_2^*(2460)^- \ell^+ \nu_\ell$ anything × B($D_2^*(2460)^- \rightarrow$ $D^0 \pi^-$)	(4.2 ± 1.5) × 10 ⁻³	—
$\bar{D}_2^*(2460)^0 \ell^+ \nu_\ell$ anything × B($\bar{D}_2^*(2460)^0 \rightarrow$ $D^- \pi^+$)	(1.6 ± 0.8) × 10 ⁻³	—
charmless $\ell \bar{\nu}_\ell$	[III] (1.7 ± 0.5) × 10 ⁻³	—
$\tau^+ \nu_\tau$ anything	(2.41 ± 0.23) %	—
$D^{*-} \tau \nu_\tau$ anything	(9 ± 4) × 10 ⁻³	—
$\bar{c} \rightarrow \ell^- \bar{\nu}_\ell$ anything	[III] (8.02 ± 0.19) %	—
$c \rightarrow \ell^+ \nu_\ell$ anything	(1.6 ± 0.5) %	—

Charmed meson and baryon modes

\bar{D}^0 anything	(58.7 ± 2.8) %	—
$D^0 D_s^\pm$ anything	[bb] (9.1 ± 4.0) %	—
$D^\mp D_s^\pm$ anything	[bb] (4.0 ± 2.3) %	—
$\bar{D}^0 D^0$ anything	[bb] (5.1 ± 2.0) %	—
$D^0 D^\pm$ anything	[bb] (2.7 ± 1.8) %	—
$D^\pm D^\mp$ anything	[bb] < 9 × 10 ⁻³ CL=90%	—
D^- anything	(22.7 ± 1.6) %	—
$D^*(2010)^+$ anything	(17.3 ± 2.0) %	—
$D_1(2420)^0$ anything	(5.0 ± 1.5) %	—
$D^*(2010)^\mp D_s^\pm$ anything	[bb] (3.3 ± 1.6) %	—
$D^0 D^*(2010)^\pm$ anything	[bb] (3.0 ± 1.1) %	—
$D^*(2010)^\pm D^\mp$ anything	[bb] (2.5 ± 1.2) %	—
$D^*(2010)^\pm D^*(2010)^\mp$ anything	[bb] (1.2 ± 0.4) %	—
$\bar{D} D$ anything	(10 ± 11) %	—
$D_2^*(2460)^0$ anything	(4.7 ± 2.7) %	—
D_s^- anything	(14.7 ± 2.1) %	—
D_s^+ anything	(10.1 ± 3.1) %	—
Λ_c^+ anything	(7.7 ± 1.1) %	—
\bar{c}/c anything	[hhaa] (116.2 ± 3.2) %	—

Charmonium modes

$J/\psi(1S)$ anything	(1.16 ± 0.10) %	—
$\psi(2S)$ anything	(2.86 ± 0.28) × 10 ⁻³	—
$\chi_{c0}(1P)$ anything	(1.5 ± 0.6) %	—
$\chi_{c1}(1P)$ anything	(1.4 ± 0.4) %	—
$\chi_{c2}(1P)$ anything	(6.2 ± 2.9) × 10 ⁻³	—
$\chi_c(2P)$ anything, $\chi_c \rightarrow \phi\phi$	< 2.8 × 10 ⁻⁷ CL=95%	—
$\eta_c(1S)$ anything	(4.5 ± 1.9) %	—
$\eta_c(2S)$ anything, $\eta_c \rightarrow \phi\phi$	(3.2 ± 1.7) × 10 ⁻⁶	—
$\chi_{c1}(3872)$ anything, $\chi_{c1} \rightarrow$ $\phi\phi$	< 4.5 × 10 ⁻⁷ CL=95%	—
$X(3915)$ anything, $X \rightarrow \phi\phi$	< 3.1 × 10 ⁻⁷ CL=95%	—

K or K* modes

$\bar{3}\gamma$	(3.1 ± 1.1) × 10 ⁻⁴	—
$\bar{3}\bar{\nu}\nu$	< 6.4 × 10 ⁻⁴ CL=90%	—
K^\pm anything	(74 ± 6) %	—
K_S^0 anything	(29.0 ± 2.9) %	—

Pion modes

π^\pm anything	(397 ± 21) %	—
π^0 anything	[hhaa] (278 ± 60) %	—
ϕ anything	(2.82 ± 0.23) %	—

Baryon modes

p/\bar{p} anything	(13.1 ± 1.1) %	—
$\Lambda/\bar{\Lambda}$ anything	(5.9 ± 0.6) %	—
b -baryon anything	(10.2 ± 2.8) %	—

Other modes

charged anything	[hhaa] (497 ± 7) %	—
hadron ⁺ hadron ⁻	(1.7 ± 1.0) × 10 ⁻⁵	—
charmless	(7 ± 21) × 10 ⁻³	—

 $\Delta B = 1$ weak neutral current ($B1$) modes

$\mu^+ \mu^-$ anything	$B1$ < 3.2 × 10 ⁻⁴ CL=90%	—
------------------------	--------------------------------------	---

 B^*

$$I(J^P) = \frac{1}{2}(1^-)$$

I, J, P need confirmation.

Quantum numbers shown are quark-model predictions.

$$\begin{aligned} \text{Mass } m_{B^*} &= 5324.70 \pm 0.21 \text{ MeV} \\ m_{B^*} - m_B &= 45.21 \pm 0.21 \text{ MeV} \\ m_{B^{*+}} - m_{B^+} &= 45.37 \pm 0.21 \text{ MeV} \end{aligned}$$

B^* DECAY MODES	Fraction (Γ_i/Γ)	p (MeV/c)
$B\gamma$	seen	45

 $B_1(5721)^+$

$$I(J^P) = \frac{1}{2}(1^+)$$

I, J, P need confirmation.

$$\begin{aligned} \text{Mass } m &= 5725.9 \pm 2.5 \text{ MeV} \\ m_{B_1^+} - m_{B^{*0}} &= 401.2 \pm 2.4 \text{ MeV} \\ \text{Full width } \Gamma &= 31 \pm 6 \text{ MeV} \quad (S = 1.1) \end{aligned}$$

Meson Summary Table

$B_1(5721)^+$ DECAY MODES	Fraction (Γ_i/Γ)	ρ (MeV/c)
$B^{*0}\pi^+$	seen	363

$B_1(5721)^0$	$I(J^P) = \frac{1}{2}(1^+)$ <i>I, J, P</i> need confirmation.
$B_1(5721)^0$ MASS = 5726.1 ± 1.3 MeV ($S = 1.2$)	
$m_{B_1^0} - m_{B^+} = 446.7 \pm 1.3$ MeV ($S = 1.2$)	
$m_{B_1^0} - m_{B^{*+}} = 401.4 \pm 1.2$ MeV ($S = 1.2$)	
Full width $\Gamma = 27.5 \pm 3.4$ MeV ($S = 1.1$)	

$B_1(5721)^0$ DECAY MODES	Fraction (Γ_i/Γ)	ρ (MeV/c)
$B^{*+}\pi^-$	seen	363

$B_2^*(5747)^+$	$I(J^P) = \frac{1}{2}(2^+)$ <i>I, J, P</i> need confirmation.
Mass $m = 5737.2 \pm 0.7$ MeV	
$m_{B_2^{*+}} - m_{B^0} = 457.5 \pm 0.7$ MeV	
Full width $\Gamma = 20 \pm 5$ MeV ($S = 2.2$)	

$B_2^*(5747)^+$ DECAY MODES	Fraction (Γ_i/Γ)	ρ (MeV/c)
$B^0\pi^+$	seen	418
$B^{*0}\pi^+$	seen	374

$B_2^*(5747)^0$	$I(J^P) = \frac{1}{2}(2^+)$ <i>I, J, P</i> need confirmation.
$B_2^*(5747)^0$ MASS = 5739.5 ± 0.7 MeV ($S = 1.4$)	
$m_{B_2^0} - m_{B^0} = 13.4 \pm 1.4$ MeV ($S = 1.3$)	
$m_{B_2^0} - m_{B^+} = 460.2 \pm 0.6$ MeV ($S = 1.4$)	
Full width $\Gamma = 24.2 \pm 1.7$ MeV	

$B_2^*(5747)^0$ DECAY MODES	Fraction (Γ_i/Γ)	ρ (MeV/c)
$B^+\pi^-$	seen	421
$B^{*+}\pi^-$	seen	376

$B_J(5970)^+$	$I(J^P) = \frac{1}{2}(?^?)$ <i>I, J, P</i> need confirmation.
Mass $m = 5964 \pm 5$ MeV	
$m_{B_J(5970)^+} - m_{B^0} = 685 \pm 5$ MeV	
Full width $\Gamma = 62 \pm 20$ MeV	

$B_J(5970)^+$ DECAY MODES	Fraction (Γ_i/Γ)	ρ (MeV/c)
$B^0\pi^+$	possibly seen	632
$B^{*0}\pi^+$	seen	591

$B_J(5970)^0$	$I(J^P) = \frac{1}{2}(?^?)$ <i>I, J, P</i> need confirmation.
Mass $m = 5971 \pm 5$ MeV	
$m_{B_J(5970)^0} - m_{B^+} = 691 \pm 5$ MeV	
Full width $\Gamma = 81 \pm 12$ MeV	

$B_J(5970)^0$ DECAY MODES	Fraction (Γ_i/Γ)	ρ (MeV/c)
$B^+\pi^-$	possibly seen	638
$B^{*+}\pi^-$	seen	596

BOTTOM, STRANGE MESONS

($B = \pm 1, S = \mp 1$)

$$B_s^0 = s\bar{b}, \bar{B}_s^0 = \bar{s}b, \text{ similarly for } B_s^{*\pm}$$

B_s^0	$I(J^P) = 0(0^-)$
---------	-------------------

I, J, P need confirmation. Quantum numbers shown are quark-model predictions.

$$\text{Mass } m_{B_s^0} = 5366.88 \pm 0.14 \text{ MeV}$$

$$m_{B_s^0} - m_B = 87.38 \pm 0.16 \text{ MeV}$$

$$\text{Mean life } \tau = (1.515 \pm 0.004) \times 10^{-12} \text{ s}$$

$$c\tau = 454.2 \text{ } \mu\text{m}$$

$$\Delta\Gamma_{B_s^0} = \Gamma_{B_{sL}^0} - \Gamma_{B_{sH}^0} = (0.085 \pm 0.004) \times 10^{12} \text{ s}^{-1}$$

$B_s^0\text{-}\bar{B}_s^0$ mixing parameters

$$\Delta m_{B_s^0} = m_{B_{sH}^0} - m_{B_{sL}^0} = (17.749 \pm 0.020) \times 10^{12} \text{ } \hbar \text{ s}^{-1}$$

$$= (1.1683 \pm 0.0013) \times 10^{-8} \text{ MeV}$$

$$\chi_s = \Delta m_{B_s^0} / \Gamma_{B_s^0} = 26.89 \pm 0.07$$

$$\chi_s = 0.499312 \pm 0.000004$$

CP violation parameters in B_s^0

$$\text{Re}(\epsilon_{B_s^0}) / (1 + |\epsilon_{B_s^0}|^2) = (-0.15 \pm 0.70) \times 10^{-3}$$

$$C_{KK}(B_s^0 \rightarrow K^+K^-) = 0.14 \pm 0.11$$

$$S_{KK}(B_s^0 \rightarrow K^+K^-) = 0.30 \pm 0.13$$

$$r_B(B_s^0 \rightarrow D_s^\mp K^\pm) = 0.37 \pm_{0.09}^{0.10}$$

$$\delta_B(B_s^0 \rightarrow D_s^\pm K^\mp) = (358 \pm 14)^\circ$$

$$\text{CP Violation phase } \beta_s = (2.55 \pm 1.15) \times 10^{-2} \text{ rad}$$

$$|\lambda| (B_s^0 \rightarrow J/\psi(1S)\phi) = 1.012 \pm 0.017$$

$$|\lambda| = 0.999 \pm 0.017$$

$$A, \text{ CP violation parameter} = -0.75 \pm 0.12$$

$$C, \text{ CP violation parameter} = 0.19 \pm 0.06$$

$$S, \text{ CP violation parameter} = 0.17 \pm 0.06$$

$$A_{CP}^L(B_s \rightarrow J/\psi \bar{K}^*(892)^0) = -0.05 \pm 0.06$$

$$A_{CP}^{\parallel}(B_s \rightarrow J/\psi \bar{K}^*(892)^0) = 0.17 \pm 0.15$$

$$A_{CP}^{\perp}(B_s \rightarrow J/\psi \bar{K}^*(892)^0) = -0.05 \pm 0.10$$

$$A_{CP}(B_s \rightarrow \pi^+ K^-) = 0.221 \pm 0.015$$

$$A_{CP}(B_s^0 \rightarrow [K^+ K^-]_D \bar{K}^*(892)^0) = -0.04 \pm 0.07$$

$$A_{CP}(B_s^0 \rightarrow [\pi^+ K^-]_D K^*(892)^0) = -0.01 \pm 0.04$$

$$A_{CP}(B_s^0 \rightarrow [\pi^+ \pi^-]_D K^*(892)^0) = 0.06 \pm 0.13$$

$$S(B_s^0 \rightarrow \phi\gamma) = 0.43 \pm 0.32$$

$$C(B_s^0 \rightarrow \phi\gamma) = 0.11 \pm 0.31$$

$$A^\Delta(B_s \rightarrow \phi\gamma) = -0.7 \pm 0.4$$

$$\Delta a_\perp < 1.2 \times 10^{-12} \text{ GeV}, \text{ CL} = 95\%$$

$$\Delta a_\parallel = (-0.9 \pm 1.5) \times 10^{-14} \text{ GeV}$$

$$\Delta a_X = (1.0 \pm 2.2) \times 10^{-14} \text{ GeV}$$

$$\Delta a_Y = (-3.8 \pm 2.2) \times 10^{-14} \text{ GeV}$$

$$\text{Re}(\xi) = -0.022 \pm 0.033$$

$$\text{Im}(\xi) = 0.004 \pm 0.011$$

These branching fractions all scale with $B(\bar{B} \rightarrow B_s^0)$.

The branching fraction $B(B_s^0 \rightarrow D_s^- \ell^+ \nu_\ell \text{ anything})$ is not a pure measurement since the measured product branching fraction $B(\bar{B} \rightarrow B_s^0) \times B(B_s^0 \rightarrow D_s^- \ell^+ \nu_\ell \text{ anything})$ was used to determine $B(\bar{B} \rightarrow B_s^0)$, as described in the note on " $B^0\text{-}\bar{B}^0$ Mixing"

For inclusive branching fractions, e.g., $B \rightarrow D^\pm \text{ anything}$, the values usually are multiplicities, not branching fractions. They can be greater than one.

B_s^0 DECAY MODES	Fraction (Γ_i/Γ)	Scale factor/ Confidence level	ρ (MeV/c)
D_s^- anything	(93 \pm 25) %		-
$\ell \nu_\ell X$	(9.6 \pm 0.8) %		-
$e^+ \nu X^-$	(9.1 \pm 0.8) %		-
$\mu^+ \nu X^-$	(10.2 \pm 1.0) %		-
$D_s^- \ell^+ \nu_\ell \text{ anything}$	[<i>jjaa</i>] (8.1 \pm 1.3) %		-
$D_s^{*-} \ell^+ \nu_\ell \text{ anything}$	(5.4 \pm 1.1) %		-
$D_{s1}(2536)^- \mu^+ \nu_\mu, D_{s1}^- \rightarrow D^{*-} K_s^0$	(2.7 \pm 0.7) $\times 10^{-3}$		-

Meson Summary Table

$D_{s1}(2536)^- X \mu^+ \nu, D_{s1}^- \rightarrow \bar{D}^0 K^+$	$(4.4 \pm 1.3) \times 10^{-3}$	-	$J/\psi(1S) f_2'(1525)_{ }, f_2' \rightarrow \pi^+ \pi^-$	$(1.3 \pm \frac{2.7}{0.9}) \times 10^{-7}$	-
$D_{s2}(2573)^- X \mu^+ \nu, D_{s2}^- \rightarrow \bar{D}^0 K^+$	$(2.7 \pm 1.0) \times 10^{-3}$	-	$J/\psi(1S) f_2'(1525)_{\perp}, f_2' \rightarrow \pi^+ \pi^-$	$(5 \pm 4) \times 10^{-7}$	-
$D_s^- \rho^+$	$(3.00 \pm 0.23) \times 10^{-3}$	2320	$J/\psi(1S) f_0(1790), f_0 \rightarrow \pi^+ \pi^-$	$(5.0 \pm \frac{11.0}{1.1}) \times 10^{-6}$	-
$D_s^- \pi^+ \pi^+$	$(6.9 \pm 1.4) \times 10^{-3}$	2249	$J/\psi(1S) \pi^+ \pi^-$ (nonresonant)	$(1.8 \pm \frac{1.1}{0.4}) \times 10^{-5}$	1775
$D_s^- \pi^+ \pi^+ \pi^-$	$(6.1 \pm 1.0) \times 10^{-3}$	2301	$J/\psi(1S) \bar{K}^0 \pi^+ \pi^-$	$< 4.4 \times 10^{-5}$	CL=90% 1675
$D_{s1}(2536)^- \pi^+, D_{s1}^- \rightarrow D_s^- \pi^+ \pi^-$	$(2.5 \pm 0.8) \times 10^{-5}$	-	$J/\psi(1S) K^+ K^-$	$(7.9 \pm 0.7) \times 10^{-4}$	1601
$D_s^{\mp} K^{\pm}$	$(2.27 \pm 0.19) \times 10^{-4}$	2293	$J/\psi(1S) K^0 K^- \pi^+ + c.c.$	$(9.2 \pm 1.3) \times 10^{-4}$	1538
$D_s^- K^+ \pi^+ \pi^-$	$(3.2 \pm 0.6) \times 10^{-4}$	2249	$J/\psi(1S) \bar{K}^0 K^+ K^-$	$< 1.2 \times 10^{-5}$	CL=90% 1333
$D_s^+ D_s^-$	$(4.4 \pm 0.5) \times 10^{-3}$	1824	$J/\psi(1S) f_2'(1525)$	$(2.6 \pm 0.6) \times 10^{-4}$	1310
$D_s^- D^+$	$(2.8 \pm 0.5) \times 10^{-4}$	1875	$J/\psi(1S) p\bar{p}$	$(3.6 \pm 0.4) \times 10^{-6}$	982
$D^+ D^-$	$(2.2 \pm 0.6) \times 10^{-4}$	1925	$J/\psi(1S) \gamma$	$< 7.3 \times 10^{-6}$	CL=90% 1790
$D^0 \bar{D}^0$	$(1.9 \pm 0.5) \times 10^{-4}$	1930	$J/\psi(1S) \pi^+ \pi^- \pi^+ \pi^-$	$(7.8 \pm 1.0) \times 10^{-5}$	1731
$D_s^{*-} \pi^+$	$(2.0 \pm 0.5) \times 10^{-3}$	2265	$J/\psi(1S) f_1(1285)$	$(7.2 \pm 1.4) \times 10^{-5}$	1460
$D_s^{*\mp} K^{\pm}$	$(1.33 \pm 0.35) \times 10^{-4}$	-	$\psi(2S) \eta$	$(3.3 \pm 0.9) \times 10^{-4}$	1338
$D_s^{*-} \rho^+$	$(9.6 \pm 2.1) \times 10^{-3}$	2191	$\psi(2S) \eta'$	$(1.29 \pm 0.35) \times 10^{-4}$	1158
$D_s^{*+} D_s^- + D_s^{*-} D_s^+$	$(1.39 \pm 0.17) \%$	1742	$\psi(2S) \pi^+ \pi^-$	$(7.1 \pm 1.3) \times 10^{-5}$	1397
$D_s^{*+} D_s^{*-}$	$(1.44 \pm 0.21) \%$	S=1.1 1655	$\psi(2S) \phi$	$(5.4 \pm 0.6) \times 10^{-4}$	1120
$D_s^{*(*)+} D_s^{*(*)-}$	$(4.5 \pm 1.4) \%$	-	$\psi(2S) K^- \pi^+$	$(3.1 \pm 0.4) \times 10^{-5}$	1310
$\bar{D}^{*0} \bar{K}^0$	$(2.8 \pm 1.1) \times 10^{-4}$	2278	$\psi(2S) \bar{K}^*(892)^0$	$(3.3 \pm 0.5) \times 10^{-5}$	1196
$\bar{D}^0 \bar{K}^0$	$(4.3 \pm 0.9) \times 10^{-4}$	2330	$\chi_{c1} \phi$	$(2.04 \pm 0.30) \times 10^{-4}$	1274
$\bar{D}^0 K^- \pi^+$	$(1.04 \pm 0.13) \times 10^{-3}$	2312	$\pi^+ \pi^-$	$(7.0 \pm 1.0) \times 10^{-7}$	2680
$\bar{D}^0 \bar{K}^*(892)^0$	$(4.4 \pm 0.6) \times 10^{-4}$	2264	$\pi^0 \pi^0$	$< 2.1 \times 10^{-4}$	CL=90% 2680
$\bar{D}^0 \bar{K}^*(1410)$	$(3.9 \pm 3.5) \times 10^{-4}$	2117	$\eta \pi^0$	$< 1.0 \times 10^{-3}$	CL=90% 2654
$\bar{D}^0 \bar{K}_0^*(1430)$	$(3.0 \pm 0.7) \times 10^{-4}$	2113	$\eta \eta$	$< 1.5 \times 10^{-3}$	CL=90% 2627
$\bar{D}^0 \bar{K}_2^*(1430)$	$(1.1 \pm 0.4) \times 10^{-4}$	2112	$\rho^0 \rho^0$	$< 3.20 \times 10^{-4}$	CL=90% 2569
$\bar{D}^0 \bar{K}^*(1680)$	$< 7.8 \times 10^{-5}$	CL=90% 1997	$\eta' \eta'$	$(3.3 \pm 0.7) \times 10^{-5}$	2507
$\bar{D}^0 \bar{K}_0^*(1950)$	$< 1.1 \times 10^{-4}$	CL=90% 1890	$\eta' \phi$	$< 8.2 \times 10^{-7}$	CL=90% 2495
$\bar{D}^0 \bar{K}_3^*(1780)$	$< 2.6 \times 10^{-5}$	CL=90% 1971	$\phi f_0(980), f_0(980) \rightarrow \pi^+ \pi^-$	$(1.12 \pm 0.21) \times 10^{-6}$	-
$\bar{D}^0 \bar{K}_4^*(2045)$	$< 3.1 \times 10^{-5}$	CL=90% 1835	$\phi f_2(1270), f_2(1270) \rightarrow \pi^+ \pi^-$	$(6.1 \pm \frac{1.8}{1.5}) \times 10^{-7}$	-
$\bar{D}^0 K^- \pi^+$ (non-resonant)	$(2.1 \pm 0.8) \times 10^{-4}$	2312	$\phi \rho^0$	$(2.7 \pm 0.8) \times 10^{-7}$	2526
$D_{s2}^*(2573)^- \pi^+, D_{s2}^* \rightarrow \bar{D}^0 K^-$	$(2.6 \pm 0.4) \times 10^{-4}$	-	$\phi \pi^+ \pi^-$	$(3.5 \pm 0.5) \times 10^{-6}$	2579
$D_{s1}^*(2700)^- \pi^+, D_{s1}^* \rightarrow \bar{D}^0 K^-$	$(1.6 \pm 0.8) \times 10^{-5}$	-	$\phi \phi$	$(1.87 \pm 0.15) \times 10^{-5}$	2482
$D_{s1}^*(2860)^- \pi^+, D_{s1}^* \rightarrow \bar{D}^0 K^-$	$(5 \pm 4) \times 10^{-5}$	-	$\phi \phi \phi$	$(2.2 \pm 0.7) \times 10^{-6}$	2165
$D_{s3}^*(2860)^- \pi^+, D_{s3}^* \rightarrow \bar{D}^0 K^-$	$(2.2 \pm 0.6) \times 10^{-5}$	-	$\pi^+ K^-$	$(5.8 \pm 0.7) \times 10^{-6}$	2659
$\bar{D}^0 K^+ K^-$	$(5.5 \pm 0.8) \times 10^{-5}$	2243	$K^+ K^-$	$(2.66 \pm 0.22) \times 10^{-5}$	2638
$\bar{D}^0 f_0(980)$	$< 3.1 \times 10^{-6}$	CL=90% 2242	$K^0 \bar{K}^0$	$(2.0 \pm 0.6) \times 10^{-5}$	2637
$\bar{D}^0 \phi$	$(3.0 \pm 0.5) \times 10^{-5}$	2235	$K^0 \pi^+ \pi^-$	$(9.5 \pm 2.1) \times 10^{-6}$	2653
$\bar{D}^{*0} \phi$	$(3.7 \pm 0.6) \times 10^{-5}$	2178	$K^0 K^{\pm} \pi^{\mp}$	$(8.4 \pm 0.9) \times 10^{-5}$	2622
$D^{*\mp} \pi^{\pm}$	$< 6.1 \times 10^{-6}$	CL=90%	$K^*(892)^- \pi^+$	$(2.9 \pm 1.1) \times 10^{-6}$	2607
$\eta_c \phi$	$(5.0 \pm 0.9) \times 10^{-4}$	1663	$K^*(892)^{\pm} K^{\mp}$	$(1.9 \pm 0.5) \times 10^{-5}$	2585
$\eta_c \pi^+ \pi^-$	$(1.8 \pm 0.7) \times 10^{-4}$	1840	$K_0^*(1430)^{\pm} K^{\mp}$	$(3.1 \pm 2.5) \times 10^{-5}$	-
$J/\psi(1S) \phi$	$(1.08 \pm 0.08) \times 10^{-3}$	1588	$K_2^*(1430)^{\pm} K^{\mp}$	$(1.0 \pm 1.7) \times 10^{-5}$	-
$J/\psi(1S) \phi \phi$	$(1.24 \pm \frac{0.17}{0.19}) \times 10^{-5}$	764	$K^*(892)^0 \bar{K}^0 + c.c.$	$(2.0 \pm 0.6) \times 10^{-5}$	2585
$J/\psi(1S) \pi^0$	$< 1.2 \times 10^{-3}$	CL=90% 1787	$K_0^*(1430) \bar{K}^0 + c.c.$	$(3.3 \pm 1.0) \times 10^{-5}$	2468
$J/\psi(1S) \eta$	$(4.0 \pm 0.7) \times 10^{-4}$	S=1.4 1733	$K_2^*(1430)^0 \bar{K}^0 + c.c.$	$(1.7 \pm 2.2) \times 10^{-5}$	2467
$J/\psi(1S) K_S^0$	$(1.88 \pm 0.15) \times 10^{-5}$	1743	$K_S^0 \bar{K}^*(892)^0 + c.c.$	$(1.6 \pm 0.4) \times 10^{-5}$	2585
$J/\psi(1S) \bar{K}^*(892)^0$	$(4.1 \pm 0.4) \times 10^{-5}$	1637	$K^0 K^+ K^-$	$(1.3 \pm 0.6) \times 10^{-6}$	2568
$J/\psi(1S) \eta'$	$(3.3 \pm 0.4) \times 10^{-4}$	1612	$\bar{K}^*(892)^0 \rho^0$	$< 7.67 \times 10^{-4}$	CL=90% 2550
$J/\psi(1S) \pi^+ \pi^-$	$(2.09 \pm 0.23) \times 10^{-4}$	S=1.3 1775	$\bar{K}^*(892)^0 K^*(892)^0$	$(1.11 \pm 0.27) \times 10^{-5}$	2531
$J/\psi(1S) f_0(500), f_0 \rightarrow \pi^+ \pi^-$	$< 4 \times 10^{-6}$	CL=90%	$\phi K^*(892)^0$	$(1.14 \pm 0.30) \times 10^{-6}$	2507
$J/\psi(1S) \rho, \rho \rightarrow \pi^+ \pi^-$	$< 4 \times 10^{-6}$	CL=90%	$p\bar{p}$	$< 1.5 \times 10^{-8}$	CL=90% 2514
$J/\psi(1S) f_0(980), f_0 \rightarrow \pi^+ \pi^-$	$(1.28 \pm 0.18) \times 10^{-4}$	S=1.7	$p\bar{p} K^+ K^-$	$(4.5 \pm 0.5) \times 10^{-6}$	2231
$J/\psi(1S) f_2(1270), f_2 \rightarrow \pi^+ \pi^-$	$(1.1 \pm 0.4) \times 10^{-6}$	-	$p\bar{p} K^+ \pi^-$	$(1.39 \pm 0.26) \times 10^{-6}$	2355
$J/\psi(1S) f_2(1270)_0, f_2 \rightarrow \pi^+ \pi^-$	$(7.5 \pm 1.8) \times 10^{-7}$	-	$p\bar{p} \pi^+ \pi^-$	$(4.3 \pm 2.0) \times 10^{-7}$	2454
$J/\psi(1S) f_2(1270)_{ }, f_2 \rightarrow \pi^+ \pi^-$	$(1.09 \pm 0.34) \times 10^{-6}$	-	$p\bar{p} K^- + c.c.$	$(5.5 \pm 1.0) \times 10^{-6}$	2358
$J/\psi(1S) f_2(1270)_{\perp}, f_2 \rightarrow \pi^+ \pi^-$	$(1.3 \pm 0.8) \times 10^{-6}$	-	$\Lambda_c^- \Lambda \pi^+$	$(3.6 \pm 1.6) \times 10^{-4}$	1979
$J/\psi(1S) f_0(1370), f_0 \rightarrow \pi^+ \pi^-$	$(4.5 \pm \frac{0.7}{4.0}) \times 10^{-5}$	-	$\Lambda_c^- \Lambda_c^+$	$< 8.0 \times 10^{-5}$	CL=95% 1405
$J/\psi(1S) f_0(1500), f_0 \rightarrow \pi^+ \pi^-$	$(2.11 \pm \frac{0.40}{0.29}) \times 10^{-5}$	-	Lepton Family number (LF) violating modes or $\Delta B = 1$ weak neutral current (BI) modes		
$J/\psi(1S) f_2'(1525)_0, f_2' \rightarrow \pi^+ \pi^-$	$(1.07 \pm 0.24) \times 10^{-6}$	-	$\gamma \gamma$	BI	$< 3.1 \times 10^{-6}$ CL=90% 2683
			$\phi \gamma$	BI	$(3.4 \pm 0.4) \times 10^{-5}$ 2587
			$\mu^+ \mu^-$	BI	$(3.0 \pm 0.4) \times 10^{-9}$ 2681
			$e^+ e^-$	BI	$< 2.8 \times 10^{-7}$ CL=90% 2683
			$\tau^+ \tau^-$	BI	$< 6.8 \times 10^{-3}$ CL=95% 2011
			$\mu^+ \mu^- \mu^+ \mu^-$	BI	$< 2.5 \times 10^{-9}$ CL=95% 2673
			$S P, S \rightarrow \mu^+ \mu^-$	BI	$[aaaa] < 2.2 \times 10^{-9}$ CL=95% -
			$P \rightarrow \mu^+ \mu^-$		
			$\phi(1020) \mu^+ \mu^-$	BI	$(8.2 \pm 1.2) \times 10^{-7}$ 2582
			$\bar{K}^*(892)^0 \mu^+ \mu^-$		$(2.9 \pm 1.1) \times 10^{-8}$ 2605
			$\pi^+ \pi^- \mu^+ \mu^-$	BI	$(8.4 \pm 1.7) \times 10^{-8}$ 2670

Meson Summary Table

$\phi\nu\bar{\nu}$	BI	< 5.4	$\times 10^{-3}$	$CL=90\%$	2587
$e^\pm\mu^\mp$	LF	$[bb] < 5.4$	$\times 10^{-9}$	$CL=90\%$	2682
$\mu^\pm\tau^\mp$		< 4.2	$\times 10^{-5}$	$CL=95\%$	2388

 B_s^*

$$I(J^P) = 0(1^-)$$

I, J, P need confirmation. Quantum numbers shown are quark-model predictions.

$$\text{Mass } m = 5415.4_{-1.5}^{+1.8} \text{ MeV} \quad (S = 2.9)$$

$$m_{B_s^*} - m_{B_s} = 48.6_{-1.5}^{+1.8} \text{ MeV} \quad (S = 2.9)$$

B_s^* DECAY MODES	Fraction (Γ_i/Γ)	ρ (MeV/c)
$B_s\gamma$	seen	48

 $B_{s1}(5830)^0$

$$I(J^P) = 0(1^+)$$

I, J, P need confirmation.

$$\text{Mass } m = 5828.70 \pm 0.20 \text{ MeV}$$

$$m_{B_{s1}^0} - m_{B^{*+}} = 504.00 \pm 0.17 \text{ MeV}$$

$$\text{Full width } \Gamma = 0.5 \pm 0.4 \text{ MeV}$$

$B_{s1}(5830)^0$ DECAY MODES	Fraction (Γ_i/Γ)	ρ (MeV/c)
$B^{*+}K^-$	seen	97

 $B_{s2}(5840)^0$

$$I(J^P) = 0(2^+)$$

I, J, P need confirmation.

$$\text{Mass } m = 5839.86 \pm 0.12 \text{ MeV}$$

$$m_{B_{s2}^0} - m_{B^{*+}} = 560.52 \pm 0.14 \text{ MeV}$$

$$\text{Full width } \Gamma = 1.49 \pm 0.27 \text{ MeV}$$

$B_{s2}(5840)^0$ DECAY MODES	Fraction (Γ_i/Γ)	ρ (MeV/c)
B^+K^-	DEFINED AS 1	252
$B^{*+}K^-$	0.093 ± 0.018	141
$B^0K_S^0$	0.43 ± 0.11	245
$B^{*0}K_S^0$	0.04 ± 0.04	-

BOTTOM, CHARMED MESONS ($B = C = \pm 1$)

$$B_c^+ = c\bar{b}, B_c^- = \bar{c}b, \quad \text{similarly for } B_c^{* \pm}$$

 B_c^+

$$I(J^P) = 0(0^-)$$

I, J, P need confirmation.

Quantum numbers shown are quark-model predictions.

$$\text{Mass } m = 6274.9 \pm 0.8 \text{ MeV}$$

$$\text{Mean life } \tau = (0.510 \pm 0.009) \times 10^{-12} \text{ s}$$

B_c^- modes are charge conjugates of the modes below.

B_c^+ DECAY MODES $\times B(\bar{b} \rightarrow B_c)$	Fraction (Γ_i/Γ)	Confidence level	ρ (MeV/c)
---	--------------------------------	------------------	----------------

The following quantities are not pure branching ratios; rather the fraction $\Gamma_i/\Gamma \times B(\bar{b} \rightarrow B_c)$.

$J/\psi(1S)\ell^+\nu_\ell\text{ anything}$	$(8.1 \pm 1.2) \times 10^{-5}$	-	-
$J/\psi(1S)\pi^+$	seen	2371	-
$J/\psi(1S)K^+$	seen	2341	-
$J/\psi(1S)\pi^+\pi^+\pi^-$	seen	2350	-
$J/\psi(1S)a_1(1260)$	< 1.2	$\times 10^{-3}$	90%
$J/\psi(1S)K^+K^-\pi^+$	seen	2203	-
$J/\psi(1S)\pi^+\pi^+\pi^+\pi^-\pi^-$	seen	2309	-
$\psi(2S)\pi^+$	seen	2052	-
$J/\psi(1S)D^0K^+$	seen	1539	-
$J/\psi(1S)D^*(2007)^0K^+$	seen	1412	-
$J/\psi(1S)D^*(2010)^+K^*$	seen	920	-
$J/\psi(1S)D^+K^*$	seen	1123	-
$J/\psi(1S)D^+$	seen	1822	-
$J/\psi(1S)D_s^{*+}$	seen	1728	-
$J/\psi(1S)D_s^+\pi^+$	seen	1792	-

$\chi_c^0\pi^+$	$(2.4_{-0.8}^{+0.9}) \times 10^{-5}$	2205	-
$\rho\bar{\rho}\pi^+$	not seen	2970	-
D^0K^+	$(3.8_{-1.1}^{+1.2}) \times 10^{-7}$	2837	-
$D^0\pi^+$	< 1.6	$\times 10^{-7}$	95%
$D^{*0}\pi^+$	< 4	$\times 10^{-7}$	95%
$D^{*0}K^+$	< 4	$\times 10^{-7}$	95%
$D_s^+\bar{D}^0$	< 1.4	$\times 10^{-7}$	90%
$D_s^+D^0$	< 6	$\times 10^{-8}$	90%
$D^+\bar{D}^0$	< 3.0	$\times 10^{-6}$	90%
D^+D^0	< 1.9	$\times 10^{-6}$	90%
$D^*(2010)^+\bar{D}^0$	< 6.2	$\times 10^{-3}$	90%
$D_s^{*+}\bar{D}^*(2007)^0$	< 1.7	$\times 10^{-6}$	90%
$D_s^{*+}D^*(2007)^0$	< 3.1	$\times 10^{-6}$	90%
$D^*(2010)^+\bar{D}^*(2007)^0$	< 1.0	$\times 10^{-4}$	90%
$D^*(2010)^+D^*(2007)^0$	< 2.0	$\times 10^{-5}$	90%
D^+K^{*0}	< 0.20	$\times 10^{-6}$	90%
D^+K^{*0}	< 0.16	$\times 10^{-6}$	90%
$D_s^+K^{*0}$	< 0.28	$\times 10^{-6}$	90%
$D_s^+K^{*0}$	< 0.4	$\times 10^{-6}$	90%
$D_s^+\phi$	< 0.32	$\times 10^{-6}$	90%
K^+K^0	< 4.6	$\times 10^{-7}$	90%
$B_s^0\pi^+ / B(\bar{b} \rightarrow B_s)$	$(2.37_{-0.35}^{+0.37}) \times 10^{-3}$	-	-

$c\bar{c}$ MESONS (including possibly non- $q\bar{q}$ states)

 $\eta_c(1S)$

$$I^G(J^PC) = 0^+(0^-)$$

$$\text{Mass } m = 2983.9 \pm 0.5 \text{ MeV} \quad (S = 1.3)$$

$$\text{Full width } \Gamma = 32.0 \pm 0.7 \text{ MeV}$$

$\eta_c(1S)$ DECAY MODES	Fraction (Γ_i/Γ)	Confidence level	ρ (MeV/c)
--------------------------	--------------------------------	------------------	----------------

Decays involving hadronic resonances

$\eta'(958)\pi\pi$	$(4.1 \pm 1.7) \%$		1323
$\rho\rho$	$(1.8 \pm 0.5) \%$		1275
$K^*(892)^0K^-\pi^+ + \text{c.c.}$	$(2.0 \pm 0.7) \%$		1278
$K^*(892)\bar{K}^*(892)$	$(7.0 \pm 1.3) \times 10^{-3}$		1196
$K^*(892)^0\bar{K}^*(892)^0\pi^+\pi^-$	$(1.1 \pm 0.5) \%$		1073
ϕK^+K^-	$(2.9 \pm 1.4) \times 10^{-3}$		1104
$\phi\phi$	$(1.77 \pm 0.19) \times 10^{-3}$		1089
$\phi 2(\pi^+\pi^-)$	< 4	$\times 10^{-3}$	90%
$a_0(980)\pi$	< 2	%	90%
$a_2(1320)\pi$	< 2	%	90%
$K^*(892)K + \text{c.c.}$	< 1.28	%	90%
$f_2(1270)\eta$	< 1.1	%	90%
$\omega\omega$	$(2.9 \pm 0.8) \times 10^{-3}$		1270
$\omega\phi$	< 2.5	$\times 10^{-4}$	90%
$f_2(1270)f_2(1270)$	$(9.8 \pm 2.5) \times 10^{-3}$		774
$f_2(1270)f_2'(1525)$	$(9.7 \pm 3.2) \times 10^{-3}$		524
$f_0(980)\eta$	seen		1264
$f_0(1500)\eta$	seen		1025
$f_0(2200)\eta$	seen		498
$a_0(980)\pi$	seen		1327
$a_0(1320)\pi$	seen		-
$a_0(1450)\pi$	seen		1123
$a_0(1950)\pi$	seen		860
$K_0^*(1430)\bar{K}$	seen		-
$K_2^*(1430)\bar{K}$	seen		-
$K_0^*(1950)\bar{K}$	seen		-

Decays into stable hadrons

$K\bar{K}\pi$	$(7.3 \pm 0.4) \%$		1381
$K\bar{K}\eta$	$(1.36 \pm 0.15) \%$		1265
$\eta\pi^+\pi^-$	$(1.7 \pm 0.5) \%$		1428
$\eta 2(\pi^+\pi^-)$	$(4.4 \pm 1.3) \%$		1386
$K^+K^-\pi^+\pi^-$	$(6.9 \pm 1.0) \times 10^{-3}$		1345
$K^+K^-\pi^+\pi^-\pi^0$	$(3.5 \pm 0.6) \%$		1304
$K^0K^-\pi^+\pi^-\pi^+ + \text{c.c.}$	$(5.6 \pm 1.5) \%$		-
$K^+K^-2(\pi^+\pi^-)$	$(7.5 \pm 2.4) \times 10^{-3}$		1254
$2(K^+K^-)$	$(1.46 \pm 0.30) \times 10^{-3}$		1056
$\pi^+\pi^-\pi^0$	< 5	$\times 10^{-4}$	90%

Meson Summary Table

$\pi^+\pi^-\pi^0\pi^0$	$(4.7 \pm 1.0) \%$	1460
$2(\pi^+\pi^-)$	$(9.7 \pm 1.2) \times 10^{-3}$	1459
$2(\pi^+\pi^-\pi^0)$	$(16.1 \pm 2.0) \%$	1409
$3(\pi^+\pi^-)$	$(1.8 \pm 0.4) \%$	1407
$\rho\bar{\rho}$	$(1.45 \pm 0.14) \times 10^{-3}$	1160
$\rho\bar{\rho}\pi^0$	$(3.6 \pm 1.3) \times 10^{-3}$	1101
$\Lambda\bar{\Lambda}$	$(1.07 \pm 0.24) \times 10^{-3}$	991
$K^+\bar{p}\Lambda$ c.c.	$(2.6 \pm 0.4) \times 10^{-3}$	772
$\bar{\Lambda}(1520)\Lambda$ c.c.	$(3.1 \pm 1.4) \times 10^{-3}$	694
$\Sigma^+\bar{\Sigma}^-$	$(2.1 \pm 0.6) \times 10^{-3}$	901
$\Xi^-\bar{\Xi}^+$	$(9.0 \pm 2.6) \times 10^{-4}$	692
$\pi^+\pi^-\rho\bar{\rho}$	$(5.3 \pm 1.8) \times 10^{-3}$	1027

Radiative decays

$\gamma\gamma$	$(1.58 \pm 0.11) \times 10^{-4}$	1492
----------------	----------------------------------	------

Charge conjugation (C), Parity (P),
Lepton family number (LF) violating modes

$\pi^+\pi^-$	$P, CP < 1.1$	$\times 10^{-4}$	90%	1485
$\pi^0\pi^0$	$P, CP < 4$	$\times 10^{-5}$	90%	1486
K^+K^-	$P, CP < 6$	$\times 10^{-4}$	90%	1408
$K_S^0 K_S^0$	$P, CP < 3.1$	$\times 10^{-4}$	90%	1407

 $J/\psi(1S)$

$$J^G(J^{PC}) = 0^-(1^{--})$$

Mass $m = 3096.900 \pm 0.006$ MeV
 Full width $\Gamma = 92.9 \pm 2.8$ keV ($S = 1.1$)
 $\Gamma_{ee} = 5.53 \pm 0.10$ keV
 $\Gamma_{ee} < 5.4$ eV, CL = 90%

$J/\psi(1S)$ DECAY MODES	Fraction (Γ_i/Γ)	Scale factor/ Confidence level (MeV/c)	p
hadrons	$(87.7 \pm 0.5) \%$	-	-
virtual $\gamma \rightarrow$ hadrons	$(13.50 \pm 0.30) \%$	-	-
ggg	$(64.1 \pm 1.0) \%$	-	-
γgg	$(8.8 \pm 1.1) \%$	-	-
e^+e^-	$(5.971 \pm 0.032) \%$	-	1548
$e^+e^-\gamma$	[kkaa] $(8.8 \pm 1.4) \times 10^{-3}$	-	1548
$\mu^+\mu^-$	$(5.961 \pm 0.033) \%$	-	1545

Decays involving hadronic resonances

$\rho\pi$	$(1.69 \pm 0.15) \%$	$S=2.4$	1448
$\rho^0\pi^0$	$(5.6 \pm 0.7) \times 10^{-3}$	-	1448
$\rho(770)^\mp K^\pm K_S^0$	$(1.9 \pm 0.4) \times 10^{-3}$	-	-
$\rho(1450)\pi \rightarrow \pi^+\pi^-\pi^0$	$(2.3 \pm 0.7) \times 10^{-3}$	-	-
$\rho(1450)^\pm \pi^\mp \rightarrow K_S^0 K^\pm \pi^\mp$	$(3.5 \pm 0.6) \times 10^{-4}$	-	-
$\rho(1450)^0 \pi^0 \rightarrow K^+ K^- \pi^0$	$(2.7 \pm 0.6) \times 10^{-4}$	-	-
$\rho(1450)\eta'(958) \rightarrow \pi^+\pi^-\eta'(958)$	$(3.3 \pm 0.7) \times 10^{-6}$	-	-
$\rho(1700)\pi \rightarrow \pi^+\pi^-\pi^0$	$(1.7 \pm 1.1) \times 10^{-4}$	-	-
$\rho(2150)\pi \rightarrow \pi^+\pi^-\pi^0$	$(8 \pm 40) \times 10^{-6}$	-	-
$a_2(1320)\rho$	$(1.09 \pm 0.22) \%$	-	1124
$\omega\pi^+\pi^+\pi^-\pi^-$	$(8.5 \pm 3.4) \times 10^{-3}$	-	1392
$\omega\pi^+\pi^-\pi^0$	$(4.0 \pm 0.7) \times 10^{-3}$	-	1418
$\omega\pi^+\pi^-$	$(7.2 \pm 1.0) \times 10^{-3}$	-	1435
$\omega f_2(1270)$	$(4.3 \pm 0.6) \times 10^{-3}$	-	1142
$K^*(892)^0 \bar{K}^*(892)^0$	$(2.3 \pm 0.6) \times 10^{-4}$	-	1266
$K^*(892)^\pm K^*(892)^\mp$	$(1.00 \pm 0.22) \times 10^{-3}$	-	1266
$K^*(892)^\pm K^*(700)^\mp$	$(1.1 \pm 1.0) \times 10^{-3}$	-	-
$K_S^0 \pi^- K^*(892)^+ + c.c.$	$(2.0 \pm 0.5) \times 10^{-3}$	-	1342
$K_S^0 \pi^- K^*(892)^+ + c.c. \rightarrow K_S^0 K_S^0 \pi^+ \pi^-$	$(6.7 \pm 2.2) \times 10^{-4}$	-	-
$K_S^0 K^*(892)^0 \rightarrow \gamma K_S^0 K_S^0$	$(6.3 \pm 0.6) \times 10^{-6}$	-	-
$K_2^*(1430)^+ K^- + c.c. \rightarrow K^+ K^- \pi^0$	$(2.69 \pm 0.25) \times 10^{-4}$	-	-
$K_2^*(1980)^+ K^- + c.c. \rightarrow K^+ K^- \pi^0$	$(1.10 \pm 0.60) \times 10^{-5}$	-	-
$K_4^*(2045)^+ K^- + c.c. \rightarrow K^+ K^- \pi^0$	$(6.2 \pm 2.9) \times 10^{-6}$	-	-
$\eta K^*(892)^0 \bar{K}^*(892)^0$	$(1.15 \pm 0.26) \times 10^{-3}$	-	1003
$\eta' K^+ \bar{K}^\mp$	$(1.48 \pm 0.13) \times 10^{-3}$	-	-
$\eta' K^+ \bar{K}^0 + c.c.$	$(1.66 \pm 0.21) \times 10^{-3}$	-	1000
$\eta' h_1(1415) \rightarrow \eta' K^* \bar{K} + c.c.$	$(2.16 \pm 0.31) \times 10^{-4}$	-	-
$\eta' h_1(1415) \rightarrow \eta' K^* \bar{K}^\mp$	$(1.51 \pm 0.23) \times 10^{-4}$	-	-
$K^*(1410) \bar{K} + c.c. \rightarrow K^\pm K^\mp \pi^0$	$(7 \pm 4) \times 10^{-5}$	-	-

$K^*(1410) \bar{K} + c.c. \rightarrow K_S^0 K^\pm \pi^\mp$	$(8 \pm 6) \times 10^{-5}$	-
$K_2^*(1430) \bar{K} + c.c. \rightarrow K^\pm K^\mp \pi^0$	$(1.0 \pm 0.5) \times 10^{-4}$	-
$K_2^*(1430) \bar{K} + c.c. \rightarrow K_S^0 K^\pm \pi^\mp$	$(4.0 \pm 1.0) \times 10^{-4}$	-
$K^*(892)^0 \bar{K}_2^*(1430)^0 + c.c.$	$(4.66 \pm 0.31) \times 10^{-3}$	1011
$K^*(892)^+ K_2^*(1430)^- + c.c.$	$(3.4 \pm 2.9) \times 10^{-3}$	1011
$K^*(892)^+ K_2^*(1430)^- + c.c. \rightarrow K^*(892)^+ K_S^0 \pi^- + c.c.$	$(4 \pm 4) \times 10^{-4}$	-
$K^*(892)^0 \bar{K}_2^*(1770)^0 + c.c. \rightarrow K^*(892)^0 K^- \pi^+ + c.c.$	$(6.9 \pm 0.9) \times 10^{-4}$	-
$\omega K^*(892) \bar{K} + c.c.$	$(6.1 \pm 0.9) \times 10^{-3}$	1097
$\bar{K} K^*(892) + c.c. \rightarrow K_S^0 K^\pm \pi^\mp$	$(5.0 \pm 0.5) \times 10^{-3}$	-
$K^+ K^*(892)^- + c.c.$	$(6.0 \pm 0.8) \times 10^{-3}$	$S=2.9$ 1373
$K^+ K^*(892)^- + c.c. \rightarrow K^+ K^- \pi^0$	$(2.69 \pm 0.13) \times 10^{-3}$	-
$K^+ K^*(892)^- + c.c. \rightarrow K^0 K^\pm \pi^\mp + c.c.$	$(3.0 \pm 0.4) \times 10^{-3}$	-
$K^0 \bar{K}^*(892)^0 + c.c.$	$(4.2 \pm 0.4) \times 10^{-3}$	1373
$K^0 \bar{K}^*(892)^0 + c.c. \rightarrow K^0 K^\pm \pi^\mp + c.c.$	$(3.2 \pm 0.4) \times 10^{-3}$	-
$K_1(1400)^\pm K^\mp$	$(3.8 \pm 1.4) \times 10^{-3}$	1170
$\bar{K}^*(892)^0 K^+ \pi^- + c.c.$	$(7.7 \pm 1.6) \times 10^{-3}$	1343
$K^*(892)^\pm K^\mp \pi^0$	$(4.1 \pm 1.3) \times 10^{-3}$	1344
$K^*(892)^0 K_S^0 \pi^0$	$(6 \pm 4) \times 10^{-4}$	1343
$\omega\pi^0\pi^0$	$(3.4 \pm 0.8) \times 10^{-3}$	1436
$\omega\pi^0\eta$	$(3.4 \pm 1.7) \times 10^{-4}$	1363
$b_1(1235)^\pm \pi^\mp$	[bb] $(3.0 \pm 0.5) \times 10^{-3}$	1300
$\omega K^\pm K_S^0 \pi^\mp$	[bb] $(3.4 \pm 0.5) \times 10^{-3}$	1210
$b_1(1235)^0 \pi^0$	$(2.3 \pm 0.6) \times 10^{-3}$	1300
$\eta K^\pm K_S^0 \pi^\mp$	[bb] $(2.2 \pm 0.4) \times 10^{-3}$	1278
$\phi K^*(892) \bar{K} + c.c.$	$(2.18 \pm 0.23) \times 10^{-3}$	969
$\omega K \bar{K}$	$(1.9 \pm 0.4) \times 10^{-3}$	1268
$\omega f_0(1710) \rightarrow \omega K \bar{K}$	$(4.8 \pm 1.1) \times 10^{-4}$	878
$\phi_2(\pi^+\pi^-)$	$(1.60 \pm 0.32) \times 10^{-3}$	1318
$\Delta(1232)^{++} \bar{p}\pi^-$	$(1.6 \pm 0.5) \times 10^{-3}$	1030
$\omega\eta$	$(1.74 \pm 0.20) \times 10^{-3}$	$S=1.6$ 1394
$\omega\eta'\pi^+\pi^-$	$(1.12 \pm 0.13) \times 10^{-3}$	1173
$\phi K \bar{K}$	$(1.77 \pm 0.16) \times 10^{-3}$	$S=1.3$ 1179
$\phi K_S^0 K_S^0$	$(5.9 \pm 1.5) \times 10^{-4}$	1176
$\phi f_0(1710) \rightarrow \phi K \bar{K}$	$(3.6 \pm 0.6) \times 10^{-4}$	875
$\phi K^+ K^-$	$(8.3 \pm 1.2) \times 10^{-4}$	1179
$\phi f_2(1270)$	$(3.2 \pm 0.6) \times 10^{-4}$	1036
$\Delta(1232)^{++} \bar{\Delta}(1232)^{--}$	$(1.10 \pm 0.29) \times 10^{-3}$	938
$\Sigma(1385)^- \bar{\Sigma}(1385)^+ (or c.c.)$	[bb] $(1.16 \pm 0.05) \times 10^{-3}$	697
$\Sigma(1385)^0 \bar{\Sigma}(1385)^0$	$(1.07 \pm 0.08) \times 10^{-3}$	697
$K^+ K^- f_2'(1525)$	$(1.05 \pm 0.35) \times 10^{-3}$	897
$\phi f_2'(1525)$	$(8 \pm 4) \times 10^{-4}$	$S=2.7$ 877
$\phi\pi^+\pi^-$	$(9.4 \pm 1.5) \times 10^{-4}$	$S=1.7$ 1365
$\phi\pi^0\pi^0$	$(5.0 \pm 1.0) \times 10^{-4}$	1366
$\phi K^\pm K_S^0 \pi^\mp$	[bb] $(7.2 \pm 0.8) \times 10^{-4}$	1114
$\omega f_1(1420)$	$(6.8 \pm 2.4) \times 10^{-4}$	1062
$\phi\eta$	$(7.4 \pm 0.8) \times 10^{-4}$	$S=1.5$ 1320
$\Xi^0 \Xi^0$	$(1.17 \pm 0.04) \times 10^{-3}$	818
$\Xi(1530)^- \Xi^+ + c.c.$	$(3.18 \pm 0.08) \times 10^{-4}$	600
$\rho K^- \bar{\Sigma}(1385)^0$	$(5.1 \pm 3.2) \times 10^{-4}$	646
$\omega\pi^0 \rightarrow \pi^+\pi^-\pi^0$	$(4.5 \pm 0.5) \times 10^{-4}$	$S=1.4$ 1446
$\phi\eta'(958)$	$(1.7 \pm 0.8) \times 10^{-5}$	-
$\phi f_0(980)$	$(4.6 \pm 0.5) \times 10^{-4}$	$S=2.2$ 1192
$\phi f_0(980) \rightarrow \phi\pi^+\pi^-$	$(3.2 \pm 0.9) \times 10^{-4}$	$S=1.9$ 1178
$\phi f_0(980) \rightarrow \phi\pi^0\pi^0$	$(2.59 \pm 0.34) \times 10^{-4}$	-
$\phi f_0(980) \rightarrow \phi\pi^0\pi^0$	$(1.8 \pm 0.5) \times 10^{-4}$	-
$\phi\eta\eta'$	$(2.32 \pm 0.17) \times 10^{-4}$	885
$\phi\pi^0 f_0(980) \rightarrow \phi\pi^0\pi^+\pi^-$	$(4.5 \pm 1.0) \times 10^{-6}$	-
$\phi\pi^0 f_0(980) \rightarrow \phi\pi^0\rho^0\pi^0$	$(1.7 \pm 0.6) \times 10^{-6}$	1045
$\eta\phi f_0(980) \rightarrow \eta\phi\pi^+\pi^-$	$(3.2 \pm 1.0) \times 10^{-4}$	-
$\phi a_0(980)^0 \rightarrow \phi\eta\pi^0$	$(4.4 \pm 1.4) \times 10^{-6}$	-
$\Xi(1530)^0 \Xi^0$	$(3.2 \pm 1.4) \times 10^{-4}$	608
$\Sigma(1385)^- \bar{\Sigma}^+ (or c.c.)$	[bb] $(3.1 \pm 0.5) \times 10^{-4}$	855
$\phi f_1(1285)$	$(2.6 \pm 0.5) \times 10^{-4}$	1032
$\phi f_1(1285) \rightarrow \phi\pi^0 f_0(980) \rightarrow \phi\pi^0\pi^+\pi^-$	$(9.4 \pm 2.8) \times 10^{-7}$	952

Meson Summary Table

$\gamma f'_2(1525)$	$(5.7 \pm_{-0.5}^{+0.8}) \times 10^{-4}$	S=1.5	1177
$\gamma f'_2(1525) \rightarrow \gamma K_S^0 K_S^0$	$(8.0 \pm_{-0.5}^{+0.7}) \times 10^{-5}$		-
$\gamma f'_2(1525) \rightarrow \gamma \eta \eta$	$(3.4 \pm 1.4) \times 10^{-5}$		-
$\gamma f_2(1640) \rightarrow \gamma \omega \omega$	$(2.8 \pm 1.8) \times 10^{-4}$		-
$\gamma f_2(1910) \rightarrow \gamma \omega \omega$	$(2.0 \pm 1.4) \times 10^{-4}$		-
$\gamma f_0(1750) \rightarrow \gamma K_S^0 K_S^0$	$(1.11 \pm_{-0.33}^{+0.20}) \times 10^{-5}$		-
$\gamma f_0(1800) \rightarrow \gamma \omega \phi$	$(2.5 \pm 0.6) \times 10^{-4}$		-
$\gamma f_2(1810) \rightarrow \gamma \eta \eta$	$(5.4 \pm_{-2.4}^{+3.5}) \times 10^{-5}$		-
$\gamma f_2(1950) \rightarrow$	$(7.0 \pm 2.2) \times 10^{-4}$		-
$\gamma K^*(892) \bar{K}^*(892)$			
$\gamma K^*(892) \bar{K}^*(892)$	$(4.0 \pm 1.3) \times 10^{-3}$	S=2.1	1266
$\gamma \phi \phi$	$(4.0 \pm 1.2) \times 10^{-4}$		1166
$\gamma \rho \bar{\rho}$	$(3.8 \pm 1.0) \times 10^{-4}$		1232
$\gamma \eta(2225)$	$(3.14 \pm_{-0.19}^{+0.50}) \times 10^{-4}$		752
$\gamma \eta(1760) \rightarrow \gamma \rho^0 \rho^0$	$(1.3 \pm 0.9) \times 10^{-4}$		1048
$\gamma \eta(1760) \rightarrow \gamma \omega \omega$	$(1.98 \pm 0.33) \times 10^{-3}$		-
$\gamma \eta(1760) \rightarrow \gamma \gamma \gamma$	$< 4.80 \times 10^{-6}$	CL=90%	-
$\gamma X(1835) \rightarrow \gamma \pi^+ \pi^- \eta'$	$(2.77 \pm_{-0.40}^{+0.34}) \times 10^{-4}$	S=1.1	1006
$\gamma X(1835) \rightarrow \gamma \rho \bar{\rho}$	$(7.7 \pm_{-0.9}^{+1.5}) \times 10^{-5}$		-
$\gamma X(1835) \rightarrow \gamma K_S^0 K_S^0 \eta$	$(3.3 \pm_{-1.3}^{+2.0}) \times 10^{-5}$		-
$\gamma X(1835) \rightarrow \gamma \gamma \gamma$	$< 3.56 \times 10^{-6}$	CL=90%	-
$\gamma X(1840) \rightarrow \gamma 3(\pi^+ \pi^-)$	$(2.4 \pm_{-0.8}^{+0.7}) \times 10^{-5}$		-
$\gamma(K \bar{K} \pi) [J^{PC} = 0^{-+}]$	$(7 \pm 4) \times 10^{-4}$	S=2.1	1442
$\gamma \pi^0$	$(3.56 \pm 0.17) \times 10^{-5}$		1546
$\gamma \rho \bar{\rho} \pi^+ \pi^-$	$< 7.9 \times 10^{-4}$	CL=90%	1107
$\gamma \Lambda \bar{\Lambda}$	$< 1.3 \times 10^{-4}$	CL=90%	1074
$\gamma f_0(2100) \rightarrow \gamma \eta \eta$	$(1.13 \pm_{-0.30}^{+0.60}) \times 10^{-4}$		-
$\gamma f_0(2100) \rightarrow \gamma \pi \pi$	$(6.2 \pm 1.0) \times 10^{-4}$		-
$\gamma f_0(2200) \rightarrow \gamma K \bar{K}$	$(5.9 \pm 1.3) \times 10^{-4}$		-
$\gamma f_0(2200) \rightarrow \gamma K_S^0 K_S^0$	$(2.72 \pm_{-0.50}^{+0.19}) \times 10^{-4}$		-
$\gamma f_J(2220) \rightarrow \gamma \pi \pi$	$< 3.9 \times 10^{-5}$	CL=90%	-
$\gamma f_J(2220) \rightarrow \gamma K \bar{K}$	$< 4.1 \times 10^{-5}$	CL=90%	-
$\gamma f_J(2220) \rightarrow \gamma \rho \bar{\rho}$	$(1.5 \pm 0.8) \times 10^{-5}$		-
$\gamma f_0(2330) \rightarrow \gamma K_S^0 K_S^0$	$(4.9 \pm 0.7) \times 10^{-5}$		-
$\gamma f_2(2340) \rightarrow \gamma \eta \eta$	$(5.6 \pm_{-2.2}^{+2.4}) \times 10^{-5}$		-
$\gamma f_2(2340) \rightarrow \gamma K_S^0 K_S^0$	$(5.5 \pm_{-1.5}^{+4.0}) \times 10^{-5}$		-
$\gamma f_0(1500) \rightarrow \gamma \pi \pi$	$(1.09 \pm 0.24) \times 10^{-4}$		1183
$\gamma f_0(1500) \rightarrow \gamma \eta \eta$	$(1.7 \pm_{-1.4}^{+0.6}) \times 10^{-5}$		-
$\gamma A \rightarrow \gamma$ invisible	$[o\bar{o}a\bar{a}] < 6.3 \times 10^{-6}$	CL=90%	-
$\gamma A^0 \rightarrow \gamma \mu^+ \mu^-$	$[p\bar{p}a\bar{a}] < 5 \times 10^{-6}$	CL=90%	-

Dalitz decays

$\pi^0 e^+ e^-$	$(7.6 \pm 1.4) \times 10^{-7}$		1546
$\eta e^+ e^-$	$(1.43 \pm 0.07) \times 10^{-5}$		1500
$\eta'(958) e^+ e^-$	$(6.59 \pm 0.18) \times 10^{-5}$		1400
$\eta U \rightarrow \eta e^+ e^-$	$< 9.11 \times 10^{-7}$	CL=90%	-
$\eta'(958) U \rightarrow \eta'(958) e^+ e^-$	$< 2.0 \times 10^{-7}$	CL=90%	-
$\phi e^+ e^-$	$< 1.2 \times 10^{-7}$	CL=90%	1381

Weak decays

$D^- e^+ \nu_e + c.c.$	$< 1.2 \times 10^{-5}$	CL=90%	984
$\bar{D}^0 e^+ e^- + c.c.$	$< 8.5 \times 10^{-8}$	CL=90%	987
$D_S^- e^+ \nu_e + c.c.$	$< 1.3 \times 10^{-6}$	CL=90%	923
$D_S^{*-} e^+ \nu_e + c.c.$	$< 1.8 \times 10^{-6}$	CL=90%	828
$D^- \pi^+ + c.c.$	$< 7.5 \times 10^{-5}$	CL=90%	977
$\bar{D}^0 \bar{K}^0 + c.c.$	$< 1.7 \times 10^{-4}$	CL=90%	898
$\bar{D}^0 \bar{K}^{*0} + c.c.$	$< 2.5 \times 10^{-6}$	CL=90%	670
$D_S^- \pi^+ + c.c.$	$< 1.3 \times 10^{-4}$	CL=90%	915
$D_S^- \rho^+ + c.c.$	$< 1.3 \times 10^{-5}$	CL=90%	663

Charge conjugation (C), Parity (P), Lepton Family number (LF) violating modes

$\gamma \gamma$	C	$< 2.7 \times 10^{-7}$	CL=90%	1548
$\gamma \phi$	C	$< 1.4 \times 10^{-6}$	CL=90%	1381
$e^\pm \mu^\mp$	LF	$< 1.6 \times 10^{-7}$	CL=90%	1547
$e^\pm \tau^\mp$	LF	$< 8.3 \times 10^{-6}$	CL=90%	1039
$\mu^\pm \tau^\mp$	LF	$< 2.0 \times 10^{-6}$	CL=90%	1035
$\Lambda_c^+ e^- + c.c.$		$< 6.9 \times 10^{-8}$	CL=90%	-

Other decays	$< 7 \times 10^{-4}$	CL=90%	-
invisible	$< 7 \times 10^{-4}$	CL=90%	-

$\chi_{c0}(1P)$

$$I^G(J^{PC}) = 0^+(0^{++})$$

Mass $m = 3414.71 \pm 0.30$ MeV
Full width $\Gamma = 10.8 \pm 0.6$ MeV

$\chi_{c0}(1P)$ DECAY MODES	Fraction (Γ_i/Γ)	Scale factor/ Confidence level	ρ (MeV/c)
-----------------------------	--------------------------------	-----------------------------------	-------------------

Hadronic decays

$2(\pi^+ \pi^-)$	$(2.34 \pm 0.18) \%$		1679
$\rho^0 \pi^+ \pi^-$	$(9.1 \pm 2.9) \times 10^{-3}$		1607
$f_0(980) f_0(980)$	$(6.6 \pm 2.1) \times 10^{-4}$		1391
$\pi^+ \pi^- \pi^0 \pi^0$	$(3.3 \pm 0.4) \%$		1680
$\rho^+ \pi^- \pi^0 + c.c.$	$(2.9 \pm 0.4) \%$		1607
$4\pi^0$	$(3.3 \pm 0.4) \times 10^{-3}$		1681
$\pi^+ \pi^- K^+ K^-$	$(1.81 \pm 0.14) \%$		1580
$K_0^*(1430) \bar{K}_0^*(1430) \rightarrow$	$(9.8 \pm_{-2.8}^{+4.0}) \times 10^{-4}$		-
$\pi^+ \pi^- K^+ K^-$			
$K_0^*(1430) \bar{K}_2^*(1430) \rightarrow$	$(8.0 \pm_{-2.4}^{+2.0}) \times 10^{-4}$		-
$\pi^+ \pi^- K^+ K^-$			
$K_1(1270)^+ K^- + c.c. \rightarrow$	$(6.3 \pm 1.9) \times 10^{-3}$		-
$\pi^+ \pi^- K^+ K^-$			
$K_1(1400)^+ K^- + c.c. \rightarrow$	$< 2.7 \times 10^{-3}$	CL=90%	-
$\pi^+ \pi^- K^+ K^-$			
$f_0(980) f_0(980)$	$(1.6 \pm_{-0.9}^{+1.0}) \times 10^{-4}$		1391
$f_0(980) f_0(2200)$	$(7.9 \pm_{-2.5}^{+2.0}) \times 10^{-4}$		586
$f_0(1370) f_0(1370)$	$< 2.7 \times 10^{-4}$	CL=90%	1019
$f_0(1370) f_0(1500)$	$< 1.7 \times 10^{-4}$	CL=90%	920
$f_0(1370) f_0(1710)$	$(6.7 \pm_{-2.3}^{+3.5}) \times 10^{-4}$		740
$f_0(1500) f_0(1370)$	$< 1.3 \times 10^{-4}$	CL=90%	920
$f_0(1500) f_0(1500)$	$< 5 \times 10^{-5}$	CL=90%	804
$f_0(1500) f_0(1710)$	$< 7 \times 10^{-5}$	CL=90%	581
$K^+ K^- \pi^+ \pi^- \pi^0$	$(8.6 \pm 0.9) \times 10^{-3}$		1545
$K_S^0 K^\pm \pi^\mp \pi^+ \pi^-$	$(4.2 \pm 0.4) \times 10^{-3}$		1543
$K^+ K^- \pi^0 \pi^0$	$(5.6 \pm 0.9) \times 10^{-3}$		1582
$K^+ \pi^- \bar{K}^0 \pi^0 + c.c.$	$(2.49 \pm 0.33) \%$		1581
$\rho^+ K^- K^0 + c.c.$	$(1.21 \pm 0.21) \%$		1458
$K^*(892) \bar{K}^+ \pi^0 \rightarrow$	$(4.6 \pm 1.2) \times 10^{-3}$		-
$K^+ \pi^- \bar{K}^0 \pi^0 + c.c.$			
$K_S^0 K_S^0 \pi^+ \pi^-$	$(5.7 \pm 1.1) \times 10^{-3}$		1579
$K^+ K^- \eta \pi^0$	$(3.0 \pm 0.7) \times 10^{-3}$		1468
$3(\pi^+ \pi^-)$	$(1.20 \pm 0.18) \%$		1633
$K^+ \bar{K}^*(892)^0 \pi^- + c.c.$	$(7.5 \pm 1.6) \times 10^{-3}$		1523
$K^*(892)^0 \bar{K}^*(892)^0$	$(1.7 \pm 0.6) \times 10^{-3}$		1456
$\pi \pi$	$(8.51 \pm 0.33) \times 10^{-3}$		1702
$\pi^0 \eta$	$< 1.8 \times 10^{-4}$		1661
$\pi^0 \eta'$	$< 1.1 \times 10^{-3}$		1570
$\pi^0 \eta_c$	$< 1.6 \times 10^{-3}$	CL=90%	383
$\eta \eta$	$(3.01 \pm 0.19) \times 10^{-3}$		1617
$\eta \eta'$	$(9.1 \pm 1.1) \times 10^{-5}$		1521
$\eta' \eta'$	$(2.17 \pm 0.12) \times 10^{-3}$		1413
$\omega \omega$	$(9.7 \pm 1.1) \times 10^{-4}$		1517
$\omega \phi$	$(1.41 \pm 0.13) \times 10^{-4}$		1447
$\omega K^+ K^-$	$(1.94 \pm 0.21) \times 10^{-3}$		1457
$K^+ K^-$	$(6.05 \pm 0.31) \times 10^{-3}$		1634
$K_S^0 K_S^0$	$(3.16 \pm 0.17) \times 10^{-3}$		1633
$\pi^+ \pi^- \eta$	$< 2.0 \times 10^{-4}$	CL=90%	1651
$\pi^+ \pi^- \eta'$	$< 4 \times 10^{-4}$	CL=90%	1560
$\bar{K}^0 K^+ \pi^- + c.c.$	$< 9 \times 10^{-5}$	CL=90%	1610
$K^+ K^- \pi^0$	$< 6 \times 10^{-5}$	CL=90%	1611
$K^+ K^- \eta$	$< 2.3 \times 10^{-4}$	CL=90%	1512
$K^+ K^- K_S^0 K_S^0$	$(1.4 \pm 0.5) \times 10^{-3}$		1331
$K_S^0 K_S^0 K_S^0 K_S^0$	$(5.8 \pm 0.5) \times 10^{-4}$		1327
$K^+ K^- K^+ K^-$	$(2.82 \pm 0.29) \times 10^{-3}$		1333
$K^+ K^- \phi$	$(9.7 \pm 2.5) \times 10^{-4}$		1381
$\bar{K}^0 K^+ \pi^- \phi + c.c.$	$(3.7 \pm 0.6) \times 10^{-3}$		1326
$K^+ K^- \pi^0 \phi$	$(1.90 \pm 0.35) \times 10^{-3}$		1329
$\phi \pi^+ \pi^- \pi^0$	$(1.18 \pm 0.15) \times 10^{-3}$		1525
$\phi \phi$	$(8.0 \pm 0.7) \times 10^{-4}$		1370
$\phi \phi \eta$	$(8.4 \pm 1.0) \times 10^{-4}$		1100
$\rho \bar{\rho}$	$(2.21 \pm 0.08) \times 10^{-4}$		1426
$\rho \bar{\rho} \pi^0$	$(7.0 \pm 0.7) \times 10^{-4}$	S=1.3	1379
$\rho \bar{\rho} \eta$	$(3.5 \pm 0.4) \times 10^{-4}$		1187

Meson Summary Table

$\rho\bar{\rho}\omega$	$(5.2 \pm 0.6) \times 10^{-4}$		1043
$\rho\bar{\rho}\phi$	$(6.0 \pm 1.4) \times 10^{-5}$		876
$\rho\bar{\rho}\pi^+\pi^-$	$(2.1 \pm 0.7) \times 10^{-3}$	S=1.4	1320
$\rho\bar{\rho}\pi^0\pi^0$	$(1.04 \pm 0.28) \times 10^{-3}$		1324
$\rho\bar{\rho}K^+K^-$ (non-resonant)	$(1.22 \pm 0.26) \times 10^{-4}$		890
$\rho\bar{\rho}K_S^0K_S^0$	$< 8.8 \times 10^{-4}$	CL=90%	884
$\rho\bar{\rho}\pi^-$	$(1.27 \pm 0.11) \times 10^{-3}$		1376
$\bar{\rho}n\pi^+$	$(1.37 \pm 0.12) \times 10^{-3}$		1376
$\rho\bar{\rho}\pi^-\pi^0$	$(2.34 \pm 0.21) \times 10^{-3}$		1321
$\bar{\rho}n\pi^+\pi^0$	$(2.21 \pm 0.18) \times 10^{-3}$		1321
$\Lambda\bar{\Lambda}$	$(3.27 \pm 0.24) \times 10^{-4}$		1292
$\Lambda\bar{\Lambda}\pi^+\pi^-$	$(1.18 \pm 0.13) \times 10^{-3}$		1153
$\Lambda\bar{\Lambda}\pi^+\pi^-$ (non-resonant)	$< 5 \times 10^{-4}$	CL=90%	1153
$\Sigma(1385)^+\bar{\Lambda}\pi^- + c.c.$	$< 5 \times 10^{-4}$	CL=90%	1083
$\Sigma(1385)^-\bar{\Lambda}\pi^+ + c.c.$	$< 5 \times 10^{-4}$	CL=90%	1083
$K^+\bar{p}\Lambda + c.c.$	$(1.25 \pm 0.12) \times 10^{-3}$	S=1.3	1132
$K^*(892)^+\bar{p}\Lambda + c.c.$	$(4.8 \pm 0.9) \times 10^{-4}$		845
$K^+\bar{p}\Lambda(1520) + c.c.$	$(2.9 \pm 0.7) \times 10^{-4}$		859
$\Lambda(1520)\bar{\Lambda}(1520)$	$(3.1 \pm 1.2) \times 10^{-4}$		780
$\Sigma^0\bar{\Sigma}^0$	$(4.68 \pm 0.32) \times 10^{-4}$		1222
$\Sigma^+\bar{p}K_S^0 + c.c.$	$(3.52 \pm 0.27) \times 10^{-4}$		1089
$\Sigma^+\bar{\Sigma}^-$	$(4.6 \pm 0.8) \times 10^{-4}$	S=2.6	1225
$\Sigma(1385)^+\bar{\Sigma}(1385)^-$	$(1.6 \pm 0.6) \times 10^{-4}$		1001
$\Sigma(1385)^-\bar{\Sigma}(1385)^+$	$(2.3 \pm 0.7) \times 10^{-4}$		1001
$K^-\Lambda\bar{\Xi}^+ + c.c.$	$(1.94 \pm 0.35) \times 10^{-4}$		873
$\Xi^0\bar{\Xi}^0$	$(3.1 \pm 0.8) \times 10^{-4}$		1089
$\Xi^-\bar{\Xi}^+$	$(4.8 \pm 0.7) \times 10^{-4}$		1081
$\eta_c\pi^+\pi^-$	$< 7 \times 10^{-4}$	CL=90%	307
Radiative decays			
$\gamma J/\psi(1S)$	$(1.40 \pm 0.05) \%$		303
$\gamma\rho^0$	$< 9 \times 10^{-6}$	CL=90%	1619
$\gamma\omega$	$< 8 \times 10^{-6}$	CL=90%	1618
$\gamma\phi$	$< 6 \times 10^{-6}$	CL=90%	1555
$\gamma\gamma$	$(2.04 \pm 0.09) \times 10^{-4}$		1707
$e^+e^- J/\psi(1S)$	$(1.33 \pm 0.29) \times 10^{-4}$		303
$\mu^+\mu^- J/\psi(1S)$	$< 1.9 \times 10^{-5}$	CL=90%	226

X_{cl}(1P)

$$I^G(J^{PC}) = 0^+(1^{++})$$

Mass $m = 3510.67 \pm 0.05$ MeV (S = 1.2)

Full width $\Gamma = 0.84 \pm 0.04$ MeV

X_{cl}(1P) DECAY MODES	Fraction (Γ_i/Γ)	Scale factor/ Confidence level	ρ (MeV/c)
Hadronic decays			
$3(\pi^+\pi^-)$	$(5.8 \pm 1.4) \times 10^{-3}$	S=1.2	1683
$2(\pi^+\pi^-)$	$(7.6 \pm 2.6) \times 10^{-3}$		1728
$\pi^+\pi^-\pi^0\pi^0$	$(1.19 \pm 0.15) \%$		1729
$\rho^+\pi^-\pi^0 + c.c.$	$(1.45 \pm 0.24) \%$		1658
$\rho^0\pi^+\pi^-$	$(3.9 \pm 3.5) \times 10^{-3}$		1657
$4\pi^0$	$(5.4 \pm 0.8) \times 10^{-4}$		1729
$\pi^+\pi^-K^+K^-$	$(4.5 \pm 1.0) \times 10^{-3}$		1632
$K^+K^-\pi^0\pi^0$	$(1.12 \pm 0.27) \times 10^{-3}$		1634
$K^+K^-\pi^+\pi^-\pi^0$	$(1.15 \pm 0.13) \%$		1598
$K_S^0K_S^0\pi^+\pi^-$	$(7.5 \pm 0.8) \times 10^{-3}$		1596
$K^{\pm}\pi^-\bar{K}^0\pi^0 + c.c.$	$(8.6 \pm 1.4) \times 10^{-3}$		1632
$\rho^-K^+\bar{K}^0 + c.c.$	$(5.0 \pm 1.2) \times 10^{-3}$		1514
$K^*(892)^0\bar{K}^0\pi^0 \rightarrow K^+\pi^-\bar{K}^0\pi^0 + c.c.$	$(2.3 \pm 0.6) \times 10^{-3}$		-
$K^+K^-\eta\pi^0$	$(1.12 \pm 0.34) \times 10^{-3}$		1523
$\pi^+\pi^-K_S^0K_S^0$	$(6.9 \pm 2.9) \times 10^{-4}$		1630
$K^+K^-\eta$	$(3.2 \pm 1.0) \times 10^{-4}$		1566
$\bar{K}^0K^+\pi^- + c.c.$	$(7.0 \pm 0.6) \times 10^{-3}$		1661
$K^*(892)^0\bar{K}^0 + c.c.$	$(10 \pm 4) \times 10^{-4}$		1602
$K^*(892)^+K^- + c.c.$	$(1.4 \pm 0.6) \times 10^{-3}$		1602
$K_S^0(1430)^0\bar{K}^0 + c.c. \rightarrow K_S^0K^+\pi^- + c.c.$	$< 8 \times 10^{-4}$	CL=90%	-
$K_S^0(1430)^+K^- + c.c. \rightarrow K_S^0K^+\pi^- + c.c.$	$< 2.1 \times 10^{-3}$	CL=90%	-
$K^+K^-\pi^0$	$(1.81 \pm 0.24) \times 10^{-3}$		1662
$\eta\pi^+\pi^-$	$(4.62 \pm 0.23) \times 10^{-3}$		1701
$a_0(980)^+\pi^- + c.c. \rightarrow \eta\pi^+\pi^-$	$(3.2 \pm 0.4) \times 10^{-3}$	S=2.2	-
$a_2(1320)^+\pi^- + c.c. \rightarrow \eta\pi^+\pi^-$	$(1.76 \pm 0.24) \times 10^{-4}$		-
$a_2(1700)^+\pi^- + c.c. \rightarrow \eta\pi^+\pi^-$	$(4.6 \pm 0.7) \times 10^{-5}$		-
$f_2(1270)\eta \rightarrow \eta\pi^+\pi^-$	$(3.5 \pm 0.6) \times 10^{-4}$		-
$f_4(2050)\eta \rightarrow \eta\pi^+\pi^-$	$(2.5 \pm 0.9) \times 10^{-5}$		-

$\pi_1(1400)^+\pi^- + c.c. \rightarrow \eta\pi^+\pi^-$	$< 5 \times 10^{-5}$	CL=90%	-
$\pi_1(1600)^+\pi^- + c.c. \rightarrow \eta\pi^+\pi^-$	$< 1.5 \times 10^{-5}$	CL=90%	-
$\pi_1(2015)^+\pi^- + c.c. \rightarrow \eta\pi^+\pi^-$	$< 8 \times 10^{-6}$	CL=90%	-
$f_2(1270)\eta$	$(6.7 \pm 1.1) \times 10^{-4}$		1467
$\pi^+\pi^-\eta'$	$(2.2 \pm 0.4) \times 10^{-3}$		1612
$K^+K^-\eta'(958)$	$(8.8 \pm 0.9) \times 10^{-4}$		1461
$K_S^*(1430)^+K^- + c.c.$	$(6.4 \pm 2.2) \times 10^{-4}$		-
$f_0(980)\eta'(958)$	$(1.6 \pm 1.4) \times 10^{-4}$		1460
$f_0(1710)\eta'(958)$	$(7 \pm 5) \times 10^{-5}$		1118
$f_2'(1525)\eta'(958)$	$(9 \pm 6) \times 10^{-5}$		1229
$\pi^0 f_0(980) \rightarrow \pi^0\pi^+\pi^-$	$(3.5 \pm 0.9) \times 10^{-7}$		-
$K^+K^*(892)^0\pi^- + c.c.$	$(3.2 \pm 2.1) \times 10^{-3}$		1577
$K^*(892)^0K^*(892)^0$	$(1.4 \pm 0.4) \times 10^{-3}$		1512
$K^+K^-\pi^0\pi^0$	$< 4 \times 10^{-4}$	CL=90%	1390
$K_S^0K_S^0K_S^0K_S^0$	$(3.5 \pm 1.0) \times 10^{-5}$		1387
$K^+K^-K^+K^-$	$(5.4 \pm 1.1) \times 10^{-4}$		1393
$K^+K^-\phi$	$(4.1 \pm 1.5) \times 10^{-4}$		1440
$\bar{K}^0K^+\pi^-\phi + c.c.$	$(3.3 \pm 0.5) \times 10^{-3}$		1387
$K^+K^-\pi^0\phi$	$(1.62 \pm 0.30) \times 10^{-3}$		1390
$\phi\pi^+\pi^-\pi^0$	$(7.5 \pm 1.0) \times 10^{-4}$		1578
$\omega\omega$	$(5.7 \pm 0.7) \times 10^{-4}$		1571
ωK^+K^-	$(7.8 \pm 0.9) \times 10^{-4}$		1513
$\omega\phi$	$(2.7 \pm 0.4) \times 10^{-5}$		1503
$\phi\phi$	$(4.2 \pm 0.5) \times 10^{-4}$		1429
$\phi\phi\eta$	$(3.0 \pm 0.5) \times 10^{-4}$		1172
$\rho\bar{\rho}$	$(7.60 \pm 0.34) \times 10^{-5}$		1484
$\rho\bar{\rho}\pi^0$	$(1.55 \pm 0.18) \times 10^{-4}$		1438
$\rho\bar{\rho}\eta$	$(1.45 \pm 0.25) \times 10^{-4}$		1254
$\rho\bar{\rho}\omega$	$(2.12 \pm 0.31) \times 10^{-4}$		1117
$\rho\bar{\rho}\phi$	$< 1.7 \times 10^{-5}$	CL=90%	962
$\rho\bar{\rho}\pi^+\pi^-$	$(5.0 \pm 1.9) \times 10^{-4}$		1381
$\rho\bar{\rho}\pi^0\pi^0$	$< 5 \times 10^{-4}$	CL=90%	1385
$\rho\bar{\rho}K^+K^-$ (non-resonant)	$(1.27 \pm 0.22) \times 10^{-4}$		974
$\rho\bar{\rho}K_S^0K_S^0$	$< 4.5 \times 10^{-4}$	CL=90%	968
$\rho\bar{\rho}\pi^-$	$(3.8 \pm 0.5) \times 10^{-4}$		1435
$\bar{\rho}n\pi^+$	$(3.9 \pm 0.5) \times 10^{-4}$		1435
$\rho\bar{\rho}\pi^-\pi^0$	$(1.03 \pm 0.12) \times 10^{-3}$		1383
$\bar{\rho}n\pi^+\pi^0$	$(1.01 \pm 0.12) \times 10^{-3}$		1383
$\Lambda\bar{\Lambda}$	$(1.14 \pm 0.11) \times 10^{-4}$		1355
$\Lambda\bar{\Lambda}\pi^+\pi^-$	$(2.9 \pm 0.5) \times 10^{-4}$		1223
$\Lambda\bar{\Lambda}\pi^+\pi^-$ (non-resonant)	$(2.5 \pm 0.6) \times 10^{-4}$		1223
$\Sigma(1385)^+\bar{\Lambda}\pi^- + c.c.$	$< 1.3 \times 10^{-4}$	CL=90%	1157
$\Sigma(1385)^-\bar{\Lambda}\pi^+ + c.c.$	$< 1.3 \times 10^{-4}$	CL=90%	1157
$K^+\bar{p}\Lambda + c.c.$	$(4.2 \pm 0.4) \times 10^{-4}$	S=1.2	1203
$K^*(892)^+\bar{p}\Lambda + c.c.$	$(4.9 \pm 0.7) \times 10^{-4}$		935
$K^+\bar{p}\Lambda(1520) + c.c.$	$(1.7 \pm 0.4) \times 10^{-4}$		951
$\Lambda(1520)\bar{\Lambda}(1520)$	$< 9 \times 10^{-5}$	CL=90%	880
$\Sigma^0\bar{\Sigma}^0$	$(4.2 \pm 0.6) \times 10^{-5}$		1288
$\Sigma^+\bar{p}K_S^0 + c.c.$	$(1.53 \pm 0.12) \times 10^{-4}$		1163
$\Sigma^+\bar{\Sigma}^-$	$(3.6 \pm 0.7) \times 10^{-5}$		1291
$\Sigma(1385)^+\bar{\Sigma}(1385)^-$	$< 9 \times 10^{-5}$	CL=90%	1081
$\Sigma(1385)^-\bar{\Sigma}(1385)^+$	$< 5 \times 10^{-5}$	CL=90%	1081
$K^-\Lambda\bar{\Xi}^+ + c.c.$	$(1.35 \pm 0.24) \times 10^{-4}$		963
$\Xi^0\bar{\Xi}^0$	$< 6 \times 10^{-5}$	CL=90%	1163
$\Xi^-\bar{\Xi}^+$	$(8.0 \pm 2.1) \times 10^{-5}$		1155
$\pi^+\pi^- + K^+K^-$	$< 2.1 \times 10^{-3}$		-
$K_S^0K_S^0$	$< 6 \times 10^{-5}$	CL=90%	1683
$\eta_c\pi^+\pi^-$	$< 3.2 \times 10^{-3}$	CL=90%	413
Radiative decays			
$\gamma J/\psi(1S)$	$(34.3 \pm 1.0) \%$		389
$\gamma\rho^0$	$(2.16 \pm 0.17) \times 10^{-4}$		1670
$\gamma\omega$	$(6.8 \pm 0.8) \times 10^{-5}$		1668
$\gamma\phi$	$(2.4 \pm 0.5) \times 10^{-5}$		1607
$\gamma\gamma$	$< 6.3 \times 10^{-6}$	CL=90%	1755
$e^+e^- J/\psi(1S)$	$(3.46 \pm 0.22) \times 10^{-3}$		389
$\mu^+\mu^- J/\psi(1S)$	$(2.33 \pm 0.29) \times 10^{-4}$		335

h_c(1P)

$$I^G(J^{PC}) = 0^-(1^{+-})$$

Mass $m = 3525.38 \pm 0.11$ MeV
Full width $\Gamma = 0.7 \pm 0.4$ MeV

Meson Summary Table

$\eta_c(1P)$ DECAY MODES	Fraction (Γ_i/Γ)	Confidence level	p (MeV/c)
$J/\psi(1S)\pi\pi$	not seen		312
$J/\psi(1S)\pi^+\pi^-$	$< 2.3 \times 10^{-3}$	90%	305
$\rho\bar{\rho}$	$< 1.5 \times 10^{-4}$	90%	1492
$\rho\bar{\rho}\pi^+\pi^-$	$(2.9 \pm 0.6) \times 10^{-3}$		1390
$\pi^+\pi^-\pi^0$	$(1.6 \pm 0.5) \times 10^{-3}$		1749
$2\pi^+2\pi^-\pi^0$	$(8.1 \pm 1.8) \times 10^{-3}$		1716
$3\pi^+3\pi^-\pi^0$	$< 9 \times 10^{-3}$	90%	1661
$K^+K^-\pi^+\pi^-$	$< 6 \times 10^{-4}$	90%	1640
Radiative decays			
$\gamma\eta$	$(4.7 \pm 2.1) \times 10^{-4}$		1720
$\gamma\eta'(958)$	$(1.5 \pm 0.4) \times 10^{-3}$		1633
$\gamma\eta_c(1S)$	$(51 \pm 6) \%$		500

 $\chi_{c2}(1P)$

$$I^G(J^{PC}) = 0^+(2^+ +)$$

Mass $m = 3556.17 \pm 0.07$ MeVFull width $\Gamma = 1.97 \pm 0.09$ MeV

$\chi_{c2}(1P)$ DECAY MODES	Fraction (Γ_i/Γ)	Confidence level	p (MeV/c)
Hadronic decays			
$2(\pi^+\pi^-)$	$(1.02 \pm 0.09) \%$		1751
$\pi^+\pi^-\pi^0$	$(1.83 \pm 0.23) \%$		1752
$\rho^+\pi^-\pi^0 + c.c.$	$(2.19 \pm 0.34) \%$		1682
$4\pi^0$	$(1.11 \pm 0.15) \times 10^{-3}$		1752
$K^+K^-\pi^0$	$(2.1 \pm 0.4) \times 10^{-3}$		1658
$K^+\pi^-\bar{K}^0\pi^0 + c.c.$	$(1.38 \pm 0.20) \%$		1657
$\rho^-K^+\bar{K}^0 + c.c.$	$(4.1 \pm 1.2) \times 10^{-3}$		1540
$K^*(892)^0K^-\pi^+ \rightarrow$ $K^-\pi^+K^0\pi^0 + c.c.$	$(2.9 \pm 0.8) \times 10^{-3}$		-
$K^*(892)^0\bar{K}^0\pi^0 \rightarrow$ $K^+\pi^-\bar{K}^0\pi^0 + c.c.$	$(3.8 \pm 0.9) \times 10^{-3}$		-
$K^*(892)^-K^+\pi^0 \rightarrow$ $K^+\pi^-\bar{K}^0\pi^0 + c.c.$	$(3.7 \pm 0.8) \times 10^{-3}$		-
$K^*(892)^+\bar{K}^0\pi^- \rightarrow$ $K^+\pi^-\bar{K}^0\pi^0 + c.c.$	$(2.9 \pm 0.8) \times 10^{-3}$		-
$K^+K^-\eta\pi^0$	$(1.3 \pm 0.4) \times 10^{-3}$		1549
$K^+K^-\pi^+\pi^-$	$(8.4 \pm 0.9) \times 10^{-3}$		1656
$K^+K^-\pi^+\pi^-\pi^0$	$(1.17 \pm 0.13) \%$		1623
$K_S^0K^\pm\pi^\mp\pi^\pm\pi^-$	$(7.3 \pm 0.8) \times 10^{-3}$		1621
$K^+\bar{K}^*(892)^0\pi^-\pi^+ + c.c.$	$(2.1 \pm 1.1) \times 10^{-3}$		1602
$K^*(892)^0\bar{K}^*(892)^0$	$(2.3 \pm 0.4) \times 10^{-3}$		1538
$3(\pi^+\pi^-)$	$(8.6 \pm 1.8) \times 10^{-3}$		1707
$\phi\phi$	$(1.06 \pm 0.09) \times 10^{-3}$		1457
$\phi\phi\eta$	$(5.3 \pm 0.6) \times 10^{-4}$		1206
$\omega\omega$	$(8.4 \pm 1.0) \times 10^{-4}$		1597
ωK^+K^-	$(7.3 \pm 0.9) \times 10^{-4}$		1540
$\omega\phi$	$(9.6 \pm 2.7) \times 10^{-6}$		1529
$\pi\pi$	$(2.23 \pm 0.09) \times 10^{-3}$		1773
$\rho^0\pi^+\pi^-$	$(3.7 \pm 1.6) \times 10^{-3}$		1682
$\pi^+\pi^-\pi^0$ (non-resonant)	$(2.0 \pm 0.4) \times 10^{-5}$		1765
$\rho(770)^\pm\pi^\mp$	$(6 \pm 4) \times 10^{-6}$		-
$\pi^+\pi^-\eta$	$(4.8 \pm 1.3) \times 10^{-4}$		1724
$\pi^+\pi^-\eta'$	$(5.0 \pm 1.8) \times 10^{-4}$		1636
$\eta\eta$	$(5.4 \pm 0.4) \times 10^{-4}$		1692
K^+K^-	$(1.01 \pm 0.06) \times 10^{-3}$		1708
$K_S^0K_S^0$	$(5.2 \pm 0.4) \times 10^{-4}$		1707
$K^*(892)^\pm K^\mp$	$(1.44 \pm 0.21) \times 10^{-4}$		1627
$K^*(892)^0\bar{K}^0 + c.c.$	$(1.24 \pm 0.27) \times 10^{-4}$		1627
$K_2^*(1430)^\pm K^\mp$	$(1.48 \pm 0.12) \times 10^{-3}$		-
$K_2^*(1430)^0\bar{K}^0 + c.c.$	$(1.24 \pm 0.17) \times 10^{-3}$		1443
$K_3^*(1780)^\pm K^\mp$	$(5.2 \pm 0.8) \times 10^{-4}$		-
$K_3^*(1780)^0\bar{K}^0 + c.c.$	$(5.6 \pm 2.1) \times 10^{-4}$		1276
$a_2(1320)^0\pi^0$	$(1.29 \pm 0.34) \times 10^{-3}$		-
$a_2(1320)^\pm\pi^\mp$	$(1.8 \pm 0.6) \times 10^{-3}$		1531
$\bar{K}^0K^+\pi^- + c.c.$	$(1.28 \pm 0.18) \times 10^{-3}$		1685
$K^+K^-\pi^0$	$(3.0 \pm 0.8) \times 10^{-4}$		1686
$K^+K^-\eta$	$< 3.2 \times 10^{-4}$	90%	1592
$K^+K^-\eta'(958)$	$(1.94 \pm 0.34) \times 10^{-4}$		1488
$\eta\eta'$	$(2.2 \pm 0.5) \times 10^{-5}$		1600
$\eta'\eta'$	$(4.6 \pm 0.6) \times 10^{-5}$		1498
$\pi^+\pi^-K_S^0K_S^0$	$(2.2 \pm 0.5) \times 10^{-3}$		1655
$K^+K^-K_S^0K_S^0$	$< 4 \times 10^{-4}$	90%	1418
$K_S^0K_S^0K_S^0K_S^0$	$(1.13 \pm 0.18) \times 10^{-4}$		1415

$K^+K^-K^+K^-$	$(1.65 \pm 0.20) \times 10^{-3}$		1421
$K^+K^-\phi$	$(1.42 \pm 0.29) \times 10^{-3}$		1468
$\bar{K}^0K^+\pi^-\phi + c.c.$	$(4.8 \pm 0.7) \times 10^{-3}$		1416
$K^+K^-\pi^0\phi$	$(2.7 \pm 0.5) \times 10^{-3}$		1419
$\phi\pi^+\pi^-\pi^0$	$(9.3 \pm 1.2) \times 10^{-4}$		1603
$\rho\bar{\rho}$	$(7.33 \pm 0.33) \times 10^{-5}$		1510
$\rho\bar{\rho}\pi^0$	$(4.7 \pm 0.4) \times 10^{-4}$		1465
$\rho\bar{\rho}\eta$	$(1.74 \pm 0.25) \times 10^{-4}$		1285
$\rho\bar{\rho}\omega$	$(3.6 \pm 0.4) \times 10^{-4}$		1152
$\rho\bar{\rho}\phi$	$(2.8 \pm 0.9) \times 10^{-5}$		1002
$\rho\bar{\rho}\pi^+\pi^-$	$(1.32 \pm 0.34) \times 10^{-3}$		1410
$\rho\bar{\rho}\pi^0\pi^0$	$(7.8 \pm 2.3) \times 10^{-4}$		1414
$\rho\bar{\rho}K^+K^-$ (non-resonant)	$(1.91 \pm 0.32) \times 10^{-4}$		1013
$\rho\bar{\rho}K_S^0K_S^0$	$< 7.9 \times 10^{-4}$	90%	1007
$\rho\bar{\rho}\pi^-$	$(8.5 \pm 0.9) \times 10^{-4}$		1463
$\bar{\rho}\pi\pi^+$	$(8.9 \pm 0.8) \times 10^{-4}$		1463
$\rho\bar{\rho}\pi^-\pi^0$	$(2.17 \pm 0.18) \times 10^{-3}$		1411
$\bar{\rho}\pi\pi^+\pi^0$	$(2.11 \pm 0.18) \times 10^{-3}$		1411
$\Lambda\bar{\Lambda}$	$(1.84 \pm 0.15) \times 10^{-4}$		1384
$\Lambda\bar{\Lambda}\pi^+\pi^-$	$(1.25 \pm 0.15) \times 10^{-3}$		1255
$\Lambda\bar{\Lambda}\pi^+\pi^-$ (non-resonant)	$(6.6 \pm 1.5) \times 10^{-4}$		1255
$\Sigma(1385)^+\bar{\Lambda}\pi^- + c.c.$	$< 4 \times 10^{-4}$	90%	1192
$\Sigma(1385)^-\bar{\Lambda}\pi^+ + c.c.$	$< 6 \times 10^{-4}$	90%	1192
$K^+\bar{\rho}\Lambda + c.c.$	$(7.8 \pm 0.5) \times 10^{-4}$		1236
$K^*(892)^+\bar{\rho}\Lambda + c.c.$	$(8.2 \pm 1.1) \times 10^{-4}$		976
$K^+\bar{\rho}\Lambda(1520) + c.c.$	$(2.8 \pm 0.7) \times 10^{-4}$		992
$\Lambda(1520)\bar{\Lambda}(1520)$	$(4.6 \pm 1.5) \times 10^{-4}$		924
$\Sigma^0\bar{\Sigma}^0$	$(3.7 \pm 0.6) \times 10^{-5}$		1319
$\Sigma^+\bar{\rho}K_S^0 + c.c.$	$(8.2 \pm 0.9) \times 10^{-5}$		1197
$\Sigma^+\bar{\Sigma}^-$	$(3.4 \pm 0.7) \times 10^{-5}$		1322
$\Sigma(1385)^+\bar{\Sigma}(1385)^-$	$< 1.6 \times 10^{-4}$	90%	1118
$\Sigma(1385)^-\bar{\Sigma}(1385)^+$	$< 8 \times 10^{-5}$	90%	1118
$K^-\Lambda\bar{\Xi}^+ + c.c.$	$(1.76 \pm 0.32) \times 10^{-4}$		1004
$\Xi^0\Xi^0$	$< 1.0 \times 10^{-4}$	90%	1197
$\Xi^-\Xi^+$	$(1.42 \pm 0.32) \times 10^{-4}$		1189
$J/\psi(1S)\pi^+\pi^-\pi^0$	$< 1.5 \%$		185
$\pi^0\eta_c$	$< 3.2 \times 10^{-3}$	90%	511
$\eta_c(1S)\pi^+\pi^-$	$< 5.4 \times 10^{-3}$	90%	459

Radiative decays

$\gamma J/\psi(1S)$	$(19.0 \pm 0.5) \%$		430
$\gamma\rho^0$	$< 1.9 \times 10^{-5}$	90%	1694
$\gamma\omega$	$< 6 \times 10^{-6}$	90%	1692
$\gamma\phi$	$< 7 \times 10^{-6}$	90%	1632
$\gamma\gamma$	$(2.85 \pm 0.10) \times 10^{-4}$		1778
$e^+e^- J/\psi(1S)$	$(2.15 \pm 0.14) \times 10^{-3}$		430
$\mu^+\mu^- J/\psi(1S)$	$(2.02 \pm 0.33) \times 10^{-4}$		381

 $\eta_c(2S)$

$$I^G(J^{PC}) = 0^+(0^- +)$$

Quantum numbers are quark model predictions.

Mass $m = 3637.5 \pm 1.1$ MeV ($S = 1.2$)Full width $\Gamma = 11.3^{+3.2}_{-2.9}$ MeV

$\eta_c(2S)$ DECAY MODES	Fraction (Γ_i/Γ)	Confidence level	p (MeV/c)
hadrons	not seen		-
$K\bar{K}\pi$	$(1.9 \pm 1.2) \%$		1729
$K\bar{K}\eta$	$(5 \pm 4) \times 10^{-3}$		1637
$2\pi^+2\pi^-$	not seen		1792
$\rho^0\rho^0$	not seen		1645
$3\pi^+3\pi^-$	not seen		1749
$K^+K^-\pi^+\pi^-$	not seen		1700
$K^*0\bar{K}^*0$	not seen		1585
$K^+K^-\pi^+\pi^-\pi^0$	$(1.4 \pm 1.0) \%$		1667
$K^+K^-\pi^+\pi^-\pi^0$	not seen		1627
$K_S^0K^-2\pi^+\pi^- + c.c.$	seen		1666
$2K^+2K^-$	not seen		1470
$\phi\phi$	not seen		1506
$\rho\bar{\rho}$	seen		1558
$\rho\bar{\rho}\pi^+\pi^-$	seen		1461
$\gamma\gamma$	$(1.9 \pm 1.3) \times 10^{-4}$		1819
$\gamma J/\psi(1S)$	$< 1.4 \%$	90%	500
$\pi^+\pi^-\eta$	not seen		1766
$\pi^+\pi^-\eta'$	not seen		1680
$\pi^+\pi^-\eta_c(1S)$	$< 25 \%$	90%	537

Meson Summary Table

$\phi f_1(1285)$	$(3.0 \pm 1.3) \times 10^{-5}$	1436
$\phi\eta(1405) \rightarrow \phi\pi^+\pi^-\eta$	$(8.5 \pm 1.7) \times 10^{-6}$	-
$\omega\eta'$	$(3.2 \pm 2.5_{-2.1}) \times 10^{-5}$	1623
$\omega\pi^0$	$(2.1 \pm 0.6) \times 10^{-5}$	1757
$\rho\eta'$	$(1.9 \pm 1.7_{-1.2}) \times 10^{-5}$	1625
$\rho\eta$	$(2.2 \pm 0.6) \times 10^{-5}$	S=1.1 1717
$\omega\eta$	$< 1.1 \times 10^{-5}$	CL=90% 1715
$\phi\pi^0$	$< 4 \times 10^{-7}$	CL=90% 1699
$\eta_c\pi^+\pi^-\pi^0$	$< 1.0 \times 10^{-3}$	CL=90% 512
$\rho\bar{\rho}K^+K^-$	$(2.7 \pm 0.7) \times 10^{-5}$	1118
$\bar{\Lambda}nK_S^0 + c.c.$	$(8.1 \pm 1.8) \times 10^{-5}$	1324
$\phi f_2'(1525)$	$(4.4 \pm 1.6) \times 10^{-5}$	1325
$\Theta(1540)\bar{\Theta}(1540) \rightarrow K_S^0\rho K^-\bar{\pi} + c.c.$	$< 8.8 \times 10^{-6}$	CL=90% -
$\Theta(1540)K^-\bar{\pi} \rightarrow K_S^0\rho K^-\bar{\pi}$	$< 1.0 \times 10^{-5}$	CL=90% -
$\Theta(1540)K_S^0\bar{\rho} \rightarrow K_S^0\bar{\rho}K^+n$	$< 7.0 \times 10^{-6}$	CL=90% -
$\bar{\Theta}(1540)K^+n \rightarrow K_S^0\bar{\rho}K^+n$	$< 2.6 \times 10^{-5}$	CL=90% -
$\bar{\Theta}(1540)K_S^0\rho \rightarrow K_S^0\rho K^-\bar{\pi}$	$< 6.0 \times 10^{-6}$	CL=90% -
$K_S^0 K_S^0$	$< 4.6 \times 10^{-6}$	1775
$\Lambda_c^+\bar{\rho}e^+e^- + c.c.$	$< 1.7 \times 10^{-6}$	CL=90% 830

Radiative decays

$\gamma\chi_{c0}(1P)$	$(9.79 \pm 0.20) \%$	261
$\gamma\chi_{c1}(1P)$	$(9.75 \pm 0.24) \%$	171
$\gamma\chi_{c2}(1P)$	$(9.52 \pm 0.20) \%$	128
$\gamma\eta_c(1S)$	$(3.4 \pm 0.5) \times 10^{-3}$	S=1.3 635
$\gamma\eta_c(2S)$	$(7 \pm 5) \times 10^{-4}$	48
$\gamma\pi^0$	$(1.04 \pm 0.22) \times 10^{-6}$	S=1.4 1841
$\gamma\eta'(958)$	$(1.24 \pm 0.04) \times 10^{-4}$	1719
$\gamma f_2(1270)$	$(2.73 \pm 0.29_{-0.25}) \times 10^{-4}$	S=1.8 1622
$\gamma f_0(1370) \rightarrow \gamma K\bar{K}$	$(3.1 \pm 1.7) \times 10^{-5}$	1588
$\gamma f_0(1500)$	$(9.3 \pm 1.9) \times 10^{-5}$	1535
$\gamma f_2'(1525)$	$(3.3 \pm 0.8) \times 10^{-5}$	1531
$\gamma f_0(1710) \rightarrow \gamma\pi\pi$	$(3.5 \pm 0.6) \times 10^{-5}$	-
$\gamma f_0(1710) \rightarrow \gamma K\bar{K}$	$(6.6 \pm 0.7) \times 10^{-5}$	-
$\gamma f_0(2100) \rightarrow \gamma\pi\pi$	$(4.8 \pm 1.0) \times 10^{-6}$	1244
$\gamma f_0(2200) \rightarrow \gamma K\bar{K}$	$(3.2 \pm 1.0) \times 10^{-6}$	1193
$\gamma f_1(2220) \rightarrow \gamma\pi\pi$	$< 5.8 \times 10^{-6}$	CL=90% 1168
$\gamma f_2(2220) \rightarrow \gamma\pi\pi$	$< 9.5 \times 10^{-6}$	CL=90% 1168
$\gamma f_2(2220) \rightarrow \gamma K\bar{K}$	$< 1.5 \times 10^{-4}$	CL=90% 1843
$\gamma\gamma$	$(9.2 \pm 1.8) \times 10^{-7}$	1802
$\gamma\eta\pi^+\pi^-$	$(8.7 \pm 2.1) \times 10^{-4}$	1791
$\gamma\eta(1405) \rightarrow \gamma K\bar{K}\pi$	$< 9 \times 10^{-5}$	CL=90% 1569
$\gamma\eta(1405) \rightarrow \eta\pi^+\pi^-$	$(3.6 \pm 2.5) \times 10^{-5}$	-
$\gamma\eta(1405) \rightarrow \gamma f_0(980)\pi^0 \rightarrow \gamma\pi^+\pi^-\pi^0$	$< 5.0 \times 10^{-7}$	CL=90% -
$\gamma\eta(1475) \rightarrow K\bar{K}\pi$	$< 1.4 \times 10^{-4}$	CL=90% -
$\gamma\eta(1475) \rightarrow \eta\pi^+\pi^-$	$< 8.8 \times 10^{-5}$	CL=90% -
$\gamma 2(\pi^+\pi^-)$	$(4.0 \pm 0.6) \times 10^{-4}$	1817
$\gamma K^{*0}K^+\pi^- + c.c.$	$(3.7 \pm 0.9) \times 10^{-4}$	1674
$\gamma K^{*0}\bar{K}^{*0}$	$(2.4 \pm 0.7) \times 10^{-4}$	1613
$\gamma K_S^0K^+\pi^- + c.c.$	$(2.6 \pm 0.5) \times 10^{-4}$	1753
$\gamma K^+K^-\pi^+\pi^-$	$(1.9 \pm 0.5) \times 10^{-4}$	1726
$\gamma\rho\bar{\rho}$	$(3.9 \pm 0.5) \times 10^{-5}$	S=2.0 1586
$\gamma f_2(1950) \rightarrow \gamma\rho\bar{\rho}$	$(1.20 \pm 0.22) \times 10^{-5}$	-
$\gamma f_2(2150) \rightarrow \gamma\rho\bar{\rho}$	$(7.2 \pm 1.8) \times 10^{-6}$	-
$\gamma X(1835) \rightarrow \gamma\rho\bar{\rho}$	$(4.6 \pm 1.8_{-4.0}) \times 10^{-6}$	-
$\gamma X \rightarrow \gamma\rho\bar{\rho}$	$[qqaa] < 2 \times 10^{-6}$	CL=90% -
$\gamma\pi^+\pi^-\rho\bar{\rho}$	$(2.8 \pm 1.4) \times 10^{-5}$	1491
$\gamma 2(\pi^+\pi^-)K^+K^-$	$< 2.2 \times 10^{-4}$	CL=90% 1654
$\gamma 3(\pi^+\pi^-)$	$< 1.7 \times 10^{-4}$	CL=90% 1774
$\gamma K^+K^-K^+K^-$	$< 4 \times 10^{-5}$	CL=90% 1499
$\gamma\gamma J/\psi$	$(3.1 \pm 1.0_{-1.2}) \times 10^{-4}$	542
$e^+e^-\eta'$	$(1.90 \pm 0.26) \times 10^{-6}$	1719
$e^+e^-\chi_{c0}(1P)$	$(1.06 \pm 0.24) \times 10^{-3}$	261
$e^+e^-\chi_{c1}(1P)$	$(8.5 \pm 0.6) \times 10^{-4}$	171
$e^+e^-\chi_{c2}(1P)$	$(7.0 \pm 0.8) \times 10^{-4}$	128

Weak decays

$D^0e^+e^- + c.c.$	$< 1.4 \times 10^{-7}$	CL=90% 1371
--------------------	------------------------	-------------

Other decays

invisible	$< 1.6 \%$	CL=90% -
-----------	------------	----------

$\psi(3770)$

$$J^G(J^{PC}) = 0^-(1^{--})$$

Mass $m = 3773.7 \pm 0.4$ MeV (S = 1.4)

Full width $\Gamma = 27.2 \pm 1.0$ MeV

$\Gamma_{ee} = 0.262 \pm 0.018$ keV (S = 1.4)

In addition to the dominant decay mode to $D\bar{D}$, $\psi(3770)$ was found to decay into the final states containing the J/ψ (BAI 05, ADAM 06). ADAMS 06 and HUANG 06A searched for various decay modes with light hadrons and found a statistically significant signal for the decay to $\phi\eta$ only (ADAMS 06).

$\psi(3770)$ DECAY MODES

DECAY MODES	Fraction (Γ_i/Γ)	Scale factor/ Confidence level	ρ (MeV/c)
$D\bar{D}$	$(93 \pm 8_{-9}) \%$	S=2.0	287
$D^0\bar{D}^0$	$(52 \pm 4_{-5}) \%$	S=2.0	287
D^+D^-	$(41 \pm 4) \%$	S=2.0	254
$J/\psi\pi^+\pi^-$	$(1.93 \pm 0.28) \times 10^{-3}$		561
$J/\psi\pi^0\pi^0$	$(8.0 \pm 3.0) \times 10^{-4}$		565
$J/\psi\eta$	$(9 \pm 4) \times 10^{-4}$		361
$J/\psi\pi^0$	$< 2.8 \times 10^{-4}$	CL=90%	604
e^+e^-	$(9.6 \pm 0.7) \times 10^{-6}$	S=1.3	1887

Decays to light hadrons

$b_1(1235)\pi$	$< 1.4 \times 10^{-5}$	CL=90%	1684
$\phi\eta'$	$< 7 \times 10^{-4}$	CL=90%	1607
$\omega\eta'$	$< 4 \times 10^{-4}$	CL=90%	1672
$\rho^0\eta'$	$< 6 \times 10^{-4}$	CL=90%	1674
$\phi\eta$	$(3.1 \pm 0.7) \times 10^{-4}$		1703
$\omega\eta$	$< 1.4 \times 10^{-5}$	CL=90%	1762
$\rho^0\eta$	$< 5 \times 10^{-4}$	CL=90%	1764
$\phi\pi^0$	$< 3 \times 10^{-5}$	CL=90%	1746
$\omega\pi^0$	$< 6 \times 10^{-4}$	CL=90%	1803
$\pi^+\pi^-\pi^0$	$< 5 \times 10^{-6}$	CL=90%	1874
$\rho\pi$	$< 5 \times 10^{-6}$	CL=90%	1805
$K^*(892)^+K^- + c.c.$	$< 1.4 \times 10^{-5}$	CL=90%	1745
$K^*(892)^0\bar{K}^0 + c.c.$	$< 1.2 \times 10^{-3}$	CL=90%	1745
$K_S^0K_L^0$	$< 1.2 \times 10^{-5}$	CL=90%	1820
$2(\pi^+\pi^-)$	$< 1.12 \times 10^{-3}$	CL=90%	1861
$2(\pi^+\pi^-)\pi^0$	$< 1.06 \times 10^{-3}$	CL=90%	1844
$2(\pi^+\pi^-\pi^0)$	$< 5.85 \%$	CL=90%	1821
$\omega\pi^+\pi^-$	$< 6.0 \times 10^{-4}$	CL=90%	1794
$3(\pi^+\pi^-)$	$< 9.1 \times 10^{-3}$	CL=90%	1820
$3(\pi^+\pi^-)\pi^0$	$< 1.37 \%$	CL=90%	1792
$3(\pi^+\pi^-)2\pi^0$	$< 11.74 \%$	CL=90%	1760
$\eta\pi^+\pi^-$	$< 1.24 \times 10^{-3}$	CL=90%	1836
$\pi^+\pi^-2\pi^0$	$< 8.9 \times 10^{-3}$	CL=90%	1862
$\rho^0\pi^+\pi^-$	$< 6.9 \times 10^{-3}$	CL=90%	1796
$\eta 3\pi$	$< 1.34 \times 10^{-3}$	CL=90%	1824
$\eta 2(\pi^+\pi^-)$	$< 2.43 \%$	CL=90%	1804
$\eta\rho^0\pi^+\pi^-$	$< 1.45 \%$	CL=90%	1708
$\eta' 3\pi$	$< 2.44 \times 10^{-3}$	CL=90%	1741
$K^+K^-\pi^+\pi^-$	$< 9.0 \times 10^{-4}$	CL=90%	1773
$\phi\pi^+\pi^-$	$< 4.1 \times 10^{-4}$	CL=90%	1737
$K^+K^-2\pi^0$	$< 4.2 \times 10^{-3}$	CL=90%	1774
$4(\pi^+\pi^-)$	$< 1.67 \%$	CL=90%	1757
$4(\pi^+\pi^-)\pi^0$	$< 3.06 \%$	CL=90%	1720
$\phi f_0(980)$	$< 4.5 \times 10^{-4}$	CL=90%	1597
$K^+K^-\pi^+\pi^-\pi^0$	$< 2.36 \times 10^{-3}$	CL=90%	1741
$K^+K^-\rho^0\pi^0$	$< 8 \times 10^{-4}$	CL=90%	1624
$K^+K^-\rho^+\pi^-$	$< 1.46 \%$	CL=90%	1623
ωK^+K^-	$< 3.4 \times 10^{-4}$	CL=90%	1664
$\phi\pi^+\pi^-\pi^0$	$< 3.8 \times 10^{-3}$	CL=90%	1723
$K^{*0}K^-\pi^+\pi^0 + c.c.$	$< 1.62 \%$	CL=90%	1694
$K^{*+}K^-\pi^+\pi^- + c.c.$	$< 3.23 \%$	CL=90%	1693
$K^+K^-\pi^+\pi^-2\pi^0$	$< 2.67 \%$	CL=90%	1705
$K^+K^-2(\pi^+\pi^-)$	$< 1.03 \%$	CL=90%	1702
$K^+K^-2(\pi^+\pi^-)\pi^0$	$< 3.60 \%$	CL=90%	1661
ηK^+K^-	$< 4.1 \times 10^{-4}$	CL=90%	1712
$\eta K^+K^-\pi^+\pi^-$	$< 1.24 \%$	CL=90%	1624
$\rho^0 K^+K^-$	$< 5.0 \times 10^{-3}$	CL=90%	1666
$2(K^+K^-)$	$< 6.0 \times 10^{-4}$	CL=90%	1552
ϕK^+K^-	$< 7.5 \times 10^{-4}$	CL=90%	1598
$2(K^+K^-)\pi^0$	$< 2.9 \times 10^{-4}$	CL=90%	1494
$2(K^+K^-)\pi^+\pi^-$	$< 3.2 \times 10^{-3}$	CL=90%	1426
$K_S^0 K^-\pi^+$	$< 3.2 \times 10^{-3}$	CL=90%	1799
$K_S^0 K^-\pi^+\pi^0$	$< 1.33 \%$	CL=90%	1773
$K_S^0 K^-\rho^+$	$< 6.6 \times 10^{-3}$	CL=90%	1665

Meson Summary Table

$K_S^0 K^- 2\pi^+ \pi^-$	< 8.7	$\times 10^{-3}$	CL=90%	1740
$K_S^0 K^- \pi^+ \rho^0$	< 1.6	%	CL=90%	1621
$K_S^0 K^- \pi^+ \eta$	< 1.3	%	CL=90%	1670
$K_S^0 K^- 2\pi^+ \pi^- \pi^0$	< 4.18	%	CL=90%	1703
$K_S^0 K^- 2\pi^+ \pi^- \eta$	< 4.8	%	CL=90%	1570
$K_S^0 K^- \pi^+ 2(\pi^+ \pi^-)$	< 1.22	%	CL=90%	1658
$K_S^0 K^- \pi^+ 2\pi^0$	< 2.65	%	CL=90%	1742
$K_S^0 K^- K^+ K^- \pi^+$	< 4.9	$\times 10^{-3}$	CL=90%	1491
$K_S^0 K^- K^+ K^- \pi^+ \pi^0$	< 3.0	%	CL=90%	1427
$K_S^0 K^- K^+ K^- \pi^+ \eta$	< 2.2	%	CL=90%	1214
$K^{*0} K^- \pi^+ + c.c.$	< 9.7	$\times 10^{-3}$	CL=90%	1722
$\rho \bar{\rho} \pi^0$	< 4	$\times 10^{-5}$	CL=90%	1595
$\rho \bar{\rho} \pi^+ \pi^-$	< 5.8	$\times 10^{-4}$	CL=90%	1544
$\Lambda \bar{\Lambda}$	< 1.2	$\times 10^{-4}$	CL=90%	1522
$\rho \bar{\rho} \pi^+ \pi^- \pi^0$	< 1.85	$\times 10^{-3}$	CL=90%	1490
$\omega \rho \bar{\rho}$	< 2.9	$\times 10^{-4}$	CL=90%	1310
$\Lambda \bar{\Lambda} \pi^0$	< 7	$\times 10^{-5}$	CL=90%	1469
$\rho \bar{\rho} 2(\pi^+ \pi^-)$	< 2.6	$\times 10^{-3}$	CL=90%	1426
$\eta \rho \bar{\rho}$	< 5.4	$\times 10^{-4}$	CL=90%	1431
$\eta \rho \bar{\rho} \pi^+ \pi^-$	< 3.3	$\times 10^{-3}$	CL=90%	1284
$\rho^0 \rho \bar{\rho}$	< 1.7	$\times 10^{-3}$	CL=90%	1314
$\rho \bar{\rho} K^+ K^-$	< 3.2	$\times 10^{-4}$	CL=90%	1186
$\eta \rho \bar{\rho} K^+ K^-$	< 6.9	$\times 10^{-3}$	CL=90%	737
$\pi^0 \rho \bar{\rho} K^+ K^-$	< 1.2	$\times 10^{-3}$	CL=90%	1094
$\phi \rho \bar{\rho}$	< 1.3	$\times 10^{-4}$	CL=90%	1178
$\Lambda \bar{\Lambda} \pi^+ \pi^-$	< 2.5	$\times 10^{-4}$	CL=90%	1405
$\Lambda \bar{\rho} K^+$	< 2.8	$\times 10^{-4}$	CL=90%	1387
$\Lambda \bar{\rho} K^+ \pi^+ \pi^-$	< 6.3	$\times 10^{-4}$	CL=90%	1234
$\Lambda \bar{\Lambda} \eta$	< 1.9	$\times 10^{-4}$	CL=90%	1263
$\Sigma^+ \bar{\Sigma}^-$	< 1.0	$\times 10^{-4}$	CL=90%	1465
$\Sigma^0 \bar{\Sigma}^0$	< 4	$\times 10^{-5}$	CL=90%	1462
$\Xi^+ \bar{\Xi}^-$	< 1.5	$\times 10^{-4}$	CL=90%	1347
$\Xi^0 \bar{\Xi}^0$	< 1.4	$\times 10^{-4}$	CL=90%	1353

Radiative decays

$\gamma \chi_{c2}$	< 6.4	$\times 10^{-4}$	CL=90%	211
$\gamma \chi_{c1}$	(2.49 ± 0.23)	$\times 10^{-3}$		254
$\gamma \chi_{c0}$	(6.9 ± 0.6)	$\times 10^{-3}$		342
$\gamma \eta_c$	< 7	$\times 10^{-4}$	CL=90%	707
$\gamma \eta_c(2S)$	< 9	$\times 10^{-4}$	CL=90%	134
$\gamma \eta'$	< 1.8	$\times 10^{-4}$	CL=90%	1765
$\gamma \eta$	< 1.5	$\times 10^{-4}$	CL=90%	1847
$\gamma \pi^0$	< 2	$\times 10^{-4}$	CL=90%	1884

 $\psi_2(3823)$

$$J^G(J^{PC}) = 0^-(2^- -)$$

I, J, P need confirmation.

was $\psi(3823)$, $X(3823)$ Mass $m = 3822.2 \pm 1.2$ MeVFull width $\Gamma < 16$ MeV, CL = 90%

$\psi_2(3823)$ DECAY MODES	Fraction (Γ_i/Γ)	ρ (MeV/c)
$\chi_{c1} \gamma$	seen	299
$\chi_{c2} \gamma$	not seen	257

 $\psi_3(3842)$

$$J^G(J^{PC}) = 0^-(3^- -)$$

J, P need confirmation.

Mass $m = 3842.71 \pm 0.20$ MeVFull width $\Gamma = 2.8 \pm 0.6$ MeV

$\psi_3(3842)$ DECAY MODES	Fraction (Γ_i/Γ)	ρ (MeV/c)
$D^+ D^-$	seen	443
$D^0 \bar{D}^0$	seen	463

 $\chi_{c1}(3872)$

$$J^G(J^{PC}) = 0^+(1^+ +)$$

also known as $X(3872)$ Mass $m = 3871.69 \pm 0.17$ MeV $m_{\chi_{c1}(3872)} - m_{J/\psi} = 775 \pm 4$ MeVFull width $\Gamma < 1.2$ MeV, CL = 90%

$\chi_{c1}(3872)$ DECAY MODES	Fraction (Γ_i/Γ)	ρ (MeV/c)
$\pi^+ \pi^- J/\psi(1S)$	> 3.2 %	650

$\omega J/\psi(1S)$	> 2.3 %	†
$D^0 \bar{D}^0 \pi^0$	>40 %	117
$\bar{D}^{*0} D^0$	>30 %	4
$\pi^0 \chi_{c1}$	> 2.8 %	319
$\gamma J/\psi$	> 7 $\times 10^{-3}$	697
$\gamma \psi(2S)$	> 4 %	181
$\pi^+ \pi^- \eta_c(1S)$	not seen	745
$\pi^+ \pi^- \chi_{c1}$	not seen	218
$\rho \bar{\rho}$	not seen	1693

 $Z_c(3900)$

$$J^G(J^{PC}) = 1^+(1^+ -)$$

was $X(3900)$ Mass $m = 3888.4 \pm 2.5$ MeV ($S = 1.7$)Full width $\Gamma = 28.3 \pm 2.5$ MeV

$Z_c(3900)$ DECAY MODES	Fraction (Γ_i/Γ)	ρ (MeV/c)
$J/\psi \pi$	seen	700
$h_c \pi^\pm$	not seen	319
$\eta_c \pi^+ \pi^-$	not seen	760
$(D \bar{D}^*)^\pm$	seen	-
$D^0 D^{*-} + c.c.$	seen	160
$D^- D^{*0} + c.c.$	seen	152
$\omega \pi^\pm$	not seen	1863
$J/\psi \eta$	not seen	511
$D^+ D^{*-} + c.c.$	seen	-
$D^0 \bar{D}^{*0} + c.c.$	seen	-

 $X(3915)$

$$J^G(J^{PC}) = 0^+(0 \text{ or } 2^+ +)$$

was $\chi_{c0}(3915)$ Mass $m = 3918.4 \pm 1.9$ MeVFull width $\Gamma = 20 \pm 5$ MeV ($S = 1.1$)

$X(3915)$ DECAY MODES	Fraction (Γ_i/Γ)	ρ (MeV/c)
$\omega J/\psi$	seen	222
$\pi^+ \pi^- \eta_c(1S)$	not seen	785
$\eta_c \eta$	not seen	665
$\eta_c \pi^0$	not seen	814
$K \bar{K}$	not seen	1896
$\gamma \gamma$	seen	1959

 $\chi_{c2}(3930)$

$$J^G(J^{PC}) = 0^+(2^+ +)$$

Mass $m = 3922.2 \pm 1.0$ MeV ($S = 1.6$)Full width $\Gamma = 35.3 \pm 2.8$ MeV ($S = 1.4$)

$\chi_{c2}(3930)$ DECAY MODES	Fraction (Γ_i/Γ)	ρ (MeV/c)
$\gamma \gamma$	seen	1961
$D \bar{D}$	seen	607
$D^+ D^-$	seen	592
$D^0 \bar{D}^0$	seen	607
$\pi^+ \pi^- \eta_c(1S)$	not seen	788
$K \bar{K}$	not seen	1898

 $X(4020)^\pm$

$$J^G(J^{PC}) = 1^+(?^- -)$$

Mass $m = 4024.1 \pm 1.9$ MeVFull width $\Gamma = 13 \pm 5$ MeV ($S = 1.7$)

$X(4020)^\pm$ DECAY MODES	Fraction (Γ_i/Γ)	ρ (MeV/c)
$h_c(1P) \pi$	seen	450
$D^* \bar{D}^*$	seen	85
$D \bar{D}^* + c.c.$	not seen	542
$\eta_c \pi^+ \pi^-$	not seen	872
$J/\psi(1S) \pi^\pm$	not seen	811

 $\psi(4040)$ [rraa]

$$J^G(J^{PC}) = 0^-(1^- -)$$

Mass $m = 4039 \pm 1$ MeVFull width $\Gamma = 80 \pm 10$ MeV $\Gamma_{ee} = 0.86 \pm 0.07$ keV

Meson Summary Table

Due to the complexity of the $c\bar{c}$ threshold region, in this listing, "seen" ("not seen") means that a cross section for the mode in question has been measured at effective \sqrt{s} near this particle's central mass value, more (less) than 2σ above zero, without regard to any peaking behavior in \sqrt{s} or absence thereof. See mode listing(s) for details and references.

$\psi(4040)$ DECAY MODES	Fraction (Γ_i/Γ)	Confidence level	ρ (MeV/c)
e^+e^-	$(1.07 \pm 0.16) \times 10^{-5}$		2019
$D\bar{D}$	seen		775
$D^0\bar{D}^0$	seen		775
D^+D^-	seen		763
$D^*\bar{D}^+$ c.c.	seen		569
$D^*(2007)^0\bar{D}^0$ + c.c.	seen		575
$D^*(2010)^+D^-$ + c.c.	seen		561
$D^*\bar{D}^*$	seen		193
$D^*(2007)^0\bar{D}^*(2007)^0$	seen		226
$D^*(2010)^+D^*(2010)^-$	seen		193
$D^0D^-\pi^+$ + c.c. (excl. $D^*(2007)^0\bar{D}^0$ + c.c., $D^*(2010)^+D^-$ + c.c.)	not seen		-
$D\bar{D}^*\pi$ (excl. $D^*\bar{D}^*$)	not seen		-
$D^0\bar{D}^{*-}\pi^+$ + c.c. (excl. $D^*(2010)^+D^*(2010)^-$)	seen		-
$D_s^+D_s^-$	seen		452
$J/\psi\pi^+\pi^-$	$< 4 \times 10^{-3}$	90%	794
$J/\psi\pi^0\pi^0$	$< 2 \times 10^{-3}$	90%	797
$J/\psi\eta$	$(5.2 \pm 0.7) \times 10^{-3}$		675
$J/\psi\pi^0$	$< 2.8 \times 10^{-4}$	90%	823
$J/\psi\pi^+\pi^-\pi^0$	$< 2 \times 10^{-3}$	90%	746
$\chi_{c1}\gamma$	$< 3.4 \times 10^{-3}$	90%	494
$\chi_{c2}\gamma$	$< 5 \times 10^{-3}$	90%	454
$\chi_{c1}\pi^+\pi^-\pi^0$	$< 1.1\%$	90%	306
$\chi_{c2}\pi^+\pi^-\pi^0$	$< 3.2\%$	90%	233
$h_c(1P)\pi^+\pi^-$	$< 3 \times 10^{-3}$	90%	403
$\phi\pi^+\pi^-$	$< 3 \times 10^{-3}$	90%	1880
$\Lambda\bar{\Lambda}\pi^+\pi^-$	$< 2.9 \times 10^{-4}$	90%	1578
$\Lambda\bar{\Lambda}\pi^0$	$< 9 \times 10^{-5}$	90%	1636
$\Lambda\bar{\Lambda}\eta$	$< 3.0 \times 10^{-4}$	90%	1452
$\Sigma^+\bar{\Sigma}^-$	$< 1.3 \times 10^{-4}$	90%	1632
$\Sigma^0\bar{\Sigma}^0$	$< 7 \times 10^{-5}$	90%	1630
$\Xi^+\bar{\Xi}^-$	$< 1.6 \times 10^{-4}$	90%	1527
$\Xi^0\bar{\Xi}^0$	$< 1.8 \times 10^{-4}$	90%	1533

$$\chi_{c1}(4140) \quad I^G(J^{PC}) = 0^+(1^{++})$$

was X(4140)

$$\text{Mass } m = 4146.8 \pm 2.4 \text{ MeV} \quad (S = 1.1)$$

$$\text{Full width } \Gamma = 22 \pm 7 \text{ MeV} \quad (S = 1.3)$$

$\chi_{c1}(4140)$ DECAY MODES	Fraction (Γ_i/Γ)	ρ (MeV/c)
$J/\psi\phi$	seen	217
$\gamma\gamma$	not seen	2073

$$\psi(4160) \text{ [rraa]} \quad I^G(J^{PC}) = 0^-(1^{--})$$

$$\text{Mass } m = 4191 \pm 5 \text{ MeV}$$

$$\text{Full width } \Gamma = 70 \pm 10 \text{ MeV}$$

$$\Gamma_{ee} = 0.48 \pm 0.22 \text{ keV}$$

Due to the complexity of the $c\bar{c}$ threshold region, in this listing, "seen" ("not seen") means that a cross section for the mode in question has been measured at effective \sqrt{s} near this particle's central mass value, more (less) than 2σ above zero, without regard to any peaking behavior in \sqrt{s} or absence thereof. See mode listing(s) for details and references.

$\psi(4160)$ DECAY MODES	Fraction (Γ_i/Γ)	Confidence level	ρ (MeV/c)
e^+e^-	$(6.9 \pm 3.3) \times 10^{-6}$		2096
$\mu^+\mu^-$	seen		2093
$D\bar{D}$	seen		956
$D^0\bar{D}^0$	seen		956
D^+D^-	seen		947
$D^*\bar{D}^+$ c.c.	seen		798
$D^*(2007)^0\bar{D}^0$ + c.c.	seen		802
$D^*(2010)^+D^-$ + c.c.	seen		792
$D^*\bar{D}^*$	seen		592

$D^*(2007)^0\bar{D}^*(2007)^0$	seen		604
$D^*(2010)^+D^*(2010)^-$	seen		592
$D^0D^-\pi^+$ + c.c. (excl. $D^*(2007)^0\bar{D}^0$ + c.c., $D^*(2010)^+D^-$ + c.c.)	not seen		-
$D\bar{D}^*\pi$ + c.c. (excl. $D^*\bar{D}^*$)	seen		-
$D^0D^{*-}\pi^+$ + c.c. (excl. $D^*(2010)^+D^*(2010)^-$)	not seen		-
$D_s^+D_s^-$	not seen		719
$D_s^{*+}D_s^-$ + c.c.	seen		385
$J/\psi\pi^+\pi^-$	$< 3 \times 10^{-3}$	90%	919
$J/\psi\pi^0\pi^0$	$< 3 \times 10^{-3}$	90%	922
$J/\psi K^+K^-$	$< 2 \times 10^{-3}$	90%	407
$J/\psi\eta$	$< 8 \times 10^{-3}$	90%	822
$J/\psi\pi^0$	$< 1 \times 10^{-3}$	90%	944
$J/\psi\eta'$	$< 5 \times 10^{-3}$	90%	457
$J/\psi\pi^+\pi^-\pi^0$	$< 1 \times 10^{-3}$	90%	879
$\psi(2S)\pi^+\pi^-$	$< 4 \times 10^{-3}$	90%	396
$\chi_{c1}\gamma$	$< 5 \times 10^{-3}$	90%	625
$\chi_{c2}\gamma$	$< 1.3\%$	90%	587
$\chi_{c1}\pi^+\pi^-\pi^0$	$< 2 \times 10^{-3}$	90%	496
$\chi_{c2}\pi^+\pi^-\pi^0$	$< 8 \times 10^{-3}$	90%	445
$h_c(1P)\pi^+\pi^-$	$< 5 \times 10^{-3}$	90%	556
$h_c(1P)\pi^0\pi^0$	$< 2 \times 10^{-3}$	90%	560
$h_c(1P)\eta$	$< 2 \times 10^{-3}$	90%	348
$h_c(1P)\pi^0$	$< 4 \times 10^{-4}$	90%	600
$\phi\pi^+\pi^-$	$< 2 \times 10^{-3}$	90%	1961
$\gamma\chi_{c1}(3872) \rightarrow \gamma J/\psi\pi^+\pi^-$	$< 6.8 \times 10^{-5}$	90%	-
$\gamma X(3915) \rightarrow \gamma J/\psi\pi^+\pi^-$	$< 1.36 \times 10^{-4}$	90%	-
$\gamma X(3930) \rightarrow \gamma J/\psi\pi^+\pi^-$	$< 1.18 \times 10^{-4}$	90%	-
$\gamma X(3940) \rightarrow \gamma J/\psi\pi^+\pi^-$	$< 1.47 \times 10^{-4}$	90%	-
$\gamma\chi_{c1}(3872) \rightarrow \gamma\gamma J/\psi$	$< 1.05 \times 10^{-4}$	90%	-
$\gamma X(3915) \rightarrow \gamma\gamma J/\psi$	$< 1.26 \times 10^{-4}$	90%	-
$\gamma X(3930) \rightarrow \gamma\gamma J/\psi$	$< 8.8 \times 10^{-5}$	90%	-
$\gamma X(3940) \rightarrow \gamma\gamma J/\psi$	$< 1.79 \times 10^{-4}$	90%	-

$$\psi(4230) \quad I^G(J^{PC}) = 0^-(1^{--})$$

also known as Y(4230); was X(4230)

$$\text{See also } \psi(4260) \text{ entry in Particle Listings.}$$

$$\text{Mass } m = 4220 \pm 15 \text{ MeV}$$

$$\text{Full width } \Gamma = 20 \text{ to } 100 \text{ MeV}$$

$\psi(4230)$ DECAY MODES	Fraction (Γ_i/Γ)	ρ (MeV/c)
$\omega\chi_{c0}$	seen	171
$\pi^+\pi^-h_c$	seen	583
$\pi^+\pi^-J/\psi$	seen	942
$\pi^+\pi^-\psi(2S)$	seen	426
$\pi^+D^0D^{*-}$ + c.c.	seen	650
$\gamma\chi_{c1}(3872)$	seen	334

$$\chi_{c1}(4274) \quad I^G(J^{PC}) = 0^+(1^{++})$$

was X(4274)

$$\text{Mass } m = 4274 \pm 8 \text{ MeV}$$

$$\text{Full width } \Gamma = 49 \pm 12 \text{ MeV}$$

$\chi_{c1}(4274)$ DECAY MODES	Fraction (Γ_i/Γ)	ρ (MeV/c)
$J/\psi\phi$	seen	503

$$\psi(4360) \quad I^G(J^{PC}) = 0^-(1^{--})$$

also known as Y(4360); was X(4360)

$$\psi(4360) \text{ MASS} = 4368 \pm 13 \text{ MeV} \quad (S = 3.7)$$

$$\psi(4360) \text{ WIDTH} = 96 \pm 7 \text{ MeV}$$

$\psi(4360)$ DECAY MODES	Fraction (Γ_i/Γ)	ρ (MeV/c)
$\psi(2S)\pi^+\pi^-$	seen	573
$\psi_2(3823)\pi^+\pi^-$	possibly seen	440
$D_1(2420)\bar{D}^+$ + c.c.	possibly seen	419

Meson Summary Table

 $\psi(4415)$ [rraa]

$$J^G(J^{PC}) = 0^-(1^{--})$$

Mass $m = 4421 \pm 4$ MeV
 Full width $\Gamma = 62 \pm 20$ MeV
 $\Gamma_{ee} = 0.58 \pm 0.07$ keV

Due to the complexity of the $c\bar{c}$ threshold region, in this listing, "seen" ("not seen") means that a cross section for the mode in question has been measured at effective \sqrt{s} near this particle's central mass value, more (less) than 2σ above zero, without regard to any peaking behavior in \sqrt{s} or absence thereof. See mode listing(s) for details and references.

$\psi(4415)$ DECAY MODES	Fraction (Γ_i/Γ)	Confidence level	ρ (MeV/c)
$D\bar{D}$	seen		1187
$D^0\bar{D}^0$	seen		1187
D^+D^-	seen		1179
$D^*\bar{D}^+$ c.c.	seen		1063
$D^*(2007)^0\bar{D}^0$ + c.c.	seen		1067
$D^*(2010)^+D^-$ + c.c.	seen		1059
$D^*\bar{D}^*$	seen		919
$D^*(2007)^0\bar{D}^*(2007)^0$ + c.c.	seen		927
$D^*(2010)^+D^*(2010)^-$ + c.c.	seen		919
$D^0D^-\pi^+$ (excl. $D^*(2007)^0\bar{D}^0$)	< 2.3 %	90%	-
+c.c., $D^*(2010)^+D^-$ + c.c.			
$D\bar{D}_2^*(2460) \rightarrow D^0D^-\pi^+$ + c.c.	(10 \pm 4) %		-
$D^0\bar{D}^*\pi^+$ + c.c.	< 11 %	90%	926
$D_1(2420)\bar{D}$ + c.c.	possibly seen		538
$D_s^+D_s^-$	not seen		1006
$\omega\chi_{c2}$	possibly seen		330
$D_s^{*+}D_s^-$ + c.c.	seen		-
$D_s^+D_s^{*-}$	not seen		652
$\psi_2(3823)\pi^+\pi^-$	possibly seen		494
$\psi(3770)\pi^+\pi^-$	possibly seen		541
$J/\psi\eta$	< 6 $\times 10^{-3}$	90%	1022
$\chi_{c1}\gamma$	< 8 $\times 10^{-4}$	90%	817
$\chi_{c2}\gamma$	< 4 $\times 10^{-3}$	90%	780
e^+e^-	(9.4 \pm 3.2) $\times 10^{-6}$		2210

 $Z_c(4430)$

$$J^G(J^{PC}) = 1^+(1^{+-})$$

G, C need confirmation.

was $X(4430)^\pm$

Quantum numbers not established.

Mass $m = 4478^{+15}_{-18}$ MeV
 Full width $\Gamma = 181 \pm 31$ MeV

$Z_c(4430)$ DECAY MODES	Fraction (Γ_i/Γ)	ρ (MeV/c)
$\pi^+\psi(2S)$	seen	711
π^+J/ψ	seen	1162

 $\psi(4660)$

$$J^G(J^{PC}) = 0^-(1^{--})$$

also known as $Y(4660)$; was $X(4660)$

$\psi(4660)$ MASS = 4633 ± 7 MeV ($S = 1.4$)
 $\psi(4660)$ WIDTH = 64 ± 9 MeV

$\psi(4660)$ DECAY MODES	Fraction (Γ_i/Γ)	ρ (MeV/c)
e^+e^-	not seen	2316
$\psi(2S)\pi^+\pi^-$	seen	812
$J/\psi\eta$	not seen	1194
$D^0D^*\pi^+$	not seen	1156
$\chi_{c1}\gamma$	not seen	986
$\chi_{c2}\gamma$	not seen	952
$A_c^+A_c^-$	seen	371
$D_s^+D_{s1}(2536)^-$	seen	539

$b\bar{b}$ MESONS

(including possibly non- $q\bar{q}$ states)

 $\eta_b(1S)$

$$J^G(J^{PC}) = 0^+(0^{-+})$$

Mass $m = 9398.7 \pm 2.0$ MeV ($S = 1.5$)
 Full width $\Gamma = 10^{+5}_{-4}$ MeV

 $\eta_b(1S)$ DECAY MODES

	Fraction (Γ_i/Γ)	Confidence level	ρ (MeV/c)
hadrons	seen		-
$3h^+3h^-$	not seen		4672
$2h^+2h^-$	not seen		4689
$4h^+4h^-$	not seen		4648
$\gamma\gamma$	not seen		4699
$\mu^+\mu^-$	< 9×10^{-3}	90%	4698
$\tau^+\tau^-$	< 8 %	90%	4350

 $T(1S)$

$$J^G(J^{PC}) = 0^-(1^{--})$$

Mass $m = 9460.30 \pm 0.26$ MeV ($S = 3.3$)
 Full width $\Gamma = 54.02 \pm 1.25$ keV
 $\Gamma_{ee} = 1.340 \pm 0.018$ keV

 $T(1S)$ DECAY MODES

	Fraction (Γ_i/Γ)	Scale factor/ Confidence level	ρ (MeV/c)
$\tau^+\tau^-$	(2.60 \pm 0.10) %		4384
e^+e^-	(2.38 \pm 0.11) %		4730
$\mu^+\mu^-$	(2.48 \pm 0.05) %		4729

Hadronic decays

$g\bar{g}g$	(81.7 \pm 0.7) %		-
$\gamma\bar{g}g$	(2.2 \pm 0.6) %		-
$\eta'(958)$ anything	(2.94 \pm 0.24) %		-
$J/\psi(1S)$ anything	(5.4 \pm 0.4) $\times 10^{-4}$	$S=1.4$	4223
$J/\psi(1S)\eta_c$	< 2.2 $\times 10^{-6}$	CL=90%	3623
$J/\psi(1S)\chi_{c0}$	< 3.4 $\times 10^{-6}$	CL=90%	3429
$J/\psi(1S)\chi_{c1}$	(3.9 \pm 1.2) $\times 10^{-6}$		3382
$J/\psi(1S)\chi_{c2}$	< 1.4 $\times 10^{-6}$	CL=90%	3359
$J/\psi(1S)\eta_c(2S)$	< 2.2 $\times 10^{-6}$	CL=90%	3317
$J/\psi(1S)X(3940)$	< 5.4 $\times 10^{-6}$	CL=90%	3148
$J/\psi(1S)X(4160)$	< 5.4 $\times 10^{-6}$	CL=90%	3018
$X(4350)$ anything, $X \rightarrow J/\psi(1S)\phi$	< 8.1 $\times 10^{-6}$	CL=90%	-
$Z_c(3900)^\pm$ anything, $Z_c \rightarrow J/\psi(1S)\pi^\pm$	< 1.3 $\times 10^{-5}$	CL=90%	-
$Z_c(4200)^\pm$ anything, $Z_c \rightarrow J/\psi(1S)\pi^\pm$	< 6.0 $\times 10^{-5}$	CL=90%	-
$Z_c(4430)^\pm$ anything, $Z_c \rightarrow J/\psi(1S)\pi^\pm$	< 4.9 $\times 10^{-5}$	CL=90%	-
X_{cs}^\pm anything, $X \rightarrow J/\psi K^\pm$	< 5.7 $\times 10^{-6}$	CL=90%	-
$\chi_{c1}(3872)$ anything, $\chi_{c1} \rightarrow J/\psi(1S)\pi^+\pi^-$	< 9.5 $\times 10^{-6}$	CL=90%	-
$\psi(4260)$ anything, $\psi \rightarrow J/\psi(1S)\pi^+\pi^-$	< 3.8 $\times 10^{-5}$	CL=90%	-
$\psi(4260)$ anything, $\psi \rightarrow J/\psi(1S)K^+K^-$	< 7.5 $\times 10^{-6}$	CL=90%	-
$\chi_{c1}(4140)$ anything, $\chi_{c1} \rightarrow J/\psi(1S)\phi$	< 5.2 $\times 10^{-6}$	CL=90%	-
χ_{c0} anything	< 4 $\times 10^{-3}$	CL=90%	-
χ_{c1} anything	(1.90 \pm 0.35) $\times 10^{-4}$		-
$\chi_{c1}(1P)X_{tetra}$	< 3.78 $\times 10^{-5}$	CL=90%	-
χ_{c2} anything	(2.8 \pm 0.8) $\times 10^{-4}$		-
$\psi(2S)$ anything	(1.23 \pm 0.20) $\times 10^{-4}$		-
$\psi(2S)\eta_c$	< 3.6 $\times 10^{-6}$	CL=90%	3345
$\psi(2S)\chi_{c0}$	< 6.5 $\times 10^{-6}$	CL=90%	3124
$\psi(2S)\chi_{c1}$	< 4.5 $\times 10^{-6}$	CL=90%	3070
$\psi(2S)\chi_{c2}$	< 2.1 $\times 10^{-6}$	CL=90%	3043
$\psi(2S)\eta_c(2S)$	< 3.2 $\times 10^{-6}$	CL=90%	2994
$\psi(2S)X(3940)$	< 2.9 $\times 10^{-6}$	CL=90%	2797
$\psi(2S)X(4160)$	< 2.9 $\times 10^{-6}$	CL=90%	2642
$\psi(4260)$ anything, $\psi \rightarrow \psi(2S)\pi^+\pi^-$	< 7.9 $\times 10^{-5}$	CL=90%	-
$\psi(4360)$ anything, $\psi \rightarrow \psi(2S)\pi^+\pi^-$	< 5.2 $\times 10^{-5}$	CL=90%	-
$\psi(4660)$ anything, $\psi \rightarrow \psi(2S)\pi^+\pi^-$	< 2.2 $\times 10^{-5}$	CL=90%	-
$X(4050)^\pm$ anything, $X \rightarrow \psi(2S)\pi^\pm$	< 8.8 $\times 10^{-5}$	CL=90%	-
$Z_c(4430)^\pm$ anything, $Z_c \rightarrow \psi(2S)\pi^\pm$	< 6.7 $\times 10^{-5}$	CL=90%	-
$Z_c(4200)^+Z_c(4200)^-$	< 2.23 $\times 10^{-5}$	CL=90%	-
$Z_c(3900)^\pm Z_c(4200)^\mp$	< 8.1 $\times 10^{-6}$	CL=90%	-
$Z_c(3900)^+Z_c(3900)^-$	< 1.8 $\times 10^{-6}$	CL=90%	-

Meson Summary Table

$X(4050)^+ X(4050)^-$	< 1.58	$\times 10^{-5}$	CL=90%	-
$X(4250)^+ X(4250)^-$	< 2.66	$\times 10^{-5}$	CL=90%	-
$X(4050)^\pm X(4250)^\mp$	< 4.42	$\times 10^{-5}$	CL=90%	-
$Z_c(4430)^+ Z_c(4430)^-$	< 2.03	$\times 10^{-5}$	CL=90%	-
$X(4055)^\pm X(4055)^\mp$	< 2.33	$\times 10^{-5}$	CL=90%	-
$X(4055)^\pm Z_c(4430)^\mp$	< 4.55	$\times 10^{-5}$	CL=90%	-
$\rho\pi$	< 3.68	$\times 10^{-6}$	CL=90%	4697
$\omega\pi^0$	< 3.90	$\times 10^{-6}$	CL=90%	4697
$\pi^+\pi^-$	< 5	$\times 10^{-4}$	CL=90%	4728
K^+K^-	< 5	$\times 10^{-4}$	CL=90%	4704
$p\bar{p}$	< 5	$\times 10^{-4}$	CL=90%	4636
$\pi^+\pi^-\pi^0$	(2.1 \pm 0.8)	$\times 10^{-6}$		4725
ϕK^+K^-	(2.4 \pm 0.5)	$\times 10^{-6}$		4622
$\omega\pi^+\pi^-$	(4.5 \pm 1.0)	$\times 10^{-6}$		4694
$K^*(892)^0 K^-\pi^+$ + c.c.	(4.4 \pm 0.8)	$\times 10^{-6}$		4667
$\phi f_2'(1525)$	< 1.63	$\times 10^{-6}$	CL=90%	4551
$\omega f_2(1270)$	< 1.79	$\times 10^{-6}$	CL=90%	4611
$\rho(770)a_2(1320)$	< 2.24	$\times 10^{-6}$	CL=90%	4605
$K^*(892)^0 K_2^*(1430)^0$ + c.c.	(3.0 \pm 0.8)	$\times 10^{-6}$		4578
$K_1(1270)^\pm K^\mp$	< 2.41	$\times 10^{-6}$	CL=90%	4634
$K_1(1400)^\pm K^\mp$	(1.0 \pm 0.4)	$\times 10^{-6}$		4613
$b_1(1235)^\pm \pi^\mp$	< 1.25	$\times 10^{-6}$	CL=90%	4649
$\pi^+\pi^-\pi^0\pi^0$	(1.28 \pm 0.30)	$\times 10^{-5}$		4720
$K_S^0 K^+\pi^-$ + c.c.	(1.6 \pm 0.4)	$\times 10^{-6}$		4696
$K^*(892)^0 \bar{K}^0$ + c.c.	(2.9 \pm 0.9)	$\times 10^{-6}$		4675
$K^*(892)^- K^+$ + c.c.	< 1.11	$\times 10^{-6}$	CL=90%	4675
$f_1(1285)$ anything	(4.6 \pm 3.1)	$\times 10^{-3}$		-
$D^*(2010)^\pm$ anything	(2.52 \pm 0.20)	%		-
$f_1(1285)X_{tetra}$	< 6.24	$\times 10^{-5}$	CL=90%	-
2H anything	(2.85 \pm 0.25)	$\times 10^{-5}$		-
Sum of 100 exclusive modes	(1.200 \pm 0.017)	%		-
Radiative decays				
$\gamma\pi^+\pi^-$	(6.3 \pm 1.8)	$\times 10^{-5}$		4728
$\gamma\pi^0\pi^0$	(1.7 \pm 0.7)	$\times 10^{-5}$		4728
$\gamma\pi\pi$ (S-wave)	(4.6 \pm 0.7)	$\times 10^{-5}$		4728
$\gamma\pi^0\eta$	< 2.4	$\times 10^{-6}$	CL=90%	4713
γK^+K^-	[ssaa] (1.14 \pm 0.13)	$\times 10^{-5}$		4704
$\gamma p\bar{p}$	[ttaa] < 6	$\times 10^{-6}$	CL=90%	4636
$\gamma 2h^+ 2h^-$	(7.0 \pm 1.5)	$\times 10^{-4}$		4720
$\gamma 3h^+ 3h^-$	(5.4 \pm 2.0)	$\times 10^{-4}$		4703
$\gamma 4h^+ 4h^-$	(7.4 \pm 3.5)	$\times 10^{-4}$		4679
$\gamma\pi^+\pi^- K^+K^-$	(2.9 \pm 0.9)	$\times 10^{-4}$		4686
$\gamma 2\pi^+ 2\pi^-$	(2.5 \pm 0.9)	$\times 10^{-4}$		4720
$\gamma 3\pi^+ 3\pi^-$	(2.5 \pm 1.2)	$\times 10^{-4}$		4703
$\gamma 2\pi^+ 2\pi^- K^+K^-$	(2.4 \pm 1.2)	$\times 10^{-4}$		4658
$\gamma\pi^+\pi^- p\bar{p}$	(1.5 \pm 0.6)	$\times 10^{-4}$		4604
$\gamma 2\pi^+ 2\pi^- p\bar{p}$	(4 \pm 6)	$\times 10^{-5}$		4563
$\gamma 2K^+ 2K^-$	(2.0 \pm 2.0)	$\times 10^{-5}$		4601
$\gamma\eta'(958)$	< 1.9	$\times 10^{-6}$	CL=90%	4682
$\gamma\eta$	< 1.0	$\times 10^{-6}$	CL=90%	4714
$\gamma f_0(980)$	< 3	$\times 10^{-5}$	CL=90%	4678
$\gamma f_2'(1525)$	(2.9 \pm 0.6)	$\times 10^{-5}$		4608
$\gamma f_2(1270)$	(1.01 \pm 0.06)	$\times 10^{-4}$		4644
$\gamma\eta(1405)$	< 8.2	$\times 10^{-5}$	CL=90%	4625
$\gamma f_0(1500)$	< 1.5	$\times 10^{-5}$	CL=90%	4610
$\gamma f_0(1500) \rightarrow \gamma K^+ K^-$	(1.0 \pm 0.4)	$\times 10^{-5}$		-
$\gamma f_0(1710)$	< 2.6	$\times 10^{-4}$	CL=90%	4577
$\gamma f_0(1710) \rightarrow \gamma K^+ K^-$	(1.01 \pm 0.32)	$\times 10^{-5}$		-
$\gamma f_0(1710) \rightarrow \gamma\pi^+\pi^-$	(5.3 \pm 2.0)	$\times 10^{-6}$		-
$\gamma f_0(1710) \rightarrow \gamma\pi^0\pi^0$	< 1.4	$\times 10^{-6}$	CL=90%	-
$\gamma f_0(1710) \rightarrow \gamma\eta\eta$	< 1.8	$\times 10^{-6}$	CL=90%	-
$\gamma f_4(2050)$	< 5.3	$\times 10^{-5}$	CL=90%	4515
$\gamma f_0(2200) \rightarrow \gamma K^+ K^-$	< 2	$\times 10^{-4}$	CL=90%	4475
$\gamma f_J(2220) \rightarrow \gamma K^+ K^-$	< 8	$\times 10^{-7}$	CL=90%	4469
$\gamma f_J(2220) \rightarrow \gamma\pi^+\pi^-$	< 6	$\times 10^{-7}$	CL=90%	-
$\gamma f_J(2220) \rightarrow \gamma p\bar{p}$	< 1.1	$\times 10^{-6}$	CL=90%	-
$\gamma\eta(2225) \rightarrow \gamma\phi\phi$	< 3	$\times 10^{-3}$	CL=90%	4469
$\gamma\eta_c(1S)$	< 5.7	$\times 10^{-5}$	CL=90%	4260
$\gamma\chi_{c0}$	< 6.5	$\times 10^{-4}$	CL=90%	4114
$\gamma\chi_{c1}$	< 2.3	$\times 10^{-5}$	CL=90%	4079
$\gamma\chi_{c2}$	< 7.6	$\times 10^{-6}$	CL=90%	4062
$\gamma\chi_{c1}(3872) \rightarrow \pi^+\pi^- J/\psi$	< 1.6	$\times 10^{-6}$	CL=90%	-
$\gamma\chi_{c1}(3872) \rightarrow \pi^+\pi^-\pi^0 J/\psi$	< 2.8	$\times 10^{-6}$	CL=90%	-
$\gamma X(3915) \rightarrow \omega J/\psi$	< 3.0	$\times 10^{-6}$	CL=90%	-
$\gamma\chi_{c1}(4140) \rightarrow \phi J/\psi$	< 2.2	$\times 10^{-6}$	CL=90%	-
γX	[uuaa] < 4.5	$\times 10^{-6}$	CL=90%	-

$\gamma X\bar{X} (m_X < 3.1 \text{ GeV})$	[waa] < 1	$\times 10^{-3}$	CL=90%	-
$\gamma X\bar{X} (m_X < 4.5 \text{ GeV})$	[xxaa] < 2.4	$\times 10^{-4}$	CL=90%	-
$\gamma X \rightarrow \gamma + \geq 4 \text{ prongs}$	[yyaa] < 1.78	$\times 10^{-4}$	CL=95%	-
$\gamma a_1^0 \rightarrow \gamma\mu^+\mu^-$	[zzaa] < 9	$\times 10^{-6}$	CL=90%	-
$\gamma a_1^0 \rightarrow \gamma\tau^+\tau^-$	[ssaa] < 1.30	$\times 10^{-4}$	CL=90%	-
$\gamma a_1^0 \rightarrow \gamma gg$	[aabb] < 1	%	CL=90%	-
$\gamma a_1^0 \rightarrow \gamma s\bar{s}$	[aabb] < 1	$\times 10^{-3}$	CL=90%	-
Lepton Family number (LF) violating modes				
$\mu^\pm\tau^\mp$	LF < 6.0	$\times 10^{-6}$	CL=95%	4563
Other decays				
invisible	< 3.0	$\times 10^{-4}$	CL=90%	-

 $\chi_{b0}(1P)$ [bbbb] $J^{PC} = 0^+(0^+ +)$
J needs confirmation.Mass $m = 9859.44 \pm 0.42 \pm 0.31 \text{ MeV}$

$\chi_{b0}(1P)$ DECAY MODES	Fraction (Γ_i/Γ)	Confidence level	P (MeV/c)
$\gamma T(1S)$	(1.94 \pm 0.27) %		391
$D^0 X$	< 10.4	%	-
$\pi^+\pi^- K^+ K^-\pi^0$	< 1.6	$\times 10^{-4}$	90% 4875
$2\pi^+\pi^- K^- K_S^0$	< 5	$\times 10^{-5}$	90% 4875
$2\pi^+\pi^- K^- K_S^0 2\pi^0$	< 5	$\times 10^{-4}$	90% 4846
$2\pi^+ 2\pi^- 2\pi^0$	< 2.1	$\times 10^{-4}$	90% 4905
$2\pi^+ 2\pi^- K^+ K^-$	(1.1 \pm 0.6)	$\times 10^{-4}$	4861
$2\pi^+ 2\pi^- K^+ K^-\pi^0$	< 2.7	$\times 10^{-4}$	90% 4846
$2\pi^+ 2\pi^- K^+ K^- 2\pi^0$	< 5	$\times 10^{-4}$	90% 4828
$3\pi^+ 2\pi^- K^- K_S^0 \pi^0$	< 1.6	$\times 10^{-4}$	90% 4827
$3\pi^+ 3\pi^-$	< 8	$\times 10^{-5}$	90% 4904
$3\pi^+ 3\pi^- 2\pi^0$	< 6	$\times 10^{-4}$	90% 4881
$3\pi^+ 3\pi^- K^+ K^-$	(2.4 \pm 1.2)	$\times 10^{-4}$	4827
$3\pi^+ 3\pi^- K^+ K^-\pi^0$	< 1.0	$\times 10^{-3}$	90% 4808
$4\pi^+ 4\pi^-$	< 8	$\times 10^{-5}$	90% 4880
$4\pi^+ 4\pi^- 2\pi^0$	< 2.1	$\times 10^{-3}$	90% 4850
$J/\psi J/\psi$	< 7	$\times 10^{-5}$	90% 3836
$J/\psi\psi(2S)$	< 1.2	$\times 10^{-4}$	90% 3571
$\psi(2S)\psi(2S)$	< 3.1	$\times 10^{-5}$	90% 3273
$J/\psi(1S)$ anything	< 2.3	$\times 10^{-3}$	90% -

 $\chi_{b1}(1P)$ [bbbb] $J^{PC} = 0^+(1^+ +)$
J needs confirmation.Mass $m = 9892.78 \pm 0.26 \pm 0.31 \text{ MeV}$

$\chi_{b1}(1P)$ DECAY MODES	Fraction (Γ_i/Γ)	Confidence level	P (MeV/c)
$\gamma T(1S)$	(35.2 \pm 2.0) %		423
$D^0 X$	(12.6 \pm 2.2) %		-
$\pi^+\pi^- K^+ K^-\pi^0$	(2.0 \pm 0.6)	$\times 10^{-4}$	4892
$2\pi^+\pi^- K^- K_S^0$	(1.3 \pm 0.5)	$\times 10^{-4}$	4892
$2\pi^+\pi^- K^- K_S^0 2\pi^0$	< 6	$\times 10^{-4}$	90% 4863
$2\pi^+ 2\pi^- 2\pi^0$	(8.0 \pm 2.5)	$\times 10^{-4}$	4921
$2\pi^+ 2\pi^- K^+ K^-$	(1.5 \pm 0.5)	$\times 10^{-4}$	4878
$2\pi^+ 2\pi^- K^+ K^-\pi^0$	(3.5 \pm 1.2)	$\times 10^{-4}$	4863
$2\pi^+ 2\pi^- K^+ K^- 2\pi^0$	(8.6 \pm 3.2)	$\times 10^{-4}$	4845
$3\pi^+ 2\pi^- K^- K_S^0 \pi^0$	(9.3 \pm 3.3)	$\times 10^{-4}$	4844
$3\pi^+ 3\pi^-$	(1.9 \pm 0.6)	$\times 10^{-4}$	4921
$3\pi^+ 3\pi^- 2\pi^0$	(1.7 \pm 0.5)	$\times 10^{-3}$	4898
$3\pi^+ 3\pi^- K^+ K^-$	(2.6 \pm 0.8)	$\times 10^{-4}$	4844
$3\pi^+ 3\pi^- K^+ K^-\pi^0$	(7.5 \pm 2.6)	$\times 10^{-4}$	4825
$4\pi^+ 4\pi^-$	(2.6 \pm 0.9)	$\times 10^{-4}$	4897
$4\pi^+ 4\pi^- 2\pi^0$	(1.4 \pm 0.6)	$\times 10^{-3}$	4867
ω anything	(4.9 \pm 1.4)	%	-
ωX_{tetra}	< 4.44	$\times 10^{-4}$	90% -
$J/\psi J/\psi$	< 2.7	$\times 10^{-5}$	90% 3857
$J/\psi\psi(2S)$	< 1.7	$\times 10^{-5}$	90% 3594
$\psi(2S)\psi(2S)$	< 6	$\times 10^{-5}$	90% 3298
$J/\psi(1S)$ anything	< 1.1	$\times 10^{-3}$	90% -
$J/\psi(1S) X_{tetra}$	< 2.27	$\times 10^{-4}$	90% -

 $h_b(1P)$ $J^{PC} = 0^-(1^+ -)$ Mass $m = 9899.3 \pm 0.8 \text{ MeV}$

Meson Summary Table

$h_b(1P)$ DECAY MODES	Fraction (Γ_i/Γ)	ρ (MeV/c)
$\eta_b(1S)\gamma$	$(52^{+6}_{-5})\%$	488

$\chi_{b2}(1P)$ ^[bbbb]

$$I^G(J^{PC}) = 0^+(2^+ +)$$

J needs confirmation.

Mass $m = 9912.21 \pm 0.26 \pm 0.31$ MeV

$\chi_{b2}(1P)$ DECAY MODES	Fraction (Γ_i/Γ)	Confidence level	ρ (MeV/c)
$\gamma T(1S)$	$(18.0 \pm 1.0)\%$		442
$D^0 X$	$< 7.9\%$	90%	-
$\pi^+ \pi^- K^+ K^- \pi^0$	$(8 \pm 5) \times 10^{-5}$		4902
$2\pi^+ \pi^- K^+ K^- K_S^0$	$< 1.0 \times 10^{-4}$	90%	4901
$2\pi^+ \pi^- K^+ K^- K_S^0 2\pi^0$	$(5.3 \pm 2.4) \times 10^{-4}$		4873
$2\pi^+ 2\pi^- 2\pi^0$	$(3.5 \pm 1.4) \times 10^{-4}$		4931
$2\pi^+ 2\pi^- K^+ K^-$	$(1.1 \pm 0.4) \times 10^{-4}$		4888
$2\pi^+ 2\pi^- K^+ K^- \pi^0$	$(2.1 \pm 0.9) \times 10^{-4}$		4872
$2\pi^+ 2\pi^- K^+ K^- 2\pi^0$	$(3.9 \pm 1.8) \times 10^{-4}$		4855
$3\pi^+ 2\pi^- K^- K_S^0 \pi^0$	$< 5 \times 10^{-4}$	90%	4854
$3\pi^+ 3\pi^-$	$(7.0 \pm 3.1) \times 10^{-5}$		4931
$3\pi^+ 3\pi^- 2\pi^0$	$(1.0 \pm 0.4) \times 10^{-3}$		4908
$3\pi^+ 3\pi^- K^+ K^-$	$< 8 \times 10^{-5}$	90%	4854
$3\pi^+ 3\pi^- K^+ K^- \pi^0$	$(3.6 \pm 1.5) \times 10^{-4}$		4835
$4\pi^+ 4\pi^-$	$(8 \pm 4) \times 10^{-5}$		4907
$4\pi^+ 4\pi^- 2\pi^0$	$(1.8 \pm 0.7) \times 10^{-3}$		4877
$J/\psi J/\psi$	$< 4 \times 10^{-5}$	90%	3869
$J/\psi \psi(2S)$	$< 5 \times 10^{-5}$	90%	3608
$\psi(2S)\psi(2S)$	$< 1.6 \times 10^{-5}$	90%	3313
$J/\psi(1S)$ anything	$(1.5 \pm 0.4) \times 10^{-3}$		-

$T(2S)$

$$I^G(J^{PC}) = 0^-(1^- -)$$

Mass $m = 10023.26 \pm 0.31$ MeV
 $m_{T(3S)} - m_{T(2S)} = 331.50 \pm 0.13$ MeV
 Full width $\Gamma = 31.98 \pm 2.63$ keV
 $\Gamma_{ee} = 0.612 \pm 0.011$ keV

$T(2S)$ DECAY MODES	Fraction (Γ_i/Γ)	Scale factor/ Confidence level	ρ (MeV/c)
$T(1S)\pi^+\pi^-$	$(17.85 \pm 0.26)\%$		475
$T(1S)\pi^0\pi^0$	$(8.6 \pm 0.4)\%$		480
$\tau^+\tau^-$	$(2.00 \pm 0.21)\%$		4686
$\mu^+\mu^-$	$(1.93 \pm 0.17)\%$	S=2.2	5011
e^+e^-	$(1.91 \pm 0.16)\%$		5012
$T(1S)\pi^0$	$< 4 \times 10^{-5}$	CL=90%	531
$T(1S)\eta$	$(2.9 \pm 0.4) \times 10^{-4}$	S=2.0	126
$J/\psi(1S)$ anything	$< 6 \times 10^{-3}$	CL=90%	4533
$J/\psi(1S)\eta_c$	$< 5.4 \times 10^{-6}$	CL=90%	3984
$J/\psi(1S)\chi_{c0}$	$< 3.4 \times 10^{-6}$	CL=90%	3808
$J/\psi(1S)\chi_{c1}$	$< 1.2 \times 10^{-6}$	CL=90%	3765
$J/\psi(1S)\chi_{c2}$	$< 2.0 \times 10^{-6}$	CL=90%	3744
$J/\psi(1S)\eta_c(2S)$	$< 2.5 \times 10^{-6}$	CL=90%	3707
$J/\psi(1S)X(3940)$	$< 2.0 \times 10^{-6}$	CL=90%	3555
$J/\psi(1S)X(4160)$	$< 2.0 \times 10^{-6}$	CL=90%	3440
χ_{c1} anything	$(2.2 \pm 0.5) \times 10^{-4}$		-
$\chi_{c1}(1P)^0 X_{tetra}$	$< 3.67 \times 10^{-5}$	CL=90%	-
χ_{c2} anything	$(2.3 \pm 0.8) \times 10^{-4}$		-
$\psi(2S)\eta_c$	$< 5.1 \times 10^{-6}$	CL=90%	3732
$\psi(2S)\chi_{c0}$	$< 4.7 \times 10^{-6}$	CL=90%	3536
$\psi(2S)\chi_{c1}$	$< 2.5 \times 10^{-6}$	CL=90%	3488
$\psi(2S)\chi_{c2}$	$< 1.9 \times 10^{-6}$	CL=90%	3464
$\psi(2S)\eta_c(2S)$	$< 3.3 \times 10^{-6}$	CL=90%	3422
$\psi(2S)X(3940)$	$< 3.9 \times 10^{-6}$	CL=90%	3250
$\psi(2S)X(4160)$	$< 3.9 \times 10^{-6}$	CL=90%	3118
$Z_c(3900)^+ Z_c(3900)^-$	$< 1.0 \times 10^{-6}$	CL=90%	-
$Z_c(4200)^+ Z_c(4200)^-$	$< 1.67 \times 10^{-5}$	CL=90%	-
$Z_c(3900)^\pm Z_c(4200)^\mp$	$< 7.3 \times 10^{-6}$	CL=90%	-
$X(4050)^+ X(4050)^-$	$< 1.35 \times 10^{-5}$	CL=90%	-
$X(4250)^+ X(4250)^-$	$< 2.67 \times 10^{-5}$	CL=90%	-
$X(4050)^\pm X(4250)^\mp$	$< 2.72 \times 10^{-5}$	CL=90%	-
$Z_c(4430)^+ Z_c(4430)^-$	$< 2.03 \times 10^{-5}$	CL=90%	-
$X(4055)^\pm X(4055)^\mp$	$< 1.11 \times 10^{-5}$	CL=90%	-
$X(4055)^\pm Z_c(4430)^\mp$	$< 2.11 \times 10^{-5}$	CL=90%	-
2H anything	$(2.78^{+0.30}_{-0.26}) \times 10^{-5}$	S=1.2	-

hadrons	$(94 \pm 11)\%$	-
ggg	$(58.8 \pm 1.2)\%$	-
γgg	$(1.87 \pm 0.28)\%$	-
$\phi K^+ K^-$	$(1.6 \pm 0.4) \times 10^{-6}$	4910
$\omega \pi^+ \pi^-$	$< 2.58 \times 10^{-6}$	CL=90% 4977
$K^*(892)^0 K^- \pi^+ + c.c.$	$(2.3 \pm 0.7) \times 10^{-6}$	4952
$\phi f_2'(1525)$	$< 1.33 \times 10^{-6}$	CL=90% 4842
$\omega f_2'(1270)$	$< 5.7 \times 10^{-7}$	CL=90% 4899
$\rho(770) a_2(1320)$	$< 8.8 \times 10^{-7}$	CL=90% 4894
$K^*(892)^0 \bar{K}_2^*(1430)^0 + c.c.$	$(1.5 \pm 0.6) \times 10^{-6}$	4869
$K_1(1270)^\pm K^\mp$	$< 3.22 \times 10^{-6}$	CL=90% 4921
$K_1(1400)^\pm K^\mp$	$< 8.3 \times 10^{-7}$	CL=90% 4901
$b_1(1235)^\pm \pi^\mp$	$< 4.0 \times 10^{-7}$	CL=90% 4935
$\rho \pi$	$< 1.16 \times 10^{-6}$	CL=90% 4981
$\pi^+ \pi^- \pi^0$	$< 8.0 \times 10^{-7}$	CL=90% 5007
$\omega \pi^0$	$< 1.63 \times 10^{-6}$	CL=90% 4980
$\pi^+ \pi^- \pi^0 \pi^0$	$(1.30 \pm 0.28) \times 10^{-5}$	5002
$K_S^0 K^+ \pi^- + c.c.$	$(1.14 \pm 0.33) \times 10^{-6}$	4979
$K^*(892)^0 \bar{K}^0 + c.c.$	$< 4.22 \times 10^{-6}$	CL=90% 4959
$K^*(892)^- K^+ + c.c.$	$< 1.45 \times 10^{-6}$	CL=90% 4960
$f_1(1285)$ anything	$(2.2 \pm 1.6) \times 10^{-3}$	-
$f_1(1285) X_{tetra}$	$< 6.47 \times 10^{-5}$	CL=90% -
Sum of 100 exclusive modes	$(2.90 \pm 0.30) \times 10^{-3}$	-

Radiative decays

$\gamma \chi_{b1}(1P)$	$(6.9 \pm 0.4)\%$	130
$\gamma \chi_{b2}(1P)$	$(7.15 \pm 0.35)\%$	110
$\gamma \chi_{b0}(1P)$	$(3.8 \pm 0.4)\%$	162
$\gamma f_0(1710)$	$< 5.9 \times 10^{-4}$	CL=90% 4867
$\gamma f_2'(1525)$	$< 5.3 \times 10^{-4}$	CL=90% 4897
$\gamma f_2'(1270)$	$< 2.41 \times 10^{-4}$	CL=90% 4930
$\gamma \eta_c(1S)$	$< 2.7 \times 10^{-5}$	CL=90% 4567
$\gamma \chi_{c0}$	$< 1.0 \times 10^{-4}$	CL=90% 4430
$\gamma \chi_{c1}$	$< 3.6 \times 10^{-6}$	CL=90% 4397
$\gamma \chi_{c2}$	$< 1.5 \times 10^{-5}$	CL=90% 4381
$\gamma \chi_{c1}(3872) \rightarrow \pi^+ \pi^- J/\psi$	$< 8 \times 10^{-7}$	CL=90% -
$\gamma \chi_{c1}(3872) \rightarrow \pi^+ \pi^- \pi^0 J/\psi$	$< 2.4 \times 10^{-6}$	CL=90% -
$\gamma X(3915) \rightarrow \omega J/\psi$	$< 2.8 \times 10^{-6}$	CL=90% -
$\gamma \chi_{c1}(4140) \rightarrow \phi J/\psi$	$< 1.2 \times 10^{-6}$	CL=90% -
$\gamma X(4350) \rightarrow \phi J/\psi$	$< 1.3 \times 10^{-6}$	CL=90% -
$\gamma \eta_b(1S)$	$(5.5^{+1.1}_{-0.9}) \times 10^{-4}$	S=1.2 605
$\gamma \eta_b(1S) \rightarrow \gamma$ Sum of 26 exclusive modes	$< 3.7 \times 10^{-6}$	CL=90% -
$\gamma X_{b\bar{b}} \rightarrow \gamma$ Sum of 26 exclusive modes	$< 4.9 \times 10^{-6}$	CL=90% -
$\gamma X \rightarrow \gamma + \geq 4$ prongs	[ccbb] $< 1.95 \times 10^{-4}$	CL=95% -
$\gamma A^0 \rightarrow \gamma$ hadrons	$< 8 \times 10^{-5}$	CL=90% -
$\gamma a_1^0 \rightarrow \gamma \mu^+ \mu^-$	$< 8.3 \times 10^{-6}$	CL=90% -

Lepton Family number (LF) violating modes

$e^\pm \tau^\mp$	LF $< 3.2 \times 10^{-6}$	CL=90% 4854
$\mu^\pm \tau^\mp$	LF $< 3.3 \times 10^{-6}$	CL=90% 4854

$T_2(1D)$

$$I^G(J^{PC}) = 0^-(2^- -)$$

was $T(1D)$

Mass $m = 10163.7 \pm 1.4$ MeV ($S = 1.7$)

$T_2(1D)$ DECAY MODES	Fraction (Γ_i/Γ)	ρ (MeV/c)
$\gamma \gamma T(1S)$	seen	679
$\gamma \chi_{bJ}(1P)$	seen	300
$\eta T(1S)$	not seen	426
$\pi^+ \pi^- T(1S)$	$(6.6 \pm 1.6) \times 10^{-3}$	623

$\chi_{b0}(2P)$ ^[bbbb]

$$I^G(J^{PC}) = 0^+(0^+ +)$$

J needs confirmation.

Mass $m = 10232.5 \pm 0.4 \pm 0.5$ MeV

$\chi_{b0}(2P)$ DECAY MODES	Fraction (Γ_i/Γ)	Confidence level	ρ (MeV/c)
$\gamma T(2S)$	$(1.38 \pm 0.30)\%$		207
$\gamma T(1S)$	$(3.8 \pm 1.7) \times 10^{-3}$		743
$D^0 X$	$< 8.2\%$	90%	-
$\pi^+ \pi^- K^+ K^- \pi^0$	$< 3.4 \times 10^{-5}$	90%	5064
$2\pi^+ \pi^- K^- K_S^0$	$< 5 \times 10^{-5}$	90%	5063
$2\pi^+ \pi^- K^- K_S^0 2\pi^0$	$< 2.2 \times 10^{-4}$	90%	5036

Meson Summary Table

$2\pi^+2\pi^-2\pi^0$	< 2.4	$\times 10^{-4}$	90%	5092
$2\pi^+2\pi^-K^+K^-$	< 1.5	$\times 10^{-4}$	90%	5050
$2\pi^+2\pi^-K^+K^-2\pi^0$	< 2.2	$\times 10^{-4}$	90%	5035
$2\pi^+2\pi^-K^+K^-2\pi^0$	< 1.1	$\times 10^{-3}$	90%	5019
$3\pi^+2\pi^-K^-K_S^02\pi^0$	< 7	$\times 10^{-4}$	90%	5018
$3\pi^+3\pi^-$	< 7	$\times 10^{-5}$	90%	5091
$3\pi^+3\pi^-2\pi^0$	< 1.2	$\times 10^{-3}$	90%	5070
$3\pi^+3\pi^-K^+K^-$	< 1.5	$\times 10^{-4}$	90%	5017
$3\pi^+3\pi^-K^+K^-2\pi^0$	< 7	$\times 10^{-4}$	90%	4999
$4\pi^+4\pi^-$	< 1.7	$\times 10^{-4}$	90%	5069
$4\pi^+4\pi^-2\pi^0$	< 6	$\times 10^{-4}$	90%	5039

 $\chi_{b1}(2P)$ ^[bbbb]

$$J^G(J^{PC}) = 0^+(1^{++})$$

J needs confirmation.

$$\text{Mass } m = 10255.46 \pm 0.22 \pm 0.50 \text{ MeV}$$

$$m_{\chi_{b1}(2P)} - m_{\chi_{b0}(2P)} = 23.5 \pm 1.0 \text{ MeV}$$

$\chi_{b1}(2P)$ DECAY MODES	Fraction (Γ_i/Γ)	ρ (MeV/c)
$\omega \mathcal{T}(1S)$	(1.63 ^{+0.40} _{-0.34}) %	135
$\gamma \mathcal{T}(2S)$	(18.1 ± 1.9) %	230
$\gamma \mathcal{T}(1S)$	(9.9 ± 1.0) %	764
$\pi\pi\chi_{b1}(1P)$	(9.1 ± 1.3) $\times 10^{-3}$	238
D^0X	(8.8 ± 1.7) %	-
$\pi^+\pi^-K^+K^-2\pi^0$	(3.1 ± 1.0) $\times 10^{-4}$	5075
$2\pi^+\pi^-K^-K_S^0$	(1.1 ± 0.5) $\times 10^{-4}$	5075
$2\pi^+\pi^-K^-K_S^02\pi^0$	(7.7 ± 3.2) $\times 10^{-4}$	5047
$2\pi^+2\pi^-2\pi^0$	(5.9 ± 2.0) $\times 10^{-4}$	5104
$2\pi^+2\pi^-K^+K^-$	(1.0 ± 0.4) $\times 10^{-5}$	5062
$2\pi^+2\pi^-K^+K^-2\pi^0$	(5.5 ± 1.8) $\times 10^{-4}$	5047
$2\pi^+2\pi^-K^+K^-2\pi^0$	(1.0 ± 0.4) $\times 10^{-4}$	5030
$3\pi^+2\pi^-K^-K_S^02\pi^0$	(6.7 ± 2.6) $\times 10^{-4}$	5029
$3\pi^+3\pi^-$	(1.2 ± 0.4) $\times 10^{-4}$	5103
$3\pi^+3\pi^-2\pi^0$	(1.2 ± 0.4) $\times 10^{-3}$	5081
$3\pi^+3\pi^-K^+K^-$	(2.0 ± 0.8) $\times 10^{-4}$	5029
$3\pi^+3\pi^-K^+K^-2\pi^0$	(6.1 ± 2.2) $\times 10^{-4}$	5011
$4\pi^+4\pi^-$	(1.7 ± 0.6) $\times 10^{-4}$	5080
$4\pi^+4\pi^-2\pi^0$	(1.9 ± 0.7) $\times 10^{-3}$	5051

 $\chi_{b2}(2P)$ ^[bbbb]

$$J^G(J^{PC}) = 0^+(2^{++})$$

J needs confirmation.

$$\text{Mass } m = 10268.65 \pm 0.22 \pm 0.50 \text{ MeV}$$

$$m_{\chi_{b2}(2P)} - m_{\chi_{b1}(2P)} = 13.10 \pm 0.24 \text{ MeV}$$

$\chi_{b2}(2P)$ DECAY MODES	Fraction (Γ_i/Γ)	Confidence level	ρ (MeV/c)	
$\omega \mathcal{T}(1S)$	(1.10 ^{+0.34} _{-0.30}) %		194	
$\gamma \mathcal{T}(2S)$	(8.9 ± 1.2) %		242	
$\gamma \mathcal{T}(1S)$	(6.6 ± 0.8) %		777	
$\pi\pi\chi_{b2}(1P)$	(5.1 ± 0.9) $\times 10^{-3}$		229	
D^0X	< 2.4	90%	-	
$\pi^+\pi^-K^+K^-2\pi^0$	< 1.1	$\times 10^{-4}$	90%	5082
$2\pi^+\pi^-K^-K_S^0$	< 9	$\times 10^{-5}$	90%	5082
$2\pi^+\pi^-K^-K_S^02\pi^0$	< 7	$\times 10^{-4}$	90%	5054
$2\pi^+2\pi^-2\pi^0$	(3.9 ± 1.6) $\times 10^{-4}$		5110	
$2\pi^+2\pi^-K^+K^-$	(9 ± 4) $\times 10^{-5}$		5068	
$2\pi^+2\pi^-K^+K^-2\pi^0$	(2.4 ± 1.1) $\times 10^{-4}$		5054	
$2\pi^+2\pi^-K^+K^-2\pi^0$	(4.7 ± 2.3) $\times 10^{-4}$		5037	
$3\pi^+2\pi^-K^-K_S^02\pi^0$	< 4	$\times 10^{-4}$	90%	5036
$3\pi^+3\pi^-$	(9 ± 4) $\times 10^{-5}$		5110	
$3\pi^+3\pi^-2\pi^0$	(1.2 ± 0.4) $\times 10^{-3}$		5088	
$3\pi^+3\pi^-K^+K^-$	(1.4 ± 0.7) $\times 10^{-4}$		5036	
$3\pi^+3\pi^-K^+K^-2\pi^0$	(4.2 ± 1.7) $\times 10^{-4}$		5017	
$4\pi^+4\pi^-$	(9 ± 5) $\times 10^{-5}$		5087	
$4\pi^+4\pi^-2\pi^0$	(1.3 ± 0.5) $\times 10^{-3}$		5058	

 $\mathcal{T}(3S)$

$$J^G(J^{PC}) = 0^-(1^{--})$$

$$\text{Mass } m = 10355.2 \pm 0.5 \text{ MeV}$$

$$m_{\mathcal{T}(3S)} - m_{\mathcal{T}(2S)} = 331.50 \pm 0.13 \text{ MeV}$$

$$\text{Full width } \Gamma = 20.32 \pm 1.85 \text{ keV}$$

$$\Gamma_{ee} = 0.443 \pm 0.008 \text{ keV}$$

 $\mathcal{T}(3S)$ DECAY MODES

	Fraction (Γ_i/Γ)	Scale factor/ Confidence level	ρ (MeV/c)
$\mathcal{T}(2S)$ anything	(10.6 ± 0.8) %		296
$\mathcal{T}(2S)\pi^+\pi^-$	(2.82 ± 0.18) %	S=1.6	177
$\mathcal{T}(2S)\pi^0\pi^0$	(1.85 ± 0.14) %		190
$\mathcal{T}(2S)\gamma\gamma$	(5.0 ± 0.7) %		327
$\mathcal{T}(2S)\pi^0$	< 5.1	$\times 10^{-4}$ CL=90%	298
$\mathcal{T}(1S)\pi^+\pi^-$	(4.37 ± 0.08) %		813
$\mathcal{T}(1S)\pi^0\pi^0$	(2.20 ± 0.13) %		816
$\mathcal{T}(1S)\eta$	< 1	$\times 10^{-4}$ CL=90%	677
$\mathcal{T}(1S)\pi^0$	< 7	$\times 10^{-5}$ CL=90%	846
$h_b(1P)\pi^0$	< 1.2	$\times 10^{-3}$ CL=90%	426
$h_b(1P)\pi^0 \rightarrow \gamma\eta_b(1S)\pi^0$	(4.3 ± 1.4) $\times 10^{-4}$		-
$h_b(1P)\pi^+\pi^-$	< 1.2	$\times 10^{-4}$ CL=90%	353
$\tau^+\tau^-$	(2.29 ± 0.30) %		4863
$\mu^+\mu^-$	(2.18 ± 0.21) %	S=2.1	5177
e^+e^-	(2.18 ± 0.20) %		5178
hadrons	(93 ± 12) %		-
$g\bar{g}g$	(35.7 ± 2.6) %		-
$\gamma\bar{g}g$	(9.7 ± 1.8) $\times 10^{-3}$		-
2H anything	(2.33 ± 0.33) $\times 10^{-5}$		-

Radiative decays

$\gamma\chi_{b2}(2P)$	(13.1 ± 1.6) %	S=3.4	86
$\gamma\chi_{b1}(2P)$	(12.6 ± 1.2) %	S=2.4	99
$\gamma\chi_{b0}(2P)$	(5.9 ± 0.6) %	S=1.4	122
$\gamma\chi_{b2}(1P)$	(10.0 ± 1.0) $\times 10^{-3}$	S=1.7	434
$\gamma\chi_{b1}(1P)$	(9 ± 5) $\times 10^{-4}$	S=1.8	452
$\gamma\chi_{b0}(1P)$	(2.7 ± 0.4) $\times 10^{-3}$		484
$\gamma\eta_b(2S)$	< 6.2	$\times 10^{-4}$ CL=90%	350
$\gamma\eta_b(1S)$	(5.1 ± 0.7) $\times 10^{-4}$		912
$\gamma A^0 \rightarrow \gamma$ hadrons	< 8	$\times 10^{-5}$ CL=90%	-
$\gamma X \rightarrow \gamma + \geq 4$ prongs	[<i>d</i> dbb] < 2.2	$\times 10^{-4}$ CL=95%	-
$\gamma a_1^0 \rightarrow \gamma\mu^+\mu^-$	< 5.5	$\times 10^{-6}$ CL=90%	-
$\gamma a_1^0 \rightarrow \gamma\tau^+\tau^-$	[<i>e</i> ebb] < 1.6	$\times 10^{-4}$ CL=90%	-

Lepton Family number (LF) violating modes

$e^+\tau^\mp$	LF	< 4.2	$\times 10^{-6}$ CL=90%	5025
$\mu^+\tau^\mp$	LF	< 3.1	$\times 10^{-6}$ CL=90%	5025

 $\chi_{b1}(3P)$

$$J^G(J^{PC}) = 0^+(1^{++})$$

$$\text{Mass } m = 10513.4 \pm 0.7 \text{ MeV}$$

 $\chi_{b1}(3P)$ DECAY MODES

	Fraction (Γ_i/Γ)	ρ (MeV/c)
$\mathcal{T}(1S)\gamma$	seen	1000
$\mathcal{T}(2S)\gamma$	seen	479
$\mathcal{T}(3S)\gamma$	seen	157

 $\chi_{b2}(3P)$

$$J^G(J^{PC}) = 0^+(2^{++})$$

$$\text{Mass } m = 10524.0 \pm 0.8 \text{ MeV}$$

 $\chi_{b2}(3P)$ DECAY MODES

	Fraction (Γ_i/Γ)	ρ (MeV/c)
$\mathcal{T}(3S)\gamma$	seen	167

 $\mathcal{T}(4S)$

$$J^G(J^{PC}) = 0^-(1^{--})$$

also known as $\mathcal{T}(10580)$

$$\text{Mass } m = 10579.4 \pm 1.2 \text{ MeV}$$

$$\text{Full width } \Gamma = 20.5 \pm 2.5 \text{ MeV}$$

$$\Gamma_{ee} = 0.272 \pm 0.029 \text{ keV} \quad (S = 1.5)$$

 $\mathcal{T}(4S)$ DECAY MODES

	Fraction (Γ_i/Γ)	Confidence level	ρ (MeV/c)	
$B\bar{B}$	> 96	%	95%	326
B^+B^-	(51.4 ± 0.6) %		331	
D^+ anything + c.c.	(17.8 ± 2.6) %		-	
$B^0\bar{B}^0$	(48.6 ± 0.6) %		326	
$J/\psi K_S^0 + (J/\psi, \eta_c) K_S^0$	< 4	$\times 10^{-7}$	90%	-
non- $B\bar{B}$	< 4	%	95%	-
e^+e^-	(1.57 ± 0.08) $\times 10^{-5}$		5290	
$\rho^+\rho^-$	< 5.7	$\times 10^{-6}$	90%	5233

Meson Summary Table

$K^*(892)^0 \bar{K}^0$	< 2.0	$\times 10^{-6}$	90%	5240
$J/\psi(1S)$ anything	< 1.9	$\times 10^{-4}$	95%	–
D^{*+} anything + c.c.	< 7.4	%	90%	5099
ϕ anything	(7.1 \pm 0.6)	%		5240
$\phi\eta$	< 1.8	$\times 10^{-6}$	90%	5226
$\phi\eta'$	< 4.3	$\times 10^{-6}$	90%	5196
$\rho\eta$	< 1.3	$\times 10^{-6}$	90%	5247
$\rho\eta'$	< 2.5	$\times 10^{-6}$	90%	5217
$\Upsilon(1S)$ anything	< 4	$\times 10^{-3}$	90%	1053
$\Upsilon(1S)\pi^+\pi^-$	(8.2 \pm 0.4)	$\times 10^{-5}$		1026
$\Upsilon(1S)\eta$	(1.81 \pm 0.18)	$\times 10^{-4}$		924
$\Upsilon(1S)\eta'$	(3.4 \pm 0.9)	$\times 10^{-5}$		–
$\Upsilon(2S)\pi^+\pi^-$	(8.2 \pm 0.8)	$\times 10^{-5}$		468
$h_b(1P)\pi^+\pi^-$	not seen			600
$h_b(1P)\eta$	(2.18 \pm 0.21)	$\times 10^{-3}$		390
2H anything	< 1.3	$\times 10^{-5}$	90%	–

Double Radiative Decays

$\gamma\gamma \Upsilon(D) \rightarrow \gamma\gamma\eta \Upsilon(1S)$	< 2.3	$\times 10^{-5}$	90%	–
--	-------	------------------	-----	---

$Z_b(10610)$

$I^G(J^{PC}) = 1^+(1^+ -)$

was $X(10610)$

Mass $m = 10607.2 \pm 2.0$ MeV
Full width $\Gamma = 18.4 \pm 2.4$ MeV

$Z_b(10610)$ DECAY MODES	Fraction (Γ_i/Γ)	p (MeV/c)
$\Upsilon(1S)\pi^+$	(5.4 $^{+1.9}_{-1.5}$) $\times 10^{-3}$	1077
$\Upsilon(1S)\pi^0$	not seen	1077
$\Upsilon(2S)\pi^+$	(3.6 $^{+1.1}_{-0.8}$) %	551
$\Upsilon(2S)\pi^0$	seen	552
$\Upsilon(3S)\pi^+$	(2.1 $^{+0.8}_{-0.6}$) %	207
$\Upsilon(3S)\pi^0$	seen	210
$h_b(1P)\pi^+$	(3.5 $^{+1.2}_{-0.9}$) %	671
$h_b(2P)\pi^+$	(4.7 $^{+1.7}_{-1.3}$) %	313
$B^+ \bar{B}^0$	not seen	505
$B^+ \bar{B}^{*0} + B^{*+} \bar{B}^0$	(85.6 $^{+2.1}_{-2.9}$) %	–

$Z_b(10650)$

$I^G(J^{PC}) = 1^+(1^+ -)$
 I, G, C need confirmation.

was $X(10650)^\pm$

Mass $m = 10652.2 \pm 1.5$ MeV
Full width $\Gamma = 11.5 \pm 2.2$ MeV

$Z_b(10650)^-$ decay modes are charge conjugates of the modes below.

$Z_b(10650)^+$ DECAY MODES	Fraction (Γ_i/Γ)	p (MeV/c)
$\Upsilon(1S)\pi^+$	(1.7 $^{+0.8}_{-0.6}$) $\times 10^{-3}$	1117
$\Upsilon(2S)\pi^+$	(1.4 $^{+0.6}_{-0.4}$) %	595
$\Upsilon(3S)\pi^+$	(1.6 $^{+0.7}_{-0.5}$) %	259
$h_b(1P)\pi^+$	(8.4 $^{+2.9}_{-2.4}$) %	714
$h_b(2P)\pi^+$	(15 \pm 4) %	360
$B^+ \bar{B}^0$	not seen	703
$B^+ \bar{B}^{*0} + B^{*+} \bar{B}^0$	not seen	–
$B^{*+} \bar{B}^{*0}$	(74 $^{+4}_{-6}$) %	122

$\Upsilon(10860)$

$I^G(J^{PC}) = 0^-(1^--)$

Mass $m = 10885.2^{+2.6}_{-1.6}$ MeV
Full width $\Gamma = 37 \pm 4$ MeV
 $\Gamma_{ee} = 0.31 \pm 0.07$ keV ($S = 1.3$)

$\Upsilon(10860)$ DECAY MODES	Fraction (Γ_i/Γ)	Confidence level	p (MeV/c)
$B\bar{B}X$	(76.2 $^{+2.7}_{-4.0}$) %	–	–
$B\bar{B}$	(5.5 \pm 1.0) %	1322	–
$B\bar{B}^* + \text{c.c.}$	(13.7 \pm 1.6) %	–	–
$B^*\bar{B}^*$	(38.1 \pm 3.4) %	1127	–

$B\bar{B}^{(*)}\pi$	< 19.7	%	90%	1015
$B\bar{B}\pi$	(0.0 \pm 1.2) %			1015
$B^*\bar{B}\pi + B\bar{B}^*\pi$	(7.3 \pm 2.3) %			–
$B^*\bar{B}^*\pi$	(1.0 \pm 1.4) %			739
$B\bar{B}\pi\pi$	< 8.9	%	90%	551
$B_s^{(*)}\bar{B}_s^{(*)}$	(20.1 \pm 3.1) %			905
$B_s\bar{B}_s$	(5 \pm 5) $\times 10^{-3}$			905
$B_s\bar{B}_s^* + \text{c.c.}$	(1.35 \pm 0.32) %			–
$B_s^*\bar{B}_s^*$	(17.6 \pm 2.7) %			543
no open-bottom	(3.8 $^{+5.0}_{-0.5}$) %			–
e^+e^-	(8.3 \pm 2.1) $\times 10^{-6}$			5443
$K^*(892)^0 \bar{K}^0$	< 1.0	$\times 10^{-5}$	90%	5395
$\Upsilon(1S)\pi^+\pi^-$	(5.3 \pm 0.6) $\times 10^{-3}$			1306
$\Upsilon(2S)\pi^+\pi^-$	(7.8 \pm 1.3) $\times 10^{-3}$			783
$\Upsilon(3S)\pi^+\pi^-$	(4.8 $^{+1.9}_{-1.7}$) $\times 10^{-3}$			440
$\Upsilon(1S)K^+K^-$	(6.1 \pm 1.8) $\times 10^{-4}$			959
$\eta \Upsilon_J(1D)$	(4.8 \pm 1.1) $\times 10^{-3}$			–
$h_b(1P)\pi^+\pi^-$	(3.5 $^{+1.0}_{-1.3}$) $\times 10^{-3}$			903
$h_b(2P)\pi^+\pi^-$	(5.7 $^{+1.7}_{-2.1}$) $\times 10^{-3}$			544
$\chi_{bJ}(1P)\pi^+\pi^-\pi^0$	(2.5 \pm 2.3) $\times 10^{-3}$			894
$\chi_{b0}(1P)\pi^+\pi^-\pi^0$	< 6.3	$\times 10^{-3}$	90%	894
$\chi_{b0}(1P)\omega$	< 3.9	$\times 10^{-3}$	90%	631
$\chi_{b0}(1P)(\pi^+\pi^-\pi^0)_{\text{non-}\omega}$	< 4.8	$\times 10^{-3}$	90%	–
$\chi_{b1}(1P)\pi^+\pi^-\pi^0$	(1.85 \pm 0.33) $\times 10^{-3}$			861
$\chi_{b1}(1P)\omega$	(1.57 \pm 0.30) $\times 10^{-3}$			582
$\chi_{b1}(1P)(\pi^+\pi^-\pi^0)_{\text{non-}\omega}$	(5.2 \pm 1.9) $\times 10^{-4}$			–
$\chi_{b2}(1P)\pi^+\pi^-\pi^0$	(1.17 \pm 0.30) $\times 10^{-3}$			841
$\chi_{b2}(1P)\omega$	(6.0 \pm 2.7) $\times 10^{-4}$			552
$\chi_{b2}(1P)(\pi^+\pi^-\pi^0)_{\text{non-}\omega}$	(6 \pm 4) $\times 10^{-4}$			–
$\gamma X_b \rightarrow \gamma \Upsilon(1S)\omega$	< 3.8	$\times 10^{-5}$	90%	–

Inclusive Decays.

These decay modes are submodes of one or more of the decay modes above.

ϕ anything	(13.8 $^{+2.4}_{-1.7}$) %	–
D^0 anything + c.c.	(108 \pm 8) %	–
D_s anything + c.c.	(46 \pm 6) %	–
J/ψ anything	(2.06 \pm 0.21) %	–
B^0 anything + c.c.	(77 \pm 8) %	–
B^+ anything + c.c.	(72 \pm 6) %	–

$\Upsilon(11020)$

$I^G(J^{PC}) = 0^-(1^--)$

Mass $m = 11000 \pm 4$ MeV
Full width $\Gamma = 24^{+8}_{-6}$ MeV
 $\Gamma_{ee} = 0.130 \pm 0.030$ keV

$\Upsilon(11020)$ DECAY MODES	Fraction (Γ_i/Γ)	p (MeV/c)
e^+e^-	(5.4 $^{+1.9}_{-2.1}$) $\times 10^{-6}$	5500
$\chi_{bJ}(1P)\pi^+\pi^-\pi^0$	(9 $^{+9}_{-8}$) $\times 10^{-3}$	1007
$\chi_{b1}(1P)\pi^+\pi^-\pi^0$	seen	975
$\chi_{b2}(1P)\pi^+\pi^-\pi^0$	seen	956

NOTES

In this Summary Table:

When a quantity has “(S = ...)” to its right, the error on the quantity has been enlarged by the “scale factor” S, defined as $S = \sqrt{\chi^2/(N-1)}$, where N is the number of measurements used in calculating the quantity. We do this when $S > 1$, which often indicates that the measurements are inconsistent. When $S > 1.25$, we also show in the Particle Listings an ideogram of the measurements. For more about S, see the Introduction.

A decay momentum p is given for each decay mode. For a 2-body decay, p is the momentum of each decay product in the rest frame of the decaying particle. For a 3-or-more-body decay, p is the largest momentum any of the products can have in this frame.

- [a] See the review on “Form Factors for Radiative Pion and Kaon Decays” for definitions and details.
- [b] Measurements of $\Gamma(e^+\nu_e)/\Gamma(\mu^+\nu_\mu)$ always include decays with γ 's, and measurements of $\Gamma(e^+\nu_e\gamma)$ and $\Gamma(\mu^+\nu_\mu\gamma)$ never include low-energy γ 's. Therefore, since no clean separation is possible, we consider the modes with γ 's to be subreactions of the modes without them, and let $[\Gamma(e^+\nu_e) + \Gamma(\mu^+\nu_\mu)]/\Gamma_{\text{total}} = 100\%$.
- [c] See the π^\pm Particle Listings for the energy limits used in this measurement; low-energy γ 's are not included.
- [d] Derived from an analysis of neutrino-oscillation experiments.
- [e] Astrophysical and cosmological arguments give limits of order 10^{-13} .
- [f] Forbidden by angular momentum conservation.
- [g] C parity forbids this to occur as a single-photon process.
- [h] The $\omega\rho$ interference is then due to $\omega\rho$ mixing only, and is expected to be small. If $e\mu$ universality holds, $\Gamma(\rho^0 \rightarrow \mu^+\mu^-) = \Gamma(\rho^0 \rightarrow e^+e^-) \times 0.99785$.
- [i] See the “Note on $a_1(1260)$ ” in the $a_1(1260)$ Particle Listings in PDG 06, Journal of Physics **G33** 1 (2006).
- [j] Our estimate. See the Particle Listings for details.
- [k] See the note on “Non- $q\bar{q}$ mesons” in the Particle Listings in PDG 06, Journal of Physics **G33** 1 (2006).
- [l] See also the $\omega(1650)$.
- [n] See also the $\omega(1420)$.
- [o] See the note in the K^\pm Particle Listings.
- [p] Neglecting photon channels. See, e.g., A. Pais and S.B. Treiman, Phys. Rev. **D12**, 2744 (1975).
- [q] The definition of the slope parameters of the $K \rightarrow 3\pi$ Dalitz plot is as follows (see also “Note on Dalitz Plot Parameters for $K \rightarrow 3\pi$ Decays” in the K^\pm Particle Listings):
- $$|M|^2 = 1 + g(s_3 - s_0)/m_{\pi^+}^2 + \dots$$
- [r] For more details and definitions of parameters see the Particle Listings.
- [s] See the K^\pm Particle Listings for the energy limits used in this measurement.
- [t] Most of this radiative mode, the low-momentum γ part, is also included in the parent mode listed without γ 's.
- [u] Structure-dependent part.
- [v] Direct-emission branching fraction.
- [x] Violates angular-momentum conservation.
- [y] Derived from measured values of ϕ_{+-} , $|\eta|$, $|m_{K_L^0} - m_{K_S^0}|$, and $\tau_{K_S^0}$, as described in the introduction to “Tests of Conservation Laws.”
- [z] The CP -violation parameters are defined as follows (see also “Note on CP Violation in $K_S \rightarrow 3\pi$ ” and “Note on CP Violation in K_L^0 Decay” in the Particle Listings):
- $$\eta_{+-} = |\eta_{+-}|e^{i\phi_{+-}} = \frac{A(K_L^0 \rightarrow \pi^+\pi^-)}{A(K_S^0 \rightarrow \pi^+\pi^-)} = \epsilon + \epsilon'$$
- $$\eta_{00} = |\eta_{00}|e^{i\phi_{00}} = \frac{A(K_L^0 \rightarrow \pi^0\pi^0)}{A(K_S^0 \rightarrow \pi^0\pi^0)} = \epsilon - 2\epsilon'$$
- $$\delta = \frac{\Gamma(K_L^0 \rightarrow \pi^-\ell^+\nu) - \Gamma(K_L^0 \rightarrow \pi^+\ell^-\nu)}{\Gamma(K_L^0 \rightarrow \pi^-\ell^+\nu) + \Gamma(K_L^0 \rightarrow \pi^+\ell^-\nu)},$$
- $$\text{Im}(\eta_{+-0})^2 = \frac{\Gamma(K_S^0 \rightarrow \pi^+\pi^-\pi^0)^{CP \text{ viol.}}}{\Gamma(K_L^0 \rightarrow \pi^+\pi^-\pi^0)},$$
- $$\text{Im}(\eta_{000})^2 = \frac{\Gamma(K_S^0 \rightarrow \pi^0\pi^0\pi^0)}{\Gamma(K_L^0 \rightarrow \pi^0\pi^0\pi^0)}.$$
- where for the last two relations CPT is assumed valid, i.e., $\text{Re}(\eta_{+-0}) \simeq 0$ and $\text{Re}(\eta_{000}) \simeq 0$.
- [aa] See the K_S^0 Particle Listings for the energy limits used in this measurement.
- [bb] The value is for the sum of the charge states or particle/antiparticle states indicated.
- [cc] $\text{Re}(\epsilon'/\epsilon) = \epsilon'/\epsilon$ to a very good approximation provided the phases satisfy CPT invariance.
- [dd] This mode includes gammas from inner bremsstrahlung but not the direct emission mode $K_L^0 \rightarrow \pi^+\pi^-\gamma(\text{DE})$.
- [ee] See the K_L^0 Particle Listings for the energy limits used in this measurement.
- [ff] Allowed by higher-order electroweak interactions.
- [gg] Violates CP in leading order. Test of direct CP violation since the indirect CP -violating and CP -conserving contributions are expected to be suppressed.
- [hh] See the “Note on $f_0(1370)$ ” in the $f_0(1370)$ Particle Listings and in the 1994 edition.
- [ii] See the note in the $L(1770)$ Particle Listings in Reviews of Modern Physics **56** S1 (1984), p. S200. See also the “Note on $K_2(1770)$ and the $K_2(1820)$ ” in the $K_2(1770)$ Particle Listings.
- [jj] See the “Note on $K_2(1770)$ and the $K_2(1820)$ ” in the $K_2(1770)$ Particle Listings.
- [kk] This result applies to $Z^0 \rightarrow c\bar{c}$ decays only. Here ℓ^+ is an average (not a sum) of e^+ and μ^+ decays.
- [ll] See the Particle Listings for the (complicated) definition of this quantity.
- [nn] The branching fraction for this mode may differ from the sum of the submodes that contribute to it, due to interference effects. See the relevant papers in the Particle Listings.
- [oo] These subfractions of the $K^-2\pi^+$ mode are uncertain: see the Particle Listings.
- [pp] Submodes of the $D^+ \rightarrow K^-2\pi^+\pi^0$ and $K_S^0 2\pi^+\pi^-$ modes were studied by ANJOS 92C and COFFMAN 92B, but with at most 142 events for the first mode and 229 for the second – not enough for precise results. With nothing new for 18 years, we refer to our 2008 edition, Physics Letters **B667** 1 (2008), for those results.
- [qq] The unseen decay modes of the resonances are included.
- [rr] This is *not* a test for the $\Delta C=1$ weak neutral current, but leads to the $\pi^+\ell^+\ell^-$ final state.
- [ss] This mode is not a useful test for a $\Delta C=1$ weak neutral current because both quarks must change flavor in this decay.
- [tt] In the 2010 *Review*, the values for these quantities were given using a measure of the asymmetry that was inconsistent with the usual definition.
- [uu] This value is obtained by subtracting the branching fractions for 2-, 4- and 6-prongs from unity.
- [vv] This is the sum of our $K^-2\pi^+\pi^-$, $K^-2\pi^+\pi^-\pi^0$, $\bar{K}^0 2\pi^+2\pi^-$, $K^+2K^-\pi^+$, $2\pi^+2\pi^-$, $2\pi^+2\pi^-\pi^0$, $K^+K^-\pi^+\pi^-$, and $K^+K^-\pi^+\pi^-\pi^0$, branching fractions.
- [xx] This is the sum of our $K^-3\pi^+2\pi^-$ and $3\pi^+3\pi^-$ branching fractions.
- [yy] The branching fractions for the $K^-e^+\nu_e$, $K^*(892)^-e^+\nu_e$, $\pi^-e^+\nu_e$, and $\rho^-e^+\nu_e$ modes add up to $6.17 \pm 0.17\%$.
- [zz] This is a doubly Cabibbo-suppressed mode.
- [aaa] Submodes of the $D^0 \rightarrow K_S^0\pi^+\pi^-\pi^0$ mode with a K^* and/or ρ were studied by COFFMAN 92B, but with only 140 events. With nothing new for 18 years, we refer to our 2008 edition, Physics Letters **B667** 1 (2008), for those results.
- [bbb] This branching fraction includes all the decay modes of the resonance in the final state.
- [ccc] This limit is for either D^0 or \bar{D}^0 to $p e^-$.
- [ddd] This limit is for either D^0 or \bar{D}^0 to $\bar{p} e^+$.
- [eee] This is the purely e^+ semileptonic branching fraction: the e^+ fraction from τ^+ decays has been subtracted off. The sum of our (non- τ) e^+ exclusive fractions — an $e^+\nu_e$ with an η , η' , ϕ , K^0 , or K^{*0} — is $5.99 \pm 0.31\%$.
- [fff] This fraction includes η from η' decays.
- [ggg] The sum of our exclusive η' fractions — $\eta'e^+\nu_e$, $\eta'\mu^+\nu_\mu$, $\eta'\pi^+$, $\eta'\rho^+$, and $\eta'K^+$ — is $11.8 \pm 1.6\%$.
- [hhh] This branching fraction includes all the decay modes of the final-state resonance.
- [iii] A test for $u\bar{u}$ or $d\bar{d}$ content in the D_s^+ . Neither Cabibbo-favored nor Cabibbo-suppressed decays can contribute, and $\omega - \phi$ mixing is an unlikely explanation for any fraction above about 2×10^{-4} .
- [jjj] We decouple the $D_s^+ \rightarrow \phi\pi^+$ branching fraction obtained from mass projections (and used to get some of the other branching fractions) from the $D_s^+ \rightarrow \phi\pi^+$, $\phi \rightarrow K^+K^-$ branching fraction obtained from the Dalitz-plot analysis of $D_s^+ \rightarrow K^+K^-\pi^+$. That is, the ratio of these two branching fractions is not exactly the $\phi \rightarrow K^+K^-$ branching fraction 0.491.

Meson Summary Table

- [kkk] This is the average of a model-independent and a K -matrix parametrization of the $\pi^+\pi^-$ S -wave and is a sum over several f_0 mesons.
- [lll] An ℓ indicates an e or a μ mode, not a sum over these modes.
- [nnn] An $CP(\pm 1)$ indicates the $CP=+1$ and $CP=-1$ eigenstates of the D^0 - \bar{D}^0 system.
- [ooo] D denotes D^0 or \bar{D}^0 .
- [ppp] D_{CP+}^{*0} decays into $D^0\pi^0$ with the D^0 reconstructed in CP -even eigenstates K^+K^- and $\pi^+\pi^-$.
- [qqq] \bar{D}^{**} represents an excited state with mass $2.2 < M < 2.8$ GeV/ c^2 .
- [rrr] $\chi_{c1}(3872)^+$ is a hypothetical charged partner of the $\chi_{c1}(3872)$.
- [sss] $\Theta(1710)^{++}$ is a possible narrow pentaquark state and $G(2220)$ is a possible glueball resonance.
- [ttt] $(\bar{\Lambda}_c^- p)_s$ denotes a low-mass enhancement near 3.35 GeV/ c^2 .
- [uuu] Stands for the possible candidates of $K^*(1410)$, $K_0^*(1430)$ and $K_2^*(1430)$.
- [vvv] B^0 and B_s^0 contributions not separated. Limit is on weighted average of the two decay rates.
- [xxx] This decay refers to the coherent sum of resonant and nonresonant $J^P = 0^+ K\pi$ components with $1.60 < m_{K\pi} < 2.15$ GeV/ c^2 .
- [yyy] $X(214)$ is a hypothetical particle of mass 214 MeV/ c^2 reported by the HyperCP experiment, Physical Review Letters **94** 021801 (2005)
- [zzz] $\Theta(1540)^+$ denotes a possible narrow pentaquark state.
- [aaa] Here S and P are the hypothetical scalar and pseudoscalar particles with masses of 2.5 GeV/ c^2 and 214.3 MeV/ c^2 , respectively.
- [bbaa] These values are model dependent.
- [ccaa] Here “anything” means at least one particle observed.
- [ddaa] This is a $B(B^0 \rightarrow D^{*-} \ell^+ \nu_\ell)$ value.
- [eeaa] D^{**} stands for the sum of the $D(1^1P_1)$, $D(1^3P_0)$, $D(1^3P_1)$, $D(1^3P_2)$, $D(2^1S_0)$, and $D(2^1S_1)$ resonances.
- [ffaa] $D^{(*)}\bar{D}^{(*)}$ stands for the sum of $D^*\bar{D}^*$, $D^*\bar{D}$, $D\bar{D}^*$, and $D\bar{D}$.
- [ggaa] $X(3915)$ denotes a near-threshold enhancement in the $\omega J/\psi$ mass spectrum.
- [hhaa] Inclusive branching fractions have a multiplicity definition and can be greater than 100%.
- [iiaa] D_j represents an unresolved mixture of pseudoscalar and tensor D^{**} (P -wave) states.
- [jjaa] Not a pure measurement. See note at head of B_s^0 Decay Modes.
- [kkaa] For $E_\gamma > 100$ MeV.
- [laa] Includes $p\bar{p}\pi^+\pi^-\gamma$ and excludes $p\bar{p}\eta$, $p\bar{p}\omega$, $p\bar{p}\eta'$.
- [naa] See the “Note on the $\eta(1405)$ ” in the $\eta(1405)$ Particle Listings.
- [oaa] For a narrow state A with mass less than 960 MeV.
- [ppaa] For a narrow scalar or pseudoscalar A^0 with mass 0.21–3.0 GeV.
- [qqaa] For a narrow resonance in the range $2.2 < M(X) < 2.8$ GeV.
- [rraa] J^{PC} known by production in e^+e^- via single photon annihilation. I^G is not known; interpretation of this state as a single resonance is unclear because of the expectation of substantial threshold effects in this energy region.
- [ssaa] $2m_\tau < M(\tau^+\tau^-) < 9.2$ GeV
- [ttaa] $2 \text{ GeV} < m_{K^+K^-} < 3 \text{ GeV}$
- [uuaa] $X = \text{scalar with } m < 8.0 \text{ GeV}$
- [vva] $X\bar{X} = \text{vectors with } m < 3.1 \text{ GeV}$
- [xxaa] $X \text{ and } \bar{X} = \text{zero spin with } m < 4.5 \text{ GeV}$
- [yyaa] $1.5 \text{ GeV} < m_X < 5.0 \text{ GeV}$
- [zzaa] $201 \text{ MeV} < M(\mu^+\mu^-) < 3565 \text{ MeV}$
- [aabb] $0.5 \text{ GeV} < m_X < 9.0 \text{ GeV}$, where m_X is the invariant mass of the hadronic final state.
- [bbbb] Spectroscopic labeling for these states is theoretical, pending experimental information.
- [ccbb] $1.5 \text{ GeV} < m_X < 5.0 \text{ GeV}$
- [ddbb] $1.5 \text{ GeV} < m_X < 5.0 \text{ GeV}$
- [eebb] For $m_{\tau^+\tau^-}$ in the ranges 4.03–9.52 and 9.61–10.10 GeV.

Meson Summary Table

See also the table of suggested $q\bar{q}$ quark-model assignments in the Quark Model section.

• Indicates particles that appear in the preceding Meson Summary Table. We do not regard the other entries as being established.

LIGHT UNFLAVORED (S = C = B = 0)		STRANGE (S = ±1, C = B = 0)		CHARMED, STRANGE (C = S = ±1)		c \bar{c} continued J^{PC}	
$J^G(J^{PC})$	$J^G(J^{PC})$	$J^G(J^{PC})$	$J^G(J^{PC})$	$J^G(J^{PC})$	$J^G(J^{PC})$	$J^G(J^{PC})$	$J^G(J^{PC})$
• π^\pm 1 ⁻ (0 ⁻)	• $\pi_2(1670)$ 1 ⁻ (2 ⁻ +) • $\phi(1680)$ 0 ⁻ (1 ⁻ -)	• K^\pm 1/2(0 ⁻)	• D_s^\pm 0(0 ⁻)	• $\psi(3770)$ 0 ⁻ (1 ⁻ -)	• $\psi_2(3823)$ 0 ⁻ (2 ⁻ -)	• $\psi_3(3842)$ 0 ⁻ (3 ⁻ -)	$\chi_{c0}(3860)$ 0 ⁺ (0 ⁺ +) • $\chi_{c1}(3872)$ 0 ⁺ (1 ⁺ +) • $Z_c(3900)$ 1 ⁺ (1 ⁺ -) • $X(3915)$ 0 ⁺ (0/2 ⁺ +) • $\chi_{c2}(3930)$ 0 ⁺ (2 ⁺ +) • $X(3940)$??(???) • $X(4020)^\pm$ 1 ⁺ (? ⁻ -) • $\psi(4040)$ 0 ⁻ (1 ⁻ -) • $X(4050)^\pm$ 1 ⁻ (? ⁺ +) • $X(4055)^\pm$ 1 ⁺ (? ⁻ -) • $X(4100)^\pm$ 1 ⁻ (? ⁺ ?) • $\chi_{c1}(4140)$ 0 ⁺ (1 ⁺ +) • $\psi(4160)$ 0 ⁻ (1 ⁻ -) • $X(4160)$??(???) • $Z_c(4200)$ 1 ⁺ (1 ⁺ -) • $\psi(4230)$ 0 ⁻ (1 ⁻ -) • $R_{c0}(4240)$ 1 ⁺ (0 ⁻ -) • $X(4250)^\pm$ 1 ⁻ (? ⁺ +) • $\psi(4260)$ 0 ⁻ (1 ⁻ -) • $\chi_{c1}(4274)$ 0 ⁺ (1 ⁺ +) • $X(4350)$ 0 ⁺ (? ⁺ +) • $\psi(4360)$ 0 ⁻ (1 ⁻ -) • $\psi(4390)$ 0 ⁻ (1 ⁻ -) • $\psi(4415)$ 0 ⁻ (1 ⁻ -) • $Z_c(4430)$ 1 ⁺ (1 ⁺ -) • $\chi_{c0}(4500)$ 0 ⁺ (0 ⁺ +) • $\psi(4660)$ 0 ⁻ (1 ⁻ -) • $\chi_{c0}(4700)$ 0 ⁺ (0 ⁺ +) • $b\bar{b}$ (+ possibly non-q \bar{q} states) • $\eta_b(1S)$ 0 ⁺ (0 ⁻ +) • $\Upsilon(1S)$ 0 ⁻ (1 ⁻ -) • $\chi_{b0}(1P)$ 0 ⁺ (0 ⁺ +) • $\chi_{b1}(1P)$ 0 ⁺ (1 ⁺ +) • $h_b(1P)$ 0 ⁻ (1 ⁺ -) • $\chi_{b2}(1P)$ 0 ⁺ (2 ⁺ +) • $\eta_b(2S)$ 0 ⁺ (0 ⁻ +) • $\Upsilon(2S)$ 0 ⁻ (1 ⁻ -) • $\Upsilon_2(1D)$ 0 ⁻ (2 ⁻ -) • $\chi_{b0}(2P)$ 0 ⁺ (0 ⁺ +) • $\chi_{b1}(2P)$ 0 ⁺ (1 ⁺ +) • $h_b(2P)$ 0 ⁻ (1 ⁺ -) • $\chi_{b2}(2P)$ 0 ⁺ (2 ⁺ +) • $\Upsilon(3S)$ 0 ⁻ (1 ⁻ -) • $\chi_{b1}(3P)$ 0 ⁺ (1 ⁺ +) • $\chi_{b2}(3P)$ 0 ⁺ (2 ⁺ +) • $\Upsilon(4S)$ 0 ⁻ (1 ⁻ -) • $Z_b(10610)$ 1 ⁺ (1 ⁺ -) • $Z_b(10650)$ 1 ⁺ (1 ⁺ -) • $\Upsilon(10753)$??(1 ⁻ -) • $\Upsilon(10860)$ 0 ⁻ (1 ⁻ -) • $\Upsilon(11020)$ 0 ⁻ (1 ⁻ -)
• π^0 1 ⁻ (0 ⁻ +) • η 0 ⁺ (0 ⁺ -) • $f_0(500)$ 0 ⁺ (0 ⁺ +) • $\rho(770)$ 1 ⁺ (1 ⁻ -) • $\omega(782)$ 0 ⁻ (1 ⁻ -) • $\eta'(958)$ 0 ⁺ (0 ⁺ -) • $f_0(980)$ 0 ⁺ (0 ⁺ +) • $a_0(980)$ 1 ⁻ (0 ⁺ +) • $\phi(1020)$ 0 ⁻ (1 ⁻ -) • $h_1(1170)$ 0 ⁻ (1 ⁺ -) • $b_1(1235)$ 1 ⁺ (1 ⁺ -) • $a_1(1260)$ 1 ⁻ (1 ⁺ +) • $f_2(1270)$ 0 ⁺ (2 ⁺ +) • $f_1(1285)$ 0 ⁺ (1 ⁺ +) • $\eta(1295)$ 0 ⁺ (0 ⁺ -) • $\pi(1300)$ 1 ⁻ (0 ⁺ -) • $a_2(1320)$ 1 ⁻ (2 ⁺ +) • $f_0(1370)$ 0 ⁺ (0 ⁺ +) • $\pi_1(1400)$ 1 ⁻ (1 ⁺ -) • $\eta(1405)$ 0 ⁺ (0 ⁺ -) • $h_1(1415)$ 0 ⁻ (1 ⁺ -) • $a_1(1420)$ 1 ⁻ (1 ⁺ +) • $f_1(1420)$ 0 ⁺ (1 ⁺ +) • $\omega(1420)$ 0 ⁻ (1 ⁻ -) • $f_2(1430)$ 0 ⁺ (2 ⁺ +) • $a_0(1450)$ 1 ⁻ (0 ⁺ +) • $\rho(1450)$ 1 ⁺ (1 ⁻ -) • $\eta(1475)$ 0 ⁺ (0 ⁺ -) • $f_0(1500)$ 0 ⁺ (0 ⁺ +) • $f_1(1510)$ 0 ⁺ (1 ⁺ +) • $f_2'(1525)$ 0 ⁺ (2 ⁺ +) • $f_2(1565)$ 0 ⁺ (2 ⁺ +) • $\rho(1570)$ 1 ⁺ (1 ⁻ -) • $h_1(1595)$ 0 ⁻ (1 ⁺ -) • $\pi_1(1600)$ 1 ⁻ (1 ⁺ -) • $a_1(1640)$ 1 ⁻ (1 ⁺ +) • $f_2(1640)$ 0 ⁺ (2 ⁺ +) • $\eta_2(1645)$ 0 ⁺ (2 ⁺ -) • $\omega(1650)$ 0 ⁻ (1 ⁻ -) • $\omega_3(1670)$ 0 ⁻ (3 ⁻ -)	• K^0 1/2(0 ⁻) • K_S^0 1/2(0 ⁻) • K_L^0 1/2(0 ⁻) • $K_0^*(700)$ 1/2(0 ⁺) • $K^*(892)$ 1/2(1 ⁻) • $K_1(1270)$ 1/2(1 ⁺) • $K_1(1400)$ 1/2(1 ⁺) • $K^*(1410)$ 1/2(1 ⁻) • $K_0^*(1430)$ 1/2(0 ⁺) • $K_2^*(1430)$ 1/2(2 ⁺) • $K(1460)$ 1/2(0 ⁻) • $K_2(1580)$ 1/2(2 ⁻) • $K(1630)$ 1/2(2 ⁻ ?) • $K_1(1650)$ 1/2(1 ⁺) • $K^*(1680)$ 1/2(1 ⁻) • $K_2(1770)$ 1/2(2 ⁻) • $K_3^*(1780)$ 1/2(3 ⁻) • $K_2(1820)$ 1/2(2 ⁻) • $K(1830)$ 1/2(0 ⁻) • $K_0^*(1950)$ 1/2(0 ⁺) • $K_2^*(1980)$ 1/2(2 ⁺) • $K_4^*(2045)$ 1/2(4 ⁺) • $K_2(2250)$ 1/2(2 ⁻) • $K_3(2320)$ 1/2(3 ⁺) • $K_5^*(2380)$ 1/2(5 ⁻) • $K_4(2500)$ 1/2(4 ⁻) • $K(3100)$??(???)	• $D_s^{*\pm}$ 0(0 ⁻) • $D_s^{*\pm}$ 0(? [?]) • $D_{s0}^*(2317)^\pm$ 0(0 ⁺) • $D_{s1}(2460)^\pm$ 0(1 ⁺) • $D_{s1}(2536)^\pm$ 0(1 ⁺) • $D_{s2}^*(2573)$ 0(2 ⁺) • $D_{s1}^*(2700)^\pm$ 0(1 ⁻) • $D_{s1}^*(2860)^\pm$ 0(1 ⁻) • $D_{s3}^*(2860)^\pm$ 0(3 ⁻) • $D_{sJ}(3040)^\pm$ 0(? [?])	• B^\pm 1/2(0 ⁻) • B^0 1/2(0 ⁻) • B^\pm/B^0 ADMIXTURE • $B^\pm/B^0/B_s^0/b$ -baryon ADMIXTURE • V_{cb} and V_{ub} CKM Matrix Elements • B^* 1/2(1 ⁻) • $B_1(5721)^+$ 1/2(1 ⁺) • $B_1(5721)^0$ 1/2(1 ⁺) • $B_2^*(5732)$?(? [?]) • $B_2^*(5747)^+$ 1/2(2 ⁺) • $B_2^*(5747)^0$ 1/2(2 ⁺) • $B_J(5840)^+$ 1/2(? [?]) • $B_J(5840)^0$ 1/2(? [?]) • $B_J(5970)^+$ 1/2(? [?]) • $B_J(5970)^0$ 1/2(? [?])	• D^\pm 1/2(0 ⁻) • D^0 1/2(0 ⁻) • $D^*(2007)^0$ 1/2(1 ⁻) • $D^*(2010)^\pm$ 1/2(1 ⁻) • $D_0^*(2300)^0$ 1/2(0 ⁺) • $D_0^*(2300)^\pm$ 1/2(0 ⁺) • $D_1(2420)^0$ 1/2(1 ⁺) • $D_1(2420)^\pm$ 1/2(? [?]) • $D_1(2430)^0$ 1/2(1 ⁺) • $D_2^*(2460)^0$ 1/2(2 ⁺) • $D_2^*(2460)^\pm$ 1/2(2 ⁺) • $D(2550)^0$ 1/2(? [?]) • $D_J^*(2600)$ 1/2(? [?]) • $D^*(2640)^\pm$ 1/2(? [?]) • $D(2740)^0$ 1/2(? [?]) • $D_3^*(2750)$ 1/2(3 ⁻) • $D(3000)^0$ 1/2(? [?])	• B_c^\pm 0(0 ⁻) • $B_c(2S)^\pm$ 0(0 ⁻)	• $\eta_c(1S)$ 0 ⁺ (0 ⁻ +) • $J/\psi(1S)$ 0 ⁻ (1 ⁻ -) • $\chi_{c0}(1P)$ 0 ⁺ (0 ⁺ +) • $\chi_{c1}(1P)$ 0 ⁺ (1 ⁺ +) • $h_c(1P)$ 0 ⁻ (1 ⁺ -) • $\chi_{c2}(1P)$ 0 ⁺ (2 ⁺ +) • $\eta_c(2S)$ 0 ⁺ (0 ⁻ +) • $\psi(2S)$ 0 ⁻ (1 ⁻ -)	
	OTHER LIGHT Further States	CHARMED (C = ±1)	BOTTOM, STRANGE (B = ±1, S = ∓1)	BOTTOM, CHARMED (B = C = ±1)			

Baryon Summary Table

This short table gives the name, the quantum numbers (where known), and the status of baryons in the Review. Only the baryons with 3- or 4-star status are included in the Baryon Summary Table. Due to insufficient data or uncertain interpretation, the other entries in the table are not established baryons. The names with masses are of baryons that decay strongly. The spin-parity J^P (when known) is given with each particle. For the strongly decaying particles, the J^P values are considered to be part of the names.

p	$1/2^+$	****	$\Delta(1232)$	$3/2^+$	****	Σ^+	$1/2^+$	****	Ξ^0	$1/2^+$	****	Ξ_{cc}^{++}	***	
n	$1/2^+$	****	$\Delta(1600)$	$3/2^+$	****	Σ^0	$1/2^+$	****	Ξ^-	$1/2^+$	****			
$N(1440)$	$1/2^+$	****	$\Delta(1620)$	$1/2^-$	****	Σ^-	$1/2^+$	****	$\Xi(1530)$	$3/2^+$	****	Λ_b^0	$1/2^+$	***
$N(1520)$	$3/2^-$	****	$\Delta(1700)$	$3/2^-$	****	$\Sigma(1385)$	$3/2^+$	****	$\Xi(1620)$	*		$\Lambda_b(5912)^0$	$1/2^-$	***
$N(1535)$	$1/2^-$	****	$\Delta(1750)$	$1/2^+$	*	$\Sigma(1580)$	$3/2^-$	*	$\Xi(1690)$	***		$\Lambda_b(5920)^0$	$3/2^-$	***
$N(1650)$	$1/2^-$	****	$\Delta(1900)$	$1/2^-$	***	$\Sigma(1620)$	$1/2^-$	*	$\Xi(1820)$	$3/2^-$	***	$\Lambda_b(6146)^0$	$3/2^+$	***
$N(1675)$	$5/2^-$	****	$\Delta(1905)$	$5/2^+$	****	$\Sigma(1660)$	$1/2^+$	***	$\Xi(1950)$	***		$\Lambda_b(6152)^0$	$5/2^+$	***
$N(1680)$	$5/2^+$	****	$\Delta(1910)$	$1/2^+$	****	$\Sigma(1670)$	$3/2^-$	****	$\Xi(2030)$	$\geq \frac{5}{2}^?$	***	Σ_b	$1/2^+$	***
$N(1700)$	$3/2^-$	***	$\Delta(1920)$	$3/2^+$	***	$\Sigma(1750)$	$1/2^-$	***	$\Xi(2120)$	*		Σ_b^*	$3/2^+$	***
$N(1710)$	$1/2^+$	****	$\Delta(1930)$	$5/2^-$	***	$\Sigma(1775)$	$5/2^-$	****	$\Xi(2250)$	**		$\Sigma_b(6097)^+$	***	
$N(1720)$	$3/2^+$	****	$\Delta(1940)$	$3/2^-$	**	$\Sigma(1780)$	$3/2^+$	*	$\Xi(2370)$	**		$\Sigma_b(6097)^-$	***	
$N(1860)$	$5/2^+$	**	$\Delta(1950)$	$7/2^+$	****	$\Sigma(1880)$	$1/2^+$	**	$\Xi(2500)$	*		Ξ_b^0, Ξ_b^-	$1/2^+$	***
$N(1875)$	$3/2^-$	***	$\Delta(2000)$	$5/2^+$	**	$\Sigma(1900)$	$1/2^-$	**				$\Xi_b'(5935)^-$	$1/2^+$	***
$N(1880)$	$1/2^+$	***	$\Delta(2150)$	$1/2^-$	*	$\Sigma(1910)$	$3/2^-$	***	Ω^-	$3/2^+$	****	$\Xi_b(5945)^0$	$3/2^+$	***
$N(1895)$	$1/2^-$	****	$\Delta(2200)$	$7/2^-$	***	$\Sigma(1915)$	$5/2^+$	****	$\Omega(2012)^-$	$?^-$	***	$\Xi_b(5955)^-$	$3/2^+$	***
$N(1900)$	$3/2^+$	****	$\Delta(2300)$	$9/2^+$	**	$\Sigma(1940)$	$3/2^+$	*	$\Omega(2250)^-$	***		$\Xi_b(6227)$	***	
$N(1990)$	$7/2^+$	**	$\Delta(2350)$	$5/2^-$	*	$\Sigma(2010)$	$3/2^-$	*	$\Omega(2380)^-$	**		Ω_b^-	$1/2^+$	***
$N(2000)$	$5/2^+$	**	$\Delta(2390)$	$7/2^+$	*	$\Sigma(2030)$	$7/2^+$	****	$\Omega(2470)^-$	**				
$N(2040)$	$3/2^+$	*	$\Delta(2400)$	$9/2^-$	**	$\Sigma(2070)$	$5/2^+$	*				$P_c(4312)^+$	*	
$N(2060)$	$5/2^-$	***	$\Delta(2420)$	$11/2^+$	****	$\Sigma(2080)$	$3/2^+$	*	Λ_c^+	$1/2^+$	****	$P_c(4380)^+$	*	
$N(2100)$	$1/2^+$	***	$\Delta(2750)$	$13/2^-$	**	$\Sigma(2100)$	$7/2^-$	*	$\Lambda_c(2595)^+$	$1/2^-$	***	$P_c(4440)^+$	*	
$N(2120)$	$3/2^-$	***	$\Delta(2950)$	$15/2^+$	**	$\Sigma(2160)$	$1/2^-$	*	$\Lambda_c(2625)^+$	$3/2^-$	***	$P_c(4457)^+$	*	
$N(2190)$	$7/2^-$	****				$\Sigma(2230)$	$3/2^+$	*	$\Lambda_c(2765)^+$	*				
$N(2220)$	$9/2^+$	****	Λ	$1/2^+$	****	$\Sigma(2250)$	***		$\Lambda_c(2860)^+$	$3/2^+$	***			
$N(2250)$	$9/2^-$	****	Λ	$1/2^-$	**	$\Sigma(2455)$	**		$\Lambda_c(2880)^+$	$5/2^+$	***			
$N(2300)$	$1/2^+$	**	$\Lambda(1405)$	$1/2^-$	****	$\Sigma(2620)$	**		$\Lambda_c(2940)^+$	$3/2^-$	***			
$N(2570)$	$5/2^-$	**	$\Lambda(1520)$	$3/2^-$	****	$\Sigma(3000)$	*		$\Sigma_c(2455)$	$1/2^+$	****			
$N(2600)$	$11/2^-$	***	$\Lambda(1600)$	$1/2^+$	****	$\Sigma(3170)$	*		$\Sigma_c(2520)$	$3/2^+$	***			
$N(2700)$	$13/2^+$	**	$\Lambda(1670)$	$1/2^-$	****				$\Sigma_c(2800)$	***				
			$\Lambda(1690)$	$3/2^-$	****				Ξ_c^+	$1/2^+$	***			
			$\Lambda(1710)$	$1/2^+$	*				Ξ_c^0	$1/2^+$	****			
			$\Lambda(1800)$	$1/2^-$	***				$\Xi_c^{'+}$	$1/2^+$	***			
			$\Lambda(1810)$	$1/2^+$	***				$\Xi_c^{'0}$	$1/2^+$	***			
			$\Lambda(1820)$	$5/2^+$	****				$\Xi_c^{'0}$	$1/2^+$	***			
			$\Lambda(1830)$	$5/2^-$	****				$\Xi_c(2645)$	$3/2^+$	***			
			$\Lambda(1890)$	$3/2^+$	****				$\Xi_c(2790)$	$1/2^-$	***			
			$\Lambda(2000)$	$1/2^-$	*				$\Xi_c(2815)$	$3/2^-$	***			
			$\Lambda(2050)$	$3/2^-$	*				$\Xi_c(2930)$	**				
			$\Lambda(2070)$	$3/2^+$	*				$\Xi_c(2970)$	***				
			$\Lambda(2080)$	$5/2^-$	*				$\Xi_c(3055)$	***				
			$\Lambda(2085)$	$7/2^+$	**				$\Xi_c(3080)$	***				
			$\Lambda(2100)$	$7/2^-$	****				$\Xi_c(3123)$	*				
			$\Lambda(2110)$	$5/2^+$	***				Ω_c^0	$1/2^+$	***			
			$\Lambda(2325)$	$3/2^-$	*				$\Omega_c(2770)^0$	$3/2^+$	***			
			$\Lambda(2350)$	$9/2^+$	***				$\Omega_c(3000)^0$	***				
			$\Lambda(2585)$	**					$\Omega_c(3050)^0$	***				
									$\Omega_c(3065)^0$	***				
									$\Omega_c(3090)^0$	***				
									$\Omega_c(3120)^0$	***				

- **** Existence is certain, and properties are at least fairly well explored.
- *** Existence ranges from very likely to certain, but further confirmation is desirable and/or quantum numbers, branching fractions, etc. are not well determined.
- ** Evidence of existence is only fair.
- * Evidence of existence is poor.

Baryon Summary Table

N BARYONS
 $(S = 0, I = 1/2)$
 $p, N^+ = uud; \quad n, N^0 = udd$

p

$$I(J^P) = \frac{1}{2}(\frac{1}{2}^+)$$

Mass $m = 1.00727646662 \pm 0.00000000009 \text{ u}$ ($S = 3.1$)
 Mass $m = 938.272081 \pm 0.000006 \text{ MeV}$ ^[a]
 $|m_p - m_{\bar{p}}|/m_p < 7 \times 10^{-10}$, CL = 90% ^[b]
 $|\frac{q_{\bar{p}}}{m_{\bar{p}}}|/(\frac{q_p}{m_p}) = 1.00000000000 \pm 0.00000000007$
 $|q_p + q_{\bar{p}}|/e < 7 \times 10^{-10}$, CL = 90% ^[b]
 $|q_p + q_e|/e < 1 \times 10^{-21}$ ^[c]
 Magnetic moment $\mu = 2.7928473446 \pm 0.0000000008 \mu_N$
 $(\mu_p + \mu_{\bar{p}}) / \mu_p = (0.002 \pm 0.004) \times 10^{-6}$
 Electric dipole moment $d < 0.021 \times 10^{-23} \text{ e cm}$
 Electric polarizability $\alpha = (11.2 \pm 0.4) \times 10^{-4} \text{ fm}^3$
 Magnetic polarizability $\beta = (2.5 \pm 0.4) \times 10^{-4} \text{ fm}^3$ ($S = 1.2$)
 Charge radius, μp Lamb shift = $0.84087 \pm 0.00039 \text{ fm}$ ^[d]
 Charge radius = $0.8409 \pm 0.0004 \text{ fm}$ ^[d]
 Magnetic radius = $0.851 \pm 0.026 \text{ fm}$ ^[e]
 Mean life $\tau > 3.6 \times 10^{29} \text{ years}$, CL = 90% ^[f] ($p \rightarrow$ invisible mode)
 Mean life $\tau > 10^{31}$ to 10^{33} years ^[f] (mode dependent)

See the "Note on Nucleon Decay" in our 1994 edition (Phys. Rev. **D50**, 1173) for a short review.

The "partial mean life" limits tabulated here are the limits on τ/B_j , where τ is the total mean life and B_j is the branching fraction for the mode in question. For N decays, p and n indicate proton and neutron partial lifetimes.

p DECAY MODES	Partial mean life (10^{30} years)	Confidence level	p (MeV/c)
Antilepton + meson			
$N \rightarrow e^+ \pi$	> 5300 (n), > 16000 (p)	90%	459
$N \rightarrow \mu^+ \pi$	> 3500 (n), > 7700 (p)	90%	453
$N \rightarrow \nu \pi$	> 1100 (n), > 390 (p)	90%	459
$p \rightarrow e^+ \eta$	> 10000	90%	309
$p \rightarrow \mu^+ \eta$	> 4700	90%	297
$n \rightarrow \nu \eta$	> 158	90%	310
$N \rightarrow e^+ \rho$	> 217 (n), > 720 (p)	90%	149
$N \rightarrow \mu^+ \rho$	> 228 (n), > 570 (p)	90%	113
$N \rightarrow \nu \rho$	> 19 (n), > 162 (p)	90%	149
$p \rightarrow e^+ \omega$	> 1600	90%	143
$p \rightarrow \mu^+ \omega$	> 2800	90%	105
$n \rightarrow \nu \omega$	> 108	90%	144
$N \rightarrow e^+ K$	> 17 (n), > 1000 (p)	90%	339
$N \rightarrow \mu^+ K$	> 26 (n), > 1600 (p)	90%	329
$N \rightarrow \nu K$	> 86 (n), > 5900 (p)	90%	338
$n \rightarrow \nu K_S^0$	> 260	90%	339
$p \rightarrow e^+ K^*(892)^0$	> 84	90%	45
$N \rightarrow \nu K^*(892)$	> 78 (n), > 51 (p)	90%	45
Antilepton + mesons			
$p \rightarrow e^+ \pi^+ \pi^-$	> 82	90%	448
$p \rightarrow e^+ \pi^0 \pi^0$	> 147	90%	449
$n \rightarrow e^+ \pi^- \pi^0$	> 52	90%	449
$p \rightarrow \mu^+ \pi^+ \pi^-$	> 133	90%	425
$p \rightarrow \mu^+ \pi^0 \pi^0$	> 101	90%	427
$n \rightarrow \mu^+ \pi^- \pi^0$	> 74	90%	427
$n \rightarrow e^+ K^0 \pi^-$	> 18	90%	319
Lepton + meson			
$n \rightarrow e^- \pi^+$	> 65	90%	459
$n \rightarrow \mu^- \pi^+$	> 49	90%	453
$n \rightarrow e^- \rho^+$	> 62	90%	150
$n \rightarrow \mu^- \rho^+$	> 7	90%	115
$n \rightarrow e^- K^+$	> 32	90%	340
$n \rightarrow \mu^- K^+$	> 57	90%	330
Lepton + mesons			
$p \rightarrow e^- \pi^+ \pi^+$	> 30	90%	448
$n \rightarrow e^- \pi^+ \pi^0$	> 29	90%	449
$p \rightarrow \mu^- \pi^+ \pi^+$	> 17	90%	425
$n \rightarrow \mu^- \pi^+ \pi^0$	> 34	90%	427
$p \rightarrow e^- \pi^+ K^+$	> 75	90%	320
$p \rightarrow \mu^- \pi^+ K^+$	> 245	90%	279

Antilepton + photon(s)			
$p \rightarrow e^+ \gamma$	> 670	90%	469
$p \rightarrow \mu^+ \gamma$	> 478	90%	463
$n \rightarrow \nu \gamma$	> 550	90%	470
$p \rightarrow e^+ \gamma \gamma$	> 100	90%	469
$n \rightarrow \nu \gamma \gamma$	> 219	90%	470
Antilepton + single massless			
$p \rightarrow e^+ X$	> 790	90%	-
$p \rightarrow \mu^+ X$	> 410	90%	-
Three (or more) leptons			
$p \rightarrow e^+ e^+ e^-$	> 793	90%	469
$p \rightarrow e^+ \mu^+ \mu^-$	> 359	90%	457
$p \rightarrow e^+ \nu \nu$	> 170	90%	469
$n \rightarrow e^+ e^- \nu$	> 257	90%	470
$n \rightarrow \mu^+ e^- \nu$	> 83	90%	464
$n \rightarrow \mu^+ \mu^- \nu$	> 79	90%	458
$p \rightarrow \mu^+ e^+ e^-$	> 529	90%	463
$p \rightarrow \mu^+ \mu^+ \mu^-$	> 675	90%	439
$p \rightarrow \mu^+ \nu \nu$	> 220	90%	463
$p \rightarrow e^- \mu^+ \mu^+$	> 6	90%	457
$n \rightarrow 3 \nu$	> 5×10^{-4}	90%	470
Inclusive modes			
$N \rightarrow e^+$ anything	> 0.6 (n, p)	90%	-
$N \rightarrow \mu^+$ anything	> 12 (n, p)	90%	-
$N \rightarrow e^+ \pi^0$ anything	> 0.6 (n, p)	90%	-

$\Delta B = 2$ dinucleon modes

The following are lifetime limits per iron nucleus.

$pp \rightarrow \pi^+ \pi^+$	> 72.2	90%	-
$pn \rightarrow \pi^+ \pi^0$	> 170	90%	-
$nn \rightarrow \pi^+ \pi^-$	> 0.7	90%	-
$nn \rightarrow \pi^0 \pi^0$	> 404	90%	-
$pp \rightarrow K^+ K^+$	> 170	90%	-
$pp \rightarrow e^+ e^+$	> 5.8	90%	-
$pp \rightarrow e^+ \mu^+$	> 3.6	90%	-
$pp \rightarrow \mu^+ \mu^+$	> 1.7	90%	-
$pn \rightarrow e^+ \bar{\nu}$	> 260	90%	-
$pn \rightarrow \mu^+ \bar{\nu}$	> 200	90%	-
$pn \rightarrow \tau^+ \bar{\nu}_\tau$	> 29	90%	-
$nn \rightarrow \nu_e \bar{\nu}_e$	> 1.4	90%	-
$nn \rightarrow \nu_\mu \bar{\nu}_\mu$	> 1.4	90%	-
$pn \rightarrow$ invisible	> 2.1×10^{-5}	90%	-
$pp \rightarrow$ invisible	> 5×10^{-5}	90%	-

\bar{p} DECAY MODES

\bar{p} DECAY MODES	Partial mean life (years)	Confidence level	\bar{p} (MeV/c)
$\bar{p} \rightarrow e^- \gamma$	> 7×10^5	90%	469
$\bar{p} \rightarrow \mu^- \gamma$	> 5×10^4	90%	463
$\bar{p} \rightarrow e^- \pi^0$	> 4×10^5	90%	459
$\bar{p} \rightarrow \mu^- \pi^0$	> 5×10^4	90%	453
$\bar{p} \rightarrow e^- \eta$	> 2×10^4	90%	309
$\bar{p} \rightarrow \mu^- \eta$	> 8×10^3	90%	297
$\bar{p} \rightarrow e^- K_S^0$	> 900	90%	337
$\bar{p} \rightarrow \mu^- K_S^0$	> 4×10^3	90%	326
$\bar{p} \rightarrow e^- K_L^0$	> 9×10^3	90%	337
$\bar{p} \rightarrow \mu^- K_L^0$	> 7×10^3	90%	326
$\bar{p} \rightarrow e^- \gamma \gamma$	> 2×10^4	90%	469
$\bar{p} \rightarrow \mu^- \gamma \gamma$	> 2×10^4	90%	463
$\bar{p} \rightarrow e^- \omega$	> 200	90%	143

n

$$I(J^P) = \frac{1}{2}(\frac{1}{2}^+)$$

Mass $m = 1.0086649159 \pm 0.0000000005 \text{ u}$
 Mass $m = 939.565413 \pm 0.000006 \text{ MeV}$ ^[a]
 $(m_n - m_{\bar{n}}) / m_n = (9 \pm 6) \times 10^{-5}$
 $m_n - m_p = 1.2933321 \pm 0.0000005 \text{ MeV}$
 $= 0.00138844919(45) \text{ u}$
 Mean life $\tau = 879.4 \pm 0.6 \text{ s}$ ($S = 1.6$)
 $c\tau = 2.6362 \times 10^8 \text{ km}$
 Magnetic moment $\mu = -1.9130427 \pm 0.0000005 \mu_N$
 Electric dipole moment $d < 0.18 \times 10^{-25} \text{ e cm}$, CL = 90%
 Mean-square charge radius $\langle r_n^2 \rangle = -0.1161 \pm 0.0022 \text{ fm}^2$ ($S = 1.3$)

Baryon Summary Table

Magnetic radius $\sqrt{\langle r_M^2 \rangle} = 0.864^{+0.009}_{-0.008}$ fm
 Electric polarizability $\alpha = (11.8 \pm 1.1) \times 10^{-4}$ fm³
 Magnetic polarizability $\beta = (3.7 \pm 1.2) \times 10^{-4}$ fm³
 Charge $q = (-0.2 \pm 0.8) \times 10^{-21}$ e
 Mean $n\bar{n}$ -oscillation time $> 8.6 \times 10^7$ s, CL = 90% (free n)
 Mean $n\bar{n}$ -oscillation time $> 2.7 \times 10^8$ s, CL = 90% [g] (bound n)
 Mean nn' -oscillation time > 448 s, CL = 90% [h]

 $p e^- \nu_e$ decay parameters [i]

$\lambda \equiv g_A / g_V = -1.2756 \pm 0.0013$ (S = 2.6)
 $A = -0.11958 \pm 0.00021$ (S = 1.2)
 $B = 0.9807 \pm 0.0030$
 $C = -0.2377 \pm 0.0026$
 $a = -0.1059 \pm 0.0028$
 $\phi_{AV} = (180.017 \pm 0.026)^\circ$ [j]
 $D = (-1.2 \pm 2.0) \times 10^{-4}$ [k]
 $R = 0.004 \pm 0.013$ [k]

n DECAY MODES	Fraction (Γ_i/Γ)	Confidence level	ρ (MeV/c)
$p e^- \bar{\nu}_e$	100	%	1
$p e^- \bar{\nu}_e \gamma$	[j] $(9.2 \pm 0.7) \times 10^{-3}$		1
hydrogen-atom $\bar{\nu}_e$	$< 2.7 \times 10^{-3}$	95%	1.19

Charge conservation (Q) violating mode

$p \nu_e \bar{\nu}_e$	Q $< 8 \times 10^{-27}$	68%	1
-----------------------	-------------------------	-----	---

 $N(1440) 1/2^+$

$$I(J^P) = \frac{1}{2}(1^+)$$

Re(pole position) = 1360 to 1380 (≈ 1370) MeV
 $-2\text{Im}(\text{pole position}) = 160$ to 190 (≈ 175) MeV
 Breit-Wigner mass = 1410 to 1470 (≈ 1440) MeV
 Breit-Wigner full width = 250 to 450 (≈ 350) MeV

$N(1440)$ DECAY MODES	Fraction (Γ_i/Γ)	ρ (MeV/c)
$N\pi$	55–75 %	398
$N\eta$	< 1 %	†
$N\pi\pi$	17–50 %	347
$\Delta(1232)\pi$, P-wave	6–27 %	147
$N\sigma$	11–23 %	–
$p\gamma$, helicity=1/2	0.035–0.048 %	414
$n\gamma$, helicity=1/2	0.02–0.04 %	413

 $N(1520) 3/2^-$

$$I(J^P) = \frac{1}{2}(3^-)$$

Re(pole position) = 1505 to 1515 (≈ 1510) MeV
 $-2\text{Im}(\text{pole position}) = 105$ to 120 (≈ 110) MeV
 Breit-Wigner mass = 1510 to 1520 (≈ 1515) MeV
 Breit-Wigner full width = 100 to 120 (≈ 110) MeV

$N(1520)$ DECAY MODES	Fraction (Γ_i/Γ)	ρ (MeV/c)
$N\pi$	55–65 %	453
$N\eta$	0.07–0.09 %	142
$N\pi\pi$	25–35 %	410
$\Delta(1232)\pi$	22–34 %	225
$\Delta(1232)\pi$, S-wave	15–23 %	225
$\Delta(1232)\pi$, D-wave	7–11 %	225
$N\sigma$	< 2 %	–
$p\gamma$	0.31–0.52 %	467
$p\gamma$, helicity=1/2	0.01–0.02 %	467
$p\gamma$, helicity=3/2	0.30–0.50 %	467
$n\gamma$	0.30–0.53 %	466
$n\gamma$, helicity=1/2	0.04–0.10 %	466
$n\gamma$, helicity=3/2	0.25–0.45 %	466

 $N(1535) 1/2^-$

$$I(J^P) = \frac{1}{2}(1^-)$$

Re(pole position) = 1500 to 1520 (≈ 1510) MeV
 $-2\text{Im}(\text{pole position}) = 110$ to 150 (≈ 130) MeV
 Breit-Wigner mass = 1515 to 1545 (≈ 1530) MeV
 Breit-Wigner full width = 125 to 175 (≈ 150) MeV

$N(1535)$ DECAY MODES	Fraction (Γ_i/Γ)	ρ (MeV/c)
$N\pi$	32–52 %	464
$N\eta$	30–55 %	176
$N\pi\pi$	3–14 %	422
$\Delta(1232)\pi$, D-wave	1–4 %	240
$N\sigma$	2–10 %	–
$N(1440)\pi$	5–12 %	†
$p\gamma$, helicity=1/2	0.15–0.30 %	477
$n\gamma$, helicity=1/2	0.01–0.25 %	477

 $N(1650) 1/2^-$

$$I(J^P) = \frac{1}{2}(1^-)$$

Re(pole position) = 1640 to 1670 (≈ 1655) MeV
 $-2\text{Im}(\text{pole position}) = 100$ to 170 (≈ 135) MeV
 Breit-Wigner mass = 1635 to 1665 (≈ 1650) MeV
 Breit-Wigner full width = 100 to 150 (≈ 125) MeV

$N(1650)$ DECAY MODES	Fraction (Γ_i/Γ)	ρ (MeV/c)
$N\pi$	50–70 %	547
$N\eta$	15–35 %	348
ΛK	5–15 %	169
$N\pi\pi$	8–36 %	514
$\Delta(1232)\pi$, D-wave	6–18 %	345
$N\sigma$	2–18 %	–
$N(1440)\pi$	6–26 %	150
$p\gamma$, helicity=1/2	0.04–0.20 %	558
$n\gamma$, helicity=1/2	0.003–0.17 %	557

 $N(1675) 5/2^-$

$$I(J^P) = \frac{1}{2}(5^-)$$

Re(pole position) = 1655 to 1665 (≈ 1660) MeV
 $-2\text{Im}(\text{pole position}) = 125$ to 150 (≈ 135) MeV
 Breit-Wigner mass = 1665 to 1680 (≈ 1675) MeV
 Breit-Wigner full width = 130 to 160 (≈ 145) MeV

$N(1675)$ DECAY MODES	Fraction (Γ_i/Γ)	ρ (MeV/c)
$N\pi$	38–42 %	564
$N\eta$	< 1 %	376
$N\pi\pi$	25–45 %	532
$\Delta(1232)\pi$, D-wave	23–37 %	366
$N\sigma$	3–7 %	–
$p\gamma$	0–0.02 %	575
$p\gamma$, helicity=1/2	0–0.01 %	575
$p\gamma$, helicity=3/2	0–0.01 %	575
$n\gamma$	0–0.15 %	574
$n\gamma$, helicity=1/2	0–0.05 %	574
$n\gamma$, helicity=3/2	0–0.10 %	574

 $N(1680) 5/2^+$

$$I(J^P) = \frac{1}{2}(5^+)$$

Re(pole position) = 1665 to 1680 (≈ 1675) MeV
 $-2\text{Im}(\text{pole position}) = 110$ to 135 (≈ 120) MeV
 Breit-Wigner mass = 1680 to 1690 (≈ 1685) MeV
 Breit-Wigner full width = 115 to 130 (≈ 120) MeV

$N(1680)$ DECAY MODES	Fraction (Γ_i/Γ)	ρ (MeV/c)
$N\pi$	60–70 %	571
$N\eta$	< 1 %	386
$N\pi\pi$	20–40 %	539
$\Delta(1232)\pi$	11–23 %	374
$\Delta(1232)\pi$, P-wave	4–10 %	374
$\Delta(1232)\pi$, F-wave	1–13 %	374
$N\sigma$	9–19 %	–
$p\gamma$	0.21–0.32 %	581
$p\gamma$, helicity=1/2	0.001–0.011 %	581
$p\gamma$, helicity=3/2	0.20–0.32 %	581
$n\gamma$	0.021–0.046 %	581
$n\gamma$, helicity=1/2	0.004–0.029 %	581
$n\gamma$, helicity=3/2	0.01–0.024 %	581

Baryon Summary Table

 $N(1700) 3/2^-$

$$I(J^P) = \frac{1}{2}(\frac{3}{2}^-)$$

Re(pole position) = 1650 to 1750 (≈ 1700) MeV
 $-2\text{Im}(\text{pole position}) = 100$ to 300 (≈ 200) MeV
 Breit-Wigner mass = 1650 to 1800 (≈ 1720) MeV
 Breit-Wigner full width = 100 to 300 (≈ 200) MeV

$N(1700)$ DECAY MODES	Fraction (Γ_i/Γ)	ρ (MeV/c)
$N\pi$	7–17 %	594
$N\eta$	seen	422
$N\omega$	10–34 %	†
$N\pi\pi$	60–90 %	564
$\Delta(1232)\pi$	55–85 %	402
$\Delta(1232)\pi$, S-wave	50–80 %	402
$\Delta(1232)\pi$, D-wave	4–14 %	402
$N(1440)\pi$	3–11 %	225
$N(1520)\pi$	<4 %	145
$N\rho$, S=3/2, S-wave	32–44 %	74
$N\sigma$	2–14 %	–
$p\gamma$	0.01–0.05 %	604
$p\gamma$, helicity=1/2	0.0–0.024 %	604
$p\gamma$, helicity=3/2	0.002–0.026 %	604
$n\gamma$	0.01–0.13 %	603
$n\gamma$, helicity=1/2	0.0–0.09 %	603
$n\gamma$, helicity=3/2	0.01–0.05 %	603

 $N(1710) 1/2^+$

$$I(J^P) = \frac{1}{2}(\frac{1}{2}^+)$$

Re(pole position) = 1680 to 1720 (≈ 1700) MeV
 $-2\text{Im}(\text{pole position}) = 80$ to 160 (≈ 120) MeV
 Breit-Wigner mass = 1680 to 1740 (≈ 1710) MeV
 Breit-Wigner full width = 80 to 200 (≈ 140) MeV

$N(1710)$ DECAY MODES	Fraction (Γ_i/Γ)	ρ (MeV/c)
$N\pi$	5–20 %	588
$N\eta$	10–50 %	412
$N\omega$	1–5 %	†
ΛK	5–25 %	269
ΣK	seen	138
$N\pi\pi$	seen	557
$\Delta(1232)\pi$, P-wave	3–9 %	394
$N(1535)\pi$	9–21 %	113
$N\rho$, S=1/2, P-wave	11–23 %	†
$p\gamma$, helicity=1/2	0.002–0.08 %	598
$n\gamma$, helicity=1/2	0.0–0.02%	597

 $N(1720) 3/2^+$

$$I(J^P) = \frac{1}{2}(\frac{3}{2}^+)$$

Re(pole position) = 1660 to 1690 (≈ 1675) MeV
 $-2\text{Im}(\text{pole position}) = 150$ to 400 (≈ 250) MeV
 Breit-Wigner mass = 1680 to 1750 (≈ 1720) MeV
 Breit-Wigner full width = 150 to 400 (≈ 250) MeV

$N(1720)$ DECAY MODES	Fraction (Γ_i/Γ)	ρ (MeV/c)
$N\pi$	8–14 %	594
$N\eta$	1–5 %	422
$N\omega$	12–40 %	†
ΛK	4–5 %	283
$N\pi\pi$	50–90 %	564
$\Delta(1232)\pi$	47–89 %	402
$\Delta(1232)\pi$, P-wave	47–77 %	402
$\Delta(1232)\pi$, F-wave	<12 %	402
$N\rho$, S=1/2, P-wave	1–2 %	74
$N\sigma$	2–14 %	–
$N(1440)\pi$	<2 %	225
$N(1520)\pi$, S-wave	1–5 %	145
$p\gamma$	0.05–0.25 %	604
$p\gamma$, helicity=1/2	0.05–0.15 %	604
$p\gamma$, helicity=3/2	0.002–0.16 %	604
$n\gamma$	0.0–0.016 %	603
$n\gamma$, helicity=1/2	0.0–0.01 %	603
$n\gamma$, helicity=3/2	0.0–0.015 %	603

 $N(1875) 3/2^-$

$$I(J^P) = \frac{1}{2}(\frac{3}{2}^-)$$

Re(pole position) = 1850 to 1950 (≈ 1900) MeV
 $-2\text{Im}(\text{pole position}) = 100$ to 220 (≈ 160) MeV
 Breit-Wigner mass = 1850 to 1920 (≈ 1875) MeV
 Breit-Wigner full width = 120 to 250 (≈ 200) MeV

$N(1875)$ DECAY MODES	Fraction (Γ_i/Γ)	ρ (MeV/c)
$N\pi$	3–11 %	695
$N\eta$	<1 %	559
$N\omega$	15–25 %	371
ΛK	seen	454
ΣK	seen	384
$N\pi\pi$		670
$\Delta(1232)\pi$	10–35 %	520
$\Delta(1232)\pi$, S-wave	7–21 %	520
$\Delta(1232)\pi$, D-wave	2–12 %	520
$N\rho$, S=3/2, S-wave	seen	379
$N\sigma$	30–60 %	–
$N(1440)\pi$	2–8 %	365
$N(1520)\pi$	<2 %	301
$p\gamma$	0.001–0.025 %	703
$p\gamma$, helicity=1/2	0.001–0.021 %	703
$p\gamma$, helicity=3/2	<0.003 %	703
$n\gamma$	<0.040 %	702
$n\gamma$, helicity=1/2	<0.007 %	702
$n\gamma$, helicity=3/2	<0.033 %	702

 $N(1880) 1/2^+$

$$I(J^P) = \frac{1}{2}(\frac{1}{2}^+)$$

Re(pole position) = 1820 to 1900 (≈ 1860) MeV
 $-2\text{Im}(\text{pole position}) = 180$ to 280 (≈ 230) MeV
 Breit-Wigner mass = 1830 to 1930 (≈ 1880) MeV
 Breit-Wigner full width = 200 to 400 (≈ 300) MeV

$N(1880)$ DECAY MODES	Fraction (Γ_i/Γ)	ρ (MeV/c)
$N\pi$	3–9 %	698
$N\eta$	5–55 %	563
$N\omega$	12–28 %	377
ΛK	12–28 %	459
ΣK	10–24 %	389
$N\pi\pi$	30–80 %	673
$\Delta(1232)\pi$	18–42 %	524
$N\sigma$	10–40 %	539
$N(1535)\pi$	4–12 %	293
$N\sigma_0(980)$	1–5 %	†
$\Lambda K^*(892)$	0.5–1 %	†
$p\gamma$, helicity=1/2	seen	706
$n\gamma$, helicity=1/2	0.002–0.63 %	705

 $N(1895) 1/2^-$

$$I(J^P) = \frac{1}{2}(\frac{1}{2}^-)$$

Re(pole position) = 1890 to 1930 (≈ 1910) MeV
 $-2\text{Im}(\text{pole position}) = 80$ to 140 (≈ 110) MeV
 Breit-Wigner mass = 1870 to 1920 (≈ 1895) MeV
 Breit-Wigner full width = 80 to 200 (≈ 120) MeV

$N(1895)$ DECAY MODES	Fraction (Γ_i/Γ)	ρ (MeV/c)
$N\pi$	2–18 %	707
$N\eta$	15–40 %	575
$N\eta'$	10–40 %	†
$N\omega$	16–40 %	395
ΛK	13–23 %	473
ΣK	6–20 %	405
$\Delta(1232)\pi$, D-wave	3–11 %	535
$N\rho$, S=1/2, S-wave	seen	403
$N\rho$, S=3/2, D-wave	3–12 %	403
$\Lambda K^*(892)$	4–9 %	†
$N\sigma$	seen	–
$N(1440)\pi$	1–4 %	382
$p\gamma$, helicity=1/2	0.01–0.06 %	715
$n\gamma$, helicity=1/2	0.003–0.05 %	715

Baryon Summary Table

 $N(1900) 3/2^+$

$$I(J^P) = \frac{1}{2}(\frac{3}{2}^+)$$

Re(pole position) = 1900 to 1940 (\approx 1920) MeV
 $-2\text{Im}(\text{pole position}) = 100$ to 200 (\approx 150) MeV
 Breit-Wigner mass = 1890 to 1950 (\approx 1920) MeV
 Breit-Wigner full width = 100 to 320 (\approx 200) MeV

$N(1900)$ DECAY MODES	Fraction (Γ_i/Γ)	ρ (MeV/c)
$N\pi$	1–20 %	723
$N\eta$	2–14 %	595
$N\eta'$	4–8 %	151
$N\omega$	7–13 %	424
ΛK	2–20 %	495
ΣK	3–7 %	431
$N\pi\pi$	40–80 %	699
$\Delta(1232)\pi$	30–70 %	553
$\Delta(1232)\pi, P\text{-wave}$	9–25 %	553
$\Delta(1232)\pi, F\text{-wave}$	21–45 %	553
$\Lambda K^*(892)$	< 0.2 %	†
$N\sigma$	1–7 %	–
$N(1520)\pi$	7–23 %	341
$N(1535)\pi$	4–10 %	328
$p\gamma$	0.001–0.025 %	731
$p\gamma, \text{helicity}=1/2$	0.001–0.021 %	731
$p\gamma, \text{helicity}=3/2$	< 0.003 %	731
$n\gamma$	< 0.040 %	730
$n\gamma, \text{helicity}=1/2$	< 0.007 %	730
$n\gamma, \text{helicity}=3/2$	< 0.033 %	730

 $N(2060) 5/2^-$

$$I(J^P) = \frac{1}{2}(\frac{5}{2}^-)$$

Re(pole position) = 2020 to 2130 (\approx 2070) MeV
 $-2\text{Im}(\text{pole position}) = 350$ to 430 (\approx 400) MeV
 Breit-Wigner mass = 2030 to 2200 (\approx 2100) MeV
 Breit-Wigner full width = 300 to 450 (\approx 400) MeV

$N(2060)$ DECAY MODES	Fraction (Γ_i/Γ)	ρ (MeV/c)
$N\pi$	7–12 %	834
$N\eta$	2–6 %	729
$N\omega$	1–7 %	600
ΛK	seen	644
ΣK	1–5 %	593
$N\pi\pi$	7–19 %	814
$\Delta(1232)\pi, D\text{-wave}$	4–10 %	680
$N\rho, S=1/2, P\text{-wave}$	seen	605
$\Lambda K^*(892)$	0.3–1.3 %	307
$N\sigma$	3–9 %	–
$N(1440)\pi$	4–14 %	544
$N(1520)\pi, P\text{-wave}$	9–21 %	490
$N(1680)\pi, S\text{-wave}$	8–22 %	353
$p\gamma$	0.03–0.19 %	840
$p\gamma, \text{helicity}=1/2$	0.02–0.08 %	840
$p\gamma, \text{helicity}=3/2$	0.01–0.10 %	840
$n\gamma$	0.003–0.07 %	840
$n\gamma, \text{helicity}=1/2$	0.001–0.02 %	840
$n\gamma, \text{helicity}=3/2$	0.002–0.05 %	840

 $N(2100) 1/2^+$

$$I(J^P) = \frac{1}{2}(\frac{1}{2}^+)$$

Re(pole position) = 2050 to 2150 (\approx 2100) MeV
 $-2\text{Im}(\text{pole position}) = 240$ to 340 (\approx 300) MeV
 Breit-Wigner mass = 2050 to 2150 (\approx 2100) MeV
 Breit-Wigner full width = 200 to 320 (\approx 260) MeV

$N(2100)$ DECAY MODES	Fraction (Γ_i/Γ)	ρ (MeV/c)
$N\pi$	8–18 %	834
$N\eta$	seen	729
$N\eta'$	5–11 %	451
$N\omega$	10–25 %	600
ΛK	seen	644
$N\pi\pi$	20–40 %	814

$\Delta(1232)\pi, P\text{-wave}$	6–14 %	680
$N\rho, S=1/2, P\text{-wave}$	seen	605
$\Lambda K^*(892)$	3–11 %	307
$N\sigma$	14–26 %	–
$N(1535)\pi$	26–34 %	478
$N\gamma, \text{helicity}=1/2$	0.001–0.012 %	840

 $N(2120) 3/2^-$

$$I(J^P) = \frac{1}{2}(\frac{3}{2}^-)$$

Re(pole position) = 2050 to 2150 (\approx 2100) MeV
 $-2\text{Im}(\text{pole position}) = 200$ to 360 (\approx 280) MeV
 Breit-Wigner mass = 2060 to 2160 (\approx 2120) MeV
 Breit-Wigner full width = 260 to 360 (\approx 300) MeV

$N(2120)$ DECAY MODES	Fraction (Γ_i/Γ)	ρ (MeV/c)
$N\pi$	5–15 %	846
$N\eta'$	2–6 %	474
$N\omega$	4–20 %	617
$N\pi\pi$	50–95 %	827
$\Delta(1232)\pi$	40–90 %	693
$\Delta(1232)\pi, S\text{-wave}$	30–70 %	693
$\Delta(1232)\pi, D\text{-wave}$	8–32 %	693
$\Lambda K^*(892)$	< 0.2 %	339
$N\sigma$	7–15 %	–
$N(1535)\pi$	7–23 %	494
$p\gamma$	0.16–2.1 %	852
$p\gamma, \text{helicity}=1/2$	0.07–0.80 %	852
$p\gamma, \text{helicity}=3/2$	0.09–1.3 %	852
$n\gamma$	0.04–0.72 %	852
$n\gamma, \text{helicity}=1/2$	0.04–0.60 %	852
$n\gamma, \text{helicity}=3/2$	0.001–0.12 %	852

 $N(2190) 7/2^-$

$$I(J^P) = \frac{1}{2}(\frac{7}{2}^-)$$

Re(pole position) = 2050 to 2150 (\approx 2100) MeV
 $-2\text{Im}(\text{pole position}) = 300$ to 500 (\approx 400) MeV
 Breit-Wigner mass = 2140 to 2220 (\approx 2180) MeV
 Breit-Wigner full width = 300 to 500 (\approx 400) MeV

$N(2190)$ DECAY MODES	Fraction (Γ_i/Γ)	ρ (MeV/c)
$N\pi$	10–20 %	882
$N\eta$	1–3 %	785
$N\omega$	8–20 %	667
$\Delta(1232)\pi, D\text{-wave}$	19–31 %	734
$N\rho, S=3/2, D\text{-wave}$	seen	672
$\Lambda K^*(892)$	0.2–0.8 %	423
$N\sigma$	3–9 %	–
$p\gamma$	0.014–0.077 %	888
$n\gamma$	< 0.04 %	888
$n\gamma, \text{helicity}=3/2$	< 0.03 %	888

 $N(2220) 9/2^+$

$$I(J^P) = \frac{1}{2}(\frac{9}{2}^+)$$

Re(pole position) = 2130 to 2200 (\approx 2170) MeV
 $-2\text{Im}(\text{pole position}) = 360$ to 480 (\approx 400) MeV
 Breit-Wigner mass = 2200 to 2300 (\approx 2250) MeV
 Breit-Wigner full width = 350 to 500 (\approx 400) MeV

$N(2220)$ DECAY MODES	Fraction (Γ_i/Γ)	ρ (MeV/c)
$N\pi$	15–30 %	924

 $N(2250) 9/2^-$

$$I(J^P) = \frac{1}{2}(\frac{9}{2}^-)$$

Re(pole position) = 2150 to 2250 (\approx 2200) MeV
 $-2\text{Im}(\text{pole position}) = 350$ to 500 (\approx 420) MeV
 Breit-Wigner mass = 2250 to 2320 (\approx 2280) MeV
 Breit-Wigner full width = 300 to 600 (\approx 500) MeV

$N(2250)$ DECAY MODES	Fraction (Γ_i/Γ)	ρ (MeV/c)
$N\pi$	0.05 to 0.15 (\approx 0.10)	941

Baryon Summary Table

 $N(2600) 11/2^-$

$$I(J^P) = \frac{1}{2}(\frac{11}{2}^-)$$

Breit-Wigner mass = 2550 to 2750 (≈ 2600) MeV
 Breit-Wigner full width = 500 to 800 (≈ 650) MeV

$N(2600)$ DECAY MODES	Fraction (Γ_i/Γ)	ρ (MeV/c)
$N\pi$	3-8 %	1126

Δ BARYONS ($S = 0, I = 3/2$)

$$\Delta^{++} = uuu, \quad \Delta^+ = uud, \quad \Delta^0 = udd, \quad \Delta^- = ddd$$

 $\Delta(1232) 3/2^+$

$$I(J^P) = \frac{3}{2}(\frac{3}{2}^+)$$

Re(pole position) = 1209 to 1211 (≈ 1210) MeV
 $-2\text{Im}(\text{pole position}) = 98$ to 102 (≈ 100) MeV
 Breit-Wigner mass (mixed charges) = 1230 to 1234 (≈ 1232) MeV
 Breit-Wigner full width (mixed charges) = 114 to 120 (≈ 117) MeV

$\Delta(1232)$ DECAY MODES	Fraction (Γ_i/Γ)	ρ (MeV/c)
$N\pi$	99.4 %	229
$N\gamma$	0.55-0.65 %	259
$N\gamma$, helicity=1/2	0.11-0.13 %	259
$N\gamma$, helicity=3/2	0.44-0.52 %	259
$p e^+ e^-$	(4.2 ± 0.7) $\times 10^{-5}$	259

 $\Delta(1600) 3/2^+$

$$I(J^P) = \frac{3}{2}(\frac{3}{2}^+)$$

Re(pole position) = 1460 to 1560 (≈ 1510) MeV
 $-2\text{Im}(\text{pole position}) = 200$ to 340 (≈ 270) MeV
 Breit-Wigner mass = 1500 to 1640 (≈ 1570) MeV
 Breit-Wigner full width = 200 to 300 (≈ 250) MeV

$\Delta(1600)$ DECAY MODES	Fraction (Γ_i/Γ)	ρ (MeV/c)
$N\pi$	8-24 %	492
$N\pi\pi$	75-90 %	454
$\Delta(1232)\pi$	73-83 %	276
$\Delta(1232)\pi$, P -wave	72-82 %	276
$\Delta(1232)\pi$, F -wave	<2 %	276
$N(1440)\pi$, P -wave	15-25 %	†
$N\gamma$	0.001-0.035 %	505
$N\gamma$, helicity=1/2	0.0-0.02 %	505
$N\gamma$, helicity=3/2	0.001-0.015 %	505

 $\Delta(1620) 1/2^-$

$$I(J^P) = \frac{3}{2}(\frac{1}{2}^-)$$

Re(pole position) = 1590 to 1610 (≈ 1600) MeV
 $-2\text{Im}(\text{pole position}) = 100$ to 140 (≈ 120) MeV
 Breit-Wigner mass = 1590 to 1630 (≈ 1610) MeV
 Breit-Wigner full width = 110 to 150 (≈ 130) MeV

$\Delta(1620)$ DECAY MODES	Fraction (Γ_i/Γ)	ρ (MeV/c)
$N\pi$	25-35 %	520
$N\pi\pi$	55-80 %	484
$\Delta(1232)\pi$, D -wave	52-72 %	311
$N\rho$, $S=1/2$, S -wave	seen	†
$N\rho$, $S=3/2$, D -wave	seen	†
$N(1440)\pi$	3-9 %	98
$N\gamma$, helicity=1/2	0.03-0.10 %	532

 $\Delta(1700) 3/2^-$

$$I(J^P) = \frac{3}{2}(\frac{3}{2}^-)$$

Re(pole position) = 1640 to 1690 (≈ 1665) MeV
 $-2\text{Im}(\text{pole position}) = 200$ to 300 (≈ 250) MeV
 Breit-Wigner mass = 1690 to 1730 (≈ 1710) MeV
 Breit-Wigner full width = 220 to 380 (≈ 300) MeV

 $\Delta(1700)$ DECAY MODES

	Fraction (Γ_i/Γ)	ρ (MeV/c)
$N\pi$	10-20 %	588
$N\pi\pi$	10-55 %	557
$\Delta(1232)\pi$	10-50 %	394
$\Delta(1232)\pi$, S -wave	5-35 %	394
$\Delta(1232)\pi$, D -wave	4-16 %	394
$N\rho$, $S=3/2$, S -wave	seen	†
$N(1520)\pi$, P -wave	1-5 %	133
$N(1535)\pi$	0.5-1.5 %	113
$\Delta(1232)\eta$	3-7 %	†
$N\gamma$	0.22-0.60 %	598
$N\gamma$, helicity=1/2	0.12-0.30 %	598
$N\gamma$, helicity=3/2	0.10-0.30 %	598

 $\Delta(1900) 1/2^-$

$$I(J^P) = \frac{3}{2}(\frac{1}{2}^-)$$

Re(pole position) = 1830 to 1900 (≈ 1865) MeV
 $-2\text{Im}(\text{pole position}) = 180$ to 300 (≈ 240) MeV
 Breit-Wigner mass = 1840 to 1920 (≈ 1860) MeV
 Breit-Wigner full width = 180 to 320 (≈ 250) MeV

 $\Delta(1900)$ DECAY MODES

	Fraction (Γ_i/Γ)	ρ (MeV/c)
$N\pi$	4-12 %	685
ΣK	seen	367
$N\pi\pi$	45-85 %	660
$\Delta(1232)\pi$, D -wave	30-70 %	509
$N\rho$, $S=1/2$, S -wave	8-16 %	360
$N\rho$, $S=3/2$, D -wave	18-28 %	360
$N(1440)\pi$	8-32 %	353
$N(1520)\pi$	2-10 %	288
$\Delta(1232)\eta$	0-2 %	251
$N\gamma$, helicity=1/2	0.06-0.43 %	693

 $\Delta(1905) 5/2^+$

$$I(J^P) = \frac{3}{2}(\frac{5}{2}^+)$$

Re(pole position) = 1770 to 1830 (≈ 1800) MeV
 $-2\text{Im}(\text{pole position}) = 260$ to 340 (≈ 300) MeV
 Breit-Wigner mass = 1855 to 1910 (≈ 1880) MeV
 Breit-Wigner full width = 270 to 400 (≈ 330) MeV

 $\Delta(1905)$ DECAY MODES

	Fraction (Γ_i/Γ)	ρ (MeV/c)
$N\pi$	9-15 %	698
$N\pi\pi$		673
$\Delta(1232)\pi$	80-100 %	524
$\Delta(1232)\pi$, P -wave	23-43 %	524
$\Delta(1232)\pi$, F -wave	56-72 %	524
$N\rho$, $S=3/2$, P -wave	seen	385
$N(1535)\pi$	<1 %	293
$N(1680)\pi$, P -wave	5-15 %	133
$\Delta(1232)\eta$	2-6 %	282
$N\gamma$	0.012-0.036 %	706
$N\gamma$, helicity=1/2	0.002-0.006 %	706
$N\gamma$, helicity=3/2	0.01-0.03 %	706

 $\Delta(1910) 1/2^+$

$$I(J^P) = \frac{3}{2}(\frac{1}{2}^+)$$

Re(pole position) = 1830 to 1890 (≈ 1860) MeV
 $-2\text{Im}(\text{pole position}) = 200$ to 400 (≈ 300) MeV
 Breit-Wigner mass = 1850 to 1950 (≈ 1900) MeV
 Breit-Wigner full width = 200 to 400 (≈ 300) MeV

 $\Delta(1910)$ DECAY MODES

	Fraction (Γ_i/Γ)	ρ (MeV/c)
$N\pi$	15-30 %	710
ΣK	4-14 %	410
$N\pi\pi$		686
$\Delta(1232)\pi$	34-66 %	539
$N(1440)\pi$	3-9 %	386
$\Delta(1232)\eta$	5-13 %	310
$N\gamma$, helicity=1/2	0.0-0.02 %	718

Baryon Summary Table

$\Delta(1920) 3/2^+$ $I(J^P) = \frac{3}{2}(\frac{3}{2}^+)$

Re(pole position) = 1850 to 1950 (≈ 1900) MeV
 $-2\text{Im}(\text{pole position}) = 200$ to 400 (≈ 300) MeV
 Breit-Wigner mass = 1870 to 1970 (≈ 1920) MeV
 Breit-Wigner full width = 240 to 360 (≈ 300) MeV

$\Delta(1920)$ DECAY MODES	Fraction (Γ_i/Γ)	ρ (MeV/c)
$N\pi$	5–20 %	723
ΣK	2–6 %	431
$N\pi\pi$		699
$\Delta(1232)\pi$	50–90 %	553
$\Delta(1232)\pi$, P -wave	8–28 %	553
$\Delta(1232)\pi$, F -wave	44–72 %	553
$N(1440)\pi$, P -wave	<4 %	403
$N(1520)\pi$, S -wave	<5 %	341
$N(1535)\pi$	<2 %	328
$N_{a_0}(980)$	seen	41
$\Delta(1232)\eta$	5–17 %	336

$\Delta(1930) 5/2^-$ $I(J^P) = \frac{3}{2}(\frac{5}{2}^-)$

Re(pole position) = 1840 to 1920 (≈ 1880) MeV
 $-2\text{Im}(\text{pole position}) = 230$ to 330 (≈ 280) MeV
 Breit-Wigner mass = 1900 to 2000 (≈ 1950) MeV
 Breit-Wigner full width = 200 to 400 (≈ 300) MeV

$\Delta(1930)$ DECAY MODES	Fraction (Γ_i/Γ)	ρ (MeV/c)
$N\pi$	5–15 %	742
$N\gamma$	0.0–0.01 %	749
$N\gamma$, helicity=1/2	0.0–0.005 %	749
$N\gamma$, helicity=3/2	0.0–0.004 %	749

$\Delta(1950) 7/2^+$ $I(J^P) = \frac{3}{2}(\frac{7}{2}^+)$

Re(pole position) = 1870 to 1890 (≈ 1880) MeV
 $-2\text{Im}(\text{pole position}) = 220$ to 260 (≈ 240) MeV
 Breit-Wigner mass = 1915 to 1950 (≈ 1930) MeV
 Breit-Wigner full width = 235 to 335 (≈ 285) MeV

$\Delta(1950)$ DECAY MODES	Fraction (Γ_i/Γ)	ρ (MeV/c)
$N\pi$	35–45 %	729
ΣK	0.3–0.5 %	441
$N\pi\pi$		706
$\Delta(1232)\pi$, F -wave	1–9 %	560
$N(1680)\pi$, P -wave	3–9 %	191
$\Delta(1232)\eta$	< 0.6 %	349

$\Delta(2200) 7/2^-$ $I(J^P) = \frac{3}{2}(\frac{7}{2}^-)$

Re(pole position) = 2050 to 2150 (≈ 2100) MeV
 $-2\text{Im}(\text{pole position}) = 260$ to 420 (≈ 340) MeV
 Breit-Wigner mass = 2150 to 2250 (≈ 2200) MeV
 Breit-Wigner full width = 200 to 500 (≈ 350) MeV

$\Delta(2200)$ DECAY MODES	Fraction (Γ_i/Γ)	ρ (MeV/c)
$N\pi$	2–8 %	894
ΣK	1–7 %	672
$\Delta\pi$, D -wave	40–100 %	747
$\Delta\pi$, G -wave	5–25 %	747
$\Delta\eta$, D -wave	seen	614

$\Delta(2420) 11/2^+$ $I(J^P) = \frac{3}{2}(\frac{11}{2}^+)$

Re(pole position) = 2300 to 2500 (≈ 2400) MeV
 $-2\text{Im}(\text{pole position}) = 350$ to 550 (≈ 450) MeV
 Breit-Wigner mass = 2300 to 2600 (≈ 2450) MeV
 Breit-Wigner full width = 300 to 700 (≈ 500) MeV

$\Delta(2420)$ DECAY MODES	Fraction (Γ_i/Γ)	ρ (MeV/c)
$N\pi$	5–10 %	1040

Λ BARYONS

$(S = -1, I = 0)$
 $\Lambda^0 = uds$

Λ $I(J^P) = 0(\frac{1}{2}^+)$

Mass $m = 1115.683 \pm 0.006$ MeV
 $(m_\Lambda - m_{\bar{\Lambda}}) / m_\Lambda = (-0.1 \pm 1.1) \times 10^{-5}$ ($S = 1.6$)
 Mean life $\tau = (2.632 \pm 0.020) \times 10^{-10}$ s ($S = 1.6$)
 $(\tau_\Lambda - \tau_{\bar{\Lambda}}) / \tau_\Lambda = -0.001 \pm 0.009$
 $c\tau = 7.89$ cm
 Magnetic moment $\mu = -0.613 \pm 0.004 \mu_N$
 Electric dipole moment $d < 1.5 \times 10^{-16}$ e cm, CL = 95%

Decay parameters

$p\pi^-$	$\alpha_- = 0.732 \pm 0.014$ ($S = 2.3$)
$\bar{p}\pi^+$	$\alpha_+ = -0.758 \pm 0.012$
$\bar{\alpha}_0$ FOR $\bar{\Lambda} \rightarrow \bar{n}\pi^0$	-0.692 ± 0.017
$p\pi^-$	$\phi_- = (-6.5 \pm 3.5)^\circ$
"	$\gamma_- = 0.76$ [n]
"	$\Delta_- = (8 \pm 4)^\circ$ [n]
$\bar{\alpha}_0 / \alpha_+$ in $\bar{\Lambda} \rightarrow \bar{n}\pi^0, \bar{\Lambda} \rightarrow \bar{p}\pi^+$	$= 0.913 \pm 0.030$
$R = G_E/G_M $ in $\Lambda \rightarrow p\pi^-, \bar{\Lambda} \rightarrow \bar{p}\pi^+$	$= 0.96 \pm 0.14$
$\Delta\Phi = \Phi_E - \Phi_M$ in $\Lambda \rightarrow p\pi^-, \bar{\Lambda} \rightarrow \bar{p}\pi^+$	$= 37 \pm 13$ degrees
$n\pi^0$	$\alpha_0 = 0.74 \pm 0.05$
$p e^- \bar{\nu}_e$	$g_A/g_V = -0.718 \pm 0.015$ [l]

Λ DECAY MODES	Fraction (Γ_i/Γ)	Confidence level	ρ (MeV/c)
$p\pi^-$	(63.9 \pm 0.5) %		101
$n\pi^0$	(35.8 \pm 0.5) %		104
$n\gamma$	(1.75 \pm 0.15) $\times 10^{-3}$		162
$p\pi^-\gamma$	[o] (8.4 \pm 1.4) $\times 10^{-4}$		101
$p e^- \bar{\nu}_e$	(8.32 \pm 0.14) $\times 10^{-4}$		163
$p\mu^- \bar{\nu}_\mu$	(1.57 \pm 0.35) $\times 10^{-4}$		131

Lepton (L) and/or Baryon (B) number violating decay modes

$\pi^+ e^-$	$L, B < 6$	$\times 10^{-7}$	90%	549
$\pi^+ \mu^-$	$L, B < 6$	$\times 10^{-7}$	90%	544
$\pi^- e^+$	$L, B < 4$	$\times 10^{-7}$	90%	549
$\pi^- \mu^+$	$L, B < 6$	$\times 10^{-7}$	90%	544
$K^+ e^-$	$L, B < 2$	$\times 10^{-6}$	90%	449
$K^+ \mu^-$	$L, B < 3$	$\times 10^{-6}$	90%	441
$K^- e^+$	$L, B < 2$	$\times 10^{-6}$	90%	449
$K^- \mu^+$	$L, B < 3$	$\times 10^{-6}$	90%	441
$K_S^0 \nu$	$L, B < 2$	$\times 10^{-5}$	90%	447
$\bar{p}\pi^+$	$B < 9$	$\times 10^{-7}$	90%	101

$\Lambda(1405) 1/2^-$ $I(J^P) = 0(\frac{1}{2}^-)$

Mass $m = 1405.1^{+1.3}_{-1.0}$ MeV
 Full width $\Gamma = 50.5 \pm 2.0$ MeV
 Below $\bar{K}N$ threshold

$\Lambda(1405)$ DECAY MODES	Fraction (Γ_i/Γ)	ρ (MeV/c)
$\Sigma\pi$	100 %	155

$\Lambda(1520) 3/2^-$ $I(J^P) = 0(\frac{3}{2}^-)$

Mass $m = 1518$ to 1520 (≈ 1519) MeV [p]
 Full width $\Gamma = 15$ to 17 (≈ 16) MeV [p]

$\Lambda(1520)$ DECAY MODES	Fraction (Γ_i/Γ)	ρ (MeV/c)
$N\bar{K}$	(45 ± 1) %	242
$\Sigma\pi$	(42 ± 1) %	268
$\Lambda\pi\pi$	(10 ± 1) %	259

Baryon Summary Table

$\Sigma \pi \pi$	(0.9 ± 0.1) %	168
$\Lambda \gamma$	(0.85 ± 0.15) %	350

 $\Lambda(1600) 1/2^+$

$$I(J^P) = 0(\frac{1}{2}^+)$$

Mass $m = 1570$ to 1630 (≈ 1600) MeV
Full width $\Gamma = 150$ to 250 (≈ 200) MeV

$\Lambda(1600)$ DECAY MODES	Fraction (Γ_i/Γ)	ρ (MeV/c)
$N\bar{K}$	15–30 %	343
$\Sigma \pi$	10–60 %	338
$\Lambda \sigma$	(19 ± 4) %	–
$\Sigma(1385)\pi$	(9 ± 4) %	158

 $\Lambda(1670) 1/2^-$

$$I(J^P) = 0(\frac{1}{2}^-)$$

Mass $m = 1670$ to 1678 (≈ 1674) MeV
Full width $\Gamma = 25$ to 35 (≈ 30) MeV

$\Lambda(1670)$ DECAY MODES	Fraction (Γ_i/Γ)	ρ (MeV/c)
$N\bar{K}$	20–30 %	418
$\Sigma \pi$	25–55 %	398
$\Lambda \eta$	10–25 %	88
$\Sigma(1385)\pi, D$ -wave	(6.0 ± 2.0) %	235
$N\bar{K}^*(892), S=3/2, D$ -wave	(5 ± 4) %	†
$\Lambda \sigma$	(20 ± 8) %	–

 $\Lambda(1690) 3/2^-$

$$I(J^P) = 0(\frac{3}{2}^-)$$

Mass $m = 1685$ to 1695 (≈ 1690) MeV
Full width $\Gamma = 60$ to 80 (≈ 70) MeV

$\Lambda(1690)$ DECAY MODES	Fraction (Γ_i/Γ)	ρ (MeV/c)
$N\bar{K}$	20–30 %	433
$\Sigma \pi$	20–40 %	410
$\Lambda \sigma$	(5.0 ± 2.0) %	–
$\Lambda \pi \pi$	~ 25 %	419
$\Sigma \pi \pi$	~ 20 %	358
$\Sigma(1385)\pi, S$ -wave	(9 ± 5) %	251
$\Sigma(1385)\pi, D$ -wave	(3.0 ± 2.0) %	251

 $\Lambda(1800) 1/2^-$

$$I(J^P) = 0(\frac{1}{2}^-)$$

Mass $m = 1750$ to 1850 (≈ 1800) MeV
Full width $\Gamma = 150$ to 250 (≈ 200) MeV

$\Lambda(1800)$ DECAY MODES	Fraction (Γ_i/Γ)	ρ (MeV/c)
$N\bar{K}$	25–40 %	528
$\Sigma \pi$	seen	494
$\Lambda \sigma$	(15 ± 4) %	–
$\Sigma(1385)\pi$	seen	349
$\Lambda \eta$	0.01 to 0.10	326
$N\bar{K}^*(892)$	seen	†

 $\Lambda(1810) 1/2^+$

$$I(J^P) = 0(\frac{1}{2}^+)$$

Mass $m = 1740$ to 1840 (≈ 1790) MeV
Full width $\Gamma = 50$ to 170 (≈ 110) MeV

$\Lambda(1810)$ DECAY MODES	Fraction (Γ_i/Γ)	ρ (MeV/c)
$N\bar{K}$	0.05 to 0.35	520
$\Sigma \pi$	(16 ± 5) %	487
$\Sigma(1385)\pi$	(40 ± 15) %	340
$N\bar{K}^*(892)$	30–60 %	†

 $\Lambda(1820) 5/2^+$

$$I(J^P) = 0(\frac{5}{2}^+)$$

Mass $m = 1815$ to 1825 (≈ 1820) MeV
Full width $\Gamma = 70$ to 90 (≈ 80) MeV

$\Lambda(1820)$ DECAY MODES	Fraction (Γ_i/Γ)	ρ (MeV/c)
$N\bar{K}$	55–65 %	545
$\Sigma \pi$	8–14 %	509
$\Sigma(1385)\pi$	5–10 %	366
$N\bar{K}^*(892), S=3/2, P$ -wave	(3.0 ± 1.0) %	†

 $\Lambda(1830) 5/2^-$

$$I(J^P) = 0(\frac{5}{2}^-)$$

Mass $m = 1820$ to 1830 (≈ 1825) MeV
Full width $\Gamma = 60$ to 120 (≈ 90) MeV

$\Lambda(1830)$ DECAY MODES	Fraction (Γ_i/Γ)	Scale factor ρ (MeV/c)
$N\bar{K}$	0.04 to 0.08	549
$\Sigma \pi$	35–75 %	512
$\Sigma(1385)\pi$	>15 %	370
$\Sigma(1385)\pi, D$ -wave	(40 ± 15) %	3.2

 $\Lambda(1890) 3/2^+$

$$I(J^P) = 0(\frac{3}{2}^+)$$

Mass $m = 1870$ to 1910 (≈ 1890) MeV
Full width $\Gamma = 80$ to 160 (≈ 120) MeV

$\Lambda(1890)$ DECAY MODES	Fraction (Γ_i/Γ)	ρ (MeV/c)
$N\bar{K}$	0.24 to 0.36	599
$\Sigma \pi$	3–10 %	560
$\Sigma(1385)\pi$	seen	423
$\Sigma(1385)\pi, P$ -wave	(6.0 ± 3.0) %	423
$\Sigma(1385)\pi, F$ -wave	(4.0 ± 2.0) %	423
$N\bar{K}^*(892)$	seen	236

 $\Lambda(2100) 7/2^-$

$$I(J^P) = 0(\frac{7}{2}^-)$$

Mass $m = 2090$ to 2110 (≈ 2100) MeV
Full width $\Gamma = 100$ to 250 (≈ 200) MeV

$\Lambda(2100)$ DECAY MODES	Fraction (Γ_i/Γ)	ρ (MeV/c)
$N\bar{K}$	25–35 %	751
$\Sigma \pi$	~ 5 %	705
$\Lambda \eta$	< 3 %	617
ΞK	< 3 %	491
$\Lambda \omega$	< 8 %	443
$N\bar{K}^*(892)$	10–20 %	515
$\Sigma(1385)\pi, G$ -wave	(1.0 ± 1.0) %	584
$N\bar{K}^*(892), S=3/2, D$ -wave	(4.0 ± 2.0) %	515

 $\Lambda(2110) 5/2^+$

$$I(J^P) = 0(\frac{5}{2}^+)$$

Mass $m = 2050$ to 2130 (≈ 2090) MeV
Full width $\Gamma = 200$ to 300 (≈ 250) MeV

$\Lambda(2110)$ DECAY MODES	Fraction (Γ_i/Γ)	ρ (MeV/c)
$N\bar{K}$	5–25 %	744
$\Sigma \pi$	10–40 %	698
$\Lambda \omega$	seen	432
$\Lambda \omega, S=3/2, P$ -wave	(5.0 ± 2.0) %	432
$\Sigma(1385)\pi$	seen	576
$N\bar{K}^*(892)$	10–60 %	505

 $\Lambda(2350) 9/2^+$

$$I(J^P) = 0(\frac{9}{2}^+)$$

Mass $m = 2340$ to 2370 (≈ 2350) MeV
Full width $\Gamma = 100$ to 250 (≈ 150) MeV

$\Lambda(2350)$ DECAY MODES	Fraction (Γ_i/Γ)	ρ (MeV/c)
$N\bar{K}$	~ 12 %	915
$\Sigma \pi$	~ 10 %	867

Baryon Summary Table

 Σ BARYONS
($S = -1, I = 1$)

$$\Sigma^+ = u u s, \quad \Sigma^0 = u d s, \quad \Sigma^- = d d s$$

 Σ^+

$$I(J^P) = 1(\frac{1}{2}^+)$$

Mass $m = 1189.37 \pm 0.07$ MeV ($S = 2.2$)
 Mean life $\tau = (0.8018 \pm 0.0026) \times 10^{-10}$ s
 $c\tau = 2.404$ cm

$(\tau_{\Sigma^+} - \tau_{\Sigma^-}) / \tau_{\Sigma^+} = -0.0006 \pm 0.0012$
 Magnetic moment $\mu = 2.458 \pm 0.010 \mu_N$ ($S = 2.1$)
 $(\mu_{\Sigma^+} + \mu_{\Sigma^-}) / \mu_{\Sigma^+} = 0.014 \pm 0.015$
 $\Gamma(\Sigma^+ \rightarrow n \ell^+ \nu) / \Gamma(\Sigma^- \rightarrow n \ell^- \bar{\nu}) < 0.043$

Decay parameters

$\rho\pi^0$ $\alpha_0 = -0.980 \pm 0.017$
 " $\phi_0 = (36 \pm 34)^\circ$
 " $\gamma_0 = 0.16$ [n]
 " $\Delta_0 = (187 \pm 6)^\circ$ [n]
 $n\pi^+$ $\alpha_+ = 0.068 \pm 0.013$
 " $\phi_+ = (167 \pm 20)^\circ$ ($S = 1.1$)
 " $\gamma_+ = -0.97$ [n]
 " $\Delta_+ = (-73 \pm 133)^\circ$ [n]
 $\rho\gamma$ $\alpha_\gamma = -0.76 \pm 0.08$

 Σ^+ DECAY MODES

	Fraction (Γ_i/Γ)	Confidence level	ρ (MeV/c)
$\rho\pi^0$	$(51.57 \pm 0.30) \%$		189
$n\pi^+$	$(48.31 \pm 0.30) \%$		185
$\rho\gamma$	$(1.23 \pm 0.05) \times 10^{-3}$		225
$n\pi^+\gamma$	[a] $(4.5 \pm 0.5) \times 10^{-4}$		185
$\Lambda e^+ \nu_e$	$(2.0 \pm 0.5) \times 10^{-5}$		71

 **$\Delta S = \Delta Q$ (SQ) violating modes or
 $\Delta S = 1$ weak neutral current (SI) modes**

$n e^+ \nu_e$	SQ	< 5	$\times 10^{-6}$	90%	224
$n\mu^+ \nu_\mu$	SQ	< 3.0	$\times 10^{-5}$	90%	202
$\rho e^+ e^-$	SI	< 7	$\times 10^{-6}$		225
$\rho\mu^+ \mu^-$	SI	$(2.4 \pm 1.7) \times 10^{-8}$			121

 Σ^0

$$I(J^P) = 1(\frac{1}{2}^+)$$

Mass $m = 1192.642 \pm 0.024$ MeV
 $m_{\Sigma^-} - m_{\Sigma^0} = 4.807 \pm 0.035$ MeV ($S = 1.1$)
 $m_{\Sigma^0} - m_\Lambda = 76.959 \pm 0.023$ MeV
 Mean life $\tau = (7.4 \pm 0.7) \times 10^{-20}$ s
 $c\tau = 2.22 \times 10^{-11}$ m
 Transition magnetic moment $|\mu_{\Sigma\Lambda}| = 1.61 \pm 0.08 \mu_N$

 Σ^0 DECAY MODES

	Fraction (Γ_i/Γ)	Confidence level	ρ (MeV/c)
$\Lambda\gamma$	100 %		74
$\Lambda\gamma\gamma$	$< 3 \%$	90%	74
$\Lambda e^+ e^-$	[a] 5×10^{-3}		74

 Σ^-

$$I(J^P) = 1(\frac{1}{2}^+)$$

Mass $m = 1197.449 \pm 0.030$ MeV ($S = 1.2$)
 $m_{\Sigma^-} - m_{\Sigma^+} = 8.08 \pm 0.08$ MeV ($S = 1.9$)
 $m_{\Sigma^-} - m_\Lambda = 81.766 \pm 0.030$ MeV ($S = 1.2$)
 Mean life $\tau = (1.479 \pm 0.011) \times 10^{-10}$ s ($S = 1.3$)
 $c\tau = 4.434$ cm
 Magnetic moment $\mu = -1.160 \pm 0.025 \mu_N$ ($S = 1.7$)
 Σ^- charge radius = 0.78 ± 0.10 fm

Decay parameters

$n\pi^-$ $\alpha_- = -0.068 \pm 0.008$
 " $\phi_- = (10 \pm 15)^\circ$
 " $\gamma_- = 0.98$ [n]
 " $\Delta_- = (249 \pm 12)^\circ$ [n]
 $n e^- \bar{\nu}_e$ $g_A/g_V = 0.340 \pm 0.017$ [i]
 " $f_2(0)/f_1(0) = 0.97 \pm 0.14$
 " $D = 0.11 \pm 0.10$
 $\Lambda e^- \bar{\nu}_e$ $g_V/g_A = 0.01 \pm 0.10$ [i] ($S = 1.5$)
 " $g_{WM}/g_A = 2.4 \pm 1.7$ [i]

 Σ^- DECAY MODES

	Fraction (Γ_i/Γ)	ρ (MeV/c)
$n\pi^-$	$(99.848 \pm 0.005) \%$	193
$n\pi^-\gamma$	[a] $(4.6 \pm 0.6) \times 10^{-4}$	193
$n e^- \bar{\nu}_e$	$(1.017 \pm 0.034) \times 10^{-3}$	230
$n\mu^- \bar{\nu}_\mu$	$(4.5 \pm 0.4) \times 10^{-4}$	210
$\Lambda e^- \bar{\nu}_e$	$(5.73 \pm 0.27) \times 10^{-5}$	79

 $\Sigma(1385) 3/2^+$

$$I(J^P) = 1(\frac{3}{2}^+)$$

$\Sigma(1385)^+$ mass $m = 1382.80 \pm 0.35$ MeV ($S = 1.9$)
 $\Sigma(1385)^0$ mass $m = 1383.7 \pm 1.0$ MeV ($S = 1.4$)
 $\Sigma(1385)^-$ mass $m = 1387.2 \pm 0.5$ MeV ($S = 2.2$)
 $\Sigma(1385)^+$ full width $\Gamma = 36.0 \pm 0.7$ MeV
 $\Sigma(1385)^0$ full width $\Gamma = 36 \pm 5$ MeV
 $\Sigma(1385)^-$ full width $\Gamma = 39.4 \pm 2.1$ MeV ($S = 1.7$)
 Below $\bar{K}N$ threshold

 $\Sigma(1385)$ DECAY MODES

	Fraction (Γ_i/Γ)	Confidence level	ρ (MeV/c)
$\Lambda\pi$	$(87.0 \pm 1.5) \%$		208
$\Sigma\pi$	$(11.7 \pm 1.5) \%$		129
$\Lambda\gamma$	$(1.25 \pm 0.13) \%$		241
$\Sigma^+\gamma$	$(7.0 \pm 1.7) \times 10^{-3}$		180
$\Sigma^-\gamma$	< 2.4	$\times 10^{-4}$	90% 173

 $\Sigma(1660) 1/2^+$

$$I(J^P) = 1(\frac{1}{2}^+)$$

Re(pole position) = 1585 ± 20 MeV
 $-2\text{Im}(\text{pole position}) = 290 \pm 140$ MeV
 Mass $m = 1640$ to 1680 (≈ 1660) MeV
 Full width $\Gamma = 100$ to 300 (≈ 200) MeV

 $\Sigma(1660)$ DECAY MODES

	Fraction (Γ_i/Γ)	ρ (MeV/c)
$\bar{N}\bar{K}$	0.05 to 0.15 (≈ 0.10)	405
$\Lambda\pi$	$(35 \pm 12) \%$	440
$\Sigma\pi$	$(37 \pm 10) \%$	387
$\Sigma\sigma$	$(20 \pm 8) \%$	-
$\Lambda(1405)\pi$	$(4.0 \pm 2.0) \%$	199

 $\Sigma(1670) 3/2^-$

$$I(J^P) = 1(\frac{3}{2}^-)$$

Mass $m = 1665$ to 1685 (≈ 1675) MeV
 Full width $\Gamma = 40$ to 100 (≈ 70) MeV

 $\Sigma(1670)$ DECAY MODES

	Fraction (Γ_i/Γ)	ρ (MeV/c)
$\bar{N}\bar{K}$	0.06 to 0.12	419
$\Lambda\pi$	5-15 %	452
$\Sigma\pi$	30-60 %	398
$\Sigma\sigma$	$(7.0 \pm 3.0) \%$	-

 $\Sigma(1750) 1/2^-$

$$I(J^P) = 1(\frac{1}{2}^-)$$

Mass $m = 1700$ to 1800 (≈ 1750) MeV
 Full width $\Gamma = 100$ to 200 (≈ 150) MeV

 $\Sigma(1750)$ DECAY MODES

	Fraction (Γ_i/Γ)	ρ (MeV/c)
$\bar{N}\bar{K}$	0.06 to 0.12	486
$\Lambda\pi$	$(14 \pm 5) \%$	507
$\Sigma\pi$	$(16 \pm 4) \%$	456
$\Sigma\eta$	15-55 %	98
$\Sigma(1385)\pi, D\text{-wave}$	< 1 %	305
$\Lambda(1520)\pi$	$(2.0 \pm 1.0) \%$	175
$\bar{N}\bar{K}^*(892), S=1/2$	$(8 \pm 4) \%$	†

 $\Sigma(1775) 5/2^-$

$$I(J^P) = 1(\frac{5}{2}^-)$$

Mass $m = 1770$ to 1780 (≈ 1775) MeV
 Full width $\Gamma = 105$ to 135 (≈ 120) MeV

Baryon Summary Table

$\Sigma(1775)$ DECAY MODES	Fraction (Γ_i/Γ)	ρ (MeV/c)
$N\bar{K}$	37-43%	508
$\Lambda\pi$	14-20%	525
$\Sigma\pi$	2-5%	475
$\Sigma(1385)\pi$	8-12%	327
$\Lambda(1520)\pi$, P -wave	17-23%	202

$\Sigma(1910) 3/2^-$ $I(J^P) = 1(\frac{3}{2}^-)$

was $\Sigma(1940)$

- Full width $\Gamma = 0.03 \pm 0.02$
- Full width $\Gamma = 0.16 \pm 0.04$
- Full width $\Gamma = 0.04 \pm 0.03$
- Full width $\Gamma = 0.01 \pm 0.01$
- Full width $\Gamma = 0.01 \pm 0.01$
- Full width $\Gamma = 0.03 \pm 0.01$
- Full width $\Gamma = 0.03 \pm 0.02$
- Full width $\Gamma = 0.02 \pm 0.01$
- Full width $\Gamma = 0.01 \pm 0.01$
- Mass $m = 1870$ to 1950 (≈ 1910) MeV
- Full width $\Gamma = 150$ to 300 (≈ 220) MeV

$\Sigma(1910)$ DECAY MODES	Fraction (Γ_i/Γ)	ρ (MeV/c)
$N\bar{K}$	0.01 to 0.05 (≈ 0.02)	615
$\Lambda\pi$	(6 \pm 4) %	619
$\Sigma\pi$	(86 \pm 21) %	574
$\Sigma(1385)\pi$	seen	439
$\Lambda(1520)\pi$	seen	329
$\Delta(1232)\bar{K}$	(3.0 \pm 1.0) %	377
$N\bar{K}^*(892)$	seen	274
$N\bar{K}^*(892)$, $S=1/2$, D -wave	(1.0 \pm 1.0) %	274

$\Sigma(1915) 5/2^+$ $I(J^P) = 1(\frac{5}{2}^+)$

Mass $m = 1900$ to 1935 (≈ 1915) MeV
Full width $\Gamma = 80$ to 160 (≈ 120) MeV

$\Sigma(1915)$ DECAY MODES	Fraction (Γ_i/Γ)	ρ (MeV/c)
$N\bar{K}$	0.05 to 0.15	618
$\Lambda\pi$	(6.0 \pm 2.0) %	623
$\Sigma\pi$	(10.0 \pm 2.0) %	577
$\Sigma(1385)\pi$, P -wave	(2.0 \pm 2.0) %	443
$\Sigma(1385)\pi$, F -wave	(4.0 \pm 2.0) %	443
$\Sigma(1385)\pi$	<5 %	443
$\Lambda(1520)\pi$, D -wave	(8.0 \pm 2.0) %	334
$N\bar{K}^*(892)$, $S=1/2$, F -wave	(5.0 \pm 3.0) %	282
$N\bar{K}^*(892)$, $S=3/2$, F -wave	(5.0 \pm 2.0) %	282
$\Delta\bar{K}$, P -wave	(16 \pm 5) %	383
$\Delta\bar{K}$, F -wave	(5.0 \pm 3.0) %	383

$\Sigma(2030) 7/2^+$ $I(J^P) = 1(\frac{7}{2}^+)$

Mass $m = 2025$ to 2040 (≈ 2030) MeV
Full width $\Gamma = 150$ to 200 (≈ 180) MeV

$\Sigma(2030)$ DECAY MODES	Fraction (Γ_i/Γ)	ρ (MeV/c)
$N\bar{K}$	17-23 %	702
$\Lambda\pi$	17-23 %	700
$\Sigma\pi$	5-10 %	657
ΞK	<2 %	422
$\Sigma(1385)\pi$	5-15 %	532
$\Sigma(1385)\pi$, F -wave	(1.0 \pm 1.0) %	532
$\Lambda(1520)\pi$	10-20 %	431
$\Delta(1232)\bar{K}$	10-20 %	498
$\Delta(1232)\bar{K}$, F -wave	(15 \pm 5) %	498
$\Delta(1232)\bar{K}$, H -wave	(1.0 \pm 1.0) %	498
$N\bar{K}^*(892)$	<5 %	439
$N\bar{K}^*(892)$, $S=3/2$, F -wave	(14 \pm 8) %	439

$\Sigma(2250)$ $I(J^P) = 1(?^?)$

Mass $m = 2210$ to 2280 (≈ 2250) MeV
Full width $\Gamma = 60$ to 150 (≈ 100) MeV

$\Sigma(2250)$ DECAY MODES	Fraction (Γ_i/Γ)	ρ (MeV/c)
$N\bar{K}$	<10 %	851
$\Lambda\pi$	seen	842
$\Sigma\pi$	seen	803

Ξ BARYONS
($S = -2, I = 1/2$)
 $\Xi^0 = uss, \Xi^- = dss$

Ξ^0 $I(J^P) = \frac{1}{2}(\frac{1}{2}^+)$

P is not yet measured; + is the quark model prediction.

Mass $m = 1314.86 \pm 0.20$ MeV
 $m_{\Xi^-} - m_{\Xi^0} = 6.85 \pm 0.21$ MeV
Mean life $\tau = (2.90 \pm 0.09) \times 10^{-10}$ s
 $c\tau = 8.71$ cm
Magnetic moment $\mu = -1.250 \pm 0.014 \mu_N$

Decay parameters

- $\Lambda\pi^0$ $\alpha = -0.356 \pm 0.011$
- " $\phi = (21 \pm 12)^\circ$
- " $\gamma = 0.85$ [n]
- " $\Delta = (218^{+12}_{-19})^\circ$ [n]
- $\Lambda\gamma$ $\alpha = -0.70 \pm 0.07$
- $\Lambda e^+ e^-$ $\alpha = -0.8 \pm 0.2$
- $\Sigma^0 \gamma$ $\alpha = -0.69 \pm 0.06$
- $\Sigma^+ e^- \bar{\nu}_e$ $g_1(0)/f_1(0) = 1.22 \pm 0.05$
- $\Sigma^+ e^- \bar{\nu}_e$ $f_2(0)/f_1(0) = 2.0 \pm 0.9$

Ξ^0 DECAY MODES	Fraction (Γ_i/Γ)	Confidence level	ρ (MeV/c)
$\Lambda\pi^0$	(99.524 \pm 0.012) %		135
$\Lambda\gamma$	(1.17 \pm 0.07) $\times 10^{-3}$		184
$\Lambda e^+ e^-$	(7.6 \pm 0.6) $\times 10^{-6}$		184
$\Sigma^0 \gamma$	(3.33 \pm 0.10) $\times 10^{-3}$		117
$\Sigma^+ e^- \bar{\nu}_e$	(2.52 \pm 0.08) $\times 10^{-4}$		120
$\Sigma^+ \mu^- \bar{\nu}_\mu$	(2.33 \pm 0.35) $\times 10^{-6}$		64

**$\Delta S = \Delta Q$ (SQ) violating modes or
 $\Delta S = 2$ forbidden (S2) modes**

$\Sigma^- e^+ \nu_e$	SQ < 9	$\times 10^{-4}$	90%	112
$\Sigma^- \mu^+ \nu_\mu$	SQ < 9	$\times 10^{-4}$	90%	49
$p\pi^-$	S2 < 8	$\times 10^{-6}$	90%	299
$p e^- \bar{\nu}_e$	S2 < 1.3	$\times 10^{-3}$		323
$p \mu^- \bar{\nu}_\mu$	S2 < 1.3	$\times 10^{-3}$		309

Ξ^- $I(J^P) = \frac{1}{2}(\frac{1}{2}^+)$

P is not yet measured; + is the quark model prediction.

Mass $m = 1321.71 \pm 0.07$ MeV
 $(m_{\Xi^-} - m_{\Xi^0}) / m_{\Xi^-} = (-3 \pm 9) \times 10^{-5}$
Mean life $\tau = (1.639 \pm 0.015) \times 10^{-10}$ s
 $c\tau = 4.91$ cm
 $(\tau_{\Xi^-} - \tau_{\Xi^0}) / \tau_{\Xi^-} = -0.01 \pm 0.07$
Magnetic moment $\mu = -0.6507 \pm 0.0025 \mu_N$
 $(\mu_{\Xi^-} + \mu_{\Xi^0}) / |\mu_{\Xi^-}| = +0.01 \pm 0.05$

Decay parameters

- $\Lambda\pi^-$ $\alpha = -0.401 \pm 0.010$
- $[\alpha(\Xi^-)\alpha_-(\Lambda) - \alpha(\Xi^+)\alpha_+(\bar{\Lambda})] / [\text{sum}] = (0 \pm 7) \times 10^{-4}$
- " $\phi = (-2.1 \pm 0.8)^\circ$
- " $\gamma = 0.89$ [n]
- " $\Delta = (175.9 \pm 1.5)^\circ$ [n]
- $\Lambda e^- \bar{\nu}_e$ $g_A/g_V = -0.25 \pm 0.05$ [l]

Baryon Summary Table

Ξ^- DECAY MODES	Fraction (Γ_i/Γ)	Confidence level	ρ (MeV/c)
$\Lambda\pi^-$	(99.887 ± 0.035) %		140
$\Sigma^- \gamma$	(1.27 ± 0.23) × 10 ⁻⁴		118
$\Lambda e^- \bar{\nu}_e$	(5.63 ± 0.31) × 10 ⁻⁴		190
$\Lambda \mu^- \bar{\nu}_\mu$	(3.5 $^{+3.5}_{-2.2}$) × 10 ⁻⁴		163
$\Sigma^0 e^- \bar{\nu}_e$	(8.7 ± 1.7) × 10 ⁻⁵		123
$\Sigma^0 \mu^- \bar{\nu}_\mu$	< 8 × 10 ⁻⁴	90%	70
$\Xi^0 e^- \bar{\nu}_e$	< 2.3 × 10 ⁻³	90%	7
$\Delta S = 2$ forbidden (S_2) modes			
$n\pi^-$	S_2 < 1.9 × 10 ⁻⁵	90%	304
$n e^- \bar{\nu}_e$	S_2 < 3.2 × 10 ⁻³	90%	327
$n \mu^- \bar{\nu}_\mu$	S_2 < 1.5 %	90%	314
$p\pi^- \pi^-$	S_2 < 4 × 10 ⁻⁴	90%	223
$p\pi^- e^- \bar{\nu}_e$	S_2 < 4 × 10 ⁻⁴	90%	305
$p\pi^- \mu^- \bar{\nu}_\mu$	S_2 < 4 × 10 ⁻⁴	90%	251
$p\mu^- \mu^-$	L < 4 × 10 ⁻⁸	90%	272

 $\Xi(1530) 3/2^+$

$$I(J^P) = \frac{1}{2}(\frac{3}{2}^+)$$

$\Xi(1530)^0$ mass $m = 1531.80 \pm 0.32$ MeV ($S = 1.3$)
 $\Xi(1530)^-$ mass $m = 1535.0 \pm 0.6$ MeV
 $\Xi(1530)^0$ full width $\Gamma = 9.1 \pm 0.5$ MeV
 $\Xi(1530)^-$ full width $\Gamma = 9.9^{+1.7}_{-1.9}$ MeV

$\Xi(1530)$ DECAY MODES	Fraction (Γ_i/Γ)	Confidence level	ρ (MeV/c)
$\Xi\pi$	100 %		158
$\Xi\gamma$	< 3.7 %	90%	202

 $\Xi(1690)$

$$I(J^P) = \frac{1}{2}(?^?)$$

Mass $m = 1690 \pm 10$ MeV [ρ]
 Full width $\Gamma < 30$ MeV

$\Xi(1690)$ DECAY MODES	Fraction (Γ_i/Γ)	ρ (MeV/c)
$\Lambda\bar{K}$	seen	240
$\Sigma\bar{K}$	seen	70
$\Xi\pi$	seen	311
$\Xi^- \pi^+ \pi^-$	possibly seen	213

 $\Xi(1820) 3/2^-$

$$I(J^P) = \frac{1}{2}(\frac{3}{2}^-)$$

Mass $m = 1823 \pm 5$ MeV [ρ]
 Full width $\Gamma = 24^{+15}_{-10}$ MeV [ρ]

$\Xi(1820)$ DECAY MODES	Fraction (Γ_i/Γ)	ρ (MeV/c)
$\Lambda\bar{K}$	large	402
$\Sigma\bar{K}$	small	324
$\Xi\pi$	small	421
$\Xi(1530)\pi$	small	237

 $\Xi(1950)$

$$I(J^P) = \frac{1}{2}(?^?)$$

Mass $m = 1950 \pm 15$ MeV [ρ]
 Full width $\Gamma = 60 \pm 20$ MeV [ρ]

$\Xi(1950)$ DECAY MODES	Fraction (Γ_i/Γ)	ρ (MeV/c)
$\Lambda\bar{K}$	seen	522
$\Sigma\bar{K}$	possibly seen	460
$\Xi\pi$	seen	519

 $\Xi(2030)$

$$I(J^P) = \frac{1}{2}(\geq \frac{5}{2}^?)$$

Mass $m = 2025 \pm 5$ MeV [ρ]
 Full width $\Gamma = 20^{+15}_{-5}$ MeV [ρ]

$\Xi(2030)$ DECAY MODES	Fraction (Γ_i/Γ)	ρ (MeV/c)
$\Lambda\bar{K}$	~ 20 %	585
$\Sigma\bar{K}$	~ 80 %	529
$\Xi\pi$	small	574
$\Xi(1530)\pi$	small	416
$\Lambda\bar{K}\pi$	small	499
$\Sigma\bar{K}\pi$	small	428

 Ω BARYONS
($S = -3, I = 0$)

$$\Omega^- = sss$$

 Ω^-

$$I(J^P) = 0(\frac{3}{2}^+)$$

$J^P = \frac{3}{2}^+$ is the quark-model prediction; and $J = 3/2$ is fairly well established.

Mass $m = 1672.45 \pm 0.29$ MeV
 $(m_{\Omega^-} - m_{\bar{\Omega}^+}) / m_{\Omega^-} = (-1 \pm 8) \times 10^{-5}$
 Mean life $\tau = (0.821 \pm 0.011) \times 10^{-10}$ s
 $c\tau = 2.461$ cm
 $(\tau_{\Omega^-} - \tau_{\bar{\Omega}^+}) / \tau_{\Omega^-} = 0.00 \pm 0.05$
 Magnetic moment $\mu = -2.02 \pm 0.05 \mu_N$

Decay parameters

$\alpha(\Omega^-) \alpha_-(\Lambda)$ FOR $\Omega^- \rightarrow \Lambda K^- = 0.0115 \pm 0.0015$
 $\Lambda K^- \quad \alpha = 0.0157 \pm 0.0021$
 $\Lambda K^-, \bar{\Lambda} K^+ \quad (\alpha + \bar{\alpha}) / (\alpha - \bar{\alpha}) = -0.02 \pm 0.13$
 $\Xi^0 \pi^- \quad \alpha = 0.09 \pm 0.14$
 $\Xi^- \pi^0 \quad \alpha = 0.05 \pm 0.21$

Ω^- DECAY MODES	Fraction (Γ_i/Γ)	Confidence level	ρ (MeV/c)
ΛK^-	(67.8 ± 0.7) %		211
$\Xi^0 \pi^-$	(23.6 ± 0.7) %		294
$\Xi^- \pi^0$	(8.6 ± 0.4) %		289
$\Xi^- \pi^+ \pi^-$	(3.7 $^{+0.7}_{-0.6}$) × 10 ⁻⁴		189
$\Xi(1530)^0 \pi^-$	< 7 × 10 ⁻⁵	90%	17
$\Xi^0 e^- \bar{\nu}_e$	(5.6 ± 2.8) × 10 ⁻³		319
$\Xi^- \gamma$	< 4.6 × 10 ⁻⁴	90%	314

 $\Delta S = 2$ forbidden (S_2) modes

$\Lambda\pi^-$	S_2 < 2.9 × 10 ⁻⁶	90%	449
----------------	--------------------------------	-----	-----

 $\Omega(2012)^-$

$$I(J^P) = 0(?^-)$$

Mass $m = 2012.4 \pm 0.9$ MeV
 Full width $\Gamma = 6.4^{+3.0}_{-2.6}$ MeV

$\Omega(2012)^-$ DECAY MODES	Fraction (Γ_i/Γ)	Confidence level	ρ (MeV/c)
$\Xi^0 K^-$	DEFINED AS 1		403
$\Xi^- K^0$	0.83 ± 0.21		392
$\Xi^0 \pi^0 K^-$	< 0.30	90%	245
$\Xi^0 \pi^- \bar{K}^0$	< 0.21	90%	230
$\Xi^- \pi^+ K^-$	< 0.08	90%	224

 $\Omega(2250)^-$

$$I(J^P) = 0(?^?)$$

Mass $m = 2252 \pm 9$ MeV
 Full width $\Gamma = 55 \pm 18$ MeV

$\Omega(2250)^-$ DECAY MODES	Fraction (Γ_i/Γ)	ρ (MeV/c)
$\Xi^- \pi^+ K^-$	seen	532
$\Xi(1530)^0 K^-$	seen	437

Baryon Summary Table

CHARMED BARYONS (C = +1)

$\Lambda_c^+ = udc, \Sigma_c^{++} = uuc, \Sigma_c^+ = udc, \Sigma_c^0 = ddc,$
 $\Xi_c^+ = usc, \Xi_c^0 = dsc, \Omega_c^0 = ssc$

Λ_c^+

$$I(J^P) = 0(\frac{1}{2}^+)$$

Mass $m = 2286.46 \pm 0.14$ MeV
Mean life $\tau = (202.4 \pm 3.1) \times 10^{-15}$ s (S = 1.7)
 $c\tau = 60.7 \mu\text{m}$

Decay asymmetry parameters

$\Lambda\pi^+$ $\alpha = -0.84 \pm 0.09$
 $\Sigma^+\pi^0$ $\alpha = -0.55 \pm 0.11$
 α FOR $\Lambda_c^+ \rightarrow \Sigma^0\pi^+ = -0.73 \pm 0.18$
 $\Lambda\ell^+\nu_\ell$ $\alpha = -0.86 \pm 0.04$
 α FOR $\Lambda_c^+ \rightarrow pK_S^0 = 0.2 \pm 0.5$
 $(\alpha + \bar{\alpha})/(\alpha - \bar{\alpha})$ in $\Lambda_c^+ \rightarrow \Lambda\pi^+, \bar{\Lambda}_c^- \rightarrow \bar{\Lambda}\pi^- = -0.07 \pm 0.31$
 $(\alpha + \bar{\alpha})/(\alpha - \bar{\alpha})$ in $\Lambda_c^+ \rightarrow \Lambda e^+\nu_e, \bar{\Lambda}_c^- \rightarrow \bar{\Lambda}e^-\bar{\nu}_e = 0.00 \pm 0.04$
 $A_{CP}(\Lambda X)$ in $\Lambda_c \rightarrow \Lambda X, \bar{\Lambda}_c \rightarrow \bar{\Lambda} X = (2 \pm 7)\%$
 $\Delta A_{CP} = A_{CP}(\Lambda_c^+ \rightarrow pK^+K^-) - A_{CP}(\Lambda_c^+ \rightarrow p\pi^+\pi^-) = (0.3 \pm 1.1)\%$

Branching fractions marked with a footnote, e.g. [a], have been corrected for decay modes not observed in the experiments. For example, the sub-mode fraction $\Lambda_c^+ \rightarrow p\bar{K}^*(892)^0$ seen in $\Lambda_c^+ \rightarrow pK^-\pi^+$ has been multiplied up to include $\bar{K}^*(892)^0 \rightarrow \bar{K}^0\pi^0$ decays.

Λ_c^+ DECAY MODES	Fraction (Γ_i/Γ)	Scale factor/ Confidence level	p (MeV/c)
Hadronic modes with a p or n: S = -1 final states			
pK_S^0	$(1.59 \pm 0.08)\%$	S=1.1	873
$pK_S^-\pi^+$	$(6.28 \pm 0.32)\%$	S=1.4	823
$p\bar{K}^*(892)^0$	[r] $(1.96 \pm 0.27)\%$		685
$\Delta(1232)^{++}K^-$	$(1.08 \pm 0.25)\%$		710
$\Lambda(1520)\pi^+$	[r] $(2.2 \pm 0.5)\%$		628
$pK^-\pi^+$ nonresonant	$(3.5 \pm 0.4)\%$		823
$pK_S^0\pi^0$	$(1.97 \pm 0.13)\%$	S=1.1	823
$nK_S^0\pi^+$	$(1.82 \pm 0.25)\%$		821
$p\bar{K}^0\eta$	$(1.6 \pm 0.4)\%$		568
$pK_S^0\pi^+\pi^-$	$(1.60 \pm 0.12)\%$	S=1.1	754
$pK^-\pi^+\pi^0$	$(4.46 \pm 0.30)\%$	S=1.5	759
$pK^*(892)^-\pi^+$	[r] $(1.4 \pm 0.5)\%$		580
$p(K^-\pi^+)_{\text{nonresonant}}\pi^0$	$(4.6 \pm 0.8)\%$		759
$\Delta(1232)\bar{K}^*(892)$	seen		419
$pK^-\pi^+\pi^-\pi^0$	$(1.4 \pm 0.9) \times 10^{-3}$		671
$pK^-\pi^+2\pi^0$	$(1.0 \pm 0.5)\%$		678
Hadronic modes with a p: S = 0 final states			
$p\pi^0$	$< 2.7 \times 10^{-4}$	CL=90%	945
$p\eta$	$(1.24 \pm 0.30) \times 10^{-3}$		856
$p\omega(782)^0$	$(9 \pm 4) \times 10^{-4}$		751
$p\pi^+\pi^-$	$(4.61 \pm 0.28) \times 10^{-3}$		927
$p f_0(980)$	[r] $(3.5 \pm 2.3) \times 10^{-3}$		614
$p2\pi^+2\pi^-$	$(2.3 \pm 1.4) \times 10^{-3}$		852
pK^+K^-	$(1.06 \pm 0.06) \times 10^{-3}$		616
$p\phi$	[r] $(1.06 \pm 0.14) \times 10^{-3}$		590
pK^+K^- non- ϕ	$(5.3 \pm 1.2) \times 10^{-4}$		616
$p\phi\pi^0$	$(10 \pm 4) \times 10^{-5}$		460
$pK^+K^-\pi^0$ nonresonant	$< 6.3 \times 10^{-5}$	CL=90%	494
Hadronic modes with a hyperon: S = -1 final states			
$\Lambda\pi^+$	$(1.30 \pm 0.07)\%$	S=1.1	864
$\Lambda\pi^+\pi^0$	$(7.1 \pm 0.4)\%$	S=1.1	844
$\Lambda\rho^+$	$< 6\%$	CL=95%	636
$\Lambda\pi^-2\pi^+$	$(3.64 \pm 0.29)\%$	S=1.4	807
$\Sigma(1385)^+\pi^+\pi^-, \Sigma^{*+} \rightarrow \Lambda\pi^+$	$(1.0 \pm 0.5)\%$		688
$\Sigma(1385)^-2\pi^+, \Sigma^{*-} \rightarrow \Lambda\pi^-$	$(7.6 \pm 1.4) \times 10^{-3}$		688
$\Lambda\pi^-\rho^0$	$(1.5 \pm 0.6)\%$		524
$\Sigma(1385)^+\rho^0, \Sigma^{*+} \rightarrow \Lambda\pi^+$	$(5 \pm 4) \times 10^{-3}$		363
$\Lambda\pi^-2\pi^+$ nonresonant	$< 1.1\%$	CL=90%	807
$\Lambda\pi^-\pi^02\pi^+$ total	$(2.3 \pm 0.8)\%$		757
$\Lambda\pi^+\eta$	[r] $(1.84 \pm 0.26)\%$		691

$\Sigma(1385)^+\eta$	[r] $(9.1 \pm 2.0) \times 10^{-3}$		570
$\Lambda\pi^+\omega$	[r] $(1.5 \pm 0.5)\%$		517
$\Lambda\pi^-\pi^02\pi^+, \text{ no } \eta \text{ or } \omega$	$< 8 \times 10^{-3}$	CL=90%	757
$\Lambda K^+\bar{K}^0$	$(5.7 \pm 1.1) \times 10^{-3}$	S=1.9	443
$\Xi(1690)^0K^+, \Xi^{*0} \rightarrow \Lambda\bar{K}^0$	$(1.6 \pm 0.5) \times 10^{-3}$		286
$\Sigma^0\pi^+$	$(1.29 \pm 0.07)\%$	S=1.1	825
$\Sigma^+\pi^0$	$(1.25 \pm 0.10)\%$		827
$\Sigma^+\eta$	$(4.4 \pm 2.0) \times 10^{-3}$		713
$\Sigma^+\eta'$	$(1.5 \pm 0.6)\%$		391
$\Sigma^+\pi^+\pi^-$	$(4.50 \pm 0.25)\%$	S=1.3	804
$\Sigma^+\rho^0$	$< 1.7\%$	CL=95%	575
$\Sigma^-2\pi^+$	$(1.87 \pm 0.18)\%$		799
$\Sigma^0\pi^+\pi^0$	$(3.5 \pm 0.4)\%$		803
$\Sigma^+\pi^0\pi^0$	$(1.55 \pm 0.15)\%$		806
$\Sigma^0\pi^-2\pi^+$	$(1.11 \pm 0.30)\%$		763
$\Sigma^+\pi^+\pi^-\pi^0$	—		767
$\Sigma^+\omega$	[r] $(1.70 \pm 0.21)\%$		569
$\Sigma^-02\pi^+$	$(2.1 \pm 0.4)\%$		762
$\Sigma^+K^+K^-$	$(3.5 \pm 0.4) \times 10^{-3}$	S=1.1	349
$\Sigma^+\phi$	[r] $(3.9 \pm 0.6) \times 10^{-3}$	S=1.1	295
$\Xi(1690)^0K^+, \Xi^{*0} \rightarrow \Sigma^+K^+K^-$ nonresonant	$< 8 \times 10^{-4}$	CL=90%	349
Ξ^0K^+	$(5.5 \pm 0.7) \times 10^{-3}$		653
$\Xi^-K^+\pi^+$	$(6.2 \pm 0.6) \times 10^{-3}$	S=1.1	565
$\Xi(1530)^0K^+$	$(4.3 \pm 0.9) \times 10^{-3}$	S=1.1	473

Hadronic modes with a hyperon: S = 0 final states

ΛK^+	$(6.1 \pm 1.2) \times 10^{-4}$		781
$\Lambda K^+\pi^+\pi^-$	$< 5 \times 10^{-4}$	CL=90%	637
Σ^0K^+	$(5.2 \pm 0.8) \times 10^{-4}$		735
$\Sigma^0K^+\pi^+\pi^-$	$< 2.6 \times 10^{-4}$	CL=90%	574
$\Sigma^+K^+\pi^-$	$(2.1 \pm 0.6) \times 10^{-3}$		670
$\Sigma^+K^*(892)^0$	[r] $(3.5 \pm 1.0) \times 10^{-3}$		470
$\Sigma^-K^+\pi^+$	$< 1.2 \times 10^{-3}$	CL=90%	664

Doubly Cabibbo-suppressed modes

$pK^+\pi^-$	$(1.11 \pm 0.18) \times 10^{-4}$		823
-------------	----------------------------------	--	-----

Semileptonic modes

$\Lambda e^+\nu_e$	$(3.6 \pm 0.4)\%$		871
$\Lambda\mu^+\nu_\mu$	$(3.5 \pm 0.5)\%$		867

Inclusive modes

e^+ anything	$(3.95 \pm 0.35)\%$		—
p anything	$(50 \pm 16)\%$		—
n anything	$(50 \pm 16)\%$		—
Λ anything	$(38.2 \pm 2.9)\%$		—
3prongs	$(24 \pm 8)\%$		—

$\Delta C = 1$ weak neutral current (CI) modes, or Lepton Family number (LF), or Lepton number (L), or Baryon number (B) violating modes

$p e^+ e^-$	CI $< 5.5 \times 10^{-6}$	CL=90%	951
$p\mu^+\mu^-$ non-resonant	CI $< 7.7 \times 10^{-8}$	CL=90%	937
$p e^+\mu^-$	LF $< 9.9 \times 10^{-6}$	CL=90%	947
$p e^-\mu^+$	LF $< 1.9 \times 10^{-5}$	CL=90%	947
$\bar{p}2e^+$	L,B $< 2.7 \times 10^{-6}$	CL=90%	951
$\bar{p}2\mu^+$	L,B $< 9.4 \times 10^{-6}$	CL=90%	937
$\bar{p}e^+\mu^+$	L,B $< 1.6 \times 10^{-5}$	CL=90%	947
$\Sigma^-\mu^+\mu^+$	L $< 7.0 \times 10^{-4}$	CL=90%	812

$\Lambda_c(2955)^+$

$$I(J^P) = 0(\frac{1}{2}^-)$$

The spin-parity follows from the fact that $\Sigma_c(2455)\pi$ decays, with little available phase space, are dominant. This assumes that $J^P = 1/2^+$ for the $\Sigma_c(2455)$.

Mass $m = 2592.25 \pm 0.28$ MeV
 $m - m_{\Lambda_c^+} = 305.79 \pm 0.24$ MeV
Full width $\Gamma = 2.6 \pm 0.6$ MeV

$\Lambda_c^+\pi\pi$ and its submode $\Sigma_c(2455)\pi$ — the latter just barely — are the only strong decays allowed to an excited Λ_c^+ having this mass; and the submode seems to dominate.

Baryon Summary Table

$\Lambda_c(2595)^+$ DECAY MODES	Fraction (Γ_i/Γ)	ρ (MeV/c)
$\Lambda_c^+ \pi^+ \pi^-$	[s] —	117
$\Sigma_c(2455)^{++} \pi^-$	24 ± 7 %	†
$\Sigma_c(2455)^0 \pi^+$	24 ± 7 %	†
$\Lambda_c^+ \pi^+ \pi^-$ 3-body	18 ± 10 %	117
$\Lambda_c^+ \pi^0$	[t] not seen	258
$\Lambda_c^+ \gamma$	not seen	288

 $\Lambda_c(2625)^+$

$$I(J^P) = 0(\frac{3}{2}^-)$$

J^P has not been measured; $\frac{3}{2}^-$ is the quark-model prediction.

$$\text{Mass } m = 2628.11 \pm 0.19 \text{ MeV} \quad (S = 1.1)$$

$$m - m_{\Lambda_c^+} = 341.65 \pm 0.13 \text{ MeV} \quad (S = 1.1)$$

$$\text{Full width } \Gamma < 0.97 \text{ MeV, CL} = 90\%$$

$\Lambda_c^+ \pi \pi$ and its submode $\Sigma(2455)\pi$ are the only strong decays allowed to an excited Λ_c^+ having this mass.

$\Lambda_c(2625)^+$ DECAY MODES	Fraction (Γ_i/Γ)	Confidence level	ρ (MeV/c)
$\Lambda_c^+ \pi^+ \pi^-$	≈ 67%		184
$\Sigma_c(2455)^{++} \pi^-$	<5	90%	102
$\Sigma_c(2455)^0 \pi^+$	<5	90%	102
$\Lambda_c^+ \pi^+ \pi^-$ 3-body	large		184
$\Lambda_c^+ \pi^0$	[i] not seen		293
$\Lambda_c^+ \gamma$	not seen		319

 $\Lambda_c(2860)^+$

$$I(J^P) = 0(\frac{3}{2}^+)$$

$$\text{Mass } m = 2856.1^{+2.3}_{-6.0} \text{ MeV}$$

$$\text{Full width } \Gamma = 68^{+12}_{-22} \text{ MeV}$$

$\Lambda_c(2860)^+$ DECAY MODES	Fraction (Γ_i/Γ)	ρ (MeV/c)
$D^0 p$	seen	259

 $\Lambda_c(2880)^+$

$$I(J^P) = 0(\frac{5}{2}^+)$$

$$\text{Mass } m = 2881.63 \pm 0.24 \text{ MeV}$$

$$m - m_{\Lambda_c^+} = 595.17 \pm 0.28 \text{ MeV}$$

$$\text{Full width } \Gamma = 5.6^{+0.8}_{-0.6} \text{ MeV}$$

$\Lambda_c(2880)^+$ DECAY MODES	Fraction (Γ_i/Γ)	ρ (MeV/c)
$\Lambda_c^+ \pi^+ \pi^-$	seen	471
$\Sigma_c(2455)^0, ++ \pi^\pm$	seen	376
$\Sigma_c(2520)^0, ++ \pi^\pm$	seen	317
ρD^0	seen	316

 $\Lambda_c(2940)^+$

$$I(J^P) = 0(\frac{3}{2}^-)$$

$J^P = 3/2^-$ is favored, but is not certain

$$\text{Mass } m = 2939.6^{+1.3}_{-1.5} \text{ MeV}$$

$$\text{Full width } \Gamma = 20^{+5}_{-6} \text{ MeV}$$

$\Lambda_c(2940)^+$ DECAY MODES	Fraction (Γ_i/Γ)	ρ (MeV/c)
ρD^0	seen	420
$\Sigma_c(2455)^0, ++ \pi^\pm$	seen	—

 $\Sigma_c(2455)$

$$I(J^P) = 1(\frac{1}{2}^+)$$

$$\Sigma_c(2455)^{++} \text{ mass } m = 2453.97 \pm 0.14 \text{ MeV}$$

$$\Sigma_c(2455)^+ \text{ mass } m = 2452.9 \pm 0.4 \text{ MeV}$$

$$\Sigma_c(2455)^0 \text{ mass } m = 2453.75 \pm 0.14 \text{ MeV}$$

$$m_{\Sigma_c^{++}} - m_{\Lambda_c^+} = 167.510 \pm 0.017 \text{ MeV}$$

$$m_{\Sigma_c^+} - m_{\Lambda_c^+} = 166.4 \pm 0.4 \text{ MeV}$$

$$m_{\Sigma_c^0} - m_{\Lambda_c^+} = 167.290 \pm 0.017 \text{ MeV}$$

$$m_{\Sigma_c^{++}} - m_{\Sigma_c^0} = 0.220 \pm 0.013 \text{ MeV}$$

$$m_{\Sigma_c^+} - m_{\Sigma_c^0} = -0.9 \pm 0.4 \text{ MeV}$$

$$\Sigma_c(2455)^{++} \text{ full width } \Gamma = 1.89^{+0.09}_{-0.18} \text{ MeV} \quad (S = 1.1)$$

$$\Sigma_c(2455)^+ \text{ full width } \Gamma < 4.6 \text{ MeV, CL} = 90\%$$

$$\Sigma_c(2455)^0 \text{ full width } \Gamma = 1.83^{+0.11}_{-0.19} \text{ MeV} \quad (S = 1.2)$$

$\Lambda_c^+ \pi$ is the only strong decay allowed to a Σ_c having this mass.

$\Sigma_c(2455)$ DECAY MODES	Fraction (Γ_i/Γ)	ρ (MeV/c)
$\Lambda_c^+ \pi$	≈ 100 %	94

 $\Sigma_c(2520)$

$$I(J^P) = 1(\frac{3}{2}^+)$$

J^P has not been measured; $\frac{3}{2}^+$ is the quark-model prediction.

$$\Sigma_c(2520)^{++} \text{ mass } m = 2518.41^{+0.21}_{-0.19} \text{ MeV} \quad (S = 1.1)$$

$$\Sigma_c(2520)^+ \text{ mass } m = 2517.5 \pm 2.3 \text{ MeV}$$

$$\Sigma_c(2520)^0 \text{ mass } m = 2518.48 \pm 0.20 \text{ MeV} \quad (S = 1.1)$$

$$m_{\Sigma_c(2520)^{++}} - m_{\Lambda_c^+} = 231.95^{+0.17}_{-0.12} \text{ MeV} \quad (S = 1.3)$$

$$m_{\Sigma_c(2520)^+} - m_{\Lambda_c^+} = 231.0 \pm 2.3 \text{ MeV}$$

$$m_{\Sigma_c(2520)^0} - m_{\Lambda_c^+} = 232.02^{+0.15}_{-0.14} \text{ MeV} \quad (S = 1.3)$$

$$m_{\Sigma_c(2520)^{++}} - m_{\Sigma_c(2520)^0} = 0.01 \pm 0.15 \text{ MeV}$$

$$\Sigma_c(2520)^{++} \text{ full width } \Gamma = 14.78^{+0.30}_{-0.40} \text{ MeV}$$

$$\Sigma_c(2520)^+ \text{ full width } \Gamma < 17 \text{ MeV, CL} = 90\%$$

$$\Sigma_c(2520)^0 \text{ full width } \Gamma = 15.3^{+0.4}_{-0.5} \text{ MeV}$$

$\Lambda_c^+ \pi$ is the only strong decay allowed to a Σ_c having this mass.

$\Sigma_c(2520)$ DECAY MODES	Fraction (Γ_i/Γ)	ρ (MeV/c)
$\Lambda_c^+ \pi$	≈ 100 %	179

 $\Sigma_c(2800)$

$$I(J^P) = 1(2^?)$$

$$\Sigma_c(2800)^{++} \text{ mass } m = 2801^{+4}_{-6} \text{ MeV}$$

$$\Sigma_c(2800)^+ \text{ mass } m = 2792^{+14}_{-5} \text{ MeV}$$

$$\Sigma_c(2800)^0 \text{ mass } m = 2806^{+5}_{-7} \text{ MeV} \quad (S = 1.3)$$

$$m_{\Sigma_c(2800)^{++}} - m_{\Lambda_c^+} = 514^{+4}_{-6} \text{ MeV}$$

$$m_{\Sigma_c(2800)^+} - m_{\Lambda_c^+} = 505^{+14}_{-5} \text{ MeV}$$

$$m_{\Sigma_c(2800)^0} - m_{\Lambda_c^+} = 519^{+5}_{-7} \text{ MeV} \quad (S = 1.3)$$

$$\Sigma_c(2800)^{++} \text{ full width } \Gamma = 75^{+22}_{-17} \text{ MeV}$$

$$\Sigma_c(2800)^+ \text{ full width } \Gamma = 62^{+60}_{-40} \text{ MeV}$$

$$\Sigma_c(2800)^0 \text{ full width } \Gamma = 72^{+22}_{-15} \text{ MeV}$$

$\Sigma_c(2800)$ DECAY MODES	Fraction (Γ_i/Γ)	ρ (MeV/c)
$\Lambda_c^+ \pi$	seen	443

 Ξ_c^+

$$I(J^P) = \frac{1}{2}(\frac{1}{2}^+)$$

J^P has not been measured; $\frac{1}{2}^+$ is the quark-model prediction.

$$\text{Mass } m = 2467.94^{+0.17}_{-0.20} \text{ MeV}$$

$$\text{Mean life } \tau = (456 \pm 5) \times 10^{-15} \text{ s}$$

$$c\tau = 136.6 \mu\text{m}$$

Branching fractions marked with a footnote, e.g. [a], have been corrected for decay modes not observed in the experiments. For example, the submode fraction $\Xi_c^+ \rightarrow \Sigma^+ \bar{K}^*(892)^0$ seen in $\Xi_c^+ \rightarrow \Sigma^+ K^- \pi^+$ has been multiplied up to include $\bar{K}^*(892)^0 \rightarrow \bar{K}^0 \pi^0$ decays.

Baryon Summary Table

Ξ_c^{\pm} DECAY MODES	Fraction (Γ_i/Γ)	Confidence level	ρ (MeV/c)
---------------------------	--------------------------------	------------------	----------------

No absolute branching fractions have been measured.
The following are branching ratios relative to $\Xi^- 2\pi^+$.

Cabibbo-favored ($S = -2$) decays — relative to $\Xi^- 2\pi^+$

$p 2K_S^0$	0.087 ± 0.021		767
$\Lambda \bar{K}^0 \pi^+$	—		852
$\Sigma(1385)^+ \bar{K}^0$	[r] 1.0 ± 0.5		746
$\Lambda K^- 2\pi^+$	0.323 ± 0.033		787
$\Lambda \bar{K}^*(892)^0 \pi^+$	[r] < 0.16	90%	608
$\Sigma(1385)^+ K^- \pi^+$	[r] < 0.23	90%	678
$\Sigma^+ K^- \pi^+$	0.94 ± 0.10		811
$\Sigma^+ \bar{K}^*(892)^0$	[r] 0.81 ± 0.15		658
$\Sigma^0 K^- 2\pi^+$	0.27 ± 0.12		735
$\Xi^0 \pi^+$	0.55 ± 0.16		877
$\Xi^- 2\pi^+$	DEFINED AS 1		851
$\Xi(1530)^0 \pi^+$	[r] < 0.10	90%	750
$\Xi(1620)^0 \pi^+$	seen		—
$\Xi(1690)^0 \pi^+$	seen		644
$\Xi^0 \pi^+ \pi^0$	2.3 ± 0.7		856
$\Xi^0 \pi^- 2\pi^+$	1.7 ± 0.5		818
$\Xi^0 e^+ \nu_e$	2.3 $^{+0.7}_{-0.8}$		884
$\Omega^- K^+ \pi^+$	0.07 ± 0.04		399

Cabibbo-suppressed decays — relative to $\Xi^- 2\pi^+$

$p K^- \pi^+$	0.0045 ± 0.0022		944
$p \bar{K}^*(892)^0$	[r] 0.0024 ± 0.0013		828
$\Sigma^+ \pi^+ \pi^-$	0.48 ± 0.20		922
$\Sigma^- 2\pi^+$	0.18 ± 0.09		918
$\Sigma^+ K^+ K^-$	0.15 ± 0.06		580
$\Sigma^+ \phi$	[r] < 0.11	90%	549
$\Xi(1690)^0 K^+, \Xi^0 \rightarrow$	< 0.05	90%	501
$\Sigma^+ K^-$			
$p \phi(1020)$	(9 ± 4) × 10 ⁻⁵		751

Ξ_c^0

$$I(J^P) = \frac{1}{2}(\frac{1}{2}^+)$$

J^P has not been measured; $\frac{1}{2}^+$ is the quark-model prediction.

Mass $m = 2470.90^{+0.22}_{-0.29}$ MeV

$$m_{\Xi_c^0} - m_{\Xi_c^+} = 2.96 \pm 0.22 \text{ MeV}$$

Mean life $\tau = (153 \pm 6) \times 10^{-15} \text{ s}$ ($S = 2.4$)

$$c\tau = 45.8 \mu\text{m}$$

Decay asymmetry parameters

$$\Xi^- \pi^+ \quad \alpha = -0.6 \pm 0.4$$

Ξ_c^0 DECAY MODES	Fraction (Γ_i/Γ)	Scale factor	ρ (MeV/c)
-----------------------	--------------------------------	--------------	----------------

Cabibbo-favored ($S = -2$) decays

$p K^- K^- \pi^+$	(4.8 ± 1.2) × 10 ⁻³	1.1	676
$p K^- \bar{K}^*(892)^0, \bar{K}^{*0} \rightarrow K^- \pi^+$	(2.0 ± 0.6) × 10 ⁻³		413
$p K^- K^- \pi^+$ (no \bar{K}^{*0})	(3.0 ± 0.9) × 10 ⁻³		676
ΛK_S^0	(3.0 ± 0.8) × 10 ⁻³		906
$\Lambda K^- \pi^+$	(1.45 ± 0.33) %	1.1	856
$\Lambda \bar{K}^0 \pi^+ \pi^-$	seen		787
$\Lambda K^- \pi^+ \pi^+ \pi^-$	seen		703
$\Xi^- \pi^+$	(1.43 ± 0.32) %	1.1	875
$\Xi^- \pi^+ \pi^+ \pi^-$	(4.8 ± 2.3) %		816
$\Omega^- K^+$	(4.2 ± 1.0) × 10 ⁻³		522
$\Xi^- e^+ \nu_e$	(1.8 ± 1.2) %		882

Cabibbo-suppressed decays

$\Xi^- K^+$	(3.9 ± 1.2) × 10 ⁻⁴		790
$\Lambda K^+ K^-$ (no ϕ)	(4.1 ± 1.4) × 10 ⁻⁴		648
$\Lambda \phi$	(4.9 ± 1.5) × 10 ⁻⁴		621

Ξ_c^{\pm}

$$I(J^P) = \frac{1}{2}(\frac{1}{2}^+)$$

J^P has not been measured; $\frac{1}{2}^+$ is the quark-model prediction.

Mass $m = 2578.4 \pm 0.5$ MeV

$$m_{\Xi_c^{\pm}} - m_{\Xi_c^{\pm}} = 110.5 \pm 0.4 \text{ MeV}$$

$$m_{\Xi_c^{\pm}} - m_{\Xi_c^0} = -0.8 \pm 0.6 \text{ MeV}$$

The $\Xi_c^{\pm} - \Xi_c^0$ mass difference is too small for any strong decay to occur.

Ξ_c^{\pm} DECAY MODES	Fraction (Γ_i/Γ)	ρ (MeV/c)
---------------------------	--------------------------------	----------------

$\Xi_c^{\pm} \gamma$

seen

108

Ξ_c^{\pm}

$$I(J^P) = \frac{1}{2}(\frac{1}{2}^+)$$

J^P has not been measured; $\frac{1}{2}^+$ is the quark-model prediction.

Mass $m = 2579.2 \pm 0.5$ MeV

$$m_{\Xi_c^0} - m_{\Xi_c^{\pm}} = 108.3 \pm 0.4 \text{ MeV}$$

The $\Xi_c^0 - \Xi_c^{\pm}$ mass difference is too small for any strong decay to occur.

Ξ_c^0 DECAY MODES	Fraction (Γ_i/Γ)	ρ (MeV/c)
-----------------------	--------------------------------	----------------

$\Xi_c^0 \gamma$

seen

106

$\Xi_c(2645)$

$$I(J^P) = \frac{1}{2}(\frac{3}{2}^+)$$

J^P has not been measured; $\frac{3}{2}^+$ is the quark-model prediction.

$\Xi_c(2645)^+$ mass $m = 2645.56^{+0.24}_{-0.30}$ MeV

$\Xi_c(2645)^0$ mass $m = 2646.38^{+0.20}_{-0.23}$ MeV ($S = 1.1$)

$$m_{\Xi_c(2645)^+} - m_{\Xi_c^0} = 174.66 \pm 0.09 \text{ MeV}$$

$$m_{\Xi_c(2645)^0} - m_{\Xi_c^+} = 178.44 \pm 0.10 \text{ MeV}$$

$$m_{\Xi_c(2645)^+} - m_{\Xi_c(2645)^0} = -0.82 \pm 0.26 \text{ MeV}$$

$\Xi_c(2645)^+$ full width $\Gamma = 2.14 \pm 0.19$ MeV ($S = 1.1$)

$\Xi_c(2645)^0$ full width $\Gamma = 2.35 \pm 0.22$ MeV

$\Xi_c \pi$ is the only strong decay allowed to a Ξ_c resonance having this mass.

$\Xi_c(2645)$ DECAY MODES	Fraction (Γ_i/Γ)	ρ (MeV/c)
---------------------------	--------------------------------	----------------

$\Xi_c^0 \pi^+$

seen

102

$\Xi_c^+ \pi^-$

seen

106

$\Xi_c(2790)$

$$I(J^P) = \frac{1}{2}(\frac{1}{2}^-)$$

J^P has not been measured; $\frac{1}{2}^-$ is the quark-model prediction.

$\Xi_c(2790)^+$ mass = 2792.4 ± 0.5 MeV

$\Xi_c(2790)^0$ mass = 2794.1 ± 0.5 MeV

$m_{\Xi_c(2790)^+} - m_{\Xi_c^0} = 213.20 \pm 0.22$ MeV

$m_{\Xi_c(2790)^0} - m_{\Xi_c^+} = 215.70 \pm 0.22$ MeV

$$m_{\Xi_c(2790)^+} - m_{\Xi_c(2790)^0} = -1.7 \pm 0.7 \text{ MeV}$$

$\Xi_c(2790)^+$ width = 8.9 ± 1.0 MeV

$\Xi_c(2790)^0$ width = 10.0 ± 1.1 MeV

$\Xi_c(2790)$ DECAY MODES	Fraction (Γ_i/Γ)	ρ (MeV/c)
---------------------------	--------------------------------	----------------

$\Xi_c^{\pm} \pi$

seen

160

$\Xi_c(2815)$

$$I(J^P) = \frac{1}{2}(\frac{3}{2}^-)$$

J^P has not been measured; $\frac{3}{2}^-$ is the quark-model prediction.

$\Xi_c(2815)^+$ mass $m = 2816.74^{+0.20}_{-0.23}$ MeV

$\Xi_c(2815)^0$ mass $m = 2820.25^{+0.25}_{-0.31}$ MeV

$$m_{\Xi_c(2815)^+} - m_{\Xi_c^+} = 348.80 \pm 0.10 \text{ MeV}$$

$$m_{\Xi_c(2815)^0} - m_{\Xi_c^0} = 349.35 \pm 0.11 \text{ MeV}$$

$$m_{\Xi_c(2815)^+} - m_{\Xi_c(2815)^0} = -3.51 \pm 0.26 \text{ MeV}$$

$\Xi_c(2815)^+$ full width $\Gamma = 2.43 \pm 0.26$ MeV

$\Xi_c(2815)^0$ full width $\Gamma = 2.54 \pm 0.25$ MeV

The $\Xi_c \pi \pi$ modes are consistent with being entirely via $\Xi_c(2645) \pi$.

$\Xi_c(2815)$ DECAY MODES	Fraction (Γ_i/Γ)	ρ (MeV/c)
---------------------------	--------------------------------	----------------

$\Xi_c^{\pm} \pi$

seen

188

$\Xi_c(2645) \pi$

seen

102

Baryon Summary Table

$$\Xi_c(2970) \quad I(J^P) = \frac{1}{2}(??)$$

was $\Xi_c(2980)$

$$\Xi_c(2970)^+ m = 2966.34^{+0.17}_{-1.00} \text{ MeV}$$

$$\Xi_c(2970)^0 m = 2970.9^{+0.4}_{-0.6} \text{ MeV}$$

$$\quad m_{\Xi_c(2970)^+} - m_{\Xi_c^+} = 498.40^{+0.27}_{-0.90} \text{ MeV}$$

$$\quad m_{\Xi_c(2970)^0} - m_{\Xi_c^0} = 500.0^{+0.4}_{-0.6} \text{ MeV}$$

$$m_{\Xi_c(2970)^+} - m_{\Xi_c(2970)^0} = -4.6^{+0.4}_{-0.6} \text{ MeV}$$

$$\Xi_c(2970)^+ \text{ width } \Gamma = 20.9^{+2.4}_{-3.5} \text{ MeV} \quad (S = 1.2)$$

$$\Xi_c(2970)^0 \text{ width } \Gamma = 28.1^{+3.4}_{-4.0} \text{ MeV} \quad (S = 1.5)$$

$\Xi_c(2970)$ DECAY MODES	Fraction (Γ_i/Γ)	ρ (MeV/c)
$\Lambda_c^+ \bar{K} \pi$	seen	228
$\Sigma_c(2455) \bar{K}$	seen	128
$\Lambda_c^+ \bar{K}$	not seen	412
$\Xi_c 2\pi$	seen	383
$\Xi_c' \pi$	seen	—
$\Xi_c(2645) \pi$	seen	275

$$\Xi_c(3055) \quad I(J^P) = ?(??)$$

$$\text{Mass } m = 3055.9 \pm 0.4 \text{ MeV}$$

$$\text{Full width } \Gamma = 7.8 \pm 1.9 \text{ MeV}$$

$\Xi_c(3055)$ DECAY MODES	Fraction (Γ_i/Γ)	ρ (MeV/c)
$\Sigma^{++} K^-$	seen	—
ΛD^+	seen	316

$$\Xi_c(3080) \quad I(J^P) = \frac{1}{2}(??)$$

$$\Xi_c(3080)^+ m = 3077.2 \pm 0.4 \text{ MeV}$$

$$\Xi_c(3080)^0 m = 3079.9 \pm 1.4 \text{ MeV} \quad (S = 1.3)$$

$$\Xi_c(3080)^+ \text{ width } \Gamma = 3.6 \pm 1.1 \text{ MeV} \quad (S = 1.5)$$

$$\Xi_c(3080)^0 \text{ width } \Gamma = 5.6 \pm 2.2 \text{ MeV}$$

$\Xi_c(3080)$ DECAY MODES	Fraction (Γ_i/Γ)	ρ (MeV/c)
$\Lambda_c^+ \bar{K} \pi$	seen	415
$\Sigma_c(2455) \bar{K}$	seen	342
$\Sigma_c(2455)^{++} K^-$	seen	342
$\Sigma_c(2520)^{++} K^-$	seen	239
$\Sigma_c(2455) \bar{K} + \Sigma_c(2520) \bar{K}$	seen	—
$\Lambda_c^+ \bar{K}$	not seen	536
$\Lambda_c^+ \bar{K} \pi^+ \pi^-$	not seen	144
ΛD^+	seen	362

$$\Omega_c^0 \quad I(J^P) = 0(\frac{1}{2}^+)$$

J^P has not been measured; $\frac{1}{2}^+$ is the quark-model prediction.

$$\text{Mass } m = 2695.2 \pm 1.7 \text{ MeV} \quad (S = 1.3)$$

$$\text{Mean life } \tau = (268 \pm 26) \times 10^{-15} \text{ s}$$

$$c\tau = 80 \text{ } \mu\text{m}$$

Ω_c^0 DECAY MODES	Fraction (Γ_i/Γ)	Confidence level	ρ (MeV/c)
--------------------------	--------------------------------	------------------	----------------

No absolute branching fractions have been measured.
The following are branching ratios relative to $\Omega^- \pi^+$.

Cabibbo-favored ($S = -3$) decays — relative to $\Omega^- \pi^+$

	DEFINED AS 1		
$\Omega^- \pi^+$	1.80 ± 0.33		821
$\Omega^- \pi^+ \pi^0$	>1.3	90%	797
$\Omega^- \rho^+$	0.31 ± 0.05		753
$\Omega^- \pi^- 2\pi^+$	2.4 ± 1.2		829
$\Omega^- e^+ \nu_e$	1.64 ± 0.29		950
$\Xi^0 \bar{K}^0$	1.20 ± 0.18		901
$\Xi^0 K^- \pi^+$	0.68 ± 0.16		764
$\Xi^0 \bar{K}^{*0}, \bar{K}^{*0} \rightarrow K^- \pi^+$	2.12 ± 0.28		895

$\Xi^- K^- 2\pi^+$	0.63 ± 0.09	830
$\Xi(1530)^0 K^- \pi^+, \Xi^{*0} \rightarrow$	0.21 ± 0.06	757
$\Xi^- \bar{K}^{*0} \pi^+$	0.34 ± 0.11	653
$\Sigma^+ K^- K^- \pi^+$	<0.32	90% 689
$\Lambda \bar{K}^0 \bar{K}^0$	1.72 ± 0.35	837

$$\Omega_c(2770)^0 \quad I(J^P) = 0(\frac{3}{2}^+)$$

J^P has not been measured; $\frac{3}{2}^+$ is the quark-model prediction.

$$\text{Mass } m = 2765.9 \pm 2.0 \text{ MeV} \quad (S = 1.2)$$

$$m_{\Omega_c(2770)^0} - m_{\Omega_c^0} = 70.7^{+0.8}_{-0.9} \text{ MeV}$$

The $\Omega_c(2770)^0 - \Omega_c^0$ mass difference is too small for any strong decay to occur.

$\Omega_c(2770)^0$ DECAY MODES	Fraction (Γ_i/Γ)	ρ (MeV/c)
$\Omega_c^0 \gamma$	presumably 100%	70

$$\Omega_c(3000)^0 \quad I(J^P) = ?(??)$$

$$\text{Mass } m = 3000.41 \pm 0.22 \text{ MeV}$$

$$\text{Full width } \Gamma = 4.5 \pm 0.7 \text{ MeV}$$

$\Omega_c(3000)^0$ DECAY MODES	Fraction (Γ_i/Γ)	ρ (MeV/c)
$\Xi_c^+ K^-$	seen	181

$$\Omega_c(3050)^0 \quad I(J^P) = ?(??)$$

$$\text{Mass } m = 3050.20 \pm 0.13 \text{ MeV}$$

$$\text{Full width } \Gamma < 1.2 \text{ MeV, CL} = 95\%$$

$\Omega_c(3050)^0$ DECAY MODES	Fraction (Γ_i/Γ)	ρ (MeV/c)
$\Xi_c^+ K^-$	seen	278

$$\Omega_c(3065)^0 \quad I(J^P) = ?(??)$$

$$\text{Mass } m = 3065.46 \pm 0.28 \text{ MeV}$$

$$\text{Full width } \Gamma = 3.5 \pm 0.4 \text{ MeV}$$

$\Omega_c(3065)^0$ DECAY MODES	Fraction (Γ_i/Γ)	ρ (MeV/c)
$\Xi_c^+ K^-$	seen	303

$$\Omega_c(3090)^0 \quad I(J^P) = ?(??)$$

$$\text{Mass } m = 3090.0 \pm 0.5 \text{ MeV}$$

$$\text{Full width } \Gamma = 8.7 \pm 1.3 \text{ MeV}$$

$\Omega_c(3090)^0$ DECAY MODES	Fraction (Γ_i/Γ)	ρ (MeV/c)
$\Xi_c^+ K^-$	seen	339

$$\Omega_c(3120)^0 \quad I(J^P) = ?(??)$$

$$\text{Mass } m = 3119.1 \pm 1.0 \text{ MeV}$$

$$\text{Full width } \Gamma < 2.6 \text{ MeV, CL} = 95\%$$

$\Omega_c(3120)^0$ DECAY MODES	Fraction (Γ_i/Γ)	ρ (MeV/c)
$\Xi_c^+ K^-$	seen	379

DOUBLY CHARMED BARYONS ($C = +2$)

$$\Xi_{cc}^{++} = ucc, \Xi_{cc}^+ = dcc, \Omega_{cc}^+ = scc$$

$$\Xi_{cc}^{++} \quad I(J^P) = ?(??)$$

$$\text{Mass } m = 3621.2 \pm 0.7 \text{ MeV}$$

$$\text{Mean life } \tau = (256 \pm 27) \times 10^{-15} \text{ s}$$

Baryon Summary Table

Ξ_{cc}^{++} DECAY MODES	Fraction (Γ_i/Γ)	ρ (MeV/c)
$\Lambda_c^+ K^- \pi^+ \pi^+$	seen	880
$\Xi_c^+ \pi^+, \Xi_c^+ \rightarrow p K^- \pi^+$	seen	-

BOTTOM BARYONS

($B = -1$)

$\Lambda_b^0 = udb, \Xi_b^0 = usb, \Xi_b^- = dsb, \Omega_b^- = ssb$

Λ_b^0

$I(J^P) = 0(\frac{1}{2}^+)$

$I(J^P)$ not yet measured; $0(\frac{1}{2}^+)$ is the quark model prediction.
 Mass $m = 5619.60 \pm 0.17$ MeV
 $m_{\Lambda_b^0} - m_{B^0} = 339.2 \pm 1.4$ MeV
 $m_{\Lambda_b^0} - m_{B^+} = 339.72 \pm 0.28$ MeV
 Mean life $\tau = (1.471 \pm 0.009) \times 10^{-12}$ s
 $c\tau = 441.0 \mu\text{m}$
 $A_{CP}(\Lambda_b \rightarrow p\pi^-) = -0.025 \pm 0.029$ ($S = 1.2$)
 $A_{CP}(\Lambda_b \rightarrow pK^-) = -0.025 \pm 0.022$
 $\Delta A_{CP}(\rho K^-/\pi^-) = 0.014 \pm 0.024$
 $A_{CP}(\Lambda_b \rightarrow p\bar{K}^0\pi^-) = 0.22 \pm 0.13$
 $\Delta A_{CP}(J/\psi p\pi^-/K^-) = (5.7 \pm 2.7) \times 10^{-2}$
 $A_{CP}(\Lambda_b \rightarrow \Lambda K^+\pi^-) = -0.53 \pm 0.25$
 $A_{CP}(\Lambda_b \rightarrow \Lambda K^+K^-) = -0.28 \pm 0.12$
 $\Delta A_{CP}(\Lambda_b^0 \rightarrow pK^- \mu^+ \mu^-) = (-4 \pm 5) \times 10^{-2}$
 $\Delta A_{CP}(\Lambda_b^0 \rightarrow p\pi^- \pi^+ \pi^-) = (1.1 \pm 2.6) \times 10^{-2}$
 $\Delta A_{CP}(\Lambda_b^0 \rightarrow (p\pi^- \pi^+ \pi^-)_{LBM}) = (4 \pm 4) \times 10^{-2}$
 $\Delta A_{CP}(\Lambda_b^0 \rightarrow \rho a_1(1260)^-) = (-1 \pm 4) \times 10^{-2}$
 $\Delta A_{CP}(\Lambda_b^0 \rightarrow N(1520)^0 \rho(770)^0) = (2 \pm 5) \times 10^{-2}$
 $\Delta A_{CP}(\Lambda_b^0 \rightarrow \Delta(1232)^{++} \pi^- \pi^-) = (0.1 \pm 3.3) \times 10^{-2}$
 $\Delta A_{CP}(\Lambda_b^0 \rightarrow pK^- \pi^+ \pi^-) = (3.2 \pm 1.3) \times 10^{-2}$
 $\Delta A_{CP}(\Lambda_b^0 \rightarrow (pK^- \pi^+ \pi^-)_{LBM}) = (3.5 \pm 1.6) \times 10^{-2}$
 $\Delta A_{CP}(\Lambda_b^0 \rightarrow N(1520)^0 K^*(892)^0) = (5.5 \pm 2.5) \times 10^{-2}$
 $\Delta A_{CP}(\Lambda_b^0 \rightarrow \Lambda(1520) \rho(770)^0) = (1 \pm 6) \times 10^{-2}$
 $\Delta A_{CP}(\Lambda_b^0 \rightarrow \Delta(1232)^{++} K^- \pi^-) = (4.4 \pm 2.7) \times 10^{-2}$
 $\Delta A_{CP}(\Lambda_b^0 \rightarrow pK_1(1410)^-) = (5 \pm 4) \times 10^{-2}$
 $\Delta A_{CP}(\Lambda_b^0 \rightarrow pK^- K^+ \pi^-) = (-7 \pm 5) \times 10^{-2}$
 $\Delta A_{CP}(\Lambda_b^0 \rightarrow pK^- K^+ K^-) = (0.2 \pm 1.9) \times 10^{-2}$
 $\Delta A_{CP}(\Lambda_b^0 \rightarrow \Lambda(1520) \phi(1020)) = (4 \pm 6) \times 10^{-2}$
 $\Delta A_{CP}(\Lambda_b^0 \rightarrow (pK^-)_{highmass} \phi(1020)) = (-0.7 \pm 3.4) \times 10^{-2}$
 $\Delta A_{CP}(\Lambda_b^0 \rightarrow (pK^- K^+ K^-)_{LBM}) = (2.7 \pm 2.4) \times 10^{-2}$
 $A_{FB}^{\ell}(\mu\mu)$ in $\Lambda_b \rightarrow \Lambda \mu^+ \mu^- = -0.39 \pm 0.04$
 $\Delta(A_{FB}^{\ell}(\mu\mu))$ in $\Lambda_b \rightarrow \Lambda \mu^+ \mu^- = -0.05 \pm 0.09$
 $A_{FB}^{\ell}(\rho\pi)$ in $\Lambda_b \rightarrow \Lambda(\rho\pi) \mu^+ \mu^- = -0.30 \pm 0.05$
 $A_{FB}^{\ell h}$ in $\Lambda_b \rightarrow \Lambda \mu^+ \mu^- = 0.25 \pm 0.04$

The branching fractions $B(b\text{-baryon} \rightarrow \Lambda_c \ell^- \bar{\nu}_{\ell} \text{anything})$ and $B(\Lambda_b^0 \rightarrow \Lambda_c^+ \ell^- \bar{\nu}_{\ell} \text{anything})$ are not pure measurements because the underlying measured products of these with $B(b \rightarrow b\text{-baryon})$ were used to determine $B(b \rightarrow b\text{-baryon})$, as described in the note "Production and Decay of b -Flavored Hadrons."

For inclusive branching fractions, e.g., $\Lambda_b \rightarrow \bar{\Lambda}_c \text{anything}$, the values usually are multiplicities, not branching fractions. They can be greater than one.

Λ_b^0 DECAY MODES	Fraction (Γ_i/Γ)	Scale factor/ Confidence level	ρ (MeV/c)
$J/\psi(1S) \Lambda \times B(b \rightarrow \Lambda_b^0)$	$(5.8 \pm 0.8) \times 10^{-5}$		1740
$pD^0 \pi^-$	$(6.3 \pm 0.7) \times 10^{-4}$		2370
$pD^0 K^-$	$(4.6 \pm 0.8) \times 10^{-5}$		2269
$pJ/\psi \pi^-$	$(2.6 \pm 0.5) \times 10^{-5}$		1755
$p\pi^- J/\psi, J/\psi \rightarrow \mu^+ \mu^-$	$(1.6 \pm 0.8) \times 10^{-6}$		-
$pJ/\psi K^-$	$(3.2 \pm 0.6) \times 10^{-4}$		1589
$P_c(4380)^+ K^-, P_c \rightarrow pJ/\psi$	[u] $(2.7 \pm 1.4) \times 10^{-5}$		-
$P_c(4450)^+ K^-, P_c \rightarrow pJ/\psi$	[u] $(1.3 \pm 0.4) \times 10^{-5}$		-
$\chi_{c1}(1P) pK^-$	$(7.6 \pm 1.5) \times 10^{-5}$		1242
$\chi_{c2}(1P) pK^-$	$(7.9 \pm 1.6) \times 10^{-5}$		1198

$\rho J/\psi(1S) \pi^+ \pi^- K^-$	$(6.6 \pm 1.3) \times 10^{-5}$		1410
$\rho\psi(2S) K^-$	$(6.6 \pm 1.2) \times 10^{-5}$		1063
$\chi_{c1}(3872) \rho K^-, \chi_{c1}(3872) \rightarrow J/\psi \pi^+ \pi^-$	$(1.23 \pm 0.33) \times 10^{-6}$		-
$\psi(2S) p \pi^-$	$(7.5 \pm 1.6) \times 10^{-6}$		1320
$p\bar{K}^0 \pi^-$	$(1.3 \pm 0.4) \times 10^{-5}$		2693
$pK^0 K^-$	$< 3.5 \times 10^{-6}$	CL=90%	2639
$\Lambda_c^+ \pi^-$	$(4.9 \pm 0.4) \times 10^{-3}$	S=1.2	2342
$\Lambda_c^+ K^-$	$(3.59 \pm 0.30) \times 10^{-4}$	S=1.2	2314
$\Lambda_c^+ a_1(1260)^-$	seen		2153
$\Lambda_c^+ D^-$	$(4.6 \pm 0.6) \times 10^{-4}$		1886
$\Lambda_c^+ D_s^-$	$(1.10 \pm 0.10) \%$		1833
$\Lambda_c^+ \pi^+ \pi^- \pi^-$	$(7.7 \pm 1.1) \times 10^{-3}$	S=1.1	2323
$\Lambda_c(2595)^+ \pi^-$	$(3.4 \pm 1.5) \times 10^{-4}$		2210
$\Lambda_c(2595)^+ \rightarrow \Lambda_c^+ \pi^+ \pi^-$			
$\Lambda_c(2625)^+ \pi^-$	$(3.3 \pm 1.3) \times 10^{-4}$		2193
$\Lambda_c(2625)^+ \rightarrow \Lambda_c^+ \pi^+ \pi^-$			
$\Sigma_c(2455)^0 \pi^+ \pi^-, \Sigma_c^0 \rightarrow \Lambda_c^+ \pi^-$	$(5.7 \pm 2.2) \times 10^{-4}$		2265
$\Sigma_c(2455)^{++} \pi^- \pi^-, \Sigma_c^{++} \rightarrow \Lambda_c^+ \pi^+$	$(3.2 \pm 1.6) \times 10^{-4}$		2265
$\Lambda_c^+ p \bar{p} \pi^-$	$(2.65 \pm 0.29) \times 10^{-4}$		1805
$\Sigma_c(2455)^0 p \bar{p}, \Sigma_c(2455)^0 \rightarrow \Lambda_c^+ \pi^-$	$(2.4 \pm 0.5) \times 10^{-5}$		-
$\Sigma_c(2520)^0 p \bar{p}, \Sigma_c(2520)^0 \rightarrow \Lambda_c^+ \pi^-$	$(3.2 \pm 0.7) \times 10^{-5}$		-
$\Lambda_c^+ \ell^- \bar{\nu}_{\ell} \text{anything}$	[v] $(10.9 \pm 2.2) \%$		-
$\Lambda_c^+ \ell^- \bar{\nu}_{\ell}$	$(6.2 \pm 1.4) \%$		2345
$\Lambda_c^+ \pi^+ \pi^- \ell^- \bar{\nu}_{\ell}$	$(5.6 \pm 3.1) \%$		2335
$\Lambda_c(2595)^+ \ell^- \bar{\nu}_{\ell}$	$(7.9 \pm 4.0) \times 10^{-3}$		2212
$\Lambda_c(2625)^+ \ell^- \bar{\nu}_{\ell}$	$(1.3 \pm 0.6) \%$		2195
$p h^-$	[x] $< 2.3 \times 10^{-5}$	CL=90%	2730
$p\pi^-$	$(4.5 \pm 0.8) \times 10^{-6}$		2730
pK^-	$(5.4 \pm 1.0) \times 10^{-6}$		2709
pD_s^-	$< 4.8 \times 10^{-4}$	CL=90%	2364
$p\mu^- \bar{\nu}_{\mu}$	$(4.1 \pm 1.0) \times 10^{-4}$		2730
$\Lambda \mu^+ \mu^-$	$(1.08 \pm 0.28) \times 10^{-6}$		2695
$p\pi^- \mu^+ \mu^-$	$(6.9 \pm 2.5) \times 10^{-8}$		2720
$\Lambda \gamma$	$(7.1 \pm 1.7) \times 10^{-6}$		2699
$\Lambda \eta$	$(9 \pm 7) \times 10^{-6}$		2670
$\Lambda \eta'(958)$	$< 3.1 \times 10^{-6}$	CL=90%	2611
$\Lambda \pi^+ \pi^-$	$(4.7 \pm 1.9) \times 10^{-6}$		2692
$\Lambda K^+ \pi^-$	$(5.7 \pm 1.3) \times 10^{-6}$		2660
$\Lambda K^+ K^-$	$(1.62 \pm 0.23) \times 10^{-5}$		2605
$\Lambda \phi$	$(9.8 \pm 2.6) \times 10^{-6}$		2599
$p\pi^- \pi^+ \pi^-$	$(2.11 \pm 0.23) \times 10^{-5}$		2715
$pK^- K^+ \pi^-$	$(4.1 \pm 0.6) \times 10^{-6}$		2612
$pK^- \pi^+ \pi^-$	$(5.1 \pm 0.5) \times 10^{-5}$		2675
$pK^- K^+ K^-$	$(1.27 \pm 0.14) \times 10^{-5}$		2524

$\Lambda_b(5912)^0$

$J^P = \frac{1}{2}^-$

Mass $m = 5912.20 \pm 0.21$ MeV
 Full width $\Gamma < 0.66$ MeV, CL = 90%

$\Lambda_b(5912)^0$ DECAY MODES	Fraction (Γ_i/Γ)	ρ (MeV/c)
$\Lambda_b^0 \pi^+ \pi^-$	seen	86

$\Lambda_b(5920)^0$

$J^P = \frac{3}{2}^-$

Mass $m = 5919.92 \pm 0.19$ MeV ($S = 1.1$)
 Full width $\Gamma < 0.63$ MeV, CL = 90%

$\Lambda_b(5920)^0$ DECAY MODES	Fraction (Γ_i/Γ)	ρ (MeV/c)
$\Lambda_b^0 \pi^+ \pi^-$	seen	108

Baryon Summary Table

$\Lambda_b(6146)^0$		$J^P = \frac{3}{2}^+$		
Mass $m = 6146.2 \pm 0.4$ MeV				
Full width $\Gamma = 2.9 \pm 1.3$ MeV				
Full width $\Gamma = 526.55 \pm 0.34$ MeV				
$\Lambda_b(6152)^0$		$J^P = \frac{5}{2}^+$		
Mass $m = 6152.5 \pm 0.4$ MeV				
Full width $\Gamma = 2.1 \pm 0.9$ MeV				
Full width $\Gamma = 532.89 \pm 0.28$ MeV				
Full width $\Gamma = 6.34 \pm 0.32$ MeV				
Σ_b		$I(J^P) = 1(\frac{1}{2}^+)$ <i>I, J, P</i> need confirmation.		
Mass $m(\Sigma_b^{*+}) = 5810.56 \pm 0.25$ MeV				
Mass $m(\Sigma_b^{*-}) = 5815.64 \pm 0.27$ MeV				
$m_{\Sigma_b^{*+}} - m_{\Sigma_b^{*-}} = -5.06 \pm 0.18$ MeV				
$\Gamma(\Sigma_b^{*+}) = 5.0 \pm 0.5$ MeV				
$\Gamma(\Sigma_b^{*-}) = 5.3 \pm 0.5$ MeV				
Σ_b DECAY MODES		Fraction (Γ_i/Γ)	ρ (MeV/c)	
$\Lambda_b^0 \pi$		dominant	133	
Σ_b^*		$I(J^P) = 1(\frac{3}{2}^+)$ <i>I, J, P</i> need confirmation.		
Mass $m(\Sigma_b^{*+}) = 5830.32 \pm 0.27$ MeV				
Mass $m(\Sigma_b^{*-}) = 5834.74 \pm 0.30$ MeV				
$m_{\Sigma_b^{*+}} - m_{\Sigma_b^{*-}} = -4.37 \pm 0.33$ MeV ($S = 1.6$)				
$m_{\Sigma_b^{*+}} - m_{\Sigma_b^+} = 19.73 \pm 0.18$				
$m_{\Sigma_b^{*-}} - m_{\Sigma_b^-} = 19.09 \pm 0.22$				
$\Gamma(\Sigma_b^{*+}) = 9.4 \pm 0.5$ MeV				
$\Gamma(\Sigma_b^{*-}) = 10.4 \pm 0.8$ MeV ($S = 1.3$)				
$m_{\Sigma_b^{*+}} - m_{\Sigma_b^+} = 21.2 \pm 2.0$ MeV				
Σ_b^* DECAY MODES		Fraction (Γ_i/Γ)	ρ (MeV/c)	
$\Lambda_b^0 \pi$		dominant	159	
$\Sigma_b(6097)^+$		$J^P = ?^?$		
Mass $m = 6095.8 \pm 1.7$ MeV				
Full width $\Gamma = 31 \pm 6$ MeV				
$\Sigma_b(6097)^+$ DECAY MODES		Fraction (Γ_i/Γ)	ρ (MeV/c)	
$\Lambda_b \pi^+ \times B(b \rightarrow \Sigma_b(6097)^+)$		seen	-	
$\Sigma_b(6097)^-$		$J^P = ?^?$		
Mass $m = 6098.0 \pm 1.8$ MeV				
Full width $\Gamma = 29 \pm 4$ MeV				
$\Sigma_b(6097)^-$ DECAY MODES		Fraction (Γ_i/Γ)	ρ (MeV/c)	
$\Lambda_b \pi^- \times B(b \rightarrow \Sigma_b(6097)^-)$		seen	-	
Ξ_b^0, Ξ_b^-		$I(J^P) = \frac{1}{2}(\frac{1}{2}^+)$ <i>I, J, P</i> need confirmation.		
$m(\Xi_b^-) = 5797.0 \pm 0.6$ MeV ($S = 1.7$)				
$m(\Xi_b^0) = 5791.9 \pm 0.5$ MeV				
$m_{\Xi_b^-} - m_{\Lambda_b^0} = 177.5 \pm 0.5$ MeV ($S = 1.6$)				
$m_{\Xi_b^0} - m_{\Lambda_b^0} = 172.5 \pm 0.4$ MeV				
$m_{\Xi_b^-} - m_{\Xi_b^0} = 5.9 \pm 0.6$ MeV				
Mean life $\tau_{\Xi_b^-} = (1.572 \pm 0.040) \times 10^{-12}$ s				
Mean life $\tau_{\Xi_b^0} = (1.480 \pm 0.030) \times 10^{-12}$ s				
Ξ_b DECAY MODES		Fraction (Γ_i/Γ)	Scale factor/ Confidence level	ρ (MeV/c)
$\Xi^- \ell^- \bar{\nu}_\ell X \times B(\bar{b} \rightarrow \Xi_b^-)$		$(3.9 \pm 1.2) \times 10^{-4}$	$S=1.4$	-
$J/\psi \Xi^- \times B(b \rightarrow \Xi_b^-)$		$(1.02^{+0.26}_{-0.21}) \times 10^{-5}$		1782
$J/\psi \Lambda K^- \times B(b \rightarrow \Xi_b^-)$		$(2.5 \pm 0.4) \times 10^{-6}$		1631
$\rho D^0 K^- \times B(\bar{b} \rightarrow \Xi_b^-)$		$(1.7 \pm 0.6) \times 10^{-6}$		2374
$\rho \bar{K}^0 \pi^- \times B(\bar{b} \rightarrow \Xi_b^-)/B(\bar{b} \rightarrow B^0)$		$< 1.6 \times 10^{-6}$	CL=90%	2783
$\rho K^0 K^- \times B(\bar{b} \rightarrow \Xi_b^-)/B(\bar{b} \rightarrow B^0)$		$< 1.1 \times 10^{-6}$	CL=90%	2730
$\rho K^- K^- \times B(\bar{b} \rightarrow \Xi_b^-)$		$(3.7 \pm 0.8) \times 10^{-8}$		2731
$\Lambda \pi^+ \pi^- \times B(b \rightarrow \Xi_b^0)/B(b \rightarrow \Lambda_b^0)$		$< 1.7 \times 10^{-6}$	CL=90%	2781
$\Lambda K^- \pi^+ \times B(b \rightarrow \Xi_b^0)/B(b \rightarrow \Lambda_b^0)$		$< 8 \times 10^{-7}$	CL=90%	2751
$\Lambda K^+ K^- \times B(b \rightarrow \Xi_b^0)/B(b \rightarrow \Lambda_b^0)$		$< 3 \times 10^{-7}$	CL=90%	2698
$\Lambda_c^+ K^- \times B(\bar{b} \rightarrow \Xi_b^-)$		$(6 \pm 4) \times 10^{-7}$		2416
$\Lambda_b^0 \pi^- \times B(b \rightarrow \Xi_b^-)/B(b \rightarrow \Lambda_b^0)$		$(5.7 \pm 2.0) \times 10^{-4}$		99
$\rho K^- \pi^+ \pi^- \times B(b \rightarrow \Xi_b^0)/B(b \rightarrow \Lambda_b^0)$		$(1.9 \pm 0.4) \times 10^{-6}$		2766
$\rho K^- K^- \pi^+ \times B(b \rightarrow \Xi_b^0)/B(b \rightarrow \Lambda_b^0)$		$(1.73 \pm 0.32) \times 10^{-6}$		2704
$\rho K^- K^+ K^- \times B(b \rightarrow \Xi_b^0)/B(b \rightarrow \Lambda_b^0)$		$(1.8 \pm 1.0) \times 10^{-7}$		2620
$\Xi_b'(5935)^-$		$J^P = \frac{1}{2}^+$		
Mass $m = 5935.02 \pm 0.05$ MeV				
$m_{\Xi_b'(5935)^-} - m_{\Xi_b^0} - m_{\pi^-} = 3.653 \pm 0.019$ MeV				
Full width $\Gamma < 0.08$ MeV, CL = 95%				
$\Xi_b'(5935)^-$ DECAY MODES		Fraction (Γ_i/Γ)	ρ (MeV/c)	
$\Xi_b^0 \pi^- \times B(\bar{b} \rightarrow \Xi_b'(5935)^-)/B(\bar{b} \rightarrow \Xi_b^0)$		$(11.8 \pm 1.8) \%$	31	
$\Xi_b(5945)^0$		$J^P = \frac{3}{2}^+$		
Mass $m = 5952.3 \pm 0.6$ MeV				
Full width $\Gamma = 0.90 \pm 0.18$ MeV				
$\Xi_b(5945)^0$ DECAY MODES		Fraction (Γ_i/Γ)	ρ (MeV/c)	
$\Xi_b^- \pi^+$		seen	78	
$\Xi_b(5955)^-$		$J^P = \frac{3}{2}^+$		
Mass $m = 5955.33 \pm 0.13$ MeV				
$m_{\Xi_b(5955)^-} - m_{\Xi_b^0} - m_{\pi^-} = 23.96 \pm 0.13$ MeV				
Full width $\Gamma = 1.65 \pm 0.33$ MeV				
$\Xi_b(5955)^-$ DECAY MODES		Fraction (Γ_i/Γ)	ρ (MeV/c)	
$\Xi_b^0 \pi^- \times B(\bar{b} \rightarrow \Xi_b(5955)^-)/B(\bar{b} \rightarrow \Xi_b^0)$		$(20.7 \pm 3.5) \%$	84	
$\Xi_b(6227)$		$J^P = ?^?$		
Mass $m = 6226.9 \pm 2.0$ MeV				
Full width $\Gamma = 18 \pm 6$ MeV				
$\Xi_b(6227)$ DECAY MODES		Fraction (Γ_i/Γ)	Scale factor (MeV/c)	
$\Lambda_b^0 K^- \times B(b \rightarrow \Xi_b(6227))/B(b \rightarrow \Lambda_b^0)$		$(3.20 \pm 0.35) \times 10^{-3}$	336	
$\Xi_b^0 \pi^- \times B(b \rightarrow \Xi_b(6227))/B(b \rightarrow \Xi_b^0)$		$(2.8 \pm 1.1) \%$	1.8	
$\Xi_b^0 \pi^- \times B(b \rightarrow \Xi_b(6227))/B(b \rightarrow \Xi_b^0)$			398	

Baryon Summary Table

 Ω_b^-

$$I(J^P) = 0(\frac{1}{2}^+)$$

I, J, P need confirmation.

Mass $m = 6046.1 \pm 1.7$ MeV
 $m_{\Omega_b^-} - m_{\Lambda_b^0} = 426.4 \pm 2.2$ MeV
 $m_{\Omega_b^-} - m_{\Xi_b^-} = 247.3 \pm 3.2$ MeV
 Mean life $\tau = (1.64^{+0.18}_{-0.17}) \times 10^{-12}$ s
 $\tau(\Omega_b^-)/\tau(\Xi_b^-)$ mean life ratio = 1.11 ± 0.16

Ω_b^- DECAY MODES	Fraction (Γ_i/Γ)	Confidence level	p (MeV/c)
$J/\psi \Omega_b^- \times B(b \rightarrow \Omega_b)$	$(2.9^{+1.1}_{-0.8}) \times 10^{-6}$		1806
$p K^- K^- \times B(\bar{b} \rightarrow \Omega_b)$	< 2.5	$\times 10^{-9}$	90% 2866
$p \pi^- \pi^- \times B(\bar{b} \rightarrow \Omega_b)$	< 1.5	$\times 10^{-8}$	90% 2943
$p K^- \pi^- \times B(\bar{b} \rightarrow \Omega_b)$	< 7	$\times 10^{-9}$	90% 2915

b-baryon ADMIXTURE ($\Lambda_b, \Xi_b, \Omega_b$)

These branching fractions are actually an average over weakly decaying b -baryons weighted by their production rates at the LHC, LEP, and Tevatron, branching ratios, and detection efficiencies. They scale with the b -baryon production fraction $B(b \rightarrow b\text{-baryon})$.

The branching fractions $B(b\text{-baryon} \rightarrow \Lambda \ell^- \bar{\nu}_\ell \text{ anything})$ and $B(\Lambda_b^0 \rightarrow \Lambda_c^+ \ell^- \bar{\nu}_\ell \text{ anything})$ are not pure measurements because the underlying measured products of these with $B(b \rightarrow b\text{-baryon})$ were used to determine $B(b \rightarrow b\text{-baryon})$, as described in the note "Production and Decay of b -Flavored Hadrons."

For inclusive branching fractions, e.g., $B \rightarrow D^\pm \text{ anything}$, the values usually are multiplicities, not branching fractions. They can be greater than one.

b-baryon ADMIXTURE DECAY MODES ($\Lambda_b, \Xi_b, \Omega_b$)	Fraction (Γ_i/Γ)	p (MeV/c)
$p \mu^- \bar{\nu}$ anything	$(5.8^{+2.3}_{-2.0}) \%$	—
$p \ell \bar{\nu}_\ell$ anything	$(5.6 \pm 1.2) \%$	—
p anything	$(70 \pm 22) \%$	—
$\Lambda \ell^- \bar{\nu}_\ell$ anything	$(3.8 \pm 0.6) \%$	—
$\Lambda \ell^+ \nu_\ell$ anything	$(3.2 \pm 0.8) \%$	—
Λ anything	$(39 \pm 7) \%$	—
$\Xi^- \ell^- \bar{\nu}_\ell$ anything	$(6.6 \pm 1.6) \times 10^{-3}$	—

EXOTIC BARYONS $P_c(4312)^+$

Mass $m = 4311.9^{+7.0}_{-0.9}$ MeV
 Full width $\Gamma = 10 \pm 5$ MeV

$P_c(4312)^+$ DECAY MODES	Fraction (Γ_i/Γ)	p (MeV/c)
$J/\psi p$	seen	658

 $P_c(4380)^+$

Mass $m = 4380 \pm 30$ MeV
 Full width $\Gamma = 205 \pm 90$ MeV

$P_c(4380)^+$ DECAY MODES	Fraction (Γ_i/Γ)	p (MeV/c)
$J/\psi p$	seen	741

 $P_c(4440)^+$

Mass $m = 4440^{+4}_{-5}$ MeV
 Full width $\Gamma = 21^{+10}_{-11}$ MeV

$P_c(4440)^+$ DECAY MODES	Fraction (Γ_i/Γ)	p (MeV/c)
$J/\psi p$	seen	810

 $P_c(4457)^+$ was $P_c(4450)$

Mass $m = 4457.3^{+4.0}_{-1.8}$ MeV
 Full width $\Gamma = 6.4^{+6.0}_{-2.8}$ MeV

$P_c(4457)^+$ DECAY MODES	Fraction (Γ_i/Γ)	p (MeV/c)
$J/\psi p$	seen	828

NOTES

This Summary Table only includes established baryons. The Particle Listings include evidence for other baryons. The masses, widths, and branching fractions for the resonances in this Table are Breit-Wigner parameters, but pole positions are also given for most of the N and Δ resonances.

For most of the resonances, the parameters come from various partial-wave analyses of more or less the same sets of data, and it is not appropriate to treat the results of the analyses as independent or to average them together. Furthermore, the systematic errors on the results are not well understood. Thus, we usually only give ranges for the parameters. We then also give a best guess for the mass (as part of the name of the resonance) and for the width. The *Note on N and Δ Resonances* and the *Note on Λ and Σ Resonances* in the Particle Listings review the partial-wave analyses.

When a quantity has "($S = \dots$)" to its right, the error on the quantity has been enlarged by the "scale factor" S , defined as $S = \sqrt{\chi^2/(N-1)}$, where N is the number of measurements used in calculating the quantity. We do this when $S > 1$, which often indicates that the measurements are inconsistent. When $S > 1.25$, we also show in the Particle Listings an ideogram of the measurements. For more about S , see the Introduction.

A decay momentum p is given for each decay mode. For a 2-body decay, p is the momentum of each decay product in the rest frame of the decaying particle. For a 3-or-more-body decay, p is the largest momentum any of the products can have in this frame. For any resonance, the *nominal* mass is used in calculating p . A dagger ("†") in this column indicates that the mode is forbidden when the nominal masses of resonances are used, but is in fact allowed due to the nonzero widths of the resonances.

- [a] The masses of the p and n are most precisely known in u (unified atomic mass units). The conversion factor to MeV, $1 u = 931.494061(21)$ MeV, is less well known than are the masses in u .
- [b] The $|m_p - m_{\bar{p}}|/m_p$ and $|q_p + q_{\bar{p}}|/e$ are not independent, and both use the more precise measurement of $|q_{\bar{p}}/m_{\bar{p}}|/(q_p/m_p)$.
- [c] The limit is from neutrality-of-matter experiments; it assumes $q_n = q_p + q_e$. See also the charge of the neutron.
- [d] The μp and $e p$ values for the charge radius are much too different to average them. The disagreement is not yet understood.
- [e] There is a lot of disagreement about the value of the proton magnetic charge radius. See the Listings.
- [f] The first limit is for $p \rightarrow$ anything or "disappearance" modes of a bound proton. The second entry, a rough range of limits, assumes the dominant decay modes are among those investigated. For antiprotons the best limit, inferred from the observation of cosmic ray \bar{p} 's is $\tau_{\bar{p}} > 10^7$ yr, the cosmic-ray storage time, but this limit depends on a number of assumptions. The best direct observation of stored antiprotons gives $\tau_{\bar{p}}/B(\bar{p} \rightarrow e^- \gamma) > 7 \times 10^5$ yr.
- [g] There is some controversy about whether nuclear physics and model dependence complicate the analysis for bound neutrons (from which the best limit comes). The first limit here is from reactor experiments with free neutrons.
- [h] Lee and Yang in 1956 proposed the existence of a mirror world in an attempt to restore global parity symmetry—thus a search for oscillations between the two worlds. Oscillations between the worlds would be maximal when the magnetic fields B and B' were equal. The limit for any B' in the range 0 to 12.5 μ T is > 12 s (95% CL).
- [i] The parameters g_A, g_V , and g_{WM} for semileptonic modes are defined by $\bar{B}_f[\gamma_\lambda(g_V + g_A\gamma_5) + i(g_{WM}/m_{B_f})\sigma_{\lambda\nu}q^\nu]B_i$, and ϕ_{AV} is defined by $g_A/g_V = |g_A/g_V|e^{i\phi_{AV}}$. See the "Note on Baryon Decay Parameters" in the neutron Particle Listings.
- [j] Time-reversal invariance requires this to be 0° or 180° .
- [k] This coefficient is zero if time invariance is not violated.
- [l] This limit is for γ energies between 0.4 and 782 keV.

Baryon Summary Table

[n] The decay parameters γ and Δ are calculated from α and ϕ using

$$\gamma = \sqrt{1-\alpha^2} \cos\phi, \quad \tan\Delta = -\frac{1}{\alpha} \sqrt{1-\alpha^2} \sin\phi.$$

See the "Note on Baryon Decay Parameters" in the neutron Particle Listings.

[o] See the Listings for the pion momentum range used in this measurement.

[p] Our estimate. See the Particle Listings for details.

[q] A theoretical value using QED.

[r] This branching fraction includes all the decay modes of the final-state resonance.

[s] See AALTONEN 11H, Fig. 8, for the calculated ratio of $\Lambda_c^+ \pi^0 \pi^0$ and $\Lambda_c^+ \pi^+ \pi^-$ partial widths as a function of the $\Lambda_c(2595)^+ - \Lambda_c^+$ mass difference. At our value of the mass difference, the ratio is about 4.

[t] A test that the isospin is indeed 0, so that the particle is indeed a Λ_c^+ .

[u] P_c^+ is a pentaquark-charmonium state.

[v] Not a pure measurement. See note at head of Λ_b^0 Decay Modes.

[x] Here h^- means π^- or K^- .

SEARCHES not in other sections

Magnetic Monopole Searches

The most sensitive experiments obtain negative results.
Best cosmic-ray supermassive monopole flux limit:
 $< 1.4 \times 10^{-16} \text{ cm}^{-2} \text{sr}^{-1} \text{s}^{-1}$ for $1.1 \times 10^{-4} < \beta < 1$

Supersymmetric Particle Searches

All supersymmetric mass bounds here are model dependent.
The limits assume:

1) $\tilde{\chi}_1^0$ is the lightest supersymmetric particle; 2) R -parity is conserved, unless stated otherwise;

See the Particle Listings for a Note giving details of supersymmetry.

$\tilde{\chi}_i^0$ — neutralinos (mixtures of $\tilde{\gamma}$, \tilde{Z}^0 , and \tilde{H}_i^0)

Mass $m_{\tilde{\chi}_1^0} > 0$ GeV, CL = 95%
[general MSSM, non-universal gaugino masses]

Mass $m_{\tilde{\chi}_1^0} > 46$ GeV, CL = 95%

[all $\tan\beta$, all m_0 , all $m_{\tilde{\chi}_2^0} - m_{\tilde{\chi}_1^0}$]

Mass $m_{\tilde{\chi}_2^0} > 62.4$ GeV, CL = 95%

[$1 < \tan\beta < 40$, all m_0 , all $m_{\tilde{\chi}_2^0} - m_{\tilde{\chi}_1^0}$]

Mass $m_{\tilde{\chi}_3^0} > 99.9$ GeV, CL = 95%

[$1 < \tan\beta < 40$, all m_0 , all $m_{\tilde{\chi}_2^0} - m_{\tilde{\chi}_1^0}$]

Mass $m_{\tilde{\chi}_4^0} > 116$ GeV, CL = 95%

[$1 < \tan\beta < 40$, all m_0 , all $m_{\tilde{\chi}_2^0} - m_{\tilde{\chi}_1^0}$]

$\tilde{\chi}_i^\pm$ — charginos (mixtures of \tilde{W}^\pm and \tilde{H}_i^\pm)

Mass $m_{\tilde{\chi}_1^\pm} > 94$ GeV, CL = 95%
[$\tan\beta < 40$, $m_{\tilde{\chi}_1^\pm} - m_{\tilde{\chi}_2^\pm} > 3$ GeV, all m_0]

Mass $m_{\tilde{\chi}_2^\pm} > 810$ GeV, CL = 95%

[$\ell^\pm \ell^\mp$, Tchi1chi1C, $m_{\tilde{\chi}_1^0} = 0$ GeV]

$\tilde{\chi}^\pm$ — long-lived chargino

Mass $m_{\tilde{\chi}^\pm} > 620$ GeV, CL = 95% [stable $\tilde{\chi}^\pm$]

$\tilde{\nu}$ — sneutrino

Mass $m > 41$ GeV, CL = 95% [model independent]

Mass $m > 94$ GeV, CL = 95%

[CMSSM, $1 \leq \tan\beta \leq 40$, $m_{\tilde{\tau}_R} - m_{\tilde{\chi}_1^0} > 10$ GeV]

Mass $m > 3400$ GeV, CL = 95% [R-Parity Violating]

[$\tilde{\nu}_\tau \rightarrow e\mu$, $\lambda_{312} = \lambda_{321} = 0.07$, $\lambda'_{311} = 0.11$]

\tilde{e} — scalar electron (selectron)

Mass $m(\tilde{e}_L) > 107$ GeV, CL = 95% [all $m_{\tilde{e}_L} - m_{\tilde{\chi}_1^0}$]

Mass $m > 410$ GeV, CL = 95% [R-Parity Violating]

[$\geq 4\ell^\pm$, $\tilde{\ell} \rightarrow I\tilde{\chi}_1^0, \tilde{\chi}_1^0 \rightarrow \ell^\pm \ell^\mp \nu$]

$\tilde{\mu}$ — scalar muon (smuon)

Mass $m > 94$ GeV, CL = 95%

[CMSSM, $1 \leq \tan\beta \leq 40$, $m_{\tilde{\mu}_R} - m_{\tilde{\chi}_1^0} > 10$ GeV]

Mass $m > 410$ GeV, CL = 95% [R-Parity Violating]

[$\geq 4\ell^\pm$, $\tilde{\ell} \rightarrow I\tilde{\chi}_1^0, \tilde{\chi}_1^0 \rightarrow \ell^\pm \ell^\mp \nu$]

$\tilde{\tau}$ — scalar tau (stau)

Mass $m > 81.9$ GeV, CL = 95%

[$m_{\tilde{\tau}_R} - m_{\tilde{\chi}_1^0} > 15$ GeV, all θ_τ , $B(\tilde{\tau} \rightarrow \tau\tilde{\chi}_1^0) = 100\%$]

Mass $m > 286$ GeV, CL = 95% [long-lived $\tilde{\tau}$]

\tilde{q} — squarks of the first two quark generations

Mass $m > 1.450 \times 10^3$ GeV, CL = 95%

[CMSSM, $\tan\beta = 30$, $A_0 = -2\max(m_0, m_{1/2})$, $\mu > 0$]

Mass $m > 1630$ GeV, CL = 95%

[mass degenerate squarks]

Mass $m > 1130$ GeV, CL = 95%

[single light squark bounds]

Mass $m > 1.600 \times 10^3$ GeV, CL = 95% [R-Parity Violating]

[$\tilde{q} \rightarrow q\tilde{\chi}_1^0, \tilde{\chi}_1^0 \rightarrow \ell\ell\nu, \lambda_{121}, \lambda_{122} \neq 0, m_{\tilde{g}} = 2400$ GeV]

\tilde{q} — long-lived squark

Mass $m > 1340$, CL = 95% [\tilde{t} R -hadrons]

Mass $m > 1250$, CL = 95% [\tilde{b} R -hadrons]

\tilde{b} — scalar bottom (sbottom)

Mass $m > 1230$ GeV, CL = 95%

[jets+ \cancel{E}_T , Tsb01, $m_{\tilde{\chi}_1^0} = 0$ GeV]

Mass $m > 307$ GeV, CL = 95% [R-Parity Violating]

[$\tilde{b} \rightarrow t d$ or $t s$, λ''_{332} or λ''_{331} coupling]

\tilde{t} — scalar top (stop)

Mass $m > 1190$ GeV, CL = 95%

[jets+ \cancel{E}_T , Tstop1, $m_{\tilde{\chi}_1^0} = 0$ GeV]

Mass $m > 1100$ GeV, CL = 95% [R-Parity Violating]

[$\tilde{t} \rightarrow b e$, Tstop2RPV, prompt]

\tilde{g} — gluino

Mass $m > 2.000 \times 10^3$ GeV, CL = 95%

[jets + \cancel{E}_T , Tglu1A, $m_{\tilde{\chi}_1^0} = 0$ GeV]

Mass $m > 2.260 \times 10^3$ GeV, CL = 95% [R-Parity Violating]

[$\geq 4\ell$, $\lambda_{12k} \neq 0$, $m_{\tilde{\chi}_1^0} > 1000$ GeV]

Technicolor

The limits for technicolor (and top-color) particles are quite varied depending on assumptions. See the Technicolor section of the full *Review* (the data listings).

Quark and Lepton Compositeness, Searches for

Scale Limits Λ for Contact Interactions

(the lowest dimensional interactions with four fermions)

If the Lagrangian has the form

$$\pm \frac{g^2}{2\Lambda^2} \bar{\psi}_L \gamma_\mu \psi_L \bar{\psi}_L \gamma^\mu \psi_L$$

(with $g^2/4\pi$ set equal to 1), then we define $\Lambda \equiv \Lambda_{LL}^\pm$. For the full definitions and for other forms, see the Note in the Listings on Searches for Quark and Lepton Compositeness in the full *Review* and the original literature.

$$\Lambda_{LL}^+(eeee) > 8.3 \text{ TeV, CL} = 95\%$$

$$\Lambda_{LL}^-(eeee) > 10.3 \text{ TeV, CL} = 95\%$$

$$\Lambda_{LL}^+(e\mu\mu\mu) > 8.5 \text{ TeV, CL} = 95\%$$

$$\Lambda_{LL}^-(e\mu\mu\mu) > 9.5 \text{ TeV, CL} = 95\%$$

$$\Lambda_{LL}^+(e\tau\tau\tau) > 7.9 \text{ TeV, CL} = 95\%$$

$$\Lambda_{LL}^-(e\tau\tau\tau) > 7.2 \text{ TeV, CL} = 95\%$$

$$\Lambda_{LL}^+(\ell\ell\ell\ell) > 9.1 \text{ TeV, CL} = 95\%$$

$$\Lambda_{LL}^-(\ell\ell\ell\ell) > 10.3 \text{ TeV, CL} = 95\%$$

$$\Lambda_{LL}^+(eeqq) > 24 \text{ TeV, CL} = 95\%$$

$$\Lambda_{LL}^-(eeqq) > 37 \text{ TeV, CL} = 95\%$$

$$\Lambda_{LL}^+(eeuu) > 23.3 \text{ TeV, CL} = 95\%$$

$$\Lambda_{LL}^-(eeuu) > 12.5 \text{ TeV, CL} = 95\%$$

$$\Lambda_{LL}^+(eedd) > 11.1 \text{ TeV, CL} = 95\%$$

$$\Lambda_{LL}^-(eedd) > 26.4 \text{ TeV, CL} = 95\%$$

$$\Lambda_{LL}^+(eccc) > 9.4 \text{ TeV, CL} = 95\%$$

$$\Lambda_{LL}^-(eccc) > 5.6 \text{ TeV, CL} = 95\%$$

$$\Lambda_{LL}^+(ebbb) > 9.4 \text{ TeV, CL} = 95\%$$

$$\Lambda_{LL}^-(ebbb) > 10.2 \text{ TeV, CL} = 95\%$$

$$\Lambda_{LL}^+(\mu\mu qq) > 20 \text{ TeV, CL} = 95\%$$

$$\Lambda_{LL}^-(\mu\mu qq) > 30 \text{ TeV, CL} = 95\%$$

$$\Lambda(\ell\nu\ell\nu) > 3.10 \text{ TeV, CL} = 90\%$$

$$\Lambda(e\nu qq) > 2.81 \text{ TeV, CL} = 95\%$$

$$\Lambda_{LL}^+(qqqq) > 13.1 \text{ none } 17.4\text{--}29.5 \text{ TeV, CL} = 95\%$$

$$\Lambda_{LL}^-(qqqq) > 21.8 \text{ TeV, CL} = 95\%$$

$$\Lambda_{LL}^+(\nu\nu qq) > 5.0 \text{ TeV, CL} = 95\%$$

$$\Lambda_{LL}^-(\nu\nu qq) > 5.4 \text{ TeV, CL} = 95\%$$

Searches Summary Table

Excited Leptons

The limits from $\ell^{*+} \ell^{*-}$ do not depend on λ (where λ is the $\ell \ell^*$ transition coupling). The λ -dependent limits assume chiral coupling.

$e^{*\pm}$ — excited electron

- Mass $m > 103.2$ GeV, CL = 95% (from $e^* e^*$)
- Mass $m > 4.800 \times 10^3$ GeV, CL = 95% (from ee^*)
- Mass $m > 356$ GeV, CL = 95% (if $\lambda_\gamma = 1$)

$\mu^{*\pm}$ — excited muon

- Mass $m > 103.2$ GeV, CL = 95% (from $\mu^* \mu^*$)
- Mass $m > 3.800 \times 10^3$ GeV, CL = 95% (from $\mu\mu^*$)

$\tau^{*\pm}$ — excited tau

- Mass $m > 103.2$ GeV, CL = 95% (from $\tau^* \tau^*$)
- Mass $m > 2.500 \times 10^3$ GeV, CL = 95% (from $\tau\tau^*$)

ν^* — excited neutrino

- Mass $m > 1.600 \times 10^3$ GeV, CL = 95% (from $\nu^* \nu^*$)
- Mass $m > 213$ GeV, CL = 95% (from $\nu^* X$)

q^* — excited quark

- Mass $m > 338$ GeV, CL = 95% (from $q^* q^*$)
- Mass $m > 6.000 \times 10^3$ GeV, CL = 95% (from $q^* X$)

Color Sextet and Octet Particles

Color Sextet Quarks (q_6)

- Mass $m > 84$ GeV, CL = 95% (Stable q_6)

Color Octet Charged Leptons (ℓ_8)

- Mass $m > 86$ GeV, CL = 95% (Stable ℓ_8)

Color Octet Neutrinos (ν_8)

- Mass $m > 110$ GeV, CL = 90% ($\nu_8 \rightarrow \nu g$)

Extra Dimensions

Please refer to the Extra Dimensions section of the full *Review* for a discussion of the model-dependence of these bounds, and further constraints.

Constraints on the radius of the extra dimensions, for the case of two-flat dimensions of equal radii

- $R < 30 \mu\text{m}$, CL = 95% (direct tests of Newton's law)
- $R < 4.8 \mu\text{m}$, CL = 95% ($pp \rightarrow j\bar{G}$)
- $R < 0.16\text{--}916$ nm (astrophysics; limits depend on technique and assumptions)

Constraints on the fundamental gravity scale

- $M_{TT} > 9.02$ TeV, CL = 95% ($pp \rightarrow$ dijet, angular distribution)
- $M_c > 4.16$ TeV, CL = 95% ($pp \rightarrow \ell\bar{\ell}$)

Constraints on the Kaluza-Klein graviton in warped extra dimensions

- $M_G > 4.25$ TeV, CL = 95% ($pp \rightarrow \gamma\gamma$)

Constraints on the Kaluza-Klein gluon in warped extra dimensions

- $M_{g_{KK}} > 3.8$ TeV, CL = 95% ($g_{KK} \rightarrow t\bar{t}$)

WIMP and Dark Matter Searches

No confirmed evidence found for galactic WIMPs from the GeV to the TeV mass scales and down to 1×10^{-10} pb spin independent cross section at $M = 100$ GeV.

Tests of Conservation Laws

Written August 2019 by A. Pich (IFIC, Valencia) and M. Ramsey-Musolf (Tsung-Dao Lee Inst.; SJTU; U. Massachusetts).

In keeping with the current interest in tests of conservation laws, we collect together a Table of experimental limits on all weak and electromagnetic decays, mass differences, and moments, and on a few reactions, whose observation would violate conservation laws. The Table is given only in the full Review of Particle Physics (RPP), not in the Particle Physics Booklet, and organizes the data in two main sections: “Discrete Space-Time Symmetries”, *i.e.*, C , P , T , CP and CPT ; and “Number Conservation Laws”, *i.e.*, lepton, baryon, flavor and charge conservation. The references for these data can be found in the Particle Listings. The following text discusses the best limits among those included in the Table and gives a brief overview of the current status. For some topics, a more extensive discussion of the framework for theoretical interpretation is provided, particularly where the analogous discussion does not appear elsewhere in the RPP. References to more extensive review articles are also included where appropriate. Unless otherwise specified, all limits quoted in this review are given at a C.L. of 90%.

DISCRETE SPACE-TIME SYMMETRIES

Charge conjugation (C), parity (P) and time reversal (T) are empirically exact symmetries of the electromagnetic (QED) and strong (QCD) interactions, but they are violated by the weak forces. Owing to the left-handed nature of the $SU(2)_L \otimes U(1)_Y$ electroweak theory, C and P are maximally violated in the fermionic couplings of the W^\pm and (up to $\sin^2 \theta_W$ corrections) the Z . However, their product CP is still an exact symmetry when only one or two fermion families are considered. With three generations of fermions, CP is violated through the single complex phase present in the Cabibbo-Kobayashi-Maskawa (CKM) quark mixing matrix. An analogous CP -violating (CPV) phase appears in the lepton sector when non-vanishing neutrino masses are taken into account (plus two additional phases if neutrinos are Majorana particles). The product of the three discrete symmetries, CPT , is an exact symmetry of any local and Lorentz-invariant quantum field theory with a positive-definite hermitian Hamiltonian that preserves micro-causality [1, 2]. Therefore, the breaking of CP implies a corresponding violation of T .

Violations of charge-conjugation symmetry have never been observed in electromagnetic and strong phenomena. The most stringent limits are extracted from C -violating transitions of neutral (self-conjugate) particles such as $\text{Br}(\pi^0 \rightarrow 3\gamma) < 3.1 \times 10^{-8}$ [3] and $\text{Br}(J/\psi \rightarrow 2\gamma) < 2.7 \times 10^{-7}$ [4]. P (and CP) conservation has been also precisely tested through forbidden decays such as $\text{Br}(\eta \rightarrow 4\pi^0) < 6.9 \times 10^{-7}$ [5], but the best limits on P and T are set by the non-observation of electric dipole moments (see section 2). Obviously, the interplay of the weak interaction puts a lower bound in sensitivity for this type of tests, beyond which violations of the corresponding conservation laws should be detected.

1 Violations of CP and T

The first evidence of CP non-invariance in particle physics was the observation in 1964 of $K_L^0 \rightarrow \pi^+\pi^-$ decays [6]. For many years afterwards, the non-zero ratio

$$\begin{aligned} |\eta_{+-}| &\equiv |\mathcal{M}(K_L^0 \rightarrow \pi^+\pi^-)/\mathcal{M}(K_S^0 \rightarrow \pi^+\pi^-)| \\ &= (2.232 \pm 0.011) \times 10^{-3} \end{aligned} \quad (1)$$

could be explained as a $K^0\text{-}\bar{K}^0$ mixing effect, $\eta_{+-} = \epsilon$ (superweak CP violation), which would imply an identical ratio $\eta_{00} \equiv \mathcal{M}(K_L^0 \rightarrow \pi^0\pi^0)/\mathcal{M}(K_S^0 \rightarrow \pi^0\pi^0)$ in the neutral decay mode and successfully predicts the observed CPV semileptonic asymmetry ($A_L(e) \approx 2\text{Re}\epsilon$)

$$\begin{aligned} A_L(e) &\equiv \frac{\Gamma(K_L^0 \rightarrow \pi^- e^+ \nu_e) - \Gamma(K_L^0 \rightarrow \pi^+ e^- \bar{\nu}_e)}{\Gamma(K_L^0 \rightarrow \pi^- e^+ \nu_e) + \Gamma(K_L^0 \rightarrow \pi^+ e^- \bar{\nu}_e)} \\ &= (3.34 \pm 0.07) \times 10^{-3}. \end{aligned} \quad (2)$$

A tiny difference between η_{+-} and η_{00} was reported for the first time in 1988 by the CERN NA31 collaboration [7], and later es-

tablished at the 7.2σ level with the full data samples from the NA31 [8], E731 [9], NA48 [10] and KTeV [11] experiments:

$$\text{Re}(\epsilon'/\epsilon) = \frac{1}{3} (1 - |\eta_{00}/\eta_{+-}|) = (1.66 \pm 0.23) \times 10^{-3}. \quad (3)$$

This important measurement confirmed that CP violation is associated with a $\Delta S = 1$ transition, as predicted by the CKM mechanism. The Standard Model (SM) prediction, $\text{Re}(\epsilon'/\epsilon) = (1.4 \pm 0.5) \times 10^{-3}$ [12, 13], is in good agreement with the measured ratio, although the theoretical uncertainty is unfortunately large.

Much larger CP asymmetries have been later measured in B meson decays, many of them involving the interference between $B^0\text{-}\bar{B}^0$ mixing and the decay amplitude. They provide many successful tests of the CKM unitarity structure, validating the SM mechanism of CP violation (see the review on CP violation in the quark sector). Prominent signals of direct CP violation have been also clearly established in several B^\pm , B_d^0 and B_s^0 decays, and, very recently, in charm decays [14]:

$$\begin{aligned} \Delta a_{CP}^{\text{dir}} &\equiv a_{CP}^{\text{dir}}(D^0 \rightarrow K^+K^-) - a_{CP}^{\text{dir}}(D^0 \rightarrow \pi^+\pi^-) \\ &= (-15.7 \pm 2.9) \times 10^{-4}. \end{aligned} \quad (4)$$

These direct CP asymmetries necessarily involve the presence of a strong phase-shift difference between (at least) two interfering amplitudes, which makes very challenging to perform reliable SM predictions for heavy-flavored mesons.

Global fits to neutrino oscillation data provide some hints of a non-zero mixing phase [15, 16]. Although the statistical significance is not yet compelling, they suggest that CP -violation effects in neutrino oscillations could be large (see the review on neutrino masses, mixings and oscillations). The future DUNE and Hyper-Kamiokande experiments are expected to confirm the presence of CP violation in the lepton sector or constrain the phase in the leptonic mixing matrix to be smaller than $O(10^\circ)$.

While CP violation implies a breaking of time-reversal symmetry, direct tests of T violation are much more difficult. The CPLEAR experiment observed longtime ago a non-zero difference between the oscillation probabilities of $K^0 \rightarrow \bar{K}^0$ and $\bar{K}^0 \rightarrow K^0$ [17]. Initial neutral kaons with defined strangeness were produced from proton-antiproton annihilations at rest, $p\bar{p} \rightarrow K^-\pi^+K^0, K^+\pi^-\bar{K}^0$, and tagged by the accompanying charged kaon, while the strangeness of the final neutral kaon was identified through its semileptonic decay: $K^0 \rightarrow e^+\pi^-\nu_e, \bar{K}^0 \rightarrow e^-\pi^+\bar{\nu}_e$. The average asymmetry over the time interval from 1 to 20 K_S^0 lifetimes was found to be different from zero at 4σ [17]:

$$\begin{aligned} \frac{R[\bar{K}^0(t=0) \rightarrow e^+\pi^-\nu_e(t)] - R[K^0(t=0) \rightarrow e^-\pi^+\bar{\nu}_e(t)]}{R[\bar{K}^0(t=0) \rightarrow e^+\pi^-\nu_e(t)] + R[K^0(t=0) \rightarrow e^-\pi^+\bar{\nu}_e(t)]} &= \\ = (6.6 \pm 1.3 \pm 1.0) \times 10^{-3}. \end{aligned} \quad (5)$$

Since this asymmetry violates also CP , its interpretation as direct evidence of T violation requires a detailed analysis of the underlying $K^0\text{-}\bar{K}^0$ mixing process [18–20].

More recently, the exchange of initial and final states has been made possible in B decays, taking advantage of the entanglement of the two daughter mesons produced in the decay $\Upsilon(4S) \rightarrow B\bar{B}$ which allows for both flavor ($B^0 \rightarrow \ell^+X, \bar{B}^0 \rightarrow \ell^-X$) and CP ($B_+ \rightarrow J/\psi K_L^0, B_- \rightarrow J/\psi K_S^0$) tagging. Selecting events where one B candidate is reconstructed in a CP eigenstate and the flavor of the other B is identified, one can compare the rates of the $\bar{B}^0 \rightarrow B_\pm$ and $B^0 \rightarrow B_\pm$ transitions with their T -reversed $B_\pm \rightarrow \bar{B}^0$ and $B_\pm \rightarrow B^0$ processes, as a function of the time difference Δt between the two B decays [21–23]. Neglecting the small width difference between the two B_d^0 mass eigenstates, each of these eight transitions has a time-dependent decay rate of the form $e^{-\Gamma_d \Delta t} \{1 + S_{\alpha,\beta}^\pm \sin(\Delta m_d \Delta t) + C_{\alpha,\beta}^\pm \cos(\Delta m_d \Delta t)\}$, where Γ_d is the average decay width, Δm_d the B_d^0 mass difference, the subindices $\alpha = \ell^+, \ell^-$ and $\beta = K_S^0, K_L^0$ stand for the reconstructed final states of the two B mesons and the superindex \pm

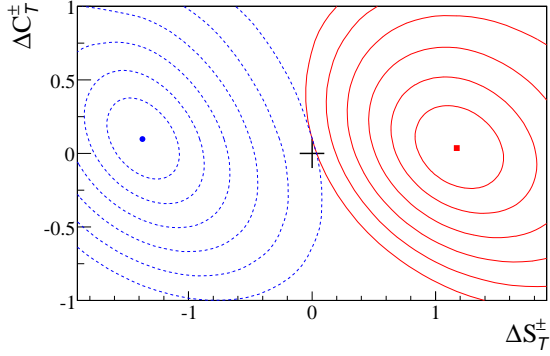


Figure 1: Measured values of ΔS_T^+ , ΔC_T^+ (blue point, dashed lines) and ΔS_T^- , ΔC_T^- (red square, solid lines) [24]. The two-dimensional contours correspond to $1 - \text{CL} = 0.317, 4.55 \times 10^{-2}, 2.70 \times 10^{-3}, 6.33 \times 10^{-5}, 5.73 \times 10^{-7},$ and 1.97×10^{-9} . The + sign indicates the T -invariant point.

or $-$ indicates whether the decay to the flavor final state α occurs before or after the decay to the CP final state β . Figure 1 shows confidence-level contours for the T -asymmetry parameters $\Delta S_T^\pm \equiv S_{\ell^-, K_L^0}^\mp - S_{\ell^+, K_S^0}^\pm$ and $\Delta C_T^\pm \equiv C_{\ell^-, K_L^0}^\mp - C_{\ell^+, K_S^0}^\pm$, reported by the BABAR experiment [24], which clearly demonstrate a violation of T in ΔS_T^\pm , with a significance of 14σ .

2 Electric dipole moments

Among the most powerful tests of CP invariance is the search for a permanent electric dipole moment (EDM) of an elementary fermion or non-degenerate quantum system. The EDM of an elementary spin-1/2 fermion f is defined by the effective, non-renormalizable interaction

$$\mathcal{L}_{\text{EDM}} = -\frac{i}{2} d_f \bar{f} \sigma_{\mu\nu} \gamma_5 f F^{\mu\nu} \quad (6)$$

where $F^{\mu\nu}$ is the QED field strength tensor. The values for d_f are conventionally expressed in units of $e \text{ cm}$. The interaction (6) is separately odd under T and P . In the non-relativistic limit, Eq. (6) reduces to

$$\mathcal{L}_{\text{EDM}} \rightarrow d_f \chi_f^\dagger \vec{\sigma} \chi \cdot \vec{E} \quad (7)$$

where χ is a two-component Pauli spinor and \vec{E} is the electric field. Note the interaction (7) is manifestly T -odd and carries no direct information on CP . The observation of a non-zero EDM of a non-relativistic (and non-degenerate) quantum system, such as the mercury atom (see below) would imply CP violation under the assumption of CPT invariance.

To date, no experimental observation of an EDM of an elementary particle or non-degenerate bound quantum system has been observed. The most stringent limits have been obtained for the EDMs of the electron, mercury atom, and neutron. A selection of the representative, most stringent limits is given in Table 1. The limits on the electron EDM are inferred from experiments involving polar molecules, paramagnetic systems with an unpaired electron spin. In contrast, the neutron and ^{199}Hg atom are diamagnetic. A variety of experimental efforts aimed at improved sensitivities are underway. For reviews of the experimental and theoretical situation, see, *e.g.* [25–28].

EDMs in the Standard Model

The SM provides two sources of d_f : the CPV phase in the CKM matrix and the P - and T -odd ‘ θ term’ in the QCD Lagrangian. The former is characterized by the Jarlskog invariant [35]

$$\mathcal{J} = \text{Im}(V_{us} V_{cs}^* V_{cb} V_{ub}^*) \sim A^2 \lambda^6 \eta < 10^{-4}, \quad (8)$$

while the latter is given by

$$\mathcal{L}_{\bar{\theta}} = -\frac{g_3^2}{16\pi^2} \bar{\theta} \text{Tr} (G^{\mu\nu} \tilde{G}_{\mu\nu}), \quad (9)$$

Table 1: Most stringent limits on electric dipole moments.

EDM	Limit ($e \text{ cm}$)	Source
Electron	1.1×10^{-29} (90% C.L.)	ThO [29]
	1.3×10^{-28} (90% C.L.)	HfF ⁺ [30]
Muon	1.8×10^{-19} (95% C.L.)	[31]
Neutron	1.8×10^{-26} (90% C.L.)	[32]
^{199}Hg Atom	7.4×10^{-30} (95% C.L.)	[33]
^{129}Xe Atom	1.5×10^{-27} (95% C.L.)	[34]

where $G_{\mu\nu}$ ($\tilde{G}_{\mu\nu} = \epsilon_{\mu\nu\alpha\beta} G^{\alpha\beta}/2$) is the QCD field strength tensor (dual).

The CKM-induced EDMs of quarks and charged leptons arise at three- and four-loop orders, respectively [36–39]. The resulting numerical impact for the experimental observables (see below) falls well below present and prospective experimental sensitivities. The most important impact of \mathcal{J} for the EDMs of the neutron and diamagnetic atoms arise via induced hadronic interactions. The resulting theoretical expectations for the electron, neutron and ^{199}Hg EDMs are

$$|d_e|_{\text{CKM}} \approx 10^{-44} e \text{ cm} \quad [39], \quad (10a)$$

$$|d_n|_{\text{CKM}} \approx (1 - 6) \times 10^{-32} e \text{ cm} \quad [40], \quad (10b)$$

$$|d_A(^{199}\text{Hg})|_{\text{CKM}} \lesssim 4 \times 10^{-34} e \text{ cm} \quad [25]. \quad (10c)$$

For d_n and $d_A(^{199}\text{Hg})$, the dominant CKM contributions arise from four-quark operators (generated after integrating out the electroweak gauge bosons) rather than from the EDMs of the individual quarks. The corresponding sensitivities to the QCD $\bar{\theta}$ parameter are given by

$$|d_n|_{\bar{\theta}} \approx (0.9 - 1.2) \times 10^{-16} \bar{\theta} e \text{ cm} \quad [40], \quad (11a)$$

$$|d_A(^{199}\text{Hg})|_{\bar{\theta}} \approx (0.07 - 8) \times 10^{-20} \bar{\theta} e \text{ cm} \quad [25, 26], \quad (11b)$$

where the ranges quoted include the impacts of hadronic, nuclear, and atomic theory uncertainties. The neutron EDM puts then a stringent limit on ‘strong’ CP violation: $\bar{\theta} \lesssim 2 \times 10^{-10}$. The corresponding limit from $d_A(^{199}\text{Hg})$ is weaker due to the large theoretical uncertainty.

EDMs Beyond the Standard Model

It is possible that the next generation of EDM searches will yield a non-zero result, arising from the $\bar{\theta}$ -term interaction and/or physics beyond the SM (BSM). Most of the considered BSM scenarios involve new particles with masses well above the electroweak scale. At energies much lower than the BSM mass scale Λ , the dynamics can be described through an effective field theory (SMEFT) involving an infinite set of non-renormalizable operators $\mathcal{O}_k^{(d)}$, with dimensions $d > 4$, that are invariant under the SM gauge group:

$$\mathcal{L}_{\text{SMEFT}} = \mathcal{L}_{\text{SM}} + \sum_{k,d} \alpha_k^{(d)} \left(\frac{1}{\Lambda}\right)^{d-4} \mathcal{O}_k^{(d)}. \quad (12)$$

The operators contain only SM fields, while all short-distance information on the BSM physics is encoded in their Wilson coefficients $\alpha_k^{(d)}$. The $d = 4$ term corresponds to the SM Lagrangian.

For the systems of Table 1 and for many BSM scenarios of recent interest, it suffices to consider the leading contributions from $d = 6$ operators. Considering only the first-generation SM fermions, there exist 12 independent CPV pertinent operators. For a complete listing, see *e.g.*, Refs. [26, 41]. For a given elementary fermion f , two of these operators reduce to the EDM interaction in Eq. (6). Of the remaining, the most relevant include the chromo-electric dipole moments (cEDMs) of the quarks; a CP -odd three gluon operator; three semileptonic, four-fermion operators; two four-quark operators; and a CPV interaction involving two Higgs fields and a right-handed quark current. For the dipole operators, it is useful to define a rescaled Wilson coefficient $\alpha_{fV_j}^{(6)} \equiv g_j C_{fV_j}$, where V_j ($j = 1, 2, 3$) denote the gauge bosons for

Table 2: Pertinent dimension-six EDM and cEDM sources (first generation fermions only).

System	$d = 6$ Source	Wilson Coefficient
Paramagnetic	Electron EDM	$\text{Im } C_{e\gamma}$
	Electron-quark	$C_{e\bar{q}}^{(\pm)}$
Diamagnetic	Quark EDM	$\text{Im } C_{q\gamma}$
	Quark cEDM	$\text{Im } C_{qG}$
	Three gluon	$C_{\bar{G}}$
	Four quark	$\text{Im } C_{quqd}^{(1,8)}$
	Quark-Higgs	$\text{Im } C_{\varphi ud}$
	Electron-quark tensor*	$\text{Im } C_{\ell e qu}^{(3)}$

*Applicable only to atoms.

the three SM gauge groups with corresponding couplings g_j ; for all other $d = 6$ operators we correspondingly identify $\alpha_k^{(6)} \equiv C_k$. In this case, one has for the EDM (d_f) and cEDM (\tilde{d}_q)

$$d_f = -(1.13 \times 10^{-16} \text{ e cm}) \left(\frac{v}{\Lambda}\right)^2 \text{Im } C_{f\gamma}, \quad (13a)$$

$$\tilde{d}_q = -(1.13 \times 10^{-16} \text{ cm}) \left(\frac{v}{\Lambda}\right)^2 \text{Im } C_{qG}, \quad (13b)$$

with $\text{Im } C_{f\gamma} = \text{Im } C_{fB} + 3I_3^f \text{Im } C_{fW}$. As the expressions (13a,13b) illustrate, the magnitude of the BSM contributions scales with two inverse powers of the scale Λ . A similar conclusion holds for the contributions from the other $d = 6$ operators to the EDMs of Table 1.

It is important to emphasize that if the BSM mediators are light, with masses below the weak scale, the effective field theory description of Eq. (12) does not apply. For recent studies along these lines, see, *e.g.* [42,43].

EDM Interpretation: From Short Distances to the Atomic Scale

The EDM limits in Table 1 are obtained using composite quantum systems, wherein the relevant dynamics involve physics at the hadronic, nuclear, atomic and molecular scales. The manifestation of a given CPV source (CKM, θ term, BSM) involves an interplay of these dynamics. In all cases, one must first evolve the Wilson coefficients from the weak scale to the hadronic scale, then match onto the relevant low-energy degrees of freedom (electrons, nucleons, pions, *etc.*). At this level, the most straightforward interpretation involves the paramagnetic systems, for which two sources dominate: the electron EDM and the electron spin-dependent semileptonic interaction $\bar{e}\gamma_5 e \bar{q}q$. The latter gives rise to a spin-independent Hamiltonian, for an atom with Z electrons/protons and N neutrons,

$$\hat{H}_S = \frac{iG_F}{\sqrt{2}} \delta(\vec{r}) \left[(Z+N) C_S^{(0)} + (Z-N) C_S^{(1)} \right] \gamma_0 \gamma_5, \quad (14)$$

where $C_S^{(0)}$ ($C_S^{(1)}$) is proportional to $C_{e\bar{q}}^{(+)}$ ($C_{e\bar{q}}^{(-)}$). The computation of $C_S^{(0,1)}$ is relatively free from theoretical uncertainty since the operator $\bar{q}q$ essentially counts the number of quarks of flavor q in the nucleus. Experimental results for paramagnetic systems, thus, often quote bounds on

$$C_S \equiv C_S^{(0)} + \left(\frac{Z-N}{Z+N} \right) C_S^{(1)} \quad (15)$$

as well as on d_e , assuming only one of these two sources is non-vanishing. Combining results from ThO and HfF⁺ (see Figure 2) allows one to obtain the global, 90% C.L. bounds

$$|d_e| < 1.8 \times 10^{-28} \text{ e cm}, \quad |C_S| < 9.8 \times 10^{-9}. \quad (16)$$

Note that the limits on d_e given in Table 1 have been obtained assuming $C_S = 0$.

For the diamagnetic systems, the situation is considerably more involved. For the neutron, a variety of approaches – including

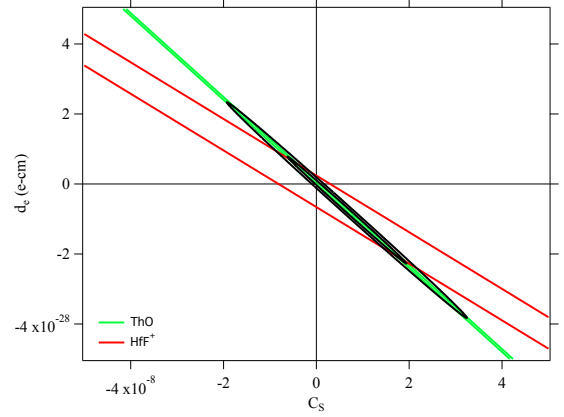


Figure 2: Constraints on d_e and C_S from EDM searches using polar molecules (updated by [44] from Ref. [25]).

lattice QCD, chiral perturbation theory, QCD sum rules, and the quark model – have been employed to compute the relevant hadronic matrix elements of the CPV sources (see, *e.g.*, [26,27,45,46]). For diamagnetic atoms, the non-leptonic sources of Table 2 give rise to the EDM of the nucleus as well as other P - and T -odd nuclear moments, as allowed by the nuclear spin. However, according to a theorem by Schiff [47], the nuclear EDM generates no contribution to the neutral-atom EDM due to screening by atomic electrons. The leading contribution from these sources, instead, arises via the nuclear Schiff moment, \vec{S} , an r^3 -weighted moment of the T - and P -odd component of the nuclear charge density. The resulting effective atomic Hamiltonian is

$$\hat{H}_{\text{Schiff}} = -4\pi \vec{\nabla} \rho_e(0) \cdot \vec{S}, \quad (17)$$

where $\vec{\nabla} \rho_e(0)$ is the gradient of the electron density at the nucleus. To date, computations of the nuclear Schiff moment have assumed that the leading contribution arises from a pion-exchange induced nuclear force, with the P - and T -odd πN interaction given by

$$\mathcal{L}_{\pi N}^{T,P} = \bar{N} \left[\bar{g}_\pi^{(0)} \vec{\tau} \cdot \vec{\pi} + \bar{g}_\pi^{(1)} \pi^0 + \bar{g}_\pi^{(2)} (3\tau_3 \pi^0 - \vec{\tau} \cdot \vec{\pi}) \right] N. \quad (18)$$

Chiral effective field theory power counting implies that in general the magnitude of $\bar{g}_\pi^{(2)}$ is suppressed with respect to the isoscalar and isovector couplings. The CPV sources then generate a diamagnetic atom EDM d_A via the sequence

$$\text{CPV source} \rightarrow \bar{g}_\pi^{(i)} \rightarrow \vec{S} \rightarrow d_A. \quad (19)$$

The steps in this sequence involve dynamics at the hadronic, nuclear, and atomic scales, respectively. In addition, d_A may receive contributions from the nuclear spin-dependent interaction generated by the semileptonic tensor interaction listed in Table 2, with the corresponding atomic Hamiltonian

$$\hat{H}_T = \frac{2iG_F}{\sqrt{2}} \delta(\vec{r}) \sum_N \left[C_T^{(0)} + C_T^{(1)} \tau_3 \right] \vec{\sigma}_N \cdot \vec{\gamma}, \quad (20)$$

where σ_N is the nucleon spin Pauli matrix and $C_T^{(0,1)} \propto \text{Im } C_{\ell e qu}^{(3)}$.

Given the large number of CPV sources and existing diamagnetic EDM limits, it is not possible to obtain a set of global constraints on the former. One may, however, do so for the low-energy effective parameters $\bar{g}_\pi^{(0,1)}$, $C_T^{(0,1)}$ and \bar{d}_n^{sr} , where the latter denotes a ‘short-range’ contribution to the neutron EDM [25,48]. In this context, the dominant source of theoretical uncertainty involves computations of the nuclear Schiff moment. From the bounds on the low-energy parameters, one may then derive constraints on the CPV sources by utilizing computations of the hadronic matrix elements. Reducing the degree of theoretical hadronic and nuclear physics uncertainty is an area of active effort.

3 Tests of CPT

CPT symmetry implies the equality of the masses and widths of a particle and its antiparticle. The most constraining limits are extracted from the neutral kaons [49, 50]:

$$2 \frac{|m_{K^0} - m_{\bar{K}^0}|}{(m_{K^0} + m_{\bar{K}^0})} < 6 \times 10^{-19}, \quad (21)$$

$$2 \frac{|\Gamma_{K^0} - \Gamma_{\bar{K}^0}|}{(\Gamma_{K^0} + \Gamma_{\bar{K}^0})} = (8 \pm 8) \times 10^{-18}.$$

The limit on the $K^0 - \bar{K}^0$ mass difference assumes that there is no other source of CPT violation. An upper bound on CPT breaking in $K_L^0 \rightarrow 2\pi$ has been also set through the measured phase difference of the CPV ratios η_{00} and η_{+-} , $\phi_{00} - \phi_{+-} = (0.34 \pm 0.32)^\circ$, thanks to the small value of $(1 - |\eta_{00}/\eta_{+-}|)$ (see the review on CP violation in K_L^0 decays).

The measured masses and electric charges of the electron, the proton and their antiparticles provide also strong limits on CPT violation [51–53]:

$$2 \frac{|m_{e^+} - m_{e^-}|}{m_{e^+} + m_{e^-}} < 8 \times 10^{-9}, \quad \frac{|q_{e^+} + q_{e^-}|}{e} < 4 \times 10^{-8},$$

$$\left| \frac{q_{\bar{p}}/m_{\bar{p}}}{q_p/m_p} - 1 \right| = (0.1 \pm 6.9) \times 10^{-11}. \quad (22)$$

Worth mentioning are also the tight constraints derived from the lepton and antilepton magnetic moments [54, 55],

$$2 \frac{g_{e^+} - g_{e^-}}{g_{e^+} + g_{e^-}} = (-0.5 \pm 2.1) \times 10^{-12}, \quad (23)$$

$$2 \frac{g_{\mu^+} - g_{\mu^-}}{g_{\mu^+} + g_{\mu^-}} = (-0.11 \pm 0.12) \times 10^{-8},$$

those of the proton and antiproton [56],

$$(\mu_p + \mu_{\bar{p}})/\mu_p = (2 \pm 4) \times 10^{-9}, \quad (24)$$

and the recent measurement of the 1S-2S atomic transition in anti-hydrogen which agrees with the corresponding frequency spectral line in hydrogen at a relative precision of 2×10^{-12} [57].

A violation of CPT in an interacting local quantum field theory would imply that Lorentz symmetry is also violated [58]. Signatures of Lorentz-invariance violation have been searched for with atomic clocks, penning traps, matter and antimatter spectroscopy, colliders and astroparticle experiments, with so far negative results [59]. A compilation of experimental bounds is given in Ref. [60], parametrized through the coefficients of the so-called Standard Model Extension (SME) Lagrangian which contains all possible Lorentz- and CPT -violating operators preserving gauge invariance, renormalizability, locality and observer causality [61].

QUANTUM-NUMBER CONSERVATION LAWS

Conservation laws of several quantum numbers have been empirically established with a very high degree of confidence. They are usually associated with some global phase symmetry. However, while some of them are deeply rooted in basic principles such as gauge invariance (charge conservation; local symmetry implies global symmetry) or Lorentz symmetry (fermion number conservation), others appear to be accidental symmetries of the SM Lagrangian and could be broken by new physics interactions.

In fact, if one only assumes the SM gauge symmetries and particle content, the most general dynamics at energies below the BSM mass scale is described by the SMEFT Lagrangian in Eq. (12). All $d = 4$ operators (*i.e.*, the SM) happen to preserve the B and L quantum numbers, but this is no-longer true for the gauge-invariant structures of higher dimensionality. There is only one operator with $d = 5$ (up to hermitian conjugation and flavor assignments), and it violates lepton number by two units [62], giving rise to Majorana neutrino masses after the electroweak spontaneous symmetry breaking. With $d = 6$, there are five operators

that violate B and L [63, 64]. Thus, violations of these quantum numbers can be generically expected, unless there is an explicit symmetry protecting them.

4 Electric charge

The conservation of electric charges is associated with the QED gauge symmetry. The most precise tests are the non-observation of the decays $e \rightarrow \nu_e \gamma$ (lifetime larger than 6.6×10^{28} yr [65]) and $n \rightarrow p \nu_e \bar{\nu}_e$ ($\text{Br} < 8 \times 10^{-27}$, 68% C.L. [66]). The neutrality of matter can be also interpreted as a test of electric charge conservation. Worth mentioning are the experimental limits on the electric charge of the neutron, $q_n/e = (-0.2 \pm 0.8) \times 10^{-21}$, and on the sum of the proton and electron charges, $|q_p + q_e|/e < 1 \times 10^{-21}$ (68% CL) [67].

The isotropy of the cosmic microwave background has been used to set stringent limits on a possible charge asymmetry of the Universe [68]. Assuming that charge asymmetries produced by different particles are not anticorrelated, this implies upper bounds on the photon ($|q_\gamma|/e < 1 \times 10^{-35}$) and neutrino ($|q_\nu|/e < 4 \times 10^{-35}$) electric charges. A much stronger upper bound on the photon charge ($|q_\gamma|/e < 1 \times 10^{-46}$) has been derived from the non-observation of Aharonov-Bohm phase differences in interferometric experiments with photons that have traversed cosmological distances, under the assumption that both positive and negative charged photons exist [69].

5 Lepton family numbers

In the SM with massless left-handed neutrinos there is a separate conservation number for each lepton family. However, neutrino oscillations show that neutrinos have tiny masses and there are sizable mixings among the different lepton flavors. Compelling evidence from solar, atmospheric, accelerator and reactor neutrino experiments has established a quite solid pattern of neutrino mass differences and mixing angles [15, 16] (see the review on neutrino masses, mixings and oscillations). Nevertheless, flavor mixing among the different charged leptons has never been observed.

If neutrino masses and mixings among the three active neutrinos were the only sources of lepton-flavor violation (LFV), neutrinoless transitions from one charged lepton flavor to another would be heavily suppressed by powers of m_{ν_i} (GIM mechanism), leading to un-observably small rates; for instance [72–77],

$$\text{Br}(\mu \rightarrow e\gamma) = \frac{3\alpha}{32\pi} \left| \sum_i U_{\mu i}^* U_{ei} \frac{m_{\nu_i}^2 - m_{\nu_1}^2}{M_W^2} \right|^2 < 10^{-54}, \quad (25)$$

where U_{ia} are the relevant elements of the PMNS mixing matrix. This contribution is clearly too small to be observed in any realistic experiment, so any experimentally accessible effect would arise from BSM physics with sources of LFV not related to m_{ν_i} . The search for charged LFV (CLFV) remains an area of active interest, which has the potential to probe physics at scales much higher than the TeV.

Among the most sensitive probes are searches for the CLFV decays of the muon, $\mu \rightarrow e\gamma$ and $\mu \rightarrow 3e$, as well as the conversion process $\mu^- + A(N, Z) \rightarrow e^- + A(N, Z)$, where $A(N, Z)$ denotes a nucleus with N neutrons and Z protons. Searches for rare τ decays such as $\tau \rightarrow \ell\gamma$ ($\ell = e, \mu$) also provide interesting probes of CLFV. A variety of BSM scenarios predict that rates for these CLFV processes could be sufficiently large to be observed in the present or planned searches. To date, no observation has been reported, and the resulting null results place strong constraints on BSM scenarios. For extensive reviews of the experimental and theoretical status and prospects, see Refs. [71, 78, 79].

A detailed set of upper bounds on CLFV branching ratios is given in the listings for the muon and tau leptons. Here we emphasize those with the strongest limits:

$$\text{Br}(\mu \rightarrow e\gamma) < 4.2 \times 10^{-13} \quad [80], \quad (26)$$

$$\text{Br}(\mu \rightarrow 3e) < 1.0 \times 10^{-12} \quad [81]$$

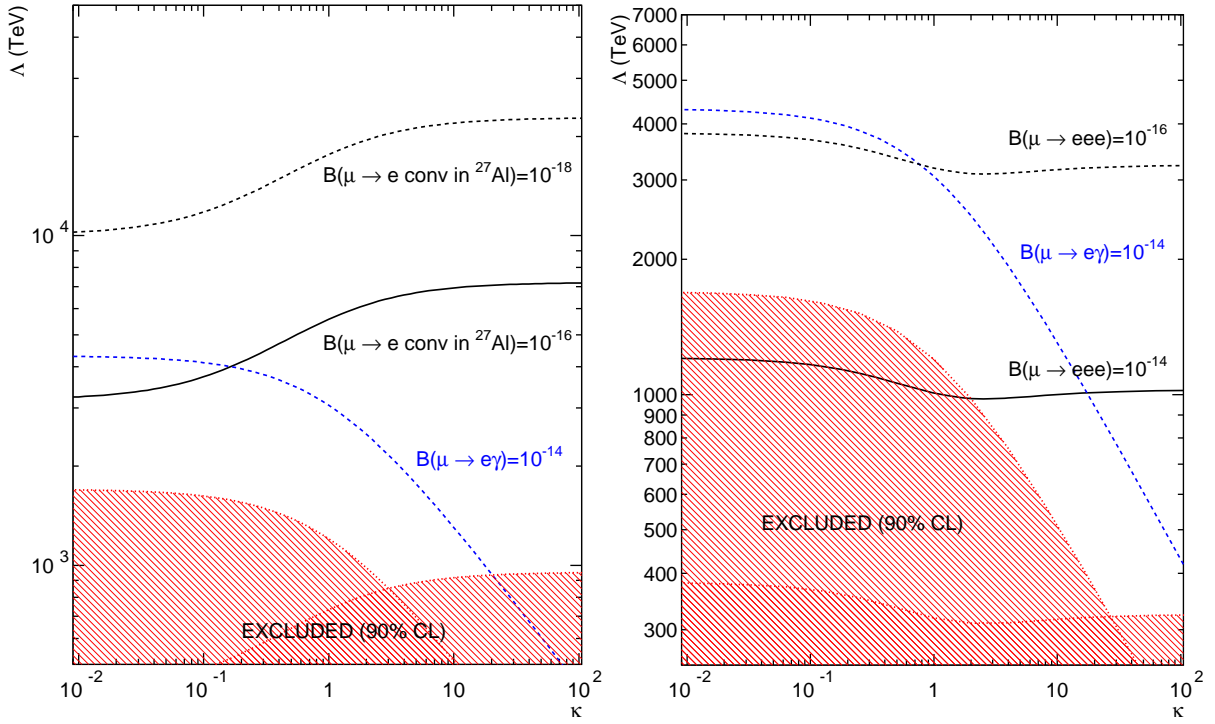


Figure 3: Model-independent CLFV sensitivities based on Eq (31). Left panel shows the comparison of present constraints with prospective future sensitivities for $\mu \rightarrow e\gamma$ and $\mu \rightarrow e$ conversion. Right panel gives analogous comparison for $\mu \rightarrow e\gamma$ and $\mu \rightarrow 3e$. Updated by [70] from Ref. [71].

and

$$B_{\mu \rightarrow e} \equiv \frac{\Gamma(\mu^- + A(N, Z) \rightarrow e^- + A(N, Z))}{\Gamma(\mu^- + A(N, Z) \rightarrow \nu + A(N+1, Z-1))} \quad (27)$$

with the best limit so far, $B_{\mu \rightarrow e} < 7 \times 10^{-13}$ [82], obtained with gold. Several proposed experiments aim to improve these limits by several orders of magnitude with different atoms.

One may interpret both $\mu \rightarrow e\gamma$ and $\mu \rightarrow e$ conversion in terms of the amplitudes to emit a real or virtual photon:

$$\begin{aligned} \mathcal{M}_{\mu \rightarrow e\gamma(*)} = & eG_\mu \varepsilon^{\alpha*} \bar{e}(p-q) \left[(q^2 \gamma_\alpha - \not{q} q_\alpha) (\tilde{A}_1^R P_R + \tilde{A}_1^L P_L) \right. \\ & \left. + im_\mu \sigma_{\alpha\beta} q^\beta (\tilde{A}_2^R P_R + \tilde{A}_2^L P_L) \right] \mu(p), \end{aligned} \quad (28)$$

where it is conventional to normalize the amplitude to the Fermi constant. One then has

$$\text{Br}(\mu \rightarrow e\gamma) = 48\pi^3 \alpha (|\tilde{A}_2^R|^2 + |\tilde{A}_2^L|^2). \quad (29)$$

For the conversion process, the virtual photon is absorbed by the quarks in the nucleus, yielding an effective four-fermion operator. In general, the exchange of other particles could lead to similar or alternate Lorentz structures, and it is not possible to distinguish between the exchange of a virtual photon or other particle. It is conventional to write the most general four-fermion amplitude, valid for energies below the electroweak scale as (adapted from Ref. [88])

$$\mathcal{M}_{\mu \rightarrow e} = G_\mu \sum_{n,a,q} a_{a,q}^{(n)} \bar{e} \Gamma^n P_a \mu \bar{q} \Gamma_n q, \quad (30)$$

where P_a ($a = L, R$) denote the left and right-handed projectors and Γ^n denotes $1, \gamma_5, \gamma^\mu, \gamma^\mu \gamma_5$, and $\sigma_{\mu\nu}$. If any of the coefficients $a_{a,q}^{(n)}$ are generated by physics at a scale $\Lambda > v$, then their effects would be encoded in the SMEFT Lagrangian (12). For scenarios in which the leading CLFV operators occur at $d = 6$,

the $a_{a,q}^{(n)}$ will scale as $(v/\Lambda)^2$. The corresponding decay and conversion rates will then scale as $(v/\Lambda)^4$. Note that the scalar and time component of the vector interactions are coherent over the nucleus, essentially counting the number of quarks. Consequently, these interactions typically yield the greatest sensitivities to high BSM mass scales.

It is sometimes convenient to compare the relative sensitivities of the decay and conversion processes using the following simplified effective Lagrangian [71]:

$$\begin{aligned} \mathcal{L}_{\text{eff}}^{\text{CLFV}} = & \frac{m_\mu}{(\kappa+1)\Lambda^2} \bar{\mu}_R \sigma_{\mu\nu} e_L F^{\mu\nu} \\ & + \frac{\kappa}{(\kappa+1)\Lambda^2} \bar{\mu} \gamma_\mu e \sum_q \bar{q} \gamma^\mu q + \text{h.c.} \end{aligned} \quad (31)$$

Note that one may replace the second term in Eq. (31) by any one of the other four-fermion interactions given in Eq. (30). An analogous expression applies to the process $\mu \rightarrow 3e$ when replacing the sum over quarks by the corresponding electron bilinear. A comparison of the present and prospective sensitivities for various muon CLFV searches in this framework is shown in Figure 3.

Stringent limits have been also set on the LFV decay modes of the τ lepton [89]. As shown in Figure 4, the large τ data samples collected at the B factories have made possible to reach a 10^{-8} sensitivity for many of its leptonic ($\tau \rightarrow \ell\gamma, \tau \rightarrow \ell'\ell^+\ell^-$) and semileptonic ($\tau \rightarrow \ell P^0, \tau \rightarrow \ell V^0, \tau \rightarrow \ell P^0 P^0, \tau \rightarrow \ell P^+ P'^-$) neutrinoless LFV decays, and BELLE-II is expected to push these limits beyond the 10^{-9} level [84]. Being a third generation lepton, the τ could be more sensitive to heavier new-physics scales, which makes his LFV decays particularly interesting. Compared to the muon, the τ decay amplitudes could be enhanced by a chirality ratio $(m_\tau/m_\mu)^2 \sim 280$ and/or by lepton-mixing factors such as $|U_{\tau 3}/U_{e 3}|^2 \sim 20$, but the exact relation is model dependent. In any case, the τ LFV decays provide a rich data set that is very complementary to the μ bounds. If LFV is finally observed, the correlations between μ and τ data, and among different LFV τ decays will allow to probe the underlying mechanism of lepton flavor breaking.

Interesting limits on LFV are also obtained in meson decays.

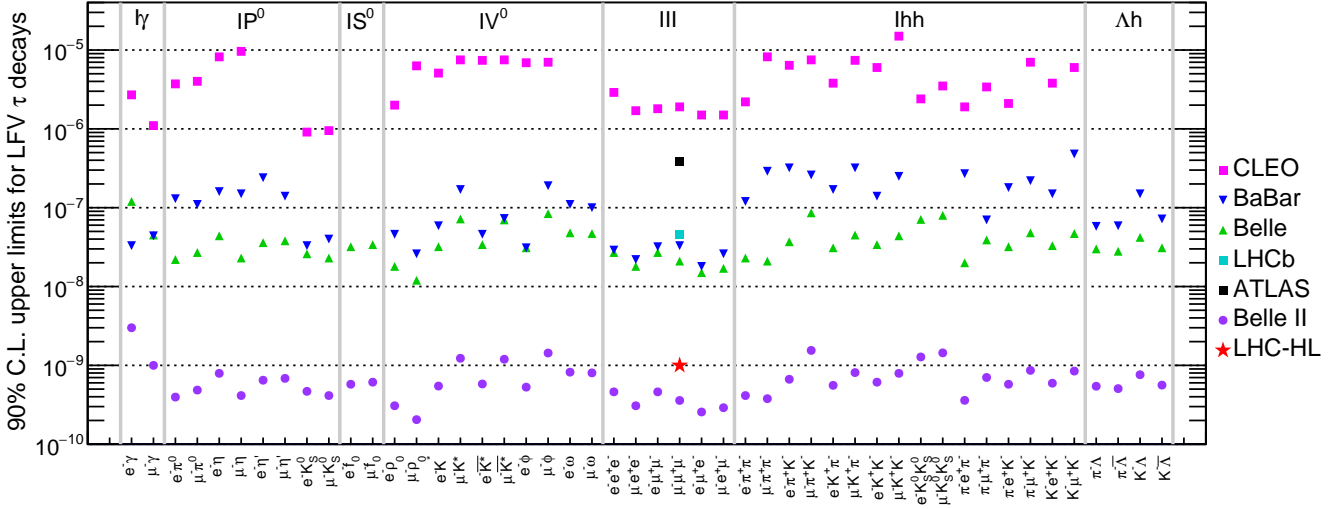


Figure 4: Current experimental limits on neutrinoless LFV τ decays [83]. Also shown are the future projections at Belle-II [84] and at the HL-LHC [85].

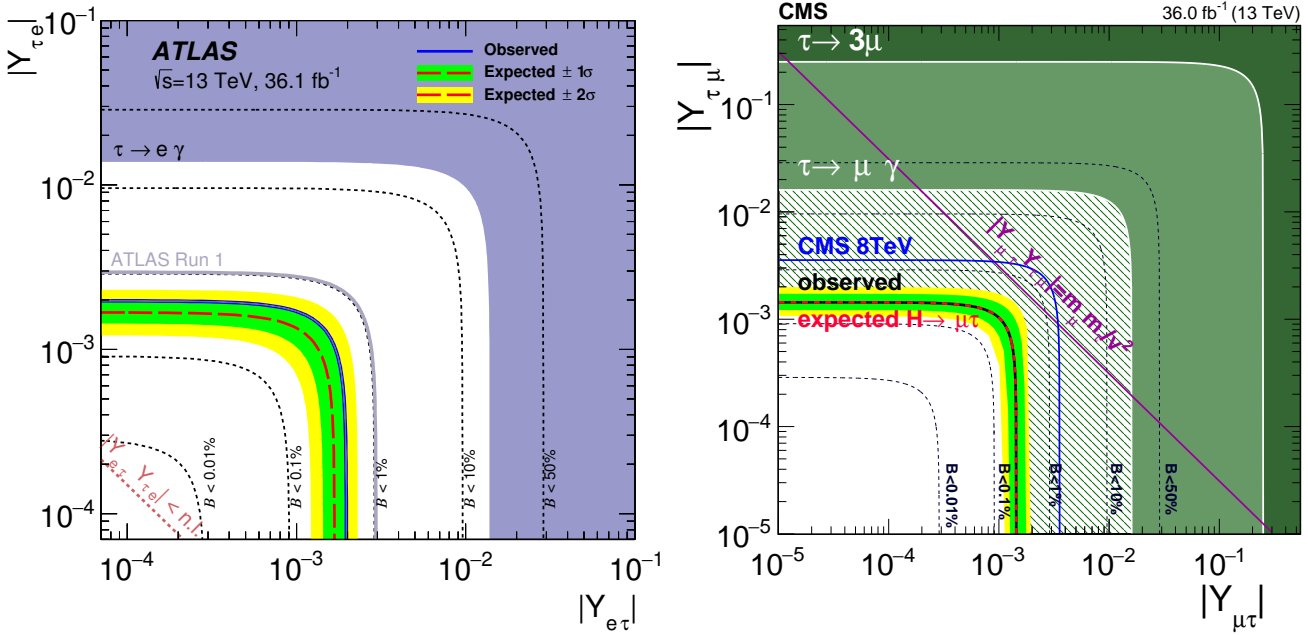


Figure 5: Current limits on the Higgs LFV τ Yukawas from direct $H^0 \rightarrow \ell^\pm \tau^\mp$ decays ($\ell = e, \mu$), and indirect constraints from τ decays [86, 87].

The best bounds come from kaon experiments, e.g., $\text{Br}(K_L^0 \rightarrow e^\pm \mu^\mp) < 4.7 \times 10^{-12}$ [90], $\text{Br}(K^+ \rightarrow \pi^+ \mu^+ e^-) < 1.3 \times 10^{-11}$ [91]. Quite strong limits have also been set in decays of B and D mesons, the best upper bounds being $\text{Br}(B^0 \rightarrow e^\pm \mu^\mp) < 1.0 \times 10^{-9}$ [92] and $\text{Br}(D^0 \rightarrow e^\pm \mu^\mp) < 1.3 \times 10^{-8}$ [93].

The LFV decays of the Z boson were probed at LEP at the 10^{-5} to 10^{-6} level. The LHC ATLAS collaboration has put recently a stronger bound on the $Z \rightarrow e^\pm \mu^\mp$ decay mode [94]. Currently, the best (95% C.L.) limits are [94–96]:

$$\begin{aligned} \text{Br}(Z \rightarrow e^\pm \mu^\mp) &< 7.5 \times 10^{-7}, & \text{Br}(Z \rightarrow e^\pm \tau^\mp) &< 9.8 \times 10^{-6}, \\ \text{Br}(Z \rightarrow \mu^\pm \tau^\mp) &< 1.2 \times 10^{-5}. \end{aligned} \quad (32)$$

LHC is now starting to test LFV in Higgs decays, within the available statistics. From the current (95% C.L.) experimental

upper bounds [86, 87, 97],

$$\begin{aligned} \text{Br}(H^0 \rightarrow e^\pm \mu^\mp) &< 6.1 \times 10^{-5}, & \text{Br}(H^0 \rightarrow e^\pm \tau^\mp) &< 0.47\%, \\ \text{Br}(H^0 \rightarrow \mu^\pm \tau^\mp) &< 0.25\%, \end{aligned} \quad (33)$$

one can derive direct limits on the LFV Yukawa couplings of the Higgs boson,

$$\mathcal{L}_Y = -H^0 \sum_{i \neq j} (Y_{\ell_i \ell_j} \bar{\ell}_i^j \ell_R^j + \text{h.c.}). \quad (34)$$

From $H^0 \rightarrow e^\pm \mu^\mp$, one obtains $\sqrt{Y_{\mu e}^2 + Y_{e\mu}^2} < 2.2 \times 10^{-4}$, which is not yet competitive with the indirect limit set by $\mu \rightarrow e\gamma$ through a (one-loop) virtual Higgs exchange:

$$\sqrt{Y_{\mu e}^2 + Y_{e\mu}^2} < 3.6 \times 10^{-6}. \quad (35)$$

However, the LHC data provides at present the strongest bounds

on the LFV τ Yukawas [86, 87]:

$$\sqrt{Y_{e\tau}^2 + Y_{\tau e}^2} < 2.0 \times 10^{-3}, \quad \sqrt{Y_{\mu\tau}^2 + Y_{\tau\mu}^2} < 1.4 \times 10^{-3}. \quad (36)$$

Figure 5 compares the Higgs exclusion limits on the τ Yukawas with the current indirect constraints from LFV τ decays.

6 Baryon and Lepton Number

The transitions discussed in the previous section preserve the total lepton number $L = L_e + L_\mu + L_\tau$. In the SM, conservation of $B - L$ is an accidental symmetry of the Lagrangian. At the classical level, $B + L$ is also conserved, though it is violated at the loop level by the anomaly. The latter is a topological effect that is highly suppressed at zero temperature and, moreover, does not contribute to the processes discussed in the review. Going beyond renormalizable interactions, there exists a tower of operators in the SMEFT Lagrangian (12), containing only SM fields, that break one or both of these symmetries. We briefly review these possibilities in turn.

Lepton Number

The lowest-dimension operator containing only SM fields that breaks baryon or lepton number is the $d = 5$, lepton-number-violating (LNV) ‘Weinberg’ neutrino-mass operator [62]:

$$\mathcal{L}^{\text{LNV}} = \frac{y}{\Lambda} \bar{L}^C H H^T L. \quad (37)$$

When the neutral component of the Higgs field obtains its vacuum expectation value, this $\Delta L = 2$ interaction yields a Majorana mass for the light, active neutrinos. The most comprehensive approach for probing this effect is the search for neutrinoless double-beta decay ($0\nu\beta\beta$) of atomic nuclei, $(Z, A) \rightarrow (Z + 2, A) + e^- + e^-$ [98, 99] (see the review on neutrinoless double- β decay). The detection of a non-zero $0\nu\beta\beta$ signal could represent a spectacular evidence of Majorana neutrinos. The current best limit, $\tau_{1/2} > 1.07 \times 10^{26}$ yr, was obtained by the KamLAND-Zen experiment with ^{136}Xe [100].

Theoretically, the interaction (37) can arise from BSM interactions in the well-known see-saw mechanism for neutrino mass (for a review, see [101]). In this context, the conventional choice for the scale Λ is of order the GUT scale, yielding light neutrino masses of order eV and below when the couplings y are of order the charged elementary fermion Yukawa couplings. BSM theories may also give rise to LNV observables in other contexts. In these scenarios, if the LNV scale is of order 1 TeV, one may observe signatures of LNV not only in $0\nu\beta\beta$ but also in collider searches for final states containing same sign dileptons. Searches for same sign dileptons plus a di-jet pair at the LHC have placed constraints on TeV-scale LNV [102, 103] that in some cases complement those obtained from $0\nu\beta\beta$.

Stringent constraints on violations of L have been also set in $\mu^- \rightarrow e^+$ conversion in muonic atoms, the best limit being $\sigma(\mu^- \text{Ti} \rightarrow e^+ \text{Ca}) / \sigma(\mu^- \text{Ti} \rightarrow \text{all}) < 3.6 \times 10^{-11}$ [104], and at the flavor factories through L -violating decays of the τ lepton and K , D and B mesons. Some representative examples are $\text{Br}(\tau^- \rightarrow e^+ \pi^- \pi^-) < 2.0 \times 10^{-8}$ [105], $\text{Br}(K^+ \rightarrow \pi^- \mu^+ \mu^+) < 4.2 \times 10^{-11}$ [106], $\text{Br}(D^+ \rightarrow \pi^- \mu^+ \mu^+) < 2.2 \times 10^{-8}$ [107] and $\text{Br}(B^+ \rightarrow K^- e^+ e^+) < 3.0 \times 10^{-8}$ [108]. All these $|\Delta L| = 2$ processes could be mediated by a massive Majorana neutrino. They provide useful bounds on the effective Majorana neutrino mass matrix $m_{\ell\ell'} \sim \sum_i U_{\ell i} U_{\ell' i} m_{\nu_i}$ [109], although not as strong as the $0\nu\beta\beta$ constraint on m_{ee} .

Baryon Number

Grand Unified Theories (GUTs) combine leptons and quarks in the same symmetry multiplets and, therefore, predict the violation of the baryon and lepton quantum numbers. Many experiments have searched for B -violating transitions, but no positive signal has been identified so far. Proton decay would be the most relevant violation of B , as it would imply the instability of matter. The current lower bound on the proton lifetime is 3.6×10^{29} yr [110]. Stronger limits have been set for particular decay modes, such as $\tau(p \rightarrow e^+ \pi^0) > 1.6 \times 10^{34}$ yr [111]. For a discussion of proton decay in the context of GUTs, see the review on Grand Unified Theories.

Another spectacular signal would be neutron-antineutron oscillations. Searches have been performed for quasi-free $n-\bar{n}$ oscillations and for $n\bar{n}$ annihilation products in a nucleus. The latter would arise when the \bar{n} produced through oscillations annihilates with another neutron in the nuclear medium. The corresponding best limits, expressed in terms of the free and bound oscillation times, $\tau_{n\bar{n}}$ and τ_m , respectively, are:

$$\tau_{n\bar{n}} > 0.86 \times 10^8 \text{ s} \quad [112], \quad (38a)$$

$$\tau_m > 1.9 \times 10^{32} \text{ yr} \quad [113]. \quad (38b)$$

From the latter, one may infer a bound $\tau_{n\bar{n}} > 2.7 \times 10^8$ s, as discussed below. See Ref. [114] for a recent review.

The theoretical interpretation of these bounds starts with an assumed, effective Hamiltonian for the free (anti-)neutron, \mathcal{H}_{eff} that contains a B -violating part, yielding matrix elements

$$\langle n | \mathcal{H}_{\text{eff}} | n \rangle = \langle \bar{n} | \mathcal{H}_{\text{eff}} | \bar{n} \rangle = m - i \frac{\lambda}{2}, \quad (39a)$$

$$\langle n | \mathcal{H}_{\text{eff}} | \bar{n} \rangle = \langle \bar{n} | \mathcal{H}_{\text{eff}} | n \rangle \equiv \delta m, \quad (39b)$$

where CPT is assumed to be conserved, the neutron lifetime $\tau_n = 1/\lambda$ and $\tau_{n\bar{n}} = 1/|\delta m|$. The rate for a neutron to oscillate into an antineutron after a time t is given by

$$\mathcal{P}_{n\bar{n}}(t) = \sin^2 \left(\frac{t}{\tau_{n\bar{n}}} \right) e^{-\lambda t}. \quad (40)$$

For $t \ll \tau_n \ll \tau_{n\bar{n}}$, one has

$$\mathcal{P}_{n\bar{n}}(t) \rightarrow (t/\tau_{n\bar{n}})^2. \quad (41)$$

In realistic experiments, there exist effects, such as background magnetic fields, that split the energies of the neutron and antineutron. One must ensure that the observation time is sufficiently short so that these effects do not overwhelm the small B -violating term δm and that Eq. (40) applies.

In nuclei, the interactions of neutrons and antineutrons with the surrounding medium are sufficiently distinct that one must take the corresponding matter potentials into account. In particular, the matrix elements in Eq. (39a) become

$$\langle n | \mathcal{H}_{\text{eff}} | n \rangle = m + V_n, \quad \langle \bar{n} | \mathcal{H}_{\text{eff}} | \bar{n} \rangle = m + V_{\bar{n}}, \quad (42)$$

with V_n being essentially real ($V_n \equiv V_{nR}$) and $V_{\bar{n}} = V_{\bar{n}R} - iV_{\bar{n}I}$. The imaginary part $V_{\bar{n}I}$ characterizes the annihilation of the antineutron with bound nucleons into secondary hadrons. The rate for a bound neutron to disappear is given by

$$\Gamma_m = \frac{2(\delta m)^2 |V_{\bar{n}I}|}{(V_{nR} - V_{\bar{n}R})^2 + V_{\bar{n}I}^2} \equiv (R\tau_{n\bar{n}}^2)^{-1}. \quad (43)$$

For the nuclei of experimental interest, nuclear theory computations yield $R \sim 10^{23} \text{ s}^{-1}$. Null results of bound $n-\bar{n}$ oscillation searches thus allow one to infer a bound on $\tau_{n\bar{n}}$ via Eq. (43).

From an elementary particle standpoint, $n-\bar{n}$ oscillations involve the conversion of three quarks into three antiquarks (and vice-versa). The lowest-dimension operators mediating such process arise at dimension nine in the SMEFT:

$$\mathcal{L}_{n-\bar{n}} = \frac{1}{\Lambda^5} \sum_j \alpha_j^{(9)} \mathcal{O}_j^{\text{BNV}}. \quad (44)$$

Consequently, one expects

$$\delta m \sim \alpha_j^{(9)} \frac{\Lambda_{\text{HAD}}^6}{\Lambda^5}, \quad (45)$$

where Λ_{HAD} is a hadronic scale set by the $n-\bar{n}$ matrix elements in Eq. (39b). Taking Λ_{HAD} to be of order the QCD scale and using the present bounds on $\tau_{n\bar{n}}$ yields a lower bound on the B -violating mass scale of ~ 100 TeV.

The search for B -violating decays of short-lived particles such as Z bosons, τ leptons and B mesons provides also relevant constraints. The best limits are $\text{Br}(Z \rightarrow pe, p\mu) < 1.8 \times 10^{-6}$ (95% C.L.) [115], $\text{Br}(\tau^- \rightarrow A\pi^-) < 7.2 \times 10^{-8}$ [116] and $\text{Br}(B^+ \rightarrow Ae^+) < 3.2 \times 10^{-8}$ [117].

7 Quark flavors

While strong and electromagnetic forces preserve the quark flavor, the charged-current weak interactions generate transitions among the different quark species (see the review on the CKM quark-mixing matrix). Since the SM flavor-changing mechanism is associated with the W^\pm fermionic vertices, the tree-level transitions satisfy a $\Delta F = \Delta Q$ rule where ΔQ denotes the change in charge of the relevant hadrons. Remember that the flavor quantum number F is defined to be +1 for positively charged quarks ($F = U, C, T$) and -1 for quarks with negative charges ($F = D, S, B$). The strongest tests on this conservation law have been obtained in kaon decays such as $\text{Br}(K^+ \rightarrow \pi^+ \pi^+ e^- \bar{\nu}_e) < 1.3 \times 10^{-8}$ [118], and $(\text{Re } x, \text{Im } x) = (-0.002 \pm 0.006, 0.0012 \pm 0.0021)$ [119, 120] where $x \equiv \mathcal{M}(K^0 \rightarrow \pi^- \ell^+ \nu) / \mathcal{M}(K^0 \rightarrow \pi^- \ell^+ \nu)$.

The $\Delta F = \Delta Q$ rule can be violated through quantum loop contributions giving rise to flavor-changing neutral-current transitions (FCNCs). Owing to the GIM mechanism, processes of this type are very suppressed in the SM, which makes them a superb tool in the search for new physics associated with the flavor dynamics. Within the SM itself, these transitions are also sensitive to the heavy-quark mass scales and have played a crucial role identifying the size of the charm (K^0 - \bar{K}^0 mixing) and top (B^0 - \bar{B}^0 mixing) masses before the discovery of those quarks. In addition to the well-established $\Delta F = 2$ mixings in neutral K and B mesons, $\Delta M_{K^0} \equiv M_{K_L^0} - M_{K_S^0} = (0.5293 \pm 0.0009) \times 10^{10} \text{ s}^{-1}$, $\Delta M_{B^0} \equiv M_{B_H^0} - M_{B_L^0} = (0.5065 \pm 0.0019) \times 10^{12} \text{ s}^{-1}$ and $\Delta M_{B_s^0} \equiv M_{B_{sH}^0} - M_{B_{sL}^0} = (17.757 \pm 0.0021) \times 10^{12} \text{ s}^{-1}$, there is now strong evidence for the mixing of the D^0 meson and its antiparticle [121],

$$x_D \equiv (M_{D_H^0} - M_{D_L^0}) / \Gamma_{D^0} = (3.9^{+1.1}_{-1.2}) \times 10^{-3}, \quad (46)$$

showing that there is a nonzero mass difference between the two neutral charm-meson eigenstates, of the expected size. The SM prediction for x_D is dominated by long-distance physics, because it involves virtual loops with down-type light quarks, and has unfortunately quite large uncertainties [122].

The FCNC kaon decays into lepton-antilepton pairs put stringent constraints on new flavor-changing interactions. The measured $K_L^0 \rightarrow \mu^+ \mu^-$ rate, $\text{Br}(K_L^0 \rightarrow \mu^+ \mu^-) = (6.84 \pm 0.11) \times 10^{-9}$, is completely dominated by the known 2γ absorptive contribution, leaving very little room for new-physics, and $\text{Br}(K_L^0 \rightarrow e^+ e^-) = (9^{+6}_{-4}) \times 10^{-12}$ [123] (the tiniest branching ratio ever measured) also agrees with the SM expectation [124]. The experimental K_S^0 upper bounds on the electron, $\text{Br}(K_S^0 \rightarrow e^+ e^-) < 9 \times 10^{-9}$ [125], and muon, $\text{Br}(K_S^0 \rightarrow \mu^+ \mu^-) < 2.1 \times 10^{-10}$ [126], modes are still five and two orders of magnitude, respectively, larger than their SM predictions [124]. Another very clean test of FCNCs will be soon provided by the decay $K^+ \rightarrow \pi^+ \nu \bar{\nu}$. With a predicted SM branching fraction of $(7.8 \pm 0.8) \times 10^{-11}$ [127], the CERN NA62 experiment is aiming to collect around one hundred events. Even more interesting is the CP -violating neutral mode $K_L^0 \rightarrow \pi^0 \nu \bar{\nu}$, expected at a rate of $(2.4 \pm 0.4) \times 10^{-11}$ [127] that is still far away from the current upper bound of 3.0×10^{-9} [128]. The KOTO experiment at KEK is expected to substantially increase the sensitivity to this mode.

The strongest bound on FCNC transitions in charm decays is $\text{Br}(D^0 \rightarrow \mu^+ \mu^-) < 6.2 \times 10^{-9}$ [129], while in B decays the LHC experiments have recently reached the SM sensitivity: $\text{Br}(B_d^0 \rightarrow \mu^+ \mu^-) = (0.14^{+0.16}_{-0.14}) \times 10^{-9}$ and $\text{Br}(B_s^0 \rightarrow \mu^+ \mu^-) = (3.0 \pm 0.4) \times 10^{-9}$. At present, there is a lot of interest on the decays $B \rightarrow K^{(*)} \ell^+ \ell^-$ where sizable discrepancies between the measured data and the SM predictions have been reported [130]. In particular, the LHCb experiment has found the ratios of produced muons versus electrons to be around 2.5σ below the SM predictions, both in $B \rightarrow K^* \ell^+ \ell^-$ [131] and in $B^+ \rightarrow K^+ \ell^+ \ell^-$ [132] (for dilepton invariant-masses squared in the range $q^2 \leq 6 \text{ GeV}^2$), suggesting a significant violation of lepton universality. The current Belle-II measurements of these ratios [133, 134] are consistent with the SM, but they are also compatible with the LHCb results. Future analyses from LHCb and Belle-II are expected to clarify the situation.

References

- [1] G. Luders, Kong. Dan. Vid. Sel. Mat. Fys. Med. **28N5**, 5, 1 (1954).
- [2] W. Pauli, in L. Rosenfeld and V. Weisskopf, editors, “Niels Bohr and the Development of Physics,” 30–51, McGraw-Hill, New York (1955).
- [3] J. McDonough *et al.*, Phys. Rev. **D38**, 2121 (1988).
- [4] M. Ablikim *et al.* (BESIII), Phys. Rev. **D90**, 9, 092002 (2014), [arXiv:1409.4040].
- [5] S. Prakhov *et al.* (Crystal Ball), Phys. Rev. Lett. **84**, 4802 (2000).
- [6] J. H. Christenson *et al.*, Phys. Rev. Lett. **13**, 138 (1964).
- [7] H. Burkhardt *et al.* (NA31), Phys. Lett. **B206**, 169 (1988).
- [8] G. D. Barr *et al.* (NA31), Phys. Lett. **B317**, 233 (1993).
- [9] L. K. Gibbons *et al.*, Phys. Rev. Lett. **70**, 1203 (1993).
- [10] J. R. Batley *et al.* (NA48), Phys. Lett. **B544**, 97 (2002), [hep-ex/0208009].
- [11] E. Abouzaid *et al.* (KTeV), Phys. Rev. **D83**, 092001 (2011), [arXiv:1011.0127].
- [12] H. Gisbert and A. Pich, Rept. Prog. Phys. **81**, 7, 076201 (2018), [arXiv:1712.06147].
- [13] V. Cirigliano *et al.*, JHEP **02**, 032 (2020), [arXiv:1911.01359].
- [14] R. Aaij *et al.* (LHCb), Phys. Rev. Lett. **122**, 21, 211803 (2019), [arXiv:1903.08726].
- [15] P. F. de Salas *et al.*, Phys. Lett. **B782**, 633 (2018), [arXiv:1708.01186].
- [16] I. Esteban *et al.*, JHEP **01**, 106 (2019), [arXiv:1811.05487].
- [17] A. Angelopoulos *et al.* (CLEAR), Phys. Lett. **B444**, 43 (1998).
- [18] L. Wolfenstein, Phys. Rev. Lett. **83**, 911 (1999).
- [19] L. Alvarez-Gaume *et al.*, Phys. Lett. **B458**, 347 (1999), [hep-ph/9812326].
- [20] H. J. Gerber, Eur. Phys. J. **C35**, 195 (2004).
- [21] M. C. Bañuls and J. Bernabeu, Phys. Lett. **B464**, 117 (1999), [hep-ph/9908353].
- [22] M. C. Bañuls and J. Bernabeu, Nucl. Phys. **B590**, 19 (2000), [hep-ph/0005323].
- [23] J. Bernabeu, F. Martinez-Vidal and P. Villanueva-Perez, JHEP **08**, 064 (2012), [arXiv:1203.0171].
- [24] J. P. Lees *et al.* (BaBar), Phys. Rev. Lett. **109**, 211801 (2012), [arXiv:1207.5832].
- [25] T. Chupp *et al.*, Rev. Mod. Phys. **91**, 1, 015001 (2019), [arXiv:1710.02504].
- [26] J. Engel, M. J. Ramsey-Musolf and U. van Kolck, Prog. Part. Nucl. Phys. **71**, 21 (2013), [arXiv:1303.2371].
- [27] M. Pospelov and A. Ritz, Annals Phys. **318**, 119 (2005), [hep-ph/0504231].
- [28] J. S. M. Ginges and V. V. Flambaum, Phys. Rept. **397**, 63 (2004), [arXiv:physics/0309054].
- [29] V. Andreev *et al.* (ACME), Nature **562**, 7727, 355 (2018).
- [30] W. B. Cairncross *et al.*, Phys. Rev. Lett. **119**, 15, 153001 (2017), [arXiv:1704.07928].
- [31] G. W. Bennett *et al.* (Muon (g-2)), Phys. Rev. **D80**, 052008 (2009), [arXiv:0811.1207].
- [32] C. Abel *et al.* (nEDM), Phys. Rev. Lett. **124**, 8, 081803 (2020), [arXiv:2001.11966].
- [33] B. Graner *et al.*, Phys. Rev. Lett. **116**, 16, 161601 (2016), [Erratum: Phys. Rev. Lett. 119, no.11, 119901 (2017)], [arXiv:1601.04339].
- [34] F. Allmendinger *et al.*, Phys. Rev. **A100**, 2, 022505 (2019), [arXiv:1904.12295].

- [35] C. Jarlskog, Phys. Rev. Lett. **55**, 1039 (1985); C. Jarlskog, Z. Phys. **C29**, 491 (1985).
- [36] E. P. Shabalin, Sov. J. Nucl. Phys. **28**, 75 (1978), [Yad. Fiz.28,151(1978)].
- [37] E. P. Shabalin, Sov. Phys. Usp. **26**, 297 (1983), [Usp. Fiz. Nauk139,561(1983)].
- [38] W. Bernreuther and M. Suzuki, Rev. Mod. Phys. **63**, 313 (1991), [Erratum: Rev. Mod. Phys.64,633(1992)].
- [39] M. Pospelov and A. Ritz, Phys. Rev. **D89**, 5, 056006 (2014), [arXiv:1311.5537].
- [40] C.-Y. Seng, Phys. Rev. **C91**, 2, 025502 (2015), [arXiv:1411.1476].
- [41] B. Grzadkowski *et al.*, JHEP **10**, 085 (2010), [arXiv:1008.4884].
- [42] S. Mantry, M. Pitschmann and M. J. Ramsey-Musolf, Phys. Rev. **D90**, 5, 054016 (2014), [arXiv:1401.7339].
- [43] B. K. Sahoo, Phys. Rev. **D95**, 1, 013002 (2017), [arXiv:1612.09371].
- [44] T. Chupp, Private Communication (2019).
- [45] J. Bsaisou *et al.*, Annals Phys. **359**, 317 (2015), [arXiv:1412.5471].
- [46] J. de Vries *et al.*, Annals Phys. **338**, 50 (2013), [arXiv:1212.0990].
- [47] L. I. Schiff, Phys. Rev. **132**, 2194 (1963).
- [48] T. Chupp and M. Ramsey-Musolf, Phys. Rev. **C91**, 3, 035502 (2015), [arXiv:1407.1064].
- [49] J. Beringer *et al.* (Particle Data Group), Phys. Rev. **D86**, 010001 (2012).
- [50] A. Angelopoulos *et al.* (CPLEAR), Phys. Lett. **B471**, 332 (1999).
- [51] M. S. Fee *et al.*, Phys. Rev. **A48**, 192 (1993).
- [52] R. J. Hughes and B. I. Deutch, Phys. Rev. Lett. **69**, 578 (1992).
- [53] S. Ulmer *et al.* (BASE), Nature **524**, 7564, 196 (2015).
- [54] R. S. Van Dyck, P. B. Schwinberg and H. G. Dehmelt, Phys. Rev. Lett. **59**, 26 (1987).
- [55] G. W. Bennett *et al.* (Muon g-2), Phys. Rev. Lett. **92**, 161802 (2004), [hep-ex/0401008].
- [56] C. Smorra *et al.* (BASE), Nature **550**, 7676, 371 (2017).
- [57] M. Ahmadi *et al.*, Nature **557**, 7703, 71 (2018).
- [58] O. W. Greenberg, Phys. Rev. Lett. **89**, 231602 (2002), [hep-ph/0201258].
- [59] S. Liberati, Class. Quant. Grav. **30**, 133001 (2013), [arXiv:1304.5795].
- [60] V. A. Kostelecky and N. Russell, Rev. Mod. Phys. **83**, 11 (2011), [arXiv:0801.0287].
- [61] D. Colladay and V. A. Kostelecky, Phys. Rev. **D58**, 116002 (1998), [hep-ph/9809521].
- [62] S. Weinberg, Phys. Rev. Lett. **43**, 1566 (1979).
- [63] F. Wilczek and A. Zee, Phys. Rev. Lett. **43**, 1571 (1979).
- [64] L. F. Abbott and M. B. Wise, Phys. Rev. **D22**, 2208 (1980).
- [65] M. Agostini *et al.* (Borexino), Phys. Rev. Lett. **115**, 231802 (2015), [arXiv:1509.01223].
- [66] E. B. Norman, J. N. Bahcall and M. Goldhaber, Phys. Rev. **D53**, 4086 (1996).
- [67] G. Bressi *et al.*, Phys. Rev. **A83**, 5, 052101 (2011), [arXiv:1102.2766].
- [68] C. Caprini, S. Biller and P. G. Ferreira, JCAP **0502**, 006 (2005), [hep-ph/0310066].
- [69] B. Altschul, Phys. Rev. Lett. **98**, 261801 (2007), [hep-ph/0703126].
- [70] A. de Gouvea, Private Communication (2019).
- [71] A. de Gouvea and P. Vogel, Prog. Part. Nucl. Phys. **71**, 75 (2013), [arXiv:1303.4097].
- [72] S. T. Petcov, Sov. J. Nucl. Phys. **25**, 340 (1977), [Erratum: Yad. Fiz.25,1336(1977)].
- [73] W. J. Marciano and A. I. Sanda, Phys. Lett. **67B**, 303 (1977).
- [74] S. M. Bilenky, S. T. Petcov and B. Pontecorvo, Phys. Lett. **67B**, 309 (1977).
- [75] T.-P. Cheng and L.-F. Li, Phys. Rev. **D16**, 1425 (1977).
- [76] B. W. Lee and R. E. Shrock, Phys. Rev. **D16**, 1444 (1977).
- [77] B. W. Lee *et al.*, Phys. Rev. Lett. **38**, 937 (1977), [Erratum: Phys. Rev. Lett.38,1230(1977)].
- [78] R. H. Bernstein and P. S. Cooper, Phys. Rept. **532**, 27 (2013), [arXiv:1307.5787].
- [79] L. Calibbi and G. Signorelli, Riv. Nuovo Cim. **41**, 2, 71 (2018), [arXiv:1709.00294].
- [80] A. M. Baldini *et al.* (MEG), Eur. Phys. J. **C76**, 8, 434 (2016), [arXiv:1605.05081].
- [81] U. Bellgardt *et al.* (SINDRUM), Nucl. Phys. **B299**, 1 (1988).
- [82] W. H. Bertl *et al.* (SINDRUM II), Eur. Phys. J. **C47**, 337 (2006).
- [83] Y. S. Amhis *et al.* (HFLAV) (2019), [arXiv:1909.12524].
- [84] W. Altmannshofer *et al.* (Belle-II), PTEP **2019**, 12, 123C01 (2019), [arXiv:1808.10567].
- [85] A. Cerri *et al.*, CERN Yellow Rep. Monogr. **7**, 867 (2019), [arXiv:1812.07638].
- [86] G. Aad *et al.* (ATLAS), Phys. Lett. **B800**, 135069 (2020), [arXiv:1907.06131].
- [87] A. M. Sirunyan *et al.* (CMS), JHEP **06**, 001 (2018), [arXiv:1712.07173].
- [88] R. Kitano, M. Koike and Y. Okada, Phys. Rev. **D66**, 096002 (2002), [Erratum: Phys. Rev.D76,059902(2007)], [hep-ph/0203110].
- [89] A. Pich, Prog. Part. Nucl. Phys. **75**, 41 (2014), [arXiv:1310.7922].
- [90] D. Ambrose *et al.* (BNL), Phys. Rev. Lett. **81**, 5734 (1998), [hep-ex/9811038].
- [91] A. Sher *et al.*, Phys. Rev. **D72**, 012005 (2005), [hep-ex/0502020].
- [92] R. Aaij *et al.* (LHCb), JHEP **03**, 078 (2018), [arXiv:1710.04111].
- [93] R. Aaij *et al.* (LHCb), Phys. Lett. **B754**, 167 (2016), [arXiv:1512.00322].
- [94] G. Aad *et al.* (ATLAS), Phys. Rev. **D90**, 7, 072010 (2014), [arXiv:1408.5774].
- [95] R. Akers *et al.* (OPAL), Z. Phys. **C67**, 555 (1995).
- [96] P. Abreu *et al.* (DELPHI), Z. Phys. **C73**, 243 (1997).
- [97] G. Aad *et al.* (ATLAS), Phys. Lett. **B801**, 135148 (2020), [arXiv:1909.10235].
- [98] S. Dell’Oro *et al.*, Adv. High Energy Phys. **2016**, 2162659 (2016), [arXiv:1601.07512].
- [99] J. Engel and J. Menéndez, Rept. Prog. Phys. **80**, 4, 046301 (2017), [arXiv:1610.06548].
- [100] A. Gando *et al.* (KamLAND-Zen), Phys. Rev. Lett. **117**, 8, 082503 (2016), [Addendum: Phys. Rev. Lett.117,no.10,109903(2016)], [arXiv:1605.02889].
- [101] P. Fileviez Perez, Phys. Rept. **597**, 1 (2015), [arXiv:1501.01886].
- [102] M. Aaboud *et al.* (ATLAS), JHEP **01**, 016 (2019), [arXiv:1809.11105].
- [103] A. M. Sirunyan *et al.* (CMS), JHEP **05**, 05, 148 (2018), [arXiv:1803.11116].

- [104] J. Kaulard *et al.* (SINDRUM II), Phys. Lett. **B422**, 334 (1998).
- [105] Y. Miyazaki *et al.* (Belle), Phys. Lett. **B719**, 346 (2013), [arXiv:1206.5595].
- [106] E. Cortina Gil *et al.* (NA62), Phys. Lett. **B797**, 134794 (2019), [arXiv:1905.07770].
- [107] R. Aaij *et al.* (LHCb), Phys. Lett. **B724**, 203 (2013), [arXiv:1304.6365].
- [108] J. P. Lees *et al.* (BaBar), Phys. Rev. **D85**, 071103 (2012), [arXiv:1202.3650].
- [109] A. Abada *et al.*, JHEP **02**, 169 (2018), [arXiv:1712.03984].
- [110] M. Anderson *et al.* (SNO+), Phys. Rev. D **99**, 3, 032008 (2019), [arXiv:1812.05552].
- [111] K. Abe *et al.* (Super-Kamiokande), Phys. Rev. **D95**, 1, 012004 (2017), [arXiv:1610.03597].
- [112] M. Baldo-Ceolin *et al.*, Z. Phys. **C63**, 409 (1994).
- [113] K. Abe *et al.* (Super-Kamiokande), Phys. Rev. **D91**, 072006 (2015), [arXiv:1109.4227].
- [114] D. G. Phillips, II *et al.*, Phys. Rept. **612**, 1 (2016), [arXiv:1410.1100].
- [115] G. Abbiendi *et al.* (OPAL), Phys. Lett. **B447**, 157 (1999), [hep-ex/9901011].
- [116] Y. Miyazaki *et al.* (Belle), Phys. Lett. **B632**, 51 (2006), [hep-ex/0508044].
- [117] P. del Amo Sanchez *et al.* (BaBar), Phys. Rev. **D83**, 091101 (2011), [arXiv:1101.3830].
- [118] P. Bloch *et al.* (Geneva-Saclay), Phys. Lett. **60B**, 393 (1976).
- [119] A. Angelopoulos *et al.* (CPLEAR), Phys. Lett. **B444**, 38 (1998).
- [120] A. Angelopoulos *et al.* (CPLEAR), Eur. Phys. J. **C22**, 55 (2001).
- [121] R. Aaij *et al.* (LHCb), Phys. Rev. Lett. **122**, 23, 231802 (2019), [arXiv:1903.03074].
- [122] A. A. Petrov, Int. J. Mod. Phys. **A21**, 5686 (2006), [hep-ph/0611361].
- [123] D. Ambrose *et al.* (BNL E871), Phys. Rev. Lett. **81**, 4309 (1998), [hep-ex/9810007].
- [124] V. Cirigliano *et al.*, Rev. Mod. Phys. **84**, 399 (2012), [arXiv:1107.6001].
- [125] F. Ambrosino *et al.* (KLOE), Phys. Lett. **B672**, 203 (2009), [arXiv:0811.1007].
- [126] R. Aaij *et al.* (LHCb) (2020), [arXiv:2001.10354].
- [127] J. Brod, M. Gorbahn and E. Stamou, Phys. Rev. **D83**, 034030 (2011), [arXiv:1009.0947].
- [128] J. K. Ahn *et al.* (KOTO), Phys. Rev. Lett. **122**, 2, 021802 (2019), [arXiv:1810.09655].
- [129] R. Aaij *et al.* (LHCb), Phys. Lett. **B725**, 15 (2013), [arXiv:1305.5059].
- [130] S. Bifani *et al.*, J. Phys. **G46**, 2, 023001 (2019), [arXiv:1809.06229].
- [131] R. Aaij *et al.* (LHCb), JHEP **08**, 055 (2017), [arXiv:1705.05802].
- [132] R. Aaij *et al.* (LHCb), Phys. Rev. Lett. **122**, 19, 191801 (2019), [arXiv:1903.09252].
- [133] A. Abdesselam *et al.* (Belle) (2019), [arXiv:1904.02440].
- [134] A. Abdesselam *et al.* (2019), [arXiv:1908.01848].

TESTS OF DISCRETE SPACE-TIME SYMMETRIES

CHARGE CONJUGATION (C) INVARIANCE

$\Gamma(\pi^0 \rightarrow 3\gamma)/\Gamma_{\text{total}}$	$<3.1 \times 10^{-8}$, CL = 90%
η C-nonconserving decay parameters	
$\pi^+ \pi^- \pi^0$ left-right asymmetry	$(0.09^{+0.11}_{-0.12}) \times 10^{-2}$
$\pi^+ \pi^- \pi^0$ sextant asymmetry	$(0.12^{+0.10}_{-0.11}) \times 10^{-2}$
$\pi^+ \pi^- \pi^0$ quadrant asymmetry	$(-0.09 \pm 0.09) \times 10^{-2}$
$\pi^+ \pi^- \gamma$ left-right asymmetry	$(0.9 \pm 0.4) \times 10^{-2}$
$\pi^+ \pi^- \gamma$ parameter β (D -wave)	-0.02 ± 0.07 ($S = 1.3$)
$\Gamma(\eta \rightarrow \pi^0 \gamma)/\Gamma_{\text{total}}$	[a] $<9 \times 10^{-5}$, CL = 90%
$\Gamma(\eta \rightarrow 2\pi^0 \gamma)/\Gamma_{\text{total}}$	$<5 \times 10^{-4}$, CL = 90%
$\Gamma(\eta \rightarrow 3\pi^0 \gamma)/\Gamma_{\text{total}}$	$<6 \times 10^{-5}$, CL = 90%
$\Gamma(\eta \rightarrow 3\gamma)/\Gamma_{\text{total}}$	$<1.6 \times 10^{-5}$, CL = 90%
$\Gamma(\eta \rightarrow \pi^0 e^+ e^-)/\Gamma_{\text{total}}$	[b] $<8 \times 10^{-6}$, CL = 90%
$\Gamma(\eta \rightarrow \pi^0 \mu^+ \mu^-)/\Gamma_{\text{total}}$	[b] $<5 \times 10^{-6}$, CL = 90%
$\Gamma(\omega(782) \rightarrow \eta \pi^0)/\Gamma_{\text{total}}$	$<2.2 \times 10^{-4}$, CL = 90%
$\Gamma(\omega(782) \rightarrow 2\pi^0)/\Gamma_{\text{total}}$	$<2.2 \times 10^{-4}$, CL = 90%
$\Gamma(\omega(782) \rightarrow 3\pi^0)/\Gamma_{\text{total}}$	$<2.3 \times 10^{-4}$, CL = 90%
asymmetry parameter for $\eta'(958) \rightarrow \pi^+ \pi^- \gamma$ decay	-0.03 ± 0.04
$\Gamma(\eta'(958) \rightarrow \pi^0 e^+ e^-)/\Gamma_{\text{total}}$	[b] $<1.4 \times 10^{-3}$, CL = 90%
$\Gamma(\eta'(958) \rightarrow \eta e^+ e^-)/\Gamma_{\text{total}}$	[b] $<2.4 \times 10^{-3}$, CL = 90%
$\Gamma(\eta'(958) \rightarrow 3\gamma)/\Gamma_{\text{total}}$	$<1.0 \times 10^{-4}$, CL = 90%
$\Gamma(\eta'(958) \rightarrow \mu^+ \mu^- \pi^0)/\Gamma_{\text{total}}$	[b] $<6.0 \times 10^{-5}$, CL = 90%
$\Gamma(\eta'(958) \rightarrow \mu^+ \mu^- \eta)/\Gamma_{\text{total}}$	[b] $<1.5 \times 10^{-5}$, CL = 90%
$\Gamma(J/\psi(1S) \rightarrow \gamma \gamma)/\Gamma_{\text{total}}$	$<2.7 \times 10^{-7}$, CL = 90%
$\Gamma(J/\psi(1S) \rightarrow \gamma \phi)/\Gamma_{\text{total}}$	$<1.4 \times 10^{-6}$, CL = 90%

PARITY (P) INVARIANCE

e electric dipole moment	$<0.11 \times 10^{-28}$ ecm, CL = 90%
μ electric dipole moment [d]	$<1.8 \times 10^{-19}$ ecm, CL = 95%
$\text{Re}(d_\tau = \tau \text{ electric dipole moment})$	$-0.220 \text{ to } 0.45 \times 10^{-16}$ ecm, CL = 95%
$\Gamma(\eta \rightarrow \pi^+ \pi^-)/\Gamma_{\text{total}}$	$<1.3 \times 10^{-5}$, CL = 90%
$\Gamma(\eta \rightarrow 2\pi^0)/\Gamma_{\text{total}}$	$<3.5 \times 10^{-4}$, CL = 90%
$\Gamma(\eta \rightarrow 4\pi^0)/\Gamma_{\text{total}}$	$<6.9 \times 10^{-7}$, CL = 90%
$\Gamma(\eta'(958) \rightarrow \pi^+ \pi^-)/\Gamma_{\text{total}}$	$<1.8 \times 10^{-5}$, CL = 90%
$\Gamma(\eta'(958) \rightarrow \pi^0 \pi^0)/\Gamma_{\text{total}}$	$<4 \times 10^{-4}$, CL = 90%
$\Gamma(\eta_c(1S) \rightarrow \pi^+ \pi^-)/\Gamma_{\text{total}}$	$<1.1 \times 10^{-4}$, CL = 90%
$\Gamma(\eta_c(1S) \rightarrow \pi^0 \pi^0)/\Gamma_{\text{total}}$	$<4 \times 10^{-5}$, CL = 90%
$\Gamma(\eta_c(1S) \rightarrow K^+ K^-)/\Gamma_{\text{total}}$	$<6 \times 10^{-4}$, CL = 90%
$\Gamma(\eta_c(1S) \rightarrow K_S^0 K_S^0)/\Gamma_{\text{total}}$	$<3.1 \times 10^{-4}$, CL = 90%
p electric dipole moment	$<0.021 \times 10^{-23}$ ecm
n electric dipole moment	$<0.18 \times 10^{-25}$ ecm, CL = 90%
Λ electric dipole moment	$<1.5 \times 10^{-16}$ ecm, CL = 95%
$a_P(\Lambda_b^0 \rightarrow p \pi^- \pi^+ \pi^-)$	$(-3.7 \pm 1.5)\%$
$a_P(\Lambda_b^0 \rightarrow p K^- \pi^+ \pi^-)$	$(-0.6 \pm 0.9)\%$
$a_P(\Lambda_b^0 \rightarrow p K^- K^+ \pi^-)$	$(4 \pm 5)\%$
$a_P(\Lambda_b^0 \rightarrow p K^- K^+ K^-)$	$(-1.6 \pm 1.5)\%$
$a_P(\Lambda_b^0 \rightarrow p K^- \mu^+ \mu^-)$	$(-5 \pm 5)\%$
$a_P(\Xi_b^0 \rightarrow p K^- K^- \pi^+)$	$(-3 \pm 5)\%$

TIME REVERSAL (T) INVARIANCE

e electric dipole moment	$<0.11 \times 10^{-28}$ ecm, CL = 90%
μ electric dipole moment [d]	$<1.8 \times 10^{-19}$ ecm, CL = 95%
μ decay parameters	
transverse e^+ polarization normal to plane of μ spin, e^+ momentum	$(-2 \pm 8) \times 10^{-3}$
α'/A	$(-10 \pm 20) \times 10^{-3}$
β'/A	$(2 \pm 7) \times 10^{-3}$
$\text{Re}(d_\tau = \tau \text{ electric dipole moment})$	$-0.220 \text{ to } 0.45 \times 10^{-16}$ ecm, CL = 95%
P_T in $K^+ \rightarrow \pi^0 \mu^+ \nu_\mu$	$(-1.7 \pm 2.5) \times 10^{-3}$
P_T in $K^+ \rightarrow \mu^+ \nu_\mu \gamma$	$(-0.6 \pm 1.9) \times 10^{-2}$
$\text{Im}(\xi)$ in $K^+ \rightarrow \pi^0 \mu^+ \nu_\mu$ decay (from transverse μ pol.)	-0.006 ± 0.008
asymmetry A_T in K^0 - \bar{K}^0 mixing	$(6.6 \pm 1.6) \times 10^{-3}$

$\text{Im}(\xi)$ in $K^0_{\mu 3}$ decay (from transverse μ pol.)	-0.007 ± 0.026
$A_T(D^\pm \rightarrow K_S^0 K^\pm \pi^+ \pi^-)$	[c] $(-12 \pm 11) \times 10^{-3}$
$A_T(D^0 \rightarrow K^+ K^- \pi^+ \pi^-)$	[c] $(2.9 \pm 2.2) \times 10^{-3}$
$A_T(D_S^\pm \rightarrow K_S^0 K^\pm \pi^+ \pi^-)$	[c] $(-14 \pm 8) \times 10^{-3}$
$\Delta S_T^+(S_{\ell^-, K_S^0}^- - S_{\ell^+, K_S^0}^+)$	-1.37 ± 0.15
$\Delta S_T^-(S_{\ell^-, K_S^0}^+ - S_{\ell^+, K_S^0}^-)$	1.17 ± 0.21
$\Delta C_T^+(C_{\ell^-, K_S^0}^- - C_{\ell^+, K_S^0}^+)$	0.10 ± 0.16
$\Delta C_T^-(C_{\ell^-, K_S^0}^+ - C_{\ell^+, K_S^0}^-)$	0.04 ± 0.16
p electric dipole moment	$<0.021 \times 10^{-23}$ ecm
n electric dipole moment	$<0.18 \times 10^{-25}$ ecm, CL = 90%
$n \rightarrow p e^- \bar{\nu}_e$ decay parameters	
ϕ_{AV} , phase of g_A relative to g_V	[d] $(180.017 \pm 0.026)^\circ$
triple correlation coefficient D	[e] $(-1.2 \pm 2.0) \times 10^{-4}$
triple correlation coefficient R	[e] 0.004 ± 0.013
Λ electric dipole moment	$<1.5 \times 10^{-16}$ ecm, CL = 95%
triple correlation coefficient D for $\Sigma^- \rightarrow n e^- \bar{\nu}_e$	0.11 ± 0.10

CP INVARIANCE

$\text{Re}(d_T^W)$	$<0.50 \times 10^{-17}$ ecm, CL = 95%
$\text{Im}(d_T^W)$	$<1.1 \times 10^{-17}$ ecm, CL = 95%
δ (CP violating phase in neutrino mixing)	1.36 ± 0.17 π rad
$\eta \rightarrow \pi^+ \pi^- e^+ e^-$ decay-plane asymmetry	$(-0.6 \pm 3.1) \times 10^{-2}$
$\Gamma(\eta \rightarrow \pi^+ \pi^-)/\Gamma_{\text{total}}$	$<1.3 \times 10^{-5}$, CL = 90%
$\Gamma(\eta \rightarrow 2\pi^0)/\Gamma_{\text{total}}$	$<3.5 \times 10^{-4}$, CL = 90%
$\Gamma(\eta \rightarrow 4\pi^0)/\Gamma_{\text{total}}$	$<6.9 \times 10^{-7}$, CL = 90%
$\Gamma(\eta'(958) \rightarrow \pi^+ \pi^-)/\Gamma_{\text{total}}$	$<1.8 \times 10^{-5}$, CL = 90%
$\Gamma(\eta'(958) \rightarrow \pi^0 \pi^0)/\Gamma_{\text{total}}$	$<4 \times 10^{-4}$, CL = 90%
$K^\pm \rightarrow \pi^\pm e^+ e^-$ rate difference/sum	$(-2.2 \pm 1.6) \times 10^{-2}$
$K^\pm \rightarrow \pi^\pm \mu^+ \mu^-$ rate difference/sum	0.010 ± 0.023
$K^\pm \rightarrow \pi^\pm \pi^0 \gamma$ rate difference/sum	$(0.0 \pm 1.2) \times 10^{-3}$
$K^\pm \rightarrow \pi^\pm \pi^+ \pi^-$ rate difference/sum	$(0.04 \pm 0.06)\%$
$K^\pm \rightarrow \pi^\pm \pi^0 \pi^0$ rate difference/sum	$(-0.02 \pm 0.28)\%$
$K^\pm \rightarrow \pi^\pm \pi^+ \pi^- (g_+ - g_-) / (g_+ + g_-)$	$(-1.5 \pm 2.2) \times 10^{-4}$
$K^\pm \rightarrow \pi^\pm \pi^0 \pi^0 (g_+ - g_-) / (g_+ + g_-)$	$(1.8 \pm 1.8) \times 10^{-4}$
$A_S = [\Gamma(K_S^0 \rightarrow \pi^- e^+ \nu_e) - \Gamma(K_S^0 \rightarrow \pi^+ e^- \bar{\nu}_e)] / \text{SUM}$	$(-4 \pm 6) \times 10^{-3}$
$\text{Im}(\eta_{+-0}) = \text{Im}(A(K_S^0 \rightarrow \pi^+ \pi^- \pi^0, CP\text{-violating}) / A(K_L^0 \rightarrow \pi^+ \pi^- \pi^0))$	-0.002 ± 0.009
$\text{Im}(\eta_{000}) = \text{Im}(A(K_S^0 \rightarrow \pi^0 \pi^0 \pi^0) / A(K_L^0 \rightarrow \pi^0 \pi^0 \pi^0))$	-0.001 ± 0.016
$ \eta_{000} = A(K_S^0 \rightarrow 3\pi^0) / A(K_L^0 \rightarrow 3\pi^0) $	<0.0088 , CL = 90%
CP asymmetry A in $K_S^0 \rightarrow \pi^+ \pi^- e^+ e^-$	$(-0.4 \pm 0.8)\%$
$\Gamma(K_S^0 \rightarrow 3\pi^0)/\Gamma_{\text{total}}$	$<2.6 \times 10^{-8}$, CL = 90%
linear coefficient j for $K_L^0 \rightarrow \pi^+ \pi^- \pi^0$	0.0012 ± 0.0008
quadratic coefficient f for $K_L^0 \rightarrow \pi^+ \pi^- \pi^0$	0.004 ± 0.006
$ \epsilon'_{+-\gamma} $ for $K_L^0 \rightarrow \pi^+ \pi^- \gamma$	<0.3 , CL = 90%
$ \delta E_1 $ for $K_L^0 \rightarrow \pi^+ \pi^- \gamma$	<0.21 , CL = 90%
$\Gamma(K_L^0 \rightarrow \pi^0 \mu^+ \mu^-)/\Gamma_{\text{total}}$	[f] $<3.8 \times 10^{-10}$, CL = 90%
$\Gamma(K_L^0 \rightarrow \pi^0 e^+ e^-)/\Gamma_{\text{total}}$	[f] $<2.8 \times 10^{-10}$, CL = 90%
$\Gamma(K_L^0 \rightarrow \pi^0 \nu \bar{\nu})/\Gamma_{\text{total}}$	[g] $<3.0 \times 10^{-9}$, CL = 90%
$A_{CP}(D^\pm \rightarrow \mu^\pm \nu)$	$(8 \pm 8)\%$
$A_{CP}(D^\pm \rightarrow K_S^0 e^\pm \nu)$	$(-0.6 \pm 1.6)\%$
$A_{CP}(D^\pm \rightarrow K_S^0 \pi^\pm)$	$(-0.41 \pm 0.09)\%$
$A_{CP}(D^\pm \rightarrow K^\mp 2\pi^\pm)$	$(-0.18 \pm 0.16)\%$
$A_{CP}(D^\pm \rightarrow K^\mp \pi^\pm \pi^\pm \pi^0)$	$(-0.3 \pm 0.7)\%$
$A_{CP}(D^\pm \rightarrow K_S^0 \pi^\pm \pi^0)$	$(-0.1 \pm 0.7)\%$
$A_{CP}(D^\pm \rightarrow K_S^0 \pi^\pm \pi^+ \pi^-)$	$(0.0 \pm 1.2)\%$
$A_{CP}(D^\pm \rightarrow \pi^\pm \pi^0)$	$(2.4 \pm 1.2)\%$
$A_{CP}(D^\pm \rightarrow \pi^\pm \eta)$	$(1.0 \pm 1.5)\%$ ($S = 1.4$)
$A_{CP}(D^\pm \rightarrow \pi^\pm \eta'(958))$	$(-0.6 \pm 0.7)\%$
$A_{CP}(D^\pm \rightarrow \bar{K}^0 / K^0 K^\pm)$	$(0.11 \pm 0.17)\%$
$A_{CP}(D^\pm \rightarrow K_S^0 K^\pm)$	$(-0.01 \pm 0.07)\%$
$A_{CP}(D^\pm \rightarrow K^+ K^- \pi^\pm)$	$(0.37 \pm 0.29)\%$
$A_{CP}(D^\pm \rightarrow K^\pm K^* 0)$	$(-0.3 \pm 0.4)\%$
$A_{CP}(D^\pm \rightarrow \phi \pi^\pm)$	$(0.01 \pm 0.09)\%$ ($S = 1.8$)
$A_{CP}(D^\pm \rightarrow K^\pm K_S^0(1430)^0)$	$(\delta_{-6}^{\pm 7})\%$

Tests of Conservation Laws

$A_{CP}(D^\pm \rightarrow K^\pm K_2^*(1430)^0)$	$(43 \pm 20)\%$	$A_{CP}(D^0 \rightarrow K^- \pi^+ \pi^0)$	$(0.1 \pm 0.5)\%$
$A_{CP}(D^\pm \rightarrow K^\pm K_0^*(700))$	$(-12 \pm 18)\%$	$A_{CP}(D^0 \rightarrow K^+ \pi^- \pi^0)$	$(0 \pm 5)\%$
$A_{CP}(D^\pm \rightarrow a_0(1450)^0 \pi^\pm)$	$(-19 \pm 16)\%$	$A_{CP}(D^0 \rightarrow K_S^0 \pi^+ \pi^-)$	$(-0.1 \pm 0.8)\%$
$A_{CP}(D^\pm \rightarrow \phi(1680) \pi^\pm)$	$(-9 \pm 26)\%$	$A_{CP}(D^0 \rightarrow K^*(892)^- \pi^+ \rightarrow K_S^0 \pi^+ \pi^-)$	$(0.4 \pm 0.5)\%$
$A_{CP}(D^\pm \rightarrow \pi^+ \pi^- \pi^\pm)$	$(-2 \pm 4)\%$	$A_{CP}(D^0 \rightarrow K^*(892)^+ \pi^- \rightarrow K_S^0 \pi^+ \pi^-)$	$(1 \pm 6)\%$
$A_{CP}(D^\pm \rightarrow K_S^0 K^\pm \pi^+ \pi^-)$	$(-4 \pm 7)\%$	$A_{CP}(D^0 \rightarrow K_S^0 \rho^0 \rightarrow K_S^0 \pi^+ \pi^-)$	$(-0.1 \pm 0.5)\%$
$A_{CP}(D^\pm \rightarrow K^\pm \pi^0)$	$(-4 \pm 11)\%$	$A_{CP}(D^0 \rightarrow K_S^0 \omega \rightarrow K_S^0 \pi^+ \pi^-)$	$(-13 \pm 7)\%$
Local CPV in $D^\pm \rightarrow \pi^+ \pi^- \pi^\pm$	78.1%	$A_{CP}(D^0 \rightarrow K_S^0 f_0(980) \rightarrow K_S^0 \pi^+ \pi^-)$	$(-0.4 \pm 2.7)\%$
Local CPV in $D^\pm \rightarrow K^+ K^- \pi^\pm$	31%	$A_{CP}(D^0 \rightarrow K_S^0 f_2(1270) \rightarrow K_S^0 \pi^+ \pi^-)$	$(-4 \pm 5)\%$
$ q/p $ of D^0 - \bar{D}^0 mixing	0.92 ± 0.12	$A_{CP}(D^0 \rightarrow K_S^0 f_0(1370) \rightarrow K_S^0 \pi^+ \pi^-)$	$(-1 \pm 9)\%$
A_Γ of D^0 - \bar{D}^0 mixing	$(-0.125 \pm 0.526) \times 10^{-3}$	$A_{CP}(D^0 \rightarrow \bar{K}^0 \rho^0(1450) \rightarrow K_S^0 \pi^+ \pi^-)$	$(-4 \pm 10)\%$
Where there is ambiguity, the CP test is labelled by the D^0 decay mode.		$A_{CP}(D^0 \rightarrow \bar{K}^0 f_0(600) \rightarrow K_S^0 \pi^+ \pi^-)$	$(-3 \pm 5)\%$
$A_{CP}(D^0 \rightarrow K^+ K^-)$	$(-0.07 \pm 0.11)\%$	$A_{CP}(D^0 \rightarrow K^*(1410)^- \pi^+ \rightarrow K_S^0 \pi^+ \pi^-)$	$(-2 \pm 9)\%$
$A_{CP}(D^0 \rightarrow K_S^0 K_S^0)$	$(0.4 \pm 1.4)\%$	$A_{CP}(D^0 \rightarrow K_S^0(1430)^- \pi^+ \rightarrow K_S^0 \pi^+ \pi^-)$	$(4 \pm 4)\%$
$A_{CP}(D^0 \rightarrow \pi^+ \pi^-)$	$(0.13 \pm 0.14)\%$	$A_{CP}(D^0 \rightarrow K_S^0(1430)^- \pi^+ \rightarrow K_S^0 \pi^+ \pi^-)$	$(12 \pm 15)\%$
$A_{CP}(D^0 \rightarrow \pi^0 \pi^0)$	$(0.0 \pm 0.6)\%$	$A_{CP}(D^0 \rightarrow K_S^0(1430)^- \pi^+ \rightarrow K_S^0 \pi^+ \pi^-)$	$(3 \pm 6)\%$
$A_{CP}(D^0 \rightarrow \rho \gamma)$	$(6 \pm 15) \times 10^{-2}$	$A_{CP}(D^0 \rightarrow K_S^0(1430)^- \pi^+ \rightarrow K_S^0 \pi^+ \pi^-)$	$(-10 \pm 32)\%$
$A_{CP}(D^0 \rightarrow \phi \gamma)$	$(-9 \pm 7) \times 10^{-2}$	$A_{CP}(D^0 \rightarrow K^*(1410)^- \pi^+ \rightarrow K_S^0 \pi^+ \pi^-)$	$(0.2 \pm 0.5)\%$
$A_{CP}(D^0 \rightarrow \bar{K}^*(892)^0 \gamma)$	$(-0.3 \pm 2.0) \times 10^{-2}$	$A_{CP}(D^0 \rightarrow K^+ \pi^- \pi^+ \pi^-)$	$(-2 \pm 4)\%$
$A_{CP}(D^0 \rightarrow \pi^+ \pi^- \pi^0)$	$(0.3 \pm 0.4)\%$	$A_{CP}(D^0 \rightarrow K^+ K^- \pi^+ \pi^-)$	$(1.3 \pm 1.7)\%$
$A_{CP}(D^0 \rightarrow \rho(770)^+ \pi^- \rightarrow \pi^+ \pi^- \pi^0)$	[h] $(1.2 \pm 0.9)\%$	$A_{CP}(D^0 \rightarrow K_1^*(1270)^+ K^- \rightarrow K^+ K^- \pi^+ \pi^-)$	$(-2.3 \pm 1.7)\%$
$A_{CP}(D^0 \rightarrow \rho(770)^0 \pi^0 \rightarrow \pi^+ \pi^- \pi^0)$	[h] $(-3.1 \pm 3.0)\%$	$A_{CP}(D^0 \rightarrow K_1^*(1270)^+ K^- \rightarrow K^*0 \pi^+ K^-)$	$(-1 \pm 10)\%$
$A_{CP}(D^0 \rightarrow \rho(770)^- \pi^+ \rightarrow \pi^+ \pi^- \pi^0)$	[h] $(-1.0 \pm 1.7)\%$	$A_{CP}(D^0 \rightarrow K_1^*(1270)^- K^+ \rightarrow \bar{K}^*0 \pi^- K^+)$	$(-10 \pm 32)\%$
$A_{CP}(D^0 \rightarrow \rho(1450)^+ \pi^- \rightarrow \pi^+ \pi^- \pi^0)$	[h] $(0 \pm 70)\%$	$A_{CP}(D^0 \rightarrow K_1^*(1270)^- K^+ \rightarrow K^+ K^- \pi^+ \pi^-)$	$(1.7 \pm 3.5)\%$
$A_{CP}(D^0 \rightarrow \rho(1450)^0 \pi^0 \rightarrow \pi^+ \pi^- \pi^0)$	[h] $(-20 \pm 40)\%$	$A_{CP}(D^0 \rightarrow K_1^*(1270)^+ K^- \rightarrow K^+ K^- \pi^+ \pi^-)$	$(-7 \pm 17)\%$
$A_{CP}(D^0 \rightarrow \rho(1450)^- \pi^+ \rightarrow \pi^+ \pi^- \pi^0)$	[h] $(6 \pm 9)\%$	$A_{CP}(D^0 \rightarrow K_1^*(1270)^+ K^- \rightarrow \rho^0 K^+ K^-)$	$(10 \pm 13)\%$
$A_{CP}(D^0 \rightarrow \rho(1700)^+ \pi^- \rightarrow \pi^+ \pi^- \pi^0)$	[h] $(-5 \pm 14)\%$	$A_{CP}(D^0 \rightarrow K_1^*(1270)^- K^+ \rightarrow \rho^0 K^- K^+)$	$(-4.4 \pm 2.1)\%$
$A_{CP}(D^0 \rightarrow \rho(1700)^0 \pi^0 \rightarrow \pi^+ \pi^- \pi^0)$	[h] $(13 \pm 9)\%$	$A_{CP}(D^0 \rightarrow K_1^*(1270)^- K^+ \rightarrow K^+ K^- \pi^+ \pi^-)$	$(-20 \pm 17)\%$
$A_{CP}(D^0 \rightarrow \rho(1700)^- \pi^+ \rightarrow \pi^+ \pi^- \pi^0)$	[h] $(8 \pm 11)\%$	$A_{CP}(D^0 \rightarrow K^*(1410)^+ K^- \rightarrow K^*0 \pi^+ K^-)$	$(-1 \pm 14)\%$
$A_{CP}(D^0 \rightarrow f_0(980) \pi^0 \rightarrow \pi^+ \pi^- \pi^0)$	[h] $(0 \pm 35)\%$	$A_{CP}(D^0 \rightarrow K^*(1410)^- K^+ \rightarrow \bar{K}^*0 \pi^- K^+)$	$(-17 \pm 29)\%$
$A_{CP}(D^0 \rightarrow f_0(1370) \pi^0 \rightarrow \pi^+ \pi^- \pi^0)$	[h] $(25 \pm 18)\%$	$A_{CP}(D^0 \rightarrow K^*(1680)^+ K^- \rightarrow K^+ K^- \pi^+ \pi^-)$	$(-5 \pm 14)\%$
$A_{CP}(D^0 \rightarrow f_0(1500) \pi^0 \rightarrow \pi^+ \pi^- \pi^0)$	[h] $(0 \pm 18)\%$	$A_{CP}(D^0 \rightarrow K^*(1410)^+ K^- \rightarrow K^*0 \pi^+ K^-)$	$(-3.9 \pm 2.2)\%$
$A_{CP}(D^0 \rightarrow f_0(1710) \pi^0 \rightarrow \pi^+ \pi^- \pi^0)$	[h] $(0 \pm 24)\%$	$A_{CP}(D^0 \rightarrow K^*(1410)^- K^+ \rightarrow K^*0 \pi^+ K^-)$	$(1 \pm 9)\%$
$A_{CP}(D^0 \rightarrow f_2(1270) \pi^0 \rightarrow \pi^+ \pi^- \pi^0)$	[h] $(-4 \pm 6)\%$	$A_{CP}(D^0 \rightarrow K^*(1680)^+ K^- \rightarrow K^+ K^- \pi^+ \pi^-)$	$(-3 \pm 5)\%$
$A_{CP}(D^0 \rightarrow \sigma(400) \pi^0 \rightarrow \pi^+ \pi^- \pi^0)$	[h] $(6 \pm 8)\%$	$A_{CP}(D^0 \rightarrow \phi \rho^0$ in $D^0, \bar{D}^0 \rightarrow \phi \rho^0$	$(-37 \pm 19)\%$
$A_{CP}(\text{nonresonant } D^0 \rightarrow \pi^+ \pi^- \pi^0)$	[h] $(-13 \pm 23)\%$	$A_{CP}(D^0 \rightarrow \phi \rho^0$ S-wave)	$(6 \pm 6)\%$
$A_{CP}(D^0, \bar{D}^0 \rightarrow 2\pi^+ 2\pi^-)$	$(0.5 \pm 1.2)\%$	$A_{CP}(D^0 \rightarrow \phi \rho^0$ D-wave)	$(-10 \pm 40)\%$
$A_{CP}(D^0 \rightarrow a_1(1260)^+ \pi^- \rightarrow 2\pi^+ 2\pi^-)$	$(5 \pm 6)\%$	$A_{CP}(D^0 \rightarrow \phi(\pi^+ \pi^-)_{S\text{-wave}})$	$(8 \pm 20)\%$
$A_{CP}(D^0 \rightarrow a_1(1260)^- \pi^+ \rightarrow 2\pi^+ 2\pi^-)$	$(14 \pm 18)\%$	$A_{CP}(D^0 \rightarrow K^*(892)^0(K^- \pi^+)_{S\text{-wave}})$	$(3 \pm 11)\%$
$A_{CP}(D^0 \rightarrow \pi(1300)^+ \pi^- \rightarrow 2\pi^+ 2\pi^-)$	$(-2 \pm 15)\%$	$A_{CP}(D^0 \rightarrow K^*(892)^0(K^- \pi^+)_{S\text{-wave}}$	$(97.3 \pm 1.7)\%$
$A_{CP}(D^0 \rightarrow \pi(1300)^- \pi^+ \rightarrow 2\pi^+ 2\pi^-)$	$(-6 \pm 30)\%$	$A_{CP}(D^0 \rightarrow K^+ K^- \pi^+ \pi^- \text{ non-resonant})$	$(73 \pm 6)\%$
$A_{CP}(D^0 \rightarrow a_1(1640)^+ \pi^- \rightarrow 2\pi^+ 2\pi^-)$	$(9 \pm 26)\%$	$A_{CP}(D^0 \rightarrow K^+ K^- \pi^+ \pi^- \text{ non-resonant})$	$(76.9 \pm 2.3)\%$
$A_{CP}(D^0 \rightarrow \pi_2(1670)^+ \pi^- \rightarrow 2\pi^+ 2\pi^-)$	$(7 \pm 18)\%$	$CP\text{-even fraction in } D^0 \rightarrow \pi^+ \pi^- \pi^0$	
$A_{CP}(D^0 \rightarrow \sigma f_0(1370) \rightarrow 2\pi^+ 2\pi^-)$	$(-15 \pm 19)\%$	decays	
$A_{CP}(D^0 \rightarrow \sigma \rho(770)^0 \rightarrow 2\pi^+ 2\pi^-)$	$(3 \pm 27)\%$	$CP\text{-even fraction in } D^0 \rightarrow K^+ K^- \pi^0$	
$A_{CP}(D^0 \rightarrow 2\rho(770)^0 \rightarrow 2\pi^+ 2\pi^-)$	$(-6 \pm 6)\%$	decays	
$A_{CP}(D^0 \rightarrow 2f_2(1270) \rightarrow 2\pi^+ 2\pi^-)$	$(-28 \pm 24)\%$	$CP\text{-even fraction in } D^0 \rightarrow \pi^+ \pi^- \pi^+ \pi^-$	
$A_{CP}(D^0 \rightarrow K^+ K^- \pi^0)$	$(-1.0 \pm 1.7)\%$	decays	
$A_{CP}(D^0 \rightarrow K^*(892)^+ K^- \rightarrow K^+ K^- \pi^0)$	[h] $(-0.9 \pm 1.3)\%$	Local CPV p-value in $D^0, \bar{D}^0 \rightarrow \pi^+ \pi^- \pi^0$	4.9%
$A_{CP}(D^0 \rightarrow K^*(1410)^+ K^- \rightarrow K^+ K^- \pi^0)$	[h] $(-21 \pm 24)\%$	Local CPV p-value in $D^0, \bar{D}^0 \rightarrow \pi^+ \pi^- \pi^+ \pi^-$	$(0.6 \pm 0.2)\%$
$A_{CP}(D^0 \rightarrow (K^+ \pi^0)_S K^- \rightarrow K^+ K^- \pi^0)$	[h] $(7 \pm 15)\%$	Local CPV p-value in $D^0, \bar{D}^0 \rightarrow K_S^0 \pi^+ \pi^-$	96%
$A_{CP}(D^0 \rightarrow \phi(1020) \pi^0 \rightarrow K^+ K^- \pi^0)$	[h] $(1.1 \pm 2.2)\%$	Local CPV p-value in $D^0, \bar{D}^0 \rightarrow K^+ K^- \pi^0$	16.6%
$A_{CP}(D^0 \rightarrow f_0(980) \pi^0 \rightarrow K^+ K^- \pi^0)$	[h] $(-3 \pm 19)\%$	Local CPV p-value in $D^0, \bar{D}^0 \rightarrow K^+ K^- \pi^+ \pi^-$	9.1%
$A_{CP}(D^0 \rightarrow a_0(980)^0 \pi^0 \rightarrow K^+ K^- \pi^0)$	[h] $(-5 \pm 16)\%$	$A_{CP}(D^\pm \rightarrow \mu^\pm \nu)$	$(5 \pm 6)\%$
$A_{CP}(D^0 \rightarrow f'_2(1525) \pi^0 \rightarrow K^+ K^- \pi^0)$	[h] $(0 \pm 160)\%$	$A_{CP}(D^\pm \rightarrow K^\pm K_S^0)$	$(0.09 \pm 0.26)\%$
$A_{CP}(D^0 \rightarrow K^*(892)^- K^+ \rightarrow K^+ K^- \pi^0)$	[h] $(-5 \pm 4)\%$	$A_{CP}(D^\pm \rightarrow K^+ K^- \pi^\pm)$	$(-0.5 \pm 0.9)\%$
$A_{CP}(D^0 \rightarrow K^*(1410)^- K^+ \rightarrow K^+ K^- \pi^0)$	[h] $(-17 \pm 29)\%$		
$A_{CP}(D^0 \rightarrow (K^- \pi^0)_{S\text{-wave}} K^+ \rightarrow K^+ K^- \pi^0)$	[h] $(-10 \pm 40)\%$		
$A_{CP}(D^0 \rightarrow K_S^0 \pi^0)$	$(-0.20 \pm 0.17)\%$		
$A_{CP}(D^0 \rightarrow K_S^0 \eta)$	$(0.5 \pm 0.5)\%$		
$A_{CP}(D^0 \rightarrow K_S^0 \eta')$	$(1.0 \pm 0.7)\%$		
$A_{CP}(D^0 \rightarrow K_S^0 \phi)$	$(-3 \pm 9)\%$		
$A_{CP}(D^0 \rightarrow K^- \pi^+)$	$(0.2 \pm 0.5)\%$		
$A_{CP}(D^0 \rightarrow K^+ \pi^-)$	$(-0.9 \pm 1.4)\%$		
$A_{CP}(D_{CP}(\pm 1) \rightarrow K^\mp \pi^\pm)$	$(12.7 \pm 1.5)\%$		

Unless otherwise stated, limits are given at the 90% confidence level, while errors are given as ± 1 standard deviation.

Tests of Conservation Laws

$A_{CP}(D_S^{\pm} \rightarrow \phi \pi^{\pm})$	$(-0.38 \pm 0.27)\%$	$A_{CP}(B^+ \rightarrow [K^+ K^-]_D \pi^+ \pi^- \pi^+)$	-0.019 ± 0.015
$A_{CP}(D_S^{\pm} \rightarrow K^{\pm} K_S^0 \pi^0)$	$(-2 \pm 6)\%$	$A_{CP}(B^+ \rightarrow [\pi^+ \pi^-]_D \pi^+ \pi^- \pi^+)$	-0.013 ± 0.019
$A_{CP}(D_S^{\pm} \rightarrow 2K_S^0 \pi^{\pm})$	$(3 \pm 5)\%$	$A_{CP}(B^+ \rightarrow [K^- \pi^+]_D \pi^+ \pi^- \pi^+)$	-0.002 ± 0.011
$A_{CP}(D_S^{\pm} \rightarrow K^+ K^- \pi^{\pm} \pi^0)$	$(0.0 \pm 3.0)\%$	$A_{CP}(B^+ \rightarrow \overline{D}^{*0} \pi^+)$	0.0010 ± 0.0028
$A_{CP}(D_S^{\pm} \rightarrow K^{\pm} K_S^0 \pi^+ \pi^-)$	$(-6 \pm 5)\%$	$A_{CP}(B^+ \rightarrow (D_{CP(+1)}^*)^0 \pi^+)$	$0.016 \pm 0.010 (S = 1.2)$
$A_{CP}(D_S^{\pm} \rightarrow K_S^0 K^{\mp} 2\pi^{\pm})$	$(4.1 \pm 2.8)\%$	$A_{CP}(B^+ \rightarrow (D_{CP(-1)}^*)^0 \pi^+)$	-0.09 ± 0.05
$A_{CP}(D_S^{\pm} \rightarrow \pi^+ \pi^- \pi^{\pm})$	$(-0.7 \pm 3.1)\%$	$A_{CP}(B^+ \rightarrow D^{*0} K^+)$	$-0.001 \pm 0.011 (S = 1.1)$
$A_{CP}(D_S^{\pm} \rightarrow \pi^{\pm} \eta)$	$(1.1 \pm 3.1)\%$	$A_{CP}(B^+ \rightarrow D_{CP(+1)}^{*0} K^+)$	$-0.11 \pm 0.08 (S = 2.7)$
$A_{CP}(D_S^{\pm} \rightarrow \pi^{\pm} \eta')$	$(-0.9 \pm 0.5)\%$	$A_{CP}(B^+ \rightarrow D_{CP(-1)}^{*0} K^+)$	0.07 ± 0.10
$A_{CP}(D_S^{\pm} \rightarrow \eta \pi^{\pm} \pi^0)$	$(-1 \pm 4)\%$	$A_{CP}(B^+ \rightarrow D_{CP(+1)} K^*(892)^+)$	0.08 ± 0.06
$A_{CP}(D_S^{\pm} \rightarrow \eta' \pi^{\pm} \pi^0)$	$(0 \pm 8)\%$	$A_{CP}(B^+ \rightarrow D_{CP(-1)} K^*(892)^+)$	-0.23 ± 0.22
$A_{CP}(D_S^{\pm} \rightarrow K^{\pm} \pi^0)$	$(-27 \pm 24)\%$	$A_{CP}(B^+ \rightarrow D_S^+ \phi)$	0.0 ± 0.4
$A_{CP}(D_S^{\pm} \rightarrow \overline{K}^0 / K^0 \pi^{\pm})$	$(0.4 \pm 0.5)\%$	$A_{CP}(B^+ \rightarrow D_S^+ \overline{D}^0)$	$(-0.4 \pm 0.7)\%$
$A_{CP}(D_S^{\pm} \rightarrow K_S^0 \pi^{\pm})$	$(0.20 \pm 0.18)\%$	$A_{CP}(B^+ \rightarrow D^{*+} \overline{D}^{*0})$	-0.15 ± 0.11
$A_{CP}(D_S^{\pm} \rightarrow K^{\pm} \pi^+ \pi^-)$	$(4 \pm 5)\%$	$A_{CP}(B^+ \rightarrow D^{*+} \overline{D}^0)$	-0.06 ± 0.13
$A_{CP}(D_S^{\pm} \rightarrow K^{\pm} \eta)$	$(9 \pm 15)\%$	$A_{CP}(B^+ \rightarrow D^+ \overline{D}^{*0})$	0.13 ± 0.18
$A_{CP}(D_S^{\pm} \rightarrow K^{\pm} \eta' (958))$	$(6 \pm 19)\%$	$A_{CP}(B^+ \rightarrow D^+ \overline{D}^0)$	0.016 ± 0.025
$A_{CP}(B^+ \rightarrow J/\psi(1S) K^+)$	$(1.8 \pm 3.0) \times 10^{-3} (S = 1.5)$	$A_{CP}(B^+ \rightarrow K_S^0 \pi^+)$	-0.017 ± 0.016
$A_{CP}(B^+ \rightarrow J/\psi(1S) \pi^+)$	$(1.8 \pm 1.2) \times 10^{-2} (S = 1.3)$	$A_{CP}(B^+ \rightarrow K^+ \pi^0)$	0.037 ± 0.021
$A_{CP}(B^+ \rightarrow J/\psi \rho^+)$	-0.05 ± 0.05	$A_{CP}(B^+ \rightarrow \eta' K^+)$	0.004 ± 0.011
$A_{CP}(B^+ \rightarrow J/\psi K^*(892)^+)$	-0.048 ± 0.033	$A_{CP}(B^+ \rightarrow \eta' K^*(892)^+)$	-0.26 ± 0.27
$A_{CP}(B^+ \rightarrow \eta_c K^+)$	$0.01 \pm 0.07 (S = 2.2)$	$A_{CP}(B^+ \rightarrow \eta' K_S^0(1430)^+)$	0.06 ± 0.20
$A_{CP}(B^+ \rightarrow \psi(2S) \pi^+)$	0.03 ± 0.06	$A_{CP}(B^+ \rightarrow \eta' K_2^*(1430)^+)$	0.15 ± 0.13
$A_{CP}(B^+ \rightarrow \psi(2S) K^+)$	$0.012 \pm 0.020 (S = 1.5)$	$A_{CP}(B^+ \rightarrow \eta K^*(892)^+)$	0.02 ± 0.06
$A_{CP}(B^+ \rightarrow \psi(2S) K^*(892)^+)$	0.08 ± 0.21	$A_{CP}(B^+ \rightarrow \eta K_0^*(1430)^+)$	0.05 ± 0.13
$A_{CP}(B^+ \rightarrow \chi_{c1}(1P) \pi^+)$	0.07 ± 0.18	$A_{CP}(B^+ \rightarrow \eta K_2^*(1430)^+)$	-0.45 ± 0.30
$A_{CP}(B^+ \rightarrow \chi_{c0} K^+)$	$-0.20 \pm 0.18 (S = 1.5)$	$A_{CP}(B^+ \rightarrow \omega K^+)$	-0.02 ± 0.04
$A_{CP}(B^+ \rightarrow \chi_{c1} K^+)$	-0.009 ± 0.033	$A_{CP}(B^+ \rightarrow \omega K^{*+})$	0.29 ± 0.35
$A_{CP}(B^+ \rightarrow \chi_{c1} K^*(892)^+)$	0.5 ± 0.5	$A_{CP}(B^+ \rightarrow \omega(K\pi)_0^{*+})$	-0.10 ± 0.09
$A_{CP}(B^+ \rightarrow \overline{D}^0 \pi^+)$	-0.007 ± 0.007	$A_{CP}(B^+ \rightarrow \omega K_2^*(1430)^+)$	0.14 ± 0.15
$A_{CP}(B^+ \rightarrow D_{CP(+1)} \pi^+)$	-0.0080 ± 0.0026	$A_{CP}(B^+ \rightarrow K^{*0} \pi^+)$	$-0.04 \pm 0.09 (S = 2.1)$
$A_{CP}(B^+ \rightarrow D_{CP(-1)} \pi^+)$	0.017 ± 0.026	$A_{CP}(B^+ \rightarrow K^*(892)^+ \pi^0)$	$-0.39 \pm 0.21 (S = 1.6)$
$A_{CP}([K^{\mp} \pi^{\pm} \pi^+ \pi^-]_D \pi^+)$	0.02 ± 0.05	$A_{CP}(B^+ \rightarrow K^+ \pi^- \pi^+)$	0.027 ± 0.008
$A_{CP}(B^+ \rightarrow [\pi^+ \pi^+ \pi^- \pi^-]_D K^+)$	0.10 ± 0.04	$A_{CP}(B^+ \rightarrow K^+ K^- K^+ \text{ nonresonant})$	0.06 ± 0.05
$A_{CP}(B^+ \rightarrow [\pi^+ \pi^- \pi^+ \pi^-]_D K^*(892)^+)$	0.02 ± 0.11	$A_{CP}(B^+ \rightarrow f(980)^0 K^+)$	-0.08 ± 0.09
$A_{CP}(B^+ \rightarrow \overline{D}^0 K^+)$	-0.017 ± 0.005	$A_{CP}(B^+ \rightarrow f_0(1500) K^+)$	0.28 ± 0.30
$A_{CP}([K^{\mp} \pi^{\pm} \pi^+ \pi^-]_D K^+)$	-0.31 ± 0.11	$A_{CP}(B^+ \rightarrow f'_2(1525)^0 K^+)$	$-0.08^{+0.05}_{-0.04}$
$A_{CP}(B^+ \rightarrow [\pi^+ \pi^+ \pi^- \pi^-]_D \pi^+)$	$(-4 \pm 8) \times 10^{-3}$	$A_{CP}(B^+ \rightarrow K_0^*(1430)^0 \pi^+)$	0.061 ± 0.032
$A_{CP}(B^+ \rightarrow [K^- \pi^+]_D K^+)$	-0.58 ± 0.21	$A_{CP}(B^+ \rightarrow K_0^*(1430)^+ \pi^0)$	$0.26^{+0.18}_{-0.14}$
$A_{CP}(B^+ \rightarrow [K^- \pi^+ \pi^0]_D K^+)$	$0.07 \pm 0.30 (S = 1.5)$	$A_{CP}(B^+ \rightarrow K_2^*(1430)^0 \pi^+)$	$0.05^{+0.29}_{-0.24}$
$A_{CP}(B^+ \rightarrow [K^+ K^- \pi^0]_D K^+)$	0.30 ± 0.20	$A_{CP}(B^+ \rightarrow K^+ \pi^0 \pi^0)$	-0.06 ± 0.07
$A_{CP}(B^+ \rightarrow [\pi^+ \pi^- \pi^0]_D K^+)$	0.05 ± 0.09	$A_{CP}(B^+ \rightarrow K^0 \rho^+)$	-0.03 ± 0.15
$A_{CP}(B^+ \rightarrow \overline{D}^0 K^*(892)^+)$	-0.007 ± 0.019	$A_{CP}(B^+ \rightarrow K^{*+} \pi^+ \pi^-)$	0.07 ± 0.08
$A_{CP}(B^+ \rightarrow [K^- \pi^+ \pi^- \pi^+]_D K^*(892)^+)$	-0.45 ± 0.25	$A_{CP}(B^+ \rightarrow \rho^0 K^*(892)^+)$	0.31 ± 0.13
$A_{CP}(B^+ \rightarrow [K^- \pi^+]_D \pi^+)$	0.00 ± 0.09	$A_{CP}(B^+ \rightarrow K^*(892)^+ f_0(980))$	-0.15 ± 0.12
$A_{CP}(B^+ \rightarrow [K^- \pi^+ \pi^0]_D \pi^+)$	0.35 ± 0.16	$A_{CP}(B^+ \rightarrow a_1^+ K^0)$	0.12 ± 0.11
$A_{CP}(B^+ \rightarrow [K^+ K^- \pi^0]_D \pi^+)$	-0.03 ± 0.04	$A_{CP}(B^+ \rightarrow b_1^+ K^0)$	-0.03 ± 0.15
$A_{CP}(B^+ \rightarrow [\pi^+ \pi^- \pi^0]_D \pi^+)$	-0.016 ± 0.020	$A_{CP}(B^+ \rightarrow K^*(892)^0 \rho^+)$	-0.01 ± 0.16
$A_{CP}(B^+ \rightarrow [K^- \pi^+]_D \pi^+)$	-0.09 ± 0.27	$A_{CP}(B^+ \rightarrow b_0^0 K^+)$	-0.46 ± 0.20
$A_{CP}(B^+ \rightarrow [K^- \pi^+]_D \gamma \pi^+)$	-0.7 ± 0.6	$A_{CP}(B^+ \rightarrow K^0 K^+)$	0.04 ± 0.14
$A_{CP}(B^+ \rightarrow [K^- \pi^+]_D \pi) K^+)$	0.8 ± 0.4	$A_{CP}(B^+ \rightarrow K^+ K_S^0 K_S^0)$	0.025 ± 0.031
$A_{CP}(B^+ \rightarrow [K^- \pi^+]_D \gamma) K^+)$	0.4 ± 1.0	$A_{CP}(B^+ \rightarrow \phi K^+)$	$0.024 \pm 0.028 (S = 2.3)$
$A_{CP}(B^+ \rightarrow [\pi^+ \pi^- \pi^0]_D K^+)$	-0.02 ± 0.15	$A_{CP}(B^+ \rightarrow X_0(1550) K^+)$	-0.04 ± 0.07
$A_{CP}(B^+ \rightarrow [K_S^0 K^+ \pi^-]_D K^+)$	0.04 ± 0.09	$A_{CP}(B^+ \rightarrow K^{*+} K^+ K^-)$	0.11 ± 0.09
$A_{CP}(B^+ \rightarrow [K_S^0 K^- \pi^+]_D K^+)$	0.23 ± 0.13	$A_{CP}(B^+ \rightarrow \phi K^*(892)^+)$	-0.01 ± 0.08
$A_{CP}(B^+ \rightarrow [K_S^0 K^- \pi^+]_D \pi^+)$	-0.052 ± 0.034	$A_{CP}(B^+ \rightarrow \phi(K\pi)_0^{*+})$	0.04 ± 0.16
$A_{CP}(B^+ \rightarrow [K_S^0 K^+ \pi^-]_D \pi^+)$	-0.025 ± 0.026	$A_{CP}(B^+ \rightarrow \phi K_1(1270)^+)$	0.15 ± 0.20
$A_{CP}(B^+ \rightarrow [K^*(892)^- K^+]_D K^+)$	0.03 ± 0.11	$A_{CP}(B^+ \rightarrow \phi K_2^*(1430)^+)$	-0.23 ± 0.20
$A_{CP}(B^+ \rightarrow [K^*(892)^+ K^-]_D K^+)$	0.34 ± 0.21	$A_{CP}(B^+ \rightarrow K^+ \phi \phi)$	-0.10 ± 0.08
$A_{CP}(B^+ \rightarrow [K^*(892)^+ K^-]_D \pi^+)$	-0.05 ± 0.05	$A_{CP}(B^+ \rightarrow K^+[\phi \phi]_{\eta_c})$	0.09 ± 0.10
$A_{CP}(B^+ \rightarrow [K^*(892)^- K^+]_D \pi^+)$	-0.012 ± 0.030	$A_{CP}(B^+ \rightarrow K^*(892)^+ \gamma)$	0.014 ± 0.018
$A_{ADS}(B^+ \rightarrow D \pi^+)$	0.100 ± 0.032	$A_{CP}(B^+ \rightarrow X_S \gamma)$	0.028 ± 0.019
$A_{ADS}(B^+ \rightarrow [K^- \pi^+]_D K^+ \pi^- \pi^+)$	-0.33 ± 0.35	$A_{CP}(B^+ \rightarrow \eta K^+ \gamma)$	-0.12 ± 0.07
$A_{ADS}(B^+ \rightarrow [K^- \pi^+]_D \pi^+ \pi^- \pi^+)$	-0.01 ± 0.09	$A_{CP}(B^+ \rightarrow \phi K^+ \gamma)$	$-0.13 \pm 0.11 (S = 1.1)$
$A_{CP}(B^+ \rightarrow D_{CP(-1)} K^+)$	-0.10 ± 0.07	$A_{CP}(B^+ \rightarrow \rho^+ \gamma)$	-0.11 ± 0.33
$A_{CP}(B^+ \rightarrow [K^+ K^-]_D K^+ \pi^- \pi^+)$	-0.04 ± 0.06	$A_{CP}(B^+ \rightarrow \pi^+ \pi^0)$	0.03 ± 0.04
$A_{CP}(B^+ \rightarrow [\pi^+ \pi^-]_D K^+ \pi^- \pi^+)$	-0.05 ± 0.10	$A_{CP}(B^+ \rightarrow \rho^0 \pi^+)$	0.009 ± 0.019
$A_{CP}(B^+ \rightarrow [K^- \pi^+]_D K^+ \pi^- \pi^+)$	0.013 ± 0.023		

Unless otherwise stated, limits are given at the 90% confidence level, while errors are given as ± 1 standard deviation.

Tests of Conservation Laws

$A_{CP}(B^+ \rightarrow \rho^0(1450)\pi^+)$	-0.11 ± 0.05	$A_{CP}(B^0 \rightarrow K^{*0}\ell^+\ell^-)$	-0.05 ± 0.10
$A_{CP}(B^+ \rightarrow \pi^+\pi^-\pi^0 \text{ nonresonant})$	$-0.14^{+0.23}_{-0.16}$	$A_{CP}(B^0 \rightarrow K^{*0}e^+e^-)$	-0.21 ± 0.19
$A_{CP}(B^+ \rightarrow \rho^+\pi^0)$	0.02 ± 0.11	$A_{CP}(B^0 \rightarrow K^{*0}\mu^+\mu^-)$	-0.034 ± 0.024
$A_{CP}(B^+ \rightarrow \rho^+\rho^0)$	-0.05 ± 0.05	$C_{D^*(2010)^-D^+}(B^0 \rightarrow D^*(2010)^-D^+)$	-0.01 ± 0.11
$A_{CP}(B^+ \rightarrow \omega\pi^+)$	-0.04 ± 0.05	$C_{D^*(2010)^+D^-}(B^0 \rightarrow D^*(2010)^+D^-)$	$0.00 \pm 0.13 (S = 1.3)$
$A_{CP}(B^+ \rightarrow \omega\rho^+)$	-0.20 ± 0.09	$C_{D^{*+}D^{*-}}(B^0 \rightarrow D^{*+}D^{*-})$	$0.01 \pm 0.09 (S = 1.6)$
$A_{CP}(B^+ \rightarrow \eta\pi^+)$	$-0.14 \pm 0.07 (S = 1.4)$	$C_+(B^0 \rightarrow D^{*+}D^{*-})$	$0.00 \pm 0.10 (S = 1.6)$
$A_{CP}(B^+ \rightarrow \eta\rho^+)$	0.11 ± 0.11	$C_-(B^0 \rightarrow D^{*+}D^{*-})$	0.19 ± 0.31
$A_{CP}(B^+ \rightarrow \eta'\pi^+)$	0.06 ± 0.16	$S_-(B^0 \rightarrow D^{*+}D^{*-})$	$0.1 \pm 1.6 (S = 3.5)$
$A_{CP}(B^+ \rightarrow \eta'\rho^+)$	0.26 ± 0.17	$C(B^0 \rightarrow D^*(2010)^+D^*(2010)^-K_S^0)$	0.01 ± 0.29
$A_{CP}(B^+ \rightarrow b_1^0\pi^+)$	0.05 ± 0.16	$S(B^0 \rightarrow D^*(2010)^+D^*(2010)^-K_S^0)$	0.1 ± 0.4
$A_{CP}(B^+ \rightarrow p\bar{p}\pi^+)$	0.00 ± 0.04	$C_{D^+D^-}(B^0 \rightarrow D^+D^-)$	$-0.22 \pm 0.24 (S = 2.5)$
$A_{CP}(B^+ \rightarrow p\bar{p}K^+)$	$0.00 \pm 0.04 (S = 2.2)$	$C_{J/\psi(1S)\pi^0}(B^0 \rightarrow J/\psi(1S)\pi^0)$	$0.03 \pm 0.17 (S = 1.5)$
$A_{CP}(B^+ \rightarrow p\bar{p}K^*(892)^+)$	$0.21 \pm 0.16 (S = 1.4)$	$C(B^0 \rightarrow J/\psi(1S)\rho^0)$	-0.06 ± 0.06
$A_{CP}(B^+ \rightarrow p\bar{p}\gamma)$	0.17 ± 0.17	$C_{D_{CP}^{(*)}h^0}(B^0 \rightarrow D_{CP}^{(*)}h^0)$	-0.02 ± 0.08
$A_{CP}(B^+ \rightarrow p\bar{p}\pi^0)$	0.01 ± 0.17	$S_{D_{CP}^{(*)}h^0}(B^0 \rightarrow D_{CP}^{(*)}h^0)$	-0.66 ± 0.12
$A_{CP}(B^+ \rightarrow K^+\ell^+\ell^-)$	-0.02 ± 0.08	$C_{K^0\pi^0}(B^0 \rightarrow K^0\pi^0)$	$0.00 \pm 0.13 (S = 1.4)$
$A_{CP}(B^+ \rightarrow K^+e^+e^-)$	0.14 ± 0.14	$C_{\eta'(958)K_S^0}(B^0 \rightarrow \eta'(958)K_S^0)$	$-0.04 \pm 0.20 (S = 2.5)$
$A_{CP}(B^+ \rightarrow K^+\mu^+\mu^-)$	0.011 ± 0.017	$S_{\eta'(958)K_S^0}(B^0 \rightarrow \eta'(958)K_S^0)$	$0.43 \pm 0.17 (S = 1.5)$
$A_{CP}(B^+ \rightarrow K^{*+}\ell^+\ell^-)$	-0.09 ± 0.14	$C_{\eta'K^0}(B^0 \rightarrow \eta'K^0)$	-0.06 ± 0.04
$A_{CP}(B^+ \rightarrow K^{*+}e^+e^-)$	-0.14 ± 0.23	$C_{\omega K_S^0}(B^0 \rightarrow \omega K_S^0)$	$0.0 \pm 0.4 (S = 3.0)$
$A_{CP}(B^+ \rightarrow K^{*+}\mu^+\mu^-)$	-0.12 ± 0.24	$S_{\omega K_S^0}(B^0 \rightarrow \omega K_S^0)$	0.70 ± 0.21
$\text{Re}(\epsilon_{B^0})/(1+ \epsilon_{B^0} ^2)$	$(-0.5 \pm 0.4) \times 10^{-3}$	$C(B^0 \rightarrow K_S^0\pi^0\pi^0)$	-0.21 ± 0.20
$A_{T/CP}(B^0 \leftrightarrow \bar{B}^0)$	0.005 ± 0.018	$S(B^0 \rightarrow K_S^0\pi^0\pi^0)$	$0.89^{+0.27}_{-0.30}$
$A_{CP}(B^0 \rightarrow D^*(2010)^+D^-)$	0.037 ± 0.034	$C_{\rho^0 K_S^0}(B^0 \rightarrow \rho^0 K_S^0)$	-0.04 ± 0.20
$A_{CP}(B^0 \rightarrow [K^+K^-]_D K^*(892)^0)$	-0.05 ± 0.10	$S_{\rho^0 K_S^0}(B^0 \rightarrow \rho^0 K_S^0)$	$0.50^{+0.17}_{-0.21}$
$A_{CP}(B^0 \rightarrow [K^+\pi^-]_D K^*(892)^0)$	0.047 ± 0.029	$C_{f_0(980)K_S^0}(B^0 \rightarrow f_0(980)K_S^0)$	0.29 ± 0.20
$A_{CP}(B^0 \rightarrow [\pi^+\pi^-]_D K^*(892)^0)$	-0.18 ± 0.14	$S_{f_0(980)K_S^0}(B^0 \rightarrow f_0(980)K_S^0)$	-0.50 ± 0.16
$A_{CP}(B^0 \rightarrow \eta'K^*(892)^0)$	-0.07 ± 0.18	$S_{f_2(1270)K_S^0}(B^0 \rightarrow f_2(1270)K_S^0)$	-0.5 ± 0.5
$A_{CP}(B^0 \rightarrow \eta'K_0^*(1430)^0)$	-0.19 ± 0.17	$C_{f_2(1270)K_S^0}(B^0 \rightarrow f_2(1270)K_S^0)$	0.3 ± 0.4
$A_{CP}(B^0 \rightarrow \eta'K_2^*(1430)^0)$	0.14 ± 0.18	$S_{f_x(1300)K_S^0}(B^0 \rightarrow f_x(1300)K_S^0)$	-0.2 ± 0.5
$A_{CP}(B^0 \rightarrow \eta K_0^*(1430)^0)$	0.06 ± 0.13	$C_{f_x(1300)K_S^0}(B^0 \rightarrow f_x(1300)K_S^0)$	0.13 ± 0.35
$A_{CP}(B^0 \rightarrow \eta K_2^*(1430)^0)$	-0.07 ± 0.19	$S_{K^0\pi^+\pi^-}(B^0 \rightarrow K^0\pi^+\pi^- \text{ nonresonant})$	-0.01 ± 0.33
$A_{CP}(B^0 \rightarrow b_1 K^+)$	-0.07 ± 0.12	$C_{K^0\pi^+\pi^-}(B^0 \rightarrow K^0\pi^+\pi^- \text{ nonresonant})$	0.01 ± 0.26
$A_{CP}(B^0 \rightarrow \omega K^{*0})$	0.45 ± 0.25	$C_{K_S^0 K_S^0}(B^0 \rightarrow K_S^0 K_S^0)$	$0.0 \pm 0.4 (S = 1.4)$
$A_{CP}(B^0 \rightarrow \omega(K\pi)_0^{*0})$	-0.07 ± 0.09	$S_{K_S^0 K_S^0}(B^0 \rightarrow K_S^0 K_S^0)$	-0.8 ± 0.5
$A_{CP}(B^0 \rightarrow \omega K_2^*(1430)^0)$	-0.37 ± 0.17	$C_{K^+K^-K_S^0}(B^0 \rightarrow K^+K^-K_S^0)$	0.06 ± 0.08
$A_{CP}(B^0 \rightarrow K^+\pi^-\pi^0)$	$(0 \pm 6) \times 10^{-2}$	$C_{K^+K^-K_S^0}(B^0 \rightarrow K^+K^-K_S^0 \text{ inclusive})$	0.01 ± 0.09
$A_{CP}(B^0 \rightarrow \rho^-K^+)$	0.20 ± 0.11	$C_{\phi K_S^0}(B^0 \rightarrow \phi K_S^0)$	0.01 ± 0.14
$A_{CP}(B^0 \rightarrow \rho(1450)^-K^+)$	-0.10 ± 0.33	$S_{\phi K_S^0}(B^0 \rightarrow \phi K_S^0)$	0.59 ± 0.14
$A_{CP}(B^0 \rightarrow \rho(1700)^-K^+)$	-0.4 ± 0.6	$C_{K_S K_S K_S}(B^0 \rightarrow K_S K_S K_S)$	-0.23 ± 0.14
$A_{CP}(B^0 \rightarrow K^+\pi^-\pi^0 \text{ nonresonant})$	0.10 ± 0.18	$S_{K_S K_S K_S}(B^0 \rightarrow K_S K_S K_S)$	$-0.5 \pm 0.6 (S = 3.0)$
$A_{CP}(B^0 \rightarrow K^0\pi^+\pi^-)$	-0.01 ± 0.05	$C_{K_S^0\pi^0\gamma}(B^0 \rightarrow K_S^0\pi^0\gamma)$	0.36 ± 0.33
$A_{CP}(B^0 \rightarrow (K\pi)_0^{*+}\pi^-)$	0.02 ± 0.04	$S_{K_S^0\pi^0\gamma}(B^0 \rightarrow K_S^0\pi^0\gamma)$	-0.8 ± 0.6
$A_{CP}(B^0 \rightarrow K_2^*(1430)^+\pi^-)$	-0.29 ± 0.24	$C_{K^*(892)^0\gamma}(B^0 \rightarrow K^*(892)^0\gamma)$	$-0.04 \pm 0.16 (S = 1.2)$
$A_{CP}(B^0 \rightarrow K^*(1680)^+\pi^-)$	-0.07 ± 0.14	$S_{K^*(892)^0\gamma}(B^0 \rightarrow K^*(892)^0\gamma)$	-0.15 ± 0.22
$A_{CP}(B^0 \rightarrow f_0(980)K_S^0)$	0.28 ± 0.31	$C_{\eta K^0\gamma}(B^0 \rightarrow \eta K^0\gamma)$	$0.1 \pm 0.4 (S = 1.4)$
$A_{CP}(B^0 \rightarrow (K\pi)_0^{*0}\pi^0)$	-0.15 ± 0.11	$S_{\eta K^0\gamma}(B^0 \rightarrow \eta K^0\gamma)$	$-0.5 \pm 0.5 (S = 1.2)$
$A_{CP}(B^0 \rightarrow K^{*0}\pi^0)$	-0.15 ± 0.13	$C_{K^0\phi\gamma}(B^0 \rightarrow K^0\phi\gamma)$	-0.3 ± 0.6
$A_{CP}(B^0 \rightarrow K^*(892)^0\pi^+\pi^-)$	0.07 ± 0.05	$S_{K^0\phi\gamma}(B^0 \rightarrow K^0\phi\gamma)$	$0.7^{+0.7}_{-1.1}$
$A_{CP}(B^0 \rightarrow K^*(892)^0\rho^0)$	-0.06 ± 0.09	$C(B^0 \rightarrow K_S^0\rho^0\gamma)$	-0.05 ± 0.19
$A_{CP}(B^0 \rightarrow K^{*0}f_0(980))$	0.07 ± 0.10	$S(B^0 \rightarrow K_S^0\rho^0\gamma)$	-0.04 ± 0.23
$A_{CP}(B^0 \rightarrow K^{*+}\rho^-)$	0.21 ± 0.15	$C(B^0 \rightarrow \rho^0\gamma)$	0.4 ± 0.5
$A_{CP}(B^0 \rightarrow K^*(892)^0 K^+K^-)$	0.01 ± 0.05	$S(B^0 \rightarrow \rho^0\gamma)$	-0.8 ± 0.7
$A_{CP}(B^0 \rightarrow a_1^- K^+)$	-0.16 ± 0.12	$C_{\pi^0\pi^0}(B^0 \rightarrow \pi^0\pi^0)$	-0.33 ± 0.22
$A_{CP}(B^0 \rightarrow K^0 K^0)$	-0.6 ± 0.7	$C_{\rho\pi}(B^0 \rightarrow \rho^+\pi^-)$	$-0.03 \pm 0.07 (S = 1.2)$
$A_{CP}(B^0 \rightarrow K^*(892)^0\phi)$	0.00 ± 0.04		
$A_{CP}(B^0 \rightarrow K^*(892)^0 K^-\pi^+)$	0.2 ± 0.4		
$A_{CP}(B^0 \rightarrow \phi(K\pi)_0^{*0})$	0.12 ± 0.08		
$A_{CP}(B^0 \rightarrow \phi K_2^*(1430)^0)$	-0.11 ± 0.10		
$A_{CP}(B^0 \rightarrow K^*(892)^0\gamma)$	-0.006 ± 0.011		
$A_{CP}(B^0 \rightarrow K_2^*(1430)^0\gamma)$	-0.08 ± 0.15		
$A_{CP}(B^0 \rightarrow X_S\gamma)$	-0.009 ± 0.018		
$A_{CP}(B^0 \rightarrow \rho^+\pi^-)$	$0.13 \pm 0.06 (S = 1.1)$		
$A_{CP}(B^0 \rightarrow \rho^-\pi^+)$	-0.08 ± 0.08		
$A_{CP}(B^0 \rightarrow a_1(1260)\pi^+\pi^-)$	-0.07 ± 0.06		
$A_{CP}(B^0 \rightarrow b_1^-\pi^+)$	-0.05 ± 0.10		
$A_{CP}(B^0 \rightarrow p\bar{p}K^*(892)^0)$	0.05 ± 0.12		
$A_{CP}(B^0 \rightarrow p\bar{p}\pi^-)$	0.04 ± 0.07		

Tests of Conservation Laws

$S_{\rho\pi}(B^0 \rightarrow \rho^+\pi^-)$	0.05 ± 0.07	$A_{CP}^1(B_S \rightarrow J/\psi \bar{K}^*(892)^0)$	-0.05 ± 0.10
$\Delta S_{\rho\pi}(B^0 \rightarrow \rho^+\pi^-)$	0.01 ± 0.08	$A_{CP}(B_S^0 \rightarrow [K^+K^-]_D \bar{K}^*(892)^0)$	-0.04 ± 0.07
$C_{\rho^0\pi^0}(B^0 \rightarrow \rho^0\pi^0)$	0.27 ± 0.24	$A_{CP}(B_S^0 \rightarrow [\pi^+K^-]_D K^*(892)^0)$	-0.01 ± 0.04
$S_{\rho^0\pi^0}(B^0 \rightarrow \rho^0\pi^0)$	-0.23 ± 0.34	$A_{CP}(B_S^0 \rightarrow [\pi^+\pi^-]_D K^*(892)^0)$	0.06 ± 0.13
$C_{a_1\pi}(B^0 \rightarrow a_1(1260)^+\pi^-)$	-0.05 ± 0.11	$\Gamma(\eta_C(1S) \rightarrow \pi^+\pi^-)/\Gamma_{\text{total}}$	$<1.1 \times 10^{-4}$, CL = 90%
$S_{a_1\pi}(B^0 \rightarrow a_1(1260)^+\pi^-)$	-0.2 ± 0.4 (S = 3.2)	$\Gamma(\eta_C(1S) \rightarrow \pi^0\pi^0)/\Gamma_{\text{total}}$	$<4 \times 10^{-5}$, CL = 90%
$\Delta C_{a_1\pi}(B^0 \rightarrow a_1(1260)^+\pi^-)$	0.43 ± 0.14 (S = 1.3)	$\Gamma(\eta_C(1S) \rightarrow K^+K^-)/\Gamma_{\text{total}}$	$<6 \times 10^{-4}$, CL = 90%
$\Delta S_{a_1\pi}(B^0 \rightarrow a_1(1260)^+\pi^-)$	-0.11 ± 0.12	$\Gamma(\eta_C(1S) \rightarrow K_S^0 K_S^0)/\Gamma_{\text{total}}$	$<3.1 \times 10^{-4}$, CL = 90%
$C(B^0 \rightarrow b_1^- K^+)$	-0.22 ± 0.24	n electric dipole moment	$<0.18 \times 10^{-25}$ ecm, CL = 90%
$\Delta C(B^0 \rightarrow b_1^- \pi^+)$	-1.04 ± 0.24	$(\alpha + \bar{\alpha})/(\alpha - \bar{\alpha})$ in $\Lambda \rightarrow p\pi^-, \bar{\Lambda} \rightarrow \bar{p}\pi^+$	-0.002 ± 0.012
$C_{\rho^0\rho^0}(B^0 \rightarrow \rho^0\rho^0)$	0.2 ± 0.9	$[\alpha(\Xi^-)\alpha_-(\Lambda) - \alpha(\Xi^+)\alpha_+(\Lambda)]$	$(0 \pm 7) \times 10^{-4}$
$S_{\rho^0\rho^0}(B^0 \rightarrow \rho^0\rho^0)$	0.3 ± 0.7	$[\alpha(\Xi^-)\alpha_-(\Lambda) + \alpha(\Xi^+)\alpha_+(\Lambda)]$	
$C_{\rho\rho}(B^0 \rightarrow \rho^+\rho^-)$	0.00 ± 0.09	$(\alpha + \bar{\alpha})/(\alpha - \bar{\alpha})$ in $\Omega^- \rightarrow \Lambda K^-, \bar{\Omega}^+ \rightarrow \bar{\Lambda} K^+$	-0.02 ± 0.13
$S_{\rho\rho}(B^0 \rightarrow \rho^+\rho^-)$	-0.14 ± 0.13	$(\alpha + \bar{\alpha})/(\alpha - \bar{\alpha})$ in $\Lambda_C^+ \rightarrow \Lambda\pi^+, \bar{\Lambda}_C^- \rightarrow \bar{\Lambda}\pi^-$	-0.07 ± 0.31
$ \lambda (B^0 \rightarrow J/\psi K^*(892)^0)$	<0.25 , CL = 95%	$(\alpha + \bar{\alpha})/(\alpha - \bar{\alpha})$ in $\Lambda_C^+ \rightarrow \Lambda e^+ \nu_e, \bar{\Lambda}_C^- \rightarrow \bar{\Lambda} e^- \bar{\nu}_e$	0.00 ± 0.04
$\cos 2\beta(B^0 \rightarrow J/\psi K^*(892)^0)$	$1.7_{-0.9}^{+0.7}$ (S = 1.6)	$A_{CP}(\Lambda_b \rightarrow p\pi^-)$	-0.025 ± 0.029 (S = 1.2)
$\cos 2\beta(B^0 \rightarrow [K_S^0 \pi^+ \pi^-]_{D^{(*)}} h^0)$	0.91 ± 0.25	$A_{CP}(\Lambda_b \rightarrow pK^-)$	-0.025 ± 0.022
$(S_+ + S_-)/2(B^0 \rightarrow D^{*-}\pi^+)$	-0.039 ± 0.011	$\Delta A_{CP}(pK^-/\pi^-)$	0.014 ± 0.024
$(S_- - S_+)/2(B^0 \rightarrow D^{*-}\pi^+)$	-0.009 ± 0.015	$A_{CP}(\Lambda_b \rightarrow p\bar{K}^0\pi^-)$	0.22 ± 0.13
$(S_+ + S_-)/2(B^0 \rightarrow D^-\pi^+)$	-0.046 ± 0.023	$\Delta A_{CP}(J/\psi p\pi^-/K^-)$	$(5.7 \pm 2.7) \times 10^{-2}$
$(S_- - S_+)/2(B^0 \rightarrow D^-\pi^+)$	-0.022 ± 0.021	$A_{CP}(\Lambda_b \rightarrow \Lambda K^+\pi^-)$	-0.53 ± 0.25
$S_+(B^0 \rightarrow D^-\pi^+)$	0.058 ± 0.023	$A_{CP}(\Lambda_b \rightarrow \Lambda K^+K^-)$	-0.28 ± 0.12
$S_-(B^0 \rightarrow D^+\pi^-)$	0.038 ± 0.021	$\Delta A_{CP}(\Lambda_b^0 \rightarrow pK^-\mu^+\mu^-)$	$(-4 \pm 5) \times 10^{-2}$
$(S_+ + S_-)/2(B^0 \rightarrow D^-\rho^+)$	-0.024 ± 0.032	$A_c(\Lambda)$	-0.22 ± 0.13
$(S_- - S_+)/2(B^0 \rightarrow D^-\rho^+)$	-0.10 ± 0.06	$A_s(\Lambda)$	0.13 ± 0.13
$C_{\eta_C K_S^0}(B^0 \rightarrow \eta_C K_S^0)$	0.08 ± 0.13	$A_c(\phi)$	-0.01 ± 0.12
$C_{c\bar{c}K^{(*)0}}(B^0 \rightarrow c\bar{c}K^{(*)0})$	$(0.5 \pm 1.7) \times 10^{-2}$	$A_s(\phi)$	-0.07 ± 0.12
$C_{J/\psi(nS)K^0}(B^0 \rightarrow J/\psi(nS)K^0)$	$(0.5 \pm 2.0) \times 10^{-2}$	$a_{CP}(\Lambda_b^0 \rightarrow p\pi^-\pi^+\pi^-)$	$(1.1 \pm 1.5)\%$
$C_{J/\psi K^{*0}}(B^0 \rightarrow J/\psi K^{*0})$	0.03 ± 0.10	$a_{CP}(\Lambda_b^0 \rightarrow pK^-\pi^+\pi^-)$	$(-0.8 \pm 0.9)\%$
$S_{J/\psi K^{*0}}(B^0 \rightarrow J/\psi K^{*0})$	0.60 ± 0.25	$a_{CP}(\Lambda_b^0 \rightarrow pK^+K^+\pi^-)$	$(-1 \pm 5)\%$
$C_{\chi_{c0} K_S^0}(B^0 \rightarrow \chi_{c0} K_S^0)$	$-0.3_{-0.4}^{+0.5}$	$a_{CP}(\Lambda_b^0 \rightarrow pK^-K^+K^-)$	$(1.1 \pm 1.5)\%$
$S_{\chi_{c0} K_S^0}(B^0 \rightarrow \chi_{c0} K_S^0)$	-0.7 ± 0.5	$a_{CP}(\Lambda_b^0 \rightarrow pK^-\mu^+\mu^-)$	$(1 \pm 5)\%$
$C_{\chi_{c1} K_S^0}(B^0 \rightarrow \chi_{c1} K_S^0)$	0.06 ± 0.07	$a_{CP}(\Xi_b^0 \rightarrow pK^-K^-\pi^+)$	$(-4 \pm 5)\%$
$\sin(2\beta_{\text{eff}})(B^0 \rightarrow \phi K^0)$	0.22 ± 0.30	CP VIOLATION OBSERVED	
$\sin(2\beta_{\text{eff}})(B^0 \rightarrow \phi K_0^*(1430)^0)$	$0.97_{-0.52}^{+0.03}$	$\text{Re}(\epsilon)$	$(1.596 \pm 0.013) \times 10^{-3}$
$\sin(2\beta_{\text{eff}})(B^0 \rightarrow [K_S^0 \pi^+ \pi^-]_{D^{(*)}} h^0)$	0.80 ± 0.16	charge asymmetry in K_{L3}^0 decays	
$ \lambda (B^0 \rightarrow [K_S^0 \pi^+ \pi^-]_{D^{(*)}} h^0)$	1.01 ± 0.08	$A_L(\mu) = \text{weighted average of } A_L(\mu) \text{ and } A_L(e)$	$(0.332 \pm 0.006)\%$
$ \sin(2\beta + \gamma) $	>0.40 , CL = 90%	$A_L(\mu) = [\Gamma(\pi^-\mu^+\nu_\mu) - \Gamma(\pi^+\mu^-\bar{\nu}_\mu)]/\text{sum}$	$(0.304 \pm 0.025)\%$
$2\beta + \gamma$	$(83 \pm 60)^\circ$	$A_L(e) = [\Gamma(\pi^-e^+\nu_e) - \Gamma(\pi^+e^-\bar{\nu}_e)]/\text{sum}$	$(0.334 \pm 0.007)\%$
$x_+(B^0 \rightarrow D K^{*0})$	0.04 ± 0.17	parameters for $K_L^0 \rightarrow 2\pi$ decay	
$x_-(B^0 \rightarrow D K^{*0})$	-0.16 ± 0.14	$ \eta_{00} = A(K_L^0 \rightarrow 2\pi^0) / A(K_S^0 \rightarrow 2\pi^0) $	$(2.220 \pm 0.011) \times 10^{-3}$ (S = 1.8)
$y_-(B^0 \rightarrow D K^{*0})$	0.20 ± 0.25 (S = 1.2)	$ \eta_{+-} = A(K_L^0 \rightarrow \pi^+\pi^-) / A(K_S^0 \rightarrow \pi^+\pi^-) $	$(2.232 \pm 0.011) \times 10^{-3}$ (S = 1.8)
$A_{CP}(B \rightarrow K^*(892)\gamma)$	-0.003 ± 0.011	$ \epsilon = (2 \eta_{+-} + \eta_{00})/3$	$(2.228 \pm 0.011) \times 10^{-3}$ (S = 1.8)
$A_{CP}(B \rightarrow s\gamma)$	0.015 ± 0.011	$ \eta_{00}/\eta_{+-} $	[i] 0.9950 ± 0.0007 (S = 1.6)
$A_{CP}(B \rightarrow (s+d)\gamma)$	0.010 ± 0.031	$\text{Re}(\epsilon'/\epsilon) = (1 - \eta_{00}/\eta_{+-})/3$	[j] $(1.66 \pm 0.23) \times 10^{-3}$ (S = 1.6)
$A_{CP}(B \rightarrow X_S \ell^+ \ell^-)$	0.04 ± 0.11	Assuming CPT	
$A_{CP}(B \rightarrow K^*e^+e^-)$	-0.18 ± 0.15	ϕ_{+-} , phase of η_{+-}	$(43.51 \pm 0.05)^\circ$ (S = 1.2)
$A_{CP}(B \rightarrow K^*\mu^+\mu^-)$	-0.03 ± 0.13	ϕ_{00} , phase of η_{00}	$(43.52 \pm 0.05)^\circ$ (S = 1.3)
$A_{CP}(B \rightarrow K^*\ell^+\ell^-)$	-0.04 ± 0.07	$\phi_\epsilon = (2\phi_{+-} + \phi_{00})/3$	$(43.52 \pm 0.05)^\circ$ (S = 1.2)
$A_{CP}(B \rightarrow \eta \text{ anything})$	$-0.13_{-0.05}^{+0.04}$	Not assuming CPT	
$\Delta A_{CP}(X_S\gamma) = A_{CP}(B^\pm \rightarrow X_S\gamma) - A_{CP}(B^0 \rightarrow X_S\gamma)$	0.041 ± 0.023	ϕ_{+-} , phase of η_{+-}	$(43.4 \pm 0.5)^\circ$ (S = 1.2)
$\bar{A}_{CP}(B \rightarrow X_S\gamma) = (A_{CP}(B^+ \rightarrow X_S\gamma) + A_{CP}(B^0 \rightarrow X_S\gamma))/2$	0.009 ± 0.012	ϕ_{00} , phase of η_{00}	$(43.7 \pm 0.6)^\circ$ (S = 1.2)
$\bar{A}_{CP}(B \rightarrow K^*\gamma) = (A_{CP}(B^+ \rightarrow K^*\gamma) + A_{CP}(B^0 \rightarrow K^*\gamma))/2$	-0.001 ± 0.014	$\phi_\epsilon = (2\phi_{+-} + \phi_{00})/3$	$(43.5 \pm 0.5)^\circ$ (S = 1.3)
$\text{Re}(\epsilon_{B_S^0}) / (1 + \epsilon_{B_S^0} ^2)$	$(-0.15 \pm 0.70) \times 10^{-3}$	CP asymmetry A in $K_L^0 \rightarrow \pi^+\pi^-e^+e^-$	$(13.7 \pm 1.5)\%$
$C_{KK}(B_S^0 \rightarrow K^+K^-)$	0.14 ± 0.11	β_{CP} from $K_L^0 \rightarrow e^+e^-e^+e^-$	-0.19 ± 0.07
$S_{KK}(B_S^0 \rightarrow K^+K^-)$	0.30 ± 0.13	γ_{CP} from $K_L^0 \rightarrow e^+e^-e^+e^-$	0.01 ± 0.11 (S = 1.6)
$r_B(B_S^0 \rightarrow D_S^\mp K^\pm)$	$0.37_{-0.09}^{+0.10}$	parameters for $K_L^0 \rightarrow \pi^+\pi^-\gamma$ decay	
$\delta_B(B_S^0 \rightarrow D_S^\pm K^\mp)$	$(358 \pm 14)^\circ$	$ \eta_{+-\gamma} = A(K_L^0 \rightarrow \pi^+\pi^-\gamma, CP \text{ violating}) / A(K_S^0 \rightarrow \pi^+\pi^-\gamma) $	$(2.35 \pm 0.07) \times 10^{-3}$
CP Violation phase β_s	$(2.55 \pm 1.15) \times 10^{-2}$ rad	$\phi_{+-\gamma} = \text{phase of } \eta_{+-\gamma}$	$(44 \pm 4)^\circ$
$A_{CP}^1(B_S \rightarrow J/\psi \bar{K}^*(892)^0)$	-0.05 ± 0.06		
$A_{CP}^1(B_S \rightarrow J/\psi \bar{K}^*(892)^0)$	0.17 ± 0.15		

Unless otherwise stated, limits are given at the 90% confidence level, while errors are given as ± 1 standard deviation.

Tests of Conservation Laws

$\Gamma(K_L^0 \rightarrow \pi^+ \pi^-) / \Gamma_{\text{total}}$	[j] $(1.967 \pm 0.010) \times 10^{-3}$ (S = 1.5)	$(m_{K^+} - m_{K^-}) / m_{\text{average}}$	$(-0.6 \pm 1.8) \times 10^{-4}$
$\Gamma(K_L^0 \rightarrow \pi^0 \pi^0) / \Gamma_{\text{total}}$	$(8.64 \pm 0.06) \times 10^{-4}$ (S = 1.8)	$(\tau_{K^+} - \tau_{K^-}) / \tau_{\text{average}}$	$(0.10 \pm 0.09)\%$ (S = 1.2)
$\Delta A_{CP}^{D^0} = A_{CP}(K^+ K^-) - A_{CP}(\pi^+ \pi^-)$	$(-0.154 \pm 0.029)\%$	$K^{\pm} \rightarrow \mu^{\pm} \nu_{\mu}$ rate difference/sum	$(-0.27 \pm 0.21)\%$
$A_{CP}(B^+ \rightarrow [K^- \pi^+]_{\overline{D}} K^*(892)^+)$	-0.75 ± 0.16	$K^{\pm} \rightarrow \pi^{\pm} \pi^0$ rate difference/sum	[k] $(0.4 \pm 0.6)\%$
$A_{CP}(B^+ \rightarrow D_{CP(+1)} K^+)$	0.120 ± 0.014 (S = 1.4)	δ in $K^0 - \overline{K}^0$ mixing	
$A_{ADS}(B^+ \rightarrow D K^+)$	-0.40 ± 0.06	real part of δ	$(2.5 \pm 2.3) \times 10^{-4}$
$A_{CP}(B^+ \rightarrow \eta K^+)$	-0.37 ± 0.08	imaginary part of δ	$(-1.5 \pm 1.6) \times 10^{-5}$
$A_{CP}(B^+ \rightarrow f_2(1270) K^+)$	$-0.68^{+0.19}_{-0.17}$	Re(y), K_{e3} parameter	$(0.4 \pm 2.5) \times 10^{-3}$
$A_{CP}(B^+ \rightarrow \rho^0 K^+)$	0.37 ± 0.10	Re(x ₋), K_{e3} parameter	$(-2.9 \pm 2.0) \times 10^{-3}$
$A_{CP}(B^+ \rightarrow K^+ K^- \pi^+)$	-0.122 ± 0.021	$ m_{K^0} - m_{\overline{K}^0} / m_{\text{average}}$	[l] $< 6 \times 10^{-19}$, CL = 90%
$A_{CP}(B^+ \rightarrow K^+ K^- K^+)$	-0.033 ± 0.008	$(\Gamma_{K^0} - \Gamma_{\overline{K}^0}) / m_{\text{average}}$	$(8 \pm 8) \times 10^{-18}$
$A_{CP}(B^+ \rightarrow \pi^+ \pi^- \pi^+)$	0.057 ± 0.013	phase difference $\phi_{00} - \phi_{+-}$	$(0.34 \pm 0.32)^\circ$
$A_{CP}(B^+ \rightarrow f_2(1270) \pi^+)$	0.40 ± 0.06	$\text{Re}(\frac{2}{3}\eta_{+-} + \frac{1}{3}\eta_{00}) - \frac{A_{\mu}}{A_{\pi}}$	$(-3 \pm 35) \times 10^{-6}$
$A_{CP}(B^+ \rightarrow f_0(1370) \pi^+)$	0.72 ± 0.22	$A_{CPT}(D^0 \rightarrow K^- \pi^+)$	0.008 ± 0.008
γ	$(71.1^{+4.6}_{-5.3})^\circ$	$\Delta S_{CPT}^+(S_{\ell^+, K_S^0}^- - S_{\ell^+, K_S^0}^+)$	0.16 ± 0.23
$r_B(B^+ \rightarrow D^0 K^+)$	0.0993 ± 0.0046	$\Delta S_{CPT}^-(S_{\ell^+, K_S^0}^+ - S_{\ell^+, K_S^0}^-)$	-0.03 ± 0.14
$\delta_B(B^+ \rightarrow D^0 K^+)$	$(129.6^{+5.0}_{-6.0})^\circ$	$\Delta C_{CPT}^+(C_{\ell^+, K_S^0}^- - C_{\ell^+, K_S^0}^+)$	0.14 ± 0.17
$r_B(B^+ \rightarrow D^0 K^{*+})$	0.076 ± 0.020	$\Delta C_{CPT}^-(C_{\ell^+, K_S^0}^+ - C_{\ell^+, K_S^0}^-)$	0.03 ± 0.14
$\delta_B(B^+ \rightarrow D^0 K^{*+})$	$(98^{+18}_{-37})^\circ$		
$r_B(B^+ \rightarrow D^{*0} K^+)$	0.140 ± 0.019	$ m_{\rho^-} - m_{\overline{\rho}^-} / m_{\rho}$	[n] $< 7 \times 10^{-10}$, CL = 90%
$\delta_B(B^+ \rightarrow D^{*0} K^+)$	$(319.2^{+7.7}_{-8.1})^\circ$	$(\frac{q_{\overline{\rho}^-}}{m_{\overline{\rho}^-}} - \frac{q_{\rho^-}}{m_{\rho^-}}) / \frac{q_{\rho^-}}{m_{\rho^-}}$	$(0.1 \pm 6.9) \times 10^{-11}$
$A_{CP}(B^0 \rightarrow K^+ \pi^-)$	-0.083 ± 0.004	$ q_{\rho^-} + q_{\overline{\rho}^-} / e$	[n] $< 7 \times 10^{-10}$, CL = 90%
$A_{CP}(B^0 \rightarrow \eta K^*(892)^0)$	0.19 ± 0.05	$(\mu_{\rho^-} + \mu_{\overline{\rho}^-}) / \mu_{\rho}$	$(0.002 \pm 0.004) \times 10^{-6}$
$A_{CP}(B^0 \rightarrow K^*(892)^+ \pi^-)$	-0.27 ± 0.04	$(m_{\eta^-} - m_{\overline{\eta}^-}) / m_{\eta}$	$(9 \pm 6) \times 10^{-5}$
$S_{D^*(2010)-D^+}(B^0 \rightarrow D^*(2010)^- D^+)$	-0.72 ± 0.15	$(m_{\Lambda^-} - m_{\overline{\Lambda}^-}) / m_{\Lambda}$	$(-0.1 \pm 1.1) \times 10^{-5}$ (S = 1.6)
$S_{D^*(2010)+D^-}(B^0 \rightarrow D^*(2010)^+ D^-)$	-0.73 ± 0.14	$(\tau_{\Lambda^-} - \tau_{\overline{\Lambda}^-}) / \tau_{\Lambda}$	-0.001 ± 0.009
$S_{D^{*+}D^{*-}}(B^0 \rightarrow D^{*+} D^{*-})$	-0.59 ± 0.14 (S = 1.8)	$(\tau_{\Sigma^+} - \tau_{\overline{\Sigma}^-}) / \tau_{\Sigma^+}$	-0.0006 ± 0.0012
$S_{+}(B^0 \rightarrow D^{*+} D^{*-})$	-0.73 ± 0.09	$(\mu_{\Sigma^+} + \mu_{\overline{\Sigma}^-}) / \mu_{\Sigma^+}$	0.014 ± 0.015
$S_{D^+D^-}(B^0 \rightarrow D^+ D^-)$	$-0.76^{+0.15}_{-0.13}$ (S = 1.2)	$(m_{\Xi^-} - m_{\overline{\Xi}^+}) / m_{\Xi^-}$	$(-3 \pm 9) \times 10^{-5}$
$S_{J/\psi(1S)\pi^0}(B^0 \rightarrow J/\psi(1S)\pi^0)$	-0.88 ± 0.32 (S = 2.2)	$(\tau_{\Xi^-} - \tau_{\overline{\Xi}^+}) / \tau_{\Xi^-}$	-0.01 ± 0.07
$S(B^0 \rightarrow J/\psi(1S)\rho^0)$	$-0.66^{+0.16}_{-0.12}$	$(\mu_{\Xi^-} + \mu_{\overline{\Xi}^+}) / \mu_{\Xi^-} $	$+0.01 \pm 0.05$
$S_{K^0\pi^0}(B^0 \rightarrow K^0\pi^0)$	0.58 ± 0.17	$(m_{\Omega^-} - m_{\overline{\Omega}^+}) / m_{\Omega^-}$	$(-1 \pm 8) \times 10^{-5}$
$S_{\eta'K^0}(B^0 \rightarrow \eta'K^0)$	0.63 ± 0.06	$(\tau_{\Omega^-} - \tau_{\overline{\Omega}^+}) / \tau_{\Omega^-}$	0.00 ± 0.05
$S_{K^+K^-K_S^0}(B^0 \rightarrow K^+K^-K_S^0)$ nonresonant)	-0.66 ± 0.11		
$S_{K^+K^-K_S^0}(B^0 \rightarrow K^+K^-K_S^0)$ inclusive)	-0.65 ± 0.12		
$C_{\pi\pi}(B^0 \rightarrow \pi^+\pi^-)$	-0.32 ± 0.04		
$S_{\pi\pi}(B^0 \rightarrow \pi^+\pi^-)$	-0.65 ± 0.04		
$\Delta C_{\rho\pi}(B^0 \rightarrow \rho^+\pi^-)$	0.27 ± 0.06		
$S_{\eta_c K_S^0}(B^0 \rightarrow \eta_c K_S^0)$	0.93 ± 0.17		
$\sin(2\beta)(B^0 \rightarrow J/\psi K_S^0)$	0.695 ± 0.019		
$S_{J/\psi(nS)K^0}(B^0 \rightarrow J/\psi(nS)K^0)$	0.701 ± 0.017		
$S_{\chi_{c1} K_S^0}(B^0 \rightarrow \chi_{c1} K_S^0)$	0.63 ± 0.10		
$\sin(2\beta_{\text{eff}})(B^0 \rightarrow K^+K^-K_S^0)$	$0.77^{+0.13}_{-0.12}$		
α	$(84.9^{+5.1}_{-4.5})^\circ$		
$r_{B^0}(B^0 \rightarrow D K^{*0})$	$0.220^{+0.041}_{-0.047}$		
$\delta_{B^0}(B^0 \rightarrow D K^{*0})$	$(194^{+30}_{-22})^\circ$		
$A_{CP}(B_S \rightarrow \pi^+ K^-)$	0.221 ± 0.015		

CPT INVARIANCE

$(m_{W^+} - m_{W^-}) / m_{\text{average}}$	$(-3.7 \pm 3.5) \times 10^{-4}$
$(m_{e^+} - m_{e^-}) / m_{\text{average}}$	$< 8 \times 10^{-9}$, CL = 90%
$ q_{e^+} + q_{e^-} / e$	$< 4 \times 10^{-8}$
$(g_{e^+} - g_{e^-}) / g_{\text{average}}$	$(-0.5 \pm 2.1) \times 10^{-12}$
$(\tau_{\mu^+} - \tau_{\mu^-}) / \tau_{\text{average}}$	$(2 \pm 8) \times 10^{-5}$
$(g_{\mu^+} - g_{\mu^-}) / g_{\text{average}}$	$(-0.11 \pm 0.12) \times 10^{-8}$
$(m_{\tau^+} - m_{\tau^-}) / m_{\text{average}}$	$< 2.8 \times 10^{-4}$, CL = 90%
$\langle \Delta m_{21}^2 - \overline{\Delta m}_{21}^2 \rangle$ in neutrino mixing	$< 1.1 \times 10^{-4}$ eV ² , CL = 99.7%
$\langle \Delta m_{32}^2 - \overline{\Delta m}_{32}^2 \rangle$ in neutrino mixing	$(-0.12 \pm 0.25) \times 10^{-3}$ eV ²
$m_t - m_{\overline{t}}$	-0.16 ± 0.19 GeV
$(m_{\pi^+} - m_{\pi^-}) / m_{\text{average}}$	$(2 \pm 5) \times 10^{-4}$
$(\tau_{\pi^+} - \tau_{\pi^-}) / \tau_{\text{average}}$	$(6 \pm 7) \times 10^{-4}$

TESTS OF NUMBER CONSERVATION LAWS

LEPTON FAMILY NUMBER

Lepton family number conservation means separate conservation of each of L_e, L_{μ}, L_{τ} .

$\Gamma(Z \rightarrow e^{\pm} \mu^{\mp}) / \Gamma_{\text{total}}$	[o] $< 7.5 \times 10^{-7}$, CL = 95%
$\Gamma(Z \rightarrow e^{\pm} \tau^{\mp}) / \Gamma_{\text{total}}$	[o] $< 9.8 \times 10^{-6}$, CL = 95%
$\Gamma(Z \rightarrow \mu^{\pm} \tau^{\mp}) / \Gamma_{\text{total}}$	[o] $< 1.2 \times 10^{-5}$, CL = 95%
$\Gamma(H^0 \rightarrow e\mu) / \Gamma_{\text{total}}$	$< 6.1 \times 10^{-5}$, CL = 95%
$\Gamma(H^0 \rightarrow e\tau) / \Gamma_{\text{total}}$	$< 4.7 \times 10^{-3}$, CL = 95%
$\Gamma(H^0 \rightarrow \mu\tau) / \Gamma_{\text{total}}$	$< 2.5 \times 10^{-3}$, CL = 95%
$\sigma(e^+e^- \rightarrow e^{\pm} \tau^{\mp}) / \sigma(e^+e^- \rightarrow \mu^{\pm} \mu^-)$	$< 8.9 \times 10^{-6}$, CL = 95%
$\sigma(e^+e^- \rightarrow \mu^{\pm} \tau^{\mp}) / \sigma(e^+e^- \rightarrow \mu^+ \mu^-)$	$< 4.0 \times 10^{-6}$, CL = 95%
limit on $\mu^- \rightarrow e^-$ conversion	
$\sigma(\mu^- 32S \rightarrow e^- 32S) / \sigma(\mu^- 32S \rightarrow \nu_{\mu} 32P^*)$	$< 7 \times 10^{-11}$, CL = 90%
$\sigma(\mu^- \text{Ti} \rightarrow e^- \text{Ti}) / \sigma(\mu^- \text{Ti} \rightarrow \text{capture})$	$< 4.3 \times 10^{-12}$, CL = 90%
$\sigma(\mu^- \text{Pb} \rightarrow e^- \text{Pb}) / \sigma(\mu^- \text{Pb} \rightarrow \text{capture})$	$< 4.6 \times 10^{-11}$, CL = 90%
$\sigma(\mu^- \text{Au} \rightarrow e^- \text{Au}) / \sigma(\mu^- \text{Au} \rightarrow \text{capture})$	$< 7 \times 10^{-13}$, CL = 90%
limit on muonium \rightarrow antimuonium conversion $R_g = G_C / G_F$	< 0.0030 , CL = 90%
$\Gamma(\mu^- \rightarrow e^- \nu_e \overline{\nu}_{\mu}) / \Gamma_{\text{total}}$	[p] $< 1.2 \times 10^{-2}$, CL = 90%
$\Gamma(\mu^- \rightarrow e^- \gamma) / \Gamma_{\text{total}}$	$< 4.2 \times 10^{-13}$, CL = 90%
$\Gamma(\mu^- \rightarrow e^- e^+ e^-) / \Gamma_{\text{total}}$	$< 1.0 \times 10^{-12}$, CL = 90%
$\Gamma(\mu^- \rightarrow e^- 2\gamma) / \Gamma_{\text{total}}$	$< 7.2 \times 10^{-11}$, CL = 90%

Tests of Conservation Laws

$\Gamma(\tau^- \rightarrow e^- \gamma)/\Gamma_{total}$	$<3.3 \times 10^{-8}$, CL = 90%	$\Gamma(D^+ \rightarrow \pi^+ e^- \mu^+)/\Gamma_{total}$	$<3.6 \times 10^{-6}$, CL = 90%
$\Gamma(\tau^- \rightarrow \mu^- \gamma)/\Gamma_{total}$	$<4.4 \times 10^{-8}$, CL = 90%	$\Gamma(D^+ \rightarrow K^+ e^+ \mu^-)/\Gamma_{total}$	$<1.2 \times 10^{-6}$, CL = 90%
$\Gamma(\tau^- \rightarrow e^- \pi^0)/\Gamma_{total}$	$<8.0 \times 10^{-8}$, CL = 90%	$\Gamma(D^+ \rightarrow K^+ e^- \mu^+)/\Gamma_{total}$	$<2.8 \times 10^{-6}$, CL = 90%
$\Gamma(\tau^- \rightarrow \mu^- \pi^0)/\Gamma_{total}$	$<1.1 \times 10^{-7}$, CL = 90%	$\Gamma(D^0 \rightarrow \mu^\pm e^\mp)/\Gamma_{total}$	[o] $<1.3 \times 10^{-8}$, CL = 90%
$\Gamma(\tau^- \rightarrow e^- K_S^0)/\Gamma_{total}$	$<2.6 \times 10^{-8}$, CL = 90%	$\Gamma(D^0 \rightarrow \pi^0 e^\pm \mu^\mp)/\Gamma_{total}$	[o] $<8.6 \times 10^{-5}$, CL = 90%
$\Gamma(\tau^- \rightarrow \mu^- K_S^0)/\Gamma_{total}$	$<2.3 \times 10^{-8}$, CL = 90%	$\Gamma(D^0 \rightarrow \eta e^\pm \mu^\mp)/\Gamma_{total}$	[o] $<1.0 \times 10^{-4}$, CL = 90%
$\Gamma(\tau^- \rightarrow e^- \eta)/\Gamma_{total}$	$<9.2 \times 10^{-8}$, CL = 90%	$\Gamma(D^0 \rightarrow \pi^+ \pi^- e^\pm \mu^\mp)/\Gamma_{total}$	[o] $<1.5 \times 10^{-5}$, CL = 90%
$\Gamma(\tau^- \rightarrow \mu^- \eta)/\Gamma_{total}$	$<6.5 \times 10^{-8}$, CL = 90%	$\Gamma(D^0 \rightarrow \rho^0 e^\pm \mu^\mp)/\Gamma_{total}$	[o] $<4.9 \times 10^{-5}$, CL = 90%
$\Gamma(\tau^- \rightarrow e^- \rho^0)/\Gamma_{total}$	$<1.8 \times 10^{-8}$, CL = 90%	$\Gamma(D^0 \rightarrow \omega e^\pm \mu^\mp)/\Gamma_{total}$	[o] $<1.2 \times 10^{-4}$, CL = 90%
$\Gamma(\tau^- \rightarrow \mu^- \rho^0)/\Gamma_{total}$	$<1.2 \times 10^{-8}$, CL = 90%	$\Gamma(D^0 \rightarrow K^- K^+ e^\pm \mu^\mp)/\Gamma_{total}$	[o] $<1.8 \times 10^{-4}$, CL = 90%
$\Gamma(\tau^- \rightarrow e^- \omega)/\Gamma_{total}$	$<4.8 \times 10^{-8}$, CL = 90%	$\Gamma(D^0 \rightarrow \phi e^\pm \mu^\mp)/\Gamma_{total}$	[o] $<3.4 \times 10^{-5}$, CL = 90%
$\Gamma(\tau^- \rightarrow \mu^- \omega)/\Gamma_{total}$	$<4.7 \times 10^{-8}$, CL = 90%	$\Gamma(D^0 \rightarrow \bar{K}^0 e^\pm \mu^\mp)/\Gamma_{total}$	[o] $<1.0 \times 10^{-4}$, CL = 90%
$\Gamma(\tau^- \rightarrow e^- K^*(892)^0)/\Gamma_{total}$	$<3.2 \times 10^{-8}$, CL = 90%	$\Gamma(D^0 \rightarrow K^- \pi^+ e^\pm \mu^\mp)/\Gamma_{total}$	[o] $<5.53 \times 10^{-4}$, CL = 90%
$\Gamma(\tau^- \rightarrow \mu^- K^*(892)^0)/\Gamma_{total}$	$<5.9 \times 10^{-8}$, CL = 90%	$\Gamma(D^0 \rightarrow \bar{K}^*(892)^0 e^\pm \mu^\mp)/\Gamma_{total}$	[o] $<8.3 \times 10^{-5}$, CL = 90%
$\Gamma(\tau^- \rightarrow e^- \bar{K}^*(892)^0)/\Gamma_{total}$	$<3.4 \times 10^{-8}$, CL = 90%	$\Gamma(D_S^+ \rightarrow \pi^+ e^+ \mu^-)/\Gamma_{total}$	$<1.2 \times 10^{-5}$, CL = 90%
$\Gamma(\tau^- \rightarrow \mu^- \bar{K}^*(892)^0)/\Gamma_{total}$	$<7.0 \times 10^{-8}$, CL = 90%	$\Gamma(D_S^+ \rightarrow \pi^+ e^- \mu^+)/\Gamma_{total}$	$<2.0 \times 10^{-5}$, CL = 90%
$\Gamma(\tau^- \rightarrow e^- \eta'(958))/\Gamma_{total}$	$<1.6 \times 10^{-7}$, CL = 90%	$\Gamma(D_S^+ \rightarrow K^+ e^+ \mu^-)/\Gamma_{total}$	$<1.4 \times 10^{-5}$, CL = 90%
$\Gamma(\tau^- \rightarrow \mu^- \eta'(958))/\Gamma_{total}$	$<1.3 \times 10^{-7}$, CL = 90%	$\Gamma(D_S^+ \rightarrow K^+ e^- \mu^+)/\Gamma_{total}$	$<9.7 \times 10^{-6}$, CL = 90%
$\Gamma(\tau^- \rightarrow e^- f_0(980) \rightarrow e^- \pi^+ \pi^-)/\Gamma_{total}$	$<3.2 \times 10^{-8}$, CL = 90%	$\Gamma(B^+ \rightarrow \pi^+ e^+ \mu^-)/\Gamma_{total}$	$<6.4 \times 10^{-3}$, CL = 90%
$\Gamma(\tau^- \rightarrow \mu^- f_0(980) \rightarrow \mu^- \pi^+ \pi^-)/\Gamma_{total}$	$<3.4 \times 10^{-8}$, CL = 90%	$\Gamma(B^+ \rightarrow \pi^+ e^- \mu^+)/\Gamma_{total}$	$<6.4 \times 10^{-3}$, CL = 90%
$\Gamma(\tau^- \rightarrow e^- \phi)/\Gamma_{total}$	$<3.1 \times 10^{-8}$, CL = 90%	$\Gamma(B^+ \rightarrow \pi^+ e^\pm \mu^\mp)/\Gamma_{total}$	$<1.7 \times 10^{-7}$, CL = 90%
$\Gamma(\tau^- \rightarrow \mu^- \phi)/\Gamma_{total}$	$<8.4 \times 10^{-8}$, CL = 90%	$\Gamma(B^+ \rightarrow \pi^+ e^\pm \tau^\mp)/\Gamma_{total}$	$<7.4 \times 10^{-5}$, CL = 90%
$\Gamma(\tau^- \rightarrow e^- e^+ e^-)/\Gamma_{total}$	$<2.7 \times 10^{-8}$, CL = 90%	$\Gamma(B^+ \rightarrow \pi^+ e^- \tau^+)/\Gamma_{total}$	$<2.0 \times 10^{-5}$, CL = 90%
$\Gamma(\tau^- \rightarrow e^- \mu^+ \mu^-)/\Gamma_{total}$	$<2.7 \times 10^{-8}$, CL = 90%	$\Gamma(B^+ \rightarrow \pi^+ e^\pm \tau^\mp)/\Gamma_{total}$	$<7.5 \times 10^{-5}$, CL = 90%
$\Gamma(\tau^- \rightarrow e^+ \mu^- \mu^-)/\Gamma_{total}$	$<1.7 \times 10^{-8}$, CL = 90%	$\Gamma(B^+ \rightarrow \pi^+ \mu^+ \tau^-)/\Gamma_{total}$	$<6.2 \times 10^{-5}$, CL = 90%
$\Gamma(\tau^- \rightarrow \mu^- e^+ e^-)/\Gamma_{total}$	$<1.8 \times 10^{-8}$, CL = 90%	$\Gamma(B^+ \rightarrow \pi^+ \mu^- \tau^+)/\Gamma_{total}$	$<4.5 \times 10^{-5}$, CL = 90%
$\Gamma(\tau^- \rightarrow \mu^+ e^- e^-)/\Gamma_{total}$	$<1.5 \times 10^{-8}$, CL = 90%	$\Gamma(B^+ \rightarrow \pi^+ \mu^\pm \tau^\mp)/\Gamma_{total}$	$<7.2 \times 10^{-5}$, CL = 90%
$\Gamma(\tau^- \rightarrow \mu^- \mu^+ \mu^-)/\Gamma_{total}$	$<2.1 \times 10^{-8}$, CL = 90%	$\Gamma(B^+ \rightarrow K^+ e^+ \mu^-)/\Gamma_{total}$	$<7.0 \times 10^{-9}$, CL = 90%
$\Gamma(\tau^- \rightarrow e^- \pi^+ \pi^-)/\Gamma_{total}$	$<2.3 \times 10^{-8}$, CL = 90%	$\Gamma(B^+ \rightarrow K^+ e^- \mu^+)/\Gamma_{total}$	$<6.4 \times 10^{-9}$, CL = 90%
$\Gamma(\tau^- \rightarrow \mu^- \pi^+ \pi^-)/\Gamma_{total}$	$<2.1 \times 10^{-8}$, CL = 90%	$\Gamma(B^+ \rightarrow K^+ e^\pm \mu^\mp)/\Gamma_{total}$	$<9.1 \times 10^{-8}$, CL = 90%
$\Gamma(\tau^- \rightarrow e^- \pi^+ K^-)/\Gamma_{total}$	$<3.7 \times 10^{-8}$, CL = 90%	$\Gamma(B^+ \rightarrow K^+ e^+ \tau^-)/\Gamma_{total}$	$<4.3 \times 10^{-5}$, CL = 90%
$\Gamma(\tau^- \rightarrow e^- \pi^- K^+)/\Gamma_{total}$	$<3.1 \times 10^{-8}$, CL = 90%	$\Gamma(B^+ \rightarrow K^+ e^- \tau^+)/\Gamma_{total}$	$<1.5 \times 10^{-5}$, CL = 90%
$\Gamma(\tau^- \rightarrow e^- K_S^0 K_S^0)/\Gamma_{total}$	$<7.1 \times 10^{-8}$, CL = 90%	$\Gamma(B^+ \rightarrow K^+ e^\pm \tau^\mp)/\Gamma_{total}$	$<3.0 \times 10^{-5}$, CL = 90%
$\Gamma(\tau^- \rightarrow e^- K^+ K^-)/\Gamma_{total}$	$<3.4 \times 10^{-8}$, CL = 90%	$\Gamma(B^+ \rightarrow K^+ \mu^+ \tau^-)/\Gamma_{total}$	$<4.5 \times 10^{-5}$, CL = 90%
$\Gamma(\tau^- \rightarrow \mu^- \pi^+ K^-)/\Gamma_{total}$	$<8.6 \times 10^{-8}$, CL = 90%	$\Gamma(B^+ \rightarrow K^+ \mu^- \tau^+)/\Gamma_{total}$	$<2.8 \times 10^{-5}$, CL = 90%
$\Gamma(\tau^- \rightarrow \mu^- \pi^- K^+)/\Gamma_{total}$	$<4.5 \times 10^{-8}$, CL = 90%	$\Gamma(B^+ \rightarrow K^+ \mu^\pm \tau^\mp)/\Gamma_{total}$	$<4.8 \times 10^{-5}$, CL = 90%
$\Gamma(\tau^- \rightarrow \mu^- K_S^0 K_S^0)/\Gamma_{total}$	$<8.0 \times 10^{-8}$, CL = 90%	$\Gamma(B^+ \rightarrow K^*(892)^+ e^+ \mu^-)/\Gamma_{total}$	$<1.3 \times 10^{-6}$, CL = 90%
$\Gamma(\tau^- \rightarrow \mu^- K^+ K^-)/\Gamma_{total}$	$<4.4 \times 10^{-8}$, CL = 90%	$\Gamma(B^+ \rightarrow K^*(892)^+ e^- \mu^+)/\Gamma_{total}$	$<9.9 \times 10^{-7}$, CL = 90%
$\Gamma(\tau^- \rightarrow e^- \pi^0 \pi^0)/\Gamma_{total}$	$<6.5 \times 10^{-6}$, CL = 90%	$\Gamma(B^+ \rightarrow K^*(892)^+ e^\pm \mu^\mp)/\Gamma_{total}$	$<1.4 \times 10^{-6}$, CL = 90%
$\Gamma(\tau^- \rightarrow \mu^- \pi^0 \pi^0)/\Gamma_{total}$	$<1.4 \times 10^{-5}$, CL = 90%	$\Gamma(B^0 \rightarrow e^\pm \mu^\mp)/\Gamma_{total}$	[o] $<1.0 \times 10^{-9}$, CL = 90%
$\Gamma(\tau^- \rightarrow e^- \eta \eta)/\Gamma_{total}$	$<3.5 \times 10^{-5}$, CL = 90%	$\Gamma(B^0 \rightarrow \pi^0 e^\pm \mu^\mp)/\Gamma_{total}$	$<1.4 \times 10^{-7}$, CL = 90%
$\Gamma(\tau^- \rightarrow \mu^- \eta \eta)/\Gamma_{total}$	$<6.0 \times 10^{-5}$, CL = 90%	$\Gamma(B^0 \rightarrow K^0 e^\pm \mu^\mp)/\Gamma_{total}$	$<2.7 \times 10^{-7}$, CL = 90%
$\Gamma(\tau^- \rightarrow e^- \pi^0 \eta)/\Gamma_{total}$	$<2.4 \times 10^{-5}$, CL = 90%	$\Gamma(B^0 \rightarrow K^*(892)^0 e^+ \mu^-)/\Gamma_{total}$	$<1.6 \times 10^{-7}$, CL = 90%
$\Gamma(\tau^- \rightarrow \mu^- \pi^0 \eta)/\Gamma_{total}$	$<2.2 \times 10^{-5}$, CL = 90%	$\Gamma(B^0 \rightarrow K^*(892)^0 e^- \mu^+)/\Gamma_{total}$	$<1.2 \times 10^{-7}$, CL = 90%
$\Gamma(\tau^- \rightarrow e^- \text{light boson})/\Gamma_{total}$	$<2.7 \times 10^{-3}$, CL = 95%	$\Gamma(B^0 \rightarrow K^*(892)^0 e^\pm \mu^\mp)/\Gamma_{total}$	$<1.8 \times 10^{-7}$, CL = 90%
$\Gamma(\tau^- \rightarrow \mu^- \text{light boson})/\Gamma_{total}$	$<5 \times 10^{-3}$, CL = 95%	$\Gamma(B^0 \rightarrow e^\pm \tau^\mp)/\Gamma_{total}$	[o] $<2.8 \times 10^{-5}$, CL = 90%
LEPTON FAMILY NUMBER VIOLATION IN NEUTRINOS			
$\sin^2(\theta_{12})$	0.307 ± 0.013	$\Gamma(B^0 \rightarrow \mu^\pm \tau^\mp)/\Gamma_{total}$	[o] $<1.4 \times 10^{-5}$, CL = 95%
Δm_{21}^2	$(7.53 \pm 0.18) \times 10^{-5} \text{ eV}^2$	$\Gamma(B \rightarrow s e^\pm \mu^\mp)/\Gamma_{total}$	[o] $<2.2 \times 10^{-5}$, CL = 90%
$\sin^2(\theta_{23})$ (Normal order)	0.545 ± 0.021	$\Gamma(B \rightarrow \pi e^\pm \mu^\mp)/\Gamma_{total}$	$<9.2 \times 10^{-8}$, CL = 90%
Δm_{32}^2 (Inverted order)	$(-2.546 \pm 0.034 - 0.040) \times 10^{-3} \text{ eV}^2$	$\Gamma(B \rightarrow \rho e^\pm \mu^\mp)/\Gamma_{total}$	$<3.2 \times 10^{-6}$, CL = 90%
Δm_{32}^2 (Normal order)	$(2.453 \pm 0.034) \times 10^{-3} \text{ eV}^2$	$\Gamma(B \rightarrow K e^\pm \mu^\mp)/\Gamma_{total}$	$<3.8 \times 10^{-8}$, CL = 90%
$\sin^2(\theta_{13})$	$(2.18 \pm 0.07) \times 10^{-2}$	$\Gamma(B \rightarrow K^*(892) e^\pm \mu^\mp)/\Gamma_{total}$	$<5.1 \times 10^{-7}$, CL = 90%
$\Gamma(\pi^+ \rightarrow \mu^+ \nu_e)/\Gamma_{total}$	[q] $<8.0 \times 10^{-3}$, CL = 90%	$\Gamma(B_S^0 \rightarrow e^\pm \mu^\mp)/\Gamma_{total}$	[o] $<5.4 \times 10^{-9}$, CL = 90%
$\Gamma(\pi^+ \rightarrow \mu^- e^+ e^+ \nu)/\Gamma_{total}$	$<1.6 \times 10^{-6}$, CL = 90%	$\Gamma(J/\psi(1S) \rightarrow e^\pm \mu^\mp)/\Gamma_{total}$	$<1.6 \times 10^{-7}$, CL = 90%
$\Gamma(\pi^0 \rightarrow \mu^+ e^-)/\Gamma_{total}$	$<3.8 \times 10^{-10}$, CL = 90%	$\Gamma(J/\psi(1S) \rightarrow e^\pm \tau^\mp)/\Gamma_{total}$	$<8.3 \times 10^{-6}$, CL = 90%
$\Gamma(\pi^0 \rightarrow \mu^- e^+)/\Gamma_{total}$	$<3.4 \times 10^{-9}$, CL = 90%	$\Gamma(J/\psi(1S) \rightarrow \mu^\pm \tau^\mp)/\Gamma_{total}$	$<2.0 \times 10^{-6}$, CL = 90%
$\Gamma(\pi^0 \rightarrow \mu^+ e^- + \mu^- e^+)/\Gamma_{total}$	$<3.6 \times 10^{-10}$, CL = 90%	$\Gamma(\Upsilon(1S) \rightarrow \mu^\pm \tau^\mp)/\Gamma_{total}$	$<6.0 \times 10^{-6}$, CL = 95%
$\Gamma(\eta \rightarrow \mu^+ e^- + \mu^- e^+)/\Gamma_{total}$	$<6 \times 10^{-6}$, CL = 90%	$\Gamma(\Upsilon(2S) \rightarrow e^\pm \tau^\mp)/\Gamma_{total}$	$<3.2 \times 10^{-6}$, CL = 90%
$\Gamma(\eta'(958) \rightarrow e \mu)/\Gamma_{total}$	$<4.7 \times 10^{-4}$, CL = 90%	$\Gamma(\Upsilon(2S) \rightarrow \mu^\pm \tau^\mp)/\Gamma_{total}$	$<3.3 \times 10^{-6}$, CL = 90%
$\Gamma(\phi(1020) \rightarrow e^\pm \mu^\mp)/\Gamma_{total}$	$<2 \times 10^{-6}$, CL = 90%	$\Gamma(\Upsilon(3S) \rightarrow e^\pm \tau^\mp)/\Gamma_{total}$	$<4.2 \times 10^{-6}$, CL = 90%
$\Gamma(K^+ \rightarrow \mu^- \nu e^+ e^+)/\Gamma_{total}$	$<2.1 \times 10^{-8}$, CL = 90%	$\Gamma(\Upsilon(3S) \rightarrow \mu^\pm \tau^\mp)/\Gamma_{total}$	$<3.1 \times 10^{-6}$, CL = 90%
$\Gamma(K^+ \rightarrow \mu^+ \nu_e)/\Gamma_{total}$	[q] $<4 \times 10^{-3}$, CL = 90%	$\Gamma(\Lambda_c^+ \rightarrow p e^+ \mu^-)/\Gamma_{total}$	$<9.9 \times 10^{-6}$, CL = 90%
$\Gamma(K^+ \rightarrow \pi^+ \mu^+ e^-)/\Gamma_{total}$	$<1.3 \times 10^{-11}$, CL = 90%	$\Gamma(\Lambda_c^+ \rightarrow p e^- \mu^+)/\Gamma_{total}$	$<1.9 \times 10^{-5}$, CL = 90%
$\Gamma(K^+ \rightarrow \pi^+ \mu^- e^+)/\Gamma_{total}$	$<5.2 \times 10^{-10}$, CL = 90%		
$\Gamma(K_L^0 \rightarrow e^\pm \mu^\mp)/\Gamma_{total}$	[o] $<4.7 \times 10^{-12}$, CL = 90%		
$\Gamma(K_L^0 \rightarrow e^\pm e^\pm \mu^\mp \mu^\mp)/\Gamma_{total}$	[o] $<4.12 \times 10^{-11}$, CL = 90%		
$\Gamma(K_L^0 \rightarrow \pi^0 \mu^\pm e^\mp)/\Gamma_{total}$	[o] $<7.6 \times 10^{-11}$, CL = 90%		
$\Gamma(K_L^0 \rightarrow \pi^0 \pi^0 \mu^\pm e^\mp)/\Gamma_{total}$	$<1.7 \times 10^{-10}$, CL = 90%		
$\Gamma(D^+ \rightarrow \pi^+ e^+ \mu^-)/\Gamma_{total}$	$<2.9 \times 10^{-6}$, CL = 90%		

Unless otherwise stated, limits are given at the 90% confidence level, while errors are given as ± 1 standard deviation.

Tests of Conservation Laws

TOTAL LEPTON NUMBER

Violation of total lepton number conservation also implies violation of lepton family number conservation.

$\Gamma(Z \rightarrow p e)/\Gamma_{\text{total}}$	$<1.8 \times 10^{-6}$, CL = 95%
$\Gamma(Z \rightarrow p \mu)/\Gamma_{\text{total}}$	$<1.8 \times 10^{-6}$, CL = 95%
limit on $\mu^- \rightarrow e^+$ conversion	
$\sigma(\mu^- 32\text{S} \rightarrow e^+ 32\text{Si}^*) / \sigma(\mu^- 32\text{S} \rightarrow \nu_\mu 32\text{P}^*)$	$<9 \times 10^{-10}$, CL = 90%
$\sigma(\mu^- 127\text{I} \rightarrow e^+ 127\text{Sb}^*) / \sigma(\mu^- 127\text{I} \rightarrow \text{anything})$	$<3 \times 10^{-10}$, CL = 90%
$\sigma(\mu^- \text{Ti} \rightarrow e^+ \text{Ca}) / \sigma(\mu^- \text{Ti} \rightarrow \text{capture})$	$<3.6 \times 10^{-11}$, CL = 90%
$\Gamma(\tau^- \rightarrow e^+ \pi^- \pi^-)/\Gamma_{\text{total}}$	$<2.0 \times 10^{-8}$, CL = 90%
$\Gamma(\tau^- \rightarrow \mu^+ \pi^- \pi^-)/\Gamma_{\text{total}}$	$<3.9 \times 10^{-8}$, CL = 90%
$\Gamma(\tau^- \rightarrow e^+ \pi^- K^-)/\Gamma_{\text{total}}$	$<3.2 \times 10^{-8}$, CL = 90%
$\Gamma(\tau^- \rightarrow e^+ K^- K^-)/\Gamma_{\text{total}}$	$<3.3 \times 10^{-8}$, CL = 90%
$\Gamma(\tau^- \rightarrow \mu^+ \pi^- K^-)/\Gamma_{\text{total}}$	$<4.8 \times 10^{-8}$, CL = 90%
$\Gamma(\tau^- \rightarrow \mu^+ K^- K^-)/\Gamma_{\text{total}}$	$<4.7 \times 10^{-8}$, CL = 90%
$\Gamma(\tau^- \rightarrow \rho \mu^- \mu^-)/\Gamma_{\text{total}}$	$<4.4 \times 10^{-7}$, CL = 90%
$\Gamma(\tau^- \rightarrow \bar{p} \mu^+ \mu^-)/\Gamma_{\text{total}}$	$<3.3 \times 10^{-7}$, CL = 90%
$\Gamma(\tau^- \rightarrow \bar{p} \gamma)/\Gamma_{\text{total}}$	$<3.5 \times 10^{-6}$, CL = 90%
$\Gamma(\tau^- \rightarrow \bar{p} \pi^0)/\Gamma_{\text{total}}$	$<1.5 \times 10^{-5}$, CL = 90%
$\Gamma(\tau^- \rightarrow \bar{p} 2\pi^0)/\Gamma_{\text{total}}$	$<3.3 \times 10^{-5}$, CL = 90%
$\Gamma(\tau^- \rightarrow \bar{p} \eta)/\Gamma_{\text{total}}$	$<8.9 \times 10^{-6}$, CL = 90%
$\Gamma(\tau^- \rightarrow \bar{p} \pi^0 \eta)/\Gamma_{\text{total}}$	$<2.7 \times 10^{-5}$, CL = 90%
$\Gamma(\tau^- \rightarrow \Lambda \pi^-)/\Gamma_{\text{total}}$	$<7.2 \times 10^{-8}$, CL = 90%
$\Gamma(\tau^- \rightarrow \bar{\Lambda} \pi^-)/\Gamma_{\text{total}}$	$<1.4 \times 10^{-7}$, CL = 90%
$t_{1/2}({}^{76}\text{Ge} \rightarrow {}^{76}\text{Se} + 2 e^-)$	$>9.0 \times 10^{25}$ yr, CL = 90%
$t_{1/2}({}^{136}\text{Xe} \rightarrow {}^{136}\text{Ba} + 2 e^-)$	$>10.7 \times 10^{25}$ yr, CL = 90%
$t_{1/2}({}^{130}\text{Te} \rightarrow {}^{130}\text{Xe} + 2 e^-)$	$>1.5 \times 10^{25}$ yr, CL = 90%
$\Gamma(\pi^+ \rightarrow \mu^+ \bar{\nu}_e)/\Gamma_{\text{total}}$	[q] $<1.5 \times 10^{-3}$, CL = 90%
$\Gamma(K^+ \rightarrow \pi^- \mu^+ e^+)/\Gamma_{\text{total}}$	$<5.0 \times 10^{-10}$, CL = 90%
$\Gamma(K^+ \rightarrow \pi^- e^+ e^+)/\Gamma_{\text{total}}$	$<2.2 \times 10^{-10}$, CL = 90%
$\Gamma(K^+ \rightarrow \pi^- \mu^+ \mu^+)/\Gamma_{\text{total}}$	[q] $<4.2 \times 10^{-11}$, CL = 90%
$\Gamma(K^+ \rightarrow \mu^+ \bar{\nu}_e)/\Gamma_{\text{total}}$	[q] $<3.3 \times 10^{-3}$, CL = 90%
$\Gamma(K^+ \rightarrow \pi^0 e^+ \bar{\nu}_e)/\Gamma_{\text{total}}$	$<3 \times 10^{-3}$, CL = 90%
$\Gamma(D^+ \rightarrow \pi^- 2e^+)/\Gamma_{\text{total}}$	$<1.1 \times 10^{-6}$, CL = 90%
$\Gamma(D^+ \rightarrow \pi^- 2\mu^+)/\Gamma_{\text{total}}$	$<2.2 \times 10^{-8}$, CL = 90%
$\Gamma(D^+ \rightarrow \pi^- e^+ \mu^+)/\Gamma_{\text{total}}$	$<2.0 \times 10^{-6}$, CL = 90%
$\Gamma(D^+ \rightarrow \rho^- 2\mu^+)/\Gamma_{\text{total}}$	$<5.6 \times 10^{-4}$, CL = 90%
$\Gamma(D^+ \rightarrow K^- 2e^+)/\Gamma_{\text{total}}$	$<9 \times 10^{-7}$, CL = 90%
$\Gamma(D^+ \rightarrow K^- 2\mu^+)/\Gamma_{\text{total}}$	$<1.0 \times 10^{-5}$, CL = 90%
$\Gamma(D^+ \rightarrow K^- e^+ \mu^+)/\Gamma_{\text{total}}$	$<1.9 \times 10^{-6}$, CL = 90%
$\Gamma(D^+ \rightarrow K^*(892)^- 2\mu^+)/\Gamma_{\text{total}}$	$<8.5 \times 10^{-4}$, CL = 90%
$\Gamma(D^0 \rightarrow 2\pi^- 2e^+ + \text{c.c.})/\Gamma_{\text{total}}$	$<1.12 \times 10^{-4}$, CL = 90%
$\Gamma(D^0 \rightarrow 2\pi^- 2\mu^+ + \text{c.c.})/\Gamma_{\text{total}}$	$<2.9 \times 10^{-5}$, CL = 90%
$\Gamma(D^0 \rightarrow K^- \pi^- 2\mu^+ + \text{c.c.})/\Gamma_{\text{total}}$	$<3.9 \times 10^{-4}$, CL = 90%
$\Gamma(D^0 \rightarrow 2K^- 2e^+ + \text{c.c.})/\Gamma_{\text{total}}$	$<1.52 \times 10^{-4}$, CL = 90%
$\Gamma(D^0 \rightarrow 2K^- 2\mu^+ + \text{c.c.})/\Gamma_{\text{total}}$	$<9.4 \times 10^{-5}$, CL = 90%
$\Gamma(D^0 \rightarrow \pi^- \pi^- e^+ \mu^+ + \text{c.c.})/\Gamma_{\text{total}}$	$<7.9 \times 10^{-5}$, CL = 90%
$\Gamma(D^0 \rightarrow K^- \pi^- e^+ \mu^+ + \text{c.c.})/\Gamma_{\text{total}}$	$<2.18 \times 10^{-4}$, CL = 90%
$\Gamma(D^0 \rightarrow 2K^- e^+ \mu^+ + \text{c.c.})/\Gamma_{\text{total}}$	$<5.7 \times 10^{-5}$, CL = 90%
$\Gamma(D^0 \rightarrow p e^-)/\Gamma_{\text{total}}$	[r] $<1.0 \times 10^{-5}$, CL = 90%
$\Gamma(D^0 \rightarrow \bar{p} e^+)/\Gamma_{\text{total}}$	[s] $<1.1 \times 10^{-5}$, CL = 90%
$\Gamma(D_S^+ \rightarrow \pi^- 2e^+)/\Gamma_{\text{total}}$	$<4.1 \times 10^{-6}$, CL = 90%
$\Gamma(D_S^+ \rightarrow \pi^- 2\mu^+)/\Gamma_{\text{total}}$	$<1.2 \times 10^{-7}$, CL = 90%
$\Gamma(D_S^+ \rightarrow \pi^- e^+ \mu^+)/\Gamma_{\text{total}}$	$<8.4 \times 10^{-6}$, CL = 90%
$\Gamma(D_S^+ \rightarrow K^- 2e^+)/\Gamma_{\text{total}}$	$<5.2 \times 10^{-6}$, CL = 90%
$\Gamma(D_S^+ \rightarrow K^- 2\mu^+)/\Gamma_{\text{total}}$	$<1.3 \times 10^{-5}$, CL = 90%
$\Gamma(D_S^+ \rightarrow K^- e^+ \mu^+)/\Gamma_{\text{total}}$	$<6.1 \times 10^{-6}$, CL = 90%
$\Gamma(D_S^+ \rightarrow K^*(892)^- 2\mu^+)/\Gamma_{\text{total}}$	$<1.4 \times 10^{-3}$, CL = 90%
$\Gamma(B^+ \rightarrow \pi^- e^+ e^+)/\Gamma_{\text{total}}$	$<2.3 \times 10^{-8}$, CL = 90%
$\Gamma(B^+ \rightarrow \pi^- \mu^+ \mu^+)/\Gamma_{\text{total}}$	$<4.0 \times 10^{-9}$, CL = 95%
$\Gamma(B^+ \rightarrow \pi^- e^+ \mu^+)/\Gamma_{\text{total}}$	$<1.5 \times 10^{-7}$, CL = 90%
$\Gamma(B^+ \rightarrow \rho^- e^+ e^+)/\Gamma_{\text{total}}$	$<1.7 \times 10^{-7}$, CL = 90%
$\Gamma(B^+ \rightarrow \rho^- \mu^+ \mu^+)/\Gamma_{\text{total}}$	$<4.2 \times 10^{-7}$, CL = 90%
$\Gamma(B^+ \rightarrow \rho^- e^+ \mu^+)/\Gamma_{\text{total}}$	$<4.7 \times 10^{-7}$, CL = 90%
$\Gamma(B^+ \rightarrow K^- e^+ e^+)/\Gamma_{\text{total}}$	$<3.0 \times 10^{-8}$, CL = 90%
$\Gamma(B^+ \rightarrow K^- \mu^+ \mu^+)/\Gamma_{\text{total}}$	$<4.1 \times 10^{-8}$, CL = 90%

$\Gamma(B^+ \rightarrow K^- e^+ \mu^+)/\Gamma_{\text{total}}$	$<1.6 \times 10^{-7}$, CL = 90%
$\Gamma(B^+ \rightarrow K^*(892)^- e^+ e^+)/\Gamma_{\text{total}}$	$<4.0 \times 10^{-7}$, CL = 90%
$\Gamma(B^+ \rightarrow K^*(892)^- \mu^+ \mu^+)/\Gamma_{\text{total}}$	$<5.9 \times 10^{-7}$, CL = 90%
$\Gamma(B^+ \rightarrow K^*(892)^- e^+ \mu^+)/\Gamma_{\text{total}}$	$<3.0 \times 10^{-7}$, CL = 90%
$\Gamma(B^+ \rightarrow D^- e^+ e^+)/\Gamma_{\text{total}}$	$<2.6 \times 10^{-6}$, CL = 90%
$\Gamma(B^+ \rightarrow D^- e^+ \mu^+)/\Gamma_{\text{total}}$	$<1.8 \times 10^{-6}$, CL = 90%
$\Gamma(B^+ \rightarrow D^- \mu^+ \mu^+)/\Gamma_{\text{total}}$	$<6.9 \times 10^{-7}$, CL = 95%
$\Gamma(B^+ \rightarrow D^{*-} \mu^+ \mu^+)/\Gamma_{\text{total}}$	$<2.4 \times 10^{-6}$, CL = 95%
$\Gamma(B^+ \rightarrow D_S^- \mu^+ \mu^+)/\Gamma_{\text{total}}$	$<5.8 \times 10^{-7}$, CL = 95%
$\Gamma(B^+ \rightarrow \bar{D}^0 \pi^- \mu^+ \mu^+)/\Gamma_{\text{total}}$	$<1.5 \times 10^{-6}$, CL = 95%
$\Gamma(B^+ \rightarrow \Lambda^0 \mu^+)/\Gamma_{\text{total}}$	$<6 \times 10^{-8}$, CL = 90%
$\Gamma(B^+ \rightarrow \Lambda^0 e^+)/\Gamma_{\text{total}}$	$<3.2 \times 10^{-8}$, CL = 90%
$\Gamma(B^+ \rightarrow \bar{\Lambda}^0 \mu^+)/\Gamma_{\text{total}}$	$<6 \times 10^{-8}$, CL = 90%
$\Gamma(B^+ \rightarrow \bar{\Lambda}^0 e^+)/\Gamma_{\text{total}}$	$<8 \times 10^{-8}$, CL = 90%
$\Gamma(B^0 \rightarrow \Lambda_C^+ \mu^-)/\Gamma_{\text{total}}$	$<1.4 \times 10^{-6}$, CL = 90%
$\Gamma(B^0 \rightarrow \Lambda_C^+ e^-)/\Gamma_{\text{total}}$	$<4 \times 10^{-6}$, CL = 90%
$\Gamma(\Lambda \rightarrow \pi^+ e^-)/\Gamma_{\text{total}}$	$<6 \times 10^{-7}$, CL = 90%
$\Gamma(\Lambda \rightarrow \pi^+ \mu^-)/\Gamma_{\text{total}}$	$<6 \times 10^{-7}$, CL = 90%
$\Gamma(\Lambda \rightarrow \pi^- e^+)/\Gamma_{\text{total}}$	$<4 \times 10^{-7}$, CL = 90%
$\Gamma(\Lambda \rightarrow \pi^- \mu^+)/\Gamma_{\text{total}}$	$<6 \times 10^{-7}$, CL = 90%
$\Gamma(\Lambda \rightarrow K^+ e^-)/\Gamma_{\text{total}}$	$<2 \times 10^{-6}$, CL = 90%
$\Gamma(\Lambda \rightarrow K^+ \mu^-)/\Gamma_{\text{total}}$	$<3 \times 10^{-6}$, CL = 90%
$\Gamma(\Lambda \rightarrow K^- e^+)/\Gamma_{\text{total}}$	$<2 \times 10^{-6}$, CL = 90%
$\Gamma(\Lambda \rightarrow K^- \mu^+)/\Gamma_{\text{total}}$	$<3 \times 10^{-6}$, CL = 90%
$\Gamma(\Lambda \rightarrow K_S^0 \nu)/\Gamma_{\text{total}}$	$<2 \times 10^{-5}$, CL = 90%
$\Gamma(\Xi^- \rightarrow p \mu^- \mu^-)/\Gamma_{\text{total}}$	$<4 \times 10^{-8}$, CL = 90%
$\Gamma(\Lambda_C^+ \rightarrow \bar{p} 2e^+)/\Gamma_{\text{total}}$	$<2.7 \times 10^{-6}$, CL = 90%
$\Gamma(\Lambda_C^+ \rightarrow \bar{p} 2\mu^+)/\Gamma_{\text{total}}$	$<9.4 \times 10^{-6}$, CL = 90%
$\Gamma(\Lambda_C^+ \rightarrow \bar{p} e^+ \mu^+)/\Gamma_{\text{total}}$	$<1.6 \times 10^{-5}$, CL = 90%
$\Gamma(\Lambda_C^+ \rightarrow \Sigma^- \mu^+ \mu^+)/\Gamma_{\text{total}}$	$<7.0 \times 10^{-4}$, CL = 90%

BARYON NUMBER

$\Gamma(Z \rightarrow p e)/\Gamma_{\text{total}}$	$<1.8 \times 10^{-6}$, CL = 95%
$\Gamma(Z \rightarrow p \mu)/\Gamma_{\text{total}}$	$<1.8 \times 10^{-6}$, CL = 95%
$\Gamma(\tau^- \rightarrow p \mu^- \mu^-)/\Gamma_{\text{total}}$	$<4.4 \times 10^{-7}$, CL = 90%
$\Gamma(\tau^- \rightarrow \bar{p} \mu^+ \mu^-)/\Gamma_{\text{total}}$	$<3.3 \times 10^{-7}$, CL = 90%
$\Gamma(\tau^- \rightarrow \bar{p} \gamma)/\Gamma_{\text{total}}$	$<3.5 \times 10^{-6}$, CL = 90%
$\Gamma(\tau^- \rightarrow \bar{p} \pi^0)/\Gamma_{\text{total}}$	$<1.5 \times 10^{-5}$, CL = 90%
$\Gamma(\tau^- \rightarrow \bar{p} 2\pi^0)/\Gamma_{\text{total}}$	$<3.3 \times 10^{-5}$, CL = 90%
$\Gamma(\tau^- \rightarrow \bar{p} \eta)/\Gamma_{\text{total}}$	$<8.9 \times 10^{-6}$, CL = 90%
$\Gamma(\tau^- \rightarrow \bar{p} \pi^0 \eta)/\Gamma_{\text{total}}$	$<2.7 \times 10^{-5}$, CL = 90%
$\Gamma(\tau^- \rightarrow \Lambda \pi^-)/\Gamma_{\text{total}}$	$<7.2 \times 10^{-8}$, CL = 90%
$\Gamma(\tau^- \rightarrow \bar{\Lambda} \pi^-)/\Gamma_{\text{total}}$	$<1.4 \times 10^{-7}$, CL = 90%
$\Gamma(D^0 \rightarrow p e^-)/\Gamma_{\text{total}}$	[r] $<1.0 \times 10^{-5}$, CL = 90%
$\Gamma(D^0 \rightarrow \bar{p} e^+)/\Gamma_{\text{total}}$	[s] $<1.1 \times 10^{-5}$, CL = 90%
$\Gamma(B^+ \rightarrow \Lambda^0 \mu^+)/\Gamma_{\text{total}}$	$<6 \times 10^{-8}$, CL = 90%
$\Gamma(B^+ \rightarrow \Lambda^0 e^+)/\Gamma_{\text{total}}$	$<3.2 \times 10^{-8}$, CL = 90%
$\Gamma(B^+ \rightarrow \bar{\Lambda}^0 \mu^+)/\Gamma_{\text{total}}$	$<6 \times 10^{-8}$, CL = 90%
$\Gamma(B^+ \rightarrow \bar{\Lambda}^0 e^+)/\Gamma_{\text{total}}$	$<8 \times 10^{-8}$, CL = 90%
$\Gamma(B^0 \rightarrow \Lambda_C^+ \mu^-)/\Gamma_{\text{total}}$	$<1.4 \times 10^{-6}$, CL = 90%
$\Gamma(B^0 \rightarrow \Lambda_C^+ e^-)/\Gamma_{\text{total}}$	$<4 \times 10^{-6}$, CL = 90%
p mean life	[t] $>3.6 \times 10^{29}$ years, CL = 90%
A few examples of proton or bound neutron decay follow. For limits on many other nucleon decay channels, see the Baryon Summary Table.	
$\tau(N \rightarrow e^+ \pi)$	$> 5300 (n), > 16000 (p) \times 10^{30}$ years, CL = 90%
$\tau(N \rightarrow \mu^+ \pi)$	$> 3500 (n), > 7700 (p) \times 10^{30}$ years, CL = 90%
$\tau(N \rightarrow e^+ K)$	$> 17 (n), > 1000 (p) \times 10^{30}$ years, CL = 90%
$\tau(N \rightarrow \mu^+ K)$	$> 26 (n), > 16000 (p) \times 10^{30}$ years, CL = 90%
limit on $n\bar{n}$ oscillations (free n)	$>0.86 \times 10^8$ s, CL = 90%
limit on $n\bar{n}$ oscillations (bound n)	[u] $>2.7 \times 10^8$ s, CL = 90%
$\Gamma(\Lambda \rightarrow \pi^+ e^-)/\Gamma_{\text{total}}$	$<6 \times 10^{-7}$, CL = 90%
$\Gamma(\Lambda \rightarrow \pi^+ \mu^-)/\Gamma_{\text{total}}$	$<6 \times 10^{-7}$, CL = 90%
$\Gamma(\Lambda \rightarrow \pi^- e^+)/\Gamma_{\text{total}}$	$<4 \times 10^{-7}$, CL = 90%
$\Gamma(\Lambda \rightarrow \pi^- \mu^+)/\Gamma_{\text{total}}$	$<6 \times 10^{-7}$, CL = 90%
$\Gamma(\Lambda \rightarrow K^+ e^-)/\Gamma_{\text{total}}$	$<2 \times 10^{-6}$, CL = 90%
$\Gamma(\Lambda \rightarrow K^+ \mu^-)/\Gamma_{\text{total}}$	$<3 \times 10^{-6}$, CL = 90%
$\Gamma(\Lambda \rightarrow K^- e^+)/\Gamma_{\text{total}}$	$<2 \times 10^{-6}$, CL = 90%

$\Gamma(\Lambda \rightarrow K^- \mu^+)/\Gamma_{\text{total}}$	$< 3 \times 10^{-6}$, CL = 90%
$\Gamma(\Lambda \rightarrow K_S^0 \nu)/\Gamma_{\text{total}}$	$< 2 \times 10^{-5}$, CL = 90%
$\Gamma(\Lambda \rightarrow \bar{p} \pi^+)/\Gamma_{\text{total}}$	$< 9 \times 10^{-7}$, CL = 90%
$\Gamma(\Lambda_C^+ \rightarrow \bar{p} 2e^+)/\Gamma_{\text{total}}$	$< 2.7 \times 10^{-6}$, CL = 90%
$\Gamma(\Lambda_C^+ \rightarrow \bar{p} 2\mu^+)/\Gamma_{\text{total}}$	$< 9.4 \times 10^{-6}$, CL = 90%
$\Gamma(\Lambda_C^+ \rightarrow \bar{p} e^+ \mu^+)/\Gamma_{\text{total}}$	$< 1.6 \times 10^{-5}$, CL = 90%

ELECTRIC CHARGE (Q)

γ charge (mixed)	$< 1 \times 10^{-46} e$
γ charge (single)	$< 1 \times 10^{-35} e$
$e \rightarrow \nu_e \gamma$ and astrophysical limits	[ν] $> 6.6 \times 10^{28}$ yr, CL = 90%
ν charge	$< 4 \times 10^{-35} e$, CL = 95%
$ q_p + q_e /e$	[X] $< 1 \times 10^{-21}$
n charge	$(-0.2 \pm 0.8) \times 10^{-21} e$
$\Gamma(n \rightarrow p \nu_e \bar{\nu}_e)/\Gamma_{\text{total}}$	$< 8 \times 10^{-27}$, CL = 68%

$\Delta S = \Delta Q$ RULE

Violations allowed in second-order weak interactions.

$\Gamma(K^+ \rightarrow \pi^+ \pi^+ e^- \bar{\nu}_e)/\Gamma_{\text{total}}$	$< 1.3 \times 10^{-8}$, CL = 90%
$\Gamma(K^+ \rightarrow \pi^+ \pi^+ \mu^- \bar{\nu}_\mu)/\Gamma_{\text{total}}$	$< 3.0 \times 10^{-6}$, CL = 95%
Re(X_+), K_{e3} parameter	$(-0.9 \pm 3.0) \times 10^{-3}$
$x = A(\bar{K}^0 \rightarrow \pi^- \ell^+ \nu)/A(K^0 \rightarrow \pi^- \ell^+ \nu) = A(\Delta S = -\Delta Q)/A(\Delta S = \Delta Q)$	
real part of x	-0.002 ± 0.006
imaginary part of x	0.0012 ± 0.0021
$\Gamma(\Sigma^+ \rightarrow n \ell^+ \nu)/\Gamma(\Sigma^- \rightarrow n \ell^- \bar{\nu})$	< 0.043
$\Gamma(\Sigma^+ \rightarrow n e^+ \nu_e)/\Gamma_{\text{total}}$	$< 5 \times 10^{-6}$, CL = 90%
$\Gamma(\Sigma^+ \rightarrow n \mu^+ \nu_\mu)/\Gamma_{\text{total}}$	$< 3.0 \times 10^{-5}$, CL = 90%
$\Gamma(\Xi^0 \rightarrow \Sigma^- e^+ \nu_e)/\Gamma_{\text{total}}$	$< 9 \times 10^{-4}$, CL = 90%
$\Gamma(\Xi^0 \rightarrow \Sigma^- \mu^+ \nu_\mu)/\Gamma_{\text{total}}$	$< 9 \times 10^{-4}$, CL = 90%

$\Delta S = 2$ FORBIDDEN

Allowed in second-order weak interactions.

$\Gamma(\Xi^0 \rightarrow p \pi^-)/\Gamma_{\text{total}}$	$< 8 \times 10^{-6}$, CL = 90%
$\Gamma(\Xi^0 \rightarrow p e^- \bar{\nu}_e)/\Gamma_{\text{total}}$	$< 1.3 \times 10^{-3}$
$\Gamma(\Xi^0 \rightarrow p \mu^- \bar{\nu}_\mu)/\Gamma_{\text{total}}$	$< 1.3 \times 10^{-3}$
$\Gamma(\Xi^- \rightarrow n \pi^-)/\Gamma_{\text{total}}$	$< 1.9 \times 10^{-5}$, CL = 90%
$\Gamma(\Xi^- \rightarrow n e^- \bar{\nu}_e)/\Gamma_{\text{total}}$	$< 3.2 \times 10^{-3}$, CL = 90%
$\Gamma(\Xi^- \rightarrow n \mu^- \bar{\nu}_\mu)/\Gamma_{\text{total}}$	$< 1.5 \times 10^{-2}$, CL = 90%
$\Gamma(\Xi^- \rightarrow p \pi^- \pi^-)/\Gamma_{\text{total}}$	$< 4 \times 10^{-4}$, CL = 90%
$\Gamma(\Xi^- \rightarrow p \pi^- e^- \bar{\nu}_e)/\Gamma_{\text{total}}$	$< 4 \times 10^{-4}$, CL = 90%
$\Gamma(\Xi^- \rightarrow p \pi^- \mu^- \bar{\nu}_\mu)/\Gamma_{\text{total}}$	$< 4 \times 10^{-4}$, CL = 90%
$\Gamma(\Omega^- \rightarrow \Lambda \pi^-)/\Gamma_{\text{total}}$	$< 2.9 \times 10^{-6}$, CL = 90%

$\Delta S = 2$ VIA MIXING

Allowed in second-order weak interactions, e.g. mixing.

$m_{K_L^0} - m_{K_S^0}$	$(0.5293 \pm 0.0009) \times 10^{10} \text{ h s}^{-1}$ ($S = 1.3$)
$m_{K_L^0} - m_{K_S^0}$	$(3.484 \pm 0.006) \times 10^{-12} \text{ MeV}$

$\Delta C = 2$ VIA MIXING

Allowed in second-order weak interactions, e.g. mixing.

$ m_{D_1^0} - m_{D_2^0} = x\Gamma$	$(0.95 \pm_{-0.44}^{0.41}) \times 10^{10} \text{ h s}^{-1}$
$(\Gamma_{D_1^0} - \Gamma_{D_2^0})/\Gamma = 2y$	$(1.29 \pm_{-0.18}^{0.14}) \times 10^{-2}$

$\Delta B = 2$ VIA MIXING

Allowed in second-order weak interactions, e.g. mixing.

x_d	0.1858 ± 0.0011
$\Delta m_{B^0} = m_{B_H^0} - m_{B_L^0}$	$(0.5065 \pm 0.0019) \times 10^{12} \text{ h s}^{-1}$
$x_d = \Delta m_{B^0}/\Gamma_{B^0}$	0.769 ± 0.004
$\Delta m_{B_s^0} = m_{B_{sH}^0} - m_{B_{sL}^0}$	$(17.749 \pm 0.020) \times 10^{12} \text{ h s}^{-1}$
$x_s = \Delta m_{B_s^0}/\Gamma_{B_s^0}$	26.89 ± 0.07
x_s	0.499312 ± 0.000004

$\Delta S = 1$ WEAK NEUTRAL CURRENT FORBIDDEN

Allowed by higher-order electroweak interactions.

$\Gamma(K^+ \rightarrow \pi^+ e^+ e^-)/\Gamma_{\text{total}}$	$(3.00 \pm 0.09) \times 10^{-7}$
$\Gamma(K^+ \rightarrow \pi^+ \mu^+ \mu^-)/\Gamma_{\text{total}}$	$(9.4 \pm 0.6) \times 10^{-8}$ ($S = 2.6$)
$\Gamma(K^+ \rightarrow \pi^+ \nu \bar{\nu})/\Gamma_{\text{total}}$	$(1.7 \pm 1.1) \times 10^{-10}$
$\Gamma(K^+ \rightarrow \pi^+ \pi^0 \nu \bar{\nu})/\Gamma_{\text{total}}$	$< 4.3 \times 10^{-5}$, CL = 90%
$\Gamma(K_S^0 \rightarrow \mu^+ \mu^-)/\Gamma_{\text{total}}$	$< 8 \times 10^{-10}$, CL = 90%
$\Gamma(K_S^0 \rightarrow e^+ e^-)/\Gamma_{\text{total}}$	$< 9 \times 10^{-9}$, CL = 90%
$\Gamma(K_S^0 \rightarrow \pi^0 e^+ e^-)/\Gamma_{\text{total}}$	[ν] $(3.0 \pm_{-1.2}^{1.5}) \times 10^{-9}$
$\Gamma(K_S^0 \rightarrow \pi^0 \mu^+ \mu^-)/\Gamma_{\text{total}}$	$(2.9 \pm_{-1.2}^{1.5}) \times 10^{-9}$
$\Gamma(K_L^0 \rightarrow \mu^+ \mu^-)/\Gamma_{\text{total}}$	$(6.84 \pm 0.11) \times 10^{-9}$
$\Gamma(K_L^0 \rightarrow e^+ e^-)/\Gamma_{\text{total}}$	$(9 \pm_{-4}^6) \times 10^{-12}$
$\Gamma(K_L^0 \rightarrow \pi^+ \pi^- e^+ e^-)/\Gamma_{\text{total}}$	[z] $(3.11 \pm 0.19) \times 10^{-7}$
$\Gamma(K_L^0 \rightarrow \pi^0 \pi^0 e^+ e^-)/\Gamma_{\text{total}}$	$< 6.6 \times 10^{-9}$, CL = 90%
$\Gamma(K_L^0 \rightarrow \pi^0 \pi^0 \mu^+ \mu^-)/\Gamma_{\text{total}}$	$< 9.2 \times 10^{-11}$, CL = 90%
$\Gamma(K_L^0 \rightarrow \mu^+ \mu^- e^+ e^-)/\Gamma_{\text{total}}$	$(2.69 \pm 0.27) \times 10^{-9}$
$\Gamma(K_L^0 \rightarrow e^+ e^- e^+ e^-)/\Gamma_{\text{total}}$	$(3.56 \pm 0.21) \times 10^{-8}$
$\Gamma(K_L^0 \rightarrow \pi^0 \mu^+ \mu^-)/\Gamma_{\text{total}}$	$< 3.8 \times 10^{-10}$, CL = 90%
$\Gamma(K_L^0 \rightarrow \pi^0 e^+ e^-)/\Gamma_{\text{total}}$	$< 2.8 \times 10^{-10}$, CL = 90%
$\Gamma(K_L^0 \rightarrow \pi^0 \nu \bar{\nu})/\Gamma_{\text{total}}$	$< 3.0 \times 10^{-9}$, CL = 90%
$\Gamma(K_L^0 \rightarrow \pi^0 \pi^0 \nu \bar{\nu})/\Gamma_{\text{total}}$	$< 8.1 \times 10^{-7}$, CL = 90%
$\Gamma(\Sigma^+ \rightarrow p e^+ e^-)/\Gamma_{\text{total}}$	$< 7 \times 10^{-6}$
$\Gamma(\Sigma^+ \rightarrow p \mu^+ \mu^-)/\Gamma_{\text{total}}$	$(2.4 \pm_{-1.3}^{1.7}) \times 10^{-8}$

$\Delta C = 1$ WEAK NEUTRAL CURRENT FORBIDDEN

Allowed by higher-order electroweak interactions.

$\Gamma(D^+ \rightarrow \pi^+ e^+ e^-)/\Gamma_{\text{total}}$	$< 1.1 \times 10^{-6}$, CL = 90%
$\Gamma(D^+ \rightarrow \pi^+ \mu^+ \mu^-)/\Gamma_{\text{total}}$	$< 7.3 \times 10^{-8}$, CL = 90%
$\Gamma(D^+ \rightarrow \rho^+ \mu^+ \mu^-)/\Gamma_{\text{total}}$	$< 5.6 \times 10^{-4}$, CL = 90%
$\Gamma(D^0 \rightarrow \gamma \gamma)/\Gamma_{\text{total}}$	$< 8.5 \times 10^{-7}$, CL = 90%
$\Gamma(D^0 \rightarrow e^+ e^-)/\Gamma_{\text{total}}$	$< 7.9 \times 10^{-8}$, CL = 90%
$\Gamma(D^0 \rightarrow \mu^+ \mu^-)/\Gamma_{\text{total}}$	$< 6.2 \times 10^{-9}$, CL = 90%
$\Gamma(D^0 \rightarrow \pi^0 e^+ e^-)/\Gamma_{\text{total}}$	$< 4 \times 10^{-6}$, CL = 90%
$\Gamma(D^0 \rightarrow \pi^0 \mu^+ \mu^-)/\Gamma_{\text{total}}$	$< 1.8 \times 10^{-4}$, CL = 90%
$\Gamma(D^0 \rightarrow \eta e^+ e^-)/\Gamma_{\text{total}}$	$< 3 \times 10^{-6}$, CL = 90%
$\Gamma(D^0 \rightarrow \eta \mu^+ \mu^-)/\Gamma_{\text{total}}$	$< 5.3 \times 10^{-4}$, CL = 90%
$\Gamma(D^0 \rightarrow \pi^+ \pi^- e^+ e^-)/\Gamma_{\text{total}}$	$< 7 \times 10^{-6}$, CL = 90%
$\Gamma(D^0 \rightarrow \rho^0 e^+ e^-)/\Gamma_{\text{total}}$	$< 1.0 \times 10^{-4}$, CL = 90%
$\Gamma(D^0 \rightarrow \pi^+ \pi^- \mu^+ \mu^-)/\Gamma_{\text{total}}$	$(9.6 \pm 1.2) \times 10^{-7}$
$\Gamma(D^0 \rightarrow \rho^0 \mu^+ \mu^-)/\Gamma_{\text{total}}$	$< 2.2 \times 10^{-5}$, CL = 90%
$\Gamma(D^0 \rightarrow \omega e^+ e^-)/\Gamma_{\text{total}}$	$< 6 \times 10^{-6}$, CL = 90%
$\Gamma(D^0 \rightarrow \omega \mu^+ \mu^-)/\Gamma_{\text{total}}$	$< 8.3 \times 10^{-4}$, CL = 90%
$\Gamma(D^0 \rightarrow K^- K^+ e^+ e^-)/\Gamma_{\text{total}}$	$< 1.1 \times 10^{-5}$, CL = 90%
$\Gamma(D^0 \rightarrow \phi e^+ e^-)/\Gamma_{\text{total}}$	$< 5.2 \times 10^{-5}$, CL = 90%
$\Gamma(D^0 \rightarrow K^- K^+ \mu^+ \mu^-)/\Gamma_{\text{total}}$	$(1.54 \pm 0.32) \times 10^{-7}$
$\Gamma(D^0 \rightarrow \phi \mu^+ \mu^-)/\Gamma_{\text{total}}$	$< 3.1 \times 10^{-5}$, CL = 90%
$\Gamma(D^0 \rightarrow K^- \pi^+ \mu^+ \mu^-)/\Gamma_{\text{total}}$	$< 3.59 \times 10^{-4}$, CL = 90%
$\Gamma(D^0 \rightarrow \pi^+ \pi^- \pi^0 \mu^+ \mu^-)/\Gamma_{\text{total}}$	$< 8.1 \times 10^{-4}$, CL = 90%
$\Gamma(D_s^+ \rightarrow K^+ e^+ e^-)/\Gamma_{\text{total}}$	$< 3.7 \times 10^{-6}$, CL = 90%
$\Gamma(D_s^+ \rightarrow K^+ \mu^+ \mu^-)/\Gamma_{\text{total}}$	$< 2.1 \times 10^{-5}$, CL = 90%
$\Gamma(D_s^+ \rightarrow K^*(892)^+ \mu^+ \mu^-)/\Gamma_{\text{total}}$	$< 1.4 \times 10^{-3}$, CL = 90%
$\Gamma(\Lambda_C^+ \rightarrow p e^+ e^-)/\Gamma_{\text{total}}$	$< 5.5 \times 10^{-6}$, CL = 90%

Tests of Conservation Laws

$$\Gamma(\Lambda_c^+ \rightarrow p \mu^+ \mu^- \text{ non-resonant})/\Gamma_{\text{total}} < 7.7 \times 10^{-8}, \text{ CL} = 90\%$$

$\Delta B = 1$ WEAK NEUTRAL CURRENT FORBIDDEN

Allowed by higher-order electroweak interactions.

$\Gamma(B^+ \rightarrow \pi^+ \ell^+ \ell^-)/\Gamma_{\text{total}}$	$< 4.9 \times 10^{-8}, \text{ CL} = 90\%$
$\Gamma(B^+ \rightarrow \pi^+ e^+ e^-)/\Gamma_{\text{total}}$	$< 8.0 \times 10^{-8}, \text{ CL} = 90\%$
$\Gamma(B^+ \rightarrow \pi^+ \mu^+ \mu^-)/\Gamma_{\text{total}}$	$(1.75 \pm 0.22) \times 10^{-8}$
$\Gamma(B^+ \rightarrow \pi^+ \nu \bar{\nu})/\Gamma_{\text{total}}$	$< 1.4 \times 10^{-5}, \text{ CL} = 90\%$
$\Gamma(B^+ \rightarrow K^+ \ell^+ \ell^-)/\Gamma_{\text{total}}$	[<i>a</i>] $(4.51 \pm 0.23) \times 10^{-7} (S = 1.1)$
$\Gamma(B^+ \rightarrow K^+ e^+ e^-)/\Gamma_{\text{total}}$	$(5.5 \pm 0.7) \times 10^{-7}$
$\Gamma(B^+ \rightarrow K^+ \mu^+ \mu^-)/\Gamma_{\text{total}}$	$(4.41 \pm 0.22) \times 10^{-7} (S = 1.2)$
$\Gamma(B^+ \rightarrow K^+ \mu^+ \mu^- \text{ nonresonant})/\Gamma_{\text{total}}$	$(4.37 \pm 0.27) \times 10^{-7}$
$\Gamma(B^+ \rightarrow K^+ \tau^+ \tau^-)/\Gamma_{\text{total}}$	$< 2.25 \times 10^{-3}, \text{ CL} = 90\%$
$\Gamma(B^+ \rightarrow K^+ \nu \bar{\nu})/\Gamma_{\text{total}}$	$< 1.6 \times 10^{-5}, \text{ CL} = 90\%$
$\Gamma(B^+ \rightarrow \rho^+ \nu \bar{\nu})/\Gamma_{\text{total}}$	$< 3.0 \times 10^{-5}, \text{ CL} = 90\%$
$\Gamma(B^+ \rightarrow K^*(892)^+ \ell^+ \ell^-)/\Gamma_{\text{total}}$	[<i>a</i>] $(1.01 \pm 0.11) \times 10^{-6} (S = 1.1)$
$\Gamma(B^+ \rightarrow K^*(892)^+ e^+ e^-)/\Gamma_{\text{total}}$	$(1.55 \pm_{-0.31}^{0.40}) \times 10^{-6}$
$\Gamma(B^+ \rightarrow K^*(892)^+ \mu^+ \mu^-)/\Gamma_{\text{total}}$	$(9.6 \pm 1.0) \times 10^{-7}$
$\Gamma(B^+ \rightarrow K^*(892)^+ \nu \bar{\nu})/\Gamma_{\text{total}}$	$< 4.0 \times 10^{-5}, \text{ CL} = 90\%$
$\Gamma(B^+ \rightarrow K^+ \pi^+ \pi^- \mu^+ \mu^-)/\Gamma_{\text{total}}$	$(4.3 \pm 0.4) \times 10^{-7}$
$\Gamma(B^+ \rightarrow \phi K^+ \mu^+ \mu^-)/\Gamma_{\text{total}}$	$(7.9 \pm_{-1.7}^{2.1}) \times 10^{-8}$
$\Gamma(B^0 \rightarrow \gamma \gamma)/\Gamma_{\text{total}}$	$< 3.2 \times 10^{-7}, \text{ CL} = 90\%$
$\Gamma(B^0 \rightarrow e^+ e^-)/\Gamma_{\text{total}}$	$< 8.3 \times 10^{-8}, \text{ CL} = 90\%$
$\Gamma(B^0 \rightarrow e^+ e^- \gamma)/\Gamma_{\text{total}}$	$< 1.2 \times 10^{-7}, \text{ CL} = 90\%$
$\Gamma(B^0 \rightarrow \mu^+ \mu^-)/\Gamma_{\text{total}}$	$(1.1 \pm_{-1.3}^{1.4}) \times 10^{-10} (S = 1.6)$
$\Gamma(B^0 \rightarrow \mu^+ \mu^- \gamma)/\Gamma_{\text{total}}$	$< 1.6 \times 10^{-7}, \text{ CL} = 90\%$
$\Gamma(B^0 \rightarrow \mu^+ \mu^- \mu^+ \mu^-)/\Gamma_{\text{total}}$	$< 6.9 \times 10^{-10}, \text{ CL} = 95\%$
$\Gamma(B^0 \rightarrow SP, S \rightarrow \mu^+ \mu^-, P \rightarrow \mu^+ \mu^-)/\Gamma_{\text{total}}$	[<i>b</i>] $< 6.0 \times 10^{-10}, \text{ CL} = 95\%$
$\Gamma(B^0 \rightarrow \tau^+ \tau^-)/\Gamma_{\text{total}}$	$< 2.1 \times 10^{-3}, \text{ CL} = 95\%$
$\Gamma(B^0 \rightarrow \pi^0 \ell^+ \ell^-)/\Gamma_{\text{total}}$	$< 5.3 \times 10^{-8}, \text{ CL} = 90\%$
$\Gamma(B^0 \rightarrow \pi^0 e^+ e^-)/\Gamma_{\text{total}}$	$< 8.4 \times 10^{-8}, \text{ CL} = 90\%$
$\Gamma(B^0 \rightarrow \pi^0 \mu^+ \mu^-)/\Gamma_{\text{total}}$	$< 6.9 \times 10^{-8}, \text{ CL} = 90\%$
$\Gamma(B^0 \rightarrow \eta \ell^+ \ell^-)/\Gamma_{\text{total}}$	$< 6.4 \times 10^{-8}, \text{ CL} = 90\%$
$\Gamma(B^0 \rightarrow \eta e^+ e^-)/\Gamma_{\text{total}}$	$< 1.08 \times 10^{-7}, \text{ CL} = 90\%$
$\Gamma(B^0 \rightarrow \eta \mu^+ \mu^-)/\Gamma_{\text{total}}$	$< 1.12 \times 10^{-7}, \text{ CL} = 90\%$
$\Gamma(B^0 \rightarrow \pi^0 \nu \bar{\nu})/\Gamma_{\text{total}}$	$< 9 \times 10^{-6}, \text{ CL} = 90\%$
$\Gamma(B^0 \rightarrow K^0 \ell^+ \ell^-)/\Gamma_{\text{total}}$	[<i>a</i>] $(3.1 \pm_{-0.7}^{0.8}) \times 10^{-7}$
$\Gamma(B^0 \rightarrow K^0 e^+ e^-)/\Gamma_{\text{total}}$	$(1.6 \pm_{-0.8}^{1.0}) \times 10^{-7}$
$\Gamma(B^0 \rightarrow K^0 \mu^+ \mu^-)/\Gamma_{\text{total}}$	$(3.39 \pm 0.34) \times 10^{-7}$
$\Gamma(B^0 \rightarrow K^0 \nu \bar{\nu})/\Gamma_{\text{total}}$	$< 2.6 \times 10^{-5}, \text{ CL} = 90\%$
$\Gamma(B^0 \rightarrow \rho^0 \nu \bar{\nu})/\Gamma_{\text{total}}$	$< 4.0 \times 10^{-5}, \text{ CL} = 90\%$
$\Gamma(B^0 \rightarrow K^*(892)^0 \ell^+ \ell^-)/\Gamma_{\text{total}}$	[<i>a</i>] $(9.9 \pm_{-1.1}^{1.2}) \times 10^{-7}$
$\Gamma(B^0 \rightarrow K^*(892)^0 e^+ e^-)/\Gamma_{\text{total}}$	$(1.03 \pm_{-0.17}^{0.19}) \times 10^{-6}$
$\Gamma(B^0 \rightarrow K^*(892)^0 \mu^+ \mu^-)/\Gamma_{\text{total}}$	$(9.4 \pm 0.5) \times 10^{-7}$
$\Gamma(B^0 \rightarrow \pi^+ \pi^- \mu^+ \mu^-)/\Gamma_{\text{total}}$	$(2.1 \pm 0.5) \times 10^{-8}$
$\Gamma(B^0 \rightarrow K^*(892)^0 \nu \bar{\nu})/\Gamma_{\text{total}}$	$< 1.8 \times 10^{-5}, \text{ CL} = 90\%$
$\Gamma(B^0 \rightarrow \text{invisible})/\Gamma_{\text{total}}$	$< 2.4 \times 10^{-5}, \text{ CL} = 90\%$
$\Gamma(B^0 \rightarrow \nu \bar{\nu} \gamma)/\Gamma_{\text{total}}$	$< 1.7 \times 10^{-5}, \text{ CL} = 90\%$
$\Gamma(B^0 \rightarrow \phi \nu \bar{\nu})/\Gamma_{\text{total}}$	$< 1.27 \times 10^{-4}, \text{ CL} = 90\%$
$\Gamma(B \rightarrow s e^+ e^-)/\Gamma_{\text{total}}$	$(6.7 \pm 1.7) \times 10^{-6} (S = 2.0)$
$\Gamma(B \rightarrow s \mu^+ \mu^-)/\Gamma_{\text{total}}$	$(4.3 \pm 1.0) \times 10^{-6}$
$\Gamma(B \rightarrow s \ell^+ \ell^-)/\Gamma_{\text{total}}$	[<i>a</i>] $(5.8 \pm 1.3) \times 10^{-6} (S = 1.8)$
$\Gamma(B \rightarrow \pi \ell^+ \ell^-)/\Gamma_{\text{total}}$	$< 5.9 \times 10^{-8}, \text{ CL} = 90\%$
$\Gamma(B \rightarrow \pi e^+ e^-)/\Gamma_{\text{total}}$	$< 1.10 \times 10^{-7}, \text{ CL} = 90\%$
$\Gamma(B \rightarrow \pi \mu^+ \mu^-)/\Gamma_{\text{total}}$	$< 5.0 \times 10^{-8}, \text{ CL} = 90\%$
$\Gamma(B \rightarrow K e^+ e^-)/\Gamma_{\text{total}}$	$(4.4 \pm 0.6) \times 10^{-7}$
$\Gamma(B \rightarrow K^*(892) e^+ e^-)/\Gamma_{\text{total}}$	$(1.19 \pm 0.20) \times 10^{-6} (S = 1.2)$
$\Gamma(B \rightarrow K \mu^+ \mu^-)/\Gamma_{\text{total}}$	$(4.4 \pm 0.4) \times 10^{-7}$
$\Gamma(B \rightarrow K^*(892) \mu^+ \mu^-)/\Gamma_{\text{total}}$	$(1.06 \pm 0.09) \times 10^{-6}$
$\Gamma(B \rightarrow K \ell^+ \ell^-)/\Gamma_{\text{total}}$	$(4.8 \pm 0.4) \times 10^{-7}$
$\Gamma(B \rightarrow K^*(892) \ell^+ \ell^-)/\Gamma_{\text{total}}$	$(1.05 \pm 0.10) \times 10^{-6}$
$\Gamma(B \rightarrow K \nu \bar{\nu})/\Gamma_{\text{total}}$	$< 1.6 \times 10^{-5}, \text{ CL} = 90\%$
$\Gamma(B \rightarrow K^* \nu \bar{\nu})/\Gamma_{\text{total}}$	$< 2.7 \times 10^{-5}, \text{ CL} = 90\%$
$\Gamma(B \rightarrow \pi \nu \bar{\nu})/\Gamma_{\text{total}}$	$< 8 \times 10^{-6}, \text{ CL} = 90\%$
$\Gamma(B \rightarrow \rho \nu \bar{\nu})/\Gamma_{\text{total}}$	$< 2.8 \times 10^{-5}, \text{ CL} = 90\%$
$\Gamma(\bar{B} \rightarrow \bar{s} \nu \bar{\nu})/\Gamma_{\text{total}}$	$< 6.4 \times 10^{-4}, \text{ CL} = 90\%$
$\Gamma(\bar{B} \rightarrow \mu^+ \mu^- \text{ anything})/\Gamma_{\text{total}}$	$< 3.2 \times 10^{-4}, \text{ CL} = 90\%$

Unless otherwise stated, limits are given at the 90% confidence level, while errors are given as ± 1 standard deviation.

$\Gamma(B_S^0 \rightarrow \gamma \gamma)/\Gamma_{\text{total}}$	$< 3.1 \times 10^{-6}, \text{ CL} = 90\%$
$\Gamma(B_S^0 \rightarrow \phi \gamma)/\Gamma_{\text{total}}$	$(3.4 \pm 0.4) \times 10^{-5}$
$\Gamma(B_S^0 \rightarrow \mu^+ \mu^-)/\Gamma_{\text{total}}$	$(3.0 \pm 0.4) \times 10^{-9}$
$\Gamma(B_S^0 \rightarrow e^+ e^-)/\Gamma_{\text{total}}$	$< 2.8 \times 10^{-7}, \text{ CL} = 90\%$
$\Gamma(B_S^0 \rightarrow \tau^+ \tau^-)/\Gamma_{\text{total}}$	$< 6.8 \times 10^{-3}, \text{ CL} = 95\%$
$\Gamma(B_S^0 \rightarrow \mu^+ \mu^- \mu^+ \mu^-)/\Gamma_{\text{total}}$	$< 2.5 \times 10^{-9}, \text{ CL} = 95\%$
$\Gamma(B_S^0 \rightarrow SP, S \rightarrow \mu^+ \mu^-, P \rightarrow \mu^+ \mu^-)/\Gamma_{\text{total}}$	[<i>b</i>] $< 2.2 \times 10^{-9}, \text{ CL} = 95\%$
$\Gamma(B_S^0 \rightarrow \phi(1020) \mu^+ \mu^-)/\Gamma_{\text{total}}$	$(8.2 \pm 1.2) \times 10^{-7}$
$\Gamma(B_S^0 \rightarrow \pi^+ \pi^- \mu^+ \mu^-)/\Gamma_{\text{total}}$	$(8.4 \pm 1.7) \times 10^{-8}$
$\Gamma(B_S^0 \rightarrow \phi \nu \bar{\nu})/\Gamma_{\text{total}}$	$< 5.4 \times 10^{-3}, \text{ CL} = 90\%$

$\Delta T = 1$ WEAK NEUTRAL CURRENT FORBIDDEN

Allowed by higher-order electroweak interactions.

$\Gamma(t \rightarrow Zq(q=u,c))/\Gamma_{\text{total}}$	[<i>cc</i>] $< 5 \times 10^{-4}, \text{ CL} = 95\%$
$\Gamma(t \rightarrow Hu)/\Gamma_{\text{total}}$	$< 1.2 \times 10^{-3}, \text{ CL} = 95\%$
$\Gamma(t \rightarrow Hc)/\Gamma_{\text{total}}$	$< 1.1 \times 10^{-3}, \text{ CL} = 95\%$
$\Gamma(t \rightarrow \ell^+ \bar{q}q' (q=d,s,b; q'=u,c))/\Gamma_{\text{total}}$	$< 1.6 \times 10^{-3}, \text{ CL} = 95\%$

NOTES

In this Summary Table:

When a quantity has “(S = ...)” to its right, the error on the quantity has been enlarged by the “scale factor” S, defined as $S = \sqrt{\chi^2/(N-1)}$, where N is the number of measurements used in calculating the quantity. We do this when $S > 1$, which often indicates that the measurements are inconsistent. When $S > 1.25$, we also show in the Particle Listings an ideogram of the measurements. For more about S, see the Introduction.

- [a] Forbidden by angular momentum conservation.
- [b] C parity forbids this to occur as a single-photon process.
- [c] See the Particle Listings for the (complicated) definition of this quantity.
- [d] Time-reversal invariance requires this to be 0° or 180° .
- [e] This coefficient is zero if time invariance is not violated.
- [f] Allowed by higher-order electroweak interactions.
- [g] Violates CP in leading order. Test of direct CP violation since the indirect CP-violating and CP-conserving contributions are expected to be suppressed.
- [h] In the 2010 Review, the values for these quantities were given using a measure of the asymmetry that was inconsistent with the usual definition.
- [i] $\text{Re}(\epsilon'/\epsilon) = \epsilon'/\epsilon$ to a very good approximation provided the phases satisfy CPT invariance.
- [j] This mode includes gammas from inner bremsstrahlung but not the direct emission mode $K_L^0 \rightarrow \pi^+ \pi^- \gamma$ (DE).
- [k] Neglecting photon channels. See, e.g., A. Pais and S.B. Treiman, Phys. Rev. **D12**, 2744 (1975).
- [l] Derived from measured values of $\phi_{+-}, \phi_{00}, |\eta|, |m_{K_L^0} - m_{K_S^0}|$, and $\tau_{K_S^0}$, as described in the introduction to “Tests of Conservation Laws.”
- [n] The $|m_p - m_{\bar{p}}|/m_p$ and $|q_p + q_{\bar{p}}|/e$ are not independent, and both use the more precise measurement of $|q_{\bar{p}}/m_{\bar{p}}|/(q_p/m_p)$.
- [o] The value is for the sum of the charge states or particle/antiparticle states indicated.
- [p] A test of additive vs. multiplicative lepton family number conservation.
- [q] Derived from an analysis of neutrino-oscillation experiments.
- [r] This limit is for either D^0 or \bar{D}^0 to $p e^-$.
- [s] This limit is for either D^0 or \bar{D}^0 to $\bar{p} e^+$.
- [t] The first limit is for $p \rightarrow$ anything or “disappearance” modes of a bound proton. The second entry, a rough range of limits, assumes the dominant decay modes are among those investigated. For antiprotons the best limit, inferred from the observation of cosmic ray \bar{p} 's is $\tau_{\bar{p}} > 10^7$ yr, the cosmic-ray storage time, but this limit depends on a number of assumptions. The best direct observation of stored antiprotons gives $\tau_{\bar{p}}/B(\bar{p} \rightarrow e^- \gamma) > 7 \times 10^5$ yr.
- [u] There is some controversy about whether nuclear physics and model dependence complicate the analysis for bound neutrons (from which the

- best limit comes). The first limit here is from reactor experiments with free neutrons.
- [v] This is the best limit for the mode $e^- \rightarrow \nu \gamma$. The best limit for Nuclear de-excitation experiments is 6.4×10^{24} yr.
- [x] The limit is from neutrality-of-matter experiments; it assumes $q_n = q_p + q_e$. See also the charge of the neutron.
- [y] See the K_S^0 Particle Listings for the energy limits used in this measurement.
- [z] See the K_L^0 Particle Listings for the energy limits used in this measurement.
- [aa] An ℓ indicates an e or a μ mode, not a sum over these modes.
- [bb] Here S and P are the hypothetical scalar and pseudoscalar particles with masses of $2.5 \text{ GeV}/c^2$ and $214.3 \text{ MeV}/c^2$, respectively.
- [cc] This limit is for $\Gamma(t \rightarrow Zq)/\Gamma(t \rightarrow Wb)$.

REVIEWS, TABLES, AND PLOTS

Constants, Units, Atomic and Nuclear Properties

1. Physical constants (rev.)	137
2. Astrophysical constants (rev.)	138
3. International system of units (SI)	140
4. Periodic table of the elements (rev.)	141
5. Electronic structure of the elements	142
6. Atomic and nuclear properties of materials	144
7. Electromagnetic relations	146
8. Naming scheme for hadrons (rev.)	148

1. Physical Constants (a major revision)

Table 1.1. Revised 2019 by C.G. Wohl (LBNL). Reviewed by P.J. Mohr and D.B. Newell (NIST). Mainly from “CODATA Recommended Values of the Fundamental Physical Constants: 2018,” E. Tiesinga, D.B. Newell, P.J. Mohr, and B.N. Taylor, NIST SP961 (May 2019). The electron charge magnitude e , and the Planck, Boltzmann, and Avogadro constants h , k , and N_A , now join c as having defined values; the free-space permittivity and permeability constants ϵ_0 and μ_0 are no longer exact. These changes affect practically everything else in the Table. Figures in parentheses after the values are the 1-standard-deviation uncertainties in the last digits; the fractional uncertainties in parts per 10^9 (ppb) are in the last column. The full 2018 CODATA Committee on Data for Science and Technology set of constants are found at <https://physics.nist.gov/constants>. The last set of constants (beginning with the Fermi coupling constant) comes from the Particle Data Group. See also “The International System of Units (SI),” 9th ed. (2019) of the International Bureau of Weights and Measures (BIPM), <https://www.bipm.org/utis/common/pdf/si-brochure/SI-Brochure-9-EN.pdf>.

Quantity	Symbol, equation	Value	Uncertainty (ppb)
speed of light in vacuum	c	299 792 458 m s ⁻¹	exact
Planck constant	h	6.626 070 15×10 ⁻³⁴ J s (or J/Hz) [‡]	exact
Planck constant, reduced	$\hbar \equiv h/2\pi$	1.054 571 817... × 10 ⁻³⁴ J s = 6.582 119 569... × 10 ⁻²² MeV s	exact* exact*
electron charge magnitude	e	1.602 176 634×10 ⁻¹⁹ C	exact
conversion constant	$\hbar c$	197.326 980 4... MeV fm	exact*
conversion constant	$(\hbar c)^2$	0.389 379 372 1... GeV ² mbarn	exact*
electron mass	m_e	0.510 998 950 00(15) MeV/c ² = 9.109 383 7015(28)×10 ⁻³¹ kg	0.30
proton mass	m_p	938.272 088 16(29) MeV/c ² = 1.672 621 923 69(51)×10 ⁻²⁷ kg = 1.007 276 466 621(53) u = 1836.152 673 43(11) m_e	0.053, 0.060
neutron mass	m_n	939.565 420 52(54) MeV/c ² = 1.008 664 915 95(49) u	0.57, 0.48
deuteron mass	m_d	1875.612 942 57(57) MeV/c ²	0.30
unified atomic mass unit**	$u = (\text{mass } ^{12}\text{C atom})/12$	931.494 102 42(28) MeV/c ² = 1.660 539 066 60(50)×10 ⁻²⁷ kg	0.30
permittivity of free space	$\epsilon_0 = 1/\mu_0 c^2$	8.854 187 8128(13) × 10 ⁻¹² F m ⁻¹	0.15
permeability of free space	$\mu_0/(4\pi \times 10^{-7})$	1.000 000 000 55(15) N A ⁻²	0.15
fine-structure constant	$\alpha = e^2/4\pi\epsilon_0\hbar c$	7.297 352 5693(11)×10 ⁻³ = 1/137.035 999 084(21) [†]	0.15
classical electron radius	$r_e = e^2/4\pi\epsilon_0 m_e c^2$	2.817 940 3262(13)×10 ⁻¹⁵ m	0.45
(e^- Compton wavelength)/2 π	$\lambda_e = \hbar/m_e c = r_e \alpha^{-1}$	3.861 592 6796(12)×10 ⁻¹³ m	0.30
Bohr radius ($m_{\text{nucleus}} = \infty$)	$a_\infty = 4\pi\epsilon_0\hbar^2/m_e e^2 = r_e \alpha^{-2}$	0.529 177 210 903(80)×10 ⁻¹⁰ m	0.15
wavelength of 1 eV/c particle	$\hbar c/(1 \text{ eV})$	1.239 841 984... × 10 ⁻⁶ m	exact*
Rydberg energy	$\hbar c R_\infty = m_e e^4/2(4\pi\epsilon_0)^2 \hbar^2 = m_e c^2 \alpha^2/2$	13.605 693 122 994(26) eV	1.9×10 ⁻³
Thomson cross section	$\sigma_T = 8\pi r_e^2/3$	0.665 245 873 21(60) barn	0.91
Bohr magneton	$\mu_B = e\hbar/2m_e$	5.788 381 8060(17)×10 ⁻¹¹ MeV T ⁻¹	0.3
nuclear magneton	$\mu_N = e\hbar/2m_p$	3.152 451 258 44(96)×10 ⁻¹⁴ MeV T ⁻¹	0.31
electron cyclotron freq./field	$\omega_{\text{cycl}}^e/B = e/m_e$	1.758 820 010 76(53)×10 ¹¹ rad s ⁻¹ T ⁻¹	0.30
proton cyclotron freq./field	$\omega_{\text{cycl}}^p/B = e/m_p$	9.578 833 1560(29)×10 ⁷ rad s ⁻¹ T ⁻¹	0.31
gravitational constant [‡]	G_N	6.674 30(15)×10 ⁻¹¹ m ³ kg ⁻¹ s ⁻² = 6.708 83(15)×10 ⁻³⁹ $\hbar c$ (GeV/c ²) ⁻²	2.2 × 10 ⁴ 2.2 × 10 ⁴
standard gravitational accel.	g_N	9.806 65 m s ⁻²	exact
Avogadro constant	N_A	6.022 140 76×10 ²³ mol ⁻¹	exact
Boltzmann constant	k	1.380 649×10 ⁻²³ J K ⁻¹ = 8.617 333 262... × 10 ⁻⁵ eV K ⁻¹	exact* exact*
molar volume, ideal gas at STP	$N_A k$ (273.15 K)/(101 325 Pa)	22.413 969 54... × 10 ⁻³ m ³ mol ⁻¹	exact*
Wien displacement law constant	$b = \lambda_{\text{max}} T$	2.897 771 955... × 10 ⁻³ m K	exact*
Stefan-Boltzmann constant	$\sigma = \pi^2 k^4/60\hbar^3 c^2$	5.670 374 419... × 10 ⁻⁸ W m ⁻² K ⁻⁴	exact*
Fermi coupling constant ^{‡‡}	$G_F/(\hbar c)^3$	1.166 378 7(6)×10 ⁻⁵ GeV ⁻²	510
weak-mixing angle	$\sin^2 \hat{\theta}(M_Z) (\overline{\text{MS}})$	0.231 21(4) ^{††}	1.7 × 10 ⁵
W^\pm boson mass	m_W	80.379(12) GeV/c ²	1.5 × 10 ⁵
Z^0 boson mass	m_Z	91.1876(21) GeV/c ²	2.3 × 10 ⁴
strong coupling constant	$\alpha_s(m_Z)$	0.1179(10)	8.5 × 10 ⁶
$\pi = 3.141 592 653 589 793 238...$		$e = 2.718 281 828 459 045 235...$	$\gamma = 0.577 215 664 901 532 860...$
1 in \equiv 0.0254 m	1 G \equiv 10 ⁻⁴ T	1 eV = 1.602 176 634 × 10 ⁻¹⁹ J (exact)	kT at 300 K = [38.681 740(22)] ⁻¹ eV
1 Å \equiv 0.1 nm	1 dyne \equiv 10 ⁻⁵ N	(1 kg)c ² = 5.609 588 603... × 10 ³⁵ eV (exact*)	0 °C \equiv 273.15 K
1 barn \equiv 10 ⁻²⁸ m ²	1 erg \equiv 10 ⁻⁷ J	1 C = 2.997 924 58 × 10 ⁹ esu	1 atmosphere \equiv 760 Torr \equiv 101 325 Pa

[‡] CODATA recommends that the unit be J/Hz to stress that in $h = E/\nu$ the frequency ν is in cycles/sec (Hz), not radians/sec.

* These are calculated from exact values and are exact to the number of places given (*i.e.* no rounding).

** The molar mass of ¹²C is 11.999 999 9958(36) g.

† At $Q^2 = 0$. At $Q^2 \approx m_W^2$ the value is $\sim 1/128$.

‡ Absolute laboratory measurements of G_N have been made only on scales of about 1 cm to 1 m.

‡‡ See the discussion in Sec. 10, “Electroweak model and constraints on new physics.”

†† The corresponding $\sin^2 \theta$ for the effective angle is 0.23153(4).

2. Astrophysical Constants and Parameters

Table 2.1: Revised August 2019 by D.E. Groom (LBNL) and D. Scott (U. of British Columbia). The figures in parentheses after some values give the $1\text{-}\sigma$ uncertainties in the last digit(s). Physical constants are from Ref. [1]. While every effort has been made to obtain the most accurate current values of the listed quantities, the table does not represent a critical review or adjustment of the constants, and is not intended as a primary reference. The values and uncertainties for the cosmological parameters depend on the exact data sets, priors, and basis parameters used in the fit. Many of the derived parameters reported in this table have non-Gaussian likelihoods. Parameters may be highly correlated, so care must be taken in propagating errors. Unless otherwise specified, cosmological parameters are derived from a 6-parameter Λ CDM cosmology fit to *Planck* cosmic microwave background 2018 temperature (TT) + polarization (TE,EE+lowE) + lensing data [2]. For more information see Ref. [3] and the original papers.

Quantity	Symbol, equation.	Value	Reference, footnote
Newtonian constant of gravitation	G_N	$6.674\,30(15) \times 10^{-11} \text{ m}^3 \text{ kg}^{-1} \text{ s}^{-2}$	[1]
Planck mass	$M_P = \sqrt{\hbar c/G_N}$	$1.220\,890(14) \times 10^{19} \text{ GeV}/c^2 = 2.176\,434(24) \times 10^{-8} \text{ kg}$	[1]
Planck length	$l_P = \sqrt{\hbar G_N/c^3}$	$1.616\,255(18) \times 10^{-35} \text{ m}$	[1]
tropical year (equinox to equinox, 2020)	yr	$31\,556\,925.1 \text{ s} = 365.242\,189 \text{ days}$	[4]
sidereal year (period of Earth around Sun relative to stars)		$31\,558\,149.8 \text{ s} \approx \pi \times 10^7 \text{ s}$	[4]
mean sidereal day (Earth rotation period relative to stars)		$23^{\text{h}}\,56^{\text{m}}\,04^{\text{s}}.090\,53$	[4]
astronomical unit	au	$149\,597\,870\,700 \text{ m}$	exact [5]
parsec (1 au/1 arc sec)	pc	$3.085\,677\,581\,49 \times 10^{16} \text{ m} = 3.261\,56 \dots \text{ ly}$	exact [6]
light year (deprecated unit)	ly	$0.306\,601 \dots \text{ pc} = 0.946\,073 \dots \times 10^{16} \text{ m}$	[7]
solid angle	deg^2	$(\pi/180)^2 \text{ sr} = 3.046\,17 \dots \times 10^{-4} \text{ sr}$	[8]
Schwarzschild radius of the Sun	$2G_N M_\odot/c^2$	$2.953\,250\,076\,100\,25 \text{ km}$	[9]
Solar mass	M_\odot	$1.988\,41(4) \times 10^{30} \text{ kg}$	[10]
nominal Solar equatorial radius	R_\odot	$6.957 \times 10^8 \text{ m}$	exact [11]
nominal Solar constant	S_\odot	1361 W m^{-2}	exact [11, 12]
nominal Solar photosphere temperature	T_\odot	5772 K	exact [11]
nominal Solar luminosity	L_\odot	$3.828 \times 10^{26} \text{ W}$	exact [11, 13]
Schwarzschild radius of the Earth	$2G_N M_\oplus/c^2$	$8.870\,055\,940 \text{ mm}$	[9]
Earth mass	M_\oplus	$5.972\,17(13) \times 10^{24} \text{ kg}$	[10]
nominal Earth equatorial radius	R_\oplus	$6.3781 \times 10^6 \text{ m}$	exact [11]
Chandrasekhar mass	M_{Ch}	$3.097\,972 \mu^{-2} M_P^3/m_H^2 = 1.433\,77(6) (\mu/2)^{-2} M_\odot$	[14, 15]
Eddington luminosity	L_{Ed}	$1.257\,065\,179\,8(12) \times 10^{31} (M/M_\odot) \text{ W}$ $= 3.283\,869\,330\,8(31) \times 10^4 (M/M_\odot) L_\odot$	[16, 17]
jansky (flux density)	Jy	$10^{-26} \text{ W m}^{-2} \text{ Hz}^{-1}$	definition
luminosity conversion	f_0	$3.0128 \times 10^{28} \times 10^{-0.4 M_{\text{Bol}}} \text{ W}$	exact [18]
flux conversion	\mathcal{F}	$(M_{\text{Bol}} = \text{absolute bolometric magnitude} = \text{bolometric magnitude at } 10 \text{ pc})$ $2.518\,021\,002 \times 10^{-8} \times 10^{-0.4 m_{\text{Bol}}} \text{ W m}^{-2}$	exact [18]
ABsolute monochromatic magnitude	AB	$(m_{\text{Bol}} = \text{apparent bolometric magnitude})$ $-2.5 \log_{10} f_\nu - 56.10 \text{ (for } f_\nu \text{ in } \text{W m}^{-2} \text{ Hz}^{-1})$ $= -2.5 \log_{10} f_\nu + 8.90 \text{ (for } f_\nu \text{ in Jy)}$	[19]
Solar angular velocity around Galactic center	Θ_0/R_0	$27.1(5) \text{ km s}^{-1} \text{ kpc}^{-1}$	[20]
Solar distance from Galactic center	R_0	$8.178 \pm 0.013(\text{stat.}) \pm 0.022(\text{sys.}) \text{ kpc}$	[21, 22]
circular velocity at R_0	v_0 or Θ_0	$240(8) \text{ km s}^{-1}$	[22, 23]
escape velocity from the Galaxy	v_{esc}	$492 \text{ km s}^{-1} < v_{\text{esc}} < 587 \text{ km s}^{-1} \text{ (90\%)}$	[24]
local disk density	ρ_{disk}	$6.6(9) \times 10^{-24} \text{ g cm}^{-3} = 3.7(5) \text{ GeV}/c^2 \text{ cm}^{-3}$	[25]
local dark matter density	ρ_χ	canonical value $0.3 \text{ GeV}/c^2 \text{ cm}^{-3}$ within factor 2–3	[26]
present-day CMB temperature	T_0	$2.7255(6) \text{ K}$	[27, 28]
present-day CMB dipole amplitude	d	$3.3621(10) \text{ mK}$	[27, 29]
Solar velocity with respect to CMB	v_\odot	$369.82(11) \text{ km s}^{-1}$ towards $(l, b) = (264.021(11)^\circ, 48.253(5)^\circ)$	[29]
Local Group velocity with respect to CMB	v_{LG}	$620(15) \text{ km s}^{-1}$ towards $(l, b) = (271.9(20)^\circ, 29.6(14)^\circ)$	[29]
number density of CMB photons	n_γ	$410.7(3) (T/2.7255)^3 \text{ cm}^{-3}$	[30]
density of CMB photons	ρ_γ	$4.645(4) (T/2.7255)^4 \times 10^{-34} \text{ g cm}^{-3} \approx 0.260 \text{ eV cm}^{-3}$	[30]
entropy density/Boltzmann constant	s/k	$2.891.2 (T/2.7255)^3 \text{ cm}^{-3}$	[30]
present-day Hubble expansion rate	H_0	$100 h \text{ km s}^{-1} \text{ Mpc}^{-1} = h \times (9.777\,752 \text{ Gyr})^{-1}$	[31]
scaling factor for Hubble expansion rate	h	$0.674(5)$	[2, 32]
Hubble length	c/H_0	$0.925\,0629 \times 10^{26} h^{-1} \text{ m} = 1.372(10) \times 10^{26} \text{ m}$	
scaling for cosmological constant	$c^2/3H_0^2$	$2.85247 \times 10^{51} h^{-2} \text{ m}^2 = 6.21(9) \times 10^{51} \text{ m}^2$	
critical density of the Universe	$\rho_{\text{crit}} = 3H_0^2/8\pi G_N$	$1.878\,34(4) \times 10^{-29} h^2 \text{ g cm}^{-3}$ $= 1.053\,672(24) \times 10^{-5} h^2 (\text{GeV}/c^2) \text{ cm}^{-3}$ $= 2.77536627 \times 10^{11} h^2 M_\odot \text{ Mpc}^{-3}$	
baryon-to-photon ratio (from BBN)	$\eta = n_b/n_\gamma$	$5.8 \times 10^{-10} \leq \eta \leq 6.5 \times 10^{-10} \text{ (95\% CL)}$	[33]
number density of baryons	n_b	$2.515(17) \times 10^{-7} \text{ cm}^{-3}$ $(2.4 \times 10^{-7} < n_b < 2.7 \times 10^{-7}) \text{ cm}^{-3} \text{ (95\% CL, } \eta \times n_\gamma)$	[2, 3, 34, 35]
CMB radiation density of the Universe	$\Omega_\gamma = \rho_\gamma/\rho_{\text{crit}}$	$2.473 \times 10^{-5} (T/2.7255)^4 h^{-2} = 5.38(15) \times 10^{-5}$	[30]
--- <i>Planck</i> 2018 6-parameter fit to flat Λ CDM cosmology ---			
baryon density of the Universe	$\Omega_b = \rho_b/\rho_{\text{crit}}$	$\ddagger 0.02237(15) h^{-2} = \dagger 0.0493(6)$	[2, 3, 27]
cold dark matter density of the Universe	$\Omega_c = \rho_c/\rho_{\text{crit}}$	$\ddagger 0.1200(12) h^{-2} = \dagger 0.265(7)$	[2, 3, 27]
100 \times approx to r_*/D_A	$100 \times \theta_{\text{MC}}$	$\ddagger 1.04092(31)$	[2, 3, 27]
reionization optical depth	τ	$\ddagger 0.054(7)$	[2, 3, 27]
ln(power prim. curv. pert.) ($k_0 = 0.05 \text{ Mpc}^{-1}$)	$\ln(10^{10} \Delta_{\mathcal{R}}^2)$	$\ddagger 3.044(14)$	[2, 3, 27]
scalar spectral index	n_s	$\ddagger 0.965(4)$	[2, 3, 27]
pressureless matter parameter	$\Omega_m = \Omega_c + \Omega_b$	$\ddagger 0.315(7)$	[2, 3]
dark energy density parameter	Ω_Λ	$\ddagger 0.685(7)$	[2, 3]
energy density of dark energy	ρ_Λ	$\ddagger 5.83(16) \times 10^{-30} \text{ g cm}^{-3}$	[2]
cosmological constant	Λ	$\ddagger 1.088(30) \times 10^{-56} \text{ cm}^{-2}$	[2]
fluctuation amplitude at $8 h^{-1} \text{ Mpc}$ scale	σ_8	$\ddagger 0.811(6)$	[2, 3]

Quantity	Symbol, equation.	Value	Reference, footnote
redshift of matter-radiation equality	z_{eq}	$\dagger 3402(26)$	[2, 36]
age at matter-radiation equality	t_{eq}	$\dagger 51.1(8)$ kyr	[2, 37]
redshift at which optical depth equals unity	z_*	$\dagger 1089.92(25)$	[2]
comoving size of sound horizon at z_*	r_*	$\dagger 144.43(26)$ Mpc	[2, 38]
age when optical depth equals unity	t_*	$\dagger 372.9(10)$ kyr	[2, 37]
redshift at half reionization	z_i	$\dagger 7.7(7)$	[2, 39]
age at half reionization	t_i	$\dagger 690(90)$ Myr	[2]
redshift when acceleration was zero	z_q	$\dagger 0.636(18)$	[2, 37]
age when acceleration was zero	t_q	$\dagger 7.70(10)$ Gyr	[2]
age of the Universe today	t_0	$\dagger 13.797(23)$ Gyr	[2]
effective number of neutrinos	N_{eff}	$\# 2.99(17)$	[2, 40, 41]
sum of neutrino masses	Σm_ν	$\# < 0.12$ eV (95%, CMB + BAO); ≥ 0.06 eV (mixing)	[2, 41–43]
neutrino density of the Universe	$\Omega_\nu = h^{-2} \Sigma m_{\nu_j} / 93.14$ eV	$\# < 0.003$ (95%, CMB + BAO); ≥ 0.0012 (mixing)	[2, 42, 43]
curvature	Ω_K	$\# 0.0007(19)$	[2]
running spectral index, $k_0 = 0.05$ Mpc $^{-1}$	$dn_s/d \ln k$	$\# -0.004(7)$	[2]
tensor-to-scalar field perturbations ratio,	$r_{0.002} = T/S$	$\# < 0.058$ (95% CL, $k_0 = 0.002$ Mpc $^{-1}$, no running)	[2, 44, 45]
dark energy equation of state parameter	w	$-1.028(31)$	[2, 46]
primordial helium fraction	Y_p	$0.245(4)$	[47]

\dagger Parameter in 6-parameter Λ CDM fit; \ddagger Derived parameter in 6-parameter Λ CDM fit; $\#$ Extended model parameter, *Planck* + BAO data [2].

References

- [1] CODATA recommended 2018 values of the fundamental physical constants: <https://physics.nist.gov/cuu/Constants/index.html>.
- [2] Planck Collab. 2018 Results VI (2018), [arXiv:1807.06209].
- [3] O. Lahav & A.R. Liddle, “The Cosmological Parameters,” Sec. 25.1 in this *Review*.
- [4] *The Astronomical Almanac for the year 2020*.
- [5] The astronomical unit of length (au) in meters is re-defined (IAU XXVIII General Assembly 2012, Resolution B2) to be a conventional unit of length in agreement with the value adopted in IAU XXVII 2009 Resolution B2. It is to be used with all time scales.
- [6] The distance at which 1 au subtends 1 arc sec: 1 au divided by $\pi/648000$.
- [7] IAU XVI GA 1976, Recommendations.
- [8] The number of square degrees on a sphere is $360^2/\pi = 41\,259.9\dots$
- [9] Observationally determined mass parameter $G_N M \times 2/c^2$ [1] for either the Sun or the Earth, where $G M_\odot = 1.327\,124\,4 \times 10^{20}$ m 3 s $^{-2}$ and $G M_\oplus = 3.986\,004 \times 10^{14}$ m 3 s $^{-2}$ [48].
- [10] $G_N M \div G_N$ [1].
- [11] IAU XXIX GA, 2015, Resolution B3, “on recommended nominal conversion constants ...” Calligraphic symbol indicates recommended nominal value.
- [12] See also G. Kopp & J.L. Lean, *Geophys. Res. Lett.* **38**, L01706 (2011), who give (1360.8 ± 0.6) W m $^{-2}$; see paper for caveats and other measurements.
- [13] $4\pi(1\text{ au})^2 \times S_\odot$, assuming isotropic irradiance.
- [14] S. Chandrasekhar, *Astrophys. J.* **74**, 81 (1931).
- [15] This value assumes an ideal Fermi gas, using a numerical constant from the Lane-Emden equation [49], and with μ the average molecular weight per electron, defined relative to the mass of the single-proton hydrogen atom.
- [16] A. S. Eddington, *Mon. Not. R. Astron. Soc.* **77**, 16 (1916).
- [17] The maximum luminosity assuming pure electron scattering for the outward force arising from radiation pressure: $4\pi G_N M m_p c / \sigma_T$.
- [18] IAU XXIX GA, 2015, Resolution B2, “on recommended zero points for the absolute and apparent bolometric magnitude scales”.
- [19] J. Oke and J. Gunn, *Astrophys. J.* **266**, 713 (1983).
- [20] J. Bovy, *Mon. Not. R. Astron. Soc.* **468**, 1, L63 (2017).
- [21] R. Abuter *et al.* (2019), [arXiv:1904.05721].
- [22] IAU XIX GA (1985) suggested that “in cases where standardization on a common set of galactic parameters is desirable” that the values $R_0 = (8.5 \pm 1.0)$ kpc and $\theta_0 = (220 \pm 20)$ km s $^{-1}$ should be used.
- [23] M. Reid *et al.*, *Astrophys. J.* **783**, 2, 130 (2014).
- [24] T. Piffl *et al.*, *Astron. Astrophys.* **562**, A91 (2014), [arXiv:1309.4293].
- [25] C. F. McKee, A. Parravano and D. J. Hollenbach, *Astrophys. J.* **814**, 1, 13 (2015); This is representative of other published estimates.
- [26] J. Read, *J. Phys.* **G41**, 063101 (2014); A. M. Green, *J. Phys.* **G44**, 8, 084001 (2017); The conclusion is $\rho_{\text{DM}}^{\text{local}} = 0.39 \pm 0.03$ GeV cm $^{-3}$.
- [27] D. Scott & G.F. Smoot, “Cosmic Microwave Background,” Sec. 29 in this *Review*.
- [28] D. J. Fixsen, *Astrophys. J.* **707**, 916 (2009).
- [29] Planck Collab. 2018 Results I (2018), [arXiv:1807.06205].
- [30] $n_\gamma = \frac{2c(3)}{\pi^2} \left(\frac{kT}{hc}\right)^3$; $\rho_\gamma = \frac{\pi^2 kT}{15 c^2} \left(\frac{kT}{hc}\right)^3$; $s/k = \frac{2.43 \cdot \pi^2}{11.45} \left(\frac{kT}{hc}\right)^3$; $kT/hc = 11.90\,235(T/2.7255)/\text{cm}$.
- [31] Conversion using length of sidereal year.
- [32] Distance-ladder estimates of H_0 tend to give higher values than derived from the CMB, *e.g.* Riess *et al.*, *Astrophys. J.* **826**, 56 (2016) give $h = 0.732 \pm 0.017$; for discussion see O. Lahav & A.R. Liddle, “The Cosmological Parameters,” Sec. 25.1 in this *Review*.
- [33] B.D. Fields, P. Molaro, & S. Sarkar, “Big-Bang Nucleosynthesis,” Sec. 24 in this *Review*.
- [34] n_b depends only upon the measured $\Omega_b h^2$, the average baryon mass at the present epoch [35], and G_N : $n_b = (\Omega_b h^2)(h^{-2} \rho_{\text{crit}})/(0.93711 \text{ GeV}/c^2 \text{ per baryon})$.
- [35] G. Steigman, *JCAP* **0610**, 016 (2006).
- [36] Here ‘radiation’ includes three species of light neutrinos as well as photons.
- [37] D. Scott, A. Narimani and D. N. Page, *Phys. Canada* **70**, 258 (2014).
- [38] D.H. Weinberg, M. White, “Dark Energy,” Sec. 28 in this *Review*.
- [39] Planck Collab. Intern. Results XLVI, *Astron. & Astrophys.* **596**, A108 (2016) extend the range by $\Delta z \approx 1$, depending on the reionization model.
- [40] Summary Tables in this *Review* list $N_\nu = 2.984(8)$ (Standard Model fits to LEP-SLC data). Because neutrinos are not completely decoupled at e^\pm annihilation, the effective number of massless neutrino species is 3.045, rather than 3.
- [41] J. Lesgourgues & L. Verde, “Neutrinos in Cosmology,” Sec. 26 in this *Review*.
- [42] The sum is over all neutrino mass eigenstates, the lower limit following from neutrino mixing results reported in this *Review* combined with the assumptions that there are three light neutrinos and that the lightest neutrino is substantially less massive than the others.
- [43] Astrophysical determinations of $\sum m_{\nu_j}$, reported in the Full Listings of this *Review* under “Sum of the neutrino masses,” range from < 0.17 eV to < 2.3 eV in papers published since 2003.
- [44] P. A. R. Ade *et al.* (BICEP2, Keck Array), *Phys. Rev. Lett.* **121**, 221301 (2018).
- [45] *Planck* data alone give $r < 0.10$; adding the BICEP/Keck data tightens the constraint.
- [46] This constraint uses BAO and SNe data, as described in Ref. [2]; see discussion in D.H. Weinberg, M. White, “Dark Energy,” Sec. 28 in this *Review*.
- [47] E. Aver, K. A. Olive and E. D. Skillman, *JCAP* **1507**, 07, 011 (2015).
- [48] IAU XXIX GA 2015, Resolution B2.
- [49] G. P. Horedt, *Astrophys. Space Sci.* **126**, 2, 357 (1986).

3. International System of Units (SI)

See “The International System of Units (SI),” NIST Special Publication **330**, B.N. Taylor, ed. (USGPO, Washington, DC, 1991); and “Guide for the Use of the International System of Units (SI),” NIST Special Publication **811**, 1995 edition, B.N. Taylor (USGPO, Washington, DC, 1995).

Physical quantity	Name of unit	Symbol
<i>Base units</i>		
length	meter	m
mass	kilogram	kg
time	second	s
electric current	ampere	A
thermodynamic temperature	kelvin	K
amount of substance	mole	mol
luminous intensity	candela	cd
<i>Derived units with special names</i>		
plane angle	radian	rad
solid angle	steradian	sr
frequency	hertz	Hz
energy	joule	J
force	newton	N
pressure	pascal	Pa
power	watt	W
electric charge	coulomb	C
electric potential	volt	V
electric resistance	ohm	Ω
electric conductance	siemens	S
electric capacitance	farad	F
magnetic flux	weber	Wb
inductance	henry	H
magnetic flux density	tesla	T
luminous flux	lumen	lm
illuminance	lux	lx
celsius temperature	degree celsius	$^{\circ}\text{C}$
activity (of a radioactive source)*	becquerel	Bq
absorbed dose (of ionizing radiation)*	gray	Gy
dose equivalent*	sievert	Sv

SI prefixes

10^{24}	yotta	(Y)
10^{21}	zetta	(Z)
10^{18}	exa	(E)
10^{15}	peta	(P)
10^{12}	tera	(T)
10^9	giga	(G)
10^6	mega	(M)
10^3	kilo	(k)
10^2	hecto	(h)
10	deca	(da)
10^{-1}	deci	(d)
10^{-2}	centi	(c)
10^{-3}	milli	(m)
10^{-6}	micro	(μ)
10^{-9}	nano	(n)
10^{-12}	pico	(p)
10^{-15}	femto	(f)
10^{-18}	atto	(a)
10^{-21}	zepto	(z)
10^{-24}	yocto	(y)

*See our section 37, on “Radioactivity and radiation protection.”

4. Periodic Table of the Elements

Table 4.1. Revised June 2019 by D.E. Groom (LBNL). The atomic number (top left) is the number of protons in the nucleus. The atomic masses (bottom) of stable elements are weighted by isotopic abundances in the Earth's surface. Atomic masses are relative to the mass of ¹²C, defined to be exactly 12 unified atomic mass units (u) (1 u ≈ 1 g/mole). The exceptions are Th, Pa, and U, which have no stable isotopes but do have characteristic terrestrial compositions. Relative isotopic abundances often vary considerably, both in natural and commercial samples; this is reflected in the number of significant figures given for the mass. Masses may be found at <https://www.nist.gov/pml/atomic-weights-and-isotopic-compositions-relative-atomic-masses>. If there is no stable isotope, the atomic mass of the most stable isotope known as of June 2019 is given in parentheses.

IUPAC announced verification of the discoveries of elements 113, 115, 117, and 118 in December 2015. The names were approved November 2016. The 7th period of the periodic table is now complete.

1		2		3		4		5		6		7		8		9		10		11		12		13		14		15		16		17		18			
IA		IIA		IIIB		IVB		VB		VIB		VIIB		VIII		VIII		VIII		IB		IIB		IIIA		IVA		VA		VIA		VIIA		VIIIA			
1	H	2	He	3	Li	4	Be	5	B	6	C	7	N	8	O	9	F	10	Ne	11	Na	12	Mg	13	Al	14	Si	15	P	16	S	17	Cl	18	Ar		
hydrogen	1.008	helium	4.002602	lithium	6.94	beryllium	9.012182	boron	10.81	carbon	12.0107	nitrogen	14.007	oxygen	15.999	fluorine	18.998403163	neon	20.1797	sodium	22.98976928	magnesium	24.305	aluminum	26.9815385	silicon	28.085	phosphorus	30.973761998	sulfur	32.06	chlorine	35.45	argon	39.948		
19	K	20	Ca	21	Sc	22	Ti	23	V	24	Cr	25	Mn	26	Fe	27	Co	28	Ni	29	Cu	30	Zn	31	Ga	32	Ge	33	As	34	Se	35	Br	36	Kr		
potassium	39.0983	calcium	40.078	scandium	44.955908	titanium	47.867	vanadium	50.9415	chromium	51.9961	manganese	54.938044	iron	55.845	cobalt	58.933195	nickel	58.6934	copper	63.546	zinc	65.38	gallium	69.723	germanium	72.630	arsenic	74.921595	selenium	78.971	bromine	79.904	krypton	83.798		
37	Rb	38	Sr	39	Y	40	Zr	41	Nb	42	Mo	43	Tc	44	Ru	45	Rh	46	Pd	47	Ag	48	Cd	49	In	50	Sn	51	Sb	52	Te	53	I	54	Xe		
rubidium	85.4678	strontium	87.62	yttrium	88.90584	zirconium	91.224	niobium	92.90637	molybdenum	95.95	technetium	(97.907212)	ruthenium	101.07	rhodium	102.90550	palladium	106.42	silver	107.8682	cadmium	112.414	indium	114.818	tin	118.710	antimony	121.760	tellurium	127.60	iodine	126.90447	xenon	131.293		
55	Cs	56	Ba	57-71	LANTHANIDES	72	Hf	73	Ta	74	W	75	Re	76	Os	77	Ir	78	Pt	79	Au	80	Hg	81	Tl	82	Pb	83	Bi	84	Po	85	At	86	Rn		
caesium	132.90545196	barium	137.327					hafnium	178.49	tantalum	180.94788	tungsten	183.84	rhenium	186.207	osmium	190.23	iridium	192.217	platinum	195.084	gold	196.966569	mercury	200.592	thallium	204.38	lead	207.2	bismuth	208.98040	polonium	(208.98243)	astatine	(209.98715)	radon	(222.01758)
87	Fr	88	Ra	89-103	ACTINIDES	104	Rf	105	Db	106	Sg	107	Bh	108	Hs	109	Mt	110	Ds	111	Rg	112	Cn	113	Nh	114	Fl	115	Mc	116	Lv	117	Ts	118	Og		
francium	(223.01974)	radium	(226.02541)					rutherfordium	(261.10116)	dubnium	(268.10267)	seaborgium	(269.10336)	bohrium	(270.103336)	hassium	(278.103375)	meitnerium	(281.103336)	darmstadtium	(282.103336)	roentgenium	(285.103336)	copernicium	(286.103336)	nihonium	(286.103336)	flerovium	(289.103336)	tennessine	(294.103336)	oganesson	(294.103336)				

Lanthanide series		Actinide series	
57	La	89	Ac
lanthanum	138.90547	actinium	(227.02775)
58	Ce	90	Th
cerium	140.116	thorium	232.0377
59	Pr	91	Pa
praseodymium	140.90766	protactinium	231.03588
60	Nd	92	U
neodymium	144.242	uranium	238.02891
61	Pm	93	Np
promethium	(144.91276)	neptunium	(237.04817)
62	Sm	94	Pu
samarium	150.36	plutonium	(244.06420)
63	Eu	95	Am
europium	151.964	americium	(243.06138)
64	Gd	96	Cm
gadolinium	157.25	curium	(247.07035)
65	Tb	97	Bk
terbium	158.92535	berkelium	(247.07031)
66	Dy	98	Cf
dysprosium	162.500	californium	(251.07959)
67	Ho	99	Es
holmium	164.93033	einsteinium	(252.08298)
68	Er	100	Fm
erbium	167.259	fermium	(257.09511)
69	Tm	101	Md
thulium	168.93422	mendelevium	(258.09844)
70	Yb	102	No
ytterbium	173.054	nobelium	(259.10103)
71	Lu	103	Lr
lutetium	174.9668	lawrencium	(262.10961)

5. Electronic Structure of the Elements

Table 5.1. Reviewed 2011 by J.E. Sansonetti (NIST). The electronic configurations and the ionization energies are from the NIST database, “Ground Levels and Ionization Energies for the Neutral Atoms,” W.C. Martin, A. Musgrove, S. Kotochigova, and J.E. Sansonetti, http://www.nist.gov/pml/data/ion_energy.cfm. The electron configuration for, say, iron indicates an argon electronic core (see argon) plus six $3d$ electrons and two $4s$ electrons.

Element	Electron configuration ($3d^5 =$ five $3d$ electrons, <i>etc.</i>)	Ground state $2S+1L_J$	Ionization energy (eV)
1 H Hydrogen	$1s$	$^2S_{1/2}$	13.5984
2 He Helium	$1s^2$	1S_0	24.5874
3 Li Lithium	(He) $2s$	$^2S_{1/2}$	5.3917
4 Be Beryllium	(He) $2s^2$	1S_0	9.3227
5 B Boron	(He) $2s^2 2p$	$^2P_{1/2}$	8.2980
6 C Carbon	(He) $2s^2 2p^2$	3P_0	11.2603
7 N Nitrogen	(He) $2s^2 2p^3$	$^4S_{3/2}$	14.5341
8 O Oxygen	(He) $2s^2 2p^4$	3P_2	13.6181
9 F Fluorine	(He) $2s^2 2p^5$	$^2P_{3/2}$	17.4228
10 Ne Neon	(He) $2s^2 2p^6$	1S_0	21.5645
11 Na Sodium	(Ne) $3s$	$^2S_{1/2}$	5.1391
12 Mg Magnesium	(Ne) $3s^2$	1S_0	7.6462
13 Al Aluminum	(Ne) $3s^2 3p$	$^2P_{1/2}$	5.9858
14 Si Silicon	(Ne) $3s^2 3p^2$	3P_0	8.1517
15 P Phosphorus	(Ne) $3s^2 3p^3$	$^4S_{3/2}$	10.4867
16 S Sulfur	(Ne) $3s^2 3p^4$	3P_2	10.3600
17 Cl Chlorine	(Ne) $3s^2 3p^5$	$^2P_{3/2}$	12.9676
18 Ar Argon	(Ne) $3s^2 3p^6$	1S_0	15.7596
19 K Potassium	(Ar) $4s$	$^2S_{1/2}$	4.3407
20 Ca Calcium	(Ar) $4s^2$	1S_0	6.1132
21 Sc Scandium	(Ar) $3d 4s^2$	$^2D_{3/2}$	6.5615
22 Ti Titanium	(Ar) $3d^2 4s^2$	3F_2	6.8281
23 V Vanadium	(Ar) $3d^3 4s^2$	$^4F_{3/2}$	6.7462
24 Cr Chromium	(Ar) $3d^5 4s$	7S_3	6.7665
25 Mn Manganese	(Ar) $3d^5 4s^2$	$^6S_{5/2}$	7.4340
26 Fe Iron	(Ar) $3d^6 4s^2$	5D_4	7.9024
27 Co Cobalt	(Ar) $3d^7 4s^2$	$^4F_{9/2}$	7.8810
28 Ni Nickel	(Ar) $3d^8 4s^2$	3F_4	7.6399
29 Cu Copper	(Ar) $3d^{10} 4s$	$^2S_{1/2}$	7.7264
30 Zn Zinc	(Ar) $3d^{10} 4s^2$	1S_0	9.3942
31 Ga Gallium	(Ar) $3d^{10} 4s^2 4p$	$^2P_{1/2}$	5.9993
32 Ge Germanium	(Ar) $3d^{10} 4s^2 4p^2$	3P_0	7.8994
33 As Arsenic	(Ar) $3d^{10} 4s^2 4p^3$	$^4S_{3/2}$	9.7886
34 Se Selenium	(Ar) $3d^{10} 4s^2 4p^4$	3P_2	9.7524
35 Br Bromine	(Ar) $3d^{10} 4s^2 4p^5$	$^2P_{3/2}$	11.8138
36 Kr Krypton	(Ar) $3d^{10} 4s^2 4p^6$	1S_0	13.9996
37 Rb Rubidium	(Kr) $5s$	$^2S_{1/2}$	4.1771
38 Sr Strontium	(Kr) $5s^2$	1S_0	5.6949
39 Y Yttrium	(Kr) $4d 5s^2$	$^2D_{3/2}$	6.2173
40 Zr Zirconium	(Kr) $4d^2 5s^2$	3F_2	6.6339
41 Nb Niobium	(Kr) $4d^4 5s$	$^6D_{1/2}$	6.7589
42 Mo Molybdenum	(Kr) $4d^5 5s$	7S_3	7.0924
43 Tc Technetium	(Kr) $4d^5 5s^2$	$^6S_{5/2}$	7.28
44 Ru Ruthenium	(Kr) $4d^7 5s$	5F_5	7.3605
45 Rh Rhodium	(Kr) $4d^8 5s$	$^4F_{9/2}$	7.4589
46 Pd Palladium	(Kr) $4d^{10}$	1S_0	8.3369
47 Ag Silver	(Kr) $4d^{10} 5s$	$^2S_{1/2}$	7.5762
48 Cd Cadmium	(Kr) $4d^{10} 5s^2$	1S_0	8.9938

49	In	Indium	(Kr)4d ¹⁰ 5s ² 5p		² P _{1/2}	5.7864
50	Sn	Tin	(Kr)4d ¹⁰ 5s ² 5p ²		³ P ₀	7.3439
51	Sb	Antimony	(Kr)4d ¹⁰ 5s ² 5p ³		⁴ S _{3/2}	8.6084
52	Te	Tellurium	(Kr)4d ¹⁰ 5s ² 5p ⁴		³ P ₂	9.0096
53	I	Iodine	(Kr)4d ¹⁰ 5s ² 5p ⁵		² P _{3/2}	10.4513
54	Xe	Xenon	(Kr)4d ¹⁰ 5s ² 5p ⁶		¹ S ₀	12.1298
55	Cs	Cesium	(Xe) 6s		² S _{1/2}	3.8939
56	Ba	Barium	(Xe) 6s ²		¹ S ₀	5.2117
57	La	Lanthanum	(Xe) 5d 6s ²		² D _{3/2}	5.5769
58	Ce	Cerium	(Xe)4f 5d 6s ²		¹ G ₄	5.5387
59	Pr	Praseodymium	(Xe)4f ³ 6s ²	L	⁴ I _{9/2}	5.473
60	Nd	Neodymium	(Xe)4f ⁴ 6s ²	a	⁵ I ₄	5.5250
61	Pm	Promethium	(Xe)4f ⁵ 6s ²	n	⁶ H _{5/2}	5.582
62	Sm	Samarium	(Xe)4f ⁶ 6s ²	t	⁷ F ₀	5.6437
63	Eu	Europium	(Xe)4f ⁷ 6s ²	h	⁸ S _{7/2}	5.6704
64	Gd	Gadolinium	(Xe)4f ⁷ 5d 6s ²	a	⁹ D ₂	6.1498
65	Tb	Terbium	(Xe)4f ⁹ 6s ²	n	⁶ H _{15/2}	5.8638
66	Dy	Dysprosium	(Xe)4f ¹⁰ 6s ²	i	⁵ I ₈	5.9389
67	Ho	Holmium	(Xe)4f ¹¹ 6s ²	d	⁴ I _{15/2}	6.0215
68	Er	Erbium	(Xe)4f ¹² 6s ²	e	³ H ₆	6.1077
69	Tm	Thulium	(Xe)4f ¹³ 6s ²	s	² F _{7/2}	6.1843
70	Yb	Ytterbium	(Xe)4f ¹⁴ 6s ²		¹ S ₀	6.2542
71	Lu	Lutetium	(Xe)4f ¹⁴ 5d 6s ²		² D _{3/2}	5.4259
72	Hf	Hafnium	(Xe)4f ¹⁴ 5d ² 6s ²	T	³ F ₂	6.8251
73	Ta	Tantalum	(Xe)4f ¹⁴ 5d ³ 6s ²	r	⁴ F _{3/2}	7.5496
74	W	Tungsten	(Xe)4f ¹⁴ 5d ⁴ 6s ²	a	⁵ D ₀	7.8640
75	Re	Rhenium	(Xe)4f ¹⁴ 5d ⁵ 6s ²	n	⁶ S _{5/2}	7.8335
76	Os	Osmium	(Xe)4f ¹⁴ 5d ⁶ 6s ²	s	⁵ D ₄	8.4382
77	Ir	Iridium	(Xe)4f ¹⁴ 5d ⁷ 6s ²	i	⁴ F _{9/2}	8.9670
78	Pt	Platinum	(Xe)4f ¹⁴ 5d ⁹ 6s	t	³ D ₃	8.9588
79	Au	Gold	(Xe)4f ¹⁴ 5d ¹⁰ 6s	i	² S _{1/2}	9.2255
80	Hg	Mercury	(Xe)4f ¹⁴ 5d ¹⁰ 6s ²	n	¹ S ₀	10.4375
81	Tl	Thallium	(Xe)4f ¹⁴ 5d ¹⁰ 6s ² 6p		² P _{1/2}	6.1082
82	Pb	Lead	(Xe)4f ¹⁴ 5d ¹⁰ 6s ² 6p ²		³ P ₀	7.4167
83	Bi	Bismuth	(Xe)4f ¹⁴ 5d ¹⁰ 6s ² 6p ³		⁴ S _{3/2}	7.2855
84	Po	Polonium	(Xe)4f ¹⁴ 5d ¹⁰ 6s ² 6p ⁴		³ P ₂	8.414
85	At	Astatine	(Xe)4f ¹⁴ 5d ¹⁰ 6s ² 6p ⁵		² P _{3/2}	
86	Rn	Radon	(Xe)4f ¹⁴ 5d ¹⁰ 6s ² 6p ⁶		¹ S ₀	10.7485
87	Fr	Francium	(Rn) 7s		² S _{1/2}	4.0727
88	Ra	Radium	(Rn) 7s ²		¹ S ₀	5.2784
89	Ac	Actinium	(Rn) 6d 7s ²		² D _{3/2}	5.3807
90	Th	Thorium	(Rn) 6d ² 7s ²		³ F ₂	6.3067
91	Pa	Protactinium	(Rn)5f ² 6d 7s ²	A	⁴ K _{11/2} *	5.89
92	U	Uranium	(Rn)5f ³ 6d 7s ²	c	⁵ L ₆ *	6.1939
93	Np	Neptunium	(Rn)5f ⁴ 6d 7s ²	t	⁶ L _{11/2} *	6.2657
94	Pu	Plutonium	(Rn)5f ⁶ 7s ²	i	⁷ F ₀	6.0260
95	Am	Americium	(Rn)5f ⁷ 7s ²	n	⁸ S _{7/2}	5.9738
96	Cm	Curium	(Rn)5f ⁷ 6d 7s ²	d	⁹ D ₂	5.9914
97	Bk	Berkelium	(Rn)5f ⁹ 7s ²	e	⁶ H _{15/2}	6.1979
98	Cf	Californium	(Rn)5f ¹⁰ 7s ²	s	⁵ I ₈	6.2817
99	Es	Einsteinium	(Rn)5f ¹¹ 7s ²		⁴ I _{15/2}	6.3676
100	Fm	Fermium	(Rn)5f ¹² 7s ²		³ H ₆	6.50
101	Md	Mendelevium	(Rn)5f ¹³ 7s ²		² F _{7/2}	6.58
102	No	Nobelium	(Rn)5f ¹⁴ 7s ²		¹ S ₀	6.65
103	Lr	Lawrencium	(Rn)5f ¹⁴ 7s ² 7p?		² P _{1/2} ?	4.9?
104	Rf	Rutherfordium	(Rn)5f ¹⁴ 6d ² 7s ² ?		³ F ₂ ?	6.0?

* The usual *LS* coupling scheme does not apply for these three elements. See the introductory note to the NIST table from which this table is taken.

6. Atomic and Nuclear Properties of Materials

Table 6.1 Abridged from pdg.lbl.gov/AtomicNuclearProperties by D.E. Groom (2017). See web pages for more detail about entries in this table and for several hundred others. Parentheses in the dE/dx and density columns indicate gases at 20°C and 1 atm. Boiling points are at 1 atm. Refractive indices n are evaluated at the sodium D line blend (589.2 nm); values $\gg 1$ in brackets indicate $(n-1) \times 10^6$ for gases at 0°C and 1 atm.

Material	Z	A	$\langle Z/A \rangle$	Nucl.coll. length λ_T {g cm ⁻² }	Nucl.inter. length λ_I {g cm ⁻² }	Rad.len. X_0 {g cm ⁻² }	$dE/dx _{\min}$ { MeV g ⁻¹ cm ² }	Density {g cm ⁻³ } ({g ℓ ⁻¹ })	Melting point (K)	Boiling point (K)	Refract. index @ Na D
H ₂	1	1.008(7)	0.99212	42.8	52.0	63.05	(4.103)	0.071(0.084)	13.81	20.28	1.11[132.]
D ₂	1	2.014101764(8)	0.49650	51.3	71.8	125.97	(2.053)	0.169(0.168)	18.7	23.65	1.11[138.]
He	2	4.002602(2)	0.49967	51.8	71.0	94.32	(1.937)	0.125(0.166)		4.220	1.02[35.0]
Li	3	6.94(2)	0.43221	52.2	71.3	82.78	1.639	0.534	453.6	1615.	
Be	4	9.0121831(5)	0.44384	55.3	77.8	65.19	1.595	1.848	1560.	2744.	
C diamond	6	12.0107(8)	0.49955	59.2	85.8	42.70	1.725	3.520			2.419
C graphite	6	12.0107(8)	0.49955	59.2	85.8	42.70	1.742	2.210	Sublimes at 4098. K		
N ₂	7	14.007(2)	0.49976	61.1	89.7	37.99	(1.825)	0.807(1.165)	63.15	77.29	1.20[298.]
O ₂	8	15.999(3)	0.50002	61.3	90.2	34.24	(1.801)	1.141(1.332)	54.36	90.20	1.22[271.]
F ₂	9	18.998403163(6)	0.47372	65.0	97.4	32.93	(1.676)	1.507(1.580)	53.53	85.03	[195.]
Ne	10	20.1797(6)	0.49555	65.7	99.0	28.93	(1.724)	1.204(0.839)	24.56	27.07	1.09[67.1]
Al	13	26.9815385(7)	0.48181	69.7	107.2	24.01	1.615	2.699	933.5	2792.	
Si	14	28.0855(3)	0.49848	70.2	108.4	21.82	1.664	2.329	1687.	3538.	3.95
Cl ₂	17	35.453(2)	0.47951	73.8	115.7	19.28	(1.630)	1.574(2.980)	171.6	239.1	[773.]
Ar	18	39.948(1)	0.45059	75.7	119.7	19.55	(1.519)	1.396(1.662)	83.81	87.26	1.23[281.]
Ti	22	47.867(1)	0.45961	78.8	126.2	16.16	1.477	4.540	1941.	3560.	
Fe	26	55.845(2)	0.46557	81.7	132.1	13.84	1.451	7.874	1811.	3134.	
Cu	29	63.546(3)	0.45636	84.2	137.3	12.86	1.403	8.960	1358.	2835.	
Ge	32	72.630(1)	0.44053	86.9	143.0	12.25	1.370	5.323	1211.	3106.	
Sn	50	118.710(7)	0.42119	98.2	166.7	8.82	1.263	7.310	505.1	2875.	
Xe	54	131.293(6)	0.41129	100.8	172.1	8.48	(1.255)	2.953(5.483)	161.4	165.1	1.39[701.]
W	74	183.84(1)	0.40252	110.4	191.9	6.76	1.145	19.300	3695.	5828.	
Pt	78	195.084(9)	0.39983	112.2	195.7	6.54	1.128	21.450	2042.	4098.	
Au	79	196.966569(5)	0.40108	112.5	196.3	6.46	1.134	19.320	1337.	3129.	
Pb	82	207.2(1)	0.39575	114.1	199.6	6.37	1.122	11.350	600.6	2022.	
U	92	[238.02891(3)]	0.38651	118.6	209.0	6.00	1.081	18.950	1408.	4404.	
Air (dry, 1 atm)			0.49919	61.3	90.1	36.62	(1.815)	(1.205)		78.80	[289]
Shielding concrete			0.50274	65.1	97.5	26.57	1.711	2.300			
Borosilicate glass (Pyrex)			0.49707	64.6	96.5	28.17	1.696	2.230			
Lead glass			0.42101	95.9	158.0	7.87	1.255	6.220			
Standard rock			0.50000	66.8	101.3	26.54	1.688	2.650			
Methane (CH ₄)			0.62334	54.0	73.8	46.47	(2.417)	(0.667)	90.68	111.7	[444.]
Ethane (C ₂ H ₆)			0.59861	55.0	75.9	45.66	(2.304)	(1.263)	90.36	184.5	
Propane (C ₃ H ₈)			0.58962	55.3	76.7	45.37	(2.262)	0.493(1.868)	85.52	231.0	
Butane (C ₄ H ₁₀)			0.59497	55.5	77.1	45.23	(2.278)	(2.489)	134.9	272.6	
Octane (C ₈ H ₁₈)			0.57778	55.8	77.8	45.00	2.123	0.703	214.4	398.8	
Paraffin (CH ₃ (CH ₂) _{n≈23} CH ₃)			0.57275	56.0	78.3	44.85	2.088	0.930			
Nylon (type 6, 6/6)			0.54790	57.5	81.6	41.92	1.973	1.18			
Polycarbonate (Lexan)			0.52697	58.3	83.6	41.50	1.886	1.20			
Polyethylene ([CH ₂ CH ₂] _n)			0.57034	56.1	78.5	44.77	2.079	0.89			
Polyethylene terephthalate (Mylar)			0.52037	58.9	84.9	39.95	1.848	1.40			
Polyimide film (Kapton)			0.51264	59.2	85.5	40.58	1.820	1.42			
Polymethylmethacrylate (acrylic)			0.53937	58.1	82.8	40.55	1.929	1.19			1.49
Polypropylene			0.55998	56.1	78.5	44.77	2.041	0.90			
Polystyrene ([C ₆ H ₅ CHCH ₂] _n)			0.53768	57.5	81.7	43.79	1.936	1.06			1.59
Polytetrafluoroethylene (Teflon)			0.47992	63.5	94.4	34.84	1.671	2.20			
Polyvinyltoluene			0.54141	57.3	81.3	43.90	1.956	1.03			1.58
Aluminum oxide (sapphire)			0.49038	65.5	98.4	27.94	1.647	3.970	2327.	3273.	1.77
Barium fluoride (BaF ₂)			0.42207	90.8	149.0	9.91	1.303	4.893	1641.	2533.	1.47
Bismuth germanate (BGO)			0.42065	96.2	159.1	7.97	1.251	7.130	1317.		2.15
Carbon dioxide gas (CO ₂)			0.49989	60.7	88.9	36.20	1.819	(1.842)			[449.]
Solid carbon dioxide (dry ice)			0.49989	60.7	88.9	36.20	1.787	1.563	Sublimes at 194.7 K		
Cesium iodide (CsI)			0.41569	100.6	171.5	8.39	1.243	4.510	894.2	1553.	1.79
Lithium fluoride (LiF)			0.46262	61.0	88.7	39.26	1.614	2.635	1121.	1946.	1.39
Lithium hydride (LiH)			0.50321	50.8	68.1	79.62	1.897	0.820	965.		
Lead tungstate (PbWO ₄)			0.41315	100.6	168.3	7.39	1.229	8.300	1403.		2.20
Silicon dioxide (SiO ₂ , fused quartz)			0.49930	65.2	97.8	27.05	1.699	2.200	1986.	3223.	1.46
Sodium chloride (NaCl)			0.47910	71.2	110.1	21.91	1.847	2.170	1075.	1738.	1.54
Sodium iodide (NaI)			0.42697	93.1	154.6	9.49	1.305	3.667	933.2	1577.	1.77
Water (H ₂ O)			0.55509	58.5	83.3	36.08	1.992	1.000	273.1	373.1	1.33
Silica aerogel			0.50093	65.0	97.3	27.25	1.740	0.200	(0.03 H ₂ O, 0.97 SiO ₂)		

Material	Dielectric constant ($\kappa = \epsilon/\epsilon_0$) () is $(\kappa-1)\times 10^6$ for gas	Young's modulus [10^6 psi]	Coeff. of thermal expansion [10^{-6} cm/cm- $^{\circ}$ C]	Specific heat [cal/g- $^{\circ}$ C]	Electrical resistivity [$\mu\Omega$ cm(@ $^{\circ}$ C)]	Thermal conductivity [cal/cm- $^{\circ}$ C-sec]
H ₂	(253.9)	—	—	—	—	—
He	(64)	—	—	—	—	—
Li	—	—	56	0.86	8.55(0 $^{\circ}$)	0.17
Be	—	37	12.4	0.436	5.885(0 $^{\circ}$)	0.38
C	—	0.7	0.6–4.3	0.165	1375(0 $^{\circ}$)	0.057
N ₂	(548.5)	—	—	—	—	—
O ₂	(495)	—	—	—	—	—
Ne	(127)	—	—	—	—	—
Al	—	10	23.9	0.215	2.65(20 $^{\circ}$)	0.53
Si	11.9	16	2.8–7.3	0.162	—	0.20
Ar	(517)	—	—	—	—	—
Ti	—	16.8	8.5	0.126	50(0 $^{\circ}$)	—
Fe	—	28.5	11.7	0.11	9.71(20 $^{\circ}$)	0.18
Cu	—	16	16.5	0.092	1.67(20 $^{\circ}$)	0.94
Ge	16.0	—	5.75	0.073	—	0.14
Sn	—	6	20	0.052	11.5(20 $^{\circ}$)	0.16
Xe	—	—	—	—	—	—
W	—	50	4.4	0.032	5.5(20 $^{\circ}$)	0.48
Pt	—	21	8.9	0.032	9.83(0 $^{\circ}$)	0.17
Pb	—	2.6	29.3	0.038	20.65(20 $^{\circ}$)	0.083
U	—	—	36.1	0.028	29(20 $^{\circ}$)	0.064

7. Electromagnetic Relations

Revised September 2005 by H.G. Spieler (LBNL).

Quantity	Gaussian CGS	SI
Conversion factors:		
Charge:	$2.997\,924\,58 \times 10^9$ esu	$= 1\text{ C} = 1\text{ A s}$
Potential:	$(1/299.792\,458)$ statvolt (ergs/esu)	$= 1\text{ V} = 1\text{ J C}^{-1}$
Magnetic field:	10^4 gauss = 10^4 dyne/esu	$= 1\text{ T} = 1\text{ N A}^{-1}\text{m}^{-1}$
	$\mathbf{F} = q(\mathbf{E} + \frac{\mathbf{v}}{c} \times \mathbf{B})$	$\mathbf{F} = q(\mathbf{E} + \mathbf{v} \times \mathbf{B})$
	$\nabla \cdot \mathbf{D} = 4\pi\rho$ $\nabla \times \mathbf{H} - \frac{1}{c} \frac{\partial \mathbf{D}}{\partial t} = \frac{4\pi}{c} \mathbf{J}$ $\nabla \cdot \mathbf{B} = 0$ $\nabla \times \mathbf{E} + \frac{1}{c} \frac{\partial \mathbf{B}}{\partial t} = 0$	$\nabla \cdot \mathbf{D} = \rho$ $\nabla \times \mathbf{H} - \frac{\partial \mathbf{D}}{\partial t} = \mathbf{J}$ $\nabla \cdot \mathbf{B} = 0$ $\nabla \times \mathbf{E} + \frac{\partial \mathbf{B}}{\partial t} = 0$
Constitutive relations:	$\mathbf{D} = \mathbf{E} + 4\pi\mathbf{P}, \quad \mathbf{H} = \mathbf{B} - 4\pi\mathbf{M}$	$\mathbf{D} = \epsilon_0\mathbf{E} + \mathbf{P}, \quad \mathbf{H} = \mathbf{B}/\mu_0 - \mathbf{M}$
Linear media:	$\mathbf{D} = \epsilon\mathbf{E}, \quad \mathbf{H} = \mathbf{B}/\mu$ 1 1	$\mathbf{D} = \epsilon\mathbf{E}, \quad \mathbf{H} = \mathbf{B}/\mu$ $\epsilon_0 = 8.854\,187 \dots \times 10^{-12}\text{ F m}^{-1}$ $\mu_0 = 4\pi \times 10^{-7}\text{ N A}^{-2}$
	$\mathbf{E} = -\nabla V - \frac{1}{c} \frac{\partial \mathbf{A}}{\partial t}$ $\mathbf{B} = \nabla \times \mathbf{A}$	$\mathbf{E} = -\nabla V - \frac{\partial \mathbf{A}}{\partial t}$ $\mathbf{B} = \nabla \times \mathbf{A}$
	$V = \sum_{\text{charges}} \frac{q_i}{r_i} = \int \frac{\rho(\mathbf{r}')}{ \mathbf{r} - \mathbf{r}' } d^3x'$ $\mathbf{A} = \frac{1}{c} \oint \frac{I d\boldsymbol{\ell}}{ \mathbf{r} - \mathbf{r}' } = \frac{1}{c} \int \frac{\mathbf{J}(\mathbf{r}')}{ \mathbf{r} - \mathbf{r}' } d^3x'$	$V = \frac{1}{4\pi\epsilon_0} \sum_{\text{charges}} \frac{q_i}{r_i} = \frac{1}{4\pi\epsilon_0} \int \frac{\rho(\mathbf{r}')}{ \mathbf{r} - \mathbf{r}' } d^3x'$ $\mathbf{A} = \frac{\mu_0}{4\pi} \oint \frac{I d\boldsymbol{\ell}}{ \mathbf{r} - \mathbf{r}' } = \frac{\mu_0}{4\pi} \int \frac{\mathbf{J}(\mathbf{r}')}{ \mathbf{r} - \mathbf{r}' } d^3x'$
	$\mathbf{E}'_{\parallel} = \mathbf{E}_{\parallel}$ $\mathbf{E}'_{\perp} = \gamma(\mathbf{E}_{\perp} + \frac{1}{c}\mathbf{v} \times \mathbf{B})$ $\mathbf{B}'_{\parallel} = \mathbf{B}_{\parallel}$ $\mathbf{B}'_{\perp} = \gamma(\mathbf{B}_{\perp} - \frac{1}{c}\mathbf{v} \times \mathbf{E})$	$\mathbf{E}'_{\parallel} = \mathbf{E}_{\parallel}$ $\mathbf{E}'_{\perp} = \gamma(\mathbf{E}_{\perp} + \mathbf{v} \times \mathbf{B})$ $\mathbf{B}'_{\parallel} = \mathbf{B}_{\parallel}$ $\mathbf{B}'_{\perp} = \gamma(\mathbf{B}_{\perp} - \frac{1}{c^2}\mathbf{v} \times \mathbf{E})$
	$\frac{1}{4\pi\epsilon_0} = c^2 \times 10^{-7}\text{ N A}^{-2} = 8.987\,55 \dots \times 10^9\text{ m F}^{-1}; \quad \frac{\mu_0}{4\pi} = 10^{-7}\text{ N A}^{-2}; \quad c = \frac{1}{\sqrt{\mu_0\epsilon_0}} = 2.997\,924\,58 \times 10^8\text{ m s}^{-1}$	

7.1. Impedances (SI units)

ρ = resistivity at room temperature in $10^{-8} \Omega \text{ m}$:
 ~ 1.7 for Cu ~ 5.5 for W
 ~ 2.4 for Au ~ 73 for SS 304
 ~ 2.8 for Al ~ 100 for Nichrome
 (Al alloys may have double the Al value.)

For alternating currents, instantaneous current I , voltage V , angular frequency ω :

$$V = V_0 e^{j\omega t} = ZI . \tag{7.1}$$

Impedance of self-inductance L : $Z = j\omega L$.

Impedance of capacitance C : $Z = 1/j\omega C$.

Impedance of free space: $Z = \sqrt{\mu_0/\epsilon_0} = 376.7 \Omega$.

High-frequency surface impedance of a good conductor:

$$Z = \frac{(1+j)\rho}{\delta} , \quad \text{where } \delta = \text{skin depth} ; \tag{7.2}$$

$$\delta = \sqrt{\frac{\rho}{\pi\nu\mu}} \approx \frac{6.6 \text{ cm}}{\sqrt{\nu \text{ (Hz)}}} \quad \text{for Cu} . \tag{7.3}$$

7.2. Capacitors, inductors, and transmission Lines

The capacitance between two parallel plates of area A spaced by the distance d and enclosing a medium with the dielectric constant ϵ is

$$C = K\epsilon A/d , \tag{7.4}$$

where the correction factor K depends on the extent of the fringing field. If the dielectric fills the capacitor volume without extending beyond the electrodes. the correction factor $K \approx 0.8$ for capacitors of typical geometry.

The inductance at high frequencies of a straight wire whose length ℓ is much greater than the wire diameter d is

$$L \approx 2.0 \left[\frac{\text{nH}}{\text{cm}} \right] \cdot \ell \left(\ln \left(\frac{4\ell}{d} \right) - 1 \right) . \tag{7.5}$$

For very short wires, representative of vias in a printed circuit board, the inductance is

$$L(\text{in nH}) \approx \ell/d . \tag{7.6}$$

A transmission line is a pair of conductors with inductance L and capacitance C . The characteristic impedance $Z = \sqrt{L/C}$ and the phase velocity $v_p = 1/\sqrt{LC} = 1/\sqrt{\mu\epsilon}$, which decreases with the inverse square root of the dielectric constant of the medium. Typical coaxial and ribbon cables have a propagation delay of about 5 ns/cm. The impedance of a coaxial cable with outer diameter D and inner diameter d is

$$Z = 60 \Omega \cdot \frac{1}{\sqrt{\epsilon_r}} \ln \frac{D}{d} , \tag{7.7}$$

where the relative dielectric constant $\epsilon_r = \epsilon/\epsilon_0$. A pair of parallel wires of diameter d and spacing $a > 2.5d$ has the impedance

$$Z = 120 \Omega \cdot \frac{1}{\sqrt{\epsilon_r}} \ln \frac{2a}{d} . \tag{7.8}$$

This yields the impedance of a wire at a spacing h above a ground plane,

$$Z = 60 \Omega \cdot \frac{1}{\sqrt{\epsilon_r}} \ln \frac{4h}{d} . \tag{7.9}$$

A common configuration utilizes a thin rectangular conductor above a ground plane with an intermediate dielectric (microstrip). Detailed calculations for this and other transmission line configurations are given by Gunston.*

7.3. Synchrotron radiation (CGS units)

For a particle of charge e , velocity $v = \beta c$, and energy $E = \gamma mc^2$, traveling in a circular orbit of radius R , the classical energy loss per revolution δE is

$$\delta E = \frac{4\pi}{3} \frac{e^2}{R} \beta^3 \gamma^4 . \tag{7.10}$$

For high-energy electrons or positrons ($\beta \approx 1$), this becomes

$$\delta E \text{ (in MeV)} \approx 0.0885 [E(\text{in GeV})]^4 / R(\text{in m}) . \tag{7.11}$$

For $\gamma \gg 1$, the energy radiated per revolution into the photon energy interval $d(\hbar\omega)$ is

$$dI = \frac{8\pi}{9} \alpha \gamma F(\omega/\omega_c) d(\hbar\omega) , \tag{7.12}$$

where $\alpha = e^2/\hbar c$ is the fine-structure constant and

$$\omega_c = \frac{3\gamma^3 c}{2R} \tag{7.13}$$

is the critical frequency. The normalized function $F(y)$ is

$$F(y) = \frac{9}{8\pi} \sqrt{3} y \int_y^\infty K_{5/3}(x) dx , \tag{7.14}$$

where $K_{5/3}(x)$ is a modified Bessel function of the third kind. For electrons or positrons,

$$\hbar\omega_c \text{ (in keV)} \approx 2.22 [E(\text{in GeV})]^3 / R(\text{in m}) . \tag{7.15}$$

Fig. 7.1 shows $F(y)$ over the important range of y .

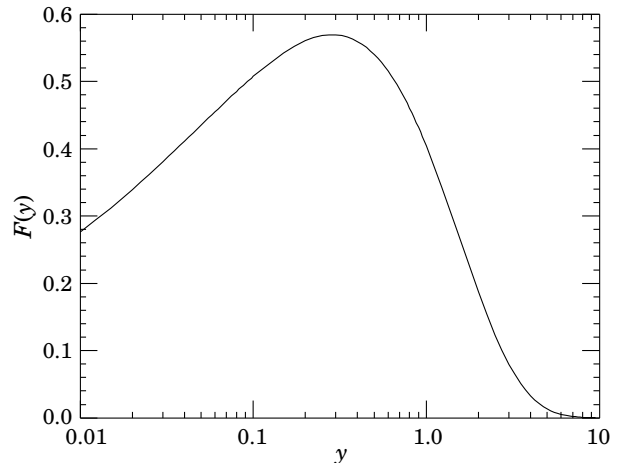


Figure 7.1: The normalized synchrotron radiation spectrum $F(y)$.

For $\gamma \gg 1$ and $\omega \ll \omega_c$,

$$\frac{dI}{d(\hbar\omega)} \approx 3.3\alpha (\omega R/c)^{1/3} , \tag{7.16}$$

whereas for

$$\gamma \gg 1 \text{ and } \omega \gtrsim 3\omega_c ,$$

$$\frac{dI}{d(\hbar\omega)} \approx \sqrt{\frac{3\pi}{2}} \alpha \gamma \left(\frac{\omega}{\omega_c} \right)^{1/2} e^{-\omega/\omega_c} \left[1 + \frac{55}{72} \frac{\omega_c}{\omega} + \dots \right] . \tag{7.17}$$

The radiation is confined to angles $\lesssim 1/\gamma$ relative to the instantaneous direction of motion. For $\gamma \gg 1$, where Eq. (7.12) applies, the mean number of photons emitted per revolution is

$$N_\gamma = \frac{5\pi}{\sqrt{3}} \alpha \gamma , \tag{7.18}$$

and the mean energy per photon is

$$\langle \hbar\omega \rangle = \frac{8}{15\sqrt{3}} \hbar\omega_c . \tag{7.19}$$

When $\langle \hbar\omega \rangle \gtrsim O(E)$, quantum corrections are important.

* M.A.R. Gunston. Microwave Transmission Line Data, Noble Publishing Corp., Atlanta (1997) ISBN 1-884932-57-6, TK6565.T73G85.

8. Naming Scheme for Hadrons

Revised August 2019 by V. Burkert (Jefferson Lab), S. Eidelman (Budker Inst., Novosibirsk; Novosibirsk U.), C. Hanhart (Jülich), E. Klempt (Bonn U.), R.E. Mitchell (Indiana U.), U. Thoma (Bonn U.), L. Tiator (KPH, JGU Mainz) and R.L. Workman (George Washington U.).

In the 1986 edition [1], the Particle Data Group extended and systematized the naming scheme for mesons and baryons. The extensions were necessary in order to name the new particles containing c or b quarks that were rapidly being discovered. With the discoveries of particles that are candidates for states with more complicated structures than just $q\bar{q}$ or qqq , it is necessary to extend the naming scheme again.

8.1 “Neutral-flavor” mesons

The naming of mesons is based on their quantum numbers. Although we use names established within the naive quark model, the name does *not* necessarily designate a (predominantly) $q\bar{q}$ state. In other words, the name provides information on the quantum numbers of a given state and not about its dominant component, which might well be $q\bar{q}$ (if allowed) or tetraquark, molecule, etc. In many cases, exotic states will be difficult to distinguish from $q\bar{q}$ states and will likely mix with them, and we make no attempt to, e.g., distinguish those that are “mostly gluonium” from those that are “mostly $q\bar{q}$.”

Table 8.1: Symbols for mesons with strangeness and heavy-flavor quantum numbers equal to zero. States that do not yet appear in the RPP are listed in parentheses.

J^{PC}	0^{-+}	1^{+-}	1^{--}	0^{++}
$J^{PC} = \left\{ \begin{array}{l} 2^{-+} \\ 3^{+-} \\ \vdots \end{array} \right.$	2^{-+}	3^{+-}	2^{--}	1^{++}
Minimal quark content	π	b	ρ	a
$u\bar{d}, u\bar{u} - d\bar{d}, d\bar{u}$ ($I = 1$)	η, η'	h, h'	ω, ϕ	f, f'
$d\bar{d} + u\bar{u}$ and/or $s\bar{s}$ ($I = 0$)	η_c	h_c	ψ^*	χ_c
$c\bar{c}$	η_b	h_b	Υ	χ_b
$b\bar{b}$	(Π_c)	Z_c	R_c	(W_c)
$I = 1$ with $c\bar{c}$	(Π_b)	Z_b	(R_b)	(W_b)
$I = 1$ with $b\bar{b}$				

*The J/ψ remains the J/ψ .

Table 8.1 shows the names for mesons having strangeness and all heavy-flavor quantum numbers equal to zero. The rows of Table 8.1 give the minimal $q\bar{q}$ content. The columns give the possible parity/charge-conjugation states,

$$PC = --, +-, --, \text{ and } ++.$$

Within the naive quark model, these combinations correspond one-to-one to the angular-momentum state $^{2S+1}L_J$ of the $q\bar{q}$ system being

$$^1(L \text{ even})_J, ^1(L \text{ odd})_J, ^3(L \text{ even})_J, \text{ or } ^3(L \text{ odd})_J,$$

respectively. Here S , L , and J are the spin, orbital, and total angular momenta of the $q\bar{q}$ system. Within the naive quark model, the quantum numbers are related by $P = (-1)^{L+1}$, $C = (-1)^{L+S}$, and G parity $= (-1)^{L+S+I}$, where the quantum number C is only relevant to neutral mesons with neutral-flavor quantum numbers and G extends to isovector mesons; see the review on the quark model. These expressions impose restrictions on the quantum numbers that are allowed for $q\bar{q}$ states. However, they do not apply to more complicated structures such as tetraquarks.

The spin J is added as a subscript in the name except for pseudoscalar and vector mesons, and the mass is added in parentheses for mesons that decay strongly. However, for some of the familiar mesons (e.g. η' , ϕ , ω), we omit the mass.

Measurements of the mass, quark content (where relevant), and quantum numbers I , J , P , and C (or G) of a meson thus deter-

mine its symbol. Conversely, these properties may be inferred unambiguously from the symbol. The name X is used for states with still unknown quantum numbers.

The mass label used in particle names is chosen using the best information available when a name is assigned. A more accurate value of a particle mass may become available at a later time. PDG will decide on a case-by-case basis whether to revise the mass label, taking into account the updated information.

With u , d , and s quarks, there are two isospin-0 mesons. A prime is used to distinguish one from the other (e.g. η and η'). Vector mesons decoupling to $u\bar{u} + d\bar{d}$ and $s\bar{s}$ (ideal mixing) are labeled ω and ϕ , respectively. As usual, we assign the spectroscopic name (e.g. $\Upsilon(1S)$) as the primary name to most of those ψ , Υ , and χ states whose spectroscopic identity is known. We use the form $\Upsilon(9460)$ as an alternative, and as the primary name when the spectroscopic identity is not known.

Since the top quark is so heavy that it decays too rapidly to form bound states, no name is assigned to structures like $t\bar{t}$.

Mesons with quantum numbers $J^{PC} = 0^{-+}, 0^{+-}, 1^{-+}, 2^{+-}, 3^{-+}$, etc. cannot be $q\bar{q}$. For such a “manifestly exotic” meson, we use the same symbol as for a $q\bar{q}$ meson; the exotic nature of the meson can be inferred from the values of the P and C quantum numbers (given by the symbol), and the spin J (given by the subscript). For example, an isospin-0 1^{-+} meson containing only u , d , and s quarks and antiquarks would be denoted η_1 and an isospin-1 0^{--} meson containing only u , d , and s quarks and antiquarks would be denoted ρ_0 .

The last two lines of Table 8.1 list isospin-1 states that also contain hidden heavy flavor, i.e. whose minimal quark content includes $c\bar{c}$ or $b\bar{b}$. We have assigned new names to these states, in keeping with the practice in the light-quark sector, where the $I = 0$ and $I = 1$ states have distinct names. The currently established $I = 1$ states in the heavy-quark sector have quantum numbers $J^{PC} = 1^{+-}$ and the proposed scheme keeps their original names Z .

8.2 Remarks on “neutral-flavor” mesons with hidden charm or bottom not classified as $q\bar{q}$

In the heavy-quark sector, there are several states with properties – such as masses, decay patterns, and widths – that are in disagreement with predictions from the naive quark model. For example, the vector state at 4260 MeV does not decay into $D\bar{D}$, although within the naive quark model its quantum numbers would call for this decay channel to be dominant. In recent literature, these states have been called X , Y , or Z , with their masses added in parentheses. This nomenclature conflicts with the rules outlined in the previous section, since the meson names are not related to their quantum numbers. However, these states have properties in conflict with the naive quark model and therefore deserve some special labeling.

Therefore in the Review of Particle Physics we will keep two names, one that carries the quantum number information and the other the original name. However, the former name will be given priority. In particular, it will be used when the particle appears as a decay product. Thus, in the Listings as well as Summary Tables from the 2018 edition onwards (listed are only some examples of the particles that appear in the Summary Tables),

- $X(3872)$ will appear as ‘ $\chi_{c1}(3872)$ also known as $X(3872)$ ’;
- $X(3900)^\pm$ will appear as ‘ $Z_c(3900)^\pm$ ’;
- $X(4260)$ will appear as ‘ $\psi(4260)$ also known as $Y(4260)$ ’;

In addition, states with quantum numbers allowed by the naive quark model but showing some peculiarities, such as an unusual decay pattern, will have the following information in the header:

This state shows properties different from a conventional $q\bar{q}$ state. A candidate for an exotic structure. See the minireview on non- $q\bar{q}$ states.

The states that cannot be classified as $q\bar{q}$ states (such as charged states with strong decays to heavy quarkonia) will have in the header:

Properties incompatible with a $q\bar{q}$ structure (exotic state). See the minireview on non- $q\bar{q}$ states.

The names Z_c and Z_b used in the literature for isovector states in the $c\bar{c}$ and $b\bar{b}$ sector, respectively, will now also be the official PDG names. No heavy isovector $PC = -+, --, \text{ or } ++$ states have yet been confirmed, but provisional names for such states – H , R , and W , respectively – are listed in Table 8.1. Note that the heavy isovector $PC = ++$ states were predicted to exist as spin partners of the Z states in [2], where the name W was also introduced.

By analogy to the light-quark sector, states with quantum numbers that are in conflict with the naive quark model are labeled according to their I , P , C , and spin J . The exotic nature can be inferred from the quantum numbers.

8.3 Mesons with nonzero S , C and/or B

Mesons with nonzero strangeness S or heavy flavor C and/or B are not eigenstates of charge conjugation, and in each of them one of the quarks is heavier than the other (as above, states containing top quarks are not considered). The rules have been and remain:

1. The main symbol is an upper-case italic letter indicating the heavier quark as follows:

$$s \rightarrow \bar{K} \quad c \rightarrow D \quad b \rightarrow \bar{B},$$

We use the convention that *the flavor quantum number and the charge of a quark have the same sign*. Thus the strangeness of the s quark is negative, the charm of the c quark is positive, and the bottomness of the b quark is negative. The effect of this convention is as follows: *any flavor carried by a charged meson has the same sign as its charge*. Thus the K^+ , D^+ , and B^+ have positive strangeness, charm, and bottomness, respectively, and all have positive I_3 . The D_s^+ has positive charm and strangeness. Furthermore, the $\Delta(\text{flavor}) = \Delta Q$ rule, best known for the strange kaons, applies to every flavor.

2. If the lighter quark is not a u or a d quark, its identity is given by a subscript. The D_s^+ is an example.
3. When the spin-parity is in the natural series, $J^P = 0^+, 1^-, 2^+, \dots$, a superscript “*” is added.
4. The spin is added as a subscript except for pseudoscalar or vector mesons.

8.4 Ordinary (3-quark) baryons

All baryons having quantum numbers consistent with a minimal quark content of three quarks are denoted by the symbols N , Δ , Λ , Σ , Ξ , and Ω introduced more than 50 years ago. These symbols are followed by J^P signifying their spin J and parity P . For those where the minimal content involves one or more heavier quarks than the light (u , d , and s) quarks, subscripts are added to their symbols, (c and b) as appropriate. The rules are:

1. Baryons with minimal content of *three* u and/or d quarks are N 's (isospin 1/2) or Δ 's (isospin 3/2).
2. Baryons with *two* u and/or d quarks are Λ 's (isospin 0) or Σ 's (isospin 1). If the third quark is a c or b quark, its identity is given by a subscript.
3. Baryons with *one* u or d quark are Ξ 's (isospin 1/2). One or two subscripts are used if one or both of the remaining quarks are heavy: thus Ξ_c , Ξ_{cc} , Ξ_b , etc.*
4. Baryons with *no* u or d quarks are Ω 's (isospin 0), and subscripts indicate any heavy-quark content.
5. A baryon that decays strongly has its mass in parentheses. Examples are the $\Delta(1232)$ $3/2^+$, $\Sigma(1385)$ $3/2^+$, $N(1440)$ $1/2^+$, $\Xi_c(2645)$ $3/2^+$.

In short, the minimal number of u plus d quarks together with the isospin determine the main symbol, and subscripts indicate any content of heavy quarks. A Σ always has isospin 1, an Ω always has isospin 0, etc.

8.5 Exotic baryons

In 2003, several experiments reported finding a strangeness $S = +1$, charge $Q = +1$ baryon, and one experiment reported finding an $S = -2$, $Q = -2$ baryon. Baryons with such quantum numbers cannot be made from three quarks, and thus they are exotic with respect to the naive quark model. However, these “discoveries” were then ruled out by many experiments with far larger statistics: See our 2008 *Review* [3].

More recently, the LHCb collaboration found a series of candidates for pentaquark states in the $J/\psi p$ system extracted from data on $\Lambda_b^0 \rightarrow J/\psi K^- p$ [4,5].** These have the quantum numbers of excited nucleons, but have a minimal quark content of $c\bar{c}uud$. Following the name established by the LHCb collaboration, we label these $P_c^+(\text{mass})J^P$, with the mass given in parentheses.

8.6 Change of meson names

For the recently discovered particles above open-flavor threshold in the charmonium and bottomonium systems (previously the “XYZ” mesons), there are a number of differences between the names newly adopted by the PDG and those that have commonly appeared in the literature. Table 8.2 maps the names now used in the PDG to former commonly used names.

Footnotes and References:

* See the “Note on Charmed Baryons” in the Charmed Baryon Listings.

** See our review “Pentaquarks” in the 2016 Edition.

Table 8.2: A comparison of current PDG names to former names commonly used in the literature.

Mesons with complete $I^G J^{PC}$ assignment	
PDG Name	Former Common Name(s)
$\psi_2(3823)^*$	$X(3823)$
$\chi_{c1}(3872)$	$X(3872)$
$Z_c(3900)$	$Z_c(3900)$
$\chi_{c2}(3930)^\dagger$	$\chi_{c2}(2P)$, $Z(3930)$
$\chi_{c1}(4140)$	$Y(4140)$
$Z_c(4200)$	$Z_c(4200)$
$\psi(4230)$	$Y(4230)$
$R_{c0}(4240)$	$Z_c(4240)$
$\psi(4260)$	$Y(4260)$
$\chi_{c1}(4274)$	$Y(4274)$
$\psi(4360)$	$Y(4360)$
$Z_c(4430)$	$Z_c(4430)$
$\chi_{c0}(4500)$	$X(4500)$
$\psi(4660)$	$X(4630)$, $Y(4660)$
$\chi_{c0}(4700)$	$X(4700)$
$Z_b(10610)$	$Z_b(10610)$
$Z_b(10650)$	$Z_b^{(l)}(10650)$
Mesons with incomplete $I^G J^{PC}$ assignment	
PDG Name	Former Common Name(s)
$X(3915)^\ddagger$	$\chi_{c0}(3915)$, $X(3915)$, $Y(3940)$
$X(3940)$	$X(3940)$
$X(4020)$	$Z_c^{(l)}(4020)$
$X(4050)^\pm$	$Z_1(4050)$
$X(4055)^\pm$	$Z_c(4055)$
$X(4160)$	$X(4160)$
$X(4250)^\pm$	$Z_2(4250)$
$X(4350)$	$X(4350)$

*The 2016 edition used $\psi(3823)$.

†The 2016 edition used $\chi_{c2}(2P)$. The mass is now used in the name following the current prescription.

‡The 2016 edition used $\chi_{c0}(3915)$. The J^{PC} have since been questioned.

References

- [1] M. Aguilar-Benitez *et al.* (Particle Data Group), *Phys. Lett.* **170B**, 1 (1986).
- [2] M. B. Voloshin, *Phys. Rev.* **D84**, 031502 (2011), [arXiv:1105.5829].

- [3] C. Amsler *et al.* (Particle Data Group), Phys. Lett. **B667**, 1 (2008). [arXiv:1507.03414].
- [4] R. Aaij *et al.* (LHCb), Phys. Rev. Lett. **115**, 072001 (2015), [arXiv:1507.03414].
- [5] R. Aaij *et al.* (LHCb), Phys. Rev. Lett. **122**, 22, 222001 (2019), [arXiv:1904.03947].

Standard Model and Related Topics

9. Quantum chromodynamics (rev.)	153
10. Electroweak model and constraints on new physics (rev.)	180
11. Higgs boson physics, status of (rev.)	203
12. CKM quark-mixing matrix (rev.)	261
13. CP violation in the quark sector (rev.)	271
14. Neutrino mass, mixing, and oscillations (new)	285
15. Quark model (rev.)	312
16. Heavy-quark & soft-collinear effective theory (rev.)	325
17. Lattice quantum chromodynamics (rev.)	333
18. Structure functions (rev.)	347
19. Fragmentation functions in e^+e^- , ep and pp collisions (rev.)	368
20. High Energy Soft QCD and Diffraction (new)	385

9. Quantum Chromodynamics

Revised August 2019 by J. Huston (Michigan State U.), K. Rabertz (KIT) and G. Zanderighi (MPI Munich).

9.1 Basics

Quantum Chromodynamics (QCD), the gauge field theory that describes the strong interactions of colored quarks and gluons, is the SU(3) component of the SU(3)×SU(2)×U(1) Standard Model of Particle Physics. The Lagrangian of QCD is given by

$$\mathcal{L} = \sum_q \bar{\psi}_{q,a} (i\gamma^\mu \partial_\mu \delta_{ab} - g_s \gamma^\mu t_{ab}^C \mathcal{A}_\mu^C - m_q \delta_{ab}) \psi_{q,b} - \frac{1}{4} F_{\mu\nu}^A F^{A\mu\nu}, \quad (9.1)$$

where repeated indices are summed over. The γ^μ are the Dirac γ -matrices. The $\psi_{q,a}$ are quark-field spinors for a quark of flavor q and mass m_q , with a color-index a that runs from $a = 1$ to $N_c = 3$, *i.e.* quarks come in three “colors.” Quarks are said to be in the fundamental representation of the SU(3) color group.

The \mathcal{A}_μ^C correspond to the gluon fields, with C running from 1 to $N_c^2 - 1 = 8$, *i.e.* there are eight kinds of gluon. Gluons transform under the adjoint representation of the SU(3) color group. The t_{ab}^C correspond to eight 3×3 matrices and are the generators of the SU(3) group (*cf.* the section on “SU(3) isoscalar factors and representation matrices” in this *Review*, with $t_{ab}^C \equiv \lambda_{ab}^C/2$). They encode the fact that a gluon’s interaction with a quark rotates the quark’s color in SU(3) space. The quantity g_s (or $\alpha_s = \frac{g_s^2}{4\pi}$) is the QCD coupling constant. Besides quark masses, who have electroweak origin, it is the only fundamental parameter of QCD. Finally, the field tensor $F_{\mu\nu}^A$ is given by

$$F_{\mu\nu}^A = \partial_\mu \mathcal{A}_\nu^A - \partial_\nu \mathcal{A}_\mu^A - g_s f_{ABC} \mathcal{A}_\mu^B \mathcal{A}_\nu^C, \quad (9.2)$$

$$[t^A, t^B] = i f_{ABC} t^C,$$

where the f_{ABC} are the structure constants of the SU(3) group.

Neither quarks nor gluons are observed as free particles. Hadrons are color-singlet (*i.e.* color-neutral) combinations of quarks, anti-quarks, and gluons.

Ab-initio predictive methods for QCD include lattice gauge theory and perturbative expansions in the coupling. The Feynman rules of QCD involve a quark-antiquark-gluon ($q\bar{q}g$) vertex, a 3-gluon vertex (both proportional to g_s), and a 4-gluon vertex (proportional to g_s^2). A full set of Feynman rules is to be found for example in Refs. [1, 2].

Useful color-algebra relations include: $t_{ab}^A t_{bc}^A = C_F \delta_{ac}$, where $C_F \equiv (N_c^2 - 1)/(2N_c) = 4/3$ is the color-factor (“Casimir”) associated with gluon emission from a quark; $f_{ACD} f_{BCD} = C_A \delta_{AB}$, where $C_A \equiv N_c = 3$ is the color-factor associated with gluon emission from a gluon; $t_{ab}^A t_{ab}^B = T_R \delta_{AB}$, where $T_R = 1/2$ is the color-factor for a gluon to split to a $q\bar{q}$ pair.

There is freedom for an additional CP-violating term to be present in the QCD Lagrangian, $\theta \frac{\alpha_s}{8\pi} F_{\mu\nu}^A \tilde{F}^{A\mu\nu}$, where $\tilde{F}^{A\mu\nu}$ is the dual of the gluon field tensor, $\frac{1}{2} \epsilon_{\mu\nu\sigma\rho} F^{A\sigma\rho}$, where $\epsilon_{\mu\nu\sigma\rho}$ is the fully antisymmetric Levi-Civita symbol. Experimental limits on ultracold neutrons [3, 4] and atomic mercury [5] constrain the QCD vacuum angle to satisfy $|\theta| \lesssim 10^{-10}$. Further discussion is to be found in Ref. [6] and in the Axions section in the Listings of this *Review*.

This section will concentrate mainly on perturbative aspects of QCD as they relate to collider physics. Related textbooks and lecture notes include Refs. [1, 2, 7–9]. Aspects specific to Monte Carlo event generators are reviewed in the dedicated section 41. Lattice QCD is also reviewed in a section of its own, Sec. 17, with further discussion of perturbative and non-perturbative aspects to be found in the sections on “Quark Masses”, “The CKM quark-mixing matrix”, “Structure Functions”, “Fragmentation Functions”, “Passage of Particles Through Matter” and “Heavy-Quark and Soft-Collinear Effective Theory” in this *Review*.

9.1.1 Running coupling

In the framework of perturbative QCD (pQCD), predictions for observables are expressed in terms of the renormalized coupling $\alpha_s(\mu_R^2)$, a function of an (unphysical) renormalization scale μ_R . When one takes μ_R close to the scale of the momentum transfer Q

in a given process, then $\alpha_s(\mu_R^2 \simeq Q^2)$ is indicative of the effective strength of the strong interaction in that process.

The coupling satisfies the following renormalization group equation (RGE):

$$\mu_R^2 \frac{d\alpha_s}{d\mu_R^2} = \beta(\alpha_s) = -(b_0 \alpha_s^2 + b_1 \alpha_s^3 + b_2 \alpha_s^4 + \dots), \quad (9.3)$$

where $b_0 = (11C_A - 4n_f T_R)/(12\pi) = (33 - 2n_f)/(12\pi)$ is referred to as the 1-loop β -function coefficient, the 2-loop coefficient is $b_1 = (17C_A^2 - n_f T_R(10C_A + 6C_F))/(24\pi^2) = (153 - 19n_f)/(24\pi^2)$, and the 3-loop coefficient is $b_2 = (2857 - \frac{5033}{9} n_f + \frac{325}{27} n_f^2)/(128\pi^3)$ for the SU(3) values of C_A and C_F . Here n_f is the number of quark flavours. The 4-loop coefficient, b_3 , is to be found in Refs. [10, 11], while the 5-loop coefficient, b_4 , is in Refs. [12–16]. The coefficients b_2 and b_3 (and beyond) are renormalization-scheme-dependent and given here in the modified minimal subtraction ($\overline{\text{MS}}$) scheme [17], by far the most widely used scheme in QCD and the one adopted in the following.

The minus sign in Eq. (9.3) is the origin of Asymptotic Freedom [18, 19], *i.e.* the fact that the strong coupling becomes weak for processes involving large momentum transfers (“hard processes”). For momentum transfers in the 0.1–1 TeV range, $\alpha_s \sim 0.1$, while the theory is strongly interacting for scales around and below 1 GeV.

The β -function coefficients, the b_i , are given for the coupling of an *effective theory* in which n_f of the quark flavors are considered light ($m_q \ll \mu_R$), and in which the remaining heavier quark flavors decouple from the theory. One may relate the coupling for the theory with $n_f + 1$ light flavors to that with n_f flavors through an equation of the form

$$\alpha_s^{(n_f+1)}(\mu_R^2) = \alpha_s^{(n_f)}(\mu_R^2) \times \left(1 + \sum_{n=1}^{\infty} \sum_{\ell=0}^n c_{n\ell} [\alpha_s^{(n_f)}(\mu_R^2)]^n \ln^\ell \frac{\mu_R^2}{m_h^2} \right), \quad (9.4)$$

where m_h is the mass of the $(n_f + 1)^{\text{th}}$ flavor, and the first few $c_{n\ell}$ coefficients are $c_{11} = \frac{1}{6\pi}$, $c_{10} = 0$, $c_{22} = c_{11}^2$, $c_{21} = \frac{11}{24\pi^2}$, and $c_{20} = -\frac{11}{72\pi^2}$ when m_h is the $\overline{\text{MS}}$ mass at scale m_h , while $c_{20} = \frac{7}{24\pi^2}$ when m_h is the pole mass (mass definitions are discussed below in Sec. (9.1.2) and in the review on “Quark Masses”). Terms up to $c_{4\ell}$ are to be found in Refs. [20, 21]. Numerically, when one chooses $\mu_R = m_h$, the matching is a modest effect, owing to the zero value for the c_{10} coefficient. Relations between n_f and (n_f+2) flavors where the two heavy flavors are close in mass are given to three loops in Ref. [22].

Working in an energy range where the number of flavors is taken constant, a simple exact analytic solution exists for Eq. (9.3) only if one neglects all but the b_0 term, giving $\alpha_s(\mu_R^2) = (b_0 \ln(\mu_R^2/\Lambda^2))^{-1}$. Here Λ is a constant of integration, which corresponds to the scale where the perturbatively-defined coupling would diverge. Its value is indicative of the energy range where non-perturbative dynamics dominates. A convenient approximate analytic solution to the RGE that includes terms up to b_4 is given by solving iteratively Eq. (9.3)

$$\alpha_s(\mu_R^2) \simeq \frac{1}{b_0 t} \left(1 - \frac{b_1 \ell}{b_0^2 t} + \frac{b_1^2 (\ell^2 - \ell - 1) + b_0 b_2}{b_0^4 t^2} + \frac{b_1^3 (-2\ell^3 + 5\ell^2 + 4\ell - 1) - 6b_0 b_2 b_1 \ell + b_0^2 b_3}{2b_0^6 t^3} + \frac{18b_0 b_2 b_1^2 (2\ell^2 - \ell - 1) + b_1^4 (6\ell^4 - 26\ell^3 - 9\ell^2 + 24\ell + 7)}{6b_0^8 t^4} + \frac{-b_0^2 b_3 b_1 (12\ell + 1) + 2b_0^2 (5b_2^2 + b_0 b_4)}{6b_0^8 t^4} \right), \quad (9.5)$$

with $t \equiv \ln \frac{\mu_R^2}{\Lambda^2}$ and $\ell = \ln t$, again parametrized in terms of a constant Λ . Note that Eq. (9.5) is one of several possible approximate 4-loop solutions for $\alpha_s(\mu_R^2)$, and that a value for Λ only defines $\alpha_s(\mu_R^2)$ once one knows which particular approximation is being used. An alternative to the use of formulas such as Eq. (9.5) is to solve the RGE exactly, numerically (including the discontinuities, Eq. (9.4), at flavor thresholds). In such cases the quantity Λ does not directly arise (though it can be defined, *cf.* Eqs. (1–3) of Ref. [23]). For these reasons, in determinations of the coupling, it has become standard practice to quote the value of α_s at a given scale (typically the mass of the Z boson, M_Z) rather than to quote a value for Λ .

A discussion of determinations of the coupling and a graph illustrating its scale dependence (“running”) are to be found in Section 9.4. The RunDec package [24–26] is often used to calculate the evolution of the coupling. For a discussion of electroweak effects in the evolution of the QCD coupling, see Ref. [27] and references therein.

9.1.2 Quark masses

Free quarks have never been observed, which is understood as a result of a long-distance, confining property of the strong QCD force: up, down, strange, charm, and bottom quarks all *hadronize*, *i.e.* become part of a meson or baryon, on a timescale $\sim 1/\Lambda$; the top quark instead decays before it has time to hadronize. This means that the question of what one means by the quark mass is a complex one, which requires one to adopt a specific prescription. A perturbatively defined prescription is the pole mass, m_q , which corresponds to the position of the divergence of the propagator. This is close to one’s physical picture of mass. However, when relating it to observable quantities, it suffers from substantial non-perturbative ambiguities (see *e.g.* Ref. [28–30]). An alternative is the $\overline{\text{MS}}$ mass, $\overline{m}_q(\mu_R^2)$, which depends on the renormalization scale μ_R .

Results for the masses of heavier quarks are often quoted either as the pole mass or as the $\overline{\text{MS}}$ mass evaluated at a scale equal to the mass, $\overline{m}_q(\overline{m}_q^2)$; light quark masses are often quoted in the $\overline{\text{MS}}$ scheme at a scale $\mu_R \sim 2 \text{ GeV}$. The pole and $\overline{\text{MS}}$ masses are related by a series that starts as $m_q = \overline{m}_q(\overline{m}_q^2)(1 + \frac{4\alpha_s(\overline{m}_q^2)}{3\pi} + \mathcal{O}(\alpha_s^2))$, while the scale-dependence of $\overline{\text{MS}}$ masses is given at lowest order by

$$\mu_R^2 \frac{d\overline{m}_q(\mu_R^2)}{d\mu_R^2} = \left[-\frac{\alpha_s(\mu_R^2)}{\pi} + \mathcal{O}(\alpha_s^2) \right] \overline{m}_q(\mu_R^2). \quad (9.6)$$

A more detailed discussion is to be found in a dedicated section of the *Review*, “Quark Masses”, with detailed formulas also in Ref. [31] and references therein.

In perturbative QCD calculations of scattering processes, it is common to work in an approximation in which one neglects (*i.e.* sets to zero) the masses of all quarks, whose mass is significantly smaller than the momentum transfer in the process.

9.2 Structure of QCD predictions

9.2.1 Fully inclusive cross sections

The simplest observables in perturbative QCD are those that do not involve initial-state hadrons and that are fully inclusive with respect to details of the final state. One example is the total cross section for $e^+e^- \rightarrow \text{hadrons}$ at center-of-mass energy Q , for which one can write

$$\frac{\sigma(e^+e^- \rightarrow \text{hadrons}, Q)}{\sigma(e^+e^- \rightarrow \mu^+\mu^-, Q)} \equiv R(Q) = R_{\text{EW}}(Q)(1 + \delta_{\text{QCD}}(Q)), \quad (9.7)$$

where $R_{\text{EW}}(Q)$ is the purely electroweak prediction for the ratio and $\delta_{\text{QCD}}(Q)$ is the correction due to QCD effects. To keep the discussion simple, we can restrict our attention to energies $Q \ll M_Z$, where the process is dominated by photon exchange (neglecting electroweak and finite-quark-mass corrections $R_{\text{EW}} = N_c \sum_q e_q^2$, where the e_q are the electric charges of the quarks) and

$$\delta_{\text{QCD}}(Q) = \sum_{n=1}^{\infty} c_n \cdot \left(\frac{\alpha_s(Q^2)}{\pi} \right)^n + \mathcal{O} \left(\frac{\Lambda^4}{Q^4} \right). \quad (9.8)$$

The first four terms in the α_s series expansion are then to be found in Ref. [32],

$$c_1 = 1, \quad c_2 = 1.9857 - 0.1152n_f, \quad (9.9a)$$

$$c_3 = -6.63694 - 1.20013n_f - 0.00518n_f^2 - 1.240\eta, \quad (9.9b)$$

$$c_4 = -156.61 + 18.775n_f - 0.7974n_f^2 + 0.0215n_f^3 - (17.828 - 0.575n_f)\eta, \quad (9.9c)$$

with $\eta = (\sum e_q)^2 / (3 \sum e_q^2)$. For corresponding expressions including also Z exchange and finite-quark-mass effects, see Refs. [33–35].

A related series holds also for the QCD corrections to the hadronic decay width of the τ lepton, which essentially involves an integral of $R(Q)$ over the allowed range of invariant masses of the hadronic part of the τ decay (see *e.g.* Ref. [36]). The series expansions for QCD corrections to Higgs-boson hadronic (partial) decay widths in the limit of heavy top quark and massless light flavours at N⁴LO are given in Ref. [37].

One characteristic feature of Eqs. (9.8) and (9.9) is that the coefficients of α_s^n increase order by order: calculations in perturbative QCD tend to converge more slowly than would be expected based just on the size of α_s . The situation is significantly worse near thresholds or in the presence of tight kinematic cuts. Another feature is the existence of an extra “power-correction” term $\mathcal{O}(\Lambda^4/Q^4)$ in Eq. (9.8), which accounts for contributions that are fundamentally non-perturbative. All high-energy QCD predictions involve power corrections $(\Lambda/Q)^p$, although typically the suppression of these corrections with Q is smaller than given in Eq. (9.8) where $p = 4$. The exact power p depends on the observable and, for many processes and observables, it is possible to introduce an operator product expansion and associate power suppressed terms with specific higher-dimension (non-perturbative) operators [38].

Scale dependence. In Eq. (9.8) the renormalization scale for α_s has been chosen equal to Q . The result can also be expressed in terms of the coupling at an arbitrary renormalization scale μ_R ,

$$\delta_{\text{QCD}}(Q) = \sum_{n=1}^{\infty} \bar{c}_n \left(\frac{\mu_R^2}{Q^2} \right) \cdot \left(\frac{\alpha_s(\mu_R^2)}{\pi} \right)^n + \mathcal{O} \left(\frac{\Lambda^4}{Q^4} \right), \quad (9.10)$$

where $\bar{c}_1(\mu_R^2/Q^2) \equiv c_1$, $\bar{c}_2(\mu_R^2/Q^2) = c_2 + \pi b_0 c_1 \ln(\mu_R^2/Q^2)$, $\bar{c}_3(\mu_R^2/Q^2) = c_3 + (2b_0 c_2 \pi + b_1 c_1 \pi^2) \times \ln(\mu_R^2/Q^2) + b_0^2 c_1 \pi^2 \ln^2(\mu_R^2/Q^2)$, *etc.* Given an infinite number of terms in the α_s expansion, the μ_R dependence of the $\bar{c}_n(\mu_R^2/Q^2)$ coefficients will exactly cancel that of $\alpha_s(\mu_R^2)$, and the final result will be independent of the choice of μ_R : physical observables do not depend on unphysical scales.¹

With just terms up to some finite $n = N$, a residual μ_R dependence will remain, which implies an uncertainty on the prediction of $R(Q)$ due to the arbitrariness of the scale choice. This uncertainty will be $\mathcal{O}(\alpha_s^{N+1})$, *i.e.* of the same order as the neglected higher-order terms. For this reason it is customary to use QCD predictions’ scale dependence as an estimate of the uncertainties due to neglected terms. One usually takes a central value for $\mu_R \sim Q$, in order to avoid the poor convergence of the perturbative series that results from the large $\ln^{n-1}(\mu_R^2/Q^2)$ terms in the \bar{c}_n coefficients when $\mu_R \ll Q$ or $\mu_R \gg Q$. Uncertainties are then

¹ With respect to pQCD there is an important caveat to this statement: at sufficiently high orders, perturbative series generally suffer from “renormalon” divergences $\alpha_s^n n!$ (reviewed in Ref. [28]). This phenomenon is not usually visible with the limited number of perturbative terms available today. However it is closely connected with non-perturbative contributions and sets a limit on the possible precision of perturbative predictions. The cancellation of scale dependence will also ultimately be affected by this renormalon-induced breakdown of perturbation theory.

commonly determined by varying μ_R by a factor of two up and down around the central scale choice. A more detailed discussion on the accuracy of theoretical predictions and on ways to estimate the theoretical uncertainties can be found in Section 9.2.4.

9.2.2 Processes with initial-state hadrons

Deep-Inelastic Scattering. To illustrate the key features of QCD cross sections in processes with initial-state hadrons, let us consider deep-inelastic scattering (DIS), $ep \rightarrow e + X$, where an electron e with four-momentum k emits a highly off-shell photon (momentum q) that interacts with the proton (momentum p). For photon virtualities $Q^2 \equiv -q^2$ far above the squared proton mass (but far below the Z mass), the differential cross section in terms of the kinematic variables Q^2 , $x = Q^2/(2p \cdot q)$ and $y = (q \cdot p)/(k \cdot p)$ is

$$\frac{d^2\sigma}{dx dQ^2} = \frac{4\pi\alpha^2}{2xQ^4} \left[(1 + (1-y)^2)F_2(x, Q^2) - y^2 F_L(x, Q^2) \right], \quad (9.11)$$

where α is the electromagnetic coupling and $F_2(x, Q^2)$ and $F_L(x, Q^2)$ are proton structure functions, which encode the interaction between the photon (in given polarization states) and the proton. In the presence of parity-violating interactions (e.g. νp scattering) an additional F_3 structure function is present. For an extended review, including equations for the full electroweak and polarized cases, see Sec. 18 of this *Review*.

Structure functions are not calculable in perturbative QCD, nor is any other cross section that involves QCD interactions and initial-state hadrons. To zeroth order in α_s , the structure functions are given directly in terms of non-perturbative parton (quark or gluon) distribution functions (PDFs),

$$F_2(x, Q^2) = x \sum_q e_q^2 f_{q/p}(x), \quad F_L(x, Q^2) = 0, \quad (9.12)$$

where $f_{q/p}(x)$ is the non-perturbative PDF for quarks of type q inside the proton, i.e. the number density of quarks of type q inside a fast-moving proton that carry a fraction x of its longitudinal momentum (the quark flavor index q , here, is not to be confused with the photon momentum q in the lines preceding Eq. (9.11)). Recently, some first determinations on lattice started to appear [39–43] but there is also some debate about the underlying methods [44]. Accordingly, for all practical uses, PDFs are currently determined from data (cf. Sec. 18 of this *Review* and also Refs. [45, 46])².

The above result, with PDFs $f_{q/p}(x)$ that are independent of the scale Q , corresponds to the “quark-parton model” picture in which the photon interacts with point-like free quarks, or equivalently, one has incoherent elastic scattering between the electron and individual constituents of the proton. As a consequence, in this picture also F_2 and F_L are independent of Q [50]. When including higher orders in pQCD,

$$F_2(x, Q^2) = x \sum_{n=0}^{\infty} \frac{\alpha_s^n(\mu_R^2)}{(2\pi)^n} \times \sum_{i=q,g} \int_x^1 \frac{dz}{z} C_{2,i}^{(n)}(z, Q^2, \mu_R^2, \mu_F^2) f_{i/p}\left(\frac{x}{z}, \mu_F^2\right) + \mathcal{O}\left(\frac{\Lambda^2}{Q^2}\right). \quad (9.13)$$

²PDFs can be determined from data in a global fit at LO, NLO and NNLO, depending on the order of the matrix elements used to describe the data. In modern global PDF fits, data are included from DIS, DY, jets and $t\bar{t}$ processes, and more LHC collider data, with the global PDF fits using 3000–4000 data points. There is a large change in the PDFs from LO to NLO, with a much smaller change from NLO to NNLO. LO PDFs can be unreliable for collider predictions, especially at low and high x . The uncertainties of the resulting PDFs are determined from the experimental uncertainties of the data that serves as input to the global PDF fits. The PDF uncertainties can either be determined through a Hessian approach or through the use of Monte Carlo replicas. It is now relatively straightforward to convert results from one approach to the other. The PDF4LHC15 PDF set is formed by combining replicas of the CT14, MMHT2014 and NNPDF3.0 PDF sets, at NLO and at NNLO [47]. Recently, theoretical uncertainties related to missing higher orders have been included in global PDF determinations but so far only at NLO [48, 49].

Just as in Eq. (9.10), we have a series in powers of $\alpha_s(\mu_R^2)$, each term involving a coefficient $C_{2,i}^{(n)}$ that can be calculated using Feynman graphs. At variance with the parton model, the PDFs in pQCD depend on an additional scale, the factorization scale μ_F , whose significance will be discussed in the following. Another important difference is the additional integral over z . The parton that comes from the proton can undergo a splitting before it interacts with the photon. As a result, the $C_{2,i}^{(n)}$ coefficients are functions that depend on the ratio, z , of the parton’s momentum before and after radiation, and one must integrate over that ratio. For the electromagnetic component of DIS with light quarks and gluons, the zeroth order coefficient functions are $C_{2,q}^{(0)} = e_q^2 \delta(1-z)$ and $C_{2,g}^{(0)} = 0$. Corrections are known up to $\mathcal{O}(\alpha_s^3)$ (next-to-next-to-next-to-leading order, N³LO) for both electromagnetic [51] and weak currents [52, 53]. For heavy-quark production they are known to $\mathcal{O}(\alpha_s^2)$ [54, 55] (next-to-leading order, NLO, insofar as the series starts at $\mathcal{O}(\alpha_s)$). For precise comparisons of LHC cross sections with theoretical predictions, the photon PDF of the proton is also needed. It has been computed precisely in Ref. [56] and has now been implemented in most global PDF fits.

The majority of the emissions that modify a parton’s momentum are collinear (parallel) to that parton, and do not depend on the fact that the parton is destined to interact with a photon. It is natural to view these emissions as modifying the proton’s structure rather than being part of the coefficient function for the parton’s interaction with the photon. Technically, one uses a procedure known as *collinear factorization* to give a well-defined meaning to this distinction, most commonly through the $\overline{\text{MS}}$ factorization scheme, defined in the context of dimensional regularization. The $\overline{\text{MS}}$ factorization scheme involves an arbitrary choice of *factorization scale*, μ_F , whose meaning can be understood roughly as follows: emissions with transverse momenta above μ_F are included in the $C_{2,q}^{(n)}(z, Q^2, \mu_R^2, \mu_F^2)$; emissions with transverse momenta below μ_F are accounted for within the PDFs, $f_{i/p}(x, \mu_F^2)$. While collinear factorization is generally believed to be valid for suitable (sufficiently inclusive) observables in processes with hard scales, Ref. [57], which reviews the factorization proofs in detail, is cautious in the statements it makes about their exhaustivity, notably for the hadron-collider processes which we shall discuss below. Further discussion is to be found in Refs. [58, 59].

The PDFs’ resulting dependence on μ_F is described by the Dokshitzer-Gribov-Lipatov-Altarelli-Parisi (DGLAP) equations [60], which to leading order (LO) read³

$$\mu_F^2 \frac{\partial f_{i/p}(x, \mu_F^2)}{\partial \mu_F^2} = \sum_j \frac{\alpha_s(\mu_F^2)}{2\pi} \int_x^1 \frac{dz}{z} P_{i \leftarrow j}^{(1)}(z) f_{j/p}\left(\frac{x}{z}, \mu_F^2\right), \quad (9.14)$$

with, for example, $P_{q \leftarrow g}^{(1)}(z) = T_R(z^2 + (1-z)^2)$. The other LO splitting functions are listed in Sec. 18 of this *Review*, while results up to NLO, α_s^2 , and NNLO, α_s^3 , are given in Refs. [61] and [62] respectively. At N³LO accuracy, only partial results are currently available Ref. [63–65].

Splitting functions for polarized PDFs are given in Ref. [66]. Beyond LO, the coefficient functions are also μ_F dependent, for example $C_{2,i}^{(1)}(x, Q^2, \mu_R^2, \mu_F^2) = C_{2,i}^{(1)}(x, Q^2, \mu_R^2, Q^2) - \ln\left(\frac{\mu_F^2}{Q^2}\right) \sum_j \int_x^1 \frac{dz}{z} \times C_{2,j}^{(0)}\left(\frac{x}{z}\right) P_{j \leftarrow i}^{(1)}(z)$. In certain contexts, higher-order QED and mixed QED-QCD corrections to the splitting functions are also needed [67].

As with the renormalization scale, the choice of factorization scale is arbitrary, but if one has an infinite number of terms in the perturbative series, the μ_F -dependencies of the coefficient functions and PDFs will compensate each other fully. Given only N terms of the series, a residual $\mathcal{O}(\alpha_s^{N+1})$ uncertainty is associated with the ambiguity in the choice of μ_F . As with μ_R , varying μ_F provides an input in estimating uncertainties on predictions. In inclusive DIS predictions, the default choice for the scales is

³ LO is generally taken to mean the lowest order at which a quantity is non-zero.

usually $\mu_R = \mu_F = Q$.

As is the case for the running coupling, in DGLAP evolution one can introduce flavor thresholds near the heavy quark masses: below a given heavy quark's mass, that quark is not considered to be part of the proton's structure, while above it is considered to be part of the proton's structure and evolves with massless DGLAP splitting kernels. With appropriate parton distribution matching terms at threshold, such a variable flavor number scheme (VFNS), when used with massless coefficient functions, gives the full heavy-quark contributions at high Q^2 scales. For scales near the threshold, it is instead necessary to appropriately adapt the standard massive coefficient functions to account for the heavy-quark contribution already included in the PDFs [68–70].

At sufficiently small x and Q^2 in inclusive DIS, resummation of small x logarithms may be necessary [71, 72]. This may in fact have been observed in Refs. [73] based on HERA data [74], in a kinematic region where useful information for PDFs for collider predictions is present. A better description of the data in this region can be gained by small x resummation matched to NNLO [73, 75], or by the inclusion of power-suppressed contributions [76] or by using an x -dependent factorization scale in the NNLO DIS predictions [77].

Hadron-hadron collisions. The extension to processes with two initial-state hadrons can be illustrated with the example of the total (inclusive) cross section for W boson production in collisions of hadrons h_1 and h_2 , which can be written as

$$\begin{aligned} \sigma(h_1 h_2 \rightarrow W + X) &= \sum_{n=0}^{\infty} \alpha_s^n(\mu_R^2) \\ &\times \sum_{i,j} \int dx_1 dx_2 f_{i/h_1}(x_1, \mu_F^2) f_{j/h_2}(x_2, \mu_F^2) \\ &\times \hat{\sigma}_{ij \rightarrow W+X}^{(n)}(x_1 x_2 s, \mu_R^2, \mu_F^2) + \mathcal{O}\left(\frac{\Lambda^2}{M_W^4}\right), \end{aligned} \quad (9.15)$$

where s is the squared center-of-mass energy of the collision. At LO, $n = 0$, the hard (partonic) cross section $\hat{\sigma}_{ij \rightarrow W+X}^{(0)}(x_1 x_2 s, \mu_R^2, \mu_F^2)$ is simply proportional to $\delta(x_1 x_2 s - M_W^2)$, in the narrow W -boson width approximation (see Sec. 5.0 of this *Review* for detailed expressions for this and other hard scattering cross sections). It is non-zero only for choices of i, j that can directly give a W , such as $i = u, j = \bar{d}$. At higher orders, $n \geq 1$, new partonic channels contribute, such as gg , and $x_1 x_2 s \geq M_W^2$ in the narrow W -boson width approximation.

Eq. (9.15) involves a collinear factorization between the hard cross section and the PDFs, just like Eq. (9.13). As long as the same factorization scheme is used in DIS and pp or $p\bar{p}$ (usually the $\overline{\text{MS}}$ scheme), then PDFs extracted in DIS can be directly used in pp and $p\bar{p}$ predictions [57, 78] (with the anti-quark distributions in an anti-proton being the same as the quark distributions in a proton).

Fully inclusive hard cross sections are known to NNLO, *i.e.* corrections up to relative order α_s^2 , for Drell-Yan (DY) lepton-pair and vector-boson production [79, 80], Higgs-boson production in association with a vector boson [81], Higgs-boson production via vector-boson fusion [82] (in an approximation that factorizes the production of the two vector bosons), Higgs-pair production with full m_t dependence [83], top-antitop production [84] and vector-boson pair production [85–87].⁴ Inclusive Higgs production through gluon fusion in the large m_t limit was calculated at N³LO [88, 89]. A calculation at this order, differential in the Higgs rapidity has also been presented recently [90]. Vector-boson fusion Higgs production is also known to N³LO [91] in the factorized approximation. A discussion of many other calculations for Higgs production processes is to be found in Ref. [92].

Photoproduction. γp (and $\gamma\gamma$) collisions are similar to pp collisions, with the subtlety that the photon can behave in two ways:

there is “direct” photoproduction, in which the photon behaves as a point-like particle and takes part directly in the hard collision, with hard subprocesses such as $\gamma g \rightarrow q\bar{q}$; there is also resolved photoproduction, in which the photon behaves like a hadron, with non-perturbative partonic substructure and a corresponding PDF for its quark and gluon content, $f_{i/\gamma}(x, Q^2)$. While useful to understand the general structure of γp collisions, the distinction between direct and resolved photoproduction is not well defined beyond leading order, as discussed for example in Ref. [93].

The high-energy (BFKL) limit. In situations in which the total center-of-mass energy \sqrt{s} is much larger than all other momentum-transfer scales in the problem (*e.g.* Q in DIS, m_b for $b\bar{b}$ production in pp collisions, *etc.*), each power of α_s beyond LO can be accompanied by a power of $\ln(s/Q^2)$ (or $\ln(s/m_b^2)$, *etc.*). This is variously referred to as the high-energy, small- x or Balitsky-Fadin-Kuraev-Lipatov (BFKL) limit [72, 94, 95]. Currently it is possible to account for the dominant and first sub-dominant [96, 97] power of $\ln s$ at each order of α_s , and also to estimate further sub-dominant contributions that are numerically large (see Refs. [98–101] and references therein). Progress towards NNLO is discussed in Ref. [102].

Physically, the summation of all orders in α_s can be understood as leading to a growth with s of the gluon density in the proton. At sufficiently high energies this implies non-linear effects (commonly referred to as parton saturation), whose treatment has been the subject of intense study (see for example Refs. [103, 104] and references thereto).

9.2.3 Cross sections with phase-space restrictions

QCD final states always consist of hadrons, while perturbative QCD calculations deal with partons. Physically, an energetic parton fragments (“showers”) into many further partons, which then, on later timescales, undergo a transition to hadrons (“hadronization”). Fixed-order perturbation theory captures only a small part of these dynamics. This does not matter for the fully inclusive cross sections discussed above: the showering and hadronization stages are approximately unitary, *i.e.* they do not substantially change the overall probability of hard scattering, because they occur long after it has taken place (they introduce at most a correction proportional to a power of the ratio of timescales involved, *i.e.* a power of Λ/Q , where Q is the hard scattering scale).

Less inclusive measurements, in contrast, may be affected by the extra dynamics. For those sensitive just to the main directions of energy flow (jet rates, event shapes, *cf.* Sec. 9.3.1) fixed-order perturbation theory is often still adequate, because showering and hadronization do not substantially change the overall energy flow. This means that one can make a prediction using just a small number of partons, which should correspond well to a measurement of the same observable carried out on hadrons. For observables that instead depend on distributions of individual hadrons (which, *e.g.*, are the inputs to detector simulations), it is mandatory to account for showering and hadronization. The range of predictive techniques available for QCD final states reflects this diversity of needs of different measurements.

While illustrating the different methods, we shall for simplicity mainly use expressions that hold for e^+e^- scattering. The extension to cases with initial-state partons will be mostly straightforward (space constraints unfortunately prevent us from addressing diffraction and exclusive hadron-production processes; extensive discussion is to be found in Refs. [105, 106]).

9.2.3.1 Soft and collinear limits

Before examining specific predictive methods, it is useful to be aware of a general property of QCD matrix elements in the soft and collinear limits. Consider a squared tree-level matrix element $|M_n^2(p_1, \dots, p_n)|$ for the process $e^+e^- \rightarrow n$ partons with momenta p_1, \dots, p_n , and a corresponding phase-space integration measure $d\Phi_n$. If particle n is a gluon, which becomes collinear (parallel) to another particle i and additionally its momentum tends to zero

⁴ Processes with jets or photons in the final state have divergent cross sections unless one places a cut on the jet or photon momentum. Accordingly, they are discussed below in Section 9.2.3.2.

(is “soft”), the matrix element simplifies as follows,

$$\lim_{\theta_{in} \rightarrow 0, E_n \rightarrow 0} d\Phi_n |M_n^2(p_1, \dots, p_n)| = d\Phi_{n-1} |M_{n-1}^2(p_1, \dots, p_{n-1})| \frac{\alpha_s C_i}{\pi} \frac{d\theta_{in}^2}{\theta_{in}^2} \frac{dE_n}{E_n}, \quad (9.16)$$

where $C_i = C_F$ (C_A) if i is a quark (gluon). This formula has non-integrable divergences both for the inter-parton angle $\theta_{in} \rightarrow 0$ and for the gluon energy $E_n \rightarrow 0$, which are mirrored also in the structure of divergences in loop diagrams. These divergences are important for at least two reasons: firstly, they govern the typical structure of events (inducing many emissions either with low energy or at small angle with respect to hard partons); secondly, they will determine which observables can be calculated within perturbative QCD.

9.2.3.2 Fixed-order predictions

Let us consider an observable \mathcal{O} that is a function $\mathcal{O}_n(p_1, \dots, p_n)$ of the four-momenta of the n final-state particles in an event (either partons or hadrons). In what follows, we shall consider the cross section for events weighted with the value of the observable, $\sigma_{\mathcal{O}}$. As examples, if $\mathcal{O}_n \equiv 1$ for all n , then $\sigma_{\mathcal{O}}$ is just the total cross section; if $\mathcal{O}_n \equiv \hat{\tau}(p_1, \dots, p_n)$ where $\hat{\tau}$ is the value of the Thrust for that event (see Sec. 9.3.1.2), then the average value of the Thrust is $\langle \tau \rangle = \sigma_{\mathcal{O}} / \sigma_{\text{tot}}$; if $\mathcal{O}_n \equiv \delta(\tau - \hat{\tau}(p_1, \dots, p_n))$ then one gets the differential cross section as a function of the Thrust, $\sigma_{\mathcal{O}} \equiv d\sigma/d\tau$.

In the expressions below, we shall omit to write the non-perturbative power correction term, which for most common observables is proportional to a single power of Λ/Q .

Leading Order. If the observable \mathcal{O} is non-zero only for events with at least n final-state particles, then the LO QCD prediction for the weighted cross section in e^+e^- annihilation is

$$\sigma_{\mathcal{O}, LO} = \alpha_s^{n-2} (\mu_R^2) \int d\Phi_n |M_n^2(p_1, \dots, p_n)| \mathcal{O}_n(p_1, \dots, p_n), \quad (9.17)$$

where the squared tree-level matrix element, $|M_n^2(p_1, \dots, p_n)|$, including relevant symmetry factors, has been summed over all subprocesses (e.g. $e^+e^- \rightarrow q\bar{q}q\bar{q}$, $e^+e^- \rightarrow q\bar{q}gg$) and has had all factors of α_s extracted in front. In processes other than e^+e^- collisions, the center-of-mass energy of the LO process is generally not fixed, and so the powers of the coupling are often brought inside the integrals, with the scale μ_R chosen event by event, as a function of the event kinematics.

Other than in the simplest cases (see the review on Cross Sections in this *Review*), the matrix elements in Eq. (9.17) are usually calculated automatically with programs such as CompHEP [107], MadGraph [108], Alpgen [109], Comix/Sherpa [110], and Helac/Phegas [111]. Some of these (CompHEP, MadGraph) use formulas obtained from direct evaluations of Feynman diagrams. Others (Alpgen, Helac/Phegas and Comix/Sherpa) use methods designed to be particularly efficient at high multiplicities, such as Berends-Giele recursion [112], which builds up amplitudes for complex processes from simpler ones (see also Refs. [113–116] for reviews on the topic and for other tree-level calculational methods).

The phase-space integration is usually carried out by Monte Carlo sampling, in order to deal with the possibly involved kinematic cuts that are used in the corresponding experimental measurements. Because of the divergences in the matrix element, Eq. (9.16), the integral converges only if the observable vanishes for kinematic configurations in which one of the n particles is arbitrarily soft or it is collinear to another particle. As an example, the cross section for producing any configuration of n partons will lead to an infinite integral, whereas a finite result will be obtained for the cross section for producing n deposits of energy (or jets, see Sec. 9.3.1.1), each above some energy threshold and well separated from each other in angle.

At a practical level, LO calculations can be carried out for $2 \rightarrow n$ processes with $n \lesssim 6 - 10$. The exact upper limit depends on the process, the method used to evaluate the matrix elements (recursive methods are more efficient), and the extent to which

the phase-space integration can be optimized to work around the large variations in the values of the matrix elements.

NLO. Given an observable that is non-zero starting from n final-state particles, its prediction at NLO involves supplementing the LO result, Eq. (9.17), with the $2 \rightarrow (n+1)$ -particle squared tree-level matrix element ($|M_{n+1}^2|$), and the interference of a $2 \rightarrow n$ tree-level and $2 \rightarrow n$ 1-loop amplitude ($2\text{Re}(M_n M_{n,1\text{-loop}}^*)$),

$$\begin{aligned} \sigma_{\mathcal{O}}^{NLO} &= \sigma_{\mathcal{O}}^{LO} + \alpha_s^{n-1} (\mu_R^2) \int d\Phi_{n+1} |M_{n+1}^2(p_1, \dots, p_{n+1})| \\ &\quad \times \mathcal{O}_{n+1}(p_1, \dots, p_{n+1}) + \alpha_s^{n-1} (\mu_R^2) \\ &\quad \times \int d\Phi_n 2\text{Re} [M_n(p_1, \dots, p_n) M_{n,1\text{-loop}}^*(p_1, \dots, p_n)] \\ &\quad \times \mathcal{O}_n(p_1, \dots, p_n). \end{aligned} \quad (9.18)$$

Relative to LO calculations, two important issues appear in the NLO calculations. Firstly, the extra complexity of loop-calculations relative to tree-level calculations means that automated calculations started to appear only about fifteen years ago (see below). Secondly, loop amplitudes are infinite in 4 dimensions, while tree-level amplitudes are finite, but their *integrals* are infinite, due to the divergences of Eq. (9.16). These two sources of infinities have the same soft and collinear origins and cancel after the integration only if the observable \mathcal{O} satisfies the property of infrared and collinear safety, which means that the observable is non-sensitive to soft emissions or to collinear splittings, *i.e.*

$$\begin{aligned} \mathcal{O}_{n+1}(p_1, \dots, p_s, \dots, p_n) &\rightarrow \mathcal{O}_n(p_1, \dots, p_{s-1}, p_{s+1}, \dots, p_n) \\ &\quad \text{if } p_s \rightarrow 0 \\ \mathcal{O}_{n+1}(p_1, \dots, p_a, p_b, \dots, p_n) &\rightarrow \mathcal{O}_n(p_1, \dots, p_a + p_b, \dots, p_n) \\ &\quad \text{if } p_a \parallel p_b. \end{aligned} \quad (9.19)$$

Examples of infrared-safe quantities include event-shape distributions and jet cross sections (with appropriate jet algorithms, see below). Unsafe quantities include the distribution of the momentum of the hardest QCD particle (which is not conserved under collinear splitting), observables that require the complete absence of radiation in some region of phase space (e.g. rapidity gaps or 100% isolation cuts, which are affected by soft emissions), or the particle multiplicity (affected by both soft and collinear emissions). The non-cancellation of divergences at NLO due to infrared or collinear unsafety compromises the usefulness not only of the NLO calculation, but also that of a LO calculation, since LO is only an acceptable approximation if one can prove that higher-order terms are smaller. Infrared and collinear unsafety usually also imply large non-perturbative effects.

As with LO calculations, the phase-space integrals in Eq. (9.18) are usually carried out by Monte Carlo integration, so as to facilitate the study of arbitrary observables. Various methods exist to obtain numerically efficient cancellation among the different infinities. These include notably dipole [117], FKS [118] and antenna [119] subtraction.

Thanks to new ideas like the OPP method [120], generalised [121] and D -dimensional [122] unitarity, onshell methods [123], and on the fly reduction algorithms [124], recent years have seen a breakthrough in the calculation of one-loop matrix elements (for reviews on unitarity based method see Ref. [125, 126]). Thanks to these innovative methods, automated NLO calculations tools have been developed and a number of programs are available publicly: Madgraph5_aMC@NLO [108] and Helac-NLO [127] provide full frameworks for NLO calculations; GoSam [128], Njet [129], OpenLoops [130] and Recola [131] calculate just the 1-loop part and are typically interfaced with an external tool such as Sherpa [132] for a combination with the appropriate tree-level amplitudes. Other tools such as NLOJet++ [133], MCFM [134], VBFNLO [135], the Phox family [136] or BlackHat [137] implement analytic calculations for a selected class of processes. Given that NLO computation for high-multiplicity final states is numerically demanding,

procedures [138–141] have been developed for *a posteriori* PDF and scale change. These methods represent NLO (or NNLO) results, for a given set of cuts and binning, as an effective coefficient function on a grid in parton momentum fractions and factorization scales.

Recently, a lot of attention has also been paid to the calculation of NLO electroweak corrections. Electroweak corrections are especially important for transverse momenta significantly above the W and Z masses, because they are enhanced by two powers of $\ln p_t/M_W$ for each power of the electroweak coupling, and close to Sudakov peaks, where most of the data lie and the best experimental precision can be achieved. In some cases the above programs (or development versions of them) can be used to calculate also NLO electroweak or beyond-standard-model corrections [142–148].

Given the progress in QCD and EW fixed-order computations, the largest unknown from fixed-order corrections is often given by the mixed QCD-electroweak corrections of $\mathcal{O}(\alpha_s\alpha)$. These mixed two-loop corrections are often available only in an approximate form [149–154] and first three-loop results $\mathcal{O}(\alpha_s^3\alpha)$ in the case of Higgs productions started to appear recently [155].

NNLO. Conceptually, NNLO and NLO calculations are similar, except that one must add a further order in α_s , consisting of: the squared $(n+2)$ -parton tree-level amplitude, the interference of the $(n+1)$ -parton tree-level and 1-loop amplitudes, the interference of the n -parton tree-level and 2-loop amplitudes, and the squared n -parton 1-loop amplitude.

Each of these elements involves large numbers of soft and collinear divergences, satisfying relations analogous to Eq. (9.16) which now involve multiple collinear or soft particles and higher loop orders (see *e.g.* Refs. [156–158]). Arranging for the cancellation of the divergences after numerical Monte Carlo integration has been one of the significant challenges of NNLO calculations, as has been the determination of the relevant 2-loop amplitudes. For the cancellations of divergences a wide range of methods has been developed. Some of them [159–163] retain the approach, inherent in NLO methods, of directly combining the separate loop and tree-level amplitudes. Others combine a suitably chosen, partially inclusive $2 \rightarrow n$ NNLO calculation with a fully differential $2 \rightarrow n+1$ NLO calculation [164–167].

Quite a number of processes have been calculated differentially at NNLO so far. The state of the art for e^+e^- collisions is $e^+e^- \rightarrow 3$ jets [168–170]. For DIS, dijet production is known at NNLO [171] and the description jet production has been recently pushed even to N^3 LO using the Projection-to-Born method [172,173]. For hadron colliders, all $2 \rightarrow 1$ processes are known, specifically vector boson [174,175] and Higgs boson production [164,176]. For most of the above calculations there exist public codes (EERAD3 for e^+e^- , DYNLO, FEWZ and MATRIX for W and Z production, Fehipro and HNNLO for Higgs production), links to which are to be found among the above references. Substantial progress has been made in the past couple of years for hadron-collider $2 \rightarrow 2$ processes, with calculations having been performed for nearly all relevant processes: ZZ [86] WW [85] and WZ [177], $\gamma\gamma$ [178,179], $Z\gamma$ [180] and $W\gamma$ [181] (many of these colour singlet processes are available also in MCFM [182] or MATRIX [87]), inclusive photon [183,184], γ +jet [184,185], W +jet [165], Z +jet [185–187] H +jet [188–191], WH [192] and ZH [193], t -channel single-top [194,195], $t\bar{t}$ production [196], dijet production [197], and HH [198] (in large-top-mass approximation, see also the exact (two-loop) NLO result [83]). One $2 \rightarrow 3$ process is known at NNLO, Higgs production through vector-boson fusion, using an approximation in which the two underlying DIS-like $q \rightarrow qV$ scatterings are factorised, the so-called structure function approximation [167,199]. Corrections beyond the structure function approximation are expected to be small, on the order of a percent or less [200].

The Les Houches precision wishlist compiles predictions needed to fully exploit the data that will be taken at the High Luminosity LHC [201]. Most of the needed calculations require accuracy of at least NNLO QCD and NLO EW, and many require the prediction of $2 \rightarrow 3$ processes, such as $W/Z+ \geq 2$ jets, $H+ \geq 2$ jets, and $t\bar{t}H$ to NNLO.

As discussed in this section, calculations at NLO can now be

relatively easily generated by non-experts using the programs described. However, many NNLO calculations can be too complex and CPU-intensive to allow such an approach. In these cases, the relevant matrix element information can be stored in a grid format (or in ROOT ntuples) allowing predictions to be generated on-the-fly, similar to what has been available at NLO.

9.2.3.3 Resummation

Many experimental measurements place tight constraints on emissions in the final state. For example, in e^+e^- events, that (one minus) the Thrust should be less than some value $\tau \ll 1$, or, in $pp \rightarrow Z$, events that the Z -boson transverse momentum or the transverse momentum of the accompanying jet should be much smaller than the Z -boson mass. A further example is the production of heavy particles or jets near threshold (so that little energy is left over for real emissions) in DIS and pp collisions.

In such cases, the constraint vetoes a significant part of the integral over the soft and collinear divergence of Eq. (9.16). As a result, there is only a partial cancellation between real emission terms (subject to the constraint) and loop (virtual) contributions (not subject to the constraint), causing each order of α_s to be accompanied by a large coefficient $\sim L^2$, where *e.g.* $L = \ln \tau$ or $L = \ln(M_Z/p_t^Z)$. One ends up with a perturbative series, whose terms go as $\sim (\alpha_s L^2)^n$. It is not uncommon that $\alpha_s L^2 \gg 1$, so that the perturbative series converges very poorly if at all.⁵ In such cases one may carry out a “resummation”, which accounts for the dominant logarithmically enhanced terms to all orders in α_s , by making use of known properties of matrix elements for multiple soft and collinear emissions, and of the all-orders properties of the divergent parts of virtual corrections, following original works such as Refs. [202–211] and also through soft-collinear effective theory [212,213] (*cf.* also the section on “Heavy-Quark and Soft-Collinear Effective Theory” in this *Review*, as well as Ref. [214]).

For cases with double logarithmic enhancements (two powers of logarithm per power of α_s), there are two classification schemes for resummation accuracy. Writing the cross section including the constraint as $\sigma(L)$ and the unconstrained (total) cross section as σ_{tot} , the series expansion takes the form

$$\sigma(L) \simeq \sigma_{\text{tot}} \sum_{n=0}^{\infty} \sum_{k=0}^{2n} R_{nk} \alpha_s^n (\mu_R^2) L^k, \quad L \gg 1, \quad (9.20)$$

and leading log (LL) resummation means that one accounts for all terms with $k = 2n$, next-to-leading-log (NLL) includes additionally all terms with $k = 2n - 1$, *etc.* Often $\sigma(L)$ (or its Fourier or Mellin transform) *exponentiates*⁶,

$$\sigma(L) \simeq \sigma_{\text{tot}} \exp \left[\sum_{n=1}^{\infty} \sum_{k=0}^{n+1} G_{nk} \alpha_s^n (\mu_R^2) L^k \right], \quad L \gg 1, \quad (9.21)$$

where one notes the different upper limit on k ($\leq n+1$) compared to Eq. (9.20). This is a more powerful form of resummation: the G_{12} term alone reproduces the full LL series in Eq. (9.20). With the form Eq. (9.21) one still uses the nomenclature LL, but this now means that all terms with $k = n+1$ are included, and NLL implies all terms with $k = n$, *etc.*

For a large number of observables, NLL resummations are available in the sense of Eq. (9.21) (see Refs. [218–220] and references therein). NNLL has been achieved for the DY and Higgs-boson p_t distributions [221–224] (also available in the CuTe [225], HRes [226] and ResBos [227] families of programs and also differentially in vector-boson decay products [228]) and related variables [229], for the p_t of vector-boson pairs [230], for the back-to-back energy-energy correlation in e^+e^- [231], the jet broadening

⁵ To be precise one should be aware of two causes of the divergence of perturbative series. That which interests us here is associated with the presence of a new large parameter (*e.g.* ratio of scales). It is distinct from the “renormalon” induced factorial divergences of perturbation theory which were discussed above.

⁶ Whether or not this happens depends on the quantity being resummed. A classic example involves two-jet rate in e^+e^- collisions as a function of a jet-resolution parameter y_{cut} . The logarithms of $1/y_{\text{cut}}$ exponentiate for the k_t (Durham) jet algorithm [215], but not [216] for the JADE algorithm [217] (both are discussed below in Sec. 9.3.1.1).

in e^+e^- collisions [232], the jet-veto survival probability in Higgs and Z boson production in pp collisions [233, 234]⁷, an event-shape type observable known as the beam Thrust [235], hadron-collider jet masses in specific limits [236] (see also Ref. [237]), the production of top anti-top pairs near threshold [238–240] (and references therein), and high- p_t W and Z production [241]. Automation of NNLL jet-veto resummations for different processes has been achieved in Ref. [242] (*cf.* also the NLL automation in Ref. [243]), while automation for a certain class of e^+e^- observables has been achieved in Ref. [244]. N³LL resummations are available for the Thrust variable, C -parameter and heavy-jet mass in e^+e^- annihilations [245–247] (confirmed for Thrust at NNLL in Ref. [248]), for p_t distribution of the Higgs boson [249] and weak gauge bosons [250] and for Higgs- and vector-boson production near threshold [251]. An extensive discussion of jet masses for heavy-quark induced jets has been given in Ref. [252] (see also Ref. [253]). In order to make better contact with experimental measurements, recent years have seen an increasing interest in resummations in exclusive phase-space regions and joint resummations [254–260]. Finally, there has also been considerable progress in resummed calculations for jet substructure, whose observables involve more complicated definitions than is the case for standard resummations [261–267], see also Refs. [268, 269]. The inputs and methods involved in these various calculations are somewhat too diverse to discuss in detail here, so we recommend that the interested reader consult the original references for further details.

9.2.3.4 Fragmentation functions

Since the parton-hadron transition is non-perturbative, it is not possible to perturbatively calculate quantities such as the energy-spectra of specific hadrons in high-energy collisions. However, one can factorize perturbative and non-perturbative contributions via the concept of fragmentation functions. These are the final-state analogue of the parton distribution functions which are used for initial-state hadrons. Like parton distribution functions, they depend on a (fragmentation) factorization scale and satisfy a DGLAP evolution equation.

It should be added that if one ignores the non-perturbative difficulties and just calculates the energy and angular spectrum of partons in perturbative QCD with some low cutoff scale $\sim \Lambda$ (using resummation to sum large logarithms of \sqrt{s}/Λ), then this reproduces many features of the corresponding hadron spectra [270]. This is often taken to suggest that hadronization is “local”, in this sense it mainly involves partons that are close both in position and in momentum.

Section 19 of this *Review* provides further information (and references) on these topics, including also the question of heavy-quark fragmentation.

9.2.3.5 Parton-shower Monte Carlo generators

Parton-shower Monte Carlo (MC) event generators like PYTHIA [271–273], HERWIG [274–276] and SHERPA [132] provide fully exclusive simulations of QCD events.⁸ Because they provide access to “hadron-level” events, they are a crucial tool for all applications that involve simulating the response of detectors to QCD events. Here we give only a brief outline of how they work and refer the reader to Sec. 41 and Ref. [278] for a full overview.

The MC generation of an event involves several stages. It starts with the random generation of the kinematics and partonic channels of whatever *hard scattering process* the user has requested at some high scale Q_0 (for complex processes, this may be carried out by an external program). This is followed by a *parton shower*, usually based on the successive random generation of gluon emissions (or $g \rightarrow q\bar{q}$ splittings). Emissions are ordered according to some ordering variable. Common choices of scale for the ordering of emissions are virtuality, transverse momentum or angle. Each emission is generated at a scale lower than the previous

emission, following a (soft and collinear resummed) perturbative QCD distribution, which depends on the momenta of all previous emissions. Parton showering stops at a scale of order 1 GeV, at which point a *hadronization model* is used to convert the resulting partons into hadrons. One widely-used model involves stretching a color “string” across quarks and gluons, and breaking it up into hadrons [279, 280]. Another breaks each gluon into a $q\bar{q}$ pair and then groups quarks and anti-quarks into colorless “clusters”, which then give the hadrons [274]. As both models are tuned primarily to LEP data, the cluster and string models provide similar results for most observables [281]. For pp and γp processes, modeling is also needed to treat the collision between the two hadron remnants, which generates an *underlying event* (UE), usually implemented via additional $2 \rightarrow 2$ scatterings (“multiple parton interactions”) at a scale of a few GeV, following Ref. [282]. The parameter values for the multiple parton interaction models must be determined from fits to the underlying event levels from LHC collision data. As the different Monte Carlo programs fit to essentially the same data, there should be similar results for each program. One complication, however, is the non-universality of the underlying event for different physics processes.

A deficiency of the soft and collinear approximations that underlie parton showers is that they may fail to reproduce the full pattern of hard wide-angle emissions, important, for example, in many new physics searches. It is therefore common to use LO multi-parton matrix elements to generate hard high-multiplicity partonic configurations as additional starting points for the showering, supplemented with some prescription (CKKW [283], MLM [284]) for consistently merging samples with different initial multiplicities. Monte Carlo generators, as described above, compute cross sections for the requested hard process that are correct at LO.

A wide variety of processes are available in MC implementations that are correct also to NLO, using the MC@NLO [285] or POWHEG [286] prescriptions, notably through the Madgraph5_aMC@NLO [108], POWHEGBox [287] and Sherpa [110] programs. Techniques have also been developed to combine NLO plus shower accuracy for different multiplicities of final-state jets [288]. Building in part on some of that work, several groups have also obtained NNLO plus shower accuracy for Drell-Yan and Higgs production [289], as well as for a handful of $2 \rightarrow 2$ processes [290–292].

In general, we expect parton-shower matched predictions to differ from the underlying fixed-order results in regions where (1) there is a large sensitivity to jet shapes (for instance small R jets), (2) there is a restriction in phase space such that soft gluon resummation effects become important, (3) the observable contains multiple disparate scales, (4) there are perturbative instabilities at fixed order, *e.g.* related to kinematical cuts, and (5) the observable is sensitive to higher multiplicity states than those described by the fixed-order calculation [281].

9.2.4 Accuracy of predictions

Estimating the accuracy of perturbative QCD predictions is not an exact science. It is often said that LO calculations are accurate to within a factor of two. This is based on experience with NLO corrections in the cases where these are available. In processes involving new partonic scattering channels at NLO and/or large ratios of scales (such as jet observables in processes with vector bosons, or the production of high- p_t jets containing B -hadrons), the ratio of the NLO to LO predictions, commonly called the “ K -factor”, can be substantially larger than two. NLO corrections tend to be large for processes for which there is a great deal of color annihilation in the interaction. In addition, NLO corrections tend to decrease as more final state legs are added.

For calculations beyond LO, a conservative approach to estimate the perturbative uncertainty is to take it to be the last known perturbative correction; a more widely used method is to estimate it from the change in the prediction when varying the renormalization and factorization scales around a central value Q that is taken close to the physical scale of the process. A conventional range of variation is $Q/2 < \mu_R, \mu_F < 2Q$, varying the two scales independently with the restriction $\frac{1}{2}\mu_R < \mu_F < 2\mu_R$ [293]. This constraint limits the risk of misleadingly small uncertainties due

⁷A veto on the jet phase space can be severe, for example by requiring exactly zero jets above a given transverse momentum cut accompanying a Higgs boson, or relatively mild, for example by placing a transverse momentum cut of 30 GeV on the measurement of the production of a Higgs boson with one or more jets. In general, inclusive cross sections are preferable, as uncertainties on both the theoretical and experimental sides are smaller.

⁸The program ARIADNE [277] has also been widely used for simulating e^+e^- and DIS collisions.

to fortuitous cancellations between the μ_F and μ_R dependence when both are varied together, while avoiding the appearance of large logarithms of μ_R^2/μ_F^2 when both are varied completely independently. Where possible, it can be instructive to examine the two-dimensional scale distributions (μ_R vs. μ_F) to obtain a better understanding of the interplay between μ_R and μ_F . This procedure should not be assumed to always estimate the full uncertainty from missing higher orders, but it does indicate the size of one important known source of higher-order ambiguity.⁹

For processes involving jets in the final state, estimates of the uncertainties at NNLO, along the lines described above, can be misleading for jets of smaller radii, due to accidental cancellations. Procedures are available to provide more reasonable estimates of the uncertainties in those cases [281, 302]. In addition, care must be taken as to the form of the central scale [303].

Calculations that involve resummations usually have an additional source of uncertainty associated with the choice of argument of the logarithms being resummed, *e.g.* $\ln(2 \frac{p_t^Z}{M_Z})$ as opposed to $\ln(\frac{1}{2} \frac{p_t^Z}{M_Z})$. In addition to varying renormalization and factorization scales, it is therefore also advisable to vary the argument of the logarithm by a suitable factor in either direction with respect to the “natural” argument.

The accuracy of QCD predictions is limited also by non-perturbative corrections, which typically scale as a power of A/Q .¹⁰ For measurements that are directly sensitive to the structure of the hadronic final state, the corrections are usually linear in A/Q . The non-perturbative corrections are further enhanced in processes with a significant underlying event (*i.e.* in pp and $p\bar{p}$ collisions) and in cases where the perturbative cross sections fall steeply as a function of p_t or some other kinematic variable, for example in inclusive jet spectra or dijet mass spectra. In general, the underlying event for a hard scattering process, such as dijet production, is of a similar order, but somewhat harder, than the average energy density in a minimum-bias event. Under high-luminosity running conditions, such as 13 TeV at the LHC, there can be on the order of 50 minimum-bias interactions occurring at each beam-beam crossing. This additional energy needs to be corrected for, and is typically removed by subtracting a rapidity-dependent transverse energy density determined on an event-by-event basis [304]. This subtraction, of necessity, also removes the underlying event, which must be added back in to restore the measured event to the hadron level.

Non-perturbative corrections are commonly estimated from the difference between Monte Carlo events at the parton level and after hadronization. An issue to be aware of with this procedure is that “parton level” is not a uniquely defined concept. For example, in an event generator it depends on a (somewhat arbitrary and tunable) internal cutoff scale that separates the parton showering from the hadronization. In contrast, no such cutoff scale exists in an NLO or NNLO partonic calculation. There exist alternative methods for estimating hadronization corrections, that attempt to analytically deduce non-perturbative effects in one observable based on measurements of other observables (see the reviews [28, 305]). While they directly address the problem of different possible definitions of parton level, it should also be said that they are far less flexible than Monte Carlo programs and not always able to provide equally good descriptions of the data.

One of the main issues is whether the fixed partonic final state of a NLO or NNLO prediction can match the parton shower in its ability to describe the experimental jet shape (minus any underlying event). NNLO calculations provide a better match to the parton shower predictions than do NLO ones, as might be expected from the additional gluon available to describe the jet shape. The hadronization predictions appear to work for both orders, but at an unknown accuracy. The impact of any error should fall as a power correction.

⁹ A number of prescriptions also exist for setting the scale automatically, *e.g.* Refs. [294–298], eliminating uncertainties from scale variation, though not from the truncation of the perturbative series itself. Recently, there have also been studies of how to estimate uncertainties from missing higher orders that go beyond scale variations [299–301].

¹⁰ In some circumstances, the scale in the denominator could be a smaller kinematic or physical scale that depends on the observable.

9.3 Experimental studies of QCD

Since we are not able to directly measure partons (quarks or gluons), but only hadrons and their decay products, a central issue for every experimental study of perturbative QCD is establishing a correspondence between observables obtained at the partonic and the hadronic level. The only theoretically sound correspondence is achieved by means of *infrared and collinear safe* quantities, which allow one to obtain finite predictions at any order of perturbative QCD.

As stated above, the simplest case of infrared- and collinear-safe observables are total cross sections. More generally, when measuring fully inclusive observables, the final state is not analyzed at all regarding its (topological, kinematical) structure or its composition. Basically the relevant information consists in the rate of a process ending up in a partonic or hadronic final state. In e^+e^- annihilation, widely used examples are the ratios of partial widths or branching ratios for the electroweak decay of particles into hadrons or leptons, such as Z or τ decays, (*cf.* Sec. 9.2.1). Such ratios are often favored over absolute cross sections or partial widths because of large cancellations of experimental and theoretical systematic uncertainties. The strong suppression of non-perturbative effects, $\mathcal{O}(A^4/Q^4)$, is one of the attractive features of such observables, however, at the same time, the sensitivity to radiative QCD corrections is small, which for example affects the statistical uncertainty when using them for the determination of the strong coupling constant. In the case of τ decays not only the hadronic branching ratio is of interest, but also moments of the spectral functions of hadronic tau decays, which sample different parts of the decay spectrum and thus provide additional information. Other examples of fully inclusive observables are structure functions (and related sum rules) in DIS. These are extensively discussed in Sec. 18 of this *Review*.

On the other hand, often the structure or composition of the final state are analyzed and cross sections differential in one or more variables characterizing this structure are of interest. Examples are jet rates, jet substructure, event shapes or transverse momentum distributions of jets or vector bosons in hadron collisions. The case of fragmentation functions, *i.e.* the measurement of hadron production as a function of the hadron momentum relative to some hard scattering scale, is discussed in Sec. 19 of this *Review*.

It is worth mentioning that, besides the correspondence between the parton and hadron level, also a correspondence between the hadron level and the actually measured quantities in the detector has to be established. The simplest examples are corrections for finite experimental acceptance and efficiencies. Whereas acceptance corrections essentially are of theoretical nature, since they involve extrapolations from the measurable (partial) to the full phase space, other corrections such as for efficiency, resolution and response are of experimental nature. For example, measurements of differential cross sections such as jet rates require corrections in order to relate, *e.g.*, the energy deposits in a calorimeter to the jets at the hadron level. Typically detector simulations and/or data-driven methods are used in order to obtain these corrections. Care should be taken here in order to have a clear separation between the parton-to-hadron level and hadron-to-detector level corrections. Finally, for the sake of an easy comparison to the results of other experiments and/or theoretical calculations, it is suggested to provide, whenever possible, measurements corrected for detector effects and/or all necessary information related to the detector response (*e.g.*, the detector response matrix).

9.3.1 Hadronic final-state observables

9.3.1.1 Jets

In hard interactions, final-state partons and hadrons appear predominantly in collimated bunches, which are generically called *jets*. To a first approximation, a jet can be thought of as a hard parton that has undergone soft and collinear showering and then hadronization. Jets are used both for testing our understanding and predictions of high-energy QCD processes, and also for identifying the hard partonic structure of decays of massive particles such as top quarks and W, Z and Higgs bosons.

In order to map observed hadrons onto a set of jets, one uses a *jet definition*. The mapping involves explicit choices: for example when a gluon is radiated from a quark, for what range of kinematics should the gluon be part of the quark jet, or instead form a separate jet? Good jet definitions are infrared and collinear safe, simple to use in theoretical and experimental contexts, applicable to any type of inputs (parton or hadron momenta, charged particle tracks, and/or energy deposits in the detectors) and lead to jets that are not too sensitive to non-perturbative effects.

An extensive treatment of the topic of jet definitions is given in Ref. [306] (for e^+e^- collisions) and Refs. [307–309]. Here we briefly review the two main classes: cone algorithms, extensively used at older hadron colliders, and sequential recombination algorithms, more widespread in e^+e^- and ep colliders and at the LHC.

Very generically, most (iterative) cone algorithms start with some seed particle i , sum the momenta of all particles j within a cone of opening-angle R , typically defined in terms of rapidity and azimuthal angle. They then take the direction of this sum as a new seed and repeat until the direction of the cone is stable, and call the contents of the resulting stable cone a jet if its transverse momentum is above some threshold $p_{t,\min}$. The parameters R and $p_{t,\min}$ should be chosen according to the needs of a given analysis.

There are many variants of the cone algorithm, and they differ in the set of seeds they use and the manner in which they ensure a one-to-one mapping of particles to jets, given that two stable cones may share particles (“overlap”). The use of seed particles is a problem w.r.t. infrared and collinear safety. Seeded algorithms are generally not compatible with higher-order (or sometimes even leading-order) QCD calculations, especially in multi-jet contexts, as well as potentially subject to large non-perturbative corrections and instabilities. Seeded algorithms (JetCLU, MidPoint, and various other experiment-specific iterative cone algorithms) are therefore to be deprecated. Such algorithms are not used at the LHC, but were at the Fermilab Tevatron, where data still provide useful information, for example for global PDF fits. A modern alternative is to use a seedless variant, SIScone [310].

Sequential recombination algorithms at hadron colliders (and in DIS) are characterized by a distance $d_{ij} = \min(k_{t,i}^{2p}, k_{t,j}^{2p}) \Delta_{ij}^2 / R^2$ between all pairs of particles i, j , where Δ_{ij} is their separation in the rapidity-azimuthal plane, $k_{t,i}$ is the transverse momentum w.r.t. the incoming beams, and R is a free parameter. At the LHC, R is typically in the range from 0.4 to 0.7. They also involve a “beam” distance $d_{iB} = k_{t,i}^{2p}$. One identifies the smallest of all the d_{ij} and d_{iB} , and if it is a d_{ij} , then i and j are merged into a new pseudo-particle (with some prescription, a recombination scheme, for the definition of the merged four-momentum). If the smallest distance is a d_{iB} , then i is removed from the list of particles and called a jet. As with cone algorithms, one usually considers only jets above some transverse-momentum threshold $p_{t,\min}$. The parameter p determines the kind of algorithm: $p = 1$ corresponds to the (*inclusive*-) k_t algorithm [215, 311, 312], $p = 0$ defines the *Cambridge-Aachen* algorithm [313, 314], while for the *anti- k_t* algorithm $p = -1$ [315]. All these variants are infrared and collinear safe. Whereas the former two lead to irregularly shaped jet boundaries, the latter results in cone-like boundaries. The *anti- k_t* algorithm has become the de-facto standard for the LHC experiments.

In e^+e^- annihilation the k_t algorithm [215] uses $y_{ij} = 2 \min(E_i^2, E_j^2) (1 - \cos \theta_{ij}) / Q^2$ as distance measure between two particles/partons i and j and repeatedly merges the pair with smallest y_{ij} , until all y_{ij} distances are above some threshold y_{cut} , the jet resolution parameter. Q is a measure of the overall hardness of the event. The (pseudo)-particles that remain at this point are called the jets. Here it is y_{cut} (rather than R and $p_{t,\min}$) that should be chosen according to the needs of the analysis. The two-jet rate in the k_t algorithm has the property that logarithms $\ln(1/y_{\text{cut}})$ exponentiate. This is one reason why it is preferred over the earlier JADE algorithm [217], which uses the distance measure $y_{ij} = 2 E_i E_j (1 - \cos \theta_{ij}) / Q^2$. Note that other variants of sequential recombination algorithms for e^+e^- annihilations, using different definitions of the resolution measure y_{ij} , exhibit

much larger sensitivities to fragmentation and hadronization effects than the k_t and JADE algorithms [316]. Efficient implementations of the above algorithms are available through the *FastJet* package [317].

9.3.1.2 Event Shapes

Event-shape variables are functions of the four momenta of the particles in the final state and characterize the topology of an event’s energy flow. They are sensitive to QCD radiation (and correspondingly to the strong coupling) insofar as gluon emission changes the shape of the energy flow.

The classic example of an event shape is the *Thrust* [318, 319] in e^+e^- annihilations, defined as

$$\hat{\tau} = \max_{\vec{n}_\tau} \frac{\sum_i |\vec{p}_i \cdot \vec{n}_\tau|}{\sum_i |\vec{p}_i|}, \quad (9.22)$$

where \vec{p}_i are the momenta of the particles or the jets in the final state and the maximum is obtained for the Thrust axis \vec{n}_τ . In the Born limit of the production of a perfect back-to-back $q\bar{q}$ pair, the limit $\hat{\tau} \rightarrow 1$ is obtained, whereas a perfectly spherical many-particle configuration leads to $\hat{\tau} \rightarrow 1/2$. Further event shapes of similar nature have been extensively measured at LEP and at HERA, and for their definitions and reviews we refer to Refs. [1, 7, 305, 320, 321]. The energy-energy correlation function [322], namely the energy-weighted angular distribution of produced hadron pairs, and its associated asymmetry are further shape variables which have been studied in detail at e^+e^- colliders. For hadron colliders the appropriate modification consists in only taking the transverse momentum component [323]. More recently, the event shape *N -jettiness* has been proposed [324], that measures the degree to which the hadrons in the final state are aligned along N jet axes or the beam direction. It vanishes in the limit of exactly N infinitely narrow jets.

Phenomenological discussions of event shapes at hadron colliders can be found in Refs. [324–328]. Measurements of hadronic event-shape distributions have been published by CDF [329], ATLAS [330–335] and CMS [336–339].

Event shapes are used for many purposes. These include measuring the strong coupling, tuning the parameters of Monte Carlo programs, investigating analytical models of hadronization and distinguishing QCD events from events that might involve decays of new particles (giving event-shape values closer to the spherical limit).

9.3.1.3 Jet substructure, quark vs. gluon jets

Jet substructure, which can be resolved by finding subjets or by measuring jet shapes, is sensitive to the details of QCD radiation in the shower development inside a jet and has been extensively used to study differences in the properties of quark and gluon induced jets, strongly related to their different color charges. In general, there is clear experimental evidence that gluon jets have a softer particle spectrum and are “broader” than (light-) quark jets (as expected from perturbative QCD) when looking at observables such as the jet shape $\Psi(r/R)$. This is the fractional transverse momentum contained within a sub-cone of cone-size r for jets of cone-size R . It is sensitive to the relative fractions of quark and gluon jets in an inclusive jet sample and receives contributions from soft-gluon initial-state radiation and the underlying event. Therefore, it has been widely employed for validation and tuning of Monte Carlo parton-shower models. Furthermore, this quantity turns out to be sensitive to the modification of the gluon radiation pattern in heavy ion collisions (see *e.g.* Ref. [340]).

The most recent jet shape measurements using proton-proton collision data have been presented for inclusive jet samples [341–343] and for top-quark production [344]. Further discussions, references and summaries can be found in Refs. [321, 345, 346] and Sec. 4 of Ref. [347].

The use of jet substructure has also been investigated in order to distinguish QCD jets from jets that originate from hadronic decays of boosted massive particles (high- p_t electroweak bosons, top quarks and hypothesized new particles). A considerable number of experimental studies have been carried out with Tevatron and LHC data, in order to investigate on the performance of the

proposed algorithms for resolving jet substructure and to apply them to searches for new physics, as well as to the reconstruction of boosted top quarks, vector bosons and the Higgs boson. For reviews of this rapidly growing field, see sec. 5.3 of Ref. [307], Ref. [348] and Refs. [347, 349–352]. Perhaps no other sub-field has benefited as much from machine learning techniques as the study of jet substructure. As a jet can have $O(100)$ constituents each with kinematic and other information, jet substructure analysis is naturally a highly multivariate problem. Deep learning techniques can use all of the available information to study jets in their natural high dimensionality. Such techniques have not only improved discrimination between different final states/types of jets, but have also improved our understanding of perturbative QCD. See for example the review in Ref. [268].

9.3.2 QCD measurements at colliders

There exists a wealth of data on QCD-related measurements in e^+e^- , ep , pp , and $p\bar{p}$ collisions, to which a short overview like this would not be able to do any justice. Extensive reviews of the subject have been published in Refs. [320, 321] for e^+e^- colliders and in Ref. [353] for ep scattering, whereas for hadron colliders comprehensive overviews are given in, e.g., Refs. [308, 346] and Refs. [2, 354–356].

Below we concentrate our discussion on measurements that are most sensitive to hard QCD processes with focus on jet production.

9.3.2.1 e^+e^- colliders

Analyses of jet production in e^+e^- collisions are mostly based on data from the JADE experiment at center-of-mass energies between 14 and 44 GeV, as well as on LEP collider data at the Z resonance and up to 209 GeV. The analyses cover the measurements of (differential or exclusive) jet rates (with multiplicities typically up to 4, 5 or 6 jets), the study of 3-jet events and particle production between the jets, as well as 4-jet production and angular correlations in 4-jet events.

Event-shape distributions from e^+e^- data have been an important input to the tuning of parton shower MC models, typically matched to matrix elements for 3-jet production. In general these models provide good descriptions of the available, highly precise data. Especially for the large LEP data sample at the Z peak, the statistical uncertainties are mostly negligible and the experimental systematic uncertainties are at the percent level or even below. These are usually dominated by the uncertainties related to the MC model dependence of the efficiency and acceptance corrections (often referred to as “detector corrections”).

Observables measured in e^+e^- collisions have been used for determinations of the strong coupling constant (cf. Section 9.4 below) and for putting constraints on the QCD color factors (cf. Sec. 9.1 for their definitions), thus probing the non-Abelian nature of QCD. Typically, cross sections can be expressed as functions of these color factors, for example $\sigma = f(\alpha_s C_F, C_A/C_F, n_f T_R/C_F)$. Angular correlations in 4-jet events give sensitivity at leading order. Some sensitivity to these color factors, although only at NLO, is also obtained from event-shape distributions. Scaling violations of fragmentation functions and the different substructure in quark and gluon induced jets also give access to these color factors. In order to extract absolute values, e.g. for C_F and C_A , certain assumptions have to be made for other parameters, such as T_R, n_f or α_s , since typically only combinations (ratios, products) of all the relevant parameters appear in the perturbative predictions. A compilation of results [321] quotes world average values of $C_A = 2.89 \pm 0.03(\text{stat}) \pm 0.21(\text{syst})$ and $C_F = 1.30 \pm 0.01(\text{stat}) \pm 0.09(\text{syst})$, with a correlation coefficient of 82%. These results are in perfect agreement with the expectations from $SU(3)$ of $C_A = 3$ and $C_F = 4/3$.

9.3.2.2 DIS and photoproduction

Jet measurements in ep collisions, both in the DIS and photoproduction regimes, allow for tests of QCD factorization (as they involve only one initial state proton and thus one PDF function), and provide sensitivity to both the gluon distribution and to the strong coupling constant. Calculations are available at NNLO in both regimes [357, 358]. Experimental uncertainties of the order of 5–10% have been achieved, mostly dominated by the jet energy

scale, whereas statistical uncertainties are negligible to a large extent. For comparison to theoretical predictions, at large jet p_t the PDF uncertainty dominates the theoretical uncertainty (typically of order 5–10%, in some regions of phase space up to 20%), therefore jet observables become useful inputs for PDF fits.

In general, the data are well described by the NLO and NNLO matrix-element calculations, combined with DGLAP evolution equations, in particular at large Q^2 and central values of jet pseudo-rapidity. At low values of Q^2 and x , in particular for large jet pseudo-rapidities, certain features of the data have been interpreted as requiring BFKL-type evolution, though the predictions for such schemes are still limited. It is worth noting that there is lack of consensus throughout the community regarding this need of BFKL-evolution at currently probed x, Q^2 values, and an alternative approach [359], which implements the merging of LO matrix-element based event generation with a parton shower (using the SHERPA framework), successfully describes the data in all kinematical regions, including the low Q^2 , low x domain. At moderately small x values, it should perhaps not be surprising that the BFKL approach and fixed-order matrix-element merging with parton showers may both provide adequate descriptions of the data, because some part of the multi-parton phase space that they model is common to both approaches.

In the case of photoproduction, a wealth of measurements with low p_t jets were performed in order to constrain the photon content of the proton. The uncertainties related to such photon PDFs play a minor role at high jet p_t , which has allowed for precise tests of pQCD calculations.

A few examples of recent measurements can be found in Refs. [360–364] for photoproduction and in Refs. [365–374] for DIS.

9.3.2.3 Hadron-hadron colliders

The spectrum of observables and the number of measurements performed at hadron colliders is enormous, probing many regions of phase space and covering a huge range of cross sections, as illustrated in Fig. 9.1 for the case of the ATLAS and CMS experiments at the LHC. In general, the theory agreement with data is excellent for a wide variety of processes, indicating the success of perturbative QCD with the PDF and strong coupling inputs. For the sake of brevity, in the following only certain classes of those measurements will be discussed, which allow addressing particular aspects of the various QCD studies performed. Most of our discussion will focus on LHC results, which are available for center-of-mass energies of 2.76, 5, 7, 8 and 13 TeV with integrated luminosities of up to 140 fb^{-1} . Generally speaking, besides representing a general test of the standard model and QCD in particular, these measurements serve several purposes, such as: (i) probing pQCD and its various approximations and implementations in MC models, in order to quantify the order of magnitude of not yet calculated contributions and to gauge their precision when used as background predictions, or (ii) extracting/constraining model parameters such as the strong coupling constant or PDFs. Indeed, data from the LHC is becoming increasingly important for the determination of both, PDFs and the strong coupling constant.

The final states measured at the LHC include single, double and triple gauge boson production, top production (single top, top pair and four top production), Higgs boson production, alone and in conjunction with a W or Z boson, and with a top quark pair. Many/most of these events are accompanied by additional jets. So far only relatively loose limits have been placed on double Higgs production. The volume of LHC results prohibits a comprehensive description in this *Review*; hence, only a few highlights will be presented.

Among the most important cross sections measured, and the one with the largest dynamic range, is the inclusive jet spectrum as a function of the jet transverse momentum (p_t), for several rapidity regions and for p_t up to 700 GeV at the Tevatron and ~ 3.5 TeV at the LHC. It is worth noting that this upper limit in p_t corresponds to a distance scale of $\sim 10^{-19}$ m: no other experiment so far is able to directly probe smaller distance scales of nature than this measurement. The Tevatron inclusive jet measurements in Run 2 (Refs. [377–380]) were carried out with the MidPoint jet clustering algorithm (or its equivalent) and with the k_t jet

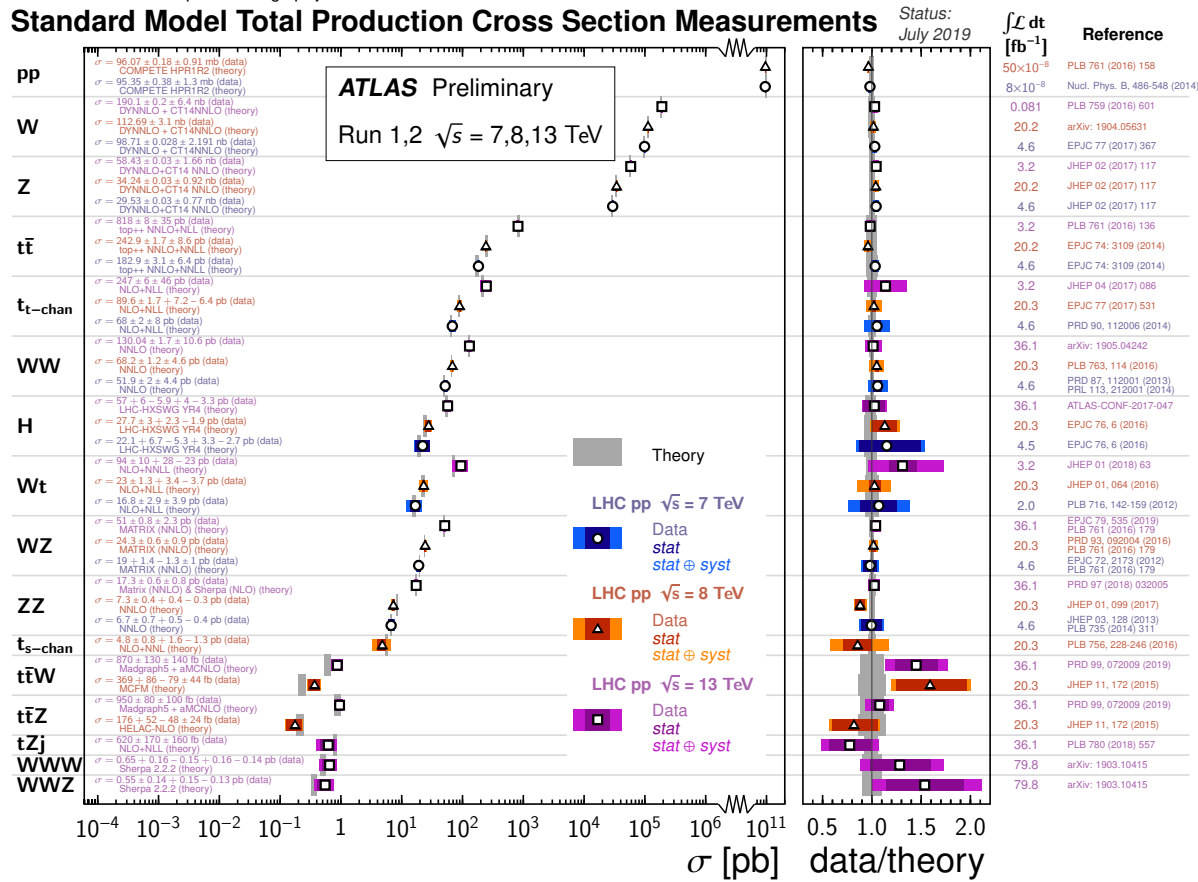
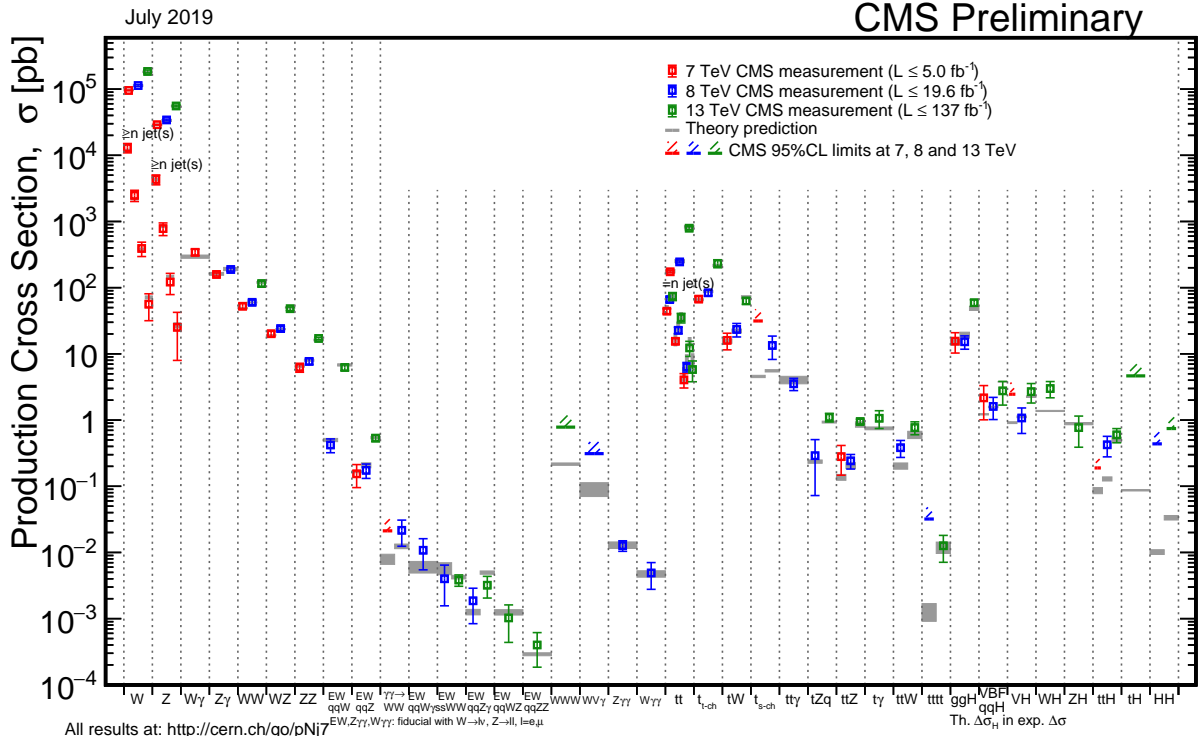


Figure 9.1: Overview of cross section measurements for a wide class of processes and observables, as obtained by the CMS [375] and ATLAS [376] experiments at the LHC, for centre-of-mass energies of 7, 8 and 13 TeV. Also shown are the theoretical predictions and their uncertainties.

clustering algorithm. Most of the LHC measurements use the *anti-k_t* algorithm, with a variety of jet radii. The use of multiple jet radii in the same analysis allows a better understanding of the underlying QCD dynamics. Measurements by ALICE, ATLAS

and CMS have been published in Refs. [381–389].

In general, we observe a good description of the data by the NLO and NNLO QCD predictions over about 11 orders of magnitude in cross section. as long as care is taken for the form of

the central scale choice [303]. The experimental systematic uncertainties are dominated by the jet energy scale uncertainty, quoted to be in the range of a few percent (see for instance the review in Ref. [390]), leading to uncertainties of $\sim 5 - 30\%$ on the cross section, increasing with p_t and rapidity. The PDF uncertainties dominate the theoretical uncertainty at large p_t and rapidity. In fact, inclusive jet data are one of the most important inputs to global PDF fits, in particular for constraining the high- x gluon PDF [77, 391]. Constraints on the PDFs can also be obtained from ratios of inclusive cross sections at different center-of-mass energies [382, 387]. In general, ratios of jet cross sections are a means to (at least partially) cancel the jet energy scale uncertainties and thus provide jet observables with significantly improved precision.

Dijet events are analyzed in terms of their invariant mass or average dijet p_t and angular distributions, which allows for tests of NLO and NNLO QCD predictions (see *e.g.* Refs. [386, 392, 393] for recent LHC results), and for setting stringent limits on deviations from the Standard Model, such as quark compositeness or contact interactions (some examples can be found in Refs. [389, 394–400]). Furthermore, dijet azimuthal correlations between the two leading jets, normalized to the total dijet cross section, are an extremely valuable tool for studying the spectrum of gluon radiation in the event. The azimuthal separation of the two leading jets is sensitive to multi-jet production, avoiding at the same time large systematic uncertainties from the jet energy calibration. For example, results from the Tevatron [401, 402] and the LHC [335, 403–407] show that the LO (non-trivial) prediction for this observable, with at most three partons in the final state, is not able to describe the data for an azimuthal separation below $2\pi/3$, where NLO contributions (with 4 partons) restore the agreement with data. In addition, this observable can be employed to tune Monte Carlo predictions of soft gluon radiation. Further examples of dijet observables that probe special corners of phase space are those that involve forward (large rapidity) jets and where a large rapidity separation, possibly also a rapidity gap, is required between the two jets. Reviews of such measurements can be found in Ref. [346], showing that no single prediction is capable of describing the data in all phase-space regions. In particular, no conclusive evidence for BFKL effects in these observables has been established so far.

Beyond dijet final states, measurements of the production of three or more jets, including cross section ratios, have been performed (see Refs. [346, 408] for recent reviews), as a means of testing perturbative QCD predictions, determining the strong coupling constant (at NLO precision so far), and probing/tuning MC models, in particular those combining multi-parton matrix elements with parton showers.

W and Z production serve as benchmark cross sections at the LHC. The large boson mass provides a stability for the perturbative predictions which results in better theoretical precision. In terms of experimental precision, measurements of inclusive vector boson (W, Z) production provide the most precisely determined observables at hadron colliders so far. This is because the experimental signatures are based on leptons which are measured much more accurately than jets or photons. At the LHC [409–416], the dominant uncertainty stems from the luminosity determination ($\leq 2-4\%$), while other uncertainties (*e.g.* statistics, lepton efficiencies) are controlled at the $\sim 0.5-3\%$ level. The uncertainty from the acceptance correction of about $\sim 1-2\%$ can be reduced by measuring so-called fiducial cross sections, *ie.* by applying kinematic cuts also to the particle level of the theoretical predictions. A further reduction or even complete elimination of particular uncertainties (*e.g.* luminosity) is achieved by measuring cross section ratios (W/Z or W^+/W^-) or differential distributions that are normalised to the inclusive cross section. On the theory side, as discussed earlier in this *Review*, the production of these color-singlet states has been calculated up to NNLO accuracy, with some progress towards N³LO. Since the dominant theoretical uncertainty is related to the choice of PDFs, these high-precision data provide useful handles for PDF determinations.

Further insights are obtained from measurements of differential vector boson production, as a function of the invariant dilepton mass, the boson's rapidity or its transverse momentum. For

example, the dilepton invariant mass distribution has been measured [417–422] for masses between 15 and 3000 GeV, covering more than 8 orders of magnitude in cross section. NNLO QCD predictions, together with modern PDF sets and including higher-order electroweak and QED final-state radiation corrections, describe the data to within 5–10% over this large range, whereas NLO predictions show larger deviations, unless matched to a parton shower.

Similar conclusions can be drawn from the observed rapidity distribution of the dilepton system (see *e.g.* Refs. [409, 418, 423]) or, in the case of W production, from the observed charged lepton rapidity distribution and its charge asymmetry. The latter is particularly sensitive to differences among PDF sets [409, 424–426], also thanks to the high precision achieved by the ATLAS and CMS experiments for central rapidity ranges. These measurements are nicely extended to the very forward region, up to 4.5 in lepton rapidity, by the LHCb experiment.

An overview of this kind of measurements can be found in Ref. [346]. There one can also find a discussion of and references to LHC results from studies of the vector boson's transverse momentum distribution, p_t^V (see also Refs. [427–429]). This observable covers a wide kinematic range and probes different aspects of higher-order QCD effects. It is sensitive to jet production in association with the vector boson, without suffering from the large jet energy scale uncertainties. In the p_t^V region of several tens of GeV to over 1 TeV, the NNLO predictions for V+jet¹¹ can be used to predict the high p_t boson transverse cross section. The NNLO predictions agree with the data to within about 10%, and agree somewhat better at high transverse momentum than do the NLO predictions [430]. At transverse momenta below ~ 20 GeV, the fixed-order predictions fail and soft-gluon resummation is needed to restore the agreement with data. The soft gluon resummation can either be performed analytically, or effectively using parton showering implemented in Monte Carlo programs.

The addition of jets to the final state extends the kinematic range as well as increasing the complexity of the calculation/measurements.¹² The number of results obtained both at the Tevatron and at the LHC is extensive. Recent summaries can be found in Refs. [346, 432]. Some more recent results can be found in Refs. [430, 433–436].

The measurements cover a very large phase space, *e.g.* with jet transverse momenta between 30 GeV and ~ 1.5 TeV and jet rapidities up to $|y| < 4.4$ [430]. Jet multiplicities as high as seven jets accompanying the vector boson have already been probed at the LHC, together with a substantial number of other kinematical observables, such as angular correlations among the various jets or among the jets and the vector boson, or the sum of jet transverse momenta, H_T . Whereas the jet p_t and H_T distributions are dominated by jet energy scale uncertainties at levels similar to those discussed above for inclusive jet production, angular correlations and jet multiplicity ratios have been measured with a precision of $\sim 10\%$, see *e.g.* Refs. [337, 437].

NLO calculations for up to five jets [438] in addition to the vector boson are in good agreement with the data over that phase space, where the calculations are applicable; that is, one can not expect such predictions to work for *e.g.* the p_t distribution of the $n + 1$ st jet with $V + n$ jets calculated at NLO. However, with the higher kinematic reach achieved by the LHC experiments, some more detailed observations can be made. NLO fixed-order predictions describe the W boson p_t distribution and the lead jet p_t distribution reasonably well at transverse momenta below around 500 GeV, but predict smaller cross sections than the data at higher transverse momenta. Predictions for V+jet at NNLO improve the description of the data. MC models that implement parton shower matching to matrix elements (either at LO or NLO) have mixed results.

The challenges get even more severe in the case of vector boson plus heavy quark (b, c) production, both because of theoretical

¹¹For these calculations, there is a requirement of the presence of a jet, but the p_t cut is typically small (30 GeV) compared to the high p_t region being discussed here.

¹²For reliable predictions, the scale used in the higher order calculations should be proportional to the sum of the transverse momenta of all of the objects in the final state [431].

issues (an additional scale is introduced by the heavy quark mass and different schemes exist for the handling of heavy quarks and their mass effects in the initial and/or final state) and because of additional experimental uncertainties related to the heavy-flavour tagging. A review of heavy quark production at the LHC can be found in Ref. [439]. There it is stated that studies of b -jet production with or without associated W and Z bosons reveal the di- b -jet p_t and mass spectra to be well modelled, within experimental and theoretical uncertainties, by most generators on the market. However, sizable differences between data and predictions are seen in the modelling of events with single b jets, particularly at large b -jet p_t , where gluon splitting processes become dominant, as also confirmed by studies of b -hadron and b -jet angular correlations.

The precision reached in photon measurements is in between that for lepton and jet measurements. The photon 4-vectors can be measured at about the same precision as the lepton 4-vectors in Drell-Yan production, but there are greater challenges encountered in photon reconstruction (for example isolation) and in purity determination. Note, though, that the photon purity approaches unity as the photon p_t increases. At high p_t , it becomes increasingly difficult for a jet to fragment into an isolated neutral electromagnetic cluster which mimics the photon signature. The inclusive photon cross section can be measured [392, 440–443], as well as the production of a photon accompanied by one or more jets [443–445, 445–448]. The kinematic range for photon production is less than that for jet production because of the presence of the electromagnetic coupling, but still reaches about 2 TeV. Better agreement is obtained with NNLO predictions for photon production than for NLO predictions, except when the latter are matched to matrix element plus parton shower predictions. Photon production in association with a heavy-flavor jet is a useful input for the determination of the b and c quark PDFs [449].

Electroweak corrections are expected to become more and more relevant now that the TeV energy range starts to be explored. For example, such corrections were found [450] to be sizable (tens of percent) when studying the ratio $(d\sigma^\gamma/dp_t)/(d\sigma^Z/dp_t)$ in $\gamma(Z)$ -jet production, p_t being the boson's transverse momentum, and might account for (some of) the differences observed in a CMS measurement [451] of this quantity.

A number of interesting developments, in terms of probing higher-order QCD effects, have occurred in the sector of diboson production, in particular for the WW and $\gamma\gamma$ cases. Regarding the former, an early disagreement of about 10% between the LHC measurements and the NLO predictions had led to a number of speculations of possible new physics effects in this channel. However, more recent ATLAS and CMS measurements [452–455] are in agreement with the NNLO prediction [85]. The statistical reach of the LHC has resulted in evidence for triple massive gauge boson production [456].

In the case of diphoton production, ATLAS [457, 458] and CMS [459] have provided accurate measurements, in particular for phase-space regions that are sensitive to radiative QCD corrections (multi-jet production), such as small azimuthal photon separation. While there are large deviations between data and NLO predictions in this region, a calculation [178] at NNLO accuracy manages to mostly fill this gap. This is an interesting example where scale variations can not provide a reliable estimate of missing contributions beyond NLO, since at NNLO new channels appear in the initial state (gluon fusion in this case). These missing channels can be included in a matrix element plus parton shower calculation in which two additional jets are included at NLO. The result is a similar level of agreement as that obtained at NNLO. Three photon production has also been measured [460].

In terms of heaviest particle involved, top-quark production at the LHC has become an important tool for probing higher-order QCD calculations, thanks to very impressive achievements both on the experimental and theoretical side, as extensively summarised in Ref. [461]. Regarding $t\bar{t}$ production, the most precise inclusive cross section measurements are achieved using the dilepton ($e\mu$) final state, with a total uncertainty of 4% [462–465]. This is of about the same size as the uncertainty on the most advanced theoretical predictions [84, 466–468], obtained at NNLO with additional soft-gluon resummation at NNLL accuracy [469]. There

is excellent agreement between data and the QCD predictions.

The $t\bar{t}$ final state allows multiple observables to be measured. A large number of differential cross section measurements have been performed at 7, 8 and 13 TeV centre-of-mass energy, studying distributions such as the top-quark p_t and rapidity, the transverse momentum and invariant mass of the $t\bar{t}$ system (probing scales up to the TeV range), or the number of additional jets. These measurements have been compared to a wide range of predictions, at fixed order up to NNLO as well as using LO or NLO matrix elements matched to parton showers. Each of the observables provides information on the high x gluon and have been used in global PDF fits. While in general there is reasonable agreement observed with data, most MC simulations predict a somewhat harder top-quark p_t distribution than seen in data.

Thanks to both the precise measurements of, and predictions for, the inclusive top-pair cross section, which is sensitive to the strong coupling constant and the top-quark mass, this observable has been used to measure the strong coupling constant at NNLO accuracy from hadron collider data [470, 471] (*cf.* Section 9.4 below), as well as to obtain a measurement of the top-quark's pole mass without employing direct reconstruction methods [470, 472, 473].

The Higgs boson lends itself to being a tool for QCD studies, especially as the dominant production mechanism is gg fusion, which is subject to very large QCD corrections. Higgs boson production has been measured in the $ZZ, \gamma\gamma, WW$ and $\tau\tau$ decay channels. The experimental cross section is now known with a precision approaching 10% [474, 475], similar to the size of the theoretical uncertainty [92], of which the PDF+ α_s uncertainty is the largest component. The experimental precision has allowed detailed fiducial and differential cross section measurements. For example, with the diphoton final state, the transverse momentum of the Higgs boson can be measured out to 350–400 GeV [476, 477], where top quark mass effects become important. The production of a Higgs boson with up to 4 jets has been measured [476, 478]. The experimental cross sections have been compared to NNLO predictions (for $H + \geq 1$ jet), NLO for 2 and 3 jets, and NNLO+NNLL for the transverse momentum distribution. In addition, finite top quark mass effects have been taken into account at NLO. The use of the boosted $H \rightarrow b\bar{b}$ topology allows probes of Higgs boson transverse momenta on the order of 600 GeV [478]. So far the agreement with the perturbative QCD corrections is good.

9.4 Determinations of the strong coupling constant

Beside the quark masses, the only free parameter in the QCD Lagrangian is the strong coupling constant α_s . The coupling constant in itself is not a physical observable, but rather a quantity defined in the context of perturbation theory, which enters predictions for experimentally measurable observables, such as R in Eq. (9.7). The value of the strong coupling constant must be inferred from such measurements and is subject to experimental and theoretical uncertainties. The incomplete knowledge of α_s propagates into uncertainties in numerous precision tests of the Standard Model. Here we present an update of the 2016 PDG average value of $\alpha_s(M_Z^2)$ and its uncertainty [479], which were retained in the 2018 edition of this *Review* [480].¹³

Many experimental observables are used to determine α_s . A number of recent determinations are collected in Ref. [484]. Further discussions and considerations on determinations of α_s can also be found in Refs. [485, 486]. Such considerations include:

- The observable's sensitivity to α_s as compared to the experimental precision. For example, for the e^+e^- cross section to hadrons (*cf.* R in Sec. 9.2.1), QCD effects are only a small correction, since the perturbative series starts at order α_s^0 ; 3-jet production or event shapes in e^+e^- annihilations are directly sensitive to α_s since they start at order α_s ; the hadronic decay width of heavy quarkonia, $\Gamma(\Upsilon \rightarrow \text{hadrons})$, is very sensitive to α_s since its leading order term is $\propto \alpha_s^3$.

¹³ The time evolution of α_s combinations can be followed by consulting Refs. [481–483] as well as earlier editions of this *Review*.

- The accuracy of the perturbative prediction, or equivalently of the relation between α_s and the value of the observable. The minimal requirement is generally considered to be an NLO prediction. Some observables (many inclusive ones as well as 3-jet rates and event shapes in e^+e^- collisions) are known to NNLO since quite some time. Recent additions to the list of processes calculated up to NNLO comprise inclusive jet and dijet production in DIS and pp or $p\bar{p}$ collisions. Likewise, $t\bar{t}$ and W/Z +jet production cross sections have been computed up to NNLO for pp and $p\bar{p}$ scattering. The e^+e^- hadronic cross section and τ branching fraction to hadrons are even known to N³LO, where one denotes the LO as the first non-trivial term. In certain cases, fixed-order predictions are supplemented with resummation. The precise magnitude of the associated theory uncertainties usually is estimated as discussed in Sec. 9.2.4.
- The size of non-perturbative effects. Sufficiently inclusive quantities, like the e^+e^- cross section to hadrons, have small non-perturbative contributions $\sim \Lambda^4/Q^4$. Others, such as event-shape distributions, have typically contributions $\sim \Lambda/Q$.
- The scale at which the measurement is performed. An uncertainty δ on a measurement of $\alpha_s(Q^2)$, at a scale Q , translates to an uncertainty $\delta' = (\alpha_s^2(M_Z^2)/\alpha_s^2(Q^2)) \cdot \delta$ on $\alpha_s(M_Z^2)$. For example, this enhances the already important impact of precise low- Q measurements, such as from τ decays, in combinations performed at the M_Z scale.

The selection of results from which to determine the world average value of $\alpha_s(M_Z^2)$ is restricted to those that are

- published in a peer-reviewed journal at the time of writing this report,
- based on the most complete perturbative QCD predictions of at least NNLO accuracy,
- accompanied by reliable estimates of all experimental and theoretical uncertainties.

We note that all determinations of $\alpha_s(M_Z^2)$ entering the average of the lattice gauge community as summarised comprehensively in the FLAG2019 report [487] are published in peer-reviewed journals, although the FLAG report itself that only describes the averaging procedure is not.

We also note that a prediction in perturbative QCD for the determination of $\alpha_s(M_Z^2)$ at NNLO accuracy requires the calculation of at least three consecutive terms in powers $p > 0$ of α_s^p . Although this condition is fulfilled, measurements from jet production in DIS and at hadron colliders (with one exception) are still excluded, because the determination of $\alpha_s(M_Z^2)$ has not yet been upgraded to NNLO. Nevertheless, the NLO analyses will be discussed in this *Review*, as they are important ingredients for the experimental evidence of the energy dependence of α_s , *i.e.* for Asymptotic Freedom, one of the key features of QCD.

In order to calculate the world average value of $\alpha_s(M_Z^2)$, as in earlier editions we apply an intermediate step of pre-averaging results within the sub-fields now labelled “Hadronic τ decays and low Q^2 continuum” (τ decays and low Q^2), “Heavy quarkonia decays” ($Q\bar{Q}$ bound states), “Deep-inelastic scattering and global PDF fits” (DIS & PDF fits), “Hadronic final states of e^+e^- annihilations” (e^+e^- jets & shapes), “Hadron collider results” (hadron collider), and “Electroweak precision fit” (electroweak) as explained in the following sections. For each sub-field, the *unweighted average* of all selected results is taken as the pre-average value of $\alpha_s(M_Z^2)$, and the unweighted average of the quoted uncertainties is assigned to be the respective overall error of this pre-average.¹⁴ At variance with previous reviews, for the “Lattice QCD” (lattice) sub-field we do not perform a pre-averaging;

¹⁴In the previous review, if this error appeared to be smaller than the unweighted standard deviation - *i.e.* the *spread* - of the results, the standard deviation was taken as the overall uncertainty instead. This was done in order to arrive at an unbiased estimator of the average value of $\alpha_s(M_Z^2)$ from a given sub-field, and to avoid that singular, optimistic estimates of systematic uncertainties unduly bias the uncertainty of the sub-field average. Here we find that, for all six sub-fields, the quoted error is larger than the standard deviation.

instead, we adopt for this sub-field the FLAG2019 average value and uncertainty derived in Ref. [487].

Assuming that the six sub-fields (excluding lattice) are largely independent of each other, we determine a non-lattice world average value using a ‘ χ^2 averaging’ method. In a last step we perform an unweighted average of the values and uncertainties of $\alpha_s(M_Z^2)$ from our non-lattice result and the lattice result presented in the FLAG 2019 report [487].

9.4.1 Hadronic τ decays and low Q^2 continuum:

Based on complete N³LO predictions [36], analyses of the τ hadronic decay width and spectral functions have been performed, *e.g.* in Refs. [36, 488–493], and lead to precise determinations of α_s at the energy scale of M_τ^2 . They are based on different approaches to treat perturbative and non-perturbative contributions, the impacts of which have been a matter of intense discussions since a long time, see *e.g.* Refs. [492–495]. In particular, in τ decays there is a significant difference between results obtained using fixed-order (FOPT) or contour improved perturbation theory (CIPT), such that analyses based on CIPT generally arrive at larger values of $\alpha_s(M_\tau^2)$ than those based on FOPT. In addition, some results show differences in $\alpha_s(M_\tau^2)$ between different groups using the same data sets and perturbative calculations, most likely due to different treatments of the non-perturbative contributions, *cf.* Ref. [493] with Refs. [492, 496].

Here, we largely keep the same input calculations as in the previous review, with only the following changes. The result of Ref. [492] has been replaced by the one of Ref. [495]. From Ref. [493] we use the values resulting from a combination of ALEPH and OPAL data instead of ALEPH data alone. Moreover, we include the new α_s determination obtained from $R(s)$ below the charm threshold [497]. Here, the average from the FOPT and CIPT results gives $\alpha_s(M_\tau^2) = 0.301 \pm 0.019$, where the difference between the two amounts to 2% at m_τ . This corresponds to $\alpha_s(M_Z^2) = 0.1162 \pm 0.0025$.

In summary, we determine the pre-average value of $\alpha_s(M_Z^2)$ for this sub-field from studies that employ both FOPT and CIPT expansions, and that account for the difference among these in the quoted overall uncertainty: $\alpha_s(M_Z^2) = 0.1202 \pm 0.0019$ [36], $\alpha_s(M_Z^2) = 0.1199 \pm 0.0015$ [496], $\alpha_s(M_Z^2) = 0.1175 \pm 0.0017$ [493], $\alpha_s(M_Z^2) = 0.1197 \pm 0.0015$ [495], and $\alpha_s(M_Z^2) = 0.1162 \pm 0.0025$ [497]. Additionally, we include the result from τ decay and lifetime measurements, obtained in Sec. *Electroweak Model and constraints on New Physics* of the 2018 edition of this *Review*, $\alpha_s(M_Z^2) = 0.1184 \pm 0.0019$. The latter result, being a global fit of τ data, involve some correlations with the other extractions of this category. However, since we perform an unweighted average of the central value and uncertainty, we do not need to worry about double counting.

All these results are summarised in Fig. 9.2. Determining the unweighted average of the central values and their overall uncertainties, we arrive at $\alpha_s(M_Z^2) = 0.1187 \pm 0.0018$, which we will use as the first input for determining the world average value of $\alpha_s(M_Z^2)$. This corresponds to $\alpha_s(M_\tau^2) = 0.325 \pm 0.016$.

9.4.2 Heavy quarkonia decays:

For a long time, the best determination of the strong coupling constant from radiative Υ decays was the one of Ref. [498], which resulted in $\alpha_s(M_Z^2) = 0.119^{+0.006}_{-0.005}$. This determination is based on QCD at NLO only, so it will not be considered for the final extraction of the world average value of α_s ; it is, however, an important ingredient for the demonstration of Asymptotic Freedom as given in Fig. 9.3. More recently, two determinations have been performed [499, 500] that are based on N³LO accurate predictions. Reference [499] performs a simultaneous fit of the strong coupling and the bottom mass \overline{m}_b , including states with principal quantum number up to $n \leq 2$ in order to break the degeneracy between α_s and \overline{m}_b , finding $\alpha_s(M_Z^2) = 0.1178 \pm 0.0051$. Reference [500] instead uses as input of the fit the renormalon-free energy combination of B_c and bottomonium η_b and charmonium η_c , $M_{B_c} - M_{\eta_b}/2 - M_{\eta_c}/2$, which is weakly dependent on the heavy quark masses, but shows a good dependence on α_s . Using this observable, they obtain $\alpha_s(M_Z^2) = 0.1178 \pm 0.0051$. These two determinations satisfy our criteria to be included in the world

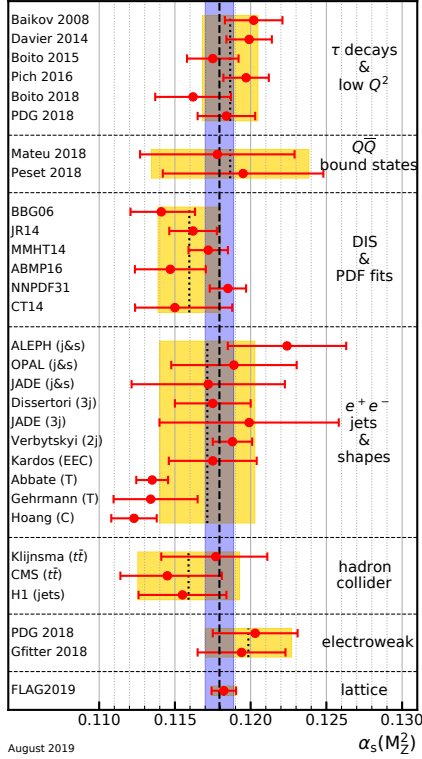


Figure 9.2: Summary of determinations of $\alpha_s(M_Z^2)$ from the seven sub-fields discussed in the text. The yellow (light shaded) bands and dotted lines indicate the pre-average values of each sub-field. The dashed line and blue (dark shaded) band represent the final world average value of $\alpha_s(M_Z^2)$.

average and are at the moment the only input values in the Heavy-quarkonia category. Their unweighted combination leads to the pre-average for this category of $\alpha_s(M_Z^2) = 0.1187 \pm 0.0052$. We note that, while we include this result in our final average, because of the large uncertainty of the two determinations in this category, removing this pre-average would not change the final result within the quoted uncertainty.

9.4.3 Deep-inelastic scattering and global PDF fits:

Studies of DIS final states have led to a number of precise determinations of α_s : a combination [501] of precision measurements at HERA, based on NLO fits to inclusive jet cross sections in neutral current DIS at high Q^2 , provides combined values of α_s at different energy scales Q , as shown in Fig. 9.3, and quotes a combined result of $\alpha_s(M_Z^2) = 0.1198 \pm 0.0032$. A more recent study of multijet production [373], based on improved reconstruction and data calibration, confirms the general picture, albeit with a somewhat smaller value of $\alpha_s(M_Z^2) = 0.1165 \pm 0.0039$, still at NLO. An evaluation of inclusive jet production, including *approximate* NNLO contributions [502], reduces the theoretical prediction for jet production in DIS, improves the description of the final HERA data in particular at high photon virtuality Q^2 and increases the central fit value of the strong coupling constant.

Another class of studies, analyzing structure functions at NNLO QCD (and partly beyond), provide results that serve as relevant inputs for the world average of α_s . Most of these studies do *not*, however, explicitly include estimates of theoretical uncertainties when quoting fit results of α_s . In such cases we add, in quadrature, half of the difference between the results obtained in NNLO and NLO to the quoted errors: a combined analysis of non-singlet structure functions from DIS [503], based on QCD predictions up to N³LO in some of its parts, results in $\alpha_s(M_Z^2) = 0.1141 \pm 0.0022$ (BBG). Studies of singlet and non-singlet structure functions, based on NNLO predictions, result in $\alpha_s(M_Z^2) = 0.1162 \pm 0.0017$ [504] (JR14). The AMBP group [505, 506] determined a set of parton distribution functions using data from HERA, NOMAD,

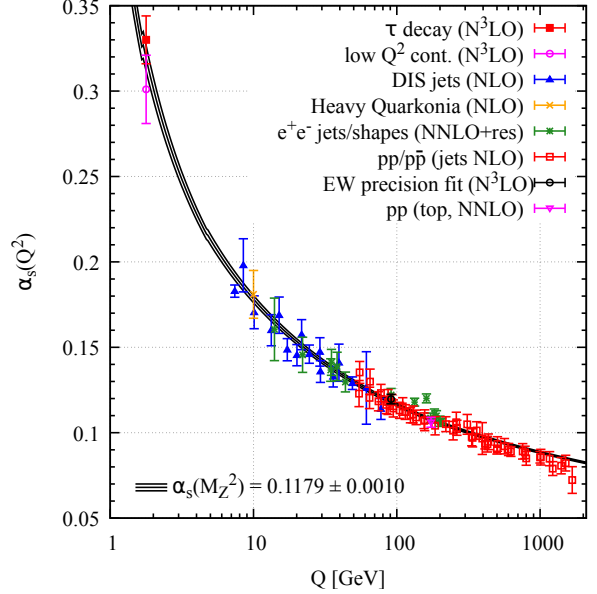


Figure 9.3: Summary of measurements of α_s as a function of the energy scale Q . The respective degree of QCD perturbation theory used in the extraction of α_s is indicated in brackets (NLO: next-to-leading order; NNLO: next-to-next-to-leading order; NNLO+res.: NNLO matched to a resummed calculation; N³LO: next-to-NNLO).

CHORUS, from Tevatron and the LHC for the Drell-Yan process and the hadro-production of single-top and top-quark pairs and determined $\alpha_s(M_Z^2) = 0.1147 \pm 0.0024$ [505]. The MMHT group [507], also including hadron collider data, determined a new set of parton density functions (MMHT2014) together with $\alpha_s(M_Z^2) = 0.1172 \pm 0.0013$. Similarly, the CT group [508] determined the CT14 parton density set together with $\alpha_s(M_Z^2) = 0.1150^{+0.0036}_{-0.0024}$. The NNPDF group [509] presented NNPDF3.1 parton distribution functions together with $\alpha_s(M_Z^2) = 0.1185 \pm 0.0012$.

We note that criticism has been expressed on some of the above extractions. Among the issues raised, we mention the neglect of singlet contributions at $x \geq 0.3$ in pure non-singlet fits [510], the impact and detailed treatment of particular classes of data in the fits [510, 511], possible biases due to insufficiently flexible parametrizations of the PDFs [512] and the use of a fixed-flavor number scheme [513, 514].

Summarizing the results from world data on structure functions, taking the *unweighted average* of the central values and errors of all selected results, leads to a pre-average value of $\alpha_s(M_Z^2) = 0.1161 \pm 0.0018$, see Fig. 9.2.

9.4.4 Hadronic final states of e^+e^- annihilations:

Re-analyses of event shapes in e^+e^- annihilation (j&s), measured around the Z peak and at LEP2 center-of-mass energies up to 209 GeV, using NNLO predictions matched to NLL resummation and Monte Carlo models to correct for hadronization effects, resulted in $\alpha_s(M_Z^2) = 0.1224 \pm 0.0039$ (ALEPH) [515], with a dominant theoretical uncertainty of 0.0035, and in $\alpha_s(M_Z^2) = 0.1189 \pm 0.0043$ (OPAL) [516]. Similarly, an analysis of JADE data [517] at center-of-mass energies between 14 and 46 GeV gives $\alpha_s(M_Z^2) = 0.1172 \pm 0.0051$, with contributions from the hadronization model and from perturbative QCD uncertainties of 0.0035 and 0.0030, respectively. Precise determinations of α_s from 3-jet production alone (3j), at NNLO, resulted in $\alpha_s(M_Z^2) = 0.1175 \pm 0.0025$ [518] from ALEPH data and in $\alpha_s(M_Z^2) = 0.1199 \pm 0.0059$ [519] from JADE. A recent determination is based on an NNLO+NNLL accurate calculation that allows to fit the region of lower 3-jet rate (2j) using data collected at LEP and PETRA at different energies. This fit gives $\alpha_s(M_Z^2) = 0.1188 \pm 0.0013$ [520], where the dominant uncertainty is the hadronization uncertainty, which is estimated

from Monte Carlo simulations. A fit of energy-energy-correlation (EEC) also based on an NNLO+NNLL calculation together with a Monte Carlo based modelling of hadronization corrections gives $\alpha_s(M_Z^2) = 0.1175 \pm 0.0029$ [521]. These results are summarized in the upper seven rows of the e^+e^- sector of Fig. 9.2.

Another class of α_s determinations is based on analytic modelling of non-perturbative and hadronization effects, rather than on Monte Carlo models [522–525], using methods like power corrections, factorization of soft-collinear effective field theory, dispersive models and low scale QCD effective couplings. In these studies, the world data on Thrust distributions (T), or - most recently - C-parameter distributions (C), are analysed and fitted to perturbative QCD predictions at NNLO matched with resummation of leading logs up to N³LL accuracy, see Sec. 9.2.3.3. The results are $\alpha_s(M_Z^2) = 0.1135 \pm 0.0011$ [523] and $\alpha_s(M_Z^2) = 0.1134^{+0.0031}_{-0.0025}$ [524] from Thrust, and $\alpha_s(M_Z^2) = 0.1123 \pm 0.0015$ [525] from C-parameter. They are displayed in the lower three rows of the e^+e^- sector of Fig. 9.2.

The determination of Ref. [522], $\alpha_s(M_Z^2) = 0.1164^{+0.0028}_{-0.0024}$, is no longer included in the average as it is superseded by other determinations that use the same Thrust data but rely on more accurate theoretical predictions. Not included in the computation of the world average but worth mentioning are a computation of the NLO corrections to 5-jet production and comparison to the measured 5-jet rates at LEP [526], giving $\alpha_s(M_Z^2) = 0.1156^{+0.0041}_{-0.0034}$, and a computation of non-perturbative and perturbative QCD contributions to the scale evolution of quark and gluon jet multiplicities, including resummation, resulting in $\alpha_s(M_Z^2) = 0.1199 \pm 0.0026$ [527].

We note that there is criticism on both classes of α_s extractions described above: those based on corrections of non-perturbative hadronization effects using QCD-inspired Monte Carlo generators (since the parton level of a Monte Carlo simulation is not defined in a manner equivalent to that of a fixed-order calculation), as well as studies based on non-perturbative analytic modelling, as their systematics have not yet been fully verified. For the latter case, Refs. [523, 525] quote surprisingly small overall experimental, hadronization, and theoretical uncertainties of only 2, 5, and 9 per-mille, respectively, which calls for an independent confirmation.

In view of these open questions, the determination of the *unweighted average* and uncertainties is intended to provide the most appropriate and unbiased estimate of the average value of $\alpha_s(M_Z^2)$ for this sub-field, which results in $\alpha_s(M_Z^2) = 0.1171 \pm 0.0031$.

9.4.5 Hadron collider results:

Until recently, determinations of α_s using hadron collider data, mostly from jet or $t\bar{t}$ production processes, could be performed at NLO only. In the meantime, NNLO calculations have become available for $t\bar{t}$ [84, 466, 468] and for inclusive jet and dijet production [197, 528, 529]. Both can be supplemented by electroweak corrections [530–532], which become important for high- p_T collisions at the LHC; for $t\bar{t}$ logarithms have been resummed [469]. Z +jet production, studied with respect to an α_s determination at NLO from multi-jet events in Ref. [533], is also known at NNLO for the 1-jet case [187, 534].

The first determination of α_s at NNLO accuracy in QCD has been reported by CMS [470] from the $t\bar{t}$ production cross section at $\sqrt{s} = 7$ TeV: $\alpha_s(M_Z^2) = 0.1151^{+0.0028}_{-0.0027}$, whereby the dominating contributions to the overall uncertainty are experimental ($^{+0.0017}_{-0.0018}$), from parton density functions ($^{+0.0013}_{-0.0011}$) and the value of the top quark pole mass (± 0.0013). In the last *Review* this opened up a new sub-field on its own. In the meantime, multiple datasets on $t\bar{t}$ production from Tevatron at $\sqrt{s} = 1.96$ TeV and from LHC at $\sqrt{s} = 7, 8,$ and 13 TeV have been analyzed simultaneously to determine α_s [471] to

$$\alpha_s(M_Z^2) = 0.1177^{+0.0034}_{-0.0036},$$

where the largest uncertainties are associated with missing higher orders and with PDFs. Since this combined analysis contains among other things an updated measurement as compared to the dataset used by CMS, the latter is replaced in the averaging by

the new combined result. A second entry into this sub-field is given by an analysis of new $t\bar{t}$ production data at $\sqrt{s} = 13$ TeV from the CMS collaboration [464]. From the four values presented for the chosen PDF sets, the unweighted average is taken:

$$\alpha_s(M_Z^2) = 0.1145^{+0.0036}_{-0.0031}.$$

From jet production only one α_s determination has been performed yet at NNLO using DIS data of the H1 Collaboration [374]. Two strategies are pursued for the extraction of α_s , one using pre-determined PDFs as input and a second strategy fitting the proton PDFs together with the strong coupling constant. From the first approach we choose the result with the smallest total uncertainty, $\alpha_s(M_Z^2) = 0.1168 \pm 0.0030$, where the analysis is restricted to the phase space with the most precise theoretical prediction at the cost of excluding numerous data points at lower scale values. The second approach gives $\alpha_s(M_Z^2) = 0.1142 \pm 0.0028$, which we combine with the first result to our unweighted input average:

$$\alpha_s(M_Z^2) = 0.1155 \pm 0.0029.$$

As unweighted pre-average for this sub-field we obtain: $\alpha_s(M_Z^2) = 0.1159 \pm 0.0034$. Also worth mentioning is a recent still unpublished extraction of $\alpha_s(M_Z^2) = 0.1170 \pm 0.0030$ [535] using HERA jet data and relying on fast interpolation grid techniques.

Many further α_s determinations from jet measurements either could not yet be advanced to NNLO accuracy or the NNLO predictions are not yet available as is the case for observables requiring three or more jets in the final state. A selection of results from inclusive jet [373, 387, 536–541] and multi-jet measurements [332, 334, 335, 373, 542–546] is presented in Fig. 9.4, where the uncertainty in most cases is dominated by the impact of missing higher orders estimated through scale variations. The multi-jet α_s determinations are based on 3-jet cross sections (m3j), 3- to 2-jet cross-section ratios (R32), dijet angular decorrelations (RdR, Rd-Phi), and transverse energy-energy-correlations and their asymmetry (TEEC, ATEEC). The H1 result is extracted from a fit to inclusive 1-, 2-, and 3-jet cross sections (nj) simultaneously.

The CMS Collaboration has also derived an α_s value at NLO from dijet production at $\sqrt{s} = 8$ TeV [393], but only in combination with a PDF fit. The last point of the inclusive jet sub-field from Ref. [541] is derived from a simultaneous fit to six datasets from different experiments and partially includes data used already for the other data points, *e.g.* the CMS result at 7 TeV.

All NLO results are within their large uncertainties in agreement with the world average and the associated analyses provide valuable new values for the scale dependence of α_s at energy scales now extending up to almost 2.0 TeV as shown in Fig. 9.3.

9.4.6 Electroweak precision fit:

For this category, we update the global electroweak fit result of Ref. [547] to the one of Ref. [548], which now includes kinematic top quark and W boson mass measurements from the LHC, new determinations of the effective leptonic electroweak mixing angles from the Tevatron, a Higgs mass measurement from ATLAS and CMS, and a new evaluation of the hadronic contribution to the running of the electromagnetic coupling at the Z-boson mass. In addition, we use the newer results of the electroweak fit at the Z mass pole from LEP and SLC data presented in Sec. *Electroweak Model and constraints on New Physics* of the 2018 edition of this *Review*. Both very similar results, $\alpha_s(M_Z^2) = 0.1203 \pm 0.0028$ [480], $\alpha_s(M_Z^2) = 0.1194 \pm 0.0029$ [548], are also in perfect agreement with the original result obtained from LEP and SLD data [549]. Our pre-averaging gives $\alpha_s(M_Z^2) = 0.1199 \pm 0.0029$.

We note, however, that results from electroweak precision data strongly depend on the strict validity of Standard Model predictions and the existence of the minimal Higgs mechanism to implement electroweak symmetry breaking. Any - even small - deviation of nature from this model could strongly influence this extraction of α_s .

9.4.7 Lattice QCD:

Several methods exist to extract the strong coupling constant from lattice QCD, as reviewed also in Sec. *Lattice QCD* of this *Review*.

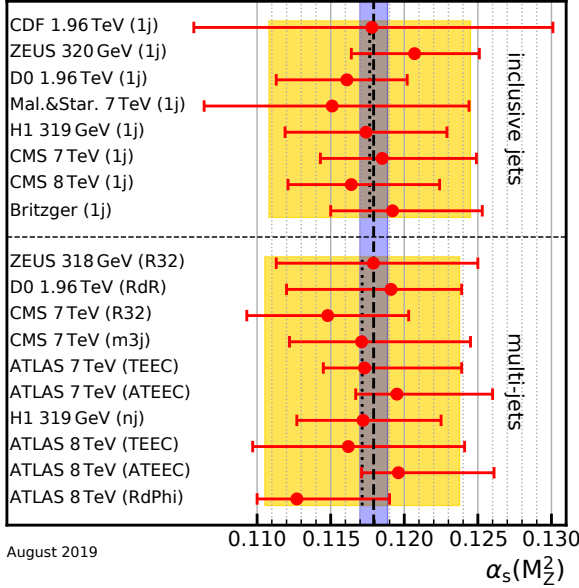


Figure 9.4: Summary of determinations of $\alpha_s(M_Z^2)$ at NLO from inclusive and multi-jet measurements at hadron colliders. The uncertainty is dominated by estimates of the impact of missing higher orders. The yellow (light shaded) bands and dotted lines indicate average values for the two sub-fields. The dashed line and blue (dark shaded) band represent the final world average value of $\alpha_s(M_Z^2)$.

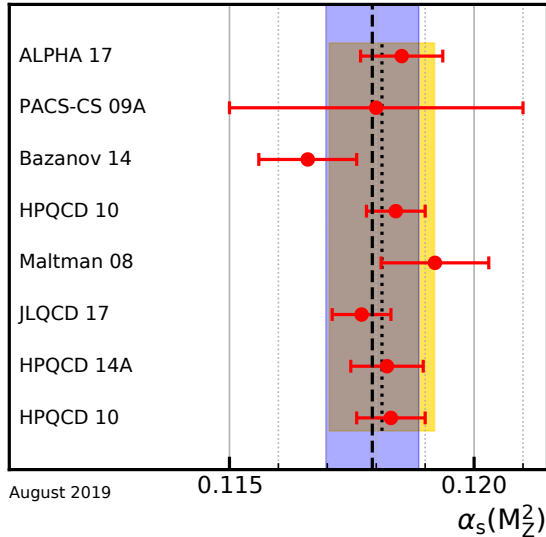


Figure 9.5: Lattice determinations that enter the FLAG2019 average. The yellow (light shaded) band and dotted line indicates the average value for this sub-field. The dashed line and blue (dark shaded) band represent the final world average value of $\alpha_s(M_Z^2)$.

The Flavour Lattice Averaging Group (FLAG) has recently considered the most up-to-date determinations and combined them to produce an update of their average α_s [487]. Their final result is obtained by considering seventeen possible input calculations [550–567] and by retaining in their final average only those eight [551–553, 556, 559–561, 563] that fulfill their predefined quality criteria. These determinations, together with their uncertainties, are displayed in Fig. 9.5. The yellow (light shaded) band and dotted line indicate the FLAG 2018 average, while the dashed line and blue (dark shaded) band represent the world average (see later). The level of agreement of individual results to the world average, or to the non-lattice world average is very similar. The criteria applied are detailed in the Sec. 9.2.1 of Ref. [487]. We

note that, as in our case, the calculation must be published in a peer-reviewed journal for it to be eligible to be included in the FLAG average. We also note that the criteria applied now are considered relatively loose by the FLAG collaboration and they have already formulated more stringent criteria. It is likely that in future FLAG averages only results satisfying these stricter criteria will be included in their averaging.

Similarly to what is done here, the FLAG collaboration built pre-averages of results that belong to different classes. The categories that currently contribute to the average are: step-scaling methods ($\alpha_s(M_Z^2) = 0.11848^{+0.00081}_{-0.00081}$), the potential at short distances ($\alpha_s(M_Z^2) = 0.11660^{+0.00160}_{-0.00160}$), Wilson loops ($\alpha_s(M_Z^2) = 0.11858^{+0.00120}_{-0.00120}$), and heavy-quark current two-point functions ($\alpha_s(M_Z^2) = 0.11824^{+0.00150}_{-0.00150}$).

Other categories like the vacuum polarization at short distances, the calculation of QCD vertices, or of the eigenvalue spectrum of the Dirac operator have not yet published results that fulfill all requirements to be included in the average. Ref. [568] has been completed after the publication of Ref. [487], hence these results have not been considered in the last FLAG average.

The final value is obtained by performing an unweighted average of the pre-averages. In order to be conservative, the final uncertainty is not the combined uncertainty of the pre-averages, rather it is taken to be the smallest uncertainty of the pre-averages, which is the uncertainty of the step-scaling category and is dominated by the ALPHA 17 result [563]. The final FLAG average (rounded to four digits) is

$$\alpha_s(M_Z^2) = 0.1182 \pm 0.0008, \quad (\text{lattice}). \quad (9.23)$$

We believe that this result expresses to a large extent the consensus of the lattice community and that the imposed criteria and the rigorous assessment of systematic uncertainties qualify for a direct inclusion of this FLAG average here. In contrast to the previous review, we therefore decided to adopt the FLAG average with its uncertainty as our value of α_s for the lattice category. Moreover, this lattice result will not be directly combined with any other sub-field average, but with our non-lattice average to give our final world average value for α_s .

9.4.8 Determination of the world average value of $\alpha_s(M_Z^2)$: Obtaining a world average value for $\alpha_s(M_Z^2)$ is a non-trivial exercise. A certain arbitrariness and subjective component is inevitable because of the choice of measurements to be included in the average, the treatment of (non-Gaussian) systematic uncertainties of mostly theoretical nature, as well as the treatment of correlations among the various inputs, of theoretical as well as experimental origin.

We have chosen to determine pre-averages for sub-fields of measurements that are considered to exhibit a maximum of independence among each other, considering experimental as well as theoretical issues. The seven pre-averages are summarized in Fig. 9.2. We recall that these are exclusively obtained from extractions that are based on (at least) full NNLO QCD predictions, and are published in peer-reviewed journals at the time of completing this *Review*. To obtain our final world average, we first combine six pre-averages, excluding the lattice result, using a χ^2 averaging method. This gives

$$\alpha_s(M_Z^2) = 0.1176 \pm 0.0011, \quad (\text{without lattice}). \quad (9.24)$$

This result is fully compatible with the lattice pre-average Eq. (9.23) and has a comparable error. In order to be conservative, we combine these two numbers using an unweighted average and take as an uncertainty the average between these two uncertainties. This gives our final world average value

$$\alpha_s(M_Z^2) = 0.1179 \pm 0.0010. \quad (9.25)$$

This world average value is in very good agreement with the last version of this *Review*, which was $\alpha_s(M_Z^2) = 0.1181 \pm 0.0011$, with only a slightly lower central value and decreased overall uncertainty. Performing a weighted average of all seven categories

gives $\alpha_s(M_Z^2) = 0.1180 \pm 0.0007$. Our uncertainty instead is about 50% larger.

Notwithstanding the many open issues still present within each of the sub-fields summarised in this *Review*, the wealth of available results provides a rather precise and reasonably stable world average value of $\alpha_s(M_Z^2)$, as well as a clear signature and proof of the energy dependence of α_s , in full agreement with the QCD prediction of Asymptotic Freedom. This is demonstrated in Fig. 9.3, where results of $\alpha_s(Q^2)$ obtained at discrete energy scales Q , now also including those based just on NLO QCD, are summarised. Thanks to the results from the Tevatron and from the LHC, the energy scales, at which α_s is determined, now extend up to almost 2 TeV.¹⁵

9.5 Acknowledgments

We are grateful to S. Bethke, G. Dissertori, D. d'Enterria, C. Glasman, A. Hoang, D. Lombardi, G.P. Salam, and B. Webber for discussions and for their comments on the manuscript, and to J. Andersen, A. Bazavov, H.-L. Win, and J. Smillie for useful discussions.

References

- [1] R. K. Ellis, W. J. Stirling and B. R. Webber, *Camb. Monogr. Part. Phys. Nucl. Phys. Cosmol.* **8**, 1 (1996).
- [2] J. Campbell, J. Huston, F. Krauss “*The Black Book of Quantum Chromodynamics, a Primer for the QCD Era*,” Oxford University Press, UK (2017).
- [3] C. A. Baker *et al.*, *Phys. Rev. Lett.* **97**, 131801 (2006), [hep-ex/0602020].
- [4] J. M. Pendlebury *et al.*, *Phys. Rev.* **D92**, 9, 092003 (2015), [arXiv:1509.04411].
- [5] B. Graner *et al.*, *Phys. Rev. Lett.* **116**, 16, 161601 (2016), [Erratum: *Phys. Rev. Lett.* 119, no.11, 119901 (2017)], [arXiv:1601.04339].
- [6] J. E. Kim and G. Carosi, *Rev. Mod. Phys.* **82**, 557 (2010), [arXiv:0807.3125].
- [7] G. Dissertori, I. G. Knowles and M. Schmelling, *High energy experiments and theory*, Oxford, UK: Clarendon (2003).
- [8] R. Brock *et al.* (CTEQ), *Rev. Mod. Phys.* **67**, 157 (1995); see also <http://www.phys.psu.edu/~cteq/handbook/v1.1/handbook.pdf>.
- [9] K. Melnikov, *CERN Yellow Rep. School Proc.* **3**, 37 (2018).
- [10] T. van Ritbergen, J. A. M. Vermaseren and S. A. Larin, *Phys. Lett.* **B400**, 379 (1997), [hep-ph/9701390].
- [11] M. Czakon, *Nucl. Phys.* **B710**, 485 (2005), [hep-ph/0411261].
- [12] P. A. Baikov, K. G. Chetyrkin and J. H. Kühn, *Phys. Rev. Lett.* **118**, 8, 082002 (2017), [arXiv:1606.08659].
- [13] T. Luthe *et al.*, *JHEP* **07**, 127 (2016), [arXiv:1606.08662].
- [14] F. Herzog *et al.*, *JHEP* **02**, 090 (2017), [arXiv:1701.01404].
- [15] T. Luthe *et al.*, *JHEP* **10**, 166 (2017), [arXiv:1709.07718].
- [16] K. G. Chetyrkin *et al.*, *JHEP* **10**, 179 (2017), [Addendum: *JHEP*12,006(2017)], [arXiv:1709.08541].
- [17] W. A. Bardeen *et al.*, *Phys. Rev.* **D18**, 3998 (1978).
- [18] D. J. Gross and F. Wilczek, *Phys. Rev. Lett.* **30**, 1343 (1973), [,271(1973)].
- [19] H. D. Politzer, *Phys. Rev. Lett.* **30**, 1346 (1973), [,274(1973)].
- [20] Y. Schroder and M. Steinhauser, *JHEP* **01**, 051 (2006), [hep-ph/0512058].
- [21] K. G. Chetyrkin, J. H. Kuhn and C. Sturm, *Nucl. Phys.* **B744**, 121 (2006), [hep-ph/0512060].
- [22] A. G. Grozin *et al.*, *JHEP* **09**, 066 (2011), [arXiv:1107.5970].
- [23] M. Dalla Brida *et al.* (ALPHA), *Phys. Rev. Lett.* **117**, 18, 182001 (2016), [arXiv:1604.06193].
- [24] K. G. Chetyrkin, J. H. Kuhn and M. Steinhauser, *Comput. Phys. Commun.* **133**, 43 (2000), [hep-ph/0004189].
- [25] B. Schmidt and M. Steinhauser, *Comput. Phys. Commun.* **183**, 1845 (2012), [arXiv:1201.6149].
- [26] F. Herren and M. Steinhauser, *Comput. Phys. Commun.* **224**, 333 (2018), [arXiv:1703.03751].
- [27] A. V. Bednyakov, *Phys. Lett.* **B741**, 262 (2015), [arXiv:1410.7603].
- [28] M. Beneke, *Phys. Rept.* **317**, 1 (1999), [hep-ph/9807443].
- [29] M. Beneke *et al.*, *Phys. Lett.* **B775**, 63 (2017), [arXiv:1605.03609].
- [30] A. H. Hoang, C. Lepenik and M. Preisser, *JHEP* **09**, 099 (2017), [arXiv:1706.08526].
- [31] P. Marquard *et al.*, *Phys. Rev. Lett.* **114**, 14, 142002 (2015), [arXiv:1502.01030].
- [32] P. A. Baikov *et al.*, *Phys. Lett.* **B714**, 62 (2012), [arXiv:1206.1288].
- [33] K. G. Chetyrkin, J. H. Kuhn and A. Kwiatkowski (1996), [Phys. Rept.277,189(1996)], [hep-ph/9503396].
- [34] Y. Kiyo *et al.*, *Nucl. Phys.* **B823**, 269 (2009), [arXiv:0907.2120].
- [35] P. A. Baikov *et al.*, *Phys. Rev. Lett.* **108**, 222003 (2012), [arXiv:1201.5804].
- [36] P. A. Baikov, K. G. Chetyrkin and J. H. Kuhn, *Phys. Rev. Lett.* **101**, 012002 (2008), [arXiv:0801.1821].
- [37] F. Herzog *et al.*, *JHEP* **08**, 113 (2017), [arXiv:1707.01044].
- [38] V. A. Novikov *et al.*, *Nucl. Phys.* **B174**, 378 (1980).
- [39] H.-W. Lin *et al.*, *Phys. Rev.* **D91**, 054510 (2015), [arXiv:1402.1462]; C. Alexandrou *et al.*, *Phys. Rev.* **D92**, 014502 (2015), [arXiv:1504.07455].
- [40] H.-W. Lin *et al.*, *Prog. Part. Nucl. Phys.* **100**, 107 (2018), [arXiv:1711.07916].
- [41] C. Alexandrou *et al.*, *Phys. Rev. Lett.* **121**, 11, 112001 (2018), [arXiv:1803.02685].
- [42] J.-W. Chen *et al.* (2018), [arXiv:1803.04393].
- [43] K. Cichy, L. Del Debbio and T. Giani (2019), [arXiv:1907.06037].
- [44] G. C. Rossi and M. Testa, *Phys. Rev.* **D96**, 1, 014507 (2017), [arXiv:1706.04428].
- [45] J. Gao, L. Harland-Lang and J. Rojo, *Phys. Rept.* **742**, 1 (2018), [arXiv:1709.04922].
- [46] K. Kovařík, P. M. Nadolsky and D. E. Soper (2019), [arXiv:1905.06957].
- [47] J. Butterworth *et al.*, *J. Phys.* **G43**, 023001 (2016), [arXiv:1510.03865].
- [48] R. Abdul Khalek *et al.* (NNPDF) (2019), [arXiv:1905.04311].
- [49] R. Abdul Khalek *et al.* (NNPDF) (2019), [arXiv:1906.10698].
- [50] J. D. Bjorken and E. A. Paschos, *Phys. Rev.* **185**, 1975 (1969).
- [51] J. A. M. Vermaseren, A. Vogt and S. Moch, *Nucl. Phys.* **B724**, 3 (2005), [hep-ph/0504242].
- [52] S. Moch, J. A. M. Vermaseren and A. Vogt, *Nucl. Phys.* **B813**, 220 (2009), [arXiv:0812.4168].
- [53] J. Davies *et al.*, *PoS DIS2016*, 059 (2016), [arXiv:1606.08907].
- [54] E. Laenen *et al.*, *Nucl. Phys.* **B392**, 162 (1993); S. Riemersma, J. Smith and W. L. van Neerven, *Phys. Lett.* **B347**, 143 (1995), [hep-ph/9411431].

¹⁵We note, however, that in many such studies, like those based on exclusive states of jet multiplicities, the relevant energy scale of the measurement is not uniquely defined. For instance, in studies of the ratio of 3- to 2-jet cross sections at the LHC, the relevant scale was taken to be the average of the transverse momenta of the two leading jets [543], but could alternatively have been chosen to be the transverse momentum of the 3rd jet.

- [55] J. Blümlein *et al.* (2019), [arXiv:1903.06155].
- [56] A. Manohar *et al.*, Phys. Rev. Lett. **117**, 24, 242002 (2016), [arXiv:1607.04266].
- [57] J. C. Collins, D. E. Soper and G. F. Sterman, Adv. Ser. Direct. High Energy Phys. **5**, 1 (1989), [hep-ph/0409313].
- [58] J.C. Collins, *Foundations of Perturbative QCD*, Cambridge University Press, 2011.
- [59] G. C. Nayak, J.-W. Qiu and G. F. Sterman, Phys. Rev. **D72**, 114012 (2005), [hep-ph/0509021].
- [60] V. N. Gribov and L. N. Lipatov, Sov. J. Nucl. Phys. **15**, 438 (1972), [Yad. Fiz.15,781(1972)]; L. N. Lipatov, Sov. J. Nucl. Phys. **20**, 94 (1975), [Yad. Fiz.20,181(1974)]; G. Altarelli and G. Parisi, Nucl. Phys. **B126**, 298 (1977); Y. L. Dokshitzer, Sov. Phys. JETP **46**, 641 (1977), [Zh. Eksp. Teor. Fiz.73,1216(1977)].
- [61] G. Curci, W. Furmanski and R. Petronzio, Nucl. Phys. **B175**, 27 (1980); W. Furmanski and R. Petronzio, Phys. Lett. **97B**, 437 (1980).
- [62] A. Vogt, S. Moch and J. A. M. Vermaseren, Nucl. Phys. **B691**, 129 (2004), [hep-ph/0404111]; S. Moch, J. A. M. Vermaseren and A. Vogt, Nucl. Phys. **B688**, 101 (2004), [hep-ph/0403192].
- [63] S. Moch *et al.*, JHEP **10**, 041 (2017), [arXiv:1707.08315].
- [64] A. Vogt *et al.*, PoS **RADCOR2017**, 046 (2018), [arXiv:1801.06085].
- [65] A. Vogt *et al.*, PoS **LL2018**, 050 (2018), [arXiv:1808.08981].
- [66] S. Moch, J. A. M. Vermaseren and A. Vogt, Nucl. Phys. **B889**, 351 (2014), [arXiv:1409.5131].
- [67] D. de Florian, G. F. R. Sborlini and G. Rodrigo, Eur. Phys. J. **C76**, 5, 282 (2016), [arXiv:1512.00612]; D. de Florian, G. F. R. Sborlini and G. Rodrigo, JHEP **10**, 056 (2016), [arXiv:1606.02887].
- [68] R. S. Thorne, Phys. Rev. **D73**, 054019 (2006), [hep-ph/0601245].
- [69] S. Forte *et al.*, Nucl. Phys. **B834**, 116 (2010), [arXiv:1001.2312].
- [70] M. Guzzi *et al.*, Phys. Rev. **D86**, 053005 (2012), [arXiv:1108.5112].
- [71] V. S. Fadin, E. A. Kuraev and L. N. Lipatov, Phys. Lett. **60B**, 50 (1975).
- [72] I. I. Balitsky and L. N. Lipatov, Sov. J. Nucl. Phys. **28**, 822 (1978), [Yad. Fiz.28,1597(1978)].
- [73] R. D. Ball *et al.*, Eur. Phys. J. **C78**, 4, 321 (2018), [arXiv:1710.05935].
- [74] H. Abramowicz *et al.* (H1, ZEUS), Eur. Phys. J. **C75**, 12, 580 (2015), [arXiv:1506.06042].
- [75] H. Abdolmaleki *et al.* (xFitter Developers' Team), Eur. Phys. J. **C78**, 8, 621 (2018), [arXiv:1802.00064].
- [76] L. A. Harland-Lang *et al.*, Eur. Phys. J. **C76**, 4, 186 (2016), [arXiv:1601.03413].
- [77] T.-J. Hou *et al.* (2019), [arXiv:1908.11238].
- [78] J. C. Collins, D. E. Soper and G. F. Sterman, Nucl. Phys. **B261**, 104 (1985).
- [79] R. Hamberg, W. L. van Neerven and T. Matsuura, Nucl. Phys. **B359**, 343 (1991), [Erratum: Nucl. Phys. B644,403(2002)].
- [80] R. V. Harlander and W. B. Kilgore, Phys. Rev. Lett. **88**, 201801 (2002), [hep-ph/0201206].
- [81] O. Brein, A. Djouadi and R. Harlander, Phys. Lett. **B579**, 149 (2004), [hep-ph/0307206].
- [82] P. Bolzoni *et al.*, Phys. Rev. Lett. **105**, 011801 (2010), [arXiv:1003.4451].
- [83] S. Borowka *et al.*, Phys. Rev. Lett. **117**, 1, 012001 (2016), [Erratum: Phys. Rev. Lett.117,no.7,079901(2016)], [arXiv:1604.06447].
- [84] M. Czakon, P. Fiedler and A. Mitov, Phys. Rev. Lett. **110**, 252004 (2013), [arXiv:1303.6254].
- [85] T. Gehrmann *et al.*, Phys. Rev. Lett. **113**, 21, 212001 (2014), [arXiv:1408.5243].
- [86] F. Cascioli *et al.*, Phys. Lett. **B735**, 311 (2014), [arXiv:1405.2219].
- [87] M. Grazzini, S. Kallweit and M. Wiesemann, Eur. Phys. J. **C78**, 7, 537 (2018), [arXiv:1711.06631].
- [88] C. Anastasiou *et al.*, Phys. Rev. Lett. **114**, 212001 (2015), [arXiv:1503.06056]; C. Anastasiou *et al.*, JHEP **05**, 058 (2016), [arXiv:1602.00695].
- [89] B. Mistlberger, JHEP **05**, 028 (2018), [arXiv:1802.00833].
- [90] F. Dulat, B. Mistlberger and A. Pelloni, Phys. Rev. **D99**, 3, 034004 (2019), [arXiv:1810.09462].
- [91] F. A. Dreyer and A. Karlberg, Phys. Rev. Lett. **117**, 7, 072001 (2016), [arXiv:1606.00840].
- [92] D. de Florian *et al.* (LHC Higgs Cross Section Working Group) (2016), [arXiv:1610.07922].
- [93] M. Greco and A. Vicini, Nucl. Phys. **B415**, 386 (1994).
- [94] L. N. Lipatov, Sov. J. Nucl. Phys. **23**, 338 (1976), [Yad. Fiz.23,642(1976)].
- [95] E. A. Kuraev, L. N. Lipatov and V. S. Fadin, Sov. Phys. JETP **45**, 199 (1977), [Zh. Eksp. Teor. Fiz.72,377(1977)].
- [96] V. S. Fadin and L. N. Lipatov, Phys. Lett. **B429**, 127 (1998), [hep-ph/9802290].
- [97] M. Ciafaloni and G. Camici, Phys. Lett. **B430**, 349 (1998), [hep-ph/9803389].
- [98] G. Altarelli, R. D. Ball and S. Forte, Nucl. Phys. **B799**, 199 (2008), [arXiv:0802.0032].
- [99] M. Ciafaloni *et al.*, JHEP **08**, 046 (2007), [arXiv:0707.1453].
- [100] C. D. White and R. S. Thorne, Phys. Rev. **D75**, 034005 (2007), [hep-ph/0611204].
- [101] E. Iancu *et al.*, Phys. Lett. **B744**, 293 (2015), [arXiv:1502.05642].
- [102] N. Gromov, F. Levkovich-Maslyuk and G. Sizov, Phys. Rev. Lett. **115**, 25, 251601 (2015), [arXiv:1507.04010]; V. N. Velizhanin (2015), [arXiv:1508.02857]; S. Caron-Huot and M. Herranen, JHEP **02**, 058 (2018), [arXiv:1604.07417].
- [103] I. Balitsky, Nucl. Phys. **B463**, 99 (1996), [hep-ph/9509348].
- [104] Y. V. Kovchegov, Phys. Rev. **D60**, 034008 (1999), [hep-ph/9901281].
- [105] A. Hebecker, Phys. Rept. **331**, 1 (2000), [hep-ph/9905226].
- [106] A. V. Belitsky and A. V. Radyushkin, Phys. Rept. **418**, 1 (2005), [hep-ph/0504030].
- [107] E. Boos *et al.* (CompHEP), Nucl. Instrum. Meth. **A534**, 250 (2004), [hep-ph/0403113]; <http://compep.sinp.su.ru/>.
- [108] J. Alwall *et al.*, JHEP **07**, 079 (2014), [arXiv:1405.0301]; <https://launchpad.net/mg5amcnlo>.
- [109] M. L. Mangano *et al.*, JHEP **07**, 001 (2003), [hep-ph/0206293]; <http://cern.ch/mlm/alpgen/>.
- [110] T. Gleisberg and S. Hoeche, JHEP **12**, 039 (2008), [arXiv:0808.3674]; <https://sherpa.hepforge.org/trac/wiki>.
- [111] A. Cafarella, C. G. Papadopoulos and M. Worek, Comput. Phys. Commun. **180**, 1941 (2009), [arXiv:0710.2427]; <http://cern.ch/helac-phegas/>.
- [112] F. A. Berends and W. T. Giele, Nucl. Phys. **B306**, 759 (1988).
- [113] L. J. Dixon, in "QCD and beyond. Proceedings, Theoretical Advanced Study Institute in Elementary Particle Physics, TASI-95, Boulder, USA, June 4-30, 1995," 539-584 (1996), [hep-ph/9601359], URL <http://www-public.slac.stanford.edu/sciDoc/docMeta.aspx?slacPubNumber=SLAC-PUB-7106>.

- [114] R. Britto, F. Cachazo and B. Feng, Nucl. Phys. **B715**, 499 (2005), [hep-th/0412308].
- [115] F. Cachazo, P. Svrcek and E. Witten, JHEP **09**, 006 (2004), [hep-th/0403047].
- [116] S. Badger *et al.*, Phys. Rev. **D87**, 3, 034011 (2013), [arXiv:1206.2381].
- [117] S. Catani and M. H. Seymour, Nucl. Phys. **B485**, 291 (1997), [Erratum: Nucl. Phys.B510,503(1998)], [hep-ph/9605323].
- [118] S. Frixione, Z. Kunszt and A. Signer, Nucl. Phys. **B467**, 399 (1996), [hep-ph/9512328].
- [119] D. A. Kosower, Phys. Rev. **D57**, 5410 (1998), [hep-ph/9710213]; J. M. Campbell, M. A. Cullen and E. W. N. Glover, Eur. Phys. J. **C9**, 245 (1999), [hep-ph/9809429]; D. A. Kosower, Phys. Rev. **D71**, 045016 (2005), [hep-ph/0311272].
- [120] G. Ossola, C. G. Papadopoulos and R. Pittau, Nucl. Phys. **B763**, 147 (2007), [hep-ph/0609007].
- [121] R. Britto, F. Cachazo and B. Feng, Nucl. Phys. **B725**, 275 (2005), [hep-th/0412103].
- [122] R. K. Ellis *et al.*, Nucl. Phys. **B822**, 270 (2009), [arXiv:0806.3467].
- [123] C. F. Berger and D. Forde, Ann. Rev. Nucl. Part. Sci. **60**, 181 (2010), [arXiv:0912.3534].
- [124] F. Cascioli, P. Maierhofer and S. Pozzorini, Phys. Rev. Lett. **108**, 111601 (2012), [arXiv:1111.5206].
- [125] Z. Bern, L. J. Dixon and D. A. Kosower, Annals Phys. **322**, 1587 (2007), [arXiv:0704.2798].
- [126] R. K. Ellis *et al.*, Phys. Rept. **518**, 141 (2012), [arXiv:1105.4319].
- [127] G. Bevilacqua *et al.*, Comput. Phys. Commun. **184**, 986 (2013), [arXiv:1110.1499]; <http://cern.ch/helax-pegas/>.
- [128] G. Cullen *et al.*, Eur. Phys. J. **C74**, 8, 3001 (2014), [arXiv:1404.7096]; <http://gosam.hepforge.org/>.
- [129] S. Badger *et al.*, Comput. Phys. Commun. **184**, 1981 (2013), [arXiv:1209.0100]; <https://bitbucket.org/njet/wiki/Home/>.
- [130] F. Buccioni, S. Pozzorini and M. Zoller, Eur. Phys. J. **C78**, 1, 70 (2018), [arXiv:1710.11452]; <https://openloops.hepforge.org/>.
- [131] S. Actis *et al.*, Comput. Phys. Commun. **214**, 140 (2017), [arXiv:1605.01090].
- [132] T. Gleisberg *et al.*, JHEP **02**, 007 (2009), [arXiv:0811.4622]; <http://projects.hepforge.org/sherpa>.
- [133] Z. Nagy, Phys. Rev. **D68**, 094002 (2003), [hep-ph/0307268]; <http://www.desy.de/~znagy/Site/NLOJet++.html>.
- [134] J. M. Campbell and R. K. Ellis, Phys. Rev. **D62**, 114012 (2000), [hep-ph/0006304].
- [135] J. Baglio *et al.* (2011), [arXiv:1107.4038]; <http://www-itp.particle.uni-karlsruhe.de/~vbf/floweb>.
- [136] T. Binoth *et al.*, Eur. Phys. J. **C16**, 311 (2000), [hep-ph/9911340]; http://lapth.in2p3.fr/PHOX_FAMILY/.
- [137] Z. Bern *et al.*, PoS **LL2012**, 018 (2012), [arXiv:1210.6684].
- [138] T. Kluge, K. Rabbertz and M. Wobisch, *FastNLO: Fast pQCD calculations for PDF fits* (2006), [hep-ph/0609285], URL http://lss.fnal.gov/cgi-bin/find_paper.pl?conf-06-352; <http://fastnlo.hepforge.org/>.
- [139] T. Carli *et al.*, Eur. Phys. J. **C66**, 503 (2010), [arXiv:0911.2985]; <https://apllgrid.hepforge.org/>.
- [140] L. Del Debbio, N. P. Hartland and S. Schumann, Comput. Phys. Commun. **185**, 2115 (2014), [arXiv:1312.4460]; <http://mcgrid.hepforge.org/>.
- [141] V. Bertone *et al.*, JHEP **08**, 166 (2014), [arXiv:1406.7693]; <https://amcfast.hepforge.org/>.
- [142] G. Cullen, N. Greiner and G. Heinrich, Eur. Phys. J. **C73**, 4, 2388 (2013), [arXiv:1212.5154].
- [143] S. Kallweit *et al.*, JHEP **04**, 012 (2015), [arXiv:1412.5157].
- [144] A. Denner *et al.*, JHEP **04**, 018 (2015), [arXiv:1412.7421].
- [145] M. Chiesa, N. Greiner and F. Tramontano, J. Phys. **G43**, 1, 013002 (2016), [arXiv:1507.08579].
- [146] S. Frixione *et al.*, JHEP **06**, 184 (2015), [arXiv:1504.03446].
- [147] B. Biedermann *et al.*, Eur. Phys. J. **C77**, 492 (2017), [arXiv:1704.05783].
- [148] R. Frederix *et al.*, JHEP **07**, 185 (2018), [arXiv:1804.10017].
- [149] C. Anastasiou, R. Boughezal and F. Petriello, JHEP **04**, 003 (2009), [arXiv:0811.3458].
- [150] S. Dittmaier, A. Huss and C. Schwinn, Nucl. Phys. **B885**, 318 (2014), [arXiv:1403.3216].
- [151] S. Dittmaier, A. Huss and C. Schwinn, Nucl. Phys. **B904**, 216 (2016), [arXiv:1511.08016].
- [152] D. de Florian, M. Der and I. Fabre, Phys. Rev. **D98**, 9, 094008 (2018), [arXiv:1805.12214].
- [153] M. Bonetti, K. Melnikov and L. Tancredi, Phys. Rev. **D97**, 5, 056017 (2018), [Erratum: Phys. Rev. **D97**, no.9, 099906(2018)], [arXiv:1801.10403].
- [154] C. Anastasiou *et al.*, JHEP **03**, 162 (2019), [arXiv:1811.11211].
- [155] M. Bonetti, K. Melnikov and L. Tancredi, Phys. Rev. **D97**, 3, 034004 (2018), [arXiv:1711.11113].
- [156] Z. Bern *et al.*, Nucl. Phys. **B425**, 217 (1994), [hep-ph/9403226].
- [157] J. M. Campbell and E. W. N. Glover, Nucl. Phys. **B527**, 264 (1998), [hep-ph/9710255].
- [158] S. Catani and M. Grazzini, Phys. Lett. **B446**, 143 (1999), [hep-ph/9810389].
- [159] T. Binoth and G. Heinrich, Nucl. Phys. **B585**, 741 (2000), [hep-ph/0004013].
- [160] C. Anastasiou, K. Melnikov and F. Petriello, Phys. Rev. **D69**, 076010 (2004), [hep-ph/0311311].
- [161] A. Gehrmann-De Ridder, T. Gehrmann and E. W. N. Glover, JHEP **09**, 056 (2005), [hep-ph/0505111].
- [162] G. Somogyi, Z. Trocsanyi and V. Del Duca, JHEP **01**, 070 (2007), [hep-ph/0609042].
- [163] M. Czakon, Phys. Lett. **B693**, 259 (2010), [arXiv:1005.0274].
- [164] S. Catani and M. Grazzini, Phys. Rev. Lett. **98**, 222002 (2007), [hep-ph/0703012]; <http://theory.fi.infn.it/grazzini/codes.html>.
- [165] R. Boughezal *et al.*, Phys. Rev. Lett. **115**, 6, 062002 (2015), [arXiv:1504.02131].
- [166] J. Gaunt *et al.*, JHEP **09**, 058 (2015), [arXiv:1505.04794].
- [167] M. Cacciari *et al.*, Phys. Rev. Lett. **115**, 8, 082002 (2015), [Erratum: Phys. Rev. Lett. **120**, no.13, 139901(2018)], [arXiv:1506.02660].
- [168] A. Gehrmann-De Ridder *et al.*, Phys. Rev. Lett. **99**, 132002 (2007), [arXiv:0707.1285]; A. Gehrmann-De Ridder *et al.*, JHEP **12**, 094 (2007), [arXiv:0711.4711]; A. Gehrmann-De Ridder *et al.*, Phys. Rev. Lett. **100**, 172001 (2008), [arXiv:0802.0813].
- [169] A. Gehrmann-De Ridder *et al.*, Comput. Phys. Commun. **185**, 3331 (2014), [arXiv:1402.4140]; <https://eerad3.epforge.org/>.
- [170] S. Weinzierl, Phys. Rev. Lett. **101**, 162001 (2008), [arXiv:0807.3241]; S. Weinzierl, JHEP **06**, 041 (2009), [arXiv:0904.1077].
- [171] J. Currie, T. Gehrmann and J. Niehues, Phys. Rev. Lett. **117**, 4, 042001 (2016), [arXiv:1606.03991].
- [172] J. Currie *et al.*, JHEP **05**, 209 (2018), [arXiv:1803.09973].

- [173] T. Gehrmann *et al.*, Phys. Lett. **B792**, 182 (2019), [arXiv:1812.06104].
- [174] K. Melnikov and F. Petriello, Phys. Rev. **D74**, 114017 (2006), [hep-ph/0609070]; <http://gate.hep.anl.gov/fpetriello/FEWZ.html>.
- [175] S. Catani *et al.*, Phys. Rev. Lett. **103**, 082001 (2009), [arXiv:0903.2120]; <http://theory.fi.infn.it/gazzani/dy.html>.
- [176] C. Anastasiou, K. Melnikov and F. Petriello, Nucl. Phys. **B724**, 197 (2005), [hep-ph/0501130]; <http://www.phys.ethz.ch/~pheno/fehipro/>.
- [177] M. Grazzini *et al.*, JHEP **05**, 139 (2017), [arXiv:1703.09065].
- [178] S. Catani *et al.*, Phys. Rev. Lett. **108**, 072001 (2012), [Erratum: Phys. Rev. Lett.117,no.8,089901(2016)], [arXiv:1110.2375].
- [179] J. M. Campbell *et al.*, JHEP **07**, 148 (2016), [arXiv:1603.02663].
- [180] M. Grazzini *et al.*, Phys. Lett. **B731**, 204 (2014), [arXiv:1309.7000].
- [181] M. Grazzini, S. Kallweit and D. Rathlev, JHEP **07**, 085 (2015), [arXiv:1504.01330].
- [182] R. Boughezal *et al.*, Eur. Phys. J. **C77**, 1, 7 (2017), [arXiv:1605.08011].
- [183] J. M. Campbell, R. K. Ellis and C. Williams, Phys. Rev. Lett. **118**, 22, 222001 (2017), [arXiv:1612.04333].
- [184] X. Chen *et al.*, Submitted to: J. High Energy Phys. (2019), [arXiv:1904.01044].
- [185] J. M. Campbell, R. K. Ellis and C. Williams, Phys. Rev. **D96**, 1, 014037 (2017), [arXiv:1703.10109].
- [186] A. Gehrmann-De Ridder *et al.*, Phys. Rev. Lett. **117**, 2, 022001 (2016), [arXiv:1507.02850].
- [187] R. Boughezal *et al.*, Phys. Rev. Lett. **116**, 15, 152001 (2016), [arXiv:1512.01291].
- [188] R. Boughezal *et al.*, Phys. Rev. Lett. **115**, 8, 082003 (2015), [arXiv:1504.07922].
- [189] R. Boughezal *et al.*, Phys. Lett. **B748**, 5 (2015), [arXiv:1505.03893].
- [190] F. Caola, K. Melnikov and M. Schulze, Phys. Rev. **D92**, 7, 074032 (2015), [arXiv:1508.02684].
- [191] X. Chen *et al.*, JHEP **10**, 066 (2016), [arXiv:1607.08817].
- [192] G. Ferrera, M. Grazzini and F. Tramontano, Phys. Rev. Lett. **107**, 152003 (2011), [arXiv:1107.1164].
- [193] G. Ferrera, M. Grazzini and F. Tramontano, Phys. Lett. **B740**, 51 (2015), [arXiv:1407.4747].
- [194] M. Brucherseifer, F. Caola and K. Melnikov, Phys. Lett. **B736**, 58 (2014), [arXiv:1404.7116].
- [195] E. L. Berger *et al.*, Phys. Rev. **D94**, 7, 071501 (2016), [arXiv:1606.08463].
- [196] M. Czakon, P. Fiedler and A. Mitov, Phys. Rev. Lett. **115**, 5, 052001 (2015), [arXiv:1411.3007].
- [197] J. Currie, E. W. N. Glover and J. Pires, Phys. Rev. Lett. **118**, 7, 072002 (2017), [arXiv:1611.01460].
- [198] D. de Florian and J. Mazzitelli, Phys. Rev. Lett. **111**, 201801 (2013), [arXiv:1309.6594].
- [199] J. Cruz-Martinez *et al.*, Phys. Lett. **B781**, 672 (2018), [arXiv:1802.02445].
- [200] T. Liu, K. Melnikov and A. A. Penin (2019), [arXiv:1906.10899].
- [201] *Les Houches 2017: Physics at TeV Colliders Standard Model Working Group Report* (2018), [arXiv:1803.07977], URL <http://lss.fnal.gov/archive/2018/conf/fermilab-conf-18-122-cd-t.pdf>.
- [202] Y. L. Dokshitzer, D. Diakonov and S. I. Troian, Phys. Rept. **58**, 269 (1980).
- [203] G. Parisi and R. Petronzio, Nucl. Phys. **B154**, 427 (1979).
- [204] G. Curci, M. Greco and Y. Srivastava, Nucl. Phys. **B159**, 451 (1979).
- [205] A. Bassetto, M. Ciafaloni and G. Marchesini, Nucl. Phys. **B163**, 477 (1980).
- [206] J. C. Collins and D. E. Soper, Nucl. Phys. **B193**, 381 (1981), [Erratum: Nucl. Phys.B213,545(1983)].
- [207] J. C. Collins and D. E. Soper, Nucl. Phys. **B197**, 446 (1982).
- [208] J. Kodaira and L. Trentadue, Phys. Lett. **112B**, 66 (1982).
- [209] J. Kodaira and L. Trentadue, Phys. Lett. **123B**, 335 (1983).
- [210] J. C. Collins, D. E. Soper and G. F. Sterman, Nucl. Phys. **B250**, 199 (1985).
- [211] S. Catani *et al.*, Nucl. Phys. **B407**, 3 (1993).
- [212] C. W. Bauer *et al.*, Phys. Rev. **D63**, 114020 (2001), [hep-ph/0011336].
- [213] C. W. Bauer, D. Pirjol and I. W. Stewart, Phys. Rev. **D65**, 054022 (2002), [hep-ph/0109045].
- [214] T. Becher, A. Broggio and A. Ferroglia, Lect. Notes Phys. **896**, pp.1 (2015), [arXiv:1410.1892].
- [215] S. Catani *et al.*, Phys. Lett. **B269**, 432 (1991).
- [216] N. Brown and W. J. Stirling, Phys. Lett. **B252**, 657 (1990).
- [217] W. Bartel *et al.* (JADE), Z. Phys. **C33**, 23 (1986), [53(1986)].
- [218] N. Kidonakis, G. Oderda and G. F. Sterman, Nucl. Phys. **B531**, 365 (1998), [hep-ph/9803241].
- [219] R. Bonciani *et al.*, Phys. Lett. **B575**, 268 (2003), [hep-ph/0307035].
- [220] A. Banfi, G. P. Salam and G. Zanderighi, JHEP **03**, 073 (2005), [hep-ph/0407286].
- [221] D. de Florian and M. Grazzini, Phys. Rev. Lett. **85**, 4678 (2000), [hep-ph/0008152].
- [222] G. Bozzi *et al.*, Nucl. Phys. **B737**, 73 (2006), [hep-ph/0508068]; <http://theory.fi.infn.it/grazzini/codes.html>.
- [223] G. Bozzi *et al.*, Phys. Lett. **B696**, 207 (2011), [arXiv:1007.2351].
- [224] T. Becher and M. Neubert, Eur. Phys. J. **C71**, 1665 (2011), [arXiv:1007.4005].
- [225] T. Becher, M. Neubert, and D. Wilhelm, <http://cute.hepforge.org/>.
- [226] D. de Florian *et al.*, JHEP **06**, 132 (2012), [arXiv:1203.6321]; <http://theory.fi.infn.it/grazzini/codes.html>.
- [227] C. Balazs and C. P. Yuan, Phys. Rev. **D56**, 5558 (1997), [hep-ph/9704258].
- [228] S. Catani *et al.*, JHEP **12**, 047 (2015), [arXiv:1507.06937].
- [229] A. Banfi *et al.*, Phys. Lett. **B715**, 152 (2012), [arXiv:1205.4760].
- [230] M. Grazzini *et al.*, JHEP **08**, 154 (2015), [arXiv:1507.02565].
- [231] D. de Florian and M. Grazzini, Nucl. Phys. **B704**, 387 (2005), [hep-ph/0407241].
- [232] T. Becher and G. Bell, JHEP **11**, 126 (2012), [arXiv:1210.0580].
- [233] A. Banfi *et al.*, Phys. Rev. Lett. **109**, 202001 (2012), [arXiv:1206.4998]; T. Becher, M. Neubert and L. Rothen, JHEP **10**, 125 (2013), [arXiv:1307.0025].
- [234] I. W. Stewart *et al.*, Phys. Rev. **D89**, 5, 054001 (2014), [arXiv:1307.1808].
- [235] I. W. Stewart, F. J. Tackmann and W. J. Waalewijn, Phys. Rev. Lett. **106**, 032001 (2011), [arXiv:1005.4060].
- [236] Y.-T. Chien *et al.*, Phys. Rev. **D87**, 1, 014010 (2013), [arXiv:1208.0010]; T. T. Jouttenus *et al.*, Phys. Rev. **D88**, 5, 054031 (2013), [arXiv:1302.0846].

- [237] M. Dasgupta *et al.*, JHEP **10**, 126 (2012), [arXiv:1207.1640].
- [238] V. Ahrens *et al.*, JHEP **09**, 097 (2010), [arXiv:1003.5827].
- [239] M. Aliev *et al.*, Comput. Phys. Commun. **182**, 1034 (2011), [arXiv:1007.1327].
- [240] N. Kidonakis, Phys. Rev. **D82**, 114030 (2010), [arXiv:1009.4935].
- [241] T. Becher, C. Lorentzen and M. D. Schwartz, Phys. Rev. Lett. **108**, 012001 (2012), [arXiv:1106.4310].
- [242] T. Becher *et al.*, Eur. Phys. J. **C75**, 4, 154 (2015), [arXiv:1412.8408].
- [243] E. Gerwick *et al.*, JHEP **02**, 106 (2015), [arXiv:1411.7325].
- [244] A. Banfi *et al.*, JHEP **05**, 102 (2015), [arXiv:1412.2126].
- [245] T. Becher and M. D. Schwartz, JHEP **07**, 034 (2008), [arXiv:0803.0342].
- [246] A. H. Hoang *et al.*, Phys. Rev. **D91**, 9, 094017 (2015), [arXiv:1411.6633].
- [247] Y.-T. Chien and M. D. Schwartz, JHEP **08**, 058 (2010), [arXiv:1005.1644].
- [248] P. F. Monni, T. Gehrmann and G. Luisoni, JHEP **08**, 010 (2011), [arXiv:1105.4560].
- [249] W. Bizon *et al.*, JHEP **02**, 108 (2018), [arXiv:1705.09127].
- [250] W. Bizon *et al.* (2019), [arXiv:1905.05171].
- [251] S. Catani *et al.*, Nucl. Phys. **B888**, 75 (2014), [arXiv:1405.4827].
- [252] S. Fleming *et al.*, Phys. Rev. **D77**, 074010 (2008), [hep-ph/0703207].
- [253] A. H. Hoang, P. Pietrulewicz and D. Samitz, Phys. Rev. **D93**, 3, 034034 (2016), [arXiv:1508.04323].
- [254] A. Banfi *et al.*, JHEP **04**, 049 (2016), [arXiv:1511.02886].
- [255] A. J. Larkoski and I. Moult, Phys. Rev. **D93**, 014017 (2016), [arXiv:1510.08459].
- [256] G. Lustermsans, W. J. Waalewijn and L. Zeune, Phys. Lett. **B762**, 447 (2016), [arXiv:1605.02740].
- [257] C. Muselli, S. Forte and G. Ridolfi, JHEP **03**, 106 (2017), [arXiv:1701.01464].
- [258] M. Bonvini and S. Marzani, Phys. Rev. Lett. **120**, 202003 (2018), [arXiv:1802.07758].
- [259] M. Procura, W. J. Waalewijn and L. Zeune, JHEP **10**, 098 (2018), [arXiv:1806.10622].
- [260] G. Lustermsans *et al.*, JHEP **03**, 124 (2019), [arXiv:1901.03331].
- [261] I. Feige *et al.*, Phys. Rev. Lett. **109**, 092001 (2012), [arXiv:1204.3898].
- [262] M. Dasgupta *et al.*, JHEP **09**, 029 (2013), [arXiv:1307.0007].
- [263] A. J. Larkoski *et al.*, JHEP **05**, 146 (2014), [arXiv:1402.2657].
- [264] M. Dasgupta, A. Powling and A. Siodmok, JHEP **08**, 079 (2015), [arXiv:1503.01088].
- [265] A. J. Larkoski, I. Moult and D. Neill, JHEP **05**, 117 (2016), [arXiv:1507.03018].
- [266] C. Frye *et al.*, JHEP **07**, 064 (2016), [arXiv:1603.09338].
- [267] A. J. Larkoski, I. Moult and D. Neill, JHEP **02**, 144 (2018), [arXiv:1710.00014].
- [268] A. J. Larkoski, I. Moult and B. Nachman (2017), [arXiv:1709.04464].
- [269] S. Marzani, G. Soyez and M. Spannowsky (2019), [Lect. Notes Phys.958,pp.(2019)], [arXiv:1901.10342].
- [270] Yu.L. Dokshitzer *et al.*, "Basics of perturbative QCD," Gif-sur-Yvette, France: Éditions frontières (1991), see also <http://www.lpthe.jussieu.fr/~yuri/BPQCD/cover.html>.
- [271] T. Sjostrand *et al.*, Comput. Phys. Commun. **135**, 238 (2001), [hep-ph/0010017].
- [272] T. Sjostrand, S. Mrenna and P. Z. Skands, JHEP **05**, 026 (2006), [hep-ph/0603175]; <http://projects.hepforge.org/pythia6/>.
- [273] T. Sjostrand *et al.*, Comput. Phys. Commun. **191**, 159 (2015), [arXiv:1410.3012]; <http://home.thep.lu.se/~torbjorn/Pythia.html>.
- [274] B. R. Webber, Nucl. Phys. **B238**, 492 (1984).
- [275] G. Corcella *et al.*, JHEP **01**, 010 (2001), [hep-ph/0011363]; <http://www.hep.phy.cam.ac.uk/theory/webber/Herwig/>.
- [276] M. Bahr *et al.*, Eur. Phys. J. **C58**, 639 (2008), [arXiv:0803.0883]; <http://projects.hepforge.org/herwig/>.
- [277] L. Lonnblad, Comput. Phys. Commun. **71**, 15 (1992).
- [278] A. Buckley *et al.*, Phys. Rept. **504**, 145 (2011), [arXiv:1101.2599].
- [279] B. Andersson *et al.*, Phys. Rept. **97**, 31 (1983).
- [280] T. Sjostrand, Nucl. Phys. **B248**, 469 (1984).
- [281] J. Bellm *et al.* (2019), [arXiv:1903.12563].
- [282] T. Sjostrand and M. van Zijl, Phys. Rev. **D36**, 2019 (1987).
- [283] S. Catani *et al.*, JHEP **11**, 063 (2001), [hep-ph/0109231].
- [284] J. Alwall *et al.*, Eur. Phys. J. **C53**, 473 (2008), [arXiv:0706.2569].
- [285] S. Frixione and B. R. Webber, JHEP **06**, 029 (2002), [hep-ph/0204244].
- [286] P. Nason, JHEP **11**, 040 (2004), [hep-ph/0409146].
- [287] S. Alioli *et al.*, JHEP **06**, 043 (2010), [arXiv:1002.2581]; <http://powhegbox.mib.infn.it/>.
- [288] S. Plätzer, JHEP **08**, 114 (2013), [arXiv:1211.5467]; R. Frederix and S. Frixione, JHEP **12**, 061 (2012), [arXiv:1209.6215]; K. Hamilton *et al.*, JHEP **05**, 082 (2013), [arXiv:1212.4504].
- [289] K. Hamilton *et al.*, JHEP **10**, 222 (2013), [arXiv:1309.0017]; A. Karlberg, E. Re and G. Zanderighi, JHEP **09**, 134 (2014), [arXiv:1407.2940]; S. Höche, Y. Li and S. Prestel, Phys. Rev. **D91**, 7, 074015 (2015), [arXiv:1405.3607]; S. Höche, Y. Li and S. Prestel, Phys. Rev. **D90**, 5, 054011 (2014), [arXiv:1407.3773]; S. Alioli *et al.*, Phys. Rev. **D92**, 9, 094020 (2015), [arXiv:1508.01475]; P. F. Monni *et al.* (2019), [arXiv:1908.06987].
- [290] W. Astill *et al.*, JHEP **06**, 154 (2016), [arXiv:1603.01620].
- [291] W. Astill *et al.*, JHEP **11**, 157 (2018), [arXiv:1804.08141].
- [292] E. Re, M. Wiesemann and G. Zanderighi, JHEP **12**, 121 (2018), [arXiv:1805.09857].
- [293] M. Cacciari *et al.*, JHEP **04**, 068 (2004), [hep-ph/0303085].
- [294] P. M. Stevenson, Phys. Lett. **100B**, 61 (1981).
- [295] P. M. Stevenson, Phys. Rev. **D23**, 2916 (1981).
- [296] G. Grunberg, Phys. Rev. **D29**, 2315 (1984).
- [297] S. J. Brodsky, G. P. Lepage and P. B. Mackenzie, Phys. Rev. **D28**, 228 (1983).
- [298] S.-Q. Wang *et al.* (2019), [arXiv:1908.00060].
- [299] M. Cacciari and N. Houdeau, JHEP **09**, 039 (2011), [arXiv:1105.5152].
- [300] A. David and G. Passarino, Phys. Lett. **B726**, 266 (2013), [arXiv:1307.1843].
- [301] E. Bagnaschi *et al.*, JHEP **02**, 133 (2015), [arXiv:1409.5036].
- [302] M. Dasgupta *et al.*, JHEP **06**, 057 (2016), [arXiv:1602.01110].
- [303] J. Currie *et al.*, JHEP **10**, 155 (2018), [arXiv:1807.03692].
- [304] G. Soyez *et al.*, Phys. Rev. Lett. **110**, 16, 162001 (2013), [arXiv:1211.2811].

- [305] M. Dasgupta and G. P. Salam, *J. Phys.* **G30**, R143 (2004), [hep-ph/0312283].
- [306] S. Moretti, L. Lonnblad and T. Sjostrand, *JHEP* **08**, 001 (1998), [hep-ph/9804296].
- [307] G. P. Salam, *Eur. Phys. J.* **C67**, 637 (2010), [arXiv:0906.1833].
- [308] S. D. Ellis *et al.*, *Prog. Part. Nucl. Phys.* **60**, 484 (2008), [arXiv:0712.2447].
- [309] M. Cacciari, *Int. J. Mod. Phys.* **A30**, 31, 1546001 (2015), [arXiv:1509.02272].
- [310] G. P. Salam and G. Soyez, *JHEP* **05**, 086 (2007), [arXiv:0704.0292].
- [311] S. Catani *et al.*, *Nucl. Phys.* **B406**, 187 (1993).
- [312] S. D. Ellis and D. E. Soper, *Phys. Rev.* **D48**, 3160 (1993), [hep-ph/9305266].
- [313] Y. L. Dokshitzer *et al.*, *JHEP* **08**, 001 (1997), [hep-ph/9707323].
- [314] M. Wobisch and T. Wengler, in “Monte Carlo generators for HERA physics. Proceedings, Workshop, Hamburg, Germany, 1998-1999,” 270–279 (1998), [hep-ph/9907280].
- [315] M. Cacciari, G. P. Salam and G. Soyez, *JHEP* **04**, 063 (2008), [arXiv:0802.1189].
- [316] S. Bethke *et al.*, *Nucl. Phys.* **B370**, 310 (1992), [Erratum: *Nucl. Phys.* B523,681(1998)].
- [317] M. Cacciari and G. P. Salam, *Phys. Lett.* **B641**, 57 (2006), [hep-ph/0512210]; M. Cacciari, G. P. Salam and G. Soyez, *Eur. Phys. J.* **C72**, 1896 (2012), [arXiv:1111.6097].
- [318] S. Brandt *et al.*, *Phys. Lett.* **12**, 57 (1964).
- [319] E. Farhi, *Phys. Rev. Lett.* **39**, 1587 (1977).
- [320] O. Biebel, *Phys. Rept.* **340**, 165 (2001).
- [321] S. Kluth, *Rept. Prog. Phys.* **69**, 1771 (2006), [hep-ex/0603011].
- [322] C. L. Basham *et al.*, *Phys. Rev. Lett.* **41**, 1585 (1978).
- [323] A. Ali, E. Pietarinen and W. J. Stirling, *Phys. Lett.* **141B**, 447 (1984).
- [324] I. W. Stewart, F. J. Tackmann and W. J. Waalewijn, *Phys. Rev. Lett.* **105**, 092002 (2010), [arXiv:1004.2489].
- [325] A. Banfi, G. P. Salam and G. Zanderighi, *JHEP* **08**, 062 (2004), [hep-ph/0407287].
- [326] A. Banfi, G. P. Salam and G. Zanderighi, *JHEP* **06**, 038 (2010), [arXiv:1001.4082].
- [327] T. Becher, X. Garcia i Tormo and J. Piclum, *Phys. Rev.* **D93**, 5, 054038 (2016), [Erratum: *Phys. Rev.* D93,no.7,079905(2016)], [arXiv:1512.00022].
- [328] A. Gao *et al.*, *Phys. Rev. Lett.* **123**, 6, 062001 (2019), [arXiv:1901.04497].
- [329] T. Aaltonen *et al.* (CDF), *Phys. Rev.* **D83**, 112007 (2011), [arXiv:1103.5143].
- [330] G. Aad *et al.* (ATLAS), *Eur. Phys. J.* **C72**, 2211 (2012), [arXiv:1206.2135].
- [331] G. Aad *et al.* (ATLAS), *Phys. Rev.* **D88**, 3, 032004 (2013), [arXiv:1207.6915].
- [332] G. Aad *et al.* (ATLAS), *Phys. Lett.* **B750**, 427 (2015), [arXiv:1508.01579].
- [333] G. Aad *et al.* (ATLAS), *Eur. Phys. J.* **C76**, 7, 375 (2016), [arXiv:1602.08980].
- [334] M. Aaboud *et al.* (ATLAS), *Eur. Phys. J.* **C77**, 12, 872 (2017), [arXiv:1707.02562].
- [335] M. Aaboud *et al.* (ATLAS), *Phys. Rev.* **D98**, 9, 092004 (2018), [arXiv:1805.04691].
- [336] V. Khachatryan *et al.* (CMS), *Phys. Lett.* **B699**, 48 (2011), [arXiv:1102.0068].
- [337] S. Chatrchyan *et al.* (CMS), *Phys. Lett.* **B722**, 238 (2013), [arXiv:1301.1646].
- [338] V. Khachatryan *et al.* (CMS), *JHEP* **10**, 87 (2014), [arXiv:1407.2856].
- [339] A. M. Sirunyan *et al.* (CMS), *JHEP* **12**, 117 (2018), [arXiv:1811.00588].
- [340] S. Chatrchyan *et al.* (CMS), *Phys. Lett.* **B730**, 243 (2014), [arXiv:1310.0878].
- [341] G. Aad *et al.* (ATLAS), *Phys. Rev.* **D83**, 052003 (2011), [arXiv:1101.0070].
- [342] S. Chatrchyan *et al.* (CMS), *JHEP* **06**, 160 (2012), [arXiv:1204.3170].
- [343] B. B. Abelev *et al.* (ALICE), *Phys. Rev.* **D91**, 11, 112012 (2015), [arXiv:1411.4969].
- [344] G. Aad *et al.* (ATLAS), *Eur. Phys. J.* **C73**, 12, 2676 (2013), [arXiv:1201.5749].
- [345] C. Glasman (H1, ZEUS), *Nucl. Phys. Proc. Suppl.* **191**, 121 (2009), [arXiv:0812.0757].
- [346] T. Carli, K. Rabbertz and S. Schumann, in T. Schörner-Sadenius, editor, “The Large Hadron Collider: Harvest of Run 1,” 139–194 (2015), [arXiv:1506.03239].
- [347] A. Abdesselam *et al.*, *Eur. Phys. J.* **C71**, 1661 (2011), [arXiv:1012.5412].
- [348] D. Krohn, J. Thaler and L.-T. Wang, *JHEP* **02**, 084 (2010), [arXiv:0912.1342].
- [349] A. Altheimer *et al.*, *J. Phys.* **G39**, 063001 (2012), [arXiv:1201.0008].
- [350] A. Altheimer *et al.*, *Eur. Phys. J.* **C74**, 3, 2792 (2014), [arXiv:1311.2708].
- [351] P. C. Stichel and W. J. Zakrzewski, *Eur. Phys. J.* **C75**, 1, 9 (2015), [arXiv:1409.1363].
- [352] D. Adams *et al.*, *Eur. Phys. J.* **C75**, 9, 409 (2015), [arXiv:1504.00679].
- [353] T. Schorner-Sadenius, *Eur. Phys. J.* **C72**, 2060 (2012), [Erratum: *Eur. Phys. J.* C72,2133(2012)].
- [354] J. M. Campbell, J. W. Huston and W. J. Stirling, *Rept. Prog. Phys.* **70**, 89 (2007), [hep-ph/0611148].
- [355] M. L. Mangano, *Phys. Usp.* **53**, 109 (2010), [*Usp. Fiz. Nauk*180,113(2010)].
- [356] J. M. Butterworth, G. Dissertori and G. P. Salam, *Ann. Rev. Nucl. Part. Sci.* **62**, 387 (2012), [arXiv:1202.0583].
- [357] J. Currie *et al.*, *JHEP* **07**, 018 (2017), [arXiv:1703.05977].
- [358] M. Klasen, G. Kramer and M. Michael, *Phys. Rev.* **D89**, 7, 074032 (2014), [arXiv:1310.1724].
- [359] T. Carli, T. Gehrmann and S. Hoeche, *Eur. Phys. J.* **C67**, 73 (2010), [arXiv:0912.3715].
- [360] S. Chekanov *et al.* (ZEUS), *Nucl. Phys.* **B792**, 1 (2008), [arXiv:0707.3749].
- [361] S. Chekanov *et al.* (ZEUS), *Phys. Rev.* **D76**, 072011 (2007), [arXiv:0706.3809].
- [362] A. Aktas *et al.* (H1), *Phys. Lett.* **B639**, 21 (2006), [hep-ex/0603014].
- [363] H. Abramowicz *et al.* (ZEUS), *Eur. Phys. J.* **C71**, 1659 (2011), [arXiv:1104.5444].
- [364] H. Abramowicz *et al.* (ZEUS), *Nucl. Phys.* **B864**, 1 (2012), [arXiv:1205.6153].
- [365] F. D. Aaron *et al.* (H1), *Eur. Phys. J.* **C65**, 363 (2010), [arXiv:0904.3870].
- [366] F. D. Aaron *et al.* (H1), *Eur. Phys. J.* **C54**, 389 (2008), [arXiv:0711.2606].
- [367] S. Chekanov *et al.* (ZEUS), *Eur. Phys. J.* **C52**, 515 (2007), [arXiv:0707.3093].
- [368] S. Chekanov *et al.* (ZEUS), *Phys. Rev.* **D78**, 032004 (2008), [arXiv:0802.3955].
- [369] H. Abramowicz *et al.* (ZEUS), *Eur. Phys. J.* **C70**, 965 (2010), [arXiv:1010.6167].

- [370] H. Abramowicz *et al.* (ZEUS), Phys. Lett. **B691**, 127 (2010), [arXiv:1003.2923].
- [371] S. Chekanov *et al.* (ZEUS), Phys. Rev. **D85**, 052008 (2012), [arXiv:0808.3783].
- [372] F. D. Aaron *et al.* (H1), Eur. Phys. J. **C67**, 1 (2010), [arXiv:0911.5678].
- [373] V. Andreev *et al.* (H1), Eur. Phys. J. **C75**, 2, 65 (2015), [arXiv:1406.4709].
- [374] V. Andreev *et al.* (H1), Eur. Phys. J. **C77**, 11, 791 (2017), [arXiv:1709.07251].
- [375] <http://twiki.cern.ch/twiki/bin/view/CMSPublic/PhysicsResultsCombined>.
- [376] <http://atlas.web.cern.ch/Atlas/GROUPS/PHYSICS/CombinedSummaryPlots/SM>.
- [377] A. Abulencia *et al.* (CDF), Phys. Rev. **D75**, 092006 (2007), [Erratum: Phys. Rev. **D75**, 119901(2007)], [hep-ex/0701051].
- [378] T. Aaltonen *et al.* (CDF), Phys. Rev. **D78**, 052006 (2008), [Erratum: Phys. Rev. **D79**, 119902(2009)], [arXiv:0807.2204].
- [379] V. M. Abazov *et al.* (D0), Phys. Rev. Lett. **101**, 062001 (2008), [arXiv:0802.2400].
- [380] V. M. Abazov *et al.* (D0), Phys. Rev. **D85**, 052006 (2012), [arXiv:1110.3771].
- [381] B. Abelev *et al.* (ALICE), Phys. Lett. **B722**, 262 (2013), [arXiv:1301.3475].
- [382] G. Aad *et al.* (ATLAS), Eur. Phys. J. **C73**, 8, 2509 (2013), [arXiv:1304.4739].
- [383] G. Aad *et al.* (ATLAS), JHEP **02**, 153 (2015), [Erratum: JHEP09,141(2015)], [arXiv:1410.8857].
- [384] M. Aaboud *et al.* (ATLAS), JHEP **09**, 020 (2017), [arXiv:1706.03192].
- [385] V. Khachatryan *et al.* (CMS), Eur. Phys. J. **C76**, 5, 265 (2016), [arXiv:1512.06212].
- [386] S. Chatrchyan *et al.* (CMS), Phys. Rev. **D87**, 11, 112002 (2013), [Erratum: Phys. Rev. **D87**, no.11, 119902(2013)], [arXiv:1212.6660].
- [387] V. Khachatryan *et al.* (CMS), JHEP **03**, 156 (2017), [arXiv:1609.05331].
- [388] V. Khachatryan *et al.* (CMS), Eur. Phys. J. **C76**, 8, 451 (2016), [arXiv:1605.04436].
- [389] M. Aaboud *et al.* (ATLAS), JHEP **05**, 195 (2018), [arXiv:1711.02692].
- [390] A. Schwartzman, Int. J. Mod. Phys. **A30**, 31, 1546002 (2015), [arXiv:1509.05459].
- [391] J. Rojo, Int. J. Mod. Phys. **A30**, 1546005 (2015), [arXiv:1410.7728].
- [392] G. Aad *et al.* (ATLAS), JHEP **05**, 059 (2014), [arXiv:1312.3524].
- [393] A. M. Sirunyan *et al.* (CMS), Eur. Phys. J. **C77**, 11, 746 (2017), [arXiv:1705.02628].
- [394] T. Aaltonen *et al.* (CDF), Phys. Rev. **D79**, 112002 (2009), [arXiv:0812.4036].
- [395] V. M. Abazov *et al.* (D0), Phys. Rev. Lett. **103**, 191803 (2009), [arXiv:0906.4819].
- [396] S. Chatrchyan *et al.* (CMS), JHEP **05**, 055 (2012), [arXiv:1202.5535].
- [397] V. Khachatryan *et al.* (CMS), Phys. Lett. **B746**, 79 (2015), [arXiv:1411.2646].
- [398] A. M. Sirunyan *et al.* (CMS), JHEP **07**, 013 (2017), [arXiv:1703.09986].
- [399] G. Aad *et al.* (ATLAS), JHEP **01**, 029 (2013), [arXiv:1210.1718].
- [400] M. Aaboud *et al.* (ATLAS), Phys. Rev. **D96**, 5, 052004 (2017), [arXiv:1703.09127].
- [401] V. M. Abazov *et al.* (D0), Phys. Rev. Lett. **94**, 221801 (2005), [hep-ex/0409040].
- [402] V. M. Abazov *et al.* (D0), Phys. Lett. **B721**, 212 (2013), [arXiv:1212.1842].
- [403] G. Aad *et al.* (ATLAS), Phys. Rev. Lett. **106**, 172002 (2011), [arXiv:1102.2696].
- [404] V. Khachatryan *et al.* (CMS), Phys. Rev. Lett. **106**, 122003 (2011), [arXiv:1101.5029].
- [405] V. Khachatryan *et al.* (CMS), Eur. Phys. J. **C76**, 10, 536 (2016), [arXiv:1602.04384].
- [406] A. M. Sirunyan *et al.* (CMS), Eur. Phys. J. **C78**, 7, 566 (2018), [arXiv:1712.05471].
- [407] A. M. Sirunyan *et al.* (CMS) (2019), [arXiv:1902.04374].
- [408] P. Kokkas, Int. J. Mod. Phys. **A30**, 31, 1546004 (2015), [arXiv:1509.02144].
- [409] M. Aaboud *et al.* (ATLAS), Eur. Phys. J. **C77**, 6, 367 (2017), [arXiv:1612.03016].
- [410] G. Aad *et al.* (ATLAS), Phys. Lett. **B759**, 601 (2016), [arXiv:1603.09222].
- [411] R. Aaij *et al.* (LHCb), JHEP **08**, 039 (2015), [arXiv:1505.07024].
- [412] S. Chatrchyan *et al.* (CMS), JHEP **10**, 132 (2011), [arXiv:1107.4789].
- [413] S. Chatrchyan *et al.* (CMS), Phys. Rev. Lett. **112**, 191802 (2014), [arXiv:1402.0923].
- [414] R. Aaij *et al.* (LHCb), JHEP **06**, 058 (2012), [arXiv:1204.1620].
- [415] R. Aaij *et al.* (LHCb), JHEP **01**, 155 (2016), [arXiv:1511.08039].
- [416] R. Aaij *et al.* (LHCb), JHEP **09**, 136 (2016), [arXiv:1607.06495].
- [417] S. Chatrchyan *et al.* (CMS), JHEP **10**, 007 (2011), [arXiv:1108.0566].
- [418] V. Khachatryan *et al.* (CMS), Eur. Phys. J. **C75**, 4, 147 (2015), [arXiv:1412.1115].
- [419] G. Aad *et al.* (ATLAS), Phys. Lett. **B725**, 223 (2013), [arXiv:1305.4192].
- [420] G. Aad *et al.* (ATLAS), JHEP **06**, 112 (2014), [arXiv:1404.1212].
- [421] G. Aad *et al.* (ATLAS), JHEP **08**, 009 (2016), [arXiv:1606.01736].
- [422] A. M. Sirunyan *et al.* (CMS), Submitted to: JHEP (2018), [arXiv:1812.10529].
- [423] M. Aaboud *et al.* (ATLAS), JHEP **12**, 059 (2017), [arXiv:1710.05167].
- [424] S. Chatrchyan *et al.* (CMS), Phys. Rev. **D90**, 3, 032004 (2014), [arXiv:1312.6283].
- [425] V. Khachatryan *et al.* (CMS), Eur. Phys. J. **C76**, 8, 469 (2016), [arXiv:1603.01803].
- [426] G. Aad *et al.* (ATLAS), Submitted to: Eur. Phys. J. (2019), [arXiv:1904.05631].
- [427] G. Aad *et al.* (ATLAS), Eur. Phys. J. **C76**, 5, 291 (2016), [arXiv:1512.02192].
- [428] V. Khachatryan *et al.* (CMS), JHEP **02**, 096 (2017), [arXiv:1606.05864].
- [429] A. M. Sirunyan *et al.* (CMS), JHEP **03**, 172 (2018), [arXiv:1710.07955].
- [430] M. Aaboud *et al.* (ATLAS), JHEP **05**, 077 (2018), [arXiv:1711.03296].
- [431] C. F. Berger *et al.*, Phys. Rev. **D80**, 074036 (2009), [arXiv:0907.1984].
- [432] U. Blumenschein, Int. J. Mod. Phys. **A30**, 31, 1546007 (2015), [arXiv:1509.04885].
- [433] G. Aad *et al.* (ATLAS) (2019), [arXiv:1907.06728].

- [434] V. Khachatryan *et al.* (CMS), Phys. Rev. **D95**, 052002 (2017), [arXiv:1610.04222].
- [435] A. M. Sirunyan *et al.* (CMS), Phys. Rev. **D96**, 7, 072005 (2017), [arXiv:1707.05979].
- [436] A. M. Sirunyan *et al.* (CMS), Eur. Phys. J. **C78**, 11, 965 (2018), [arXiv:1804.05252].
- [437] G. Aad *et al.* (ATLAS), JHEP **07**, 032 (2013), [arXiv:1304.7098].
- [438] Z. Bern *et al.*, Phys. Rev. **D88**, 1, 014025 (2013), [arXiv:1304.1253].
- [439] M. Voutilainen, Int. J. Mod. Phys. **A30**, 31, 1546008 (2015), [arXiv:1509.05026].
- [440] G. Aad *et al.* (ATLAS), JHEP **08**, 005 (2016), [arXiv:1605.03495].
- [441] G. Aad *et al.* (ATLAS) (2019), [arXiv:1908.02746].
- [442] S. Chatrchyan *et al.* (CMS), Phys. Rev. **D84**, 052011 (2011), [arXiv:1108.2044].
- [443] S. Chatrchyan *et al.* (CMS), JHEP **06**, 009 (2014), [arXiv:1311.6141].
- [444] G. Aad *et al.* (ATLAS), Phys. Rev. **D89**, 5, 052004 (2014), [arXiv:1311.1440].
- [445] M. Aaboud *et al.* (ATLAS), Phys. Lett. **B780**, 578 (2018), [arXiv:1801.00112].
- [446] M. Aaboud *et al.* (ATLAS), Nucl. Phys. **B918**, 257 (2017), [arXiv:1611.06586].
- [447] A. M. Sirunyan *et al.* (CMS), Eur. Phys. J. **C79**, 1, 20 (2019), [arXiv:1807.00782].
- [448] A. M. Sirunyan *et al.* (CMS) (2019), [arXiv:1907.08155].
- [449] M. Aaboud *et al.* (ATLAS), Phys. Lett. **B776**, 295 (2018), [arXiv:1710.09560].
- [450] J. H. Kuhn *et al.*, JHEP **03**, 059 (2006), [hep-ph/0508253].
- [451] V. Khachatryan *et al.* (CMS), JHEP **10**, 128 (2015), [Erratum: JHEP04,010(2016)], [arXiv:1505.06520].
- [452] G. Aad *et al.* (ATLAS), JHEP **09**, 029 (2016), [arXiv:1603.01702].
- [453] M. Aaboud *et al.* (ATLAS), Phys. Lett. **B773**, 354 (2017), [arXiv:1702.04519].
- [454] M. Aaboud *et al.* (ATLAS) (2019), [arXiv:1905.04242].
- [455] V. Khachatryan *et al.* (CMS), Eur. Phys. J. **C76**, 7, 401 (2016), [arXiv:1507.03268].
- [456] G. Aad *et al.* (ATLAS) (2019), [arXiv:1903.10415].
- [457] G. Aad *et al.* (ATLAS), JHEP **01**, 086 (2013), [arXiv:1211.1913].
- [458] M. Aaboud *et al.* (ATLAS), Phys. Rev. **D95**, 11, 112005 (2017), [arXiv:1704.03839].
- [459] S. Chatrchyan *et al.* (CMS), Eur. Phys. J. **C74**, 11, 3129 (2014), [arXiv:1405.7225].
- [460] M. Aaboud *et al.* (ATLAS), Phys. Lett. **B781**, 55 (2018), [arXiv:1712.07291].
- [461] K. Kröninger, A. B. Meyer and P. Uwer, in T. Schörner-Sadenius, editor, “The Large Hadron Collider: Harvest of Run 1,” 259–300 (2015), [arXiv:1506.02800].
- [462] M. Aaboud *et al.* (ATLAS), Phys. Rev. **D94**, 9, 092003 (2016), [arXiv:1607.07281].
- [463] M. Aaboud *et al.* (ATLAS), Eur. Phys. J. **C77**, 5, 292 (2017), [arXiv:1612.05220].
- [464] A. M. Sirunyan *et al.* (CMS), Eur. Phys. J. **C79**, 5, 368 (2019), [arXiv:1812.10505].
- [465] A. M. Sirunyan *et al.* (CMS), Submitted to: Eur. Phys. J. (2019), [arXiv:1904.05237].
- [466] M. Czakon, D. Heymes and A. Mitov, Phys. Rev. Lett. **116**, 8, 082003 (2016), [arXiv:1511.00549].
- [467] S. Catani *et al.*, Phys. Rev. **D99**, 5, 051501 (2019), [arXiv:1901.04005].
- [468] S. Catani *et al.*, JHEP **07**, 100 (2019), [arXiv:1906.06535].
- [469] M. Czakon *et al.*, JHEP **05**, 149 (2018), [arXiv:1803.07623].
- [470] S. Chatrchyan *et al.* (CMS), Phys. Lett. **B728**, 496 (2014), [Erratum: Phys. Lett. B738,526(2014)], [arXiv:1307.1907].
- [471] T. Klijnsma *et al.*, Eur. Phys. J. **C77**, 11, 778 (2017), [arXiv:1708.07495].
- [472] G. Aad *et al.* (ATLAS), Eur. Phys. J. **C74**, 10, 3109 (2014), [Addendum: Eur. Phys. J. C76,no.11,642(2016)], [arXiv:1406.5375].
- [473] A. M. Sirunyan *et al.* (CMS), JHEP **09**, 051 (2017), [arXiv:1701.06228].
- [474] M. Aaboud *et al.* (ATLAS), Phys. Lett. **B786**, 114 (2018), [arXiv:1805.10197].
- [475] A. M. Sirunyan *et al.* (CMS), Phys. Lett. **B792**, 369 (2019), [arXiv:1812.06504].
- [476] M. Aaboud *et al.* (ATLAS), Phys. Rev. **D98**, 052005 (2018), [arXiv:1802.04146].
- [477] A. M. Sirunyan *et al.* (CMS), JHEP **01**, 183 (2019), [arXiv:1807.03825].
- [478] A. M. Sirunyan *et al.* (CMS Collaboration), Phys. Lett. B **792**, arXiv:1812.06504. CMS-HIG-17-028-003, 369. 28 p (2018), submitted to Phys.Lett., URL <http://cds.cern.ch/record/2651932>.
- [479] C. Patrignani *et al.* (Particle Data Group), Chin. Phys. **C40**, 10, 100001 (2016).
- [480] M. Tanabashi *et al.* (Particle Data Group), Phys. Rev. **D98**, 3, 030001 (2018).
- [481] S. Bethke, Prog. Part. Nucl. Phys. **58**, 351 (2007), [hep-ex/0606035].
- [482] S. Bethke, Eur. Phys. J. **C64**, 689 (2009), [111(2009)], [arXiv:0908.1135].
- [483] S. Bethke, J. Phys. **G26**, R27 (2000), [hep-ex/0004021].
- [484] D. d’Enterria *et al.*, in “Workshop on precision measurements of the QCD coupling constant (alphas-2019) Trento, Trentino, Italy, February 11-15, 2019,” (2019), [arXiv:1907.01435].
- [485] G. P. Salam, in A. Levy, S. Forte and G. Ridolfi, editors, “From My Vast Repertoire ...: Guido Altarelli’s Legacy,” 101–121 (2019), [arXiv:1712.05165].
- [486] A. Pich *et al.*, in “13th Conference on Quark Confinement and the Hadron Spectrum (Confinement XIII) Maynooth, Ireland, July 31-August 6, 2018,” (2018), [arXiv:1811.11801].
- [487] S. Aoki *et al.* (Flavour Lattice Averaging Group) (2019), [arXiv:1902.08191].
- [488] M. Beneke and M. Jamin, JHEP **09**, 044 (2008), [arXiv:0806.3156].
- [489] K. Maltman and T. Yavin, Phys. Rev. **D78**, 094020 (2008), [arXiv:0807.0650].
- [490] S. Narison, Phys. Lett. **B673**, 30 (2009), [arXiv:0901.3823].
- [491] I. Caprini and J. Fischer, Eur. Phys. J. **C64**, 35 (2009), [arXiv:0906.5211].
- [492] A. Pich, Prog. Part. Nucl. Phys. **75**, 41 (2014), [arXiv:1310.7922].
- [493] D. Boito *et al.*, Phys. Rev. **D91**, 3, 034003 (2015), [arXiv:1410.3528].
- [494] G. Altarelli, PoS **Corfu2012**, 002 (2013), [arXiv:1303.6065].
- [495] A. Pich and A. Rodríguez-Sánchez, Phys. Rev. **D94**, 3, 034027 (2016), [arXiv:1605.06830].
- [496] M. Davier *et al.*, Eur. Phys. J. **C74**, 3, 2803 (2014), [arXiv:1312.1501].
- [497] D. Boito *et al.*, Phys. Rev. **D98**, 7, 074030 (2018), [arXiv:1805.08176].

- [498] N. Brambilla *et al.*, Phys. Rev. **D75**, 074014 (2007), [hep-ph/0702079].
- [499] V. Mateu and P. G. Ortega, JHEP **01**, 122 (2018), [arXiv:1711.05755].
- [500] C. Peset, A. Pineda and J. Segovia, JHEP **09**, 167 (2018), [arXiv:1806.05197].
- [501] C. Glasman (H1, ZEUS), J. Phys. Conf. Ser. **110**, 022013 (2008), [arXiv:0709.4426].
- [502] T. Biekötter, M. Klasen and G. Kramer, Phys. Rev. **D92**, 7, 074037 (2015), [arXiv:1508.07153].
- [503] J. Blumlein, H. Bottcher and A. Guffanti, Nucl. Phys. **B774**, 182 (2007), [hep-ph/0607200].
- [504] P. Jimenez-Delgado and E. Reya, Phys. Rev. **D89**, 7, 074049 (2014), [arXiv:1403.1852].
- [505] S. Alekhin *et al.*, Phys. Rev. **D96**, 1, 014011 (2017), [arXiv:1701.05838].
- [506] S. Alekhin, J. Blümlein and S. Moch, Eur. Phys. J. **C78**, 6, 477 (2018), [arXiv:1803.07537].
- [507] L. A. Harland-Lang *et al.*, Eur. Phys. J. **C75**, 9, 435 (2015), [arXiv:1506.05682].
- [508] S. Dulat *et al.*, Phys. Rev. **D93**, 3, 033006 (2016), [arXiv:1506.07443].
- [509] R. D. Ball *et al.* (NNPDF), Eur. Phys. J. **C78**, 5, 408 (2018), [arXiv:1802.03398].
- [510] R. S. Thorne and G. Watt, JHEP **08**, 100 (2011), [arXiv:1106.5789].
- [511] S. Alekhin, J. Blumlein and S. Moch, Eur. Phys. J. **C71**, 1723 (2011), [arXiv:1101.5261].
- [512] R. D. Ball *et al.* (NNPDF), Phys. Lett. **B704**, 36 (2011), [arXiv:1102.3182].
- [513] R. D. Ball *et al.* (NNPDF), Phys. Lett. **B723**, 330 (2013), [arXiv:1303.1189].
- [514] R. S. Thorne, PoS **DIS2013**, 042 (2013), [arXiv:1306.3907].
- [515] G. Dissertori *et al.*, JHEP **08**, 036 (2009), [arXiv:0906.3436].
- [516] G. Abbiendi *et al.* (OPAL), Eur. Phys. J. **C71**, 1733 (2011), [arXiv:1101.1470].
- [517] S. Bethke *et al.* (JADE), Eur. Phys. J. **C64**, 351 (2009), [arXiv:0810.1389].
- [518] G. Dissertori *et al.*, Phys. Rev. Lett. **104**, 072002 (2010), [arXiv:0910.4283].
- [519] J. Schieck *et al.* (JADE), Eur. Phys. J. **C73**, 3, 2332 (2013), [arXiv:1205.3714].
- [520] A. Verbitskiy *et al.*, JHEP **08**, 129 (2019), [arXiv:1902.08158].
- [521] A. Kardos *et al.*, Eur. Phys. J. **C78**, 6, 498 (2018), [arXiv:1804.09146].
- [522] R. A. Davison and B. R. Webber, Eur. Phys. J. **C59**, 13 (2009), [arXiv:0809.3326].
- [523] R. Abbate *et al.*, Phys. Rev. **D83**, 074021 (2011), [arXiv:1006.3080].
- [524] T. Gehrmann, G. Luisoni and P. F. Monni, Eur. Phys. J. **C73**, 1, 2265 (2013), [arXiv:1210.6945].
- [525] A. H. Hoang *et al.*, Phys. Rev. **D91**, 9, 094018 (2015), [arXiv:1501.04111].
- [526] R. Frederix *et al.*, JHEP **11**, 050 (2010), [arXiv:1008.5313].
- [527] P. Bolzoni, B. A. Kniehl and A. V. Kotikov, Nucl. Phys. **B875**, 18 (2013), [arXiv:1305.6017].
- [528] J. Currie *et al.*, Phys. Rev. Lett. **119**, 15, 152001 (2017), [arXiv:1705.10271].
- [529] M. Czakon *et al.* (2019), [arXiv:1907.12911].
- [530] S. Dittmaier, A. Huss and C. Speckner, JHEP **11**, 095 (2012), [arXiv:1210.0438].
- [531] R. Frederix *et al.*, JHEP **04**, 076 (2017), [arXiv:1612.06548].
- [532] M. Czakon *et al.*, JHEP **10**, 186 (2017), [arXiv:1705.04105].
- [533] M. Johnson and D. Maître, Phys. Rev. **D97**, 5, 054013 (2018), [arXiv:1711.01408].
- [534] A. Gehrmann-De Ridder *et al.*, JHEP **07**, 133 (2016), [arXiv:1605.04295].
- [535] D. Britzger *et al.* (2019), [arXiv:1906.05303].
- [536] T. Affolder *et al.* (CDF), Phys. Rev. Lett. **88**, 042001 (2002), [hep-ex/0108034].
- [537] S. Chekanov *et al.* (ZEUS), Phys. Lett. B **649**, 12 (2007), [hep-ex/0701039].
- [538] V. M. Abazov *et al.* (D0), Phys. Rev. **D80**, 111107 (2009), [arXiv:0911.2710].
- [539] B. Malaescu and P. Starovoitov, Eur. Phys. J. **C72**, 2041 (2012), [arXiv:1203.5416].
- [540] V. Khachatryan *et al.* (CMS), Eur. Phys. J. **C75**, 6, 288 (2015), [arXiv:1410.6765].
- [541] D. Britzger *et al.*, Eur. Phys. J. **C79**, 1, 68 (2019), [arXiv:1712.00480].
- [542] S. Chekanov *et al.* (ZEUS), Eur. Phys. J. **C44**, 183 (2005), [hep-ex/0502007].
- [543] S. Chatrchyan *et al.* (CMS), Eur. Phys. J. **C73**, 10, 2604 (2013), [arXiv:1304.7498].
- [544] V. M. Abazov *et al.* (D0), Phys. Lett. **B718**, 56 (2012), [arXiv:1207.4957].
- [545] V. Khachatryan *et al.* (CMS), Eur. Phys. J. **C75**, 5, 186 (2015), [arXiv:1412.1633].
- [546] V. Andreev *et al.* (H1), Eur. Phys. J. C **77**, 4, 215 (2017), [arXiv:1611.03421].
- [547] M. Baak *et al.* (Gfitter Group), Eur. Phys. J. **C74**, 3046 (2014), [arXiv:1407.3792].
- [548] J. Haller *et al.*, Eur. Phys. J. **C78**, 8, 675 (2018), [arXiv:1803.01853].
- [549] S. Schael *et al.* (ALEPH, DELPHI, L3, OPAL, SLD, LEP Electroweak Working Group, SLD Electroweak Group, SLD Heavy Flavour Group), Phys. Rept. **427**, 257 (2006), [hep-ex/0509008].
- [550] I. Allison *et al.* (HPQCD), Phys. Rev. **D78**, 054513 (2008), [arXiv:0805.2999].
- [551] K. Maltman *et al.*, Phys. Rev. **D78**, 114504 (2008), [arXiv:0807.2020].
- [552] S. Aoki *et al.* (PACS-CS), JHEP **10**, 053 (2009), [arXiv:0906.3906].
- [553] C. McNeile *et al.*, Phys. Rev. **D82**, 034512 (2010), [arXiv:1004.4285].
- [554] E. Shintani *et al.*, Phys. Rev. **D82**, 7, 074505 (2010), [Erratum: Phys. Rev. D89, no.9, 099903(2014)], [arXiv:1002.0371].
- [555] B. Blossier *et al.*, Phys. Rev. **D85**, 034503 (2012), [arXiv:1110.5829].
- [556] A. Bazavov *et al.*, Phys. Rev. **D86**, 114031 (2012), [arXiv:1205.6155].
- [557] B. Blossier *et al.*, Phys. Rev. Lett. **108**, 262002 (2012), [arXiv:1201.5770].
- [558] B. Blossier *et al.* (ETM), Phys. Rev. **D89**, 1, 014507 (2014), [arXiv:1310.3763].
- [559] B. Chakraborty *et al.*, Phys. Rev. **D91**, 5, 054508 (2015), [arXiv:1408.4169].
- [560] A. Bazavov *et al.*, Phys. Rev. **D90**, 7, 074038 (2014), [arXiv:1407.8437].
- [561] K. Nakayama, B. Fahy and S. Hashimoto, Phys. Rev. **D94**, 5, 054507 (2016), [arXiv:1606.01002].
- [562] Y. Maezawa and P. Petreczky, Phys. Rev. **D94**, 3, 034507 (2016), [arXiv:1606.08798].
- [563] M. Bruno *et al.* (ALPHA), Phys. Rev. Lett. **119**, 10, 102001 (2017), [arXiv:1706.03821].

- [564] R. J. Hudspith *et al.* (2018), [arXiv:1804.10286].
- [565] H. Takaura *et al.*, Phys. Lett. **B789**, 598 (2019), [arXiv:1808.01632].
- [566] H. Takaura *et al.*, JHEP **04**, 155 (2019), [arXiv:1808.01643].
- [567] K. Nakayama, H. Fukaya and S. Hashimoto, Phys. Rev. **D98**, 1, 014501 (2018), [arXiv:1804.06695].
- [568] A. Bazavov *et al.* (2019), [arXiv:1907.11747].

10. Electroweak Model and Constraints on New Physics

Revised March 2020 by J. Erler (IF-UNAM; U. of Mainz) and A. Freitas (Pittsburg U.).

10.1	Introduction	180
10.2	Renormalization and radiative corrections	180
10.2.1	The Fermi constant	181
10.2.2	The electromagnetic coupling	181
10.2.3	Quark masses	182
10.2.4	The weak mixing angle	182
10.2.5	Radiative corrections	183
10.3	Low energy electroweak observables	184
10.3.1	Neutrino scattering	184
10.3.2	Parity violating lepton scattering	185
10.3.3	Atomic parity violation	186
10.4	Precision flavor physics	187
10.4.1	The τ lifetime	187
10.4.2	The muon anomalous magnetic moment	187
10.5	Physics of the massive electroweak bosons	188
10.5.1	Electroweak physics off the Z pole	189
10.5.2	Z pole physics	189
10.5.3	W and Z decays	190
10.6	Global fit results	192
10.7	Constraints on new physics	194

10.1 Introduction

The standard model of the electroweak interactions (SM) [1–4] is based on the gauge group $SU(2) \times U(1)$, with gauge bosons W_μ^i , $i = 1, 2, 3$, and B_μ for the $SU(2)$ and $U(1)$ factors, respectively, and the corresponding gauge coupling constants g and g' . The left-handed fermion fields of the i^{th} fermion family transform as doublets $\Psi_i = \begin{pmatrix} \nu_i \\ d_i' \end{pmatrix}$ and $\begin{pmatrix} u_i \\ d_i' \end{pmatrix}$ under $SU(2)$, where $d_i' \equiv \sum_j V_{ij} d_j$, and V is the Cabibbo-Kobayashi-Maskawa mixing [5, 6] matrix¹. The right-handed fields are $SU(2)$ singlets. From Higgs and electroweak precision data it is known that there are precisely three sequential fermion families.

A complex scalar Higgs doublet, ϕ , is added to the model for mass generation through spontaneous symmetry breaking with potential² given by,

$$V(\phi) = \mu^2 \phi^\dagger \phi + \frac{\lambda^2}{2} (\phi^\dagger \phi)^2, \quad \phi \equiv \begin{pmatrix} \phi^+ \\ \phi^0 \end{pmatrix}. \quad (10.1)$$

For μ^2 negative, ϕ develops a vacuum expectation value, $v/\sqrt{2} = |\mu|/\lambda$, where $v = 246.22$ GeV, breaking part of the electroweak (EW) gauge symmetry, after which only one neutral Higgs scalar, H , remains in the physical particle spectrum. In non-minimal models there are additional charged and neutral scalar Higgs particles. Higgs boson physics is reviewed in the Section on the ‘‘Status of Higgs Boson Physics’’ in this *Review*.

After symmetry breaking the Lagrangian for the fermion fields,

ψ_i , is

$$\begin{aligned} \mathcal{L}_F = & \sum_i \bar{\psi}_i \left(i \not{\partial} - m_i - \frac{m_i H}{v} \right) \psi_i \\ & - \frac{g}{2\sqrt{2}} \sum_i \bar{\Psi}_i \gamma^\mu (1 - \gamma^5) (T^+ W_\mu^+ + T^- W_\mu^-) \Psi_i \\ & - e \sum_i Q_i \bar{\psi}_i \gamma^\mu \psi_i A_\mu \\ & - \frac{g}{2 \cos \theta_W} \sum_i \bar{\psi}_i \gamma^\mu (g_V^i - g_A^i \gamma^5) \psi_i Z_\mu. \end{aligned} \quad (10.2)$$

Here $\theta_W \equiv \tan^{-1}(g'/g)$ is the weak mixing angle and $e = g \sin \theta_W$ is the positron electric charge. Furthermore,

$$A_\mu \equiv B_\mu \cos \theta_W + W_\mu^3 \sin \theta_W, \quad (10.3a)$$

$$W_\mu^\pm \equiv \frac{W_\mu^1 \mp i W_\mu^2}{\sqrt{2}}, \quad (10.3b)$$

$$Z_\mu \equiv -B_\mu \sin \theta_W + W_\mu^3 \cos \theta_W, \quad (10.3c)$$

are the photon field (γ) and the charged (W^\pm) and neutral (Z) weak boson fields, respectively.

The Yukawa coupling of H to ψ_i in the first term in \mathcal{L}_F , which is flavor diagonal in the minimal model, is $gm_i/2M_W$. The boson masses in the EW sector are given (at tree level, *i.e.*, to lowest order in perturbation theory) by,

$$M_H = \lambda v, \quad (10.4a)$$

$$M_W = \frac{gv}{2} = \frac{ev}{2 \sin \theta_W}, \quad (10.4b)$$

$$M_Z = \sqrt{g^2 + g'^2} \frac{v}{2} = \frac{ev}{2 \sin \theta_W \cos \theta_W}, \quad (10.4c)$$

$$M_\gamma = 0. \quad (10.4d)$$

The second term in \mathcal{L}_F represents the charged-current weak interaction [8–10], where T^+ and T^- are the weak isospin raising and lowering operators. For example, the coupling of a W to an electron and a neutrino is

$$-\frac{e}{2\sqrt{2} \sin \theta_W} \left[W_\mu^- \bar{e} \gamma^\mu (1 - \gamma^5) \nu + W_\mu^+ \bar{\nu} \gamma^\mu (1 - \gamma^5) e \right]. \quad (10.5)$$

For momenta small compared to M_W , this term gives rise to the effective four-fermion interaction with the Fermi constant given by $G_F/\sqrt{2} = 1/2v^2 = g^2/8M_W^2$. CP violation is incorporated into the EW model by a single observable phase in V_{ij} .

The third term in \mathcal{L}_F describes electromagnetic interactions (QED) [11, 12], and the last is the weak neutral-current interaction [9, 10, 13]. The vector and axial-vector couplings are

$$g_V^i \equiv t_{3L}(i) - 2Q_i \sin^2 \theta_W, \quad (10.6a)$$

$$g_A^i \equiv t_{3L}(i), \quad (10.6b)$$

where $t_{3L}(i)$ is the weak isospin of fermion i ($+1/2$ for u_i and ν_i ; $-1/2$ for d_i and e_i) and Q_i is the charge of ψ_i in units of e .

The first term in Eq. (10.2) also gives rise to fermion masses, and in the presence of right-handed neutrinos to Dirac neutrino masses. The possibility of Majorana masses is discussed in the Section on ‘‘Neutrino Mass, Mixing, and Oscillations’’ in this *Review*.

10.2 Renormalization and radiative corrections

In addition to the Higgs boson mass, M_H , the fermion masses and mixings, and the strong coupling constant, α_s , the SM has three parameters. The set with the smallest experimental errors contains the Z mass³, the Fermi constant, and the fine structure

³We emphasize that in the fits described in Sec. 10.6 and Sec. 10.7 the values of the SM parameters are affected by all observables that depend on

¹Constraints on V and tests of universality are discussed in Ref. [7] and in the Section on the ‘‘CKM Quark-Mixing Matrix’’ in this *Review*. The extension of the formalism to allow an analogous leptonic mixing matrix is discussed in the Section on ‘‘Neutrino Masses, Mixing, and Oscillations’’ in this *Review*.

²There is no generally accepted convention to write the quartic term. Our numerical coefficient simplifies Eq. (10.4a) below and the squared coupling preserves the relation between the number of external legs and the power counting of couplings at a given loop order. This structure also naturally emerges from physics beyond the SM, such as Supersymmetry.

constant, to be discussed in turn (the numerical values quoted in Sections 10.2–10.4 correspond to the main fit result in Table 10.7).

The Z boson mass, $M_Z = 91.1876 \pm 0.0021$ GeV, has been determined from the Z lineshape scan at LEP 1 [14]. This value of M_Z corresponds to a definition based on a Breit-Wigner shape with an energy-dependent width⁴ (see the Section on the “ Z Boson” in this *Review*).

10.2.1 The Fermi constant

The Fermi constant, $G_F = 1.1663787(6) \times 10^{-5}$ GeV⁻², is derived from the μ lifetime formula⁵,

$$\frac{\hbar}{\tau_\mu} = \frac{G_F^2 m_\mu^5}{192\pi^3} F(\rho) \left[1 + H_1(\rho) \frac{\hat{\alpha}(m_\mu)}{\pi} + H_2(\rho) \frac{\hat{\alpha}^2(m_\mu)}{\pi^2} \right], \quad (10.7)$$

where $\rho = m_e^2/m_\mu^2$, and where

$$F(\rho) = 1 - 8\rho + 8\rho^3 - \rho^4 - 12\rho^2 \ln \rho = 0.99981295, \quad (10.8a)$$

$$\begin{aligned} H_1(\rho) &= \frac{25}{8} - \frac{\pi^2}{2} - (9 + 4\pi^2 + 12 \ln \rho) \rho + 16\pi^2 \rho^{3/2} + \mathcal{O}(\rho^2) \\ &= -1.80793, \end{aligned} \quad (10.8b)$$

$$\begin{aligned} H_2(\rho) &= \frac{156815}{5184} - \frac{518}{81} \pi^2 - \frac{895}{36} \zeta(3) + \frac{67}{720} \pi^4 + \frac{53}{6} \pi^2 \ln 2 \\ &\quad - (0.042 \pm 0.002)_{\text{had}} - \frac{5}{4} \pi^2 \sqrt{\rho} + \mathcal{O}(\rho) = 6.64, \end{aligned} \quad (10.8c)$$

$$\hat{\alpha}(m_\mu)^{-1} = \alpha^{-1} + \frac{1}{3\pi} \ln \rho + \mathcal{O}(\alpha) = 135.901. \quad (10.8d)$$

H_1 and H_2 capture the QED corrections within the Fermi model. The results for $\rho = 0$ have been obtained in Refs. [16] and [17, 18] for H_1 and H_2 , respectively, where the term in parentheses is from the hadronic vacuum polarization [17]. The mass corrections to H_1 have been known for some time [19], while those to H_2 are more recent [20]. Notice the term linear in m_e whose appearance was unforeseen and can be traced to the use of the muon pole mass in the prefactor [20]. The remaining uncertainty in G_F is mostly experimental and has been reduced by an order of magnitude by the MuLan collaboration [15] at the PSI.

10.2.2 The electromagnetic coupling

The fine structure constant, α , can be extracted from the e^\pm anomalous magnetic moment [21], $a_e = (1159652180.91 \pm 0.26) \times 10^{-12}$ [22], which gives the value $\alpha^{-1} = 137.035999150(33)$. Another approach combines measurements of the Rydberg constant and atomic masses with interferometry of atomic recoil kinematics. Applied to ^{87}Rb [23] and ^{133}Cs [24], this method implies the results $\alpha^{-1} = 137.035998997(85)$ and $\alpha^{-1} = 137.035999047(28)$, respectively, which can be combined to give $\alpha^{-1} = 137.035999042(26)$. Finally, combining the anomalous magnetic moment and atomic interferometry methods leads to the world average of $\alpha^{-1} = 137.035999084(21)$, but notice that they also show a 2.6σ discrepancy. If this is interpreted as due to physics beyond the SM (BSM), the new physics would contribute to a_e with opposite sign compared to the μ^\pm anomalous magnetic moment, a_μ , to be discussed in Section 10.4.2.

In most EW renormalization schemes, it is convenient to define a running α dependent on the energy scale of the process, with

them. This is of no practical consequence for α and G_F , however, since they are very precisely known.

⁴The theoretically consistent and gauge-invariant definition of the Z -boson mass through the complex pole of the propagator would instead lead to a Breit-Wigner with a constant width. The two definitions differ numerically, and this difference has to be accounted for in theoretical calculations.

⁵In the spirit of the Fermi theory, we incorporated the small propagator correction, $3/5 m_\mu^2/M_W^2$, into Δr (see below). This is also the convention adopted by the MuLan collaboration [15]. While this breaks with historical consistency, the numerical difference was negligible in the past.

$\alpha^{-1} \approx 137.036$ appropriate at very low energy, *i.e.* close to the Thomson limit. The OPAL [25] and L3 [26] collaborations at LEP could also observe the running directly in small and large angle Bhabha scattering, respectively. For scales above a few hundred MeV the low energy hadronic contribution to vacuum polarization introduces a theoretical uncertainty in α . In the modified minimal subtraction ($\overline{\text{MS}}$) scheme⁶ [27] (used for this *Review*), and with $\alpha_s(M_Z) = 0.1185 \pm 0.0016$ we have $\hat{\alpha}^{(4)}(m_\tau)^{-1} = 133.472 \pm 0.007$ and $\hat{\alpha}^{(5)}(M_Z)^{-1} = 127.952 \pm 0.009$. The latter corresponds to a quark sector contribution (without the top) to the conventional (on-shell) QED coupling,

$$\alpha(M_Z) = \frac{\alpha}{1 - \Delta\alpha(M_Z)}, \quad (10.9)$$

of $\Delta\alpha_{\text{had}}^{(5)}(M_Z) = 0.02766 \pm 0.00007$. These values are updated from Ref. [28] with $\Delta\alpha_{\text{had}}^{(5)}(M_Z)$ moved downwards and its uncertainty reduced (partly due to a more precise charm quark mass). Its correlation with a_μ , as well as the non-linear α_s dependence of $\hat{\alpha}(M_Z)$ and the resulting correlation with the input variable α_s , are fully taken into account in the fits. This is done by using as actual input (fit constraint) instead of $\Delta\alpha_{\text{had}}^{(5)}(M_Z)$ the low energy contribution by the three light quarks, $\Delta\alpha_{\text{had}}^{(3)}(2.0 \text{ GeV}) = (58.84 \pm 0.51) \times 10^{-4}$ [29], and by calculating the perturbative and heavy quark contributions to $\hat{\alpha}(M_Z)$ in each call of the fits according to [28]. Part of the error ($\pm 0.37 \times 10^{-4}$) is from e^+e^- annihilation data below 2 GeV, as well as isospin rotated data from τ decays into two- and four-pion final states [30] (including uncertainties from isospin breaking effects [31]), but uncalculated higher order perturbative ($\pm 0.21 \times 10^{-4}$) and non-perturbative ($\pm 0.28 \times 10^{-4}$ [29]) QCD corrections and the $\overline{\text{MS}}$ quark mass values (see below) also contribute. Various evaluations of $\Delta\alpha_{\text{had}}^{(5)}(M_Z)$ are summarized in Table 10.1, where the relation⁷ between the $\overline{\text{MS}}$ and on-shell definitions (obtained using Ref [34]) is given by,

$$\begin{aligned} \Delta\hat{\alpha}(M_Z) &= \Delta\alpha(M_Z) + \frac{\alpha}{\pi} \left[\frac{100}{27} - \frac{1}{6} - \frac{7}{4} \ln \frac{M_Z^2}{M_W^2} \right. \\ &\quad \left. + \frac{\alpha_s(M_Z)}{\pi} \left(\frac{605}{108} - \frac{44}{9} \zeta(3) \right) \right. \\ &\quad \left. + \frac{\alpha_s^2}{\pi^2} \left(\frac{976481}{23328} - \frac{253}{36} \zeta(2) - \frac{781}{18} \zeta(3) + \frac{275}{27} \zeta(5) \right) \right] \\ &= 0.007127(2), \end{aligned} \quad (10.10)$$

and where the first entry of the lowest order term is from fermions and the other two are from W^\pm loops, which are usually excluded from the on-shell definition. Fermion mass effects and corrections of $\mathcal{O}(\alpha\alpha_s^3)$ and $\mathcal{O}(\alpha^2)$ contributing to Eq. (10.10) are small, partly cancel each other and are not included here. The most recent results on $\Delta\alpha_{\text{had}}^{(5)}(M_Z)$ [29, 35–37] typically assume the validity of perturbative QCD (PQCD) at scales of ~ 2 GeV or above and are in good agreement with each other. In regions where PQCD is not trusted, one can use $e^+e^- \rightarrow$ hadrons cross-section data and τ decay spectral functions [38], where the latter derive from OPAL [39], CLEO [40], ALEPH [41], and Belle [42]. Recently, new data for various $e^+e^- \rightarrow$ hadrons channels was obtained from BaBar, BES III, CLEO, the SND and CMD-3 experiments at VEPP-2000, and the KEDR experiments at VEPP-4M (for a list of references see, *e.g.*, Ref. [29]). While VEPP-2000 and VEPP-4M scanned center-of-mass (CM) energies up to 2 GeV and between about 3 and 4 GeV, respectively, the BaBar collaboration studied multi-hadron events radiatively returned from the $\Upsilon(4S)$,

⁶In this Section we denote quantities defined in the $\overline{\text{MS}}$ scheme by a caret; the exception is the strong coupling constant, α_s , which will always correspond to the $\overline{\text{MS}}$ definition and where the caret will be dropped.

⁷In practice, $\alpha(M_Z)$ is directly evaluated in the $\overline{\text{MS}}$ scheme using the FORTRAN package GAPP [32], including the QED contributions of both leptons and quarks. The leptonic three-loop contribution in the on-shell scheme has been obtained in Ref. [33].

reconstructing the radiated photon and normalizing to $\mu^\pm\gamma$ final states. The precision of these results generally exceeds those from τ decays. There are significant discrepancies between the older (CMD-2) and newer (CMD-3) measurements of $e^+e^- \rightarrow K^+K^-$, which could be due to difficulties in determining the detection efficiency of low-momentum kaons. The radiative return data from BaBar is expected to be more reliable for this channel owing to an additional boost of the final-state hadrons.

10.2.3 Quark masses

Further free parameters entering into Eq. (10.2) are the quark and lepton masses, where m_i is the mass of the i^{th} fermion ψ_i . For the light quarks, as described in the Section on “Quark Masses” in this Review, $\hat{m}_u = 2.16^{+0.49}_{-0.26}$ MeV, $\hat{m}_d = 4.67^{+0.48}_{-0.17}$ MeV, and $\hat{m}_s = 93^{+11}_{-5}$ MeV. These are running $\overline{\text{MS}}$ masses evaluated at the scale $\mu = 2$ GeV. For the charm mass we use the constraint [51],

$$\hat{m}_c(\hat{m}_c) = 1274 \pm 8 + 2616[\alpha_s(M_Z) - 0.1182] \text{ MeV}, \quad (10.11)$$

which is based on QCD sum rules [52, 53], and recalculate \hat{m}_c in each call of our fits to account for its α_s dependence. Similarly, for the bottom quark mass we use,

$$\hat{m}_b(\hat{m}_b) = 4180 \pm 8 + 108[\alpha_s(M_Z) - 0.1182] \text{ MeV}, \quad (10.12)$$

with a theoretical correlation of about 60% arising mostly from the PQCD truncation uncertainty which is similar for $\hat{m}_c(\hat{m}_c)$ and $\hat{m}_b(\hat{m}_b)$. To improve the precisions in $\hat{m}_c(\hat{m}_c)$ and $\hat{m}_b(\hat{m}_b)$ in the future it would help to remeasure the threshold regions of the heavy quarks, as well as the electronic decay widths of the narrow $c\bar{c}$ and $b\bar{b}$ resonances.

The top quark “pole” mass (the quotation marks are a reminder that the experiments do not strictly measure the pole mass and that quarks do not form asymptotic states), has been kinematically reconstructed by the Tevatron collaborations, CDF and DØ, in leptonic, hadronic, and mixed channels with the result $m_t = 174.30 \pm 0.35_{\text{stat.}} \pm 0.54_{\text{syst.}}$ GeV [54]. Likewise, using data from CM energies $\sqrt{s} = 7$ and 8 TeV (Run 1), ATLAS and CMS (including alternative technique measurements) at the LHC obtained $m_t = 172.69 \pm 0.25_{\text{stat.}} \pm 0.41_{\text{syst.}}$ GeV [55] and $m_t = 172.43 \pm 0.13_{\text{stat.}} \pm 0.46_{\text{syst.}}$ GeV [56], respectively. In addition, there are first results with $\sqrt{s} = 13$ TeV data (Run 2). CMS obtained $m_t = 172.26 \pm 0.07_{\text{mostly stat.}} \pm 0.61_{\text{syst.}}$ GeV [57] in the lepton + jets and all-jets channels, and $m_t = 172.33 \pm 0.14_{\text{stat.}} \pm 0.69_{\text{syst.}}$ GeV [58] in the di-lepton channel. Using a leptonic invariant mass and thus featuring reduced correlation with the more traditional analysis approaches, ATLAS quotes $m_t = 174.48 \pm 0.40_{\text{stat.}} \pm 0.67_{\text{syst.}}$ GeV [59] from the lepton + jets channel. While there seems to be generally good agreement between all these measurements, we observe a 2.8σ discrepancy (or more in case of correlated systematics) between the two most precise determinations, 174.98 ± 0.76 GeV [60] (by the DØ collaboration) and 172.25 ± 0.63 GeV [61] (by the CMS collaboration), both from the lepton + jets channels. In addition, the latter is also 2.2σ lower than the preliminary result of Ref. [59]. Assuming a systematic error component of 0.17 GeV (the QCD, PDF and Monte Carlo type errors at ATLAS at Run 1) is common to all six results, we arrive at the combination,

$$m_t = 172.89 \pm 0.28_{\text{exp.}} \text{ GeV} + \Delta m_{\text{MC}}, \quad (10.13)$$

where Δm_{MC} is defined to account for any difference between the top pole mass, m_t , and the mass parameter implemented in the Monte Carlo event generators employed by the experimental groups. Δm_{MC} is expected to be of order $\alpha_s(Q_0)Q_0$ with a low scale $Q_0 \sim \mathcal{O}(1 \text{ GeV})$ [62], but its value is unknown in hadron collider environments so that we will treat it as an uncertainty instead, and choose for definiteness $Q_0 = \Gamma_t = 1.42$ GeV to arrive at $\Delta m_{\text{MC}} = 0 \pm 0.52$ GeV. We further assume that an uncertainty [63] of ± 0.32 GeV in the relation [64] between m_t and the $\overline{\text{MS}}$ definition, $\hat{m}_t(\hat{m}_t)$, entering electroweak radiative correction libraries, including the renormalon ambiguity [65], is already included in Δm_{MC} , as m_t merely serves as an intermediate book-keeping device in Ref. [62]. A promising future direction to arrive

at a competitive independent constraint on m_t is to analyze differential top quark pair production cross-sections at next-to-next-to-leading order (NNLO) [66], as m_t extraction based on them are easier to interpret, and experimentally they have become much more precise recently [67, 68]. The combination in Eq. (10.13) differs slightly from the average, $m_t = 172.9 \pm 0.4_{\text{exp.}}$ GeV, which appears in the Top Quark Listings in this Review, as its uncertainty has been scaled up by a factor of 1.3. For more details and references, see the Section on the “Top Quark” and the Quarks Listings in this Review.

10.2.4 The weak mixing angle

The observables $\sin^2\theta_W$ and M_W can be calculated from M_Z , $\hat{\alpha}(M_Z)$, and G_F , when values for m_t and M_H are given, or conversely, M_H can be constrained by $\sin^2\theta_W$ and M_W . The value of $\sin^2\theta_W$ is extracted from neutral-current processes (see Sec. 10.3) and Z pole observables (see Sec. 10.5.3) and depends on the renormalization prescription. There are a number of popular schemes [9] leading to values which differ by small factors depending on m_t and M_H . The notation for these schemes is shown in Table 10.2.

- (i) The on-shell scheme [70] promotes the tree-level formula $\sin^2\theta_W = 1 - M_W^2/M_Z^2$ to a definition of the renormalized $\sin^2\theta_W$ to all orders in perturbation theory, *i.e.*,

$$\sin^2\theta_W \rightarrow s_W^2 \equiv 1 - \frac{M_W^2}{M_Z^2}, \quad (10.14a)$$

$$M_W = \frac{A_0}{s_W(1 - \Delta r)^{1/2}}, \quad M_Z = \frac{M_W}{c_W}, \quad (10.14b)$$

where $c_W \equiv \cos\theta_W$, $A_0 = (\pi\alpha/\sqrt{2}G_F)^{1/2} = 37.28038(1)$ GeV, and Δr includes the radiative corrections relating α , $\alpha(M_Z)$, G_F , M_W , and M_Z . One finds $\Delta r \sim \Delta r_0 - \rho_t \tan^{-2}\theta_W$, where $\Delta r_0 = 1 - \alpha/\hat{\alpha}(M_Z) = 0.06629(7)$ is due to the running of α , and

$$\rho_t = \frac{3G_F m_t^2}{8\sqrt{2}\pi^2} = 0.00937 \times \frac{m_t^2}{(172.89 \text{ GeV})^2}, \quad (10.15)$$

represents the dominant (quadratic) m_t dependence. There are additional contributions to Δr from bosonic loops, including those which depend logarithmically on M_H and higher-order corrections⁸. One has $\Delta r = 0.03652 \mp 0.00021 \pm 0.00007$, where the first uncertainty is from m_t and the second is from $\alpha(M_Z)$. Thus the value of s_W^2 extracted from M_Z includes an uncertainty (∓ 0.00007) from the currently allowed range of m_t . This scheme is simple conceptually. However, the relatively large ($\sim 3\%$) correction from ρ_t causes large spurious contributions in higher orders. s_W^2 depends not only on the gauge couplings but also on the spontaneous-symmetry breaking, and it is awkward in the presence of any extension of the SM which perturbs the value of M_Z (or M_W). Other definitions are motivated by the tree-level coupling constant definition $\theta_W = \tan^{-1}(g'/g)$:

- (ii) In particular, the $\overline{\text{MS}}$ scheme introduces the quantity,

$$\sin^2\hat{\theta}_W(\mu) \equiv \frac{\hat{g}'^2(\mu)}{\hat{g}^2(\mu) + \hat{g}'^2(\mu)}, \quad (10.16)$$

where the couplings \hat{g} and \hat{g}' are defined by modified minimal subtraction and the scale μ is conveniently chosen to be M_Z for many EW processes. The value of $\hat{s}_Z^2 \equiv \sin^2\hat{\theta}_W(M_Z)$ extracted from M_Z is less sensitive than s_W^2 to m_t (by a factor of $\tan^2\theta_W$), and is less sensitive to most types of new physics. It is also very useful for comparing with the predictions of grand unification. There are actually several variant definitions of $\sin^2\hat{\theta}_W(M_Z)$, differing according

⁸All explicit numbers quoted here and below include the two- and three-loop corrections described near the end of Sec. 10.2.

Table 10.1: Evaluations of the on-shell $\Delta\alpha_{\text{had}}^{(5)}(M_Z)$ by different groups (for a more complete list of evaluations see the 2012 edition of this *Review*). For better comparison we adjusted central values and errors to correspond to a common and fixed value of $\alpha_s(M_Z) = 0.120$. References quoting results without the top quark decoupled are converted to the five flavor definition. Ref. [43] uses $\Lambda_{\text{QCD}} = 380 \pm 60$ MeV; for the conversion we assumed $\alpha_s(M_Z) = 0.118 \pm 0.003$.

Reference	Result	Comment
Geshkenbein, Morgunov [44]	0.02780 ± 0.00006	$\mathcal{O}(\alpha_s)$ resonance model
Swartz [45]	0.02754 ± 0.00046	use of fitting function
Krasnikov, Rodenberg [46]	0.02737 ± 0.00039	PQCD for $\sqrt{s} > 2.3$ GeV
Kühn & Steinhauser [47]	0.02778 ± 0.00016	full $\mathcal{O}(\alpha_s^2)$ for $\sqrt{s} > 1.8$ GeV
Groote <i>et al.</i> [43]	0.02787 ± 0.00032	use of QCD sum rules
Martin <i>et al.</i> [48]	0.02741 ± 0.00019	incl. new BES data
de Troconiz, Yndurain [49]	0.02754 ± 0.00010	PQCD for $s > 2$ GeV ²
Burkhardt, Pietrzyk [50]	0.02750 ± 0.00033	PQCD for $\sqrt{s} > 12$ GeV
Erlar, Ferro-Hernández [35]	0.02761 ± 0.00010	conv. from $\overline{\text{MS}}$ scheme
Jegerlehner [36]	0.02755 ± 0.00013	Euclidean split technique
Davier <i>et al.</i> [29]	0.02760 ± 0.00010	PQCD for $\sqrt{s} = 1.8\text{--}3.7$ & > 5 GeV
Keshavarzi <i>et al.</i> [37]	0.02761 ± 0.00011	PQCD for $\sqrt{s} > 11.2$ GeV

Table 10.2: Notations used to indicate the various schemes discussed in the text. Each definition of $\sin^2\theta_W$ leads to values that differ by small factors depending on m_t and M_H . Numerical values and the uncertainties induced by the imperfectly known SM parameters and unknown higher orders [69] are also given for illustration.

Scheme	Notation	Value	Uncertainty
On-shell	s_W^2	0.22337	± 0.00010
$\overline{\text{MS}}$	\widehat{s}_Z^2	0.23121	± 0.00004
$\overline{\text{MS}}_{\text{ND}}$	$\widehat{s}_{\text{ND}}^2$	0.23141	± 0.00004
$\overline{\text{MS}}$	\widehat{s}_0^2	0.23857	± 0.00005
Effective angle	\widehat{s}_ℓ^2	0.23153	± 0.00004

to whether or how finite $\alpha \ln(m_t/M_Z)$ terms are decoupled (subtracted from the couplings). One cannot entirely decouple the $\alpha \ln(m_t/M_Z)$ terms from all EW quantities because $m_t \gg m_b$ breaks SU(2) symmetry. The scheme that will be adopted here decouples the $\alpha \ln(m_t/M_Z)$ terms from the γ - Z mixing [27, 71], essentially eliminating any $\ln(m_t/M_Z)$ dependence in the formulae for asymmetries at the Z pole when written in terms of \widehat{s}_Z^2 . (A similar definition is used for $\widehat{\alpha}$.) The on-shell and $\overline{\text{MS}}$ definitions are related by

$$\widehat{s}_Z^2 = c(m_t, M_H) s_W^2 = (1.0351 \pm 0.0003) s_W^2. \quad (10.17)$$

The quadratic m_t dependence is given by $c \sim 1 + \rho_t / \tan^2\theta_W$. The expressions for M_W and M_Z in the $\overline{\text{MS}}$ scheme are

$$M_W = \frac{A_0}{\widehat{s}_Z(1 - \Delta\widehat{r}_W)^{1/2}}, \quad M_Z = \frac{M_W}{\widehat{\rho}^{1/2} \widehat{c}_Z}, \quad (10.18)$$

and one predicts $\Delta\widehat{r}_W = 0.06918 \pm 0.00007$. $\Delta\widehat{r}_W$ has no quadratic m_t dependence, because shifts in M_W are absorbed into the observed G_F , so that the error in $\Delta\widehat{r}_W$ is almost entirely due to $\Delta r_0 = 1 - \alpha/\widehat{\alpha}(M_Z)$. The quadratic m_t dependence has been shifted into $\widehat{\rho} \sim 1 + \rho_t$, where including bosonic loops, $\widehat{\rho} = 1.01019 \pm 0.00009$.

- (iii) A variant $\overline{\text{MS}}$ quantity $\widehat{s}_{\text{ND}}^2$ (used in the 1992 edition of this *Review*) does not decouple the $\alpha \ln(m_t/M_Z)$ terms [72]. It is related to \widehat{s}_Z^2 by

$$\widehat{s}_Z^2 = \frac{\widehat{s}_{\text{ND}}^2}{1 + \frac{\alpha}{\pi} d}, \quad (10.19)$$

$$d = \frac{1}{3} \left(\frac{1}{\widehat{s}^2} - \frac{8}{3} \right) \left[\left(1 + \frac{\alpha_s}{\pi} \right) \ln \frac{m_t}{M_Z} - \frac{15\alpha_s}{8\pi} \right].$$

Thus, $\widehat{s}_Z^2 - \widehat{s}_{\text{ND}}^2 = -0.0002$.

- (iv) Some of the low-energy experiments discussed in the next section are sensitive to the weak mixing angle at almost vanishing momentum transfer [35, 73–75]. Thus, Table 10.2 also includes $\widehat{s}_0^2 \equiv \sin^2\widehat{\theta}_W(0)$.

- (v) Yet another definition, the effective angle [76, 77], $\widehat{s}_f^2 \equiv \sin\theta_{\text{eff}}^f$, for the Z vector coupling to fermion f , is based on Z pole observables and described in Sec. 10.5.

10.2.5 Radiative corrections

Experiments are at such level of precision [69] that complete one-loop, dominant two-loop, and partial three and four-loop radiative corrections must be applied. For neutral-current and Z pole processes, these corrections are conveniently divided into two classes:

1. QED diagrams involving the emission of real photons or the exchange of virtual photons in loops, but not including vacuum polarization diagrams. These graphs often yield finite and gauge-invariant contributions to observable processes. However, they are dependent on energies, experimental cuts, *etc.*, and must be calculated individually for each experiment.
2. EW corrections, including $\gamma\gamma$, γZ , ZZ , and WW vacuum polarization diagrams, as well as vertex corrections, box graphs, *etc.*, involving virtual W and Z bosons. One-loop corrections [78] are included for all processes, and many two-loop corrections are also important. In particular, two-loop corrections involving the top quark modify ρ_t in $\widehat{\rho}$, Δr , and elsewhere by

$$\rho_t \rightarrow \rho_t \left[1 + R(M_H, m_t) \frac{\rho_t}{3} \right]. \quad (10.20)$$

$R(M_H, m_t)$ can be described as an expansion in M_Z^2/m_t^2 , for which the leading m_t^4/M_Z^4 [79, 80] and next-to-leading m_t^2/M_Z^2 [81, 82] terms are known. The complete two-loop calculation of Δr (without further approximation) has been performed in Refs. [83–87]. More recently, Ref. [88] obtained

the $\overline{\text{MS}}$ quantities $\Delta\widehat{\nu}_W$ and $\widehat{\rho}$ to two-loop accuracy, confirming the prediction of M_W in the on-shell scheme from Refs. [85, 89] within about 4 MeV. Similarly, the EW two-loop corrections for the relation between $\widehat{s}_{\ell,b}^2$ and s_W^2 are known [90–95], as well as for the partial decay and total decay widths and the effective couplings of the Z boson [96–99]. For $\widehat{s}_{s,c}$ only two-loop corrections from diagrams with closed fermion loops are available [100], but given the experimental precision this is more than adequate.

The mixed QCD-EW contributions to gauge boson self-energies of order $\alpha\alpha_s m_t^2$ [101, 102], $\alpha\alpha_s^2 m_t^2$ [103, 104], and $\alpha\alpha_s^3 m_t^2$ [105–107] increase the predicted value of m_t by 6%. This is, however, almost entirely an artifact of using the pole mass definition for m_t . The equivalent corrections when using the $\overline{\text{MS}}$ definition \widehat{m}_t increase m_t by less than 0.5%. The sub-leading $\alpha\alpha_s$ corrections [108–111] are also included. Further three-loop corrections of order $\alpha\alpha_s^2$ [112, 113], $\alpha^3 m_t^6$, and $\alpha^2\alpha_s m_t^4$ [114, 115], are rather small. The same is true for $\alpha^3 M_H^4$ [116] corrections unless M_H approaches 1 TeV. The theoretical uncertainty from unknown higher-order corrections [69] is estimated to amount to 4 MeV for the prediction of M_W [89] and 4.5×10^{-5} for \widehat{s}_ℓ^2 [100].

Throughout this *Review* we utilize EW radiative corrections from the program GAPP [32], which works entirely in the $\overline{\text{MS}}$ scheme, and which is independent of the package ZFITTER [117].

10.3 Low energy electroweak observables

In the following we discuss EW precision observables obtained at low momentum transfers [118], *i.e.*, $Q^2 \ll M_Z^2$. It is convenient to write the four-fermion interactions relevant to ν -hadron, ν - e , as well as parity violating e -hadron and e - e neutral-current processes, in a form that is valid in an arbitrary gauge theory (assuming massless left-handed neutrinos). One has⁹,

$$-\mathcal{L}^{\nu e} = \frac{G_F}{\sqrt{2}} \bar{\nu}\gamma_\mu(1-\gamma^5)\nu \bar{e}\gamma^\mu(g_{LV}^{\nu e} - g_{LA}^{\nu e}\gamma^5)e, \quad (10.21a)$$

$$-\mathcal{L}^{\nu h} = \frac{G_F}{\sqrt{2}} \bar{\nu}\gamma_\mu(1-\gamma^5)\nu \sum_q \left[g_{LL}^{\nu q} \bar{q}\gamma^\mu(1-\gamma^5)q + g_{LR}^{\nu q} \bar{q}\gamma^\mu(1+\gamma^5)q \right] \quad (10.21b)$$

$$-\mathcal{L}^{ee} = -\frac{G_F}{\sqrt{2}} g_{AV}^{ee} \bar{e}\gamma_\mu\gamma^5 e \bar{e}\gamma^\mu e, \quad (10.21c)$$

$$-\mathcal{L}^{eh} = -\frac{G_F}{\sqrt{2}} \sum_q \left[g_{AV}^{eq} \bar{e}\gamma_\mu\gamma^5 e \bar{q}\gamma^\mu q + g_{VA}^{eq} \bar{e}\gamma_\mu e \bar{q}\gamma^\mu\gamma^5 q \right], \quad (10.21d)$$

where one must include the charged-current contribution for ν_e - e and $\bar{\nu}_e$ - e and the parity conserving QED contribution for electron scattering. The SM tree level expressions for the four-Fermi couplings are given in Table 10.3. Note that they differ from the respective products of the gauge couplings in (10.6) in the radiative corrections and in the presence of possible physics beyond the SM.

10.3.1 Neutrino scattering

The cross-section in the laboratory system for $\nu_\mu e \rightarrow \nu_\mu e$ or $\bar{\nu}_\mu e \rightarrow \bar{\nu}_\mu e$ elastic scattering [9, 119] is (in this subsection we drop

⁹We use here slightly different definitions (and to avoid confusion also a different notation) for the coefficients of these four-Fermi operators than we did in previous editions of this *Review*. The new couplings [13] are defined in the static limit, $Q^2 \rightarrow 0$, with specific radiative corrections included, while others (more experiment specific ones) are assumed to be removed by the experimentalist. They are convenient in that their determinations from very different types of processes can be straightforwardly combined.

the redundant index L in the effective neutrino couplings),

$$\frac{d\sigma_{\nu,\bar{\nu}}}{dy} = \frac{G_F^2 m_e E_\nu}{2\pi} \left[(g_V^{\nu e} \pm g_A^{\nu e})^2 + (g_V^{\bar{\nu} e} \mp g_A^{\bar{\nu} e})^2 (1-y)^2 - (g_V^{\nu e 2} - g_A^{\nu e 2}) \frac{y m_e}{E_\nu} \right], \quad (10.22)$$

where the upper (lower) sign refers to ν_μ ($\bar{\nu}_\mu$), and $y \equiv T_e/E_\nu$ (which runs from 0 to $(1+m_e/2E_\nu)^{-1}$) is the ratio of the kinetic energy of the recoil electron to the incident ν or $\bar{\nu}$ energy. For $E_\nu \gg m_e$ this yields a total cross-section

$$\sigma = \frac{G_F^2 m_e E_\nu}{2\pi} \left[(g_V^{\nu e} \pm g_A^{\nu e})^2 + \frac{1}{3} (g_V^{\bar{\nu} e} \mp g_A^{\bar{\nu} e})^2 \right]. \quad (10.23)$$

The most accurate measurements of $\sin^2 \theta_W$ from ν -lepton scattering (see Sec. 10.6) are from the ratio $R \equiv \sigma_{\nu_\mu e}/\sigma_{\bar{\nu}_\mu e}$, in which many of the systematic uncertainties cancel. The results are $\sin^2 \theta_W = 0.211 \pm 0.037$ [120], $\sin^2 \theta_W = 0.195 \pm 0.022$ [121], and $\sin^2 \theta_W = 0.2324 \pm 0.0083$ [122], where radiative corrections (other than m_t effects) are small compared to the precision of present experiments and have negligible effect. As shown in Fig. 10.1, one can determine $g_{V,A}^{\nu e}$ from the experimental data as well. The cross-sections for ν_e - e and $\bar{\nu}_e$ - e may be obtained from Eq. (10.22) by replacing $g_{V,A}^{\nu e}$ by $g_{V,A}^{\nu e} + 1$, where the 1 is due to the charged-current contribution.

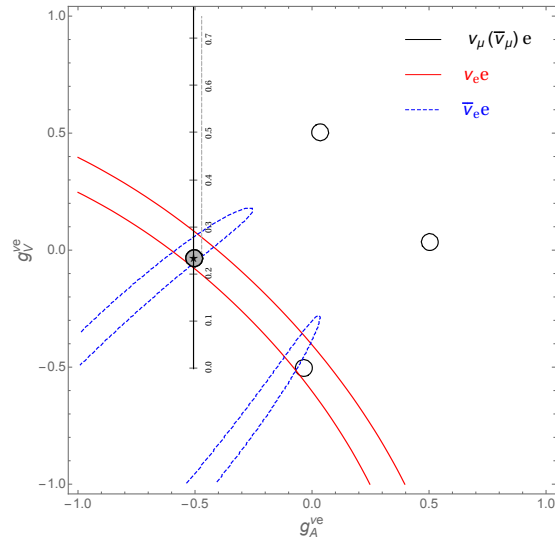


Figure 10.1: Allowed contours in $g_A^{\nu e}$ vs. $g_V^{\nu e}$ from neutrino-electron scattering and the SM prediction as a function of \widehat{s}_Z^2 . (The SM best fit value, $\widehat{s}_Z^2 = 0.23121$, is also indicated.) The ν_e - e [123, 124] and $\bar{\nu}_e$ - e [125] constraints are at 1 σ , while each of the four equivalent ν_μ ($\bar{\nu}_\mu$)- e [120–122] solutions ($g_{V,A} \rightarrow -g_{V,A}$ and $g_{V,A} \rightarrow g_{A,V}$) are at the 90% CL. The global best fit region (shaded) almost exactly coincides with the corresponding ν_μ ($\bar{\nu}_\mu$)- e region. The solution near $g_A = 0$ and $g_V = -0.5$ is eliminated by $e^+e^- \rightarrow \ell^+\ell^-$ data under the weak additional assumption that the neutral current is dominated by the exchange of a single Z boson.

A precise determination of the on-shell s_W^2 , which depends only very weakly on m_t and M_H , is obtained from deep inelastic scattering (DIS) of neutrinos [119, 126] from (approximately) isoscalar targets. The ratio $R_\nu \equiv \sigma_{\nu N}^{NC}/\sigma_{\nu N}^{CC}$ of neutral-to-charged-current cross-sections has been measured to 1% accuracy by CDHS [127] and CHARM [128] at CERN. CCFR [129] at Fermilab has obtained an even more precise result, so it is important to obtain theoretical expressions for R_ν and $R_{\bar{\nu}} \equiv \sigma_{\bar{\nu} N}^{NC}/\sigma_{\bar{\nu} N}^{CC}$ to comparable accuracy. Fortunately, many of the uncertainties from the strong interactions and neutrino spectra cancel in the ratio. A large theoretical uncertainty is associated with the c -threshold,

Table 10.3: SM tree level expressions for the neutral-current parameters for ν -hadron, ν - e , and e^- scattering processes. To obtain the SM values in the last column, the tree level expressions have to be multiplied by the low-energy neutral-current ρ parameter, $\rho_{NC} = 1.00063$, and further vertex and box corrections need to be added as detailed in Ref. [13]. The dominant m_t dependence is again given by $\rho_{NC} \sim 1 + \rho_t$.

Quantity	SM tree level	SM value
$g_{LV}^{\nu\mu e}$	$-\frac{1}{2} + 2\widehat{s}_0^2$	-0.0398
$g_{LA}^{\nu\mu e}$	$-\frac{1}{2}$	-0.5064
$g_{LL}^{\nu\mu u}$	$\frac{1}{2} - \frac{2}{3}\widehat{s}_0^2$	0.3458
$g_{LL}^{\nu\mu d}$	$-\frac{1}{2} + \frac{1}{3}\widehat{s}_0^2$	-0.4288
$g_{LR}^{\nu\mu u}$	$-\frac{2}{3}\widehat{s}_0^2$	-0.1552
$g_{LR}^{\nu\mu d}$	$\frac{1}{3}\widehat{s}_0^2$	0.0777
g_{AV}^{ee}	$\frac{1}{2} - 2\widehat{s}_0^2$	0.0227
g_{AV}^{eu}	$-\frac{1}{2} + \frac{4}{3}\widehat{s}_0^2$	-0.1888
g_{AV}^{ed}	$\frac{1}{2} - \frac{2}{3}\widehat{s}_0^2$	0.3419
g_{VA}^{eu}	$-\frac{1}{2} + 2\widehat{s}_0^2$	-0.0352
g_{VA}^{ed}	$\frac{1}{2} - 2\widehat{s}_0^2$	0.0249

which mainly affects σ^{CC} . Using the slow rescaling prescription [130, 131] the central value of $\sin^2 \theta_W$ from CCFR varies as $0.0111(m_c/\text{GeV} - 1.31)$, where m_c is the effective mass which is numerically close to the $\overline{\text{MS}}$ mass $\widehat{m}_c(\widehat{m}_c)$, but their exact relation is unknown at higher orders. For $m_c = 1.31 \pm 0.24$ GeV, which was determined from ν -induced di-muon production [132], this contributes ± 0.003 to the total uncertainty of $\Delta \sin^2 \theta_W = \pm 0.004$, where the experimental uncertainty was also ± 0.003 . This uncertainty largely cancels, however, in the Paschos-Wolfenstein ratio [133],

$$R^- = \frac{\sigma_{\nu N}^{NC} - \sigma_{\bar{\nu} N}^{NC}}{\sigma_{\nu N}^{CC} - \sigma_{\bar{\nu} N}^{CC}}. \quad (10.24)$$

It was measured by Fermilab's NuTeV collaboration [134] for the first time, and required a high-intensity and high-energy anti-neutrino beam.

A simple zeroth-order approximation is,

$$R_\nu = g_L^2 + g_R^2 r, \quad R_{\bar{\nu}} = g_L^2 + \frac{g_R^2}{r}, \quad (10.25a)$$

$$R^- = g_L^2 - g_R^2, \quad r \equiv \frac{\sigma_{\bar{\nu} N}^{CC}}{\sigma_{\nu N}^{CC}}, \quad (10.25b)$$

where r is the ratio of $\bar{\nu}$ to ν charged-current cross-sections which can be measured directly¹⁰, and

$$g_L^2 \equiv (g_{LL}^{\nu\mu u})^2 + (g_{LL}^{\nu\mu d})^2 \approx \frac{1}{2} - \sin^2 \theta_W + \frac{5}{9} \sin^4 \theta_W, \quad (10.26a)$$

$$g_R^2 \equiv (g_{LR}^{\nu\mu u})^2 + (g_{LR}^{\nu\mu d})^2 \approx \frac{5}{9} \sin^4 \theta_W. \quad (10.26b)$$

In practice, Eq. (10.25b) must be corrected for quark mixing, quark sea effects, c quark threshold effects, non-isoscalarity, W - Z propagator differences, the finite muon mass, QED and EW radiative corrections. Details of the neutrino spectra, experimental cuts, x and Q^2 dependence of structure functions, and longitudinal structure functions, enter only at the level of these corrections and therefore lead to very small uncertainties. CCFR quotes $s_W^2 = 0.2236 \pm 0.0041$ for the reference values $(m_t, M_H) = (175, 150)$ GeV with very little sensitivity to (m_t, M_H) .

The NuTeV collaboration found $s_W^2 = 0.2277 \pm 0.0016$ (for the same reference values), which was 3.0σ higher than the SM prediction [134]. However, since then several groups have raised concerns about the interpretation of the NuTeV result, which could

affect the extracted $g_{L,R}^2$ (and thus s_W^2) including their uncertainties and correlation. These include the assumption of symmetric strange and anti-strange sea quark distributions, the electron neutrino contamination from K_{e3} decays, isospin symmetry violation in the parton distribution functions and from QED splitting effects, nuclear shadowing effects, and a more complete treatment of EW and QCD radiative corrections. A more detailed discussion and a list of references can be found in the 2016 edition of this *Review*. The precise impact of these effects would need to be evaluated carefully by the collaboration, but in the absence of such an effort we do not include the ν DIS constraints in our default set of fits.

Very recently, the COHERENT collaboration was the first to observe the coherent elastic neutrino nucleus scattering (CE ν NS) process [135] on a target consisting mostly of ^{133}Cs and ^{127}I , and at the opposite end of the kinematic scale where the momentum transfer is significantly smaller than the inverse of the nuclear radius. The coherence enhances the process roughly proportional to the square of the number of neutrons in the nuclei, but the process is difficult to observe as the experimental signature is a mere keV scale nuclear recoil.

10.3.2 Parity violating lepton scattering

Reviews on weak polarized electron scattering may be found in Refs. [9, 136]. The SLAC polarized electron-deuteron DIS (eDIS) experiment [137] measured the parity violating right-left asymmetry,

$$A_{RL} \equiv \frac{\sigma_R - \sigma_L}{\sigma_R + \sigma_L}, \quad (10.27)$$

where $\sigma_{R,L}$ is the cross-section for the deep-inelastic scattering of a right- or left-handed electron, $e_{R,L}N \rightarrow eX$. In the quark parton model,

$$\frac{A_{RL}}{Q^2} = a_1 + a_2 \frac{1 - (1-y)^2}{1 + (1-y)^2}, \quad (10.28)$$

where $Q^2 > 0$ is the momentum transfer and y is the fractional energy transfer from the electron to the hadrons. For the deuteron or other isoscalar targets, one has, neglecting the s quark and anti-quarks,

$$a_1 = \frac{3G_F}{5\sqrt{2}\pi\alpha} \left(g_{AV}^{eu} - \frac{1}{2}g_{AV}^{ed} \right) \approx \frac{3G_F}{5\sqrt{2}\pi\alpha} \left(-\frac{3}{4} + \frac{5}{3}\widehat{s}_0^2 \right), \quad (10.29a)$$

$$a_2 = \frac{3G_F}{5\sqrt{2}\pi\alpha} \left(g_{VA}^{eu} - \frac{1}{2}g_{VA}^{ed} \right) \approx \frac{9G_F}{5\sqrt{2}\pi\alpha} \left(\widehat{s}_0^2 - \frac{1}{4} \right). \quad (10.29b)$$

The Jefferson Lab Hall A collaboration [138, 139] improved on the SLAC result by measuring A_{RL} at $Q^2 = 1.085$ GeV² and

¹⁰In the simple parton model, ignoring hadron energy cuts, $r \approx (1 + 3\epsilon)/(3 + \epsilon)$, where $\epsilon \sim 0.125$ is the ratio of the fraction of the nucleon's momentum carried by anti-quarks to that carried by quarks.

1.901 GeV², and determined the weak mixing angle to 2% precision, $\hat{s}^2(161 \text{ MeV}) = 0.2403 \pm 0.0043$. In another polarized electron scattering experiment on deuterons, but in the quasi-elastic kinematic regime, the SAMPLE experiment [140, 141] at MIT-Bates extracted the combination $g_{V_A}^{eu} - g_{V_A}^{ed}$ at Q^2 values of 0.038 GeV² and 0.091 GeV². What was actually determined were nucleon form factors from which the quoted results were obtained by the removal of a multi-quark radiative correction [142]. Other linear combinations of the effective couplings have been determined in polarized lepton scattering at CERN in μ -¹²C DIS [143] (the observable was the double charge-helicity cross-section asymmetry), at Mainz in e -⁹Be (quasi-elastic) [144], and at Bates in e -¹²C (elastic) [145]. More recent polarized electron scattering experiments, *i.e.*, SAMPLE, the PVA4 experiment at Mainz, and the HAPPEX and GØ experiments at Jefferson Lab, have focussed on the strange quark content of the nucleon [146].

A_{RL} can also be measured in fixed target polarized Møller scattering, $e^-e^- \rightarrow e^-e^-$, and reads [147],

$$\frac{A_{RL}}{Q^2} = -2g_{AV}^{ee} \frac{G_F}{\sqrt{2}\pi\alpha} \frac{1-y}{1+y^4+(1-y)^4}. \quad (10.30)$$

It has been determined at low $Q^2 = 0.026 \text{ GeV}^2$ in the SLAC E158 experiment [148], with the result, $A_{RL} = (-1.31 \pm 0.14_{\text{stat.}} \pm$

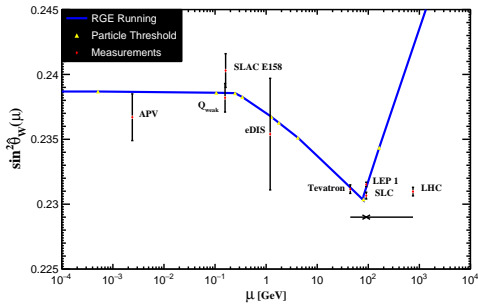


Figure 10.2: Scale dependence of the weak mixing angle defined in the $\overline{\text{MS}}$ scheme [35, 74] (for the scale dependence in a mass-dependent renormalization scheme, see Ref. [73]). The minimum of the curve corresponds to $\mu = M_W$, below which we switch to an effective theory with the W^\pm bosons integrated out, and where the β -function for $\hat{s}^2(\mu)$ changes sign. At M_W and each fermion mass there are also discontinuities arising from scheme dependent matching terms, which are necessary to ensure that the various effective field theories within a given loop order describe the same physics. However, in the $\overline{\text{MS}}$ scheme these are very small numerically and barely visible in the figure provided one decouples quarks at $\mu = \hat{m}_q(\hat{m}_q)$. The width of the curve exceeds the theory uncertainty from strong interaction effects which at low energies is at the level of $\pm 2 \times 10^{-5}$ [35]. The Tevatron and LHC measurements are strongly dominated by invariant masses of the final-state di-lepton pair of $\mathcal{O}(M_Z)$ and can thus be considered as additional Z pole data points. For clarity we displayed the Tevatron and LHC points horizontally to the left and right, respectively.

$0.10_{\text{sys.}}) \times 10^{-7}$. Expressed in terms of the weak mixing angle in the $\overline{\text{MS}}$ scheme this yields $\hat{s}^2(161 \text{ MeV}) = 0.2403 \pm 0.0013$, and as shown in Fig. 10.2 established the scale dependence of the weak mixing angle at the level of 6.4σ . One also extracts the model-independent effective coupling, $g_{AV}^{ee} = 0.0190 \pm 0.0027$ [13]. One-loop radiative corrections and implications are discussed in Ref. [73].

In a similar experiment and at about the same $Q^2 = 0.0248 \text{ GeV}^2$, the Q_{weak} collaboration at Jefferson Lab obtained $A_{RL} = (-2.265 \pm 0.073_{\text{stat.}} \pm 0.058_{\text{sys.}}) \times 10^{-7}$ [149, 150] in elastic $e^-p \rightarrow e^-p$ scattering. To extract the physical quantity of interest, the weak charge of the proton [151], a large ($\approx 30\%$) correction had to be applied to A_{RL} arising from electromagnetic, strange, and axial form factors. This was achieved by

performing a global fit [152] including a large number of A_{RL} data points at larger Q^2 , dominated by the HAPPEX result at $Q^2 = 0.109 \text{ GeV}^2$ [153]. Finally, the constraint, $2g_{AV}^{eu} + g_{AV}^{ed} = 0.0356 \pm 0.0023$, which translates into a weak mixing angle measurement of $\hat{s}^2(157 \text{ MeV}) = 0.2382 \pm 0.0011$, could be deduced, after correcting for a relatively large and uncertain contribution from the γZ box diagram [154–157].

10.3.3 Atomic parity violation

There are precise measurements of atomic parity violation (APV) [9, 158, 159] in ¹³³Cs [160, 161] (at the 0.4% level [160]), ²⁰⁵Tl [162, 163], ²⁰⁸Pb [164], and ²⁰⁹Bi [165]. The EW physics is contained in the nuclear weak charges $Q_W(Z, N)$, where Z and N are the numbers of protons and neutrons in the nucleus. In terms of the nucleon vector couplings,

$$g_{AV}^{ep} \equiv 2g_{AV}^{eu} + g_{AV}^{ed} \approx -\frac{1}{2} + 2\hat{s}_0^2, \quad (10.31a)$$

$$g_{AV}^{en} \equiv g_{AV}^{eu} + 2g_{AV}^{ed} \approx +\frac{1}{2}, \quad (10.31b)$$

one has,

$$Q_W(Z, N) \equiv -2 \left[Z(g_{AV}^{ep} + 0.00005) + N(g_{AV}^{en} + 0.00006) \right] \times \left(1 - \frac{\alpha}{2\pi} \right), \quad (10.32)$$

where the numerically small adjustments are discussed in Ref. [13] and include the result of the γZ -box correction from Ref. [166].

E.g., $Q_W(^{133}\text{Cs})$ is extracted by measuring experimentally the ratio of the parity violating amplitude, E_{PNC} , to the Stark vector transition polarizability, β , and by calculating theoretically E_{PNC} in terms of Q_W . One can then write,

$$Q_W(^{133}\text{Cs}) = N \left(\frac{\text{Im } E_{\text{PNC}}}{\beta} \right)_{\text{exp.}} \left(\frac{|e|a_B Q_W}{\text{Im } E_{\text{PNC}} N} \right)_{\text{th.}} \times \left(\frac{\beta}{a_B^3} \right)_{\text{exp.+th.}} \left(\frac{a_B^2}{|e|} \right), \quad (10.33)$$

where a_B is the Bohr radius. There are currently two semi-empirical approaches to β of similar precision. The ratio of the off-diagonal hyperfine amplitude to the vector polarizability was measured directly by the Boulder group [167]. Combined with the hyperfine amplitude, computed precisely in Ref. [168], one finds $\beta = (26.957 \pm 0.044_{\text{exp.}} \pm 0.027_{\text{th.}}) a_B^3$. Alternatively, one can combine [169] the measurement of the ratio of scalar to vector transition polarizabilities [170] with the recent calculation of the scalar polarizability [171] to obtain $\beta = (27.139 \pm 0.030_{\text{exp.}} \pm 0.030_{\text{th.}}) a_B^3$, in agreement with earlier results [172, 173] based on this approach. The two determinations average to $\beta = (27.064 \pm 0.025_{\text{exp.}} \pm 0.021_{\text{th.}}) a_B^3$, while they differ by 2.7σ .

The uncertainties associated with the atomic wave function calculations are relatively small for cesium [9, 174–176]. State-of-the-art many-body atomic structure computations of the parity non-conserving amplitude, $\text{Im } E_{\text{PNC}} = (0.8977 \pm 0.0040) \times 10^{-11} |e| a_B Q_W/N$ [177–182], together with the measurements [160, 161] which can be combined to give $\text{Im } E_{\text{PNC}}/\beta = -1.5924 \pm 0.0055 \text{ mV/cm}$, imply,

$$Q_W(^{133}\text{Cs}) = -72.82 \pm 0.26_{\text{exp.}} \pm 0.33_{\text{th.}}, \quad (10.34)$$

or equivalently the constraint, $55g_{AV}^{ep} + 78g_{AV}^{en} = 36.46 \pm 0.21$. Within the SM this can also be translated into a determination of the weak mixing angle, $\hat{s}^2(2.4 \text{ MeV}) = 0.2367 \pm 0.0018$, where the scale setting follows the estimate in Ref. [183] for the typical momentum transfer for parity violation experiments in Cs (the corresponding estimate for Tl amounts to 8 MeV). By comparing different hyperfine transitions, the Boulder experiment in cesium also observed the parity violating weak corrections to the nuclear electromagnetic vertex, called the nuclear anapole moment [184–186].

The theoretical atomic structure uncertainties are 3% for thallium [187] and even larger for the other atoms. However, they mostly cancel if one takes ratios of parity violation in different isotopes [188]. The first result of this type of experiment was announced very recently by the Mainz group [189], who studied APV in ^{100}Yb , ^{102}Yb , ^{104}Yb , and ^{106}Yb , at the 0.5% level. The resulting three ratios can be interpreted as a measurement of $\widehat{s}_0^2 = 0.258 \pm 0.052$, and represent a very complementary approach to search for BSM physics [190]. If the precision increases in the future, one would ultimately face uncertainties from differences in the neutron charge radii [191, 192]. These can be constrained experimentally [193], *e.g.*, by measuring A_{RL} in heavier nuclei as done by the PREX collaboration at Jefferson Lab on ^{208}Pb [194].

10.4 Precision flavor physics

In addition to cross-sections, asymmetries, parity violation, W , Z , Higgs and other collider physics, there is a large number of experiments and observables testing the flavor structure of the SM. These are addressed elsewhere in this *Review*, and are generally not included in this Section. However, we identify three precision observables with sensitivity to similar types of new physics as the other processes discussed here. The branching fraction of the flavor changing transition $b \rightarrow s\gamma$ is of comparatively low precision, but since it is a loop-level process (in the SM) its sensitivity to new physics (and SM parameters, such as heavy quark masses) is enhanced. A discussion can be found in the 2010 edition of this *Review*.

The τ lepton lifetime and leptonic branching ratios are primarily sensitive to α_s and not affected significantly by many types of new physics. However, having an independent and reliable low energy measurement of α_s in a global analysis allows the comparison with the Z lineshape determination of α_s which shifts easily in the presence of new physics contributions. By far the most precise observable discussed here is the anomalous magnetic moment of the muon. Its combined experimental and theoretical uncertainty is smaller than typical electroweak scale contributions. The electron magnetic moment is measured to even greater precision, and as discussed in Sec. 10.2.2 can be used to determine α . Its new physics sensitivity, however, is suppressed by an additional factor of m_e^2/m_μ^2 , unless there is a new light degree of freedom such as a dark Z [195] boson.

10.4.1 The τ lifetime

The extraction of α_s from the τ lifetime τ_τ [196, 197] is standing out from other determinations because of a variety of independent reasons:

- (i) The τ -scale is low, so that upon extrapolation to the Z scale (where it can be compared to the theoretically clean Z lineshape determinations) the α_s error shrinks by about an order of magnitude.
- (ii) Yet, this scale is high enough that perturbation theory and the operator product expansion (OPE) can be applied.
- (iii) These observables are fully inclusive and thus free of fragmentation and hadronization effects that would have to be modeled or measured.
- (iv) Duality violation (DV) effects are most problematic near the branch cut but there they are suppressed by a double zero at $s = m_\tau^2$.
- (v) There are data [39, 41, 198] to constrain non-perturbative effects both within and breaking the OPE.
- (vi) A complete four-loop order QCD calculation is available [199–203] in the massless limit.
- (vii) Large effects associated with the QCD β -function can be re-summed [204] in what has become known as contour improved perturbation theory (CIPT).

However, while CIPT certainly shows faster convergence in the lower (calculable) orders, doubts have been cast on the method by the observation that at least in a specific model [205], which includes the exactly known coefficients and theoretical constraints on the large-order behavior, ordinary fixed order perturbation theory (FOPT) may nevertheless give a better approximation to the

full result. We therefore use the expressions [53, 203, 206],

$$\tau_\tau = \hbar \frac{1 - \mathcal{B}_\tau^s}{\Gamma_\tau^e + \Gamma_\tau^\mu + \Gamma_\tau^{ud}} = 290.75 \pm 0.36 \text{ fs} , \quad (10.35)$$

and

$$\Gamma_\tau^{ud} = \frac{G_F^2 m_\tau^5 |V_{ud}|^2}{64\pi^3} S(m_\tau, M_Z) \left(1 + \frac{3}{5} \frac{m_\tau^2 - m_\mu^2}{M_W^2} \right) \times \left[1 + \frac{\alpha_s(m_\tau)}{\pi} + 5.202 \frac{\alpha_s^2}{\pi^2} + 26.37 \frac{\alpha_s^3}{\pi^3} + 127.1 \frac{\alpha_s^4}{\pi^4} + \widehat{\alpha} \left(\frac{85}{24} - \frac{\pi^2}{2} \right) + \delta_{\text{NP}} \right] , \quad (10.36)$$

where Γ_τ^e and Γ_τ^μ can be taken from Eq. (10.7) with obvious replacements. The relative fraction of strangeness changing ($\Delta S = -1$) decays, $\mathcal{B}_\tau^s = 0.0292 \pm 0.0004$, is based on experimental data since the value for the strange quark mass, $\widehat{m}_s(m_\tau)$, is not well known and the QCD expansion proportional to \widehat{m}_s^2 converges poorly and cannot be trusted. $S(m_\tau, M_Z) = 1.01907 \pm 0.0003$ is a logarithmically enhanced EW correction factor [207] with higher orders re-summed [208].

δ_{NP} collects non-perturbative and quark-mass suppressed contributions, including the dimension four, six and eight terms in the OPE, as well as DV effects. We use the average $\delta_{\text{NP}} = 0.0141 \pm 0.0072$ derived from the τ decay spectral functions provided by OPAL [39] and ALEPH [41, 198], which give $\delta_{\text{NP}} = 0.000 \pm 0.012$ and $\delta_{\text{NP}} = 0.022 \pm 0.009$, respectively. These numbers are based on the original analyses in Refs. [209, 210], but are modified to correspond to a strict FOPT analysis as is appropriate for our purpose¹¹ (for alternative analyses, see Refs. [197, 198, 211]).

The dominant uncertainty arises from the truncation of the FOPT series and is conservatively taken as the α_s^4 term (this is re-calculated in each call of the fits, leading to an α_s -dependent and thus asymmetric error) until a better understanding of the numerical differences between FOPT and CIPT has been gained. Our perturbative error covers almost the entire range from using CIPT to assuming that the nearly geometric series in Eq. (10.36) continues to higher orders. The experimental uncertainty in Eq. (10.35) is from the combination of the two leptonic branching ratios with the direct τ_τ . Included are also various smaller uncertainties (± 0.15 fs) from other sources. Based on the method of Refs. [53, 212], we obtain in total

$$\alpha_s^{(4)}(m_\tau) = 0.312_{-0.013}^{+0.016} , \quad \alpha_s^{(5)}(M_Z) = 0.1170_{-0.0017}^{+0.0019} , \quad (10.37)$$

which represents a 1.5% determination of $\alpha_s(M_Z)$. For more details, see Refs. [209, 210] where the τ spectral functions themselves and an estimate of the unknown α_s^5 term were used as additional inputs.

10.4.2 The muon anomalous magnetic moment

The world average of the muon anomalous magnetic moment¹²,

$$a_\mu^{\text{exp}} = \frac{g_\mu - 2}{2} = (1165920.91 \pm 0.63) \times 10^{-9} , \quad (10.38)$$

is dominated by the final result of the BNL E821 collaboration [213]. The QED contribution has been calculated to five loops [214–216] (fully analytic to three loops [217–221] and semi-analytic to four loops [222]). The estimated SM EW contribution [223–228], $a_\mu^{\text{EW}} = (1.54 \pm 0.01) \times 10^{-9}$, includes two

¹¹We are indebted to Diogo Boito, Maarten Golterman, Kim Maltman and Santiago Peris for privately communicating these results to us.

¹²In what follows, we summarize the most important aspects of a_μ and give some details on the evaluation in our fits. For more details and references, see the Section on the ‘‘Muon Anomalous Magnetic Moment’’ in this *Review*. There are some numerical differences, which are well understood and arise because internal consistency of the fits requires the calculation of all observables from analytical expressions and common inputs and fit parameters, so that an independent evaluation is necessary for this Section. Note, that in the spirit of a global analysis based on all available information we have chosen here to also include τ decay data [30], corrected for isospin breaking effects [31].

loop [229–233] and leading three-loop [234, 235] corrections and is at the level of twice the current uncertainty.

The limiting factor in the interpretation of the result are the uncertainties from hadronic effects. The most recent evaluations of the leading-order (two-loop) hadronic vacuum polarization contribution obtained $a_\mu^{\text{had,VP}}(\alpha^2) = (68.81 \pm 0.41) \times 10^{-9}$ [236], $a_\mu^{\text{had,VP}}(\alpha^2) = (69.39 \pm 0.40) \times 10^{-9}$ [29], and $a_\mu^{\text{had,VP}}(\alpha^2) = (69.28 \pm 0.24) \times 10^{-9}$ [37]. These are mainly based on data from $e^+e^- \rightarrow \text{hadrons}$ (see, *e.g.*, Ref. [29] for references). Our analysis combines the e^+e^- [29] and τ -decay data [30, 31] for contributions up to $\sqrt{s} = 2$ GeV, $a_\mu^{\text{had,VP}}(\alpha^2, 2 \text{ GeV}) = (64.49 \pm 0.33) \times 10^{-9}$, with analytical PQCD expressions for energies beyond 2 GeV and for the c and b quark contributions [221]. By now there are also precise results for the determination of $a_\mu^{\text{had,VP}}(\alpha^2)$ from lattice QCD calculations [237] at the 2–3% level [238–242], while the most recent one has a 0.6% quoted uncertainty [243] (for a comparative appraisal and further references, see Ref. [244]). The result of Ref. [243], $(71.24 \pm 0.45) \times 10^{-9}$, has a more than 3σ conflict with the data-driven evaluations, while there is very good statistical agreement among the different lattice results, assuming them to be uncorrelated ($\chi^2/\text{d.o.f.} = 5.1/5$). If confirmed, the recent lattice determinations for $a_\mu^{\text{had,VP}}(\alpha^2)$ may point to a problem with the data-driven approach to this quantity.

The other hadronic uncertainty is induced by the three-loop light-by-light scattering amplitude, where a number of independent model calculations yield results which are in reasonable agreement with each other, $a_\mu^{\text{had,\gamma}\times\gamma}(\alpha^3) = (1.36 \pm 0.25) \times 10^{-9}$ [245], $a_\mu^{\text{had,\gamma}\times\gamma}(\alpha^3) = 1.37^{+0.15}_{-0.27} \times 10^{-9}$ [246], $a_\mu^{\text{had,\gamma}\times\gamma}(\alpha^3) = (1.05 \pm 0.26) \times 10^{-9}$ [247], and $a_\mu^{\text{had,\gamma}\times\gamma}(\alpha^3) = (1.03 \pm 0.29) \times 10^{-9}$ [236], but the sign of this effect is opposite [248] to the one quoted in the 2002 edition of this *Review*. There is also an upper bound given by $a_\mu^{\text{had,\gamma}\times\gamma}(\alpha^3) < 1.59 \times 10^{-9}$ [246] but this requires an *ad hoc* assumption, too. An effort to improve the evaluation of the light-by-light contribution by using experimental input where available yields a slightly lower value, $a_\mu^{\text{had,\gamma}\times\gamma}(\alpha^3) = (0.87 \pm 0.13) \times 10^{-9}$ [249]. A first complete result from lattice simulations, $a_\mu^{\text{had,\gamma}\times\gamma}(\alpha^3) = (0.79 \pm 0.35) \times 10^{-9}$ [250], accounting for all systematic errors, is consistent with the model and data-driven calculations. For the fits, we take the result from Ref. [236], shifted by 2×10^{-11} to account for the more accurate charm quark treatment of Ref. [246], and with increased error to cover all recent evaluations, resulting in $a_\mu^{\text{had,\gamma}\times\gamma}(\alpha^3) = (1.05 \pm 0.33) \times 10^{-9}$.

Sub-leading hadronic vacuum polarization effects at three-loop [251] and four-loop order [252] contribute $a_\mu^{\text{had,VP}}(\alpha^3) = (-0.983 \pm 0.004) \times 10^{-9}$ [37] and $a_\mu^{\text{had,VP}}(\alpha^4) = (0.124 \pm 0.001) \times 10^{-9}$ [252], respectively. The correlations with the two-loop hadronic contribution and with $\Delta\alpha(M_Z)$ (see Sec. 10.2) were considered in Ref. [221]. The contributions with a hadronic light-by-light scattering subgraph have been estimated in Ref. [253], with the result, $a_\mu^{\text{had,\gamma}\times\gamma}(\alpha^4) = (0.03 \pm 0.02) \times 10^{-9}$.

Altogether, the SM prediction is

$$a_\mu^{\text{theory}} = (1165918.46 \pm 0.47) \times 10^{-9}, \quad (10.39)$$

where the error is from the hadronic uncertainties excluding parametric ones such as from α_s and the heavy quark masses. We evaluate the correlation of the total (experimental plus theoretical) uncertainty in a_μ with $\Delta\alpha(M_Z)$ to amount to roughly 30%. The overall 3.1σ discrepancy between a_μ^{theory} and a_μ^{exp} could be due to fluctuations (the E821 result is statistics dominated) or underestimates of the theoretical uncertainties. On the other hand, the deviation could also arise from physics beyond the SM, such as supersymmetric models with large $\tan\beta$ and moderately light superparticle masses [254], or a dark Z boson [195].

10.5 Physics of the massive electroweak bosons

If the CM energy \sqrt{s} is large compared to the fermion mass m_f , the unpolarized Born cross-section for $e^+e^- \rightarrow f\bar{f}$ [255] can

be written as,

$$\frac{d\sigma}{d\cos\theta} = \frac{\pi\alpha^2(s)}{2s} [F_1(1 + \cos^2\theta) + 2F_2\cos\theta] + B, \quad (10.40a)$$

$$F_1 = Q_e^2 Q_f^2 - 2\chi Q_e Q_f \bar{g}_V^e \bar{g}_V^f \cos\delta_R + \chi^2 (\bar{g}_V^e{}^2 + \bar{g}_A^e{}^2) (\bar{g}_V^f{}^2 + \bar{g}_A^f{}^2), \quad (10.40b)$$

$$F_2 = -2\chi Q_e Q_f \bar{g}_A^e \bar{g}_A^f \cos\delta_R + 4\chi^2 \bar{g}_V^e \bar{g}_A^e \bar{g}_V^f \bar{g}_A^f, \quad (10.40c)$$

where,

$$\tan\delta_R = \frac{\bar{M}_Z \bar{\Gamma}_Z}{\bar{M}_Z^2 - s}, \quad \chi = \frac{G_F}{2\sqrt{2}\pi\alpha(s)} \frac{s\bar{M}_Z^2}{\left[(\bar{M}_Z^2 - s)^2 + \bar{M}_Z^2 \bar{\Gamma}_Z^2\right]^{1/2}}. \quad (10.41)$$

B accounts for box graphs involving virtual Z and W bosons, and the $\bar{g}_{V,A}^f$ are defined in Eq. (10.42) below. \bar{M}_Z and $\bar{\Gamma}_Z$ correspond to mass and width definitions based on a Breit-Wigner shape with an energy-independent width (see the Section on the “ Z Boson” in this *Review*). The differential cross-section receives important corrections from QED effects in the initial and final state, and interference between the two [256]. For $q\bar{q}$ production, there are additional final-state QCD corrections, which are relatively large. Note also that the equations above are written in the CM frame of the incident e^+e^- system, which may be boosted due to the initial-state QED radiation.

Some of the leading virtual EW corrections are captured by the running QED coupling $\alpha(s)$ and the Fermi constant G_F . The remaining corrections to the $Zf\bar{f}$ interactions are absorbed by replacing the tree-level couplings in Eq. (10.6) with the s -dependent *effective couplings* [14],

$$\bar{g}_V^f = \sqrt{\rho_f} (t_{3L}^f - 2Q_f \kappa_f \sin^2\theta_W), \quad (10.42a)$$

$$\bar{g}_A^f = \sqrt{\rho_f} t_{3L}^f. \quad (10.42b)$$

In these equations, the effective couplings are to be taken at the scale \sqrt{s} , but for notational simplicity we do not show this explicitly. At tree-level, $\rho_f = \kappa_f = 1$, but inclusion of EW radiative corrections leads to $\rho_f \neq 1$ and $\kappa_f \neq 1$, which depend on the fermion f and on the renormalization scheme. In the on-shell scheme, the quadratic m_t dependence is given by,

$$\rho_f \sim 1 + \rho_t, \quad \kappa_f \sim 1 + \frac{\rho_t}{\tan^2\theta_W}, \quad (10.43)$$

while in $\overline{\text{MS}}$, $\hat{\rho}_f \sim \hat{\kappa}_f \sim 1$, for $f \neq b$, and

$$\hat{\rho}_b \sim 1 - \frac{4}{3}\rho_t, \quad \hat{\kappa}_b \sim 1 + \frac{2}{3}\rho_t. \quad (10.44)$$

In the $\overline{\text{MS}}$ scheme the normalization is changed according to $G_F M_Z^2 / 2\sqrt{2}\pi \rightarrow \hat{\alpha} / 4\hat{s}_Z^2 \hat{c}_Z^2$ in the second Eq. (10.41).

As reviewed in Sec. 10.2.5, for the high precision Z pole observables discussed below, many additional bosonic and fermionic loop effects, vertex corrections, and higher order contributions, *etc.*, must be included. For example, in the $\overline{\text{MS}}$ scheme one has $\hat{\rho}_e = 0.9977$, $\hat{\kappa}_e = 1.0014$, $\hat{\rho}_b = 0.9866$, and $\hat{\kappa}_b = 1.0068$.

To connect to measured quantities, it is convenient to define an effective angle

$$\bar{s}_f^2 \equiv \sin^2\bar{\theta}_{Wf} \equiv \hat{\kappa}_f \hat{s}_Z^2 = \kappa_f s_W^2, \quad (10.45)$$

in terms of which \bar{g}_V^f and \bar{g}_A^f are given by $\sqrt{\rho_f}$ times their tree-level formulae. One finds that the $\hat{\kappa}_f$ ($f \neq b$) are almost independent of m_t and M_H , and thus one can write,

$$\bar{s}_f^2 = \hat{s}_Z^2 + 0.00032, \quad (10.46)$$

while the κ_f for the on-shell scheme are m_t dependent.

10.5.1 Electroweak physics off the Z pole

Experiments at PEP, PETRA and TRISTAN have measured the unpolarized forward-backward asymmetry, A_{FB} , and the total cross-section relative to pure QED, R , for $e^+e^- \rightarrow \ell^+\ell^-$, $\ell = \mu$ or τ at CM energies $\sqrt{s} < M_Z$. They are defined as

$$A_{FB} \equiv \frac{\sigma_F - \sigma_B}{\sigma_F + \sigma_B}, \quad R = \frac{\sigma}{\mathcal{R}_{\text{ini}} \otimes 4\pi\alpha^2/3s}, \quad (10.47)$$

where σ_F (σ_B) is the cross-section for ℓ^- to travel forward (backward) with respect to the e^- direction, and $\mathcal{R}_{\text{ini}} \otimes$ denotes convolution with initial-state QED corrections. Neglecting box graph contributions, they are given by,

$$A_{FB} = \frac{3}{4} \frac{F_2}{F_1}, \quad R = F_1. \quad (10.48)$$

For the available data, it is sufficient to approximate the EW corrections through the leading running $\alpha(s)$ and quadratic m_t contributions [257], as described above. Reviews and formulae for $e^+e^- \rightarrow$ hadrons may be found in [9, 258, 259].

LEP 2 [260] ran at several energies above the Z pole up to ~ 209 GeV. Measurements were made of a number of observables, including the total production cross-sections of $f\bar{f}$ pairs for $f = \mu, \tau$, and q (hadrons), of four-fermion final states, of $\gamma\gamma$, ZZ , WW , $WW\gamma$, and WWZ , as well as of single resonant W and Z bosons. The differential cross-sections for all three lepton flavors, and the leptonic and hadronic W branching ratios were also extracted.

Among the most important LEP 2 results were the measurements [260] of the W boson mass,

$$M_W = 80.376 \pm 0.025_{\text{stat.}} \pm 0.022_{\text{syst.}} \text{ GeV (LEP 2)}, \quad (10.49)$$

which were dominated by kinematic reconstruction, but included the complementary albeit statistics limited and thus much less precise determination from a WW threshold cross section scan. The kinematic method was also employed at the Tevatron [261] and by ATLAS [263]. They quote,

$$M_W = 80.387 \pm 0.016 \text{ GeV (Tevatron)}, \quad (10.50a)$$

$$M_W = 80.3695 \pm 0.0068_{\text{stat.}} \pm 0.0106_{\text{syst.}} \pm 0.0136_{\text{th.}} \text{ GeV (ATLAS)}. \quad (10.50b)$$

We assume an error component of 7 MeV to be common between the two hadron collider determinations. This is smaller than the 10 MeV PDF uncertainty quoted by CDF, because the larger CM energy at the LHC enhances the sensitivity to second generation quark PDFs, in addition to the greater sea quark PDF dependence of the Drell-Yan process in the pp environment. There may also be some correlation due to other production modeling uncertainties. This implies for the average,

$$M_W = 80.379 \pm 0.012 \text{ GeV (world average)}. \quad (10.51)$$

For details and references, see the Section on the ‘‘Mass and Width of the W Boson’’ in this *Review*.

Strong constraints on anomalous triple and quartic gauge couplings have been obtained at LEP 2, the Tevatron, and the LHC. These are described in detail in the three Sections on the ‘‘Extraction of Triple Gauge Couplings (TGCs)’’, ‘‘Anomalous W/Z Quartic Couplings (QGCs)’’, and ‘‘Anomalous $ZZ\gamma$, $Z\gamma\gamma$, and ZZV Couplings’’ in this *Review*.

After their discovery of the Higgs boson [264, 265], the LHC experiments are now performing high precision measurements of its mass. We average the results, $M_H = 124.97 \pm 0.16_{\text{stat.}} \pm 0.18_{\text{syst.}} \text{ GeV}$ from ATLAS [266], and $M_H = 125.38 \pm 0.11_{\text{stat.}} \pm 0.09_{\text{syst.}} \text{ GeV}$ from CMS [267], by conservatively treating the smaller systematic error as common among the two determinations, and arrive at,

$$M_H = 125.30 \pm 0.09_{\text{stat.}} \pm 0.09_{\text{syst.}} \text{ GeV (LHC)}. \quad (10.52)$$

For further references and many more details on Higgs boson properties, see the Section on the ‘‘Status of Higgs Boson Physics’’ in this *Review*. The principal non- Z pole observables discussed here and in Sections 10.2–10.4 are summarized in Table 10.4.

10.5.2 Z pole physics

High precision measurements of various Z pole ($\sqrt{s} \approx M_Z$) observables [9, 276, 277] have been performed at LEP 1 and SLC [14, 273, 274, 278, 279], as summarized in Table 10.5. These include the Z mass and total width, Γ_Z , and partial widths $\Gamma_{f\bar{f}}$ for $Z \rightarrow f\bar{f}$, where $f = e, \mu, \tau$, light hadrons, b , and c . It is convenient to use the variables M_Z, Γ_Z ,

$$\sigma_{\text{had}} \equiv \frac{12\pi\Gamma_{e^+e^-}\Gamma_{\text{had}}}{M_Z^2\Gamma_Z^2}, \quad R_\ell \equiv \frac{\Gamma_{\text{had}}}{\Gamma_{\ell^+\ell^-}}, \quad R_q \equiv \frac{\Gamma_{q\bar{q}}}{\Gamma_{\text{had}}}, \quad (10.53)$$

for $\ell = e, \mu$ or τ , and $q = b$ or c , where Γ_{had} is the partial width into hadrons. Most of these are weakly correlated experimentally. The three values for R_ℓ are consistent with lepton universality (although R_τ is somewhat low compared to R_e and R_μ), but we use the general analysis in which the three observables are treated as independent. Similar remarks apply to $A_{FB}^{0,\ell}$ defined through Eq. (10.54) with $P_e = 0$, where $A_{FB}^{0,\tau}$ is somewhat high. Initial-state radiation reduces the peak cross section by more than 25%, where $\mathcal{O}(\alpha^3)$ QED effects induce a large anti-correlation (-30%) between Γ_Z and σ_{had} . The anti-correlation between R_b and R_c amounts to -18% [14]. The R_ℓ are insensitive to m_t except for the $Z \rightarrow b\bar{b}$ vertex, final-state corrections, and the implicit dependence through $\sin^2\theta_W$. Thus, they are especially useful for constraining α_s .

Very important constraints follow from measurements of various Z pole asymmetries. These include the forward-backward asymmetry, A_{FB} , and the polarization or left-right asymmetry, A_{LR} , defined analogously to Eq. (10.27). The latter was measured precisely by the SLD collaboration at the SLC [273], and has the advantages of being very sensitive to \bar{s}_ℓ^2 and that systematic uncertainties largely cancel. After removing initial-state QED corrections and contributions from photon exchange, γ - Z interference, as well as the EW boxes in Eq. (10.40a), one can use the effective tree-level expressions,

$$A_{LR} = A_e P_e, \quad A_{FB} = \frac{3}{4} A_f \frac{A_e + P_e}{1 + P_e A_e}, \quad (10.54)$$

where,

$$A_f \equiv \frac{2\bar{g}_V^f \bar{g}_A^f}{\bar{g}_V^{f2} + \bar{g}_A^{f2}} = \frac{1 - 4|Q_f|\bar{s}_f^2}{1 - 4|Q_f|\bar{s}_f^2 + 8(|Q_f|\bar{s}_f^2)^2}. \quad (10.55)$$

P_e is the initial e^- polarization, so that the second equality in Eq. (10.56) is reproduced for $P_e = 1$, and the Z pole forward-backward asymmetries at LEP 1 ($P_e = 0$) are given by $A_{FB}^{(0,f)} = \frac{3}{4} A_e A_f$ for $f = e, \mu, \tau, b, c, s$ [14], and q , and where $A_{FB}^{(0,q)}$ refers to the hadronic charge asymmetry. Corrections for t -channel exchange and s/t -channel interference cause $A_{FB}^{(0,e)}$ to be strongly anti-correlated with R_e (-37%). Very recently, the m_b -dependence [280] of the $\mathcal{O}(\alpha_s^2)$ QCD correction [281], affecting the reference axis of the b quark asymmetry [282], increased the extracted¹³ $A_{FB}^{(0,b)}$ by about 0.2σ . The correlation between $A_{FB}^{(0,b)}$ and $A_{FB}^{(0,c)}$ amounts to 15%.

In addition, SLD extracted the final-state couplings A_b, A_c [14], A_s [278], A_τ , and A_μ [274], from left-right forward-backward asymmetries, using

$$A_{LR}^{FB}(f) = \frac{\sigma_{LF}^f - \sigma_{LB}^f - \sigma_{RF}^f + \sigma_{RB}^f}{\sigma_{LF}^f + \sigma_{LB}^f + \sigma_{RF}^f + \sigma_{RB}^f} = \frac{3}{4} A_f, \quad (10.56)$$

where, for example, σ_{LF}^f is the cross-section for a left-handed incident electron to produce a fermion f traveling in the forward hemisphere. Similarly, A_τ and A_e were measured at LEP 1 [14] through the τ polarization, \mathcal{P}_τ , as a function of the scattering

¹³We are grateful to Werner Bernreuther and Long Chen for the recalculation of their result employing the more appropriate $\overline{\text{MS}}$ mixing angle, \bar{s}_Z^2 , instead of the on-shell quantity, s_W^2 .

Table 10.4: Non- Z pole observables, compared with the SM best fit predictions. The first M_W and Γ_W values are from the Tevatron [261, 262], the second ones from LEP 2 [260], while the third M_W is from ATLAS [263]. The entry of m_t differs from the one in the Particle Listings as it includes an additional theory error. The world averages for $g_{V,A}^{\nu e}$ are dominated by the CHARM II [122] results, $g_V^{\nu e} = -0.035 \pm 0.017$ and $g_A^{\nu e} = -0.503 \pm 0.017$. The τ_τ value is the τ lifetime world average computed by combining the direct measurements with values derived from the leptonic branching ratios [53]; in this case, the theory error is included in the SM prediction. In all other SM predictions, the uncertainty is parametric from M_Z , M_H , m_t , m_b , m_c , $\hat{\alpha}(M_Z)$, and α_s , and theoretical from unknown higher orders [69], where correlations due to both types have been accounted for. The column denoted by Pull gives the standard deviations.

Quantity	Value	Standard Model	Pull
m_t [GeV]	172.89 ± 0.59	173.19 ± 0.55	-0.5
M_H [GeV]	125.30 ± 0.13	125.30 ± 0.13	0.0
M_W [GeV]	80.387 ± 0.016	80.361 ± 0.006	1.6
	80.376 ± 0.033		0.5
	80.370 ± 0.019		0.5
Γ_W [GeV]	2.046 ± 0.049	2.090 ± 0.001	-0.9
	2.195 ± 0.083		1.3
$g_V^{\nu e}$	-0.040 ± 0.015	-0.0398 ± 0.0001	0.0
$g_A^{\nu e}$	-0.507 ± 0.014	-0.5064	0.0
$Q_W(e)$	-0.0403 ± 0.0053	-0.0476 ± 0.0002	1.4
$Q_W(p)$	0.0719 ± 0.0045	0.0711 ± 0.0002	0.2
$Q_W(Cs)$	-72.82 ± 0.42	-73.23 ± 0.01	1.0
$Q_W(Tl)$	-116.4 ± 3.6	-116.88 ± 0.02	0.1
$\hat{s}_Z^2(\text{eDIS})$	0.2299 ± 0.0043	0.23121 ± 0.00004	-0.3
τ_τ [fs]	290.75 ± 0.36	288.90 ± 2.24	0.8
$\frac{1}{2}(g_\mu - 2 - \frac{\alpha}{\pi})$	$(4511.18 \pm 0.78) \times 10^{-9}$	$(4508.74 \pm 0.03) \times 10^{-9}$	3.1

angle θ , which can be written as,

$$\mathcal{P}_\tau = -\frac{A_\tau(1 + \cos^2 \theta) + 2A_e \cos \theta}{(1 + \cos^2 \theta) + 2A_\tau A_e \cos \theta}. \quad (10.57)$$

The average polarization, $\langle \mathcal{P}_\tau \rangle$, obtained by integrating over $\cos \theta$ in the numerator and denominator of Eq. (10.57), yields $\langle \mathcal{P}_\tau \rangle = -A_\tau$, and A_e can be extracted from the \mathcal{P}_τ angular distribution. The initial-state coupling, A_e , was also determined through the left-right charge asymmetry [279] and in polarized Bhabba scattering [274] at the SLC. Because \hat{g}_V^f is very small, not only $A_{LR}^0 = A_e$, $A_{FB}^{(0,\ell)}$, and \mathcal{P}_τ , but also $A_{FB}^{(0,q)}$ for $q = b, c$, and s , as well as the hadronic asymmetries are mainly sensitive to \hat{s}_ℓ^2 .

As an example of the precision of the Z pole observables, the values of \hat{g}_A^f and \hat{g}_V^f for $f = e, \mu, \tau$, and ℓ , extracted from the LEP and SLC lineshape and asymmetry data, are shown in Fig. 10.3. It may be compared with Fig. 10.1 as the two sets of parameters coincide at the SM at tree-level.

As for hadron colliders, the forward-backward asymmetry, A_{FB} , for e^+e^- and $\mu^+\mu^-$ final states (with invariant masses restricted to or dominated by values around M_Z) in $p\bar{p}$ collisions has been measured by the CDF [283] and DØ [284] collaborations, and the values $\hat{s}_\ell^2 = 0.23221 \pm 0.00046$ and $\hat{s}_\ell^2 = 0.23095 \pm 0.00040$ were extracted, respectively. The combination of these measurements (which differ by more than 2σ) yields [268],

$$\hat{s}_\ell^2 = 0.23148 \pm 0.00033 \text{ (Tevatron)}. \quad (10.58)$$

By varying the invariant mass and the scattering angle (and assuming the electron couplings), information on the effective Z couplings to light quarks, $\hat{g}_{V,A}^{u,d}$, could also be obtained [285, 286], but with large uncertainties, mutual correlations, and not independently of \hat{s}_ℓ^2 above. Similar analyses have also been reported by the H1 [287] and ZEUS [288] collaborations at HERA and by the LEP collaborations [14]. This kind of measurement is harder in the pp environment due to the difficulty to assign the initial quark and antiquark in the underlying Drell-Yan process to the protons, thus requiring excellent control of uncertainties from parton distribution functions. ATLAS obtained $\hat{s}_\ell^2 = 0.2308 \pm 0.0012$ using 7 TeV data [269] and $\hat{s}_\ell^2 = 0.23140 \pm 0.00036$ at 8 TeV [270],

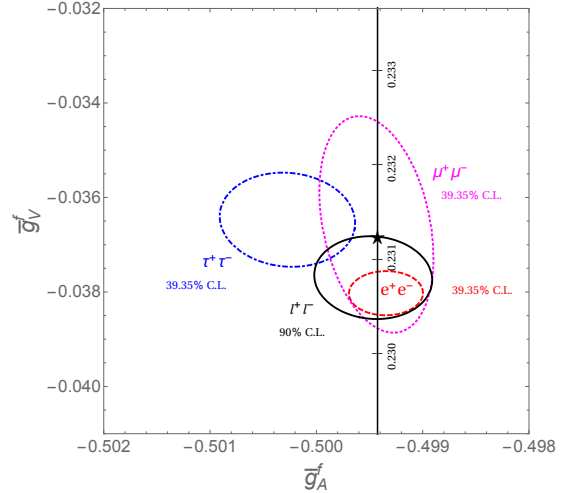


Figure 10.3: 1σ (39.35% CL) contours of the effective couplings \hat{g}_A^f and \hat{g}_V^f for $f = e, \mu$ and τ from LEP and SLC, compared to the SM expectation as a function of \hat{s}_Z^2 . (The SM best fit value $\hat{s}_Z^2 = 0.23121$ is also indicated.) Also shown is the 90% CL allowed region in $\hat{g}_{A,V}^f$ obtained assuming lepton universality.

while CMS measured $\hat{s}_\ell^2 = 0.23101 \pm 0.00053$ (8 TeV) [271] and LHCb reported $\hat{s}_\ell^2 = 0.23142 \pm 0.00106$ (from both 7 and 8 TeV data, but only analyzing $\mu^+\mu^-$ final state) [272]. Assuming that the smallest theoretical and PDF uncertainty (± 0.00024 from ATLAS [270]) is fully correlated among the four determinations, they combine to

$$\hat{s}_\ell^2 = 0.23129 \pm 0.00033 \text{ (LHC)}. \quad (10.59)$$

10.5.3 W and Z decays

The partial decay widths for gauge bosons to decay into massless fermions $f_1\bar{f}_2$ (the numerical values include the small EW

Table 10.5: Principal Z pole observables and their SM predictions (*cf.* Table 10.4). The first \bar{s}_ℓ^2 is the effective weak mixing angle extracted from the hadronic charge asymmetry at LEP 1 [14], the second is the combined value from the Tevatron [268], and the third is from the LHC [269–272]. The values of A_e are (i) from A_{LR} for hadronic final states [273]; (ii) from A_{LR} for leptonic final states and from polarized Bhabba scattering [274]; and (iii) from the angular distribution of the τ polarization at LEP 1 [14]. The A_τ values are from SLD [274] and the total τ polarization, respectively. Note that the SM errors in Γ_Z , the R_ℓ , and σ_{had} are largely dominated by the uncertainty in α_s .

Quantity	Value	Standard Model	Pull
M_Z [GeV]	91.1876 ± 0.0021	91.1882 ± 0.0020	-0.3
Γ_Z [GeV]	2.4955 ± 0.0023	2.4942 ± 0.0009	0.6
σ_{had} [nb]	41.481 ± 0.033	41.482 ± 0.008	0.0
R_e	20.804 ± 0.050	20.736 ± 0.010	1.4
R_μ	20.784 ± 0.034	20.735 ± 0.010	1.4
R_τ	20.764 ± 0.045	20.781 ± 0.010	-0.4
R_b	0.21629 ± 0.00066	0.21581 ± 0.00002	0.7
R_c	0.1721 ± 0.0030	0.17221 ± 0.00003	0.0
$A_{FB}^{(0,e)}$	0.0145 ± 0.0025	0.01619 ± 0.00007	-0.7
$A_{FB}^{(0,\mu)}$	0.0169 ± 0.0013		0.5
$A_{FB}^{(0,\tau)}$	0.0188 ± 0.0017		1.5
$A_{FB}^{(0,b)}$	0.0996 ± 0.0016	0.1030 ± 0.0002	-2.1
$A_{FB}^{(0,c)}$	0.0707 ± 0.0035	0.0736 ± 0.0002	-0.8
$A_{FB}^{(0,s)}$	0.0976 ± 0.0114	0.1031 ± 0.0002	-0.5
\bar{s}_ℓ^2	0.2324 ± 0.0012	0.23153 ± 0.00004	0.7
	0.23148 ± 0.00033		-0.2
	0.23129 ± 0.00033		-0.7
A_e	0.15138 ± 0.00216	0.1469 ± 0.0003	2.1
	0.1544 ± 0.0060		1.2
	0.1498 ± 0.0049		0.6
A_μ	0.142 ± 0.015		-0.3
A_τ	0.136 ± 0.015		-0.7
	0.1439 ± 0.0043		-0.7
A_b	0.923 ± 0.020	0.9347	-0.6
A_c	0.670 ± 0.027	0.6677 ± 0.0001	0.1
A_s	0.895 ± 0.091	0.9356	-0.4

Table 10.6: Results derived from Table 10.5 and the corresponding covariance matrices [14, 275], and the SM predictions for the partial and total Z decay widths [in MeV]. In the (second) third column lepton universality is (not) assumed.

Quantity	Value	Value (universal)	Standard Model
$\Gamma_{e^+e^-}$	83.87 ± 0.12	83.942 ± 0.085	83.964 ± 0.009
$\Gamma_{\mu^+\mu^-}$	83.95 ± 0.18	83.941 ± 0.085	83.963 ± 0.009
$\Gamma_{\tau^+\tau^-}$	84.03 ± 0.21	83.759 ± 0.085	83.780 ± 0.009
Γ_{inv}	498.9 ± 2.5	500.5 ± 1.5	501.464 ± 0.047
$\Gamma_{u\bar{u}}$	—	—	299.91 ± 0.20
$\Gamma_{c\bar{c}}$	300.3 ± 5.3	300.0 ± 5.2	299.83 ± 0.20
$\Gamma_{d\bar{d}}, \Gamma_{s\bar{s}}$	—	—	382.79 ± 0.14
$\Gamma_{b\bar{b}}$	377.4 ± 1.3	377.0 ± 1.2	375.75 ± 0.18
Γ_{had}	1744.8 ± 2.6	1743.2 ± 1.9	1741.06 ± 0.85
Γ_Z	2495.5 ± 2.3	2495.5 ± 2.3	2494.23 ± 0.86

radiative corrections and final-state mass effects) are given by,

$$\Gamma(W^+ \rightarrow e^+\nu_e) = \frac{M_W^3}{12\pi v^2} = 226.35 \pm 0.05 \text{ MeV}, \quad (10.60a)$$

$$\Gamma(W^+ \rightarrow u_i\bar{d}_j) = \frac{M_W^3}{12\pi v^2} |V_{ij}|^2 \mathcal{R}_V^q = (705.4 \pm 0.4 \text{ MeV}) |V_{ij}|^2, \quad (10.60b)$$

$$\Gamma(Z \rightarrow f\bar{f}) = \frac{M_Z^3}{12\pi v^2} [\mathcal{R}_V^f \bar{g}_V^{f2} + \mathcal{R}_A^f \bar{g}_A^{f2}], \quad (10.60c)$$

where the result for the latter are shown in Table 10.6. Final-state QED and QCD corrections [289] to the vector and axial-vector form factors are given by,

$$\mathcal{R}_{V,A}^f = N_C \left[1 + \frac{3}{4} \left(Q_f^2 \frac{\alpha(s)}{\pi} + \frac{N_C^2 - 1}{2N_C} \frac{\alpha_s(s)}{\pi} \right) + \dots \right], \quad (10.61)$$

where $N_C = 3$ (1) is the color factor for quarks (leptons) and the dots indicate finite fermion mass effects proportional to m_f^2/s which are different for \mathcal{R}_V^f and \mathcal{R}_A^f , as well as higher-order QCD corrections [290], which are known to $\mathcal{O}(\alpha_s^4)$ [203]. These include

singlet contributions starting from two-loop order which are large, strongly top quark mass dependent, family universal, and flavor non-universal [291–295]. The $\mathcal{O}(\alpha^2)$ self-energy corrections from Ref. [296] are also taken into account.

For the W decay into quarks, Eq. (10.60b), only the universal massless part (non-singlet and $m_q = 0$) of the final-state QCD radiator function in \mathcal{R}_V from Eq. (10.61) is used, and the QED corrections are modified. Expressing the widths in terms of $G_F M_{W,Z}^3$ incorporates the largest radiative corrections from the running QED coupling. EW corrections to the Z widths are then taken into account through the effective couplings $\bar{g}_{V,A}^i$. Hence, in the on-shell scheme the Z widths are proportional to $\rho_i \sim 1 + \rho_t$. There is additional (negative) quadratic m_t dependence in the $Z \rightarrow b\bar{b}$ vertex corrections [297, 298] which causes $\Gamma_{b\bar{b}}$ to decrease with m_t . The dominant effect is to multiply $\Gamma_{b\bar{b}}$ by the vertex correction $1 + \delta\rho_{b\bar{b}}$, where $\delta\rho_{b\bar{b}} \sim 10^{-2}(-\frac{1}{2}m_t^2/M_Z^2 + \frac{1}{5})$. In practice, the corrections are included in $\hat{\rho}_b$ and $\hat{\kappa}_b$, as discussed in Sec. 10.5.

Starting at $\mathcal{O}(\alpha\alpha_s)$, the factorized form indicated in Eq. (10.60) is violated and corrections need to be included [299–301]. They add coherently, resulting in a sizable effect, and shift $\alpha_s(M_Z)$ when extracted from Z lineshape observables by about $+0.0007$. Similar non-factorizable corrections are also known for mixed QED-EW corrections [97, 98, 100, 302].

For three fermion families the total widths of the Z [303–307] and W [308, 309] bosons are predicted to be,

$$\Gamma_Z = 2.4942 \pm 0.0009 \text{ GeV}, \quad \Gamma_W = 2.0896 \pm 0.0008 \text{ GeV}. \quad (10.62)$$

The uncertainties in these predictions are almost entirely induced by the parametric error in $\alpha_s(M_Z) = 0.1185 \pm 0.0016$ from the global fit. These predictions can be compared with the experimental results, $\Gamma_Z = 2.4955 \pm 0.0023 \text{ GeV}$ [14, 275] and $\Gamma_W = 2.085 \pm 0.042 \text{ GeV}$ [260, 262] (see the Gauge & Higgs Bosons Particle Listings). The measurements of the total and partial widths are generally in good agreement with the SM. The exception is the branching ratio $W \rightarrow \tau + \nu_\tau$ from LEP 2, which is 2.6σ larger than the electron-muon average [260].

The invisible decay width, $\Gamma_{\text{inv}} = \Gamma_Z - \Gamma_{e^+e^-} - \Gamma_{\mu^+\mu^-} - \Gamma_{\tau^+\tau^-} - \Gamma_{\text{had}}$, can be used to determine the number of neutrino flavors, N_ν , much lighter than $M_Z/2$. The hadronic peak cross section, and therefore the extracted Γ_{had} , depends strongly on the knowledge of the LEP 1 luminosity derived from small-angle Bhabha scattering. However, the prediction for the Bhabha cross-section was very recently found to be overestimated, and consequently the luminosity underestimated [275]. The updated analysis involved an improved Z lineshape fit, significantly reducing σ_{had} , while slightly increasing Γ_Z , with the result, $N_\nu = 2.9963 \pm 0.0074$ [275]. In practice, we determine N_ν by allowing it as an additional fit parameter and obtain,

$$N_\nu = 3.0026 \pm 0.0061, \quad (10.63)$$

which is now in perfect agreement with the observed number of fermion generations and $N_\nu = 3$ (a 1.3σ deviation was observed in the 2018 edition of this *Review* before including the correction in the luminosity determination).

10.6 Global fit results

In this section, we present the results of global fits, subject to the experimental data and theoretical constraints discussed in Section 10.2–10.4. For earlier analyses, see Refs. [14, 69, 310–313] and previous editions of this *Review*. The values for m_t , M_W [260, 261, 263], Γ_W [260, 262], the weak charges of the electron [148], the proton [149], cesium [160, 161] and thallium [162, 163], the weak mixing angle extracted from eDIS [138], $\nu_\mu(\bar{\nu}_\mu)$ - e scattering [120–122], the τ lifetime, and the μ anomalous magnetic moment [213] are listed in Table 10.4. Likewise, Table 10.5 summarizes the principal Z pole observables, where the LEP 1 averages of the ALEPH, DELPHI, L3, and OPAL results include common systematic uncertainties and correlations [14, 275]. The heavy flavor results [14, 280] of LEP 1 and SLD are based on common inputs, and are thus correlated, as well.

Also shown in both tables are the SM predictions for the values of M_Z , M_H , $\alpha_s(M_Z)$, $\Delta\alpha_{\text{had}}^{(3)}$ and the heavy quark masses shown in Table 10.7. The predictions result from a global least-square (χ^2) fit to all data using the minimization package MINUIT [314] and the EW library GAPP [32]. In most cases, we treat all input errors (the uncertainties of the values) as Gaussian. The reason is not that we assume that theoretical and systematic errors are intrinsically bell-shaped (which they are not) but because in most cases the input errors are either dominated by the statistical components or they are combinations of many different (including statistical) error sources, which should yield approximately Gaussian combined errors by the large number theorem. An exception is the theory dominated error on the τ lifetime, which we recalculate in each χ^2 -function call since it depends itself on α_s . Sizes and shapes of the output errors (the uncertainties of the predictions and the SM fit parameters) are fully determined by the fit, and 1σ errors are defined to correspond to $\Delta\chi^2 = \chi^2 - \chi_{\text{min}}^2 = 1$, and do not necessarily correspond to the 68.3% probability range or the 39.3% probability contour (for 2 parameters).

The agreement is generally very good. Despite the few discrepancies addressed in the following, the global electroweak fit describes the data very well, with an excellent $\chi^2/\text{d.o.f.} = 40.8/41$. The probability of a larger χ^2 is 48%, and only $g_\mu - 2$ is currently showing a larger (3.1σ) conflict. In addition, A_{LR}^0 (SLD) from hadronic final states and $A_{FB}^{(0,b)}$ (LEP 1) deviate at the 2σ level. g_L^2 from NuTeV is nominally in conflict with the SM, as well, but the precise status is unresolved (see Sec. 10.3.1). We also emphasize that there are a number of discrepancies among individual measurements of certain quantities, as discussed in previous sections, but that they are not reflected in the overall χ^2 of the fit as only the corresponding combinations are used as constraints.

A_b can be extracted from $A_{FB}^{(0,b)}$ when $A_e = 0.1501 \pm 0.0016$ is taken from a fit to leptonic asymmetries (using lepton universality). The result, $A_b = 0.885 \pm 0.017$, is 2.9σ below the SM prediction¹⁴ and also 1.4σ below $A_b = 0.923 \pm 0.020$ obtained from $A_{LR}^{FB}(b)$ at SLD. Thus, it appears that at least some of the problem in A_b is due to a statistical fluctuation or other experimental effect in one of the asymmetries. Note, however, that the uncertainty in $A_{FB}^{(0,b)}$ is strongly statistics dominated. The combined value, $A_b = 0.901 \pm 0.013$ deviates by 2.6σ .

The left-right asymmetry, $A_{LR}^0 = 0.15138 \pm 0.00216$ [273], from hadronic decays at SLD, differs by 2.1σ from the SM expectation of 0.1469 ± 0.0003 . The combined value of $A_\ell = 0.1513 \pm 0.0021$ from SLD (using lepton-family universality and including correlations) is also 2.1σ above the SM prediction; but there is experimental agreement between this SLD value and the LEP 1 value, $A_\ell = 0.1481 \pm 0.0027$, obtained from a fit to $A_{FB}^{(0,\ell)}$, $A_e(\mathcal{P}_\tau)$, and $A_\tau(\mathcal{P}_\tau)$, again assuming universality.

The observables in Table 10.4 and Table 10.5, as well as some other less precise observables, are used in the global fits described below. In all fits, the errors include full statistical, systematic, and theoretical uncertainties. The correlations from the LEP 1 lineshape and τ polarization measurements, the LEP/SLD heavy flavor observables, the SLD lepton asymmetries, and the ν - e scattering observables, are included. The theoretical correlations between $\Delta\alpha_{\text{had}}^{(5)}$, \hat{s}_0^2 , and $g_\mu - 2$, and between the M_W extractions from ATLAS and the Tevatron, are also accounted for.

The electroweak data allow a simultaneous determination of M_Z , m_t , and $\alpha_s(M_Z)$. The direct measurements of M_H at the LHC [266, 267] have reached a precision that the global fit result for M_H coincides with the constraint in Eq. (10.52) with negligible correlations with the other fit parameters. \hat{m}_c , \hat{m}_b , and $\Delta\alpha_{\text{had}}^{(3)}$ are also allowed to float in the fits, subject to the theoretical constraints [28, 51] described in Sec. 10.2, and are correlated with α_s , which in turn is determined mainly through R_ℓ , Γ_Z , σ_{had} , and τ_τ . The global fit to all data, including the hadron collider m_t average in Eq. (10.13), yields the results in Table 10.7, while those

¹⁴Alternatively, one can use $A_\ell = 0.1481 \pm 0.0027$, which is from LEP 1 alone and in excellent agreement with the SM, and obtain $A_b = 0.897 \pm 0.022$ which is 1.7σ low. This illustrates that some of the discrepancy is related to the one in A_{LR} .

Table 10.7: Principal SM fit result including mutual correlations.

M_Z [GeV]	91.1882 ± 0.0020	1.00	-0.07	0.00	0.00	0.02	0.02
$\widehat{m}_t(\widehat{m}_t)$ [GeV]	163.51 ± 0.55	-0.07	1.00	0.00	-0.11	-0.22	0.04
$\widehat{m}_b(\widehat{m}_b)$ [GeV]	4.180 ± 0.008	0.00	0.00	1.00	0.20	-0.02	0.00
$\widehat{m}_c(\widehat{m}_c)$ [GeV]	1.275 ± 0.009	0.00	-0.11	0.20	1.00	0.47	0.00
$\alpha_s(M_Z)$	0.1185 ± 0.0016	0.02	-0.22	-0.02	0.47	1.00	-0.03
$\Delta\alpha_{\text{had}}^{(3)}(2 \text{ GeV})$	0.00592 ± 0.00005	0.02	0.04	0.00	0.00	-0.03	1.00

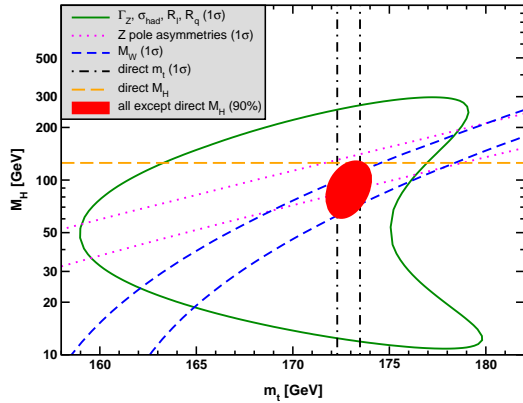


Figure 10.4: Fit result and one-standard-deviation (39.35% for the closed contours and 68% for the others) uncertainties in M_H as a function of m_t for various inputs, and the 90% CL region ($\Delta\chi^2 = 4.605$) allowed by all data. $\alpha_s(M_Z) = 0.1185$ is assumed except for the fits including the Z lineshape. The width of the horizontal dashed band is not visible on the scale of the plot.

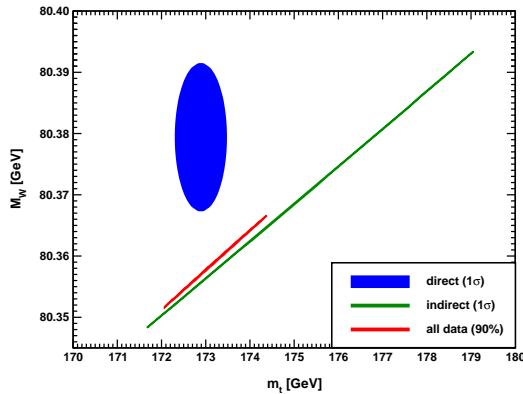


Figure 10.5: One-standard-deviation (39.35%) regions in M_W as a function of m_t for the direct and indirect data, and the 90% CL region ($\Delta\chi^2 = 4.605$) allowed by all data.

for the weak mixing angle in various schemes are summarized in Table 10.2.

Removing the kinematic constraint on M_H from LHC gives the loop-level determination from the precision data,

$$M_H = 90_{-16}^{+18} \text{ GeV}, \quad (10.64)$$

which is 1.8σ below the value in Eq. (10.52). The latter is also slightly outside the 90% central confidence range,

$$64 \text{ GeV} < M_H < 122 \text{ GeV}. \quad (10.65)$$

This is mostly a reflection of the Tevatron determination of M_W , which is 1.6σ higher than the SM best fit value in Table 10.4. This is shown in Fig. 10.4 where one sees that the precision data

together with M_H from the LHC prefer m_t to be closer to the upper end of its 1σ allowed range.

Conversely, one can remove the explicit M_W and Γ_W constraints from the global fit and use $M_H = 125.30 \pm 0.13 \text{ GeV}$ to obtain $M_W = 80.357 \pm 0.006 \text{ GeV}$, which is 1.7σ below the world average in Eq. (10.51). Finally, one can carry out a fit without including the direct constraint, $m_t = 172.89 \pm 0.59 \text{ GeV}$, from the hadron colliders. One obtains $m_t = 176.3 \pm 1.9 \text{ GeV}$, which is 1.7σ higher than the collider average. (The indirect prediction is for the $\overline{\text{MS}}$ mass definition, $\widehat{m}_t(\widehat{m}_t) = 166.4 \pm 1.8 \text{ GeV}$, which is in the end converted to the pole mass.) The situation is summarized in Fig. 10.5 showing the 1σ contours in the M_W - m_t plane from the direct and indirect determinations, as well as the combined 90% CL region.

In view of these tensions it is instructive to study the effect of doubling the uncertainty in $\Delta\alpha_{\text{had}}^{(3)}(2 \text{ GeV}) = (58.84 \pm 0.51) \times 10^{-4}$ (see Sec. 10.2) on the loop-level determination of the Higgs boson mass. The result, $M_H = 88_{-17}^{+18} \text{ GeV}$, deviates even slightly *more* (1.9σ) than Eq. (10.64), and demonstrates that the uncertainty in $\Delta\alpha_{\text{had}}$ is currently of only secondary importance. Note also that a shift of $\pm 10^{-4}$ in $\Delta\alpha_{\text{had}}^{(3)}(2 \text{ GeV})$ corresponds to a shift of $\mp 4.4 \text{ GeV}$ in M_H . The hadronic contribution to $\alpha(M_Z)$ is correlated with $g_\mu - 2$ (see Sec. 10.4). The measurement of the latter is higher than the SM prediction, and its inclusion in the fit favors a larger $\alpha(M_Z)$ and a lower M_H from the precision data (currently by 2.3 GeV).

The weak mixing angle can be determined from Z pole observables, M_W , and a variety of neutral-current processes spanning a very wide Q^2 range. The results (for older low energy neutral-current data see Refs. [310–313], as well as earlier editions of this *Review*) shown in Table 10.8 are in reasonable agreement with each other, indicating the quantitative success of the SM. One of the largest discrepancies is the value $\widehat{s}_Z^2 = 0.23176 \pm 0.00027$ from $A_{FB}^{(0,b)}$ and $A_{FB}^{(0,c)}$, which is 2.0σ above the value 0.23121 ± 0.00004 from the global fit to all data. Similarly, $\widehat{s}_Z^2 = 0.23064 \pm 0.00028$ from the SLD asymmetries (in both cases when combined with M_Z , Γ_Z , and m_t) is 2.0σ low.

The extracted Z pole value of $\alpha_s(M_Z)$ is based on a formula with negligible theoretical uncertainty if one assumes the exact validity of the SM. One should keep in mind, however, that this value, $\alpha_s(M_Z) = 0.1221 \pm 0.0027$, which increased after the updated analysis in Ref. [275], is very sensitive to certain types of new physics such as non-universal vertex corrections. In contrast, the value derived from τ decays, $\alpha_s(M_Z) = 0.1170_{-0.0017}^{+0.0019}$, is theory dominated but less sensitive to new physics. The agreement between the two values is only marginal, but the latter does agree well with the averages deduced from DIS and global PDF fits (0.1161 ± 0.0018), hadronic final states of e^+e^- annihilations (0.1171 ± 0.0031), hadron colliders (0.1159 ± 0.0034), as well as lattice QCD simulations (0.1182 ± 0.0008). For more details, other determinations, and references, see the Section on “Quantum Chromodynamics” in this *Review*.

Using $\alpha(M_Z)$ and \widehat{s}_Z^2 as inputs, one can predict $\alpha_s(M_Z)$ assuming grand unification. One finds $\alpha_s(M_Z) = 0.13 \pm 0.01$ [317, 318] for the simplest theories based on the minimal supersymmetric extension of the SM, where the uncertainty is from the unknown particle thresholds. This is slightly larger, but consistent with $\alpha_s(M_Z) = 0.1185 \pm 0.0016$ from our fit and most other determinations, while minimal non-supersymmetric theories predict much lower and excluded values (see the Section on “Grand Unified The-

Table 10.8: Values of \widehat{s}_Z^2 , s_W^2 , α_s , m_t and M_H for various data sets. In the fit to the LHC data, the α_s constraint is from a combined NNLO analysis of inclusive electroweak boson production cross-sections at the LHC [315]. Likewise, for the Tevatron fit we use the α_s result from the inclusive jet cross-section at DØ [316].

data set	\widehat{s}_Z^2	s_W^2	$\alpha_s(M_Z)$	m_t [GeV]	M_H [GeV]
all data	0.23121(4)	0.22337(10)	0.1185(16)	173.2 ± 0.6	125
all data except M_H	0.23107(9)	0.22309(19)	0.1189(17)	172.9 ± 0.6	90_{-16}^{+18}
all data except M_Z	0.23111(6)	0.22334(10)	0.1185(16)	172.9 ± 0.6	125
all data except M_W	0.23123(4)	0.22345(11)	0.1189(17)	172.9 ± 0.6	125
all data except m_t	0.23113(6)	0.22305(21)	0.1190(17)	176.3 ± 1.9	125
$M_{H,Z} + \Gamma_Z + m_t$	0.23126(8)	0.22351(17)	0.1215(47)	172.9 ± 0.6	125
LHC	0.23113(10)	0.22337(13)	0.1188(16)	172.7 ± 0.6	125
Tevatron + M_Z	0.23102(13)	0.22295(30)	0.1160(44)	174.3 ± 0.8	99_{-26}^{+32}
LEP 1 + LEP 2	0.23137(18)	0.22353(46)	0.1235(29)	178 ± 11	201_{-113}^{+279}
LEP 1 + SLD	0.23116(17)	0.22348(58)	0.1221(27)	169 ± 10	80_{-39}^{+101}
SLD + $M_Z + \Gamma_Z + m_t$	0.23064(28)	0.22227(54)	0.1188(48)	172.9 ± 0.6	37_{-21}^{+30}
$A_{FB}^{(b,c)} + M_Z + \Gamma_Z + m_t$	0.23176(27)	0.22467(66)	0.1266(46)	172.9 ± 0.6	280_{-100}^{+145}
$M_{W,Z} + \Gamma_{W,Z} + m_t$	0.23103(12)	0.22302(25)	0.1198(44)	172.9 ± 0.6	84_{-20}^{+24}
low energy + $M_{H,Z}$	0.23176(94)	0.2254(35)	0.1171(18)	156 ± 29	125

Table 10.9: Values of model-independent neutral-current parameters, compared with the SM predictions, where the uncertainties in the latter are $\lesssim 0.0001$, throughout.

Quantity	Experimental Value	Standard Model	Correlation
$g_{LV}^{\nu e}$	-0.040 ± 0.015	-0.0398	-0.05
$g_{LA}^{\nu e}$	-0.507 ± 0.014	-0.5064	
$g_{AV}^{eu} + 2g_{AV}^{ed}$	0.4927 ± 0.0031	0.4950	-0.88 0.20
$2g_{AV}^{eu} - g_{AV}^{ed}$	-0.7165 ± 0.0068	-0.7195	-0.22
$2g_{VA}^{eu} - g_{VA}^{ed}$	-0.13 ± 0.06	-0.0954	
g_{VA}^{ee}	0.0190 ± 0.0027	0.0227	

ories” in this *Review*).

Most of the parameters relevant to ν -hadron, ν - e , e -hadron, and e - e processes are determined uniquely and precisely from the data in “model-independent” fits, *i.e.*, fits allowing for an arbitrary EW gauge theory. The values for the parameters defined in Eq. (10.21) are given in Table 10.9 along with the predictions of the SM. The agreement is very good. (The ν -hadron results including NuTeV [134] and other ν -DIS data can be found in the 2006 edition of this *Review*, and fits with modified NuTeV constraints in the 2008 and 2010 editions.)

10.7 Constraints on new physics

The masses and decay properties of the electroweak bosons and low energy data can be used to search for and set limits on deviations from the SM. We will mainly discuss the effects of exotic particles (with heavy masses $M_{\text{new}} \gg M_Z$ in an expansion in M_Z/M_{new}) on the gauge boson self-energies. (Brief remarks are made on new physics which is not of this type.) Most of the effects on precision measurements can be described by three gauge self-energy parameters S , T , and U . We will define these, as well as the related parameters ρ_0 , ϵ_i , and $\widehat{\epsilon}_i$, to arise from new physics only. In other words, they are equal to zero ($\rho_0 = 1$) exactly in the SM, and do not include any (loop induced) contributions that depend on m_t or M_H , which are treated separately. Our treatment differs from most of the original papers.

The dominant effect of many extensions of the SM can be described by the ρ_0 parameter,

$$\rho_0 \equiv \frac{M_W^2}{M_Z^2 \widehat{c}_Z^2 \widehat{\rho}}, \quad (10.66)$$

which describes new sources of SU(2) breaking that cannot be accounted for by the SM Higgs doublet or by m_t effects. $\widehat{\rho}$ is calculated as in Eq. (10.18) assuming the validity of the SM. In the

presence of $\rho_0 \neq 1$, Eq. (10.66) generalizes the second Eq. (10.18) while the first remains unchanged. Provided that the new physics which yields $\rho_0 \neq 1$ is a small perturbation which does not significantly affect other radiative corrections, ρ_0 can be regarded as a phenomenological parameter which multiplies G_F in Eqs. (10.21) and (10.41), as well as Γ_Z in Eq. (10.60c). There are enough data to determine ρ_0 , M_H , m_t , and α_s , simultaneously. From the global fit,

$$\rho_0 = 1.00038 \pm 0.00020, \quad (10.67a)$$

$$\alpha_s(M_Z) = 0.1188 \pm 0.0017, \quad (10.67b)$$

where as before the uncertainty is from the experimental inputs and includes an estimate of the error from unknown higher-order electroweak corrections. The result in Eq. (10.67a) is 1.9 σ above the SM expectation, $\rho_0 = 1$. It can be used to constrain higher-dimensional Higgs representations to have vacuum expectation values of less than a few percent of those of the doublets. Indeed, the relation between M_W and M_Z is modified if there are Higgs multiplets with weak isospin $> 1/2$ and significant vacuum expectation values. For a general (charge-conserving) Higgs structure,

$$\rho_0 = \frac{\sum_i [t_i(t_i + 1) - t_{3i}^2] |v_i|^2}{2 \sum_i t_{3i}^2 |v_i|^2}, \quad (10.68)$$

where v_i is the expectation value of the neutral component of a Higgs multiplet with weak isospin t_i and third component t_{3i} . In order to calculate to higher orders in such theories one must define a set of four fundamental renormalized parameters which one may conveniently choose to be α , G_F , M_Z , and M_W , since M_W and M_Z are directly measurable. Then \widehat{s}_Z^2 and ρ_0 can be considered dependent parameters.

Eq. (10.67a) can also be used to constrain other types of new physics. For example, non-degenerate multiplets of heavy

fermions or scalars break the vector part of weak SU(2) and lead to a decrease in the value of M_Z/M_W . Each non-degenerate SU(2) doublet $\begin{pmatrix} f_1 \\ f_2 \end{pmatrix}$ yields a positive contribution to ρ_0 [319–321] of

$$\frac{N_C G_F}{8\sqrt{2}\pi^2} \Delta m^2, \quad (10.69)$$

where

$$\Delta m^2 \equiv m_1^2 + m_2^2 - \frac{4m_1^2 m_2^2}{m_1^2 - m_2^2} \ln \frac{m_1}{m_2} \geq (m_1 - m_2)^2, \quad (10.70)$$

and $N_C = 1$ (3) for color singlets (triplets). Eq. (10.67a) taken together with Eq. (10.69) implies the following constraint on the mass splitting at the 90% CL,

$$(14 \text{ GeV})^2 < \sum_i \frac{N_C^i}{3} \Delta m_i^2 < (48 \text{ GeV})^2, \quad (10.71)$$

where the sum runs over all new-physics doublets, for example fourth-family quarks or leptons, $\begin{pmatrix} t' \\ b' \end{pmatrix}$ or $\begin{pmatrix} \nu' \\ e' \end{pmatrix}$, vector-like fermion doublets (which contribute to the sum in Eq. (10.71) with an extra factor of 2), and scalar doublets such as $\begin{pmatrix} \xi \\ \eta \end{pmatrix}$ in Supersymmetry (in the absence of L - R mixing).

Non-degenerate multiplets usually imply $\rho_0 > 1$. Similarly, heavy Z' bosons decrease the prediction for M_Z due to mixing and generally lead to $\rho_0 > 1$ [322]. On the other hand, extra Higgs doublets participating in spontaneous symmetry breaking [323–325] or heavy lepton doublets involving Majorana neutrinos [326], both of which have more complicated expressions, and the v_i of higher-dimensional Higgs representations can contribute to ρ_0 with either sign.

A number of authors [327–329] have considered the general effects on neutral-current, Z and W boson observables of various types of heavy (*i.e.*, $M_{\text{new}} \gg M_Z$) physics which contribute to the W and Z self-energies but which do not have any direct coupling to the ordinary fermions (an alternative formulation is given by Ref. [330]). In addition to non-degenerate multiplets, which break the vector part of weak SU(2), these include heavy degenerate multiplets of chiral fermions which break the axial generators.

Such effects can be described by just three parameters, S , T , and U [331], at the (EW) one-loop level¹⁵. T is proportional to the difference between the W and Z self-energies at $Q^2 = 0$ (*i.e.*, vector SU(2)-breaking), while S ($S + U$) is associated with the difference between the Z (W) self-energy at $Q^2 = M_{Z,W}^2$ and $Q^2 = 0$ (axial SU(2)-breaking). Denoting the contributions of new physics to the various self-energies by Π_{ij}^{new} , we have

$$\widehat{\alpha}(M_Z)T \equiv \frac{\Pi_{WW}^{\text{new}}(0)}{M_W^2} - \frac{\Pi_{ZZ}^{\text{new}}(0)}{M_Z^2}, \quad (10.72a)$$

$$\begin{aligned} \frac{\widehat{\alpha}(M_Z)}{4\widehat{s}_Z^2\widehat{c}_Z^2} S \equiv & \frac{\Pi_{ZZ}^{\text{new}}(M_Z^2) - \Pi_{ZZ}^{\text{new}}(0)}{M_Z^2} - \frac{\widehat{c}_Z^2 - \widehat{s}_Z^2}{\widehat{c}_Z\widehat{s}_Z} \frac{\Pi_{Z\gamma}^{\text{new}}(M_Z^2)}{M_Z^2} \\ & - \frac{\Pi_{\gamma\gamma}^{\text{new}}(M_Z^2)}{M_Z^2}, \end{aligned} \quad (10.72b)$$

$$\begin{aligned} \frac{\widehat{\alpha}(M_Z)}{4\widehat{s}_Z^2} (S + U) \equiv & \frac{\Pi_{WW}^{\text{new}}(M_W^2) - \Pi_{WW}^{\text{new}}(0)}{M_W^2} - \frac{\widehat{c}_Z}{\widehat{s}_Z} \frac{\Pi_{Z\gamma}^{\text{new}}(M_Z^2)}{M_Z^2} \\ & - \frac{\Pi_{\gamma\gamma}^{\text{new}}(M_Z^2)}{M_Z^2}. \end{aligned} \quad (10.72c)$$

S , T , and U are defined with a factor proportional to $\widehat{\alpha}$ removed, so that they are expected to be of order unity in the presence of new physics. In the $\overline{\text{MS}}$ scheme as defined in Ref. [71], the last

¹⁵Three additional parameters are needed if the new physics scale is comparable to M_Z [332]. Further generalizations, including effects relevant to LEP 2 and Drell-Yan production at the LHC, are described in Refs. [333] and [334], respectively.

two terms in Eqs. (10.72b) and (10.72c) can be omitted, as was done in some earlier editions of this *Review*. These parameters are related to other parameter sets, S_i [71], $\widehat{\epsilon}_i$ [335], and h_i [336], by

$$T = h_V = \frac{\widehat{\epsilon}_1}{\widehat{\alpha}(M_Z)}, \quad (10.73a)$$

$$S = h_{AZ} = S_Z = 4\widehat{s}_Z^2 \frac{\widehat{\epsilon}_3}{\widehat{\alpha}(M_Z)}, \quad (10.73b)$$

$$U = h_{AW} - h_{AZ} = S_W - S_Z = -4\widehat{s}_Z^2 \frac{\widehat{\epsilon}_2}{\widehat{\alpha}(M_Z)}. \quad (10.73c)$$

A heavy non-degenerate multiplet of fermions or scalars contributes positively to T as

$$\rho_0 - 1 = \frac{1}{1 - \widehat{\alpha}(M_Z)T} - 1 \approx \widehat{\alpha}(M_Z)T, \quad (10.74)$$

where $\rho_0 - 1$ is given in Eq. (10.69). The effects of non-standard Higgs representations cannot be separated from heavy non-degenerate multiplets unless the new physics has other consequences, such as vertex corrections. Most of the original papers defined T to include the effects of loops only. However, we will redefine T to include all new sources of SU(2) breaking, including non-standard Higgs, so that T and ρ_0 are equivalent by Eq. (10.74).

A multiplet of heavy degenerate chiral fermions yields

$$S = \frac{N_C}{3\pi} \sum_i (t_{3i}^L - t_{3i}^R)^2, \quad (10.75)$$

where $t_{3i}^{L,R}$ is the 3rd component of weak isospin of the left-(right)-handed component of fermion i . For example, a heavy degenerate ordinary or mirror family would contribute $2/3\pi$ to S . In models with warped extra dimensions [337], sizeable corrections to the S parameter are generated through mixing between the SM gauge bosons and their Kaluza-Klein (KK) excitations, and one finds $S \approx 30 v^2 M_{KK}^{-2}$ [338], where M_{KK} is the mass scale of the KK gauge bosons. Large positive values of S can also be generated in models with dynamical electroweak symmetry breaking, where the Higgs boson is composite. In simple composite Higgs models, the dominant contribution stems from heavy spin-1 resonances of the strong dynamics leading to $S \approx 4\pi v^2 (M_V^{-2} + M_A^{-2})$, where $M_{V,A}$ are the masses of the lightest vector and axial-vector resonances, respectively [339].

Negative values of S are possible, for example, in models of walking Technicolor [340–347], or from loops involving scalars or Majorana particles [348, 349]. The simplest origin of $S < 0$ would probably be an additional heavy Z' boson [322]. Supersymmetric extensions of the SM [350, 351] generally give very small effects. For more details and references, see Refs. [352–361] and the Sections on “Supersymmetry” in this *Review*. Most simple types of new physics yield $U = 0$, although there are counter-examples, such as the effects of anomalous triple gauge vertices [335].

The SM expressions for observables are replaced by,

$$M_Z^2 = M_{Z0}^2 \frac{1 - \widehat{\alpha}(M_Z)T}{1 - G_F M_{Z0}^2 S / 2\sqrt{2}\pi}, \quad (10.76a)$$

$$M_W^2 = M_{W0}^2 \frac{1}{1 - G_F M_{W0}^2 (S + U) / 2\sqrt{2}\pi}, \quad (10.76b)$$

where M_{Z0} and M_{W0} are the SM expressions (as functions of m_t and M_H) in the $\overline{\text{MS}}$ scheme. Furthermore,

$$\Gamma_Z = \frac{M_Z^3 \beta_Z}{1 - \widehat{\alpha}(M_Z)T}, \quad (10.77a)$$

$$\Gamma_W = M_W^3 \beta_W, \quad (10.77b)$$

$$A_i = \frac{A_{i0}}{1 - \widehat{\alpha}(M_Z)T}, \quad (10.77c)$$

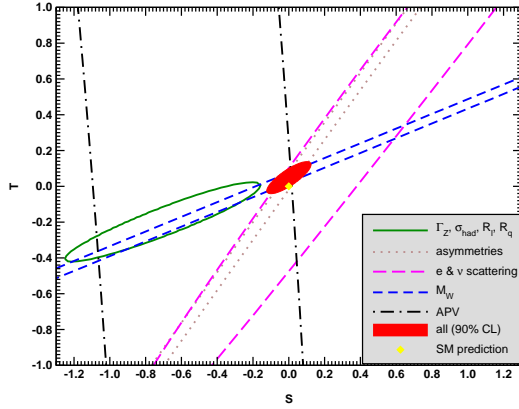


Figure 10.6: 1σ constraints (39.35% for the closed contours and 68% for the others) on S and T (for $U = 0$) from various inputs combined with M_Z . S and T represent the contributions of new physics only. Data sets not involving M_W or Γ_W are insensitive to U . With the exception of the fit to all data, we fix $\alpha_s = 0.1185$. The black dot indicates the Standard Model values $S = T = 0$.

where $\beta_{Z,W}$ are the SM expressions for the reduced widths Γ_{Z0}/M_{Z0}^3 and Γ_{W0}/M_{W0}^3 , M_Z and M_W are the physical masses, and A_i (A_{i0}) is a neutral-current amplitude (in the SM).

The data allows for a simultaneous determination of M_H and m_t (from the hadron colliders), S (from M_Z), T (mainly from Γ_Z), U (from M_W), $\hat{s}_Z^2 = 0.23112 \pm 0.00013$ (from the Z pole asymmetries), and $\alpha_s(M_Z) = 0.1189 \pm 0.0018$ (from R_ℓ , σ_{had} , and τ_τ), giving,

$$S = -0.01 \pm 0.10, \quad (10.78a)$$

$$T = 0.03 \pm 0.12, \quad (10.78b)$$

$$U = 0.02 \pm 0.11, \quad (10.78c)$$

with little correlation among the SM parameters, where the uncertainties are from unknown higher orders in the SM predictions and the inputs. The parameters in Eq. (10.78), which by definition are due to new physics only, are in excellent agreement with the SM values of zero. Fixing $U = 0$, which is motivated by the fact that U is suppressed by an additional factor M_{new}^2/M_Z^2 compared to S and T [362], greatly improves the precision on S and particularly T ,

$$S = 0.00 \pm 0.07, \quad (10.79a)$$

$$T = 0.05 \pm 0.06. \quad (10.79b)$$

If only any one of the three parameters is allowed, then this parameter would deviate at the 1.6 to 1.9 σ level, reflecting the deviation in M_W . Using Eq. (10.74), the value of ρ_0 corresponding to T in Eqs. (10.78) is 1.0002 ± 0.0009 , while the one corresponding to Eqs. (10.79) is 1.0004 ± 0.0005 . Thus, the multi-parameter fits are consistent with $\rho_0 = 1$, in contrast to the fit with $S = U = 0$ in Eq. (10.67a). There is a strong correlation (92%) between the S and T parameters. The U parameter is -80% (-93%) anticorrelated with S (T). The allowed regions in S - T (for $U = 0$) are shown in Fig. 10.6. From Eq. (10.78) one obtains $S < 0.14$ and $T < 0.22$ at 95% CL, where the former puts the constraint $M_{KK} \gtrsim 3.6$ TeV on the masses of KK gauge bosons in warped extra dimensions. In minimal composite Higgs models, the bound on S requires $M_V \gtrsim 4$ TeV [363], but this constraint can be relaxed, *e.g.*, if the fermionic sector is also allowed to be partially composite [364, 365].

The S parameter can also be used to constrain the number of fermion families, *under the assumption* that there are no new contributions to T or U and therefore that any new families are degenerate; then an extra generation of SM fermions is excluded at the 8σ level corresponding to $N_F = 2.75 \pm 0.15$. This can be compared to the fit to the number of light neutrinos given in Eq. (10.63),

$N_\nu = 3.0026 \pm 0.0061$, but the S parameter fits are valid even for a very heavy fourth family neutrino. Allowing T to vary as well, the constraint on a fourth family is weaker [366]. However, a heavy fourth family would increase the Higgs production cross-section through gluon fusion by a factor of about 9 [367], which is in considerable tension with the observed Higgs signal at the LHC [368]. Combining the limits from electroweak precision data with the measured Higgs production rate and limits from direct searches for heavy quarks [369], a fourth family of chiral fermions is now excluded by more than five standard deviations [370, 371]. Similar remarks apply to a heavy mirror family [372] involving right-handed $SU(2)$ doublets and left-handed singlets. In contrast, new doublets that receive most of their mass from a different source than the Higgs vacuum expectation value, such as vector-like fermion doublets or scalar doublets in Supersymmetry, give small or no contribution to S , T , U , and the Higgs production cross-section and are therefore still allowed. Partial or complete vector-like fermion families are predicted in many Grand Unified Theories [373] (see the Section on “Grand Unified Theories” in this *Review*), and many other models including supersymmetric and superstring inspired ones [374–377].

As discussed in Sec. 10.6, there is a 3.6% deviation in the asymmetry parameter A_b . Assuming that this is due to new physics affecting preferentially the third generation, we can perform a fit allowing additional $Z \rightarrow b\bar{b}$ vertex corrections ρ_b and κ_b as in Eq. (10.42) (here defined to be due to new physics only with the SM contributions removed), as well as S , T , U , and the SM parameters, with the result,

$$\rho_b = 0.058 \pm 0.020, \quad (10.80a)$$

$$\kappa_b = 0.185 \pm 0.067, \quad (10.80b)$$

with an almost perfect correlation of 99% (because R_b is much better determined than A_b). The central values of the oblique parameters are consistent with their SM values of zero, and there is little change in the SM parameters, except that the value of $\alpha_s(M_Z)$ is lower by 0.0008 compared to the SM fit. Given that an $\mathcal{O}(20\%)$ correction to κ_b would be necessary, it would be difficult to account for the deviation in A_b by new physics that enters only at the level of radiative corrections. Thus, if it is due to new physics, it is most likely of tree-level type affecting preferentially the third generation. Examples include the decay of a scalar neutrino resonance [378], mixing of the b quark with heavy exotics [379], and a heavy Z' with family non-universal couplings [380, 381]. It is difficult, however, to simultaneously account for R_b without tuning, which has been measured on the Z peak and off-peak [382] at LEP 1.

There is no simple parametrization to describe the effects of every type of new physics on every possible observable. The S , T , and U formalism describes many types of heavy physics which affect only the gauge self-energies, and it can be applied to all precision observables. However, new physics which couples directly to ordinary fermions cannot be fully parametrized in the S , T , and U framework. Examples include heavy Z' bosons [322], mixing with exotic fermions [9, 383, 384], leptoquark exchange [260, 385, 386], supersymmetric models, strong EW dynamics [364], Little Higgs models [387, 388], and TeV-scale extra spatial dimensions [389–392] (for more details and references, see the Section on “Extra Dimensions” in this *Review*). These types of new physics can be parametrized in a model-independent way by using an effective field theory description [393–396]. Here the SM is extended by a set of higher-dimensional operators, denoted \mathcal{O}_i ,

$$\mathcal{L} = \mathcal{L}_{\text{SM}} + \sum_{d>4} \sum_i \frac{C_i}{\Lambda^{d-4}} \mathcal{O}_i, \quad (10.81)$$

where Λ is the characteristic scale of the new physics sector, which is assumed to satisfy $\Lambda \gg v$. For EW precision observables, the leading new operators enter at dimension $d = 6$. Note that S and T can be identified with two of these operators (or linear combinations thereof, depending on the chosen operator basis), while U corresponds to a dimension-8 operator [362, 397]. With current data on M_W and Z pole observables, Λ is constrained to

be larger than $\mathcal{O}(\text{TeV})$ if the Wilson coefficients C_i are of order unity [398–402].

An alternate formalism [403] defines parameters, $\epsilon_1, \epsilon_2, \epsilon_3$, and ϵ_b in terms of the specific observables $M_W/M_Z, \Gamma_{\ell\ell}, A_{FB}^{(0,\ell)}$, and R_b . The definitions coincide with those for $\hat{\epsilon}_i$ in Eqs. (10.72) and (10.73c) for physics which affects gauge self-energies only, but the ϵ 's now parametrize arbitrary types of new physics. However, the ϵ_i are not related to other observables unless additional model-dependent assumptions are made.

Limits on new four-Fermi operators and on leptoquarks using LEP 2 and lower energy data are given in Refs. [260, 404–406], while constraints on various types of new physics are addressed in Refs. [9, 151, 277, 407, 408]. For a particularly well motivated and explored type of physics beyond the SM, see the Section on “ Z' -Boson Searches” in this Review.

Acknowledgments

It is a pleasure to thank Rodolfo Ferro-Hernández for discussions, for performing some of the calculations and checks, and for producing the plot in Fig. 10.2. J.E. is supported by the German–Mexican research collaboration grant SP 778/4–1 (DFG) and 278017 (CONACyT). A.F. is supported in part by the National Science Foundation under grant no. PHY–1820760.

References

- [1] S. Glashow, Nucl. Phys. **22**, 579 (1961).
- [2] S. Weinberg, Phys. Rev. Lett. **19**, 1264 (1967).
- [3] A. Salam, Conf. Proc. C **680519**, 367 (1968).
- [4] S. Glashow, J. Iliopoulos and L. Maiani, Phys. Rev. D **2**, 1285 (1970).
- [5] N. Cabibbo, Phys. Rev. Lett. **10**, 531 (1963).
- [6] M. Kobayashi and T. Maskawa, Prog. Theor. Phys. **49**, 652 (1973).
- [7] S. Descotes-Genon and P. Koppenburg, Ann. Rev. Nucl. Part. Sci. **67**, 97 (2017), [arXiv:1702.08834].
- [8] E. Commins and P. Bucksbaum, *Weak Interactions of Leptons and Quarks*, Cambridge Univ. Pr., Cambridge, USA (1983), ISBN 978-0-521-27370-1.
- [9] P. Langacker, editor, *Precision tests of the standard electroweak model*, volume 14, WSP, Singapore (1996).
- [10] P. Langacker, *The standard model and beyond*, CRC Pr., Boca Raton, USA (2010), ISBN 978-1-4200-7906-7.
- [11] T. Kinoshita, editor, *Quantum electrodynamics*, volume 7, WSP, Singapore (1990).
- [12] S. G. Karshenboim, Phys. Rept. **422**, 1 (2005), [hep-ph/0509010].
- [13] J. Erler and S. Su, Prog. Part. Nucl. Phys. **71**, 119 (2013), [arXiv:1303.5522].
- [14] S. Schael *et al.* (ALEPH, DELPHI, L3, OPAL, SLD, LEP Electroweak Working Group, SLD Electroweak Group, SLD Heavy Flavour Group), Phys. Rept. **427**, 257 (2006), [hep-ex/0509008].
- [15] D. Webber *et al.* (MuLan), Phys. Rev. Lett. **106**, 041803 (2011), [arXiv:1010.0991].
- [16] T. Kinoshita and A. Sirlin, Phys. Rev. **113**, 1652 (1959).
- [17] T. van Ritbergen and R. G. Stuart, Nucl. Phys. B **564**, 343 (2000), [hep-ph/9904240].
- [18] M. Steinhauser and T. Seidensticker, Phys. Lett. B **467**, 271 (1999), [hep-ph/9909436].
- [19] Y. Nir, Phys. Lett. B **221**, 184 (1989).
- [20] A. Pak and A. Czarnecki, Phys. Rev. Lett. **100**, 241807 (2008), [arXiv:0803.0960].
- [21] T. Aoyama, T. Kinoshita and M. Nio, Atoms **7**, 1, 28 (2019).
- [22] P. J. Mohr, D. B. Newell and B. N. Taylor, Rev. Mod. Phys. **88**, 3, 035009 (2016), [arXiv:1507.07956].
- [23] R. Bouchendira *et al.*, Phys. Rev. Lett. **106**, 080801 (2011), [arXiv:1012.3627].
- [24] R. H. Parker *et al.*, Science **360**, 191 (2018), [arXiv:1812.04130].
- [25] G. Abbiendi *et al.* (OPAL), Eur. Phys. J. C **45**, 1 (2006), [hep-ex/0505072].
- [26] P. Achard *et al.* (L3), Phys. Lett. B **623**, 26 (2005), [hep-ex/0507078].
- [27] S. Fanchiotti, B. A. Kniehl and A. Sirlin, Phys. Rev. D **48**, 307 (1993), [hep-ph/9212285].
- [28] J. Erler, Phys. Rev. D **59**, 054008 (1999), [hep-ph/9803453].
- [29] M. Davier *et al.*, Eur. Phys. J. C **80**, 3, 241 (2020), [arXiv:1908.00921].
- [30] F. Jegerlehner, EPJ Web Conf. **118**, 01016 (2016), [arXiv:1511.04473].
- [31] F. Jegerlehner and R. Szafron, Eur. Phys. J. C **71**, 1632 (2011), [arXiv:1101.2872].
- [32] J. Erler (1999), [hep-ph/0005084].
- [33] M. Steinhauser, Phys. Lett. B **429**, 158 (1998), [hep-ph/9803313].
- [34] K. Chetyrkin, J. H. Kuhn and M. Steinhauser, Nucl. Phys. B **482**, 213 (1996), [hep-ph/9606230].
- [35] J. Erler and R. Ferro-Hernández, JHEP **03**, 196 (2018), [arXiv:1712.09146].
- [36] *Theory report on the 11th FCC-ee workshop* (2019), [arXiv:1905.05078].
- [37] A. Keshavarzi, D. Nomura and T. Teubner, Phys. Rev. D **101**, 1, 014029 (2020), [arXiv:1911.00367].
- [38] M. Davier *et al.*, Eur. Phys. J. C **71**, 1515 (2011), [Erratum: Eur.Phys.J.C **72**, 1874 (2012)], [arXiv:1010.4180].
- [39] K. Ackerstaff *et al.* (OPAL), Eur. Phys. J. C **7**, 571 (1999), [hep-ex/9808019].
- [40] S. Anderson *et al.* (CLEO), Phys. Rev. D **61**, 112002 (2000), [hep-ex/9910046].
- [41] S. Schael *et al.* (ALEPH), Phys. Rept. **421**, 191 (2005), [hep-ex/0506072].
- [42] M. Fujikawa *et al.* (Belle), Phys. Rev. D **78**, 072006 (2008), [arXiv:0805.3773].
- [43] S. Groote *et al.*, Phys. Lett. B **440**, 375 (1998), [hep-ph/9802374].
- [44] B. Geshkenbein and V. Morgunov, Phys. Lett. B **352**, 456 (1995).
- [45] M. L. Swartz, Phys. Rev. D **53**, 5268 (1996), [hep-ph/9509248].
- [46] N. Krasnikov and R. Rodenberg, Nuovo Cim. A **111**, 217 (1998), [hep-ph/9711367].
- [47] J. H. Kuhn and M. Steinhauser, Phys. Lett. B **437**, 425 (1998), [hep-ph/9802241].
- [48] A. D. Martin, J. Outhwaite and M. Ryskin, Phys. Lett. B **492**, 69 (2000), [hep-ph/0008078].
- [49] J. de Troconiz and F. Yndurain, Phys. Rev. D **65**, 093002 (2002), [hep-ph/0107318].
- [50] H. Burkhardt and B. Pietrzyk, Phys. Rev. D **84**, 037502 (2011), [arXiv:1106.2991].
- [51] J. Erler, P. Masjuan and H. Spiesberger, Eur. Phys. J. C **77**, 2, 99 (2017), [arXiv:1610.08531].
- [52] V. Novikov *et al.*, Phys. Rept. **41**, 1 (1978).
- [53] J. Erler and M. Luo, Phys. Lett. B **558**, 125 (2003), [hep-ph/0207114].
- [54] T. Aaltonen *et al.* (CDF, DØ, Tevatron Electroweak Working Group) (2016), [arXiv:1608.01881].
- [55] M. Aaboud *et al.* (ATLAS), Eur. Phys. J. C **79**, 4, 290 (2019), [arXiv:1810.01772].
- [56] Technical Report CMS-PAS-TOP-15-012, CERN, Geneva (2016), URL <https://cds.cern.ch/record/2235162>.

- [57] A. M. Sirunyan *et al.* (CMS), *Eur. Phys. J. C* **79**, 4, 313 (2019), [arXiv:1812.10534].
- [58] A. M. Sirunyan *et al.* (CMS), *Eur. Phys. J. C* **79**, 5, 368 (2019), [arXiv:1812.10505].
- [59] Technical Report ATLAS-CONF-2019-046, CERN, Geneva (2019), URL <https://cds.cern.ch/record/2693954>.
- [60] V. M. Abazov *et al.* (DØ), *Phys. Rev. Lett.* **113**, 032002 (2014), [arXiv:1405.1756].
- [61] A. M. Sirunyan *et al.* (CMS), *Eur. Phys. J. C* **78**, 11, 891 (2018), [arXiv:1805.01428].
- [62] A. H. Hoang, S. Plätzer and D. Samitz, *JHEP* **10**, 200 (2018), [arXiv:1807.06617].
- [63] M. Beneke *et al.*, *Phys. Lett. B* **775**, 63 (2017), [arXiv:1605.03609].
- [64] P. Marquard *et al.*, *Phys. Rev. Lett.* **114**, 14, 142002 (2015), [arXiv:1502.01030].
- [65] M. Beneke, *Phys. Rept.* **317**, 1 (1999), [hep-ph/9807443].
- [66] S. Catani *et al.*, *JHEP* **07**, 100 (2019), [arXiv:1906.06535].
- [67] Technical Report CMS-PAS-TOP-18-004, CERN, Geneva (2018), URL <https://cds.cern.ch/record/2647989>.
- [68] G. Aad *et al.* (ATLAS), *JHEP* **11**, 150 (2019), [arXiv:1905.02302].
- [69] J. Erler and M. Schott, *Prog. Part. Nucl. Phys.* **106**, 68 (2019), [arXiv:1902.05142].
- [70] A. Sirlin, *Phys. Rev. D* **22**, 971 (1980).
- [71] W. J. Marciano and J. L. Rosner, *Phys. Rev. Lett.* **65**, 2963 (1990), [Erratum: *Phys.Rev.Lett.* 68, 898 (1992)].
- [72] G. Degrassi, S. Fanchiotti and A. Sirlin, *Nucl. Phys. B* **351**, 49 (1991).
- [73] A. Czarnecki and W. J. Marciano, *Int. J. Mod. Phys. A* **15**, 2365 (2000), [hep-ph/0003049].
- [74] J. Erler and M. J. Ramsey-Musolf, *Phys. Rev. D* **72**, 073003 (2005), [hep-ph/0409169].
- [75] K. Kumar *et al.*, *Ann. Rev. Nucl. Part. Sci.* **63**, 237 (2013), [arXiv:1302.6263].
- [76] G. Degrassi and A. Sirlin, *Nucl. Phys. B* **352**, 342 (1991).
- [77] P. Gambino and A. Sirlin, *Phys. Rev. D* **49**, 1160 (1994), [hep-ph/9309326].
- [78] W. Hollik, *Fortsch. Phys.* **38**, 165 (1990).
- [79] R. Barbieri *et al.*, *Nucl. Phys. B* **409**, 105 (1993).
- [80] J. Fleischer, O. Tarasov and F. Jegerlehner, *Phys. Lett. B* **319**, 249 (1993).
- [81] G. Degrassi, P. Gambino and A. Vicini, *Phys. Lett. B* **383**, 219 (1996), [hep-ph/9603374].
- [82] G. Degrassi, P. Gambino and A. Sirlin, *Phys. Lett. B* **394**, 188 (1997), [hep-ph/9611363].
- [83] A. Freitas *et al.*, *Phys. Lett. B* **495**, 338 (2000), [Erratum: *Phys.Lett.B* 570, 265 (2003)], [hep-ph/0007091].
- [84] M. Awramik and M. Czakon, *Phys. Lett. B* **568**, 48 (2003), [hep-ph/0305248].
- [85] A. Freitas *et al.*, *Nucl. Phys. B* **632**, 189 (2002), [Erratum: *Nucl.Phys.B* 666, 305–307 (2003)], [hep-ph/0202131].
- [86] M. Awramik and M. Czakon, *Phys. Rev. Lett.* **89**, 241801 (2002), [hep-ph/0208113].
- [87] A. Onishchenko and O. Veretin, *Phys. Lett. B* **551**, 111 (2003), [hep-ph/0209010].
- [88] G. Degrassi, P. Gambino and P. P. Giardino, *JHEP* **05**, 154 (2015), [arXiv:1411.7040].
- [89] M. Awramik *et al.*, *Phys. Rev. D* **69**, 053006 (2004), [hep-ph/0311148].
- [90] M. Awramik *et al.*, *Phys. Rev. Lett.* **93**, 201805 (2004), [hep-ph/0407317].
- [91] W. Hollik, U. Meier and S. Uccirati, *Nucl. Phys. B* **731**, 213 (2005), [hep-ph/0507158].
- [92] M. Awramik, M. Czakon and A. Freitas, *Phys. Lett. B* **642**, 563 (2006), [hep-ph/0605339].
- [93] W. Hollik, U. Meier and S. Uccirati, *Nucl. Phys. B* **765**, 154 (2007), [hep-ph/0610312].
- [94] M. Awramik *et al.*, *Nucl. Phys. B* **813**, 174 (2009), [arXiv:0811.1364].
- [95] I. Dubovyk *et al.*, *Phys. Lett. B* **762**, 184 (2016), [arXiv:1607.08375].
- [96] A. Freitas, *Phys. Lett. B* **730**, 50 (2014), [arXiv:1310.2256].
- [97] A. Freitas, *JHEP* **04**, 070 (2014), [arXiv:1401.2447].
- [98] I. Dubovyk *et al.*, *Phys. Lett. B* **783**, 86 (2018), [arXiv:1804.10236].
- [99] I. Dubovyk *et al.*, *JHEP* **08**, 113 (2019), [arXiv:1906.08815].
- [100] M. Awramik, M. Czakon and A. Freitas, *JHEP* **11**, 048 (2006), [hep-ph/0608099].
- [101] A. Djouadi and C. Verzegnassi, *Phys. Lett. B* **195**, 265 (1987).
- [102] A. Djouadi, *Nuovo Cim. A* **100**, 357 (1988).
- [103] K. Chetyrkin, J. H. Kuhn and M. Steinhauser, *Phys. Lett. B* **351**, 331 (1995), [hep-ph/9502291].
- [104] L. Avdeev *et al.*, *Phys. Lett. B* **336**, 560 (1994), [Erratum: *Phys.Lett.B* 349, 597–598 (1995)], [hep-ph/9406363].
- [105] Y. Schroder and M. Steinhauser, *Phys. Lett. B* **622**, 124 (2005), [hep-ph/0504055].
- [106] K. Chetyrkin *et al.*, *Phys. Rev. Lett.* **97**, 102003 (2006), [hep-ph/0605201].
- [107] R. Boughezal and M. Czakon, *Nucl. Phys. B* **755**, 221 (2006), [hep-ph/0606232].
- [108] B. A. Kniehl, J. H. Kuhn and R. Stuart, *Phys. Lett. B* **214**, 621 (1988).
- [109] B. A. Kniehl, *Nucl. Phys. B* **347**, 86 (1990).
- [110] F. Halzen and B. A. Kniehl, *Nucl. Phys. B* **353**, 567 (1991).
- [111] A. Djouadi and P. Gambino, *Phys. Rev. D* **49**, 3499 (1994), [Erratum: *Phys.Rev.D* 53, 4111 (1996)], [hep-ph/9309298].
- [112] A. Anselm, N. Dombey and E. Leader, *Phys. Lett. B* **312**, 232 (1993).
- [113] K. Chetyrkin, J. H. Kuhn and M. Steinhauser, *Phys. Rev. Lett.* **75**, 3394 (1995), [hep-ph/9504413].
- [114] J. van der Bij *et al.*, *Phys. Lett. B* **498**, 156 (2001), [hep-ph/0011373].
- [115] M. Faisst *et al.*, *Nucl. Phys. B* **665**, 649 (2003), [hep-ph/0302275].
- [116] R. Boughezal, J. Tausk and J. van der Bij, *Nucl. Phys. B* **725**, 3 (2005), [hep-ph/0504092].
- [117] A. Arbuzov *et al.*, *Comput. Phys. Commun.* **174**, 728 (2006), [hep-ph/0507146].
- [118] J. Erler and M. J. Ramsey-Musolf, *Prog. Part. Nucl. Phys.* **54**, 351 (2005), [hep-ph/0404291].
- [119] J. Formaggio and G. Zeller, *Rev. Mod. Phys.* **84**, 1307 (2012), [arXiv:1305.7513].
- [120] J. Dorenbosch *et al.* (CHARM), *Z. Phys. C* **41**, 567 (1989), [Erratum: *Z.Phys.C* 51, 142 (1991)].
- [121] L. Ahrens *et al.*, *Phys. Rev. D* **41**, 3297 (1990).
- [122] P. Vilain *et al.* (CHARM-II), *Phys. Lett. B* **335**, 246 (1994).
- [123] R. Allen *et al.*, *Phys. Rev. D* **47**, 11 (1993).
- [124] L. Auerbach *et al.* (LSND), *Phys. Rev. D* **63**, 112001 (2001), [hep-ex/0101039].
- [125] M. Deniz *et al.* (TEXONO), *Phys. Rev. D* **81**, 072001 (2010), [arXiv:0911.1597].
- [126] J. M. Conrad, M. H. Shaevitz and T. Bolton, *Rev. Mod. Phys.* **70**, 1341 (1998), [hep-ex/9707015].

- [127] A. Blondel *et al.*, *Z. Phys. C* **45**, 361 (1990).
- [128] J. Allaby *et al.* (CHARM), *Z. Phys. C* **36**, 611 (1987).
- [129] K. S. McFarland *et al.* (CCFR, E744, E770), *Eur. Phys. J. C* **1**, 509 (1998), [hep-ex/9701010].
- [130] R. Barnett, *Phys. Rev. D* **14**, 70 (1976).
- [131] H. Georgi and H. Politzer, *Phys. Rev. D* **14**, 1829 (1976).
- [132] S. Rabinowitz *et al.*, *Phys. Rev. Lett.* **70**, 134 (1993).
- [133] E. Paschos and L. Wolfenstein, *Phys. Rev. D* **7**, 91 (1973).
- [134] G. Zeller *et al.* (NuTeV), *Phys. Rev. Lett.* **88**, 091802 (2002), [Erratum: *Phys.Rev.Lett.* 90, 239902 (2003)], [hep-ex/0110059].
- [135] D. Akimov *et al.* (COHERENT), *Science* **357**, 6356, 1123 (2017), [arXiv:1708.01294].
- [136] J. Erler *et al.*, *Ann. Rev. Nucl. Part. Sci.* **64**, 269 (2014), [arXiv:1401.6199].
- [137] C. Prescott *et al.*, *Phys. Lett. B* **84**, 524 (1979).
- [138] D. Wang *et al.* (PVDIS), *Nature* **506**, 7486, 67 (2014).
- [139] D. Wang *et al.*, *Phys. Rev. C* **91**, 4, 045506 (2015), [arXiv:1411.3200].
- [140] R. Hasty *et al.* (SAMPLE), *Science* **290**, 2117 (2000), [arXiv:nucl-ex/0102001].
- [141] E. Beise, M. Pitt and D. Spayde, *Prog. Part. Nucl. Phys.* **54**, 289 (2005), [arXiv:nucl-ex/0412054].
- [142] S.-L. Zhu *et al.*, *Phys. Rev. D* **62**, 033008 (2000), [hep-ph/0002252].
- [143] A. Argento *et al.*, *Phys. Lett. B* **120**, 245 (1983).
- [144] W. Heil *et al.*, *Nucl. Phys. B* **327**, 1 (1989).
- [145] P. Souder *et al.*, *Phys. Rev. Lett.* **65**, 694 (1990).
- [146] D. Armstrong and R. McKeown, *Ann. Rev. Nucl. Part. Sci.* **62**, 337 (2012), [arXiv:1207.5238].
- [147] E. Derman and W. J. Marciano, *Annals Phys.* **121**, 147 (1979).
- [148] P. Anthony *et al.* (SLAC E158), *Phys. Rev. Lett.* **95**, 081601 (2005), [hep-ex/0504049].
- [149] D. Androić *et al.* (Qweak), *Nature* **557**, 7704, 207 (2018), [arXiv:1905.08283].
- [150] R. D. Carlini *et al.*, *Ann. Rev. Nucl. Part. Sci.* **69**, 191 (2019).
- [151] J. Erler, A. Kurylov and M. J. Ramsey-Musolf, *Phys. Rev. D* **68**, 016006 (2003), [hep-ph/0302149].
- [152] R. D. Young *et al.*, *Phys. Rev. Lett.* **99**, 122003 (2007), [arXiv:0704.2618].
- [153] A. Acha *et al.* (HAPPEX), *Phys. Rev. Lett.* **98**, 032301 (2007), [arXiv:nucl-ex/0609002].
- [154] M. Gorchtein and C. Horowitz, *Phys. Rev. Lett.* **102**, 091806 (2009), [arXiv:0811.0614].
- [155] M. Gorchtein, C. Horowitz and M. J. Ramsey-Musolf, *Phys. Rev. C* **84**, 015502 (2011), [arXiv:1102.3910].
- [156] N. Hall *et al.*, *Phys. Lett. B* **753**, 221 (2016), [arXiv:1504.03973].
- [157] J. Erler *et al.*, *Phys. Rev. D* **100**, 5, 053007 (2019), [arXiv:1907.07928].
- [158] M. Bouchiat and C. Bouchiat, *Phys. Lett. B* **48**, 111 (1974).
- [159] M. Safronova *et al.*, *Rev. Mod. Phys.* **90**, 2, 025008 (2018), [arXiv:1710.01833].
- [160] C. Wood *et al.*, *Science* **275**, 1759 (1997).
- [161] J. Guena, M. Lintz and M. Bouchiat, *Phys. Rev. A* **71**, 042108 (2005), [arXiv:physics/0412017].
- [162] N. Edwards *et al.*, *Phys. Rev. Lett.* **74**, 2654 (1995).
- [163] P. Vetter *et al.*, *Phys. Rev. Lett.* **74**, 2658 (1995).
- [164] D. Meekhof *et al.*, *Phys. Rev. Lett.* **71**, 3442 (1993).
- [165] M. Macpherson *et al.*, *Phys. Rev. Lett.* **67**, 20, 2784 (1991).
- [166] P. Blunden, W. Melnitchouk and A. Thomas, *Phys. Rev. Lett.* **109**, 262301 (2012), [arXiv:1208.4310].
- [167] S. Bennett and C. E. Wieman, *Phys. Rev. Lett.* **82**, 2484 (1999), [Erratum: *Phys.Rev.Lett.* 82, 4153 (1999), Erratum: *Phys.Rev.Lett.* 83, 889 (1999)], [hep-ex/9903022].
- [168] V. Dzuba and V. Flambaum., *Phys. Rev. A* **62**, 052101 (2000), [arXiv:physics/0005038].
- [169] V. Dzuba, V. Flambaum and O. Sushkov, *Phys. Rev. A* **56**, 4357 (1997), [hep-ph/9709251].
- [170] D. Cho *et al.*, *Phys. Rev. A* **55**, 1007 (1997).
- [171] G. Toh *et al.*, *Phys. Rev. Lett.* **123**, 7, 073002 (2019), [arXiv:1905.02768].
- [172] A. A. Vasilyev *et al.*, *Phys. Rev. A* **66**, 020101 (2002).
- [173] V. Dzuba, V. Flambaum and J. Ginges, *Phys. Rev. D* **66**, 076013 (2002), [hep-ph/0204134].
- [174] J. Ginges and V. Flambaum, *Phys. Rept.* **397**, 63 (2004), [arXiv:physics/0309054].
- [175] A. Derevianko and S. G. Porsev, *Eur. Phys. J. A* **32**, 4, 517 (2007), [hep-ph/0608178].
- [176] B. Roberts, V. Dzuba and V. Flambaum, *Ann. Rev. Nucl. Part. Sci.* **65**, 63 (2015), [arXiv:1412.6644].
- [177] A. Derevianko, *Phys. Rev. Lett.* **85**, 1618 (2000), [hep-ph/0005274].
- [178] W. Johnson, I. Bednyakov and G. Soff, *Phys. Rev. Lett.* **87**, 233001 (2001), [Erratum: *Phys.Rev.Lett.* 88, 079903 (2002)], [hep-ph/0110262].
- [179] M. Kuchiev and V. Flambaum, *Phys. Rev. Lett.* **89**, 283002 (2002), [hep-ph/0206124].
- [180] A. Milstein, O. Sushkov and I. Terekhov, *Phys. Rev. Lett.* **89**, 283003 (2002), [hep-ph/0208227].
- [181] S. Porsev, K. Beloy and A. Derevianko, *Phys. Rev. Lett.* **102**, 181601 (2009), [arXiv:0902.0335].
- [182] V. Dzuba *et al.*, *Phys. Rev. Lett.* **109**, 203003 (2012), [arXiv:1207.5864].
- [183] C. Bouchiat and C. Piketty, *Phys. Lett. B* **128**, 73 (1983).
- [184] I. Zel'dovich, *J. Exp. Theor. Phys.* **6**, 1184 (1958).
- [185] V. Flambaum and D. Murray, *Phys. Rev. C* **56**, 1641 (1997), [arXiv:nucl-th/9703050].
- [186] W. Haxton and C. E. Wieman, *Ann. Rev. Nucl. Part. Sci.* **51**, 261 (2001), [arXiv:nucl-th/0104026].
- [187] V. Dzuba *et al.*, *J. Phys. B* **20**, 3297 (1987).
- [188] J. L. Rosner, *Phys. Rev. D* **53**, 2724 (1996), [hep-ph/9507375].
- [189] D. Antypas *et al.*, *Nature Phys.* **15**, 2, 120 (2019), [arXiv:1804.05747].
- [190] M. Ramsey-Musolf, *Phys. Rev. C* **60**, 015501 (1999), [hep-ph/9903264].
- [191] S. Pollock, E. Fortson and L. Wilets, *Phys. Rev. C* **46**, 2587 (1992), [arXiv:nucl-th/9211004].
- [192] B. Chen and P. Vogel, *Phys. Rev. C* **48**, 1392 (1993), [arXiv:nucl-th/9303003].
- [193] C. Horowitz *et al.*, *Phys. Rev. C* **63**, 025501 (2001), [arXiv:nucl-th/9912038].
- [194] S. Abrahamyan *et al.*, *Phys. Rev. Lett.* **108**, 112502 (2012), [arXiv:1201.2568].
- [195] H. Davoudiasl, H.-S. Lee and W. J. Marciano, *Phys. Rev. D* **86**, 095009 (2012), [arXiv:1208.2973].
- [196] E. Braaten, S. Narison and A. Pich, *Nucl. Phys. B* **373**, 581 (1992).
- [197] A. Pich, *Prog. Part. Nucl. Phys.* **75**, 41 (2014), [arXiv:1310.7922].
- [198] M. Davier *et al.*, *Eur. Phys. J. C* **74**, 3, 2803 (2014), [arXiv:1312.1501].

- [199] K. Chetyrkin, A. Kataev and F. Tkachov, *Phys. Lett. B* **85**, 277 (1979).
- [200] M. Dine and J. Sapirstein, *Phys. Rev. Lett.* **43**, 668 (1979).
- [201] S. Gorishnii, A. Kataev and S. Larin, *Phys. Lett. B* **259**, 144 (1991).
- [202] L. R. Surguladze and M. A. Samuel, *Phys. Rev. Lett.* **66**, 560 (1991), [Erratum: *Phys.Rev.Lett.* 66, 2416 (1991)].
- [203] P. Baikov, K. Chetyrkin and J. H. Kuhn, *Phys. Rev. Lett.* **101**, 012002 (2008), [arXiv:0801.1821].
- [204] F. Le Diberder and A. Pich, *Phys. Lett. B* **286**, 147 (1992).
- [205] M. Beneke and M. Jamin, *JHEP* **09**, 044 (2008), [arXiv:0806.3156].
- [206] E. Braaten and C.-S. Li, *Phys. Rev. D* **42**, 3888 (1990).
- [207] W. Marciano and A. Sirlin, *Phys. Rev. Lett.* **61**, 1815 (1988).
- [208] J. Erler, *Rev. Mex. Fis.* **50**, 200 (2004), [hep-ph/0211345].
- [209] D. Boito *et al.*, *Phys. Rev. D* **85**, 093015 (2012), [arXiv:1203.3146].
- [210] D. Boito *et al.*, *Phys. Rev. D* **91**, 3, 034003 (2015), [arXiv:1410.3528].
- [211] A. Pich and A. Rodríguez-Sánchez, *Phys. Rev. D* **94**, 3, 034027 (2016), [arXiv:1605.06830].
- [212] J. Erler (2011), [arXiv:1102.5520].
- [213] G. Bennett *et al.* (Muon g-2), *Phys. Rev. Lett.* **92**, 161802 (2004), [hep-ex/0401008].
- [214] T. Aoyama *et al.*, *Phys. Rev. Lett.* **109**, 111808 (2012), [arXiv:1205.5370].
- [215] T. Aoyama *et al.*, *PTEP* **2012**, 01A107 (2012).
- [216] P. Baikov, A. Maier and P. Marquard, *Nucl. Phys. B* **877**, 647 (2013), [arXiv:1307.6105].
- [217] G. Li, R. Mendel and M. A. Samuel, *Phys. Rev. D* **47**, 1723 (1993).
- [218] S. Laporta and E. Remiddi, *Phys. Lett. B* **301**, 440 (1993).
- [219] S. Laporta and E. Remiddi, *Phys. Lett. B* **379**, 283 (1996), [hep-ph/9602417].
- [220] A. Czarnecki and M. Skrzypek, *Phys. Lett. B* **449**, 354 (1999), [hep-ph/9812394].
- [221] J. Erler and M. Luo, *Phys. Rev. Lett.* **87**, 071804 (2001), [hep-ph/0101010].
- [222] S. Laporta, *Phys. Lett. B* **772**, 232 (2017), [arXiv:1704.06996].
- [223] S. J. Brodsky and J. D. Sullivan, *Phys. Rev.* **156**, 1644 (1967).
- [224] T. Burnett and M. Levine, *Phys. Lett. B* **24**, 467 (1967).
- [225] R. Jackiw and S. Weinberg, *Phys. Rev. D* **5**, 2396 (1972).
- [226] I. Bars and M. Yoshimura, *Phys. Rev. D* **6**, 374 (1972).
- [227] K. Fujikawa, B. Lee and A. Sanda, *Phys. Rev. D* **6**, 2923 (1972).
- [228] W. A. Bardeen, R. Gastmans and B. Lautrup, *Nucl. Phys. B* **46**, 319 (1972).
- [229] T. Kukhto *et al.*, *Nucl. Phys. B* **371**, 567 (1992).
- [230] S. Peris, M. Perrottet and E. de Rafael, *Phys. Lett. B* **355**, 523 (1995), [hep-ph/9505405].
- [231] A. Czarnecki, B. Krause and W. J. Marciano, *Phys. Rev. D* **52**, 2619 (1995), [hep-ph/9506256].
- [232] A. Czarnecki, B. Krause and W. J. Marciano, *Phys. Rev. Lett.* **76**, 3267 (1996), [hep-ph/9512369].
- [233] C. Gnendiger, D. Stöckinger and H. Stöckinger-Kim, *Phys. Rev. D* **88**, 053005 (2013), [arXiv:1306.5546].
- [234] G. Degrossi and G. Giudice, *Phys. Rev. D* **58**, 053007 (1998), [hep-ph/9803384].
- [235] A. Czarnecki, W. J. Marciano and A. Vainshtein, *Phys. Rev. D* **67**, 073006 (2003), [Erratum: *Phys.Rev.D* 73, 119901 (2006)], [hep-ph/0212229].
- [236] F. Jegerlehner, *EPJ Web Conf.* **166**, 00022 (2018), [arXiv:1705.00263].
- [237] H. B. Meyer and H. Wittig, *Prog. Part. Nucl. Phys.* **104**, 46 (2019), [arXiv:1807.09370].
- [238] T. Blum *et al.* (RBC, UKQCD), *Phys. Rev. Lett.* **121**, 2, 022003 (2018), [arXiv:1801.07224].
- [239] D. Giusti *et al.*, *Phys. Rev. D* **99**, 11, 114502 (2019), [arXiv:1901.10462].
- [240] E. Shintani and Y. Kuramashi (PACS), *Phys. Rev. D* **100**, 3, 034517 (2019), [arXiv:1902.00885].
- [241] C. Davies *et al.* (Fermilab Lattice, LATTICE-HPQCD, MILC), *Phys. Rev. D* **101**, 3, 034512 (2020), [arXiv:1902.04223].
- [242] A. Gérardin *et al.*, *Phys. Rev. D* **100**, 1, 014510 (2019), [arXiv:1904.03120].
- [243] S. Borsanyi *et al.* (2020), [arXiv:2002.12347].
- [244] C. Lehner and A. S. Meyer (2020), [arXiv:2003.04177].
- [245] K. Melnikov and A. Vainshtein, *Phys. Rev. D* **70**, 113006 (2004), [hep-ph/0312226].
- [246] J. Erler and G. Toledo Sanchez, *Phys. Rev. Lett.* **97**, 161801 (2006), [hep-ph/0605052].
- [247] J. Prades, E. de Rafael and A. Vainshtein **20**, 303 (2009), [arXiv:0901.0306].
- [248] M. Knecht and A. Nyffeler, *Phys. Rev. D* **65**, 073034 (2002), [hep-ph/0111058].
- [249] I. Danilkin, C. F. Redmer and M. Vanderhaeghen, *Prog. Part. Nucl. Phys.* **107**, 20 (2019), [arXiv:1901.10346].
- [250] T. Blum *et al.* (2019), [arXiv:1911.08123].
- [251] B. Krause, *Phys. Lett. B* **390**, 392 (1997), [hep-ph/9607259].
- [252] A. Kurz *et al.*, *Phys. Lett. B* **734**, 144 (2014), [arXiv:1403.6400].
- [253] G. Colangelo *et al.*, *Phys. Lett. B* **735**, 90 (2014), [arXiv:1403.7512].
- [254] J. L. Lopez, D. V. Nanopoulos and X. Wang, *Phys. Rev. D* **49**, 366 (1994), [hep-ph/9308336].
- [255] G. Passarino and M. Veltman, *Nucl. Phys. B* **160**, 151 (1979).
- [256] W. Hollik and G. Duckeck, *Springer Tracts Mod. Phys.* **162**, 1 (2000).
- [257] B. Lynn and R. Stuart, *Nucl. Phys. B* **253**, 216 (1985).
- [258] S. L. Wu, *Phys. Rept.* **107**, 59 (1984).
- [259] R. Marshall, *Z. Phys. C* **43**, 607 (1989).
- [260] S. Schael *et al.* (ALEPH, DELPHI, L3, OPAL, LEP Electroweak), *Phys. Rept.* **532**, 119 (2013), [arXiv:1302.3415].
- [261] T. A. Aaltonen *et al.* (CDF, DØ), *Phys. Rev. D* **88**, 5, 052018 (2013), [arXiv:1307.7627].
- [262] Technical Report TEVEWWG/WZ 2010/01, FERMILAB, Batavia (2010), [arXiv:1003.2826], URL <https://www-d0.fnal.gov/Run2Physics/WWW/results/prelim/EW/E34>.
- [263] M. Aaboud *et al.* (ATLAS), *Eur. Phys. J. C* **78**, 2, 110 (2018), [Erratum: *Eur.Phys.J.C* 78, 898 (2018)], [arXiv:1701.07240].
- [264] G. Aad *et al.* (ATLAS), *Phys. Lett. B* **716**, 1 (2012), [arXiv:1207.7214].
- [265] S. Chatrchyan *et al.* (CMS), *Phys. Lett. B* **716**, 30 (2012), [arXiv:1207.7235].
- [266] M. Aaboud *et al.* (ATLAS), *Phys. Lett. B* **784**, 345 (2018), [arXiv:1806.00242].
- [267] A. M. Sirunyan *et al.* (CMS) (2020), [arXiv:2002.06398].
- [268] T. A. Aaltonen *et al.* (CDF, DØ), *Phys. Rev. D* **97**, 11, 112007 (2018), [arXiv:1801.06283].

- [269] G. Aad *et al.* (ATLAS), JHEP **09**, 049 (2015), [arXiv:1503.03709].
- [270] Technical Report ATLAS-CONF-2018-037, CERN, Geneva (2018), URL <https://cds.cern.ch/record/2630340>.
- [271] A. M. Sirunyan *et al.* (CMS), Eur. Phys. J. C **78**, 9, 701 (2018), [arXiv:1806.00863].
- [272] R. Aaij *et al.* (LHCb), JHEP **11**, 190 (2015), [arXiv:1509.07645].
- [273] K. Abe *et al.* (SLD), Phys. Rev. Lett. **84**, 5945 (2000), [hep-ex/0004026].
- [274] K. Abe *et al.* (SLD), Phys. Rev. Lett. **86**, 1162 (2001), [hep-ex/0010015].
- [275] P. Janot and S. Jadach, Phys. Lett. B **803**, 135319 (2020), [arXiv:1912.02067].
- [276] D. Kennedy *et al.*, Nucl. Phys. B **321**, 83 (1989).
- [277] S. Riemann, Rept. Prog. Phys. **73**, 126201 (2010).
- [278] K. Abe *et al.* (SLD), Phys. Rev. Lett. **85**, 5059 (2000), [hep-ex/0006019].
- [279] K. Abe *et al.* (SLD), Phys. Rev. Lett. **78**, 17 (1997), [hep-ex/9609019].
- [280] W. Bernreuther *et al.*, JHEP **01**, 053 (2017), [arXiv:1611.07942].
- [281] S. Catani and M. H. Seymour, JHEP **07**, 023 (1999), [hep-ph/9905424].
- [282] A. Djouadi, J. H. Kuhn and P. Zerwas, Z. Phys. C **46**, 411 (1990).
- [283] T. A. Aaltonen *et al.* (CDF), Phys. Rev. D **93**, 11, 112016 (2016), [Addendum: Phys.Rev.D 95, 119901 (2017)], [arXiv:1605.02719].
- [284] V. M. Abazov *et al.* (DØ), Phys. Rev. Lett. **120**, 24, 241802 (2018), [arXiv:1710.03951].
- [285] V. Abazov *et al.* (DØ), Phys. Rev. D **84**, 012007 (2011), [arXiv:1104.4590].
- [286] D. Acosta *et al.* (CDF), Phys. Rev. D **71**, 052002 (2005), [hep-ex/0411059].
- [287] A. Aktas *et al.* (H1), Phys. Lett. B **632**, 35 (2006), [hep-ex/0507080].
- [288] H. Abramowicz *et al.* (ZEUS), Phys. Rev. D **93**, 9, 092002 (2016), [arXiv:1603.09628].
- [289] D. Albert *et al.*, Nucl. Phys. B **166**, 460 (1980).
- [290] K. Chetyrkin, J. H. Kuhn and A. Kwiatkowski, Phys. Rept. **277**, 189 (1996), [hep-ph/9503396].
- [291] B. A. Kniehl and J. H. Kuhn, Nucl. Phys. B **329**, 547 (1990).
- [292] K. Chetyrkin and A. Kwiatkowski, Phys. Lett. B **319**, 307 (1993), [hep-ph/9310229].
- [293] S. Larin, T. van Ritbergen and J. Vermaseren, Phys. Lett. B **320**, 159 (1994), [hep-ph/9310378].
- [294] K. Chetyrkin and O. Tarasov, Phys. Lett. B **327**, 114 (1994), [hep-ph/9312323].
- [295] P. Baikov *et al.*, Phys. Rev. Lett. **108**, 222003 (2012), [arXiv:1201.5804].
- [296] A. Kataev, Phys. Lett. B **287**, 209 (1992).
- [297] B. W. Lynn and R. G. Stuart, Phys. Lett. B **252**, 676 (1990).
- [298] J. Bernabeu, A. Pich and A. Santamaria, Nucl. Phys. B **363**, 326 (1991).
- [299] A. Czarnecki and J. H. Kuhn, Phys. Rev. Lett. **77**, 3955 (1996), [hep-ph/9608366].
- [300] R. Harlander, T. Seidensticker and M. Steinhauser, Phys. Lett. B **426**, 125 (1998), [hep-ph/9712228].
- [301] J. Fleischer *et al.*, Phys. Lett. B **459**, 625 (1999), [hep-ph/9904256].
- [302] P. A. Grassi, B. A. Kniehl and A. Sirlin, Phys. Rev. Lett. **86**, 389 (2001), [hep-th/0005149].
- [303] A. Akhundov, D. Bardin and T. Riemann, Nucl. Phys. B **276**, 1 (1986).
- [304] F. Jegerlehner, Z. Phys. C **32**, 425 (1986), [Erratum: Z.Phys.C 38, 519 (1988)].
- [305] W. Beenakker and W. Hollik, Z. Phys. C **40**, 141 (1988).
- [306] D. Bardin *et al.*, Z. Phys. C **44**, 493 (1989).
- [307] A. Borrelli *et al.*, Nucl. Phys. B **333**, 357 (1990).
- [308] A. Denner and T. Sack, Z. Phys. C **46**, 653 (1990).
- [309] A. Denner, Fortsch. Phys. **41**, 307 (1993), [arXiv:0709.1075].
- [310] U. Amaldi *et al.*, Phys. Rev. D **36**, 1385 (1987).
- [311] G. Costa *et al.*, Nucl. Phys. B **297**, 244 (1988).
- [312] P. Langacker and M. Luo, Phys. Rev. D **44**, 817 (1991).
- [313] J. Erler and P. Langacker, Phys. Rev. D **52**, 441 (1995), [hep-ph/9411203].
- [314] F. James and M. Roos, Comput. Phys. Commun. **10**, 343 (1975).
- [315] D. d'Enterria and A. Poldaru (2019), [arXiv:1912.11733].
- [316] V. Abazov *et al.* (DØ), Phys. Rev. D **80**, 111107 (2009), [arXiv:0911.2710].
- [317] J. Bagger, K. T. Matchev and D. Pierce, Phys. Lett. B **348**, 443 (1995), [hep-ph/9501277].
- [318] P. Langacker and N. Polonsky, Phys. Rev. D **52**, 3081 (1995), [hep-ph/9503214].
- [319] M. Veltman, Nucl. Phys. B **123**, 89 (1977).
- [320] M. S. Chanowitz, M. Furman and I. Hinchliffe, Phys. Lett. B **78**, 285 (1978).
- [321] J. van der Bij and F. Hoogeveen, Nucl. Phys. B **283**, 477 (1987).
- [322] P. Langacker and M. Luo, Phys. Rev. D **45**, 278 (1992).
- [323] A. Denner, R. Guth and J. H. Kuhn, Phys. Lett. B **240**, 438 (1990).
- [324] W. Grimus *et al.*, J. Phys. G **35**, 075001 (2008), [arXiv:0711.4022].
- [325] H. E. Haber and D. O'Neil, Phys. Rev. D **83**, 055017 (2011), [arXiv:1011.6188].
- [326] S. Bertolini and A. Sirlin, Phys. Lett. B **257**, 179 (1991).
- [327] M. Golden and L. Randall, Nucl. Phys. B **361**, 3 (1991).
- [328] B. Holdom and J. Terning, Phys. Lett. B **247**, 88 (1990).
- [329] M. E. Peskin and T. Takeuchi, Phys. Rev. Lett. **65**, 964 (1990).
- [330] K. Hagiwara *et al.*, Z. Phys. C **64**, 559 (1994), [Erratum: Z.Phys.C 68, 352 (1995)], [hep-ph/9409380].
- [331] M. E. Peskin and T. Takeuchi, Phys. Rev. D **46**, 381 (1992).
- [332] I. Maksymyk, C. Burgess and D. London, Phys. Rev. D **50**, 529 (1994), [hep-ph/9306267].
- [333] R. Barbieri *et al.*, Nucl. Phys. B **703**, 127 (2004), [hep-ph/0405040].
- [334] M. Farina *et al.*, Phys. Lett. B **772**, 210 (2017), [arXiv:1609.08157].
- [335] G. Altarelli and R. Barbieri, Phys. Lett. B **253**, 161 (1991).
- [336] D. Kennedy and P. Langacker, Phys. Rev. D **44**, 1591 (1991).
- [337] L. Randall and R. Sundrum, Phys. Rev. Lett. **83**, 3370 (1999), [hep-ph/9905221].
- [338] M. Carena *et al.*, Nucl. Phys. B **759**, 202 (2006), [hep-ph/0607106].
- [339] R. Contino (2011), [arXiv:1005.4269].
- [340] E. Gates and J. Terning, Phys. Rev. Lett. **67**, 1840 (1991).
- [341] R. Sundrum, Nucl. Phys. B **395**, 60 (1993), [hep-ph/9205203].
- [342] R. Sundrum and S. D. Hsu, Nucl. Phys. B **391**, 127 (1993), [hep-ph/9206225].

- [343] M. A. Luty and R. Sundrum, *Phys. Rev. Lett.* **70**, 529 (1993), [hep-ph/9209255].
- [344] T. Appelquist and J. Terning, *Phys. Lett. B* **315**, 139 (1993), [hep-ph/9305258].
- [345] D. D. Dietrich, F. Sannino and K. Tuominen, *Phys. Rev. D* **72**, 055001 (2005), [hep-ph/0505059].
- [346] N. D. Christensen and R. Shrock, *Phys. Lett. B* **632**, 92 (2006), [hep-ph/0509109].
- [347] M. Harada, M. Kurachi and K. Yamawaki, *Prog. Theor. Phys.* **115**, 765 (2006), [hep-ph/0509193].
- [348] H. Georgi, *Nucl. Phys. B* **363**, 301 (1991).
- [349] M. J. Dugan and L. Randall, *Phys. Lett. B* **264**, 154 (1991).
- [350] H. E. Haber and G. L. Kane, *Phys. Rept.* **117**, 75 (1985).
- [351] A. Djouadi, *Phys. Rept.* **459**, 1 (2008), [hep-ph/0503173].
- [352] R. Barbieri *et al.*, *Nucl. Phys. B* **341**, 309 (1990).
- [353] R. Barbieri, M. Frigeni and F. Caravaglios, *Phys. Lett. B* **279**, 169 (1992).
- [354] J. Erler and D. M. Pierce, *Nucl. Phys. B* **526**, 53 (1998), [hep-ph/9801238].
- [355] G.-C. Cho and K. Hagiwara, *Nucl. Phys. B* **574**, 623 (2000), [hep-ph/9912260].
- [356] G. Altarelli *et al.*, *JHEP* **06**, 018 (2001), [hep-ph/0106029].
- [357] S. Heinemeyer, W. Hollik and G. Weiglein, *Phys. Rept.* **425**, 265 (2006), [hep-ph/0412214].
- [358] S. P. Martin, K. Tobe and J. D. Wells, *Phys. Rev. D* **71**, 073014 (2005), [hep-ph/0412424].
- [359] M. Ramsey-Musolf and S. Su, *Phys. Rept.* **456**, 1 (2008), [hep-ph/0612057].
- [360] S. Heinemeyer *et al.*, *JHEP* **04**, 039 (2008), [arXiv:0710.2972].
- [361] O. Buchmuller *et al.*, *Eur. Phys. J. C* **72**, 2020 (2012), [arXiv:1112.3564].
- [362] B. Grinstein and M. B. Wise, *Phys. Lett. B* **265**, 326 (1991).
- [363] A. Pich, I. Rosell and J. Sanz-Cillero, *JHEP* **01**, 157 (2014), [arXiv:1310.3121].
- [364] C. T. Hill and E. H. Simmons, *Phys. Rept.* **381**, 235 (2003), [Erratum: *Phys.Rept.* 390, 553–554 (2004)], [hep-ph/0203079].
- [365] G. Panico and A. Wulzer **913** (2016), [arXiv:1506.01961].
- [366] J. Erler and P. Langacker, *Phys. Rev. Lett.* **105**, 031801 (2010), [arXiv:1003.3211].
- [367] J. Gunion, D. W. McKay and H. Pois, *Phys. Rev. D* **53**, 1616 (1996), [hep-ph/9507323].
- [368] A. Lenz, *Adv. High Energy Phys.* **2013**, 910275 (2013).
- [369] S. Chatrchyan *et al.* (CMS), *Phys. Rev. D* **86**, 112003 (2012), [arXiv:1209.1062].
- [370] A. Djouadi and A. Lenz, *Phys. Lett. B* **715**, 310 (2012), [arXiv:1204.1252].
- [371] O. Eberhardt *et al.*, *Phys. Rev. Lett.* **109**, 241802 (2012), [arXiv:1209.1101].
- [372] J. Maalampi and M. Roos, *Phys. Rept.* **186**, 53 (1990).
- [373] P. Langacker, *Phys. Rept.* **72**, 185 (1981).
- [374] J. L. Hewett and T. G. Rizzo, *Phys. Rept.* **183**, 193 (1989).
- [375] J. Kang, P. Langacker and B. D. Nelson, *Phys. Rev. D* **77**, 035003 (2008), [arXiv:0708.2701].
- [376] S. P. Martin, *Phys. Rev. D* **81**, 035004 (2010), [arXiv:0910.2732].
- [377] P. W. Graham *et al.*, *Phys. Rev. D* **81**, 055016 (2010), [arXiv:0910.3020].
- [378] J. Erler, J. L. Feng and N. Polonsky, *Phys. Rev. Lett.* **78**, 3063 (1997), [hep-ph/9612397].
- [379] D. Choudhury, T. M. Tait and C. Wagner, *Phys. Rev. D* **65**, 053002 (2002), [hep-ph/0109097].
- [380] J. Erler and P. Langacker, *Phys. Rev. Lett.* **84**, 212 (2000), [hep-ph/9910315].
- [381] P. Langacker and M. Plumacher, *Phys. Rev. D* **62**, 013006 (2000), [hep-ph/0001204].
- [382] P. Abreu *et al.* (DELPHI), *Eur. Phys. J. C* **10**, 415 (1999).
- [383] P. Langacker and D. London, *Phys. Rev. D* **38**, 886 (1988).
- [384] F. del Aguila, J. de Blas and M. Perez-Victoria, *Phys. Rev. D* **78**, 013010 (2008), [arXiv:0803.4008].
- [385] M. Chemtob, *Prog. Part. Nucl. Phys.* **54**, 71 (2005), [hep-ph/0406029].
- [386] R. Barbieri *et al.*, *Phys. Rept.* **420**, 1 (2005), [hep-ph/0406039].
- [387] T. Han, H. E. Logan and L.-T. Wang, *JHEP* **01**, 099 (2006), [hep-ph/0506313].
- [388] M. Perelstein, *Prog. Part. Nucl. Phys.* **58**, 247 (2007), [hep-ph/0512128].
- [389] I. Antoniadis (2001), [hep-th/0102202].
- [390] M. Carena *et al.*, *Phys. Rev. D* **68**, 035010 (2003), [hep-ph/0305188].
- [391] K. Agashe *et al.*, *JHEP* **08**, 050 (2003), [hep-ph/0308036].
- [392] I. Gogoladze and C. Macesanu, *Phys. Rev. D* **74**, 093012 (2006), [hep-ph/0605207].
- [393] S. Weinberg, *Phys. Rev. Lett.* **43**, 1566 (1979).
- [394] W. Buchmuller and D. Wyler, *Nucl. Phys. B* **268**, 621 (1986).
- [395] B. Grzadkowski *et al.*, *JHEP* **10**, 085 (2010), [arXiv:1008.4884].
- [396] R. Contino *et al.*, *JHEP* **07**, 035 (2013), [arXiv:1303.3876].
- [397] K. Hagiwara *et al.*, *Phys. Rev. D* **48**, 2182 (1993).
- [398] A. Falkowski, F. Riva and A. Urbano, *JHEP* **11**, 111 (2013), [arXiv:1303.1812].
- [399] A. Pomarol and F. Riva, *JHEP* **01**, 151 (2014), [arXiv:1308.2803].
- [400] J. Ellis, V. Sanz and T. You, *JHEP* **03**, 157 (2015), [arXiv:1410.7703].
- [401] A. Efrati, A. Falkowski and Y. Soreq, *JHEP* **07**, 018 (2015), [arXiv:1503.07872].
- [402] J. de Blas *et al.*, *PoS EPS-HEP2017*, 467 (2017), [arXiv:1710.05402].
- [403] G. Altarelli, R. Barbieri and S. Jadach, *Nucl. Phys. B* **369**, 3 (1992), [Erratum: *Nucl.Phys.B* 376, 444 (1992)].
- [404] G.-C. Cho, K. Hagiwara and S. Matsumoto, *Eur. Phys. J. C* **5**, 155 (1998), [hep-ph/9707334].
- [405] K. Cheung, *Phys. Lett. B* **517**, 167 (2001), [hep-ph/0106251].
- [406] Z. Han and W. Skiba, *Phys. Rev. D* **71**, 075009 (2005), [hep-ph/0412166].
- [407] P. Langacker, M. Luo and A. K. Mann, *Rev. Mod. Phys.* **64**, 87 (1992).
- [408] P. Langacker, *Rev. Mod. Phys.* **81**, 1199 (2009), [arXiv:0801.1345].

11. Status of Higgs Boson Physics

Revised August 2019 by M. Carena (FNAL; Chicago U.; Chicago U., Kavli Inst.), C. Grojean (Theoriegruppe, DESY, Hamburg; Physik, Humboldt U.), M. Kado (Rome U. Sapienza; INFN, Rome; U. Paris-Saclay, IJCLab) and V. Sharma (UC San Diego).

11.1	Introduction	203
11.2	The Standard Model and the mechanism of electroweak symmetry breaking	204
11.2.1	The SM Higgs boson mass, couplings and quantum numbers	204
11.2.2	The SM custodial symmetry	205
11.2.3	Stability of the Higgs potential	205
11.2.4	Higgs boson production and decay mechanisms	205
11.3	The experimental profile of the Higgs boson	209
11.3.1	The principal decay channels to vector bosons	209
11.3.2	Decays to third generation fermions ($b\bar{b}$ and $\tau^+\tau^-$)	212
11.3.3	Higgs boson production in association with top quarks or in top decays	214
11.3.4	Higgs boson pair production	215
11.3.5	Searches for rare decays of the Higgs boson	216
11.3.6	Searches for non-SM decay channels	218
11.4	Combining the main channels	220
11.4.1	Principles of the combination	220
11.4.2	Main decay modes	221
11.4.3	Main production modes	222
11.5	Main quantum numbers and width of the Higgs boson	222
11.5.1	Main quantum numbers J^{PC}	222
11.5.2	Off-shell couplings of the Higgs boson	225
11.5.3	The Higgs boson width	226
11.6	Probing the coupling properties of the Higgs boson	227
11.6.1	Effective Lagrangian framework	228
11.6.2	Probing coupling properties	228
11.7	New physics models of EWSB in the light of the Higgs boson discovery	234
11.7.1	Higgs bosons in the minimal supersymmetric standard model (MSSM)	235
11.7.2	Supersymmetry with singlet extensions	238
11.7.3	Supersymmetry with extended gauge sectors	238
11.7.4	Effects of CP violation	239
11.7.5	Non-supersymmetric extensions of the Higgs sector	240
11.7.6	Composite Higgs models	242
11.7.7	Searches for signatures of extended Higgs sectors	245
11.8	Summary and outlook	250

11.1 Introduction

Understanding the mechanism that breaks the electroweak symmetry and generates the masses of the known elementary particles has been one of the fundamental endeavours in particle physics for several decades. The discovery in 2012 by the ATLAS [1] and the CMS [2] collaborations of a new resonance with a mass of approximately 125 GeV and the subsequent studies of its properties with the full data set from Run 1, from 2009 to 2012, with a centre-of-mass energy of 7 TeV and 8 TeV, conclusively provided a first portrait of the Electroweak Symmetry Breaking (EWSB) mechanism. The data collected during the LHC Run 2, from 2015 to 2018, with a higher centre-of-mass energy of 13 TeV and more conspicuous dataset, put in solid grounds the compatibility of the measured resonance with the Higgs boson of the Standard Model (SM) [3].

In the SM, the electroweak interactions are described by a gauge field theory invariant under the $SU(2)_L \times U(1)_Y$ symmetry group. The mechanism of EWSB [4] provides a general framework to keep untouched the structure of these gauge interactions at high energies and still generate the observed masses of the W and Z gauge bosons. The EWSB mechanism posits a self-interacting complex

EW doublet scalar field, whose CP -even neutral component acquires a vacuum expectation value (VEV) $v \approx 246$ GeV, which sets the scale of the symmetry breaking. Three massless Goldstone bosons are generated and are absorbed to give masses to the W and Z gauge bosons. The remaining component of the complex doublet becomes the Higgs boson – a new, and so far unique, fundamental scalar particle. The masses of all fermions are also a consequence of EWSB since the Higgs doublet is postulated to couple to the fermions through Yukawa interactions

The initial measurements during the LHC Run 1 were accessible mainly through production and decay channels related to the couplings of the Higgs boson to the vector gauge bosons (the mediators of the electroweak interactions, W^\pm , Z and γ , as well as the gluons, g , mediators of the strong interactions).

The outstanding performance of the LHC Run 2, made it possible for the ATLAS and CMS experiments to independently and unambiguously establish the couplings of the Higgs boson to the charged fermions of the third generation (the top quark, the bottom quark, and the tau). These observations of fundamental importance were made with partial Run 2 datasets.

In all observed production and decay modes measured so far, the rates and differential measurements are found to be consistent, within experimental and theoretical uncertainties, with the SM predictions. In high resolution decay channels, such as the ones with four leptons (electrons or muons) or diphoton final states, the mass of the Higgs boson has been measured at the permill precision level.

Nevertheless, several channels are still out of reach experimentally and the couplings of the Higgs boson to light fermions are yet to be proven. Moreover, within the current precision, a more complex sector with additional states is not ruled out, nor has it been established whether the Higgs boson is an elementary particle or whether it has an internal structure like any other scalar particles observed before it.

Without the Higgs boson, the calculability of the SM would have been spoiled. In particular, perturbative unitarity [5] would be lost at high energies since the longitudinal W/Z boson scattering amplitude would grow with the centre-of-mass energy. In addition, the radiative corrections to the gauge boson self-energies would exhibit dangerous logarithmic divergences that would be difficult to reconcile with EW precision data. With the discovery of the Higgs boson, the SM is a spontaneously broken gauge theory and, as such, it could a priori be consistently extrapolated well above the masses of the W and Z bosons. Hence, formally there is no need for new physics at the EW scale. However, as the SM Higgs boson is a scalar particle, at the quantum level it has sensitivity to possible new physics scales. Quite generally, the Higgs boson mass is affected by the presence of heavy particles and receives quantum corrections which destabilise the weak scale barring a large fine tuning of unrelated parameters. This is known as the Higgs naturalness or hierarchy problem [6]. It has been the prime argument for expecting new physics right at the TeV scale. New theoretical paradigms have been imagined, such as a new fermion-boson symmetry called supersymmetry (SUSY) [7] (for recent reviews, see Refs. [8, 9]), or the existence of strong interactions at a scale of the order of a TeV from which the Higgs boson would emerge as a composite state [10] (see Refs. [11, 12] for recent reviews). Alternatively, new agents stabilising the weak scale could also be light but elusive, like in models of neutral naturalness [13, 14]. Other more recent scenarios [15], instead, rely on the cosmological evolution of the Universe to drive the Higgs boson mass to a value much smaller than the cutoff of the theory and aim at alleviating the hierarchy problem without the need for TeV scale new physics, even though there might still be interesting and spectacular signatures [15, 16]. Beyond the naturalness problem, extensions of the SM Higgs sector without other low-energy particles have been proposed, for example, to provide explanations for the fermion mass hierarchies, see e.g. Ref. [17], to account for the Dark Matter abundance, see e.g. Ref. [18], or to modify the properties of the electroweak phase transition [19]. Such models with additional scalars provide grounds to explore new Higgs boson signals in concrete and complete scenarios, with different types of coupling structure to fermions and gauge bosons.

The Higgs boson is anyway special and, in the eight years since its discovery, it became a powerful tool to explore the manifestations of the SM and to probe the physics landscape beyond it. It might offer direct insights on what comes beyond the weak scale through possible sizeable effects on the Higgs boson properties. The Higgs boson couplings, however, are observed to be in good agreement with their SM predictions. This, together with the strong bounds from precision electroweak and flavour data, leaves open the possibility that the Higgs boson may well be elementary, weakly coupled and solitary up to the Planck scale, rendering the EW vacuum potentially metastable [20].

After completion of the first two runs, the LHC has only gathered approximately 5% of its projected full dataset. During the second long shut down currently underway, the LHC is undergoing important upgrades in order to prepare for its high luminosity phase. The foreseen larger datasets to be collected during Run 3 and ultimately during the High Luminosity LHC (HL-LHC), will enable yet more fundamental and challenging measurements to explore new physics.

This review is organised as follows. Section 11.2 is a theoretical review of the SM Higgs boson, its properties, production mechanisms and decay rates. In Section 11.3, the experimental measurements are described. In Section 11.4, the combination of the main Higgs boson production and decay channels is presented. In Section 11.5, measurements of the main quantum numbers and CP properties of the Higgs boson are reported and the bounds on its total width are discussed. In Section 11.6, a general theoretical framework to describe the deviations of the Higgs boson couplings from the SM predictions is introduced and the experimental measurements of these Higgs couplings is reviewed. Measurements of differential cross sections are outlined. Section 11.7 presents, in detail, some interesting models proposed for extensions of the SM Higgs sector, addressing the hierarchy problem or not, and considers their experimental signatures. Section 11.8 provides a short summary and a brief outlook.

11.2 The Standard Model and the mechanism of electroweak symmetry breaking

In the SM [3], electroweak symmetry breaking [4] is responsible for generating mass for the W and Z gauge bosons rendering the weak interactions short ranged. The SM scalar potential reads:

$$V(\Phi) = m^2 \Phi^\dagger \Phi + \lambda (\Phi^\dagger \Phi)^2 \quad (11.1)$$

with the Higgs field Φ being a self-interacting $SU(2)_L$ complex doublet (four real degrees of freedom) with weak hypercharge $Y=1$ (the hypercharge is normalised such that $Q = T_{3L} + Y/2$, Q being the electric charge and T_{3L} the eigenvalue of the diagonal generator of $SU(2)_L$):

$$\Phi = \frac{1}{\sqrt{2}} \begin{pmatrix} \sqrt{2}\phi^+ \\ \phi^0 + ia^0 \end{pmatrix}, \quad (11.2)$$

where ϕ^0 and a^0 are the CP -even and CP -odd neutral components, and ϕ^+ is the complex charged component of the Higgs doublet, respectively. $V(\Phi)$ is the most general renormalisable scalar potential. If the quadratic term is negative, the neutral component of the scalar doublet acquires a non-zero vacuum expectation value (VEV)

$$\langle \Phi \rangle = \frac{1}{\sqrt{2}} \begin{pmatrix} 0 \\ v \end{pmatrix}, \quad (11.3)$$

with $\phi^0 = H + \langle \phi^0 \rangle$ and $\langle \phi^0 \rangle \equiv v$, inducing the spontaneous breaking of the SM gauge symmetry $SU(3)_C \times SU(2)_L \times U(1)_Y$ into $SU(3)_C \times U(1)_{\text{em}}$. The global minimum of the theory defines the ground state, and spontaneous symmetry breaking implies that there is a (global and/or local) symmetry of the system that is not respected by the ground state. From the four generators of the $SU(2)_L \times U(1)_Y$ SM gauge group, three are spontaneously broken, implying that they lead to non-trivial transformations of the ground state and indicate the existence of three massless Goldstone bosons identified with three of the four Higgs field degrees of freedom. The Higgs field couples to the W_μ and B_μ gauge fields associated with the $SU(2)_L \times U(1)_Y$ local symmetry through the

covariant derivative appearing in the kinetic term of the Higgs Lagrangian,

$$\mathcal{L}_{\text{Higgs}} = (D_\mu \Phi)^\dagger (D^\mu \Phi) - V(\Phi), \quad (11.4)$$

where $D_\mu \Phi = (\partial_\mu + ig\sigma^a W_\mu^a/2 + ig'YB_\mu/2)\Phi$, g and g' are the $SU(2)_L$ and $U(1)_Y$ gauge couplings, respectively, and $\sigma^a, a = 1, 2, 3$ are the usual Pauli matrices. As a result, the neutral and the two charged massless Goldstone degrees of freedom mix with the gauge fields corresponding to the broken generators of $SU(2)_L \times U(1)_Y$ and become, in the unitarity gauge, the longitudinal components of the Z and W physical gauge bosons, respectively. The Z and W gauge bosons acquire masses,

$$m_W^2 = \frac{g^2 v^2}{4}, \quad m_Z^2 = \frac{(g^2 + g'^2)v^2}{4}. \quad (11.5)$$

The fourth generator remains unbroken since it is the one associated to the conserved $U(1)_{\text{em}}$ gauge symmetry, and its corresponding gauge field, the photon, remains massless. Similarly the eight color gauge bosons, the gluons, corresponding to the conserved $SU(3)_C$ gauge symmetry with 8 unbroken generators, also remain massless (though confined inside hadrons and mesons as the result of the asymptotic freedom behaviour of QCD). Hence, from the initial four degrees of freedom of the Higgs field, two are absorbed by the W^\pm gauge bosons, one by the Z gauge boson, and there is one remaining degree of freedom, H , that is the physical Higgs boson — a new scalar particle first imagined by P. Higgs [4]. The Higgs boson is neutral under the electromagnetic interactions and transforms as a singlet under $SU(3)_C$ and hence does not couple at tree level to the massless photons and gluons.

The fermions of the SM acquire mass through renormalisable interactions between the Higgs field and the fermions: the Yukawa interactions,

$$\mathcal{L}_{\text{Yukawa}} = -\hat{h}_{d_{ij}} \bar{q}_{L_i} \Phi d_{R_j} - \hat{h}_{u_{ij}} \bar{q}_{L_i} \tilde{\Phi} u_{R_j} - \hat{h}_{l_{ij}} \bar{l}_{L_i} \Phi e_{R_j} + h.c., \quad (11.6)$$

which respect the symmetries of the SM but generate fermion masses once EWSB occurs. In the Lagrangian above, $\tilde{\Phi} = i\sigma_2 \Phi^*$ and q_L (l_L) and u_R , d_R (e_R) are the quark (lepton) $SU(2)_L$ doublets and singlets, respectively, while in each term, $\hat{h}_{X_{ij}}$ is parametrised by a 3×3 matrix in family space. The mass term for neutrinos is omitted, but could be added in an analogous manner to the up-type quarks when right-handed neutrinos are supplementing the SM particle content (neutrinos can also acquire Majorana masses via non-renormalisable dimension-5 interactions with the Higgs field [21]). Once the Higgs field acquires a VEV, and after rotation to the fermion mass eigenstate basis that also diagonalises the Higgs-fermion interactions, $\hat{h}_{f_{ij}} \rightarrow h_{f_i} \delta_{ij}$, all fermions acquire a mass given by $m_{f_i} = h_{f_i} v / \sqrt{2}$. The indices $i, j = 1, 2, 3$ refer to the three families in the up-quark, down-quark or charged lepton sectors. It should be noted that the EWSB mechanism provides no additional insight on possible underlying reasons for the large variety of masses of the fermions, often referred to as the flavour hierarchy. The fermion masses, accounting for a large number of the free parameters of the SM, are simply translated into Yukawa couplings.

11.2.1 The SM Higgs boson mass, couplings and quantum numbers

The SM Higgs boson is a CP -even scalar of spin 0. Its mass is given by $m_H = \sqrt{2\lambda} v$, where λ is the self coupling parameter in $V(\Phi)$. The expectation value of the Higgs field, $v = (\sqrt{2}G_F)^{-1/2} \approx 246 \text{ GeV}$, is fixed by the Fermi coupling G_F , which is determined with a precision of 0.6 ppm from muon decay measurements [22]. The quartic coupling λ is a free parameter in the SM, and hence, there is no a priori prediction for the Higgs mass. Moreover the sign of the mass parameter $m^2 = -\lambda v^2$ has to be negative for the EW symmetry breaking to take place, but there is no a priori understanding of what decides of this sign. The experimentally measured Higgs boson mass, $m_H = 125.10 \pm 0.14 \text{ GeV}$ [22], implies that $\lambda \simeq 0.13$ and $|m| \simeq 88.4 \text{ GeV}$.

The Higgs boson couplings to the fundamental particles are set by their masses. This is a new type of interaction; very weak for light particles, such as up and down quarks, and electrons, but strong for heavy particles such as the W and Z bosons and the top quark. More precisely, the SM Higgs couplings to fundamental fermions are linearly proportional to the fermion masses, whereas the couplings to bosons are proportional to the square of the boson masses. The SM Higgs boson couplings to gauge bosons and fermions, as well as the Higgs boson self coupling, are summarised in the following Lagrangian:

$$\mathcal{L} = -g_{Hf\bar{f}}\bar{f}fH + \frac{g_{HHH}}{6}H^3 + \frac{g_{HHHH}}{24}H^4 + \delta_V V_\mu V^\mu \left(g_{HVV}H + \frac{g_{HHVV}}{2}H^2 \right) \quad (11.7)$$

with

$$g_{Hf\bar{f}} = \frac{m_f}{v}, \quad g_{HVV} = \frac{2m_V^2}{v}, \quad g_{HHVV} = \frac{2m_V^2}{v^2}, \quad (11.8)$$

$$g_{HHH} = \frac{3m_H^2}{v}, \quad g_{HHHH} = \frac{3m_H^2}{v^2},$$

where $V = W^\pm$ or Z and $\delta_W = 1, \delta_Z = 1/2$. As a result, the dominant mechanisms for Higgs boson production and decay involve the coupling of H to W, Z and/or the third generation quarks and leptons. The Higgs boson coupling to gluons [23, 24] is induced at leading order by a one-loop process in which H couples to a virtual $t\bar{t}$ pair (with minor contributions from the other lighter quarks). Likewise, the Higgs boson coupling to photons is also generated via loops, although in this case the one-loop graph with a virtual W^+W^- pair provides the dominant contribution [25] and it is interfering with the smaller contribution involving a virtual $t\bar{t}$ pair (as such, the Higgs coupling to photons is sensitive to the relative phase of the interactions between bosons and fermions).

11.2.2 The SM custodial symmetry

The SM Higgs Lagrangian, $\mathcal{L}_{\text{Higgs}} + \mathcal{L}_{\text{Yukawa}}$ of Eq. (11.4) and Eq. (11.6), is, by construction, $SU(2)_L \times U(1)_Y$ gauge invariant, but it also has an approximate global symmetry. In the limit $g' \rightarrow 0$ and $h_f \rightarrow 0$, the Higgs sector has a global $SU(2)_R$ symmetry, and hence it is invariant under a global $SU(2)_L \times SU(2)_R$ symmetry, with $SU(2)_L$ just being the global variant of the SM chiral gauge symmetry. This symmetry is preserved for non-vanishing Yukawa couplings, provided $h_u = h_d$. Once the Higgs acquires a VEV, both the $SU(2)_L$ and $SU(2)_R$ symmetry groups are broken but the diagonal subgroup $SU(2)_{L+R}$ remains unbroken and it is the subgroup that defines the custodial symmetry of the SM [26].

In the limit $g' \rightarrow 0$, the W and Z gauge bosons have equal mass and form a triplet of the $SU(2)_{L+R}$ unbroken global symmetry. Using the expressions for the W and Z gauge boson masses in term of the gauge couplings, one obtains at tree level

$$\frac{m_W^2}{m_Z^2} = \frac{g^2}{g'^2 + g^2} = \cos^2 \theta_W \quad \text{or} \quad \rho \equiv \frac{m_W^2}{m_Z^2 \cos^2 \theta_W} = 1. \quad (11.9)$$

The custodial symmetry protects the above relation from large radiative corrections. All corrections to the ρ parameter are therefore proportional to terms that break the custodial symmetry. For instance, radiative corrections involving the Higgs boson are proportional to $\sin^2 \theta_W$, $\delta\rho = -11G_F m_Z^2 \sin^2 \theta_W \log(m_H^2/m_Z^2)/(24\sqrt{2}\pi^2)$, and vanish in the limit $g' \rightarrow 0$. Since $m_t \neq m_b$, there are also relevant radiative corrections generated by massive fermions. They are proportional to $m_t^2 + m_b^2 - 2(m_t^2 m_b^2) \log(m_t^2/m_b^2)/(m_t^2 - m_b^2)$ and would indeed vanish for $m_t = m_b$ [27].

11.2.3 Stability of the Higgs potential

The discovery of the Higgs boson with $m_H \approx 125$ GeV has far reaching consequences within the SM framework. In particular, the precise value of m_H determines the value of the quartic coupling λ at the electroweak scale and makes it possible to study its behavior up to high energy scales. A larger value of m_H would have implied that the self coupling λ would become non-perturbative at some scale Λ that could be well below the Planck scale [28].

However, for the value of Higgs boson mass experimentally measured, the EW vacuum of the Higgs potential is most likely metastable [20]. The high energy evolution of λ shows that it becomes negative at energies $\Lambda = \mathcal{O}(10^{11})$ GeV (even though λ could remain positive till higher energy, maybe all the way to the Planck scale, if the top quark mass exceeds its current measured value by 3σ). When this occurs, the SM Higgs potential develops an instability and the long term existence of the EW vacuum is challenged. This behaviour may call for new physics at an intermediate scale before the instability develops, i.e., below M_{Planck} , even though new physics at M_{Planck} could influence the stability of the EW vacuum and possibly modify this conclusion [29]. The consequences of the instability of the EW vacuum on high-scale inflation have been discussed in Ref. [30]. It was also noticed that Higgs field fluctuations during inflation could seed the formation of primordial black holes, possibly making up the Dark Matter relic abundance [31] or they could produce a stochastic background of gravitational waves with characteristic structures [32], offering a probe of the EW vacuum near criticality.

The lifetime of the EW metastable vacuum is determined by the rate of quantum tunnelling from this vacuum into the true vacuum of the theory (for the most recent computation of the EW vacuum lifetime within the SM, see Ref. [33]). Within the SM, the running of the Higgs self coupling slows down at high energies with a cancellation of its β -function at energies just one to two orders of magnitude below the Planck scale [34]. This slow evolution of the quartic coupling is responsible for saving the EW vacuum from premature collapse. It might also help the Higgs boson to play the role of an inflaton [35] (see, however, Ref. [36] for potential issues with this Higgs-boson-as-an-inflaton idea).

11.2.4 Higgs boson production and decay mechanisms

Reviews of the SM Higgs boson's properties and phenomenology, with an emphasis on the impact of loop corrections to the Higgs boson decay rates and cross sections, can be found in Refs. [37–44].

11.2.4.1 Production mechanisms at hadron colliders

The main production mechanisms at the Tevatron collider and the LHC are gluon fusion (ggF), weak-boson fusion (VBF), associated production with a gauge boson (VH), and associated production with a pair of $t\bar{t}$ quarks ($t\bar{t}H$) or with a single top quark (tHq). Figure 11.1 depicts representative diagrams for these dominant Higgs boson production processes.

The state-of-the-art of the theoretical calculations in the main different production channels is summarized in Table 11.1.

The cross sections for the production of a SM Higgs boson as a function of \sqrt{s} , the center of mass energy, for pp collisions, including bands indicating the theoretical uncertainties, are summarised in Fig. 11.2 (left) [45]. A detailed discussion, including uncertainties in the theoretical calculations due to missing higher-order effects and experimental uncertainties on the determination of SM parameters involved in the calculations, can be found in Refs. [41–44]. These references also contain state-of-the-art discussions on the impact of PDF uncertainties, QCD scale uncertainties and uncertainties due to different procedures for including higher-order corrections matched to parton shower simulations, as well as uncertainties due to hadronisation and parton-shower events.

Table 11.2 summarises the Higgs boson production cross sections and relative uncertainties for a Higgs boson mass of 125 GeV, for $\sqrt{s} = 7, 8, 13$ and 14 TeV. The Higgs boson production cross sections in pp collisions at $\sqrt{s} = 1.96$ TeV for the Tevatron are obtained from Ref. [46].

i. Gluon fusion production mechanism

At high-energy hadron colliders, the Higgs boson production mechanism with the largest cross section is the gluon-fusion process, $gg \rightarrow H + X$, mediated by the exchange of a virtual, heavy top quark [47]. Contributions from lighter quarks propagating in the loop are suppressed proportionally to m_q^2 . QCD radiative corrections to the gluon-fusion process are very important and have been studied in detail. Including the full dependence on the

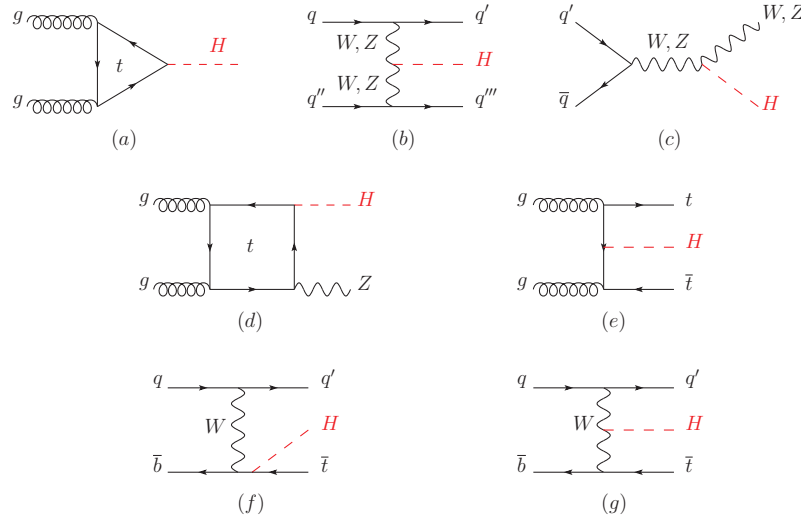


Figure 11.1: Main leading order Feynman diagrams contributing to the Higgs boson production in (a) gluon fusion, (b) Vector-boson fusion, (c) Higgs-strahlung (or associated production with a gauge boson at tree level from a quark-quark interaction), (d) associated production with a gauge boson (at loop level from a gluon-gluon interaction), (e) associated production with a pair of top quarks (there is a similar diagram for the associated production with a pair of bottom quarks), (f-g) production in association with a single top quark

Table 11.1: State-of-the-art of the theoretical calculations in the main Higgs boson production channels in the SM, and the major MC tools used in the simulations

ggF	VBF	VH	ttH
Fixed order: N3LO QCD + NLO EW (HIGLU, iHixs, FeHiPro, HNNLO)	Fixed order: NNLO QCD (VBF@NNLO)	Fixed order: NLO QCD+EW (V2HV and HAWK)	Fixed order: NLO QCD+EW (Powheg)
Resummed: NNLO + NNLL QCD (HRes)	Fixed order: NLO QCD + NLO EW (HAWK)	Fixed order: NNLO QCD (VH@NNLO)	(MG5_aMC@NLO)
Higgs p_T : NNLO+NNLL (HqT, HRes)			
Jet Veto: N3LO+NNLL			

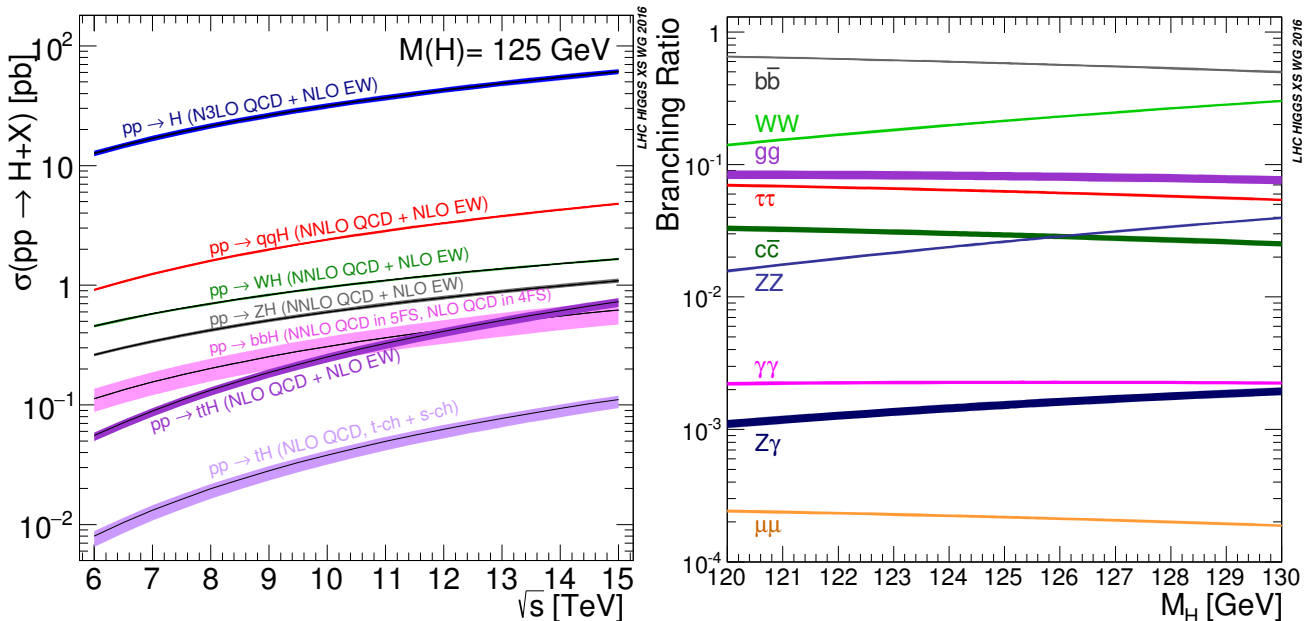


Figure 11.2: (Left) The SM Higgs boson production cross sections as a function of the center of mass energy, \sqrt{s} , for pp collisions [45]. The VBF process is indicated here as qqH . The theoretical uncertainties are indicated as bands. (Right) The branching ratios for the main decays of the SM Higgs boson near $m_H = 125$ GeV [43, 44]. The theoretical uncertainties are indicated as bands.

(top, bottom, charm) quark and Higgs boson masses, the cross section has been calculated at the next-to-leading order (NLO)

Table 11.2: The SM Higgs boson production cross sections for $m_H = 125$ GeV in pp collisions ($p\bar{p}$ collisions at $\sqrt{s} = 1.96$ TeV for the Tevatron), as a function of the center of mass energy, \sqrt{s} . The predictions for the LHC energies are taken from Refs. [41–44], the ones for the Tevatron energy are from Ref. [46]. The predictions for the ggF channel at the LHC include the latest N3LO results leading to reduced theoretical uncertainties by a factor around 2 compared to the NNLO+NLL results. The total uncertainties are estimated assuming no correlations between α_s and PDF uncertainties.

\sqrt{s} (TeV)	Production cross section (in pb) for $m_H = 125$ GeV					
	ggF	VBF	WH	ZH	$t\bar{t}H$	total
1.96	$0.95^{+17\%}_{-17\%}$	$0.065^{+8\%}_{-7\%}$	$0.13^{+8\%}_{-8\%}$	$0.079^{+8\%}_{-8\%}$	$0.004^{+10\%}_{-10\%}$	1.23
7	$16.9^{+4.4\%}_{-7.0\%}$	$1.24^{+2.1\%}_{-2.1\%}$	$0.58^{+2.2\%}_{-2.3\%}$	$0.34^{+3.1\%}_{-3.0\%}$	$0.09^{+5.6\%}_{-10.2\%}$	19.1
8	$21.4^{+4.4\%}_{-6.9\%}$	$1.60^{+2.3\%}_{-2.1\%}$	$0.70^{+2.1\%}_{-2.2\%}$	$0.42^{+3.4\%}_{-2.9\%}$	$0.13^{+5.9\%}_{-10.1\%}$	24.2
13	$48.6^{+4.6\%}_{-6.7\%}$	$3.78^{+2.2\%}_{-2.2\%}$	$1.37^{+2.6\%}_{-2.6\%}$	$0.88^{+4.1\%}_{-3.5\%}$	$0.50^{+6.8\%}_{-9.9\%}$	55.1
14	$54.7^{+4.6\%}_{-6.7\%}$	$4.28^{+2.2\%}_{-2.2\%}$	$1.51^{+1.9\%}_{-2.0\%}$	$0.99^{+4.1\%}_{-3.7\%}$	$0.60^{+6.9\%}_{-9.8\%}$	62.1

in α_s [48, 49]. To a very good approximation, the leading top-quark contribution can be evaluated in the limit $m_t \rightarrow \infty$ by matching the SM to an effective theory. The gluon-fusion amplitude is then evaluated from an effective Lagrangian containing a local $HG_{\mu\nu}^a G^{a\mu\nu}$ operator [23, 24]. In this approximation, the cross section is known at next-to-next-to-next-to-leading order (N3LO) [50]. The validity of the effective theory with infinite m_t is greatly enhanced by rescaling the result by the exact LO result: $\sigma = (\sigma_{m_t}^{\text{LO}}/\sigma_{m_t=\infty}^{\text{LO}}) \times \sigma_{m_t=\infty}$ [44]. The large top-quark mass approximation, after this rescaling of the cross section, yields a NNLO result that has been established to be at the percent level accuracy [51]. Further progress is made to include full top mass dependence at NNLO [52].

The LO and NLO QCD corrections [53] amount to about 80% of the total N3LO cross section. The NNLO corrections [54] further enhance the cross section by approximately 30% of the LO plus NLO result (at $\mu_f = \mu_r = m_H/2$). Electroweak radiative corrections have been computed at NLO and increase the LO cross section by about 5% for $m_H \simeq 125$ GeV [55]. Mixed QCD-EW corrections are now being investigated with encouraging results on the computation of the exact 3-loop amplitude [56] complementing the results obtained in either limit of heavy [57] or massless [58] gauge bosons.

At N3LO, the perturbation series is rather stable with a mere enhancement of 3% of the total cross section, with a central value quite insensitive to threshold resummation effects with the scale choice mentioned above [44, 50, 59]. At the LHC with a center-of-mass energy of 13 TeV, the most up-to-date value for the production cross section of a 125 GeV Higgs boson amounts to [44]

$$\sigma_{\text{ggF}}^{\text{N3LO}} = 48.6 \text{ pb}^{+2.2 \text{ pb} (+4.6\%)}_{-3.3 \text{ pb} (-6.7\%)} \text{ (theory)} \pm 1.6 \text{ pb} (3.2\%) \text{ (PDF} + \alpha_s \text{)}. \quad (11.10)$$

Besides considering the inclusive Higgs boson production cross section at the LHC, it is important to study differential distributions in order to probe the properties of the Higgs boson in a detailed way. A more exclusive account of Higgs boson production is also required because experimental analyses often impose cuts on the final states in order to improve the signal-to-background ratio. To this end, it is useful to define benchmark cuts and compare the differential distributions obtained at various levels of theoretical accuracy (i.e., at NLO or NNLO) with Monte-Carlo generators. In the infinite top mass limit, the Higgs

boson p_T distribution is known at NNLO [60, 61] (see Ref. [62] for a recent reappraisal) and heavy quark mass effects, including top-bottom interferences, have been computed at NLO [63], revealing a non-trivial logarithmic structure that will make resummation difficult [64]. A programmatic approach for a fixed-order/resummation matching of the top-bottom interferences has been proposed [65]. Many search modes for the Higgs boson are carried out by separating the events according to the number of jets or the transverse momentum and rapidity of the Higgs boson. For $p_T < 35$ GeV, predictions for the transverse-momentum distribution can only be trusted after large logarithms of the form $\alpha_s^n \ln^k(m_H/p_T^{\text{veto}})$, $k \leq 2n - 1$, and (non-Sudakov) double logarithms of the form $g_{Hq\bar{q}} m_q/m_H [\ln^2(m_H/m_q), \ln^2(p_T/m_q)]$ have been resummed. This has been accomplished with N3LL accuracy [66] and the results have been matched onto the fixed-order prediction at NNLO [67]. In addition, impressive progress is made to improve the calculation of the Higgs boson production cross section with a jet veto (the “0-jet bin” or in the presence of a veto bounding the transverse momentum of the hardest accompanying jet) [68], reaching N2LL accuracy matched to N3LO. These accurate predictions for the jet-veto cross section are required, e.g., to suppress the $t\bar{t}$ background in the $H \rightarrow WW$ channel [69]. Electroweak corrections have been studied in Ref. [70]. Note that in the boosted regime, at $p_T \sim 1$ TeV, VH takes over ggF as the dominant channel [71].

ii. Vector boson fusion production mechanism

The SM Higgs boson production mode with the second-largest cross section at the LHC is vector boson fusion. At the Tevatron collider, VBF also occurred, but for $m_H = 125$ GeV had a smaller cross section than Higgs boson production in association with a W or Z boson. Higgs boson production via VBF, $qq \rightarrow qqH$, proceeds by the scattering of two (anti-)quarks, mediated by t - or u -channel exchange of a W or Z boson, with the Higgs boson radiated off the weak-boson propagator. The scattered quarks give rise to two back-to-back hard jets in the forward and backward regions of the detector [72]. Because of the color-singlet nature of the weak-gauge boson exchange, gluon radiation from the central-rapidity regions is strongly suppressed. These characteristic features of VBF processes can be exploited to distinguish them from overwhelming QCD backgrounds, including gluon-fusion induced Higgs boson + 2 jet production, and from s -channel WH or ZH production with a hadronically decaying weak gauge boson. After the application of specific selection cuts, the VBF channel provides a clean environment, not only for the Higgs boson searches originally performed, but also for the subsequent determination of Higgs boson couplings at the LHC.

At the inclusive level, the cross-section is known at N3LO [73], with a residual uncertainty of the order of few permill. However, this result is obtained in the DIS/factorised approximation [74] where the fusing gauge bosons are emitted from the two quark legs independently. While, the exact NNLO VBF calculation will remain out-of-reach in the near future, the leading non-factorisable contributions with two forward jets have been estimated [75]. They give some corrections, also of the order of few permill, to inclusive quantities, but they are an order of magnitude larger for differential observables. Full NNLO QCD and NLO EW results in the DIS approximation are known [76] and the residual uncertainty is of the order of a few percent but is quite sensitive to the tagging jet cuts and jet radius modelling [77].

iii. WH and ZH associated production mechanism

The next most relevant Higgs boson production mechanisms after ggF and VBF at the LHC, and the most relevant ones after ggF at the Tevatron collider, are associated production with W and Z gauge bosons. The cross sections for the associated production processes, $pp \rightarrow VH + X$, with $V = W^\pm, Z$ receive contributions at NLO given by NLO QCD corrections to the Drell–Yan cross section [78, 79] and from NLO EW corrections. The latter, unlike the QCD corrections, do not respect the factorisation into Drell–Yan production since there are irreducible box contributions already at one loop [80]. At NNLO, the Drell–Yan-like corrections

to WH production also give the bulk of the corrections to ZH production [81]. For ZH production there are, however, gluon-gluon induced contributions that do not involve a virtual Z gauge boson but are such that the Z gauge boson and H boson couple to gluons via top-quark loops [82], see diagram (d) in Fig. 11.1. In addition, WH and ZH production receive non Drell–Yan-like corrections in the $q\bar{q}'$ and $q\bar{q}$ initiated channels, respectively, at the NNLO level, where the Higgs boson is radiated off top-quark loops [83]. The full QCD corrections up to NNLO order, the NLO EW corrections and the NLO corrections to the gluon-gluon channel are available in $\overline{\text{VH@NNLO}}$ [84].

As neither the Higgs boson nor the weak gauge bosons are stable particles, their decays also have to be taken into account. Providing full kinematical information for the decay products can furthermore help in the suppression of large QCD backgrounds. Differential distributions for the processes $pp \rightarrow WH \rightarrow \bar{\nu}_\ell \ell H$ and $pp \rightarrow ZH \rightarrow \ell^+ \ell^- H / \nu_\ell \bar{\nu}_\ell H$, including NLO QCD and EW corrections, have been presented in Ref. [85]. The NNLO QCD corrections to differential observables for WH production at the LHC, including the leptonic decays of the W boson and the decay of the Higgs boson into a $b\bar{b}$ pair, are presented in Ref. [86]. Calculations at the same level, including also the ZH process have been performed [87]. The WH production mode has also been matched to a parton shower at NNLO accuracy [88]. Full NNLO results for both the production and decay are available [89] and show a large impact of radiation from the final-state bottoms. The WH and ZH production modes, especially in the boosted regime, provide a relatively clean environment for studying the decay of the Higgs boson into bottom quarks [90].

iv. Higgs boson production in association with $t\bar{t}$

Higgs boson radiation off top quarks, $pp \rightarrow t\bar{t}H$, provides a direct probe of the top-Higgs Yukawa coupling. The LO cross section for this production process was computed in Ref. [91]. Later, the NLO(+NNLL) QCD [92] and NLO EW corrections [93] were evaluated yielding a moderate increase in the total cross section of at most 20%, but significantly reducing the scale dependence of the inclusive cross section. The EW corrections can be enhanced by large electroweak Sudakov logarithms in particular in the boosted regime often used in the phenomenological analyses [94]. The total theoretical errors, estimated by combining the uncertainties from factorisation and renormalisation scales, strong gauge coupling, and parton distributions, amount to 10–15% of the corresponding inclusive cross section. Interfaces between NLO QCD calculations for $t\bar{t}H$ production with parton-shower Monte-Carlo programs have been provided in Ref. [95]. These programs provide the most flexible tools to date for the computation of differential distributions, including experimental selection cuts and vetoes on the final-state particles and their decay products. The fixed-order NLO QCD calculation have been interfaced with the standard Parton Shower Monte-Carlo generators, allowing an accurate description of the $t\bar{t}H$ signal, from the energy scale of the hard scattering to the hadronisation energy scale. The exploitation of this channel requires, however, a proper description of the background, in particular $t\bar{t}b\bar{b}$, which exhibits a huge k-factor¹ enhancement from shower effects, see Ref. [44] for a detailed discussion.

v. Other single Higgs boson production mechanisms at the LHC

The Higgs boson production in association with a single top quark, though subdominant, can bring valuable information, in particular regarding the sign of the top Yukawa coupling. This is due to an almost totally destructive interference between two large contributions, one where the Higgs boson couples to a space-like W boson and the other where it couples to the top quark. This process has been computed at NLO in a five-flavour scheme [96] and amounts to about 90 fb at $\sqrt{s} = 14$ TeV (with the opposite sign of the top Yukawa coupling, the cross section increases by one or

der of magnitude while the cross section for associated production with a pair of top quarks is unaffected).

The Higgs boson production in association with a pair of bottom quarks ($b\bar{b}H$) is known at NNLO in the case of five quark flavours [97–99]. The coupling of the Higgs boson to a b -quark is suppressed in the SM by the bottom-quark mass over the Higgs VEV, m_b/v , implying that associated production of a SM Higgs boson with b -quarks is small at the LHC. Yet, at high energy, large logarithms are present and need to be resummed, leading to an enhancement of the inclusive cross section. At $\sqrt{s} = 14$ TeV, the $b\bar{b}H$ cross section can be as large as 550 fb, still two orders of magnitude below the ggF production cross section. In a two Higgs doublet model or a SUSY model, which will be discussed in Section 11.7, this coupling is proportional to the ratio of neutral Higgs boson vacuum expectation values, $\tan \beta$, and can be significantly enhanced for large values of this ratio. Consequently, the $b\bar{b}H$ mode can even become the dominant production process for the Higgs boson, unlike in the SM.

The Higgs boson production in association with charm quarks is also known at NNLO and its cross section is approximately 85 fb at $\sqrt{s} = 13$ TeV [44].

vi. Double Higgs boson production at the LHC

The main interest in the double Higgs boson production is that it can provide invaluable information on the Higgs potential. In particular, it gives access to the Higgs trilinear self coupling. The dominant production is via gluon fusion $gg \rightarrow HH$. It accounts for more than 90% of the total inclusive cross-section, the sub-leading production mechanisms are VBF $HHjj$ (around 1.7 fb at 13 TeV), HHW (0.50 fb), HHZ (0.36 fb) and $t\bar{t}HH$ (0.8 fb). The fixed order QCD corrections, computed in the infinite top mass limit, are large, typically doubling the cross section from LO to NLO [100] and further enhancing it by 20% from NLO to NNLO [101] to reach at 13 TeV [45]

$$\begin{aligned} \sigma(gg \rightarrow HH)_{\text{ggF}}^{\text{NNLO, FTa}} &= 31.05 \text{ fb}_{-5.0\%}^{+2.2\%} \text{ (theory)} \\ &\pm 3\% \text{ (PDF} + \alpha_s) \pm 2.6\% (m_t). \end{aligned} \quad (11.11)$$

Recently, the complete NLO corrections with all top quark mass effects also became available numerically [102, 103], intriguingly revealing a k-factor much less flat than predicted in the large top mass approximations. The non-trivial dependence of the results on the renormalisation scheme and scale for the top quark mass [103] questions the assessment of the scale uncertainty and would warrant a proper NNLO computation that will however remain out of reach for quite some time. At the differential level, the destructive interference between the box and the triangle contributions complicates the predictions made in the infinite top mass limit for both the HH invariant mass and the leading Higgs boson p_T distributions. With an inclusive cross section of about 35 fb at $\sqrt{s} = 13$ TeV and a difficult signal vs background discrimination, the double Higgs boson production remains a challenging channel to probe and will greatly benefit from the high-luminosity run of the LHC [104].

11.2.4.2 Production mechanisms at e^+e^- colliders

The dominant Higgs boson production cross sections at an e^+e^- collider are from the Higgs-strahlung process [23, 105], $e^+e^- \rightarrow ZH$, and the WW fusion process [106], $e^+e^- \rightarrow \bar{\nu}_e \nu_e W^* W^* \rightarrow \bar{\nu}_e \nu_e H$. The cross-section for the Higgs-strahlung process scales as s^{-1} and is predominant at low energies, while the cross-section for the WW fusion process scales as $\ln(s/m_H^2)$ and dominates at high energies [107]. The ZZ fusion mechanism, $e^+e^- \rightarrow e^+e^- Z^* Z^* \rightarrow e^+e^- H$, also contributes to the Higgs boson production, with a cross-section suppressed by an order of magnitude with respect to that of WW fusion. The process $e^+e^- \rightarrow t\bar{t}H$ [108] becomes important for $\sqrt{s} \geq 500$ GeV. For a more detailed discussion of Higgs boson production properties at lepton colliders, see for example Ref. [109].

¹the k-factor is defined as the ratio of a physical quantity with and without radiative corrections included.

11.2.4.3 SM Higgs boson branching ratios and total width

For the understanding and interpretation of the experimental results, the computation of all relevant Higgs boson decay widths is essential, including an estimate of their uncertainties and, when appropriate, the effects of Higgs boson decays into off-shell particles with successive decays into lighter SM ones. A Higgs boson mass of about 125 GeV allows to explore the Higgs boson couplings to many SM particles. In particular the dominant decay modes are $H \rightarrow b\bar{b}$ and $H \rightarrow WW^*$, followed by $H \rightarrow gg$, $H \rightarrow \tau^+\tau^-$, $H \rightarrow c\bar{c}$ and $H \rightarrow ZZ^*$. With much smaller rates follow the Higgs boson decays into $H \rightarrow \gamma\gamma$, $H \rightarrow \gamma Z$ and $H \rightarrow \mu^+\mu^-$. Since the decays into gluons, diphotons and $Z\gamma$ are loop induced, they provide indirect information on the Higgs boson couplings to WW , ZZ and $t\bar{t}$ in different combinations. The uncertainties in the branching ratios include the missing higher-order corrections in the theoretical calculations as well as the errors in the SM input parameters, in particular fermion masses and the QCD gauge coupling, involved in the decay. In the following the state-of-the-art of the theoretical calculations will be discussed and the reader is referred to Refs. [41–44, 110] for detail.

The evaluation of the radiative corrections to the fermionic decays of the SM Higgs boson are implemented in HDECAY [111] at different levels of accuracy. The computations of the $H \rightarrow b\bar{b}$ and $H \rightarrow c\bar{c}$ decays include the complete massless QCD corrections up to N4LO, with a corresponding scale dependence of about 0.1% [112]. Both the electroweak corrections to $H \rightarrow b\bar{b}$, $c\bar{c}$ as well as $H \rightarrow \tau^+\tau^-$ are known at NLO [113] providing predictions with an overall accuracy of about 1–2% for $m_H \simeq 125$ GeV.

The loop induced decays of the SM Higgs boson are known fully at NLO and partially beyond that approximation. For $H \rightarrow gg$, the QCD corrections are known up to N3LO in the limit of heavy top quarks [49, 114] and the uncertainty from the scale dependence is about 3%. For the $H \rightarrow \gamma\gamma$, the full NLO QCD corrections are available [49, 115] and the three-loop QCD corrections have also been evaluated [116]. The NLO electroweak corrections to $H \rightarrow gg$ and $H \rightarrow \gamma\gamma$ have been computed in Ref. [117]. All these corrections are implemented in HDECAY [111]. For $m_H \simeq 125$ GeV, the overall impact of known QCD and EW radiative effects turns out to be well below 1%. In addition, the contribution of the $H \rightarrow \gamma e^+e^-$ decay via virtual photon conversion has been computed in Ref. [118]. The partial decay width $H \rightarrow Z\gamma$ is only implemented at LO in HDECAY, including the virtual W , top-, bottom-, and τ -loop contributions. The QCD corrections have been calculated and are at the percent level [119]. The theoretical uncertainty due to unknown electroweak corrections is estimated to be less than 5%, an accuracy that will be hard to achieve in the measurement of this process at the LHC.

Table 11.3: The branching ratios and the relative uncertainty [43, 44] for a SM Higgs boson with $m_H = 125$ GeV.

Decay channel	Branching ratio	Rel. uncertainty
$H \rightarrow \gamma\gamma$	2.27×10^{-3}	2.1%
$H \rightarrow ZZ$	2.62×10^{-2}	$\pm 1.5\%$
$H \rightarrow W^+W^-$	2.14×10^{-1}	$\pm 1.5\%$
$H \rightarrow \tau^+\tau^-$	6.27×10^{-2}	$\pm 1.6\%$
$H \rightarrow b\bar{b}$	5.82×10^{-1}	+1.2% –1.3%
$H \rightarrow c\bar{c}$	2.89×10^{-2}	+5.5% –2.0%
$H \rightarrow Z\gamma$	1.53×10^{-3}	$\pm 5.8\%$
$H \rightarrow \mu^+\mu^-$	2.18×10^{-4}	$\pm 1.7\%$

The decays $H \rightarrow WW/ZZ \rightarrow 4f$ can be simulated with the

Prophecy4f Monte-Carlo generator [120] that includes complete NLO QCD and EW corrections for Higgs decays into any possible four-fermion final state. All calculations are consistently performed with off-shell gauge bosons, without any on-shell approximation. For the SM Higgs boson, the missing higher-order corrections are estimated to be roughly 0.5%. Such uncertainties will have to be combined with the parametric uncertainties, in particular those associated to the bottom-quark mass and the strong gauge coupling, to arrive at the full theory uncertainty. A detailed treatment of the differential distributions for a Higgs boson decay into four charged leptons in the final state is discussed in Refs. [43, 121].

The total width of a 125 GeV SM Higgs boson is $\Gamma_H = 4.07 \times 10^{-3}$ GeV, with a relative uncertainty of $^{+4.0\%}_{-3.9\%}$. The branching ratios for the most relevant decay modes of the SM Higgs boson as a function of m_H , including the most recent theoretical uncertainties, are shown in Fig. 11.2 (right) and listed for $m_H = 125$ GeV in Table 11.3. Further details of these calculations can be found in the reviews [41–44] and references therein.

11.3 The experimental profile of the Higgs boson

The observation [1, 2] at the LHC of a narrow resonance with a mass of about 125 GeV was an important landmark in the decades-long direct search [46, 122] for the SM Higgs boson. This was followed by a detailed exploration of properties of the Higgs boson at the different runs of the LHC at $\sqrt{s} = 7, 8$ and 13 TeV.

The dataset at $\sqrt{s} = 13$ TeV in the Run 2 phase of the LHC operation corresponds to an integrated luminosity of about 156 fb^{-1} see Table 11.4. The datasets effectively useful for analysis need to take into account the data-taking efficiency with fully operational detectors and the data quality efficiency. The typical total inefficiency for both ATLAS and CMS is approximately 10%, where approximately half is due to the data taking inefficiency and half from data quality.

In this section, most of the references for the Run 1 measurements that have been updated at the Run 2 are given in the previous version of this review [123] and are not repeated herein.

Table 11.4: The LHC pp collision centre-of-mass energies and delivered data samples.

Year	\sqrt{s} (TeV)	$\int \text{L.d.t}$ (fb^{-1})	Period
2010	7	0.04	Run 1
2011	7	6.1	Run 1
2012	8	23.3	Run 1
2015	13	4.2	Run 2
2016	13	40.8	Run 2
2017	13	50.2	Run 2
2018	13	60.6	Run 2

11.3.1 The principal decay channels to vector bosons

For a given m_H , the sensitivity of a channel depends on the production cross section of the Higgs boson, its decay branching fraction, the reconstructed mass resolution, the selection efficiency and the level of background in the final state. For a low-mass Higgs boson ($110 \text{ GeV} < m_H < 150 \text{ GeV}$) for which the SM width would be only a few MeV, five decay channels play an important role at the LHC. In the $H \rightarrow \gamma\gamma$ and $H \rightarrow ZZ^* \rightarrow 4\ell$ channels, all final state particles can be very precisely measured and the reconstructed m_H resolution is excellent (typically 1–2%). While the $H \rightarrow W^+W^- \rightarrow \ell^+\nu_\ell\ell'^-\bar{\nu}_{\ell'}$ channel has relatively large branching fraction, however, due to the presence of neutrinos which are not reconstructed in the final state, the m_H resolution, obtained through observables sensitive to the Higgs boson mass such as the transverse mass, is poor (approximately 20%). The $H \rightarrow b\bar{b}$ and the $H \rightarrow \tau^+\tau^-$ channels suffer from large backgrounds and lead to an intermediate mass resolution of about 10% and 15% respectively.

With the increase in the size of datasets, measurements in the most sensitive channels are now carried out differentially or in exclusive modes depending on specific production characteristics. These measurements are discussed in Section 11.6.2.4.

The candidate events in each Higgs boson decay channel are split into several mutually exclusive categories (or event tags) based on the specific topological, kinematic or other features present in the event. The categorization of events increases the sensitivity of the overall analysis and allows a separation of different Higgs boson production processes. Most categories are dominated by signal from one Higgs boson decay mode but contain an admixture of various Higgs boson production processes. For example, a typical VBF selection requires Higgs boson candidates to be accompanied by two energetic jets (≥ 30 GeV) with a large dijet mass (≥ 400 GeV) and separated by a large pseudo-rapidity ($\Delta\eta_{jj} \geq 3.5$) [124]. While such a category is enriched in Higgs bosons produced via VBF, the contamination from the ggF production mechanism can be significant. Hence, a measurement of the signal rate in the VBF category does not imply a measurement of VBF production cross section since one cannot resolve the contamination from ggF. Simulations are used to determine the relative contributions of the various Higgs boson production modes in each specific categories.

An important difference between the Run 1 and Run 2 results, in particular when comparing signal strengths, and therefore in the measurement of the couplings of the Higgs boson as discussed in Section 11.4, is that values and errors of the predicted cross sections have been improved (mostly the scale and PDF uncertainties). The theoretical predictions are however compatible and therefore, the signal strengths can be compared on a sound basis.

11.3.1.1 $H \rightarrow \gamma\gamma$

In the $H \rightarrow \gamma\gamma$ channel, a search is performed for a narrow peak over a smoothly falling background in the invariant mass distribution of two high p_T photons. The background in this channel is conspicuous and stems from prompt $\gamma\gamma$ processes for the irreducible backgrounds, and the γ +jet and dijet processes for the reducible backgrounds where one jet fragments typically into a leading π^0 . In order to optimise search sensitivity and also to separate the various Higgs boson production modes, ATLAS and CMS split events into several mutually exclusive categories. Diphoton events containing a high p_T muon or electron, or missing energy (E_T^{miss}) consistent with the decay of a W or Z boson, are tagged in the VH production category. Diphoton events containing energetic dijets with a large mass and pseudo-rapidity difference are assigned to the VBF production category, and the remaining events are considered either in the VH category when the two jets are compatible with the hadronic decay of a W or a Z , or in the ggF production category. While the leptonic VH category is relatively pure, the VBF category has significant contamination from the gluon fusion process. Events which are not picked by any of the above selections are further categorised according to their expected $m_{\gamma\gamma}$ resolution and signal-to-background ratio. Categories with good m_H resolution and larger signal-to-background ratio contribute most to the sensitivity of the search.

Both ATLAS and CMS have studied in detail the calibration of the energy response of photons, in particular using $Z \rightarrow e^+e^-$, $Z \rightarrow \mu^+\mu^-$ and the response of muons in the calorimeter (for ATLAS) from $Z \rightarrow \mu^+\mu^-$ events. This information is used to correct the simulated signal mass line-shapes. In each category, parametric signal models are adjusted to these line-shapes to provide a functional form for the signal. Simple monotonic functional forms of the backgrounds are determined by a fit to the $m_{\gamma\gamma}$ distribution in each category (typically exponential, Bernstein polynomials, Laurent series or power laws). All categories are fitted simultaneously to determine the signal yield at the measured combined Run 1 mass of 125.09 ± 0.17 GeV [127] discussed in Section 11.3.2. The $m_{\gamma\gamma}$ distribution after combining all categories is shown in Fig. 11.3, using the full ATLAS Run 2 dataset.

The signal strength, $\mu = (\sigma \cdot \text{BR})_{\text{obs}} / (\sigma \cdot \text{BR})_{\text{SM}}$, which is the observed product of the Higgs boson production cross section (σ) and its branching ratio (BR) normalised to the corresponding SM values, is 1.17 ± 0.27 for ATLAS in Run 1 and 1.02 ± 0.14 in Run 2 [128] (where this signal strength measurement is estimated from the measured fiducial cross sections and thus neglects acceptance systematic uncertainties, which are not expected to be dominant in particular given that the measurement is inclusive).

The signal strengths 2 measured in Run 1 and Run 2 by the CMS collaboration are $1.18_{-0.23}^{+0.26}$ and $1.18_{-0.14}^{+0.17}$ [129] respectively.

11.3.1.2 $H \rightarrow ZZ^* \rightarrow \ell^+\ell^-\ell^+\ell^-$

In the $H \rightarrow ZZ^* \rightarrow \ell^+\ell^-\ell^+\ell^-$ channel, a search is performed for a narrow mass peak over a small continuous background dominated by non-resonant ZZ^* production from $q\bar{q}$ annihilation and gg fusion processes. The contribution and the shape of this irreducible background is taken from simulation. The subdominant and reducible backgrounds stem from $Z+b\bar{b}$, $t\bar{t}$ and Z +jets events. Their contribution is suppressed by requirements on lepton isolation and lepton impact parameter and their yield is estimated from control samples in data.

To help to distinguish the Higgs boson signal from the dominant non-resonant ZZ^* background, both ATLAS and CMS [130] use a matrix element likelihood approach to construct a kinematic discriminant built for each 4ℓ event based on the ratio of complete leading-order matrix elements $|\mathcal{M}_{\text{sig}}|^2 / |\mathcal{M}_{\text{bkg}}|^2$ for the signal ($gg \rightarrow H \rightarrow 4\ell$) and background ($q\bar{q} \rightarrow ZZ \rightarrow 4\ell$) hypotheses. To further enhance the sensitivity, experiments also use multivariate techniques.

To improve the sensitivity to more exclusive production processes such as VBF, VH and $t\bar{t}H$, the experiments divide 4ℓ events into mutually exclusive categories. Events are categorised in terms of the number of reconstructed jets, the number of additional leptons (from the decay of a vector boson in the associated production mode), number of jet tagged as containing a b -hadron, the transverse momentum of the Higgs boson (or e.g. its associated vector boson) and missing transverse momentum. The exclusive processes are also further separated in different kinematic regions in a framework referred to as Simplified Template Cross Sections (see Section 11.6.2.4). Dijets with a large mass and pseudo-rapidity difference populate the VBF category. ATLAS requires the presence of an additional lepton in the VH category. In events with less than two jets, CMS uses the $p_T^{4\ell}$ to distinguish between production via the gluon fusion and the VH /VBF processes.

Since the $m_{4\ell}$ resolutions and the reducible background levels are different in the 4μ , $4e$ and $2e2\mu$ sub-channels, they are analysed separately and the results are then combined. The distribution of the reconstructed invariant mass of the four leptons for CMS [126] is given in Fig. 11.3 (right), showing a clear excess at a mass of approximately $m_H = 125$ GeV. Both experiments also observe a clear peak at $m_{4\ell} = 91$ GeV from the production of a Z boson on-mass-shell and decaying to four leptons due typically to the emission of an off-shell photon from one of the primary leptons from the Z boson decay.

The signal strengths μ for the inclusive $H \rightarrow 4\ell$ production measured by ATLAS and CMS are $1.44_{-0.33}^{+0.40}$ at $m_H = 125.36$ GeV and $0.93_{-0.25}^{+0.29}$ at $m_H = 125.6$ GeV respectively, in Run 1. The signal strengths measured by ATLAS and CMS in Run 2 are 1.04 ± 0.10 [131] and 0.94 ± 0.10 [126] respectively (the ATLAS measurement is made at the combined Run 1 Higgs boson mass of $m_H = 125.09$ GeV while the m_H is profiled in the CMS analysis). The dominant uncertainty in these measurements remains the statistical uncertainty.

11.3.1.3 Measurement of the Higgs boson mass

To measure the mass of the Higgs boson, ATLAS and CMS collaborations rely on the two high mass-resolution and sensitive channels, $\gamma\gamma$ and $ZZ^*/4\ell$. The ATLAS and CMS approaches are very similar in these two analyses with small differences on the usage of categories, additional discriminating variables and per-event errors. In these two channels, the mass resolutions range from 1.4 GeV to 2 GeV for ATLAS and from 1.0 GeV to 2.8 GeV for CMS (see Ref. [127] and the reconstruction-performance references therein). The best mass resolution is obtained for both experiments in the diphoton channel for central diphoton pairs (typically for events where both photons are not converted). The signal strengths in the $\gamma\gamma$ and ZZ channels are assumed to be

²The Run 1 results for ATLAS and CMS are at fixed values of $m_H = 125.4$ GeV and 124.7 GeV, respectively.

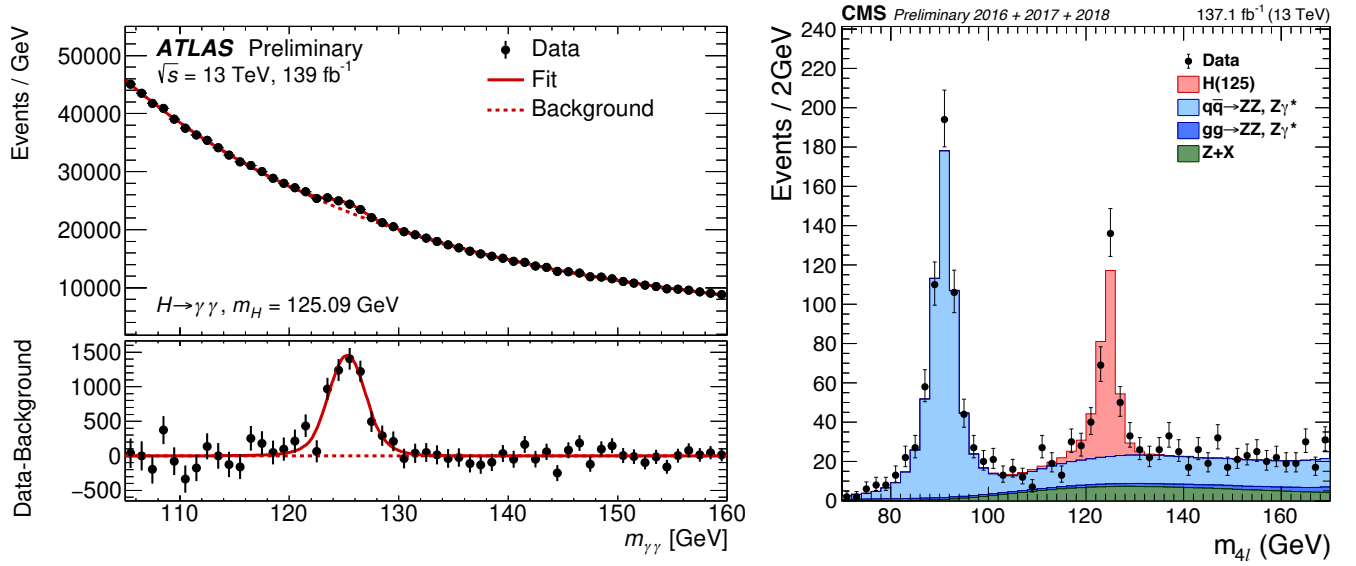


Figure 11.3: (Left) The invariant mass distribution of diphoton candidates, with each event weighted by the ratio of signal-to-background in each event category, observed by ATLAS [125] at Run 2. The residuals of the data with respect to the fitted background are displayed in the lower panel. (Right) The $m_{4\ell}$ distribution from CMS [126] Run 2 data.

independent and not constrained to the expected rate ($\mu = 1$) for the SM Higgs boson.

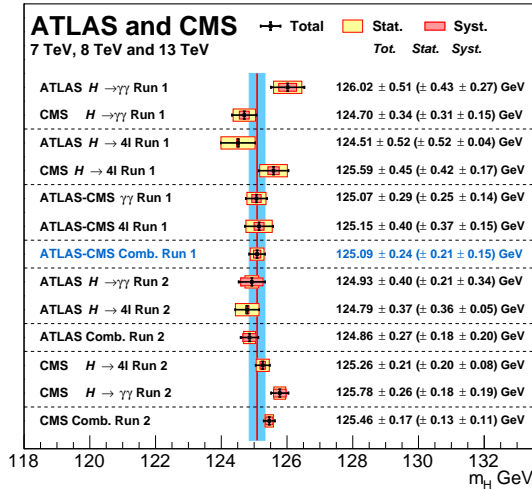


Figure 11.4: Summary of the CMS and ATLAS mass measurements in the $\gamma\gamma$ and ZZ channels in Run 1 and Run 2.

Figure 11.4 summarizes all measurements of the Higgs boson mass, including the individual and combined Run 1 measurements [127] and the Run 2 measurement by ATLAS [132] and CMS [130, 133] for both the diphoton and the 4ℓ channels.

In the diphoton channel, as discussed in Section 11.5.3.2, a mass shift is expected to be induced by the deformation of the mass line-shape of the signal in presence of background, from the interference between the Higgs boson production and the continuum irreducible background. It is a small but non negligible effect of approximately 35 MeV [134] for a Higgs boson width close to that of the SM. This effect could be larger if the width of the Higgs boson were to be substantially larger. This effect estimated by ATLAS with a full simulation is still relatively small with respect to the total uncertainty on the mass and is therefore neglected.

11.3.1.4 $H \rightarrow W^+W^- \rightarrow \ell^+\nu\ell^-\bar{\nu}$

In this intricate channel, experiments search for an excess of events with two leptons of opposite charge accompanied by missing energy and/or jets. A typical event selection is described below in order to give an idea of the main challenges. Specific se-

lections vary between experiments and between Run 1 and Run 2 analyses. Events are divided into several categories depending on the lepton flavour combination (e^+e^- , $\mu^+\mu^-$ and $e^\pm\mu^\mp$) and the number of accompanying jets ($N_{\text{jet}} = 0, 1, \geq 2$). In the ATLAS analysis, the $N_{\text{jet}} \geq 2$ category is optimised for the VBF production process by selecting two leading jets with a large pseudorapidity difference and with a large mass ($m_{jj} > 500$ GeV).

Backgrounds contributing to this channel are numerous and depend on the category of selected events. Reducing them and accurately estimating the remainder is a major challenge in this analysis. For events with opposite-flavour leptons and no accompanying high p_T jets, the dominant background stems from non-resonant WW production. Events with same-flavour leptons suffer from large Drell–Yan contamination (note that also the opposite-flavour leptons analysis has Drell–Yan $\tau\tau$ background in 0-jet category). The $t\bar{t}$, tW and W +jets (with the jet misidentified as a lepton) events contaminate all categories. Non-resonant WZ , ZZ and $W\gamma$ processes also contribute to the background at a sub-leading level.

A requirement of large missing transverse energy (E_T^{miss}) is used to reduce the Drell–Yan and multijet backgrounds. In the e^+e^- and $\mu^+\mu^-$ categories, events with $m_{\ell\ell}$ consistent with the Z mass are vetoed. The $t\bar{t}$ background is suppressed by a veto against identified b -jets or low p_T muons assumed to be coming from semi-leptonic b -hadron decays within jets (this soft muon veto was not applied anymore in Run 2 analysis) and tight isolation requirements diminish the W +jets background. The scalar nature of the Higgs boson and the $V-A$ nature of the W boson decay implies that the two charged leptons in the final state are preferentially emitted at small angles with respect to each other. Therefore the dilepton invariant mass ($m_{\ell\ell}$) and the azimuthal angle difference between the leptons ($\Delta\phi_{\ell\ell}$) are used to discriminate between the signal and non-resonant WW events [135]. The transverse mass, constructed from the dilepton p_T ($p_T^{\ell\ell}$), E_T^{miss} and the azimuthal angle between E_T^{miss} and $p_T^{\ell\ell}$, is defined as

$$m_T = \sqrt{2p_T^{\ell\ell}E_T^{\text{miss}}(1 - \cos\Delta\phi_{E_T^{\text{miss}}\ell\ell})}$$

and serves as an effective discriminant against backgrounds. The transverse mass variable also tracks the Higgs boson mass but with a poor mass resolution. Background rates except for the small contributions typically from non-resonant WZ , ZZ and $W\gamma$ are evaluated from data control samples with floating normalisation.

ATLAS fitted the m_T distributions and observed an excess at $m_H = 125.36$ GeV with a local significance of 6.1σ similar to that expected from a 125 GeV SM Higgs boson. The measured inclusive

signal strength is $\mu = 1.09_{-0.21}^{+0.23}$. In the VBF category, an excess with a significance of 3.2σ corresponding to a signal strength of $\mu = 1.27_{-0.45}^{+0.53}$ is observed. The CMS analysis of 0- and 1-jet categories, using all lepton flavour combinations, shows an excess with an observed significance of 4.3σ , lower than the expected sensitivity of 5.8σ for a 125.6 GeV SM Higgs boson. CMS observes no significant excess in the VBF production mode and sets a 95% CL limit on the signal strength of $\mu_{\text{VBF}} < 1.7$ for $m_H = 125.6$ GeV.

ATLAS and CMS have also searched for the associated Higgs boson production in this channel. The signal consists of up to three (WH) or four (ZH) high p_T isolated leptons with missing transverse energy and low hadronic activity. The major backgrounds stem from triboson and diboson production where each boson decays leptonically. ATLAS observes [136] an excess at $m_H = 125.36$ GeV with a local significance of 2.5σ corresponding to a $\mu_{\text{VH}} = 3.0_{-1.0}^{+1.6}$. CMS instead sets a 95% CL limit of $\mu_{\text{VH}} < 4.7$.

In this difficult channel, the full Run 2 dataset has not yet been analysed by ATLAS nor CMS. There have been partial analyses made with Run 2 data at 13 TeV by both ATLAS and CMS. ATLAS has analysed the $WW \rightarrow e\nu\mu\nu$ decay mode in the gluon fusion, the VBF and VH production modes with 2015 and 2016 datasets [137, 138]. With this limited dataset the measured gluon fusion signal strength yielded [138] $\mu_{\text{ggF}} = 1.10 \pm 0.20$, with the largest uncertainties being the experimental systematic uncertainties.

CMS has performed a more complete analysis with the full 2016 dataset, with most production channels covering both the opposite- and same-flavour final states of opposite charge leptons (electrons or muons), obtaining a combined signal strength of $\mu_{\text{WW}} = 1.28 \pm 0.18$ [139]. This analysis aims at several production modes (ggF, VBF and VH – with the vector boson reconstructed both in jet and leptonic decay modes).

11.3.2 Decays to third generation fermions ($b\bar{b}$ and $\tau^+\tau^-$)

In the SM, fermions acquire a mass through gauge invariant interactions with the Higgs field which is also responsible for the electroweak symmetry breaking and thus for generating the masses of gauge bosons (see Section 11.2 for more details). While this minimal solution is very elegant, there is no fundamental reason for it to be the case, and probing the couplings of the Higgs boson to fermions is therefore of fundamental importance, in particular since BSM physics can largely change the SM predictions.

The discovery of the Higgs boson was made essentially through bosonic final states. These decays probed mostly the couplings of the Higgs boson to vector bosons (the decay of the Higgs boson to photons occurring only through loops is also dominated in the SM by the coupling of the Higgs boson to W bosons). However, the predominant Higgs boson production mode is the gluon fusion, occurring only through loops dominated by the coupling of the Higgs boson to fermions. The observation of the Higgs boson in the two photons or two gluons decay modes is also an indirect evidence for the coupling of the Higgs boson to fermions (and in particular to the top quark). Nevertheless, the observation of either decays to fermions or production modes which unambiguously proceed through fermion couplings provide direct probes of the coupling of the Higgs boson to fermions and is thus of fundamental importance.

At hadron colliders, the most promising channel for probing the coupling of the Higgs field to the quarks and leptons are $H \rightarrow b\bar{b}$ and $H \rightarrow \tau^+\tau^-$, respectively. For a Higgs boson with $m_H \approx 125$ GeV, the branching fraction to $b\bar{b}$ is about 58% and to $\tau^+\tau^-$ is about 6%. Nevertheless, the presence of very large backgrounds makes the isolation of a Higgs boson signal in these channels quite challenging.

One of the most prominent goals of the LHC Run 2 for ATLAS and CMS was the direct observation of the Yukawa coupling of the Higgs boson to fermions of the third generation (bottom quarks, tau leptons and top quarks). This goal has been reached independently by both ATLAS and CMS and with only partial Run 2 datasets.

11.3.2.1 $H \rightarrow \tau^+\tau^-$

In the $H \rightarrow \tau^+\tau^-$ search, τ leptons decaying to electrons (τ_e), muons (τ_μ) and hadrons (τ_{had}) are considered. The $\tau^+\tau^-$ invariant mass ($m_{\tau\tau}$) is reconstructed from a kinematic fit of the visible products from the two τ leptons and the missing energy observed in the event. Due to the presence of missing neutrinos, the $m_{\tau\tau}$ resolution is poor ($\approx 15\%$). As a result, a broad excess over the expected background in the $m_{\tau\tau}$ distribution is searched for. The major sources of background stem from Drell–Yan $Z \rightarrow \tau^+\tau^-$ and $Z \rightarrow e^+e^-$, W +jets, $t\bar{t}$ and multijet production. Events in all sub-channels are divided into categories based on the number and kinematic properties of additional energetic jets in the event and the transverse momentum of the reconstructed Higgs boson and the distance ΔR distance between the two τ 's. The sensitivity of the search is generally higher for categories with one or more additional jets. The VBF category, consisting of a τ pair with two energetic jets separated by a large pseudo-rapidity, has the best signal-to-background ratio and search sensitivity, followed by the $\tau^+\tau^-+1$ jet category. The signal to background discrimination relies in part on the $m_{\tau\tau}$ resolution, which improves with the boost of the Higgs boson. The non-VBF categories are further subdivided according to the observed boost of the $\tau^+\tau^-$ system. CMS primarily uses the reconstructed $m_{\tau\tau}$ as the final discriminating variable while ATLAS combines various kinematic properties of each event categories with multivariate techniques to build the final discriminant [140].

Searches for $H \rightarrow \tau^+\tau^-$ decays in the VH production mode are also performed in final states where the W or Z boson decays into leptons or jets. The irreducible background in this search arises from non-resonant WZ and ZZ diboson production. The reducible backgrounds originate from W , Z , and $t\bar{t}$ events that contain at least one fake lepton in the final state due to a misidentified jet. The shape and yield of the major backgrounds in each category are estimated from control samples in data. Contributions from non-resonant WZ and ZZ diboson production are estimated from simulations but corrected for reconstruction efficiency using control samples formed from observed data.

For CMS, the significance of the observed excess at $m_H = 125$ GeV in Run 1 is 3.2σ , close to the expected 3.7σ sensitivity, and corresponds to a signal strength of $\mu = 0.86 \pm 0.29$. The observed (expected) deviation from the background-only hypothesis in ATLAS corresponds to a local significance of 4.5σ (3.4σ) and the best fit value of the signal strength is $\mu = 1.43_{-0.37}^{+0.43}$ [140].

When the ATLAS and CMS $H \rightarrow \tau\tau$ Run 1 measurements are combined [141], the significance of the observed excess corresponding to $m_H = 125.09$ GeV is 5.5σ and the combined signal strength is $\mu = 1.11_{-0.22}^{+0.24}$, consistent with the SM expectation.

The Run 1 evidence was strong only through the combination of the two experiments. The Run 2 larger dataset at a greater centre-of-mass energy is essential to further confirm this observation and perform first precision measurements in this important channel.

ATLAS has analysed its 2015 and 2016 dataset so far, providing further evidence at the 4.4σ level with an expected significance of 4.1σ . When combined with the Run 1 data the single experiment observation significance is 6.4σ (5.4σ expected) [142].

In the CMS analysis of the 2016 data [143], the strategy was improved using additional categories aiming at the inclusive production of the Higgs boson and binned in transverse momentum of the $\tau^+\tau^-$ system, and for the VBF production, the analysis is binned as a function of the dijet mass. This analysis reached a sensitivity of 4.7σ with a dataset corresponding to an integrated luminosity of 35.9 fb^{-1} . CMS observes an excess with a significance of 4.9σ . In combination with the Run 1 results, this provides an unambiguous observation of the direct coupling of the Higgs boson to taus, in the VBF production mode.

CMS has then also extended to additional production modes via the associated production with a vector boson [144] and analysed a larger dataset corresponding to an integrated luminosity of almost 80 fb^{-1} of data collected in 2016 and 2017, providing results which complete the Run 1 search for an unambiguous observation of the direct decay of the Higgs bosons to a pair of taus (and measurements of cross sections times branching-fractions) [145].

11.3.2.2 $H \rightarrow b\bar{b}$

In the search for the decay of the Higgs boson to a pair of b -quarks, the most sensitive production modes are the associated WH and ZH processes allowing use of the leptonic W and Z decays for triggering, and to purify the signal and reject QCD backgrounds. The W bosons are reconstructed via their leptonic decay $W \rightarrow \ell\bar{\nu}_\ell$ where $\ell = e, \mu$ or τ . The Z bosons are reconstructed via their decay into e^+e^- , $\mu^+\mu^-$ or $\nu\bar{\nu}$. The Higgs boson candidate mass is reconstructed from two b -tagged jets in the event. Backgrounds arise from production of W and Z bosons in association with gluon, light and heavy-flavoured jets (V +jets), $t\bar{t}$, diboson (ZZ and WZ with $Z \rightarrow b\bar{b}$) and QCD multi-jet processes. Due to the limited $m_{b\bar{b}}$ mass resolution, a SM Higgs boson signal is expected to appear as a broad enhancement in the reconstructed dijet mass distribution. The crucial elements in this search are b -jet tagging with high efficiency and low fake rate, accurate estimate of b -jet momentum and estimate of backgrounds from various signal depleted control samples constructed from data.

At the Tevatron, the $H \rightarrow b\bar{b}$ channel contributes the majority of the Higgs boson search sensitivity below $m_H = 130$ GeV. To separate signal from background, CDF and D0 use multivariate analysis (MVA) techniques that combine several discriminating variables into a single final discriminant. Each channel is divided into exclusive sub-channels according to various lepton, jet multiplicity, and b -tagging characteristics in order to group events with similar signal-to-background ratio and thus optimise the overall search sensitivity. The combined CDF and D0 data show [46, 146] an excess of events with respect to the predicted background in the 115–140 GeV mass range in the most sensitive bins of the discriminant distributions suggesting the potential presence of a signal. At $m_H = 125$ GeV, the observed signal strength is $\mu = 1.59^{+0.69}_{-0.72}$.

At the LHC, in order to reduce the dominant V +jets background, following Ref. [90], experiments select a region in the VH production phase space where the vector boson is significantly boosted and recoils from the $H \rightarrow b\bar{b}$ candidate with a large azimuthal angle $\Delta\phi_{VH}$. For each channel, events are categorised into different $p_T(V)$ regions with varying signal/background ratios. Events with higher $p_T(V)$ have smaller backgrounds and better $m_{b\bar{b}}$ resolution. CMS uses MVA classifiers based on kinematic, topological and quality of b -jet tagging and trained on different values of m_H to separate Higgs boson signal in each category from backgrounds. The MVA outputs for all categories are then fit simultaneously.

The nominal results from ATLAS are also based on a combination of (i) a multivariate analysis of their 8 TeV data, incorporating various kinematic variables in addition to $m_{b\bar{b}}$ and b -tagging information and (ii) a statistical analysis of their 7 TeV data centred on $m_{b\bar{b}}$ as the main discriminant. In both cases, customised control samples devised from data are used to constrain the contributions of the dominant background processes.

The direct observation of the Higgs boson decaying to a pair of b -quarks, a major result of Run 2, was obtained by both ATLAS and CMS independently after the update of their search with similar analyses as those performed at Run 1 but with a larger dataset of approximately 80 fb^{-1} of data collected in 2015, 2016 and 2017. The increase in signal cross sections of nearly a factor of 3 at the centre-of-mass energy of 13 TeV with respect to 7 TeV, has also been instrumental in bringing the two experiments to the required sensitivity to claim an evidence for this decay mode in the VH production mode (in the high transverse momentum of the vector boson fiducial region of interest for this channel). The expected significance for a SM Higgs boson is 4.3σ for ATLAS [147] and 4.9σ for CMS [148]. Both ATLAS and CMS observe significant excesses corresponding to 4.9σ and 4.8σ respectively with Run 2 data only. When combined with results obtained in Run 1, the observed (expected) significance of the excesses are 5.4σ (5.5σ) and 5.6σ (5.5σ) respectively. These results provide direct evidence for the Higgs boson decay to a $b\bar{b}$ through the VH production mode. All these results are summarised in Table 11.5. It should be noted that the sensitivity of these analyses are already limited by systematic uncertainties.

This channel has also been exploited by ATLAS to produce a

measurement at higher transverse momentum of the vector boson in the framework of Simplified Template Cross Sections (STXS) discussed in Section 11.6.2.4 [149]. In this case, at higher transverse momentum, the statistical uncertainty still dominates.

Also, the LHCb collaboration has performed a search for the VH production with subsequent decay of the Higgs boson to a pair of b -quarks [150] with 1.98 fb^{-1} of data taken at a centre-of-mass energy of 8 TeV. The final state is required to have two reconstructed b quarks and one lepton in the LHCb acceptance of $2 < \eta < 5$. The sensitivity of this search is an expected 95% CL exclusion of 84 times the SM production rate. This analysis is also used to set a limit on the VH production with the subsequent decay of the Higgs boson in a pair of c quarks with a 95% CL limit at 6.4×10^3 times the SM production rate, while the expected sensitivity corresponds to an exclusion of 7.9×10^3 times the SM production rate.

ATLAS and CMS have also searched for $H \rightarrow b\bar{b}$ in the VBF production mode. The event topology consists of two VBF-tagging energetic light-quark jets in the forward and backward direction relative to the beam direction and two b -tagged jets in the central region of the detector. Due to the electroweak nature of the process, for the signal events, no additional energetic jet activity (excluding that from the Higgs boson) is expected in the rapidity gap between the two VBF-tagging jets. The dominant background in this search stems from QCD production of multi-jet events and the hadronic decays of vector bosons accompanied by additional jets. A contribution of Higgs boson events produced in the ggF process but with two or more associated jets is expected in the signal sample. The signal is expected as a broad enhancement in the $m_{b\bar{b}}$ distribution over the smoothly falling contribution from the SM background processes. Both ATLAS [151] and CMS [152] have produced results in this channel with Run 1 data, but with limited sensitivity. Both experiments performed a similar analysis with Run 2 data [153]. The results are summarised in Table 11.5.

Two of the main difficulties for the VBF production mode are the large QCD background and the difficulty in triggering events fully hadronic events. Both difficulties are addressed, by the proposal made in Ref. [154], where the requirement of an additional photon in the final state reduces the background through an interference effect and enhances the possibilities for triggering. This analysis has been carried out by ATLAS at Run 2 [153] (see Table 11.5).

The sensitivity in the inclusive search for the Higgs boson in the ggF production mode with $H \rightarrow b\bar{b}$ is limited by the overwhelming background from the inclusive production of $pp \rightarrow b\bar{b} + X$ via the strong interaction. For this reason, no meaningful results exist with the Run 1 dataset for this production mode. With the increase in centre-of-mass energy to 13 TeV, and by taking advantage of the harder transverse momentum spectrum of the $gg \rightarrow H$ production mode with respect to the QCD background, a search for high p_T Higgs boson decaying to a pair of b quarks in association with an energetic Initial State Radiation (ISR) jet, has been performed by ATLAS [155] and CMS [156]. For this analysis with the Run 2 data, ATLAS and CMS require jets clustered with the anti- k_T algorithm [157] with a distance parameter of 1.0 and 0.8 respectively, with a transverse momentum in excess of 480 GeV and 450 GeV respectively. As in the case of VH production mode, this analysis is sensitive also to the VZ , $Z \rightarrow b\bar{b}$ production, which is an important step in the validation of the analysis chain. The $Z \rightarrow b\bar{b}$ decay is observed with a significance of 5.8σ , in good agreement with the expected sensitivity of 5.1σ . CMS provides an expected sensitivity to the observation of a Higgs boson of 0.7σ . This estimate has a non negligible uncertainty from the precise estimate of the fiducial signal cross section in the specific acceptance of this analysis. Both ATLAS and CMS observe small and non significant excesses at $m_H = 125$ GeV of 1.6σ and 1.5σ respectively. These results are reported in Table 11.5.

Another important production mode sensitive to the decay of the Higgs boson to bottom quarks, is the associated production with a pair of top quarks. The results of the searches for this process have been combined with the channels described above, to provide an additional constraint on the Yukawa coupling of

Table 11.5: Summary of the results of measurements for a Higgs boson decaying to a pair of b -quarks by ATLAS and CMS. The results are given in terms of measured signal strength. When available, the statistical and systematic contributions to the total uncertainty are reported separately and in this order.

$H \rightarrow b\bar{b}$	Tevatron	ATLAS Run 1	CMS Run 1	ATLAS Run 2	CMS Run 2
VH	1.6 ± 0.7	$0.52 \pm 0.32 \pm 0.24$	1.0 ± 0.5	$1.16 \pm 0.16^{+0.21}_{-0.19}$	1.01 ± 0.22
VBF (γ)	—	-0.8 ± 2.3	$2.8 \pm 1.4 \pm 0.8$	2.5 ± 1.3	1.3 ± 1.2
$t\bar{t}H$	—	$1.4 \pm 0.6 \pm 0.8$	0.7 ± 1.9	$0.79 \pm 0.29 \pm 0.53$	$1.49 \pm 0.21 \pm 0.39$
Inclusive	—	—	—	$5.8 \pm 3.1 \pm 2.5$	2.3 ± 1.7

the Higgs boson to bottom quarks. The channels corresponding to this production mode are described in Section 11.3.3. The results are, however, also reported in Table 11.5.

11.3.3 Higgs boson production in association with top quarks or in top decays

11.3.3.1 The associated production with top quark pairs

As discussed in Section 11.2, the coupling of the Higgs boson to top quarks plays a special role in the electroweak symmetry breaking mechanism in the SM, as well as in its possible extensions. Substantial indirect evidence of this coupling is provided by the compatibility of observed rates of the Higgs boson in the principal discovery channels, given that the main production process – the gluon fusion – is dominated by a top quark loop. Direct evidence of this coupling at the LHC and the future e^+e^- colliders will be mainly available through the $t\bar{t}H$ final state and will permit a clean measurement of the top quark-Higgs boson Yukawa coupling. The $t\bar{t}H$ production cross section at the LHC is small in comparison with the ggF or even VH production modes. The production cross section for a 125 GeV Higgs boson in pp collisions at $\sqrt{s} = 8$ TeV of about 130 fb made it challenging to measure the $t\bar{t}H$ process with the LHC Run 1 dataset. However, in Run 2, the increase in cross section at $\sqrt{s} = 13$ TeV is substantial, reaching approximately 500 fb. For a sensitive search, at Run 1, it was important to target as many accessible experimental signatures as possible. The analysis channels for such complex final states can be separated in four classes according to the decays of the Higgs boson. In each of these classes, most of the decay final states of the top quarks are considered (fully hadronic, semi-leptonic and dilepton decay final states).

The first analysis in this ensemble is the search for $t\bar{t}H$ production in the $H \rightarrow \gamma\gamma$ channel. This analysis relies on the search for a narrow mass peak in the $m_{\gamma\gamma}$ distribution. The background is estimated from the $m_{\gamma\gamma}$ sidebands. The sensitivity in this channel is mostly limited by the available statistics. The second analysis is the search for the Higgs boson decaying to ZZ^* and subsequently to four leptons (electrons and/or muons). This channel is currently limited by the low statistics due to the small branching fraction of the Z decays to leptons. The third analysis is the search in the $H \rightarrow b\bar{b}$ channel. This search is intricate due to the large backgrounds, both physical and combinatorial in resolving the $b\bar{b}$ system from the Higgs boson decay, in events with six jets and four b -tagged jets. Already with the Run 1 dataset, the sensitivity of this analysis was strongly impacted by the systematic uncertainties on the background predictions. The fourth analysis channel is a specific search for $\tau^+\tau^-$ where the two tau leptons decay to hadrons. Finally, the W^+W^- , $\tau^+\tau^-$ and ZZ^* final states can be searched for inclusively in multilepton event topologies (not including the resonant $H \rightarrow 4\ell$ channel that is covered in a more specific analysis). The corresponding $t\bar{t}H$ modes can be decomposed in terms of the decays of the Higgs boson and those of the top quarks as having two b -quarks and four W bosons (or two W and two taus, or two W and two Z) in the final state.

ATLAS and CMS have provided a complete set of results in these channels and their combination with the Run 1 data [158, 159]. Results for most of these channels have been updated with Run 2 data.

With the large increase in production cross section for the $t\bar{t}H$ associated production process of a factor of 3.9 from 7 TeV to 13 TeV, an outstanding goal of the Run 2 physics program was the direct observation of the top Yukawa coupling through this production mode. As could be seen in the Run 1 results, the $H \rightarrow b\bar{b}$ channel sensitivity was already dominated by systematic uncertainties and the multilepton channel had already large systematic uncertainties, while channels such as the $H \rightarrow \gamma\gamma$ had very limited sensitivity due to the low statistics. With a conspicuous amount of data, the hierarchy of channels was therefore bound to change.

ATLAS and CMS have analysed Run 2 data in all the sensitive decay channels for this production mode, with datasets of variable size of up to the full Run 2 dataset in the case where it matters the most, i.e., the $t\bar{t}(H \rightarrow \gamma\gamma)$ channel. With this partial analysis of the Run 2 data, ATLAS and CMS were able to independently observe the production of the Higgs boson in association with a pair of top quarks, and therefore the Yukawa coupling of the Higgs boson to the top quark [160]. This observation is particularly important in comparison to the indirect evidence through the gluon fusion production process dominated by the top quark loop.

The observation made independently by the two experiments was based on all the channels that were studied at the Run 1. ATLAS used up to 79.8 fb^{-1} of Run 2 data and CMS has used its 2016 dataset of 35.9 fb^{-1} . ATLAS reached an expected sensitivity of 4.9σ and an observed significance of 5.8σ with the Run 2 partial dataset alone, and 6.3σ (with 5.1σ expected) in combination with the Run 1 results. CMS reached a sensitivity of 4.2σ and observed an excess with respect to the background-only hypothesis of 5.2σ , combining the Run 1 and Run 2 results.

With the larger Run 2 dataset, the dominant mode is the $t\bar{t}(H \rightarrow \gamma\gamma)$ channel, where a narrow peak over a continuous background is searched for. At Run 2, this channel has reached a signal-to-background ratio in excess of 1 in the most signal-like categories. This is in contrast with the inclusive diphoton channel Higgs channels where the signal-to-background ratios are of the order of a few percent. ATLAS has analysed the entire Run 2 dataset reaching an observed (expected) sensitivity of 4.9σ (4.2σ) [161] and CMS has utilised 77.4 fb^{-1} of Run 2 data for this channel with an observed (expected) sensitivity of 4.1σ (2.7σ) [162], providing nearly unambiguous observations in this channel alone. These results are largely dominated by statistical uncertainty and are therefore expected to improve significantly with more data. These results with the full dataset from ATLAS [161] and with a larger Run 2 dataset for CMS [162] are not part of the ATLAS and CMS combinations and therefore provide substantially more evidence for the direct coupling of the Higgs boson to the top quark.

The resonant search for the resonant Higgs boson decay to four leptons in the associated production with a pair of top quarks has also been updated in ATLAS [131] with the full Run 2 dataset and reported in Table 11.6, but it is also not included in the combination.

An update of the $H \rightarrow b\bar{b}$ channel made by CMS with a partial Run 2 dataset of 41.5 fb^{-1} [163], using in particular the fully hadronic channel, is not in combination either. It is nevertheless reported in Table 11.5.

For the so-called “multi-lepton” channels which cover mostly

the WW , ZZ and $\tau\tau$ decay modes, ATLAS and CMS have analysed only part of the Run 2 datasets [164].

All results are summarized in Table 11.6.

11.3.3.2 The associated production with a single top quark

An additional production mode of the Higgs boson in association with a top quark is the single top associated production mode. There is an interesting similarity between this production mode and the $H \rightarrow \gamma\gamma$ decay mode. Both processes proceed through either the top Yukawa coupling or the interaction of the Higgs boson with the W boson, with a negative interference between the two. Representative Feynman diagrams for this production process are shown in Fig. 11.1. Contrary to the diphoton decay channel, in this production mode the interference occurs at the tree level and is dominant. This process can therefore be used to further discriminate a negative relative sign between the couplings of the Higgs boson to fermions and its couplings to gauge bosons [165].

ATLAS and CMS have produced specific searches for the tH production mode with the Run 1 and Run 2 data exploiting a variety of Higgs boson decay modes resulting in final states with photons, bottom quarks, and multiple charged leptons, including tau leptons. In particular, with the Run 2 data, CMS has searched for multi-lepton decay signatures from the $H \rightarrow WW^*$, $H \rightarrow \tau^+\tau^-$ and $H \rightarrow ZZ^*$ modes [166]. This analysis restricts values of κ_t , the top-Higgs coupling normalized to its SM value, to $[-1.25, 1.60]$ at 95% CL. CMS has also performed an analysis of the 2015 dataset to search for the $H \rightarrow b\bar{b}$ mode [167], yielding much less stringent constraints.

The diphoton channel has also been used to search specifically for this production mode by ATLAS using Run 1 data, yielding the restricted range of allowed values of κ_t at the 95% CL to $[-1.3, 8]$.

The strongest constraint on the negative (relative) sign of κ_t was obtained by CMS with a recent analysis of the 2016 dataset [168] in the multilepton ($H \rightarrow WW$, $H \rightarrow ZZ$, $H \rightarrow \tau\tau$) and $H \rightarrow b\bar{b}$ channels, all combined with a reinterpretation of the $H \rightarrow \gamma\gamma$ analysis channel aiming at measuring the $pp \rightarrow t\bar{t}H$ production mode. Negative values of κ_t are disfavoured at approximately 1.5σ and values of κ_t below -0.9 are excluded at 95% CL.

11.3.3.3 Flavour changing neutral current decays of the top quark

The discovery of the Higgs boson at a mass smaller than the top quark mass opened a new decay channel for the top quark. The decays of the top quark to a Higgs boson and a charm or an up quark proceed through a Flavour Changing Neutral Current (FCNC) which are forbidden at tree level and suppressed at higher orders through the Glashow–Iliopoulos–Maiani (GIM) mechanism [3]. The SM prediction for these branching fractions is $\text{BR}(t \rightarrow Hc) = 10^{-15}$ and two orders of magnitude less for the Hu final state. These decay channels of the top quark are, therefore, very interesting to probe possible FCNC interactions in the Yukawa couplings to the quark sector, see Section 11.7.

ATLAS has searched for FCNC top decays specifically in channels involving a Higgs boson with subsequent decays to two photons and a pair of b -quarks [169]. It has also reinterpreted a search for the $t\bar{t}H$ production in the multilepton final state (discussed in Section 11.3.6.1) [159]. The latter channel covers Higgs boson decays to a pair of W bosons and a pair of taus. No significant excess was observed in any of the specific channels (as discussed in Section 11.3.6.1, a slight excess is observed in the $t\bar{t}H$ multilepton channel) and 95% CL upper limits are set on $\text{BR}(t \rightarrow Hc) < 0.46\%$ with an expected sensitivity of 0.25% and $\text{BR}(t \rightarrow Hu) < 0.45\%$ with an expected sensitivity of 0.29%. CMS has performed a search for these FCNC top decays in the diphoton and multi-lepton channels [170], placing a 95% CL upper limit on $\text{BR}(t \rightarrow Hc) < 0.40\%$ with an expected sensitivity of 0.43%.

From these limits on branching fractions, constraints on non-flavour-diagonal Yukawa couplings of a FCNC Lagrangian of the form:

$$\mathcal{L}_{\text{FCNC}} = \lambda_{tc}H\bar{t}Hc + \lambda_{tu}H\bar{t}Hu + h.c. \quad (11.12)$$

can be derived. The 95% CL observed (expected) upper limits from ATLAS on the $|\lambda_{tc}H|$ and $|\lambda_{tu}H|$ couplings are 0.13 (0.10)

and 0.13 (0.10), respectively.

The results above are derived from the combination of several channels for searches performed with Run 1 data. Both ATLAS and CMS have produced updates of individual channels with Run 2 data. ATLAS has searched for FCNC top decays with subsequent decays of the Higgs boson to a pair of photons [171], yielding a 95% CL upper limit on $\text{BR}(t \rightarrow Hc) < 0.22\%$ with an expected sensitivity of 0.16%. CMS has searched for FCNC top decays with subsequent decays of the Higgs boson to a pair of b -quarks [172], yielding a 95% CL upper limit on $\text{BR}(t \rightarrow Hc) < 0.47\%$ with an expected sensitivity of 0.44%.

11.3.4 Higgs boson pair production

Higgs boson pair production in the SM is a rare but very important mode to measure and search for. The measurement of Higgs boson pair production is essential to directly constrain the trilinear Higgs boson self coupling and the search for Higgs boson pair resonances is key in a variety of BSM models. The latter searches are discussed in Section 11.7.7.

In the SM, the main non-resonant production mode of two Higgs bosons proceeds through a loop, mainly of top quarks, see Fig. 11.5(a). Another production mode is via the trilinear coupling of the Higgs boson, see Fig. 11.5(b), whose amplitude is not negligible compared to the former. These diagrams interfere negatively, making the overall production rate smaller than what would be expected in the absence of a trilinear coupling.

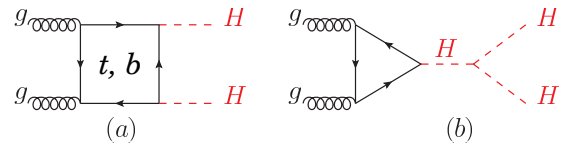


Figure 11.5: Feynman diagrams contributing at leading order to Higgs boson pair production through (a) a top- and bottom-quark loop and (b) through the self coupling of the Higgs boson.

11.3.4.1 Searches for Higgs boson pair production

The searches for Higgs boson pair production both resonant and non-resonant are very interesting probes for a variety of BSM theories, and they can be done in a large number of Higgs boson decay channels. At Run 1, ATLAS and CMS have searched for both resonant and non resonant Higgs boson pair production in the following channels: (i) $HH \rightarrow b\bar{b}\gamma\gamma$; (ii) $HH \rightarrow b\bar{b}\tau^+\tau^-$; (iii) $HH \rightarrow b\bar{b}b\bar{b}$; (iv) $HH \rightarrow WW^*\gamma\gamma$; (v) in final states containing multiple leptons (electrons or muons) covering the WW^*WW^* , WW^*ZZ^* , ZZ^*ZZ^* , $ZZ^*\tau^+\tau^-$, $WW^*\tau^+\tau^-$, $ZZ^*b\bar{b}$, $\tau^+\tau^-\tau^+\tau^-$ channels; and (vi) $\gamma\gamma\tau^+\tau^-$ channels.

At Run 2, similarly to the $t\bar{t}H$ production process, the di-Higgs production gains a substantial increase in production cross section of a factor in excess of 3 from 8 TeV to 13 TeV, and most of these channels have been updated both by ATLAS [173] and CMS [174] using the 2016 datasets with the addition of the (vii) $HH \rightarrow b\bar{b}b\bar{b}$ channels. The detailed description of the analyses can be found in references within the combination results published by the collaborations [173, 174]. All the results and their combinations are summarised in Table 11.7.

11.3.4.2 The Higgs boson self coupling

The Higgs boson self coupling is an extremely important direct probe of the Higgs potential with implications on our understanding of the electroweak phase transition. Constraints on the trilinear self coupling from HH processes is an outstanding long term goal of the LHC and the reach in sensitivity has been reappraised in the light of the recent HH analyses from ATLAS and CMS, shedding a different light on the achievable sensitivity [104]. Constraints from the HHH final state on the quartic Higgs boson self coupling are out of reach at the LHC due mostly to the very small production rates and intricate final states.

In the SM, the Higgs boson pair production through the trilinear Higgs boson self coupling has an on-shell component and a large off-shell component. The on-shell $H \rightarrow H^*H^*$ is strongly disfavoured, requiring two off-shell Higgs bosons in the final state.

Table 11.6: Summary of the results of searches for a Higgs boson in association with a top quark pair by ATLAS and CMS. The results are given in terms of a measured signal strength. When available, the statistical and systematic contributions to the total uncertainty are reported separately and in this order. The ATLAS [161] and CMS [162] diphoton results indicated by (*) are not included in the overall combinations which include versions of the diphoton analyses with smaller Run2 datasets. The combination includes the $t\bar{t}(H \rightarrow b\bar{b})$ channels reported in Table 11.5.

$t\bar{t}H$	ATLAS Run 1	CMS Run 1	ATLAS Run 2	CMS Run 2
$H \rightarrow \gamma\gamma$	$1.3^{+2.6}_{-1.7}{}^{+2.5}_{-1.7}$	$1.2^{+2.5}_{-1.7}{}^{+2.6}_{-1.8}$	$1.38^{+0.33}_{-0.31}{}^{+0.26}_{-0.18}$ (*)	$2.27^{+0.86}_{-0.74}$ (*)
$H \rightarrow 4\ell$	—	—	$1.2^{+1.4}_{-0.8}$ (*)	0.0 ± 1.2 (*)
$WW/\tau\tau/ZZ$	$1.4 \pm 0.6 \pm 1.0$	3.3 ± 1.4	$1.56^{+0.30}_{-0.29}{}^{+0.30}_{-0.27}$	$0.96^{+0.34}_{-0.31}$
Comb.	$1.7 \pm 0.5 \pm 0.8$	$2.6^{+1.0}_{-0.9}$	$1.32 \pm 0.18^{+0.21}_{-0.19}$	$1.49 \pm 0.16^{+0.27}_{-0.21}$

Table 11.7: Summary of the final states investigated in the search for Higgs boson pair production by ATLAS and CMS, most analyses make use of the 2016 Run2 dataset corresponding to integrated luminosities of up to 36 fb^{-1} . For ATLAS, the result indicated by (*) uses mostly the $b\bar{b}W^+W^-$ channel. Results are 95% CL upper limits on the observed (expected) SM signal strengths.

Channel	ATLAS	CMS
$b\bar{b}\gamma\gamma$	20.3 (26)	23.6 (18.8)
$b\bar{b}b\bar{b}$	12.9 (21)	74.6 (36.9)
$b\bar{b}\tau^+\tau^-$	12.5 (15)	31.4 (25.1)
$W^+W^-W^+W^-$	160 (120)	—
$W^+W^-\gamma\gamma$	230 (170)	—
$b\bar{b}VV$	305 (305)*	79 (89)
Combination	6.9 (10)	22.2 (12.8)

The sensitivity region to the trilinear coupling production as in Fig. 11.5(b), is mainly in the kinematic region where the two Higgs boson in the final state are on-shell and the Higgs boson acts as a propagator (off-shell). As discussed in the introduction to this section, this process interferes negatively with the background Higgs boson pair production (Fig. 11.5(a)).

The measurement of the trilinear coupling requires separating the contributions of the diagram of Fig. 11.5(b) from the box diagram of Fig. 11.5(b), and therefore a precise knowledge of the top-Yukawa coupling is needed. Each diagram alone would produce rather distinct m_{HH} distribution. And, for values of the trilinear coupling close to the SM value, an additional discriminating feature of the signal with respect to one obtained with the box contribution alone is a deficit in the number of events. With large variations of the trilinear coupling, an excess of events over the SM prediction would be observed (for a value of the trilinear coupling about 6 times larger than its SM value, the number of events is equal to the SM expectation). Additional sensitivity to the trilinear coupling is also obtained from the kinematical distributions of the signal taking in particular into account the effect of the HH mass distribution which discriminates the main contributions of Fig. 11.5. This further discrimination is instrumental in resolving the degeneracy in the total cross section mentioned above. The bounds obtained by ATLAS [173] and CMS [174] are

the following:

$$\begin{aligned}
 & \text{(ATLAS)} - 5.0 < \kappa_\lambda < 12.0 \text{ (observed),} \\
 & \quad \quad \quad - 5.8 < \kappa_\lambda < 12.0 \text{ (expected),} \\
 & \text{(CMS)} - 11.8 < \kappa_\lambda < 18.8 \text{ (observed),} \\
 & \quad \quad \quad - 7.1 < \kappa_\lambda < 13.6 \text{ (expected),}
 \end{aligned} \tag{11.13}$$

where κ_λ is the ratio between the trilinear coupling value left free in the fit and its expected value in the SM ($\kappa_\lambda = 1$ corresponds to the SM). These results are also illustrated in Fig. 11.6.

The analyses performed at Run2 bring substantial improvements from those of Run1, and they were used to reappraise the sensitivity of the LHC in the High Luminosity regime in the framework of the update of the European Strategy for Particle Physics [104]. The result in terms of bounds on the trilinear coupling are shown in Fig. 11.6, indicating that the significance of the observation of the HH process reaches 4σ . It is also apparent that the degeneracy of secondary minimum at intermediate values of κ_λ is resolved by the use of the kinematic discriminants. Indeed, this secondary minimum is expected to be excluded at 99.4% CL. This is very important to allow the measurement in the vicinity of the SM value at one standard deviation and to provide a meaningful confidence interval. At HL-LHC, the foreseen precision on κ_λ is approximately 50%.

Significantly higher precisions can be reached at pp colliders (and e^+e^- colliders) at higher centre-of-mass energies. The foreseen precision for a High-Energy (HE) LHC at a centre-of-mass energy of 27 TeV is expected to be within 10% to 20% [104]. At a very large hadron collider at a centre-of-mass energy of 100 TeV, a 5% sensitivity is expected to be reached, provided that the theoretical and parametric uncertainties are kept at the 1% level.

Indirect constraints on the Higgs boson trilinear coupling from single Higgs boson production processes will be discussed in Section 11.6.2.5.

11.3.5 Searches for rare decays of the Higgs boson

11.3.5.1 $H \rightarrow Z\gamma$ and the Dalitz $H \rightarrow \ell^+\ell^-\gamma$ decay

The search for $H \rightarrow Z\gamma$ is performed in the final states where the Z boson decays into opposite sign and same flavour leptons ($\ell^+\ell^-$), ℓ here refers to e or μ . While the branching fraction for $H \rightarrow Z\gamma$ is comparable to $H \rightarrow \gamma\gamma$ (about 10^{-3}) at $m_H = 125 \text{ GeV}$, the observable signal yield is brought down by the small branching ratio of $Z \rightarrow (e^+e^- + \mu^+\mu^-) = 6.7 \times 10^{-2}$. In these channels, the $m_{\ell\ell\gamma}$ mass resolution is excellent (1–3%), therefore the analyses search for a narrow mass peak over a continuous background. The major backgrounds arise from the $Z + \gamma$ final state radiation in Drell–Yan decays and from the $Z + \text{jets}$ processes where a jet is misidentified as a photon. The ratio of signal over background in this channel is typically of the order of 0.5%. In a narrow window of a few GeV around 125 GeV, several hundreds of events are expected in a Run 2 dataset corresponding to approximately 36 fb^{-1} .

Events are divided into mutually exclusive categories on the basis of the expected $m_{Z\gamma}$ resolution and the signal-to-background ratio. A VBF category is formed for $H \rightarrow Z\gamma$ candidates which

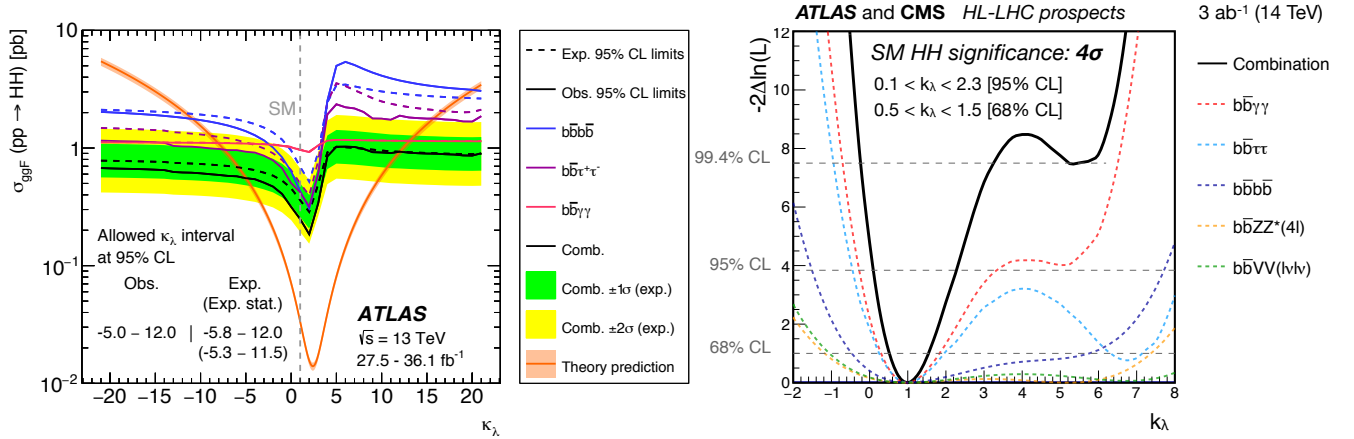


Figure 11.6: (Left) Upper limit obtained by ATLAS on the total $pp \rightarrow HH$ production cross section as a function of the trilinear coupling modifier κ_λ . The variation of the limit corresponds to variations in the signal acceptance. The expected total production cross section is also illustrated (red). (Right) Expected combined ATLAS and CMS likelihood for the searches for the $pp \rightarrow HH$ production at the High Luminosity LHC. The channels used in the combination are indicated in the figure.

are accompanied by two energetic jets separated by a large pseudorapidity. While this category contains only about 2% of the total event count, the signal-to-noise ratio is about an order of magnitude higher. The search for a Higgs boson is conducted independently in each category and the results from all categories are then combined.

No excess of events is observed in either ATLAS or CMS in the Run 1 data. The CMS expected and observed 95% CL upper limits for $m_H = 125$ GeV on the signal strength μ are 10.0 and 9.5 respectively. The ATLAS expected and observed upper limits on the signal strength μ are 9.0 and 11.0 respectively, for $m_H = 125.5$ GeV.

The CMS analysis also extended the search for the so-called Dalitz Higgs boson decays $H \rightarrow \gamma^* \gamma \rightarrow \ell^+ \ell^- \gamma$ in the low mass γ^* range of $m_{\ell\ell} < 20$ GeV. This decay mode has a substantially larger branching fraction compared to the $Z\gamma$ decay, as $\Gamma(H \rightarrow \gamma^* \gamma \rightarrow e^+ e^- \gamma) \sim 3.5\% \times \Gamma(H \rightarrow \gamma\gamma)$ and $\Gamma(H \rightarrow \gamma^* \gamma \rightarrow \mu^+ \mu^- \gamma) \sim 1.7\% \times \Gamma(H \rightarrow \gamma\gamma)$, while $\Gamma(H \rightarrow Z\gamma) = 2.3\% \times \Gamma(H \rightarrow \gamma\gamma)$ (which does not account for the subsequent decay of the Z boson to electrons or muons). The limits in this channel are therefore stronger and CMS has observed an upper limit of 6.7 times the SM branching ratio [175].

ATLAS has performed an analysis of the full 2015 and 2016 Run 2 data to search for the $Z\gamma$ decay mode [176]. No significant excess was observed and 95% CL observed (expected) upper limits on the signal strength are 6.6 (5.2).

CMS has repeated its $Z\gamma$ and $\gamma^* \gamma$ analyses with the 2016 dataset and obtained much more stringent observed limits on cross section times the corresponding branching fractions of 1.4 and 4.0 (6.1 and 11.4) times the SM cross section for $H \rightarrow \gamma^* \gamma$ ($H \rightarrow Z\gamma$) [177]. CMS also performed a combination of the two modes, obtaining a combined observed (expected) limit of 3.9 (2.0) times the SM branching fractions.

11.3.5.2 $H \rightarrow \mu^+ \mu^-$

The branching fraction in the $H \rightarrow \mu^+ \mu^-$ channel for a 125 GeV SM Higgs boson is 2.2×10^{-4} , about ten times smaller than that for $H \rightarrow \gamma\gamma$. The dominant and irreducible background arises from the $Z/\gamma^* \rightarrow \mu^+ \mu^-$ process which has a rate several orders of magnitude larger than that from the SM Higgs boson signal. Due to the precise muon momentum measurement achieved by ATLAS and CMS, the $m_{\mu^+ \mu^-}$ mass resolution is very good ($\approx 2-3\%$ for ATLAS and $\approx 1-3\%$ for CMS depending on the selected categories; a better resolution is expected for CMS due its higher field in the inner detector). A search is performed for a narrow peak over a large but smoothly falling background. For optimal search sensitivity, events are divided into several categories. Either taking advantage of the superior muon momentum measurement in the central region, events can be subdivided by the pseudo-rapidity of the muons, or designing selections aiming

at specific production processes such in particular as the vector boson fusion.

No excess in the $m_{\mu^+ \mu^-}$ spectrum is observed near 125 GeV. From an analysis of the Run 1 data, ATLAS sets an observed (expected) 95% CL upper limit on the signal strength $\mu < 7.0$ (7.2). The CMS analysis of its 7 and 8 TeV data sets an observed (expected) limit of $\mu < 7.4$ (6.5).

ATLAS performed a reoptimised analysis using the full Run 2 dataset and categorising events in number of jets including VBF-topology specific categories [178]. The data showed a non-significance excess with a best-fit value of the signal strength for Higgs boson with a mass of 125 GeV, $\mu = 0.5 \pm 0.7$. The data subsequently yielded an observed (expected) 95% CL upper limit on the signal strength of 1.7 (1.3), assuming $\text{BR}(H \rightarrow \mu\mu) = 0$, (while the expected limit assuming the SM value for $\text{BR}(H \rightarrow \mu\mu)$ is 2.2).

CMS, having analysed its 2016 dataset of Run 2, has obtained an observed (expected) limit on the production cross section times the branching fraction to a pair of muons of 3.0 (2.5) times the SM expectation [179]. In combination with the Run 1 data, the limit improves to 2.2 times the SM expectation. A non significant excess is also observed (with a significance of approximately 1σ) and the best fit signal strength is 1.0 ± 1.0 (stat) ± 0.1 (syst).

11.3.5.3 $H \rightarrow e^+ e^-$

A search similar to the $H \rightarrow \mu^+ \mu^-$ is performed by CMS in the di-electron channel. In this search channel, the contribution from the peaking background from Higgs boson decays to diphotons mis-identified as di-electrons (when mostly converted photons are faking electrons) needs to be assessed. The sensitivity to the SM Higgs decays is negligible given the extremely small branching fraction to $e^+ e^-$, approximately 40'000 times smaller than the branching fraction to dimuons. It is nevertheless interesting to probe this decay channel to search for potential large anomalous couplings. Assuming a SM Higgs boson production cross section, the observed limit on the branching fraction at the 95% CL is 0.0019, five orders of magnitude larger than the expected SM prediction. It is also important to note that processes not depending on the electron Yukawa coupling such as the $H \rightarrow e^+ e^- \gamma$ (where the photon is soft), are sizeably larger than the direct Yukawa coupling process, but also much smaller than the current constraints, making any interpretation in terms of constraint on the electron Yukawa couplings far from straightforward.

At Run 2, ATLAS has also performed a search for the $H \rightarrow e^+ e^-$ decay mode with the full dataset, improving the current limit by a factor of approximately 5, with a limit of 3.6×10^{-4} on the branching fraction [180].

11.3.5.4 Lepton flavour violating (LFV) Higgs boson decays

Given the Yukawa suppression of the couplings of the Higgs boson to quarks and leptons of the first two generations and the small total width of the Higgs boson, new physics contributions could easily have sizable branching fractions. One very interesting possibility is the Lepton Flavour Violating (LFV) decays of the Higgs boson, in particular in the $\tau\mu$ and τe modes. These decays are suppressed in the SM but they could easily be enhanced in theories such as two-Higgs-doublet models (discussed in Section 11.7).

There are already constraints on LFV Yukawa couplings $|Y_{\tau\mu}|$ from channels such as the $\tau \rightarrow 3\mu$ or $\tau \rightarrow \mu\gamma$, or a re-interpretation of the search for Higgs boson decays to $\tau^+\tau^-$. A direct search at the LHC, however, complements these indirect limits. The search for LFV decays in the $\tau\mu$ channel have been done with the Run 1 dataset in several channels according to the subsequent decay of the τ . The results from CMS [181] and from ATLAS for the hadronic [182], the leptonic [183] decays of the tau, and their combination [183] are reported in Table 11.8. It is interesting to note that the analysis strategies at Run 1 for the di-lepton $\tau_{\text{lep}}\mu$ channel are very different between ATLAS [183] and CMS [181].

As shown in Table 11.8, an excess was observed in this channel by CMS with a significance of 2.5σ , while in ATLAS analysis, the excess is smaller, about 1σ at Run 1. CMS has performed the search again with the full 2016 Run 2 dataset [184], relying on a multivariate analysis. The observed best fit branching fraction is $(0.00 \pm 0.12)\%$. These limits are reported in Table 11.8.

ATLAS and CMS have also performed a search for the LFV Higgs boson decays in the τe and μe channels [183–185]. No significant excess was observed and 95% CL limits are reported in Table 11.8, for the τe channel only. For the μe channel, the constraints from the $\mu \rightarrow e\gamma$ experiments [186] are much stronger than those from the direct LFV Higgs boson decay search. However these indirect constraints can be relaxed by the cancellation of LFV effects from new physics.

At Run 2, ATLAS has performed searches for LFV decays of the Higgs boson in the $e\tau$ and $\mu\tau$ channels [187] as well as in the $e\mu$ channel [180]. The searches for the $H \rightarrow e\tau$ and $H \rightarrow \mu\tau$ decays where done with the 2016 data only and yielded upper limits on the LFV decay branching fraction of 0.47% (0.34%) and 0.28% (0.37%), respectively.

CMS has also searched for LFV decays with the 2016 dataset at Run 2 and obtained observed (expected) limits on the LFV branching fraction of $\text{BR}(H \rightarrow \mu\tau) < 0.25\%$ (0.25%) and $\text{BR}(H \rightarrow e\tau) < 0.61\%$ (0.37%), at the 95% CL [188]. These limits were also interpreted in terms of constraints on the corresponding off-diagonal Yukawa couplings.

The results obtained by ATLAS and CMS at Run 2 do not confirm the excesses observed at Run 1.

11.3.5.5 Probing charm- and light-quark-Yukawa couplings

Probing the Yukawa couplings to quarks of the second or even the first generation is extremely challenging given the overwhelming backgrounds and very small rates.

The possibility of probing the Yukawa coupling to the charm has been discussed in Ref. [189] where indirect bounds are estimated from a combined fit to the Higgs data and the importance of using charm tagging is emphasised. Searches in the VH production mode have then been carried out, in the channels very similarly to those aiming at the b -quark Yukawa coupling, by both ATLAS [190] and CMS [191] with Run 2 data. The upper limits obtained (expected) on the VH production cross section times the charm quark decay branching fraction of the Higgs boson are:

$$\text{(ATLAS)} \quad \sigma(ZH) \times \text{BR}(H \rightarrow c\bar{c}) < 2.7 \quad (3.9^{+2.1}_{-1.1}) \text{ pb}, \quad (11.14)$$

$$\text{(CMS)} \quad \frac{\sigma(VH) \times \text{BR}(H \rightarrow c\bar{c})}{\sigma(VH)_{SM} \times \text{BR}(H \rightarrow c\bar{c})_{SM}} < 70 \quad (37^{+16}_{-10}). \quad (11.15)$$

The ATLAS search [190] was done in the ZH channel where the Z boson decays to a pair of leptons (electrons or muons) only. The expected cross section times branching fraction $\sigma(ZH) \times \text{BR}(H \rightarrow c\bar{c})$ is 26 fb^{-1} .

Another possibility to access the charm Yukawa coupling has been discussed in Ref. [192]. It relies on the decays of the Higgs boson to a final state with charmonium: $H \rightarrow J/\Psi\gamma$. Higgs boson decays in this final state have been searched for by ATLAS [193]. The sensitivity of this analysis is, however, several orders of magnitude above the branching fraction estimated in the SM: $\text{BR}(H \rightarrow J/\Psi\gamma) = (2.8 \pm 0.2) \times 10^{-6}$. ATLAS [193] has also searched for Higgs boson decays to $\Upsilon(nS)\gamma$ where ($n = 1, 2, 3$), a channel with much lower sensitivity than the $H \rightarrow b\bar{b}$ to the Yukawa coupling to b -quarks.

More recently, ATLAS has searched, , with a specific trigger, for another quarkonia final state where the Higgs boson decays to $\phi\gamma$ [194] at the LHC Run 2 and a center-of-mass energy of 13 TeV. This channel could probe deviations from the strange-quark Yukawa coupling. Its sensitivity is several orders of magnitude above the SM expectation. Other quarkonia final states, such as the $\rho\gamma$, which could potentially probe the Yukawa coupling to light quarks, can also be searched for.

CMS has also performed a search of the decays of the Higgs boson in the $J/\Psi J/\Psi$ and $\Upsilon\Upsilon$ decay to cover the cases where the photon in the $J/\Psi\gamma$ decay is virtual and transforms into a J/Ψ meson. These decays provide an additional channel potentially sensitive to BSM phenomena [195].

11.3.5.6 Rare decays outlook

Rare decays such as those described in the above sections have clearly a limited sensitivity. However, they already deliver interesting messages. For example, if the coupling of the Higgs boson to muons was as strong as it is to top quarks, this mode should have been observed. Therefore, it can be concluded that the observed couplings of the Higgs boson are manifestly non-universal. Further developing these rare decay modes is an important component of the High Luminosity program of the LHC in order to directly probe the couplings of the Higgs boson, and to potentially measure the Yukawa coupling to the fermions of the second generation, in particular to muons. It is also an integral part of the physics program of the discussed potential future Higgs boson factories.

11.3.6 Searches for non-SM decay channels

The main decay and production properties of the observed Higgs boson are consistent with the SM predictions. The Higgs boson may, however, have other decay channels beyond those anticipated in the SM. Among these, and of great interest, are the invisible decays into stable particles, such as DM particle candidates, that interact very weakly with the detector, and that remain undetected. Other non standard decay channels that have been investigated are the decays of the Higgs particle to hidden valley or dark particles.

11.3.6.1 Invisible decays of the Higgs boson

The discovery of the Higgs boson immediately raised the question of its couplings to DM and how it could be used to reveal at colliders the existence of a dark sector coupled to the SM via the Higgs boson portal, see Ref. [196] and references therein. If kinematically accessible and with a sufficiently large coupling to the Higgs boson, DM particles, such as, e.g., neutralinos in SUSY models, graviscalars in models with extra dimensions or heavy neutrinos in the context of four-generation fermion models, would manifest themselves as invisible decays of the Higgs boson, thus strongly motivating searches for the invisible decays of the Higgs boson.

To identify an invisibly decaying Higgs boson at the LHC, it must be produced in association with other particles. Searches for invisible decays of the Higgs particle at the LHC have been carried out in the three associated production modes of the Higgs boson with the highest SM cross sections and target events with large missing energy.

The ggF production mode has the largest SM cross section but it usually results in the Higgs boson being created alone and hence leaving no characteristic signature in the detector of its invisible decay. One way to search for invisible decays in ggF production mode is to look for events with the monojet topology arising from initial state gluon radiation and containing missing energy. The major irreducible background in such searches stems from $Z + \text{jets}$

Table 11.8: Summary of the results of searches for lepton flavour violating decays of the Higgs boson in the $\tau\mu$ and τe channels from ATLAS and CMS. For the result with *, the expected sensitivity was not reported but appears consistent with the observed one.

	ATLAS (Run 1)	CMS (Run 1)	CMS (Run 2)
$\text{BR}(H \rightarrow \tau\mu)$	$(0.53 \pm 0.51)\%$	$(0.84^{+0.39}_{-0.37})\%$	$(0.00 \pm 0.12)\%$
95% CL Obs. (Exp.)	1.43% (1.01%)	1.51% (0.75%)	0.25% (0.25%)
$H \rightarrow \tau e$ 95% CL Obs. (Exp.)	1.02% (1.21%)	0.69%*	0.61% (0.37%)

events where the Z boson decays into a pair of neutrinos [197]. The analysis with the best sensitivity targets the VBF production topology but it suffers from large backgrounds arising from events with two jets and large missing energy. The VH mode has much smaller cross section but the presence of a W or Z boson allows a variety of final states that can be tagged with relatively low background.

ATLAS and CMS have searched for such final states at Run 1 and have observed no significant excess over the predicted backgrounds (for references, see the previous edition of this review [123]). Table 11.9 summarizes the 95% CL limits on the invisible decays of the Higgs boson assuming a SM Higgs boson production cross section and the corresponding detector acceptances.

ATLAS has performed the search for invisible decays of the Higgs boson at Run 2 with the 2015 and 2016 datasets, corresponding to an integrated luminosity of approximately 36 fb^{-1} , in the VBF production [198], the ZH associated production where the Z boson subsequently decays to a pair of leptons [199], and the VH associated production where the vector boson (a W or a Z) subsequently decays hadronically [200]. The most stringent constraint is obtained through the VBF channel. All results and their combination [201] are reported in Table 11.9. Combined with the Run 1 results, the ATLAS limit on the invisible branching fraction reaches 26%, with an expected sensitivity of 17% [201].

CMS has updated the search for invisible decays of the Higgs boson in the vector boson fusion and the associated production with a vector boson channels (both with subsequent leptonic [202] and hadronic decays [203]) using Run 2 data collected in 2016 [204]. It has produced a combination with Run 1 channels, yielding a limit on the invisible branching fraction of 19%, with an expected sensitivity of 15% [204].

CMS has also reinterpreted a search for scalar top quarks in the all-hadronic, semi-leptonic and fully leptonic final state with the 2016 data of Run 2 to set limits on the invisible Higgs decays through the $pp \rightarrow t\bar{t}H$ production mode [205]. The results of the search are reported in Table 11.9.

This constraint can then be further used to probe Higgs portal models to DM [196], where an additional weakly interacting particle χ with mass lower than $m_H/2$ is introduced as DM candidate and where the Higgs boson is considered as the only mediator between the SM particles and DM. In this model, it is interesting to express the limit on the invisible branching fraction in terms of strength of interaction of DM with standard matter, i.e., in terms of its interaction cross section with nucleons $\sigma_{\chi-N}$. In this model, the couplings of the Higgs boson to SM particles are assumed to be those of the SM and the interaction of the Higgs boson with the nucleon is parametrised in a Higgs-Nucleon form factor estimated using lattice QCD calculations [196]. The exclusion limits from the constraints on invisible Higgs boson decays, both direct and indirect from the measurement of the coupling properties of the Higgs boson can be compared to direct detection experiments. For comparison, the limit at 90% CL on the invisible branching fraction of $\text{BR}_{\text{inv}} < 0.16$ [204] is used and converted into limits on $\sigma_{\chi-N}$ under several hypotheses on the nature of DM particles depending mainly on their spin (scalar- or fermion-like). The vector DM hypothesis is not included since (renormalisable) models of vectorial DM require an extended dark sector that could imply modifications of the signal. The results are shown in Fig. 11.7.

11.3.6.2 Exotic Higgs boson decays

The 125 GeV Higgs boson serves not only as a probe for potential DM candidates, but also to search for other exotic particles arising from fields associated with a low-mass hidden sector. Such

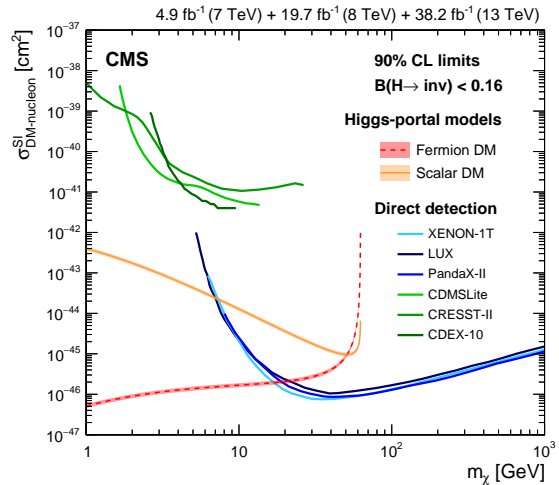


Figure 11.7: 90% CL upper limits on the WIMP-nucleon scattering cross section as a function of the DM particle mass. Spin-independent results excluded and favored regions from direct detection experiments are also shown.

hidden sectors are composed of fields that are singlet under the SM gauge group $SU(3) \times SU(2) \times U(1)$. These models are referred to as hidden valley models [206]. Since a light Higgs boson is a particle with a narrow width, even modest couplings to new states can give rise to a significant modification of the Higgs boson phenomenology through exotic decays. Simple hidden valley models exist in which the Higgs boson decays to an invisible fundamental particle, which has a long lifetime to decay back to SM particles through a small mixing with the SM Higgs boson, see Ref. [206] for a concrete example. The Higgs boson may also decay to a pair of hidden valley “ v -quarks,” which subsequently hadronise in the hidden sector, forming “ v -mesons.” These mesons often prefer to decay to the heaviest state kinematically available, so that a possible signature is $H \rightarrow 4b$. Some of the v -mesons may be stable, implying a mixed missing energy plus heavy flavour final state. In other cases, the v -mesons may decay to leptons, implying the presence of low mass lepton resonances in high- H_T events [207]. Other scenarios have been studied [208] in which the Higgs boson decays predominantly into light hidden sector particles, either directly, or through light SUSY states, and with subsequent cascades that increase the multiplicity of hidden sector particles. In such scenarios, the high-multiplicity hidden-sector particles, after decaying back into the SM, appear in the detector as clusters of collimated leptons known as “lepton jets”.

A variety of models have been investigated searching for final states involving dark photons and hidden valley scalars. The resulting topologies typically have leptons or light hadrons which in some cases can be prompt (i.e., originating from the hard process interaction point) or not and are in some cases collimated and reconstructed as jets [209, 210], and long lived weakly interacting particles. The latter occur not only in hidden valley scenarios, but also in gauge-mediated extensions of the minimal SUSY standard model (MSSM), the MSSM with R-parity violation, and inelastic DM scenarios [211]. Finally, CMS has performed a search for pair production of light bosons [212]. Such a scenario can occur in SUSY models with additional hidden (or dark) valleys.

Table 11.9: Summary of the channels searched for and the corresponding 95% CL limits from ATLAS and CMS on the branching fraction for the Higgs boson decay to invisible particles assuming a SM Higgs boson production cross section. The results in parentheses are the expected exclusions.

	ATLAS (Run 1)	ATLAS (Run 2)	CMS (Run 1)	CMS (Run 2)
ggF (monojet); $H \rightarrow \text{inv.}$	–	–	67 (71) %	66 (59) %
VBF; $H \rightarrow \text{inv.}$	28 (31) %	37 (28) %	57 (40) %	33 (25) %
ZH; $Z \rightarrow \ell^+ \ell^-$; $H \rightarrow \text{inv.}$	75 (62) %	67 (39) %	75 (91) %	40 (42) %
VH; $Z, W \rightarrow jj$; $H \rightarrow \text{inv.}$	78 (86) %	83 (58) %	–	50 (48) %
ZH; $Z \rightarrow b\bar{b}$; $H \rightarrow \text{inv.}$	–	–	182 (189) %	–
Combination	25 (27) %	38 (21) %	–	26 (20) %
Run 1 & 2 Combination	–	26 (17) %	19 (15) %	–
$t\bar{t}H$; $H \rightarrow \text{inv.}$	–	–	–	46 (48) %

11.4 Combining the main channels

The analysis strategy used by the LHC experiments to perform the searches for the Higgs boson has been based on the Higgs boson decay modes. It is a natural choice given that it focusses on the decay products of the object searched for. However, for each channel, exclusive sub-channels have been defined according to the Higgs boson production processes and, in the results presented, these sub-channels have been combined. The natural extension of this approach in order to probe further the production and decay modes of the Higgs boson is to combine the analysis channels together. Such a combination is also used in Section 11.6 to further measure the coupling properties of the Higgs boson.

At the LHC, the total cross section cannot be measured in any of the production modes. As a consequence, neither the absolute branching fractions nor the total width of the Higgs boson can be directly measured, at least if the width is of the SM size. However, a combined measurement of the large variety of categories described in Section 11.3, with different sensitivities to various production and decay modes, permits a wide variety of measurements of the production, decay and coupling properties. These measurements require, in general, a limited but nevertheless restrictive number of assumptions.

In this section, three sets of results will be given. The first one is the ATLAS and CMS Run 1 combination [141]. The other two are the individual combinations of ATLAS and CMS independently with partial Run 2 dataset. It is important to note that, between the Run 1 and the Run 2 results, the signal theoretical systematic uncertainties have improved significantly.

The Run 1 full combination results were derived by the two collaborations, taking rigorously into account all correlations in the systematic uncertainties and in the large number of channels and their categories.

At Run 2, ATLAS [213] and CMS [214] have already produced combined measurements of the coupling properties of the Higgs boson with partial datasets, of up to 80 fb^{-1} and up to 36 fb^{-1} respectively.

In this section, only the results on the main Higgs boson production and decay modes will be discussed. Only a brief presentation of the combination framework is given here (a more detailed description is given in Ref. [215]). This framework will also be used in Section 11.6 to discuss the measurements of the coupling properties of the Higgs boson.

11.4.1 Principles of the combination

The combination of the Higgs boson analysis channels in each experiment and for the two experiments together was done using a fit of a signal and background model to the data. As described above, the data was made of a large number of categories, aiming at reconstructing exclusive production and decay modes. In the combination of ATLAS and CMS [141], there were approximately 600 categories. The combination was a simultaneous fit to all these categories, using a reduced number of parameters of interest and a Higgs boson mass fixed at its measured value (see Section 11.3.2). The much larger number of categories present in the ATLAS and CMS combination [141] is due to additional separation in terms of finer exclusive production regions, decay channels of the Z and the W bosons, and taus, control regions where

little-to-no signal is present, and different center-of-mass energies. It should be noted that the individual combination performed by ATLAS [216] included two additional decay channels: the $\mu^+ \mu^-$ and $Z\gamma$. For the sake of simplicity these channels were omitted in the ATLAS–CMS combination. In addition, a $H \rightarrow b\bar{b}$ analysis performed by CMS, see the reference in Ref [123], and included in its own combination, has been omitted from the ATLAS–CMS combination.

In their Run 2 individual combinations, ATLAS and CMS have not considered the $Z\gamma$ channel. The CMS experiment has included the $\mu\mu$ channel.

The key to understand how the combination of channels works relies on the combination master formula, which expresses for each category, indexed by c , of a given channel (typically a category covers mostly one decay mode, but possibly various production modes), the measured number of signal events n_s^c as a function of a limited number of parameters as follows:

$$n_s^c = \left(\sum_{i,f} \mu_i \sigma_i^{\text{SM}} \times A_{if}^c \times \varepsilon_{if}^c \times \mu_f \text{BR}_f^{\text{SM}} \right) \times \mathcal{L}^c. \quad (11.16)$$

The production index is defined as $i \in \{\text{ggF}, \text{VBF}, \text{VH}, \text{t}\bar{t}H\}$ and the decay index is defined as $f \in \{\gamma\gamma, WW, ZZ, b\bar{b}, \tau\tau\}$, while σ_i^{SM} and BR_f^{SM} are the corresponding production cross sections and decay branching fractions, estimated as described in Section 11.2, assuming that the Higgs boson is that of the SM. A_{if}^c and ε_{if}^c are the signal acceptance and the reconstruction efficiency for the given production and decay modes in the category c . \mathcal{L}^c is the integrated luminosity used for that specific category. For the purpose of this review, these parameters can be considered as fixed³.

The parameters of interest in the master formula are the signal strength parameters μ_i and μ_f . It is important to note that the formula relies on the factorisation of the production cross section and decay branching fraction, which assumes the narrow width approximation. The width of the Higgs boson will be discussed in Section 11.5, however, for the precision needed here, the fact that the Higgs boson has been observed in decay channels with high mass resolution as a resonance is sufficient to validate this hypothesis. It is also manifest in the above equation that the ten parameters for the production modes (μ_i) and decay modes (μ_f) cannot be determined simultaneously. This illustrates that total cross sections or branching fractions cannot be measured without further assumptions in this fit.

The master formula also illustrates an important caveat to the measurement of signal strength parameters. In case these are interpreted as scale factors of the production cross sections or branching fractions, then all the other quantities such as the acceptances and efficiencies, A_{if}^c and ε_{if}^c , need to be assumed as independent and fixed to their estimated values for the SM Higgs boson. An additional important caveat to note concerning these combined results is that only the normalisation is varied, while the discriminating variables for the signal are not modified and

³In the combination performed by ATLAS and CMS, the systematic uncertainties on these parameters are taken into account by allowing these parameters to vary in the fit.

Table 11.10: Summary of the observation significances (with respect to the background only hypothesis) for the main production and decay processes at the LHC. Measured signal strengths are reported when the observation has been established unambiguously. Measured signal strengths are reported with the uncertainty of statistical nature first and systematic last, ATLAS has not reported these results in its Run 2 combination (NR). *The Run 2 VH significances reported in this table are obtained from the observation of the Higgs boson decays to b quarks, while the Run 1 combination corresponds to combination of all channels.

	Decay modes			
	ATLAS (Run 1)	CMS (Run 1)	ATLAS (Run 2)	CMS (Run 2)
$\gamma\gamma$	4.6 σ (5.3 σ)	5.2 σ (4.6 σ)	NR	1.20 $^{+0.13}_{-0.11}$ $^{+0.12}_{-0.09}$
ZZ	6.2 σ (6.3 σ)	8.1 σ (6.5 σ)	NR	1.06 $^{+0.16}_{-0.15}$ $^{+0.11}_{-0.08}$
WW	5.9 σ (5.4 σ)	6.5 σ (4.7 σ)	NR	1.28 $^{+0.09}_{-0.09}$ $^{+0.14}_{-0.13}$
$\tau^+\tau^-$	3.4 σ (3.9 σ)	4.5 σ (3.8 σ)	6.4 σ (5.4 σ)	5.9 σ (5.9 σ)
	Comb. 5.0 σ (5.5 σ)			
$b\bar{b}$	2.6 σ (2.5 σ)	1.4 σ (2.1 σ)	5.4 σ (5.5 σ)	5.5 σ (5.6 σ)
	Comb. 3.7 σ (2.6 σ)			
	Production modes			
	ATLAS and CMS (Run 1)		ATLAS (Run 2)	CMS (Run 2)
$qq \rightarrow qqH$ (VBF)	Comb. 5.4 σ (4.6 σ)		1.21 $^{+0.18}_{-0.17}$ $^{+0.16}_{-0.13}$	0.73 $^{+0.24}_{-0.23}$ $^{+0.17}_{-0.15}$
$pp \rightarrow VH$	Comb. 3.5 σ (4.2 σ)		5.3 σ (4.8 σ)*	4.8 σ (4.9 σ)*
$pp \rightarrow t\bar{t}H$	Comb. 4.4 σ (2.2 σ)		5.8 σ (4.9 σ)	5.2 σ (4.2 σ)

are still used in the fit. These caveats are of particular importance in the use of the combination to measure the coupling properties of the Higgs boson, as discussed in Section 11.6. For relatively small perturbations of the couplings of the Higgs boson from the SM values, this hypothesis is valid.

However, the products $\mu_i \times \mu_f$ can be considered as free parameters and in principle measurable (if there is sufficient sensitivity from specific categories). Measuring the products of signal strengths can be viewed as measuring the cross sections times the branching fraction, $\sigma \cdot \text{BR}$. An illustration of the results for the Run 2 combinations of ATLAS and CMS is presented in Fig. 11.8 for the combination of ATLAS and CMS.

A coherent picture emerges (including the Run 1 results, see Ref. [123]) where an excellent consistency between the observation in each channel and the SM expectation. This multi-parameter fit quantifies the current experimental knowledge of the main production and decays modes. Run 2 results are also available [213, 214]. These are not included in the figure for the sake of simplicity. The Run 2 results are already competitive with the Run 1 results. In Fig. 11.8, the Run 1 results are kept for illustration purposes. The theoretical uncertainty in the aforementioned fit is not included in the measured values of the signal strengths but is illustrated on the unit value corresponding to the SM expectation.

Other fits involving ratios of cross sections, which are less sensitive to theory uncertainties, are performed and reported in Ref. [215].

The most constrained fit in the combination allows for only one single parameter to vary, i.e., $\forall(i, f), \mu_i = \mu_f = \mu$. This global-signal-strength model provides the simplest probe of the compatibility of the signal with the SM Higgs boson. Indeed, it is sensitive to any deviation from the SM Higgs boson couplings provided that these deviations do not cancel overall. The full Run 1 combination determines the global signal strength to be

$$\mu = 1.09 \pm 0.11 = 1.09 \pm 0.07 \text{ (stat.)} \pm 0.04 \text{ (expt.)} \pm 0.03 \text{ (th. bkg.)} \pm 0.07 \text{ (th. sig.)}, \quad (11.17)$$

where the statistical, experimental uncertainties as well as the theoretical uncertainties on the background and on the signal are reported separately. The ATLAS Run 2 combination of the global

signal strength yields [213]:

$$\mu = 1.11^{+0.09}_{-0.08} = 1.11 \pm 0.05 \text{ (stat.)}^{+0.05}_{-0.04} \text{ (expt.)} \pm 0.03 \text{ (th. bkg.)}^{+0.05}_{-0.04} \text{ (th. sig.)}, \quad (11.18)$$

while the CMS Run 2 combination yields [214]:

$$\mu = 1.17 \pm 0.10 = 1.17 \pm 0.06 \text{ (stat.)}^{+0.06}_{-0.05} \text{ (th. sig.)} \pm 0.06 \text{ (other. syst.)}. \quad (11.19)$$

These overall signal strengths are fully compatible with the SM expectation, $\mu = 1$, with a precision of 10%. It is interesting to note that the main uncertainty in these measurements arises from the limited precision in the theoretical predictions for the signal production processes. The precision reached with the individual experiments combinations using partial Run 2 data sets have already exceeded the full Run 1 ATLAS and CMS combination precision.

11.4.2 Main decay modes

Despite the large number of decay channels, since the cross sections cannot be independently measured, from the measurements described in this section it is impossible to measure the decay branching fractions without a loss of generality. The simplest assumption that can be made is that the production cross sections are those of the SM, which is equivalent to assume that, for all i indices, $\mu_i = 1$. All branching fractions μ_f can then be measured in a simple 5 parameter fit. The results of these fits are reported in Table 11.10 in terms of significances to highlight their unambiguous observations: all the measured branching fractions are compatible with the SM values.

For the $\tau^+\tau^-$ channel, ATLAS and CMS were both only mildly sensitive at the Run 1 and have observed excesses in their data. The individual results were not sufficiently significant to claim an observation, however, in combination the evidence was very strong. It is really with the addition of the Run 2 data that the decay of the Higgs boson to tau pairs has been established by the two experiments independently and unambiguously (see Table 11.10 and Section 11.3.2).

As illustrated in Table 11.10, ATLAS and CMS were both less sensitive in the $H \rightarrow b\bar{b}$ decay mode. The available sensitivity

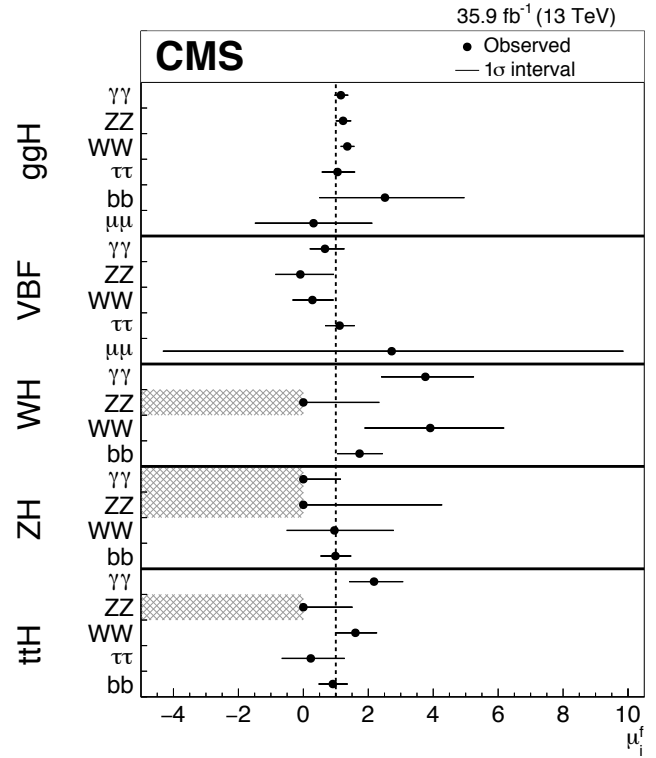
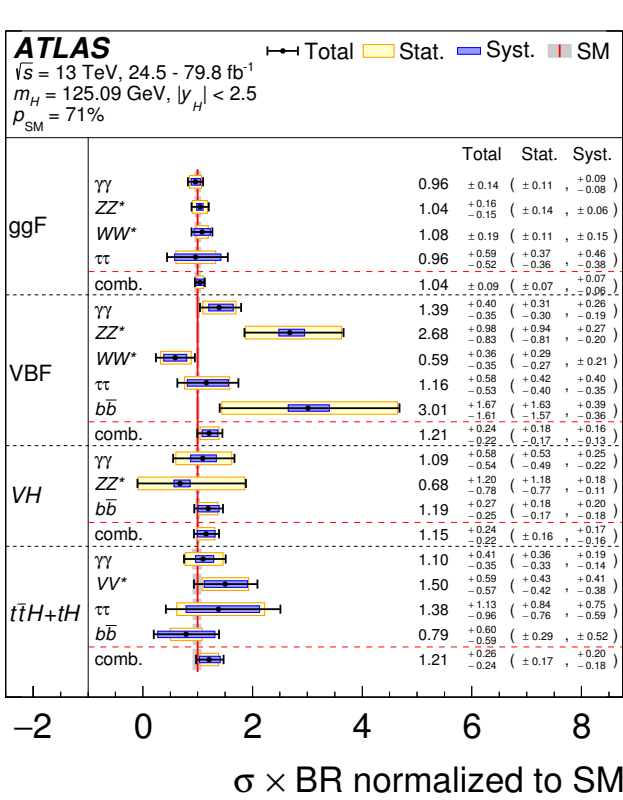


Figure 11.8: Combined measurements of the products $\sigma \cdot \text{BR}$, normalised to the SM predictions, for the five main production and five main decay modes. The hatched combinations require more data for a meaningful confidence interval to be provided.

came mostly from the VH process. The combined significance of 3.7σ at Run 1 was sufficient to suggest evidence, however ATLAS and CMS observations were both low with respect to the rate expected in the SM. At Run 2, this channel benefited largely from the increased production cross sections at 13 TeV and the much larger dataset. In this case as well, it is with the addition of the Run 2 data that both experiments were able to establish a measurement in this channel (as discussed in Section 11.3.2).

These are major milestones of the LHC physics program.

11.4.3 Main production modes

Most analysis channels are divided into exclusive categories allowing for an increased overall sensitivity and permitting to access the various Higgs boson production modes. The cross sections of the main production modes can be measured assuming that the branching fractions are those of the SM, i.e., for all f indices $\mu_f = 1$. These assumptions lead to a 5 parameter combination. The results are reported in terms of significances of observation of the production modes in Table 11.10.

The gluon fusion production process is the dominant production mode. Although no numerical estimate of combined significance of observation for this process has been given by the experiments, it is considered as established due to the overwhelming evidence from the three main discovery channels. None of the other production modes have been firmly established by the experiments individually. However, the table shows that, for the VBF production mode, the combination had a large sensitivity and produced a combined observation of 5.4σ , therefore establishing this process with a rate compatible with that expected in the SM.

The VH production mode has only very recently been unambiguously observed by ATLAS and CMS independently (as discussed in Section 11.3.2) through the $V(H \rightarrow b\bar{b})$ channel. This is illustrated in the relative contributions of all channels to the VH process shown in Figure 11.8.

With the Run 2 data, all production processes have been established, and in particular the $pp \rightarrow t\bar{t}H$ process, which provides direct evidence of the coupling of the Higgs boson to top quarks. This is another milestone in the LHC physics program.

11.5 Main quantum numbers and width of the Higgs boson

11.5.1 Main quantum numbers J^{PC}

Probing the Higgs boson quantum numbers is essential to further unveiling its coupling properties. The measurements of the signal event yields in all the channels discussed in Sections 11.3 and 11.4, and their compatibility with the SM Higgs boson predictions, give a qualitative but, nonetheless, compelling indication of its nature. This qualitative picture is further complemented by the implications of the observation of the particle in the diphoton channel. According to the Landau–Yang theorem [217], the observation made in the diphoton channel excludes the spin-1 hypothesis and restricts possibilities for the spin to 0 or 2.

The Landau–Yang theorem does not apply if the observed state is not decaying to a pair of photons but to a pair of scalars subsequently decaying to two very collimated pairs of photons (as for example in the case of $H \rightarrow a_1 a_1 \rightarrow 4\gamma$). This possibility has not been rigorously excluded but is not experimentally favoured since tight selection criteria are applied on the electromagnetic shower shapes of the reconstructed photons. A more systematic analysis of shower shapes and the fraction of conversions could be performed to further discriminate between the single prompt photon and the two overlapping photons hypotheses. There are also potential theoretical loopholes concerning the applicability of the Landau–Yang theorem, such as off-shell vector boson decays. However, for the observed particle not to be of spin 0 and +1 parity would require an improbable conspiracy of effects. It is nevertheless important to test this hypothesis independently, in particular since the measurements of coupling properties of the Higgs boson assume that it is a CP -even state.

11.5.1.1 Charge conjugation

The charge conjugation quantum number is multiplicative, therefore given that the Higgs-like particle is observed in the $H \rightarrow \gamma\gamma$ channel, and given that photons are C -odd eigenstates, assuming C conservation, the observed neutral particle should be C -even.

11.5.1.2 Spin and parity

To probe the spin and parity quantum numbers of the discovered particle, a systematic analysis of its production and decay processes is performed in several analyses. These analyses are designed to be independent of the measured event yields and they rely instead on the production and the decay angles, and on the threshold distributions as long as a significant signal is observed, i.e., in situations when an excess over the expected background can be used to further discriminate between signal hypotheses. These analyses are based on probing various alternative models of spin and parity [218]. These models can be expressed in terms of an effective Lagrangian [219] or in terms of helicity amplitudes [220]. The two approaches are equivalent. In the following, the effective Lagrangian formalism is chosen to describe the models considered and a restricted number of models are discussed [219]. In the analysis performed by CMS [220], a larger number of models have been investigated, however, the main channels studied by both experiments are essentially the same and the main conclusions are similar and fully consistent.

i. Spin-0 model

The interaction Lagrangian relevant for the analysis of spin-0 particle interaction with a pair of W or Z bosons with either fixed or mixed SM and BSM CP -even couplings or CP -odd couplings, is the following [221]:

$$\begin{aligned} \mathcal{L}_0^{W,Z} \supset & \left\{ \cos(\alpha)\kappa_{SM} \left[\frac{1}{2}g_{HZZ}Z_\mu Z^\mu + g_{HWW}W_\mu^+ W^{-\mu} \right] \right. \\ & - \frac{1}{4\Lambda} \left[\cos(\alpha)\kappa_{HZZ}Z_{\mu\nu}Z^{\mu\nu} + \sin(\alpha)\kappa_{AZZ}Z_{\mu\nu}\tilde{Z}^{\mu\nu} \right] \\ & \left. - \frac{1}{2\Lambda} \left[\cos(\alpha)\kappa_{HWW}W_{\mu\nu}^+ W^{-\mu\nu} + \sin(\alpha)\kappa_{AWW}W_{\mu\nu}^+\tilde{W}^{-\mu\nu} \right] \right\} H, \end{aligned} \quad (11.20)$$

where $V^\mu = Z^\mu, W^{+\mu}$ are the vector boson fields, $V^{\pm\mu\nu}$ are the reduced field tensors and $\tilde{V}^{\pm\mu\nu} = 1/2 \varepsilon^{\mu\nu\rho\sigma} V_{\rho\sigma}$ are the dual tensor fields. And Λ defines an effective theory energy scale. The factors $\kappa_{SM}, \kappa_{HZZ}, \kappa_{HWW}, \kappa_{AZZ}, \kappa_{AWW}$ denote the coupling constants corresponding of the coupling of the SM and BSM CP -even and CP -odd components of the Higgs boson to the W and Z fields. The mixing angle α allows for the production of a CP -mixed state and the CP -symmetry is broken when $\alpha \neq 0, \pi$.

This formalism can be used to probe both CP -mixing for a spin-0 state, as discussed in Section 11.5.1.4 or specific alternative hypotheses, as discussed below in Section 11.5.1.3, such as a pure CP -odd state ($J^P = 0^-$) corresponding to $\alpha = \pi/2$, $\kappa_{SM} = \kappa_{HVV} = 0$ and $\kappa_{AVV} = 1$. A BSM CP -even state $J^P = 0^+$ corresponds to $\alpha = 0$, $\kappa_{AVV} = 0$, $\kappa_{HVV} = 1$ and κ_{SM} arbitrary. These hypotheses are compared to the SM Higgs boson hypothesis corresponding to $\alpha = 0$ and $\kappa_{HVV} = \kappa_{AVV} = 0$ and $\kappa_{SM} = 1$. This formalism has been adopted by the ATLAS experiment. The analysis of these benchmarks are illustrated in Fig. 11.9.

A different parametrisation of anomalous couplings of a spin-zero boson with two gauge bosons VV can also be expressed in the general form of the scattering amplitude A :

$$\begin{aligned} A \sim & \left[a_1^{VV} - \frac{\kappa_1^{VV} q_1^2 + \kappa_2^{VV} q_2^2}{(A_1^{VV})^2} - \frac{\kappa_3^{VV} (q_1 + q_2)^2}{(A_Q^{VV})^2} \right] m_{V_1}^2 \varepsilon_{V_1}^* \varepsilon_{V_2}^* \\ & + a_2^{VV} f_{\mu\nu}^{*(1)} f^{*(2)\mu\nu} + a_3^{VV} f_{\mu\nu}^{*(1)} \tilde{f}^{*(2)\mu\nu} \end{aligned} \quad (11.21)$$

where ε_i is the polarization vector of the boson V_i , $f_{\mu\nu}^{*(i)} = \varepsilon_i^\mu q^\nu - \varepsilon_i^\nu q^\mu$ is a scalar tensor constructed from the vector boson V_i polarization and four momentum, $\tilde{f}_{\mu\nu}^{*(i)} = \frac{1}{2} \varepsilon_{\mu\nu\rho\sigma} f^{*(i)\rho\sigma}$ is the corresponding pseudo-scalar tensor. A_1 and A_Q are new physics scales, $a_{1,2,3}$ are coupling strength modifiers and $|\kappa_{(1,2,3)}^{VV}| = 0$ or 1. The custodial symmetry would require that $a^{WW} = a^{ZZ}$ and, at tree-level, the only non-zero contributions would come from the a_1 term. This parametrisation is used by CMS. It is fully equivalent to the interaction Lagrangian approach described above.

ii. Spin-2 model

The graviton-inspired interaction Lagrangian for a spin-2 boson $X^{\mu\nu}$ that does not carry any color, weak and electromagnetic charge and that uniquely interacts with the energy momentum tensor $\mathcal{T}^{V,f}$ of vector bosons V or fermions f , can be written as follows [221]:

$$\mathcal{L}_2 \supset \frac{1}{\Lambda} \left[\sum_V \xi_V \mathcal{T}_{\mu\nu}^V X^{\mu\nu} + \sum_f \xi_f \mathcal{T}_{\mu\nu}^f X^{\mu\nu} \right], \quad (11.22)$$

where the strength of the interaction is determined by the couplings ξ_V and ξ_f . The simplest scenarios, referred to as universal couplings (UC), correspond to $\xi_V = \xi_f$. They predict a large branching ratio to photons (of approximately 5%) and negligible couplings to massive gauge bosons (W and Z). They are therefore disfavoured, and other models are investigated where the couplings of the W , Z and γ are assumed to be independent. Universality of the couplings refers to $\xi_g = \xi_q$. Two other scenarios are considered: $\xi_q = 0$ and $\xi_q = 2\xi_g$. In these scenarios, a large enhancement of the tail of the transverse momentum of the spin-2 state is expected and requires a further selection requirement in order to probe the models within the range of validity of the effective field theory. Two requirements are considered, $p_T^X < 300$ GeV and $p_T^X < 125$ GeV [219]. The analysis of these benchmarks are discussed below and results are illustrated in Fig. 11.9.

11.5.1.3 Probing fixed J^P scenarios

At the LHC, the determination of the spin and CP properties of the Higgs boson is done independently from the total rates measurement, it uses a global angular helicity analysis and, when applicable, the study of threshold effects. The channels used for this analysis, $H \rightarrow \gamma\gamma$, $H \rightarrow WW^{(*)} \rightarrow \ell\nu\ell\nu$ and $H \rightarrow ZZ^{(*)} \rightarrow 4\ell$, are those where the observation of a signal is unambiguous.

At the Tevatron, an analysis using the threshold distribution in the associated production mode VH with subsequent decay to a pair of b quarks was performed by the D0 collaboration.

i. The VH production at D0

The mass of the VH system is a powerful discriminant to distinguish a $J^P = 0^+$, with a threshold behaviour in $d\sigma/dM^2 \sim \beta, \beta^3, \beta^5$ from a $0^+, 0^-$ and 2^+ state, respectively [222]. The VH mass observable not only discriminates signal hypotheses, but also has an increased separation between the 0^- and 2^+ hypotheses with respect to the backgrounds, thus allowing, with a small and not yet significant signal yield, to exclude that the observed state is 0^- at 98% CL [223] and 2^+ at the 99.9% CL [224], assuming a signal produced with their best fit signal strength (which was $\mu = 1.23$).

ii. The $\gamma\gamma$ channel at the LHC

In the $H \rightarrow \gamma\gamma$ channel, the analysis is performed inclusively using the production angle $\cos\theta_{CS}^*$ and the transverse momentum of the diphoton pair [219]. The polar angle in the rest frame is defined with respect to the bisector axis of the momenta of the incoming protons and is referred to as the polar angle in the Collins-Soper frame [225]. The SM Higgs boson signal distribution is expected to be uniform with a cutoff due to the selection requirements on the photons transverse momentum. The $H \rightarrow \gamma\gamma$ channel is mostly sensitive to the gluon-initiated spin-2 production scenarios, which yield a $\cos\theta_{CS}^*$ distribution peaking at values close to 1. The ATLAS limits are derived from a fit of the signal in bins of $\cos\theta_{CS}^*$ and diphoton transverse momentum and are summarised in Fig. 11.9 (right) (only combined results are shown). The data shows a good compatibility with the SM 0^+ hypothesis and contributes strongly to the exclusion of several spin-2 scenarios. The conclusions are the same from CMS results [220].

iii. The $H \rightarrow WW^{(*)} \rightarrow \ell\nu\ell\nu$ channel at the LHC

In the $H \rightarrow WW^{(*)} \rightarrow \ell\nu\ell\nu$ channel, the production and decay angles cannot be easily reconstructed due to the presence of neu-

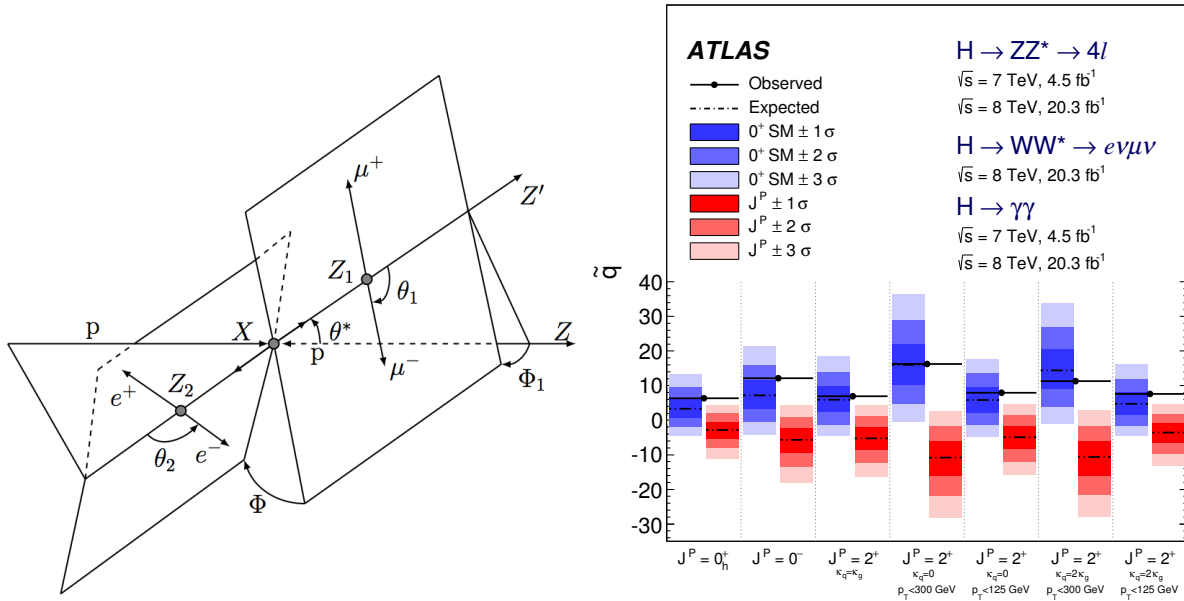


Figure 11.9: (Left) Definition of the production and decay angles defined for the $H \rightarrow ZZ^{(*)} \rightarrow 4\ell$ final state [220]. (Right) Expected distributions of the test statistic for the SM hypothesis (in blue) and several alternative spin and parity hypotheses (in red).

trinos in the final state, however, sensitivity arises from the $V-A$ structure of the decay of the W bosons. A scalar state thus yields a clear spin correlation pattern that implies that the charged leptons e or μ from the decays of the W bosons are produced close to one another in the transverse plane. This feature impacts observables such as the azimuthal angle between the two leptons $\Delta\Phi_{\ell\ell}$ or their invariant mass $m_{\ell\ell}$ in addition to the threshold behaviour of the decay. It can be used to discriminate between various spin and parity hypotheses. The approach adopted by ATLAS uses a multivariate discriminant, whereas CMS uses a 2D-fit of the dilepton mass and the transverse mass. Figure 11.9 (right) summarises the ATLAS results of the $H \rightarrow WW^{(*)} \rightarrow \ell\nu\ell\nu$ analyses alone and in combination with other channels. Spin-1 hypotheses (1^+ and 1^-) have also been tested in this channel by ATLAS and CMS. ATLAS and CMS exclude the 1^+ and 1^- hypotheses at more than 95% CL.

iv. The $H \rightarrow ZZ^{(*)} \rightarrow 4\ell$ channel at the LHC

The $H \rightarrow ZZ^{(*)} \rightarrow 4\ell$ coupling analysis, as described in Section 11.3, also uses a discriminant based on the 0^+ nature of the Higgs boson to further separate signal and background. In this analysis, this feature is used to discriminate between signal hypotheses. The observables sensitive to the spin and parity are [226] the masses of the two Z bosons (due to the threshold dependence of the mass of the off-shell Z boson), two production angle θ^* and Φ_1 , and three decay angles, Φ , θ_1 and θ_2 . The production and decay angles are defined as:

- θ_1 and θ_2 , the angles between the negative final state lepton and the direction of flight of Z_1 and Z_2 in the rest frame.
- Φ , the angle between the decay planes of the four final state leptons expressed in the four lepton rest frame.
- Φ_1 , the angle defined between the decay plane of the leading lepton pair and a plane defined by the vector of the Z_1 in the four lepton rest frame and the positive direction of the proton axis.
- θ^* , the production angle of the Z_1 defined in the four lepton rest frame with respect to the proton axis.

These angles are illustrated in Fig. 11.9 (left). There are two approaches to this analysis. The first, used by CMS, is a matrix element likelihood approach where a kinematic discriminant is defined based on the ratio of the signal and background probabilities. These probabilities are defined using the leading-order matrix elements. A similar approach is also performed by ATLAS as a cross check of their main result. The main approach adopted by ATLAS is the combination of sensitive observables

with a Boosted Decision Tree. These analyses are sensitive to various J^P hypotheses and in particular discriminate the 0^+ hypothesis from the 0^- . In all scenarios investigated, and for both ATLAS and CMS, the data is compatible with the 0^+ hypothesis. ATLAS and CMS exclude a pure pseudo-scalar nature of the observed boson at CL_S levels of 98% and 99.8% [220].

11.5.1.4 Probing CP -mixing and anomalous HVV couplings

The careful study of the kinematic properties of the events observed in the $H \rightarrow ZZ^{(*)} \rightarrow 4\ell$ and $H \rightarrow WW^{(*)} \rightarrow \ell\nu\ell\nu$ channel, and in particular the angular distributions described above, allows one to further probe the HVV coupling beyond testing fixed hypotheses. Assuming that the observed particle is a spin-0 state, and using several discriminating observables in the $H \rightarrow ZZ^{(*)} \rightarrow 4\ell$ and $H \rightarrow WW^{(*)} \rightarrow \ell\nu\ell\nu$ channels, the anomalous terms in the formalism of Eq. (11.20) can be probed. In the approach of helicity amplitudes used by CMS [220], all terms are essentially equivalent, except for one additional phase which is neglected in Eq. (11.20).

Results are derived in terms of the parameters $\tilde{\kappa}_{HVV} = v\kappa_{HVV}/\Lambda$ and $\tilde{\kappa}_{AVV} = v\kappa_{AVV}/\Lambda$, and, more precisely, as measurements of $\tilde{\kappa}_{HVV}/\kappa_{SM}$ and $\tan\alpha \cdot \tilde{\kappa}_{AVV}/\kappa_{SM}$, as shown in Fig. 11.10. These parameters can be interpreted as mixing parameters of a tensor anomalous CP -even coupling and a CP -odd component. The measurements are made in the $H \rightarrow ZZ^{(*)} \rightarrow 4\ell$ and $H \rightarrow WW^{(*)} \rightarrow \ell\nu\ell\nu$ channels independently and then combined assuming that the $\tilde{\kappa}_{HVV}/\kappa_{SM}$ and $\tan\alpha \cdot \tilde{\kappa}_{AVV}/\kappa_{SM}$ are the same for the W and Z vector bosons. Only the combination of the WW and ZZ channels is shown in Fig. 11.10. The asymmetric shape of the likelihood as a function of $\tilde{\kappa}_{HWW}, HZZ/\kappa_{SM}$ is mainly due to the interference between the BSM and the SM contributions that gives a maximal deviation from the SM predictions for negative relative values of the BSM couplings. In Fig. 11.10, the expected likelihood profiles for a SM Higgs boson are also displayed. While no significant deviation from the SM expectation is observed, the precision of the measurements of the mixing parameters is fairly low. The results and conclusions from the CMS measurements [220] are very similar.

An individual ZZ^* channel measurement has also been carried out with a partial Run2 dataset by ATLAS [227]. CMS has performed a CP -mixing analysis of a partial Run2 dataset of 36 pb^{-1} combined with the full Run1 data using the ZZ^* channel [228]. In this analysis the CMS experiment sets constraints on the following parameters defined in the scattering amplitude

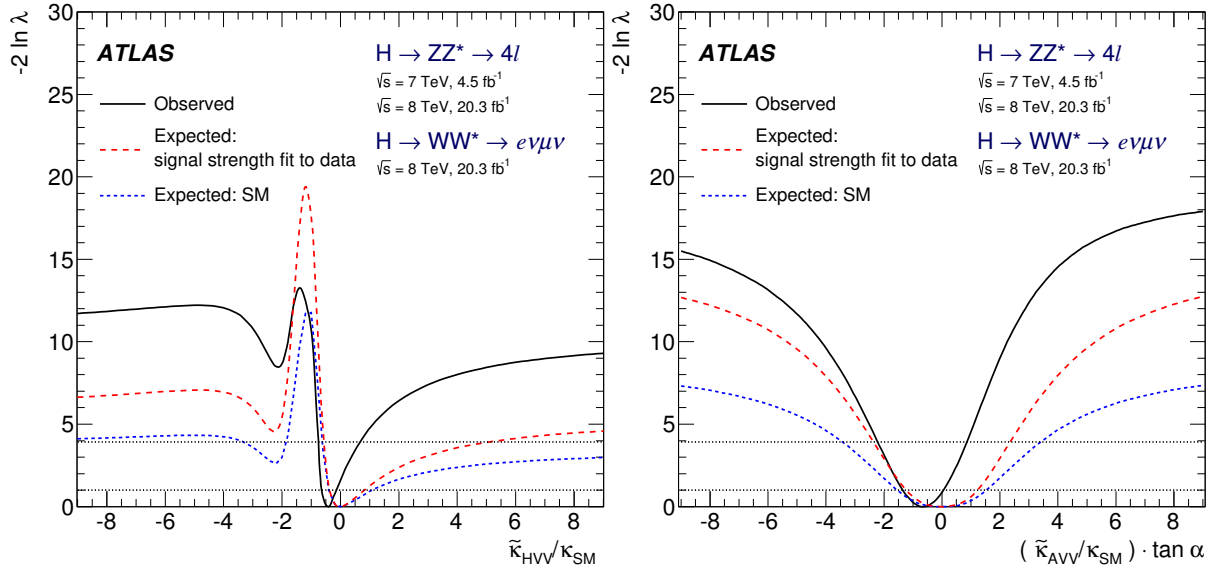


Figure 11.10: Likelihood profiles for the $\tilde{\kappa}_{HV V}$ and $\tilde{\kappa}_{AVV} \cdot \tan \alpha$ parameters, representing respectively CP -even and CP -odd anomalous couplings of the Higgs boson.

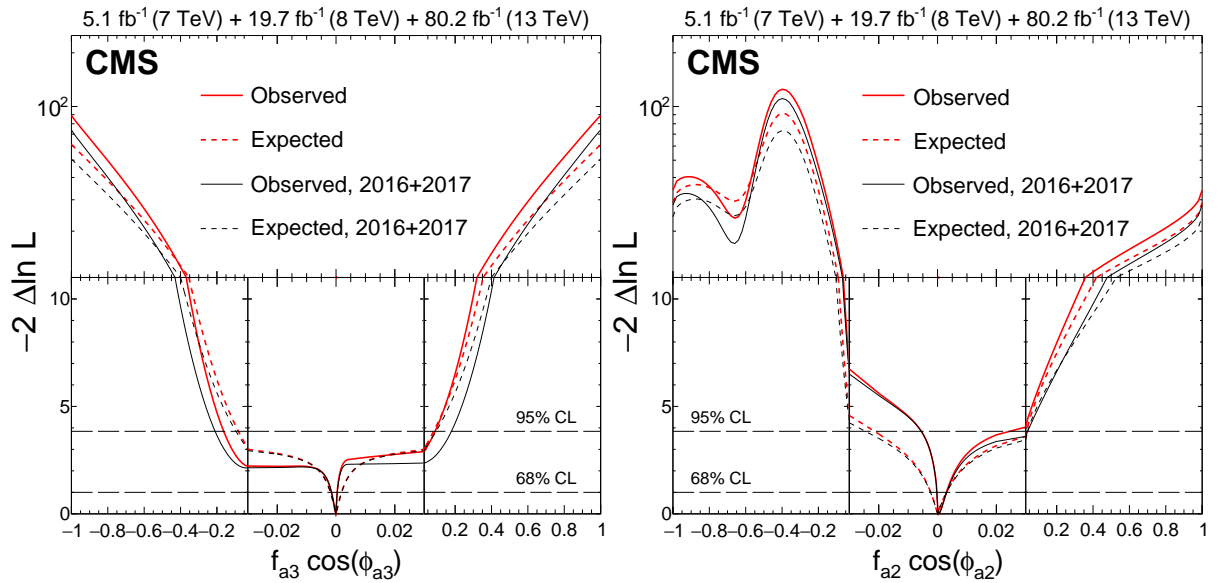


Figure 11.11: Observed (solid) and expected (dashed) likelihoods as a function of $f_{a_3} \cos(\phi_{a_3})$ (left), $f_{a_2} \cos(\phi_{a_2})$ (right) for the Run 1 and Run 2 datasets separately and combined.

parametrisation (11.21):

$$f_{a_i} = \frac{|a_i|^2 \sigma_i}{\sum_{j=1,2,3} |a_j|^2 \sigma_j}, \quad \phi_{a_i} = \arg\left(\frac{a_i}{a_1}\right), \quad (11.23)$$

where σ_i is the cross section for process with $a_i = 1$ and $a_{j \neq i} = 0$. The constraints on these parameters are shown in Fig. 11.11.

CP invariance in the HVV coupling can also be probed with the VBF production process in the $H \rightarrow \tau^+ \tau^-$ channel. CMS has performed an analysis in this channel and has combined its results with the aforementioned ZZ^* channel using the same dataset [229].

ATLAS has also performed an analysis using optimal observables [230], defined as the ratio of the interference between the CP -odd and the SM contributions normalised to the SM matrix element squared, using the Run1 data. In this study, the CP -mixing contributions are described in the framework of an effective field theory governed by a single parameter \tilde{d} , found to be consistent with its SM value of $\tilde{d} = 0$ and constrained to the interval $[-0.11, 0.05]$ at the 68% CL.

11.5.2 Off-shell couplings of the Higgs boson

In the dominant ggF production mode with a subsequent decay of the Higgs boson into a pair of Z bosons, the production cross section of an off-shell Higgs boson is known to be sizeable. This follows as a consequence of the enhanced couplings of the Higgs boson to the longitudinal polarisation of the massive vector bosons at high energy.

The off-shell to on-shell cross section ratio is approximately 8% in the SM [231]. Still the Higgs contribution to VV production at large invariant mass remains small compared to the background. It is nevertheless interesting to probe Higgs production in this regime as it is sensitive to new physics beyond the SM.

The difficulty in the off-shell VV analysis, beyond the small signal-to-background ratio, is due to a large negative interference between the signal and the $gg \rightarrow VV$ background.

The resulting presence of a SM Higgs boson signal in the far off-shell domain results in a deficit of events with respect to the expectation from background only events. It is only when the off-shell couplings of the Higgs boson are larger than expected in

the SM that the presence of a signal appears as an excess over the background expectation. One additional intricacy arises from the precision in the prediction of the rate for $gg \rightarrow VV$, a loop process at lowest order, and its interference with the signal. At the time of the publication of the original ATLAS and CMS results, a full NLO prediction had not been computed.

It is interesting to note that, in this regime, the Higgs boson is studied as a propagator and not as a particle. The measurement of its off-shell couplings is therefore absolute and does not rely on the knowledge of the total Higgs boson width. The off-shell coupling constraints can then be used to indirectly constrain the width of the Higgs boson, under specific assumptions detailed in Section 11.5.3.3.

This measurement has been carried out in the $H \rightarrow ZZ \rightarrow 4\ell$, $H \rightarrow ZZ \rightarrow \ell\nu\nu$ and $H \rightarrow WW \rightarrow \ell\nu\nu$ channels. To enhance the sensitivity of the analysis, the knowledge of the full kinematics of the events is important. In particular the signal and the background can be further distinguished by the invariant mass of the VV system, which is more accurately accessible in the $H \rightarrow ZZ \rightarrow 4\ell$ channel. Angular distributions also play an important role in this analysis. For these reasons, the $H \rightarrow ZZ^{(*)} \rightarrow 4\ell$ channel is significantly more sensitive than $H \rightarrow WW^{(*)} \rightarrow \ell\nu\nu$. The CMS results in Refs. [232] include the VBF and VH processes through the selection of two additional jets in the final state. The ATLAS results do not have a specific selection for the VBF or VH production processes, but their contributions are taken into account.

Limits on the off-shell rates have been reported for the two channels by ATLAS [233] and CMS [232]. The combined results, assuming that the off-shell rates in the ZZ and WW channels scale equally, are given for two different hypotheses on the VBF production rate: fixing it to its SM value or scaling it as the gluon fusion rate. The observed (expected) limits on the off-shell rate fraction with respect to its SM expectation is 6.7 (9.1) for ATLAS [233] with the VBF rate fixed to its SM value and 2.4 (6.2) for CMS [232] where no assumption is made on the relative production rates of gluon-fusion and VBF. In both cases, the custodial symmetry is assumed and the ratio of the rates in the ZZ and WW decays are fixed to those of the SM. Results without this assumption have also been reported in Ref. [232].

Both ATLAS [234] and CMS [228] have performed off-shell Higgs boson analyses to constrain the off-shell Higgs boson production rates with partial Run 2 datasets, corresponding respectively to luminosities of 36.1 fb^{-1} and 80.2 fb^{-1} . With the increase in centre-of-mass energy and luminosities, significantly better sensitivities are achieved. The ATLAS analysis is based on two decay channels, $H \rightarrow 4\ell$ and $H \rightarrow 2\ell 2\nu$, and the two main ggF and VBF production modes, while the CMS analysis is based on the $H \rightarrow 4\ell$ channel exclusively, but uses the exclusive VH categories. The results obtained have already reached an impressive sensitivity, with 95% CL upper limits on the off shell signal strength $\mu_{\text{off-shell}}$:

$$\begin{aligned} (\text{ATLAS}) \quad \mu_{\text{off-shell}} &< 3.8 \text{ (obs)} \quad [3.4 \text{ (exp)}], \\ (\text{CMS}) \quad \mu_{\text{off-shell}} &< 2.28 \text{ (obs)} \quad [3.2 \text{ (exp)}]. \end{aligned} \quad (11.24)$$

11.5.3 The Higgs boson width

In the SM, the Higgs boson width is very precisely predicted once the Higgs boson mass is known. For a mass of 125 GeV, the Higgs boson has a very narrow width of 4.1 MeV [44]. It is dominated by the fermionic decays partial width at approximately 75%, while the vector boson modes are suppressed and contribute 25% only.

At the LHC or the Tevatron, in all production modes, only the cross sections times branching fractions can be measured. As a consequence, the total width of the Higgs boson cannot be inferred from measurements of Higgs boson rates. Direct constraints on the Higgs boson width are much larger than the expected width of the SM Higgs boson.

11.5.3.1 Direct constraints

Analyses of the reconstructed mass line-shape in the two channels with a good mass resolution, the $H \rightarrow \gamma\gamma$ and $H \rightarrow ZZ^{(*)} \rightarrow 4\ell$ channels, allow for a direct measurement of the

width of the SM Higgs boson. The intrinsic mass resolution in these channels is about 1–2 GeV, much larger than the expected width of the SM Higgs boson. As a result, only upper limits on the Higgs boson width have been set by ATLAS [235] and CMS [236]. The two main challenges of direct constraints on the width through the measurement of the line-shape are: (i) the modelling of resolution uncertainties and (ii) the modelling of the interference between the signal and the continuum background which can be sizeable for large widths, in particular in the range where direct constraints are set. Given that these interference effects are small with respect to the individual channels sensitivity, they are neglected in deriving constraints on the total width. The combined constraints, however, being more precise, could be affected by the interference. ATLAS [235] has therefore not combined the constraints on the width from the two channels. The results are reported in Table 11.11. These constraints are still three orders of magnitude larger than the expected SM width and are fully compatible with the SM hypothesis.

Another direct constraint on the Higgs boson width can be obtained, in the $H \rightarrow ZZ^{(*)} \rightarrow 4\ell$ channel, from the measurement of the average lifetime of the Higgs boson calculated from the displacement of the four-lepton vertex from the beam spot. This analysis has been carried out by CMS (see references in Ref. [123]), using the measured decay length. The measured $c\tau_H$ is $2_{-2}^{+25} \mu\text{m}$, yielding an observed (and expected) limit at the 95% CL of $c\tau_H < 57(56) \mu\text{m}$. From this upper limit on the lifetime of the Higgs boson, the 95% CL lower limit on its width is $\Gamma_H > 3.5 \times 10^{-12} \text{ GeV}$.

11.5.3.2 Indirect constraints from mass shift in the diphoton channel

In the diphoton channel, it was noticed in Ref. [237], that the effect of the interference between the main signal $gg \rightarrow H \rightarrow \gamma\gamma$ and the continuum irreducible background $gg \rightarrow \gamma\gamma$, taking into account detector resolution effects, is responsible for a non negligible mass shift. The size of the mass shift depends on the total width of the Higgs boson and it was suggested that measuring this mass shift could provide a constraint on the width [237]. It was further noticed that the mass shift has a dependence also on the diphoton transverse momentum. The total width of the Higgs boson could therefore be constrained using the diphoton channel alone.

Further studies were performed by ATLAS to estimate the size of the expected mass shift [134]. The expected shift in mass in the diphoton channel is $35 \pm 9 \text{ MeV}$ for the SM Higgs boson. Very preliminary studies of the sensitivity of this method to estimate the width of the Higgs boson in the High-Luminosity regime have been made by ATLAS [238] and yield an expected 95% CL upper limit on the total width of approximately 200 MeV from 3 ab^{-1} of 14 TeV data.

11.5.3.3 Indirect constraints from on-shell rate in the diphoton channel

In the diphoton channel, it was noticed in Ref. [239], that the interference between the main signal $gg \rightarrow H \rightarrow \gamma\gamma$ amplitude and the continuum irreducible background $gg \rightarrow \gamma\gamma$ amplitude generates non-negligible change in the on-shell cross sections, as a result of the existence of a relative phase between these amplitudes. The size of this on-shell interference effect depends on the total width of the Higgs boson and it was suggested that measuring this on-shell cross section precisely could provide a constraint on the Higgs total width. This interference effect yields around 2% reduction for the $gg \rightarrow H \rightarrow \gamma\gamma$ cross section measurement. The current evaluation of this interference effect is performed at NLO and has a $^{+50\%}_{-30\%}$ uncertainty, due to the fact that the large relative phase is driven by the two-loop $gg \rightarrow \gamma\gamma$ background amplitude [237, 239]. This on-shell interference effect has a dependence on the p_T of the diphoton system and the photon polar angle in the diphoton rest frame, which can be further exploited to improve the measurement to constrain the Higgs total width.

Taking the ratios of the on-shell cross section of Higgs boson to diphoton channel and the cross section of Higgs boson to four-leptons channel where the interference effect is negligible could put bound on the Higgs boson total width. This ratio is free

Table 11.11: Run 1 observed (expected) direct 95% CL constraints on the width of the 125 GeV resonance from fits to the $\gamma\gamma$ and ZZ mass spectra and to the 4ℓ vertex lifetime. *The CMS measurement from the 4ℓ mass line-shape was performed using Run 2 data.

Exp.	$M_{\gamma\gamma}$ mass spectrum	$M_{4\ell}$ spectrum	4ℓ vertex lifetime
ATLAS	< 5.0 (6.2) GeV	< 2.6 (6.2) GeV	—
CMS	< 2.4 (3.1) GeV	< 1.1 (1.6) GeV*	$> 3.5 \times 10^{-12}$ GeV

from many dominant sources of systematic uncertainties for cross section measurements, i.e., PDF uncertainty and luminosity uncertainty, and can be further improved by the accumulation of the LHC data. From this cross section ratio measurement alone, a preliminary estimation of the current limit from this interference effect with current 30% precision puts an upper bound of 800 MeV on the Higgs boson total width and the limit improves to 60 MeV with 3 ab^{-1} of 14 TeV data [239,240].

11.5.3.4 Indirect constraints from off-shell couplings

Using simultaneously on-shell and off-shell measurements in the VV channels, it was noticed [231,241] that the total width of the Higgs boson could be constrained. This can be illustrated from the parametrisation of the signal strength measurements both on-shell ($\mu_{\text{on-shell}}$) and off-shell ($\mu_{\text{off-shell}}$) as a function of the couplings modifiers κ_g and κ_V parameterising the main process $gg \rightarrow H \rightarrow VV$ (see Section 11.6.2 for the definition of these coupling modifiers). The on-shell and off-shell signal strengths can be written as:

$$\begin{aligned}\mu_{\text{on-shell}} &= \frac{\kappa_{g,\text{on-shell}}^2 \kappa_{V,\text{on-shell}}^2}{\Gamma_H/\Gamma_{\text{SM}}}, \\ \mu_{\text{off-shell}} &= \kappa_{g,\text{off-shell}}^2 \kappa_{V,\text{off-shell}}^2.\end{aligned}\quad (11.25)$$

A bound on the Higgs boson width can then be obtained from the measurements of the on-shell and off-shell signal strengths. This assumes that no new physics alters the Higgs boson couplings in the off-shell regime, i.e., that the running of its couplings is negligible in the off-shell regime [242,243]. Both ATLAS [233] and CMS [232] have used their off-shell production limits to constrain the width of the Higgs boson.

Both ATLAS and CMS analyses use the kinematic event characteristics to further gain in sensitivity to discriminate between the signal and background. The ATLAS analysis assumed that there are no anomalous couplings of the Higgs boson to vector bosons, and obtains 95% CL observed (expected) upper limit on the total width of $5.7 \times \Gamma_{\text{SM}}$ ($9.0 \times \Gamma_{\text{SM}}$) with the Run 1 dataset. In the CMS analysis, the observed (expected) limit on the total width is $6.2 \times \Gamma_{\text{SM}}$ ($9.8 \times \Gamma_{\text{SM}}$) for the ZZ channel only at Run 1.

In addition, in the CMS analysis, results are also derived allowing for anomalous couplings of the Higgs boson, therefore reducing the discriminating power of the kinematic variables used in the analysis but reducing the model dependence. The observed (expected) limit on the total width is $10.9 \times \Gamma_{\text{SM}}$ ($17.4 \times \Gamma_{\text{SM}}$).

CMS has also combined the ZZ and W^+W^- channels while keeping the gluon-fusion and VBF production processes separate. For the gluon fusion mode, the observed (expected) combined upper limit at the 95% CL on the total width of the Higgs boson is $2.4 \times \Gamma_{\text{SM}}$ ($6.2 \times \Gamma_{\text{SM}}$) [232], while for the VBF production mode the exclusion limits are $19.3 \times \Gamma_{\text{SM}}$ ($34.4 \times \Gamma_{\text{SM}}$) [232].

At Run 2, using the ATLAS [234] and CMS [228] analyses described in Section 11.5.2, the following bounds were obtained:

$$(\text{ATLAS}) \quad \Gamma_H/\Gamma_H^{\text{SM}} < 3.5 \quad [3.7 \text{ (exp)}], \quad (11.26)$$

$$\begin{aligned}(\text{CMS}) \quad \Gamma_H &< 9.16 \quad [13.7 \text{ (exp)}] \text{ MeV} \\ \text{or } \Gamma_H \Gamma_H^{\text{SM}} &= 3.2_{-2.2}^{+2.8} \quad [4.1_{-4.0}^{+5.0} \text{ (exp)}].\end{aligned}\quad (11.27)$$

CMS has also performed this analysis considering possible anomalous HZZ couplings as discussed in Section 11.5.1.4. Neither the results nor the sensitivities are significantly affected by allowing specific anomalous coupling parameters to float in the fits.

ATLAS and CMS have also performed a study of the prospects for measuring the Higgs boson width mainly in the four lepton channel. Projecting to a luminosity of 3 ab^{-1} , it was concluded that, within assumptions similar to the ones mentioned above and assuming the SM central value, the observed (expected) combined

upper limit at the 95% CL on the total width of the Higgs boson would be $3.8 \times \Gamma_{\text{SM}}$ ($3.4 \times \Gamma_{\text{SM}}$), i.e., the width of the Higgs boson could be constrained with the following precision [104]:

$$\Gamma_H = 4.1_{-0.8}^{+0.7} \text{ MeV}. \quad (11.28)$$

11.6 Probing the coupling properties of the Higgs boson

As discussed in Section 11.2, within the SM, all the Higgs boson couplings are fixed unambiguously once all the particle masses are known. Any deviation in the measurement of the couplings of the Higgs boson could therefore signal BSM physics.

Measuring the Higgs boson couplings without relying on the SM assumption requires a general framework treating deviations from the SM coherently at the quantum level in order to provide theoretical predictions for relevant observables to be confronted with experimental data. An attempt in that direction has been formalised in the so-called κ -formalism [244], following earlier attempts [245] and initial phenomenological studies of the first hints of the existence of the Higgs boson [246]. In this LO-inspired approach, the SM Higgs boson couplings are rescaled by arbitrary factors, κ 's, keeping the same Lorentz structure of the interactions. This formalism allows for simple interpretation of the signal strengths measured in the various Higgs channels. It has been utilised to test various physics scenarios, like the existence of additional new particles contributing to the radiative Higgs boson production and decays, or to probe various symmetries of the SM itself, as for example the custodial symmetry. It only compares the experimental measurements to their best SM predictions and does not require any new BSM computations per se. And, from a more theoretical perspective, its relevance arises from the fact that it actually fully captures the leading effects in single Higgs processes of well motivated scenarios. Still, the κ -formalism has obvious limitations and certainly does not capture the most general deformations of the SM, even under the assumptions of heavy and decoupling new physics. A particularly acute shortcoming at the time Higgs physics is entering a precision era is the lack of proficiency to assert the richness of kinematical distributions beyond simple signal strength measurements. Several extensions and alternative approaches are being developed as part of the activities of the LHC Higgs Cross Section Working Group [45].

The Higgs Pseudo-Observable (HPO) approach [247] allows one to report the data in terms of a finite set of on-shell form factors parameterising amplitudes of physical processes subject to constraints from Lorentz invariance and other general requirements like analyticity, unitarity, and crossing symmetry. These form factors are expanded in powers of kinematical invariants of the process around the known poles of SM particles, assuming that poles from BSM particles are absent in the relevant energy regime. A set of HPOs have been proposed to characterise both the Higgs boson decays and the EW Higgs boson production channels, thus exploring different kinematical regimes. Prospective studies concluded that these HPOs can be measured/bounded at the percent level at the HL-LHC and could therefore be used to constrain some explicit models of new physics.

Another systematic approach to characterise the possible Higgs boson coupling deviations induced by BSM physics is the use of Effective Field Theories (EFT) [248,249]. This approach assumes again that the new physics degrees of freedom are sufficiently heavy to be integrated out and they give rise to effective interactions among the light SM particles. By construction, the effective Lagrangians cannot account for deviations in Higgs physics induced by light degrees of freedom, unless they are added themselves as extra fields in the effective Lagrangians. In Section 11.7, several examples of models with light degrees of freedom affect-

ing Higgs boson production and decay rates will be presented. The main advantage of EFTs is their prowess to relate different observables in different sectors and at different energies to constrain a finite set of effective interactions among the SM degrees of freedom. In an EFT, the SM Lagrangian is extended by a set of higher-dimensional operators, and it reproduces the low-energy limit of a more fundamental UV description. It will be assumed that the Higgs boson is part of a CP -even EW doublet, Φ , and that the Lagrangian is an analytic function of the gauge invariant $\Phi^\dagger\Phi$. This scenario is commonly referred to as SMEFT. Even though it is not fully established experimentally, this set-up is motivated by the measurements of the Higgs couplings to the different SM particles that show an alignment with their masses, such an alignment naturally follows under this assumption of a linear realisation of the $SU(2)_L \times U(1)_Y$ symmetry of the SM but would require an ad-hoc tuning otherwise. General Lagrangians bypassing this linear assumption have been explicitly written down, see for instance Ref. [250]. They rely on a chiral expansion with a specific power-counting, effectively resumming the expansion in powers of the Higgs field, usually referred to as HEFT as opposed to SMEFT.

11.6.1 Effective Lagrangian framework

The SMEFT has the same field content and it respects the same linearly-realised $SU(3)_C \times SU(2)_L \times U(1)_Y$ local symmetry as the SM. The difference is the presence of operators with canonical mass-dimension d larger than 4. These are organised in a systematic expansion in d , where each consecutive term is suppressed by a larger power of a high mass scale. Assuming baryon and lepton number conservation, the most general Lagrangian takes the form

$$\mathcal{L}_{\text{eff}} = \mathcal{L}_{\text{SM}} + \sum_i c_i^{(6)} \mathcal{O}_i^{(6)} + \sum_j c_j^{(8)} \mathcal{O}_j^{(8)} + \dots \quad (11.29)$$

The contribution of the higher order operators of dimension d to physical amplitudes is suppressed by $(E/\Lambda)^{d-4}$, where E is the relevant energy scale of the process and Λ is the energy scale suppressing the higher-dimensional operators. The Wilson coefficients $c_i^{(d)}$ encode the virtual effects of the heavy new physics in low-energy observables. Their precise forms in terms of masses and couplings of the new particles can be obtained via matching with the ultraviolet (UV) completion of the SM, see, e.g., Ref. [251], or inferred using specific power-counting rules [248, 252].

The list of dimension-6 operators was first classified in a systematic way in Ref. [253] after the works of Ref. [254]. Subsequent analyses pointed out the presence of redundant operators, and a minimal and complete list of operators was finally provided in Ref. [255]⁴. For a single family of fermions, there are 76 real ways to deform the SM generated by 59 independent operators. With the 3 families of fermions of the SM, flavour indices can be added to these 59 operators, and furthermore, new operator structures, that have been dismissed by means of Fierz transformations in the single family case, have to be considered, for a total of 2499 real deformations [258]. When considering Higgs data, one can reasonably focus on a relatively small subset of the 2499 operators of dimension 6. In particular the vast subset of 4-fermion operators, whether flavour and CP preserving or not, can be more strongly constrained by other processes. Thus, it makes sense to neglect this whole class, with the exception of one particular four-fermion interaction that contributes to the muon decay and thus directly affects the Fermi constant. The dipole operators, instead do directly affect Higgs boson production, however, under very general and plausible assumptions on the flavour structure of new physics, the coefficients of these operators display the same structure and the same chiral suppression of the Yukawa couplings. The consequence is that, with the possible exception of processes involving the top quark, their effect in Higgs boson production is expected to be negligible. Furthermore, as far as Higgs boson decays

are concerned, the dipole operators only contribute to three (or more)-body final states (for instance $H \rightarrow b\bar{b}\gamma$) and as such they can easily be neglected too. Eliminating these two classes, there remain three other classes: 1) purely bosonic operators, 2) generalised Yukawas, 3) Higgs-fermion current operators. Operators in class 2 and 3, per se, can still contain CP - or flavour-violating terms, on which experimental constraints are rather strong. Under the assumption of flavour universality (respectively diagonality), one is left with 12 (14) parameters affecting EW precision measurements, diboson processes and single- and double-Higgs data and 7 (17) other parameters modifying the EW gauge boson couplings to fermions, see Ref. [44] for further technical details. Working in the unitary gauge and performing suitable redefinition of fields and input parameters the effective Lagrangian can be conveniently expressed in the parameterisation of Ref. [259], the so-called *Higgs basis* that conveniently single out these special less constrained parameters. Such a classification reflects the current experimental situation and the hierarchy in the sensitivity of the experimental measurements in the various sectors of the SM. As the sensitivity of the measurements in the Higgs sector improves, another and more general parametrisation of the SM deformation will have to be retained, in particular a parametrisation more suited for a treatment at the quantum level. In other bases of operators, in particular the so-called Warsaw basis [255] used in some experimental EFT analyses [128, 260, 261], one finds strong correlations among the operators affecting the EW gauge couplings to fermions, leaving 12 (14) linear combinations of operators with weaker constraints.

Section 11.6.2 illustrates how the Higgs data accumulated at the LHC can (partially) constrain the SM deformations, i.e., the dimension-6 operators of the SEMFT Lagrangian. Automatic tools are being developed to analyse the experimental data within an EFT framework, see the report [262] and references therein.

11.6.2 Probing coupling properties

As described in Section 11.3, a framework was developed by ATLAS and CMS [141], individually and together, to combine the very large number of exclusive categories aimed at reconstructing the five main decay modes and the five main production modes of the Higgs boson. The general conclusion of this combination, illustrating the compatibility of the observation with the SM expectations, is given in Section 11.3. The same framework with its master formula, Eq. (11.16), can be used to further measure coupling properties of the Higgs boson under specific additional assumptions.

11.6.2.1 Combined measurements of the Higgs boson coupling properties

i. From effective Lagrangians to Higgs observables

The κ framework, described in detail in Ref. [43, 244], facilitates the characterisation of Higgs coupling properties in terms of a series of Higgs coupling strength modifier parameters κ_i , which are defined as the ratios of the couplings of the Higgs bosons to particles i to their corresponding SM values. The κ framework assumes a single narrow resonance so that the zero-width approximation can be used to decompose the cross section as a product of two factors characterising the production and the decay of the Higgs boson. The κ parameters are introduced by expressing each of these factors as their SM expectation multiplied by the square of a coupling strength modifier for the corresponding process at leading order:

$$\begin{aligned} (\sigma \cdot \text{BR})(i \rightarrow H \rightarrow f) &= \frac{\sigma_i^{\text{SM}} \kappa_i^2 \cdot \Gamma_f^{\text{SM}} \kappa_f^2}{\Gamma_H^{\text{SM}} \kappa_H^2} \rightarrow \\ &\rightarrow \mu_i^f \equiv \frac{\sigma \cdot \text{BR}}{\sigma_{\text{SM}} \cdot \text{BR}_{\text{SM}}} = \frac{\kappa_i^2 \cdot \kappa_f^2}{\kappa_H^2}, \end{aligned} \quad (11.30)$$

where μ_i^f is the rate relative to the SM expectation and κ_H^2 is an expression that adjusts the SM Higgs width to take into account the modifications induced by the deformed Higgs boson couplings. When all κ_i are set to 1, the SM is reproduced. For loop-induced processes, e.g. $H \rightarrow \gamma\gamma$, there is a choice of either resolving the coupling strength modification in its SM expectation,

⁴Complete enumerations of $d=8$ operators have been obtained [256] and some preliminary constraints on peculiar subsets of these operators have been derived from experimental measurements [257]. Still, in this review, the EFT Lagrangians will be truncated at the level of dimension-6 operators.

i.e., $\kappa_\gamma(\kappa_t, \kappa_W)$ or keeping κ_γ as an effective coupling strength parameter.

The κ -framework is the simplest parametrisation directly related to experimental measurements of the Higgs boson production and decay modes. For this reason, it has been widely used by the community. It can also be connected to the SMEFT formalism as follows. Restricting to the EFT directions not probed outside Higgs physics [263], the Higgs boson couplings are written in the unitary gauge as:

$$\begin{aligned} \mathcal{L} = & \kappa_Z \frac{m_Z^2}{v} Z_\mu Z^\mu H + \kappa_W \frac{2m_W^2}{v} W_\mu^+ W^{-\mu} H \\ & + \kappa_{VV} \frac{\alpha}{2\pi v} (\cos^2 \theta_W Z_{\mu\nu} Z^{\mu\nu} + 2W_{\mu\nu}^+ W^{-\mu\nu}) H \\ & + \kappa_g \frac{\alpha_s}{12\pi v} G_{\mu\nu}^a G^{a\mu\nu} H + \kappa_\gamma \frac{\alpha}{2\pi v} A_{\mu\nu} A^{\mu\nu} H + \kappa_{Z\gamma} \frac{\alpha}{\pi v} A_{\mu\nu} Z^{\mu\nu} H \\ & + \kappa_3 \frac{m_H^2}{2v} H^3 \\ & - \left(\kappa_t \sum_{f=u,c,t} \frac{m_f}{v} + \kappa_b \sum_{f=d,s,b} \frac{m_f}{v} + \kappa_\tau \sum_{f=e,\mu,\tau} \frac{m_f}{v} \right) f\bar{f}H. \end{aligned} \quad (11.31)$$

The exact correspondence between the effective coefficients of the dimension-6 operators and the κ 's can be found for instance in Ref. [44]. In the SM, the Higgs boson does not couple to massless gauge bosons at tree level, hence $\kappa_g = \kappa_\gamma = \kappa_{Z\gamma} = 0$. Nonetheless, the contact operators are generated radiatively by SM particles loops. In particular, the top quark gives a contribution to the 3 coefficients $\kappa_g, \kappa_\gamma, \kappa_{Z\gamma}$ that does not decouple in the infinite top mass limit. For instance, in that limit $\kappa_\gamma = \kappa_g = 1$ [23, 24, 264].

The coefficient for the contact interactions of the Higgs boson to the W and Z field strengths is not independent but obeys the relation

$$(1 - \cos^4 \theta_W) \kappa_{VV} = \sin 2\theta_W \kappa_{Z\gamma} + \sin^2 \theta_W \kappa_{\gamma\gamma}. \quad (11.32)$$

This relation is a general consequence of the custodial symmetry [265], which also imposes $\kappa_Z = \kappa_W$ at leading order ($\kappa_Z/\kappa_W - 1$ is a measure of custodial symmetry breaking and, as such, is already constrained by electroweak precision data and the bounds on anomalous gauge couplings). When the Higgs boson is part of a $SU(2)_L$ doublet, the custodial symmetry in the bosonic sector could only be broken by the $\mathcal{O}_T = \frac{1}{2} (\Phi^\dagger \overleftrightarrow{D}^\mu \Phi)^2$ operator at the level of dimension-6 operators and it is accidentally realised among the interactions with four derivatives, like the contact interactions considered.

The coefficient κ_3 can be accessed directly only through double Higgs boson production processes, hence it will remain largely unconstrained at the LHC. Before the associated production of a Higgs boson with a pair of top quarks was observed, the Higgs boson coupling to the top quark was only probed indirectly via the one-loop gluon fusion production or the radiative decay into two photons. However, these two processes are only sensitive to the combinations of couplings ($\kappa_t + \kappa_g$) and ($\kappa_t + \kappa_\gamma$) and not to the individual couplings. Therefore a deviation in the Higgs boson coupling to the top quark can in principle always be masked by new contact interactions to photons and gluons (and this is precisely what is happening in minimal incarnations of composite Higgs models [266]). The current and still limited sensitivity, of the order of 20%, in the $t\bar{t}H$ channel leaves elongated ellipses in the direction $\kappa_g = \kappa_\gamma = 1 - \kappa_t$.

The operators already bounded by EW precision data and the limits on anomalous gauge couplings modify in general the Lorentz structure of the Higgs couplings and hence induce some modifications of the kinematical differential distributions [267]. A promising way to have a direct access to the effective coefficients of these operators in Higgs physics is to study the VH associated production with a W or a Z at large invariant mass of the VH system [268]. These differential distributions could also be a way to test the hypothesis that the Higgs boson belongs to a $SU(2)_L$ doublet together with the longitudinal components of the massive electroweak gauge bosons.

ii. Interpretations of the experimental data

The measurements of the coupling properties of the Higgs boson are entirely based on the formalism of the effective Lagrangian described above. Measurements of coupling properties in this framework implies assessing the parameters of the model Eq. (11.31) or combinations of these parameters with different sets of assumptions.

These measurements are carried out with the combination framework described in Section 11.4, where the μ_i and μ_f signal strength parameters are further interpreted in terms of modifiers of the SM couplings κ_k where $k \in \{Z, W, f, g, \gamma, Z\gamma\}$ as in Eq. (11.31). The number of signal events per category for the various production modes are typically estimated at higher orders in the analyses but are scaled by these single LO-inspired factors, thus not taking into account possible intricacies and correlations of these parameters through the higher-order corrections. This approximation is valid within the level of precision of current results and their compatibility with the SM expectation.

In this formalism, further assumptions are explicitly made: (i) the signals observed in the different search channels originate from a single narrow resonance with a mass of 125 GeV; (ii) similarly to the combination described in Section 11.4, the narrow width approximation is assumed (to allow the decomposition of signal yields into products of production and decay signal strengths); (iii) the tensor structure of the couplings is assumed to be the same as that of a SM Higgs boson. This means in particular that the observed state is assumed to be a CP -even scalar as in the SM.

Loop-level couplings such as the $gg \rightarrow H$, $H \rightarrow \gamma\gamma$ and $H \rightarrow Z\gamma$ can either be treated effectively, with κ_g, κ_γ and $\kappa_{Z\gamma}$ as free parameters in the fit or these parameters can be expressed in terms of the know SM field content and as a function of the SM coupling modifiers, in the following way [269]:

$$\begin{aligned} \kappa_g^2(\kappa_t, \kappa_b, \kappa_c) = & 1.042 \kappa_t^2 - 0.040 \kappa_t \kappa_b + 0.002 \kappa_b^2 \\ & - 0.005 \kappa_t \kappa_c + 0.0005 \kappa_b \kappa_c + 0.00002 \kappa_c^2, \\ \kappa_\gamma^2(\kappa_F, \kappa_V) = & 1.59 \kappa_V^2 - 0.66 \kappa_V \kappa_F + 0.07 \kappa_F^2, \\ \kappa_{Z\gamma}^2(\kappa_F, \kappa_V) = & 1.12 \kappa_V^2 - 0.15 \kappa_V \kappa_F + 0.03 \kappa_F^2. \end{aligned} \quad (11.33)$$

The $\kappa_{Z\gamma}$ parametrisation has been used only in the ATLAS Run 1 combined measurements of the coupling properties of the Higgs boson. The $\mu^+\mu^-$ channels is included neither in the CMS and ATLAS-CMS Run 1 combinations, nor in the ATLAS [213] Run 2 individual combination, while it is included in the CMS [214] Run 2 combination.

The parametrisations are given for a Higgs boson mass hypothesis of 125.09 GeV (and in the last two expressions, all the Higgs-fermion couplings are assumed to be rescaled by an universal multiplicative factor κ_F). It can be noted from the expression of κ_γ that the coupling of the Higgs boson to photons is dominated by the loop of W bosons, and it is affected by the top quark loop mostly through its interference with the W loop. The sensitivity of the current measurements to the relative sign of the fermion and vector boson couplings to the Higgs boson is due to this large negative interference term. The κ_g parameter is expressed in terms of the scaling of production cross sections and therefore also depends on the pp collisions centre-of-mass energy. The parametrisations of κ_γ and $\kappa_{Z\gamma}$ are obtained from the scaling of partial widths and are only dependent on the Higgs boson mass hypothesis. Experiments use a more complete parametrisation with the contributions from the b -quarks, τ -leptons in the loops [43, 244].

The global fit is then performed expressing the μ_i and μ_f parameters in terms of a limited number of κ_k parameters or their ratios, under various assumptions. The parametrisation for the main production modes are: (i) $\mu_{\text{ggF}} = \kappa_g^2$ for the gluon fusion and an effective coupling of the Higgs boson to the gluons; (ii) $\mu_{\text{VBF}, VH} = \kappa_V^2$ for the VBF and VH processes when the W and Z couplings are assumed to scale equally, and $\mu_{\text{VBF}}^2(\kappa_W, \kappa_Z) = (\kappa_W^2 \sigma_{WWH} + \kappa_Z^2 \sigma_{ZZH}) / (\sigma_{WWH} + \sigma_{ZZH})$, when the couplings to the W and Z bosons are varied independently (σ_{WWH} and

σ_{ZZH} denote the VBF cross sections via the fusion of a W and a Z boson respectively, the small interference term is neglected); (iii) $\mu_{t\bar{t}H} = \kappa_t^2$ for the $t\bar{t}H$ production mode. Numerically the production modes signal strengths as a function of the coupling modifiers to the SM fields are:

$$\begin{aligned}\mu_{\text{ggF}} &= 1.06\kappa_t^2 + 0.01\kappa_b^2 - 0.07\kappa_t\kappa_b, \quad \text{and} \\ \mu_{\text{VBF}} &= 0.74\kappa_W^2 + 0.26\kappa_Z^2.\end{aligned}\quad (11.34)$$

The decay mode signal strengths are parametrised as $\mu_k = \kappa_k^2/\kappa_H^2$ where $k \in \{Z, W, f, g, \gamma, Z\gamma\}$ denotes the decay mode and κ_H , the overall modifier of the total width that affects all the signal yields. κ_H is a priori an independent parameter. However, when it is assumed that the Higgs boson cannot decay to new particles beyond those of the SM, κ_H can also be treated as an effective parameter and expressed in terms of the coupling modifiers to the SM field content. Its general expression is:

$$\begin{aligned}\kappa_H^2 &= 0.57\kappa_b^2 + 0.06\kappa_\tau^2 + 0.03\kappa_c^2 + 0.22\kappa_W^2 + 0.03\kappa_Z^2 + 0.09\kappa_g^2 \\ &\quad + 0.0023\kappa_\gamma^2.\end{aligned}\quad (11.35)$$

The general expression of the total width of the Higgs boson can be written as follows:

$$\Gamma_H = \frac{\kappa_H^2 \Gamma_H^{\text{SM}}}{1 - \text{BR}_{\text{BSM}}}\quad (11.36)$$

where Γ_H^{SM} is the total width of the SM Higgs boson and BR_{BSM} is the branching fraction of the Higgs boson to new particles beyond the SM.

Specific parametrisations will be made in order to address the following aspects of the coupling properties of the Higgs boson under different assumptions: (i) the relative couplings of the Higgs boson to fermions and bosons; (ii) the potential impact of the presence of new particles beyond the SM either in the loops or both in the loops and the decay of the H ; and (iii) also, more general models either of coupling modifiers or their ratios, under different assumptions.

iii. Couplings to bosons and fermions

As it will be discussed in Section 11.7.6.3, it is interesting to probe a model where no additional field content is considered in the decay width of the Higgs boson and where the relative couplings of the Higgs boson to W - and Z -bosons is fixed to its SM value, i.e., $\kappa_W = \kappa_Z$, and where all Yukawa couplings scale with one coupling modifier. In this model, only the SM particles are assumed to contribute to the gluon fusion and the diphoton loops, and all fermion couplings modifiers are required to scale simultaneously with a unique factor κ_F while all vector boson couplings modifiers also scale with a common factor κ_V . It is a two-parameter fit with κ_V and κ_F as free variables of interest. The ATLAS-CMS combined results for each channel independently, the combinations of all channels for the two experiments separately and the results of the overall combination are all shown in Fig. 11.12.

The global fit is only sensitive to the relative sign of κ_V and κ_F . By convention, either κ_F or κ_V can be considered positive and negative values of κ_V or κ_F respectively can be considered. Such values are not excluded a priori, but would imply the existence of new physics at a light scale and would also raise questions about the validity of the perturbative treatment of the SM deformations and also about the stability of the vacuum [271]. Among the five main Higgs boson decay channels, only the $\gamma\gamma$ is sensitive to the sign of κ_F (or κ_V) through the interference of the W and t loops as shown in Eq. (11.33). The current global fit disfavors a negative value of κ_F at more than five standard deviations. A specific analysis for the Higgs boson production in association with a single top quark has been proposed in order to more directly probe the sign of κ_F (see references in Ref. [123]). All available experimental data show a fair agreement of the SM prediction of the couplings of the Higgs boson to fermions and gauge bosons. The results shown in Fig. 11.12 assume that $\kappa_F \geq 0$, however, in Ref. [141], a similar combination is done without this assumption.

The observed exclusion is fully compatible with the SM expectation. The ATLAS and CMS combined measurements with the Run 1 dataset lead to

$$\kappa_V = 1.04 \pm 0.05 \quad \text{and} \quad \kappa_F = 0.98_{-0.10}^{+0.11}, \quad (11.37)$$

and were already at an impressive 5% level of accuracy for the κ_V parameter. The ATLAS Run 2 combination yielded:

$$\kappa_V = 1.05 \pm 0.04 \quad \text{and} \quad \kappa_F = 1.05 \pm 0.09. \quad (11.38)$$

And the results for the CMS Run 2 are reported as likelihood contours shown in Fig. 11.12.

iv. Probing new physics in the loops (and the decay)

A more constrained model fully focussing on BSM scenarios with new heavy particles contributing to the loops and where all couplings to the SM particles are assumed to be the same as in the SM ($\kappa_W = \kappa_Z = \kappa_t = \kappa_b = \kappa_\tau = 1$) is also used to constrain the κ_g and κ_γ parameters only. In this model, it can be assumed that the new physics affecting the loops are either introducing new decay channels (i.e., BR_{BSM} allowed to vary in the fit) or not (i.e., $\text{BR}_{\text{BSM}} = 0$). In the two cases, the results on the couplings through loops (to gluons and photons) do not change significantly. The constraints on BR_{BSM} will be discussed in the next section, while here the focus will be on the effective couplings of the Higgs boson to gluons and photons. The contours of the combined likelihood in the $(\kappa_\gamma, \kappa_g)$ plane for the ATLAS and CMS experiments and their combination are shown in Fig. 11.13. The measured values of these parameters for the ATLAS and CMS Run 1 combination are:

$$\kappa_g = 0.78_{-0.10}^{+0.13} \quad \text{and} \quad \kappa_\gamma = 0.87_{-0.09}^{+0.14}. \quad (11.39)$$

At Run 2, the ATLAS combination yielded:

$$\kappa_g = 1.03_{-0.06}^{+0.07} \quad \text{and} \quad \kappa_\gamma = 1.00 \pm 0.06. \quad (11.40)$$

The CMS results are reported as likelihood contours in the $(\kappa_g, \kappa_\gamma)$ plane only, as shown in Fig. 11.13.

In this model as well, all results are fully compatible with the SM expectations.

v. Coupling measurements and probing BSM physics in loops and in the decay

In the models described above, it was either assumed that no new latent BSM degree of freedom distorts neither the loop-induced Higgs boson couplings to gluons and photons nor the total Higgs boson width, or that all tree level couplings to SM particles are SM-like. These assumptions can be relaxed.

In order to probe simultaneously the Higgs boson couplings to massive and massless particles, only the assumption $\text{BR}_{\text{BSM}} = 0$ is kept. The couplings to photons and gluons are then parametrised by independent effective couplings, κ_g and κ_γ , and κ_Z , κ_W , κ_t , $|\kappa_\tau|$, and $|\kappa_b|$ are measured simultaneously. The absolute values of certain coupling modifiers only indicate the degeneracy of combined likelihood for the two signs. It can be noted that when the coupling to gluons is not considered effective, there is some sensitivity to the sign of κ_b through the interference between the top- and bottom-quark loops in the gluon fusion process. In this analysis, the constraint on the top quark Yukawa coupling comes from the $t\bar{t}H$ direct search channels only. The complete set of results from this model is given in Table 11.12 for the ATLAS-CMS combination using the full Run 1 dataset [270] and for the ATLAS [213] and CMS [214] individual combinations using partial Run 2 datasets. Figure 11.14 also displays the results of the individual ATLAS and CMS combinations. A negative relative sign is allowed for the κ_W and κ_Z parameters without loss of generality. This convention is used in the ATLAS and CMS Run 1 combination and in the CMS Run 2 combination. Neglecting the very small interference between the W and Z exchanges in the VBF production and when treating the photon and gluon couplings as effective, the sensitivity to the negative signs of the

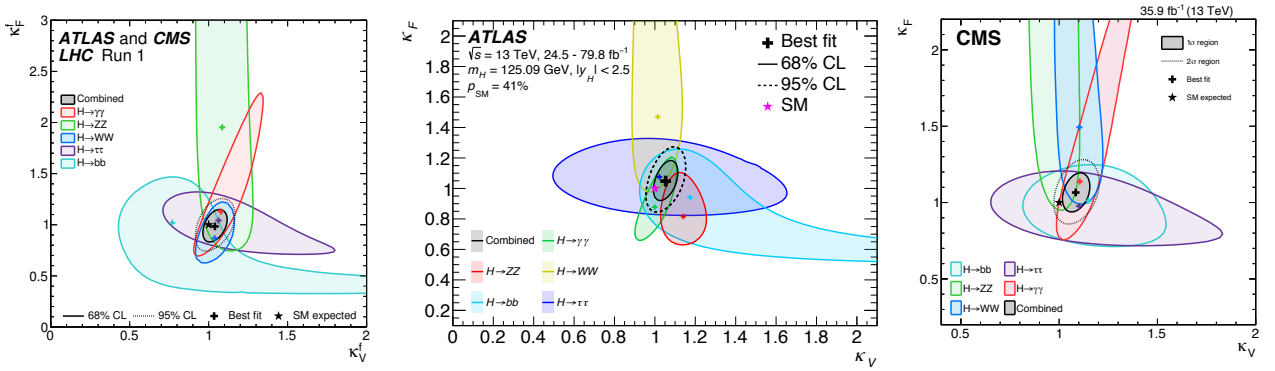


Figure 11.12: Likelihood contours in the (κ_F, κ_V) plane for the ATLAS-CMS Run 1 combination [270] (left) and the ATLAS [213] (center) and CMS [214] (right) individual Run 2 combinations.

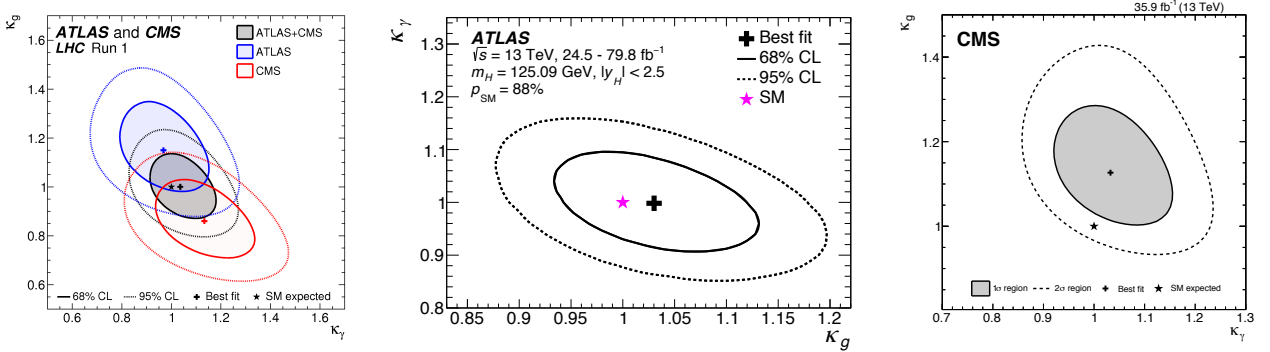


Figure 11.13: Likelihood contours in the $(\kappa_g, \kappa_\gamma)$ plane for the ATLAS-CMS [270] combination (left) and for the ATLAS [213] (center) and CMS [214] (right) individual Run 2 combinations.

couplings of the Higgs boson to the W and the top quark and that of the Z to the gluon come respectively from the tH and the $ggHZ$ production processes. In the case of the ATLAS Run 2 combination, only a relative negative sign of the coupling of the Higgs boson to the top quark is allowed. The cases reported in Table 11.12 of negative values of the couplings correspond to *quasi*-degenerate cases and the choice of sign is therefore not significant. For instance, the negative value of κ_W obtained by CMS in its Run 2 combination is due to tH contribution to the $t\bar{t}H$ channels as the specific tH analyses described in Section 11.3.3 are not included in the combination.

It is interesting to note that, with a partial Run 2 dataset, the sensitivity of individual experiments is already better than the one obtained at Run 1. This is in large part due to the improved systematic uncertainties related to the predictions of the Higgs boson production and decay that have been discussed in Section 11.2.

The results above are obtained under the assumption that the Higgs boson decays only to SM particles. This assumption is necessary since the signal rates cannot resolve separately κ_H and the absolute couplings of the Higgs boson to the SM particles. This degeneracy can, however, be resolved using an independent constraint on the Higgs boson width as the one derived from off-shell couplings measurements. This approach was used by the ATLAS experiment (see references in Ref. [123]), thus yielding a priori an absolute measurement of the couplings of the Higgs boson. The validity of the results obtained still relies on assumptions that have been discussed in Section 11.5.2. Another well-motivated assumption to resolve the aforementioned degeneracy preventing the determination of κ_H is inspired by unitarity conditions. Requiring that $\kappa_V \leq 1$ allows to free the BR_{BSM} parameter and further probe new physics in the decay of the Higgs boson. An intuitive understanding of how this constraint works can be given by a simple example. In the VBF $H \rightarrow W^+W^-$ channel, the number of signal events compared to the SM prediction is rescaled by $(1 - \text{BR}_{\text{BSM}})\kappa_W^4/\kappa_H^2$, and, an observed signal close to the SM expectation cannot accommodate a large value of

BR_{BSM} since the depletion factor $(1 - \text{BR}_{\text{BSM}})$ cannot be compensated by an enhanced value $\kappa_W > 1$. Or, in other terms, if $\kappa_W \sim 1$ is preferred from other channels, a low signal in the VBF $H \rightarrow W^+W^-$ channel would be a sign of the presence of BSM physics in the Higgs boson decays. Within this framework, all the Higgs boson couplings to massive and massless SM particles can be measured in addition to BR_{BSM} . The results of this combination are shown in Fig. 11.14 (left). The results for all parameters do not change significantly with respect to the previous fit that assumed $\text{BR}_{\text{BSM}} = 0$. But a 95% CL bound on this parameter can now be obtained:

$$\text{BR}_{\text{BSM}} < 34\% \text{ (ATLAS)}, \quad \text{BR}_{\text{BSM}} < 38\% \text{ (CMS)}. \quad (11.41)$$

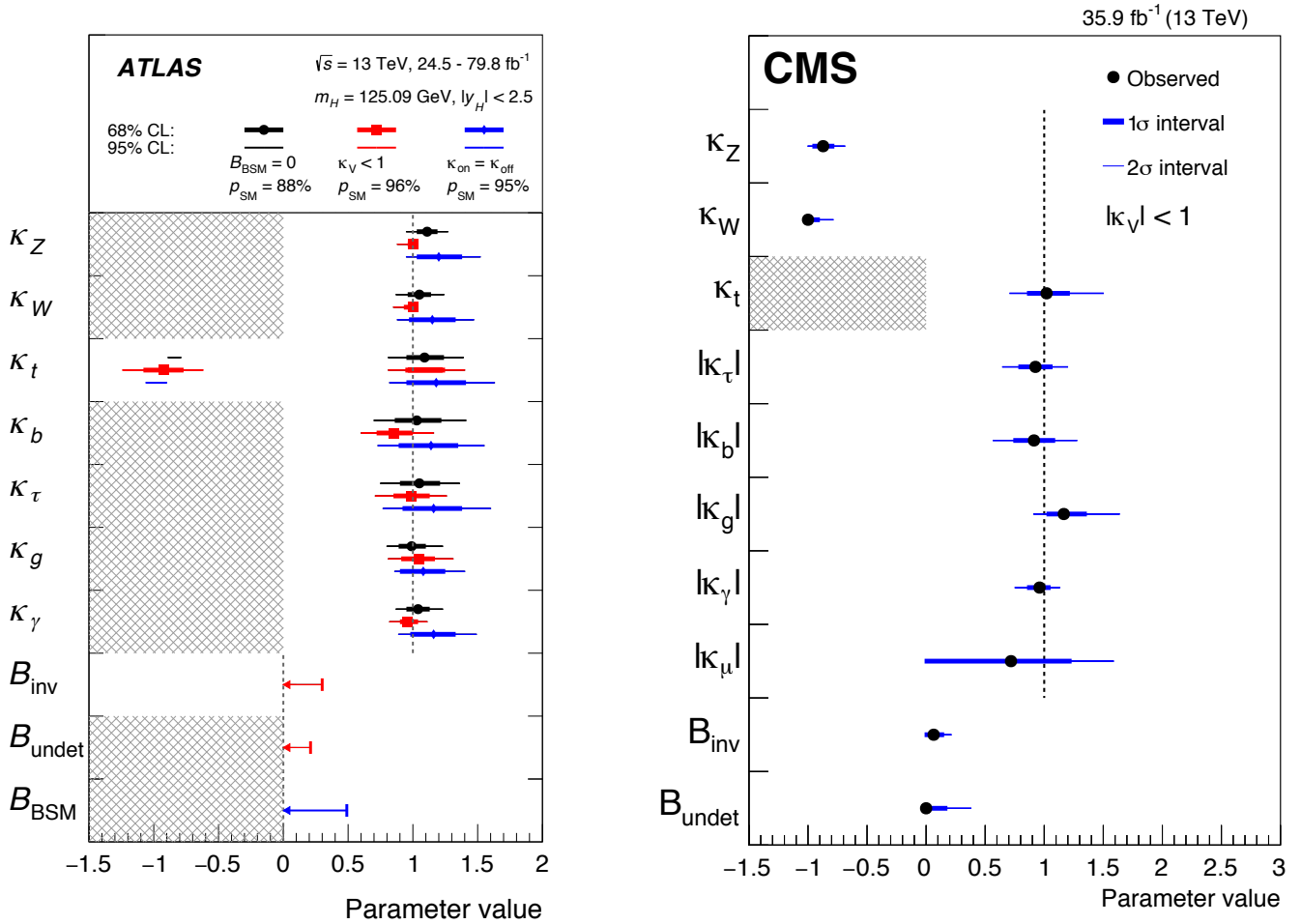
Both ATLAS and CMS in their Run 2 combinations have included the search for invisible decays of the Higgs boson [213, 214], described in Section 11.3. This allows for a coherent interpretation of the constraints on invisible decays and the measurements in the visible channels as well as simultaneously constraining BR_{inv} and the overall branching fraction to potentially “visible” particles but to which none of the considered measurements are sensitive, as for example Higgs boson decays to light quarks or BSM particles decaying subsequently mainly to light quarks (BR_{und} referred to as branching fraction to undetected particles). The limits obtained on the invisible branching fractions are:

$$\text{BR}_{\text{inv}} < 30\% \text{ (ATLAS)}, \quad \text{BR}_{\text{inv}} < 22\% \text{ (CMS)}. \quad (11.42)$$

Models which are less sensitive to modelling systematic uncertainties and requiring no constraints on the natural width of the Higgs bosons have been considered, either through the ratio of cross section and branching ratios (see results in Ref. [123]) or through a more generic approach to avoid the degeneracy in the measurement of the coupling modifiers, probing the coupling properties of the Higgs boson through ratio of couplings. In the latter model, the cross section times branching fraction of the $gg \rightarrow H \rightarrow ZZ$ process is parametrised as a function of a single

Table 11.12: Coupling modifier combined measurements assuming the absence of perceptible new physics in the decay of the Higgs boson. No assumption is made for the loop level couplings of the Higgs boson to gluons and photons which are considered as effective.

	LHC Run 1	ATLAS Run 2	CMS Run 2	HL-LHC (expected)
κ_γ	$0.87^{+0.14}_{-0.09}$	1.05 ± 0.09	$1.07^{+0.10+0.09}_{-0.14-0.05}$	1.8%
κ_W	$0.87^{+0.13}_{-0.09}$	1.05 ± 0.09	$-1.13^{+0.15+0.06}_{-0.10-0.08}$	1.7%
κ_Z	-0.98 ± 0.10	1.11 ± 0.08	$1.00^{+0.09+0.06}_{-0.09-0.07}$	1.5%
κ_g	$0.78^{+0.13}_{-0.10}$	$0.99^{+0.11}_{-0.10}$	$1.18^{+0.10+0.12}_{-0.09-0.10}$	2.5%
κ_t	$1.40^{+0.24}_{-0.21}$	$1.09^{+0.15}_{-0.14}$	$0.98^{+0.08+0.12}_{-0.08-0.11}$	3.4%
κ_b	$0.49^{+0.27}_{-0.15}$	$1.03^{+0.19}_{-0.18}$	$1.17^{+0.18+0.20}_{-0.29-0.10}$	3.7%
κ_τ	$0.84^{+0.15}_{-0.11}$	$1.05^{+0.16}_{-0.15}$	$0.80^{+0.56+0.17}_{-0.81-0.00}$	1.9%

Figure 11.14: ATLAS [213] (left) and CMS [214] (right) combined measurements of coupling modifiers in the $\kappa_V < 1$ scenario, and in the case of the ATLAS measurements with the assumption $\text{BR}_{\text{BSM}} = 0$ and using the off-shell Higgs measurements.

coupling modifier:

$$\kappa_{gZ} = \kappa_g \times \frac{\kappa_Z}{\kappa_H} \quad (11.43)$$

Then all combination signals can be parametrised with the following ratios of coupling modifiers: (i) the $\lambda_{Zg} = \kappa_Z/\kappa_g$ ratio which is mainly probed by the measurements of the VBF and ZH production; (ii) the $\lambda_{tg} = \kappa_t/\kappa_g$ ratio constrained by the $t\bar{t}H$ production process; (iii) the $\lambda_{WZ} = \kappa_W/\kappa_Z$ ratio mainly probed by the WW and ZZ decay modes; (iv) the $\lambda_{\tau Z} = \kappa_\tau/\kappa_Z$ ratio constrained by the $\tau^+\tau^-$ channel; (v) the $\lambda_{bZ} = \kappa_b/\kappa_Z$ ratio probed mainly by the $VH(b\bar{b})$ channels; and (vi) the $\lambda_{\gamma Z} = \kappa_\gamma/\kappa_Z$ ratio constrained by the diphoton channel. In this parametrisation, the

ZZ channel plays an important normalisation role (the results are discussed in detail in the previous edition of this review [123]).

11.6.2.2 Differential cross sections

To further characterise the production and decay properties of the Higgs boson, with the increase in size of the LHC datasets, measurements of fiducial and differential cross sections are being carried out by ATLAS and CMS both at Run 1 (the references can be found in the previous edition of this review [123]) and Run 2 [260, 272] and in several channels: (i) the diphoton, (ii) the four leptons, and (iii) the WW channels.

The definition of a fiducial volume as close as possible to the reconstruction level selection criteria is very important as it will

minimise the model dependence from possible variations in the signal reconstruction efficiencies. Minimising model dependence of unfolded fiducial differential cross section measurements is also key to ensure their usefulness to further probe and tune more accurate models in the future.

As an example in the diphoton channel for the ATLAS Run 1 analysis (similar criteria are used at Run 2 and by CMS), the selection criteria defining the fiducial volume are the following: the two highest transverse momentum (E_T), isolated final state photons, within $|\eta| < 2.37$ and with $105 \text{ GeV} < M_{\gamma\gamma} < 160 \text{ GeV}$ are selected (the transition region between the barrel and end-cap calorimeters is not removed); after the pair is selected, the same cut on $E_T/M_{\gamma\gamma}$ as in the event selection, i.e., in excess of 0.35 (0.25) for the two photons is applied. The requirement of the isolation of the photon to define the fiducial volume is particularly important to avoid potentially large variations of the reconstruction efficiency within this volume for production processes as different as the gluon fusion and $t\bar{t}H$.

While strict fiducial requirements are key to minimise model dependence, these make combinations of decay channels impossible. To gain precision in the measurement of the production properties of the Higgs boson, the fiducial volume defined on the decay products of the Higgs boson can be removed and channels can be combined relying on the extrapolation from the reconstruction acceptance using Monte Carlo simulations. This has been used to combine differential cross section for instance in the transverse momentum of the Higgs boson. Such hybrid approaches are also discussed in Section 11.6.2.4.

A large number of observables have been studied aiming at probing the accuracy of the modelling of the Higgs boson production simulations. Some examples include (i) the transverse momentum and pseudo rapidity of the objects, such as jets or leptons, produced in association with the Higgs boson in several modes, the principal distributions of the Higgs boson decay products such for instance in the diphoton channel; (ii) the production angle in the Collins–Soper frame [225] in the diphoton channel; (iii) the overall distribution of the Higgs boson transverse momentum.

The measured differential cross section in the Higgs boson transverse momentum by ATLAS and CMS using the full Run 2 datasets are illustrated in Fig. 11.15.

11.6.2.3 Constraints on non-SM Higgs boson interactions in an effective Lagrangian

An example of the possible use of differential cross sections in constraining non-SM Higgs boson couplings in an EFT is given by ATLAS [273]. In this analysis, differential cross section measured in the diphoton channel are used to constrain an effective Lagrangian where the SM is supplemented by dimension six CP -even operators of the Strongly Interacting Light Higgs (SILH) formulation [248] and corresponding CP -odd operators. The diphoton differential cross sections are mainly sensitive to the operators that affect the Higgs boson interactions with gauge bosons. CMS has also recently analysed [260] the Higgs boson transverse momentum distribution to constrain the Higgs boson couplings to top, bottom, and charm quarks as well as the effective coupling to gluons. This analysis is, however, not performed in an EFT framework.

The differential distributions used in this combination are: (i) the transverse momentum of the Higgs boson, (ii) the number of reconstructed jets produced in association with the diphoton pair, (iii) the invariant mass of the diphoton system and (iv) the difference in azimuthal angle of the leading and sub-leading jets in events with two or more jets. This analysis shows how differential information significantly improves the sensitivity to dimension-6 operators.

11.6.2.4 Simplified Template Cross Sections (STXS)

An overarching subject of discussion between the theory and experimental communities in the field of Higgs physics has been how experimentalists could best communicate their results for them to be most efficiently used by others for further interpretation.

In the field of precision SM measurements, the commonly used practise is that results are given at particle level within a well

defined fiducial volume of phase space. The fiducial volume is usually defined close enough to the experimental reconstruction to minimise the possible variations of the reconstruction efficiency within the particle level fiducial volume. In this way, results minimise their dependence on theoretical uncertainties.

ATLAS and CMS have produced fiducial and unfolded cross sections based on all objects reconstructed in the events. These measurements could be used for further interpretation. However, performing a proper combination of channels taking into account all experimental systematic uncertainties is non trivial. A proposal [44, 274] was made by the LHC Higgs Cross Section Working Group to produce results in each decay channel with a well defined fiducial phase space of the Higgs boson (and not its decay products) and for other associated objects pertaining to all channels, such as jets and missing transverse momentum (MET). The definition of the fiducial regions is motivated by maximising the experimental sensitivity, isolating possible BSM effects, and minimising the dependence on theoretical uncertainties. The number of regions is also minimised to avoid the loss of experimental sensitivity. The observables that are measured in this approach are still the standard production cross sections (the gluon fusion, the vector boson fusion, the VH and $t\bar{t}H$ associated production modes) within the defined fiducial volumes.

In summary, this approach is hybrid. It is fiducial on specific objects to reduce the theory dependence and inclusive in the Higgs kinematics in order to allow for a more straightforward combination. This approach also allows the use of multivariate techniques to enhance the sensitivity within given fiducial regions, at the expense of a greater extrapolation and therefore increased model dependence.

The currently used Simplified Template Cross Sections (STXS) scheme covers, with a limited number of bins, the ggF process in four categories in number of jets (0, 1, 2 and 2 VBF-like jets, where VBF-like means a selection of two high invariant mass jets with large pseudo rapidity difference) further subdivided in four transverse momentum categories covering the full spectrum with the last bin being inclusive for $p_T > 200 \text{ GeV}$. The VH process is subdivided two categories depending on the number of reconstructed charged leptons corresponding to the decays of either a W boson or a Z boson, and two bins in transverse momentum. VBF and hadronic VH categories are defined using jet cuts and two bins in transverse momentum.

Measurements in this framework have been made in various decay channels. The first measurements have been performed in the main Higgs boson discovery channels. ATLAS has produced measurements of the diphoton and the 4ℓ channels with Run 2 data [125, 227, 236, 275, 276]. And full Run 2 results are available for the $H \rightarrow 4\ell$ channel from ATLAS [131] and CMS [277].

CMS has carried out a measurement of the STXS in the $H \rightarrow \tau^+\tau^-$ decay channel targeting the high transverse momentum of the Higgs boson [145], in particular in the channel where the Higgs boson is produced with one jet of transverse energy in excess of 200 GeV.

ATLAS [149] has made a measurement of the STXS aiming at the VH production mode in the $H \rightarrow b\bar{b}$ decay mode at high transverse momentum of the vector boson above 250 GeV, where the discrimination of the background further increases.

A combination of STXS across decay channels has also been carried out by ATLAS with a dataset corresponding to an integrated luminosity of up to 80 fb^{-1} [213].

11.6.2.5 Indirect constraints on the Higgs boson couplings

The direct measurements at the LHC provide direct probes of the Higgs boson couplings to the vector bosons (photons, W , Z and gluons) and to a limited number of Yukawa couplings to fermions. Currently these include essentially the third generation fermions – tau leptons, bottom and top quarks. For the High-Luminosity run, prospective studies [104] have shown that a good precision will be reached in the measurement of the coupling of the Higgs boson to muons and an evidence of the Higgs boson trilinear self-coupling with a precision of the order of 50% can be achieved. For the couplings of the Higgs boson to the other light SM fermions, direct evidences will be hard to reach at the LHC. However, from the measurements of the main observed Higgs final

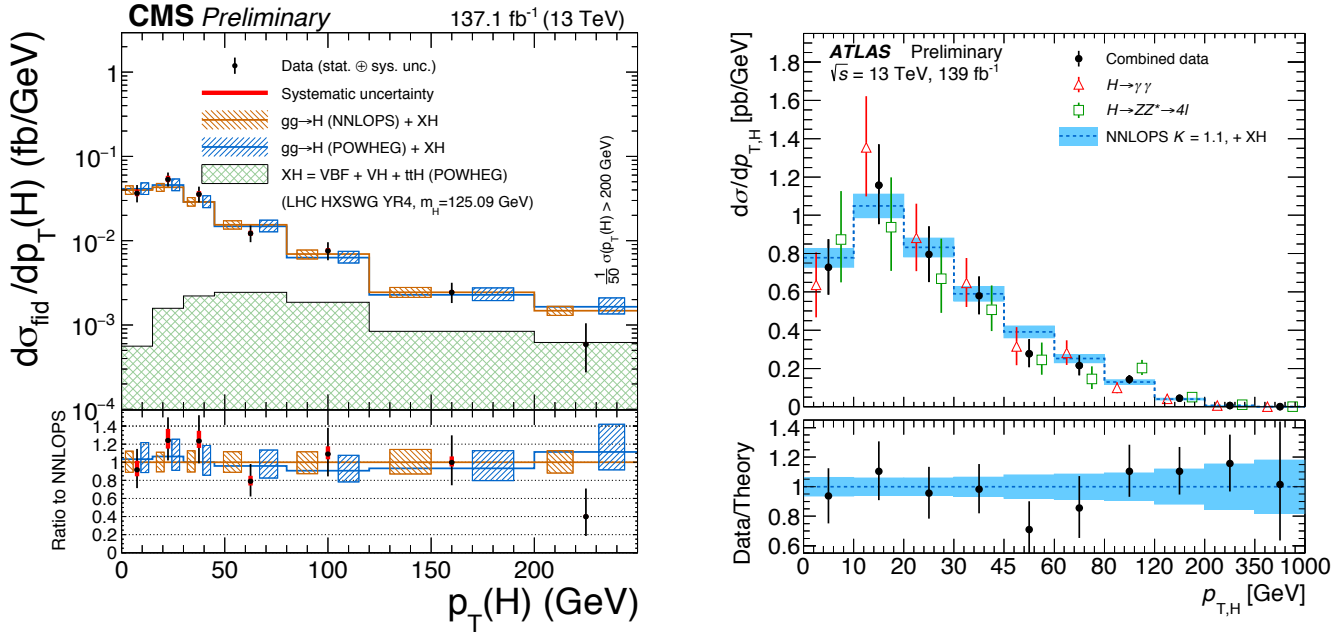


Figure 11.15: (Left) Fiducial differential, closely matching the reconstruction level selections, cross sections in Higgs boson transverse momentum in the $H \rightarrow 4\ell$ channel from the CMS experiment [126]. (Right) Partially fiducial combined cross sections using the $H \rightarrow \gamma\gamma$ and $H \rightarrow 4\ell$ channels from the ATLAS experiment [272].

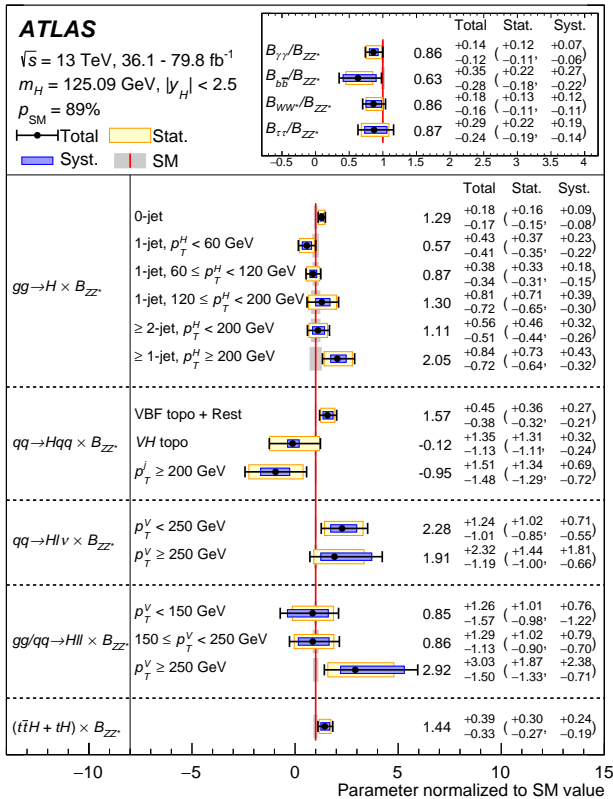


Figure 11.16: Simultaneous measurement of the simplified template cross sections times the branching fraction $\text{BR}(H \rightarrow ZZ)$ (normalised to their Standard Model expectations) and the ratios of branching fractions $\text{BR}(f)/\text{BR}(ZZ)$ [213].

states, it is possible to constrain specific couplings through their radiative corrections to dominant processes. Two prime examples are: (i) the trilinear self-coupling can be constrained through loop corrections to the single Higgs boson production [278–280], see the interpretation carried out by ATLAS of the combination of

the main decay channels [281]; (ii) the charm Yukawa coupling can be constrained from the differential cross section in Higgs boson transverse momentum [282], see the ATLAS [283] and CMS [260] analyses in the diphoton channel. These indirect constraints, however, require assumptions on the possible variations of all the other couplings.

ATLAS has also performed a preliminary combination of the single Higgs boson production measurements [284], using the approach and parametrisations of Ref. [279], which yield the following constraint:

$$-3.2 < \kappa_\lambda < 11.9. \quad (11.44)$$

When combined with results of the double Higgs boson production searches, the following combined constraint on the Higgs boson trilinear coupling yields:

$$-2.3 < \kappa_\lambda < 10.3 \text{ (obs)} \quad [-5.1 < \kappa_\lambda < 11.2 \text{ (exp)}]. \quad (11.45)$$

The *direct* and *indirect* constraints on the Higgs boson trilinear self-coupling are currently of similar strength. The double Higgs boson measurements are dominated by statistical uncertainties and are expected to improve much more rapidly than the precision on single Higgs boson measurements. Furthermore, it should be stressed that the constraints on the trilinear self-coupling obtained via the NLO fit of single Higgs boson data are less robust and more model-dependent since the NLO effects induced by a shift of the trilinear self-coupling compete with possible LO effects sourced by the deviations of the Higgs boson couplings to the other SM particles. The different effects can be disentangled by the measurements of various kinematical differential distributions in addition to the study of the inclusive rates [285], but the expected sensitivity in such global fits is not as promising as the one obtained when only the Higgs boson self-coupling is allowed to deviate from its SM value [286].

11.7 New physics models of EWSB in the light of the Higgs boson discovery

The discovery of a light scalar with couplings to gauge bosons and fermions that are consistent with SM predictions, together with the slow running of the Higgs boson self-coupling at high energies allow one to consider the SM as a valid perturbative description of nature all the way to the Planck scale. This picture is admittedly very attractive, but it posits that the Higgs boson

is an elementary scalar field, whose mass has quantum sensitivity to possible new physics scales. This EW/Higgs naturalness problem [6] has become much more definite after the Higgs boson discovery.

There are two broad classes of models addressing the naturalness problem⁵. One is based on SUSY [7] (for recent reviews, see Refs. [8, 9]). This is a weakly coupled approach to EWSB, maintaining the perturbativity of the SM, and, the Higgs boson remains elementary and the corrections to its mass are screened at the scale at which SUSY is broken so the value of the weak scale remains insensitive to the details of the physics at higher scales. These theories predict at least three neutral Higgs particles and a pair of charged Higgs particles [25]. One of the neutral Higgs bosons, most often the lightest CP -even one, has properties that could resemble those of the SM Higgs boson (at least in some regions of the parameter space). It is referred to as a SM-like Higgs boson, meaning that its couplings are close to the ones predicted in the SM. The other approach invokes the existence of strong interactions at a scale of the order of one TeV or above and these new interactions induce the breaking of the electroweak symmetry [288]. In the original incarnation, dubbed technicolor, the strong interactions themselves trigger EWSB without the need of a Higgs boson. Another possibility, more compatible with the ATLAS and CMS discovery, is that the strong interactions produce four light resonances identified with the Higgs doublet and EWSB proceeds through vacuum misalignment [10] (see Refs. [11, 12] for recent reviews). In that case, the Higgs boson itself has a finite size and thus never feels the UV degrees of freedom that would otherwise have dragged its mass to much higher scales. The Higgs boson could also correspond to the Goldstone boson associated with the spontaneous breaking of scale invariance, see Ref. [289] and references therein. However, this dilaton/radion scenario now requires a jumbled model-building to be consistent with the constraints from the coupling measurements. All these BSM scenarios can have important effects on the phenomenology of the Higgs boson. Also, in each case, the role of the Higgs boson in the unitarisation of scattering amplitudes is shared by other particles which remain targets of experimental searches.

The realisation of SUSY at low energies has many good qualities that render it attractive as a model of new physics. First of all since, for every SM degree of freedom, there is a superpartner of different spin but of equal mass and effective coupling to the SM-like Higgs boson, in the case of exact SUSY, an automatic cancellation of quantum corrections to the Higgs mass parameter holds. In practice, it is known that SUSY must be broken since no superpartners of the SM particles have been observed so far. The mass difference between the precise value of the mass of any particle and that of its corresponding superpartner is proportional to the correlated soft SUSY breaking parameter, generically called M_{SUSY} . The quantum corrections to the Higgs boson mass parameter are proportional to M_{SUSY}^2 , and provided M_{SUSY} is of order of a few TeV, the low energy mass parameters of the Higgs sector become insensitive to physics at the GUT or Planck scale. Another interesting feature of SUSY theories is related to the dynamical generation of EWSB [290]. In the SM, a negative Higgs mass parameter, m^2 , needs to be inserted by hand to induce EWSB, see Eq. (11.1). In SUSY, instead, even if the relevant Higgs mass parameter is positive in the ultraviolet, it may become negative and induce EWSB radiatively through the strong effect of the top quark-Higgs boson coupling in its renormalisation group evolution [290].

In the following, the Higgs sector will be explored in specific SUSY models. In all of them, it is often possible to find regions of the parameter space that accommodate one neutral Higgs boson with properties that resemble those of the SM Higgs boson, whereas additional neutral and charged Higgs bosons are also predicted and are intensively being sought for at the LHC (see Section 11.7.7). In the simplest SUSY model, accommodating a SM-like Higgs boson mass of about 125 GeV results in constraints on the stop sector, with at least one stop mass in the few TeV

mass range. In non-minimal SUSY extensions of the SM (details and related references can be found in the previous edition of this review [123]), a SM-like Higgs boson with mass of 125 GeV can be accommodated with less restrictions on the stop sector. While naturalness dictates relatively light stops and - at the two loop level - also gluinos, the first and second generation of squarks and sleptons couple weakly to the Higgs sector and may be heavy. Moreover, small values of the μ parameter and therefore light Higgsinos, the fermionic superpartners of the Higgs bosons, would be a signature of a natural realization of electroweak symmetry breaking [291]. Such SUSY spectra, consisting of TeV range stop masses and light Higgsinos, continue to be under intense scrutiny by the experimental collaborations [292] in order to understand if such natural SUSY scenarios endure and can explain why the Higgs boson remains light.

In the context of weakly coupled models of EWSB, one can also consider multiple Higgs $SU(2)_L$ doublets as well as additional Higgs singlets, triplets or even more complicated multiplet structures, with or without low energy SUSY. In general, for such models, one needs to take into account experimental constraints from precision measurements and flavour changing neutral currents. The LHC signatures of such extended Higgs sectors are largely shaped by the role of the exotic scalar fields in EWSB.

The idea that the Higgs boson itself could be a composite bound state emerging from a new strongly-coupled sector has been reconsidered thanks to the insights gained from the AdS/CFT duality. The composite Higgs boson idea is an incarnation of EWSB via strong dynamics that smoothly interpolates between the standard technicolor approach and the true SM limit. To avoid the usual conflict with EW data, it is sufficient, if not necessary, that a mass gap separates the Higgs resonance from the other resonances of the strong sector. Such a mass gap can naturally follow from dynamics if the strongly-interacting sector exhibits a global symmetry, G , broken dynamically to a subgroup H at the scale f , such that, in addition to the three Nambu-Goldstone bosons of $SO(4)/SO(3)$ that describe the longitudinal components of the massive W and Z , the coset G/H contains a fourth Nambu-Goldstone boson that can be identified with the physical Higgs boson. Simple examples of such a coset are $SU(3)/SU(2)$ or $SO(5)/SO(4)$, the latter being favoured since it is invariant under the custodial symmetry. It is also possible to have non-minimal custodial cosets with extra Goldstone bosons leading to additional Higgs bosons in the spectrum, see for instance Ref. [293]. Modern incarnations of composite Higgs models have been recently investigated in the framework of 5D warped models where, according to the principles of the AdS/CFT correspondence, the holographic composite Higgs boson then originates from a component of a gauge field along the 5th dimension with appropriate boundary conditions.

A last crucial ingredient in the construction of viable composite Higgs boson models is the concept of partial compositeness [294], i.e., the idea that there are only linear mass mixings between elementary fields and composite states. After diagonalisation of the mass matrices, the SM particles, fermions and gauge bosons, are admixtures of elementary and composite states and thus they interact with the strong sector, and in particular with the Higgs boson, through their composite component. This setup has important consequences on the flavour properties, chiefly the suppression of large flavour changing neutral currents involving light fermions. It also plays an important role in dynamically generating a potential for the would-be Goldstone bosons. Partial compositeness also links the properties of the Higgs boson to the spectrum of the fermionic resonances, i.e., the partners of the top quark. As in the MSSM, these top partners are really the agents that trigger the EWSB and also generate the mass of the Higgs boson that otherwise would remain an exact Goldstone boson and hence massless. The bounds from the direct searches for the top partners, in addition to the usual constraints from EW precision data, force the minimal composite Higgs models into some unnatural corners of their parameter spaces [295].

11.7.1 Higgs bosons in the minimal supersymmetric standard model (MSSM)

The particle masses and interactions in a SUSY theory are uniquely defined as a function of the superpotential and the Kähler

⁵Another solution to the naturalness problem is to lower the fundamental scale of quantum gravity, like for instance in models with large extra-dimensions, see Ref. [287].

ler potential [9]. A fundamental theory of SUSY breaking, however, is unknown at this time. Nevertheless, one can parametrise the low-energy theory in terms of the most general set of soft SUSY-breaking operators [9]. The simplest realistic model of low-energy SUSY is the minimal SUSY extension of the SM (MSSM) [9, 296], that associates a SUSY partner to each gauge boson and chiral fermion of the SM, and provides a realistic model of physics at the weak scale. However, even in this minimal model with the most general set of soft SUSY-breaking terms, more than 100 new parameters are introduced. Fortunately, only a subset of these parameters impact the Higgs boson phenomenology either directly at tree-level or through quantum effects.

The MSSM contains the particle spectrum of a two-Higgs-doublet model (2HDM) extension of the SM and the corresponding SUSY partners. Two Higgs doublets, Φ_1 and Φ_2 , with hypercharge $Y = -1$ and $Y = 1$, respectively, are required to ensure an anomaly-free SUSY extension of the SM and to generate mass for down-type quarks/charged leptons (Φ_1) and up-type quarks (Φ_2) [25]. The Higgs potential reads

$$\begin{aligned}
 V = & m_1^2 \Phi_1^\dagger \Phi_1 + m_2^2 \Phi_2^\dagger \Phi_2 - m_3^2 (\Phi_1^T i \sigma_2 \Phi_2 + \text{h.c.}) \\
 & + \frac{1}{2} \lambda_1 (\Phi_1^\dagger \Phi_1)^2 + \frac{1}{2} \lambda_2 (\Phi_2^\dagger \Phi_2)^2 + \lambda_3 (\Phi_1^\dagger \Phi_1) (\Phi_2^\dagger \Phi_2) \\
 & + \lambda_4 |\Phi_1^T i \sigma_2 \Phi_2|^2 + \frac{1}{2} \lambda_5 [(\Phi_1^T i \sigma_2 \Phi_2)^2 + \text{h.c.}] \\
 & + [[\lambda_6 (\Phi_1^\dagger \Phi_1) + \lambda_7 (\Phi_2^\dagger \Phi_2)] \Phi_1^T i \sigma_2 \Phi_2 + \text{h.c.}],
 \end{aligned} \tag{11.46}$$

where $m_i^2 = \mu^2 + m_{H_i}^2$ ($i = 1, 2$), with μ being the supersymmetric Higgsino mass parameter and m_i the soft supersymmetric breaking mass parameters of the two Higgs doublets; $m_3^2 \equiv B\mu$ is associated to the B-term soft SUSY breaking parameter; and λ_i , for $i = 1$ to 7 , are all the Higgs quartic couplings.

After the spontaneous breaking of the electroweak symmetry, five physical Higgs particles are left in the MSSM spectrum: one charged Higgs pair, H^\pm , one CP -odd neutral scalar, A , and two CP -even neutral states, H and h , with h being the lightest.⁶ The Higgs sector at tree level depends on the electroweak gauge coupling constants and the vacuum expectation value v – or equivalently the Z gauge boson mass – and is determined by only two free parameters: $\tan \beta$ – the ratio of the two Higgs doublets' vacuum expectation values v_2/v_1 – and one Higgs boson mass, conventionally chosen to be the CP -odd Higgs boson mass, m_A . The other tree-level Higgs boson masses are then given in terms of these parameters. The tree level value of m_h is maximised not only for $m_A \gg m_Z$ but also for $\tan \beta \gg 1$. For $m_A \gg m_Z$ it acquires a maximum value $m_h = m_Z \cos 2\beta$.

Radiative corrections have a significant impact on the values of Higgs boson masses and couplings in the MSSM. The dominant radiative effects to the SM-like Higgs boson mass arise from the incomplete cancellation between top and scalar-top (stop) loops and at large $\tan \beta$ also from sbottom and stau loops. The stop, sbottom and stau masses and mixing angles depend on the SUSY Higgsino mass parameter μ and on the soft-SUSY-breaking parameters [9, 296]: M_Q , M_U , M_D , M_L , M_E , and A_t , A_b , A_τ . The first three of these are the left-chiral and the right-chiral top and bottom scalar quark mass parameters. The next two are the left-chiral stau/sneutrino and the right-chiral stau mass parameters, and the last three are the trilinear parameters that enter in the off-diagonal squark/slepton mixing elements: $X_t \equiv A_t - \mu \cot \beta$ and $X_{b,\tau} \equiv A_{b,\tau} - \mu \tan \beta$. At one-loop, the electroweak gauginos yield a small contribution to the Higgs boson mass, and at the two-loop level, the masses of the gluinos also enter in the calculations. Radiative corrections to the Higgs boson masses have been computed using a number of techniques, with a variety of approximations; for a discussion see for example Refs. [39, 297, 298]

⁶Observe that in the SM sections of this review, H denotes the SM Higgs boson, whereas in the sections about SUSY, or extensions of the SM with two Higgs doublets, H is used for the heaviest CP -even Higgs boson, since this is the standard notation in the literature, and the 125 GeV SM-like light Higgs boson will be denoted by h . Generically, in the MSSM, the lightest CP -even Higgs boson is indeed SM-like and thus it is naturally identified with the 125 GeV Higgs boson discovered by ATLAS and CMS, while in 2HDM extensions, with or without SUSY, there could still be lighter scalar states below 125 GeV.

and the corresponding section of the previous edition of this review [123].

The discovered SM-like Higgs boson, if interpreted as the lightest MSSM Higgs boson with a mass of about 125 GeV, provides information on the possible MSSM parameter space, see Fig. 11.17.

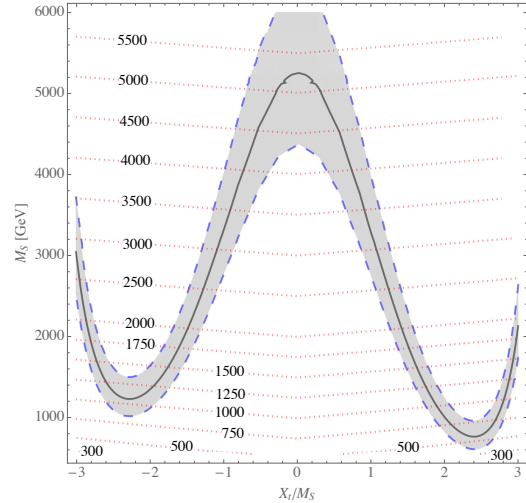


Figure 11.17: Values of the SUSY mass scale $M_{\text{SUSY}} = M_S$ versus the stop mixing parameter normalised by the SUSY mass scale X_t/M_{SUSY} , for fixed $\tan \beta = 20$, $\mu = 200$ GeV and $M_A = A_t = A_b = A_\tau = M_{\text{SUSY}}$. The solid black line corresponds to $m_h = 125$ GeV while in the grey band m_h varies by ± 1 GeV. The red dotted lines are iso-values of the stop mass. This figure is based on Ref. [299].

The phenomenology of the Higgs sector depends on the couplings of the Higgs bosons to gauge bosons and fermions. At tree-level, the couplings of the two CP -even Higgs bosons to W and Z bosons are given in terms of the angles α , that diagonalises the CP -even Higgs boson squared-mass matrix, and β

$$g_{hVV} = g_V m_V \sin(\beta - \alpha), \quad g_{HVV} = g_V m_V \cos(\beta - \alpha), \tag{11.47}$$

where $g_V \equiv 2m_V/v$, for $V = W$ or Z ($g_V m_V$ is the SM hVV coupling). Observe that in the limit $\cos(\beta - \alpha) \rightarrow 0$, the lightest CP -even Higgs boson h behaves as the SM Higgs boson. This situation is called alignment and is achieved in specific regions of parameter space for $m_A \geq m_Z$ [300] or in the large $m_A \gg m_Z$ limit, in which alignment is achieved through decoupling [300, 301]. There are no tree-level couplings of A or H^\pm to VV . The couplings of the Z boson to two neutral Higgs bosons are given by $g_{\phi AZ}(p_\phi - p_A)$, where $\phi = H$ or h , the momenta p_ϕ and p_A point into the vertex, and

$$g_{hAZ} = g_Z \cos(\beta - \alpha)/2, \quad g_{HAZ} = -g_Z \sin(\beta - \alpha)/2. \tag{11.48}$$

The expressions of the couplings between a charged Higgs boson, a neutral Higgs boson and the W boson as well as the expressions of the four-point couplings of vector bosons and Higgs bosons can be found in Ref. [25].

The tree-level Higgs boson couplings to fermions obey the following property: the neutral components of one Higgs doublet, Φ_1 , couple exclusively to down-type fermion pairs while the neutral components of the other doublet, Φ_2 , couple exclusively to up-type fermion pairs [25]. This Higgs-fermion coupling structure defines the Type-II 2HDM. In the MSSM, fermion masses are generated when both neutral Higgs components acquire a vacuum expectation value, and the relations between Yukawa couplings and fermion masses are (in third-generation notation)

$$h_{b,\tau} = \sqrt{2} m_{b,\tau} / (v \cos \beta), \quad h_t = \sqrt{2} m_t / (v \sin \beta). \tag{11.49}$$

The couplings of the neutral Higgs bosons to $f\bar{f}$, relative to their

SM values, $g m_f / (2m_W)$, are given by

$$\begin{aligned} h\bar{b}b &: -\sin\alpha/\cos\beta, & ht\bar{t} &: \cos\alpha/\sin\beta, \\ H\bar{b}b &: \cos\alpha/\cos\beta, & Ht\bar{t} &: \sin\alpha/\sin\beta, \\ A\bar{b}b &: \gamma_5 \tan\beta, & At\bar{t} &: \gamma_5 \cot\beta. \end{aligned} \quad (11.50)$$

In each relation above, the factor listed for $b\bar{b}$ also pertains to $\tau^+\tau^-$. The charged Higgs boson couplings to fermion pairs, normalised to $g/(\sqrt{2}m_W)$, are given by

$$\begin{aligned} g_{H-t\bar{b}} &: m_t \cot\beta \frac{1+\gamma_5}{2} + m_b \tan\beta \frac{1-\gamma_5}{2}, \\ g_{H-\tau+\nu} &: m_\tau \tan\beta \frac{1-\gamma_5}{2}. \end{aligned} \quad (11.51)$$

The non-standard neutral Higgs bosons have significantly enhanced couplings to down-type fermions at sizeable $\tan\beta$. Radiative corrections can modify significantly the values of the Higgs boson couplings to fermion pairs and to vector boson pairs, through a radiatively-corrected value for $\cos(\beta-\alpha)$ as well as from the one-loop vertex corrections to tree-level Higgs-fermion Yukawa couplings, see Ref. [9] and references therein, for a detailed discussion.

11.7.1.1 MSSM Higgs boson phenomenology

The MSSM parameters have to be arranged such that the mass, the CP properties, the decay and production properties of one of the neutral Higgs bosons agree with the LHC Higgs data. Given that present data allows only for moderate departures from the SM predictions, it implies that some degree of alignment is necessary.

The SM-like branching ratios of h can be modified if decays into SUSY particles are kinematically allowed, and, in particular, decays into a pair of the lightest SUSY particles – i.e., the lightest neutralinos, $\tilde{\chi}_1^0$ – can become dominant and would be invisible if R -parity is conserved [302]. Moreover, if light superpartners exist and couple to photons and/or gluons, the h loop-induced coupling to gg and $\gamma\gamma$ could deviate sizeably from the corresponding SM predictions (see for instance the review [297]), and would be in conflict with present data (see Section 11.3). For the heavier Higgs states, there are two possibilities to be considered⁷:

- i) Alignment triggered by decoupling, hence $m_A \geq$ several hundred GeV: The HWW and HZZ couplings are very small. The dominant H, A decay branching ratios strongly depend on $\tan\beta$. The decay modes $H, A \rightarrow b\bar{b}, \tau^+\tau^-$ dominate when $\tan\beta$ is large (this holds even away from decoupling). For small $\tan\beta$, the $t\bar{t}$ decay mode dominates above its kinematic threshold. For the charged Higgs boson, $H^\pm \rightarrow t\bar{b}$ dominates.
- ii) Some degree of alignment without decoupling, hence $m_A \leq$ a few hundred GeV: The main difference with the previous case is that, in the low $\tan\beta$ regime ($\tan\beta \leq 5$), additional decay channels may be allowed which involve decays into the lightest SM-like Higgs boson; $A \rightarrow Zh, H \rightarrow hh$ as well as $H \rightarrow WW/ZZ$ decay modes are available (they are suppressed in the strict alignment limit). When kinematically open, the decays $A/H \rightarrow t\bar{t}$ become relevant or even dominant for sufficiently small $\tan\beta$. For the charged Higgs boson, $H^\pm \rightarrow \tau^+\nu_\tau$ dominates below the $t\bar{b}$ threshold, and also $H^\pm \rightarrow W^\pm h$ may be searched for.

In both cases i) and ii), the heavier Higgs states, H, A and H^\pm , are roughly mass degenerate (with masses ± 20 GeV or less apart). If kinematically allowed, the heavy Higgs boson decays into charginos, neutralinos and third-generation squarks and sleptons can be important [305].

At hadron colliders, the dominant neutral Higgs boson production mechanism at moderate values of $\tan\beta$ is gluon fusion, mediated by loops containing heavy top and bottom quarks and the corresponding SUSY partners. The effect of light stops that may

contribute to the gluon fusion production can be partially cancelled by mixing effects. Higgs boson radiation off bottom quarks becomes important for large $\tan\beta$, where at least two of the three neutral Higgs bosons have enhanced couplings to bottom-type fermions [306, 307]. Detailed discussions of the impact of radiative corrections in these search modes are presented for instance in Ref. [308]. The vector boson fusion and Higgs-strahlung production of the CP -even Higgs bosons as well as the associated production of neutral Higgs bosons with top quark pairs have lower production cross sections by at least an order of magnitude with respect to the dominant ones, depending on the precise region of MSSM parameter space [41–44]. Higgs boson pair production of non-standard MSSM Higgs bosons has been studied in Ref. [309]. For a discussion of charged Higgs boson production at LHC, see Refs. [42, 43, 310].

Strong production of a heavy neutral Higgs boson followed by its decay into top-quark pairs is a challenging channel, only most recently being searched for by ATLAS and CMS. Interference effects between the signal and the SM $t\bar{t}$ background need to be carefully taken into account [311].

Summarising, the additional Higgs bosons are sought for mainly via the channels:

$$\begin{aligned} pp &\rightarrow A/H \rightarrow \tau^+\tau^- \text{ (inclusive)}, \\ \bar{b}\bar{b}A/H, A/H &\rightarrow \tau^+\tau^- \text{ (with } b\text{-tag)}, \\ \bar{b}\bar{b}A/H, A/H &\rightarrow b\bar{b} \text{ (with } b\text{-tag)}, \\ pp &\rightarrow t\bar{t} \rightarrow H^\pm W^\mp b\bar{b}, H^\pm \rightarrow \tau\nu_\tau, \\ gb &\rightarrow H^-t \text{ or } g\bar{b} \rightarrow H^+\bar{t}, H^\pm \rightarrow \tau\nu_\tau. \end{aligned} \quad (11.52)$$

After the Higgs boson discovery, updated MSSM benchmark scenarios have been defined to highlight interesting conditions for the MSSM Higgs boson searches [43, 304, 312]. The latest benchmark scenarios update [304], partly based in MSSM parameter space discussions in Ref. [312], considers six benchmarks to illustrate different aspects of Higgs phenomenology in the MSSM. They include one case with complex parameters, but they all assume R -parity conservation and no flavour mixing. Each scenario contains one CP -even scalar with mass around 125 GeV and SM-like couplings. These scenarios include a M_h^{125} scenario with relatively heavy superparticles, so the Higgs phenomenology at the LHC resembles that of a 2HDM with MSSM-inspired Higgs boson couplings. Other two scenarios are characterised by some of the superparticles – staus or electroweakinos – being relatively light, that in turn is of relevance for heavy neutral Higgs boson searches. In particular, the traditional $A/H \rightarrow \tau^+\tau^-$ search channel varies depending on the values of μ and M_2 , that may enable the A/H decays into electroweakinos. Another two scenarios are characterised by the phenomenon of alignment without decoupling, in which one of the two neutral CP -even scalars has SM-like couplings independently of the mass spectrum of the remaining Higgs bosons, hence allowing for all the Higgs bosons to have relatively low mass values (about few hundred GeV). Finally there is one scenario which incorporates CP violation in the Higgs sector and gives rise to a strong admixture of the two heavier neutral states. All the above scenarios assume all parameters in the mass range from 1 to a few TeV, hence they are not applicable for values of $\tan\beta$ of order a few, for which a Higgs boson mass value of 125 GeV is out of reach. An additional study, EFTMSSM [313], proposes two scenarios specifically designed for the low $\tan\beta$ region and ensures a 125 GeV Higgs boson mass in almost the entire parameter space by employing a flexible supersymmetric mass scale, reaching values of up to 10^{16} GeV.

An alternative approach to reduce the large number of parameters relevant to the Higgs sector is to consider that, in the Higgs basis, the only important radiative corrections are those affecting the Higgs boson mass [314]. This approximation is called hMSSM and works well in large regions of parameter space but it breaks down for sizeable values of μ and A_t , and moderate values of $\tan\beta$, for which the radiative corrections to the mixing between the two CP even eigenstates become relevant. The effect of such radiative corrections is to allow for alignment for small to intermediate values of $\tan\beta$, independent of the specific value of m_A [315]. In

⁷In very special regions of the parameter space, there is still the possibility that the heavier CP -even Higgs state is identified with the 125 GeV Higgs boson discovered by ATLAS and CMS, see for instance the discussion in Ref. [303] and the benchmark M_H^{125} defined in Ref. [304].

addition, the hMSSM assumption that the right value of the Higgs boson mass may be obtained for all values of m_A and $\tan\beta$ is in conflict with the MSSM predictions for the Higgs boson mass for small values of m_A and $\tan\beta \simeq \mathcal{O}(1)$. The recent M_h^{125} [304] and EFTMSSM benchmarks [313], are designed to address the limitations of the hMSSM, in particular the low $\tan\beta$ region for the EFTMSSM.

The M_h^{125} scenarios are aiming at treating more rigorously all radiative correction to the observed Higgs boson mass as well as specifically taking into possibly intermediate to light MSSM colorless states as electroweakinos or staus [304]. The main M_h^{125} benchmark, however, assumes that super partners are heavy, so that the phenomenology of the observed Higgs boson is not altered except in its couplings due to the existence of another doublet. Another important example scenario, referred to as $M_h^{125}(\tilde{\chi})$, considers light electroweakinos and therefore the heavy Higgs bosons H and A can have sizeable decay rates to charginos and neutralinos, consequently suppressing the $\tau^+\tau^-$ decay rate. It is interesting to note that in this scenario the branching fraction of the Higgs boson to photons is enhanced for small values of $\tan\beta$ due to the presence of electroweakinos in the loop. These two scenarios are illustrated in Fig. 11.18.

The compatibility between the predicted and measured Higgs boson mass is an important constraint in these scenarios. The predictions are illustrated in Fig. 11.18. To use the predicted Higgs boson mass as a constraint (exclusion at nearly constant $\tan\beta$ at high M_A in the $(M_A, \tan\beta)$ plane), it is important to account for the theoretical uncertainty on the prediction which is in excess of an order of magnitude larger than the experimental uncertainty on the measured mass of the Higgs boson. The theoretical uncertainty depends itself on the specific SUSY spectrum for a given MSSM parameter set and should be estimated accordingly, however, a more generic estimate of ± 3 GeV is made and found to be a conservative choice.

Reviews of the properties and phenomenology of the Higgs bosons of the MSSM can be found for example in Refs. [9, 39, 297]. Future precision measurements of the Higgs boson couplings to fermions and gauge bosons together with information on heavy Higgs boson searches will provide powerful information on the SUSY parameter space [315, 316].

Improvements in our understanding of B -physics observables put indirect constraints on additional Higgs bosons in mass ranges that would be accessible in direct LHC searches. In particular, $\text{BR}(B_s \rightarrow \mu^+\mu^-)$, $\text{BR}(b \rightarrow s\gamma)$, and $\text{BR}(B_u \rightarrow \tau\nu)$ play an important role within minimal flavour-violating (MFV) models [317], in which flavor effects proportional to the CKM matrix elements are induced as in the SM.

11.7.2 Supersymmetry with singlet extensions

The Higgs mass parameter μ is a SUSY parameter, and as such, it should naturally be of order M_{GUT} or M_{Planck} . The fact that phenomenologically it is required that μ be at the electroweak/TeV scale is known as the μ problem [318]. SUSY models with additional singlets can provide a solution to the μ problem, by promoting the μ parameter to a dynamical singlet superfield S that only interacts with the MSSM Higgs doublets through a coupling λ_S at the level of the superpotential. An effective μ is generated when the real scalar component of S acquires a vacuum expectation value v_S , yielding $\mu_{\text{eff}} = \lambda_S v_S$. After the minimization of the Higgs potential, the vacuum state relates the vacuum expectation values of the three CP -even neutral scalars, v_1 , v_2 and v_S , to the scalar doublet and singlet soft SUSY breaking masses, hence, one expects that these VEVs should all be of order M_{SUSY} and therefore the μ problem is solved.

The addition of a singlet superfield to the MSSM may come along with additional symmetries imposed to the theory. Depending on such symmetries, different models with singlet extensions of the MSSM (xMSSM) have been proposed, see Ref. [319] for a general review. Among the most studied examples are the NMSSM with an additional discrete Z_3 symmetry (first introduced in Ref. [320]), the Nearly-Minimal SUSY SM (nMSSM), with additional discrete Z_5^R , and Z_7^R symmetries [321], and the $U(1)'$ -extended MSSM (UMSSM) [322]. A Secluded $U(1)'$ -extended MSSM (sMSSM) [323] contains three singlets in addition to the

standard UMSSM Higgs boson singlet; this model is equivalent to the nMSSM in the limit that the additional singlet VEV's are large, and the trilinear singlet coupling, λ_S , is small [324].

A singlet extended SUSY Higgs sector opens new avenues for discovery. Since the singlet pseudoscalar particle may be identified as the pseudo-Goldstone boson of a spontaneously broken Peccei–Quinn symmetry, it may become naturally light [325]. Generally, there is mixing of the singlet sector with the MSSM Higgs sector, and for a sufficiently light, singlet-dominated scalar or pseudoscalar, h_S or A_S , respectively, the SM-like Higgs boson h may decay to pairs of h_S or A_S . The light scalar and/or pseudoscalar may subsequently decay to $\tau\tau$ or $b\bar{b}$ pairs. Such cascade decays are more difficult to detect than in standard searches due to the potentially soft decay products. There is also a rich phenomenology for the decays of the heavy CP -even and CP -odd doublets, H and A into two lighter Higgs bosons such as $H \rightarrow hh_S$, hh , $h_S h_S$ or $A \rightarrow A_S h_S$, $A_S h$ as well as into a light Higgs boson and a gauge boson: $H \rightarrow A_S Z$; $A \rightarrow h_S Z$, hZ . If kinematically allowed, the heavy Higgs bosons decay into $t\bar{t}$. If the singlet-dominated scalar or pseudoscalar are somewhat heavier, the decays $h_S \rightarrow WW$ or $A_S \rightarrow h_S Z$ will be allowed.

In addition, the light singlet scenario in the NMSSM or nMSSM is typically associated with a light singlino-dominated neutralino. The recently discovered SM-like Higgs boson can then decay to pairs of this neutralino [326], opening an invisible decay mode that is not excluded by present data. All of the Higgs bosons can decay into electroweakinos depending on kinematics and on the singlino or Higgsino composition of the electroweakinos.

In models with extended singlets, at low $\tan\beta$, it is possible to trade the requirement of a large stop mixing by a sizeable trilinear Higgs-singlet Higgs coupling λ_S , rendering more freedom on the requirements for gluon fusion production. As in the MSSM, mixing in the Higgs sector – additionally triggered by the extra new parameter λ_S – can produce variations in the Higgs– $b\bar{b}$ and Higgs– $\tau^-\tau^+$ couplings that can alter the Higgs to ZZ/WW and to diphoton rates. Light charginos at low $\tan\beta$ can independently contribute to enhance the di-photon rate, without altering any other of the Higgs boson decay rates, see for instance Ref. [327].

There is much activity in exploring the NMSSM phenomenology in the light of the 125 GeV Higgs boson as well as in defining benchmark scenarios with new topologies including Higgs decay chains, see Refs. [44, 328] and references therein. An analytic understanding of the alignment condition in the NMSSM is presented in Ref. [329]. The NMSSM with a Higgs boson of mass 125 GeV can be compatible with stop masses of order of the electroweak/TeV scale, thereby reducing the degree of fine tuning necessary to achieve electroweak symmetry breaking. Interestingly, the alignment conditions point toward a more natural region of parameter space for electroweak symmetry breaking, while allowing for perturbativity of the theory up to the Planck scale and yielding a rich and interesting Higgs boson phenomenology at the LHC.

11.7.3 Supersymmetry with extended gauge sectors

In the MSSM, the tree-level value of the lightest CP -even Higgs boson mass originates from the D-term dependence of the scalar potential that comes from the SUSY kinetic terms in the Kähler potential. The D-terms lead to tree-level quartic couplings which are governed by the squares of the gauge couplings of the weak interactions, under which the Higgs boson has non-trivial charges. Hence, the lightest Higgs mass is bounded to be smaller than M_Z . In the presence of new gauge interactions at the TeV scale, and if the Higgs fields had non-trivial charges under them, new D-term contributions would lead to an enhancement of the tree-level Higgs boson mass value. Since the low energy gauge interactions reduce to the known $SU(3)_c \times SU(2)_L \times U(1)_Y$ ones, in order for this mechanism to work, the extended gauge and Higgs sectors should be integrated out in a non-SUSY way. This means that there must be SUSY breaking terms that are of the order of, or larger than, the new gauge boson masses. The tree-level quartic couplings would then be enhanced through their dependence on the square of the gauge couplings of the extended Higgs sector. This effect will be suppressed when the heavy gauge boson masses are larger than the SUSY breaking scale and will acquire its full

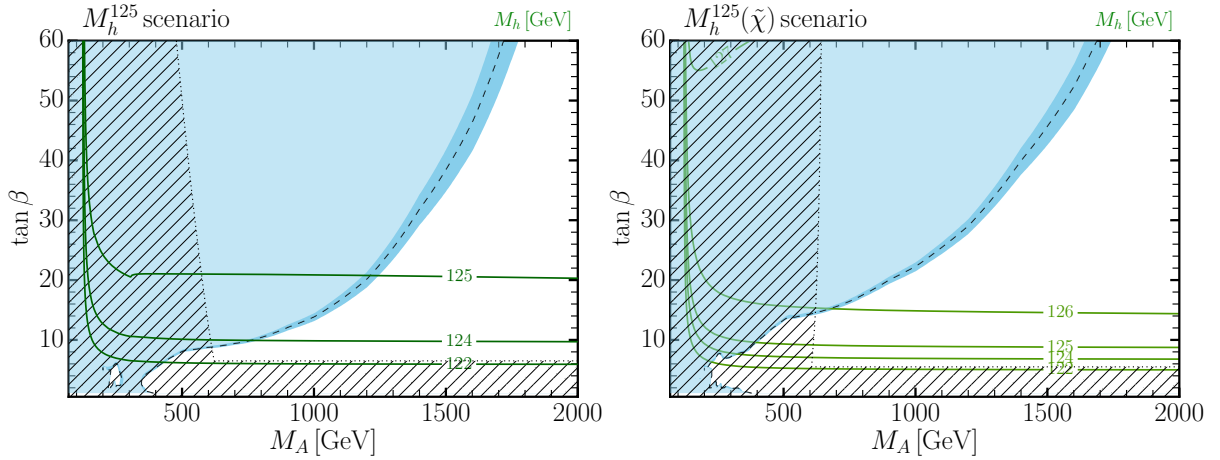


Figure 11.18: The 95% CL exclusion contours in the $(M_A, \tan\beta)$ parameter space for the M_h^{125} (right) and $M_h^{125}(\tilde{\chi})$ (left) benchmark scenarios. The nearly vertical dotted line illustrated the lower limit on the mass of the A boson and the close-to horizontal dotted line represents the limit on $\tan\beta$ from the compatibility of the measured mass of the observed Higgs boson and the prediction using radiative corrections (mostly from the stop sector).

potential only for large values of this scale.

One of the simplest possibilities is to extend the weak interactions to a $SU(2)_1 \times SU(2)_2$ sector, such that the known weak interactions are obtained after the spontaneous breaking of these groups to $SU(2)_L$ [330]. This example is briefly summarized in the previous editions of this review [123]. Assuming SUSY breaking terms of the order of the new gauge boson masses, enhancements of order 50% of the MSSM D-term contribution to the Higgs boson mass may be obtained. Such enhancements are sufficient to obtain the measured Higgs mass without the need for very heavy stops or large stop mixing parameters. This gauge extension leads to new, heavy gauge and Higgs bosons, as well as new neutralinos and charginos, that depending on the region of parameter space can induce novel phenomenology at the LHC. Gauge extensions including new abelian gauge groups have also been considered.

Gauge extensions of the MSSM can also lead to an enhancement of the Higgs boson mass value by modifying the renormalisation group evolution of the Higgs quartic coupling to low energies. In the MSSM, the evolution of the quartic coupling is governed by the top-quark Yukawa interactions and depends on the fourth power of the top-quark Yukawa coupling. The neutralino and chargino contributions, which depend on the fourth power of the weak gauge couplings, are small due to the smallness of these couplings. Depending on the values of the soft SUSY breaking parameters in the gaugino and Higgsino sectors, the $SU(2)_1$ gauginos may become light, with masses of the order of the weak scale. Since the $SU(2)_1$ coupling may be significantly larger than the $SU(2)_L$ one, for small values of the Higgsino mass parameter μ , the associated charginos and neutralinos may modify the evolution of the quartic coupling in a significant way [331]. This may lead to a significant increase of the lightest CP -even Higgs boson mass, even for small values of $\tan\beta \simeq 1$ for which the D-term contributions become small. Radiative corrections should be properly taken into account in this scenario as they might modify the tree-level result.

11.7.4 Effects of CP violation

SUSY scenarios with CP -violation (CPV) phases are theoretically appealing, since additional CPV beyond that observed in the K , D , and B meson systems is required to explain the observed cosmic matter-antimatter asymmetry. In the MSSM, CP -violation effects in the Higgs sector appear at the quantum level, while in singlet extensions of the MSSM CP -violation effects can already be effective at tree level. In general, CP -violation effects in the Higgs sector have significant constraints from electric dipole moments data [332].

In the MSSM, the gaugino mass parameters $(M_{1,2,3})$, the Higgsino mass parameter, μ , the bilinear Higgs squared-mass parameter, m_{12}^2 , and the trilinear couplings of the squark and

slepton fields to the Higgs fields, A_f , may carry non-trivial phases. The two parameter combinations $\arg[\mu A_f (m_{12}^2)^*]$ and $\arg[\mu M_i (m_{12}^2)^*]$ are invariant under phase redefinitions of the MSSM fields [333, 334]. Therefore, if one of these quantities is non-zero, there would be new sources of CP -violation affecting the Higgs sector through radiative corrections, see Ref. [335] and references therein. The mixing of the neutral CP -odd and CP -even Higgs boson states is no longer forbidden. Hence, m_A is no longer a physical parameter. However, the charged Higgs boson mass m_{H^\pm} is still physical and can be used as an input for the computation of the neutral Higgs boson spectrum of the theory. For large values of m_{H^\pm} , corresponding to the decoupling limit, the properties of the lightest neutral Higgs boson state approach those of the SM Higgs boson. In particular, the upper bound on the lightest neutral Higgs boson mass takes the same value as in the CP -conserving case [334]. Nevertheless, there still can be significant mixing between the two heavier neutral mass eigenstates. For a detailed study of the Higgs boson mass spectrum and parametric dependence of the associated radiative corrections, see Ref. [335] and references therein.

Major variations to the Higgs boson phenomenology occur in the presence of explicit CPV phases. In the CPV case, vector boson pairs couple to all three neutral Higgs boson mass eigenstates, H_i ($i = 1, 2, 3$), with couplings

$$\begin{aligned} g_{H_i V V} &= \cos\beta \mathcal{O}_{1i} + \sin\beta \mathcal{O}_{2i}, \\ g_{H_i H_j Z} &= \mathcal{O}_{3i} (\cos\beta \mathcal{O}_{2j} - \sin\beta \mathcal{O}_{1j}) \\ &\quad - \mathcal{O}_{3j} (\cos\beta \mathcal{O}_{2i} - \sin\beta \mathcal{O}_{1i}), \end{aligned} \quad (11.53)$$

where the $g_{H_i V V}$ couplings are normalised to the analogous SM coupling and the $g_{H_i H_j Z}$ have been normalised to $g_Z^{\text{SM}}/2$. The orthogonal matrix \mathcal{O}_{ij} , only defined in the $p^2 \rightarrow 0$ limit, is relating the weak eigenstates to the mass eigenstates. It has non-zero off-diagonal entries mixing the CP -even and CP -odd components of the weak eigenstates. Moreover, CPV phases imply that all neutral Higgs bosons can couple to both scalar and pseudoscalar fermion bilinear densities. The couplings of the mass eigenstates H_i to fermions depend on the loop-corrected fermion Yukawa couplings (similarly to the CP conserving (CPC) case), on $\tan\beta$ and on \mathcal{O}_{ji} [336].

The production processes of neutral MSSM Higgs bosons in the CPV scenario are similar to those in the CPC scenario. Regarding the decay properties, the lightest mass eigenstate, H_1 , predominantly decays to $b\bar{b}$ if kinematically allowed, with a smaller fraction decaying to $\tau^+\tau^-$. If kinematically allowed, a SM-like neutral Higgs boson, H_2 or H_3 can decay predominantly to $H_1 H_1$ leading to many new interesting signals both at lepton and hadron colliders; otherwise it will decay preferentially to $b\bar{b}$.

The discovery of a 125 GeV Higgs boson has put strong constraints on the realisation of the CPV scenario within the MSSM. This is partly due to the fact that the observed Higgs boson rates are close to the SM values, and a large CP -violating component would necessarily induce a large variation in the rate of the SM-like Higgs boson decays into the weak gauge bosons W^\pm and Z . The measured Higgs mass imposes additional constraints on the realisation of this scenario. Once all effects are considered, the CP -odd Higgs boson A component of the lightest Higgs boson tends to be smaller than about 10% [337]. This restriction can be alleviated in the NMSSM or more general two Higgs doublet models. CP -violating effects can still be significant in the heavy Higgs sector. For instance, the Higgs bosons H_2 and H_3 may be admixtures of CP -even and CP -odd scalars, and therefore both may be able to decay into pairs of weak gauge bosons. The observation of such decays would be a clear signal of CP -violation. In the MSSM, the proximity of the masses of H_2 and H_3 makes the measurement of such effect quite challenging, but in generic two Higgs doublet models, the mass splitting between the two heavy mass eigenstates may become larger, facilitating the detection of CP -violating effects at collider experiments [338].

11.7.5 Non-supersymmetric extensions of the Higgs sector

There are many ways to extend the minimal Higgs sector of the SM. In the preceding sections the phenomenology of SUSY Higgs sectors is considered, which at tree level implies a constrained type-II 2HDM (with restrictions on the Higgs boson masses and couplings). In the following discussion, more generic 2HDM's are presented (for some comprehensive reviews, see Ref. [339]). These models are theoretically less compelling since they do not provide an explanation for the SM Higgs naturalness problem, but can lead to different patterns of Higgs-fermion couplings, hence, to different phenomenology. It is also possible to consider models with a SM Higgs boson and one or more additional scalar $SU(2)$ doublets that acquire no VEV and hence play no role in the EWSB mechanism. Such models are dubbed Inert Higgs Doublet Models (IHD) [340]. Without a VEV associated to it, a Higgs boson from an inert doublet has no tree-level coupling to gauge bosons and hence cannot decay into a pair of them. Moreover, imposing a Z_2 symmetry that prevents them from coupling to the fermions, it follows that, if the lightest inert Higgs boson is neutral, it becomes a good DM candidate with interesting associated collider signals. Various studies of IHD models in the light of a 125 GeV Higgs boson have been performed, see for instance Ref. [341], showing an interesting interplay between collider and direct DM detection signals.

An interesting type of 2HDMs are those in which an abelian flavour symmetry broken at the electroweak scale creates the fermion mass hierarchies and mixing angles [17]. This idea is based on the Froggatt–Nielsen model [342], where a flavon field couples differently to the SM fermions of different flavour charges. Such flavon acquires a vacuum expectation value, breaking the flavour symmetry but leaving both the flavour breaking and the new physics scales undetermined. In Refs. [343], it was proposed to relate the flavour breaking scale to the electroweak scale by identifying the flavon with the modulus square of the Higgs field. A 2HDM, however, provides a more compelling realisation of the electroweak scale flavour breaking idea. In the most ambitious constructions of two Higgs doublet flavour models (2HDFM), the textures of the Yukawa couplings are a result of an abelian flavour symmetry that only allows renormalisable Yukawa couplings of the top quark to the Higgs bosons. All other Yukawa couplings are generated by higher dimensional operators that produce hierarchical entries of the Yukawa matrices, explaining the observed quark masses and mixing angles. Flavour observables, LHC Higgs signal strength measurements, electroweak precision measurements, unitarity and perturbativity bounds, as well as collider searches for new scalar resonances result in precise predictions for the parameters of these 2HDFMs. In particular, correlated departures from SM Higgs boson couplings, as well as additional Higgs bosons with masses < 700 GeV must be observed at the LHC. Other incarnations of 2HDFMs can aim at only partially explaining the fermion mass hierarchies but are therefore less restrictive.

Other extensions of the Higgs sector can include multiple copies

of $SU(2)_L$ doublets [344], additional Higgs singlets [345], triplets or more complicated combinations of Higgs multiplets. It is also possible to enlarge the gauge symmetry beyond $SU(2)_L \times U(1)_Y$ along with the necessary Higgs field structure to generate gauge boson and fermion masses. There are two main experimental constraints on these extensions: (i) precision measurements which constrain $\rho = m_W^2/(m_Z^2 \cos^2 \theta_W)$ to be very close to 1 and (ii) flavour changing neutral current (FCNC) effects. In electroweak models based on the SM gauge group, the tree-level value of ρ is determined by the Higgs multiplet structure. By suitable choices for the hypercharges, and in some cases the mass splitting between the charged and neutral Higgs sector or the vacuum expectation values of the Higgs fields, it is possible to obtain a richer combination of singlets, doublets, triplets and higher multiplets compatible with precision measurements. Concerning the constraints coming from FCNC effects, the Glashow–Weinberg (GW) criterion [346] states that, in the presence of multiple Higgs doublets, the tree-level FCNC's mediated by neutral Higgs bosons will be absent if all fermions of a given electric charge couple to no more than one Higgs doublet. An alternative way of suppressing FCNC in a two Higgs doublet model has been considered in Ref. [347], where it is shown that it is possible to have tree level FCNC completely fixed by the CKM matrix, as a result of an abelian symmetry.

11.7.5.1 Two-Higgs-doublet models

General two Higgs doublet models [339] can have a more diverse Higgs-fermion coupling structure than in SUSY, and can be viewed as a simple extension of the SM to realise the spontaneous breakdown of $SU(2)_L \times U(1)_Y$ to $U(1)_{em}$. Quite generally, if the two Higgs doublets contain opposite hypercharges, the scalar potential will contain mixing mass parameters of the kind $m_{12}^2 \Phi_1^T i\sigma_2 \Phi_2 + h.c.$. In the presence of such terms, both Higgs doublets will acquire vacuum expectation values, $v_1/\sqrt{2}$ and $v_2/\sqrt{2}$, respectively, and the gauge boson masses will keep their SM expressions with the Higgs VEV v replaced by $\sqrt{v_1^2 + v_2^2}$. Apart from the mass terms, the most generic renormalisable and gauge invariant scalar potential for two Higgs doublets with opposite hypercharges contains seven quartic couplings, as presented in Eq. (11.46).

Just as in the MSSM case, after electroweak symmetry breaking and in the absence of CP -violation, the physical spectrum contains a pair of charged Higgs bosons H^\pm , a CP -odd Higgs boson A and two neutral CP -even Higgs bosons, h and H . The angles α and β diagonalise the CP -even, and the CP -odd and charged Higgs sectors, respectively. The complete 2HDM is defined only after considering the interactions of the Higgs fields to fermions. Yukawa couplings of the generic form

$$-h_{ij}^a \bar{\Psi}_L^i H_a \Psi_R^j + h.c. \quad (11.54)$$

may be added to the renormalisable Lagrangian of the theory. Contrary to the SM, the two Higgs doublet structure does not ensure the alignment of the fermion mass terms $m_{ij} = h_{ij}^a v_a/\sqrt{2}$ with the Yukawa couplings h_{ij}^a . This implies that quite generally the neutral Higgs boson will mediate flavour changing interactions between the different mass eigenstates of the fermion fields. Such flavour changing interactions should be suppressed in order to describe properly the Kaon, D and B meson phenomenology. Based on the Glashow–Weinberg criterion, it is clear that the simplest way of avoiding such transitions is to assume the existence of a symmetry that ensures the couplings of the fermions of each given quantum number (up-type and down-type quarks, charged and neutral leptons) to only one of the two Higgs doublets. Different models may be defined depending on which of these fermion fields couple to a given Higgs boson, see Table 11.13. Models of type-I are those in which all SM fermions couple to a single Higgs field. In type-II models, down-type quarks and charged leptons couple to a common Higgs field, while the up-type quarks and neutral leptons couple to the other. In models of type-III (lepton-specific), quarks couple to one of the Higgs bosons, while leptons couple to the other. Finally, in models of type-IV (flipped), up-type quarks and charged leptons couple to one of the Higgs fields while down-quarks and neutral leptons couple to the other.

Table 11.13: Higgs boson couplings to up, down and charged lepton-type $SU(2)_L$ singlet fermions in the four discrete types of 2HDM models that satisfy the Glashow–Weinberg criterion.

Model	2HDM I	2HDM II	2HDM III	2HDM IV
u	Φ_2	Φ_2	Φ_2	Φ_2
d	Φ_2	Φ_1	Φ_2	Φ_1
e	Φ_2	Φ_1	Φ_1	Φ_2

The two Higgs doublet model phenomenology depends strongly on the size of the mixing angle α and therefore on the quartic couplings. For large values of m_A , $\sin \alpha \rightarrow -\cos \beta$, $\cos \alpha \rightarrow \sin \beta$, $\cos(\beta - \alpha) \rightarrow 0$, and the lightest CP -even Higgs boson h behaves as the SM Higgs boson. The same behaviour is obtained if the quartic couplings are such that $\mathcal{M}_{12}^2 \sin \beta = -(\mathcal{M}_{11}^2 - m_h^2) \cos \beta$. The latter condition represents a situation in which the couplings of h to fermions and weak gauge bosons become the same as in the SM, without decoupling the rest of the non-standard scalars and it is of particular interest due to the fact that the discovered Higgs boson has SM-like properties. This situation will be referred to as alignment, as in the MSSM case.

In analogy to the effects of CP violation in the SUSY 2HDM, some parameters of the Higgs potential can be complex and one has a model that is explicitly CP violating. The three neutral mass eigenstates mixed with each other and the Higgs phenomenology is analogous to the one described for the SUSY case above, with the caveat that when considering the neutral Higgs boson couplings to the scalar and pseudoscalar fermion bilinear densities, the proper weight should be considered for the respective 2HDM's.

In type-II Higgs doublet models, at large values of $\tan \beta$ and moderate values of m_A , the non-standard Higgs bosons H , A and H^\pm couple strongly to bottom quarks and τ leptons. Hence the decay modes of the non-standard Higgs bosons tend to be dominated by the b -quark and τ -lepton modes, including top quarks or neutrinos in the case of the charged Higgs boson. However, for large and negative values of λ_4 , the charged Higgs boson mass may be sufficiently heavy to allow on-shell decays $H^\pm \rightarrow W^\pm + (H, A)$, via a trilinear coupling

$$g_{H^\pm W^\mp H, A} \simeq \frac{M_W}{v} \sin(\beta - \alpha)(p_{H^\pm} - p_{H, A}), \quad (11.55)$$

where p_{H^\pm} and $p_{H, A}$ are the charged and neutral scalar Higgs boson momenta pointing into the vertex. On the other hand, for large and positive values of λ_5 , the above charged Higgs boson decay into a W^\pm and the CP -odd Higgs boson may be allowed, but the heavy Higgs boson H may be sufficiently heavy to decay into a CP -odd Higgs boson and an on-shell Z , $H \rightarrow Z + A$, via

$$g_{HZA} \simeq \frac{M_Z}{v} \sin(\beta - \alpha)(p_H - p_A). \quad (11.56)$$

The decay $H^\pm \rightarrow W^\pm + H$, on the other hand may be allowed only if $\lambda_4 < -\lambda_5$. The couplings controlling all the above decay modes are proportional to $\sin(\beta - \alpha)$ and therefore they are unsuppressed in the alignment limit. Moreover, these could still be the dominant decay modes at moderate values of $\tan \beta$, offering a way to evade the current bounds obtained assuming a dominant decay into b -quarks or τ -leptons.

The quartic couplings are restricted by the condition of stability of the effective potential as well as by the restriction of obtaining the proper value of the lightest CP -even Higgs boson mass. Close to the alignment limit, the lightest CP -even Higgs boson mass becomes approximately independent of m_A and is given by

$$m_h^2 \simeq v^2(\lambda_1 \cos^4 \beta + \lambda_2 \sin^4 \beta + 2\tilde{\lambda}_3 v^2 \cos^2 \beta \sin^2 \beta + 4\lambda_6 \cos^3 \beta \sin \beta + 4\lambda_7 \sin^3 \beta \cos \beta), \quad (11.57)$$

where $\tilde{\lambda}_3 = \lambda_3 + \lambda_4 + \lambda_5$.

The stability conditions imply the positiveness of all masses, as well as the avoidance of run-away solutions to large negative

values of the fields in the scalar potential. These conditions imply

$$\begin{aligned} \lambda_1 &\geq 0, \quad \lambda_2 \geq 0, \quad \lambda_3 + \lambda_4 - |\lambda_5| \geq -\sqrt{\lambda_1 \lambda_2}, \quad \lambda_3 \geq -\sqrt{\lambda_1 \lambda_2}, \\ 2|\lambda_6 + \lambda_7| &< \frac{\lambda_1 + \lambda_2}{2} + \tilde{\lambda}_3, \end{aligned} \quad (11.58)$$

where the first four conditions are necessary and sufficient conditions in the case of $\lambda_6 = \lambda_7 = 0$, while the last one is a necessary condition in the case all couplings are non-zero. Therefore, to obtain the conditions that allow the decays $H^\pm \rightarrow W^\pm H$, A and $H \rightarrow ZA$, λ_3 should take large positive values in order to compensate for the effects of λ_4 and λ_5 . For more detailed discussions about 2HDM phenomenology, see for example Refs. [44, 339].

11.7.5.2 Higgs triplets

Electroweak triplet scalars are the simplest non-doublet extension of the SM that can participate in the spontaneous breakdown of $SU(2)_L \times U(1)_Y$ to $U(1)_{\text{em}}$. Two types of model have been developed in enough detail to make a meaningful comparison to LHC data: the Higgs triplet model (HTM) [348] and the Georgi–Machacek model (GM) [349].

The Higgs triplet model extends the SM by the addition of a complex $SU(2)_L$ triplet scalar field Δ with hypercharge $Y = 2$, and a general gauge-invariant renormalisable potential $V(\Phi, \Delta)$ for Δ and the SM Higgs doublet Φ . The components of the triplet field can be parameterised as

$$\Delta = \frac{1}{\sqrt{2}} \begin{pmatrix} \Delta^+ & \sqrt{2}\Delta^{++} \\ v_\Delta + \delta + i\xi & -\Delta^+ \end{pmatrix}. \quad (11.59)$$

where Δ^+ is a singly-charged field, Δ^{++} is a doubly-charged field, δ is a neutral CP -even scalar, ξ is a neutral CP -odd scalar, and v_Δ is the triplet VEV. The general scalar potential mixes the doublet and triplet components. After electroweak symmetry breaking there are seven physical mass eigenstates, denoted $H^{\pm\pm}$, H^\pm , A , H , and h .

A distinguishing feature of the HTM is that it violates the custodial symmetry of the SM; thus the ρ parameter deviates from 1 even at tree level. Letting x denote the ratio of triplet and doublet VEVs, the tree level expression is

$$\rho = \frac{1 + 2x^2}{1 + 4x^2}. \quad (11.60)$$

The measured value of the ρ parameter then limits the triplet VEV to be quite small, $x \lesssim 0.03$, or $v_\Delta < 8$ GeV. This constraint severely limits the role of the triplet scalar in the EWSB mechanism.

The small VEV of the Higgs triplet in the HTM is a virtue from the point of view of generating neutrino masses without the necessity for introducing right-handed neutrino fields. The gauge invariant dimension four interaction

$$h_{\nu_{ij}} \ell_i^T C^{-1} i\sigma_2 \Delta \ell_j, \quad (11.61)$$

where ℓ_i are the lepton doublets, C is the charge conjugation matrix, and $h_{\nu_{ij}}$ is a complex symmetric coupling matrix, generates a Majorana mass matrix for the neutrinos:

$$m_{\nu_{ij}} = \sqrt{2} h_{\nu_{ij}} v_\Delta. \quad (11.62)$$

This can be combined with the usual neutrino seesaw to produce what is known as the type-II seesaw [350].

The HTM suggests the exciting possibility of measuring parameters of the neutrino mass matrix at the LHC. If the doubly-charged Higgs boson is light enough and/or its couplings to W^+W^+ are sufficiently suppressed, then its primary decay is into same-sign lepton pairs: $H^{++} \rightarrow \ell_i^+ \ell_j^+$; from Eq. (11.61) and Eq. (11.62), it is apparent that these decays are in general lepton-flavor violating with branchings proportional to elements of the neutrino mass matrix [351].

Precision electroweak data constrain the mass spectrum as well as the triplet VEV of the HTM [352]. These constraints favour a spectrum where H^{++} is the lightest of the exotic bosons, and

where the mass difference between H^+ and H^{++} is a few hundred GeV. The favoured triplet VEV is a few GeV, which also favours H^{++} decays into W^+W^+ over same-sign dileptons.

The GM model addresses the ρ parameter constraint directly by building in custodial symmetry. Writing the complex scalar doublet of the SM as a $(2, 2)$ under $SU(2)_L \times SU(2)_R$, it is obvious that the next simplest construction respecting custodial symmetry is a scalar transforming like a $(3, 3)$ [353]. These nine real degrees of freedom correspond to a complex electroweak triplet combined with a real triplet, with the scalar potential required to be invariant under $SU(2)_R$. Under the custodial $SU(2)_{L+R}$, they transform as $1 \oplus 3 \oplus 5$, with a CP -even neutral scalar as the custodial singlet (thus matching the SM Higgs boson), a CP -odd neutral scalar in the custodial triplet, and another CP -even neutral scalar in the custodial 5-plet.

The scalar components can be decomposed as

$$\Xi = \begin{pmatrix} \chi_3^* & \xi_1 & \chi_1 \\ -\chi_2^* & \xi_2 & \chi_2 \\ \chi_1^* & -\xi_1^* & \chi_3 \end{pmatrix}, \quad (11.63)$$

where ξ_2 is a real scalar and the others are complex scalars. Linear combinations of these scalars account for the neutral custodial singlet, a neutral and singly-charged field making up the custodial triplet, and neutral, singly-charged, and doubly-charged fields making up the custodial 5-plet.

When combined with the usual SM doublet field Φ , the electroweak scale v is now related to the doublet and triplet VEVs by

$$v^2 = v_\Phi^2 + 8v_\Xi^2. \quad (11.64)$$

Note that the GM triplets by themselves are sufficient to explain electroweak symmetry breaking and the existence of a 125 GeV neutral boson along with a custodial triplet of Goldstone bosons; the complex doublet field in the GM model is required to generate fermion masses via the usual dimension four Yukawa couplings. This raises the question of whether one can rule out the possibility that the 125 GeV boson is the neutral member of a custodial 5-plet rather than a custodial singlet, without invoking decays to fermions. A conclusive answer is given by observing that the ratio of the branching fractions to W versus Z bosons is completely determined by the custodial symmetry properties of the boson. For a custodial 5-plet, the ratio of the signal strength to WW over that to ZZ is predicted to be $1/4$ that of a SM Higgs boson [353], and thus already ruled out by the experimental results presented in Section 11.6.

Another interesting general feature of Higgs triplet models is that, after mixing, the SM-like neutral boson can have stronger couplings to WW and ZZ than predicted by the SM [354]; this is in contrast to mixing with additional doublets and singlet, which can only reduce the WW and ZZ couplings versus the SM. This emphasises that LHC Higgs data cannot extract model independent coupling strengths for the Higgs boson [244].

Because of the built-in custodial symmetry, the triplet VEV in the GM model can be large compared to the doublet VEV. The custodial singlet neutral boson from the triplets mixes with the neutral boson from the doublet. Two interesting special cases are (i) the triplet VEV is small and the 125 GeV boson is SM-like except for small deviations, and (ii) the 125 GeV boson is mostly the custodial singlet neutral boson from the electroweak triplets. The phenomenology of the doubly-charged and singly-charged bosons is similar to that of the HTM. The constraints on the GM model from precision electroweak data, LEP data, and current LHC data are summarised in Ref. [44].

11.7.6 Composite Higgs models

Within the SM, EWSB is posited but has no dynamical origin. Furthermore, the Higgs boson appears to be unnaturally light. A scenario that remedies these two catches is to consider the Higgs boson as a bound state of new dynamics becoming strong around the weak scale. The Higgs boson can be made significantly lighter than the other resonances of the strong sector if it appears as a pseudo-Nambu-Goldstone boson, see Refs. [11] for reviews.

11.7.6.1 Little Higgs models

The idea behind the Little Higgs boson models [355] is to identify the Higgs doublet as a (pseudo) Nambu-Goldstone boson while keeping some sizeable non-derivative interactions, in particular a largish Higgs quartic interaction. By analogy with QCD where the pions $\pi^{\pm,0}$ appear as Nambu-Goldstone bosons associated to the breaking of the chiral symmetry $SU(2)_L \times SU(2)_R/SU(2)$, switching on some interactions that break explicitly the global symmetry will generate masses for the would-be massless Nambu-Goldstone bosons of the order of $g\Lambda_{G/H}/(4\pi)$, where g is the coupling of the symmetry breaking interaction and $\Lambda_{G/H} = 4\pi f_{G/H}$ is the dynamical scale of the global symmetry breaking G/H . In the case of the Higgs boson, the top Yukawa interaction or the gauge interactions themselves will certainly break explicitly (part of) the global symmetry since they act non-linearly on the Higgs boson. Therefore, obtaining a Higgs boson mass around 125 GeV would demand a dynamical scale $\Lambda_{G/H}$ of the order of 1 TeV, which is known to lead to too large oblique corrections. Raising the strong dynamical scale by at least one order of magnitude requires an additional selection rule to ensure that a Higgs boson mass is generated at the 2-loop level only

$$m_H^2 = \frac{g^2}{16\pi^2} \Lambda_{G/H}^2 \rightarrow m_H^2 = \frac{g^2 g_2^2}{(16\pi^2)^2} \Lambda_{G/H}^2. \quad (11.65)$$

The way to enforce this selection rule is through a ‘‘collective breaking’’ of the global symmetry:

$$\mathcal{L} = \mathcal{L}_{G/H} + g_1 \mathcal{L}_1 + g_2 \mathcal{L}_2. \quad (11.66)$$

Each interaction \mathcal{L}_1 or \mathcal{L}_2 individually preserves a subset of the global symmetry such that the Higgs boson remains an exact Nambu-Goldstone boson whenever either g_1 or g_2 is vanishing. A mass term for the Higgs boson can be generated only by diagrams involving simultaneously both interactions. At one-loop, such diagrams are not quadratically divergent, so the Higgs boson mass is not UV sensitive. Explicitly, the cancellation of the SM quadratic divergences is achieved by a set of new particles around the Fermi scale: gauge bosons, vector-like quarks, and extra massive scalars, which are related, by the original global symmetry, to the SM particles with the same spin. Contrary to SUSY, the cancellation of the quadratic divergences is achieved by same-spin particles. These new particles, with definite couplings to SM particles as dictated by the global symmetries of the theory, are perfect goals for the LHC.

The simplest incarnation of the collective breaking idea, the so-called littlest Higgs boson model, is based on a non-linear σ -model describing the spontaneous breaking $SU(5)$ down to $SO(5)$. A subgroup $SU(2)_1 \times U(1)_1 \times SU(2)_2 \times U(1)_2$ is weakly gauged. This model contains a weak doublet, that is identified with the Higgs doublet, and a complex weak triplet whose mass is not protected by collective breaking. Other popular little Higgs models are based on different coset spaces: minimal moose ($SU(3)^2/SU(3)$), the simplest little Higgs ($SU(3)^2/SU(2)^2$), the bestest little Higgs ($SO(6)^2/SO(6)$). For comprehensive reviews, see Ref. [356].

Generically, oblique corrections in Little Higgs models are reduced either by increasing the coupling of one of the gauge groups (in the case of product group models) or by increasing the masses of the W and Z partners, leading ultimately to a fine-tuning of the order of a few percents (see for instance Ref. [357] and references therein). The compatibility of Little Higgs models with experimental data is significantly improved when the global symmetry involves a custodial symmetry as well as a T -parity [358] under which, in analogy with R -parity in SUSY models, the SM particles are even and their partners are odd. Such Little Higgs models would therefore appear in colliders as jet(s) with missing transverse energy [359] and the ATLAS and CMS searches for squarks and gluinos (see ‘‘Supersymmetry, Part II’’ in this review) can be recast to obtain limits on the masses of the heavy vector-like quarks. The T -even top partner, with an expected mass below 1 TeV to cancel the top loop quadratic divergence without too much fine-tuning, would decay dominantly into a $t + Z$ pair or into a $b + W$ pair or even into $t + H$. The latest CMS and ATLAS direct searches [360] for vector-like top partners put a lower bound

around 1.1–1.3 TeV (for various branching fraction combinations), excluding the most natural region of the parameter space of these models, i.e., imposing a fine-tuning below the percent level.

The motivation for Little Higgs models is to solve the little hierarchy problem, i.e., to push the need for new physics (responsible for the stability of the weak scale) up to around 10 TeV. Per se, Little Higgs models are effective theories valid up to their cut-off scale $\Lambda_{G/H}$. Their UV completions could either be weakly or strongly coupled.

11.7.6.2 Models of partial compositeness

Even in composite models, the Higgs boson cannot appear as a regular resonance of the strong sector without endangering the viability of the setup when confronted to data. The way out is that the Higgs boson appears as a pseudo Nambu–Goldstone boson: the new strongly coupled sector is supposed to be invariant under a global symmetry G spontaneously broken to a subgroup H at the scale f (the typical mass scale of the resonances of the strong sector is $m_\rho \sim g_\rho f$ with g_ρ the characteristic coupling of the strong sector). To avoid conflict with EW precision measurements, the strong interactions themselves should better not break the EW symmetry. Hence the SM gauge symmetry itself should be contained in H . See Table 11.14 for a few examples of coset spaces.

Table 11.14: Global symmetry breaking patterns and the corresponding Goldstone boson contents of the SM, the minimal composite Higgs model, the next to minimal composite Higgs model, and the minimal composite two Higgs doublet model. Note that the SU(3) model does not have a custodial invariance. a denotes a CP-odd scalar while h and H are CP-even scalars.

Model	Symmetry Pattern	Goldstones
SM	SO(4)/SO(3)	W_L, Z_L
–	SU(3)/SU(2)×U(1)	W_L, Z_L, H
MCHM	SO(5)/SO(4)	W_L, Z_L, H
NMCHM	SO(6)/SO(5)	W_L, Z_L, H, a
MC2HM	SO(6)/SO(4)×SO(2)	W_L, Z_L, h, H, H^\pm, a

The SM (light) fermions and gauge bosons cannot be part of the strong sector itself since LEP data have already put stringent bounds on the compositeness scale of these particles far above the TeV scale. The gauge bosons couple to the strong sector by a weak gauging of a SU(2)×U(1) subgroup of the global symmetry G . Inspiration for the construction of such models comes from the AdS/CFT correspondence: the components of a gauge field along an extra warped space dimension can be interpreted as the Goldstone bosons resulting from the breaking of global symmetry of the strong sector. The couplings of the SM fermions to the strong sector could a priori take two different forms:

- (i) a bilinear coupling of two SM fermions to a composite scalar operator, \mathcal{O} , of the form $\mathcal{L} = y \bar{q}_L u_R \mathcal{O} + h.c.$, in simple analogy with the SM Yukawa interactions. This is the way fermion masses were introduced in technicolor theories and it generically comes with severe flavour problems and calls for extended model-building gymnastics [12] to circumvent them;
- (ii) a linear mass mixing with fermionic vector-like operators: $\mathcal{L} = \lambda_L \bar{q}_L \mathcal{Q}_R + \lambda_R \bar{U}_L u_R$. \mathcal{Q} and \mathcal{U} are two fermionic composite operators of mass M_Q and M_U .

Being part of the composite sector, the composite fermionic operators can have a direct coupling of generic order Y_* to the Higgs boson. In analogy with the photon- ρ mixing in QCD, once the linear mixings are diagonalised, the physical states are a linear combination of elementary and composite fields. Effective Yukawa couplings are generated and read for instance for the up-type quark

$$y = Y_* \sin \theta_L \sin \theta_R \tag{11.67}$$

where $\sin \theta_i = \lambda_i / \sqrt{M_{Q,U}^2 + \lambda_i^2}$, $i = L, R$, measure the amount of compositeness of the SM left- and right-handed up-type quark.

If the strong sector is flavour-anarchic, i.e., if the couplings of the Higgs boson to the composite fermions does not exhibit any particular flavour structure, the relation Eq. (11.67) implies that the light fermions are mostly elementary states ($\sin \theta_i \ll 1$), while the third generation quarks need to have a sizable degree of compositeness. The partial compositeness paradigm offers an appealing dynamical explanation of the hierarchies in the fermion masses. In fact, assuming the strong sector to be almost conformal above the confinement scale, the low-energy values of the mass-mixing parameters $\lambda_{L,R}$ are determined by the (constant) anomalous dimension of the composite operator they mix with. If the UV scale at which the linear mixings are generated is large, then $\mathcal{O}(1)$ differences in the anomalous dimensions can generate naturally large hierarchies in the fermion masses via renormalisation group running [361]. While the introduction of partial compositeness greatly ameliorated the flavor problem of the original composite Higgs models, nevertheless, it did not solve the issue completely, at least in the case where the strong sector is assumed to be flavour-anarchic [362]. While the partial compositeness set-up naturally emerges in models built in space-times with extra dimensions, no fully realistic microscopic realisation of partial compositeness has been proposed in the literature.

Another nice aspect of the partial compositeness structure is the dynamical generation of the Higgs potential that is not arbitrary like in the SM. The Higgs boson being a pseudo-Nambu–Goldstone boson, its mass does not receive any contribution from the strong sector itself but it is generated at the one-loop level via the couplings of the SM particles to the strong sector since these interactions are breaking the global symmetries under which the Higgs doublet transforms non-linearly. Obtaining $v \ll f$, as required phenomenologically, requires some degree of tuning, which scales like $\xi \equiv v^2/f^2$. A mild tuning of the order of 10% ($\xi \approx 0.1$) is typically enough to comply with electroweak precision constraints. This is an important point: in partial compositeness models, the entire Higgs potential is generated at one loop, therefore the separation between v and f can only be obtained at a price of a tuning. This marks a difference with respect to the Little Higgs models which realise a parametric hierarchy between the quartic and mass terms through the collective symmetry breaking mechanism. In fact in Little Higgs models, the quartic coupling is a tree-level effect, leading to a potential

$$V(H) \approx \frac{g_{SM}^2}{16\pi^2} m_\rho^2 H^2 + g_{SM}^2 H^4, \tag{11.68}$$

where g_{SM} generically denotes the SM couplings. The minimisation condition reads $v^2/f^2 \sim g_\rho^2/(16\pi^2)$, therefore v is formally loop suppressed with respect to f . This is the major achievement of the Little Higgs constructions, which however comes at the price of the presence of sub-TeV vectors carrying EW quantum numbers and therefore giving rise generically to large oblique corrections to the propagators of the W and the Z gauge bosons.

After minimisation, the dynamically generated potential leads to an estimate of the Higgs boson mass as

$$m_H^2 \approx g_\rho^3 y_t^2 \pi^2 v^2. \tag{11.69}$$

It follows that the limit $f \rightarrow \infty$, i.e., $\xi \rightarrow 0$, is a true decoupling limit: all the resonances of the strong sector become heavy but the Higgs boson whose mass is protected by the symmetries of the coset G/H . When compared to the experimentally measured Higgs boson mass, this estimate puts an upper bound on the strength of the strong interactions: $g_\rho \lesssim 2$. In this limit of not so large coupling, the Higgs potential receives additional contributions. In particular, the fermionic resonances in the top sector which follow from the global symmetry structure of the new physics sector can help raising the Higgs boson mass. Using some dispersion relation techniques, the mass of the Higgs is connected to the resonance masses. In the minimal SO(5)/SO(4) model, it was shown [363] that a 125 GeV mass can be obtained if at least one of the fermionic resonances is lighter than $\sim 1.4 f$. As in SUSY scenarios, the top sector is playing a crucial role in the dynamics of EWSB and can provide the first direct signs of new physics. The direct searches for these top partners, in particular

the ones with exotic electric charges 5/3, are already exploring the natural parameter spaces of these models [364].

The main physics properties of a pseudo Nambu–Goldstone Higgs boson can be captured in a model-independent way by a small number of higher-dimensional operators. Indeed, the strong dynamics at the origin of the composite Higgs boson singles out a few operators among the complete list discussed earlier in Section 11.6: these are the operators that involve extra powers of the Higgs doublets and they are therefore generically suppressed by a factor $1/f^2$ as opposed to the operators that involve extra derivatives or gauge bosons that are suppressed by a factor $1/(g_\rho^2 f^2)$. The relevant effective Lagrangian describing a strongly interacting light Higgs boson is:

$$\begin{aligned} \mathcal{L}_{\text{SILH}} = & \frac{c_H}{2f^2} (\partial_\mu (\Phi^\dagger \Phi))^2 + \frac{c_T}{2f^2} (\Phi^\dagger \overleftrightarrow{D}^\mu \Phi)^2 - \frac{c_6 \lambda}{f^2} (\Phi^\dagger \Phi)^3 \\ & + \left(\sum_f \frac{c_f y_f}{f^2} \Phi^\dagger \Phi \bar{f}_L \Phi f_R + \text{h.c.} \right). \end{aligned} \tag{11.70}$$

Typically, these new interactions induce deviations in the Higgs boson couplings that scale like $\mathcal{O}(v^2/f^2)$. Hence the measurements of the Higgs boson couplings can be translated into some constraints on the compositeness scale, $4\pi f$, of the Higgs boson. The peculiarity of these composite models is that, due to the Goldstone nature of the Higgs boson, the direct couplings to photons and gluons are further suppressed and generically the coupling modifiers scale like

$$\begin{aligned} \kappa_{W,Z,f} & \sim 1 + \mathcal{O}\left(\frac{v^2}{f^2}\right), \quad \kappa_{Z,\gamma} \sim \mathcal{O}\left(\frac{v^2}{f^2}\right), \\ \kappa_{\gamma,g} & \sim \mathcal{O}\left(\frac{v^2}{f^2} \times \frac{y_t^2}{g_\rho^2}\right), \end{aligned} \tag{11.71}$$

where g_ρ denotes the typical coupling strength among the states of the strongly coupled sector and y_t is the top Yukawa coupling, the largest interaction that breaks the Goldstone symmetry. The $\kappa_{Z,\gamma,g}$ coupling modifiers are not generated by the strong coupling operators of Eq. (11.70) but by some subleading form-factor operator generated by loops of heavy resonances of the strong sector. The coupling modifiers also receive additional contributions from the other resonances of the strong sector, in particular the fermionic resonances of the top sector that are required to be light to generate a 125 GeV Higgs boson mass. Some indirect information on the resonance spectrum could thus be inferred by a precise measurement of the Higgs boson coupling deviations. However, it was realised, see in particular Ref. [266], that the task is actually complicated by the fact that, in the minimal models, these top partners give a contribution to both κ_t (resulting from a modification of the top Yukawa coupling) and κ_γ and κ_g (resulting from new heavy particles running into the loops) and the structure of interactions is such that the net effect vanishes for inclusive quantities like $\sigma(gg \rightarrow H)$ or $\Gamma(H \rightarrow \gamma\gamma)$ as a consequence of the Higgs low energy theorem [23, 24, 264]. So, one would need to rely on differential distribution, like the Higgs boson p_T distribution discussed in Section 11.2.4.1, to see the top partner effects in Higgs data [365]. The off-shell channel $gg \rightarrow H^* \rightarrow 4\ell$ [243] and the double Higgs boson production $gg \rightarrow HH$ [366] can also help to resolve the gluon loop and separate the top and top-partner contributions.

11.7.6.3 Minimal composite Higgs models

The minimal composite Higgs models (MCHM) are concrete examples of the partial compositeness paradigm. The Higgs doublet is described by the coset space $\text{SO}(5)/\text{SO}(4)$ where a subgroup $\text{SU}(2)_L \times \text{U}(1)_Y$ is weakly gauged and under which the four Goldstone bosons transform as a doublet of hypercharge 1. There is some freedom on how the global symmetry is acting on the SM fermions: in MCHM4 the quarks and leptons are embedded into spinorial representations of $\text{SO}(5)$, while in MCHM5 they are part of fundamental representations (it might also be interesting phenomenologically to consider larger representations

like MCHM14 [367] with the SM fermions inside a representation of dimension 14). It is also possible to consider that fermions of different chirality and flavour are in different representations of $\text{SO}(5)$, leading to a more varied phenomenology [368]. The non-linearly realised symmetry acting on the Goldstone bosons leads to general predictions of the coupling of the Higgs boson to the EW gauge bosons. For instance, it can be shown that the quadratic terms in the W and Z bosons read

$$m_W^2(H) \left(W_\mu W^\mu + \frac{1}{2 \cos^2 \theta_W} Z_\mu Z^\mu \right), \tag{11.72}$$

with $m_W(H) = \frac{gf}{2} \sin \frac{H}{f}$. Expanding around the EW vacuum, the expression of the weak scale is $v = f \sin(\langle H \rangle / f)$. And the values of the modified Higgs boson couplings to the W and Z become:

$$g_{HVV} = \frac{2m_V^2}{v} \sqrt{1 - v^2/f^2}, \quad g_{HHVV} = \frac{2m_V^2}{v^2} (1 - 2v^2/f^2). \tag{11.73}$$

Note that the Higgs boson couplings to gauge bosons is always suppressed compared to the SM prediction. This is a general result [369] that holds as long as the coset space is compact.

The Higgs boson couplings to the fermions depend on the representation which the SM fermions are embedded into. The most commonly used embeddings consider all fermion doublets and singlets in the same representations. While, in MCHM4 and MCHM5, the modifications of the couplings depend only on the Higgs boson compositeness scale, in MCHM14 the leading corrections depend also on the mass spectrum of the resonances [367]. This is due to the fact that more than one $\text{SO}(5)$ invariant gives rise to SM fermion masses. The (κ_V, κ_f) experimental fit of the Higgs boson couplings can be used to derive a lower bound on the Higgs boson compositeness scale $4\pi f \gtrsim 9 \text{ TeV}$, which is less stringent than the indirect bound obtained from EW precision data, $4\pi f \gtrsim 15 \text{ TeV}$ [370] but more robust and less subject on assumptions [371].

11.7.6.4 Twin Higgs models

In all composite models presented above, the particles responsible for canceling the quadratic divergences in the Higgs boson mass are charged under the SM gauge symmetries. In particular, the top partner carries color charge, implying a reasonably large minimal production cross section at the LHC. An alternative scenario, which is experimentally quite challenging and might explain the null result in various new physics searches, is the case nowadays referred to as “neutral naturalness” [13, 14], where the particles canceling the 1-loop quadratic divergences are neutral under the SM. The canonical example for such theories is the Twin Higgs model of Ref. [13]. This is an example of a pseudo-Goldstone boson model with an approximate global $\text{SU}(4)$ symmetry broken to $\text{SU}(3)$. The Twin Higgs model is obtained by gauging the $\text{SU}(2)_A \times \text{SU}(2)_B$ subgroup of $\text{SU}(4)$, where $\text{SU}(2)_A$ is identified with the SM $\text{SU}(2)_L$, while $\text{SU}(2)_B$ is the twin $\text{SU}(2)$ group. Gauging this subgroup breaks the $\text{SU}(4)$ symmetry explicitly, but quadratically divergent corrections do not involve the Higgs boson when the gauge couplings of the two $\text{SU}(2)$ subgroups are equal, $g_A = g_B$. The $\text{SU}(4) \rightarrow \text{SU}(3)$ breaking will also result in the breaking of the twin $\text{SU}(2)_B$ group and, as a result, three of the seven Goldstone bosons will be eaten, leaving 4 Goldstone bosons corresponding to the SM Higgs doublet. In fact, imposing the Z_2 symmetry on the full model will ensure the cancellation of all 1-loop quadratic divergences to the Higgs boson mass. Logarithmically divergent terms can, however, arise for example from gauge loops, leading to a Higgs boson mass of order $g^2 f / 4\pi$, which is of the order of the physical Higgs boson mass for $f \sim 1 \text{ TeV}$. The quadratic divergences from the top sector can be eliminated if the Z_2 protecting the Higgs boson mass remains unbroken by the couplings that result in the top Yukawa coupling. This can be achieved by introducing top partners charged under a twin $\text{SU}(3)_C$. In this case, the quadratic divergences are cancelled by top partners that are neutral under the SM gauge symmetries.

Twin Higgs models are low-energy effective theories valid up to a cutoff scale of order $\Lambda \sim 4\pi f \sim 5\text{--}10 \text{ TeV}$, beyond which a UV

completion has to be specified. The simplest such possibility is to also make the Higgs boson composite, and to UV complete the twin Higgs model via gauge and top partners at masses of the order of a few TeV. A concrete implementation is the holographic twin Higgs model [372], which also incorporates a custodial symmetry to protect the T -parameter from large corrections. It is based on a warped extra dimensional theory with a bulk $SO(8)$ gauge group, which incorporates the $SU(4)$ global symmetry discussed above enlarged to contain the $SU(2)_L \times SU(2)_R$ custodial symmetry. In addition the bulk contains either a full $SU(7)$ group or an $SU(3) \times SU(3) \times U(1) \times U(1) \times Z_2$ subgroup of it to incorporate the QCD, its twin, and the hypercharge local symmetries. The breaking on the UV brane is to the SM symmetries and their twin symmetries, while on the IR brane $SO(8) \rightarrow SO(7)$, giving rise to the 7 Goldstone bosons, three of which will be again eaten by the twin W, Z . The main difference compared to ordinary composite Higgs models is that, in composite twin Higgs models, the cancellation of the one-loop quadratic divergences is achieved by the twin partners. They have a mass of order $700 \text{ GeV} - 1 \text{ TeV}$ and they are uncharged under the SM gauge group. This allows the IR scale of the warped extra dimension to be raised to the multi-TeV range without reintroducing the hierarchy problem. The role of the composite partners is to UV complete the theory, rather than to cancel the one-loop quadratic divergences. For more details about the composite twin Higgs models, see Refs. [373].

11.7.7 Searches for signatures of extended Higgs sectors

The measurements described in Sections 11.3 to 11.6 have established the existence of one state of the electroweak symmetry breaking sector, compatible with a SM Higgs boson, but not that it is the only one. As was discussed above, several classes of models beyond the SM require extended Higgs sectors. The searches are typically designed to be as model-independent as possible⁸ and can be categorised in the classes summarised as follows:

- (i) the search for an additional CP -even state mostly in the high mass domain decaying to vector bosons, which would correspond either to the heavy CP -even state in a generic 2HDM where the light state would be the discovered Higgs boson at 125 GeV or to a generic additional singlet;
- (ii) the search for a state in the high mass domain decaying to pairs of fermions, which would correspond to the CP -odd A or the heavy CP -even state H in a generic 2HDM;
- (iii) the search for charged Higgs bosons, which also appear in generic 2HDMs;
- (iv) the search for a CP -odd state a in the low mass region which appears in the NMSSM in a variety of final states, e.g., with one or two a bosons decaying to pairs of photons, muons, taus, and b -quarks;
- (v) the search for doubly charged Higgs bosons which are expected in extensions of the Higgs sector with triplets.

Below is a concise description of the most recent searches performed at the LHC and elsewhere. A summary of these searches in terms of final states is given in Table 11.15 where the corresponding references are given for more details.

11.7.7.1 Searches for an additional CP -even state

(a) Exclusion limits from LEP

The searches for the SM Higgs boson at LEP provided an absolute lower limit of 114 GeV on its mass. These searches are also relevant for non-SM Higgs bosons. These searches were interpreted as 95% CL upper bounds on the ratio of the coupling g_{HZZ} to its SM prediction as a function of the Higgs boson mass [122, 436]. These results have an impact on MSSM benchmarks such as the low- m_H scenario, which is also nearly ruled out by current direct constraints and charged Higgs boson limits from LHC. These results also impact scenarios of light CP -even Higgs boson of the NMSSM which are constrained to project predominantly onto the

⁸Still, most non-SUSY models are likely to include further states and dynamics above the weak scale to stabilise the scalar sector and this new and unknown physics may influence the searches described in this section in a way difficult to estimate.

EW singlet component. Additional interest for these scenarios is due to the slight excess observed at LEP [122] at a Higgs boson mass hypothesis of approximately 98 GeV .

(b) Searches at the LHC

At the LHC, the searches for the SM Higgs boson before the 2012 discovery covered a wide range of mass hypotheses up to approximately 1 TeV . After the discovery, the SM Higgs boson searches have been reappraised to search for a heavy CP -even state, extending progressively the search mass range beyond 1 TeV . This state could be the heavy CP -even Higgs boson of a 2HDM, or a generic additional singlet. In both cases, the natural width of the additional H state can be very different from that of the SM Higgs boson. To preserve unitarity of the longitudinal vector boson scattering and the longitudinal vector boson scattering into fermion pairs, the couplings of the additional CP -even Higgs boson to gauge bosons and fermions should not be too large and should constrain the natural width to be smaller than that of a unique Higgs boson at high mass with couplings to fermions and gauge bosons as predicted by the SM (and provided that trilinear and quartic couplings are not too large and that no new state affects the heavy state total width). It is therefore reasonable to consider total widths for the high mass CP -even state smaller than the equivalent SM width. Two specific cases have been considered: (i) the SM width using the complex pole scheme (CPS), and (ii) the narrow width approximation. For the sake of generality, these searches are now done as a function of the Higgs boson mass and total width.

Searches for the Higgs boson in the channels $H \rightarrow \gamma\gamma$, $H \rightarrow Z\gamma$, $H \rightarrow WW^{(*)}$ leptonic and semi-leptonic, and in the $H \rightarrow ZZ^{(*)}$ searches in the 4ℓ , $\ell\ell q\bar{q}$ and $\ell\ell\nu\nu$ channels have also been done, but some of them are simple reinterpretations of the SM Higgs boson search in the CPS scheme. References for these searches are summarised in Table 11.15.

(c) Searches for an additional resonance decaying to a pair of Higgs bosons

In addition to the rare and expected Higgs boson pair production mode, high mass CP -even Higgs bosons can be searched for in the resonant double Higgs boson mode. Searches for such processes, where the Higgs boson is used as a tool for searches for BSM phenomena, have been carried out in a variety of distinct modes depending on the subsequent decays of each Higgs bosons. ATLAS and CMS have searched for the $H \rightarrow hh \rightarrow b\bar{b}\tau\tau$, $b\bar{b}\gamma\gamma$, $H \rightarrow hh \rightarrow 4b$, $H \rightarrow hh \rightarrow \gamma\gamma WW^{*}$, $H \rightarrow hh \rightarrow b\bar{b}WW^{*}$, $H \rightarrow hh \rightarrow WW^{*}WW^{*}$ and $H \rightarrow hh \rightarrow b\bar{b}ZZ^{*}$ final states. For mass hypotheses of an additional Higgs boson below 500 GeV , the two dominant search channels are the $b\bar{b}\gamma\gamma$ and the $b\bar{b}\tau\tau$ channels. For masses above 500 GeV , the most powerful search is with the $4b$ final state. As illustrated in Figure 11.19, these searches provide useful limits in the low $\tan\beta$ and high mass domain. The list of references for these searches is given in Table 11.15.

(d) Searches for an additional state with the presence of the Higgs boson

In the post-discovery era, analyses searching for additional Higgs bosons need to take into account the presence of the 125 GeV Higgs boson. For searches with sufficiently high mass resolution to disentangle the additional states which are not degenerate in mass, the strength of the observed state and limits on the signal strength of a potential additional state can be set independently, as discussed in the next section. However, in some cases where channels do not have a sufficiently fine mass resolution to resolve states nearly degenerate in mass, specific analyses need to be designed. There are two examples of such analyses: (i) the search for an additional state in the $H \rightarrow WW^{(*)} \rightarrow \nu\ell\nu$ channel in ATLAS, and (ii) the search for nearly degenerate states in the $H \rightarrow \gamma\gamma$ channel with the CMS detector.

In the $H \rightarrow WW^{(*)} \rightarrow \nu\ell\nu$ channel, the search for an additional state is done using a boosted decision tree combining several discriminating kinematic characteristics to separate both the signal from the background and a high mass signal H from the lower mass state h [437]. A simultaneous fit of the two states h

Table 11.15: Summary of references to the searches for additional states from extended Higgs sectors. (BBr) denotes the BaBar experiment and (TeV), the Tevatron experiments. Results using the full Run 2 dataset are indicated by (*). V denotes either the W or the Z boson. Only Run 2 searches references are indicated except when searches have been carried out using Run 1 data only. References for Run 1 searches are available in Ref. [123].

	ATLAS	CMS	Other experiments
<i>CP-even H</i>			
$H \rightarrow \gamma\gamma$	[374]	[375]	—
$H \rightarrow \gamma\gamma$ (low mass)	[374]	[376]	—
$H \rightarrow Z\gamma$	[176]	[377]	—
$H \rightarrow ZZ \rightarrow 4\ell$	[378]	[379]	—
$H \rightarrow ZZ \rightarrow \ell\nu\nu$	[378]	[380]	—
$H \rightarrow ZZ \rightarrow \ell\ell q\bar{q}$	[381]	[382]	—
$H \rightarrow ZZ \rightarrow \nu\nu q\bar{q}$	[381]	—	—
$H \rightarrow WW \rightarrow \ell\nu\ell\nu$	[383]	* [384]	—
$H \rightarrow WW \rightarrow \ell\nu q\bar{q}'$	[385]	[384]	—
$H \rightarrow VV \rightarrow q\bar{q}'q\bar{q}'(JJ)$	[386, 387]	—	—
$H \rightarrow VV$ combination	[388]	—	—
$H \rightarrow hh \rightarrow b\bar{b}\tau\tau, b\bar{b}\gamma\gamma, 4b,$ $\gamma\gamma WW^*, bbWW^*, WW^*WW^*, bbZZ^*$	* [389, 390]	[391–393]	—
<i>CP-odd A (and/or CP-even H)</i>			
$H, A \rightarrow \tau^+\tau^-$	* [394]	* [395]	[396, 397] (TeV) [398] (LHCb)
$A \rightarrow \tau^+\tau^-$ (low mass)	—	[399]	—
$H, A \rightarrow \mu^+\mu^-$	[400]	[401]	—
$H \rightarrow \mu\tau, e\tau$ LFV	—	[402]	—
$bj\mu^+\mu^-$ (low $\mu^+\mu^-$ mass)	* [403]	[404]	—
$H, A \rightarrow t\bar{t}$	* [387, 405]	[406]	—
$H, A \rightarrow b\bar{b}$	[407]	[408]	[409, 410] (TeV)
$A \rightarrow hV \rightarrow b\bar{b}q\bar{q}', b\bar{b}\ell\nu, b\bar{b}\ell\ell, \ell\ell\tau\tau, \nu\bar{\nu}b\bar{b}$	* [411]	[392, 412]	—
$H \rightarrow ZA \rightarrow b\bar{b}\ell^+\ell^-$	—	[413]	—
<i>Charged H^\pm</i>			
$H^\pm \rightarrow \tau^\pm\nu$	* [414, 415]	* [416]	—
$H^\pm \rightarrow cs$	[417]	[418]	—
$H^\pm \rightarrow tb$	* [419]	[420]	—
$H^\pm \rightarrow W^\pm Z$	[421]	* [422]	—
$H^\pm \rightarrow W^\pm A$	—	* [423]	—
$H^\pm \rightarrow cb$	—	* [424]	—
<i>CP-odd NMSSM a</i>			
$a \rightarrow \mu^+\mu^-$	[425]	* [426]	—
$h \rightarrow aa \rightarrow 4\mu, 4\tau, 2\mu 2\tau, 4\gamma,$ $aa \rightarrow \mu^+\mu^-\mu^+\mu^-$	[427]	* [428] [430]	[429] (TeV)
$bb\mu\mu, bb\tau\tau$	—	—	[431] (LEP)
$\Upsilon_{1s,3s} \rightarrow a\gamma$	—	—	[432, 433] (BBr)
Doubly charged $H^{\pm\pm}$	* [434]	* [435]	—

and H is then made to test the presence of an additional state. In this case, the usual null hypothesis of background includes the SM signal.

The CMS search for nearly degenerate mass states decaying to a pair of photons [438] is more generic and could for instance apply to CP -odd Higgs bosons as well. It consists of a fit to the diphoton mass spectrum using two nearly degenerate mass templates.

(e) *Type I 2HDM and fermiophobia*

The measurements of coupling properties of the 125 GeV Higgs boson directly establish its couplings to fermions. However, the presence of an additional fermiophobic state, as predicted by Type I 2HDMs, is not excluded. Prior to the discovery, ATLAS and CMS have performed searches for a fermiophobic Higgs boson, i.e., produced through couplings with vector bosons only (VBF and VH) and decaying in two photons. CMS has further combined these results with searches in the W^+W^- and ZZ channels, assuming fermiophobic production and decay. This way, CMS excluded a fermiophobic Higgs boson in the range $110 \text{ GeV} < m_H < 188 \text{ GeV}$ at the 95% CL. References for these Run 1 measurements can be found in Ref. [123]

11.7.7.2 *Searches for additional neutral states ($\phi \equiv h, H, A$) decaying to fermions*

(a) *Exclusion limits from LEP*

In e^+e^- collisions, around the centre-of-mass energies reached by LEP, the main production mechanisms of the neutral MSSM Higgs bosons were the Higgs-strahlung processes $e^+e^- \rightarrow hZ$, HZ and the pair production processes $e^+e^- \rightarrow hA$, HA , while the vector boson fusion processes played a marginal role. Higgs boson decays to $b\bar{b}$ and $\tau^+\tau^-$ were used in these searches.

The searches and limits from the four LEP experiments are described in Refs. [439]. The combined LEP data did not contain any excess of events which would imply the production of a Higgs boson. Combined limits were derived [436]. For $m_A \gg M_Z$, the limit on m_h is nearly that of the SM searches, as $\sin^2(\beta - \alpha) \approx 1$. For high values of $\tan\beta$ and low m_A ($m_A \leq m_h^{max}$), the $e^+e^- \rightarrow hA$ searches become the most important, and the lightest Higgs boson h is non SM-like. In this region, the 95% CL mass bounds are $m_h > 92.8 \text{ GeV}$ and $m_A > 93.4 \text{ GeV}$. In the m_h^{max} scenario [440], values of $\tan\beta$ from 0.7 to 2.0 are excluded taking $m_t = 174.3 \text{ GeV}$, while a much larger $\tan\beta$ region is excluded for other benchmark scenarios such as the no-mixing one.

A flavour-independent limit for Higgs bosons in the Higgs-strahlung process at LEP has also been set at 112 GeV [441].

Neutral Higgs bosons may also be produced by Yukawa processes $e^+e^- \rightarrow f\bar{f}\phi$, where the Higgs particle $\phi \equiv h, H, A$, is radiated off a massive fermion ($f \equiv b$ or τ^\pm). These processes can be dominant at low masses, and whenever the $e^+e^- \rightarrow hZ$ and hA processes are suppressed. The corresponding ratios of

the $f\bar{f}h$ and $f\bar{f}A$ couplings to the SM coupling are $-\sin\alpha/\cos\beta$ and $\tan\beta$, respectively. The LEP data have been used to search for $b\bar{b}b\bar{b}$, $b\bar{b}\tau^+\tau^-$, and $\tau^+\tau^-\tau^+\tau^-$ final states [442]. Regions of low mass and high enhancement factors are excluded by these searches.

The searches for the Higgs boson at LEP also included the case where it does not predominantly decay to a pair of b quarks. All four collaborations conducted dedicated searches for the Higgs boson with reduced model dependence, assuming it is produced via the Higgs-strahlung process, and not addressing its flavour of decay, a lower limit on the Higgs boson mass of 112.9 GeV is set by combining the data of all four experiments [441].

Using an effective Lagrangian approach and combining results sensitive to the $h\gamma\gamma$, $hZ\gamma$ and hZZ couplings, an interpretation of several searches for the Higgs boson was made and set a lower limit of 106.7 GeV on the mass of a Higgs boson that can couple anomalously to photons [441].

(b) Searches at the Tevatron and the LHC

The best sensitivity is in the regime with low to moderate m_A and with large $\tan\beta$ which enhances the couplings of the Higgs bosons to down-type fermions. The corresponding limits on the Higgs boson production cross section times the branching ratio of the Higgs boson into down-type fermions can be interpreted in MSSM benchmark scenarios [443]. If $\phi = A, H$ for $m_A > m_h^{\max}$, and $\phi = A, h$ for $m_A < m_h^{\max}$, the most promising channels at the Tevatron are the inclusive $p\bar{p} \rightarrow \phi \rightarrow \tau^+\tau^-$ process, with contributions from both $gg \rightarrow \phi$ and $b\bar{b}\phi$ production, and $b\bar{b}\phi, \phi \rightarrow \tau^+\tau^-$ or $\phi \rightarrow b\bar{b}$, with $b\tau\tau$ or three tagged b -jets in the final state, respectively. Although the Higgs boson production via gluon fusion has a higher cross section in general than via associated production, it cannot be used to study the $\phi \rightarrow b\bar{b}$ decay mode since the signal is overwhelmed by the QCD background.

CDF and D0 have searched for neutral Higgs bosons produced in association with bottom quarks and which decay into $b\bar{b}$ [409, 410], or into $\tau^+\tau^-$ [396, 397]. The most recent searches in the $b\bar{b}\phi$ channel with $\phi \rightarrow b\bar{b}$ analyse approximately 2.6 fb^{-1} (CDF) and 5.2 fb^{-1} (D0) of data, seeking events with at least three b -tagged jets. The cross section is defined such that at least one b quark not from ϕ decay is required to have $p_T > 20\text{ GeV}$ and $|\eta| < 5$. The invariant mass of the two leading jets as well as b -tagging variables are used to discriminate the signal from the backgrounds. The QCD background rates and shapes are inferred from data control samples, in particular, the sample with two b -tagged jets and a third, untagged jet. Separate-signal hypotheses are tested and limits are placed on $\sigma(p\bar{p} \rightarrow b\bar{b}\phi) \times \text{BR}(\phi \rightarrow b\bar{b})$. A local excess of approximately 2.5σ significance has been observed in the mass range of 130–160 GeV, but D0's search is more sensitive and sets stronger limits. The D0 result had a $\mathcal{O}(2\sigma)$ local upward fluctuation in the 110 to 125 GeV mass range. These results have been superseded by the LHC searches and the excess seen by D0 has not been confirmed elsewhere.

A substantially larger sensitivity in the search for the $\phi \rightarrow \tau^+\tau^-$ is obtained with the ATLAS and CMS analyses. The higher centre-of-mass energy reached at the Run 2 brings a substantial, though not excessively large, increase in sensitivity due to the intermediate masses probed. Both ATLAS and CMS have reported the result of their searches in this important channel with the full 2016 dataset. The searches are performed in categories of the decays of the two tau leptons: $e\tau_{\text{had}}, \mu\tau_{\text{had}}, e\mu$, and $\mu\mu$, where τ_{had} denotes a tau lepton which decays to one or more hadrons plus a tau neutrino, e denotes $\tau \rightarrow e\nu\nu$, and μ denotes $\tau \rightarrow \mu\nu\nu$. The dominant background comes from $Z \rightarrow \tau^+\tau^-$ decays, although $t\bar{t}$, W +jets and Z +jets events contribute as well. Separating events into categories based on the number of b -tagged jets improves the sensitivity in the MSSM. The $b\bar{b}$ annihilation process and radiation of a Higgs boson from a b quark gives rise to events in which the Higgs boson is accompanied by a $b\bar{b}$ pair in the final state. Requiring the presence of one or more b -jets reduces the background from Z +jets. Data control samples are used to constrain background rates. The rates for jets to be identified as a hadronically decaying tau lepton are measured in dijet samples, and W +jets samples provide a measurement of the rate of

events that, with a fake hadronic tau, can pass the signal selection requirements. Lepton fake rates are measured using samples of isolated lepton candidates and same-sign lepton candidates. Constraints from the ATLAS searches are shown in Fig. 11.19 (left) in the hMSSM approximation defined in Ref. [314]. The neutral Higgs boson searches consider the contributions of both the CP -odd and CP -even neutral Higgs bosons with enhanced couplings to bottom quarks, similarly to was done for the Tevatron results. In Fig. 11.19, decays of the charged Higgs boson into $\tau\nu$ and decays of the heavy Higgs boson into a pair of SM-like Higgs bosons or gauge bosons, or decays of A into hZ are also being constrained. In addition, decays of the neutral Higgs bosons into muon pairs are also being explored. In the m_h -mod+ scenario the region of $\tan\beta$ lower than 5 does not allow for a Higgs boson mass m_h close to 125 GeV. For the hMSSM scenario, instead, the SM-like Higgs boson mass is fixed as an input and hence the requirement that it is close to 125 GeV is always fulfilled, although this may imply other limitations as discussed in Section 11.7.1.1.

A search for $\phi \rightarrow \mu^+\mu^-$ has also been performed by ATLAS [400] and CMS [401].

Finally searches for a resonance decaying to a top quark pair were done by ATLAS [405, 444] and CMS [406, 445]. These searches were interpreted as searches for scalar resonances by ATLAS [405], however, an important component of these searches is an accurate treatment of the interference effects between the signal and the continuum background. These effects can yield a dip and peak structure instead of a simple peak [311]. ATLAS has performed a search for a high mass state decaying to a pair of top quarks taking into account the deformation in mass shape of the signal in the presence of the continuum background [446].

The LHC has the potential to explore a broad range of SUSY parameter space through the search for non-SM-like Higgs bosons. As illustrated in Fig. 11.19, the parameter space corresponding to large $\tan\beta$ values and large masses of the A boson are covered mostly by the searches in the $A, H \rightarrow \tau^+\tau^-$ channel. A projection of the combined sensitivity of ATLAS and CMS at the HL-LHC has been performed in Ref. [104], showing that, compared to the current sensitivity, the full HL-LHC luminosity can expand the exclusion domain by nearly 1 TeV. In the low $\tan\beta$ limit, the parameter space spanning large A boson masses is best excluded indirectly from the observed Higgs boson measurements. This is illustrated in the Mh125 scenario by the nearly horizontal exclusion which is due to the compatibility of the Higgs boson mass measurement with its prediction from radiative corrections (mostly from the stop sector). Nevertheless, Fig. 11.19 (right) shows a broad region with intermediate $\tan\beta$ and large values of m_A that is not accessed by current searches, and in which the most promising channel is the very difficult search for $t\bar{t}$ decays with its aforementioned intricacies. In this region of parameter space, it is possible that only the SM-like Higgs boson can be within the LHC's reach. If no other state of the EWSB sector than the 125 GeV state is discovered, it may be challenging to determine only from the Higgs sector whether there is a SUSY extension of the SM in nature.

11.7.7.3 Searches for a CP -odd state decaying to hZ

Similarly to the search for a CP -even high mass Higgs boson decaying to a pair of Higgs bosons, the search for a CP -odd states decaying to hZ was carried out at the LHC by ATLAS and CMS in various channels:

- (i) $(Z \rightarrow \ell\ell)(h \rightarrow b\bar{b})$,
- (ii) $(Z \rightarrow \nu\nu)(h \rightarrow b\bar{b})$,
- (iii) $(Z \rightarrow \ell\ell)(h \rightarrow \tau\tau)$,
- (iv) and $(Z \rightarrow \ell\ell)(h \rightarrow \tau\tau)$.

The searches where the A boson decays to a pair of b quarks have been performed both in the regime where both b -jets are resolved and in the boosted regime where the two b -jets are merged in a single larger radius jet. These searches have been used to constrain the parameter space of 2HDMS. In the MSSM, these searches place limits on small values of $\tan\beta$ for masses of A between 220 GeV and 360 GeV.

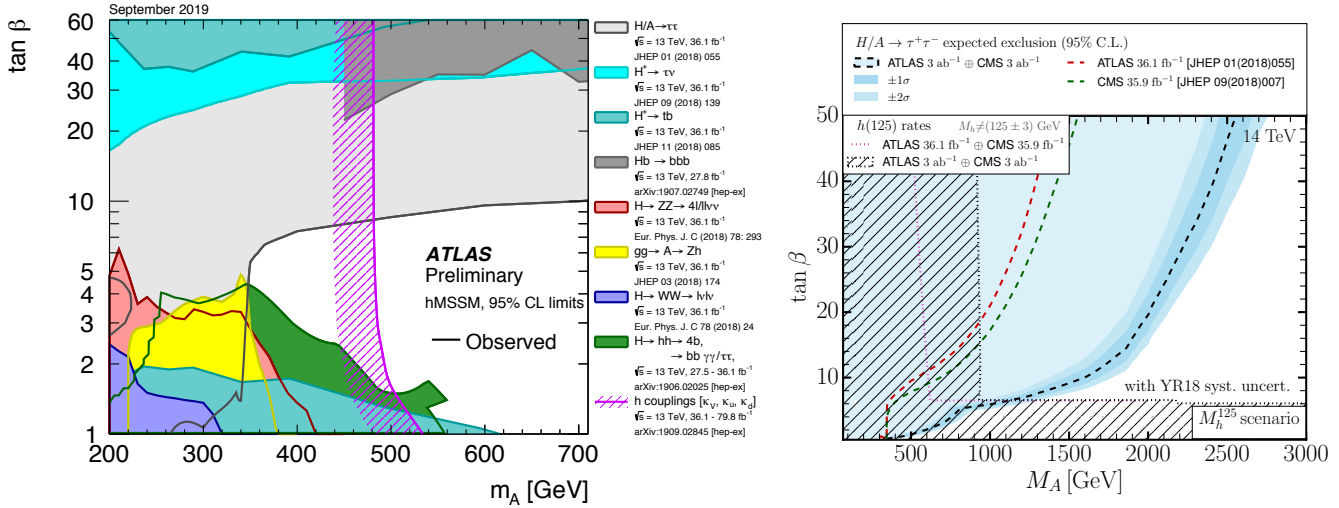


Figure 11.19: The 95% CL exclusion contours in the $(M_A, \tan\beta)$ parameter space for: (left) a summary of ATLAS Run 2 searches in the hMSSM and (right) the projected sensitivity for the combination of ATLAS and CMS searches in the $A, H \rightarrow \tau^+\tau^-$ channel at HL-LHC and the interpretation of the constraints from the measurements of the Higgs boson couplings in the M_h^{125} benchmark (the projected ATLAS sensitivity in the $A, H \rightarrow \tau^+\tau^-$ channel used for this projection was not optimised for high masses, when re-optimised similar sensitivities are obtained between ATLAS and CMS).

11.7.7.4 Searches for low mass states

Searches for pseudo-scalar Higgs boson at intermediate to low masses, below the Z mass (in the 25 GeV to 80 GeV mass range) have been performed by CMS both in the $\tau^+\tau^-$ [447] and the $\mu^+\mu^-$ [448] decay channels. A light pseudo-scalar in this mass range is excluded by current direct constraints in the MSSM but not in general 2HDMs [449]. These searches are done in the decay channels where the pseudo-scalar Higgs boson is produced in association with a pair of b -quarks and decays into a pair of taus or muons.

CMS has also reported an anomaly observed in the search for $\mu^+\mu^-$ resonances produced with one jet tagged as containing a b -hadron and a forward jet in the Run 1 data. A mild excess appeared in the di-muon mass distribution at approximately 28 GeV. Another very mild excess was then also found in the 2016 Run 2 data [404]. ATLAS then performed a similar analysis with the full Run 2 dataset corresponding to an integrated luminosity of approximately 139 fb⁻¹, and no significant excess was found [403].

Searches for low mass Higgs bosons were also performed in the diphoton channel by both ATLAS and CMS [450, 451] at Run 1. CMS has updated the results of this search with the full 2016 dataset [452]. A modest excess has been observed by CMS at a mass of 95.3 GeV with a local significance of 2.8σ (the corresponding global significance is 1.3σ). A slight excess was also seen by CMS in the 8 TeV data at a slightly higher mass of 97.6 GeV with a local significance of 2.0σ (1.47σ global). No significant excess has been observed in this region by ATLAS neither in the Run 1 nor Run 2 [374] data. It should, however, be noted that the ATLAS search does not reach the level of sensitivity to exclude at the 95% CL the excess seen in CMS. This mildly significant excess also coincides in mass with the excess observed at LEP and discussed in Section 11.7.7.1. It has therefore raised interest and speculations on its possible nature, see for instance Ref. [453] and references therein.

11.7.7.5 Searches for charged Higgs bosons H^\pm

At e^+e^- colliders, charged Higgs bosons can be pair produced in the s -channel via γ or Z boson exchange. This process is dominant in the LEP centre-of-mass energies range, i.e., up to 209 GeV. At higher centre-of-mass energies, other processes can play an important role such as the production in top quark decays via $t \rightarrow b + H^\pm$ if $m_{H^\pm} < m_t - m_b$ or via the one-loop process $e^+e^- \rightarrow W^\pm H^\mp$ [454, 455], which allows the production of a charged Higgs boson with $m_{H^\pm} > \sqrt{s}/2$, even when H^+H^- production is kinematically forbidden. Other single charged Higgs boson production mechanisms include $t\bar{b}H^-/\bar{t}bH^+$

production [108], $\tau^+\nu H^-/\tau^-\bar{\nu}H^+$ production [456], and a variety of processes in which H^\pm is produced in association with a one or two other gauge and/or Higgs bosons [457].

At hadron colliders, charged Higgs bosons can be produced in several different modes depending on the value of its mass with respect to the top-quark mass. For light values of the charged Higgs boson mass, defined by Higgs boson masses smaller than the mass of the top quark (with experimental analyses typically considering masses up to $m_{H^\pm} \leq 160$ GeV), the top-quark decay $t \rightarrow Hb$ is allowed and the charged Higgs boson is light enough so that top-quark off-shell effects can be neglected. The cross section for the production of a light charged Higgs boson is simply given by the product of the top-pair production cross section and the branching ratio of a top quark into a charged Higgs boson. The top-pair production cross section is known up to NNLO in perturbative QCD [458], and relevant QCD and SUSY-QCD including NLO corrections to the branching ratio for $t \rightarrow H^+b$ have been computed in the literature, see Refs. [459–461] and references therein. At present, the theoretical accuracy for the production of a light charged Higgs boson is at the few percent level. For the intermediate mass range, values of m_{H^\pm} near m_t , the finite top-width effects as well as the interplay between top-quark resonant and non-resonant diagrams cannot be neglected. Hence, the full process $pp \rightarrow H^\pm W^\mp b\bar{b}$ (with massive b -quarks) must be considered to perform a reliable perturbative calculation of the charged Higgs boson production cross section [461]. For heavy charged Higgs boson scenarios, with charged Higgs boson masses larger than the top-quark mass (typically above 180 GeV), the dominant charged Higgs boson production channel is the associated production with a top quark/antiquark and a (possibly low transverse momentum) bottom antiquark/quark. Theoretical calculation at NLO have been computed both at the inclusive and fully-differential level in the five-flavour scheme and in the four-flavour scheme, see Ref. [44] and references therein. Charged Higgs bosons can also be produced via associated production with W^\pm bosons through $b\bar{b}$ annihilation and gg -fusion annihilation [462].

For charged Higgs boson production cross section predictions for the Tevatron and the LHC, see Refs. [42, 43, 310].

(a) Exclusion limits from LEP

Charged Higgs bosons have been searched for at LEP, where the combined data of the four experiments, ALEPH, DELPHI, L3, and OPAL, were sensitive to masses of up to about 90 GeV [436] in two decay channels, $\tau\nu$ and $c\bar{s}$. The combined LEP data exclude, at 95% CL, charged Higgs bosons with mass below 80 GeV (Type II scenario) or 72.5 GeV (Type I scenario) [463].

(b) Exclusion limits from Tevatron

Compared to the mass domain covered by LEP searches, the Tevatron covered a complementary range of charged Higgs boson masses. CDF and D0 have also searched for charged Higgs bosons in top quark decays with subsequent decays to $\tau\nu$ or to $c\bar{s}$ [464]. For the $H^+ \rightarrow c\bar{s}$ channel, the limits on $\text{BR}(t \rightarrow H^+b)$ from CDF and D0 are $\approx 20\%$ in the mass range $90 \text{ GeV} < m_{H^+} < 160 \text{ GeV}$ and assuming a branching fraction of 100% in this specific final state. $H^+ \rightarrow \tau^+\nu_\tau$ channel, D0's limits on $\text{BR}(t \rightarrow H^+b)$ are also $\approx 20\%$ in the same mass range and assuming a branching fraction of 100% in this final state. These limits are valid in general 2HDMs, and they have also been interpreted in terms of the MSSM [464].

(c) Exclusion limits from LHC

Similarly to the Tevatron, at the LHC, light charged Higgs bosons can be searched for in the decays of top quarks. The main initial production mode for light charged Higgs bosons ($m_{H^\pm} < m_t - m_b$) is top pair production. The subsequent decay modes of the charged Higgs boson for these searches are $\tau\nu$ and $c\bar{s}$. More recently, ATLAS and CMS have also searched for higher mass charged Higgs bosons ($m_{H^\pm} > m_t + m_b$) in $H^+ \rightarrow t\bar{b}$. The main production modes are the associated production of a charged Higgs boson in association with a top and a bottom quark or in association with a top quark only.

The decay $H^+ \rightarrow \tau^+\nu_\tau$ is searched typically in three final state topologies:

- (i) lepton+jets: with $t\bar{t} \rightarrow \bar{b}WH^+ \rightarrow \bar{b}\bar{b}(q\bar{q}')(\tau_{\text{lep}}\nu)$, i.e., the W boson decays hadronically and the tau decays into an electron or a muon, with two neutrinos;
- (ii) τ +lepton: with $t\bar{t} \rightarrow \bar{b}WH^+ \rightarrow \bar{b}\bar{b}(\ell\nu)(\tau_{\text{had}}\nu)$, i.e., the W boson decays leptonically (with $\ell = e, \mu$) and the tau decays hadronically;
- (iii) τ +jets: $t\bar{t} \rightarrow \bar{b}WH^+ \rightarrow \bar{b}\bar{b}(q\bar{q}')(\tau_{\text{had}}\nu)$, i.e., both the W boson and the τ decay hadronically.

CMS has also searched for the charged Higgs boson in the decay products of top quark pairs: $t\bar{t} \rightarrow H^\pm W^\mp b\bar{b}$ and $t\bar{t} \rightarrow H^+ H^- b\bar{b}$ as well. Three types of final states with large missing transverse energy and jets originating from b -quark hadronisation have been analysed: the fully-hadronic channel with a hadronically decaying tau in association with jets, the dilepton channel with a hadronically decaying tau in association with an electron or muon and the dilepton channel with an electron-muon pair. The results of the searches at the LHC are illustrated in Figure 11.19.

Both ATLAS and CMS have also searched for high mass charged Higgs bosons decaying to a top and bottom quarks. The main production mode for this search is the associated production with one top quark (5-flavour scheme) or a top quark and a bottom quark (4-flavour scheme) in the final state. The s -channel production mode where the charged Higgs boson is produced alone in the final state at tree level is also considered. This search is particularly intricate and it is sensitive to the modelling of the top pair production background produced in association with additional partons and in particular b -quarks. No excess was found and the results are expressed in terms of exclusion limits of cross section times branching fractions.

ATLAS and CMS have also searched for charged Higgs bosons in top quark decays assuming $\text{BR}(H^+ \rightarrow c\bar{s}) = 100\%$ [417, 418], and sets limits of $\approx 20\%$ on $\text{BR}(t \rightarrow H^+b)$ in the $90 \text{ GeV} < m_{H^+} < 160 \text{ GeV}$ mass range.

In 2HDMs, the decay of the charged Higgs boson to a W and a Z boson is allowed only at loop level and is therefore suppressed. However the $H^\pm \rightarrow W^\pm Z$ decay channel is allowed in Higgs triplet models. ATLAS [421] has searched for such decays, requiring that the charged Higgs boson is produced through the fusion of vector bosons. No excess with respect to the SM backgrounds has been observed in this channel, and the results are interpreted in the Georgi–Machacek model [349] discussed in Section 11.7.5.2.

At the LHC, various other channels still remain to be explored, in particular searches involving additional neutral scalars in particular in the WH , WA channels (A is the pseudo-scalar MSSM

Higgs boson), and in the Wa channel (a is the light CP -odd scalars of the NMSSM).

11.7.7.6 Interpretation of the measurements of the coupling properties of the Higgs boson

The 125 GeV Higgs boson being part of any hypothetically extended EWSB sector, it can be used through the compatibility of its measured couplings and mass with those predicted in specific models to provide constraints on these specific models parameters.

As discussed in Section 11.7.1.1, the mass of the Higgs boson limits drastically the MSSM parameter space and can be used to set limits on specific MSSM benchmarks. This is the case for the Mh125 scenario as illustrated in Figure 11.18 and in Figure 11.19, corresponding approximately to a lower limit on $\tan\beta$ in this model [104].

The measurements of the Higgs boson couplings, discussed in Section 11.6, can be interpreted in the framework of a constrained model where the couplings of the Higgs boson to vector bosons, up-type quarks, down-type quarks and leptons, are varied. In 2HDMs, these couplings are functions of the mixing angle α between the observed Higgs boson and the heavy CP -even neutral scalar, and of the ratio of the vacuum expectation values of the two doublets, $\tan\beta$. In the case of the MSSM, the two parameters are the A boson mass and $\tan\beta$ (the sole two parameters needed to describe the MSSM Higgs sector at tree level). The coupling measurements have been interpreted both by ATLAS [213] and CMS [214] in specific MSSM benchmarks and in 2HDMs. The exclusion contour in the hMSSM for the ATLAS combination [213] is illustrated in Figure 11.19.

11.7.7.7 Searches for a light CP -odd Higgs boson

A light pseudo-scalar boson a is present in any two Higgs doublet model enhanced with an additional singlet field. A prominent example is the NMSSM. The theoretical motivations for singlet extensions of the MSSM are discussed in Section 11.7.2. There is also a variety of other models with light additional spin-0 bosons such as two Higgs doublet models with a scalar, Little Higgs models or light scalar mediator to a dark sector.

In the framework of the NMSSM, the searches now focus on the low a mass region for several reasons:

- (i) in the NMSSM, the light pseudo-scalar a boson can, as a pseudo-Goldstone boson, be a natural candidate for an axion;
- (ii) scenarios where $m_a > 2m_b$ and a CP -even state h decaying to a pair of a ($m_h > 2m_a$) are excluded by direct searches at LEP in the four b 's channel [429, 436, 465];
- (iii) in the pre-discovery era, LEP limits on a CP -even Higgs boson resulted in fine tuning MSSM constraints [466] which could be evaded through non standard decays of the Higgs boson to aa ;
- (iv) in the NMSSM, a CP -odd a boson with a mass in the range 9.2–12 GeV can also account for the difference observed between the measured anomalous muon magnetic moment and its prediction [467].

The benchmark scenarios have also changed in the light of the Higgs boson discovery. The 125 GeV state could be the lightest or the next-to-lightest of the three CP -even states of the NMSSM. Light pseudo-scalar scenarios are still very interesting in particular for the potential axion candidate. There are three main types of direct searches for the light a boson:

- (i) for masses below the Υ resonance, the search is for radiative decays $\Upsilon \rightarrow a\gamma$ at B-factories;
- (ii) the inclusive search in high energy pp collisions at the LHC;
- (iii) the search for decays of the observed CP -even Higgs h boson into a pair of a bosons.

Radiative decays $\Upsilon \rightarrow a\gamma$ have been searched for in various colliders, the most recent results are searches for radiative decays of the $\Upsilon(1s)$ to $a\gamma$ with a subsequent decay of the a boson to a pair of taus at CLEO [468], and the radiative decays of the $\Upsilon(1s, 2s, 3s)$ to $a\gamma$ with subsequent decays to a pair of muons or taus by BaBar [432, 433].

Direct inclusive searches for the light pseudo scalar a boson were performed in the $a \rightarrow \mu\mu$ channel at the Tevatron by D0 [429] and by ATLAS [425], CMS [426], and LHCb [151] at the LHC.

Finally, searches for the decays of the Higgs boson to a pair of a bosons were performed with subsequent decays to four photons, in the four muons final state, in the two muons and two taus final state, and in the four taus final state.

No significant excess in the searches for a light CP -odd a boson was found and limits on the production times branching fractions of the a boson have been set.

References for all these searches are summarised in Table 11.15.

11.7.7.8 Searches for doubly charged Higgs bosons $H^{\pm\pm}$

As discussed in Section 11.7.5, the generation of small neutrino masses via the standard EWSB mechanism described in Section 11.2 requires unnaturally small Yukawa couplings, provided that neutrinos are Dirac-type fermions. A Majorana mass term with a see-saw mechanism for neutrinos, would allow for naturally small masses and would also yield a framework for the appealing scenario of leptogenesis. However, within the SM, Majorana mass terms correspond to (non-renormalizable) dimension-5 operators. Such effective interactions can be generated via renormalisable interactions with an electroweak triplet of complex scalar fields (corresponding to a type-II see-saw mechanism). Other models such as the Zee–Babu model, with the introduction of two $SU(2)_L$ singlets, also generate Majorana mass terms. The signature of such models would be the presence of doubly charged Higgs bosons $H^{\pm\pm}$.

The main production mechanisms of $H^{\pm\pm}$ bosons at hadron colliders are the pair production in the s -channel through the exchange of a Z boson or a photon and the associated production with a charged Higgs boson through the exchange of a W boson. Various searches for doubly charged Higgs bosons have been performed by ATLAS and CMS at Run 1 [469] and Run 2 [434, 435]. Typically, these searches aim at low values of the Higgs triplet vacuum expectation for which the doubly charged Higgs boson will decay mostly to leptons (for high values, the decay to W bosons will become predominant). These searches assume that the coupling to W bosons is negligible and that the main production mode is through the Drell–Yan process.

11.7.7.9 Searches for non-standard production processes of the Higgs boson

The discovery of the Higgs boson has also allowed for searches of BSM processes involving standard decays of the Higgs boson. One example directly pertaining to the search for additional states of the EWSB sector is the search for Higgs bosons in the cascade decay of a heavy CP -even Higgs boson decaying to charged Higgs boson and a W boson, and the charged Higgs boson subsequently decaying to H and another W boson. This search has been performed by ATLAS in $b\bar{b}$ decays of the 125 GeV Higgs boson [470].

11.7.7.10 Outlook on searches for additional states

The LHC program of searches for additional states covers a large variety of decay and production channels. Since the Higgs boson discovery, many new channels have been explored at the LHC, e.g., the searches for additional states decaying into hh or Vh or ZA . The search for charged Higgs bosons has been extended to include the WZ , WA and the very difficult $t\bar{b}$ decay channel.

11.8 Summary and outlook

Summary– The discovery of the Higgs boson is a major milestone in the history of particle physics as well as an extraordinary achievement of the LHC machine and the ATLAS and CMS experiments. Seven years after the discovery, substantial progress in the field of Higgs boson physics has been accomplished and a significant number of measurements probing the nature of this unique particle have been made. They are revealing an increasingly precise profile of the Higgs boson.

The LHC has now concluded its Run 2, delivering a dataset of 13 TeV pp collisions corresponding to an integrated luminosity of approximately 140 fb^{-1} of data collected by ATLAS and CMS. With the substantial increase in production rates at the higher

center-of-mass energy and the larger datasets, new landmark results in Higgs physics have been achieved.

Three new results of fundamental importance have been achieved with partial Run 2 datasets by ATLAS and CMS independently: (i) the clear and unambiguous observation of the Higgs boson decay to taus; (ii) the clear and unambiguous observation of the Higgs boson decay to a pair of b quarks; (iii) the clear and unambiguous observation of the production of the Higgs boson through the $t\bar{t}H$ process. These results provide direct evidence for the Yukawa coupling of the Higgs boson to fermions of the third generation: taus, bottom quarks and top quarks, at rates compatible with those expected in the SM. These, and all other experimental measurements, are consistent with the EWSB mechanism of the SM.

New theoretical calculations and developments in Monte-Carlo simulation pertaining to Higgs physics are still occurring at a rapid pace. For example, the theoretical prediction for the dominant gluon fusion production mode now includes the latest N3LO result, which is twice as precise as previous N2LO calculations. With these improvements in the state-of-the-art theory predictions and the increase in luminosity and center-of-mass energy, Higgs physics has definitively entered a precision era. Its impact can already be seen on the latest Run 2 combined measurements of the Higgs boson couplings (see Section 11.6).

Since the discovery of the Higgs boson, new ideas have emerged to probe its rare decays and production modes, as well as to indirectly measure the Higgs boson width through the study of its off-shell couplings, or via on-shell interference effects. The Higgs boson has now become part of the standard toolkit in searches for new physics.

Many extensions of the SM at higher energies call for an enlargement of the EWSB sector. Hence, direct searches for additional scalar states can provide valuable insights on the dynamics of the EWSB mechanism. The ATLAS and CMS experiments have searched for additional Higgs bosons in the Run 2 data, and have imposed constraints in broad ranges of mass and couplings for various scenarios with an extended Higgs sector.

The landscape of Higgs physics has been extended extraordinarily since its discovery. The current dataset is approximately only five percent of the total dataset foreseen for the High Luminosity phase of the LHC project. The current precisions on the measurements of the couplings of the Higgs boson to gauge bosons and third generation fermions are typically of the order of 10–20%. The uncertainty on the Higgs boson coupling to the muon is approximately 100%, and the upper limits on the branching fraction to new invisible or undetected particles are approximately 20%. The sensitivity to the Higgs boson self-coupling has not reached the SM value yet and there is no information on how the Higgs field acquired its VEV in the early times of the Universe. This situation allows for new challenges to ultimately increase further the reach in precision and it also widens the possibilities of unveiling the true nature and the dynamics of the electroweak symmetry breaking.

Outlook– The unitarisation of the vector boson scattering (VBS) amplitudes, dominated at high energies by their longitudinal polarisation, has been the basis of the *no lose* theorem at the LHC, and was a determining consideration in the building of the accelerator and detectors. It motivated the existence of a Higgs boson or the observability of manifestations of strong dynamics at the TeV scale. Now that a Higgs boson has been found and its couplings to gauge bosons are consistent with the SM predictions, perturbative unitarity is preserved to a large extent with the sole exchange of the Higgs boson, and without the need for any additional states. VBS is, however, still an important channel to further investigate in order to better understand the nature of the Higgs sector and the possible completion of the SM at the TeV scale. In association with the double Higgs boson production channel by vector boson fusion, VBS could, for instance, confirm that the Higgs boson is part of a weak doublet and also establish whether it is an elementary object or a composite state that could emerge as a pseudo-Nambu–Goldstone boson from a new underlying broken symmetry.

The fermion-Higgs boson couplings are not governed by local

gauge symmetry. Thus, in addition to a new particle, the LHC has also discovered a new force, different in nature from the other fundamental interactions since it is non-universal and distinguishes between the three families of quarks and leptons. The existence of the Higgs boson embodies the problem of an unnatural cancellation among the quantum corrections to its mass if new physics is present at scales significantly higher than the EW scale. The non-observation of additional states which could stabilise the Higgs boson mass is a challenge for natural scenarios like SUSY or models with a new strong interaction in which the Higgs boson is not a fundamental particle. This increasingly pressing paradox starts questioning the principle of naturalness.

The search for the Higgs boson has occupied the particle physics community for the last 50 years. Its discovery has shaped and sharpened the physics programs of the LHC and of prospective future accelerators [471]. With the HL-LHC, the precision will improve by a factor 5–10 on all observables with respect to current data. Table 11.12 displays the expected sensitivities in the characterization of the Higgs boson at HL-LHC: in this table, the parameters κ_i specify by how much the coupling of the Higgs boson to a given particle i deviates from the SM expectation. The only channels which are expected to be limited by data statistics are the rare decays to muons and $Z\gamma$. In all other cases, the experimental systematic uncertainties are similar to the statistical uncertainties, but the dominant source of uncertainty arises from theory, and this remains the case even after assuming that, by the end of the HL-LHC run, the theory uncertainties can be reduced by a factor two compared to the current uncertainties, a hypothesis that appears realistic but still requires dedicated and concerted work [104]. For both hadron and lepton colliders, some theoretical progress is crucial to fully exploit and capitalise on the experimental data. In particular, the expected HL-LHC data together with rapid ongoing progress in theoretical calculations are defining a new era of precision Higgs boson measurements.

Acknowledgements

We would like to thank many of our colleagues for proofreading this review, for useful criticism and for their input in general: W. Altmannshofer, J. de Blas, G. Branco, J. Campbell, F. Caola, F. Cerutti, C. Csáki, R. Contino, J. Conway, N. Craig, A. David, S. Dawson, J.B. De Vivie, J. D’Hondt, G. Durieux, C. Englert, J.R. Espinosa, A. Falkowski, L. Fayard, W. Fischer, S. Forte, M. Grazzini, J. Gu, H. Haber, B. Heinemann, S. Heinemeyer, J. Hubisz, A. Korytov, B. Jäger, H. Ji, T. Junk, P. Langacker, J. Lykken, F. Maltoni, M.L. Mangano, B. Mansoulié, M. McCullough, R. Mishra, M. Mühlleitner, B. Murray, M. Neubert, A. Nisati, Y. Paul, G. Perez, G. Petruccianni, A. Pomarol, E. Pontón, R. Rattazzi, D. Rebutti, F. Riva, R. Salerno, E. Salvioni, N. Shah, G. Shaughnessy, M. Spira, O. Stål, A. Strumia, K. Tackmann, R. Tanaka, J. Terning, A. Vartak, C. Wagner, A. Weiler, A. Wulzer, and G. Zanderighi. We are also most grateful to the ATLAS, CDF, CMS and D0 collaborations for their help with this review.

M.C. is supported by Fermilab, that is operated by Fermi Research Alliance, LLC under Contract No. DE-AC02-07CH11359 with the United States Department of Energy. C.G. is supported by the Helmholtz Association and by the Deutsche Forschungsgemeinschaft under Germany’s Excellence Strategy – EXC 2121 “Quantum Universe” – 390833306. V.S. is supported by the grant DE-SC0009919 of the United States Department of Energy.

References

- [1] G. Aad *et al.* (ATLAS), Phys. Lett. **B716**, 1 (2012), [arXiv:1207.7214].
- [2] S. Chatrchyan *et al.* (CMS), Phys. Lett. **B716**, 30 (2012), [arXiv:1207.7235].
- [3] S.L. Glashow, Nucl. Phys. **20**, 579 (1961); S. Weinberg, Phys. Rev. Lett. **19**, 1264 (1967); A. Salam, *Elementary Particle Theory*, eds.: Svartholm, Almqvist and Wiksells, Stockholm, 1968; S. L. Glashow, J. Iliopoulos and L. Maiani, Phys. Rev. **D2**, 1285 (1970).
- [4] F. Englert and R. Brout, Phys. Rev. Lett. **13**, 321 (1964), [157(1964)]; P. W. Higgs, Phys. Rev. **145**, 1156 (1966); G. S. Guralnik, C. R. Hagen and T. W. B. Kibble, Phys. Rev. Lett. **13**, 585 (1964), [162(1964)].
- [5] J. M. Cornwall, D. N. Levin and G. Tiktopoulos, Phys. Rev. Lett. **30**, 1268 (1973), [Erratum: Phys. Rev. Lett. **31**, 572 (1973)]; J. M. Cornwall, D. N. Levin and G. Tiktopoulos, Phys. Rev. **D10**, 1145 (1974), [Erratum: Phys. Rev. **D11**, 972 (1975)]; C. H. Llewellyn Smith, Phys. Lett. **46B**, 233 (1973); B. W. Lee, C. Quigg and H. B. Thacker, Phys. Rev. **D16**, 1519 (1977).
- [6] K. G. Wilson, Phys. Rev. **D3**, 1818 (1971); G. ’t Hooft, in *Proc. of 1979 Cargèse Institute on Recent Developments in Gauge Theories*, p. 135 Press, New York 1980; For a recent review, see G.F. Giudice, PoS EPS-HEP2013, 163 (2013).
- [7] J. Wess and B. Zumino, Phys. Lett. **49B**, 52 (1974).
- [8] S. P. Martin, Adv. Ser. Direct. High Energy Phys. 1–98 (1998), [hep-ph/9709356].
- [9] B.C. Allanach and H.E. Haber, *Supersymmetry, Part I (Theory)*, in this volume.
- [10] D. B. Kaplan and H. Georgi, Phys. Lett. **136B**, 183 (1984).
- [11] B. Bellazzini, C. Csaki and J. Serra, Eur. Phys. J. **C74**, 5, 2766 (2014), [arXiv:1401.2457]; G. Panico and A. Wulzer, Lect. Notes Phys. **913**, pp.1 (2016), [arXiv:1506.01961]; C. Csaki, C. Grojean and J. Terning, Rev. Mod. Phys. **88**, 4, 045001 (2016), [arXiv:1512.00468].
- [12] K.M. Black, R.S. Chivukula and M. Narain, *Dynamical Electroweak Symmetry Breaking: Implications of the H0*, in this volume.
- [13] Z. Chacko, H.-S. Goh and R. Harnik, Phys. Rev. Lett. **96**, 231802 (2006), [hep-ph/0506256]; Z. Chacko, H.-S. Goh and R. Harnik, JHEP **01**, 108 (2006), [hep-ph/0512088].
- [14] N. Craig *et al.*, JHEP **07**, 105 (2015), [arXiv:1501.05310]; N. Craig, S. Knapen and P. Longhi, Phys. Rev. Lett. **114**, 6, 061803 (2015), [arXiv:1410.6808].
- [15] P. W. Graham, D. E. Kaplan and S. Rajendran, Phys. Rev. Lett. **115**, 22, 221801 (2015), [arXiv:1504.07551]; J. R. Espinosa *et al.*, Phys. Rev. Lett. **115**, 25, 251803 (2015), [arXiv:1506.09217]; G. Dvali (2019), [arXiv:1908.05984].
- [16] T. Flacke *et al.*, JHEP **06**, 050 (2017), [arXiv:1610.02025].
- [17] M. Bauer, M. Carena and K. Gemmler, JHEP **11**, 016 (2015), [arXiv:1506.01719]; M. Bauer, M. Carena and K. Gemmler, Phys. Rev. **D94**, 11, 115030 (2016), [arXiv:1512.03458].
- [18] R. Barbieri, L. J. Hall and V. S. Rychkov, Phys. Rev. **D74**, 015007 (2006), [hep-ph/0603188].
- [19] D. E. Morrissey and M. J. Ramsey-Musolf, New J. Phys. **14**, 125003 (2012), [arXiv:1206.2942].
- [20] G. Degrandi *et al.*, JHEP **08**, 098 (2012), [arXiv:1205.6497]; S. Alekhin, A. Djouadi and S. Moch, Phys. Lett. **B716**, 214 (2012), [arXiv:1207.0980]; D. Buttazzo *et al.*, JHEP **12**, 089 (2013), [arXiv:1307.3536].
- [21] S. Weinberg, Phys. Rev. Lett. **43**, 1566 (1979).
- [22] See the particle listing section at <http://pdg.lbl.gov>.
- [23] J. R. Ellis, M. K. Gaillard and D. V. Nanopoulos, Nucl. Phys. **B106**, 292 (1976).
- [24] M. A. Shifman *et al.*, Sov. J. Nucl. Phys. **30**, 711 (1979), [Yad. Fiz.30,1368(1979)].
- [25] J. F. Gunion *et al.*, *The Higgs Hunter’s Guide*, Addison-Wesley (1990).
- [26] P. Sikivie *et al.*, Nucl. Phys. **B173**, 189 (1980); H. Georgi, Ann. Rev. Nucl. Part. Sci. **43**, 209 (1993).
- [27] M. J. G. Veltman, Nucl. Phys. **B123**, 89 (1977).
- [28] M. Luscher and P. Weisz, Nucl. Phys. **B290**, 25 (1987); M. Luscher and P. Weisz, Nucl. Phys. **B295**, 65 (1988).
- [29] V. Branchina, E. Messina and M. Sher, Phys. Rev. **D91**, 013003 (2015), [arXiv:1408.5302].

- [30] A. Hook *et al.*, JHEP **01**, 061 (2015), [arXiv:1404.5953]; J. Kearney, H. Yoo and K. M. Zurek, Phys. Rev. **D91**, 12, 123537 (2015), [arXiv:1503.05193].
- [31] J. R. Espinosa, D. Racco and A. Riotto, Phys. Rev. Lett. **120**, 12, 121301 (2018), [arXiv:1710.11196].
- [32] J. R. Espinosa, D. Racco and A. Riotto, JCAP **1809**, 09, 012 (2018), [arXiv:1804.07732].
- [33] A. Andreassen, W. Frost and M. D. Schwartz, Phys. Rev. **D97**, 5, 056006 (2018), [arXiv:1707.08124]; S. Chigusa, T. Moroi and Y. Shoji, Phys. Rev. Lett. **119**, 21, 211801 (2017), [arXiv:1707.09301].
- [34] M. Shaposhnikov and C. Wetterich, Phys. Lett. **B683**, 196 (2010), [arXiv:0912.0208]; M. Holthausen, K. S. Lim and M. Lindner, JHEP **02**, 037 (2012), [arXiv:1112.2415].
- [35] F. L. Bezrukov and M. Shaposhnikov, Phys. Lett. **B659**, 703 (2008), [arXiv:0710.3755]; F. L. Bezrukov, A. Magnin and M. Shaposhnikov, Phys. Lett. **B675**, 88 (2009), [arXiv:0812.4950].
- [36] C. P. Burgess, H. M. Lee and M. Trott, JHEP **09**, 103 (2009), [arXiv:0902.4465]; J. L. F. Barbon and J. R. Espinosa, Phys. Rev. **D79**, 081302 (2009), [arXiv:0903.0355]; M. P. Hertzberg, JHEP **11**, 023 (2010), [arXiv:1002.2995].
- [37] B. A. Kniehl, Phys. Rept. **240**, 211 (1994).
- [38] M. Spira, Fortsch. Phys. **46**, 203 (1998), [hep-ph/9705337].
- [39] M. Carena and H. E. Haber, Prog. Part. Nucl. Phys. **50**, 63 (2003), [hep-ph/0208209].
- [40] A. Djouadi, Phys. Rept. **457**, 1 (2008), [hep-ph/0503172].
- [41] S. Dittmaier *et al.* (LHC Higgs Cross Section Working Group), CERN Report **2011-002** (2011), [arXiv:1101.0593].
- [42] S. Dittmaier *et al.* (LHC Higgs Cross Section Working Group), CERN Report **2012-002** (2012), [arXiv:1201.3084].
- [43] S. Heinemeyer *et al.* (LHC Higgs Cross Section Working Group), CERN Report **2013-004** (2013), [arXiv:1307.1347].
- [44] D. de Florian *et al.* (LHC Higgs Cross Section Working Group), CERN Report **2017-002** (2016), [arXiv:1610.07922].
- [45] LHC Higgs Cross Section Working Group, <https://twiki.cern.ch/twiki/bin/view/LHCPhysics/LHCHXSWG>.
- [46] T. Aaltonen *et al.* (CDF, D0), Phys. Rev. **D88**, 5, 052014 (2013), [arXiv:1303.6346].
- [47] H. M. Georgi *et al.*, Phys. Rev. Lett. **40**, 692 (1978).
- [48] D. Graudenz, M. Spira and P. M. Zerwas, Phys. Rev. Lett. **70**, 1372 (1993).
- [49] M. Spira *et al.*, Nucl. Phys. **B453**, 17 (1995), [hep-ph/9504378].
- [50] C. Anastasiou *et al.*, Phys. Rev. Lett. **114**, 212001 (2015), [arXiv:1503.06056]; C. Anastasiou *et al.*, JHEP **05**, 058 (2016), [arXiv:1602.00695].
- [51] R. V. Harlander and K. J. Ozeren, JHEP **11**, 088 (2009), [arXiv:0909.3420]; A. Pak, M. Rogal and M. Steinhauser, JHEP **02**, 025 (2010), [arXiv:0911.4662].
- [52] J. Davies *et al.*, Phys. Rev. **D100**, 3, 034017 (2019), [arXiv:1906.00982].
- [53] S. Dawson, Nucl. Phys. **B359**, 283 (1991); A. Djouadi, M. Spira and P. M. Zerwas, Phys. Lett. **B264**, 440 (1991).
- [54] R. V. Harlander and W. B. Kilgore, Phys. Rev. Lett. **88**, 201801 (2002), [hep-ph/0201206]; C. Anastasiou and K. Melnikov, Nucl. Phys. **B646**, 220 (2002), [hep-ph/0207004]; V. Ravindran, J. Smith and W. L. van Neerven, Nucl. Phys. **B665**, 325 (2003), [hep-ph/0302135].
- [55] A. Djouadi and P. Gambino, Phys. Rev. Lett. **73**, 2528 (1994), [hep-ph/9406432]; S. Actis *et al.*, Phys. Lett. **B670**, 12 (2008), [arXiv:0809.1301]; U. Aglietti *et al.*, Phys. Lett. **B595**, 432 (2004), [hep-ph/0404071]; G. Degrandi and F. Maltoni, Phys. Lett. **B600**, 255 (2004), [hep-ph/0407249].
- [56] M. Bonetti, K. Melnikov and L. Tancredi, Phys. Rev. **D97**, 5, 056017 (2018), [Erratum: Phys. Rev. **D97**, 9, 099906 (2018)], [arXiv:1801.10403].
- [57] C. Anastasiou, R. Boughezal and F. Petriello, JHEP **04**, 003 (2009), [arXiv:0811.3458].
- [58] C. Anastasiou *et al.*, JHEP **03**, 162 (2019), [arXiv:1811.11211].
- [59] M. Bonvini *et al.*, JHEP **08**, 105 (2016), [arXiv:1603.08000]; B. Mistlberger, JHEP **05**, 028 (2018), [arXiv:1802.00833].
- [60] R. Boughezal *et al.*, Phys. Rev. Lett. **115**, 8, 082003 (2015), [arXiv:1504.07922].
- [61] X. Chen *et al.*, Phys. Lett. **B740**, 147 (2015), [arXiv:1408.5325].
- [62] J. M. Campbell, R. K. Ellis and S. Seth (2019), [arXiv:1906.01020].
- [63] J. M. Lindert *et al.*, Phys. Rev. Lett. **118**, 25, 252002 (2017), [arXiv:1703.03886]; J. M. Lindert *et al.*, Phys. Lett. **B782**, 210 (2018), [arXiv:1801.08226]; S. P. Jones, M. Kerner and G. Luisoni, Phys. Rev. Lett. **120**, 16, 162001 (2018), [arXiv:1802.00349]; T. Neumann, J. Phys. Comm. **2**, 9, 095017 (2018), [arXiv:1802.02981].
- [64] S. Forte and C. Muselli, JHEP **03**, 122 (2016), [arXiv:1511.05561]; K. Melnikov and A. Penin, JHEP **05**, 172 (2016), [arXiv:1602.09020]; T. Liu and A. Penin, JHEP **11**, 158 (2018), [arXiv:1809.04950].
- [65] F. Caola *et al.*, JHEP **09**, 035 (2018), [arXiv:1804.07632].
- [66] W. Bizon *et al.*, JHEP **02**, 108 (2018), [arXiv:1705.09127]; X. Chen *et al.*, Phys. Lett. **B788**, 425 (2019), [arXiv:1805.00736].
- [67] S. Catani and M. Grazzini, Eur. Phys. J. **C72**, 2013 (2012), [Erratum: Eur. Phys. J. **C72**, 2132 (2012)], [arXiv:1106.4652].
- [68] A. Banfi, G. P. Salam and G. Zanderighi, JHEP **06**, 159 (2012), [arXiv:1203.5773]; T. Becher, M. Neubert and D. Wilhelm, JHEP **05**, 110 (2013), [arXiv:1212.2621]; A. Banfi *et al.*, JHEP **04**, 049 (2016), [arXiv:1511.02886]; J. K. L. Michel, P. Pietrulewicz and F. J. Tackmann, JHEP **04**, 142 (2019), [arXiv:1810.12911]; P. F. Monni, L. Rottoli and P. Torrielli (2019), [arXiv:1909.04704].
- [69] I. Moulton and I. W. Stewart, JHEP **09**, 129 (2014), [arXiv:1405.5534].
- [70] W.-Y. Keung and F. J. Petriello, Phys. Rev. **D80**, 013007 (2009), [arXiv:0905.2775]; S. Bühler *et al.*, JHEP **07**, 115 (2012), [arXiv:1204.4415].
- [71] LHC Higgs Cross Section Working Group, "Recommended predictions for the boosted-Higgs cross section", Note LHCHXSWG-2019-002, <https://cds.cern.ch/record/2669113>.
- [72] V. D. Barger *et al.*, Phys. Rev. **D44**, 1426 (1991).
- [73] F. A. Dreyer and A. Karlberg, Phys. Rev. Lett. **117**, 7, 072001 (2016), [arXiv:1606.00840].
- [74] T. Han, G. Valencia and S. Willenbrock, Phys. Rev. Lett. **69**, 3274 (1992), [hep-ph/9206246].
- [75] T. Liu, K. Melnikov and A. A. Penin (2019), [arXiv:1906.10899].
- [76] M. Cacciari *et al.*, Phys. Rev. Lett. **115**, 8, 082002 (2015), [Erratum: Phys. Rev. Lett. **120**, 13, 139901 (2018)], [arXiv:1506.02660]; J. Cruz-Martinez *et al.*, Phys. Lett. **B781**, 672 (2018), [arXiv:1802.02445].
- [77] M. Rauch and D. Zeppenfeld, Phys. Rev. **D95**, 11, 114015 (2017), [arXiv:1703.05676].

- [78] S. L. Glashow, D. V. Nanopoulos and A. Yildiz, *Phys. Rev.* **D18**, 1724 (1978); T. Han and S. Willenbrock, *Phys. Lett.* **B273**, 167 (1991); T. Han, G. Valencia, and S. Willenbrock, *Phys. Rev. Lett.* **69**, 3274 (1992); H. Baer, B. Bailey and J. F. Owens, *Phys. Rev.* **D47**, 2730 (1993); J. Ohnemus and W. J. Stirling, *Phys. Rev.* **D47**, 2722 (1993).
- [79] A. Stange, W. J. Marciano and S. Willenbrock, *Phys. Rev.* **D49**, 1354 (1994), [hep-ph/9309294]; A. Stange, W. J. Marciano and S. Willenbrock, *Phys. Rev.* **D50**, 4491 (1994), [hep-ph/9404247].
- [80] M. L. Ciccolini, S. Dittmaier and M. Kramer, *Phys. Rev.* **D68**, 073003 (2003), [hep-ph/0306234]; A. Denner *et al.*, *JHEP* **03**, 075 (2012), [arXiv:1112.5142].
- [81] R. Hamberg, W. L. van Neerven and T. Matsuura, *Nucl. Phys.* **B359**, 343 (1991), [Erratum: *Nucl. Phys.* **B644**, 403 (2002)].
- [82] O. Brein, A. Djouadi and R. Harlander, *Phys. Lett.* **B579**, 149 (2004), [hep-ph/0307206]; L. Altenkamp *et al.*, *JHEP* **02**, 078 (2013), [arXiv:1211.5015].
- [83] O. Brein *et al.*, *Eur. Phys. J.* **C72**, 1868 (2012), [arXiv:1111.0761].
- [84] O. Brein, R.V. Harlander, and T.J. Zirke, *Comp. Phys. Comm.* **184**, 998 (2013).
- [85] A. Denner *et al.*, *JHEP* **03**, 075 (2012), [arXiv:1112.5142].
- [86] G. Ferrera, M. Grazzini, and F. Tramontano, *Phys. Rev. Lett.* **107**, 152003 (2011).
- [87] G. Ferrera, M. Grazzini and F. Tramontano, *Phys. Lett.* **B740**, 51 (2015), [arXiv:1407.4747]; J. M. Campbell, R. K. Ellis and C. Williams, *JHEP* **06**, 179 (2016), [arXiv:1601.00658].
- [88] W. Astill *et al.*, *JHEP* **06**, 154 (2016), [arXiv:1603.01620].
- [89] F. Caola *et al.*, *Phys. Rev.* **D97**, 7, 074022 (2018), [arXiv:1712.06954]; R. Gauld *et al.* (2019), [arXiv:1907.05836].
- [90] J. M. Butterworth *et al.*, *Phys. Rev. Lett.* **100**, 242001 (2008), [arXiv:0802.2470].
- [91] R. Raitio and W. W. Wada, *Phys. Rev.* **D19**, 941 (1979); Z. Kunszt, *Nucl. Phys.* **B247**, 339 (1984); J. F. Gunion, *Phys. Lett.* **B261**, 510 (1991); W. J. Marciano and F. E. Paige, *Phys. Rev. Lett.* **66**, 2433 (1991).
- [92] W. Beenakker *et al.*, *Phys. Rev. Lett.* **87**, 201805 (2001), [hep-ph/0107081]; L. Reina and S. Dawson, *Phys. Rev. Lett.* **87**, 201804 (2001), [hep-ph/0107101]; S. Dawson *et al.*, *Phys. Rev.* **D67**, 071503 (2003), [hep-ph/0211438]; W. Beenakker *et al.*, *Nucl. Phys.* **B653**, 151 (2003), [hep-ph/0211352]; S. Dawson *et al.*, *Phys. Rev.* **D68**, 034022 (2003), [hep-ph/0305087].
- [93] Y. Zhang *et al.*, *Phys. Lett.* **B738**, 1 (2014), [arXiv:1407.1110]; S. Frixione *et al.*, *JHEP* **09**, 065 (2014), [arXiv:1407.0823].
- [94] T. Plehn, G. P. Salam and M. Spannowsky, *Phys. Rev. Lett.* **104**, 111801 (2010), [arXiv:0910.5472].
- [95] R. Frederix *et al.*, *Phys. Lett.* **B701**, 427 (2011), [arXiv:1104.5613]; M. V. Garzelli *et al.*, *EPL* **96**, 1, 11001 (2011), [arXiv:1108.0387].
- [96] F. Demartin *et al.*, *Eur. Phys. J.* **C75**, 6, 267 (2015), [arXiv:1504.00611].
- [97] K.A. Assamagan *et al.*, [Higgs Working Group, “Physics at TeV Colliders” workshop, Les Houches, 2003], arXiv:hep-ph/0406152 (2004).
- [98] R. V. Harlander and W. B. Kilgore, *Phys. Rev.* **D68**, 013001 (2003), [hep-ph/0304035]; J. M. Campbell *et al.*, *Phys. Rev.* **D67**, 095002 (2003), [hep-ph/0204093]; S. Dawson *et al.*, *Phys. Rev. Lett.* **94**, 031802 (2005), [hep-ph/0408077]; S. Dittmaier, M. Krämer and M. Spira, *Phys. Rev.* **D70**, 074010 (2004), [hep-ph/0309204]; S. Dawson *et al.*, *Phys. Rev.* **D69**, 074027 (2004), [hep-ph/0311067].
- [99] W. J. Stirling and D. J. Summers, *Phys. Lett.* **B283**, 411 (1992); F. Maltoni *et al.*, *Phys. Rev.* **D64**, 094023 (2001), [hep-ph/0106293].
- [100] S. Dawson, S. Dittmaier and M. Spira, *Phys. Rev.* **D58**, 115012 (1998), [hep-ph/9805244].
- [101] D. de Florian and J. Mazzitelli, *Phys. Rev. Lett.* **111**, 201801 (2013), [arXiv:1309.6594].
- [102] S. Borowka *et al.*, *Phys. Rev. Lett.* **117**, 1, 012001 (2016), [Erratum: *Phys. Rev. Lett.* **117**, 7, 079901 (2016)], [arXiv:1604.06447].
- [103] J. Baglio *et al.*, *Eur. Phys. J.* **C79**, 6, 459 (2019), [arXiv:1811.05692].
- [104] M. Cepeda *et al.* (HL/HE WG2 group) (2019), [arXiv:1902.00134].
- [105] B.L. Ioffe and V.A. Khoze, *Sov. J. Nucl. Phys.* **9**, 50 (1978).
- [106] D. R. T. Jones and S. T. Petcov, *Phys. Lett.* **84B**, 440 (1979); R. N. Cahn and S. Dawson, *Phys. Lett.* **136B**, 196 (1984), [Erratum: *Phys. Lett.* **138B**, 464 (1984)]; G. L. Kane, W. W. Repko and W. B. Rolnick, *Phys. Lett.* **148B**, 367 (1984); G. Altarelli, B. Mele and F. Pitolli, *Nucl. Phys.* **B287**, 205 (1987); W. Kilian, M. Kramer and P. M. Zerwas, *Phys. Lett.* **B373**, 135 (1996), [hep-ph/9512355].
- [107] B. A. Kniehl, *Z. Phys.* **C55**, 605 (1992); J. Fleischer and F. Jegerlehner, *Nucl. Phys.* **B216**, 469 (1983); A. Denner *et al.*, *Z. Phys.* **C56**, 261 (1992); B. A. Kniehl, *Int. J. Mod. Phys.* **A17**, 1457 (2002), [hep-ph/0112023].
- [108] K. J. F. Gaemers and G. J. Gounaris, *Phys. Lett.* **77B**, 379 (1978); A. Djouadi, J. Kalinowski and P. M. Zerwas, *Z. Phys.* **C54**, 255 (1992); B. A. Kniehl, F. Madricardo and M. Steinhauser, *Phys. Rev.* **D66**, 054016 (2002), [hep-ph/0205312]; S. Dittmaier *et al.*, *Phys. Lett.* **B441**, 383 (1998), [hep-ph/9808433]; S. Dittmaier *et al.*, *Phys. Lett.* **B478**, 247 (2000), [hep-ph/0002035]; S. Dawson and L. Reina, *Phys. Rev.* **D59**, 054012 (1999), [hep-ph/9808443].
- [109] A. Arbey *et al.*, *Eur. Phys. J.* **C75**, 8, 371 (2015), [arXiv:1504.01726].
- [110] A. Denner *et al.*, *Eur. Phys. J.* **C71**, 1753 (2011), [arXiv:1107.5909].
- [111] A. Djouadi, J. Kalinowski, and M. Spira, *Comp. Phys. Comm.* **108**, 56 (1998); A. Djouadi *et al.*, arXiv:1003.1643 [hep-ph] (2010).
- [112] S. G. Gorishnii *et al.*, *Mod. Phys. Lett.* **A5**, 2703 (1990); S. G. Gorishnii *et al.*, *Phys. Rev.* **D43**, 1633 (1991); A. L. Kataev and V. T. Kim, *Mod. Phys. Lett.* **A9**, 1309 (1994); L. R. Surguladze, *Phys. Lett.* **B341**, 60 (1994), [hep-ph/9405325]; S. A. Larin, T. van Ritbergen and J. A. M. Vermaseren, *Phys. Lett.* **B362**, 134 (1995), [hep-ph/9506465]; K. G. Chetyrkin and A. Kwiatkowski, *Nucl. Phys.* **B461**, 3 (1996), [hep-ph/9505358]; K. G. Chetyrkin, *Phys. Lett.* **B390**, 309 (1997), [hep-ph/9608318]; P. A. Baikov, K. G. Chetyrkin and J. H. Kuhn, *Phys. Rev. Lett.* **96**, 012003 (2006), [hep-ph/0511063].
- [113] J. Fleischer and F. Jegerlehner, *Phys. Rev.* **D23**, 2001 (1981); D. Yu. Bardin, B. M. Vilensky and P. K. Khristova, *Sov. J. Nucl. Phys.* **53**, 152 (1991), [*Yad. Fiz.*53,240(1991)]; A. Dabelstein and W. Hollik, *Z. Phys.* **C53**, 507 (1992); B. A. Kniehl, *Nucl. Phys.* **B376**, 3 (1992); A. Djouadi *et al.*, in “In *Munich/Annecy/Hamburg 1991, Proceedings, e+ e- collisions at 500-GeV, pt. A* 11-30,” (1991).
- [114] T. Inami, T. Kubota and Y. Okada, *Z. Phys.* **C18**, 69 (1983); K. G. Chetyrkin, B. A. Kniehl and M. Steinhauser, *Phys. Rev. Lett.* **79**, 353 (1997), [hep-ph/9705240]; P. A. Baikov and K. G. Chetyrkin, *Phys. Rev. Lett.* **97**, 061803 (2006), [hep-ph/0604194].
- [115] H.-Q. Zheng and D.-D. Wu, *Phys. Rev.* **D42**, 3760 (1990); A. Djouadi *et al.*, *Phys. Lett.* **B257**, 187 (1991); S. Dawson and R. P. Kauffman, *Phys. Rev.* **D47**, 1264 (1993); A. Djouadi, M. Spira and P. M. Zerwas, *Phys. Lett.*

- B311**, 255 (1993), [hep-ph/9305335]; K. Melnikov and O. I. Yakovlev, Phys. Lett. **B312**, 179 (1993), [hep-ph/9302281]; M. Inoue *et al.*, Mod. Phys. Lett. **A9**, 1189 (1994).
- [116] P. Maierhöfer and P. Marquard, Phys. Lett. **B721**, 131 (2013), [arXiv:1212.6233].
- [117] U. Aglietti *et al.*, Phys. Lett. **B595**, 432 (2004), [hep-ph/0404071]; G. Degrossi and F. Maltoni, Phys. Lett. **B600**, 255 (2004), [hep-ph/0407249]; S. Actis *et al.*, Phys. Lett. **B670**, 12 (2008), [arXiv:0809.1301]; U. Aglietti *et al.*, Phys. Lett. **B600**, 57 (2004), [hep-ph/0407162]; G. Degrossi and F. Maltoni, Nucl. Phys. **B724**, 183 (2005), [hep-ph/0504137]; U. Aglietti *et al.*, FERMI LAB-CONF (2006), [hep-ph/0612172].
- [118] A. Abbasabadi *et al.*, Phys. Rev. **D55**, 5647 (1997), [hep-ph/9611209]; A. Abbasabadi and W. W. Repko, Phys. Rev. **D71**, 017304 (2005), [hep-ph/0411152]; A. Abbasabadi and W. W. Repko, JHEP **08**, 048 (2006), [hep-ph/0602087]; D. A. Dicus and W. W. Repko, Phys. Rev. **D87**, 7, 077301 (2013), [arXiv:1302.2159]; L.-B. Chen, C.-F. Qiao and R.-L. Zhu, Phys. Lett. **B726**, 306 (2013), [arXiv:1211.6058]; Y. Sun, H.-R. Chang and D.-N. Gao, JHEP **05**, 061 (2013), [arXiv:1303.2230]; G. Passarino, Phys. Lett. **B727**, 424 (2013), [arXiv:1308.0422].
- [119] M. Spira, A. Djouadi and P. M. Zerwas, Phys. Lett. **B276**, 350 (1992).
- [120] A. Bredenstein *et al.*, Phys. Rev. **D74**, 013004 (2006), [hep-ph/0604011]; A. Bredenstein *et al.*, JHEP **02**, 080 (2007), [hep-ph/0611234]; A. Bredenstein *et al.*, Prophecy4f: A Monte Carlo generator for a proper description of the Higgs decay into 4 fermions, <http://omnibus.uni-freiburg.de/~sd565/programs/prophecy4f/prophecy4f.html>.
- [121] A. Ghinculov, Phys. Lett. **B337**, 137 (1994), [Erratum: Phys. Lett. **B346**, 426 (1995)], [hep-ph/9405394]; L. Durand, B. A. Kniehl and K. Riesselmann, Phys. Rev. **D51**, 5007 (1995), [hep-ph/9412311]; L. Durand, K. Riesselmann and B. A. Kniehl, Phys. Rev. Lett. **72**, 2534 (1994), [Erratum: Phys. Rev. Lett. **74**, 1699 (1995)].
- [122] R. Barate *et al.* (LEP Working Group for Higgs boson searches, ALEPH, DELPHI, L3, OPAL), Phys. Lett. **B565**, 61 (2003), [hep-ex/0306033].
- [123] M. Tanabashi *et al.* (Particle Data Group), Phys. Rev. **D98**, 3, 030001 (2018).
- [124] Y. L. Dokshitzer, S. I. Troian and V. A. Khoze, Sov. J. Nucl. Phys. **46**, 712 (1987), [Yad. Fiz. **46**, 1220 (1987)].
- [125] ATLAS Collaboration, ATLAS-CONF-2017-045 (2017).
- [126] CMS Collaboration, CMS-PAS-HIG-19-001 (2019).
- [127] G. Aad *et al.* (ATLAS, CMS), Phys. Rev. Lett. **114**, 191803 (2015), [arXiv:1503.07589].
- [128] ATLAS Collaboration, ATLAS-CONF-2019-029 (2019).
- [129] A. M. Sirunyan *et al.* (CMS), JHEP **11**, 185 (2018), [arXiv:1804.02716].
- [130] A. M. Sirunyan *et al.* (CMS), JHEP **11**, 047 (2017), [arXiv:1706.09936].
- [131] ATLAS Collaboration, ATLAS-CONF-2019-025 (2019).
- [132] M. Aaboud *et al.* (ATLAS), Phys. Lett. **B784**, 345 (2018), [arXiv:1806.00242].
- [133] CMS Collaboration, CMS-PAS-HIG-18-029 (2019).
- [134] ATLAS Collaboration, ATLAS-CONF-2016-009 (2016).
- [135] M. Dittmar and H. K. Dreiner, Phys. Rev. **D55**, 167 (1997), [hep-ph/9608317].
- [136] G. Aad *et al.* (ATLAS), JHEP **08**, 137 (2015), [arXiv:1506.06641].
- [137] ATLAS Collaboration, ATLAS-CONF-2016-112 (2016).
- [138] M. Aaboud *et al.* (ATLAS), Phys. Lett. **B789**, 508 (2019), [arXiv:1808.09054].
- [139] A. M. Sirunyan *et al.* (CMS), Phys. Lett. **B791**, 96 (2019), [arXiv:1806.05246].
- [140] G. Aad *et al.* (ATLAS), JHEP **04**, 117 (2015), [arXiv:1501.04943].
- [141] ATLAS and CMS Collaboration, ATLAS-CONF-2015-044 and CMS-PAS-HIG-15-002 (2015).
- [142] M. Aaboud *et al.* (ATLAS), Phys. Rev. **D99**, 072001 (2019), [arXiv:1811.08856].
- [143] A. M. Sirunyan *et al.* (CMS), Phys. Lett. **B779**, 283 (2018), [arXiv:1708.00373].
- [144] A. M. Sirunyan *et al.* (CMS), JHEP **06**, 093 (2019), [arXiv:1809.03590].
- [145] CMS Collaboration, CMS-PAS-HIG-18-032 (2019).
- [146] T. Aaltonen *et al.* (CDF, D0), Phys. Rev. Lett. **109**, 071804 (2012), [arXiv:1207.6436].
- [147] M. Aaboud *et al.* (ATLAS), Phys. Lett. **B786**, 59 (2018), [arXiv:1808.08238].
- [148] A. M. Sirunyan *et al.* (CMS), Phys. Rev. Lett. **121**, 12, 121801 (2018), [arXiv:1808.08242].
- [149] M. Aaboud *et al.* (ATLAS), JHEP **05**, 141 (2019), [arXiv:1903.04618].
- [150] LHCb Collaboration, LHCb-CONF-2016-006, CERN-LHCb-CONF-2016-006 (2016).
- [151] M. Aaboud *et al.* (ATLAS), JHEP **11**, 112 (2016), [arXiv:1606.02181].
- [152] V. Khachatryan *et al.* (CMS), Phys. Rev. **D92**, 3, 032008 (2015), [arXiv:1506.01010].
- [153] M. Aaboud *et al.* (ATLAS), Phys. Rev. **D98**, 5, 052003 (2018), [arXiv:1807.08639]; CMS Collaboration, CMS-PAS-HIG-16-003 (2019).
- [154] E. Gabrielli *et al.*, Nucl. Phys. **B781**, 64 (2007), [hep-ph/0702119].
- [155] ATLAS Collaboration, ATLAS-CONF-2018-052 (2018).
- [156] A. M. Sirunyan *et al.* (CMS), Phys. Rev. Lett. **120**, 7, 071802 (2018), [arXiv:1709.05543].
- [157] M. Cacciari, G. P. Salam and G. Soyez, JHEP **04**, 063 (2008), [arXiv:0802.1189].
- [158] V. Khachatryan *et al.* (CMS), Eur. Phys. J. **C75**, 6, 251 (2015), [arXiv:1502.02485].
- [159] G. Aad *et al.* (ATLAS), Phys. Lett. **B749**, 519 (2015), [arXiv:1506.05988].
- [160] M. Aaboud *et al.* (ATLAS), Phys. Lett. **B784**, 173 (2018), [arXiv:1806.00425]; A. M. Sirunyan *et al.* (CMS), Phys. Rev. Lett. **120**, 23, 231801 (2018), [arXiv:1804.02610].
- [161] ATLAS Collaboration, ATLAS-CONF-2019-004 (2019).
- [162] CMS Collaboration, CMS-PAS-HIG-18-018 (2019).
- [163] CMS Collaboration, CMS-PAS-HIG-18-030 (2019).
- [164] ATLAS Collaboration, ATLAS-CONF-2017-077 (2017); A. M. Sirunyan *et al.* (CMS), JHEP **08**, 066 (2018), [arXiv:1803.05485]; CMS Collaboration, CMS-PAS-HIG-18-019 (2018); ATLAS Collaboration, ATLAS-CONF-2019-045 (2019).
- [165] M. Farina *et al.*, JHEP **05**, 022 (2013), [arXiv:1211.3736].
- [166] CMS Collaboration, CMS-PAS-HIG-17-005 (2017).
- [167] CMS Collaboration, CMS-PAS-HIG-16-019 (2016).
- [168] A. M. Sirunyan *et al.* (CMS), Phys. Rev. **D99**, 9, 092005 (2019), [arXiv:1811.09696].
- [169] G. Aad *et al.* (ATLAS), JHEP **12**, 061 (2015), [arXiv:1509.06047].
- [170] V. Khachatryan *et al.* (CMS), JHEP **02**, 079 (2017), [arXiv:1610.04857].
- [171] ATLAS Collaboration, JHEP **129**, 010 (2017).
- [172] CMS Collaboration, CMS-PAS-TOP-2017-003 (2017).
- [173] G. Aad *et al.* (ATLAS) (2019), [arXiv:1906.02025].

- [174] A. M. Sirunyan *et al.* (CMS), Phys. Rev. Lett. **122**, 12, 121803 (2019), [arXiv:1811.09689].
- [175] V. Khachatryan *et al.* (CMS), Phys. Lett. **B753**, 341 (2016), [arXiv:1507.03031].
- [176] M. Aaboud *et al.* (ATLAS), JHEP **10**, 112 (2017), [arXiv:1708.00212].
- [177] A. M. Sirunyan *et al.* (CMS), JHEP **11**, 152 (2018), [arXiv:1806.05996].
- [178] ATLAS Collaboration, ATLAS-CONF-2019-028 (2019).
- [179] A. M. Sirunyan *et al.* (CMS), Phys. Rev. Lett. **122**, 2, 021801 (2019), [arXiv:1807.06325].
- [180] ATLAS Collaboration, ATLAS-CONF-2019-037 (2019).
- [181] V. Khachatryan *et al.* (CMS), Phys. Lett. **B749**, 337 (2015), [arXiv:1502.07400].
- [182] G. Aad *et al.* (ATLAS), JHEP **11**, 211 (2015), [arXiv:1508.03372].
- [183] G. Aad *et al.* (ATLAS), Eur. Phys. J. **C77**, 2, 70 (2017), [arXiv:1604.07730].
- [184] CMS Collaboration, CMS-PAS-HIG-17-001 (2017).
- [185] V. Khachatryan *et al.* (CMS), Phys. Lett. **B763**, 472 (2016), [arXiv:1607.03561].
- [186] R. Harnik, J. Kopp and J. Zupan, JHEP **03**, 026 (2013), [arXiv:1209.1397].
- [187] G. Aad *et al.* (ATLAS) (2019), [arXiv:1907.06131].
- [188] A. M. Sirunyan *et al.* (CMS), JHEP **06**, 001 (2018), [arXiv:1712.07173].
- [189] C. Delaunay *et al.*, Phys. Rev. **D89**, 3, 033014 (2014), [arXiv:1310.7029].
- [190] M. Aaboud *et al.* (ATLAS), Phys. Rev. Lett. **120**, 21, 211802 (2018), [arXiv:1802.04329].
- [191] CMS Collaboration, CMS-PAS-HIG-18-031 (2019).
- [192] G. Isidori, A. V. Manohar and M. Trott, Phys. Lett. **B728**, 131 (2014), [arXiv:1305.0663]; G. T. Bodwin *et al.*, Phys. Rev. **D88**, 5, 053003 (2013), [arXiv:1306.5770]; M. König and M. Neubert, JHEP **08**, 012 (2015), [arXiv:1505.03870].
- [193] G. Aad *et al.* (ATLAS), Phys. Rev. Lett. **114**, 12, 121801 (2015), [arXiv:1501.03276].
- [194] M. Aaboud *et al.* (ATLAS), Phys. Rev. Lett. **117**, 11, 111802 (2016), [arXiv:1607.03400].
- [195] A. M. Sirunyan *et al.* (CMS), Phys. Lett. **B797**, 134811 (2019), [arXiv:1905.10408].
- [196] A. Djouadi *et al.*, Eur. Phys. J. **C73**, 6, 2455 (2013), [arXiv:1205.3169].
- [197] O. J. P. Eboli and D. Zeppenfeld, Phys. Lett. **B495**, 147 (2000), [hep-ph/0009158].
- [198] M. Aaboud *et al.* (ATLAS), Phys. Lett. **B793**, 499 (2019), [arXiv:1809.06682].
- [199] M. Aaboud *et al.* (ATLAS), Phys. Lett. **B776**, 318 (2018), [arXiv:1708.09624].
- [200] M. Aaboud *et al.* (ATLAS), JHEP **10**, 180 (2018), [arXiv:1807.11471].
- [201] M. Aaboud *et al.* (ATLAS), Phys. Rev. Lett. **122**, 23, 231801 (2019), [arXiv:1904.05105].
- [202] A. M. Sirunyan *et al.* (CMS), Eur. Phys. J. **C78**, 4, 291 (2018), [arXiv:1711.00431].
- [203] A. M. Sirunyan *et al.* (CMS), Phys. Rev. **D97**, 9, 092005 (2018), [arXiv:1712.02345].
- [204] A. M. Sirunyan *et al.* (CMS), Phys. Lett. **B793**, 520 (2019), [arXiv:1809.05937].
- [205] CMS Collaboration, CMS-PAS-HIG-18-008 (2019).
- [206] M. J. Strassler and K. M. Zurek, Phys. Lett. **B651**, 374 (2007), [hep-ph/0604261]; M. J. Strassler and K. M. Zurek, Phys. Lett. **B661**, 263 (2008), [hep-ph/0605193].
- [207] T. Han *et al.*, JHEP **07**, 008 (2008), [arXiv:0712.2041].
- [208] A. Falkowski *et al.*, Phys. Rev. Lett. **105**, 241801 (2010), [arXiv:1007.3496].
- [209] G. Aad *et al.* (ATLAS) (2019), [arXiv:1909.01246].
- [210] CMS Collaboration, CMS-PAS-EXO-19-007 (2019).
- [211] D. Tucker-Smith and N. Weiner, Phys. Rev. **D64**, 043502 (2001), [hep-ph/0101138].
- [212] S. Chatrchyan *et al.* (CMS), Phys. Lett. **B726**, 564 (2013), [arXiv:1210.7619].
- [213] G. Aad *et al.* (ATLAS) (2019), [arXiv:1909.02845].
- [214] A. M. Sirunyan *et al.* (CMS), Eur. Phys. J. **C79**, 5, 421 (2019), [arXiv:1809.10733].
- [215] C. Patrignani *et al.* (Particle Data Group), Chin. Phys. **C40**, 10, 100001 (2016).
- [216] G. Aad *et al.* (ATLAS), Eur. Phys. J. **C76**, 1, 6 (2016), [arXiv:1507.04548].
- [217] L. D. Landau, Dokl. Akad. Nauk Ser. Fiz. **60**, 2, 207 (1948); C.-N. Yang, Phys. Rev. **77**, 242 (1950).
- [218] S. Bolognesi *et al.*, Phys. Rev. **D86**, 095031 (2012), [arXiv:1208.4018].
- [219] G. Aad *et al.* (ATLAS), Eur. Phys. J. **C75**, 10, 476 (2015), [Erratum: Eur. Phys. J. **C76**, 3, 152 (2016)], [arXiv:1506.05669].
- [220] V. Khachatryan *et al.* (CMS), Phys. Rev. **D92**, 1, 012004 (2015), [arXiv:1411.3441]; G. Aad *et al.* (ATLAS), Phys. Lett. **B726**, 120 (2013), [arXiv:1307.1432].
- [221] P. Artoisenet *et al.*, JHEP **11**, 043 (2013), [arXiv:1306.6464].
- [222] J. Ellis *et al.*, JHEP **11**, 134 (2012), [arXiv:1208.6002].
- [223] D0 Collaboration, Note 6387-CONF (2013).
- [224] D0 Collaboration, Note 6406-CONF (2013).
- [225] J. C. Collins and D. E. Soper, Phys. Rev. **D16**, 2219 (1977).
- [226] A. De Rijula *et al.*, Phys. Rev. **D82**, 013003 (2010), [arXiv:1001.5300].
- [227] ATLAS Collaboration, ATLAS-CONF-2017-043 (2017).
- [228] A. M. Sirunyan *et al.* (CMS), Phys. Rev. **D99**, 11, 112003 (2019), [arXiv:1901.00174].
- [229] A. M. Sirunyan *et al.* (CMS), Submitted to: Phys. Rev. (2019), [arXiv:1903.06973].
- [230] G. Aad *et al.* (ATLAS), Eur. Phys. J. **C76**, 12, 658 (2016), [arXiv:1602.04516].
- [231] N. Kauer and G. Passarino, JHEP **08**, 116 (2012), [arXiv:1206.4803].
- [232] V. Khachatryan *et al.* (CMS), JHEP **09**, 051 (2016), [arXiv:1605.02329].
- [233] G. Aad *et al.* (ATLAS), Eur. Phys. J. **C75**, 7, 335 (2015), [arXiv:1503.01060].
- [234] M. Aaboud *et al.* (ATLAS), Phys. Lett. **B786**, 223 (2018), [arXiv:1808.01191].
- [235] G. Aad *et al.* (ATLAS), Phys. Rev. **D90**, 5, 052004 (2014), [arXiv:1406.3827].
- [236] CMS Collaboration, CMS-PAS-HIG-16-041 (2017).
- [237] L. J. Dixon and M. S. Siu, Phys. Rev. Lett. **90**, 252001 (2003), [hep-ph/0302233]; S. P. Martin, Phys. Rev. **D86**, 073016 (2012), [arXiv:1208.1533]; L. J. Dixon and Y. Li, Phys. Rev. Lett. **111**, 111802 (2013), [arXiv:1305.3854].
- [238] ATLAS Collaboration, ATL-PHYS-PUB-2013-014 (2013).
- [239] J. Campbell *et al.*, Phys. Rev. Lett. **119**, 18, 181801 (2017), [Addendum: Phys. Rev. Lett. **119**, 19, 199901 (2017)], [arXiv:1704.08259].
- [240] ATLAS Collaboration, ATL-PHYS-PUB-2014-016 (2014).

- [241] F. Caola and K. Melnikov, *Phys. Rev.* **D88**, 054024 (2013), [arXiv:1307.4935]; J. M. Campbell, R. K. Ellis and C. Williams, *JHEP* **04**, 060 (2014), [arXiv:1311.3589]; J. M. Campbell, R. K. Ellis and C. Williams, *Phys. Rev.* **D89**, 5, 053011 (2014), [arXiv:1312.1628].
- [242] C. Englert and M. Spannowsky, *Phys. Rev.* **D90**, 053003 (2014), [arXiv:1405.0285].
- [243] A. Azatov *et al.*, *Zh. Eksp. Teor. Fiz.* **147**, 410 (2015), [*J. Exp. Theor. Phys.* 120,354(2015)], [arXiv:1406.6338]; A. Azatov *et al.*, *JHEP* **09**, 123 (2016), [arXiv:1608.00977].
- [244] A. David *et al.* (LHC Higgs Cross Section Working Group), “LHC HXSWG interim recommendations to explore the coupling structure of a Higgs-like particle,” (2012), [arXiv:1209.0040].
- [245] M. Dührssen, “Prospects for the measurement of Higgs boson coupling parameters in the mass range from 110–190 GeV,” (2003); M. Dührssen *et al.*, *Phys. Rev.* **D70**, 113009 (2004), [hep-ph/0406323]; R. Lafaye *et al.*, *JHEP* **08**, 009 (2009), [arXiv:0904.3866].
- [246] J. R. Espinosa *et al.*, *JHEP* **05**, 097 (2012), [arXiv:1202.3697]; A. Azatov, R. Contino and J. Galloway, *JHEP* **04**, 127 (2012), [Erratum: *JHEP* **04**, 140 (2013)], [arXiv:1202.3415]; D. Carmi *et al.*, *JHEP* **07**, 136 (2012), [arXiv:1202.3144]; J. R. Espinosa *et al.*, *JHEP* **12**, 045 (2012), [arXiv:1207.1717].
- [247] M. Gonzalez-Alonso *et al.*, *Eur. Phys. J.* **C75**, 128 (2015), [arXiv:1412.6038]; A. Greljo *et al.*, *Eur. Phys. J.* **C76**, 3, 158 (2016), [arXiv:1512.06135].
- [248] G. F. Giudice *et al.*, *JHEP* **06**, 045 (2007), [hep-ph/0703164].
- [249] S. Willenbrock and C. Zhang, *Ann. Rev. Nucl. Part. Sci.* **64**, 83 (2014), [arXiv:1401.0470]; I. Brivio and M. Trott, *Phys. Rept.* **793**, 1 (2019), [arXiv:1706.08945]; S. Dawson, C. Englert and T. Plehn, *Phys. Rept.* **816**, 1 (2019), [arXiv:1808.01324]; T. Cohen, *PoS TASI2018*, 011 (2019), [arXiv:1903.03622].
- [250] F. Feruglio, *Int. J. Mod. Phys.* **A8**, 4937 (1993), [hep-ph/9301281]; G. Buchalla, O. Catà and C. Krause, *Nucl. Phys.* **B880**, 552 (2014), [Erratum: *Nucl. Phys.* **B913**, 475 (2016)], [arXiv:1307.5017]; R. Alonso *et al.*, *Phys. Lett.* **B722**, 330 (2013), [Erratum: *Phys. Lett.* **B726**, 926 (2013)], [arXiv:1212.3305]; A. V. Manohar, in “Les Houches summer school: EFT in Particle Physics and Cosmology Les Houches, Chamonix Valley, France, July 3-28, 2017,” (2018), [arXiv:1804.05863]; I. Brivio *et al.*, *JHEP* **03**, 024 (2014), [arXiv:1311.1823].
- [251] J. de Blas *et al.*, *JHEP* **03**, 109 (2018), [arXiv:1711.10391].
- [252] A. Manohar and H. Georgi, *Nucl. Phys.* **B234**, 189 (1984); M. A. Luty, *Phys. Rev.* **D57**, 1531 (1998), [hep-ph/9706235]; D. Liu *et al.*, *JHEP* **11**, 141 (2016), [arXiv:1603.03064].
- [253] W. Buchmuller and D. Wyler, *Nucl. Phys.* **B268**, 621 (1986).
- [254] C. J. C. Burges and H. J. Schnitzer, *Nucl. Phys.* **B228**, 464 (1983); C. N. Leung, S. T. Love and S. Rao, *Z. Phys.* **C31**, 433 (1986).
- [255] B. Grzadkowski *et al.*, *JHEP* **10**, 085 (2010), [arXiv:1008.4884].
- [256] L. Lehman and A. Martin, *JHEP* **02**, 081 (2016), [arXiv:1510.00372]; B. Henning *et al.*, *JHEP* **08**, 016 (2017), [arXiv:1512.03433].
- [257] C. Hays *et al.*, *JHEP* **02**, 123 (2019), [arXiv:1808.00442].
- [258] R. Alonso *et al.*, *JHEP* **04**, 159 (2014), [arXiv:1312.2014].
- [259] A. Falkowski, LHCHSWG-INT-2015-001 (2015); A. Falkowski, *Pramana* **87**, 3, 39 (2016), [arXiv:1505.00046].
- [260] A. M. Sirunyan *et al.* (CMS), *Phys. Lett.* **B792**, 369 (2019), [arXiv:1812.06504].
- [261] M. Aaboud *et al.* (ATLAS), *Phys. Rev.* **D98**, 052005 (2018), [arXiv:1802.04146].
- [262] F. Maltoni *et al.* (2019), [arXiv:1906.12310].
- [263] R. S. Gupta, A. Pomarol and F. Riva, *Phys. Rev.* **D91**, 3, 035001 (2015), [arXiv:1405.0181].
- [264] B. A. Kniehl and M. Spira, *Z. Phys.* **C69**, 77 (1995), [hep-ph/9505225].
- [265] R. Contino *et al.*, *JHEP* **07**, 035 (2013), [arXiv:1303.3876].
- [266] A. Azatov and J. Galloway, *Phys. Rev.* **D85**, 055013 (2012), [arXiv:1110.5646].
- [267] G. Isidori and M. Trott, *JHEP* **02**, 082 (2014), [arXiv:1307.4051]; A. Pomarol and F. Riva, *JHEP* **01**, 151 (2014), [arXiv:1308.2803].
- [268] J. Ellis, V. Sanz and T. You, *JHEP* **07**, 036 (2014), [arXiv:1404.3667]; A. Biekötter *et al.*, *Phys. Rev.* **D91**, 055029 (2015), [arXiv:1406.7320].
- [269] LHC Higgs Cross Section Working Group, <https://twiki.cern.ch/twiki/bin/view/LHCPhysics/LHCHSWG2KAPPA>.
- [270] ATLAS and C. Collaboration (CMS) (2015).
- [271] M. Reece, *New J. Phys.* **15**, 043003 (2013), [arXiv:1208.1765].
- [272] ATLAS Collaboration, ATLAS-CONF-2019-032 (2019).
- [273] G. Aad *et al.* (ATLAS), *Phys. Lett.* **B753**, 69 (2016), [arXiv:1508.02507].
- [274] N. Berger *et al.* (2019), [arXiv:1906.02754].
- [275] CMS Collaboration, CMS-PAS-HIG-16-040 (2017).
- [276] ATLAS Collaboration, ATLAS-CONF-2018-028 (2018).
- [277] ATLAS Collaboration, CMS-PAS-HIG-19-001 (2019).
- [278] M. McCullough, *Phys. Rev.* **D90**, 1, 015001 (2014), [Erratum: *Phys. Rev.* **D92**, 3, 039903 (2015)], [arXiv:1312.3322].
- [279] G. Degrossi *et al.*, *JHEP* **12**, 080 (2016), [arXiv:1607.04251].
- [280] M. Gorbahn and U. Haisch, *JHEP* **10**, 094 (2016), [arXiv:1607.03773].
- [281] ATLAS Collaboration, ATLAS-PHYS-PUB-2019-009 (2019).
- [282] F. Bishara *et al.*, *Phys. Rev. Lett.* **118**, 12, 121801 (2017), [arXiv:1606.09253].
- [283] T. A. collaboration (ATLAS) (2019).
- [284] ATLAS Collaboration, ATLAS-CONF-2019-049 (2019).
- [285] S. Di Vita *et al.*, *JHEP* **09**, 069 (2017), [arXiv:1704.01953]; F. Maltoni *et al.*, *Eur. Phys. J.* **C77**, 12, 887 (2017), [arXiv:1709.08649].
- [286] B. Di Micco *et al.* (2019), [arXiv:1910.00012].
- [287] J. Parsons, and A. Pomarol, *Extra Dimensions*, in this volume.
- [288] S. Weinberg, *Phys. Rev.* **D13**, 974 (1976), [Addendum: *Phys. Rev.* D19,1277(1979)]; L. Susskind, *Phys. Rev.* **D20**, 2619 (1979); For a review, see C. T. Hill and E. H. Simmons, *Phys. Reports* **381**, 235 (2003) [Erratum: 390, 553 (2004)], [arXiv:hep-ph/0203079].
- [289] Z. Chacko, R. Franceschini and R. K. Mishra, *JHEP* **04**, 015 (2013), [arXiv:1209.3259].
- [290] L. E. Ibanez and G. G. Ross, *Phys. Lett.* **110B**, 215 (1982); L. E. Ibanez, *Phys. Lett.* **118B**, 73 (1982); J. R. Ellis, D. V. Nanopoulos and K. Tamvakis, *Phys. Lett.* **121B**, 123 (1983); L. Alvarez-Gaume, J. Polchinski and M. B. Wise, *Nucl. Phys.* **B221**, 495 (1983).
- [291] S. Dimopoulos and G. F. Giudice, *Phys. Lett.* **B357**, 573 (1995), [hep-ph/9507282]; M. Papucci, J. T. Ruderman and A. Weiler, *JHEP* **09**, 035 (2012), [arXiv:1110.6926].
- [292] ATLAS Collaboration, <https://twiki.cern.ch/twiki/bin/view/AtlasPublic/Publications>; CMS Collaboration, <http://cms-results.web.cern.ch/cms-results/public-results/publications/SUS/STOP.html>.

- [293] J. Mrazek *et al.*, Nucl. Phys. **B853**, 1 (2011), [arXiv:1105.5403].
- [294] D. B. Kaplan, Nucl. Phys. **B365**, 259 (1991).
- [295] G. Panico *et al.*, JHEP **03**, 051 (2013), [arXiv:1210.7114].
- [296] H. E. Haber and G. L. Kane, Phys. Rept. **117**, 75 (1985).
- [297] A. Djouadi, Phys. Rept. **459**, 1 (2008), [hep-ph/0503173].
- [298] S. Heinemeyer, W. Hollik and G. Weiglein, Phys. Rept. **425**, 265 (2006), [hep-ph/0412214].
- [299] P. Draper, G. Lee and C. E. M. Wagner, Phys. Rev. **D89**, 5, 055023 (2014), [arXiv:1312.5743].
- [300] J. F. Gunion and H. E. Haber, Phys. Rev. **D67**, 075019 (2003), [hep-ph/0207010].
- [301] H. E. Haber and Y. Nir, Nucl. Phys. **B335**, 363 (1990).
- [302] E. L. Berger *et al.*, Phys. Rev. **D66**, 095001 (2002), [hep-ph/0205342].
- [303] P. Bechtle *et al.*, Eur. Phys. J. **C77**, 2, 67 (2017), [arXiv:1608.00638].
- [304] E. Bagnaschi *et al.*, Eur. Phys. J. **C79**, 7, 617 (2019), [arXiv:1808.07542].
- [305] A. Djouadi, J. Kalinowski and P. M. Zerwas, Z. Phys. **C57**, 569 (1993).
- [306] G. Lee and C. E. M. Wagner, Phys. Rev. **D92**, 7, 075032 (2015), [arXiv:1508.00576].
- [307] D. Dicus *et al.*, Phys. Rev. **D59**, 094016 (1999), [hep-ph/9811492].
- [308] M. Carena *et al.*, JHEP **07**, 091 (2012), [arXiv:1203.1041].
- [309] A. A. Barrientos Bendezu and B. A. Kniehl, Phys. Rev. **D64**, 035006 (2001), [hep-ph/0103018].
- [310] LHC Higgs Cross Section Working Group, <https://twiki.cern.ch/twiki/bin/view/LHCPhysics/LHCHXSWGSMSSMCharged>.
- [311] A. Djouadi, J. Ellis and J. Quevillon, JHEP **07**, 105 (2016), [arXiv:1605.00542]; M. Carena and Z. Liu, JHEP **11**, 159 (2016), [arXiv:1608.07282].
- [312] M. Carena *et al.*, Eur. Phys. J. **C26**, 601 (2003), [hep-ph/0202167]; M. Carena *et al.*, Eur. Phys. J. **C73**, 9, 2552 (2013), [arXiv:1302.7033].
- [313] H. Bahl, S. Liebler and T. Stefaniak, Eur. Phys. J. **C79**, 3, 279 (2019), [arXiv:1901.05933].
- [314] L. Maiani, A. D. Polosa and V. Riquer, Phys. Lett. **B718**, 465 (2012), [arXiv:1209.4816]; A. Djouadi and J. Quevillon, JHEP **10**, 028 (2013), [arXiv:1304.1787]; A. Djouadi *et al.*, Eur. Phys. J. **C73**, 2650 (2013), [arXiv:1307.5205].
- [315] M. Carena *et al.*, Phys. Rev. **D91**, 3, 035003 (2015), [arXiv:1410.4969].
- [316] M. Carena *et al.*, JHEP **04**, 015 (2014), [arXiv:1310.2248]; K. Blum, R. T. D'Agnolo and J. Fan, JHEP **01**, 057 (2013), [arXiv:1206.5303]; A. Djouadi *et al.*, JHEP **06**, 168 (2015), [arXiv:1502.05653].
- [317] R. S. Chivukula and H. Georgi, Phys. Lett. **B188**, 99 (1987); L. J. Hall and L. Randall, Phys. Rev. Lett. **65**, 2939 (1990); A. J. Buras *et al.*, Phys. Lett. **B500**, 161 (2001), [hep-ph/0007085]; G. D'Ambrosio *et al.*, Nucl. Phys. **B645**, 155 (2002), [hep-ph/0207036].
- [318] L. J. Hall, J. D. Lykken and S. Weinberg, Phys. Rev. **D27**, 2359 (1983); J. E. Kim and H. P. Nilles, Phys. Lett. **138B**, 150 (1984); G. F. Giudice and A. Masiero, Phys. Lett. **B206**, 480 (1988).
- [319] U. Ellwanger, C. Hugonie and A. M. Teixeira, Phys. Rept. **496**, 1 (2010), [arXiv:0910.1785].
- [320] P. Fayet, Nucl. Phys. **B90**, 104 (1975).
- [321] C. Panagiotakopoulos and K. Tamvakis, Phys. Lett. **B469**, 145 (1999), [hep-ph/9908351]; A. Dedes *et al.*, Phys. Rev. **D63**, 055009 (2001), [hep-ph/0009125]; A. Menon, D. E. Morrissey and C. E. M. Wagner, Phys. Rev. **D70**, 035005 (2004), [hep-ph/0404184].
- [322] M. Cvetič *et al.*, Phys. Rev. **D56**, 2861 (1997), [Erratum: Phys. Rev. **D58**, 119905 (1998)], [hep-ph/9703317]; P. Langacker and J. Wang, Phys. Rev. **D58**, 115010 (1998), [hep-ph/9804428].
- [323] J. Erler, P. Langacker and T.-j. Li, Phys. Rev. **D66**, 015002 (2002), [hep-ph/0205001]; T. Han, P. Langacker and B. McElrath, Phys. Rev. **D70**, 115006 (2004), [hep-ph/0405244]; V. Barger *et al.*, Phys. Rev. **D73**, 115010 (2006), [hep-ph/0603247].
- [324] V. Barger, P. Langacker and G. Shaughnessy, Phys. Rev. **D75**, 055013 (2007), [hep-ph/0611239].
- [325] B. A. Dobrescu, G. L. Landsberg and K. T. Matchev, Phys. Rev. **D63**, 075003 (2001), [hep-ph/0005308]; R. Dermisek and J. F. Gunion, Phys. Rev. Lett. **95**, 041801 (2005), [hep-ph/0502105].
- [326] O. J. P. Eboli and D. Zeppenfeld, Phys. Lett. **B495**, 147 (2000), [hep-ph/0009158]; H. Davoudiasl, T. Han and H. E. Logan, Phys. Rev. **D71**, 115007 (2005), [hep-ph/0412269].
- [327] J.-J. Cao *et al.*, JHEP **03**, 086 (2012), [arXiv:1202.5821].
- [328] LHC Higgs Cross Section Working Group, Beyond the Standard Model Higgs – NMSSM, <https://twiki.cern.ch/twiki/bin/view/LHCPhysics/LHCHXSWGSMSSM>.
- [329] M. Carena *et al.*, Phys. Rev. **D93**, 3, 035013 (2016), [arXiv:1510.09137].
- [330] P. Batra *et al.*, JHEP **02**, 043 (2004), [hep-ph/0309149].
- [331] R. Huo *et al.*, Phys. Rev. **D87**, 5, 055011 (2013), [arXiv:1212.0560].
- [332] J. Engel, M. J. Ramsey-Musolf and U. van Kolck, Prog. Part. Nucl. Phys. **71**, 21 (2013), [arXiv:1303.2371].
- [333] S. Dimopoulos and S. D. Thomas, Nucl. Phys. **B465**, 23 (1996), [hep-ph/9510220]; S. D. Thomas, Int. J. Mod. Phys. **A13**, 2307 (1998), [hep-ph/9803420].
- [334] A. Pilaftsis and C. E. M. Wagner, Nucl. Phys. **B553**, 3 (1999), [hep-ph/9902371].
- [335] M. Frank *et al.*, JHEP **02**, 047 (2007), [hep-ph/0611326].
- [336] M. Carena *et al.*, Nucl. Phys. **B586**, 92 (2000), [hep-ph/0003180].
- [337] B. Li and C. E. M. Wagner, Phys. Rev. **D91**, 095019 (2015), [arXiv:1502.02210].
- [338] M. D. Goodsell and F. Staub, Eur. Phys. J. **C77**, 1, 46 (2017), [arXiv:1604.05335]; A. Chakraborty *et al.*, Phys. Rev. **D90**, 5, 055005 (2014), [arXiv:1301.2745]; M. Carena *et al.*, JHEP **02**, 123 (2016), [arXiv:1512.00437].
- [339] J. F. Gunion and H. E. Haber, Phys. Rev. **D67**, 075019 (2003), [hep-ph/0207010]; G. C. Branco *et al.*, Phys. Rept. **516**, 1 (2012), [arXiv:1106.0034].
- [340] N. G. Deshpande and E. Ma, Phys. Rev. **D18**, 2574 (1978).
- [341] A. Goudelis, B. Herrmann and O. Stål, JHEP **09**, 106 (2013), [arXiv:1303.3010].
- [342] C. D. Froggatt and H. B. Nielsen, Nucl. Phys. **B147**, 277 (1979).
- [343] K. S. Babu and S. Nandi, Phys. Rev. **D62**, 033002 (2000), [hep-ph/9907213]; G. F. Giudice and O. Lebedev, Phys. Lett. **B665**, 79 (2008), [arXiv:0804.1753].
- [344] E. Accomando *et al.*, CERN Report **2006-009** (2006), [hep-ph/0608079].
- [345] T. Robens and T. Stefaniak, Eur. Phys. J. **C75**, 104 (2015), [arXiv:1501.02234].
- [346] S. L. Glashow and S. Weinberg, Phys. Rev. **D15**, 1958 (1977); E. A. Paschos, Phys. Rev. **D15**, 1966 (1977).
- [347] G. C. Branco, W. Grimus and L. Lavoura, Phys. Lett. **B380**, 119 (1996), [hep-ph/9601383]; F. J. Botella, G. C. Branco and M. N. Rebelo, Phys. Lett. **B687**, 194 (2010), [arXiv:0911.1753].

- [348] J. Schechter and J. W. F. Valle, Phys. Rev. **D22**, 2227 (1980); T. P. Cheng and L.-F. Li, Phys. Rev. **D22**, 2860 (1980).
- [349] H. Georgi and M. Machacek, Nucl. Phys. **B262**, 463 (1985); M. S. Chanowitz and M. Golden, Phys. Lett. **165B**, 105 (1985); J. F. Gunion, R. Vega and J. Wudka, Phys. Rev. **D42**, 1673 (1990).
- [350] P. Nath *et al.*, Nucl. Phys. Proc. Suppl. **200-202**, 185 (2010), [arXiv:1001.2693].
- [351] J. Garayoa and T. Schwetz, JHEP **03**, 009 (2008), [arXiv:0712.1453].
- [352] H. E. Haber and H. E. Logan, Phys. Rev. **D62**, 015011 (2000), [hep-ph/9909335]; J. F. Gunion, R. Vega and J. Wudka, Phys. Rev. **D43**, 2322 (1991); S. Kanemura and K. Yagyu, Phys. Rev. **D85**, 115009 (2012), [arXiv:1201.6287].
- [353] I. Low and J. Lykken, JHEP **10**, 053 (2010), [arXiv:1005.0872]; I. Low, J. Lykken and G. Shaughnessy, Phys. Rev. **D86**, 093012 (2012), [arXiv:1207.1093].
- [354] H. E. Logan and M.-A. Roy, Phys. Rev. **D82**, 115011 (2010), [arXiv:1008.4869]; A. Falkowski, S. Rychkov and A. Urbano, JHEP **04**, 073 (2012), [arXiv:1202.1532].
- [355] N. Arkani-Hamed *et al.*, JHEP **07**, 034 (2002), [hep-ph/0206021]; N. Arkani-Hamed, A. G. Cohen and H. Georgi, Phys. Lett. **B513**, 232 (2001), [hep-ph/0105239].
- [356] M. Perelstein, Prog. Part. Nucl. Phys. **58**, 247 (2007), [hep-ph/0512128]; M. Schmaltz and D. Tucker-Smith, Ann. Rev. Nucl. Part. Sci. **55**, 229 (2005), [hep-ph/0502182].
- [357] J. A. Casas, J. R. Espinosa and I. Hidalgo, JHEP **03**, 038 (2005), [hep-ph/0502066].
- [358] H.-C. Cheng and I. Low, JHEP **09**, 051 (2003), [hep-ph/0308199].
- [359] M. Carena *et al.*, Phys. Rev. **D75**, 091701 (2007), [hep-ph/0610156].
- [360] M. Aaboud *et al.* (ATLAS), Phys. Rev. Lett. **121**, 21, 211801 (2018), [arXiv:1808.02343]; A. M. Sirunyan *et al.* (CMS), Eur. Phys. J. **C79**, 4, 364 (2019), [arXiv:1812.09768].
- [361] H. Georgi, A. E. Nelson and A. Manohar, Phys. Lett. **126B**, 169 (1983); A. E. Nelson and M. J. Strassler, JHEP **09**, 030 (2000), [hep-ph/0006251]; S. Davidson, G. Isidori and S. Uhlig, Phys. Lett. **B663**, 73 (2008), [arXiv:0711.3376].
- [362] C. Csaki, A. Falkowski and A. Weiler, JHEP **09**, 008 (2008), [arXiv:0804.1954]; B. Keren-Zur *et al.*, Nucl. Phys. **B867**, 394 (2013), [arXiv:1205.5803].
- [363] O. Matsedonskyi, G. Panico and A. Wulzer, JHEP **01**, 164 (2013), [arXiv:1204.6333]; M. Redi and A. Tesi, JHEP **10**, 166 (2012), [arXiv:1205.0232]; D. Marzocca, M. Serone and J. Shu, JHEP **08**, 013 (2012), [arXiv:1205.0770]; A. Pomarol and F. Riva, JHEP **08**, 135 (2012), [arXiv:1205.6434].
- [364] R. Contino and G. Servant, JHEP **06**, 026 (2008), [arXiv:0801.1679]; J. Mrazek and A. Wulzer, Phys. Rev. **D81**, 075006 (2010), [arXiv:0909.3977]; A. De Simone *et al.*, JHEP **04**, 004 (2013), [arXiv:1211.5663]; A. Azatov *et al.*, Phys. Rev. **D89**, 7, 075001 (2014), [arXiv:1308.6601].
- [365] A. Banfi, A. Martin and V. Sanz, JHEP **08**, 053 (2014), [arXiv:1308.4771]; A. Azatov and A. Paul, JHEP **01**, 014 (2014), [arXiv:1309.5273]; C. Grojean *et al.*, JHEP **05**, 022 (2014), [arXiv:1312.3317].
- [366] A. Azatov *et al.*, Phys. Rev. **D92**, 3, 035001 (2015), [arXiv:1502.00539].
- [367] K. Agashe, R. Contino and A. Pomarol, Nucl. Phys. **B719**, 165 (2005), [hep-ph/0412089]; R. Contino, L. Da Rold and A. Pomarol, Phys. Rev. **D75**, 055014 (2007), [hep-ph/0612048]; D. Pappadopulo, A. Thamm and R. Torre, JHEP **07**, 058 (2013), [arXiv:1303.3062]; M. Montull *et al.*, Phys. Rev. **D88**, 095006 (2013), [arXiv:1308.0559].
- [368] M. Carena, L. Da Rold and E. Pontón, JHEP **06**, 159 (2014), [arXiv:1402.2987]; D. Liu, I. Low and C. E. M. Wagner, Phys. Rev. **D96**, 3, 035013 (2017), [arXiv:1703.07791].
- [369] I. Low, R. Rattazzi and A. Vichi, JHEP **04**, 126 (2010), [arXiv:0907.5413].
- [370] M. Ciuchini *et al.*, JHEP **08**, 106 (2013), [arXiv:1306.4644].
- [371] C. Grojean, O. Matsedonskyi and G. Panico, JHEP **10**, 160 (2013), [arXiv:1306.4655].
- [372] M. Geller and O. Telem, Phys. Rev. Lett. **114**, 191801 (2015), [arXiv:1411.2974].
- [373] P. Batra and Z. Chacko, Phys. Rev. **D79**, 095012 (2009), [arXiv:0811.0394]; R. Barbieri *et al.*, JHEP **08**, 161 (2015), [arXiv:1501.07803]; M. Low, A. Tesi and L.-T. Wang, Phys. Rev. **D91**, 095012 (2015), [arXiv:1501.07890].
- [374] M. Aaboud *et al.* (ATLAS), Phys. Lett. **B775**, 105 (2017), [arXiv:1707.04147].
- [375] CMS Collaboration, CMS-PAS-HIG-17-13 (2017); V. Khachatryan *et al.* (CMS), Phys. Lett. **B767**, 147 (2017), [arXiv:1609.02507].
- [376] A. M. Sirunyan *et al.* (CMS), Phys. Lett. **B793**, 320 (2019), [arXiv:1811.08459].
- [377] CMS Collaboration, CMS-PAS-HIG-16-014 (2016).
- [378] ATLAS Collaboration, ATLAS-CONF-2017-058 (2017).
- [379] CMS Collaboration, CMS-PAS-HIG-16-033 (2016).
- [380] CMS Collaboration, CMS-PAS-HIG-16-023 (2016).
- [381] ATLAS Collaboration, ATLAS-CONF-2016-082 (2016).
- [382] CMS Collaboration, CMS-PAS-HIG-16-034 (2017).
- [383] ATLAS Collaboration, ATLAS-CONF-2013-067 (2013).
- [384] CMS Collaboration, CMS-PAS-HIG-17-033 (2019).
- [385] ATLAS Collaboration, ATLAS-CONF-2012-018 (2012).
- [386] M. Aaboud *et al.* (ATLAS), Phys. Lett. **B777**, 91 (2018), [arXiv:1708.04445].
- [387] G. Aad *et al.* (ATLAS), JHEP **09**, 091 (2019), [arXiv:1906.08589].
- [388] M. Aaboud *et al.* (ATLAS), Phys. Rev. **D98**, 5, 052008 (2018), [arXiv:1808.02380].
- [389] ATLAS Collaboration, ATLAS-CONF-2016-004 (2016); M. Aaboud *et al.* (ATLAS), JHEP **05**, 124 (2019), [arXiv:1811.11028]; M. Aaboud *et al.* (ATLAS), Eur. Phys. J. **C78**, 12, 1007 (2018), [arXiv:1807.08567].
- [390] ATLAS Collaboration, ATLAS-CONF-2019-030 (2019); M. Aaboud *et al.* (ATLAS), Phys. Rev. Lett. **121**, 19, 191801 (2018), [Erratum: Phys. Rev. Lett. **122**, 089901 (2019)], [arXiv:1808.00336]; G. Aad *et al.* (ATLAS) (2019), [arXiv:1908.06765].
- [391] CMS Collaboration, CMS-PAS-HIG-2017-008 (2016).
- [392] V. Khachatryan *et al.* (CMS), Phys. Lett. **B755**, 217 (2016), [arXiv:1510.01181].
- [393] CMS Collaboration, CMS-PAS-HIG-18-013 (2019).
- [394] M. Aaboud *et al.* (ATLAS), JHEP **01**, 055 (2018), [arXiv:1709.07242].
- [395] A. M. Sirunyan *et al.* (CMS), JHEP **09**, 007 (2018), [arXiv:1803.06553].
- [396] V. M. Abazov *et al.* (D0), Phys. Rev. Lett. **104**, 151801 (2010), [arXiv:0912.0968].
- [397] D0 Collaboration, D0Note 5974-CONF (2011).
- [398] R. Aaij *et al.* (LHCb), JHEP **05**, 132 (2013), [arXiv:1304.2591].
- [399] A. M. Sirunyan *et al.* (CMS), JHEP **05**, 210 (2019), [arXiv:1903.10228].
- [400] M. Aaboud *et al.* (ATLAS), JHEP **07**, 117 (2019), [arXiv:1901.08144].
- [401] A. M. Sirunyan *et al.* (CMS) (2019), [arXiv:1907.03152].

- [402] CMS Collaboration, CMS-PAS-HIG-18-017 (2019).
- [403] ATLAS Collaboration, ATLAS-CONF-2019-036 (2019).
- [404] A. M. Sirunyan *et al.* (CMS), JHEP **11**, 161 (2018), [arXiv:1808.01890].
- [405] G. Aad *et al.* (ATLAS), JHEP **08**, 148 (2015), [arXiv:1505.07018].
- [406] A. M. Sirunyan *et al.* (CMS) (2019), [arXiv:1908.01115].
- [407] G. Aad *et al.* (ATLAS) (2019), [arXiv:1907.02749].
- [408] S. Chatrchyan *et al.* (CMS), Phys. Lett. **B722**, 207 (2013), [arXiv:1302.2892]; CMS Collaboration, CMS-PAS-HIG-16-025 (2016); A. M. Sirunyan *et al.* (CMS), JHEP **08**, 113 (2018), [arXiv:1805.12191].
- [409] V. M. Abazov *et al.* (D0), Phys. Lett. **B698**, 97 (2011), [arXiv:1011.1931].
- [410] T. Aaltonen *et al.* (CDF), Phys. Rev. **D85**, 032005 (2012), [arXiv:1106.4782].
- [411] ATLAS Collaboration, ATLAS-CONF-2017-055 (2017); G. Aad *et al.* (ATLAS), Phys. Lett. **B744**, 163 (2015), [arXiv:1502.04478].
- [412] A. M. Sirunyan *et al.* (CMS), Eur. Phys. J. **C79**, 7, 564 (2019), [arXiv:1903.00941].
- [413] CMS Collaboration, CMS-PAS-HIG-18-012 (2019).
- [414] M. Aaboud *et al.* (ATLAS), Phys. Lett. **B759**, 555 (2016), [arXiv:1603.09203].
- [415] M. Aaboud *et al.* (ATLAS), JHEP **09**, 139 (2018), [arXiv:1807.07915].
- [416] CMS Collaboration, CMS-PAS-HIG-16-031 (2016); A. M. Sirunyan *et al.* (CMS), JHEP **07**, 142 (2019), [arXiv:1903.04560].
- [417] ATLAS Collaboration, ATLAS-CONF-2012-010 (2012).
- [418] V. Khachatryan *et al.* (CMS), JHEP **12**, 178 (2015), [arXiv:1510.04252].
- [419] ATLAS Collaboration, ATLAS-CONF-2016-089 (2016); M. Aaboud *et al.* (ATLAS), JHEP **11**, 085 (2018), [arXiv:1808.03599].
- [420] V. Khachatryan *et al.* (CMS), JHEP **11**, 018 (2015), [arXiv:1508.07774]; A. M. Sirunyan *et al.* (CMS) (2019), [arXiv:1908.09206].
- [421] G. Aad *et al.* (ATLAS), Phys. Rev. Lett. **114**, 23, 231801 (2015), [arXiv:1503.04233].
- [422] A. M. Sirunyan *et al.* (CMS), Phys. Rev. Lett. **119**, 14, 141802 (2017), [arXiv:1705.02942].
- [423] A. M. Sirunyan *et al.* (CMS), Phys. Rev. Lett. **123**, 13, 131802 (2019), [arXiv:1905.07453].
- [424] CMS Collaboration, CMS-PAS-HIG-16-030 (2016).
- [425] ATLAS Collaboration, ATLAS-CONF-2011-020 (2011).
- [426] CMS Collaboration, CMS-PAS-HIG-15-009 (2016).
- [427] G. Aad *et al.* (ATLAS), Phys. Rev. **D92**, 5, 052002 (2015), [arXiv:1505.01609]; ATLAS Collaboration, ATLAS-CONF-2012-079 (2012).
- [428] CMS Collaboration, CMS-PAS-HIG-16-055 (2016); V. Khachatryan *et al.* (CMS), JHEP **10**, 076 (2017), [arXiv:1701.02032]; A. M. Sirunyan *et al.* (CMS), Phys. Lett. **B795**, 398 (2019), [arXiv:1812.06359]; A. M. Sirunyan *et al.* (CMS) (2019), [arXiv:1907.07235]; A. M. Sirunyan *et al.* (CMS), Phys. Lett. **B785**, 462 (2018), [arXiv:1805.10191]; A. M. Sirunyan *et al.* (CMS), JHEP **11**, 018 (2018), [arXiv:1805.04865]; CMS Collaboration, CMS-PAS-HIG-18-015 (2019).
- [429] V. M. Abazov *et al.* (D0), Phys. Rev. Lett. **103**, 061801 (2009), [arXiv:0905.3381].
- [430] A. M. Sirunyan *et al.* (CMS), Phys. Lett. **B796**, 131 (2019), [arXiv:1812.00380].
- [431] S. Schael *et al.* (ALEPH), JHEP **05**, 049 (2010), [arXiv:1003.0705].
- [432] B. Aubert *et al.* (BaBar), Phys. Rev. Lett. **103**, 081803 (2009), [arXiv:0905.4539].
- [433] B. Aubert *et al.* (BaBar), Phys. Rev. Lett. **103**, 181801 (2009), [arXiv:0906.2219].
- [434] ATLAS Collaboration, ATLAS-CONF-2016-051 (2016); ATLAS Collaboration, ATLAS-CONF-2017-053 (2017); M. Aaboud *et al.* (ATLAS), Eur. Phys. J. **C79**, 1, 58 (2019), [arXiv:1808.01899].
- [435] CMS Collaboration, CMS-PAS-HIG-16-036 (2017).
- [436] S. Schael *et al.* (ALEPH, DELPHI, L3, OPAL, LEP Working Group for Higgs Boson Searches), Eur. Phys. J. **C47**, 547 (2006), [hep-ex/0602042].
- [437] ATLAS Collaboration, ATLAS-CONF-2013-027 (2013).
- [438] CMS Collaboration, CMS-PAS-HIG-13-016 (2013).
- [439] A. Heister *et al.* (ALEPH), Phys. Lett. **B526**, 191 (2002), [hep-ex/0201014]; P. Achard *et al.* (L3), Phys. Lett. **B545**, 30 (2002), [hep-ex/0208042].
- [440] M. Carena *et al.* (1999), [hep-ph/9912223].
- [441] M. M. Kado and C. G. Tully, Ann. Rev. Nucl. Part. Sci. **52**, 65 (2002).
- [442] G. Abbiendi *et al.* (OPAL), Eur. Phys. J. **C23**, 397 (2002), [hep-ex/0111010]; J. Abdallah *et al.* (DELPHI), Eur. Phys. J. **C38**, 1 (2004), [hep-ex/0410017].
- [443] M. Carena *et al.*, Eur. Phys. J. **C45**, 797 (2006), [hep-ph/0511023].
- [444] ATLAS Collaboration, ATLAS-CONF-2016-104 (2016).
- [445] S. Chatrchyan *et al.* (CMS), JHEP **09**, 029 (2012), [Erratum: JHEP **03**, 132 (2014)], [arXiv:1204.2488].
- [446] M. Aaboud *et al.* (ATLAS), Phys. Rev. Lett. **119**, 19, 191803 (2017), [arXiv:1707.06025].
- [447] V. Khachatryan *et al.* (CMS), Phys. Lett. **B758**, 296 (2016), [arXiv:1511.03610].
- [448] A. M. Sirunyan *et al.* (CMS), JHEP **11**, 010 (2017), [arXiv:1707.07283].
- [449] J. Bernon *et al.*, Phys. Rev. **D91**, 7, 075019 (2015), [arXiv:1412.3385].
- [450] G. Aad *et al.* (ATLAS), Phys. Rev. Lett. **113**, 17, 171801 (2014), [arXiv:1407.6583].
- [451] CMS Collaboration, CMS-PAS-HIG-14-037 (2015).
- [452] CMS Collaboration, CMS-PAS-HIG-17-013 (2017).
- [453] S. Heinemeyer, Int. J. Mod. Phys. **A33**, 31, 1844006 (2018).
- [454] S. H. Zhu, arXiv preprint (1999), [hep-ph/9901221].
- [455] H. E. Logan and S.-f. Su, Phys. Rev. **D66**, 035001 (2002), [hep-ph/0203270].
- [456] A. Gutierrez-Rodriguez and O. A. Sampayo, Phys. Rev. **D62**, 055004 (2000).
- [457] S. Kanemura, S. Moretti and K. Odagiri, JHEP **02**, 011 (2001), [hep-ph/0012030].
- [458] M. Czakon, P. Fiedler and A. Mitov, Phys. Rev. Lett. **110**, 252004 (2013), [arXiv:1303.6254].
- [459] M. Carena *et al.*, Nucl. Phys. **B577**, 88 (2000), [hep-ph/9912516].
- [460] J. M. Campbell, R. K. Ellis and F. Tramontano, Phys. Rev. **D70**, 094012 (2004), [hep-ph/0408158].
- [461] C. Degrande *et al.*, Phys. Lett. **B772**, 87 (2017), [arXiv:1607.05291].
- [462] A. A. Barrientos Bendezu and B. A. Kniehl, Phys. Rev. **D63**, 015009 (2001), [hep-ph/0007336]; A. A. Barrientos Bendezu and B. A. Kniehl, Nucl. Phys. **B568**, 305 (2000), [hep-ph/9908385].
- [463] G. Abbiendi *et al.* (ALEPH, DELPHI, L3, OPAL, LEP), Eur. Phys. J. **C73**, 2463 (2013), [arXiv:1301.6065].

- [464] B. Abbott *et al.* (D0), Phys. Rev. Lett. **82**, 4975 (1999), [hep-ex/9902028]; A. Abulencia *et al.* (CDF), Phys. Rev. Lett. **96**, 042003 (2006), [hep-ex/0510065]; V. M. Abazov *et al.* (D0), Phys. Lett. **B682**, 278 (2009), [arXiv:0908.1811].
- [465] J. Abdallah *et al.* (DELPHI), Eur. Phys. J. **C54**, 1 (2008), [Erratum: Eur. Phys. J. **C56**, 165 (2008)], [arXiv:0801.3586].
- [466] R. Dermisek, Mod. Phys. Lett. **A24**, 1631 (2009), [arXiv:0907.0297].
- [467] J. F. Gunion, JHEP **08**, 032 (2009), [arXiv:0808.2509].
- [468] W. Love *et al.* (CLEO), Phys. Rev. Lett. **101**, 151802 (2008), [arXiv:0807.1427].
- [469] G. Aad *et al.* (ATLAS), Eur. Phys. J. **C72**, 2244 (2012), [arXiv:1210.5070]; S. Chatrchyan *et al.* (CMS), Eur. Phys. J. **C72**, 2189 (2012), [arXiv:1207.2666].
- [470] G. Aad *et al.* (ATLAS), Phys. Rev. **D89**, 3, 032002 (2014), [arXiv:1312.1956].
- [471] J. de Blas *et al.*, JHEP **01**, 139 (2020), [arXiv:1905.03764].

12. CKM Quark-Mixing Matrix

Revised March 2020 by A. Ceccucci (CERN), Z. Ligeti (LBNL) and Y. Sakai (KEK).

12.1 Introduction

The masses and mixings of quarks have a common origin in the Standard Model (SM). They arise from the Yukawa interactions with the Higgs condensate,

$$\mathcal{L}_Y = -Y_{ij}^d \overline{Q_{Li}^I} \phi d_{Rj}^I - Y_{ij}^u \overline{Q_{Li}^I} \epsilon \phi^* u_{Rj}^I + \text{h.c.}, \quad (12.1)$$

where $Y^{u,d}$ are 3×3 complex matrices, ϕ is the Higgs field, i, j are generation labels, and ϵ is the 2×2 antisymmetric tensor. Q_L^I are left-handed quark doublets, and d_R^I and u_R^I are right-handed down- and up-type quark singlets, respectively, in the weak-eigenstate basis. When ϕ acquires a vacuum expectation value, $\langle \phi \rangle = (0, v/\sqrt{2})$, Eq. (12.1) yields mass terms for the quarks. The physical states are obtained by diagonalizing $Y^{u,d}$

by four unitary matrices, $V_{L,R}^{u,d}$, as $M_{\text{diag}}^f = V_L^f Y^f V_R^{f\dagger} (v/\sqrt{2})$, $f = u, d$. As a result, the charged-current W^\pm interactions couple to the physical u_{Lj} and d_{Lk} quarks with couplings given by

$$\frac{-g}{\sqrt{2}} (\overline{u_L}, \overline{c_L}, \overline{t_L}) \gamma^\mu W_\mu^+ V_{\text{CKM}} \begin{pmatrix} d_L \\ s_L \\ b_L \end{pmatrix} + \text{h.c.}, \quad (12.2)$$

$$V_{\text{CKM}} \equiv V_L^u V_L^{d\dagger} = \begin{pmatrix} V_{ud} & V_{us} & V_{ub} \\ V_{cd} & V_{cs} & V_{cb} \\ V_{td} & V_{ts} & V_{tb} \end{pmatrix}.$$

This Cabibbo-Kobayashi-Maskawa (CKM) matrix [1,2] is a 3×3 unitary matrix. It can be parameterized by three mixing angles and the CP -violating KM phase [2]. Of the many possible conventions, a standard choice has become [3]

$$V_{\text{CKM}} = \begin{pmatrix} 1 & 0 & 0 \\ 0 & c_{23} & s_{23} \\ 0 & -s_{23} & c_{23} \end{pmatrix} \begin{pmatrix} c_{13} & 0 & s_{13} e^{-i\delta} \\ 0 & 1 & 0 \\ -s_{13} e^{i\delta} & 0 & c_{13} \end{pmatrix} \begin{pmatrix} c_{12} & s_{12} & 0 \\ -s_{12} & c_{12} & 0 \\ 0 & 0 & 1 \end{pmatrix} \quad (12.3)$$

$$= \begin{pmatrix} c_{12} c_{13} & s_{12} c_{13} & s_{13} e^{-i\delta} \\ -s_{12} c_{23} - c_{12} s_{23} s_{13} e^{i\delta} & c_{12} c_{23} - s_{12} s_{23} s_{13} e^{i\delta} & s_{23} c_{13} \\ s_{12} s_{23} - c_{12} c_{23} s_{13} e^{i\delta} & -s_{12} s_{23} - c_{12} c_{23} s_{13} e^{i\delta} & c_{23} c_{13} \end{pmatrix},$$

where $s_{ij} = \sin \theta_{ij}$, $c_{ij} = \cos \theta_{ij}$, and δ is the phase responsible for all CP -violating phenomena in flavor-changing processes in the SM. The angles θ_{ij} can be chosen to lie in the first quadrant, so $s_{ij}, c_{ij} \geq 0$.

It is known experimentally that $s_{13} \ll s_{23} \ll s_{12} \ll 1$, and it is convenient to exhibit this hierarchy using the Wolfenstein parameterization. We define [4–6]

$$s_{12} = \lambda = \frac{|V_{us}|}{\sqrt{|V_{ud}|^2 + |V_{us}|^2}}, \quad s_{23} = A\lambda^2 = \lambda \left| \frac{V_{cb}}{V_{us}} \right|,$$

$$s_{13} e^{i\delta} = V_{ub}^* = A\lambda^3 (\rho + i\eta) = \frac{A\lambda^3 (\bar{\rho} + i\bar{\eta}) \sqrt{1 - A^2 \lambda^4}}{\sqrt{1 - \lambda^2} [1 - A^2 \lambda^4 (\bar{\rho} + i\bar{\eta})]}. \quad (12.4)$$

These relations ensure that $\bar{\rho} + i\bar{\eta} = -(V_{ud} V_{ub}^*) / (V_{cd} V_{cb}^*)$ is phase convention independent, and the CKM matrix written in terms of $\lambda, A, \bar{\rho}$, and $\bar{\eta}$ is unitary to all orders in λ . The definitions of $\bar{\rho}, \bar{\eta}$ reproduce all approximate results in the literature; *i.e.*, $\bar{\rho} = \rho(1 - \lambda^2/2 + \dots)$ and $\bar{\eta} = \eta(1 - \lambda^2/2 + \dots)$, and one can write V_{CKM} to $\mathcal{O}(\lambda^4)$ either in terms of $\bar{\rho}, \bar{\eta}$ or, traditionally,

$$V_{\text{CKM}} = \begin{pmatrix} 1 - \lambda^2/2 & \lambda & A\lambda^3 (\rho - i\eta) \\ -\lambda & 1 - \lambda^2/2 & A\lambda^2 \\ A\lambda^3 (1 - \rho - i\eta) & -A\lambda^2 & 1 \end{pmatrix} + \mathcal{O}(\lambda^4). \quad (12.5)$$

The CKM matrix elements are fundamental parameters of the SM, so their precise determination is important. The unitarity of the CKM matrix imposes $\sum_i V_{ij} V_{ik}^* = \delta_{jk}$ and $\sum_j V_{ij} V_{kj}^* = \delta_{ik}$. The six vanishing combinations can be represented as triangles in a complex plane, of which those obtained by taking scalar products of neighboring rows or columns are nearly degenerate. The areas of all triangles are the same, half of the Jarlskog invariant, J [7], which is a phase-convention-independent measure of CP violation, defined by $\text{Im} [V_{ij} V_{kl} V_{il}^* V_{kj}^*] = J \sum_{m,n} \epsilon_{ikm} \epsilon_{jln}$.

The most commonly used unitarity triangle arises from

$$V_{ud} V_{ub}^* + V_{cd} V_{cb}^* + V_{td} V_{tb}^* = 0, \quad (12.6)$$

by dividing each side by the best-known one, $V_{cd} V_{cb}^*$ (see Fig. 12.1). Its vertices are exactly $(0, 0)$, $(1, 0)$, and, due to the definition in Eq. (12.4), $(\bar{\rho}, \bar{\eta})$. An important goal of flavor physics is to overconstrain the CKM elements, and many measurements can be conveniently displayed and compared in the $\bar{\rho}, \bar{\eta}$ plane. While

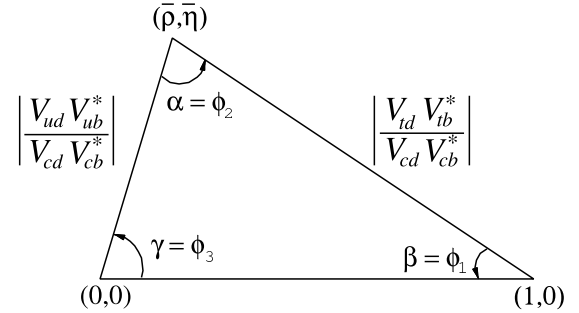


Figure 12.1: Sketch of the unitarity triangle.

the Lagrangian in Eq. (12.1) is normalized, and the CKM matrix has a well known scale dependence above the weak scale [8], below $\mu = m_W$ the CKM elements can be treated as constants, with all μ -dependence contained in the running of quark masses and higher-dimension operators.

Unless explicitly stated otherwise, we describe all measurements assuming the SM, to extract magnitudes and phases of CKM elements in Sec. 12.2 and 12.3. Processes dominated by loop-level contributions in the SM are particularly sensitive to new physics beyond the SM (BSM). We give the global fit results for the CKM elements in Sec. 12.4, and discuss some implications for beyond standard model physics in Sec. 12.5.

12.2 Magnitudes of CKM elements

12.2.1 $|V_{ud}|$

The most precise determination of $|V_{ud}|$ comes from the study of superallowed $0^+ \rightarrow 0^+$ nuclear beta decays, which are pure vector transitions. Taking the average of the fourteen most precise determinations [9] yields [10]

$$|V_{ud}| = 0.97370 \pm 0.00014. \quad (12.7)$$

This value is about 2σ smaller than in the review two years ago, mainly due to adopting a recent calculation of electroweak corrections based on dispersion relations [11]. The dominant and comparable uncertainties are the experimental ones, and from the estimates of the radiative corrections. A less precise determination of $|V_{ud}|$ can be obtained from the measurement of the neutron lifetime. The theoretical uncertainties are very small, but the determination is limited by the knowledge of the ratio of the axial-

vector and vector couplings, $g_A = G_A/G_V$ [10]. The PIBETA experiment [12] has improved the measurement of the $\pi^+ \rightarrow \pi^0 e^+ \nu$ branching ratio to 0.6%, and quotes $|V_{ud}| = 0.9739 \pm 0.0029$, in agreement with the more precise result listed above. The interest in this measurement is that the determination of $|V_{ud}|$ is very clean theoretically, because it is a pure vector transition and is free from nuclear-structure uncertainties.

12.2.2 $|V_{us}|$

The product of $|V_{us}|$ and the form factor at $q^2 = 0$, $|V_{us}| f_+(0)$, has been extracted traditionally from $K_L^0 \rightarrow \pi e \nu$ decays in order to avoid isospin-breaking corrections ($\pi^0 - \eta$ mixing) that affect K^\pm semileptonic decay, and the complications induced by a second (scalar) form factor present in the muonic decays. The last round of measurements has led to enough experimental constraints to justify the comparison between different decay modes. Systematic errors related to the experimental quantities, *e.g.*, the lifetime of neutral or charged kaons, and the form factor determinations for electron and muonic decays, differ among decay modes, and the consistency between different determinations enhances the confidence in the final result. For this reason, we follow the prescription [13] to average $K_L^0 \rightarrow \pi e \nu$, $K_L^0 \rightarrow \pi \mu \nu$, $K^\pm \rightarrow \pi^0 e^\pm \nu$, $K^\pm \rightarrow \pi^0 \mu^\pm \nu$ and $K_S^0 \rightarrow \pi e \nu$. The average of these five decay modes yields $|V_{us}| f_+(0) = 0.2165 \pm 0.0004$. Results obtained from each decay mode, and exhaustive references to the experimental data, are listed for instance in Ref. [10]. The form factor average $f_+(0) = 0.9706 \pm 0.0027$ [14] from $N_f = 2 + 1 + 1$ lattice QCD calculations gives $|V_{us}| = 0.2231 \pm 0.0007$ [10].¹ The broadly used classic calculation of $f_+(0)$ [16] is in good agreement with this value, while other calculations [18] differ by as much as 2%.

The calculation of the ratio of the kaon and pion decay constants enables one to extract $|V_{us}/V_{ud}|$ from $K \rightarrow \mu \nu(\gamma)$ and $\pi \rightarrow \mu \nu(\gamma)$, where (γ) indicates that radiative decays are included [19]. The value of $\Gamma(K \rightarrow \mu \nu(\gamma))$ [10] derived from the KLOE measurement of the corresponding branching ratio [20], combined with the lattice QCD result, $f_K/f_\pi = 1.1932 \pm 0.0019$ [14], leads to $|V_{us}| = 0.2252 \pm 0.0005$, where the accuracy is limited by the knowledge of the ratio of the decay constants. The average of these two determinations, with the error scaled according to the PDG prescription [21] by $\sqrt{\chi^2} = 2.0$, is quoted as [10]

$$|V_{us}| = 0.2245 \pm 0.0008. \quad (12.8)$$

It is important to include both QED and QCD isospin violations in the lattice QCD calculations.

The latest determination from hyperon decays can be found in Ref. [22]. The authors focus on the analysis of the vector form factor, protected from first order $SU(3)$ breaking effects by the Ademollo-Gatto theorem [23], and treat the ratio between the axial and vector form factors g_1/f_1 as experimental input, thus avoiding first order $SU(3)$ breaking effects in the axial-vector contribution. They find $|V_{us}| = 0.2250 \pm 0.0027$, although this does not include an estimate of the theoretical uncertainty due to second-order $SU(3)$ breaking, contrary to Eq. (12.8). Concerning hadronic τ decays to strange particles, averaging the inclusive decay and the exclusive $\tau \rightarrow h \nu$ ($h = \pi, K$) measurements yields $|V_{us}| = 0.2221 \pm 0.0013$ [24].

12.2.3 $|V_{cd}|$

The magnitude of V_{cd} can be extracted from semileptonic charm decays, using theoretical knowledge of the form factors. In semileptonic D decays, lattice QCD calculations have predicted the normalization of the $D \rightarrow \pi \ell \nu$ and $D \rightarrow K \ell \nu$ form factors [14]. The dependence on the invariant mass of the lepton pair, q^2 , is determined from lattice QCD and theoretical constraints from analyticity [15]. Using $N_f = 2 + 1 + 1$ lattice QCD calculations for $D \rightarrow \pi \ell \nu$, $f_+^{D\pi}(0) = 0.612 \pm 0.035$ [14], and the average [24] of the measurements of $D \rightarrow \pi \ell \nu$ decays by

¹For lattice QCD inputs, we use the averages from Ref. [14], unless the minireviews [10,15] choose different values. We only use unquenched results, and if both $N_f = 2 + 1 + 1$ and $2 + 1$ calculations are available, we use the former.

BABAR [25], *BESIII* [26,27], *CLEO-c* [28], and *Belle* [29], one obtains $|V_{cd}| = 0.2330 \pm 0.0029 \pm 0.0133$, where the first uncertainty is experimental, and the second is from the theoretical uncertainty of the form factor.

The determination of $|V_{cd}|$ is also possible from the leptonic decay $D^+ \rightarrow \mu^+ \nu$. The experimental uncertainties have not decreased significantly recently. Averaging the *BESIII* [30] and earlier *CLEO* [31] measurements, and using the $N_f = 2 + 1 + 1$ lattice QCD result, $f_D = 212.0 \pm 0.7$ MeV [14], yields $|V_{cd}| = 0.2173 \pm 0.0051 \pm 0.0007$ [24].²

Earlier determinations of $|V_{cd}|$ came from neutrino scattering data. The difference of the ratio of double-muon to single-muon production by neutrino and antineutrino beams is proportional to the charm cross section off valence d quarks, and therefore to $|V_{cd}|^2$ times the average semileptonic branching ratio of charm mesons, \mathcal{B}_μ . The method was used first by CDHS [32] and then by CCFR [33,34] and CHARM II [35]. Averaging these results is complicated, because it requires assumptions about the scale of the QCD corrections, and because \mathcal{B}_μ is an effective quantity, which depends on the specific neutrino beam characteristics. With no recent experimental input available, we quote the average from a past review, $\mathcal{B}_\mu |V_{cd}|^2 = (0.463 \pm 0.034) \times 10^{-2}$ [36]. Analysis cuts make these experiments insensitive to neutrino energies smaller than 30 GeV. Thus, \mathcal{B}_μ should be computed using only neutrino interactions with visible energy larger than 30 GeV. An appraisal [37] based on charm-production fractions measured in neutrino interactions [38,39] gives $\mathcal{B}_\mu = 0.088 \pm 0.006$. Data from the CHORUS experiment [40] are sufficiently precise to extract \mathcal{B}_μ directly, by comparing the number of charm decays with a muon to the total number of charmed hadrons found in the nuclear emulsions. Requiring the visible energy to be larger than 30 GeV, CHORUS found $\mathcal{B}_\mu = 0.085 \pm 0.009 \pm 0.006$. We use the average of these two determinations, $\mathcal{B}_\mu = 0.087 \pm 0.005$, and obtain $|V_{cd}| = 0.230 \pm 0.011$. Averaging the three determinations above, we find

$$|V_{cd}| = 0.221 \pm 0.004. \quad (12.9)$$

12.2.4 $|V_{cs}|$

The direct determination of $|V_{cs}|$ is possible from semileptonic D or leptonic D_s decays, using lattice QCD calculations of the semileptonic D form factor or the D_s decay constant. For muonic decays, the average of *Belle* [41], *CLEO-c* [42], *BABAR* [43], and *BESIII* [44,45] is $\mathcal{B}(D_s^+ \rightarrow \mu^+ \nu) = (5.51 \pm 0.16) \times 10^{-3}$ [24]. For decays to τ leptons, the average of *CLEO-c* [42,46,47], *BABAR* [43], *Belle* [41], and *BESIII* [44] gives $\mathcal{B}(D_s^+ \rightarrow \tau^+ \nu) = (5.52 \pm 0.24) \times 10^{-2}$ [24]. From each of these values, determinations of $|V_{cs}|$ can be obtained using the PDG values for the mass and lifetime of the D_s , the masses of the leptons, and $f_{D_s} = (249.9 \pm 0.5)$ MeV [14]. The average of these determinations gives $|V_{cs}| = 0.992 \pm 0.012$, where the error is dominated by the experimental uncertainty. In semileptonic D decays, lattice QCD calculations of the $D \rightarrow K \ell \nu$ form factor are available [14]. Using $f_+^{DK}(0) = 0.765 \pm 0.031$ and the average [24] of *CLEO-c* [28], *Belle* [29], *BABAR* [48], and recent *BESIII* [26,49] measurements of $D \rightarrow K \ell \nu$ decays, one obtains $|V_{cs}| = 0.939 \pm 0.038$, where the dominant uncertainty is from the theoretical calculation of the form factor. Averaging the determinations from leptonic and semileptonic decays, we find

$$|V_{cs}| = 0.987 \pm 0.011. \quad (12.10)$$

Measurements of on-shell W^\pm decays sensitive to $|V_{cs}|$ were made by LEP-2. The W branching ratios depend on the six CKM elements involving quarks lighter than m_W . The W branching ratio to each lepton flavor is $1/\mathcal{B}(W \rightarrow \ell \bar{\nu}_\ell) = 3[1 + \sum_{u,c,d,s,b} |V_{ij}|^2 (1 + \alpha_s(m_W)/\pi) + \dots]$. Assuming lepton universality, the measurement $\mathcal{B}(W \rightarrow \ell \bar{\nu}_\ell) = (10.83 \pm 0.07 \pm 0.07)\%$ [50] implies $\sum_{u,c,d,s,b} |V_{ij}|^2 = 2.002 \pm 0.027$. This is a precise test of unitarity; however, only flavor-tagged W -decays determine $|V_{cs}|$

²Hereafter the first error is statistical and the second is systematic, unless mentioned otherwise.

directly, such as DELPHI's tagged $W^+ \rightarrow c\bar{s}$ analysis, yielding $|V_{cs}| = 0.94_{-0.26}^{+0.32} \pm 0.13$ [51].

12.2.5 $|V_{cb}|$

This matrix element can be determined from exclusive and inclusive semileptonic decays of B mesons to charm. The inclusive determinations use the semileptonic decay rate measurement, together with (certain moments of) the lepton energy and the hadronic invariant-mass spectra. The theoretical basis is the operator product expansion [52, 53], which allows calculation of the decay rate and various spectra as expansions in α_s and inverse powers of the heavy-quark mass. The dependence on m_b , m_c , and the parameters that occur at subleading order is different for different moments, and a large number of measured moments overconstrain all the parameters, and tests the consistency of the determination. The precise extraction of $|V_{cb}|$ requires using a "threshold" quark mass definition [54, 55]. Inclusive measurements have been performed using B mesons from Z^0 decays at LEP, and at e^+e^- machines operated at the $\Upsilon(4S)$. At LEP, the large boost of B mesons from the Z^0 decay allows the determination of the moments throughout phase space, which is not possible otherwise, but the large statistics available at the B factories lead to more precise determinations. An average of the measurements and a compilation of the references are provided in Ref. [15]: $|V_{cb}| = (42.2 \pm 0.8) \times 10^{-3}$.

Complementary determinations are based on exclusive semileptonic B decays to D and D^* . In the $m_{b,c} \gg \Lambda_{\text{QCD}}$ limit, all form factors are given by a single Isgur-Wise function [56], which depends on the product of the four-velocities of the B and $D^{(*)}$ mesons, $w = v \cdot v'$. Heavy-quark symmetry determines the rate at $w = 1$, the maximum momentum transfer to the $\ell\bar{\nu}$ pair, and $|V_{cb}|$ is obtained from an extrapolation to $w = 1$. The current update of the V_{cb} and V_{ub} minireview quotes from exclusive decays $|V_{cb}| = (39.5 \pm 0.9) \times 10^{-3}$ [15], based on the only unfolded measurement of $B \rightarrow D^*$ semileptonic decay distributions [57], and using a more general fit [58] than in earlier B factory measurements. With the uncertainty scaled by $\sqrt{\chi^2} = 2.4$, this yields the combination [15],

$$|V_{cb}| = (41.0 \pm 1.4) \times 10^{-3}. \quad (12.11)$$

Less precise measurements of $|V_{cb}|$, not included in this average, can be obtained from $\mathcal{B}(B \rightarrow D^{(*)}\tau\bar{\nu})$. The most precise data involving τ leptons are the $|V_{cb}|$ -independent ratios, $\mathcal{B}(B \rightarrow D^{(*)}\tau\bar{\nu})/\mathcal{B}(B \rightarrow D^{(*)}\ell\bar{\nu})$ measured by BaBar, Belle, and LHCb. If the current, approximately 3σ [24], hint of lepton non-universality prevails, the determination of $|V_{cb}|$ becomes more complicated.

12.2.6 $|V_{ub}|$

The determination of $|V_{ub}|$ from inclusive $B \rightarrow X_u\ell\bar{\nu}$ decay is complicated due to large $B \rightarrow X_c\ell\bar{\nu}$ backgrounds. In most regions of phase space where the charm background is kinematically forbidden, the hadronic physics enters via unknown nonperturbative functions, so-called shape functions. (In contrast, the nonperturbative physics for $|V_{cb}|$ is encoded in a few parameters.) At leading order in Λ_{QCD}/m_b , there is only one shape function, which can be extracted from the photon energy spectrum in $B \rightarrow X_s\gamma$ [59, 60], and applied to several spectra in $B \rightarrow X_u\ell\bar{\nu}$. The subleading shape functions are modeled in the current determinations. Phase space cuts for which the rate has only subleading dependence on the shape function are also possible [61]. The measurements of both the hadronic and the leptonic systems are important for an optimal choice of phase space. A different approach is to make the measurements more inclusive by extending them deeper into the $B \rightarrow X_c\ell\bar{\nu}$ region, and thus reduce the theoretical uncertainties. Analyses of the electron-energy endpoint from CLEO [62], BABAR [63], and Belle [64] quote $B \rightarrow X_u e\bar{\nu}$ partial rates for $|\vec{p}_e| \geq 2.0 \text{ GeV}$ and 1.9 GeV , which are well below the charm endpoint. The large and pure $B\bar{B}$ samples at the B factories permit the selection of $B \rightarrow X_u\ell\bar{\nu}$ decays in events where the other B is fully reconstructed [65]. With this full-reconstruction tag method, the four-momenta of both the leptonic and the hadronic final states can be measured. It also gives access to a wider kinematic region, because of improved signal purity. Ref. [15] quotes the inclusive average, $|V_{ub}| = (4.25 \pm 0.12_{-0.14}^{+0.15} \pm 0.23) \times 10^{-3}$, where the first error is experimental, the second arises from the model dependence quoted by the individual measurements, and the third is an additional one estimated in Ref. [15].

To extract $|V_{ub}|$ from exclusive decays, the form factors have to be known. Experimentally, better signal-to-background ratios are offset by smaller yields. The $B \rightarrow \pi\ell\bar{\nu}$ branching ratio is now known to 5%. Lattice QCD calculations of the $B \rightarrow \pi\ell\bar{\nu}$ form factor are available [66] for the high q^2 region ($q^2 > 16$ or 18 GeV^2). A fit to the experimental partial rates and lattice QCD results versus q^2 yields $|V_{ub}| = (3.70 \pm 0.10 \pm 0.12) \times 10^{-3}$ [24]. Light-cone QCD sum rules are supposed to be applicable for $q^2 < 12 \text{ GeV}^2$ [67], yielding a combination, $|V_{ub}| = (3.67 \pm 0.09 \pm 0.12) \times 10^{-3}$ [15, 24].

The uncertainties in extracting $|V_{ub}|$ from inclusive and exclusive decays are different to a large extent. An average of these determinations, with the uncertainty scaled by $\sqrt{\chi^2} = 1.6$, is [15]

$$|V_{ub}| = (3.82 \pm 0.24) \times 10^{-3}. \quad (12.12)$$

A determination of $|V_{ub}|$ not included in this average can be obtained from $\mathcal{B}(B \rightarrow \tau\bar{\nu}) = (1.06 \pm 0.19) \times 10^{-4}$ [24]. Using $f_B = (190.0 \pm 1.3) \text{ MeV}$ [14] and $\tau_{B^\pm} = (1.638 \pm 0.004) \text{ ps}$ [68], we find the remarkably consistent result, $|V_{ub}| = (4.05 \pm 0.36) \times 10^{-3}$. This decay is sensitive, for example, to tree-level charged Higgs contributions, and the measured rate is consistent with the SM expectation. The LHCb measurement $|V_{ub}/V_{cb}| = 0.079 \pm 0.006$ [69] from the ratio of $\Lambda_b \rightarrow p^+\mu^-\bar{\nu}$ and $\Lambda_b \rightarrow \Lambda_c^+\mu^-\bar{\nu}$ in different regions of q^2 , provides another complementary determination.

12.2.7 $|V_{td}|$ and $|V_{ts}|$

The CKM elements $|V_{td}|$ and $|V_{ts}|$ are not likely to be precisely measurable in tree-level processes involving top quarks, so one has to rely on determinations from $B-\bar{B}$ oscillations dominated by box diagrams with top quarks, or loop-mediated rare K and B decays. Theoretical uncertainties in hadronic effects limit the accuracy of the current determinations. These can be reduced by taking ratios of processes that are equal in the flavor $SU(3)$ limit to determine $|V_{td}/V_{ts}|$.

The mixing of the two B^0 mesons was discovered by ARGUS [70], and the mass difference is now precisely measured as $\Delta m_d = (0.5065 \pm 0.0019) \text{ ps}^{-1}$ [71]. In the B_s^0 system, Δm_s was first measured significantly by CDF [72] and the world average, dominated by an LHCb measurement [73], is $\Delta m_s = (17.749 \pm 0.020) \text{ ps}^{-1}$ [71]. Neglecting corrections suppressed by $|V_{tb}| - 1$, and using the lattice QCD results $f_{B_d}\sqrt{\widehat{B}_{B_d}} = (225 \pm 9) \text{ MeV}$ and $f_{B_s}\sqrt{\widehat{B}_{B_s}} = (274 \pm 8) \text{ MeV}$ [14],

$$|V_{td}| = (8.0 \pm 0.3) \times 10^{-3}, \quad |V_{ts}| = (38.8 \pm 1.1) \times 10^{-3}. \quad (12.13)$$

The uncertainties are dominated by lattice QCD. Several uncertainties are reduced in the calculation of the ratio $\xi = (f_{B_s}\sqrt{\widehat{B}_{B_s}})/(f_{B_d}\sqrt{\widehat{B}_{B_d}}) = 1.206 \pm 0.038$ [14] and therefore the constraint on $|V_{td}/V_{ts}|$ from $\Delta m_d/\Delta m_s$ is more reliable theoretically. These provide a theoretically clean and significantly improved determination,

$$|V_{td}/V_{ts}| = 0.205 \pm 0.001 \pm 0.006. \quad (12.14)$$

The inclusive branching ratio $\mathcal{B}(B \rightarrow X_s\gamma) = (3.32 \pm 0.15) \times 10^{-4}$ extrapolated to $E_\gamma > E_0 = 1.6 \text{ GeV}$ [24] is also sensitive to $|V_{tb}V_{ts}|$. In addition to t -quark penguins, a substantial part of the rate comes from charm contributions proportional to $V_{cb}V_{cs}^*$ via the application of 3×3 CKM unitarity (which is used here). With the NNLO calculation of $\mathcal{B}(B \rightarrow X_s\gamma)_{E_\gamma > E_0}/\mathcal{B}(B \rightarrow X_c e\bar{\nu})$ [74], we obtain $|V_{ts}/V_{cb}| = 0.98 \pm 0.04$. The $B_s \rightarrow \mu^+\mu^-$ rate is also proportional to $|V_{tb}V_{ts}|^2$ in the SM, and the world average, $\mathcal{B}(B_s \rightarrow \mu^+\mu^-) = (3.1 \pm 0.6) \times 10^{-9}$ [24], is consistent with the SM, with sizable uncertainties.

A complementary determination of $|V_{td}/V_{ts}|$ is possible from the ratio of $B \rightarrow \rho\gamma$ and $K^*\gamma$ rates. The ratio of the neutral modes

is theoretically cleaner than that of the charged ones, because the poorly known spectator-interaction contribution is expected to be smaller (W -exchange vs. weak annihilation). For now, because of low statistics, we average the charged and neutral rates assuming the isospin symmetry and heavy-quark limit motivated relation, $|V_{td}/V_{ts}|^2/\xi_\gamma^2 = [\Gamma(B^+ \rightarrow \rho^+\gamma) + 2\Gamma(B^0 \rightarrow \rho^0\gamma)]/[\Gamma(B^+ \rightarrow K^{*+}\gamma) + \Gamma(B^0 \rightarrow K^{*0}\gamma)] = (3.37 \pm 0.49)\%$ [24]. Here ξ_γ contains the poorly known hadronic physics. Using $\xi_\gamma = 1.2 \pm 0.2$ [75] gives $|V_{td}/V_{ts}| = 0.220 \pm 0.016 \pm 0.037$, where the first uncertainty is experimental and the second is theoretical.

A theoretically clean determination of $|V_{td}V_{ts}^*|$ is possible from $K^+ \rightarrow \pi^+\nu\bar{\nu}$ decay [76]. Experimentally, only a handful of events have been observed [77, 78] and the rate is consistent with the SM with large uncertainties. Much more data are needed for a precision measurement.

12.2.8 $|V_{tb}|$

The determination of $|V_{tb}|$ from top decays uses the ratio of branching fractions $R = \mathcal{B}(t \rightarrow Wb)/\mathcal{B}(t \rightarrow Wq) = |V_{tb}|^2/(\sum_q |V_{tq}|^2) = |V_{tb}|^2$, where $q = b, s, d$. The CDF and DØ measurements performed on data collected during Run II of the Tevatron give $|V_{tb}| > 0.78$ [79] and $0.99 > |V_{tb}| > 0.90$ [80], respectively, at 95% CL. CMS measured the same quantity at 8 TeV and obtained $|V_{tb}| > 0.975$ [81] at 95% CL.

The direct determination of $|V_{tb}|$, without assuming unitarity, is possible from the single top quark production cross section. The $(3.30^{+0.52}_{-0.40})$ pb combined cross section [82] of DØ and CDF measurements implies $|V_{tb}| = 1.02^{+0.06}_{-0.05}$. The LHC experiments, ATLAS and CMS, have measured single top quark production cross sections (and extracted $|V_{tb}|$) in t -channel, Wt -channel, and s -channel at 7 TeV, 8 TeV, and 13 TeV [83]. The average of these $|V_{tb}|$ values is calculated to be $|V_{tb}| = 1.010 \pm 0.036$, where all systematic errors and theoretical errors are treated to be fully correlated. The average of Tevatron and LHC values gives

$$|V_{tb}| = 1.013 \pm 0.030. \quad (12.15)$$

The experimental systematic uncertainties dominate, and a dedicated combination would be welcome.

A weak constraint on $|V_{tb}|$ can be obtained from precision electroweak data, where top quarks enter in loops. The sensitivity is best in $\Gamma(Z \rightarrow b\bar{b})$ and yields $|V_{tb}| = 0.77^{+0.18}_{-0.24}$ [84].

12.3 Phases of CKM elements

As can be seen from Fig. 12.1, the angles of the unitarity triangle are

$$\begin{aligned} \beta &= \phi_1 = \arg\left(-\frac{V_{cd}V_{cb}^*}{V_{td}V_{tb}^*}\right), \\ \alpha &= \phi_2 = \arg\left(-\frac{V_{td}V_{tb}^*}{V_{ud}V_{ub}^*}\right), \\ \gamma &= \phi_3 = \arg\left(-\frac{V_{ud}V_{ub}^*}{V_{cd}V_{cb}^*}\right). \end{aligned} \quad (12.16)$$

Since CP violation involves phases of CKM elements, many measurements of CP -violating observables can be used to constrain these angles and the $\bar{\rho}, \bar{\eta}$ parameters.

12.3.1 ϵ and ϵ'

The measurement of CP violation in $K^0-\bar{K}^0$ mixing, $|\epsilon| = (2.228 \pm 0.011) \times 10^{-3}$ [85], provides important information about the CKM matrix. The phase of ϵ is determined by long-distance physics, $\epsilon = \frac{1}{2} e^{i\phi_\epsilon} \sin\phi_\epsilon \arg(-M_{12}/\Gamma_{12})$, where $\phi_\epsilon = \arctan[2\Delta m_K/\Delta\Gamma_K] \simeq 43.5^\circ$. The SM prediction can be written as

$$\begin{aligned} \epsilon &= \kappa_\epsilon e^{i\phi_\epsilon} \frac{G_F^2 m_W^2 m_K}{12\sqrt{2}\pi^2 \Delta m_K} f_K^2 \hat{B}_K \left\{ \eta_{tt} S(x_t) \text{Im}[(V_{ts}V_{td}^*)^2] \right. \\ &\quad \left. + 2\eta_{ct} S(x_c, x_t) \text{Im}(V_{cs}V_{cd}^*V_{ts}V_{td}^*) + \eta_{cc} x_c \text{Im}[(V_{cs}V_{cd}^*)^2] \right\}, \end{aligned} \quad (12.17)$$

where $\kappa_\epsilon \simeq 0.94 \pm 0.02$ [86] includes the effects of strangeness changing $\Delta s = 1$ operators and additional dependence on $\phi_\epsilon \neq$

$\pi/4$ (see also Ref. [87]). The displayed terms are the short-distance $\Delta s = 2$ contribution to $\text{Im}M_{12}$ in the usual phase convention, S is an Inami-Lim function [88], $x_q = m_q^2/m_W^2$, and η_{ij} are perturbative QCD corrections. The constraint from ϵ in the $\bar{\rho}, \bar{\eta}$ plane is bounded by approximate hyperbolas. Lattice QCD determined the bag parameter $\hat{B}_K = 0.717 \pm 0.024$ [14], and the main uncertainties are from $(V_{ts}V_{td}^*)^2$ (approximately given by that of $|V_{cb}|^4$ or A^4), the η_{ij} coefficients, and estimates of κ_ϵ .

The measurement of $6 \text{Re}(\epsilon'/\epsilon) = 1 - |\eta_{00}/\eta_{+-}|^2$, where each $\eta_{ij} = \langle \pi^i \pi^j | \mathcal{H}(K_L) / \langle \pi^i \pi^j | \mathcal{H}(K_S) \rangle$ violates CP , provides a qualitative test of the CKM mechanism, and strong constraints on many BSM scenarios. Its nonzero value, $\text{Re}(\epsilon'/\epsilon) = (1.67 \pm 0.23) \times 10^{-3}$ [85], demonstrated the existence of direct CP violation, a prediction of the KM ansatz. While $\text{Re}(\epsilon'/\epsilon) \propto \text{Im}(V_{td}V_{ts}^*)$, this quantity cannot easily be used to extract CKM parameters, because cancellations between the electromagnetic and gluonic penguin contributions for large m_t [89] enhance the hadronic uncertainties. Most SM estimates [90] agree with the observed value, indicating that $\bar{\eta}$ is positive. Progress in lattice QCD [91] may yield a precise SM prediction in the future, and trigger new work on assessing the consistency of the SM with the measured value [92, 93].

12.3.2 β / ϕ_1

12.3.2.1 Charmonium modes

CP -violation measurements in B -meson decays provide direct information on the angles of the unitarity triangle, shown in Fig. 12.1. These overconstraining measurements serve to improve the determination of the CKM elements, and to reveal possible effects beyond the SM.

The time-dependent CP asymmetry of neutral B decays to a final state f common to B^0 and \bar{B}^0 is given by [94–96]

$$\begin{aligned} \mathcal{A}_f &= \frac{\Gamma(\bar{B}^0(t) \rightarrow f) - \Gamma(B^0(t) \rightarrow f)}{\Gamma(\bar{B}^0(t) \rightarrow f) + \Gamma(B^0(t) \rightarrow f)}, \\ &= S_f \sin(\Delta m_d t) - C_f \cos(\Delta m_d t), \end{aligned} \quad (12.18)$$

where

$$S_f = \frac{2 \text{Im}\lambda_f}{1 + |\lambda_f|^2}, \quad C_f = \frac{1 - |\lambda_f|^2}{1 + |\lambda_f|^2}, \quad \lambda_f = \frac{q}{p} \frac{\bar{A}_f}{A_f}. \quad (12.19)$$

Here, q/p describes $B^0-\bar{B}^0$ mixing and, to a good approximation in the SM, $q/p = V_{tb}^*V_{td}/V_{tb}V_{td}^* = e^{-2i\beta + \mathcal{O}(\lambda^4)}$ in the usual phase convention. A_f (\bar{A}_f) is the amplitude of the $B^0 \rightarrow f$ ($\bar{B}^0 \rightarrow f$) decay. If f is a CP eigenstate, and amplitudes with one CKM phase dominate the decay, then $|A_f| = |\bar{A}_f|$, $C_f = 0$, and $S_f = \sin(\arg\lambda_f) = \eta_f \sin 2\phi$, where η_f is the CP eigenvalue of f and 2ϕ is the phase difference between the $B^0 \rightarrow f$ and $B^0 \rightarrow \bar{B}^0 \rightarrow f$ decay paths. A contribution of another amplitude to the decay with a different CKM phase makes the value of S_f sensitive to relative strong-interaction phases between the decay amplitudes (it also makes $C_f \neq 0$ possible).

The $b \rightarrow c\bar{c}s$ decays to CP eigenstates ($B^0 \rightarrow$ charmonium $K_{S,L}^0$) are the theoretically cleanest examples, measuring $S_f = -\eta_f \sin 2\beta$. The $b \rightarrow s$ penguin amplitudes have dominantly the same weak phase as the $b \rightarrow c\bar{c}s$ tree amplitude. Since only λ^2 -suppressed penguin amplitudes introduce a different CP -violating phase, amplitudes with a single weak phase dominate, and we expect $|\bar{A}_{\psi K}/A_{\psi K} - 1| < 0.01$. The e^+e^- asymmetric-energy B -factory experiments, $BABAR$ [97] and Belle [98], and LHCb [99] provided precise measurements. The world average, including some other measurements, is [24]

$$\sin 2\beta = 0.699 \pm 0.017. \quad (12.20)$$

This measurement has a four-fold ambiguity in β , which can be resolved by a global fit as mentioned in Sec. 12.4. Experimentally, the two-fold ambiguity $\beta \rightarrow \pi/2 - \beta$ (but not $\beta \rightarrow \pi + \beta$) can be resolved by a time-dependent angular analysis of $B^0 \rightarrow J/\psi K^{*0}$ [100, 101], or a time-dependent Dalitz plot analysis of $B^0 \rightarrow \bar{D}^0 h^0$. The time-dependent Dalitz plot analysis of $B^0 \rightarrow \bar{D}^0 h^0$ ($h^0 = \pi^0, \eta, \omega$) with $\bar{D}^0 \rightarrow K_S^0 \pi^+ \pi^-$, jointly performed by Belle and $BABAR$, excludes the $\pi/2 - \beta$ solution with 7.3σ confidence level

[102]. These results indicate that negative $\cos 2\beta$ solutions are very unlikely, in agreement with the global CKM fit result.

The $b \rightarrow c\bar{c}d$ mediated transitions, such as $B^0 \rightarrow J/\psi\pi^0$ and $B^0 \rightarrow D^{(*)+}D^{(*)-}$, also measure approximately $\sin 2\beta$. However, the dominant component of the $b \rightarrow d$ penguin amplitude has a different CKM phase ($V_{tb}^*V_{td}$) than the tree amplitude ($V_{cb}^*V_{cd}$), and their magnitudes are of the same order in λ . Therefore, the effect of penguins could be large, resulting in $S_f \neq -\eta_f \sin 2\beta$ and $C_f \neq 0$. Such decay modes have been measured by *BABAR*, Belle, and LHCb. The world averages [24], $S_{J/\psi\pi^0} = -0.86 \pm 0.14$, $S_{J/\psi\rho^0} = -0.66^{+0.16}_{-0.12}$, $S_{D^+D^-} = -0.84 \pm 0.12$, and $S_{D^{*+}D^{*-}} = -0.71 \pm 0.09$ (where $\eta_f = +1$ for the $J/\psi\pi^0$ and D^+D^- modes, while $J/\psi\rho^0$ and $D^{*+}D^{*-}$ are mixtures of CP even and odd states), are consistent with $\sin 2\beta$ obtained from $B^0 \rightarrow$ charmium K^0 decays, and the C_f 's are consistent with zero, although the uncertainties are sizable.

The $b \rightarrow c\bar{u}d$ decays $B^0 \rightarrow \bar{D}^0(*)h^0$, with $\bar{D}^0 \rightarrow CP$ eigenstates and $\bar{D}^0 \rightarrow K_S^0\pi^+\pi^-$ with Dalitz plot analysis, have no penguin contributions, and provide theoretically clean $\sin 2\beta$ measurements. The average of joint analyses of *BABAR* and Belle data [102, 103] give $\sin 2\beta = 0.71 \pm 0.09$ [24, 104].

12.3.2.2 Penguin-dominated modes

The $b \rightarrow s\bar{q}q$ penguin-dominated decays have the same CKM phase as the $b \rightarrow c\bar{c}s$ tree level decays, up to corrections suppressed by λ^2 , since $V_{tb}^*V_{ts} = -V_{cb}^*V_{cs}[1 + \mathcal{O}(\lambda^2)]$. Therefore, decays such as $B^0 \rightarrow \phi K^0$ and $\eta' K^0$ provide $\sin 2\beta$ measurements in the SM. Any BSM contribution to the amplitude with a different weak phase would give rise to $S_f \neq -\eta_f \sin 2\beta$, and possibly $C_f \neq 0$. Therefore, the main interest in these modes is not simply to measure $\sin 2\beta$, but to search for new physics. Measurements of many other decay modes in this category, such as $B \rightarrow \pi^0 K_S^0$, $K_S^0 K_S^0 K_S^0$, etc., have also been performed by *BABAR* and Belle. The results and their uncertainties are summarized in Fig. 12.3 and Table 12.1 of Ref. [95]. The comparison of CP violation measurements between tree-dominated and penguin-dominated modes in B_s^0 decays provides similar sensitivity to new physics.

12.3.3 α / ϕ_2

Since α is the phase between $V_{tb}^*V_{td}$ and $V_{ub}^*V_{ud}$, only time-dependent CP asymmetries in decay modes dominated by $b \rightarrow u\bar{u}d$ transition can directly measure $\sin 2\alpha$, in contrast to $\sin 2\beta$, where several different quark-level transitions can be used. Since $b \rightarrow d$ penguin amplitudes have a different CKM phase than $b \rightarrow u\bar{u}d$ tree amplitudes, and their magnitudes are of the same order in λ , the penguin contribution can be sizable, which makes the determination of α complicated. To date, α has been measured in $B \rightarrow \pi\pi$, $\rho\pi$ and $\rho\rho$ decay modes.

12.3.3.1 $B \rightarrow \pi\pi$

It is well established from the data that there is a sizable contribution of $b \rightarrow d$ penguin amplitudes in $B \rightarrow \pi\pi$ decays. Thus, $S_{\pi^+\pi^-}$ in the time-dependent $B^0 \rightarrow \pi^+\pi^-$ analysis does not measure $\sin 2\alpha$, but

$$S_{\pi^+\pi^-} = \sqrt{1 - C_{\pi^+\pi^-}^2} \sin(2\alpha + 2\Delta\alpha), \quad (12.21)$$

where $2\Delta\alpha$ is the phase difference between $e^{2i\gamma}\bar{A}_{\pi^+\pi^-}$ and $A_{\pi^+\pi^-}$. The value of $\Delta\alpha$, and hence α , can be extracted using the isospin relation among the amplitudes of $B^0 \rightarrow \pi^+\pi^-$, $B^0 \rightarrow \pi^0\pi^0$, and $B^+ \rightarrow \pi^+\pi^0$ decays [105],

$$\frac{1}{\sqrt{2}} A_{\pi^+\pi^-} + A_{\pi^0\pi^0} - A_{\pi^+\pi^0} = 0, \quad (12.22)$$

and a similar expression for the $\bar{A}_{\pi\pi}$'s. This method utilizes the fact that a pair of pions from $B \rightarrow \pi\pi$ decay must be in a zero angular momentum state, and, because of Bose statistics, they must have even isospin. Consequently, $\pi^\pm\pi^0$ is in a pure isospin-2 state, while the penguin amplitudes only contribute to the isospin-0 final state. The latter does not hold for the electroweak penguin amplitudes, but their effect is expected to be small. The isospin

analysis uses the world averages of *BABAR*, Belle, and LHCb measurements, $S_{\pi^+\pi^-} = -0.63 \pm 0.04$, $C_{\pi^+\pi^-} = -0.32 \pm 0.04$, the decay widths of all three modes, and the direct CP asymmetry $C_{\pi^0\pi^0} = -0.33 \pm 0.22$ [24]. This analysis leads to 16 mirror solutions for $0 \leq \alpha < 2\pi$. Because of this, and due to the experimental uncertainties, some of these solutions are not well separated [96].

12.3.3.2 $B \rightarrow \rho\rho$

The decay $B^0 \rightarrow \rho^+\rho^-$ contains two vector mesons in the final state, and so in general is a mixture of CP -even and CP -odd components. Therefore, it was thought that extracting α from this mode would be complicated.

However, the longitudinal polarization fractions in $B^+ \rightarrow \rho^+\rho^0$ and $B^0 \rightarrow \rho^+\rho^-$ decays were measured to be close to unity [106], which implies that the final states are almost purely CP -even. Furthermore, $\mathcal{B}(B^0 \rightarrow \rho^0\rho^0) = (0.95 \pm 0.16) \times 10^{-6}$ is much smaller than $\mathcal{B}(B^0 \rightarrow \rho^+\rho^-) = (27.7 \pm 1.9) \times 10^{-6}$ and $\mathcal{B}(B^+ \rightarrow \rho^+\rho^0) = (24.0_{-2.0}^{+1.9}) \times 10^{-6}$ [24], which implies that the effect of the penguin contributions is small. The isospin analysis using the world averages, $S_{\rho^+\rho^-} = -0.14 \pm 0.13$ and $C_{\rho^+\rho^-} = 0.00 \pm 0.09$ [24], together with the time-dependent CP asymmetry, $S_{\rho^0\rho^0} = -0.3 \pm 0.7$ and $C_{\rho^0\rho^0} = -0.2 \pm 0.9$ [107], and the above mentioned branching fractions and longitudinal polarization fractions, gives two solutions (with mirror solutions at $3\pi/2 - \alpha$) [96]. A possible small violation of Eq. (12.22) due to the finite width of the ρ [108] is so far neglected.

12.3.3.3 $B \rightarrow \rho\pi$

The final state in $B^0 \rightarrow \rho^+\pi^-$ decay is not a CP eigenstate, but this decay proceeds via the same quark-level diagrams as $B^0 \rightarrow \pi^+\pi^-$, and both B^0 and \bar{B}^0 can decay to $\rho^+\pi^-$, while the final state in $B^0 \rightarrow \rho^0\pi^0$ is a CP eigenstate. Consequently, mixing-induced CP violation can occur in B^0 and \bar{B}^0 decays to $\rho^\pm\pi^\mp$ and $\rho^0\pi^0$. The time-dependent Dalitz plot analysis of $B^0 \rightarrow \pi^+\pi^-\pi^0$ decays permits the extraction of α with a single discrete ambiguity, $\alpha \rightarrow \alpha + \pi$, since one knows the variation of the strong phases in the interference regions of the $\rho^+\pi^-$, $\rho^-\pi^+$, and $\rho^0\pi^0$ amplitudes in the Dalitz plot [109]. The combination of Belle [110] and *BABAR* [111] measurements gives only moderate constraints [96].

Combining the $B \rightarrow \pi\pi$, $\rho\pi$, and $\rho\rho$ decay modes [24, 96], α is constrained as

$$\alpha = (84.9_{-4.5}^{+5.1})^\circ. \quad (12.23)$$

Similar results can be found in Refs. [112, 113].

12.3.4 γ / ϕ_3

By virtue of Eq. (12.16), γ does not depend on CKM elements involving the top quark, so it can be measured in tree-level B decays. This is an important distinction from the measurements of α and β , and implies that measurements of γ are unlikely to be affected by physics beyond the SM.

12.3.4.1 $B_{(s)} \rightarrow D_{(s)}K^{(*)}$

The interference of $B^- \rightarrow D^0K^-$ ($b \rightarrow c\bar{u}s$) and $B^- \rightarrow \bar{D}^0K^-$ ($b \rightarrow u\bar{c}s$) transitions can be studied in final states accessible in both D^0 and \bar{D}^0 decays [94]. In principle, it is possible to extract the B and D decay amplitudes, the relative strong phases, and the weak phase γ from the data [96].

A practical complication is that the precision depends sensitively on the ratio of the interfering amplitudes

$$r_B = \left| A(B^- \rightarrow \bar{D}^0K^-) / A(B^- \rightarrow D^0K^-) \right|, \quad (12.24)$$

which is around 0.1. The original GLW method [114, 115] considers D decays to CP eigenstates, such as $B^\pm \rightarrow D_{CP}^{(*)}(\rightarrow \pi^+\pi^-)K^{(*)\pm}$. To alleviate the smallness of r_B and make the interfering amplitudes (which are products of the B and D decay amplitudes) comparable in magnitude, the ADS method [116] considers final states where Cabibbo-allowed \bar{D}^0 and doubly-Cabibbo-suppressed D^0 decays interfere. Measurements have been made by the B factories, CDF, and LHCb, using both methods [24]. The GLW method currently gives only a loose constraint on γ , $14.9^\circ < \gamma < 30.8^\circ$, $69.9^\circ < \gamma < 87.9^\circ$, $92.1^\circ < \gamma < 110.1^\circ$,

and $149.2^\circ < \gamma < 165.1^\circ$ at 68% CL; while the ADS method provides $\gamma = (72^{+12}_{-14})^\circ$ [24, 104].

The BPGGSZ method [117, 118] utilizes that both D^0 and \bar{D}^0 can have large branching fractions to CP self-conjugate three-body final states, such as $K_S^0 \pi^+ \pi^-$, and the analysis can be optimized by studying the Dalitz plot dependence of the interferences. The best present determination of γ comes from this method. Combining the measurements by Belle [119], *BABAR* [120] and LHCb [121], $\gamma = (73.8^{+6.8}_{-7.0})^\circ$ is obtained [24, 104]. The error is sensitive to the central value of the amplitude ratio r_B (and r_B^* for the $D^* K$ mode), for which Belle found somewhat larger central values than *BABAR* and LHCb. The same values of $r_B^{(*)}$ enter the ADS analyses, and the data can be combined to fit for $r_B^{(*)}$ and γ . The effect of D^0 - \bar{D}^0 mixing on γ is far below the present experimental accuracy [122], unless D^0 - \bar{D}^0 mixing is due to CP -violating new physics, in which case it can be included in the analysis [123].

The amplitude ratio is much larger in the analogous $B_s^0 \rightarrow D_s^\pm K^\mp$ decays, which allows a model-independent extraction of $\gamma - 2\beta_s$ [124] (here $\beta_s = \arg(-V_{ts} V_{tb}^* / V_{cs} V_{cb}^*)$ is related to the phase of B_s mixing). A recent measurement by LHCb [125] gives $\gamma = (127^{+17}_{-22})^\circ$ using a constraint on $2\beta_s$ (see Sec. 12.5).

Combining all the above measurements [24, 96], γ is constrained as

$$\gamma = (72.1^{+4.1}_{-4.5})^\circ. \quad (12.25)$$

Similar results can be found in Refs. [112, 113].

12.3.4.2 $B^0 \rightarrow D^{(*)\pm} \pi^\mp$

The interference of $b \rightarrow u$ and $b \rightarrow c$ transitions can be studied in $\bar{B}^0 \rightarrow D^{(*)+} \pi^-$ ($b \rightarrow \bar{c} \bar{u}$) and $\bar{B}^0 \rightarrow B^0 \rightarrow D^{(*)+} \pi^-$ ($\bar{b} \rightarrow \bar{u} \bar{c}$) decays and their CP conjugates, since both B^0 and \bar{B}^0 decay to $D^{(*)\pm} \pi^\mp$ (or $D^\pm \rho^\mp$, etc.). Since there are only tree and no penguin contributions to these decays, in principle, it is possible to extract from the four time-dependent rates the magnitudes of the two hadronic amplitudes, their relative strong phase, and the weak phase between the two decay paths, which is $2\beta + \gamma$.

A complication is that the ratio of the interfering amplitudes is very small, $r_{D\pi} = A(B^0 \rightarrow D^+ \pi^-) / A(\bar{B}^0 \rightarrow D^+ \pi^-) = \mathcal{O}(0.01)$ (and similarly for $r_{D^* \pi}$ and $r_{D\rho}$), and therefore it has not been possible to measure it. To obtain $2\beta + \gamma$, $SU(3)$ flavor symmetry and dynamical assumptions have been used to relate $A(\bar{B}^0 \rightarrow D^- \pi^+)$ to $A(\bar{B}^0 \rightarrow D_s^- \pi^+)$, so this measurement is not model independent at present. Combining the $D^\pm \pi^\mp$, $D^{*\pm} \pi^\mp$ and $D^\pm \rho^\mp$ measurements [126] gives $\sin(2\beta + \gamma) > 0.68$ at 68% CL [112], consistent with the previously discussed results for β and γ .

12.4 Global fit in the Standard Model

Using the independently measured CKM elements mentioned in the previous sections, the unitarity of the CKM matrix can be checked. We obtain $|V_{ud}|^2 + |V_{us}|^2 + |V_{ub}|^2 = 0.9985 \pm 0.0005$ (1st row), $|V_{cd}|^2 + |V_{cs}|^2 + |V_{cb}|^2 = 1.025 \pm 0.022$ (2nd row), $|V_{ud}|^2 + |V_{cd}|^2 + |V_{td}|^2 = 0.9970 \pm 0.0018$ (1st column), and $|V_{us}|^2 + |V_{cs}|^2 + |V_{ts}|^2 = 1.026 \pm 0.022$ (2nd column), respectively. Due to the recent reduction of the value of $|V_{ud}|$, there is a 3σ tension with unitarity in the 1st row, leading also to poor consistency of the SM fit below. The uncertainties in the second row and column are dominated by that of $|V_{cs}|$. For the second row, another check is obtained from the measurement of $\sum_{u,c,d,s,b} |V_{ij}|^2$ in Sec. 12.2.4, minus the sum in the first row above: $|V_{cd}|^2 + |V_{cs}|^2 + |V_{cb}|^2 = 1.002 \pm 0.027$. These provide strong tests of the unitarity of the CKM matrix. With the significantly improved direct determination of $|V_{tb}|$, the unitarity checks for the third row and column have also become fairly precise, leaving decreasing room for mixing with other states. The sum of the three angles of the unitarity triangle, $\alpha + \beta + \gamma = (179^{+7}_{-6})^\circ$, is also consistent with the SM expectation.

The CKM matrix elements can be most precisely determined using a global fit to all available measurements and imposing the SM constraints (i.e., three generation unitarity). The fit must also use theory predictions for hadronic matrix elements, which

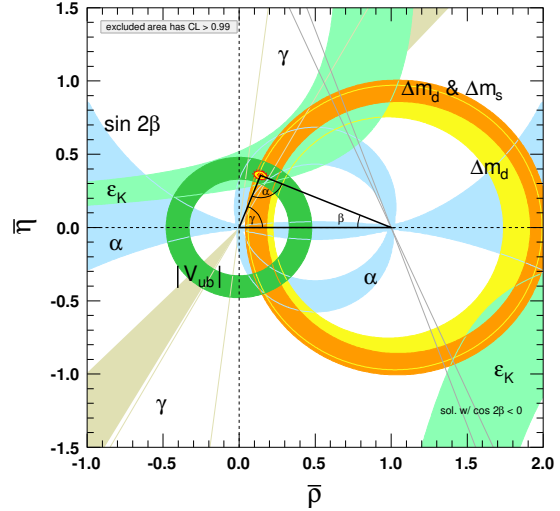


Figure 12.2: Constraints on the $\bar{\rho}, \bar{\eta}$ plane. The shaded areas have 99% CL.

sometimes have significant uncertainties. There are several approaches to combining the experimental data. CKMfitter [6, 112] and Ref. [127] (which develops [128, 129] further) use frequentist statistics, while UFit [113, 130] uses a Bayesian approach. These approaches provide similar results.

The constraints implied by the unitarity of the three generation CKM matrix significantly reduce the allowed range of some of the CKM elements. The fit for the Wolfenstein parameters defined in Eq. (12.4) gives

$$\begin{aligned} \lambda &= 0.22650 \pm 0.00048, & A &= 0.790^{+0.017}_{-0.012}, \\ \bar{\rho} &= 0.141^{+0.016}_{-0.017}, & \bar{\eta} &= 0.357 \pm 0.011. \end{aligned} \quad (12.26)$$

These values are obtained using the method of Refs. [6, 112]. Using the prescription of Refs. [113, 130] gives $\lambda = 0.22658 \pm 0.00044$, $A = 0.818 \pm 0.012$, $\bar{\rho} = 0.139 \pm 0.014$, $\bar{\eta} = 0.356 \pm 0.010$ [131]. The fit results for the magnitudes of all nine CKM elements are

$$V_{\text{CKM}} = \begin{pmatrix} 0.97401 \pm 0.00011 & 0.22650 \pm 0.00048 & 0.00361^{+0.00011}_{-0.00009} \\ 0.22636 \pm 0.00048 & 0.97320 \pm 0.00011 & 0.04053^{+0.00083}_{-0.00061} \\ 0.00854^{+0.00023}_{-0.00016} & 0.03978^{+0.00082}_{-0.00060} & 0.999172^{+0.00024}_{-0.00035} \end{pmatrix}, \quad (12.27)$$

and the Jarlskog invariant is $J = (3.00^{+0.15}_{-0.09}) \times 10^{-5}$. The parameters in Eq. (12.3) are

$$\begin{aligned} \sin \theta_{12} &= 0.22650 \pm 0.00048, & \sin \theta_{13} &= 0.00361^{+0.00011}_{-0.00009}, \\ \sin \theta_{23} &= 0.04053^{+0.00083}_{-0.00061}, & \delta &= 1.196^{+0.045}_{-0.043}. \end{aligned} \quad (12.28)$$

Fig. 12.2 illustrates the constraints on the $\bar{\rho}, \bar{\eta}$ plane from various measurements, and the global fit result. The CL of each of the shaded regions was increased from 95% to 99% for this edition, because the reduction in $|V_{ud}|$ discussed above leads to poor consistency between the fit result (for $\bar{\rho}$ and $\bar{\eta}$) and the individual constraints shown in the plot. The shaded 99% CL regions all overlap consistently around the global fit region.

If one uses only tree-level inputs (magnitudes of CKM elements not coupling to the top quark and the angle γ), the resulting fit is almost identical for λ in Eq. (12.26), while the other parameters' central values can change by about a sigma and their uncertainties double, yielding $\lambda = 0.22653 \pm 0.00048$, $A = 0.799^{+0.027}_{-0.028}$, $\bar{\rho} = 0.123^{+0.032}_{-0.028}$, and $\bar{\eta} = 0.382^{+0.029}_{-0.028}$. This illustrates how the constraints can be less tight in the presence of BSM physics.

12.5 Implications beyond the SM

The effects in B , B_s , K , and D decays and mixings due to high-scale physics (W , Z , t , H in the SM, and unknown heavier particles) can be parameterized by operators composed of SM fields, obeying the $SU(3) \times SU(2) \times U(1)$ gauge symmetry. Flavor-changing neutral currents, suppressed in the SM, are especially sensitive to beyond SM contributions. Processes studied in great detail, both experimentally and theoretically, include neutral meson mixings, $B_{(s)} \rightarrow X\gamma$, $X\ell^+\ell^-$, $\ell^+\ell^-$, $K \rightarrow \pi\nu\bar{\nu}$, etc. The BSM contributions to these operators are suppressed by powers of the scale at which they are generated. Already at lowest order, there are many dimension-6 operators, and the observable effects of BSM interactions are encoded in their coefficients. In the SM, these coefficients are determined by just the four CKM parameters, and the W , Z , and quark masses. For example, Δm_d , $\Gamma(B \rightarrow \rho\gamma)$, $\Gamma(B \rightarrow \pi\ell^+\ell^-)$, and $\Gamma(B \rightarrow \ell^+\ell^-)$ are all proportional to $|V_{td}V_{tb}|^2$ in the SM, however, they may receive unrelated BSM contributions. These BSM contributions may or may not obey the SM relations. (For example, the flavor sector of the MSSM contains 69 CP -conserving parameters and 41 CP -violating phases, *i.e.*, 40 new ones [132]). Thus, similar to the measurements of $\sin 2\beta$ in tree- and loop-dominated decay modes, overconstraining measurements of the magnitudes and phases of flavor-changing neutral-current amplitudes gives good sensitivity to BSM.

To illustrate the level of suppression required for BSM contributions, consider a class of models in which the unitarity of the CKM matrix is maintained, and the dominant BSM effects modify the neutral meson mixing amplitudes [133] by $(z_{ij}/\Lambda^2)(\bar{q}_i\gamma^\mu P_L q_j)^2$, where z_{ij} is an unknown coefficient and Λ is the scale suppressing this BSM contribution (see, [134, 135]). It is only known since the measurements of γ and α that the SM gives the leading contribution to $B^0 - \bar{B}^0$ mixing [6, 136]. Nevertheless, new physics with a generic weak phase may still contribute to neutral meson mixings at a significant fraction of the SM [130, 137, 138]. The existing data imply that $\Lambda/|z_{ij}|^{1/2}$ has to exceed about 10^4 TeV for $K^0 - \bar{K}^0$ mixing, 10^3 TeV for $D^0 - \bar{D}^0$ mixing, 500 TeV for $B^0 - \bar{B}^0$ mixing, and 100 TeV for $B_s^0 - \bar{B}_s^0$ mixing [130, 135]. (Some other operators are even better constrained [130].) The constraints are the strongest in the kaon sector, because the CKM suppression is the most severe. Thus, if there is new physics at the TeV scale, $|z_{ij}| \ll 1$ is required. Even if $|z_{ij}|$ are suppressed by a loop factor and $|V_{ti}^*V_{tj}|^2$ (in the down quark sector), similar to the SM, one expects percent-level effects, which may be observable in forthcoming flavor physics experiments. To constrain such extensions of the SM, many measurements irrelevant for the SM-CKM fit, such as the CP asymmetry in semileptonic $B_{d,s}^0$ decays, $A_{SL}^{d,s}$, are important [139]. The current world averages [24] are consistent with the SM, with experimental uncertainties far greater than those of the theory predictions.

There are many key measurements sensitive to BSM physics, which do not constrain the unitarity triangle in Fig. 12.1. For example, a key quantity in the B_s system is $\beta_s = \arg(-V_{ts}V_{tb}^*/V_{cs}V_{cb}^*)$, which is the small, λ^2 -suppressed, angle of a “squashed” unitarity triangle, obtained by taking the scalar product of the second and third columns of the CKM matrix. This angle can be measured via time-dependent CP violation in $B_s^0 \rightarrow J/\psi\phi$, similar to β in $B^0 \rightarrow J/\psi K^0$. Since the $J/\psi\phi$ final state is not a CP eigenstate, an angular analysis of the decay products is needed to separate the CP -even and CP -odd components, which give opposite asymmetries. In the SM, the asymmetry for the CP -even part is $2\beta_s$, when one neglects subdominant amplitudes with a weak phase V_{ub} . (Sometimes the notation $\phi_s = -2\beta_s$ plus a possible BSM contribution to the B_s mixing phase is used.) Testing if the data agree with the SM prediction, $2\beta_s = 0.0383_{-0.0011}^{+0.0012}$ [112], is another sensitive probe of the SM. The current world average, dominated by LHC measurements [140] including the $B_s \rightarrow J/\psi K^+ K^-$ and $J/\psi \pi^+ \pi^-$ decay modes, is $2\beta_s = 0.051 \pm 0.023$ [71]. Since the uncertainty is much larger than that in the SM, a lot will be learned from more precise future measurements. Searches for CP violation in the charm sector, in particular in $D^0 - \bar{D}^0$ mixing, provide complementary sensitivity to BSM.

In the kaon sector, the CP -violating observables, ϵ and ϵ' , are tiny, so models in which all sources of CP violation are small were viable before the B -factory measurements. Since the measurement of $\sin 2\beta$, we know that CP violation can be an $\mathcal{O}(1)$ effect, and only flavor mixing is suppressed between the three quark generations. Thus, many models with spontaneous CP violation were excluded. In the kaon sector, clean tests of the SM can come from measurements of $K^+ \rightarrow \pi^+\nu\bar{\nu}$ [78] and $K_L^0 \rightarrow \pi^0\nu\bar{\nu}$ [141]. These loop-induced rare decays are sensitive to BSM, and will allow precise tests [142] of the CKM paradigm, independent of B decays.

The CKM elements are fundamental parameters, so they should be measured as precisely as possible. The overconstraining measurements of CP asymmetries, mixing, semileptonic, and rare decays severely constrain the magnitudes and phases of possible BSM contributions to flavor-changing interactions. If new particles are observed at the LHC, it will be important to explore their flavor parameters as precisely as possible to understand the underlying physics.

References

- [1] N. Cabibbo, Phys. Rev. Lett. **10**, 531 (1963).
- [2] M. Kobayashi and T. Maskawa, Prog. Theor. Phys. **49**, 652 (1973).
- [3] L.-L. Chau and W.-Y. Keung, Phys. Rev. Lett. **53**, 1802 (1984).
- [4] L. Wolfenstein, Phys. Rev. Lett. **51**, 1945 (1983).
- [5] A. J. Buras, M. E. Lautenbacher and G. Ostermaier, Phys. Rev. **D50**, 3433 (1994), [hep-ph/9403384].
- [6] J. Charles *et al.* (CKMfitter Group), Eur. Phys. J. **C41**, 1, 1 (2005), [hep-ph/0406184].
- [7] C. Jarlskog, Phys. Rev. Lett. **55**, 1039 (1985).
- [8] W. J. Marciano and A. Sirlin, Nucl. Phys. **B93**, 303 (1975); K. S. Babu, Z. Phys. **C35**, 69 (1987).
- [9] J. Hardy and I. S. Towner, PoS **CKM2016**, 028 (2016).
- [10] E. Blucher and W.J. Marciano, “ V_{ud} , V_{us} , the Cabibbo Angle and CKM Unitarity,” in this *Review*.
- [11] C.-Y. Seng *et al.*, Phys. Rev. Lett. **121**, 24, 241804 (2018), [arXiv:1807.10197].
- [12] D. Poganec *et al.*, Phys. Rev. Lett. **93**, 181803 (2004), [hep-ex/0312030].
- [13] M. Antonelli *et al.* (FlaviaNet Working Group on Kaon Decays), Eur. Phys. J. **C69**, 399 (2010), [arXiv:1005.2323]; see also <http://www.lnf.infn.it/wg/vus>.
- [14] S. Aoki *et al.* (Flavour Lattice Averaging Group), Eur. Phys. J. **C80**, 2, 113 (2020), [arXiv:1902.08191]; The original papers that led to the quoted averages are cited in this reference or on the web page <http://flag.unibe.ch/>.
- [15] T. Mannel and P. Urquijo, “Semileptonic b -Hadron Decays, Determination of V_{cb} and V_{ub} ,” in this *Review*.
- [16] H. Leutwyler and M. Roos, Z. Phys. **C25**, 91 (1984); For earlier fits for $|V_{ud}|$ and $|V_{us}|$ in the 3-generation SM, see Ref. [17].
- [17] R. E. Shrock and L.-L. Wang, Phys. Rev. Lett. **41**, 1692 (1978).
- [18] J. Bijnens and P. Talavera, Nucl. Phys. **B669**, 341 (2003), [hep-ph/0303103]; M. Jamin, J. A. Oller and A. Pich, JHEP **02**, 047 (2004), [hep-ph/0401080]; V. Cirigliano *et al.*, JHEP **04**, 006 (2005), [hep-ph/0503108]; C. Dawson *et al.*, PoS **LAT2005**, 337 (2006), [hep-lat/0510018]; N. Tsutsui *et al.* (JLQCD), PoS **LAT2005**, 357 (2006), [hep-lat/0510068]; M. Okamoto (Fermilab Lattice, MILC, HPQCD), in “3rd Conference on Flavor Physics and CP Violation (FPCP 2004) Daegu, Korea, October 4-9, 2004,” (2004), [hep-lat/0412044].
- [19] W. J. Marciano, Phys. Rev. Lett. **93**, 231803 (2004), [hep-ph/0402299].
- [20] F. Ambrosino *et al.* (KLOE), Phys. Lett. **B632**, 76 (2006), [hep-ex/0509045].

- [21] See Sec. 5.2, “Averages and fits,” in the Introduction to this *Review*, <http://pdg.lbl.gov/2019/reviews/rpp2019-rev-rpp-intro.pdf>.
- [22] N. Cabibbo, E. C. Swallow and R. Winston, *Ann. Rev. Nucl. Part. Sci.* **53**, 39 (2003), [hep-ph/0307298]; N. Cabibbo, E. C. Swallow and R. Winston, *Phys. Rev. Lett.* **92**, 251803 (2004), [hep-ph/0307214].
- [23] M. Ademollo and R. Gatto, *Phys. Rev. Lett.* **13**, 264 (1964).
- [24] Y. S. Amhis *et al.* (HFLAV) (2019), [arXiv:1909.12524]; and updates at <https://hflav.web.cern.ch/>.
- [25] J. P. Lees *et al.* (BaBar), *Phys. Rev.* **D91**, 5, 052022 (2015), [arXiv:1412.5502].
- [26] M. Ablikim *et al.* (BESIII), *Phys. Rev.* **D92**, 7, 072012 (2015), [arXiv:1508.07560].
- [27] M. Ablikim *et al.* (BESIII), *Phys. Rev.* **D96**, 1, 012002 (2017), [arXiv:1703.09084].
- [28] D. Besson *et al.* (CLEO), *Phys. Rev.* **D80**, 032005 (2009), [arXiv:0906.2983].
- [29] L. Widhalm *et al.* (Belle), *Phys. Rev. Lett.* **97**, 061804 (2006), [hep-ex/0604049].
- [30] M. Ablikim *et al.* (BESIII), *Phys. Rev.* **D89**, 5, 051104 (2014), [arXiv:1312.0374].
- [31] B. I. Eisenstein *et al.* (CLEO), *Phys. Rev.* **D78**, 052003 (2008), [arXiv:0806.2112].
- [32] H. Abramowicz *et al.*, *Z. Phys.* **C15**, 19 (1982).
- [33] S. A. Rabinowitz *et al.*, *Phys. Rev. Lett.* **70**, 134 (1993).
- [34] A. O. Bazarko *et al.* (CCFR), *Z. Phys.* **C65**, 189 (1995), [hep-ex/9406007].
- [35] P. Vilain *et al.* (CHARM II), *Eur. Phys. J.* **C11**, 19 (1999).
- [36] F. J. Gilman, K. Kleinknecht and B. Renk (2004).
- [37] G. De Lellis, P. Migliozi and P. Santorelli, *Phys. Rept.* **399**, 227 (2004), [Erratum: *Phys. Rept.* 411,323(2005)].
- [38] N. Ushida *et al.* (Fermilab E531), *Phys. Lett.* **B206**, 380 (1988).
- [39] T. Bolton (1997), [hep-ex/9708014].
- [40] A. Kayis-Topaksu *et al.* (CHORUS), *Phys. Lett.* **B626**, 24 (2005).
- [41] A. Zupanc *et al.* (Belle), *JHEP* **09**, 139 (2013), [arXiv:1307.6240].
- [42] J. P. Alexander *et al.* (CLEO), *Phys. Rev.* **D79**, 052001 (2009), [arXiv:0901.1216].
- [43] P. del Amo Sanchez *et al.* (BaBar), *Phys. Rev.* **D82**, 091103 (2010), [Erratum: *Phys. Rev.* D91,no.1,019901(2015)], [arXiv:1008.4080].
- [44] M. Ablikim *et al.* (BESIII), *Phys. Rev.* **D94**, 7, 072004 (2016), [arXiv:1608.06732].
- [45] M. Ablikim *et al.* (BESIII), *Phys. Rev. Lett.* **122**, 7, 071802 (2019), [arXiv:1811.10890].
- [46] P. U. E. Onyisi *et al.* (CLEO), *Phys. Rev.* **D79**, 052002 (2009), [arXiv:0901.1147].
- [47] P. Naik *et al.* (CLEO), *Phys. Rev.* **D80**, 112004 (2009), [arXiv:0910.3602].
- [48] B. Aubert *et al.* (BaBar), *Phys. Rev.* **D76**, 052005 (2007), [arXiv:0704.0020].
- [49] M. Ablikim *et al.* (BESIII), *Phys. Rev. Lett.* **122**, 1, 011804 (2019), [arXiv:1810.03127].
- [50] LEP *W* branching fraction results for this Review of Particle Physics, LEPEWWG/XSEC/2005-01, <http://lepewwg.web.cern.ch/LEPEWWG/lepww/4f/Winter05>.
- [51] P. Abreu *et al.* (DELPHI), *Phys. Lett.* **B439**, 209 (1998).
- [52] I. I. Y. Bigi *et al.*, *Phys. Rev. Lett.* **71**, 496 (1993), [hep-ph/9304225].
- [53] A. V. Manohar and M. B. Wise, *Phys. Rev.* **D49**, 1310 (1994), [hep-ph/9308246].
- [54] I. I. Y. Bigi *et al.*, *Phys. Rev.* **D56**, 4017 (1997), [hep-ph/9704245].
- [55] A. H. Hoang, Z. Ligeti and A. V. Manohar, *Phys. Rev.* **D59**, 074017 (1999), [hep-ph/9811239]; A. H. Hoang, Z. Ligeti and A. V. Manohar, *Phys. Rev. Lett.* **82**, 277 (1999), [hep-ph/9809423]; A. H. Hoang and T. Teubner, *Phys. Rev.* **D60**, 114027 (1999), [hep-ph/9904468].
- [56] N. Isgur and M. B. Wise, *Phys. Lett.* **B237**, 527 (1990); N. Isgur and M. B. Wise, *Phys. Lett.* **B232**, 113 (1989).
- [57] A. Abdesselam *et al.* (Belle) (2017), [arXiv:1702.01521].
- [58] C. G. Boyd, B. Grinstein and R. F. Lebed, *Phys. Rev.* **D56**, 6895 (1997), [hep-ph/9705252]; C. G. Boyd, B. Grinstein and R. F. Lebed, *Nucl. Phys.* **B461**, 493 (1996), [hep-ph/9508211].
- [59] M. Neubert, *Phys. Rev.* **D49**, 3392 (1994), [hep-ph/9311325]; M. Neubert, *Phys. Rev.* **D49**, 4623 (1994), [hep-ph/9312311].
- [60] I. I. Y. Bigi *et al.*, *Int. J. Mod. Phys.* **A9**, 2467 (1994), [hep-ph/9312359].
- [61] C. W. Bauer, Z. Ligeti and M. E. Luke, *Phys. Lett.* **B479**, 395 (2000), [hep-ph/0002161]; C. W. Bauer, Z. Ligeti and M. E. Luke, *Phys. Rev.* **D64**, 113004 (2001), [hep-ph/0107074].
- [62] A. Bornheim *et al.* (CLEO), *Phys. Rev. Lett.* **88**, 231803 (2002), [hep-ex/0202019].
- [63] B. Aubert *et al.* (BaBar), *Phys. Rev.* **D73**, 012006 (2006), [hep-ex/0509040].
- [64] A. Limosani *et al.* (Belle), *Phys. Lett.* **B621**, 28 (2005), [hep-ex/0504046].
- [65] P. Urquijo *et al.* (Belle), *Phys. Rev. Lett.* **104**, 021801 (2010), [arXiv:0907.0379]; J. P. Lees *et al.* (BaBar), *Phys. Rev.* **D86**, 032004 (2012), [arXiv:1112.0702].
- [66] J. A. Bailey *et al.* (Fermilab Lattice, MILC), *Phys. Rev.* **D92**, 1, 014024 (2015), [arXiv:1503.07839]; J. M. Flynn *et al.*, *Phys. Rev.* **D91**, 7, 074510 (2015), [arXiv:1501.05373]; B. Colquhoun *et al.*, *Phys. Rev.* **D93**, 3, 034502 (2016), [arXiv:1510.07446].
- [67] P. Ball and R. Zwicky, *Phys. Rev.* **D71**, 014015 (2005), [hep-ph/0406232]; A. Khodjamirian *et al.*, *Phys. Rev.* **D83**, 094031 (2011), [arXiv:1103.2655].
- [68] Particle listing, in this *Review*.
- [69] R. Aaij *et al.* (LHCb), *Nature Phys.* **11**, 743 (2015), [arXiv:1504.01568].
- [70] H. Albrecht *et al.* (ARGUS), *Phys. Lett.* **B192**, 245 (1987).
- [71] O. Schneider, “ $B^0-\bar{B}^0$ mixing,” in this *Review*.
- [72] A. Abulencia *et al.* (CDF), *Phys. Rev. Lett.* **97**, 242003 (2006), [hep-ex/0609040].
- [73] R. Aaij *et al.* (LHCb), *New J. Phys.* **15**, 053021 (2013), [arXiv:1304.4741].
- [74] M. Misiak *et al.*, *Phys. Rev. Lett.* **114**, 22, 221801 (2015), [arXiv:1503.01789]; M. Czakon *et al.*, *JHEP* **04**, 168 (2015), [arXiv:1503.01791].
- [75] B. Grinstein and D. Pirjol, *Phys. Rev.* **D62**, 093002 (2000), [hep-ph/0002216]; A. Ali, E. Lunghi and A. Ya. Parkhomenko, *Phys. Lett.* **B595**, 323 (2004), [hep-ph/0405075]; M. Beneke, T. Feldmann and D. Seidel, *Nucl. Phys.* **B612**, 25 (2001), [hep-ph/0106067]; S. W. Bosch and G. Buchalla, *Nucl. Phys.* **B621**, 459 (2002), [hep-ph/0106081]; Z. Ligeti and M. B. Wise, *Phys. Rev.* **D60**, 117506 (1999), [hep-ph/9905277]; D. Becirevic *et al.*, *JHEP* **05**, 007 (2003), [hep-lat/0301020]; P. Ball, G. W. Jones and R. Zwicky, *Phys. Rev.* **D75**, 054004 (2007), [hep-ph/0612081]; W. Wang, R.-H. Li and C.-D. Lu (2007), [arXiv:0711.0432]; C.-D. Lu, W. Wang and Z.-T. Wei, *Phys. Rev.* **D76**, 014013 (2007), [hep-ph/0701265].
- [76] A. J. Buras *et al.*, *Phys. Rev. Lett.* **95**, 261805 (2005), [hep-ph/0508165].

- [77] A. V. Artamonov *et al.* (E949), Phys. Rev. Lett. **101**, 191802 (2008), [arXiv:0808.2459]; A. V. Artamonov *et al.* (BNL-E949), Phys. Rev. **D79**, 092004 (2009), [arXiv:0903.0030].
- [78] E. Cortina Gil *et al.* (NA62), Phys. Lett. **B791**, 156 (2019), [arXiv:1811.08508].
- [79] D. Acosta *et al.* (CDF), Phys. Rev. Lett. **95**, 102002 (2005), [hep-ex/0505091].
- [80] V. M. Abazov *et al.* (D0), Phys. Rev. Lett. **107**, 121802 (2011), [arXiv:1106.5436].
- [81] V. Khachatryan *et al.* (CMS), Phys. Lett. **B736**, 33 (2014), [arXiv:1404.2292].
- [82] T. A. Aaltonen *et al.* (CDF, D0), Phys. Rev. Lett. **115**, 15, 152003 (2015), [arXiv:1503.05027].
- [83] LHC Top Working Group summary plots, single top quark production, Nov. 2017, <https://twiki.cern.ch/twiki/bin/view/LHCPhysics/LHCTopWGSummaryPlots>.
- [84] J. Swain and L. Taylor, Phys. Rev. **D58**, 093006 (1998), [hep-ph/9712420].
- [85] “ K_L^0 meson” particle listing, in this *Review*.
- [86] A. J. Buras, D. Guadagnoli and G. Isidori, Phys. Lett. **B688**, 309 (2010), [arXiv:1002.3612]; For earlier discussions, see Ref. [87].
- [87] E. A. Andriyash, G. G. Ovanesyan and M. I. Vysotsky, Phys. Lett. **B599**, 253 (2004), [hep-ph/0310314]; K. Anikeev *et al.*, in “Workshop on B Physics at the Tevatron: Run II and Beyond Batavia, Illinois, September 23-25, 1999,” (2001), [hep-ph/0201071]; A. J. Buras and D. Guadagnoli, Phys. Rev. **D78**, 033005 (2008), [arXiv:0805.3887].
- [88] T. Inami and C. S. Lim, Prog. Theor. Phys. **65**, 297 (1981), [Erratum: Prog. Theor. Phys. **65**, 1772 (1981)].
- [89] J. M. Flynn and L. Randall, Phys. Lett. **B224**, 221 (1989), [Erratum: Phys. Lett. **B235**, 412 (1990)]; G. Buchalla, A. J. Buras and M. K. Harlander, Nucl. Phys. **B337**, 313 (1990).
- [90] M. Ciuchini *et al.*, Phys. Lett. **B301**, 263 (1993), [hep-ph/9212203]; A. J. Buras, M. Jamin and M. E. Lautenbacher, Nucl. Phys. **B408**, 209 (1993), [hep-ph/9303284]; T. Hambye *et al.*, Nucl. Phys. **B564**, 391 (2000), [hep-ph/9906434]; S. Bertolini, J. O. Eeg and M. Fabbrichesi, Phys. Rev. **D63**, 056009 (2001), [hep-ph/0002234]; V. Cirigliano *et al.*, Phys. Rev. Lett. **91**, 162001 (2003), [hep-ph/0307030].
- [91] Z. Bai *et al.* (RBC, UKQCD), Phys. Rev. Lett. **115**, 21, 212001 (2015), [arXiv:1505.07863].
- [92] A. J. Buras *et al.*, JHEP **11**, 202 (2015), [arXiv:1507.06345].
- [93] V. Cirigliano *et al.*, JHEP **02**, 032 (2020), [arXiv:1911.01359].
- [94] A. B. Carter and A. I. Sanda, Phys. Rev. Lett. **45**, 952 (1980); A. B. Carter and A. I. Sanda, Phys. Rev. **D23**, 1567 (1981).
- [95] A more detailed discussion and references can be found in: T. Gershon and Y. Nir, “ CP violation in meson decays,” in this *Review*.
- [96] T. Gershon, M. Kenzie and K. Trabelsi, “Determination of CKM angles from B hadrons,” in this *Review*.
- [97] B. Aubert *et al.* (BaBar), Phys. Rev. **D79**, 072009 (2009), [arXiv:0902.1708].
- [98] I. Adachi *et al.* (Belle), Phys. Rev. Lett. **108**, 171802 (2012), [arXiv:1201.4643].
- [99] R. Aaij *et al.* (LHCb), Phys. Rev. Lett. **115**, 3, 031601 (2015), [arXiv:1503.07089].
- [100] B. Aubert *et al.* (BaBar), Phys. Rev. **D71**, 032005 (2005), [hep-ex/0411016].
- [101] R. Itoh *et al.* (Belle), Phys. Rev. Lett. **95**, 091601 (2005), [hep-ex/0504030].
- [102] I. Adachi *et al.* (BaBar, Belle), Phys. Rev. Lett. **121**, 26, 261801 (2018), [arXiv:1804.06152]; I. Adachi *et al.* (BaBar, Belle), Phys. Rev. **D98**, 11, 112012 (2018), [arXiv:1804.06153].
- [103] A. Abdesselam *et al.* (BaBar, Belle), Phys. Rev. Lett. **115**, 12, 121604 (2015), [arXiv:1505.04147].
- [104] Heavy Flavor Averaging Group [24], Moriond 2020 updates for Unitarity Triangle Parameters: <https://hflav-eos.web.cern.ch/hflav-eos/triangle/PDG2020/>.
- [105] M. Gronau and D. London, Phys. Rev. Lett. **65**, 3381 (1990).
- [106] J. Zhang *et al.* (Belle), Phys. Rev. Lett. **91**, 221801 (2003), [hep-ex/0306007]; A. Somov *et al.* (Belle), Phys. Rev. Lett. **96**, 171801 (2006), [hep-ex/0601024]; B. Aubert *et al.* (BaBar), Phys. Rev. Lett. **97**, 261801 (2006), [hep-ex/0607092]; B. Aubert *et al.* (BaBar), Phys. Rev. **D76**, 052007 (2007), [arXiv:0705.2157].
- [107] B. Aubert *et al.* (BaBar), Phys. Rev. **D78**, 071104 (2008), [arXiv:0807.4977].
- [108] A. F. Falk *et al.*, Phys. Rev. **D69**, 011502 (2004), [hep-ph/0310242].
- [109] A. E. Snyder and H. R. Quinn, Phys. Rev. **D48**, 2139 (1993).
- [110] A. Kusaka *et al.* (Belle), Phys. Rev. Lett. **98**, 221602 (2007), [hep-ex/0701015].
- [111] J. P. Lees *et al.* (BaBar), Phys. Rev. **D88**, 1, 012003 (2013), [arXiv:1304.3503].
- [112] A. Hocker *et al.*, Eur. Phys. J. **C21**, 225 (2001), [hep-ph/0104062]; and updates at <http://ckmfitter.in2p3.fr/>.
- [113] M. Bona *et al.* (UTfit), JHEP **07**, 028 (2005), [hep-ph/0501199]; and updates at <http://www.utfit.org>.
- [114] M. Gronau and D. London, Phys. Lett. **B253**, 483 (1991).
- [115] M. Gronau and D. Wyler, Phys. Lett. **B265**, 172 (1991).
- [116] D. Atwood, I. Dunietz and A. Soni, Phys. Rev. Lett. **78**, 3257 (1997), [hep-ph/9612433]; D. Atwood, I. Dunietz and A. Soni, Phys. Rev. **D63**, 036005 (2001), [hep-ph/0008090].
- [117] A. Bondar, talk at the Belle analysis workshop, Novosibirsk, September 2002; A. Poluektov *et al.* (Belle), Phys. Rev. **D70**, 072003 (2004), [hep-ex/0406067].
- [118] A. Giri *et al.*, Phys. Rev. **D68**, 054018 (2003), [hep-ph/0303187].
- [119] A. Poluektov *et al.* (Belle), Phys. Rev. **D81**, 112002 (2010), [arXiv:1003.3360].
- [120] P. del Amo Sanchez *et al.* (BaBar), Phys. Rev. Lett. **105**, 121801 (2010), [arXiv:1005.1096].
- [121] R. Aaij *et al.* (LHCb), JHEP **10**, 097 (2014), [arXiv:1408.2748].
- [122] Y. Grossman, A. Soffer and J. Zupan, Phys. Rev. **D72**, 031501 (2005), [hep-ph/0505270].
- [123] A. Amorim, M. G. Santos and J. P. Silva, Phys. Rev. **D59**, 056001 (1999), [hep-ph/9807364].
- [124] R. Aleksan, I. Dunietz and B. Kayser, Z. Phys. **C54**, 653 (1992).
- [125] R. Aaij *et al.* (LHCb), JHEP **03**, 059 (2018), [arXiv:1712.07428].
- [126] B. Aubert *et al.* (BaBar), Phys. Rev. **D71**, 112003 (2005), [hep-ex/0504035]; B. Aubert *et al.* (BaBar), Phys. Rev. **D73**, 111101 (2006), [hep-ex/0602049]; F. J. Ronga *et al.* (Belle), Phys. Rev. **D73**, 092003 (2006), [hep-ex/0604013]; S. Bahinipati *et al.* (Belle), Phys. Rev. **D84**, 021101 (2011), [arXiv:1102.0888]; R. Aaij *et al.* (LHCb), JHEP **06**, 084 (2018), [arXiv:1805.03448].
- [127] G. P. Dubois-Felsmann *et al.*, *Sensitivity of CKM fits to theoretical uncertainties and their representation* (2003), [hep-ph/0308262]; G. Eigen *et al.*, Phys. Rev. **D89**, 3, 033004 (2014), [arXiv:1301.5867].

- [128] D. Boutigny *et al.* (BaBar), in “Workshop on Physics at an Asymmetric B Factory (BaBar Collaboration Meeting) Pasadena, California, September 22-24, 1997,” (1998), URL <http://www-public.slac.stanford.edu/sciDoc/docMeta.aspx?slacPubNumber=SLAC-R-504>.
- [129] S. Plaszczynski and M.-H. Schune hf8/019 (1999), [PoShf8,019(1999)], [hep-ph/9911280].
- [130] M. Bona *et al.* (UTfit), JHEP **03**, 049 (2008), [arXiv:0707.0636].
- [131] We thank the CKMfitter and UTfit groups for performing fits and preparing plots using input values from this *Review*.
- [132] H. E. Haber, Nucl. Phys. Proc. Suppl. **62**, 469 (1998), [hep-ph/9709450]; Y. Nir, *CP violation: A New era* (2001), [hep-ph/0109090].
- [133] J. M. Soares and L. Wolfenstein, Phys. Rev. **D47**, 1021 (1993); T. Goto *et al.*, Phys. Rev. **D53**, 6662 (1996), [hep-ph/9506311]; J. P. Silva and L. Wolfenstein, Phys. Rev. **D55**, 5331 (1997), [hep-ph/9610208].
- [134] Y. Grossman, Z. Ligeti and Y. Nir, Prog. Theor. Phys. **122**, 125 (2009), [arXiv:0904.4262].
- [135] G. Isidori, Y. Nir and G. Perez, Ann. Rev. Nucl. Part. Sci. **60**, 355 (2010), [arXiv:1002.0900]; G. Isidori, in “Proceedings, 2012 European School of High-Energy Physics (ES-HEP 2012): La Pommeraye, Anjou, France, June 06-19, 2012,” 69–105 (2014), [arXiv:1302.0661].
- [136] Z. Ligeti, Int. J. Mod. Phys. **A20**, 5105 (2005), [hep-ph/0408267].
- [137] J. Charles *et al.*, Phys. Rev. **D89**, 3, 033016 (2014), [arXiv:1309.2293].
- [138] K. Agashe *et al.* (2005), [hep-ph/0509117].
- [139] S. Laplace *et al.*, Phys. Rev. **D65**, 094040 (2002), [hep-ph/0202010].
- [140] R. Aaij *et al.* (LHCb), JHEP **08**, 037 (2017), [arXiv:1704.08217]; G. Aad *et al.* (ATLAS) (2020), [arXiv:2001.07115]; V. Khachatryan *et al.* (CMS), Phys. Lett. **B757**, 97 (2016), [arXiv:1507.07527].
- [141] J. K. Ahn *et al.* (KOTO), Phys. Rev. Lett. **122**, 2, 021802 (2019), [arXiv:1810.09655].
- [142] A. J. Buras *et al.*, JHEP **11**, 033 (2015), [arXiv:1503.02693].

13. CP Violation in the Quark Sector

Revised August 2019 by T. Gershon (Warwick U.) and Y. Nir (Weizmann Inst.).

The CP transformation combines charge conjugation C with parity P . Under C , particles and antiparticles are interchanged, by conjugating all internal quantum numbers, *e.g.*, $Q \rightarrow -Q$ for electromagnetic charge. Under P , the handedness of space is reversed, $\vec{x} \rightarrow -\vec{x}$. Thus, for example, a left-handed electron e_L^- is transformed under CP into a right-handed positron, e_R^+ .

If CP were an exact symmetry, the laws of Nature would be the same for matter and for antimatter. We observe that most phenomena are C - and P -symmetric, and therefore, also CP -symmetric. In particular, these symmetries are respected by the gravitational, electromagnetic, and strong interactions. The weak interactions, on the other hand, violate C and P in the strongest possible way. For example, the charged W bosons couple to left-handed electrons, e_L^- , and to their CP -conjugate right-handed positrons, e_R^+ , but to neither their C -conjugate left-handed positrons, e_L^+ , nor their P -conjugate right-handed electrons, e_R^- . While weak interactions violate C and P separately, CP is still preserved in most weak interaction processes. The CP symmetry is, however, violated in certain rare processes, as discovered in neutral K decays in 1964 [1], and established later in B (2001) and D (2019) decays. A K_L meson decays more often to $\pi^- e^+ \nu_e$ than to $\pi^+ e^- \bar{\nu}_e$, thus allowing electrons and positrons to be unambiguously distinguished, but the decay-rate asymmetry is only at the 0.003 level. The CP -violating effects observed in the B system are larger: the parameter describing the CP asymmetry in the decay time distribution of B^0/\bar{B}^0 meson transitions to CP eigenstates like $J/\psi K_S$ is about 0.7 [2, 3]. These effects are related to $K^0-\bar{K}^0$ and $B^0-\bar{B}^0$ mixing, but CP violation arising solely from decay amplitudes has also been observed, first in $K \rightarrow \pi\pi$ decays [4–6], subsequently in B^0 [7, 8], B^+ [9–11], and B_s^0 [12] decays, and most recently in charm decays [13]. Similar effects could also occur in decays of baryons, but have not yet been observed. Moreover, CP violation has not yet been observed in processes involving the top quark, nor in flavor-conserving processes such as electric dipole moments, nor in the lepton sector; for all of these any significant observation would be a clear indication of physics beyond the Standard Model.

In addition to parity and to continuous Lorentz transformations, there is one other spacetime operation that could be a symmetry of the interactions: time reversal T , $t \rightarrow -t$. Violations of T symmetry have been observed in neutral K decays [14]. More recently, exploiting the fact that for neutral B mesons both flavor tagging and CP tagging can be used [15], T violation has been observed between states that are not CP -conjugate [16]. Moreover, T violation is expected as a corollary of CP violation if the combined CPT transformation is a fundamental symmetry of Nature [17]. All observations indicate that CPT is indeed a symmetry of Nature. Furthermore, one cannot build a locally Lorentz-invariant quantum field theory with a Hermitian Hamiltonian that violates CPT . (At several points in our discussion, we avoid assumptions about CPT , in order to identify cases where evidence for CP violation relies on assumptions about CPT .)

Within the Standard Model, CP symmetry is broken by complex phases in the Yukawa couplings (that is, the couplings of the Higgs scalar to quarks). When all manipulations to remove unphysical phases in this model are exhausted, one finds that there is a single CP -violating parameter [18]. In the basis of mass eigenstates, this single phase appears in the 3×3 unitary matrix that gives the W -boson couplings to an up-type antiquark and a down-type quark. (If the Standard Model is supplemented with Majorana mass terms for the neutrinos, the analogous mixing matrix for leptons has three CP -violating phases.) The beautifully consistent and economical Standard-Model description of CP violation in terms of Yukawa couplings, known as the Kobayashi-Maskawa (KM) mechanism [18], agrees with all measurements to date. (Some measurements are in tension with the predictions, and are discussed in more detail below. Pending verification, the results are not considered to change the overall picture of agreement with the Standard Model.) Furthermore, one can fit

the data allowing new physics contributions to loop processes to compete with, or even dominate over, the Standard Model amplitudes [19, 20]. Such an analysis provides model-independent proof that the KM phase is different from zero, and that the matrix of three-generation quark mixing is the dominant source of CP violation in meson decays.

The current level of experimental accuracy and the theoretical uncertainties involved in the interpretation of the various observations leave room, however, for additional subdominant sources of CP violation from new physics. Indeed, almost all extensions of the Standard Model imply that there are such additional sources. Moreover, CP violation is a necessary condition for baryogenesis, the process of dynamically generating the matter-antimatter asymmetry of the Universe [21]. Despite the phenomenological success of the KM mechanism, it fails (by several orders of magnitude) to accommodate the observed asymmetry [22]. This discrepancy strongly suggests that Nature provides additional sources of CP violation beyond the KM mechanism. The evidence for neutrino masses implies that CP can be violated also in the lepton sector. This situation makes leptogenesis [23, 24], a scenario where CP -violating phases in the Yukawa couplings of the neutrinos play a crucial role in the generation of the baryon asymmetry, a very attractive possibility. The expectation of new sources motivates the large ongoing experimental effort to find deviations from the predictions of the KM mechanism.

CP violation can be experimentally searched for in a variety of processes, such as hadron decays, electric dipole moments of neutrons, electrons and nuclei, and neutrino oscillations. Hadron decays via the weak interaction probe flavor-changing CP violation. The search for electric dipole moments may find (or constrain) sources of CP violation that, unlike the KM phase, are not related to flavor-changing couplings. Following the discovery of the Higgs boson [25, 26], searches for CP violation in the Higgs sector are becoming feasible. Future searches for CP violation in neutrino oscillations might provide further input on leptogenesis.

The present measurements of CP asymmetries provide some of the strongest constraints on the weak couplings of quarks. Future measurements of CP violation in K , D , B , and B_s^0 meson decays will provide additional constraints on the flavor parameters of the Standard Model, and can probe new physics. In this review, we give the formalism and basic physics that are relevant to present and near future measurements of CP violation in the quark sector.

Before going into details, we list here the observables where CP violation has been observed at a level above 5σ [27–29]:

- Indirect CP violation in $K \rightarrow \pi\pi$ and $K \rightarrow \pi\ell\nu$ decays, and in the $K_L \rightarrow \pi^+\pi^-e^+e^-$ decay, is given by

$$|\epsilon| = (2.228 \pm 0.011) \times 10^{-3}. \quad (13.1)$$

- Direct CP violation in $K \rightarrow \pi\pi$ decays is given by

$$\mathcal{R}e(\epsilon'/\epsilon) = (1.65 \pm 0.26) \times 10^{-3}. \quad (13.2)$$

- CP violation in the interference of mixing and decay in the tree-dominated $b \rightarrow c\bar{c}s$ transitions, such as $B^0 \rightarrow \psi K^0$, is given by (we use K^0 throughout to denote results that combine K_S and K_L modes, but use the sign appropriate to K_S):

$$S_{\psi K^0} = +0.699 \pm 0.017. \quad (13.3)$$

- CP violation in the interference of mixing and decay in modes governed by the tree-dominated $b \rightarrow c\bar{u}d$ transitions is given by

$$S_{D^{(*)}h^0} = +0.71 \pm 0.09, \quad (13.4)$$

- CP violation in the interference of mixing and decay in various modes related to $b \rightarrow c\bar{c}d$ transitions is given by

$$\begin{aligned} S_{\psi\pi^0} &= -0.86 \pm 0.14, \\ S_{D^+D^-} &= -0.84 \pm 0.12, \\ S_{D^{*+}D^{*-}} &= -0.71 \pm 0.09. \end{aligned} \quad (13.5)$$

- CP violation in the interference of mixing and decay in various modes related to $b \rightarrow q\bar{q}s$ (penguin) transitions is given by

$$\begin{aligned} S_{\phi K^0} &= +0.74^{+0.11}_{-0.13}, \\ S_{\eta' K^0} &= +0.63 \pm 0.06, \\ S_{f_0 K^0} &= +0.69^{+0.10}_{-0.12}, \\ S_{K^+ K^- K_S} &= +0.68^{+0.09}_{-0.10}. \end{aligned} \quad (13.6)$$

- CP violation in the interference of mixing and decay in the $B^0 \rightarrow \pi^+ \pi^-$ mode is given by

$$S_{\pi^+ \pi^-} = -0.63 \pm 0.04. \quad (13.7)$$

- Direct CP violation in the $B^0 \rightarrow \pi^+ \pi^-$ mode is given by

$$C_{\pi^+ \pi^-} = -0.32 \pm 0.04. \quad (13.8)$$

- Direct CP violation in $B^+ \rightarrow D_+ K^+$ decays (D_+ is the CP-even neutral D state) is given by

$$\mathcal{A}_{B^+ \rightarrow D_+ K^+} = +0.129 \pm 0.012, \quad (13.9)$$

while the corresponding quantity in the case that the neutral D meson is reconstructed in the suppressed $K^- \pi^+$ final state is

$$\mathcal{A}_{B^+ \rightarrow D K^- \pi^+ K^+} = -0.41 \pm 0.06, \quad (13.10)$$

- Direct CP violation has also been observed in $B^+ \rightarrow DK^+$ decays through differences between the Dalitz plot distributions of subsequent $D \rightarrow K_S \pi^+ \pi^-$ decays.
- Direct CP violation in the $\bar{B}^0 \rightarrow K^- \pi^+$ mode is given by

$$\mathcal{A}_{\bar{B}^0 \rightarrow K^- \pi^+} = -0.084 \pm 0.004. \quad (13.11)$$

- Direct CP violation in the $\bar{B}_s^0 \rightarrow K^+ \pi^-$ mode is given by

$$\mathcal{A}_{\bar{B}_s^0 \rightarrow K^+ \pi^-} = +0.213 \pm 0.017. \quad (13.12)$$

- Direct CP violation in $B^+ \rightarrow K^+ K^- \pi^+$ decays is given by

$$\mathcal{A}_{B^+ \rightarrow K^+ K^- \pi^+} = -0.118 \pm 0.022. \quad (13.13)$$

An amplitude analysis has established a large CP violation effect associated with $\pi\pi \leftrightarrow KK$ S-wave rescattering in $B^+ \rightarrow K^+ K^- \pi^+$ decays.

- Large CP violation effects have also been observed in certain regions of the phase space of $B^+ \rightarrow K^+ K^- K^+$, $\pi^+ \pi^- K^+$ and $\pi^+ \pi^- \pi^+$ decays.
- Direct CP violation has been established in the difference of asymmetries for $D^0 \rightarrow K^+ K^-$ and $D^0 \rightarrow \pi^+ \pi^-$ decays

$$\Delta a_{CP} = (-0.164 \pm 0.028) \times 10^{-3}. \quad (13.14)$$

13.1 Formalism

The phenomenology of CP violation for neutral flavored mesons is particularly interesting, since many of the observables can be cleanly interpreted. Although the phenomenology is superficially different for K^0 , D^0 , B^0 , and B_s^0 decays, this is primarily because each of these systems is governed by a different balance between decay rates, oscillations, and lifetime splitting. However, the general considerations presented in this section are identical for all flavored neutral pseudoscalar mesons. The phenomenology of CP violation for neutral mesons that do not carry flavor quantum numbers (such as the $\eta^{(l)}$ state) is quite different: such states are their own antiparticles and have definite CP eigenvalues, so the signature of CP violation is simply the decay to a final state with the opposite CP. Such decays are mediated by the electromagnetic or (OZI-suppressed) strong interaction, where CP violation is not expected and has not yet been observed. In the remainder of this review, we restrict ourselves to considerations of weakly decaying hadrons.

In this section, we present a general formalism for, and classification of, CP violation in the decay of a weakly decaying hadron,

denoted M . We pay particular attention to the case that M is a K^0 , D^0 , B^0 , or B_s^0 meson. Subsequent sections describe the CP-violating phenomenology, approximations, and alternative formalisms that are specific to each system.

13.1.1 Charged- and neutral-hadron decays

We define decay amplitudes of M (which could be charged or neutral) and its CP conjugate \bar{M} to a multi-particle final state f and its CP conjugate \bar{f} as

$$A_f = \langle f | \mathcal{H} | M \rangle, \quad \bar{A}_f = \langle f | \mathcal{H} | \bar{M} \rangle, \quad (13.15a)$$

$$\bar{A}_{\bar{f}} = \langle \bar{f} | \mathcal{H} | M \rangle, \quad \bar{A}_{\bar{f}} = \langle \bar{f} | \mathcal{H} | \bar{M} \rangle, \quad (13.15b)$$

where \mathcal{H} is the Hamiltonian governing weak interactions. The action of CP on these states introduces phases ξ_M and ξ_f that depend on their flavor content, according to

$$CP|M\rangle = e^{+i\xi_M} |\bar{M}\rangle, \quad CP|f\rangle = e^{+i\xi_f} |\bar{f}\rangle, \quad (13.16a)$$

$$CP|\bar{M}\rangle = e^{-i\xi_M} |M\rangle, \quad CP|\bar{f}\rangle = e^{-i\xi_f} |f\rangle, \quad (13.16b)$$

so that $(CP)^2 = 1$. The phases ξ_M and ξ_f are arbitrary and unobservable because of the flavor symmetry of the strong interaction. If CP is conserved by the dynamics, $[CP, \mathcal{H}] = 0$, then A_f and $\bar{A}_{\bar{f}}$ have the same magnitude and an arbitrary unphysical relative phase

$$\bar{A}_{\bar{f}} = e^{i(\xi_f - \xi_M)} A_f. \quad (13.17)$$

13.1.2 Neutral-meson mixing

A state that is initially a superposition of M^0 and \bar{M}^0 , say

$$|\psi(0)\rangle = a(0)|M^0\rangle + b(0)|\bar{M}^0\rangle, \quad (13.18)$$

will evolve in time acquiring components that describe all possible decay final states $\{f_1, f_2, \dots\}$, that is,

$$|\psi(t)\rangle = a(t)|M^0\rangle + b(t)|\bar{M}^0\rangle + c_1(t)|f_1\rangle + c_2(t)|f_2\rangle + \dots \quad (13.19)$$

If we are interested in computing only the values of $a(t)$ and $b(t)$ (and not the values of all $c_i(t)$), and if the times t in which we are interested are much larger than the typical strong interaction scale, then we can use a much simplified formalism [30]. The simplified time evolution is determined by a 2×2 effective Hamiltonian \mathbf{H} that is not Hermitian, since otherwise the mesons would only oscillate and not decay. Any complex matrix, such as \mathbf{H} , can be written in terms of Hermitian matrices \mathbf{M} and $\mathbf{\Gamma}$ as

$$\mathbf{H} = \mathbf{M} - \frac{i}{2} \mathbf{\Gamma}. \quad (13.20)$$

\mathbf{M} and $\mathbf{\Gamma}$ are associated with $(M^0, \bar{M}^0) \leftrightarrow (M^0, \bar{M}^0)$ transitions via off-shell (dispersive), and on-shell (absorptive) intermediate states, respectively. Diagonal elements of \mathbf{M} and $\mathbf{\Gamma}$ are associated with the flavor-conserving transitions $M^0 \rightarrow M^0$ and $\bar{M}^0 \rightarrow \bar{M}^0$, while off-diagonal elements are associated with flavor-changing transitions $M^0 \leftrightarrow \bar{M}^0$.

The eigenvectors of \mathbf{H} have well-defined masses and decay widths. To specify the components of the strong interaction eigenstates, M^0 and \bar{M}^0 , in the light (M_L) and heavy (M_H) mass eigenstates, we introduce three complex parameters: p , q , and, for the case that both CP and CPT are violated in mixing, z :

$$|M_L\rangle \propto p\sqrt{1-z}|M^0\rangle + q\sqrt{1+z}|\bar{M}^0\rangle, \quad (13.21a)$$

$$|M_H\rangle \propto p\sqrt{1+z}|M^0\rangle - q\sqrt{1-z}|\bar{M}^0\rangle, \quad (13.21b)$$

with the normalization $|q|^2 + |p|^2 = 1$ when $z = 0$. (Another possible choice of labelling, which is in standard usage for K mesons, defines the mass eigenstates according to their lifetimes: K_S for the short-lived and K_L for the long-lived state. The K_L is experimentally found to be the heavier state. Yet another choice is often used for the D mesons [31]: the eigenstates are labelled according to their dominant CP content.)

The real and imaginary parts of the eigenvalues $\omega_{L,H}$ corresponding to $|M_{L,H}\rangle$ represent their masses and decay widths, respectively. The mass and width splittings are

$$\Delta m \equiv m_H - m_L = \mathcal{R}e(\omega_H - \omega_L), \quad (13.22a)$$

$$\Delta\Gamma \equiv \Gamma_H - \Gamma_L = -2\mathcal{I}m(\omega_H - \omega_L). \quad (13.22b)$$

Note that here Δm is positive by definition, while the sign of $\Delta\Gamma$ must be experimentally determined. The sign of $\Delta\Gamma$ has not yet been established for B^0 mesons, while $\Delta\Gamma < 0$ is established for K and B_s^0 mesons. The Standard Model predicts $\Delta\Gamma < 0$ for $B_{(s)}^0$ mesons; for this reason, $\Delta\Gamma = \Gamma_L - \Gamma_H$, which is still a signed quantity, is often used in the $B_{(s)}^0$ literature and is the convention used in the PDG experimental summaries.

Solving the eigenvalue problem for \mathbf{H} yields

$$\left(\frac{q}{p}\right)^2 = \frac{\mathbf{M}_{12}^* - (i/2)\mathbf{\Gamma}_{12}^*}{\mathbf{M}_{12} - (i/2)\mathbf{\Gamma}_{12}} \quad (13.23)$$

and

$$z \equiv \frac{\delta m - (i/2)\delta\Gamma}{\Delta m - (i/2)\Delta\Gamma}, \quad (13.24)$$

where

$$\delta m \equiv \mathbf{M}_{11} - \mathbf{M}_{22}, \quad \delta\Gamma \equiv \mathbf{\Gamma}_{11} - \mathbf{\Gamma}_{22} \quad (13.25)$$

are the differences in effective mass and decay-rate expectation values for the strong interaction states M^0 and \bar{M}^0 .

If either CP or CPT is a symmetry of \mathbf{H} (independently of whether T is conserved or violated), then the values of δm and $\delta\Gamma$ are both zero, and hence $z = 0$. We also find that

$$\omega_H - \omega_L = 2\sqrt{\left(\mathbf{M}_{12} - \frac{i}{2}\mathbf{\Gamma}_{12}\right)\left(\mathbf{M}_{12}^* - \frac{i}{2}\mathbf{\Gamma}_{12}^*\right)}. \quad (13.26)$$

If either CP or T is a symmetry of \mathbf{H} (independently of whether CPT is conserved or violated), then $\mathbf{\Gamma}_{12}/\mathbf{M}_{12}$ is real, leading to

$$\left(\frac{q}{p}\right)^2 = e^{2i\xi_M} \Rightarrow \left|\frac{q}{p}\right| = 1, \quad (13.27)$$

where ξ_M is the arbitrary unphysical phase introduced in Eq. (13.16). If, and only if, CP is a symmetry of \mathbf{H} (independently of CPT and T), then both of the above conditions hold, with the result that the mass eigenstates are orthogonal

$$\langle M_H | M_L \rangle = |p|^2 - |q|^2 = 0. \quad (13.28)$$

13.1.3 CP-violating observables

All CP -violating observables in M and \bar{M} decays to final states f and \bar{f} can be expressed in terms of phase-convention-independent combinations of A_f , \bar{A}_f , $A_{\bar{f}}$, and $\bar{A}_{\bar{f}}$, together with, for neutral meson decays only, q/p . CP violation in charged meson and all baryon decays depends only on the combination $|\bar{A}_{\bar{f}}/A_f|$, while CP violation in flavored neutral meson decays is complicated by $M^0 \leftrightarrow \bar{M}^0$ oscillations, and depends, additionally, on $|q/p|$ and on $\lambda_f \equiv (q/p)(\bar{A}_{\bar{f}}/A_f)$.

The decay rates of the two neutral kaon mass eigenstates, K_S and K_L , are different enough ($\Gamma_S/\Gamma_L \sim 500$) that one can, in most cases, actually study their decays independently. For D^0 , B^0 , and B_s^0 mesons, however, values of $\Delta\Gamma/\Gamma$ (where $\Gamma \equiv (\Gamma_H + \Gamma_L)/2$) are relatively small, and so both mass eigenstates must be considered in their evolution. We denote the state of an initially pure $|M^0\rangle$ or $|\bar{M}^0\rangle$ after an elapsed proper time t as $|M_{\text{phys}}^0(t)\rangle$ or $|\bar{M}_{\text{phys}}^0(t)\rangle$, respectively. Using the effective Hamiltonian approximation, but not assuming CPT to be a good symmetry, we obtain

$$|M_{\text{phys}}^0(t)\rangle = (g_+(t) + z g_-(t)) |M^0\rangle - \sqrt{1 - z^2} \frac{q}{p} g_-(t) |\bar{M}^0\rangle, \quad (13.29a)$$

$$|\bar{M}_{\text{phys}}^0(t)\rangle = (g_+(t) - z g_-(t)) |\bar{M}^0\rangle - \sqrt{1 - z^2} \frac{p}{q} g_-(t) |M^0\rangle, \quad (13.29b)$$

where

$$g_{\pm}(t) \equiv \frac{1}{2} \left[\exp\left(-im_H t - \frac{1}{2}\Gamma_H t\right) \pm \exp\left(-im_L t - \frac{1}{2}\Gamma_L t\right) \right] \quad (13.30)$$

and $z = 0$ if either CPT or CP is conserved.

Defining $x \equiv \Delta m/\Gamma$ and $y \equiv \Delta\Gamma/(2\Gamma)$, and assuming $z = 0$, one obtains the following time-dependent decay rates:

$$\begin{aligned} \frac{d\Gamma[M_{\text{phys}}^0(t) \rightarrow f]/dt}{e^{-\Gamma t}\mathcal{N}_f} &= (|A_f|^2 + |(q/p)\bar{A}_f|^2) \cosh(y\Gamma t) \\ &+ (|A_f|^2 - |(q/p)\bar{A}_f|^2) \cos(x\Gamma t) \\ &+ 2\mathcal{R}e((q/p)A_f^* \bar{A}_f) \sinh(y\Gamma t) \\ &- 2\mathcal{I}m((q/p)A_f^* \bar{A}_f) \sin(x\Gamma t), \end{aligned} \quad (13.31a)$$

$$\begin{aligned} \frac{d\Gamma[\bar{M}_{\text{phys}}^0(t) \rightarrow \bar{f}]/dt}{e^{-\Gamma t}\mathcal{N}_{\bar{f}}} &= (|(p/q)A_f|^2 + |\bar{A}_f|^2) \cosh(y\Gamma t) \\ &- (|(p/q)A_f|^2 - |\bar{A}_f|^2) \cos(x\Gamma t) \\ &+ 2\mathcal{R}e((p/q)A_f \bar{A}_f^*) \sinh(y\Gamma t) \\ &- 2\mathcal{I}m((p/q)A_f \bar{A}_f^*) \sin(x\Gamma t), \end{aligned} \quad (13.31b)$$

where \mathcal{N}_f is a common, time-independent, normalization factor that can be determined bearing in mind that the range of t is $0 < t < \infty$. Decay rates to the CP -conjugate final state \bar{f} are obtained analogously, with $\mathcal{N}_f = \mathcal{N}_{\bar{f}}$ and the substitutions $A_f \rightarrow A_{\bar{f}}$ and $\bar{A}_f \rightarrow \bar{A}_{\bar{f}}$ in Eqs. (13.31a) and (13.31b). Terms proportional to $|A_f|^2$ or $|\bar{A}_f|^2$ are associated with decays that occur without any net $M^0 \leftrightarrow \bar{M}^0$ oscillation, while terms proportional to $|(q/p)\bar{A}_f|^2$ or $|(p/q)A_f|^2$ are associated with decays following a net oscillation. The $\sinh(y\Gamma t)$ and $\sin(x\Gamma t)$ terms of Eqs. (13.31a) and (13.31b) are associated with the interference between these two cases. Note that, in multi-body decays, amplitudes are functions of variables that describe the phase-space of the final state. Interference may be present in some regions but not others, and is strongly influenced by resonant substructure.

When neutral pseudoscalar mesons are produced coherently in pairs from the decay of a vector resonance, $V \rightarrow M^0 \bar{M}^0$ (for example, $\Upsilon(4S) \rightarrow B^0 \bar{B}^0$, $\psi(3770) \rightarrow D^0 \bar{D}^0$ or $\phi \rightarrow K^0 \bar{K}^0$), the time-dependence of their subsequent decays to final states f_1 and f_2 has a similar form to Eqs. (13.31a) and (13.31b):

$$\begin{aligned} \frac{d\Gamma[V_{\text{phys}}(t_1, t_2) \rightarrow f_1 f_2]/d(\Delta t)}{e^{-\Gamma|\Delta t|}\mathcal{N}_{f_1 f_2}} &= (|a_+|^2 + |a_-|^2) \cosh(y\Gamma\Delta t) \\ &+ (|a_+|^2 - |a_-|^2) \cos(x\Gamma\Delta t) \\ &- 2\mathcal{R}e(a_+^* a_-) \sinh(y\Gamma\Delta t) \\ &+ 2\mathcal{I}m(a_+^* a_-) \sin(x\Gamma\Delta t), \end{aligned} \quad (13.32)$$

where $\Delta t \equiv t_2 - t_1$ is the difference in the production times, t_1 and t_2 , of f_1 and f_2 , respectively, and the dependence on the average decay time and on decay angles has been integrated out. The normalisation factor $\mathcal{N}_{f_1 f_2}$ can be evaluated, noting that the range of Δt is $-\infty < \Delta t < \infty$. The coefficients in Eq. (13.32) are determined by the amplitudes for no net oscillation from $t_1 \rightarrow t_2$, $\bar{A}_{f_1} A_{f_2}$, and $A_{f_1} \bar{A}_{f_2}$, and for a net oscillation, $(q/p)\bar{A}_{f_1} \bar{A}_{f_2}$ and $(p/q)A_{f_1} A_{f_2}$, via

$$a_+ \equiv \bar{A}_{f_1} A_{f_2} - A_{f_1} \bar{A}_{f_2}, \quad (13.33a)$$

$$\begin{aligned} a_- \equiv & -\sqrt{1 - z^2} \left(\frac{q}{p} \bar{A}_{f_1} \bar{A}_{f_2} - \frac{p}{q} A_{f_1} A_{f_2} \right) \\ & + z \left(\bar{A}_{f_1} A_{f_2} + A_{f_1} \bar{A}_{f_2} \right). \end{aligned} \quad (13.33b)$$

Assuming CPT conservation, $z = 0$, and identifying $\Delta t \rightarrow t$ and $f_2 \rightarrow f$, we find that Eqs. (13.32) and (13.33) reduce to

Eq. (13.31a) with $A_{f_1} = 0$, $\bar{A}_{f_1} = 1$, or to Eq. (13.31b) with $\bar{A}_{f_1} = 0$, $A_{f_1} = 1$. Indeed, such a situation plays an important role in experiments that exploit the coherence of $V \rightarrow M^0 \bar{M}^0$ production. Final states f_1 with $A_{f_1} = 0$ or $\bar{A}_{f_1} = 0$ are called tagging states, because they identify the decaying pseudoscalar meson as, respectively, \bar{M}^0 or M^0 . Before one of M^0 or \bar{M}^0 decays, they evolve in phase, so that there is always one M^0 and one \bar{M}^0 present. A tagging decay of one meson sets the clock for the time evolution of the other: it starts at t_1 as purely M^0 or \bar{M}^0 , with time evolution that depends only on $t_2 - t_1$.

When f_1 is a state that both M^0 and \bar{M}^0 can decay into, then Eq. (13.32) contains interference terms proportional to $A_{f_1} \bar{A}_{f_1} \neq 0$ that are not present in Eqs. (13.31a) and (13.31b). Even when f_1 is dominantly produced by M^0 decays rather than \bar{M}^0 decays, or vice versa, $A_{f_1} \bar{A}_{f_1}$ can be non-zero owing to doubly-CKM-suppressed decays (with amplitudes suppressed by at least two powers of λ relative to the dominant amplitude, in the language of Section 13.3), and these terms should be considered for precision studies of CP violation in coherent $V \rightarrow M^0 \bar{M}^0$ decays [32]. The correlations in $V \rightarrow M^0 \bar{M}^0$ decays can also be exploited to determine strong phase differences between favored and suppressed decay amplitudes [33].

13.1.4 Classification of CP-violating effects

We distinguish three types of CP -violating effects that can occur in the quark sector:

- I. CP violation in decay is defined by

$$|\bar{A}_{\bar{f}}/A_f| \neq 1. \quad (13.34)$$

In charged meson (and all baryon) decays, where mixing effects are absent, this is the only possible source of CP asymmetries:

$$\mathcal{A}_{f\pm} \equiv \frac{\Gamma(M^- \rightarrow f^-) - \Gamma(M^+ \rightarrow f^+)}{\Gamma(M^- \rightarrow f^-) + \Gamma(M^+ \rightarrow f^+)} = \frac{|\bar{A}_{f-}/A_{f+}|^2 - 1}{|\bar{A}_{f-}/A_{f+}|^2 + 1}. \quad (13.35)$$

Note that the usual sign convention for CP asymmetries of hadrons is for the difference between the rate involving the particle that contains a heavy quark and that which contains an antiquark. Hence Eq. (13.35) corresponds to the definition for B^\pm mesons, but the opposite sign is used for $D_{(s)}^\pm$ decays.

- II. CP (and T) violation in mixing is defined by

$$|q/p| \neq 1. \quad (13.36)$$

In charged-current semileptonic neutral meson decays $M, \bar{M} \rightarrow \ell^\pm X$ (taking $|\mathcal{A}_{\ell^+ X}| = |\mathcal{A}_{\ell^- X}|$ and $\mathcal{A}_{\ell^- X} = \bar{\mathcal{A}}_{\ell^+ X} = 0$, as is the case in the Standard Model, to lowest order in G_F , and in most of its reasonable extensions), this is the only source of CP violation, and can be measured via the asymmetry of “wrong-sign” decays induced by oscillations:

$$\begin{aligned} \mathcal{A}_{\text{SL}}(t) & \equiv \frac{d\Gamma/dt[\bar{M}_{\text{phys}}^0(t) \rightarrow \ell^+ X] - d\Gamma/dt[M_{\text{phys}}^0(t) \rightarrow \ell^- X]}{d\Gamma/dt[\bar{M}_{\text{phys}}^0(t) \rightarrow \ell^+ X] + d\Gamma/dt[M_{\text{phys}}^0(t) \rightarrow \ell^- X]}, \\ & \quad (13.37a) \end{aligned}$$

$$= \frac{1 - |q/p|^4}{1 + |q/p|^4}. \quad (13.37b)$$

Note that this asymmetry of time-dependent decay rates is actually time-independent.

- III. CP violation in interference between a decay without mixing, $M^0 \rightarrow f$, and a decay with mixing, $M^0 \rightarrow \bar{M}^0 \rightarrow f$ (such an effect occurs only in decays to final states that are common to M^0 and \bar{M}^0 , including all CP eigenstates), is defined by

$$\arg(\lambda_f) + \arg(\lambda_{\bar{f}}) \neq 0, \quad \text{with} \quad \lambda_f \equiv \frac{q \bar{A}_{\bar{f}}}{p A_f}. \quad (13.38)$$

For final CP eigenstates, f_{CP} , the condition Eq. (13.38) simplifies to

$$\text{Im}(\lambda_{f_{CP}}) \neq 0, \quad (13.39)$$

This form of CP violation can be observed, for example, using the asymmetry of neutral meson decays into CP eigenstates

$$\begin{aligned} \mathcal{A}_{f_{CP}}(t) & \equiv \\ & \equiv \frac{d\Gamma/dt[\bar{M}_{\text{phys}}^0(t) \rightarrow f_{CP}] - d\Gamma/dt[M_{\text{phys}}^0(t) \rightarrow f_{CP}]}{d\Gamma/dt[\bar{M}_{\text{phys}}^0(t) \rightarrow f_{CP}] + d\Gamma/dt[M_{\text{phys}}^0(t) \rightarrow f_{CP}]}. \end{aligned} \quad (13.40)$$

If $\Delta\Gamma = 0$, as expected to a good approximation for B^0 mesons but not for K^0 and B_s^0 mesons, and $|q/p| = 1$, then $\mathcal{A}_{f_{CP}}$ has a particularly simple form (see Eq. (13.89), below). If, in addition, the decay amplitudes fulfill $|\bar{A}_{f_{CP}}| = |A_{f_{CP}}|$, the interference between decays with and without mixing is the only source of asymmetry and $\mathcal{A}_{f_{CP}}(t) = \text{Im}(\lambda_{f_{CP}}) \sin(x\Gamma t)$.

Examples of these three types of CP violation will be given in Sections 13.4, 13.5, and 13.6.

13.2 Theoretical Interpretation: General Considerations

Consider the $M \rightarrow f$ decay amplitude A_f , and the CP conjugate process, $\bar{M} \rightarrow \bar{f}$, with decay amplitude $\bar{A}_{\bar{f}}$. There are two types of phases that may appear in these decay amplitudes. Complex parameters in any Lagrangian term that contributes to the amplitude will appear in complex conjugate form in the CP -conjugate amplitude. Thus, their phases appear in A_f and $\bar{A}_{\bar{f}}$ with opposite signs. In the Standard Model, these phases occur only in the couplings of the W^\pm bosons, and hence, are often called “weak phases.” The weak phase of any single term is convention-dependent. However, the difference between the weak phases in two different terms in A_f is convention-independent. A second type of phase can appear in scattering or decay amplitudes, even when the Lagrangian is real. This phase originates from the possible contribution from intermediate on-shell states in the decay process. Since such phases are generated by CP -invariant interactions, they are the same in A_f and $\bar{A}_{\bar{f}}$. Usually the dominant rescattering is due to strong interactions; hence the designation “strong phases” for the phase shifts so induced. Again, only the relative strong phases between different terms in the amplitude are physically meaningful.

The “weak” and “strong” phases discussed here appear in addition to the spurious CP -transformation phases of Eq. (13.17). Those spurious phases are due to an arbitrary choice of phase convention, and do not originate from any dynamics or induce any CP violation. For simplicity, we set them to zero from here on.

It is useful to write each contribution a_i to A_f in three parts: its magnitude $|a_i|$, its weak phase ϕ_i , and its strong phase δ_i . If, for example, there are two such contributions, $A_f = a_1 + a_2$, we have

$$A_f = |a_1|e^{i(\delta_1 + \phi_1)} + |a_2|e^{i(\delta_2 + \phi_2)}, \quad (13.41a)$$

$$\bar{A}_{\bar{f}} = |a_1|e^{i(\delta_1 - \phi_1)} + |a_2|e^{i(\delta_2 - \phi_2)}. \quad (13.41b)$$

Similarly, for neutral mesons, it is useful to write

$$\mathbf{M}_{12} = |\mathbf{M}_{12}|e^{i\phi_M}, \quad \mathbf{\Gamma}_{12} = |\mathbf{\Gamma}_{12}|e^{i\phi_\Gamma}. \quad (13.42)$$

Each of the phases appearing in Eqs. (13.41) and (13.42) is convention-dependent, but combinations such as $\delta_1 - \delta_2$, $\phi_1 - \phi_2$, $\phi_M - \phi_\Gamma$, and $\phi_M + \phi_1 - \bar{\phi}_1$ (where $\bar{\phi}_1$ is a weak phase contributing to $\bar{A}_{\bar{f}}$) are physical.

It is now straightforward to evaluate the various asymmetries in terms of the theoretical parameters introduced here. We will do so with approximations that are often relevant to the most interesting measured asymmetries.

1. The CP asymmetry in charged meson and all baryon decays [Eq. (13.35)] is given by

$$\mathcal{A}_f = - \frac{2|a_1 a_2| \sin(\delta_2 - \delta_1) \sin(\phi_2 - \phi_1)}{|a_1|^2 + |a_2|^2 + 2|a_1 a_2| \cos(\delta_2 - \delta_1) \cos(\phi_2 - \phi_1)}. \quad (13.43)$$

The quantity of most interest to theory is the weak phase difference $\phi_2 - \phi_1$. Its extraction from the asymmetry requires, however, that the amplitude ratio $|a_2/a_1|$ and the strong phase difference $\delta_2 - \delta_1$ are known. Both quantities depend on non-perturbative hadronic parameters that are difficult to calculate, but in some cases can be obtained from experiment.

2. In the approximation that $|\Gamma_{12}/\mathbf{M}_{12}| \ll 1$ (valid for B^0 and B_s^0 mesons), the CP asymmetry in semileptonic neutral-meson decays [Eq. (13.37)] is given by

$$A_{\text{SL}} = - \left| \frac{\Gamma_{12}}{\mathbf{M}_{12}} \right| \sin(\phi_M - \phi_\Gamma). \quad (13.44)$$

The quantity of most interest to theory is the weak phase $\phi_M - \phi_\Gamma$. Its extraction from the asymmetry requires, however, that $|\Gamma_{12}/\mathbf{M}_{12}|$ is known. State of the art calculations of this quantity for the B^0 and B_s^0 mesons have uncertainties of around 15–20% [34].

3. In the approximations that only a single weak phase contributes to decay, $A_f = |a_f|e^{i(\delta_f + \phi_f)}$, and that $|\Gamma_{12}/\mathbf{M}_{12}| = 0$, we obtain $|\lambda_f| = 1$, and the CP asymmetries in decays to a final CP eigenstate f [Eq. (13.40)] with eigenvalue $\eta_f = \pm 1$ are given by

$$A_{fCP}(t) = \mathcal{I}m(\lambda_f) \sin(\Delta mt) \quad \text{with} \quad \mathcal{I}m(\lambda_f) = \eta_f \sin(\phi_M + 2\phi_f). \quad (13.45)$$

Note that the phase measured is purely a weak phase, and no hadronic parameters are involved in the extraction of its value from $\mathcal{I}m(\lambda_f)$.

The discussion above allows us to introduce another classification of CP -violating effects:

1. *Indirect CP violation* is consistent with taking $\phi_M \neq 0$ and setting all other CP violating phases to zero. CP violation in mixing (type II) belongs to this class.
2. *Direct CP violation* cannot be accounted for by just $\phi_M \neq 0$. CP violation in decay (type I) belongs to this class.

The historical significance of this classification is related to theory. In superweak models [35], CP violation appears only in diagrams that contribute to \mathbf{M}_{12} , hence they predict that there is no direct CP violation. In most models and, in particular, in the Standard Model, CP violation is both direct and indirect. As concerns type III CP violation, a single observation of such an

effect would be consistent with indirect CP violation, but observing $\eta_{f_1} \mathcal{I}m(\lambda_{f_1}) \neq \eta_{f_2} \mathcal{I}m(\lambda_{f_2})$ (for the same decaying meson and two different final CP eigenstates f_1 and f_2) would establish direct CP violation. The experimental observation of $\epsilon' \neq 0$, which was achieved by establishing that $\mathcal{I}m(\lambda_{\pi^+\pi^-}) \neq \mathcal{I}m(\lambda_{\pi^0\pi^0})$ (see Section 13.4), excluded the superweak scenario.

13.3 Theoretical Interpretation: The KM Mechanism

Of all the Standard Model quark parameters, only the Kobayashi-Maskawa (KM) phase is CP -violating. Having a single source of CP violation, the Standard Model is very predictive for CP asymmetries: some vanish, and those that do not are correlated.

To be precise, CP could be violated also by strong interactions. The experimental upper bound on the electric-dipole moment of the neutron implies, however, that θ_{QCD} , the non-perturbative parameter that determines the strength of this type of CP violation, is tiny, if not zero. (The smallness of θ_{QCD} constitutes a theoretical puzzle, known as “the strong CP problem.”) In particular, it is irrelevant to our discussion of hadron decays.

The charged current interactions (that is, the W^\pm interactions) for quarks are given by

$$-\mathcal{L}_{W^\pm} = \frac{g}{\sqrt{2}} \bar{u}_L^i \gamma^\mu (V_{\text{CKM}})_{ij} d_{Lj} W_\mu^\pm + \text{h.c.} \quad (13.46)$$

Here $i, j = 1, 2, 3$ are generation numbers. The Cabibbo-Kobayashi-Maskawa (CKM) mixing matrix for quarks is a 3×3 unitary matrix [36]. Ordering the quarks by their masses, *i.e.*, $(u_1, u_2, u_3) \rightarrow (u, c, t)$ and $(d_1, d_2, d_3) \rightarrow (d, s, b)$, the elements of V_{CKM} are written as follows:

$$V_{\text{CKM}} = \begin{pmatrix} V_{ud} & V_{us} & V_{ub} \\ V_{cd} & V_{cs} & V_{cb} \\ V_{td} & V_{ts} & V_{tb} \end{pmatrix}. \quad (13.47)$$

While a general 3×3 unitary matrix depends on three real angles and six phases, the freedom to redefine the phases of the quark mass eigenstates can be used to remove five of the phases, leaving a single physical phase, the Kobayashi-Maskawa phase, that is responsible for all CP violation in the Standard Model.

The fact that one can parametrize V_{CKM} by three real and only one imaginary physical parameters can be made manifest by choosing an explicit parametrization. The Wolfenstein parametrization [37, 38] is particularly useful:

$$V_{\text{CKM}} = \begin{pmatrix} 1 - \frac{1}{2}\lambda^2 - \frac{1}{8}\lambda^4 & \lambda & A\lambda^3(\rho - i\eta) \\ -\lambda + \frac{1}{2}A^2\lambda^5[1 - 2(\rho + i\eta)] & 1 - \frac{1}{2}\lambda^2 - \frac{1}{8}\lambda^4(1 + 4A^2) & A\lambda^2 \\ A\lambda^3[1 - (1 - \frac{1}{2}\lambda^2)(\rho + i\eta)] & -A\lambda^2 + \frac{1}{2}A\lambda^4[1 - 2(\rho + i\eta)] & 1 - \frac{1}{2}A^2\lambda^4 \end{pmatrix}. \quad (13.48)$$

Here $\lambda \approx 0.23$ (not to be confused with λ_f), the sine of the Cabibbo angle, plays the role of an expansion parameter, and η represents the CP -violating phase. Terms of $\mathcal{O}(\lambda^6)$ have been neglected.

The unitarity of the CKM matrix, $(VV^\dagger)_{ij} = (V^\dagger V)_{ij} = \delta_{ij}$, leads to twelve distinct complex relations among the matrix elements. The six relations with $i \neq j$ can be represented geometrically as triangles in the complex plane. Two of these,

$$V_{ud}V_{ub}^* + V_{cd}V_{cb}^* + V_{td}V_{tb}^* = 0, \quad (13.49a)$$

$$V_{td}V_{ud}^* + V_{ts}V_{us}^* + V_{tb}V_{ub}^* = 0, \quad (13.49b)$$

have terms of equal order, $\mathcal{O}(A\lambda^3)$, and so have corresponding triangles whose interior angles are all $\mathcal{O}(1)$ physical quantities that can be independently measured. The angles of the first triangle

(see Fig. 13.1) are given by

$$\alpha \equiv \varphi_2 \equiv \arg \left(-\frac{V_{td}V_{tb}^*}{V_{ud}V_{ub}^*} \right) \simeq \arg \left(-\frac{1 - \rho - i\eta}{\rho + i\eta} \right), \quad (13.50a)$$

$$\beta \equiv \varphi_1 \equiv \arg \left(-\frac{V_{cd}V_{cb}^*}{V_{td}V_{tb}^*} \right) \simeq \arg \left(\frac{1}{1 - \rho - i\eta} \right), \quad (13.50b)$$

$$\gamma \equiv \varphi_3 \equiv \arg \left(-\frac{V_{ud}V_{ub}^*}{V_{cd}V_{cb}^*} \right) \simeq \arg(\rho + i\eta). \quad (13.50c)$$

The angles of the second triangle are equal to (α, β, γ) up to corrections of $\mathcal{O}(\lambda^2)$. The notations (α, β, γ) and $(\varphi_1, \varphi_2, \varphi_3)$ are both in common usage but, for convenience, we only use the first convention in the following.

Another relation that can be represented as a triangle,

$$V_{us}V_{ub}^* + V_{cs}V_{cb}^* + V_{ts}V_{tb}^* = 0, \quad (13.51)$$

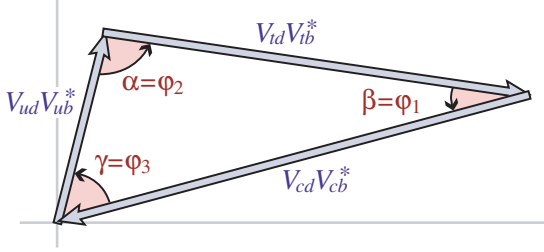


Figure 13.1: Graphical representation of the unitarity constraint $V_{ud}V_{ub}^* + V_{cd}V_{cb}^* + V_{td}V_{tb}^* = 0$ as a triangle in the complex plane.

and, in particular, its small angle, of $\mathcal{O}(\lambda^2)$,

$$\beta_s \equiv \arg\left(-\frac{V_{ts}V_{tb}^*}{V_{cs}V_{cb}^*}\right), \quad (13.52)$$

is convenient for analyzing CP violation in the B_s^0 sector.

All unitarity triangles have the same area, commonly denoted by $J/2$ [39]. If CP is violated, J is different from zero and can be taken as the single CP -violating parameter. In the Wolfenstein parametrization of Eq. (13.48), $J \simeq \lambda^6 A^2 \eta$.

13.4 Kaons

CP violation was discovered in $K \rightarrow \pi\pi$ decays in 1964 [1]. The same mode provided the first observation of direct CP violation [4–6].

The decay amplitudes actually measured in neutral K decays refer to the mass eigenstates K_L and K_S , rather than to the K and \bar{K} states referred to in Eq. (13.15). The final $\pi^+\pi^-$ and $\pi^0\pi^0$ states are CP -even. In the CP conservation limit, K_S (K_L) would be CP -even (odd), and therefore would (would not) decay to two pions. We define CP -violating amplitude ratios for two-pion final states,

$$\eta_{00} \equiv \frac{\langle \pi^0\pi^0 | \mathcal{H} | K_L \rangle}{\langle \pi^0\pi^0 | \mathcal{H} | K_S \rangle}, \quad \eta_{+-} \equiv \frac{\langle \pi^+\pi^- | \mathcal{H} | K_L \rangle}{\langle \pi^+\pi^- | \mathcal{H} | K_S \rangle}. \quad (13.53)$$

Another important observable is the asymmetry of time-integrated semileptonic decay rates:

$$\delta_L \equiv \frac{\Gamma(K_L \rightarrow \ell^+\nu_\ell\pi^-) - \Gamma(K_L \rightarrow \ell^-\bar{\nu}_\ell\pi^+)}{\Gamma(K_L \rightarrow \ell^+\nu_\ell\pi^-) + \Gamma(K_L \rightarrow \ell^-\bar{\nu}_\ell\pi^+)}. \quad (13.54)$$

CP violation has been observed as an appearance of K_L decays to two-pion final states [27],

$$|\eta_{00}| = (2.220 \pm 0.011) \times 10^{-3}, \quad (13.55a)$$

$$|\eta_{+-}| = (2.232 \pm 0.011) \times 10^{-3}, \quad (13.55b)$$

$$|\eta_{00}/\eta_{+-}| = 0.9950 \pm 0.0007, \quad (13.55c)$$

where the phase ϕ_{ij} of the amplitude ratio η_{ij} has been determined both assuming CPT invariance:

$$\phi_{00} = (43.52 \pm 0.05)^\circ, \quad \phi_{+-} = (43.51 \pm 0.05)^\circ, \quad (13.56)$$

and without assuming CPT invariance:

$$\phi_{00} = (43.7 \pm 0.6)^\circ, \quad \phi_{+-} = (43.4 \pm 0.5)^\circ. \quad (13.57)$$

CP violation has also been observed in semileptonic K_L decays [27]

$$\delta_L = (3.32 \pm 0.06) \times 10^{-3}, \quad (13.58)$$

where δ_L is a weighted average of muon and electron measurements, as well as in K_L decays to $\pi^+\pi^-\gamma$ and $\pi^+\pi^-e^+e^-$ [27]. CP violation in $K \rightarrow 3\pi$ decays has not yet been observed [27,40].

Historically, CP violation in neutral K decays has been described in terms of the complex parameters ϵ and ϵ' . The observables η_{00} , η_{+-} , and δ_L are related to these parameters, and to

those of Section 13.1, by

$$\eta_{00} = \frac{1 - \lambda_{\pi^0\pi^0}}{1 + \lambda_{\pi^0\pi^0}} = \epsilon - 2\epsilon', \quad (13.59a)$$

$$\eta_{+-} = \frac{1 - \lambda_{\pi^+\pi^-}}{1 + \lambda_{\pi^+\pi^-}} = \epsilon + \epsilon', \quad (13.59b)$$

$$\delta_L = \frac{1 - |q/p|^2}{1 + |q/p|^2} = \frac{2\mathcal{R}e(\epsilon)}{1 + |\epsilon|^2}, \quad (13.59c)$$

where, in the last line, we have assumed that $|A_{\ell^+\nu_\ell\pi^-}| = |\bar{A}_{\ell^-\bar{\nu}_\ell\pi^+}|$ and $|A_{\ell^-\bar{\nu}_\ell\pi^+}| = |\bar{A}_{\ell^+\nu_\ell\pi^-}| = 0$. (The convention-dependent parameter $\tilde{\epsilon} \equiv (1 - q/p)/(1 + q/p)$, sometimes used in the literature, is, in general, different from ϵ but yields a similar expression, $\delta_L = 2\mathcal{R}e(\tilde{\epsilon})/(1 + |\tilde{\epsilon}|^2)$.) A fit to the $K \rightarrow \pi\pi$ data yields [27]

$$|\epsilon| = (2.228 \pm 0.011) \times 10^{-3}, \quad (13.60a)$$

$$\mathcal{R}e(\epsilon'/\epsilon) = (1.66 \pm 0.23) \times 10^{-3}. \quad (13.60b)$$

In discussing two-pion final states, it is useful to express the amplitudes $A_{\pi^0\pi^0}$ and $A_{\pi^+\pi^-}$ in terms of their isospin components via

$$A_{\pi^0\pi^0} = \sqrt{\frac{1}{3}} |A_0| e^{i(\delta_0 + \phi_0)} - \sqrt{\frac{2}{3}} |A_2| e^{i(\delta_2 + \phi_2)}, \quad (13.61a)$$

$$A_{\pi^+\pi^-} = \sqrt{\frac{2}{3}} |A_0| e^{i(\delta_0 + \phi_0)} + \sqrt{\frac{1}{3}} |A_2| e^{i(\delta_2 + \phi_2)}, \quad (13.61b)$$

where we parameterize the amplitude $A_I(\bar{A}_I)$ for $K^0(\bar{K}^0)$ decay into two pions with total isospin $I = 0$ or 2 as

$$A_I \equiv \langle (\pi\pi)_I | \mathcal{H} | K^0 \rangle = |A_I| e^{i(\delta_I + \phi_I)}, \quad (13.62a)$$

$$\bar{A}_I \equiv \langle (\pi\pi)_I | \mathcal{H} | \bar{K}^0 \rangle = |\bar{A}_I| e^{i(\delta_I - \phi_I)}. \quad (13.62b)$$

The smallness of $|\eta_{00}|$ and $|\eta_{+-}|$ allows us to approximate

$$\epsilon \simeq \frac{1}{2}(1 - \lambda_{(\pi\pi)_{I=0}}), \quad \epsilon' \simeq \frac{1}{6}(\lambda_{\pi^0\pi^0} - \lambda_{\pi^+\pi^-}). \quad (13.63)$$

The parameter ϵ represents indirect CP violation, while ϵ' parameterizes direct CP violation: $\mathcal{R}e(\epsilon')$ measures CP violation in decay (type I), $\mathcal{R}e(\epsilon)$ measures CP violation in mixing (type II), and $\mathcal{I}m(\epsilon)$ and $\mathcal{I}m(\epsilon')$ measure the interference between decays with and without mixing (type III).

The following expressions for ϵ and ϵ' are useful for theoretical evaluations:

$$\epsilon \simeq \frac{e^{i\pi/4} \mathcal{I}m(\mathbf{M}_{12})}{\sqrt{2} \Delta m}, \quad \epsilon' = \frac{i}{\sqrt{2}} \left| \frac{A_2}{A_0} \right| e^{i(\delta_2 - \delta_0)} \sin(\phi_2 - \phi_0). \quad (13.64)$$

The expression for ϵ is only valid in a phase convention where $\phi_2 = 0$, corresponding to a real $V_{ud}V_{us}^*$, and in the approximation that also $\phi_0 = 0$. The phase of ϵ , $\arg(\epsilon) \approx \arctan(-2\Delta m/\Delta\Gamma)$, is determined by non-perturbative QCD dynamics and is experimentally determined to be about $\pi/4$. The calculation of ϵ benefits from the fact that $\mathcal{I}m(\mathbf{M}_{12})$ is dominated by short distance physics. Consequently, the main sources of uncertainty in theoretical interpretations of ϵ are the values of matrix elements, such as $\langle K^0 | (\bar{s}d)_{V-A} (\bar{s}d)_{V-A} | \bar{K}^0 \rangle$. The expression for ϵ' is valid to first order in $|A_2/A_0| \sim 1/20$. The phase of ϵ' is experimentally determined, $\pi/2 + \delta_2 - \delta_0 \approx \pi/4$, and is independent of the electroweak model. Note that, accidentally, ϵ'/ϵ is real to a good approximation. Determination of weak phase information from the measurement of $\mathcal{R}e(\epsilon'/\epsilon)$ given in Eq. (13.60) has until now been precluded by uncertainties in the hadronic parameters, but recent advances in lattice QCD calculations [41, 42] suggest that it may become possible [43].

A future measurement of much interest is that of CP violation in the rare $K \rightarrow \pi\nu\bar{\nu}$ decays. The signal for CP violation is simply observing the $K_L \rightarrow \pi^0\nu\bar{\nu}$ decay. The effect here is that

of interference between decays with and without mixing (type III) [44]:

$$\frac{\Gamma(K_L \rightarrow \pi^0 \nu \bar{\nu})}{\Gamma(K^+ \rightarrow \pi^+ \nu \bar{\nu})} = \frac{1}{2} [1 + |\lambda_{\pi \nu \bar{\nu}}|^2 - 2 \mathcal{R}e(\lambda_{\pi \nu \bar{\nu}})] \quad (13.65)$$

$$\simeq 1 - \mathcal{R}e(\lambda_{\pi \nu \bar{\nu}}),$$

where in the last equation we neglect CP violation in decay and in mixing (expected, model-independently, to be of order 10^{-5} and 10^{-3} , respectively). Such a measurement is experimentally very challenging but would be theoretically very rewarding [45]. Similar to the CP asymmetry in $B^0 \rightarrow J/\psi K_S$, the CP violation in $K \rightarrow \pi \nu \bar{\nu}$ decay is predicted to be large (that is, the ratio in Eq. (13.65) is neither CKM- nor loop-suppressed) and can be very cleanly interpreted.

Within the Standard Model, the $K_L \rightarrow \pi^0 \nu \bar{\nu}$ decay is dominated by an intermediate top quark contribution and, consequently, can be interpreted in terms of CKM parameters [46]. (For the charged mode, $K^+ \rightarrow \pi^+ \nu \bar{\nu}$, the contribution from an intermediate charm quark is not negligible, and constitutes a source of hadronic uncertainty.) In particular, $\mathcal{B}(K_L \rightarrow \pi^0 \nu \bar{\nu})$ provides a theoretically clean way to determine the Wolfenstein parameter η [47]:

$$\mathcal{B}(K_L \rightarrow \pi^0 \nu \bar{\nu}) = \kappa_L [X(m_t^2/m_W^2)]^2 A^4 \eta^2, \quad (13.66)$$

where the hadronic parameter $\kappa_L \sim 2 \times 10^{-10}$ incorporates the value of the four-fermion matrix element which is deduced, using isospin relations, from $\mathcal{B}(K^+ \rightarrow \pi^0 e^+ \nu_e)$, and $X(m_t^2/m_W^2)$ is a known function of the top mass. An explicit calculation gives $\mathcal{B}(K_L \rightarrow \pi^0 \nu \bar{\nu}) = (3.00 \pm 0.30) \times 10^{-11}$ [48].

The currently tightest experimental limit is $\mathcal{B}(K_L \rightarrow \pi^0 \nu \bar{\nu}) < 3.0 \times 10^{-9}$ [49], which does not yet reach the bound that can be derived from Eq. (13.65), $\mathcal{B}(K_L \rightarrow \pi^0 \nu \bar{\nu}) < 4.4 \times \mathcal{B}(K^+ \rightarrow \pi^+ \nu \bar{\nu})$ [44]. Significant further progress is anticipated from experiments searching for $K \rightarrow \pi \nu \bar{\nu}$ decays in the next few years [50,51].

13.5 Charm

The existence of $D^0-\bar{D}^0$ mixing is well established [52–55], with the latest experimental constraints giving [29, 56] $x \equiv \Delta m/\Gamma = (0.39_{-0.12}^{+0.11}) \times 10^{-2}$ and $y \equiv \Delta\Gamma/(2\Gamma) = (0.65_{-0.07}^{+0.06}) \times 10^{-2}$. Thus, the data clearly show that $y \neq 0$, but improved measurements are needed to be sure of the size of x . Long-distance contributions make it difficult to calculate Standard Model predictions for the $D^0-\bar{D}^0$ mixing parameters. Therefore, the goal of the search for $D^0-\bar{D}^0$ mixing is not to constrain the CKM parameters, but rather to probe new physics. Here CP violation plays an important role. Within the Standard Model, the CP -violating effects are predicted to be small, since the mixing and the relevant decays are described, to an excellent approximation, by the physics of the first two generations only. The expectation is that the Standard Model size of CP violation in D decays is $\mathcal{O}(10^{-3})$ or less. At present, the most sensitive searches involve the $D^0 \rightarrow K^+ K^-$, $D^0 \rightarrow \pi^+ \pi^-$ and $D^0 \rightarrow K^\pm \pi^\mp$ modes.

The neutral D mesons decay via a singly-Cabibbo-suppressed transition to the CP eigenstates $K^+ K^-$ and $\pi^+ \pi^-$. These decays are dominated by Standard-Model tree diagrams. Thus, we can write, for $f = K^+ K^-$ or $\pi^+ \pi^-$,

$$A_f = A_f^T e^{+i\phi_f^T} [1 + r_f e^{i(\delta_f + \phi_f)}], \quad (13.67a)$$

$$\bar{A}_f = A_f^T e^{-i\phi_f^T} [1 + r_f e^{i(\delta_f - \phi_f)}], \quad (13.67b)$$

where $A_f^T e^{\pm i\phi_f^T}$ is the Standard Model tree-level contribution, ϕ_f^T and ϕ_f are weak, CP violating phases, δ_f is a strong phase difference, and r_f is the ratio between a subleading ($r_f \ll 1$) contribution with a weak phase different from ϕ_f^T and the Standard Model tree-level contribution. Neglecting r_f , λ_f is universal, and we can define an observable phase ϕ_D via

$$\lambda_f \equiv -|q/p| e^{i\phi_D}. \quad (13.68)$$

(In the limit of CP conservation, choosing $\phi_D = 0$ is equivalent to defining the mass eigenstates by their CP eigenvalue: $|D_\mp\rangle =$

$p|D^0\rangle \pm q|\bar{D}^0\rangle$, with D_- (D_+) being the CP -odd (CP -even) state; that is, the state that does not (does) decay into $K^+ K^-$.)

We define the time integrated CP asymmetry for a final CP eigenstate f as follows:

$$a_f \equiv \frac{\int_0^\infty \Gamma(D_{\text{phys}}^0(t) \rightarrow f) dt - \int_0^\infty \Gamma(\bar{D}_{\text{phys}}^0(t) \rightarrow f) dt}{\int_0^\infty \Gamma(D_{\text{phys}}^0(t) \rightarrow f) dt + \int_0^\infty \Gamma(\bar{D}_{\text{phys}}^0(t) \rightarrow f) dt}. \quad (13.69)$$

(This expression corresponds to the D meson being tagged at production, hence the integration goes from 0 to $+\infty$; measurements are also possible with $\psi(3770) \rightarrow D^0 \bar{D}^0$, in which case the integration goes from $-\infty$ to $+\infty$ giving slightly different results; see the discussion in Section 13.1.3.) We take $x, y, r_f \ll 1$ and expand to leading order in these parameters. We can then separate the contribution to a_f into three parts [57],

$$a_f = a_f^d + a_f^m + a_f^i, \quad (13.70)$$

with the following underlying mechanisms:

1. a_f^d signals CP violation in decay (similar to Eq. (13.35)):

$$a_f^d = 2r_f \sin \phi_f \sin \delta_f. \quad (13.71)$$

2. a_f^m signals CP violation in mixing (similar to Eq. (13.44)).

With our approximations, it is universal:

$$a^m = -\frac{y}{2} \left(\left| \frac{q}{p} \right| - \left| \frac{p}{q} \right| \right) \cos \phi_D. \quad (13.72)$$

3. a_f^i signals CP violation in the interference of mixing and decay (similar to Eq. (13.45)). With our approximations, it is universal:

$$a^i = \frac{x}{2} \left(\left| \frac{q}{p} \right| + \left| \frac{p}{q} \right| \right) \sin \phi_D. \quad (13.73)$$

One can isolate the effects of direct CP violation by taking the difference between the CP asymmetries in the $K^+ K^-$ and $\pi^+ \pi^-$ modes:

$$\Delta a_{CP} \equiv a_{K^+ K^-} - a_{\pi^+ \pi^-} = a_{K^+ K^-}^d - a_{\pi^+ \pi^-}^d, \quad (13.74)$$

where we neglected a residual, experiment-dependent, contribution from indirect CP violation due to the fact that there may be a decay time-dependent acceptance function that can be different for the $K^+ K^-$ and $\pi^+ \pi^-$ channels. The current average gives [29]:

$$a_{K^+ K^-}^d - a_{\pi^+ \pi^-}^d = (-0.164 \pm 0.028) \times 10^{-3}, \quad (13.75)$$

demonstrating CP violation in charm decay.

One can also isolate the effects of indirect CP violation in the following way. Consider the time-dependent decay rates in Eq. (13.31a) and Eq. (13.31b). The mixing processes modify the time dependence from a pure exponential. However, given the small values of x and y , the time dependences can be recast, to a good approximation, into purely exponential form, but with modified decay-rate parameters [58,59] (given here for the $K^+ K^-$ final state):

$$\Gamma_{D^0 \rightarrow K^+ K^-} = \Gamma \times [1 + |q/p| (y \cos \phi_D - x \sin \phi_D)], \quad (13.76a)$$

$$\Gamma_{\bar{D}^0 \rightarrow K^+ K^-} = \Gamma \times [1 + |p/q| (y \cos \phi_D + x \sin \phi_D)]. \quad (13.76b)$$

One can define CP -conserving and CP -violating combinations of these two observables (normalized to the true width Γ):

$$y_{CP} \equiv \frac{\Gamma_{\bar{D}^0 \rightarrow K^+ K^-} + \Gamma_{D^0 \rightarrow K^+ K^-}}{2\Gamma} - 1$$

$$= (y/2) (|q/p| + |p/q|) \cos \phi_D - (x/2) (|q/p| - |p/q|) \sin \phi_D, \quad (13.77a)$$

$$A_\Gamma \equiv \frac{\Gamma_{D^0 \rightarrow K^+ K^-} - \Gamma_{\bar{D}^0 \rightarrow K^+ K^-}}{2\Gamma}$$

$$= -(a^m + a^i). \quad (13.77b)$$

In the limit of CP conservation (and, in particular, within the Standard Model), $y_{CP} = (\Gamma_+ - \Gamma_-)/2\Gamma = y$ (where $\Gamma_+(\Gamma_-)$ is the decay width of the CP -even (-odd) mass eigenstate) and $A_\Gamma = 0$. Indeed, present measurements imply that CP violation is small [29],

$$y_{CP} = (+0.72 \pm 0.11) \times 10^{-2}, \quad (13.78a)$$

$$A_\Gamma = (-0.032 \pm 0.026) \times 10^{-2}. \quad (13.78b)$$

The $K^\pm\pi^\mp$ states are not CP eigenstates, but they are still common final states for D^0 and \bar{D}^0 decays. Since $D^0(\bar{D}^0) \rightarrow K^-\pi^+$ is a Cabibbo-favored (doubly-Cabibbo-suppressed) process, these processes are particularly sensitive to x and/or $y = \mathcal{O}(\lambda^2)$. Taking into account that $|\lambda_{K^-\pi^+}|, |\lambda_{K^+\pi^-}^{-1}| \ll 1$ and $x, y \ll 1$, assuming that there is no direct CP violation (these are Standard Model tree-level decays dominated by a single weak phase, and there is no contribution from penguin-like and chromomagnetic operators), and expanding the time-dependent rates for $xt, yt \lesssim \Gamma^{-1}$, one obtains

$$\begin{aligned} \Gamma[D_{\text{phys}}^0(t) \rightarrow K^+\pi^-] &= e^{-\Gamma t} |\bar{A}_{K^-\pi^+}|^2 \\ &\times \left[r_d^2 + r_d \left| \frac{q}{p} \right| (y' \cos \phi_D - x' \sin \phi_D) \Gamma t + \left| \frac{q}{p} \right|^2 \frac{y^2 + x^2}{4} (\Gamma t)^2 \right], \end{aligned} \quad (13.79a)$$

$$\begin{aligned} \Gamma[\bar{D}_{\text{phys}}^0(t) \rightarrow K^-\pi^+] &= e^{-\Gamma t} |\bar{A}_{K^-\pi^+}|^2 \\ &\times \left[r_d^2 + r_d \left| \frac{p}{q} \right| (y' \cos \phi_D + x' \sin \phi_D) \Gamma t + \left| \frac{p}{q} \right|^2 \frac{y^2 + x^2}{4} (\Gamma t)^2 \right], \end{aligned} \quad (13.79b)$$

where

$$y' \equiv y \cos \delta - x \sin \delta \quad \text{and} \quad x' \equiv x \cos \delta + y \sin \delta. \quad (13.80)$$

The weak phase ϕ_D is the same as that of Eq. (13.68) (a consequence of neglecting direct CP violation) and $r_d = \mathcal{O}(\tan^2 \theta_c)$ is the amplitude ratio, $r_d = |\bar{A}_{K^-\pi^+}/A_{K^-\pi^+}| = |A_{K^+\pi^-}/\bar{A}_{K^+\pi^-}|$, that is, $\lambda_{K^-\pi^+} = r_d |q/p| e^{-i(\delta - \phi_D)}$ and $\lambda_{K^+\pi^-}^{-1} = r_d |p/q| e^{-i(\delta + \phi_D)}$. The parameter δ is a strong-phase difference for these processes, that can be obtained from measurements of quantum correlated $\psi(3770) \rightarrow D^0 \bar{D}^0$ decays [60,61]. By fitting to the six coefficients of the various time-dependences, one can determine $r_d, |q/p|, (x^2 + y^2), y' \cos \phi_D$, and $x' \sin \phi_D$. In particular, finding CP violation ($|q/p| \neq 1$ and/or $\sin \phi_D \neq 0$) at a level much higher than 10^{-3} would constitute evidence for new physics. The most stringent constraints to date on CP violation in charm mixing have been obtained with this method [62] and from the A_Γ measurement [63].

A fit to all data [29], including also results from time-dependent analyses of $D^0 \rightarrow K_S \pi^+ \pi^-$ decays, from which $x, y, |q/p|$ and ϕ_D can be determined directly, yields no evidence for indirect CP violation:

$$1 - |q/p| = +0.031_{-0.050}^{+0.045}, \quad (13.81a)$$

$$\phi_D = (-3.9_{-4.6}^{+4.5})^\circ. \quad (13.81b)$$

With the additional assumption of no direct CP violation in doubly-Cabibbo-suppressed D decays [64–66], tighter constraints are obtained:

$$1 - |q/p| = +0.002 \pm 0.008, \quad (13.82a)$$

$$\phi_D = (+0.08 \pm 0.31)^\circ. \quad (13.82b)$$

More details on various theoretical and experimental aspects of $D^0\text{--}\bar{D}^0$ mixing can be found in Ref. [31].

Searches for CP violation in charged $D_{(s)}$ decays have been performed in many modes. Searches in decays mediated by Cabibbo-suppressed amplitudes are particularly interesting, since in other channels effects are likely to be too small to be observable in current experiments. Examples of relevant two-body modes are $D^+ \rightarrow \pi^+ \pi^0, K_S K^+, \phi \pi^+$ and $D_s^+ \rightarrow K^+ \pi^0, K_S \pi^+, \phi K^+$. The

most precise results are $\mathcal{A}_{D^+ \rightarrow K_S K^+} = +0.0011 \pm 0.0017$ and $\mathcal{A}_{D_s^+ \rightarrow K_S \pi^+} = +0.0038 \pm 0.0048$ [29]. The precision of experiments is now sufficient that the effect from CP violation in the neutral kaon system can be seen in $D^+ \rightarrow K_S \pi^+$ decays [67,68].

Three- and four-body final states provide additional possibilities to search for CP violation, since effects may vary over the phase-space [69]. A number of methods have been proposed to exploit this feature and search for CP violation in ways that do not require modelling of the decay distribution [70–73]. Such methods are useful for analysis of charm decays since they are less sensitive to biases from production asymmetries, and are well suited to address the issue of whether or not CP violation effects are present. They can also be applied to tagged neutral D meson as well as to charged $D_{(s)}$ decays (flavor tagging is typically achieved from the charge of the pion produced in $D^{*+} \rightarrow D^0 \pi^+$ decays). The results of all searches to date are consistent with the absence of CP violation, with the most significant hint at the level of 2.7σ [74].

13.6 Beauty

13.6.1 CP violation in mixing of B^0 and B_s^0 mesons

The upper bound on the CP asymmetry in semileptonic B decays [28] implies that CP violation in $B^0\text{--}\bar{B}^0$ mixing is a small effect (we use $\mathcal{A}_{\text{SL}}/2 \approx 1 - |q/p|$, see Eq. (13.37)):

$$\mathcal{A}_{\text{SL}}^d = (-2.1 \pm 1.7) \times 10^{-3} \implies |q/p| = 1.0010 \pm 0.0008. \quad (13.83)$$

The Standard Model prediction is

$$\mathcal{A}_{\text{SL}}^d = \mathcal{O}[(m_c^2/m_t^2) \sin \beta] \lesssim 0.001. \quad (13.84)$$

An explicit calculation gives $(-4.7 \pm 0.6) \times 10^{-4}$ [34].

The experimental constraint on CP violation in $B_s^0\text{--}\bar{B}_s^0$ mixing is somewhat weaker than that in the $B^0\text{--}\bar{B}^0$ system [28]

$$\mathcal{A}_{\text{SL}}^s = (-0.6 \pm 2.8) \times 10^{-3} \implies |q/p| = 1.0003 \pm 0.0014. \quad (13.85)$$

The Standard Model prediction is $\mathcal{A}_{\text{SL}}^s = \mathcal{O}[(m_c^2/m_t^2) \sin \beta_s] \lesssim 10^{-4}$, with an explicit calculation giving $(2.22 \pm 0.27) \times 10^{-5}$ [34].

The fit to experimental data that results in the averages quoted above has a χ^2 probability of 4.5% indicating some tension between the different measurements [29]. This originates in part from a result from the D0 collaboration for the inclusive same-sign dimuon asymmetry that deviates from the Standard Model prediction by 3.6σ [75]. As yet, this has not been confirmed by independent studies.

In models where $\Gamma_{12}/\mathbf{M}_{12}$ is approximately real, such as the Standard Model, an upper bound on $\Delta\Gamma/\Delta m \approx \mathcal{R}e(\Gamma_{12}/\mathbf{M}_{12})$ provides yet another upper bound on the deviation of $|q/p|$ from one. This constraint does not hold if $\Gamma_{12}/\mathbf{M}_{12}$ is approximately imaginary. (An alternative parameterization uses $q/p = (1 - \bar{\epsilon}_B)/(1 + \bar{\epsilon}_B)$, leading to $\mathcal{A}_{\text{SL}} \simeq 4\mathcal{R}e(\bar{\epsilon}_B)$.)

13.6.2 CP violation in interference of B^0 decays with and without mixing

The small deviation (less than one percent) of $|q/p|$ from 1 implies that, at the present level of experimental precision, CP violation in B^0 mixing is a negligible effect. Thus, for the purpose of analyzing CP asymmetries in hadronic B^0 decays, we can use

$$\lambda_f = e^{-i\phi_{M(B^0)}} (\bar{A}_f/A_f), \quad (13.86)$$

where $\phi_{M(B^0)}$ refers to the phase of \mathbf{M}_{12} appearing in Eq. (13.42) that is appropriate for $B^0\text{--}\bar{B}^0$ oscillations. Within the Standard Model, the corresponding phase factor is given by

$$e^{-i\phi_{M(B^0)}} = (V_{tb}^* V_{td}) / (V_{tb} V_{td}^*). \quad (13.87)$$

The class of CP violation effects in interference between mixing and decay is studied with final states that are common to B^0 and \bar{B}^0 decays [76–78]. It is convenient to rewrite Eq. (13.40) for B^0 decays as [79–81]

$$\mathcal{A}_f(t) = S_f \sin(\Delta m t) - C_f \cos(\Delta m t), \quad (13.88)$$

$$S_f \equiv \frac{2\text{Im}(\lambda_f)}{1 + |\lambda_f|^2}, \quad C_f \equiv \frac{1 - |\lambda_f|^2}{1 + |\lambda_f|^2}, \quad (13.89)$$

where we assume that $\Delta\Gamma = 0$ and $|q/p| = 1$. An alternative notation in use is $A_f \equiv -C_f$ – this A_f should not be confused with the A_f of Eq. (13.15), but in the limit that $|q/p| = 1$ is equivalent with the A_f of Eq. (13.35).

A large class of interesting processes proceed via quark transitions of the form $\bar{b} \rightarrow \bar{q}q\bar{q}'$ with $q' = s$ or d . For $q = c$ or u , there are contributions from both tree (t) and penguin (p^{qu} , where $q_u = u, c, t$ is the quark in the loop) diagrams (see Fig. 13.2) which carry different weak phases:

$$A_f = (V_{qb}^* V_{qq'}) t_f + \sum_{q_u=u,c,t} (V_{q_u b}^* V_{q_u q'}) p_f^{q_u}. \quad (13.90)$$

(The distinction between tree and penguin contributions is a heuristic one; the separation by the operator that enters is more precise. A more detailed discussion of the operator product expansion approach, which also includes higher order QCD corrections, can be found in Ref. [82] for example.) Using CKM unitarity, these decay amplitudes can always be written in terms of just two CKM combinations. For example, for $f = \pi\pi$, which proceeds via a $\bar{b} \rightarrow \bar{u}u\bar{d}$ transition, we can write

$$A_{\pi\pi} = (V_{ub}^* V_{ud}) T_{\pi\pi} + (V_{tb}^* V_{td}) P_{\pi\pi}^t, \quad (13.91)$$

where $T_{\pi\pi} = t_{\pi\pi} + p_{\pi\pi}^u - p_{\pi\pi}^c$ and $P_{\pi\pi}^t = p_{\pi\pi}^t - p_{\pi\pi}^c$. CP -violating phases in Eq. (13.91) appear only in the CKM elements, so that

$$\frac{\bar{A}_{\pi\pi}}{A_{\pi\pi}} = \frac{(V_{ub} V_{ud}^*) T_{\pi\pi} + (V_{tb} V_{td}^*) P_{\pi\pi}^t}{(V_{ub}^* V_{ud}) T_{\pi\pi} + (V_{tb}^* V_{td}) P_{\pi\pi}^t}. \quad (13.92)$$

For $f = J/\psi K$, which proceeds via a $\bar{b} \rightarrow \bar{c}c\bar{s}$ transition, we can write

$$A_{\psi K} = (V_{cb}^* V_{cs}) T_{\psi K} + (V_{ub}^* V_{us}) P_{\psi K}^u, \quad (13.93)$$

where $T_{\psi K} = t_{\psi K} + p_{\psi K}^c - p_{\psi K}^t$ and $P_{\psi K}^u = p_{\psi K}^u - p_{\psi K}^t$. A subtlety arises in this decay that is related to the fact that B^0 decays into a final $J/\psi K^0$ state while \bar{B}^0 decays into a final $J/\psi \bar{K}^0$ state. A common final state, *e.g.*, $J/\psi K_S$, is reached only via K^0 – \bar{K}^0 mixing. Consequently, the phase factor (defined in Eq. (13.42)) corresponding to neutral K mixing, $e^{-i\phi_M(K)} = (V_{cd}^* V_{cs}) / (V_{cd} V_{cs}^*)$, plays a role:

$$\frac{\bar{A}_{\psi K_S}}{A_{\psi K_S}} = - \frac{(V_{cb} V_{cs}^*) T_{\psi K} + (V_{ub} V_{us}^*) P_{\psi K}^u}{(V_{cb}^* V_{cs}) T_{\psi K} + (V_{ub}^* V_{us}) P_{\psi K}^u} \times \frac{V_{cd}^* V_{cs}}{V_{cd} V_{cs}^*}. \quad (13.94)$$

For $q = s$ or d , there are only penguin contributions to A_f , that is, $t_f = 0$ in Eq. (13.90). (The tree $\bar{b} \rightarrow \bar{u}u\bar{q}'$ transition followed by $\bar{u}u \rightarrow \bar{q}q$ rescattering is included below in the P^u terms.) Again, CKM unitarity allows us to write A_f in terms of two CKM combinations. For example, for $f = \phi K_S$, which proceeds via a $\bar{b} \rightarrow \bar{s}s\bar{s}$ transition, we can write

$$\frac{\bar{A}_{\phi K_S}}{A_{\phi K_S}} = - \frac{(V_{cb} V_{cs}^*) P_{\phi K}^c + (V_{ub} V_{us}^*) P_{\phi K}^u}{(V_{cb}^* V_{cs}) P_{\phi K}^c + (V_{ub}^* V_{us}) P_{\phi K}^u} \times \frac{V_{cd}^* V_{cs}}{V_{cd} V_{cs}^*}, \quad (13.95)$$

where $P_{\phi K}^c = p_{\phi K}^c - p_{\phi K}^t$ and $P_{\phi K}^u = p_{\phi K}^u - p_{\phi K}^t$.

Since in general the amplitude A_f involves two different weak phases, the corresponding decays can exhibit both CP violation in the interference of decays with and without mixing, $S_f \neq 0$, and CP violation in decay, $C_f \neq 0$. (At the present level of experimental precision, the contribution to C_f from CP violation in mixing is negligible, see Eq. (13.83).) If the contribution from a second weak phase is suppressed, then the interpretation of S_f in terms of Lagrangian CP -violating parameters is clean, while C_f is small. If such a second contribution is not suppressed, S_f depends on hadronic parameters and, if the relevant strong phase difference is large, C_f is large.

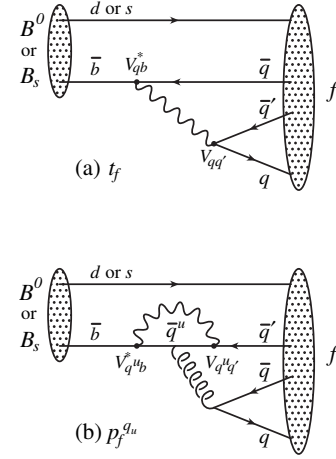


Figure 13.2: Feynman diagrams for (a) tree and (b) penguin amplitudes contributing to $B^0 \rightarrow f$ or $B_s^0 \rightarrow f$ via a $\bar{b} \rightarrow \bar{q}q\bar{q}'$ quark-level process.

A summary of $\bar{b} \rightarrow \bar{q}q\bar{q}'$ modes with $q' = s$ or d is given in Table 13.1. The $\bar{b} \rightarrow \bar{d}d\bar{q}$ transitions lead to final states that are similar to those from $\bar{b} \rightarrow \bar{u}u\bar{q}$ transitions and have similar phase dependence. Final states that consist of two vector mesons ($\psi\phi$ and $\phi\phi$) are not CP eigenstates, and angular analysis is needed to separate the CP -even from the CP -odd contributions.

The cleanliness of the theoretical interpretation of S_f can be assessed from the information in the last column of Table 13.1. In case of small uncertainties, the expression for S_f in terms of CKM phases can be deduced from the fourth column of Table 13.1 in combination with Eq. (13.87) (and, for $b \rightarrow q\bar{q}s$ decays, the example in Eq. (13.94)). Here we consider several interesting examples.

For $B^0 \rightarrow J/\psi K_S$ and other $\bar{b} \rightarrow \bar{c}c\bar{s}$ processes, we can neglect the P^u contribution to A_f , in the Standard Model, to an approximation that is better than one percent, giving:

$$\lambda_{\psi K_S} = -e^{-2i\beta} \Rightarrow S_{\psi K_S} = \sin 2\beta, \quad C_{\psi K_S} = 0. \quad (13.96)$$

It is important to verify experimentally the level of suppression of the penguin contribution. Methods based on flavor symmetries [83–86] allow limits to be obtained. All are currently consistent with the P^u term being negligible. Explicit calculations [86–89] also support this conclusion.

In the presence of new physics, A_f is still likely to be dominated by the T term, but the mixing amplitude might be modified. We learn that, model-independently, $C_f \approx 0$ while S_f cleanly determines the mixing phase ($\phi_M - 2\arg(V_{cb} V_{cd}^*)$). The experimental measurement [29], $S_{\psi K} = +0.699 \pm 0.017$, gave the first precision test of the Kobayashi-Maskawa mechanism, and its consistency with the predictions for $\sin 2\beta$ makes it very likely that this mechanism is indeed the dominant source of CP violation in the quark sector.

For $B^0 \rightarrow \phi K_S$ and other $\bar{b} \rightarrow \bar{s}s\bar{s}$ processes (as well as some $\bar{b} \rightarrow \bar{u}u\bar{s}$ processes), we can neglect the subdominant contributions, in the Standard Model, to an approximation that is good to the order of a few percent:

$$\lambda_{\phi K_S} = -e^{-2i\beta} \Rightarrow S_{\phi K_S} = \sin 2\beta, \quad C_{\phi K_S} = 0. \quad (13.97)$$

A review of explicit calculations of the effects of subleading amplitudes can be found in Ref. [90]. In the presence of new physics, both A_f and M_{12} can have contributions that are comparable in size to those of the Standard Model and carry new weak phases. Such a situation gives several interesting consequences for penguin-dominated $\bar{b} \rightarrow \bar{q}q\bar{s}$ decays ($q = u, d, s$) to a final state f :

1. The value of $-\eta_f S_f$ may be different from $S_{\psi K_S}$ by more than a few percent, where η_f is the CP eigenvalue of the final state.

Table 13.1: Summary of $\bar{b} \rightarrow \bar{q}q\bar{q}'$ modes with $q' = s$ or d . The second and third columns give examples of hadronic final states (usually those which are experimentally most convenient to study). The fourth column gives the CKM dependence of the amplitude A_f , using the notation of Eqs. ((13.91), (13.93), (13.95)), with the dominant term first and the subdominant second. The suppression factor of the second term compared to the first is given in the last column. “Loop” refers to a penguin versus tree-suppression factor (it is mode-dependent and roughly $\mathcal{O}(0.2 - 0.3)$) and $\lambda \simeq 0.23$ is the expansion parameter of Eq. (13.48).

$\bar{b} \rightarrow \bar{q}q\bar{q}'$	$B^0 \rightarrow f$	$B_s^0 \rightarrow f$	CKM dependence of A_f	Suppression
$\bar{b} \rightarrow \bar{c}c\bar{s}$	ψK_S	$\psi\phi$	$(V_{cb}^* V_{cs})T + (V_{ub}^* V_{us})P^u$	loop $\times \lambda^2$
$\bar{b} \rightarrow \bar{s}s\bar{s}$	ϕK_S	$\phi\phi$	$(V_{cb}^* V_{cs})P^c + (V_{ub}^* V_{us})P^u$	λ^2
$\bar{b} \rightarrow \bar{u}u\bar{s}$	$\pi^0 K_S$	$K^+ K^-$	$(V_{cb}^* V_{cs})P^c + (V_{ub}^* V_{us})T$	λ^2/loop
$\bar{b} \rightarrow \bar{c}c\bar{d}$	$D^+ D^-$	ψK_S	$(V_{cb}^* V_{cd})T + (V_{tb}^* V_{td})P^t$	loop
$\bar{b} \rightarrow \bar{s}s\bar{d}$	$K_S K_S$	ϕK_S	$(V_{tb}^* V_{td})P^t + (V_{cb}^* V_{cd})P^c$	$\lesssim 1$
$\bar{b} \rightarrow \bar{u}u\bar{d}$	$\pi^+ \pi^-$	$\rho^0 K_S$	$(V_{ub}^* V_{ud})T + (V_{tb}^* V_{td})P^t$	loop
$\bar{b} \rightarrow \bar{c}c\bar{u}$	$D_{CP}\pi^0$	$D_{CP}K_S$	$(V_{cb}^* V_{ud})T + (V_{ub}^* V_{cd})T'$	λ^2
$\bar{b} \rightarrow \bar{c}u\bar{s}$	$D_{CP}K_S$	$D_{CP}\phi$	$(V_{cb}^* V_{us})T + (V_{ub}^* V_{cs})T'$	$\lesssim 1$

- The values of $\eta_f S_f$ for different final states f may be different from each other by more than a few percent (for example, $S_{\phi K_S} \neq S_{\eta' K_S}$).
- The value of C_f may be different from zero by more than a few percent.

While a clear interpretation of such signals in terms of Lagrangian parameters will be difficult because, under these circumstances, hadronic parameters play a role, any of the above three options will clearly signal new physics. In addition flavor symmetry relations, such as those which relate observables in $B \rightarrow K\pi$ decays [91,92] can be used to provide further tests of the Standard Model. Fig. 13.3 summarizes the present experimental results: none of the possible signatures listed above is unambiguously established, but there is definitely still room for new physics.

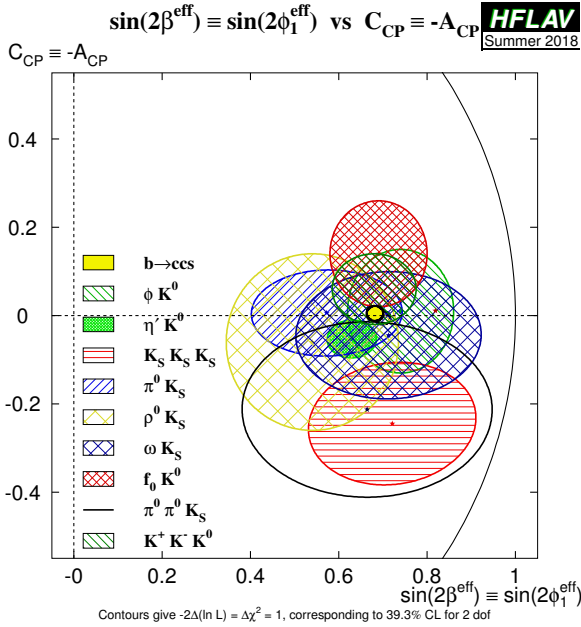


Figure 13.3: Summary of the results [29] of time-dependent analyses of $b \rightarrow \bar{q}q\bar{s}$ decays, which are potentially sensitive to new physics.

For the $\bar{b} \rightarrow \bar{u}u\bar{d}$ process $B \rightarrow \pi\pi$ and other related channels, the penguin-to-tree ratio can be estimated using SU(3) relations and experimental data on related $B \rightarrow K\pi$ decays. The result (for $\pi\pi$) is that the suppression is at the level of 0.2 – 0.3 and so cannot be neglected. The expressions for $S_{\pi\pi}$ and $C_{\pi\pi}$ to leading order in $R_{PT} \equiv (|V_{tb}V_{td}|P_{\pi\pi}^t)/(|V_{ub}V_{ud}|T_{\pi\pi})$ are:

$$\lambda_{\pi\pi} = e^{2i\alpha} \left[(1 - R_{PT}e^{-i\alpha}) / (1 - R_{PT}e^{+i\alpha}) \right] \Rightarrow \quad (13.98)$$

$$S_{\pi\pi} \approx \sin 2\alpha + 2 \operatorname{Re}(R_{PT}) \cos 2\alpha \sin \alpha, \quad C_{\pi\pi} \approx 2 \operatorname{Im}(R_{PT}) \sin \alpha. \quad (13.99)$$

Note that R_{PT} is mode-dependent and, in particular, could be different for $\pi^+\pi^-$ and $\pi^0\pi^0$. If strong phases can be neglected, then R_{PT} is real, resulting in $C_{\pi\pi} = 0$. The size of $C_{\pi\pi}$ is an indicator of how large the strong phase is. The present experimental average is $C_{\pi^+\pi^-} = -0.32 \pm 0.04$ [29]. As concerns $S_{\pi\pi}$, it is clear from Eq. (13.99) that the relative size or strong phase of the penguin contribution must be known to extract α . This is the problem of penguin pollution.

The cleanest solution involves isospin relations among the $B \rightarrow \pi\pi$ amplitudes [93]:

$$\frac{1}{\sqrt{2}} A_{\pi^+\pi^-} + A_{\pi^0\pi^0} = A_{\pi^+\pi^0}. \quad (13.100)$$

The method exploits the fact that the penguin contribution to $P_{\pi\pi}^t$ is pure $\Delta I = 1/2$ (this is not true for the electroweak penguins which, however, are expected to be small), while the tree contribution to $T_{\pi\pi}$ contains pieces that are both $\Delta I = 1/2$ and $\Delta I = 3/2$. A simple geometric construction then allows one to find R_{PT} and extract α cleanly from $S_{\pi^+\pi^-}$. The key experimental difficulty is that one must measure accurately the separate rates for B^0 and $\bar{B}^0 \rightarrow \pi^0\pi^0$.

CP asymmetries in $B \rightarrow \rho\pi$ and $B \rightarrow \rho\rho$ can also be used to determine α . In particular, the $B \rightarrow \rho\rho$ measurements are presently very significant in constraining α . The extraction proceeds via isospin analysis similar to that of $B \rightarrow \pi\pi$. There are, however, several important differences. First, due to the finite width of the ρ mesons, a final $(\rho\rho)_{I=1}$ state is possible [94]. The effect is, however, of the order of $(\Gamma_\rho/m_\rho)^2 \sim 0.04$. Second, due to the presence of three helicity states for the two vector mesons, angular analysis is needed to separate the CP -even and CP -odd components. The theoretical expectation is that the CP -odd component is small, which is supported by experiments which find that the $\rho^+\rho^-$ and $\rho^\pm\rho^0$ modes are dominantly longitudinally polarized. Third, an important advantage of the $\rho\rho$ modes is that the penguin contribution is expected to be small due to different hadronic dynamics. This expectation is confirmed by the smallness of $\mathcal{B}(B^0 \rightarrow \rho^0\rho^0) = (0.95 \pm 0.16) \times 10^{-6}$ [29,95] compared to $\mathcal{B}(B^0 \rightarrow \rho^+\rho^-) = (24.2 \pm 3.1) \times 10^{-6}$ [29]. Thus, $S_{\rho^+\rho^-}$ is far from $\sin 2\alpha$. Finally, both $S_{\rho^0\rho^0}$ and $C_{\rho^0\rho^0}$ are experimentally accessible, which may allow a precision determination of α . However, a full isospin analysis should allow that the fractions of longitudinal polarisation in B and \bar{B} decays may differ, which has not yet been done by the experiments.

Detailed discussion of the determination of α with these methods, and the latest world average, can be found in Refs. [36,96]. The consistency between the range of α determined by the $B \rightarrow \pi\pi$, $\rho\pi$ and $\rho\rho$ measurements and the range allowed by CKM fits (excluding these direct determinations) provides further support to the Kobayashi-Maskawa mechanism.

All modes discussed in this Section so far have possible contributions from penguin amplitudes. As shown in Table 13.1, CP violation can also be studied with final states, typically containing charmed mesons, where no such contribution is possible. The neutral charmed meson must be reconstructed in a final state, such as a CP eigenstate, common to D^0 and \bar{D}^0 so that the am-

plitudes for the B and \bar{B} meson decays interfere. Although there is a second tree amplitude with a different weak phase, the contributions of the different diagrams can in many cases be separated experimentally (for example by exploiting different decays of the neutral D mesons) making these channels very clean theoretically. The first determination of $\sin(2\beta)$, with significance of CP violation over 5σ , with this method has recently been reported [97]. Moreover, the interference between the two tree diagrams gives sensitivity to γ , as will be discussed in Section 13.6.4.

13.6.3 CP violation in interference of B_s^0 decays with and without mixing

As discussed in Section 13.6.1, the world average for $|q/p|$ in the B_s^0 system currently deviates from the Standard Model expectation due to an anomalous value of the dimuon asymmetry. Attributing the dimuon asymmetry result to a fluctuation, we again neglect the deviation of $|q/p|$ from 1, and use

$$\lambda_f = e^{-i\phi_M(B_s^0)} (\bar{A}_f/A_f). \quad (13.101)$$

Within the Standard Model,

$$e^{-i\phi_M(B_s^0)} = (V_{tb}^* V_{ts}) / (V_{tb} V_{ts}^*). \quad (13.102)$$

Note that $\Delta\Gamma/\Gamma = 0.132 \pm 0.008$ [29] and therefore y should not be put to zero in Eqs. (13.31a) and (13.31b). However, $|q/p| = 1$ is expected to hold to an even better approximation than for B^0 mesons. One therefore obtains

$$\mathcal{A}_f(t) = \frac{S_f \sin(\Delta mt) - C_f \cos(\Delta mt)}{\cosh(\Delta\Gamma t/2) - A_f^{\Delta\Gamma} \sinh(\Delta\Gamma t/2)}, \quad (13.103)$$

$$A_f^{\Delta\Gamma} \equiv \frac{-2\mathcal{R}e(\lambda_f)}{1 + |\lambda_f|^2}. \quad (13.104)$$

The presence of the $A_f^{\Delta\Gamma}$ term implies that information on λ_f can be obtained from analyses that do not use tagging of the initial flavor, through so-called effective lifetime measurements [98].

The $B_s^0 \rightarrow J/\psi\phi$ decay proceeds via the $\bar{b} \rightarrow \bar{c}\bar{c}\bar{s}$ transition. The CP asymmetry in this mode thus determines (with angular analysis to disentangle the CP -even and CP -odd components of the final state) $\sin 2\beta_s$, where β_s is defined in Eq. (13.52) [99]. The $B_s^0 \rightarrow J/\psi\pi^+\pi^-$ decay, which has a large contribution from $J/\psi f_0(980)$ and is assumed to also proceed dominantly via the $\bar{b} \rightarrow \bar{c}\bar{c}\bar{s}$ transition, has also been used to determine β_s . In this case no angular analysis is necessary, since the final state has been shown to be dominated by the CP -odd component [100]. The combination of measurements yields [29]

$$-2\beta_s = -0.021 \pm 0.031, \quad (13.105)$$

consistent with the Standard Model prediction, $\beta_s = 0.0184 \pm 0.0004$ [19].

The experimental investigation of CP violation in the B_s^0 sector is still at a relatively early stage, and far fewer modes have been studied than in the B^0 system. First results on the $\bar{b} \rightarrow \bar{q}q\bar{s}$ decays $B_s^0 \rightarrow \phi\phi$, K^+K^- and $K^{*0}\bar{K}^{*0}$ have been reported. More channels are expected to be studied in the near future.

13.6.4 Direct CP violation in the B system

An interesting class of decay modes is that of the tree-level decays $B^\pm \rightarrow D^{(*)}K^\pm$. These decays provide golden methods for a clean determination of the angle γ [101–106]. The method uses the decays $B^+ \rightarrow D^0K^+$, which proceeds via the quark transition $\bar{b} \rightarrow \bar{u}\bar{c}\bar{s}$, and $B^+ \rightarrow \bar{D}^0K^+$, which proceeds via the quark transition $\bar{b} \rightarrow \bar{c}\bar{u}\bar{s}$, with the D^0 and \bar{D}^0 decaying into a common final state. The decays into common final states, such as $(\pi^0 K_S)DK^+$, involve interference effects between the two amplitudes, with sensitivity to the relative phase, $\delta + \gamma$ (δ is the relevant strong phase difference). The CP -conjugate processes are sensitive to $\delta - \gamma$. Measurements of branching ratios and CP asymmetries allow the determination of γ and δ from amplitude triangle relations. The method suffers from discrete ambiguities but, since all hadronic parameters can be determined from the data, has negligible theoretical uncertainty [107].

Unfortunately, the smallness of the CKM-suppressed $b \rightarrow u$ transitions makes it difficult to use the simplest methods alone [101–103] to determine γ . These difficulties are overcome (and the discrete ambiguities are removed) by performing a Dalitz plot analysis for multi-body D decays [104–106]. Detailed discussion of the determination of γ with these methods can be found in Ref. [36].

Constraints on γ from combinations of results on various $B \rightarrow D^{(*)}K^{(*)}$ processes have been obtained by experiments [108, 109]. The latest world average is [29]:

$$\gamma = (71.1_{-5.3}^{+4.6})^\circ. \quad (13.106)$$

The consistency between the range of γ determined by the $B \rightarrow DK$ measurements and the range allowed by CKM fits (excluding these direct determinations) provides further support to the Kobayashi-Maskawa mechanism. As more data become available, determinations of γ from $B_s^0 \rightarrow D_s^\mp K^\pm$ [110, 111] and $B^0 \rightarrow DK^{*0}$ [112–115] are expected to also give competitive measurements.

Decays to the final state $K^\mp\pi^\pm$ provided the first observations of direct CP violation in both B^0 and B_s^0 systems. The asymmetry arises due to interference between tree and penguin diagrams [116], similar to the effect discussed in Section 13.6.2. In principle, measurements of $\mathcal{A}_{\bar{B}^0 \rightarrow K^-\pi^+}$ and $\mathcal{A}_{B^0 \rightarrow K^+\pi^-}$ could be used to determine the weak phase difference γ , but lack of knowledge of the relative magnitude and strong phase of the contributing amplitudes limits the achievable precision. The uncertainties on these hadronic parameters can be reduced by exploiting flavor symmetries, which predict a number of relations between asymmetries in different modes. One such relation is that the partial rate differences for B^0 and B_s^0 decays to $K^\mp\pi^\pm$ are expected to be approximately equal and opposite [117], which is consistent with current data. It is also expected that the partial rate asymmetries for $\bar{B}^0 \rightarrow K^-\pi^+$ and $B^- \rightarrow K^-\pi^0$ should be approximately equal; however, the experimental results currently show a significant discrepancy [29]:

$$\mathcal{A}_{\bar{B}^0 \rightarrow K^-\pi^+} = -0.084 \pm 0.004, \quad \mathcal{A}_{B^- \rightarrow K^-\pi^0} = +0.040 \pm 0.021. \quad (13.107)$$

It is therefore of great interest to understand whether this originates from Standard Model QCD corrections, or whether it is a signature of new dynamics. Improved tests of a more precise relation between the partial rate differences of all four $K\pi$ final states [118–121], currently limited by knowledge of the CP asymmetry in $\bar{B}^0 \rightarrow K_S\pi^0$ decays, may help to resolve the situation.

It is also of interest to investigate whether similar patterns appear among the CP violating asymmetries in B meson decays to final states containing one pseudoscalar and one vector meson. Since the vector resonance decays to two particles, such channels can be studied through Dalitz plot analysis of the three-body final state. Model-independent analyses of $B^+ \rightarrow K^+K^-K^+$, $\pi^+\pi^-K^+$, $\pi^+\pi^-K^+$ and $K^+K^-\pi^+$ decays have revealed large CP violation effects in certain regions of phase space [122]. For the $B^+ \rightarrow K^+K^-\pi^+$ decay, an amplitude analysis has established a large CP violation effect associated with $\pi\pi \leftrightarrow KK$ S-wave rescattering [123]. For the other channels it remains to be seen whether the CP violation effects are associated to particular resonances or to interference effects, which will be necessary to understand the underlying dynamics.

13.7 Summary and Outlook

CP violation has been experimentally established in K , D and B meson decays. A full list of CP asymmetries that have been measured at a level higher than 5σ is given in the introduction to this review. In Section 13.1.4 we introduced three types of CP -violating effects. Examples of these three types include the following:

1. All three types of CP violation have been observed in $K \rightarrow \pi\pi$

decays:

$$\begin{aligned} \mathcal{R}e(\epsilon') &= \frac{1}{6} \left(\left| \frac{\bar{A}_{\pi^0\pi^0}}{A_{\pi^0\pi^0}} \right| - \left| \frac{\bar{A}_{\pi^+\pi^-}}{A_{\pi^+\pi^-}} \right| \right) \\ &= (2.5 \pm 0.4) \times 10^{-6}, \quad (\text{I}) \quad (13.108a) \end{aligned}$$

$$\begin{aligned} \mathcal{R}e(\epsilon) &= \frac{1}{2} \left(1 - \left| \frac{q}{p} \right| \right) \\ &= (1.66 \pm 0.02) \times 10^{-3}, \quad (\text{II}) \quad (13.108b) \end{aligned}$$

$$\begin{aligned} \mathcal{I}m(\epsilon) &= -\frac{1}{2} \mathcal{I}m(\lambda_{(\pi\pi)_{I=0}}) \\ &= (1.57 \pm 0.02) \times 10^{-3}. \quad (\text{III}) \quad (13.108c) \end{aligned}$$

2. For D mesons, CP violation in decay has been established in the difference of asymmetries for $D^0 \rightarrow K^+K^-$ and $D^0 \rightarrow \pi^+\pi^-$ decays.

$$\begin{aligned} \Delta a_{CP} &= \frac{|\bar{A}_{K^+K^-}/A_{K^+K^-}|^2 - 1}{|\bar{A}_{K^+K^-}/A_{K^+K^-}|^2 + 1} - \frac{|\bar{A}_{\pi^+\pi^-}/A_{\pi^+\pi^-}|^2 - 1}{|\bar{A}_{\pi^+\pi^-}/A_{\pi^+\pi^-}|^2 + 1} \\ &= (-0.164 \pm 0.028) \times 10^{-3}, \quad (\text{I}) \quad (13.109) \end{aligned}$$

3. In the B meson system, CP violation in decay has been observed in, for example, $B^0 \rightarrow K^+\pi^-$ transitions, while CP violation in interference of decays with and without mixing has been observed in, for example, the $B^0 \rightarrow J/\psi K_S$ channel:

$$\begin{aligned} \mathcal{A}_{K^+\pi^-} &= \frac{|\bar{A}_{K^-\pi^-}/A_{K^+\pi^-}|^2 - 1}{|\bar{A}_{K^-\pi^-}/A_{K^+\pi^-}|^2 + 1} \\ &= -0.084 \pm 0.004, \quad (\text{I}) \quad (13.110a) \end{aligned}$$

$$\begin{aligned} S_{\psi K} &= \mathcal{I}m(\lambda_{\psi K}) \\ &= +0.699 \pm 0.017. \quad (\text{III}) \quad (13.110b) \end{aligned}$$

Based on Standard Model predictions, further observations of CP violation in B^0 , B^+ and B_s^0 decays seem likely in the near future, at both LHCb and its upgrades [124–126] as well as the Belle II experiment [127]. The first observation of CP violation in b baryons is also likely to be within reach of LHCb. Further improvements in the sensitivity to CP violation effects in the charm sector can also be anticipated, though uncertainty in the Standard Model predictions makes it difficult to forecast whether or not additional discoveries will be forthcoming. A number of upcoming experiments have potential to make significant progress on rare kaon decays. Observables that are subject to clean theoretical interpretation, such as β from $S_{\psi K_S}$, β_s from $B_s^0 \rightarrow J/\psi\phi$, $\mathcal{B}(K_L \rightarrow \pi^0\nu\bar{\nu})$ and γ from CP violation in $B \rightarrow DK$ decays, are of particular value for constraining the values of the CKM parameters and probing the flavor sector of extensions to the Standard Model. Progress in lattice QCD calculations is also needed to complement the anticipated experimental results. Other probes of CP violation now being pursued experimentally include the electric dipole moments of the neutron and electron, and the decays of tau leptons. Additional processes that are likely to play an important role in future CP studies include top-quark production and decay, Higgs boson decays and neutrino oscillations.

All measurements of CP violation to date are consistent with the predictions of the Kobayashi-Maskawa mechanism of the Standard Model. In fact, it is now established that the KM mechanism plays a major role in the CP violation measured in the quark sector. However, a dynamically-generated matter-antimatter asymmetry of the universe requires additional sources of CP violation, and such sources are naturally generated by extensions to the Standard Model. New sources might eventually reveal themselves as small deviations from the predictions of the KM mechanism, or else might not be observable in the quark sector at all, but observable with future probes such as neutrino oscillations or electric dipole moments. The fundamental nature of CP violation demands a vigorous search.

A number of excellent reviews of CP violation are available [128–135], where the interested reader may find a detailed discussion of the various topics that are briefly reviewed here.

We thank David Kirkby for significant contributions to earlier versions of this review.

References

- [1] J. H. Christenson *et al.*, Phys. Rev. Lett. **13**, 138 (1964).
- [2] B. Aubert *et al.* (BaBar), Phys. Rev. Lett. **87**, 091801 (2001), [hep-ex/0107013].
- [3] K. Abe *et al.* (Belle), Phys. Rev. Lett. **87**, 091802 (2001), [hep-ex/0107061].
- [4] H. Burkhardt *et al.* (NA31), Phys. Lett. **B206**, 169 (1988).
- [5] V. Fanti *et al.* (NA48), Phys. Lett. **B465**, 335 (1999), [hep-ex/9909022].
- [6] A. Alavi-Harati *et al.* (KTeV), Phys. Rev. Lett. **83**, 22 (1999), [hep-ex/9905060].
- [7] B. Aubert *et al.* (BaBar), Phys. Rev. Lett. **93**, 131801 (2004), [hep-ex/0407057].
- [8] Y. Chao *et al.* (Belle), Phys. Rev. Lett. **93**, 191802 (2004), [hep-ex/0408100].
- [9] A. Poluektov *et al.* (Belle), Phys. Rev. **D81**, 112002 (2010), [arXiv:1003.3360].
- [10] P. del Amo Sanchez *et al.* (BaBar), Phys. Rev. **D82**, 072004 (2010), [arXiv:1007.0504].
- [11] R. Aaij *et al.* (LHCb), Phys. Lett. **B712**, 203 (2012), [Erratum: Phys. Lett. **B713**, 351 (2012)], [arXiv:1203.3662].
- [12] R. Aaij *et al.* (LHCb), Phys. Rev. Lett. **110**, 22, 221601 (2013), [arXiv:1304.6173].
- [13] R. Aaij *et al.* (LHCb), Phys. Rev. Lett. **122**, 21, 211803 (2019), [arXiv:1903.08726].
- [14] See results on the “Time reversal invariance,” within the review on “Tests of Conservation Laws,” in this *Review*.
- [15] J. Bernabeu, F. Martinez-Vidal and P. Villanueva-Perez, JHEP **08**, 064 (2012), [arXiv:1203.0171].
- [16] J. P. Lees *et al.* (BaBar), Phys. Rev. Lett. **109**, 211801 (2012), [arXiv:1207.5832].
- [17] See, for example, R. F. Streater and A. S. Wightman, *CPT, Spin and Statistics, and All That*, reprinted by Addison-Wesley, New York (1989).
- [18] M. Kobayashi and T. Maskawa, Prog. Theor. Phys. **49**, 652 (1973).
- [19] J. Charles *et al.* (CKMfitter Group), Eur. Phys. J. **C41**, 1, 1 (2005), updated results and plots available at: <http://ckmfitter.in2p3.fr>, [hep-ph/0406184].
- [20] M. Bona *et al.* (UTfit), JHEP **10**, 081 (2006), updated results and plots available at: <http://www.utfit.org/UTfit>, [hep-ph/0606167].
- [21] A. D. Sakharov, Pisma Zh. Eksp. Teor. Fiz. **5**, 32 (1967), [Usp. Fiz. Nauk **161**, no.5, 61 (1991)].
- [22] A. Riotto, in “Proceedings, Summer School in High-energy physics and cosmology: Trieste, Italy, June 29–July 17, 1998,” 326–436 (1998), [hep-ph/9807454].
- [23] M. Fukugita and T. Yanagida, Phys. Lett. **B174**, 45 (1986).
- [24] S. Davidson, E. Nardi and Y. Nir, Phys. Rept. **466**, 105 (2008), [arXiv:0802.2962].
- [25] G. Aad *et al.* (ATLAS), Phys. Lett. **B716**, 1 (2012), [arXiv:1207.7214].
- [26] S. Chatrchyan *et al.* (CMS), Phys. Lett. **B716**, 30 (2012), [arXiv:1207.7235].
- [27] See the K -meson Listings in this *Review*.
- [28] See the B -meson Listings in this *Review*.
- [29] Y. Amhis *et al.* (HFLAV), Eur. Phys. J. **C77**, 12, 895 (2017), [arXiv:1612.07233].
- [30] V. Weisskopf and E. P. Wigner, Z. Phys. **63**, 54 (1930).
- [31] See the review on “ $D^0 - \bar{D}^0$ Mixing” in this *Review*.
- [32] O. Long *et al.*, Phys. Rev. **D68**, 034010 (2003), [hep-ex/0303030].

- [33] M. Gronau, Y. Grossman and J. L. Rosner, Phys. Lett. **B508**, 37 (2001), [hep-ph/0103110].
- [34] M. Artuso, G. Borissov and A. Lenz, Rev. Mod. Phys. **88**, 4, 045002 (2016), [arXiv:1511.09466].
- [35] L. Wolfenstein, Phys. Rev. Lett. **13**, 562 (1964).
- [36] See the review on “Cabibbo-Kobayashi-Maskawa Mixing Matrix,” in this *Review*.
- [37] L. Wolfenstein, Phys. Rev. Lett. **51**, 1945 (1983).
- [38] A. J. Buras, M. E. Lautenbacher and G. Ostermaier, Phys. Rev. **D50**, 3433 (1994), [hep-ph/9403384].
- [39] C. Jarlskog, Phys. Rev. Lett. **55**, 1039 (1985).
- [40] See the review on “CP violation in $K_S \rightarrow 3\pi$,” in this *Review*.
- [41] T. Blum *et al.*, Phys. Rev. **D91**, 7, 074502 (2015), [arXiv:1502.00263].
- [42] Z. Bai *et al.* (RBC, UKQCD), Phys. Rev. Lett. **115**, 21, 212001 (2015), [arXiv:1505.07863].
- [43] A. J. Buras *et al.*, JHEP **11**, 202 (2015), [arXiv:1507.06345].
- [44] Y. Grossman and Y. Nir, Phys. Lett. **B398**, 163 (1997), [hep-ph/9701313].
- [45] L. S. Littenberg, Phys. Rev. **D39**, 3322 (1989).
- [46] A. J. Buras, Phys. Lett. **B333**, 476 (1994), [hep-ph/9405368].
- [47] G. Buchalla and A. J. Buras, Nucl. Phys. **B400**, 225 (1993).
- [48] A. J. Buras *et al.*, JHEP **11**, 033 (2015), [arXiv:1503.02693].
- [49] J. K. Ahn *et al.* (KOTO), Phys. Rev. Lett. **122**, 2, 021802 (2019), [arXiv:1810.09655].
- [50] T. Yamanaka (KOTO), PTEP **2012**, 02B006 (2012).
- [51] M. Mirra [NA62 Collab.], Nuovo Cimento **C038**, 13 (2015).
- [52] B. Aubert *et al.* (BaBar), Phys. Rev. Lett. **98**, 211802 (2007), [hep-ex/0703020].
- [53] M. Staric *et al.* (BELLE), Phys. Rev. Lett. **98**, 211803 (2007), [65(2007)], [hep-ex/0703036].
- [54] T. Aaltonen *et al.* (CDF), Phys. Rev. Lett. **100**, 121802 (2008), [arXiv:0712.1567].
- [55] R. Aaij *et al.* (LHCb), Phys. Rev. Lett. **110**, 10, 101802 (2013), [arXiv:1211.1230].
- [56] See the *D*-meson Listings in this *Review*.
- [57] Y. Grossman, A. L. Kagan and Y. Nir, Phys. Rev. **D75**, 036008 (2007), [hep-ph/0609178].
- [58] S. Bergmann *et al.*, Phys. Lett. **B486**, 418 (2000), [hep-ph/0005181].
- [59] M. Gersabeck *et al.*, J. Phys. **G39**, 045005 (2012), [arXiv:1111.6515].
- [60] D. M. Asner *et al.* (CLEO), Phys. Rev. **D78**, 012001 (2008), [arXiv:0802.2268].
- [61] M. Ablikim *et al.* (BESIII), Phys. Lett. **B734**, 227 (2014), [arXiv:1404.4691].
- [62] R. Aaij *et al.* (LHCb), Phys. Rev. Lett. **111**, 25, 251801 (2013), [arXiv:1309.6534].
- [63] R. Aaij *et al.* (LHCb), Phys. Rev. Lett. **118**, 26, 261803 (2017), [arXiv:1702.06490].
- [64] M. Ciuchini *et al.*, Phys. Lett. **B655**, 162 (2007), [hep-ph/0703204].
- [65] Y. Grossman, Y. Nir and G. Perez, Phys. Rev. Lett. **103**, 071602 (2009), [arXiv:0904.0305].
- [66] A. L. Kagan and M. D. Sokoloff, Phys. Rev. **D80**, 076008 (2009), [arXiv:0907.3917].
- [67] Y. Grossman and Y. Nir, JHEP **04**, 002 (2012), [arXiv:1110.3790].
- [68] B. R. Ko *et al.* (Belle), Phys. Rev. Lett. **109**, 021601 (2012), [Erratum: Phys. Rev. Lett.109,119903(2012)], [arXiv:1203.6409].
- [69] See the “Review of Multibody Charm Analyses” in this *Review*.
- [70] B. Aubert *et al.* (BaBar), Phys. Rev. **D78**, 051102 (2008), [arXiv:0802.4035].
- [71] I. Bediaga *et al.*, Phys. Rev. **D80**, 096006 (2009), [arXiv:0905.4233].
- [72] I. Bediaga *et al.*, Phys. Rev. **D86**, 036005 (2012), [arXiv:1205.3036].
- [73] M. Williams, Phys. Rev. **D84**, 054015 (2011), [arXiv:1105.5338].
- [74] R. Aaij *et al.* (LHCb), Phys. Lett. **B769**, 345 (2017), [arXiv:1612.03207].
- [75] V. M. Abazov *et al.* (D0), Phys. Rev. **D82**, 032001 (2010), [arXiv:1005.2757].
- [76] A. B. Carter and A. I. Sanda, Phys. Rev. Lett. **45**, 952 (1980).
- [77] A. B. Carter and A. I. Sanda, Phys. Rev. **D23**, 1567 (1981).
- [78] I. I. Y. Bigi and A. I. Sanda, Nucl. Phys. **B193**, 85 (1981).
- [79] I. Dunietz and J. L. Rosner, Phys. Rev. **D34**, 1404 (1986).
- [80] Y. I. Azimov, N. G. Uraltsev and V. A. Khoze, Sov. J. Nucl. Phys. **45**, 878 (1987), [Yad. Fiz.45,1412(1987)].
- [81] I. I. Y. Bigi and A. I. Sanda, Nucl. Phys. **B281**, 41 (1987).
- [82] G. Buchalla, A. J. Buras and M. E. Lautenbacher, Rev. Mod. Phys. **68**, 1125 (1996), [hep-ph/9512380].
- [83] R. Fleischer, Eur. Phys. J. **C10**, 299 (1999), [hep-ph/9903455].
- [84] M. Ciuchini, M. Pierini and L. Silvestrini, Phys. Rev. Lett. **95**, 221804 (2005), [hep-ph/0507290].
- [85] S. Faller *et al.*, Phys. Rev. **D79**, 014030 (2009), [arXiv:0809.0842].
- [86] M. Jung, Phys. Rev. **D86**, 053008 (2012), [arXiv:1206.2050].
- [87] H.-n. Li and S. Mishima, JHEP **03**, 009 (2007), [hep-ph/0610120].
- [88] K. De Bruyn and R. Fleischer, JHEP **03**, 145 (2015), [arXiv:1412.6834].
- [89] P. Frings, U. Nierste and M. Wiebusch, Phys. Rev. Lett. **115**, 6, 061802 (2015), [arXiv:1503.00859].
- [90] L. Silvestrini, Ann. Rev. Nucl. Part. Sci. **57**, 405 (2007), [arXiv:0705.1624].
- [91] R. Fleischer *et al.*, Phys. Rev. **D78**, 111501 (2008), [arXiv:0806.2900].
- [92] R. Fleischer *et al.*, Eur. Phys. J. **C78**, 11, 943 (2018), [arXiv:1806.08783].
- [93] M. Gronau and D. London, Phys. Rev. Lett. **65**, 3381 (1990).
- [94] A. F. Falk *et al.*, Phys. Rev. **D69**, 011502 (2004), [hep-ph/0310242].
- [95] R. Aaij *et al.* (LHCb), Phys. Lett. **B747**, 468 (2015), [arXiv:1503.07770].
- [96] J. Charles *et al.*, Eur. Phys. J. **C77**, 8, 574 (2017), [arXiv:1705.02981].
- [97] A. Abdesselam *et al.* (BaBar, Belle), Phys. Rev. Lett. **115**, 12, 121604 (2015), [arXiv:1505.04147].
- [98] R. Fleischer and R. Knegjens, Eur. Phys. J. **C71**, 1789 (2011), [arXiv:1109.5115].
- [99] A. S. Dighe, I. Dunietz and R. Fleischer, Eur. Phys. J. **C6**, 647 (1999), [hep-ph/9804253].
- [100] R. Aaij *et al.* (LHCb), Phys. Rev. **D89**, 9, 092006 (2014), [arXiv:1402.6248].
- [101] M. Gronau and D. London, Phys. Lett. **B253**, 483 (1991).
- [102] M. Gronau and D. Wyler, Phys. Lett. **B265**, 172 (1991).
- [103] D. Atwood, I. Dunietz and A. Soni, Phys. Rev. Lett. **78**, 3257 (1997), [hep-ph/9612433].

- [104] D. Atwood, I. Dunietz and A. Soni, Phys. Rev. **D63**, 036005 (2001), [hep-ph/0008090].
- [105] A. Giri *et al.*, Phys. Rev. **D68**, 054018 (2003), [hep-ph/0303187].
- [106] A. Bondar, *Proceedings of BINP special analysis meeting on Dalitz analysis*, 24-26 Sep. 2002, unpublished.
- [107] J. Brod and J. Zupan, JHEP **01**, 051 (2014), [arXiv:1308.5663].
- [108] J. P. Lees *et al.* (BaBar), Phys. Rev. **D87**, 5, 052015 (2013), [arXiv:1301.1029].
- [109] R. Aaij *et al.* (LHCb), JHEP **12**, 087 (2016), [arXiv:1611.03076].
- [110] R. Aleksan, I. Dunietz and B. Kayser, Z. Phys. **C54**, 653 (1992).
- [111] R. Fleischer, Nucl. Phys. **B671**, 459 (2003), [hep-ph/0304027].
- [112] I. Dunietz, Phys. Lett. **B270**, 75 (1991).
- [113] M. Gronau, Phys. Lett. **B557**, 198 (2003), [hep-ph/0211282].
- [114] T. Gershon, Phys. Rev. **D79**, 051301 (2009), [arXiv:0810.2706].
- [115] T. Gershon and M. Williams, Phys. Rev. **D80**, 092002 (2009), [arXiv:0909.1495].
- [116] M. Bander, D. Silverman and A. Soni, Phys. Rev. Lett. **43**, 242 (1979).
- [117] X.-G. He, Eur. Phys. J. **C9**, 443 (1999), [hep-ph/9810397].
- [118] D. Atwood and A. Soni, Phys. Rev. **D58**, 036005 (1998), [hep-ph/9712287].
- [119] M. Gronau and J. L. Rosner, Phys. Rev. **D59**, 113002 (1999), [hep-ph/9809384].
- [120] H. J. Lipkin, Phys. Lett. **B445**, 403 (1999), [hep-ph/9810351].
- [121] M. Gronau, Phys. Lett. **B627**, 82 (2005), [hep-ph/0508047].
- [122] R. Aaij *et al.* (LHCb), Phys. Rev. **D90**, 11, 112004 (2014), [arXiv:1408.5373].
- [123] R. Aaij *et al.* (LHCb) (2019), [arXiv:1905.09244].
- [124] A. A. Alves, Jr. *et al.* (LHCb), JINST **3**, S08005 (2008).
- [125] I. Bediaga *et al.* (LHCb) (2012).
- [126] R. Aaij *et al.* [LHCb Collab.], CERN-LHCC-2017-003.
- [127] T. Aushev *et al.* (2010), [arXiv:1002.5012].
- [128] G. C. Branco, L. Lavoura and J. P. Silva, Int. Ser. Monogr. Phys. **103**, 1 (1999).
- [129] I. I. Bigi and A. I. Sanda (2000), [Camb. Monogr. Part. Phys. Nucl. Phys. Cosmol.9,1(2009)].
- [130] A. J. Bevan *et al.* (BaBar, Belle), Eur. Phys. J. **C74**, 3026 (2014), [arXiv:1406.6311].
- [131] H.R. Quinn and Y. Nir, “*The Mystery of the Missing Antimatter*,” Princeton University Press, Princeton (2008).
- [132] T. E. Browder *et al.*, Rev. Mod. Phys. **81**, 1887 (2009), [arXiv:0802.3201].
- [133] M. Ciuchini and A. Stocchi, Ann. Rev. Nucl. Part. Sci. **61**, 491 (2011), [arXiv:1110.3920].
- [134] R. Aaij *et al.* (LHCb), Eur. Phys. J. **C73**, 4, 2373 (2013), [arXiv:1208.3355].
- [135] T. Gershon and V. V. Gligorov, Rept. Prog. Phys. **80**, 4, 046201 (2017), [arXiv:1607.06746].

14. Neutrino Masses, Mixing, and Oscillations

Written August 2019 by M.C. Gonzalez-Garcia (YITP, Stony Brook; ICREA, Barcelona; ICC, U. of Barcelona) and M. Yokoyama (Tokyo U.; Kavli IPMU (WPI), U. Tokyo).

14.1	Neutrinos in the Standard Model: Massless Neutrinos	285
14.2	Extending the Standard Model to Introduce Massive Neutrinos	285
14.2.1	Dirac Neutrinos	286
14.2.2	The See-saw Mechanism	286
14.2.3	Light Sterile Neutrinos	287
14.2.4	Neutrino Masses from Generic New Physics	287
14.3	Lepton Mixing	287
14.4	Mass-Induced Flavour Oscillations in Vacuum	288
14.5	Propagation of Massive Neutrinos in Matter	289
14.5.1	The Mikheev-Smirnov-Wolfenstein Effect for Solar Neutrinos	291
14.6	Experimental Study of Neutrino Oscillations	291
14.6.1	Solar Neutrinos	291
14.6.2	Atmospheric Neutrinos	293
14.6.3	Accelerator Neutrinos	294
14.6.4	Reactor Antineutrinos	297
14.7	Combined Analysis of Experimental Results: The 3ν Paradigm	300
14.7.1	3ν Oscillation Probabilities	301
14.7.2	3ν Oscillation Analysis	302
14.7.3	Convention-independent Measures of Leptonic CP Violation in 3ν Mixing	302
14.8	Beyond 3ν : Additional Neutrinos at the eV Scale	304
14.9	Laboratory Probes of ν Mass Scale and its Nature	305
14.9.1	Constraints from Kinematics of Weak Decays	305
14.9.2	Dirac vs Majorana: Neutrinoless Double-beta Decay	306
14.9.3	Experimental Search for Neutrinoless Double-beta Decay	307

14.1 Neutrinos in the Standard Model: Massless Neutrinos

The gauge symmetry principle is one of the pillars of the great success of modern particle physics as it establishes an unambiguous connection between local (gauge) symmetries and forces mediated by spin-1 particles. In the Standard Model (SM) of particle physics the strong, weak, and electromagnetic interactions are connected to gauge symmetry under $SU(3)_C \times SU(2)_L \times U(1)_Y$ where C stands for colour, L for left-handedness, and Y for hypercharge. The SM gauge symmetry is spontaneously broken to $SU(3)_C \times U(1)_{EM}$ where $U(1)_{EM}$ couples to the electromagnetic charge $Q_{EM} = T_{L3} + Y$ (T_{L3} is the weak isospin which is the third generator of $SU(2)_L$). The model explains all the interactions of the known fermions once they are assigned to well defined representation of the gauge group. The construction and tests of the Standard Model as a gauge theory are covered in the review sections on “Quantum chromodynamics” and “Electroweak model and constraints on new physics” respectively. In here we emphasize that the gauge invariance principle requires that all terms in the Lagrangian, including the mass terms, respect the local symmetry. This has important implications for the neutrino and in particular for the question of the neutrino mass ¹.

In the SM, neutrinos are fermions that do not have strong nor electromagnetic interactions. Consequently they are singlets of the subgroup $SU(3)_C \times U(1)_{EM}$. They are part of the lepton doublets $L_{L\ell} = \begin{pmatrix} \nu_\ell \\ \ell \end{pmatrix}_L$ where f_L is the left-handed component of the fermion f , $f_L = P_L f \equiv \frac{1-\gamma_5}{2} f$. In what follows we will refer as *active* neutrinos to neutrinos that are part of these lepton doublets. In the SM there is one active neutrino for each charged

leptons, $\ell = e, \mu, \tau$. $SU(2)_L$ gauge invariance dictates the form of weak charged current (CC) interactions between the neutrinos and their corresponding charged leptons and neutral current (NC) among themselves to be:

$$-\mathcal{L}_{CC} = \frac{g}{\sqrt{2}} \sum_{\ell} \bar{\nu}_{L\ell} \gamma^\mu \ell_L^- W_\mu^+ + \text{h.c.}, \quad (14.1)$$

$$-\mathcal{L}_{NC} = \frac{g}{2 \cos \theta_W} \sum_{\ell} \bar{\nu}_{L\ell} \gamma^\mu \nu_{L\ell} Z_\mu^0. \quad (14.2)$$

In the above equations g is the coupling constant associated to $SU(2)$ and θ_W is the Weinberg angle.

Equations(14.1) and (14.2) describe all the neutrino interactions in the SM. In particular, Eq.(14.2) determines the decay width of the Z^0 boson into light ($m_\nu \leq m_{Z^0}/2$) left-handed neutrinos states. Thus from the measurement of the total decay width of the Z^0 one can infer the number of such states. At present the measurement implies $N_\nu = 2.984 \pm 0.008$ (see Particle Listing). As a result any extension of the SM should contain three, and only three, light active neutrinos.

Sterile neutrinos are defined as having no SM gauge interactions, that is, they are singlets of the complete SM gauge group. Thus the SM, as the gauge theory able to describe all known particle interactions, contains no sterile neutrinos.

The SM with its gauge symmetry and the particle content required for the gauge interactions, that is, in the absence of SM singlets, respects an accidental global symmetry which is not imposed but appears as consequence of the gauge symmetry and the representation of the matter fields:

$$G_{SM}^{\text{global}} = U(1)_B \times U(1)_{L_e} \times U(1)_{L_\mu} \times U(1)_{L_\tau}, \quad (14.3)$$

where $U(1)_B$ is the baryon number symmetry, and $U(1)_{L_e, L_\mu, L_\tau}$ are the three lepton flavour symmetries. The total lepton number, $L_e + L_\mu + L_\tau$, is then also an accidental symmetry since is a subgroup of G_{SM}^{global} . This fact has consequences which are relevant to the question of the neutrino mass as we argue next.

In the SM, the masses of the fermions are generated via a Yukawa coupling of the scalar Higgs doublet ϕ with a fermion right-handed and left-handed component. The former is an $SU(2)_L$ singlet, the latter is part of a doublet. For leptons, we can one can build such term coupling the left-handed lepton doublets L_L with the right-handed charged lepton fields E_R :

$$-\mathcal{L}_{\text{Yukawa,lep}} = Y_{ij}^\ell \bar{L}_{Li} \phi E_{Rj} + \text{h.c.} \quad (14.4)$$

After spontaneous symmetry breaking these terms lead to charged lepton masses

$$m_{ij}^\ell = Y_{ij}^\ell \frac{v}{\sqrt{2}}, \quad (14.5)$$

where v is the vacuum expectation value of the Higgs field. However, since the model does not contain right-handed neutrinos, no such Yukawa interaction can be built for the neutrinos, which are consequently massless at the Lagrangian level.

In principle, a neutrino mass term could be generated at loop level. With the particle content of the SM the only possible neutrino mass term that could be constructed is the bilinear $\bar{L}_L L_L^c$, where L_L^c is the charge conjugated field, $L_L^c = C \bar{L}_L^T$ and C is the charge conjugation matrix. However this term is forbidden in the SM because it violates the total lepton symmetry by two units and therefore it cannot be induced by loop corrections because it breaks the accidental symmetry of the model. Also, because $U(1)_{B-L}$ is a non-anomalous subgroup of G_{SM}^{global} , the bilinear $\bar{L}_L L_L^c$, cannot be induced by nonperturbative corrections either since it breaks $B - L$.

We conclude that within the SM neutrinos are precisely massless. Consequently one must go beyond the SM in order to add a mass to the neutrino.

14.2 Extending the Standard Model to Introduce Massive Neutrinos

From the above discussion we conclude that it is not possible to construct a renormalizable mass term for the neutrinos with the

¹The physics of massive neutrinos has been the subject of excellent books such as [1–5] and multiple review articles. The contents of the present review is built upon the structure and the contents of the review articles [6, 7].

fermionic content and gauge symmetry of the SM. The obvious consequence is that in order to introduce a neutrino mass in the theory one must extend the particle content of the model, depart from gauge invariance and/or renormalizability, or do both.

As a matter of fact, neutrino mass terms can be constructed in different ways. In the following we shall assume to maintain the gauge symmetry and explore the different possibilities to introduce a neutrino mass term adding to the SM an arbitrary number of sterile neutrinos ν_{si} ($i = 1, \dots, m$).

In the SM extended with the addition of m number of sterile neutrinos one can construct two gauge invariant renormalizable operators leading to two type of mass terms

$$-\mathcal{L}_{M_\nu} = M_{Dij} \bar{\nu}_{si} \nu_{Lj} + \frac{1}{2} M_{Nij} \bar{\nu}_{si} \nu_{sj}^c + \text{h.c.}, \quad (14.6)$$

where ν^c is the neutrino charge conjugated field (defined in section 14.1). M_D is a complex matrix of dimension $m \times 3$ and M_N is a symmetric $m \times m$ matrix.

The first term is generated after spontaneous electroweak symmetry breaking from Yukawa interactions,

$$Y_{ij}^\nu \bar{\nu}_{si} \tilde{\phi}^\dagger L_{Lj} \Rightarrow M_{Dij} = Y_{ij}^\nu \frac{v}{\sqrt{2}}, \quad (14.7)$$

in similarity to Eqs.(14.4) and (14.5) for the charged fermion masses. It is correspondingly called a Dirac mass term. It conserves total lepton number but it can break the lepton flavour number symmetries.

The second term in Eq.(14.6) is a Majorana mass term and it differs from the Dirac mass terms in several relevant aspects. First, it is a singlet of the SM gauge group and, as such, it can appear as a bare mass term in the Lagrangian. Second, since it involves two neutrino fields (right-handed in this case), it breaks lepton number by two units. In general such a term is not allowed if the neutrinos carry any additive conserved charge.

It is possible to rewrite Eq.(14.6) as:

$$-\mathcal{L}_{M_\nu} = \frac{1}{2} (\bar{\nu}_L^c, \bar{\nu}_s^c) \begin{pmatrix} 0 & M_D^T \\ M_D & M_N \end{pmatrix} \begin{pmatrix} \bar{\nu}_L \\ \bar{\nu}_s^c \end{pmatrix} + \text{h.c.} \equiv \bar{\nu}^c M_\nu \bar{\nu} + \text{h.c.}, \quad (14.8)$$

where $\bar{\nu} = (\bar{\nu}_L, \bar{\nu}_s^c)^T$ is a $(3+m)$ -dimensional vector. The matrix M_ν is complex and symmetric². Thus it can be diagonalized by a unitary matrix V^ν of dimension $(3+m)$, so

$$(V^\nu)^T M_\nu V^\nu = \text{diag}(m_1, m_2, \dots, m_{3+m}). \quad (14.9)$$

One can express the original weak eigenstates in terms of the resulting $3+m$ mass eigenstates

$$\bar{\nu}_{\text{mass}} = (V^\nu)^\dagger \bar{\nu}, \quad (14.10)$$

and in terms of the mass eigenstates Eq.(14.8) takes the form:

$$\begin{aligned} -\mathcal{L}_{M_\nu} &= \frac{1}{2} \sum_{k=1}^{3+m} m_k (\bar{\nu}_{\text{mass},k}^c \nu_{\text{mass},k} + \bar{\nu}_{\text{mass},k} \nu_{\text{mass},k}^c) \\ &= \frac{1}{2} \sum_{k=1}^{3+m} m_k \bar{\nu}_{Mk} \nu_{Mk}, \end{aligned} \quad (14.11)$$

where

$$\nu_{Mk} = \nu_{\text{mass},k} + \nu_{\text{mass},k}^c = (V^\nu)^\dagger \bar{\nu}_k + (V^\nu)^\dagger \bar{\nu}_k^c. \quad (14.12)$$

So these states obey the Majorana condition

$$\nu_M = \nu_M^c, \quad (14.13)$$

and are referred to as Majorana neutrinos. The Majorana condition implies that only one field describes both neutrino and antineutrino states, unlike in the case of a charge for which particle

²Notice that Eq.(14.8) corresponds to the tree-level neutrino mass matrix. Corrections are induced at the loop level, which in particular lead to non-vanishing $\bar{\nu}_L^c \nu_L$ entry [8].

and antiparticle are described by two different fields. So a Majorana neutrino can be described by a two-component spinor unlike the charged fermions, which are Dirac particles, and are represented by four-component spinors.

Inverting Eq.(14.12) we can write the weak-doublet components of the neutrino fields as:

$$\nu_{Li} = P_L \sum_{j=1}^{3+m} V_{ij}^\nu \nu_{Mj} \quad i = 1, 2, 3, \quad (14.14)$$

where P_L is the left projector.

In what follows we will discuss some interesting particular cases of this general framework: light Dirac neutrinos in Sec.14.2.1, and light Majorana neutrinos and the see-saw mechanism in Sec.14.2.2. A special case of the second one is the possibility of light-sterile neutrinos discussed in Sec.14.2.3. In Sec.14.2.4 we shall discuss the effective generation of neutrino masses from non-renormalizable operators (of which the see-saw mechanism is a particular realization).

14.2.1 Dirac Neutrinos

Imposing $M_N = 0$ is equivalent to imposing lepton number symmetry on the model. Doing so only the first term in Eq.(14.6), the Dirac mass term, is allowed. If sterile neutrinos are three ($m = 3$), we can identify them with the right-handed component of a four-spinor neutrino field. In this case the Dirac mass term can be diagonalized with two 3×3 unitary matrices, V^ν and V_R^ν as:

$$V_R^{\nu\dagger} M_D V^\nu = \text{diag}(m_1, m_2, m_3). \quad (14.15)$$

The neutrino mass term can be written as:

$$-\mathcal{L}_{M_\nu} = \sum_{k=1}^3 m_k \bar{\nu}_{Dk} \nu_{Dk}, \quad (14.16)$$

where

$$\nu_{Dk} = (V^\nu)^\dagger \bar{\nu}_k + (V_R^{\nu\dagger}) \bar{\nu}_s^c, \quad (14.17)$$

so the weak-doublet components of the neutrino fields are

$$\nu_{Li} = P_L \sum_{j=1}^3 V_{ij}^\nu \nu_{Dj}. \quad i = 1, 2, 3. \quad (14.18)$$

Let's stress that in this case both the low energy matter content and the assumed symmetries are different from those of the SM. Consequently the SM is not even a good low-energy effective theory. Furthermore, this scenario does not explain the fact that neutrinos are much lighter than the corresponding charged fermions, because all acquire their mass via the same mechanism.

14.2.2 The See-saw Mechanism

If the mass eigenvalues of M_N are much higher than the scale of electroweak symmetry breaking v , the diagonalization of M_ν leads to three light neutrinos, ν_l , and m heavy neutrinos, N :

$$-\mathcal{L}_{M_\nu} = \frac{1}{2} \bar{\nu}_l M^l \nu_l + \frac{1}{2} \bar{N} M^h N, \quad (14.19)$$

with

$$M^l \simeq -V_l^T M_D^T M_N^{-1} M_D V_l, \quad M^h \simeq V_h^T M_N V_h, \quad (14.20)$$

and

$$V^\nu \simeq \begin{bmatrix} \left(1 - \frac{1}{2} M_D^\dagger M_N^* - 1 M_N^{-1} M_D\right) V_l & M_D^\dagger M_N^* V_h \\ -M_N^{-1} M_D V_l & \left(1 - \frac{1}{2} M_N^{-1} M_D M_D^\dagger M_N^* - 1\right) V_h \end{bmatrix}, \quad (14.21)$$

where V_l and V_h are 3×3 and $m \times m$ unitary matrices respectively. From Eq.(14.20) we see that the masses of the heavier states are proportional to M_N while those of the lighter ones to M_N^{-1} , hence the name of *see-saw mechanism* [9–13]. Also, as seen from Eq.(14.21), the heavy states are mostly right-handed while the light ones are mostly left-handed. Both the light and the heavy neutrinos are Majorana particles. Two well-known examples of extensions of the SM leading to a see-saw mechanism for neutrino masses are SO(10) Grand Unified Theories [10, 11] and left-right symmetry [13].

In this case the SM is a good effective low energy theory. Indeed the see-saw mechanism is a particular example of a full theory whose low energy effective realization is the SM with three light Majorana neutrinos which we describe in Sec.14.2.4.

14.2.3 Light Sterile Neutrinos

If the scale of some $n_s \leq m$ eigenvalues of M_N are not higher than the electroweak scale, the low energy spectrum contains n_s additional light states with large admixture of sterile component. As in the case with Dirac Neutrinos, the SM is not a good low energy effective theory: there are more than three ($3+n_s$) light neutrinos, and they are admixtures of doublet and singlet fields. As in the general case, both light and heavy neutrinos are Majorana particles.

14.2.4 Neutrino Masses from Generic New Physics

Under the generic hypothesis that new physics (NP) beyond the SM only manifests itself directly above some scale Λ_{NP} , we can consider that the SM is an effective low energy theory which is valid to describe the physical world at energies well below Λ_{NP} with the same gauge group, fermionic spectrum, and the pattern of spontaneous symmetry breaking of the SM. However, this is an effective theory, holding only till energy below Λ_{NP} , and consequently does not need to be renormalizable. In this case the low energy Lagrangian can contain non-renormalizable higher dimensional terms whose effect will be suppressed by powers $1/\Lambda_{\text{NP}}^{\text{dim}-4}$.

In this approach, the least suppressed NP effects at low energy are expected to come from $\text{dim}=5$ operators. With the SM fields an gauge symmetry one can only construct the following set of dimension-five terms

$$\mathcal{O}_5 = \frac{Z_{ij}^\nu}{\Lambda_{\text{NP}}} (\bar{L}_{Li} \tilde{\phi}) (\tilde{\phi}^T L_{Lj}^C) + \text{h.c.} \quad (14.22)$$

This set violates (14.3) which poses no problem since in general there is no reason for the NP to respect the accidental symmetries of the SM. In particular it violates total lepton number by two units and after spontaneous symmetry breaking it generates a bilinear neutrino field term:

$$-\mathcal{L}_{M_\nu} = \frac{Z_{ij}^\nu}{2} \frac{v^2}{\Lambda_{\text{NP}}} \bar{\nu}_{Li} \nu_{Lj}^c + \text{h.c.} \quad (14.23)$$

This is a Majorana mass term (see Eq.(14.8)). It is built with the left-handed neutrino fields and with mass matrix:

$$(M_\nu)_{ij} = Z_{ij}^\nu \frac{v^2}{\Lambda_{\text{NP}}}. \quad (14.24)$$

We conclude that Eq.(14.24) would arise in a generic extension of the SM and that neutrino masses are very likely to appear if there is NP. Comparing Eq.(14.24) and Eq.(14.5), we also find that the scale of neutrino masses is suppressed by v/Λ_{NP} when compared to the scale of charged fermion masses providing an explanation for their smallness. Furthermore, both total lepton number and the lepton flavour symmetry $U(1)_e \times U(1)_\mu \times U(1)_\tau$ are broken by Eq.(14.24) which means that, generically, in the absence of additional symmetries on the coefficients Z_{ij} , we can expect lepton flavour mixing and CP violation as we discuss in next section.

Finally, we notice that, as mentioned in Sec.14.2.2, a theory where the NP is composed of m heavy sterile neutrinos, provides an specific example of a theory which at low energy theory contains three light mass eigenstates with an effective dim-5 interaction of the form (14.22) with $\Lambda_{\text{NP}} = M_N$. This is, in this case the NP scale is the characteristic mass scale of the heavy sterile neutrinos.

14.3 Lepton Mixing

Let us start by considering $n = 3 + m$ massive neutrino states and denote the neutrino mass eigenstates by $(\nu_1, \nu_2, \nu_3, \dots, \nu_n)$. The neutrino interaction eigenstates are denoted by $\tilde{\nu} = (\nu_{Le}, \nu_{L\mu}, \nu_{L\tau}, \nu_{s1}, \dots, \nu_{sm})$. We label the corresponding mass and interaction eigenstates for the charged leptons as (e, μ, τ) and (e^I, μ^I, τ^I) respectively. The Lagrangian for the leptonic charged current interactions in the mass basis takes the form:

$$-\mathcal{L}_{\text{CC}} = \frac{g}{\sqrt{2}} (\bar{e}_L, \bar{\mu}_L, \bar{\tau}_L) \gamma^\mu U \begin{pmatrix} \nu_1 \\ \nu_2 \\ \nu_3 \\ \vdots \\ \nu_n \end{pmatrix} W_\mu^+ + \text{h.c.}, \quad (14.25)$$

where U is a $3 \times n$ matrix [14–16]. It satisfies the unitary condition

$$UU^\dagger = I_{3 \times 3}. \quad (14.26)$$

However, in general $U^\dagger U \neq I_{n \times n}$.

In the interaction basis, the mass terms for the leptons are:

$$-\mathcal{L}_M = [(\bar{e}_L^I, \bar{\mu}_L^I, \bar{\tau}_L^I) M_\ell \begin{pmatrix} e_R^I \\ \mu_R^I \\ \tau_R^I \end{pmatrix} + \text{h.c.}] - \mathcal{L}_{M_\nu}, \quad (14.27)$$

with \mathcal{L}_{M_ν} given in Eq.(14.8). M_ℓ can be diagonalize with two 3×3 unitary matrices V^ℓ and V_R^ℓ which satisfy

$$V^{\ell\dagger} M_\ell V_R^\ell = \text{diag}(m_e, m_\mu, m_\tau). \quad (14.28)$$

Then for the charged leptons we have

$$-\mathcal{L}_{M_\ell} = \sum_{k=1}^3 m_{\ell k} \bar{\ell}_k \ell_k, \quad (14.29)$$

with

$$\ell_k = (V^{\ell\dagger} \ell_L^I)_k + (V_R^\ell \ell_R^I)_k. \quad (14.30)$$

Inverting the equation above we find that the weak-doublet components of the charged lepton fields are

$$\ell_{Li}^I = P_L \sum_{j=1}^3 V_{ij}^\ell \ell_{Lj}. \quad i = 1, 2, 3 \quad (14.31)$$

From Eqs.(14.14), (14.18) and (14.31) we find that the mixing matrix U can be expressed as:

$$U_{ij} = \mathcal{P}_{\ell,ii} V_{ik}^{\ell\dagger} V_{kj}^\nu (\mathcal{P}_{\nu,jj}). \quad (14.32)$$

The matrix $V^{\ell\dagger} V^\nu$ contains a number of phases that are not physical. Three of them are eliminated by the diagonal 3×3 phase matrix \mathcal{P}_ℓ that absorbs them in the charged lepton mass eigenstates. If neutrinos are Dirac states, further $n-1$ are similarly eliminated by absorbing them in the neutrino mass eigenstates with the diagonal $n \times n$ phase matrix \mathcal{P}_ν . For Majorana neutrinos, $\mathcal{P}_\nu = I_{n \times n}$ because one cannot rotate by an arbitrary phase a Majorana field without physical effects. If one rotates a Majorana neutrino by a phase, this phase will appear in its mass term which will no longer be real. Consequently the number of phases

that can be absorbed by redefining the mass eigenstates depends on whether the neutrinos are Dirac or Majorana particles. Altogether for $n \geq 3$ Majorana [Dirac] neutrinos the U matrix contains a total of $6(n-2)$ [$5n-11$] real parameters, of which $3(n-2)$ are angles and $3(n-2)$ [$2n-5$] can be interpreted as physical phases.

The possibility of arbitrary mixing between massive neutrino states was first discussed in the context of two neutrinos introduced in Ref. [17] (the possibility of two mixed massless flavour neutrino states had been previously considered in the literature [18], and even before the possibility of mixing between neutrino

and antineutrino states in the seminal paper of Pontecorvo [19]). For that case, in which only mixing between two generations is considered with $n = 2$ distinct neutrino masses, the U matrix is 2×2 and contains one mixing angle if the neutrinos are Dirac and an additional physical phase if they are Majorana.

If there are only $n = 3$ Majorana neutrinos, U is a 3×3 matrix analogous to the CKM matrix for the quarks [20,21] but due to the Majorana nature of the neutrinos it depends on six independent parameters: three mixing angles and three phases. In this case the mixing matrix can be conveniently parametrized as:

$$U = \begin{pmatrix} 1 & 0 & 0 \\ 0 & c_{23} & s_{23} \\ 0 & -s_{23} & c_{23} \end{pmatrix} \cdot \begin{pmatrix} c_{13} & 0 & s_{13}e^{-i\delta_{CP}} \\ 0 & 1 & 0 \\ -s_{13}e^{i\delta_{CP}} & 0 & c_{13} \end{pmatrix} \cdot \begin{pmatrix} c_{21} & s_{12} & 0 \\ -s_{12} & c_{12} & 0 \\ 0 & 0 & 1 \end{pmatrix} \cdot \begin{pmatrix} e^{i\eta_1} & 0 & 0 \\ 0 & e^{i\eta_2} & 0 \\ 0 & 0 & 1 \end{pmatrix}, \quad (14.33)$$

where $c_{ij} \equiv \cos \theta_{ij}$ and $s_{ij} \equiv \sin \theta_{ij}$. The angles θ_{ij} can be taken without loss of generality to lie in the first quadrant, $\theta_{ij} \in [0, \pi/2]$ and the phases $\delta_{CP}, \eta_i \in [0, 2\pi]$. This is to be compared to the case of three Dirac neutrinos. In this case the Majorana phases,

η_1 and η_2 , can be absorbed in the neutrino states so number of physical phases is one (similar to the CKM matrix). Thus we can write U as:

$$U = \begin{pmatrix} c_{12} c_{13} & s_{12} c_{13} & s_{13} e^{-i\delta_{CP}} \\ -s_{12} c_{23} - c_{12} s_{13} s_{23} e^{i\delta_{CP}} & c_{12} c_{23} - s_{12} s_{13} s_{23} e^{i\delta_{CP}} & c_{13} s_{23} \\ s_{12} s_{23} - c_{12} s_{13} c_{23} e^{i\delta_{CP}} & -c_{12} s_{23} - s_{12} s_{13} c_{23} e^{i\delta_{CP}} & c_{13} c_{23} \end{pmatrix}. \quad (14.34)$$

This matrix is often called the Pontecorvo-Maki-Nakagawa-Sakata (PMNS) mixing matrix.

Notice that when the charged leptons have no other interactions than the SM ones, one can identify their interaction eigenstates with the corresponding mass eigenstates up to phase redefinition. This implies that, in this case, U is just a $3 \times n$ sub-matrix of the unitary neutrino mass diagonalizing matrix V^ν .

Finally, let us point out that for the case of 3 light Dirac neutrinos the procedure above leads to a unitary U matrix for the light states. But for three light Majorana neutrinos this is not the case when the full spectrum contains states which are heavy and are not in the low energy spectrum as seen, for example, in Eq.(14.21). This implies that, strictly speaking, the parametrization in Eq.(14.33) is not valid to describe the flavour mixing of the three light Majorana neutrinos in the see-saw mechanism. The violation of unitarity, however, is rather small, of the order $\mathcal{O}(M_D/M_N)$ as seen in Eq.(14.21). It is also severely constrained experimentally [22,23]. For all these reasons, for all practical purposes, we will consider the U matrix for the 3ν mixing case to be unitary independently of whether neutrinos are Dirac or Majorana particles.

14.4 Mass-Induced Flavour Oscillations in Vacuum

If neutrinos have masses and lepton flavours are mixed in the weak CC interactions, lepton flavour is not conserved in neutrino propagation [19,24]. This phenomenon is usually referred to as *neutrino oscillations*. In brief, a weak eigenstates, ν_α , which by default is the state produced in the weak CC interaction of a charged lepton ℓ_α , is the linear combination determined by the mixing matrix U

$$|\nu_\alpha\rangle = \sum_{i=1}^n U_{\alpha i}^* |\nu_i\rangle, \quad (14.35)$$

where ν_i are the mass eigenstates and here n is the number of light neutrino species (implicit in our definition of the state $|\nu\rangle$ is its energy-momentum and space-time dependence). After travelling a distance L ($L \simeq ct$ for relativistic neutrinos), that state evolves as:

$$|\nu_\alpha(t)\rangle = \sum_{i=1}^n U_{\alpha i}^* |\nu_i(t)\rangle. \quad (14.36)$$

This neutrino can then undergo a charged-current (CC) interaction producing a charge lepton ℓ_β , $\nu_\alpha(t)N' \rightarrow \ell_\beta N$, with a

probability

$$P_{\alpha\beta} = |\langle \nu_\beta | \nu_\alpha(t) \rangle|^2 = \left| \sum_{i=1}^n \sum_{j=1}^n U_{\alpha i}^* U_{\beta j} \langle \nu_j | \nu_i(t) \rangle \right|^2. \quad (14.37)$$

Assuming that $|\nu\rangle$ is a plane wave, $|\nu_i(t)\rangle = e^{-i E_i t} |\nu_i(0)\rangle$,³ with $E_i = \sqrt{p_i^2 + m_i^2}$ and m_i being, respectively, the energy and the mass of the neutrino mass eigenstate ν_i . In all practical cases neutrinos are very relativistic, so $p_i \simeq p_j \equiv p \simeq E$. We can then write

$$E_i = \sqrt{p_i^2 + m_i^2} \simeq p + \frac{m_i^2}{2E}, \quad (14.38)$$

and use the orthogonality of the mass eigenstates, $\langle \nu_j | \nu_i \rangle = \delta_{ij}$, to arrive to the following form for $P_{\alpha\beta}$:

$$P_{\alpha\beta} = \delta_{\alpha\beta} - 4 \sum_{i<j} \text{Re}[U_{\alpha i} U_{\beta i}^* U_{\alpha j}^* U_{\beta j}] \sin^2 X_{ij} + 2 \sum_{i<j} \text{Im}[U_{\alpha i} U_{\beta i}^* U_{\alpha j}^* U_{\beta j}] \sin 2X_{ij}, \quad (14.39)$$

where

$$X_{ij} = \frac{(m_i^2 - m_j^2)L}{4E} = 1.267 \frac{\Delta m_{ij}^2}{\text{eV}^2} \frac{L/E}{\text{m/MeV}}. \quad (14.40)$$

If we had made the same derivation for antineutrino states we would have ended with a similar expression but with the exchange $U \rightarrow U^*$. Consequently we conclude that the first term in the right-hand-side of Eq.(14.39) is CP conserving since it is the same for neutrinos and antineutrinos, while the last one is CP violating because it has opposite sign for neutrinos and antineutrinos.

Equation (14.39) oscillatory in distance with oscillation lengths

$$L_{0,ij}^{\text{osc}} = \frac{4\pi E}{|\Delta m_{ij}^2|}, \quad (14.41)$$

and with amplitudes proportional to products of elements in the mixing matrix. Thus, neutrinos must have different masses

³ For a pedagogical discussion of the quantum mechanical description of flavour oscillations in the wave package approach see for example Ref. [3]. A recent review of the quantum mechanical aspects and subtleties on neutrino oscillations can be found in Ref. [25].

($\Delta m_{ij}^2 \neq 0$) and they must have not vanishing mixing ($U_{\alpha_i} U_{\beta_i} \neq 0$) in order to undergo flavour oscillations. Also, from Eq.(14.39) we see that the Majorana phases cancel out in the oscillation probability. This is expected because flavour oscillation is a total lepton number conserving process.

Ideally, a neutrino oscillation experiment would like to measure an oscillation probability over a distance L between the source and the detector, for neutrinos of a definite energy E . In practice, neutrino beams, both from natural or artificial sources, are never monoenergetic, but have an energy spectrum $\Phi(E)$. In addition each detector has a finite energy resolution. Under these circumstances what is measured is an average probability

$$\begin{aligned} \langle P_{\alpha\beta} \rangle &= \frac{\int dE \frac{d\Phi}{dE} \sigma(E) P_{\alpha\beta}(E) \epsilon(E)}{\int dE \frac{d\Phi}{dE} \sigma_{CC}(E) \epsilon(E)} \\ &= \delta_{\alpha\beta} - 4 \sum_{i < j}^n \text{Re}[U_{\alpha i} U_{\beta i}^* U_{\alpha j}^* U_{\beta j}] \langle \sin^2 X_{ij} \rangle \\ &\quad + 2 \sum_{i < j}^n \text{Im}[U_{\alpha i} U_{\beta i}^* U_{\alpha j}^* U_{\beta j}] \langle \sin 2X_{ij} \rangle. \end{aligned} \quad (14.42)$$

σ is the cross section for the process in which the neutrino flavour is detected, and $\epsilon(E)$ is the detection efficiency. The minimal range of the energy integral is determined by the energy resolution of the experiment.

It is clear from the above expression that if $(E/L) \gg |\Delta m_{ij}^2|$ ($L \ll L_{0,ij}^{\text{osc}}$) so $\sin^2 X_{ij} \ll 1$, the oscillation phase does not give any appreciable effect. Conversely if $L \gg L_{0,ij}^{\text{osc}}$, many oscillation cycles occur between production and detection so the oscillating term is averaged to $\langle \sin^2 X_{ij} \rangle = 1/2$.

We summarize in Table 14.1. the typical values of L/E for different types of neutrino sources and experiments and the corresponding ranges of Δm^2 to which they can be most sensitive.

Table 14.1: Characteristic values of L and E for experiments performed using various neutrino sources and the corresponding ranges of $|\Delta m^2|$ to which they can be most sensitive to flavour oscillations in vacuum. SBL stands for Short Baseline and LBL for Long Baseline.

Experiment	L (m)	E (MeV)	$ \Delta m^2 $ (eV ²)
Solar	10^{10}	1	10^{-10}
Atmospheric	$10^4 - 10^7$	$10^2 - 10^5$	$10^{-1} - 10^{-4}$
Reactor	SBL $10^2 - 10^3$	1	$10^{-2} - 10^{-3}$
	LBL $10^4 - 10^5$		$10^{-4} - 10^{-5}$
Accelerator	SBL 10^2	$10^3 - 10^4$	> 0.1
	LBL $10^5 - 10^6$	$10^3 - 10^4$	$10^{-2} - 10^{-3}$

Historically, the results of neutrino oscillation experiments were interpreted assuming two-neutrino states so there is only one oscillating phase, the mixing matrix depends on a single mixing angle θ and no CP violation effect in oscillations is possible. At present, as we will discuss in Sec.14.7, we need at least the mixing among three-neutrino states to fully describe the bulk of experimental results. However, in many cases, the observed results can be understood in terms of oscillations dominantly driven by one Δm^2 . In this limit $P_{\alpha\beta}$ of Eq.(14.39) takes the form [24]

$$P_{\alpha\beta} = \delta_{\alpha\beta} - (2\delta_{\alpha\beta} - 1) \sin^2 2\theta \sin^2 X. \quad (14.43)$$

In this effective $2 - \nu$ limit, changing the sign of the mass difference, $\Delta m^2 \rightarrow -\Delta m^2$, and changing the octant of the mixing angle, $\theta \rightarrow \frac{\pi}{2} - \theta$, is just redefining the mass eigenstates, $\nu_1 \leftrightarrow \nu_2$:

$P_{\alpha\beta}$ must be invariant under such transformation. So the physical parameter space can be covered with either $\Delta m^2 \geq 0$ with $0 \leq \theta \leq \frac{\pi}{2}$, or, alternatively, $0 \leq \theta \leq \frac{\pi}{4}$ with either sign for Δm^2 .

However, from Eq.(14.43) we see that $P_{\alpha\beta}$ is actually invariant under the change of sign of the mass splitting and the change of octant of the mixing angle separately. This implies that there is a two-fold discrete ambiguity since the two different sets of physical parameters, $(\Delta m^2, \theta)$ and $(\Delta m^2, \frac{\pi}{2} - \theta)$, give the same transition probability in vacuum. In other words, one could not tell from a measurement of, say, $P_{e\mu}$ in vacuum whether the larger component of ν_e resides in the heavier or in the lighter neutrino mass eigenstate. This symmetry is broken when one considers mixing of three or more neutrinos in the flavour evolution and/or when the neutrinos traverse regions of dense matter as we describe in Sec.14.7.1 and Sec.14.5 respectively.

14.5 Propagation of Massive Neutrinos in Matter

Neutrinos propagating in a dense medium can interact with the particles in the medium. The probability of an incoherent inelastic scattering is very small. For example the characteristic cross section for ν -proton scattering is of the order

$$\sigma \sim \frac{G_F^2 s}{\pi} \sim 10^{-43} \text{ cm}^2 \left(\frac{E}{\text{MeV}} \right)^2, \quad (14.44)$$

where G_F is the Fermi constant and s is the square of the center of mass energy of the collision.

But when neutrinos propagate in dense matter, they can also interact coherently with the particles in the medium. By definition, in coherent interactions, the medium remains unchanged so it is possible to have interference of the forward scattered and the unscattered neutrino waves which enhances the effect of matter in the neutrino propagation. In this case the effect of the medium is not on the intensity of the propagating neutrino beam, which remains unchanged, but on the phase velocity of the neutrino wave, and for this reason the effect is proportional to G_F , instead of the G_F^2 dependence of the incoherent scattering. Coherence also allows decoupling the evolution equation of the neutrinos from those of the medium. In this limit the effect of the medium is introduced in the evolution equation for the neutrinos in the form of an effective potential which depends on the density and composition of the matter [26].

As an example, let us consider the evolution of ν_e in a medium with electrons, protons and neutrons with corresponding n_e , n_p and n_n number densities. The effective low-energy Hamiltonian describing the relevant neutrino interactions at point x is given by

$$H_W = \frac{G_F}{\sqrt{2}} \left[J^{(+)\alpha}(x) J_{\alpha}^{(-)}(x) + \frac{1}{4} J^{(N)\alpha}(x) J_{\alpha}^{(N)}(x) \right], \quad (14.45)$$

where the J_{α} 's are the standard fermionic currents

$$J_{\alpha}^{(+)}(x) = \bar{\nu}_e(x) \gamma_{\alpha} (1 - \gamma_5) e(x), \quad (14.46)$$

$$J_{\alpha}^{(-)}(x) = \bar{e}(x) \gamma_{\alpha} (1 - \gamma_5) \nu_e(x), \quad (14.47)$$

$$\begin{aligned} J_{\alpha}^{(N)}(x) &= \bar{\nu}_e(x) \gamma_{\alpha} (1 - \gamma_5) \nu_e(x) \\ &\quad - \bar{e}(x) [\gamma_{\alpha} (1 - \gamma_5) - 4 \sin^2 \theta_W \gamma_{\alpha}] e(x) \\ &\quad + \bar{p}(x) [\gamma_{\alpha} (1 - g_A^{(p)} \gamma_5) - 4 \sin^2 \theta_W \gamma_{\alpha}] p(x) \\ &\quad - \bar{n}(x) \gamma_{\alpha} (1 - g_A^{(n)} \gamma_5) n(x), \end{aligned} \quad (14.48)$$

and $g_A^{(n,p)}$ are the axial couplings for neutrons and protons, respectively.

Let us focus first on the the effect of the charged current interactions. The effective CC Hamiltonian due to electrons in the medium is

$$\begin{aligned}
H_C^{(e)} &= \frac{G_F}{\sqrt{2}} \int d^3 p_e f(E_e, T) \times \left\langle \langle e(s, p_e) | \bar{e}(x) \gamma^\alpha (1 - \gamma_5) \nu_e(x) \bar{\nu}_e(x) \gamma_\alpha (1 - \gamma_5) e(x) | e(s, p_e) \rangle \right\rangle \\
&= \frac{G_F}{\sqrt{2}} \bar{\nu}_e(x) \gamma_\alpha (1 - \gamma_5) \nu_e(x) \int d^3 p_e f(E_e, T) \left\langle \langle e(s, p_e) | \bar{e}(x) \gamma_\alpha (1 - \gamma_5) e(x) | e(s, p_e) \rangle \right\rangle.
\end{aligned} \tag{14.49}$$

In the above equation we denote by s the electron spin, and by p_e its momentum and $f(E_e, T)$, is the energy distribution function of the electrons in the medium which is assumed to be homogeneous and isotropic and is normalized as

$$\int d^3 p_e f(E_e, T) = 1. \tag{14.50}$$

We denote by $\langle \dots \rangle$ the averaging over electron spinors and summing over all electrons in the medium. Coherence dictates that s, p_e are the same for initial and final electrons. The axial current reduces to the spin in the non-relativistic limit and therefore averages to zero for a background of non-relativistic electrons. The spatial components of the vector current cancel because of isotropy. Therefore the only non trivial average is

$$\int d^3 p_e f(E_e, T) \left\langle \langle e(s, p_e) | \bar{e}(x) \gamma_0 e(x) | e(s, p_e) \rangle \right\rangle = n_e(x), \tag{14.51}$$

which gives a contribution to the effective Hamiltonian

$$H_C^{(e)} = \sqrt{2} G_F n_e \bar{\nu}_{eL}(x) \gamma_0 \nu_{eL}(x). \tag{14.52}$$

This can be interpreted as a contribution to the ν_{eL} potential energy

$$V_C = \sqrt{2} G_F n_e. \tag{14.53}$$

Should we have considered antineutrino states we would have ended up with $V_C = -\sqrt{2} G_F n_e$. For a more detailed derivation of the matter potentials see, for example, Ref. [3].

With an equivalent derivation we find that for ν_μ and ν_τ , the potential due to its CC interactions is zero for most media since neither μ 's nor τ 's are present, while the effective potential for any active neutrino due to the neutral current interactions is found to be

$$V_{NC} = \frac{\sqrt{2}}{2} G_F \left[-n_e (1 - 4 \sin^2 \theta_w) + n_p (1 - 4 \sin^2 \theta_w) - n_n \right]. \tag{14.54}$$

In neutral matter $n_e = n_p$ and the contribution from electrons and protons cancel each other. So we are left only with the neutron contribution

$$V_{NC} = -1/\sqrt{2} G_F n_n. \tag{14.55}$$

After including these effects, the evolution equation for n ultrarelativistic neutrinos propagating in matter written in the mass basis is (see for instance Ref. [27–29] for the derivation):

$$i \frac{d\vec{\nu}}{dx} = H \vec{\nu}, \quad H = H_m + U^{\nu\dagger} V U^\nu. \tag{14.56}$$

Here $\vec{\nu} \equiv (\nu_1, \nu_2, \dots, \nu_n)^T$, H_m is the kinetic Hamiltonian,

$$H_m = \frac{1}{2E} \text{diag}(m_1^2, m_2^2, \dots, m_n^2), \tag{14.57}$$

and V is the effective neutrino potential in the interaction basis. U^ν is the $n \times n$ submatrix of the unitary V^ν matrix corresponding to the n ultrarelativistic neutrino states. For the three SM active neutrinos with purely SM interactions crossing a neutral medium with electrons, protons and neutrons, the evolution equation takes the form (14.56) with $U^\nu \equiv U$, and the effective potential:

$$V = \text{diag}(\pm\sqrt{2} G_F n_e(x), 0, 0) \equiv \text{diag}(V_e, 0, 0). \tag{14.58}$$

The sign $+$ ($-$) in Eq.(14.58) applies to neutrinos (antineutrinos), and $n_e(x)$ is the electron number density in the medium, which

in general is not constant along the neutrino trajectory so the potential is not constant. Characteristic value of the potential at the Earth core is $V_e \sim 10^{-13}$ eV while at the solar core $V_e \sim 10^{-12}$ eV. Since the neutral current potential Eq.(14.55) is flavour diagonal, it can be eliminated from the evolution equation as it only contributes to an overall unobservable phase.

The instantaneous mass eigenstates in matter, ν_i^m , are the eigenstates of the Hamiltonian H in (14.56) for a fixed value of x , and they are related to the interaction basis by

$$\vec{\nu} = \tilde{U}(x) \vec{\nu}^m. \tag{14.59}$$

The corresponding instantaneous eigenvalues of H are $\mu_i(x)^2/(2E)$ with $\mu_i(x)$ being the instantaneous effective neutrino masses.

Let us take for simplicity a neutrino state which is an admixture of only two neutrino species $|\nu_\alpha\rangle$ and $|\nu_\beta\rangle$, so the two instantaneous mass eigenstates in matter ν_1^m and ν_2^m have instantaneous effective neutrino masses

$$\mu_{1,2}^2(x) = \frac{m_1^2 + m_2^2}{2} + E[V_\alpha + V_\beta] \tag{14.60}$$

$$\mp \frac{1}{2} \sqrt{[\Delta m^2 \cos 2\theta - A]^2 + [\Delta m^2 \sin 2\theta]^2},$$

and $\tilde{U}(x)$ is a 2x2 rotation matrix with the instantaneous mixing angle in matter given by

$$\tan 2\theta_m = \frac{\Delta m^2 \sin 2\theta}{\Delta m^2 \cos 2\theta - A}. \tag{14.61}$$

In the Eqs.(14.60) and (14.61) A is

$$A \equiv 2E(V_\alpha - V_\beta), \tag{14.62}$$

and its sign depends on depends on the composition of the medium and on the flavour composition of the neutrino state considered. From the expressions above we see that for a given sign of A the mixing angle in matter is larger(smaller) than in vacuum if this last one is in the first (second) octant. We see that the symmetry about 45 degrees which existing in vacuum oscillations between two neutrino states is broken by the matter potential in propagation in a medium. The expressions above show that very important effects are present when A , is close to $\Delta m^2 \cos 2\theta$. In particular, as seen in Eq.(14.61), the tangent of the mixing angle changes sign if, along its path, the neutrino passes by some matter density region satisfying, for its energy, the *resonance condition*

$$A_R = \Delta m^2 \cos 2\theta. \tag{14.63}$$

This implies that if the neutrino is created in a region where the relevant potential satisfies $A_0 > A_R$ (A_0 here is the value of the relevant potential at the production point), then the effective mixing angle in matter at the production point is such that $\text{sgn}(\cos 2\theta_{m,0}) = -\text{sgn}(\cos 2\theta)$. So the flavour component of the mass eigenstates is inverted as compared to their composition in vacuum. In particular, if at production point we have $A_0 = 2A_R$, then $\theta_{m,0} = \frac{\pi}{2} - \theta$. Asymptotically, for $A_0 \gg A_R$, $\theta_{m,0} \rightarrow \frac{\pi}{2}$. In other words, if in vacuum the lightest (heaviest) mass eigenstate has a larger projection on the flavour α (β), inside a matter with density and composition such that $A > A_R$, the opposite holds. So if the neutrino system is travelling across a monotonically varying matter potential, the dominant flavour component of a given mass eigenstate changes when crossing the region with $A = A_R$. This phenomenon is known as *level crossing*.

Taking the derivative of Eq.(14.59) with respect to x and using Eq.(14.56), we find that in the instantaneous mass basis the evolution equation reads:

$$i \frac{d\tilde{\nu}^m}{dx} = \left[\frac{1}{2E} \text{diag} (\mu_1^2(x), \mu_2^2(x), \dots, \mu_n^2(x)) - i \tilde{U}^\dagger(x) \frac{d\tilde{U}(x)}{dx} \right] \tilde{\nu}^m. \quad (14.64)$$

The presence of the last term, Eq.(14.64) implies that this is a system of coupled equations. So in general, the instantaneous mass eigenstates, ν_i^m are not energy eigenstates. For constant or slowly enough varying matter potential this last term can be neglected and the instantaneous mass eigenstates, ν_i^m , behave approximately as energy eigenstates and they do not mix in the evolution. This is the *adiabatic* transition approximation. On the contrary, when the last term in Eq.(14.64) cannot be neglected, the instantaneous mass eigenstates mix along the neutrino path. This implies there can be *level-jumping* [30–33] and the evolution is *non-adiabatic*.

For adiabatic evolution in matter the oscillation probability take a form very similar to the vacuum oscillation expression, Eq.(14.39). For example, neglecting CP violation:

$$P_{\alpha\beta} = \left| \sum_i \tilde{U}_{\alpha i}(0) \tilde{U}_{\beta i}(L) \exp \left(-\frac{i}{2E} \int_0^L \mu_i^2(x') dx' \right) \right|^2. \quad (14.65)$$

To compute $P_{\alpha\beta}$ in a varying potential one can always solve the evolution equation numerically. Also several analytic approximations for specific profiles of the matter potential can be found in the literature [34].

14.5.1 The Mikheev-Smirnov-Wolfenstein Effect for Solar Neutrinos

The matter effects discussed in the previous section are of special relevance for solar neutrinos. As the Sun produces ν_e 's in its core, here we shall consider the propagation of a $\nu_e - \nu_X$ neutrino system (X is some superposition of μ and τ , which is arbitrary because ν_μ and ν_τ have only and equal neutral current interactions) in the matter density of the Sun.

The density of solar matter is a monotonically decreasing function of the distance R from the center of the Sun, and it can be approximated by an exponential for $R < 0.9R_\odot$

$$n_e(R) = n_e(0) \exp(-R/r_0), \quad (14.66)$$

with $r_0 = R_\odot/10.54 = 6.6 \times 10^7 \text{ m} = 3.3 \times 10^{14} \text{ eV}^{-1}$.

As mentioned above, the nuclear reactions in the Sun produce electron neutrinos. After crossing the Sun, the composition of the neutrino state exiting the Sun will depend on the relative size of $\Delta m^2 \cos 2\theta$ versus $A_0 = 2E G_F n_{e,0}$ (here 0 refers to the neutrino production point which is near but not exactly at the center of the Sun, $R = 0$).

If the relevant matter potential at production is well below the resonant value, $A_R = \Delta m^2 \cos 2\theta \gg A_0$, matter effects are negligible. With the characteristic matter density and energy of the solar neutrinos, this condition is fulfilled for values of Δm^2 such that $\Delta m^2/E \gg L_{\text{Sun-Earth}}$. So the propagation occurs as in vacuum with the oscillating phase averaged to $1/2$ and the survival probability at the exposed surface of the Earth is

$$P_{ee}(\Delta m^2 \cos 2\theta \gg A_0) = 1 - \frac{1}{2} \sin^2 2\theta > \frac{1}{2}. \quad (14.67)$$

If the relevant matter potential at production is only slightly below the resonant value, $A_R = \Delta m^2 \cos 2\theta \gtrsim A_0$, the neutrino does not cross a region with resonant density, but matter effects are sizable enough to modify the mixing. The oscillating phase is averaged in the propagation between the Sun and the Earth. This regime is well described by an adiabatic propagation, Eq.(14.65). Using that $\tilde{U}(0)$ is a 2×2 rotation of angle $\theta_{m,0}$ – the mixing

angle in matter at the neutrino production point–, and $\tilde{U}(L)$ is the corresponding rotation with vacuum mixing angle θ , we get

$$P_{ee}(\Delta m^2 \cos 2\theta \geq A_0) = \cos^2 \theta_{m,0} \cos^2 \theta + \sin^2 \theta_{m,0} \sin^2 \theta = \frac{1}{2} [1 + \cos 2\theta_{m,0} \cos 2\theta]. \quad (14.68)$$

This expression reflects that an electron neutrino produced at A_0 is an admixture of ν_1 with fraction $P_{e1,0} = \cos^2 \theta_{m,0}$ and ν_2 with fraction $P_{e2,0} = \sin^2 \theta_{m,0}$. On exiting the Sun, ν_1 consists of ν_e with fraction $P_{1e} = \cos^2 \theta$, and ν_2 consists of ν_e with fraction $P_{2e} = \sin^2 \theta$ so $P_{ee} = P_{e1,0}P_{1e} + P_{e2,0}P_{2e} = \cos^2 \theta_{m,0} \cos^2 \theta + \sin^2 \theta_{m,0} \sin^2 \theta$ [35–37], exactly as given in Eq.(14.68). Since $A_0 < A_R$ the resonance is not crossed so $\cos 2\theta_{m,0}$ has the same sign as $\cos 2\theta$ and still $P_{ee} \geq 1/2$.

Finally, in the case that $A_R = \Delta m^2 \cos 2\theta < A_0$, the neutrino can cross the resonance on its way out. In the convention of $\Delta m^2 > 0$ this occurs if $\cos 2\theta > 0$ ($\theta < \pi/4$). which means that in vacuum ν_e is a combination of ν_1 and ν_2 with larger ν_1 component, while at the production point ν_e is a combination of ν_1^m and ν_2^m with larger ν_2^m component. In particular, if the density at the production point is much higher than the resonant density, $\Delta m^2 \cos 2\theta \ll A_0$,

$$\theta_{m,0} = \frac{\pi}{2} \Rightarrow \cos 2\theta_{m,0} = -1, \quad (14.69)$$

and the produced ν_e is purely ν_2^m .

In this regime, the evolution of the neutrino ensemble can be adiabatic or non-adiabatic depending on the particular values of Δm^2 and the mixing angle. The oscillation parameters (see Secs.14.6.1 and 14.7) happen to be such that the transition is adiabatic in all ranges of solar neutrino energies. Thus the survival probability at the exposed surface of the Earth is given by Eq.(14.68) but now with mixing angle (14.69) so

$$P_{ee}(\Delta m^2 \cos 2\theta < A_0) = \frac{1}{2} [1 + \cos 2\theta_{m,0} \cos 2\theta] = \sin^2 \theta. \quad (14.70)$$

So in this case P_{ee} can be much smaller than $1/2$ because $\cos 2\theta_{m,0}$ and $\cos 2\theta$ have opposite signs. This is referred to as the Mikheev-Smirnov-Wolfenstein (MSW) effect [26, 38] which plays a fundamental role in the interpretation of the solar neutrino data.

The resulting energy dependence of the survival probability of solar neutrinos is shown in Fig.14.3 (together with a compilation of data from solar experiments). The plotted curve corresponds to $\Delta m^2 \sim 7.5 \times 10^{-5} \text{ eV}^2$ and $\sin^2 \theta \sim 0.3$ (the so-called large mixing angle, LMA, solution). The figure illustrates the regimes described above. For these values of the oscillation parameters, neutrinos with $E \ll 1 \text{ MeV}$ are in the regime with $\Delta m^2 \cos 2\theta \gg A_0$ so the curve represents the value of vacuum averaged survival probability, Eq.(14.67), and therefore $P_{ee} > 0.5$. For $E > 10 \text{ MeV}$, on the contrary, $\Delta m^2 \cos 2\theta \ll A_0$ and the survival probability is given by Eq.(14.70), so $P_{ee} = \sin^2 \theta \sim 0.3$. In between, the survival probability is given by Eq.(14.68) with θ_0 changing rapidly from its vacuum value to the asymptotic matter value (14.69), 90° .

14.6 Experimental Study of Neutrino Oscillations

Neutrino flavour transitions, or neutrino oscillations, have been experimentally studied using various neutrino sources and detection techniques. Intense sources and large detectors are mandatory because of a large distance necessary for observable oscillation effects in addition to the small cross sections. Also, the relevant neutrino flux before oscillations should be known with sufficient precision for a definitive measurement. Here, the experimental status of neutrino oscillations with the different neutrino sources, the Sun, Earth's atmosphere, accelerators and nuclear reactors, are reviewed.

14.6.1 Solar Neutrinos

14.6.1.1 Solar neutrino flux

In the Sun, electron neutrinos are produced in the thermonuclear reactions which generate the solar energy. These reac-

tions occur via two main chains, the pp chain and the CNO cycle. The pp chain includes reactions $p + p \rightarrow d + e^+ + \nu$ (pp), $p + e^- + p \rightarrow d + \nu$ (pep), ${}^3\text{He} + p \rightarrow {}^4\text{He} + e^+ + \nu$ (hep), ${}^7\text{Be} + e^- \rightarrow {}^7\text{Li} + \nu$ (${}^7\text{Be}$), and ${}^8\text{B} \rightarrow {}^8\text{Be}^* + e^+ + \nu$ (${}^8\text{B}$). The CNO cycle involves ${}^{13}\text{N} \rightarrow {}^{13}\text{C} + e^+ + \nu$ (${}^{13}\text{N}$), ${}^{15}\text{O} \rightarrow {}^{15}\text{N} + e^+ + \nu$ (${}^{15}\text{O}$), and ${}^{17}\text{F} \rightarrow {}^{17}\text{O} + e^+ + \nu$ (${}^{17}\text{F}$). Those reactions result in the overall fusion of protons into ${}^4\text{He}$, $4p \rightarrow {}^4\text{He} + 2e^+ + 2\nu_e$, where the energy released in the reaction, $Q = 4m_p - m_{{}^4\text{He}} - 2m_e \sim 26$ MeV, is mostly radiated through the photons and only a small fraction is carried by the neutrinos, $\langle E_{2\nu_e} \rangle = 0.59$ MeV. In addition, electron capture on ${}^{13}\text{N}$, ${}^{15}\text{O}$, and ${}^{17}\text{F}$ produces line spectra of neutrinos called ecCNO neutrinos. Dividing the solar luminosity by the energy released per neutrino production, the total neutrino flux can be estimated. At the Earth, the pp solar neutrino flux is about $6 \times 10^{10} \text{ cm}^{-2}\text{s}^{-1}$.

The detailed calculation of the solar neutrino fluxes has been done based on the Standard Solar Model (SSM). The SSM describes the structure and evolution of the Sun based on a variety of inputs such as the mass, luminosity, radius, surface temperature, age, and surface elemental abundances. In addition, the knowledge of the absolute nuclear reaction cross sections for the relevant fusion reactions and the radiative opacities are necessary. John Bahcall and his collaborators continuously updated the SSM calculations over several decades [39,40]. Figure 14.1 shows the solar neutrino fluxes predicted by the SSM calculation in [41] and ecCNO neutrinos in [42].

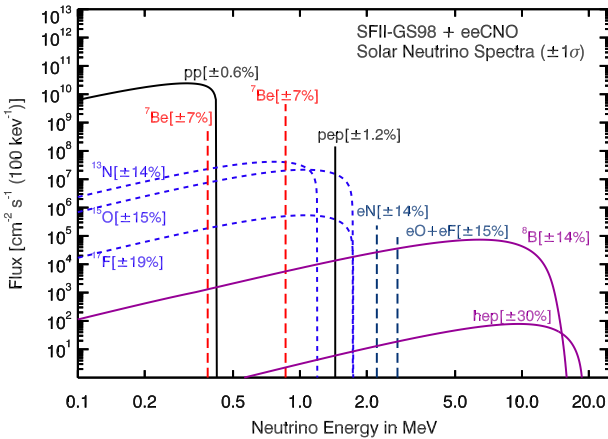


Figure 14.1: Spectrum of solar neutrino fluxes predicted by SSM calculation in [41]. In addition to standard fluxes, ecCNO neutrinos have been added based on [42]. Electron capture fluxes are given in $\text{cm}^{-2}\text{s}^{-1}$. Taken from [43]

14.6.1.2 Detection of solar neutrinos and the solar neutrino problem

Experiments which observed solar neutrinos are summarized in Table 14.2.

A pioneering solar neutrino experiment was carried out by R. Davis, Jr. and collaborators at Homestake starting in the late 1960s [44]. The Davis' experiment utilizes the reaction $\nu_e + {}^{37}\text{Cl} \rightarrow e^- + {}^{37}\text{Ar}$. Because this process has an energy threshold of 814 keV, the most relevant fluxes are the ${}^7\text{Be}$ and ${}^8\text{B}$ neutrinos. The detector contained ~ 615 t of C_2Cl_4 . The produced ${}^{37}\text{Ar}$, which has a half life of 34.8 d, was chemically extracted and introduced into a low-background proportional chamber every few months. The Auger electrons from electron capture of ${}^{37}\text{Ar}$ were counted to determine the reaction rate.

From the beginning, the observed number of neutrinos in the Homestake mine experiment was significantly smaller than the prediction by SSM — it was almost one third. After thorough check of both experimental and theoretical work, the discrepancy remained. This became to be known as the solar neutrino problem. The final result from Homestake experiment is $2.56 \pm 0.16 \pm 0.16$ SNU [45], where SNU (solar neutrino unit) is a unit of event rate, $1 \text{ SNU} = 10^{-36} \text{ captures}/(\text{s atom})$. On the other hand, prediction based on SSM is $8.46^{+0.87}_{-0.88}$ SNU [46].

The detection of neutrinos from other production processes was recognized as an important input to investigate the origin of the solar neutrino problem. In particular, the pp neutrino is most abundant, and its flux prediction has the smallest uncertainty. Using the radiochemical technique with gallium, the reaction $\nu_e + {}^{71}\text{Ga} \rightarrow e^- + {}^{71}\text{Ge}$ has an energy threshold of 233 keV and can be used for the pp neutrino detection. According to the SSM, more than a half of the events on ${}^{71}\text{Ga}$ are due to the pp neutrinos, with the second dominant contribution coming from the ${}^7\text{Be}$ neutrinos. ${}^{71}\text{Ge}$ decays via electron capture with a half life of 11.4 d. The SAGE experiment in Baksan [47] used about 50 t of liquid metallic gallium as a target. The GALLEX experiment in LNGS [48] used 101 t of GaCl_3 , containing 30.3 t of gallium. Both experiments used natural gallium, containing 39.9% of ${}^{71}\text{Ga}$ isotope. GALLEX was followed by its successor GNO experiment. The measured capture rate is $69.3 \pm 4.1 \pm 3.6$ SNU for GALLEX+GNO [49] and $65.4^{+3.1+2.6}_{-3.0-2.8}$ SNU for SAGE [50]. A SSM prediction is $127.9^{+8.1}_{-8.2}$ SNU [46].

The radiochemical detectors measure the reaction rate integrated between extractions. The real time measurement of solar neutrino was realized by the Kamiokande experiment [51]. The Kamiokande detector was a 3,000-t water-Cherenkov detector in the Kamioka mine. An array of 50 cm diameter PMTs were attached onto the inner wall of the detector to detect Cherenkov light. Although the original purpose of the Kamiokande detector was search for nucleon decays, with an upgrade of detector Kamiokande-II achieved an energy threshold sufficiently low to allow for the observation of solar neutrinos using ν_e - e elastic scattering (ES), $\nu_x + e^- \rightarrow \nu_x + e^-$. The signal and background from radioactivity can be statistically separated by using the directional correlation between the incoming neutrino and the recoil electron. The Super-Kamiokande, the successor of Kamiokande, started operation in April 1996. It is a large upright cylindrical water Cherenkov detector containing 50 kt of pure water. An inner detector volume corresponding to 32 kt water mass is viewed by more than 11,000 inward-facing 50 cm diameter PMTs.

The ES reaction occurs via both charged and neutral current interactions. Consequently, it is sensitive to all active neutrino flavours, although the cross section for ν_e , which is the only flavour to interact via charged current, is about six times larger than that for ν_μ or ν_τ . Because the energy threshold is 6.5 MeV for Kamiokande and 3.5 MeV for the present Super-Kamiokande (for the kinetic energy of recoil electron), these experiments are sensitive to primarily to ${}^8\text{B}$ neutrinos.

The results from Kamiokande [52, 53] and Super-Kamiokande [54, 55] showed significantly smaller numbers of observed solar neutrinos compared to the prediction. The latest ${}^8\text{B}$ neutrino flux measured by Super-Kamiokande is $(2.345 \pm 0.014 \pm 0.036) \times 10^6 \text{ cm}^{-2}\text{s}^{-1}$ [56], while a prediction based on the SSM is $(5.46 \pm 0.66) \times 10^6 \text{ cm}^{-2}\text{s}^{-1}$ [57]. In addition, no significant zenith angle variation nor spectrum distortion were observed in the initial phase of Super-Kamiokande, which placed strong constraints on the solution of the solar neutrino problem [58, 59].

14.6.1.3 Solution of the solar neutrino problem

SNO experiment in Canada used 1,000 t of heavy water (D_2O) contained in a spherical acrylic vessel which was surrounded by an H_2O shield. An array of PMTs installed on a stainless steel structure detected Cherenkov radiation produced in both the D_2O and H_2O . The SNO detector observed ${}^8\text{B}$ neutrinos via three different reactions. In addition to the ES scattering with an electron, with D_2O target the charged current (CC) $\nu_e + d \rightarrow e^- + p + p$ and the neutral current (NC) $\nu_x + d \rightarrow \nu_x + p + n$ interactions are possible. The CC reaction is sensitive to only ν_e , while NC reaction is sensitive to all active flavours of neutrinos with equal cross sections. Therefore, by comparing the measurements of different reactions, SNO could provide a model independent test of the neutrino flavour change.

In 2001, SNO reported the initial result of CC measurement [62]. Combined with the high statistics measurement of ν_e - e elastic scattering from Super-Kamiokande [58], it provided a direct evidence for existence of non- ν_e component in solar neutrino flux. The result of NC measurement in 2002 [63] established it

Table 14.2: List of solar neutrino experiments

Name	Target material	Energy threshold (MeV)	Mass (ton)	Years
Homestake	C ₂ Cl ₄	0.814	615	1970–1994
SAGE	Ga	0.233	50	1989–
GALEX	GaCl ₃	0.233	100 [30.3 for Ga]	1991–1997
GNO	GaCl ₃	0.233	100 [30.3 for Ga]	1998–2003
Kamiokande	H ₂ O	6.5	3,000	1987–1995
Super-Kamiokande	H ₂ O	3.5	50,000	1996–
SNO	D ₂ O	3.5	1,000	1999–2006
KamLAND	Liquid scintillator	0.5/5.5	1,000	2001–2007
Borexino	Liquid scintillator	0.19	300	2007–

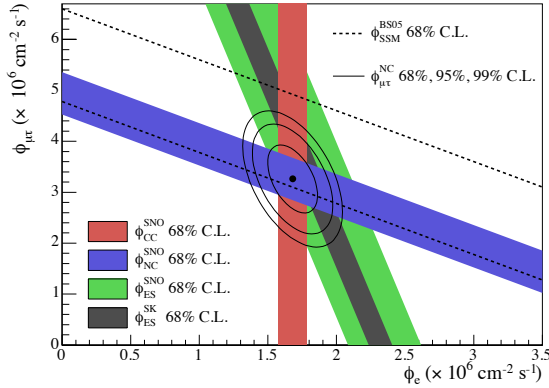


Figure 14.2: Fluxes of ^8B solar neutrinos, $\phi(\nu_e)$, and $\phi(\nu_{\mu,\tau})$, deduced from the SNO's CC, ES, and NC results [60]. The Super-Kamiokande ES flux is from [61]. The BS05(OP) standard solar model prediction [40] is also shown. The bands represent the 1σ error. The contours show the 68%, 95%, and 99% joint probability for $\phi(\nu_e)$ and $\phi(\nu_{\mu,\tau})$. The figure is from [60].

with 5.3σ of statistical significance. Figure 14.2 shows the fluxes of electron neutrinos ($\phi(\nu_e)$) and muon and tau neutrinos ($\phi(\nu_{\mu,\tau})$) with the 68%, 95%, and 99% joint probability contours, obtained with the SNO data. Finally, together with the reactor neutrino experiment KamLAND (see Sec.14.6.4), the solution of solar neutrino problem was found to be the MSW adiabatic flavour transitions in the solar matter, the so-called large mixing angle (LMA) solution, with parameters $\Delta m^2 \sim 7.5 \times 10^{-5} \text{ eV}^2$ and $\sin^2 \theta \sim 0.3$.

From a combined result of three phases of SNO [64], the total flux of ^8B solar neutrino is found to be $(5.25 \pm 0.16^{+0.11}_{-0.13}) \text{ cm}^{-2} \text{ s}^{-1}$, consistent with the SSM prediction. This consistency is one of major accomplishments of SSM.

In order to understand the SSM as well as to study the MSW effect for the solar neutrino, measurements of solar neutrinos other than ^8B are important. The Borexino experiment at Gran Sasso, Italy, detects solar neutrino via ν - e scattering in real time with a low energy threshold. The Borexino detector consists of 300 t of ultra-pure liquid scintillator, which achieved 0.19 MeV of energy threshold and 5% energy resolution at 1 MeV. Borexino reported the first real time detection of ^7Be solar neutrinos [66]. They also measured the fluxes of pep [67] and pp neutrino [68] for the first time. Together with ^8B [69] neutrino measurement, Borexino provides important data to study the MSW effect. The KamLAND experiment also measured ^8B [70] and ^7Be [71] solar neutrinos. Figure 14.3 shows the survival probability of solar ν_e as a function of neutrino energy. The data points are from the Borexino results [72, 73] except the SNO+SK ^8B data. The theoretical curve shows the prediction of the MSW-LMA solution. All the data shown in this plot are consistent with the theoretically calculated curve. This indicates that these solar neutrino measurements are consistent with the MSW-LMA solution of the solar neutrino problem.

The matter effects can also be relevant to the propagation of solar neutrinos through the Earth. Because solar neutrinos go through the Earth before interaction in the detector during the

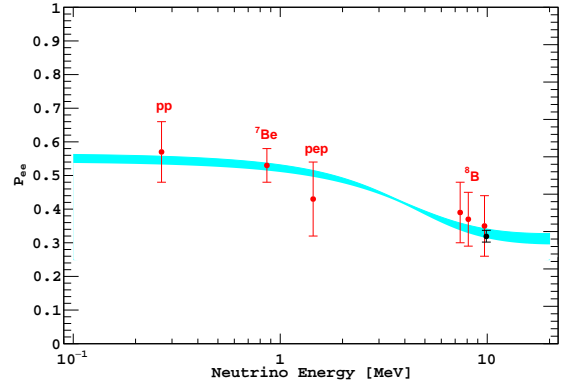


Figure 14.3: Electron neutrino survival probability as a function of neutrino energy. The points represent, from left to right, the Borexino pp , ^7Be , pep , and ^8B data (red points) and the SNO+SK ^8B data (black point). The three Borexino ^8B data points correspond, from left to right, to the low-energy (LE) range, LE+HE range, and the high-energy (HE) range. The electron neutrino survival probabilities from experimental points are determined using a high metallicity SSM from Ref. [57]. The error bars represent the $\pm 1\sigma$ experimental + theoretical uncertainties. The curve corresponds to the $\pm 1\sigma$ prediction of the MSW-LMA solution using the parameter values given in [65]. This figure is provided by A. Ianni.

nighttime, a comparison of measured event rate between daytime and nighttime provides a clean and direct test of matter effects on neutrino oscillations. Super-Kamiokande reported the first indication of the day/night asymmetry in ^8B solar neutrinos [74]. The measured asymmetry, defined as the difference of the average day rate and average night rate divided by the average of those two rates, is $(-3.2 \pm 1.1 \pm 0.5)\%$, corresponding to a statistical significance of 2.7σ . The measured value of the asymmetry is consistent with the LMA solution.

14.6.2 Atmospheric Neutrinos

14.6.2.1 Atmospheric neutrino flux

Atmospheric neutrinos are produced by the decays of pions and kaons generated in the interaction of cosmic rays and nucleons in the Earth's atmosphere. They have a broad range of energy ($\sim 0.1 \text{ GeV}$ to $> \text{TeV}$) and long travel distances before detection (~ 10 to $1.3 \times 10^4 \text{ km}$). As shown in Table 14.1, atmospheric neutrino oscillation experiments are most sensitive to flavour oscillations with $\Delta m^2 \sim 10^{-1}$ to 10^{-4} eV^2 .

Considering their dominant production modes, some generic relations for flux ratios of different flavour of neutrinos can be derived without detailed calculations. From the decay chain of a charged pion $\pi^+ \rightarrow \mu^+ \nu_\mu$ followed by $\mu^+ \rightarrow e^+ \nu_e \bar{\nu}_\mu$ (and the charge conjugate for π^-), the ratio $(\nu_\mu + \bar{\nu}_\mu)/(\nu_e + \bar{\nu}_e)$ is expected to be around 2 at low energies ($\sim 1 \text{ GeV}$) where most muons decay in the atmosphere. For higher energies, some of muons reach the Earth before they decay and the ratio increases. One can also expect that the zenith angle distributions of atmospheric neutrinos are symmetric between upward-going and downward-going

neutrinos. It is true for the energy above 1 GeV, but at lower energies, the Earth's geomagnetic field induces up-down asymmetries in the primary cosmic ray. The zenith angle corresponds to the flight length of atmospheric neutrinos. Vertically upward-going neutrinos come from the other side of the Earth with flight lengths of $\sim 10^4$ km, while downward-going neutrinos produced just above the experimental site travel ~ 10 km before detection.

The atmospheric neutrino fluxes are calculated in detail based on the energy spectrum and composition of primary cosmic rays and their hadronic interactions in the atmosphere. The effects of solar activity and geomagnetic field should be also taken into account. Results of calculations by several groups are available [75–78]. A typical uncertainty of the absolute flux is 10–20%, while the ratio of fluxes between different flavour has much smaller uncertainty ($< 5\%$).

14.6.2.2 Observation of atmospheric neutrino oscillations

The first detection of atmospheric neutrinos was reported in the 1960's by the underground experiments in the Kolar Gold Field experiment in India [79] and in South Africa [80]. In the 1980's, experiments searching for nucleon decays started operation. They used large underground detectors which could also observe atmospheric neutrinos. In these experiments, atmospheric neutrinos were studied as backgrounds to nucleon decays. Among the early experiments were Kamiokande [81] and IMB [82] using water Cherenkov detectors, and Frejus [83] and NUSEX [84] using iron tracking calorimeters.

The flavour of atmospheric neutrino can be identified in charged current interaction with nuclei, which produces the corresponding charged lepton. In order to study the neutrino oscillations, the identification of charged lepton is essential. Those detectors originally designed for nucleon decay search had capability to distinguish muons and electrons. For example, a water Cherenkov detector can utilize the information from Cherenkov ring patterns for particle identification; e -like particles (e^\pm , γ) produce more diffuse ring than μ -like particles (μ^\pm , π^\pm) because of electromagnetic cascades and multiple Coulomb scattering effects.

To reduce the uncertainty, in early results the flux ratio $\nu_\mu/\nu_e \equiv (\nu_\mu + \bar{\nu}_\mu)/(\nu_e + \bar{\nu}_e)$ was measured, and the double ratio between observation and expectation $(\nu_\mu/\nu_e)_{\text{obs}}/(\nu_\mu/\nu_e)_{\text{exp}}$ was reported. The Kamiokande experiment reported an indication of a deficit of $(\nu_\mu + \bar{\nu}_\mu)$ flux [81]. IMB also observed similar deficit [82], but measurements by Frejus [83] and NUSEX [84] were consistent with the expectations. This was the original formulation of the atmospheric neutrino anomaly. Kamiokande reported studies with an increased data set of the sub-GeV (< 1.33 GeV) [85] as well as the multi-GeV (> 1.33 GeV) [86] samples. In the latter, they reported an analysis of zenith angle distributions, which showed an indication that the muon disappearance probability is dependent on the zenith angle, hence the travel length of neutrinos. However, the statistical significance was not sufficient to provide a conclusive interpretation.

The solution to the atmospheric neutrino anomaly was brought by Super-Kamiokande, which reported compelling evidence for neutrino oscillations in atmospheric neutrinos in 1998 [87]. The zenith angle (θ_z , with $\theta_z = 0$ for vertically downward-going) distributions of μ -like events showed a clear deficit of upward-going events, while no significant asymmetry was observed for e -like events. The asymmetry is defined as $A = (U - D)/(U + D)$, where U is the number of upward-going ($-1 < \cos \theta_z < -0.2$) events and D is the number of downward-going ($0.2 < \cos \theta_z < 1.0$) events. With multi-GeV (visible energy > 1.33 GeV) μ -like events alone, the measured asymmetry was $A = -0.296 \pm 0.048 \pm 0.001$, deviating from zero by more than 6σ . The sub-GeV (< 1.33 GeV) μ -like, upward through going, and upward stopping μ samples, which correspond to different energy range of neutrino, show the consistent behaviour, strengthening the credibility of the observation. The corresponding oscillation parameters were found to be $\Delta m^2 \sim 2.5 \times 10^{-3} \text{ eV}^2$ and $\theta \sim 45^\circ$. Super-Kamiokande's results were confirmed by other atmospheric neutrino observations MACRO [88] and Soudan2 [89].

Although the energy and zenith-angle dependent muon neutrino disappearance observed with atmospheric neutrinos could be consistently explained by the neutrino oscillations between ν_μ

and ν_τ , other exotic explanations such as neutrino decay or de-coherence were not initially ruled out. By using a selected sample from Super-Kamiokande's atmospheric data with good L/E resolution, the L/E dependence of the survival probability was measured [90]. The observed dip in the L/E distribution was consistent with the expectation from neutrino oscillation, while alternative models were strongly disfavored.

As an experimental proof of ν_μ - ν_τ oscillation, appearance signal of ν_τ was searched for in the atmospheric neutrino data. Because of the high energy threshold (> 3.5 GeV) of ν_τ CC interaction and the short lifetime of τ lepton (0.3 ps), the identification of ν_τ appearance is experimentally very difficult. Super-Kamiokande reported evidence of tau neutrino appearance using atmospheric neutrino data with 4.6σ significance [91]. The definitive observation of ν_τ appearance was made by the long-baseline experiment, OPERA [92] (See Sec.14.6.3.3), and recently IceCube also reported the ν_τ appearance analysis [93] using atmospheric neutrinos.

14.6.2.3 Neutrino oscillation measurements using atmospheric neutrinos

Figure 14.4 shows the zenith angle distributions of atmospheric neutrino data from Super-Kamiokande. For wide range of neutrino energy and path length, the observed distributions are consistent with the expectation from neutrino oscillation. Atmospheric neutrinos in the energy region of a few to ~ 10 GeV provide information for the determination of the neutrino mass ordering [94].

The neutrino telescopes primarily built for the high energy neutrino astronomy such as ANTARES [95] and IceCube [96] can also measure neutrino oscillations with atmospheric neutrinos. ANTARES consists of a sparse array of PMTs deployed under the Mediterranean Sea at a depth of about 2.5 km to instrument a 10^5 m^3 volume. IceCube is a detector deployed in ice in Antarctica at the South Pole, at depth between 1.45 and 2.45 km. In the bottom center of IceCube there is a region of $\sim 10^7 \text{ m}^3$ volume with denser PMT spacing called DeepCore to extend the observable energies to lower energy region. By observing the charged current interaction of up-going ν_μ , they measure the ν_μ disappearance. ANTARES reported a measurement of ν_μ disappearance with 20 GeV threshold [97]. With analysis of events with 6–56 GeV energy range, the results on ν_μ disappearance measurements from IceCube DeepCore [98] provided a precision comparable to the measurements by Super-Kamiokande and long-baseline experiments.

There are several projects for atmospheric neutrino observations either proposed or under preparation. The atmospheric neutrino observation program is included in the plans for future neutrino telescopes, ORCA in the second phase of KM3NeT project [99] in the Mediterranean Sea, and PINGU in the upgrade of IceCube [100]. In India, a 50 kt magnetized iron tracking calorimeter ICAL is planned at the INO [101]. Future large underground detectors, Hyper-Kamiokande in Japan [102] and DUNE in US [103] can also study the atmospheric neutrinos.

14.6.3 Accelerator Neutrinos

14.6.3.1 Accelerator neutrino beams

A comprehensive description of the accelerator neutrino beams is found in [104]. Conventional neutrino beams from accelerators are produced by colliding high energy protons onto a target, producing π and K which then decay into neutrinos, and stopping undecayed mesons and muons in the beam dump and soil. Because pions are the most abundant product in the high energy collisions, a conventional neutrino beam contains dominantly muon-type neutrinos (or antineutrinos).

Focusing devices called magnetic horns are used to concentrate the neutrino beam flux towards the desired direction. A magnetic horn is a pulsed electromagnet with toroidal magnetic fields to focus charged particles that are parents of neutrinos. One can choose the dominant component of the beam to be either neutrinos or antineutrinos by selecting the direction of current in the magnetic horns. Even with the focusing with horns, *wrong sign* neutrinos contaminate in the beam. Also, there is small amount of contamination of ν_e and $\bar{\nu}_e$ coming primarily from kaon and

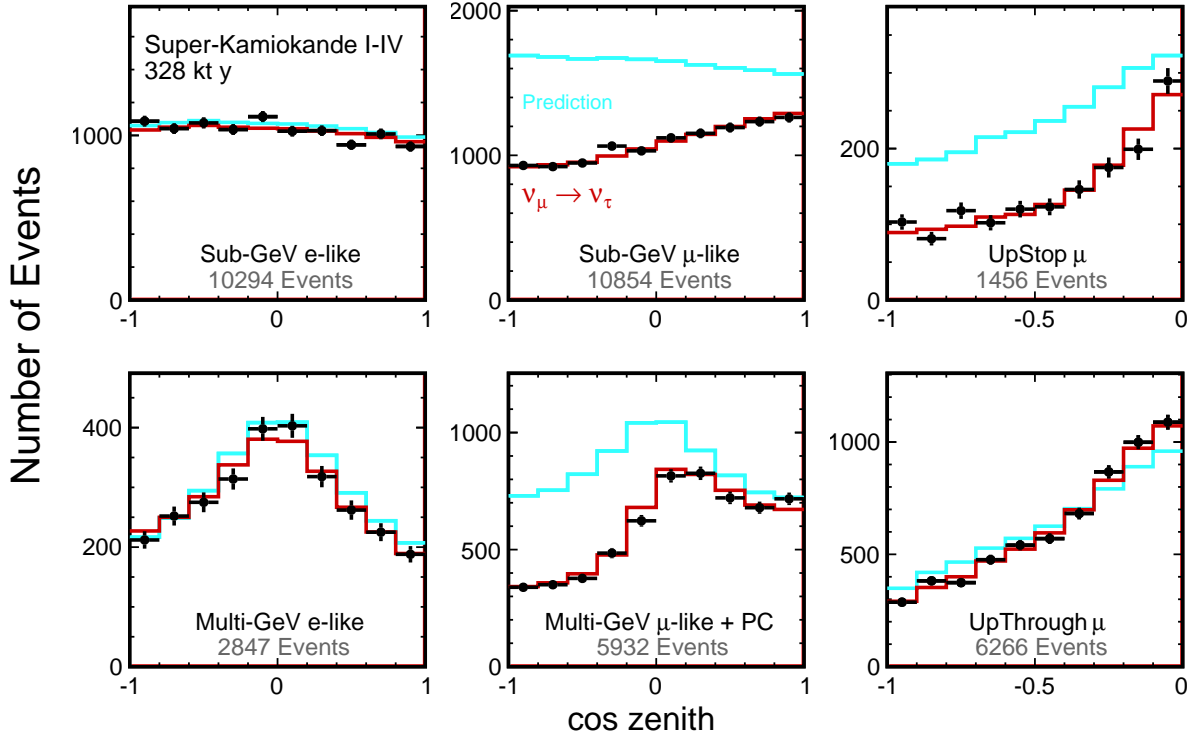


Figure 14.4: The zenith angle distributions of Super-Kamiokande atmospheric neutrino events. Fully contained 1-ring e -like and μ -like events with visible energy < 1.33 GeV (sub-GeV) and > 1.33 GeV (multi-GeV), as well as upward stopping and upward stopping μ samples are shown. Partially contained (PC) events are combined with multi-GeV μ -like events. The blue histograms show the non-oscillated Monte Carlo events, and the red histograms show the best-fit expectations for ν_μ - ν_τ oscillations. (This figure is provided by the Super-Kamiokande Collaboration)

Table 14.3: List of long-baseline neutrino oscillation experiments

Name	Beamline	Far Detector	L (km)	E_ν (GeV)	Year
K2K	KEK-PS	Water Cherenkov	250	1.3	1999–2004
MINOS	NuMI	Iron-scintillator	735	3	2005–2013
MINOS+	NuMI	Iron-scintillator	735	7	2013–2016
OPERA	CNGS	Emulsion	730	17	2008–2012
ICARUS	CNGS	Liquid argon TPC	730	17	2010–2012
T2K	J-PARC	Water Cherenkov	295	0.6	2010–
NOvA	NuMI	Liquid scint. tracking calorimeter	810	2	2014–

muon decays.

In order to maximize the sensitivity of the experiment, the ratio of baseline and neutrino energy (L/E) should be chosen to match the oscillation effects to be studied. In addition to maximizing the flux of neutrinos with relevant energy, neutrinos with irrelevant energy that result in unwanted background process should be suppressed. The energy of neutrino from a pion decay is

$$E_\nu = \frac{[1 - (m_\mu/m_\pi)^2]E_\pi}{1 + \gamma^2\theta^2}, \quad (14.71)$$

where E_ν and E_π are the energy of neutrino and pion, respectively, θ is the angle between the pion and neutrino direction, and $\gamma = E_\pi/m_\pi$. For $\theta = 0$, the energy of neutrino is linearly proportional to the energy of pion. In this case, a narrow band beam can be made by selecting the momentum of pions. On the other hand, for $\theta \neq 0$, the energy of neutrino is not strongly dependent on the parent energy for a wide range of pion energy, but dependent on the off-axis angle θ . Using this relation, a neutrino beam with narrow energy spectrum, around the energy determined by θ , can be produced. This off-axis beam method was first introduced for BNL E889 proposal [105] and adopted in T2K and NOvA experiments. For a list of neutrino beamlines, see also the review 32. Neutrino Beam Lines at High-Energy Proton Synchrotrons.

As indicated in Table 14.1, there are two different scales of base-

lines for accelerator-based experiments to study different ranges of Δm^2 . The atmospheric mass splitting $\Delta m^2 \sim 2.5 \times 10^{-3} \text{ eV}^2$ gives rise to the first oscillation maximum at $L/E \sim 500 \text{ GeV/km}$. In order to study this parameter region with ~ 1 GeV accelerator neutrino beam, a long baseline of a few hundreds to thousand km is necessary. On the other hand, there have been reports of possible neutrino oscillations at ~ 1 eV scale, which can be studied at ~ 1 km baseline with neutrinos from accelerators. These experiments are called short-baseline oscillation experiments.

The flux of a neutrino beam is calculated using Monte Carlo simulation based on the configuration of the beamline. An important ingredient of the neutrino flux prediction is the hadron production cross section. Data from dedicated hadron production experiments [106–108] are used to tune the beam simulation and constrain the uncertainty. The uncertainty of predicted neutrino flux for the most relevant energy region is ~ 5 – 10% with the latest hadron production data.

14.6.3.2 Near detectors and neutrino interaction cross sections

Many long-baseline experiments use two detectors to reduce the systematic uncertainties arising from neutrino flux and neutrino-nucleus interactions. The near detectors either use the same technology as the far detector or consist of sub-detectors with complementary functions to obtain detailed information of the neutrino beam and interactions. The near detectors provide information

for the neutrino flux, energy spectrum, and the interaction cross sections, which is used as an input to make predictions of observables at the far detector. However, even with the two-detector configuration, one should note that the neutrino flux is inevitably different between the near and the far detectors. In addition to the fact that the neutrino source looks like a line source for the near detector while it looks as a point source for the far detector, the neutrino oscillations alter the flavour composition of the neutrino beam quite significantly, as the design of a neutrino oscillation experiment requires.

For the precision measurements of neutrino oscillations with long-baseline experiments, the understanding of the neutrino-nucleus interaction becomes crucial. Because heavy nuclei are used as the interaction target, the nuclear effects complicate the understanding of the neutrino-nucleus interaction. For more information on the neutrino cross sections, see also the review 50. Neutrino Cross Section Measurements.

14.6.3.3 Long-baseline experiments

The first long-baseline experiment was the K2K experiment which used a neutrino beam from the KEK 12 GeV proton synchrotron directed towards Super-Kamiokande with a baseline of 250 km [109]. The beam had an average energy of 1.3 GeV. The K2K near detectors, located 300 m downstream of the production target, consisted of a combination of a 1 kt water Cherenkov detector and a set of fine grained detectors. K2K reported the confirmation of muon neutrino disappearance originally reported by Super-Kamiokande atmospheric neutrino observation [110].

The MINOS experiment used a beam from Fermilab and a detector in Soudan mine 735 km away [111]. The neutrino beam is produced in NuMI beamline [112] with 120 GeV proton beam from the Main Injector. The MINOS detectors are both iron-scintillator tracking calorimeters with toroidal magnetic fields. The far detector was 5.4 kt, while the near detector had a total mass of 0.98 kt and was located 1 km downstream of the production target. The NuMI beamline can vary the neutrino energy spectrum by changing the relative position of target and horns. Most of MINOS data were taken with the “low energy” configuration with the peak energy of around 3 GeV. MINOS combined accelerator and atmospheric neutrino data in both disappearance and appearance modes to measure oscillation parameters [113, 114]. Utilizing the separation of μ^- and μ^+ with the magnetic field in the far detector, MINOS also reported separate measurements of atmospheric neutrinos and antineutrinos [115].

When the NuMI beamline started operation for the NOvA experiment in 2013, it was set to the “medium energy” configuration which provided a beam with the peak neutrino energy of around 7 GeV to the MINOS+ experiment, which used the same MINOS near and far detectors. MINOS+ verified the energy dependence of ν_μ disappearance at energies above the first oscillation maximum. Utilizing the wide neutrino energy spectrum and high intensity in the medium energy configuration, limits on sterile neutrinos is reported [116].

In Europe, the CNGS neutrino beamline provided a beam with mean energy of 17 GeV from CERN to LNGS for long-baseline experiments with 732 km of baseline. The beam energy was chosen so that charged current (CC) interaction of ν_τ can occur for direct confirmation of ν_τ appearance. There was no near detector in CNGS because it was not necessary for the ν_τ appearance search. The OPERA experiment used a detector consisted of an emulsion/lead target with about 1.25 kt total mass complemented by electronic detectors. The excellent spatial resolution of emulsion enabled the event-by-event identification of τ leptons. OPERA observed ten ν_τ CC candidate events with 2.0 ± 0.4 expected background [92] and confirmed $\nu_\mu \rightarrow \nu_\tau$ oscillation in appearance mode with a statistical significance of 6.1σ . Another neutrino experiment, ICARUS [117], which used 600 t liquid argon time projection chambers, was operated in Gran Sasso from 2010 to 2012.

The first generation of long-baseline experiments confirmed the existence of neutrino oscillation. The major initial goal of second generation experiments was the observation of $\nu_\mu \rightarrow \nu_e$ oscillation. Using this appearance mode, by comparison of neutrino and antineutrino oscillation probabilities, search for CP violation

in the neutrino mixing becomes possible.

The T2K experiment started in 2010 using a newly constructed high-intensity proton synchrotron J-PARC and the Super-Kamiokande detector. It is the first long-baseline experiment to employ the off-axis neutrino beam. The off-axis angle of 2.5° was chosen to set the peak of neutrino energy spectrum at 0.6 GeV, matching the first maximum of oscillation probability at the 295 km baseline for $\Delta m^2 \sim 2.5 \times 10^{-3} \text{ eV}^2$. T2K employs a set of near detectors at about 280 m from the production target. The on-axis detector, called INGRID, is an array of iron-scintillator sandwich trackers to monitor the beam intensity, direction and profile. The off-axis detector ND280, consisting of several sub-detectors inside a magnet, is placed in the direction of far detector to measure the neutrino beam properties and to study neutrino interactions.

In 2011, T2K reported the first indication of $\nu_\mu \rightarrow \nu_e$ oscillation with a statistical significance of 2.5σ [118]. In the framework of 3ν mixing, it corresponds to detecting non-zero amplitude generated by the mixing angle θ_{13} (see Eq.14.33). Later $\nu_\mu \rightarrow \nu_e$ oscillation was established by T2K with more than 7σ in 2014 [119]. Figure 14.5 shows the reconstructed energy distributions from T2K, for neutrino and anti-neutrino beam mode and also for muon and electron candidates. The muon type events show clear deficit in both neutrino and antineutrino mode, consistent with the energy-dependent disappearance probability expected from neutrino oscillations. By a combined analysis of the neutrino and antineutrino data, T2K reported a hint of CP violation with more than 2σ [120, 121].

The NOvA experiment uses the NuMI beamline with an off-axis configuration. The 14 kt NOvA far detector is located near Ash River, Minnesota, 810 km away from the source. At 14.6 mrad off-axis from the central axis of the NuMI beam, the neutrino energy spectrum at the far detector has a peak around 2 GeV, corresponding to the first oscillation maximum at 810 km baseline. The near detector, located around 1 km from the source, has a functionally identical design to the far detector with a total active mass of 193 t. Both detectors are tracking calorimeters consisting of planes of polyvinyl chloride cells alternating in vertical and horizontal orientation filled with liquid scintillator.

The physics run of NOvA was started in 2014. Although the initial data indicated non-maximal mixing [122], later analysis with increased data and improved analysis resulted in the allowed region consistent with maximal mixing [123]. After confirmation of ν_e appearance from ν_μ beam [124, 125], NOvA started data taking with antineutrino beam in 2016. Using the antineutrino beam data, NOvA has reported the observation of $\bar{\nu}_e$ appearance from $\bar{\nu}_\mu$ beam with 4.4σ significance [126]. Figure 14.6 shows the reconstructed neutrino energy distributions from NOvA. Some values of the CP-violating phase δ_{CP} (see Eq.14.33) have been excluded for the inverted mass ordering ($m_3 < m_2 < m_1$, see Sec.14.7 for definitions), while no significant limit has been set for the case of normal mass ordering ($m_1 < m_2 < m_3$, see Sec.14.7 for definitions).

Two large-scale long-baseline experiments are under preparation or proposed in future. DUNE [103] will be a 1,300 km long-baseline experiment based in US. The DUNE far detector will consist of four modules of at least 10 kt fiducial mass liquid argon time projection chambers, located 1.5 km underground at the Sanford Underground Research Facility in South Dakota. The beamline for DUNE, 1.2 MW at start and upgradable to 2.4 MW, as well as the facility for near detectors will be newly constructed at Fermilab. In Japan, Hyper-Kamiokande [102] is proposed as the successor of the Super-Kamiokande detector. It will be a water Cherenkov detector with 260 (190) kt total (fiducial) mass. With upgrade of existing accelerator and beamline, J-PARC will provide a 1.3 MW neutrino beam to Hyper-Kamiokande. Both DUNE and Hyper-Kamiokande will have a rich physics program besides the long-baseline experiment, such as searches for nucleon decays and study of supernova neutrinos.

14.6.3.4 Short-baseline experiments

The LSND experiment searched for neutrino oscillation using neutrinos from stopped pions at Los Alamos. A 800 MeV linac was used to produce pions which stopped in the target. Most of

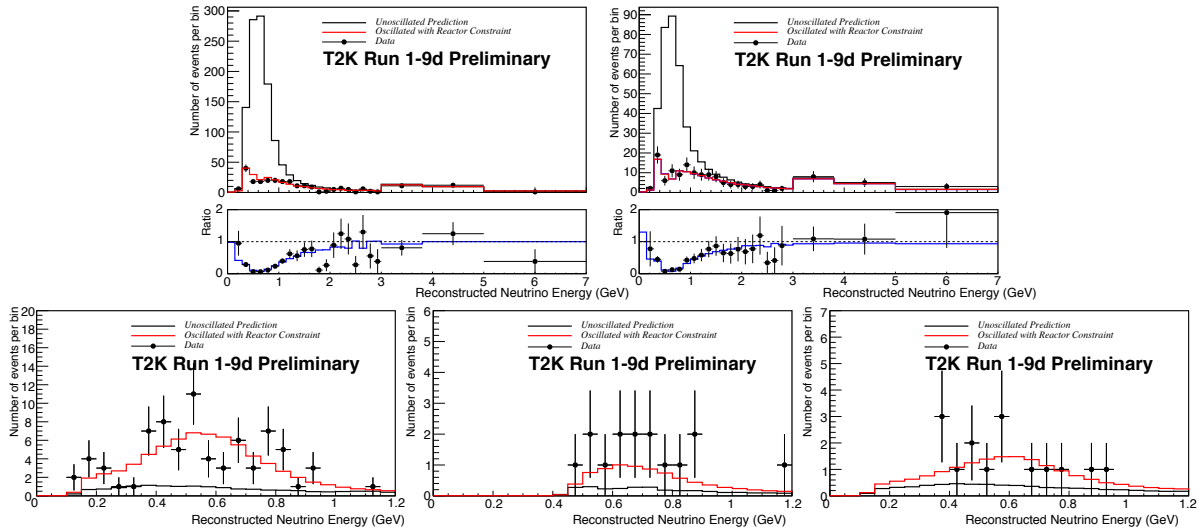


Figure 14.5: Reconstructed neutrino energy distributions from T2K. Data points with statistical error bars are shown together with the prediction without (black line) and including (red line) neutrino oscillation. Top: Single ring μ -like events. The left and right plot is for neutrino and antineutrino beam mode, respectively. Below each plot, the ratio to the prediction without oscillation is also shown. Bottom: Single ring e -like events. From left to right, 0 decay electron sample for neutrino beam, 1 decay electron sample for neutrino beam, and 0 decay electron sample for antineutrino beam. (This figure is provided by the T2K Collaboration)

π^- s are absorbed by the nuclei inside the target, while π^+ s and their daughter μ^+ s decay and produce neutrinos. Therefore, the produced neutrinos are mostly ν_μ , $\bar{\nu}_\mu$, and ν_e with very small contamination of $\bar{\nu}_e$. The detector was a tank filled with 167 t of diluted liquid scintillator, located about 30 m from the neutrino source. LSND searched for $\bar{\nu}_\mu \rightarrow \bar{\nu}_e$ appearance using the inverse beta decay process, $\bar{\nu}_e + p \rightarrow e^+ + n$, and found an excess of $87.9 \pm 22.4 \pm 6.0$ events over the expected background [127].

The KARMEN experiment was performed at the neutron spallation facility ISIS of the Rutherford Appleton Laboratory. The KARMEN 2 detector was a segmented liquid scintillation calorimeter with total volume of 65 m^3 located at a mean distance of 17.7 m from the ISIS target. KARMEN found a number of events consistent with the total background expectation, showing no signal for $\bar{\nu}_\mu \rightarrow \bar{\nu}_e$ oscillations [128]. The resulting limits exclude large regions of the parameter area favored by LSND.

The MiniBooNE experiment at Fermilab used a conventional neutrino beam to search for ν_e and $\bar{\nu}_e$ appearance in the same parameter region as LSND. The booster neutrino beamline (BNB) with a single magnetic horn uses a 8 GeV proton beam from the Fermilab booster to produce a neutrino (antineutrino) beam with energy spectrum peak of 600 (400) MeV. The MiniBooNE detector consists of a 12.2 m diameter sphere filled with 818 t of mineral and oil located 541 m from the target. MiniBooNE reported ν_e and $\bar{\nu}_e$ event excess in both neutrino and antineutrino running modes. In total, 460.5 ± 99.0 excess events are observed over the expected backgrounds, corresponding to 4.7σ significance [129].

Both LSND and MiniBooNE are single detector experiments. The reported excess will be further investigated with the multi-detector short-baseline neutrino (SBN) program at Fermilab BNB [130]. The SBN program comprises three liquid argon time projection chambers at different baselines in the same neutrino beamline. The 112 t Short-Baseline Near Detector will be located at 110 m from the target. The 85 t MicroBooNE detector has been operated at 470 m from the target. The ICARUS detector has been transported from Europe after refurbishment at CERN and is located at a baseline of 600 m.

JSNS² experiment at J-PARC will search for neutrino oscillations with $\Delta m^2 \sim 1 \text{ eV}^2$ [131]. 1MW proton beam from the 3 GeV Rapid Cycling Synchrotron of J-PARC will produce neutrinos from muon decay at rest. With a detector filled with gadolinium loaded liquid scintillator of 17 t fiducial mass at 24 m from the target, JSNS² is aiming to provide a direct test of the LSND anomaly.

14.6.4 Reactor Antineutrinos

14.6.4.1 Reactor antineutrino flux

Nuclear reactors are very intense sources of $\bar{\nu}_e$'s in the MeV energy region, which are generated in nuclear fission of heavy isotopes (mainly ^{235}U , ^{238}U , ^{239}Pu , and ^{241}Pu). The $\bar{\nu}_e$ flux from a reactor can be estimated based on the thermal power output and fuel composition as a function of time. On average, about six $\bar{\nu}_e$'s are emitted and about 200 MeV of energy is released per fission. Therefore, a 1 GW_{th} (thermal power) reactor produces about 2×10^{20} $\bar{\nu}_e$'s per second.

The detailed estimate of $\bar{\nu}_e$ flux and energy spectrum can be obtained by either summing up the spectra of beta decays involved using available nuclear data information of each fission fragment and its decays, or using measurements of cumulative electron spectra associated with the beta decays of fission fragments. Because the fission of four main fuel isotopes involves thousands of beta-decay branches, a completely *ab initio* calculation is challenging. The cumulative electron spectra for ^{235}U , ^{239}Pu , and ^{241}Pu were measured at the Institut Laue-Langevin (ILL) reactor in Grenoble, France in the 1980s [132–134]. For the prediction of $\bar{\nu}_e$ flux from ^{238}U , a summation calculation in [135] was often used together with the ILL results.

A recent calculation of the reactor $\bar{\nu}_e$ flux [136] uses an improved *ab initio* approach for ^{238}U and combined information from nuclear databases and electron spectra measured at ILL for ^{235}U , ^{239}Pu , and ^{241}Pu . Another calculation [137] is provided for ^{235}U , ^{239}Pu , and ^{241}Pu based on the ILL measurement of electron spectra, taking into account higher order corrections and minimizing the use of nuclear databases. Both calculations predict about 3% higher normalization for the energy-averaged antineutrino fluxes of ^{235}U , ^{239}Pu , and ^{241}Pu compared to the original analyses of ILL data. However, the reactor antineutrino flux measurement at Daya Bay [138] is consistent with the old flux predictions and the flux measurement results. Also, an excess of $\bar{\nu}_e$ flux around 5 MeV, compared to the prediction, has been observed by recent reactor experiments [139–142]. Measurements of a fuel-dependent reactor $\bar{\nu}_e$ rate by Daya Bay [143] and RENO [144], and individual antineutrino spectra from ^{235}U and ^{239}Pu by Daya Bay [145] showed a discrepancy between the observed and predicted rate and spectrum from ^{235}U .

14.6.4.2 Reactor antineutrino oscillation experiments

Charged current interaction cannot happen if a reactor $\bar{\nu}_e$ changes its flavour to $\bar{\nu}_\mu$ or $\bar{\nu}_\tau$, because its energy is not sufficient to produce heavier charged leptons. Thus, $\bar{\nu}_e$ disappearance is the

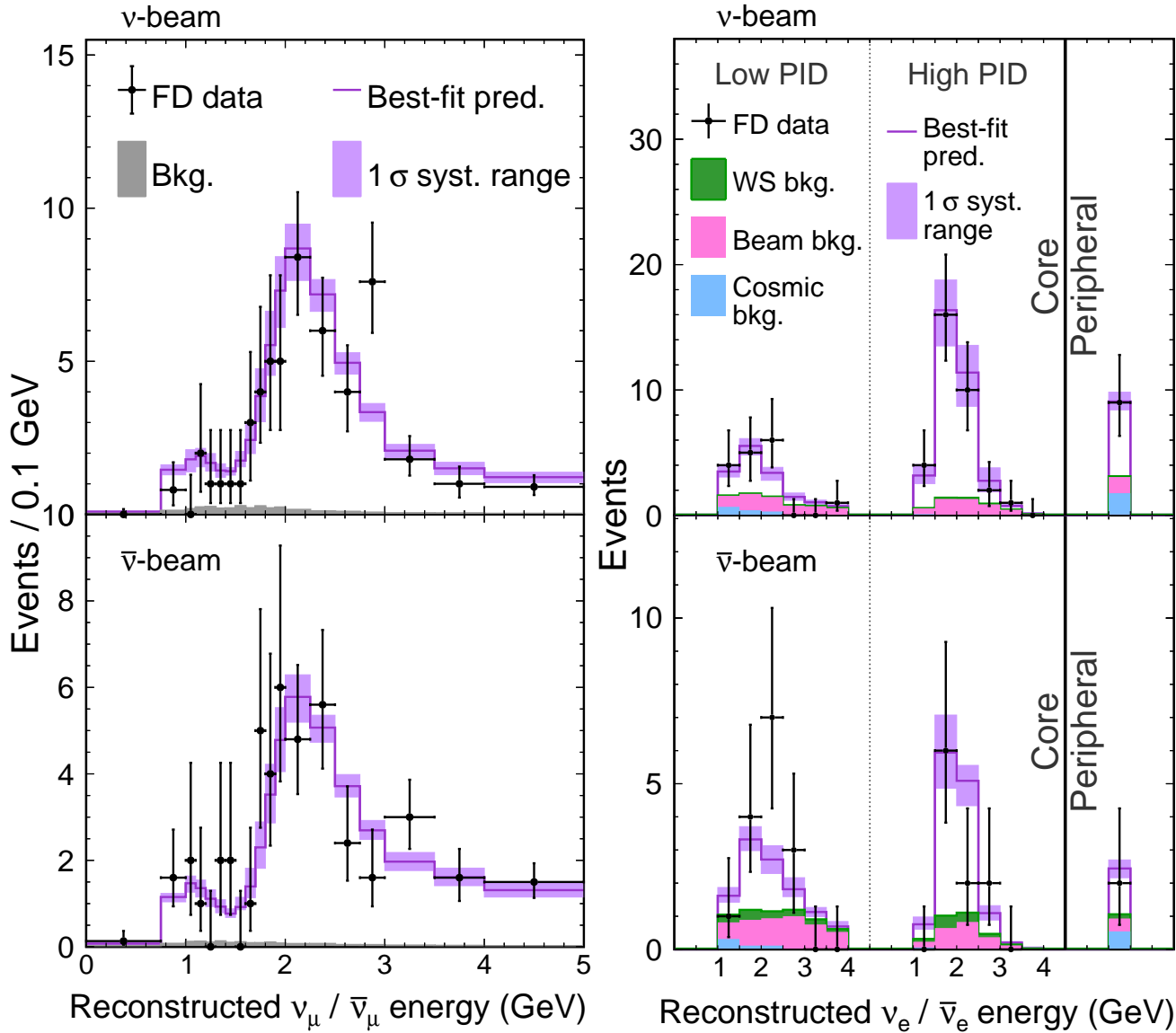


Figure 14.6: Reconstructed neutrino energy distributions from the NOvA far detector [126]. Top plots are for neutrino beam mode and bottom plots are for antineutrino beam mode. Left: muon-type candidates. Right: electron-type candidates, split into a low and high purity sample as well as the event counts in the peripheral sample which occurred near the edge of the detector.

Table 14.4: List of reactor antineutrino oscillation experiments

Name	Reactor power (GW _{th})	Baseline (km)	Detector mass (t)	Year
KamLAND	various	180 (ave.)	1,000	2001–
Double Chooz	4.25×2	1.05	8.3	2011–2018
Daya Bay	2.9×6	1.65	20×4	2011–
RENO	2.8×6	1.38	16	2011–
JUNO	26.6 (total)	53	20,000	

only channel to study neutrino flavour change with reactor experiments. The inverse beta decay $\bar{\nu}_e + p \rightarrow e^+ + n$ provides a way to detect $\bar{\nu}_e$ in the relevant energy region. The energy of prompt signal from e^+ , E_p , is related to the energy of $\bar{\nu}_e$, $E_{\bar{\nu}} \sim E_p + 0.8$ MeV. The delayed coincidence with the signal from γ ray emitted by neutron capture on nucleus after thermalization very efficiently suppresses the backgrounds. Liquid scintillator is often used to realize large detectors containing hydrogen as the target of inverse beta decay. In order to increase the neutron detection efficiency, liquid scintillator is sometimes loaded with gadolinium because of large neutron capture cross section and higher energy of emitted γ rays, the total energy of about 8 MeV, by gadolinium, in contrast

to 2.2 MeV for the capture by hydrogen.

Early reactor experiments that searched for neutrino oscillations at short or intermediate baselines reported negative results. The CHOOZ [146] and Palo Verde [147] experiments in 1990's searched for neutrino oscillations in the $\Delta m^2 \sim 10^{-2}$ – 10^{-3} eV² range and set a limit on the corresponding mixing angle $\sin^2 2\theta < 0.1$ at 90% CL.

Table 14.4 shows a list of reactor antineutrino experiments measuring neutrino oscillation. As was also shown in Table 14.1, experiments are designed with different baselines because of the different scale of mass splittings found by solar and atmospheric neutrino experiments. Experiments with O(100) km baseline are

sensitive to Δm^2 of 10^{-4} – 10^{-5} eV², while ~ 1 km of baseline results in a sensitivity in a range of 10^{-2} – 10^{-3} eV².

The KamLAND detector consists of 1,000 t of ultra-pure liquid scintillator contained in a 13-m diameter spherical balloon [148]. The detector is located in the original Kamiokande cavern, where the $\bar{\nu}_e$ flux was dominated by a few reactors at an average distance of ~ 180 km until 2011. KamLAND reported the first results in 2002 showing that the ratio of the observed number of $\bar{\nu}_e$ events and expectation without disappearance is $0.611 \pm 0.085 \pm 0.041$, evidence for reactor $\bar{\nu}_e$ disappearance at the 99.95% confidence level [148]. It confirmed a large value of the mixing angle corresponding to the LMA solution, which was reported by solar neutrino experiments. It is noted that there is a $\sim 2\sigma$ level tension between the global solar neutrino data and KamLAND reactor data regarding the best-fit value of Δm^2 , while the mixing angle is consistent. KamLAND also showed the evidence of $\bar{\nu}_e$ spectrum distortion consistent with the expectation from neutrino oscillations [149]. Figure 14.7 shows the ratio of observed $\bar{\nu}_e$ spectrum to the expectation for no-oscillation as a function of L_0/E ($L_0 = 180$ km) for the KamLAND data. A clear oscillatory signature can be seen.

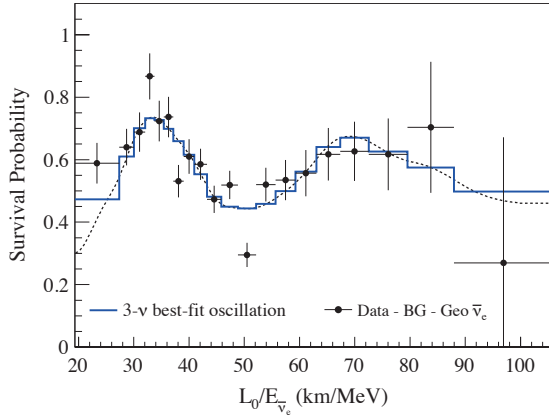


Figure 14.7: Ratio of the observed $\bar{\nu}_e$ spectrum to the expectation for no-oscillation versus L_0/E for the KamLAND data. $L_0 = 180$ km is the flux-weighted average reactor baseline. The 3- ν histogram is the best-fit survival probability curve from the three-flavour unbinned maximum-likelihood analysis using only the KamLAND data. This figure is taken from [150].

Following the establishment of neutrino oscillations with atmospheric, solar, accelerator, and reactor experiments, the measurement of the remaining mixing angle θ_{13} was recognized as the next major milestone. A reactor neutrino experiment with a baseline of ~ 1 km can make an almost pure measurement of $\sin^2 2\theta_{13}$ from disappearance of $\bar{\nu}_e$. To be sensitive to a small value below the limit set by CHOOZ and Palo Verde, experiments with two detectors were proposed. Among several proposals, three experiments have been realized: Double Chooz in France [151], Daya Bay in China [152], and RENO in Korea [153].

These three experiments employ similar detector design optimized for the precise measurement of reactor antineutrino. An antineutrino detector consists of a cylindrical stainless steel vessel that houses two nested acrylic cylindrical vessels. The innermost vessel is filled with gadolinium-doped liquid scintillator as the primary antineutrino target. It is surrounded by a liquid scintillator layer to contain γ rays from the target volume. A buffer layer of mineral oil is placed an outside to shield inner volumes from radioactivity of PMTs and surrounding rock. The light from liquid scintillator is detected by an array of PMTs mounted on the stainless steel vessel. Optically separated by the stainless steel vessel, outside region is instrumented as a veto detector with either liquid scintillator (Double Chooz) or water Cherenkov (Daya Bay and RENO) detector.

The Double Chooz detector has gadolinium-doped liquid scintillator with mass of 8.3 t. The far detector at a baseline of ~ 1050 m from the two 4.25 GW_{th} reactors started physics data taking in

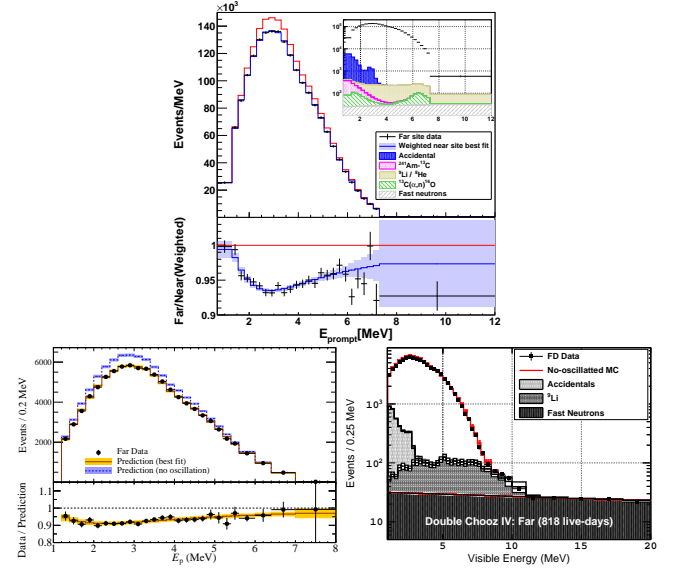


Figure 14.8: Energy spectra for prompt events at the far detectors for Daya Bay [139], RENO [140], and Double Chooz [141].

2011. The near detector, located at ~ 400 m from the reactors, was completed in the end of 2014. Double Chooz finished data taking in early 2018. Daya Bay has two near (flux-weighted baseline 470 m and 576 m) and one far (1648 m) underground experimental halls near six reactors with 2.9 GW_{th} each. Daya Bay has eight antineutrino detectors in total; two detectors in each of the near detector halls, and four detectors in the far detector hall. Each detector contains 20 t of gadolinium-loaded liquid scintillator. RENO has two identical detectors located at 294 m and 1383 m from the center of an array of six 2.8 GW_{th} reactors. The mass of gadolinium-loaded liquid scintillator is 16 t per detector. RENO started data taking with both near and far detectors from August 2011.

All the three reactor neutrino experiments published first results in 2012. First, Double Chooz reported an indication of reactor electron antineutrino disappearance with the ratio of observed to expected events of $R = 0.944 \pm 0.016 \pm 0.04$, ruling out the no-oscillation hypothesis at the 94.6% CL [154]. Daya Bay observed $R = 0.940 \pm 0.011 \pm 0.004$, corresponding to 5.2σ significance of non-zero value of θ_{13} [155]. RENO also reported $R = 0.920 \pm 0.009 \pm 0.014$, indicating a non-zero value of θ_{13} with a significance of 4.9σ [156]. These results established non-zero value of θ_{13} .

In the latest analysis, both Daya Bay [139] and RENO [140] report results constraining mass-squared difference as well as the mixing angle by using both relative $\bar{\nu}_e$ rate and energy spectra information. Double Chooz has reported the first analysis based on both far and near detectors [141] for the mixing angle, using neutron capture on any elements (primarily gadolinium and hydrogen) to increase the effective target mass. Figure 14.8 shows the energy spectra of the prompt signals observed in the far detector of three experiments.

In all three experiments as well as in the NEOS experiment [142], an excess of $\bar{\nu}_e$ events over expected energy spectrum have been observed around 5 MeV as mentioned earlier. This excess is observed in both near and far detectors and scales with the reactor power. Thanks to the cancellation between the near and far detectors, the neutrino oscillation measurements are not affected in multi-detector setup.

With a baseline of ~ 50 km and an excellent energy measurement, reactor antineutrino experiments have significant sensitivity to the mass ordering. The JUNO experiment [157] aims to determine the mass ordering with this technique as its primary goal. It can also provide precision measurements of neutrino mixing parameters as well as a broad non-oscillation program. The JUNO detector, which is under construction, will consist of 20 kt

Table 14.5: List of reactor antineutrino experiments for $O(eV^2)$ oscillations

Name	Reactor power (MW _{th})	Baseline (m)	Detector mass (t)	Detector technology	S/B
NEOS	2,800	24	1	Gd-LS	22
DANSS	3,100	10–12	0.9	Gd-PS	~30
STEREO	57	9–11	1.7	Gd-LS	0.9
PROSPECT	85	7–9	4	⁶ Li-LS	1.3
NEUTRINO-4	100	6–12	1.5	Gd-LS	0.5
SoLid	80	6–9	1.6	⁶ Li-PS	

liquid scintillator and be located at 53 km from two nuclear power plants in China.

14.6.4.3 New reactor experiments sensitive to $O(1)$ eV^2 oscillations

Possible hints of neutrino oscillation at a scale of $\Delta m^2 \sim 1 eV^2$ (see Sec.14.8) have motivated reactor experiments at a distance of ~ 10 m from the core. Recent experiments searching for $\sim 1 eV^2$ oscillation at reactors are summarized in Table 14.5.

As the antineutrino source, some use industrial reactors which can provide a large flux leading to a high statistical precision. On the other hand, though the flux is orders of magnitude smaller, a research reactor could have favorable conditions, such as relatively easier access to a short baseline, simpler fuel composition, and compact size of the core.

The detectors are based on organic scintillators, either liquid scintillator (LS) or solid plastic scintillator (PS), which contain hydrogen as the target for inverse beta decay ($\bar{\nu}_e + p \rightarrow e^+ + n$). To identify the signal, neutron capture on either gadolinium (Gd) or ⁶Li is detected with delayed coincidence. When a neutron is captured by Gd, γ rays with a total energy of 8 MeV are emitted. After neutron capture, ⁶Li decays into triton and α . The effect of neutrino oscillation appears as a distortion of energy spectrum. To be independent from the reactor neutrino spectrum uncertainties, some experiments compare the spectra at different baselines by using a segmented detector or moving the detector.

The NEOS [142] uses about 1 t of gadolinium-loaded liquid scintillator in an unsegmented detector. It is located at 23.7 m from the center of a commercial reactor and covered by an overburden of about 20 meters of water equivalent. Thanks to the high power reactor, NEOS observes antineutrino events at a rate of 1976 per day, with a signal to background ratio of about 22. The energy resolution is 5% at 1 MeV.

DANSS [158] is another experiment using a commercial reactor. The detector is highly segmented, consisting of 2,500 plastic scintillator strips, each with the size of $1 \times 4 \times 100$ cm³ and coated with a thin gadolinium-loaded reflective layer. The detector is placed on a movable platform below the reactor core. The overburden of 50 m water-equivalent reduces the cosmic muon flux by a factor of six. Data are taken with three baselines, 10.7, 11.7, and 12.7 m for a comparison between different baselines. The energy resolution of $\sigma_E/E \sim 34\%$ at 1 MeV and the large size of the reactor core, 3.7 m in height and 3.2 m in diameter, somewhat smear the oscillation pattern. However it is compensated by high statistics due to the high power reactor. The observed event rate is 4899 events per day, with less than 3% cosmic background contamination, at 10.7 m position.

The STEREO detector [159] has six identical target cells of 37 cm length, $\sim 2m^3$ of volume in total, filled with gadolinium-loaded liquid scintillator. They are placed from 9.4 to 11.1 m from the compact (80 cm high, 40 cm diameter) core of the ILL research reactor. The reconstructed energy resolution (σ_E/E) is about 9% at 0.835 MeV. The antineutrino event rate is 396 events per day with a signal to background ratio of about 0.9.

The PROSPECT detector [160] consists of a segmented 4 t ⁶Li-doped liquid scintillator detector covering a baseline range of 7–9 m from the reactor core. Thin reflecting panels divide the LS volume into an 11×14 two-dimensional array of 154 optically isolated rectangular segments ($14.5 \times 14.5 \times 117.6$ cm³). The energy resolution is 4.5% at 1 MeV. The detector is placed on the ground floor with an overburden of less than 1 m water-equivalent. With

efficient background suppression by using pulse shape discrimination and 3D position reconstruction, a signal to background ratio of 1.3 is achieved. The antineutrino rate is 771 events per day.

NEUTRINO-4 [161] uses a gadolinium-loaded liquid scintillator detector segmented in 10×5 sections with a total volume of 1.8 m³. The detector is installed on a movable platform and moved to various positions with baselines of 6–12 m. With the detector location close to the surface and no pulse shape discrimination capability, the signal to background ratio is about 0.5. The energy resolution is 16% at 1 MeV.

The SoLid detector [162] is a finely segmented detector made of $5 \times 5 \times 5$ cm³ plastic scintillator cubes and ⁶LiF:ZnS sheets. A detector with 1.6 t of active volume is installed at a distance of 6–9 m from the research reactor core with an overburden of 10 m water-equivalent. The triton and α from neutron capture by ⁶Li are detected by scintillation of ZnS. A high n - γ separation capability is achieved using the difference of time constant of scintillation between ZnS and plastic scintillator. Very fine segmentation of the detector allows 3D reconstruction of events, which also provide effective background discrimination. The energy resolution (σ_E/E) is expected to be $\sim 14\%$ at 1 MeV.

14.7 Combined Analysis of Experimental Results: The 3ν Paradigm

From the experimental situation described in Sec.14.6 we conclude that

- Atmospheric ν_μ and $\bar{\nu}_\mu$ disappear most likely converting to ν_τ and $\bar{\nu}_\tau$. The results show an energy and distance dependence perfectly described by mass-induced oscillations.
- Accelerator ν_μ and $\bar{\nu}_\mu$ disappear over distances of ~ 200 to 800 km. The energy spectrum of the results show a clear oscillatory behaviour also in accordance with mass-induced oscillations with wavelength in agreement with the effect observed in atmospheric neutrinos.
- Accelerator ν_μ and $\bar{\nu}_\mu$ appear as ν_e and $\bar{\nu}_e$ at distances ~ 200 to 800 km.
- Solar ν_e convert to ν_μ and/or ν_τ . The observed energy dependence of the effect is well described by massive neutrino conversion in the Sun matter according to the MSW effect
- Reactor $\bar{\nu}_e$ disappear over distances of ~ 200 km and ~ 1.5 km with different probabilities. The observed energy spectra show two different mass-induced oscillation wavelengths: at short distances in agreement with the one observed in accelerator ν_μ disappearance, and a long distance compatible with the required parameters for MSW conversion in the Sun.

The minimum scenario to describe these results requires the mixing between the three flavour neutrinos of the standard model in three distinct mass eigenstates. In this case U in Eq. (14.32) is a 3×3 matrix analogous to the CKM matrix for the quarks [21] but due to the possible Majorana nature of the neutrinos it can depend on six independent parameters: three mixing angles and three phases. There are several possible conventions for the ranges of the angles and ordering of the states. The community finally agreed to a parametrization of the leptonic mixing matrix as in Eq. (14.33). The angles θ_{ij} can be taken without loss of generality to lie in the first quadrant, $\theta_{ij} \in [0, \pi/2]$, and the phase $\delta_{CP} \in [0, 2\pi]$. Values of δ_{CP} different from 0 and π imply CP violation in neutrino oscillations in vacuum [163–165]. The Majorana phases η_1 and η_2 play no role in neutrino oscillations [164, 166].

Hence for the study of neutrino oscillations in the 3ν mixing scenario one can use the parametrization in Eq. (14.34) irrespective of whether neutrinos are Dirac or Majorana particles. Indeed, Majorana phases are very hard to measure since they are only physical if neutrino mass is non-zero and therefore the amplitude of any process involving them is suppressed a factor m_ν/E to some power where E is the energy involved in the process which is typically much larger than the neutrino mass. The most sensitive experimental probe of Majorana phases is the rate of neutrinoless $\beta\beta$ decay as discussed in Secs. 14.9.3 and 14.9.2.

In this convention there are two non-equivalent orderings for the spectrum of neutrino masses:

- Spectrum with Normal Ordering (NO) with $m_1 < m_2 < m_3$
- Spectrum Inverted ordering (IO) with $m_3 < m_1 < m_2$.

Furthermore the data show a hierarchy between the mass splittings, $\Delta m_{21}^2 \ll |\Delta m_{31}^2| \simeq |\Delta m_{32}^2|$ with $\Delta m_{ij}^2 \equiv m_i^2 - m_j^2$.

In this section we follow the convention used in the listing section of the PDG and discuss the results for both, NO and IO, using Δm_{21}^2 , which is always the smallest mass splitting, and Δm_{32}^2 which, up to a sign, is the largest mass splitting for IO, while for NO the largest mass splitting is $\Delta m_{31}^2 = \Delta m_{32}^2 + \Delta m_{21}^2$.

With what we know of the mass differences (see table 14.7) and the neutrino mass scale (see Sec. 14.9), depending on the value of the lightest neutrino mass, the neutrino mass spectrum can be further classified in:

- Normal Hierarchical Spectrum (NH): $m_1 \ll m_2 < m_3$,
 $\Rightarrow m_2 \simeq \sqrt{\Delta m_{21}^2} \sim 8.6 \times 10^{-3} \text{eV}$, $m_3 \simeq \sqrt{\Delta m_{32}^2 + \Delta m_{21}^2} \sim 0.05 \text{eV}$,
- Inverted Hierarchical Spectrum (IH): $m_3 \ll m_1 < m_2$,
 $\Rightarrow m_1 \simeq \sqrt{|\Delta m_{32}^2 + \Delta m_{21}^2|} \sim 0.0492 \text{eV}$, $m_2 \simeq \sqrt{|\Delta m_{32}^2|} \sim 0.05 \text{eV}$,
- Quasidegenerate Spectrum (QD): $m_1 \simeq m_2 \simeq m_3 \gg \sqrt{|\Delta m_{32}^2|}$.

Sometimes in the literature the determination of the neutrino mass spectrum is referred to as determination of the neutrino hierarchy. However, as described above, with what we know so far of the neutrino mass scale, the neutrino spectrum may or may not be hierarchical. Therefore determination of neutrino mass ordering is a more precise expression and it is the one used in this review.

In total the 3ν oscillation analysis of the existing data involves six parameters: 2 mass differences (one of which can be positive or negative), 3 mixing angles, and the CP phase. The different experiments described in Sec.14.6 provide information on different subsets of these parameters. The precise statistical analysis of the data requires the numerical evaluation of the corresponding oscillation probabilities by solving the evolution equation of the neutrino ensemble from their source to the experiment. Nevertheless the dominant effects in the different experiments can be qualitatively understood in terms of approximate expressions for the oscillation probabilities which, for convenience, we briefly summarize here.

14.7.1 3ν Oscillation Probabilities

The relevant survival probabilities for solar and KamLAND experiments in the framework of three neutrino oscillations can be written as:

$$P_{ee}^{3\nu} = \sin^4 \theta_{13} + \cos^4 \theta_{13} P_{ee}^{2\nu}(\Delta m_{21}^2, \theta_{12}), \quad (14.72)$$

where we have used the fact that $L_{0,32}^{\text{osc}} = 4\pi E_\nu / \Delta m_{32}^2$ is much shorter than the distance travelled by both solar and KamLAND neutrinos, so that the oscillations related to $L_{0,32}^{\text{osc}}$ are averaged. In presence of matter effects $P_{ee}^{2\nu}(\Delta m_{21}^2, \theta_{12})$ should be calculated taking into account the evolution in an effective matter density $n_e^{\text{eff}} = n_e \cos^2 \theta_{13}$. For $10^{-5} \lesssim \Delta m^2 / \text{eV}^2 \lesssim$

10^{-4} , $P_{ee}^{2\nu}(\Delta m_{21}^2, \theta_{12})$ presents the following asymptotic behaviours [167]:

$$P_{ee}^{2\nu, \text{sun}} \simeq 1 - \frac{1}{2} \sin^2(2\theta_{12}) \quad \text{for } E_\nu \lesssim \text{few} \times 100 \text{ keV}, \quad (14.73)$$

$$P_{ee}^{2\nu, \text{sun}} \simeq \sin^2(\theta_{12}) \quad \text{for } E_\nu \gtrsim \text{few} \times 1 \text{ MeV}, \quad (14.74)$$

$$P_{ee}^{2\nu, \text{kam}} = 1 - \frac{1}{2} \sin^2(2\theta_{12}) \sin^2 \frac{\Delta m_{21}^2 L}{2E_\nu}. \quad (14.75)$$

At present most of the precision of the solar analysis is provided by SNO and SK for which the relevant MSW survival probability provides a direct measurement of $\sin^2 \theta_{12}$, as seen in Eq. (14.74). In the MSW regime the determination of Δm_{21}^2 in solar experiments comes dominantly from the ratio between the solar potential and the Δm_{21}^2 term required to simultaneously describe the CC/NC data at SNO and the undistorted spectra of ^8B neutrinos as measured in both SK and SNO. Conversely, KamLAND $\bar{\nu}_e$ survival probability proceeds dominantly as vacuum oscillations and provides a most precise determination of Δm_{21}^2 via the strong effect of the oscillating phase in the distortion of the reactor energy spectrum. On the contrary it yields a weaker constraint on θ_{12} as the vacuum oscillation probability depends on the double-valued and “flatter” function $\sin^2(2\theta_{12})$.

In what respects the interpretation of ν_μ disappearance data at LBL experiments, the ν_μ survival probability can be expanded in the small parameters $\sin \theta_{13}$ and $\alpha \equiv \Delta m_{21}^2 / \Delta m_{31}^2$ to good accuracy as [168, 169]

$$\begin{aligned} P_{\nu_\mu \rightarrow \nu_\mu} &\approx 1 - \sin^2 2\theta_{\mu\mu} \sin^2 \frac{\Delta m_{\mu\mu}^2 L}{4E_\nu} \\ &\approx 1 - \cos^2 \theta_{13} \sin^2(2\theta_{23}) \sin^2 \frac{\Delta m_{32}^2 L}{4E_\nu} + \mathcal{O}(\alpha, s_{13}^2), \end{aligned} \quad (14.76)$$

with

$$\begin{aligned} \sin^2 \theta_{\mu\mu} &= \cos^2 \theta_{13} \sin^2 \theta_{23}, \\ \Delta m_{\mu\mu}^2 &= \sin^2 \theta_{12} \Delta m_{31}^2 + \cos^2 \theta_{12} \Delta m_{32}^2 \\ &\quad + \cos \delta_{\text{CP}} \sin \theta_{13} \sin 2\theta_{12} \tan \theta_{23} \Delta m_{21}^2. \end{aligned}$$

At present ν_μ disappearance results at LBL provide the best determination of $|\Delta m_{32}^2|$ and θ_{23} but as seen above, the probability is symmetric with respect to the octant of $\theta_{\mu\mu}$ which implies symmetry around $s_{23}^2 = 0.5/c_{13}^2$.

The relevant oscillation probability for ν_e appearance at LBL experiments can be expanded at the second order in the small parameters $\sin \theta_{13}$ and α , and assuming a constant matter density it takes the form [170–172]:

$$\begin{aligned} P_{\nu_\mu \rightarrow \nu_e}(\bar{\nu}_\mu \rightarrow \bar{\nu}_e) &\approx 4 \sin^2 \theta_{13} \sin^2 \theta_{23} \frac{\sin^2 \Delta}{(1-A)^2} \\ &\quad + \alpha^2 \sin^2 2\theta_{12} \cos^2 \theta_{23} \frac{\sin^2 A \Delta}{A^2} \\ &\quad + 8\alpha J_{\text{CP}}^{\text{max}} \cos(\Delta \pm \delta_{\text{CP}}) \frac{\sin \Delta A}{A} \frac{\sin \Delta(1-A)}{1-A}, \end{aligned} \quad (14.77)$$

with

$$J_{\text{CP}}^{\text{max}} = \cos \theta_{12} \sin \theta_{12} \cos \theta_{23} \sin \theta_{23} \cos^2 \theta_{13} \sin \theta_{13}, \quad (14.78)$$

and

$$\Delta \equiv \frac{\Delta m_{31}^2 L}{4E_\nu}, \quad A \equiv \frac{2E_\nu V}{\Delta m_{31}^2}, \quad (14.79)$$

where V is the effective matter potential in the Earth crust. Results on ν_e appearance at LBL provide us with the dominant information on leptonic CP violation. Furthermore α , Δ , and A are sensitive to the sign of Δm_{32}^2 (*i.e.*, the type of the neutrino mass ordering). The plus (minus) sign in Eq. (14.77) applies for

neutrinos (antineutrinos), and for antineutrinos $V \rightarrow -V$, which implies $A \rightarrow -A$. Numerically one finds for a typical Earth crust matter density of 3 g/cm^3 that at T2K with $E \sim 0.7 \text{ GeV}$, matter effects are of order few percent, whereas in NOvA with $E \sim 2 \text{ GeV}$ we can have $|A| \sim 0.2$. Also $\alpha^2 \approx 10^{-3}$, which implies that the second term in the first line of Eq. (14.77) gives a very small contribution compared to the other terms. Also, the first term in Eq. (14.77) (which dominates for large θ_{13}) depends on $\sin^2 \theta_{23}$ and therefore is sensitive to the octant.

The ν_e survival probability relevant for reactor experiments with medium baseline (MBL), $L \sim 1 \text{ km}$, can be approximated as [169, 173]:

$$P_{\nu_e \rightarrow \nu_e} = 1 - \sin^2 2\theta_{13} \sin^2 \frac{\Delta m_{ee}^2 L}{4E\nu} + \mathcal{O}(\alpha^2), \quad (14.80)$$

where

$$\Delta m_{ee}^2 = \cos^2 \theta_{12} \Delta m_{31}^2 + \sin^2 \theta_{12} \Delta m_{32}^2. \quad (14.81)$$

These MBL reactor experiments provide the most precise determination of θ_{13} . Furthermore there is an additional effect sensitive to the mass ordering when comparing the disappearance of ν_μ at LBL experiments – which is symmetric with respect to the sign of $\Delta m_{\mu\mu}^2$ given in Eq.(14.7.1)–, with that of ν_e disappearance at MBL reactors which is symmetric with respect to the slightly different effective mass-squared difference Δm_{ee}^2 given in Eq. (14.81)

Finally for atmospheric neutrinos the fluxes contain ν_e , ν_μ , $\bar{\nu}_e$ and $\bar{\nu}_\mu$ and for a good fraction of the events, neutrinos travel through the Earth matter. In the context of 3ν mixing, the dominant oscillation channel of atmospheric neutrinos is $\nu_\mu \rightarrow \nu_\tau$ driven by $|\Delta m_{32}^2|$ with an amplitude controlled by θ_{23} with sub-leading oscillation modes, triggered by Δm_{21}^2 and/or θ_{13} , which depend on the octant of θ_{23} , on the mass ordering and on δ_{CP} . In that respect an interesting observable is the deviation of e -like events relative to the no-oscillation prediction N_e^0 , since in the two-flavour limit one expects $N_e = N_e^0$. Such deviation can be written in the following way (see, e.g., [174]):

$$\begin{aligned} \frac{N_e}{N_e^0} - 1 &\approx (r \sin^2 \theta_{23} - 1) P_{2\nu}(\Delta m_{32}^2, \theta_{13}) \\ &+ (r \cos^2 \theta_{23} - 1) P_{2\nu}(\Delta m_{21}^2, \theta_{12}) \\ &- \sin \theta_{13} \sin 2\theta_{23} r \Re(A_{ee}^* A_{\mu e}). \end{aligned} \quad (14.82)$$

Here $r \equiv \Phi_\mu/\Phi_e$ is the flux ratio with $r \approx 2$ in the sub-GeV range and $r \approx 2.6 \rightarrow 4.5$ in the multi-GeV range. $P_{2\nu}(\Delta m^2, \theta)$ is an effective two-flavour oscillation probability and $A_{ee}, A_{\mu e}$ are elements of a transition amplitude matrix. The three terms appearing in Eq. (14.82) have a well defined physical interpretation. The first term is important in the multi-GeV range and is controlled by the mixing angle θ_{13} in $P_{2\nu}(\Delta m_{32}^2, \theta_{13})$. This probability can be strongly affected by resonant matter effects [175–180]. Depending on the mass ordering the resonance will occur either for neutrinos or antineutrinos. The second term is important for sub-GeV events and it takes into account the effect of oscillations due to Δm_{21}^2 and θ_{12} [181–184]. Via the pre-factor containing the flux ratio r both, the first and second terms in Eq. (14.82) depend on the octant of θ_{23} , though in opposite directions: the multi-GeV (sub-GeV) excess is suppressed (enhanced) for $\theta_{23} < 45^\circ$. Finally, the last term in Eq. (14.82) is an interference term between θ_{13} and Δm_{21}^2 amplitudes and this term shows also dependence on the CP phase δ_{CP} [174, 184].

Subdominant three neutrino effects can also affect μ -like events. For example for multi-GeV muon events one can write the excess in μ -like events as [185, 186]

$$\begin{aligned} \frac{N_\mu}{N_\mu^0} - 1 &\approx \sin^2 \theta_{23} \left(\frac{1}{r} - \sin^2 \theta_{23} \right) P_{2\nu}(\Delta m_{32}^2, \theta_{13}) \\ &- \frac{1}{2} \sin^2 2\theta_{23} [1 - \Re(A_{33})]. \end{aligned} \quad (14.83)$$

The first term is controlled by θ_{13} and is subject to resonant matter effects, similar to the first term in Eq. (14.82), though with a different dependence on θ_{23} and the flux ratio. In the second term,

A_{33} is a probability amplitude satisfying $P_{2\nu}(\Delta m_{32}^2, \theta_{13}) = 1 - |A_{33}|^2$. In the limit $\theta_{13} = 0$ we have $\Re(A_{33}) = \cos(\Delta m_{32}^2 L/2E)$, such that the second term in Eq. (14.83) just describes two-flavour $\nu_\mu \rightarrow \nu_\mu$ vacuum oscillations.

14.7.2 3ν Oscillation Analysis

We summarize in Table 14.6 the different experiments which dominantly contribute to the present determination of the different parameters in the chosen convention.

The table illustrates that the determination of the leptonic parameters requires global analysis of the data from the different experiments. Over the years these analyses have been in the hands of a few phenomenological groups. We show in Table 14.7 the results from the latest analyses in Refs. [187–190]. For the sake of comparison all results are presented in the convention of the listing section as described above.

The table illustrates the dependence of the present determination of the parameters on variations of the statistical analysis performed by the different groups and on the data samples included. In that last respect the main difference resides on the results from Super-Kamiokande atmospheric data [94] which, at present, can only be included in these analysis by directly adding the χ^2 tabulated χ^2 map provided by the experiment.

Altogether the different analysis find consistent results, in particular on the better known parameters, θ_{12} , θ_{13} and Δm_{21}^2 and $|\Delta m_{32}^2|$. The issues which still require clarification are: the mass ordering discrimination, the determination of θ_{23} and the leptonic CP phase δ_{CP} :

- In all analyses the best fit is for the normal mass ordering. Inverted ordering is disfavoured with a $\Delta\chi^2$ which ranges from slightly above 2σ – driven by the interplay of long-baseline accelerator and short-baseline reactor data – to 3σ when adding the atmospheric χ^2 table from Ref. [94].
- All analyses find some preference for the second octant of θ_{23} but with statistical significance still well below 3σ .
- The best fit for the complex phase in NO is at $\delta_{\text{CP}} \sim 120^\circ$ but CP conservation (for $\delta_{\text{CP}} \sim 180^\circ$) is still allowed at a confidence level (CL) of $1-2\sigma$. We notice that, at present, the significance of CP violation in the global analysis is reduced with respect to that reported by T2K [191] because NOvA data does not show a significant indication of CP violation.

14.7.3 Convention-independent Measures of Leptonic CP Violation in 3ν Mixing

In the framework of 3ν mixing leptonic CP violation can also be quantified in terms of the leptonic Jarlskog invariant [192], defined by:

$$\begin{aligned} \Im[U_{\alpha i} U_{\alpha j}^* U_{\beta i} U_{\beta j}] &\equiv \sum_{\gamma=e,\mu,\tau} \sum_{k=1,2,3} J_{\text{CP}} \epsilon_{\alpha\beta\gamma} \epsilon_{ijk} \\ &\equiv J_{\text{CP}}^{\text{max}} \sin \delta_{\text{CP}}. \end{aligned} \quad (14.84)$$

With the convention in Eq. (14.33) $J_{\text{CP}}^{\text{max}}$ is the combination of mixing angles in Eq. (14.78). For example from the analysis in Ref. [187, 188]

$$J_{\text{CP}}^{\text{max}} = 0.03359 \pm 0.0006 (\pm 0.0019), \quad (14.85)$$

at 1σ (3σ) for both orderings, and the preference of the present data for non-zero δ_{CP} implies a non-zero best fit value $J_{\text{CP}}^{\text{best}} = -0.019$.

The status of the determination of leptonic CP violation can also be graphically displayed by projecting the results of the global analysis in terms of leptonic unitarity triangles [193–195]. Since in the analysis U is unitary by construction, any given pair of rows or columns can be used to define a triangle in the complex plane. There a total of six possible triangles corresponding to the unitary conditions

$$\sum_{i=1,2,3} U_{\alpha i} U_{\beta i}^* = 0 \text{ with } \alpha \neq \beta, \quad \sum_{\alpha=e,\mu,\tau} U_{\alpha i} U_{\alpha j}^* = 0 \text{ with } i \neq j. \quad (14.86)$$

Table 14.6: Experiments contributing to the present determination of the oscillation parameters.

Experiment	Dominant	Important
Solar Experiments	θ_{12}	$\Delta m_{21}^2, \theta_{13}$
Reactor LBL (KamLAND)	Δm_{21}^2	θ_{12}, θ_{13}
Reactor MBL (Daya-Bay, Reno, D-Chooz)	$\theta_{13}, \Delta m_{31,32}^2 $	
Atmospheric Experiments (SK, IC-DC)		$\theta_{23}, \Delta m_{31,32}^2 , \theta_{13}, \delta_{CP}$
Accel LBL $\nu_\mu, \bar{\nu}_\mu$, Disapp (K2K, MINOS, T2K, NO ν A)	$ \Delta m_{31,32}^2 , \theta_{23}$	
Accel LBL $\nu_e, \bar{\nu}_e$ App (MINOS, T2K, NO ν A)	δ_{CP}	θ_{13}, θ_{23}

Table 14.7: 3ν oscillation parameters obtained from different global analysis of neutrino data. In all cases the numbers labeled as NO (IO) are obtained assuming NO (IO), *i.e.*, relative to the respective local minimum. SK-ATM makes reference to the tabulated χ^2 map from the Super-Kamiokande analysis of their data in Ref. [94].

Param	Ref. [188] w/o SK-ATM		Ref. [188] w SK-ATM		Ref. [189] w SK-ATM		Ref. [190] w SK-ATM	
	Best Fit Ordering		Best Fit Ordering		Best Fit Ordering		Best Fit Ordering	
	bfp $\pm 1\sigma$	3σ range	bfp $\pm 1\sigma$	3σ range	bfp $\pm 1\sigma$	3σ range	bfp $\pm 1\sigma$	3σ range
$\sin^2 \theta_{12}$	$3.10^{+0.13}_{-0.12}$	2.75 \rightarrow 3.50	$3.10^{+0.13}_{-0.12}$	2.75 \rightarrow 3.50	$3.04^{+0.14}_{-0.13}$	2.65 \rightarrow 3.46	$3.20^{+0.20}_{-0.16}$	2.73 \rightarrow 3.79
$\theta_{12}/^\circ$	$33.82^{+0.78}_{-0.76}$	31.61 \rightarrow 36.27	$33.82^{+0.78}_{-0.76}$	31.61 \rightarrow 36.27	$33.46^{+0.87}_{-0.88}$	30.98 \rightarrow 36.03	$34.5^{+1.2}_{-1.0}$	31.5 \rightarrow 38.0
$\sin^2 \theta_{23}$	$5.58^{+0.20}_{-0.33}$	4.27 \rightarrow 6.09	$5.63^{+0.18}_{-0.24}$	4.33 \rightarrow 6.09	$5.51^{+0.19}_{-0.80}$	4.30 \rightarrow 6.02	$5.47^{+0.20}_{-0.30}$	4.45 \rightarrow 5.99
$\theta_{23}/^\circ$	$48.3^{+1.2}_{-1.9}$	40.8 \rightarrow 51.3	$48.6^{+1.0}_{-1.4}$	41.1 \rightarrow 51.3	$47.9^{+1.1}_{-4.0}$	41.0 \rightarrow 50.9	$47.7^{+1.2}_{-1.7}$	41.8 \rightarrow 50.7
$\sin^2 \theta_{13}$	$2.241^{+0.066}_{-0.065}$	2.046 \rightarrow 2.440	$2.237^{+0.066}_{-0.065}$	2.044 \rightarrow 2.435	$2.14^{+0.09}_{-0.07}$	1.90 \rightarrow 2.39	$2.160^{+0.083}_{-0.069}$	1.96 \rightarrow 2.41
$\theta_{13}/^\circ$	$8.61^{+0.13}_{-0.13}$	8.22 \rightarrow 8.99	$8.60^{+0.13}_{-0.13}$	8.22 \rightarrow 8.98	$8.41^{+0.18}_{-0.14}$	7.9 \rightarrow 8.9	$8.45^{+0.16}_{-0.14}$	8.0 \rightarrow 8.9
$\delta_{CP}/^\circ$	222^{+38}_{-28}	141 \rightarrow 370	221^{+39}_{-28}	144 \rightarrow 357	238^{+41}_{-33}	149 \rightarrow 358	218^{+38}_{-27}	157 \rightarrow 349
Δm_{21}^2	$7.39^{+0.21}_{-0.20}$	6.79 \rightarrow 8.01	$7.39^{+0.21}_{-0.20}$	6.79 \rightarrow 8.01	$7.34^{+0.17}_{-0.14}$	6.92 \rightarrow 7.91	$7.55^{+0.20}_{-0.16}$	7.05 \rightarrow 8.24
Δm_{32}^2	$2.449^{+0.032}_{-0.030}$	2.358 \rightarrow 2.544	$2.454^{+0.029}_{-0.031}$	2.362 \rightarrow 2.544	$2.419^{+0.035}_{-0.032}$	2.319 \rightarrow 2.521	2.424 ± 0.03	2.334 \rightarrow 2.524
IO	$\Delta\chi^2 = 6.2$		$\Delta\chi^2 = 10.4$		$\Delta\chi^2 = 9.5$		$\Delta\chi^2 = 11.7$	
$\sin^2 \theta_{12}$	$3.10^{+0.13}_{-0.12}$	2.75 \rightarrow 3.50	$3.10^{+0.13}_{-0.12}$	2.75 \rightarrow 3.50	$3.03^{+0.14}_{-0.13}$	2.64 \rightarrow 3.45	$3.20^{+0.20}_{-0.16}$	2.73 \rightarrow 3.79
$\theta_{12}/^\circ$	$33.82^{+0.78}_{-0.76}$	31.61 \rightarrow 36.27	$33.82^{+0.78}_{-0.75}$	31.62 \rightarrow 36.27	$33.40^{+0.87}_{-0.81}$	30.92 \rightarrow 35.97	$34.5^{+1.2}_{-1.0}$	31.5 \rightarrow 38.0
$\sin^2 \theta_{23}$	$5.63^{+0.19}_{-0.26}$	4.30 \rightarrow 6.12	$5.65^{+0.17}_{-0.22}$	4.36 \rightarrow 6.10	$5.57^{+0.17}_{-0.24}$	4.44 \rightarrow 6.03	$5.51^{+0.18}_{-0.30}$	4.53 \rightarrow 5.98
$\theta_{23}/^\circ$	$48.6^{+1.1}_{-1.5}$	41.0 \rightarrow 51.5	$48.8^{+1.0}_{-1.2}$	41.4 \rightarrow 51.3	$48.2^{+1.0}_{-1.4}$	41.8 \rightarrow 50.9	$47.9^{+1.0}_{-1.7}$	42.3 \rightarrow 50.7
$\sin^2 \theta_{13}$	$2.261^{+0.067}_{-0.064}$	2.066 \rightarrow 2.461	$2.259^{+0.065}_{-0.065}$	2.064 \rightarrow 2.457	$2.18^{+0.08}_{-0.07}$	1.95 \rightarrow 2.43	$2.220^{+0.074}_{-0.076}$	1.99 \rightarrow 2.44
$\theta_{13}/^\circ$	$8.65^{+0.13}_{-0.12}$	8.26 \rightarrow 9.02	$8.64^{+0.12}_{-0.13}$	8.26 \rightarrow 9.02	$8.49^{+0.15}_{-0.14}$	8.0 \rightarrow 9.0	$8.53^{+0.14}_{-0.15}$	8.1 \rightarrow 9.0
$\delta_{CP}/^\circ$	285^{+24}_{-26}	205 \rightarrow 354	282^{+23}_{-25}	205 \rightarrow 348	247^{+26}_{-27}	193 \rightarrow 346	281^{+23}_{-27}	202 \rightarrow 349
Δm_{21}^2	$7.39^{+0.21}_{-0.20}$	6.79 \rightarrow 8.01	$7.39^{+0.21}_{-0.20}$	6.79 \rightarrow 8.01	$7.34^{+0.17}_{-0.14}$	6.92 \rightarrow 7.91	$7.55^{+0.20}_{-0.16}$	7.05 \rightarrow 8.24
Δm_{32}^2	$-2.509^{+0.032}_{-0.032}$	-2.603 \rightarrow -2.416	$-2.510^{+0.030}_{-0.031}$	-2.601 \rightarrow -2.419	$-2.478^{+0.035}_{-0.033}$	-2.577 \rightarrow -2.375	-2.50 ± 0.04	-2.59 \rightarrow -2.39

As illustration we show in Fig. 14.9 the recasting of the allowed regions of the analysis in Ref. [187, 188] in terms of one leptonic unitarity triangle. We show the triangle corresponding to the unitarity conditions on the first and third columns (after the shown rescaling) which is the equivalent to the one usually shown for the quark sector. In this figure the absence of CP violation would imply a flat triangle, *i.e.*, $\Im(z) = 0$. So the CL at which leptonic CP violation is being observed would be given by the CL at which the region crosses the horizontal axis. Notice however, that this representation is made *under the assumption of a unitary U matrix* and therefore does not provide any test of unitarity in the leptonic sector.

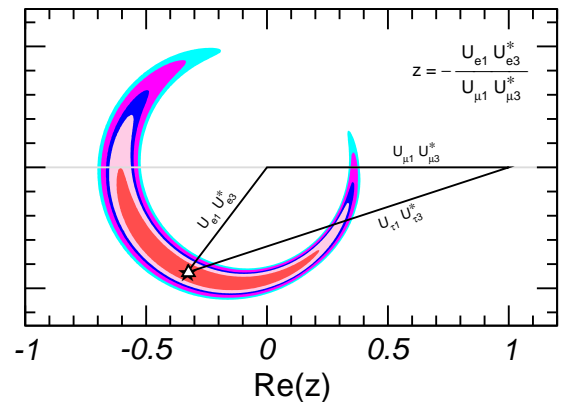


Figure 14.9: Leptonic unitarity triangle for the first and third columns of the mixing matrix. After scaling and rotating the triangle so that two of its vertices always coincide with (0, 0) and (1, 0) the figure shows the 1σ , 90%, 2σ , 99%, 3σ CL (2 dof) allowed regions of the third vertex for the NO from the analysis in Ref. [187, 188].

14.8 Beyond 3ν : Additional Neutrinos at the eV Scale

Besides the huge success of three-flavour oscillations described in Sec.14.7, as mentioned in Secs.14.6.3 and 14.6.4, there are some anomalies which cannot be explained within the 3ν framework and which might point towards the existence of additional neutrino states with masses at the eV scale. In brief:

- the LSND experiment [127] reports evidence for $\bar{\nu}_\mu \rightarrow \bar{\nu}_e$ transitions with $E/L \sim 1 \text{ eV}^2$, where E and L are the neutrino energy and the distance between source and detector, respectively (see *Short Baseline Experiments* subsection of Sec.14.6.3).
- this effect has also been searched for by the MiniBooNE experiment [196], which reports a yet unexplained event excess in the low-energy region of the electron neutrino and anti-neutrino event spectra. No significant excess is found at higher neutrino energies. Interpreting the data in terms of oscillations, parameter values consistent with the ones from LSND are obtained, but the test is not definitive;
- radioactive source experiments at the Gallium solar neutrino experiments both in SAGE and GALLEX/GNO have obtained an event rate which is somewhat lower than expected. If not due to uncertainties in the interaction cross section, this effect can be explained by the hypothesis of ν_e disappearance due to oscillations with $\Delta m^2 \gtrsim 1 \text{ eV}^2$ (“Gallium anomaly”) [197, 198];
- new calculations of the neutrino flux emitted by nuclear reactors [136, 137] predict a neutrino rate which is a few percent higher than observed in short-baseline ($L \lesssim 100 \text{ m}$) reactor experiments⁴. If not due to systematic or theoretical uncertainties, a decrease rate at those distances can be explained by assuming $\bar{\nu}_e$ disappearance due to oscillations with $\Delta m^2 \sim 1 \text{ eV}^2$ (“reactor anomaly”) [200]. This reactor anomaly is under study both by the experimental community – with a set of follow-up measurements performed at SBL both at reactors and accelerators (see the corresponding subsections in Sec.14.6.4 and Sec.14.6.3)–, and by the theory community for improvements of the reactor flux calculations.

As mentioned in Sec.14.1 whatever the extension of the SM we want to consider it must contain only three light active neutrinos. Therefore if we need more than three light massive neutrinos we must add sterile neutrinos to the particle content of the model.

The most immediate question as these anomalies were reported was whether they could all be consistently described in combination with the rest of the neutrino data – in particular with the negative results on disappearance of ν_μ at short distances – if one adds those additional sterile states. Quantitatively one can start by adding a fourth massive neutrino state to the spectrum, and perform a global data analysis to answer this question. Although the answer is always the same the physical reason behind it depends on ordering assumed for the states. In brief, there are six possible four-neutrino schemes which can in principle accommodate the results of solar+KamLAND and atmospheric+LBL neutrino experiments as well as the SBL result. They can be divided in two classes: (2+2) and (3+1). In the (3+1) schemes, there is a group of three close-by neutrino masses (as on the 3ν schemes described in the previous section) that is separated from the fourth one by a gap of the order of 1 eV, which is responsible for the SBL oscillations. In (2+2) schemes, there are two pairs of close masses (one pair responsible for solar results and the other for atmospheric [201]) separated by the $\mathcal{O}(\text{eV})$ gap. The main difference between these two classes is the following: if a (2+2)-spectrum is realized in nature, the transition into the sterile neutrino is a solution of either the solar or the atmospheric neutrino problem, or the sterile neutrino takes part in both. Consequently a (2+2)-spectrum is easier to test because the required mixing of sterile neutrinos in either solar and/or atmospheric oscillations would modify their effective matter potential in the Sun

⁴However, as discussed in Sec.14.6.4, the reactor antineutrino flux measurement at Daya Bay [143, 199] is consistent with the old flux predictions and the flux measurement results in the previous short-baseline reactor neutrino oscillation experiments.

and in the Earth and giving distinctive effects in the solar and/or atmospheric neutrino observables. Those distinctive effects were not observed so oscillations into sterile neutrinos did not describe well either solar or atmospheric data. Consequently as soon as the early 2000’s 2+2 spectra could be ruled out already beyond $3\text{--}4 \sigma$ as seen in the left panel in Fig.14.10 taken from Ref. [202].

On the contrary, for a (3+1)-spectrum (and more generally for a $3+N$ -spectrum with an arbitrary N number of sterile states), the sterile neutrino(s) could be only slightly mixed with the active ones and mainly provide a description of the SBL results. In this case the oscillation probabilities for experiments working at $E/L \sim 1 \text{ eV}^2$ take a simple form:

$$P_{\alpha\alpha} = 1 - \sin^2 2\theta_{\alpha\alpha} \sin^2 \Delta, \quad P_{\mu e} = \sin^2 2\theta_{\mu e} \sin^2 \Delta, \quad (14.87)$$

where $\Delta \equiv \Delta m_{41}^2 L/4E$ and one can define effective mixing angles

$$\sin^2 2\theta_{\alpha\alpha} \equiv 4|U_{\alpha 4}|^2(1 - |U_{\alpha 4}|^2), \quad \sin^2 2\theta_{\mu e} \equiv 4|U_{\mu 4}|^2|U_{e 4}|^2. \quad (14.88)$$

In here $\alpha = e, \mu$ and $U_{\alpha 4}$ are the elements of the lepton mixing matrix describing the mixing of the 4th neutrino mass state with the electron and muon flavour. In this scenario there is no sensitivity to CP violation in the Δ driven oscillations, so the relations above are valid for both neutrinos and antineutrinos. At linear order in the mixing elements one can derive a relation between the amplitudes of appearance and disappearance probabilities:

$$4 \sin^2 2\theta_{\mu e} \approx \sin^2 2\theta_{ee} \sin^2 2\theta_{\mu\mu}. \quad (14.89)$$

This relation implies a constraint between the possible results in disappearance and appearance experiments. Consequently it is not trivial to find a consistent description to all the SBL anomalies. Over the years, different groups have performed a variety of such global analysis leading to quantitative different conclusions on the statistical quality of the global fit (see for example [203–208], see also Refs. [209, 210] for recent reviews on the subject). Generically the results of the global analysis show that there is significant tension between groups of different data sets – in particular between appearance and disappearance results – and Eq.(14.89) makes it difficult to obtain a good global fit as illustrated in the right panel in Fig.14.10 taken from Ref. [203] which concluded that 3+1 scenario is excluded at 4.7σ level.

A straightforward question to ask is whether the situation improves if more neutrino states at the eV scale are introduced. Simplest extension is the introduction of 2 states with eV scale mass splittings, ν_4 and ν_5 . The ordering of the states can be such that Δm_{41}^2 and Δm_{51}^2 are both positive (“3+2”) or one of them is negative (“1+3+1”). From the point of view of the description of the data the most important new qualitative feature is that now non-zero CP violation at $E/L \sim \text{eV}^2$ is possibly observable [206, 211–213]. This allows some additional freedom in fitting neutrino versus anti-neutrino data from LSND and MiniBooNE together. However, it still holds that a non-zero $\nu_\mu \rightarrow \nu_e$ appearance at SBL necessarily predicts SBL disappearance for both ν_e and ν_μ . So, generically, the tension between appearance and disappearance results remains, thought differences in the methodology of statistical quantification of the degree of agreement/disagreement in these scenarios can lead to different conclusions on whether they can provide a successful description of all the data [203, 209, 210]. Cosmological observations can provide complementary information on the number of relativistic neutrino states in thermal equilibrium in the early Universe and on the sum of their masses which sets further constraints on light sterile neutrino scenarios (see Section 26, Neutrinos in cosmology).

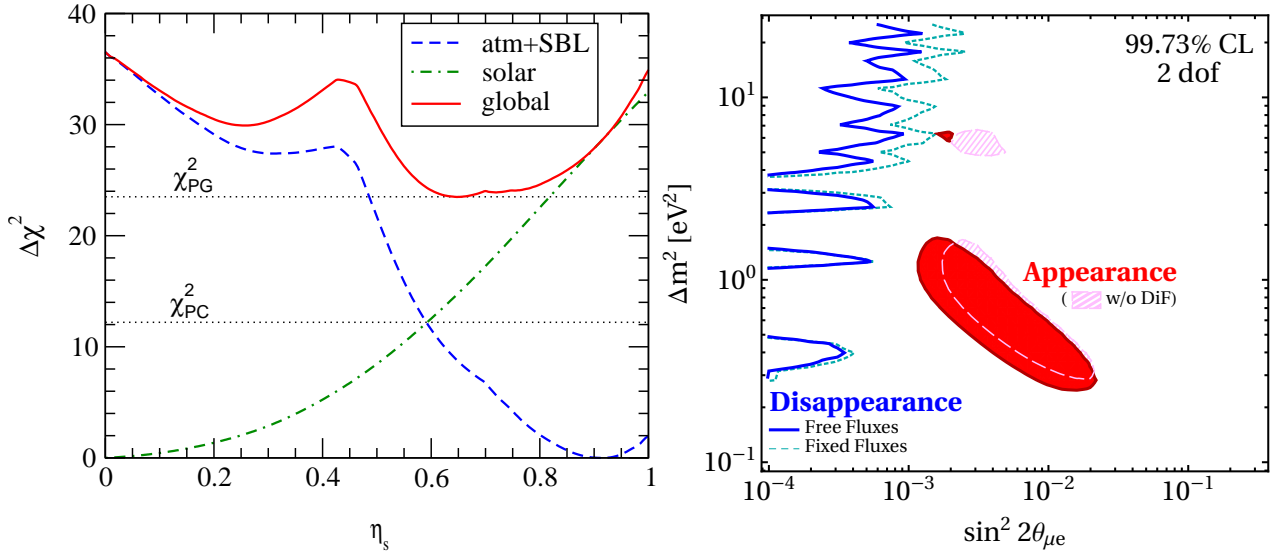


Figure 14.10: *Left*: Status of the 2+2 oscillation scenarios from Ref. [202] ($\eta_S = \sum_i |U_{is}|^2$ where i runs over the two massive states mostly relevant for solar neutrino oscillations). In the figure also shown are the values of χ_{PC}^2 and χ_{PG}^2 relevant for parameter consistency test and parameter goodness of fit respectively. *Right*: Present status of 3+1 oscillation scenarios from Ref. [203].

14.9 Laboratory Probes of ν Mass Scale and its Nature

As described in Secs.14.4 and 14.5 neutrino flavour oscillations in vacuum and flavour transitions in matter only depend on the differences between the neutrino masses-squared, Δm_{ij}^2 , and on the mixing matrix elements, U_{ij} . But they are insensitive to the absolute mass scale for the neutrinos, m_i . They also give us no information on whether they are Dirac or Majorana particles.

Clearly the observation of flavour oscillations imply a lower bound on the mass of the heavier neutrino in Δm_{ij}^2 , $|m_i| \geq \sqrt{\Delta m_{ij}^2}$ for $\Delta m_{ij}^2 > 0$. But there is no upper bound on m_i . In particular, oscillation results allow neutrino spectrum to be approximately degenerate at a mass scale that is much higher than the $\sqrt{\Delta m_{ij}^2}$ that they determine. Information of the mass scale of the neutrino is provided by other type of experiments. In here we briefly summarize the most sensitive laboratory probes of the neutrino mass scale and on whether they are Dirac or Majorana particles. Cosmological observations provide, albeit indirectly, complementary information on the neutrino mass scale as it is reviewed in Section 26, Neutrinos in cosmology.

14.9.1 Constraints from Kinematics of Weak Decays

The only model independent information on the neutrino masses, rather than mass differences, can be extracted from energy-momentum conservation relation in reactions in which a neutrino or an anti-neutrino is involved.

Historically these bounds were labeled as limits on the mass of the flavour neutrino states corresponding to the charged flavour involved in the decay. Fermi proposed in 1933 such a kinematic search for the ν_e neutrino mass (which we will label here as $m_{\nu_e}^{\text{eff}}$) in the end part of the beta spectra in ${}^3\text{H}$ beta decay ${}^3\text{H} \rightarrow {}^3\text{He} + e^- + \bar{\nu}_e$.

Because ${}^3\text{H}$ beta decay is a superallowed transition, the nuclear matrix elements are energy independent so the electron spectrum is determined exclusively by the phase space

$$\begin{aligned} \frac{dN}{dE} &= C p E (Q - T) \sqrt{(Q - T)^2 - (m_{\nu_e}^{\text{eff}})^2} F(E) \\ &\equiv R(E) \sqrt{(E_0 - E)^2 - (m_{\nu_e}^{\text{eff}})^2}. \end{aligned} \quad (14.90)$$

E_0 is the mass difference between the initial and final nucleus, $E = T + m_e$ is the total electron energy, p its momentum, $Q \equiv E_0 - m_e$ is the maximum kinetic energy of the electron and Final state Coulomb interactions are contained in the Fermi

function $F(E)$. $R(E)$ in the second equality contains all the m_{ν} -independent factors.

The Kurie function is defined as $K(T) \equiv \sqrt{\frac{dN}{dE} \frac{1}{pEF(E)}}$. From Eq.(14.90) we see that if $m_{\nu_e}^{\text{eff}}=0$ $K(T)$ would depend linearly on T . A non-vanishing neutrino mass then provokes a distortion from the straight-line T -dependence at the end point, So for $m_{\nu_e}^{\text{eff}} = 0$, $T_{\text{max}} = Q$, while for $m_{\nu_e}^{\text{eff}} \neq 0$, $T_{\text{max}} = Q - m_{\nu_e}^{\text{eff}}$. In ${}^3\text{H}$ beta decay $Q = 18.6$ KeV is very small and therefore this decay is more sensitive to this $m_{\nu_e}^{\text{eff}}$ -induced distortion.

The most recent result on the kinematic search for neutrino mass in tritium decay is from KATRIN [214], experiment which has found so far no indication of $m_{\nu_e} \neq 0$ and sets an upper limit

$$m_{\nu_e}^{\text{eff}} < 1.1 \text{ eV}, \quad (14.91)$$

at 90% CL improving over the previous bound from the Mainz [215] and Troitsk [216] experiments which constrained $m_{\nu_e}^{\text{eff}} < 2.2$ eV at 95% CL. KATRIN continues running with an estimated sensitivity limit of $m_{\nu_e}^{\text{eff}} \sim 0.2$ eV. Project 8 is exploring a new technique for β -spectrometry based on cyclotron radiation [217].

An alternative isotope to Tritium is ${}^{163}\text{Ho}$ [218] which presents the advantage of a smaller $Q = 2.8$ KeV. It decays via electron-capture to ${}^{163}\text{Dy}$. Currently, there are three experiments exploring this decay to probe the neutrino mass: ECHO [219], HOLMES [220], and NuMECS [221]. These experiments are complementary to tritium-based searches from a technical point-of-view. Also the decay of ${}^{163}\text{Ho}$ determines the effective electron neutrino mass as opposed to anti-neutrino in Tritium.

For the other flavours the present limits compiled in the listing section of the PDG read

$$m_{\nu_\mu}^{\text{eff}} < 190 \text{ keV (90\% CL)} \quad \text{from} \quad \pi^- \rightarrow \mu^- + \bar{\nu}_\mu, \quad (14.92)$$

$$m_{\nu_\tau}^{\text{eff}} < 18.2 \text{ MeV (95\% CL)} \quad \text{from} \quad \tau^- \rightarrow n\pi + \nu_\tau. \quad (14.93)$$

In the presence of mixing and for neutrinos with small mass differences the distortion of the beta spectrum is given by the sum of the individual spectra generated incoherently by each neutrino massive state weighted with the relevant mixing matrix element squared [222]:

$$\frac{dN}{dE} = R(E) \sum_i |U_{ei}|^2 \sqrt{(E_0 - E)^2 - m_i^2} \Theta(E_0 - E - m_i). \quad (14.94)$$

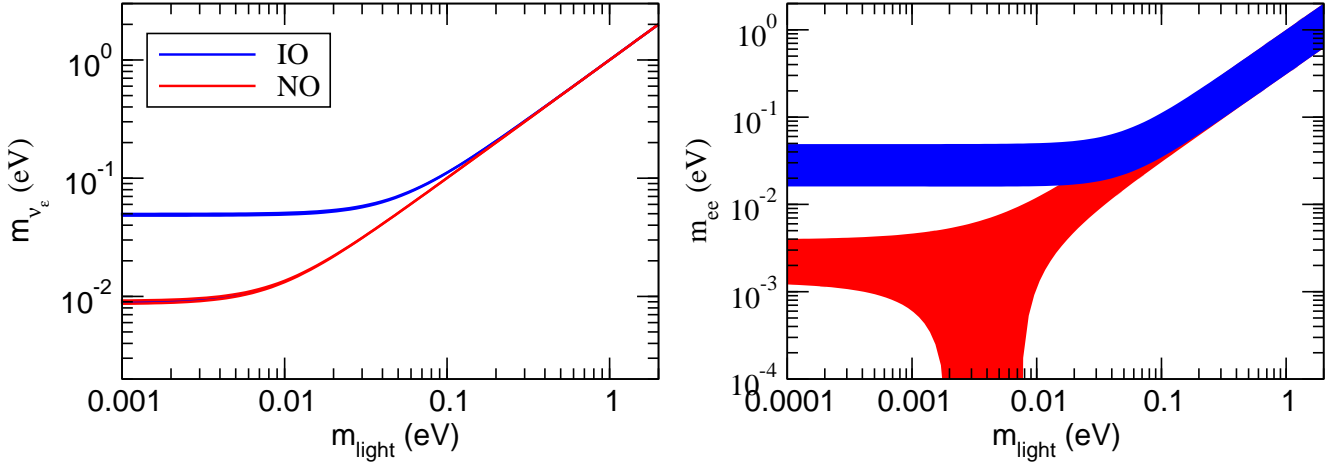


Figure 14.11: Allowed 95% CL ranges (1 dof) for the neutrino mass observable determined in ${}^3\text{H}$ beta decay (left panel) and in $0\nu\beta\beta$ (right panel) in the framework of 3ν mixing as a function of the lightest neutrino mass. The ranges are obtained by projecting the results of the global analysis of oscillation data (w/o SK-atm) in Ref. [187]. The region for each ordering is defined with respect to its local minimum.

The step function, $\Theta(E_0 - E - m_i)$ arises because a neutrino with a given mass m_i can only be produced if the available energy is larger than its mass. Equation (14.94) shows the two main effects of the neutrino masses and mixings on the electron energy spectrum: First kinks appear at the electron energies $E_e^{(i)} = E \sim E_0 - m_i$ with sizes that are determined by $|U_{ei}|^2$. Second the end point shifts to $E_{ep} = E_0 - m_0$, where m_0 is the lightest neutrino mass. Corrections are induced once the the energy resolution of the experiment is considered [223,224]

In the 3ν mixing scenario the distortion of the spectrum can still be effectively described by a single parameter – which we will still denote as m_{ν_e} – if for all neutrino states $E_0 - E = Q - T \gg m_i$. In this case one can expand Eq.(14.94) as:

$$\frac{dN}{dE} \simeq R(E) \sum_i |U_{ei}|^2 \sqrt{(E_0 - E)^2 - (m_{\nu_e}^{\text{eff}})^2}, \quad (14.95)$$

with

$$(m_{\nu_e}^{\text{eff}})^2 = \frac{\sum_i m_i^2 |U_{ei}|^2}{\sum_i |U_{ei}|^2} = \sum_i m_i^2 |U_{ei}|^2, \quad (14.96)$$

where unitarity is assumed in the second equality. In this approximation the distortion of the end point of the spectrum is described by a single parameter, and with the present results from KATRIN it is bounded to be

$$1.1 \text{ eV} \geq m_{\nu_e}^{\text{eff}} = \sqrt{\sum_i m_i^2 |U_{ei}|^2} = \begin{cases} \sqrt{m_0^2 + \Delta m_{21}^2 (1 - c_{13}^2 c_{12}^2) + \Delta m_{32}^2 s_{13}^2} & \text{in NO,} \\ \sqrt{m_0^2 + \Delta m_{21}^2 c_{13}^2 c_{12}^2 - \Delta m_{32}^2 c_{13}^2} & \text{in IO,} \end{cases} \quad (14.97)$$

where $m_0 = m_1$ (m_3) is the lightest neutrino mass in NO (IO) spectrum. Correspondingly the bounds in Eqs.(14.92) and (14.93) apply to the combinations $\sum_i m_i^2 |U_{\alpha i}|^2$ for $\alpha = \mu$ and τ respectively. So with the values known of the mixing matrix elements the strongest constraint on the absolute value of the neutrino mass comes from Tritium beta decay.

From Eq.(14.97) we see that, given the present knowledge of the neutrino mass differences and their mixing from oscillation experiments, it is possible to translate the experimental information of m_{ν_e} on a corresponding range for the lightest neutrino mass and that such relation depends on the ordering of the states. We plot in Fig.14.11 the recasting of the allowed regions of the analysis

in Ref. [187] in terms of the allowed range m_{ν_e} as a function of $m_{\text{light}} \equiv m_0$. In particular one finds that the results of oscillation experiments imply a lower bound on $m_{\nu_e} > 0.048$ (0.0085) eV for IO (NO) at 95% CL.

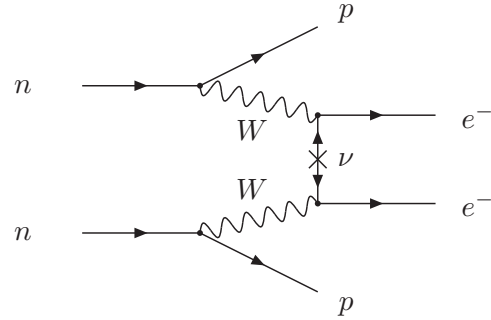


Figure 14.12: Feynman diagram for neutrinoless double-beta decay.

14.9.2 Dirac vs Majorana: Neutrinoless Double-beta Decay

The most sensitive probe to whether neutrinos are Dirac or Majorana states is the neutrinoless double beta decay ($0\nu\beta\beta$):

$$(A, Z) \rightarrow (A, Z + 2) + e^- + e^-. \quad (14.98)$$

In the presence of neutrino masses and mixing the process in Eq.(14.98) can be generated at lower order in perturbation theory by the term represented in Fig.14.12. The corresponding amplitude is proportional to the product of the two leptonic currents

$$M_{\alpha\beta} \propto [\bar{e}\gamma_\alpha(1 - \gamma_5)\nu_e] [\bar{e}\gamma_\beta(1 - \gamma_5)\nu_e] \propto \sum_i (U_{ei})^2 [\bar{e}\gamma_\alpha(1 - \gamma_5)\nu_i] [\bar{e}\gamma_\beta(1 - \gamma_5)\nu_i]. \quad (14.99)$$

The neutrino propagator in Fig.14.12 can only arise from the contraction $\langle 0 | \nu_i(x) \nu_i(y)^T | 0 \rangle$. But if the neutrino is a Dirac particle ν_i field annihilates a neutrino states and creates an antineutrino state which are different, so the contraction $\langle 0 | \nu_i(x) \nu_i(y)^T | 0 \rangle = 0$ and $M_{\alpha\beta} = 0$. On the other hand, if ν_i is a Majorana particle, neutrino and antineutrino are described by the same field and $\langle 0 | \nu_i(x) \nu_i(y)^T | 0 \rangle \neq 0$.

The conclusion is that in order to induce the $0\nu\beta\beta$ decay, neutrinos must be Majorana particles. This is consistent with the fact that the process (14.98) violates total lepton number by two

units. Conversely, if $0\nu\beta\beta$ decay is observed, massive neutrinos cannot be Dirac states [225].

It is important to stress that neutrinoless double beta decay could be dominantly induced by other new physics effects beyond that of Majorana neutrino masses. Consequently the connection between the observation or limitation of the neutrinoless double beta decay and the neutrino mass can only be made under some assumption about the source of total lepton number violation in the model.

The observable determined by the experiments is the half-life of

$$m_{ee} = \left| \sum_i m_i U_{ei}^2 \right| = \begin{cases} \left| m_0 c_{12}^2 c_{13}^2 + \sqrt{\Delta m_{21}^2 + m_0^2} s_{12}^2 c_{13}^2 e^{2i(\eta_2 - \eta_1)} + \sqrt{\Delta m_{32}^2 + \Delta m_{21}^2 + m_0^2} s_{13}^2 e^{-2i(\delta_{CP} + \eta_1)} \right| & \text{in NO,} \\ \left| m_0 s_{13}^2 + \sqrt{m_0^2 - \Delta m_{32}^2} s_{12}^2 c_{13}^2 e^{2i(\eta_2 + \delta_{CP})} + \sqrt{m_0^2 - \Delta m_{32}^2 - \Delta m_{21}^2} c_{12}^2 c_{13}^2 e^{2i(\eta_1 + \delta_{CP})} \right| & \text{in IO,} \end{cases}$$

which, in addition to the masses and mixing parameters that affect the tritium beta decay spectrum, depends also on the leptonic CP violating phases. We plot in Fig.14.11 the the recasting of the allowed regions of the analysis in Ref. [187] in terms of the allowed range m_{ee} as a function of $m_{\text{light}} \equiv m_0$ for the two orderings. As a consequence of the dependence on the unknown Majorana phases, the allowed range of m_{ee} for a given value of m_{light} and ordering is substantially broader than that of m_{ν_e} . Nevertheless, the results of oscillation experiments imply a lower bound on the effective Majorana mass for the IO, which at 95%CL reads $m_{ee} > 0.016$ eV.

From Eq.(14.100) we see that nuclear structure details enter relation between the decay rate (or lifetime) and the effective Majorana mass. As a consequence uncertainties in the nuclear structure calculations result in a spread of m_{ee} values for a given $T_{1/2}^{0\nu}$ by a factor of 2–3 [226].

We present in Sec.14.9.3 a brief description of the experimental searches for neutrinoless double-beta decay. At the time of writing of this review the strongest bound on $0\nu\beta\beta$ decay lifetime comes from the search in KamLAND-Zen experiment [227] (see Sec.14.9.3) which uses 13 Tons of Xe-loaded liquid scintillator to search for the decay $0\nu\beta\beta$ of ^{136}Xe and has set a bound on the half-life of $T_{1/2}^{0\nu} > 1.07 \times 10^{26}$ yr at 90% CL. Using a variety of nuclear matrix element calculations, the corresponding upper bound on the effective Majorana mass is

$$m_{ee} < 61 - 165 \text{ meV}. \quad (14.101)$$

14.9.3 Experimental Search for Neutrinoless Double-beta Decay

The signature of $0\nu\beta\beta$ is that the sum of energy of two electrons is equal to the Q -value of the nuclear transition. Various requirements must be met to achieve high sensitivity such as a large source mass with isotopic enrichment, underground location to shield cosmic-ray induced background, and ultra-low background techniques to reduce radioactive background. The sensitivity to the half-life is proportional to εMt in the case of a background-free measurement and $\varepsilon \sqrt{\frac{Mt}{b\Delta E}}$ for the case background exists, where ε is the detection efficiency of the signal, M is the source mass, t is the measurement time, b is the background rate, and ΔE is the energy resolution.

There are 35 candidate nuclei for double-beta decay. Currently, experiments using ^{136}Xe and ^{76}Ge have reported the most sensitive results of $0\nu\beta\beta$ search. Because of the uncertainties related to the nuclear matrix element, complementarity of technologies, different background, and the investigation of the mechanism behind the $0\nu\beta\beta$ in case of a positive signal, it is important to pursue the searches with various isotopes.

The energy from electrons is measured with either ionization, scintillation, or through phonons. In some experiments a combination of two techniques is used. Among those using

the decay. Under the assumption that the Majorana neutrino mass is the only source of lepton number violation at low energies, the decay half-life is given by:

$$(T_{1/2}^{0\nu})^{-1} = G^{0\nu} |M^{0\nu}|^2 \left(\frac{m_{ee}}{m_e} \right)^2, \quad (14.100)$$

where $G^{0\nu}$ is the phase space integral taking into account the final atomic state, $|M^{0\nu}|$ is the nuclear matrix element of the transition, and m_{ee} is the *effective Majorana mass of ν_e* ,

ionization detection, ultra-high-purity germanium detector provides the best sensitivity thanks to high energy resolution and low background. GERDA uses total 20.0 kg of broad energy germanium (BEGe) and 15.6 kg of coaxial detectors, both enriched in ^{76}Ge , for the second phase. Background levels of $(5.6^{+3.4}_{-2.4}) \times 10^{-4}$ counts/(keV·kg·year) for BEGe detectors and $(5.7^{+4.1}_{-2.6}) \times 10^{-4}$ counts/(keV·kg·year) for coaxial detectors have been achieved [228], which enable a background-free search. The Majorana-Demonstrator [229] consists of 44.1 kg of Ge (29.7 kg enriched to 88% in ^{76}Ge) detectors split between two modules. It has achieved energy resolution of 2.5 keV FWHM at the Q -value (2.039 MeV).

Liquid scintillator detectors have simple structure and can utilize existing large detectors with low background environments. By adding an inner balloon to contain xenon-loaded liquid scintillator to the KamLAND detector, KamLAND-Zen used 380 kg of xenon with 90.1% enrichment in ^{136}Xe . Reducing the background level by purification of scintillator, KamLAND-Zen reported the half-life limit above 10^{26} years at 90% CL [227]. The SNO detector has been also upgraded to be filled with liquid scintillator in SNO+ experiment [230]. The SNO+ detector will be loaded with 0.5% natural tellurium, corresponding to approximately 1330 kg of ^{130}Te to search for $0\nu\beta\beta$.

With a time projection chamber, one can utilize both ionization and scintillation. EXO-200 uses a liquid xenon time projection chamber with enrichment to 80.6%, corresponding to 74.7 kg of ^{136}Xe in the fiducial mass [231]. An energy resolution of 1.15% (σ/E) is achieved at the Q -value of ^{136}Xe $0\nu\beta\beta$. The NEXT collaboration has been developing a high-pressure xenon gas time projection chamber with electroluminescent amplification and optical readouts. An energy resolution of 1% FWHM at the Q -value of ^{136}Xe $0\nu\beta\beta$ is demonstrated with NEXT-White detector [232].

CUORE uses cryogenic bolometer to measure the energy in a calorimetric way. The detector is located in Gran Sasso and composed of 988 TeO_2 bolometers for a total mass of 742 kg, corresponding to 206 kg of ^{130}Te . An effective energy resolution of (7.7 ± 0.5) keV FWHM is achieved for the first result [233]. For further reduction of background towards future search based on the CUORE technology, CUPID proposes to simultaneously measure the calorimetric signal and the scintillation light. Using the prototype CUPID-0, the technology is demonstrated and also $0\nu\beta\beta$ is searched for with ^{82}Se [234].

AMoRE also uses the simultaneous detection of heat and scintillation. Six ^{100}Mo -enriched and ^{48}Ca -depleted CaMoO_4 crystals with a total mass of 1.9 kg (AMoRE-Pilot) are operated in Yangyang underground laboratory located in South Korea, searching for $0\nu\beta\beta$ of ^{100}Mo [235].

A tracker-calorimeter technique is employed in NEMO. Source isotopes are hosted in thin foils surrounded by a tracking detector, which in turn is surrounded by a calorimeter. Full topological event reconstruction with this configuration enables background rejection and gives additional information after discovery. The

NEMO-3 experiment used 7 isotopes, with the largest mass comprised of ^{100}Mo (7 kg) [236]. NEMO-3 also reported a first search for neutrinoless quadruple- β decay of ^{150}Nd [237].

References

- [1] J. N. Bahcall, *NEUTRINO ASTROPHYSICS* (1989), ISBN 9780521379755.
- [2] R. N. Mohapatra and P. B. Pal, World Sci. Lect. Notes Phys. **60**, 1 (1998), [World Sci. Lect. Notes Phys.72,1(2004)].
- [3] C. W. Kim and A. Pevsner, *Contemp. Concepts Phys.* **8**, 1 (1993).
- [4] B. Kayser, F. Gibrat-Debu and F. Perrier, World Sci. Lect. Notes Phys. **25**, 1 (1989).
- [5] C. Giunti and C. W. Kim, *Fundamentals of Neutrino Physics and Astrophysics* (2007), ISBN 9780198508717.
- [6] M. C. Gonzalez-Garcia and Y. Nir, *Rev. Mod. Phys.* **75**, 345 (2003), [hep-ph/0202058].
- [7] M. C. Gonzalez-Garcia and M. Maltoni, *Phys. Rept.* **460**, 1 (2008), [arXiv:0704.1800].
- [8] A. Pilaftsis, *Z. Phys.* **C55**, 275 (1992), [hep-ph/9901206].
- [9] P. Minkowski, *Phys. Lett.* **67B**, 421 (1977).
- [10] P. Ramond, in “International Symposium on Fundamentals of Quantum Theory and Quantum Field Theory Palm Coast, Florida, February 25-March 2, 1979,” 265–280 (1979), [hep-ph/9809459].
- [11] M. Gell-Mann, P. Ramond and R. Slansky, *Conf. Proc.* **C790927**, 315 (1979), [arXiv:1306.4669].
- [12] T. Yanagida, *Conf. Proc.* **C7902131**, 95 (1979).
- [13] R. N. Mohapatra and G. Senjanovic, *Phys. Rev. Lett.* **44**, 912 (1980), [231(1979)].
- [14] J. Schechter and J. W. F. Valle, *Phys. Rev.* **D21**, 309 (1980).
- [15] J. Schechter and J. W. F. Valle, *Phys. Rev.* **D22**, 2227 (1980).
- [16] J. Schechter and J. W. F. Valle, *Phys. Rev.* **D24**, 1883 (1981), [Erratum: *Phys. Rev.* **D25**, 283(1982)].
- [17] Z. Maki, M. Nakagawa and S. Sakata, *Prog. Theor. Phys.* **28**, 870 (1962), [34(1962)].
- [18] Y. Katayama *et al.*, *Prog. Theor. Phys.* **28**, 675 (1962).
- [19] B. Pontecorvo, *Sov. Phys. JETP* **26**, 984 (1968), [*Zh. Eksp. Teor. Fiz.* 53,1717(1967)].
- [20] N. Cabibbo, *Phys. Rev. Lett.* **10**, 531 (1963), [648(1963)].
- [21] M. Kobayashi and T. Maskawa, *Prog. Theor. Phys.* **49**, 652 (1973).
- [22] S. Antusch *et al.*, *JHEP* **10**, 084 (2006), [hep-ph/0607020].
- [23] S. Antusch and O. Fischer, *JHEP* **10**, 094 (2014), [arXiv:1407.6607].
- [24] V. N. Gribov and B. Pontecorvo, *Phys. Lett.* **28B**, 493 (1969).
- [25] E. Akhmedov, in “International Conference on History of the Neutrino: 1930-2018 Paris, France, September 5-7, 2018,” (2019), [arXiv:1901.05232].
- [26] L. Wolfenstein, *Phys. Rev.* **D17**, 2369 (1978), [294(1977)].
- [27] A. Halprin, *Phys. Rev.* **D34**, 3462 (1986).
- [28] A. J. Baltz and J. Weneser, *Phys. Rev.* **D37**, 3364 (1988).
- [29] P. D. Mannheim, *Phys. Rev.* **D37**, 1935 (1988).
- [30] L. Landau, *Phys. Z. Sov.* **2**, 46 (1932).
- [31] C. Zener, *Proc. Roy. Soc. Lond.* **A137**, 696 (1932).
- [32] E. Majorana, *Nuovo Cim.* **9**, 43 (1932).
- [33] E. C. G. Stueckelberg, *Helv. Phys. Acta* **5**, 369 (1932).
- [34] T.-K. Kuo and J. T. Pantaleone, *Rev. Mod. Phys.* **61**, 937 (1989).
- [35] S. J. Parke, *Phys. Rev. Lett.* **57**, 1275 (1986), [328(1986)].
- [36] W. C. Haxton, *Phys. Rev. Lett.* **57**, 1271 (1986), [332(1986)].
- [37] S. T. Petcov, *Phys. Lett.* **B191**, 299 (1987), [427(1987)].
- [38] S. P. Mikheyev and A. Yu. Smirnov, *Sov. J. Nucl. Phys.* **42**, 913 (1985), [305(1986)].
- [39] J. N. Bahcall *et al.*, *Rev. Mod. Phys.* **54**, 767 (1982).
- [40] J. N. Bahcall, A. M. Serenelli and S. Basu, *Astrophys. J.* **621**, L85 (2005), [arXiv:astro-ph/0412440].
- [41] A. M. Serenelli, W. C. Haxton and C. Pena-Garay, *Astrophys. J.* **743**, 24 (2011), [arXiv:1104.1639].
- [42] F. L. Villante, *Phys. Lett.* **B742**, 279 (2015), [arXiv:1410.2796].
- [43] A. Serenelli, *Eur. Phys. J.* **A52**, 4, 78 (2016), [arXiv:1601.07179].
- [44] R. Davis, Jr., D. S. Harmer and K. C. Hoffman, *Phys. Rev. Lett.* **20**, 1205 (1968).
- [45] B. T. Cleveland *et al.*, *Astrophys. J.* **496**, 505 (1998).
- [46] C. Pena-Garay and A. Serenelli (2008), [arXiv:0811.2424].
- [47] J. N. Abdurashitov *et al.* (SAGE), *J. Exp. Theor. Phys.* **95**, 181 (2002), [*Zh. Eksp. Teor. Fiz.* 122,211(2002)], [arXiv:astro-ph/0204245].
- [48] W. Hampel *et al.* (GALLEX), *Phys. Lett.* **B447**, 127 (1999).
- [49] M. Altmann *et al.* (GNO), *Phys. Lett.* **B616**, 174 (2005), [hep-ex/0504037].
- [50] J. N. Abdurashitov *et al.* (SAGE), *Phys. Rev.* **C80**, 015807 (2009), [arXiv:0901.2200].
- [51] K. S. Hirata *et al.* (Kamiokande-II), *Phys. Rev. Lett.* **63**, 16 (1989).
- [52] K. S. Hirata *et al.* (Kamiokande-II), *Phys. Rev.* **D44**, 2241 (1991), [Erratum: *Phys. Rev.* **D45**, 2170(1992)].
- [53] Y. Fukuda *et al.* (Kamiokande), *Phys. Rev. Lett.* **77**, 1683 (1996).
- [54] Y. Fukuda *et al.* (Super-Kamiokande), *Phys. Rev. Lett.* **81**, 1158 (1998), [Erratum: *Phys. Rev. Lett.* **81**, 4279(1998)], [hep-ex/9805021].
- [55] Y. Fukuda *et al.* (Super-Kamiokande), *Phys. Rev. Lett.* **82**, 2430 (1999), [hep-ex/9812011].
- [56] K. Abe *et al.* (Super-Kamiokande), *Phys. Rev.* **D94**, 5, 052010 (2016), [arXiv:1606.07538].
- [57] N. Vinyoles *et al.*, *Astrophys. J.* **835**, 2, 202 (2017), [arXiv:1611.09867].
- [58] S. Fukuda *et al.* (Super-Kamiokande), *Phys. Rev. Lett.* **86**, 5651 (2001), [hep-ex/0103032].
- [59] S. Fukuda *et al.* (Super-Kamiokande), *Phys. Rev. Lett.* **86**, 5656 (2001), [hep-ex/0103033].
- [60] B. Aharmim *et al.* (SNO), *Phys. Rev.* **C72**, 055502 (2005), [arXiv:nucl-ex/0502021].
- [61] S. Fukuda *et al.* (Super-Kamiokande), *Phys. Lett.* **B539**, 179 (2002), [hep-ex/0205075].
- [62] Q. R. Ahmad *et al.* (SNO), *Phys. Rev. Lett.* **87**, 071301 (2001), [arXiv:nucl-ex/0106015].
- [63] Q. R. Ahmad *et al.* (SNO), *Phys. Rev. Lett.* **89**, 011301 (2002), [arXiv:nucl-ex/0204008].
- [64] B. Aharmim *et al.* (SNO), *Phys. Rev.* **C88**, 025501 (2013), [arXiv:1109.0763].
- [65] J. Bergstrom *et al.*, *JHEP* **03**, 132 (2016), [arXiv:1601.00972].
- [66] C. Arpesella *et al.* (Borexino), *Phys. Lett.* **B658**, 101 (2008), [arXiv:0708.2251].
- [67] G. Bellini *et al.* (Borexino), *Phys. Rev. Lett.* **108**, 051302 (2012), [arXiv:1110.3230].
- [68] M. Agostini *et al.* (BOREXINO), *Nature* **562**, 7728, 505 (2018).
- [69] G. Bellini *et al.* (Borexino), *Phys. Rev.* **D82**, 033006 (2010), [arXiv:0808.2868].

- [70] S. Abe *et al.* (KamLAND), Phys. Rev. **C84**, 035804 (2011), [arXiv:1106.0861].
- [71] A. Gando *et al.* (KamLAND), Phys. Rev. **C92**, 5, 055808 (2015), [arXiv:1405.6190].
- [72] M. Agostini *et al.* (Borexino) (2017), [arXiv:1707.09279].
- [73] M. Agostini *et al.* (Borexino) (2017), [arXiv:1709.00756].
- [74] A. Renshaw *et al.* (Super-Kamiokande), Phys. Rev. Lett. **112**, 9, 091805 (2014), [arXiv:1312.5176].
- [75] M. Honda *et al.*, Phys. Rev. **D92**, 2, 023004 (2015), [arXiv:1502.03916].
- [76] G. D. Barr *et al.*, Phys. Rev. **D74**, 094009 (2006), [arXiv:astro-ph/0611266].
- [77] G. Battistoni *et al.*, Astropart. Phys. **19**, 269 (2003), [Erratum: Astropart. Phys.19,291(2003)], [hep-ph/0207035].
- [78] J. Evans *et al.*, Phys. Rev. **D95**, 2, 023012 (2017), [arXiv:1612.03219].
- [79] C. V. Achar *et al.*, Phys. Lett. **18**, 196 (1965).
- [80] F. Reines *et al.*, Phys. Rev. Lett. **15**, 429 (1965).
- [81] K. S. Hirata *et al.* (Kamiokande-II), Phys. Lett. **B205**, 416 (1988), [447(1988)].
- [82] D. Casper *et al.*, Phys. Rev. Lett. **66**, 2561 (1991).
- [83] K. Daum *et al.* (Frejus), Z. Phys. **C66**, 417 (1995).
- [84] M. Aglietta *et al.* (NUSEX), Europhys. Lett. **8**, 611 (1989).
- [85] K. S. Hirata *et al.* (Kamiokande-II), Phys. Lett. **B280**, 146 (1992).
- [86] Y. Fukuda *et al.* (Kamiokande), Phys. Lett. **B335**, 237 (1994).
- [87] Y. Fukuda *et al.* (Super-Kamiokande), Phys. Rev. Lett. **81**, 1562 (1998), [hep-ex/9807003].
- [88] M. Ambrosio *et al.* (MACRO), Phys. Lett. **B517**, 59 (2001), [hep-ex/0106049].
- [89] M. C. Sanchez *et al.* (Soudan 2), Phys. Rev. **D68**, 113004 (2003), [hep-ex/0307069].
- [90] Y. Ashie *et al.* (Super-Kamiokande), Phys. Rev. Lett. **93**, 101801 (2004), [hep-ex/0404034].
- [91] Z. Li *et al.* (Super-Kamiokande), Phys. Rev. **D98**, 5, 052006 (2018), [arXiv:1711.09436].
- [92] N. Agafonova *et al.* (OPERA), Phys. Rev. Lett. **120**, 21, 211801 (2018), [Erratum: Phys. Rev. Lett.121,no.13,139901(2018)], [arXiv:1804.04912].
- [93] M. G. Aartsen *et al.* (IceCube), Phys. Rev. **D99**, 3, 032007 (2019), [arXiv:1901.05366].
- [94] K. Abe *et al.* (Super-Kamiokande), Phys. Rev. **D97**, 7, 072001 (2018), [arXiv:1710.09126].
- [95] M. Ageron *et al.* (ANTARES), Nucl. Instrum. Meth. **A656**, 11 (2011), [arXiv:1104.1607].
- [96] M. G. Aartsen *et al.* (IceCube), JINST **12**, 03, P03012 (2017), [arXiv:1612.05093].
- [97] A. Albert *et al.* (ANTARES), JHEP **06**, 113 (2019), [arXiv:1812.08650].
- [98] M. G. Aartsen *et al.* (IceCube), Phys. Rev. Lett. **120**, 7, 071801 (2018), [arXiv:1707.07081].
- [99] S. Adrian-Martinez *et al.* (KM3Net), J. Phys. **G43**, 8, 084001 (2016), [arXiv:1601.07459].
- [100] M. G. Aartsen *et al.* (IceCube), J. Phys. **G44**, 5, 054006 (2017), [arXiv:1607.02671].
- [101] S. Ahmed *et al.* (ICAL), Pramana **88**, 5, 79 (2017), [arXiv:1505.07380].
- [102] K. Abe *et al.* (Hyper-Kamiokande) (2018), [arXiv:1805.04163].
- [103] B. Abi *et al.* (DUNE) (2018), [arXiv:1807.10334].
- [104] S. E. Kopp, Phys. Rept. **439**, 101 (2007), [arXiv:physics/0609129].
- [105] D. Beavis *et al.* (E899) (1995).
- [106] M. G. Catanesi *et al.* (HARP), Nucl. Instrum. Meth. **A571**, 527 (2007).
- [107] J. M. Paley *et al.* (MIPP), Phys. Rev. **D90**, 3, 032001 (2014), [arXiv:1404.5882].
- [108] N. Abgrall *et al.* (NA61), JINST **9**, P06005 (2014), [arXiv:1401.4699].
- [109] S. H. Ahn *et al.* (K2K), Phys. Lett. **B511**, 178 (2001), [hep-ex/0103001].
- [110] M. H. Ahn *et al.* (K2K), Phys. Rev. **D74**, 072003 (2006), [hep-ex/0606032].
- [111] D. G. Michael *et al.* (MINOS), Nucl. Instrum. Meth. **A596**, 190 (2008), [arXiv:0805.3170].
- [112] P. Adamson *et al.*, Nucl. Instrum. Meth. **A806**, 279 (2016), [arXiv:1507.06690].
- [113] P. Adamson *et al.* (MINOS), Phys. Rev. Lett. **110**, 25, 251801 (2013), [arXiv:1304.6335].
- [114] P. Adamson *et al.* (MINOS), Phys. Rev. Lett. **112**, 191801 (2014), [arXiv:1403.0867].
- [115] P. Adamson *et al.* (MINOS), Phys. Rev. **D86**, 052007 (2012), [arXiv:1208.2915].
- [116] P. Adamson *et al.* (MINOS+), Phys. Rev. Lett. **122**, 9, 091803 (2019), [arXiv:1710.06488].
- [117] C. Rubbia *et al.*, JINST **6**, P07011 (2011), [arXiv:1106.0975].
- [118] K. Abe *et al.* (T2K), Phys. Rev. Lett. **107**, 041801 (2011), [arXiv:1106.2822].
- [119] K. Abe *et al.* (T2K), Phys. Rev. Lett. **112**, 061802 (2014), [arXiv:1311.4750].
- [120] K. Abe *et al.* (T2K), Phys. Rev. Lett. **121**, 17, 171802 (2018), [arXiv:1807.07891].
- [121] K. Abe *et al.* (T2K) (2019), [arXiv:1910.03887].
- [122] P. Adamson *et al.* (NOvA), Phys. Rev. Lett. **118**, 15, 151802 (2017), [arXiv:1701.05891].
- [123] M. A. Acero *et al.* (NOvA), Phys. Rev. **D98**, 032012 (2018), [arXiv:1806.00096].
- [124] P. Adamson *et al.* (NOvA), Phys. Rev. Lett. **116**, 15, 151806 (2016), [arXiv:1601.05022].
- [125] P. Adamson *et al.* (NOvA), Phys. Rev. Lett. **118**, 23, 231801 (2017), [arXiv:1703.03328].
- [126] M. A. Acero *et al.* (NOvA), Phys. Rev. Lett. **123**, 151803 (2019), [arXiv:1906.04907].
- [127] A. Aguilar-Arevalo *et al.* (LSND), Phys. Rev. **D64**, 112007 (2001), [hep-ex/0104049].
- [128] B. Armbruster *et al.* (KARMEN), Phys. Rev. **D65**, 112001 (2002), [hep-ex/0203021].
- [129] A. A. Aguilar-Arevalo *et al.* (MiniBooNE), Phys. Rev. Lett. **121**, 22, 221801 (2018), [arXiv:1805.12028].
- [130] M. Antonello *et al.* (MicroBooNE, LAr1-ND, ICARUS-WA104) (2015), [arXiv:1503.01520].
- [131] S. Ajimura *et al.* (2017), [arXiv:1705.08629].
- [132] F. Von Feilitzsch, A. A. Hahn and K. Schreckenbach, Phys. Lett. **118B**, 162 (1982).
- [133] K. Schreckenbach *et al.*, Phys. Lett. **160B**, 325 (1985).
- [134] A. A. Hahn *et al.*, Phys. Lett. **B218**, 365 (1989).
- [135] P. Vogel *et al.*, Phys. Rev. **C24**, 1543 (1981).
- [136] T. A. Mueller *et al.*, Phys. Rev. **C83**, 054615 (2011), [arXiv:1101.2663].
- [137] P. Huber, Phys. Rev. **C84**, 024617 (2011), [Erratum: Phys. Rev. C85,029901(2012)], [arXiv:1106.0687].
- [138] D. Adey *et al.* (Daya Bay), Phys. Rev. **D100**, 5, 052004 (2019), [arXiv:1808.10836].

- [139] D. Adey *et al.* (Daya Bay), Phys. Rev. Lett. **121**, 24, 241805 (2018), [arXiv:1809.02261].
- [140] G. Bak *et al.* (RENO), Phys. Rev. Lett. **121**, 20, 201801 (2018), [arXiv:1806.00248].
- [141] H. de Kerret *et al.* (Double Chooz) (2019), [arXiv:1901.09445].
- [142] Y. J. Ko *et al.* (NEOS), Phys. Rev. Lett. **118**, 12, 121802 (2017), [arXiv:1610.05134].
- [143] F. P. An *et al.* (Daya Bay), Phys. Rev. Lett. **118**, 25, 251801 (2017), [arXiv:1704.01082].
- [144] G. Bak *et al.* (RENO), Phys. Rev. Lett. **122**, 23, 232501 (2019), [arXiv:1806.00574].
- [145] D. Adey *et al.* (Daya Bay), Phys. Rev. Lett. **123**, 11, 111801 (2019), [arXiv:1904.07812].
- [146] M. Apollonio *et al.* (CHOOZ), Eur.Phys.J. **C27**, 331 (2003), [hep-ex/0301017].
- [147] F. Boehm *et al.*, Phys. Rev. **D64**, 112001 (2001), [hep-ex/0107009].
- [148] K. Eguchi *et al.* (KamLAND), Phys. Rev. Lett. **90**, 021802 (2003), [hep-ex/0212021].
- [149] T. Araki *et al.* (KamLAND), Phys. Rev. Lett. **94**, 081801 (2005), [hep-ex/0406035].
- [150] A. Gando *et al.* (KamLAND), Phys. Rev. **D88**, 3, 033001 (2013), [arXiv:1303.4667].
- [151] F. Ardellier *et al.* (Double Chooz) (2006), [hep-ex/0606025].
- [152] X. Guo *et al.* (Daya Bay) (2007), [hep-ex/0701029].
- [153] J. K. Ahn *et al.* (RENO) (2010), [arXiv:1003.1391].
- [154] Y. Abe *et al.* (Double Chooz), Phys. Rev. Lett. **108**, 131801 (2012), [arXiv:1112.6353].
- [155] F. P. An *et al.* (Daya Bay), Phys. Rev. Lett. **108**, 171803 (2012), [arXiv:1203.1669].
- [156] J. K. Ahn *et al.* (RENO), Phys. Rev. Lett. **108**, 191802 (2012), [arXiv:1204.0626].
- [157] F. An *et al.* (JUNO), J. Phys. **G43**, 3, 030401 (2016), [arXiv:1507.05613].
- [158] I. Alekseev *et al.* (DANSS), Phys. Lett. **B787**, 56 (2018), [arXiv:1804.04046].
- [159] H. Almazán *et al.* (STEREO), Phys. Rev. Lett. **121**, 16, 161801 (2018), [arXiv:1806.02096].
- [160] J. Ashenfelter *et al.* (PROSPECT), Phys. Rev. Lett. **121**, 25, 251802 (2018), [arXiv:1806.02784].
- [161] A. P. Serebrov *et al.* (NEUTRINO-4), Pisma Zh. Eksp. Teor. Fiz. **109**, 4, 209 (2019), [JETP Lett.109,no.4,213(2019)], [arXiv:1809.10561].
- [162] Y. Abreu *et al.* (SoLid), JINST **12**, 04, P04024 (2017), [arXiv:1703.01683].
- [163] N. Cabibbo, Phys. Lett. **72B**, 333 (1978).
- [164] S. M. Bilenky, J. Hosek and S. T. Petcov, Phys. Lett. **94B**, 495 (1980).
- [165] V. D. Barger, K. Whisnant and R. J. N. Phillips, Phys. Rev. Lett. **45**, 2084 (1980).
- [166] P. Langacker *et al.*, Nucl. Phys. **B282**, 589 (1987).
- [167] S. Goswami and A. Yu. Smirnov, Phys. Rev. **D72**, 053011 (2005), [hep-ph/0411359].
- [168] N. Okamura, Prog. Theor. Phys. **114**, 1045 (2006), [hep-ph/0411388].
- [169] H. Nunokawa, S. J. Parke and R. Zukanovich Funchal, Phys. Rev. **D72**, 013009 (2005), [hep-ph/0503283].
- [170] A. Cervera *et al.*, Nucl. Phys. **B579**, 17 (2000), [Erratum: Nucl. Phys. B593,731(2001)], [hep-ph/0002108].
- [171] M. Freund, Phys. Rev. **D64**, 053003 (2001), [hep-ph/0103300].
- [172] E. K. Akhmedov *et al.*, JHEP **04**, 078 (2004), [hep-ph/0402175].
- [173] H. Minakata *et al.*, Phys. Rev. **D74**, 053008 (2006), [hep-ph/0607284].
- [174] O. L. G. Peres and A. Yu. Smirnov, Nucl. Phys. **B680**, 479 (2004), [hep-ph/0309312].
- [175] S. Petcov, Phys.Lett. **B434**, 321 (1998), [hep-ph/9805262].
- [176] E. K. Akhmedov *et al.*, Nucl.Phys. **B542**, 3 (1999), [hep-ph/9808270].
- [177] E. K. Akhmedov, Nucl.Phys. **B538**, 25 (1999), [hep-ph/9805272].
- [178] M. Chizhov, M. Maris and S. Petcov (1998), [hep-ph/9810501].
- [179] M. Chizhov and S. Petcov, Phys.Rev.Lett. **83**, 1096 (1999), [hep-ph/9903399].
- [180] E. K. Akhmedov, M. Maltoni and A. Y. Smirnov, JHEP **0705**, 077 (2007), [hep-ph/0612285].
- [181] C. Kim and U. Lee, Phys.Lett. **B444**, 204 (1998), [hep-ph/9809491].
- [182] O. Peres and A. Y. Smirnov, Phys.Lett. **B456**, 204 (1999), [hep-ph/9902312].
- [183] M. Gonzalez-Garcia, M. Maltoni and A. Y. Smirnov, Phys.Rev. **D70**, 093005 (2004), [hep-ph/0408170].
- [184] E. K. Akhmedov, M. Maltoni and A. Y. Smirnov, JHEP **0806**, 072 (2008), [arXiv:0804.1466].
- [185] J. Bernabeu, S. Palomares Ruiz and S. Petcov, Nucl.Phys. **B669**, 255 (2003), [hep-ph/0305152].
- [186] S. Petcov and T. Schwetz, Nucl.Phys. **B740**, 1 (2006), [hep-ph/0511277].
- [187] I. Esteban *et al.*, JHEP **01**, 106 (2019), [arXiv:1811.05487].
- [188] I. Esteban *et al.*, “Nufit4.1 at nufit webpage,” <http://www.nu-fit.org>.
- [189] F. Capozzi *et al.*, Prog. Part. Nucl. Phys. **102**, 48 (2018), [arXiv:1804.09678].
- [190] P. F. de Salas *et al.*, Phys. Lett. **B782**, 633 (2018), [arXiv:1708.01186].
- [191] M. Friend, “Updated Results from the T2K Experiment with 3.13×10^{21} Protons on Target,” (2019), KEK/J-PARC Physics seminar, January 10, 2019, URL <https://t2k.org/docs/talk/335/2019kekseminar>.
- [192] C. Jarlskog, Phys. Rev. Lett. **55**, 1039 (1985).
- [193] M. C. Gonzalez-Garcia, M. Maltoni and T. Schwetz, JHEP **11**, 052 (2014), [arXiv:1409.5439].
- [194] Y. Farzan and A. Yu. Smirnov, Phys. Rev. **D65**, 113001 (2002), [hep-ph/0201105].
- [195] A. Dueck, S. Petcov and W. Rodejohann, Phys. Rev. **D82**, 013005 (2010), [arXiv:1006.0227].
- [196] A. Aguilar-Arevalo *et al.* (MiniBooNE) (2012), [arXiv:1207.4809].
- [197] M. A. Acero, C. Giunti and M. Laveder, Phys. Rev. **D78**, 073009 (2008), [arXiv:0711.4222].
- [198] C. Giunti and M. Laveder, Phys. Rev. **C83**, 065504 (2011), [arXiv:1006.3244].
- [199] F. P. An *et al.* (Daya Bay), Phys. Rev. Lett. **116**, 6, 061801 (2016), [Erratum: Phys. Rev. Lett.118,no.9,099902(2017)], [arXiv:1508.04233].
- [200] G. Mention *et al.*, Phys. Rev. **D83**, 073006 (2011), [arXiv:1101.2755].
- [201] J. J. Gomez-Cadenas and M. C. Gonzalez-Garcia, Z. Phys. **C71**, 443 (1996), [hep-ph/9504246].
- [202] M. Maltoni *et al.*, Nucl. Phys. **B643**, 321 (2002), [hep-ph/0207157].
- [203] M. Dentler *et al.*, JHEP **08**, 010 (2018), [arXiv:1803.10661].
- [204] C. Giunti and M. Laveder, Phys. Rev. **D84**, 093006 (2011), [arXiv:1109.4033].

- [205] J. M. Conrad *et al.*, Adv. High Energy Phys. **2013**, 163897 (2013), [arXiv:1207.4765].
- [206] J. Kopp *et al.*, JHEP **05**, 050 (2013), [arXiv:1303.3011].
- [207] G. H. Collin *et al.*, Phys. Rev. Lett. **117**, 22, 221801 (2016), [arXiv:1607.00011].
- [208] S. Gariazzo *et al.*, JHEP **06**, 135 (2017), [arXiv:1703.00860].
- [209] A. Diaz *et al.* (2019), [arXiv:1906.00045].
- [210] S. Böser *et al.* (2019), [arXiv:1906.01739].
- [211] G. Karagiorgi *et al.*, Phys. Rev. **D75**, 013011 (2007), [Erratum: Phys. Rev.D80,099902(2009)], [hep-ph/0609177].
- [212] M. Maltoni and T. Schwetz, Phys. Rev. **D76**, 093005 (2007), [arXiv:0705.0107].
- [213] C. Giunti and M. Laveder, Phys. Rev. **D84**, 073008 (2011), [arXiv:1107.1452].
- [214] M. Aker *et al.* (KATRIN) (2019), [arXiv:1909.06048].
- [215] J. Bonn *et al.*, Nucl. Phys. Proc. Suppl. **91**, 273 (2001), [PoShep2001,192(2001)].
- [216] V. M. Lobashev *et al.*, Nucl. Phys. Proc. Suppl. **91**, 280 (2001), [280(2001)].
- [217] B. Monreal and J. A. Formaggio, Phys. Rev. **D80**, 051301 (2009), [arXiv:0904.2860].
- [218] A. De Rujula and M. Lusignoli, Phys. Lett. **118B**, 429 (1982).
- [219] L. Gastaldo *et al.*, J. Low Temp. Phys. **176**, 5-6, 876 (2014), [arXiv:1309.5214].
- [220] B. Alpert *et al.*, Eur. Phys. J. **C75**, 3, 112 (2015), [arXiv:1412.5060].
- [221] M. P. Croce *et al.*, J. Low. Temp. Phys. **184**, 3-4, 958 (2016), [arXiv:1510.03874].
- [222] R. E. Shrock, Phys. Lett. **96B**, 159 (1980).
- [223] F. Vissani, Nucl. Phys. Proc. Suppl. **100**, 273 (2001), [273(2000)], [hep-ph/0012018].
- [224] Y. Farzan, O. L. G. Peres and A. Yu. Smirnov, Nucl. Phys. **B612**, 59 (2001), [hep-ph/0105105].
- [225] J. Schechter and J. W. F. Valle, Phys. Rev. **D25**, 2951 (1982), [289(1981)].
- [226] J. Engel and J. Menendez, Rept. Prog. Phys. **80**, 4, 046301 (2017), [arXiv:1610.06548].
- [227] A. Gando *et al.* (KamLAND-Zen), Phys. Rev. Lett. **117**, 8, 082503 (2016), [Addendum: Phys. Rev. Lett.117,no.10,109903(2016)], [arXiv:1605.02889].
- [228] M. Agostini *et al.* (GERDA), Science **365**, 1445 (2019), [arXiv:1909.02726].
- [229] S. I. Alvis *et al.* (Majorana) (2019), [arXiv:1902.02299].
- [230] S. Andringa *et al.* (SNO+), Adv. High Energy Phys. **2016**, 6194250 (2016), [arXiv:1508.05759].
- [231] G. Anton *et al.* (EXO-200) (2019), [arXiv:1906.02723].
- [232] J. Renner *et al.* (NEXT), JINST **13**, 10, P10020 (2018), [arXiv:1808.01804].
- [233] C. Alduino *et al.* (CUORE), Phys. Rev. Lett. **120**, 13, 132501 (2018), [arXiv:1710.07988].
- [234] O. Azzolini *et al.* (CUPID), Phys. Rev. Lett. **123**, 3, 032501 (2019), [arXiv:1906.05001].
- [235] V. Alenkov *et al.*, Eur. Phys. J. **C79**, 9, 791 (2019), [arXiv:1903.09483].
- [236] R. Arnold *et al.* (NEMO-3), Phys. Rev. **D92**, 7, 072011 (2015), [arXiv:1506.05825].
- [237] R. Arnold *et al.* (NEMO-3), Phys. Rev. Lett. **119**, 4, 041801 (2017), [arXiv:1705.08847].

15. Quark Model

Revised August 2019 by C. Amsler (Stefan Meyer Inst.), T. De-Grand (Colorado U., Boulder) and B. Krusche (Basel U.).

15.1 Quantum numbers of the quarks

Quantum chromodynamics (QCD) is the theory of strong interactions. QCD is a quantum field theory and its constituents are a set of fermions, the quarks, and gauge bosons, the gluons. Strongly interacting particles, the hadrons, are bound states of quark and gluon fields. As gluons carry no intrinsic quantum numbers beyond color charge, and because color is believed to be permanently confined, most of the quantum numbers of strongly interacting particles are given by the quantum numbers of their constituent quarks and antiquarks. The description of hadronic properties which strongly emphasizes the role of the minimum-quark-content part of the wave function of a hadron is generically called the quark model. It exists on many levels: from the simple, almost dynamics-free picture of strongly interacting particles as bound states of quarks and antiquarks, to more detailed descriptions of dynamics, either through models or directly from QCD itself. The different sections of this review survey the many approaches to the spectroscopy of strongly interacting particles which fall under the umbrella of the quark model.

Quarks are strongly interacting fermions with spin 1/2 and, by convention, positive parity. Antiquarks have negative parity. Quarks have the additive baryon number 1/3, antiquarks -1/3. Table 15.1 gives the other additive quantum numbers (flavors) for the three generations of quarks. They are related to the charge Q (in units of the elementary charge e) through the generalized Gell-Mann-Nishijima formula

$$Q = I_z + \frac{B + S + C + B + T}{2}, \quad (15.1)$$

where B is the baryon number. The convention is that the quark flavor (I_z , S , C , B , or T) has the same sign as its charge Q . With this convention, any flavor carried by a charged meson has

Table 15.1

	d	u	s	c	b	t
Q - electric charge	$-\frac{1}{3}$	$+\frac{2}{3}$	$-\frac{1}{3}$	$+\frac{2}{3}$	$-\frac{1}{3}$	$+\frac{2}{3}$
I - isospin	$\frac{1}{2}$	$\frac{1}{2}$	0	0	0	0
I_z - isospin z -component	$-\frac{1}{2}$	$+\frac{1}{2}$	0	0	0	0
S - strangeness	0	0	-1	0	0	0
C - charm	0	0	0	+1	0	0
B - bottomness	0	0	0	0	-1	0
T - topness	0	0	0	0	0	+1

the same sign as its charge, e.g., the strangeness of the K^+ is +1, the bottomness of the B^+ is +1, and the charm and strangeness of the D_s^- are each -1. Antiquarks have the opposite flavor signs. The hypercharge is defined as

$$Y = B + S - \frac{C - B + T}{3}. \quad (15.2)$$

Thus Y is equal to $\frac{1}{3}$ for the u and d quarks, $-\frac{2}{3}$ for the s quark, and 0 for all other quarks. More details and derivations on the quark structure of mesons and baryons can be found in Ref. [1].

15.2 Mesons

Mesons have baryon number $B = 0$. In the quark model, they are $q\bar{q}'$ bound states of quarks q and antiquarks \bar{q}' (the flavors of q and q' may be different). If the orbital angular momentum of the $q\bar{q}'$ state is ℓ , then the parity P is $(-1)^{\ell+1}$. The meson spin J is given by the usual relation $|\ell - s| \leq J \leq |\ell + s|$, where s is 0 (antiparallel quark spins) or 1 (parallel quark spins). The charge conjugation, or C -parity $C = (-1)^{\ell+s}$, is defined only for the $q\bar{q}$ states made of quarks and their own antiquarks. The C -parity can be generalized to the G -parity $G = (-1)^{I+\ell+s}$ for mesons made of quarks and their own antiquarks (isospin $I_z = 0$), and for the charged $u\bar{d}$ and $d\bar{u}$ states (isospin $I = 1$).

The mesons are classified in J^{PC} multiplets. The $\ell = 0$ states are the pseudoscalars (0^{-+}) and the vectors (1^{--}). The orbital

excitations $\ell = 1$ are the scalars (0^{++}), the axial vectors (1^{+-}) and (1^{+}), and the tensors (2^{++}). Assignments for many of the known mesons are given in Tables 15.2, 15.3 and 15.4. Radial excitations are denoted by the principal quantum number n . The very short lifetime of the t quark makes it likely that bound-state hadrons containing t quarks and/or antiquarks do not exist.

States in the natural spin-parity series $P = (-1)^J$ must, according to the above, have $s = 1$ and hence, $CP = +1$. Thus, mesons with natural spin-parity and $CP = -1$ (0^{+-} , 1^{+-} , 2^{+-} , 3^{-+} , etc.) are forbidden in the $q\bar{q}'$ model. The $J^{PC} = 0^{-}$ state is forbidden as well. Mesons with such exotic quantum numbers may exist, but would lie outside the $q\bar{q}'$ model (see section below on exotic mesons).

Following $SU(3)$, the nine possible $q\bar{q}'$ combinations containing the light u , d , and s quarks are grouped into an octet and a singlet of light quark mesons:

$$3 \otimes \bar{3} = 8 \oplus 1. \quad (15.3)$$

A fourth quark such as charm c can be included by extending $SU(3)$ to $SU(4)$. However, $SU(4)$ is badly broken owing to the much heavier c quark. Nevertheless, in an $SU(4)$ classification, the sixteen mesons are grouped into a 15-plet and a singlet:

$$4 \otimes \bar{4} = 15 \oplus 1. \quad (15.4)$$

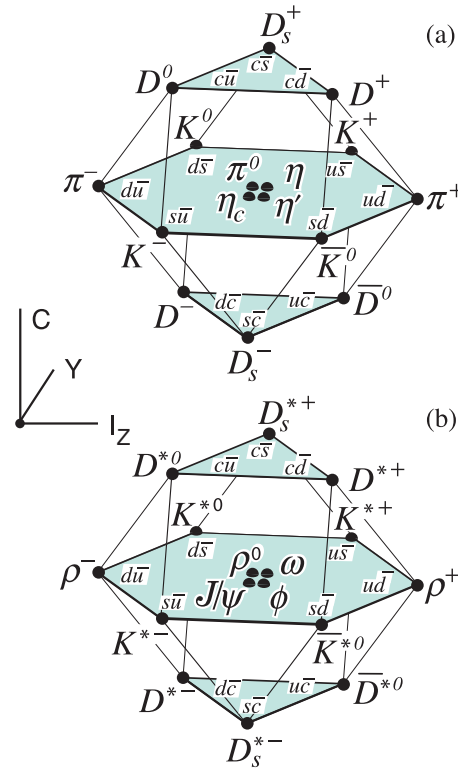


Figure 15.1: $SU(4)$ weight diagram showing the 16-plets for the pseudoscalar (a) and vector mesons (b) made of the u , d , s , and c quarks as a function of isospin I_z , charm C , and hypercharge $Y = B + S - \frac{C}{3}$. The nonets of light mesons occupy the central planes to which the $c\bar{c}$ states have been added.

The weight diagrams for the ground-state pseudoscalar (0^{-+}) and vector (1^{--}) mesons are depicted in Fig. 15.1. The light quark mesons are members of nonets building the middle plane in Fig. 15.1(a) and (b).

Isoscalar states with the same J^{PC} mix, but mixing between the two light quark isoscalar mesons, and the much heavier charmonium or bottomonium states, are generally assumed to be negligible. In the following, we shall use the generic names a for the $I = 1$, K for the $I = 1/2$, and f and f' for the $I = 0$ members of

Table 15.2: Suggested $q\bar{q}$ quark-model assignments for some of the observed light mesons. Mesons in bold face are included in the Meson Summary Table. The wave functions f and f' are given in the text (Eqn. 15.9). The singlet-octet mixing angles from the linear mass formula (15.12) and its quadratic version (in which the masses are squared) are also given for the well established nonets. The classification of the 0^{++} mesons is tentative: the light scalars $a_0(980)$, $f_0(980)$, $f_0(500)$ and $K_0^*(700)$ are often considered to be four-quark states, and are omitted from the table, see Eqn. (15.26) below. The isoscalar 0^{++} mesons $f_0(1370)$, $f_0(1500)$ (not shown) and $f_0(1710)$ are expected to mix, see the “Note on Non- $q\bar{q}$ mesons” and the “Note on Scalar Mesons below 2 GeV” in the Meson Listings for details. The isoscalar assignments in the 2^1S_0 (0^{-+}) nonet are also tentative. The $\eta(1405)$ (not shown) and $\eta(1475)$ may be manifestations of the same state, see the “Note on Pseudoscalar and Pseudovector Mesons in the 1400 MeV Region” in the Meson Listings.
[†] The $1^{+\pm}$ and $2^{-\pm}$ isospin $\frac{1}{2}$ states mix. In particular, the K_{1A} and K_{1B} are nearly equal (45°) mixtures of the $K_1(1270)$ and $K_1(1400)$ (see [2] and references therein).
[‡] The physical vector mesons may be mixtures of 1^3D_1 and 2^3S_1 [3].

$n^{2s+1}\ell_J$	J^{PC}	$l = 1$	$l = \frac{1}{2}$	$l = 0$	$l = 0$	θ_{quad} [$^\circ$]	θ_{lin} [$^\circ$]
		$u\bar{d}, \bar{u}d,$ $\frac{1}{\sqrt{2}}(d\bar{d} - u\bar{u})$	$u\bar{s}, d\bar{s};$ $\bar{d}s, \bar{u}s$	f'	f		
1^1S_0	0^{-+}	π	K	η	$\eta'(958)$	-11.3	-24.5
1^3S_1	1^{--}	$\rho(770)$	$K^*(892)$	$\phi(1020)$	$\omega(782)$	39.2	36.5
1^1P_1	1^{+-}	$b_1(1235)$	K_{1B}^\dagger	$h_1(1415)$	$h_1(1170)$		
1^3P_0	0^{++}	$a_0(1450)$	$K_0^*(1430)$	$f_0(1710)$	$f_0(1370)$		
1^3P_1	1^{++}	$a_1(1260)$	K_{1A}^\dagger	$f_1(1420)$	$f_1(1285)$		
1^3P_2	2^{++}	$a_2(1320)$	$K_2^*(1430)$	$f_2'(1525)$	$f_2(1270)$	29.6	28.0
1^1D_2	2^{-+}	$\pi_2(1670)$	$K_2(1770)^\dagger$	$\eta_2(1870)$	$\eta_2(1645)$		
1^3D_1	1^{--}	$\rho(1700)$	$K^*(1680)^\ddagger$		$\omega(1650)$		
1^3D_2	2^{--}		$K_2(1820)^\dagger$				
1^3D_3	3^{--}	$\rho_3(1690)$	$K_3^*(1780)$	$\phi_3(1850)$	$\omega_3(1670)$	31.8	30.8
1^3F_4	4^{++}	$a_4(1970)$	$K_4^*(2045)$	$f_4(2300)$	$f_4(2050)$		
1^3G_5	5^{--}	$\rho_5(2350)$	$K_5^*(2380)$				
2^1S_0	0^{-+}	$\pi(1300)$	$K(1460)$	$\eta(1475)$	$\eta(1295)$		
2^3S_1	1^{--}	$\rho(1450)$	$K^*(1410)^\ddagger$	$\phi(1680)$	$\omega(1420)$		
2^3P_1	1^{++}	$a_1(1640)$					
2^3P_2	2^{++}	$a_2(1700)$	$K_2^*(1980)$	$f_2(1950)$	$f_2(1640)$		

Table 15.3: $c\bar{c}$ quark-model assignments for the charmonium and open charm mesons with established J^{PC} . Mesons in bold face are included in the Meson Summary Table. The open flavor states in the 1^{+-} and 1^{++} rows are mixtures of the $1^{+\pm}$ states.
[†] The masses are considerably smaller than most theoretical predictions.
These states have also been considered as four-quark states.
[‡] Mixtures of the 1^3D_1 and 2^3S_1 states.

$n^{2s+1}\ell_J$	J^{PC}	$l = 0$	$l = \frac{1}{2}$	$l = 0$
		$c\bar{c}$	$c\bar{u}, c\bar{d};$ $\bar{c}u, \bar{c}d$	$c\bar{s};$ $\bar{c}s$
1^1S_0	0^{-+}	$\eta_c(1S)$	D	D_s^\pm
1^3S_1	1^{--}	$J/\psi(1S)$	D^*	$D_s^{*\pm}$
1^3P_0	0^{++}	$\chi_{c0}(1P)$	$D_0^*(2300)$	$D_{s0}^*(2317)^\pm$
1^3P_1	1^{++}	$\chi_{c1}(1P)$	$D_1(2430)$	$D_{s1}(2460)^\pm$
1^1P_1	1^{+-}	$h_c(1P)$	$D_1(2420)$	$D_{s1}(2536)^\pm$
1^3P_2	2^{++}	$\chi_{c2}(1P)$	$D_2^*(2460)$	$D_{s2}^*(2573)$
2^1S_0	0^{-+}	$\eta_c(2S)$		
2^3S_1	1^{--}	$\psi(2S)$		$D_{s1}^*(2700)^\pm$
1^3D_1	1^{--}	$\psi(3770)$		$D_{s1}^*(2860)^\pm$
1^3D_2	2^{--}	$\psi_2(3823)$		
2^3P_J	$0, 1^{++}$	$\chi_{c0}(3860)$		
	2^{++}	$\chi_{c2}(3930)$		
3^3S_1	1^{--}	$\psi(4040)$		
2^3D_1	1^{--}	$\psi(4160)$		
4^3S_1	1^{--}	$\psi(4415)$		
1^3D_3	3^{--}		$D_3^*(2750)$	$D_{s3}^*(2860)^\pm$

Table 15.4: $b\bar{b}$ quark-model assignments for the bottomonium and B mesons with established J^{PC} .

$n^{2s+1}\ell_J$	J^{PC}	$l = 0$ $b\bar{b}$	$l = \frac{1}{2}$ $b\bar{u}, b\bar{d};$ $\bar{b}u, \bar{b}d$	$l = 0$ $b\bar{s};$ $\bar{b}s$	$l = 0$ $b\bar{c};$ $\bar{b}c$
1^1S_0	0^{-+}	$\eta_b(1S)$	B	B_s^0	B_c^\pm
1^3S_1	1^{--}	$\Upsilon(1S)$	B^*	B_s^*	
1^3P_0	0^{++}	$\chi_{b0}(1P)$			
1^3P_1	1^{++}	$\chi_{b1}(1P)$			
1^1P_1	1^{+-}	$h_b(1P)$	$B_1(5721)$	$B_{s1}(5830)^0$	
1^3P_2	2^{++}	$\chi_{b2}(1P)$	$B_2^*(5747)$	$B_{s2}^*(5840)^0$	
2^1S_0	0^{-+}	$\eta_b(2S)$			$B_c(2S)^\pm$
2^3S_1	1^{--}	$\Upsilon(2S)$			$B_c^*(2S)^\pm$
1^3D_2	2^{--}	$\Upsilon_2(1D)$			
2^3P_J	$0, 1, 2^{++}$	$\chi_{b0,1,2}(2P)$			
2^1P_1	1^{+-}	$h_b(2P)$			
3^3S_1	1^{--}	$\Upsilon(3S)$			
3^3P_J	$0, 1, 2^{++}$	$\chi_{b1,2}(3P)$			
4^3S_1	1^{--}	$\Upsilon(4S)$			

the light quark nonets. Thus, the physical isoscalars are mixtures of the SU(3) wave function ψ_8 and ψ_1 :

$$f' = \psi_8 \cos \theta - \psi_1 \sin \theta, \tag{15.5}$$

$$f = \psi_8 \sin \theta + \psi_1 \cos \theta, \tag{15.6}$$

where θ is the nonet mixing angle and

$$\psi_8 = \frac{1}{\sqrt{6}}(u\bar{u} + d\bar{d} - 2s\bar{s}), \tag{15.7}$$

$$\psi_1 = \frac{1}{\sqrt{3}}(u\bar{u} + d\bar{d} + s\bar{s}). \tag{15.8}$$

These mixing relations are often rewritten to exhibit the $u\bar{u} + d\bar{d}$ and $s\bar{s}$ components which decouple for the “ideal” mixing angle θ_i , such that $\tan \theta_i = 1/\sqrt{2}$ (or $\theta_i = 35.3^\circ$). Defining $\alpha = \theta + 54.7^\circ$, one obtains the physical isoscalar in the flavor basis

$$f' = \frac{1}{\sqrt{2}}(u\bar{u} + d\bar{d}) \cos \alpha - s\bar{s} \sin \alpha, \tag{15.9}$$

and its orthogonal partner f (replace α by $\alpha - 90^\circ$). Thus for ideal mixing ($\alpha_i = 90^\circ$), the f' becomes pure $s\bar{s}$ and the f pure $u\bar{u} + d\bar{d}$. The mixing angle θ can be derived by diagonalizing the mass matrix

$$\begin{pmatrix} m_8 & m_{81} \\ m_{18} & m_1 \end{pmatrix} \tag{15.10}$$

The mass eigenvalues are $m_{f'}$ and m_f . The mixing angle is given by

$$\tan \theta = \frac{m_8 - m_{f'}}{m_{81}}. \tag{15.11}$$

Calculating m_8 and m_{81} from the wave functions Eq. 15.7 and Eq. 15.8, and expressing the quark masses as a function of the $l = 1/2$ and $l = 1$ meson masses, one obtains

$$\tan \theta = \frac{4m_K - m_a - 3m_{f'}}{2\sqrt{2}(m_a - m_K)}, \tag{15.12}$$

which also determines the sign of θ . Alternatively, one can express the mixing angle as a function of all nonet masses. The octet mass is given by

$$m_8 = m_{f'} \cos^2 \theta + m_f \sin^2 \theta \tag{15.13}$$

whence

$$\tan^2 \theta = \frac{4m_K - m_a - 3m_{f'}}{-4m_K + m_a + 3m_f}. \tag{15.14}$$

Eliminating θ from Eq. (15.12) and Eq. (15.14) leads to the sum rule [4]

$$(m_f + m_{f'})(4m_K - m_a) - 3m_f m_{f'} = 8m_K^2 - 8m_K m_a + 3m_a^2. \tag{15.15}$$

This relation is verified for the ground-state vector mesons. We identify the $\phi(1020)$ with the f' and the $\omega(783)$ with the f . Thus

$$\begin{aligned} \phi(1020) &= \psi_8 \cos \theta_V - \psi_1 \sin \theta_V, \\ \omega(782) &= \psi_8 \sin \theta_V + \psi_1 \cos \theta_V, \end{aligned} \tag{15.16}$$

with the vector mixing angle $\theta_V = 36.4^\circ$ from Eq. (15.14), very close to ideal mixing. Thus $\phi(1020)$ is nearly pure $s\bar{s}$. For ideal mixing, Eq. (15.12) and Eq. (15.14) lead to the relations

$$m_K = \frac{m_f + m_{f'}}{2}, \quad m_a = m_f, \tag{15.17}$$

which are satisfied for the vector mesons.

The situation for the pseudoscalar and scalar mesons is not so clear cut, either theoretically or experimentally. For the pseudoscalars, the mixing angle is small. This can be understood qualitatively via gluon-line counting of the mixing process. The size of the mixing process between the nonstrange and strange mass bases scales as α_s^2 , not α_s^3 , because of two rather than three gluon exchange as it does for the vector mesons. It may also be that the lightest isoscalar pseudoscalars mix more strongly with excited states or with states of substantial non- $\bar{q}q$ content, as will be discussed below.

A variety of analysis methods lead to similar results: First, for these states, Eqn. 15.15 is satisfied only approximately. Then Eqn. 15.12 and Eqn. 15.14 lead to somewhat different values for the mixing angle. Identifying the η with the f' one gets

$$\eta = \psi_8 \cos \theta_P - \psi_1 \sin \theta_P, \tag{15.18}$$

$$\eta' = \psi_8 \sin \theta_P + \psi_1 \cos \theta_P. \tag{15.19}$$

Following chiral perturbation theory, the meson masses in the mass formulae (Eq. (15.12) and Eq. (15.14)) might be replaced by their squares. Table 15.5 lists the mixing angle θ_{lin} from Eqn. 15.14 (using the neutral members of the nonets) and the corresponding θ_{quad} obtained by replacing the meson masses by their squares throughout.

Table 15.5: Singlet-octet mixing angles for the well established nonets from the linear mass formula (15.12) and its quadratic version in which the masses are squared.

$n^{2s+1}\ell_J$	J^{PC}	θ_{quad} [$^\circ$]	θ_{lin} [$^\circ$]
1^1S_0	0^{-+}	-11.3	-24.5
1^3S_1	1^{--}	39.2	36.5
1^3P_2	2^{++}	29.6	28.0
1^3D_3	3^{--}	31.8	30.8

The pseudoscalar mixing angle θ_P can also be measured by comparing the partial widths for radiative J/ψ decay into a vector and a pseudoscalar [5], radiative $\phi(1020)$ decay into η and η' [6], radiative decays between pseudoscalar and vector mesons [7], or $p\bar{p}$ annihilation at rest into a pair of vector and pseudoscalar or into two pseudoscalars [8,9]. One obtains a mixing angle between -10° and -20° . More recently, a lattice QCD simulation, Ref. [10], has successfully reproduced the masses of the η and η' , and as a byproduct find a mixing angle $\theta_{lin} = -14.1(2.8)^\circ$. We return to this point in Sec. 15.6.

The nonet mixing angles can be measured in $\gamma\gamma$ collisions, *e.g.*, for the 0^{-+} , 0^{++} , and 2^{++} nonets. In the quark model, the amplitude for the coupling of neutral mesons to two photons is proportional to $\sum_i Q_i^2$, where Q_i is the charge of the i -th quark. The 2γ partial width of an isoscalar meson with mass m is then given in terms of the mixing angle α by

$$\Gamma_{2\gamma} = C(5 \cos \alpha - \sqrt{2} \sin \alpha)^2 m^3, \quad (15.20)$$

- for f' and f ($\alpha \rightarrow \alpha - 90^\circ$). The coupling C may depend on the meson mass. It is often assumed to be a constant in the nonet. For the isovector a , one then finds $\Gamma_{2\gamma} = 9 C m^3$. Thus the members of an ideally mixed nonet couple to 2γ with partial widths in the ratios $f : f' : a = 25 : 2 : 9$. For tensor mesons, one finds from the ratios of the measured 2γ partial widths for the $f_2(1270)$ and $f'_2(1525)$ mesons a mixing angle α_T of $(81 \pm 1)^\circ$, or $\theta_T = (27 \pm 1)^\circ$, in accord with the linear mass formula. For the pseudoscalars, one finds from the ratios of partial widths $\Gamma(\eta' \rightarrow 2\gamma)/\Gamma(\eta \rightarrow 2\gamma)$ a mixing angle $\theta_P = (-18 \pm 2)^\circ$, while the ratio $\Gamma(\eta' \rightarrow 2\gamma)/\Gamma(\pi^0 \rightarrow 2\gamma)$ leads to $\sim -24^\circ$. SU(3) breaking effects for pseudoscalars are discussed in [11].

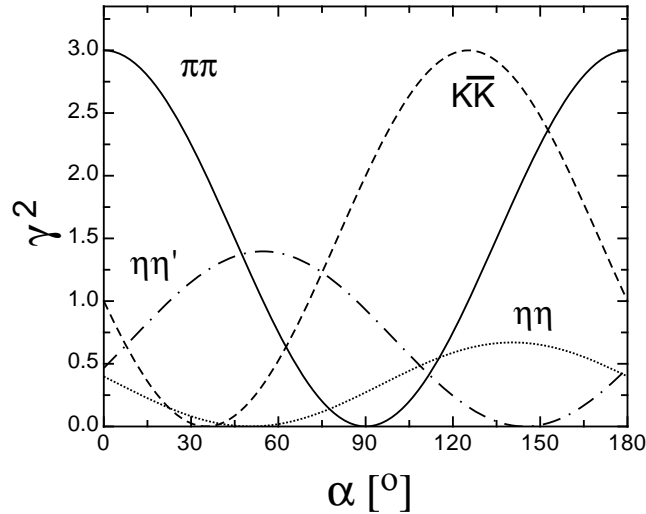


Figure 15.2: SU(3) couplings as a function of mixing angle α for isoscalar decays, up to a common multiplicative factor C and for $\theta_P = -17.3^\circ$.

The partial width for the decay of a scalar or a tensor meson into a pair of pseudoscalar mesons is model-dependent. Following Ref. [13],

$$\Gamma = C \times \gamma^2 \times |F(q)|^2 \times q. \quad (15.21)$$

C is a nonet constant, q the momentum of the decay products, $F(q)$ a form factor, and γ^2 the SU(3) coupling. The model-dependent form factor may be written as

$$|F(q)|^2 = q^{2\ell} \times \exp\left(-\frac{q^2}{8\beta^2}\right), \quad (15.22)$$

where ℓ is the relative angular momentum between the decay products. The decay of a $q\bar{q}$ meson into a pair of mesons involves the creation of a $q\bar{q}$ pair from the vacuum, and SU(3) symmetry assumes that the matrix elements for the creation of $s\bar{s}$, $u\bar{u}$, and $d\bar{d}$ pairs are equal. The couplings γ^2 are given in Table 15.6, and

Table 15.6: SU(3) couplings γ^2 for quarkonium decays as a function of nonet mixing angle α , up to a common multiplicative factor C ($\phi = 54.7^\circ + \theta_P$).

Isospin	Decay channel	γ^2
0	$\pi\pi$	$3 \cos^2 \alpha$
	$K\bar{K}$	$(\cos \alpha - \sqrt{2} \sin \alpha)^2$
	$\eta\eta$	$(\cos \alpha \cos^2 \phi - \sqrt{2} \sin \alpha \sin^2 \phi)^2$
	$\eta\eta'$	$\frac{1}{2} \sin^2 2\phi (\cos \alpha + \sqrt{2} \sin \alpha)^2$
1	$\eta\pi$	$2 \cos^2 \phi$
	$\eta'\pi$	$2 \sin^2 \phi$
	$K\bar{K}$	1
$\frac{1}{2}$	$K\pi$	$\frac{3}{2}$
	$K\eta$	$(\sin \phi - \frac{\cos \phi}{\sqrt{2}})^2$
	$K\eta'$	$(\cos \phi + \frac{\sin \phi}{\sqrt{2}})^2$

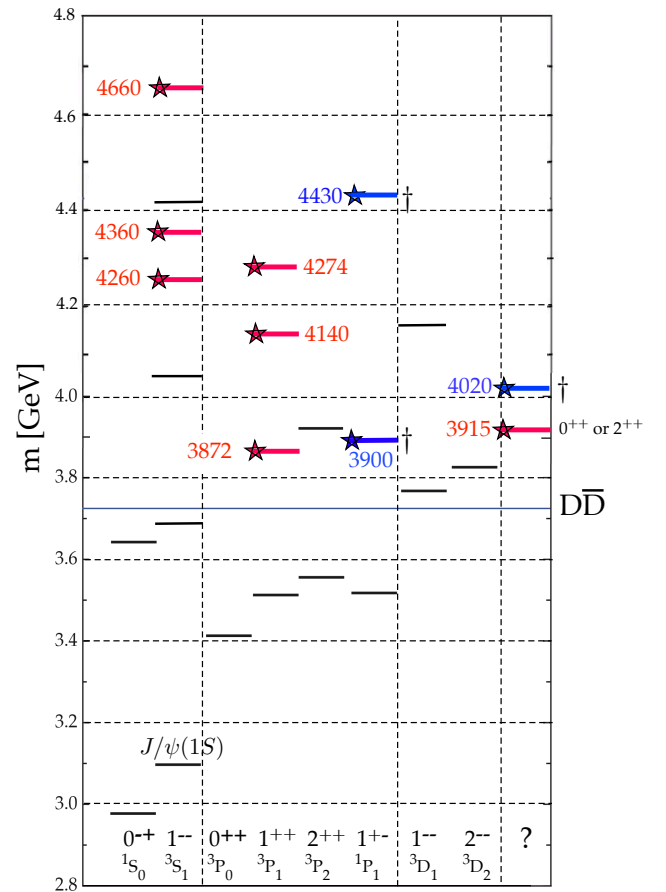


Figure 15.3: Established states populating the charmonium spectrum that are listed in the Summary Tables. The $c\bar{c}$ states are shown in black, the exotic ones are tagged by stars (red for the isoscalars, blue for the isovectors). The quantum numbers of the two states in the right column are not firmly established.

their dependence upon the mixing angle α is shown in Fig. 15.2 for isoscalar decays. The generalization to unequal $s\bar{s}$, $u\bar{u}$, and $d\bar{d}$ couplings is given in Ref. [13]. An excellent fit to the tensor meson decay widths is obtained assuming SU(3) symmetry, with $\beta \simeq 0.5$ GeV/c, $\theta_V \simeq 26^\circ$ and $\theta_P \simeq -17^\circ$ [13].

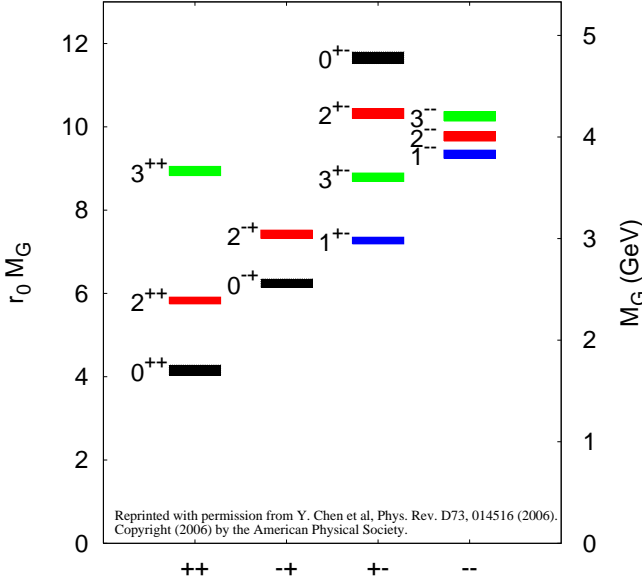


Figure 15.4: Predicted glueball mass spectrum from the lattice in quenched approximation (from [12]).

15.3 Exotic mesons

The existence of a light nonet composed of four quarks (tetraquarks) with masses below 1 GeV was suggested a long time ago [14] [15]. Coupling two triplets of light quarks u , d , and s , one obtains nine states, of which the six symmetric (uu , dd , ss , $ud + du$, $us + su$, $ds + sd$) form the six dimensional representation $\mathbf{6}$, while the three antisymmetric ($ud - du$, $us - su$, $ds - sd$) form the three dimensional representation $\bar{\mathbf{3}}$ of SU(3):

$$\mathbf{3} \otimes \mathbf{3} = \mathbf{6} \oplus \bar{\mathbf{3}}. \quad (15.23)$$

Hence for tetraquarks one gets the reduction

$$\begin{aligned} \mathbf{3} \otimes \mathbf{3} \otimes \bar{\mathbf{3}} \otimes \bar{\mathbf{3}} \\ &= \mathbf{6} \oplus \bar{\mathbf{3}} \otimes \bar{\mathbf{6}} \otimes \bar{\mathbf{3}} \\ &= \bar{\mathbf{3}} \otimes \mathbf{3} \oplus \mathbf{6} \otimes \bar{\mathbf{6}} \oplus \mathbf{6} \otimes \mathbf{3} \oplus \bar{\mathbf{3}} \otimes \bar{\mathbf{6}} \\ &= \mathbf{9} \oplus \mathbf{36} \oplus \mathbf{18} \oplus \bar{\mathbf{18}}. \end{aligned} \quad (15.24)$$

$$(15.25)$$

Combining with spin and color and requiring antisymmetry for diquarks and antidiquarks, one finds for ground states (zero angular momenta) that the most deeply bound tetraquarks (and hence the lightest ones) lie in the nonet and are scalar mesons (see also [1]). The average mass is estimated to be around 900 MeV from the mass differences between the ρ and π masses. Letting the strange quark determine the mass splittings one obtains a mass inverted spectrum with a light isosinglet, a medium heavy isodoublet and a heavy isotriplet + isosinglet. It is then tempting to identify these mesons as the lightest scalars

$$\begin{aligned} f_0(500) &= \bar{u}\bar{d}ud, \quad K_0^*(700) = (\bar{s}\bar{d}ud, \bar{s}\bar{u}ud) \quad \text{and} \quad (\bar{u}\bar{d}us, \bar{u}\bar{d}ds), \\ a_0(980) &= (us\bar{d}\bar{s}, \frac{1}{\sqrt{2}}[u\bar{u} - d\bar{d}]s\bar{s}, \bar{u}\bar{s}ds), \\ f_0(980) &= \frac{1}{\sqrt{2}}[u\bar{u} + d\bar{d}]s\bar{s}. \end{aligned} \quad (15.26)$$

A plethora of new states have been reported in the charmonium and bottomonium spectra. The most prominent one is the $\chi_{c1}(3872)$ (formerly $X(3872)$), first observed in 2003 in B -decays in the final state $J/\psi \pi^+ \pi^-$ (see Fig. 15.3). Even more remarkable is the observation of isovector (charged) mesons decaying into $c\bar{c}$ plus a charged pion, such as the $Z^\pm(4430)$ decaying into $\psi(2S)\pi^\pm$, which a priori excludes an interpretation as true $c\bar{c}$ (charmonium) state. Similar states are also observed in the bottomonium spectrum. Some of these states may be tetraquarks (e.g. $cq\bar{c}\bar{q}$), molecular structures (e.g. $c\bar{q}c\bar{q}$) made of pairs of

mesons such as D , D_s and D^* , D_s^* excitations, or their B and B^* counterparts. They could also be mimicked by kinematical effects. Details and references can be found in recent reviews [16], [17] and in the “Note on Non- $q\bar{q}$ Mesons” in the Meson Listings.

QCD predicts the existence of extra isoscalar mesons. In the pure gauge theory they contain only gluons, and are called glueballs. The ground state glueball is predicted by lattice gauge theories to be 0^{++} , the first excited state 2^{++} . Errors on the mass predictions are large. From Ref. [18] one obtains 1750 (50) (80) MeV for the mass of the lightest 0^{++} glueball from quenched QCD. As an example for the glueball mass spectrum, we show in Fig. 15.4 a calculation from Ref. [12]. A mass of 1710 MeV is predicted for the ground state, also with an error of about 100 MeV. Earlier work by other groups produced masses at 1650 MeV [19] and 1550 MeV [20] (see also [21]). The first excited state has a mass of about 2.4 GeV, and the lightest glueball with exotic quantum numbers (2^{+-}) has a mass of about 4 GeV.

These calculations are made in the so-called “quenched approximation” which neglects $q\bar{q}$ loops. However, both glue and $q\bar{q}$ states couple to singlet scalar mesons. Therefore glueballs will mix with nearby $q\bar{q}$ states of the same quantum numbers. For example, the two isoscalar 0^{++} mesons around 1500 MeV will mix with the pure ground state glueball to generate the observed physical states $f_0(1370)$, $f_0(1500)$, and $f_0(1710)$ [13, 22]. The first results from lattice calculations, which include these effects, indicate that the mass shifts are small. We return to a discussion of this point in Sec. 15.6.

The existence of three singlet scalar mesons around 1.5 GeV suggests additional degrees of freedom such as glue, since only two mesons are predicted in this mass range. The $f_0(1500)$ [13, 22] or, alternatively, the $f_0(1710)$ [19], have been proposed as candidates for the scalar glueball, both states having considerable mixing also with the $f_0(1370)$. Other mixing schemes, in particular with the $f_0(500)$ and the $f_0(980)$, have also been proposed [23]. According to a holographic model of low-energy QCD scalar glueballs decay strongly into kaons and η mesons, in good agreement with data on the $f_0(1710)$ [24]. Details can be found in the “Note on Non- $q\bar{q}$ Mesons” in the Meson Listings and in Ref. [25]. See also the “Note on Scalar Mesons below 2 GeV”.

Mesons made of $q\bar{q}$ pairs bound by excited gluons g , the hybrid states $q\bar{q}g$, are also predicted. They should lie in the 1.9 GeV mass region, according to gluon flux tube models [26]. Lattice QCD also predicts the lightest hybrid, an exotic 1^{-+} , at a mass of 1.8 to 1.9 GeV [27]. However, the bag model predicts four nonets, among them an exotic 1^{-+} around or above 1.4 GeV [28, 29]. There are so far two candidates for exotic states with quantum numbers 1^{-+} , the $\pi_1(1400)$ and $\pi_1(1600)$, which could be hybrids or four-quark states (see the “Note on Non- $q\bar{q}$ Mesons” in the Meson Listings and in [25]).

15.4 Baryons: qqq states

Baryons are fermions with baryon number $B = 1$, *i.e.*, in the most general case, they are composed of three quarks plus any number of quark - antiquark pairs. Until recently, all established baryons were 3-quark (qqq) configurations, which we mainly discuss in this section. However, in 2015 the LHCb collaboration published first evidence for charmed ‘pentaquark’ states of minimal quark content $c\bar{c}uud$ at invariant masses close to 4.4 GeV [30]. More refined LHCb experiments have revealed evidence for three such states called $P_c(4312)^+$, $P_c(4440)^+$, and $P_c(4457)^+$ [31]. These states are located close to the thresholds of the production of ordinary baryon-meson pairs like $\Sigma_c^+ \bar{D}^0$ and $\Sigma_c^+ \bar{D}^{*0}$ and are discussed in terms of molecular-like states. A nice overview on the discussion of pentaquark and tetraquark states is given in Ref. [32].

The color part of baryon state functions is an SU(3) singlet, a completely antisymmetric state of the three colors. Since the quarks are fermions, the state function must be antisymmetric under interchange of any two equal-mass quarks (up and down quarks in the limit of isospin symmetry). Thus it can be written as

$$|qqq\rangle_A = |\text{color}\rangle_A \times |\text{space, spin, flavor}\rangle_S, \quad (15.27)$$

where the subscripts S and A indicate symmetry or antisymme-

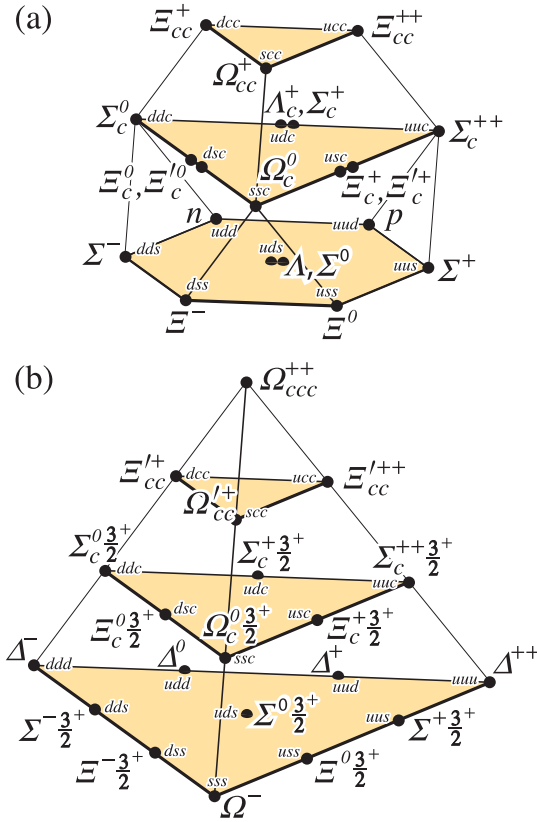


Figure 15.5: SU(4) multiplets of baryons made of u , d , s , and c quarks. (a) The spin 1/2 20-plet with an SU(3) octet. (b) The spin 3/2 20-plet with an SU(3) decuplet.

try under interchange of any two equal-mass quarks. Note the contrast with the state function for the three nucleons in ${}^3\text{H}$ or ${}^3\text{He}$:

$$|NNN\rangle_A = |\text{space, spin, isospin}\rangle_A. \quad (15.28)$$

This difference has major implications for internal structure, magnetic moments, *etc.* (For a nice discussion, see Ref. [33])

The “ordinary” baryons are made up of u , d , and s quarks. The three flavors imply an approximate flavor SU(3), which requires that baryons made of these quarks belong to the multiplets on the right side of

$$\mathbf{3} \otimes \mathbf{3} \otimes \mathbf{3} = \mathbf{10}_S \oplus \mathbf{8}_M \oplus \mathbf{8}_M \oplus \mathbf{1}_A \quad (15.29)$$

(see the section on “SU(n) Multiplets and Young Diagrams”). Here the subscripts indicate symmetric, mixed-symmetry, or antisymmetric states under interchange of any two quarks. The $\mathbf{1}$ is a uds state (A_1), and the octet contains a similar state (A_8). If these have the same spin and parity, they can mix. The mechanism is the same as for the mesons (see above). In the ground state multiplet, the SU(3) flavor singlet A_1 is forbidden by Fermi statistics. The section on “SU(3) Isoscalar Factors and Representation Matrices,” shows how relative decay rates in, say, $\mathbf{10} \rightarrow \mathbf{8} \otimes \mathbf{8}$ decays may be calculated.

The addition of the c quark to the light quarks extends the flavor symmetry to SU(4). However, due to the large mass of the c quark, this symmetry is much more strongly broken than the SU(3) of the three light quarks. Figures 15.5(a) and 15.5(b) show the SU(4) baryon multiplets that have as their bottom levels an SU(3) octet, such as the octet that includes the nucleon, or an SU(3) decuplet, such as the decuplet that includes the $\Delta(1232)$. All particles in a given SU(4) multiplet have the same spin and parity. The charmed baryons are discussed in more detail in the “Note on Charmed Baryons” in the Particle Listings. The same multiplets as shown in Fig. 15.5 can be constructed when the c quark is replaced by the b quark, or they can be embedded in

a larger SU(5) group that accounts for all baryons that can be constructed from the five quark flavors. The existence of baryons with t -quarks is very unlikely due to the short lifetime of the t -quark. The heavy quark baryons have recently gained a lot of interest [34]. Their relatively narrow widths allow to isolate the states much easier than the light quark baryon resonances which require intricate partial wave analyses. The only problem on the experimental side are the small production cross sections, but the recent measurements at the e^+e^- colliding B factories, at the $p\bar{p}$ Tevatron collider, and at LHCb at CERN have boosted this field. The LHCb collaboration has published evidence for five new narrow Ω_c^0 states (css) [35] and for a doubly charmed Ξ_{cc}^{++} (ccu) [36] baryon. Doubly charmed baryons have a much different structure from light baryons, more resembling a heavy ‘double-star’ system with an attached light ‘planet’ and open a new window for QCD properties. Another candidate for a doubly charmed baryon (Ξ_{cc}^+ , ccd) had been earlier reported by the SELEX experiment [37, 38] but could so far not be confirmed by other experiments and the difference in mass between the LHCb Ξ_{cc}^{++} and the SELEX Ξ_{cc}^+ would be much larger than predicted. Quark model predictions for baryons with two heavy quarks are given in Ref. [39] and lattice results for doubly and triply charmed states are discussed in Sec. 15.6 of this review.

For the “ordinary” baryons (no c or b quark), flavor and spin may be combined in an approximate flavor-spin SU(6), in which the six basic states are $d \uparrow$, $d \downarrow$, \dots , $s \downarrow$ ($\uparrow, \downarrow =$ spin up, down). Then the baryons belong to the multiplets on the right side of

$$\mathbf{6} \otimes \mathbf{6} \otimes \mathbf{6} = \mathbf{56}_S \oplus \mathbf{70}_M \oplus \mathbf{70}_M \oplus \mathbf{20}_A.$$

These SU(6) multiplets decompose into flavor SU(3) multiplets as follows:

$$\mathbf{56} = \mathbf{4}\mathbf{10} \oplus \mathbf{2}\mathbf{8} \quad (15.30)$$

$$\mathbf{70} = \mathbf{2}\mathbf{10} \oplus \mathbf{4}\mathbf{8} \oplus \mathbf{2}\mathbf{8} \oplus \mathbf{2}\mathbf{1} \quad (15.31)$$

$$\mathbf{20} = \mathbf{2}\mathbf{8} \oplus \mathbf{4}\mathbf{1}, \quad (15.32)$$

where the superscript ($2S+1$) gives the net spin S of the quarks for each particle in the SU(3) multiplet. The $J^P = 1/2^+$ octet containing the nucleon and the $J^P = 3/2^+$ decuplet containing the $\Delta(1232)$ together make up the “ground-state” 56-plet, in which the orbital angular momenta between the quark pairs are zero (so that the spatial part of the state function is trivially symmetric). The $\mathbf{70}$ and $\mathbf{20}$ require some excitation of the spatial part of the state function in order to make the overall state function symmetric. States with nonzero orbital angular momenta are classified in SU(6) \otimes O(3) supermultiplets.

It is useful to classify the baryons into bands that have the same number N of quanta of excitation. Each band consists of a number of supermultiplets, specified by (D, L_N^P) , where D is the dimensionality of the SU(6) representation, L is the total quark orbital angular momentum, and P is the total parity. Supermultiplets contained in bands up to $N = 12$ are given in Ref. [40]. The $N = 0$ band, which contains the nucleon and $\Delta(1232)$, consists only of the $(56, 0_0^+)$ supermultiplet. The $N = 1$ band consists only of the $(70, 1_1^-)$ multiplet and contains the negative-parity baryons with masses below about 1.9 GeV. The $N = 2$ band contains five supermultiplets: $(56, 0_2^+)$, $(70, 0_2^+)$, $(56, 2_2^+)$, $(70, 2_2^+)$, and $(20, 1_2^+)$.

The wave functions of the non-strange baryons in the harmonic oscillator basis are often labeled by $|X^{2S+1}L_\pi J^P\rangle$, where S, L, J, P are as above, $X = N$ or Δ , and $\pi = S, M$ or A denotes the symmetry of the spatial wave function. The possible model states for the bands with $N=0,1,2$ are given in Table 15.8. The assignment of experimentally observed states is only complete and well established up to the $N=1$ band. Some more tentative assignments for higher multiplets are suggested in [41].

In Table 15.7, quark-model assignments are given for many of the established baryons whose SU(6) \otimes O(3) compositions are relatively unmixed. One must, however, keep in mind that apart from the mixing of the A singlet and octet states, states with same J^P but different L, S combinations can also mix. In the quark model with one-gluon exchange motivated interactions, the size of the mixing is determined by the relative strength of the tensor term with respect to the contact term (see below). The

Table 15.7: Quark-model assignments for some of the known baryons in terms of a flavor-spin SU(6) basis. Only the dominant representation is listed. Assignments for several states, especially for the $\Lambda(1810)$, $\Lambda(2350)$, $\Xi(1820)$, and $\Xi(2030)$, are merely educated guesses. [†] suggestions for assignments and re-assignments from Ref. [42]. For assignments of the charmed baryons, see the “Note on Charmed Baryons” in the Particle Listings.

J^P	(D, L_N^P)	S	Octet members				Singlets
1/2 ⁺	(56, 0 ₀ ⁺)	1/2	$N(939)$	$\Lambda(1116)$	$\Sigma(1193)$	$\Xi(1318)$	
1/2 ⁺	(56, 0 ₂ ⁺)	1/2	$N(1440)$	$\Lambda(1600)$	$\Sigma(1660)$	$\Xi(1690)$ [†]	
1/2 ⁻	(70, 1 ₁ ⁻)	1/2	$N(1535)$	$\Lambda(1670)$	$\Sigma(1620)$	$\Xi(?)$	$\Lambda(1405)$
					$\Sigma(1560)$ [†]		
3/2 ⁻	(70, 1 ₁ ⁻)	1/2	$N(1520)$	$\Lambda(1690)$	$\Sigma(1670)$	$\Xi(1820)$	$\Lambda(1520)$
1/2 ⁻	(70, 1 ₁ ⁻)	3/2	$N(1650)$	$\Lambda(1800)$	$\Sigma(1750)$	$\Xi(?)$	
					$\Sigma(1620)$ [†]		
3/2 ⁻	(70, 1 ₁ ⁻)	3/2	$N(1700)$	$\Lambda(?)$	$\Sigma(1940)$ [†]	$\Xi(?)$	
5/2 ⁻	(70, 1 ₁ ⁻)	3/2	$N(1675)$	$\Lambda(1830)$	$\Sigma(1775)$	$\Xi(1950)$ [†]	
1/2 ⁺	(70, 0 ₂ ⁺)	1/2	$N(1710)$	$\Lambda(1810)$	$\Sigma(1880)$	$\Xi(?)$	$\Lambda(1810)$ [†]
3/2 ⁺	(56, 2 ₂ ⁺)	1/2	$N(1720)$	$\Lambda(1890)$	$\Sigma(?)$	$\Xi(?)$	
5/2 ⁺	(56, 2 ₂ ⁺)	1/2	$N(1680)$	$\Lambda(1820)$	$\Sigma(1915)$	$\Xi(2030)$	
7/2 ⁻	(70, 3 ₃ ⁻)	1/2	$N(2190)$	$\Lambda(?)$	$\Sigma(?)$	$\Xi(?)$	$\Lambda(2100)$
9/2 ⁻	(70, 3 ₃ ⁻)	3/2	$N(2250)$	$\Lambda(?)$	$\Sigma(?)$	$\Xi(?)$	
9/2 ⁺	(56, 4 ₄ ⁺)	1/2	$N(2220)$	$\Lambda(2350)$	$\Sigma(?)$	$\Xi(?)$	

Decuplet members						
3/2 ⁺	(56, 0 ₀ ⁺)	3/2	$\Delta(1232)$	$\Sigma(1385)$	$\Xi(1530)$	$\Omega(1672)$
3/2 ⁺	(56, 0 ₂ ⁺)	3/2	$\Delta(1600)$	$\Sigma(1690)$ [†]	$\Xi(?)$	$\Omega(?)$
1/2 ⁻	(70, 1 ₁ ⁻)	1/2	$\Delta(1620)$	$\Sigma(1750)$ [†]	$\Xi(?)$	$\Omega(?)$
3/2 ⁻	(70, 1 ₁ ⁻)	1/2	$\Delta(1700)$	$\Sigma(?)$	$\Xi(?)$	$\Omega(?)$
5/2 ⁺	(56, 2 ₂ ⁺)	3/2	$\Delta(1905)$	$\Sigma(?)$	$\Xi(?)$	$\Omega(?)$
7/2 ⁺	(56, 2 ₂ ⁺)	3/2	$\Delta(1950)$	$\Sigma(2030)$	$\Xi(?)$	$\Omega(?)$
11/2 ⁺	(56, 4 ₄ ⁺)	3/2	$\Delta(2420)$	$\Sigma(?)$	$\Xi(?)$	$\Omega(?)$

Table 15.8: N and Δ states in the $N=0,1,2$ harmonic oscillator bands. L^P denotes angular momentum and parity, S the three-quark spin and ‘sym’=A,S,M the symmetry of the spatial wave function. Listed are all possible spin/parity combinations and assignments of experimentally observed states. Only dominant components are indicated. Assignments in the $N=2$ band are partly tentative.

N	sym	L^P	S	$N(I = 1/2)$			
2	A	1 ⁺	1/2	1/2 ⁺	3/2 ⁺	-	-
2	M	2 ⁺	3/2	1/2 ⁺	3/2 ⁺	5/2 ⁺	7/2 ⁺
2	M	2 ⁺	1/2	-	3/2 ⁺	5/2 ⁺	-
2	M	0 ⁺	3/2	-	3/2 ⁺	-	-
2	M	0 ⁺	1/2	1/2 ⁺	$N(1710)$	-	-
2	S	2 ⁺	3/2	-	-	-	-
2	S	2 ⁺	1/2	-	3/2 ⁺	$N(1720)$	5/2 ⁺
2	S	0 ⁺	3/2	-	-	-	-
2	S	0 ⁺	1/2	1/2 ⁺	$N(1440)$	-	-
1	M	1 ⁻	3/2	1/2 ⁻	$N(1650)$	3/2 ⁻	$N(1700)$
1	M	1 ⁻	1/2	1/2 ⁻	$N(1535)$	3/2 ⁻	$N(1520)$
0	S	0 ⁺	3/2	-	-	-	-
0	S	0 ⁺	1/2	1/2 ⁺	$N(938)$	-	-

N	sym	L^P	S	$\Delta(I = 3/2)$			
2	A	1 ⁺	1/2	-	-	-	-
2	M	2 ⁺	3/2	-	-	-	-
2	M	2 ⁺	1/2	-	3/2 ⁺	5/2 ⁺	-
2	M	0 ⁺	3/2	-	-	-	-
2	M	0 ⁺	1/2	1/2 ⁺	$\Delta(1750)$	-	-
2	S	2 ⁺	3/2	1/2 ⁺	$\Delta(1910)$	3/2 ⁺	$\Delta(1920)$
2	S	2 ⁺	1/2	-	-	5/2 ⁺	$\Delta(1905)$
2	S	0 ⁺	3/2	-	3/2 ⁺	$\Delta(1600)$	-
2	S	0 ⁺	1/2	-	-	-	-
1	M	1 ⁻	3/2	-	-	-	-
1	M	1 ⁻	1/2	1/2 ⁻	$\Delta(1620)$	3/2 ⁻	$\Delta(1700)$
0	S	0 ⁺	3/2	-	3/2 ⁺	$\Delta(1232)$	-
0	S	0 ⁺	1/2	-	-	-	-

mixing is more important for the decay patterns of the states than for their positions. An example are the lowest lying $(70, 1_1^-)$ states with $J^P=1/2^-$ and $3/2^-$. The physical states are:

$$|N(1535)1/2^-\rangle = \cos(\Theta_S)|N^2P_M1/2^-\rangle - \sin(\Theta_S)|N^4P_M1/2^-\rangle \quad (15.33)$$

$$|N(1520)3/2^-\rangle = \cos(\Theta_D)|N^2P_M3/2^-\rangle - \sin(\Theta_D)|N^4P_M3/2^-\rangle \quad (15.34)$$

and the orthogonal combinations for $N(1650)1/2^-$ and $N(1700)3/2^-$. The mixing is large for the $J^P=1/2^-$ states ($\Theta_S \approx -32^\circ$), but small for the $J^P=3/2^-$ states ($\Theta_D \approx +6^\circ$) [43–45].

All baryons of the ground state multiplets are known. Many of their properties, in particular their masses, are in good agreement even with the most basic versions of the quark model, including harmonic (or linear) confinement and a spin-spin interaction, which is responsible for the octet - decuplet mass shifts. A consistent description of the ground-state electroweak properties, however, requires refined relativistic constituent quark models.

The situation for the excited states is much less clear. The assignment of some experimentally observed states with strange quarks to model configurations is only tentative and in many cases candidates are completely missing. Melde, Plessas and Sengl [42] have calculated baryon properties in relativistic constituent quark models, using one-gluon exchange and Goldstone-boson exchange for the modeling of the hyperfine interactions (see Sec. 15.5 on Dynamics). Both types of models give qualitatively comparable results, and underestimate in general experimentally observed decay widths. Nevertheless, in particular on the basis of the observed decay patterns, the authors have assigned some additional states with strangeness to the SU(3) multiplets and suggest re-assignments for a few others. Among the new assignments are states with weak experimental evidence (two or three star ratings) and partly without firm spin/parity assignments, so that further experimental efforts are necessary before final conclusions can be drawn. We have added their suggestions in Table 15.7.

In the non-strange sector there are two main problems which are illustrated in Fig. 15.6, where the experimentally observed excitation spectrum of the nucleon (N and Δ resonances) is compared to the results of a typical quark model calculation [46]. The lowest states from the N=2 band, the $N(1440)1/2^+$, and the $\Delta(1600)3/2^+$, appear lower than the negative parity states from the N=1 band (see Table 15.8) and much lower than predicted by most models. Also negative parity Δ states from the N=3 band ($\Delta(1900)1/2^-$, $\Delta(1940)3/2^-$, and $\Delta(1930)5/2^-$) are too low in energy. Part of the problem could be experimental. Among the negative parity Δ states, only the $\Delta(1930)5/2^-$ has three stars and the uncertainty in the position of the $\Delta(1600)3/2^+$ is large (1550 - 1700 MeV).

Furthermore, many more states are predicted than observed. This has been known for a long time as the ‘missing resonance’ problem [43]. Up to an excitation energy of 2.4 GeV, about 45 N states are predicted, but only 20 are established (four- or three-star; see Note on N and Δ Resonances for the rating of the status of resonances) and 5 are tentative (two- or one-star). Even for the N=2 band, up to now only half of the predicted states have been observed. However, there is some recent progress. The total number of states has not much changed but the number of states with four- or three-star rating has increased from 14 to 20 compared to the 2018 PDG particle listings. Most of this progress is due to the programs concentrating on the study of meson photoproduction reactions, while the most recent partial wave analysis of elastic pion scattering and charge exchange data by Arndt and collaborators [47] found no evidence for almost half of the states listed in this review (and included in Fig. 15.6). Such analyses are of course biased against resonances which couple only weakly to the $N\pi$ channel. Quark model predictions for the couplings to other hadronic channels and to photons are given in Ref. [46]. The large experimental effort ongoing at several electron accelerators to study the baryon resonance spectrum with real and virtual photon-induced meson production reactions includes the search for as-yet-unobserved states, as well as detailed studies of the properties of the low lying states (decay patterns, electromagnetic couplings, magnetic moments, *etc.*) (see Ref. [48] for

reviews). There are two major new aspects of this program. The investigation of single and double polarization observables allows via the study of interference terms access to small partial waves that do not leave a footprint in unpolarized cross sections. An example for the impact of such data is given by a comparison of results from different multipole analyses of pion photoproduction [49]. It shows clearly that with the inclusion of polarization observables the reaction model results start to converge. This will in the near future much improve the data basis for excited baryons in the light quark sector.

The other aspect is the study of final states with meson pairs, in particular $\pi\pi$ and $\pi\eta$ pairs, which made large progress during the last few years. This is important for higher lying states, which in the quark model may have both possible oscillations excited. Such states can be expected to decay in sequential processes de-exciting the two oscillations step-by-step so that they couple strongly to multiple-meson final states but not to single-meson production. Detailed analyses of such data are for example given in [50, 51] and had already significant impact on partial wave analyses.

In quark models, the number of excited states is determined by the effective degrees of freedom, while their ordering and decay properties are related to the residual quark - quark interaction. An overview of quark models for baryons is given in [52], recent discussions of baryon spectroscopy are given in [34, 41]. The effective degrees of freedom in the standard nonrelativistic quark model are three equivalent valence quarks with one-gluon exchange-motivated, flavor-independent color-magnetic interactions. The QCD aspect of gluon-gluon interactions is emphasized by the hypercentral quark model [53, 54], which includes in a natural way three-body forces between the quarks. A different class of models uses interactions which give rise to a quark - diquark clustering of the baryons: for a review see [55]. If there is a tightly bound diquark, only two degrees of freedom are available at low energies, and thus *fewer* states are predicted. Furthermore, selection rules in the decay pattern may arise from the quantum numbers of the diquark. *More* states are predicted by collective models of the baryon like the algebraic approach in [56]. In this approach, the quantum numbers of the valence quarks are distributed over a Y-shaped string-like configuration, and additional states arise *e.g.*, from vibrations of the strings. *More* states are also predicted in the framework of flux-tube models, see [57], which are motivated by lattice QCD. In addition to the quark degrees of freedom, flux-tubes responsible for the confinement of the quarks are considered as degrees of freedom. These models include hybrid baryons containing explicit excitations of the gluon fields. However, since all half integral J^P quantum numbers are possible for ordinary baryons, such ‘exotics’ will be very hard to identify, and probably always mix with ordinary states. So far, the experimentally observed number of states is still far lower even than predicted by the quark-diquark models.

The influence of chiral symmetry on the excitation spectrum of the nucleon has been debated from a somewhat different perspective. Chiral symmetry, the fundamental symmetry of QCD, is strongly broken for the low lying states, resulting in large mass differences of parity partners like the $J^P=1/2^+$ $N(938)1/2^+$ ground state and the $J^P=1/2^-$ $N(1535)1/2^-$ excitation. However, at higher excitation energies there is some evidence for parity doublets and even some very tentative suggestions for full chiral multiplets of N^* and Δ resonances. An effective restoration of chiral symmetry at high excitation energies due to a decoupling from the quark condensate of the vacuum has been discussed (see Ref. [58] for recent reviews) as a possible cause. In this case, the mass generating mechanisms for low and high lying states would be essentially different. As a further consequence, the parity doublets would decouple from pions, so that experimental bias would be worse. However, parity doublets might also arise from the spin-orbital dynamics of the 3-quark system. Presently, the status of data does not allow final conclusions.

The most recent developments on the theory side are the first unquenched lattice calculations for the excitation spectrum discussed in Sec15.6. The results are basically consistent with the level counting of $SU(6)\otimes O(3)$ in the standard non-relativistic quark model and show no indication for quark-diquark structures

or parity doubling. Consequently, there is as yet no indication from lattice that the mis-match between the excitation spectrum predicted by the standard quark model and experimental observations is due to inappropriate degrees of freedom in the quark model.

15.5 Dynamics

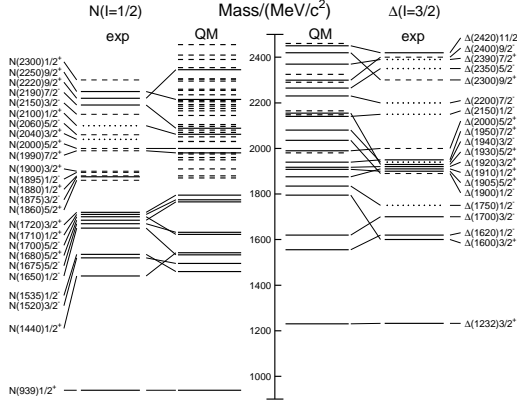


Figure 15.6: Excitation spectrum of the nucleon. Compared are the positions of the excited states identified in experiment, to those predicted by a relativized quark model calculation. Left hand side: isospin $I = 1/2$ N -states, right hand side: isospin $I = 3/2$ Δ -states. Experimental: (columns labeled 'exp'), three- and four-star states are indicated by full lines (two-star dashed lines, one-star dotted lines). At the very left and right of the figure, the spectroscopic notation of these states is given. Quark model [46, 59]: (columns labeled 'QM'), all states for the $N=1,2$ bands, low-lying states for the $N=3,4,5$ bands. Full lines: at least tentative assignment to observed states, dashed lines: so far no observed counterparts. Many of the assignments between predicted and observed states are highly tentative.

Quantum chromodynamics (QCD) is well-established as the theory for the strong interactions. As such, one of the goals of QCD is to predict the spectrum of strongly-interacting particles. To date, the only first-principles calculations of spectroscopy from QCD use lattice methods. These are the subject of Sec. 15.6. These calculations are difficult and unwieldy, and many interesting questions do not have a good lattice-based method of solution. Therefore, it is natural to build models, whose ingredients are abstracted from QCD, or from the low-energy limit of QCD (such as chiral Lagrangians) or from the data itself. The words “quark model” are a shorthand for such phenomenological models. Many specific quark models exist, but most contain a similar basic set of dynamical ingredients. These include:

1. A confining interaction, which is generally spin-independent (e.g., harmonic oscillator or linear confinement);
2. Different types of spin-dependent interactions:
 - a) commonly used is a color-magnetic flavor-independent interaction modeled after the effects of gluon exchange in QCD (see e.g., Ref. [60]). For example, in the S -wave states, there is a spin-spin hyperfine interaction of the form

$$H_{HF} = -\alpha_S M \sum_{i>j} (\vec{\sigma}\lambda_a)_i (\vec{\sigma}\lambda_a)_j, \quad (15.35)$$

where M is a constant with units of energy, λ_a ($a = 1, \dots, 8$) is the set of SU(3) unitary spin matrices, defined in the review “SU(3) Isoscalar Factors and Representation Matrices,” and the sum runs over constituent quarks or antiquarks. Spin-orbit interactions, although allowed, seem to be small in general, but a tensor term is responsible for the mixing of states with the same J^P but different L, S combinations.

b) other approaches include flavor-dependent short-range quark forces from instanton effects (see e.g., [61, 62]). This interaction acts only on scalar, isoscalar pairs of quarks in a relative S -wave state:

$$\langle q^2; S, L, T | W | q^2; S, L, T \rangle = -4g\delta_{S,0}\delta_{L,0}\delta_{T,0}W \quad (15.36)$$

where W is the radial matrix element of the contact interaction.

c) a rather different and controversially discussed approach is based on flavor-dependent spin-spin forces arising from one-boson exchange. The interaction term is of the form:

$$H_{HF} \propto \sum_{i<j} V(\vec{r}_{ij}) \lambda_i^F \cdot \lambda_j^F \vec{\sigma}_i \cdot \vec{\sigma}_j \quad (15.37)$$

where the λ_i^F are in flavor space (see e.g., Ref. [63]).

3. A strange quark mass somewhat larger than the up and down quark masses, in order to split the SU(3) multiplets;
4. In the case of spin-spin interactions (iia,c), a flavor-symmetric interaction for mixing $q\bar{q}$ configurations of different flavors (e.g., $u\bar{u} \leftrightarrow d\bar{d} \leftrightarrow s\bar{s}$), in isoscalar channels, so as to reproduce e.g., the $\eta - \eta'$ and $\omega - \phi$ mesons.

These ingredients provide the basic mechanisms that determine the hadron spectrum in the standard quark model.

15.6 Lattice Calculations of Hadronic Spectroscopy

Lattice calculations are a major source of information about QCD masses and matrix elements. The necessary theoretical background is given in Sec. 17 of this *Review*. Here we confine ourselves to some general comments and illustrations of lattice calculations for spectroscopy.

In general, the cleanest lattice results come from computations of processes in which there is only one particle in the simulation volume. These quantities include masses of hadrons, simple decay constants, like pseudoscalar meson decay constants, and semileptonic form factors (such as the ones appropriate to $B \rightarrow D\nu, K\nu, \pi\nu$). The cleanest predictions for masses are for states which have narrow decay widths and are far below any thresholds to open channels, since the effects of final state interactions are not yet under complete control on the lattice. As a simple corollary, the lightest state in a channel is easier to study than the heavier ones. “Difficult” states for the quark model (such as exotics) are also difficult for the lattice because of the lack of simple operators which couple well to them.

Good-quality modern lattice calculations will present multi-part error budgets with their predictions. A small part of the uncertainty is statistical, from sample size. Typically, the quoted statistical uncertainty includes uncertainty from a fit: it is rare that a simulation computes one global quantity which is the desired observable. Simulations which include virtual quark-antiquark pairs (also known as “dynamical quarks” or “sea quarks”) are often done at up and down quark mass values heavier than the experimental ones, and it is then necessary to extrapolate in these quark masses. Simulations can work at the physical values of the heavier quarks’ masses. They are always done at nonzero lattice spacing, and so it is necessary to extrapolate to zero lattice spacing. Some theoretical input is needed to do this. Much of the uncertainty in these extrapolations is systematic, from the choice of fitting function. Other systematics include the effect of finite simulation volume, the number of flavors of dynamical quarks actually simulated, and technical issues with how these dynamical quarks are included. The particular choice of a fiducial mass (to normalize other predictions) is not standardized; there are many possible choices, each with its own set of strengths and weaknesses, and determining it usually requires a second lattice simulation from that used to calculate the quantity under consideration.

A systematic error of major historical interest is the “quenched approximation,” in which dynamical quarks are simply left out of the simulation. This was done because the addition of these

virtual pairs presented an expensive computational problem. No generally-accepted methodology has ever allowed one to correct for quenching effects, short of redoing all calculations with dynamical quarks. Recent advances in algorithms and computer hardware have rendered it obsolete.

With these brief remarks, we turn to examples. The field of lattice QCD simulations is vast, and so it is not possible to give a comprehensive review of them in a small space. The history of lattice QCD simulations is a story of thirty years of incremental improvements in physical understanding, algorithm development, and ever faster computers, which have combined to bring the field to a present state where it is possible to carry out very high quality calculations. We present a few representative illustrations, to show the current state of the art.

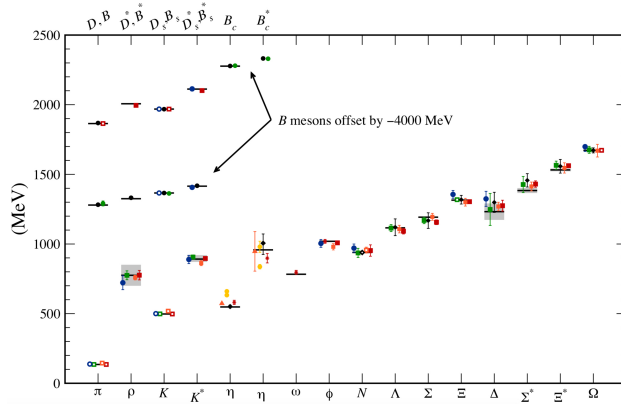


Figure 15.7: Hadron spectrum from lattice QCD. Comprehensive results for mesons and baryons are from MILC [64, 65], PACS-CS [66], BMW [67], QCDSF [68], and ETM [69]. Results for η and η' are from RBC & UKQCD [10], Hadron Spectrum [70] (also the only ω mass), UKQCD [71], and Michael, Otnad, and Urbach [72]. Results for heavy-light hadrons from Fermilab-MILC [73], HPQCD [74, 75], and Mohler and Woloshyn [76]. Circles, squares, diamonds, and triangles stand for staggered, Wilson, twisted-mass Wilson, and chiral sea quarks, respectively. Asterisks represent anisotropic lattices. Open symbols denote the masses used to fix parameters. Filled symbols (and asterisks) denote results. Red, orange, yellow, green, and blue stand for increasing numbers of ensembles (i.e., lattice spacing and sea quark mass) Black symbols stand for results with 2+1+1 flavors of sea quarks. Horizontal bars (gray boxes) denote experimentally measured masses (widths). b -flavored meson masses are offset by -4000 MeV.

By far, the major part of all lattice spectroscopy is concerned with that of the light hadrons, and so we illustrate results in Fig. 15.7, a comprehensive summary provided by A. Kronfeld (private communication; see also [77]).

Flavor singlet mesons are at the frontier of lattice QCD calculations, because one must include the effects of “annihilation graphs,” for the valence q and \bar{q} . Recently, several groups, Refs. [10,71,78], have reported calculations of the η and η' mesons. The numbers of [10] are typical, finding masses of 573(6) and 947(142) MeV for the η and η' . The singlet-octet mixing angle (in the conventions of Table 15.2) is $\theta_{lin} = -14.1(2.8)^\circ$.

The spectroscopy of mesons containing heavy quarks has become a truly high-precision endeavor. These simulations use Non-Relativistic QCD (NRQCD) or Heavy Quark Effective Theory (HQET), systematic expansions of the QCD Lagrangian in powers of the heavy quark velocity, or the heavy quark mass. Terms in the Lagrangian have obvious quark model analogs, but are derived directly from QCD. For example, the heavy quark potential is a derived quantity, extracted from simulations. Fig. 15.8 shows the mass spectrum for mesons containing at least one heavy (b or c) quark from Ref. [75]. It also contains results from Ref. [79,80]. The calculations use a discretization of nonrelativistic QCD for bottom quarks with charm and lighter quarks being handled with an improved relativistic action. Four flavors (u, d, s, c) of dynam-

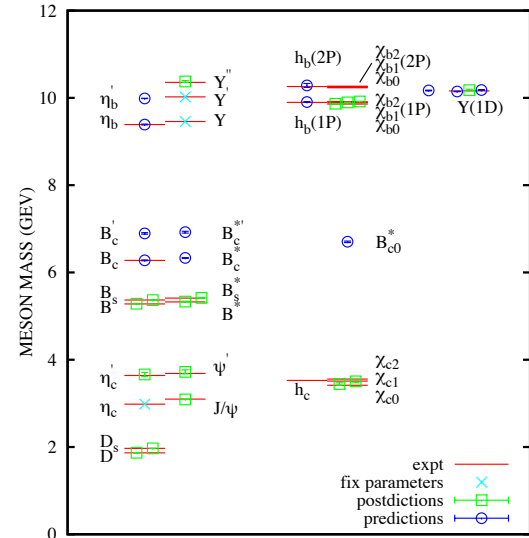


Figure 15.8: Spectroscopy for mesonic systems containing one or more heavy quarks (adapted from Ref. [75]). Particles whose masses are used to fix lattice parameters are shown with crosses; the authors distinguish between “predictions” and “postdictions” of their calculation. Lines represent experiment.

ical quarks are included.

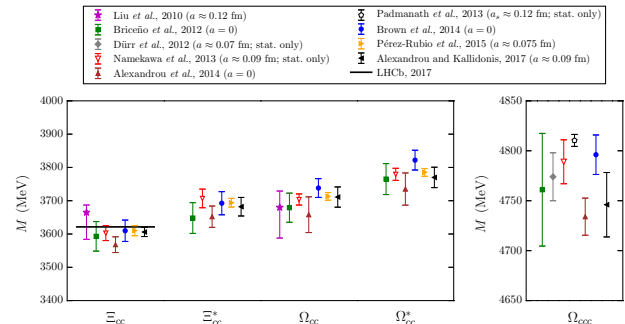


Figure 15.9: Comparison of lattice QCD results for the doubly and triply charmed baryon masses. Labels are Liu, *et al.*, [81]; Briceno, *et al.*, [82]; Namekawa, *et al.*, [83]; Padmanath, *et al.*, [84]; Alexandrou, *et al.*, [69]; Brown, *et al.*, [85]; Perez-Rubio *et al.*, [86]; Alexandrou and Kallidonis 2017, [87]. Only calculations with dynamical light quarks are included; for the doubly charmed baryons, only calculations were performed at or extrapolated to the physical pion mass are shown. Results without estimates of systematic uncertainties are labeled “stat. only”. The lattice spacing values used in the calculations are also given; $a = 0$ indicates that the results have been extrapolated to the continuum limit. In the plot of the doubly charmed baryons, the recently announced experimental result for the Ξ_{cc}^+ mass from LHCb [36] is shown with a horizontal line.

Fig. 15.9 shows a compilation of recent lattice results for doubly and triply charmed baryons, provided by S. Meinel [88]. The state recently announced by LHCb [36] is also shown. Note that the lattice calculations for the mass of this state were predictions, not postdictions.

Recall that lattice calculations take operators which are interpolating fields with quantum numbers appropriate to the desired states, compute correlation functions of these operators, and fit the correlation functions to functional forms parametrized by a set of masses and matrix elements. As we move away from hadrons which can be created by the simplest quark model operators (appropriate to the lightest meson and baryon multiplets) we encounter a host of new problems: either no good interpolating fields, or too many possible interpolating fields, and many states

with the same quantum numbers. Techniques for dealing with these interrelated problems vary from collaboration to collaboration, but all share common features: typically, correlation functions from many different interpolating fields are used, and the signal is extracted in what amounts to a variational calculation using the chosen operator basis. In addition to mass spectra, wave function information can be garnered from the form of the best variational wave function. Of course, the same problems which are present in the spectroscopy of the lightest hadrons (the need to extrapolate to infinite volume, physical values of the light quark masses, and zero lattice spacing) are also present. We briefly touch on three different kinds of hadrons: excited states of mesons (including hybrids), excited states of baryons, and glueballs. The quality of the data is not as good as for the ground states, and so the results continue to evolve.

Modern calculations use a large bases of trial states, which allow them to probe many quantum number channels simultaneously. This is vital for studying “difficult sectors” of QCD, such as the isoscalar mesons. A recent example of meson spectroscopy where this is done, by [89], is shown in Fig. 15.10. The quark masses are still heavier than their physical values, so the pion is at 392 MeV. The authors can assign a relative composition of nonstrange and strange quark content to their states, observing, for example, a nonstrange ω and a strange ϕ . Some states also have a substantial component of gluonic excitation. Note especially the three exotic channels $J^{PC} = 1^{-+}$, 0^{+-} , and 2^{+-} , with states around 2 GeV. These calculations will continue to improve as the quark masses are carried lower.

The interesting physics questions of excited baryon spectroscopy to be addressed are precisely those enumerated in the last section. An example of a recent calculation, due to Ref. [90] is shown in Fig. 15.11. Notice that the pion is not yet at its physical value. The lightest positive parity state is the nucleon, and the Roper resonance has not yet appeared as a light state.

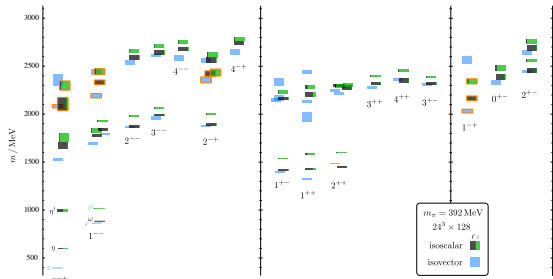


Figure 15.10: Isoscalar (green and black) and isovector (blue) spectrum from Ref. [89]. States are labeled J^{PC} . The quark mass is heavier than its physical value; $m_\pi = 392$ MeV. The vertical height of each box indicates the statistical uncertainty in the mass. Black and green indicate relative nonstrange and strange composition. Orange outlines show states with a large chromomagnetic component to their wave function, which the authors argue are hybrid states. Note the exotic states in the three right-most columns.

Most hadrons are resonances, and lattice calculations will have to deal with this fact as the quark masses are taken ever smaller. The actual calculation is of the combined mass of two (or more) hadrons in a box of finite size. The combined mass is shifted from being the sum of the individual masses because the finite box forces the hadrons to interact with each other. The volume-dependent mass shift yields the phase shift for the continuum scattering amplitude, which in turn can be used to extract the resonance mass and width, with some degree of modeling. So far only two-body resonances, the rho meson and a few others, have been well studied. This is an active research area. A recent review, [91], summarizes the situation, and example of a calculation of the rho meson decay width is [92]. The mass and decay width of the $f_0(500)$ have recently been computed in [93]. Ref. [94] studies the decay width of the $\Delta(1238)$. Lattice calculations relevant to the extra states observed in the charmonium spectrum (Sec. 15.3)

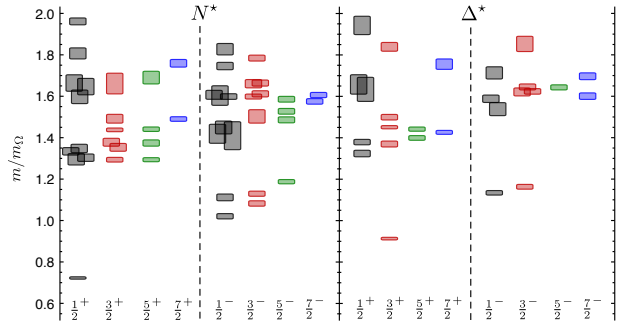


Figure 15.11: Spin-identified spectrum of nucleons and deltas, from lattices where $m_\pi = 396$ MeV, in units of the calculated Ω mass, from Ref. [90]. The colors just correspond to the different J assignments: grey for $J = 1/2$, red for $J = 3/2$, green for $5/2$, blue for $J = 7/2$.

are difficult, because the states sit high in the spectrum of most channels and due to the number of nearby multiparticle states.

In Fig. 15.4 we showed a figure from [12] presenting a lattice prediction for the glueball mass spectrum in quenched approximation. A true QCD prediction of the glueball spectrum requires dynamical light quarks and (because glueball operators are intrinsically noisy) high statistics. Only recently have the first useful such calculations appeared, in [95, 96]. Fig. 15.12 shows results from [95], done with dynamical u , d and s quarks at two lattice spacings, 0.123 and 0.092 fm, along with comparisons to the quenched lattice calculation of [18] and to experimental isosinglet mesons. The dynamical simulation is, of course, not the last word on this subject, but it shows that the effects of quenching seem to be small.

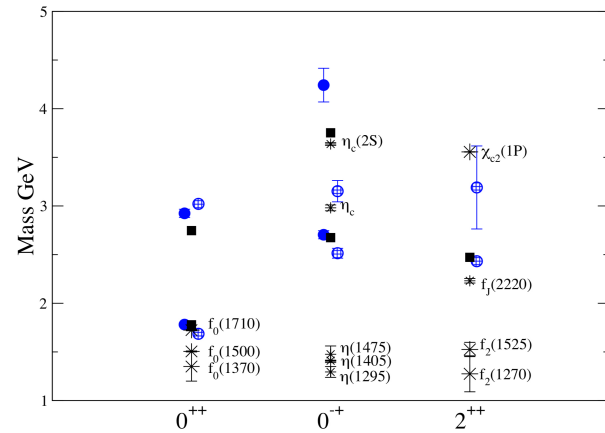


Figure 15.12: Lattice QCD predictions for glueball masses. The open and closed circles are the larger and smaller lattice spacing data of the full QCD calculation of glueball masses of Ref. [95]. Squares are the quenched data for glueball masses of Ref. [18]. The bursts labeled by particle names are experimental states with the appropriate quantum numbers.

As a final part of spectroscopy we mention electromagnetic mass splittings (such as the neutron - proton mass difference). They are interesting but difficult. These calculations are important for determining the values of the quark masses (for a discussion see the review in the PDG). Knowing that the neutron is heavier than the proton tells us that these splittings have a complicated origin. One part of the shift is because the up and down quarks have slightly different masses. The second is that the quarks have (different) charges. Phenomenologists (compare Ref. [97]) combine Coulomb forces and spin-dependent electromagnetic hyperfine interactions to model their charge effects. In order to compute hadronic mass differences on the lattice, electromagnetic interactions must be included in the simulations. This creates a host of technical is-

sues. An important one is that electromagnetic interactions are long range, but lattice simulations are done in finite volumes. The theoretical situation is summarized in the recent review [98]. A recent calculation, Ref. [99], has presented the first results for electromagnetic mass splittings in the baryon octet, with good agreement with observation. Ref. [100] has calculations for meson splittings.

References

- [1] C. Amsler in the Quark Structure of Hadrons, Lecture Notes in Physics **949** (2018), ed. Springer.
- [2] K.-C. Yang, Nucl. Phys. **B776**, 187 (2007), [arXiv:0705.0692].
- [3] L. Burakovsky and J. T. Goldman, Nucl. Phys. **A625**, 220 (1997), [hep-ph/9703272].
- [4] J. Schwinger, Phys. Rev. **135**, B816 (1964).
- [5] A. Bramon, R. Escribano and M. D. Scadron, Phys. Lett. **B403**, 339 (1997), [hep-ph/9703313].
- [6] A. Aloisio *et al.* (KLOE), Phys. Lett. **B541**, 45 (2002), [hep-ex/0206010].
- [7] F. Ambrosino *et al.*, JHEP **07**, 105 (2009), [arXiv:0906.3819].
- [8] C. Amsler *et al.* (Crystal Barrel), Phys. Lett. **B294**, 451 (1992).
- [9] C. Amsler, Rev. Mod. Phys. **70**, 1293 (1998), [hep-ex/9708025].
- [10] N. H. Christ *et al.*, Phys. Rev. Lett. **105**, 241601 (2010), [arXiv:1002.2999].
- [11] T. Feldmann, Int. J. Mod. Phys. **A915**, 159 (2000).
- [12] Y. Chen *et al.*, Phys. Rev. **D73**, 014516 (2006), [hep-lat/0510074].
- [13] C. Amsler and F. E. Close, Phys. Rev. **D53**, 295 (1996), [hep-ph/9507326].
- [14] R. L. Jaffe, Phys. Rev. **D15**, 267 (1977).
- [15] R. L. Jaffe, Phys. Rev. **D15**, 281 (1977).
- [16] S.L. Olsen, Front. Phys. **10**, 121 (2015).
- [17] S. L. Olsen, T. Skwarnicki and D. Zieminska, Rev. Mod. Phys. **90**, 1, 015003 (2018), [arXiv:1708.04012].
- [18] C. J. Morningstar and M. J. Peardon, Phys. Rev. **D60**, 034509 (1999), [hep-lat/9901004].
- [19] W.-J. Lee and D. Weingarten, Phys. Rev. **D61**, 014015 (2000), [hep-lat/9910008].
- [20] G. S. Bali *et al.* (UKQCD), Phys. Lett. **B309**, 378 (1993), [hep-lat/9304012].
- [21] C. Michael, AIP Conf. Proc. **432**, 1, 657 (1998), [hep-ph/9710502].
- [22] F. E. Close and A. Kirk, Eur. Phys. J. **C21**, 531 (2001), [hep-ph/0103173].
- [23] W. Ochs, J. Phys. **G40**, 043001 (2013), [arXiv:1301.5183].
- [24] F. Brünner and A. Rebhan, Phys. Rev. Lett. **115**, 13, 131601 (2015), [arXiv:1504.05815].
- [25] C. Amsler and N. A. Tornqvist, Phys. Rept. **389**, 61 (2004).
- [26] N. Isgur and J. E. Paton, Phys. Rev. **D31**, 2910 (1985).
- [27] P. Lacock *et al.* (UKQCD), Phys. Lett. **B401**, 308 (1997), [hep-lat/9611011].
- [28] M. S. Chanowitz and S. R. Sharpe, Nucl. Phys. **B222**, 211 (1983), [Erratum: Nucl. Phys. **B228**, 588 (1983)].
- [29] T. Barnes *et al.*, Nucl. Phys. **B224**, 241 (1983).
- [30] R. Aaij *et al.* (LHCb), Phys. Rev. Lett. **115**, 072001 (2015), [arXiv:1507.03414].
- [31] R. Aaij *et al.* (LHCb), Phys. Rev. Lett. **122**, 22, 222001 (2019), [arXiv:1904.03947].
- [32] Y.-R. Liu *et al.*, Prog. Part. Nucl. Phys. **107**, 237 (2019), [arXiv:1903.11976].
- [33] F.E. Close, in *Quarks and Nuclear Forces* (Springer-Verlag, 1982), p. 56.
- [34] V. Crede and W. Roberts, Rept. on Prog. in Phys. **76**, 076301 (2013).
- [35] R. Aaij *et al.* (LHCb), Phys. Rev. Lett. **118**, 18, 182001 (2017), [arXiv:1703.04639].
- [36] R. Aaij *et al.* (LHCb), Phys. Rev. Lett. **119**, 11, 112001 (2017), [arXiv:1707.01621].
- [37] M. Mattson *et al.* (SELEX), Phys. Rev. Lett. **89**, 112001 (2002), [hep-ex/0208014].
- [38] A. Ocherashvili *et al.* (SELEX), Phys. Lett. **B628**, 18 (2005), [hep-ex/0406033].
- [39] M. Karliner and J. L. Rosner, Phys. Rev. **D90**, 9, 094007 (2014), [arXiv:1408.5877].
- [40] R.H. Dalitz and L.J. Reinders, in “Hadron Structure as Known from Electromagnetic and Strong Interactions,” *Proceedings of the Hadron ’77 Conference* (Veda, 1979), p. 11.
- [41] E. Klempt and J.-M. Richard, Rev. Mod. Phys. **82**, 1095 (2010), [arXiv:0901.2055].
- [42] T. Melde, W. Plessas and B. Sengl, Phys. Rev. **D77**, 114002 (2008), [arXiv:0806.1454].
- [43] N. Isgur and G. Karl, Phys. Rev. **D18**, 4187 (1978).
- [44] N. Isgur and G. Karl, Phys. Rev. **D19**, 2653 (1979), [Erratum: Phys. Rev. **D23**, 817 (1981)].
- [45] S. Capstick and W. Roberts, Prog. Part. Nucl. Phys. **45**, S241 (2000), [arXiv:nucl-th/0008028].
- [46] S. Capstick and W. Roberts, Phys. Rev. **D58**, 074011 (1998), [arXiv:nucl-th/9804070].
- [47] R. A. Arndt *et al.*, Phys. Rev. **C74**, 045205 (2006), [arXiv:nucl-th/0605082].
- [48] B. Krusche and S. Schadmand, Prog. Part. Nucl. Phys. **51**, 399 (2003), [arXiv:nucl-ex/0306023].
- [49] A. V. Anisovich *et al.*, Eur. Phys. J. **A52**, 9, 284 (2016), [arXiv:1604.05704].
- [50] E. Gutz *et al.* (CBELSA/TAPS), Eur. Phys. J. **A50**, 74 (2014), [arXiv:1402.4125].
- [51] V. Sokhoyan *et al.* (CBELSA/TAPS), Eur. Phys. J. **A51**, 8, 95 (2015), [Erratum: Eur. Phys. J. **A51**, no.12, 187 (2015)], [arXiv:1507.02488].
- [52] S. Capstick and W. Roberts, Prog. in Part. Nucl. Phys. **45**, 241 (2000).
- [53] M. Ferraris *et al.*, Phys. Lett. **B364**, 231 (1995).
- [54] M. M. Giannini and E. Santopinto, Chin. J. Phys. **53**, 020301 (2015), [arXiv:1501.03722].
- [55] M. Anselmino *et al.*, Rev. Mod. Phys. **65**, 1199 (1993).
- [56] R. Bijker, F. Iachello and A. Leviatan, Annals Phys. **236**, 69 (1994), [arXiv:nucl-th/9402012].
- [57] S. Capstick and P. R. Page, Phys. Rev. **C66**, 065204 (2002), [arXiv:nucl-th/0207027].
- [58] R. L. Jaffe, D. Pirjol and A. Scardicchio, Phys. Rept. **435**, 157 (2006), [hep-ph/0602010].
- [59] S. Capstick, Phys. Rev. **D46**, 2864 (1992).
- [60] A. De Rujula, H. Georgi and S. L. Glashow, Phys. Rev. **D12**, 147 (1975).
- [61] W. H. Blask *et al.*, Z. Phys. **A337**, 327 (1990).
- [62] U. Loring *et al.*, Eur. Phys. J. **A10**, 309 (2001), [hep-ph/0103287].
- [63] L. Ya. Glozman and D. O. Riska, Phys. Rept. **268**, 263 (1996), [hep-ph/9505422].
- [64] C. Aubin *et al.*, Phys. Rev. **D70**, 094505 (2004), [hep-lat/0402030].
- [65] A. Bazavov *et al.* (MILC), Rev. Mod. Phys. **82**, 1349 (2010), [arXiv:0903.3598].

- [66] S. Aoki *et al.* (PACS-CS), Phys. Rev. **D79**, 034503 (2009), [arXiv:0807.1661].
- [67] S. Durr *et al.*, Science **322**, 1224 (2008), [arXiv:0906.3599].
- [68] W. Bietenholz *et al.*, Phys. Rev. **D84**, 054509 (2011), [arXiv:1102.5300].
- [69] C. Alexandrou *et al.*, Phys. Rev. **D90**, 7, 074501 (2014), [arXiv:1406.4310].
- [70] J. J. Dudek *et al.*, Phys. Rev. **D83**, 111502 (2011), [arXiv:1102.4299].
- [71] E. B. Gregory *et al.* (UKQCD), Phys. Rev. **D86**, 014504 (2012), [arXiv:1112.4384].
- [72] C. Michael, K. Ottnad and C. Urbach (ETM), Phys. Rev. Lett. **111**, 18, 181602 (2013), [arXiv:1310.1207].
- [73] C. Bernard *et al.* (Fermilab Lattice, MILC), Phys. Rev. **D83**, 034503 (2011), [arXiv:1003.1937].
- [74] E. B. Gregory *et al.*, Phys. Rev. **D83**, 014506 (2011), [arXiv:1010.3848].
- [75] R. J. Dowdall *et al.*, Phys. Rev. **D86**, 094510 (2012), [arXiv:1207.5149].
- [76] D. Mohler and R. M. Woloshyn, Phys. Rev. **D84**, 054505 (2011), [arXiv:1103.5506].
- [77] A. S. Kronfeld, Ann. Rev. Nucl. Part. Sci. **62**, 265 (2012), [arXiv:1203.1204].
- [78] K. Ottnad, C. Urbach and F. Zimmermann (OTM), Nucl. Phys. **B896**, 470 (2015), [arXiv:1501.02645].
- [79] J. O. Daldrop, C. T. H. Davies and R. J. Dowdall (HPQCD), Phys. Rev. Lett. **108**, 102003 (2012), [arXiv:1112.2590].
- [80] G. C. Donald *et al.*, Phys. Rev. **D86**, 094501 (2012), [arXiv:1208.2855].
- [81] L. Liu *et al.*, Phys. Rev. **D81**, 094505 (2010), [arXiv:0909.3294].
- [82] R. A. Briceno, H.-W. Lin and D. R. Bolton, Phys. Rev. **D86**, 094504 (2012), [arXiv:1207.3536].
- [83] Y. Namekawa *et al.* (PACS-CS), Phys. Rev. **D87**, 9, 094512 (2013), [arXiv:1301.4743].
- [84] M. Padmanath *et al.*, Phys. Rev. **D90**, 7, 074504 (2014), [arXiv:1307.7022].
- [85] Z. S. Brown *et al.*, Phys. Rev. **D90**, 9, 094507 (2014), [arXiv:1409.0497].
- [86] P. Pérez-Rubio, S. Collins and G. S. Bali, Phys. Rev. **D92**, 3, 034504 (2015), [arXiv:1503.08440].
- [87] C. Alexandrou and C. Kallidonis, Phys. Rev. **D96**, 3, 034511 (2017), [arXiv:1704.02647].
- [88] S. Meinel, private communication .
- [89] J. J. Dudek *et al.* (Hadron Spectrum), Phys. Rev. **D88**, 9, 094505 (2013), [arXiv:1309.2608].
- [90] R. G. Edwards *et al.*, Phys. Rev. **D84**, 074508 (2011), [arXiv:1104.5152].
- [91] R. A. Briceno, J. J. Dudek and R. D. Young, Rev. Mod. Phys. **90**, 2, 025001 (2018), [arXiv:1706.06223].
- [92] J. Bulava *et al.*, Nucl. Phys. **B910**, 842 (2016), [arXiv:1604.05593].
- [93] R. A. Briceno *et al.*, Phys. Rev. Lett. **118**, 2, 022002 (2017), [arXiv:1607.05900].
- [94] C. W. Andersen *et al.*, Phys. Rev. **D97**, 1, 014506 (2018), [arXiv:1710.01557].
- [95] C. M. Richards *et al.* (UKQCD), Phys. Rev. **D82**, 034501 (2010), [arXiv:1005.2473].
- [96] E. Gregory *et al.*, JHEP **10**, 170 (2012), [arXiv:1208.1858].
- [97] M. Karliner and J. L. Rosner (2019), [arXiv:1906.07799].
- [98] A. Patella, PoS **LATTICE2016**, 020 (2017), [arXiv:1702.03857].
- [99] S. Borsanyi *et al.*, Science **347**, 1452 (2015), [arXiv:1406.4088].
- [100] D. Giusti *et al.*, Phys. Rev. **D95**, 11, 114504 (2017), [arXiv:1704.06561].

16. Heavy-Quark and Soft-Collinear Effective Theory

Revised August 2019 by C.W. Bauer (LBNL) and M. Neubert (PRISMA, Mainz Inst. for Theor. Physics, JG U.).

16.1 Effective Field Theories

Quantum field theories provide the most precise computational tools for describing physics at the highest energies. One of their characteristic features is that they almost inevitably involve multiple length scales. When trying to determine the value of an observable, quantum field theory demands that all possible virtual states and hence all particles be included in the calculation. Since these particles have widely different masses, the final prediction is sensitive to many scales. This fact represents a formidable challenge from a practical point of view. No realistic quantum field theories can be solved exactly, so that one needs to resort to approximation schemes; these, however, are typically most straightforward when only a single scale is involved at a time.

Effective field theories (EFTs) provide a general theoretical framework to deal with the multi-scale problems of realistic quantum field theories. This framework aims at reducing such problems to a combination of separate and simpler single-scale problems; simultaneously, however, it provides an organization scheme whereby the other scales are not omitted but allowed to play their role in a separate step of the computation. The philosophy and basic principles of this approach are very generic, and correspondingly EFTs represent a widely used method in many different areas of high-energy physics, from the low-energy scales of atomic and nuclear physics to the high-energy scales of (partly yet unknown) elementary-particle physics, see [1–3] for some early references. EFTs can play a role both within analytic perturbative computations and in the context of non-perturbative numerical simulations; One of the simplest applications of EFTs to particle physics concerns the description of an underlying theory that is only probed at energy scales $E < \Lambda$. Any particle with mass $m > \Lambda$ cannot be produced as a real state and therefore only leads to short-distance virtual effects. Thus, one can construct an effective theory in which the quantum fluctuations of such heavy particles are “integrated out” from the generating functional for Green functions. This results in a simpler theory containing only those degrees of freedom that are relevant to the energy scales under consideration. In fact, the standard model of particle physics itself is widely viewed as an EFT of some yet unknown, more fundamental theory.

The development of any effective theory starts by identifying the degrees of freedom that are relevant to describe the physics at a given energy (or length) scale and constructing the Lagrangian describing the interactions among these fields. Short-distance quantum fluctuations associated with much smaller length scales are absorbed into the coefficients of the various operators in the effective theory. These coefficients are determined in a matching procedure, by requiring that the EFT reproduces the matrix elements of the full theory up to power corrections. In many cases the effective Lagrangian exhibits enhanced symmetries compared with the fundamental theory, allowing for simple and sometimes striking predictions relating different observables.

16.2 Heavy-Quark Effective Theory

Heavy-quark systems provide prime examples for applications of the EFT technology, because the hierarchy $m_Q \gg \Lambda_{\text{QCD}}$ (with $Q = b, c$) provides a natural separation of scales. Physics at the scale m_Q is of a short-distance nature and can be treated perturbatively, while for heavy-quark systems there is always also some hadronic physics governed by the confinement scale Λ_{QCD} of the strong interaction. Being able to separate the short-distance and long-distance effects associated with these two scales is crucial for any quantitative description. For instance, if the long-distance hadronic matrix elements are obtained from lattice QCD, then it is necessary to analytically compute the effects of short-wavelength modes that do not fit on the lattice. In many other instances, the long-distance physics can be encoded in a small number of hadronic parameters.

16.2.1 General idea and derivation of the effective Lagrangian

The simplest effective theory for heavy-quark systems is the heavy-quark effective theory (HQET) [4–7] (see [8, 9] for detailed discussions). It provides a simplified description of the soft interactions of a single heavy quark with light partons. This includes the interactions that bind the heavy quark with other light partons inside heavy mesons and baryons.

A softly interacting heavy quark is nearly on-shell. Its momentum may be decomposed as $p_Q = m_Q v + k$, where v is the 4-velocity of the hadron containing the heavy quark. The “residual momentum” k results from the soft interactions of the heavy quark with its environment and satisfies $v \cdot k \sim \Lambda_{\text{QCD}}$ and $k^2 \sim \Lambda_{\text{QCD}}^2$, which in the rest frame of the heavy hadron reduces to $k^\mu \sim \Lambda_{\text{QCD}}$. In the limit $m_Q \gg \Lambda_{\text{QCD}}$, the soft interactions do not change the 4-velocity of the heavy quark, which is therefore a conserved quantum number that is often used as a label on the effective heavy-quark fields. A nearly on-shell Dirac spinor has two large and two small components. We define

$$Q(x) = e^{-im_Q v \cdot x} [h_v(x) + H_v(x)], \quad (16.1)$$

where

$$h_v(x) = e^{im_Q v \cdot x} \frac{1 + \not{v}}{2} Q(x), \quad H_v(x) = e^{im_Q v \cdot x} \frac{1 - \not{v}}{2} Q(x) \quad (16.2)$$

are the large (“upper”) and small (“lower”) components of the spinor field, respectively. The extraction of the phase factor in (16.1) implies that the fields h_v and H_v carry the residual momentum k . The field H_v is $1/m_Q$ suppressed relative to h_v and describes quantum fluctuations far off the mass shell. Integrating it out using its equations of motion yields the HQET Lagrangian

$$\begin{aligned} \mathcal{L}_{\text{HQET}} = & \bar{h}_v i v \cdot D_s h_v \\ & + \frac{1}{2m_Q} \left[\bar{h}_v (iD_s)^2 h_v + C_{\text{mag}}(\mu) \frac{g}{2} \bar{h}_v \sigma_{\mu\nu} G_s^{\mu\nu} h_v \right] + \dots \end{aligned} \quad (16.3)$$

The covariant derivative $iD_s^\mu = i\partial^\mu + gA_s^\mu$ and the field strength $G_s^{\mu\nu}$ contain only the soft gluon field. Hard gluons have been integrated out, and their effects are contained in the Wilson coefficients of the operators in the effective Lagrangian. From the leading operator one derives the Feynman rules of HQET. The new operators entering at subleading order are referred to as the “kinetic energy” and “chromo-magnetic interaction”. The kinetic-energy operator corresponds to the first correction term in the Taylor expansion of the relativistic energy $E = m_Q + \vec{p}^2/2m_Q + \dots$. Lorentz invariance, which is encoded as a reparametrization invariance of the effective Lagrangian [10], ensures that its Wilson coefficient is not renormalized ($C_{\text{kin}} \equiv 1$). The coefficient C_{mag} of the chromo-magnetic operator receives corrections starting at one-loop order.

16.2.2 Spin-flavor symmetry

The leading term in the HQET Lagrangian exhibits a global spin-flavor symmetry. Its physical meaning is that, in the infinite mass limit, the properties of hadronic systems containing a single heavy quark are insensitive to the spin and flavor of the heavy quark [11, 12]. The spin symmetry results from the fact that there are no Dirac matrices in the leading term of the effective Lagrangian in (16.3), implying that the interactions of the heavy quark with soft gluons leave its spin unchanged. The flavor symmetry arises since the mass of the heavy quark does not appear at leading order. For n_Q heavy quarks moving at the same velocity, one can simply extend (16.3) by summing over n_Q identical terms for heavy-quark fields h_v^i . The result is invariant under rotations in flavor space. When combined with the spin symmetry, the symmetry group becomes promoted to $SU(2n_Q)$. These symmetries are broken by the operators at subleading power in the $1/m_Q$ expansion.

The spin-flavor symmetry leads to many interesting relations between the properties of hadrons containing a heavy quark. The most direct consequences concern the spectroscopy of such states

[13]. In the heavy-quark limit, the spin of the heavy quark and the total angular momentum j of the light degrees of freedom are separately conserved by the strong interactions. Because of heavy-quark symmetry, the dynamics is independent of the spin and mass of the heavy quark. Hadronic states can thus be classified by the quantum numbers (flavor, spin, parity, etc.) of the light degrees of freedom. The spin symmetry predicts that, for fixed $j \neq 0$, there is a doublet of degenerate states with total spin $J = j \pm \frac{1}{2}$. The flavor symmetry relates the properties of states with different heavy-quark flavor.

16.2.3 Weak decay form factors

Of particular interest are the relations between the weak decay form factors of heavy mesons, which parametrize hadronic matrix elements of currents between two mesons containing a heavy quark. These relations have been derived by Isgur and Wise [12], generalizing ideas developed by Nussinov and Wetzel [14] and Voloshin and Shifman [15]. For the purpose of this discussion, it is convenient to work with a mass-independent normalization of meson states and use velocity rather than momentum variables.

Consider the elastic scattering of a pseudoscalar meson, $P(v) \rightarrow P(v')$, induced by an external vector current coupled to the heavy quark contained in P , which acts as a color source moving with the meson's velocity v . The action of the current is to replace instantaneously the color source by one moving at velocity v' . Soft gluons need to be exchanged in order to rearrange the light degrees of freedom and build up the final state meson moving at velocity v' . This rearrangement leads to a form-factor suppression. The important observation is that, in the $m_Q \rightarrow \infty$ limit, the form factor can only depend on the Lorentz boost $\gamma = v \cdot v'$ connecting the rest frames of the initial and final-state mesons (as long as $\gamma = \mathcal{O}(1)$). In the effective theory the hadronic matrix element describing the scattering process can therefore be written as

$$\langle P(v') | \bar{h}_{v'} \gamma^\mu h_v | P(v) \rangle = \xi(v \cdot v') (v + v')^\mu, \quad (16.4)$$

with a form factor $\xi(v \cdot v')$ that is real and independent of m_Q . By flavor symmetry, the form factor remains identical when one replaces the heavy quark Q in one of the meson states by a heavy quark Q' of a different flavor, thereby turning P into another pseudoscalar meson P' . At the same time, the current becomes a flavor-changing vector current. This universal form factor is called the Isgur-Wise function [12]. For equal velocities the vector current $J^\mu = \bar{h}_v \gamma^\mu h_v$ is conserved in the effective theory, irrespective of the flavor of the heavy quarks. The corresponding conserved charges are the generators of the flavor symmetry. It follows that the Isgur-Wise function is normalized at the point of equal velocities: $\xi(1) = 1$. Since the recoil energy of the daughter meson P' in the rest frame of the parent meson P is $E_{\text{recoil}} = m_{P'} (v \cdot v' - 1)$, the point $v \cdot v' = 1$ is referred to as the zero-recoil limit. The heavy-quark spin symmetry leads to additional relations among weak decay form factors. It can be used to relate matrix elements involving vector mesons to those involving pseudoscalar mesons, which once again can be described completely in terms of the universal Isgur-Wise function.

The form factor relations imposed by heavy-quark symmetry describe the semileptonic decay processes $\bar{B} \rightarrow D \ell \bar{\nu}$ and $\bar{B} \rightarrow D^* \ell \bar{\nu}$ in the limit of infinite heavy-quark masses. They are model-independent consequences of QCD. The known normalization of the Isgur-Wise function at zero recoil can be used to obtain a model-independent measurement of the element $|V_{cb}|$ of the Cabibbo-Kobayashi-Maskawa (CKM) matrix. The semileptonic decay $\bar{B} \rightarrow D^* \ell \bar{\nu}$ is particularly well suited for this purpose [16]. Experimentally this is a very clean mode, since the reconstruction of the D^* meson mass provides a powerful rejection against background. From the theoretical point of view, it is ideal since the decay rate at zero recoil is protected by Luke's theorem against first-order power corrections in $1/m_Q$ [17]. This is described in more detail in Section 12. Corrections to the heavy-quark symmetry relations for the $\bar{B} \rightarrow D^{(*)}$ form factors near zero recoil can also be constrained using sum rules derived in the small-velocity limit [18, 19].

16.2.4 Decoupling transformation

At leading order in $1/m_Q$, the couplings of soft gluons to heavy quarks in the effective Lagrangian (16.3) can be removed by the field redefinition $h_v(x) = Y_v(x) \bar{h}_v^{(0)}(x)$, where $Y_v(x)$ is a soft Wilson line along the direction of v , extending from minus infinity to the point x . In terms of the new fields the leading-order HQET Lagrangian becomes $\mathcal{L}_{\text{HQET}} = \bar{h}_v^{(0)} i v \cdot \partial h_v^{(0)}$. It describes a free theory as far as the strong interactions of heavy quarks are concerned. However, the theory is nevertheless non-trivial in the presence of external sources. Consider, e.g., the case of a weak-interaction heavy-quark current

$$\bar{h}_{v'} \gamma^\mu (1 - \gamma_5) h_v = \bar{h}_{v'}^{(0)} \gamma^\mu (1 - \gamma_5) Y_{v'}^\dagger Y_v h_v^{(0)}, \quad (16.5)$$

where v and v' are the velocities of the heavy mesons containing the heavy quarks. Unless the two velocities are equal, corresponding to the zero-recoil limit discussed above, the object $Y_{v'}^\dagger Y_v$ is non-trivial, and hence the soft gluons do not decouple from the heavy quarks inside the current operator. One may interpret $Y_{v'}^\dagger Y_v$ as a Wilson loop with a cusp at the point x , where the two paths parallel to the different velocity vectors intersect. The presence of the cusp leads to non-trivial ultra-violet behavior (for $v \neq v'$), which is described by a cusp anomalous dimension $\Gamma_{\text{cusp}}(v \cdot v')$ that was calculated at two-loop order in [20]. It coincides with the velocity-dependent anomalous dimension of heavy-quark currents, which was introduced in the context of HQET in [21]. The interpretation of heavy quarks as Wilson lines is a useful tool, which was put forward in one of the very first papers on the subject [4]. This technology will be useful in the study of the interactions of heavy quarks with collinear degrees of freedom discussed later in this review.

16.2.5 Heavy-quark expansion for inclusive decays

The theoretical description of inclusive decays of hadrons containing a heavy quark exploits two observations [22–26]: bound-state effects related to the initial state can be calculated using the heavy-quark expansion, and the fact that the final state consists of a sum over many hadronic channels eliminates the sensitivity to the properties of individual final-state hadrons. The second feature rests on the hypothesis of quark-hadron duality, i.e. the assumption that decay rates are calculable in QCD after a smearing procedure has been applied [27]. In semileptonic decays, the integration over the lepton spectrum provides a smearing over the invariant hadronic mass of the final state (global duality). For nonleptonic decays, where the total hadronic mass is fixed, the summation over many hadronic final states provides an averaging (local duality). Since global duality is a much weaker assumption, the theoretical control of inclusive semileptonic decays is on firmer footing.

Using the optical theorem, the inclusive decay width of a hadron H_b containing a b quark can be written in the form

$$\Gamma(H_b) = \frac{1}{M_{H_b}} \text{Im} \langle H_b | i \int d^4x T \{ \mathcal{H}_{\text{eff}}(x), \mathcal{H}_{\text{eff}}(0) \} | H_b \rangle. \quad (16.6)$$

The effective weak Hamiltonian for b -quark decays consists of dimension-6 four-fermion operators and dipole operators [28]. Because of the large mass of the b quark, it follows that the separation of fields in the time-ordered product in (16.6) is small, of order $x \sim 1/m_b$. It is thus possible to construct an operator-product expansion (OPE) for the time-ordered product, in which it is represented as a series of local operators in HQET. The leading operator $\bar{h}_v h_v$ has a trivial matrix element. The next contributions arise at $\mathcal{O}(1/m_b^2)$ and give rise to two parameters $\mu_\pi^2(H_b)$ and $\mu_G^2(H_b)$, which are defined as the matrix elements of the heavy-quark kinetic energy and chromo-magnetic interaction inside the hadron H_b , respectively [29]. For the ground-state heavy mesons and baryons, one has $\mu_G^2(B) = 3(m_{B^*}^2 - m_B^2)/4 \simeq 0.36 \text{ GeV}^2$ and $\mu_G^2(\Lambda_b) = 0$. Thus, the total inclusive decay rate of a hadron H_b

can be written as [23, 24]

$$\Gamma(H_b) = \frac{G_F^2 m_b^5 |V_{cb}|^2}{192\pi^3} \left[c_1 + c_2 \frac{\mu_\pi^2(H_b)}{2m_b^2} + c_3 \frac{\mu_G^2(H_b)}{2m_b^2} + \mathcal{O}\left(\frac{1}{m_b^3}\right) + \dots \right], \quad (16.7)$$

where the prefactor arises from the loop integrations and is proportional to the fifth power of the b -quark mass. The coefficient functions c_i are calculable order by order in perturbation theory. While c_1 corresponds to the decay rate of a free heavy quark, the higher-order coefficients systematically account for bound-state effects. The coefficients of the subleading operators and of the leading operator at third order in $1/m_b$ have recently been calculated at NLO [30–34], and the heavy-quark expansion has been pushed to fifth order in $1/m_b$ [35].

From the fully inclusive width in (16.7) one can obtain the lifetime of a heavy hadron via $\tau(H_b) = 1/\Gamma(H_b)$. Due to the universality of the leading term in the heavy-quark expansion, lifetime ratios such as $\tau(B^-)/\tau(B^0)$, $\tau(\bar{B}_s^0)/\tau(B^0)$ and $\tau(A_b)/\tau(\bar{B}^0)$ are particularly sensitive to the hadronic parameters determining the power corrections in the expansion. In order to understand these ratios theoretically, it is necessary to include phase-space enhanced power corrections of order $(\Lambda_{\text{QCD}}/m_b)^3$ [36, 37] as well as short-distance perturbative effects [38] in the calculation (see [39] for a recent discussion of the status of the corresponding calculations).

A formula analogous to (16.7) can be derived for differential distributions in specific inclusive decay processes, assuming that these distributions are integrated over a sufficiently large region of phase space to ensure quark-hadron duality. Important examples are the distributions in the lepton energy and the lepton invariant mass, as well as moments of the invariant hadronic mass distribution in the semileptonic processes $\bar{B} \rightarrow X_u \ell \bar{\nu}$ and $\bar{B} \rightarrow X_c \ell \bar{\nu}$. A global fit of semileptonic decay distributions can be used to determine the CKM matrix elements $|V_{ub}|$ and $|V_{cb}|$ along with heavy-quark parameters such as the masses m_b , m_c and the hadronic parameters $\mu_\pi^2(B)$, $\mu_G^2(B)$. These determinations provide some of the most accurate values for these parameters (see e.g. [40–42]).

16.2.6 Shape functions and non-local power corrections

In certain regions of phase space, in which the hadronic final state in an inclusive heavy-hadron decay is made up of light energetic partons, the local OPE for inclusive decays must be replaced by a more complicated expansion involving hadronic matrix elements of non-local light-ray operators [43, 44]. Prominent examples are the radiative decay $\bar{B} \rightarrow X_s \gamma$ for large photon energy E_γ near $m_B/2$, and the semileptonic decay $\bar{B} \rightarrow X_u \ell \bar{\nu}$ at large lepton energy or small hadronic invariant mass. In these cases, the differential decay rates at leading order in the heavy-quark expansion can be written in the factorized form $d\Gamma = H J \otimes S$ [45], where the hard function H and the jet function J are calculable in perturbation theory. The characteristic scales for these functions are set by m_b and $(m_b \Lambda_{\text{QCD}})^{1/2}$, respectively. The soft function

$$S(\omega) = \int \frac{dt}{4\pi} e^{-i\omega t} \langle \bar{B}(v) | \bar{h}_v(tn) Y_n(tn) Y_n^\dagger(0) h_v(0) | \bar{B}(v) \rangle \quad (16.8)$$

is a non-perturbative object called the shape function [43, 44]. Here Y_n are soft Wilson lines along a light-like direction n aligned with the momentum of the hadronic final-state jet. The jet function and the shape function share a common variable $\omega \sim \Lambda_{\text{QCD}}$, and the symbol \otimes denotes a convolution in this variable.

While the hard functions are different for the decays $\bar{B} \rightarrow X_s \gamma$ and $\bar{B} \rightarrow X_u \ell \bar{\nu}$, the jet and soft functions are identical at leading order in Λ_{QCD}/m_Q . This is particularly important for the shape function, which introduces non-perturbative physics into the theoretical predictions for the decay rates in the regions of experimental interest. The fact that both processes depend on the same non-perturbative function makes it possible to use the measured shape of the $\bar{B} \rightarrow X_s \gamma$ photon spectrum to reduce the theoretical uncertainties in the determination of the CKM element $|V_{ub}|$ from semileptonic decays. In higher orders of the heavy-quark

expansion, an increasing number of subleading jet and soft functions are required to describe the decay distributions [46]. These have been analyzed in detail at order $1/m_b$ [47–49]. In the case of $\bar{B} \rightarrow X_s \gamma$ (and also in the related case of $\bar{B} \rightarrow X_s \ell \bar{\ell}$), some of these non-local effects survive in the total decay rate and give rise to irreducible hadronic uncertainties [50]. The technology for deriving the corresponding factorization theorems relies on the soft-collinear effective theory, to which we now turn.

16.3 Soft-Collinear Effective Theory

As discussed in the previous section, soft gluons that bind a heavy quark inside a heavy meson cannot change the virtuality of that heavy quark by a significant amount. The ratio Λ_{QCD}/m_Q provides the expansion parameter in HQET, which is a small parameter since $m_Q \gg \Lambda_{\text{QCD}}$. This obviously does not work when considering light quarks. However, if the energy Q of the quarks is large, the ratio Λ_{QCD}/Q provides a small parameter, which can be used to construct an effective theory. One major difference to HQET is that light energetic quarks cannot only emit soft gluons, but they can also emit collinear gluons (an energetic gluon in the same direction as the original quark), without parametrically changing their virtuality. Thus, to fully reproduce the long-distance physics of energetic quarks requires that one includes their interactions with both soft and collinear particles. The resulting effective theory is therefore called soft-collinear effective theory (SCET) [51–53] (see [54] for a review).

A single energetic particle can always be boosted to a frame where all momentum components have similar size, in which case there is no small expansion parameter. Thus the presence of energetic particles must refer to a reference frame defined by external kinematics. SCET has a wide range of applications; some examples are the production of energetic, light states in the decay of a heavy particle in its rest frame, the production of energetic jets in collider environments, and the scattering of energetic particles off a target at rest. In this brief review we will outline the main features of this effective theory and mention a few selected applications.

16.3.1 General idea of the expansion

Consider a quark with virtuality much less than its energy Q , moving along the direction \vec{n} . It is convenient to parameterize the momentum p_n of this particle in terms of its light-cone components, defined by $(p_n^-, p_n^+, p_n^\perp) = (\vec{n} \cdot p_n, n \cdot p_n, p_n^\perp)$, where $n^\mu = (1, \vec{n})$ and $\bar{n}^\mu = (1, -\vec{n})$ are light-like vectors, and $n \cdot p_n^\perp = \bar{n} \cdot p_n^\perp = 0$. The subscript n on the momentum indicates the direction of the collinear particle. In terms of these light-cone components, the virtuality satisfies $p_n^2 = p_n^+ p_n^- + p_n^{\perp 2}$. The individual components of the momentum obey

$$(p_n^-, p_n^+, p_n^\perp) \sim Q(1, \lambda^2, \lambda), \quad (16.9)$$

where $\lambda^2 = p^2/Q^2$ is the expansion parameter of SCET. The virtuality of such an energetic particle remains parametrically unchanged if it interacts with energetic particles in the same direction n , or with soft particles with momentum scaling as

$$(p_s^-, p_s^+, p_s^\perp) \sim Q(\lambda^2, \lambda^2, \lambda^2). \quad (16.10)$$

SCET is constructed in such a way as to reproduce the long-distance dynamics arising from the interactions of collinear and soft degrees of freedom.

In the above power counting the transverse momenta of soft degrees of freedom scale as $p_s^\perp \sim Q\lambda^2$, which is much smaller than the transverse momenta $p_c^\perp \sim Q\lambda$ of collinear fields. This theory is usually called SCET_I. If the external kinematics require that the transverse momenta of both soft and collinear fields are of the same size, $p_c^\perp \sim p_s^\perp$, then the appropriate degrees of freedom have the scaling $p_c \sim Q(1, \lambda^2, \lambda)$ and $p_s \sim Q(\lambda, \lambda, \lambda)$. This theory is usually called SCET_{II} and is required, e.g., for exclusive hadronic decays such as $\bar{B} \rightarrow D\pi$, where the virtuality of both collinear and soft degrees of freedom are set by Λ_{QCD} , or for the description of transverse-momentum distributions at colliders. SCET_I power counting is assumed in the following sections, while SCET_{II} is discussed in more detail in 16.3.6.

16.3.2 Leading-order Lagrangian

The derivation of the SCET Lagrangian follows similar steps as described for HQET in Section 16.2.1. One begins by deriving the Lagrangian for a theory containing only a single collinear sector. Similar to HQET, one separates the full QCD field into two components, $q_n(x) = \psi_n(x) + \Xi_n(x)$, where (with $n \cdot \bar{n} = 2$)

$$\psi_n(x) = \frac{\not{n}\not{\bar{n}}}{4} q_n(x), \quad \Xi_n(x) = \frac{\not{\bar{n}}\not{n}}{4} q_n(x). \quad (16.11)$$

The degrees of freedom described by the field Ξ_n are far off shell and can therefore be eliminated using its equation of motion. This gives

$$\mathcal{L}_n = \bar{\psi}_n(x) \left[in \cdot D + i\mathcal{D}^\perp \frac{1}{i\bar{n} \cdot D} i\mathcal{D}^\perp \right] \frac{\not{n}}{2} \psi_n(x). \quad (16.12)$$

As a next step, one separates the large and residual momentum components by decomposing the collinear momentum into a “label” and a residual momentum, $p^\mu = P^\mu + k^\mu$ with $n \cdot P = 0$. One then performs a phase redefinition on the collinear fields, such that $\psi_n(x) = e^{iP \cdot x} \xi_n(x)$. Derivatives acting on the fields $\xi_n(x)$ now only pick out the residual momentum. Since unlike in HQET the label momentum in SCET is not conserved, one defines a label operator \mathcal{P}^μ acting as $\mathcal{P}^\mu \xi_n(x) = P^\mu \xi_n(x)$ [52], as well as a corresponding covariant label operator $i\mathcal{D}_n^\mu = \mathcal{P}^\mu + gA_n^\mu(x)$. Note that at leading order in power counting $i\mathcal{D}_n^\mu$ does not contain the soft gluon field. This leads to the final SCET Lagrangian [52,53,55,56]

$$\mathcal{L}_n = \bar{\xi}_n(x) \left[in \cdot D_n + gn \cdot A_s + i\mathcal{P}_n^\perp \frac{1}{i\bar{n} \cdot \mathcal{D}_n} i\mathcal{P}_n^\perp \right] \frac{\not{n}}{2} \xi_n(x) + \dots, \quad (16.13)$$

where we have split $in \cdot D$ into a collinear piece $in \cdot D_n = in \cdot \partial + gn \cdot A_n$ and a soft piece $gn \cdot A_s$. This latter term gives rise to the only interaction between a collinear quark and soft gluons at leading power in λ . The ellipses represent higher-order interactions between soft and collinear particles.

The Lagrangian describing collinear fields in different light-like directions is simply given by the sum of the Lagrangians for each direction n , i.e. $\mathcal{L} = \sum_n \mathcal{L}_n$. The soft gluons are the same in each individual Lagrangian. An alternative way to understand the separation between large and small momentum components is to derive the Lagrangian of SCET in position space [56]. In this case no label operators are required, and the dependence on short-distance effects is contained in non-localities at short distances. An important difference between SCET and HQET is that the SCET Lagrangian is not corrected by short distance fluctuations. The physical reason is that in the construction described above no high-momentum modes have been integrated out [56]. Such hard modes arise when different collinear sectors are coupled via some external current (e.g. in jet production at e^+e^- or hadron colliders), or when collinear particles are produced in the rest frame of a decaying heavy object (such as in B decays). Short-distance effects are then incorporated in the Wilson coefficients of the external source operators.

16.3.3 Collinear gauge invariance and Wilson lines

An important aspect of SCET is the implementation of local gauge invariance. Because the effective field operators describe modes with certain momentum scalings, the effective Lagrangian respects only residual gauge symmetries. One of them satisfies the collinear scaling

$$(\bar{n} \cdot \partial, n \cdot \partial, \partial^\perp) U_n(x) \sim Q(\lambda^2, \lambda) U_n(x), \quad (16.14)$$

and one the soft scaling

$$(\bar{n} \cdot \partial, n \cdot \partial, \partial^\perp) U_s(x) \sim Q(\lambda^2, \lambda^2, \lambda^2) U_s(x). \quad (16.15)$$

While the soft gauge transformation is common for all fields, collinear fields in different directions each transform under their own collinear gauge transformation, which means that each collinear sector, containing particles with large momenta along a certain direction, has to be separately gauge invariant under its

collinear gauge transformation. This requires the introduction of collinear Wilson lines [52]

$$W_n(x) = \text{P exp} \left[-ig \int_{-\infty}^0 ds \bar{n} \cdot A_n(s\bar{n} + x) \right], \quad (16.16)$$

which transform under collinear gauge transformations according to $W_n \rightarrow U_n W_n$. Thus, the combination $\chi_n \equiv W_n^\dagger \psi_n$ is gauge invariant. In a similar manner, one can define the gauge-invariant gluon field $B_n^\mu = g^{-1} W_n^\dagger iD_n^\mu W_n$ [57, 58]. Collinear operators in SCET are typically constructed from such collinearly gauge-invariant building blocks.

16.3.4 Derivation of factorization theorems

One of the important applications of SCET is to understand how to factorize cross sections involving energetic particles moving in different directions into simpler pieces that can either be calculated perturbatively or determined from data. Factorization theorems have been around for much longer than SCET (see [59] for a review). However, the effective theory allows for a conceptually simpler understanding of certain classes of factorization theorems [57], since most simplifications happen already at the level of the Lagrangian. The discussion in this section is valid to leading order in the power counting of the effective theory.

As discussed in the previous section, the Lagrangian of SCET does not involve any couplings between collinear particles moving in different directions. Soft gluons couple to collinear quarks only through the term $\xi_n gn \cdot A_s (\not{n}/2) \xi_n$ in the effective Lagrangian in (16.13). This coupling is similar to the coupling of soft gluons to heavy quarks in HQET, see Section 16.2.4. It can be removed by means of the field redefinition [53]

$$\psi_n(x) = Y_n(x) \psi_n^{(0)}(x), \quad A_n^a(x) = Y_n^{ab}(x) A_n^{b(0)}(x), \quad (16.17)$$

where Y_n and Y_n^{ab} live in the fundamental and adjoint representations of $SU(3)$, respectively. This fact greatly facilitates proofs of factorization theorems in SCET. A QCD operator $O(x)$ describing the interactions of collinear partons moving in different directions can thus be written as (omitting color indices for simplicity)

$$\begin{aligned} \langle O(x) \rangle &= \\ C_O(\mu) \langle [C_{n_a}^{(0)} C_{n_b}^{(0)} C_{n_1}^{(0)} \dots C_{n_N}^{(0)}](x) [\mathcal{Y}_{n_a} \mathcal{Y}_{n_b} \mathcal{Y}_{n_1} \dots \mathcal{Y}_{n_N}](x) \rangle_\mu. \end{aligned} \quad (16.18)$$

Here $C_{n_i}^{(0)}(x)$ denotes a gauge-invariant combination of collinear fields (either quark or gluon fields) in the direction n_i . The hard matching coefficient C_O accounts for short-distance effects at the scale Q . The soft Wilson lines can either be in a color triplet or color octet representation, and are collectively denoted by \mathcal{Y}_{n_i} . Both the matrix elements and the coefficient C_O depend on the renormalization scale μ .

Having defined the operator mediating a given process, one can calculate the cross section by squaring the operator, taking the forward matrix element and integrating over the phase space of all final-state particles. The absence of interactions between collinear degrees of freedom moving along different directions or soft degrees of freedom implies that the forward matrix element can be factorized as

$$\begin{aligned} \langle \text{in} | O(x) O^\dagger(0) | \text{in} \rangle &= |C_O(\mu)|^2 \langle \text{in}_a | C_{n_a}(x) C_{n_a}^\dagger(0) | \text{in}_a \rangle_\mu \\ &\times \langle \text{in}_b | C_{n_b}(x) C_{n_b}^\dagger(0) | \text{in}_b \rangle_\mu \\ &\times \langle 0 | C_{n_1}(x) C_{n_1}^\dagger(0) | 0 \rangle_\mu \dots \langle 0 | C_{n_N}(x) C_{n_N}^\dagger(0) | 0 \rangle_\mu \\ &\times \langle 0 | [\mathcal{Y}_{n_a} \dots \mathcal{Y}_{n_N}](x) [\mathcal{Y}_{n_a} \dots \mathcal{Y}_{n_N}]^\dagger(0) | 0 \rangle_\mu. \end{aligned} \quad (16.19)$$

Thus, the matrix element can be written as a product of simpler structures, each of which can be evaluated separately.

The vacuum matrix elements of the outgoing collinear fields are determined by jet functions $J_i(\mu)$. As long as the relevant scale (for example the jet mass) is sufficiently large, these functions can

be calculated perturbatively. The matrix elements of the incoming collinear fields are non-perturbative objects $B_{p/N}(\mu)$ called beam functions for parton p in nucleon N [60]. For many applications they can be related perturbatively to the well-known parton distribution functions. Finally, the vacuum matrix element of the soft Wilson lines defines a so-called soft function $S_{ab\dots N}(\mu)$. The shared dependence on x in the above equation implies that in momentum space the various components of the factorization theorem are convoluted with one another. Deriving this convolution requires a careful treatment of the phase-space integration and the factorization of the measurement defining the cross section of interest, in particular treating the large and residual components of each momentum appropriately.

Putting all information together, the differential cross section for a proton-proton collision with N jet-like objects can schematically be written as

$$d\sigma \sim \sum_{ab} H_{ab}(\mu) [B_{a/P}(\mu) B_{b/P}(\mu)] \otimes [J_1(\mu) \dots J_N(\mu)] \otimes S_{ab\dots N}(\mu). \quad (16.20)$$

The hard function is equal to the square of the matching coefficient, $H_{ab}(\mu) = |C_O(\mu)|^2$, and the beam, jet, and soft functions and their convolution structure depend on the specific N -jet measurement. It should be mentioned that the most difficult part of traditional factorization proofs involves showing that so-called Glauber gluons do not spoil the above factorization theorem [61]. Significant progress toward the description of Glauber effects within SCET has been made in [62], where a closed form for the effective Lagrangian describing these interactions was derived. In this context, a proof of factorization requires demonstrating that this Lagrangian has no impact on a particular cross section, and such proofs have not yet been fully derived within SCET.

16.3.5 Resummation of large logarithms

SCET can be used to sum the large logarithms arising in perturbative calculations to all orders in the strong coupling constant α_s . In general, perturbation theory will generate a logarithmic dependence on any ratio of scales r in a problem. For processes that involve initial or final states with energy much in excess of their mass, there are two powers of logarithms for every power of α_s . These are referred to as Sudakov logarithms. For widely separated scales these large logarithms can spoil the convergence of fixed-order perturbation theory. One thus needs to reorganize the expansion in such a way that $\alpha_s L = \mathcal{O}(1)$ is kept fixed, with $L = \ln r$. More precisely, a proper resummation requires summing logarithms of the form $\alpha_s^n L^m$ with $m \leq (n+1)$ in the logarithm of a cross section, by writing $\ln \sigma \sim L g_0(\alpha_s L) + g_1(\alpha_s L) + \alpha_s g_2(\alpha_s L) + \dots$, with functions $g_n(x)$ that need to be determined.

The important ingredient in achieving this resummation is the fact that SCET factorizes a given cross section into simpler pieces, each of which depends on a single physical scale. The only dependence on that scale can arise through logarithms of its ratio with the renormalization scale μ . Thus, for each of the components in the factorization theorem one can choose a renormalization scale μ for which the large logarithmic terms are absent. Of course, the factorization formula requires a common renormalization scale μ in all its components, and one therefore has to use the renormalization group (RG) to evolve the various component functions from their preferred scale to the common scale μ . A novel feature of RG equations in SCET, as opposed to other EFTs, is that the anomalous dimensions entering the evolution equations of the hard, beam, jet and soft functions in a factorization formula such as (16.20) contain a single power of the logarithm of the relevant energy scale. For example, the anomalous dimension γ_H of the hard function has the form

$$\gamma_H(\mu) = c_H \Gamma_{\text{cusp}}(\alpha_s) \ln \frac{Q^2}{\mu^2} + \gamma(\alpha_s), \quad (16.21)$$

where c_H is a process-dependent coefficient and Γ_{cusp} denotes the

so-called cusp anomalous dimension [20, 63]. Collinear and soft functions have similar anomalous dimensions, which also involve a cusp and a non-cusp part. The non-cusp part γ of the anomalous dimensions is process (and observable) dependent. The presence of a logarithm in the anomalous dimension is characteristic of Sudakov problems and arises since the perturbative series contains double logarithms of scale ratios.

Solving the RG equations one can systematically resum all large logarithms of scale ratios in the factorized cross section and express the functions $g_n(\alpha_s L)$ introduced above in terms of ratios of running coupling constants. In order to compute the first two terms $L g_0(\alpha_s L) + g_1(\alpha_s L)$ in $\ln \sigma$, corresponding to the next-to-leading logarithmic (NLL) approximation, one needs two-loop expressions for the cusp anomalous dimension and β function, one-loop expressions for the non-cusp pieces in the anomalous dimensions, and tree-level matching conditions for all component functions at their characteristic scales. To calculate the next term $\alpha_s g_2(\alpha_s L)$ in the expansion, corresponding to NNLL order, one needs to go one order higher in the loop expansion, and so on.

16.3.6 Factorization and resummation in SCET_{II}

The effective theory SCET_{II} contains collinear and soft particles with momenta scaling as $(p_n^-, p_n^+, p_n^\perp) \sim Q(1, \lambda^2, \lambda)$ and $(p_s^-, p_s^+, p_s^\perp) \sim Q(\lambda, \lambda, \lambda)$. They have the same small virtuality ($p_n^2 \sim p_s^2 \sim Q^2 \lambda^2$) but differ in their rapidities. An important class of observables, for which this scaling is relevant, contains cross sections for processes in which the transverse momenta of particles are constrained by external kinematics. The prime example are the transverse-momentum distributions of electroweak gauge bosons or Higgs bosons produced at hadron colliders. The parton transverse momenta are constrained by the fact that their vector sum must be equal and opposite to the transverse momentum q_T of the boson. Standard RG evolution in the effective theory controls the logarithms arising from the fact that the virtualities of the collinear and soft modes are much smaller than the hard scale Q in the process (the boson mass). However, additional large logarithms arise since the rapidities of collinear and soft modes are parametrically different, such that $e^{|\ln \eta - \ln \eta_s|} \sim 1/\lambda$. These logarithms can be traced to a new source of divergences and an unusual failure of dimensional regularization. They need to be factorized in the cross section and resummed by other means.

Two equivalent approaches exist for how to deal with the additional rapidity logarithms in SCET. In the approach of [64], they are interpreted as a consequence of a ‘‘collinear anomaly’’ of the effective theory SCET_{II}, resulting from the fact that a classical rescaling symmetry of the effective Lagrangian is broken by quantum effects. The extra large logarithms can be resummed by means of simple differential equations, which typically state that to all orders in perturbation theory (and in an appropriate space) the logarithm of the cross section contains only a single extra logarithm of $\lambda \sim q_T/Q$ not contained in the hard function. Another approach to resum the rapidity logarithms uses the ‘‘rapidity renormalization group’’ [65], in which the relevant differential equations are obtained by considering a new type of scale variation in a parameter ν , which separates the phase space for collinear and soft particles along a hyperbola in the (p_-, p_+) plane. In contrast to the standard RG, there is no running coupling involved in the ν evolution, since the different contributions live at the same virtuality.

SCET_{II} also plays an important role in the study of factorization for a variety of exclusive B meson decays, such as $\bar{B} \rightarrow \pi \ell \bar{\nu}$, $\bar{B} \rightarrow K^* \gamma$ and $\bar{B} \rightarrow \pi \pi$, for which the virtualities of energetic (collinear) final-state particles are of order Λ_{QCD} , which is also the scale for the soft light degrees of freedom contained in the initial-state B meson.

16.3.7 Applications

Most of the applications of SCET are either in flavor physics, where the decay of a heavy B meson can give rise to energetic light partons, or in collider physics, where the presence of jets naturally leads to collimated sets of energetic particles. For some of these applications alternative approaches existed before the invention of SCET, but the effective theory has opened up alternative ways to understand the physics of these processes. For

many examples, however, SCET has allowed new insights and new applications. The investigation of heavy-to-light form factors has been instrumental for understanding factorization in exclusive semileptonic B decays [66]. SCET has also provided a field-theoretic basis for the QCD factorization approach to exclusive, non-leptonic decays of B mesons [67]. Using SCET methods, proofs of factorization were derived for the color-allowed decay $\bar{B}^0 \rightarrow D^+\pi^-$ [68], the color-suppressed decay $\bar{B}^0 \rightarrow D^0\pi^0$ [69], and the radiative decay $\bar{B} \rightarrow K^*\gamma$ [70]. Further examples are factorization theorems and the resummation of endpoint logarithms for quarkonia production [71], the resummation of large logarithmic terms for the thrust [72] and jet broadening [73] distributions in e^+e^- annihilation beyond NLL order, the development of new factorizable observables to veto extra jets [60, 74], all-orders factorization theorems for processes containing electroweak Sudakov logarithms [75], and the resummation of threshold (soft gluon) logarithms in momentum space for several important processes at hadron colliders [76–78]. There has also been a lot of activity describing p_T -based resummation at hadron colliders. Prominent examples are the transverse-momentum distributions of electroweak bosons [64, 65, 79]. Finally, SCET has given new insights into the jet substructure methods (see [80] for a recent review). We now describe a few of these applications in more detail.

Event-shape distributions, in particular the thrust distribution, have been measured to high accuracy at LEP [81]. They can be used for a determination of the strong coupling constant α_s . SCET has increased the theoretical accuracy in the calculations of the thrust and C-parameter distributions significantly. First, it has allowed to increase the perturbative accuracy of the thrust spectrum. The resummation of logarithms of τ , which become important for $\tau \ll 1$, has been performed to $N^3\text{LL}$ [72], two orders beyond what was previously available. Combining this resummation with the known two-loop spectrum [82, 83] gives precise perturbative predictions both at small and large values of τ . Second, the factorization of the cross section in SCET has made it possible to include non-perturbative physics through a shape function, in analogy with the B -physics case discussed in Section 16.2.6. Comparing the theoretical predictions to the measured thrust and C-parameter distributions yields a precise value of the strong coupling constant $\alpha_s(m_Z)$, which however is lower than the average value cited in Section 9 by several standard deviations [84, 85]. For more discussions on this, see Section 9.

The Higgs-boson production cross section in gluon fusion at the LHC, defined with a jet veto stating that no jet in the final state has transverse momentum above a threshold p_T^{veto} , can be factorized in the form [86, 87] (see [88] for a corresponding calculation outside the SCET framework)

$$\begin{aligned} \sigma(p_T^{\text{veto}}) = & H(m_H, \mu) \left(\frac{\nu_B}{\nu_S}\right)^{-2F_{gg}(R, p_T^{\text{veto}}, \mu)} S_{gg}(R, p_T^{\text{veto}}, \mu, \frac{\nu_S}{p_T^{\text{veto}}}) \\ & \times \int_{\tau}^1 \frac{dz}{z} B_{g/P}\left(z, R, p_T^{\text{veto}}, \mu, \frac{\nu_B}{m_H}\right) B_{g/P}\left(\frac{\tau}{z}, R, p_T^{\text{veto}}, \mu, \frac{\nu_B}{m_H}\right), \end{aligned} \quad (16.22)$$

where $\tau = m_H^2/s$, and $\mu \sim p_T^{\text{veto}}$ is a common factorization scale. The beam functions $B_{g/P}$, the soft function S_{gg} and the exponent F_{gg} all depend on the jet radius R as well as the jet clustering algorithm. The scale dependence of the hard function H is controlled by standard RG evolution in SCET. The beam functions can be factorized further into calculable collinear kernels convoluted with parton distribution functions. In addition to the renormalization scale μ , the beam and soft functions depend on two rapidity scales $\nu_B \sim m_H$ and $\nu_S \sim p_T^{\text{veto}}$, respectively. In [86] the default values $\nu_B = m_H$ and $\nu_S = p_T^{\text{veto}}$ are used for these scales, and the soft function S_{gg} is absorbed into the beam functions. In [87] the exponent F_{gg} is called $-\gamma_g^g/2$. The second factor on the right-hand side of the factorization formula (16.22), which resums large rapidity logarithms, implies that the logarithm of the jet-veto cross section contains a single large logarithm $\ln \sigma = -2F_{gg}(R, p_T^{\text{veto}}, \mu) \ln(m_H/p_T^{\text{veto}}) + \dots$ not contained in the hard function. Its coefficient can be calculated in fixed-order per-

turbation theory.

Obtaining more precise fixed-order calculations has been an important goal for many years. A major difficulty in these calculations is the proper handling of the infrared singularities that arise in both virtual and real contributions. A method based on N -jettiness (\mathcal{T}_N) slicing [89, 90] allows one to obtain the NNLO result from a much easier NLO calculation, combined with information about the singular dependence of the cross section on the \mathcal{T}_N resolution variable [74]. This has been used to compute various processes with final states containing up to one hard, colored particle [91–95]. While the NLO calculations can be performed using well established techniques, the singular dependence on \mathcal{T}_N can be calculated using SCET at NNLO. Calculations of the leading power corrections in \mathcal{T}_0/Q [96, 97] have helped to improve the numerical stability for several processes. The N -jettiness (\mathcal{T}_N) slicing method has been used prior to the fixed-order application in the combination of higher order resummation with parton showers [98, 99].

More generally, there is currently a strong effort to push the applications of SCET toward factorization and resummation at subleading power in the expansion in λ . The subleading SCET Lagrangian [56, 100] and current operators arising in B -meson decays and their anomalous dimensions [55, 56, 101–103] have been studied a long time ago. More recently, the focus has shifted to subleading operators arising in important collider processes, such as Drell-Yan or Higgs production. The general set of operators for such processes have been identified [104–106], and several of their anomalous dimensions have been calculated [106, 107]. First resummed results at subleading power have been presented for event shapes [108] and the Drell-Yan process [109].

16.4 Open issues and perspectives

HQET has successfully passed many experimental tests, and there are not many open questions that still need to be addressed. One concept that has not been derived from first principles is the notion of quark-hadron duality, which underlies the application of HQET to the description of inclusive decays of B mesons. The validity of global duality (at energies even lower than those relevant in B decays) has been tested experimentally using high-precision data on semileptonic B decays and on hadronic τ decays. However, assigning a theoretical uncertainty due to possible duality violations remains a difficult task. Another known issue is that the measured values of the CKM element $|V_{ub}|$ extracted from exclusive or inclusive decays of B mesons differ from each other by several standard deviations (see Section 75). This measurement relies on the heavy-quark limit, and the uncertainty quoted includes a theoretical estimate of the effect of power corrections arising from the finite b -quark mass. It remains an open question whether the discrepancy is due to underestimated theoretical or experimental uncertainties, or whether it may hint to the existence of new physics.

SCET, on the other hand, is still an active field of research, and new results are being obtained regularly. An important example concerns the understanding of non-global logarithms arising in hadron-collider processes with jets [110, 111]. For a long time a fully factorized form of non-global jet cross sections has not been available, despite significant progress towards this goal [112, 113]. A consistent factorization formula for non-global jet observables was developed in [114, 115]. It requires the introduction of a collinear-soft mode in the SCET Lagrangian. The first application of this formalism was to the light jet mass distribution [116], and significant steps toward an extension to NLL accuracy have been taken in [117]. It is believed that the results obtained from the factorization theorem derived in [114, 115] are equivalent to those obtained using the approaches proposed in [112, 113]. The various methods differ in the way in which they organize the all-order expansion for the appearing complicated multi-Wilson-line structures.

Another active field concerns the study of Glauber gluons in SCET [118] and their relation to the BFKL equation familiar from small- x physics [119]. A systematic account of the effects of Glauber gluons in the context of the SCET Lagrangian has been developed in [62]. The formalism has been extended to Glauber quarks in [120]. These developments set the basis for

a solid understanding of the impact of Glauber exchanges on factorization theorems. Glauber gluons also play an important role in SCET-based analysis of jet propagation in dense QCD media [121, 122], which gives rise to the jet-quenching phenomenon in heavy-ion collisions. An important open question facing some applications of SCET concerns factorized expressions containing endpoint-divergent convolution integrals.

We close this short review by mentioning a particularly nice application combining the methods of heavy-particle EFTs such as HQET and non-relativistic QCD with SCET in the context of describing the interactions of heavy dark matter (with mass $M \gg v$) with SM particles. In [123] it was realized that the interactions of heavy, weakly interacting massive particles (WIMPs) with nuclear targets can be described in a model-independent way using heavy-particle EFTs. The WIMPs are charged under $SU(2)_L$ and can interact with electroweak gauge bosons and the Higgs boson. The WIMP EFT was later extended by describing the produced, highly energetic electroweak gauge bosons in terms of soft or collinear fields in SCET [124–126]. This allows one to systematically separate all relevant mass scales, resum electroweak Sudakov logarithms and disentangle the so-called Sommerfeld enhancement from the short-distance hard annihilation process.

References

- [1] E. Witten, Nucl. Phys. **B122**, 109 (1977).
- [2] S. Weinberg, Phys. Lett. **91B**, 51 (1980).
- [3] L. J. Hall, Nucl. Phys. **B178**, 75 (1981).
- [4] E. Eichten and B. R. Hill, Phys. Lett. **B234**, 511 (1990).
- [5] H. Georgi, Phys. Lett. **B240**, 447 (1990).
- [6] B. Grinstein, Nucl. Phys. **B339**, 253 (1990).
- [7] T. Mannel, W. Roberts and Z. Ryzak, Nucl. Phys. **B368**, 204 (1992).
- [8] M. Neubert, Phys. Rept. **245**, 259 (1994), [hep-ph/9306320].
- [9] A. V. Manohar and M. B. Wise, Camb. Monogr. Part. Phys. Nucl. Phys. Cosmol. **10**, 1 (2000).
- [10] M. E. Luke and A. V. Manohar, Phys. Lett. **B286**, 348 (1992), [hep-ph/9205228].
- [11] E. V. Shuryak, Phys. Lett. **93B**, 134 (1980).
- [12] N. Isgur and M. B. Wise, Phys. Lett. **B232**, 113 (1989).
- [13] N. Isgur and M. B. Wise, Phys. Rev. Lett. **66**, 1130 (1991).
- [14] S. Nussinov and W. Wetzel, Phys. Rev. **D36**, 130 (1987).
- [15] M. A. Shifman and M. B. Voloshin, Sov. J. Nucl. Phys. **45**, 292 (1987), [Yad. Fiz.45,463(1987)].
- [16] M. Neubert, Phys. Lett. **B264**, 455 (1991).
- [17] M. E. Luke, Phys. Lett. **B252**, 447 (1990).
- [18] I. I. Y. Bigi *et al.*, Phys. Rev. **D52**, 196 (1995), [hep-ph/9405410].
- [19] N. Uraltsev, Phys. Lett. **B501**, 86 (2001), [195(2000)], [hep-ph/0011124].
- [20] G. P. Korchemsky and A. V. Radyushkin, Nucl. Phys. **B283**, 342 (1987).
- [21] A. F. Falk *et al.*, Nucl. Phys. **B343**, 1 (1990).
- [22] J. Chay, H. Georgi and B. Grinstein, Phys. Lett. **B247**, 399 (1990).
- [23] I. I. Y. Bigi, N. G. Uraltsev and A. I. Vainshtein, Phys. Lett. **B293**, 430 (1992), [Erratum: Phys. Lett. B297,477(1992)], [hep-ph/9207214].
- [24] A. V. Manohar and M. B. Wise, Phys. Rev. **D49**, 1310 (1994), [hep-ph/9308246].
- [25] T. Mannel, Nucl. Phys. **B413**, 396 (1994), [hep-ph/9308262].
- [26] A. F. Falk, M. E. Luke and M. J. Savage, Phys. Rev. **D49**, 3367 (1994), [hep-ph/9308288].
- [27] E. C. Poggio, H. R. Quinn and S. Weinberg, Phys. Rev. **D13**, 1958 (1976).
- [28] G. Buchalla, A. J. Buras and M. E. Lautenbacher, Rev. Mod. Phys. **68**, 1125 (1996), [hep-ph/9512380].
- [29] A. F. Falk and M. Neubert, Phys. Rev. **D47**, 2965 (1993), [hep-ph/9209268].
- [30] T. Becher, H. Boos and E. Lunghi, JHEP **12**, 062 (2007), [arXiv:0708.0855].
- [31] A. Alberti, P. Gambino and S. Nandi, JHEP **01**, 147 (2014), [arXiv:1311.7381].
- [32] T. Mannel, A. A. Pivovarov and D. Rosenthal, Phys. Lett. **B741**, 290 (2015), [arXiv:1405.5072].
- [33] T. Mannel, A. A. Pivovarov and D. Rosenthal, Phys. Rev. **D92**, 5, 054025 (2015), [arXiv:1506.08167].
- [34] T. Mannel and A. A. Pivovarov, Phys. Rev. **D100**, 9, 093001 (2019), [arXiv:1907.09187].
- [35] T. Mannel, S. Turczyk and N. Uraltsev, JHEP **11**, 109 (2010), [arXiv:1009.4622].
- [36] M. Neubert and C. T. Sachrajda, Nucl. Phys. **B483**, 339 (1997), [hep-ph/9603202].
- [37] M. Beneke, G. Buchalla and I. Dunietz, Phys. Rev. **D54**, 4419 (1996), [Erratum: Phys. Rev. D83,119902(2011)], [hep-ph/9605259].
- [38] M. Beneke *et al.*, Phys. Lett. **B459**, 631 (1999), [hep-ph/9808385].
- [39] M. Kirk, A. Lenz and T. Rauh, JHEP **12**, 068 (2017), [arXiv:1711.02100].
- [40] P. Gambino and C. Schwanda, Phys. Rev. **D89**, 1, 014022 (2014), [arXiv:1307.4551].
- [41] Y. Amhis *et al.* (HFLAV), Eur. Phys. J. **C77**, 12, 895 (2017), [arXiv:1612.07233].
- [42] P. Gambino, M. Jung and S. Schacht, Phys. Lett. **B795**, 386 (2019), [arXiv:1905.08209].
- [43] M. Neubert, Phys. Rev. **D49**, 3392 (1994), [hep-ph/9311325].
- [44] I. I. Y. Bigi *et al.*, Int. J. Mod. Phys. **A9**, 2467 (1994), [hep-ph/9312359].
- [45] G. P. Korchemsky and G. F. Sterman, Phys. Lett. **B340**, 96 (1994), [hep-ph/9407344].
- [46] C. W. Bauer, M. E. Luke and T. Mannel, Phys. Rev. **D68**, 094001 (2003), [hep-ph/0102089].
- [47] K. S. M. Lee and I. W. Stewart, Nucl. Phys. **B721**, 325 (2005), [hep-ph/0409045].
- [48] S. W. Bosch, M. Neubert and G. Paz, JHEP **11**, 073 (2004), [hep-ph/0409115].
- [49] M. Beneke *et al.*, JHEP **06**, 071 (2005), [hep-ph/0411395].
- [50] M. Benzke *et al.*, JHEP **08**, 099 (2010), [arXiv:1003.5012].
- [51] C. W. Bauer, S. Fleming and M. E. Luke, Phys. Rev. **D63**, 014006 (2000), [hep-ph/0005275].
- [52] C. W. Bauer and I. W. Stewart, Phys. Lett. **B516**, 134 (2001), [hep-ph/0107001].
- [53] C. W. Bauer, D. Pirjol and I. W. Stewart, Phys. Rev. **D65**, 054022 (2002), [hep-ph/0109045].
- [54] T. Becher, A. Broggio and A. Ferroglia, Lect. Notes Phys. **896**, pp.1 (2015), [arXiv:1410.1892].
- [55] J. Chay and C. Kim, Phys. Rev. **D65**, 114016 (2002), [hep-ph/0201197].
- [56] M. Beneke *et al.*, Nucl. Phys. **B643**, 431 (2002), [hep-ph/0206152].
- [57] C. W. Bauer *et al.*, Phys. Rev. **D66**, 014017 (2002), [hep-ph/0202088].
- [58] R. J. Hill and M. Neubert, Nucl. Phys. **B657**, 229 (2003), [hep-ph/0211018].
- [59] J. C. Collins, D. E. Soper and G. F. Sterman, Adv. Ser. Direct. High Energy Phys. **5**, 1 (1989), [hep-ph/0409313].

- [60] I. W. Stewart, F. J. Tackmann and W. J. Waalewijn, Phys. Rev. **D81**, 094035 (2010), [arXiv:0910.0467].
- [61] J. C. Collins, D. E. Soper and G. F. Sterman, Nucl. Phys. **B261**, 104 (1985).
- [62] I. Z. Rothstein and I. W. Stewart, JHEP **08**, 025 (2016), [arXiv:1601.04695].
- [63] I. A. Korchemskaya and G. P. Korchemsky, Phys. Lett. **B287**, 169 (1992).
- [64] T. Becher and M. Neubert, Eur. Phys. J. **C71**, 1665 (2011), [arXiv:1007.4005].
- [65] J.-Y. Chiu *et al.*, JHEP **05**, 084 (2012), [arXiv:1202.0814].
- [66] M. Beneke and T. Feldmann, Nucl. Phys. **B685**, 249 (2004), [hep-ph/0311335].
- [67] M. Beneke *et al.*, Phys. Rev. Lett. **83**, 1914 (1999), [hep-ph/9905312].
- [68] C. W. Bauer, D. Pirjol and I. W. Stewart, Phys. Rev. Lett. **87**, 201806 (2001), [hep-ph/0107002].
- [69] S. Mantry, D. Pirjol and I. W. Stewart, Phys. Rev. **D68**, 114009 (2003), [hep-ph/0306254].
- [70] T. Becher, R. J. Hill and M. Neubert, Phys. Rev. **D72**, 094017 (2005), [hep-ph/0503263].
- [71] S. Fleming, A. K. Leibovich and T. Mehen, Phys. Rev. **D68**, 094011 (2003), [hep-ph/0306139].
- [72] T. Becher and M. D. Schwartz, JHEP **07**, 034 (2008), [arXiv:0803.0342].
- [73] T. Becher and G. Bell, JHEP **11**, 126 (2012), [arXiv:1210.0580].
- [74] I. W. Stewart, F. J. Tackmann and W. J. Waalewijn, Phys. Rev. Lett. **105**, 092002 (2010), [arXiv:1004.2489].
- [75] J.-y. Chiu, R. Kelley and A. V. Manohar, Phys. Rev. **D78**, 073006 (2008), [arXiv:0806.1240].
- [76] T. Becher, M. Neubert and G. Xu, JHEP **07**, 030 (2008), [arXiv:0710.0680].
- [77] V. Ahrens *et al.*, Eur. Phys. J. **C62**, 333 (2009), [arXiv:0809.4283].
- [78] X. Liu, S. Mantry and F. Petriello, Phys. Rev. **D86**, 074004 (2012), [arXiv:1205.4465].
- [79] M. G. Echevarria, A. Idilbi and I. Scimemi, JHEP **07**, 002 (2012), [arXiv:1111.4996].
- [80] A. J. Larkoski, I. Moult and B. Nachman (2017), [arXiv:1709.04464].
- [81] S. Kluth, Rept. Prog. Phys. **69**, 1771 (2006), [hep-ex/0603011].
- [82] A. Gehrmann-De Ridder *et al.*, Phys. Rev. Lett. **99**, 132002 (2007), [arXiv:0707.1285].
- [83] S. Weinzierl, Phys. Rev. Lett. **101**, 162001 (2008), [arXiv:0807.3241].
- [84] R. Abbate *et al.*, Phys. Rev. **D83**, 074021 (2011), [arXiv:1006.3080].
- [85] A. H. Hoang *et al.*, Phys. Rev. **D91**, 9, 094018 (2015), [arXiv:1501.04111].
- [86] T. Becher and M. Neubert, JHEP **07**, 108 (2012), [arXiv:1205.3806].
- [87] I. W. Stewart *et al.*, Phys. Rev. **D89**, 5, 054001 (2014), [arXiv:1307.1808].
- [88] A. Banfi *et al.*, Phys. Rev. Lett. **109**, 202001 (2012), [arXiv:1206.4998].
- [89] R. Boughezal, X. Liu and F. Petriello, Phys. Rev. **D91**, 9, 094035 (2015), [arXiv:1504.02540].
- [90] J. Gaunt *et al.*, JHEP **09**, 058 (2015), [arXiv:1505.04794].
- [91] R. Boughezal *et al.*, Phys. Lett. **B748**, 5 (2015), [arXiv:1505.03893].
- [92] R. Boughezal *et al.*, Phys. Rev. Lett. **116**, 15, 152001 (2016), [arXiv:1512.01291].
- [93] J. M. Campbell, R. K. Ellis and C. Williams, JHEP **06**, 179 (2016), [arXiv:1601.00658].
- [94] J. M. Campbell *et al.*, JHEP **07**, 148 (2016), [arXiv:1603.02663].
- [95] G. Heinrich *et al.*, JHEP **03**, 142 (2018), [arXiv:1710.06294].
- [96] I. Moult *et al.*, Phys. Rev. **D95**, 7, 074023 (2017), [arXiv:1612.00450].
- [97] R. Boughezal, X. Liu and F. Petriello, JHEP **03**, 160 (2017), [arXiv:1612.02911].
- [98] S. Alioli *et al.*, JHEP **09**, 120 (2013), [arXiv:1211.7049].
- [99] S. Alioli *et al.*, Phys. Rev. **D92**, 9, 094020 (2015), [arXiv:1508.01475].
- [100] C. W. Bauer, D. Pirjol and I. W. Stewart, Phys. Rev. **D68**, 034021 (2003), [hep-ph/0303156].
- [101] D. Pirjol and I. W. Stewart, Phys. Rev. **D67**, 094005 (2003), [Erratum: Phys. Rev. **D69**, 019903 (2004)], [hep-ph/0211251].
- [102] R. J. Hill *et al.*, JHEP **07**, 081 (2004), [hep-ph/0404217].
- [103] M. Beneke and D. Yang, Nucl. Phys. **B736**, 34 (2006), [hep-ph/0508250].
- [104] I. Moult, I. W. Stewart and G. Vita, JHEP **07**, 067 (2017), [arXiv:1703.03408].
- [105] I. Feige *et al.*, JHEP **11**, 142 (2017), [arXiv:1703.03411].
- [106] M. Beneke *et al.*, JHEP **03**, 001 (2018), [arXiv:1712.04416].
- [107] S. Alte, M. König and M. Neubert, JHEP **08**, 095 (2018), [arXiv:1806.01278].
- [108] I. Moult *et al.*, JHEP **08**, 013 (2018), [arXiv:1804.04665].
- [109] M. Beneke *et al.*, JHEP **03**, 043 (2019), [arXiv:1809.10631].
- [110] M. Dasgupta and G. P. Salam, Phys. Lett. **B512**, 323 (2001), [hep-ph/0104277].
- [111] R. B. Appleby and M. H. Seymour, JHEP **12**, 063 (2002), [hep-ph/0211426].
- [112] S. Caron-Huot, JHEP **03**, 036 (2018), [arXiv:1501.03754].
- [113] A. J. Larkoski, I. Moult and D. Neill, JHEP **09**, 143 (2015), [arXiv:1501.04596].
- [114] T. Becher *et al.*, Phys. Rev. Lett. **116**, 19, 192001 (2016), [arXiv:1508.06645].
- [115] T. Becher *et al.*, JHEP **11**, 019 (2016), [Erratum: JHEP05,154(2017)], [arXiv:1605.02737].
- [116] T. Becher, B. D. Pecjak and D. Y. Shao, JHEP **12**, 018 (2016), [arXiv:1610.01608].
- [117] M. Balsiger, T. Becher and D. Y. Shao, JHEP **04**, 020 (2019), [arXiv:1901.09038].
- [118] C. W. Bauer, B. O. Lange and G. Ovanesyan, JHEP **07**, 077 (2011), [arXiv:1010.1027].
- [119] S. Fleming, Phys. Lett. **B735**, 266 (2014), [arXiv:1404.5672].
- [120] I. Moult *et al.*, JHEP **02**, 134 (2018), [arXiv:1709.09174].
- [121] A. Idilbi and A. Majumder, Phys. Rev. **D80**, 054022 (2009), [arXiv:0808.1087].
- [122] G. Ovanesyan and I. Vitev, JHEP **06**, 080 (2011), [arXiv:1103.1074].
- [123] R. J. Hill and M. P. Solon, Phys. Lett. **B707**, 539 (2012), [arXiv:1111.0016].
- [124] M. Bauer *et al.*, JHEP **01**, 099 (2015), [arXiv:1409.7392].
- [125] M. Baumgart, I. Z. Rothstein and V. Vaidya, Phys. Rev. Lett. **114**, 211301 (2015), [arXiv:1409.4415].
- [126] G. Ovanesyan, T. R. Slatyer and I. W. Stewart, Phys. Rev. Lett. **114**, 21, 211302 (2015), [arXiv:1409.8294].

17. Lattice Quantum Chromodynamics

Revised August 2019 by S. Hashimoto (KEK), J. Laiho (Syracuse U.) and S.R. Sharpe (U. Washington).

17.1	Lattice regularization of QCD	333
17.1.1	Gauge invariance, gluon fields and the gluon action	333
17.1.2	Lattice fermions	334
17.1.3	Heavy quarks on the lattice	335
17.1.4	QED on the lattice	336
17.1.5	Basic inputs for lattice calculations	336
17.1.6	Sources of systematic error	337
17.2	Methods and status	337
17.2.1	Monte-Carlo method	338
17.2.2	Two-point functions	338
17.2.3	Three-point functions	339
17.2.4	Scattering amplitudes and resonances	339
17.2.5	Recent advances	339
17.2.6	Status of LQCD simulations	340
17.3	Physics applications	340
17.3.1	Spectrum	340
17.3.2	Decay constants and bag parameters	340
17.3.3	Form factors ($K \rightarrow \pi \ell \nu$, $D \rightarrow K \ell \nu$, $B \rightarrow \pi \ell \nu$, $B \rightarrow D^{(*)} \ell \nu$)	341
17.3.4	Strong coupling constant	341
17.3.5	Quark masses	342
17.3.6	Other applications	342
17.4	Outlook	342

Many physical processes considered in the Review of Particle Properties (RPP) involve hadrons. The properties of hadrons—which are composed of quarks and gluons—are governed primarily by Quantum Chromodynamics (QCD) (with small corrections from Quantum Electrodynamics [QED]). Theoretical calculations of these properties require non-perturbative methods, and Lattice Quantum Chromodynamics (LQCD) is a tool to carry out such calculations. It has been successfully applied to many properties of hadrons. Most important for the RPP are the calculation of electroweak form factors, which are needed to extract Cabibbo-Kobayashi-Maskawa (CKM) matrix elements when combined with the corresponding experimental measurements. LQCD has also been used to determine other fundamental parameters of the standard model, in particular the strong coupling constant and quark masses, as well as to predict hadronic contributions to the anomalous magnetic moment of the muon, $g_\mu - 2$.

This review describes the theoretical foundations of LQCD and sketches the methods used to calculate the quantities relevant for the RPP. It also describes the various sources of error that must be controlled in a LQCD calculation. Results for hadronic quantities are given in the corresponding dedicated reviews.

17.1 Lattice regularization of QCD

Gauge theories form the building blocks of the Standard Model. While the SU(2) and U(1) parts have weak couplings and can be studied accurately with perturbative methods, the SU(3) component—QCD—is only amenable to a perturbative treatment at high energies. The growth of the coupling constant in the infrared—the flip-side of asymptotic freedom—requires the use of non-perturbative methods to determine the low energy properties of QCD. Lattice gauge theory, proposed by K. Wilson in 1974 [1], provides such a method, for it gives a non-perturbative definition of vector-like gauge field theories like QCD. In lattice regularized QCD—commonly called lattice QCD or LQCD—Euclidean space-time is discretized, usually on a hypercubic lattice with lattice spacing a , with quark fields placed on sites and gauge fields on the links between sites. The lattice spacing plays the role of the ultraviolet regulator, rendering the quantum field theory finite. The continuum theory is recovered by taking the limit of vanishing lattice spacing, which can be reached by tuning the bare coupling constant to zero according to the renormalization group.

Unlike dimensional regularization, which is commonly used in continuum QCD calculations, the definition of LQCD does not

rely on the perturbative expansion. Indeed, LQCD allows non-perturbative calculations by numerical evaluation of the path integral that defines the theory.

Practical LQCD calculations are limited by the availability of computational resources and the efficiency of algorithms. Because of this, LQCD results come with both statistical and systematic errors, the former arising from the use of Monte-Carlo integration, the latter, for example, from the use of non-zero values of a . There are also different ways in which the QCD action can be discretized, and all must give consistent results in the continuum limit, $a \rightarrow 0$. It is the purpose of this review to provide an outline of the methods of LQCD, with particular focus on applications to particle physics, and an overview of the various sources of error. This should allow the reader to better understand the LQCD results that are presented in other reviews, primarily those on “Quark Masses,” “Quantum Chromodynamics,” “CKM quark-mixing matrix,” “ V_{ud} , V_{us} , Cabibbo angle and CKM Unitarity,” “Leptonic Decays of Charged Pseudoscalar Mesons,” “ $B^0 - \bar{B}^0$ Mixing,” and “Semileptonic b -Hadron Decays, Determination of V_{cb} and V_{ub} .” For more extensive explanations the reader should consult the available textbooks or lecture notes, the most up-to-date of which are Refs. [2–4].

17.1.1 Gauge invariance, gluon fields and the gluon action

A key feature of the lattice formulation of QCD is that it preserves gauge invariance. This is in contrast to perturbative calculations, where gauge fixing is an essential step. The preservation of gauge invariance leads to considerable simplifications, e.g. restricting the form of operators that can mix under renormalization.

The gauge transformations of lattice quark fields are just as in the continuum: $q(x) \rightarrow V(x)q(x)$ and $\bar{q}(x) \rightarrow \bar{q}(x)V^\dagger(x)$, with $V(x)$ an arbitrary element of SU(3). The only difference is that the Euclidean space-time positions x are restricted to lie on the sites of the lattice, i.e. $x = a(n_1, n_2, n_3, n_4)$ for a hypercubic lattice, with the n_j being integers. Quark bilinears involving different lattice points can be made gauge invariant by introducing the gluon field $U_\mu(x)$. For example, for adjacent points the bilinear is $\bar{q}(x)U_\mu(x)q(x+a\hat{\mu})$, with $\hat{\mu}$ the unit vector in the μ 'th direction. (This form is used in the construction of the lattice covariant derivative.) This is illustrated in Fig. 17.1. The gluon field (or “gauge link”) is an element of the group, SU(3), in contrast to the continuum field A_μ which takes values in the Lie algebra. The bilinear is invariant if U_μ transforms as $U_\mu(x) \rightarrow V(x)U_\mu(x)V^\dagger(x+a\hat{\mu})$. The lattice gluon field is naturally associated with the link joining x and $x+a\hat{\mu}$, and corresponds in the continuum to a Wilson line connecting these two points, $P \exp(i \int_x^{x+a\hat{\mu}} dx_\mu A_\mu^{\text{cont}}(x))$ (where P indicates a path-ordered integral, and the superscript on A_μ indicates that it is a continuum field). The trace of a product of the $U_\mu(x)$ around any closed loop is easily seen to be gauge invariant and is the lattice version of a Wilson loop.

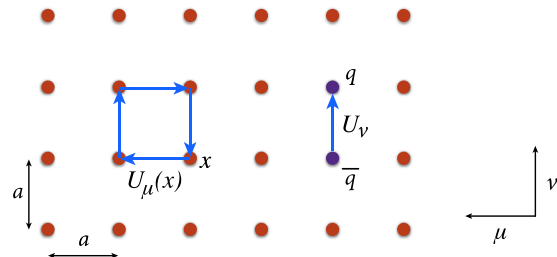


Figure 17.1: Sketch of a two-dimensional slice through the $\mu - \nu$ plane of a lattice, showing gluon fields lying on links and forming either the plaquette product appearing in the gauge action or a component of the covariant derivative connecting quark and antiquark fields.

The simplest possible gauge action, usually called the Wilson gauge action, is given by the product of gauge links around elementary plaquettes:

$$S_g = \beta \sum_{x,\mu,\nu} \left[1 - \frac{1}{3} \text{ReTr}[U_\mu(x)U_\nu(x+a\hat{\mu})U_\mu^\dagger(x+a\hat{\nu})U_\nu^\dagger(x)] \right]. \quad (17.1)$$

This is illustrated in Fig. 17.1. For small a , assuming that the fields are slowly varying, one can expand the action in powers of a using $U_\mu(x) = \exp(iaA_\mu(x))$. Keeping only the leading non-vanishing term, and replacing the sum with an integral, one finds the continuum form,

$$S_g \longrightarrow \int d^4x \frac{1}{4g_{\text{lat}}^2} \text{Tr}[F_{\mu\nu}^2(x)], \quad (F_{\mu\nu} = \partial_\mu A_\nu - \partial_\nu A_\mu + i[A_\mu, A_\nu]) \quad (17.2)$$

as long as one chooses $\beta = 6/g_{\text{lat}}^2$ for the lattice coupling. In this expression, g_{lat} is the bare coupling constant in the lattice scheme, which can be related (by combining continuum and lattice perturbation theory) to a more conventional coupling constant such as that in the $\overline{\text{MS}}$ scheme (see Sec. 17.3.4 below).

In practice, the lattice spacing a is non-zero, leading to discretization errors. In particular, the lattice breaks Euclidean rotational invariance (which is the Euclidean version of Lorentz invariance) down to a discrete hypercubic subgroup. One wants to reduce discretization errors as much as possible. A very useful tool for understanding and then reducing discretization errors is the Symanzik effective action: the interactions of quarks and gluons with momenta low compared to the lattice cutoff ($|p| \ll 1/a$) are described by a continuum action consisting of the standard continuum terms (e.g. the gauge action given in Eq. (17.2)) augmented by higher dimensional operators suppressed by powers of a [5]. For the Wilson lattice gauge action, the leading corrections come in at $\mathcal{O}(a^2)$. They take the form $\sum_j a^2 c_j \mathcal{O}_6^{(j)}$, with the sum running over all dimension-six operators $\mathcal{O}_6^{(j)}$ allowed by the lattice symmetries, and c_j unknown coefficients. Some of these operators violate Euclidean rotational invariance, and all of them lead to discretization errors of the form $a^2 \Lambda^2$, where Λ is a typical momentum scale for the quantity being calculated. These errors can, however, be reduced by adding corresponding operators to the lattice action and tuning their coefficients to eliminate the dimension-six operators in the effective action to a given order in perturbation theory or even non-perturbatively. This is the idea of the Symanzik improvement program [5]. In the case of the gauge action, one adds Wilson loops involving six gauge links (as opposed to the four links needed for the original plaquette action, Eq. (17.1)) to define the $\mathcal{O}(a^2)$ improved (or ‘‘Symanzik’’) action [6]. In practical implementations, the improvement is either at tree-level (so that residual errors are proportional to $\alpha_s a^2$, where the coupling is evaluated at a scale $\sim 1/a$), or at one loop order (errors proportional to $\alpha_s^2 a^2$). Another popular choice is motivated by studies of renormalization group (RG) flow. It has the same terms as the $\mathcal{O}(a^2)$ improved action but with different coefficients, and is called the RG-improved or ‘‘Iwasaki’’ action [7].

17.1.2 Lattice fermions

Discretizing the fermion action turns out to involve subtle issues, and the range of actions being used is more extensive than for gauge fields. Recall that the continuum fermion action is $S_f = \int d^4x \bar{q}[iD_\mu \gamma_\mu + m_q]q$, where $D_\mu = \partial_\mu + iA_\mu$ is the gauge-covariant derivative. The simplest discretization replaces the derivative with a symmetric difference:

$$D_\mu q(x) \longrightarrow \frac{1}{2a} [U_\mu(x)q(x+a\hat{\mu}) - U_\mu(x-a\hat{\mu})^\dagger q(x-a\hat{\mu})]. \quad (17.3)$$

The factors of U_μ ensure that $D_\mu q(x)$ transforms under gauge transformations in the same way as $q(x)$, so that the discretized version of $\bar{q}(x)D_\mu \gamma_\mu q(x)$ is gauge invariant. The choice in Eq. (17.3) leads to the so-called naive fermion action. This, however, suffers from the fermion doubling problem—in d dimensions it describes 2^d equivalent fermion fields in the continuum limit. The appearance of the extra ‘‘doubler’’ fermions is related to the deeper theoretical problem of formulating chirally symmetric fermions on the lattice. This is encapsulated by the Nielsen-Ninomiya theorem [8]: one cannot define lattice fermions having

exact, continuum-like chiral symmetry without producing doublers. Naive lattice fermions do have chiral symmetry but at the cost of introducing 15 unwanted doublers (for $d = 4$).

There are a number of different strategies for dealing with the doubling problem, each with their own theoretical and computational advantages and disadvantages. Wilson fermions [1] add a term proportional to $a\bar{q}\Delta q$ to the fermion action (the ‘‘Wilson term’’—in which Δ is a covariant lattice Laplacian). This gives a mass of $\mathcal{O}(1/a)$ to the doublers, so that they decouple in the continuum limit. The Wilson term, however, violates chiral symmetry, and also introduces discretization errors linear in a . A commonly used variant that eliminates the $\mathcal{O}(a)$ discretization error is the $\mathcal{O}(a)$ -improved Wilson (or ‘‘clover’’) fermion [9]. In this application of Symanzik improvement, methods have been developed to remove $\mathcal{O}(a)$ terms non-perturbatively using auxiliary simulations to tune parameters [10]. Such ‘‘non-perturbative improvement’’ is of great practical importance as it brings the discretization error from the fermion action down to the same level as that from the gauge action.

The advantages of Wilson fermions are their theoretical simplicity and relatively low computational cost. Their main disadvantage is the lack of chiral symmetry, which makes them difficult to use in cases where mixing with wrong chirality operators can occur, particularly if this involves divergences proportional to powers of $1/a$. A related problem is the presence of potential numerical instabilities due to spurious near-zero modes of the lattice Dirac operator. There are, however, studies that successfully ameliorate these problems and increase the range of quantities for which Wilson fermions can be used (see, e.g., Refs. [11–14]).

Twisted-mass fermions [15] are a variant of Wilson fermions in which two flavors are treated together with an isospin-breaking mass term (the ‘‘twisted mass’’ term). The main advantage of this approach is that all errors linear in a are automatically removed (without the need for tuning of parameters) by a clever choice of twisted mass and operators [16]. A disadvantage is the presence of isospin breaking effects (such as a splitting between charged and neutral pion masses even when up and down quarks are degenerate), which, however, vanish as $a^2 \Lambda^2$ in the continuum limit. Strange and charm quarks can be added as a second pair, with a term added to split their masses [17, 18].

Staggered fermions are a reduced version of naive fermions in which there is only a single fermion Dirac component on each lattice site, with the full Dirac structure built up from neighboring sites [19]. They have the advantages of being somewhat faster to simulate than Wilson-like fermions, of preserving some chiral symmetry, and of having discretization errors of $\mathcal{O}(a^2)$. Their disadvantage is that they retain some of the doublers (3 for $d = 4$). The action thus describes four degenerate fermions in the continuum limit. These are usually called ‘‘tastes’’, to distinguish them from physical flavors, and the corresponding $\text{SU}(4)$ symmetry is referred to as the ‘‘taste symmetry’’. The preserved chiral symmetry in this formulation has non-singlet taste. Practical applications usually introduce one staggered fermion for each physical flavor, and remove contributions from the unwanted tastes by taking the fourth-root of the fermion determinant appearing in the path integral. The validity of this ‘‘rooting’’ procedure is not obvious because taste symmetry is violated for non-zero lattice spacing. Theoretical arguments, supported by numerical evidence, suggest that the procedure is valid as long as one takes the continuum limit before approaching the light quark mass region [20]. Additional issues arise for the valence quarks (those appearing in quark propagators, as described in Sec. 17.2 below), where rooting is not possible, and one must ignore the extra tastes, or account for them by dividing by appropriate factors of four [21].

Just as for Wilson fermions, the staggered action can be improved, so as to reduce discretization errors. The Asqtad (a -squared tadpole improved) action [22] was used until recently in many large scale simulations [23]. More recent calculations use the HISQ (highly improved staggered quark) action, introduced in Ref. [24]. At tree-level it removes both $\mathcal{O}(a^2)$ errors and, to lowest order in the quark speed v/c , $\mathcal{O}([am]^4)$ errors. It also substantially reduces effects caused by taste-symmetry breaking. This makes it attractive not only for light quarks, but means that it is

also quite accurate for heavy quarks because it suppresses $(am)^n$ errors. It is being used to directly simulate charm quarks and to approach direct simulations of bottom quarks (see, e.g. [25, 26]).

There is an important class of lattice fermions, “Ginsparg-Wilson fermions,” that possess a continuum-like chiral symmetry without introducing unwanted doublers. The lattice Dirac operator D for these fermions satisfies the Ginsparg-Wilson relation $D\gamma_5 + \gamma_5 D = aD\gamma_5 D$ [27]. In the continuum, the right-hand-side vanishes, leading to chiral symmetry. On the lattice, it is non-vanishing, but with a particular form (with two factors of D) that restricts the violations of chiral symmetry in Ward-Takahashi identities to short-distance terms that do not contribute to physical matrix elements [28]. In fact, one can define a modified chiral transformation on the lattice (by including dependence on the gauge fields) such that Ginsparg-Wilson fermions have an exact chiral symmetry for on-shell quantities [29]. The net result is that such fermions essentially have the same properties under chiral transformations as do continuum fermions, including the index theorem [28]. Their leading discretization errors are of $\mathcal{O}(a^2)$.

Two types of Ginsparg-Wilson fermions are currently being used in large-scale numerical simulations. The first is Domain-wall fermions (DWF). These are defined on a five-dimensional space, in which the fifth dimension is fictitious [30]. The action is chosen so that the low-lying modes are chiral, with left- and right-handed modes localized on opposite four-dimensional surfaces. For an infinite fifth dimension, these fermions satisfy the Ginsparg-Wilson relation. In practice, the fifth dimension is kept finite, and there remains a small, controllable violation of chiral symmetry. The second type is Overlap fermions. These appeared from a completely different context and have an explicit form that exactly satisfies the Ginsparg-Wilson relation [31]. Their numerical implementation requires an approximation of the matrix sign function of a Wilson-like fermion operator, and various approaches are being used. In fact, it is possible to rewrite these approximations in terms of a five-dimensional formulation, showing that the DWF and Overlap approaches are essentially equivalent [32, 33]. Numerically, the five-dimensional approach appears to be more computationally efficient.

The various lattice fermion formulations are often combined with the technique of link smearing. Here one couples the fermions to a smoother gauge link, defined by averaging with adjacent links in a gauge invariant manner. Several closely related implementations are being used. All reduce the coupling of fermions to the short-distance fluctuations in the gauge field, leading to an improvement in the numerical stability and speed of algorithms. One cannot perform this smearing too aggressively, however, since the smearing may distort short distance physics and enhance discretization errors.

As noted above, each fermion formulation has its own advantages and disadvantages. For instance, domain-wall and overlap fermions are theoretically preferred as they have chiral symmetry without doublers, but their computational cost is greater than for other choices. If the physics application of interest and the target precision do not require near-exact chiral symmetry, there is no strong motivation to use these expensive formulations. On the other hand, there is a class of applications (including the calculation of the $\Delta I = 1/2$ amplitude for $K \rightarrow \pi\pi$ decays and the S-parameter [34]) where chiral symmetry plays an essential role and for which the use of Ginsparg-Wilson fermions is strongly favored.

17.1.3 Heavy quarks on the lattice

The fermion formulations described in the previous subsection can be used straightforwardly only for quarks whose masses are small compared to the lattice cutoff, $m_q \lesssim 1/a$. This is because there are discretization errors proportional to powers of am_q , and if $am_q \gtrsim 1$ these errors are large and uncontrolled. Present LQCD simulations typically have cutoffs in the range of $1/a = 2 - 4$ GeV (corresponding to $a \approx 0.1 - 0.05$ fm). Thus, while for the up, down and strange quarks one has $am_q \ll 1$, for bottom quarks (with $m_b \approx 4.5$ GeV) one must use alternative approaches. Charm quarks ($m_c \approx 1.5$ GeV) are an intermediate case, allowing simulations using both direct and alternative approaches.

For the charm quark, the straightforward approach is to simul-

aneously reduce the lattice spacing and to improve the fermion action so as to reduce the size of errors proportional to powers of am_c . This approach has been followed successfully using the HISQ, twisted-mass and domain-wall actions [24–26, 35, 36]. It is important to note, however, that reducing a increases the computational cost because an increased number of lattice points are needed for the same physical volume. One cannot reduce the spatial size below $2 - 3$ fm without introducing finite volume errors. Present lattices have typical sizes of $\sim 64^3 \times 128$ (with the long direction being Euclidean time), and thus allow a lattice cutoff up to $1/a \sim 4$ GeV.

This approach can, to some extent, be extended to the bottom quark, by the use of simulations with small lattice spacings [37]. This has been pursued with the HISQ action, using lattices of size up to $144^3 \times 288$ and lattice spacings down to $a \approx 0.03$ fm ($1/a \approx 6.6$ GeV) [38]. Extrapolation in m_b is still needed [39], however, and this makes use of the mass dependence predicted by Heavy Quark Effective Theory (HQET).

Alternative approaches for discretizing heavy quarks are motivated by effective field theories. For a bottom quark in heavy-light hadrons, one can use HQET to expand about the infinite quark-mass limit. In this limit, the bottom quark is a static color source, and one can straightforwardly write the corresponding lattice action [40]. Corrections, proportional to powers of $1/m_b$, can be introduced as operator insertions, with coefficients that can be determined non-perturbatively using existing techniques [41]. This method allows the continuum limit to be taken controlling all $1/m_b$ corrections.

Another way of introducing the $1/m_b$ corrections is to include the relevant terms in the effective action. This leads to a non-relativistic QCD (NRQCD) action, in which the heavy quark is described by a two-component spinor [42]. This approach has the advantage over HQET that it can also be used for heavy-heavy systems, such as the Upsilon states. Moreover, the bottom quark can be treated without any extrapolation in m_b . A disadvantage is that some of the parameters in this effective theory are determined perturbatively (originally at tree-level, but more recently at one-loop [43]), which limits the precision of the final results. Although discretization effects can be controlled with good numerical precision for a range of lattice spacings, these artifacts cannot be extrapolated away by taking the lattice spacing to zero. This is because NRQCD is a nonrelativistic effective field theory and so ceases to work when the cutoff π/a becomes much larger than the heavy-quark mass. In practice these effects are accounted for in the error budget.

This problem can be avoided if one uses HQET power counting to analyze and reduce discretization effects for heavy quarks while using conventional fermion actions [44]. For instance, one can tune the parameters of an improved Wilson quark action so that the leading HQET corrections to the static quark limit are correctly accounted for. As the lattice spacing becomes finer, the action smoothly goes over to that of a light Wilson quark action, where the continuum limit can be taken as usual. In principle, one can improve the action in the heavy quark regime up to arbitrarily high orders using HQET, but so far large-scale simulations have typically used clover improved Wilson quarks, where tuning the parameters of the action corresponds to including all corrections through next-to-leading order in HQET. Three different methods for tuning the parameters of the clover action are being used: the Fermilab [44], Tsukuba [45] and Columbia [46] approaches. An advantage of this HQET approach is that the c and b quarks can be treated on the same footing. Parameter tuning has typically been done perturbatively, as in NRQCD, but recent work using the Columbia approach has used non-perturbative tuning of some of the parameters [47, 48]. One can improve the effective theory including the terms beyond the next-to-leading order. The Oktay-Kronfeld action that includes dimension-six and -seven operators has been constructed [49] and recently used in large-scale numerical calculations [50].

Another approach is the “ratio method” introduced in Ref. [51]. Here one uses quarks with masses lying at, or slightly above, the charm mass m_c , which can be simulated with a relativistic action, and extrapolates to m_b incorporating the behavior predicted by

HQET. The particular implementation relies on the use of ratios. As an example, consider the B meson decay constant f_B . According to HQET, this scales as $1/\sqrt{m_B}$ for $m_B \gg \Lambda_{\text{QCD}}$, up to a logarithmic dependence that is calculable in perturbative QCD (but will be suppressed in the following). Here m_B is the B meson mass, which differs from m_b by $\sim \Lambda_{\text{QCD}}$. One considers the ratio $y(\lambda, m_{b'}) \equiv f_B'' \sqrt{m_{B'}}/f_{B'} \sqrt{m_{B'}}$ for fictitious B mesons containing b quarks with unphysical masses $m_{b'}$ and $m_{b'} = \lambda m_b$. HQET implies that $y(\lambda, m_{b'})$ approaches unity for large $m_{b'}$ and any fixed $\lambda > 1$. The ratios are evaluated on the lattice for the sequence of masses $m_{b'} = m_c, \lambda m_c, \lambda^2 m_c$, all well below the physical m_b , and for each the continuum limit is taken. The form of the ratio for larger values of $m_{b'}$ is obtained by fitting, incorporating the constraints implied by HQET. The result for $f_B \sqrt{m_B}$ is then obtained as a product of y 's with $f_D \sqrt{m_D}$.

17.1.4 QED on the lattice

Quarks in nature are electrically charged, and the resultant coupling to photons leads to shifts in the properties of hadrons that are generically of $\mathcal{O}(\alpha_{\text{EM}})$. Thus, for example, the proton mass is increased by ~ 1 MeV relative to that of the neutron due to its overall charge although this effect is more than compensated for by the ~ 2.5 MeV relative decrease due to the up quark being lighter than the down quark [52]. This example shows that once pure QCD, isospin-symmetric lattice calculations reach percent level accuracy, further improvement requires the inclusion of effects due to both electromagnetism and the up-down mass difference. This level of accuracy has in fact been obtained for various quantities, e.g. light hadron masses and decay constants (see Ref. [53]), and simulations including QED in addition to QCD are becoming more common.

The extension of lattice methods to include QED is straightforward, although some new subtleties arise. The essential change is that the quark must now propagate through a background field containing both gluons and photons. The gauge field U_μ that appears in the covariant derivative of Eq. (17.3) is extended from an SU(3) matrix to one living in U(3): $U_\mu \rightarrow U_\mu e^{iaq_e A_\mu^{\text{EM}}}$. Here A_μ^{EM} is the photon field, e the electromagnetic coupling, and q the charge of the quark, e.g. $q = 2/3$ for up and $-1/3$ for down and strange quarks. The lattice action for the photon that is typically used is a discretized version of the continuum action Eq. (17.2), rather than the form used for the gluons, Eq. (17.1). This “non-compact” action has the advantage that it is quadratic in A_μ^{EM} , which simplifies the QED part of the generation of configurations.

One subtlety that arises is that Gauss’ law forbids a charged particle in a box with periodic boundary conditions. This finite volume effect can be overcome by including a uniform background charge, and this can be shown to be equivalent to removing the zero-momentum mode from the photon field. This is an example of the enhanced finite-volume effects that arise in the presence of the massless photon.

Simulations including QED have progressed over the last few years, and now a full inclusion of QED has been achieved with almost physical quark masses [52, 54]. Alternative approaches have also been used: reweighting the QCD fields *a posteriori* [55, 56], and keeping only the linear term in an expansion in α_{EM} about the QCD only case [57]. In addition, some calculations have included QED effects for the valence quarks but not the sea quarks (the “electroquenched approximation”)—for a recent example see Ref. [58].

The QED corrections to processes including leptons, such as the leptonic and semileptonic decays of hadrons, involve additional diagrams in which a photon propagator bridges between a hadron and a lepton. Such diagrams induce infrared divergences that cancel against soft photon radiation (Bloch-Nordsieck theorem [59]). Methods have been developed to implement this cancellation in lattice calculations, treating the soft photon analytically [60], with first results reported recently for leptonic pion and kaon decays [61, 62].

17.1.5 Basic inputs for lattice calculations

Since LQCD is nothing but a regularization of QCD, the renormalizability of QCD implies that the number of input parameters in LQCD is the same as for continuum QCD—the strong coupling

constant $\alpha_s = g^2/(4\pi)$, the quark masses for each flavor, and the CP violating phase θ . The θ parameter is usually assumed to be zero, while the other parameters must be determined using experimental inputs.

17.1.5.1 Lattice spacing

In QCD, the coupling constant is a function of scale. With lattice regularization, this scale is the inverse lattice spacing $1/a$, and choosing the bare coupling constant is equivalent to fixing the lattice spacing.

In principle, a can be determined using any dimensionful quantity measured by experiments. For example, using the mass of hadron H one has $a = (am_H)^{\text{lat}}/m_H^{\text{exp}}$. One chooses quantities that can be calculated accurately on the lattice, and that are only weakly dependent on the light quark masses. The latter property minimizes errors from extrapolating or interpolating to the physical light quark masses or from mistuning of these masses.

Commonly used choices are the spin-averaged 1S-1P or 1S-2S splittings in the Upsilon system, the mass of the Ω^- baryon, and the pion decay constant f_π . Ultimately, all choices must give consistent results for a , and that this is the case provides a highly non-trivial check of both the calculational method and of QCD.

17.1.5.2 Light quark masses

In LQCD simulations, the up, down and strange quarks are usually referred to as the light quarks, in the sense that $m_q < \Lambda_{\text{QCD}}$. (The standard definition of Λ_{QCD} is given in the “Quantum Chromodynamics” review; in this review we are using it only to indicate the approximate non-perturbative scale of QCD.) This condition is stronger than that used above to distinguish quarks with small discretization errors, $m_q < 1/a$. Loop effects from light quarks must be included in the simulations to accurately represent QCD. At present, most simulations are done in the isospin symmetric limit $m_u = m_d \equiv m_\ell < m_s$, and are often referred to as “ $N_f = 2 + 1$ ” simulations. Increasingly, simulations also include loops of charm quarks (denoted $N_f = 2 + 1 + 1$ simulations), although the effect of charmed sea quarks on low-energy physics is generically expected to be at the sub-percent level [63–66]. Precision is now reaching the point where isospin breaking effects must be included. To do so without approximation requires simulating with nondegenerate up and down quarks (leading to $N_f = 1 + 1 + 1$ or $1 + 1 + 1 + 1$ simulations) as well as including electromagnetism (as described above). This has been done in Ref. [52]. Alternatively, one can use a perturbative approach, expanding about the isospin symmetric theory and working to linear order in α_{EM} and $m_u - m_d$ [57, 67].

We now describe the tuning of m_ℓ , m_s and m_c to their physical values. (For brevity, we ignore isospin violation in the following discussion.) The most commonly used quantities for these tunings are, respectively, m_π , m_K and m_{η_c} . If the scale is being set by m_Ω , then one adjusts the lattice quark masses until the ratios m_π/m_Ω , m_K/m_Ω and m_{η_c}/m_Ω take their physical values. In the past, most calculations needed to extrapolate to the physical value of m_ℓ (typically using forms based on chiral perturbation theory [ChPT]), while simulating directly at or near to the physical values of m_s and m_c . Present calculations are increasingly done with physical or near physical values of m_ℓ , requiring at most only a short extrapolation.

17.1.5.3 Heavy quark masses

The b quark is usually treated only as a valence quark, with no loop effects included. The errors introduced by this approximation can be estimated to be $\sim \alpha_s(m_b) \Lambda_{\text{QCD}}^2/m_b^2$ and are likely to be very small. In the past, the same approximation has been made for the c quark, leading to errors $\sim \alpha_s(m_c) \Lambda_{\text{QCD}}^2/m_c^2$. (See Ref. [63] for a quantitative estimate of the effects of including the charm quark on some low energy physical quantities, and Ref. [68] for similar estimates for B -meson matrix elements.) For high precision, however, dynamical charm quarks are necessary, and some of the most recent simulations now include them.

The b quark mass can be tuned by setting heavy-heavy (\mathcal{Y}) or heavy-light (B) meson masses to their experimental values. Consistency between these two determinations provides an important check that the determination of parameters in the heavy quark lat-

tice formulations is being done correctly (see, e.g., Ref. [37,69,70])

17.1.6 Sources of systematic error

Lattice results have statistical and systematic errors that must be quantified for any calculation in order for the result to be a useful input to phenomenology. The statistical error is due to the use of Monte Carlo importance sampling to evaluate the path integral (a method discussed below). There are, in addition, a number of systematic errors that are always present to some degree in lattice calculations, although the size of any given error depends on the particular quantity under consideration and the parameters of the ensembles being used. The most common lattice errors are reviewed below.

Although not strictly a systematic error, it is important to note that the presence of long autocorrelations in the sequence of lattice configurations generated by the Monte Carlo method can lead to underestimates of statistical errors [71]. It is known that the global topological charge of the gauge fields decorrelates very slowly with certain algorithms [71,72]. The effect of poorly sampling topological charge is expected to be most significant for the pion mass and related quantities [73,74]. This issue becomes more relevant as the precision of the final results increases.

17.1.6.1 Continuum limit

Physical results are obtained in the limit that the lattice spacing a goes to zero. The Symanzik effective theory determines the scaling of lattice artefacts with a . Most lattice calculations use improved actions with leading discretization errors of $\mathcal{O}(a^2\Lambda^2)$, $\mathcal{O}(\alpha_s a^2\Lambda^2)$, or $\mathcal{O}(\alpha_s a\Lambda)$, where Λ is a typical momentum scale in the system. Knowledge of the scaling of the leading discretization errors allows controlled extrapolation to $a = 0$ when multiple lattice spacings are available, as in current state-of-the-art calculations. Residual errors arise from the exclusion of subleading a dependence from the fits.

For many quantities the typical momentum scale in the system is $\sim \Lambda_{\text{QCD}} \approx 300$ MeV. Discretization errors are expected to be larger for quantities involving larger scales, for example form factors or decays involving particles with momenta larger than Λ_{QCD} .

17.1.6.2 Infinite volume limit

LQCD calculations are necessarily carried out in finite space-time boxes, leading to departures of physical quantities (masses, decay constants, etc.) from their measured, infinite volume values. These finite-volume shifts are an important systematic that must be estimated and minimized.

Typical lattices are asymmetric, with N_s points in the three spatial directions and N_t in the (Euclidean) temporal direction. The spatial and temporal sizes in physical units are thus $L_s = aN_s$ and $L_t = aN_t$, respectively. (Anisotropic lattice spacings are also sometimes used, as discussed below in Sec. 17.2.2.) Typically, $L_t \geq 2L_s$, a longer temporal direction being used to allow excited-state contributions to correlators to decay. This means that the dominant impact of using finite volume is from the presence of a finite spatial box.

High-precision LQCD calculations are of quantities involving no more than a single particle in initial and final states (with the exception of the $K \rightarrow \pi\pi$ decay amplitudes). For such quantities, once the volume exceeds about 2 fm (so that the particle is not “squeezed”), the dominant finite-volume effect comes from virtual pions wrapping around the lattice in the spatial directions. This effect is exponentially suppressed as the volume becomes large, roughly as $\sim \exp(-m_\pi L_s)$, and has been estimated using ChPT [75] or other methods [76]. The estimates suggest that finite volume shifts are sub-percent effects when $m_\pi L_s \gtrsim 4$, and most large-scale simulations use lattices satisfying this condition. This becomes challenging as one approaches the physical pion mass, for which $L_s \gtrsim 5$ fm is required.

Finite volume errors are usually determined by repeating the simulations on two or more different volumes (with other parameters fixed). If different volumes are not available, the ChPT estimate can be used, often inflated to account for the fact that the ChPT calculation is truncated at some order.

In the future, LQCD calculations involving more than a single hadron will become increasingly precise. Examples include

the calculation of resonance parameters and the above-mentioned $K \rightarrow \pi\pi$ amplitudes. Finite volume effects are much larger in these cases, with power-law terms (e.g. $1/L_s^3$) in addition to exponential dependence. Indeed, as will be discussed in Sec. 17.2.4, one can use the volume dependence to indirectly extract infinite-volume quantities such as scattering lengths. Doing so, however, requires a set of lattice volumes satisfying $m_\pi L_s \gtrsim 4$ and is thus more challenging than for single-particle quantities.

17.1.6.3 Chiral extrapolation

Until recently, an important source of systematic error in LQCD calculations was the need to extrapolate in m_u and m_d (or, equivalently, in m_π). This extrapolation was usually done using functional forms based on ChPT, or with analytic functions, with the difference between different fits used as an estimate of the systematic error, which was often substantial. Increasingly, however, calculations work directly at, or very close to, the physical quark masses. This either removes entirely, or greatly reduces, the uncertainties in the extrapolation, such that this error is subdominant.

17.1.6.4 Operator matching

Many of the quantities that LQCD can precisely calculate involve hadronic matrix elements of operators from the electroweak Hamiltonian. Examples include the pion and kaon decay constants, semileptonic form factors and the kaon mixing parameter B_K (the latter defined in Eq. (17.13)). The operators in the lattice matrix elements are defined in the lattice regularization scheme. To be used in tests of the Standard Model, however, they must be matched to the continuum regularization scheme in which the corresponding Wilson coefficients have been calculated. The only case in which such matching is not needed is if the operator is a conserved or partially conserved current. Similar matching is also needed for the conversion of lattice bare quark masses to those in the continuum $\overline{\text{MS}}$ scheme.

Several methods are used to calculate the matching factors: perturbation theory (usually to one- or two-loop order), non-perturbative renormalization (NPR) using Landau-gauge quark and gluon external states [77], NPR using gauge-invariant methods based on the Schrödinger functional [78], NPR using gauge-invariant short-distance hadron correlators [79], and NPR using gauge-invariant heavy-heavy correlators [26,80]. The NPR methods replace truncation errors (which can only be approximately estimated) by statistical and systematic errors that can be determined reliably and systematically reduced.

An issue that arises in some of such calculations (e.g. for quark masses and B_K) is that, using NPR with Landau-gauge quark and gluon external states, one ends up with operators regularized in a MOM-like scheme (or a Schrödinger-functional scheme), rather than the $\overline{\text{MS}}$ scheme mostly used for calculating the Wilson coefficients. To make contact with this scheme requires a purely continuum perturbative matching calculation. The resultant truncation error can, however, be minimized by pushing up the momentum scale at which the matching is done using step-scaling techniques as part of the NPR calculation [81]. It should also be noted that this final step in the conversion to the $\overline{\text{MS}}$ scheme could be avoided if continuum calculations used a MOM-like scheme or if one imposes a renormalization condition for quantities that are calculable both in the $\overline{\text{MS}}$ scheme and in LQCD, such as the hadron correlators at short distances (see, e.g., Ref. [82]).

17.2 Methods and status

Once the lattice action is chosen, it is straightforward to define the quantum theory using the path integral formulation. The Euclidean-space partition function is

$$Z = \int [dU] \prod_f [dq_f][d\bar{q}_f] e^{-S_g[U] - \sum_f \bar{q}_f (D[U] + m_f) q_f}, \quad (17.4)$$

where link variables are integrated over the SU(3) manifold, q_f and \bar{q}_f are Grassmann (anticommuting) quark and antiquark fields of flavor f , and $D[U]$ is the chosen lattice Dirac operator with m_f the quark mass in lattice units. Integrating out the quark

and antiquark fields, one arrives at a form suitable for simulation:

$$Z = \int [dU] e^{-S_g[U]} \prod_f \det(D[U] + m_f). \quad (17.5)$$

$$\langle \mathcal{O}(U, q, \bar{q}) \rangle = (1/Z) \int [dU] \prod_f [dq_f][d\bar{q}_f] \mathcal{O}(U, q, \bar{q}) e^{-S_g[U] - \sum_f \bar{q}_f (D[U] + m_f) q_f}. \quad (17.6)$$

If the operators depend on the (anti-)quark fields q_f and \bar{q}_f , then integrating these fields out leads not only to the fermion determinant but also, through Wick's theorem, to a series of quark "propagators", $(D[U] + m_f)^{-1}$, connecting the positions of the fields.

This set-up allows one to choose, by hand, the masses of the quarks in the determinant (the sea quarks) differently from those in the propagators (valence quarks). This is called "partial quenching", and is used by some calculations as a way of obtaining more data points from which to extrapolate both sea and valence quarks to their physical values.

17.2.1 Monte-Carlo method

Since the number of integration variables U is huge ($N_s^3 \times N_t \times 4 \times 9$), direct numerical integration is impractical and one has to use Monte-Carlo techniques. In this method, one generates a Markov chain of gauge configurations (a "configuration" being the set of U 's on all links) distributed according to the probability measure $[dU] e^{-S_g[U]} \prod_f \det(D[U] + m_f)$. Once the configurations are generated, expectation values $\langle \mathcal{O}(U, q, \bar{q}) \rangle$ are calculated by averaging over those configurations. In this way the configurations can be used repeatedly for many different calculations, and there are several large collections of ensembles of configurations (with a range of values of a , lattice sizes and quark masses) that are publicly available through the International Lattice Data Grid (ILDG). As the number of the configurations, N , is increased, the error decreases as $1/\sqrt{N}$.

The most challenging part of the generation of gauge configurations is the need to include the fermion determinant. Direct evaluation of the determinant is not feasible, as it requires $\mathcal{O}((N_s^3 \times N_t)^3)$ computations. Instead, one rewrites it in terms of "pseudofermion" fields ϕ (auxiliary fermion fields with bosonic statistics). For example, for two degenerate quarks one has

$$\det(D[U] + m_f)^2 = \int [d\phi] e^{-\phi^\dagger (D[U] + m_f)^{-2} \phi}. \quad (17.7)$$

By treating the pseudofermions as additional integration variables in the path integral, one obtains a totally bosonic representation. The price one pays is that the pseudofermion effective action is highly non-local since it includes the inverse Dirac operator $(D[U] + m_f)^{-1}$. Thus, the large sparse matrix $(D[U] + m)$ has to be inverted every time one needs an evaluation of the effective action.

Present simulations generate gauge configurations using the Hybrid Monte Carlo (HMC) algorithm [83], or variants thereof. This algorithm combines molecular dynamics (MD) evolution in a fictitious time (which is also discretized) with a Metropolis "accept-reject" step. It makes a global update of the configuration, and is made exact by the Metropolis step. In its original form it can be used only for two degenerate flavors, but extensions (particularly the rational HMC [84]) are available for single flavors. Considerable speed-up of the algorithms has been achieved over the last two decades using a variety of techniques.

All these algorithms spend the bulk of their computational time on the repeated inversion of $(D[U] + m)$ acting on a source (which is required at every step of the MD evolution). Inversions are done using a variety of iterative algorithms, *e.g.* the conjugate gradient algorithm. In this class of algorithms, computational cost is proportional to the condition number of the matrix, which is the ratio of maximum and minimum eigenvalues. For $(D[U] + m)$ the smallest eigenvalue is $\approx m$, so the condition number and cost are

The building blocks for calculations are expectation values of multi-local gauge-invariant operators, also known as "correlation functions",

inversely proportional to the quark mass. This is a major reason why simulations at the physical quark mass are challenging.

Recent algorithmic improvements have significantly reduced this problem. The main idea is to separate different length scales. Since the low eigenvalues of $(D[U] + m)$ are associated with long wavelength quark modes, one may project the problem onto that of a coarse-grained lattice by averaging the field within a block of sublattices and carrying out the inversion on this coarse lattice. The result is then fed back to the original lattice as an efficient *preconditioner* for the iterative solver, and the whole procedure may be nested multiple times. Variants of such methods have been implemented, specifically domain-decomposition [11, 12], deflation [85–88] and multigrid [89, 90]. They are increasingly used in large-scale lattice simulations.

A practical concern is the inevitable presence of correlations between configurations in the Markov chain. These are characterized by an autocorrelation length in the fictitious MD time. One aims to use configurations separated in MD time by greater than this autocorrelation length. In practice, it is difficult to measure this length accurately, see, *e.g.*, [91], and this leads to some uncertainty in the resulting statistical errors, as well as the possibility of insufficient equilibration.

For most of the applications of LQCD discussed in this review, the cost of generating gauge configurations is larger than or similar to that of performing the "measurements" on those configurations. The computational cost of gauge generation grows with the lattice volume, $V_{\text{lat}} = N_s^3 N_t$, as $V_{\text{lat}}^{1+\delta}$. Here $\delta = 1/4$ for the HMC algorithm [92] and can be reduced slightly using modern variants. Such growth with V_{lat} provides a (time-dependent) limit on the largest lattice volumes that can be simulated. At present, the largest lattices being used have $N_s = 144$ and $N_t = 288$. Typically one aims to create an ensemble of $\sim 10^3$ statistically independent configurations at each choice of parameters (a , m_q and V_{lat}). For most physical quantities of interest, this is sufficient to make the resulting statistical errors smaller than or comparable to the systematic errors.

17.2.2 Two-point functions

One can extract properties of stable hadrons using two-point correlation functions, $\langle O_X(x) O_Y^\dagger(0) \rangle$. Here $O_{X,Y}(x)$ are operators that have non-zero overlaps with the hadronic state of interest $|H\rangle$, *i.e.* $\langle 0|O_{X,Y}(x)|H\rangle \neq 0$. One usually Fourier transforms in the spatial directions and considers correlators as a function of Euclidean time:

$$C_{XY}(t; \vec{p}) = \sum_{\vec{x}} \langle O_X(t, \vec{x}) O_Y^\dagger(0) \rangle e^{-i\vec{p}\cdot\vec{x}}. \quad (17.8)$$

(Here and throughout this section all quantities are expressed in dimensionless lattice units, so that, for example, $\vec{p} = a\vec{p}_{\text{phys}}$.) By inserting a complete set of states having spatial momentum \vec{p} , the two-point function can be written as

$$C_{XY}(t; \vec{p}) = \sum_{i=0}^{\infty} \frac{1}{2E_i(\vec{p})} \langle 0|O_X(0)|H_i(\vec{p})\rangle \langle H_i(\vec{p})|O_Y^\dagger(0)|0\rangle e^{-E_i(\vec{p})t}, \quad (17.9)$$

where the energy of the i -th state $E_i(\vec{p})$ appears as an eigenvalue of the time evolution operator e^{-Ht} in the Euclidean time direction. The factor of $1/[2E_i(\vec{p})]$ is due to the relativistic normalization used for the states. For large enough t , the dominant contribution

is that of the lowest energy state $|H_0(\vec{p})\rangle$:

$$C_{XY}(t) \xrightarrow{t \rightarrow \infty} \frac{1}{2E_0(\vec{p})} \langle 0|O_X(0)|H_0(\vec{p})\rangle \langle H_0(\vec{p})|O_Y^\dagger(0)|0\rangle e^{-E_0(\vec{p})t}. \quad (17.10)$$

One can thus obtain the energy $E_0(\vec{p})$, which equals the hadron mass m_H when $\vec{p} = 0$, and the product of matrix elements $\langle 0|O_X(0)|H_i(\vec{p})\rangle \langle H_i(\vec{p})|O_Y^\dagger(0)|0\rangle$.

This method can be used to determine the masses of all the stable mesons and baryons by making appropriate choices of operators. For example, if one uses the axial current, $O_X = O_Y = A_\mu = \bar{d}\gamma_\mu\gamma_5 u$, then one can determine m_{π^+} from the rate of exponential fall-off, and in addition the decay constant f_π from the coefficient of the exponential. A complication arises for states with high spins ($j \geq 4$ for bosons) because the spatial rotation group on the lattice is a discrete subgroup of the continuum group $SO(3)$. This implies that lattice operators, even when chosen to lie in irreducible representations of the lattice rotation group, have overlap with states that have a number of values of j in the continuum limit [93]. For example $j = 0$ operators can also create mesons with $j = 4$. Methods to overcome this problem in practice are available [94, 95] and have been used successfully.

The expression given above for the correlator $C_{XY}(t; \vec{p})$ shows how, in principle, one can determine the energies of the excited hadron states having the same quantum numbers as the operators $O_{X,Y}$, by fitting the correlation function to a sum of exponentials, which is also important to precisely determine the ground-state exponential. In practice, in order to reliably identify the excited state, one often needs to use a large basis of operators and to adopt the variational approach such as that of Ref. [96]. One can also use an anisotropic lattice in which a_t , the lattice spacing in the time direction, is smaller than its spatial counterpart a_s . Using a combination of these and other technical improvements extensive excited-state spectra have been obtained [95, 97–100].

17.2.3 Three-point functions

Hadronic matrix elements needed to calculate semileptonic form factors and neutral meson mixing amplitudes can be computed from three-point correlation functions. We discuss here, as a representative example, the $D \rightarrow K$ amplitude. As in the case of two-point correlation functions one constructs operators O_D and O_K having overlap, respectively, with the D and K mesons. We are interested in calculating the matrix element $\langle K|V_\mu|D\rangle$, with $V_\mu = \bar{c}\gamma_\mu s$ the vector current calculations of this contribution.

To obtain this, we use the three-point correlator

$$C_{KV_\mu D}(t_x, t_y; \vec{p}) = \sum_{\vec{x}, \vec{y}} \langle O_K(t_x, \vec{x}) V_\mu(0) O_D^\dagger(t_y, \vec{y}) \rangle e^{-i\vec{p}\cdot\vec{x}}, \quad (17.11)$$

and focus on the limit $t_x \rightarrow \infty$, $t_y \rightarrow -\infty$. In this example we set the D -meson at rest while the kaon carries three-momentum \vec{p} . Momentum conservation then implies that the weak operator V_μ inserts three-momentum $-\vec{p}$. Inserting a pair of complete sets of states between each pair of operators, we find

$$C_{KV_\mu D}(t_x, t_y; \vec{p}) = \sum_{i,j} \frac{1}{2m_{D_i} 2E_{K_j}(\vec{p})} e^{-m_{D_i} t_x - E_{K_j}(\vec{p}) |t_y|} \langle 0|O_K(0)|K_i(\vec{p})\rangle \langle K_i(\vec{p})|V_\mu(0)|D_j(\vec{0})\rangle \langle D_j(\vec{0})|O_D^\dagger(0)|0\rangle. \quad (17.12)$$

The matrix element $\langle K_i(\vec{p})|V_\mu(0)|D_j(\vec{0})\rangle$ can then be extracted, since all other quantities in this expression can be obtained from two-point correlation functions. Typically one is interested in the weak matrix elements of ground states, such as the lightest pseudoscalar mesons. In the limit of large separation between the three operators in Euclidean time, the three-point correlation function yields the weak matrix element of the transition between ground states.

17.2.4 Scattering amplitudes and resonances

The methods described thus far yield matrix elements involving single, stable particles (where by stable we mean here absolutely stable to strong interaction decays). Most of the particles listed in the Review of Particle Properties are, however, unstable—they

are resonances decaying into final states consisting of multiple strongly interacting particles. LQCD simulations cannot directly calculate resonance properties, but methods have been developed to do so indirectly for resonances coupled to two-particle final states in the elastic regime, starting from the seminal work of Lüscher [101].

The difficulty faced by LQCD calculations is that, to obtain resonance properties, or, more generally, scattering phase-shifts, one must calculate multiparticle scattering amplitudes in momentum space and put the external particles on their mass-shells. This requires analytically continuing from Euclidean to Minkowski momenta. Although it is straightforward in LQCD to generalize the methods described above to calculate four- and higher-point correlation functions, one necessarily obtains them at a discrete and finite set of Euclidean momenta. Analytic continuation to $p_E^2 = -m^2$ is then an ill-posed and numerically unstable problem. The same problem arises for single-particle states, but can be largely overcome by picking out the exponential fall-off of the Euclidean correlator, as described above. With a multi-particle state there is no corresponding trick, except for two particles at threshold [102], although recent ideas using smeared correlators and advanced spectral-reconstruction methods offer hope for future progress [103–105].

What LQCD can calculate are the energies of the eigenstates of the QCD Hamiltonian in a finite box. The energies of states containing two stable particles, e.g. two pions, clearly depend on the interactions between the particles. It is possible to invert this dependence and, with plausible assumptions, determine the scattering phase-shifts at a discrete set of momenta from a calculation of the two-particle energy levels for a variety of spatial volumes [101]. This is a challenging calculation, but it has recently been carried through in several channels with quark masses approaching physical values. Channels studied include $\pi\pi$ (for $I = 2, 1$ and 0), $\bar{K}K$, $K\pi$, $\pi\omega$, $\pi\phi$, KD , DD^* and $B\pi$. For recent comprehensive reviews see [106, 107]. Extensions to nucleon interactions are also being actively studied [108]. The generalization of the formalism to the case of three particles is under active development [109–111]. For a recent review, see [112].

It is also possible to extend the methodology to calculate electroweak decay amplitudes to two particles below the inelastic threshold, e.g. $\Gamma(K \rightarrow \pi\pi)$ [113]. Results for both the $\Delta I = 3/2$ and $1/2$ amplitudes with physical quark masses have been obtained [114, 115], the former now including a controlled continuum limit [116]. First results for the CP-violating quantity ϵ' have been obtained [115].

Partial extensions of the formalism above the elastic threshold have been worked out, in particular for the case of multiple two-particle channels [117]. Another theoretical extension is to allow the calculation of form factors between a stable particle and a resonance [118], and between two resonances [119]. The former has been used to calculate the $\gamma\pi \rightarrow \rho$ amplitude, albeit for unphysically large quark masses [120].

While a systematic extension to decays with many multiparticle channels, e.g. hadronic B decays, has, however, yet to be formulated, some interesting new ideas have been recently proposed [121, 122].

17.2.5 Recent advances

In some physics applications, one is interested in the two-point correlation function $\langle O_X(x) O_Y^\dagger(0) \rangle$ for all values of the separation x , not just its asymptotic form for large separations (which is used to determine the hadron spectrum as sketched above). A topical example is the hadronic vacuum polarization function $\Pi_{\mu\nu}(x) = \langle V_\mu(x) V_\nu(0) \rangle$ and its Fourier transform $\Pi_{\mu\nu}(q^2)$. Since the lattice is in Euclidean space-time, only space-like momenta, $q^2 = -Q^2 < 0$, are accessible. Nevertheless, this quantity is of significant interest. It is related by a dispersion relation to the cross section for $e^+e^- \rightarrow$ hadrons, and is needed for a first-principles calculation of the “hadronic vacuum polarization” contribution to the muon anomalous magnetic moment a_μ . This is the contribution with the largest theoretical uncertainty at present. There are a number of lattice calculations of this contribution (see, e.g., Refs. [123–138] following the pioneering work Ref. [139]). Since the relevant scale is set by the muon mass m_μ , this quantity is

most sensitive to the low-energy region $Q^2 \simeq m_\mu^2$ of $\Pi_{\mu\nu}(-Q^2)$, where the long-range contribution of multibody states become relevant. The lattice calculation is challenging because of this and also because the necessary precision is high (below 1%). Many systematic effects must be carefully studied and controlled in order to achieve this precision, including finite volume errors and QED corrections.

Calculations of the light-by-light scattering contribution to a_μ are also underway. These involve the calculations of four-point correlation functions with various external momenta. Clever ways to sum over them to evaluate the contribution to a_μ are developed and first results have been reported [140–144]. Another approach to the light-by-light scattering is to decompose the amplitude to components using ChPT or phenomenological models, and to calculate the components in LQCD. Calculations of the $\pi \rightarrow \gamma^* \gamma^*$ amplitudes follow similar directions [145–147].

There are other processes for which lattice calculations can make a significant contribution to establishing a quantitative understanding. One example is the long-distance contribution to the neutral kaon mass splitting, ΔM_K . This also requires the evaluation of a four-point function, constructed from the two-point functions described above by the insertion of two electroweak Hamiltonians [148]. Rare kaon decays $K \rightarrow \pi \ell^+ \ell^-$ and $K \rightarrow \pi \nu \bar{\nu}$ are also important processes for which first lattice studies have recently appeared [149–153].

17.2.6 Status of LQCD simulations

Until the 1990s, most large-scale lattice simulations were limited to the “quenched” approximation, wherein the fermion determinant is omitted from the path integral. While much of the basic methodology was developed in this era, the results obtained had uncontrolled systematic errors and were not suitable for use in placing precision constraints on the Standard Model. During the 1990s, more extensive simulations including the fermion determinant (also known as simulations with “dynamical” fermions) were begun, but with unphysically heavy quark masses ($m_\ell \sim 50 - 100$ MeV), such that the extrapolation to the physical light quark masses was a source of large systematic errors [154]. During the 2000s, advances in both algorithms and computers allowed simulations to reach much smaller quark masses ($m_\ell \sim 10 - 20$ MeV) such that LQCD calculations of selected quantities with all sources of error controlled and small became available. Their results played an important role in constraints on the CKM matrix and other phenomenological analyses. In the last few years, simulations directly at the physical isospin-symmetric light quark masses have become standard, removing the need for a chiral extrapolation and thus significantly reducing the overall error. The present frontier, as noted above, is the inclusion of isospin breaking. This will be needed to push the accuracy of calculations below the percent level.

On a more qualitative level, analytic and numerical results from LQCD have demonstrated that QCD confines color and spontaneously breaks chiral symmetry. Confinement can be seen as a linearly rising potential between heavy quark and anti-quark in the absence of quark loops. Analytically, this can be shown in the strong coupling limit $g_{\text{lat}} \rightarrow \infty$ [1]. At weaker couplings there are precise numerical calculations of the potential that clearly show that this behavior persists in the continuum limit [155–157].

Chiral symmetry breaking was also demonstrated in the strong coupling limit on the lattice [19, 158], and there have been a number of numerical studies showing that this holds also in the continuum limit. The accumulation of low-lying modes of the Dirac operator, which is the analog of Cooper pair condensation in superconductors, has been observed, yielding a determination of the chiral condensate [159–164]. Many relations among physical quantities that can be derived under the assumption of broken chiral symmetry have been confirmed by a number of lattice groups [165].

17.3 Physics applications

In this section we describe the main applications of LQCD that are both computationally mature and relevant for the determination of particle properties.

A general feature to keep in mind is that, since there are many

different choices for lattice actions, all of which lead to the same continuum theory, a crucial test is that results for any given quantity are consistent. In many cases, different lattice calculations are completely independent and often have very different systematic errors. Thus final agreement, if found, is a highly non-trivial check, just as it is for different experimental measurements.

The number, variety and precision of the calculations has progressed to the point that an international “Flavour Lattice Averaging Group” (FLAG) has been formed. The main aims of FLAG include collecting all lattice results of relevance for a variety of phenomenologically interesting quantities and providing averages of those results which pass appropriate quality criteria. The averages attempt to account for possible correlations between results (which can arise, for example, if they use common gauge configurations). The quantities considered are those we discuss in this section, with the exception of the hadron spectrum. The most recent FLAG review is from 2019 [53] (see also an older edition, Ref. [165]). The interested reader can consult this review for very extensive discussions of the details of the calculations and of the sources of systematic errors.

We stress that the results we quote below are those obtained using the physical complement of light quarks (i.e. $N_f = 2 + 1$ or $2 + 1 + 1$ simulations).

17.3.1 Spectrum

The most basic prediction of LQCD is of the hadron spectrum. Once the input parameters are fixed as described in Sec. 17.1.5, the masses or resonance parameters of all other states can be predicted. This includes hadrons composed of light (u , d and s) quarks, as well as heavy-light and heavy-heavy hadrons. It also includes quark-model exotics (e.g. $J^{PC} = 1^{-+}$ mesons) and glueballs. Thus, in principle, LQCD calculations should be able to reproduce many of the experimental results compiled in the Review of Particle Properties. Doing so would test both that the error budgets of LQCD calculations are accurate and that QCD indeed describes the strong interactions in the low-energy domain. The importance of the latter test can hardly be overstated.

What is the status of this fundamental test? As discussed in Sec. 1.2, LQCD calculations are most straightforward for stable, low-lying hadrons. Calculations of the properties of resonances that can decay into only two particles are more challenging, though substantial progress has been made. First theoretical work on decays to more than two particles has begun, but the methodology is not yet practical. It is also more technically challenging to calculate masses of flavor singlet states (which can annihilate into purely gluonic intermediate states) than those of flavor non-singlets, although again algorithmic and computational advances have begun to make such calculations accessible, although not yet for physical quark masses. The present status for light hadrons is that fully controlled results are available for the masses of the octet light baryons, while results with less than complete control are available for the decuplet baryon resonances, the vector meson resonances and the η and η' . In addition, it has been possible to calculate the isospin splitting in light mesons and baryons (due to the up-down mass difference and the incorporation of QED). There are also extensive results for heavy-light (D and B systems) and heavy-heavy (J/ψ and Υ systems). All present results, which are discussed in the “Quark Model” review, are consistent with experimental values, and several predictions have been made. We refer the reader to that review for references to the relevant work.

17.3.2 Decay constants and bag parameters

The pseudoscalar decay constants can be determined from two-point correlation functions involving the axial-vector current, as discussed in Sec. 17.2.2. The decay constant f_P of a meson P is extracted from the weak matrix element involving the axial-vector current using the relation $\langle 0 | A_\mu(x) | P(\vec{p}) \rangle = f_P p_\mu \exp(-ip \cdot x)$, where p_μ is the momentum of P and $A_\mu(x)$ is the axial-vector current. Since they are among the simplest quantities to calculate, decay constants provide good benchmarks for lattice methods, in addition to being important inputs for flavor physics phenomenology in their own right. Results from many lattice groups for the pion and kaon decay constants now have errors at the percent level or better. The decay constants in the charm and bottom sectors,

f_D , f_{D_s} , f_B , and f_{B_s} , have also been calculated to high precision. Lattice results for all of these decay constants are discussed in detail in the review “Leptonic Decays of Charged Pseudoscalar Mesons.”

Another important lattice quantity is the kaon bag parameter, B_K , which is needed to turn the precise measurement of CP-violation in kaon mixing into a constraint on the Standard Model. It is defined by

$$\frac{8}{3} m_K^2 f_K^2 B_K(\mu) = \langle \bar{K}^0 | Q_{\Delta S=2}(\mu) | K^0 \rangle, \quad (17.13)$$

where m_K is the kaon mass, f_K is the kaon decay constant, $Q_{\Delta S=2} = \bar{s}\gamma_\mu(1-\gamma_5)d\bar{s}\gamma_\mu(1-\gamma_5)d$ is the four-quark operator of the effective electroweak Hamiltonian and μ is the renormalization scale. The short distance contribution to the electroweak Hamiltonian can be calculated perturbatively, but the hadronic matrix element parameterized by B_K must be computed using non-perturbative methods. In order to be of use to phenomenology, the renormalization factor of the four-quark operator must be matched to a continuum renormalization scheme, e.g. to $\overline{\text{MS}}$, as described in Sec. 17.1.6.4. Determinations with percent-level precision using different fermion actions and $N_f = 2 + 1$ light sea quarks are now available using DWF [166], staggered fermions [167], DWF valence on staggered sea quarks [168], and Wilson fermions [13]. The results are all consistent, and the present FLAG average is $\hat{B}_K = 0.7625(97)$ [53].

The bag parameters for B and B_s meson mixing are defined analogously to that for kaon mixing. The B and B_s mesons contain a valence b -quark so that calculations of these quantities must use one of the methods for heavy quarks described above. Calculations with $N_f = 2 + 1$ light fermions have been done using NRQCD [169], the Fermilab formalism [68], and static heavy quarks [170]. All results are consistent. The FLAG averages for the quantities relevant for B_s and B mixing are $f_{B_s}\sqrt{B_{B_s}} = 274(8)$ MeV and $f_B\sqrt{B_B} = 225(9)$ MeV, with their ratio (which is somewhat better determined) being $\xi = 1.206(17)$ [53]. Note that the errors for quantities involving b quarks are larger than those for quantities involving only light quarks, although the difference has decreased over the last two years.

For the K , D and B systems, one can also consider the matrix elements of four-fermion operators that arise in beyond-the-standard-model (BSM) theories, which can have a different chiral structure. Knowledge of these matrix elements allows one to constrain the parameters of the BSM theories, and is complementary to direct searches at the LHC. Reliable results are now available from lattice calculations, and are reviewed by FLAG in the case of kaon mixing [53]. Complete results for D and B mixing are presented in Ref. [171] and Ref. [68], respectively.

The results for mixing matrix elements are used in the reviews “The CKM Quark-Mixing Matrix,” and “ $B^0 - \bar{B}^0$ Mixing.”

17.3.3 Form factors ($K \rightarrow \pi\ell\nu$, $D \rightarrow K\ell\nu$, $B \rightarrow \pi\ell\nu$, $B \rightarrow D^{(*)}\ell\nu$)

Semileptonic decay rates can be used to extract CKM matrix elements once the semileptonic form factors are known from lattice calculations. For example, the matrix element of a pseudoscalar meson P undergoing semileptonic decay to another pseudoscalar meson D is mediated by the vector current, and can be written in terms of form factors as

$$\langle D(p_D) | V_\mu | P(p_P) \rangle = f_+(q^2)(p_D + p_P - \Delta)_\mu + f_0(q^2)\Delta_\mu, \quad (17.14)$$

where $q = p_D - p_P$, $\Delta_\mu = (m_D^2 - m_P^2)q_\mu/q^2$ and V_μ is the quark vector current. The shape of the form factor is typically well determined by experiment, and the value of $f_+(q^2)$ at some reference value of q^2 is needed from the lattice in order to extract CKM matrix elements. Typically $f_+(q^2)$ dominates the decay rate, since the contribution from $f_0(q^2)$ is suppressed when the final state lepton is light.

The form factor $f_+(0)$ for $K \rightarrow \pi\ell\nu$ decays is highly constrained by the Ademollo-Gatto theorem [172] and chiral symmetry. Old estimates using chiral perturbation theory combined with quark models quote sub-percent precision [173], though they suffer from

some model dependence. Utilizing the constraint from the vector current conservation that $f_+(0)$ is normalized to unity in the limit of degenerate up and strange quark masses, the lattice calculation can be made very precise and has now matched the precision of the phenomenological estimates [174–181]. The present FLAG average (from $N_f = 2 + 1$ simulations) is $f_+(0) = 0.9677(27)$ [53].

Charm meson semileptonic decays have been calculated by different groups using methods similar to those used for charm decay constants, and results are steadily improving in precision [182–185]. For semileptonic decays involving a bottom quark, one uses HQET or NRQCD to control the discretization errors of the bottom quark. The form factors for the semileptonic decay $B \rightarrow \pi\ell\nu$ have been calculated in unquenched lattice QCD by a number of groups [186–191]. These B semileptonic form factors are difficult to calculate at low q^2 , *i.e.* when the mass of the B -meson must be balanced by a large pion momentum, in order to transfer a large momentum to the lepton pair. The low q^2 region has large discretization errors and very large statistical errors, while the high q^2 region is much more accessible to the lattice. For experiment, the opposite is true. To combine lattice and experimental results it has proved helpful to use the z -parameter expansion [192]. This provides a theoretically constrained parameterization of the entire q^2 range, and allows one to obtain $|V_{ub}|$ without model dependence [193, 194].

The semileptonic decays $B \rightarrow D\ell\nu$ and $B \rightarrow D^*\ell\nu$ can be used to extract $|V_{cb}|$ once the corresponding form factors are known. The lattice calculation is most precise at zero recoil since the bulk of the systematic error cancels for appropriate ratios between $B \rightarrow D^{(*)}$ and $B \rightarrow B$ or $D^{(*)} \rightarrow D^{(*)}$ [195, 196]. The unquenched calculation of the $B \rightarrow D^{(*)}\ell\nu$ form factor at zero recoil has been performed with various formulations for the heavy quark [197–201]. Calculations at non-zero recoil have also been performed to constrain the functional form of the form factor, which can be used to extrapolate the experimental data to the zero-recoil point or to determine $|V_{cb}|$ directly at the non-zero recoil points [202–205]. Semileptonic decays of the Λ_b baryon can also be used to constrain $|V_{cb}|$ and $|V_{ub}|$ using lattice calculations of the relevant form factors [206, 207].

The rare decays $B \rightarrow K^{(*)}\ell^+\ell^-$ involve matrix elements similar to those needed for semileptonic decays, Eq. (17.14), except that the vector current V_μ is replaced by the operators $\bar{s}\gamma^\mu(1-\gamma_5)b$ or $\bar{s}\sigma^{\mu\nu}(1+\gamma_5)b$. Lattice calculations of the corresponding form factors involve similar techniques to those for the semileptonic form factors. The values of q^2 for which lattice calculations can be done are limited as for B semileptonic decays, and, in addition, the region of $c\bar{c}$ resonances has to be avoided. Recent lattice calculations [190, 208–210] have been used to constrain the standard model and new physics contributions.

The results discussed in this section are used in the reviews “The CKM Quark-Mixing Matrix,” “ V_{ud} , V_{us} , the Cabibbo Angle and CKM Unitarity,” and “ V_{cb} and V_{ub} CKM Matrix Elements.”

17.3.4 Strong coupling constant

As explained in Sec. 17.1.5.1, for a given lattice action, the choice of bare lattice coupling constant, g_{lat} , determines the lattice spacing a . If one then calculates a as described in Sec. 17.1.5.1, one knows the strong coupling constant in the bare lattice scheme at the scale $1/a$, $\alpha_{\text{lat}} = g_{\text{lat}}^2/(4\pi)$. This is not, however, useful for comparing to results for α_s obtained from other inputs, such as deep inelastic scattering or jet shape variables. This is because the latter results give α_s in the $\overline{\text{MS}}$ scheme, which is commonly used in such analyses, and the conversion factor between these two schemes is known to converge extremely poorly in perturbation theory. Instead one must use a method which directly determines α_s on the lattice in a scheme closer to $\overline{\text{MS}}$.

Several such methods have been used, all following a similar strategy. One calculates a short-distance quantity K both perturbatively (K^{PT}) and non-perturbatively (K^{NP}) on the lattice, and requires equality: $K^{\text{NP}} = K^{\text{PT}} = \sum_{i=0}^n c_i \alpha_s^i$. Solving this equation one obtains α_s at a scale related to the quantity being used. Often, α_s thus obtained is not defined in the conventional $\overline{\text{MS}}$ scheme, and one has to convert among the different schemes using perturbation theory. Unlike for the bare lattice scheme, the required conversion factors are reasonably convergent. As a fi-

nal step, one uses the renormalization group to run the resulting coupling to a canonical scale (such as M_Z).

In the work of the HPQCD collaboration [211, 212], the short-distance quantities are Wilson loops of several sizes and their ratios. These quantities are perturbatively calculated through $\mathcal{O}(\alpha_s^3)$ using the V -scheme defined through the heavy quark potential. The coefficients of even higher orders are estimated using the data at various values of a . In addition, this work obtains a result for α_s by matching with α_{lat} in a tadpole-improved scheme that improves convergence.

Another choice of short-distance quantities is to use current-current correlators. Appropriate moments of these correlators are ultraviolet finite, and by matching lattice results to the *continuum* perturbative predictions, one can directly extract the $\overline{\text{MS}}$ coupling. The method can be applied for light meson correlators [213, 214] as well as heavy meson correlators [36, 212, 215–217]. Yet another choice of short-distance quantity is the static-quark potential, where the lattice result for the potential is compared to perturbative calculations; this method was used to compute α_s within 2+1 flavor QCD [218–222]. There is also a determination of α_s from a comparison of lattice data for the ghost-gluon coupling with that of perturbation theory [223, 224].

With a definition of α_s given using the Schrödinger functional, one can non-perturbatively control the evolution of α_s to high-energy scales, such as 100 GeV, where the perturbative expansion converges very well. This method developed by the ALPHA collaboration [81] has been applied to 2+1-flavor QCD in [225–227].

The various lattice methods for calculating α_s have significantly different sources of systematic error. The FLAG review [53] reported an estimate $\alpha_{\overline{\text{MS}}}^{(5)}(M_Z) = 0.11823(81)$ based on these various lattice calculations. A comparison to other phenomenological determinations can be found in the “Quantum Chromodynamics” review.

17.3.5 Quark masses

Once the quark mass parameters are tuned in the lattice action, the remaining task is to convert them to those of the conventional definition. Since the quarks do not appear as asymptotic states due to confinement, the pole mass of the quark propagator is not a physical quantity. Instead, one defines the quark mass after subtracting the ultra-violet divergences in some particular way. The conventional choice is again the $\overline{\text{MS}}$ scheme at a canonical scale such as 2 or 3 GeV. Ratios such as m_c/m_s and m_b/m_c are also useful as they are free from multiplicative renormalization (in a mass-independent scheme).

As discussed in Sec. 17.1.6.4, one must convert the lattice bare quark mass to that in the $\overline{\text{MS}}$ scheme. Older calculations did so directly using perturbation theory; most recent calculations use an intermediate NPR method (e.g. RI/MOM or RI/SMOM) which is then converted to the $\overline{\text{MS}}$ scheme using perturbation theory (see, e.g., [166, 228, 229]).

Alternatively, one can use a definition based on the Schrödinger functional, which allows one to evolve the quark mass to a high scale non-perturbatively [230]. In practice, one can reach scales as high as ~ 100 GeV, at which matching to the $\overline{\text{MS}}$ scheme can be reliably calculated in perturbation theory.

Another approach available for heavy quarks is to match current-current correlators at short distances calculated on the lattice to those obtained in continuum perturbation theory in the $\overline{\text{MS}}$ scheme [36, 212, 215–217]. This has allowed an accurate determination of m_c and m_b [80, 212, 216].

The ratio method for heavy quarks (discussed earlier) can also be used to determine m_b [231].

Results are summarized in the review of “Quark Masses.”

17.3.6 Other applications

In this review we have concentrated on applications of LQCD that are relevant to the quantities discussed in the Review of Particle Properties. We have not discussed at all several other applications that are being actively pursued by simulations. Here we list the major such applications. The reader can consult the aforementioned texts [2–4] for further details, as well as the proceedings of recent lattice conferences [232], and several recent white

papers [233–239].

LQCD can be used, in principle, to simulate QCD at non-zero temperature and density, and in particular to study how confinement and chiral-symmetry breaking are lost as T and μ (the chemical potential) are increased. This is of relevance to heavy-ion collisions, the early Universe and neutron-star structure. In practice, finite temperature simulations are computationally tractable and relatively mature, while simulations at finite μ suffer from a “sign problem” and are at a rudimentary stage.

Another topic under active investigation is nucleon structure and inter-nucleon interactions. The simplest nucleon matrix elements are calculable with a precision that is now starting to rival that for some mesonic quantities. Of particular interest are those of the axial current (leading to g_A) and of the scalar density (with $\langle N|\bar{s}s|N\rangle$ needed for dark matter searches). Other such matrix elements provide information on the parton distribution functions (PDFs) including their low moments. More recently, methods to directly access PDFs are being developed (see, e.g., Ref. [233] for a recent summary).

Finally, we note that there is much recent interest in studying QCD-like theories with more fermions, possibly in other representations of the gauge group (see, e.g., [235]). The main interest is to find nearly conformal theories which might be candidates for “walking technicolor” models.

17.4 Outlook

While LQCD calculations have made major strides in the last decade, and are now playing an important role in constraining the Standard Model, there are many calculations that could be done in principle but are not yet mature due to limitations in computational resources. As we move to exascale resources (10^{18} floating point operations per second), the list of mature calculations will grow. Examples that we expect to mature in the next few years are results for B meson and Λ_b baryon form factors covering the full range of q^2 ; results for excited hadrons, including quark-model exotics, at close to physical light-quark masses; results for moments of structure functions; results for the simplest nucleon matrix elements; $K \rightarrow \pi\pi$ amplitudes (allowing a prediction of ϵ'/ϵ from the Standard Model); hadronic vacuum polarization contributions to $g_\mu - 2$, the running of α_{EM} and α_s ; $\pi \rightarrow \gamma\gamma$ and related amplitudes; long-distance contributions to $\overline{K} \leftrightarrow K$ mixing; the light-by-light contribution to $g_\mu - 2$; and determinations of long distance contributions to rare kaon decays such as $K \rightarrow \pi\nu\bar{\nu}$. There will also be steady improvement in the precision attained for the mature quantities discussed above. As already noted, this will ultimately require simulations with $m_u \neq m_d$ and including electromagnetic effects.

References

- [1] K. G. Wilson, Phys. Rev. **D10**, 2445 (1974).
- [2] T. DeGrand & C. DeTar, “Lattice Methods for Quantum Chromodynamics,” World Scientific (2006).
- [3] C. Gattringer & C.B. Lang, “Quantum Chromodynamics on the Lattice: An Introductory Presentation,” Springer (2009).
- [4] “Modern Perspectives in Lattice QCD: quantum field theory and high performance computing” (Lecture notes of the Les Houches Summer School, Vol. 93) eds. L. Lellouch *et al.*, Oxford Univ. Press. (Aug. 2011).
- [5] W. Zimmermann, in “Lectures on Elementary Particles and Quantum Field Theory”, ed. S. Deser *et al.*, MIT Press, Cambridge, MA (1971); K. Symanzik, Nucl. Phys. **B226**, 187 (1983); K. Symanzik, Nucl. Phys. **B226**, 205 (1983).
- [6] M. Luscher and P. Weisz, Commun. Math. Phys. **97**, 59 (1985), [Erratum: Commun. Math. Phys.98,433(1985)].
- [7] Y. Iwasaki, UT-HEP-118.
- [8] H. B. Nielsen and M. Ninomiya, Phys. Lett. **105B**, 219 (1981).
- [9] B. Sheikholeslami and R. Wohlert, Nucl. Phys. **B259**, 572 (1985).
- [10] K. Jansen *et al.*, Phys. Lett. **B372**, 275 (1996), [hep-lat/9512009].

- [11] M. Luscher, JHEP **05**, 052 (2003), [hep-lat/0304007].
- [12] M. Luscher, Comput. Phys. Commun. **156**, 209 (2004), [hep-lat/0310048]; M. Luscher, Comput. Phys. Commun. **165**, 199 (2005), [hep-lat/0409106]; M. Hasenbusch, Phys. Lett. **B519**, 177 (2001), [hep-lat/0107019]; C. Urbach *et al.*, Comput. Phys. Commun. **174**, 87 (2006), [hep-lat/0506011].
- [13] S. Durr *et al.*, Phys. Lett. **B705**, 477 (2011), [arXiv:1106.3230].
- [14] N. Ishizuka *et al.*, Phys. Rev. **D92**, 7, 074503 (2015), [arXiv:1505.05289].
- [15] R. Frezzotti *et al.* (Alpha), JHEP **08**, 058 (2001), [hep-lat/0101001].
- [16] R. Frezzotti and G. C. Rossi, JHEP **08**, 007 (2004), [hep-lat/0306014].
- [17] R. Frezzotti and G. C. Rossi, Nucl. Phys. Proc. Suppl. **128**, 193 (2004), [hep-lat/0311008].
- [18] R. Frezzotti and G. C. Rossi, JHEP **10**, 070 (2004), [hep-lat/0407002].
- [19] L. Susskind, Phys. Rev. **D16**, 3031 (1977).
- [20] M. Golterman, PoS **CONFINEMENT8**, 014 (2008).
- [21] C. Bernard, Phys. Rev. **D73**, 114503 (2006), [hep-lat/0603011]; S. R. Sharpe, PoS **LAT2006**, 022 (2006), [hep-lat/0610094].
- [22] G. P. Lepage, Phys. Rev. **D59**, 074502 (1999), [hep-lat/9809157].
- [23] A. Bazavov *et al.* (MILC), Rev. Mod. Phys. **82**, 1349 (2010), [arXiv:0903.3598].
- [24] E. Follana *et al.* (HPQCD, UKQCD), Phys. Rev. **D75**, 054502 (2007), [hep-lat/0610092].
- [25] C. T. H. Davies *et al.*, Phys. Rev. **D82**, 114504 (2010), [arXiv:1008.4018].
- [26] G. C. Donald *et al.*, Phys. Rev. **D86**, 094501 (2012), [arXiv:1208.2855].
- [27] P. H. Ginsparg and K. G. Wilson, Phys. Rev. **D25**, 2649 (1982).
- [28] P. Hasenfratz, V. Laliena and F. Niedermayer, Phys. Lett. **B427**, 125 (1998), [hep-lat/9801021].
- [29] M. Luscher, Phys. Lett. **B428**, 342 (1998), [hep-lat/9802011].
- [30] D. B. Kaplan, Phys. Lett. **B288**, 342 (1992), [hep-lat/9206013]; Y. Shamir, Nucl. Phys. **B406**, 90 (1993), [hep-lat/9303005]; Y. Shamir, Nucl. Phys. **B417**, 167 (1994), [hep-lat/9310006].
- [31] H. Neuberger, Phys. Lett. **B417**, 141 (1998), [hep-lat/9707022]; H. Neuberger, Phys. Lett. **B427**, 353 (1998), [hep-lat/9801031].
- [32] A. Borici, NATO Sci. Ser. C **553**, 41 (2000), [hep-lat/9912040].
- [33] A. D. Kennedy (2006), [hep-lat/0607038].
- [34] E. Shintani *et al.* (JLQCD), Phys. Rev. Lett. **101**, 242001 (2008), [arXiv:0806.4222].
- [35] P. A. Boyle *et al.*, JHEP **12**, 008 (2017), [arXiv:1701.02644].
- [36] K. Nakayama, B. Fahy and S. Hashimoto, Phys. Rev. **D94**, 5, 054507 (2016), [arXiv:1606.01002].
- [37] C. McNeile *et al.*, Phys. Rev. **D85**, 031503 (2012), [arXiv:1110.4510].
- [38] A. Bazavov *et al.*, Phys. Rev. **D98**, 7, 074512 (2018), [arXiv:1712.09262].
- [39] A. Bazavov *et al.* (Fermilab Lattice, MILC, TUMQCD), Phys. Rev. **D98**, 5, 054517 (2018), [arXiv:1802.04248].
- [40] E. Eichten and B. R. Hill, Phys. Lett. **B234**, 511 (1990).
- [41] J. Heitger and R. Sommer (ALPHA), JHEP **02**, 022 (2004), [hep-lat/0310035]; B. Blossier *et al.* (ALPHA), JHEP **12**, 039 (2010), [arXiv:1006.5816].
- [42] B. A. Thacker and G. P. Lepage, Phys. Rev. **D43**, 196 (1991); G. P. Lepage *et al.*, Phys. Rev. **D46**, 4052 (1992), [hep-lat/9205007].
- [43] R. J. Dowdall *et al.* (HPQCD), Phys. Rev. **D85**, 054509 (2012), [arXiv:1110.6887].
- [44] A. X. El-Khadra, A. S. Kronfeld and P. B. Mackenzie, Phys. Rev. **D55**, 3933 (1997), [hep-lat/9604004].
- [45] S. Aoki, Y. Kuramashi and S.-i. Tominaga, Prog. Theor. Phys. **109**, 383 (2003), [hep-lat/0107009].
- [46] N. H. Christ, M. Li and H.-W. Lin, Phys. Rev. **D76**, 074505 (2007), [hep-lat/0608006].
- [47] Y. Aoki *et al.* (RBC, UKQCD), Phys. Rev. **D86**, 116003 (2012), [arXiv:1206.2554].
- [48] N. H. Christ *et al.*, Phys. Rev. **D91**, 5, 054502 (2015), [arXiv:1404.4670].
- [49] M. B. Oktay and A. S. Kronfeld, Phys. Rev. **D78**, 014504 (2008), [arXiv:0803.0523].
- [50] J. A. Bailey *et al.*, Eur. Phys. J. **C77**, 11, 768 (2017), [arXiv:1701.00345].
- [51] B. Blossier *et al.* (ETM), JHEP **04**, 049 (2010), [arXiv:0909.3187].
- [52] S. Borsanyi *et al.*, Science **347**, 1452 (2015), [arXiv:1406.4088].
- [53] S. Aoki *et al.* (Flavour Lattice Averaging Group) (2019), [arXiv:1902.08191].
- [54] R. Horsley *et al.*, J. Phys. G **43**, no. 10, 10LT02 (2016).
- [55] S. Aoki *et al.* [PACS-CS Collab.], PTEP **2012**, 01A102 (2012).
- [56] T. Ishikawa *et al.*, Phys. Rev. Lett. **109**, 072002 (2012), [arXiv:1202.6018].
- [57] G. M. de Divitiis *et al.* (RM123), Phys. Rev. **D87**, 11, 114505 (2013), [arXiv:1303.4896].
- [58] P. Boyle *et al.*, JHEP **09**, 153 (2017), [arXiv:1706.05293].
- [59] F. Bloch and A. Nordsieck, Phys. Rev. **52**, 54 (1937).
- [60] N. Carrasco *et al.*, Phys. Rev. **D91**, 7, 074506 (2015), [arXiv:1502.00257].
- [61] D. Giusti *et al.*, Phys. Rev. Lett. **120**, 7, 072001 (2018), [arXiv:1711.06537].
- [62] M. Di Carlo *et al.* (2019), [arXiv:1904.08731].
- [63] M. Bruno *et al.* (ALPHA), Phys. Rev. Lett. **114**, 10, 102001 (2015), [arXiv:1410.8374].
- [64] F. Knechtli *et al.* (ALPHA), Phys. Lett. **B774**, 649 (2017), [arXiv:1706.04982].
- [65] A. Athenodorou *et al.* (ALPHA), Nucl. Phys. **B943**, 114612 (2019), [arXiv:1809.03383].
- [66] S. Cali, F. Knechtli and T. Korzec, Eur. Phys. J. **C79**, 7, 607 (2019), [arXiv:1905.12971].
- [67] D. Giusti *et al.*, Phys. Rev. **D95**, 11, 114504 (2017), [arXiv:1704.06561].
- [68] A. Bazavov *et al.* (Fermilab Lattice, MILC), Phys. Rev. **D93**, 11, 113016 (2016), [arXiv:1602.03560].
- [69] R. J. Dowdall *et al.*, Phys. Rev. **D86**, 094510 (2012), [arXiv:1207.5149].
- [70] C. McNeile *et al.*, Phys. Rev. **D86**, 074503 (2012), [arXiv:1207.0994].
- [71] S. Schaefer, R. Sommer and F. Virotta (ALPHA), Nucl. Phys. **B845**, 93 (2011), [arXiv:1009.5228].
- [72] M. Luscher, PoS **LATTICE2010**, 015 (2010), [arXiv:1009.5877].
- [73] R. Brower *et al.*, Phys. Lett. **B560**, 64 (2003), [hep-lat/0302005].
- [74] S. Aoki *et al.*, Phys. Rev. **D76**, 054508 (2007), [arXiv:0707.0396].

- [75] G. Colangelo, S. Durr and C. Haefeli, Nucl. Phys. **B721**, 136 (2005), [hep-lat/0503014].
- [76] M. Luscher, Commun. Math. Phys. **104**, 177 (1986).
- [77] G. Martinelli *et al.*, Nucl. Phys. **B445**, 81 (1995), [hep-lat/9411010].
- [78] M. Luscher *et al.*, Nucl. Phys. **B384**, 168 (1992), [hep-lat/9207009].
- [79] G. Martinelli *et al.*, Phys. Lett. **B411**, 141 (1997), [hep-lat/9705018].
- [80] B. Colquhoun *et al.*, Phys. Rev. **D91**, 7, 074514 (2015), [arXiv:1408.5768].
- [81] M. Luscher *et al.*, Nucl. Phys. **B413**, 481 (1994), [hep-lat/9309005]; M. Della Morte *et al.* (ALPHA), Nucl. Phys. **B713**, 378 (2005), [hep-lat/0411025].
- [82] M. Tomii *et al.* (JLQCD), Phys. Rev. **D94**, 5, 054504 (2016), [arXiv:1604.08702].
- [83] S. Duane *et al.*, Phys. Lett. **B195**, 216 (1987).
- [84] M. A. Clark and A. D. Kennedy, Phys. Rev. Lett. **98**, 051601 (2007), [hep-lat/0608015].
- [85] M. Luscher, JHEP **07**, 081 (2007), [arXiv:0706.2298].
- [86] M. Luscher, JHEP **12**, 011 (2007), [arXiv:0710.5417].
- [87] A. Stathopoulos and K. Orginos, SIAM J. Sci. Comput. **32**, 439 (2010), [arXiv:0707.0131].
- [88] P. A. Boyle (2014), [arXiv:1402.2585].
- [89] R. Babich *et al.*, Phys. Rev. Lett. **105**, 201602 (2010), [arXiv:1005.3043].
- [90] A. Frommer *et al.*, SIAM J. Sci. Comput. **36**, A1581 (2014), [arXiv:1303.1377].
- [91] M. Bruno, S. Schaefer and R. Sommer (ALPHA), JHEP **08**, 150 (2014), [arXiv:1406.5363].
- [92] M. Creutz, Phys. Rev. **D38**, 1228 (1988); R. Gupta, G. W. Kilcup and S. R. Sharpe, Phys. Rev. **D38**, 1278 (1988).
- [93] J. E. Mandula, G. Zweig and J. Govaerts, Nucl. Phys. **B228**, 91 (1983); J. E. Mandula and E. Shpiz, Nucl. Phys. **B232**, 180 (1984).
- [94] H. B. Meyer and M. J. Teper, Nucl. Phys. **B658**, 113 (2003), [hep-lat/0212026].
- [95] J. J. Dudek *et al.*, Phys. Rev. **D82**, 034508 (2010), [arXiv:1004.4930]; J. J. Dudek *et al.*, Phys. Rev. **D83**, 111502 (2011), [arXiv:1102.4299]; R. G. Edwards *et al.*, Phys. Rev. **D84**, 074508 (2011), [arXiv:1104.5152].
- [96] M. Luscher and U. Wolff, Nucl. Phys. **B339**, 222 (1990).
- [97] G. P. Engel *et al.* (BGR [Bern-Graz-Regensburg]), Phys. Rev. **D82**, 034505 (2010), [arXiv:1005.1748]; D. Mohler *et al.*, Phys. Rev. Lett. **111**, 22, 222001 (2013), [arXiv:1308.3175].
- [98] M. S. Mahbub *et al.*, Annals Phys. **342**, 270 (2014), [arXiv:1310.6803].
- [99] J. Bulava *et al.*, Nucl. Phys. **B910**, 842 (2016), [arXiv:1604.05593].
- [100] R. Brett *et al.*, Nucl. Phys. **B932**, 29 (2018), [arXiv:1802.03100].
- [101] M. Luscher, Commun. Math. Phys. **105**, 153 (1986); M. Luscher, Nucl. Phys. **B364**, 237 (1991).
- [102] L. Maiani and M. Testa, Phys. Lett. **B245**, 585 (1990).
- [103] M. T. Hansen, H. B. Meyer and D. Robaina, Phys. Rev. **D96**, 9, 094513 (2017), [arXiv:1704.08993].
- [104] M. Hansen, A. Lupo and N. Tantalo, Phys. Rev. **D99**, 9, 094508 (2019), [arXiv:1903.06476].
- [105] J. Bulava and M. T. Hansen (2019), [arXiv:1903.11735].
- [106] R. A. Briceño, J. J. Dudek and R. D. Young, Rev. Mod. Phys. **90**, 2, 025001 (2018), [arXiv:1706.06223].
- [107] N. Brambilla *et al.* (2019), [arXiv:1907.07583].
- [108] M. J. Savage, Prog. Part. Nucl. Phys. **67**, 140 (2012), [arXiv:1110.5943]; T. Inoue *et al.* (HAL QCD), Phys. Rev. **C91**, 1, 011001 (2015), [arXiv:1408.4892].
- [109] K. Polejaeva and A. Rusetsky, Eur. Phys. J. **A48**, 67 (2012), [arXiv:1203.1241]; R. A. Briceño and Z. Davoudi, Phys. Rev. **D87**, 9, 094507 (2013), [arXiv:1212.3398]; M. T. Hansen and S. R. Sharpe, Phys. Rev. **D90**, 11, 116003 (2014), [arXiv:1408.5933]; M. T. Hansen and S. R. Sharpe, Phys. Rev. **D92**, 11, 114509 (2015), [arXiv:1504.04248]; R. A. Briceño, M. T. Hansen and S. R. Sharpe, Phys. Rev. **D95**, 7, 074510 (2017), [arXiv:1701.07465]; H. W. Hammer, J. Y. Pang and A. Rusetsky, JHEP **10**, 115 (2017), [arXiv:1707.02176].
- [110] R. A. Briceño, M. T. Hansen and S. R. Sharpe, Phys. Rev. **D99**, 1, 014516 (2019), [arXiv:1810.01429].
- [111] M. Mai and M. Döring, Eur. Phys. J. **A53**, 12, 240 (2017), [arXiv:1709.08222].
- [112] M. T. Hansen and S. R. Sharpe (2019), [arXiv:1901.00483].
- [113] L. Lellouch and M. Luscher, Commun. Math. Phys. **219**, 31 (2001), [hep-lat/0003023].
- [114] T. Blum *et al.*, Phys. Rev. Lett. **108**, 141601 (2012), [arXiv:1111.1699]; T. Blum *et al.*, Phys. Rev. **D86**, 074513 (2012), [arXiv:1206.5142].
- [115] Z. Bai *et al.* (RBC, UKQCD), Phys. Rev. Lett. **115**, 21, 212001 (2015), [arXiv:1505.07863].
- [116] T. Blum *et al.*, Phys. Rev. **D91**, 7, 074502 (2015), [arXiv:1502.00263].
- [117] V. Bernard *et al.*, JHEP **01**, 019 (2011), [arXiv:1010.6018]; M. Doring *et al.*, Eur. Phys. J. **A47**, 139 (2011), [arXiv:1107.3988]; M. T. Hansen and S. R. Sharpe, Phys. Rev. **D86**, 016007 (2012), [arXiv:1204.0826]; R. A. Briceño and Z. Davoudi, Phys. Rev. **D88**, 9, 094507 (2013), [arXiv:1204.1110].
- [118] R. A. Briceño, M. T. Hansen and A. Walker-Loud, Phys. Rev. **D91**, 3, 034501 (2015), [arXiv:1406.5965].
- [119] R. A. Briceño and M. T. Hansen, Phys. Rev. **D94**, 1, 013008 (2016), [arXiv:1509.08507].
- [120] R. A. Briceño *et al.*, Phys. Rev. **D93**, 11, 114508 (2016), [arXiv:1604.03530].
- [121] D. Agadjanov *et al.*, JHEP **06**, 043 (2016), [arXiv:1603.07205].
- [122] S. Hashimoto, PTEP **2017**, 5, 053B03 (2017), [arXiv:1703.01881].
- [123] X. Feng *et al.*, Phys. Rev. Lett. **107**, 081802 (2011), [arXiv:1103.4818].
- [124] P. Boyle *et al.*, Phys. Rev. **D85**, 074504 (2012), [arXiv:1107.1497].
- [125] M. Della Morte *et al.*, JHEP **03**, 055 (2012), [arXiv:1112.2894].
- [126] F. Burger *et al.* (ETM), JHEP **02**, 099 (2014), [arXiv:1308.4327].
- [127] B. Chakraborty *et al.* (HPQCD), Phys. Rev. **D89**, 11, 114501 (2014), [arXiv:1403.1778].
- [128] F. Burger, K. Jansen, M. Petschlies and G. Pientka, Eur. Phys. J. **C76**, 464 (2016).
- [129] B. Chakraborty *et al.*, Phys. Rev. **D93**, 7, 074509 (2016), [arXiv:1512.03270].
- [130] B. Chakraborty *et al.*, Phys. Rev. **D96**, 3, 034516 (2017), [arXiv:1601.03071].
- [131] T. Blum *et al.* (RBC/UKQCD), JHEP **04**, 063 (2016), [Erratum: JHEP05,034(2017)], [arXiv:1602.01767].
- [132] S. Borsanyi *et al.*, Phys. Rev. **D96**, 7, 074507 (2017), [arXiv:1612.02364].
- [133] M. Della Morte *et al.*, JHEP **10**, 020 (2017), [arXiv:1705.01775].

- [134] S. Borsanyi *et al.* (Budapest-Marseille-Wuppertal), Phys. Rev. Lett. **121**, 2, 022002 (2018), [arXiv:1711.04980].
- [135] T. Blum *et al.* (RBC, UKQCD), Phys. Rev. Lett. **121**, 2, 022003 (2018), [arXiv:1801.07224].
- [136] B. Chakraborty *et al.*, Phys. Rev. **D98**, 9, 094503 (2018), [arXiv:1806.08190].
- [137] D. Giusti, F. Sanfilippo and S. Simula, Phys. Rev. **D98**, 11, 114504 (2018), [arXiv:1808.00887].
- [138] C. T. H. Davies *et al.* (Fermilab Lattice, LATTICE-HPQCD, MILC) (2019), [arXiv:1902.04223].
- [139] T. Blum, Phys. Rev. Lett. **91**, 052001 (2003), [hep-lat/0212018].
- [140] T. Blum *et al.*, Phys. Rev. Lett. **114**, 1, 012001 (2015), [arXiv:1407.2923].
- [141] T. Blum *et al.*, Phys. Rev. **D93**, 1, 014503 (2016), [arXiv:1510.07100].
- [142] J. Green *et al.*, Phys. Rev. Lett. **115**, 22, 222003 (2015), [arXiv:1507.01577].
- [143] T. Blum *et al.*, Phys. Rev. Lett. **118**, 2, 022005 (2017), [arXiv:1610.04603].
- [144] T. Blum *et al.*, Phys. Rev. **D96**, 3, 034515 (2017), [arXiv:1705.01067].
- [145] X. Feng *et al.*, Phys. Rev. Lett. **109**, 182001 (2012), [arXiv:1206.1375].
- [146] A. Gérardin, H. B. Meyer and A. Nyffeler, Phys. Rev. **D94**, 7, 074507 (2016), [arXiv:1607.08174].
- [147] A. Gérardin *et al.*, Phys. Rev. **D98**, 7, 074501 (2018), [arXiv:1712.00421].
- [148] Z. Bai *et al.*, Phys. Rev. Lett. **113**, 112003 (2014), [arXiv:1406.0916].
- [149] N. H. Christ *et al.* (RBC, UKQCD), Phys. Rev. **D92**, 9, 094512 (2015), [arXiv:1507.03094].
- [150] N. H. Christ *et al.* (RBC, UKQCD), Phys. Rev. **D93**, 11, 114517 (2016), [arXiv:1605.04442].
- [151] N. H. Christ *et al.*, Phys. Rev. **D94**, 11, 114516 (2016), [arXiv:1608.07585].
- [152] Z. Bai *et al.*, Phys. Rev. Lett. **118**, 25, 252001 (2017), [arXiv:1701.02858].
- [153] Z. Bai *et al.*, Phys. Rev. **D98**, 7, 074509 (2018), [arXiv:1806.11520].
- [154] C. Bernard *et al.*, Nucl. Phys. Proc. Suppl. **119**, 170 (2003), [hep-lat/0209086].
- [155] S. Perantonis and C. Michael, Nucl. Phys. **B347**, 854 (1990).
- [156] G. S. Bali and K. Schilling, Phys. Rev. **D46**, 2636 (1992).
- [157] S. Necco and R. Sommer, Nucl. Phys. **B622**, 328 (2002), [hep-lat/0108008].
- [158] J. M. Blairon *et al.*, Nucl. Phys. **B180**, 439 (1981).
- [159] H. Fukaya *et al.* (JLQCD), Phys. Rev. Lett. **104**, 122002 (2010), [Erratum: Phys. Rev. Lett.105,159901(2010)], [arXiv:0911.5555].
- [160] H. Fukaya *et al.* (JLQCD, TWQCD), Phys. Rev. **D83**, 074501 (2011), [arXiv:1012.4052].
- [161] L. Giusti and M. Luscher, JHEP **03**, 013 (2009), [arXiv:0812.3638].
- [162] K. Cichy, E. Garcia-Ramos and K. Jansen, JHEP **10**, 175 (2013), [arXiv:1303.1954].
- [163] G. P. Engel *et al.*, Phys. Rev. Lett. **114**, 11, 112001 (2015), [arXiv:1406.4987].
- [164] G. P. Engel *et al.*, Phys. Rev. **D91**, 5, 054505 (2015), [arXiv:1411.6386].
- [165] S. Aoki *et al.*, Eur. Phys. J. **C77**, 2, 112 (2017), [arXiv:1607.00299].
- [166] T. Blum *et al.* (RBC, UKQCD), Phys. Rev. **D93**, 7, 074505 (2016), [arXiv:1411.7017].
- [167] B. J. Choi *et al.* (SWME), Phys. Rev. **D93**, 1, 014511 (2016), [arXiv:1509.00592].
- [168] J. Laiho and R. S. Van de Water, PoS **LATTICE2011**, 293 (2011), [arXiv:1112.4861].
- [169] E. Gamiz *et al.* (HPQCD), Phys. Rev. **D80**, 014503 (2009), [arXiv:0902.1815].
- [170] Y. Aoki *et al.*, Phys. Rev. **D91**, 11, 114505 (2015), [arXiv:1406.6192].
- [171] A. Bazavov *et al.*, Phys. Rev. **D97**, 3, 034513 (2018), [arXiv:1706.04622].
- [172] M. Ademollo and R. Gatto, Phys. Rev. Lett. **13**, 264 (1964).
- [173] H. Leutwyler and M. Roos, Z. Phys. **C25**, 91 (1984).
- [174] P. A. Boyle *et al.*, Phys. Rev. Lett. **100**, 141601 (2008), [arXiv:0710.5136].
- [175] V. Lubicz *et al.* (ETM), Phys. Rev. **D80**, 111502 (2009), [arXiv:0906.4728]; V. Lubicz *et al.* (ETM), PoS **LATTICE2010**, 316 (2010), [arXiv:1012.3573].
- [176] P. A. Boyle *et al.* (RBC-UKQCD), Eur. Phys. J. **C69**, 159 (2010), [arXiv:1004.0886].
- [177] A. Bazavov *et al.*, Phys. Rev. **D87**, 073012 (2013), [arXiv:1212.4993].
- [178] T. Kaneko *et al.* (JLQCD), PoS **LATTICE2012**, 111 (2012), [arXiv:1211.6180].
- [179] P. A. Boyle *et al.*, JHEP **08**, 132 (2013), [arXiv:1305.7217].
- [180] P. A. Boyle *et al.* (RBC/UKQCD), JHEP **06**, 164 (2015), [arXiv:1504.01692].
- [181] N. Carrasco *et al.*, Phys. Rev. **D93**, 11, 114512 (2016), [arXiv:1602.04113].
- [182] H. Na *et al.*, Phys. Rev. **D82**, 114506 (2010), [arXiv:1008.4562].
- [183] H. Na *et al.*, Phys. Rev. **D84**, 114505 (2011), [arXiv:1109.1501].
- [184] V. Lubicz *et al.* (ETM), Phys. Rev. **D96**, 5, 054514 (2017), [Erratum: Phys. Rev.D99,no.9,099902(2019)], [arXiv:1706.03017].
- [185] T. Kaneko *et al.* (JLQCD), EPJ Web Conf. **175**, 13007 (2018), [arXiv:1711.11235].
- [186] E. Dalgic *et al.*, Phys. Rev. **D73**, 074502 (2006), [Erratum: Phys. Rev.D75,119906(2007)], [hep-lat/0601021].
- [187] J. M. Flynn *et al.*, Phys. Rev. **D91**, 7, 074510 (2015), [arXiv:1501.05373].
- [188] J. A. Bailey *et al.* (Fermilab Lattice, MILC), Phys. Rev. **D92**, 1, 014024 (2015), [arXiv:1503.07839].
- [189] B. Colquhoun *et al.*, Phys. Rev. **D93**, 3, 034502 (2016), [arXiv:1510.07446].
- [190] Z. Gelzer *et al.*, EPJ Web Conf. **175**, 13024 (2018), [arXiv:1710.09442].
- [191] B. Colquhoun, S. Hashimoto and T. Kaneko, PoS **LATTICE2018**, 274 (2018), [arXiv:1811.00227].
- [192] C. Burrely, B. Machet and E. de Rafael, Nucl. Phys. **B189**, 157 (1981); C. G. Boyd, B. Grinstein and R. F. Lebed, Phys. Rev. Lett. **74**, 4603 (1995), [hep-ph/9412324]; T. Becher and R. J. Hill, Phys. Lett. **B633**, 61 (2006), [hep-ph/0509090]; C. Burrely, I. Caprini and L. Lellouch, Phys. Rev. **D79**, 013008 (2009), [Erratum: Phys. Rev.D82,099902(2010)], [arXiv:0807.2722].
- [193] M. C. Arnesen *et al.*, Phys. Rev. Lett. **95**, 071802 (2005), [hep-ph/0504209].
- [194] J. A. Bailey *et al.*, Phys. Rev. **D79**, 054507 (2009), [arXiv:0811.3640].
- [195] S. Hashimoto *et al.*, Phys. Rev. **D61**, 014502 (1999), [hep-ph/9906376].

- [196] S. Hashimoto *et al.*, Phys. Rev. **D66**, 014503 (2002), [hep-ph/0110253].
- [197] C. Bernard *et al.*, Phys. Rev. **D79**, 014506 (2009), [arXiv:0808.2519].
- [198] J. A. Bailey *et al.* (Fermilab Lattice, MILC), Phys. Rev. **D89**, 11, 114504 (2014), [arXiv:1403.0635].
- [199] J. Harrison, C. Davies and M. Wingate (HPQCD), Phys. Rev. **D97**, 5, 054502 (2018), [arXiv:1711.11013].
- [200] E. McLean *et al.*, Phys. Rev. **D99**, 11, 114512 (2019), [arXiv:1904.02046].
- [201] T. Bhattacharya *et al.* (LANL/SWME), PoS **LATTICE2018**, 283 (2018).
- [202] J. A. Bailey *et al.* (MILC), Phys. Rev. **D92**, 3, 034506 (2015), [arXiv:1503.07237].
- [203] H. Na *et al.* (HPQCD), Phys. Rev. **D92**, 5, 054510 (2015), [Erratum: Phys. Rev.D93,no.11,119906(2016)], [arXiv:1505.03925].
- [204] A. V. Avilés-Casco *et al.* (Fermilab Lattice, MILC), PoS **LATTICE2018**, 282 (2019), [arXiv:1901.00216].
- [205] T. Kaneko *et al.* (JLQCD), PoS **LATTICE2018**, 311 (2018), [arXiv:1811.00794].
- [206] W. Detmold, C. Lehner and S. Meinel, Phys. Rev. **D92**, 3, 034503 (2015), [arXiv:1503.01421].
- [207] W. Detmold and S. Meinel, Phys. Rev. **D93**, 7, 074501 (2016), [arXiv:1602.01399].
- [208] R. R. Horgan *et al.*, Phys. Rev. **D89**, 9, 094501 (2014), [arXiv:1310.3722].
- [209] J. A. Bailey *et al.*, Phys. Rev. **D93**, 2, 025026 (2016), [arXiv:1509.06235].
- [210] D. Du *et al.*, Phys. Rev. **D93**, 3, 034005 (2016), [arXiv:1510.02349].
- [211] C. T. H. Davies *et al.* (HPQCD), Phys. Rev. **D78**, 114507 (2008), [arXiv:0807.1687].
- [212] C. McNeile *et al.*, Phys. Rev. **D82**, 034512 (2010), [arXiv:1004.4285].
- [213] E. Shintani *et al.*, Phys. Rev. **D82**, 7, 074505 (2010), [Erratum: Phys. Rev.D89,no.9,099903(2014)], [arXiv:1002.0371].
- [214] R. J. Hudspith *et al.*, Mod. Phys. Lett. **A31**, 32, 1630037 (2016).
- [215] I. Allison *et al.* (HPQCD), Phys. Rev. **D78**, 054513 (2008), [arXiv:0805.2999].
- [216] B. Chakraborty *et al.*, Phys. Rev. **D91**, 5, 054508 (2015), [arXiv:1408.4169].
- [217] Y. Maezawa and P. Petreczky, Phys. Rev. **D94**, 3, 034507 (2016), [arXiv:1606.08798].
- [218] Q. Mason *et al.* (HPQCD, UKQCD), Phys. Rev. Lett. **95**, 052002 (2005), [hep-lat/0503005].
- [219] A. Bazavov *et al.*, Phys. Rev. **D86**, 114031 (2012), [arXiv:1205.6155].
- [220] A. Bazavov *et al.*, Phys. Rev. **D90**, 7, 074038 (2014), [arXiv:1407.8437].
- [221] F. Karbstein, M. Wagner and M. Weber, Phys. Rev. **D98**, 11, 114506 (2018), [arXiv:1804.10909].
- [222] H. Takaura *et al.*, JHEP **04**, 155 (2019), [arXiv:1808.01643].
- [223] B. Blossier *et al.*, Phys. Rev. **D85**, 034503 (2012), [arXiv:1110.5829]; B. Blossier *et al.*, Phys. Rev. Lett. **108**, 262002 (2012), [arXiv:1201.5770].
- [224] S. Zafeiropoulos *et al.*, Phys. Rev. Lett. **122**, 16, 162002 (2019), [arXiv:1902.08148].
- [225] S. Aoki *et al.* (PACS-CS), JHEP **10**, 053 (2009), [arXiv:0906.3906].
- [226] P. Fritzsche *et al.*, PoS **LATTICE2014**, 291 (2014), [arXiv:1411.7648].
- [227] M. Bruno *et al.* (ALPHA), Phys. Rev. Lett. **119**, 10, 102001 (2017), [arXiv:1706.03821].
- [228] S. Durr *et al.*, Phys. Lett. **B701**, 265 (2011), [arXiv:1011.2403].
- [229] S. Durr *et al.*, JHEP **08**, 148 (2011), [arXiv:1011.2711].
- [230] S. Capitani *et al.*, Nucl. Phys. **B544**, 669 (1999), [Erratum: Nucl. Phys.B582,762(2000)], [hep-lat/9810063].
- [231] A. Bussone *et al.* (ETM), Phys. Rev. **D93**, 11, 114505 (2016), [arXiv:1603.04306].
- [232] SISSA, *Proceedings, 36th International Symposium on Lattice Field Theory (Lattice 2018)*, volume LATTICE2018, SISSA (2019), URL <https://pos.sissa.it/334/>.
- [233] W. Detmold *et al.* (USQCD) (2019), [arXiv:1904.09512].
- [234] A. S. Kronfeld *et al.* (USQCD) (2019), [arXiv:1904.09931].
- [235] R. C. Brower *et al.* (USQCD) (2019), [arXiv:1904.09964].
- [236] C. Lehner *et al.* (USQCD) (2019), [arXiv:1904.09479].
- [237] A. Bazavov *et al.* (USQCD) (2019), [arXiv:1904.09951].
- [238] V. Cirigliano *et al.* (USQCD) (2019), [arXiv:1904.09704].
- [239] B. Joó *et al.* (USQCD) (2019), [arXiv:1904.09725].

18. Structure Functions

Revised August 2019 by E.C. Aschenauer (BNL), R.S. Thorne (UCL) and R. Yoshida (Jefferson Lab).

18.1 Deep inelastic scattering

High-energy lepton-nucleon scattering plays a key role in determining the partonic structure of the proton. The process $\ell N \rightarrow \ell' X$ is illustrated in Fig. 18.1. The filled circle in this figure represents the internal structure of the proton which can be expressed in terms of structure functions.

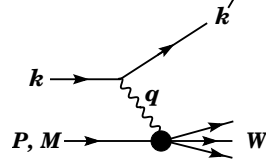


Figure 18.1: Kinematic quantities for the description of deep inelastic scattering. The quantities k and k' are the four-momenta of the incoming and outgoing leptons, P is the four-momentum of a nucleon with mass M , and W is the mass of the recoiling system X . The exchanged particle is a γ , W^\pm , or Z ; it transfers four-momentum $q = k - k'$ to the nucleon.

Invariant quantities:

$\nu = \frac{q \cdot P}{M} = E - E'$ is the lepton's energy loss in the nucleon rest frame (in earlier literature sometimes $\nu = q \cdot P$). Here, E and E' are the initial and final lepton energies in the nucleon rest frame.

$Q^2 = -q^2 = 2(E E' - \vec{k} \cdot \vec{k}') - m_\ell^2 - m_{\ell'}^2$, where m_ℓ ($m_{\ell'}$) is the initial (final) lepton mass. If $E E' \sin^2(\theta/2) \gg m_\ell^2, m_{\ell'}^2$, then

$\approx 4E E' \sin^2(\theta/2)$, where θ is the lepton's scattering angle with respect to the lepton beam direction.

$x = \frac{Q^2}{2M\nu}$ where, in the parton model, x is the fraction of the nucleon's momentum carried by the struck quark. Beyond leading order the equation remains the definition of x , but this is no longer identical to nucleon momentum fraction.

$y = \frac{q \cdot P}{k \cdot P} = \frac{\nu}{E}$ is the fraction of the lepton's energy lost in the nucleon rest frame.

$W^2 = (P + q)^2 = M^2 + 2M\nu - Q^2$ is the mass squared of the system X recoiling against the scattered lepton.

$s = (k + P)^2 = \frac{Q^2}{xy} + M^2 + m_\ell^2$ is the center-of-mass energy squared of the lepton-nucleon system.

The process in Fig. 18.1 is called deep ($Q^2 \gg M^2$) inelastic ($W^2 \gg M^2$) scattering (DIS). In what follows, the masses of the initial and scattered leptons, m_ℓ and $m_{\ell'}$, are neglected.

18.1.1 DIS cross sections

The double-differential cross section for deep inelastic scattering can be expressed in terms of kinematic variables in several ways.

$$\frac{d^2\sigma}{dx dy} = x(s - M^2) \frac{d^2\sigma}{dx dQ^2} = \frac{2\pi M\nu}{E'} \frac{d^2\sigma}{d\Omega_{N\text{rest}} dE'} \quad (18.1)$$

In lowest-order perturbation theory, the cross section for the scattering of polarized leptons on polarized nucleons can be expressed in terms of the products of leptonic and hadronic tensors associated with the coupling of the exchanged bosons at the upper and lower vertices in Fig. 18.1 (see Refs. [1–4])

$$\frac{d^2\sigma}{dx dy} = \frac{2\pi y \alpha^2}{Q^4} \sum_j \eta_j L_j^{\mu\nu} W_{\mu\nu}^j \quad (18.2)$$

For neutral-current processes, the summation is over $j = \gamma, Z$ and γZ representing photon and Z exchange and the interference

between them, whereas for charged-current interactions there is only W exchange, $j = W$. (For transverse nucleon polarization, there is a dependence on the azimuthal angle of the scattered lepton.) The lepton tensor $L_{\mu\nu}$ is associated with the coupling of the exchange boson to the leptons. For incoming leptons of charge $e = \pm 1$ and helicity $\lambda = \pm 1$,

$$\begin{aligned} L_{\mu\nu}^\gamma &= 2(k_\mu k'_\nu + k'_\mu k_\nu - (k \cdot k' - m_\ell^2)g_{\mu\nu} - i\lambda \varepsilon_{\mu\nu\alpha\beta} k^\alpha k'^\beta), \\ L_{\mu\nu}^{\gamma Z} &= (g_V^e + e\lambda g_A^e) L_{\mu\nu}^\gamma, \quad L_{\mu\nu}^Z = (g_V^e + e\lambda g_A^e)^2 L_{\mu\nu}^\gamma, \\ L_{\mu\nu}^W &= (1 + e\lambda)^2 L_{\mu\nu}^\gamma, \end{aligned} \quad (18.3)$$

where $g_V^e = -\frac{1}{2} + 2\sin^2\theta_W$, $g_A^e = -\frac{1}{2}$.

Although here the helicity formalism is adopted, an alternative approach is to express the tensors in Eq. (18.3) in terms of the polarization of the lepton.

The factors η_j in Eq. (18.2) denote the ratios of the corresponding propagators and couplings to the photon propagator and coupling squared

$$\begin{aligned} \eta_\gamma &= 1; \quad \eta_{\gamma Z} = \left(\frac{G_F M_Z^2}{2\sqrt{2}\pi\alpha} \right) \left(\frac{Q^2}{Q^2 + M_Z^2} \right); \\ \eta_Z &= \eta_{\gamma Z}^2; \quad \eta_W = \frac{1}{2} \left(\frac{G_F M_W^2}{4\pi\alpha} \frac{Q^2}{Q^2 + M_W^2} \right)^2. \end{aligned} \quad (18.4)$$

The hadronic tensor, which describes the interaction of the appropriate electroweak currents with the target nucleon, is given by

$$W_{\mu\nu} = \frac{1}{4\pi} \int d^4z e^{iq \cdot z} \langle P, S | [J_\mu^\dagger(z), J_\nu(0)] | P, S \rangle, \quad (18.5)$$

where J_α is the hadronic contribution to the electromagnetic, or weak current and S denotes the nucleon-spin 4-vector, with $S^2 = -M^2$ and $S \cdot P = 0$.

18.2 Structure functions of the proton

The structure functions are defined in terms of the hadronic tensor (see Refs. [1–3])

$$\begin{aligned} W_{\mu\nu} &= \left(-g_{\mu\nu} + \frac{q_\mu q_\nu}{q^2} \right) F_1(x, Q^2) + \frac{\hat{P}_\mu \hat{P}_\nu}{P \cdot q} F_2(x, Q^2) \\ &- i\varepsilon_{\mu\nu\alpha\beta} \frac{q^\alpha P^\beta}{2P \cdot q} F_3(x, Q^2) \\ &+ i\varepsilon_{\mu\nu\alpha\beta} \frac{q^\alpha}{P \cdot q} \left[S^\beta g_1(x, Q^2) + \left(S^\beta - \frac{S \cdot q}{P \cdot q} P^\beta \right) g_2(x, Q^2) \right] \\ &+ \frac{1}{P \cdot q} \left[\frac{1}{2} (\hat{P}_\mu \hat{S}_\nu + \hat{S}_\mu \hat{P}_\nu) - \frac{S \cdot q}{P \cdot q} \hat{P}_\mu \hat{P}_\nu \right] g_3(x, Q^2) \\ &+ \frac{S \cdot q}{P \cdot q} \left[\frac{\hat{P}_\mu \hat{P}_\nu}{P \cdot q} g_4(x, Q^2) + \left(-g_{\mu\nu} + \frac{q_\mu q_\nu}{q^2} \right) g_5(x, Q^2) \right] \end{aligned} \quad (18.6)$$

where

$$\hat{P}_\mu = P_\mu - \frac{P \cdot q}{q^2} q_\mu, \quad \hat{S}_\mu = S_\mu - \frac{S \cdot q}{q^2} q_\mu \quad (18.7)$$

In [2], the definition of $W_{\mu\nu}$ with $\mu \leftrightarrow \nu$ is adopted, which changes the sign of the $\varepsilon_{\mu\nu\alpha\beta}$ terms in Eq. (18.6), although the formulae given below are unchanged. Ref. [1] tabulates the relation between the structure functions defined in Eq. (18.6) and other choices available in the literature.

The cross sections for neutral- and charged-current deep inelastic scattering on unpolarized nucleons can be written in terms of

the structure functions in the generic form

$$\begin{aligned} \frac{d^2\sigma^i}{dx dy} &= \frac{4\pi\alpha^2}{xyQ^2} \eta^i \left\{ \left(1 - y - \frac{x^2 y^2 M^2}{Q^2} \right) F_2^i \right. \\ &\quad \left. + y^2 x F_1^i \mp \left(y - \frac{y^2}{2} \right) x F_3^i \right\}, \end{aligned} \quad (18.8)$$

where $i = \text{NC, CC}$ corresponds to neutral-current ($eN \rightarrow eX$) or charged-current ($eN \rightarrow \nu X$ or $\nu N \rightarrow eX$) processes, respectively. For incoming neutrinos, $L_{\mu\nu}^W$ of Eq. (18.3) is still true, but with e, λ corresponding to the outgoing charged lepton. In the last term of Eq. (18.8), the $-$ sign is taken for an incoming e^+ or $\bar{\nu}$ and the $+$ sign for an incoming e^- or ν . The factor $\eta^{\text{NC}} = 1$ for unpolarized e^\pm beams, whereas

$$\eta^{\text{CC}} = (1 \pm \lambda)^2 \eta_W \quad (18.9)$$

with \pm for ℓ^\pm ; and where λ is the helicity of the incoming lepton and η_W is defined in Eq. (18.4); for incoming neutrinos $\eta^{\text{CC}} = 4\eta_W$. The CC structure functions, which derive exclusively from W exchange, are

$$F_1^{\text{CC}} = F_1^W, \quad F_2^{\text{CC}} = F_2^W, \quad xF_3^{\text{CC}} = xF_3^W. \quad (18.10)$$

The NC structure functions $F_2^\gamma, F_2^{\gamma Z}, F_2^Z$ are, for $e^\pm N \rightarrow e^\pm X$, given by [5],

$$F_2^{\text{NC}} = F_2^\gamma - (g_V^e \pm \lambda g_A^e) \eta_{\gamma Z} F_2^{\gamma Z} + (g_V^e \mp \lambda g_A^e)^2 \pm 2\lambda g_V^e g_A^e \eta_Z F_2^Z \quad (18.11)$$

and similarly for F_1^{NC} , whereas

$$xF_3^{\text{NC}} = -(g_A^e \pm \lambda g_V^e) \eta_{\gamma Z} x F_3^{\gamma Z} + [2g_V^e g_A^e \pm \lambda (g_V^e \mp \lambda g_A^e)] \eta_Z x F_3^Z. \quad (18.12)$$

The polarized cross-section difference

$$\Delta\sigma = \sigma(\lambda_n = -1, \lambda_\ell) - \sigma(\lambda_n = 1, \lambda_\ell), \quad (18.13)$$

where λ_ℓ, λ_n are the helicities (± 1) of the incoming lepton and nucleon, respectively, may be expressed in terms of the five structure functions $g_{1,\dots,5}(x, Q^2)$ of Eq. (18.6). Explicitly,

$$\begin{aligned} \frac{d^2\Delta\sigma^i}{dx dy} &= \frac{8\pi\alpha^2}{xyQ^2} \eta^i \left\{ -\lambda_\ell y \left(2 - y - 2x^2 y^2 \frac{M^2}{Q^2} \right) x g_1^i \right. \\ &\quad \left. + \lambda_\ell 4x^3 y^2 \frac{M^2}{Q^2} g_2^i + 2x^2 y \frac{M^2}{Q^2} \left(1 - y - x^2 y^2 \frac{M^2}{Q^2} \right) g_3^i \right. \\ &\quad \left. - \left(1 + 2x^2 y \frac{M^2}{Q^2} \right) \left[\left(1 - y - x^2 y^2 \frac{M^2}{Q^2} \right) g_4^i + x y^2 g_5^i \right] \right\} \end{aligned} \quad (18.14)$$

with $i = \text{NC or CC}$ as before. The Eq. (18.13) corresponds to the difference of antiparallel minus parallel spins of the incoming particles for e^- or ν initiated reactions, but the difference of parallel minus antiparallel for e^+ or $\bar{\nu}$ initiated processes. For longitudinal nucleon polarization, the contributions of g_2 and g_3 are suppressed by powers of M^2/Q^2 . These structure functions give an unsuppressed contribution to the cross section for transverse polarization [1], but in this case the cross-section difference vanishes as $M/Q \rightarrow 0$.

Because the same tensor structure occurs in the spin-dependent and spin-independent parts of the hadronic tensor of Eq. (18.6) in the $M^2/Q^2 \rightarrow 0$ limit, the differential cross-section difference of Eq. (18.14) may be obtained from the differential cross section Eq. (18.8) by replacing

$$F_1 \rightarrow -g_5, \quad F_2 \rightarrow -g_4, \quad F_3 \rightarrow 2g_1, \quad (18.15)$$

and multiplying by two, since the total cross section is the average over the initial-state polarizations. In this limit, Eq. (18.8) and Eq. (18.14) may be written in the form

$$\begin{aligned} \frac{d^2\sigma^i}{dx dy} &= \frac{2\pi\alpha^2}{xyQ^2} \eta^i \left[Y_+ F_2^i \mp Y_- x F_3^i - y^2 F_L^i \right], \\ \frac{d^2\Delta\sigma^i}{dx dy} &= \frac{4\pi\alpha^2}{xyQ^2} \eta^i \left[-Y_+ g_4^i \mp Y_- 2x g_1^i + y^2 g_L^i \right], \end{aligned} \quad (18.16)$$

with $i = \text{NC or CC}$, where $Y_\pm = 1 \pm (1 - y)^2$ and

$$F_L^i = F_2^i - 2x F_1^i, \quad g_L^i = g_4^i - 2x g_5^i. \quad (18.17)$$

In the naive quark-parton model, the analogy with the Callan-Gross relations [6] $F_L^i = 0$, are the Dicus relations [7] $g_L^i = 0$. Therefore, there are only two independent polarized structure functions: g_1 (parity conserving) and g_5 (parity violating), in analogy with the unpolarized structure functions F_1 and F_3 .

18.2.1 Structure functions in the quark-parton model

In the naive quark-parton model [8, 9], contributions to the structure functions F^i and g^i can be expressed in terms of the quark distribution functions $q(x, Q^2)$ of the proton, where $q = u, \bar{u}, d, \bar{d}$ etc. The quantity $q(x, Q^2) dx$ is the number of quarks (or antiquarks) of designated flavor that carry a momentum fraction between x and $x + dx$ of the proton's momentum in a frame in which the proton momentum is large.

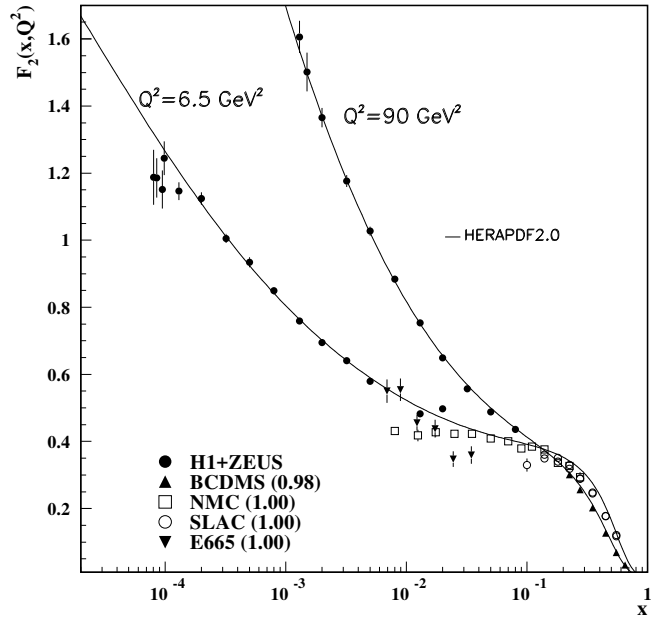


Figure 18.2: The proton structure function F_2^p given at two Q^2 values (6.5 GeV^2 and 90 GeV^2), which exhibit scaling at the ‘pivot’ point $x \sim 0.14$. See the captions in Fig. 18.8 and Fig. 18.10 for the references of the data. The various data sets have been renormalized by the factors shown in brackets in the key to the plot, which were globally determined in a previous HERAPDF analysis [10]. The curves were obtained using the PDFs from the HERAPDF analysis [11]. In practice, data for the reduced cross section, $F_2(x, Q^2) - (y^2/Y_+)F_L(x, Q^2)$, were fitted, rather than F_2 and F_L separately. The agreement between data and theory at low Q^2 and x can be improved by a positive higher-twist correction to $F_L(x, Q^2)$ [12, 13] (see Fig. 8 of Ref. [13]), or small- x resummation [14, 15].

For the neutral-current processes $ep \rightarrow eX$,

$$\begin{aligned} [F_2^\gamma, F_2^{\gamma Z}, F_2^Z] &= x \sum_q [e_q^2, 2e_q g_V^q, g_V^{q^2} + g_A^{q^2}] (q + \bar{q}), \\ [F_3^\gamma, F_3^{\gamma Z}, F_3^Z] &= \sum_q [0, 2e_q g_A^q, 2g_V^q g_A^q] (q - \bar{q}), \\ [g_1^\gamma, g_1^{\gamma Z}, g_1^Z] &= \frac{1}{2} \sum_q [e_q^2, 2e_q g_V^q, g_V^{q^2} + g_A^{q^2}] (\Delta q + \Delta \bar{q}), \\ [g_5^\gamma, g_5^{\gamma Z}, g_5^Z] &= \sum_q [0, e_q g_A^q, g_V^q g_A^q] (\Delta \bar{q} - \Delta q), \end{aligned} \quad (18.18)$$

where $g_V^q = \pm \frac{1}{2} - 2e_q \sin^2 \theta_W$ and $g_A^q = \pm \frac{1}{2}$, with \pm according to whether q is a u - or d -type quark respectively. The quantity Δq is the difference $q \uparrow - q \downarrow$ of the distributions with the quark spin parallel and antiparallel to the proton spin.

For the charged-current processes $e^- p \rightarrow \nu X$ and $\bar{\nu} p \rightarrow e^+ X$, the structure functions are:

$$\begin{aligned} F_2^{W^-} &= 2x(u + \bar{d} + \bar{s} + c \dots), \\ F_3^{W^-} &= 2(u - \bar{d} - \bar{s} + c \dots), \\ g_1^{W^-} &= (\Delta u + \Delta \bar{d} + \Delta \bar{s} + \Delta c \dots), \\ g_5^{W^-} &= (-\Delta u + \Delta \bar{d} + \Delta \bar{s} - \Delta c \dots), \end{aligned} \quad (18.19)$$

where only the active flavors have been kept and where CKM mixing has been neglected. For $e^+ p \rightarrow \bar{\nu} X$ and $\nu p \rightarrow e^- X$, the structure functions $F_i^{W^+}, g_i^{W^+}$ are obtained by the flavor interchanges $d \leftrightarrow u, s \leftrightarrow c$ in the expressions for $F_i^{W^-}, g_i^{W^-}$. The structure functions for scattering on a neutron are obtained from those of the proton by the interchange $u \leftrightarrow d$. For both the neutral- and charged-current processes, the quark-parton model predicts $2xF_1^i = F_2^i$ and $g_4^i = 2xg_5^i$.

Neglecting masses, the structure functions g_2 and g_3 contribute only to scattering from transversely polarized nucleons, and have no simple interpretation in terms of the quark-parton model. They arise from off-diagonal matrix elements $\langle P, \lambda' | [J_\mu^\dagger(z), J_\nu(0)] | P, \lambda \rangle$, where the proton helicities satisfy $\lambda' \neq \lambda$. In fact, the leading-twist contributions to both g_2 and g_3 are both twist-2 and twist-3, which contribute at the same order of Q^2 . The Wandzura-Wilczek relation [16] expresses the twist-2 part of g_2 in terms of g_1 as

$$g_2^i(x) = -g_1^i(x) + \int_x^1 \frac{dy}{y} g_1^i(y). \quad (18.20)$$

However, the twist-3 component of g_2 is unknown. Similarly, there is a relation expressing the twist-2 part of g_3 in terms of g_4 . A complete set of relations, including M^2/Q^2 effects, can be found in [17].

18.2.2 Structure functions and QCD

One of the most striking predictions of the quark-parton model is that the structure functions F_i, g_i scale, i.e., $F_i(x, Q^2) \rightarrow F_i(x)$ in the Bjorken limit that Q^2 and $\nu \rightarrow \infty$ with x fixed [18]. This property is related to the assumption that the transverse momentum of the partons in the infinite-momentum frame of the proton is small. In QCD, however, the radiation of hard gluons from the quarks violates this assumption, leading to logarithmic scaling violations, which are particularly large at small x , see Fig. 18.2. The radiation of gluons produces the evolution of the structure functions. As Q^2 increases, more and more gluons are radiated, which in turn split into $q\bar{q}$ pairs. This process leads both to the softening of the initial quark momentum distributions and to the growth of the gluon density and the $q\bar{q}$ sea as x decreases.

In QCD, the above processes are described in terms of scale-dependent parton distributions $f_a(x, \mu^2)$, where $a = g$ or q and, typically, μ is the scale of the probe Q . For parton distributions

x always refers to the nucleon momentum fraction of the parton, whereas for structure functions it retains the definition in Sec. 18.1. For $Q^2 \gg M^2$, the structure functions are of the form

$$F_i = \sum_a C_i^a \otimes f_a + \mathcal{O}(M^2/Q^2), \quad (18.21)$$

where \otimes denotes the convolution integral

$$C \otimes f = \int_x^1 \frac{dy}{y} C(y) f\left(\frac{x}{y}\right), \quad (18.22)$$

and where the coefficient functions C_i^a are given as a power series in α_s . The parton distribution f_a corresponds, at a given x , to the density of parton a in the proton integrated over transverse momentum k_t up to μ . Its evolution in μ is described in QCD by a DGLAP equation (see Refs. [19–22]) which has the schematic form

$$\frac{\partial f_a}{\partial \ln \mu^2} \sim \frac{\alpha_s(\mu^2)}{2\pi} \sum_b (P_{ab} \otimes f_b), \quad (18.23)$$

where the P_{ab} , which describe the parton splitting $b \rightarrow a$, are also given as a power series in α_s . Although perturbative QCD can predict, via Eq. (18.23), the evolution of the parton distribution functions from a particular scale, μ_0 , these DGLAP equations cannot predict them *a priori* at any particular μ_0 . Thus they must be measured at a starting point μ_0 before the predictions of QCD can be compared to the data at other scales, μ . In general, all observables involving a hard hadronic interaction (such as structure functions) can be expressed as a convolution of calculable, process-dependent coefficient functions and these universal parton distributions, e.g. Eq. (18.21).

It is often convenient to write the evolution equations in terms of the gluon, non-singlet (q^{NS}) and singlet (q^S) quark distributions, such that

$$q^{NS} = q_i - \bar{q}_i \quad (\text{or } q_i - q_j), \quad q^S = \sum_i (q_i + \bar{q}_i). \quad (18.24)$$

The non-singlet distributions have non-zero values of flavor quantum numbers, such as isospin and baryon number. The DGLAP evolution equations then take the form

$$\begin{aligned} \frac{\partial q^{NS}}{\partial \ln \mu^2} &= \frac{\alpha_s(\mu^2)}{2\pi} P_{qq} \otimes q^{NS}, \\ \frac{\partial}{\partial \ln \mu^2} \begin{pmatrix} q^S \\ g \end{pmatrix} &= \frac{\alpha_s(\mu^2)}{2\pi} \begin{pmatrix} P_{qq} & 2n_f P_{qg} \\ P_{gq} & P_{gg} \end{pmatrix} \otimes \begin{pmatrix} q^S \\ g \end{pmatrix}, \end{aligned} \quad (18.25)$$

where P are splitting functions that describe the probability of a given parton splitting into two others, and n_f is the number of (active) quark flavors. The leading-order Altarelli-Parisi [21]

Table 18.1: The main processes relevant to global PDF analyses, ordered in three groups: fixed-target experiments, HERA and the $p\bar{p}$ Tevatron / pp LHC. For each process we give an indication of their dominant partonic subprocesses, the primary partons which are probed and the approximate range of x constrained by the data.

Process	Subprocess	Partons	x range
$\ell^\pm \{p, n\} \rightarrow \ell^\pm X$	$\gamma^* q \rightarrow q$	q, \bar{q}, g	$x \gtrsim 0.01$
$\ell^\pm n/p \rightarrow \ell^\pm X$	$\gamma^* d/u \rightarrow d/u$	d/u	$x \gtrsim 0.01$
$pp \rightarrow \mu^+ \mu^- X$	$u\bar{u}, d\bar{d} \rightarrow \gamma^*$	\bar{q}	$0.015 \lesssim x \lesssim 0.35$
$pn/pp \rightarrow \mu^+ \mu^- X$	$(u\bar{d})/(u\bar{u}) \rightarrow \gamma^*$	\bar{d}/\bar{u}	$0.015 \lesssim x \lesssim 0.35$
$\nu(\bar{\nu}) N \rightarrow \mu^-(\mu^+) X$	$W^* q \rightarrow q'$	q, \bar{q}	$0.01 \lesssim x \lesssim 0.5$
$\nu N \rightarrow \mu^- \mu^+ X$	$W^* s \rightarrow c$	s	$0.01 \lesssim x \lesssim 0.2$
$\bar{\nu} N \rightarrow \mu^+ \mu^- X$	$W^* \bar{s} \rightarrow \bar{c}$	\bar{s}	$0.01 \lesssim x \lesssim 0.2$
$e^\pm p \rightarrow e^\pm X$	$\gamma^* q \rightarrow q$	g, q, \bar{q}	$10^{-4} \lesssim x \lesssim 0.1$
$e^+ p \rightarrow \bar{\nu} X$	$W^+ \{d, s\} \rightarrow \{u, c\}$	d, s	$x \gtrsim 0.01$
$e^\pm p \rightarrow e^\pm c\bar{c}X, e^\pm b\bar{b}X$	$\gamma^* c \rightarrow c, \gamma^* g \rightarrow c\bar{c}$	c, b, g	$10^{-4} \lesssim x \lesssim 0.01$
$e^\pm p \rightarrow \text{jet}+X$	$\gamma^* g \rightarrow q\bar{q}$	g	$0.01 \lesssim x \lesssim 0.1$
$p\bar{p}, pp \rightarrow \text{jet}+X$	$gg, qg, q\bar{q} \rightarrow 2j$	g, q	$0.00005 \lesssim x \lesssim 0.5$
$p\bar{p} \rightarrow (W^\pm \rightarrow \ell^\pm \nu) X$	$ud \rightarrow W^+, \bar{u}\bar{d} \rightarrow W^-$	u, d, \bar{u}, \bar{d}	$x \gtrsim 0.05$
$pp \rightarrow (W^\pm \rightarrow \ell^\pm \nu) X$	$u\bar{d} \rightarrow W^+, d\bar{u} \rightarrow W^-$	$u, d, \bar{u}, \bar{d}, g$	$x \gtrsim 0.001$
$p\bar{p}(pp) \rightarrow (Z \rightarrow \ell^+ \ell^-) X$	$uu, dd, ..(u\bar{u}, ..) \rightarrow Z$	$u, d, ..(g)$	$x \gtrsim 0.001$
$pp \rightarrow W^- c, W^+ \bar{c}$	$gs \rightarrow W^- c$	s, \bar{s}	$x \sim 0.01$
$pp \rightarrow (\gamma^* \rightarrow \ell^+ \ell^-) X$	$u\bar{u}, d\bar{d}, .. \rightarrow \gamma^*$	\bar{q}, g	$x \gtrsim 10^{-5}$
$pp \rightarrow (\gamma^* \rightarrow \ell^+ \ell^-) X$	$u\gamma, d\gamma, .. \rightarrow \gamma^*$	γ	$x \gtrsim 10^{-2}$
$pp \rightarrow b\bar{b} X, t\bar{t} X$	$gg \rightarrow b\bar{b}, t\bar{t}$	g	$x \gtrsim 10^{-5}, 10^{-2}$
$pp \rightarrow \text{exclusive } J/\psi, \Upsilon$	$\gamma^*(gg) \rightarrow J/\psi, \Upsilon$	g	$x \gtrsim 10^{-5}, 10^{-4}$
$pp \rightarrow \gamma X$	$gq \rightarrow \gamma q, g\bar{q} \rightarrow \gamma\bar{q}$	g	$x \gtrsim 0.005$

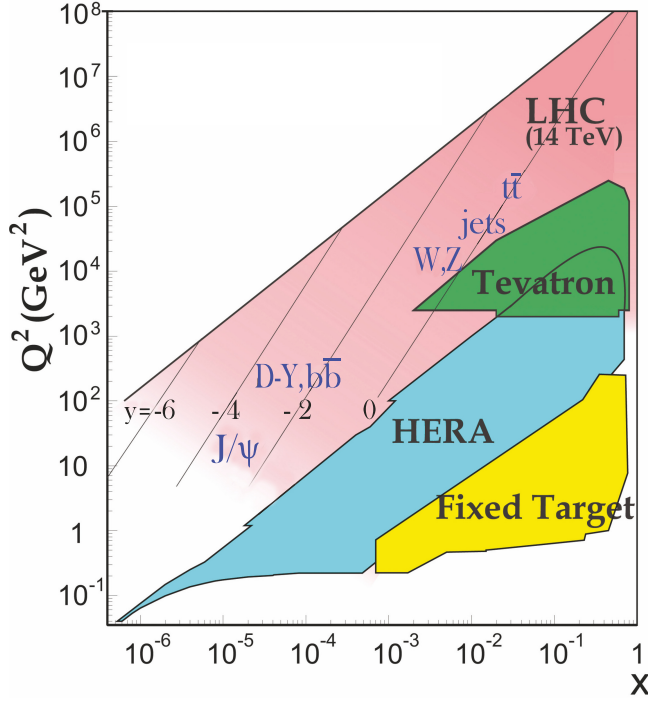


Figure 18.3: Kinematic domains in x and Q^2 probed by fixed-target and collider experiments, where here Q^2 can refer either the literal Q^2 for deep inelastic scattering, or the hard scale of the process in hadron-hadron collisions, e.g. invariant mass or transverse momentum p_T^2 . Some of the final states accessible at the LHC are indicated in the appropriate regions, where y is the rapidity. The incoming partons have $x_{1,2} = (Q/14 \text{ TeV})e^{\pm y}$ where Q is the hard scale of the process shown in blue in the figure. For example, open charm production [23] and exclusive J/ψ and Υ production [24] at high $|y|$ at the LHC may probe the PDF down to $x \sim 10^{-5}$.

splitting functions are

$$P_{qq} = \frac{4}{3} \left[\frac{1+x^2}{(1-x)_+} \right] = \frac{4}{3} \left[\frac{1+x^2}{(1-x)_+} \right] + 2\delta(1-x), \quad (18.26)$$

$$P_{gq} = \frac{1}{2} [x^2 + (1-x)^2], \quad P_{gq} = \frac{4}{3} \left[\frac{1+(1-x)^2}{x} \right], \quad (18.27)$$

$$P_{gg} = 6 \left[\frac{1-x}{x} + x(1-x) + \frac{x}{(1-x)_+} \right] + \left[\frac{11}{2} - \frac{n_f}{3} \right] \delta(1-x), \quad (18.28)$$

where the notation $[F(x)]_+$ defines a distribution such that for any sufficiently regular test function, $f(x)$,

$$\int_0^1 dx f(x) [F(x)]_+ = \int_0^1 dx (f(x) - f(1)) F(x). \quad (18.29)$$

In general, the splitting functions can be expressed as a power series in α_s . The series contains both terms proportional to $\ln \mu^2$ and to $\ln(1/x)$ and $\ln(1-x)$. The leading-order DGLAP evolution sums up the $(\alpha_s \ln \mu^2)^n$ contributions, while at next-to-leading order (NLO) the sum over the $\alpha_s (\alpha_s \ln \mu^2)^{n-1}$ terms is included [28, 29]. The NNLO contributions to the splitting functions and the DIS coefficient functions are also all known [30–32].

In the kinematic region of very small x , one may also sum leading terms in $\ln(1/x)$, independent of the value of $\ln \mu^2$. At leading order, LLx, this is done by the BFKL equation for the unintegrated distributions (see Refs. [33, 34]). The leading-order $(\alpha_s \ln(1/x))^n$ terms result in a power-like growth, $x^{-\omega}$ with

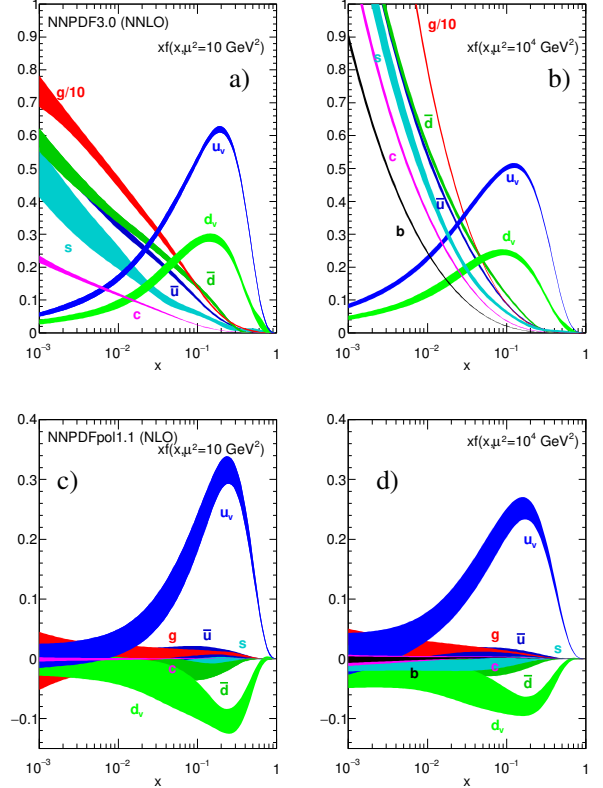


Figure 18.4: The bands are x times the unpolarized (a,b) parton distributions $f(x)$ (where $f = u_v, d_v, \bar{u}, \bar{d}, s \simeq \bar{s}, c = \bar{c}, b = \bar{b}, g$) obtained in NNLO NNPDF3.0 global analysis [25] at scales $\mu^2 = 10 \text{ GeV}^2$ (left) and $\mu^2 = 10^4 \text{ GeV}^2$ (right), with $\alpha_s(M_Z^2) = 0.118$. The analogous results obtained in the NNLO MMHT analysis can be found in Fig. 1 of Ref [26]. The corresponding polarized parton distributions are shown (c,d), obtained in NLO with NNPDFpol1.1 [27].

$\omega = (12\alpha_s \ln 2)/\pi$, at asymptotic values of $\ln 1/x$. The next-to-leading $\ln 1/x$ (NLLx) contributions are also available [35, 36]. They are so large (and negative) that the results initially appeared to be perturbatively unstable. Methods, based on a combination of collinear and small- x resummations, have been developed which reorganize the perturbative series into a more stable hierarchy [37–40], and this has been used as the basis for a framework for including the corrections in phenomenological studies [41, 42]. There are some limited indications that small- x resummations become necessary for sufficient precision for $x \lesssim 10^{-3}$ at low scales [14, 15]. There is not yet any very convincing indication for a ‘non-linear’ regime, for $Q^2 \gtrsim 2 \text{ GeV}^2$, in which the gluon density would be so high that gluon-gluon recombination effects would become significant.

The precision of the experimental data demands that at least NLO, and preferably NNLO, DGLAP evolution be used in comparisons between QCD theory and experiment. Beyond the leading order, it is necessary to specify, and to use consistently, both a renormalization and a factorization scheme. The renormalization scheme used almost universally is the modified minimal subtraction ($\overline{\text{MS}}$) scheme [43, 44]. The most popular choices for the factorization scheme is also $\overline{\text{MS}}$ [45]. However, sometimes the DIS [46] scheme is adopted, in which there are no higher-order corrections to the F_2 structure function. The two schemes differ in how the non-divergent pieces are assimilated in the parton distribution functions.

The discussion above relates to the Q^2 behavior of leading-twist (twist-2) contributions to the structure functions. Higher-twist terms, which involve their own non-perturbative input, exist. These die off as powers of Q ; specifically twist- n terms are damped by $1/Q^{n-2}$. Provided a cut, say $W^2 > 15 \text{ GeV}^2$ is imposed, the

higher-twist terms appear to be numerically unimportant for Q^2 above a few GeV^2 , except possibly for very small x and more definitely for x close to 1 [47–49], though it is important to note that they are likely to be larger in $xF_3(x, Q^2)$ than in $F_2(x, Q^2)$ (see e.g. [50]) due to a lack of a constraining sum rule for $xF_3(x, Q^2)$.

18.3 Determination of parton distributions

The parton distribution functions (PDFs) can be determined from an analysis of data for deep inelastic lepton-nucleon scattering and for related hard-scattering processes initiated by nucleons; see Refs. [51–56] for reviews. Table 18.1 highlights some of the processes, where LHC data are playing an increasing role [57], and their primary sensitivity to PDFs. Fixed-target and collider experiments have complementary kinematic reach (as is shown in Fig. 18.3), which enables the determination of PDFs over a wide range in x and μ^2 . As more precise LHC data for W^\pm , Z , γ , jet, $b\bar{b}$, $t\bar{t}$ and J/ψ production become available, tighter constraints on the PDFs are expected in a wider kinematic range.

Recent determinations and releases of the unpolarized PDFs up to NNLO have been made by six groups: MMHT [26], NNPDF [58], CT(EQ) [59], HERAPDF [11], ABMP [60] and JR [61]. JR generate ‘dynamical’ PDFs from a valence-like input at a very low starting scale, $Q_0^2 = 0.5 \text{ GeV}^2$, whereas other groups start evolution at $Q_0^2 = 1\text{--}4 \text{ GeV}^2$. Most groups use input PDFs of the form $xf = x^a(\dots)(1-x)^b$ with 14–28 free parameters in total. In these cases the PDF uncertainties are made available using the ‘Hessian’ formulation. The free parameters are expanded around their best fit values, and orthogonal eigenvector sets of PDFs depending on linear combinations of the parameter variations are obtained. The uncertainty is then the quadratic sum of the uncertainties arising from each eigenvector. The NNPDF group combines a Monte Carlo representation of the probability measure in the space of PDFs with the use of neural networks. Fits are performed to a number of ‘replica’ data sets obtained by allowing individual data points to fluctuate randomly by amounts determined by the size of the data uncertainties. This results in a set of replicas of unbiased PDF sets. In this case the best prediction is the average obtained using all PDF replicas and the uncertainty is the standard deviation over all replicas. It is now possible to convert the eigenvectors of Hessian-based PDFs to Monte Carlo replicas [62] and *vice versa* [63].

In these analyses, the u , d and s quarks are taken to be massless, but the treatment of the heavy c and b quark masses, m_Q , differs, and has a long history, which may be traced from Refs. [64–75]. The MSTW, CT, NNPDF and HERAPDF analyses use different variants of the General-Mass Variable-Flavour-Number Scheme (GM-VFNS). This combines fixed-order contributions to the coefficient functions (or partonic cross sections) calculated with the full m_Q dependence, with the all-order resummation of contributions via DGLAP evolution in which the heavy quarks are treated as massless after starting evolution at some transition point. Transition matrix elements are computed, following [67], which provide the boundary conditions between n_f and $n_f + 1$ PDFs. The ABMP and JR analyses use a FFNS where only the three light (massless) quarks enter the evolution, while the heavy quarks enter the partonic cross sections with their full m_Q dependence. The GM-VFNS and FFNS approaches yield different results: in particular $\alpha_s(M_Z^2)$ and the large- x gluon PDF at large Q^2 are both significantly smaller in the FFNS. It has been argued [48, 49, 74] that the difference is due to the slow convergence of the $\ln^n(Q^2/m_Q^2)$ terms in certain regions in a FFNS. The final HERA combination of heavy flavour structure function data has recently been published [76], and the evolution of these measurements and their interpretation may be traced in [77].

The most recent determinations of the groups fitting a variety of data and using a GM-VFNS (MMHT, NNPDF and CT) have converged, so that now a good agreement has been achieved between the resulting PDFs. Indeed, the CT14 [59], MMHT2014 [26], and NNPDF3.0 [25] PDF sets have been combined [78] using the Monte Carlo approach [62] mentioned above. The single combined set of PDFs is discussed in detail in Ref. [78].

For illustration, we show in Fig. 18.4 the PDFs obtained in the NNLO NNPDF analysis [25] at scales $\mu^2 = 10$ and 10^4 GeV^2 . The

values of α_s found by MMHT [79] may be taken as representative of those resulting from the GM-VFNS analyses

$$\text{NLO} : \alpha_s(M_Z^2) = 0.1201 \pm 0.0015,$$

$$\text{NNLO} : \alpha_s(M_Z^2) = 0.1172 \pm 0.0012,$$

where the error (at 68% C.L.) corresponds to the uncertainties resulting from the data fitted (the uncertainty that might be expected from the neglect of higher orders is at least as large). A similar result is found by the NNPDF group [80], who find $\alpha_s(M_Z^2) = 0.1185 \pm 0.0005$ at NNLO. The ABMP analysis [60], which uses a FFNS, finds $\alpha_s(M_Z^2) = 0.1147 \pm 0.0011$ at NNLO.

As a first step towards the inclusion of higher order electroweak corrections a recent development has been a vastly increased understanding of the photon content of the proton. Sets of PDFs with a photon contribution were first considered in Ref. [81] and then in subsequent PDF sets [82, 83]. However, due to weak data constraints, the uncertainty was extremely large. Subsequently, there has been a much improved understanding of the separation into elastic and inelastic contributions [84–86]. This gives much more theoretical precision, since the elastic contribution, arising from coherent emission of a photon from the proton, can be directly related to the well-known proton electric and magnetic form factors; the model dependence of the inelastic (incoherent) contribution, related to the quark PDFs, is at the level of tens of percent. A final development directly relating the entire photon contribution to the proton structure function [87] resulted in a determination of the photon content of the proton as precise as that of the light quarks. The framework has been applied within global fits to PDFs via an iterative procedure in [88] and to provide the low-scale input photon PDF in [89].

Nuclear PDFs: The study of the parton distributions for nucleons within nuclei, so-called nuclear parton distribution functions (nPDFs), is now reaching a level of maturity and sophistication similar to nucleon PDFs. The PDFs are now also a function of the nucleon number of the nucleus, A . The nPDFs are obtained via fits to deep inelastic scattering data and dilepton (Drell-Yan) and pion production from proton-nucleus. There are a number of recent examples of NLO analyses, DSSZ [90], nCTEQ15 [91], EPPS16 [92], while an NNLO analysis with a smaller selection of data types now also exists [93]. Much of the heavy-nucleus data included are in the form of ratios to proton or deuteron measurements. And most nuclear PDFs are related to a particular proton PDF via a nuclear modification factor, i.e.

$$f_i^{p/A}(x, Q^2) = R_i^A(x, Q^2) f_i^p(x, Q^2). \quad (18.30)$$

An exception is the PDFs in [91] which parameterise the nuclear PDFs directly but are equal to proton PDFs in the limit $A = 1$. There is some variation in whether charged current neutrino DIS data is used as well as neutral current DIS data since there is no clear compatibility in the modification factors obtained [94, 95]. Recently, LHC data from vector boson production [96, 97] in proton-lead collisions has been studied [98] or used directly [92], and LHC jet data [99] has been included [92], giving extra constraint on the gluon within nuclei. Further information at smaller x values should soon be extracted from heavy meson production at LHCb [100] and pion production [101]. All the PDF extractions above are based on the Hessian formulation, but the first NNPDF study of nPDFs has appeared [102], so far based on neutral current DIS data only. As well as improved constraints from further LHC data, nPDFs would be significantly improved by data from a potential high-energy Electron-Ion Collider [103].

Polarized PDFs: For spin-dependent structure functions, data exists for a more restricted range of Q^2 and has lower precision, so that the scaling violations are not seen so clearly. However, spin-dependent (or polarized) parton distributions have been extracted by comparison to data using NLO global analyses which include measurements of the g_1 structure function in inclusive polarized

DIS, ‘flavour-tagged’ semi-inclusive DIS data, open-charm production in DIS and results from polarized pp scattering at RHIC. There are recent results on DIS from JLAB [104] (for g_1^n/F_1^n), COMPASS [105,106] and CLAS [107]. NLO analyses are given in Refs. [108–111] and more recent extractions [112,113]. Improved parton-to-hadron fragmentation functions, needed to describe the semi-inclusive DIS (SIDIS) data, can be found in Refs. [114–117]. Only the DSSV collaboration includes in their NLO analysis to extract polarized PDFs all the world data, inclusive and semi-inclusive DIS, double spin asymmetries in jet, dijet and inclusive

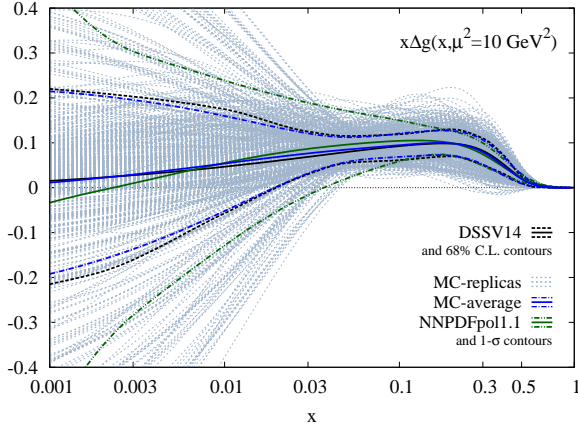


Figure 18.5: Ensemble of replicas (dotted blue lines) for the NLO gluon helicity density $\Delta g(x, Q^2)$ at $Q^2 = 10 \text{ GeV}^2$ shown along with its statistical average (solid blue line) and variance (dot-dashed blue lines). The corresponding results from the DSSV14 fit (black lines) [112] and the NNPDFpol1.1 analysis (green lines) [27] are shown for comparison. Figure taken from Ref. [118].

π^0 -production as well as the single spin asymmetries in W^\pm, Z^0 production. A determination [119], using the NNPDF methodology, concentrates just on the inclusive polarized DIS data, and finds the uncertainties on the polarized gluon PDF have been underestimated in the earlier analyses. An update to this [27], where jet and W^\pm data from pp collisions and open-charm DIS data have been included via reweighting, reduces the uncertainty and suggests a positive polarized gluon PDF. The DSSV group has recently implemented a Monte Carlo sampling strategy to extract helicity parton densities and their uncertainties from a reference set of longitudinally polarized scattering data [118].

A comparison of the polarized gluon PDFs obtained in the NLO analyses of NNPDF [27] and DSSV [118] is shown in Fig. 18.5 at scale $\mu^2 = 10 \text{ GeV}^2$. The world data of the inclusive structure function g_1 for proton and deuterium included in these analysis are shown in Fig. 18.14 and Fig. 18.15.

Comprehensive sets of PDFs are available from the LHAPDF library [120], which can be linked directly into a user’s programme to provide access to recent PDFs in a standard format.

18.4 The hadronic structure of the photon

Besides the *direct* interactions of the photon, it is possible for it to fluctuate into a hadronic state via the process $\gamma \rightarrow q\bar{q}$. While in this state, the partonic content of the photon may be *resolved*, for example, through the process $e^+e^- \rightarrow e^+e^-\gamma^* \rightarrow e^+e^-X$, where the virtual photon emitted by the DIS lepton probes the hadronic structure of the quasi-real photon emitted by the other lepton. The perturbative LO QED contributions to this process with $\gamma \rightarrow q\bar{q}$ in conjunction with $\gamma^*q(\bar{q}) \rightarrow q(\bar{q})$, are subject to QCD corrections due to the radiation of gluons from these quarks.

Often the equivalent-photon approximation is used to express the differential cross section for deep inelastic electron–photon scattering in terms of the structure functions of the transverse quasi-real photon times a flux factor N_γ^T (for these incoming

quasi-real photons of transverse polarization)

$$\frac{d^2\sigma}{dx dQ^2} = N_\gamma^T \frac{2\pi\alpha^2}{xQ^4} \left[(1 + (1-y)^2) F_2^\gamma(x, Q^2) - y^2 F_L^\gamma(x, Q^2) \right], \quad (18.31)$$

where we have used $F_2^\gamma = 2xF_T^\gamma + F_L^\gamma$ (where F_T is the transverse structure function), not to be confused with F_2^γ of Sec. 18.2. Complete formulae are given, for example, in the comprehensive review of [121].

The hadronic photon structure function, F_2^γ , evolves with increasing Q^2 from the ‘hadron-like’ behavior, calculable via the vector-meson-dominance model, to the dominating ‘point-like’ behaviour, calculable in perturbative QCD. Due to the point-like coupling, the logarithmic evolution of F_2^γ with Q^2 has a *positive* slope for all values of x , see Fig. 18.16. The ‘loss’ of quarks at large x due to gluon radiation is over-compensated by the ‘creation’ of quarks via the point-like $\gamma \rightarrow q\bar{q}$ coupling. The logarithmic evolution was first predicted in the quark–parton model ($\gamma^* \gamma \rightarrow q\bar{q}$) [122,123], and then an improved expression was obtained using QCD corrections in the limit of large Q^2 [124]. The evolution is now known to NLO [125–127]. The NLO data analyses to determine the parton densities of the photon can be found in Refs. [128–130].

18.5 Diffractive DIS (DDIS)

Some 10% of DIS events are diffractive, $\gamma^*p \rightarrow X + p$, in which the slightly deflected proton and the cluster X of outgoing hadrons are well-separated in rapidity [131]. Besides x and Q^2 , two extra

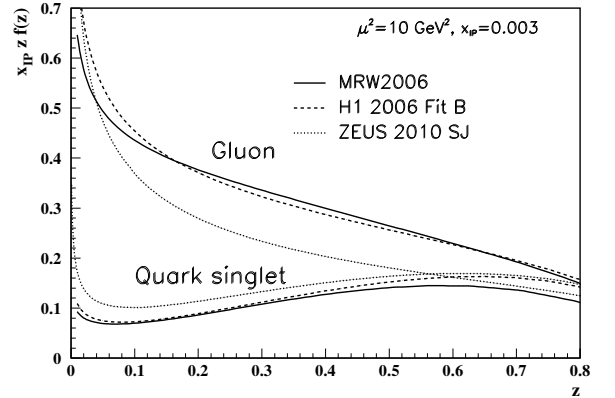


Figure 18.6: Diffractive parton distributions, $x_{IP} z f_{a/p}^D$, obtained from fitting to the ZEUS data with $Q^2 > 5 \text{ GeV}^2$ [132], H1 data with $Q^2 > 8.5 \text{ GeV}^2$ assuming Regge factorization [133], and from MRW2006 [134] using a more perturbative QCD approach [134]. Only the Pomeron contributions are shown and not the secondary Reggeon contributions, which are negligible at the value of $x_{IP} = 0.003$ chosen here. The H1 2007 Jets distribution [135] is similar to H1 2006 Fit B.

variables are needed to describe a DDIS event: the fraction x_{IP} of the proton’s momentum transferred across the rapidity gap and t , the square of the 4-momentum transfer of the proton. The DDIS data [136,137] are usually analysed using two levels of factorization. First, the diffractive structure function F_2^D satisfies *collinear factorization*, and can be expressed as the convolution [138]

$$F_2^D = \sum_{a=q,g} C_2^a \otimes f_{a/p}^D, \quad (18.32)$$

with the same coefficient functions as in DIS (see Eq. (18.21)), and where the diffractive parton distributions $f_{a/p}^D$ ($a = q, g$) satisfy DGLAP evolution. Second, *Regge factorization* is assumed [139],

$$f_{a/p}^D(x_{IP}, t, z, \mu^2) = f_{IP/p}(x_{IP}, t) f_{a/IP}(z, \mu^2), \quad (18.33)$$

where $f_{a/IP}$ are the parton densities of the Pomeron, which itself is treated like a hadron, and $z \in [x/x_{IP}, 1]$ is the fraction of the Pomeron’s momentum carried by the parton entering the

hard subprocess. The Pomeron flux factor $f_{\mathbb{P}/p}(x_{\mathbb{P}}, t)$ is taken from Regge phenomenology. There are also secondary Reggeon contributions to Eq. (18.33). A sample of the t -integrated diffractive parton densities, obtained in this way, is shown in Fig. 18.6. A more recent extraction of the parton densities may be found in [140].

Although collinear factorization holds as $\mu^2 \rightarrow \infty$, there are non-negligible corrections for finite μ^2 and small $x_{\mathbb{P}}$. Besides the *resolved* interactions of the Pomeron, the perturbative QCD Pomeron may also interact *directly* with the hard subprocess, giving rise to an inhomogeneous evolution equation for the diffractive parton densities analogous to the photon case. The results of the MRW analysis [134], which includes these contributions, are also shown in Fig. 18.6.

Unlike the inclusive case, the diffractive parton densities cannot be directly used to calculate diffractive hadron-hadron cross sections, since account must first be taken of “soft” rescattering effects.

18.6 Generalized parton distributions

The parton distributions of the proton of Sec. 18.3 are given by the diagonal matrix elements $\langle P, \lambda | \hat{O} | P, \lambda \rangle$, where P and λ are the 4-momentum and helicity of the proton, and \hat{O} is a twist-2 quark or gluon operator. However, there is new information in the so-called generalised parton distributions (GPDs) defined in terms of the off-diagonal matrix elements $\langle P', \lambda' | \hat{O} | P, \lambda \rangle$; see Refs. [141–146] for reviews. Unlike the diagonal PDFs, the GPDs cannot be regarded as parton densities, but are to be interpreted as probability amplitudes.

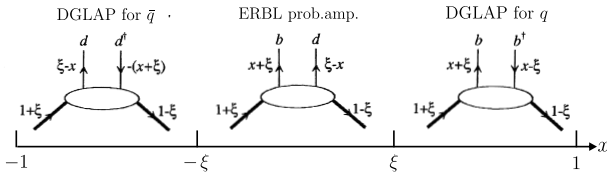


Figure 18.7: Schematic diagrams of the three distinct kinematic regions of the imaginary part of H_q . The proton and quark momentum fractions refer to \bar{P}^+ , and x covers the interval $(-1, 1)$. In the ERBL domain the GPDs are generalisations of distribution amplitudes which occur in processes such as $p\bar{p} \rightarrow J/\psi$.

The physical significance of GPDs is best seen using light-cone coordinates, $z^\pm = (z^0 \pm z^3)/\sqrt{2}$, and in the light-cone gauge, $A^+ = 0$. It is conventional to define the generalised quark distributions in terms of quark operators at light-like separation

$$F_q(x, \xi, t) = \frac{1}{2} \int \frac{dz^-}{2\pi} e^{ix\bar{P}^+z^-} \langle P' | \bar{\psi}(-z/2) \gamma^+ \psi(z/2) | P \rangle \Big|_{z^+=z^1=z^2=0} = \frac{1}{2\bar{P}^+} \times \left(H_q(x, \xi, t) \bar{u}(P') \gamma^+ u(P) + E_q(x, \xi, t) \bar{u}(P') \frac{i\sigma^{+\alpha} \Delta_\alpha}{2m} u(P) \right) \quad (18.34)$$

with $\bar{P} = (P + P')/2$ and $\Delta = P' - P$, and where we have suppressed the helicity labels of the protons and spinors. We now have two extra kinematic variables:

$$t = \Delta^2, \quad \xi = -\Delta^+ / (P + P')^+. \quad (18.35)$$

We see that $-1 \leq \xi \leq 1$. Similarly, we may define GPDs \tilde{H}_q and \tilde{E}_q with an additional γ_5 between the quark operators in Eq. (18.34); and also an analogous set of gluon GPDs, H_g, E_g, \tilde{H}_g and \tilde{E}_g . After a Fourier transform with respect to the transverse components of Δ , we are able to describe the spatial distribution of partons in the impact parameter plane in terms of GPDs [147, 148].

For $P' = P, \lambda' = \lambda$ the matrix elements reduce to the ordinary PDFs of Sec. 18.2.1

$$H_q(x, 0, 0) = q(x), \quad H_q(-x, 0, 0) = -\bar{q}(x), \quad H_g(x, 0, 0) = xg(x), \quad (18.36)$$

$$\tilde{H}_q(x, 0, 0) = \Delta q(x), \quad \tilde{H}_q(-x, 0, 0) = \Delta \bar{q}(x), \quad \tilde{H}_g(x, 0, 0) = x\Delta g(x), \quad (18.37)$$

where $\Delta q = q \uparrow - q \downarrow$ as in Eq. (18.18). No corresponding relations exist for E, \tilde{E} as they decouple in the forward limit, $\Delta = 0$.

The functions H_g, E_g are even in x , and \tilde{H}_g, \tilde{E}_g are odd functions of x . We can introduce valence and ‘singlet’ quark distributions which are even and odd functions of x respectively. For example

$$H_q^V(x, \xi, t) \equiv H_q(x, \xi, t) + H_q(-x, \xi, t) = H_q^V(-x, \xi, t), \quad (18.38)$$

$$H_q^S(x, \xi, t) \equiv H_q(x, \xi, t) - H_q(-x, \xi, t) = -H_q^S(-x, \xi, t). \quad (18.39)$$

All the GPDs satisfy relations of the form

$$H(x, -\xi, t) = H(x, \xi, t) \quad \text{and} \quad H(x, -\xi, t)^* = H(x, \xi, t), \quad (18.40)$$

and so are real-valued functions. Moreover, the moments of GPDs, that is the x integrals of $x^n H_q$ etc., are *polynomials* in ξ of order $n + 1$. Another important property of GPDs are Ji’s sum rule [141]

$$\frac{1}{2} \int_{-1}^1 dx x (H_q(x, \xi, t) + E_q(x, \xi, t)) = J_q(t), \quad (18.41)$$

where $J_q(0)$ is the total angular momentum carried by quarks and antiquarks of flavour q , with a similar relation for gluons.

To visualize the physical content of H_q , we Fourier expand ψ in terms of quark, antiquark creation (b, d) and annihilation (b^\dagger, d^\dagger) operators, and sketch the result in Fig. 18.7. There are two types of domain: (i) the time-like or ‘annihilation’ domain, with $|x| < |\xi|$, where the GPDs describe the wave functions of a t -channel $q\bar{q}$ (or gluon) pair and evolve according to modified ERBL equations [149, 150]; (ii) the space-like or ‘scattering’ domain, with $|x| > |\xi|$, where the GPDs generalise the familiar \bar{q}, q (and gluon) PDFs and describe processes such as ‘deeply virtual Compton scattering’ ($\gamma^* p \rightarrow \gamma p$), $\gamma p \rightarrow J/\psi p$, etc., and evolve according to modified DGLAP equations. The splitting functions for the evolution of GPDs are known to NLO [151–153].

GPDs describe new aspects of proton structure and must be determined from experiment. We can parametrise them in terms of ‘double distributions’ [154, 155], which reduce to diagonal PDFs as $\xi \rightarrow 0$. Alternatively, flexible $SO(3)$ -based parametrisations have been used to determine GPDs from DVCS data [156, 157]; a more recent summary may be found in Ref. [158, 159].

18.7 Transverse momentum dependent distributions

Transverse momentum dependent distributions (TMDs) are complementary to GPDs. Together, they describe the three-dimensional structure of hadrons. In contrast to GPDs that encode the transverse position of a parton in a nucleon, TMDs encompassing both the parton distributions (TMD PDF) and fragmentation functions (TMD FF) encode the transverse momenta and lead to observable transverse momenta in the final state. Both TMDs and GPDs derive, via integration over the appropriate variable, from Wigner distributions [160–162] that depend on the average transverse momentum and position of partons.

For a proton, there are eight independent TMD PDFs, at leading twist, three of which correspond to the usual unpolarized, longitudinally polarized and transversely polarized quark parton distributions [163, 164]. The novel TMD PDFs have physical interpretations. For example, the Sivers function [165] represents the distribution of unpolarized partons inside a transversely polarized hadron. For (pseudo)scalar particles, such as kaon and pions, there are two independent leading-twist TMD FFs, one being the ordinary unpolarized fragmentation function and the other the Collins FF [166] which is related to the probability of a polarized quark fragmenting into an unpolarized hadron.

Factorization of TMDs have been shown for semi-inclusive DIS, for the Drell-Yan process as well as for electron-position annihilation into dihadrons [167–172]. Recently first TMD global fits have become available [173–180], although problems with consistent descriptions still remain [181,182].

Because TMD PDFs encode nonperturbative information about transverse momentum and polarization degrees of freedom, they are important for descriptions of multi-scale, non-inclusive collider observables, for example, production of electroweak gauge bosons at LHC [183] and can have an effect on determination of the W boson mass [184]. The combination of TMD PDFs and FFs can give consistent global description of spin and azimuthal asymmetries and provide predictions. Some recent reviews of this rapidly developing field are given here [183,185–187].

References

- [1] J. Blumlein and N. Kochelev, Nucl. Phys. **B498**, 285 (1997), [hep-ph/9612318].
- [2] S. Forte, M. L. Mangano and G. Ridolfi, Nucl. Phys. **B602**, 585 (2001), [hep-ph/0101192].
- [3] M. Anselmino, P. Gambino and J. Kalinowski, Z. Phys. **C64**, 267 (1994), [hep-ph/9401264].
- [4] M. Anselmino, A. Efremov and E. Leader, Phys. Rept. **261**, 1 (1995), [Erratum: Phys. Rept.281,399(1997)], [hep-ph/9501369].
- [5] M. Klein and T. Riemann, Z. Phys. **C24**, 151 (1984).
- [6] C. G. Callan, Jr. and D. J. Gross, Phys. Rev. Lett. **22**, 156 (1969).
- [7] D. A. Dicus, Phys. Rev. **D5**, 1367 (1972).
- [8] J. D. Bjorken and E. A. Paschos, Phys. Rev. **185**, 1975 (1969).
- [9] R.P. Feynman, Photon Hadron Interactions (Benjamin, New York, 1972).
- [10] A.M. Cooper-Sarkar, private communication.
- [11] H. Abramowicz *et al.* (H1, ZEUS), Eur. Phys. J. **C75**, 12, 580 (2015), [arXiv:1506.06042].
- [12] L. A. Harland-Lang *et al.*, Eur. Phys. J. **C76**, 4, 186 (2016), [arXiv:1601.03413].
- [13] I. Abt *et al.*, Phys. Rev. **D94**, 3, 034032 (2016), [arXiv:1604.02299].
- [14] R. D. Ball *et al.*, Eur. Phys. J. **C78**, 4, 321 (2018), [arXiv:1710.05935].
- [15] H. Abdolmaleki *et al.* (xFitter Developers' Team), Eur. Phys. J. **C78**, 8, 621 (2018), [arXiv:1802.00064].
- [16] S. Wandzura and F. Wilczek, Phys. Lett. **72B**, 195 (1977).
- [17] J. Blumlein and A. Tkabladze, Nucl. Phys. **B553**, 427 (1999), [hep-ph/9812478].
- [18] J. D. Bjorken, Phys. Rev. **179**, 1547 (1969).
- [19] V. N. Gribov and L. N. Lipatov, Sov. J. Nucl. Phys. **15**, 438 (1972), [Yad. Fiz.15,781(1972)].
- [20] L.N. Lipatov, Sov. J. Nucl. Phys. **20**, 95 (1975).
- [21] G. Altarelli and G. Parisi, Nucl. Phys. **B126**, 298 (1977).
- [22] Y. L. Dokshitzer, Sov. Phys. JETP **46**, 641 (1977), [Zh. Eksp. Teor. Fiz.73,1216(1977)].
- [23] O. Zenaiev *et al.* (PROSA), Eur. Phys. J. **C75**, 8, 396 (2015), [arXiv:1503.04581].
- [24] R. Aaij *et al.* (LHCb), J. Phys. **G41**, 055002 (2014), [arXiv:1401.3288].
- [25] R. D. Ball *et al.* (NNPDF), JHEP **04**, 040 (2015), [arXiv:1410.8849].
- [26] L. A. Harland-Lang *et al.*, Eur. Phys. J. **C75**, 5, 204 (2015), [arXiv:1412.3989].
- [27] E. R. Nocera *et al.* (NNPDF), Nucl. Phys. **B887**, 276 (2014), [arXiv:1406.5539].
- [28] G. Curci, W. Furmanski and R. Petronzio, Nucl. Phys. **B175**, 27 (1980); W. Furmanski and R. Petronzio, Phys. Lett. **97B**, 437 (1980).
- [29] R.K. Ellis *et al.*, QCD and Collider Physics (Cambridge UP, 1996).
- [30] W. L. van Neerven and E. B. Zijlstra, Phys. Lett. **B272**, 127 (1991); E. B. Zijlstra and W. L. van Neerven, Phys. Lett. **B273**, 476 (1991); E. B. Zijlstra and W. L. van Neerven, Phys. Lett. **B297**, 377 (1992); E. B. Zijlstra and W. L. van Neerven, Nucl. Phys. **B383**, 525 (1992).
- [31] S. Moch and J. A. M. Vermaseren, Nucl. Phys. **B573**, 853 (2000), [hep-ph/9912355].
- [32] S. Moch, J. A. M. Vermaseren and A. Vogt, Nucl. Phys. **B688**, 101 (2004), [hep-ph/0403192]; A. Vogt, S. Moch and J. A. M. Vermaseren, Nucl. Phys. **B691**, 129 (2004), [hep-ph/0404111]; S. Moch, J. A. M. Vermaseren and A. Vogt, Phys. Lett. **B606**, 123 (2005), [hep-ph/0411112]; J. A. M. Vermaseren, A. Vogt and S. Moch, Nucl. Phys. **B724**, 3 (2005), [hep-ph/0504242].
- [33] V. S. Fadin, E. A. Kuraev and L. N. Lipatov, Phys. Lett. **60B**, 50 (1975); E. A. Kuraev, L. N. Lipatov and V. S. Fadin, Sov. Phys. JETP **44**, 443 (1976), [Zh. Eksp. Teor. Fiz.71,840(1976)]; E. A. Kuraev, L. N. Lipatov and V. S. Fadin, Sov. Phys. JETP **45**, 199 (1977), [Zh. Eksp. Teor. Fiz.72,377(1977)].
- [34] I. I. Balitsky and L. N. Lipatov, Sov. J. Nucl. Phys. **28**, 822 (1978), [Yad. Fiz.28,1597(1978)].
- [35] V. S. Fadin and L. N. Lipatov, Phys. Lett. **B429**, 127 (1998), [hep-ph/9802290].
- [36] G. Camici and M. Ciafaloni, Phys. Lett. **B412**, 396 (1997), [Erratum: Phys. Lett. B417,390(1998)], [hep-ph/9707390]; M. Ciafaloni and G. Camici, Phys. Lett. **B430**, 349 (1998), [hep-ph/9803389].
- [37] M. Ciafaloni, D. Colferai and G. P. Salam, Phys. Rev. **D60**, 114036 (1999), [hep-ph/9905566]; M. Ciafaloni, D. Colferai and G. P. Salam, JHEP **07**, 054 (2000), [hep-ph/0007240].
- [38] M. Ciafaloni *et al.*, Phys. Lett. **B576**, 143 (2003), [hep-ph/0305254]; M. Ciafaloni *et al.*, Phys. Rev. **D68**, 114003 (2003), [hep-ph/0307188].
- [39] G. Altarelli, R. D. Ball and S. Forte, Nucl. Phys. **B742**, 1 (2006), [hep-ph/0512237]; G. Altarelli, R. D. Ball and S. Forte, Nucl. Phys. **B799**, 199 (2008), [arXiv:0802.0032].
- [40] C. D. White and R. S. Thorne, Phys. Rev. **D75**, 034005 (2007), [hep-ph/0611204].
- [41] M. Bonvini, S. Marzani and T. Peraro, Eur. Phys. J. **C76**, 11, 597 (2016), [arXiv:1607.02153].
- [42] M. Bonvini, S. Marzani and C. Muselli, JHEP **12**, 117 (2017), [arXiv:1708.07510].
- [43] G. 't Hooft and M. J. G. Veltman, Nucl. Phys. **B44**, 189 (1972).
- [44] G. 't Hooft, Nucl. Phys. **B61**, 455 (1973).
- [45] W. A. Bardeen *et al.*, Phys. Rev. **D18**, 3998 (1978).
- [46] G. Altarelli, R. K. Ellis and G. Martinelli, Nucl. Phys. **B143**, 521 (1978), [Erratum: Nucl. Phys. B146,544(1978)].
- [47] A. D. Martin *et al.*, Eur. Phys. J. **C35**, 325 (2004), [hep-ph/0308087].
- [48] R. D. Ball *et al.* (NNPDF), Phys. Lett. **B723**, 330 (2013), [arXiv:1303.1189].
- [49] R. S. Thorne, Eur. Phys. J. **C74**, 7, 2958 (2014), [arXiv:1402.3536].
- [50] M. Dasgupta and B. R. Webber, Phys. Lett. **B382**, 273 (1996), [hep-ph/9604388].
- [51] A. De Roeck and R. S. Thorne, Prog. Part. Nucl. Phys. **66**, 727 (2011), [arXiv:1103.0555].
- [52] S. Forte and G. Watt, Ann. Rev. Nucl. Part. Sci. **63**, 291 (2013), [arXiv:1301.6754].

- [53] J. Blumlein, *Prog. Part. Nucl. Phys.* **69**, 28 (2013), [arXiv:1208.6087].
- [54] E. Perez and E. Rizvi, *Rept. Prog. Phys.* **76**, 046201 (2013), [arXiv:1208.1178].
- [55] R. D. Ball *et al.*, *JHEP* **04**, 125 (2013), [arXiv:1211.5142].
- [56] J. Gao, L. Harland-Lang and J. Rojo, *Phys. Rept.* **742**, 1 (2018), [arXiv:1709.04922].
- [57] J. Rojo *et al.*, *J. Phys.* **G42**, 103103 (2015), [arXiv:1507.00556].
- [58] R. D. Ball *et al.* (NNPDF), *Eur. Phys. J.* **C77**, 10, 663 (2017), [arXiv:1706.00428].
- [59] CT₁₄, S. Dulat *et al.*, *Phys. Rev.* **D93**, 3, 033006 (2016), [arXiv:1506.07443].
- [60] S. Alekhin *et al.*, *Phys. Rev.* **D96**, 1, 014011 (2017), [arXiv:1701.05838].
- [61] P. Jimenez-Delgado and E. Reya, *Phys. Rev.* **D89**, 7, 074049 (2014), [arXiv:1403.1852].
- [62] G. Watt and R. S. Thorne, *JHEP* **08**, 052 (2012), [arXiv:1205.4024].
- [63] S. Carrazza *et al.*, *Eur. Phys. J.* **C75**, 8, 369 (2015), [arXiv:1505.06736].
- [64] J. C. Collins, F. Wilczek and A. Zee, *Phys. Rev.* **D18**, 242 (1978).
- [65] E. Laenen *et al.*, *Nucl. Phys.* **B392**, 162 (1993).
- [66] M. A. G. Aivazis *et al.*, *Phys. Rev.* **D50**, 3102 (1994), [hep-ph/9312319].
- [67] M. Buza *et al.*, *Eur. Phys. J.* **C1**, 301 (1998), [hep-ph/9612398].
- [68] J. C. Collins, *Phys. Rev.* **D58**, 094002 (1998), [hep-ph/9806259].
- [69] A. Chuvakin, J. Smith and W. L. van Neerven, *Phys. Rev.* **D61**, 096004 (2000), [hep-ph/9910250].
- [70] R. S. Thorne, *Phys. Rev.* **D73**, 054019 (2006), [hep-ph/0601245].
- [71] R. S. Thorne and W. K. Tung, in “Proceedings, HERA and the LHC Workshop Series on the implications of HERA for LHC physics: 2006-2008,” 332–351 (2008), [2(2008)], [arXiv:0809.0714].
- [72] S. Alekhin and S. Moch, *Phys. Lett.* **B699**, 345 (2011), [arXiv:1011.5790].
- [73] S. Forte *et al.*, *Nucl. Phys.* **B834**, 116 (2010), [arXiv:1001.2312].
- [74] R. S. Thorne, *Phys. Rev.* **D86**, 074017 (2012), [arXiv:1201.6180].
- [75] E. G. de Oliveira *et al.*, *Eur. Phys. J.* **C73**, 10, 2616 (2013), [arXiv:1307.3508].
- [76] H. Abramowicz *et al.* (H1, ZEUS), *Eur. Phys. J.* **C78**, 6, 473 (2018), [arXiv:1804.01019].
- [77] O. Behnke, A. Geiser and M. Lisovsky, *Prog. Part. Nucl. Phys.* **84**, 1 (2015), [arXiv:1506.07519].
- [78] J. Butterworth *et al.*, *J. Phys.* **G43**, 023001 (2016), [arXiv:1510.03865].
- [79] L. A. Harland-Lang *et al.*, *Eur. Phys. J.* **C75**, 9, 435 (2015), [arXiv:1506.05682].
- [80] R. D. Ball *et al.* (NNPDF), *Eur. Phys. J.* **C78**, 5, 408 (2018), [arXiv:1802.03398].
- [81] A. D. Martin *et al.*, *Eur. Phys. J.* **C39**, 155 (2005), [hep-ph/0411040].
- [82] R. D. Ball *et al.* (NNPDF), *Nucl. Phys.* **B877**, 290 (2013), [arXiv:1308.0598].
- [83] C. Schmidt *et al.*, *Phys. Rev.* **D93**, 11, 114015 (2016), [arXiv:1509.02905].
- [84] M. Gluck, C. Pisano and E. Reya, *Phys. Lett.* **B540**, 75 (2002), [hep-ph/0206126].
- [85] A. D. Martin and M. G. Ryskin, *Eur. Phys. J.* **C74**, 3040 (2014), [arXiv:1406.2118].
- [86] L. A. Harland-Lang, V. A. Khoze and M. G. Ryskin, *Phys. Rev.* **D94**, 7, 074008 (2016), [arXiv:1607.04635].
- [87] A. Manohar *et al.*, *Phys. Rev. Lett.* **117**, 24, 242002 (2016), [arXiv:1607.04266].
- [88] V. Bertone *et al.* (NNPDF), *SciPost Phys.* **5**, 1, 008 (2018), [arXiv:1712.07053].
- [89] L. A. Harland-Lang *et al.*, *Eur. Phys. J.* **C79**, 10, 811 (2019), [arXiv:1907.02750].
- [90] D. de Florian *et al.*, *Phys. Rev.* **D85**, 074028 (2012), [arXiv:1112.6324].
- [91] K. Kovarik *et al.*, *Phys. Rev.* **D93**, 8, 085037 (2016), [arXiv:1509.00792].
- [92] H. Paukkunen, *Nucl. Phys.* **A967**, 241 (2017), [arXiv:1704.04036].
- [93] H. Khanpour and S. Atashbar Tehrani, *Phys. Rev.* **D93**, 1, 014026 (2016), [arXiv:1601.00939].
- [94] K. Kovarik *et al.*, *Phys. Rev. Lett.* **106**, 122301 (2011), [arXiv:1012.0286].
- [95] H. Paukkunen and C. A. Salgado, *Phys. Rev. Lett.* **110**, 21, 212301 (2013), [arXiv:1302.2001].
- [96] G. Aad *et al.* (ATLAS), *Phys. Rev.* **C92**, 4, 044915 (2015), [arXiv:1507.06232].
- [97] V. Khachatryan *et al.* (CMS), *Phys. Lett.* **B750**, 565 (2015), [arXiv:1503.05825].
- [98] A. Kusina *et al.*, *Eur. Phys. J.* **C77**, 7, 488 (2017), [arXiv:1610.02925].
- [99] S. Chatrchyan *et al.* (CMS), *Eur. Phys. J.* **C74**, 7, 2951 (2014), [arXiv:1401.4433].
- [100] R. Aaij *et al.* (LHCb), *JHEP* **10**, 090 (2017), [arXiv:1707.02750].
- [101] S. Acharya *et al.* (ALICE), *Eur. Phys. J.* **C78**, 8, 624 (2018), [arXiv:1801.07051].
- [102] R. Abdul Khalek, J. J. Ethier and J. Rojo (NNPDF), *Eur. Phys. J.* **C79**, 6, 471 (2019), [arXiv:1904.00018].
- [103] E. C. Aschenauer *et al.*, *Phys. Rev.* **D96**, 11, 114005 (2017), [arXiv:1708.05654].
- [104] D. Flay *et al.* (Jefferson Lab Hall A), *Phys. Rev.* **D94**, 5, 052003 (2016), [arXiv:1603.03612].
- [105] C. Adolph *et al.* (COMPASS), *Phys. Lett.* **B753**, 18 (2016), [arXiv:1503.08935].
- [106] C. Adolph *et al.* (COMPASS), *Phys. Lett.* **B769**, 34 (2017), [arXiv:1612.00620].
- [107] R. Fersch *et al.* (CLAS), *Phys. Rev.* **C96**, 6, 065208 (2017), [arXiv:1706.10289].
- [108] M. Hirai and S. Kumano (Asymmetry Analysis), *Nucl. Phys.* **B813**, 106 (2009), [arXiv:0808.0413].
- [109] D. de Florian *et al.*, *Phys. Rev. Lett.* **101**, 072001 (2008), [arXiv:0804.0422]; D. de Florian *et al.*, *Phys. Rev.* **D80**, 034030 (2009), [arXiv:0904.3821].
- [110] E. Leader, A. V. Sidorov and D. B. Stamenov, *Phys. Rev.* **D82**, 114018 (2010), [arXiv:1010.0574].
- [111] J. Blumlein and H. Bottcher, *Nucl. Phys.* **B841**, 205 (2010), [arXiv:1005.3113].
- [112] D. de Florian *et al.*, *Phys. Rev. Lett.* **113**, 1, 012001 (2014), [arXiv:1404.4293].
- [113] N. Sato *et al.* (Jefferson Lab Angular Momentum), *Phys. Rev.* **D93**, 7, 074005 (2016), [arXiv:1601.07782].
- [114] D. de Florian *et al.*, *Phys. Rev.* **D91**, 1, 014035 (2015), [arXiv:1410.6027].
- [115] D. de Florian *et al.*, *Phys. Rev.* **D95**, 9, 094019 (2017), [arXiv:1702.06353].

- [116] V. Bertone *et al.* (NNPDF), *Eur. Phys. J.* **C77**, 8, 516 (2017), [arXiv:1706.07049].
- [117] V. Bertone *et al.* (NNPDF), *Eur. Phys. J.* **C78**, 8, 651 (2018), [arXiv:1807.03310].
- [118] D. De Florian *et al.* (2019), [arXiv:1902.10548].
- [119] R. D. Ball *et al.* (NNPDF), *Nucl. Phys.* **B874**, 36 (2013), [arXiv:1303.7236].
- [120] A. Buckley *et al.*, *Eur. Phys. J.* **C75**, 132 (2015), [arXiv:1412.7420].
- [121] R. Nisius, *Phys. Rept.* **332**, 165 (2000), [hep-ex/9912049].
- [122] T. F. Walsh and P. M. Zerwas, *Phys. Lett.* **44B**, 195 (1973).
- [123] R. L. Kingsley, *Nucl. Phys.* **B60**, 45 (1973).
- [124] E. Witten, *Nucl. Phys.* **B120**, 189 (1977).
- [125] W. A. Bardeen and A. J. Buras, *Phys. Rev.* **D20**, 166 (1979), [Erratum: *Phys. Rev.*D21,2041(1980)].
- [126] M. Fontannaz and E. Pilon, *Phys. Rev.* **D45**, 382 (1992).
- [127] M. Gluck, E. Reya and A. Vogt, *Phys. Rev.* **D45**, 3986 (1992).
- [128] F. Cornet, P. Jankowski and M. Krawczyk, *Phys. Rev.* **D70**, 093004 (2004), [hep-ph/0404063].
- [129] P. Aurenche, M. Fontannaz and J. P. Guillet, *Eur. Phys. J.* **C44**, 395 (2005), [hep-ph/0503259].
- [130] W. Slominski, H. Abramowicz and A. Levy, *Eur. Phys. J.* **C45**, 633 (2006), [hep-ph/0504003].
- [131] H. Abramowicz and A. Caldwell, *Rev. Mod. Phys.* **71**, 1275 (1999), [hep-ex/9903037].
- [132] S. Chekanov *et al.* (ZEUS), *Nucl. Phys.* **B831**, 1 (2010), [arXiv:0911.4119].
- [133] A. Aktas *et al.* (H1), *Eur. Phys. J.* **C48**, 715 (2006), [hep-ex/0606004].
- [134] A. D. Martin, M. G. Ryskin and G. Watt, *Phys. Lett.* **B644**, 131 (2007), [hep-ph/0609273].
- [135] A. Aktas *et al.* (H1), *JHEP* **10**, 042 (2007), [arXiv:0708.3217].
- [136] F. D. Aaron *et al.* (H1, ZEUS), *Eur. Phys. J.* **C72**, 2175 (2012), [arXiv:1207.4864].
- [137] F. D. Aaron *et al.* (H1), *Eur. Phys. J.* **C72**, 2074 (2012), [arXiv:1203.4495].
- [138] J. C. Collins, *Phys. Rev.* **D57**, 3051 (1998), [Erratum: *Phys. Rev.*D61,019902(2000)], [hep-ph/9709499].
- [139] G. Ingelman and P. E. Schlein, *Phys. Lett.* **152B**, 256 (1985).
- [140] M. Goharipour, H. Khanpour and V. Guzey, *Eur. Phys. J.* **C78**, 4, 309 (2018), [arXiv:1802.01363].
- [141] X.-D. Ji, *J. Phys.* **G24**, 1181 (1998), [hep-ph/9807358].
- [142] K. Goeke, M. V. Polyakov and M. Vanderhaeghen, *Prog. Part. Nucl. Phys.* **47**, 401 (2001), [hep-ph/0106012].
- [143] M. Diehl, *Phys. Rept.* **388**, 41 (2003), [hep-ph/0307382].
- [144] A. V. Belitsky and A. V. Radyushkin, *Phys. Rept.* **418**, 1 (2005), [hep-ph/0504030].
- [145] S. Boffi and B. Pasquini, *Riv. Nuovo Cim.* **30**, 387 (2007), [arXiv:0711.2625].
- [146] K. Kumericki, S. Liuti and H. Moutarde, *Eur. Phys. J.* **A52**, 6, 157 (2016), [arXiv:1602.02763].
- [147] M. Burkardt, *Int. J. Mod. Phys.* **A18**, 173 (2003), [hep-ph/0207047].
- [148] M. Diehl, *Eur. Phys. J.* **C25**, 223 (2002), [Erratum: *Eur. Phys. J.*C31,277(2003)], [hep-ph/0205208].
- [149] A. V. Efremov and A. V. Radyushkin, *Phys. Lett.* **94B**, 245 (1980).
- [150] G. P. Lepage and S. J. Brodsky, *Phys. Rev.* **D22**, 2157 (1980).
- [151] A. V. Belitsky, A. Freund and D. Mueller, *Phys. Lett.* **B493**, 341 (2000), [hep-ph/0008005].
- [152] A. V. Belitsky, A. Freund and D. Mueller, *Nucl. Phys.* **B574**, 347 (2000), [hep-ph/9912379].
- [153] V. M. Braun *et al.*, *JHEP* **06**, 037 (2017), [arXiv:1703.09532].
- [154] A. V. Radyushkin, *Phys. Rev.* **D59**, 014030 (1999), [hep-ph/9805342].
- [155] A. V. Radyushkin, *Phys. Lett.* **B449**, 81 (1999), [hep-ph/9810466].
- [156] K. Kumericki and D. Mueller, *Nucl. Phys.* **B841**, 1 (2010), [arXiv:0904.0458].
- [157] N. d'Hose, S. Niccolai and A. Rostomyan, *Eur. Phys. J.* **A52**, 6, 151 (2016).
- [158] M. Guidal, H. Moutarde and M. Vanderhaeghen, *Rept. Prog. Phys.* **76**, 066202 (2013), [arXiv:1303.6600].
- [159] M. Anselmino, M. Guidal and P. Rossi, *The European Physical Journal A* **52**, 6, 149 (2016), ISSN 1434-601X, URL <https://doi.org/10.1140/epja/i2016-16164-4>.
- [160] X. Ji, *Phys. Rev. Lett.* **91**, 062001 (2003), [hep-ph/0304037].
- [161] A. V. Belitsky, X. Ji and F. Yuan, *Phys. Rev.* **D69**, 074014 (2004), [hep-ph/0307383].
- [162] C. Lorce, B. Pasquini and M. Vanderhaeghen, *JHEP* **05**, 041 (2011), [arXiv:1102.4704].
- [163] P. J. Mulders and R. D. Tangerman, *Nucl. Phys.* **B461**, 197 (1996), [Erratum: *Nucl. Phys.*B484,538(1997)], [hep-ph/9510301].
- [164] D. Boer and P. J. Mulders, *Phys. Rev.* **D57**, 5780 (1998), [hep-ph/9711485].
- [165] D. W. Sivers, *Phys. Rev.* **D41**, 83 (1990).
- [166] J. C. Collins, *Nucl. Phys.* **B396**, 161 (1993), [hep-ph/9208213].
- [167] X. Ji, J. Ma and F. Yuan, *Phys. Rev.* **D71**, 034005 (2005), [hep-ph/0404183].
- [168] J. Collins, *Foundations of perturbative QCD Camb. Monogr. Part. Phys. Nucl. Phys. Cosmol.* **32** (2011) 1-624 and references therein.
- [169] S. M. Aybat and T. C. Rogers, *Phys. Rev.* **D83**, 114042 (2011), [arXiv:1101.5057].
- [170] M. G. Echevarria, A. Idilbi and I. Scimemi, *JHEP* **07**, 002 (2012), [arXiv:1111.4996].
- [171] M. G. A. Buffing, A. Mukherjee and P. J. Mulders, *Phys. Rev.* **D88**, 054027 (2013), [arXiv:1306.5897].
- [172] T. C. Rogers and P. J. Mulders, *Phys. Rev.* **D81**, 094006 (2010), [arXiv:1001.2977].
- [173] A. Signori *et al.*, *JHEP* **11**, 194 (2013), [arXiv:1309.3507].
- [174] M. Anselmino *et al.*, *JHEP* **04**, 005 (2014), [arXiv:1312.6261].
- [175] U. D'Alesio *et al.*, *JHEP* **11**, 098 (2014), [arXiv:1407.3311].
- [176] M. G. Echevarria *et al.*, *Phys. Rev.* **D89**, 074013 (2014), [arXiv:1401.5078].
- [177] P. Sun *et al.*, *Int. J. Mod. Phys.* **A33**, 11, 1841006 (2018), [arXiv:1406.3073].
- [178] A. Bacchetta *et al.*, *JHEP* **06**, 081 (2017), [Erratum: *JHEP*06,051(2019)], [arXiv:1703.10157].
- [179] I. Scimemi and A. Vladimirov, *Eur. Phys. J.* **C78**, 2, 89 (2018), [arXiv:1706.01473].
- [180] V. Bertone, I. Scimemi and A. Vladimirov, *JHEP* **06**, 028 (2019), [arXiv:1902.08474].
- [181] J. O. Gonzalez-Hernandez *et al.*, *Phys. Rev.* **D98**, 11, 114005 (2018), [arXiv:1808.04396].
- [182] A. Bacchetta *et al.*, *Phys. Rev.* **D100**, 1, 014018 (2019), [arXiv:1901.06916].

- [183] R. Angeles-Martinez *et al.*, *Acta Phys. Polon.* **B46**, 12, 2501 (2015), [arXiv:1507.05267].
- [184] A. Bacchetta *et al.*, *Phys. Lett.* **B788**, 542 (2019), [arXiv:1807.02101].
- [185] M. Diehl, *Eur. Phys. J.* **A52**, 6, 149 (2016), [arXiv:1512.01328].
- [186] A. Bacchetta, *Eur. Phys. J.* **A52**, 6, 163 (2016).
- [187] <http://hepdata.cedar.ac.uk/pdfs>.

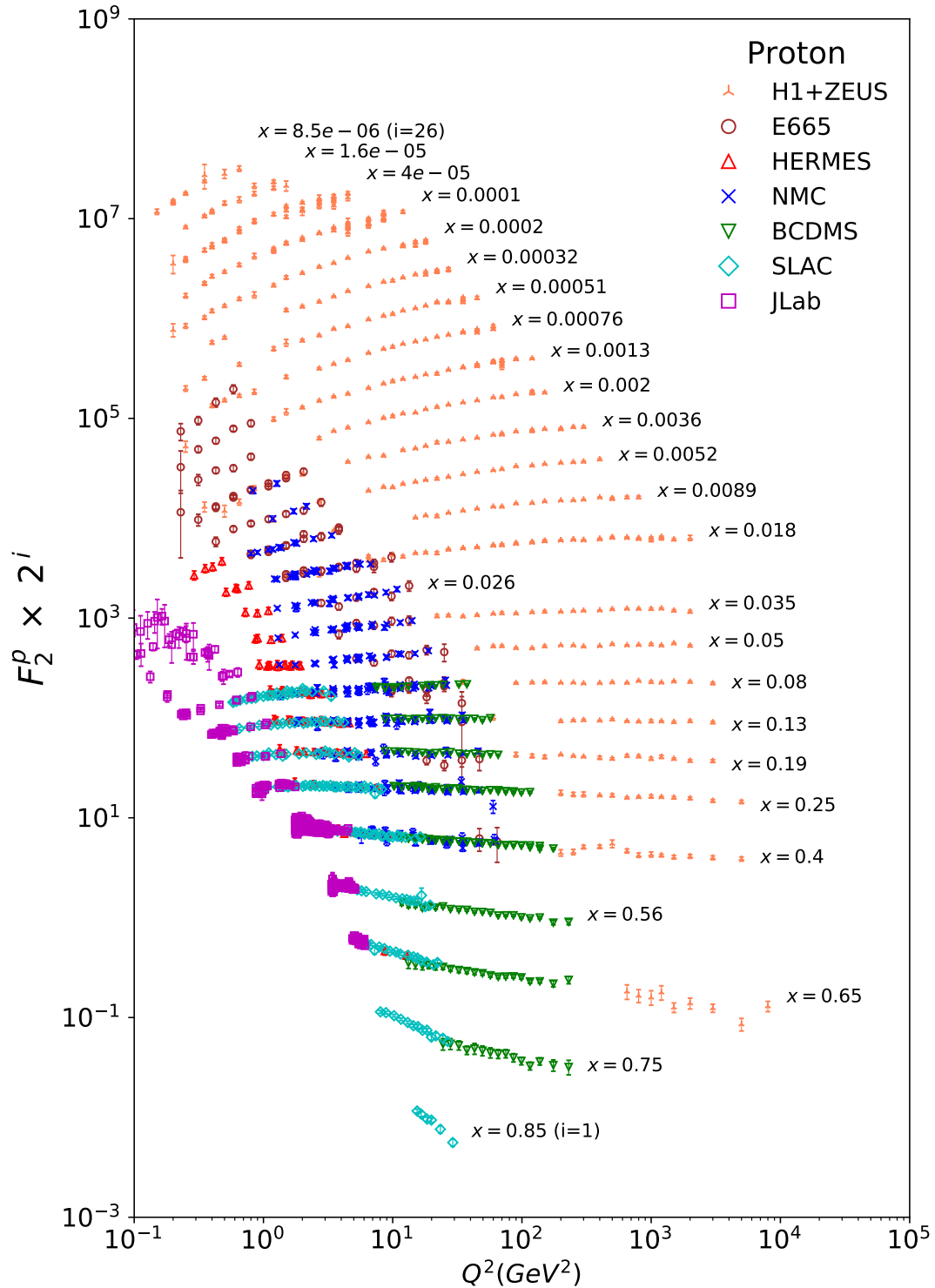


Figure 18.8: The proton structure function F_2^p measured in electromagnetic scattering of electrons and positrons on protons, and for electrons/positrons (SLAC, HERMES, JLAB) and muons (BCDMS, E665, NMC) on a fixed target. Statistical and systematic errors added in quadrature are shown. The H1+ZEUS combined values are obtained from the measured reduced cross section and converted to F_2^p with a HERAPDF NLO fit, for all measured points where the predicted ratio of F_2^p to reduced cross-section was within 10% of unity. The data are plotted as a function of Q^2 in bins of fixed x . Some points have been slightly offset in Q^2 for clarity. The H1+ZEUS combined binning in x is used in this plot; all other data are rebinned to the x values of these data. For the purpose of plotting, F_2^p has been multiplied by 2^{i_x} , where i_x is the number of the x bin, ranging from $i_x = 1$ ($x = 0.85$) to $i_x = 26$ ($x = 0.0000085$). Only data with $W^2 > 3.5 \text{ GeV}^2$ is included. Plot from CJ collaboration (Shujie Li – private communication). References: **H1 and ZEUS**—H. Abramowicz *et al.*, Eur. Phys. J. **C75**, 580 (2015) (for both data and HERAPDF parameterization); **BCDMS**—A.C. Benvenuti *et al.*, Phys. Lett. **B223**, 485 (1989) (as given in [187]); **E665**—M.R. Adams *et al.*, Phys. Rev. **D54**, 3006 (1996); **NMC**—M. Arneodo *et al.*, Nucl. Phys. **B483**, 3 (1997); **SLAC**—L.W. Whitlow *et al.*, Phys. Lett. **B282**, 475 (1992); **HERMES**—A. Airapetian *et al.*, JHEP **1105**, 126 (2011); **JLAB**—Y. Liang *et al.*, Jefferson Lab Hall C E94-110 collaboration, nucl-ex/0410027, M.E. Christy *et al.*, Jefferson Lab Hall C E94-110 Collaboration, Phys. Rev. **C70**, 015206 (2004), S. Malace *et al.*, Jefferson Lab Hall C E00-116 Collaboration, Phys. Rev. **C80**, 035207 (2009), V. Tvaskis *et al.*, Jefferson Lab Hall C E99-118 Collaboration, Phys. Rev. **C81**, 055207 (2010), M. Osipenko *et al.*, Jefferson Lab Hall B CLAS6 Collaboration, Phys. Rev. **D67**, 092001 (2003).

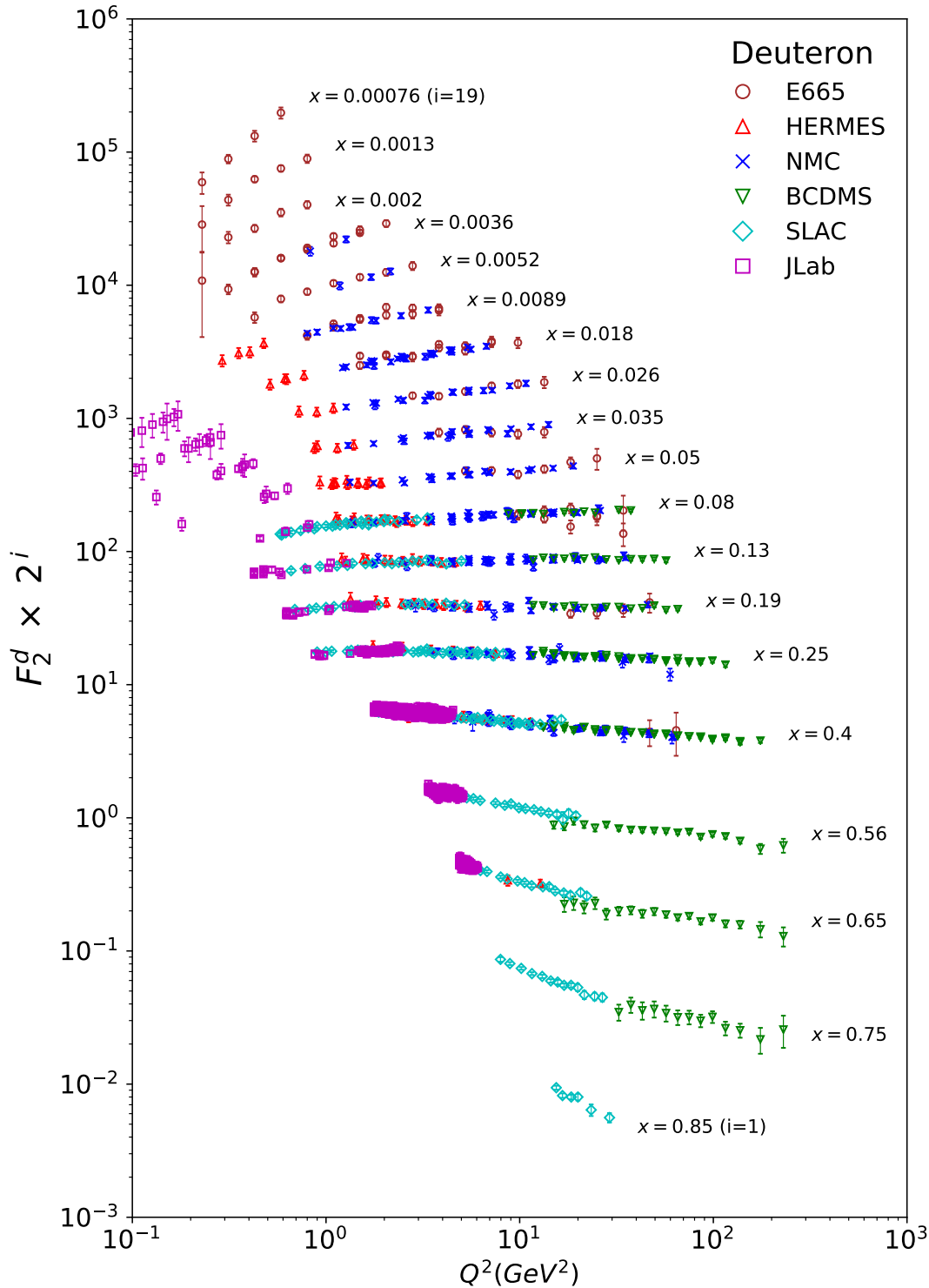


Figure 18.9: The deuteron structure function F_2^d measured in electromagnetic scattering of electrons/positrons (SLAC, HERMES, JLAB) and muons (BCDMS, E665, NMC) on a fixed target, shown as a function of Q^2 for bins of fixed x . Statistical and systematic errors added in quadrature are shown. For the purpose of plotting, F_2^d has been multiplied by 2^{i_x} , where i_x is the number of the x bin, ranging from 1 ($x = 0.85$) to 29 ($x = 0.00076$). Only data with $W^2 > 3.5$ GeV² is included. Plot from CJ collaboration (Shujie Li – private communication) References: **BCDMS**—A.C. Benvenuti *et al.*, Phys. Lett. **B237**, 592 (1990). **E665**, **NMC**, **SLAC**, **HERMES**—same references as Fig. 18.8; **JLAB**—S. Malace *et al.*, Jefferson Lab Hall C E00-116 Collaboration, Phys. Rev. **C80**, 035207 (2009), V. Tvaskis *et al.*, Jefferson Lab Hall C E99-118 Collaboration, Phys. Rev. **C81**, 055207 (2010), J. Seely (MIT, LNS) *et al.*, Jefferson Lab Hall C E03-103 Collaboration, Phys. Rev. Lett. **103**, 202301 (2009), M. Osipenko *et al.*, Jefferson Lab Hall B CLAS6 Collaboration, Phys. Rev. **C73**, 045205 (2006).

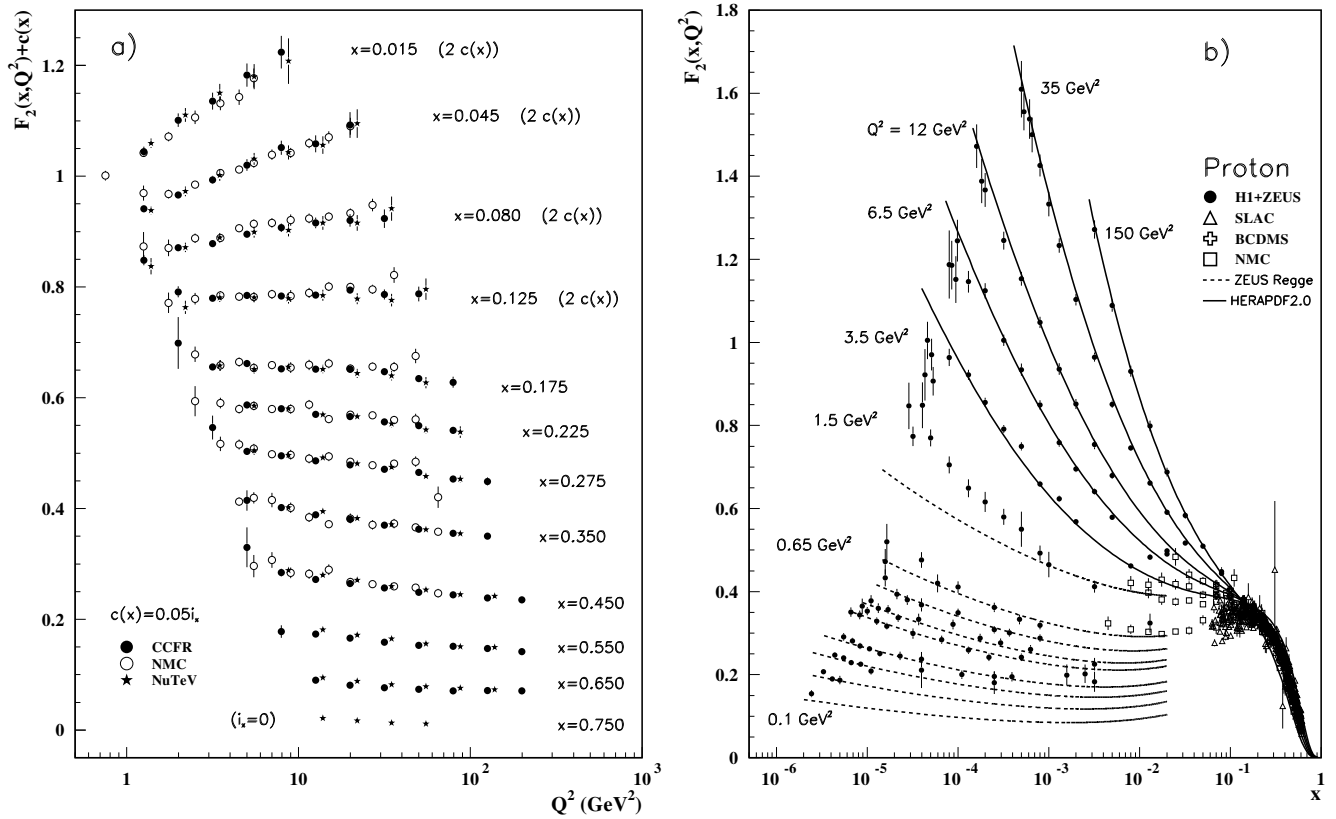


Figure 18.10: a) The deuteron structure function F_2 measured in deep inelastic scattering of muons on a fixed target (NMC) is compared to the structure function F_2 from neutrino-iron scattering (CCFR and NuTeV) using $F_2^{\mu} = (5/18)F_2^{\nu} - x(s + \bar{s})/6$, where heavy-target effects have been taken into account. The data are shown versus Q^2 , for bins of fixed x . The NMC data have been rebinned to CCFR and NuTeV x values. For the purpose of plotting, a constant $c(x) = 0.05i_x$ is added to F_2 , where i_x is the number of the x bin, ranging from 0 ($x = 0.75$) to 7 ($x = 0.175$). For $i_x = 8$ ($x = 0.125$) to 11 ($x = 0.015$), $2c(x)$ has been added. References: **NMC**—M. Arneodo *et al.*, Nucl. Phys. **B483**, 3 (1997); **CCFR/NuTeV**—U.K. Yang *et al.*, Phys. Rev. Lett. **86**, 2741 (2001); **NuTeV**—M. Tzanov *et al.*, Phys. Rev. **D74**, 012008 (2006).

b) The proton structure function F_2^p mostly at small x and Q^2 , measured in electromagnetic scattering of electrons and positrons (H1, ZEUS), electrons (SLAC), and muons (BCDMS, NMC) on protons. Lines are ZEUS Regge and HERAPDF parameterizations for lower and higher Q^2 , respectively. The width of the bins can be up to 10% of the stated Q^2 . Some points have been slightly offset in x for clarity. The H1+ZEUS combined values for $Q^2 \geq 3.5$ GeV² are obtained from the measured reduced cross section and converted to F_2^p with a HERAPDF NLO fit, for all measured points where the predicted ratio of F_2^p to reduced cross-section was within 10% of unity. A turn-over is visible in the low- x points at medium Q^2 (3.5 GeV² and 6 GeV²) for the H1+ZEUS combined values. In order to obtain F_2^p from the measured reduced cross-section, F_L must be estimated; for the points shown, this estimate is obtained from HERAPDF2.0. No F_L value consistent with the HERA data can eliminate the turn-over. This may indicate that at low x and Q^2 there are contributions to the structure functions that cannot be described in standard DGLAP evolution.

References: **H1 and ZEUS**—F.D. Aaron *et al.*, JHEP **1001**, 109 (2010) (data for $Q^2 < 3.5$ GeV²), H. Abramowicz *et al.*, Eur. Phys. J. **C75**, 580 (2015) (data for $Q^2 \geq 3.5$ GeV² and HERAPDF parameterization); **ZEUS**—J. Breitweg *et al.*, Phys. Lett. **B487**, 53 (2000) (ZEUS Regge parameterization); **BCDMS, NMC, SLAC**—same references as Fig. 18.8.

Statistical and systematic errors added in quadrature are shown for both plots.

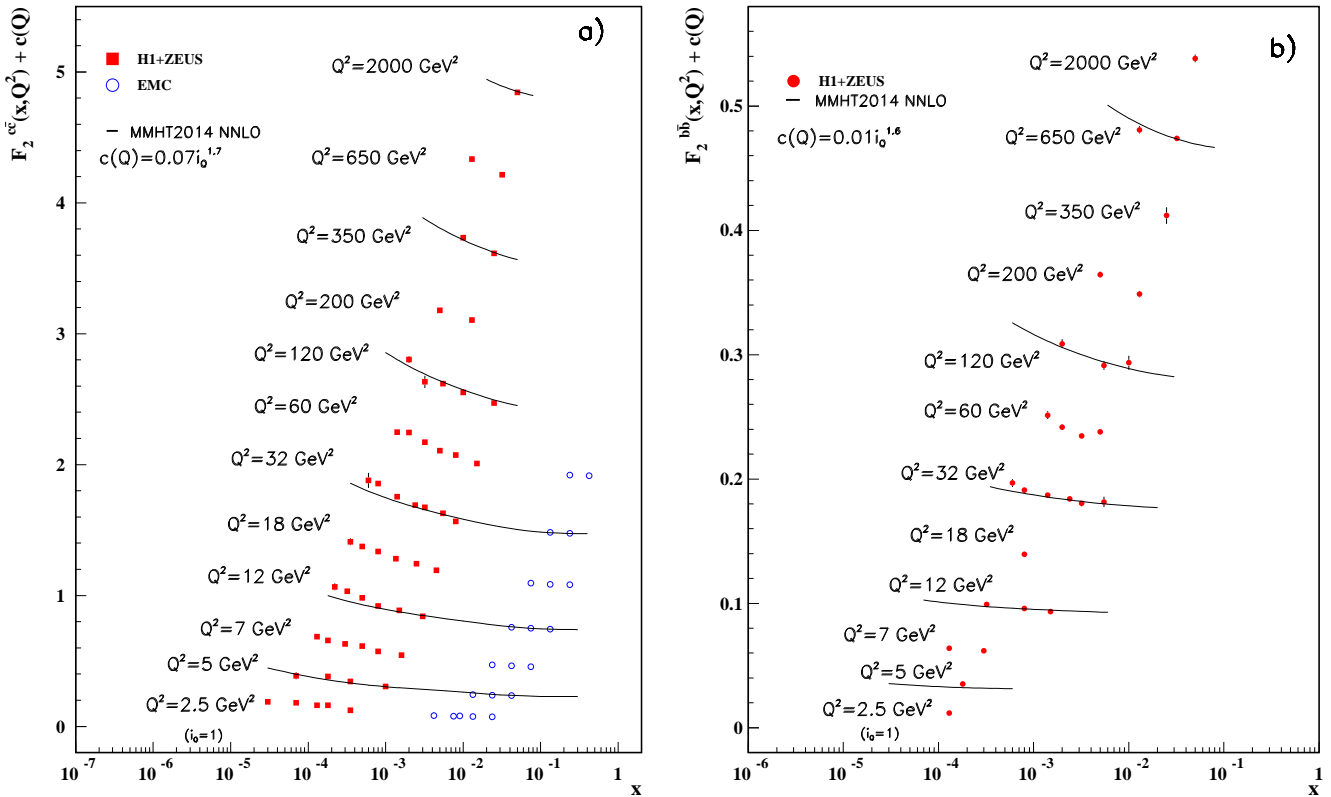


Figure 18.11: a) The charm-quark structure function $F_2^{c\bar{c}}(x)$, i.e. that part of the inclusive structure function F_2^P arising from the production of charm quarks, measured in electromagnetic scattering of positrons on protons (H1, ZEUS) (the values are obtained from the measured reduced cross section and converted to $F_2^{c\bar{c}}$ using the PDFs from the MMHT NNLO fit) and muons on iron (EMC). For the purpose of plotting, a constant $c(Q) = 0.07i_Q^{1.7}$ is added to $F_2^{c\bar{c}}$ where i_Q is the number of the Q^2 bin, ranging from 1 ($Q^2 = 2.5 \text{ GeV}^2$) to 12 ($Q^2 = 2000 \text{ GeV}^2$). References: **H1 and ZEUS run I +II combination**—H. Abramowicz *et al.*, *Eur. Phys. J. C* **78**, 473 (2018); **EMC**—J.J. Aubert *et al.*, *Nucl. Phys. B* **213**, 31 (1983).

b) The bottom-quark structure function $F_2^{b\bar{b}}(x)$. For the purpose of plotting, a constant $c(Q) = 0.01i_Q^{1.6}$ is added to $F_2^{b\bar{b}}$ where i_Q is the number of the Q^2 bin, ranging from 1 ($Q^2 = 2.5 \text{ GeV}^2$) to 12 ($Q^2 = 2000 \text{ GeV}^2$). References: **H1 and ZEUS run I combination**—H. Abramowicz *et al.*, *Eur. Phys. J. C* **78**, 473 (2018).

For both plots, statistical and systematic errors added in quadrature are shown. The data are given as a function of x in bins of Q^2 . Points may have been slightly offset in x for clarity. Some data have been rebinned to common Q^2 values. Also shown is the MMHT2014 parameterization given at several Q^2 values (L. A. Harland-Lang *et al.*, *Eur. Phys. J. C* **75**, 204 (2015)).

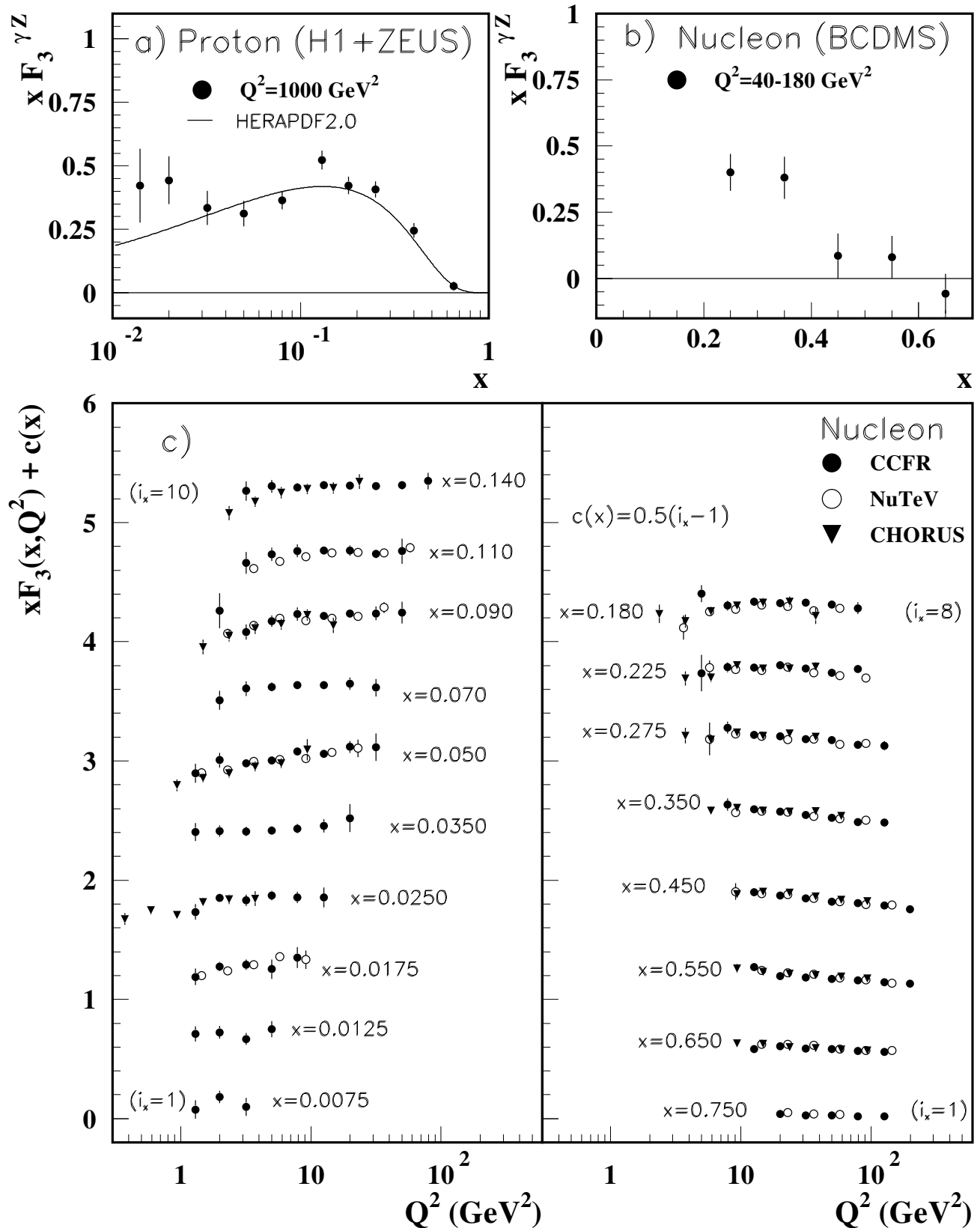


Figure 18.12: The structure function $x F_3^{\gamma Z}$ measured in electroweak scattering of **a)** electrons on protons (H1 and ZEUS) and **b)** muons on carbon (BCDMS). The line in **a)** is the HERAPDF parameterization. References: **H1 and ZEUS**—H. Abramowicz *et al.*, Eur. Phys. J. **C75**, 580 (2015) (for both data and HERAPDF parameterization); **BCDMS**—A. Argento *et al.*, Phys. Lett. **B140**, 142 (1984). **c)** The structure function $x F_3$ of the nucleon measured in ν -Fe scattering. The data are plotted as a function of Q^2 in bins of fixed x . For the purpose of plotting, a constant $c(x) = 0.5(i_x - 1)$ is added to $x F_3$, where i_x is the number of the x bin as shown in the plot. The NuTeV and CHORUS points have been shifted to the nearest corresponding x bin as given in the plot and slightly offset in Q^2 for clarity. References: **CCFR**—W.G. Seligman *et al.*, Phys. Rev. Lett. **79**, 1213 (1997); **NuTeV**—M. Tzanov *et al.*, Phys. Rev. **D74**, 012008 (2006); **CHORUS**—G. Öngüt *et al.*, Phys. Lett. **B632**, 65 (2006).

Statistical and systematic errors added in quadrature are shown for all plots.

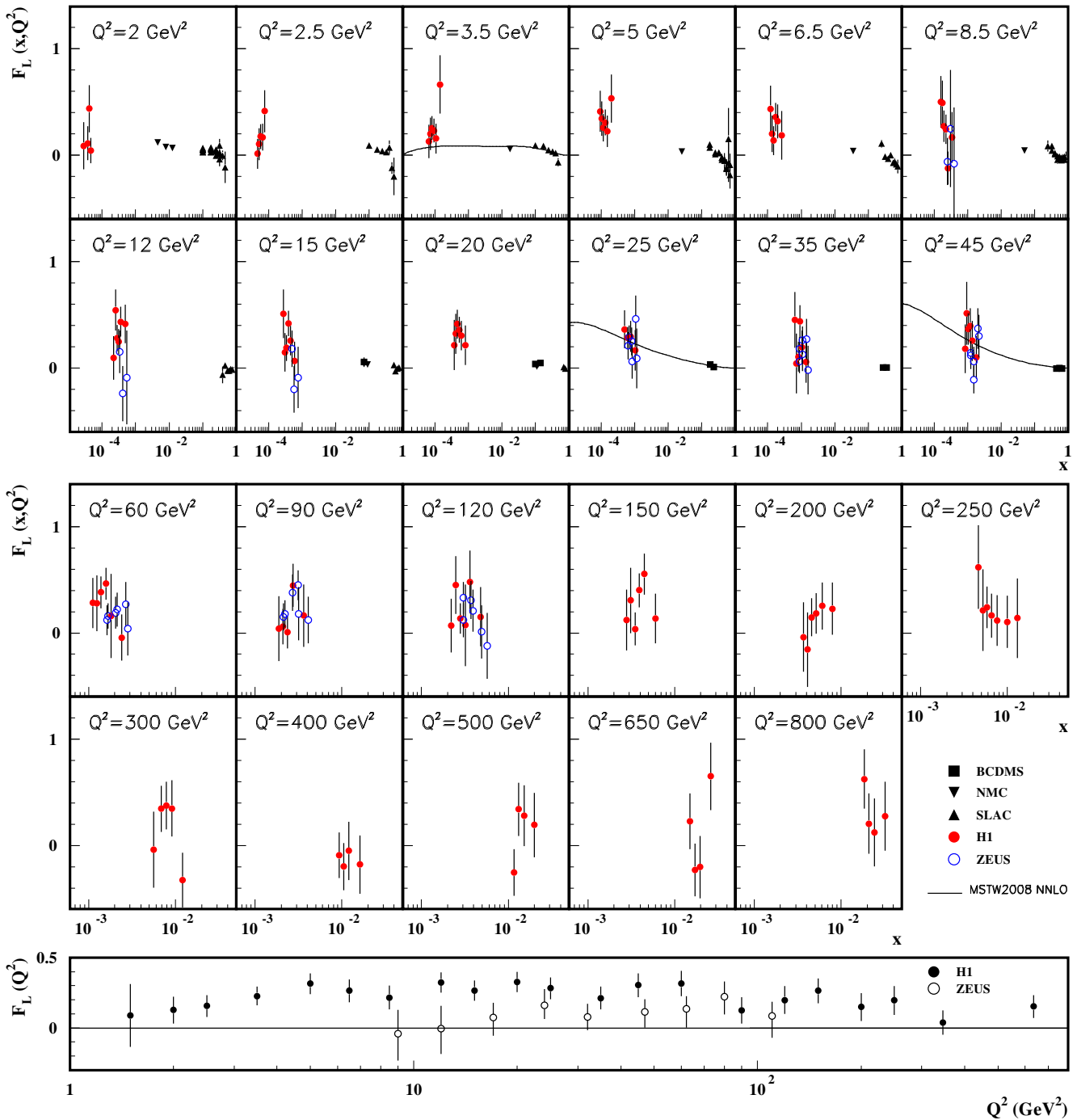


Figure 18.13: Top panels: The longitudinal structure function F_L as a function of x in bins of fixed Q^2 measured on the proton (except for the SLAC data which also contain deuterium data). BCDMS, NMC, and SLAC results are from measurements of R (the ratio of longitudinal to transverse photon absorption cross sections) which are converted to F_L by using the BCDMS parameterization of F_2 (A.C. Benvenuti *et al.*, Phys. Lett. **B223**, 485 (1989)). It is assumed that the Q^2 dependence of the fixed-target data is small within a given Q^2 bin. Some of the other data may have been rebinned to common Q^2 values. Some points have been slightly offset in x for clarity. Also shown is the MSTW2008 parameterization given at three Q^2 values (A.D. Martin *et al.*, Eur. Phys. J. **C63**, 189 (2009)). References: **H1**—V. Andreev *et al.*, Eur. Phys. J. **C74**, 2814 (2014); **ZEUS**—S. Chekanov *et al.*, Phys. Lett. **B682**, 8 (2009); H. Abramowicz *et al.*, Phys. Rev. **D90**, 072002 (2014); **BCDMS**—A. Benvenuti *et al.*, Phys. Lett. **B223**, 485 (1989); **NMC**—M. Arneodo *et al.*, Nucl. Phys. **B483**, 3 (1997); **SLAC**—L.W. Whitlow *et al.*, Phys. Lett. **B250**, 193 (1990) and numerical values from the thesis of L.W. Whitlow (SLAC-357). Bottom panel: The longitudinal structure function F_L as a function of Q^2 . Some points have been slightly offset in Q^2 for clarity. References: **H1**—V. Andreev *et al.*, Eur. Phys. J. **C74**, 2814 (2014); **ZEUS**—H. Abramowicz *et al.*, Phys. Rev. **D90**, 072002 (2014). The results shown in the bottom plot require the assumption of the validity of the QCD form for the F_2 structure function in order to extract F_L . Statistical and systematic errors added in quadrature are shown for both plots.

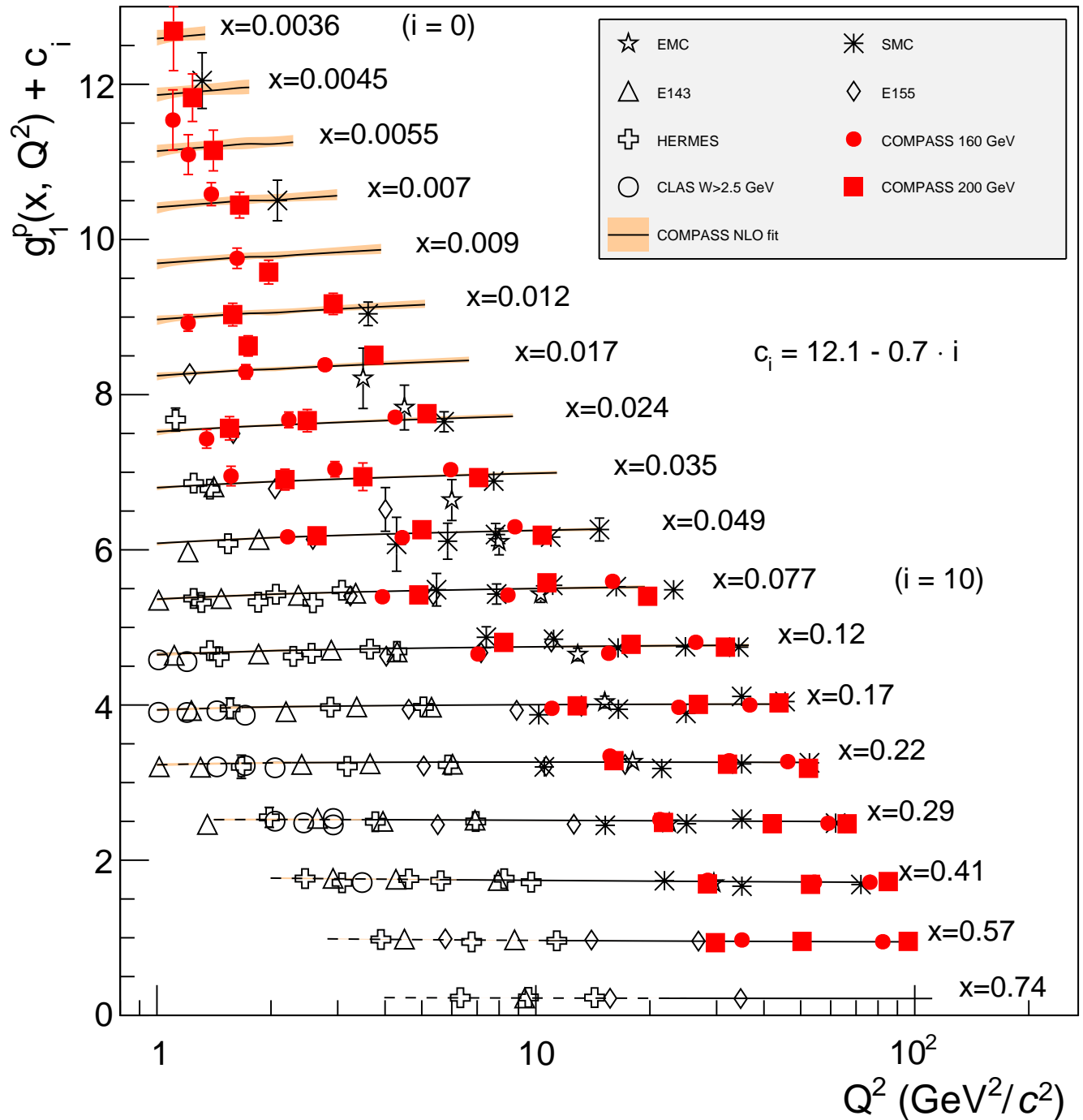


Figure 18.14: World data on the spin-dependent structure function g_1^p as a function of Q^2 for various values of x . The lines represent the Q^2 dependence for each value of x , as determined from a NLO QCD fit. The dashed ranges represent the region with $W^2 < 10$ (GeV/c^2)². References: **EMC**—J. Ashman *et al.*, Phys. Lett. **B206**, 363 (1988); Nucl. Phys. **B328**, 1 (1989); **E143**—K. Abe *et al.*, Phys. Rev. **D58**, 112003 (1998); **SMC**—B. Adeva *et al.*, Phys. Rev. **D58**, 112001 (1998); **HERMES**—A. Airapetian *et al.*, Phys. Rev. **D75**, 012007 (2007); **E155**—P.L. Anthony *et al.*, Phys. Lett. **B493**, 19 (2000); **COMPASS**—M.G. Alekseev *et al.*, Phys. Lett. **B690**, 466 (2010), C. Adolph, *et al.*, Phys. Lett. **B753**, 18 (2016); **CLAS**—K.V. Dharmawardane *et al.*, Phys. Lett. **B641**, 11 (2006) (which also includes resonance region data not shown on this plot — there is also low W^2 CLAS data in Y. Prok *et al.*, Phys. Rev. **C90**, 025212 (2014) and N. Guler *et al.*, Phys. Rev. **C92**, 055201 (2015)).

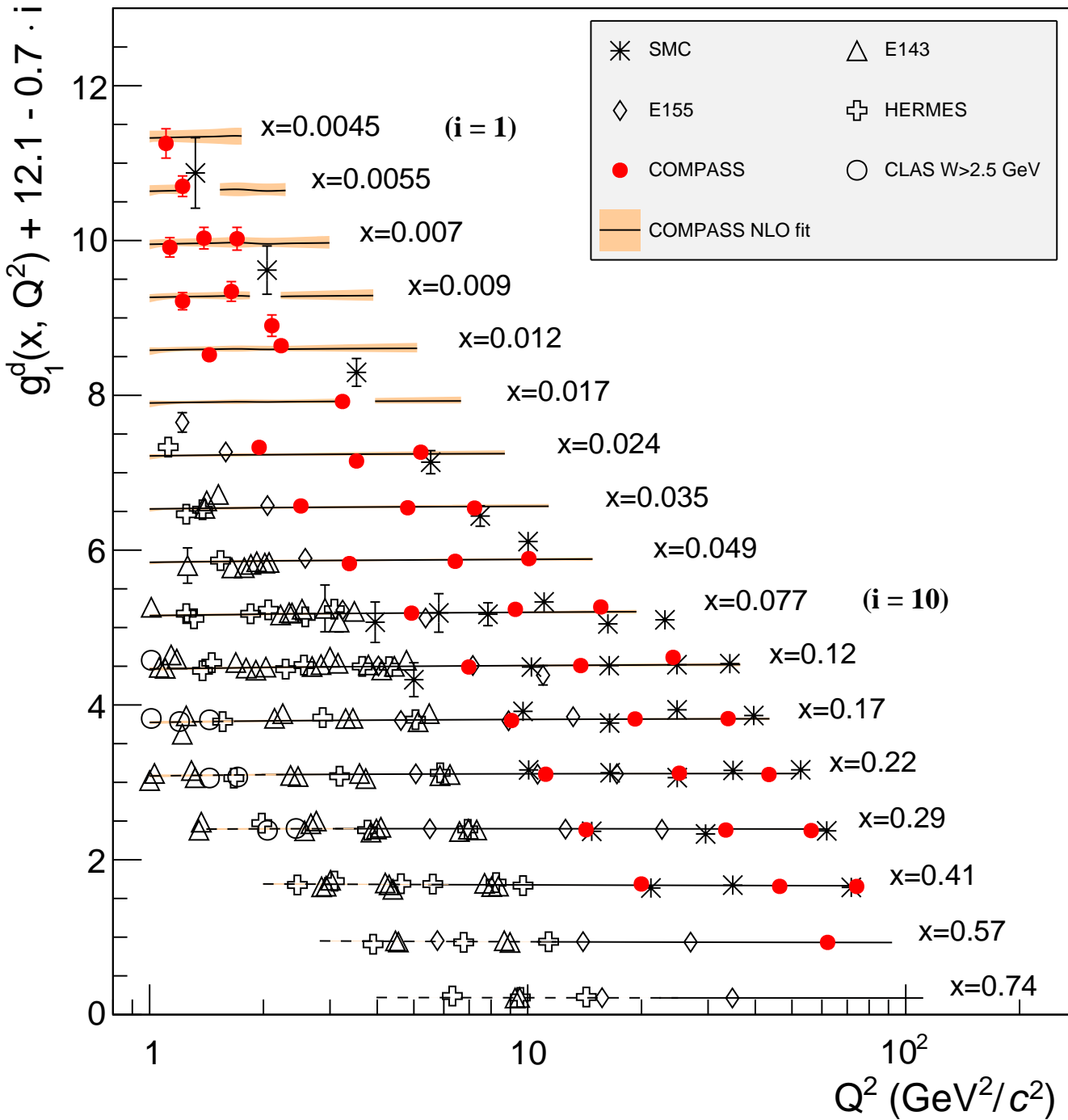


Figure 18.15: World data on the spin-dependent structure function g_1^d as a function of Q^2 for various values of x . The lines represent the Q^2 dependence for each value of x , as determined from a NLO QCD fit. The dashed ranges represent the region with $W^2 < 10$ $(\text{GeV}/c^2)^2$. **CLAS**—K.V. Dharmawardane *et al.*, Phys. Lett. **B641**, 11 (2006); **HERMES**—A. Airapetian *et al.*, Phys. Rev. **D75**, 012007 (2007); **SMC**—B. Adeva *et al.*, Phys. Rev. **D58**, 112001 (1998); **E155**—P.L. Anthony *et al.*, Phys. Lett. **B463**, 339 (1999); **E143**—K. Abe *et al.*, Phys. Rev. **D58**, 112003 (1998); **COMPASS**—C. Adolph, *et al.*, Phys. Lett. **B769**, 34 (2017);

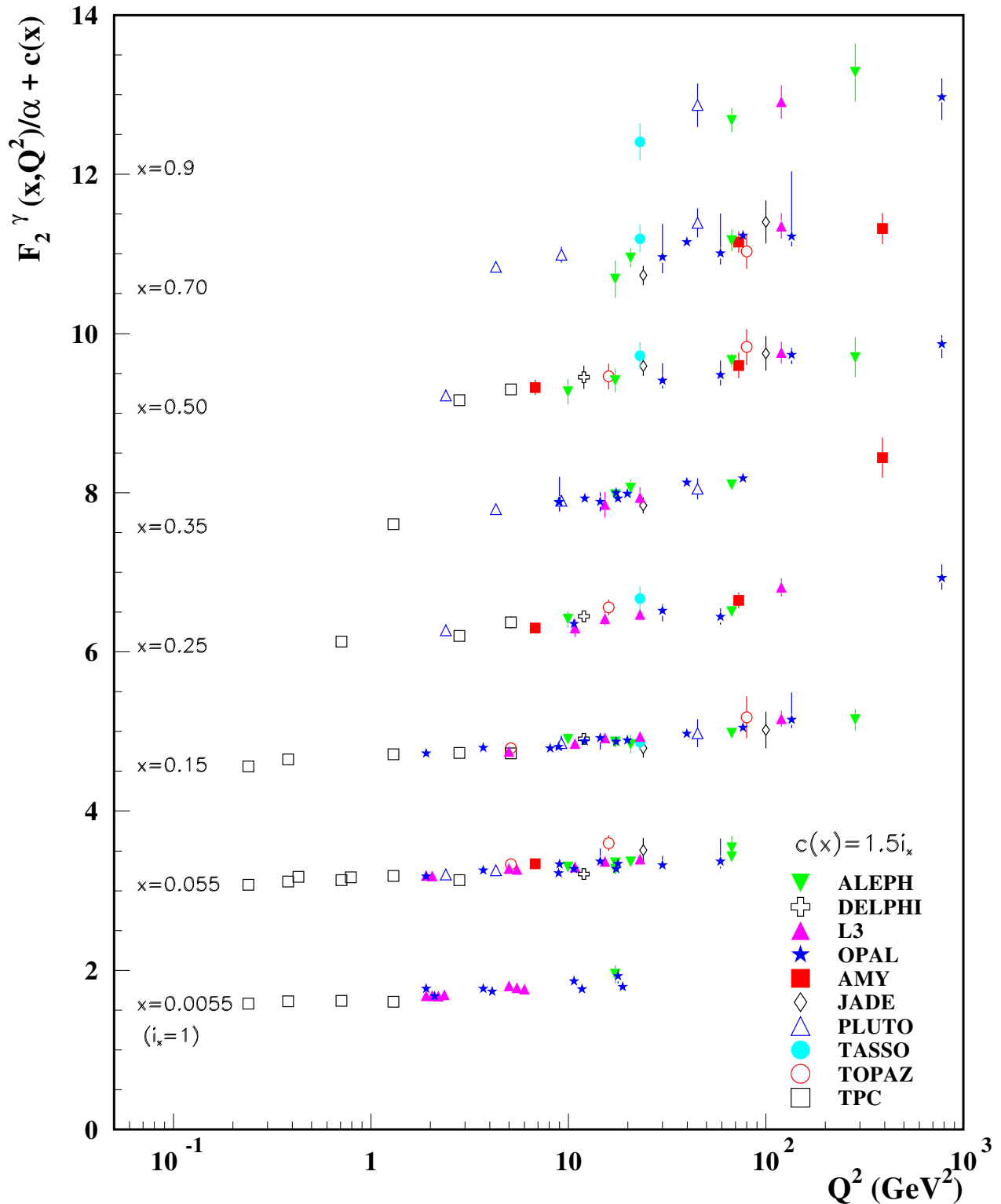


Figure 18.16: The hadronic structure function of the photon F_2^γ divided by the fine structure constant α measured in e^+e^- scattering, shown as a function of Q^2 for bins of x . Data points have been shifted to the nearest corresponding x bin as given in the plot. Some points have been offset in Q^2 for clarity. Statistical and systematic errors added in quadrature are shown. For the purpose of plotting, a constant $c(x) = 1.5i_x$ is added to F_2^γ/α where i_x is the number of the x bin, ranging from 1 ($x = 0.0055$) to 8 ($x = 0.9$). References: **ALEPH**–R. Barate *et al.*, Phys. Lett. **B458**, 152 (1999); A. Heister *et al.*, Eur. Phys. J. **C30**, 145 (2003); **DELPHI**–P. Abreu *et al.*, Z. Phys. **C69**, 223 (1995); **L3**–M. Acciarri *et al.*, Phys. Lett. **B436**, 403 (1998); M. Acciarri *et al.*, Phys. Lett. **B447**, 147 (1999); M. Acciarri *et al.*, Phys. Lett. **B483**, 373 (2000); **OPAL**–A. Ackerstaff *et al.*, Phys. Lett. **B411**, 387 (1997); A. Ackerstaff *et al.*, Z. Phys. **C74**, 33 (1997); G. Abbiendi *et al.*, Eur. Phys. J. **C18**, 15 (2000); G. Abbiendi *et al.*, Phys. Lett. **B533**, 207 (2002) (note that there is overlap of the data samples in these last two papers); **AMY**–S.K. Sahu *et al.*, Phys. Lett. **B346**, 208 (1995); T. Kojima *et al.*, Phys. Lett. **B400**, 395 (1997); **JADE**–W. Bartel *et al.*, Z. Phys. **C24**, 231 (1984); **PLUTO**–C. Berger *et al.*, Phys. Lett. **142B**, 111 (1984); C. Berger *et al.*, Nucl. Phys. **B281**, 365 (1987); **TASSO**–M. Althoff *et al.*, Z. Phys. **C31**, 527 (1986); **TOPAZ**–K. Muramatsu *et al.*, Phys. Lett. **B332**, 477 (1994); **TPC/Two Gamma**–H. Aihara *et al.*, Z. Phys. **C34**, 1 (1987).

19. Fragmentation Functions in e^+e^- , ep , and pp Collisions

Revised August 2019 by O. Biebel (Ludwig-Maximilians U.), D. de Florian (ICAS and ICIFI, UNSAM), D. Milstead (Stockholm U.) and W. Vogelsang (Tübingen U.).

19.1 Introduction to fragmentation

Quarks and gluons produced in hard-scattering reactions will ultimately give rise to the colorless hadronic bound states that may be observed in the detector. The associated hadronization process is described by fragmentation functions $D_i^h(x, \mu^2)$ ($i = q, \bar{q}, g$) which are universal functions representing, in the simplest picture, a measure of the probability density that an outgoing parton produces a hadron h . Here, x is the fraction of the parton's momentum transferred to the hadron, and μ is a 'resolution' scale known as factorization scale. The $D_i^h(x, \mu^2)$ may be viewed as the final-state analogs of the initial-state parton distribution functions (PDFs) addressed in Section 18 of this *Review*. They are also sometimes referred to as *timelike* distributions since they are primarily accessed in e^+e^- annihilation via a timelike intermediate boson. (See Refs. [1,2] for introductory reviews, and Refs. [3–5] for summaries of experimental and theoretical research in this field.)

The cleanest laboratory for the study of fragmentation functions is provided by semi-inclusive electron-positron annihilation, $e^+e^- \rightarrow \gamma/Z \rightarrow h+X$. The cross section for this reaction may be expressed in terms of 'fragmentation structure functions' $F_{T,L,A}$ that are directly related to the fragmentation functions. At center-of-mass (CM) energy $\sqrt{s} = q^2$ we have

$$\begin{aligned} \frac{1}{\sigma_0} \frac{d^2\sigma^h}{dx d\cos\theta} &= \frac{3}{8}(1 + \cos^2\theta)F_T^h(x, q^2) + \frac{3}{4}\sin^2\theta F_L^h(x, q^2) \\ &+ \frac{3}{4}\cos\theta F_A^h(x, q^2). \end{aligned} \quad (19.1)$$

Here, q is the four-momentum of the intermediate photon or Z -boson, with $q^2 > 0$, and $x = 2P_h \cdot q/q^2$ with the hadron's four-momentum P_h is the fragmentation counterpart of the familiar DIS Bjorken variable. (Note that $x = 2E_h/\sqrt{s} \leq 1$ in terms of the energy E_h of the produced hadron in the CM frame of the electron positron pair.) Furthermore, in the same frame, θ is the hadron's angle relative to the electron beam direction. Eq. (19.1) is the most general form for unpolarized inclusive single-particle production via vector bosons [6]. The fragmentation structure functions F_T and F_L represent the contributions from γ/Z polarizations transverse or longitudinal with respect to the direction of motion of the hadron. The parity-violating term with the asymmetric fragmentation function F_A arises from the interference between vector and axial-vector contributions. Various normalization factors σ_0 are used in the literature, ranging from the total cross section σ_{tot} for $e^+e^- \rightarrow \text{hadrons}$, including all weak and QCD contributions, to $\sigma_0 = 4\pi\alpha^2 N_c/3s$ with $N_c = 3$, the lowest-order QED cross section for $e^+e^- \rightarrow \mu^+\mu^-$ times the number of colors N_c . LEP1 measurements of the three fragmentation structure functions are shown in Fig. 19.1.

Integration of Eq. (19.1) over all θ yields the total fragmentation structure function $F^h = F_T^h + F_L^h$:

$$\begin{aligned} \frac{1}{\sigma_0} \frac{d\sigma^h}{dx} &= F^h(x, q^2) \\ &= \sum_i \int_x^1 \frac{dz}{z} C_i \left(z, \alpha_s(\mu), \frac{q^2}{\mu^2} \right) D_i^h \left(\frac{x}{z}, \mu^2 \right). \end{aligned} \quad (19.2)$$

On the right we have written the factorized expression for the structure function in terms of a sum over convolutions of the fragmentation functions D_i^h for partons $i = u, \bar{u}, d, \bar{d}, \dots, g$ with perturbative coefficient functions C_i . Since photons and Z bosons do not distinguish between quarks and antiquarks, e^+e^- annihilation primarily constrains the combinations $D_q^h + D_{\bar{q}}^h$. Gluon fragmentation contributes only at higher order in perturbation theory or by scaling violations. Corrections to the factorized expression in Eq. (19.2) are suppressed by inverse powers of q^2 . They arise from quark and hadron mass terms and from non-perturbative effects.

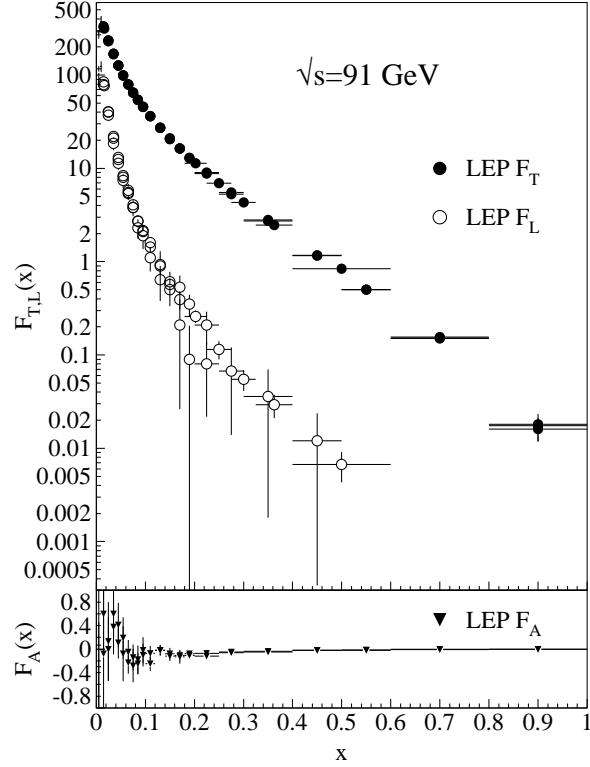


Figure 19.1: LEP1 measurements of total transverse (F_T), longitudinal (F_L), and asymmetric (F_A) fragmentation structure functions [7]. Data points with relative errors greater than 100% are omitted.

Analogous factorized expressions as in Eq. (19.2) may be written for each of the structure functions $F_{T,L,A}$ individually.

The fragmentation functions obey the momentum sum rule constraint

$$\sum_h \int_0^1 dx x D_i^h(x, \mu^2) = 1, \quad (19.3)$$

separately for each flavor i . Note that the sum rule involves a sum over all possible produced hadrons. The dependence of the functions D_i^h on the factorization scale μ^2 will be discussed in the next section.

Measurements of hadron production in deeply-inelastic lepton-proton scattering and hadron-hadron scattering are complementary to those in e^+e^- annihilation. The former process, $\ell p \rightarrow \ell' + h + X$, is known as *semi-inclusive deep-inelastic scattering (SIDIS)*. Here, in analogy with Eq. (19.2), the high virtuality of the photon in DIS also permits factorization of the cross section in terms of fragmentation functions, PDFs for the incoming proton, and perturbative hard-scattering cross sections. Likewise, factorization also occurs for $pp \rightarrow h + X$ at large transverse momentum of the produced hadron, and for $pp \rightarrow \text{jet}(h) + X$, where the hadron is part of a fully reconstructed jet. The fragmentation functions contributing to $e^+e^- \rightarrow h + X$, $\ell p \rightarrow \ell' + h + X$, and $pp \rightarrow h + X$, $pp \rightarrow \text{jet}(h) + X$ are universal in the sense that the same functions appear in the factorized expressions for the three reactions. Modern QCD analyses of fragmentation functions ‘globally’ take into account experimental data sets for all three types of processes in order to obtain optimal sets of fragmentation functions.

Electron-positron annihilation has the advantage that there is no hadronic initial state and hence no beam remnant. This is in contrast to $\ell p \rightarrow \ell' + h + X$ or $pp \rightarrow h + X$, which are affected by hadron remnant contributions associated with the partons of the initial-state hadron(s) which are collaterally involved in the hard lepton-parton or parton-parton collision. On the other hand,

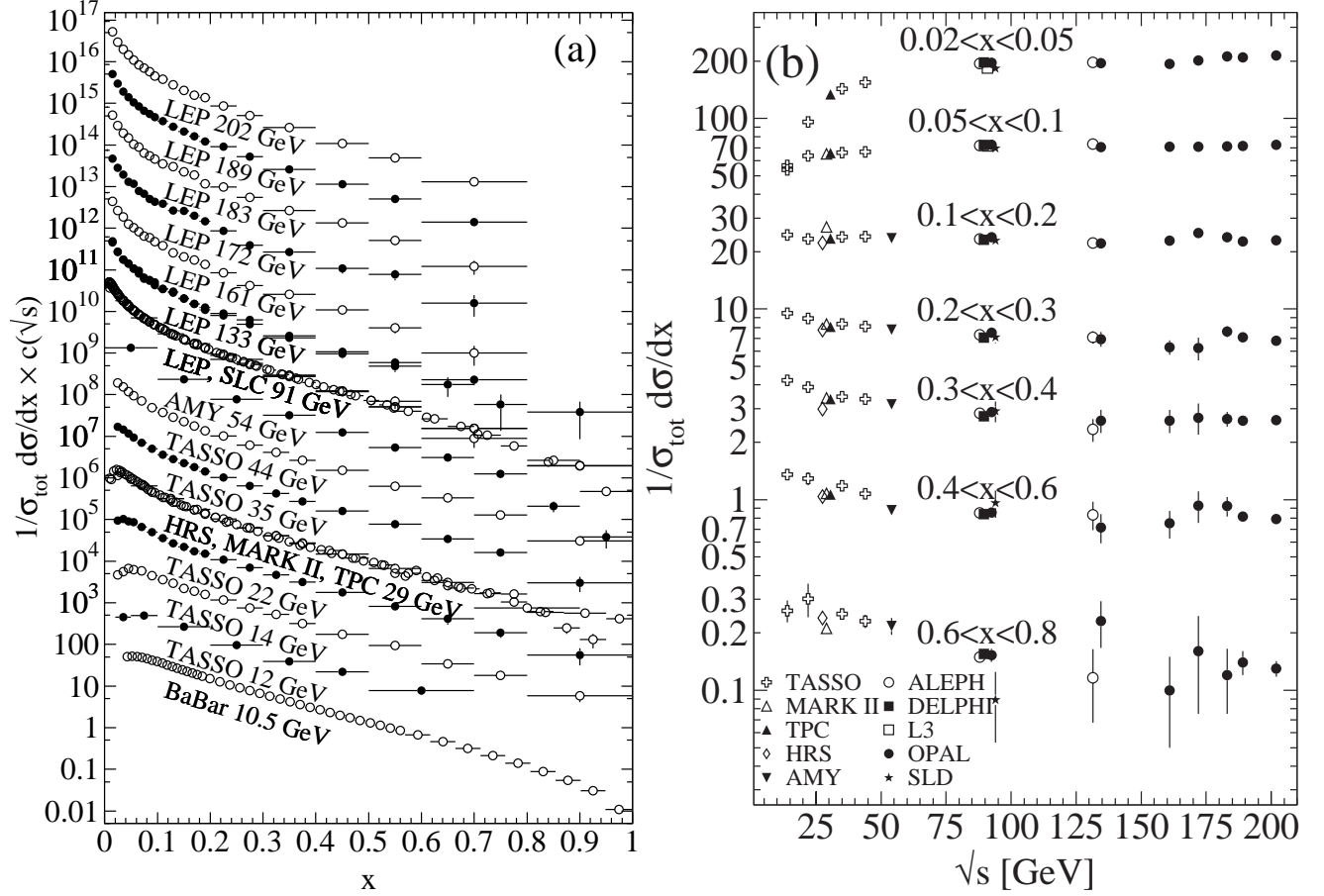


Figure 19.2: Cross section for $e^+e^- \rightarrow h + X$ for all charged hadrons [8–26], (a) for different CM energies \sqrt{s} versus x , and (b) for various ranges of x versus \sqrt{s} . For (a) the distributions have been scaled by $c(\sqrt{s}) = 10^i$ with i ranging from $i = 0$ ($\sqrt{s} = 12$ GeV) to $i = 13$ ($\sqrt{s} = 202$ GeV).

$e^+e^- \rightarrow h + X$ has little sensitivity to D_q^h and is insensitive to the charge asymmetries $D_q^h - D_{\bar{q}}^h$. These quantities are best constrained in proton-(anti-)proton and electron-proton scattering, respectively. Especially the latter provides an environment that allows the study of the influence of initial-state QCD radiation on the fragmentation process, of the partonic and spin structure of the hadron target, and of the target remnant system. (See Ref. [27] for a comprehensive review of the measurements and models of fragmentation in lepton-hadron scattering).

Moreover, unlike e^+e^- annihilation where $q^2 = s$ is fixed by the collider energy, lepton-hadron scattering has two independent scales, $Q^2 = -q^2$ and the invariant mass squared, $W^2 \approx Q^2(1-x)/x$, of the hadronic final state, which both can vary by several orders of magnitudes for a given CM energy, thus allowing the study of fragmentation in different environments by a single experiment. For example, in photoproduction the exchanged photon is quasi-real ($Q^2 \approx 0$), leading to processes akin to hadron-hadron scattering. In DIS ($Q^2 \gg 1$ GeV²), using factorization, the hadronic fragments of the struck quark can be directly compared with quark fragmentation in e^+e^- in a suitable frame. Results from lepton-hadron experiments quoted in this report primarily concern fragmentation in the DIS regime. Studies performed by lepton-hadron experiments of fragmentation with photoproduction data containing high transverse momentum jets or particles are also reported, when these are directly comparable to DIS and e^+e^- results.

Fragmentation studies in lepton-hadron collisions are usually performed in one of two frames in which the target hadron and the exchanged boson are collinear. The hadronic center-of-mass frame (HCMS) is defined as the rest system of the exchanged boson and incoming hadron, with the z^* -axis defined along the direction of the exchanged boson. The positive z^* direction de-

fines the so-called current fragmentation region. Fragmentation measurements performed in the HCMS often use the Feynman- x variable $x_F = 2p_z^*/W$, where p_z^* is the longitudinal momentum of the particle in this frame. As W is the invariant mass of the hadronic final state, x_F ranges between -1 and 1 .

The Breit system [28, 29] is related to the HCMS by a longitudinal boost such that the time component of q vanishes, i.e., $q = (0, 0, 0, -Q)$. In the parton model, the struck parton then has the longitudinal momentum $Q/2$ which becomes $-Q/2$ after the collision. As compared with the HCMS, the current fragmentation region of the Breit frame is more closely matched to the partonic scattering process, and is thus appropriate for direct comparisons of fragmentation functions in DIS with those from e^+e^- annihilation. The variable $x_p = 2p^*/Q$, where p^* is the particle's momentum in the current region of the Breit frame, is used at HERA for measurements in the Breit frame, enabling rather direct comparisons of DIS and e^+e^- results.

19.2 Scaling violations and QCD corrections

As mentioned, the coefficient functions for the fragmentation structure functions in $e^+e^- \rightarrow h + X$ are amenable to QCD perturbation theory. For each of the structure functions $F_{T,L,A}(x, q^2)$ in Eq. (19.1) (and hence for the total structure function F^h in Eq. (19.2)) the coefficient function has an expansion of the form

$$C_{a,i} \left(z, \alpha_s(\mu), \frac{q^2}{\mu^2} \right) = (1 - \delta_{aL}) \delta_{iq} \delta(1-z) + \frac{\alpha_s(\mu)}{2\pi} c_{a,i}^{(1)} \left(z, \frac{q^2}{\mu^2} \right) + \left(\frac{\alpha_s(\mu)}{2\pi} \right)^2 c_{a,i}^{(2)} \left(z, \frac{q^2}{\mu^2} \right) + \dots (19.4)$$

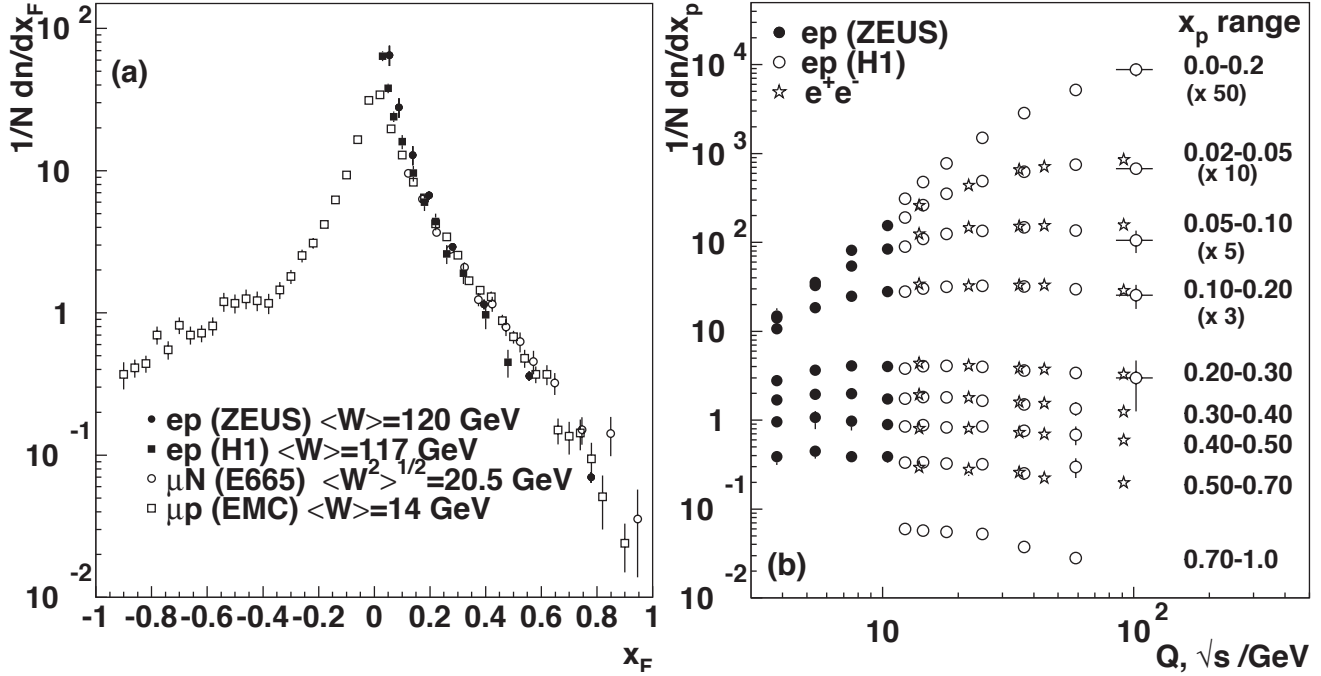


Figure 19.3: (a) The distribution $1/N \cdot dn/dx_F$ for all charged particles in DIS lepton-hadron experiments at different values of W , measured in the HCMS [30–33]. (b) Scaling violations of the fragmentation structure function for all charged particles in the current region of the Breit frame of DIS [34, 35] and in e^+e^- interactions [19, 36]. The data are shown as a function of \sqrt{s} for e^+e^- results, and as a function of Q for the DIS results, each within the same indicated intervals of the scaled momentum x_p . The data for the four lowest intervals of x_p are multiplied by factors 50, 10, 5, and 3, respectively for better visibility.

where $a = T, L, A$. At the zeroth order in the strong coupling α_s the coefficient functions C_g for gluons vanish, while for (anti-) quarks $C_i = g_i(s) \delta(1-z)$ (except for F_L for which the leading contribution is of order α_s , as indicated in Eq. (19.4)). Here $g_i(s)$ is the appropriate electroweak coupling. In particular, $g_i(s)$ is proportional to the squared charge of the quark i at $s \ll M_Z^2$, when weak effects can be neglected. The full electroweak prefactors $g_i(s)$ can be found in Ref. [6]. The first-order QCD corrections to the coefficient functions have been calculated in Refs. [37, 38], and the second-order terms in [39–41]. Thus, the coefficient functions are known to NNLO, except for F_L . We note that beyond the leading order the coefficient functions, and hence the fragmentation functions, start to depend on the choice of factorization scheme. The standard choice in the literature is the $\overline{\text{MS}}$ scheme.

The simplest parton-model approach would predict scale-independent (‘scaling’) x -distributions for both the structure function F^h and the parton fragmentation functions D_i^h . Perturbative QCD corrections lead to logarithmic scaling violations via the evolution equations [42]

$$\frac{\partial}{\partial \ln \mu^2} D_i^h(x, \mu^2) = \sum_j \int_x^1 \frac{dz}{z} P_{ji}(z, \alpha_s(\mu^2)) D_j^h\left(\frac{x}{z}, \mu^2\right), \quad (19.5)$$

where the functions $P_{ij}(z, \alpha_s(\mu^2))$ describe the splitting process $i \rightarrow j + X$, where parton j carries the longitudinal momentum fraction z of parton i . Note that for fragmentation the relevant splitting functions are P_{ji} (rather than P_{ij} as for the PDFs) since D_j^h represents the fragmentation of the final parton. Usually the system of evolution equations is decomposed into a 2×2 flavor-singlet sector comprising the gluon and the sum of all quark and antiquark fragmentation functions, and scalar (‘non-singlet’) equations for quark-antiquark and flavor differences.

The splitting functions in Eq. (19.5) have the perturbative expansion

$$P_{ji}(z, \alpha_s) = \frac{\alpha_s}{2\pi} P_{ji}^{(0)}(z) + \left(\frac{\alpha_s}{2\pi}\right)^2 P_{ji}^{(1)}(z) + \left(\frac{\alpha_s}{2\pi}\right)^3 P_{ji}^{(2)}(z) + \dots, \quad (19.6)$$

where the leading-order (LO) functions $P^{(0)}(z)$ [42, 43] are the same as those for the initial-state parton distributions. The next-to-leading order (NLO) corrections $P^{(1)}(z)$ have been calculated in Refs. [44–48] (there are well-known misprints in the journal version of Ref. [45]). Ref. [48] also includes the spin-dependent case. The timelike functions are different from, but related to, their spacelike counterparts, see also Ref. [49]. The connections between the two sets of functions has facilitated recent calculations of the next-to-next-to-leading order (NNLO) quantities $P_{qq}^{(2)}(z)$ and $P_{gg}^{(2)}(z)$ in Eq. (19.6) [40, 50]. In the same way, the corresponding off-diagonal quantities $P_{qg}^{(2)}$ and $P_{gq}^{(2)}$ were recently obtained in Ref. [51] with the help of constraints from the momentum sum rule Eq. (19.3) [50] and of the limit of $C_A = C_F = n_f$ for which QCD becomes supersymmetric. An uncertainty still remains for the $P_{qg}^{(2)}$ kernel, which however does not affect the logarithmic behavior at small and large momentum fractions. With the exception of Ref. [47], all these higher-order results refer to the standard $\overline{\text{MS}}$ scheme with a fixed number n_f of light flavors. When the threshold for the production of a heavier quark flavor is crossed in the course of the scale evolution, fragmentation functions change. The NLO treatment of these flavor thresholds in the evolution has been addressed in Ref. [52].

The phenomenological effect of scale evolution is similar in the timelike and spacelike cases: As the scale increases, one observes a scaling violation in which the x -distribution is shifted towards lower values. This can be seen from Fig. 19.2 where a set of measurements of the total fragmentation structure function in e^+e^- annihilation are shown. In particular, the figure on the right exhibits the dependence on $\sqrt{q^2} = \sqrt{s}$ at fixed values of x . QCD analyses of these data are discussed in Section 19.5 below.

The NLO coefficient functions for SIDIS, $ep \rightarrow e + h + X$, have been presented in Refs. [37, 38] Corresponding results have also been obtained for the case that a non-vanishing hadron transverse momentum is required in the HCMS frame [53, 54].

Scaling violations in DIS are shown in Fig. 19.3 for both the HCMS and the Breit frames. In Fig. 1.3(a) the distribution in terms of $x_F = 2p_F^z/W$ shows a steeper slope in ep data than for the lower-energy μp data for $x_F > 0.15$, indicating the scaling

violations. At smaller values of x_F in the current jet region, the multiplicity of particles substantially increases with W , owing to the increased phase space available for the fragmentation process. The EMC data access both the current region and the region of the fragmenting target remnant system. At higher values of $|x_F|$, due to the extended nature of the remnant, the multiplicity in the target region far exceeds that in the current region. For acceptance reasons the remnant hemisphere of the HCMS is only accessible by the lower-energy fixed-target experiments.

Using hadrons from the current hemisphere in the Breit frame, measurements of fragmentation functions and the production properties of particles in ep scattering have been reported in Refs. [34, 35, 55–58]. Fig. 19.3(b) compares results from ep scattering and e^+e^- experiments; the latter results have been divided by two as they cover both event hemispheres. The agreement between the DIS and e^+e^- results is fairly good. However, processes in DIS which are not present in e^+e^- annihilation, such as boson-gluon fusion and initial-state QCD radiation, can depopulate the current region. These effects become most prominent at low values of Q and x_p . Hence, when compared with e^+e^- annihilation data at $\sqrt{s} = 5.2, 6.5$ GeV [59] not shown here, the DIS particle rates tend to lie below those observed in e^+e^- annihilation. A ZEUS study [60] finds that the direct comparability of the ep data to e^+e^- results at low scales is improved if twice the energy in the current hemisphere of the Breit frame, $2E_B^{\text{cr}}$, is used instead of $Q/2$ as the fragmentation scale. Choosing $2E_B^{\text{cr}}$ for the fragmentation scale approximates QCD radiation effects relevant at low scales, as detailed in Ref. [29].

19.3 Fragmentation functions for small particle momenta

The higher-order timelike splitting functions in Eq. (19.6) are singular at small values of x . They show a double-logarithmic enhancement, with leading terms of the form $\alpha_s^k (\ln^{2k-2} x)/x$ at the k th order of perturbation theory, corresponding to poles $\alpha_s^k (N-1)^{1-2k}$ for the Mellin moments

$$P^{(k)}(N) = \int_0^1 dx x^{N-1} P^{(k)}(x). \quad (19.7)$$

Despite large cancellations between leading and non-leading logarithms at non-asymptotic values of x , the resulting small- x rise in the timelike splitting functions dwarfs that of their spacelike counterparts for the evolution of the parton distributions in Section 18 of this *Review*, see Fig. 1 of Ref. [50]. Consequently, in fragmentation the fixed-order approximation to the evolution breaks down orders of magnitude earlier in x than in DIS.

The pattern of the known coefficients and other considerations suggest that the double-logarithmic terms sum to all-order expressions without any pole at $N = 1$, such as [61, 62]

$$P_{gg}^{\text{LL}}(N) = -\frac{1}{4} \left(N-1 - \sqrt{(N-1)^2 \cdot 24\alpha_s/\pi} \right) \quad (19.8)$$

for the gluon-to-gluon splitting function at leading logarithmic order. Keeping the first three terms in the resulting expansion of Eq. (19.5) around $N = 1$ and taking the Mellin inverse yields a Gaussian in the variable $\xi = \ln(1/x)$ for the small- x fragmentation functions,

$$xD(x, q^2 = s) \propto \exp \left[-\frac{1}{2\sigma^2} (\xi - \xi_p)^2 \right], \quad (19.9)$$

with the peak position and width varying with the energy as [63] (see also Ref. [2])

$$\xi_p \simeq \frac{1}{4} \ln \left(\frac{s}{\Lambda^2} \right), \quad \sigma \propto \left[\ln \left(\frac{s}{\Lambda^2} \right) \right]^{3/4}. \quad (19.10)$$

Next-to-leading logarithmic corrections to the above predictions have been calculated [64]. In the method of Ref. [65], see also Refs. [66, 67], the corrections are included in an analytical form known as the ‘modified leading logarithmic approximation’ (MLLA). Alternatively they can be used to compute higher-moment correc-

tions to the shape in Eq. (19.9) [68]. The small- x resummation of the coefficient functions for semi-inclusive e^+e^- annihilation and of the timelike spitting functions in the standard $\overline{\text{MS}}$ scheme was extended in Refs. [69–73] and has reached full next-to-next-to-leading logarithmic accuracy. Applications of these results to gluon and quark jet multiplicities have been presented in Refs. [74].

Fig. 19.4 shows the ξ distribution for charged particles produced in the current region of the Breit frame in DIS and in e^+e^- annihilation. Consistently with Eq. (19.9) (the ‘hump backed plateau’) and Eq. (19.10) the distributions have a Gaussian shape, with the peak position and area increasing with CM energy (e^+e^-) and Q^2 (DIS).

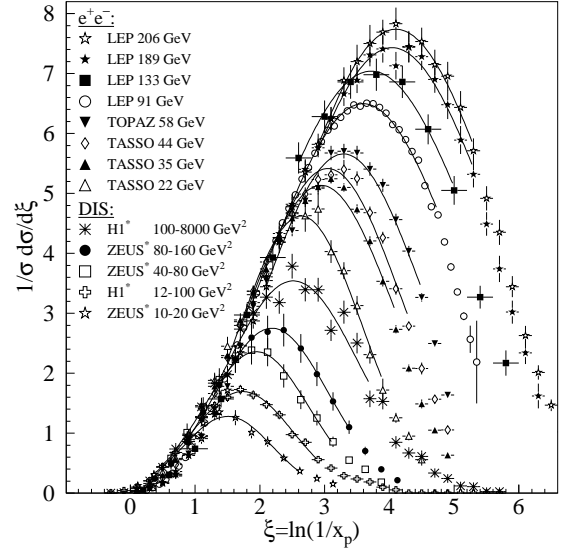


Figure 19.4: Distribution of the normalized fragmentation cross sections in $\xi = \ln(1/x_p)$ at several CM energies (e^+e^-) [10, 11, 16–19, 57, 58, 75–78] and for intervals of Q^2 (DIS). At each energy only one representative measurement is displayed. For clarity some measurements at intermediate CM energies (e^+e^-) or Q^2 ranges (DIS) are not shown. The DIS measurements (*) have been scaled by a factor of 2 for direct comparability with the e^+e^- results. Fits of simple Gaussian functions are overlaid for illustration.

The predicted energy dependence of the peak in the ξ distribution (see Eq. (19.10)) is explained by soft gluon coherence (angular ordering), *i.e.*, the destructive interference of the color wavefunction of low energy gluon radiation, which correctly predicts the suppression of hadron production at small x . Of course, a decrease at very small x is expected on purely kinematical grounds, but this would occur at particle energies proportional to their masses, *i.e.*, at $x \propto m/\sqrt{s}$ and hence $\xi \sim \frac{1}{2} \ln s$. Thus, if the suppression were purely kinematic, the peak position ξ_p would vary twice as rapidly with the energy, which is ruled out by the data in Fig. 19.5. The e^+e^- and DIS data agree well with each other, demonstrating the universality of hadronization and the MLLA prediction. Measurements of the higher moments of the ξ distribution in e^+e^- [19, 78–80] and DIS [58] have also been performed and show consistency with each other.

The average charged-particle multiplicity is another observable sensitive to fragmentation functions for small particle momenta. Perturbative predictions using both NLO [89] and MLLA [90, 91] have been obtained by solving Eq. (19.5) yielding

$$\langle n_G(Q^2) \rangle \propto \alpha_s^b(Q^2) \exp \left[\frac{c}{4\pi b_0 \sqrt{\alpha_s(Q^2)}} \cdot \left(1 + 6a_2 \frac{\alpha_s(Q^2)}{\pi} \right) \right], \quad (19.11)$$

where $b = \frac{1}{4} + \frac{10}{27} \frac{n_f}{4\pi b_0}$, $c = \sqrt{96\pi}$, with $b_0 = (33 - 2n_f)/(12\pi)$, *cf.* Section 9 of this *Review*, for n_f contributing quark flavors. Higher-order corrections to Eq. (19.11) are known up to next-to-next-to-next-to-leading order (N³LO), for details and references

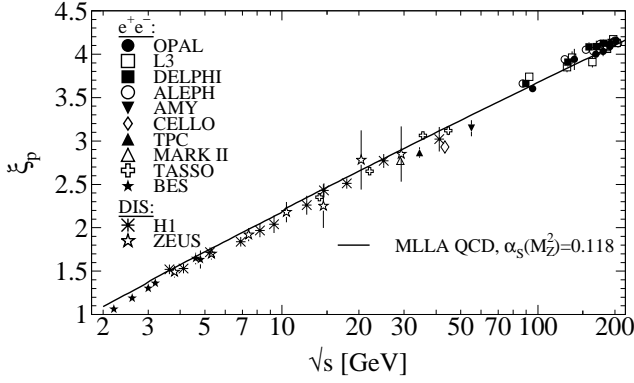


Figure 19.5: Evolution of the peak position, ξ_p , of the ξ distribution with the CM energy \sqrt{s} . The MLLA QCD prediction using $\alpha_s(s = M_Z^2) = 0.118$ is superimposed to the data of Refs. [10, 12, 15, 19, 56, 57, 76, 77, 80–88].

see [92]. The term proportional to $a_2 \approx -0.502 + 0.0421 n_f - 0.00036 n_f^2$ in Eq. (19.11) is the contribution due to NNLO corrections [93]. The quantity $\langle n_G(Q^2) \rangle$ refers to the average number of gluons, while for $\langle n_q(Q^2) \rangle$ for quarks a correction factor $1/r$ is required due to the different color factors in quark and gluon couplings, so that $\langle n_q(Q^2) \rangle = \langle n_G(Q^2) \rangle / r$. The correction factor depends only weakly on Q^2 ; higher-order corrections up to N³LO on the asymptotic value $r = C_A/C_F = 9/4$ [94] are quoted in [92].

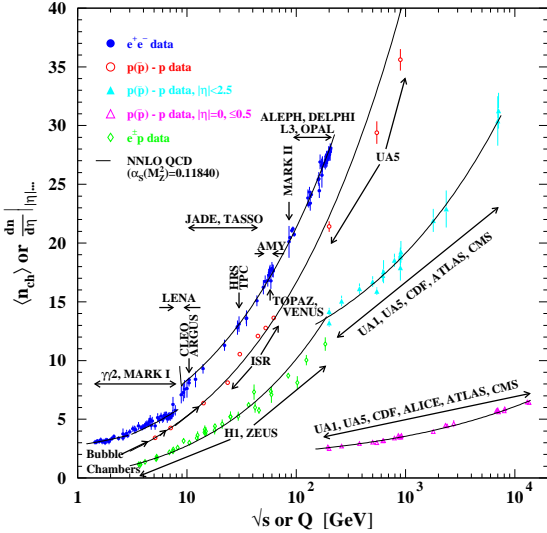


Figure 19.6: Average charged-particle multiplicity $\langle n_{\text{ch}} \rangle$ as a function of \sqrt{s} or Q for e^+e^- and $p\bar{p}$ annihilations, and pp and ep collisions. The indicated errors are statistical and systematic uncertainties added in quadrature, except when no systematic uncertainties are given. All NNLO QCD curves are from Eq. (19.11) with fitted normalization, K_{LHPD} , and offset, n_0 , using a fixed $\alpha_s(M_Z^2) = 0.1184$ [95] and for e^+e^- annihilation data $n_f = 3, 4$, or 5 depending on \sqrt{s} , else $n_f = 3$. e^+e^- : Contributions from K_S^0 and Λ decays included. Data compiled from Refs. [8, 10, 16, 16, 22, 77, 83, 96–106]; $e^\pm p$: Multiplicities have been measured in the current fragmentation region of the Breit frame. Data compiled from Refs. [35, 57, 58, 60, 107]; $p(\bar{p})$: Measured values above 20 GeV refer to non-single diffractive (NSD) processes. Central pseudorapidity multiplicities $(dn/d\eta)|_{|\eta| \dots}$ refer to either $|\eta| < 2.5$ (CMS: $|\eta| < 2.4$) or $|\eta| = 0$ (UA5, CMS, ALICE: $|\eta| < 0.5$). Data compiled from Refs. [108–123].

Employing the hypothesis of ‘Local Parton-Hadron Duality’ (LPHD) [90], *i.e.*, that the color charge of partons is balanced locally in phase space and, hence, their hadronization occurs locally such that (Mellin transformed) parton and hadron inclusive

distributions directly correspond, Eq. (19.11) can be applied to describe average charged particle multiplicities obtained in e^+e^- annihilation. The equation can also be applied to $e^\pm p$ scattering if the current fragmentation region of the Breit frame is considered for measuring the average charged-particle multiplicity. Fig. 19.6 shows corresponding data and fits of Eq. (19.11) where apart from an LPHD normalization factor a constant offset has been allowed for, so that $\langle n_{\text{ch}}(Q) \rangle = K_{\text{LHPD}} \cdot \langle n_G(Q) \rangle / r + n_0$.

In hadron-hadron collisions beam remnants, *e.g.* from single-diffractive (SD) scattering where one colliding proton is negligibly deflected while hadrons related with the other colliding proton are well-separated in rapidity from the former proton, contribute to the measurement of the hadron multiplicity from a hard parton-parton scattering, making interpretation of the data more model dependent. Experimental results are usually given for inelastic processes or for non-single diffractive processes (NSD). Due to the large beam particle momenta at Tevatron and LHC, not all final state particles can be detected within the limited detector acceptance. Therefore, experiments at Tevatron and LHC quote particle multiplicities for limited ranges of pseudo-rapidity $\eta = -\ln \tan(\vartheta/2)$ or at central rapidity, *i.e.* $\eta = 0$, as shown in Fig. 19.6.

A universality of the average particle multiplicities in e^+e^- and $p(\bar{p})$ processes has been reported in Ref. [124] when considering an effective collision energy $Q_{\text{eff}} = \sqrt{s}/k$ in $p(\bar{p})$ reduced by a factor of $k \approx 3$, plus a constant offset of $n_0 \approx 2$. A more detailed review is available in Ref. [125]. According to the investigations presented in Ref. [126] the universality of the energy dependence of average particle multiplicities also applies to hadron-hadron and nucleus-nucleus collisions for both full and central rapidity multiplicities. Evidence for this universality is given by the good agreement for the energy dependence of Eq. (19.11) when fit to the $p(\bar{p})$ data as shown in Fig. 19.6.

19.4 Fragmentation models

Although the scaling violations can be calculated perturbatively, the actual form of the parton fragmentation functions is non-perturbative. Perturbative evolution gives rise to a shower of quarks and gluons (partons). Multi-parton final states from leading and higher order matrix element calculations are linked to these parton showers using factorization prescriptions, also called matching schemes, see Ref. [127] for an overview.

Phenomenological schemes are then used to model the carry-over of parton momenta and flavor to the hadrons. Implemented in Monte Carlo event generators (see Section 42 of this Review), these schemes have been tuned using e^+e^- data and provide good description of hadron collisions as well, thus providing evidence of the universality of fragmentation. However, e^+e^- mainly fix the quark jet fragmentation while it provides less constraints for modelling the gluon jet fragmentation.

19.5 Phenomenology of quark and gluon fragmentation functions

The fragmentation functions are solutions to the evolution equations Eq. (19.5), but need to be specified at some initial scale μ_0^2 (usually around 1 GeV² for light quarks and gluons, and at m_Q^2 for heavy quarks). A typical parameterization for a given light hadron is [128, 129, 131–137]

$$D_i^h(x, \mu_0^2) = N_i x^{\alpha_i} (1-x)^{\beta_i} (1 + \gamma_i(1-x)^{\delta_i}), \quad (19.12)$$

where as indicated the normalization N_i , and the parameters α_i , β_i , γ_i and δ_i depend on the type i of the fragmenting parton. Heavy flavor fragmentation into heavy mesons is discussed in Sec. 19.8 below. The parameters of Eq. (19.12) are obtained by performing global fits to data on various hadron types for different combinations of partons and hadrons in e^+e^- , lepton-hadron and hadron-hadron collisions. We note that the choice of parameterization of the fragmentation functions at the initial scale necessarily introduces a bias since it imposes a certain form of the functions. This bias is largely avoided in neural network approaches which offer a wide flexibility of the initial functions and have recently been applied to fragmentation functions as well [130]. Sets of fragmentation functions are now available for

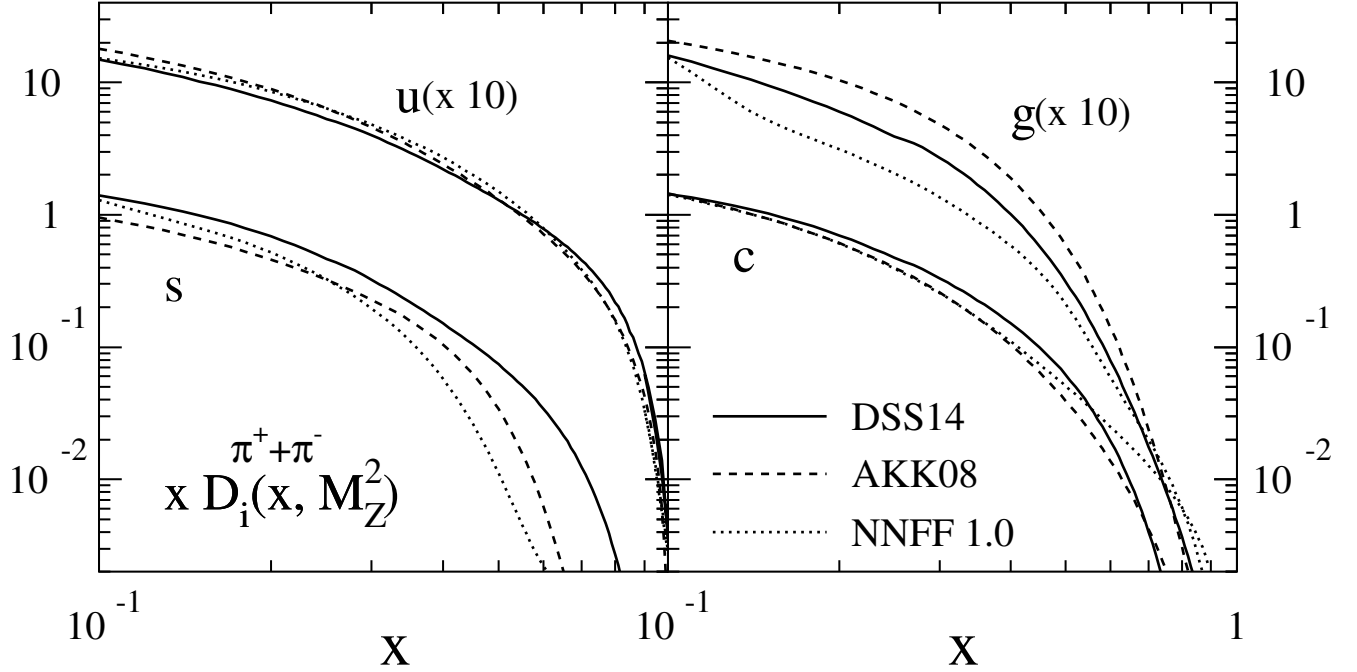


Figure 19.7: Comparison of up, strange, charm and gluon NLO fragmentation functions for $\pi^+ + \pi^-$ at the mass of the Z . The different lines correspond to the results of the analyses performed in Refs. [128–130].

pions, kaons, protons, neutrons, η mesons, Λ baryons, and charged hadrons [128–130, 132–140]. They are all at NLO level, except for Refs. [130, 139] which have been performed at NNLO level. The latter sets are restricted to the analysis of e^+e^- annihilation data. Recently, data from hadron-hadron collisions have been added in the framework of the neural network approach at NLO accuracy for charged hadrons [141]. It is noteworthy that the NNLO effects lead to an improvement in the theoretical description of the data in e^+e^- annihilation.

Data from e^+e^- annihilation present the cleanest experimental source for the measurement of fragmentation functions, but cannot be used to disentangle quark from antiquark fragmentation. Since the bulk of the e^+e^- annihilation data is obtained at the mass of the Z -boson, where the electroweak couplings are roughly the same for the different partons, it provides the most precise determination of the flavor-singlet combination of quark and antiquark fragmentation functions. Flavor-tagged results [142], distinguishing between the light quark, charm and bottom contributions are of particular value for flavor decomposition, even though those measurements cannot be unambiguously interpreted in perturbative QCD.

The most relevant source for quark-antiquark (and also flavor) separation is provided by SIDIS data. Semi-inclusive measurements are usually performed at much lower scales than for e^+e^- annihilation. The inclusion of SIDIS data in global fits allows for a wider coverage in the evolution of the fragmentation functions, resulting at the same time in a stringent test of the universality of the distributions. Charged-hadron production data in hadronic collisions also have sensitivity to (anti-)quark fragmentation functions.

The gluon fragmentation function $D_g^h(x)$ can be extracted, in principle, from the longitudinal fragmentation structure function F_L in Eq. (19.2), as the coefficient functions $C_{L,i}$ for quarks and gluons are comparable at order α_s . However at NLO, *i.e.*, including the $\mathcal{O}(\alpha_s^2)$ coefficient functions $C_{L,i}^{(2)}$ [39], quark fragmentation is dominant in F_L over a large part of the kinematic range, reducing the sensitivity to D_g^h . This distribution could be determined also by analyzing the scale evolution of the fragmentation functions. This possibility is limited by the lack of sufficiently precise data at energy scales away from the Z -resonance and the dominance of the quark contributions at medium and large values of x . In e^+e^- annihilation, D_g^h can also be deduced from the study

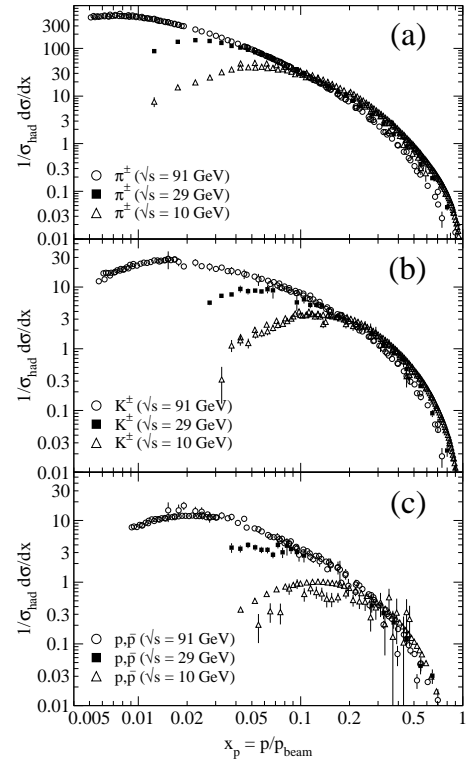


Figure 19.8: Scaled momentum spectra of (a) π^\pm , (b) K^\pm , and (c) p, \bar{p} at $\sqrt{s} = 10, 29, \text{ and } 91$ GeV [24, 26, 85, 143, 144].

of three-jet events in which the gluon jet is identified, for example, by tagging the other two jets with heavy quark decays. To leading order, the measured distributions of $x = E_{\text{had}}/E_{\text{jet}}$ for particles in gluon jets can be identified directly with the gluon fragmentation function $D_g^h(x)$.

Data for $p(\bar{p}) \rightarrow h + X$ provide much more direct constraint on D_g^h . At variance with e^+e^- annihilation and SIDIS, here gluon

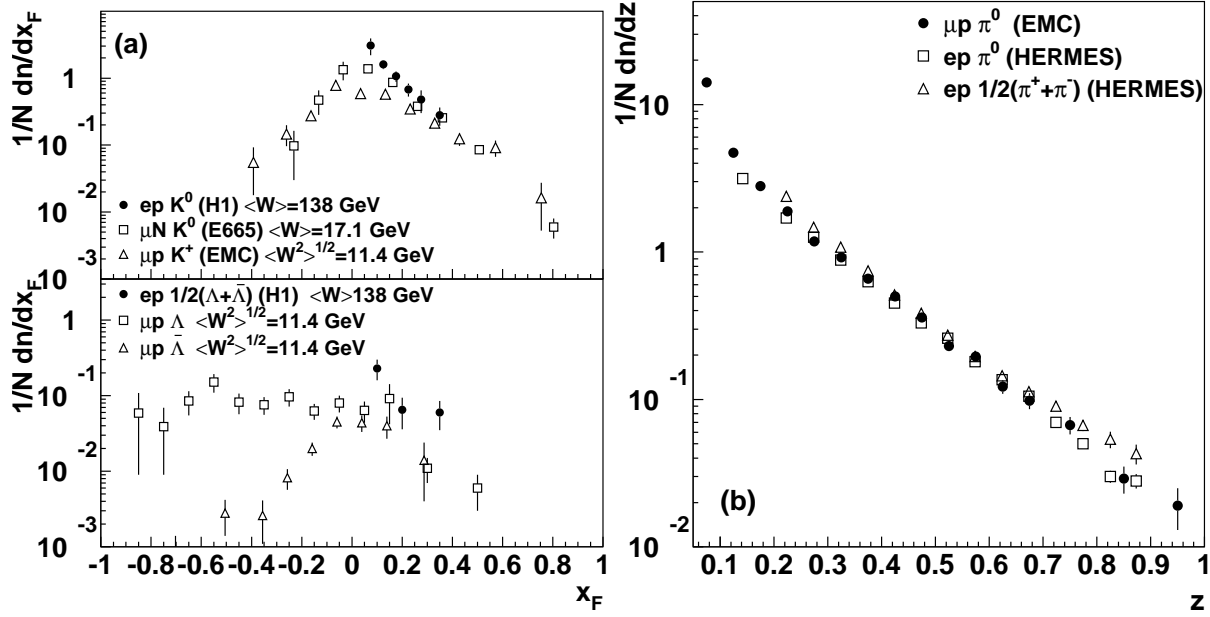


Figure 19.9: (a) $1/N \cdot dn/dx_F$ for identified strange particles in DIS at various values of W [145–147]. (b) $1/N \cdot dn/dz$ for measurements of pions in fixed-target DIS experiments [148–150].

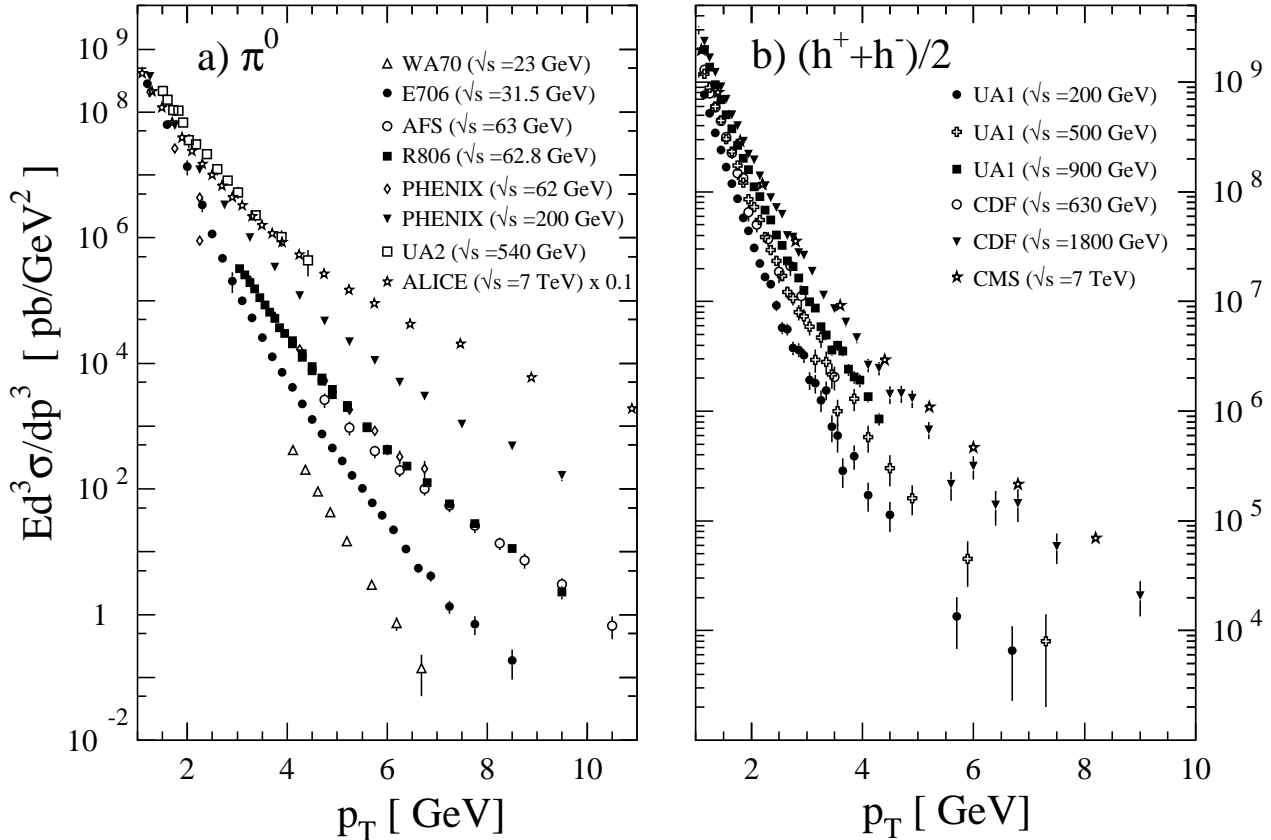


Figure 19.10: Selection of inclusive (a) π^0 and (b) charged-hadron production data from pp [118, 151–156] and $p\bar{p}$ [114, 157, 158] collisions.

fragmentation contributes already at the lowest order in the coupling constant. At large $x \gtrsim 0.5$, where information from e^+e^- is sparse, data from hadronic colliders significantly improve extractions of D_g^h [128, 129, 131, 138]. Recent LHC data has been included in the NLO analyses [129, 137] of pion-fragmentation functions; see Sec. (17.7) for more details. Note that these analyses are currently the only ones that ‘globally’ incorporate available data

from all sources, $e^+e^- \rightarrow h + X$, $ep \rightarrow e'h + X$ and $pp \rightarrow h + X$.

We note that recently a ‘hybrid’ type of high- p_T jet/hadron observable has also been considered both theoretically [159–165] and experimentally [166–173]. It is defined by an identified specific hadron found inside a fully reconstructed jet. This gives rise to a *same-side* hadron-jet momentum correlation that may be addressed using perturbative methods. One of several rele-

Table 19.1: Classification of spin- and transverse-momentum dependent quark fragmentation functions. For simplicity we have left out the ubiquitous label for flavor i of the fragmenting quark and for hadron species h . Each of the functions carries the argument $(x, x^2 k_T^2)$ (plus dependence on a factorization scale), where $xk_T = p_T^h$ is the hadron's transverse momentum. λ and Λ are the quark's and hadron's helicities, respectively, and \vec{s}_T and \vec{S}_T are their transverse spin vectors. We have defined $[\vec{a} \times \vec{b}] \equiv a^1 b^2 - a^2 b^1$. Finally, m_h is the mass of the produced hadron.

hadron pol.	quark polarization		
	unpolarized	long. polarized	transv. polarized
unpol.	D	–	$\frac{[\vec{k}_T \times \vec{s}_T]}{m_h} H^\perp$
long. pol.	–	$\lambda \Lambda G_L$	$\frac{\vec{k}_T \cdot \vec{s}_T}{m_h} \Lambda H_L^\perp$
transv. pol.	$\frac{[\vec{k}_T \times \vec{S}_T]}{m_h} D_T^\perp$	$\frac{\vec{k}_T \cdot \vec{S}_T}{m_h} \lambda G_T^\perp$	$(\vec{s}_T \cdot \vec{S}_T) H_T + \frac{\vec{k}_T \cdot \vec{S}_T}{m_h} \frac{\vec{k}_T \cdot \vec{s}_T}{m_h} H_T^\perp$

variant kinematical variables (see [164] for an overview) is $z_h \equiv (\vec{p}_T^h \cdot \vec{p}_T^{\text{jet}}) / (p_T^{\text{jet}})^2$, where \vec{p}_T^h and \vec{p}_T^{jet} are the transverse momenta of the hadron and the jet, respectively. The observable provides an alternative window on fragmentation functions in a more exclusive setting, enabling novel tests of the universality of fragmentation functions. Varying z_h and/or the hadron species, one can map out the fragmentation functions ‘locally’ as functions of x . This is in contrast to the single-inclusive observable $pp \rightarrow h + X$, which inevitably samples over a broad range of x . Although hadron-in-jet data are not yet routinely included in analyses of fragmentation functions, a ‘proof-of-principle’ analysis does exist [174] that shows the potential of the observable in providing constraint on fragmentation functions.

A comparison of recent NLO fits of fragmentation functions for $\pi^+ + \pi^-$ obtained by DSS14 [129], AKK08 [128] and NNPDF1.0 [130] is shown in Fig. 19.7. Differences among the functions for these sets are large, especially for the gluon fragmentation function over the full range of x and for the quark functions at large momentum fractions. The differences are even larger for other species of hadrons like kaons and protons [128, 131, 135, 138]. Recent analyses [129, 130, 135, 137, 175, 176] estimate the uncertainties involved in the extraction of fragmentation functions.

Photonic fragmentation functions play a relevant role in the theoretical understanding of inclusive photon production in (leptonic and hadronic) high energy processes. In the spirit of the analogy between parton fragmentation functions and parton distribution functions, also photonic fragmentation functions are analogous to the photon structure function F_2^γ and to the proton's photonic parton distributions (see review on structure functions in Section 18 of this *Review*). Since photons have a pointlike coupling to quarks [177], the corresponding fragmentation functions obey inhomogeneous evolution equations and are generally decomposed into a perturbative and a non-perturbative component [134, 178, 179]. The hadronic part, sometimes approximated by the Vector Meson Dominance Model, can in principle be obtained by performing a global analysis to the available prompt photon production data [7, 12, 15, 19–21, 85, 143, 180, 181], although in practice this has not been done. We note that also the cross section for photons produced in fully reconstructed jets has been proposed [182] as a new tool for obtaining access to photon fragmentation functions, in analogy to the hadron-in-jet cross section discussed above.

19.6 Identified particles in e^+e^- and semi-inclusive DIS

There is a great wealth of measurements of e^+e^- fragmentation into identified particles. A collection of references for data on fragmentation into identified particles is provided in Table 52.1 of this *Review*. As a representative example, Figure 19.8 shows differential charged-hadron spectra as functions of the scaled hadron momentum at several CM energies.

Quantitative results of studies of scaling violations in e^+e^- fragmentation have been reported in [7, 21, 183, 184]. Scaling viola-

tions may be used to extract a value of α_s ; the values obtained are consistent with the world average (see review on QCD in Section 9 of this *Review*).

Many studies have been made of production of identified particles in lepton-hadron scattering, although fewer particle species have been measured than in e^+e^- collisions. References [145, 146, 148–150, 185–187] and [147, 188–193] are representative of the data from fixed target and ep collider experiments, respectively. QCD calculations performed at NLO provide an overall good description of the HERA data [33, 34, 58, 193–195], both for SIDIS [196] and for the hadron transverse momentum distribution [53, 197] in the kinematic regions in which the calculations are predictive. A first step towards an NNLO calculation for SIDIS has been presented in [198].

Fig. 19.9(a) compares lower-energy fixed-target and HERA data on strangeness production, showing that the HERA spectra have substantially increased multiplicities, albeit with statistical precision that is insufficient to study scaling violations. The fixed-target data show that the Λ rate substantially exceeds the $\bar{\Lambda}$ rate in the remnant region, owing to the conserved baryon number from the baryon target. Fig. 19.9(b) shows $1/N \cdot dn/dz$ for neutral and charged pion production, where z is defined as the ratio of the pion energy to that of the exchanged boson, both measured in the laboratory frame. Results are shown from the HERMES and the EMC experiments, where the HERMES data have been evolved to $\langle Q^2 \rangle = 25 \text{ GeV}^2$ at NLO QCD, in order to be comparable with the EMC data. Each of the experiments uses various kinematic cuts to ensure that the measured particles lie in the region that is expected to be associated with the struck quark. In the DIS kinematic regime accessed at these experiments, and over the range in z shown in Fig. 19.9, the z and x_F variables have similar values [30]. The precision data on identified particles can be used in the study of the quark flavor content of the proton [175, 214, 215].

Data on identified particle production can aid the investigation of the universality of jet fragmentation in e^+e^- and DIS. The strangeness suppression factor γ_s , as derived principally from tuning the Lund string model [216] within JETSET [217], is typically found to be around 0.3 in e^+e^- experiments [75], although values closer to 0.2 [218] have also been obtained. A number of measurements of so-called V^0 -particles (K^0 , Λ^0) and the relative rates of V^0 's and inclusively produced charged particles have been performed at HERA [147, 188, 219] and fixed target experiments [145]. These typically favour a stronger suppression ($\gamma_s \approx 0.2$) than usually obtained from e^+e^- data, although values close to 0.3 have also been obtained [220, 221].

However, when comparing the description of QCD-based models for lepton-hadron interactions and e^+e^- collisions, it is important to note that the overall description by event generators of inclusively produced hadronic final states is more accurate in e^+e^- collisions than in lepton-hadron interactions [222]. Predictions of particle rates in lepton-hadron scattering are affected by uncertainties in the modelling of the parton composition of the

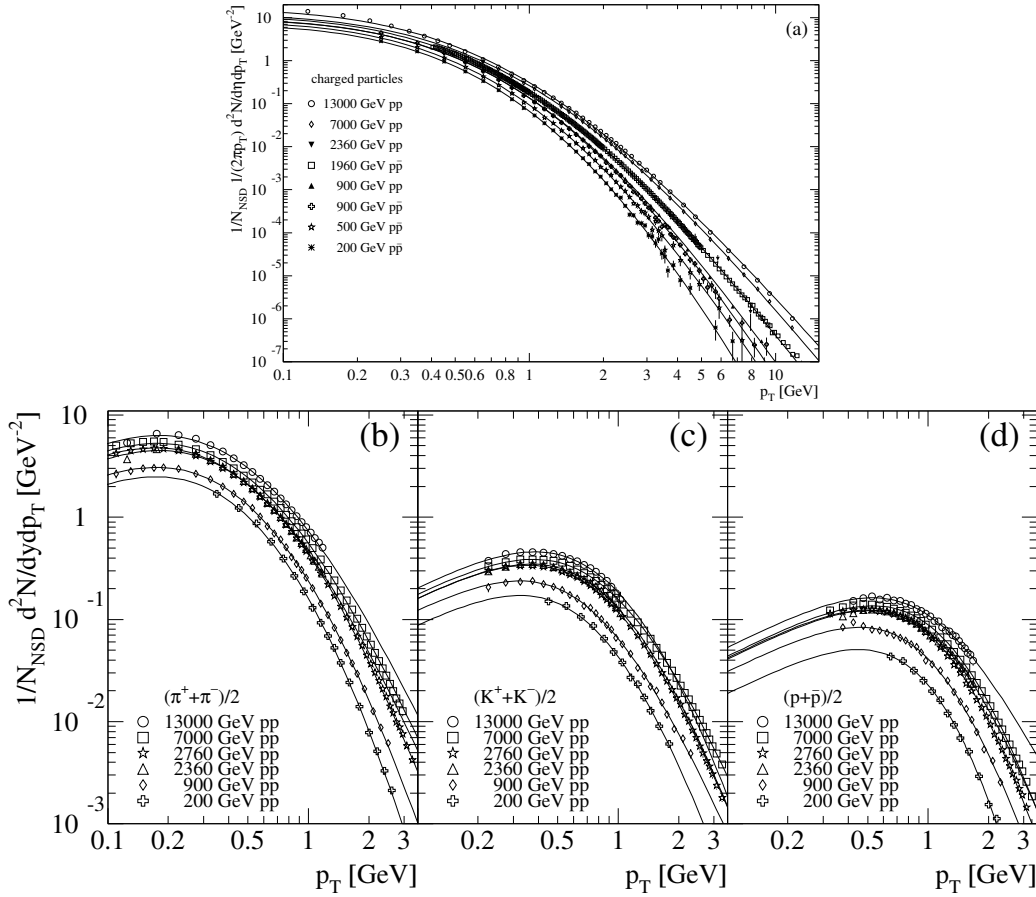


Figure 19.11: (a) Selection of inclusive charged-particle transverse momentum spectra [114, 117, 119, 121, 157, 199, 200], normalized to the non-single diffractive cross section (NSD). (b)–(d) Selection of identified charged-particle transverse momentum spectra [201–206] normalized to the NSD cross section. All spectra are scaled to the NSD cross-section using measurements of total, inelastic, elastic, single, or non-single diffractive cross sections from [207–211, 211–213]. The overall normalization uncertainty of about 3% is not shown. Superimposed are fits of the Tsallis distribution in Eq. (19.13).

proton and photon, the extended target remnant, and initial and final-state QCD radiation. Furthermore, the tuning of event generators for e^+e^- collisions is typically based on a larger set of parameters and uses more observables [75] than are used when optimizing models for lepton-hadron data [223].

19.7 Fragmentation in hadron-hadron collisions

An extensive set on high-transverse momentum (p_T) single-inclusive hadron data has been collected in $h_1 h_2 \rightarrow hX$ scattering processes, both at high energy colliders and fixed-target experiments [151–158, 181, 224–246]. Fig. 19.10 shows the invariant cross sections $Ed^3\sigma/dp^3$ for a compilation of neutral-pion and charged-hadron production data for energies in the range $\sqrt{s} \approx 23 - 7000$ GeV.

The differential cross section for high-transverse momentum hadron production has been computed to NLO accuracy in perturbative QCD [247]. The NLO corrections are typically large and can even double the prediction for the cross section at fixed-target energies. Nevertheless, the NLO calculations significantly under-predict the cross-section for several fixed-target energy data sets [242, 248, 249]. Different strategies have been developed to ameliorate the theoretical description at fixed-target energies. A possible phenomenological approach involves the introduction of a non-perturbative intrinsic partonic transverse momentum [156, 242, 250, 251]. Furthermore, the resummation of the dominant higher order corrections at threshold produces an enhancement of the theoretical calculation that significantly improves the description of the data [252, 253].

Data collected at high energy colliders are either included in global fit analyses or used as a test for the universality of fragmentation functions. A certain tension has been observed between

data sets from RHIC and the LHC [254]. The tension can be largely resolved [129] by excluding data with transverse momentum smaller than ~ 5 GeV from the analysis, where fixed-order pQCD calculations are not expected to provide an accurate description of the process. Still, after removing these smaller p_T values where the data sets appear to be mutually exclusive in the global fit, the RHIC data show a preference towards harder gluon fragmentation at large x than the LHC data.

Transverse momentum distributions can usually be fit by power laws [255]. An approach to describe the low p_T particle spectra is the Tsallis distribution [256–258], which is based on a non-extensive generalization of the Boltzmann-Gibbs statistics. The functional form [259]

$$\frac{d^2N}{dp_T dy} = p_T \frac{dN}{dy} \frac{(n-1)(n-2)}{nT(nT+m_0(n-2))} \left[1 + \frac{m_T - m_0}{nT} \right]^{-n} \quad (19.13)$$

is frequently used to fit the transverse momentum spectra, where dN/dy is the particle's multiplicity, T and n are fit parameters of the Tsallis distribution, m_0 is the either the mass of the most abundant particle, i.e. the pion for inclusive spectra, or the mass of an identified particle, and $m_T = \sqrt{p_T^2 + m_0^2}$. The parameter n is related to the non-extensive parameter $q = n/(n-1)$ of the original Tsallis formula [260], and T is connected to the temperature in the Boltzmann-Gibbs statistics. The Tsallis distribution has been very successfully fit to measured transverse momentum distributions of both inclusive charged particles and identified particle spectra for hadron-hadron collisions, see for example [261–263], for collisions of heavy nuclei, see for example [264], and also for e^+e^- collisions, see for example [265]. The energy dependence of

the fitted Tsallis parameters has also been investigated in detail, see [259, 266]. Fig. 19.11 shows examples of hadron production data in pp and $p\bar{p}$ collisions compared to Tsallis distributions.

Hadron production provides a critical observable for probing the high energy-density matter produced in heavy-ion collisions. Measurements at colliders show a suppression of inclusive hadron yields at high transverse momentum for AA collisions compared to pp scattering, indicating the formation of a dense medium opaque to quark and gluons, see e.g. [267].

19.8 Heavy quark fragmentation

It was recognized very early [268] that a heavy flavored meson should retain a large fraction of the momentum of the primordial heavy quark, and therefore its fragmentation function should be much harder than that of a light hadron. In the limit of a very heavy quark, one expects the fragmentation function for a heavy quark to go into any heavy hadron to be peaked near $x = 1$.

When the heavy quark is produced at a momentum much larger than its mass, one expects important perturbative effects, enhanced by powers of the logarithm of the transverse momentum over the heavy quark mass, to intervene and modify the shape of the fragmentation function. In leading logarithmic order (*i.e.*, including all powers of $\alpha_s \log(m_Q/p_T)$), the total (*i.e.*, summed over all hadron types) perturbative fragmentation function is simply obtained by solving the leading evolution equation for fragmentation functions, Eq. (19.5), with the initial condition due to the finite mass of the heavy quark given by $D_Q(x, \mu^2)|_{\mu^2=m_Q^2} = \delta(1-x)$ and $D_i(x, \mu^2)|_{\mu^2=m_Q^2} = 0$ for $i \neq Q$ (here $D_i(x, \mu^2)$, stands for the probability to produce a heavy quark Q from parton i with a fraction x of the parton momentum).

Several extensions of the leading logarithmic result have appeared in the literature. Next-to-leading-log (NLL) order results for the perturbative heavy quark fragmentation function have been obtained in [272]. The resummation of the dominant logarithmic contributions at large x was performed in [273] to next-to-leading-log accuracy. Fixed-order calculations of the fragmentation function at order α_s^2 in e^+e^- annihilation have appeared in [274] while the initial condition for the perturbative heavy quark fragmentation function has been extended to NNLO in [275].

Inclusion of non-perturbative effects in the calculation of the heavy-quark fragmentation function is done by convoluting the perturbative result with a phenomenological non-perturbative form. This form follows from the simple kinematical consideration that the formation of a hadron by attaching light quarks/anti-quarks to the heavy quark will slightly decelerate the heavy quark. Thus its shape will show a peak that becomes increasingly centered next to $x = 1$ the higher the quark mass. Among the most popular parameterizations we have the following:

$$\text{Peterson } et al. [276]: D_{np}(x) \propto \frac{1}{x} \left(1 - \frac{1}{x} - \frac{\epsilon}{1-x}\right)^{-2}, \quad (19.14)$$

$$\text{Kartvelishvili } et al. [277]: D_{np}(x) \propto x^\alpha(1-x), \quad (19.15)$$

$$\begin{aligned} \text{Collins \& Spiller [278]: } D_{np}(x) \propto & \left(\frac{1-x}{x} + \frac{(2-x)\epsilon_C}{1-x}\right) \times \\ & (1+x^2) \times \left(1 - \frac{1}{x} - \frac{\epsilon_C}{1-x}\right)^{-2} \end{aligned} \quad (19.16)$$

$$\text{Colangelo \& Nason [279]: } D_{np}(x) \propto (1-x)^\alpha x^\beta \quad (19.17)$$

$$\begin{aligned} \text{Bowler [280]: } D_{np}(x) \propto & x^{-(1+bm_{h,\perp}^2)} \times \\ & (1-x)^a \exp\left(-\frac{bm_{h,\perp}^2}{x}\right) \end{aligned} \quad (19.18)$$

$$\text{Braaten } et al. [281]: \text{ (see Eqs. (31), (32) in [281]) } \quad (19.19)$$

where ϵ , ϵ_C , a , $bm_{h,\perp}^2$, α , and β are non-perturbative param-

eters that depend on the heavy hadron considered. The parameters entering the non-perturbative forms are fitted together with some model of hard radiation, which can be either a shower Monte Carlo, a leading-log or NLL calculation (which may or may not include Sudakov resummation), or a fixed order calculation. In [274], for example, the Peterson *et al.* [276] ϵ parameter for charm and bottom production is fitted from the measured distributions of Refs. [282, 283] for charm, and of [284] for bottom. If the leading-logarithmic approximation (LLA) is used for the perturbative part, one finds $\epsilon_c \approx 0.05$ and $\epsilon_b \approx 0.006$; if a second order calculation is used one finds $\epsilon_c \approx 0.035$ and $\epsilon_b \approx 0.0033$; if a NLL improved fixed order $\mathcal{O}(\alpha_s^2)$ calculation is used instead of NLO $\mathcal{O}(\alpha_s)$ one finds $\epsilon_c \approx 0.022$ and $\epsilon_b \approx 0.0023$. The larger values found in the LL approximation are consistent with what is obtained in the context of parton shower models [285], as expected. The ϵ parameter for charm and bottom scales roughly with the inverse square of the heavy flavor mass. This behavior can be justified by several arguments [268, 286, 287]. It can be used to relate the non-perturbative parts of the fragmentation functions of charm and bottom quarks [274, 279, 288].

A more conventional approach [289] involves the introduction of a unique set of heavy quark fragmentation functions of non-perturbative nature that obey the usual massless evolution equations in Eq. (19.5). Finite mass terms of the form $(m_Q/p_T)^n$ are kept in the corresponding short distance coefficient function for each scattering process. Within this approach, the initial condition for the perturbative fragmentation function provides the term needed to define the correct subtraction scheme to match the massless limit for the coefficient function (see e.g. [290]). Such an implementation is in line with the variable flavor number scheme introduced for parton distributions functions, as described in Section 18 of this *Review*.

High statistics data for charmed-meson production near the Υ resonance (excluding decay products of B mesons) have been published [269, 270]. They include results for D and D^* , D_s (see also [291, 292]) and Λ_c . Shown in Fig. 19.12(a) are the CLEO and BELLE inclusive cross-sections times branching ratio \mathcal{B} , $s\mathcal{B}d\sigma/dx_p$, for the production of D^0 and D^{*+} . The variable x_p approximates the light-cone momentum fraction x , but is not identical to it. The two measurements are consistent with each other.

The branching ratio \mathcal{B} represents $D^0 \rightarrow K^-\pi^+$ for the D^0 results and for the D^{*+} the product of the branching fractions for $D^{*+} \rightarrow D^0\pi^+$ and $D^0 \rightarrow K^-\pi^+$. Given the high precision of CLEO's and BELLE's data, a superposition of different parametric forms for the non-perturbative contribution is needed to obtain a good fit [52]. Older studies are reported in Refs. [283, 293, 294]. Charmed meson spectra on the Z peak have been published by OPAL and ALEPH [295, 296].

Charm quark production has also been extensively studied at HERA by the H1 and ZEUS collaborations. Measurements have been made of $D^{*\pm}$, D^\pm , and D_s^\pm mesons and the Λ_c baryon. See, for example, Refs. [297, 298].

Experimental studies of the fragmentation function for b quarks, shown in Fig. 19.12(b), have been performed at LEP and SLD [271, 284, 299]. Commonly used methods identify the B meson through its semileptonic decay or based upon tracks emerging from the B secondary vertex. Heavy flavor contributions from gluon splitting are usually explicitly removed before fitting the fragmentation functions. The studies in [271] fit the B spectrum using a Monte Carlo shower model supplemented with non-perturbative fragmentation functions yielding consistent results.

The experiments measure primarily the spectrum of B mesons. This defines a fragmentation function that includes the effect of the decay of higher mass excitations, like the B^* and B^{**} . In the literature (cf. details in Ref. [300]), there is sometimes ambiguity in what is defined to be the bottom fragmentation function. Instead of using what is directly measured (*i.e.*, the B meson spectrum), in some cases corrections are applied to account for B^* or B^{**} production.

Heavy-flavor production in e^+e^- collisions is the primary source of information for the role of fragmentation effects in heavy-flavor production in hadron-hadron and lepton-hadron collisions. The

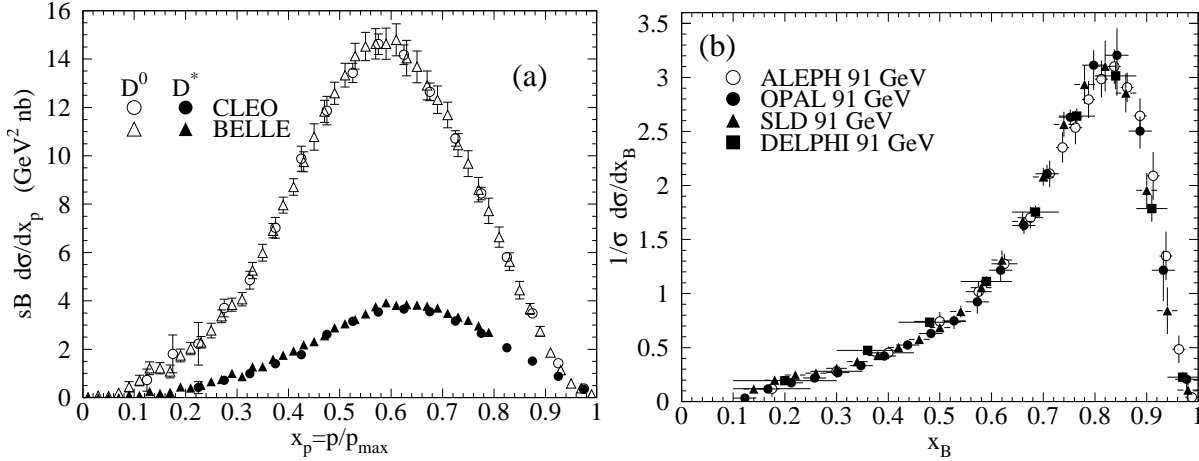


Figure 19.12: (a) Efficiency-corrected inclusive cross-section measurements for the production of D^0 and D^{*+} in e^+e^- measurements at $\sqrt{s} \approx 10.6$ GeV, excluding B decay products [269] [270]. (b) Measured e^+e^- fragmentation function of b quarks into B hadrons at $\sqrt{s} \approx 91$ GeV [271].

QCD calculations tend to underestimate the data in certain regions of phase space. Some experimental results from LHC summarized in [301] show such deviations e.g. at high transverse jet momentum and also at low di-jet separation angles, see [302] for details, and were already theoretically investigated in [303].

Both bottomed- and charmed-meson spectra have been measured at the Tevatron with unprecedented accuracy [304]. The measured spectra are in good agreement with QCD calculations (including non-perturbative fragmentation effects inferred from e^+e^- data [305]).

The HERA collaborations have produced a number of measurements of beauty production; see, for example, Refs. [297, 306–309]. As for the Tevatron data, the HERA results are described well by QCD-based calculations using fragmentation models optimised with e^+e^- data.

Besides degrading the fragmentation function by gluon radiation, QCD evolution can also generate soft heavy quarks, increasing in the small x region as \sqrt{s} increases. Several theoretical studies are available on the issue of how often $b\bar{b}$ or $c\bar{c}$ pairs are produced indirectly via a gluon splitting mechanism [310–312]. Experimental results from studies on charm and bottom production via gluon splitting, given in [296, 313–317], yield weighted averages of $\bar{n}_{g \rightarrow c\bar{c}} = 3.05 \pm 0.45\%$ and $\bar{n}_{g \rightarrow b\bar{b}} = 0.277 \pm 0.072\%$, respectively. The production of bottom-antibottom quark pairs via gluon splitting has also been investigated at hadron colliders, see for example [318–320].

19.9 Spin-dependent and transverse-momentum dependent fragmentation functions

The fragmentation functions we have considered so far apply to the spin-averaged case in which the polarization of the produced hadron is not observed, or the hadron has spin-0. We have also only considered ‘collinear’ fragmentation functions $D_i^h(x, \mu^2)$ which carry only one kinematical variable, the momentum fraction x . New insights into fragmentation and hadronization become available when also the dependence of fragmentation functions on the spin of the produced hadron and/or its relative transverse momentum with respect to the fragmenting parton are considered. In the latter case, one refers to the fragmentation functions as ‘transverse-momentum dependent (TMD)’ fragmentation functions.

Staying first with collinear fragmentation functions, two types of spin-dependent fragmentation functions to spin-1/2 hadrons can be considered. The helicity-dependent fragmentation function measures the transfer of longitudinal spin from the fragmenting parton to the hadron [38, 321–324]. It is given by

$$\Delta D_i^h(x, \mu^2) \equiv D_{i+}^{h+}(x, \mu^2) - D_{i+}^{h-}(x, \mu^2), \quad (19.20)$$

where the superscripts \pm refer to the helicities of the parton and

hadron. Λ hyperons are ideally suited for measurements of the ΔD_i^h , thanks to their self-analyzing weak decay $\Lambda \rightarrow \pi p$. Measurements of the longitudinal spin transfer to Lambda hyperons have been presented in e^+e^- (on the Z resonance), ℓp , and pp scattering in Refs. [325–331]. One may readily extend Eq. (19.20) to the case of transverse polarization of hadrons and quarks [332], where the corresponding fragmentation functions are known as ‘transversity’ fragmentation functions. There are also measurements constraining these fragmentation functions [326, 333, 334].

If the transverse-momentum (k_T) dependence of fragmentation functions is considered, there are eight types of leading-twist functions, defined by the correlations among the hadronic and partonic spin vectors and transverse-momentum vectors they represent. (For review, see [5]). We note that the eight fragmentation functions given in the table below exist separately for each quark and antiquark flavor, and a similar set may be introduced for gluons. Upon integration over the transverse momentum k_T the collinear unpolarized, helicity, and transversity fragmentation functions are reproduced.

The various fragmentation functions may be obtained from spin asymmetries and angular distributions in hadron production processes. There is a large body of precision data by now on transverse-momentum distributions in e^+e^- annihilation [335] and SIDIS [186, 336] that provide constraints on the unpolarized TMD fragmentation functions D_i^h , which have been analyzed theoretically, partly also including TMD evolution effects and high orders of perturbation theory [337–342].

Besides the unpolarized functions D most of the attention in experiment and theory has been on the function H^\perp which describes the production of unpolarized (or spin-0) hadrons by transversely polarized quarks. This function is known as the ‘Collins function’ [343]. Its importance also derives from the fact that it may be used to probe the quark transversity PDF of the nucleon [344] which gives the probability of finding a transversely polarized quark with its spin aligned or anti-aligned with the spin of a transversely polarized nucleon. The transversity function is chiral-odd, and therefore not accessible through measurements of inclusive lepton-hadron scattering. The Collins effect in semi-inclusive DIS, on the other hand, provides an avenue for accessing transversity. The Collins fragmentation function is chiral-odd and T-odd, leading to a characteristic single-spin asymmetry in the azimuthal angular distribution of the produced hadron in the hadron scattering plane. A number of SIDIS [345–356] and e^+e^- experiments [357–361] have performed measurements of the Collins effect, for charged pions and kaons. These have been analyzed theoretically [362, 363], leading to an extraction of the nucleon’s transversity distributions [363]. The Collins effect has also been studied in pp scattering, where one considers azimuthal transverse single-spin asymmetries for distributions of hadrons inside

jets [173, 364, 365].

In the context of extractions of transversity PDFs also fragmentation functions for same-side pairs of hadrons with small invariant mass, *dihadrons*, have been introduced and studied [366–374]. Compared to the Collins effect, dihadron fragmentation functions have the advantage that they may be defined purely in collinear factorization. The relevant spin-dependent dihadron fragmentation function exploits a correlation between the transverse polarization of the fragmenting quark and the relative momentum of the two hadrons. In SIDIS with a transversely polarized hadron beam, the dihadron cross section then contains a specific modulation in the azimuthal orientation of the plane containing the momenta of the two hadrons. The coefficient of this modulation is a product of the spin-dependent dihadron fragmentation function and the target’s transversity PDF. The dihadron fragmentation functions may be separately extracted from measurements in e^+e^- annihilation, and the Belle experiment has presented data [375] that have been analyzed theoretically [376, 377]. In lepton scattering, HERMES [378] and COMPASS [379, 380] have reported data sensitive to the spin-dependent dihadron fragmentation functions, and recently the STAR experiment at RHIC has presented data in the azimuthal distribution of $\pi^+\pi^-$ pairs produced in pp scattering with one transversely polarized proton [381]. The results have been successfully used for the extraction of transversity PDFs [377, 382–384].

References

- [1] G. Altarelli, Phys. Rept. **81**, 1 (1982).
- [2] R.K. Ellis *et al.*, *QCD and Collider Physics*, Cambridge University Press (1996).
- [3] S. Albino *et al.* (2008), [arXiv:0804.2021].
- [4] F. Arleo, Eur. Phys. J. **C61**, 603 (2009), [arXiv:0810.1193].
- [5] A. Metz and A. Vossen, Prog. Part. Nucl. Phys. **91**, 136 (2016), [arXiv:1607.02521].
- [6] P. Nason and B. R. Webber, Nucl. Phys. **B421**, 473 (1994), [Erratum: Nucl. Phys. **B480**, 755 (1996)].
- [7] D. Buskalic *et al.* (ALEPH), Phys. Lett. **B357**, 487 (1995), [Erratum: Phys. Lett. **B364**, 247 (1995)].
- [8] P. Abreu *et al.* (DELPHI), Eur. Phys. J. **C6**, 19 (1999).
- [9] R. Barate *et al.* (ALEPH), Phys. Rept. **294**, 1 (1998).
- [10] D. Buskalic *et al.* (ALEPH), Z. Phys. **C73**, 409 (1997).
- [11] B. Adeva *et al.* (L3), Phys. Lett. **B259**, 199 (1991).
- [12] Y. K. Li *et al.* (AMY), Phys. Rev. **D41**, 2675 (1990).
- [13] D. Bender *et al.*, Phys. Rev. **D31**, 1 (1985).
- [14] G. S. Abrams *et al.*, Phys. Rev. Lett. **64**, 1334 (1990).
- [15] A. Petersen *et al.*, Phys. Rev. **D37**, 1 (1988).
- [16] G. Alexander *et al.* (OPAL), Z. Phys. **C72**, 191 (1996).
- [17] K. Ackerstaff *et al.* (OPAL), Z. Phys. **C75**, 193 (1997).
- [18] G. Abbiendi *et al.* (OPAL), Eur. Phys. J. **C16**, 185 (2000), [hep-ex/0002012].
- [19] W. Braunschweig *et al.* (TASSO), Z. Phys. **C47**, 187 (1990).
- [20] K. Ackerstaff *et al.* (OPAL), Eur. Phys. J. **C7**, 369 (1999), [hep-ex/9807004].
- [21] P. Abreu *et al.* (DELPHI), Phys. Lett. **B398**, 194 (1997).
- [22] G. Abbiendi *et al.* (OPAL), Eur. Phys. J. **C37**, 1, 25 (2004), [hep-ex/0404026].
- [23] R. Brandelik *et al.* (TASSO), Phys. Lett. **114B**, 65 (1982).
- [24] K. Abe *et al.* (SLD), Phys. Rev. **D69**, 072003 (2004), [hep-ex/0310017].
- [25] H. Aihara *et al.* (TPC/Two Gamma), Phys. Rev. Lett. **61**, 1263 (1988).
- [26] M. Leitgab *et al.* (Belle), Phys. Rev. Lett. **111**, 062002 (2013), [arXiv:1301.6183].
- [27] W. Kittel and E.A. De Wolf, *Soft Multihadron Dynamics*, World Scientific (2005).
- [28] H.F. Jones, Nuovo Cimento **40A**, 1018 (1965).
- [29] K. H. Streng, T. F. Walsh and P. M. Zerwas, Z. Phys. **C2**, 237 (1979).
- [30] M. R. Adams *et al.* (E-665), Phys. Lett. **B272**, 163 (1991).
- [31] M. Arneodo *et al.* (European Muon), Z. Phys. **C35**, 417 (1987).
- [32] I. Abt *et al.* (H1), Z. Phys. **C63**, 377 (1994).
- [33] M. Derrick *et al.* (ZEUS), Z. Phys. **C70**, 1 (1996), [hep-ex/9511010].
- [34] J. Breitweg *et al.* (ZEUS), Phys. Lett. **B414**, 428 (1997), [hep-ex/9710011].
- [35] F. D. Aaron *et al.* (H1), Phys. Lett. **B654**, 148 (2007), [arXiv:0706.2456].
- [36] P. Abreu *et al.* (DELPHI), Phys. Lett. **B311**, 408 (1993).
- [37] G. Altarelli *et al.*, Nucl. Phys. **B160**, 301 (1979); R. Baier and K. Fey, Z. Phys. **C2**, 339 (1979).
- [38] D. de Florian, M. Stratmann and W. Vogelsang, Phys. Rev. **D57**, 5811 (1998), [hep-ph/9711387].
- [39] P. J. Rijken and W. L. van Neerven, Phys. Lett. **B386**, 422 (1996), [hep-ph/9604436]; P. J. Rijken and W. L. van Neerven, Phys. Lett. **B392**, 207 (1997), [hep-ph/9609379]; P. J. Rijken and W. L. van Neerven, Nucl. Phys. **B487**, 233 (1997), [hep-ph/9609377].
- [40] A. Mitov, S. Moch and A. Vogt, Phys. Lett. **B638**, 61 (2006), [hep-ph/0604053].
- [41] A. Mitov and S.-O. Moch, Nucl. Phys. **B751**, 18 (2006), [hep-ph/0604160].
- [42] V. N. Gribov and L. N. Lipatov, Sov. J. Nucl. Phys. **15**, 438 (1972), [Yad. Fiz. **15**, 781 (1972)]; V. N. Gribov and L. N. Lipatov, Sov. J. Nucl. Phys. **15**, 675 (1972), [Yad. Fiz. **15**, 1218 (1972)]; L.N. Lipatov, Sov. J. Nucl. Phys. **20**, 95 (1975); Yu.L. Dokshitzer, Sov. Phys. JETP Lett. **46**, 641 (1977); G. Altarelli and G. Parisi, Nucl. Phys. **B126**, 298 (1977).
- [43] H. Georgi and H. D. Politzer, Nucl. Phys. **B136**, 445 (1978); J. F. Owens, Phys. Lett. **76B**, 85 (1978); T. Uematsu, Phys. Lett. **79B**, 97 (1978).
- [44] G. Curci, W. Furmanski and R. Petronzio, Nucl. Phys. **B175**, 27 (1980).
- [45] W. Furmanski and R. Petronzio, Phys. Lett. **97B**, 437 (1980).
- [46] E. G. Floratos, C. Kounnas and R. Lacaze, Nucl. Phys. **B192**, 417 (1981).
- [47] J. Kalinowski, K. Konishi and T. R. Taylor, Nucl. Phys. **B181**, 221 (1981).
- [48] M. Stratmann and W. Vogelsang, Nucl. Phys. **B496**, 41 (1997), [hep-ph/9612250].
- [49] Yu. L. Dokshitzer, G. Marchesini and G. P. Salam, Phys. Lett. **B634**, 504 (2006), [hep-ph/0511302].
- [50] S. Moch and A. Vogt, Phys. Lett. **B659**, 290 (2008), [arXiv:0709.3899].
- [51] A. A. Almasy, S. Moch and A. Vogt, Nucl. Phys. **B854**, 133 (2012), [arXiv:1107.2263].
- [52] M. Cacciari, P. Nason and C. Oleari, JHEP **04**, 006 (2006), [hep-ph/0510032]; M. Cacciari, P. Nason and C. Oleari, JHEP **10**, 034 (2005), [hep-ph/0504192].
- [53] P. Aurenche *et al.*, Eur. Phys. J. **C34**, 277 (2004), [hep-ph/0312359]; A. Daleo, D. de Florian and R. Sassot, Phys. Rev. **D71**, 034013 (2005), [hep-ph/0411212]; B. A. Kniehl, G. Kramer and M. Maniatis, Nucl. Phys. **B711**, 345 (2005), [Erratum: Nucl. Phys. **B720**, 231 (2005)], [hep-ph/0411300].
- [54] B. Wang *et al.*, Phys. Rev. **D99**, 9, 094029 (2019), [arXiv:1903.01529].
- [55] S. Aid *et al.* (H1), Nucl. Phys. **B445**, 3 (1995), [hep-ex/9505003].
- [56] M. Derrick *et al.* (ZEUS), Z. Phys. **C67**, 93 (1995), [hep-ex/9501012].

- [57] C. Adloff *et al.* (H1), Nucl. Phys. **B504**, 3 (1997), [hep-ex/9707005].
- [58] J. Breitweg *et al.* (ZEUS), Eur. Phys. J. **C11**, 251 (1999), [hep-ex/9903056].
- [59] J. F. Patrick *et al.*, Phys. Rev. Lett. **49**, 1232 (1982).
- [60] S. Chekanov *et al.* (ZEUS), JHEP **06**, 061 (2008), [arXiv:0803.3878].
- [61] A. H. Mueller, Phys. Lett. **104B**, 161 (1981).
- [62] A. Bassetto *et al.*, Nucl. Phys. **B207**, 189 (1982).
- [63] Yu.L. Dokshitzer *et al.*, Z. Phys. **C15**, 324 (1982).
- [64] A. H. Mueller, Nucl. Phys. **B213**, 85 (1983); A. H. Mueller, Nucl. Phys. **B241**, 141 (1984).
- [65] Y. L. Dokshitzer, V. A. Khoze and S. I. Troian, Int. J. Mod. Phys. **A7**, 1875 (1992).
- [66] Yu.L. Dokshitzer *et al.*, *Basics of Perturbative QCD*, Editions Frontières (1991).
- [67] V. A. Khoze and W. Ochs, Int. J. Mod. Phys. **A12**, 2949 (1997), [hep-ph/9701421].
- [68] C. P. Fong and B. R. Webber, Nucl. Phys. **B355**, 54 (1991).
- [69] S. Albino *et al.*, Phys. Rev. Lett. **95**, 232002 (2005), [hep-ph/0503170].
- [70] S. Albino *et al.*, Phys. Rev. **D73**, 054020 (2006), [hep-ph/0510319].
- [71] S. Albino *et al.*, Nucl. Phys. **B851**, 86 (2011), [arXiv:1104.3018]; S. Albino *et al.*, Nucl. Phys. **B855**, 801 (2012), [arXiv:1108.3948].
- [72] A. Vogt, JHEP **10**, 025 (2011), [arXiv:1108.2993]; C. H. Kom, A. Vogt and K. Yeats, JHEP **10**, 033 (2012), [arXiv:1207.5631].
- [73] D. P. Anderle *et al.*, Phys. Rev. **D95**, 5, 054003 (2017), [arXiv:1611.03371].
- [74] P. Bolzoni, B. A. Kniehl and A. V. Kotikov, Phys. Rev. Lett. **109**, 242002 (2012), [arXiv:1209.5914]; P. Bolzoni, B. A. Kniehl and A. V. Kotikov, Nucl. Phys. **B875**, 18 (2013), [arXiv:1305.6017].
- [75] P. Abreu *et al.* (DELPHI), Z. Phys. **C73**, 11 (1996).
- [76] P. Abreu *et al.* (DELPHI), Z. Phys. **C73**, 229 (1997).
- [77] P. Achard *et al.* (L3), Phys. Rept. **399**, 71 (2004), [hep-ex/0406049].
- [78] R. Itoh *et al.* (TOPAZ), Phys. Lett. **B345**, 335 (1995), [hep-ex/9412015].
- [79] M. Althoff *et al.* (TASSO), Z. Phys. **C22**, 307 (1984).
- [80] M. Z. Akrawy *et al.* (OPAL), Phys. Lett. **B247**, 617 (1990).
- [81] W. Dunwoodie *et al.* (BES), Phys. Rev. **D69**, 072002 (2004), [hep-ex/0306055].
- [82] D. Buskulic *et al.* (ALEPH), Z. Phys. **C55**, 209 (1992).
- [83] A. Heister *et al.* (ALEPH), Eur. Phys. J. **C35**, 457 (2004).
- [84] P. Abreu *et al.* (DELPHI), Phys. Lett. **B275**, 231 (1992).
- [85] P. Abreu *et al.* (DELPHI), Eur. Phys. J. **C5**, 585 (1998).
- [86] P. Abreu *et al.* (DELPHI), Phys. Lett. **B459**, 397 (1999).
- [87] M. Acciarri *et al.* (L3), Phys. Lett. **B444**, 569 (1998).
- [88] TPC/TWO-GAMMA Collab.: H. Aihara *et al.*, LBL 23737.
- [89] B. R. Webber, Phys. Lett. **143B**, 501 (1984).
- [90] Y. I. Azimov *et al.*, Z. Phys. **C27**, 65 (1985).
- [91] Y. I. Azimov *et al.*, Z. Phys. **C31**, 213 (1986).
- [92] I. M. Dremin and J. W. Gary, Phys. Rept. **349**, 301 (2001), [hep-ph/0004215].
- [93] I. M. Dremin and V. A. Nechitailo, Mod. Phys. Lett. **A9**, 1471 (1994), [hep-ex/9406002].
- [94] S. J. Brodsky and J. F. Gunion, Phys. Rev. Lett. **37**, 402 (1976).
- [95] J. Beringer *et al.* (Particle Data Group), Phys. Rev. **D86**, 010001 (2012).
- [96] R. Akers *et al.* (OPAL), Z. Phys. **C68**, 203 (1995).
- [97] P. D. Acton *et al.* (OPAL), Z. Phys. **C53**, 539 (1992).
- [98] D. Buskulic *et al.* (ALEPH), Z. Phys. **C69**, 15 (1995).
- [99] P. Abreu *et al.* (DELPHI), Phys. Lett. **B372**, 172 (1996).
- [100] P. Abreu *et al.* (DELPHI), Phys. Lett. **B416**, 233 (1998).
- [101] P. Abreu *et al.* (DELPHI), Eur. Phys. J. **C18**, 203 (2000), [Erratum: Eur. Phys. J. **C25**, 493 (2002)], [hep-ex/0103031].
- [102] M. Acciarri *et al.* (L3), Phys. Lett. **B371**, 137 (1996).
- [103] M. Acciarri *et al.* (L3), Phys. Lett. **B404**, 390 (1997).
- [104] K. Nakabayashi *et al.* (TOPAZ), Phys. Lett. **B413**, 447 (1997).
- [105] K. Okabe *et al.* (VENUS), Phys. Lett. **B423**, 407 (1998).
- [106] H. Albrecht *et al.* (ARGUS), Z. Phys. **C54**, 13 (1992).
- [107] S. Chekanov *et al.* (ZEUS), Phys. Lett. **B510**, 36 (2001), [hep-ex/0104036].
- [108] J. Benecke *et al.* (Bonn-Hamburg-Munich), Nucl. Phys. **B76**, 29 (1974).
- [109] W. M. Morse *et al.*, Phys. Rev. **D15**, 66 (1977).
- [110] W. Thome *et al.* (Aachen-CERN-Heidelberg-Munich), Nucl. Phys. **B129**, 365 (1977).
- [111] A. Breakstone *et al.* (Ames-Bologna-CERN-Dortmund-Heidelberg-Warsaw), Phys. Rev. **D30**, 528 (1984).
- [112] G. J. Alner *et al.* (UA5), Phys. Rept. **154**, 247 (1987).
- [113] R. E. Ansorge *et al.* (UA5), Z. Phys. **C43**, 357 (1989).
- [114] C. Albajar *et al.* (UA1), Nucl. Phys. **B335**, 261 (1990).
- [115] F. Abe *et al.* (CDF), Phys. Rev. **D41**, 2330 (1990), [119(1989)].
- [116] K. Aamodt *et al.* (ALICE), Eur. Phys. J. **C68**, 89 (2010), [arXiv:1004.3034].
- [117] V. Khachatryan *et al.* (CMS), JHEP **02**, 041 (2010), [arXiv:1002.0621].
- [118] V. Khachatryan *et al.* (CMS), JHEP **01**, 079 (2011), [arXiv:1011.5531].
- [119] V. Khachatryan *et al.* (CMS), Phys. Rev. Lett. **105**, 022002 (2010), [arXiv:1005.3299].
- [120] G. Aad *et al.* (ATLAS), Eur. Phys. J. **C76**, 7, 403 (2016), [arXiv:1603.02439].
- [121] M. Aaboud *et al.* (ATLAS), Eur. Phys. J. **C76**, 9, 502 (2016), [arXiv:1606.01133].
- [122] J. Adam *et al.* (ALICE), Phys. Lett. **B753**, 319 (2016), [arXiv:1509.08734].
- [123] J. Adam *et al.* (ALICE), Eur. Phys. J. **C77**, 1, 33 (2017), [arXiv:1509.07541].
- [124] P. V. Chliapnikov and V. A. Uvarov, Phys. Lett. **B251**, 192 (1990).
- [125] J. F. Grosse-Oetringhaus and K. Reygers, J. Phys. **G37**, 083001 (2010), [arXiv:0912.0023].
- [126] E. K. G. Sarkisyan and A. S. Sakharov (2004), [hep-ph/0410324]; E. K. G. Sarkisyan and A. S. Sakharov, AIP Conf. Proc. **828**, 1, 35 (2006), [hep-ph/0510191]; E. K. G. Sarkisyan and A. S. Sakharov, Eur. Phys. J. **C70**, 533 (2010), [arXiv:1004.4390].
- [127] S. Hoeche *et al.*, in "HERA and the LHC: A Workshop on the implications of HERA for LHC physics: Proceedings Part A," 288–289 (2005), [hep-ph/0602031]; S. Mrenna and P. Richardson, JHEP **05**, 040 (2004), [hep-ph/0312274]; J. Alwall *et al.*, Eur. Phys. J. **C53**, 473 (2008), [arXiv:0706.2569].
- [128] S. Albino, B. A. Kniehl and G. Kramer, Nucl. Phys. **B803**, 42 (2008), [arXiv:0803.2768].

- [129] D. de Florian *et al.*, Phys. Rev. **D91**, 1, 014035 (2015), [arXiv:1410.6027].
- [130] V. Bertone *et al.* (NNPDF), Eur. Phys. J. **C77**, 8, 516 (2017), [arXiv:1706.07049].
- [131] D. de Florian, R. Sassot and M. Stratmann, Phys. Rev. **D76**, 074033 (2007), [arXiv:0707.1506].
- [132] S. Kretzer, E. Leader and E. Christova, Eur. Phys. J. **C22**, 269 (2001), [hep-ph/0108055].
- [133] S. Kretzer, Phys. Rev. **D62**, 054001 (2000), [hep-ph/0003177].
- [134] L. Bourhis *et al.*, Eur. Phys. J. **C19**, 89 (2001), [hep-ph/0009101].
- [135] M. Hirai *et al.*, Phys. Rev. **D75**, 094009 (2007), [hep-ph/0702250].
- [136] C. A. Aidala *et al.*, Phys. Rev. **D83**, 034002 (2011), [arXiv:1009.6145].
- [137] D. de Florian *et al.*, Phys. Rev. **D95**, 9, 094019 (2017), [arXiv:1702.06353].
- [138] D. de Florian, R. Sassot and M. Stratmann, Phys. Rev. **D75**, 114010 (2007), [hep-ph/0703242].
- [139] D. P. Anderle, F. Ringer and M. Stratmann, Phys. Rev. **D92**, 11, 114017 (2015), [arXiv:1510.05845].
- [140] E. Leader, A. V. Sidorov and D. B. Stamenov, Phys. Rev. **D93**, 7, 074026 (2016), [arXiv:1506.06381].
- [141] V. Bertone *et al.* (NNPDF), Eur. Phys. J. **C78**, 8, 651 (2018), [arXiv:1807.03310].
- [142] R. Barate *et al.* (ALEPH), Eur. Phys. J. **C17**, 1 (2000); R. Akers *et al.* (OPAL), Z. Phys. **C68**, 179 (1995); G. Abbiendi *et al.* (OPAL), Eur. Phys. J. **C11**, 217 (1999), [hep-ex/9903027].
- [143] K. Abe *et al.* (SLD), Phys. Rev. **D59**, 052001 (1999), [hep-ex/9805029].
- [144] D. Buskulic *et al.* (ALEPH), Z. Phys. **C66**, 355 (1995); H. Albrecht *et al.* (ARGUS), Z. Phys. **C44**, 547 (1989); R. Akers *et al.* (OPAL), Z. Phys. **C63**, 181 (1994).
- [145] M. R. Adams *et al.* (E665), Z. Phys. **C61**, 539 (1994).
- [146] M. Arneodo *et al.* (European Muon), Z. Phys. **C34**, 283 (1987).
- [147] S. Aid *et al.* (H1), Nucl. Phys. **B480**, 3 (1996), [hep-ex/9607010].
- [148] J. J. Aubert *et al.* (European Muon), Z. Phys. **C18**, 189 (1983).
- [149] A. Airapetian *et al.* (HERMES), Eur. Phys. J. **C21**, 599 (2001), [hep-ex/0104004].
- [150] T. P. McPharlin *et al.*, Phys. Lett. **90B**, 479 (1980).
- [151] S. S. Adler *et al.* (PHENIX), Phys. Rev. Lett. **91**, 241803 (2003), [hep-ex/0304038].
- [152] B. Abelev *et al.* (ALICE), Phys. Lett. **B717**, 162 (2012), [arXiv:1205.5724].
- [153] M. Bonesini *et al.* (WA70), Z. Phys. **C38**, 371 (1988).
- [154] T. Akesson *et al.* (Axial Field Spectrometer), Sov. J. Nucl. Phys. **51**, 836 (1990), [Yad. Fiz.51,1314(1990)].
- [155] C. Kourkoumelis *et al.*, Z. Phys. **C5**, 95 (1980).
- [156] L. Apanasevich *et al.* (Fermilab E706), Phys. Rev. **D68**, 052001 (2003), [hep-ex/0204031].
- [157] F. Abe *et al.* (CDF), Phys. Rev. Lett. **61**, 1819 (1988).
- [158] M. Banner *et al.* (UA2), Phys. Lett. **115B**, 59 (1982).
- [159] M. Procura and I. W. Stewart, Phys. Rev. **D81**, 074009 (2010), [Erratum: Phys. Rev.D83,039902(2011)], [arXiv:0911.4980].
- [160] A. Jain, M. Procura and W. J. Waalewijn, JHEP **05**, 035 (2011), [arXiv:1101.4953].
- [161] M. Procura and W. J. Waalewijn, Phys. Rev. **D85**, 114041 (2012), [arXiv:1111.6605].
- [162] F. Arleo *et al.*, JHEP **04**, 147 (2014), [arXiv:1311.7356].
- [163] M. Ritzmann and W. J. Waalewijn, Phys. Rev. **D90**, 5, 054029 (2014), [arXiv:1407.3272].
- [164] T. Kaufmann, A. Mukherjee and W. Vogelsang, Phys. Rev. **D92**, 5, 054015 (2015), [arXiv:1506.01415].
- [165] Y.-T. Chien *et al.*, JHEP **05**, 125 (2016), [arXiv:1512.06851].
- [166] F. Abe *et al.* (CDF), Phys. Rev. Lett. **65**, 968 (1990).
- [167] T. A. collaboration (ATLAS) (2015).
- [168] S. Chatrchyan *et al.* (CMS), JHEP **10**, 087 (2012), [arXiv:1205.5872].
- [169] X. Lu (ALICE), Nucl. Phys. **A931**, 428 (2014), [arXiv:1407.8385].
- [170] C. Bianchin (ALICE), J. Phys. Conf. Ser. **612**, 1, 012020 (2015).
- [171] F. Krizek (ALICE), J. Phys. Conf. Ser. **668**, 1, 012018 (2016), [arXiv:1509.02024].
- [172] M. Aaboud *et al.* (ATLAS), Nucl. Phys. **A978**, 65 (2018), [arXiv:1706.02859].
- [173] L. Adamczyk *et al.* (STAR), Phys. Rev. **D97**, 3, 032004 (2018), [arXiv:1708.07080].
- [174] D. P. Anderle *et al.*, Phys. Rev. **D96**, 3, 034028 (2017), [arXiv:1706.09857].
- [175] N. Sato *et al.* (JAM) (2019), [arXiv:1905.03788].
- [176] M. Epele *et al.*, Phys. Rev. **D86**, 074028 (2012), [arXiv:1209.3240].
- [177] E. Witten, Nucl. Phys. **210**, 189 (1977).
- [178] L. Bourhis, M. Fontannaz and J. P. Guillet, Eur. Phys. J. **C2**, 529 (1998), [hep-ph/9704447].
- [179] M. Gluck, E. Reya and A. Vogt, Phys. Rev. **D48**, 116 (1993), [Erratum: Phys. Rev.D51,1427(1995)]; Erratum *ibid.* **D51**, 1427 (1995).
- [180] G. Abbiendi *et al.* (OPAL), Eur. Phys. J. **C27**, 467 (2003), [hep-ex/0209048].
- [181] G. Bocquet *et al.*, Phys. Lett. **B366**, 434 (1996).
- [182] T. Kaufmann, A. Mukherjee and W. Vogelsang, Phys. Rev. **D93**, 11, 114021 (2016), [arXiv:1604.07175].
- [183] P. Abreu *et al.* (DELPHI), Eur. Phys. J. **C13**, 573 (2000).
- [184] B. A. Kniehl, G. Kramer and B. Potter, Phys. Rev. Lett. **85**, 5288 (2000), [hep-ph/0003297].
- [185] M. Arneodo *et al.* (European Muon), Z. Phys. **C33**, 167 (1986).
- [186] A. Airapetian *et al.* (HERMES), Phys. Rev. **D87**, 074029 (2013), [arXiv:1212.5407].
- [187] C. Adolph *et al.* (COMPASS), Phys. Lett. **B764**, 1 (2017), [arXiv:1604.02695].
- [188] F. D. Aaron *et al.* (H1), Phys. Lett. **B673**, 119 (2009), [arXiv:0901.0477].
- [189] M. Derrick *et al.* (ZEUS), Z. Phys. **C68**, 29 (1995), [hep-ex/9505011].
- [190] S. Chekanov *et al.* (ZEUS), Phys. Lett. **B553**, 141 (2003), [hep-ex/0211025].
- [191] S. Chekanov *et al.* (ZEUS), Nucl. Phys. **B786**, 181 (2007), [arXiv:0705.3770].
- [192] F. D. Aaron *et al.* (H1), Eur. Phys. J. **C61**, 185 (2009), [arXiv:0810.4036].
- [193] A. Aktas *et al.* (H1), Eur. Phys. J. **C36**, 413 (2004), [hep-ex/0403056].
- [194] P. Dixon, D. Kant and G. Thompson, J. Phys. **G25**, 1453 (1999).
- [195] C. Adloff *et al.* (H1), Phys. Lett. **B462**, 440 (1999), [hep-ex/9907030].

- [196] D. Graudenz, Fortsch. Phys. **45**, 629 (1997), [hep-ph/9701334].
- [197] P. M. Nadolsky, D. R. Stump and C. P. Yuan, Phys. Rev. **D61**, 014003 (2000), [Erratum: Phys. Rev.D64,059903(2001)], [hep-ph/9906280].
- [198] D. de Florian *et al.*, Phys. Rev. **D95**, 0334027 (2017).
- [199] T. Aaltonen *et al.* (CDF), Phys. Rev. **D79**, 112005 (2009), [Erratum: Phys. Rev.D82,119903(2010)], [arXiv:0904.1098].
- [200] G. Aad *et al.* (ATLAS), New J. Phys. **13**, 053033 (2011), [arXiv:1012.5104].
- [201] B. I. Abelev *et al.* (STAR), Phys. Rev. **C75**, 064901 (2007), [arXiv:nucl-ex/0607033].
- [202] K. Aamodt *et al.* (ALICE), Eur. Phys. J. **C71**, 1655 (2011), [arXiv:1101.4110].
- [203] B. B. Abelev *et al.* (ALICE), Phys. Lett. **B736**, 196 (2014), [arXiv:1401.1250].
- [204] J. Adam *et al.* (ALICE), Eur. Phys. J. **C75**, 5, 226 (2015), [arXiv:1504.00024].
- [205] S. Chatrchyan *et al.* (CMS), Eur. Phys. J. **C72**, 2164 (2012), [arXiv:1207.4724].
- [206] A. M. Sirunyan *et al.* (CMS), Phys. Rev. **D96**, 11, 112003 (2017), [arXiv:1706.10194].
- [207] G. J. Alner *et al.* (UA5), Z. Phys. **C32**, 153 (1986).
- [208] B. Abelev *et al.* (ALICE), Eur. Phys. J. **C73**, 6, 2456 (2013), [arXiv:1208.4968].
- [209] G. Antchev *et al.* (TOTEM), EPL **101**, 2, 21004 (2013).
- [210] A. M. Sirunyan *et al.* (CMS), JHEP **07**, 161 (2018), [arXiv:1802.02613].
- [211] F. Abe *et al.* (CDF), Phys. Rev. **D50**, 5550 (1994).
- [212] F. Abe *et al.* (CDF), Phys. Rev. **D50**, 5518 (1994).
- [213] S. S. Adler *et al.* (PHENIX), Phys. Rev. **C74**, 024904 (2006), [arXiv:nucl-ex/0603010].
- [214] S. Albino *et al.*, Phys. Rev. **D75**, 034018 (2007), [hep-ph/0611029].
- [215] I. Borsa, R. Sassot and M. Stratmann, Phys. Rev. **D96**, 9, 094020 (2017), [arXiv:1708.01630].
- [216] B. Andersson *et al.*, Phys. Rept. **97**, 31 (1983).
- [217] T. Sjostrand and M. Bengtsson, Comput. Phys. Commun. **43**, 367 (1987); T. Sjostrand, Comput. Phys. Commun. **82**, 74 (1994).
- [218] P. D. Acton *et al.* (OPAL), Phys. Lett. **B305**, 407 (1993).
- [219] J. Breitweg *et al.* (ZEUS), Eur. Phys. J. **C2**, 77 (1998), [hep-ex/9711018].
- [220] D. DeProspero *et al.* (E632), Phys. Rev. **D50**, 6691 (1994).
- [221] S. Chekanov *et al.* (ZEUS), Eur. Phys. J. **C51**, 1 (2007), [hep-ex/0612023].
- [222] G. Grindhammer *et al.*, in: *Proceedings of the Workshop on Monte Carlo Generators for HERA Physics*, Hamburg, Germany, 1998/1999.
- [223] N. Brook *et al.*, in: *Proceedings of the Workshop for Future HERA Physics at HERA*, Hamburg, Germany, 1996.
- [224] D. Acosta *et al.* (CDF), Phys. Rev. **D72**, 052001 (2005), [hep-ex/0504048].
- [225] G. Arnison *et al.* (UA1), Phys. Lett. **118B**, 167 (1982).
- [226] M. Banner *et al.* (UA2), Phys. Lett. **122B**, 322 (1983).
- [227] M. Banner *et al.* (UA2, Bern-CERN-Copenhagen-Osaka-Pavia-Saclay), Z. Phys. **C27**, 329 (1985).
- [228] A. Adare *et al.* (PHENIX), Phys. Rev. **D76**, 051106 (2007), [arXiv:0704.3599].
- [229] A. Adare *et al.* (PHENIX), Phys. Rev. **D83**, 032001 (2011), [arXiv:1009.6224].
- [230] A. Adare *et al.* (PHENIX), Phys. Rev. **D86**, 092006 (2012), [arXiv:1202.4020].
- [231] A. Adare *et al.* (PHENIX), Phys. Rev. **D88**, 3, 032006 (2013), [arXiv:1209.3283].
- [232] A. Adare *et al.* (PHENIX), Phys. Rev. **D91**, 3, 032001 (2015), [arXiv:1409.1907].
- [233] A. Adare *et al.* (PHENIX), Phys. Rev. **D90**, 7, 072008 (2014), [arXiv:1406.3541].
- [234] A. Adare *et al.* (PHENIX), Phys. Rev. **D93**, 1, 011501 (2016), [arXiv:1510.02317].
- [235] I. Arsene *et al.* (BRAHMS), Phys. Rev. Lett. **98**, 252001 (2007), [hep-ex/0701041].
- [236] J. Adams *et al.* (STAR), Phys. Rev. Lett. **97**, 152302 (2006), [arXiv:nucl-ex/0602011].
- [237] J. Adams *et al.* (STAR), Phys. Lett. **B637**, 161 (2006), [arXiv:nucl-ex/0601033].
- [238] B. I. Abelev *et al.* (STAR), Phys. Rev. **D80**, 111108 (2009), [arXiv:0911.2773].
- [239] G. Agakishiev *et al.* (STAR), Phys. Rev. Lett. **108**, 072302 (2012), [arXiv:1110.0579].
- [240] L. Adamczyk *et al.* (STAR), Phys. Rev. **D89**, 1, 012001 (2014), [arXiv:1309.1800].
- [241] B. B. Abelev *et al.* (ALICE), Eur. Phys. J. **C73**, 12, 2662 (2013), [arXiv:1307.1093].
- [242] L. Apanasevich *et al.* (Fermilab E706), Phys. Rev. Lett. **81**, 2642 (1998), [hep-ex/9711017].
- [243] G. Balocchi *et al.* (UA6), Phys. Lett. **B436**, 222 (1998).
- [244] K. Aamodt *et al.* (ALICE), Eur. Phys. J. **C71**, 1594 (2011), [arXiv:1012.3257].
- [245] R. Aaij *et al.* (LHCb), Phys. Lett. **B703**, 267 (2011), [arXiv:1107.3935].
- [246] G. Aad *et al.* (ATLAS), Phys. Lett. **B758**, 67 (2016), [arXiv:1602.01633].
- [247] F. Aversa *et al.*, Nucl. Phys. **B327**, 105 (1989); D. de Florian, Phys. Rev. **D67**, 054004 (2003), [hep-ph/0210442]; B. Jager *et al.*, Phys. Rev. **D67**, 054005 (2003), [hep-ph/0211007].
- [248] U. Baur *et al.*, in "QCD and weak boson physics in Run II. Proceedings, Batavia, USA, March 4-6, June 3-4, November 4-6, 1999," 115-164 (2000), [115(2000)], [hep-ph/0005226], URL <http://lss.fnal.gov/archive/preprint/fermilab-conf-00-411-ae.shtml>.
- [249] P. Aurenche *et al.*, Eur. Phys. J. **C13**, 347 (2000), [hep-ph/9910252].
- [250] L. Apanasevich *et al.*, Phys. Rev. **D59**, 074007 (1999), [hep-ph/9808467].
- [251] U. D'Alesio and F. Murgia, Phys. Rev. **D70**, 074009 (2004), [hep-ph/0408092].
- [252] D. de Florian and W. Vogelsang, Phys. Rev. **D71**, 114004 (2005), [hep-ph/0501258].
- [253] P. Hinderer *et al.*, Phys. Rev. **D99**, 5, 054019 (2019), [arXiv:1812.00915].
- [254] D. d'Enterria *et al.*, Nucl. Phys. **B883**, 615 (2014), [arXiv:1311.1415].
- [255] G. Wilk and Z. Wlodarczyk, Eur. Phys. J. **A40**, 299 (2009), [arXiv:0810.2939].
- [256] C. Tsallis, J. Statist. Phys. **52**, 479 (1988).
- [257] C. Tsallis, Braz. J. Phys. **29**, 1 (1999).
- [258] C. Tsallis, Eur. Phys. J. **A40**, 257 (2009), [arXiv:0812.4370].
- [259] M. D. Azmi and J. Cleymans, J. Phys. **G41**, 065001 (2014), [arXiv:1401.4835].
- [260] G. Wilk and Z. Wlodarczyk, Phys. Rev. Lett. **84**, 2770 (2000), [hep-ph/9908459].
- [261] T. Bhattacharyya *et al.*, J. Phys. **G45**, 5, 055001 (2018), [arXiv:1709.07376].

- [262] S. Grigoryan, Phys. Rev. **D95**, 5, 056021 (2017), [arXiv:1702.04110].
- [263] T. Wibig, Int. J. Mod. Phys. **A29**, 1450021 (2014).
- [264] K. Saraswat, P. Shukla and V. Singh, J. Phys. Comm. **2**, 3, 035003 (2018), [arXiv:1706.04860].
- [265] K. Urmossy, G. G. Barnafoldi and T. S. Biro, Phys. Lett. **B701**, 111 (2011), [arXiv:1101.3023].
- [266] A. S. Parvan, O. V. Teryaev and J. Cleymans, Eur. Phys. J. **A53**, 5, 102 (2017), [arXiv:1607.01956].
- [267] K. Adcox *et al.* (PHENIX), Phys. Rev. Lett. **88**, 022301 (2002), [arXiv:nucl-ex/0109003]; C. Adler *et al.* (STAR), Phys. Rev. Lett. **90**, 082302 (2003), [arXiv:nucl-ex/0210033].
- [268] V.A. Khoze *et al.*, *Proceedings, Conference on High-Energy Physics, Tbilisi 1976*; J. D. Bjorken, Phys. Rev. **D17**, 171 (1978).
- [269] M. Artuso *et al.* (CLEO), Phys. Rev. **D70**, 112001 (2004), [hep-ex/0402040].
- [270] R. Seuster *et al.* (Belle), Phys. Rev. **D73**, 032002 (2006), [hep-ex/0506068].
- [271] A. Heister *et al.* (ALEPH), Phys. Lett. **B512**, 30 (2001), [hep-ex/0106051]; J. Abdallah *et al.* (DELPHI), Eur. Phys. J. **C71**, 1557 (2011), [arXiv:1102.4748]; G. Abbiendi *et al.* (OPAL), Eur. Phys. J. **C29**, 463 (2003), [hep-ex/0210031]; K. Abe *et al.* (SLD), Phys. Rev. **D65**, 092006 (2002), [Erratum: Phys. Rev.D66,079905(2002)], [hep-ex/0202031].
- [272] B. Mele and P. Nason, Phys. Lett. **B245**, 635 (1990); B. Mele and P. Nason, Nucl. Phys. **B361**, 626 (1991), [Erratum: Nucl. Phys.B921,841(2017)].
- [273] M. Cacciari and S. Catani, Nucl. Phys. **B617**, 253 (2001), [hep-ph/0107138].
- [274] P. Nason and C. Oleari, Phys. Lett. **B418**, 199 (1998), [hep-ph/9709358]; P. Nason and C. Oleari, Phys. Lett. **B447**, 327 (1999), [hep-ph/9811206]; P. Nason and C. Oleari, Nucl. Phys. **B565**, 245 (2000), [hep-ph/9903541].
- [275] K. Melnikov and A. Mitov, Phys. Rev. **D70**, 034027 (2004), [hep-ph/0404143].
- [276] C. Peterson *et al.*, Phys. Rev. **D27**, 105 (1983).
- [277] V. G. Kartvelishvili, A. K. Likhoded and V. A. Petrov, Phys. Lett. **78B**, 615 (1978).
- [278] P. D. B. Collins and T. P. Spiller, J. Phys. **G11**, 1289 (1985).
- [279] G. Colangelo and P. Nason, Phys. Lett. **B285**, 167 (1992).
- [280] M. G. Bowler, Z. Phys. **C11**, 169 (1981).
- [281] E. Braaten *et al.*, Phys. Rev. **D51**, 4819 (1995), [hep-ph/9409316].
- [282] R. Akers *et al.* (OPAL), Z. Phys. **C67**, 27 (1995).
- [283] H. Albrecht *et al.* (ARGUS), Z. Phys. **C52**, 353 (1991).
- [284] D. Buskulic *et al.* (ALEPH), Phys. Lett. **B357**, 699 (1995).
- [285] J. Chrin, Z. Phys. **C36**, 163 (1987).
- [286] R. L. Jaffe and L. Randall, Nucl. Phys. **B412**, 79 (1994), [hep-ph/9306201].
- [287] M. Cacciari and E. Gardi, Nucl. Phys. **B664**, 299 (2003), [hep-ph/0301047].
- [288] L. Randall and N. Rius, Nucl. Phys. **B441**, 167 (1995), [hep-ph/9405217].
- [289] J. C. Collins, Phys. Rev. **D58**, 094002 (1998), [hep-ph/9806259].
- [290] B. A. Kniehl *et al.*, Eur. Phys. J. **C41**, 199 (2005), [hep-ph/0502194].
- [291] S. Ahmed *et al.* (CLEO), Phys. Rev. **D62**, 112003 (2000), [hep-ex/0008015].
- [292] B. Aubert *et al.* (BaBar), Phys. Rev. **D65**, 091104 (2002), [hep-ex/0201041].
- [293] D. Bortoletto *et al.* (CLEO), Phys. Rev. **D37**, 1719 (1988), [Erratum: Phys. Rev.D39,1471(1989)].
- [294] H. Albrecht *et al.* (ARGUS), Z. Phys. **C54**, 1 (1992).
- [295] G. Alexander *et al.* (OPAL), Z. Phys. **C69**, 543 (1996).
- [296] A. Heister *et al.* (ALEPH), Phys. Lett. **B561**, 213 (2003), [hep-ex/0302003].
- [297] F. D. Aaron *et al.* (H1), Eur. Phys. J. **C65**, 89 (2010), [arXiv:0907.2643].
- [298] S. Chekanov *et al.* (ZEUS), JHEP **07**, 074 (2007), [arXiv:0704.3562]; ZEUS Collab: H. Abramowicz *et al.*, JHEP, 1309 (2013); A. Aktas *et al.* (H1), Eur. Phys. J. **C51**, 271 (2007), [hep-ex/0701023]; F. D. Aaron *et al.* (H1), Eur. Phys. J. **C59**, 589 (2009), [arXiv:0808.1003].
- [299] B. Adeva *et al.* (L3), Phys. Lett. **B261**, 177 (1991).
- [300] O. Biebel, P. Nason and B. R. Webber (2001), [hep-ph/0109282].
- [301] H. Evans (ALICE, ATLAS, CMS, LHCb), in “Proceedings, 14th International Conference on Hadron spectroscopy (Hadron 2011): Munich, Germany, June 13-17, 2011,” (2011), [arXiv:1110.5294]; E. Aguilo, in “Proceedings, 47th Rencontres de Moriond on QCD and High Energy Interactions: La Thuile, France, March 10-17, 2012,” 115–120 (2012), [arXiv:1205.5678]; F. Simonetto, Journal of Physics: Conference Series **347**, 012014 (2012).
- [302] V. Khachatryan *et al.* (CMS), JHEP **03**, 136 (2011), [arXiv:1102.3194]; G. Aad *et al.* (ATLAS), Eur. Phys. J. **C71**, 1846 (2011), [arXiv:1109.6833]; S. Chatrchyan *et al.* (CMS), JHEP **04**, 084 (2012), [arXiv:1202.4617]; G. Aad *et al.* (ATLAS), Eur. Phys. J. **C73**, 2, 2301 (2013), [arXiv:1210.0441].
- [303] H. Jung *et al.*, Phys. Rev. **D85**, 034035 (2012), [arXiv:1111.1942].
- [304] D. Acosta *et al.* (CDF), Phys. Rev. Lett. **91**, 241804 (2003), [hep-ex/0307080]; D. Acosta *et al.* (CDF), Phys. Rev. **D71**, 032001 (2005), [hep-ex/0412071].
- [305] M. Cacciari and P. Nason, JHEP **09**, 006 (2003), [hep-ph/0306212]; M. Cacciari *et al.*, JHEP **07**, 033 (2004), [hep-ph/0312132]; B. A. Kniehl *et al.*, Phys. Rev. Lett. **96**, 012001 (2006), [hep-ph/0508129].
- [306] H. Abramowicz *et al.* (ZEUS), Eur. Phys. J. **C71**, 1573 (2011), [arXiv:1101.3692].
- [307] S. Chekanov *et al.* (ZEUS), Phys. Rev. **D78**, 072001 (2008), [arXiv:0805.4390].
- [308] S. Chekanov *et al.* (ZEUS), JHEP **02**, 032 (2009), [arXiv:0811.0894].
- [309] F. D. Aaron *et al.* (H1), Eur. Phys. J. **C72**, 2148 (2012), [arXiv:1206.4346].
- [310] M. L. Mangano and P. Nason, Phys. Lett. **B285**, 160 (1992).
- [311] M. H. Seymour, Nucl. Phys. **B436**, 163 (1995).
- [312] D. J. Miller and M. H. Seymour, Phys. Lett. **B435**, 213 (1998), [hep-ph/9805414].
- [313] R. Barate *et al.* (ALEPH), Phys. Lett. **B434**, 437 (1998).
- [314] P. Abreu *et al.* (DELPHI), Phys. Lett. **B405**, 202 (1997).
- [315] M. Acciarri *et al.* (L3), Phys. Lett. **B476**, 243 (2000), [hep-ex/9911016].
- [316] G. Abbiendi *et al.* (OPAL), Eur. Phys. J. **C13**, 1 (2000), [hep-ex/9908001].
- [317] K. Abe *et al.* (SLD) (1999), [hep-ex/9908028], URL <http://www-public.slac.stanford.edu/sciDoc/docMeta.aspx?slacPubNumber=SLAC-PUB-8157>.
- [318] C. Albajar *et al.* (UA1 Collaboration), Z. Phys. **C 61**, 41 (1993), URL <http://cds.cern.ch/record/253028>.
- [319] R. Aaij *et al.* (LHCb), JHEP **11**, 030 (2017), [arXiv:1708.05994].
- [320] M. Aaboud *et al.* (ATLAS), Phys. Rev. **D99**, 5, 052004 (2019), [arXiv:1812.09283].

- [321] M. Burkardt and R. L. Jaffe, Phys. Rev. Lett. **70**, 2537 (1993), [hep-ph/9302232].
- [322] P. J. Mulders and R. D. Tangerman, Nucl. Phys. **B461**, 197 (1996), [Erratum: Nucl. Phys. **B484**, 538 (1997)], [hep-ph/9510301].
- [323] R. Jakob, Nucl. Phys. **A711**, 35 (2002), [hep-ph/0206271].
- [324] D. de Florian, M. Stratmann and W. Vogelsang, Phys. Rev. Lett. **81**, 530 (1998), [hep-ph/9802432].
- [325] D. Buskulic *et al.* (ALEPH), Phys. Lett. **B374**, 319 (1996).
- [326] K. Ackerstaff *et al.* (OPAL), Eur. Phys. J. **C2**, 49 (1998), [hep-ex/9708027].
- [327] G. Abbiendi *et al.* (OPAL), Phys. Lett. **B444**, 539 (1998), [hep-ex/9808006].
- [328] M. Alekseev *et al.* (COMPASS), Eur. Phys. J. **C64**, 171 (2009), [arXiv:0907.0388].
- [329] A. Airapetian *et al.* (HERMES), Phys. Rev. **D74**, 072004 (2006), [hep-ex/0607004].
- [330] G. Karyan (HERMES), Int. J. Mod. Phys. Conf. Ser. **40**, 1660067 (2016).
- [331] J. Adam *et al.* (STAR), Phys. Rev. **D98**, 11, 112009 (2018), [arXiv:1808.07634].
- [332] R. L. Jaffe, Phys. Rev. **D54**, 11, R6581 (1996), [hep-ph/9605456].
- [333] A. Airapetian *et al.* (HERMES), Phys. Rev. **D76**, 092008 (2007), [arXiv:0704.3133].
- [334] A. Moretti (COMPASS), PoS **SPIN2018**, 138 (2018), [arXiv:1901.01735].
- [335] R. Seidl *et al.* (Belle), Phys. Rev. **D99**, 11, 112006 (2019), [arXiv:1902.01552].
- [336] C. Adolph *et al.* (COMPASS), Eur. Phys. J. **C73**, 8, 2531 (2013), [Erratum: Eur. Phys. J. **C75**, no. 2, 94 (2015)], [arXiv:1305.7317].
- [337] A. Signori *et al.*, JHEP **11**, 194 (2013), [arXiv:1309.3507].
- [338] M. Anselmino *et al.*, JHEP **04**, 005 (2014), [arXiv:1312.6261].
- [339] M. G. Echevarria *et al.*, Phys. Rev. **D89**, 074013 (2014), [arXiv:1401.5078].
- [340] M. G. Echevarria, I. Scimemi and A. Vladimirov, Phys. Rev. **D93**, 1, 011502 (2016), [Erratum: Phys. Rev. **D94**, no. 9, 099904 (2016)], [arXiv:1509.06392].
- [341] M. G. Echevarria, I. Scimemi and A. Vladimirov, JHEP **09**, 004 (2016), [arXiv:1604.07869].
- [342] A. Bacchetta *et al.*, JHEP **06**, 081 (2017), [Erratum: JHEP **06**, 051 (2019)], [arXiv:1703.10157].
- [343] J. C. Collins, Nucl. Phys. **B396**, 161 (1993), [hep-ph/9208213].
- [344] J. P. Ralston and D. E. Soper, Nucl. Phys. **B152**, 109 (1979).
- [345] H. Avakian *et al.* (CLAS), Phys. Rev. **D69**, 112004 (2004), [hep-ex/0301005].
- [346] A. Airapetian *et al.* (HERMES), Phys. Rev. Lett. **84**, 4047 (2000), [hep-ex/9910062].
- [347] A. Airapetian *et al.* (HERMES), Phys. Rev. **D64**, 097101 (2001), [hep-ex/0104005].
- [348] A. Airapetian *et al.* (HERMES), Phys. Rev. Lett. **94**, 012002 (2005), [hep-ex/0408013].
- [349] A. Airapetian *et al.* (HERMES), Phys. Lett. **B693**, 11 (2010), [arXiv:1006.4221].
- [350] V. Yu. Alexakhin *et al.* (COMPASS), Phys. Rev. Lett. **94**, 202002 (2005), [hep-ex/0503002].
- [351] E. S. Ageev *et al.* (COMPASS), Nucl. Phys. **B765**, 31 (2007), [hep-ex/0610068].
- [352] M. Alekseev *et al.* (COMPASS), Phys. Lett. **B673**, 127 (2009), [arXiv:0802.2160].
- [353] M. G. Alekseev *et al.* (COMPASS), Phys. Lett. **B692**, 240 (2010), [arXiv:1005.5609].
- [354] M. G. Alekseev *et al.* (COMPASS), Eur. Phys. J. **C70**, 39 (2010), [arXiv:1007.1562].
- [355] C. Adolph *et al.* (COMPASS), Phys. Lett. **B717**, 376 (2012), [arXiv:1205.5121].
- [356] C. Adolph *et al.* (COMPASS), Phys. Lett. **B744**, 250 (2015), [arXiv:1408.4405].
- [357] K. Abe *et al.* (Belle), Phys. Rev. Lett. **96**, 232002 (2006), [hep-ex/0507063].
- [358] R. Seidl *et al.* (Belle), Phys. Rev. **D78**, 032011 (2008), [Erratum: Phys. Rev. **D86**, 039905 (2012)], [arXiv:0805.2975].
- [359] J. P. Lees *et al.* (BaBar), Phys. Rev. **D90**, 5, 052003 (2014), [arXiv:1309.5278].
- [360] J. P. Lees *et al.* (BaBar), Phys. Rev. **D92**, 11, 111101 (2015), [arXiv:1506.05864].
- [361] M. Ablikim *et al.* (BESIII), Phys. Rev. Lett. **116**, 4, 042001 (2016), [arXiv:1507.06824].
- [362] M. Anselmino *et al.*, Phys. Rev. **D92**, 11, 114023 (2015), [arXiv:1510.05389].
- [363] Z.-B. Kang *et al.*, Phys. Rev. **D93**, 1, 014009 (2016), [arXiv:1505.05589].
- [364] F. Yuan, Phys. Rev. Lett. **100**, 032003 (2008), [arXiv:0709.3272].
- [365] Z.-B. Kang *et al.*, JHEP **11**, 068 (2017), [arXiv:1705.08443].
- [366] K. Konishi, A. Ukawa and G. Veneziano, Phys. Lett. **78B**, 243 (1978).
- [367] I. Vendramin, Nuovo Cim. **A66**, 339 (1981).
- [368] J. C. Collins, S. F. Heppelmann and G. A. Ladinsky, Nucl. Phys. **B420**, 565 (1994), [hep-ph/9305309].
- [369] R. L. Jaffe, X.-m. Jin and J. Tang, Phys. Rev. Lett. **80**, 1166 (1998), [hep-ph/9709322].
- [370] R. L. Jaffe, X.-m. Jin and J.-a. Tang, Phys. Rev. **D57**, 5920 (1998), [hep-ph/9710561].
- [371] A. Bianconi *et al.*, Phys. Rev. **D62**, 034008 (2000), [hep-ph/9907475].
- [372] M. Radici, R. Jakob and A. Bianconi, Phys. Rev. **D65**, 074031 (2002), [hep-ph/0110252].
- [373] D. de Florian and L. Vanni, Phys. Lett. **B578**, 139 (2004), [hep-ph/0310196].
- [374] A. Bacchetta and M. Radici, Phys. Rev. **D67**, 094002 (2003), [hep-ph/0212300].
- [375] A. Vossen *et al.* (Belle), Phys. Rev. Lett. **107**, 072004 (2011), [arXiv:1104.2425].
- [376] A. Courtoy *et al.*, Phys. Rev. **D85**, 114023 (2012), [arXiv:1202.0323].
- [377] M. Radici *et al.*, JHEP **05**, 123 (2015), [arXiv:1503.03495].
- [378] A. Airapetian *et al.* (HERMES), JHEP **06**, 017 (2008), [arXiv:0803.2367].
- [379] C. Adolph *et al.* (COMPASS), Phys. Lett. **B713**, 10 (2012), [arXiv:1202.6150].
- [380] C. Adolph *et al.* (COMPASS), Phys. Lett. **B736**, 124 (2014), [arXiv:1401.7873].
- [381] L. Adamczyk *et al.* (STAR), Phys. Rev. Lett. **115**, 242501 (2015), [arXiv:1504.00415].
- [382] A. Bacchetta, A. Courtoy and M. Radici, Phys. Rev. Lett. **107**, 012001 (2011), [arXiv:1104.3855].
- [383] A. Bacchetta, A. Courtoy and M. Radici, JHEP **03**, 119 (2013), [arXiv:1212.3568].
- [384] M. Radici and A. Bacchetta, Phys. Rev. Lett. **120**, 19, 192001 (2018), [arXiv:1802.05212].

20. High Energy Soft QCD and Diffraction

Written February 2020 by V.A. Khoze (Durham U.; Petersburg Nuclear Phys. Inst.), M. Ryskin (Petersburg Nuclear Phys. Inst.) and M. Taševský (Prague, Inst. Phys.).

20.1 Introduction

Despite the enormous successes of Quantum Chromodynamics (QCD) (see Section 9 in [1] and [2]) there remain a number of deep questions to be answered in the domain of strong interaction physics. These concern first of all small momentum transfer processes which are generically called soft interactions.

One of the most challenging problems is the high-energy behaviour of hadronic scattering processes. At high collision energies, \sqrt{s} , soft interactions play a dominant role. Unfortunately, soft interactions cannot be described in terms of perturbative QCD. These are non-perturbative phenomena related to confinement which are generally considered in the context of the analytic S -matrix, based on *first principles*, such as analyticity, crossing symmetry and unitarity of partial waves, see e.g. [3, 4]. At high energies the most self-consistent way to perform the calculations and to describe the data is the Regge approach (see for example [5–7]), which will be considered below. As discussed in Section 20.5, this formalism could be smoothly matched with perturbative QCD calculations at larger transverse momenta. Therefore, here we will concentrate on the properties of high energy soft interactions that can be expected from the extension of the perturbative QCD domain.

The main aim of this review is to present the well-established theoretical framework, based on Regge theory and QCD, used for describing high-energy collisions. A limited number of some new experimental results, mainly from the LHC, are shown in order to demonstrate that the gross features of the data are in agreement with this approach. We are not focussing on any particular phenomenological or Monte Carlo model, which are covered in the dedicated reviews and books, see e.g. Section 41 in [1], [2, 8–14] and Chapter 2 in [15].

Typically, in multiparticle production, the secondaries¹ fill the whole available rapidity interval.² However, there exists an important class of events in which a large interval of rapidity (typically at least 4 units) is devoid of any hadronic activity. Such an interval is called a Large Rapidity Gap (LRG). The most frequent case with a LRG is elastic scattering. There are also events in which one of the incoming protons (or both) is transformed (dissociates) into a set of two or more final state particles with the mass $M \ll \sqrt{s}$ and proton quantum number. All these events have properties similar to those of the well-known from optics pattern of diffraction of a beam of light on an obstacle. By analogy, in high-energy physics, the corresponding processes are usually called diffractive. The classic example is the elastic scattering of hadrons on nuclei (see e.g. [16]), which manifests an angular distribution with a series of minima and maxima, analogous to the diffraction of light on a black disk. At LHC energies diffractive processes constitute up to 40% of the total (pp) cross section, σ_{tot} . Therefore, we will pay special attention to the description of the elastic scattering amplitude and proton diffractive dissociation. Diffraction dissociation can be considered as a quantum mechanical process caused by the fact that different components of the incoming hadron wave function have different probabilities for interaction with a target [17]. This feature allows us to probe the transverse size of the interaction region.

Note that besides being of a fundamental interest in their own right for understanding the high energy behaviour of the QCD amplitude, there are several reasons why it is important to study soft and diffractive processes. Firstly, soft interactions unavoidably give an underlying component to rare ‘hard’ events, from which we hope to extract signals for New Physics. Secondly, we should be able to estimate the probability that rapidity gaps, which oc-

cur in ‘hard’ diffractive events, survive rescattering effects, that is, survive the population of the gaps by the secondary particles from the underlying event. Thirdly, an understanding of diffractive processes is very important for evaluation of pile-up backgrounds in high-luminosity pp collisions, which have a direct impact on various experimental measurements. Pile-up corresponds to soft independent interactions in the same bunch crossing whose number rises with increasing instantaneous luminosity. And, finally, studies of diffractive processes should help in the understanding of the structure of high-energy cosmic ray cascades, which requires a very detailed knowledge of the spectra of particles carrying a large fraction x of the incoming momentum in proton-air and nucleus-air interactions, see for instance [18].

Experimentally, diffractive processes are selected using two distinct features:

1. large regions (typically at least $\Delta\eta > 4$) in the detector are devoid of hadronic activity (LRG) and/or
2. one or both incoming particles stay intact after collision and are registered by the dedicated forward detectors placed a few hundred meters from the interaction point. The momentum loss of the initial particle, $\xi = 1 - x$, is typically smaller than 0.15.

Thus, in the case of proton-proton collisions, diffractive events correspond to elastic $pp \rightarrow pp$ scattering and to $pp \rightarrow p + X$ (Single Dissociation, SD) and $pp \rightarrow X + Y$ (Double Dissociation, DD) processes, where the + sign denotes a large rapidity gap. Note that strictly speaking in high energy physics it is impossible to define (and select) rigorously purely diffractive events. We can always have some admixture of events of different origin. As a rule we call ‘diffractive’ the events with sufficiently large gap (with say $\Delta y > 4$, see above) and the vacuum quantum numbers transferred across the gap. Typically at the LHC the integrated cross sections of diffractive dissociation, σ_{SD} , σ_{DD} , are of the order of 5–10 mb depending on the gap size. Schematic diagrams of all discussed processes are shown in Fig. 20.1.

20.2 Regge pole approach

In pre-QCD times, in order to describe the behaviour of scattering amplitudes at high energy, \sqrt{s} , and small momentum-transfer squared, $-t$, Regge theory was developed and successfully applied in a wide range of energies. The Regge approach [5–7] is based on the singularities of amplitudes in the complex angular momentum, j , plane.

For instance, the measured $\pi^- p \rightarrow \pi^0 n$ amplitude behaves as

$$T_{\pi p}(s, t) \propto s^{\alpha_\rho(t)}, \quad (20.1)$$

where the process is described by the exchange of the ρ -trajectory, $j = \alpha_\rho(t) \simeq 0.5 + 0.9t$ (with $t = (p_{\pi^-} - p_{\pi^0})^2$ in GeV^2). This trajectory passes through the spin-1 ρ -meson resonance in the ‘crossed’ t -channel $\pi^- \pi^0 \rightarrow \bar{p}n$; that is, $\alpha_\rho(t = m_\rho^2) = 1$. The corresponding cross section decreases with increasing s .

On the other hand, high-energy total and elastic pp cross sections are observed to grow slowly with energy (see e.g. Section 52 in [1]) and in terms of Regge theory are dominated by the exchange of a trajectory with vacuum quantum numbers, $\sigma_{\text{tot}} \propto s^{j-1}$. The simplest possibility is to assume that the rightmost singularity in the j -plane, which drives the high-energy behaviour of the cross section, is the leading (at $t \leq 0$) Regge pole at $j = \alpha(t)$. Then the pp elastic amplitude reads

$$T_{\text{el}}(s, t) \propto s^{\alpha_{\text{P}}(t)}. \quad (20.2)$$

The total cross section can then be conveniently expressed using the so called optical theorem which states that

$$s\sigma_{\text{tot}} = \text{Im}T_{\text{el}}(s, t = 0), \quad (20.3)$$

as illustrated in the upper part of Fig. 20.2, and thus

$$\sigma_{\text{tot}} \propto s^{\alpha_{\text{P}}(0)-1}. \quad (20.4)$$

¹Here and in what follows, we call secondaries the new particles produced in the course of the interaction.

²For definition of particle rapidity (pseudorapidity), see Section 48.5.2 in [1]; $y = \frac{1}{2} \ln \frac{E+p_z}{E-p_z}$ ($\eta = -\ln(\tan(\theta/2))$); the correct variable is the rapidity y , however, experimentally it is simpler to use the pseudorapidity η which does not require identifying the particles, setting $m = 0$. For $p_T \gg m$, $\eta \simeq y$.

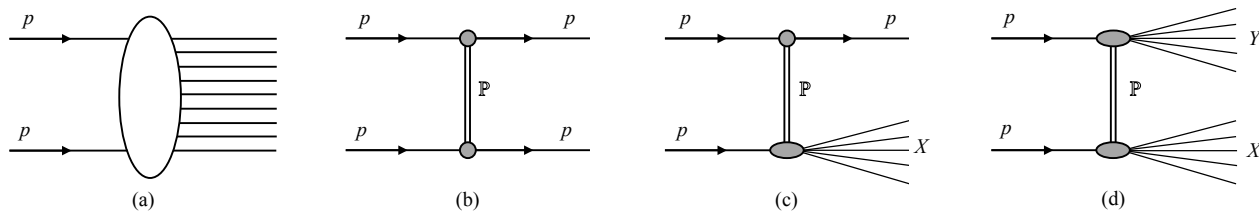


Figure 20.1: Schematic diagrams of soft pp processes. (a) non-diffractive processes, (b) elastic scattering, (c) single dissociation and (d) double dissociation. The double line corresponds to the Pomeron exchange.

$$\sigma_{\text{tot}} = \sum_X \left| \begin{array}{c} \text{Diagram: incoming proton, Pomeron, outgoing particles X} \end{array} \right|^2 = \text{Im} \left[\begin{array}{c} \text{Diagram: Pomeron exchange, outgoing particles X} \end{array} \right] = \alpha_{\mathbb{P}}(0) \sim g_N^2 \left(\frac{s}{s_0} \right)^{\alpha_{\mathbb{P}}(0)-1}$$

$$M^2 \frac{d\sigma}{dM^2} = \left| \begin{array}{c} \text{Diagram: t-channel Pomeron exchange, incoming proton, outgoing proton and X} \end{array} \right|^2 = \alpha_{\mathbb{P}}(t) \alpha_{\mathbb{P}}(t) = \alpha_{\mathbb{P}}(t) \alpha_{\mathbb{P}}(0)$$

$$= \underbrace{g_{3P} g_N^3 \left(\frac{M^2}{s_0} \right)^{\alpha_{\mathbb{P}}(0)-1} \left(\frac{s}{M^2} \right)^{2\alpha_{\mathbb{P}}(t)-2}}_{\text{Approximation}}$$

Figure 20.2: Illustration of the optical theorem for the total cross section and for high-mass diffractive dissociation in the absence of absorptive corrections.

The pole with the largest intercept, originally assumed to be $\alpha_{\mathbb{P}}(0) = 1$ since high-energy total cross sections were thought to have a constant asymptotic behaviour, is called the *Pomeron*³

Prior to the LHC, the energy behaviour of pp , $p\bar{p}$, πp , Kp cross sections was satisfactorily reproduced by the sum of the Pomeron and secondary Reggeons (the poles at lower values of j , typically with $\alpha_{\rho}(0) \simeq 0.5$, see [22, 23] and Section 51 in [24]). However, above Tevatron energies the secondary Reggeon contributions (which all have intercepts $\alpha(0) \simeq 0.5$) are highly suppressed, which enables us to study the properties of the Pomeron only.

A popular parameterization of the elastic pp -scattering amplitude by Donnachie-Landshoff (DL) is the Regge form [25]

$$T_{\text{el}}(s, t) = \eta_P \sigma_0 F_1^2(t) s^{\alpha_{\mathbb{P}}(t)}, \quad (20.5)$$

where $\sigma_0 = 21.7$ mb [26] and η_P is the signature factor

$$\eta_P = \frac{1 + \exp(-i\pi\alpha_{\mathbb{P}}(t))}{\sin(-\pi\alpha_{\mathbb{P}}(t))}, \quad (20.6)$$

F_1 is the Dirac electromagnetic form factor of the proton and the *effective* Pomeron trajectory

$$\alpha_{\mathbb{P}}(t) = 1 + \Delta + \alpha' t \simeq 1 + 0.0808 + 0.25t, \quad (20.7)$$

with t given in GeV^2 . The intercept $\alpha_{\mathbb{P}}(0)$ just above 1 reproduces the observed slow growth of the total hadron-hadron cross sections at high energies.

However, this simple parameterization is becoming increasingly deficient at higher energies. This is because due to unitarity we have to take into account not only Regge poles, but also the cuts in the j -plane [27, 28], which correspond to the multiple exchange of Regge poles in the t -channel, see for instance [29–31]. A powerful technique to evaluate Reggeon diagrams was developed by Gribov [7, 32] (Reggeon calculus or Reggeon Field Theory (RFT)), which allows us to calculate the multi-Pomeron contributions.

³Pomeron pole was named after I. Y. Pomeranchuk. The history of the Pomeron is discussed in [19–21].

20.3 Theoretical description of high-energy diffraction

Diffractive processes (see e.g. reviews [33–37]) represent a rich testing ground for the dynamics of soft interactions as well as Monte Carlo models for soft hadron-hadron physics (see for reviews e.g. [8], Section 41 in [1] and Chapter 2 in [15]).

There is no universally agreed definition of diffractive processes. Theoretically, diffraction is the effect caused by the absorption of the incoming plane-wave in some region of impact parameter, b . After a decomposition of the distorted plane-wave over the outgoing momentum, q , due to absorption we arrive at some set of plane-waves with non-zero transverse momentum, $q_t \neq 0$. Experimentally, we call diffractive the events with large rapidity gaps (LRG) in the distribution of the final state particles. However, this definition is appropriate only for the events with very large gap sizes ($\Delta\eta > 4 - 5$); otherwise gaps can also be caused by fluctuations in the hadronization process [38].

In the case of proton-proton collisions, diffraction corresponds to elastic $pp \rightarrow pp$ scattering and to the $pp \rightarrow p + X$ and $pp \rightarrow X_1 + X_2$ processes where one or both protons are allowed to dissociate into a system X with the quantum numbers of the proton. The $p \rightarrow X$ dissociation is caused by the fact that the individual components of the incoming proton wave function interact differently with the target (see Section 20.3.1).

Theoretically, high-energy diffraction may be studied from either the s -channel or the t -channel viewpoint.

20.3.1 Diffraction from the s -channel viewpoint

Unitarity plays a central role in diffractive processes. To discuss unitarity effects it is convenient to work in terms of impact parameter, b . The total cross section is closely related to the elastic scattering amplitude and the scattering into inelastic final states via the s -channel unitarity of the S -matrix (see Sections 49 and 52 in [1]), $SS^\dagger = I$, or

$$\text{disc } T \equiv T - T^\dagger = iT^\dagger T \quad (20.8)$$

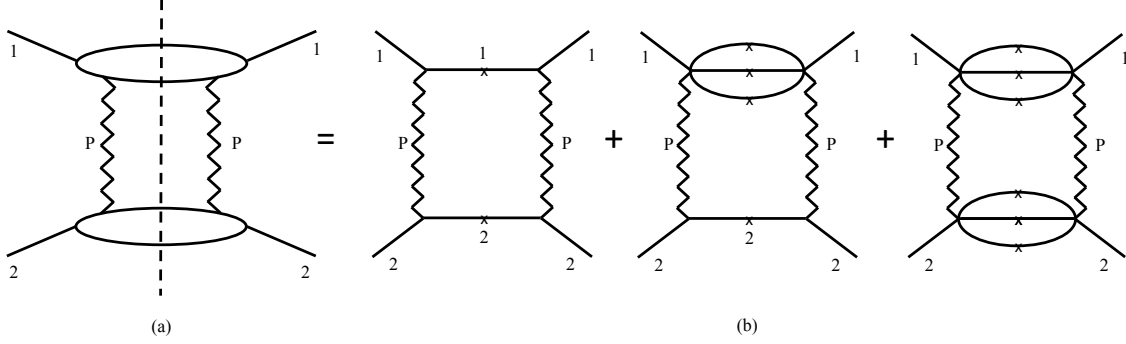


Figure 20.3: Two-Pomeron exchange in the t channel expressed as a sum over all diffractive intermediate states in the s -channel. The crosses indicate that the particles are on the mass shell.

with $S = I + iT$. If we were to focus, for example, on the unitarity for elastic and quasielastic processes, then *disc* T would simply denote a cut in s -channel between incoming and outgoing particles as visualized by crosses in Fig. 20.3.

At high energies, the s -channel unitarity relation is diagonal in the b basis such that

$$2\text{Im} T_{\text{el}}(s, b) = |T_{\text{el}}(s, b)|^2 + G_{\text{inel}}(s, b) \quad (20.9)$$

with

$$\sigma_{\text{tot}} = 2 \int d^2b \text{Im} T_{\text{el}}(s, b) \quad (20.10)$$

$$\sigma_{\text{el}} = \int d^2b |T_{\text{el}}(s, b)|^2 \quad (20.11)$$

$$\sigma_{\text{inel}} = \int d^2b [2\text{Im} T_{\text{el}}(s, b) - |T_{\text{el}}(s, b)|^2]. \quad (20.12)$$

The general solution of Eq. (20.9) is

$$T_{\text{el}}(b) = i(1 - e^{-\Omega(b)/2}) \quad (20.13)$$

and

$$G_{\text{inel}}(s, b) = 1 - e^{-\text{Re}\Omega(b)} = 1 - P_{\text{nointer}}(s, b), \quad (20.14)$$

where G_{inel} is the sum over all inelastic intermediate states and P_{nointer} is a probability to have no inelastic interactions. $G_{\text{inel}}(s, b)$ describes the b -profile of inelastic particle collisions. It satisfies the condition $0 \leq G_{\text{inel}} \leq 1$ and determines how absorptive the interaction region is at a given impact parameter (with $G_{\text{inel}} = 1$ for full absorption and $G_{\text{inel}} = 0$ for the complete dominance of elastic scattering). As seen from Eq. (20.14), $\exp(-\text{Re}\Omega(s, b))$ is the probability that no inelastic interactions occur at impact parameter b . Ω ($\text{Re}\Omega \geq 0$) is called the opacity (optical density) or eikonal. The quantity

$$S^2(b) \equiv e^{-\text{Re}\Omega(b)} = P_{\text{nointer}}(b) \quad (20.15)$$

is the so-called survival factor, which enables us to calculate the probability that the LRG survives soft rescattering.

In terms of the opacity the elastic cross section takes the form

$$\begin{aligned} \frac{d\sigma_{\text{el}}}{dt} &= \frac{1}{16\pi s^2} |T_{\text{el}}(s, t)|^2 = \frac{1}{4\pi} \left| \int d^2b e^{i\vec{q}_t \cdot \vec{b}} (1 - e^{-\Omega(b)/2}) \right|^2 \\ &= \pi \left| \int b db J_0(q_t b) (1 - e^{-\Omega(b)/2}) \right|^2, \end{aligned} \quad (20.16)$$

where $q_t = \sqrt{|t|}$ and J_0 is the zeroth-order Bessel function.

To describe the elastic scattering at one fixed energy we can always find an appropriate parameterization for the opacity $\Omega(b)$ and tune the parameters to reproduce the observed $d\sigma_{\text{el}}/dt$ cross

section. Moreover, we can fix the form of the parameterization, but choose, at each particular energy, the corresponding values of parameters; see, e.g. [39]. Alternatively, we may simply take the Fourier-Bessel transform from the experimental data [33, 40, 41]

$$\text{Im} T_{\text{el}}(b) = \int \frac{q_t dq_t}{4\pi} \sqrt{\frac{d\sigma_{\text{el}}}{dt} \frac{16\pi}{1+\rho^2}} J_0(q_t b), \quad (20.17)$$

where the square root represents $\text{Im} T_{\text{el}}(q_t)$, with $\rho \equiv \text{Re} T_{\text{el}}/\text{Im} T_{\text{el}}$. In this way, we first determine T_{el} from the data for $d\sigma_{\text{el}}/dt$, and then calculate $\Omega(b)$ using Eq. (20.13), assuming in accordance with data that ρ is small (or $\rho(t) = \text{constant}$).

At high energies $\rho^2 \ll 1$, which is usually well justified except in the diffractive dip region (see Section 20.3.3.1 for discussion of the dip region).

The value of ρ can be derived via the dispersion relation, see [3]:

$$\frac{1}{s} \text{Re} T_{\text{el}}(s) = \frac{1}{\pi} \int_{-\infty}^{+\infty} \frac{ds'}{s' - s} \sigma_{\text{tot}}(|s'|) = \frac{1}{\pi} \int_0^{\infty} \sigma_{\text{tot}}(s') \frac{2s ds'}{s'^2 - s^2}. \quad (20.18)$$

Since we consider just the charge-parity C -even amplitude, here for negative s' we put $\sigma_{p\bar{p}} = \sigma_{pp}$. That is, for negative s' , which corresponds to the interaction with an *antiparticle*, we use the same $\sigma_{pp}(|s'|)$. The major contribution comes from $s' \simeq s$. Thus, with a good accuracy we can evaluate $\rho(t = 0)$ as

$$\rho \simeq \frac{\pi}{2} \frac{\partial \ln \sigma_{\text{tot}}(s)}{\partial \ln s}. \quad (20.19)$$

20.3.2 Diffractive dissociation

The elastic cross section probes the optical density of the proton. The well known example of scattering on a black disk, with $G_{\text{inel}} = 1$ for $b < R$, gives $\sigma_{\text{el}} = \sigma_{\text{inel}} = \pi R^2$ and $\sigma_{\text{tot}} = 2\pi R^2$. In general, the absorption of the initial wave (due to inelastic channels) leads, via s -channel unitarity, to elastic scattering.

Inelastic diffraction (i.e. proton dissociation) is a consequence of the *internal structure* of hadrons. This can be conveniently described at high energies, where the lifetimes of each particular Fock component of the incoming hadron/proton wave function (the hadronic fluctuations) are large, $\tau \sim E/m^2$, and during these time intervals the corresponding Fock states can be considered as ‘frozen’. Each hadronic constituent can undergo a scattering with its own probability and thus destroys coherence of the fluctuations⁴. As a result, the outgoing superposition of states will be different from the incident particle, and will most likely contain multiparticle states, so we will have *inelastic*, as well as elastic scattering.

To calculate diffractive dissociation we can enlarge the set of intermediate states (p, N_a^*), from just the single elastic channel, and introduce a multichannel eikonal. However, it is more convenient

⁴At high energies the configurations with different transverse separation, r , between the quarks (valence partons) can serve as an example of such Fock states. An interaction with the QCD Pomeron does not change the value of r , while the cross section $\sigma \propto \alpha_s^2 r^2$ (see Section 20.4.2 and [42–44]).

to follow Good and Walker [45], and to introduce states ϕ_k diagonalising the T matrix (which e.g. in the proton case describes different $p \rightarrow N^*$, $N_a^* \rightarrow N_b^*$ transitions). Such eigenstates only undergo elastic scattering. Since there are no off-diagonal transitions,

$$\langle \phi_i | T | \phi_k \rangle = 0 \quad \text{for } i \neq k, \quad (20.20)$$

a state k cannot diffractively dissociate into a state $j \neq k$. Working in terms of the Good-Walker eigenstates ϕ_i , we have a simple one-channel eikonal for each state. We denote the orthogonal matrix which diagonalizes T by a , so that

$$T = a F a^T \quad \text{with} \quad \langle \phi_i | F | \phi_k \rangle = F_k \delta_{ik}, \quad (20.21)$$

where F_k is the probability amplitude of the hadronic process proceeding via the diffractive eigenstate ϕ_k .

Now consider the diffractive dissociation of an incoming state $|h\rangle$. We can write

$$|h\rangle = \sum_k a_{hk} |\phi_k\rangle. \quad (20.22)$$

The elastic scattering amplitude satisfies

$$\langle h | T | h \rangle = \sum_k |a_{hk}|^2 F_k = \langle F \rangle, \quad (20.23)$$

where $F_k \equiv \langle \phi_k | F | \phi_k \rangle$ and where the brackets of $\langle F \rangle$ mean that we take the average of F over the initial probability distribution of diffractive eigenstates. After the diffractive scattering described by T_{fh} , the final state $|f\rangle$ will, in general, be a different superposition of eigenstates from that of $|h\rangle$, which was shown in Eq. (20.22). Neglecting the real parts, for the cross sections at a given impact parameter b , we have

$$\begin{aligned} \frac{d\sigma_{\text{tot}}}{d^2b} &= 2 \text{Im} \langle h | T | h \rangle = 2 \sum_k |a_{hk}|^2 \text{Im} F_k = 2 \langle \text{Im} F \rangle \\ \frac{d\sigma_{\text{el}}}{d^2b} &= |\langle h | T | h \rangle|^2 = \left| \sum_k |a_{hk}|^2 F_k \right|^2 = \langle |F|^2 \rangle \\ \frac{d\sigma_{\text{el}} + \text{SD}}{d^2b} &= \sum_k |\langle \phi_k | T | h \rangle|^2 = \sum_k |a_{hk}|^2 |F_k|^2 = \langle |F^2| \rangle. \end{aligned} \quad (20.24)$$

It follows that the cross section for the single diffractive dissociation of a proton,

$$\frac{d\sigma_{\text{SD}}}{d^2b} = \langle |F^2| \rangle - \langle |F|^2 \rangle, \quad (20.25)$$

is given by the statistical dispersion in the absorption probabilities of the diffractive eigenstates. Here the average is taken over the components k of the incoming proton which dissociates. If the averages are taken over the components of both of the incoming particles, then Eq. (20.25) is the sum of the cross sections for single and double dissociation, see Fig. 20.3.

Note that if all the components ϕ_k of the incoming proton $|h\rangle$ were absorbed equally, then the diffracted superposition would be proportional to the incident one and the probability of the inelastic diffraction would be zero. Thus if, at very high energies, the amplitudes F_k at small impact parameters are equal to the black disk limit, $F_k = i$, then diffractive production will be equal to zero in this impact parameter domain, and so will only occur in the peripheral b region where the edge of the disk becomes not completely black. Hence the impact parameter structure of diffractive dissociation and elastic scattering is drastically different in the presence of absorptive s -channel unitarity effects (see the G_{inel} term in Eq. (20.9)). Under the assumption that amplitudes F_k at high energies cannot exceed the black disk limit, $\text{Im} F_k \leq 1$, equations 20.24 lead to the following bound

$$\frac{d\sigma_{\text{el}} + \text{SD}_1 + \text{SD}_2 + \text{DD}}{d^2b} \leq \frac{1}{2} \frac{d\sigma_{\text{tot}}}{d^2b}. \quad (20.26)$$

known as the Pumplin bound [46]⁵.

20.3.3 Diffraction from the t -channel viewpoint

The t -channel approach is based on the Regge model (see Section 20.2), where high-energy diffractive processes are mediated by the exchange of a Pomeron (\mathbb{P}). In the case of the elastic pp -scattering amplitude in the eikonal model (see Eq. (20.13)), the opacity corresponding to the exchange of one Pomeron is

$$\Omega(s, b) = \int \frac{d^2q_t}{4\pi^2} \Omega(s, q_t) e^{i\vec{q}_t \cdot \vec{b}} \quad (20.27)$$

with

$$\Omega(s, q_t) = \frac{1}{s} T'_{\text{el}} = -i\eta_P(t) g_N(t) g_N(t) \left(\frac{s}{s_0} \right)^{\alpha_{\mathbb{P}}(t)-1}, \quad (20.28)$$

where T'_{el} is the two-particle s -channel irreducible elastic amplitude, cf. Eq. (20.5), and $g_N(t)$ is the proton-Pomeron coupling.

If we assume an exponential t -dependence of the coupling, $g_N(t) = g_N(0) \exp(B_0 t)$, and neglect the Pomeron phase, then the opacity is

$$\Omega(s, q_t) = g_N(0) g_N(0) \left(\frac{s}{s_0} \right)^{\alpha_{\mathbb{P}}(0)-1} e^{Bt}, \quad (20.29)$$

with the t -slope given by

$$B = 2B_0 + \alpha'_{\mathbb{P}} \ln \left(\frac{s}{s_0} \right). \quad (20.30)$$

At high energies the opacity has a Gaussian form in the b -space:

$$\Omega(s, b) = \frac{g_N^2(0)}{4\pi B} \left(\frac{s}{s_0} \right)^{\alpha_{\mathbb{P}}(0)-1} e^{-b^2/4B}. \quad (20.31)$$

In terms of opacity the effective radius of interaction increases at high energies as $\sqrt{\alpha'_{\mathbb{P}} \ln(s/s_0)}$. This means that with energy increasing the differential cross section becomes steeper (the so called *shrinkage* of the diffractive peak).

If we were to take for the Pomeron the DL parametrisation [25, 26], that is to keep just the first, $T(b) = \Omega(b)/2$, term in the elastic amplitude (Eq. (20.13)) then, at LHC energies, the Gaussian would exceed the black disk limit at small b . However, the eikonal unitarization reduces the power growth of the one-Pomeron exchange cross section. Thus, in Eq. (20.31) $\Omega(s, b) \propto (s/s_0)^{\alpha_{\mathbb{P}}-1}$ gives an amplitude $\text{Im} T_{\text{el}}(s, b) = 1 - e^{-\Omega/2} < 1$. Hence the total cross section is limited by the size of the effective interaction area $\sigma_{\text{tot}} < 2\pi R^2$, where the interaction radius R can be estimated from Eq. (20.31) as the value of b where $\text{Re}\Omega(b)$ becomes ~ 1 .

For the parameterization of Eq. (20.31) the corresponding radius grows at very large energies as

$$b^2 = R^2 = 4B \ln \left[\frac{g_N^2(0)}{4\pi B} \left(\frac{s}{s_0} \right)^{\alpha_{\mathbb{P}}(0)-1} \right] \simeq 4\Delta \alpha'_{\mathbb{P}} \ln^2(s/s_0). \quad (20.32)$$

That is for $\Delta = 0.1$ and $\alpha'_{\mathbb{P}} = 0.25 \text{ GeV}^{-2}$ we may expect that the cross section increases as

$$\sigma_{\text{tot}} = 2\pi R^2 \simeq c \cdot \ln^2 s, \quad (20.33)$$

with $c = 8\pi \Delta \alpha'_{\mathbb{P}} = 0.24 \text{ mb}$. This value is close to that obtained by the COMPETE parameterization ($c = 0.27 \text{ mb}$ [22, 24]) but much smaller than the Froissart-Lukaszk-Martin (FLM) bound [47–49]. With $c^{\text{FLM}} = \pi/m_{\pi}^2 \simeq 60 \text{ mb}$, see Section 20.7,

$$\sigma_{\text{tot}} \leq \frac{\pi}{m_{\pi}^2} \ln^2 \left(\frac{s}{s_0} \right). \quad (20.34)$$

⁵Strictly speaking the proof of the Pumplin bound is justified only for low mass dissociation. When the masses $M_{1,2}$ become so large (say, $M_i^2 > \sqrt{ss_0}$) that the Good-Walker states $|\phi_i\rangle$, corresponding to two incoming protons overlap, we may face double counting. Therefore, the high mass dissociation will be considered in the next Section, in terms of the multi-Pomeron diagram. Here and in what follows s_0 is a constant which should be defined for a particular theoretical model or fitted from experiment.

The fact that $c = (0.24\text{--}0.27) \text{ mb} \ll c^{\text{FLM}} = 60 \text{ mb}$ demonstrates that even at the LHC we are very far from true high-energy asymptotics⁶, and the observed growth of the cross section is driven by the interactions at relatively large transverse momenta $k_t \gg m_\pi$ rather than the smallest hadron mass m_π in the denominator of Eq. (20.34).

20.3.3.1 The t -slope and dip in the elastic cross section

We first start with a relatively small one-Pomeron amplitude and consider the two-Pomeron contribution corresponding to the Ω^2 term in the expansion of the eikonal $1 - \exp(-\Omega/2)$. In this term the momentum transferred, $q_t = \sqrt{|t|}$, is divided between the two Pomerons so that each Pomeron carries about a momentum $q_t/2$. Correspondingly, the t dependence of the whole ‘two-Pomeron’ amplitude will be $\exp(2B(t/4)) = \exp(Bt/2)$ ⁷.

Since the two-Pomeron contribution has an opposite sign in comparison with the one-Pomeron exchange, their interference will result in the appearance of the first diffractive minimum which moves to smaller $|t|$ with energy increasing. Such interference effects are largely responsible for the zero in the imaginary part of the amplitude (with the minimum filled by the real part).

It is worth mentioning that the one-channel eikonal discussed so far is a rather oversimplified approximation. It provides some indications about the behaviour we may expect for the elastic cross section, but clearly it does not give the whole story. Moreover, even within the framework of the one-channel eikonal, the expectation for the elastic slope t -dependence could be masked by other effects. Firstly, there is no reason why the t -dependence of the proton-Pomeron coupling $g_N(t)$ has to be a pure exponent. Next, there exists a two-pion singularity at $t = 4m_\pi^2$ (close to the physical region) in the Pomeron trajectory which generates some curvature in the behaviour of $d\sigma_{\text{el}}/dt$ [50–52]. So there may be some compensation between the effects caused by the eikonal (arising from the interference between the different multi-Pomeron contributions), and the curvatures coming from the form of the proton-Pomeron coupling and the two-pion singularity of the Pomeron trajectory. However, an exact compensation looks quite non-trivial and a *pure* exponential behaviour of $d\sigma_{\text{el}}/dt$ looks highly unlikely.

Indeed, the measurements by the TOTEM collaboration at 8 TeV [53] and at 13 TeV [54] clearly demonstrate that the local slope of the elastic pp cross section,

$$B = d[\ln(d\sigma_{\text{el}}/dt)]/dt, \quad (20.35)$$

at $-t \lesssim 0.3 \text{ GeV}^2$ varies with t .

20.3.3.2 High mass dissociation

Let us turn to inelastic diffractive processes that is, to single and double proton dissociations, $pp \rightarrow X+p$ and $pp \rightarrow X_1+X_2$, where the $+$ sign denotes the presence of a LRG in the distribution of final state particles. For example, for the diffractive dissociation of a proton into a system of mass M , the rapidity gap between the incoming proton and the remaining hadrons is

$$\Delta y = \ln\left(\frac{s}{M^2}\right) = \ln\left(\frac{1}{\xi}\right), \quad (20.36)$$

where $\xi = 1-x$ and x is the initial momentum fraction (Feynman variable) carried by the outgoing proton. The masses, M , of the diffractively excited states, produced in high \sqrt{s} collisions, can be large. To separate dissociation from the common inelastic process, usually the condition $M^2 \ll s$ is imposed.

The simplest multi-Pomeron diagram used to describe the diffractive dissociation is the so-called triple-Pomeron graph, shown at the end of Fig. 20.2.

In the Regge pole model, the cross section for the inclusive single diffractive (SD) dissociation process [55–57] can be written

⁶As usual, we assume $s_0 = 1 \text{ GeV}^2$, but the qualitative conclusion does not depend on any realistic choice of s_0 .

⁷The two-Pomeron contribution has a factor of two smaller t -slope, and in terms of the impact parameter, the $\Omega^2(b)$ term is concentrated in the domain of a smaller radius. In such a simplified picture, the impact parameters corresponding to an exchange of n Pomerons will rapidly decrease with n increasing.

in the form (see Fig. 20.2)

$$\begin{aligned} \frac{\xi d\sigma_{\text{SD}}}{dtd\xi} &= \frac{M^2 d\sigma_{\text{SD}}}{dtdM^2} \\ &= \frac{g_{3\mathbb{P}}(t)g_N(0)g_N^2(t)}{16\pi^2} \left(\frac{s}{M^2}\right)^{2\alpha_{\mathbb{P}}(t)-2} \left(\frac{M^2}{s_0}\right)^{\alpha_{\mathbb{P}}(0)-1}, \end{aligned} \quad (20.37)$$

where $g_{3\mathbb{P}}(t)$ is the triple-Pomeron coupling. The value of the coupling $g_{3\mathbb{P}}$ is usually obtained from a triple-Regge analysis of lower energy data (see e.g. [34]).

In an analogous way the cross section for double dissociation reads

$$\begin{aligned} \frac{\xi_1\xi_2 d\sigma_{\text{DD}}}{dtd\xi_1\xi_2} &= \frac{M_1^2 M_2^2 d\sigma_{\text{DD}}}{dtdM_1^2 dM_2^2} \\ &= \frac{g_{3\mathbb{P}}^2(t)g_N^2(0)}{16\pi^3} \left(\frac{ss_0}{M_1^2 M_2^2}\right)^{2\alpha_{\mathbb{P}}(t)-2} \left(\frac{M_1^2 M_2^2}{s_0^2}\right)^{\alpha_{\mathbb{P}}(0)-1}, \end{aligned} \quad (20.38)$$

where t is the momentum squared transferred through the LRG. As discussed in Section 20.5, from a microscopic point of view the

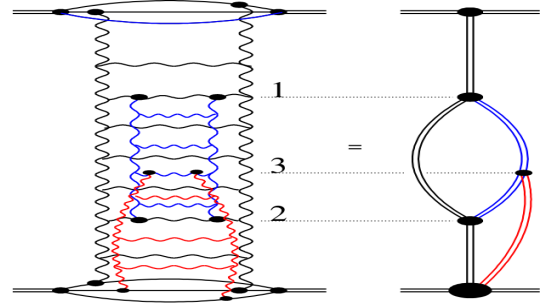


Figure 20.4: Pomeron exchange with schematic diagrams for the enhanced and semi-enhanced exchanges.

Pomeron exchange is described by a set of ladder-type diagrams (see [58–60]), which can lead to a rescattering of the intermediate partons (inside this ladder during the evolution), see Fig. 20.4. The left plot shows the Pomeron exchange complemented with the rescattering of partons 1 and 2 and the scattering of a parton 3 on the target. In terms of multi-Pomeron exchanges this corresponds to the diagram on the right hand side, where the Pomeron exchange is shown by the double line of a corresponding colour. The blue one is called ‘‘enhanced’’ (its contribution is integrated over the rapidities of both upper and lower vertices, i.e. of partons 1 and 2). The loop formed by the Pomerons shown in red is called ‘‘semi-enhanced’’ (it is integrated over the rapidity of one intermediate parton).

While the rescattering of the incoming hadron (proton) is already embedded in the eikonal formula (Eq. (20.13)), the rescattering of the intermediate partons in RFT is accounted for by the so-called enhanced diagrams⁸ with multi-Pomeron vertices, g_m^n , which couple m to n Pomerons. It is quite a challenging task to resum all the enhanced diagrams, however this was successfully performed within the framework of the QGSJET Monte Carlo [61]. An elegant approach to sum up all enhanced diagrams in the case when each extra effective Pomeron contribution is very large was proposed in [62], assuming the analyticity of the g_m^n vertices in n and m in the right half of the complex n - and m -planes. The resulting amplitude becomes a black disk.

The simplest triple-Pomeron vertex $g_3^1 = g_{3\mathbb{P}}$ produces the first multi-Pomeron graph considered above (see the end of Fig. 20.2). However, numerically the multi-Pomeron vertices are relatively small. Note also that the value of $g_{3\mathbb{P}}$, determined from the fit to

⁸This contribution is *enhanced* due to the large parton multiplicity.

experimental data (e.g. [63]), is actually an effective vertex with coupling

$$g_{\text{eff}} = g_{3\mathbb{P}} \langle S^2 \rangle, \quad (20.39)$$

which already includes the survival factor $S^2(b)$, see Eq. (20.15).

Since the opacity Ω increases with energy, at large Ω the number of multiple interactions grows as $N \propto \Omega$, leading to a smaller S^2 . An explicit analysis [64] accounting for the survival effects gives a coupling $g_{3\mathbb{P}}$ about a factor of 3 larger than g_{eff} , namely $g_{3\mathbb{P}} \simeq 0.2g_N$.

Recall that the Pomeron exchange simultaneously describes both the elastic scattering amplitude, T_{el} , and the multiparticle production cross section, G_{inel} . The discontinuity (*disc* T_{el}) of the ladder diagram corresponds to the production of secondary particles, practically homogeneously distributed over the whole available rapidity interval covered by the Pomeron, as illustrated by the right-hand diagram in Fig. 20.5.

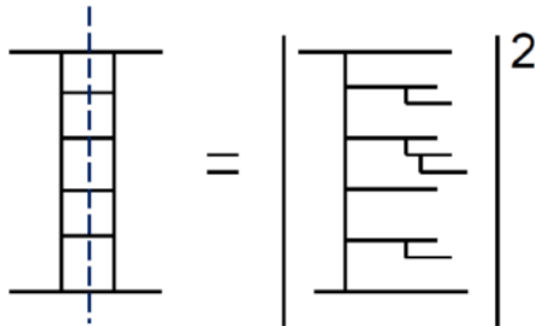


Figure 20.5: Cut Pomeron contribution to the inelastic cross section.

For the one-Pomeron case this discontinuity is called the ‘‘cut Pomeron’’. Correspondingly each multi-Pomeron diagram describes a series of different processes. Cutting k Pomerons in the diagram with n Pomerons we get the inelastic interaction with the multiplicity (density of secondaries) k times larger than that, N_0 , produced by one cut Pomeron, $dN/dy = k \cdot N_0$. The remaining $n - k$ (elastic) Pomerons account for the absorptive corrections to the subprocess with k cut Pomerons. Indeed, the contribution of the diagram with n Pomerons includes also the processes with larger, $(k + i) \cdot N_0$ multiplicities (cut Pomerons), where $(i = 1, 2, \dots, n - k)$. Absorptive corrections, described by the remaining elastic Pomerons, play a role of the survival factor S^2 for the process with the fixed particle density $k \cdot N_0$. They ensure probability conservation (the sum of the probabilities of all possible different channels is equal to one) and restore unitarity. Note that the multi-Pomeron diagrams represent all possible interactions between partons from the protons and partons from the Pomerons. In the case of Monte Carlo generators, the non-enhanced multi-Pomeron contributions are included in terms of the multiple parton interaction (MPI) option, see [13,65] and Section 7.2 in [2]. However, as a rule, this option accounts mainly for the multiple interactions between the partons from the protons (incoming hadrons). The energy-momentum sharing between the various inelastic rescattering processes (including the cut and uncut Pomerons) was performed at the amplitude level within the EPOS Monte Carlo [66].

20.3.3.3 AGK cutting rules

The relation between the cross sections of subprocesses with a different number of cut Pomerons within a given diagram with n Pomerons is given by the AGK (Abramovsky-Gribov-Kancheli [67]) cutting rules. These rules include also the cut *between* the Pomerons with $k = 0$ which corresponds to the contribution of the particular diagram to the elastic cross section. By applying these rules, it is possible to show the self-consistency of the approach, which was lacking in the pure Regge-pole model.

Consider a diagram where the elastic scattering amplitude is mediated by an exchange of n Pomerons. The AGK cutting rules specify the coefficients c_n^k arising when k of these Pomerons are cut. Recall that the Pomeron cut discontinuities give the

corresponding inelastic contributions to σ_{tot} . The terms with $k = 0$ correspond to the diffractive cutting of the diagram (that is, the cut is between the Pomeron exchanges, and not through the Pomerons themselves), while the terms with $k = 1, 2, \dots$ describe the processes with k cut Pomerons. The coefficients $c_n^k = \sigma_n^k / |\sigma_{\text{tot}}^{(n)}|$ are ⁹

$$c_n^{k=0} = (-1)^n (2^{n-1} - 1), \quad c_n^{k \neq 0} = (-2)^{n-1} \frac{(-1)^{k-1} n!}{k!(n-k)!} \quad (20.40)$$

where $\sigma_{\text{tot}}^{(n)}$ denotes the contribution of the n -Pomeron diagram to the total cross section. Note the alternating sign of $\sigma_{\text{tot}}^{(n)}$ expressed as $(-1)^{n-1}$.

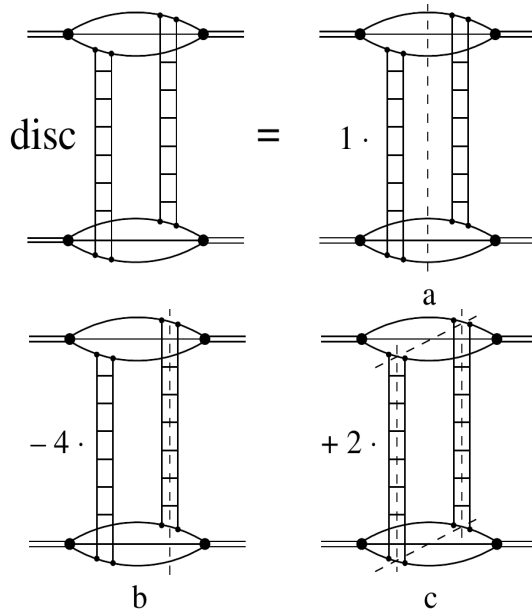


Figure 20.6: Two-Pomeron exchange diagram as a sum of different AGK cuts shown by the dashed lines.

For the two-Pomeron exchange, $n = 2$, the coefficients are +1, -4, or +2 according to whether $k = 0, 1$ or 2 Pomerons are cut, respectively. As shown in Fig. 20.6, the amplitude of the two-Pomeron exchange corresponds to a sum of three processes: i) inelastic interaction with particle density twice that caused by one Pomeron (see Fig. 20.6(c)) which enters with the coefficient ‘2’, ii) shadowing (absorptive) correction to the one-Pomeron exchange contribution, which corresponds to events with a single Pomeron density (only one Pomeron is cut), see Fig. 20.6 (b), which enters with a factor ‘-4’, and iii) diffractive elastic scattering or proton dissociation (when different components of the proton wave function correspond to different interaction cross sections), caused by the distortion of the incoming plane wave, see Fig. 20.6(a).

Note that the inclusive cross section is not affected by the multi-Pomeron contribution: $2 \times (2) + 1 \times (-4) = 0$. This is a general property of the AGK rules valid for any number of Pomerons n . Thus in order to calculate the inclusive single-particle cross section, it is sufficient to consider just the *one*-Pomeron exchange diagram.

Let us emphasize that the AGK rules provide a framework to consistently work with multi-Pomeron diagrams, that is, with the Regge cuts, accounting for their contributions to different processes (elastic scattering and diffractive dissociation, inelastic events with different densities, dN/dy , of secondaries, etc.).

Measurements of diffractive dissociation cross sections have been made in a wide range of pre-LHC energies, see e.g. [68–73]. At the LHC, cross sections of events with a LRG were measured by the ATLAS, CMS and ALICE collaborations at 7 and 8 TeV,

⁹In their complete form the AGK cutting rules were implemented in the QGSJET Monte Carlo [61].

see [74–77]. ATLAS [78] and CMS and TOTEM [79] presented first measurements of SD cross sections at 8 TeV with a tagged forward proton. While ATLAS measured inclusive SD cross section, CMS and TOTEM studied SD dijet production. Note that in [78] the measured slope $B = 7.65 \pm 0.34 \text{ GeV}^{-2}$ of the inclusive SD cross section as well as the differential distributions $\frac{d\sigma_{SD}}{dtd\xi}$ for $0.0001 \leq \xi \leq 0.025$ are (within the experimental uncertainties) in a good agreement with the theoretical expectations [29,80]. Moreover a relatively small (in comparison with the $d\sigma_{el}/dt$) slope B indicates that the size of the triple-Pomeron vertex is much smaller than the proton size.

20.3.4 Central Diffractive processes

Processes $pp \rightarrow p + X + p$, where an object X , produced in the central rapidity region, is separated from the outgoing protons by a LRG on each side, are called Central Exclusive Production (CEP). They are described by the double Pomeron exchange (DPE) diagrams. When the mass of the central system, M_X , is large and the interaction in the M_X region can be described by Pomeron exchange, the corresponding cross section reads

$$\frac{\xi_1 \xi_2 d\sigma^{\text{CEP}}}{d\xi_1 dt_1 d\xi_2 dt_2} = \frac{g_N^2(t_1)g_N^2(t_2)}{(16\pi^2)^2} \left(\frac{1}{\xi_1}\right)^{2\alpha_P(t_1)-2} \left(\frac{1}{\xi_2}\right)^{2\alpha_P(t_2)-2} \times g_{3P}^2(0) \left(\frac{M_X^2}{s_0}\right)^{\alpha_P(0)-1} \tag{20.41}$$

If the mass M_X is not too large or for the cases (such as exclusive Higgs boson or dijet production) where the mass M_X is comparable with the corresponding hard scale, the last factor $g_{3P}^2(0)(M_X^2/s_0)^{\alpha_P(0)-1}$ should be replaced by the corresponding ‘Pomeron-Pomeron cross section’, see for instance [81,82].

Note that equations (20.37), (20.38) and (20.41) are written in a simplified way without accounting for absorptive corrections. That is, the cross sections in equations (20.37) (20.38) and (20.41) should be multiplied by the gap survival factor S^2 (see Eq. (20.15)).

Since the QCD Pomeron is built mainly from gluons it is natural to search for glueballs in double Pomeron exchange processes, and in particular, in CEP.

Resonance production in the Pomeron-Pomeron fusion was extensively studied at the CERN ISR at \sqrt{s} from 22 GeV to 63 GeV (see for reviews [82–84]) and, after the ISR closure in 1983, in fixed target experiments at the CERN SPS [85] and E690 at the Tevatron [86,87]. Glueballs were actively searched for and the properties of the f_0 and f_2 production studied in detail using multiparticle spectrometers, such as the Omega facility at the CERN SPS experiments (WA76, WA91 and WA102), see for a review [85].

An important property of CEP processes, which can be expected from matching with the perturbative QCD LO (leading order) calculation, is the $J_z = 0$ dominance. Perturbatively, for the CEP of a heavy object, the leading contribution comes from a configuration with the projection of this object spin onto the beam axis $J_z = 0$ [81]. Note that the CEP cross section is suppressed at large M_X by a strong bremsstrahlung off the incoming gluons (from the Pomeron) which would violate the ‘exclusivity’. The small probability of not having such radiation is described by the Sudakov suppression factor, T_{Sud} , [88], see [81] for details.

20.3.5 Diffractive parton distributions

Selecting in Deep Inelastic Scattering (DIS) events with a LRG (see e.g. [89,90]) or detecting the leading proton (see Section V.C. in the review [91]) we can study the parton (quark and gluon) distributions of the Pomeron ¹⁰. In other words, such events can be treated as DIS on the Pomeron target with the incoming Pomeron flux given by

$$f_{\mathbb{P}}(x_{\mathbb{P}}) = \int dt \frac{g_N^2(t)}{16\pi^2} x_{\mathbb{P}}^{2(1-\alpha_{\mathbb{P}}(t))} \tag{20.42}$$

¹⁰see also Section 18.5 in [1]

where the proton momentum fraction transferred through the Pomeron $x_{\mathbb{P}} = \xi = M^2/s$.

These Pomeron PDFs were extracted from the HERA measurements of ep scattering with leading protons or a LRG and can be used to describe the inclusive production of high E_T dijets or another hard process based on the collinear factorization theorem in the same way as that in non-diffractive collisions (see [91]). The inclusive measurements of these PDFs are described in [92–94], with the combined H1 and ZEUS data using tagged protons analyzed in [95]. The impact of diffractive jet measurements is addressed e.g. in [96] and the measured charm contribution is presented in [97,98]. As far as the parton distributions are known, we can calculate the corresponding inelastic cross section of the Pomeron-proton interaction using one of the ‘general purpose’ Monte Carlo generators (see e.g. [13]), multiply it by the Pomeron flux and compare the obtained result with the Regge formula in Eq. (20.37). This approach provides another way to evaluate the triple-Pomeron vertex $g_{3\mathbb{P}}$. The corresponding analysis was performed in [99] and leads to practically the same (within the error bars) value of $g_{3\mathbb{P}} = 0.2g_N(0)$.

It is worth mentioning that in DIS at large Q^2 we are dealing with small-size objects and the rescattering effects are small. Therefore, the survival factor $S^2 \simeq 1$ and does not affect the results.

20.4 Experimental data on diffraction at high energies

20.4.1 Total and elastic cross sections

The elastic scattering of protons is a process with a special and rather simple experimental signature: the central detector is empty while the incoming protons after the collisions are detected in the dedicated forward proton detectors (FPD) placed far from the interaction point (IP). Elastic scattering data are taken in special runs in order to be able to reach different ranges of t -values and thanks to the very large value of the cross section the data can be collected with a relatively low instantaneous luminosity and hence a negligible pile-up.¹¹

These special runs usually have very few proton bunches and differ in the t range covered, which is governed roughly by the relation $t_{\text{min}} \propto d^2/\beta^*$. Here d is the distance, expressed in multiples of the beam size at the detector, from the centre of the LHC beam and β^* is defined as the distance from the IP to the point where the transverse area of the beam is twice as wide as that at the IP (see Section 31 in [1]). Note that if we work at large β^* , the incoming protons have very small angular divergence leading to small average transverse momentum, which allows us to measure very small $|t|$ values. The lowest $|t|$ values measured so far at the LHC are $4 \times 10^{-4} \text{ GeV}^2$ (ALFA) and $6 \times 10^{-4} \text{ GeV}^2$ (TOTEM) reached with the 8 TeV LHC beam configured with $\beta^* = 1 \text{ km}$ optics. The largest t values of about 4 GeV^2 were measured by TOTEM at 8 and 13 TeV with $\beta^* = 90 \text{ m}$ thanks to special triggers. Other β^* values used in special runs are 3.5 m, 11 m and 2.5 km.

There are four ways to determine the σ_{tot} value:

- 1. Elastic and Inelastic.** This method does not require the optical theorem and hence no extrapolation of $d\sigma_{el}/dt$ to $t = 0$ and no ρ (defined below Eq. (20.17)) but rather the luminosity and measuring rates N_{el} (elastic) and N_{inel} (inelastic). The total cross section is then simply:

$$\sigma_{\text{tot}} = \frac{1}{\mathcal{L}}(N_{el} + N_{inel}). \tag{20.43}$$

Of course, both N_{el} and N_{inel} should be corrected for the detector acceptance and efficiency. This is especially important for N_{inel} since the detectors never cover the whole rapidity region (i.e. the whole 4π).

- 2. Elastic only.** This approach necessitates measuring $d\sigma_{el}/dt$ and using the optical theorem with a known value of ρ . As explained in Section 20.2, the optical theorem states that

¹¹The pile-up is formed by additional pp collisions which typically produce low- p_T particles. These may affect the signal sample and worsen various reconstruction and identification efficiencies.

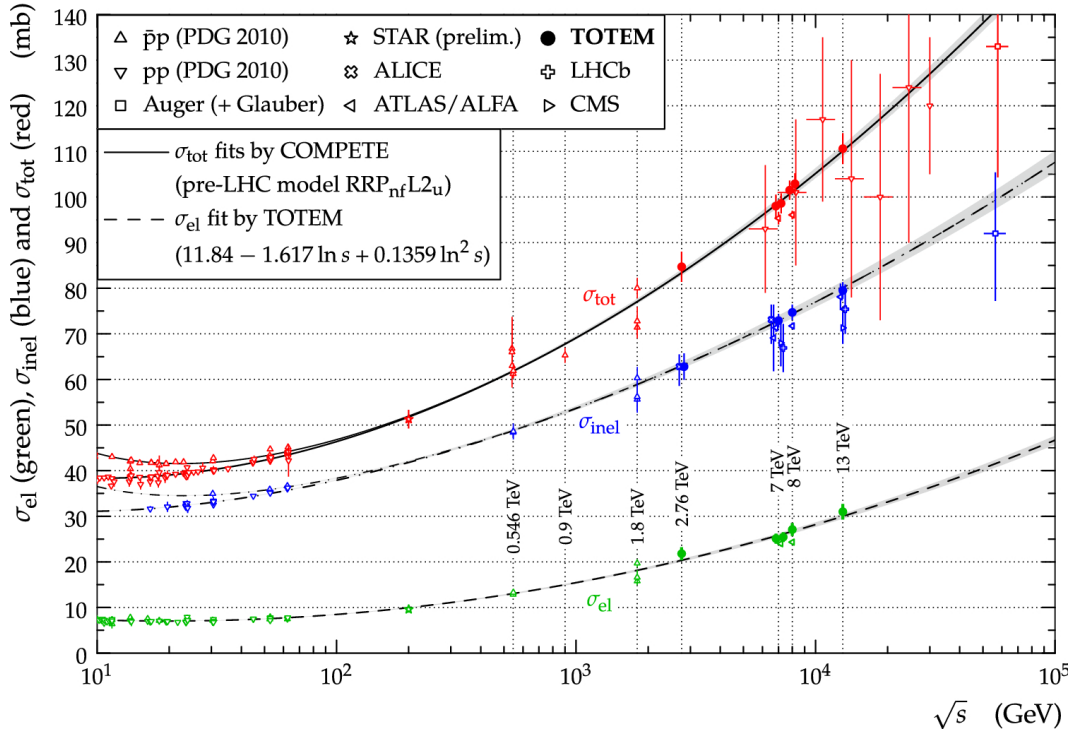


Figure 20.7: Overview of elastic (σ_{el}), inelastic (σ_{inel}) and total (σ_{tot}) cross section data for pp and $p\bar{p}$ collisions as a function of \sqrt{s} . The continuous black lines (lower for pp , upper for $p\bar{p}$) represent the best fits of the total cross section data by the COMPETE collaboration [22]. The dashed line is a fit of the elastic cross section data. The dashed-dotted lines refer to the inelastic cross section and are obtained from the difference between the continuous and dashed lines. Figure from Ref. [100].

$\sigma_{\text{tot}} \propto \text{Im}[T_{\text{el}}(t \rightarrow 0)]$, see Eq. (20.3). Since in practice it is not possible to measure down to $t = 0$, we need to extrapolate. To minimize the model dependence when extrapolating, it is vital to measure down to as low $|t|$ values as possible (i.e. high β^*). This method requires an independent luminosity measurement. Once the luminosity is known, $d\sigma_{\text{el}}/dt$ can be normalized and used to extract σ_{tot} using the formula:

$$\sigma_{\text{tot}}^2 = \frac{16\pi}{1 + \rho^2} \left. \frac{d\sigma_{\text{el}}}{dt} \right|_{t \rightarrow 0}. \quad (20.44)$$

3. Coulomb normalization. Similarly to the previous method, this approach relies on the elastic observables only and requires a measurement of the elastic cross section at very low values of $|t|$, where it is sensitive to the theoretically well known Coulomb QED contribution $4\pi\alpha_{\text{QED}}^2/t^2$. The normalization of $d\sigma_{\text{el}}/dt$ is then determined by fitting the experimental data at very low $|t|$ using a formula including the Coulomb amplitude and its interference with the strongly interacting (the so-called nuclear) term. This method has been successfully used by UA4/2 [101] and TOTEM [102].

4. Luminosity-independent. This method does not rely on the knowledge of luminosity but rather on the knowledge of N_{el} and N_{inel} and on the optical theorem: combining equations (20.43) and (20.44) with $\frac{d\sigma_{\text{el}}}{dt} = \frac{1}{L} \frac{dN_{\text{el}}}{dt}$ we get

$$\sigma_{\text{tot}} = \frac{16\pi}{1 + \rho^2} \frac{dN_{\text{el}}/dt|_{t=0}}{N_{\text{el}} + N_{\text{inel}}}, \quad (20.45)$$

where $dN_{\text{el}}/dt|_{t=0}$ corresponds to the extrapolation to $t = 0$ of the nuclear term only. By independently and simultaneously measuring N_{el} and N_{inel} , and applying the optical theorem, we can also determine the luminosity.

The TOTEM [100, 103–105] and ATLAS [106, 107] collaborations at CERN have covered an energy range from $\sqrt{s}=2.76$ TeV to 13 TeV. A compilation of high energy total pp and $p\bar{p}$ cross section measurements is shown in Fig. 20.7 (for discussion of the pre-LHC elastic scattering data see review [108]).

Despite some tension between the Tevatron CDF [109] and E811 [110] data¹² and to a lesser extent between the TOTEM [104, 105] and ATLAS [106, 107] measurements, the data clearly indicate that in the Tevatron – LHC energy interval the total cross section starts to grow *faster* than the power-law parametrization [26] describing the data below the Tevatron energy. In particular, while the DL fit [26] predicts $\sigma_{\text{tot}} = 90.7$ mb at $\sqrt{s} = 7$ TeV, the TOTEM experiment observes 98.6 ± 2.2 mb [104].

A compilation of the high-energy data on the elastic slope is shown in Fig. 20.8. It is clearly seen that in the TeV energy range the slope increases with \sqrt{s} more rapidly than the logarithmic behaviour expected in the case of one-Pomeron exchange, see Eq. (20.30). Such an acceleration of the t -slope derivative, $dB/d\ln s$, is a clear manifestation of the increasing role of the multi-Pomeron exchanges, where asymptotically the slope should rise as $\ln^2 s$, see [117]. Finally, Fig. 20.9 illustrates the energy dependence of the differential elastic pp cross section. As expected (see Section 20.3.3.1), the diffractive dip moves to smaller $|t|$ with increasing energy.

20.4.2 Diffractive vector meson production

The exclusive production of vector mesons was studied in detail at HERA (see for a review [91]). It is well described within the ‘dipole model’ (see for review and references [120]), where the incoming photon first fluctuates into a quark-antiquark, which then interacts with the target proton and, finally, with the probability given by the overlap integral between the vector meson wave function and the outgoing $q\bar{q}$ -pair, the vector meson is produced. The crucial quantity is the value of cross section, $\sigma(q\bar{q} - p)$, of elastic scattering of the $q\bar{q}$ -pair on the proton. The energy behaviour of $\sigma(q\bar{q} - p)$ is driven by the intercept, $\alpha_{\text{eff}}(0)$, of the effective Pomeron¹³ (rightmost singularity in the j -plane), while

¹²The CDF 1.8 TeV point [109] is 2.8σ higher than the corresponding E811 result [110].

¹³Effective Pomeron means that this is not an original pole in the j -plane, but it includes the corrections (renormalizations) caused by the enhanced diagrams (see e.g. [121]).

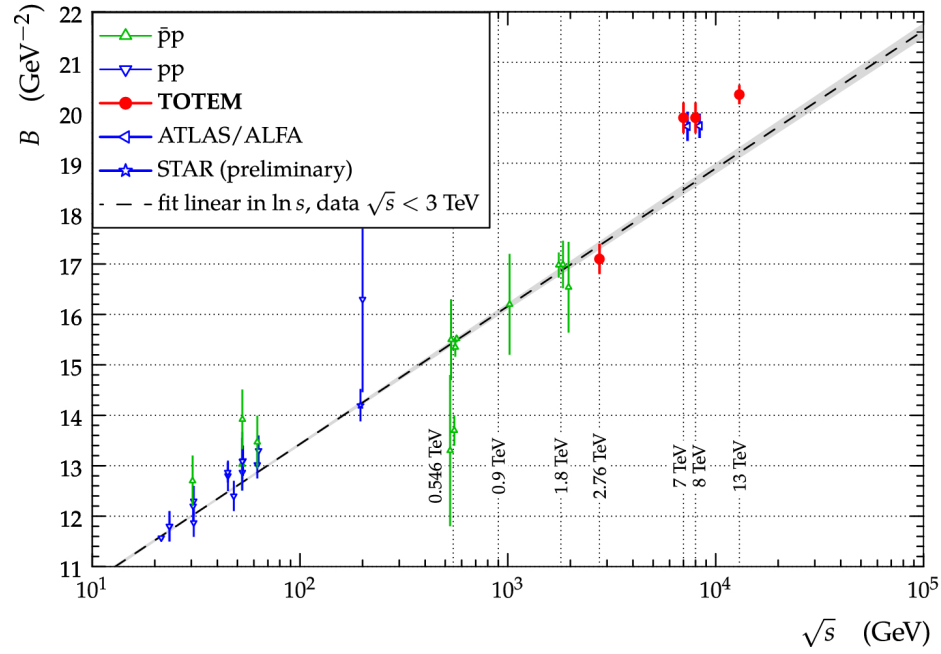


Figure 20.8: The diffractive slope B for pp and $p\bar{p}$ elastic scattering as a function of \sqrt{s} . The experimental uncertainties represent the quadratic sum of statistical and systematic uncertainties. The dashed line is a result of a linear fit to data at $\sqrt{s} < 3$ TeV. The data points come from [103–107, 111–113]. Figure from Ref. [100].

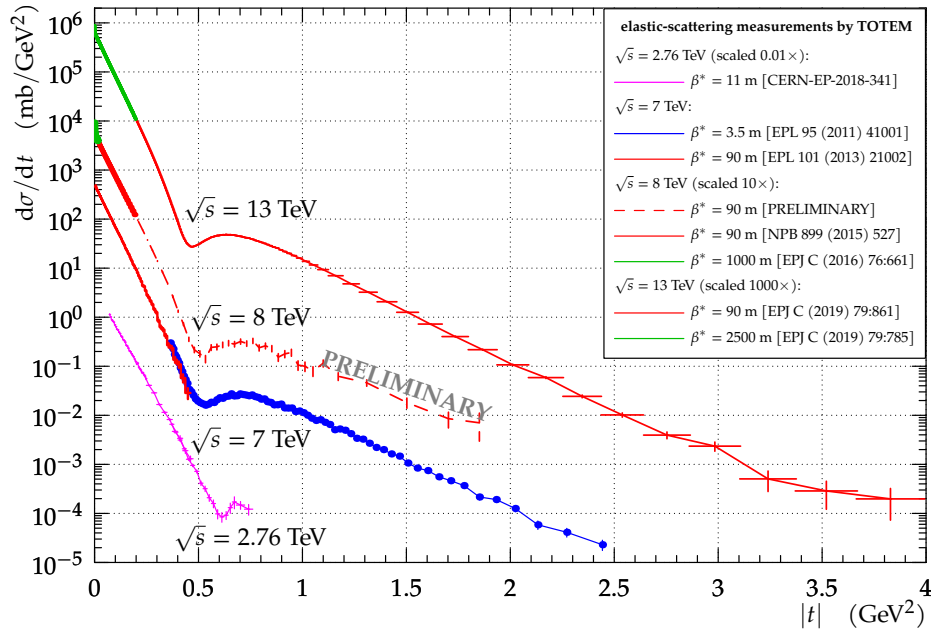


Figure 20.9: The t -dependence of the pp elastic cross section for collision energies $\sqrt{s} = 2.76$ TeV [103], 7 TeV [104, 114], 8 TeV [53, 115, 116] and 13 TeV [54, 102]. The experimental uncertainties represent the quadratic sum of statistical and systematic uncertainties. Figure from Ref. [116].

the value of the cross section depends on the quark separation, r , in the transverse plane, $\sigma(q\bar{q} - p) \propto \alpha_s^2 \langle r^2 \rangle$ [43, 44]. Thus different processes with the same $\langle r^2 \rangle$ are driven by the same $\sigma(q\bar{q} - p)$ cross section.

In the DIS case this separation in turn is controlled by the photon virtuality, Q^2 , and the quark mass, m_q : $\langle r^2 \rangle \simeq 1/(z(1-z)Q^2 + m_q^2)$ (z is the photon momentum fraction carried by the quark). Indeed, the cross section of the ρ meson diffractive production in DIS at $Q^2 = M_{J/\psi}^2$ is close (up to the difference in the quark electric charges) to that for the J/ψ photoproduction, see Fig. 20.10 (Left).

The production cross section depends non-trivially on W , the

energy of the γ^*p center of mass system. It increases with W as W^n , where $n = 0.2$ for ρ, ω and ϕ (light quark)-mesons but $n = 0.8$ for J/ψ . Note that in the J/ψ case the energy dependence is close to that of the BFKL (Balitsky-Fadin-Kuraev-Lipatov) Pomeron [59, 122, 123], that is, the singularity calculated within the leading (and next-to-leading) approximation in perturbative QCD. But at lower scales the absorptive (multi-Pomeron) corrections tame the growth which leads to smaller values of n ([124–127]), see Fig. 20.10 (Right).

A similar situation reveals in the dependence of α_{eff} on Q^2 , as can be seen in Fig. 47 of [91]. At a large scale $\mu^2 = (Q^2 + M_\rho^2)/4$ the value of $\alpha_{\text{eff}} \simeq 1.3$ is close to the prediction for the QCD

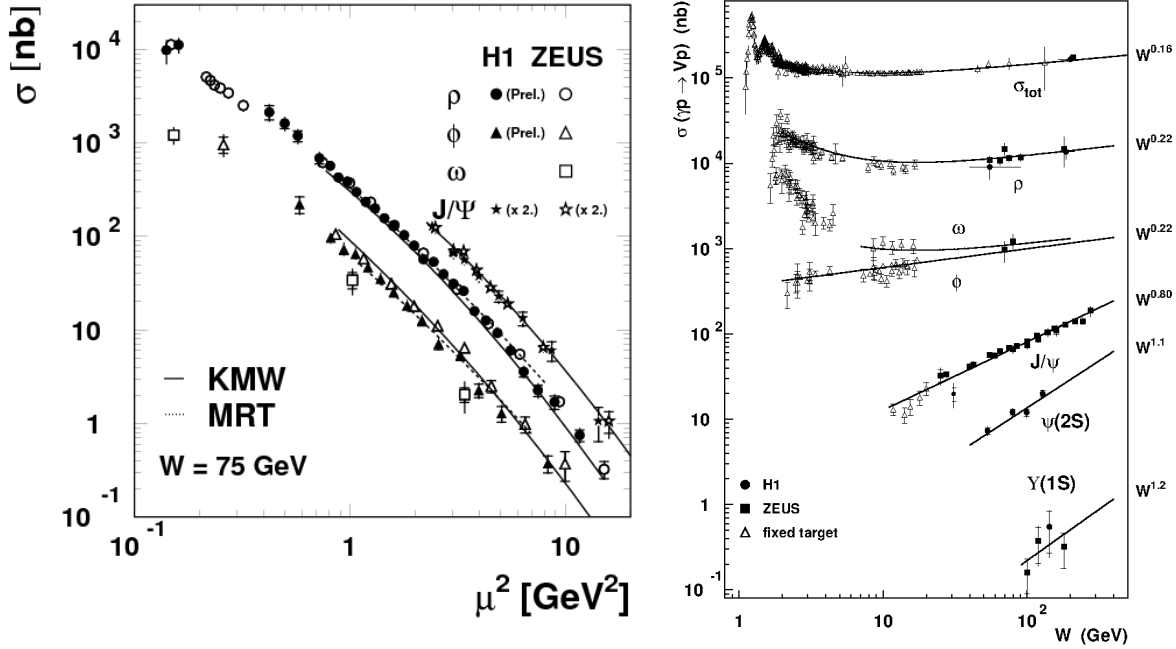


Figure 20.10: (Left) The ρ, ω, ϕ and J/ψ elastic production cross sections as a function of the scale $\mu^2 = (Q^2 + M_V^2)/4$. For readability of the figure, the J/ψ cross sections are multiplied by a factor 2. Figure from Ref. [118]. (Right) Compilation of photoproduction cross section measurements as a function of the γp centre-of-mass energy, W . The total cross section and various vector meson production cross sections are included, with the approximate power law dependences $\sigma \propto W^\delta$ indicated for each process. Figure from Ref. [119].

Pomeron, while for a smaller scale, the absorptive corrections described by the multi-Pomeron diagrams start to reduce the cross section, and α_{eff} decreases.

20.5 Pomeron in QCD

All features described in the previous Sections were based on *first principles*, such as analyticity (based on causality), unitarity, crossing symmetry, etc. Since QCD theory satisfies all these principles it should reveal a corresponding ‘‘Regge’’ behaviour. Indeed, within perturbative QCD there is a Pomeron: an even-signature singularity in the j -plane with vacuum quantum numbers. While in the old Regge theory the Regge trajectories and their couplings were phenomenological numbers fitted from experiment, perturbative QCD allows one to calculate the positions of the singularities and the corresponding couplings with $O(\alpha_s)$ and even with $O(\alpha_s^2)$ accuracy [59, 122, 123, 128–131].

In terms of Feynman diagrams, the QCD Pomeron may be viewed as a sum of multi-particle ladders built by the exchange of two t -channel (reggeized¹⁴) gluons, see the left-hand side of Fig. 20.5.

The sum of ladder diagrams of the type of Fig. 20.5 is the simplest multiparticle structure which reproduces the power-like s^α behaviour of the Pomeron pole. In other words it corresponds to a sum of completely inelastic $2 \rightarrow n$ processes, that is, to the last term $G_{\text{inel}} = 1 - \exp(-\Omega)$ in the unitarity equation (20.9). This set of diagrams was resummed in the limit of a small QCD coupling, $\alpha_s \ll 1$, but large energy, such that $\alpha_s \ln(s/s_0) \sim O(1)$ [59]. The summation results in the right-most singularity at $j = 1 + \omega_0 > 1$. After accounting for the next-to-leading logarithmic (NLL) corrections, the position of the singularity (Pomeron intercept) corresponds to $\omega_0 = 0.25\text{--}0.3$ depending only weakly on the scale [122, 123, 132–136], whose value is characterized by the transverse momentum, k_t , of gluons in the ladder.

It was demonstrated (see e.g. [137]) that the resummation of

the $(\alpha_s \ln(1/x))^n$ terms based on the QCD Pomeron results essentially improves the description of low- x inclusive HERA data within the framework of the NNLO DGLAP evolution.

At this stage the singularity is the cut in the j -plane. However we have to account for the boundary conditions at relatively small k_t . Imposing a reasonable boundary, we arrive at a series of Regge poles in the interval from $j = 1$ to $j = 1 + \omega_0$ instead of the cut [134]. Note that the first (corresponding to the rightmost pole in the j -plane, i.e. to the pole with the largest $\text{Re } j$) eigenfunction consists of gluons with relatively small k_t , while for the next poles the k_t increases. DIS inclusive $\gamma^* p$ cross sections were fitted in [135] using the QCD based approach in which Pomeron is represented by series of Regge poles obtained within the perturbative QCD BFKL approach. It was concluded that the first pole has a small coupling to the proton. It is possible that this small value of the coupling to the proton is related to the fact that the enhanced multi-Pomeron diagrams (i.e. the rescattering of intermediate partons) were neglected in the fit. The main effect of this enhanced contribution is the ‘‘renormalization’’ of the intercept which diminishes the effective value of ω_0 . Besides this, the enhanced diagrams provide a saturation by reducing the rise of the parton densities in the (b, k_t, y) -space (see e.g. [138, 139]).

Note that perturbative QCD allows us to understand why the values of the phenomenological multi-Pomeron vertices and the shift, ω_0 , of the intercept, are small (due to $\alpha_s \ll 1$ and some numerical factors such as N_c and π). Indeed, at the lowest α_s orders we get for the ω_0 value and the simplest multi-Pomeron vertices (see e.g. [59, 139, 140]):

$$\omega_0 \propto \frac{N_c \alpha_s}{\pi}, \quad g_{3\mathbb{P}} \propto \frac{N_c \alpha_s^2}{(N_c^2 - 1)\pi^2} \quad \text{and} \quad g_2^2 \propto \frac{N_c \alpha_s}{(N_c^2 - 1)^2}, \quad (20.46)$$

where g_2^2 is the coupling corresponding to the transition of 2 into 2 Pomerons.

20.5.1 BFKL evolution in the ‘dipole’ representation

It was shown in [141–144] that the LO BFKL Pomeron equation [59] can be written in terms of the evolution of the dipole

¹⁴That is, the virtual loop corrections to the one-gluon exchanges are included. These corrections are important in order to provide infrared stability of the results.

density, $N(x_d, y_d; y)$, in rapidity y (here x_d and y_d are the transverse coordinates of two t -channel gluons which form the colour singlet dipole). Indeed, after the emission of a new gluon at point z_d , the initial colour dipole with coordinates (x_d, y_d) turns into a pair of dipoles (x_d, z_d) and (z_d, y_d) . This can be considered as a development of a ‘dipole cascade’. Moreover in this formalism it is easy to include the non-linear absorptive corrections (last term in the square brackets in Eq. (20.47)), which accounts for the rescattering of the intermediate partons (gluons) on the target proton. The corresponding contribution is described by the so-called ‘fan’ diagrams and these are the most important corrections to the linear DGLAP (Dokshitzer-Gribov-Lipatov-Altarelli-Parisi) evolution [145] in the case of DIS at not large scales but at very small momentum fraction [139].

The resulting non-linear evolution (Balitsky-Kovchegov equation [146–148]) reads

$$\begin{aligned} \frac{d}{dy} N(x_d, y_d; y) &= \frac{\alpha_s N_c}{2\pi^2} \int d^2 z_d \frac{(x_d - y_d)^2}{(x_d - z_d)^2 (y_d - z_d)^2} \\ &\times [N(x_d, z_d; y) + N(y_d, z_d; y) - N(x_d, y_d; y) \\ &\quad - N(x_d, z_d; y) N(y_d, z_d; y)] . \end{aligned} \quad (20.47)$$

For a small density N the last term in the square brackets can be neglected, and the first three terms in Eq. (20.47) reproduce the conventional BFKL equation in the coordinate representation. However, for large $N \rightarrow 1$ the right-hand side of Eq. (20.47) vanishes and we reach the saturation $N = 1$. It is worth mentioning that, as shown in [149], in terms of ‘dipole’ formalism, with the triple-Pomeron vertex generated by the ‘one dipole to two dipoles’ transition, it is possible to relate the Good-Walker approach to high mass diffraction with the triple-Pomeron diagram.

20.5.2 Distribution of secondaries: theory versus experiment

As already discussed, in terms of Feynman diagrams the cut Pomeron can be viewed as a set of ladder diagrams corresponding to a sum of completely inelastic $2 \rightarrow n$ processes, that is, to the last term $G_{\text{inel}} = 1 - \exp(-\Omega)$ in the unitarity equation (20.9). Here $n > 2$ means the production of additional $(n - 2)$ gluons which, after hadronization, form minijets.¹⁵ Therefore, in the final state driven by one Pomeron we expect to observe gluon minijets with a flat rapidity distribution in the central (plateau) rapidity region. This would correspond to a flat pseudorapidity distribution of produced particles if they were massless. A typical pseudorapidity distribution of charged particles in inclusive events (up to $|\eta| = 7$) is shown in Fig. 20.11 (left) [150] (see also Fig. 52.1 in [1]). The central part ($|\eta| < 2.5$) was measured by CMS, while the forward region was covered by TOTEM. The dip observed at $\eta = 0$ is explained by the presence of massive particles (the Jacobian $J(p_T, m, \eta) = p_T/E \rightarrow p_T/\sqrt{p_T^2 + m^2}$ at $\eta = 0$). A photon energy spectrum is shown in Fig. 20.11 (right) [151], measured by LHCf inclusively and in events with a diffraction topology, i.e. no charged particles with $p_T > 100$ MeV and $|\eta| < 2.5$ observed by ATLAS. As expected in diffractive events the energy flow decreases with E_γ more slowly than that in the inclusive case.

The energy dependence of the particle density $dN_{\text{ch}}/d\eta$ at $\eta = 0$ is shown in Fig. 20.12 (left). Neglecting absorptive corrections given by the enhanced diagrams (which mainly change (‘renormalize’) the effective Pomeron intercept $\alpha_{\text{eff}}(0) = 1 + \Delta$ [121]), we conclude that according to the AGK rules the plateau height $d\sigma/d\eta \propto s^\Delta$ is driven just by the one-Pomeron exchange with effective $\Delta \sim 0.2$ (see Section 20.3.3.3). That is, the density of secondaries observed in the inclusive process increases with increasing energy faster than the total cross section, whose growth is tamed by the multi-Pomeron diagrams. Indeed, as is seen from Fig. 20.12 (left), in the interval of collider energies $dN_{\text{ch}}/d\eta = (1/\sigma_{\text{inel}})d\sigma/d\eta \propto s^{0.115}$ (i.e. $d\sigma/d\eta \propto s^{0.215}$), while $\sigma_{\text{inel}} \propto s^{0.1}$.

¹⁵Minijets result from hadronization of partons emitted from the cut QCD Pomeron. Typically these are groups of hadrons with comparatively low overall $E_T \lesssim 5\text{--}10$ GeV.

Contrary to the ‘old’ Regge theory where it was *assumed* (based on the experimental data existing in the 1950s and 1960s) that all transverse momenta are limited, in QCD the k_t distributions of jets (charged particles) have a long k_t tail ($d\sigma/dk_t^2 \propto \alpha_s^2(k_t^2)/k_t^4$ at large k_t and very large energy $s \gg k_t^2$). An example of the p_T distribution of charged secondaries is shown in Fig. 20.12 (right).

Note that the mean transverse momentum of secondaries, produced via jet fragmentation, slowly increases with collision energy, see Fig. 20.13 (right). This is caused by the stronger absorption (at larger \sqrt{s}) of the gluons with a smaller k_t ($\sigma^{\text{abs}} \propto 1/k_t^2$). The growth of $\langle p_T \rangle$ with multiplicity (see Fig. 20.13 (left)) can be explained by the fact that events with larger N_{ch} correspond to a smaller impact parameter, b , where the absorption of a low k_t component is stronger and, next, larger multiplicity can be originated by the events with jets/minijets with higher p_T . Since the mean p_T of secondaries grows with \sqrt{s} , the increase with \sqrt{s} of transverse energy flow is a bit faster than that of particle density.

The model [162] based on a modification of the classic RFT allows one to trace the smooth transition from the pure perturbative, large k_t , region into the *soft* domain. A strong absorption of the low k_t partons plays a crucial role here since it produces an effective infrared cutoff, k_{sat} , and provides the possibility of extending the parton approach, used for ‘hard’ processes, to also describe high-energy soft and semihard interactions. This approach combines a description of soft physics and diffraction with jet physics in a coherent self-consistent way.

Another way is to include the soft and hard components independently [37, 66, 163, 164]. In this approach the soft part is described in terms of RFT with the phenomenological ‘soft’ Pomeron pole while the hard part is calculated in terms of the parton model for minijet production with the energy dependent cutoff $k_t > k_0(s)$. A combined description of soft and hard processes in hadronic collisions is reached within the QGSJET Monte Carlo model (e.g. [61]) in the framework of the so-called ‘semihard Pomeron’ approach (see e.g. [165]).

In [166] a model was constructed, which incorporated the attractive features of the two successful theoretical approaches to high energy QCD: BFKL Pomeron calculus [59, 60] and the Colour Glass Condensate/saturation [167].

20.5.2.1 Correlations

All LHC experiments routinely measure tracks with $p_T > p_{\text{min}}$, where p_{min} can vary in different studies. Typically, $p_{\text{min}} = 200$ MeV, where tracking reconstruction efficiencies are larger than 70%. In order to identify particle species, each experiment has sophisticated identification procedures usually based on the ionization energy loss, dE/dx , or other techniques, with different regions of applicability for different particle species. Thanks to usually relatively large cross sections of soft QCD processes, most of the results below come from event samples with very low or negligible pile-up.

Following the notation in [168], symmetrized inclusive particle number densities for q points at y_1, \dots, y_q (where y_i represents the 4-momentum of the i th particle, $\rho_q(y_1, \dots, y_q)$, are related to the inclusive differential cross section by

$$\frac{1}{\sigma_{\text{inel}}} d\sigma = \rho_1(y) dy, \quad \frac{1}{\sigma_{\text{inel}}} d^2\sigma = \rho_2(y_1, y_2) dy_1 dy_2 \quad \text{etc.} \quad (20.48)$$

By integrating we get

$$\int \rho_1(y) dy = \langle n \rangle, \quad \int \int \rho_2(y_1, y_2) dy_1 dy_2 = \langle n(n-1) \rangle \quad \text{etc.}, \quad (20.49)$$

where the angular brackets denote averaging over the event sample and n is the particle multiplicity.

Since the inclusive q -particle densities in general contain trivial contributions from lower-order densities, it is convenient to consider quantities C_q which vanish when one of their arguments becomes statistically independent of (uncorrelated with) the others. These quantities C_q , called correlation functions (or cumulant

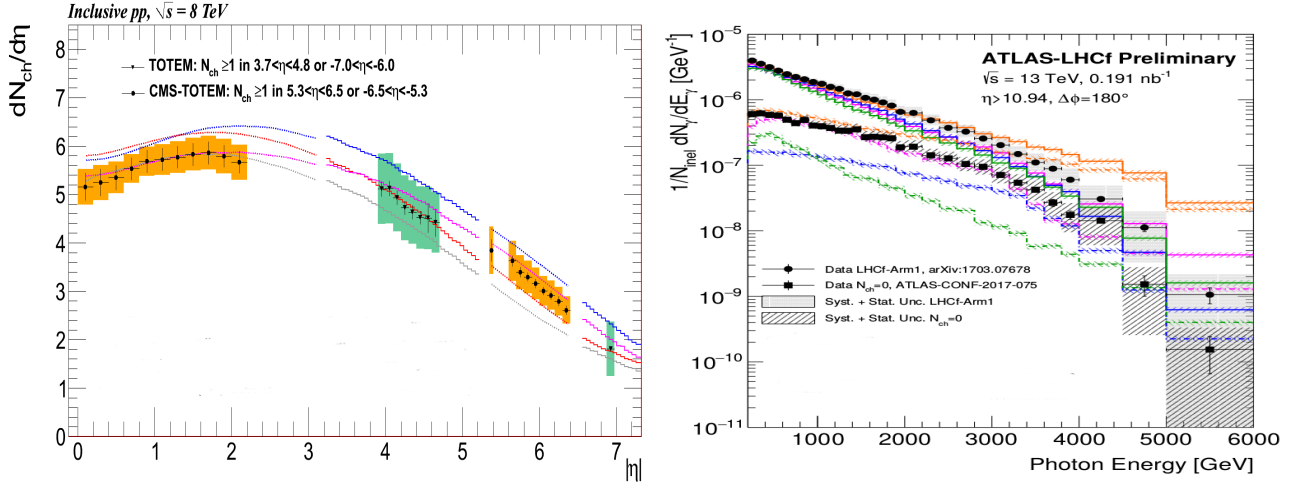


Figure 20.11: (Left) Charged-particle pseudorapidity distribution for inclusive events measured by CMS and TOTEM [150]. The error bars represent the statistical and uncorrelated systematic uncertainties between neighboring bins, while the shaded areas denote the combined statistical and full systematic uncertainties. The coloured lines indicate model predictions. (Right) Photon energy spectrum measured by LHCf at $|\eta| > 10.94$. The filled circles show the inclusive photon spectrum measured by LHCf [152] and filled squares the spectrum for $N_{ch} = 0$ events where no charged particles with $p_T > 100$ MeV and $|\eta| < 2.5$ are observed by ATLAS [153]. The coloured lines indicate model predictions. The error bars correspond to the statistical uncertainties and the shaded areas denote the combined statistical and systematic uncertainties. Figure from Ref. [151].

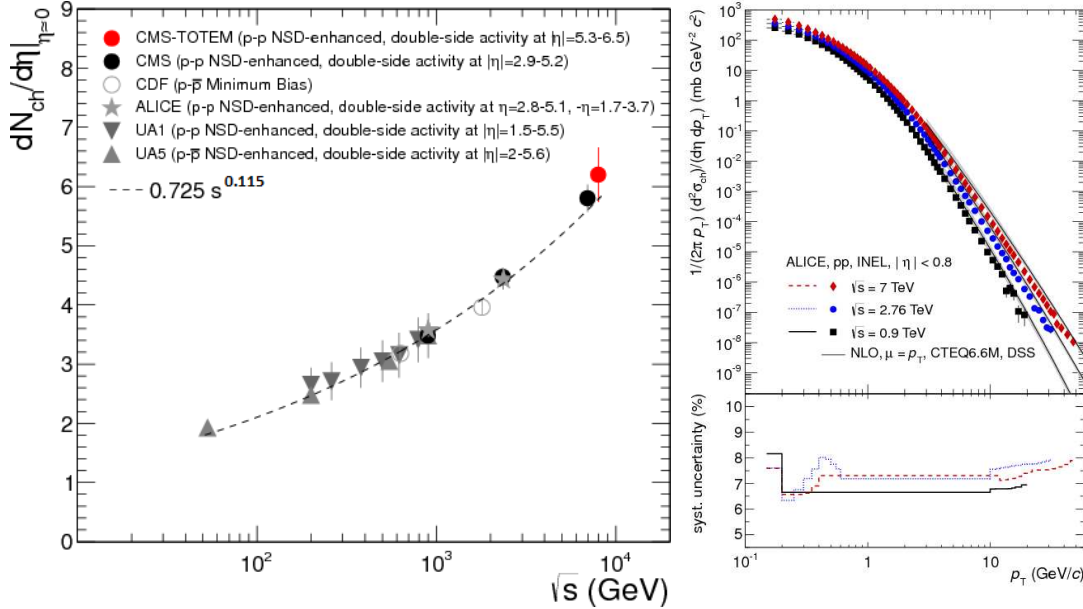


Figure 20.12: (Left) Energy dependence of the charged particle density $dN_{ch}/d\eta$ at $\eta \approx 0$ for pp and $p\bar{p}$ collisions. Shown are measurements performed with different Non-SD event selections from UA1 [154], UA5 [155], CDF [156,157], ALICE [158] and CMS [159]. The dashed line is a power-law fit to the data. Figure from Ref. [150]. (Right) Differential cross section of charged particles with $|\eta| < 0.8$ in inelastic pp collisions at $\sqrt{s} = 0.9, 2.76$ and 7 TeV as a function of p_T . Only statistical uncertainties are shown. Figure from Ref. [160].

functions), are defined as:

$$\begin{aligned}
 C_2(1, 2) &= \rho_2(1, 2) - \rho_1(1)\rho_1(2), \quad C_3(1, 2, 3) \\
 &= \rho_3(1, 2, 3) - \sum_{(3)} \rho_1(1)\rho_2(2, 3) + 2\rho_1(1)\rho_1(2)\rho_1(3), \\
 C_4(1, 2, 3, 4) &= \rho_4(1, 2, 3, 4) - \sum_{(4)} \rho_1(1)\rho_3(1, 2, 3) \\
 &\quad - \sum_{(3)} \rho_2(1, 2)\rho_2(3, 4) + 2 \sum_{(6)} \rho_1(1)\rho_1(2)\rho_2(3, 4) \\
 &\quad - 6\rho_1(1)\rho_1(2)\rho_1(3)\rho_1(4).
 \end{aligned} \tag{20.50}$$

The 2D two-particle correlation function is defined as

$$C(\Delta\eta, \Delta\phi) = \frac{\rho_2(\Delta\eta, \Delta\phi)}{\rho_1(\eta_a, \phi_a)\rho_1(\eta_b, \phi_b)}. \tag{20.51}$$

The distribution $\rho_2(\Delta\eta, \Delta\phi)$ is usually interpreted as a conditional probability to observe a particle a at the phase-space point (η_a, ϕ_a) if a particle b at (η_b, ϕ_b) is observed as well, and $\Delta\eta = \eta_a - \eta_b$ and $\Delta\phi = \phi_a - \phi_b$. The distributions $\rho_1(\eta_a, \phi_a)$ and $\rho_1(\eta_b, \phi_b)$ are probabilities to observe a single particle at (η_a, ϕ_a) and (η_b, ϕ_b) , respectively. The denominator of Eq. (20.51) is constructed as a product of two single-particle distributions using an event mixing technique, where each particle in the pair comes from a different event. Experimentally, each reconstructed track

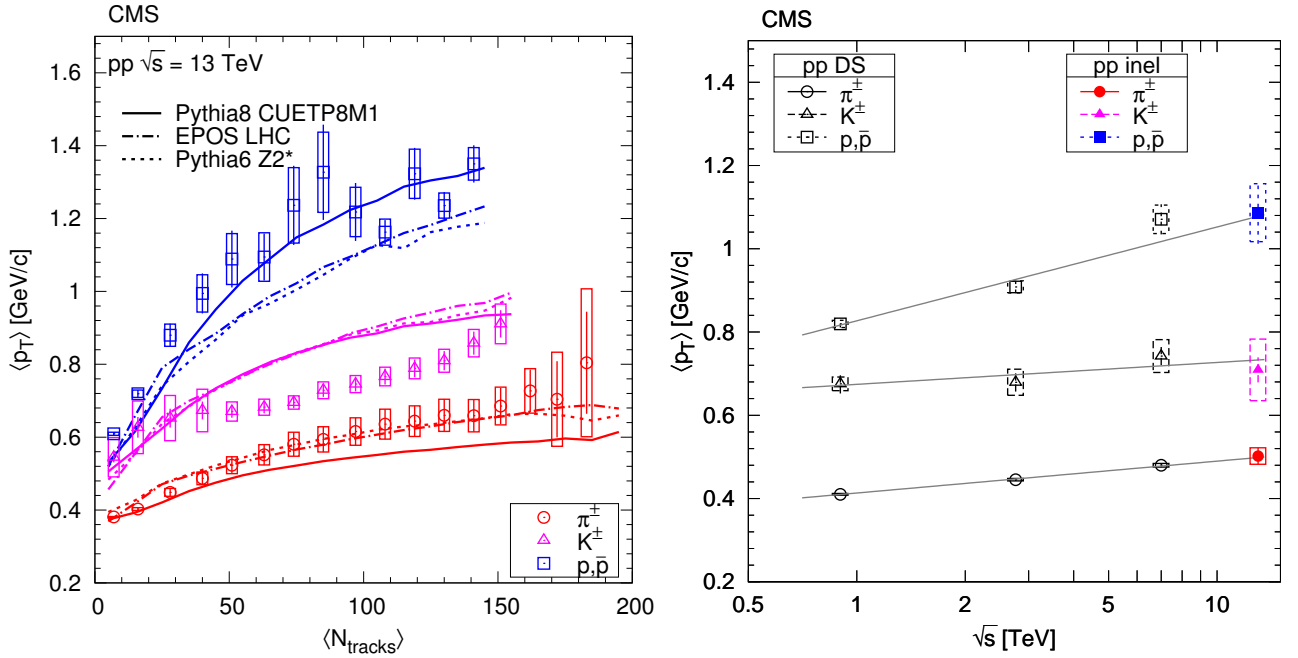


Figure 20.13: Average p_T of pions, kaons and protons in the range $|\eta| < 1.0$ as a function of (left) track multiplicity at $|\eta| < 2.4$ and (right) of center-of-mass energy where the curves show linear fits using lns. The error bars indicate the uncorrelated combined uncertainties, while the boxes show the uncorrelated systematic uncertainties. Figures from Ref. [161].

is weighted by the inverse of an efficiency factor which accounts for the detector acceptance, the reconstruction and particle identification efficiencies, the contamination by secondary particles and the fraction of misreconstructed tracks.

An example of two-particle correlation functions measured in pp collisions at 7 TeV is shown in Fig. 20.14 for identical-particle pairs (right panel) and for particle–anti-particle pairs (left panel) [169].

We observe two distinct features which can be explained by short-range (in rapidity) correlations: 1) a near-side peak at $\Delta\phi \approx 0$ and 2) an away-side peak or rather a ridge at $\Delta\phi \approx \pi$. The near-side peak is considered to be caused by at least three effects:

- *fragmentation of partons scattered at a hard scale.* These relatively high p_T partons produce showers which after the hadronization form the mini-jets which create a broad structure extending over at least one unit in $\Delta\eta$ and $\Delta\phi$.
- *resonance decays.* The decay of resonances contributes to the near-side peak at $\Delta\eta \sim 0$ and extended in $\Delta\phi$ [170–172], depending on the released kinetic energy of the given resonance. This effect is mostly visible for unlike-sign particle pairs.
- *femtoscopic correlations.* The term “femtoscopic” refers to a length scale of the order of 10^{-15} m. These correlations are present at low relative momenta of the particles in a pair (representing a very small phase-space corner, so they are practically invisible in terms of $(\Delta\eta, \Delta\phi)$) and give rise to an enhancement of the correlation function (due to Bose-Einstein quantum statistics for identical bosons) or its suppression (due to Fermi-Dirac quantum statistics for identical fermions). Besides this, at low relative momenta there are correlations caused by Coulomb and/or other final state interactions. The shape of all these effects in $(\Delta\eta, \Delta\phi)$ space depend strongly on the mass of the particle type as well as on the size of the particle-emitting system. The latter is traditionally measured in Bose-Einstein correlation (BEC) analyses and is not part of this review.

The away-side peak originates from energy-momentum conservation which manifests itself by the quark and the anti-quark going back-to-back in ϕ . In this case the rapidity width of the away-side peak is much larger than the near-side peak since in the original matrix element the quark and the antiquark can be separated by some $\Delta\eta$ interval.

As discussed in Sections 20.3.3.2 and 20.3.3.3, there may be several cut Pomerons in the same event, each giving rise to particle sets which are, in general, independent of each other (except for small Bose-Einstein correlations). This leads to long-range (in rapidity) correlations. Since the density of secondaries, dN/dy , is proportional to the number of cut Pomerons, k , the probability to observe at least one particle is proportional to $\langle k \rangle$, while the probability to observe simultaneously two particles separated by some (rather large) rapidity interval is proportional to $\langle k^2 \rangle$. Thus the long-range correlations are predicted to be $C_2 = \langle k^2 \rangle / \langle k \rangle^2 - 1 > 0$ which depends weakly on the separation $\Delta\eta$ between the two particles [173, 174]. In the case of the pure eikonal approach, neglecting the enhanced diagrams and the conservation law effects in the proton fragmentation region, we expect that these long-range correlations,

$$C_2(\Delta y) = \frac{\sigma_{\text{inel}} d^2\sigma/dy_1 dy_2}{d\sigma/dy_1 d\sigma/dy_2} - 1 \sim \text{const}, \quad (20.52)$$

do not depend on the rapidity separation, $\Delta y = |y_1 - y_2|$, between the two particles. The contribution of the processes with more cut Pomerons also results in a much wider multiplicity distribution and in a larger density of soft particles coming from the ‘underlying event’.

20.5.2.2 Color reconnection

In this context, we have to mention also the so-called ‘colour reconnection’ phenomenon. This is a pure ‘soft QCD’ effect. The point is that after a number of coloured secondary partons are produced, there are different possibilities to form the colour flow between these partons and to group the partons into colourless clusters. In the process of reconnection, one rearranges the colour flow in such a way as to minimize the size of the clusters. This is especially important when dealing with MPI contributions. The reconnection between the different cut Pomerons diminishes the final multiplicity and can change the form of the N_{ch} distributions (see e.g. Section 41.3.3 of [1] and [2, 13, 177, 178]).

20.5.2.3 Double parton scattering

The probability of MPI depends on the spatial distribution of partons in the incoming protons. The effects of MPI are suppressed if the density of partons is low and the partons from the incoming beam particles are separated from each other by a large

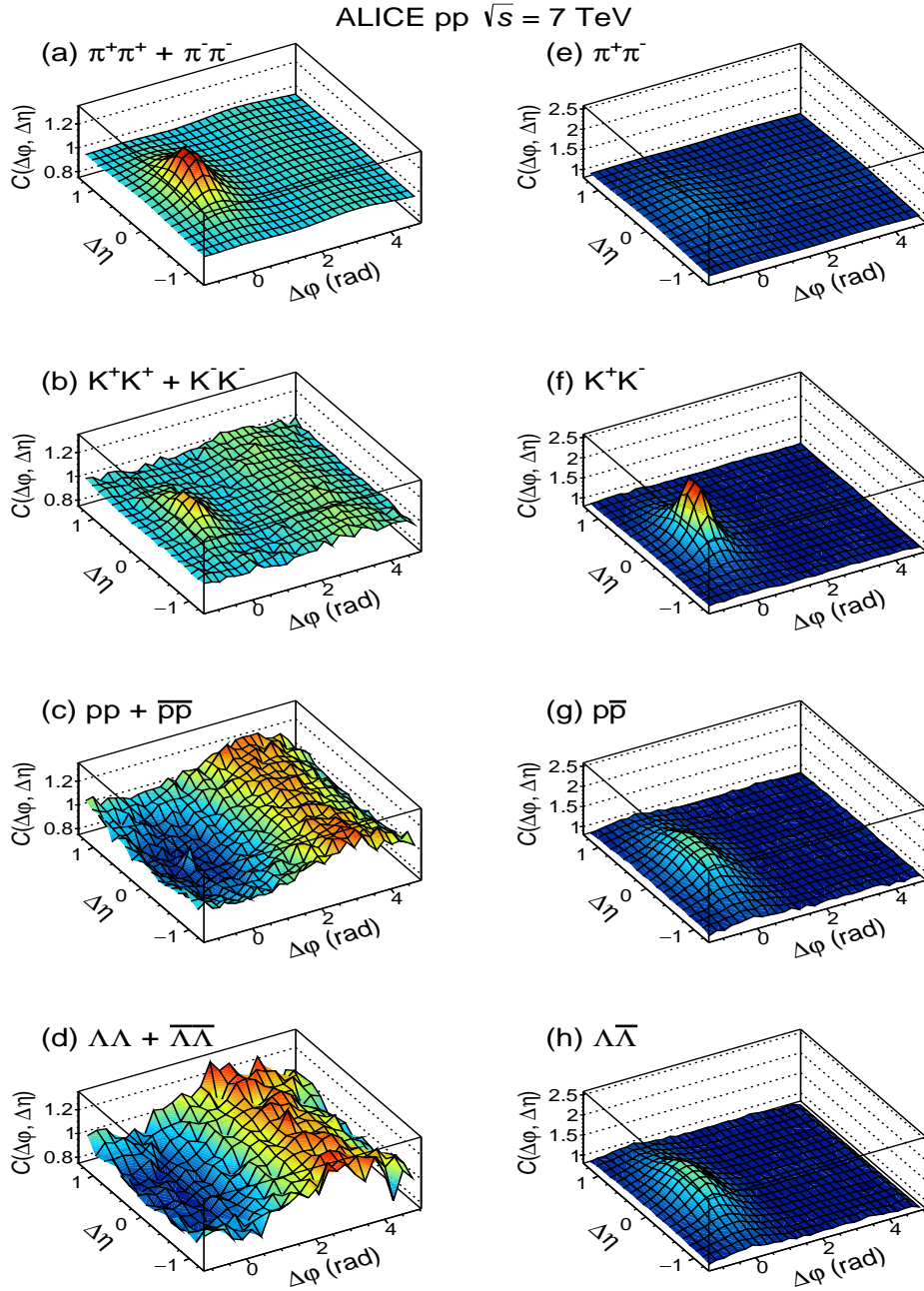


Figure 20.14: Two-particle correlation functions for identical-particle pairs: $\pi^+\pi^+ + \pi^-\pi^-$, $K^+K^+ + K^-K^-$, $pp + \bar{p}\bar{p}$, and $\Lambda\Lambda + \bar{\Lambda}\bar{\Lambda}$ (left panel) and particle-anti-particle pairs: $\pi^+\pi^-$, K^+K^- , $p\bar{p}$ and $\Lambda\bar{\Lambda}$ (right panel). Figure from Ref. [169].

interval in transverse coordinate space \vec{x}_t . Events in which two hard subprocesses, caused by interactions of two different parton pairs (say, (a_1b_1) and (a_2b_2)), take place simultaneously, are called Double Parton Scattering (DPS). The DPS cross section is driven by the ‘double parton distributions’, $D(y_{a_1}, y_{a_2}, \dots)$, where y_{a_1} and y_{a_2} are momentum fractions carried by the partons from the proton a and the dots denote all other coordinates. As a rule, experiments study DPS processes at relatively small momentum fractions y_i . Here, correlations due to momentum conservation (like $y_{a_1} + y_{a_2} < 1$) are not so important, and with a reasonable accuracy we can assume a factorization

$$D(y_{a_1}, y_{a_2}, \dots) \propto F(y_{a_1}) \cdot F(y_{a_2}), \quad (20.53)$$

where $F(y_{a_i})$ are the single parton distributions. In such a case the DPS cross section takes the form

$$\sigma^{\text{DPS}} = c \cdot \frac{\sigma_{a_1b_1} \sigma_{a_2b_2}}{\sigma_{\text{eff}}}, \quad (20.54)$$

where $\sigma_{a_1b_1}$ and $\sigma_{a_2b_2}$ are cross sections for the two *independent* hard processes, while σ_{eff} characterizes the mean area occupied by the partons a_1 and b_1 ; the constant factor $c = 1/2$ if both hard processes (a_1b_1) and (a_2b_2) are identical, otherwise $c = 1$. Thus the DPS cross section is sensitive to the spatial separations between partons in the proton (see Section 7.2.3 in [2] and [179, 180] for more explanations and reviews).

One problem is that within this approach we *assume* that the partons a_1 and a_2 are produced by two independent parton showers (and similarly for the other incoming proton). On the other hand, there is a probability that from the beginning we start with the evolution of a single shower which further splits into two different branches. In this case the separation between the two partons (two shower branches) becomes very small – of the order of the inverse scale ($\sim 1/\sqrt{q^2}$) at which the splitting occurs. The exact value of this ‘splitting’ scale q^2 depends on the particular kinematics of the DPS process. So, different experiments (with

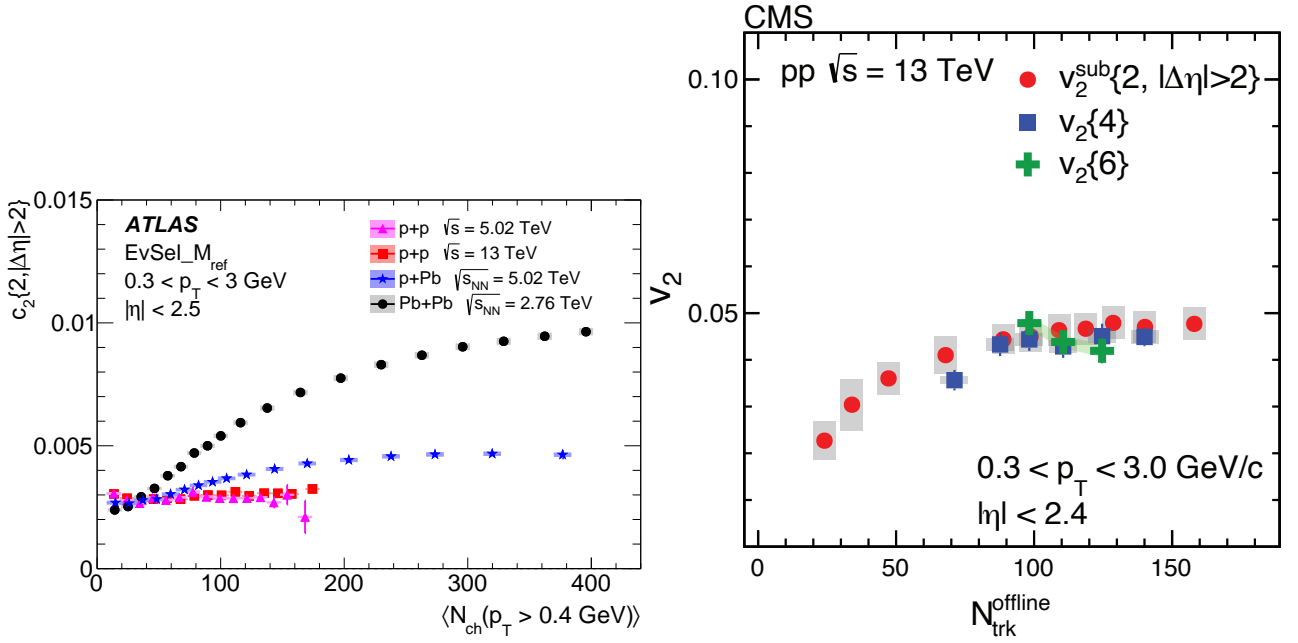


Figure 20.15: (Left) The two-particle cumulant, $c_2\{2, |\Delta\eta| > 2\}$, as a function of $\langle N_{\text{ch}}(p_T > 0.4 \text{ GeV}) \rangle$ for pp collisions at $\sqrt{s} = 5.02$ and 13 TeV , pPb collisions at $\sqrt{s_{NN}} = 5.02 \text{ TeV}$ and low-multiplicity $PbPb$ collisions at $\sqrt{s_{NN}} = 2.76 \text{ TeV}$. The data are constructed from particles with $0.3 < p_T < 3.0 \text{ GeV}$. Figure from Ref. [175]. (Right) The $v_2\{2, |\Delta\eta| > 2\}$, $v_2\{4\}$ and $v_2\{6\}$ values as a function of charged particles, averaged over $0.3 < p_T < 3.0 \text{ GeV}$ and $|\eta| < 2.4$, in pp collisions at $\sqrt{s} = 13 \text{ TeV}$. Figure from Ref. [176]. The error bars correspond to the statistical uncertainties, while the shaded areas denote the systematic uncertainties.

different kinematical conditions) can give somewhat different values of σ_{eff} . In general, the value of σ_{eff} depends on the following features: a) on the measured process since the spatial (b_i) distributions of different incoming partons (light quarks, heavy quarks, gluons) can be different; b) on the splitting scale, $\sqrt{q^2}$, of one parton cascade into two branches. The typically high value of the splitting scale then explains the fact that the experimentally measured values of $\sigma_{\text{eff}} \sim 7\text{--}25 \text{ mb}$ (see Fig. 4 of [181]) are smaller than σ_{tot} or mostly even lower than the proton area $\pi R_p^2 \sim 22\text{--}24 \text{ mb}$ (see e.g. [182]); c) on the p_T balance, k_T , in the individual hard process (e.g. for two dijet productions $k_T = |\vec{p}_{T1}| + |\vec{p}_{T2}|$ where p_{T1} and p_{T2} are jet p_T 's of the first hard process (similarly for the second hard process)). A small value of k_T indicates that there were no splittings or the splitting scale $\sqrt{q^2}$ was small and, therefore, we expect larger σ_{eff} ; d) on the contribution of single parton scatterings misidentified as DPS. For a lower scale of the hard process this contribution is larger (see [183] for more detailed discussion).

20.5.2.4 Final state interactions

The formalism of the RFT does not include ‘final state interactions’¹⁶. Therefore, besides the correlations considered in the previous Section 20.5.2.1 we have to expect the correlation caused by partons and hadrons rescattering in the final state. These effects are not crucial at lower energies, but become more important at high LHC energies, in particular in heavy-ion collisions where the particle density is large. For example, the final state interactions (FSI) lead to the formation of the collective flow of secondaries (see e.g. [185] for a review), especially in high-multiplicity events. To study the collective flow experimentally, one has to subtract correlations coming from few-particle sources such as resonance decays, mini-jets, multi-jets and BEC (so called “non-flow”). The non-flow can efficiently be suppressed using the sub-event method, that is by studying the azimuthal correlations between particles separated in η [186], or subtracted using the multi-particle correlation (or cumulant) techniques.

The cumulant method is based on calculating $2k$ -particle

azimuthal correlations, $\text{corr}_n\{2k\}$, and cumulants $c_n\{2k\}$ (where $k = 1, 2, \dots$), for n th Fourier harmonics. The $\text{corr}_n\{2k\}$ are defined as [187, 188]:

$$\begin{aligned} \langle\langle \text{corr}_n\{2\} \rangle\rangle &= \langle\langle e^{in(\phi_1 - \phi_2)} \rangle\rangle, & \langle\langle \text{corr}_n\{4\} \rangle\rangle &= \langle\langle e^{in(\phi_1 + \phi_2 - \phi_3 - \phi_4)} \rangle\rangle, \\ \langle\langle \text{corr}_n\{6\} \rangle\rangle &= \langle\langle e^{in(\phi_1 + \phi_2 + \phi_3 - \phi_4 - \phi_5 - \phi_6)} \rangle\rangle \end{aligned}$$

and similarly for higher numbers of correlated particles. The double-brackets $\langle\langle \rangle\rangle$ denote averaging first over particles in an event and then over events within a given event class. For every event, the average is taken over all possible combinations of azimuthal angles ϕ_l ($l = 1, \dots, 2k$) of the $2k$ particles. The cumulants are then obtained from multi-particle azimuthal correlations after subtracting correlations between $2(k-1)$ particles according to the following formulae [187, 188]:

$$\begin{aligned} c_n\{2\} &= \langle\langle \text{corr}_n\{2\} \rangle\rangle, & c_n\{4\} &= \langle\langle \text{corr}_n\{4\} \rangle\rangle - 2\langle\langle \text{corr}_n\{2\} \rangle\rangle^2, \\ c_n\{6\} &= \langle\langle \text{corr}_n\{6\} \rangle\rangle - 9\langle\langle \text{corr}_n\{2\} \rangle\rangle \times \langle\langle \text{corr}_n\{4\} \rangle\rangle + 12\langle\langle \text{corr}_n\{2\} \rangle\rangle^3. \end{aligned}$$

The cumulants for higher particle multiplicities are calculated in [187, 188]. The cumulants then serve to estimate the Fourier harmonics v_n as follows [187]:

$$v_n\{2\} = \sqrt{c_n\{2\}}, \quad v_n\{4\} = \sqrt[4]{-c_n\{4\}}, \quad v_n\{6\} = \sqrt[6]{c_n\{6\}}/4.$$

Some of the long-range correlation ($|\Delta\eta| > 2$) results obtained on a sample of charged particles with $0.3 < p_T < 3.0 \text{ GeV}$ and $|\eta| < 2.4$ are summarized in Fig. 20.15. The left plot shows the cumulant c_2 measured for pp , pPb and $PbPb$ collisions [175], while the right plot shows the elliptical harmonics v_2 measured for pp collisions [176], both as functions of multiplicities of charged particles. The two-particle correlations are observed to be strongest and rising with N_{ch} for $PbPb$ collisions, and weakest and rather flat for pp collisions. The elliptical-flow harmonics for 4- and 6-particle correlations show again a rather flat multiplicity dependence (at least for large multiplicities). Within experimental uncertainties, the values of $v_2\{2\}$, $v_2\{4\}$ and $v_2\{6\}$ measured in pp collisions at 13 TeV are consistent with each other. The similarity between $v_2\{4\}$ and $v_2\{6\}$ suggests that some collective effects are occurring in pp collisions at high multiplicity and the obser-

¹⁶In general, final state interactions can be included into the detailed structure of the multi-Pomeron vertices. However these vertices are phenomenological objects which are not well known experimentally.

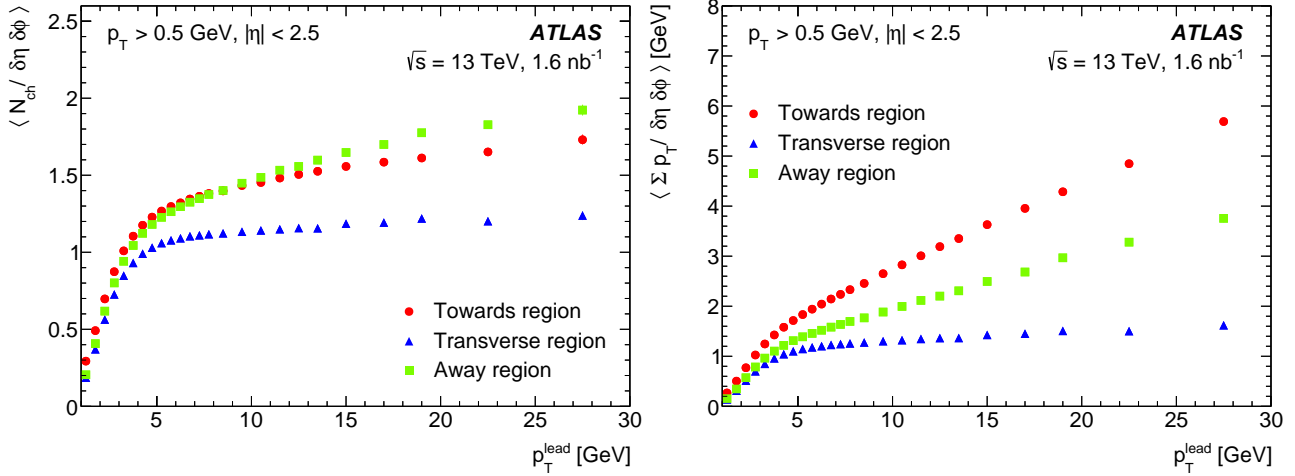


Figure 20.16: Mean charged particle density (left) and the sum of transverse momenta of secondaries (right) in events with the ‘leading’ high p_T particle as a function of p_T^{lead} in the transverse, towards and away azimuthal regions. Secondaries with $p_T > 0.5$ GeV and $|\eta| < 2.5$ are registered. The error bars (mostly hidden by the data markers) represent combined statistical and systematic uncertainties. Figures from [184].

vations are similar to those in $PbPb$ collisions, where the $v_2\{4\}$ values were measured to be close to $v_2\{6\}$ but they are both lower than $v_2\{2\}$ (not shown here).

Another example of long-range correlations is the so-called ‘ridge effect’. Here not only the ‘back-to-back’ jet correlations are registered, but also an excess of particles going in the same (in the azimuthal plane) direction as the leading (relatively high p_T) hadron. Moreover, this excess is seen at the rapidities separated from the leading hadron by a rather large interval (see e.g. [189] for a review).

It is popular to describe such FSI effects within the hydrodynamic model [190], which operates with collective (thermodynamic) variables. In terms of microscopic interactions, the collective flow can be caused by the geometry of a particular collision (the absorption is smaller for the secondaries flying in the direction orthogonal to the impact parameter vector \vec{b} [191, 192]), or by the colour reconnection at the hadronization stage [193], or accounting for the rescattering of secondaries directly, as was done, for example, in the AMPT model [194].

20.5.3 The underlying event

Except for the exclusive case, any ‘hard’ subprocess is accompanied by soft secondaries coming from initial state radiation (ISR), final state radiation (FSR) and multiple parton interaction (MPI), see Subsection 7.2.2 in [2]. These extra particles distort the signal we are looking for. In particular, they affect the isolation criteria applied to photons and charged leptons and the vertex reconstruction efficiency. In general, also the effects of colour reconnection (discussed in Section 20.5.2.2) contribute to the underlying event.

The usual procedure of estimating the amount of underlying event (UE) is to spatially divide tracks in each event according to their azimuthal angle into the Toward region (where the highest p_T jet points), the Away region (opposite to the Toward region) and to two Transverse regions. The standard observables are the average track multiplicity per unit area and the average scalar sum of track p_T per unit area. Figure 20.16 shows the particle density and the sum of p_T for the UE in ATLAS events containing at least one charged particle with $p_T > 0.5$ GeV and $|\eta| < 2.5$ [184].

Note that by construction the largest values of $\langle p_T \rangle$ are observed in the ‘Toward’ region, while in the ‘Away’ region we observe a slightly larger density than in the Toward region. These are results of the ‘leading’ and ‘backward’ jet fragmentation. In the transverse region, mostly filled by particles from the UE, the particle density and sum of p_T per unit $(\Delta\eta, \Delta\phi)$ area practically do not depend on the p_T^{lead} since these secondaries come from the other cut Pomeron(s), that is, from other ‘multiple interactions’. For low $p_T^{lead} < 2$ GeV the distributions in all three regions are close to each other. These events actually do not contain a ‘hard’

subprocess. Moreover, for a very small $p_T^{lead} \rightarrow 1$ GeV we start to select soft events with abnormally low $p_T < p_T^{lead}$ particles. Since only particles with $p_T > 0.5$ GeV are registered, the signal drops fast for $p_T^{lead} \rightarrow 1$ GeV. As a function of collision energy \sqrt{s} , the energy flow in the transverse region increases as $\sum p_T \sim s^{0.2}$ (as follows from Fig. 7 (right) in [184]) due to the larger number of MPI collisions and larger $\langle p_T \rangle$ in each collision¹⁷. As follows from this and other UE-dedicated LHC studies [195], from the comparisons of the data to the models with and without MPI, the necessity of MPI is convincingly demonstrated.

20.6 The Odderon

Apart from the even-signature singularity (Pomeron), in QCD with $N_c = 3$ there exists its counterpart, the odd-signature singularity placed at $j \simeq 1$ and formed by three t-channel reggeized gluons connected in colour space by the symmetric d^{abc} tensor of the colour $SU(3)$ group [196, 197]. This object is called the Odderon. The Odderon exchange amplitude has opposite sign for pp and $p\bar{p}$ scatterings. Its intercept is predicted to be very close to $j = 1$ [198–200], while according to perturbative estimates the coupling to the nucleon is rather small [201, 202]. The corresponding amplitude is mainly real and is about 100 times smaller than the imaginary part of the Pomeron exchange amplitude. Calculating the elastic amplitude via the eikonal formula (20.13) we have to replace the opacity $\Omega(b)$ by the sum $\Omega = \Omega_{\text{even}} + \Omega_{\text{odd}}$, where Ω_{even} is mainly real and Ω_{odd} is imaginary. Note that at $t = 0$ this QCD Odderon does not couple to mesons, and the t -slope of the Odderon amplitude is expected to be smaller than that for the Pomeron; instead of the singularity at $t = 4m_\pi^2$ in the Pomeron case, the nearest singularity in the Odderon channel is at $t = 9m_\pi^2$, see for instance [200]. Thus, in the impact parameter b space the QCD Odderon occupies an area of a smaller radius, see e.g. [203].

Experimentally an indication in favour of a manifestation of the high energy C-odd amplitude was observed by comparing the elastic pp and $p\bar{p}$ cross sections in the dip region (where the contribution from the C-even amplitude has a minimum) at the CERN-ISR [205], see Fig. 20.17 (left)¹⁸.

To get a better understanding of the Odderon effects it would be very instructive to have the $d\sigma_{el}/dt$ data for both pp and $p\bar{p}$ reactions at the same but higher energy ~ 1 TeV (ideally in the same apparatus) and, in the ideal case, to study the energy de-

¹⁷Recall the stronger absorption of the low k_t partons.

¹⁸Note that a qualitatively similar behaviour to the $p\bar{p}$ ISR data, namely a filling in of the dip in the t -distribution, was observed by the UA4 collaboration at the CERN $Spp\bar{S}$ collider at $\sqrt{s}=546$ and 630 GeV (see [208, 209] and in particular Fig. 2 in [209]) and by the $D0$ collaboration at the Tevatron at 1.96 TeV [207].

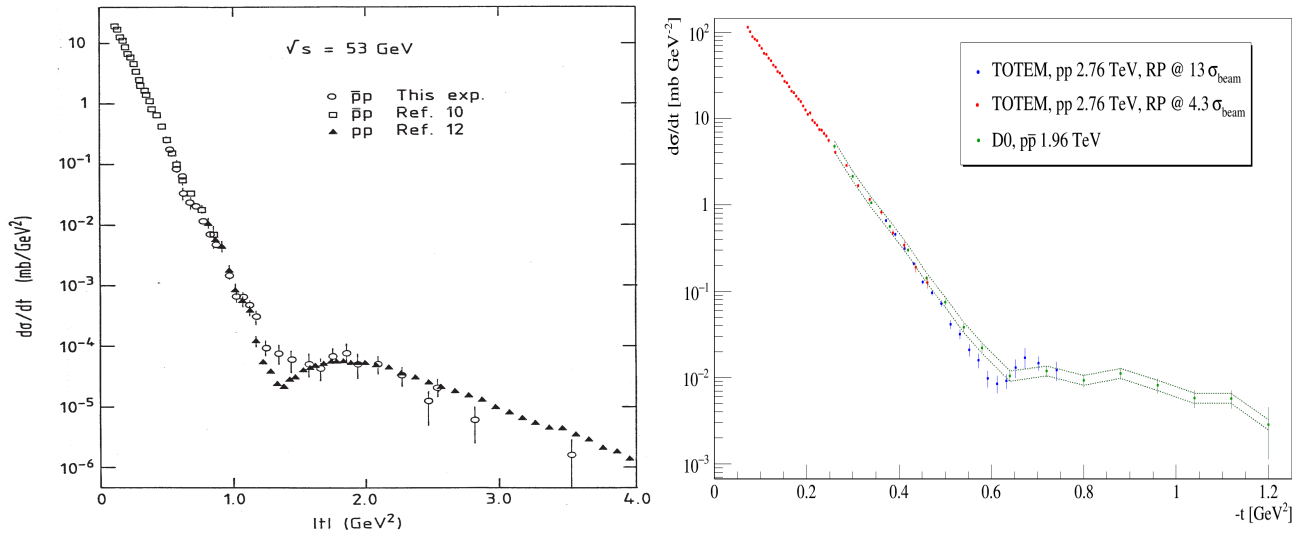


Figure 20.17: Comparison of the t -dependence of the elastic cross sections from pp and $p\bar{p}$ collisions. (Left) Data from the ISR energy of 53 GeV are shown by closed triangles [204] for pp collisions and by open circles [205] and open squares [206] for $p\bar{p}$ collisions. Only t -dependent uncertainties are shown and the systematic scale uncertainty is estimated to be $\pm 30\%$. Figure from Ref. [205]. (Right) Data from the D0 experiment at 1.96 TeV [207] are compared with data from the TOTEM experiment [103]. The green dashed line indicates the normalization uncertainty of the D0 measurement. Figure from Ref. [103].

pendence.

At the moment we can only compare the pp cross section measured by TOTEM at $\sqrt{s} = 2.76 \text{ TeV}$ [103] with the $d\sigma/dt$ values measured by the D0 collaboration at 1.96 TeV in $p\bar{p}$ collisions [207], see Fig. 20.17 (right).

The situation looks quite intriguing, but needs further investigation. Note that in the TeV energy range the ω, ρ and $\omega P, \rho P$ exchange contributions, which may be responsible for the difference between the pp and $p\bar{p}$ cross sections in the dip region at the ISR energies, are practically negligible.

Another way to search for the Odderon is to measure the real part of the elastic pp scattering amplitude via the interference with the pure QED one-photon exchange. Since the one-photon exchange amplitude contribution is sizeable only at very small $|t|$, this way we can study the Odderon at or near to $t = 0$. Indeed, the value of the ratio $\rho \equiv \text{Re}T_{\text{el}}/\text{Im}T_{\text{el}}$, obtained by TOTEM at 13 TeV ($\rho = 0.10 \pm 0.01$ [102]), turns out to be smaller than that expected for the pure even-signature amplitude, see Fig. 20.18.

Based on dispersion relations and assuming the C -even contribution only, from the known total cross sections we would rather expect $\rho \simeq 0.13$ – 0.14 . The difference could indicate that the rise of the total cross section at energies above those of the LHC slows down (see the dispersion relation, Eq. (20.19)) or this could be attributed to an Odderon contribution (see e.g. [210]). However, the Odderon exchange amplitude extracted in this analysis has opposite sign to that for the lowest- α_s -order QCD Odderon, see e.g. [201, 202, 211, 212]. Besides this, the Odderon contribution to ρ , obtained in [210], grows with \sqrt{s} (for $\sqrt{s} > 0.5 \text{ TeV}$), while in QCD we expect that the Odderon contribution to ρ decreases with energy, since the QCD Odderon intercept is smaller than that of the QCD Pomeron.

It is worth mentioning also that the Odderon contribution is strongly screened by the multi-Pomeron diagrams, which facilitate the falling-off of ρ with energy increasing, see [213, 214]. On the other hand, analyzing the whole ensemble of high energy elastic pp ($p\bar{p}$) low $|t|$ data, a reasonable description can be obtained using the even-signature amplitude only, that is, without the Odderon. In particular, the RR(PL2)qc model/version of the COMPETE parameterization is consistent with the TOTEM 13 TeV data on σ_{tot} and ρ within 1σ ¹⁹. Another example is the recent analysis in [212] of the low $|t| < 0.1 \text{ GeV}^2$ elastic data. Fitting all the low- t pp and $p\bar{p}$ data in the range of \sqrt{s} between 13 GeV and 13 TeV without Odderon, Donnachie and Landshoff [212] succeeded to

describe the TOTEM cross section with less than 1σ deviation in each $d\sigma_{\text{el}}/dt$ point (see Fig. 8 of [212]). Note that in this analysis, they get a larger value of ρ close to 0.14 at 13 TeV.

It was proposed also to search for the Odderon in exclusive C -even meson ($\pi^0, \eta, f_2, \eta_c, \dots$) photoproduction (see e.g. [215, 216]). However the expected cross sections are small (e.g. for η_c) and in each channel there is a large background caused either by Pomeron-Pomeron fusion (such as CEP of the f_2 meson production in pp or pPb collisions) or due to the vector meson radiative decay (such as $\omega \rightarrow \pi^0\gamma$ for the case of pion) [217]. Up to now, no definitive Odderon signal in the C -even meson production has been observed. At the moment there exist only upper limits on the photoproduction cross sections obtained in the measurements at HERA with $\sqrt{s} \simeq 200 \text{ GeV}$ [218–220].

To conclude, let us emphasize that the existence of the C -odd singularity with intercept

$\alpha_{\text{odd}}(0) \simeq 1$ is a firm prediction of QCD. At least in the high k_t region there is a well established C -odd three-gluon contribution to the scattering amplitude. However the expected coupling of such an Odderon singularity is numerically very small. Therefore it is quite challenging to observe its manifestation experimentally. Currently it seems to be a bit premature to draw any definite conclusion about an experimental observation of the Odderon signal.

20.7 Asymptotics

The high-energy behaviour of total hadronic cross sections has been one of the oldest problems of strong interactions over many decades, beginning from Heisenberg [221]. The most important bound obtained based on general analytical properties of scattering amplitudes is the FLM bound [47–49]. It states that the growth of the total hadronic cross section with energy does not exceed $\ln^2 s$, see Eq. (20.34).

Recall that we neglected the photon contribution as well as the whole electro-weak sector, and that the parameter in Eq. (20.34) s_0 is an *a priori* unknown scale. However, if we were to assume a reasonable hadronic scale, $s_0 \simeq 1 \text{ GeV}^2$, we would find that Eq. (20.34) implies an unrealistically high upper bound in comparison with the cross sections observed at present collider energies. Nevertheless there is a common trend in the literature (see for instance, reviews [222, 223] and references therein) to fit phenomenologically the total cross section with $\ln^2 s$, keeping in mind the saturation of the FLM bound. Such an asymptotic behaviour is assumed also by the COMPETE collaboration [22], which achieved a comprehensive description of all soft pre-LHC data measured at $\sqrt{s} \geq 4 \text{ GeV}$ as well as total pp cross sections

¹⁹We thank Jean-Rene Cudell for clarifying this issue.

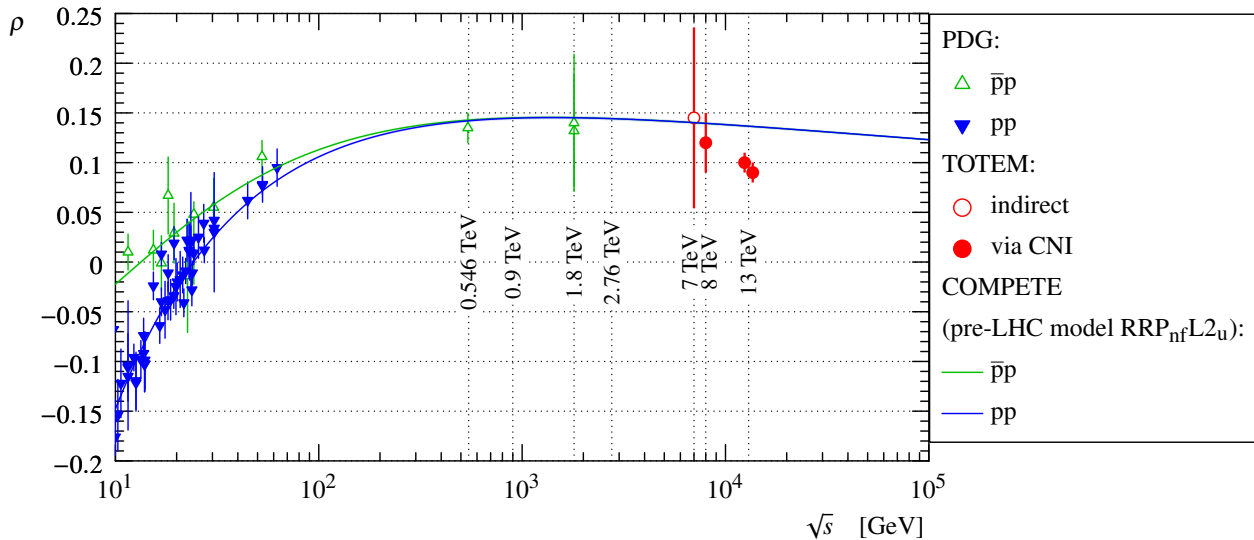


Figure 20.18: The dependence of the ρ parameter on the collision energy. The pp (blue) and $p\bar{p}$ (green) data are taken from [1]. The TOTEM measurements are marked in red. The two points at 13 TeV correspond to two fit cases, discussed in [102], using the same data. The lines represent fits to the data using the COMPETE parameterization [22]. Figure from Ref. [102].

from the LHC available in the first half of 2015 (see Section 51 in [24]).

It is interesting that the Froissart-type $\ln^2 s$ asymptotics of the pp total cross section are also supported by numerical results in lattice QCD [224]. Such a behaviour is also observed in the approach [225] based on Colour Glass Condensate saturation.

Finally, it is worth mentioning that the possibility that *asymptotically* the Pomeron intercept becomes smaller than 1, $\alpha_{\mathbb{P}}(0) < 1$, and at very high energies the total cross section starts to decrease with energy, though highly unlikely, is not yet completely rejected. For instance, such a behaviour is expected in a theory with only the triple-Pomeron coupling, $g_{3\mathbb{P}}$, and which neglects the more complicated multi-Pomeron vertices g_m^n , such as the $2 \rightarrow 2$ Pomeron coupling [226, 227].

It was also argued that in the case of an increasing (with energy) cross section the only regime consistent asymptotically with both the s - and the t -channel unitarities is that of a *black disc* whose radius increases as $R = c \cdot \ln s$ [228] (i.e. $R \propto (\ln s)^\gamma$, with $\gamma = 1$ exactly).

20.8 Acknowledgements

It is a pleasure to thank Michael Albrow, Robert Cahn, Robert Ciesielski, Per Grafstrom, Frank Krauss, Paul Newman, Sergey Ostapchenko and Edward Sarkisyan-Grinbaum for discussions, suggestions and comments on this review. Special thanks to Graeme Watt who read the article through and helped to improve the presentation. MT is supported by MEYS of the Czech Republic within project LTT17018. VAK thanks the Institute of Physics of the Czech Academy of Sciences in Prague for hospitality.

References

- [1] M. Tanabashi *et al.* (Particle Data Group), *Phys. Rev.* **D98**, 3, 030001 (2018).
- [2] J. Campbell, J. Huston and F. Krauss, *The Black Book of Quantum Chromodynamics*, Oxford University Press (2017), ISBN 9780199652747, URL <https://global.oup.com/academic/product/the-black-book-of-quantum-chromodynamics-9780199652747>.
- [3] R. J. Eden *et al.*, *The analytic S-matrix*, Cambridge Univ. Press, Cambridge (1966).
- [4] A. Martin, *Lect. Notes Phys.* **3**, 1 (1969).
- [5] P. D. B. Collins, *An Introduction to Regge Theory and High-Energy Physics*, Cambridge Monographs on Mathematical Physics, Cambridge Univ. Press, Cambridge, UK (2009), ISBN 9780521110358, URL <http://www-spires.fnal.gov/spires/find/books/www?cl=QC793.3.R4C695>.
- [6] S. Donnachie *et al.*, *Camb. Monogr. Part. Phys. Nucl. Phys. Cosmol.* **19**, 1 (2002).
- [7] V. N. Gribov, *The theory of complex angular momenta: Gribov lectures on theoretical physics*, Cambridge Monographs on Mathematical Physics, Cambridge University Press (2007), ISBN 9780521037037, 9780521818346, 9780511055041, URL <http://www.cambridge.org/uk/catalogue/catalogue.asp?isbn=0521307848>.
- [8] S. Ostapchenko, in “25th European Cosmic Ray Symposium (ECRS 2016) Turin, Italy, September 04-09, 2016,” (2016), [arXiv:1612.09461].
- [9] T. Sjostrand, *Int. J. Mod. Phys.* **A3**, 751 (1988).
- [10] B. Andersson, *Camb. Monogr. Part. Phys. Nucl. Phys. Cosmol.* **7**, 1 (1997).
- [11] W. Kittel and E. A. De Wolf, *Soft multihadron dynamics* (2005), ISBN 9789812562951.
- [12] I. M. Dremin and A. B. Kaidalov, *Phys. Usp.* **49**, 263 (2006), [*Usp. Fiz. Nauk*176,275(2006)].
- [13] A. Buckley *et al.*, *Phys. Rept.* **504**, 145 (2011), [arXiv:1101.2599].
- [14] R. Ciesielski and K. Goulianos, *PoS ICHEP2012*, 301 (2013), [arXiv:1205.1446].
- [15] K. Akiba *et al.* (LHC Forward Physics Working Group), *J. Phys.* **G43**, 110201 (2016), [arXiv:1611.05079].
- [16] G. D. Alkhalov, S. L. Belostotsky and A. A. Vorobev, *Phys. Rept.* **42**, 89 (1978).
- [17] E. L. Feinberg and I. Y. Pomeranchuk, *Doklady Akad. Nauk SSSR* **93**, 439 (1953); E. L. Feinberg and I. Y. Pomeranchuk, *Suppl. Nuovo Cimento* **III**, serie X, 652 (1956).
- [18] R. Engel, D. Heck and T. Pierog, *Ann. Rev. Nucl. Part. Sci.* **61**, 467 (2011).
- [19] M. Gell-Mann, in “High-energy physics. Proceedings, 11th International Conference, ICHEP’62, Geneva, Switzerland, Jul 4-11, 1962,” 533–542 (1962).
- [20] S. Frautschi, M. Gell-Mann and F. Zachariasen, *Phys. Rev.* **126**, 6, 2204 (1962).
- [21] K. G. Borekov, A. B. Kaidalov and O. V. Kancheli, *Phys. Atom. Nucl.* **69**, 1765 (2006), [*Yad. Fiz.*69,1802(2006)].
- [22] J. R. Cudell *et al.* (COMPETE), *Phys. Rev. Lett.* **89**, 201801 (2002), [hep-ph/0206172].

- [23] C. Bourrely, J. Soffer and T. T. Wu, *Eur. Phys. J.* **C28**, 97 (2003), [hep-ph/0210264].
- [24] C. Patrignani *et al.* (Particle Data Group), *Chin. Phys.* **C40**, 10, 100001 (2016).
- [25] A. Donnachie and P. V. Landshoff, *Nucl. Phys.* **B231**, 189 (1984).
- [26] A. Donnachie and P. V. Landshoff, *Phys. Lett.* **B296**, 227 (1992), [hep-ph/9209205].
- [27] S. Mandelstam, *Nuovo Cim.* **30**, 1148 (1963).
- [28] V. N. Gribov, I. Ya. Pomeranchuk and K. A. Ter-Martirosian, *Phys. Lett.* **9**, 269 (1964).
- [29] V. A. Khoze, A. D. Martin and M. G. Ryskin, *Int. J. Mod. Phys.* **A30**, 08, 1542004 (2015), [arXiv:1402.2778].
- [30] E. Gotsman, E. Levin and U. Maor, *Int. J. Mod. Phys.* **A30**, 08, 1542005 (2015), [arXiv:1403.4531].
- [31] S. Ostapchenko, *Phys. Rev.* **D81**, 114028 (2010), [arXiv:1003.0196].
- [32] V. N. Gribov, *Sov. Phys. JETP* **26**, 414 (1968), [*Zh. Eksp. Teor. Fiz.* 53,654(1967)].
- [33] U. Amaldi, M. Jacob and G. Matthiae, *Ann. Rev. Nucl. Part. Sci.* **26**, 385 (1976).
- [34] A. B. Kaidalov, *Phys. Rept.* **50**, 157 (1979).
- [35] V. Barone and E. Predazzi, *High-Energy Particle Diffraction*, volume v.565 of *Texts and Monographs in Physics*, Springer-Verlag, Berlin Heidelberg (2002), ISBN 3540421076, URL <http://www-spires.fnal.gov/spires/find/books/www?cl=QC794.6.C6B37::2002>.
- [36] A. B. Kaidalov *et al.*, *Acta Phys. Polon.* **B34**, 3163 (2003), [hep-ph/0303111].
- [37] L. Frankfurt and M. Strikman, in E. M. Henley and S. D. Ellis, editors, "100 Years of Subatomic Physics," 363–423 (2013), [arXiv:1304.4308].
- [38] V. A. Khoze *et al.*, *Eur. Phys. J.* **C69**, 85 (2010), [arXiv:1005.4839].
- [39] D. A. Fagundes *et al.*, *Phys. Rev.* **D88**, 9, 094019 (2013), [arXiv:1306.0452].
- [40] R. Fiore *et al.*, *Int. J. Mod. Phys.* **A24**, 2551 (2009), [arXiv:0810.2902].
- [41] I. M. Dremin, *Phys. Usp.* **56**, 3 (2013), [*Usp. Fiz. Nauk* 183, 3 (2013)], [arXiv:1206.5474].
- [42] L. Frankfurt *et al.*, *Phys. Rev. Lett.* **101**, 202003 (2008), [arXiv:0808.0182].
- [43] G. Bertsch *et al.*, *Phys. Rev. Lett.* **47**, 297 (1981).
- [44] B. Z. Kopeliovich, L. I. Lapidus and A. B. Zamolodchikov, *JETP Lett.* **33**, 595 (1981), [*Pisma Zh. Eksp. Teor. Fiz.* 33, 612 (1981)].
- [45] M. L. Good and W. D. Walker, *Phys. Rev.* **120**, 1855 (1960).
- [46] J. Pumplin, *Phys. Rev.* **D8**, 2899 (1973).
- [47] M. Froissart, *Phys. Rev.* **123**, 1053 (1961).
- [48] A. Martin, *Nuovo Cim.* **A42**, 930 (1965).
- [49] L. Lukaszuk and A. Martin, *Nuovo Cim.* **A52**, 122 (1967).
- [50] A. A. Anselm and V. N. Gribov, *Phys. Lett.* **40B**, 487 (1972).
- [51] G. Cohen-Tannoudji, V. V. Ilyin and L. L. Jenkovszky, *Lett. Nuovo Cim.* **5S2**, 957 (1972), [*Lett. Nuovo Cim.* 5,957(1972)].
- [52] V. A. Khoze, A. D. Martin and M. G. Ryskin, *Eur. Phys. J.* **C18**, 167 (2000), [hep-ph/0007359].
- [53] G. Antchev *et al.* (TOTEM), *Nucl. Phys.* **B899**, 527 (2015), [arXiv:1503.08111].
- [54] G. Antchev *et al.* (TOTEM), *Eur. Phys. J.* **C79**, 10, 861 (2019), [arXiv:1812.08283].
- [55] L. Caneschi and A. Pignotti, *Phys. Rev. Lett.* **22**, 1219 (1969).
- [56] O. V. Kancheli, *JETP Lett.* **11**, 267 (1970), [*Pisma Zh. Eksp. Teor. Fiz.* 11, 397 (1970)].
- [57] A. H. Mueller, *Phys. Rev.* **D4**, 150 (1971).
- [58] D. Amati, A. Stanghellini and S. Fubini, *Nuovo Cim.* **26**, 896 (1962).
- [59] V. S. Fadin, E. A. Kuraev and L. N. Lipatov, *Phys. Lett.* **60B**, 50 (1975); E. A. Kuraev, L. N. Lipatov and V. S. Fadin, *Sov. Phys. JETP* **44**, 443 (1976), [*Zh. Eksp. Teor. Fiz.* 71,840(1976)]; E. A. Kuraev, L. N. Lipatov and V. S. Fadin, *Sov. Phys. JETP* **45**, 199 (1977), [*Zh. Eksp. Teor. Fiz.* 72,377(1977)]; I. I. Balitsky and L. N. Lipatov, *Sov. J. Nucl. Phys.* **28**, 822 (1978), [*Yad. Fiz.* 28,1597(1978)].
- [60] B. L. Ioffe, V. S. Fadin and L. N. Lipatov, *Quantum chromodynamics: Perturbative and nonperturbative aspects*, volume 30, Cambridge Univ. Press (2010), ISBN 9781107424753, 9780521631488, 9780511717444, URL <http://www.cambridge.org/de/knowledge/isbn/item2710695>.
- [61] S. Ostapchenko, *Phys. Rev.* **D83**, 014018 (2011), [arXiv:1010.1869].
- [62] J. L. Cardy, *Nucl. Phys.* **B75**, 413 (1974).
- [63] A. B. Kaidalov *et al.*, *Phys. Lett.* **45B**, 493 (1973).
- [64] E. G. S. Luna *et al.*, *Eur. Phys. J.* **C59**, 1 (2009), [arXiv:0807.4115].
- [65] T. Sjöstrand, *Adv. Ser. Direct. High Energy Phys.* **29**, 191 (2018), [arXiv:1706.02166].
- [66] K. Werner, F.-M. Liu and T. Pierog, *Phys. Rev.* **C74**, 044902 (2006), [hep-ph/0506232].
- [67] V. A. Abramovsky, V. N. Gribov and O. V. Kancheli, *Yad. Fiz.* **18**, 595 (1973), [*Sov. J. Nucl. Phys.* 18, 308 (1974)].
- [68] G. Alberi and G. Goggi, *Phys. Rept.* **74**, 1 (1981).
- [69] K. A. Goulianos, *Phys. Rept.* **101**, 169 (1983).
- [70] D. Bernard *et al.* (UA4), *Phys. Lett.* **B186**, 227 (1987).
- [71] R. E. Ansorge *et al.* (UA5), *Z. Phys.* **C33**, 175 (1986).
- [72] N. A. Amos *et al.* (E710), *Phys. Lett.* **B301**, 313 (1993).
- [73] F. Abe *et al.* (CDF), *Phys. Rev.* **D50**, 5535 (1994).
- [74] G. Aad *et al.* (ATLAS), *Eur. Phys. J.* **C72**, 1926 (2012), [arXiv:1201.2808].
- [75] V. Khachatryan *et al.* (CMS), *Phys. Rev.* **D92**, 1, 012003 (2015), [arXiv:1503.08689].
- [76] B. Abelev *et al.* (ALICE), *Eur. Phys. J.* **C73**, 6, 2456 (2013), [arXiv:1208.4968].
- [77] G. Aad *et al.* (ATLAS), *Phys. Lett.* **B754**, 214 (2016), [arXiv:1511.00502].
- [78] G. Aad *et al.* (ATLAS), *JHEP* **02**, 042 (2020), [arXiv:1911.00453].
- [79] A. M. Sirunyan *et al.* (CMS and TOTEM) (2020), [arXiv:2002.12146].
- [80] V. A. Khoze, A. D. Martin and M. G. Ryskin, *Eur. Phys. J.* **C73**, 2503 (2013), [arXiv:1306.2149].
- [81] V. A. Khoze, A. D. Martin and M. G. Ryskin, *Eur. Phys. J.* **C23**, 311 (2002), [hep-ph/0111078].
- [82] M. G. Albrow, T. D. Coughlin and J. R. Forshaw, *Prog. Part. Nucl. Phys.* **65**, 149 (2010), [arXiv:1006.1289].
- [83] M. Albrow, *Int. J. Mod. Phys.* **A29**, 1402006 (2014).
- [84] H. G. Fischer, W. Geist and M. Makariev, *Int. J. Mod. Phys.* **A29**, 28, 1446005 (2014).
- [85] A. Kirk, *Int. J. Mod. Phys.* **A29**, 28, 1446001 (2014), [arXiv:1408.1196].
- [86] M. A. Reyes *et al.* (E690), *Phys. Rev. Lett.* **81**, 4079 (1998).
- [87] G. Gutierrez and M. A. Reyes, *Int. J. Mod. Phys.* **A29**, 28, 1446008 (2014), [arXiv:1409.8243].
- [88] Y. L. Dokshitzer, D. Diakonov and S. I. Troian, *Phys. Rept.* **58**, 269 (1980).

- [89] M. Derrick *et al.* (ZEUS), Phys. Lett. **B315**, 481 (1993).
- [90] T. Ahmed *et al.* (H1), Nucl. Phys. **B429**, 477 (1994).
- [91] P. Newman and M. Wing, Rev. Mod. Phys. **86**, 3, 1037 (2014), [arXiv:1308.3368].
- [92] A. Aktas *et al.* (H1), Eur. Phys. J. **C48**, 715 (2006), [hep-ex/0606004].
- [93] S. Chekanov *et al.* (ZEUS), Nucl. Phys. **B816**, 1 (2009), [arXiv:0812.2003].
- [94] F. D. Aaron *et al.* (H1), Eur. Phys. J. **C72**, 2074 (2012), [arXiv:1203.4495].
- [95] F. D. Aaron *et al.* (H1, ZEUS), Eur. Phys. J. **C72**, 2175 (2012), [arXiv:1207.4864].
- [96] A. Aktas *et al.* (H1), JHEP **10**, 042 (2007), [arXiv:0708.3217].
- [97] A. Aktas *et al.* (H1), Eur. Phys. J. **C50**, 1 (2007), [hep-ex/0610076].
- [98] S. Chekanov *et al.* (ZEUS), Nucl. Phys. **B672**, 3 (2003), [hep-ex/0307068].
- [99] E. G. de Oliveira, A. D. Martin and M. G. Ryskin, Phys. Lett. **B695**, 162 (2011), [arXiv:1010.1366].
- [100] G. Antchev *et al.* (TOTEM), Eur. Phys. J. **C79**, 2, 103 (2019), [arXiv:1712.06153].
- [101] C. Augier *et al.* (UA4/2), Phys. Lett. **B316**, 448 (1993).
- [102] G. Antchev *et al.* (TOTEM), Eur. Phys. J. **C79**, 9, 785 (2019), [arXiv:1812.04732].
- [103] G. Antchev *et al.* (TOTEM), Eur. Phys. J. **C80**, 2, 91 (2020), [arXiv:1812.08610].
- [104] G. Antchev *et al.* (TOTEM), EPL **101**, 2, 21002 (2013).
- [105] G. Antchev *et al.* (TOTEM), Phys. Rev. Lett. **111**, 1, 012001 (2013).
- [106] G. Aad *et al.* (ATLAS), Nucl. Phys. **B889**, 486 (2014), [arXiv:1408.5778].
- [107] M. Aaboud *et al.* (ATLAS), Phys. Lett. **B761**, 158 (2016), [arXiv:1607.06605].
- [108] M. M. Block and R. N. Cahn, Rev. Mod. Phys. **57**, 563 (1985).
- [109] F. Abe *et al.* (CDF), Phys. Rev. **D50**, 5550 (1994).
- [110] C. Avila *et al.* (E811), Phys. Lett. **B445**, 419 (1999).
- [111] W. Guryn, "Invited talk at the Workshop on Diffraction and Low-x Physics, Reggio Calabria, Italy, August 26th–September 1st, 2018," .
- [112] K. Nakamura *et al.* (Particle Data Group), J. Phys. **G37**, 075021 (2010).
- [113] F. J. Nemes, PoS **DIS2017**, 059 (2018).
- [114] G. Antchev *et al.* (TOTEM), EPL **95**, 4, 41001 (2011), [arXiv:1110.1385].
- [115] G. Antchev *et al.* (TOTEM), Eur. Phys. J. **C76**, 12, 661 (2016), [arXiv:1610.00603].
- [116] J. Kaspar, "Invited talk at the meeting of the LHC Working Group on Forward Physics and Diffraction, CERN, Switzerland, December 16-17th, 2019," .
- [117] V. A. Schegelsky and M. G. Ryskin, Phys. Rev. **D85**, 094024 (2012), [arXiv:1112.3243].
- [118] A. Bruni, X. Janssen and P. Marage, in "Proceedings, HERA and the LHC Workshop Series on the implications of HERA for LHC physics: 2006-2008," 427–439 (2008), [arXiv:0812.0539].
- [119] A. Levy, in "Proceedings, 17th International Workshop on Deep-Inelastic Scattering and Related Subjects (DIS 2009): Madrid, Spain, April 26-30, 2009," 177 (2009), [arXiv:0907.2178].
- [120] J. R. Forshaw, R. Sandapen and G. Shaw, JHEP **11**, 025 (2006), [hep-ph/0608161].
- [121] A. Capella *et al.*, Nucl. Phys. **B593**, 336 (2001), [hep-ph/0005049].
- [122] V. S. Fadin and L. N. Lipatov, Phys. Lett. **B429**, 127 (1998), [hep-ph/9802290].
- [123] M. Ciafaloni and G. Camici, Phys. Lett. **B430**, 349 (1998), [hep-ph/9803389].
- [124] F. D. Aaron *et al.* (H1), JHEP **05**, 032 (2010), [arXiv:0910.5831].
- [125] C. Adloff *et al.* (H1), Eur. Phys. J. **C13**, 371 (2000), [hep-ex/9902019].
- [126] J. Breitweg *et al.* (ZEUS), Eur. Phys. J. **C6**, 603 (1999), [hep-ex/9808020].
- [127] S. Chekanov *et al.* (ZEUS), PMC Phys. **A1**, 6 (2007), [arXiv:0708.1478].
- [128] M. Ciafaloni, Nucl. Phys. **B296**, 49 (1988).
- [129] S. Catani, F. Fiorani and G. Marchesini, Phys. Lett. **B234**, 339 (1990).
- [130] S. Catani, F. Fiorani and G. Marchesini, Nucl. Phys. **B336**, 18 (1990).
- [131] G. Marchesini, Nucl. Phys. **B445**, 49 (1995), [hep-ph/9412327].
- [132] G. P. Salam, JHEP **07**, 019 (1998), [hep-ph/9806482].
- [133] M. Ciafaloni and D. Colferai, Phys. Lett. **B452**, 372 (1999), [hep-ph/9812366].
- [134] H. Kowalski, L. N. Lipatov and D. A. Ross, Eur. Phys. J. **C76**, 1, 23 (2016), [arXiv:1508.05744].
- [135] H. Kowalski *et al.*, Eur. Phys. J. **C77**, 11, 777 (2017), [arXiv:1707.01460].
- [136] S. J. Brodsky *et al.*, JETP Lett. **70**, 155 (1999), [hep-ph/9901229].
- [137] R. D. Ball *et al.*, Eur. Phys. J. **C78**, 4, 321 (2018), [arXiv:1710.05935].
- [138] E. M. Levin and M. G. Ryskin, Phys. Rept. **189**, 267 (1990).
- [139] L. V. Gribov, E. M. Levin and M. G. Ryskin, Phys. Rept. **100**, 1 (1983).
- [140] E. M. Levin, M. G. Ryskin and A. G. Shuvaev, Nucl. Phys. **B387**, 589 (1992).
- [141] A. H. Mueller, Phys. Rept. **73**, 237 (1981).
- [142] A. H. Mueller, Nucl. Phys. **B415**, 373 (1994).
- [143] A. H. Mueller and B. Patel, Nucl. Phys. **B425**, 471 (1994), [hep-ph/9403256].
- [144] N. N. Nikolaev, B. G. Zakharov and V. R. Zoller, JETP Lett. **59**, 6 (1994), [hep-ph/9312268].
- [145] V. N. Gribov and L. N. Lipatov, Sov. J. Nucl. Phys. **15**, 438 (1972), [Yad. Fiz.15,781(1972)]; G. Altarelli and G. Parisi, Nucl. Phys. **B126**, 298 (1977); Y. L. Dokshitzer, Sov. Phys. JETP **46**, 641 (1977), [Zh. Eksp. Teor. Fiz. 73, 1216 (1977)].
- [146] I. Balitsky, Nucl. Phys. **B463**, 99 (1996), [hep-ph/9509348].
- [147] I. Balitsky, Phys. Rev. **D60**, 014020 (1999), [hep-ph/9812311].
- [148] Y. V. Kovchegov, Phys. Rev. **D60**, 034008 (1999), [hep-ph/9901281].
- [149] G. Gustafson, Phys. Lett. **B718**, 1054 (2013), [arXiv:1206.1733].
- [150] S. Chatrchyan *et al.* (CMS, TOTEM), Eur. Phys. J. **C74**, 10, 3053 (2014), [arXiv:1405.0722].
- [151] Q.-D. Zhou (LHCF, ATLAS), EPJ Web Conf. **208**, 05008 (2019).
- [152] O. Adriani *et al.* (LHCf), Phys. Lett. **B780**, 233 (2018), [arXiv:1703.07678].
- [153] M. Aaboud *et al.* (ATLAS), ATLAS-CONF-2017-075.
- [154] C. Albajar *et al.* (UA1), Nucl. Phys. **B335**, 261 (1990).
- [155] G. J. Alner *et al.* (UA5), Z. Phys. **C33**, 1 (1986).

- [156] T. Aaltonen *et al.* (CDF), Phys. Rev. **D79**, 112005 (2009), [Erratum: Phys. Rev. **D82**, 119903(2010)], [arXiv:0904.1098].
- [157] F. Abe *et al.* (CDF), Phys. Rev. **D41**, 2330 (1990), [119(1989)].
- [158] K. Aamodt *et al.* (ALICE), Eur. Phys. J. **C68**, 89 (2010), [arXiv:1004.3034].
- [159] V. Khachatryan *et al.* (CMS), Phys. Rev. Lett. **105**, 022002 (2010), [arXiv:1005.3299].
- [160] B. B. Abelev *et al.* (ALICE), Eur. Phys. J. **C73**, 12, 2662 (2013), [arXiv:1307.1093].
- [161] A. M. Sirunyan *et al.* (CMS), Phys. Rev. **D96**, 11, 112003 (2017), [arXiv:1706.10194].
- [162] M. G. Ryskin, A. D. Martin and V. A. Khoze, Eur. Phys. J. **C71**, 1617 (2011), [arXiv:1102.2844].
- [163] X.-N. Wang, Phys. Rept. **280**, 287 (1997), [hep-ph/9605214].
- [164] S. Ostepchenko and M. Bleicher, Universe **5**, 5, 106 (2019).
- [165] F. M. Liu *et al.*, J. Phys. **G28**, 2597 (2002), [hep-ph/0109104].
- [166] E. Gotsman, E. Levin and U. Maor, Acta Phys. Polon. Supp. **8**, 777 (2015).
- [167] Y. V. Kovchegov and E. Levin, Camb. Monogr. Part. Phys. Nucl. Phys. Cosmol. **33**, 1 (2012).
- [168] E. A. De Wolf, I. M. Dremin and W. Kittel, Phys. Rept. **270**, 1 (1996), [hep-ph/9508325].
- [169] J. Adam *et al.* (ALICE), Eur. Phys. J. **C77**, 8, 569 (2017), [arXiv:1612.08975].
- [170] V. Khachatryan *et al.* (CMS), JHEP **09**, 091 (2010), [arXiv:1009.4122].
- [171] K. Eggert *et al.*, Nucl. Phys. **B86**, 201 (1975).
- [172] B. Alver *et al.* (PHOBOS), Phys. Rev. **C75**, 054913 (2007), [arXiv:0704.0966].
- [173] E. M. Levin and M. G. Ryskin, Sov. J. Nucl. Phys. **20**, 280 (1975), [Yad. Fiz. **20**, 519(1974)].
- [174] A. Capella and A. Krzywicki, Phys. Rev. **D18**, 4120 (1978).
- [175] M. Aaboud *et al.* (ATLAS), Eur. Phys. J. **C77**, 6, 428 (2017), [arXiv:1705.04176].
- [176] V. Khachatryan *et al.* (CMS), Phys. Lett. **B765**, 193 (2017), [arXiv:1606.06198].
- [177] S. Gieseke, "Invited talk at the Workshop on Multiple Partonic Interactions at the LHC, Prague, Czech Republic, November 18th–26th, 2019," .
- [178] S. Kundu, B. Mohanty and D. Mallick (2019), [arXiv:1912.05176].
- [179] M. Diehl, D. Ostermeier and A. Schafer, JHEP **03**, 089 (2012), [Erratum: JHEP **03**, 001(2016)], [arXiv:1111.0910].
- [180] T. Sjostrand and P. Z. Skands, JHEP **03**, 053 (2004), [hep-ph/0402078].
- [181] M. Aaboud *et al.* (ATLAS), Phys. Lett. **B790**, 595 (2019), [Phys. Lett. **790**, 595(2019)], [arXiv:1811.11094].
- [182] M. G. Ryskin and A. M. Snigirev, Phys. Rev. **D83**, 114047 (2011), [arXiv:1103.3495].
- [183] B. Blok *et al.*, Eur. Phys. J. **C74**, 2926 (2014), [arXiv:1306.3763].
- [184] M. Aaboud *et al.* (ATLAS), JHEP **03**, 157 (2017), [arXiv:1701.05390].
- [185] R. Snellings, New J. Phys. **13**, 055008 (2011), [arXiv:1102.3010].
- [186] M. Aaboud *et al.* (ATLAS), Phys. Rev. **C97**, 2, 024904 (2018), [arXiv:1708.03559].
- [187] N. Borghini, P. M. Dinh and J.-Y. Ollitrault, Phys. Rev. **C63**, 054906 (2001), [arXiv:nucl-th/0007063].
- [188] A. Bilandzic, R. Snellings and S. Voloshin, Phys. Rev. **C83**, 044913 (2011), [arXiv:1010.0233].
- [189] W. Li, Mod. Phys. Lett. **A27**, 1230018 (2012), [arXiv:1206.0148].
- [190] B. Schenke, J. Phys. **G38**, 124009 (2011), [arXiv:1106.6012].
- [191] K. G. Boreskov, A. B. Kaidalov and O. V. Kancheli, Eur. Phys. J. **C58**, 445 (2008), [arXiv:0809.0625].
- [192] K. G. Boreskov, A. B. Kaidalov and O. V. Kancheli, Phys. Atom. Nucl. **72**, 361 (2009), [Yad. Fiz. **72**, 390(2009)].
- [193] C. Bierlich and J. R. Christiansen, Phys. Rev. **D92**, 9, 094010 (2015), [arXiv:1507.02091].
- [194] Z.-W. Lin *et al.*, Phys. Rev. **C72**, 064901 (2005), [arXiv:nucl-th/0411110].
- [195] V. Khachatryan *et al.* (CMS), CMS-PAS-FSQ-16-008.
- [196] J. Bartels, Nucl. Phys. **B175**, 365 (1980).
- [197] J. Kwiecinski and M. Praszalowicz, Phys. Lett. **94B**, 413 (1980).
- [198] M. A. Braun (1998), [hep-ph/9805394].
- [199] J. Bartels, L. N. Lipatov and G. P. Vacca, Phys. Lett. **B477**, 178 (2000), [hep-ph/9912423].
- [200] C. Ewerz (2003), [hep-ph/0306137].
- [201] M. Fukugita and J. Kwiecinski, Phys. Lett. **83B**, 119 (1979), [625(1979)].
- [202] M. G. Ryskin, Sov. J. Nucl. Phys. **46**, 337 (1987), [Yad. Fiz. **46**, 611(1987)].
- [203] J. Bartels, C. Contreras and G. P. Vacca (2019), [arXiv:1910.04588].
- [204] E. Nagy *et al.*, Nucl. Phys. **B150**, 221 (1979).
- [205] A. Breakstone *et al.*, Phys. Rev. Lett. **54**, 2180 (1985).
- [206] A. Breakstone *et al.* (AMES-BOLOGNA-CERN-DORTMUND-HEIDELBERG-WARSAW), Nucl. Phys. **B248**, 253 (1984).
- [207] V. M. Abazov *et al.* (D0), Phys. Rev. **D86**, 012009 (2012), [arXiv:1206.0687].
- [208] M. Bozzo *et al.* (UA4), Phys. Lett. **155B**, 197 (1985).
- [209] D. Bernard *et al.* (UA4), Phys. Lett. **B171**, 142 (1986).
- [210] E. Martynov and B. Nicolescu, Eur. Phys. J. **C79**, 6, 461 (2019), [arXiv:1808.08580].
- [211] A. Donnachie and P. V. Landshoff, Phys. Lett. **123B**, 345 (1983).
- [212] A. Donnachie and P. V. Landshoff, Phys. Lett. **B798**, 135008 (2019), [arXiv:1904.11218].
- [213] J. Finkelstein *et al.*, Phys. Lett. **B232**, 257 (1989).
- [214] V. A. Khoze, A. D. Martin and M. G. Ryskin, Phys. Lett. **B780**, 352 (2018), [arXiv:1801.07065].
- [215] W. Kilian and O. Nachtmann, Eur. Phys. J. **C5**, 317 (1998), [hep-ph/9712371].
- [216] J. Bartels *et al.*, Eur. Phys. J. **C20**, 323 (2001), [hep-ph/0102221].
- [217] L. A. Harland-Lang *et al.*, Phys. Rev. **D99**, 3, 034011 (2019), [arXiv:1811.12705].
- [218] J. Olsson (H1), in "New trends in high-energy physics: Experiment, phenomenology, theory. Proceedings, International Conference, Yalta, Crimea, Ukraine, September 22-29, 2001," 79–87 (2001), [hep-ex/0112012].
- [219] C. Adloff *et al.* (H1), Phys. Lett. **B544**, 35 (2002), [hep-ex/0206073].
- [220] T. Berndt (H1), Acta Phys. Polon. **B33**, 3499 (2002), [182(2002)].
- [221] W. Heisenberg, Z. Phys. **133**, 65 (1952).
- [222] G. Pancheri and Y. N. Srivastava, Eur. Phys. J. **C77**, 3, 150 (2017), [arXiv:1610.10038].
- [223] M. M. Block, Phys. Rept. **436**, 71 (2006), [hep-ph/0606215].
- [224] M. Giordano, E. Meggiolaro and N. Moretti, JHEP **09**, 031 (2012), [arXiv:1203.0961].

- [225] E. Ferreiro *et al.*, Nucl. Phys. **A710**, 373 (2002), [hep-ph/0206241].
- [226] P. Grassberger and K. Sundermeyer, Phys. Lett. **77B**, 220 (1978).
- [227] K. G. Boreskov, in M. Olshanetsky and A. Vainshtein, editors, “Multiple facets of quantization and supersymmetry,” 322–351 (2001), [hep-ph/0112325].
- [228] V. A. Khoze, A. D. Martin and M. G. Ryskin, Phys. Lett. **B787**, 167 (2018), [arXiv:1809.10406].

Astrophysics and Cosmology

21. Experimental tests of gravitational theory (rev.)	409
22. Big-Bang cosmology (rev.)	422
23. Inflation (rev.)	435
24. Big-Bang nucleosynthesis (rev.)	451
25. Cosmological parameters (rev.)	458
26. Neutrinos in cosmology (new)	467
27. Dark matter (new)	474
28. Dark energy (rev.)	490
29. Cosmic microwave background (rev.)	499
30. Cosmic rays (rev.)	510

21. Experimental Tests of Gravitational Theory

Revised August 2019 by T. Damour (IHES, Bures-sur-Yvette).

21.1 General Relativity

Einstein's theory of General Relativity (GR), the current “standard” theory of gravitation, describes gravity as a universal deformation of the Minkowski metric:

$$g_{\mu\nu}(x^\lambda) = \eta_{\mu\nu} + h_{\mu\nu}(x^\lambda), \text{ where } \eta_{\mu\nu} = \text{diag}(-1, +1, +1, +1). \quad (21.1)$$

GR is classically defined by two postulates, embodied in the total action defining the theory:

$$S_{\text{tot}}[g_{\mu\nu}, \psi, A_\mu, H] = c^{-1} \int d^4x (\mathcal{L}_{\text{Ein}} + \mathcal{L}_{\text{SM}}). \quad (21.2)$$

The first postulate states that the Lagrangian density describing the propagation and self-interaction of the gravitational field is

$$\mathcal{L}_{\text{Ein}}[g_{\alpha\beta}] = \frac{c^4}{16\pi G} \sqrt{g} g^{\mu\nu} R_{\mu\nu}(g_{\alpha\beta}), \quad (21.3)$$

where G denotes Newton's constant, $g = -\det(g_{\mu\nu})$, $g^{\mu\nu}$ is the matrix inverse of $g_{\mu\nu}$, and where the Ricci tensor $R_{\mu\nu} \equiv R^\alpha{}_{\mu\alpha\nu}$ is the only independent trace of the curvature tensor

$$R^\alpha{}_{\mu\beta\nu} = \partial_\beta \Gamma_{\mu\nu}^\alpha - \partial_\nu \Gamma_{\mu\beta}^\alpha + \Gamma_{\sigma\beta}^\alpha \Gamma_{\mu\nu}^\sigma - \Gamma_{\sigma\nu}^\alpha \Gamma_{\mu\beta}^\sigma, \quad (21.4)$$

$$\Gamma_{\mu\nu}^\lambda = \frac{1}{2} g^{\lambda\sigma} (\partial_\mu g_{\nu\sigma} + \partial_\nu g_{\mu\sigma} - \partial_\sigma g_{\mu\nu}). \quad (21.5)$$

The second postulate states that $g_{\mu\nu}$ (and its associated connection) couples universally, and minimally, to all the bosonic (respectively fermionic) fields of the Standard Model by replacing everywhere the Minkowski metric $\eta_{\mu\nu}$ (respectively the flat Minkowski connection). Schematically (suppressing matrix indices and labels for the various gauge fields and fermions and for the Higgs doublet),

$$\begin{aligned} \mathcal{L}_{\text{SM}}[\psi, A_\mu, H, g_{\mu\nu}] = & \\ & - \frac{1}{4} \sum \sqrt{g} g^{\mu\alpha} g^{\nu\beta} F_{\mu\nu}^\alpha F_{\alpha\beta}^\nu - \sum \sqrt{g} \bar{\psi} \gamma^\mu (D_\mu + \frac{1}{4} \omega_{ij\mu} \gamma^{ij}) \psi \\ & - \frac{1}{2} \sqrt{g} g^{\mu\nu} \bar{D}_\mu \bar{H} D_\nu H - \sqrt{g} V(H) - \sum \lambda \sqrt{g} \bar{\psi} H \psi. \end{aligned} \quad (21.6)$$

Here $F_{\mu\nu}^\alpha = \partial_\mu A_\nu^\alpha - \partial_\nu A_\mu^\alpha + g_A f_{bc}^\alpha A_\mu^b A_\nu^c$ and the (representation-dependent) gauge-field covariant derivative $D_\mu = \partial_\mu + g_A A_\mu^\alpha T_\alpha^{\text{rep}}$ are defined as in Special Relativity, while the derivative of spin- $\frac{1}{2}$ fermions also includes a coupling to the gravitational “spin-connection” $\omega_{ij\mu} = -\omega_{ji\mu}$, via its contraction with $\gamma^{ij} = \frac{1}{2}(\gamma^i \gamma^j - \gamma^j \gamma^i)$, where $i, j = 0, 1, 2, 3$ and $\gamma^i = e^\mu{}_{i\mu} \gamma^\mu$ are usual (numerical) Dirac matrices satisfying $\gamma^i \gamma^j + \gamma^j \gamma^i = 2\eta^{ij}$. The connection components $\omega_{ij\mu}$ are defined in terms of the local orthonormal frame (vierbein) $e^i{}_\mu$ (such that $g_{\mu\nu} = \eta_{ij} e^i{}_\mu e^j{}_\nu$) used to describe the components of the various fermions ψ , and of its inverse $e_i{}^\mu$ (such that $e_i{}^\mu e^j{}_\mu = \delta_i^j$), by $\omega_{ij\mu} = \frac{1}{2} (C_{i[jk]} + C_{j[ki]} - C_{k[ij]}) e^k{}_\mu$ where $C_{i[jk]} = \eta_{is} C^s{}_{[jk]}$, with $C^i{}_{[jk]} \equiv (\partial_\mu e^i{}_\nu - \partial_\nu e^i{}_\mu) e_j{}^\mu e_k{}^\nu$. From the total action follow Einstein's field equations,

$$R_{\mu\nu} - \frac{1}{2} R g_{\mu\nu} = \frac{8\pi G}{c^4} T_{\mu\nu}. \quad (21.7)$$

Here $R = g^{\mu\nu} R_{\mu\nu}$ is the scalar curvature, and $T_{\mu\nu} \equiv g_{\mu\alpha} g_{\nu\beta} T^{\alpha\beta}$ where $T^{\mu\nu} = (2/\sqrt{g}) \delta \mathcal{L}_{\text{SM}} / \delta g_{\mu\nu}$ is the (symmetric) energy-momentum tensor of the Standard Model matter. The theory is invariant under arbitrary coordinate transformations: $x^\mu = f^\mu(x^\nu)$ (as well as under arbitrary local $\text{SO}(3,1)$ rotations of the vierbein, $e^i{}_\mu = \Lambda^i{}_j(x) e'^j{}_\mu$). To solve the field equations Eq. (21.7), one needs to fix the coordinate gauge freedom, e.g., the “harmonic gauge” (which is the analogue of the Lorenz gauge, $\partial_\mu A^\mu = 0$, in electromagnetism) corresponds to imposing the condition $\partial_\nu (\sqrt{g} g^{\mu\nu}) = 0$.

In this *Review*, we only consider the classical limit of gravitation (i.e. classical matter and classical gravity). Quantum

gravitational effects are expected (when considered at low energy) to correct the classical action Eq. (21.2) by additional terms involving quadratic and higher powers of the curvature tensor. This suggests that the validity of classical gravity extends (at most) down to length scales of order the Planck length $L_P = \sqrt{\hbar G/c^3} \simeq 1.62 \times 10^{-33}$ cm, i.e., up to energy scales of order the Planck energy $E_P = \sqrt{\hbar c^5/G} \simeq 1.22 \times 10^{19}$ GeV. Considering quantum matter in a classical gravitational background also poses interesting challenges, notably the possibility that the zero-point fluctuations of the matter fields generate a nonvanishing vacuum energy density ρ_{vac} , corresponding to a term $-\sqrt{g} \rho_{\text{vac}}$ in \mathcal{L}_{SM} [1]. This is equivalent to adding a “cosmological constant” term $+\Lambda g_{\mu\nu}$ on the left-hand side of Einstein's equations, Eq. (21.7), with $\Lambda = 8\pi G \rho_{\text{vac}}/c^4$. Recent cosmological observations (see the following *Reviews*) suggest a positive value of Λ corresponding to $\rho_{\text{vac}} \approx (2.3 \times 10^{-3} \text{eV})^4$. Such a small value has a negligible effect on the non-cosmological tests discussed below.

21.2 Key features and predictions of GR

The definition of GR recalled above makes predictions both about the coupling of gravity to matter, and about the structure of the gravitational field beyond its previously known Newtonian aspects.

21.2.1 Equivalence Principle

First, the universal nature of the coupling between $g_{\mu\nu}$ and the Standard Model matter postulated in Eq. (21.6) entails many observable consequences that go under the generic name of “Equivalence Principle”.

A first aspect of the Equivalence Principle is that the outcome of a local non-gravitational experiment, referred to local standards, should not depend on where, when, and in which locally inertial frame, the experiment is performed. This means, for instance, that local experiments should neither feel the cosmological evolution of the Universe (constancy of the “constants”), nor exhibit preferred directions in spacetime (isotropy of space, local Lorentz invariance).

A second aspect of the Equivalence Principle is that the kinetic terms, $g^{\mu\nu} \partial_\mu \phi \partial_\nu \phi$ or $\bar{\psi} \gamma^i e_i{}^\mu \partial_\mu \psi$, of all the fields of Nature (including the gravitational field itself) are universally coupled to the same curved spacetime metric $g_{\mu\nu}(x) = \eta_{ij} e^i{}_\mu e^j{}_\nu$. This implies in particular that all massless fields should propagate with the same speed.

A third aspect of the Equivalence Principle is that two (electrically neutral) test bodies dropped at the same location and with the same velocity in an external gravitational field should fall in the same way, independently of their masses and compositions (“universality of free fall” or “Weak Equivalence Principle”). In addition, the study (using the nonlinear structure of GR) of the motion, in an external gravitational field, of bodies having a non-negligible, or even strong, self-gravity (such as planets, neutron stars, or black holes) has shown that the latter property of free-fall universality holds equally well for self-gravitating bodies (“Strong Equivalence Principle”).

A last aspect of the Equivalence Principle concerns various universality features of the gravitational redshift of clock rates. GR predicts that, when intercomparing them by means of electromagnetic signals, two (non gravity-based) clocks located along two different spacetime worldlines should exhibit a universal difference in clock rate that depends on their worldlines, but that is independent of their nature and constitution. For instance, two clocks located at two different positions in a static external Newtonian potential $U(\mathbf{x}) = \sum Gm/r$ should exhibit, when intercompared by electromagnetic signals, the difference in clock rate, $\tau_1/\tau_2 = \nu_2/\nu_1 = 1 + [U(\mathbf{x}_1) - U(\mathbf{x}_2)]/c^2 + O(1/c^4)$, (“universal gravitational redshift of clock rates”). Similarly, the comparison of atomic-transition frequencies when observing on Earth a transition that took place on a far-away galaxy should involve (at lowest order in cosmological perturbations) the universal cosmological redshift factor $1+z = a(t_{\text{reception}})/a(t_{\text{emission}})$ between the Friedmann scale factors $a(t)$ (see below).

21.2.2 Quasi-stationary, weak-field (post-Newtonian) gravity

When applied to quasi-stationary, weak-field gravitational fields, Einstein equations, Eq. (21.7), entail a spacetime structure which predicts deviations from Newtonian gravity of the first post-Newtonian (1PN) order, *i.e.*, fractionally smaller than Newtonian effects by a factor $O(v^2/c^2) \sim O(GM/(c^2 r))$. The 1PN-accurate solution of Eq. (21.7) reads (in harmonic gauge)

$$\begin{aligned} g_{00} &= -1 + \frac{2}{c^2}V - \frac{2}{c^4}V^2 + O\left(\frac{1}{c^6}\right), \\ g_{0i} &= -\frac{4}{c^3}V_i + O\left(\frac{1}{c^5}\right), \\ g_{ij} &= \delta_{ij}\left[1 + \frac{2}{c^2}V\right] + O\left(\frac{1}{c^4}\right), \end{aligned} \quad (21.8)$$

where $x^0 = ct$, $i, j = 1, 2, 3$, and where the scalar, V , and vector, V_i , (retarded) potentials are defined in terms of the sources $\sigma = \frac{T^{00} + T^{ii}}{c^2}$, $\sigma_i = \frac{T^{0i}}{c}$ by

$$V = \square_{\text{ret}}^{-1}[-4\pi G\sigma]; \quad V_i = \square_{\text{ret}}^{-1}[-4\pi G\sigma_i]. \quad (21.9)$$

In GR the gravitational interaction of N moving point masses (labelled by $A = 1, \dots, N$) is described by a reduced (classical) action that admits a diagrammatic expansion:

$$S_{\text{reduced}} = S^{\text{free}} + S^{\text{tree-level}} + S^{\text{one-loop}} + \dots \quad (21.10)$$

where the free (special-relativistic) action reads

$$\begin{aligned} S^{\text{free}} &= -\sum_A \int m_A c \sqrt{-\eta_{\mu\nu} dx_A^\mu dx_A^\nu} \\ &= -\sum_A \int dt m_A c^2 \sqrt{1 - \mathbf{v}_A^2/c^2}, \end{aligned} \quad (21.11)$$

while the tree-level (one-graviton-exchange) interaction term reads

$$S^{\text{tree-level}} = -\frac{8\pi G}{c^4} \int d^4x T^{\mu\nu} \square^{-1}(T_{\mu\nu} - \frac{1}{2}T\eta_{\mu\nu}) = \int dt L^{(2)}. \quad (21.12)$$

Corresponding to the 1PN-accurate metric of Eq. (21.8), the 1PN-accurate expansion of the latter tree-level, two-body interaction Lagrangian $L^{(2)}$ reads (with $r_{AB} \equiv |\mathbf{x}_A - \mathbf{x}_B|$, $\mathbf{n}_{AB} \equiv (\mathbf{x}_A - \mathbf{x}_B)/r_{AB}$)

$$\begin{aligned} L^{(2)} &= \frac{1}{2} \sum_{A \neq B} \frac{G m_A m_B}{r_{AB}} \left[1 + \frac{3}{2c^2}(v_A^2 + v_B^2) - \frac{7}{2c^2}(\mathbf{v}_A \cdot \mathbf{v}_B) \right. \\ &\quad \left. - \frac{1}{2c^2}(\mathbf{n}_{AB} \cdot \mathbf{v}_A)(\mathbf{n}_{AB} \cdot \mathbf{v}_B) + O\left(\frac{1}{c^4}\right) \right] \end{aligned} \quad (21.13)$$

The two-body interactions, Eq. (21.13), exhibit v^2/c^2 corrections to Newton's $1/r$ potential induced by spin-2 exchange ("gravitomagnetism"). Consistency at the 1PN level, $v^2/c^2 \sim Gm/rc^2$, requires that one also considers the three-body interactions contained in the one-loop contribution $S^{\text{one-loop}}$, corresponding to terms induced by some of the three-graviton vertices and other non-linearities (terms $O(h^2)$ and $O(hT)$ in Eq. (21.15) below), *i.e.*, to the $O(V^2)$ term in Eq. (21.8):

$$L^{(3)} = -\frac{1}{2} \sum_{B \neq A \neq C} \frac{G^2 m_A m_B m_C}{r_{AB} r_{AC} c^2} + O\left(\frac{1}{c^4}\right). \quad (21.14)$$

21.2.3 Gravitational Waves in GR

The linearized approximation to Einstein's field equations, Eq. (21.7), in harmonic gauge $\partial^\nu(h_{\mu\nu} - \frac{1}{2}h\eta_{\mu\nu}) = 0$ (with $h \equiv \eta^{\mu\nu}h_{\mu\nu}$), reads

$$\square h_{\mu\nu} = -\frac{16\pi G}{c^4}(T_{\mu\nu} - \frac{1}{2}T\eta_{\mu\nu}) + O(h^2) + O(hT). \quad (21.15)$$

Outside of any source (*i.e.*, when $T_{\mu\nu} = 0$), this yields $\square h_{\mu\nu} = 0$, with $\partial^\nu(h_{\mu\nu} - \frac{1}{2}h\eta_{\mu\nu}) = 0$. The generic linearized solution (modulo the diffeomorphism freedom) of the latter vacuum Einstein equations can be written as (with $k^2 = k \cdot k = \eta_{\mu\nu}k^\mu k^\nu$, $k \cdot x = k_\mu x^\mu$)

$$h_{\mu\nu}(x) = \int d^4k \delta(k^2) \epsilon_{\mu\nu}(k) e^{ik \cdot x}, \quad (21.16)$$

where the polarization tensor $\epsilon_{\mu\nu}(k)$ must be transverse ($\epsilon_{\mu\nu}k^\nu = 0$) and traceless ($\eta^{\mu\nu}\epsilon_{\mu\nu} = 0$). In addition, $\epsilon_{\mu\nu}(k)$ can be freely submitted to the gauge freedom $\epsilon'_{\mu\nu} = \epsilon_{\mu\nu} + \xi_\mu k_\nu + \xi_\nu k_\mu$. This implies that gravitational waves (GW) propagate with the speed of light, and (like electromagnetic waves) have only two independent polarizations. In a frame where, say, $k^\mu = (ck, 0, 0, k)$, the two independent linear polarization tensors can be taken to have components only in the transverse 1-2 plane, of the following form: $\epsilon_{11}^+ = -\epsilon_{22}^+ = \epsilon^+$, with $\epsilon_{12}^+ = \epsilon_{21}^+ = 0$; or $\epsilon_{11}^\times = +\epsilon_{22}^\times = \epsilon^\times$, with $\epsilon_{12}^\times = \epsilon_{21}^\times = 0$. Under a little-group rotation of angle θ in the 1-2 plane, the two circular polarization amplitudes $\epsilon^{(\pm)} = \epsilon^+ \mp i\epsilon^\times$ vary as $\epsilon'^{(\pm)} = e^{\pm 2i\theta} \epsilon^{(\pm)}$, thereby characterizing the helicity-2 nature of GWs.

When solving the inhomogeneous equation Eq. (21.15), taking into account the nonlinear contributions $O(h^2) + O(hT)$, one finds that, to lowest order, the GW amplitude emitted at large distances by a matter distribution is given by the following "quadrupole formula"

$$h_{ij}^{\text{TT}}(T, \mathbf{X}) \approx \frac{2G}{c^4} P_{ijab}^{\text{TT}}(\mathbf{N}) \frac{\dot{Q}_{ab}(T - R/c)}{R}, \quad (21.17)$$

where $Q_{ij}(t) = \int d^3x \sigma(t, \mathbf{x})(x^i x^j - \frac{1}{3}\delta_{ij}x^2)$ ($a, b, i, j = 1, 2, 3$) is the quadrupole moment of the source, $R = |\mathbf{X}|$ the distance to the source, $\mathbf{N} = \mathbf{X}/R$ the unit direction from the source to the observer, and $P_{ijab}^{\text{TT}}(\mathbf{N}) = (\delta_{ia} - N_i N_a)(\delta_{jb} - N_j N_b) - \frac{1}{2}(\delta_{ij} - N_i N_j)(\delta_{ab} - N_a N_b)$ the transverse-traceless projector onto the 2-plane orthogonal to \mathbf{N} .

21.2.4 Strong gravitational fields: neutron stars and black holes

The nonlinear structure of Einstein's equations implies many predictions for strong gravitational fields that distinguish GR from Newtonian gravity. For instance, in Newtonian gravity, there is no upper limit to the dimensionless gravitational potential U/c^2 , with U satisfying Poisson's equation $\Delta U = -4\pi G\rho$, where ρ denotes the Newtonian mass density. By contrast, in GR, the dimensionless surface gravitational potential $GM/(c^2 R)$ of a spherically symmetric (perfect fluid) body cannot exceed $\frac{4}{9}[2]$.

Given an equation of state $p = f(\rho)$ modeling the interior of a (cold) spherically symmetric body (say a non-rotating neutron star), Einstein equations, Eq. (21.7), with $T^{\mu\nu} = (\rho + p)u^\mu u^\nu + pg^{\mu\nu}$, and

$$g_{\mu\nu} dx^\mu dx^\nu = -e^{2\Phi(r)} c^2 dt^2 + \frac{dr^2}{1 - \frac{2GM(r)}{c^2 r}} + r^2 (d\theta^2 + \sin^2 \theta d\phi^2), \quad (21.18)$$

yield the following Tolman-Oppenheimer-Volkoff radial equations:

$$p'(r) = -\frac{G(\rho + p/c^2)(M(r) + 4\pi r^3 p/c^2)}{r^2(1 - 2GM(r)/(c^2 r))}; \quad (21.19)$$

$$M'(r) = 4\pi r^2 \rho; \quad (21.20)$$

$$\Phi'(r) = \frac{G(M(r) + 4\pi r^3 p/c^2)}{r^2(1 - 2GM(r)/(c^2 r))}. \quad (21.21)$$

In the exterior of the star ($r \geq R$), the metric takes the Schwarzschild form

$$\begin{aligned} g_{\mu\nu} dx^\mu dx^\nu &= -\left(1 - \frac{2GM}{c^2 r}\right) c^2 dt^2 + \frac{dr^2}{1 - \frac{2GM}{c^2 r}} \\ &\quad + r^2 (d\theta^2 + \sin^2 \theta d\phi^2), \end{aligned} \quad (21.22)$$

where $M \equiv M(R)$ is the total gravitational mass of the star. GR predicts, for any given $p = f(\rho)$, several (in principle) observable

features of neutron stars, such as: (i) the maximum mass of a neutron star; (ii) the relation between the radius R and the total mass M ; (iii) the dimensionless surface gravitational potential $GM/(c^2R)$ (linked to the surface redshift $\sqrt{-g_{00}} = \sqrt{1 - \frac{2GM}{c^2R}}$ measured by an observer at infinity); (iv) the moment of inertia; and (v) the Love number (tidal polarizability). The current uncertainty on the equation of state of a neutron star yields the GR-predicted approximate range for the maximum mass of non-rotating neutron stars $1.5 M_\odot \lesssim M_{\max} \lesssim 2.5 M_\odot$, and the absolute upper bound $M_{\max} < 3 M_\odot$ [3]. The surface gravitational potential of a typical neutron star is $GM/c^2 R_{\text{NS}} \simeq 0.17$, which is a factor $\sim 10^8$ higher than the surface potential of the Earth, and a mere factor 3 below the black hole limit $GM/c^2 R_{\text{BH}} = \frac{1}{2}$ to be discussed next.

The existence of a maximum mass for a neutron star led Oppenheimer and Snyder [4] to predict that the end point of stellar evolution for sufficiently heavy stars, after exhaustion of all thermonuclear sources of energy, will be what are now called “black holes.” The latter are solutions of Einstein’s equations whose past structure involves a gravitationally collapsing star, but whose presently observable structure is essentially described (for non-rotating black holes) by the vacuum Schwarzschild solution Eq. (21.22). It took many years for theoretical (and mathematical) physicists to understand that the apparent singularity of the Schwarzschild solution at $r = \frac{2GM}{c^2}$ was a coordinate singularity and that the Schwarzschild spacetime was regular at the “black hole horizon”, $R_{\text{BH}} \equiv \frac{2GM}{c^2}$. The rotating analog of the Schwarzschild spacetime is the Kerr black hole [5].

Black holes are outstanding consequences of GR which enjoy many remarkable properties, notably: (i) presence of a one-way surface (the horizon) for all waves and particles; (ii) absence of “hair” (*i.e.*, barring a possible electric charge, their structure is fully described by only two parameters, total mass, M , and total angular momentum, $J \leq GM^2/c$); (iii) existence of a spectrum of damped quasi-normal vibrational modes; and (iv) a behavior under external perturbations similar to ordinary physical objects satisfying the laws of (dissipative) thermodynamics. Moreover, though no classical waves or particles can get out of the horizon, black holes are predicted to slowly evaporate via quantum particle creation.

21.2.5 Cosmology

To complete our short tour of the main predictions of GR, let us mention that GR offers the current standard framework for describing the large-scale structure of the Cosmos, from the nearly homogeneous Big Bang (and its plausible inflationary beginning) to the current inhomogeneous Universe undergoing an accelerated expansion. The spacetime structure on large (temporal and spatial) scales is well described by a solution of Einstein’s equations of the form

$$ds^2 = -(1 + 2\Phi(t, \mathbf{x}))c^2 dt^2 + 2W_i(t, \mathbf{x})dt dx^i + a^2(t)((1 - 2\Psi(t, \mathbf{x}))\delta_{ij} + h_{ij}(t, \mathbf{x}))dx^i dx^j, \quad (21.23)$$

where, after a suitable gauge-fixing [6], $W_i(t, \mathbf{x})$ is transverse, while $h_{ij}(t, \mathbf{x})$ is transverse and traceless. The source $T^{\mu\nu}$ must involve a certain number of postulated ingredients: an inflaton field; the matter of the Standard Model; a dark matter component; and a cosmological constant contribution $T_\Lambda^{\mu\nu} = -\rho_{\text{vac}}g^{\mu\nu}$, with $\rho_{\text{vac}} \equiv c^4\Lambda/(8\pi G)$. The scale factor $a(t)$ of the Friedmann background metric $ds_0^2 = -c^2 dt^2 + a^2(t)\delta_{ij}dx^i dx^j$ satisfies the GR-predicted Friedmann equations (with vanishing spatial curvature $k = 0$),

$$H^2 \equiv \left(\frac{\dot{a}}{a}\right)^2 = \frac{8\pi G}{3}\rho_{\text{tot}}, \quad (21.24)$$

$$\frac{\ddot{a}}{a} = -\frac{4\pi G}{3}\left(\rho_{\text{tot}} + \frac{3}{c^2}p_{\text{tot}}\right), \quad (21.25)$$

while the scalar $(\Phi(t, \mathbf{x}), \Psi(t, \mathbf{x}))$, vector $(W_i(t, \mathbf{x}))$, and tensor $(h_{ij}(t, \mathbf{x}))$ inhomogeneous perturbations satisfy some GR-predicted propagation equations (coupled to matter perturbations); see [6] and the following *Reviews*. When the cosmic fluid is

well approximated by a perfect fluid, Einstein’s equations predict the following link between the scalar perturbations

$$\Phi(t, \mathbf{x}) = \Psi(t, \mathbf{x}). \quad (21.26)$$

21.3 A roadmap of parametrizations of deviations from GR, and of modified gravity

As will be discussed below, all currently performed gravitational experiments are compatible with GR. However, similarly to what is done in discussions of precision electroweak experiments, it is useful to quantify the significance of precision gravitational experiments by parameterizing possible deviations from GR. One can distinguish two main approaches to considering, and parameterizing, deviations from GR: (i) theory-agnostic phenomenological approaches; or, (ii) the study of the predictions of specific classes of alternative theories of gravity. Both types have led to useful ways of discussing tests of gravity. Both types also have their limitations. Considering them together leads to cross-fertilization.

21.3.1 Theory-agnostic phenomenological approaches to parameterizing deviations from GR

The theory-agnostic phenomenological approach is the oldest, and, arguably, the most robust one. It essentially consists in starting from specific observable predictions within the considered standard theory, and of deforming them by introducing some free parameters measuring either deviations from effects already present within the standard theory, or new effects absent from the standard theory. A classic example is the periastron advance of Mercury (and the other planets). When working within Newtonian gravity as a standard theory of gravity, the rate of periastron advance of Mercury, $\dot{\omega}$, is (when neglecting the quadrupole moment of the Sun) a calculable function of the masses and semi-major axes of the other planets of the solar system, say $\dot{\omega}^{\text{Newton}}(m_i, a_i)$. However, $\dot{\omega}$ is also a directly observable quantity, so that one can parameterize the periastron advance of Mercury by writing

$$\dot{\omega}^{\text{obs}} = \dot{\omega}^{\text{Newton}}(m_i, a_i) + \Delta\dot{\omega}. \quad (21.27)$$

Using other observable data to determine some “observed” values of the m_i ’s and a_i ’s, one can then measure the anomalous periastron precession $\Delta\dot{\omega}$ and see whether it is compatible with zero, or not. As is well-known, Leverrier used such a methodology and, in 1859, measured an anomalous periastron precession of about $\Delta\dot{\omega} \simeq 38$ arcsec/century (later re-estimated at 43 arcsec/century), which was explained in 1915 as a GR prediction. Let us discuss further examples of the use of such theory-agnostic approaches for discussing deviations from GR.

21.3.2 Parameterized post-Newtonian (PPN) formalism.

When considering the weak-field slow-motion limit appropriate to describing gravitational experiments in the solar system, it has been traditional to parameterize possible (long-range) deviations from the GR-predicted 1PN metric by introducing extra dimensionless coefficients in the various terms of the metric of Eq. (21.8). The minimal version of the parameterized post-Newtonian (PPN) formalism (essentially due to Eddington) involves only two parameters β and γ , namely

$$g_{00} = -1 + \frac{2}{c^2}V - \frac{2\beta}{c^4}V^2 + O\left(\frac{1}{c^6}\right), \quad (21.28)$$

$$g_{0i} = -\frac{2(\gamma+1)}{c^3}V_i + O\left(\frac{1}{c^5}\right), \quad (21.29)$$

$$g_{ij} = \delta_{ij}\left[1 + \frac{2\gamma}{c^2}V\right] + O\left(\frac{1}{c^4}\right), \quad (21.30)$$

with V and V_i defined by Eq. (21.9), with the same vectorial source $\sigma_i = \frac{T^{0i}}{c}$, but a modified scalar source

$$\sigma^{\text{PPN}} = \frac{1}{c^2}\left[\left(1 + (3\gamma - 2\beta - 1)\frac{V}{c^2}\right)T^{00} + \gamma T^{ii}\right]. \quad (21.31)$$

In GR, $\beta^{\text{GR}} = 1$ and $\gamma^{\text{GR}} = 1$, so that deviations from GR are parameterized by $\bar{\beta} \equiv \beta - 1$ and $\bar{\gamma} \equiv \gamma - 1$. Richer versions of the

PPN formalism (involving up to ten parameters) were developed in interaction with the study of classes of alternative theories of gravity [7, 8]. This led to parameterizing new types of contributions to the IPN metric that are absent in the GR framework.

When deriving the IPN-accurate dynamics of N point masses predicted by the PPN-modified metric, Eq. (21.28), one finds that the free Lagrangian is not modified (because we are considering here a Lorentz-invariant subclass of PPN metrics), while there are modifications of both the two-body Lagrangian, $L^{(2)}$, Eq. (21.13), and the three-body one, $L^{(3)}$, Eq. (21.14). More precisely, denoting $\eta \equiv 4\bar{\beta} - \bar{\gamma}$, the Newtonian interaction energy term in Eq. (21.13) is modified into $G_{AB}m_A m_B/r_{AB}$, with a body-dependent gravitational “constant”

$$G_{AB} = G[1 + \eta(E_A^{\text{grav}}/m_A c^2 + E_B^{\text{grav}}/m_B c^2) + O(1/c^4)], \quad (21.32)$$

where E_A^{grav} denotes the gravitational binding energy of body A . In addition, there is the additional contribution $+\bar{\gamma}(\mathbf{v}_A - \mathbf{v}_B)^2/c^2$ in the brackets on the right-hand side of $L^{(2)}$, Eq. (21.13). As for the three-body interaction term $L^{(3)}$, Eq. (21.14), it is modified by the overall factor $1 + 2\bar{\beta}$.

These results show how the introduction of the two minimal PPN deviation parameters $\bar{\beta} \equiv \beta - 1$ and $\bar{\gamma} \equiv \gamma - 1$ suffices to introduce many different observable effects. Some of them (the ones linked with $\bar{\gamma}$) concern deviations at the linearized (one-graviton-exchange) level (and affect, for instance, light deflection and time-delay effects), while the deviation parameter $\bar{\beta}$ parameterizes effects linked to the cubic vertex of Einstein’s gravity (and affects, for instance, periastron precession). Of particular interest is the fact that Eq. (21.32) shows that the combination $\eta \equiv 4\bar{\beta} - \bar{\gamma}$ parameterizes a violation of the Strong Equivalence Principle, because the gravitational interaction between self-gravitating bodies is seen to be influenced by the gravitational binding energy of each body [9]. As stated above, this effect is absent in GR (where $\eta^{\text{GR}} = 0$). This is an example where the fact of contrasting GR with some deviations from it gives physical significance to a null effect in GR (namely the universality of free fall of self-gravitating bodies).

Finally, one can extend the PPN formalism by allowing for a slow, phenomenological time variation of Newton’s constant:

$$G(t) = G_0 \left[1 + \frac{\dot{G}_0}{G_0}(t - t_0) \right]. \quad (21.33)$$

Here, one assumes that there exist units in which the masses, m_i , of elementary particles stay constant, and that G is measured in such units. A possible time variation of G then corresponds to a possible common variation of the dimensionless couplings $Gm_i^2/(\hbar c)$.

21.3.3 Parameterized post-Keplerian (PPK) formalism.

The discovery of pulsars (*i.e.*, rotating neutron stars emitting a beam of radio noise) in gravitationally bound orbits [10, 11] has given us our first experimental handle on a regime of relativistic gravity going significantly beyond the uniformly weak-field, and quasi-stationary regime of solar-system gravity. Binary pulsars allow us to probe some radiative effects, and also some strong-gravitational-field effects. In these systems, the finite speed of propagation of the gravitational interaction between the pulsar and its companion generates damping-like terms at order $(v/c)^5$ in the equations of motion [12]. These damping forces are the local counterparts of the gravitational radiation emitted at infinity by the system (“gravitational radiation reaction”). They cause the binary orbit to shrink and its orbital period P_b to decrease. The remarkable stability of pulsar clocks has allowed one to measure the corresponding very small orbital period decay $\dot{P}_b \equiv dP_b/dt \sim -(v/c)^5 \sim -10^{-12} - 10^{-14}$ in several binary systems, thereby giving us a direct experimental handle on the propagation properties of the gravitational field. In addition, the large surface gravitational potential of a neutron star allows one to probe the quasi-static strong-gravitational-field regime, as is discussed below.

It is possible to extract phenomenological (theory-independent) tests of gravity from binary pulsar data by using the parameter-

ized post-Keplerian (PPK) formalism [13]. The basis of this formalism is the fact that, after correcting for the Earth’s motion around the Sun and for the dispersion due to propagation in the interstellar plasma, the time of arrival of the N th pulse t_N can be described by a generic, parameterized “timing formula” [13, 14], whose functional form is common to the whole class of tensor-scalar gravitation theories:

$$t_N - t_0 = F[T_N(\nu_p, \dot{\nu}_p, \ddot{\nu}_p); \{p^K\}; \{p^{PK}\}]. \quad (21.34)$$

Here, T_N is the pulsar proper time corresponding to the N th turn given by $N/2\pi = \nu_p T_N + \frac{1}{2}\dot{\nu}_p T_N^2 + \frac{1}{6}\ddot{\nu}_p T_N^3$ (with $\nu_p \equiv 1/P_p$ the spin frequency of the pulsar, *etc.*), $\{p^K\} = \{P_b, T_0, e, \omega_0, x\}$ is the set of “Keplerian” parameters (notably, orbital period P_b , eccentricity e , periastron longitude ω_0 and projected semi-major axis $x = a \sin i/c$), and $\{p^{PK}\} = \{k, \gamma_{\text{timing}}, \dot{P}_b, r, s, \delta_\theta, \dot{e}, \dot{x}\}$ denotes the set of (separately measurable) “post-Keplerian” parameters. Most important among these are: the fractional periastron advance per orbit $k \equiv \dot{\omega} P_b/2\pi$; a dimensionful time-dilation parameter γ_{timing} ; the orbital period derivative \dot{P}_b ; and the “range” and “shape” parameters of the gravitational time delay caused by the companion, r and s .

Without assuming any specific theory of gravity, one can phenomenologically analyze the data from any binary pulsar by least-squares fitting the observed sequence of pulse arrival times to the timing formula of Eq. (21.34). This fit yields the “measured” values of the parameters $\{\nu_p, \dot{\nu}_p, \ddot{\nu}_p\}$, $\{p^K\}$, $\{p^{PK}\}$. Now, each specific relativistic theory of gravity predicts that, for instance, k , γ_{timing} , \dot{P}_b , r , and s (to quote parameters that have been successfully measured from some binary pulsar data) are some theory-dependent functions of the Keplerian parameters and of the (unknown) masses m_1, m_2 of the pulsar and its companion. For instance, in GR, one finds (with $M \equiv m_1 + m_2$, $n \equiv 2\pi/P_b$),

$$\begin{aligned} k^{\text{GR}}(m_1, m_2) &= 3(1 - e^2)^{-1}(GMn/c^3)^{2/3}, \\ \gamma_{\text{timing}}^{\text{GR}}(m_1, m_2) &= en^{-1}(GMn/c^3)^{2/3}m_2(m_1 + 2m_2)/M^2, \\ \dot{P}_b^{\text{GR}}(m_1, m_2) &= -(192\pi/5)(1 - e^2)^{-7/2} \left(1 + \frac{73}{24}e^2 + \frac{37}{96}e^4 \right) \\ &\quad \times (GMn/c^3)^{5/3}m_1m_2/M^2, \\ r^{\text{GR}}(m_1, m_2) &= Gm_2/c^3, \\ s^{\text{GR}}(m_1, m_2) &= nx(GMn/c^3)^{-1/3}M/m_2. \end{aligned} \quad (21.35)$$

In alternative gravity theories each of the functions $k^{\text{theory}}(m_1, m_2)$, $\gamma_{\text{timing}}^{\text{theory}}(m_1, m_2)$, $\dot{P}_b^{\text{theory}}(m_1, m_2)$, *etc.*, is modified by quasi-static strong field effects (associated with the self-gravities of the pulsar and its companion), while the particular function $\dot{P}_b^{\text{theory}}(m_1, m_2)$ is further modified by radiative effects [15–18]. If one measures $N > 2$ PPK parameters from the data of a specific binary pulsar, these N measurements determine, for each given theory, N curves (defined by the N equations $k_i^{\text{theory}}(m_1, m_2) = k_i^{\text{obs}}$) in the two-dimensional mass plane (m_1, m_2) . This yields $N - 2$ tests of the specified theory, according to whether the N curves (or strips) have one point in common, as they should.

21.3.4 Parameterized-post-Friedmannian (PPF) formalisms.

We have recalled above that, in GR, the two functions, $\Phi(t, \mathbf{x})$, and $\Psi(t, \mathbf{x})$, parameterizing (in the “longitudinal gauge”) the scalar perturbations of the background Friedmann metric are related (in absence of anisotropic stresses) by Eq. (21.26). Several authors [19–28] have defined various types of parameterized-post-Friedmannian (PPF) formalisms involving (generally space and time dependent) phenomenological parameters. The simplest versions of these formalisms involve two phenomenological parameters measuring: (i) the ratio between $\Phi(t, \mathbf{x})$, and $\Psi(t, \mathbf{x})$, say (using a parametrization which parallels the usual PPN parametrization)

$$\Psi(t, \mathbf{x}) = \gamma_{\text{cosmo}}(t, \mathbf{x})\Phi(t, \mathbf{x}); \quad (21.36)$$

and (ii) the effective gravitational constant entering the Poisson equation for $\Phi(t, \mathbf{x})$, say

$$\Delta\Phi(t, \mathbf{x}) = 4\pi G_{\Phi}(t, \mathbf{x})\delta\rho(t, \mathbf{x}). \quad (21.37)$$

However, the peculiarities of cosmological observables limit the domain of applicability of such phenomenological approaches [26] (notably because the strong dependence of cosmological probes on epochs and scales obliges one to rely on specific parameterizations of the functions $\gamma_{\text{cosmo}}(t, \mathbf{x})$ and $G_{\Phi}(t, \mathbf{x})$, *e.g.*, [25, 28]). Approaches based on specific classes of modified-gravity theories allow for a more complete treatment involving, in principle, all existing cosmological observables: Big Bang nucleosynthesis, cosmic microwave background, large-scale structure, Hubble diagram, weak lensing, etc. Discussing the current cosmological tests using either such PPF formalisms, or comparisons with the predictions of modified-gravity theories, is beyond the scope of this review. See [29] for a comprehensive recent discussion. The bottom line is that all present cosmological data have been found to be compatible with GR (within the Friedmann-Lemaître-based Λ CDM model). Beyond the quantitative limits on various parameterized theoretical models [29], one should remember the striking (strong-field-type) qualitative verification of GR embodied in the fact that relativistic cosmological models give an accurate picture of the Universe over a period during which the spatial metric has been blown up by a gigantic factor, say $(1+z)^2 \sim 10^{19}$ between Big Bang nucleosynthesis and now.

21.3.5 Various phenomenological tests of GR from gravitational wave (GW) data

The observation by the US-based Laser Interferometer Gravitational-wave Observatory (LIGO), later joined by the Europe-based Virgo detector, of gravitational-wave (GW) signals [30–34], has opened up a novel testing ground for relativistic gravity. The first two observing runs of the LIGO-Virgo Collaboration (LVC) have led to the detection of GW signals from ten binary black-hole coalescences, and one binary neutron-star merger [35].

Several approaches have been used to either test consistency with GR, or to look for special types of possible deviations. Making accurate predictions for GW signals from coalescing black holes within GR took years of both analytical [36, 37] and numerical [38] work. Some works have started (both analytically [15, 39–43] and numerically [44–46]) to derive the corresponding predictions within some modified-gravity theories. Phenomenological approaches are very useful for parameterizing general, conceivable deviations from GR when analyzing the GW signals emitted by coalescing black holes or neutron stars.

A first phenomenological, global consistency test simply consists of measuring the noise-weighted correlation \mathcal{C} between each detected strain signal and the corresponding best-fit GR-predicted waveform. \mathcal{C}^{obs} should be equal to 1, modulo statistical (and/or systematic) errors.

Various other phenomenological tests of the structure of the GR-predicted waveforms emitted by coalescing compact binaries have been suggested. One general idea [47–49] (dubbed “parameterized post-Einsteinian formalism” in [50]) is to deform the existing phenomenological representation [51] of the GR-predicted phase $\psi(f)$ of the Fourier-space black-hole coalescence GW signals $h(f) = A(f)e^{i\psi(f)}$ by introducing GR-deviation parameters, say

$$\psi(f) = \sum_i p_i^{\text{GR}}(m_1, m_2, S_1, S_2)(1 + \delta\hat{p}_i)u_i(f). \quad (21.38)$$

Here, the $u_i(f)$ ’s define a basis of functions of the GW frequency f (*e.g.* $u_0(f) = f^{-5/3}\theta[0.018 - G(m_1 + m_2)f/c^3]$, where θ denotes the step function, parameterizes the leading-order (LO) term in the phase evolution during the early inspiral) while the corresponding mass- and spin-dependent GR-predicted coefficients are denoted $p_i^{\text{GR}}(m_1, m_2, S_1, S_2)$ (*e.g.*, $p_0^{\text{GR}} = \frac{3(m_1+m_2)^2}{128m_1m_2}(\pi G(m_1+m_2)/c^3)^{-5/3}$). In GR the next-to-leading-order (NLO) term is a $O(v^2/c^2)$ correction $p_2^{\text{GR}}u_2(f)$ with $u_2(f) = f^{-1}\theta[0.018 - G(m_1 + m_2)f/c^3]$. Each dimensionless

parameter $\delta\hat{p}_i$ introduces a fractional deviation from the corresponding individual phasing GR effect having the frequency dependence $u_i(f)$, and can, in principle, be extracted by fitting the inspiral part of the observed waveform to the deformed template of Eq. (21.38). However, one must also use this deformed template for simultaneously extracting the values of m_1, m_2, S_1 , and S_2 . Together with signal-to-noise ratio (SNR) considerations, and parameter-correlation issues, this limits the applicability of such a test to introducing only one deformation parameter $\delta\hat{p}_i$ at a time. A particularly meaningful test [47] is to leave undeformed the LO and NLO terms $p_0^{\text{GR}}u_0(f) + p_2^{\text{GR}}u_2(f)$ and to vary the third coefficient p_3 parameterizing the next, “GW tail”-related $O(v^3/c^3)$ correction, with $u_3(f) = f^{-2/3}\theta[0.018 - G(m_1 + m_2)f/c^3]$. Another well-motivated test [50] is to introduce a new coefficient $\delta\hat{p}_{-2}$, which is absent in GR, and which parameterizes an $O((v/c)^{-2})$ fractional correction to the LO, quadrupolar term, thereby allowing for a possible dipolar GW flux (indeed, dipolar GW radiation generally exists in theories containing scalar excitations). As p_{-2}^{GR} vanishes, $\delta\hat{p}_{-2}$ is added as an absolute deviation, scaled by the LO term p_0^{GR} .

The coalescence of two black holes, or of a black hole and a neutron star (or of two heavy-enough neutron stars) leads to the formation of a black hole that is initially formed in a perturbed state. The relaxation of the latter perturbed black hole into its stationary, equilibrium state leads to the emission of characteristic (rapidly decaying) ringing GW modes (a.k.a. quasi-normal modes) [52, 53], whose frequencies and decay times are functions of the mass (M_f) and spin ($S_f \equiv GM_f^2 a_f/c$) of the final black hole, say

$$\omega_a = (c^3/GM_f)[2\pi\hat{f}_a^{\text{QNM}}(a_f) - i/\hat{\tau}_a^{\text{QNM}}(a_f)], \quad (21.39)$$

where $a = 1, 2, \dots$ labels the various ringing modes, starting from the least-damped one. In principle, if the SNR is large enough, one can directly test for the presence of one or several of these modes in the post-merger signal, and measure both $\text{Re}(\omega_a)$ and $\text{Im}(\omega_a)$ in a theory-independent way. These phenomenological measurements then lead to null tests of GR, from which one can extract theoretical information about eventual deviations from GR [54, 55].

As recalled above, GR predicts that GWs propagate (in vacuum) at exactly the same speed as light (*i.e.*, they have the same dispersion law $g^{\mu\nu}k_\mu k_\nu = 0$ in curved spacetime). Deviations from such a universal, scale-free dispersion law can be phenomenologically parameterized in several ways. If one phenomenologically assumes that the graviton dispersion law includes a mass term, say $g^{\mu\nu}k_\mu k_\nu + m_g^2/h^2 = 0$, or some more general type of frequency-dependent modification, such changes affect the phasing of the inspiral GW signal and can be directly tested [56]. When one observes *both* GWs and electromagnetic waves emitted by the same system, one can also directly test whether both types of waves propagate in the same way.

Let us now present some examples of theory-dependent discussions of experimental tests based on considering specific classes of alternative theories. The most conservative deviations from Einstein’s pure spin-2 theory are defined by adding new, bosonic, light or massless, macroscopically coupled fields.

21.3.6 Gravity tests within classes of tensor-scalar theories of gravity

The possible existence of new gravitational-strength couplings leading to deviations from Einsteinian (and Newtonian) gravity has been suggested by many natural extensions of GR, starting with the classic Kaluza-Klein idea, and continuing up to now with the study of extended supergravity theories, and of (super)string theory. In particular, a recurrent suggestion of such theories (which dates back to pioneering work by Jordan, and by Fierz [57]) is the existence of a scalar field φ coupled both to the scalar curvature R and to the various $F_{\mu\nu}^a$ gauge-field actions. Such fields (“dilaton” or “moduli”) generically appear in string theory and are massless at the tree-level, but could acquire a self-interaction potential $V(\varphi)$ beyond the tree-level.

The exchange of such a dilaton-like field leads to several types of observational deviations from GR. For experimental limits on the

gravitational inverse-square-law (down to the micrometer range) see Refs. [58–60]. If the potential $V(\varphi)$ is zero or negligible for the considered range, the coupling of φ to $F_{\mu\nu}^a$ leads to apparent violations of the weak equivalence principle, with rather specific composition-dependence [61]. Next, when neglecting the fractionally small composition-dependent effects, such a field approximately couples to the trace of the energy-momentum tensor $T = g_{\mu\nu}T^{\mu\nu}$. The most general such theory contains (after suitable field redefinitions) two arbitrary functions of the scalar field, namely the self-interaction potential $V(\varphi)$, and a matter-coupling function $a(\varphi)$:

$$\mathcal{L}_{\text{tot}}[g_{\mu\nu}, \varphi, \psi, A_\mu, H] = \frac{c^4}{16\pi G_*} \sqrt{g}(R(g_{\mu\nu}) - 2g^{\mu\nu}\partial_\mu\varphi\partial_\nu\varphi) - \sqrt{g}V(\varphi) + \mathcal{L}_{\text{SM}}[\psi, A_\mu, H, \tilde{g}_{\mu\nu}]. \quad (21.40)$$

Here G_* is a “bare” Newton constant, and the Standard Model matter is coupled not to the “Einstein” (pure spin-2) metric $g_{\mu\nu}$, but to the conformally related (“Jordan-Fierz”) metric

$$\tilde{g}_{\mu\nu} = \exp(2a(\varphi))g_{\mu\nu}. \quad (21.41)$$

The scalar field equation

$$\square_g\varphi = \frac{4\pi G}{c^4} \left(-\alpha(\varphi)T + \frac{\partial V(\varphi)}{\partial\varphi} \right), \quad (21.42)$$

features

$$\alpha(\varphi) \equiv \partial a(\varphi)/\partial\varphi, \quad (21.43)$$

as the basic (field-dependent) coupling between φ and matter [15, 62]. The best-known, special case of these theories is the one-parameter (ω) Jordan-Fierz-Brans-Dicke theory [63], with $V(\varphi) = 0$ and $a(\varphi) = \alpha_0\varphi$, leading to a field-independent coupling $\alpha(\varphi) = \alpha_0$ (with $\alpha_0^2 = 1/(2\omega + 3)$). More generally, if we consider the massless theories ($V(\varphi) = 0$) with arbitrary (non-linear) coupling function $a(\varphi)$, they modify Einstein’s predictions in the weak-field slow-motion limit appropriate to describing gravitational experiments in the solar system (1PN approximation) only through the appearance of exactly the same two “post-Einstein” dimensionless parameters $\bar{\gamma} = \gamma - 1$ and $\bar{\beta} = \beta - 1$ that entered the minimal (Eddington) PPN formalism presented above. However, we now have the following theoretical expressions relating the latter phenomenological parameters to the coupling functions entering the tensor-scalar action Eq. (21.40):

$$\bar{\gamma} = -2\frac{\alpha_0^2}{1 + \alpha_0^2}; \quad (21.44)$$

$$\bar{\beta} = +\frac{1}{2}\frac{\beta_0\alpha_0^2}{(1 + \alpha_0^2)^2}. \quad (21.45)$$

Here $\alpha_0 \equiv \alpha(\varphi_0)$, and $\beta_0 \equiv \partial\alpha(\varphi_0)/\partial\varphi_0$, with φ_0 denoting the vacuum expectation value (VEV) of φ around the solar system. In addition, the observable value G^{obs} of the gravitational constant is found to be field-dependent and given (at a place where $\varphi = \varphi_0$) by

$$G^{\text{obs}} = G(\varphi_0) \equiv G_* \exp[2a(\varphi_0)](1 + \alpha_0^2). \quad (21.46)$$

This makes it clear that the parameter $\bar{\gamma}$ is the basic post-Einstein parameter, which measures the admixture of an additional field (here a spin-0 field) to the pure spin-2 GR. One also sees how the parameter $\bar{\beta}$ is linked to non-linear effects (here coupling terms $\beta_0(\varphi - \varphi_0)^2 T$ in the action), and how the Nordtvedt parameter $\eta \equiv 4\bar{\beta} - \bar{\gamma}$ is related to the field-dependence of G^{obs} ($\eta = (\alpha_0/(1 + \alpha_0^2))\partial \ln G(\varphi_0)/\partial\varphi_0$).

The advantage of a theory-dependent approach, such as Eq. (21.40), over the phenomenological minimal PPN approach of Eq. (21.28), is that it allows one to consistently predict the observational deviations from GR in all possible gravity regimes: the quasi-stationary weak-field regime; the wavelike weak-field regime; the strong-field regime; the cosmological regime, etc. All such observational deviations can be consistently worked out once one

chooses specific forms of the coupling function $a(\varphi)$, and of $V(\varphi)$. The simple choice of a two-parameter quadratic coupling function, say $a(\varphi) = \alpha_0(\varphi - \varphi_0) + \frac{1}{2}\beta_0(\varphi - \varphi_0)^2$, has been found useful for describing many possible observable deviations from GR.

The observable consequences for binary pulsar observations of the strong-field and radiative effects linked to the coupling to φ have been explicitly worked out in Refs. [15, 42] in the case where φ is massless (see Ref. [64] for the case where φ is massive). In particular, the strong-field nature of the pulsar tests is demonstrated by the fact that some tensor-scalar theories can be as close as desired to GR in the weak-field regime of the solar-system (*i.e.*, $\bar{\gamma}$ and $\bar{\beta}$ can be as small as desired, or even exactly zero), while developing (via a “spontaneous scalarization” mechanism) differences of order unity with GR in binary pulsar experiments [17, 18].

21.3.7 Attractor and screening mechanisms in modified gravity

As will follow from the discussion of experimental data below, the comparison between the predictions of general massless tensor-scalar theories and current data shows that the basic coupling parameter α_0 must be tuned to a small value (especially when allowing for composition-dependent effects). This raises the issue of the naturalness of such small coupling parameters. It has been shown in this respect that, in many tensor-scalar theories, there is an *attractor mechanism* by which the cosmological evolution naturally drives the VEV $\varphi_0(t)$ towards a value for which the coupling parameter $\alpha_0 = \alpha(\varphi_0)$ vanishes, thereby making it natural to expect only small deviations from GR (at least for the weak-field regime) at our current cosmological epoch [65, 66].

There are other theoretical mechanisms (generically called “screening mechanisms”) that could explain why a theory of gravity whose theoretical content significantly differs from that of GR could naturally pass all the stringent, GR-compatible experimental limits that will be discussed below. In particular, when considering a self-interacting scalar field ($V(\varphi) \neq 0$), the interplay between the two terms on the right-hand side of Eq. (21.42) tends to drive the local VEV φ_0 of φ to a density-dependent value. In turn, this leads to a corresponding density-dependent effective mass $m_0(\varphi_0) = \sqrt{4\pi G\partial^2 V(\varphi_0)/\partial\varphi_0^2}$ of the φ field, and to density-dependent matter couplings [67]. Various choices of the functions $V(\varphi)$ and $a(\varphi)$ can then reduce the φ -induced deviations from GR in dense environments while still allowing for significant deviations in different (*e.g.*, cosmological) regimes [68–72].

Other screening mechanisms have been invoked, based on an environment dependence mediated by (first or second) derivatives of a scalar degree of freedom. Roughly speaking, such mechanisms involve a (possibly effective) scalar degree of freedom φ that satisfies a field equation that is more general than Eq. (21.42) in that the left-hand side, $\square_g\varphi$, is replaced by a non-linear function of φ , $\partial\varphi$ and $\partial^2\varphi$. The presence of non-linear derivative self-interactions of φ can weaken the effective coupling of φ to matter. A simple toy-model showing this weakening would be to replace Eq. (21.42) by an equation of the form

$$Z(\varphi, \partial\varphi, \partial^2\varphi)\square_g\varphi = \frac{4\pi G}{c^4} \left(-\alpha(\varphi)T + \frac{\partial V(\varphi)}{\partial\varphi} \right). \quad (21.47)$$

Such an equation is equivalent, at a first level of approximation, to replacing the gravitational constant G entering Eq. (21.42) by $G_{\text{eff}}(\varphi_0, \partial\varphi_0, \partial^2\varphi_0) \equiv G/Z_0$, where $Z_0 \equiv Z(\varphi_0, \partial\varphi_0, \partial^2\varphi_0)$. This has a screening effect if $Z_0 \gg 1$. Indeed, the replacement $G \rightarrow G_{\text{eff}}$ diminishes the strength of the interaction potential due to φ exchange by a factor of $1/Z_0$. In addition, the range of this interaction is also affected: $m_0(\varphi_0) = \sqrt{4\pi G\partial^2 V(\varphi_0)/\partial\varphi_0^2} \rightarrow m_{0\text{eff}}(\varphi_0, \partial\varphi_0, \partial^2\varphi_0) = \sqrt{4\pi G_{\text{eff}}\partial^2 V(\varphi_0)/\partial\varphi_0^2} = Z_0^{-1/2}m_0$.

Screening mechanisms based on such non-linear derivative self-interactions are often referred to as being “Vainshtein-like” because a similar mechanism was first invoked in Ref. [73] as a conjectural way to ensure that the extra degrees of freedom associated with a massive (rather than massless) graviton become effectively weakly coupled to matter within a large domain around gravitational sources. Here, one is considering massive deformations of the massless spin-2 metric field of GR by a very small mass,

possibly of cosmological scale: $m_g \sim \hbar H_0 \sim 10^{-33}$ eV. The construction of ghost-free potential terms for a spin-2 field has turned out to be a delicate matter [74]. The phenomenology of a very-low-mass graviton is still partly uncontrolled, both because of the unknown extent to which the Vainshtein screening is really active, and because of subtle constraints linked to an eventual UV completion of the theory beyond the unusually low energy scale where it becomes strongly coupled:

$$\Lambda_{\text{strong coupling}} \sim (M_{\text{Planck}} m_0^2)^{1/3} \sim 10^{-13} \left(\frac{m_0}{\hbar H_0} \right)^{2/3} \text{ eV}. \quad (21.48)$$

The search for modified gravity theories incorporating an extra scalar degree of freedom potentially able to yield a Vainshtein-like screening led to writing down the following general class of tensor-scalar Lagrangian [75, 76]:

$$\begin{aligned} L_{\text{tot}}[g_{\mu\nu}, \varphi, \psi] = & G_2(\varphi, X) - G_3(\varphi, X) \square_g \varphi + G_4(\varphi, X) R \\ & + G_{4X}(\varphi, X) [(\square_g \varphi)^2 - \varphi^{\mu\nu} \varphi_{\mu\nu}] \\ & + G_5(\varphi, X) G^{\mu\nu} \varphi_{\mu\nu} - \frac{1}{6} G_{5X}(\varphi, X) (\square_g \varphi)^3 \\ & - 3 \square_g \varphi \varphi^{\mu\nu} + 2 \varphi_{\mu\nu} \varphi^{\mu\lambda} \varphi_{\lambda}^{\nu} + L_{\text{matter}}[g_{\mu\nu}, \psi]. \end{aligned} \quad (21.49)$$

Here $g_{\mu\nu}$ denotes the matter-coupled metric, $X \equiv -\frac{1}{2} g^{\mu\nu} \partial_\mu \varphi \partial_\nu \varphi$, $\varphi_{\mu\nu} \equiv \nabla_\mu \nabla_\nu \varphi$, $G^{\mu\nu} \equiv R^{\mu\nu} - \frac{1}{2} R g^{\mu\nu}$, and the various coefficients $G_n(\varphi, X)$ are arbitrary functions of two variables (with $G_{nX} \equiv \partial G_n / \partial X$). The field equations derived from the Lagrangian of Eq. (21.49) are only of second order in derivatives in spite of the non-linear structure of L_{tot} . This implies that the tensor-scalar theories defined by Eq. (21.49) feature three degrees of freedom, corresponding to a massless spin-2 excitation (GW) and a spin-0 excitation. Contrary to the simpler tensor-scalar theories of Eq. (21.40), it is found that the speed of propagation of GWs implied by Eq. (21.49) is generically different from the speed of light:

$$\frac{c_{\text{GW}}^2}{c^2} = \frac{G_4 - X(\ddot{\varphi} G_{5X} + G_{5\varphi})}{G_4 - 2XG_{4X} - X(H\dot{\varphi} G_{5X} - G_{5\varphi})}. \quad (21.50)$$

More general modified gravity models have been proposed (see, e.g. Refs. [77, 78]). Apart from the simplest of them, most of these models have a rather artificial flavor, and do not lead to convincing alternative explanations either of dark matter or of dark energy. In addition, many of them do not lead (contrary to GR) to mathematically “well-posed” evolution problems [79–81]. This entails a serious challenge to deriving strong-field predictions for such models. It has been argued that many of these (dark-energy motivated) models should be viewed as effective field theory (EFT) approximations that need some sort of UV completion at an unusually low frequency scale [82]. In spite of these shortcomings, such models are conceptually interesting because they give examples of deviations for various predictions of GR, existing independently from each other, in various regimes. For instance, some special tensor-scalar models lead to black hole solutions modified by scalar-hair [83, 84]. For other types of black holes with scalar-hair, see Ref. [85]. This shows the interest of phenomenologically testing, in a democratic and agnostic way, all conceivable deviations from GR.

Let us now turn to briefly presenting current experimental results of various phenomenological tests of the main GR predictions recalled in Section 21.2 above.

21.4 Experimental tests of the Equivalence Principle (i.e., of the matter-gravity coupling)

21.4.1 Tests of the constancy of constants

Stringent limits on a possible time variation of the basic coupling constants have been obtained by analyzing a natural fission reactor phenomenon that took place at Oklo, Gabon, two billion years ago [86, 87]. These limits are at the 1×10^{-8} level for the fractional variation of the fine-structure constant α_{em} [87], and at the

4×10^{-9} level for the fractional variation of the ratio $m_q / \Lambda_{\text{QCD}}$ between the light quark masses and Λ_{QCD} [88]. The determination of the lifetime of Rhenium 187 from isotopic measurements of some meteorites dating back to the formation of the solar system (about 4.6 Gyr ago) yields comparably strong limits [89]. Measurements of absorption lines in astronomical spectra also give stringent limits on the variability of both α_{em} and $\mu = m_p / m_e$ at cosmological redshifts, e.g.,

$$\Delta \alpha_{\text{em}} / \alpha_{\text{em}} = (1.2 \pm 1.7_{\text{stat}} \pm 0.9_{\text{sys}}) \times 10^{-6}, \quad (21.51)$$

at redshifts $z = 1.0$ – 2.4 [90], and

$$|\Delta \mu / \mu| < 4 \times 10^{-7} (95\% \text{ CL}), \quad (21.52)$$

at a redshift $z = 0.88582$ [91]. There are also significant limits on the variation of α_{em} and $\mu = m_p / m_e$ at redshift $z \sim 10^3$ from cosmic microwave background data, e.g., $\Delta \alpha_{\text{em}} / \alpha_{\text{em}} = (3.6 \pm 3.7) \times 10^{-3}$ [92]. Direct laboratory limits (based on monitoring the frequency ratio of several different atomic clocks) on the present time variation of α_{em} , $\mu = m_p / m_e$, and $m_q / \Lambda_{\text{QCD}}$ have reached the levels [93]

$$\begin{aligned} d \ln(\alpha_{\text{em}}) / dt &= (-2.5 \pm 2.6) \times 10^{-17} \text{ yr}^{-1}, \\ d \ln(\mu) / dt &= (-1.5 \pm 3.0) \times 10^{-16} \text{ yr}^{-1}, \\ d \ln(m_q / \Lambda_{\text{QCD}}) / dt &= (7.1 \pm 4.4) \times 10^{-15} \text{ yr}^{-1}. \end{aligned} \quad (21.53)$$

There are also experimental limits on a possible dependence of coupling constants on the gravitational potential [93, 94].

Experimental limits on the present time variation of the gravitational constant, Eq. (21.33), have been derived from planetary ephemerides [95], lunar laser ranging [96], and binary-pulsar data [97, 98]. The most stringent limits come from lunar-laser-ranging data [96]:

$$\frac{\dot{G}_0}{G_0} = (7.1 \pm 7.6) \times 10^{-14} \text{ yr}^{-1}. \quad (21.54)$$

21.4.2 Tests of the isotropy of space and of Local Lorentz invariance

The highest precision tests of the isotropy of space have been performed by looking for possible quadrupolar shifts of nuclear energy levels [99]. The (null) results can be interpreted as testing the fact that the various pieces in the matter Lagrangian, Eq. (21.6), are indeed coupled to one and the same external metric $g_{\mu\nu}$ to the 10^{-29} level.

Stringent tests of possible violations of local Lorentz invariance in gravitational interactions have been obtained both from solar-system data [8] and pulsar data [100, 101]. For astrophysical constraints on possible Planck-scale violations of Lorentz invariance, see Ref. [102].

21.4.3 Tests of the universality of free fall (weak, and strong equivalence principles)

The universality of the acceleration of free fall has been verified, for laboratory bodies, both on the ground [103, 104] (at the 10^{-13} level), and in space [105, 106] (at the 10^{-14} level):

$$\begin{aligned} (\Delta a/a)_{\text{BeTi}} &= (0.3 \pm 1.8) \times 10^{-13}; \\ (\Delta a/a)_{\text{BeAl}} &= (-0.7 \pm 1.3) \times 10^{-13}; \\ (\Delta a/a)_{\text{TiPt}} &= (-1 \pm 9(\text{stat}) \pm 9(\text{syst})) \times 10^{-15}. \end{aligned} \quad (21.55)$$

The universality of free fall has also been verified when comparing the fall of classical and quantum objects (6×10^{-9} level [107]), or of two quantum objects ($(1 \pm 1.4) \times 10^{-9}$ level [108]; including a test that atoms prepared in a quantum superposition of two hyperfine states fall in the same way).

The universality of free fall of self-gravitating bodies (strong equivalence principle) has been verified in both the weak-gravity, and the strong-gravity regimes. The gravitational accelerations of the Earth and the Moon toward the Sun have been checked to agree at the 10^{-13} level [96]

$$(\Delta a/a)_{\text{EarthMoon}} = (-3 \pm 5) \times 10^{-14}. \quad (21.56)$$

The latter result constrains the Nordtvedt PPN parameter [9] $\eta \equiv 4\bar{\beta} - \bar{\gamma}$ to the 10^{-4} level:

$$\eta = (-0.2 \pm 1.1) \times 10^{-4}. \quad (21.57)$$

See below for strong-field tests of the strong equivalence principle.

Finally, the universality of the gravitational redshift of clock rates has been verified at the 10^{-4} level by comparing a hydrogen-maser clock flying on a rocket up to an altitude of about 10,000 km to a similar clock on the ground [109]. The redshift due to a height change of only 33 cm has been detected by comparing two optical clocks based on $^{27}\text{Al}^+$ ions [110]. The gravitational redshift has also been detected in the orbit of a star near the supermassive black hole at the center of our Galaxy [111, 112], and its universality has been verified at the 5% level [113].

21.5 Tests of quasi-stationary, weak-field gravity

All currently performed gravitational experiments in the solar system, including perihelion advances of planetary orbits, the bending and delay of electromagnetic signals passing near the Sun, and very accurate ranging data to the Moon obtained by laser echoes, are compatible with the post-Newtonian results of Eq. (21.15), Eq. (21.13), and Eq. (21.14). The “gravito-magnetic” interactions $\propto v_{AVB}$ contained in Eq. (21.13) are involved in many of these experimental tests. They have been particularly tested in lunar-laser-ranging data [114], in the combined LAGEOS-LARES satellite data [115, 116], and in the dedicated Gravity Probe B mission [117].

To assess in a quantitative manner the results of the various solar-system tests of gravity it is convenient to express them in terms of the PPN parameters defined above. The best current limit on the post-Einstein parameter $\bar{\gamma} \equiv \gamma - 1$ is

$$\bar{\gamma} = (2.1 \pm 2.3) \times 10^{-5}, \quad (21.58)$$

as deduced from the additional Doppler shift experienced by radio-wave beams connecting the Earth to the Cassini spacecraft when they passed near the Sun [118].

The (cubic-vertex-related) post-Einstein parameter $\bar{\beta} \equiv \beta - 1$ is constrained at the 10^{-4} level both from a study of the global sensitivity of planetary ephemerides to post-Einstein parameters [95],

$$|\bar{\beta}| < 7 \times 10^{-5}, \quad (21.59)$$

and from lunar-laser-ranging data [96]

$$\bar{\beta} = (-4.5 \pm 5.6) \times 10^{-5}. \quad (21.60)$$

More stringent limits on $\bar{\gamma}$ (*i.e.* the coupling of φ to matter) are obtained in dilaton-like models where scalar couplings violate the Equivalence Principle [119].

21.6 Tests of strong-field gravity (neutron stars and black holes)

Experimental tests of strong-field gravity have been obtained in various physical systems, notably binary pulsars and coalescing binary black holes.

It is convenient to quantitatively express binary-pulsar tests of strong-field gravity by using the PPK formalism defined above. We recall that the measurement of N phenomenological PPK parameters leads to $N - 2$ tests of strong-field gravity. In all, *thirteen* tests of strong-field and/or radiative gravity have been obtained in the four different (double neutron-star) binary pulsar systems PSR1913+16 [10, 11, 120], PSR1534+12 [121–123], PSR J1141–6545 [124–127], and PSR J0737–3039 A,B [128–132]. These consist of $N - 2 = 5 - 2 = 3$ tests from PSR1913+16; $5 - 2 = 3$ tests from PSR1534+12; $4 - 2 = 2$ tests from PSR J1141–6545; and $7 - 2 = 5$ tests from PSR J0737–3039 (see, also, Ref. [133] for additional, less accurate tests of relativistic gravity). Among these tests, four of them (those involving the measurement of the PPK parameter \dot{P}_b) probe radiative effects, and will be discussed in the following section. The four binary pulsar systems PSR1913+16, PSR1534+12, PSR J1141–6545, and PSR J0737–3039 A,B have given nine tests of quasi-static, strong-field gravity. GR passes all these tests within the measurement

accuracy. Let us only highlight here some of the most accurate strong-field tests.

In the binary pulsar PSR 1534+12 [121] one has measured *five* post-Keplerian parameters: k , γ_{timing} , r , s , and (with less accuracy) \dot{P}_b [122, 123]. This yields *three* tests of relativistic gravity. Among these tests, the two involving the measurements of k , γ_{timing} , r , and s accurately probe strong field gravity, without mixing of radiative effects [122]. The most precise (10^{-3} level) of these pure strong-field tests is the one obtained by combining the measurements of k , γ_{timing} , and s ; namely, [123],

$$\left[\frac{s^{\text{obs}}}{s^{\text{GR}}[k^{\text{obs}}, \gamma_{\text{timing}}^{\text{obs}}]} \right]_{1534+12} = 1.002 \pm 0.002. \quad (21.61)$$

The discovery of the remarkable *double* binary pulsar PSR J0737–3039 A and B [128, 129] has led to the measurement of *seven* independent parameters [130–132]: five of them are the post-Keplerian parameters k , γ_{timing} , r , s , and \dot{P}_b entering the relativistic timing formula of the fast-spinning pulsar PSR J0737–3039 A; a sixth is the ratio $R = x_B/x_A$ between the projected semi-major axis of the more slowly spinning companion pulsar PSR J0737–3039 B, and that of PSR J0737–3039 A (the theoretical prediction for the ratio $R = x_B/x_A$, considered as a function of the (inertial) masses $m_1 = m_A$ and $m_2 = m_B$, is $R^{\text{theory}} = m_1/m_2 + O((v/c)^4)$ [13, 14], independently of the gravitational theory considered). Finally, the seventh parameter $\Omega_{\text{SO,B}}$ is the angular rate of (spin-orbit) precession of PSR J0737–3039 B around the total angular momentum vector [131, 132]. These seven measurements give us *five* tests of relativistic gravity [130, 134, 135], four of which are quasi-static, strong-field tests. GR passes all those tests with flying colors [135]. The most accurate is at the 5×10^{-4} level:

$$\left[\frac{s^{\text{obs}}}{s^{\text{GR}}[k^{\text{obs}}, R^{\text{obs}}]} \right]_{0737-3039} = 1.0000 \pm 0.0005. \quad (21.62)$$

Binary pulsar data on other types of pulsar systems can be used to test strong-field aspects of the “strong equivalence principle,” namely the GR prediction that strong-self-gravity objects (such as neutron stars) should fall with the same acceleration as weak-self-gravity objects (such as white-dwarfs) in the (external) gravitational field created by other objects (such as the Galaxy, or another white dwarf). The first binary-pulsar tests of this property have been obtained in nearly circular binary systems (made of a neutron star and a white dwarf) falling in the field of the Galaxy, and have led to strong-field confirmations (at the 2×10^{-3} level) of the strong equivalence principle [98, 136–138]. The remarkable discovery of the pulsar PSR J0337+1715 in a hierarchical triple system [139] has allowed one to derive a much more accurate test of the strong equivalence principle because the inner binary (comprising a pulsar and a close white-dwarf companion) falls toward the outer white-dwarf companion with an acceleration that is 10^8 times larger than the Galactic acceleration. This leads to a 95% confidence level limit on a possible fractional difference in free-fall acceleration of the pulsar and its close companion of [140]

$$|\Delta a/a| < 2.6 \times 10^{-6}. \quad (21.63)$$

This limit yields strong constraints on tensor-scalar gravity models.

Measurements over several years of the pulse profiles of various pulsars have detected secular changes compatible with the prediction [141] that the general relativistic spin-orbit coupling should cause a secular change in the orientation of the pulsar beam with respect to the line of sight (“geodetic precession”). Such confirmations of general-relativistic spin-orbit effects were obtained in PSR 1913+16 [142], PSR B1534+12 [123], PSR J1141–6545 [143], PSR J0737–3039 [131, 132], and PSR J1906+0746 [144, 145]. In some cases (notably PSR 1913+16 and PSR J1906+0746) the secular change in the orientation of the pulsar beam is expected to lead to the disappearance of the beam (as seen on the Earth) on a human time scale (the second pulsar in the double system PSR J0737–3039 already disappeared in March 2008 and is expected to reappear around 2035 [132]).

Recently, the ultimate strong-field regime of black holes has started to be quantitatively probed via GW observations. The LIGO-Virgo collaboration has detected (starting in September 2015) GW signals [146], which, besides testing the radiative structure of gravity (see next section), are in excellent qualitative and quantitative agreement with the structure and dynamics of black-hole horizons in GR. Because of the mixing of strong-field effects with radiative effects during the coalescence of two black holes, and because of the lack of detailed alternative-theory predictions for this process (see, however, Refs. [44–46]), it is not easy to set quantitative limits on possible strong-field deviations from GR, independently of radiative effects. Direct tests of the existence of black-hole horizons are scarce (see, however, the suggestion to look for GW echoes as a negative test [147]). The only sharp quantitative assessment on possible deviations from GR concerns the global agreement between the full observed GW signal of coalescing binary black holes, and the GR-predicted one. In particular, the noise-weighted correlation between the first observed strain signal GW150914 and the best-fit GR-predicted waveform was found to be $\geq 96\%$ [49]. In other words, GR-violation effects that cannot be reabsorbed in a redefinition of physical parameters are limited (in a noise-weighted sense) to less than 4%.

Let us also mention that the Event Horizon Telescope collaboration has obtained event-horizon-scale images of the supermassive black hole candidate in the center of the giant elliptical galaxy M87 that are “consistent with expectations for the shadow of a Kerr black hole as predicted by general relativity” [148]. However, in view of modeling uncertainties, and of the limited accuracy of the imaging, no quantitative assessment of eventual deviations from GR can be made at this stage.

21.7 Tests of radiative gravity (both in binary-pulsar data and in GW data)

Experimental confirmations of the GR predictions for the radiative structure of gravity have been obtained both in binary-pulsar data and in the observation of GW signals from coalescing compact binaries (binary black holes and binary neutron stars).

Binary-pulsar observations involving the measurement of the orbital period derivative \dot{P}_b give *direct* experimental tests of the reality of gravitational radiation, and, in particular, an experimental confirmation that the speed of propagation of gravity c_g is equal to the speed of light c (indeed, as recalled above, \dot{P}_b is a consequence of the propagation of the gravitational interaction between the two neutron stars [12]). Even in the presence of screening mechanisms within the binary system, the value of \dot{P}_b yields a measurement of the speed of propagation of GWs at the 10^{-2} level [149]. The currently most accurate binary-pulsar tests of the radiative properties of gravity come from the binary neutron-star systems PSR1913+16 and PSR J0737–3039 A,B, as well as from several neutron-star-white-dwarf systems, notably PSR J1738+0333.

After subtracting a small ($\sim 10^{-14}$ level in $\dot{P}_b^{\text{obs}} = (-2.423 \pm 0.001) \times 10^{-12}$), but significant, “Galactic” perturbing effect (linked to Galactic accelerations and to the pulsar proper motion) [150], one finds that the phenomenological test obtained by combining the measurements of the three PPK parameters ($k - \gamma_{\text{timing}} - \dot{P}_b$)₁₉₁₃₊₁₆ is passed by GR with complete success [120]:

$$\left[\frac{\dot{P}_b^{\text{obs}} - \dot{P}_b^{\text{gal}}}{\dot{P}_b^{\text{GR}}[k^{\text{obs}}, \gamma_{\text{timing}}^{\text{obs}}]} \right]_{1913+16} = 0.9983 \pm 0.0016. \quad (21.64)$$

Here $\dot{P}_b^{\text{GR}}[k^{\text{obs}}, \gamma_{\text{timing}}^{\text{obs}}]$ is the result of inserting in $\dot{P}_b^{\text{GR}}(m_1, m_2)$ the values of the masses predicted by the two equations $k^{\text{obs}} = k^{\text{GR}}(m_1, m_2)$, and $\gamma_{\text{timing}}^{\text{obs}} = \gamma_{\text{timing}}^{\text{GR}}(m_1, m_2)$. This yields experimental evidence for the reality of gravitational radiation damping forces at the $(-1.7 \pm 1.6) \times 10^{-3}$ level.

Similarly, the combined measurement in PSR J0737–3039 A,B of the three parameters k , $R \equiv x_B/x_A$, and \dot{P}_b yields another experimental test of the radiative structure of gravity at the 10^{-3}

level [130–132]:

$$\left[\frac{\dot{P}_b^{\text{obs}}}{\dot{P}_b^{\text{GR}}[k^{\text{obs}}, R^{\text{obs}}]} \right]_{0737-3039} = 1.000 \pm 0.001. \quad (21.65)$$

In addition to the above tests, further very stringent tests of radiative gravity follow from the measurement of the orbital period decay \dot{P}_b of low-eccentricity pulsar-white dwarf systems. Notably, the system PSR J1738+0333 yields an intrinsic orbital decay of [151]

$$\left[\dot{P}_b^{\text{obs}} - \dot{P}_b^{\text{gal}} \right]_{1738+0333} = (-25.9 \pm 3.2) \times 10^{-15}, \quad (21.66)$$

to be compared to

$$\left[\dot{P}_b^{\text{GR}} \right]_{1738+0333} = (-27.7^{+1.5}_{-1.9}) \times 10^{-15}. \quad (21.67)$$

The fractional agreement between the (corrected) observed period decay and the GR-predicted one seems to be quantitatively less impressive than the double-neutron-star results cited above, but the crucial point is that asymmetric binary systems (such as neutron-star-white-dwarf ones) are strong emitters of dipolar gravitational radiation in tensor-scalar theories, with \dot{P}_b scaling (modulo matter-scalar couplings) like $m_1 m_2 / (m_1 + m_2)^2 (v/c)^3$, instead of the parametrically smaller GR-predicted quadrupolar radiation $\dot{P}_b \sim (v/c)^5$ [7, 15]. In view of the very small absolute value of \dot{P}_b , this makes such systems (and notably PSR J1738+0333) very sensitive probes of tensor-scalar gravity [97, 151–154]. It is then useful to turn to a theory-dependent analysis of pulsar data. Such an analysis (see, *e.g.*, [17, 122, 151, 154]) leads to excluding a large portion of the parameter space of tensor-scalar gravity allowed by solar-system tests. As a result, the basic matter-scalar coupling α_0^2 is more strongly constrained, over most of the parameter space, than the best current solar-system limits of Eq. (21.58) (namely below the 10^{-5} level) [151, 154].

We now turn to the tests of radiative gravity that can be deduced from the first two observing runs of the LIGO-Virgo collaboration (LVC) (the third observing run of the LVC has started on April 1, 2019, and has already issued many alerts). The first two observing runs of the LVC have reported the detection of GW signals emitted by the inspiral and coalescence of ten binary black hole systems, and one binary neutron star system [146] (see [155] for more claimed detections from the public LVC data). The network signal-to-noise ratio (SNR) of the reported events varies between 10 and 24 for binary black hole coalescences, and is equal to 33 for the binary neutron star event. All currently detected GW signals are consistent with GR predictions. Several phenomenological approaches were used and led to setting limits on possible deviations from GR.

Besides checking the agreement between the *full* observed GW signals and the corresponding best-fit full signals predicted by GR, attempts were made to test the consistency between two separate parts of the signals. A first attempt [156] separated: (i) the lower-frequency (LF) signal emitted during the inspiral phase (considered up to the innermost stable circular orbit); and (ii) the higher-frequency (HF) remaining signal emitted during the late-inspiral, the merger, and the ringdown. Separately fitting each of these partial signals to GR-based templates then leads to separate estimates of the binary’s parameters, leading to separate estimates of the mass M_f and dimensionless spin parameter $a_f = J_f / (GM_f^2)$ of the final black hole that would be formed (in GR) by the coalescence of the two initial black holes. The consistency with GR then consists in testing whether the two estimates $(M_f, a_f)_{\text{LF}}$ and $(M_f, a_f)_{\text{HF}}$ are compatible with each other. They were found to be consistent within statistical errors of order 30% for seven selected binary black hole events (see Fig. 2 in [156]). A second attempt [157] separately considered the *post-merger signal* of coalescing black holes, and tried to quantify the presence and structure of the GR-predicted ringing modes in the latter post-merger signal. Measuring, for the first event GW150914 (by using a model of the post-merger signal including the first two ringing modes), the mass and spin of the final black hole, $(M_f, a_f)_{\text{post-merger}}$, has shown consistency, at the $\sim 20\%$

level, with the corresponding values inferred (using GR predictions) from fitting the entire signal [157].

The parametrization of Eq. (21.38) for possible deviations in the frequency dependence of the Fourier-domain phase $\psi(f)$ of the black hole coalescence GW signal was used to measure best-fit values for each fractional deviation parameter $\delta\hat{p}_i$, considered separately (the other ones being set to zero). In all cases, the posterior distribution for each $\delta\hat{p}_i$ is consistent with the GR value, *i.e.*, $\delta\hat{p}_i^{\text{GR}} = 0$ (see figures 3 and 4 in Ref. [156]). The current limits on $\delta\hat{p}_i$ are (roughly) of order unity, except for the two parameters highlighted above: $\delta\hat{p}_3$ (parameterizing the $O((\frac{v}{c})^3)$ fractional correction to the LO, quadrupolar term); and $\delta\hat{p}_{-2}$ (parameterizing a possible dipolar-radiation-related $O((\frac{v}{c})^{-2})$ fractional correction to the LO, quadrupolar term). The current combined 90% upper bound on $\delta\hat{p}_3$ is $\sim 10\%$, while the corresponding bound on $\delta\hat{p}_{-2}$ is 2×10^{-3} (see figure 4 in Ref. [156]). See Ref. [158] for examples of the translation of these phenomenological constraints into bounds on specific theories.

As recalled above, GR predicts that the polarization content of GWs is pure helicity-2, *i.e.* described by the two independent components of a traceless tensor transverse to the propagation direction. A (massless) scalar excitation would add a pure-trace “breathing mode” in the plane transverse to the propagation direction. A phenomenological approach to generic metric theories of gravity would allow for up to six polarizations for a GW [159], namely two tensor, two vector and two scalar modes. The LVC tested possible polarization deviations from GR in the following way [33, 156]: they assumed that the phase evolution of the GW signal was the one predicted by GR, but they replaced the polarization structure of the signal either by a generic vector-like one, or by a generic scalar-like one. The best polarization constraints have been obtained from the GW170817 event. The latter very long (~ 100 s) and very loud (SNR $\simeq 33$) event was convincingly interpreted as coming from a binary neutron star inspiral (~ 40 Mpc away), and was associated with a subsequent γ -ray burst, followed by transient counterparts across the electromagnetic spectrum [160]. The polarization analysis of the GW170817 data has given overwhelming evidence in favor of pure tensor polarization modes in comparison to pure vector or pure scalar modes with a base-ten logarithm of the Bayes factor of $+20.81 \pm 0.08$ and $+23.09 \pm 0.08$, respectively [156].

GR also predicts that GWs are non dispersive, and propagate at the same speed as light. One can phenomenologically modify the GR-predicted GW phase evolution by adding the putative effect of an anomalous dispersion relation of the form $E^2 = p^2 c^2 + A p^\alpha c^\alpha$. GW data have been used to set bounds on the anomalous coefficient A for various values of the exponent α . The best bounds come from the analysis of the GW170104 event (see figure 5 in [32]). The case $\alpha = 0$ is equivalent to assuming that gravitons disperse as a massive particle [56]. Combined GW data lead to the following phenomenological limit on the graviton mass: $m_g \leq 7.7 \times 10^{-23} \text{ eV}/c^2$ [32]. See Refs. [161, 162] for other graviton mass bounds.

Finally, a very constraining bound on the speed of propagation of gravity c_{GW} was derived from the observed time delay of 1.7 s between GW170817 and the associated γ -ray burst. Namely, the fractional difference between c_{GW} and $c_{\text{light}} \equiv c$ is constrained to be [163]

$$-3 \times 10^{-15} < \frac{c_{\text{GW}} - c}{c} < +7 \times 10^{-16}. \quad (21.68)$$

When comparing the latter bound to the prediction Eq. (21.50) from general second-order tensor-scalar theories, Eq. (21.49), one is led to conclude that the coupling function $G_5(\varphi, X)$ has to be ignored and that the coupling function $G_4(\varphi, X)$ has to be restricted to depend only on φ . This drastically reduces the viable tensor-scalar modified-gravity models [164–167]. Observations from future GW detectors (both on the ground and in space) are expected to considerably strengthen the testing power of GW data [168, 169].

21.8 Conclusions

All present experimental tests are compatible with the predictions of the current “standard” theory of gravitation, Einstein’s General Relativity. Let us recap the main tests. The universality of the coupling between matter and gravity (Equivalence Principle) has been verified at around the 10^{-14} level. Solar system experiments have tested the weak-field predictions of Einstein’s theory at the few times 10^{-5} level. The propagation properties (in the near zone) of relativistic gravity, as well as several of its static strong-field aspects, have been verified at the 10^{-3} level (or better) in several binary pulsar experiments. Interferometric detectors of gravitational radiation have given direct observational proofs of the existence, and properties, of gravitational waves (in the wave zone), and of the existence of coalescing black holes, and they have already set strong limits on possible deviations; in particular: an upper bound $|\delta\hat{p}_{-2}| < 2 \times 10^{-3}$ on a possible dipolar contribution to the GW flux; the $O(10^{-15})$ bound of Eq. (21.68) on the speed of gravity; and strong evidence for the pure-tensor polarization structure of gravitational waves. In addition, laboratory experiments have set strong constraints on sub-millimeter modifications of Newtonian gravity, while many different cosmological data sets have been used to set limits on possible GR deviations on cosmological scales [29]. In spite of the uneasiness of having to assume the existence of dark matter, and the presence of an unaturally small cosmological constant (as dark energy), General Relativity stands out as a uniquely successful description of gravity on all the scales that have been explored so far. There are no modified-gravity models which naturally pass all existing experimental tests, while either explaining away the need for dark matter or for dark energy.

References

- [1] S. Weinberg, *Rev. Mod. Phys.* **61**, 1 (1989).
- [2] H. A. Buchdahl, *Phys. Rev.* **116**, 1027 (1959).
- [3] N. Chamel *et al.*, *Int. J. Mod. Phys. E* **22**, 1330018 (2013), [arXiv:1307.3995].
- [4] J. R. Oppenheimer and H. Snyder, *Phys. Rev.* **56**, 455 (1939).
- [5] R. P. Kerr, *Phys. Rev. Lett.* **11**, 237 (1963).
- [6] V. F. Mukhanov, H. A. Feldman and R. H. Brandenberger, *Phys. Rept.* **215**, 203 (1992).
- [7] C. M. Will, *Theory and Experiment in Gravitational Physics*, Cambridge University Press (2018).
- [8] C. M. Will, *Living Rev. Rel.* **17**, 4 (2014), [arXiv:1403.7377].
- [9] K. Nordvedt, *Phys. Rev.* **170**, 1186 (1968).
- [10] R. A. Hulse, *Rev. Mod. Phys.* **66**, 699 (1994).
- [11] J. H. Taylor, *Rev. Mod. Phys.* **66**, 711 (1994).
- [12] T. Damour and N. Deruelle, *Phys. Lett.* **A87**, 81 (1981); T. Damour, *C.R. Acad. Sci. Paris* **294**, 1335 (1982).
- [13] T. Damour and J. H. Taylor, *Phys. Rev.* **D45**, 1840 (1992).
- [14] T. Damour and N. Deruelle, *Ann. Inst. H. Poincaré A*, **44**, 263 (1986).
- [15] T. Damour and G. Esposito-Farese, *Class. Quant. Grav.* **9**, 2093 (1992).
- [16] C. M. Will and H. W. Zaglauer, *Astrophys. J.* **346**, 366 (1989).
- [17] T. Damour and G. Esposito-Farese, *Phys. Rev.* **D54**, 1474 (1996), [arXiv:gr-qc/9602056].
- [18] T. Damour and G. Esposito-Farese, *Phys. Rev.* **D58**, 042001 (1998), [arXiv:gr-qc/9803031].
- [19] J.-P. Uzan, *Gen. Rel. Grav.* **39**, 307 (2007), [arXiv:astro-ph/0605313].
- [20] R. Caldwell, A. Cooray and A. Melchiorri, *Phys. Rev.* **D76**, 023507 (2007), [arXiv:astro-ph/0703375].
- [21] P. Zhang *et al.*, *Phys. Rev. Lett.* **99**, 141302 (2007), [arXiv:0704.1932].
- [22] L. Amendola, M. Kunz and D. Sapone, *JCAP* **0804**, 013 (2008), [arXiv:0704.2421].

- [23] W. Hu and I. Sawicki, Phys. Rev. **D76**, 104043 (2007), [arXiv:0708.1190].
- [24] S. F. Daniel *et al.*, Phys. Rev. **D77**, 103513 (2008), [arXiv:0802.1068].
- [25] G.-B. Zhao *et al.*, Phys. Rev. **D79**, 083513 (2009), [arXiv:0809.3791].
- [26] J.-P. Uzan, Gen. Rel. Grav. **42**, 2219 (2010), [arXiv:0908.2243].
- [27] E. Bertschinger, Phil. Trans. Roy. Soc. Lond. **A369**, 4947 (2011), [arXiv:1111.4659].
- [28] T. Baker, P. G. Ferreira and C. Skordis, Phys. Rev. **D87**, 2, 024015 (2013), [arXiv:1209.2117].
- [29] M. Ishak, Living Rev. Rel. **22**, 1, 1 (2019), [arXiv:1806.10122].
- [30] B. P. Abbott *et al.* (LIGO Scientific, Virgo), Phys. Rev. Lett. **116**, 6, 061102 (2016), [arXiv:1602.03837].
- [31] B. P. Abbott *et al.* (LIGO Scientific, Virgo), Phys. Rev. Lett. **116**, 24, 241103 (2016), [arXiv:1606.04855].
- [32] B. P. Abbott *et al.* (LIGO Scientific, VIRGO), Phys. Rev. Lett. **118**, 22, 221101 (2017), [Erratum: Phys. Rev. Lett.121,no.12,129901(2018)], [arXiv:1706.01812].
- [33] B. P. Abbott *et al.* (LIGO Scientific, Virgo), Phys. Rev. Lett. **119**, 14, 141101 (2017), [arXiv:1709.09660].
- [34] B. P. Abbott *et al.* (LIGO Scientific, Virgo), Phys. Rev. Lett. **119**, 16, 161101 (2017), [arXiv:1710.05832].
- [35] B. P. Abbott *et al.* (LIGO Scientific, Virgo), Phys. Rev. **X6**, 4, 041015 (2016), [erratum: Phys. Rev.X8,no.3,039903(2018)], [arXiv:1606.04856].
- [36] A. Buonanno and T. Damour, Phys. Rev. **D62**, 064015 (2000), [arXiv:gr-qc/0001013].
- [37] L. Blanchet, Living Rev. Rel. **17**, 2 (2014), [arXiv:1310.1528].
- [38] F. Pretorius, Phys. Rev. Lett. **95**, 121101 (2005), [arXiv:gr-qc/0507014]; M. Campanelli *et al.*, Phys. Rev. Lett. **96**, 111101 (2006), [arXiv:gr-qc/0511048]; J. G. Baker *et al.*, Phys. Rev. Lett. **96**, 111102 (2006), [arXiv:gr-qc/0511103].
- [39] K. Yagi *et al.*, Phys. Rev. **D85**, 064022 (2012), [Erratum: Phys. Rev.D93,no.2,029902(2016)], [arXiv:1110.5950].
- [40] K. Yagi, L. C. Stein and N. Yunes, Phys. Rev. **D93**, 2, 024010 (2016), [arXiv:1510.02152].
- [41] K. Prabhu and L. C. Stein, Phys. Rev. **D98**, 2, 021503 (2018), [arXiv:1805.02668].
- [42] L. Bernard, Phys. Rev. **D98**, 4, 044004 (2018), [arXiv:1802.10201].
- [43] F.-L. Julié and E. Berti (2019), [arXiv:1909.05258].
- [44] M. Okounkova *et al.*, Phys. Rev. **D96**, 4, 044020 (2017), [arXiv:1705.07924].
- [45] H. Witek *et al.*, Phys. Rev. **D99**, 6, 064035 (2019), [arXiv:1810.05177].
- [46] M. Okounkova *et al.* (2019), [arXiv:1906.08789].
- [47] L. Blanchet and B. S. Sathyaprakash, Phys. Rev. Lett. **74**, 1067 (1995).
- [48] K. G. Arun *et al.*, Phys. Rev. **D74**, 024006 (2006), [arXiv:gr-qc/0604067].
- [49] B. P. Abbott *et al.* (LIGO Scientific, Virgo), Phys. Rev. Lett. **116**, 22, 221101 (2016), [Erratum: Phys. Rev. Lett.121,no.12,129902(2018)], [arXiv:1602.03841].
- [50] N. Yunes and F. Pretorius, Phys. Rev. **D80**, 122003 (2009), [arXiv:0909.3328].
- [51] S. Khan *et al.*, Phys. Rev. **D93**, 4, 044007 (2016), [arXiv:1508.07253].
- [52] C. V. Vishveshwara, Nature **227**, 936 (1970).
- [53] S. L. Detweiler, Astrophys. J. **239**, 292 (1980).
- [54] V. Cardoso *et al.*, Phys. Rev. **D99**, 10, 104077 (2019), [arXiv:1901.01265].
- [55] R. McManus *et al.*, Phys. Rev. **D100**, 4, 044061 (2019), [arXiv:1906.05155].
- [56] C. M. Will, Phys. Rev. **D57**, 2061 (1998), [arXiv:gr-qc/9709011].
- [57] M. Fierz, Helv. Phys. Acta **29**, 128 (1956).
- [58] E. G. Adelberger, B. R. Heckel and A. E. Nelson, Ann. Rev. Nucl. Part. Sci. **53**, 77 (2003), [hep-ph/0307284].
- [59] D. J. Kapner *et al.*, Phys. Rev. Lett. **98**, 021101 (2007), [hep-ph/0611184].
- [60] A. O. Sushkov *et al.*, Phys. Rev. Lett. **107**, 171101 (2011), [arXiv:1108.2547].
- [61] T. Damour and J. F. Donoghue, Phys. Rev. **D82**, 084033 (2010), [arXiv:1007.2792].
- [62] R. V. Wagoner, Phys. Rev. **D1**, 3209 (1970).
- [63] C. Brans and R. H. Dicke, Phys. Rev. **124**, 925 (1961), [142(1961)].
- [64] J. Alsing *et al.*, Phys. Rev. **D85**, 064041 (2012), [arXiv:1112.4903].
- [65] T. Damour and K. Nordtvedt, Phys. Rev. Lett. **70**, 2217 (1993).
- [66] T. Damour and A. M. Polyakov, Nucl. Phys. **B423**, 532 (1994), [hep-th/9401069].
- [67] K. A. Olive and M. Pospelov, Phys. Rev. **D77**, 043524 (2008), [arXiv:0709.3825].
- [68] J. Khoury and A. Weltman, Phys. Rev. Lett. **93**, 171104 (2004), [arXiv:astro-ph/0309300].
- [69] K. Hinterbichler and J. Khoury, Phys. Rev. Lett. **104**, 231301 (2010), [arXiv:1001.4525].
- [70] P. Brax *et al.*, Phys. Rev. **D82**, 063519 (2010), [arXiv:1005.3735].
- [71] A. Joyce *et al.*, Phys. Rept. **568**, 1 (2015), [arXiv:1407.0059].
- [72] C. Burrage and J. Sakstein, Living Rev. Rel. **21**, 1, 1 (2018), [arXiv:1709.09071].
- [73] A. I. Vainshtein, Phys. Lett. **39B**, 393 (1972).
- [74] C. de Rham, Living Rev. Rel. **17**, 7 (2014), [arXiv:1401.4173].
- [75] G. W. Horndeski, Int. J. Theor. Phys. **10**, 363 (1974).
- [76] C. Deffayet *et al.*, Phys. Rev. **D84**, 064039 (2011), [arXiv:1103.3260].
- [77] L. Heisenberg, Phys. Rept. **796**, 1 (2019), [arXiv:1807.01725].
- [78] T. Kobayashi, Rept. Prog. Phys. **82**, 8, 086901 (2019), [arXiv:1901.07183].
- [79] G. Papallo and H. S. Reall, Phys. Rev. **D96**, 4, 044019 (2017), [arXiv:1705.04370].
- [80] L. Bernard, L. Lehner and R. Luna, Phys. Rev. **D100**, 2, 024011 (2019), [arXiv:1904.12866].
- [81] A. D. Kovács, Phys. Rev. **D100**, 2, 024005 (2019), [arXiv:1904.00963].
- [82] C. de Rham and S. Melville, Phys. Rev. Lett. **121**, 22, 221101 (2018), [arXiv:1806.09417].
- [83] D. D. Doneva and S. S. Yazadjiev, Phys. Rev. Lett. **120**, 13, 131103 (2018), [arXiv:1711.01187].
- [84] H. O. Silva *et al.*, Phys. Rev. Lett. **120**, 13, 131104 (2018), [arXiv:1711.02080].
- [85] C. A. R. Herdeiro and E. Radu, Int. J. Mod. Phys. **D24**, 09, 1542014 (2015), [arXiv:1504.08209].
- [86] A.I. Shlyakhter, Nature **264**, 340 (1976).

- [87] T. Damour and F. Dyson, Nucl. Phys. **B480**, 37 (1996), [hep-ph/9606486]; C. R. Gould, E. I. Sharapov and S. K. Lamoreaux, Phys. Rev. **C74**, 024607 (2006), [arXiv:nucl-ex/0701019]; E. D. Davis and L. Hamdan, Phys. Rev. **C92**, 1, 014319 (2015), [arXiv:1503.06011]; Yu. V. Petrov *et al.*, Phys. Rev. **C74**, 064610 (2006), [hep-ph/0506186].
- [88] V. V. Flambaum and R. B. Wiringa, Phys. Rev. **C79**, 034302 (2009), [arXiv:0807.4943].
- [89] K. A. Olive *et al.*, Phys. Rev. **D69**, 027701 (2004), [arXiv:astro-ph/0309252].
- [90] M. T. Murphy, A. L. Malec and J. X. Prochaska, Mon. Not. Roy. Astron. Soc. **461**, 3, 2461 (2016), [arXiv:1606.06293].
- [91] N. Kanekar *et al.*, Mon. Not. Roy. Astron. Soc. **448**, 1, L104 (2015), [arXiv:1412.7757].
- [92] P. A. R. Ade *et al.* (Planck), Astron. Astrophys. **580**, A22 (2015), [arXiv:1406.7482].
- [93] T. Rosenband *et al.*, Science **319**, 1808 (2008); J. Guena *et al.*, Phys. Rev. Lett. **109**, 080801 (2012); R. M. Godun *et al.*, Phys. Rev. Lett. **113**, 21, 210801 (2014), [arXiv:1407.0164].
- [94] T. M. Fortier *et al.*, Phys. Rev. Lett. **98**, 070801 (2007); S. Blatt *et al.*, Phys. Rev. Lett. **100**, 140801 (2008), [arXiv:0801.1874]; T. Dent, Phys. Rev. Lett. **101**, 041102 (2008), [arXiv:0805.0318].
- [95] A. Fienga *et al.*, Cel. Mech. Dyn. Astr. **123**, Issue 2, 1 (2015).
- [96] F. Hofmann and J. Müller, Class. Quant. Grav. **35**, 3, 035015 (2018).
- [97] K. Lazaridis *et al.*, Mon. Not. R. Astron. Soc. **400**, 805 (2009), [arXiv:0908.0285].
- [98] W. W. Zhu *et al.*, Mon. Not. Roy. Astron. Soc. **482**, 3, 3249 (2019), [arXiv:1802.09206].
- [99] M. Smiciklas *et al.*, Phys. Rev. Lett. **107**, 171604 (2011), [arXiv:1106.0738].
- [100] J. F. Bell and T. Damour, Class. Quant. Grav. **13**, 3121 (1996), [arXiv:gr-qc/9606062].
- [101] L. Shao and N. Wex, Class. Quant. Grav. **29**, 215018 (2012), [arXiv:1209.4503].
- [102] S. Liberati, J. Phys. Conf. Ser. **631**, 1, 012011 (2015).
- [103] S. Schlamminger *et al.*, Phys. Rev. Lett. **100**, 041101 (2008), [arXiv:0712.0607].
- [104] T. A. Wagner *et al.*, Class. Quant. Grav. **29**, 184002 (2012), [arXiv:1207.2442].
- [105] P. Touboul *et al.*, Phys. Rev. Lett. **119**, 23, 231101 (2017), [arXiv:1712.01176].
- [106] P. Touboul *et al.* (MICROSCOPE), Class. Quant. Grav. **36**, 22, 225006 (2019), [arXiv:1909.10598].
- [107] S. Merlet *et al.*, Metrologia, **47**, L9-L11 (2010).
- [108] G. Rosi *et al.*, Nature Commun. **8**, 5529 (2017), [arXiv:1704.02296].
- [109] R.F.C. Vessot and M.W. Levine, Gen. Rel. Grav. **10**, 181 (1978); R. F. C. Vessot *et al.*, Phys. Rev. Lett. **45**, 2081 (1980).
- [110] C. W. Chou *et al.*, Science **329**, 1630 (2010).
- [111] R. Abuter *et al.* (GRAVITY), Astron. Astrophys. **615**, L15 (2018), [arXiv:1807.09409].
- [112] T. Do *et al.*, Science **365**, 6454, 664 (2019), [arXiv:1907.10731].
- [113] A. Amorim *et al.* (GRAVITY), Phys. Rev. Lett. **122**, 10, 101102 (2019), [arXiv:1902.04193].
- [114] J.G. Williams, S.G. Turyshev, and D.H. Boggs, Class. Quantum Grav. **29**, 184004 (2012).
- [115] I. Ciufolini and E. C. Pavlis, Nature **431**, 958 (2004).
- [116] I. Ciufolini *et al.*, Eur. Phys. J. **C76**, 3, 120 (2016), [arXiv:1603.09674].
- [117] C. W. F. Everitt *et al.*, Phys. Rev. Lett. **106**, 221101 (2011), [arXiv:1105.3456].
- [118] B. Bertotti, L. Iess and P. Tortora, Nature **425**, 374 (2003).
- [119] J. Bergé *et al.*, Phys. Rev. Lett. **120**, 14, 141101 (2018), [arXiv:1712.00483].
- [120] J. M. Weisberg and Y. Huang, Astrophys. J. **829**, 1, 55 (2016), [arXiv:1606.02744].
- [121] A. Wolszczan, Nature **350**, 688 (1991).
- [122] J. N. Taylor, A. Wolszczan and T. Damour, Nature **355**, 132 (1993).
- [123] E. Fonseca, I. H. Stairs and S. E. Thorsett, Astrophys. J. **787**, 82 (2014), [arXiv:1402.4836].
- [124] V. M. Kaspi *et al.*, Astrophys. J. **528**, 445 (2000), [arXiv:astro-ph/9906373].
- [125] S. M. Ord, M. Bailes and W. van Straten, Astrophys. J. **574**, L75 (2002), [arXiv:astro-ph/0204421].
- [126] M. Bailes *et al.*, Astrophys. J. **595**, L49 (2003), [arXiv:astro-ph/0307468].
- [127] N. D. R. Bhat, M. Bailes and J. P. W. Verbiest, Phys. Rev. **D77**, 124017 (2008), [arXiv:0804.0956].
- [128] M. Burgay *et al.*, Nature **426**, 531 (2003), [arXiv:astro-ph/0312071].
- [129] A. G. Lyne *et al.*, Science **303**, 1153 (2004), [arXiv:astro-ph/0401086].
- [130] M. Kramer *et al.*, Science **314**, 97 (2006), [arXiv:astro-ph/0609417].
- [131] R. P. Breton *et al.*, Science **321**, 104 (2008), [arXiv:0807.2644].
- [132] B. Perera *et al.*, Astrophys. J. **721**, 1193 (2010), [arXiv:1008.1097].
- [133] R. D. Ferdman *et al.*, Mon. Not. Roy. Astron. Soc. **443**, 3, 2183 (2014), [arXiv:1406.5507].
- [134] M. Kramer and N. Wex, Class. Quant. Grav. **26**, 073001 (2009).
- [135] M. Kramer, in *Neutron Stars and Pulsars: Challenges and Opportunities after 80 Years*; M. Kramer, IAU Symp. **291**, 19 (2013), [arXiv:1211.2457].
- [136] T. Damour and G. Schaefer, Phys. Rev. Lett. **66**, 2549 (1991).
- [137] M. E. Gonzalez *et al.*, Astrophys. J. **743**, 102 (2011), [arXiv:1109.5638].
- [138] P. C. C. Freire, M. Kramer and N. Wex, Class. Quant. Grav. **29**, 184007 (2012), [arXiv:1205.3751].
- [139] S. M. Ransom *et al.*, Nature **505**, 520 (2014), [arXiv:1401.0535].
- [140] A. M. Archibald *et al.*, Nature **559**, 7712, 73 (2018), [arXiv:1807.02059].
- [141] T. Damour and R. Ruffini, C. R. Acad. Sc. Paris **279**, série A, 971 (1974); B. M. Barker and R. F. O'Connell, Phys. Rev. **D12**, 329 (1975).
- [142] M. Kramer, Astrophys. J. **509**, 856 (1998), [arXiv:astro-ph/9808127]; J. M. Weisberg and J. H. Taylor, Astrophys. J. **576**, 942 (2002), [arXiv:astro-ph/0205280].
- [143] R. N. Manchester *et al.*, Astrophys. J. **710**, 1694 (2010), [arXiv:1001.1483].
- [144] J. van Leeuwen *et al.*, Astrophys. J. **798**, 2, 118 (2015), [arXiv:1411.1518].
- [145] G. Desvignes *et al.*, Science **365**, 6457, 1013 (2019).
- [146] B. P. Abbott *et al.* (LIGO Scientific, Virgo), Phys. Rev. **X9**, 3, 031040 (2019), [arXiv:1811.12907].
- [147] V. Cardoso and P. Pani, Nat. Astron. **1**, 9, 586 (2017), [arXiv:1709.01525].
- [148] K. Akiyama *et al.* (Event Horizon Telescope), Astrophys. J. **875**, 1, L1 (2019), [arXiv:1906.11238].

- [149] J. Beltran Jimenez, F. Piazza and H. Velten, *Phys. Rev. Lett.* **116**, 6, 061101 (2016), [arXiv:1507.05047].
- [150] T. Damour and J. H. Taylor, *Astrophys. J.* **366**, 501 (1991).
- [151] P. C. C. Freire *et al.*, *Mon. Not. Roy. Astron. Soc.* **423**, 3328 (2012), [arXiv:1205.1450].
- [152] J. Antoniadis *et al.*, *Science* **340**, 6131 (2013), [arXiv:1304.6875].
- [153] W. W. Zhu *et al.*, *Astrophys. J.* **809**, 1, 41 (2015), [arXiv:1504.00662].
- [154] L. Shao *et al.*, *Phys. Rev.* **X7**, 4, 041025 (2017), [arXiv:1704.07561].
- [155] T. Venumadhav *et al.* (2019), [arXiv:1904.07214].
- [156] B. P. Abbott *et al.* (LIGO Scientific, Virgo) (2019), [arXiv:1903.04467].
- [157] M. Isi *et al.*, *Phys. Rev. Lett.* **123**, 11, 111102 (2019), [arXiv:1905.00869].
- [158] N. Yunes, K. Yagi and F. Pretorius, *Phys. Rev.* **D94**, 8, 084002 (2016), [arXiv:1603.08955].
- [159] D. M. Eardley, D. L. Lee and A. P. Lightman, *Phys. Rev.* **D8**, 3308 (1973).
- [160] B. P. Abbott *et al.*, *Astrophys. J.* **848**, 2, L12 (2017), [arXiv:1710.05833].
- [161] C. de Rham *et al.*, *Rev. Mod. Phys.* **89**, 2, 025004 (2017), [arXiv:1606.08462].
- [162] C. M. Will, *Class. Quant. Grav.* **35**, 17, 17LT01 (2018), [arXiv:1805.10523].
- [163] B. P. Abbott *et al.* (LIGO Scientific, Virgo, Fermi-GBM, INTEGRAL), *Astrophys. J.* **848**, 2, L13 (2017), [arXiv:1710.05834].
- [164] T. Baker *et al.*, *Phys. Rev. Lett.* **119**, 25, 251301 (2017), [arXiv:1710.06394].
- [165] P. Creminelli and F. Vernizzi, *Phys. Rev. Lett.* **119**, 25, 251302 (2017), [arXiv:1710.05877].
- [166] J. Sakstein and B. Jain, *Phys. Rev. Lett.* **119**, 25, 251303 (2017), [arXiv:1710.05893].
- [167] J. M. Ezquiaga and M. Zumalacárregui, *Phys. Rev. Lett.* **119**, 25, 251304 (2017), [arXiv:1710.05901].
- [168] E. Barausse, N. Yunes and K. Chamberlain, *Phys. Rev. Lett.* **116**, 24, 241104 (2016), [arXiv:1603.04075].
- [169] K. Chamberlain and N. Yunes, *Phys. Rev.* **D96**, 8, 084039 (2017), [arXiv:1704.08268].

22. Big-Bang Cosmology

Revised August 2019 by K.A. Olive (Minnesota U.) and J.A. Peacock (Edinburgh U.).

22.1 Introduction to Standard Big-Bang Model

The observed expansion of the Universe [1–3] is a natural (almost inevitable) result of any homogeneous and isotropic cosmological model based on general relativity. However, by itself, the Hubble expansion does not provide sufficient evidence for what we generally refer to as the Big-Bang model of cosmology. While general relativity is in principle capable of describing the cosmology of any given distribution of matter, it is extremely fortunate that our Universe appears to be homogeneous and isotropic on large scales. Together, homogeneity and isotropy allow us to extend the Copernican Principle to the Cosmological Principle, stating that all spatial positions in the Universe are essentially equivalent.

The formulation of the Big-Bang model began in the 1940s with the work of George Gamow and his collaborators, Ralph Alpher and Robert Herman. In order to account for the possibility that the abundances of the elements had a cosmological origin, they proposed that the early Universe was once very hot and dense (enough so as to allow for the nucleosynthetic processing of hydrogen), and has subsequently expanded and cooled to its present state [4, 5]. In 1948, Alpher and Herman predicted that a direct consequence of this model is the presence of a relic background radiation with a temperature of order a few K [6, 7]. Of course this radiation was observed 16 years later as the Cosmic Microwave Background (CMB) [8]. Indeed, it was the observation of this radiation that singled out the Big-Bang model as the prime candidate to describe our Universe. Subsequent work on Big-Bang nucleosynthesis further confirmed the necessity of our hot and dense past. (See Sec. 22.3.7 for a brief discussion of BBN and the review on BBN – Sec. 24 of this *Review* for a detailed discussion of BBN.) These relativistic cosmological models face severe problems with their initial conditions, to which the best modern solution is inflationary cosmology, discussed in Sec. 22.3.5 and in – Sec. 23 of this *Review*. If correct, these ideas would strictly render the term ‘Big Bang’ redundant, since it was first coined by Hoyle to represent a criticism of the lack of understanding of the initial conditions.

22.1.1 The Robertson-Walker Universe

The observed homogeneity and isotropy enable us to describe the overall geometry and evolution of the Universe in terms of two cosmological parameters accounting for the spatial curvature and the overall expansion (or contraction) of the Universe. These two quantities appear in the most general expression for a space-time metric that has a (3D) maximally symmetric subspace of a 4D space-time, known as the Robertson-Walker metric:

$$ds^2 = dt^2 - R^2(t) \left[\frac{dr^2}{1 - kr^2} + r^2 (d\theta^2 + \sin^2 \theta d\phi^2) \right]. \quad (22.1)$$

Note that we adopt $c = 1$ throughout. By rescaling the radial coordinate, we can choose the curvature constant k to take only the discrete values $+1$, -1 , or 0 corresponding to closed, open, or spatially flat geometries. In this case, it is often more convenient to re-express the metric as

$$ds^2 = dt^2 - R^2(t) [d\chi^2 + S_k^2(\chi) (d\theta^2 + \sin^2 \theta d\phi^2)], \quad (22.2)$$

where the function $S_k(\chi)$ is $(\sin \chi, \chi, \sinh \chi)$ for $k = (+1, 0, -1)$. The coordinate r [in Eq. (22.1)] and the ‘angle’ χ [in Eq. (22.2)] are both dimensionless; the dimensions are carried by the cosmological scale factor, $R(t)$, which determines proper distances in terms of the comoving coordinates. A common alternative is to define a dimensionless scale factor, $a(t) = R(t)/R_0$, where $R_0 \equiv R(t_0)$ is R at the present epoch. It is also sometimes convenient to define a dimensionless or conformal time coordinate, η , by $d\eta = dt/R(t)$. Along constant spatial sections, the proper time is defined by the time coordinate, t . Similarly, for $dt = d\theta = d\phi = 0$, the proper distance is given by $R(t)\chi$. For standard texts on cosmological models see *e.g.*, Refs. [9–16].

22.1.2 The redshift

The cosmological redshift is a direct consequence of the Hubble expansion, determined by $R(t)$. A local observer detecting light from a distant emitter sees a redshift in frequency. We can define the redshift as

$$z \equiv \frac{\nu_1 - \nu_2}{\nu_2} \simeq v_{12}, \quad (22.3)$$

where ν_1 is the frequency of the emitted light, ν_2 is the observed frequency, and v_{12} is the relative velocity between the emitter and the observer. While the definition, $z = (\nu_1 - \nu_2)/\nu_2$ is valid in general, relating the redshift to a simple relative velocity is only correct on small scales (*i.e.*, less than cosmological scales) such that the expansion velocity is non-relativistic. For light signals, we can use the metric given by Eq. (22.1) and $ds^2 = 0$ to write

$$v_{12} = \dot{R} \delta r = \frac{\dot{R}}{R} \delta t = \frac{\delta R}{R} = \frac{R_2 - R_1}{R_1}, \quad (22.4)$$

where $\delta r(\delta t)$ is the radial coordinate (temporal) separation between the emitter and observer. Noting that physical distance, D , is $R\delta r$ or δt , Eq. (22.4) gives us Hubble’s law, $v = HD$. In addition, we obtain the simple relation between the redshift and the scale factor

$$1 + z = \frac{\nu_1}{\nu_2} = \frac{R_2}{R_1}. \quad (22.5)$$

This result does not depend on the non-relativistic approximation.

22.1.3 The Friedmann equations of motion

The cosmological equations of motion are derived from Einstein’s equations

$$\mathcal{R}_{\mu\nu} - \frac{1}{2} g_{\mu\nu} \mathcal{R} = 8\pi G_N T_{\mu\nu} + \Lambda g_{\mu\nu} \quad (22.6)$$

Gliner [17] and Zeldovich [18] have pioneered the modern view, in which the Λ term is set on the rhs and interpreted as an effective energy – momentum tensor $T_{\mu\nu}$ for the vacuum of $\Lambda g_{\mu\nu}/8\pi G_N$. It is common to assume that the matter content of the Universe is a perfect fluid, for which

$$T_{\mu\nu} = -p g_{\mu\nu} + (p + \rho) u_\mu u_\nu, \quad (22.7)$$

where $g_{\mu\nu}$ is the space-time metric described by Eq. (22.1), p is the isotropic pressure, ρ is the energy density and $u = (1, 0, 0, 0)$ is the velocity vector for the isotropic fluid in co-moving coordinates. With the perfect fluid source, Einstein’s equations lead to the Friedmann equations

$$H^2 \equiv \left(\frac{\dot{R}}{R} \right)^2 = \frac{8\pi G_N \rho}{3} - \frac{k}{R^2} + \frac{\Lambda}{3}, \quad (22.8)$$

and

$$\frac{\ddot{R}}{R} = \frac{\Lambda}{3} - \frac{4\pi G_N}{3} (\rho + 3p), \quad (22.9)$$

where $H(t)$ is the Hubble parameter and Λ is the cosmological constant. The first of these is sometimes called the Friedmann equation. Energy conservation via $T^{\mu\nu}_{;\mu} = 0$, leads to a third useful equation [which can also be derived from Eq. (22.8) and Eq. (22.9)]

$$\dot{\rho} = -3H(\rho + p). \quad (22.10)$$

Eq. (22.10) can also be simply derived as a consequence of the first law of thermodynamics.

Eq. (22.8) has a simple classical mechanical analog if we neglect (for the moment) the cosmological term Λ . By interpreting $-k/R^2$ Newtonianly as a ‘total energy’, then we see that the evolution of the Universe is governed by a competition between the potential energy, $8\pi G_N \rho/3$, and the kinetic term $(\dot{R}/R)^2$. For $\Lambda = 0$, it is clear that the Universe must be expanding or contracting (except at the turning point prior to collapse in a closed Universe). The ultimate fate of the Universe is determined by the curvature constant k . For $k = +1$, the Universe will recollapse in a finite time, whereas for $k = 0, -1$, the Universe will expand indefinitely. These simple conclusions can be altered when $\Lambda \neq 0$ or more generally with some component with $(\rho + 3p) < 0$.

22.1.4 Definition of cosmological parameters

In addition to the Hubble parameter, it is useful to define several other measurable cosmological parameters. The Friedmann equation can be used to define a critical density such that $k = 0$ when $\Lambda = 0$,

$$\begin{aligned}\rho_c &\equiv \frac{3H^2}{8\pi G_N} = 1.88 \times 10^{-26} h^2 \text{ kg m}^{-3} \\ &= 1.05 \times 10^{-5} h^2 \text{ GeV cm}^{-3},\end{aligned}\quad (22.11)$$

where the scaled Hubble parameter, h , is defined by

$$\begin{aligned}H &\equiv 100 h \text{ km s}^{-1} \text{ Mpc}^{-1} \\ \Rightarrow H^{-1} &= 9.778 h^{-1} \text{ Gyr} \\ &= 2998 h^{-1} \text{ Mpc}.\end{aligned}\quad (22.12)$$

The cosmological density parameter Ω_{tot} is defined as the energy density relative to the critical density,

$$\Omega_{\text{tot}} = \rho/\rho_c. \quad (22.13)$$

Note that one can now rewrite the Friedmann equation as

$$k/R^2 = H^2(\Omega_{\text{tot}} - 1). \quad (22.14)$$

From Eq. (22.14), one can see that when $\Omega_{\text{tot}} > 1$, $k = +1$ and the Universe is closed, when $\Omega_{\text{tot}} < 1$, $k = -1$ and the Universe is open, and when $\Omega_{\text{tot}} = 1$, $k = 0$, and the Universe is spatially flat.

It is often necessary to distinguish different contributions to the density. It is therefore convenient to define present-day density parameters for pressureless matter (Ω_m) and relativistic particles (Ω_r), plus the quantity $\Omega_\Lambda = \Lambda/3H^2$. In more general models, we may wish to drop the assumption that the vacuum energy density is constant, and we therefore denote the present-day density parameter of the vacuum by Ω_v . The Friedmann equation then becomes

$$k/R_0^2 = H_0^2(\Omega_m + \Omega_r + \Omega_v - 1), \quad (22.15)$$

where the subscript 0 indicates present-day values. Thus, it is the sum of the densities in matter, relativistic particles, and vacuum that determines the overall sign of the curvature. Note that the quantity $-k/R_0^2 H_0^2$ is sometimes referred to as Ω_K . This usage is unfortunate: it encourages one to think of curvature as a contribution to the energy density of the Universe, which is not correct.

22.1.5 Standard Model solutions

Much of the history of the Universe in the standard Big-Bang model can be easily described by assuming that either matter or radiation dominates the total energy density. During inflation and again today the expansion rate for the Universe is accelerating, and domination by a cosmological constant or some other form of dark energy should be considered. In the following, we shall delineate the solutions to the Friedmann equation when a single component dominates the energy density. Each component is distinguished by an equation of state parameter $w = p/\rho$. We concentrate on solutions that expand at early times, although the Friedmann equation also permits a time-reversed contracting solution.

22.1.5.1 Solutions for a general equation of state

Let us first assume a general equation of state parameter for a single component, w , which is constant. In this case, Eq. (22.10) can be written as $\dot{\rho} = -3(1+w)\rho\dot{R}/R$ and is easily integrated to yield

$$\rho \propto R^{-3(1+w)}. \quad (22.16)$$

Note that at early times when R is small, the less singular curvature term k/R^2 in the Friedmann equation can be neglected so long as $w > -1/3$. Curvature domination occurs at rather late times (if a cosmological constant term does not dominate sooner). For $w \neq -1$, one can insert this result into the Friedmann equation Eq. (22.8), and if one neglects the curvature and cosmological constant terms, it is easy to integrate the equation to obtain,

$$R(t) \propto t^{2/[3(1+w)]}. \quad (22.17)$$

22.1.5.2 A Radiation-dominated Universe

In the early hot and dense Universe, it is appropriate to assume an equation of state corresponding to a gas of radiation (or relativistic particles) for which $w = 1/3$. In this case, Eq. (22.16) becomes $\rho \propto R^{-4}$. The ‘extra’ factor of $1/R$ is due to the cosmological redshift; not only is the number density of particles in the radiation background decreasing as R^{-3} since volume scales as R^3 , but in addition each particle’s energy is decreasing as $E \propto \nu \propto R^{-1}$. Similarly, one can substitute $w = 1/3$ into Eq. (22.17) to obtain

$$R(t) \propto t^{1/2}; \quad H = 1/2t. \quad (22.18)$$

22.1.5.3 A Matter-dominated Universe

At relatively late times, non-relativistic matter eventually dominates the energy density over radiation [see Eq. (22.3.8)]. A pressureless gas ($w = 0$) leads to the expected dependence $\rho \propto R^{-3}$ from Eq. (22.16) and, if $k = 0$, we obtain

$$R(t) \propto t^{2/3}; \quad H = 2/3t. \quad (22.19)$$

22.1.5.4 A Universe dominated by vacuum energy

If there is a dominant source of vacuum energy, V_0 , it would act as a cosmological constant with $\Lambda = 8\pi G_N V_0$ and equation of state $w = -1$. In this case, the solution to the Friedmann equation when curvature is neglected is particularly simple and leads to an exponential expansion of the Universe:

$$R(t) \propto e^{\sqrt{\Lambda/3}t}. \quad (22.20)$$

More generally we could write

$$a(t) = \sinh^{2/3}(\sqrt{3\Lambda}t/2), \quad (22.21)$$

which describes a flat Universe containing both matter and vacuum energy, with $a(t)$ being the scale factor normalized to unity when both components are equal.

A key parameter is the equation of state of the vacuum, $w \equiv p/\rho$: this need not be the $w = -1$ of Λ , and may not even be constant [19–21]. There is much interest in the more general possibility of a dynamically evolving vacuum energy, for which the name ‘dark energy’ has become commonly used. A variety of techniques exist whereby the vacuum density as a function of time may be measured, usually expressed as the value of w as a function of epoch [22, 23]. The best current measurement of the equation of state (assumed constant, but without assuming zero curvature) is $w = -1.028 \pm 0.031$ [24]. Unless stated otherwise, we will assume that the vacuum energy is a cosmological constant with $w = -1$ exactly.

The presence of vacuum energy can dramatically alter the fate of the Universe. For example, if $\Lambda < 0$, the Universe will eventually recollapse independent of the sign of k . For large values of $\Lambda > 0$ (larger than the Einstein static value needed to halt any cosmological expansion or contraction), even a closed Universe will expand forever. One way to quantify this is the deceleration parameter, q_0 , defined as

$$q_0 = - \left. \frac{R\ddot{R}}{\dot{R}^2} \right|_0 = \frac{1}{2}\Omega_m + \Omega_r + \frac{(1+3w)}{2}\Omega_v. \quad (22.22)$$

This equation shows us that $w < -1/3$ for the vacuum may lead to an accelerating expansion. To the continuing astonishment of cosmologists, such an effect has been observed; one piece of direct evidence is the supernova Hubble diagram [25–30] (see Fig. 22.1 below). Current data indicate that vacuum energy is indeed the largest contributor to the cosmological density budget, with $\Omega_v = 0.685 \pm 0.007$ and $\Omega_m = 0.315 \pm 0.007$ if $k = 0$ is assumed [24].

The existence of this constituent is without doubt the greatest puzzle raised by the current cosmological model; the final section of this review discusses some of the ways in which the vacuum-energy problem is being addressed. For more details, see the review on Dark Energy – Sec. 28.

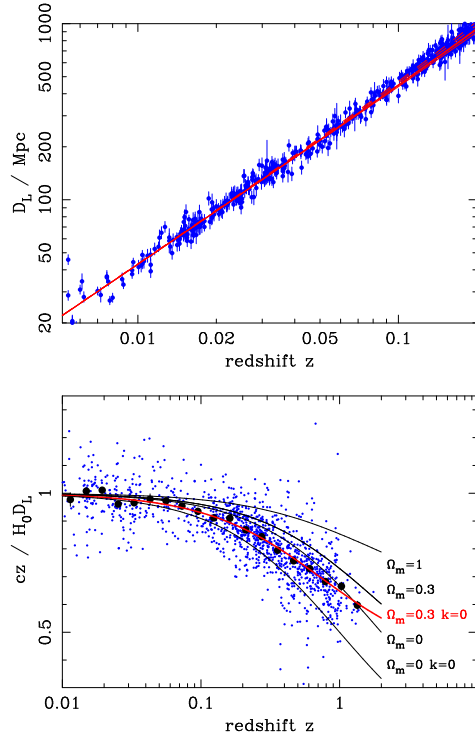


Figure 22.1: The type Ia supernova Hubble diagram, based on over 1200 publicly available supernova distance estimates [28–30]. The first panel shows that for $z \ll 1$ the large-scale Hubble flow is indeed linear and uniform; the second panel shows an expanded scale, with the linear trend divided out, and with the redshift range extended to show how the Hubble law becomes nonlinear. ($\Omega_r = 0$ is assumed.) Larger points with errors show median values in redshift bins. Comparison with the prediction of Friedmann models favors a vacuum-dominated Universe.

22.2 Introduction to Observational Cosmology

22.2.1 Fluxes, luminosities, and distances

The key quantities for observational cosmology can be deduced quite directly from the metric.

(1) The *proper* transverse size of an object seen by us to subtend an angle $d\psi$ is its comoving size $d\psi S_k(\chi)$ times the scale factor at the time of emission:

$$d\ell = d\psi R_0 S_k(\chi) / (1+z). \quad (22.23)$$

(2) The apparent flux density of an object is deduced by allowing its photons to flow through a sphere of current radius $R_0 S_k(\chi)$; but photon energies and arrival rates are redshifted, and the bandwidth $d\nu$ is reduced. The observed photons at frequency ν_0 were emitted at frequency $\nu_0(1+z)$, so the flux density is the luminosity at this frequency, divided by the total area, divided by $1+z$:

$$S_\nu(\nu_0) = \frac{L_\nu([1+z]\nu_0)}{4\pi R_0^2 S_k^2(\chi)(1+z)}. \quad (22.24)$$

These relations lead to the following common definitions:

$$\begin{aligned} \text{angular-diameter distance: } D_A &= (1+z)^{-1} R_0 S_k(\chi) \\ \text{luminosity distance: } D_L &= (1+z) R_0 S_k(\chi). \end{aligned} \quad (22.25)$$

These distance-redshift relations are expressed in terms of observables by using the equation of a null radial geodesic ($R(t)d\chi =$

dt) plus the Friedmann equation:

$$\begin{aligned} R_0 d\chi &= \frac{1}{H(z)} dz = \frac{1}{H_0} [(1 - \Omega_m - \Omega_v - \Omega_r)(1+z)^2 \\ &\quad + \Omega_v(1+z)^{3+3w} + \Omega_m(1+z)^3 \\ &\quad + \Omega_r(1+z)^4]^{-1/2} dz. \end{aligned} \quad (22.26)$$

The main scale for the distance here is the Hubble length, $1/H_0$.

The flux density is the product of the specific intensity I_ν and the solid angle $d\Omega$ subtended by the source: $S_\nu = I_\nu d\Omega$. Combining the angular size and flux-density relations thus gives the relativistic version of surface-brightness conservation:

$$I_\nu(\nu_0) = \frac{B_\nu([1+z]\nu_0)}{(1+z)^3}, \quad (22.27)$$

where B_ν is surface brightness (luminosity emitted into unit solid angle per unit area of source). We can integrate over ν_0 to obtain the corresponding total or bolometric formula:

$$I_{\text{tot}} = \frac{B_{\text{tot}}}{(1+z)^4}. \quad (22.28)$$

This cosmology-independent form expresses Liouville's Theorem: photon phase-space density is conserved along rays.

22.2.2 Distance data and geometrical tests of cosmology

In order to confront these theoretical predictions with data, we have to bridge the divide between two extremes. Nearby objects may have their distances measured quite easily, but their radial velocities are dominated by deviations from the ideal Hubble flow, which typically have a magnitude of several hundred km s^{-1} . On the other hand, objects at redshifts $z \gtrsim 0.01$ will have observed recessional velocities that differ from their ideal values by $\lesssim 10\%$, but absolute distances are much harder to supply in this case. The traditional solution to this problem is the construction of the distance ladder: an interlocking set of methods for obtaining relative distances between various classes of object, which begins with absolute distances at the 10 to 100 pc level, and terminates with galaxies at significant redshifts. This is discussed in the article on Cosmological Parameters – Sec. 25.1 of this *Review*.

One of the key developments in this area has been the use of type Ia supernovae (SNe), which now allow measurement of relative distances with 5% precision. In combination with improved Cepheid data from the HST plus improved measurements of the distance to the LMC (or alternatively a direct geometrical distance to the maser galaxy NGC4258), SNe results extend the distance ladder to the point where deviations from uniform expansion are negligible, leading to the best existing Cepheid-based value for H_0 : $74.03 \pm 1.42 \text{ km s}^{-1} \text{ Mpc}^{-1}$ [31]. Better still, the analysis of high- z SNe has allowed a simple and direct test of cosmological geometry to be carried out: as shown in Fig. 22.1 and Fig. 22.2, supernova data and measurements of CMB anisotropies strongly favor a $k = 0$ model dominated by vacuum energy. It is worth noting that there is some tension (3.7σ) between the Cepheid and CMB determinations of H_0 (the latter is 67.4 ± 0.5 [24]). While it is remarkable that the two very different methods give such similar results, the formal disagreement shows that either there are unidentified systematic errors or that some new post-CDM physics is required; there is no current consensus in the community on these alternatives. We do note that a recent analysis of SNe Ia with a calibration of the tip of the red-giant branch gives a result close to that of the CMB: 69.8 ± 0.8 (stat.) ± 1.7 (sys.) $\text{km s}^{-1} \text{ Mpc}^{-1}$ [32]. (See the review on Cosmological Parameters – Sec. 25.1 of this *Review* for a more comprehensive review of Hubble parameter determinations.)

22.2.3 Age of the Universe

The most striking conclusion of relativistic cosmology is that the Universe has not existed forever. The dynamical result for

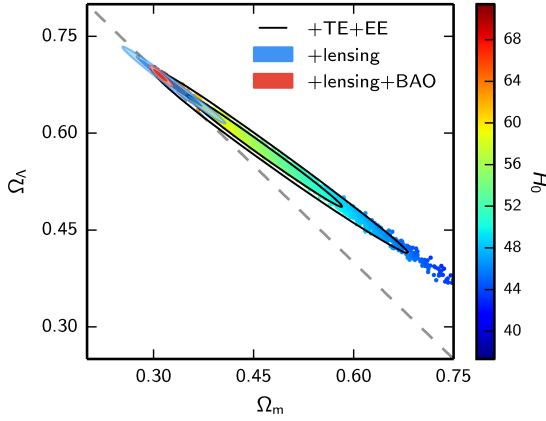


Figure 22.2: Likelihood-based probability densities over the plane Ω_Λ (i.e., Ω_ν assuming $w = -1$) vs Ω_m . The colored locus derives from *Planck* [33] and shows that the CMB alone requires a flat Universe $\Omega_\nu + \Omega_m \simeq 1$ if the Hubble constant is not too high. The SNe Ia results [34] very nearly constrain the orthogonal combination $\Omega_\nu - \Omega_m$, and the intersection of these constraints directly favors a flat model with $\Omega_m \simeq 0.3$, as does the measurement of the Baryon Acoustic Oscillation lengthscale (for which a joint constraint is shown on this plot). The CMB alone is capable of breaking the degeneracy with H_0 by using the measurements of gravitational lensing that can be made with modern high-resolution CMB data.

the age of the Universe may be written as

$$\begin{aligned} H_0 t_0 &= \int_0^\infty \frac{dz}{(1+z)H(z)} \\ &= \int_0^\infty \frac{dz}{(1+z) [(1+z)^2(1+\Omega_m z) - z(2+z)\Omega_\nu]^{1/2}}, \end{aligned} \quad (22.29)$$

where we have neglected Ω_r and chosen $w = -1$. Over the range of interest ($0.1 \lesssim \Omega_m \lesssim 1$, $|\Omega_\nu| \lesssim 1$), this exact answer may be approximated to a few per cent accuracy by

$$H_0 t_0 \simeq \frac{2}{3} (0.7\Omega_m + 0.3 - 0.3\Omega_\nu)^{-0.3}. \quad (22.30)$$

For the special case that $\Omega_m + \Omega_\nu = 1$, the integral in Eq. (22.29) can be expressed analytically as

$$H_0 t_0 = \frac{2}{3\sqrt{\Omega_\nu}} \ln \frac{1 + \sqrt{\Omega_\nu}}{\sqrt{1 - \Omega_\nu}} \quad (\Omega_m < 1). \quad (22.31)$$

The most accurate means of obtaining ages for astronomical objects is based on the natural clocks provided by radioactive decay. The use of these clocks is complicated by a lack of knowledge of the initial conditions of the decay. In the Solar System, chemical fractionation of different elements helps pin down a precise age for the pre-Solar nebula of 4.6 Gyr, but for stars it is necessary to attempt an a priori calculation of the relative abundances of nuclei that result from supernova explosions. In this way, a lower limit for the age of stars in the local part of the Milky Way of about 11 Gyr is obtained [35, 36].

The other major means of obtaining cosmological age estimates is based on the theory of stellar evolution. In principle, the main-sequence turnoff point in the color-magnitude diagram of a globular cluster should yield a reliable age. But these have been controversial, owing to theoretical uncertainties in the evolution model – as well as observational uncertainties in the distance, dust extinction, and metallicity of clusters. The present consensus favors ages for the oldest clusters of about 13 Gyr [37].

These methods are all consistent with the age deduced from studies of structure formation, using the microwave background and large-scale structure: $t_0 = 13.80 \pm 0.02$ Gyr [24], where the extra accuracy comes at the price of assuming the simple 6-parameter Λ CDM model to be true.

22.2.4 Horizon, isotropy, flatness problems

For photons, the radial equation of motion is just $c dt = R d\chi$. How far can a photon get in a given time? The answer is clearly

$$\Delta\chi = \int_{t_1}^{t_2} \frac{dt}{R(t)} \equiv \Delta\eta, \quad (22.32)$$

i.e., just the interval of conformal time. We can replace dt by dR/R , which the Friedmann equation says is $\propto dR/\sqrt{\rho R^2}$ at early times. Thus, this integral converges if $\rho R^2 \rightarrow \infty$ as $t_1 \rightarrow 0$, otherwise it diverges. Provided the equation of state is such that ρ changes faster than R^{-2} , light signals can only propagate a finite distance between the Big Bang and the present; there is then said to be a particle horizon. Such a horizon therefore exists in conventional Big-Bang models, which are dominated by radiation ($\rho \propto R^{-4}$) at early times.

At late times, the integral for the horizon is largely determined by the matter-dominated phase, for which

$$D_H = R_0 \chi_H \equiv R_0 \int_0^{t(z)} \frac{dt}{R(t)} \simeq \frac{6000}{\sqrt{\Omega_m z}} h^{-1} \text{Mpc} \quad (z \gg 1). \quad (22.33)$$

The horizon at the time of formation of the microwave background ('last scattering': $z \simeq 1100$) was thus of order 100 Mpc in size, subtending an angle of about 1° . Why then are the large number of causally disconnected regions we see on the microwave sky all at the same temperature? The Universe is very nearly isotropic and homogeneous, even though the initial conditions appear not to permit such a state to be constructed.

A related problem is that the $\Omega = 1$ Universe is unstable:

$$\Omega(a) - 1 = \frac{\Omega - 1}{1 - \Omega + \Omega_\nu a^2 + \Omega_m a^{-1} + \Omega_r a^{-2}}, \quad (22.34)$$

where Ω with no subscript is the total density parameter, and $a(t) = R(t)/R_0$. This requires $\Omega(t)$ to be unity to arbitrary precision as the initial time tends to zero; a Universe of non-zero curvature today requires very finely tuned initial conditions.

22.3 The Hot Thermal Universe

22.3.1 Thermodynamics of the early Universe

As alluded to above, we expect that much of the early Universe can be described by a radiation-dominated equation of state. In addition, through much of the radiation-dominated period, thermal equilibrium is established by the rapid rate of particle interactions relative to the expansion rate of the Universe (see Sec. 22.3.3 below). In equilibrium, it is straightforward to compute the thermodynamic quantities, ρ , p , and the entropy density, s . In general, the energy density for a given particle type i can be written as

$$\rho_i = \int E_i dn_{q_i}, \quad (22.35)$$

with the density of states given by

$$dn_{q_i} = \frac{g_i}{2\pi^2} (\exp[(E_{q_i} - \mu_i)/T_i] \pm 1)^{-1} q_i^2 dq_i, \quad (22.36)$$

where g_i counts the number of degrees of freedom for particle type i , $E_{q_i}^2 = m_i^2 + q_i^2$, μ_i is the chemical potential, and the \pm corresponds to either Fermi or Bose statistics. Similarly, we can define the pressure of a perfect gas as

$$p_i = \frac{1}{3} \int \frac{q_i^2}{E_i} dn_{q_i}. \quad (22.37)$$

The number density of species i is simply

$$n_i = \int dn_{q_i}, \quad (22.38)$$

and the entropy density is

$$s_i = \frac{\rho_i + p_i - \mu_i n_i}{T_i}. \quad (22.39)$$

In the Standard Model, a chemical potential is often associated with baryon number, and since the net baryon density relative to the photon density is known to be very small (of order 10^{-9}), we can neglect any such chemical potential when computing total thermodynamic quantities.

For photons, we can compute all of the thermodynamic quantities rather easily. Taking $g_i = 2$ for the 2 photon polarization states, we have (in units where $\hbar = k_B = 1$)

$$\rho_\gamma = \frac{\pi^2}{15} T^4, \quad p_\gamma = \frac{1}{3} \rho_\gamma, \quad s_\gamma = \frac{4\rho_\gamma}{3T}, \quad n_\gamma = \frac{2\zeta(3)}{\pi^2} T^3, \quad (22.40)$$

with $2\zeta(3)/\pi^2 \simeq 0.2436$. Note that Eq. (22.10) can be converted into an equation for entropy conservation. Recognizing that $\dot{p} = s\dot{T}$, Eq. (22.10) becomes

$$d(sR^3)/dt = 0. \quad (22.41)$$

For radiation, this corresponds to the relationship between expansion and cooling, $T \propto R^{-1}$ in an adiabatically expanding Universe. Note also that both s and n_γ scale as T^3 .

22.3.2 Radiation content of the Early Universe

At the very high temperatures associated with the early Universe, massive particles are pair produced, and are part of the thermal bath. If for a given particle species i we have $T \gg m_i$, then we can neglect the mass in Eq. (22.35) to Eq. (22.39), and the thermodynamic quantities are easily computed as in Eq. (22.40). In general, we can approximate the energy density (at high temperatures) by including only those particles with $m_i \ll T$. In this case, we have

$$\rho = \left(\sum_B g_B + \frac{7}{8} \sum_F g_F \right) \frac{\pi^2}{30} T^4 \equiv \frac{\pi^2}{30} N(T) T^4, \quad (22.42)$$

where $g_{B(F)}$ is the number of degrees of freedom of each boson (fermion) and the sum runs over all boson and fermion states with $m \ll T$. The factor of $7/8$ is due to the difference between the Fermi and Bose integrals. Eq. (22.42) defines the effective number of degrees of freedom, $N(T)$, by taking into account new particle degrees of freedom as the temperature is raised. This quantity, calculated from high temperature lattice QCD, is plotted in Fig. 22.3 [38]. Near the QCD transition, there is a slight difference between the coefficient of T^4 for ρ and the coefficient of T^3 for the entropy density $s = (2\pi^2/45)N_s(T)T^3$ [39], as seen in the figure.

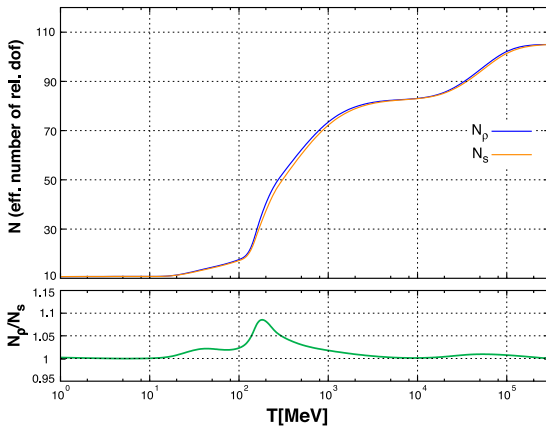


Figure 22.3: The effective numbers of relativistic degrees of freedom as a function of temperature. The sharp drop corresponds to the quark-hadron transition. The bottom panel shows the relative ratio between the number of degrees of freedom characterizing the energy density and the entropy.

The value of $N(T)$ at any given temperature depends on the particle physics model. In the standard $SU(3) \times SU(2) \times U(1)$ model, we can specify $N(T)$ up to temperatures of $O(100)$ GeV.

The change in N (ignoring mass effects) can be seen in the table below.

Temperature	New Particles	$4N(T)$
$T < m_e$	γ 's + ν 's	29
$m_e < T < m_\mu$	e^\pm	43
$m_\mu < T < m_\pi$	μ^\pm	57
$m_\pi < T < T_c^\dagger$	π 's	69
$T_c < T < m_{\text{strange}}$	π 's + u, \bar{u}, d, \bar{d} + gluons	205
$m_s < T < m_{\text{charm}}$	s, \bar{s}	247
$m_c < T < m_\tau$	c, \bar{c}	289
$m_\tau < T < m_{\text{bottom}}$	τ^\pm	303
$m_b < T < m_{W,Z}$	b, \bar{b}	345
$m_{W,Z} < T < m_{\text{Higgs}}$	W^\pm, Z	381
$m_H < T < m_{\text{top}}$	H^0	385
$m_t < T$	t, \bar{t}	427

$^\dagger T_c$ corresponds to the confinement-deconfinement transition between quarks and hadrons.

At higher temperatures, $N(T)$ will be model-dependent. For example, in the minimal $SU(5)$ model, one needs to add 24 states to $N(T)$ for the charged and colored X and Y gauge bosons, another 24 from the adjoint Higgs, and another 6 scalar degrees of freedom (in addition to the 4 associated with the complex Higgs doublet already counted in the longitudinal components of W^\pm and Z , and in H) from the $\mathbf{5}$ of Higgs. Hence for $T > m_X$ in minimal $SU(5)$, $N(T) = 160.75$. In a supersymmetric model this would at least double.

In the radiation-dominated epoch, Eq. (22.10) can be integrated (neglecting the T -dependence of N) giving us a relationship between the age of the Universe and its temperature

$$t = \left(\frac{90}{32\pi^3 G_N N(T)} \right)^{1/2} T^{-2}. \quad (22.43)$$

Put into a more convenient form

$$t T_{\text{MeV}}^2 = 2.4 [N(T)]^{-1/2}, \quad (22.44)$$

where t is measured in seconds and T_{MeV} in units of MeV.

22.3.3 Neutrinos and equilibrium

Due to the expansion of the Universe, certain rates may be too slow to either establish or maintain equilibrium. Quantitatively, for each particle i , as a minimal condition for equilibrium, we will require that some rate Γ_i involving that type be larger than the expansion rate of the Universe, or

$$\Gamma_i > H. \quad (22.45)$$

Recalling that the age of the Universe is determined by H^{-1} , this condition is equivalent to requiring that on average, at least one interaction has occurred over the lifetime of the Universe.

A good example for a process that goes in and out of equilibrium is the weak interaction of neutrinos. On dimensional grounds, one can estimate the thermally averaged scattering cross-section:

$$\langle \sigma v \rangle \sim O(10^{-2}) T^2 / m_W^4 \quad (22.46)$$

for $T \lesssim m_W$. Recalling that the number density of leptons is $n \propto T^3$, we can compare the weak interaction rate, $\Gamma_{\text{wk}} \sim n \langle \sigma v \rangle$, with the expansion rate,

$$H = \left(\frac{8\pi G_N \rho}{3} \right)^{1/2} = \left(\frac{8\pi^3}{90} N(T) \right)^{1/2} T^2 / M_P \quad (22.47) \\ \simeq 1.66 N(T)^{1/2} T^2 / M_P,$$

where the Planck mass $M_P = G_N^{-1/2} = 1.22 \times 10^{19}$ GeV.

Neutrinos will be in equilibrium when $\Gamma_{\text{wk}} > H$ or

$$T > (500 m_W^4 / M_P)^{1/3} \sim 1 \text{ MeV}. \quad (22.48)$$

However, this condition assumes $T \ll m_W$; for higher temperatures, we should write $\langle \sigma v \rangle \sim O(10^{-2})/T^2$, so that $\Gamma \sim 10^{-2} T$. Thus, in the very early stages of expansion, at temperatures $T \gtrsim 10^{-2} M_P / \sqrt{N}$, equilibrium will not have been established.

Having attained a quasi-equilibrium stage, the Universe then cools further to the point where the interaction and expansion timescales match once again. The temperature at which these rates are equal is commonly referred to as the neutrino decoupling or freeze-out temperature and is defined by $T_{\text{wk}}(T_d) = H(T_d)$. For $T < T_d$, neutrinos drop out of equilibrium. The Universe becomes transparent to neutrinos and their momenta simply redshift with the cosmic expansion. The effective neutrino temperature will simply fall with $T \sim 1/R$.

Soon after decoupling, e^\pm pairs in the thermal background begin to annihilate (when $T \lesssim m_e$). Because the neutrinos are decoupled, the energy released due to annihilation heats up the photon background relative to the neutrinos. The change in the photon temperature can be easily computed from entropy conservation. The neutrino entropy must be conserved separately from the entropy of interacting particles. A straightforward computation yields

$$T_\nu = (4/11)^{1/3} T_\gamma \simeq 1.9 \text{ K}. \quad (22.49)$$

The total entropy density is therefore given by the contribution from photons and 3 flavors of neutrinos

$$s = \frac{4}{3} \frac{\pi^2}{30} \left(2 + \frac{21}{4} (T_\nu/T_\gamma)^3 \right) T_\gamma^3 = \frac{4}{3} \frac{\pi^2}{30} \left(2 + \frac{21}{11} \right) T_\gamma^3 = 7.04 n_\gamma. \quad (22.50)$$

Similarly, the total relativistic energy density is given by

$$\rho_r = \frac{\pi^2}{30} \left[2 + \frac{21}{4} (T_\nu/T_\gamma)^4 \right] T_\gamma^4 \simeq 1.68 \rho_\gamma. \quad (22.51)$$

In practice, a small correction is needed to this, since neutrinos are not totally decoupled at e^\pm annihilation: the effective number of massless neutrino species is 3.045, rather than 3 [40, 41].

This expression ignores neutrino rest masses, but current oscillation data require at least one neutrino eigenstate to have a mass exceeding 0.05 eV. In this minimal case, $\Omega_\nu h^2 = 6 \times 10^{-4}$, so the neutrino contribution to the matter budget would be negligibly small (which is our normal assumption). However, a nearly degenerate pattern of mass eigenstates could allow larger densities, since oscillation experiments only measure differences in m^2 values. Note that a 0.05-eV neutrino has $T_\nu = m_\nu$ at $z \simeq 296$, so the above expression for the total present relativistic density is really only an extrapolation. However, neutrinos are almost certainly relativistic at all epochs where the radiation content of the Universe is dynamically significant.

22.3.4 Field Theory and Phase transitions

It is very likely that the Universe has undergone one or more phase transitions during the course of its evolution [42–45]. Our current vacuum state is described by $SU(3)_c \times U(1)_{\text{em}}$, which in the Standard Model is a remnant of an unbroken $SU(3)_c \times SU(2)_L \times U(1)_Y$ gauge symmetry. Symmetry breaking occurs when a non-singlet gauge field (the Higgs field in the Standard Model) picks up a non-vanishing vacuum expectation value, determined by a scalar potential. For example, a simple (non-gauged) potential describing symmetry breaking is $V(\phi) = \frac{1}{4} \lambda \phi^4 - \frac{1}{2} \mu^2 \phi^2 + V(0)$. The resulting expectation value is simply $\langle \phi \rangle = \mu/\sqrt{\lambda}$.

In the early Universe, finite temperature radiative corrections typically add terms to the potential of the form $\phi^2 T^2$. Thus, at very high temperatures, the symmetry is restored and $\langle \phi \rangle = 0$. As the Universe cools, depending on the details of the potential, symmetry breaking will occur via a first-order phase transition in which the field tunnels through a potential barrier, or via a second-order transition in which the field evolves smoothly from one state to another (as would be the case for the above example potential).

The evolution of scalar fields can have a profound impact on the early Universe. The equation of motion for a scalar field ϕ can be derived from the energy-momentum tensor

$$T_{\mu\nu} = \partial_\mu \phi \partial_\nu \phi - \frac{1}{2} g_{\mu\nu} \partial_\rho \phi \partial^\rho \phi - g_{\mu\nu} V(\phi). \quad (22.52)$$

By associating $\rho = T_{00}$ and $p = R^{-2}(t)T_{ii}$ we have

$$\begin{aligned} \rho &= \frac{1}{2} \dot{\phi}^2 + \frac{1}{2} R^{-2}(t) (\nabla \phi)^2 + V(\phi) \\ p &= \frac{1}{2} \dot{\phi}^2 - \frac{1}{6} R^{-2}(t) (\nabla \phi)^2 - V(\phi), \end{aligned} \quad (22.53)$$

and from Eq. (22.10) we can write the equation of motion (by considering a homogeneous region, we can ignore the gradient terms)

$$\ddot{\phi} + 3H\dot{\phi} = -\partial V/\partial \phi. \quad (22.54)$$

22.3.5 Inflation

Inflation of early universe In Sec. 22.2.4, we discussed some of the problems associated with the standard Big-Bang model. However, during a phase transition, our assumptions of an adiabatically expanding Universe are generally not valid. If, for example, a phase transition occurred in the early Universe such that the field evolved slowly from the symmetric state to the global minimum, the Universe may have been dominated by the vacuum energy density associated with the potential near $\phi \simeq 0$. During this period of slow evolution, the energy density due to radiation will fall below the vacuum energy density, $\rho \ll V(0)$. When this happens, the expansion rate will be dominated by the constant $V(0)$, and we obtain the exponentially expanding solution given in Eq. (22.20). When the field evolves towards the global minimum it will begin to oscillate about the minimum, energy will be released during its decay, and a hot thermal Universe will be restored. If released fast enough, it will produce radiation at a temperature $NT_{\text{R}}^4 \lesssim V(0)$. In this reheating process, entropy has been created and the final value of RT is greater than the initial value of RT . Thus, we see that, during a phase transition, the relation $RT \sim \text{constant}$ need not hold true. This is the basis of the inflationary Universe scenario [46–48].

If, during the phase transition, the value of RT changed by a factor of $O(10^{29})$, the cosmological problems discussed above would be solved. The observed isotropy would be generated by the immense expansion; one small causal region could get blown up, and thus our entire visible Universe would have been in thermal contact some time in the past. In addition, the density parameter Ω would have been driven to 1 (with exponential precision). Density perturbations will be stretched by the expansion, $\lambda \sim R(t)$. Thus it will appear that $\lambda \gg H^{-1}$ or that the perturbations have left the horizon, where in fact the size of the causally connected region is now no longer simply H^{-1} . However, not only does inflation offer an explanation for large scale perturbations, it also offers a source for the perturbations themselves through quantum fluctuations.

Problems with early models of inflation based on either a first-order [49] or second-order [50, 51] phase transition of a Grand Unified Theory led to models invoking a completely new scalar field: the inflaton, ϕ . The potential of this field, $V(\phi)$, needs to have a very low gradient and curvature in order to match observed metric fluctuations. For a more thorough discussion of the problems of early models and a host of current models being studied see the review on inflation – Sec. 23 of this *Review*. In most current inflation models, reheated bubbles typically do not percolate, so inflation is ‘eternal’ and continues with exponential expansion in the region outside bubbles. These causally disconnected bubble Universes constitute a ‘multiverse’, where low-energy physics can vary between different bubbles. This has led to a controversial ‘anthropic’ approach to cosmology [52–54], where observer selection within the multiverse can be introduced as a means of understanding e.g. why the observed level of vacuum energy is so low (because larger values suppress growth of structure).

22.3.6 Baryogenesis

The Universe appears to be populated exclusively with matter rather than antimatter. Indeed antimatter is only detected in accelerators or in cosmic rays. However, the presence of antimatter in the latter is understood to be the result of collisions of primary particles in the interstellar medium. There is in fact strong evidence against primary forms of antimatter in the Universe. Furthermore, the density of baryons compared to the density of photons is extremely small, $\eta \sim 10^{-9}$.

The production of a net baryon asymmetry requires baryon number violating interactions, C and CP violation, and a departure from thermal equilibrium [55]. The first two of these ingredients are expected to be contained in Grand Unified Theories (GUTs) as well as in the non-perturbative sector of the Standard Model; the third can be realized in an expanding Universe where, as we have seen, interactions come in and out of equilibrium.

There are several interesting and viable mechanisms for the production of the baryon asymmetry. While we can not review any of them here in any detail, we mention some of the important scenarios. In all cases, all three ingredients listed above are incorporated. One of the first mechanisms was based on the out of equilibrium decay of a massive particle such as a superheavy GUT gauge or Higgs boson [56, 57]. A novel mechanism involving the decay of flat directions in supersymmetric models is known as the Affleck-Dine scenario [58]. There is also the possibility of generating the baryon asymmetry at the electro-weak scale using the non-perturbative interactions of sphalerons [59]. Because these interactions conserve the sum of baryon and lepton number, $B + L$, it is possible to first generate a lepton asymmetry (*e.g.*, by the out-of-equilibrium decay of a superheavy right-handed neutrino), which is converted to a baryon asymmetry at the electro-weak scale [60]. This mechanism is known as leptobaryogenesis.

22.3.7 Nucleosynthesis

An essential element of the standard cosmological model is Big-Bang nucleosynthesis (BBN), the theory that predicts the abundances of the light element isotopes D, ^3He , ^4He , and ^7Li . Nucleosynthesis takes place at a temperature scale of order 1 MeV. The nuclear processes lead primarily to ^4He , with a primordial mass fraction of about 25%. Lesser amounts of the other light elements are produced: about 10^{-5} of D and ^3He and about 10^{-10} of ^7Li by number relative to H. The abundances of the light elements depend almost solely on one key parameter, the baryon-to-photon ratio, η . The nucleosynthesis predictions can be compared with observational determinations of the abundances of the light elements. Consistency between theory and observations driven primarily by recent D/H measurements [61, 62] leads to a range of

$$5.8 \times 10^{-10} < \eta < 6.5 \times 10^{-10}. \quad (22.55)$$

η is related to the fraction of Ω contained in baryons:

$$\Omega_b = 3.66 \times 10^7 \eta h^{-2}, \quad (22.56)$$

or $10^{10} \eta = 274 \Omega_b h^2$. The *Planck* result [24] for $\Omega_b h^2$ of 0.0224 ± 0.0002 translates into a value of $\eta = 6.12 \pm 0.04$. This result can be used to ‘predict’ the light element abundances, which can in turn be compared with observation [63]. The resulting D/H abundance is in excellent agreement with that found in quasar absorption systems. It is in reasonable agreement with the helium abundance observed in extragalactic HII regions (once systematic uncertainties are accounted for), but is in poor agreement with the Li abundance observed in the atmospheres of halo dwarf stars [64]. See the review on BBN – Sec. 24 of this *Review* for a detailed discussion of BBN or references [65–68].

22.3.8 The transition to a matter-dominated Universe

In the Standard Model, the temperature (or redshift) at which the Universe undergoes a transition from a radiation-dominated to a matter-dominated Universe is determined by the amount of dark matter. Assuming three nearly massless neutrinos, the energy density in radiation at temperatures $T \ll 1$ MeV, is given by

$$\rho_r = \frac{\pi^2}{30} \left[2 + \frac{21}{4} \left(\frac{4}{11} \right)^{4/3} \right] T^4. \quad (22.57)$$

In the absence of non-baryonic dark matter, the matter density can be written as

$$\rho_m = m_N \eta n_\gamma, \quad (22.58)$$

where m_N is the nucleon mass. Recalling that $n_\gamma \propto T^3$ [cf. Eq. (22.40)], we can solve for the temperature or redshift at the matter-radiation equality when $\rho_r = \rho_m$,

$$T_{\text{eq}} = 0.22 m_N \eta \quad \text{or} \quad (1 + z_{\text{eq}}) = 0.22 \eta \frac{m_N}{T_0}, \quad (22.59)$$

where T_0 is the present temperature of the microwave background. For $\eta = 6.1 \times 10^{-10}$, this corresponds to a temperature $T_{\text{eq}} \simeq 0.13$ eV or $(1 + z_{\text{eq}}) \simeq 550$. A transition this late would be problematic for structure formation (see Sec. 22.4.5).

The redshift of matter domination can be pushed back significantly if non-baryonic dark matter is present. If instead of Eq. (22.58), we write

$$\rho_m = \Omega_m \rho_c \left(\frac{T}{T_0} \right)^3, \quad (22.60)$$

we find that

$$T_{\text{eq}} = 0.9 \frac{\Omega_m \rho_c}{T_0^3} \quad \text{or} \quad (1 + z_{\text{eq}}) = 2.4 \times 10^4 \Omega_m h^2. \quad (22.61)$$

22.4 The Universe at late times

22.4.1 The CMB

One form of the infamous Olbers’ paradox says that, in Euclidean space, surface brightness is independent of distance. Every line of sight will terminate on matter that is hot enough to be ionized and so scatter photons: $T \gtrsim 10^3$ K, and the sky should therefore shine as brightly as the surface of the Sun. The reason the night sky is dark is entirely due to the expansion, which cools the radiation temperature to 2.73 K. This gives a Planck function peaking at around 1 mm to produce the CMB.

The CMB spectrum is a very accurate match to a Planck function [69]. (See the review on CMB – Sec. 29 of this *Review*.) The COBE estimate of the temperature is [70]

$$T = 2.7255 \pm 0.0006 \text{ K}. \quad (22.62)$$

The lack of any distortion of the Planck spectrum is a strong physical constraint. It is very difficult to account for in any expanding Universe other than one that passes through a hot stage. Alternative schemes for generating the radiation, such as thermalization of starlight by dust grains, inevitably generate a superposition of temperatures. What is required in addition to thermal equilibrium is that $T \propto 1/R$, so that radiation from different parts of space arrive at an observer with the same apparent temperature.

Although it is common to speak of the CMB as originating at ‘recombination’, a more accurate terminology is the era of ‘last scattering’. In practice, this takes place at $z \simeq 1100$, almost independently of the main cosmological parameters, at which time the fractional ionization is very small. This occurred when the age of the Universe was about 370,000 years. But the CMB photons themselves were not generated at this point, and were the result of thermalization at $z \sim 10^7$. (See the review on CMB – Sec. 29 of this *Review* for a full discussion of the CMB.)

22.4.2 Matter in the Universe

One of the main tasks of cosmology is to measure the density of the Universe, and how this is divided between dark matter and baryons. The baryons consist partly of stars, with $0.002 \lesssim \Omega_* \lesssim 0.003$ [71] but mainly inhabit the intergalactic medium (IGM). One powerful way in which this can be studied is via the absorption of light from distant luminous objects such as quasars. Even very small amounts of neutral hydrogen can absorb rest-frame UV photons (the Gunn-Peterson effect), and should suppress the continuum by a factor $\exp(-\tau)$, where

$$\tau \simeq 10^{4.62} h^{-1} \left[\frac{n_{\text{HI}}(z)/m^{-3}}{(1+z)\sqrt{1+\Omega_m z}} \right], \quad (22.63)$$

and this expression applies while the Universe is matter dominated ($z \gtrsim 1$ in the $\Omega_m = 0.3$ $\Omega_v = 0.7$ model). At $z < 6$, the dominant effect on quasar spectra is a ‘forest’ of narrow absorption lines, which produce a mean $\tau = 1$ in the Ly α forest at about $z = 3$, and so we have $\Omega_{\text{HI}} \simeq 10^{-6.7} h^{-1}$. This is such a small number that the IGM must be very highly ionized at these redshifts, apart from a few high-density clumps. But at $z > 6$ there is good evidence for a ‘reionization’ era at which the general IGM is not so strongly ionized [72]. As discussed below, this ionized IGM at low z is also detectable via the secondary Compton scattering of CMB photons.

The Ly α forest is of great importance in pinning down the abundance of deuterium. Because electrons in deuterium differ in reduced mass by about 1 part in 4000 compared to hydrogen, each absorption system in the Ly α forest is accompanied by an offset deuterium line. By careful selection of systems with an optimal HI column density, a measurement of the D/H ratio can be made. This has now been done with high accuracy in 10 quasars, with consistent results [61]. Combining these determinations with the theory of primordial nucleosynthesis yields a baryon density of $\Omega_b h^2 = 0.021 - 0.024$ (95% confidence) in excellent agreement with the Planck result. (See also the review on BBN – Sec. 24 of this *Review*.)

Ionized IGM can also be detected in emission when it is densely clumped, via bremsstrahlung radiation. This generates the spectacular X-ray emission from rich clusters of galaxies. Studies of this phenomenon allow us to achieve an accounting of the total baryonic material in clusters. Within the central $\simeq 1$ Mpc, the masses in stars, X-ray emitting gas, and total dark matter can be determined with reasonable accuracy (perhaps 20% rms), and this allows a minimum baryon fraction to be determined [73, 74]:

$$\frac{M_{\text{baryons}}}{M_{\text{total}}} \gtrsim 0.009 + (0.066 \pm 0.003) h^{-3/2}. \quad (22.64)$$

Because clusters are the largest collapsed structures, it is reasonable to take this as applying to the Universe as a whole. This equation implies a minimum baryon fraction of perhaps 12% (for reasonable h), which is too high for $\Omega_m = 1$ if we take $\Omega_b h^2 \simeq 0.02$ from nucleosynthesis. This is therefore one of the more robust arguments in favor of $\Omega_m \simeq 0.3$. (See the review on Cosmological Parameters – Sec. 25.1 of this *Review*.) This argument is also consistent with the inference on Ω_m that can be made from Fig. 22.2.

This method is much more robust than the older classical technique for weighing the Universe: ‘ $L \times M/L$ ’. The overall light density of the Universe is reasonably well determined from redshift surveys of galaxies, so that a good determination of mass M and luminosity L for a single object suffices to determine Ω_m – but only *if* the mass-to-light ratio were universal.

22.4.3 Gravitational lensing

A robust method for determining masses in cosmology is to use gravitational light deflection. Most systems can be treated as a geometrically thin gravitational lens, where the light bending is assumed to take place only at a single distance. Simple geometry then determines a mapping between the coordinates in the intrinsic source plane (S) and the observed image plane (I):

$$\alpha(D_L \theta_I) = \frac{D_S}{D_{LS}} (\theta_I - \theta_S), \quad (22.65)$$

where the angles θ_I, θ_S , and α are in general two-dimensional vectors on the sky. The distances D_{LS} etc. are given by an extension of the usual distance-redshift formula:

$$D_{LS} = \frac{R_0 S_k (\chi_S - \chi_L)}{1 + z_S}. \quad (22.66)$$

This is the angular-diameter distance for objects on the source plane as perceived by an observer on the lens.

Solutions of this equation divide into weak lensing, where the mapping between source plane and image plane is one-to-one, and strong lensing, in which multiple imaging is possible. For circularly-symmetric lenses, an on-axis source is multiply imaged into a ‘caustic’ ring, whose radius is the Einstein radius:

$$\begin{aligned} \theta_E &= \left(4GM \frac{D_{LS}}{D_L D_S} \right)^{1/2} \\ &= \left(\frac{M}{10^{11.09} M_\odot} \right)^{1/2} \left(\frac{D_L D_S / D_{LS}}{\text{Gpc}} \right)^{-1/2} \text{arcsec}. \end{aligned} \quad (22.67)$$

The observation of ‘arcs’ (segments of near-perfect Einstein rings) in rich clusters of galaxies has thus given very accurate masses for the central parts of clusters – generally in good agreement with other indicators, such as analysis of X-ray emission from the cluster IGM [75, 76].

Gravitational lensing has also developed into a particularly promising probe of cosmological structure on 10-Mpc to 100-Mpc scales. Weak image distortions manifest themselves as an additional ellipticity of galaxy images (‘shear’), which can be observed by averaging many images together (the corresponding flux amplification is less readily detected). The result is a ‘cosmic shear’ field of order 1% ellipticity, coherent over scales of around 30 arcmin, which is directly related to the cosmic mass field. For this reason, weak lensing is seen as potentially the cleanest probe of matter fluctuations, next to the CMB. Already, impressive results have been obtained in measuring cosmological parameters, based on survey data from only $\sim 10^3 \text{ deg}^2$ [77, 78]. A particular strength of lensing is its ability to measure the amplitude of mass fluctuations; this can be deduced from the amplitude of CMB fluctuations, but only with low precision on account of the poorly-known optical depth due to Compton scattering after reionization. However, the effect of weak lensing on the CMB map itself can be detected via the induced non-Gaussian signal, and this gives the CMB greater internal power [79]. The main difficulty of principle with lensing is that part of the signal is generated by small-scale density fluctuations; thus a model is required for nonlinear evolution, including astrophysical effects that separate baryons and dark matter. In this respect, the CMB is a cleaner probe of the primordial fluctuations.

22.4.4 Density Fluctuations

The overall properties of the Universe are very close to being homogeneous; and yet telescopes reveal a wealth of detail on scales varying from single galaxies to large-scale structures of size exceeding 100 Mpc. The existence of these structures must be telling us something important about the initial conditions of the Big Bang, and about the physical processes that have operated subsequently. This motivates the study of the density perturbation field, defined as

$$\delta(\mathbf{x}) \equiv \frac{\rho(\mathbf{x}) - \langle \rho \rangle}{\langle \rho \rangle}. \quad (22.68)$$

A critical feature of the δ field is that it inhabits a Universe that is isotropic and homogeneous in its large-scale properties. This suggests that the statistical properties of δ should also be statistically homogeneous – *i.e.*, it is a stationary random process.

It is often convenient to describe δ as a Fourier superposition:

$$\delta(\mathbf{x}) = \sum \delta_{\mathbf{k}} e^{-i\mathbf{k} \cdot \mathbf{x}}. \quad (22.69)$$

We avoid difficulties with an infinite Universe by applying periodic boundary conditions in a cube of some large volume V . The cross-terms vanish when we compute the variance in the field, which is just a sum over modes of the power spectrum:

$$\langle \delta^2 \rangle = \sum |\delta_{\mathbf{k}}|^2 \equiv \sum P(k). \quad (22.70)$$

Note that the statistical nature of the fluctuations must be isotropic, so we write $P(k)$ rather than $P(\mathbf{k})$. The $\langle \dots \rangle$ average here is a volume average. Cosmological density fields are an example of an ergodic process, in which the average over a large volume tends to the same answer as the average over a statistical ensemble.

The statistical properties of discrete objects sampled from the density field are often described in terms of N -point correlation functions, which represent the excess probability over random for finding one particle in each of N boxes in a given configuration. For the 2-point case, the correlation function is readily shown to be identical to the autocorrelation function of the δ field: $\xi(r) = \langle \delta(x)\delta(x+r) \rangle$.

The power spectrum and correlation function are Fourier conjugates, and thus are equivalent descriptions of the density field (similarly, k -space equivalents exist for the higher-order correlations). It is convenient to take the limit $V \rightarrow \infty$ and use k -space integrals, defining a dimensionless power spectrum, which measures the contribution to the fractional variance in density per unit logarithmic range of scale, as $\Delta^2(k) = d\langle \delta^2 \rangle / d \ln k =$

$Vk^3P(k)/2\pi^2$:

$$\xi(r) = \int \Delta^2(k) \frac{\sin kr}{kr} d \ln k; \quad \Delta^2(k) = \frac{2}{\pi} k^3 \int_0^\infty \xi(r) \frac{\sin kr}{kr} r^2 dr. \quad (22.71)$$

For many years, an adequate approximation to observational data on galaxies was $\xi = (r/r_0)^{-\gamma}$, with $\gamma \simeq 1.8$ and $r_0 \simeq 5 h^{-1}$ Mpc. Modern surveys are now able to probe into the large-scale linear regime where unaltered traces of the curved post-recombination spectrum can be detected [80–82].

22.4.5 Formation of cosmological structure

The simplest model for the generation of cosmological structure is gravitational instability acting on some small initial fluctuations (for the origin of which a theory such as inflation is required). If the perturbations are adiabatic (*i.e.*, fractionally perturb number densities of photons and matter equally), the linear growth law for matter perturbations is simple:

$$\delta \propto \begin{cases} a^2(t) & (\text{radiation domination; } \Omega_r = 1); \\ a(t) & (\text{matter domination; } \Omega_m = 1). \end{cases} \quad (22.72)$$

For low-density Universes, the growth is slower:

$$d \ln \delta / d \ln a \simeq \Omega_m^\gamma(a), \quad (22.73)$$

where the parameter γ is close to 0.55 independent of the vacuum density [83, 84].

The alternative perturbation mode is isocurvature: only the equation of state changes, and the total density is initially unperturbed. These modes perturb the total entropy density, and thus induce additional large-scale CMB anisotropies [85]. Although the character of perturbations in the simplest inflationary theories are purely adiabatic, correlated adiabatic and isocurvature modes are predicted in many models; the simplest example is the curvaton, which is a scalar field that decays to yield a perturbed radiation density. If the matter content already exists at this time, the overall perturbation field will have a significant isocurvature component. Such a prediction is inconsistent with current CMB data [86], and most analyses of CMB and large-scale structure (LSS) data assume the adiabatic case to hold exactly.

Linear evolution preserves the shape of the power spectrum. However, a variety of processes mean that growth actually depends on the matter content.

1. Pressure opposes gravity effectively for wavelengths below the horizon length while the Universe is radiation dominated. The *comoving* horizon size at z_{eq} is therefore an important scale:

$$D_H(z_{\text{eq}}) = \frac{2(\sqrt{2}-1)}{(\Omega_m z_{\text{eq}})^{1/2} H_0} = \frac{16.0}{\Omega_m h^2} \text{Mpc}. \quad (22.74)$$

2. At early times, dark matter particles will undergo free streaming at the speed of light, and so erase all scales up to the horizon – a process that only ceases when the particles go nonrelativistic. For light massive neutrinos, this happens at z_{eq} ; all structure up to the horizon-scale power-spectrum break is in fact erased. Hot(cold) dark matter models are thus sometimes dubbed large(small)-scale damping models.
3. A further important scale arises where photon diffusion can erase perturbations in the matter – radiation fluid; this process is named Silk damping.

The overall effect is encapsulated in the transfer function, which gives the ratio of the late-time amplitude of a mode to its initial value (see Fig. 22.4). The overall power spectrum is thus the primordial scalar-mode power law, times the square of the transfer function:

$$P(k) \propto k^{n_s} T_k^2. \quad (22.75)$$

The most generic power-law index is $n_s = 1$: the ‘Zeldovich’ or ‘scale-invariant’ spectrum. Inflationary models tend to predict a small ‘tilt’: $|n_s - 1| \lesssim 0.05$ [12, 13]. On the assumption that the dark matter is cold, the power spectrum then depends on 5 parameters: n_s , h , Ω_b , Ω_c ($\equiv \Omega_m - \Omega_b$), and an overall amplitude.

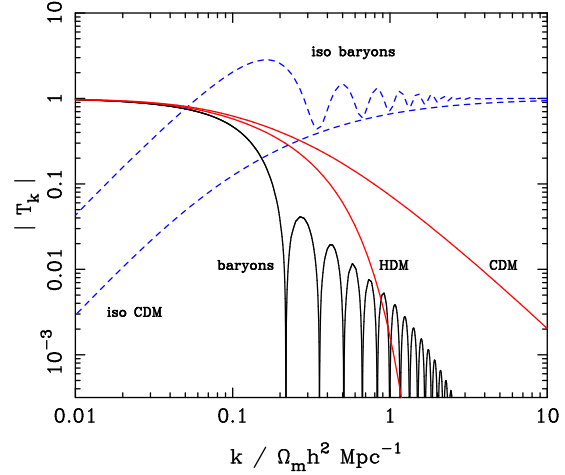


Figure 22.4: A plot of transfer functions for various models. For adiabatic models, $T_k \rightarrow 1$ at small k , whereas the opposite is true for isocurvature models. For dark-matter models, the characteristic wavenumber scales proportional to $\Omega_m h^2$. The scaling for baryonic models does not obey this exactly; the plotted cases correspond to $\Omega_m = 1$, $h = 0.5$.

The latter is often specified as σ_8 , the linear-theory fractional rms in density when a spherical filter of radius $8 h^{-1}$ Mpc is applied in linear theory. This scale can be probed directly via weak gravitational lensing, and also via its effect on the abundance of rich galaxy clusters. The favored value from the latter is approximately [87]

$$\sigma_8 \simeq [0.746 \pm 0.012 (\text{stat.}) \pm 0.022 (\text{sys.})] (\Omega_m/0.3)^{-0.47}, \quad (22.76)$$

which is rather similar to the normalization inferred from weak lensing: $\sigma_8 \simeq [0.745 \pm 0.039] (\Omega_m/0.3)^{-0.5}$ [77]; or $[0.782 \pm 0.027] (\Omega_m/0.3)^{-0.5}$ [78]. These figures are in $> 2\sigma$ tension with the *Planck* values of $(\sigma_8, \Omega_m) = (0.811 \pm 0.006, 0.315 \pm 0.007)$. If real, such a discrepancy could indicate interesting new physics; but the current evidence is not strong enough to make such a claim.

A direct measure of mass inhomogeneity is valuable, since the galaxies inevitably are biased with respect to the mass. This means that the fractional fluctuations in galaxy number, $\delta n/n$, may differ from the mass fluctuations, $\delta\rho/\rho$. It is commonly assumed that the two fields obey some proportionality on large scales where the fluctuations are small, $\delta n/n = b\delta\rho/\rho$, but even this is not guaranteed [88].

The main shape of the transfer function is a break around the horizon scale at z_{eq} , which depends just on $\Omega_m h$ when wavenumbers are measured in observable units ($h \text{Mpc}^{-1}$). For reasonable baryon content, weak oscillations in the transfer function are also expected, and these BAOs (Baryon Acoustic Oscillations) have been clearly detected [89, 90]. As well as directly measuring the baryon fraction, the scale of the oscillations directly measures the acoustic horizon at decoupling; this can be used as an additional standard ruler for cosmological tests, and the BAO signature has become one of the most important applications of large galaxy surveys. Overall, current power-spectrum data [80–82] favor $\Omega_m h \simeq 0.20$ and a baryon fraction of about 0.15 for $n_s \simeq 1$ (see Fig. 22.5).

In principle, accurate data over a wide range of k could determine both $\Omega_m h$ and n_s , but in practice there is a strong degeneracy between these. In order to constrain n_s itself, it is necessary to examine data on anisotropies in the CMB.

22.4.6 CMB anisotropies

The CMB has a clear dipole anisotropy, of magnitude 1.23×10^{-3} . This is interpreted as being due to the Earth’s motion, which is equivalent to a peculiar velocity for the Milky Way of

$$v_{\text{MW}} \simeq 600 \text{ km s}^{-1} \quad \text{towards } (\ell, b) \simeq (270^\circ, 30^\circ). \quad (22.77)$$

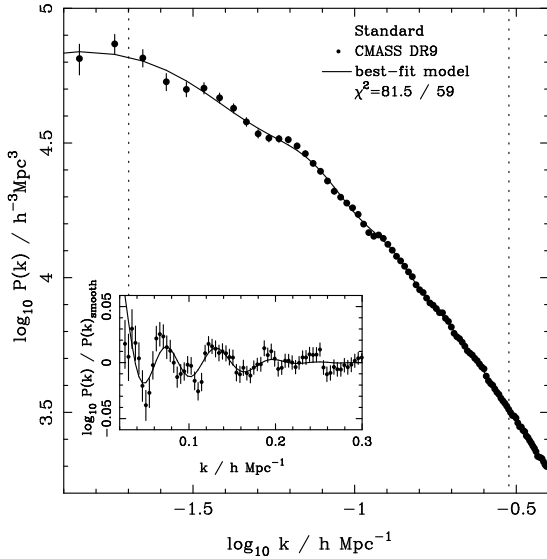


Figure 22.5: The galaxy power spectrum from the SDSS BOSS survey [82]. The solid points with error bars show the power estimate. The solid line shows a standard Λ CDM model with $\Omega_b h^2 \simeq 0.02$ and $\Omega_m h \simeq 0.2$. The inset amplifies the region where BAO features are visible. The fact that these perturb the power by $\sim 20\%$ rather than order unity is direct evidence that the matter content of the Universe is dominated by collisionless dark matter.

All higher-order multipole moments of the CMB are however much smaller (of order 10^{-5}), and interpreted as signatures of density fluctuations at last scattering ($\simeq 1100$). To analyze these, the sky is expanded in spherical harmonics as explained in the review on the CMB – Sec. 29 of this *Review*. The dimensionless power per $\ln k$ or ‘bandpower’ for the CMB is defined as

$$\mathcal{T}^2(\ell) = \frac{\ell(\ell+1)}{2\pi} C_\ell. \quad (22.78)$$

This function encodes information from the three distinct mechanisms that cause CMB anisotropies:

- (1) Gravitational (Sachs – Wolfe) perturbations. Photons from high-density regions at last scattering have to climb out of potential wells, and are thus redshifted.
- (2) Intrinsic (adiabatic) perturbations. In high-density regions, the coupling of matter and radiation can compress the radiation also, giving a higher temperature.
- (3) Velocity (Doppler) perturbations. The plasma has a non-zero velocity at recombination, which leads to Doppler shifts in frequency and hence shifts in brightness temperature.

Because the potential fluctuations obey Poisson’s equation, $\nabla^2 \Phi = 4\pi G \rho \delta$, and the velocity field satisfies the continuity equation $\nabla \cdot \mathbf{u} = -\dot{\delta}$, the resulting different powers of k ensure that the Sachs-Wolfe effect dominates on large scales and adiabatic effects on small scales.

The relation between angle and comoving distance on the last-scattering sphere requires the comoving angular-diameter distance to the last-scattering sphere; because of its high redshift, this is effectively identical to the horizon size at the present epoch, D_H :

$$\begin{aligned} D_H &= \frac{2}{\Omega_m H_0} \quad (\Omega_\nu = 0) \\ D_H &\simeq \frac{2}{\Omega_m^{0.4} H_0} \quad (\text{flat} : \Omega_m + \Omega_\nu = 1). \end{aligned} \quad (22.79)$$

These relations show how the CMB is strongly sensitive to curvature: the horizon length at last scattering is $\propto 1/\sqrt{\Omega_m}$, so that this subtends an angle that is virtually independent of Ω_m for a flat model. Observations of a peak in the CMB power spectrum

at relatively large scales ($\ell \simeq 221$) are thus strongly inconsistent with zero- Λ models with low density: current CMB + BAO + lensing data require $\Omega_m + \Omega_\nu = 0.999 \pm 0.004$ (95%) [24]. (See e.g., Fig. 22.2).

In addition to curvature, the CMB encodes information about several other key cosmological parameters. Within the compass of simple adiabatic CDM models, there are 9 of these:

$$\omega_c, \omega_b, \Omega_{\text{tot}}, h, \tau, n_s, n_t, r, Q. \quad (22.80)$$

The symbol ω denotes the physical density, Ωh^2 : the transfer function depends only on the densities of CDM (ω_c) and baryons (ω_b). Transcribing the power spectrum at last scattering into an angular power spectrum brings in the total density parameter ($\Omega_{\text{tot}} \equiv \Omega_m + \Omega_\nu = \Omega_c + \Omega_b + \Omega_\nu$) and h : there is a near-exact geometrical degeneracy [91] between these that keeps the angular-diameter distance to last scattering invariant, so that models with substantial spatial curvature and large vacuum energy cannot be ruled out without prior knowledge of the Hubble parameter. Alternatively, the CMB alone cannot measure the Hubble parameter without taking into account the line-of-sight information from CMB lensing.

A further possible degeneracy involves the tensor contribution to the CMB anisotropies. These are important at large scales (up to the horizon scales); for smaller scales, only scalar fluctuations (density perturbations) are important. Each of these components is characterized by a spectral index, n , and a ratio between the power spectra of tensors and scalars (r). See the review on Cosmological Parameters – Sec. 25.1 of this *Review* for a technical definition of the r parameter. Finally, the overall amplitude of the spectrum must be specified (Q), together with the optical depth to Compton scattering owing to recent reionization (τ). Adding a large tensor contribution reduces the contrast between low ℓ and the peak at $\ell \simeq 221$ (because the tensor spectrum has no acoustic component). The previous relative height of the peak can be recovered by increasing n_s to increase the small-scale power in the scalar component; this in turn over-predicts the power at $\ell \sim 1000$, but this effect can be counteracted by raising the baryon density [92]. This approximate 3-way degeneracy is broken as we increase the range of multipoles sampled.

The reason the tensor component is introduced, and why it is so important, is that it is the only non-generic prediction of inflation. Slow-roll models of inflation involve two dimensionless parameters:

$$\epsilon \equiv \frac{M_{\text{P}}^2}{16\pi} \left(\frac{V'}{V} \right)^2, \quad \eta \equiv \frac{M_{\text{P}}^2}{8\pi} \left(\frac{V''}{V} \right), \quad (22.81)$$

where V is the inflaton potential, and dashes denote derivatives with respect to the inflation field. In terms of these, the tensor-to-scalar ratio is $r \simeq 16\epsilon$, and the spectral indices are $n_s = 1 - 6\epsilon + 2\eta$ and $n_t = -2\epsilon$. The natural expectation of inflation is that the quasi-exponential phase ends once the magnitudes of the slow-roll parameters become of order unity, so that both $n_s \neq 1$ and a significant tensor component are expected. These predictions can be avoided in some models, but it is undeniable that observation of such features would be a great triumph for inflation. Cosmology therefore stands at a fascinating point given that the most recent CMB data reject the zero-tensor $n_s = 1$ model at more than 8σ : $n_s = 0.965 \pm 0.004$ [24]. This rejection is strong enough that it is also able to break the tensor degeneracy, so that no model with $n_s = 1$ is acceptable, whatever the value of r .

The current limit on r is < 0.06 at 95% confidence [93]. In conjunction with the measured value of n_s , this upper limit sits close to the prediction of a linear potential (i.e. $|\eta| \ll |\epsilon|$). Any further reduction in the limit on r will force η to be negative – i.e. a convex potential at the point where LSS scales were generated (sometimes called a ‘hilltop’), in contrast to simple early models such as $V(\phi) = m^2 \phi^2$ or $\lambda \phi^4$, which are now excluded. Examples of models that are currently in excellent agreement with the Planck results are the Starobinsky model of $\mathcal{R} + \mathcal{R}^2$ gravity [94], or the Higgs-inflation model where the Higgs field is non-minimally coupled [95]. Assuming 55 e-foldings of inflation, these models predict $n_s = 0.965$ and $r = 0.0035$. Assuming that no systematic error in the CMB data can be identified, cosmology has thus

passed a critical hurdle in rejecting scale-invariant fluctuations. The years ahead will be devoted to the task of searching for the tensor fluctuations – for which the main tool will be the polarization of the CMB [14].

22.4.6.1 CMB foregrounds

As the quality of CMB data improves, there is a growing interest in effects that arise along the line of sight. The CMB temperature is perturbed by dark-matter structures and by Compton scattering from ionized gas. In the former case, we have the integrated Sachs-Wolfe effect, which is sensitive to the time derivative of the gravitational potential. In the linear regime, this is damped when the Universe becomes Λ -dominated, and this is an independent way of detecting Λ [96]. The potential also causes gravitational lensing of the CMB: structures at $z \simeq 1-2$ displace features on the CMB sky by about 2 arcmin over coherent degree-scale patches. Detection of these distortions allows a map to be made of overdensity projected from $z = 0$ to 1100 [79]. This is a very powerful calibration for direct studies of gravitational lensing using galaxies. Finally, Comptonization affects the CMB in two ways: the thermal Sunyaev-Zeldovich effect measures the blurring of photon energies by hot gas, and the kinetic Sunyaev-Zeldovich effect is sensitive to the bulk velocity of the gas. Both these effects start to dominate over the intrinsic CMB fluctuations at multipoles $\ell \gtrsim 2000$ [97].

22.4.7 Probing dark energy and the nature of gravity

The most radical element of our current cosmological model is the dark energy that accelerates the expansion. The energy density of this component is approximately $(2.2 \text{ meV})^4$ (for $w = -1$, $\Omega_v = 0.68$, $h = 0.67$), or roughly $10^{-123} M_{\text{p}}^4$, and such an unnaturally small number is hard to understand. Various quantum effects (most simply, zero-point energy) should make contributions to the vacuum energy density. These may be truncated by new physics at high energy, but this presumably occurs at $> 1 \text{ TeV}$ scales, not meV; thus the apparent energy scale of the vacuum is at least 10^{15} times smaller than its natural value. A classic review of this situation is given by Weinberg [52], which lists extreme escape routes – especially the multiverse viewpoint, according to which low values of Λ are rare, but high values suppress the formation of structure and observers. It is certainly impressive that Weinberg used such reasoning to predict the value of Λ before any data strongly indicated a non-zero value.

But it may be that the phenomenon of dark energy is entirely illusory. The necessity for this constituent arises from using the Friedmann equation to describe the evolution of the cosmic expansion; if this equation is incorrect, it would require the replacement of Einstein's relativistic theory of gravity with some new alternative. A frontier of current cosmological research is to distinguish these possibilities [98, 99]. We also note that it has been suggested that dark energy might be an illusion even within general relativity, owing to an incorrect treatment of averaging in an inhomogeneous Universe [100, 101]. Most would argue that a standard Newtonian treatment of such issues should be adequate inside the cosmological horizon, but debate on this issue continues.

Dark Energy can differ from a classical cosmological constant in being a dynamical phenomenon [102, 103], *e.g.*, a rolling scalar field (sometimes dubbed 'quintessence'). Empirically, this means that it is endowed with two thermodynamic properties that astronomers can try to measure: the bulk equation of state, and the sound speed. If the sound speed is close to the speed of light, the effect of this property is confined to very large scales, and mainly manifests itself in the large-angle multipoles of the CMB anisotropies [104]. The equation of state parameter governs the rate of change of the vacuum density: $d \ln \rho_v / d \ln a = -3(1+w)$, so it can be accessed via the evolving expansion rate, $H(a)$. This can be measured most cleanly by using the inbuilt natural ruler of large-scale structure: the BAO horizon scale [105]:

$$D_{\text{BAO}} \simeq 147 (\Omega_{\text{m}} h^2 / 0.13)^{-0.25} (\Omega_{\text{b}} h^2 / 0.023)^{-0.08} \text{ Mpc}. \quad (22.82)$$

$H(a)$ is measured by radial clustering, since $dr/dz = c/H$; clustering in the plane of the sky measures the integral of this. The expansion rate is also measured by the growth of density fluctuations, where the pressure-free growth equation for the density

perturbation is $\ddot{\delta} + 2H(a)\dot{\delta} = 4\pi G\rho_0 \delta$. Thus, both the scale and amplitude of density fluctuations are sensitive to $w(a)$ – but only weakly. These observables change by only typically 0.2% for a 1% change in w . Current constraints [24] place a constant w to within 5–10% of -1 , depending on the data combination chosen. A substantial improvement in this precision will require us to limit systematics in data to a few parts in 1000.

Testing whether theories of gravity require revision can also be done using data on cosmological inhomogeneities. Two separate issues arise, concerning the metric perturbation potentials Ψ and Φ , which affect respectively the time and space parts of the metric. In Einstein gravity, these potentials are both equal to the Newtonian gravitational potential, which satisfies Poisson's equation: $\nabla^2 \Phi / a^2 = 4\pi G \bar{\rho} \delta$. Empirically, modifications of gravity require us to explore a change with scale and with time of the 'slip' (Ψ/Φ) and the effective G on the rhs of the Poisson equation. The former aspect can only be probed via gravitational lensing, whereas the latter can be addressed on 10–100 Mpc scales via the growth of clustering. Various schemes for parameterising modified gravity exist, but a practical approach is to assume that the growth rate can be tied to the density parameter: $d \ln \delta / d \ln a = \Omega_{\text{m}}^{\gamma}(a)$ [83, 84]. The parameter γ is close to 0.55 for standard relativistic gravity, but can differ by around 0.1 from this value in many non-standard models. Clearly this parameterization is incomplete, since it explicitly rejects the possibility of early dark energy ($\Omega_{\text{m}}(a) \rightarrow 1$ as $a \rightarrow 0$), but it is a convenient way of capturing the power of various experiments. Current data are consistent with standard Λ CDM [106], and exclude variations in slip or effective G of larger than a few times 10%.

Current planning envisages a set of satellite probes that, a decade hence, will have pursued these fundamental tests via gravitational lensing measurements over thousands of square degrees, $> 10^8$ redshifts, and photometry of > 1000 supernovae (Euclid in Europe, WFIRST in the USA) [22, 23]. These experiments will measure both w and the perturbation growth rate to an accuracy of around 1%. The outcome will be either a validation of the standard relativistic vacuum-dominated Big Bang cosmology at a level of precision far beyond anything attempted to date, or the opening of entirely new directions in cosmological models. For a more complete discussion of dark energy and future probes see the review on Dark Energy – Sec. 28

References

- [1] V.M. Slipher, *Pop. Astr.* **23**, 21 (1915).
- [2] K. Lundmark, *Mon. Not. R. Astron. Soc* **84**, 747 (1924).
- [3] E. Hubble and M. L. Humason, *Astrophys. J.* **74**, 43 (1931).
- [4] G. Gamow, *Phys. Rev.* **70**, 572 (1946).
- [5] R. A. Alpher, H. Bethe and G. Gamow, *Phys. Rev.* **73**, 803 (1948).
- [6] R.A. Alpher and R.C. Herman, *Phys. Rev.* **74**, 1737 (1948).
- [7] R.A. Alpher and R.C. Herman, *Phys. Rev.* **75**, 1089 (1949).
- [8] A. A. Penzias and R. W. Wilson, *Astrophys. J.* **142**, 419 (1965).
- [9] P.J.E. Peebles, *Principles of Physical Cosmology*, Princeton University Press (1993).
- [10] G. Börner, *The Early Universe: Facts and Fiction*, Springer-Verlag (1988).
- [11] E.W. Kolb and M.S. Turner, *The Early Universe*, Addison-Wesley (1990).
- [12] J.A. Peacock, *Cosmological Physics*, Cambridge Univ. Press (1999).
- [13] A.R. Liddle and D. Lyth, *Cosmological Inflation and Large-Scale Structure*, Cambridge University Press (2000).
- [14] S. Dodelson, *Modern Cosmology*, Academic Press (2003).
- [15] V. Mukhanov, *Physical Foundations of Cosmology*, Cambridge University Press (2005).
- [16] S. Weinberg, *Cosmology*, Oxford Press (2008).
- [17] E.B. Gliner, *Sov. Phys. JETP* **22**, 378 (1966).

- [18] Ya. B. Zel'dovich, A. Krasinski and Ya. B. Zeldovich, *Sov. Phys. Usp.* **11**, 381 (1968), [*Usp. Fiz. Nauk*95,209(1968)].
- [19] P.M. Garnavich *et al.*, *Astrophys. J.* **507**, 74 (1998).
- [20] S. Perlmutter, M. S. Turner and M. J. White, *Phys. Rev. Lett.* **83**, 670 (1999), [*arXiv:astro-ph/9901052*].
- [21] I. Maor *et al.*, *Phys. Rev.* **D65**, 123003 (2002), [*arXiv:astro-ph/0112526*].
- [22] A. Albrecht *et al.* (2006), [*arXiv:astro-ph/0609591*].
- [23] J. A. Peacock *et al.* (2006), [*arXiv:astro-ph/0610906*].
- [24] N. Aghanim *et al.* (Planck) (2018), [*arXiv:1807.06209*].
- [25] A.G. Riess *et al.*, *Astrophys. J.* **116**, 1009 (1998).
- [26] S. Perlmutter *et al.* (Supernova Cosmology Project), *Astrophys. J.* **517**, 565 (1999), [*arXiv:astro-ph/9812133*].
- [27] A. G. Riess, *Publ. Astron. Soc. Pac.* **112**, 1284 (2000), [*arXiv:astro-ph/0005229*].
- [28] J. L. Tonry *et al.* (Supernova Search Team), *Astrophys. J.* **594**, 1 (2003), [*arXiv:astro-ph/0305008*].
- [29] R. Amanullah *et al.*, *Astrophys. J.* **716**, 712 (2010), [*arXiv:1004.1711*].
- [30] M. Betoul *et al.*, *Astron. & Astrophys.* **568**, A22 (2014).
- [31] A. G. Riess *et al.*, "*Astrophys. J.*" **876**, 85 (2019), [*arXiv:1903.07603*].
- [32] W. L. Freedman *et al.* (2019), [*arXiv:1907.05922*].
- [33] Planck Collab. 2015 Results XIII, *Astron. & Astrophys.* **594**, A13 (2016).
- [34] P. Astier *et al.*, *Astron. & Astrophys.* **447**, 31 (2006).
- [35] J. A. Johnson and M. Bolte, *Astrophys. J.* **554**, 888 (2001), [*arXiv:astro-ph/0103299*].
- [36] R. Cayrel *et al.*, *Nature* **409**, 691 (2001), [*arXiv:astro-ph/0104357*].
- [37] D. A. Vandenberg *et al.*, *Astrophys. J.* **775**, 134 (2013), [*arXiv:1308.2257*].
- [38] S. Borsanyi *et al.*, *Nature* **539**, 7627, 69 (2016), [*arXiv:1606.07494*].
- [39] M. Srednicki, R. Watkins and K. A. Olive, *Nucl. Phys.* **B310**, 693 (1988), [*247(1988)*].
- [40] G. Mangano *et al.*, *Phys. Lett.* **B534**, 8 (2002), [*arXiv:astro-ph/0111408*].
- [41] P. F. de Salas and S. Pastor, *JCAP* **7**, 051 (2016), [*arXiv:1606.06986*].
- [42] A. D. Linde, *Phys. Rev.* **D14**, 3345 (1976).
- [43] A. Linde, *Rept. on Prog. in Phys.* **42**, 389 (1979).
- [44] C.E. Vayonakis, *Surv. High Energy Physics* **5**, 87 (1986).
- [45] S.A. Bonometto and A. Masiero, *Nuovo Cimento* **9N5**, 1 (1986).
- [46] A. Linde, *Particle Physics And Inflationary Cosmology*, Harwood (1990).
- [47] K. A. Olive, *Phys. Rept.* **190**, 307 (1990).
- [48] D. H. Lyth and A. Riotto, *Phys. Rept.* **314**, 1 (1999), [*hep-ph/9807278*].
- [49] A. H. Guth, *Phys. Rev.* **D23**, 347 (1981), [*Adv. Ser. Astrophys. Cosmol.*3,139(1987)].
- [50] A. D. Linde, *Phys. Lett.* **108B**, 389 (1982), [*Adv. Ser. Astrophys. Cosmol.*3,149(1987)].
- [51] A. Albrecht and P. J. Steinhardt, *Phys. Rev. Lett.* **48**, 1220 (1982), [*Adv. Ser. Astrophys. Cosmol.*3,158(1987)].
- [52] S. Weinberg, *Rev. Mod. Phys.* **61**, 1 (1989).
- [53] L. Susskind 247–266 (2003), [*hep-th/0302219*].
- [54] B. Carr, *Universe or multiverse?* C.U.P. (2007).
- [55] A. D. Sakharov, *Pisma Zh. Eksp. Teor. Fiz.* **5**, 32 (1967), [*Usp. Fiz. Nauk*161,no.5,61(1991)].
- [56] S. Weinberg, *Phys. Rev. Lett.* **42**, 850 (1979).
- [57] D. Toussaint *et al.*, *Phys. Rev.* **D19**, 1036 (1979).
- [58] I. Affleck and M. Dine, *Nucl. Phys.* **B249**, 361 (1985).
- [59] V. A. Kuzmin, V. A. Rubakov and M. E. Shaposhnikov, *Phys. Lett.* **155B**, 36 (1985).
- [60] M. Fukugita and T. Yanagida, *Phys. Lett.* **B174**, 45 (1986).
- [61] S. Riemer-Sorensen and S. Jenssen, *Universe* **3**, 44 (2017).
- [62] R. J. Cooke, M. Pettini and C. C. Steidel, *Astrophys. J.* **855**, 2, 102 (2018), [*arXiv:1710.11129*].
- [63] R. H. Cyburt, B. D. Fields and K. A. Olive, *Phys. Lett.* **B567**, 227 (2003), [*arXiv:astro-ph/0302431*].
- [64] R. H. Cyburt, B. D. Fields and K. A. Olive, *JCAP* **0811**, 012 (2008), [*arXiv:0808.2818*].
- [65] K. A. Olive, G. Steigman and T. P. Walker, *Phys. Rept.* **333**, 389 (2000), [*arXiv:astro-ph/9905320*].
- [66] F. Iocco *et al.*, *Phys. Rept.* **472**, 1 (2009), [*arXiv:0809.0631*].
- [67] R. H. Cyburt *et al.*, *Rev. Mod. Phys.* **88**, 015004 (2016), [*arXiv:1505.01076*].
- [68] C. Pitrou *et al.*, *Phys. Rept.* **754**, 1 (2018), [*arXiv:1801.08023*].
- [69] D. J. Fixsen *et al.*, *Astrophys. J.* **473**, 576 (1996), [*arXiv:astro-ph/9605054*].
- [70] J. C. Mather *et al.*, *Astrophys. J.* **512**, 511 (1999), [*arXiv:astro-ph/9810373*].
- [71] S. Cole *et al.* (2dFGRS), *Mon. Not. Roy. Astron. Soc.* **326**, 255 (2001), [*arXiv:astro-ph/0012429*].
- [72] J. Schroeder, A. Mesinger and Z. Haiman, *Mon. Not. R. Astron. Soc.* **428**, 3058 (2012).
- [73] S. D. M. White *et al.*, *Nature* **366**, 429 (1993).
- [74] S. W. Allen, R. W. Schmidt and A. C. Fabian, *Mon. Not. Roy. Astron. Soc.* **334**, L11 (2002), [*arXiv:astro-ph/0205007*].
- [75] S. W. Allen, *Mon. Not. Roy. Astron. Soc.* **296**, 392 (1998), [*arXiv:astro-ph/9710217*].
- [76] G. P. Smith *et al.*, *Mon. Not. Roy. Astron. Soc.* **456**, 1, L74 (2016), [*arXiv:1511.01919*].
- [77] H. Hildebrandt *et al.*, *Mon. Not. Roy. Astron. Soc.* **465**, 1454 (2017), [*arXiv:1606.05338*].
- [78] M. A. Troxel *et al.*, "*Phys. Rev.*" **98**, 4, 043528 (2018), [*arXiv:1708.01538*].
- [79] Planck Collab. 2015 Results XV, *Astron. & Astrophys.* **594**, A15 (2016).
- [80] S. Cole *et al.* (2dFGRS), *Mon. Not. Roy. Astron. Soc.* **362**, 505 (2005), [*arXiv:astro-ph/0501174*].
- [81] W. J. Percival *et al.*, *Astrophys. J.* **657**, 645 (2007), [*arXiv:astro-ph/0608636*].
- [82] L. Anderson *et al.*, *Mon. Not. Roy. Astron. Soc.* **427**, 4, 3435 (2013), [*arXiv:1203.6594*].
- [83] E. Linder, *Phys. Rev.* **D72**, 43529 (2005).
- [84] D. Polarski and R. Gannouji, *Phys. Lett.* **B660**, 439 (2008), [*arXiv:0710.1510*].
- [85] G. Efstathiou and J. R. Bond, *Mon. Not. Roy. Astron. Soc.* **218**, 1, 103 (1986).
- [86] C. Gordon and A. Lewis, *Phys. Rev.* **D67**, 123513 (2003), [*arXiv:astro-ph/0212248*].
- [87] A. Vikhlinin *et al.*, *Astrophys. J.* **692**, 1060 (2009), [*arXiv:0812.2720*].
- [88] A. Dekel and O. Lahav, *Astrophys. J.* **520**, 24 (1999), [*arXiv:astro-ph/9806193*].
- [89] W. J. Percival *et al.*, *Mon. Not. Roy. Astron. Soc.* **381**, 1053 (2007), [*arXiv:0705.3323*].
- [90] W. J. Percival *et al.* (SDSS), *Mon. Not. Roy. Astron. Soc.* **401**, 2148 (2010), [*arXiv:0907.1660*].

- [91] G. Efstathiou and J. R. Bond, *Mon. Not. Roy. Astron. Soc.* **304**, 75 (1999), [arXiv:astro-ph/9807103].
- [92] G. Efstathiou *et al.* (2dFGRS), *Mon. Not. Roy. Astron. Soc.* **330**, L29 (2002), [arXiv:astro-ph/0109152].
- [93] P. A. R. Ade *et al.* (BICEP2, Keck Array), *Phys. Rev. Lett.* **121**, 221301 (2018), [arXiv:1810.05216].
- [94] A. A. Starobinsky, *Phys. Lett.* **B91**, 99 (1980), [771(1980)].
- [95] F. Bezrukov and M. Shaposhnikov, *JHEP* **07**, 089 (2009), [arXiv:0904.1537].
- [96] Planck Collab. 2015 Results XXI, *Astron. & Astrophys.* **594**, A21 (2016).
- [97] Planck Collab. 2015 Results XXII, *Astron. & Astrophys.* **594**, A22 (2016).
- [98] W. Hu and I. Sawicki, *Phys. Rev.* **D76**, 4043 (2007).
- [99] B. Jain and P. Zhang, *Phys. Rev.* **D78**, 3503 (2008).
- [100] D. L. Wiltshire, *Phys. Rev. Lett.* **99**, 251101 (2007), [arXiv:0709.0732].
- [101] T. Buchert, *Gen. Rel. Grav.* **40**, 467 (2008), [arXiv:0707.2153].
- [102] I. Zlatev, L.-M. Wang and P. J. Steinhardt, *Phys. Rev. Lett.* **82**, 896 (1999), [arXiv:astro-ph/9807002].
- [103] C. Armendariz-Picon, V. Mukhanov, and P.J. Steinhardt, *Phys. Rev.* **D63**, 3510 (2001).
- [104] S. DeDeo, R.R. Caldwell, and P.J. Steinhardt, *Phys. Rev.* **D67**, 3509 (2003).
- [105] W. Hu, *ASP Conf. Ser.* **339**, 215 (2005), [arXiv:astro-ph/0407158].
- [106] S. F. Daniel *et al.*, *Phys. Rev.* **D81**, 123508 (2010), [arXiv:1002.1962].

23. Inflation

Revised August 2019 by J. Ellis (King's Coll. London; CERN) and D. Wands (Portsmouth U.).

23.1 Motivation and Introduction

The standard Big-Bang model of cosmology provides a successful framework in which to understand the thermal history of our Universe and the growth of cosmic structure, but it is essentially incomplete. As described in Sec. 22.2.4, Big-Bang cosmology requires very specific initial conditions. It postulates a uniform cosmological background, described by a spatially-flat, homogeneous and isotropic Robertson-Walker (RW) metric (Eq. (22.1) in “Big Bang Cosmology” review), with scale factor $R(t)$. Within this setting, it also requires an initial almost scale-invariant distribution of primordial density perturbations as seen, for example, in the cosmic microwave background (CMB) radiation (described in Chap. 29, “Cosmic Microwave Background” review), on scales far larger than the causal horizon at the time the CMB photons last scattered.

The Hubble expansion rate, $H \equiv \dot{R}/R$, in a RW cosmology is given by the Friedmann constraint equation (Eq. (22.8) in “Big Bang Cosmology” review)

$$H^2 = \frac{8\pi\rho}{3M_P^2} + \frac{\Lambda}{3} - \frac{k}{R^2}, \quad (23.1)$$

where k/R^2 is the intrinsic spatial curvature. We use natural units such that the speed of light $c = 1$ and hence we have the Planck mass $M_P = G_N^{-1/2} \simeq 10^{19}$ GeV (see “Astrophysical Constants and Parameters”). A cosmological constant, Λ , of the magnitude required to accelerate the Universe today (see Chap. 28, “Dark Energy” review) would have been completely negligible in the early Universe where the energy density $\rho \gg M_P^2 \Lambda \sim 10^{-12}(\text{eV})^4$. The standard early Universe cosmology, described in Sec. 22.1.5 in “Big Bang Cosmology” review, is thus dominated by non-relativistic matter ($p_m \ll \rho_m$) or radiation ($p_r = \rho_r/3$ for an isotropic distribution). This leads to a decelerating expansion with $\ddot{R} < 0$.

The hypothesis of inflation [1, 2] postulates a period of accelerated expansion, $\ddot{R} > 0$, in the very early Universe, preceding the standard radiation-dominated era, which offers a physical model for the origin of these initial conditions, as reviewed in [3–7]. Such a period of accelerated expansion (i) drives a curved Robertson-Walker spacetime (with spherical or hyperbolic spatial geometry) towards spatial flatness, and (ii) it also expands the causal horizon beyond the present Hubble length, so as to encompass all the scales relevant to describe the large-scale structure observed in our Universe today, via the following two mechanisms.

1. A spatially-flat universe with vanishing spatial curvature, $k = 0$, has the dimensionless density parameter $\Omega_{tot} = 1$, where we define (Eq. (22.13) in “Big Bang Cosmology” review; see Chap. 25.1, “Cosmological Parameters” review for more complete definitions)

$$\Omega_{tot} \equiv \frac{8\pi\rho_{tot}}{3M_P^2 H^2}, \quad (23.2)$$

with $\rho_{tot} \equiv \rho + \Lambda M_P^2/8\pi$. If we re-write the Friedmann constraint (Eq. (23.1)) in terms of Ω_{tot} we have

$$1 - \Omega_{tot} = -\frac{k}{R^2}. \quad (23.3)$$

Observations require $|1 - \Omega_{tot,0}| < 0.005$ today [8], where the subscript 0 denotes the present-day value. Taking the time derivative of Eq. (23.3) we obtain

$$\frac{d}{dt}(1 - \Omega_{tot}) = -2\frac{\ddot{R}}{\dot{R}}(1 - \Omega_{tot}). \quad (23.4)$$

Thus in a decelerating expansion, $\dot{R} > 0$ and $\ddot{R} < 0$, any small initial deviation from spatial flatness grows, $(d/dt)|1 - \Omega_{tot}| > 0$. A small value such as $|1 - \Omega_{tot,0}| < 0.005$ today requires an even smaller value at earlier times, e.g., $|1 - \Omega_{tot}| < 10^{-5}$ at

the last scattering of the CMB, which appears unlikely, unless for some reason space is exactly flat. However, an extended period of accelerated expansion in the very early Universe, with $\dot{R} > 0$ and $\ddot{R} > 0$ and hence $(d/dt)|1 - \Omega_{tot}| < 0$, can drive Ω_{tot} sufficiently close to unity, so that $|1 - \Omega_{tot,0}|$ remains unobservably small today, even after the radiation- and matter-dominated eras, for a wide range of initial values of Ω_{tot} .

2. The comoving distance (the present-day proper distance) traversed by light between cosmic time t_1 and t_2 in an expanding universe can be written, (see Eq. (22.32) in “Big Bang Cosmology” review), as

$$D_0(t_1, t_2) = R_0 \int_{t_1}^{t_2} \frac{dt}{R(t)} = R_0 \int_{\ln R_1}^{\ln R_2} \frac{d(\ln R)}{\dot{R}}. \quad (23.5)$$

In standard decelerated (radiation- or matter-dominated) cosmology the integrand, $1/\dot{R}$, decreases towards the past, and there is a finite comoving distance traversed by light (a particle horizon) since the Big Bang ($R_1 \rightarrow 0$). For example, the comoving size of the particle horizon at the CMB last-scattering surface ($R_2 = R_{lss}$) corresponds to $D_0 \sim 100$ Mpc, or approximately 1° on the CMB sky today (see Sec. 22.2.4 in “Big Bang Cosmology” review). However, during a period of inflation, $1/\dot{R}$ increases towards the past, and hence the integral (Eq. (23.5)) diverges as $R_1 \rightarrow 0$, allowing an arbitrarily large causal horizon, dependent only upon the duration of the accelerated expansion. Assuming that the Universe inflates with a finite Hubble rate H_* at $t_1 = t_*$, ending with $H_{end} < H_*$ at $t_2 = t_{end}$, we have

$$D_0(t_*, t_{end}) > \left(\frac{R_0}{R_{end}}\right) H_*^{-1} (e^{N_*} - 1), \quad (23.6)$$

where $N_* \equiv \ln(R_{end}/R_*)$ describes the duration of inflation, measured in terms of the logarithmic expansion (or “e-folds”) from $t_1 = t_*$ up to the end of inflation at $t_2 = t_{end}$, and R_0/R_{end} is the subsequent expansion from the end of inflation to the present day. If inflation occurs above the TeV scale, the comoving Hubble scale at the end of inflation, $(R_0/R_{end})H_{end}^{-1}$, is less than one astronomical unit ($\sim 10^{11}$ m), and a causally-connected patch can encompass our entire observable Universe today, which has a size $D_0 > 30$ Gpc, if there were more than 40 e-folds of inflation ($N_* > 40$). If inflation occurs at the GUT scale (10^{15} GeV) then we require more than 60 e-folds.

Producing an accelerated expansion in general relativity requires an energy-momentum tensor with negative pressure, $p < -\rho/3$ (see Eq. (22.9) in “Big Bang Cosmology” review and Chap. 28, “Dark Energy” review), quite different from the hot dense plasma of relativistic particles in the hot Big Bang. However a positive vacuum energy $V > 0$ does exert a negative pressure, $p_V = -\rho_V$. The work done by the cosmological expansion must be negative in this case so that the local vacuum energy density remains constant in an expanding universe, $\dot{\rho}_V = -3H(\rho_V + p_V) = 0$. Therefore, a false vacuum state can drive an exponential expansion, corresponding to a de Sitter spacetime with a constant Hubble rate $H^2 = 8\pi\rho_V/3M_P^2$ on spatially-flat hypersurfaces.

A constant vacuum energy V , equivalent to a cosmological constant Λ in the Friedmann equation Eq. (23.1), cannot provide a complete description of inflation in the early Universe, since inflation must necessarily have come to an end in order for the standard Big-Bang cosmology to follow. A phase transition to the present true vacuum is required to release the false vacuum energy into the energetic plasma of the hot Big Bang and produce the large total entropy of our observed Universe today. Thus we must necessarily study dynamical models of inflation, where the time-invariance of the false vacuum state is broken by a time-dependent field. A first-order phase transition would produce a very inhomogeneous Universe [9] unless a time-dependent scalar field leads to a rapidly changing percolation rate [10–12]. However,

a second-order phase transition [13, 14], controlled by a slowly-rolling scalar field, can lead to a smooth classical exit from the vacuum-dominated phase.

As a spectacular bonus, quantum fluctuations in that scalar field could provide a source of almost scale-invariant density fluctuations [15, 16], as detected in the CMB (see Chap. 29), which are thought to be the origin of the structures seen in the Universe today.

Accelerated expansion and primordial perturbations can also be produced in some modified gravity theories (e.g., [1, 17]), which introduce additional non-minimally coupled degrees of freedom. Such inflation models can often be conveniently studied by transforming variables to an ‘Einstein frame’ in which Einstein’s equations apply with minimally coupled scalar fields [18–20].

In the following we will review scalar field cosmology in general relativity and the spectra of primordial fluctuations produced during inflation, before studying selected inflation models.

23.2 Scalar Field Cosmology

The energy-momentum tensor for a canonical scalar field ϕ with self-interaction potential $V(\phi)$ is given in Eq. (22.52) in “Big Bang Cosmology” review. In a homogeneous background this corresponds to a perfect fluid with density

$$\rho = \frac{1}{2}\dot{\phi}^2 + V(\phi), \tag{23.7}$$

and isotropic pressure

$$p = \frac{1}{2}\dot{\phi}^2 - V(\phi), \tag{23.8}$$

while the 4-velocity is proportional to the gradient of the field, $u^\mu \propto \nabla^\mu \phi$.

A field with vanishing potential energy acts like a stiff fluid with $p = \rho = \dot{\phi}^2/2$, whereas if the time-dependence vanishes we have $p = -\rho = -V$ and the scalar field is uniform in time and space. Thus a classical, potential-dominated scalar-field cosmology, with $p \simeq -\rho$, can naturally drive a quasi-de Sitter expansion; the slow time-evolution of the energy density weakly breaks the exact $O(1, 3)$ symmetry of four-dimensional de Sitter spacetime down to a Robertson-Walker (RW) spacetime, where the scalar field plays the role of the cosmic time coordinate.

In a scalar-field RW cosmology the Friedmann constraint equation (Eq. (23.1)) reduces to

$$H^2 = \frac{8\pi}{3M_P^2} \left(\frac{1}{2}\dot{\phi}^2 + V \right) - \frac{k}{R^2}, \tag{23.9}$$

while energy conservation (Eq. (22.10) in “Big Bang Cosmology” review) for a homogeneous scalar field reduces to the Klein-Gordon equation of motion (Eq. (22.54) in “Big Bang Cosmology” review)

$$\ddot{\phi} = -3H\dot{\phi} - V'(\phi). \tag{23.10}$$

The evolution of the scalar field is thus driven by the potential gradient $V' = dV/d\phi$, subject to damping by the Hubble expansion $3H\dot{\phi}$.

If we define the Hubble slow-roll parameter

$$\epsilon_H \equiv -\frac{\dot{H}}{H^2}, \tag{23.11}$$

then we see that inflation ($\dot{R} > 0$ and hence $\dot{H} > -H^2$) requires $\epsilon_H < 1$. In this case the spatial curvature decreases relative to the scalar field energy density as the Universe expands. Hence in the following we drop the spatial curvature and consider a spatially-flat RW cosmology, assuming that inflation has lasted sufficiently long that our observable universe is very close to spatially flatness. However, we note that bubble nucleation, leading to a first-order phase transition during inflation, can lead to homogeneous hypersurfaces with a hyperbolic (‘open’) geometry, effectively resetting the spatial curvature inside the bubble [21]. This is the basis of so-called open inflation models [22–24], where inflation inside the bubble has a finite duration, leaving a finite negative spatial curvature.

In a scalar field-dominated cosmology (Eq. (23.11)) gives

$$\epsilon_H = \frac{3\dot{\phi}^2}{2V + \dot{\phi}^2}, \tag{23.12}$$

in which case we see that inflation requires a potential-dominated expansion, $\dot{\phi}^2 < V$.

23.2.1 Slow-Roll Inflation

It is commonly assumed that the field acceleration term, $\ddot{\phi}$, in (Eq. (23.10)) can be neglected, in which case one can give an approximate solution for the inflationary attractor [25]. This slow-roll approximation reduces the second-order Klein-Gordon equation (Eq. (23.10)) to a first-order system, which is over-damped, with the potential gradient being approximately balanced against to the Hubble damping:

$$3H\dot{\phi} \simeq -V', \tag{23.13}$$

and at the same time that the Hubble expansion (Eq. (23.9)) is dominated by the potential energy

$$H^2 \simeq \frac{8\pi}{3M_P^2} V(\phi), \tag{23.14}$$

corresponding to $\epsilon_H \ll 1$.

A necessary condition for the validity of the slow-roll approximation is that the potential slow-roll parameters

$$\epsilon \equiv \frac{M_P^2}{16\pi} \left(\frac{V'}{V} \right)^2, \quad \eta \equiv \frac{M_P^2}{8\pi} \left(\frac{V''}{V} \right), \tag{23.15}$$

are small, i.e., $\epsilon \ll 1$ and $|\eta| \ll 1$, requiring the potential to be correspondingly flat. If we identify V'' with the effective mass of the field, we see that the slow-roll approximation requires that the mass of the scalar field must be small compared with the Hubble scale. We note that the Hubble slow-roll parameter (Eq. (23.11)) coincides with the potential slow-roll parameter, $\epsilon_H \simeq \epsilon$, to leading order in the slow-roll approximation.

The slow-roll approximation allows one to determine the Hubble expansion rate as a function of the scalar field value, and vice versa. In particular, we can express, in terms of the scalar field value during inflation, the total logarithmic expansion, or number of “e-folds”:

$$\begin{aligned} N_* &\equiv \ln \left(\frac{R_{end}}{R_*} \right) \\ &= \int_{t_*}^{t_{end}} H dt \simeq - \int_{\phi_*}^{\phi_{end}} \sqrt{\frac{4\pi}{\epsilon}} \frac{d\phi}{M_P} \text{ for } V' > 0. \end{aligned} \tag{23.16}$$

Given that the slow-roll parameters are approximately constant during slow-roll inflation, $d\epsilon/dN \simeq 2\epsilon(\eta - 2\epsilon) = \mathcal{O}(\epsilon^2)$, we have

$$N_* \simeq \frac{4}{\sqrt{\epsilon}} \frac{\Delta\phi}{M_P}. \tag{23.17}$$

Since we require $N > 40$ to solve the flatness, horizon and entropy problems of the standard Big Bang cosmology, we require either very slow roll, $\epsilon < 0.01$, or a large change in the value of the scalar field relative to the Planck scale, $\Delta\phi > M_P$.

23.2.2 Reheating

Slow-roll inflation can lead to an exponentially large universe, close to spatial flatness and homogeneity, but the energy density is locked in the potential energy of the scalar field, and needs to be converted to particles and thermalised to recover a hot Big Bang cosmology at the end of inflation [26, 27]. This process is usually referred to as reheating, although there was not necessarily any preceding thermal era. Reheating can occur when the scalar field evolves towards the minimum of its potential, converting the potential energy first to kinetic energy. This can occur either through the breakdown of the slow-roll condition in single-field models, or due to an instability triggered by the inflaton reaching

a critical value, in multi-field models known as hybrid inflation models [28].

Close to a simple minimum, the scalar field potential can be described by a quadratic function, $V = m^2\phi^2/2$, where m is the mass of the field. We can obtain slow-roll inflation in such a potential at large field values, $\phi \gg M_P$. However, for $\phi \ll M_P$ the field approaches an oscillatory solution:

$$\phi(t) \simeq \frac{M_P}{\sqrt{3\pi}} \frac{\sin(mt)}{mt}. \quad (23.18)$$

For $|\phi| < M_P$ the Hubble rate drops below the inflaton mass, $H < m$, and the field oscillates many times over a Hubble time. Averaging over several oscillations, $\Delta t \gg m^{-1}$, we find $\langle \dot{\phi}^2/2 \rangle_{\Delta t} \simeq \langle m^2\phi^2/2 \rangle_{\Delta t}$ and hence

$$\langle \rho \rangle_{\Delta t} \simeq \frac{M_P^2}{6\pi t^2}, \quad \langle p \rangle_{\Delta t} \simeq 0. \quad (23.19)$$

This coherent oscillating field corresponds to a condensate of non-relativistic massive inflaton particles, driving a matter-dominated era at the end of inflation, with scale factor $R \propto t^{2/3}$.

The inflaton condensate can lose energy through perturbative decays due to terms in the interaction Lagrangian, such as

$$\mathcal{L}_{int} \subset -\lambda_i \sigma \phi \chi_i^2 - \lambda_j \phi \bar{\psi}_j \psi_j \quad (23.20)$$

that couple the inflation to scalar fields χ_i or fermions ψ_j , where σ has dimensions of mass and the λ_i are dimensionless couplings. When the mass of the inflaton is much larger than the decay products, the decay rate is given by [29]

$$\Gamma_i = \frac{\lambda_i^2 \sigma^2}{8\pi m}, \quad \Gamma_j = \frac{\lambda_j^2 m}{8\pi}. \quad (23.21)$$

These decay products must in turn thermalise with Standard Model particles before we recover conventional hot Big Bang cosmology. An upper limit on the reheating temperature after inflation is given by [27]

$$T_{rh} = 0.2 \left(\frac{100}{g_*} \right)^{1/4} \sqrt{M_P \Gamma_{tot}}, \quad (23.22)$$

where g_* is the effective number of degrees of freedom and Γ_{tot} is the total decay rate for the inflaton, which is required to be less than m for perturbative decay.

The baryon asymmetry of the Universe must be generated after the main release of entropy during inflation, which is an important constraint on possible models. Also, the fact that the inflaton mass is much larger than the mass scale of the Standard Model opens up the possibility that it may decay into massive stable or metastable particles that could be connected with dark matter, constraining possible models. For example, in the context of supergravity models the reheat temperature is constrained by the requirement that gravitinos are not overproduced, potentially destroying the successes of Big Bang nucleosynthesis. For a range of gravitino masses one must require $T_{rh} < 10^9$ GeV [30, 31].

The process of inflaton decay and reheating can be significantly altered by interactions leading to space-time dependences in the effective masses of the fields. In particular, parametric resonance can lead to explosive, non-perturbative decay of the inflaton in some cases, a process often referred to as preheating [26, 32]. For example, an interaction term of the form

$$\mathcal{L}_{int} \subset -\lambda^2 \phi^2 \chi^2, \quad (23.23)$$

leads to a time-dependent effective mass for the χ field as the inflaton ϕ oscillates. This can lead to non-adiabatic particle production if the bare mass of the χ field is small for large couplings or for rapid changes of the inflaton field. The process of preheating is highly model-dependent, but it highlights the possible role of non-thermal particle production after and even during inflation.

23.3 Primordial Perturbations from Inflation

Although inflation was originally discussed as a solution to the problem of initial conditions required for homogeneous and isotropic hot Big Bang cosmology, it was soon realised that inflation also offered a mechanism to generate the inhomogeneous initial conditions required for the formation of large-scale structure [15–17, 33].

23.3.1 Metric Perturbations

In a homogeneous classical inflationary cosmology driven by a scalar field, the inflaton field is uniform on constant-time hypersurfaces, $\phi = \phi_0(t)$. However, quantum fluctuations inevitably break the spatial symmetry leading to an inhomogeneous field:

$$\phi(t, x^i) = \phi_0(t) + \delta\phi(t, x^i). \quad (23.24)$$

At the same time, one should consider inhomogeneous perturbations of the RW spacetime metric (see, e.g., [34–36]):

$$ds^2 = (1 + 2A)dt^2 - 2RB_i dt dx^i - R^2 [(1 + 2C)\delta_{ij} + \partial_i \partial_j E + h_{ij}] dx^i dx^j, \quad (23.25)$$

where A , B , E and C are scalar perturbations while h_{ij} represents transverse and tracefree, tensor metric perturbations. Vector metric perturbations can be eliminated using Einstein constraint equations in a scalar field cosmology.

The tensor perturbations remain invariant under a temporal gauge transformation $t \rightarrow t + \delta t(t, x^i)$, but both the scalar field and the scalar metric perturbations transform. For example, we have

$$\delta\phi \rightarrow \delta\phi - \dot{\phi}_0 \delta t, \quad C \rightarrow C - H \delta t. \quad (23.26)$$

However, there are gauge invariant combinations, such as [37]

$$Q = \delta\phi - \frac{\dot{\phi}_0}{H} C, \quad (23.27)$$

which describes the scalar field perturbations on spatially-flat ($C = 0$) hypersurfaces. This is simply related to the curvature perturbation on uniform-field ($\delta\phi = 0$) hypersurfaces:

$$\mathcal{R} = C - \frac{H}{\dot{\phi}_0} \delta\phi = -\frac{H}{\dot{\phi}_0} Q, \quad (23.28)$$

which coincides in slow-roll inflation, $\rho \simeq \rho(\phi)$, with the curvature perturbation on uniform-density hypersurfaces [16]

$$\zeta = C - \frac{H}{\dot{\rho}_0} \delta\rho. \quad (23.29)$$

Thus scalar field and scalar metric perturbations are coupled by the evolution of the inflaton field.

23.3.2 Gravitational waves from inflation

The tensor metric perturbation, h_{ij} in Eq. (23.25), is gauge-invariant and decoupled from the scalar perturbations at first order. This represents the free excitations of the spacetime, i.e., gravitational waves, which are the simplest metric perturbations to study at linear order.

Each tensor mode, with wavevector \vec{k} , has two linearly-independent transverse and trace-free polarization states:

$$h_{ij}(\vec{k}) = h_{\vec{k}} q_{ij} + \bar{h}_{\vec{k}} \bar{q}_{ij}. \quad (23.30)$$

The linearised Einstein equations then yield the same evolution equation for the amplitude as that for a massless field in RW spacetime:

$$\ddot{h}_{\vec{k}} + 3H\dot{h}_{\vec{k}} + \frac{k^2}{R^2} h_{\vec{k}} = 0, \quad (23.31)$$

(and similarly for $\bar{h}_{\vec{k}}$). This can be re-written in terms of the conformal time, $\eta = \int dt/R$, and the conformally rescaled field:

$$u_{\vec{k}} = \frac{M_P R h_{\vec{k}}}{\sqrt{32\pi}}. \quad (23.32)$$

This conformal field then obeys the wave equation for a canonical scalar field in Minkowski spacetime with a time-dependent mass:

$$u_{\vec{k}}'' + \left(k^2 - \frac{R''}{R}\right) u_{\vec{k}} = 0. \quad (23.33)$$

During slow-roll

$$\frac{R''}{R} \simeq (2 - \epsilon)R^2 H^2. \quad (23.34)$$

This makes it possible to quantise the linearised metric fluctuations, $u_{\vec{k}} \rightarrow \hat{u}_{\vec{k}}$, on sub-Hubble scales, $k^2/R^2 \gg H^2$, where the background expansion can be neglected.

Crucially, in an inflationary expansion, where $\dot{R} > 0$, the comoving Hubble length $H^{-1}/R = 1/\dot{R}$ decreases with time. Thus all modes start inside the Hubble horizon and it is possible to take the initial field fluctuations to be in a vacuum state at early times or on small scales:

$$\langle u_{\vec{k}_1} u_{\vec{k}_2} \rangle = \frac{i}{2} (2\pi)^3 \delta^{(3)}(\vec{k}_1 + \vec{k}_2). \quad (23.35)$$

In terms of the amplitude of the tensor metric perturbations, this corresponds to

$$\langle h_{\vec{k}_1} h_{\vec{k}_2} \rangle = \frac{1}{2} \frac{\mathcal{P}_t(k_1)}{4\pi k_1^3} (2\pi)^3 \delta^{(3)}(\vec{k}_1 + \vec{k}_2), \quad (23.36)$$

where the factor 1/2 appears due to the two polarization states that contribute to the total tensor power spectrum:

$$\mathcal{P}_t(k) = \frac{64\pi}{M_P^2} \left(\frac{k}{2\pi R}\right)^2. \quad (23.37)$$

On super-Hubble scales, $k^2/R^2 \ll H^2$, we have the growing mode solution to Eq. (23.33), $u_{\vec{k}} \propto R$, corresponding to $h_{\vec{k}} \rightarrow$ constant, i.e., tensor modes are frozen-in on super-Hubble scales, both during and after inflation. Thus, connecting the initial vacuum fluctuations on sub-Hubble scales to the late-time power spectrum for tensor modes at Hubble exit during inflation, $k = R_* H_*$, we obtain

$$\mathcal{P}_t(k) \simeq \frac{64\pi}{M_P^2} \left(\frac{H_*}{2\pi}\right)^2. \quad (23.38)$$

In the de Sitter limit, $\epsilon \rightarrow 0$, the Hubble rate becomes time-independent and the tensor spectrum on super-Hubble scales becomes scale-invariant [39]. However slow-roll evolution leads to weak time dependence of H_* and thus a scale-dependent spectrum on large scales, with a spectral tilt

$$n_t \equiv \frac{d \ln \mathcal{P}_T}{d \ln k} \simeq -2\epsilon_*. \quad (23.39)$$

23.3.3 Density Perturbations from single-field inflation

The inflaton field fluctuations on spatially-flat hypersurfaces are coupled to scalar metric perturbations at first order, but these can be eliminated using the Einstein constraint equations to yield an evolution equation

$$\ddot{Q}_{\vec{k}} + 3H\dot{Q}_{\vec{k}} + \left[\frac{k^2}{R^2} + V'' - \frac{8\pi}{M_P^2 R^3} \frac{d}{dt} \left(\frac{R^3 \dot{\phi}^2}{H} \right) \right] Q_{\vec{k}} = 0. \quad (23.40)$$

Terms proportional to M_P^{-2} represent the effect on the field fluctuations of gravity at first order. As can be seen, this vanishes in the limit of a constant background field, and hence is suppressed in the slow-roll limit, but it is of the same order as the effective mass, $V'' = 3\eta H^2$, so must be included if we wish to model deviations from exact de Sitter symmetry.

This wave equation can also be written in the canonical form for a free field in Minkowski spacetime if we define [37]

$$v_{\vec{k}} \equiv RQ_{\vec{k}}, \quad (23.41)$$

to yield

$$v_{\vec{k}}'' + \left(k^2 - \frac{z''}{z}\right) v_{\vec{k}} = 0, \quad (23.42)$$

where we define

$$z \equiv \frac{R\dot{\phi}}{H}, \quad \frac{z''}{z} \simeq (2 + 5\epsilon - 3\eta)R^2 H^2, \quad (23.43)$$

where the last approximate equality holds to leading order in the slow-roll approximation.

As previously done for gravitational waves, we quantise the linearised field fluctuations $v_{\vec{k}} \rightarrow \hat{v}_{\vec{k}}$ on sub-Hubble scales, $k^2/R^2 \gg H^2$, where the background expansion can be neglected. Thus we impose

$$\langle v_{\vec{k}_1} v_{\vec{k}_2}' \rangle = \frac{i}{2} \delta^{(3)}(\vec{k}_1 + \vec{k}_2). \quad (23.44)$$

In terms of the field perturbations, this corresponds to

$$\langle Q_{\vec{k}_1} Q_{\vec{k}_2} \rangle = \frac{\mathcal{P}_Q(k_1)}{4\pi k_1^3} (2\pi)^3 \delta^{(3)}(\vec{k}_1 + \vec{k}_2), \quad (23.45)$$

where the power spectrum for vacuum field fluctuations on sub-Hubble scales, $k^2/R^2 \gg H^2$, is simply

$$\mathcal{P}_Q(k) = \left(\frac{k}{2\pi R}\right)^2, \quad (23.46)$$

yielding the classic result for the vacuum fluctuations for a massless field in de Sitter at Hubble exit, $k = R_* H_*$:

$$\mathcal{P}_Q(k) \simeq \left(\frac{H}{2\pi}\right)_*^2. \quad (23.47)$$

In practice there are slow-roll corrections due to the small but finite mass (η) and field evolution (ϵ) [40].

Slow-roll corrections to the field fluctuations are small on sub-Hubble scales, but can become significant as the field and its perturbations evolve over time on super-Hubble scales. Thus it is helpful to work instead with the curvature perturbation, ζ defined in equation (Eq. (23.29)), which remains constant on super-Hubble scales for adiabatic density perturbations both during and after inflation [16,41]. Thus we have an expression for the primordial curvature perturbation on super-Hubble scales produced by single-field inflation:

$$\mathcal{P}_\zeta(k) = \left[\left(\frac{H}{\dot{\phi}}\right)^2 \mathcal{P}_Q(k) \right]_* \simeq \frac{4\pi}{M_P^2} \left[\frac{1}{\epsilon} \left(\frac{H}{2\pi}\right)^2 \right]_*. \quad (23.48)$$

Comparing this with the primordial gravitational wave power spectrum (Eq. (23.38)) we obtain the tensor-to-scalar ratio for single-field slow-roll inflation

$$r \equiv \frac{\mathcal{P}_t}{\mathcal{P}_\zeta} \simeq 16\epsilon_*. \quad (23.49)$$

Note that the scalar amplitude is boosted by a factor $1/\epsilon_*$ during slow-roll inflation, because small scalar field fluctuations can lead to relatively large curvature perturbations on hypersurfaces defined with respect to the density if the potential energy is only weakly dependent on the scalar field, as in slow-roll. Indeed, the de Sitter limit is singular, since the potential energy becomes independent of the scalar field at first order, $\epsilon \rightarrow 0$, and the curvature perturbation on uniform-density hypersurfaces becomes ill-defined.

We note that in single-field inflation the tensor-to-scalar ratio and the tensor tilt (Eq. (23.39)) at the same scale are both determined by the first slow-roll parameter at Hubble exit, ϵ_* , giving rise to an important consistency test for single-field inflation:

$$n_t = -\frac{r}{8}. \quad (23.50)$$

This may be hard to verify if r is small, making any tensor tilt n_t difficult to measure. On the other hand, it does offer a way to rule out single-field slow-roll inflation if either r or n_t is large.

Given the relatively large scalar power spectrum, it has proved easier to measure the scalar tilt, conventionally defined as $n_s - 1$.

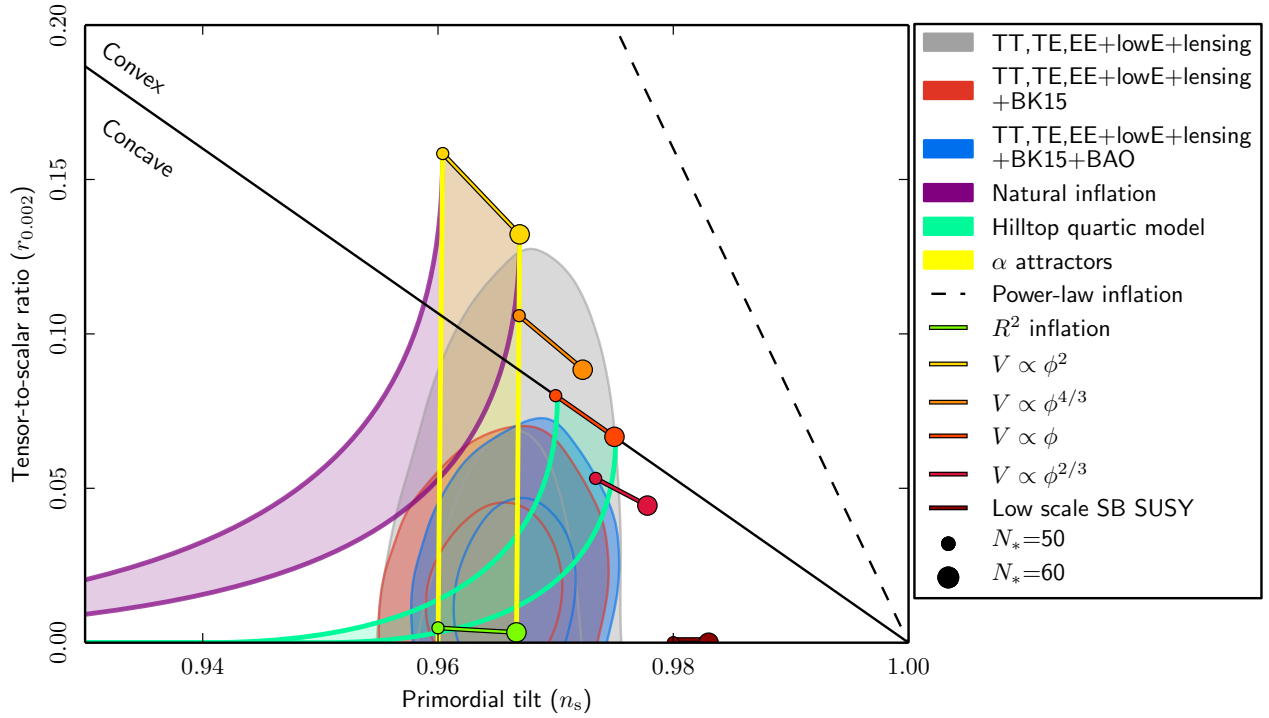


Figure 23.1: The marginalized joint 68 and 95% CL regions for the tilt in the scalar perturbation spectrum, n_s , and the relative magnitude of the tensor perturbations, r , obtained from the *Planck* 2018 and lensing data alone, and their combinations with BICEP2/Keck Array (BK15) and (optionally) BAO data, confronted with the predictions of some of the inflationary models discussed in this review. This figure is taken from [38].

Slow-roll corrections lead to slow time-dependence of both H_* and ϵ_* , giving a weak scale-dependence of the scalar power spectrum:

$$n_s - 1 \equiv \frac{d \ln \mathcal{P}_\zeta}{d \ln k} \simeq -6\epsilon_* + 2\eta_*, \quad (23.51)$$

and a running of this tilt at second-order in slow-roll:

$$\frac{dn_s}{d \ln k} \simeq -8\epsilon_*(3\epsilon_* - 2\eta_*) - 2\xi_*^2, \quad (23.52)$$

where the running introduces a new slow-roll parameter at second-order:

$$\xi^2 = \frac{M_P^4}{64\pi^2} \frac{V'V'''}{V^2}. \quad (23.53)$$

23.3.4 Observational Bounds

The observed scale-dependence of the power spectrum makes it necessary to specify the comoving scale, k , at which quantities are constrained and hence the Hubble-exit time, $k = a_* H_*$, when the corresponding theoretical quantities are calculated during inflation. This is usually expressed in terms of the number of e-folds from the end of inflation [42]:

$$N_*(k) \simeq 67 - \ln \left(\frac{k}{a_0 H_0} \right) + \frac{1}{4} \ln \left(\frac{V_*^2}{M_P^4 \rho_{end}} \right) + \frac{1}{12} \ln \left(\frac{\rho_{rh}}{\rho_{end}} \right) - \frac{1}{12} \ln(g_*), \quad (23.54)$$

where H_0^{-1}/a_0 is the present comoving Hubble length. Different models of reheating and and thus different reheat temperatures and densities, ρ_{rh} in Eq. (23.54), lead to a range of possible values for N_* corresponding to a fixed physical scale, and hence we have a range of observational predictions for a given inflation model, as seen in Fig. 23.1.

The *Planck* 2018 temperature and polarization data (see Chap. 29, “Cosmic Microwave Background” review) are consistent with a smooth featureless power spectrum over a range of comoving

wavenumbers, $0.008 h^{-1} \text{ Mpc}^{-1} \leq k \leq 0.1 h \text{ Mpc}^{-1}$. In the absence of running, the data measure the spectral index to be [38]

$$n_s = 0.9649 \pm 0.0042, \quad (23.55)$$

corresponding to a deviation from scale-invariance exceeding the 7σ level. If running of the spectral tilt is included in the model, this is constrained to be [38]

$$\frac{dn_s}{d \ln k} = -0.0045 \pm 0.0067 \quad (23.56)$$

at the 95% CL, assuming no running of the running. A combined analysis of the *Planck* 2018 and BICEP2/Keck Array 2015 data [43] places an upper bound on the tensor-to-scalar ratio at $k = 0.002 \text{ Mpc}^{-1}$ [38]

$$r < 0.06 \quad (23.57)$$

at the 95% CL.

These observational bounds can be converted into bounds on the slow-roll parameters and hence the potential during slow-roll inflation. Setting higher-order slow-roll parameters (beyond second-order in horizon-flow parameters [44]) to zero, the *Planck* collaboration obtain the following 95% CL bounds when lensing and BK15 data are included [38]

$$\epsilon < 0.0044, \quad (23.58)$$

$$\eta = -0.015 \pm 0.006, \quad (23.59)$$

$$\xi^2 = 0.0029_{-0.0069}^{+0.0073}, \quad (23.60)$$

which can be used to constrain models, as discussed in the next Section.

Fig. 23.1, which is taken from [38], compares observational CMB constraints on the tilt, n_s , in the spectrum of scalar perturbations and the ratio, r , between the magnitudes of tensor and scalar perturbations. Important rôles are played by data from the *Planck* satellite and on lensing, the BICEP2/Keck Array (BK15) and measurements of baryon acoustic oscillations (BAO). The reader is referred to [38] for technical details. These experimental constraints are compared with the predictions of some

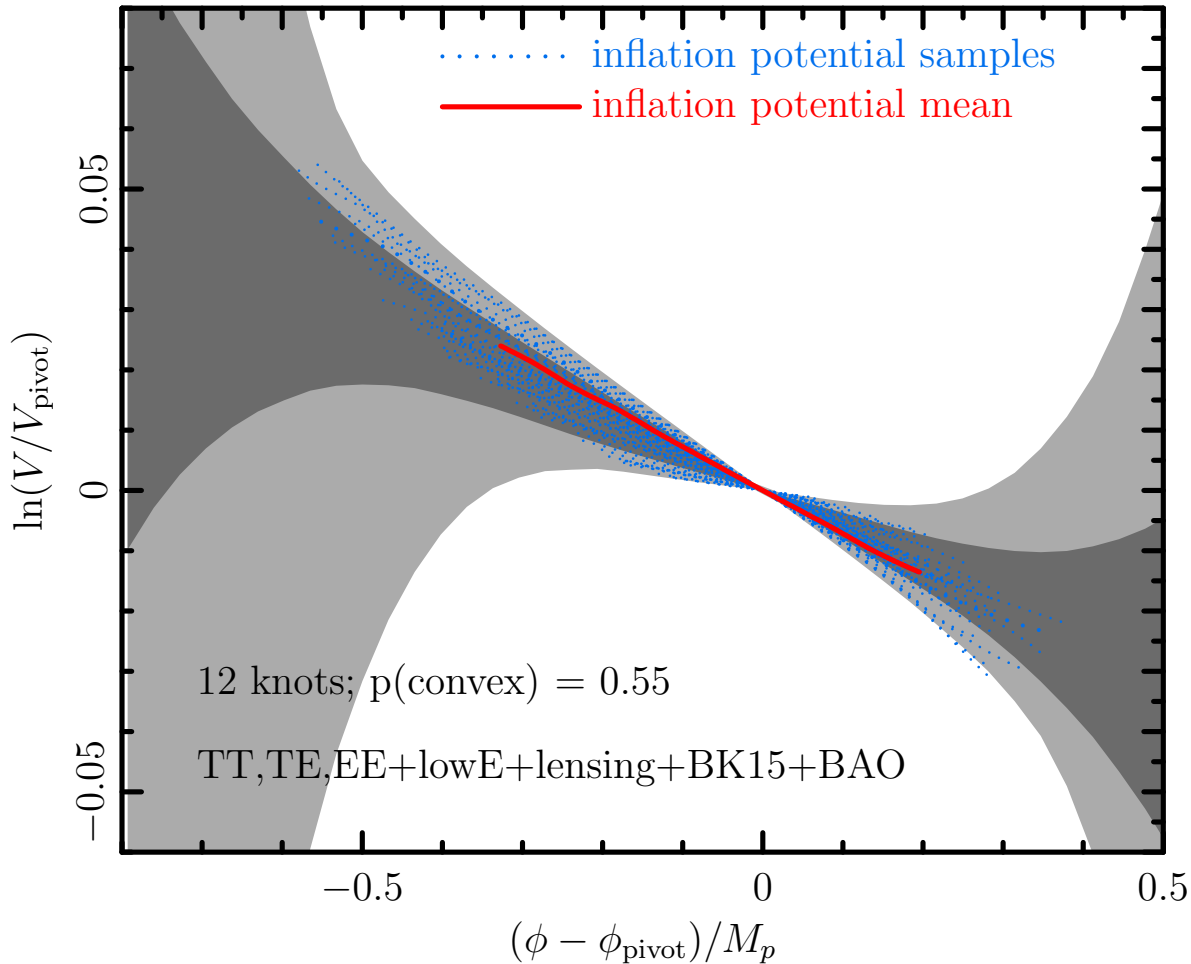


Figure 23.2: The result of reconstructing a single-field inflaton potential using a cubic-spline power-spectrum mode expansion and the the full *Planck*, lensing, BK15 and BAO data set. This figure is taken from [38].

of the inflationary models discussed in this review. Generally speaking, models with a concave potential are favored over those with a convex potential, and models with power-law inflation are now excluded, as opposed to models with de Sitter-like (quasi-)exponential expansion.

There is no significant evidence for local features within the range of inflaton field values probed by the data [38]. However, the data may be used to reconstruct partially the effective inflationary potential over a range of inflaton field values, assuming that it is suitably smooth. The result of one such exercise by the *Planck* collaboration [38] in the framework of a generic single-field inflaton potential is shown in Fig. 23.2. This reconstruction assumes a cubic-spline power-spectrum mode expansion and employs the full *Planck*, lensing, BK15 and BAO data set. The reader is again referred to [38] for technical details. We see that the effective inflaton potential is relatively well reconstructed over field values ϕ within ± 0.5 of the chosen pivot value, but the potential is only very weakly constrained for larger values of $|\phi - \phi_{pivot}|$, providing wide scope for inflationary model-builders.

23.4 Models

23.4.1 Pioneering Models

The paradigm of the inflationary Universe was proposed in [2], where it was pointed out that an early period of (near-)exponential expansion, in addition to resolving the horizon and flatness problems of conventional Big-Bang cosmology as discussed above (the possibility of a de Sitter phase in the early history of the Universe was also proposed in the non-minimal gravity model of [1], with the motivation of avoiding an initial singularity), would also dilute the prior abundance of any unseen heavy, (meta-)stable particles, as exemplified by monopoles

in grand unified theories (GUTs; see Chap. 94, “Grand Unified Theories” review). The original proposal was that this inflationary expansion took place while the Universe was in a metastable state (a similar suggestion was made in [45, 46], where in [45] it was also pointed out that such a mechanism could address the horizon problem) and was terminated by a first-order transition due to tunnelling through a potential barrier. However, it was recognized already in [2] that this ‘old inflation’ scenario would need modification if the transition to the post-inflationary universe were to be completed smoothly without generating unacceptable inhomogeneities.

This ‘graceful exit’ problem was addressed in the ‘new inflation’ model of [13] (see also [14] and footnote [39] of [2]), which studied models based on an SU(5) GUT with an effective potential of the Coleman-Weinberg type (i.e., dominated by radiative corrections), in which inflation could occur during the roll-down from the local maximum of the potential towards a global minimum. However, it was realized that the Universe would evolve to a different minimum from the Standard Model [47], and it was also recognized that density fluctuations would necessarily be too large [15], since they were related to the GUT coupling strength.

These early models of inflation assumed initial conditions enforced by thermal equilibrium in the early Universe. However, this assumption was questionable: indeed, it was not made in the model of [1], in which a higher-order gravitational curvature term was assumed to arise from quantum corrections, and the assumption of initial thermal equilibrium was jettisoned in the ‘chaotic’ inflationary model of [48]. These are the inspirations for much recent inflationary model building, so we now discuss them in more detail, before reviewing contemporary models.

In this section we will work in natural units where we set the reduced Planck mass to unity, i.e., $8\pi/M_P^2 = 1$. All masses are thus relative to the reduced Planck scale.

23.4.2 R^2 Inflation

The first-order Einstein-Hilbert action, $(1/2) \int d^4x \sqrt{-g} R$, where R is the Ricci scalar curvature, is the minimal possible theory consistent with general coordinate invariance. However, it is possible that there might be non-minimal corrections to this action, and the unique second-order possibility is

$$S = \frac{1}{2} \int d^4x \sqrt{-g} \left(R + \frac{R^2}{6M^2} \right). \quad (23.61)$$

It was pointed out in [1] that an R^2 term could be generated by quantum effects, and that (Eq. (23.61)) could lead to de Sitter-like expansion of the Universe. Scalar density perturbations in this model were calculated in [17]. Because the initial phase was (almost) de Sitter, these perturbations were (approximately) scale-invariant, with magnitude $\propto M$. It was pointed out in [17] that requiring the scalar density perturbations to lie in the range 10^{-3} to 10^{-5} , consistent with upper limits at that time, would require $M \sim 10^{-3}$ to 10^{-5} in Planck units, and it was further suggested that these perturbations could lead to the observed large-scale structure of the Universe, including the formation of galaxies.

Although the action (Eq. (23.61)) does not contain an explicit scalar field, [17] reduced the calculation of density perturbations to that of fluctuations in the scalar curvature R , which could be identified (up to a factor) with a scalar field of mass M . The formal equivalence of R^2 gravity (Eq. (23.61)) to a theory of gravity with a massive scalar ϕ had been shown in [18], see also [19]. The effective scalar potential for what we would nowadays call the ‘inflaton’ [49] takes the form

$$S = \frac{1}{2} \int d^4x \sqrt{-g} \left[R + (\partial_\mu \phi)^2 - \frac{3}{2} M^2 (1 - e^{-\sqrt{2/3} \phi})^2 \right] \quad (23.62)$$

when the action is written in the Einstein frame, and the potential is shown as the solid black line in Fig. 23.3. Using (Eq. (23.48)), one finds that the amplitude of the scalar density perturbations in this model is given by

$$\Delta_{\mathcal{R}} = \frac{3M^2}{8\pi^2} \sinh^4 \left(\frac{\phi}{\sqrt{6}} \right), \quad (23.63)$$

The measured magnitude of the density fluctuations in the CMB requires $M \simeq 1.3 \times 10^{-5}$ in Planck units (assuming $N_* \simeq 55$), so one of the open questions in this model is why M is so small. Obtaining $N_* \simeq 55$ also requires an initial value of $\phi \simeq 5.5$, i.e., a super-Planckian initial condition, and another issue for this and many other models is how the form of the effective potential is protected and remains valid at such large field values. Using Eq. (23.51) one finds that $n_s \simeq 0.965$ for $N_* \simeq 55$ and using (Eq. (23.49)) one finds that $r \simeq 0.0035$. These predictions are consistent with the present data from *Planck* and other experiments, as seen in Fig. 23.1.

23.4.3 Chaotic Models with Power-Law Potentials

As has already been mentioned, a key innovation in inflationary model-building was the suggestion to abandon the questionable assumption of a thermal initial state, and consider ‘chaotic’ initial conditions with very general forms of potential [48]. (Indeed, the R^2 model discussed above can be regarded as a prototype of this approach.) The chaotic approach was first proposed in the context of a simple power-law potential of the form $\mu^{4-\alpha} \phi^\alpha$, and the specific example of $\lambda \phi^4$ was studied in [48]. Such models make the following predictions for the slow-roll parameters ϵ and η :

$$\epsilon = \frac{1}{2} \left(\frac{\alpha}{\phi} \right)^2, \quad \eta = \frac{\alpha(\alpha-1)}{\phi^2}, \quad (23.64)$$

leading to the predictions

$$r \approx \frac{4\alpha}{N_*}, \quad n_s - 1 \approx -\frac{\alpha+2}{2N_*}, \quad (23.65)$$

which are shown in Fig. 23.1 for some illustrative values of α . We note that the prediction of the original ϕ^4 model lies out of the frame, with values of r that are too large and values of n_s that are too small. The ϕ^3 model has similar problems, and would in any case require modification in order to have a well-defined minimum. The simplest possibility is ϕ^2 , but this is now also disfavored by the data, at the 95% CL if only the *Planck* data are considered, and more strongly if other data are included, as seen in Fig. 23.1. (For non-minimal models of quadratic inflation that avoid this problem, see, e.g., [51].)

Indeed, as can be seen in Fig. 23.1, all single-field models with a convex potential (i.e., one curving upwards) are disfavored compared to models with a concave potential.

23.4.4 Hilltop Models

This preference for a concave potential motivates interest in ‘hilltop’ models [52], whose starting-point is a potential of the form

$$V(\phi) = \Lambda^4 \left[1 - \left(\frac{\phi}{\mu} \right)^p + \dots \right], \quad (23.66)$$

where the \dots represent extra terms that yield a positive semi-definite potential. To first order in the slow-roll parameters, when $x \equiv \phi/\mu$ is small, one has

$$n_s \simeq 1 - p(p-1)\mu^{-2} \frac{x^{p-2}}{(1-x^p)} - \frac{3}{8}r, \quad r \simeq 8p^2\mu^{-2} \frac{x^{2p-2}}{(1-x^p)^2}. \quad (23.67)$$

As seen in Fig. 23.1, a hilltop model with $p = 4$ can be compatible with the *Planck* and other measurements, if $\mu \gg M_P$.

23.4.5 D-Brane Inflation

Many scenarios for inflation involving extra dimensions have been proposed, e.g., the possibility that observable physics resides on a three-dimensional brane, and that there is an inflationary potential that depends on the distance between our brane and an antibrane, with a potential of the form [53]

$$V(\phi) = \Lambda^4 \left[1 - \left(\frac{\mu}{\phi} \right)^p + \dots \right]. \quad (23.68)$$

In this scenario the effective potential vanishes in the limit $\phi \rightarrow \infty$, corresponding to complete separation between our brane and the antibrane. The predictions for n_s and r in this model can be obtained from (Eq. 23.67) by exchanging $p \leftrightarrow -p$, and are also consistent with the *Planck* and other data.

23.4.6 Natural Inflation

Also seen in Fig. 23.1 are the predictions of ‘natural inflation’ [54], in which one postulates a non-perturbative shift symmetry that suppresses quantum corrections, so that a hierarchically small scale of inflation, $H \ll M_P$, is technically natural. In the simplest models, there is a periodic potential of the form

$$V(\phi) = \Lambda^4 \left[1 + \cos \left(\frac{\phi}{f} \right) \right], \quad (23.69)$$

where f is a dimensional parameter reminiscent of an axion decay constant (see the next subsection) [55], which must have a value $> M_P$. Natural inflation can yield predictions similar to quadratic inflation (which are no longer favored, as already discussed), but can also yield an effective convex potential. Thus, it may lead to values of r that are acceptably small, but for values of n_s that are in tension with the data, as seen in Fig. 23.1.

23.4.7 Axion Monodromy Models

The effective potentials in stringy models [56,57] motivated by axion monodromy may be of the form

$$V(\phi) = \mu^{4-\alpha} \phi^\alpha + \Lambda^4 e^{-C \left(\frac{\phi}{\phi_0} \right)^{p_\Lambda}} \cos \left[\gamma + \frac{\phi}{f} \left(\frac{\phi}{\phi_0} \right)^{p_f+1} \right], \quad (23.70)$$

where μ, Λ, f and ϕ_0 are parameters with the dimension of mass, and C, p, p_Λ, p_f and γ are dimensionless constants, generalizing the potential ([54]) in the simplest models of natural inflation. The oscillations in (Eq. 23.70) are associated with the axion field, and powers $p_\Lambda, p_f \neq 0$ may arise from ϕ -dependent evolutions of

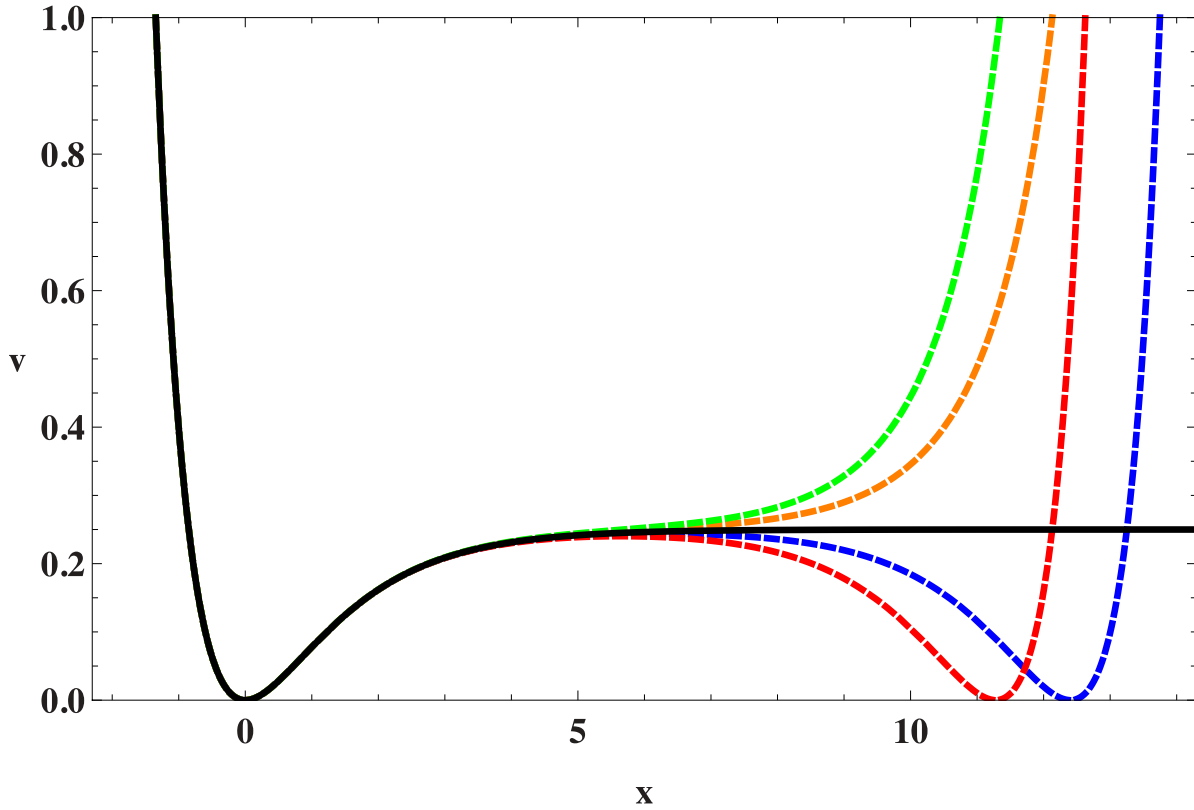


Figure 23.3: The inflationary potential V in the R^2 model (solid black line) compared with its form in various no-scale models discussed in detail in [50] (dashed coloured lines).

string moduli. Since the exponential prefactor in (Eq. 23.70) is due to non-perturbative effects that may be strongly suppressed, the oscillations may be unobservably small. Specific string models having ϕ^α with $\alpha = 4/3, 1$ or $2/3$ have been constructed in [56,57], providing some motivation for the low-power models mentioned above.

As seen in Fig. 23.1, the simple axion monodromy models with the power $\alpha = 4/3$ or 1 are no longer compatible with the current CMB data at the 95% CL, while $\alpha = 2/3$ is only marginally compatible at 95% CL. The *Planck* Collaboration has also searched for characteristic effects associated with the second term in (Eq. (23.70)), such as a possible drift in the modulation amplitude (setting $p_A = C = 0$), and a possible drifting frequency generated by $p_f \neq 0$, without finding any compelling evidence [38].

23.4.8 Higgs Inflation

Since the energy scale during inflation is commonly expected to lie between the Planck and TeV scales, it may serve as a useful bridge with contacts both to string theory or some other quantum theory of gravity, on the one side, and particle physics on the other side. However, as the above discussion shows, much of the activity in building models of inflation has been largely independent of specific connections with these subjects, though some examples of string-motivated models of inflation were mentioned above.

The most economical scenario for inflation might be to use as inflaton the only established scalar field, namely the Higgs field (see Chap.11, “Status of Higgs boson physics” review). A specific model assuming a non-minimal coupling of the Higgs field h to gravity was constructed in [58]. Its starting-point is the action

$$S = \int d^4x \sqrt{-g} \left[\frac{M^2 + \xi h^2}{2} R + \frac{1}{2} \partial_\mu h \partial^\mu h - \frac{\lambda}{4} (h^2 - v^2)^2 \right], \tag{23.71}$$

where v is the Higgs vacuum expectation value. The model requires $\xi \gg 1$, in which case it can be rewritten in the Einstein

frame as

$$S = \int d^4x \sqrt{-g} \left[\frac{1}{2} R + \frac{1}{2} \partial_\mu \chi \partial^\mu \chi - U(\chi) \right], \tag{23.72}$$

where the effective potential for the canonically-normalized inflaton field χ has the form

$$U(\chi) = \frac{\lambda}{4\xi^2} \left[1 + \exp\left(-\frac{2\chi}{\sqrt{6}M_P}\right) \right]^{-2}, \tag{23.73}$$

which is similar to the effective potential of the R^2 model at large field values. As such, the model inflates successfully if $\xi \simeq 5 \times 10^4 m_h/(\sqrt{2}v)$, with predictions for n_s and r that are indistinguishable from the predictions of the R^2 model shown in Fig. 23.1.

This model is very appealing, but must confront several issues. One is to understand the value of ξ , and another is the possibility of unitarity violation. However, a more fundamental issue is whether the effective quartic Higgs coupling is positive at the scale of the Higgs field during inflation. Extrapolations of the effective potential in the Standard Model using the measured values of the masses of the Higgs boson and the top quark indicate that probably $\lambda < 0$ at this scale [59], though there are still significant uncertainties associated with the appropriate input value of the top mass and the extrapolation to high renormalization scales.

23.4.9 Supersymmetric Models of Inflation

Supersymmetry [60] is widely considered to be a well-motivated possible extension of the Standard Model that might become apparent at the TeV scale. It is therefore natural to consider supersymmetric models of inflation. These were originally proposed because of the problems of the the new inflationary theory [13,14] based on the one-loop (Coleman-Weinberg) potential for breaking $SU(5)$. Several of these problems are related to the magnitude of the effective potential parameters: in any model of inflation based on an elementary scalar field, some parameter in the effective potential must be small in natural units, e.g., the quartic coupling

λ in a chaotic model with a quartic potential, or the mass parameter μ in a model of chaotic quadratic inflation. These parameters are renormalized multiplicatively in a supersymmetric theory, so that the quantum corrections to small values would be under control. Hence it was suggested that inflation cries out for supersymmetry [61], though non-supersymmetric resolutions of the problems of Coleman-Weinberg inflation are also possible: see, e.g., Ref. [62].

In the Standard Model there is only one scalar field that could be a candidate for the inflaton, namely the Higgs field discussed above, but even the minimal supersymmetric extension of the Standard Model (MSSM) contains many scalar fields. However, none of these is a promising candidate for the inflaton. The minimal extension of the MSSM that may contain a suitable candidate is the supersymmetric version of the minimal seesaw model of neutrino masses, which contains the three supersymmetric partners of the heavy singlet (right-handed) neutrinos. One of these singlet sneutrinos $\tilde{\nu}$ could be the inflaton [63]: it would have a quadratic potential, the mass coefficient required would be $\sim 10^{13}$ GeV, very much in the expected ball-park for singlet (right-handed) neutrino masses, and sneutrino inflaton decays also could give rise to the cosmological baryon asymmetry via leptogenesis. However, as seen in Fig. 23.1 and already discussed, a purely quadratic inflationary potential is no longer favored by the data. This difficulty could in principle be resolved in models with multiple sneutrinos [64], or by postulating a trilinear sneutrino coupling and hence a superpotential of Wess-Zumino type [65], which can yield successful inflation with predictions intermediate between those of natural inflation and hilltop inflation in Fig. 23.1.

Finally, we note that it is also possible to obtain inflation via supersymmetry breaking, as in the model [66] whose predictions are illustrated in Fig. 23.1.

23.4.10 Supergravity Models

Any model of early-Universe cosmology, and specifically inflation, must necessarily incorporate gravity. In the context of supersymmetry this requires an embedding in some supergravity theory [67, 68]. An $\mathcal{N} = 1$ supergravity theory is specified by three functions: a Hermitian function of the matter scalar fields ϕ^i , called the Kähler potential K , that describes its geometry, a holomorphic function of the superfields, called the superpotential W , which describes their interactions, and another holomorphic function $f_{\alpha\beta}$, which describes their couplings to gauge fields V_α [69].

The simplest possibility is that the Kähler metric is flat:

$$K = \phi^i \phi_i^*, \quad (23.74)$$

where the sum is over all scalar fields in the theory, and the simplest inflationary model in minimal supergravity had the superpotential [70]

$$W = m^2(1 - \phi)^2, \quad (23.75)$$

Where ϕ is the inflaton. However, this model predicts a tilted scalar perturbation spectrum, $n_s = 0.933$, which is now in serious disagreement with the data from *Planck* and other experiments shown in Fig. 23.1.

Moreover, there is a general problem that arises in any supergravity theory coupled to matter, namely that, since its effective scalar potential contains a factor of e^K , scalars typically receive squared masses $\propto H^2 \sim V$, where H is the Hubble parameter [71], an issue called the ‘ η problem’. The theory given by (Eq. (23.75)) avoids this η problem, but a generic supergravity inflationary model encounters this problem of a large inflaton mass. Moreover, there are additional challenges for supergravity inflation associated with the spontaneous breaking of local supersymmetry [72–74].

Various approaches to the η problem in supergravity have been proposed, including the possibility of a shift symmetry [75], and one possibility that has attracted renewed attention recently is no-scale supergravity [76, 77]. This is a form of supergravity with a Kähler potential that can be written in the form [78]

$$K = -3 \ln \left(T + T^* - \frac{\sum_i |\phi^i|^2}{3} \right), \quad (23.76)$$

which has the special property that it naturally has a flat potential, at the classical level and before specifying a non-trivial superpotential. As such, no-scale supergravity is well-suited for constructing models of inflation. Adding to its attraction is the feature that compactifications of string theory to supersymmetric four-dimensional models yield effective supergravity theories of the no-scale type [79]. There are many examples of superpotentials that yield effective inflationary potentials for either the T field (which is akin to a modulus field in some string compactification) or a ϕ field (generically representing matter) that are of the same form as the effective potential of the R^2 model (Eq. (23.62)) when the magnitude of the inflaton field $\gg 1$ in Planck units, as required to obtain sufficiently many e-folds of inflation, N_* [80, 81]. This framework also offers the possibility of using a suitable superpotential to construct models with effective potentials that are similar, but not identical, to the R^2 model, as shown by the dashed coloured lines in Fig. 23.3.

23.4.11 Other Exponential Potential Models

This framework also offers the possibility [80] of constructing models in which the asymptotic constant value of the potential at large inflaton field values is approached via a different exponentially-suppressed term:

$$V(\phi) = A \left[1 - \delta e^{-B\phi} + \mathcal{O}(e^{-2B\phi}) \right], \quad (23.77)$$

where the magnitude of the scalar density perturbations fixes A , but δ and B are regarded as free parameters. In the case of R^2 inflation $\delta = 2$ and $B = \sqrt{2/3}$. In a model such as (Eq. (23.77)), one finds at leading order in the small quantity $e^{-B\phi}$ that

$$\begin{aligned} n_s &= 1 - 2B^2 \delta e^{-B\phi}, \\ r &= 8B^2 \delta^2 e^{-2B\phi}, \\ N_* &= \frac{1}{B^2 \delta} e^{+B\phi}. \end{aligned} \quad (23.78)$$

yielding the relations

$$n_s = 1 - \frac{2}{N_*}, \quad r = \frac{8}{B^2 N_*^2}. \quad (23.79)$$

This model leads to the class of predictions labelled by ‘ α attractors’ [82] in Fig. 23.1. There are generalizations of the simplest no-scale model (Eq. (23.76)) with prefactors before the $\ln(\dots)$ that are 1 or 2, leading to larger values of $B = \sqrt{2}$ or 1, respectively, and hence smaller values of r than in the R^2 model.

23.5 Model Comparison

Given a particular inflationary model, one can obtain constraints on the model parameters, informed by the likelihood, corresponding to the probability of the data given a particular choice of parameters (see Sec. 40, ‘Statistics’ review). In the light of the detailed constraints on the statistical distribution of primordial perturbations now inferred from high-precision observations of the cosmic microwave background, it is also possible to make quantitative comparison of the statistical evidence for or against different inflationary models. This can be done either by comparing the logarithm of the maximum likelihood that can be obtained for the data using each model, i.e., the minimum χ^2 (with some correction for the number of free parameters in each model), or by a Bayesian model comparison [83] (see also Sec. 40.3.3 in ‘Statistics’ review).

In such a Bayesian model comparison one computes [7] the evidence, $\mathcal{E}(\mathcal{D}|\mathcal{M}_A)$ for a model, \mathcal{M}_A , given the data \mathcal{D} . This corresponds to the likelihood, $\mathcal{L}(\theta_{Aj}) = p(\mathcal{D}|\theta_{Aj}, \mathcal{M}_A)$, integrated over the assumed prior distribution, $\pi(\theta_{Aj}|\mathcal{M}_A)$, for all the model parameters θ_{Aj} :

$$\mathcal{E}(\mathcal{D}|\mathcal{M}_A) = \int \mathcal{L}(\theta_{Aj}) \pi(\theta_{Aj}|\mathcal{M}_A) d\theta_{Aj}. \quad (23.80)$$

The posterior probability of the model given the data follows from Bayes’ theorem

$$p(\mathcal{M}_A|\mathcal{D}) = \frac{\mathcal{E}(\mathcal{D}|\mathcal{M}_A) \pi(\mathcal{M}_A)}{p(\mathcal{D})}, \quad (23.81)$$

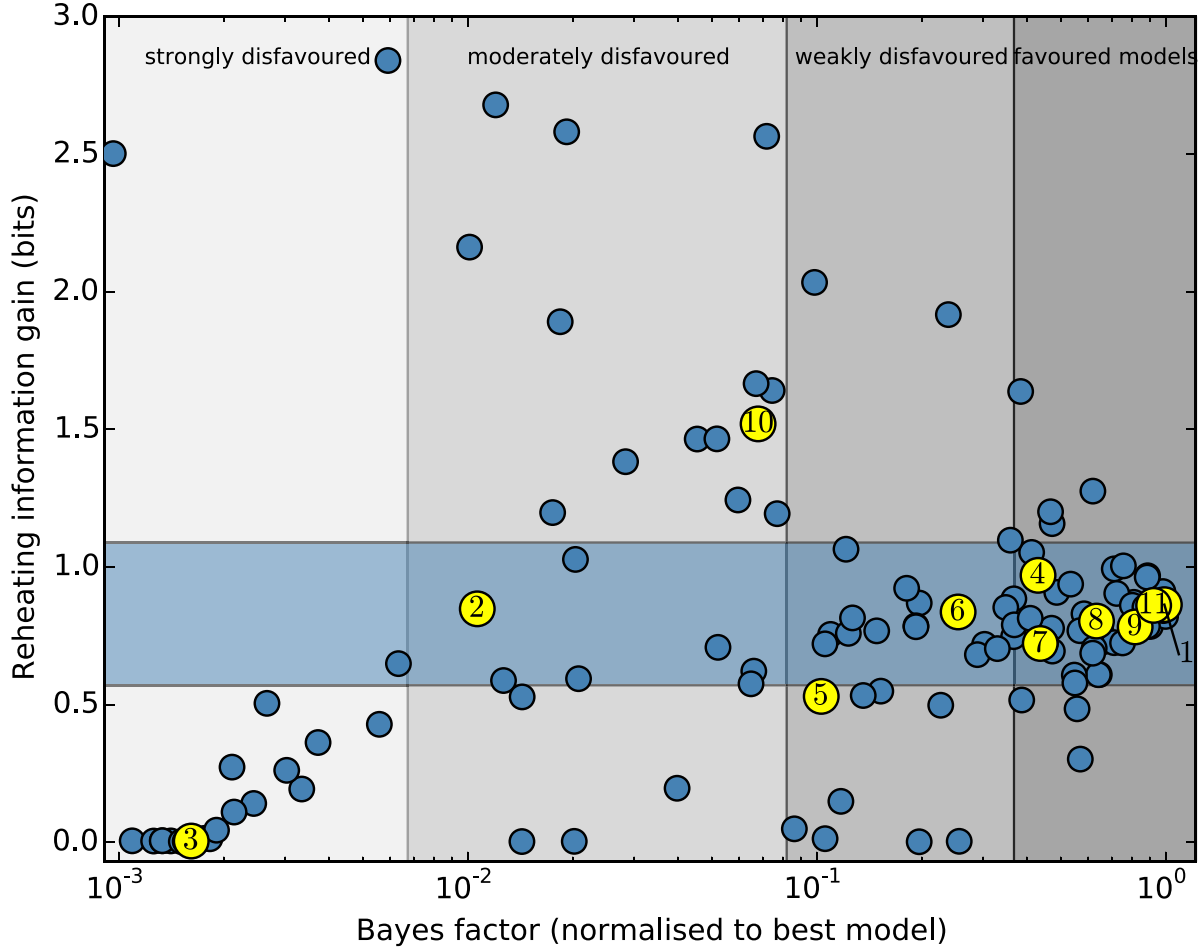


Figure 23.4: The Bayes factors calculated in [84] for a large sample of inflationary models using *Planck* 2015 data [85]. Those highlighted in yellow are featured in this review, according to the numbers listed in the text.

where the prior probability of the model is given by $\pi(\mathcal{M}_A)$. Assuming that all models are equally likely a priori, $\pi(\mathcal{M}_A) = \pi(\mathcal{M}_B)$, the relative probability of model A relative to a reference model, in the light of the data, is thus given by the Bayes factor

$$B_{A,ref} = \frac{\mathcal{E}(\mathcal{D}|\mathcal{M}_A)}{\mathcal{E}(\mathcal{D}|\mathcal{M}_{ref})}. \quad (23.82)$$

Computation of the multi-dimensional integral (Eq. (23.80)) is a challenging numerical task. Even using an efficient sampling algorithm requires hundreds of thousands of likelihood computations for each model, though slow-roll approximations can be used to calculate rapidly the primordial power spectrum using the APSIC numerical library [7] for a large number of single-field, slow-roll inflation models.

The change in χ^2 for selected slow-roll models relative to the Starobinsky R^2 inflationary model, used as a reference, is given in Table 23.1 (taken from [38]). All the other inflation models require a substantial amplitude of tensor modes, and so have an increased χ^2 with respect to the Starobinsky and other models with a scalar tilt but small tensor modes. Table 23.1 also shows the Bayesian evidence for ($\ln B_{A,ref} > 0$) or against ($\ln B_{A,ref} < 0$) a selection of inflation models using the *Planck* analysis priors [38]. The Starobinsky R^2 inflationary model may be chosen as a reference [38] that provides a good fit to current data. Higgs inflation [58] is indistinguishable using current data, making the model comparison “inconclusive” on the Jeffrey’s scale ($|\ln B_{A,ref}| < 1$). (Recall, though, that this model is disfavoured by the measured values of the Higgs and top quark masses [59].) We note that although α -attractor models can provide a good fit to the data, they are disfavoured relative to the Starobinsky model due to their larger prior volume. There is now strong evidence

($|\ln B_{A,ref}| > 5$) against large-field models such as chaotic inflation with a quadratic or a quartic potential. Indeed, over 30% of the slow-roll inflation models considered in Ref. [7] are strongly disfavoured by the *Planck* data.

Table 23.1: Observational evidence for and against selected inflation models: $\Delta\chi^2$ and the Bayes factors are calculated relative to the Starobinsky R^2 inflationary model, which is treated as a reference. Results from *Planck* 2018 analysis [38].

Model	$\Delta\chi^2$	$\ln B_{A,ref}$
R^2 inflation	0	0
Power-law potential $\phi^{2/3}$	+4.0	-4.6
Power-law potential ϕ^2	+21.6	< -10
Power-law potential ϕ^4	+75.3	< -10
Natural inflation	+9.9	-6.6
Hilltop quartic model	-0.3	-1.4

The Bayes factors for a wide selection of slow-roll inflationary models are displayed in Fig. 23.4, which is adapted from Fig. 3 in [84], where more complete descriptions of the models and the calculations of the Bayes factors using *Planck* 2015 data [85] are given. Models discussed in this review are highlighted in yellow, and numbered as follows: (1) R^2 inflation (Sec. 23.4.2) and models with similar predictions, such as Higgs inflation (Sec. 23.4.8) and no-scale supergravity inflation (Sec. 23.4.10); chaotic inflation models (2) with a ϕ^2 potential; (3) with a ϕ^4 potential; (4) with a $\phi^{2/3}$ potential, and (5) with a ϕ^p potential marginalising over $p \in [0.2, 6]$ (Sec. 23.4.3); hilltop inflation models (6) with $p = 2$;

(7) with $p = 4$ and (8) marginalising over p (Sec. 23.4.4); (9) brane inflation (Sec. 23.4.5); (10) natural inflation (Sec. 23.4.6); (11) exponential potential models such as α -attractors (Sec. 23.4.11). As seen in Fig. 23.4 and discussed in the next Section, constraints on reheating are starting to provide additional information about models of inflation.

23.6 Constraints on Reheating

One connection between inflation and particle physics is provided by inflaton decay, whose products are expected to have thermalized subsequently. As seen in (Eq. (23.54)), the number of e-folds required during inflation depends on details of this reheating process, including the matter density upon reheating, denoted by ρ_{th} , which depends in turn on the inflaton decay rate Γ_ϕ . We see in Fig. 23.1 that, within any specific inflationary model, both n_s and particularly r are sensitive to the value of N_* . In particular, the one- σ uncertainty in the experimental measurement of n_s is comparable to the variation in many model predictions for $N_* \in [50, 60]$. This implies that the data start to constrain scenarios for inflaton decay in many models. For example, it is clear from Fig. 23.1 that $N_* = 60$ would be preferred over $N_* = 50$ in a chaotic inflationary model with a quadratic potential.

As a specific example, let us consider R^2 models and related models such as Higgs and no-scale inflation models that predict small values of r [86]. As seen in Fig. 23.1, within these models the combination of *Planck*, BICEP2/Keck Array and BAO data would require a limited range of n_s , corresponding to a limited range of N_* , as seen by comparing the left and right vertical axes in Fig. 23.5:

$$N_* \gtrsim 52 \quad (68\% \text{ CL}), \quad N_* \gtrsim 44 \quad (95\% \text{ CL}). \quad (23.83)$$

Within any specific model for inflaton decay, these bounds can be translated into constraints on the effective decay coupling. For example, if one postulates a two-body inflaton decay coupling y , the bounds (Eq. (23.83)) can be translated into bounds on y . This is illustrated in Fig. 23.5, where any value of N_* (on the left vertical axis), projected onto the diagonal line representing the correlation predicted in R^2 -like models, corresponds to a specific value of the inflaton decay rate Γ_ϕ/m (lower horizontal axis) and hence y (upper horizontal axis):

$$y \gtrsim 10^{-5} \quad (68\% \text{ CL}), \quad y \gtrsim 10^{-15} \quad (95\% \text{ CL}). \quad (23.84)$$

These bounds are not very constraining – although the 68% CL lower bound on y is already comparable with the electron Yukawa coupling – but can be expected to improve significantly in the coming years and thereby provide significant information on the connections between inflation and particle physics.

23.7 Beyond Single-Field Slow-Roll Inflation

There are numerous possible scenarios beyond the simplest single-field models of slow-roll inflation. These include theories in which non-canonical fields are considered, such as k-inflation [87] or DBI inflation [88], and multiple-field models, such as the curvaton scenario [89]. As well as altering the single-field predictions for the primordial curvature power spectrum (Eq. (23.48)) and the tensor-scalar ratio (Eq. (23.49)), they may introduce new quantities that vanish in single-field slow-roll models, such as isocurvature matter perturbations, corresponding to entropy fluctuations in the photon-to-matter ratio, at first order:

$$S_m = \frac{\delta n_m}{n_m} - \frac{\delta n_\gamma}{n_\gamma} = \frac{\delta \rho_m}{\rho_m} - \frac{3}{4} \frac{\delta \rho_\gamma}{\rho_\gamma}. \quad (23.85)$$

Another possibility is non-Gaussianity in the distribution of the primordial curvature perturbation (see Chap. 29, “Cosmic Microwave Background” review), encoded in higher-order correlators such as the primordial bispectrum [90]

$$\langle \zeta(\mathbf{k})\zeta(\mathbf{k}')\zeta(\mathbf{k}'') \rangle \equiv (2\pi)^3 \delta(\mathbf{k} + \mathbf{k}' + \mathbf{k}'') B_\zeta(k, k', k''), \quad (23.86)$$

which is often expressed in terms of a dimensionless non-linearity parameter

$$f_{NL} \propto B_\zeta(k, k', k'')/P_\zeta(k)P_\zeta(k').$$

The three-point function (Eq. (23.86)) can be thought of as defined on a triangle whose sides are $\mathbf{k}, \mathbf{k}', \mathbf{k}''$, of which only two are independent, since they sum to zero. Further assuming statistical isotropy ensures that the bispectrum depends only on the magnitudes of the three vectors, k, k' and k'' . The search for f_{NL} and other non-Gaussian effects was a prime objective of the *Planck* data analysis [91, 92].

23.7.1 Effective Field Theory of Inflation

Since slow-roll inflation is a phase of accelerated expansion with an almost constant Hubble parameter, one may think of inflation in terms of an effective theory where the de Sitter spacetime symmetry is spontaneously broken down to RW symmetry by the time-evolution of the Hubble rate, $\dot{H} \neq 0$. There is then a Goldstone boson, π , associated with the spontaneous breaking of time-translation invariance, which can be used to study model-independent properties of inflation. The Goldstone boson describes a spacetime-dependent shift of the time coordinate, corresponding to an adiabatic perturbation of the matter fields:

$$\delta\phi_i(t, \vec{x}) = \phi_i(t + \pi(t, \vec{x})) - \phi_i(t). \quad (23.87)$$

Thus adiabatic field fluctuations can be absorbed into the spatial metric perturbation, \mathcal{R} in Eq. (23.28) at first order, in the comoving gauge:

$$\mathcal{R} = -H\pi, \quad (23.88)$$

where we define π on spatially-flat hypersurfaces. In terms of inflaton field fluctuations, we can identify $\pi \equiv \delta\phi/\dot{\phi}$, but in principle this analysis is not restricted to inflation driven by scalar fields.

The low-energy effective action for π can be obtained by writing down the most general Lorentz-invariant action and expanding in terms of π . The second-order effective action for the free-field wave modes, π_k , to leading order in slow roll is then

$$S_\pi^{(2)} = - \int d^4x \sqrt{-g} \frac{M_P^2 \dot{H}}{c_s^2} \left[\dot{\pi}_k^2 - \frac{c_s^2}{R^2} (\nabla\pi)^2 \right], \quad (23.89)$$

where ϵ_H is the Hubble slow-roll parameter (Eq. (23.11)). We identify c_s^2 with an effective sound speed, generalising canonical slow-roll inflation, which is recovered in the limit $c_s^2 \rightarrow 1$.

The scalar power spectrum on super-Hubble scales (Eq. (23.48)) is enhanced for a reduced sound speed, leading to a reduced tensor-scalar ratio (Eq. (23.49))

$$\mathcal{P}_\zeta(k) \simeq \frac{4\pi}{M_P^2} \frac{1}{c_s^2 \epsilon} \left(\frac{H}{2\pi} \right)^2, \quad r \simeq 16(c_s^2 \epsilon)_*. \quad (23.90)$$

At third perturbative order and to lowest order in derivatives, one obtains [94]

$$S_\pi^{(3)} = \int d^4x \sqrt{-g} \frac{M_P^2 (1 - c_s^2) \dot{H}}{c_s^2} \left[\frac{\dot{\pi} (\nabla\pi)^2}{R^2} - \left(1 + \frac{2}{3} \frac{\tilde{c}_3}{c_s^2} \right) \dot{\pi}^3 \right]. \quad (23.91)$$

Note that this expression vanishes for canonical fields with $c_s^2 = 1$. For $c_s^2 \neq 1$ the cubic action is determined by the sound speed and an additional parameter \tilde{c}_3 . Both terms in the cubic action give rise to primordial bispectra that are well approximated by equilateral bispectra. However, the shapes are not identical, so one can find a linear combination for which the equilateral bispectra of each term cancel, giving rise to a distinctive orthogonal-type bispectrum [94].

Analysis based on *Planck* 2018 temperature and polarization data has placed bounds on several bispectrum shapes including equilateral and orthogonal shapes [92]:

$$f_{NL}^{equil} = -26 \pm 47, \quad f_{NL}^{orthog} = -38 \pm 24 \quad (68\% \text{ CL}). \quad (23.92)$$

For the simplest case of a constant sound speed, and marginalising over \tilde{c}_3 , this provides a bound on the inflaton sound speed [92]

$$c_s \geq 0.021 \quad (95\% \text{ CL}). \quad (23.93)$$

For a specific model such as DBI inflation [88], corresponding to $\tilde{c}_3 = 3(1 - c_s^2)/2$, one obtains a tighter bound [92]:

$$c_s^{DBI} \geq 0.086 \quad (95\% \text{ CL}). \quad (23.94)$$

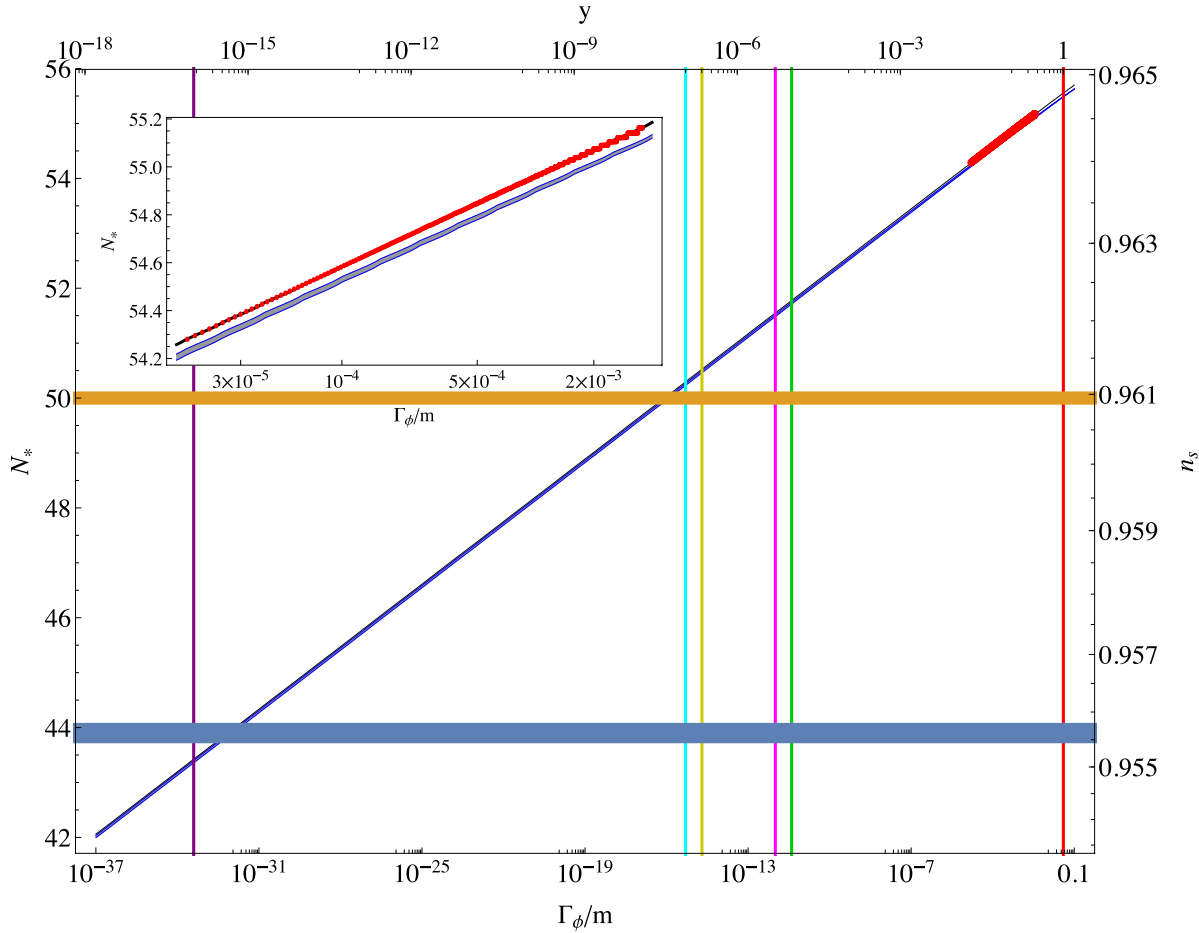


Figure 23.5: The values of N_* (left axis) and n_s (right axis) in R^2 inflation and related models for a wide range of decay rates, Γ_ϕ/m , (bottom axis) and corresponding two-body couplings, y (top axis). The diagonal red line segment shows full numerical results over a restricted range of Γ_ϕ/m (which are shown in more detail in the insert), while the diagonal blue strip represents an analytical approximation described in [86]. The difference between these results is indistinguishable in the main plot, but is visible in the insert. The horizontal yellow and blue lines show the 68 and 95% CL lower limits from the *Planck* 2015 data [85], and the vertical coloured lines correspond to specific models of inflaton decay. Figure taken from [93].

The *Planck* team have analysed a wide range of non-Gaussian templates from different inflation models, including tests for deviations from an initial Bunch-Davies vacuum state, direction-dependent non-Gaussianity, and feature models with oscillatory bispectra [92]. No individual feature or resonance is above the three- σ significance level after accounting for the look-elsewhere effect. These results are consistent with the simplest canonical, slow-roll inflation models, but do not rule out most alternative models; rather, bounds on primordial non-Gaussianity place important constraints on the parameter space for non-canonical models.

23.7.2 Multi-Field Fluctuations

There is a very large literature on two- and multi-field models of inflation, most of which lies beyond the scope of this review [95, 96]. However, two important general topics merit being mentioned here, namely residual isocurvature perturbations and the possibility of non-Gaussian effects in the primordial perturbations.

One might expect that other scalar fields besides the inflaton might have non-negligible values that evolve and fluctuate in parallel with the inflaton, without necessarily making the dominant contribution to the energy density during the inflationary epoch. However, the energy density in such a field might persist beyond the end of inflation before decaying, at which point it might come to dominate (or at least make a non-negligible contribution to) the total energy density. In such a case, its perturbations could end up generating the density perturbations detected in the CMB.

This could occur due to a late-decaying scalar field [89] or a field fluctuation that modulates the end of inflation [97] or the inflaton decay [98].

23.7.2.1 Isocurvature Perturbations

Primordial perturbations arising in single-field slow-roll inflation are necessarily adiabatic, i.e., they affect the overall density without changing the ratios of different contributions, such as the photon-matter ratio, $\delta(n_\gamma/n_m)/(n_\gamma/n_m)$. This is because inflaton perturbations represent a local shift of the time, as described in section Sec. 23.7.1:

$$\pi = \frac{\delta n_\gamma}{\dot{n}_\gamma} = \frac{\delta n_m}{\dot{n}_m}. \quad (23.95)$$

However, any light scalar field (i.e., one with effective mass less than the Hubble scale) acquires a spectrum of nearly scale-invariant perturbations during inflation. Fluctuations orthogonal to the inflaton in field space are decoupled from the inflaton at Hubble-exit, but can affect the subsequent evolution of the density perturbation. In particular, they can give rise to local variations in the equation of state (non-adiabatic pressure perturbations) that can alter the primordial curvature perturbation ζ on super-Hubble scales. Since these fluctuations are statistically independent of the inflaton perturbations at leading order in slow-roll [96], non-adiabatic field fluctuations can only increase the scalar power spectrum with respect to adiabatic perturbations at Hubble exit, while leaving the tensor modes unaffected at first perturbative order. Thus the single-field result for the

tensor-scalar ratio (Eq. (23.49)) becomes an inequality [99]

$$r \leq 16\epsilon_* . \quad (23.96)$$

Hence an observational upper bound on the tensor-scalar ratio does not bound the slow-roll parameter ϵ in multi-field models.

If all the scalar fields present during inflation eventually decay completely into fully thermalized radiation, these field fluctuations are converted fully into adiabatic perturbations in the primordial plasma [100]. On the other hand, non-adiabatic field fluctuations can also leave behind primordial isocurvature perturbations (Eq. (23.85)) after inflation. In multi-field inflation models it is thus possible for non-adiabatic field fluctuations to generate both curvature and isocurvature perturbations leading to correlated primordial perturbations [101].

The amplitudes of any primordial isocurvature perturbations (Eq. (23.85)) are strongly constrained by the current CMB data, especially on large angular scales. Using temperature and low- ℓ polarization data yields the following bound on the amplitude of cold dark matter isocurvature perturbations at scale $k = 0.002h^{-1}\text{Mpc}^{-1}$ (marginalising over the correlation angle and in the absence of primordial tensor perturbations) [38]:

$$\frac{\mathcal{P}_{S_m}}{\mathcal{P}_\zeta + \mathcal{P}_{S_m}} < 0.025 \text{ (95\% CL)} . \quad (23.97)$$

For fully (anti-)correlated isocurvature perturbations, corresponding to a single isocurvature field providing a source for both the curvature and residual isocurvature perturbations, the bounds become significantly tighter [38]:

$$\frac{\mathcal{P}_{S_m}}{\mathcal{P}_\zeta + \mathcal{P}_{S_m}} < 0.0002 \text{ (95\% CL), correlated} , \quad (23.98)$$

$$\frac{\mathcal{P}_{S_m}}{\mathcal{P}_\zeta + \mathcal{P}_{S_m}} < 0.003 \text{ (95\% CL), anti-correlated} \quad (23.99)$$

23.7.2.2 Local-Type Non-Gaussianity

Since non-adiabatic field fluctuations in multi-field inflation may lead to the evolution of the primordial curvature perturbation at all orders, it becomes possible to generate significant non-Gaussianity in the primordial curvature perturbation. Non-linear evolution on super-Hubble scales leads to local-type non-Gaussianity, where the local integrated expansion is a non-linear function of the local field values during inflation, $N(\phi_i)$. While the field fluctuations at Hubble exit, $\delta\phi_{i*}$, are Gaussian in the slow-roll limit, the curvature perturbation, $\zeta = \delta N$, becomes a non-Gaussian distribution [102]:

$$\zeta = \sum_i \frac{\partial N}{\partial \phi_i} \delta\phi_i + \frac{1}{2} \sum_{i,j} \frac{\partial^2 N}{\partial \phi_i \partial \phi_j} \delta\phi_i \delta\phi_j + \dots \quad (23.100)$$

with non-vanishing bispectrum in the squeezed limit ($k_1 \approx k_2 \gg k_3$):

$$B_\zeta(k_1, k_2, k_3) \approx \frac{12}{5} f_{NL}^{local} \frac{\mathcal{P}_\zeta(k_1)}{4\pi k_1^3} \frac{\mathcal{P}_\zeta(k_3)}{4\pi k_3^3} , \quad (23.101)$$

where

$$\frac{6}{5} f_{NL}^{local} = \frac{\sum_{i,j} \frac{\partial^2 N}{\partial \phi_i \partial \phi_j}}{\left(\sum_i \frac{\partial N}{\partial \phi_i}\right)^2} . \quad (23.102)$$

Both equilateral and orthogonal bispectra, discussed above in the context of generalised single field inflation, vanish in the squeezed limit, enabling the three types of non-Gaussianity to be distinguished by observations, in principle.

Non-Gaussianity during multi-field inflation is highly model dependent, though f_{NL}^{local} can often be smaller than unity in multi-field slow-roll inflation [103]. Scenarios where a second light field plays a role during or after inflation can make distinctive predictions for f_{NL}^{local} , such as $f_{NL}^{local} = -5/4$ in some curvaton scenarios [102, 104] or $f_{NL}^{local} = 5$ in simple modulated reheating scenarios [98, 105]. By contrast the constancy of ζ on super-Hubble

scales in single-field slow-roll inflation leads to a very small non-Gaussianity [106, 107], and in the squeezed limit we have the simple result $f_{NL}^{local} = 5(1 - n_s)/12$ [108, 109].

A combined analysis of the *Planck* 2018 temperature and polarization data [92] yields the following range for f_{NL}^{local} defined in (Eq. (23.102)):

$$f_{NL}^{local} = -1 \pm 5 \text{ (68\% CL)} . \quad (23.103)$$

This sensitivity is sufficient to rule out parameter regimes giving rise to relatively large non-Gaussianity, but insufficient to probe $f_{NL}^{local} = \mathcal{O}(\epsilon)$, as expected in single-field models, or the range $f_{NL}^{local} = \mathcal{O}(1)$ found in the simplest two-field models.

Local-type primordial non-Gaussianity can also give rise to a striking scale-dependent bias in the distribution of collapsed dark matter halos and thus the galaxy distribution [110, 111]. However, bounds from high-redshift galaxy surveys are not yet competitive with the best CMB constraints.

23.8 Initial Conditions and Fine-tuning

This review is based on the assumption that the inflationary paradigm is valid. However, it remains the object of many criticisms (see, e.g., [112]), many of them related to the perceived unnaturalness of the required initial conditions.

Most work on inflation is done in the context of RW cosmology, which assumes a high degree of symmetry, or small inhomogeneous perturbations (usually first order) about an RW cosmology. The isotropic RW space-time is an attractor for many homogeneous but anisotropic cosmologies in the presence of a false vacuum energy density [113], or a scalar field with suitable self-interaction potential energy [114, 115]. However it is much harder to establish the range of highly inhomogeneous initial conditions that yield a successful RW Universe, with only limited studies initially (see, e.g., [116, 117]). A related open question is the general nature of the pre-inflationary state of the inflaton and other fields that could have provided initial conditions suitable for inflation [112]. They would need to have satisfied non-trivial homogeneity and isotropy conditions, and one may ask how these could have arisen, whether these are plausible, and whether there may be some observable signature of the pre-inflationary state. These and other criticisms of inflation were addressed in [118], which presented studies of the sensitivity of inflation to the initial conditions. Complementing the studies reported in [118], there have been numerical relativity investigations of highly inhomogeneous initial conditions [119–121]. The general conclusion is that inflation is rather robust with respect to inhomogeneities in the initial conditions in both the scalar field profile and the extrinsic curvature, including large tensor perturbations.

To quantify the fine-tuning of initial conditions requires a measure in the space of possible cosmologies [122], however it has been argued that some of the measures historically used to frame this problem are formally invalid [123]. It is sometimes also objected that inflationary models predict the existence of a multiverse, and potentially a loss of predictive power [124], if it undergoes the process termed eternal inflation [125–127]. However, whether this is actually a bug or a feature remains a topic of debate [128, 129]. The existence of the multiverse is a purely philosophical problem, unless it has observable consequences, e.g., in the CMB.

One might expect signatures of any pre-inflationary state to appear at large angular scales, i.e., low multipoles ℓ . Indeed, various anomalies have been noted in the large-scale CMB anisotropies, as also discussed in Chap. 29, the ‘‘Cosmic Microwave Background’’ review, including a possible suppression of the quadrupole and other very large-scale anisotropies, an apparent feature in the range $\ell \approx 20$ to 30, and a possible hemispheric asymmetry. However, none of these are highly significant statistically, in view of the limitations due to cosmic variance [85]. They cannot yet be regarded as signatures of initial conditions, the multiverse or some pre-inflationary dynamics, such as might emerge from string theory.

A different kind of initial condition problem, called the trans-Planckian problem [130], is that the perturbations now seen in the CMB would have had wavelengths shorter than the Planck length at the onset of inflation. However, under quite general and

conservative assumptions the usual inflationary predictions would be quite robust [131], with the possibility of $\mathcal{O}((H/m_P)^n)$ corrections that might have interesting signatures in the CMB [132].

When inflation was first proposed [1] [2] there was no evidence for the existence of scalar fields or the accelerated expansion of the universe. The situation has changed dramatically in recent years with the observational evidence that the cosmic expansion is currently accelerating and with the discovery of a scalar particle, namely the Higgs boson (see Chap. 11, “Status of Higgs boson physics” review). Combined with the lack of any widely accepted alternative model for the origin of cosmic structure, these discoveries have lent support to the idea of a primordial accelerated expansion driven by a scalar field, i.e., cosmological inflation. In parallel, successive CMB experiments have been consistent with generic predictions of inflationary models, although without yet providing irrefutable evidence. It was concluded in [118] that the inflationary paradigm is not currently in trouble. However, we note that inflation via a formally elementary scalar inflaton should probably only be regarded as an effective field theory valid at energy densities hierarchically smaller than the Planck scale. It should eventually be embedded in a suitable ultraviolet completion, on which inflationary dynamics may be our clearest window.

23.9 Future Probes of Inflation

Prospective future CMB experiments, both ground- and space-based are reviewed in the separate PDG “Cosmic Microwave Background” review, Chap. 29. The main emphasis in CMB experiments in the coming years will be on ground-based experiments providing improved measurements of B -mode polarization and greater sensitivity to the tensor-to-scalar ratio r , and more precise measurements at higher ℓ that will constrain n_s better. As is apparent from Fig. 23.1 and the discussion of models such as R^2 inflation, there is a strong incentive to reach a $5\text{-}\sigma$ sensitivity to $r \sim 3$ to 4×10^{-3} . This could be achieved with a moderately-sized space mission with large sky coverage [133], improvements in de-lensing and foreground measurements. The discussion in Sec. 23.3 (see also Fig. 23.5), also brought out the importance of reducing the uncertainty in n_s , as a way to constrain post-inflationary reheating and the connection to particle physics. CMB temperature anisotropies probe primordial density perturbations down to comoving scales of order 50 Mpc, beyond which scale secondary sources of anisotropy dominate. CMB spectral distortions could potentially constrain the amplitude and shape of primordial density perturbations on comoving scales from Mpc to kpc due to distortions caused by the Silk damping of pressure waves in the radiation dominated era, before the last scattering of the CMB photons but after the plasma can be fully thermalised [134].

Improved sensitivity to non-Gaussianities is also a priority. In addition to CMB measurements, future large-scale structure surveys will also have roles to play as probes into models of inflation, for which there are excellent prospects. High-redshift galaxy surveys are sensitive to local-type non-Gaussianity due to the scale-dependent bias induced on large scales. Current surveys such as eBOSS, probing out to redshift $z \sim 2$, can reach a precision $\Delta f_{NL} \sim 15$, from measurements of the galaxy power spectrum, or possibly $\Delta f_{NL} \sim 10$, if the galaxy bias can be determined independently [135]. Upcoming surveys such as DESI may reach $\Delta f_{NL} \sim 4$ [136] comparable with the *Planck* sensitivity. In the future, radio surveys such as SKA will measure large-scale structure out to redshift $z \sim 3$ [137], initially through mapping the intensity of the neutral hydrogen 21-cm line, and eventually through radio galaxy surveys which will probe local-type non-Gaussianity to $f_{NL} \sim 1$.

Galaxy clustering using DESI and *Euclid* satellite data could also constrain the running of the scalar tilt to a precision of $\Delta\alpha_s \approx 0.0028$, a factor of 2 improvement on *Planck* constraints, or a precision of 0.0016 using LSST data [136].

As an example of a proposed future satellite mission, *SPHEREx* [138] will use measurements of the galaxy power spectrum to target a measurement of the running of the scalar spectral index with a sensitivity $\Delta\alpha_s \sim 10^{-3}$ and local-type primordial non-Gaussianity, $\Delta f_{NL} \sim 1$. Including information from the galaxy bispectrum one might reduce the measurement error on non-Gaussianity to $\Delta f_{NL} \sim 0.2$, making it possible to distin-

guish between single-field slow-roll models and alternatives such as the curvaton scenario for the origin of structure, which generate $f_{NL} \sim 1$.

Acknowledgements

The authors are grateful to Vincent Vennin for his careful reading of this manuscript and preparing Fig. 23.4 for this review. The work of J.E. was supported in part by the UK STFC via the research grant ST/L000258/1 and in part by the Estonian Research Council via a Mobilitas Plus grant. The work of D.W. was supported in part by the UK STFC research grants ST/N000668/1 and ST/S000550/1.

References

- [1] A. A. Starobinsky, Phys. Lett. **B91**, 99 (1980), [771(1980)].
- [2] A. H. Guth, Phys. Rev. **D23**, 347 (1981), [Adv. Ser. Astrophys. Cosmol.3,139(1987)].
- [3] K. A. Olive, Phys. Rept. **190**, 307 (1990).
- [4] D. H. Lyth and A. Riotto, Phys. Rept. **314**, 1 (1999), [hep-ph/9807278].
- [5] A.R. Liddle and D.H. Lyth, *Cosmological inflation and large-scale structure* (Cambridge University Press, 2000).
- [6] D. Baumann, in “Physics of the large and the small, TASI 09, proceedings of the Theoretical Advanced Study Institute in Elementary Particle Physics, Boulder, Colorado, USA, 1-26 June 2009,” 523–686 (2011), [arXiv:0907.5424].
- [7] J. Martin, C. Ringeval and V. Vennin, Phys. Dark Univ. **5-6**, 75 (2014), [arXiv:1303.3787]; J. Martin *et al.*, JCAP **1403**, 039 (2014), [arXiv:1312.3529]; J. Martin, Astrophys. Space Sci. Proc. **45**, 41 (2016), [arXiv:1502.05733].
- [8] P. A. R. Ade *et al.* (Planck), Astron. Astrophys. **594**, A13 (2016), [arXiv:1502.01589].
- [9] A. H. Guth and E. J. Weinberg, Nucl. Phys. **B212**, 321 (1983).
- [10] D. La and P. J. Steinhardt, Phys. Rev. Lett. **62**, 376 (1989), [Erratum: Phys. Rev. Lett.62,1066(1989)].
- [11] A. D. Linde, Phys. Lett. **B249**, 18 (1990).
- [12] F. C. Adams and K. Freese, Phys. Rev. **D43**, 353 (1991), [hep-ph/0504135].
- [13] A. D. Linde, Phys. Lett. **108B**, 389 (1982), [Adv. Ser. Astrophys. Cosmol.3,149(1987)].
- [14] A. Albrecht and P. J. Steinhardt, Phys. Rev. Lett. **48**, 1220 (1982), [Adv. Ser. Astrophys. Cosmol.3,158(1987)].
- [15] W. H. Press, Phys. Scripta **21**, 702 (1980); S. W. Hawking, Phys. Lett. **115B**, 295 (1982); A. A. Starobinsky, Phys. Lett. **117B**, 175 (1982); A. H. Guth and S. Y. Pi, Phys. Rev. Lett. **49**, 1110 (1982).
- [16] J. M. Bardeen, P. J. Steinhardt and M. S. Turner, Phys. Rev. **D28**, 679 (1983).
- [17] V. F. Mukhanov and G. V. Chibisov, JETP Lett. **33**, 532 (1981), [Pisma Zh. Eksp. Teor. Fiz.33,549(1981)].
- [18] K. S. Stelle, Gen. Rel. Grav. **9**, 353 (1978).
- [19] B. Whitt, Phys. Lett. **145B**, 176 (1984).
- [20] D. Wands, Class. Quant. Grav. **11**, 269 (1994), [arXiv:gr-qc/9307034].
- [21] S. R. Coleman and F. De Luccia, Phys. Rev. **D21**, 3305 (1980).
- [22] M. Sasaki *et al.*, Phys. Lett. **B317**, 510 (1993).
- [23] M. Bucher, A. S. Goldhaber and N. Turok, Phys. Rev. **D52**, 3314 (1995), [hep-ph/9411206].
- [24] A. D. Linde and A. Mezhlumian, Phys. Rev. **D52**, 6789 (1995), [arXiv:astro-ph/9506017].
- [25] A. R. Liddle, P. Parsons and J. D. Barrow, Phys. Rev. **D50**, 7222 (1994), [arXiv:astro-ph/9408015].
- [26] L. Kofman, A. D. Linde and A. A. Starobinsky, Phys. Rev. **D56**, 3258 (1997), [hep-ph/9704452].

- [27] B. A. Bassett, S. Tsujikawa and D. Wands, *Rev. Mod. Phys.* **78**, 537 (2006), [arXiv:astro-ph/0507632].
- [28] A. D. Linde, *Phys. Rev.* **D49**, 748 (1994), [arXiv:astro-ph/9307002].
- [29] A. D. Dolgov and A. D. Linde, *Phys. Lett.* **116B**, 329 (1982).
- [30] J. R. Ellis *et al.*, *Nucl. Phys.* **B238**, 453 (1984), [223(1983)].
- [31] M. Kawasaki and T. Moroi, *Prog. Theor. Phys.* **93**, 879 (1995), [hep-ph/9403364].
- [32] J. H. Traschen and R. H. Brandenberger, *Phys. Rev.* **D42**, 2491 (1990).
- [33] G. V. Chibisov and V. F. Mukhanov, *Mon. Not. Roy. Astron. Soc.* **200**, 535 (1982).
- [34] H. Kodama and M. Sasaki, *Prog. Theor. Phys. Suppl.* **78**, 1 (1984).
- [35] V.F. Mukhanov, H.A. Feldman and R.H. Brandenberger, *Phys. Rept.* **215**, 203 (1992).
- [36] K. A. Malik and D. Wands, *Phys. Rept.* **475**, 1 (2009), [arXiv:0809.4944].
- [37] V. F. Mukhanov, *Sov. Phys. JETP* **67**, 1297 (1988), [*Zh. Eksp. Teor. Fiz.* 94N7,1(1988)].
- [38] Y. Akrami *et al.* (Planck) (2018), [arXiv:1807.06211].
- [39] A. A. Starobinsky, *JETP Lett.* **30**, 682 (1979), [767(1979)].
- [40] E. D. Stewart and D. H. Lyth, *Phys. Lett.* **B302**, 171 (1993), [arXiv:gr-qc/9302019].
- [41] D. Wands *et al.*, *Phys. Rev.* **D62**, 043527 (2000), [arXiv:astro-ph/0003278].
- [42] A. R. Liddle and S. M. Leach, *Phys. Rev.* **D68**, 103503 (2003), [arXiv:astro-ph/0305263].
- [43] P. A. R. Ade *et al.* (BICEP2, Keck Array), *Phys. Rev. Lett.* **121**, 221301 (2018), [arXiv:1810.05216].
- [44] S.M. Leach, A.R. Liddle, J. Martin, and D.J. Schwarz, *Phys. Rev.* **D66**, 23515 (2002).
- [45] D. Kazanas, *Astrophys. J.* **241**, L59 (1980).
- [46] K. Sato, *Mon. Not. Roy. Astron. Soc.* **195**, 467 (1981).
- [47] A. Billoire and K. Tamvakis, *Nucl. Phys.* **B200**, 329 (1982); J. D. Breit, S. Gupta and A. Zaks, *Phys. Rev. Lett.* **51**, 1007 (1983).
- [48] A. D. Linde, *Phys. Lett.* **129B**, 177 (1983).
- [49] D. V. Nanopoulos, K. A. Olive and M. Srednicki, *Phys. Lett.* **127B**, 30 (1983).
- [50] J. Ellis, D. V. Nanopoulos and K. A. Olive, *Phys. Rev. Lett.* **111**, 111301 (2013), [Erratum: *Phys. Rev. Lett.* 111,no.12,129902(2013)], [arXiv:1305.1247].
- [51] T. S. Koivisto and F. R. Urban, *JCAP* **1503**, 03, 003 (2015), [arXiv:1407.3445].
- [52] L. Boubekeur and D. H. Lyth, *JCAP* **0507**, 010 (2005), [hep-ph/0502047].
- [53] G. R. Dvali, Q. Shafi and S. Solganik, in "4th European Meeting From the Planck Scale to the Electroweak Scale (Planck 2001) La Londe les Maures, Toulon, France, May 11-16, 2001," (2001), [hep-th/0105203]; J. Garcia-Bellido, R. Rabadan and F. Zamora, *JHEP* **01**, 036 (2002), [hep-th/0112147]; S. Kachru *et al.*, *JCAP* **0310**, 013 (2003), [hep-th/0308055].
- [54] F. C. Adams *et al.*, *Phys. Rev.* **D47**, 426 (1993), [hep-ph/9207245].
- [55] E. Pajer and M. Peloso, *Class. Quant. Grav.* **30**, 214002 (2013), [arXiv:1305.3557].
- [56] E. Silverstein and A. Westphal, *Phys. Rev.* **D78**, 106003 (2008), [arXiv:0803.3085].
- [57] L. McAllister, E. Silverstein and A. Westphal, *Phys. Rev.* **D82**, 046003 (2010), [arXiv:0808.0706].
- [58] F. L. Bezrukov and M. Shaposhnikov, *Phys. Lett.* **B659**, 703 (2008), [arXiv:0710.3755].
- [59] D. Buttazzo *et al.*, *JHEP* **12**, 089 (2013), [arXiv:1307.3536].
- [60] H. P. Nilles, *Phys. Rept.* **110**, 1 (1984); H. E. Haber and G. L. Kane, *Phys. Rept.* **117**, 75 (1985).
- [61] J.R. Ellis *et al.*, *Phys. Lett.* **118B**, 335 (1982).
- [62] N. Okada and Q. Shafi (2013), [arXiv:1311.0921].
- [63] H. Murayama *et al.*, *Phys. Rev. Lett.* **70**, 1912 (1993).
- [64] J. Ellis, M. Fairbairn and M. Sueiro, *JCAP* **1402**, 044 (2014), [arXiv:1312.1353].
- [65] D. Croon, J. Ellis and N. E. Mavromatos, *Phys. Lett.* **B724**, 165 (2013), [arXiv:1303.6253].
- [66] G. R. Dvali, Q. Shafi and R. K. Schaefer, *Phys. Rev. Lett.* **73**, 1886 (1994), [hep-ph/9406319].
- [67] D. V. Nanopoulos *et al.*, *Phys. Lett.* **123B**, 41 (1983).
- [68] A. B. Goncharov and A. D. Linde, *Phys. Lett.* **139B**, 27 (1984).
- [69] E. Cremmer *et al.*, *Nucl. Phys.* **B212**, 413 (1983), [413(1982)].
- [70] R. Holman, P. Ramond and G. G. Ross, *Phys. Lett.* **137B**, 343 (1984).
- [71] E. J. Copeland *et al.*, *Phys. Rev.* **D49**, 6410 (1994), [arXiv:astro-ph/9401011]; E. D. Stewart, *Phys. Rev.* **D51**, 6847 (1995), [hep-ph/9405389].
- [72] G. D. Coughlan *et al.*, *Phys. Lett.* **131B**, 59 (1983); A. S. Goncharov, A. D. Linde and M. I. Vysotsky, *Phys. Lett.* **147B**, 279 (1984); T. Banks, D. B. Kaplan and A. E. Nelson, *Phys. Rev.* **D49**, 779 (1994), [hep-ph/9308292]; B. de Carlos *et al.*, *Phys. Lett.* **B318**, 447 (1993), [hep-ph/9308325]; M. Kawasaki, T. Moroi and T. Yanagida, *Phys. Lett.* **B370**, 52 (1996), [hep-ph/9509399].
- [73] J. R. Ellis, D. V. Nanopoulos and M. Quiros, *Phys. Lett.* **B174**, 176 (1986).
- [74] T. Moroi, M. Yamaguchi and T. Yanagida, *Phys. Lett.* **B342**, 105 (1995), [hep-ph/9409367].
- [75] M. Kawasaki, M. Yamaguchi and T. Yanagida, *Phys. Rev. Lett.* **85**, 3572 (2000), [hep-ph/0004243]; K. Nakayama, F. Takahashi and T. T. Yanagida, *JCAP* **1308**, 038 (2013), [arXiv:1305.5099].
- [76] E. Cremmer *et al.*, *Phys. Lett.* **133B**, 61 (1983).
- [77] A. S. Goncharov and A. D. Linde, *Class. Quant. Grav.* **1**, L75 (1984); C. Kounnas and M. Quiros, *Phys. Lett.* **151B**, 189 (1985).
- [78] J. R. Ellis, C. Kounnas and D. V. Nanopoulos, *Nucl. Phys.* **B247**, 373 (1984).
- [79] E. Witten, *Phys. Lett.* **155B**, 151 (1985).
- [80] J. Ellis, D. V. Nanopoulos and K. A. Olive, *JCAP* **1310**, 009 (2013), [arXiv:1307.3537].
- [81] J. Ellis *et al.*, *Class. Quant. Grav.* **33**, 9, 094001 (2016), [arXiv:1507.02308].
- [82] R. Kallosh, A. Linde and D. Roest, *JHEP* **11**, 198 (2013), [arXiv:1311.0472].
- [83] A. R. Liddle, *Mon. Not. Roy. Astron. Soc.* **377**, L74 (2007), [arXiv:astro-ph/0701113].
- [84] J. Martin, C. Ringeval and V. Vennin, *Phys. Rev.* **D93**, 10, 103532 (2016), [arXiv:1603.02606].
- [85] P. A. R. Ade *et al.* (Planck), *Astron. Astrophys.* **594**, A20 (2016), [arXiv:1502.02114].
- [86] C. T. Byrnes and E. R. M. Tarrant, *JCAP* **1507**, 007 (2015), [arXiv:1502.07339].
- [87] C. Armendariz-Picon, T. Damour and V. F. Mukhanov, *Phys. Lett.* **B458**, 209 (1999), [hep-th/9904075].
- [88] M. Alishahiha, E. Silverstein and D. Tong, *Phys. Rev.* **D70**, 123505 (2004), [hep-th/0404084].

- [89] K. Enqvist and M. S. Sloth, Nucl. Phys. **B626**, 395 (2002), [hep-ph/0109214]; D. H. Lyth and D. Wands, Phys. Lett. **B524**, 5 (2002), [hep-ph/0110002]; T. Moroi and T. Takahashi, Phys. Lett. **B522**, 215 (2001), [Erratum: Phys. Lett. **B539**, 303(2002)], [hep-ph/0110096].
- [90] N. Bartolo *et al.*, Phys. Rept. **402**, 103 (2004), [arXiv:astro-ph/0406398].
- [91] P. A. R. Ade *et al.* (Planck), Astron. Astrophys. **594**, A17 (2016), [arXiv:1502.01592].
- [92] Y. Akrami *et al.* (Planck) (2019), [arXiv:1905.05697].
- [93] J. Ellis *et al.*, JCAP **1507**, 07, 050 (2015), [arXiv:1505.06986].
- [94] L. Senatore, K. M. Smith and M. Zaldarriaga, JCAP **1001**, 028 (2010), [arXiv:0905.3746].
- [95] C. Gordon *et al.*, Phys. Rev. **D63**, 023506 (2001), [arXiv:astro-ph/0009131]; R. Easther *et al.*, Phys. Rev. Lett. **112**, 161302 (2014), [arXiv:1312.4035]; J. Ellis *et al.*, JCAP **1501**, 010 (2015), [arXiv:1409.8197]; S. Renaux-Petel and K. Turzynski, JCAP **1506**, 06, 010 (2015), [arXiv:1405.6195].
- [96] C. T. Byrnes and D. Wands, Phys. Rev. **D74**, 043529 (2006), [arXiv:astro-ph/0605679].
- [97] D. H. Lyth, JCAP **0511**, 006 (2005), [arXiv:astro-ph/0510443].
- [98] G. Dvali, A. Gruzinov and M. Zaldarriaga, Phys. Rev. **D69**, 023505 (2004), [arXiv:astro-ph/0303591].
- [99] D. Wands *et al.*, Phys. Rev. **D66**, 043520 (2002), [arXiv:astro-ph/0205253].
- [100] S. Weinberg, Phys. Rev. **D67**, 123504 (2003), [arXiv:astro-ph/0302326].
- [101] D. Langlois, Phys. Rev. **D59**, 123512 (1999), [arXiv:astro-ph/9906080].
- [102] D. H. Lyth and Y. Rodriguez, Phys. Rev. Lett. **95**, 121302 (2005), [arXiv:astro-ph/0504045].
- [103] F. Vernizzi and D. Wands, JCAP **0605**, 019 (2006), [arXiv:astro-ph/0603799].
- [104] M. Sasaki, J. Valiviita and D. Wands, Phys. Rev. **D74**, 103003 (2006), [arXiv:astro-ph/0607627].
- [105] G. Dvali, A. Gruzinov and M. Zaldarriaga, Phys. Rev. **D69**, 083505 (2004), [arXiv:astro-ph/0305548].
- [106] D. S. Salopek and J. R. Bond, Phys. Rev. **D43**, 1005 (1991).
- [107] A. Gangui *et al.*, Astrophys. J. **430**, 447 (1994), [arXiv:astro-ph/9312033].
- [108] J. M. Maldacena, JHEP **05**, 013 (2003), [arXiv:astro-ph/0210603].
- [109] V. Acquaviva *et al.*, Nucl. Phys. **B667**, 119 (2003), [arXiv:astro-ph/0209156].
- [110] N. Dalal *et al.*, Phys. Rev. **D77**, 123514 (2008), [arXiv:0710.4560].
- [111] S. Matarrese and L. Verde, Astrophys. J. **677**, L77 (2008), [arXiv:0801.4826].
- [112] A. Ijjas, P. J. Steinhardt and A. Loeb, Phys. Lett. **B723**, 261 (2013), [arXiv:1304.2785].
- [113] R. M. Wald, Phys. Rev. **D28**, 2118 (1983).
- [114] M. Heusler, Phys. Lett. **B253**, 33 (1991).
- [115] Y. Kitada and K.-i. Maeda, Phys. Rev. **D45**, 1416 (1992).
- [116] D. S. Goldwirth and T. Piran, Phys. Rept. **214**, 223 (1992).
- [117] T. Vachaspati and M. Trodden, Phys. Rev. **D61**, 023502 (1999), [arXiv:gr-qc/9811037].
- [118] D. Chowdhury *et al.* (2019), [arXiv:1902.03951].
- [119] W. E. East *et al.*, JCAP **1609**, 09, 010 (2016), [arXiv:1511.05143].
- [120] K. Clough *et al.*, JCAP **1709**, 09, 025 (2017), [arXiv:1608.04408].
- [121] K. Clough, R. Flauger and E. A. Lim, JCAP **1805**, 05, 065 (2018), [arXiv:1712.07352].
- [122] G. W. Gibbons, S. W. Hawking and J. M. Stewart, Nucl. Phys. **B281**, 736 (1987).
- [123] J. S. Schiffrin and R. M. Wald, Phys. Rev. **D86**, 023521 (2012), [arXiv:1202.1818].
- [124] A. Ijjas, P. J. Steinhardt and A. Loeb, Phys. Lett. **B736**, 142 (2014), [arXiv:1402.6980].
- [125] A. Vilenkin, Phys. Rev. **D27**, 2848 (1983).
- [126] A. D. Linde, Phys. Lett. **B175**, 395 (1986).
- [127] A. S. Goncharov, A. D. Linde and V. F. Mukhanov, Int. J. Mod. Phys. **A2**, 561 (1987).
- [128] A. H. Guth, D. I. Kaiser and Y. Nomura, Phys. Lett. **B733**, 112 (2014), [arXiv:1312.7619].
- [129] A. Linde, in “Proceedings, 100th Les Houches Summer School: Post-Planck Cosmology: Les Houches, France, July 8 - August 2, 2013,” 231–316 (2015), [arXiv:1402.0526].
- [130] J. Martin and R. H. Brandenberger, Phys. Rev. **D63**, 123501 (2001), [hep-th/0005209].
- [131] R. H. Brandenberger and J. Martin, Mod. Phys. Lett. **A16**, 999 (2001), [arXiv:astro-ph/0005432].
- [132] J. Martin and R. H. Brandenberger, in “Recent developments in theoretical and experimental general relativity, gravitation and relativistic field theories. Proceedings, 9th Marcel Grossmann Meeting, MG’9, Rome, Italy, July 2-8, 2000. Pts. A-C,” 2001–2002 (2000), [arXiv:astro-ph/0012031].
- [133] A. Kogut *et al.*, JCAP **1107**, 025 (2011), [arXiv:1105.2044].
- [134] J. Chluba, J. Hamann and S. P. Patil, Int. J. Mod. Phys. **D24**, 10, 1530023 (2015), [arXiv:1505.01834].
- [135] G.-B. Zhao *et al.*, Mon. Not. Roy. Astron. Soc. **457**, 3, 2377 (2016), [arXiv:1510.08216].
- [136] A. Font-Ribera *et al.*, JCAP **1405**, 023 (2014), [arXiv:1308.4164].
- [137] R. Maartens *et al.* (SKA Cosmology SWG), PoS **AASKA14**, 016 (2015), [arXiv:1501.04076].
- [138] O. Doré *et al.* (2014), [arXiv:1412.4872].

24. Big Bang Nucleosynthesis

Revised October 2019 by B.D. Fields (Astronomy, Illinois U.; Physics, Illinois U.), P. Molaro (INAF-OATS Trieste) and S. Sarkar (Rudolf Peierls, Oxford U.).

counting argument

$$Y_p = \frac{2(n/p)}{1 + n/p} \simeq 0.25 \quad (24.1)$$

24.1 Abstract

Big-Bang nucleosynthesis (BBN) offers the deepest reliable probe of the early Universe, being based on well-understood Standard Model physics [1]. Predictions of the abundances of the light elements, D, ^3He , ^4He , and ^7Li , synthesized at the end of the *first three minutes*, are in good overall agreement with the primordial abundances inferred from observational data, thus validating the standard hot Big-Bang cosmology (see [2–5] for reviews). This is particularly impressive given that these abundances span nine orders of magnitude – from $^4\text{He}/\text{H} \sim 0.08$ down to $^7\text{Li}/\text{H} \sim 10^{-10}$ (ratios by number). Thus BBN provides powerful constraints on possible deviations from the standard cosmology, and on new physics beyond the Standard Model [6–9].

24.2 Theory

The synthesis of the light elements is sensitive to physical conditions in the early radiation-dominated era at a temperature $T \sim 1$ MeV, corresponding to an age $t \sim 1$ s. At higher temperatures, weak interactions were in thermal equilibrium, thus fixing the ratio of the neutron and proton number densities to be $n/p = e^{-Q/T}$, where $Q = 1.293$ MeV is the neutron-proton mass difference. As the temperature dropped, the neutron-proton inter-conversion rate per nucleon, $\Gamma_{n \leftrightarrow p} \sim G_F^2 T^5$, fell faster than the Hubble expansion rate, $H \sim \sqrt{g_*} G_N T^2$, where g_* counts the number of relativistic particle species determining the energy density in radiation (see The Cosmological Parameters—Sec. 22 of this *Review*). This resulted in departure from chemical equilibrium (*freeze-out*) at $T_{\text{fr}} \sim (g_* G_N / G_F^4)^{1/6} \simeq 1$ MeV. The neutron fraction at this time, $n/p = e^{-Q/T_{\text{fr}}} \simeq 1/6$, is thus sensitive to every known physical interaction, since Q is determined by both strong and electromagnetic interactions while T_{fr} depends on the weak as well as gravitational interactions. Moreover, the sensitivity to the Hubble expansion rate affords a probe of, *e.g.*, the number of relativistic neutrino species [10]. After freeze-out, the neutrons were free to β -decay, so the neutron fraction dropped to $n/p \simeq 1/7$ by the time nuclear reactions began. A simplified analytic model of freeze-out yields the n/p ratio to an accuracy of $\sim 1\%$ [11, 12].

The rates of these reactions depend on the density of baryons (strictly speaking, nucleons), which is usually expressed normalized to the relic blackbody photon density as $\eta \equiv n_b/n_\gamma$. As we shall see, all the light-element abundances can be explained with $\eta_{10} \equiv \eta \times 10^{10}$ in the range 5.8–6.5 (95% CL). With n_γ fixed by the present CMB temperature 2.7255 K (see The Cosmological Parameters—Sec. 29 of this *Review*), this can be stated as the allowed range for the baryon mass density today, $\rho_b = (3.9\text{--}4.6) \times 10^{-31}$ g cm $^{-3}$, or as the baryonic fraction of the critical density, $\Omega_b = \rho_b/\rho_{\text{crit}} \simeq \eta_{10} h^{-2}/274 = (0.021\text{--}0.024) h^{-2}$, where $h \equiv H_0/100$ km s $^{-1}$ Mpc $^{-1}$ is the present Hubble parameter (see The Cosmological Parameters—Sec. 25.1 of this *Review*).

The nucleosynthesis chain begins with the formation of deuterium in the process $p(n, \gamma)\text{D}$. However, photo-dissociation by the high number density of photons delays production of deuterium (and other complex nuclei) until well after T drops below the binding energy of deuterium, $\Delta_{\text{D}} = 2.23$ MeV. The quantity $\eta^{-1} e^{-\Delta_{\text{D}}/T}$, *i.e.*, the number of photons per baryon above the deuterium photo-dissociation threshold, falls below unity at $T \simeq 0.1$ MeV; nuclei can then begin to form without being immediately photo-dissociated again. Only 2-body reactions, such as $\text{D}(p, \gamma)^3\text{He}$ and $^3\text{He}(\text{D}, p)^4\text{He}$ are important because the density by this time has become rather low – comparable to that of air!

Nearly all neutrons end up bound in the most stable light element ^4He . Heavier nuclei do not form in any significant quantity both because of the absence of stable nuclei with mass number 5 or 8 (which impedes nucleosynthesis via $n^4\text{He}$, $p^4\text{He}$ or $^4\text{He}^4\text{He}$ reactions), and the large Coulomb barriers for reactions such as $^3\text{He}(^4\text{He}, \gamma)^7\text{Li}$ and $^3\text{He}(^4\text{He}, \gamma)^7\text{Be}$. Hence the primordial mass fraction of ^4He , $Y_p \equiv \rho(^4\text{He})/\rho_b$, can be estimated by the simple

where strictly speaking this gives the baryon fraction in ^4He , which is what we will quote throughout. This differs slightly from the mass fraction due to small binding energy corrections.

There is little sensitivity here to the actual nuclear reaction rates, which are, however, important in determining the other ‘left-over’ abundances: D and ^3He at the level of a few times 10^{-5} by number relative to H, and $^7\text{Li}/\text{H}$ at the level of about 10^{-10} (when η_{10} is in the range 1–10). These values can be understood in terms of approximate analytic arguments [12, 13]. The experimental parameter most important in determining Y_p is the neutron lifetime, τ_n , which normalizes (the inverse of) $\Gamma_{n \leftrightarrow p}$. Its value has recently been significantly revised downwards to $\tau_n = 879.4 \pm 0.6$ s (see *N Baryons Listing*).

The elemental abundances shown in Fig. 24.1 as a function of η_{10} were calculated [14] using an updated version [15] of the Wagoner code [1]; other versions [16–19] too are publicly available. The ^4He curve includes small corrections due to radiative processes at zero and finite temperatures [20], non-equilibrium neutrino heating during e^\pm annihilation [21], and finite nucleon mass effects [22]; the range primarily reflects the 2σ uncertainty in the neutron lifetime. The spread in the curves for D, ^3He , and ^7Li corresponds to the 2σ uncertainties in nuclear cross sections, as estimated by Monte Carlo methods [15, 23–25]. The input nuclear data have been carefully reassessed [2, 14, 15, 23–25, 25–29, 29], leading to improved precision for the abundance predictions. In particular, the uncertainty in $^7\text{Li}/\text{H}$ at interesting values of η has been reduced recently by a factor ~ 2 , a consequence of a similar reduction in the error budget [30] for the dominant mass-7 production channel $^3\text{He}(^4\text{He}, \gamma)^7\text{Be}$. Polynomial fits to the predicted abundances and the error correlation matrix have been given in refs. [24, 31]. The boxes in Fig 24.1 show the observationally inferred primordial abundances with their associated uncertainties, as discussed below.

24.3 Light Element Abundances

BBN theory predicts the universal abundances of D, ^3He , ^4He , and ^7Li which are essentially fixed by $t \sim 180$ s. However, abundances are observed at much later epochs, after stellar nucleosynthesis commenced. Stars produce heavy elements such as C, N, O, and Fe (“metals”), while the ejected remains of stellar processing alters the light element abundances from their primordial values. Thus, one seeks astrophysical sites with low metal abundances to measure light element abundances that are closer to primordial.

BBN is the only significant source of deuterium which is entirely destroyed when it is cycled into stars [32]. Thus, any detection provides a lower limit to primordial D/H, and an upper limit on η_{10} . The best proxy to the primordial value of D is its measure in distant and chemically unprocessed matter, where stellar processing (astration) is minimal [32]. This has become possible with the advent of large telescopes, but after two decades of observational efforts we have only about a dozen determinations listed in Table 24.1 [33–46].

High-resolution spectra reveal the presence of D in high-redshift, low-metallicity quasar absorption systems via its isotope-shifted Lyman- α absorption features, though, unfortunately, these are often obscured or contaminated by the hydrogen features of the Lyman- α forest.

The nuclear reaction cross sections important for BBN have all been measured at the relevant energies. Recently however there have been substantial advances in the precision of light element observations (*e.g.*, D/H) and in the determination of cosmological parameters (*e.g.*, from *Planck*). This motivates corresponding improvement in BBN predictions and thus in the key reaction cross sections. For example, it has been suggested [48, 49] that $\text{D}(p, \gamma)^3\text{He}$ measurements may suffer from systematic errors and be inferior to *ab initio* theory; if so, this could alter D/H abundances at a level that is now significant. Ongoing low-background cross section measurements should resolve this issue [50].

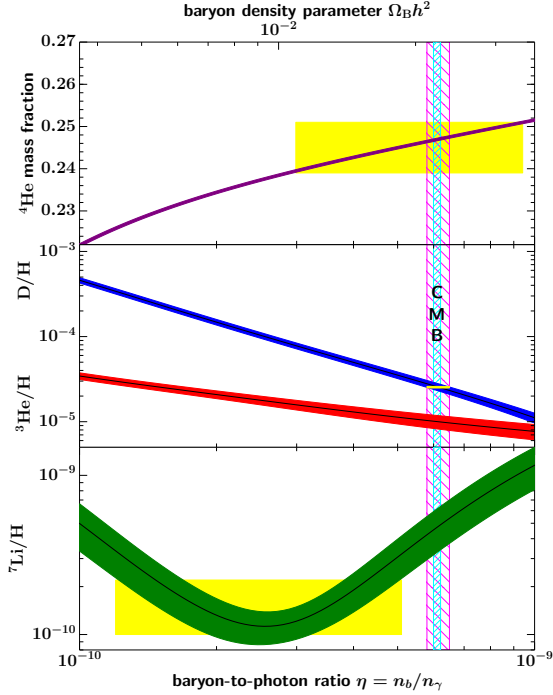


Figure 24.1: The primordial abundances of ${}^4\text{He}$, D, ${}^3\text{He}$, and ${}^7\text{Li}$ as predicted by the standard model of Big-Bang nucleosynthesis — the bands show the 95% CL range [47]. Boxes indicate the observed light element abundances. The narrow vertical band indicates the CMB measure of the cosmic baryon density, while the wider band indicates the BBN D+ ${}^4\text{He}$ concordance range (both at 95% CL).

A few DLA systems show D lines resolved up to the higher members of the Lyman series. Recent determinations [37, 39] and re-analyses [38, 46, 51] provide strikingly improved precision over earlier work. A weighted mean of the 11 most precise measurements in Table 24.1 provides a value with a one percent precision:

$$D/H|_p \times 10^6 = (25.47 \pm 0.25). \quad (24.2)$$

Considering all the 16 extant determinations, the weighted mean is $D/H|_p \times 10^6 = (25.36 \pm 0.26)$, while different selections provide $D/H|_p \times 10^6 = (25.27 \pm 0.30)$ [51] or $D/H|_p \times 10^6 = (25.45 \pm 0.25)$ [52], all consistent with each other within 1σ . Metallicities of the absorbers are $(0.001 - 0.03) \times \text{Solar}$, i.e. at a level where no significant astration is expected [34, 53]. D/H shows no correlation with metallicity, redshift, or the hydrogen column density $N(\text{H}) (= \int_{\text{los}} n_{\text{H}} ds)$ integrated over the line-of-sight through the absorber. In the Galaxy D/H measurements are anti-correlated with metal abundances, which suggests that interstellar D partly resides in dust particles [54]. However, in the absorbers where deuterium is measured, the dust content is quite small as implied by Solar proportions of the abundances of refractory and non refractory elements. This is consistent with the measured D/H being truly representative of the primordial value.

The primordial ${}^4\text{He}$ abundance is best determined through recombination emission lines of He and H in the most metal-poor extragalactic HII (ionized) regions, *viz.* blue compact galaxies, generally found at low redshift. There is now a large body of data on ${}^4\text{He}$ and CNO in these galaxies, with over 1000 such systems in the Sloan Digital Sky Survey alone [59]. These data confirm that the stellar contribution to the helium abundance is positively correlated with metal production, so extrapolation to zero metallicity gives the primordial ${}^4\text{He}$ abundance Y_p . However, HII regions are complex systems and several physical parameters enter in the He/H determination, notably the electron density and temperature, as well as reddening. Thus, systematic effects dominate the uncertainties in the abundance deter-

mination [60, 61]. A major step forward has been the inclusion of the He $\lambda 10830$ infrared emission line which shows a strong dependence on the electron density and is thus useful to break the degeneracy with the temperature, allowing for a more robust helium abundance determination. In recent works the underlying ${}^4\text{He}$ stellar absorption, and/or the newly derived values of the HeI-recombination and H-excitation-collisional coefficients are addressed and the ${}^4\text{He}$ abundances have increased significantly. Some recent results are $Y_p = 0.2451 \pm 0.0026$ [62], $Y_p = 0.2449 \pm 0.0040$ [63] and $Y_p = 0.2551 \pm 0.0022$ [59] — see Ref. [64] and references therein for previous determinations. Taking all this into account our recommended ${}^4\text{He}$ abundance is

$$Y_p = 0.245 \pm 0.003, \quad (24.3)$$

but the matter is far from settled given that the measurements are only marginally consistent.

The best suited objects for the primordial ${}^7\text{Li}$ determination are metal-poor stars in the Galactic halo, which have metallicities going down to 10^{-6} of the Solar value [65]. Observations have long shown [66–69] that ${}^7\text{Li}$ does not vary significantly in halo dwarfs with metallicities $\lesssim 1/30$ of Solar — the *Spite plateau* [66, 70]. Recent observations show a puzzling drop in the Li/H abundance in metal-poor stars with $[\text{Fe}/\text{H}] < -3.0$ [71–73]. This becomes particularly acute at the very low metallicity end where only one star out of the seven dwarfs with metallicities $[\text{Fe}/\text{H}] \lesssim -4.5$ shows a ${}^7\text{Li}$ abundance close to the Spite Plateau, while in the others where it ought to be present it is either lower or totally absent [65, 74]. The reason for the increase in scatter at low metallicity is unknown and prevents derivation of the primordial ${}^7\text{Li}$ value by extrapolating to zero metallicity [72, 73].

The primordial ${}^7\text{Li}$ in different samples of stars or globular clusters has been reported as $\text{Li}/\text{H}|_p = (1.7 \pm 0.3) \times 10^{-10}$ [69], $\text{Li}/\text{H}|_p = (2.19 \pm 0.28) \times 10^{-10}$ [75], and $\text{Li}/\text{H}|_p = (1.86 \pm 0.23) \times 10^{-10}$ [76]. We note that different parameters (*e.g.*, the temperature) of the stellar atmosphere in which the ${}^7\text{Li}$ absorption line is formed lead to slightly different values. To estimate the primordial ${}^7\text{Li}$ value we consider only stars with metallicity in the range $-2.8 < [\text{Fe}/\text{H}] < -1.5$ [73], where no scatter in excess of the observational errors is observed. This yields:

$$\text{Li}/\text{H}|_p = (1.6 \pm 0.3) \times 10^{-10}. \quad (24.4)$$

Strictly speaking the suggested primordial ${}^7\text{Li}$ abundance should be considered a *lower bound* rather than a measure. In fact, ${}^7\text{Li}$ in Pop II stars may have been partially destroyed due to mixing of the outer layers with the hotter interior [77]. Such processes can be constrained by the absence of significant scatter in ${}^7\text{Li}$ versus T_{eff} [68], but ${}^7\text{Li}$ depletion by a factor as large as ~ 1.8 may have occurred [68, 78]. A recent model predicts that an initial ${}^7\text{Li}$ abundance of $\text{Li}/\text{H}|_p = 5.3 \times 10^{-10}$, corresponding to the baryon density indicated by CMB and D/H abundance, is significantly destroyed in the pre-main-sequence phase and then partially restored by late accretion of fresh ${}^7\text{Li}$ material ending onto the Spite Plateau [79, 80].

A ${}^6\text{Li}$ plateau (analogous to the ${}^7\text{Li}$ plateau) has also been claimed [81]. This has however been challenged by new observations and analyses which show that stellar convective motions can generate asymmetries in the line shape that mimic the presence of ${}^6\text{Li}$ [82–84]. Recent high-precision measurements are sensitive to the tiny isotopic shift in absorption indicate ${}^6\text{Li}/{}^7\text{Li} \leq 0.05$, thus confirming that ${}^7\text{Li}$ is dominant [81, 82].

The primordial abundance of ${}^3\text{He}$ has the poorest observational determination of all of the light nuclides. The only data available come from the Solar system and from solar-metallicity HII regions in the Galaxy [85]. Therefore, inferring the primordial ${}^3\text{He}$ abundance is problematic, compounded by the fact that stellar nucleosynthesis models for ${}^3\text{He}$ are in conflict with observations. Consequently, we consider it inappropriate to use ${}^3\text{He}$ (and also D+ ${}^3\text{He}$) as a cosmological probe.

Table 24.1: D/H measurements. For systems with multiple measurements we used the most recent one which is generally more precise.

QSO	z_{em}	z_{em}	$\log(NHI)$	[X/H]	(D/H) $\times 10^6$	Ref
QSO 2206–199	2.56	2.076	20.436 \pm 0.008	-2.04	16.5 \pm 3.5	[55]
QSO 0347–3819	3.22	3.025	20.63 \pm 0.09	-1.25	22.4 \pm 6.7	[56]
SDSS J1134+5742	3.52	3.411	17.95 \pm 0.05	<-4.2	20.4 \pm 6.1	[41]
QSO CTQ 247	3.02	2.621	20.45 \pm 0.10	-1.99	28.0 \pm 8.0	[43]
SDSS 1337+3152	3.17	3.168	20.41 \pm 0.15	-2.68	12.0 \pm 5.0	[57]
SDSS J1419+0829	3.03	3.049	20.392 \pm 0.003	-1.92	25.1 \pm 0.5	[36]
HS 0105+1619	2.65	2.536	19.40 \pm 0.01	-1.77	25.8 \pm 1.5	[36]
QSO B0913+0715	2.78	2.618	20.312 \pm 0.008	-2.40	25.3 \pm 1.0	[36]
SDSS J1358+0349	2.89	2.853	20.524 \pm 0.006	-2.33	26.2 \pm 0.7	[37]
SDSS J1358+6522	3.17	3.067	20.50 \pm 0.01	-2.33	25.8 \pm 1.0	[36]
SDSS J1558–0031	2.82	2.702	20.75 \pm 0.03	-1.55	24.0 \pm 1.4	[36]
PKS 1937–1009	3.78	3.256	18.09 \pm 0.03	-1.87	24.5 \pm 2.8	[58]
QSO J1444+2919	2.66	2.437	19.983 \pm 0.010	-2.04	19.7 \pm 3.3	[39]
PKS 1937–1009	3.78	3.572	17.925 \pm 0.006	-2.26	26.2 \pm 0.5	[46]
QSO 1009+2956	2.63	2.504	17.362 \pm 0.005	-2.50	24.8 \pm 4.1	[52]
QSO 1243+307	2.55	2.525	19.761 \pm 0.026	-2.77	23.9 \pm 1.0	[51]
Weighted mean of all 16					25.38 \pm 0.25	
Weighted mean of the most recent 11					25.47 \pm 0.25	

24.4 Concordance, Dark Matter, and the CMB

We now use the observed light element abundances to test the theory. We first consider standard BBN, which is based on Standard Model physics alone, so $N_\nu = 3$ and the only free parameter is the baryon-to-photon ratio η . (The implications of BBN for physics beyond the Standard Model will be considered below). Thus, any abundance measurement determines η , and additional measurements overconstrain the theory and thereby provide a consistency check.

While the η ranges spanned by the boxes in Fig 24.1 do not all overlap, they are all within a factor ~ 2 of each other. In particular, the lithium abundance corresponds to η values that are inconsistent with that of the (now very precise) D/H abundance as well as the less-constraining ^4He abundance. This discrepancy marks the *lithium problem*. The problem could simply reflect difficulty in determining the primordial lithium abundance, or could hint at a more fundamental omission in the theory. The possibility that lithium reveals new physics is addressed in detail in the next section. If however we exclude the lithium constraint because its inferred abundance may suffer from systematic uncertainties, then D/H and ^4He are in agreement. The concordant η range is essentially that implied by D/H, namely

$$5.8 \leq \eta_{10} \leq 6.5 \text{ (95\% CL)}. \quad (24.5)$$

Despite the lithium problem, the overall concordance remains remarkable: using only well-established microphysics we can extrapolate back to $t \sim 1$ s to predict light element abundances spanning nine orders of magnitude, in approximate agreement with observation. This is a major success for the standard cosmology, and inspires confidence in extrapolation back to such early times.

This concordance provides a measure of the baryon content:

$$0.021 \leq \Omega_b h^2 \leq 0.024 \text{ (95\% CL)}, \quad (24.6)$$

a result that plays a key role in our understanding of the matter budget of the Universe. First of all $\Omega_b \ll 1$, *i.e.*, baryons cannot close the Universe [86]. Furthermore, the cosmic density of (optically) luminous matter is $\Omega_{\text{lum}} \simeq 0.0024 h^{-1}$ [87], so that $\Omega_b \gg \Omega_{\text{lum}}$: most baryons are optically dark, probably in the form of a diffuse intergalactic medium [88]. Finally, given that $\Omega_m \sim 0.3$ (see Dark Matter and Cosmological Parameters reviews), we infer that most matter in the Universe is not only dark, but also takes some non-baryonic (more precisely, non-nucleonic) form.

The BBN prediction for the cosmic baryon density can be tested through precision measurements of CMB temperature fluctuations (see Cosmic Microwave Background review). One can de-

termine η from the amplitudes of the acoustic peaks in the CMB angular power spectrum [89], making it possible to compare two measures of η using very different physics, at two widely separated epochs. In the standard cosmology, there is no change in η between BBN and CMB decoupling, thus, a comparison of η_{BBN} and η_{CMB} is a key test. Agreement would endorse the standard picture, while disagreement could point to new physics during/between the BBN and CMB epochs.

The analysis described in the Cosmic Microwave Background review, based on *Planck* TT, TE, EE + lowE data and lensing, yields $\Omega_b h^2 = 0.02237 \pm 0.00015$ [90], which corresponds to $\eta_{10} = 6.12 \pm 0.04$ [91]. This result depends weakly on the primordial helium abundance, and the fiducial *Planck* analysis uses BBN theory to fix $Y_p(\eta)$. Without BBN theory, the *Planck* TT, TE, EE + lowE data plus lensing give $\Omega_b h^2 = 0.02230 \pm 0.00020$, corresponding to $\eta_{10} = 6.105 \pm 0.055$. As shown in Fig. 24.1, this CMB estimate of the baryon density (narrow vertical band) is consistent with the BBN range, *i.e.*, in good agreement with the value inferred from high-redshift D/H measurements and local ^4He determinations; together these observations span diverse environments from redshifts $z \sim 1000$ to the present.

The ^4He abundance is proportional to the n/p ratio when the weak-interaction rate falls behind the Hubble expansion rate at $T_{\text{fr}} \sim 1$ MeV. The presence of additional neutrino flavors (or of any other relativistic species) at this time increases g_* , hence the expansion rate, leading to a larger value of T_{fr} , n/p , and therefore Y_p [10, 92]. In the Standard Model at $T = 1$ MeV, $g_* = 5.5 + \frac{7}{4}N_\nu$, where N_ν is the *effective* number of (nearly) massless neutrino flavors. The helium curves in 24.1 were computed taking $N_\nu = 3$; small corrections for non-equilibrium neutrino heating [21] are included in the thermal evolution and lead to an effective $N_\nu = 3.045$ compared to assuming instantaneous neutrino freezeout (see The Cosmological Parameters—Sec. 22 of this Review). The computed ^4He abundance scales as $\Delta Y_p \simeq 0.013 \Delta N_\nu$ [11]. Clearly the central value for N_ν from BBN will depend on η , which is independently determined (with weaker sensitivity to N_ν) by the adopted D or ^7Li abundance. For example, if the best value for the observed primordial ^4He abundance is 0.249, then, for $\eta_{10} \sim 6$, the central value for N_ν is very close to 3. A maximum likelihood analysis on η and N_ν based on ^4He and D abundances nearly identical to those above finds the (correlated) 95% CL ranges to be $5.6 < \eta_{10} < 6.6$ and $2.3 < N_\nu < 3.4$ [5]. Identical results are obtained using a simpler method to extract such bounds based on χ^2 statistics, given a set of input abundances [93].

The CMB damping tail is sensitive to the primordial ^4He abundance independently of both BBN and local ^4He measurements

[94]. The *Planck* analysis using TT, TE, EE+lowE and lensing but not the BBN $Y_p(\eta)$ relation gives a ${}^4\text{He}$ mass fraction $0.239^{+0.024}_{-0.025}$, and nucleon fraction $Y_p = 0.240^{+0.24}_{-0.25}$, both at 95% CL [90]. This is consistent with the HII region helium abundance determination. Moreover, this value is consistent with the Standard ($N_\nu = 3$) BBN prediction for Y_p with the *Planck*-determined baryon density.

This concordance represents a successful CMB-only test of BBN.

The precision determination of the baryon density using the CMB motivates using this as an input to BBN calculations. Within the context of the Standard Model, BBN then becomes a zero-parameter theory, and the light element abundances are completely determined to within the uncertainties in η_{CMB} and the BBN theoretical errors. Comparison with the observed abundances then can be used to test the astrophysics of post-BBN light element evolution [95]. Alternatively, one can consider possible physics beyond the Standard Model (*e.g.*, which might change the expansion rate during BBN) and then use all of the abundances to test such models; this is discussed in 23.6 below.

24.5 The Lithium Problem

As Fig. 24.1 shows, stellar Li/H measurements are inconsistent with the D/H (and CMB), given the error budgets we have quoted. Recent updates in nuclear cross sections and stellar abundance systematics *increase* the discrepancy to over 5σ , depending on the stellar abundance analysis adopted [14]. For instance it is found $\text{Li}/\text{H}|_p = (5.623 \pm 0.247) \times 10^{-10}$ in [96], *i.e.* a factor 3.5 higher than equation 24.4 and at a 10σ CL.

The question then becomes pressing as to whether this mismatch comes from systematic errors in the observed abundances, and/or uncertainties in stellar astrophysics or nuclear inputs, or whether there might be new physics at work [9]. Nuclear inputs (cross sections) for BBN reactions are constrained by extensive laboratory measurements; to increase ${}^7\text{Be}$ destruction requires enhancement of otherwise subdominant processes that can be attained by missed resonances in a few reactions such as ${}^7\text{Be}(d, p)2\alpha$ if the compound nuclear state properties are particularly favorable [29, 97–99]. However, experimental searches have now closed off these possibilities [100–102], making a *nuclear fix* increasingly unlikely.

Another conventional means to solve the lithium problem is by *in situ* destruction over the long lifetimes of the host halo stars. Stellar depletion mechanisms include diffusion, rotationally induced mixing, or pre-main-sequence depletion. These effects certainly occur, but to reduce lithium to the required levels generally requires some *ad hoc* mechanism and fine tuning of the initial stellar parameters [79, 80, 103]. A putative signature of diffusion has been reported for the globular clusters NGC 6397 and NGC 6752, where the “turnoff” stars exhibit slightly lower (by a factor ~ 1.3) abundances of Fe II TiII, ScII, CaI and MgI, than in more evolved stars [78, 104]. General features of diffusive models are a dispersion in the Li abundances and a pronounced downturn in the Li abundances at the hot end of the Li plateau. Some extra turbulence needs to be invoked to limit diffusion in the hotter stars and to restore uniform Li abundance along the Spite plateau [103]. Li destruction in the pre-Main sequence phase and partially restored by the accretion has been also proposed [80]

As nuclear and astrophysical solutions to the lithium problem become increasingly constrained (even if difficult to rule out definitively), the possibility of new physics arises. Nucleosynthesis models in which the baryon-to-photon ratio is inhomogeneous can alter abundances for a given η_{BBN} , but will overproduce ${}^7\text{Li}$ [105]. Entropy generation by some non-standard process could have decreased η between the BBN era and CMB decoupling, however the lack of spectral distortions in the CMB rules out any significant energy injection up to a redshift $z \sim 10^7$ [106]. The most intriguing resolution of the lithium problem thus involves new physics during BBN [7–9]

We summarize the general features of such solutions here, and later consider examples in the context of specific particle physics models. Many proposed solutions introduce perturbations to light-element formation during BBN; while all element abun-

dances may suffer perturbations, the interplay of ${}^7\text{Li}$ and D is often the most important *i.e.* observations of D often provide the strongest constraints on the allowed perturbations to ${}^7\text{Li}$. In this connection it is important to note that the new, very precise determination of D/H will significantly constrain the ability of such models to ameliorate or solve the lithium problem.

A well studied class of models invokes the injection of suprathermal hadronic or electromagnetic particles due to decays of dark matter particles. The effects are complex and depend on the nature of the decaying particles and their branchings and spectra. However, the models that most successfully solve the lithium problem generally feature non-thermal nucleons, which dissociate all light elements. Dissociation of even a small fraction of ${}^4\text{He}$ introduces a large abundance of free neutrons, which quickly thermalize. The thermal neutrons drive the ${}^7\text{Be}(n, p){}^7\text{Li}$ conversion of ${}^7\text{Be}$. The resulting ${}^7\text{Li}$ has a lower Coulomb barrier relative to ${}^7\text{Be}$ and is readily destroyed via ${}^7\text{Li}(p, \alpha){}^4\text{He}$ [107, 108]. But ${}^4\text{He}$ dissociation also produces D directly as well as via nonthermal neutron $n(p, \gamma)d$ reactions. This introduces a tension between Li/H reduction and D/H enhancement that becomes increasingly restrictive with the increasing precision of deuterium observations. Indeed, this now forces particle injection scenarios to make very small ${}^7\text{Li}$ perturbations — far short of the level needed. An exception is a recent model wherein MeV-scale decays by construction avoid ${}^4\text{He}$ dissociation and associated D/H overproduction, instead *borrowing* neutrons by dissociating only deuterons [109].

Another important class of models retains the standard cosmic particle content, but changes their interactions via time variations in the fundamental constants [110–115]. Here too, the details are model-dependent, but scenarios that solve or alleviate the lithium problem often feature perturbations to the deuteron binding energy. A weaker D binding leads to the D bottleneck being overcome later, so that element formation commences at a lower temperature and lower density. This leads in turn to slower nuclear rates that freeze out earlier. The net result is a *higher* final D/H, due to less efficient processing into ${}^4\text{He}$, but also *lower* Li, due to suppressed production via ${}^3\text{He}(\alpha, \gamma){}^7\text{Be}$.

The *cosmological lithium problem* remains an unresolved issue in BBN. Nevertheless, the remarkable concordance between the CMB and the D (as well as ${}^4\text{He}$) abundance, is a non-trivial success, and provides important constraints on the early Universe.

24.6 Beyond the Standard Model

Given the simple physics underlying BBN, it is remarkable that it still provides the most effective test for the cosmological viability of ideas concerning physics beyond the Standard Model. Although baryogenesis and inflation must have occurred at higher temperatures in the early Universe, we do not as yet have ‘standard models’ for these, so BBN still marks the boundary between the established and the speculative in Big Bang cosmology. It might appear possible to push the boundary back to the quark-hadron transition at $T \sim \Lambda_{\text{QCD}}$, or electroweak symmetry breaking at $T \sim 1/\sqrt{G_F}$; however, so far no observable relics of these epochs have been identified, either theoretically or observationally. Thus, although the Standard Model provides a precise description of physics up to the Fermi scale, cosmology cannot be traced in detail before the BBN era.

The CMB power spectrum in the damping tail is independently sensitive to N_ν (*e.g.* [116]). The CMB value N_ν^{CMB} probes the cosmic radiation content at (re)combination, so a discrepancy would imply new physics or astrophysics. Indeed, observations by the South Pole Telescope implied $N_\nu^{\text{CMB}} = 3.85 \pm 0.62$ [117], prompting discussion of *dark radiation* such as sterile neutrinos [118]. However, *Planck* 2018 results give $N_\nu^{\text{CMB}} = 2.92^{+0.36}_{+0.37}$, 95% CL, when using *Planck* TT, TE, EE+lowE, a result quite consistent with the 3.045 of the Standard Model neutrinos [90].

Just as one can use the measured helium abundance to place limits on g_* [92, 111, 119–121], any changes in the strong, weak, electromagnetic, or gravitational coupling constants, arising *e.g.*, from the dynamics of new dimensions, can be similarly constrained [122], as can any speed-up of the expansion rate in, *e.g.*, scalar-tensor theories of gravity [123].

The limits on N_ν can be translated into limits on other types of particles or particle masses that would affect the expansion rate

of the Universe during nucleosynthesis. For example, consider *sterile* neutrinos with only right-handed interactions of strength $G_R < G_F$. Such particles would decouple at higher temperature than (left-handed) neutrinos, so their number density ($\propto T^3$) relative to neutrinos would be reduced by any subsequent entropy release, *e.g.*, due to annihilations of massive particles that become non-relativistic between the two decoupling temperatures. Thus (relativistic) particles with less than full strength weak interactions contribute less to the energy density than particles that remain in equilibrium up to the time of nucleosynthesis [124]. If we impose $N_\nu < 4$ as an illustrative constraint, then the three right-handed neutrinos must have a temperature $3(T_{\nu_R}/T_{\nu_L})^4 < 1$. Since the temperature of the decoupled ν_R is determined by entropy conservation (see The Cosmological Parameters—Sec. 22 of this Review), $T_{\nu_R}/T_{\nu_L} = [(43/4)/g_*(T_d)]^{1/3} < 0.76$, where T_d is the decoupling temperature of the ν_R . This requires $g_*(T_d) > 24$, so decoupling must have occurred at $T_d > 140$ MeV. The decoupling temperature is related to G_R through $(G_R/G_F)^2 \sim (T_d/3 \text{ MeV})^{-3}$, where 3 MeV is the decoupling temperature for ν_L s. This yields a limit $G_R \lesssim 10^{-2}G_F$. The above argument sets lower limits on the masses of new Z' gauge bosons to which right-handed neutrinos would be coupled in models of superstrings [125], or extended technicolour [126]. Similarly a Dirac magnetic moment for neutrinos, which would allow the right-handed states to be produced through scattering and thus increase g_* , can be significantly constrained [127], as can any new interactions for neutrinos that have a similar effect [128–130]. Right-handed states can be populated directly by helicity-flip scattering if the neutrino mass is large enough, and this property has been used to infer a bound of $m_{\nu_\tau} \lesssim 1$ MeV (taking $N_\nu < 4$) [131]. If there is mixing between active and sterile neutrinos then the effect on BBN is more complicated [132, 133].

BBN limits on the cosmic expansion rate constrain supersymmetric scenarios in which the neutralino or gravitino are very light, so that they contribute to g_* [134]. A gravitino in the mass range $\sim 10^{-4} - 10$ eV will affect the expansion rate of the Universe similarly to a light neutralino (which is however now probably ruled out by collider data, especially the decays of the Higgs-like boson). The net contribution to N_ν then ranges between 0.74 and 1.69, depending on the gravitino and slepton masses [135].

The limit on the expansion rate during BBN can also be translated into bounds on the mass/lifetime of non-relativistic particles that decay during BBN. This results in an even faster speed-up rate, and typically also changes the entropy [136–138]. If the decays include Standard Model particles, the resulting electromagnetic [139] [95, 125, 140] and/or hadronic [141, 142] cascades can strongly perturb the light elements, which leads to even stronger constraints. Such arguments have been applied to rule out an MeV mass for ν_τ , which decays during nucleosynthesis [143].

Decaying-particle arguments have proved very effective in probing supersymmetry. Light-element abundances generally are complementary to accelerator data in constraining SUSY parameter space, with BBN reaching to values kinematically inaccessible to the LHC. Much recent interest has focused on the case in which the next-to-lightest supersymmetric particle is metastable and decays during or after BBN. The constraints on unstable particles discussed above imply stringent bounds on the allowed abundance of such particles [107]; if the metastable particle is charged (*e.g.*, the stau), then it is possible for it to form atom-like electromagnetic bound states with nuclei, and the resulting impact on light elements can be quite complex [8, 97, 144]. Moreover, SUSY decays can destroy ${}^7\text{Li}$ and/or produce ${}^6\text{Li}$, leading to a possible supersymmetric solution to the lithium problems noted above [145] (see [7] for a review).

These arguments impose powerful constraints on supersymmetric inflationary cosmology [95, 125, 140–142], particularly thermal leptogenesis [146]. These limits can be evaded only if the gravitino is massive enough to decay before BBN, *i.e.*, $m_{3/2} \gtrsim 50$ TeV [147] (which would be unnatural), or if it is in fact the lightest supersymmetric particle and thus stable [125, 140, 148, 149]. Similar constraints apply to moduli – very weakly coupled fields in string theory that obtain an electroweak-scale mass from supersymmetry breaking [150].

Finally, we mention that BBN places powerful constraints on the possibility that there are new large dimensions in nature, perhaps enabling the scale of quantum gravity to be as low as the electroweak scale [151]. Thus, Standard Model fields may be localized on a *brane*, while gravity alone propagates in the *bulk*. It has been further noted that the new dimensions may be non-compact, even infinite [152], and the cosmology of such models has attracted considerable attention. The expansion rate in the early Universe can be significantly modified, so BBN is able to set interesting constraints on such possibilities [153, 154].

References

- [1] R. V. Wagoner, W. A. Fowler and F. Hoyle, *Astrophys. J.* **148**, 3 (1967).
- [2] D. N. Schramm and M. S. Turner, *Rev. Mod. Phys.* **70**, 303 (1998), [arXiv:astro-ph/9706069].
- [3] G. Steigman, *Ann. Rev. Nucl. Part. Sci.* **57**, 463 (2007), [arXiv:0712.1100].
- [4] F. Iocco *et al.*, *Phys. Rept.* **472**, 1 (2009), [arXiv:0809.0631].
- [5] R. H. Cyburt *et al.*, *Rev. Mod. Phys.* **88**, 015004 (2016), [arXiv:1505.01076].
- [6] S. Sarkar, *Rept. on Prog. in Phys.* **59**, 1493 (1996).
- [7] K. Jedamzik and M. Pospelov, *New J. Phys.* **11**, 105028 (2009), [arXiv:0906.2087].
- [8] M. Pospelov and J. Pradler, *Ann. Rev. Nucl. Part. Sci.* **60**, 539 (2010), [arXiv:1011.1054].
- [9] B. D. Fields, *Ann. Rev. Nucl. Part. Sci.* **61**, 47 (2011), [arXiv:1203.3551].
- [10] P.J.E. Peebles, *Phys. Rev. Lett.* **16**, 411 (1966).
- [11] J. Bernstein, L. S. Brown and G. Feinberg, *Rev. Mod. Phys.* **61**, 25 (1989).
- [12] S. Mukhanov, *Int. J. Theor. Phys.* **143**, 669 (2004).
- [13] R. Esmailzadeh, G. D. Starkman and S. Dimopoulos, *Astrophys. J.* **378**, 504 (1991).
- [14] R. H. Cyburt, B. D. Fields and K. A. Olive, *JCAP* **0811**, 012 (2008), [arXiv:0808.2818].
- [15] R. H. Cyburt, B. D. Fields and K. A. Olive, *New Astron.* **6**, 215 (2001), [arXiv:astro-ph/0102179].
- [16] L. Kawano, Technical Report FERMILAB-PUB-92-004-A (1992), URL <https://ui.adsabs.harvard.edu/abs/1992STIN...9225163K>.
- [17] O. Pisanti *et al.*, *Comput. Phys. Commun.* **178**, 956 (2008), [arXiv:0705.0290].
- [18] A. Arbey, *Comput. Phys. Commun.* **183**, 1822 (2012), [arXiv:1106.1363].
- [19] R. Consiglio *et al.*, *Computer Physics Communications* **233**, 237 (2018), [arXiv:1712.04378].
- [20] S. Esposito *et al.*, *Nucl. Phys.* **B568**, 421 (2000), [arXiv:astro-ph/9906232].
- [21] S. Dodelson and M. S. Turner, *Phys. Rev.* **D46**, 3372 (1992).
- [22] D. Seckel (1993), [hep-ph/9305311].
- [23] M. S. Smith, L. H. Kawano and R. A. Malaney, *Astrophys. J. Suppl.* **85**, 219 (1993).
- [24] G. Fiorentini *et al.*, *Phys. Rev.* **D58**, 063506 (1998), [arXiv:astro-ph/9803177].
- [25] A. Coc *et al.*, *Astrophys. J.* **744**, 158 (2012), [arXiv:1107.1117].
- [26] K. M. Nollett and S. Burles, *Phys. Rev.* **D61**, 123505 (2000), [arXiv:astro-ph/0001440].
- [27] R. H. Cyburt, *Phys. Rev.* **D70**, 023505 (2004), [arXiv:astro-ph/0401091].
- [28] P. D. Serpico *et al.*, *JCAP* **0412**, 010 (2004), [arXiv:astro-ph/0408076].
- [29] R. N. Boyd *et al.*, *Phys. Rev.* **D82**, 105005 (2010), [arXiv:1008.0848].

- [30] R.H. Cyburt and B. Davids, *Phys. Rev.* **C78**, 012 (2008).
- [31] S. Burles, K. M. Nollett and M. S. Turner, *Astrophys. J.* **552**, L1 (2001), [arXiv:astro-ph/0010171].
- [32] R. I. Epstein, J. M. Lattimer and D. N. Schramm, *Nature* **263**, 198 (1976).
- [33] S. D’Odorico *et al.*, *Astron. & Astrophys.* **368**, L21 (2001).
- [34] D. Romano *et al.*, *Mon. Not. Roy. Astron. Soc.* **369**, 295 (2006), [arXiv:astro-ph/0603190].
- [35] M. Pettini and D. V. Bowen, *Astrophys. J.* **560**, 41 (2001), [arXiv:astro-ph/0104474].
- [36] R. Cooke *et al.*, *Astrophys. J.* **781**, 1, 31 (2014), [arXiv:1308.3240].
- [37] R. J. Cooke *et al.*, *Astrophys. J.* **830**, 2, 148 (2016), [arXiv:1607.03900].
- [38] E.O. Zavarygin *et al.*, arXiv:1706.09512(2017).
- [39] S. A. Balashev *et al.*, *Mon. Not. Roy. Astron. Soc.* **458**, 2, 2188 (2016), [arXiv:1511.01797].
- [40] S. A. Levshakov *et al.*, *Astrophys. J.* **565**, 696 (2002), [arXiv:astro-ph/0105529].
- [41] M. Fumagalli, J. M. O’Meara and J. X. Prochaska, *Science* **334**, 1245 (2011), [arXiv:1111.2334].
- [42] R. Srianand *et al.*, *Mon. Not. Roy. Astron. Soc.* **405**, 1888 (2010), [arXiv:1002.4620].
- [43] P. Noterdaeme *et al.*, *Astron. & Astrophys.* **542**, L33 (2012), [arXiv:1205.3777].
- [44] M. Pettini and R. Cooke, *Mon. Not. Roy. Astron. Soc.* **425**, 2477 (2012), [arXiv:1205.3785].
- [45] S. Riemer-Sørensen *et al.*, *Mon. Not. Roy. Astron. Soc.* **447**, 2925 (2015), [arXiv:1412.4043].
- [46] S. Riemer-Sørensen *et al.*, *Mon. Not. Roy. Astron. Soc.* **468**, 3, 3239 (2017), [arXiv:1703.06656].
- [47] B. D. Fields *et al.*, *JCAP* (2019).
- [48] K. M. Nollett and G. P. Holder (2011), [arXiv:1112.2683].
- [49] L. E. Marcucci *et al.*, *Phys. Rev. Lett.* **116**, 10, 102501 (2016), [Erratum: *Phys. Rev. Lett.* **117**, no.4, 049901(2016)], [arXiv:1510.07877].
- [50] C. Gustavino, *Euro. Phys. J. Web of Conferences*, 136, 01009 (2017).
- [51] R. J. Cooke, M. Pettini and C. C. Steidel, *Astrophys. J.* **855**, 2, 102 (2018), [arXiv:1710.11129].
- [52] E. O. Zavarygin *et al.*, *Mon. Not. R. Astron. Soc* **477**, 4, 5536 (2018), [arXiv:1706.09512].
- [53] F. van de Voort *et al.*, *Mon. Not. R. Astron. Soc* **477**, 1, 80 (2018), [arXiv:1704.08254].
- [54] J. L. Linsky *et al.*, *Astrophys. J.* **647**, 1106 (2006), [arXiv:astro-ph/0608308].
- [55] M. Pettini and D. V. Bowen, *Astrophys. J.* **560**, 1, 41 (2001), [arXiv:astro-ph/0104474].
- [56] S. D’Odorico, M. Dessauges-Zavadsky and P. Molaro, *Astron. & Astrophys.* **368**, L21 (2001), [arXiv:astro-ph/0102162].
- [57] R. Srianand *et al.*, *Mon. Not. R. Astron. Soc* **405**, 3, 1888 (2010), [arXiv:1002.4620].
- [58] S. Riemer-Sørensen *et al.*, *Mon. Not. R. Astron. Soc* **447**, 3, 2925 (2015), [arXiv:1412.4043].
- [59] Y. I. Izotov, T. X. Thuan and N. G. Guseva, *Mon. Not. Roy. Astron. Soc.* **445**, 1, 778 (2014), [arXiv:1408.6953].
- [60] Y. I. Izotov *et al.*, *Astrophys. J.* **527**, 757 (1999), [arXiv:astro-ph/9907228].
- [61] K. A. Olive and E. D. Skillman, *Astrophys. J.* **617**, 29 (2004), [arXiv:astro-ph/0405588].
- [62] M. Valerdi *et al.*, *Astrophys. J.* **876**, 2, 98 (2019), [arXiv:1904.01594].
- [63] E. Aver, K. A. Olive and E. D. Skillman, *JCAP* **1507**, 07, 011 (2015), [arXiv:1503.08146].
- [64] Y.I. Izotov *et al.*, *Astron. & Astrophys.* **558**, A57 (2013).
- [65] D. S. Aguado *et al.*, *Astrophys. J. Lett.* **874**, 2, L21 (2019), [arXiv:1904.04892].
- [66] M. Spite and F. Spite, *Nature* **297**, 483 (1982).
- [67] E. Vangioni-Flam *et al.*, *New Astron.* **4**, 245 (1999), [arXiv:astro-ph/9811327].
- [68] S. G. Ryan *et al.*, *Astrophys. J.* **530**, L57 (2000), [arXiv:astro-ph/9905211].
- [69] P. Bonifacio and P. Molaro, *Mon. Not. Roy. Astron. Soc.* **285**, 847 (1997), [arXiv:astro-ph/9611043].
- [70] R. Rebolo, P. Molaro and J. E. Beckman, *Astron. & Astrophys.* **192**, 192 (1988).
- [71] P. Bonifacio *et al.*, *Astron. & Astrophys.* **462**, 851 (2007).
- [72] W. Aoki *et al.*, *Astrophys. J.* **698**, 1803 (2009), [arXiv:0904.1448].
- [73] L. Sbordone *et al.*, *Astron. & Astrophys.* **522**, A26 (2010).
- [74] P. Bonifacio *et al.*, *Astron. & Astrophys.* **612**, A65 (2018), [arXiv:1801.03935].
- [75] P. Bonifacio *et al.*, *Astron. & Astrophys.* **390**, 91 (2002), [arXiv:astro-ph/0204332].
- [76] J. Melendez *et al.*, *Astron. & Astrophys.* **515**, L3 (2010).
- [77] M.H. Pinsonneault *et al.*, *Astrophys. J.* **574**, 389 (2002).
- [78] A. J. Korn *et al.*, *Nature* **442**, 657 (2006), [arXiv:astro-ph/0608201].
- [79] P. Molaro *et al.*, *Memorie della Soc. Astronomica Italiana Supp.* **22**, 233 (2012).
- [80] X. Fu *et al.*, *Mon. Not. R. Astron. Soc* **452**, 325 (2015).
- [81] M. Asplund *et al.*, *Astrophys. J.* **644**, 229 (2006), [arXiv:astro-ph/0510636].
- [82] K. Lind *et al.*, *Astron. & Astrophys.* **554**, 96 (2013).
- [83] R. Cayrel *et al.*, *Astron. & Astrophys.* **473**, L37 (2007).
- [84] M. Steffen *et al.*, *Memorie della Soc. Astronomica Italiana Supp.* **22**, 152 (2012).
- [85] D. S. Balsa and T. M. Bania, *Astrophys. J.* **156**, 6, 280 (2018), [arXiv:1810.09422].
- [86] H. Reeves *et al.*, *Astrophys. J.* **179**, 909 (1973).
- [87] M. Fukugita and P. J. E. Peebles, *Astrophys. J.* **616**, 643 (2004), [arXiv:astro-ph/0406095].
- [88] R. Cen and J. P. Ostriker, *Astrophys. J.* **514**, 1 (1999), [arXiv:astro-ph/9806281].
- [89] G. Jungman *et al.*, *Phys. Rev.* **D54**, 1332 (1996), [arXiv:astro-ph/9512139].
- [90] Planck Collaboration *et al.*, arXiv e-prints arXiv:1807.06209 (2018), [arXiv:1807.06209].
- [91] P.A.R. Ade *et al.*, *Astron. & Astrophys.* **594**, A13 (2016).
- [92] G. Steigman, D. N. Schramm and J. E. Gunn, *Phys. Lett.* **B66**, 202 (1977), [159(1977)].
- [93] E. Lisi, S. Sarkar and F. L. Villante, *Phys. Rev.* **D59**, 123520 (1999), [hep-ph/9901404].
- [94] R. Trotta and S. H. Hansen, *Phys. Rev.* **D69**, 023509 (2004), [arXiv:astro-ph/0306588].
- [95] R. H. Cyburt, B. D. Fields and K. A. Olive, *Phys. Lett.* **B567**, 227 (2003), [arXiv:astro-ph/0302431].
- [96] C. Pitrou *et al.*, *Phys. Rept.* **754**, 1 (2018), [arXiv:1801.08023].
- [97] R. H. Cyburt *et al.*, *JCAP* **1305**, 014 (2013), [arXiv:1303.0574].
- [98] N. Chakraborty, B. D. Fields and K. A. Olive, *Phys. Rev.* **D83**, 063006 (2011), [arXiv:1011.0722].
- [99] C. Brogгинi *et al.*, *JCAP* **1206**, 030 (2012), [arXiv:1202.5232].

- [100] P. D. O'Malley *et al.*, Phys. Rev. **C84**, 042801 (2011).
- [101] F. Hammache *et al.*, Phys. Rev. **C88**, 6, 062802 (2013), [arXiv:1312.0894].
- [102] M. W. Paris *et al.*, Nucl. Data Sheets **120**, 184 (2014), [arXiv:1304.3153].
- [103] O. Richard, G. Michaud and J. Richer, Astrophys. J. **619**, 538 (2005), [arXiv:astro-ph/0409672].
- [104] P. Gruyters *et al.*, Astron. Astrophys. **555**, 31 (2013).
- [105] K. Jedamzik and J. B. Rehm, Phys. Rev. **D64**, 023510 (2001), [arXiv:astro-ph/0101292].
- [106] D. J. Fixsen *et al.*, Astrophys. J. **473**, 576 (1996), [arXiv:astro-ph/9605054].
- [107] M. Kawasaki, K. Kohri and T. Moroi, Phys. Rev. **D71**, 083502 (2005), [arXiv:astro-ph/0408426].
- [108] K. Jedamzik, Phys. Rev. **D70**, 063524 (2004), [arXiv:astro-ph/0402344].
- [109] A. Goudelis, M. Pospelov and J. Pradler, Phys. Rev. Lett. **116**, 21, 211303 (2016), [arXiv:1510.08858].
- [110] J. D. Barrow, Phys. Rev. **D35**, 1805 (1987).
- [111] B. A. Campbell and K. A. Olive, Phys. Lett. **B345**, 429 (1995), [hep-ph/9411272].
- [112] L. Bergstrom, S. Iguri and H. Rubinstein, Phys. Rev. **D60**, 045005 (1999), [arXiv:astro-ph/9902157].
- [113] V. V. Flambaum and E. V. Shuryak, Phys. Rev. **D65**, 103503 (2002), [hep-ph/0201303].
- [114] A. Coc *et al.*, Phys. Rev. **D76**, 023511 (2007), [arXiv:astro-ph/0610733].
- [115] J. C. Berengut *et al.*, Phys. Rev. **D87**, 8, 085018 (2013), [arXiv:1301.1738].
- [116] Z. Hou *et al.*, Phys. Rev. **D87**, 083008 (2013), [arXiv:1104.2333].
- [117] R. Keisler *et al.*, Astrophys. J. **743**, 28 (2011), [arXiv:1105.3182].
- [118] J. Hamann *et al.*, Phys. Rev. Lett. **105**, 181301 (2010), [arXiv:1006.5276].
- [119] F. S. Accetta, L. M. Krauss and P. Romanelli, Phys. Lett. **B248**, 146 (1990).
- [120] K. M. Nollett and R. E. Lopez, Phys. Rev. **D66**, 063507 (2002), [arXiv:astro-ph/0204325].
- [121] C. Bambi, M. Giannotti and F. L. Villante, Phys. Rev. **D71**, 123524 (2005), [arXiv:astro-ph/0503502].
- [122] E. W. Kolb, M. J. Perry and T. P. Walker, Phys. Rev. **D33**, 869 (1986).
- [123] A. Coc *et al.*, Phys. Rev. **D73**, 083525 (2006), [arXiv:astro-ph/0601299].
- [124] K. A. Olive, D. N. Schramm and G. Steigman, Nucl. Phys. **B180**, 497 (1981).
- [125] J. R. Ellis *et al.*, Phys. Lett. **167B**, 457 (1986).
- [126] L. M. Krauss, J. Terning and T. Appelquist, Phys. Rev. Lett. **71**, 823 (1993), [hep-ph/9305265].
- [127] J. A. Morgan, Phys. Lett. **102B**, 247 (1981).
- [128] E. W. Kolb, M. S. Turner and T. P. Walker, Phys. Rev. **D34**, 2197 (1986).
- [129] J. A. Grifols and E. Masso, Mod. Phys. Lett. **A2**, 205 (1987).
- [130] K. S. Babu, R. N. Mohapatra and I. Z. Rothstein, Phys. Rev. Lett. **67**, 545 (1991).
- [131] A. D. Dolgov, S. H. Hansen and D. V. Semikoz, Nucl. Phys. **B524**, 621 (1998), [hep-ph/9712284].
- [132] K. Enqvist, K. Kainulainen and M. J. Thomson, Nucl. Phys. **B373**, 498 (1992).
- [133] A. D. Dolgov, Phys. Rept. **370**, 333 (2002), [hep-ph/0202122].
- [134] J. A. Grifols, R. N. Mohapatra and A. Riotto, Phys. Lett. **B400**, 124 (1997), [hep-ph/9612253].
- [135] H. K. Dreiner *et al.*, Phys. Rev. **D85**, 065027 (2012), [arXiv:1111.5715].
- [136] K. Sato and M. Kobayashi, Prog. Theor. Phys. **58**, 1775 (1977).
- [137] D. A. Dicus *et al.*, Phys. Rev. **D17**, 1529 (1978).
- [138] R. J. Scherrer and M. S. Turner, Astrophys. J. **331**, 19 (1988), [Astrophys. J.331,33(1988)].
- [139] D. Lindley, Mon. Not. R. Astron. Soc **188**, 15 (1979).
- [140] J. R. Ellis *et al.*, Nucl. Phys. **B373**, 399 (1992).
- [141] M. H. Reno and D. Seckel, Phys. Rev. **D37**, 3441 (1988).
- [142] S. Dimopoulos *et al.*, Nucl. Phys. **B311**, 699 (1989).
- [143] S. Sarkar and A. M. Cooper-Sarkar, Phys. Lett. **148B**, 347 (1984), [L.362(1984)].
- [144] M. Kawasaki, K. Kohri and T. Moroi, Phys. Lett. **B649**, 436 (2007), [hep-ph/0703122].
- [145] K. Jedamzik *et al.*, JCAP **0607**, 007 (2006), [hep-ph/0512044].
- [146] S. Davidson *et al.*, Phys. Rev. **466**, 105 (2008).
- [147] S. Weinberg, Phys. Rev. Lett. **48**, 1303 (1982).
- [148] R. H. Cyburt *et al.*, Phys. Rev. **D67**, 103521 (2003), [arXiv:astro-ph/0211258].
- [149] M. Bolz, A. Brandenburg and W. Buchmuller, Nucl. Phys. **B606**, 518 (2001), [Erratum: Nucl. Phys. B790,336(2008)], [hep-ph/0012052].
- [150] G. D. Coughlan *et al.*, Physics Letters B **131**, 1-3, 59 (1983).
- [151] N. Arkani-Hamed, S. Dimopoulos and G. R. Dvali, Phys. Rev. **D59**, 086004 (1999), [hep-ph/9807344].
- [152] L. Randall and R. Sundrum, Phys. Rev. Lett. **83**, 3370 (1999), [hep-ph/9905221].
- [153] J. M. Cline, C. Grojean and G. Servant, Phys. Rev. Lett. **83**, 4245 (1999), [hep-ph/9906523].
- [154] P. Binetruy *et al.*, Phys. Lett. **B477**, 285 (2000), [hep-th/9910219].

25. Cosmological Parameters

Updated September 2019, by O. Lahav (University College London) and A.R. Liddle (Perimeter Institute for Theoretical Physics and Universidade de Lisboa).

25.1 Parametrizing the Universe

Rapid advances in observational cosmology have led to the establishment of a precision cosmological model, with many of the key cosmological parameters determined to one or two significant figure accuracy. Particularly prominent are measurements of cosmic microwave background (CMB) anisotropies, with the highest precision observations being those of the *Planck* Satellite [1, 2] which supersede the landmark *WMAP* results [3, 4]. However the most accurate model of the Universe requires consideration of a range of observations, with complementary probes providing consistency checks, lifting parameter degeneracies, and enabling the strongest constraints to be placed.

The term ‘cosmological parameters’ is forever increasing in its scope, and nowadays often includes the parameterization of some functions, as well as simple numbers describing properties of the Universe. The original usage referred to the parameters describing the global dynamics of the Universe, such as its expansion rate and curvature. Now we wish to know how the matter budget of the Universe is built up from its constituents: baryons, photons, neutrinos, dark matter, and dark energy. We also need to describe the nature of perturbations in the Universe, through global statistical descriptors such as the matter and radiation power spectra. There may be additional parameters describing the physical state of the Universe, such as the ionization fraction as a function of time during the era since recombination. Typical comparisons of cosmological models with observational data now feature between five and ten parameters.

25.1.1 The global description of the Universe

Ordinarily, the Universe is taken to be a perturbed Robertson–Walker space-time, with dynamics governed by Einstein’s equations. This is described in detail in the Big-Bang Cosmology chapter in this volume. Using the density parameters Ω_i for the various matter species and Ω_Λ for the cosmological constant, the Friedmann equation can be written

$$\sum_i \Omega_i + \Omega_\Lambda - 1 = \frac{k}{R^2 H^2}, \quad (25.1)$$

where the sum is over all the different species of material in the Universe. This equation applies at any epoch, but later in this article we will use the symbols Ω_i and Ω_Λ to refer specifically to the present-epoch values.

The complete present-epoch state of the homogeneous Universe can be described by giving the current-epoch values of all the density parameters and the Hubble constant h (the present-day Hubble parameter being written $H_0 = 100h \text{ km s}^{-1} \text{ Mpc}^{-1}$). A typical collection would be baryons Ω_b , photons Ω_γ , neutrinos Ω_ν , and cold dark matter Ω_c (given charge neutrality, the electron density is guaranteed to be too small to be worth considering separately and is effectively included with the baryons). The spatial curvature can then be determined from the other parameters using Eq. (25.1). The total present matter density $\Omega_m = \Omega_c + \Omega_b$ may be used in place of the cold dark matter density Ω_c .

These parameters also allow us to track the history of the Universe, at least back until an epoch where interactions allow interchanges between the densities of the different species; this is believed to have last happened at neutrino decoupling, shortly before Big-Bang Nucleosynthesis (BBN). To probe further back into the Universe’s history requires assumptions about particle interactions, and perhaps about the nature of physical laws themselves.

The standard neutrino sector has three flavors. For neutrinos of mass in the range $5 \times 10^{-4} \text{ eV}$ to 1 MeV, the density parameter in neutrinos is predicted to be

$$\Omega_\nu h^2 = \frac{\sum m_\nu}{93.14 \text{ eV}}, \quad (25.2)$$

where the sum is over all families with mass in that range (higher masses need a more sophisticated calculation). We use units with

$c = 1$ throughout. Results on atmospheric and Solar neutrino oscillations [5] imply non-zero mass-squared differences between the three neutrino flavors. These oscillation experiments cannot tell us the absolute neutrino masses, but within the simple assumption of a mass hierarchy suggest a lower limit of approximately 0.06 eV for the sum of the neutrino masses (see the Neutrino chapter).

Even a mass this small has a potentially observable effect on the formation of structure, as neutrino free-streaming damps the growth of perturbations. Analyses commonly now either assume a neutrino mass sum fixed at this lower limit, or allow the neutrino mass sum to be a variable parameter. To date there is no decisive evidence of any effects from either neutrino masses or an otherwise non-standard neutrino sector, and observations impose quite stringent limits; see the Neutrinos in Cosmology chapter. However, we note that the inclusion of the neutrino mass sum as a free parameter can affect the derived values of other cosmological parameters.

25.1.2 Inflation and perturbations

A complete model of the Universe should include a description of deviations from homogeneity, at least in a statistical way. Indeed, some of the most powerful probes of the parameters described above come from the evolution of perturbations, so their study is naturally intertwined with the determination of cosmological parameters.

There are many different notations used to describe the perturbations, both in terms of the quantity used to and the definition of the statistical measure. We use the dimensionless power spectrum Δ^2 as defined in the Big Bang Cosmology section (also denoted \mathcal{P} in some of the literature). If the perturbations obey Gaussian statistics, the power spectrum provides a complete description of their properties.

From a theoretical perspective, a useful quantity to describe the perturbations is the curvature perturbation \mathcal{R} , which measures the spatial curvature of a comoving slicing of the space-time. A simple case is the Harrison–Zeldovich spectrum, which corresponds to a constant $\Delta_{\mathcal{R}}^2$. More generally, one can approximate the spectrum by a power law, writing

$$\Delta_{\mathcal{R}}^2(k) = \Delta_{\mathcal{R}}^2(k_*) \left[\frac{k}{k_*} \right]^{n_s - 1}, \quad (25.3)$$

where n_s is known as the spectral index, always defined so that $n_s = 1$ for the Harrison–Zeldovich spectrum, and k_* is an arbitrarily chosen scale. The initial spectrum, defined at some early epoch of the Universe’s history, is usually taken to have a simple form such as this power law, and we will see that observations require n_s close to one. Subsequent evolution will modify the spectrum from its initial form.

The simplest mechanism for generating the observed perturbations is the inflationary cosmology, which posits a period of accelerated expansion in the Universe’s early stages [6, 7]. It is a useful working hypothesis that this is the sole mechanism for generating perturbations, and it may further be assumed to be the simplest class of inflationary model, where the dynamics are equivalent to that of a single scalar field ϕ with canonical kinetic energy slowly rolling on a potential $V(\phi)$. One may seek to verify that this simple picture can match observations and to determine the properties of $V(\phi)$ from the observational data. Alternatively, more complicated models, perhaps motivated by contemporary fundamental physics ideas, may be tested on a model-by-model basis (see more in the Inflation chapter in this volume).

Inflation generates perturbations through the amplification of quantum fluctuations, which are stretched to astrophysical scales by the rapid expansion. The simplest models generate two types, density perturbations that come from fluctuations in the scalar field and its corresponding scalar metric perturbation, and gravitational waves that are tensor metric fluctuations. The former experience gravitational instability and lead to structure formation, while the latter can influence the CMB anisotropies. Defining slow-roll parameters (with primes indicating derivatives with

respect to the scalar field) as

$$\epsilon = \frac{m_{\text{Pl}}^2}{16\pi} \left(\frac{V'}{V} \right)^2, \quad \eta = \frac{m_{\text{Pl}}^2}{8\pi} \frac{V''}{V}, \quad (25.4)$$

which should satisfy $\epsilon, |\eta| \ll 1$, the spectra can be computed using the slow-roll approximation as

$$\Delta_{\mathcal{R}}^2(k) \simeq \frac{8}{3m_{\text{Pl}}^4} \frac{V}{\epsilon} \Big|_{k=aH}, \quad \Delta_{\mathcal{t}}^2(k) \simeq \frac{128}{3m_{\text{Pl}}^4} V \Big|_{k=aH}. \quad (25.5)$$

In each case, the expressions on the right-hand side are to be evaluated when the scale k is equal to the Hubble radius during inflation. The symbol ‘ \simeq ’ here indicates use of the slow-roll approximation, which is expected to be accurate to a few percent or better.

From these expressions, we can compute the spectral indices [8]:

$$n_s \simeq 1 - 6\epsilon + 2\eta \quad ; \quad n_t \simeq -2\epsilon. \quad (25.6)$$

Another useful quantity is the ratio of the two spectra, defined by

$$r \equiv \frac{\Delta_{\mathcal{t}}^2(k_*)}{\Delta_{\mathcal{R}}^2(k_*)}. \quad (25.7)$$

We have

$$r \simeq 16\epsilon \simeq -8n_t, \quad (25.8)$$

which is known as the consistency equation.

One could consider corrections to the power-law approximation, which we discuss later. However, for now we make the working assumption that the spectra can be approximated by such power laws. The consistency equation shows that r and n_t are not independent parameters, and so the simplest inflation models give initial conditions described by three parameters, usually taken as $\Delta_{\mathcal{R}}^2$, n_s , and r , all to be evaluated at some scale k_* , usually the ‘statistical center’ of the range explored by the data. Alternatively, one could use the parametrization V , ϵ , and η , all evaluated at a point on the putative inflationary potential.

After the perturbations are created in the early Universe, they undergo a complex evolution up until the time they are observed in the present Universe. When the perturbations are small, this can be accurately followed using a linear theory numerical code such as CAMB or CLASS [9]. This works right up to the present for the CMB, but for density perturbations on small scales non-linear evolution is important and can be addressed by a variety of semi-analytical and numerical techniques. However the analysis is made, the outcome of the evolution is in principle determined by the cosmological model and by the parameters describing the initial perturbations, and hence can be used to determine them.

Of particular interest are CMB anisotropies. Both the total intensity and two independent polarization modes are predicted to have anisotropies. These can be described by the radiation angular power spectra C_ℓ as defined in the CMB article in this volume, and again provide a complete description if the density perturbations are Gaussian.

25.1.3 The standard cosmological model

We now have most of the ingredients in place to describe the cosmological model. Beyond those of the previous subsections, we need a measure of the ionization state of the Universe. The Universe is known to be highly ionized at low redshifts (otherwise radiation from distant quasars would be heavily absorbed in the ultra-violet), and the ionized electrons can scatter microwave photons, altering the pattern of observed anisotropies. The most convenient parameter to describe this is the optical depth to scattering τ (*i.e.*, the probability that a given photon scatters once); in the approximation of instantaneous and complete reionization, this could equivalently be described by the redshift of reionization z_{ion} .

As described in Sec. 25.4, models based on these parameters are able to give a good fit to the complete set of high-quality data available at present, and indeed some simplification is possible. Observations are consistent with spatial flatness, and the

inflation models so far described automatically generate negligible spatial curvature, so we can set $k = 0$; the density parameters then must sum to unity, and so one of them can be eliminated. The neutrino energy density is often not taken as an independent parameter; provided that the neutrino sector has the standard interactions, the neutrino energy density, while relativistic, can be related to the photon density using thermal physics arguments, and a minimal assumption takes the neutrino mass sum to be that of the lowest mass solution to the neutrino oscillation constraints, namely 0.06 eV. In addition, there is no observational evidence for the existence of tensor perturbations (though the upper limits are fairly weak), and so r could be set to zero. This leaves seven parameters, which is the smallest set that can usefully be compared to the present cosmological data. This model is referred to by various names, including Λ CDM, the concordance cosmology, and the standard cosmological model.

Of these parameters, only Ω_γ is accurately measured directly. The radiation density is dominated by the energy in the CMB, and the COBE satellite FIRAS experiment determined its temperature to be $T = 2.7255 \pm 0.0006$ K [10],¹ corresponding to $\Omega_\gamma = 2.47 \times 10^{-5} h^{-2}$. It typically can be taken as fixed when fitting other data. Hence the minimum number of cosmological parameters varied in fits to data is six, though as described below there may additionally be many ‘nuisance’ parameters necessary to describe astrophysical processes influencing the data.

In addition to this minimal set, there is a range of other parameters that might prove important in future as the data-sets further improve, but for which there is so far no direct evidence, allowing them to be set to specific values for now. We discuss various speculative options in the next section. For completeness at this point, we mention one other interesting quantity, the helium fraction, which is a non-zero parameter that can affect the CMB anisotropies at a subtle level. It is usually fixed in microwave anisotropy studies, but the data are approaching a level where allowing its variation may become mandatory.

Most attention to date has been on parameter estimation, where a set of parameters is chosen by hand and the aim is to constrain them. Interest has been growing towards the higher-level inference problem of model selection, which compares different choices of parameter sets. Bayesian inference offers an attractive framework for cosmological model selection, setting a tension between model predictiveness and ability to fit the data [11].

25.1.4 Derived parameters

The parameter list of the previous subsection is sufficient to give a complete description of cosmological models that agree with observational data. However, it is not a unique parameterization, and one could instead use parameters derived from that basic set. Parameters that can be obtained from the set given above include the age of the Universe, the present horizon distance, the present neutrino background temperature, the epoch of matter–radiation equality, the epochs of recombination and decoupling, the epoch of transition to an accelerating Universe, the baryon-to-photon ratio, and the baryon-to-dark-matter density ratio. In addition, the physical densities of the matter components, $\Omega_i h^2$, are often more useful than the density parameters. The density perturbation amplitude can be specified in many different ways other than the large-scale primordial amplitude, for instance, in terms of its effect on the CMB, or by specifying a short-scale quantity, a common choice being the present linear-theory mass dispersion on a scale of $8 h^{-1}$ Mpc, known as σ_8 .

Different types of observation are sensitive to different subsets of the full cosmological parameter set, and some are more naturally interpreted in terms of some of the derived parameters of this subsection than on the original base parameter set. In particular, most types of observation feature degeneracies whereby they are unable to separate the effects of simultaneously varying specific combinations of several of the base parameters.

¹Unless stated otherwise, all quoted uncertainties in this article are $1\sigma/68\%$ confidence and all upper limits are 95% confidence. Cosmological parameters sometimes have significantly non-Gaussian uncertainties. Throughout we have rounded central values, and especially uncertainties, from original sources, in cases where they appear to be given to excessive precision.

25.2 Extensions to the standard model

At present, there is no positive evidence in favor of extensions of the standard model. These are becoming increasingly constrained by the data, though there always remains the possibility of trace effects at a level below present observational capability.

25.2.1 More general perturbations

The standard cosmology assumes adiabatic, Gaussian perturbations. Adiabaticity means that all types of material in the Universe share a common perturbation, so that if the space-time is foliated by constant-density hypersurfaces, then all fluids and fields are homogeneous on those slices, with the perturbations completely described by the variation of the spatial curvature of the slices. Gaussianity means that the initial perturbations obey Gaussian statistics, with the amplitudes of waves of different wavenumbers being randomly drawn from a Gaussian distribution of width given by the power spectrum. Note that gravitational instability generates non-Gaussianity; in this context, Gaussianity refers to a property of the initial perturbations, before they evolve.

The simplest inflation models, based on one dynamical field, predict adiabatic perturbations and a level of non-Gaussianity that is too small to be detected by any experiment so far conceived. For present data, the primordial spectra are usually assumed to be power laws.

25.2.1.1 Non-power-law spectra

For typical inflation models, it is an approximation to take the spectra as power laws, albeit usually a good one. As data quality improves, one might expect this approximation to come under pressure, requiring a more accurate description of the initial spectra, particularly for the density perturbations. In general, one can expand $\ln \Delta_{\mathcal{R}}^2$ as

$$\ln \Delta_{\mathcal{R}}^2(k) = \ln \Delta_{\mathcal{R}}^2(k_*) + (n_{s,*} - 1) \ln \frac{k}{k_*} + \frac{1}{2} \frac{dn_s}{d \ln k} \Big|_* \ln^2 \frac{k}{k_*} + \dots, \quad (25.9)$$

where the coefficients are all evaluated at some scale k_* . The term $dn_s/d \ln k|_*$ is often called the running of the spectral index [12]. Once non-power-law spectra are allowed, it is necessary to specify the scale k_* at which the spectral index is defined.

25.2.1.2 Isocurvature perturbations

An isocurvature perturbation is one that leaves the total density unperturbed, while perturbing the relative amounts of different materials. If the Universe contains N fluids, there is one growing adiabatic mode and $N-1$ growing isocurvature modes (for reviews see Ref. [7] and Ref. [13]). These can be excited, for example, in inflationary models where there are two or more fields that acquire dynamically-important perturbations. If one field decays to form normal matter, while the second survives to become the dark matter, this will generate a cold dark matter isocurvature perturbation.

In general, there are also correlations between the different modes, and so the full set of perturbations is described by a matrix giving the spectra and their correlations. Constraining such a general construct is challenging, though constraints on individual modes are beginning to become meaningful, with no evidence that any other than the adiabatic mode must be non-zero.

25.2.1.3 Seeded perturbations

An alternative to laying down perturbations at very early epochs is that they are seeded throughout cosmic history, for instance by topological defects such as cosmic strings. It has long been excluded that these are the sole original of structure, but they could contribute part of the perturbation signal, current limits being just a few percent [14]. In particular, cosmic defects formed in a phase transition ending inflation is a plausible scenario for such a contribution.

25.2.1.4 Non-Gaussianity

Multi-field inflation models can also generate primordial non-Gaussianity (reviewed, *e.g.*, in Ref. [7]). The extra fields can either be in the same sector of the underlying theory as the inflaton, or completely separate, an interesting example of the latter being the curvaton model [15]. Current upper limits on non-Gaussianity are

becoming stringent, but there remains strong motivation to push down those limits and perhaps reveal trace non-Gaussianity in the data. If non-Gaussianity is observed, its nature may favor an inflationary origin, or a different one such as topological defects.

25.2.2 Dark matter properties

Dark matter properties are discussed in the Dark Matter chapter in this volume. The simplest assumption concerning the dark matter is that it has no significant interactions with other matter, and that its particles have a negligible velocity as far as structure formation is concerned. Such dark matter is described as ‘cold,’ and candidates include the lightest supersymmetric particle, the axion, and primordial black holes. As far as astrophysicists are concerned, a complete specification of the relevant cold dark matter properties is given by the density parameter Ω_c , though those seeking to detect it directly need also to know its interaction properties.

Cold dark matter is the standard assumption and gives an excellent fit to observations, except possibly on the shortest scales where there remains some controversy concerning the structure of dwarf galaxies and possible substructure in galaxy halos. It has long been excluded for all the dark matter to have a large velocity dispersion, so-called ‘hot’ dark matter, as it does not permit galaxies to form; for thermal relics the mass must be above about 1 keV to satisfy this constraint, though relics produced non-thermally, such as the axion, need not obey this limit. However, in future further parameters might need to be introduced to describe dark matter properties relevant to astrophysical observations. Suggestions that have been made include a modest velocity dispersion (warm dark matter) and dark matter self-interactions. There remains the possibility that the dark matter is comprised of two separate components, *e.g.*, a cold one and a hot one, an example being if massive neutrinos have a non-negligible effect.

25.2.3 Relativistic species

The number of relativistic species in the young Universe (omitting photons) is denoted N_{eff} . In the standard cosmological model only the three neutrino species contribute, and its baseline value is assumed fixed at 3.045 (the small shift from 3 is because of a slight predicted deviation from a thermal distribution [16]). However other species could contribute, for example an extra neutrino, possibly of sterile type, or massless Goldstone bosons or other scalars. It is hence interesting to study the effect of allowing this parameter to vary, and indeed although 3.045 is consistent with the data, most analyses currently suggest a somewhat higher value (*e.g.*, Ref. [17]).

25.2.4 Dark energy

While the standard cosmological model given above features a cosmological constant, in order to explain observations indicating that the Universe is presently accelerating, further possibilities exist under the general headings of ‘dark energy’ and ‘modified gravity’. These topics are described in detail in the Dark Energy chapter in this volume. This article focuses on the case of the cosmological constant, since this simple model is a good match to existing data. We note that more general treatments of dark energy/modified gravity will lead to weaker constraints on other parameters.

25.2.5 Complex ionization history

The full ionization history of the Universe is given by the ionization fraction as a function of redshift z . The simplest scenario takes the ionization to have the small residual value left after recombination up to some redshift z_{ion} , at which point the Universe instantaneously reionizes completely. Then there is a one-to-one correspondence between τ and z_{ion} (that relation, however, also depending on other cosmological parameters). An accurate treatment of this process will track separate histories for hydrogen and helium. While currently rapid ionization appears to be a good approximation, as data improve a more complex ionization history may need to be considered.

25.2.6 Varying ‘constants’

Variation of the fundamental constants of Nature over cosmological times is another possible enhancement of the standard cosmology. There is a long history of study of variation of the

gravitational constant G_N , and more recently attention has been drawn to the possibility of small fractional variations in the fine-structure constant. There is presently no observational evidence for the former, which is tightly constrained by a variety of measurements. Evidence for the latter has been claimed from studies of spectral line shifts in quasar spectra at redshift $z \approx 2$ [18], but this is presently controversial and in need of further observational study.

25.2.7 Cosmic topology

The usual hypothesis is that the Universe has the simplest topology consistent with its geometry, for example that a flat universe extends forever. Observations cannot tell us whether that is true, but they can test the possibility of a non-trivial topology on scales up to roughly the present Hubble scale. Extra parameters would be needed to specify both the type and scale of the topology; for example, a cuboidal topology would need specification of the three principal axis lengths and orientation. At present, there is no evidence for non-trivial cosmic topology [19].

25.3 Cosmological Probes

The goal of the observational cosmologist is to utilize astronomical information to derive cosmological parameters. The transformation from the observables to the parameters usually involves many assumptions about the nature of the data, as well as of the dark sector. Below we outline the physical processes involved in each of the major probes, and the main recent results. The first two subsections concern probes of the homogeneous Universe, while the remainder consider constraints from perturbations.

In addition to statistical uncertainties we note three sources of systematic uncertainties that will apply to the cosmological parameters of interest: (i) due to the assumptions on the cosmological model and its priors (*i.e.*, the number of assumed cosmological parameters and their allowed range); (ii) due to the uncertainty in the astrophysics of the objects (*e.g.*, light-curve fitting for supernovae or the mass–temperature relation of galaxy clusters); and (iii) due to instrumental and observational limitations (*e.g.*, the effect of ‘seeing’ on weak gravitational lensing measurements, or beam shape on CMB anisotropy measurements).

These systematics, the last two of which appear as ‘nuisance parameters’, pose a challenging problem to the statistical analysis. We attempt a statistical fit to the whole Universe with 6 to 12 parameters, but we might need to include hundreds of nuisance parameters, some of them highly correlated with the cosmological parameters of interest (for example time-dependent galaxy biasing could mimic the growth of mass fluctuations). Fortunately, there is some astrophysical prior knowledge on these effects, and a small number of physically-motivated free parameters would ideally be preferred in the cosmological parameter analysis.

25.3.1 Measures of the Hubble constant

In 1929, Edwin Hubble discovered the law of expansion of the Universe by measuring distances to nearby galaxies. The slope of the relation between the distance and recession velocity is defined to be the present-epoch Hubble constant, H_0 . Astronomers argued for decades about the systematic uncertainties in various methods and derived values over the wide range $40 \text{ km s}^{-1} \text{ Mpc}^{-1} \lesssim H_0 \lesssim 100 \text{ km s}^{-1} \text{ Mpc}^{-1}$.

One of the most reliable results on the Hubble constant came from the Hubble Space Telescope (HST) Key Project [20]. This study used the empirical period–luminosity relation for Cepheid variable stars, and calibrated a number of secondary distance indicators—Type Ia Supernovae (SNe Ia), the Tully–Fisher relation, surface-brightness fluctuations, and Type II Supernovae. This approach was further extended, based on HST observations of 70 long-period Cepheids in the Large Magellanic Cloud, combined with Milky Way parallaxes and masers in NGC4258, to yield $H_0 = 74.0 \pm 1.4 \text{ km s}^{-1} \text{ Mpc}^{-1}$ [21] (the SH0ES project). The major sources of uncertainty in this result are thought to be due to the heavy element abundance of the Cepheids and the distance to the fiducial nearby galaxy, the Large Magellanic Cloud, relative to which all Cepheid distances are measured.

Three other methods have been used recently. One is a calibration of the tip of the red-giant branch applied to Type Ia

supernovae, the Carnegie–Chicago Hubble Programme (CCHP) finding $H_0 = 69.8 \pm 0.8 \text{ (stat.)} \pm 1.7 \text{ (sys.) km s}^{-1} \text{ Mpc}^{-1}$ [22]. The second uses the method of time delay in six gravitationally-lensed quasars, with the result $H_0 = 73.3^{+1.7}_{-1.8} \text{ km s}^{-1} \text{ Mpc}^{-1}$ [23] (HOLiCOW). A third method that came to fruition recently is based on gravitational waves; the ‘bright standard siren’ applied to the binary neutron star GW170817 and the ‘dark standard siren’ implemented on the binary black hole GW170814 yield $H_0 = 70^{+12}_{-8} \text{ km s}^{-1} \text{ Mpc}^{-1}$ [24] and $H_0 = 75^{+40}_{-32} \text{ km s}^{-1} \text{ Mpc}^{-1}$ [25] respectively. With many more gravitational-wave events the future uncertainties on H_0 from standard sirens will get smaller.

The determination of H_0 by the *Planck* Collaboration [2] gives a lower value, $H_0 = 67.4 \pm 0.5 \text{ km s}^{-1} \text{ Mpc}^{-1}$. As discussed in their paper, there is strong degeneracy of H_0 with other parameters, *e.g.*, Ω_m and the neutrino mass. It is worth noting that using the ‘inverse distance ladder’ method gives a result $H_0 = 67.8 \pm 1.3 \text{ km s}^{-1} \text{ Mpc}^{-1}$ [26], close to the *Planck* result. The inverse distance ladder relies on absolute-distance measurements from baryon acoustic oscillations (BAOs) to calibrate the intrinsic magnitude of the SNe Ia (rather than by nearby Cepheids and parallax). This measurement was derived from 207 spectroscopically-confirmed Type Ia supernovae from the Dark Energy Survey (DES), an additional 122 low-redshift SNe Ia, and measurements of BAOs. A combination of DES Y1 clustering and weak lensing with BAO and BBN (assuming Λ CDM) gives $H_0 = 67.4^{+1.1}_{-1.2} \text{ km s}^{-1} \text{ Mpc}^{-1}$ [27].

The tension between the H_0 values from *Planck* and the traditional cosmic distance ladder methods is of great interest and under investigation. For example, the SH0ES and HOLiCOW+SH0ES results deviate from *Planck* by 4.4σ and 5.3σ respectively, while the TRGB and standard-siren results lie between the *Planck* and cosmic ladder H_0 values. There is possibly a trend for higher H_0 derived from the nearby Universe and a lower H_0 from the early Universe, which has led some researchers to propose a time-variation of the dark energy component or other exotic scenarios. Ongoing studies are addressing the question of whether the Hubble tension is due to systematics in at least one of the probes, or a signature of new physics.

Figure 25.1 shows a selection of recent H_0 values, adapted from Ref. [28] which provides a very useful summary of the current status of the Hubble constant tension.

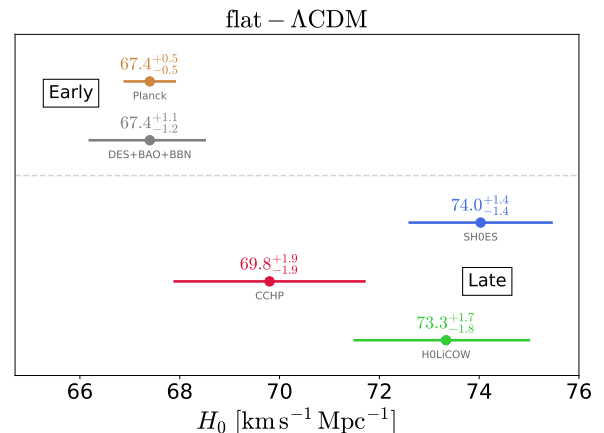


Figure 25.1: A selection of recent H_0 measurements from the various projects as described in the text, divided into early and late Universe probes. The standard-siren determinations are omitted as they are too wide for the plot. Figure courtesy of Vivien Bonvin and Martin Millon, adapted from Ref. [28].

25.3.2 Supernovae as cosmological probes

Empirically, the peak luminosity of SNe Ia can be used as an efficient distance indicator (*e.g.*, Ref. [29]), thus allowing cosmology to be constrained via the distance–redshift relation. The favorite theoretical explanation for SNe Ia is the thermonuclear disruption

of carbon–oxygen white dwarfs. Although not perfect ‘standard candles’, it has been demonstrated that by correcting for a relation between the light-curve shape, color, and luminosity at maximum brightness, the dispersion of the measured luminosities can be greatly reduced. There are several possible systematic effects that may affect the accuracy of the use of SNe Ia as distance indicators, *e.g.*, evolution with redshift and interstellar extinction in the host galaxy and in the Milky Way.

Two major studies, the Supernova Cosmology Project and the High- z Supernova Search Team, found evidence for an accelerating Universe [30], interpreted as due to a cosmological constant or a dark energy component. When combined with the CMB data (which indicate near flatness, *i.e.*, $\Omega_m + \Omega_\Lambda \simeq 1$), the best-fit values were $\Omega_m \approx 0.3$ and $\Omega_\Lambda \approx 0.7$. Most results in the literature are consistent with the $w = -1$ cosmological constant case. One study [31] deduced, from a sample of 740 spectroscopically-confirmed SNe Ia, that $\Omega_m = 0.295 \pm 0.034$ (stat+sym) for an assumed flat Λ CDM model. An analysis of a sample of spectroscopically-confirmed 207 DES SNe Ia combined with 122 low-redshift SNe [32] yielded $\Omega_m = 0.331 \pm 0.038$ for an assumed flat Λ CDM model. In combination with the CMB, for a flat w CDM these data give $w = -0.978 \pm 0.059$ and $\Omega_m = 0.321 \pm 0.018$, consistent with results from the JLA and Pantheon SNe Ia samples. Future experiments will refine constraints on the cosmic equation of state $w(z)$.

25.3.3 Cosmic microwave background

The physics of the CMB is described in detail in the CMB chapter in this volume. Before recombination, the baryons and photons are tightly coupled, and the perturbations oscillate in the potential wells generated primarily by the dark matter perturbations. After decoupling, the baryons are free to collapse into those potential wells. The CMB carries a record of conditions at the time of last scattering, often called primary anisotropies. In addition, it is affected by various processes as it propagates towards us, including the effect of a time-varying gravitational potential (the integrated Sachs–Wolfe effect), gravitational lensing, and scattering from ionized gas at low redshift.

The primary anisotropies, the integrated Sachs–Wolfe effect, and the scattering from a homogeneous distribution of ionized gas, can all be calculated using linear perturbation theory. Available codes include CAMB and CLASS [9], the former widely used embedded within the analysis package CosmoMC [33] and in higher-level analysis packages such as CosmoSIS [34] and CosmoLike [35]. Gravitational lensing is also calculated in these codes. Secondary effects, such as inhomogeneities in the reionization process, and scattering from gravitationally-collapsed gas (the Sunyaev–Zeldovich or SZ effect), require more complicated, and more uncertain, calculations.

The upshot is that the detailed pattern of anisotropies depends on all of the cosmological parameters. In a typical cosmology, the anisotropy power spectrum [usually plotted as $\ell(\ell + 1)C_\ell$] features a flat plateau at large angular scales (small ℓ), followed by a series of oscillatory features at higher angular scales, the first and most prominent being at around one degree ($\ell \simeq 200$). These features, known as acoustic peaks, represent the oscillations of the photon–baryon fluid around the time of decoupling. Some features can be closely related to specific parameters—for instance, the location in multipole space of the set of peaks probes the spatial geometry, while the relative heights of the peaks probe the baryon density—but many other parameters combine to determine the overall shape.

The 2018 data release from the *Planck* satellite [1] gives the most powerful results to date on the spectrum of CMB temperature anisotropies, with a precision determination of the temperature power spectrum to beyond $\ell = 2000$. The Atacama Cosmology Telescope (ACT) and South Pole Telescope (SPT) experiments extend these results to higher angular resolution, though without full-sky coverage. *Planck* and the polarisation-sensitive versions of ACT and SPT give the state of the art in measuring the spectrum of E -polarization anisotropies and the correlation spectrum between temperature and polarization. These are consistent with models based on the parameters we have described, and provide accurate determinations of many of those param-

eters [2]. Primordial B -mode polarization has not been detected (although the gravitational lensing effect on B modes has been measured).

The data provide an exquisite measurement of the location of the set of acoustic peaks, determining the angular-diameter distance of the last-scattering surface. In combination with other data this strongly constrains the spatial geometry, in a manner consistent with spatial flatness and excluding significantly-curved Universes. CMB data give a precision measurement of the age of the Universe. The CMB also gives a baryon density consistent with, and at higher precision than, that coming from BBN. It affirms the need for both dark matter and dark energy. It shows no evidence for dynamics of the dark energy, being consistent with a pure cosmological constant ($w = -1$). The density perturbations are consistent with a power-law primordial spectrum, and there is no indication yet of tensor perturbations. The current best-fit for the reionization optical depth from CMB data, $\tau = 0.054$, is in line with models of how early structure formation induces reionization.

Planck has also made the first all-sky map of the CMB lensing field, which probes the entire matter distribution in the Universe and adds some additional constraining power to the CMB-only data-sets. These measurements are compatible with the expected effect in the standard cosmology.

25.3.4 Galaxy clustering

The power spectrum of density perturbations is affected by the nature of the dark matter. Within the Λ CDM model, the power spectrum shape depends primarily on the primordial power spectrum and on the combination $\Omega_m h$, which determines the horizon scale at matter–radiation equality, with a subdominant dependence on the baryon density. The matter distribution is most easily probed by observing the galaxy distribution, but this must be done with care since the galaxies do not perfectly trace the dark matter distribution. Rather, they are a ‘biased’ tracer of the dark matter [36]. The need to allow for such bias is emphasized by the observation that different types of galaxies show bias with respect to each other. In particular, scale-dependent and stochastic biasing may introduce a systematic effect on the determination of cosmological parameters from redshift surveys [37]. Prior knowledge from simulations of galaxy formation or from gravitational lensing data could help to quantify biasing. Furthermore, the observed 3D galaxy distribution is in redshift space, *i.e.*, the observed redshift is the sum of the Hubble expansion and the line-of-sight peculiar velocity, leading to linear and non-linear dynamical effects that also depend on the cosmological parameters. On the largest length scales, the galaxies are expected to trace the location of the dark matter, except for a constant multiplier b to the power spectrum, known as the linear bias parameter. On scales smaller than 20 Mpc or so, the clustering pattern is ‘squashed’ in the radial direction due to coherent infall, which depends approximately on the parameter $\beta \equiv \Omega_m^{0.6}/b$ (on these shorter scales, more complicated forms of biasing are not excluded by the data). On scales of a few Mpc, there is an effect of elongation along the line of sight (colloquially known as the ‘finger of God’ effect) that depends on the galaxy velocity dispersion.

25.3.4.1 Baryon acoustic oscillations

The power spectra of the 2-degree Field (2dF) Galaxy Redshift Survey and the Sloan Digital Sky Survey (SDSS) are well fit by a Λ CDM model and both surveys showed first evidence for baryon acoustic oscillations (BAOs) [38,39]. The Baryon Oscillation Spectroscopic Survey (BOSS) of luminous red galaxies (LRGs) in the SDSS (DR 12) found, using a sample of 1.2 million galaxies, consistency with $w = -1.01 \pm 0.06$ [40] when combined with *Planck* 2015. Similar results for w were obtained by the WiggleZ survey [41].

25.3.4.2 Redshift distortion

There is renewed interest in the ‘redshift distortion’ effect. This distortion depends on cosmological parameters [42] via the perturbation growth rate in linear theory $f(z) = d \ln \delta / d \ln a \approx \Omega^\gamma(z)$, where $\gamma \simeq 0.55$ for the Λ CDM model and may be different for modified gravity models. By measuring $f(z)$ it is feasible to constrain γ and rule out certain modified gravity models [43,44].

We note the degeneracy of the redshift-distortion pattern and the geometric distortion (the so-called Alcock–Paczynski effect [45]) *e.g.*, as illustrated by the WiggleZ survey [46] and the BOSS Survey [47].

25.3.4.3 Limits on neutrino mass from galaxy surveys and other probes

Large-scale structure data place constraints on Ω_ν due to the neutrino free-streaming effect [48]. Presently there is no clear detection, and upper limits on neutrino mass are commonly estimated by comparing the observed galaxy power spectrum with a four-component model of baryons, cold dark matter, a cosmological constant, and massive neutrinos. Such analyses also assume that the primordial power spectrum is adiabatic, scale-invariant, and Gaussian. Potential systematic effects include biasing of the galaxy distribution and non-linearities of the power spectrum. An upper limit can also be derived from CMB anisotropies alone, while combination with additional cosmological data-sets can improve the results.

The most recent results on neutrino mass upper limits and other neutrino properties are summarised in the Neutrinos in Cosmology chapter in this volume. While the latest cosmological data do not yet constrain the sum of neutrino masses to below 0.2 eV, since the lower limit on this sum from oscillation experiments is 0.06 eV it is expected that future cosmological surveys will soon detect effects from the neutrino mass. Also, current cosmological datasets are in good agreement with the standard value for the effective number of neutrino species $N_{\text{eff}} = 3.045$.

25.3.5 Clustering in the inter-galactic medium

It is commonly assumed, based on hydrodynamic simulations, that the neutral hydrogen in the inter-galactic medium (IGM) can be related to the underlying mass distribution. It is then possible to estimate the matter power spectrum on scales of a few megaparsecs from the absorption observed in quasar spectra, the so-called Lyman- α forest. The usual procedure is to measure the power spectrum of the transmitted flux, and then to infer the mass power spectrum. Photo-ionization heating by the ultraviolet background radiation and adiabatic cooling by the expansion of the Universe combine to give a simple power-law relation between the gas temperature and the baryon density. It also follows that there is a power-law relation between the optical depth τ and ρ_b . Therefore, the observed flux $F = \exp(-\tau)$ is strongly correlated with ρ_b , which itself traces the mass density. The matter and flux power spectra can be related by a biasing function that is calibrated from simulations.

A study of 266,590 quasars in the range $1.77 < z < 3$ from SDSS was used to measure the BAO scale from the 3D correlation of Lyman- α and quasars [49]. Combined with the Lyman- α auto-correlation measurement presented in a companion paper [50] the BAO measurements at $z = 2.34$ are within 1.7σ of the *Planck* 2018 Λ CDM model. The Lyman- α flux power spectrum has also been used to constrain the nature of dark matter, for example limiting the amount of warm dark matter [51].

25.3.6 Weak gravitational lensing

Images of background galaxies are distorted by the gravitational effect of mass variations along the line of sight. Deep gravitational potential wells, such as galaxy clusters, generate ‘strong lensing’ leading to arcs, arcllets, and multiple images, while more moderate perturbations give rise to ‘weak lensing’. Weak lensing is now widely used to measure the mass power spectrum in selected regions of the sky (see Ref. [55] for reviews). Since the signal is weak, the image of deformed galaxy shapes (the ‘shear map’) must be analyzed statistically to measure the power spectrum, higher moments, and cosmological parameters. There are various systematic effects in the interpretation of weak lensing, *e.g.*, due to atmospheric distortions during observations, the redshift distribution of the background galaxies (usually depending on the accuracy of photometric redshifts), the intrinsic correlation of galaxy shapes, and non-linear modeling uncertainties.

As one example, the ‘Kilo-Degree Survey’ (KiDS), combined with the VISTA VIKING survey, used weak-lensing measure-

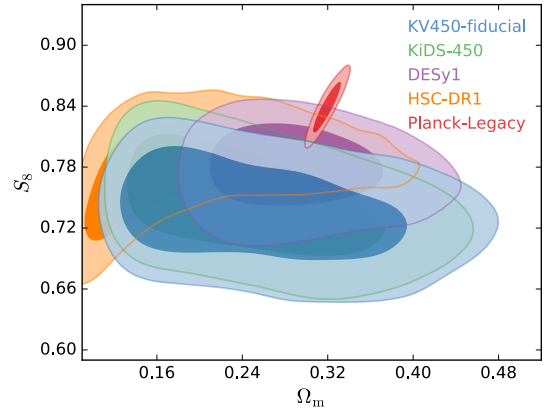


Figure 25.2: Marginalised posterior contours (inner 68% confidence level, outer 95% confidence level) in the Ω_m - S_8 plane. Shown are the optical-only KiDS-450 analysis (green; Ref. [52]), the fiducial KiDS+VISTA-450 setup (blue; Ref. [52]), DES Year 1 using cosmic shear only (purple; Ref. [53]), HSC-DR1 cosmic shear (orange; Ref. [54]) and the *Planck* Legacy analysis (red; *Planck* Collaboration [2] using TT+TE+EE+lowE). Figure from Ref. [52].

ments over 450 deg^2 to constrain the clumpiness parameter $S_8 \equiv \sigma_8(\Omega_m/0.3)^{0.5} = 0.737^{+0.040}_{-0.036}$ [52]. This is lower by 2.3σ than S_8 derived from *Planck*. Figure 25.2 (which is Figure 4 from Ref. [52]) shows the Ω_m - S_8 constraints derived from weak lensing of KiDS, DES, and HPC versus the CMB constraint from *Planck*. Variations in S_8 among the weak-lensing surveys are mainly due to difference in the procedures for photometric redshift determinations. Results from weak lensing from DES, combined with other probes, are shown in the next section.

25.3.7 Other probes

Other probes that have been used to constrain cosmological parameters, but that are not presently competitive in terms of accuracy, are the integrated Sachs–Wolfe effect [56] [57], the number density or composition of galaxy clusters [58], and galaxy peculiar velocities, which probe the mass fluctuations in the local Universe [59].

25.4 Bringing probes together

Although it contains two ingredients—dark matter and dark energy—which have not yet been verified by laboratory experiments, the Λ CDM model is almost universally accepted by cosmologists as the best description of the present data. The approximate values of some of the key parameters are $\Omega_b \approx 0.05$, $\Omega_c \approx 0.25$, $\Omega_\Lambda \approx 0.70$, and a Hubble constant $h \approx 0.70$. The spatial geometry is very close to flat (and usually assumed to be precisely flat), and the initial perturbations Gaussian, adiabatic, and nearly scale-invariant.

The most powerful data source is the CMB, which on its own supports all these main tenets. Values for some parameters, as given in Ref. [2], are reproduced in Table 25.1. These particular results presume a flat Universe. The constraints are somewhat strengthened by adding additional data-sets, BAO being shown in the Table as an example, though most of the constraining power resides in the CMB data. Similar constraints at lower precision were previously obtained by the *WMAP* collaboration.

If the assumption of spatial flatness is lifted, it turns out that the primary CMB on its own constrains the spatial curvature fairly weakly, due to a parameter degeneracy in the angular-diameter distance. However, inclusion of other data readily removes this degeneracy. Simply adding the *Planck* lensing measurement, and with the assumption that the dark energy is a cosmological constant, yields a 68% confidence constraint on $\Omega_{\text{tot}} \equiv \sum \Omega_i + \Omega_\Lambda = 1.011 \pm 0.006$ and further adding BAO makes it 0.9993 ± 0.0019 [2]. Results of this type are normally taken as justifying the restriction to flat cosmologies.

One derived parameter that is very robust is the age of the

Table 25.1: Parameter constraints reproduced from Ref. [2] (Table 2, column 5), with some additional rounding. Both columns assume the Λ CDM cosmology with a power-law initial spectrum, no tensors, spatial flatness, a cosmological constant as dark energy, and the sum of neutrino masses fixed to 0.06 eV. Above the line are the six parameter combinations actually fit to the data (θ_{MC} is a measure of the sound horizon at last scattering); those below the line are derived from these. The first column uses *Planck* primary CMB data plus the *Planck* measurement of CMB lensing. This column gives our present recommended values. The second column adds in data from a compilation of BAO measurements described in Ref. [2]. The perturbation amplitude $\Delta_{\mathcal{R}}^2$ (denoted A_s in the original paper) is specified at the scale 0.05 Mpc^{-1} . Uncertainties are shown at 68% confidence.

	<i>Planck</i> TT,TE,EE+lowE+lensing	+BAO
$\Omega_b h^2$	0.02237 ± 0.00015	0.02242 ± 0.00014
$\Omega_c h^2$	0.1200 ± 0.0012	0.1193 ± 0.0009
$100 \theta_{\text{MC}}$	1.0409 ± 0.0003	1.0410 ± 0.0003
n_s	0.965 ± 0.004	0.966 ± 0.004
τ	0.054 ± 0.007	0.056 ± 0.007
$\ln(10^{10} \Delta_{\mathcal{R}}^2)$	3.044 ± 0.014	3.047 ± 0.014
h	0.674 ± 0.005	0.677 ± 0.004
σ_8	0.811 ± 0.006	0.810 ± 0.006
Ω_m	0.315 ± 0.007	0.311 ± 0.006
Ω_Λ	0.685 ± 0.007	0.689 ± 0.006

Universe, since there is a useful coincidence that for a flat Universe the position of the first peak is strongly correlated with the age. The CMB data give 13.797 ± 0.023 Gyr (assuming flatness). This is in good agreement with the ages of the oldest globular clusters and with radioactive dating.

The baryon density Ω_b is now measured with high accuracy from CMB data alone, and is consistent with and much more precise than the determination from BBN. The value quoted in the Big-Bang Nucleosynthesis chapter in this volume is $0.021 \leq \Omega_b h^2 \leq 0.024$ (95% confidence).

While Ω_Λ is measured to be non-zero with very high confidence, there is no evidence of evolution of the dark energy density. As described in the Dark Energy chapter in this volume, from a combination of CMB, weak gravitational lensing, SN, and BAO measurements, assuming a flat universe, Ref. [2] found $w = -1.028 \pm 0.031$, consistent with the cosmological constant case $w = -1$. Allowing more complicated forms of dark energy weakens the limits.

The data provide strong support for the main predictions of the simplest inflation models: spatial flatness and adiabatic, Gaussian, nearly scale-invariant density perturbations. But it is disappointing that there is no sign of primordial gravitational waves, with a 95% confidence upper limit from combining *Planck* with BICEP2/Keck Array BK15 data of $r < 0.06$ at the scale 0.002 Mpc^{-1} [60] (weakening somewhat if running is allowed). The spectral index is clearly required to be less than one by current data, though the strength of that conclusion can weaken if additional parameters are included in the model fits.

Tests have been made for various types of non-Gaussianity, a particular example being a parameter f_{NL} that measures a quadratic contribution to the perturbations. Various non-Gaussian shapes are possible (see Ref. [61] for details), and current constraints on the popular ‘local’, ‘equilateral’, and ‘orthogonal’ types (combining temperature and polarization data) are $f_{\text{NL}}^{\text{local}} = -1 \pm 5$, $f_{\text{NL}}^{\text{equil}} = -26 \pm 47$, and $f_{\text{NL}}^{\text{ortho}} = -38 \pm 24$ respectively (these look weak, but prominent non-Gaussianity requires the product $f_{\text{NL}} \Delta_{\mathcal{R}}$ to be large, and $\Delta_{\mathcal{R}}$ is of order 10^{-5}). Clearly none of these give any indication of primordial non-gaussianity.

While the above results come from the CMB alone, other probes are becoming competitive (especially when considering more complex cosmological models), and so combination of data from different sources is of growing importance. We note that it has become fashionable to combine probes at the level of power-spectrum data vectors, taking into account nuisance parameters in each type of measurement. Recent examples include KiDS+GAMA [62] and Dark Energy Survey (DES) Year 1 [63]. For example, the DES analysis includes galaxy position–position clustering, galaxy–galaxy lensing, and weak lensing shear. Discussions on ‘tension’ in resulting cosmological parameters depend on the statistical approaches used. Commonly the cosmology community works within the Bayesian framework, and assesses agreement amongst data sets with respect to a model via Bayesian Evidence, essentially the denominator in Bayes’s theorem. As an example of results, combining DES Y1 with *Planck*, BAO measurements from SDSS, 6dF, and BOSS, and type Ia supernovae from the Joint Lightcurve Analysis (JLA) dataset has shown the datasets to be mutually compatible and yields very tight constraints on cosmological parameters: $S_8 \equiv \sigma_8 (\Omega_m/0.3)^{0.5} = 0.799_{-0.009}^{+0.014}$, and $\Omega_m = 0.301_{-0.008}^{+0.006}$ in Λ CDM, and $w = -1.00_{-0.05}^{+0.04}$ in w CDM [63]. The combined measurement of the Hubble constant within Λ CDM gives $H_0 = 68.2 \pm 0.6 \text{ km s}^{-1} \text{ Mpc}^{-1}$, still leaving some level of tension with the local measurements described earlier. Future analyses and the next generation of surveys will test for deviations from Λ CDM, for example epoch-dependent $w(z)$ and modifications to General Relativity.

25.5 Outlook for the future

The concordance model is now well established, and there seems little room left for any dramatic revision of this paradigm. A measure of the strength of that statement is how difficult it has proven to formulate convincing alternatives.

Should there indeed be no major revision of the current paradigm, we can expect future developments to take one of two directions. Either the existing parameter set will continue to prove sufficient to explain the data, with the parameters subject to ever-tightening constraints, or it will become necessary to deploy new parameters. The latter outcome would be very much the more interesting, offering a route towards understanding new physical processes relevant to the cosmological evolution. There are many possibilities on offer for striking discoveries, for example:

- the cosmological effects of a neutrino mass may be unambiguously detected, shedding light on fundamental neutrino properties;
- detection of primordial non-Gaussianities would indicate that non-linear processes influence the perturbation generation mechanism;
- detection of variation in the dark-energy density (*i.e.*, $w \neq -1$) would provide much-needed experimental input into its nature.

These provide more than enough motivation for continued efforts to test the cosmological model and improve its accuracy. Over the coming years, there are a wide range of new observations that will bring further precision to cosmological studies. Indeed, there are far too many for us to be able to mention them all here, and so we will just highlight a few areas.

The CMB observations will improve in several directions. A current frontier is the study of polarization, for which power spectrum measurements have now been made by several experiments. Detection of primordial B -mode anisotropies is the next major goal and a variety of projects are targeting this, though theory gives little guidance as to the likely signal level. Future CMB projects that are approved include *LiteBIRD* and the Simons Observatory.

An impressive array of cosmology surveys are already operational, under construction, or proposed, including the ground-based Hyper Suprime Camera (HSC) and Large Synoptic Survey Telescope (LSST) imaging surveys, spectroscopic surveys such as the Dark Energy Spectroscopic Instrument (DESI), and space missions *Euclid* and the Wide-Field Infrared Survey (WFIRST).

An exciting area for the future is radio surveys of the redshifted 21-cm line of hydrogen. Because of the intrinsic narrowness of this line, by tuning the bandpass the emission from narrow redshift slices of the Universe will be measured to extremely high redshift, probing the details of the reionization process at redshifts up to perhaps 20, as well as measuring large-scale features such as the BAOs. LOFAR and CHIME are the first instruments able to do this and have begun operations. In the longer term, the Square Kilometre Array (SKA) will take these studies to a precision level.

The development of the first precision cosmological model is a major achievement. However, it is important not to lose sight of the motivation for developing such a model, which is to understand the underlying physical processes at work governing the Universe's evolution. From that perspective, progress has been much less dramatic. For instance, there are many proposals for the nature of the dark matter, but no consensus as to which is correct. The nature of the dark energy remains a mystery. Even the baryon density, now measured to an accuracy of a percent, lacks an underlying theory able to predict it within orders of magnitude. Precision cosmology may have arrived, but at present many key questions remain to motivate and challenge the cosmology community.

References

- [1] Y. Akrami *et al.* (Planck) (2018), [arXiv:1807.06205].
- [2] N. Aghanim *et al.* (Planck) (2018), [arXiv:1807.06209].
- [3] C. L. Bennett *et al.* (WMAP), *Astrophys. J. Suppl.* **208**, 20 (2013), [arXiv:1212.5225].
- [4] G. Hinshaw *et al.* (WMAP), *Astrophys. J. Suppl.* **208**, 19 (2013), [arXiv:1212.5226].
- [5] S. Fukuda *et al.* (Super-Kamiokande), *Phys. Rev. Lett.* **85**, 3999 (2000), [hep-ex/0009001]; Q. R. Ahmad *et al.* (SNO), *Phys. Rev. Lett.* **87**, 071301 (2001), [arXiv:nucl-ex/0106015].
- [6] E.W. Kolb and M.S. Turner, *The Early Universe*, Addison-Wesley (Redwood City, 1990).
- [7] D.H. Lyth and A.R. Liddle, *The Primordial Density Perturbation*, Cambridge University Press (2009).
- [8] A. R. Liddle and D. H. Lyth, *Phys. Lett.* **B291**, 391 (1992), [arXiv:astro-ph/9208007].
- [9] A. Lewis, A. Challinor and A. Lasenby, *Astrophys. J.* **538**, 473 (2000), [arXiv:astro-ph/9911177]; D. Blas, J. Lesgourgues and T. Tram, *JCAP* **1107**, 034 (2011), [arXiv:1104.2933].
- [10] D. J. Fixsen, *Astrophys. J.* **707**, 916 (2009), [arXiv:0911.1955].
- [11] M. Hobson *et al.* (eds), *Bayesian Methods in Cosmology*, Cambridge University Press (2009).
- [12] A. Kosowsky and M. S. Turner, *Phys. Rev.* **D52**, R1739 (1995), [arXiv:astro-ph/9504071].
- [13] K. A. Malik and D. Wands, *Phys. Rept.* **475**, 1 (2009), [arXiv:0809.4944].
- [14] P. A. R. Ade *et al.* (Planck), *Astron. Astrophys.* **571**, A25 (2014), [arXiv:1303.5085].
- [15] D. H. Lyth and D. Wands, *Phys. Lett.* **B524**, 5 (2002), [hep-ph/0110002]; K. Enqvist and M. S. Sloth, *Nucl. Phys.* **B626**, 395 (2002), [hep-ph/0109214]; T. Moroi and T. Takahashi, *Phys. Lett.* **B522**, 215 (2001), [Erratum: *Phys. Lett.* **B539**, 303(2002)], [hep-ph/0110096].
- [16] P. F. de Salas and S. Pastor, *JCAP* **1607**, 07, 051 (2016), [arXiv:1606.06986].
- [17] S. Riemer-Sørensen, D. Parkinson, and T.M. Davis, *Publications of Astronomical Society of the Pacific* **30**, e029 (2013).
- [18] J. K. Webb *et al.*, *Phys. Rev. Lett.* **107**, 191101 (2011), [arXiv:1008.3907]; J. A. King *et al.*, *Mon. Not. Roy. Astron. Soc.* **422**, 3370 (2012), [arXiv:1202.4758]; P. Molaro *et al.*, *Astron. & Astrophys.* **555**, 68 (2013).
- [19] P. A. R. Ade *et al.* (Planck), *Astron. Astrophys.* **594**, A18 (2016), [arXiv:1502.01593].
- [20] W. L. Freedman *et al.* (HST), *Astrophys. J.* **553**, 47 (2001), [arXiv:astro-ph/0012376].
- [21] A. G. Riess *et al.*, *Astrophys. J.* **876**, 1, 85 (2019), [arXiv:1903.07603].
- [22] W.L. Freedman *et al.*, *Astrophys. J.* **882**, 34(2019).
- [23] K. C. Wong *et al.* (2019), [arXiv:1907.04869].
- [24] B. P. Abbott *et al.* (LIGO Scientific, Virgo, 1M2H, Dark Energy Camera GW-E, DES, DLT40, Las Cumbres Observatory, VINROUGE, MASTER), *Nature* **551**, 7678, 85 (2017), [arXiv:1710.05835].
- [25] M. Soares-Santos *et al.* (DES, LIGO Scientific, Virgo), *Astrophys. J.* **876**, 1, L7 (2019), [arXiv:1901.01540].
- [26] E. Macaulay *et al.* (DES), *Mon. Not. Roy. Astron. Soc.* **486**, 2, 2184 (2019), [arXiv:1811.02376].
- [27] T. M. C. Abbott *et al.* (DES), *Mon. Not. Roy. Astron. Soc.* **480**, 3, 3879 (2018), [arXiv:1711.00403].
- [28] L. Verde, T. Treu and A. G. Riess, in "Nature Astronomy 2019," (2019), [arXiv:1907.10625].
- [29] B. Leibundgut, *Ann. Rev. Astron. Astrophys.* **39**, 67 (2001).
- [30] A. G. Riess *et al.* (Supernova Search Team), *Astron. J.* **116**, 1009 (1998), [arXiv:astro-ph/9805201]; P. M. Garnavich *et al.* (Supernova Search Team), *Astrophys. J.* **509**, 74 (1998), [arXiv:astro-ph/9806396]; S. Perlmutter *et al.* (Supernova Cosmology Project), *Astrophys. J.* **517**, 565 (1999), [arXiv:astro-ph/9812133].
- [31] M. Betoule *et al.* (SDSS), *Astron. Astrophys.* **568**, A22 (2014), [arXiv:1401.4064].
- [32] T. M. C. Abbott *et al.* (DES), *Astrophys. J.* **872**, 2, L30 (2019), [arXiv:1811.02374].
- [33] A. Lewis and S. Bridle, *Phys. Rev.* **D66**, 103511 (2002), [arXiv:astro-ph/0205436].
- [34] J. Zuntz *et al.*, *Astron. Comput.* **12**, 45 (2015), [arXiv:1409.3409].
- [35] E. Krause and T. Eifler, *Mon. Not. Roy. Astron. Soc.* **470**, 2, 2100 (2017), [arXiv:1601.05779].
- [36] N. Kaiser, *Astrophys. J.* **284**, L9 (1984).
- [37] A. Dekel and O. Lahav, *Astrophys. J.* **520**, 24 (1999), [arXiv:astro-ph/9806193].
- [38] D. J. Eisenstein *et al.* (SDSS), *Astrophys. J.* **633**, 560 (2005), [arXiv:astro-ph/0501171].
- [39] S. Cole *et al.* (2dFGRS), *Mon. Not. Roy. Astron. Soc.* **362**, 505 (2005), [arXiv:astro-ph/0501174].
- [40] S. Alam *et al.* (BOSS), *Mon. Not. Roy. Astron. Soc.* **470**, 3, 2617 (2017), [arXiv:1607.03155].
- [41] D. Parkinson *et al.*, *Phys. Rev.* **D86**, 103518 (2012), [arXiv:1210.2130].
- [42] N. Kaiser, *Mon. Not. Roy. Astron. Soc.* **227**, 1 (1987).
- [43] L. Guzzo *et al.*, *Nature* **451**, 541 (2008), [arXiv:0802.1944].
- [44] A. Nusser and M. Davis, *Astrophys. J.* **736**, 93 (2011), [arXiv:1101.1650].
- [45] C. Alcock and B. Paczynski, *Nature* **281**, 358 (1979).
- [46] C. Blake *et al.*, *Mon. Not. Roy. Astron. Soc.* **425**, 405 (2012), [arXiv:1204.3674].
- [47] H. Gil-Marín *et al.*, *Mon. Not. Roy. Astron. Soc.* **465**, 2, 1757 (2017), [arXiv:1606.00439].
- [48] J. Lesgourgues and S. Pastor, *Phys. Rept.* **429**, 307 (2006), [arXiv:astro-ph/0603494].
- [49] M. Blomqvist *et al.*, *Astron. Astrophys.* **629**, A86 (2019), [arXiv:1904.03430].
- [50] V. de Sainte Agathe *et al.*, *Astron. Astrophys.* **629**, A85 (2019), [arXiv:1904.03400].
- [51] M. Viel *et al.*, *Phys. Rev.* **D88**, 043502 (2013), [arXiv:1306.2314].

- [52] H. Hildebrandt *et al.*, *Astron. Astrophys.* **633**, A69 (2020), [arXiv:1812.06076].
- [53] M. A. Troxel *et al.* (DES), *Phys. Rev.* **D98**, 4, 043528 (2018), [arXiv:1708.01538].
- [54] Higake M. *et al.*, *Pub. Astron. Soc. Japan* **71**, 43 (2018).
- [55] A. Refregier, *Ann. Rev. Astron. Astrophys.* **41**, 645 (2003), [arXiv:astro-ph/0307212]; R. Massey *et al.*, *Nature* **445**, 286 (2007), [arXiv:astro-ph/0701594]; H. Hoekstra and B. Jain, *Ann. Rev. Nucl. Part. Sci.* **58**, 99 (2008), [arXiv:0805.0139].
- [56] R. G. Crittenden and N. Turok, *Phys. Rev. Lett.* **75**, 2642 (1995), [arXiv:astro-ph/9505120].
- [57] Planck Collab. 2015 Results XIX, *Astron. & Astrophys.* **594**, A21 (2016).
- [58] P. A. R. Ade *et al.* (Planck), *Astron. Astrophys.* **594**, A24 (2016), [arXiv:1502.01597].
- [59] A. Dekel, *Ann. Rev. Astron. Astrophys.* **32**, 371 (1994), [arXiv:astro-ph/9401022].
- [60] Y. Akrami *et al.* (Planck) (2018), [arXiv:1807.06211].
- [61] Y. Akrami *et al.* (Planck) (2019), [arXiv:1905.05697].
- [62] E. van Uitert *et al.*, *Mon. Not. Roy. Astron. Soc.* **476**, 4, 4662 (2018), [arXiv:1706.05004].
- [63] T. M. C. Abbott *et al.* (DES), *Phys. Rev.* **D98**, 4, 043526 (2018), [arXiv:1708.01530].

26. Neutrinos in Cosmology

Revised August 2019 by J. Lesgourgues (TTK, RWTH) and L. Verde (ICC, U. of Barcelona; ICREA, Barcelona).

26.1 Standard neutrino cosmology

Neutrino properties leave detectable imprints on cosmological observations that can then be used to constrain neutrino properties. This is a great example of the remarkable interconnection and interplay between nuclear physics, particle physics, astrophysics and cosmology (for general reviews see *e.g.*, [1–4]). Present cosmological data are already providing constraints on neutrino properties not only complementary but also competitive with terrestrial experiments; for instance, upper bounds on the total neutrino mass have shrunk by a factor of about 14 in the past 17 years. Forthcoming cosmological data may soon provide key information, not obtainable in other ways like *e.g.*, a measurement of the absolute neutrino mass scale. This new section is motivated by this exciting prospect.

A relic neutrino background pervading the Universe (the Cosmic Neutrino background, $\nu\bar{\nu}$) is a generic prediction of the standard hot Big Bang model (see Big Bang Nucleosynthesis – Chap. 24 of this *Review*). While it has not yet been detected directly, it has been indirectly confirmed by the accurate agreement of predictions and observations of: *a*) the primordial abundance of light elements (see Big Bang Nucleosynthesis – Chap. 24 of this *Review*; *b*) the power spectrum of Cosmic Microwave Background (CMB) anisotropies (see Cosmic Microwave Background – Chap. 29 of this *Review*); and *c*) the large scale clustering of cosmological structures. Within the hot Big Bang model such good agreement would fail dramatically without a $\nu\bar{\nu}$ with properties matching closely those predicted by the standard neutrino decoupling process (*i.e.*, involving only weak interactions).

We will illustrate below that cosmology is sensitive to the following neutrino properties: their density, related to the number of active (*i.e.*, left-handed, see Neutrino Mass, Mixing, and Oscillations – Chap. 14 of this *Review*) neutrino species, and their masses. At first order, cosmology is sensitive to the total neutrino mass, but is blind to the mixing angles and CP violation phase as discussed in Neutrino Mass, Mixing, and Oscillations (Chap. 14 of this *Review*). This makes cosmological constraints nicely complementary to measurements from terrestrial neutrino experiments.

The minimal cosmological model, Λ CDM, currently providing a good fit to most cosmological data sets (up to moderate tensions discussed in The Cosmological Parameters Chap. 25.1 of this *Review*), assumes that the only massless or light (sub-keV) relic particles since the Big Bang Nucleosynthesis (BBN) epoch are photons and active neutrinos. Extended models with light sterile neutrinos, light thermal axions or other light relics – sometimes referred to as “dark radiation” – would produce effects similar to, and potentially degenerate with, those of active neutrinos. Thus neutrino bounds are often discussed together with limits on such scenarios. In case of anomalies in cosmological data, it might not be obvious to discriminate between interpretation in terms of active neutrinos with non-standard decoupling, additional production mechanisms, non-standard interactions, etc., or in terms of some additional light particles. Such extensions are currently being explored as a possible way to resolve the H_0 tension between late and early universe determinations, but are not widely favoured [5–8].

Hence neutrino density and mass bounds can be derived under the assumption of no additional massless or light relic particles, and the neutrino density measured in that way provides a test of standard (*i.e.*, involving only weak interactions) neutrino decoupling.

In that model, the three active neutrino types thermalize in the early Universe, with a negligible leptonic asymmetry. Then they can be viewed as three propagating mass eigenstates sharing the same temperature and identical Fermi-Dirac distributions, thus with no visible effects of flavour oscillations. Neutrinos decouple gradually from the thermal plasma at temperatures $T \sim 2$ MeV. In the instantaneous neutrino decoupling limit, *i.e.*, assuming that neutrinos were fully decoupled at the time when electron-positrons annihilate and release entropy in the thermal bath, the neutrino-

to-photon density ratio between the time of electron-positron annihilation and the non-relativistic transition of neutrinos would be given by

$$\frac{\rho_\nu}{\rho_\gamma} = \frac{7}{8} N_{\text{eff}} \left(\frac{4}{11} \right)^{4/3}, \quad (26.1)$$

with $N_{\text{eff}} = 3$, and the last factor comes from the fourth power of the temperature ratio $T_\nu/T_\gamma = (4/11)^{1/3}$ (see Big Bang Cosmology – Chap. 22 in this *Review*). In the above formula, N_{eff} is called the effective number of neutrino species because it can be viewed as a convenient parametrisation of the relativistic energy density of the Universe beyond that of photons, in units of one neutrino in the instantaneous decoupling limit. Precise simulations of neutrino decoupling and electron-positron annihilation, taking into account flavor oscillations, provide precise predictions for the actual phase-space distribution of relic neutrinos [9–12]. These distributions differ from the instantaneous decoupling approximation through a combination of a small shift in the photon temperature and small non-thermal distortions, all at the percent level. The final result for the density ratio ρ_ν/ρ_γ in the relativistic regime can always be expressed as in Eq. (26.1), but with a different value of N_{eff} . The most recent analysis, that includes the effect of neutrino oscillations with the present values of the mixing parameters and an improved calculation of the collision terms, gives $N_{\text{eff}} = 3.045$ [12]. The precise number density ratio n_ν/n_γ can also be derived from such studies, and is important for computing the ratio $\Omega_\nu h^2 / \sum_i m_i$ (ratio of the physical density of neutrinos in units of the critical density to the sum of neutrino masses) in the non-relativistic regime.

The neutrino temperature today, $T_\nu^0 \simeq 1.7 \times 10^{-4}$ eV $\simeq 1.9$ K, is smaller than at least two of the neutrino masses, since the two squared-mass differences are $|\Delta m_{31}^2|^{1/2} > |\Delta m_{21}^2|^{1/2} > T_\nu^0$ (see Neutrino mass, Mixing, and oscillations – Chap. 14 of this *Review*). Thus at least two neutrino mass eigenstates are non-relativistic today and behave as a small “hot” fraction of the total dark matter (they cannot be all the dark matter, as explained in Chap. 27 in this *Review*). This fraction of hot dark matter can be probed by cosmological experiments, for two related reasons, as we now describe.

First, neutrinos are the only known particles behaving as radiation at early times (during the CMB acoustic oscillations) and dark matter at late times (during structure formation), which has consequences on the background evolution. Neutrinos become non-relativistic when their mass is equal to their average momentum, given for any Fermi-Dirac-distributed particle by $\langle p \rangle = 3.15 T$. Thus the redshift of the non-relativistic transition is given by $z_i^{\text{nr}} = m_i / (3.15 T_\nu^0) - 1 = m_i / [0.53 \text{ meV}] - 1$ for each eigenstate of mass m_i , giving for instance $z_i^{\text{nr}} = 110$ for $m_i = 60$ meV, corresponding to a time deep inside the matter-dominated regime. Second, until the non-relativistic transition, neutrinos travel at the speed of light, and later on they move at a typical velocity $\langle v_i/c \rangle = 3.15 T_\nu(z) / m_i = 0.53(1+z) \text{ meV} / m_i$, which is several orders of magnitude larger than that of the dominant cold (or even of possibly warm) dark matter component(s). This brings their characteristic diffusion scale, called the “free-streaming length”, to cosmological relevant values, with consequences on gravitational clustering and the growth of structure.

Once neutrinos are non-relativistic, their energy density is given by $\rho_\nu \simeq \sum m_i n_i$. Since the number densities n_i are equal to each other (up to negligible corrections coming from flavour effects in the decoupling phase), the total mass ($\sum m_\nu$) = $m_1 + m_2 + m_3$ can be factorized out. It is possible that the lightest neutrino is still relativistic today, in which case this relation is slightly incorrect, but given that the total density is always strongly dominated by that of non-relativistic neutrinos, the error made is completely negligible. Using the expression for n_i/n_γ obtained from precise neutrino decoupling studies, and knowing n_γ from the measurement of the CMB temperature, one can compute ρ_ν^0 , the total neutrino density today, in units of the critical density ρ_{crit}^0 [12]:

$$\Omega_\nu = \frac{\rho_\nu^0}{\rho_{\text{crit}}^0} = \frac{\sum m_\nu}{93.14 h^2 \text{ eV}}, \quad (26.2)$$

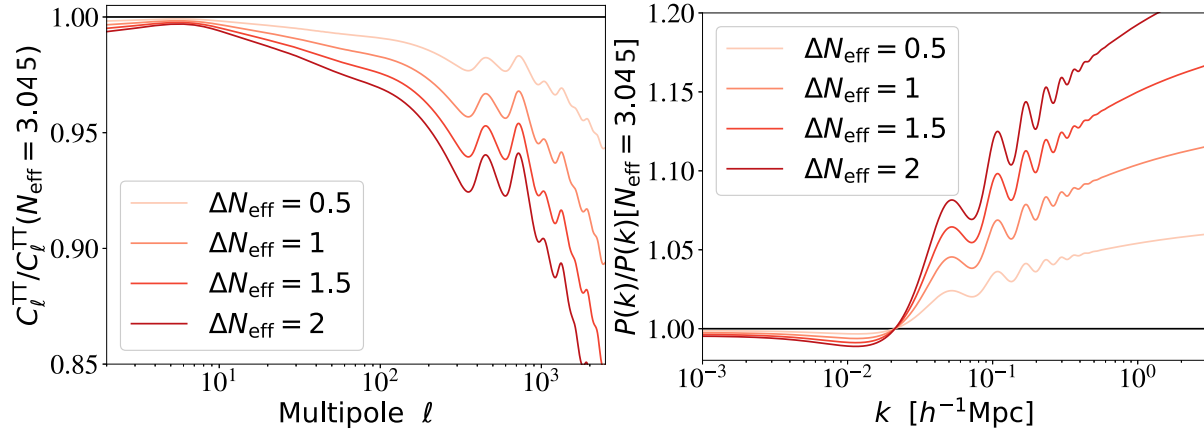


Figure 26.1: Ratio of the CMB C_ℓ^{TT} (left, including lensing effects) and matter power spectrum $P(k)$ (right, computed for each model in units of $(h^{-1}\text{Mpc})^3$) for different values of $\Delta N_{\text{eff}} \equiv N_{\text{eff}} - 3.045$ over those of a reference model with $\Delta N_{\text{eff}} = 0$. In order to minimize and better characterise the effect of N_{eff} on the CMB, the parameters that are kept fixed are $\{z_{\text{eq}}, z_\Lambda, \omega_b, \tau\}$ and the primordial spectrum parameters. Fixing $\{z_{\text{eq}}, z_\Lambda\}$ is equivalent to fixing the fractional density of total radiation, of total matter and of cosmological constant $\{\Omega_r, \Omega_m, \Omega_\Lambda\}$ while increasing the Hubble parameter as a function of N_{eff} . The statistical errors on the C_ℓ are $\sim 1\%$ for a band power of $\Delta\ell = 30$ at $\ell \sim 1000$. The error on $P(k)$ is estimated to be of the order of 5%.

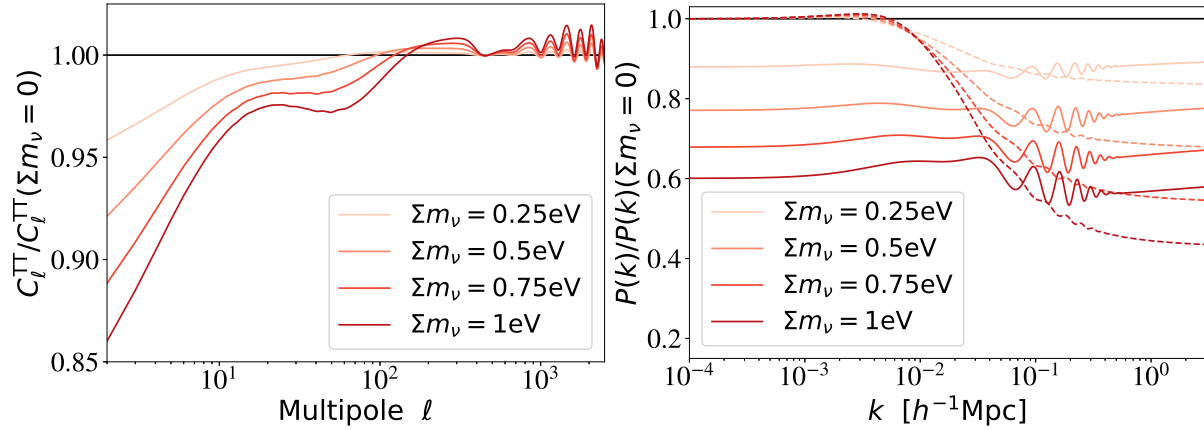


Figure 26.2: Ratio of the CMB C_ℓ^{TT} and matter power spectrum $P(k)$ (computed for each model in units of $(h^{-1}\text{Mpc})^3$) for different values of $\sum m_\nu$ over those of a reference model with massless neutrinos. In order to minimize and better characterise the effect of $\sum m_\nu$ on the CMB, the parameters that are kept fixed are ω_b, ω_c, τ , the angular scale of the sound horizon θ_s and the primordial spectrum parameters (solid lines). This implies that we are increasing the Hubble parameter h as a function of $\sum m_\nu$. For the matter power spectrum, in order to single out the effect of neutrino free-streaming on $P(k)$, the dashed lines show the spectrum ratio when $\{\omega_m, \omega_b, \Omega_\Lambda\}$ are kept fixed. For comparison, the error on $P(k)$ is of the order of 5% with current observations, and the fractional C_ℓ errors are of the order of $1/\sqrt{\ell}$ at low ℓ .

and the total neutrino average number density today: $n_\nu^0 = 339.5 \text{ cm}^{-3}$. Here h is the Hubble constant in units of $100 \text{ km s}^{-1} \text{ Mpc}^{-1}$.

26.2 Effects of neutrino properties on cosmological observables

As long as they are relativistic, *i.e.*, until some time deep inside the matter-dominated regime for neutrinos with a mass $m_i \ll 3.15 T_\nu^{\text{eq}} \sim 1.5 \text{ eV}$ (see Big Bang Cosmology, Chap. 22 in this *Review*), neutrinos enhance the density of radiation: this effect is parameterised by N_{eff} and can be discussed separately from the effect of the mass that will be described later in this section. Increasing N_{eff} impacts the observable spectra of CMB anisotropies and matter fluctuations through background and perturbation effects.

26.2.1 Effect of N_{eff} on the CMB

The background effects depend on what is kept fixed when increasing N_{eff} . If the densities of other species are kept fixed, a higher N_{eff} implies a smaller redshift of radiation-to-matter equality, with very strong effects on the CMB spectrum: when the amount of expansion between radiation-to-matter equality and

photon decoupling is larger, the CMB peaks are suppressed. This effect is not truly characteristic of the neutrino density, since it can be produced by varying several other parameters. Hence, to characterise the effect of N_{eff} , it is more useful and illuminating to enhance the density of total radiation, of total matter and of Λ by exactly the same amount, in order to keep the redshift of radiation-to-matter equality z_{eq} and matter-to- Λ equality z_Λ fixed [4, 13, 14]. The primordial spectrum parameters, the baryon density $\omega_b \equiv \Omega_b h^2$ and the optical depth to reionization τ can be kept fixed at the same time, since we can simply vary N_{eff} together with the Hubble parameter h with fixed $\{\omega_b, \Omega_c, \Omega_\Lambda\}$. The impact of such a transformation is shown in Fig. 26.1 for the CMB temperature spectrum C_ℓ^{TT} (defined in Chap. 29 in this *Review*) and for the matter power spectrum $P(k)$ (defined in Chap. 22 in this *Review*) for several representative values of N_{eff} . These effects are within the reach of cosmological observations given current error bars, as discussed in Section 26.3.1 (for instance, with the *Planck* satellite data, the statistical error on the C_ℓ 's is of the order of one per cent for a band power of $\Delta\ell = 30$ at $\ell \sim 1000$).

With this transformation, the main background effect of N_{eff}

is an increase in the diffusion scale (or Silk damping scale, see Cosmic Microwave Background – Chap. 29 in this *Review*) at the time of decoupling, responsible for the decrease in C_ℓ^{TT} at high ℓ , plus smaller effects coming from a slight increase in the redshift of photon decoupling [4, 13, 14]. At the level of perturbations, a higher N_{eff} implies that photons feel gravitational forces from a denser neutrino component; this tends to decrease the acoustic peaks (because neutrinos are distributed in a smoother way than photons) and to shift them to larger scales / smaller multipoles (because photon perturbations traveling at the speed of sound in the photon-baryon fluid feel some dragging effect from neutrino perturbations travelling at the speed of light) [4, 13, 15]. The effect of increasing N_{eff} on the polarization spectrum features are the same as on the temperature spectrum: an increased Silk damping, and a shift in the acoustic peak amplitude and location - the latter effect is even more clear in the polarization spectrum, in which the location of acoustic peaks does not get further influenced by a Doppler effect like for temperature. The combination of these effects is truly characteristic of the radiation density parameter N_{eff} and cannot be mimicked by other parameters; thus N_{eff} can be accurately measured from the CMB alone. However, there are correlations between N_{eff} and other parameters. In particular, we have seen (Fig. 26.1) that in order to minimise the effect of N_{eff} on the CMB spectrum, one should vary h at the same time, hence there is a correlation between N_{eff} and h , which implies that independent measurements reducing the error bar on h also reduce that on N_{eff} . Note that this correlation is not equivalent to a perfect degeneracy, so both parameters can anyway be constrained with CMB data alone.

26.2.2 Effect of N_{eff} on the matter spectrum

We have discussed the effect of increasing N_{eff} while keeping z_{eq} and ω_b fixed, because the latter two quantities are very accurately constrained by CMB data. This implies that ω_c increases with N_{eff} , and that the ratio $\omega_b/\omega_c = \Omega_b/\Omega_c$ decreases. However, the ratio of baryonic-to-dark matter has a strong impact on the shape of the matter power spectrum, because until the time of decoupling of the baryons from the photons, CDM experiences gravitational collapse, while baryons are kept smoothly distributed by photon pressure and affected by acoustic oscillations. The decrease of Ω_b/Ω_c following from the increase of N_{eff} gives more weight to the most clustered of the two components, namely the dark matter one, and produces an enhancement of the small-scale matter power spectrum and a damping of the amplitude of baryon acoustic oscillations (BAOs), clearly visible in Fig. 26.1 (right plot). The scale of BAOs is also slightly shifted by the same neutrino dragging effect as for CMB peaks [19].

The increase in the small-scale matter power spectrum is also responsible for a last effect on the CMB spectra: the CMB last scattering surface is slightly more affected by weak lensing from large-scale structures. This tends to smooth the maxima, the minima, and the damping scale of the CMB spectra [20].

26.2.3 Effect of neutrino masses on the CMB

Neutrino eigenstates with a mass $m_i \ll 0.57$ eV become non-relativistic after photon decoupling. They contribute to the non-relativistic matter budget today, but not at the time of equality or recombination. If we increase the neutrino mass while keeping fixed the density of baryons and dark matter (ω_b and ω_c), the early cosmological evolution remains fixed and independent of the neutrino mass, until the time of the non-relativistic transition. Thus one might expect that the CMB temperature and polarisation power spectra are left invariant. This is not true for four reasons.

First, the neutrino density enhances the total non-relativistic density at late times, $\omega_m = \omega_b + \omega_c + \omega_\nu$, where $\omega_\nu \equiv \Omega_\nu h^2$ is given as a function of the total mass $\sum m_\nu$ by Eq. (26.2). The late background evolution impacts the CMB spectrum through the relation between scales on the last scattering surface and angles on the sky, and through the late ISW effect (see Cosmic Microwave Background – Chap. 29 of this *Review*). These two effects depend respectively on the angular diameter distance to recombination, $d_A(z_{\text{rec}})$, and on the redshift of matter-to- Λ equality. Increasing $\sum m_\nu$ tends to modify these two quantities. By playing with h

and Ω_Λ , it is possible to keep one of them fixed, but not both at the same time. Since the CMB measures the angular scale of acoustic oscillations with exquisite precision, and is only loosely sensitive to the late ISW effect due to cosmic variance, we choose in Fig. 26.2 to play with the Hubble parameter in order to maintain a fixed scale $d_A(z_{\text{rec}})$. With such a choice, an increase in neutrino mass comes together with a decrease in the late ISW effect explaining the depletion of the CMB spectrum for $l \leq 20$. The fact that both $\sum m_\nu$ and h enter the expression of $d_A(z_{\text{rec}})$ implies that measurements of the neutrino mass from CMB data are strongly correlated with h . Second, the non-relativistic transition of neutrinos affects the total pressure-to-density ratio of the universe, and causes a small variation of the metric fluctuations. If this transition takes place not too long after photon decoupling, this variation is observable through the early ISW effect [4, 21, 22]. It is responsible for the dip seen in Fig. 26.2 for $20 \leq \ell \leq 200$. Third, when the neutrino mass is higher, the CMB spectrum is less affected by the weak lensing effect induced by the large-scale structure at small redshift. This is due to a decrease in the matter power spectrum described in the next paragraphs. This reduced lensing effect is responsible for most of the oscillatory patterns visible in Fig. 26.2 (left plot) for $\ell \geq 200$. Fourth, the neutrinos with the smallest momenta start to be non-relativistic earlier than the average ones. The photon perturbations feel this through their gravitational coupling with neutrinos. This leads to a small enhancement of C_ℓ^{TT} for $\ell \geq 500$, hardly visible on Fig. 26.2 because it is balanced by the lensing effect.

26.2.4 Effect of neutrino masses on the matter spectrum

The physical effect of neutrinos on the matter power spectrum is related to their velocity dispersion. Neutrinos free-stream over large distances without falling into small potential wells. The free-streaming scale is roughly defined as the distance travel by neutrinos over a Hubble time scale $t_H = (a/\dot{a})$, and approximates the scale below which neutrinos remain very smooth. On larger scales, they cluster in the same way as cold dark matter. The power spectrum of total matter fluctuations, related to the squared fluctuation δ_m^2 with $\delta_m \equiv \delta_b + \delta_c + \delta_\nu$, gets a negligible contribution from the neutrino component on small scales, and is reduced by a factor $(1 - 2f_\nu)$, where $f_\nu = \omega_\nu/\omega_m$. Additionally, on scales below the free-streaming scale, the growth of ordinary cold dark matter and baryon fluctuations is modified by the fact that neutrinos contribute to the background density, but not to the density fluctuations. This changes the balance between the gravitational forces responsible for clustering, and the Hubble friction term slowing it down. Thus the growth rate of CDM and baryon fluctuations is reduced [23]. This results today in an additional suppression of the small-scale linear matter power spectrum by approximately $(1 - 6f_\nu)$. These two effects sum up to a factor $(1 - 8f_\nu)$ [24] (more precise approximations can be found in [2, 4]). The non-linear spectrum is even more suppressed on mildly non-linear scales [3, 25–29].

This effect is often illustrated by plots of the matter power spectrum ratio with fixed parameters $\{\omega_m, \omega_b, \Omega_\Lambda\}$ and varying f_ν , *i.e.*, with the CDM density adjusted to get a fixed total dark matter density [2, 4, 24] (see Fig. 26.2, right plot, dashed lines). This transformation does not leave the redshift of equality z_{eq} invariant, and has very large effects on the CMB spectra. If one follows the logic of minimizing CMB variations and fixing z_{eq} like in the previous paragraphs, the increase in $\sum m_\nu$ must take place together with an increase of h , which tends to suppress the large-scale power spectrum, by approximately the same amount as the neutrino free-streaming effect [30]. In that case, the impact of neutrino masses on the matter power spectrum appears as an overall amplitude suppression, which can be seen in Fig. 26.2 (right plot, solid lines). The oscillations on intermediate wavenumbers come from a small shift in the BAO scale [30]. This global effect is not degenerate with a variation of the primordial spectrum amplitude A_s , because it only affects the matter power spectrum, and not the CMB spectra. However, the amplitude of the CMB temperature and polarization spectrum is given by the combination $A_s e^{-2\tau}$. Hence a measurement of τ is necessary in order to fix A_s from CMB data, and avoid a parameter degeneracy between $\sum m_\nu$ and A_s [30–32].

Table 26.1: Summary of N_{eff} constraints.

	Model	95%CL	Ref.
CMB alone			
P118[TT,TE,EE+lowE]	$\Lambda\text{CDM}+N_{\text{eff}}$	$2.92^{+0.36}_{-0.37}$	[16]
CMB + background evolution + LSS			
P118[TT,TE,EE+lowE+lensing] + BAO	$\Lambda\text{CDM}+N_{\text{eff}}$	$2.99^{+0.34}_{-0.33}$	[16]
” + BAO + R18	$\Lambda\text{CDM}+N_{\text{eff}}$	3.27 ± 0.15 (68%CL)	[17]
”	” +5-params.	2.85 ± 0.23 (68%CL)	[18]

A few of the neutrino mass effects described above –free-streaming scale, early ISW– depend on individual masses m_i , but most of them depend only on the total mass through f_ν –suppression of the matter power spectrum, CMB lensing, shift in angular diameter distance–. Because the latter effects are easier to measure, cosmology is primarily sensitive to the total mass $\sum m_\nu$ [33,34]. The possibility that future data sets might be able to measure individual masses or the mass hierarchy, despite systematic errors and parameter degeneracies, has recently become a subject of investigation [35,36].

26.3 Cosmological Constraints on neutrino properties

In this review we focus on cosmological constraints on the abundance and mass of ordinary active neutrinos. Several stringent but model-dependent constraints on non-standard neutrinos (*e.g.*, sterile neutrinos, active neutrinos with interactions beyond the weak force, unstable neutrinos with invisible decay, etc.) can also be found in the literature.

26.3.1 Neutrino abundance

Table 26.1 shows a list of constraints on N_{eff} obtained with several combination of data sets. ‘P118’ denotes the *Planck* 2018 data, composed of a high- ℓ temperature+polarization likelihood (TT,TE,EE), low- ℓ polarization (low E) and CMB lensing spectrum likelihood (lensing) based on lensing extraction from quadratic estimators [16]. ‘BAO’ refers to measurements of the BAO scale (and hence of the angular diameter distance) from various recent data sets, described in detail in the references given in the table. ‘R18’ refers to the distance ladder local measurement of the Hubble scale from cepheids and supernovae [37].

Within the framework of a 7-parameter cosmological model ($\Lambda\text{CDM}+N_{\text{eff}}$), the constraint on N_{eff} comes from the *Planck* 2018 data release [TT,TE,EE+lowE] is $N_{\text{eff}} = 2.92^{+0.36}_{-0.37}$ (95%CL). This number is perfectly compatible with the prediction of the standard neutrino decoupling model, $N_{\text{eff}} = 3.045$, and can be viewed as a proof of self-consistency of the cosmological model.

The bounds can be tightened by adding information on the low-redshift background expansion from BAOs, or local H_0 measurements. Finally, one can also add information on large scale structure (LSS), *i.e.*, on the growth rate and clustering amplitude of matter as a function of scale. However, LSS data are not very constraining for the N_{eff} parameter, and the only LSS data included in Table 26.1 is the measurement of the CMB lensing spectrum. All combinations of *Planck* 2018 data with BAO or CMB lensing constraints return measurements consistent with the standard expectation.

The situation is different with the inclusion of the low-redshift measurement of H_0 , [37], known to be in tension with *Planck* in the ΛCDM framework. As explained in Section 26.2, the positive correlation between N_{eff} and h means that inclusion of the H_0 measurement pushes N_{eff} to higher values, $N_{\text{eff}} = 3.27 \pm 0.15$ (68%CL, P118[TT,TE,EE+lowE+lensing] + BAO+R18), but still compatible with the standard expectation at the $\sim 1.5\sigma$ level.

It remains to be seen whether the $> 3\sigma$ tension between CMB data and direct measurements of H_0 results from systematics, or from a departure from the ΛCDM model [38,39].

The error bars on N_{eff} degrade mildly when the data are analysed in the context of more extended cosmological scenarios. Adding only the total neutrino mass as an 8th free parameter has a negligible impact on the bounds.

The authors of Ref. [18] take a more extreme point of view

and fit a 12-parameter model to P118[TT,TE,EE+lowE+lensing] data; they obtain $N_{\text{eff}} = 2.95 \pm 0.24$ (68% CL), showing that it is very difficult with current cosmological data to accommodate shifts of more than 0.5 from the standard N_{eff} value, and to obtain good fits with, for instance, a fourth (sterile) thermalized neutrino. This is interesting since the anomalies in some oscillation data could be interpreted as evidence for at least one sterile neutrino with a large mixing angle, which would need to be thermalised unless non-standard interactions come into play [5]. In other words cosmology disfavors the explanation of the oscillations anomalies in terms of 1 or more extra neutrinos if they are thermalized.

26.3.2 Are they really neutrinos, as expected?

While a value of N_{eff} significantly different from zero (at more than 15σ) and consistent with the expected number 3.045 yields a powerful indirect confirmation of the $C\nu B$, departures from standard N_{eff} could be caused by any ingredient affecting the early-time expansion rate of the Universe. Extra relativistic particles (either decoupled, self-interacting, or interacting with a dark sector), a background of gravitational waves, an oscillating scalar field with quartic potential, departures from Einstein gravity, or large extra dimensions are some of the possibilities for such ingredients. In principle one could even assume that the cosmic neutrino background never existed or has decayed (like in the “neutrinoless universe” model of [40]) while another dark radiation component is responsible for N_{eff} . At least, cosmological data allow to narrow the range of possible interpretations of $N_{\text{eff}} \simeq 3$ to the presence of decoupled relativistic relics like standard neutrinos. Indeed, free-streaming particles leave specific signatures in the CMB and LSS spectra, because their density and pressure perturbations, bulk velocities and anisotropic stress also source the metric perturbations. These signatures can be tested in several ways.

A first approach consists of introducing a self-interaction term in the neutrino equations [6,7]. Ref. [8] finds that current CMB and BAO data are compatible with no self-interactions. The upper limit to the effective coupling constant G_{eff} for a Fermi-like four-fermions interaction at 95% confidence is $\log_{10}(G_{\text{eff}}\text{MeV}^2) < -0.8$ for P115+BAO. Note however that neutrino self-interactions as strong as $\log_{10}(G_{\text{eff}}\text{MeV}^2) \simeq -1.4$ could reconcile CMB+BAO data with the direct H_0 measurement of Ref [37], but such interactions seem to be hardly compatible with BBN and laboratory constraints [41].

A second approach consists of introducing two phenomenological parameters, c_{eff} and c_{vis} (see *e.g.*, [42–44]): c_{eff}^2 generalizes the linear relation between isotropic pressure perturbations and density perturbations, while c_{vis}^2 modifies the neutrino anisotropic stress equation. While relativistic free-streaming species have $(c_{\text{eff}}^2, c_{\text{vis}}^2) = (1/3, 1/3)$, a perfect relativistic fluid would have $(c_{\text{eff}}^2, c_{\text{vis}}^2) = (1/3, 0)$. Other values do not necessarily refer to a concrete model, but make it possible to interpolate between these limits. *Planck* data strongly suggests $(c_{\text{eff}}^2, c_{\text{vis}}^2) = (1/3, 1/3)$ [45,46].

Finally, Ref. [15] (resp. [19]) shows that current data are precise enough to detect the “neutrino drag” effect mentioned in Sec. 26.2 through the measurement of the CMB peak (resp. BAO) scale. These findings show that current cosmological data are able to detect not just the average density of some relativistic relics, but also their anisotropies.

Table 26.2: Summary of $\sum m_\nu$ constraints.

	Model	95% CL (eV)	Ref.
CMB alone			
P118[TT+lowE]	$\Lambda\text{CDM} + \sum m_\nu$	< 0.54	[16]
P118[TT,TE,EE+lowE]	$\Lambda\text{CDM} + \sum m_\nu$	< 0.26	[16]
CMB + probes of background evolution			
P118[TT+lowE] + BAO	$\Lambda\text{CDM} + \sum m_\nu$	< 0.16	[16]
P118[TT,TE,EE+lowE] + BAO	$\Lambda\text{CDM} + \sum m_\nu$	< 0.13	[16]
P118[TT,TE,EE+lowE]+BAO	$\Lambda\text{CDM} + \sum m_\nu + 5$ params.	< 0.515	[18]
CMB + LSS			
P118[TT+lowE+lensing]	$\Lambda\text{CDM} + \sum m_\nu$	< 0.44	[16]
P118[TT,TE,EE+lowE+lensing]	$\Lambda\text{CDM} + \sum m_\nu$	< 0.24	[16]
CMB + probes of background evolution + LSS			
P118[TT+lowE+lensing] + BAO	$\Lambda\text{CDM} + \sum m_\nu$	< 0.13	[16]
P118[TT,TE,EE+lowE+lensing] + BAO	$\Lambda\text{CDM} + \sum m_\nu$	< 0.12	[16]
P118[TT,TE,EE+lowE+lensing] + BAO+Pantheon	$\Lambda\text{CDM} + \sum m_\nu$	< 0.11	[16]

26.3.3 Neutrino masses

Table 26.2 shows a list of constraints on $\sum m_\nu$ obtained with several combinations of data sets. The acronyms “P118”, “BAO” and “R18” have been described in the previous subsection, while “Pantheon” refers to the supernovae Type Ia compilation of [47].

Given that most determinations of N_{eff} are compatible with the standard prediction, $N_{\text{eff}} = 3.045$, it is reasonable to adopt this value as a theoretical prior and to investigate neutrino mass constraints in the context of a minimal 7-parameter model, $\Lambda\text{CDM} + \sum m_\nu$. Under this assumption, the most robust constraints come from *Planck* 2018 temperature and polarization data alone: $\sum m_\nu < 0.26$ eV (95%CL). Among the four effects of neutrino masses on the CMB spectra described before, current bounds are dominated by the first and the third effects (modified late background evolution, and distortions of the temperature and polarisation spectra through weak lensing).

Adding measurements of the BAO scale is crucial, since the measurement of the angular diameter distance at small redshift allows us to break parameter degeneracies, for instance between $\sum m_\nu$ and h . Combined *Planck* 2018 data, BAO experiments give $\sum m_\nu < 0.13$ eV (95%CL). Supernovae data are less constraining than BAO data for the neutrino mass determination.

Because the parameter correlation between $\sum m_\nu$ and H_0 is negative, the inclusion of R18 data provides stronger bounds on neutrinos masses, down to $\sum m_\nu < 0.097$ eV (95% CL) when including P118[TT,TE,EE+lowE]+R18 [16], but such bounds are subject to caution, since they come from a combination of discrepant data sets (at the $> 3\sigma$ level).

It is interesting to add LSS data sets, sensitive to the small-scale suppression of the matter power spectrum due to neutrino free-streaming. The bound from *Planck* 18 including lensing plus BAO is very strong, $\sum m_\nu < 0.12$ eV (95%CL), which is comparable to previous bounds derived from *Planck* 15 in combination with Ly α forest data or other large-scale structure data [48–50]. It can even be tightened down to $\sum m_\nu < 0.11$ eV by further adding supernovae data from the “Pantheon” compilation. The latter bound puts some pressure on the inverted mass hierarchy that requires $\sum m_\nu > 0.11$ eV. It should however be noticed that the full DES 1-year data [51] prefer a lower σ_8 value than the *Planck* best fit, relaxing the bound to $\sum m_\nu < 0.14$ eV (95%CL, P118[TT,TE,EE+lowE+lensing] + BAO + DES) [16].

Upper bounds on neutrino masses become weaker when the data are analysed in the context of extended cosmological models, but only by a small amount. Floating N_{eff} instead of fixing it to 3.045 has no significant impact on the neutrino mass bounds reported in the previous paragraphs. Even in the extreme case considered by Ref. [18], with 12 free cosmological parameters, one can see in Table 26.2 that the bound from *Planck* 2018 (without lensing) + BAO increases from 0.13 eV to 0.52 eV (95% CL) only. This shows that current cosmological data are precise enough to disentangle the effect of several extended cosmological parameters, and that neutrino mass bounds are becoming increasingly robust.

26.4 Future prospects and outlook

The cosmic neutrino background has been detected indirectly at very high statistical significance. Direct detection experiments are now being planned, *e.g.*, at the Princeton Tritium Observatory for Light, Early-universe, Massive-neutrino Yield (PTOLEMY) [52]. The detection prospects crucially depend on the exact value of neutrino masses and on the enhancement of their density at the location of the Earth through gravitational clustering in the Milky Way and its sub-halos – an effect however expected to be small [53–55].

Over the past few years the upper limit on the sum of neutrino masses has become increasingly stringent, first indicating that the mass ordering is hierarchical and recently putting the inverted hierarchy under pressure and favouring the normal hierarchy (although quantitative estimates of how disfavoured the inverted hierarchy is vary depending on assumptions, see *e.g.* [56–58]) which has consequences for planning future double beta decay experiments.

Neutrino mass and density bounds are expected to keep improving significantly over the next years, thanks to new LSS experiments like DESI [59], Euclid [60], LSST [61], and SKA [62], or possible new CMB experiments like CMB-S4 [63], Pixie [64], CMBPol or CORE [65]. If the ΛCDM model is confirmed, and if neutrinos have standard properties, the total neutrino mass should be detected at the level of at least $3\text{--}4\sigma$ even at the minimum level allowed by oscillations. This is the conclusion reached by several independent studies, using different dataset combinations (see *e.g.*, [32,66–71]). One should note that at the minimum level allowed by oscillations $\sum m_\nu \sim 0.06$, neutrinos constitute $\sim 0.5\%$ of the Universe matter density, and their effects on the matter power spectrum is only at the 5% level, implying that exquisite control of systematic errors will be crucial to achieve the required accuracy. At this level, the information coming from the power spectrum shape is more powerful than that coming from geometrical measurements (*e.g.*, BAO). But exploiting the shape information requires improved understanding of the non-linear regime, and of galaxy bias for galaxy surveys. The fact that different surveys and different data set combinations have enough statistical power to reach this level, offers a much needed redundancy and the possibility to perform consistency checks which in turns helps immensely with the control of systematic errors and in making the measurement robust. Using the entire Universe as a particle detector, the on-going and future observational efforts hold the exciting prospect to provide a measurement of the sum of neutrino masses and possibly indication of their mass hierarchy.

References

- [1] A. D. Dolgov, Phys. Rept. **370**, 333 (2002), [hep-ph/0202122].
- [2] J. Lesgourgues and S. Pastor, Phys. Rept. **429**, 307 (2006), [arXiv:astro-ph/0603494].

- [3] S. Hannestad, *Prog. Part. Nucl. Phys.* **65**, 185 (2010), [arXiv:1007.0658].
- [4] J. Lesgourgues *et al.*, *Neutrino cosmology* (Cambridge University Press, 2013).
- [5] M. Archidiacono *et al.*, *JCAP* **1608**, 08, 067 (2016), [arXiv:1606.07673].
- [6] L. Lancaster *et al.*, *JCAP* **1707**, 07, 033 (2017), [arXiv:1704.06657].
- [7] I. M. Oldengott *et al.*, *JCAP* **1711**, 11, 027 (2017), [arXiv:1706.02123].
- [8] M. Park *et al.* (2019), [arXiv:1904.02625].
- [9] J. Birrell, C.-T. Yang and J. Rafelski, *Nucl. Phys.* **B890**, 481 (2014), [arXiv:1406.1759].
- [10] G. Mangano *et al.*, *Nucl. Phys.* **B729**, 221 (2005), [hep-ph/0506164].
- [11] E. Grohs *et al.*, *Phys. Rev.* **D93**, 8, 083522 (2016), [arXiv:1512.02205].
- [12] P. F. de Salas and S. Pastor, *JCAP* **1607**, 07, 051 (2016), [arXiv:1606.06986].
- [13] S. Bashinsky and U. Seljak, *Phys. Rev.* **D69**, 083002 (2004), [arXiv:astro-ph/0310198].
- [14] Z. Hou *et al.*, *Phys. Rev.* **D87**, 083008 (2013), [arXiv:1104.2333].
- [15] B. Follin *et al.*, *Phys. Rev. Lett.* **115**, 9, 091301 (2015), [arXiv:1503.07863].
- [16] N. Aghanim *et al.* (Planck) (2018), [arXiv:1807.06209].
- [17] Planck 2018 explanatory supplement, wiki.cosmos.esa.int/planckpla2018/, “Mission Products: Cosmological parameters: Parameter Tables”.
- [18] E. Di Valentino, A. Melchiorri and J. Silk, arXiv:1908.01391 *Phys. Rev.* **D92**, 12,1302 (2015).
- [19] D. Baumann *et al.*, *Nature Phys.* **15**, 465 (2019), [arXiv:1803.10741].
- [20] A. Lewis and A. Challinor, *Phys. Rept.* **429**, 1 (2006), [arXiv:astro-ph/0601594].
- [21] J. Lesgourgues and S. Pastor, *Adv. High Energy Phys.* **2012**, 608515 (2012), [arXiv:1212.6154].
- [22] Z. Hou *et al.*, *Astrophys. J.* **782**, 74 (2014), [arXiv:1212.6267].
- [23] J. R. Bond, G. Efstathiou and J. Silk, *Phys. Rev. Lett.* **45**, 1980 (1980), [61(1980)].
- [24] W. Hu, D. J. Eisenstein and M. Tegmark, *Phys. Rev. Lett.* **80**, 5255 (1998), [arXiv:astro-ph/9712057].
- [25] S. Bird, M. Viel and M. G. Haehnelt, *Mon. Not. R. Astron. Soc.* **420**, 2551 (2012).
- [26] C. Wagner, L. Verde and R. Jimenez, *Astrophys. J.* **752**, L31 (2012), [arXiv:1203.5342].
- [27] C. J. Toderó Peixoto, V. de Souza and P. L. Biermann, *JCAP* **1507**, 07, 042 (2015), [arXiv:1502.00305].
- [28] J. Brandbyge and S. Hannestad, *JCAP* **1710**, 10, 015 (2017), [arXiv:1706.00025].
- [29] J. Adamek, R. Durrer and M. Kunz, *JCAP* **1711**, 11, 004 (2017), [arXiv:1707.06938].
- [30] M. Archidiacono *et al.*, *JCAP* **1702**, 02, 052 (2017), [arXiv:1610.09852].
- [31] A. Liu *et al.*, *Phys. Rev.* **D93**, 4, 043013 (2016), [arXiv:1509.08463].
- [32] R. Allison *et al.*, *Phys. Rev.* **D92**, 12, 123535 (2015), [arXiv:1509.07471].
- [33] J. Lesgourgues, S. Pastor and L. Perotto, *Phys. Rev.* **D70**, 045016 (2004), [hep-ph/0403296].
- [34] A. Slosar, *Phys. Rev.* **D73**, 123501 (2006), [arXiv:astro-ph/0602133].
- [35] R. Jimenez *et al.*, *JCAP* **1005**, 035 (2010), [arXiv:1003.5918].
- [36] R. Jimenez, C. P. Garay and L. Verde, *Phys. Dark Univ.* **15**, 31 (2017), [arXiv:1602.08430].
- [37] A. G. Riess *et al.*, *Astrophys. J.* **855**, 2, 136 (2018), [arXiv:1801.01120].
- [38] J. L. Bernal, L. Verde and A. G. Riess, *JCAP* **1610**, 10, 019 (2016), [arXiv:1607.05617].
- [39] L. Verde, T. Treu and A. G. Riess (2019), [arXiv:1907.10625].
- [40] J. F. Beacom, N. F. Bell and S. Dodelson, *Phys. Rev. Lett.* **93**, 121302 (2004), [arXiv:astro-ph/0404585].
- [41] N. Blinov *et al.* (2019), [arXiv:1905.02727].
- [42] W. Hu, *Astrophys. J.* **506**, 485 (1998), [arXiv:astro-ph/9801234].
- [43] W. Hu *et al.*, *Phys. Rev.* **D59**, 023512 (1999), [arXiv:astro-ph/9806362].
- [44] M. Gerbino, E. Di Valentino and N. Said, *Phys. Rev.* **D88**, 6, 063538 (2013), [arXiv:1304.7400].
- [45] B. Audren *et al.*, *JCAP* **1503**, 036 (2015), [arXiv:1412.5948].
- [46] P. A. R. Ade *et al.* (Planck), *Astron. Astrophys.* **594**, A13 (2016), [arXiv:1502.01589].
- [47] D. M. Scolnic *et al.*, *Astrophys. J.* **859**, 2, 101 (2018), [arXiv:1710.00845].
- [48] N. Palanque-Desabrouille *et al.*, *JCAP* **1511**, 11, 011 (2015), [arXiv:1506.05976].
- [49] A. J. Cuesta, V. Niro and L. Verde, *Phys. Dark Univ.* **13**, 77 (2016).
- [50] S. Vagnozzi *et al.*, *Phys. Rev.* **D96**, 12, 123503 (2017), [arXiv:1701.08172].
- [51] T. M. C. Abbott *et al.* (DES), *Phys. Rev.* **D98**, 4, 043526 (2018), [arXiv:1708.01530].
- [52] S. Betts *et al.*, in “Proceedings, 2013 Community Summer Study on the Future of U.S. Particle Physics: Snowmass on the Mississippi (CSS2013): Minneapolis, MN, USA, July 29-August 6, 2013,” (2013), [arXiv:1307.4738], URL <http://www.slac.stanford.edu/econf/C1307292/docs/submittedArxivFiles/1307.4738.pdf>.
- [53] A. Ringwald and Y. Y. Y. Wong, *JCAP* **0412**, 005 (2004), [hep-ph/0408241].
- [54] F. Villaescusa-Navarro *et al.*, *JCAP* **1303**, 019 (2013), [arXiv:1212.4855].
- [55] P. F. de Salas *et al.*, *JCAP* **1709**, 09, 034 (2017), [arXiv:1706.09850].
- [56] F. Simpson *et al.*, *JCAP* **1706**, 06, 029 (2017), [arXiv:1703.03425].
- [57] S. Hannestad and T. Schwetz, *JCAP* **1611**, 11, 035 (2016), [arXiv:1606.04691].
- [58] S. Roy Choudhury and S. Hannestad (2019), [arXiv:1907.12598].
- [59] A. Aghamousa *et al.* (DESI) (2016), [arXiv:1611.00036].
- [60] R. Laureijs *et al.* (EUCLID) (2011), [arXiv:1110.3193].
- [61] Paul A. Abell *et al.*, LSST Science and LSST Project Collaborations, <http://lss.fnal.gov/archive/test-tm/2000/fermilab-tm-2495-a.pdf> (2009) arXiv:0912.0201.
- [62] <http://www.skatelescope.org>.
- [63] K. N. Abazajian *et al.* (CMB-S4) (2016), [arXiv:1610.02743].
- [64] A. Kogut *et al.*, *JCAP* **1107**, 025 (2011), [arXiv:1105.2044].
- [65] J. Delabrouille *et al.* (CORE), *JCAP* **1804**, 04, 014 (2018), [arXiv:1706.04516].
- [66] C. Carbone *et al.*, *JCAP* **1103**, 030 (2011), [arXiv:1012.2868].
- [67] J. Hamann, S. Hannestad and Y. Y. Y. Wong, *JCAP* **1211**, 052 (2012), [arXiv:1209.1043].
- [68] B. Audren *et al.*, *JCAP* **1301**, 026 (2013), [arXiv:1210.2194].

- [69] R. Pearson and O. Zahn, Phys. Rev. **D89**, 4, 043516 (2014), [arXiv:1311.0905].
- [70] F. Villaescusa-Navarro, P. Bull and M. Viel, Astrophys. J. **814**, 2, 146 (2015), [arXiv:1507.05102].
- [71] T. Brinckmann *et al.*, JCAP **1901**, 059 (2019), [arXiv:1808.05955].

27. Dark Matter

Written August 2019 by L. Baudis (Zurich U.) and S. Profumo (UC Santa Cruz).

27.1 The case for dark matter

Modern cosmological models invariably include an electromagnetically close-to-neutral, non-baryonic matter species with negligible velocity from the standpoint of structure formation, generically referred to as “cold dark matter” (CDM; see The Big-Bang Cosmology—Sec. 22 of this *Review*). For the benchmark Λ CDM cosmology adopted in the Cosmological Parameters—Sec. 25.1 of this *Review*, the DM accounts for 26.4% of the critical density in the universe, or 84.4% of the total matter density. The nature of only a small fraction, between at least 0.5% (given neutrino oscillations) and at most 1.6% (from combined cosmological constraints), of the non-baryonic matter content of the universe is known: the three Standard Model neutrinos (see the Neutrino Masses, Mixing, and Oscillations—Sec. 14 of this *Review*). The fundamental makeup of the large majority of the DM is, as of yet, unknown.

Assuming the validity of General Relativity, DM is observed to be ubiquitous in gravitationally collapsed structures of size ranging from the smallest known galaxies [1] to galaxies of size comparable to the Milky Way [2], to groups and clusters of galaxies [3]. The mass-to-light ratio is observed to saturate at the largest collapsed scales to a value indicative, and close to, what inferred from other cosmological observations for the universe as a whole [4]. In such collapsed structures, the existence of DM is inferred directly using tracers of mass enclosed within a certain radius such as stellar velocity dispersion, rotation curves in axisymmetric systems, the virial theorem, gravitational lensing, and measures of the amount of non-dark, i.e. baryonic, mass such as stellar number counts and tracers of gas density such as X-ray emission [5]. The global DM abundance as determined from cosmological probes is discussed in Sec. 22.

The picture of structure formation in modern cosmology heavily relies on, and can be considered an independent and exceptionally strong motivation for, DM. Baryonic density fluctuations at CMB decoupling are observed to be at most on the order of $\delta\rho_b/\rho_b|_{\text{rec}} \approx 10^{-3}$; since density perturbations grow linearly with the scale factor in the linear regime, absent any other matter fluid, one would predict that

$$\delta\rho_b/\rho_b|_{\text{today}} \approx \frac{\delta\rho_b/\rho_b|_{\text{rec}}}{a_{\text{rec}}} \approx 10^{-2}, \quad (27.1)$$

at odds with the observed highly non-linear structures in the universe, $\delta\rho_b/\rho_b|_{\text{obs}} \gg 1$. The presence of a dominant non-relativistic (“cold”) pressure-less matter component decoupled from the thermal bath well before recombination allows instead for the prediction of a matter power spectrum in remarkable agreement with observations [6].

Assuming deviations of gravitational interactions on large scales from general relativity or from its Newtonian limit, certain effects, attributed in the standard scenario to DM, can be explained by modified gravity [7]. Usually such theories mimic the effects otherwise attributed to DM on a limited range of scales, but fail globally, and especially at the largest scales. Key issues that at present appear highly problematic in the framework of theories of modified gravity without DM include (i) predicting the correct spectrum of density perturbations, (ii) predicting the observed anisotropy power spectrum of the CMB, and (iii) explaining weak lensing and X-ray observations of merging clusters such as 1E 0657-558 (the “Bullet” cluster) [8]. The inferred relative speed of gravitational and electromagnetic radiation in GW170817 additionally excludes a significant swath of modified theories of gravity where the two speeds (of gravitational and electromagnetic waves) differ [9].

27.2 Properties of dark matter candidates

Electric charge: The “darkness” of DM can be quantified based on constraints from the CMB and large-scale structure: if the DM is charged, or “milli-charged” (for instance via a kinetic mixing with a dark photon field, producing an effective

suppressed coupling to the visible photon field), it might impact the baryon-photon plasma during recombination; in turn, DM density fluctuations can be suppressed by radiation pressure and photon diffusion, additionally altering the baryon acoustic peak structure. [10] finds that the most stringent constraints stem from the requirement that the DM be completely decoupled from the baryon-photon plasma at recombination, yielding a maximal “milli-electric” charge, in units of the electron charge, of $3.5 \times 10^{-7} (m_{\text{DM}}/1 \text{ GeV})^{0.58}$ for $m_{\text{DM}} > 1 \text{ GeV}$, and of $4.0 \times 10^{-7} (m_{\text{DM}}/1 \text{ GeV})^{0.35}$ for $m_{\text{DM}} < 1 \text{ GeV}$. Limits also exist from structure formation on how optically dark and dissipationless the DM should be.

Self-interactions: Observations of merging clusters [8] and of the ellipticity of certain galaxies as inferred from X-rays [11] constrain the level of DM-DM self interactions. The figure of merit is the ratio of the DM-DM cross section and the DM mass [12] (see Ref. [13] for a review), $\sigma_{\text{DM-DM}}/m_{\text{DM}} < 0.47 \text{ cm}^2/\text{g} \simeq 0.84 \text{ barn}/\text{GeV}$ at 95% C.L.. Assuming a velocity dependence in $\sigma_{\text{DM-DM}}$, “self-interacting DM” has been advocated as a possible solution to certain possible small-scale structure issues in the standard non-collisional ($\sigma_{\text{DM-DM}} \simeq 0$) setup [13, 14] (see Sec. 27.4).

Mass: Lower Limits: Model-independent lower limits for very small DM masses are due to quantum effects: for fermionic DM particles, the phase-space density $f(\vec{x}, \vec{p})$ is bounded from above due to Pauli’s exclusion principle, $f < gh^{-3}$, with g the number of internal degrees of freedom and h Planck’s constant; observations of the velocity dispersion (or, equivalently, measures of the enclosed mass) and physical density in dwarf galaxies, lead to a lower limit on fermionic DM masses, sometimes known as the Tremaine-Gunn limit [15]. Using the Fornax dwarf, Ref. [16] finds $m_F > 70 \text{ eV}$. More stringent limits can be drawn from Lyman- α observations, although such limits depend on the thermal history of the DM. In the case of bosonic DM, the Compton wavelength of an ultra-light species might erase small-scale structure, in conflict with CMB and large-scale structure [17], Lyman- α observations [18, 19], and measurements of high-redshift galaxy luminosity functions and the Milky Way satellite luminosity function [20–22]: these observations indicate that $m_B \gtrsim 10^{-22} \text{ eV}$.

Mass: Upper Limits: General upper limits exist on the mass of the DM constituent from the stability against tidal disruption of structures immersed in DM halos, such as galactic disks and globular clusters, and of individual small galaxies. The most stringent limits can be derived using wide halo binaries [23] and the stability of the star cluster within Eridanus II [24]. Such limits constrain an individual, point-like DM constituent, assuming it makes up 100% of the DM, to be lighter than around $5 M_{\odot}$. (Notice that the mass limits discussed here do not assume any specific production mechanism, and do not depend on the observed cosmological DM density).

Stability: The DM lifetime must be long compared to cosmological timescales [25].

27.3 Genesis of dark matter

The generation of DM in the early universe can proceed via thermal or non-thermal production, or both, or it may result from a particle-antiparticle asymmetry.

Freeze-out: The process of chemical decoupling from the high-temperature, high-density thermal bath (freeze-out) as a paradigm for particle production in the early universe is both a predictive and a successful one. The possibility that just like light elements, neutrinos, and CMB photons, particle DM also originated from a thermal decoupling process has thus garnered significant attention.

A particle species *chemically* decouples when the rate Γ for the species’ number-changing processes drops below the Hubble rate H . Rough estimates for the abundance of relics can be obtained by (i) calculating the freeze-out (i.e. “decoupling”) temperature $T_{\text{f.o.}}$, corresponding to $H(T_{\text{f.o.}}) \sim \Gamma(T_{\text{f.o.}})$, (ii) equating the comoving number density at freeze-out and today, eventually (iii) obtaining the physical density of relic particles today. This procedure assumes that entropy is conserved between $T_{\text{f.o.}}$ and today, an assumption that could well be violated, especially for

heavy relics that decouple early, for instance by entropy injection episodes [26]. Notice also that the freeze-out calculation strongly depends on the assumed background cosmology, and changes e.g. if the early universe is not radiation-dominated around DM decoupling.

The calculation of the freeze-out relic abundance hinges on a Boltzmann equation relating the Liouville operator to the collision operator acting on the phase space density. Under a variety of simplifying assumptions including homogeneity and isotropy, it is possible to reduce the relevant equation for the number density n of a single species pair-annihilating with particles in the thermal bath via 2-to-2 processes to

$$\frac{dn}{dt} - 3Hn = -\langle\sigma v\rangle (n^2 - n_{\text{eq}}^2), \quad (27.2)$$

where $\langle\sigma v\rangle$ is the thermally-averaged pair-annihilation cross section times relative velocity (see Ref. [27]), and n_{eq} is the equilibrium number density. Relics for which the freeze-out temperature is much larger than the particle mass (and thus that freeze-out as ultra-relativistic) are called *hot* relics; if the opposite is true, the relic is instead considered *cold*.

A straightforward calculation shows that to leading order the frozen-out density of *hot* relics is *linearly proportional to the relic particle mass*. The comoving number density $Y = n/s$, where s is the entropy density, for a hot relic is approximately given by its equilibrium value,

$$Y_{\text{f.o.}} \simeq Y_{\text{eq}} \simeq 0.278 \frac{g_{\text{eff}}}{g_{*s}}, \quad (27.3)$$

where g_{eff} is the relic's effective number of degrees of freedom, and g_{*s} is the number of entropic relativistic degrees of freedom, both calculated at $T_{\text{f.o.}}$. The resulting relic abundance, assuming an iso-entropic expansion, is

$$\Omega_{\text{hot}} h^2 = \frac{m Y_{\text{f.o.}} s_0 h^2}{\rho_c} \simeq \frac{m}{93 \text{ eV}}, \quad (27.4)$$

with s_0 the entropy density today, and with the latter equality holding for the case of SM neutrinos, with a freeze-out temperature around 1 MeV (which enters in the final relic abundance through the degrees of freedom dependence on the right-hand-side of Eq. (27.3)).

For *cold* relics, the leading-order dependence of the relic abundance on the DM particle properties is an *inverse proportionality relation to the pair-annihilation cross section*,

$$\Omega_{\text{cold}} h^2 \simeq 0.1 \left(\frac{x_{\text{f.o.}}}{20} \right) \left(\frac{10^{-8} \text{ GeV}^{-2}}{\sigma_{DM+DM \leftrightarrow \text{anything}}} \right), \quad (27.5)$$

where $x \equiv m_{\text{DM}}/T$. In turn, the freeze-out temperature is approximately given by the solution to the equation

$$\sqrt{x} \cdot e^{-x} = (m_{\text{DM}} \cdot M_P \cdot \sigma_{DM+DM \leftrightarrow \text{anything}})^{-1}, \quad (27.6)$$

where $M_P \simeq 2.435 \times 10^{18}$ GeV is the reduced Planck mass. As a result, $T_{\text{f.o.}} \simeq m_{\text{DM}}/x_{\text{f.o.}}$, with $x_{\text{f.o.}}$ a number between 10 and 50, depending on the cross section, with only a logarithmic dependence on the DM mass. Since for electroweak-scale cross sections and masses $\sigma_{DM+DM} \simeq 10^{-8} \text{ GeV}^{-2}$, “weakly-interacting massive particles”, or WIMPs have gained exceptional popularity. Notice that Eq. (27.5) bears, however, no connection to the weak scale [28], despite the relation being known as “WIMP miracle”.

Numerous scenarios exist, including notably supersymmetry [29,30] and models with universal extra dimensions [31,32] where the relic abundance of the DM is controlled by processes involving a slightly heavier, unstable, co-annihilating species [33]. In this case the calculation of the abundance of the stable species proceeds similarly to what outlined above, with an effective pair-annihilation cross section that captures the effects of co-annihilation replacing the pair-annihilation cross section [30].

Freeze-in: Collisional processes can lead to the production of out-of-equilibrium particles that progressively accumulate over cosmic time, a process sometimes called *freeze-in*. The abundance

of the frozen-in particles produced at a given redshift depends on the product of the production rate times the Hubble time at that redshift. Freeze-in generally implies that the lightest observable-sector particles decay to the DM with relatively long lifetimes, giving peculiar signals at colliders (see e.g. [34]). Gravitinos are an example of DM candidates possibly produced via a freeze-in type scenario, albeit the portal coupling is in that case via a higher dimensional, Planck-suppressed operator [35].

Cannibalization and other dark-sector number-changing processes: Thermal processes can drive the abundance of the DM beyond simple 2-to-2 number-changing interactions. For instance, DM can “cannibalize” [36,37] itself if $n \rightarrow 2$ processes exist. In this case, a critical aspect is whether or not the DM sector is in thermal contact with the Standard Model thermal bath. If it is, $n \rightarrow 2$ processes can drive the relic abundance, e.g. in the Strongly Interacting Massive Particles (SIMP) scenario [38]. Models exist where the *kinetic decoupling* (i.e. the decoupling from the *thermal equilibrium velocity distribution*) of the two sectors drives the abundance of the DM (elastically decoupling relics, or ELDERS [39]). When the two sectors are not in thermal contact, $n \rightarrow 2$ processes heat the DM sector dramatically, rapidly affecting the temperature ratio between the visible and dark sectors [36,38]. If the relevant cross sections are large enough, and the DM mass light enough, significant effects can arise in structure formation [36].

Non-thermal production: DM production can proceed via processes out of thermal equilibrium (“non-thermal” production). These include DM production via the decay of a “mother” particle [40,41] (or of topological defects [42], moduli [43] etc.) to the DM, or production via gravitational effects.

Asymmetric DM: An enticing alternative possibility for DM production is that of *asymmetric* DM [44,45]: the relic DM abundance arises from an asymmetry between anti-DM and DM. This asymmetry may or may not be related to the baryon-antibaryon asymmetry. If it is, then depending on the model and its thermal history, a relation exists between the mass of the DM and the proton mass. A variety of proposals have been put forward where alternately baryogenesis is explained from a DM sector asymmetry, or vice-versa (see e.g. Ref. [46] for a review).

Primordial Black Holes production: A qualitatively stand-alone class of DM candidates, primordial black holes (PBHs), arises from entirely different mechanisms from what reviewed above. PBHs are thought to originate from gravitational collapse of large density fluctuations in the early universe [47,48]. The over-densities could be produced in a variety of ways, such as topological defects like cosmic strings, necklaces or domain walls, curvature fluctuations from a period of ultra-slow-roll, a sound speed “resonance”, an early phase of matter domination, or sub-horizon phenomena including a phase transition and preheating. Albeit the calculation depends on the details of gravitational collapse, the formation time is connected to the PBH mass via $M = \gamma M_{\text{PBH}} \simeq 2 \times 10^5 \gamma \left(\frac{t}{1 \text{ s}} \right) M_{\odot}$, with $\gamma \simeq (1/\sqrt{3})^3$ during radiation domination [49].

27.4 Density and velocity distribution of dark matter

27.4.1 Local density and velocity distribution

The density and distribution of DM in the Milky Way encipher relevant dynamical information about our Galaxy, and are particularly important for direct and indirect detection experiments. The *local density* (ρ_0) is an average over a volume of a few hundred parsecs in the Solar neighbourhood.

To determine the local density from observations, two classes of methods are used [50]. So-called *local measures* rely on the vertical motion of tracer stars in the vicinity of the Sun, while *global measures* extrapolate ρ_0 from the measured rotation curve, with additional assumptions about the Galactic halo shape. Conversely, by comparing the extrapolated local density with the one obtained from local measures, one can constrain the local shape of the Milky Way halo. A major source of uncertainty on ρ_0 is the contribution of baryons (stars, gas, stellar remnants) to the local dynamical mass. For instance, the motion of tracer stars used in local measures is dictated by the total potential generated by

baryons and DM, and a robust baryonic census must be available to infer the additional contribution from DM. Recent determinations from global methods lie in the range $(0.2 - 0.6) \text{ GeV/cm}^3$, while new studies of the local DM density from *Gaia* satellite data yield $(0.4 - 1.5) \text{ GeV/cm}^3$, depending on the type of stars used in the study [51].

Other observational quantities that enter in the phase space distribution of DM, and provide constraints on mass models of the Milky Way are the local circular speed v_c and the escape velocity v_{esc} . The local circular speed is measured by various methods, roughly divided into measurements of the Sun's velocity with respect to an object assumed to be at rest with respect to the Galactic centre or direct measurements of the local radial force [52]. These methods yield values of $v_c = (218 - 246) \text{ km/s}$. A recent estimate of the escape velocity, defined as the speed above which objects are not gravitationally bound to our galaxy, is $v_{esc} = 533^{+54}_{-41} \text{ km/s}$ [53].

The local velocity distribution of DM particles can not be measured directly at present, and is mostly derived from simulations. In general, experiments use the simplest, so-called *Standard Halo Model (SHM)* for their data analysis. It assumes an isotropic, isothermal sphere of DM particles with a density profile of $\rho(r) \propto r^{-2}$, for which the velocity distribution is Maxwellian, with a velocity dispersion $\sigma_v = v_c/\sqrt{2}$. This distribution, which formally extends to infinity, is truncated at v_{esc} [54]. Earlier high resolution, dark-matter-only simulations found velocity distributions that markedly deviated from a Maxwell-Boltzmann distribution [55] and in addition revealed components above the dominant smooth distribution, including narrow spikes due to tidal streams. Recent hydrodynamical simulations of Milky Way-like galaxies including baryons, which have a non-negligible effect on the DM distribution in the Solar neighbourhood, find velocity distributions that are indeed close to Maxwellian, arguing that the SHM is a good approximation [56–58].

Ultimately the goal is to determine the velocity distribution from observations (for example by studying the motion of stars that share the same kinematics as the DM), and the *Gaia* satellite data offers a unique opportunity to study the various stellar populations. Recently it was revealed that the local stellar halo has two components: a quasi-spherical, weakly rotating structure with metal-poor stars, and a flattened, radially anisotropic structure of metal-rich stars, which arose due to accretion of a large $(10^{11-12} M_\odot)$ dwarf galaxy around $(8-10) \times 10^9$ y ago [59]. The expectation is that the local DM halo shows a similar bimodal structure, and first velocity distributions of the two components - using the stellar populations as tracers - were inferred in [60]. In Ref. [61], an updated halo model is introduced: it includes the anisotropic structure seen in the *Gaia* data and provides an analytic expression for the velocity distribution. The value of the local DM density is updated to $(0.55 \pm 0.17) \text{ GeV/cm}^3$, where the 30% error accounts for the systematics. The circular rotation and the escape speeds are updated to $v_c = (233 \pm 3) \text{ km/s}$ and $v_{esc} = 528^{+24}_{-25} \text{ km/s}$.

27.4.2 Small-scale challenges

The Λ CDM framework is tremendously successful at explaining the observed large-scale structures of the Universe (corresponding to distances $\geq 1 \text{ Mpc}$, the typical inter-galactic distance), as well as the main properties of galaxies that form within DM haloes, see [62]. The observed large-scale structure is consistent with point-like, cold DM particles that interact purely via the gravitational force. But in the past decades, observations at scales below $\sim 1 \text{ Mpc}$, where structure formation becomes strongly nonlinear, turned out more problematic to be described within the Λ CDM model. The main *small-scale challenges* which received much attention in the recent literature [13, 62] are known as: the missing satellites problem, the cusp-core problem and the too-big-to-fail problem. Initially these issues, which are not all independent of one another, arose by comparing theoretical predictions from dark-matter-only simulations to observation. While their most likely solutions are in dissipative, baryonic physics (such as gas cooling, star formation, supernovae feedback), see the recent review in Ref. [63], the small-scale problems could in addition call for a

modification or an extension of the Λ CDM paradigm. Most importantly, the ever increasing amount of data on the satellites of the MW and M31 are used to constrain alternative DM models.

The missing satellites problem: High-resolution cosmological simulations of DM haloes the size of the MW predict hundreds or thousands of subhaloes with masses that are in principle large enough to allow for galaxy formation ($> 10^7 M_\odot$). Yet less than ~ 100 satellite galaxies with masses down to $\sim 300 M_\odot$ are known to orbit our galaxy within 300 kpc. Galaxies in the field show a similar under-abundance. One solution could be that galaxy formation becomes increasingly inefficient as the halo mass drops, and thus the smallest DM haloes have naturally failed to form galaxies.

The cusp-core problem: The mass density profiles of DM haloes in Λ CDM simulations rise steeply at small radii, $\rho(r) \propto r^{-\gamma}$, with $\gamma \simeq 0.8 - 1.4$ [64]. This is in contrast to the observed density profiles of many low-mass galaxies (albeit not all), the rotation curves of which are best fit with constant-density cores, $\gamma \simeq 0 - 0.5$. A related issue is that simulations predict more DM than measured in the central regions of galaxies (also known as the central density problem). A likely solution is that baryonic feedback modifies the structure of DM haloes. Hydrodynamic simulations which include the effects of baryons on galaxy formation have shown that baryonic feedback (e.g., supernova-driven blowouts) can erase the central cusps and produce core-like density profiles.

The too-big-to-fail problem: This problem is related to the fact that the local Universe contains fewer galaxies with large central densities ($\simeq 10^{10} M_\odot$) compared to Λ CDM predictions. DM haloes of such masses are thought to be too massive to have failed to form stars (hence the name of the problem), especially if lower-mass subhaloes are capable of doing so. The bright MW satellites are generally associated with subhaloes (e.g., from the Aquarius and Via Lactea II Λ CDM simulations), however not with the most massive ones [65]. A similar issue is present in Andromeda and in field galaxies outside the Local Group. The solutions that were briefly mentioned above do not require modifications to the Λ CDM framework. Other solutions involve either modifications of linear theory predictions (via the nature of the DM particle, e.g., Warm DM - WDM) or modifications of nonlinear predictions (via DM models that involve a self-interaction of DM particles - SIDM) [62]. WDM models postulate particles with masses at the keV-scale, and the observed number of dark-matter-dominated satellites is used to set a lower limit on the number of subhaloes in the MW and thus a lower limit on the particle's mass [63]. Current constraints are in the range $m_{WDM} > (1.6 - 2.3) \text{ keV}$. Cosmological simulations with SIDM find that $\sigma/m_{SIDM} \simeq (0.5-10) \text{ cm}^2/\text{g}$ can alleviate the cusp-core and too-big-to-fail problems, giving rise to DM cores in dwarf galaxies with sizes of $(0.3-1.5) \text{ kpc}$ [13]. Galaxy clusters provide important constraints, and their large central DM densities prefer models with $\sigma/m_{DM} \lesssim 0.1 \text{ cm}^2/\text{g}$ [66]. Thus, if SIDM is to solve the small-scale CDM problems (without considering the baryonic feedback however) and obey the constraints observed on the scales of clusters, σ must depend on the velocity of the particle: it must increase as the rms speed of the particle decreases from the scale of clusters ($v \sim 10^3 \text{ km/s}$) to the scale of dwarf galaxies ($v \sim 10 \text{ km/s}$).

27.5 Dark matter models

Particle DM model building is deeply intertwined with the question of the nature of physics beyond the Standard Model (BSM) of particle physics¹. Directions in this area have followed a few strategies, including, but not limited to (1) pursuing DM candidates embedded in frameworks that include solutions to other open issues in particle physics, for example WIMPs in connection with electroweak-scale new physics that addresses the hierarchy problem, such as supersymmetry (see the Supersymmetry reviews Sec. 89 and 89); axions in connection with frameworks that address the strong CP problem (see Axions and Other Similar Particles—Sec. 91); sterile neutrinos in connection with the

¹Notice that this includes the case of PBHs, as successful formation of the correct number density of PBHs involves new ingredients beyond standard cosmology and particle physics

problem of neutrino masses and mixing (see the Neutrino Masses, Mixing, and Oscillations—Sec. 14); or (2) *ad hoc*, or *bottom-up* models built with the intent of addressing or explaining a putative experimental (e.g. particle physical anomalies) or observational (e.g. astronomical) signal.

WIMPs: The WIMP paradigm has been a preferred framework chiefly because it often arises in beyond the Standard Model scenarios that address the hierarchy problem whilst also providing a simple mechanism to explain the observed relic abundance via the “WIMP miracle” described above. Perhaps the most notable example of a framework containing a paradigmatic WIMP is the minimal supersymmetric extension to the Standard Model, if the lightest supersymmetric particle is a neutralino (the mass eigenstate resulting from the mixing of the supersymmetric partners to the Higgses and to the SU(2) and hypercharge gauge bosons, and, possibly, of additional singlet scalars); purely SU(2) sneutrinos have long been ruled out by direct detection, but with suitable mixing with “inert” (gauge-singlet) sneutrinos they can also play the role of WIMP candidates. For more details see the the Supersymmetry—Sec. 89 and 90 in this *Review*. Other non-supersymmetric WIMP models include models with a Higgs or Z (or Z') portal, universal extra dimensions [32], and other models with extra (warped or flat) dimensions, little Higgs theories, technicolor and composite Higgs theories, among others (see e.g. the review in [67]).

Axions and axion-like particles: Axions are an especially compelling example of a broad category of DM candidates encompassing very light scalar or pseudoscalar fields. The QCD axion provides a solution to the strong CP problem, and is at present a viable DM candidate (see Sec. 91 for details on motivations, production mechanisms, and detection prospects for the QCD axion). Ultra-light, bosonic DM generally implies the imprint of quantum effects on macroscopic scales (hence the name of *wave* or *fuzzy* DM). Specifically, some of the small-scale issues mentioned in sec. 27.4 can be addressed if the de Broglie wavelength of the DM, of mass m_a and velocity v_a ,

$$\frac{\lambda}{2\pi} = \frac{\hbar}{m_a v_a} \simeq 1.9 \text{ kpc} \left(\frac{10^{-22} \text{ eV}}{m_a} \right) \left(\frac{10 \text{ km/s}}{v_a} \right) \quad (27.7)$$

is comparable to the size of the smallest observed gravitationally collapsed structures, roughly, for a self-gravitating system of mass M , a scale $r \simeq GM/v^2$. The typical expectation is the formation of a soliton-like core in the DM density profile of size λ , thus inversely proportional to the DM mass, with an upper limit on the central density of around

$$\rho_s \lesssim 7 M_\odot/\text{pc}^3 \left(\frac{m_a}{10^{-22} \text{ eV}} \right)^6 \left(\frac{M}{10^9 M_\odot} \right) \quad (27.8)$$

for a halo of virial mass M . Additionally, wave DM predicts that halos lighter than around $10^7 (m_a/10^{-22} \text{ eV})^{-3/2} M_\odot$ should not exist [68], and that the number of halos in the local universe with a mass at or less $10^9 (m_a/10^{-22} \text{ eV})^{-4/3} M_\odot$ [69] be significantly depleted, addressing in part the too big to fail and missing satellite problems (see Sec. 27.4 above). Light bosonic DM is necessarily produced non-thermally [70], and the connection with the visible sector need not, but might, exist.

Dark photons: Light *vector* bosons such as a “dark photon” V with a mass below $m_V < 2m_e$, can be cosmologically stable (depending upon its kinetic mixing coupling with the visible photon) and be a viable DM candidate. Light dark photons can be produced in the early universe through scattering or annihilation via processes such as $\gamma e^\pm \rightarrow V e^\pm$ or $e^+ e^- \rightarrow V \gamma$, or via resonant photon-dark photon conversion, or from a condensate seeded by inflationary perturbations [71], or from a misalignment mechanism similar to the one commonly invoked for axion production; constraints on the parameter space stem from a combination of direct detection experiments, where the dark photon is absorbed and leads to a large ionization signal, from stellar cooling constraints from the Sun, horizontal branch stars, and red giants, and from CMB and the diffuse radiation from the $V \rightarrow 3\gamma$ decay mode. More broadly, light dark (pseudo-)scalars and vectors can be best constrained with experiments that rely on their

wave-like behaviour and/or on their possible “portal” with the visible sector. A broad assortment of experiments is sensitive to the range of masses between 10^{-22} eV and 10^{-2} eV . Among these experimental efforts, the lowest masses are probed by torsion balance experiments [72, 73], atom interferometry [74], comagnetometers [75, 76], and even gravitational wave detectors [77]; at increasing masses, if the light bosons couple electromagnetically, they can generate effective currents which are detectable with different apparatus depending on the relevant, mass-dependent target frequency. The experimental portfolio includes the broadband axion search ABRACADABRA [78, 79], the LC resonator DM Radio [80], lumped-element LC resonators [81], and cavity resonators such as HAYSTAC [82] and ADMX [83].

Sterile Neutrinos: Sterile (gauge-singlet) neutrinos, assumed to share a Dirac mass term with ordinary, SU(2) $_L$ -active neutrinos, have long been considered viable DM candidates [84]. The mostly-sterile mass eigenstate participates in SU(2) $_L$ interactions via a mixing parameter $\theta \ll 1$ that controls much of the particle’s phenomenology. In particular, the sterile neutrino possesses an inverse-lifetime on the order of $\tau^{-1} \sim G_F^2 m_\nu^5 \theta^2$, forcing the mixing to not exceed

$$\theta < 3.3 \times 10^{-4} \left(\frac{10 \text{ keV}}{m_\nu} \right)^5 \quad (27.9)$$

in order for the lifetime to exceed the age of the universe. While the main decay channel is to three active neutrinos, observationally the radiative decay mode to one neutrino plus a photon is much more relevant, giving rise to a quasi-monochromatic photon line at half the sterile neutrino mass. A recent tentative signal at 3.5 keV was reported from stacked observations of clusters of galaxies, individual clusters [85, 86], and the Galactic center [87] with both the XMM and Chandra X-ray observatories. The signal however was not detected in a large sample of galaxies and groups of galaxies [88] and dwarf galaxies [89], and especially Draco [90], shedding strong doubts on its sterile neutrino decay origin. Future observations with increased energy resolution might conclusively pinpoint the origin of the 3.5 keV emission [91].

Models with rich dark sectors: The absence of any conclusive signals from DM as a particle thus far motivates the hypothesis that the DM be charged under some new “hidden” dark-sector force, an idea that dates back many decades [92], including in the guise of “mirror DM” (more recently in the context of “neutral naturalness”). Top-down motivation for hidden-sector DM comes from string theory [93], although TeV-scale BSM framework such as supersymmetry and composite Higgs models can also naturally accommodate hidden sectors [94]. Although no coupling of the visible sector to the hidden sector need exist in principle, there are a few reasons to expect it [95]. The mass scale for hidden-sector DM is broader than, but overlapping with, that for WIMPs (this latter being limited to roughly between a few GeV and a few TeV). In particular, while some motivation exists for electroweak-scale hidden sectors, light, sub-GeV hidden sectors have a strong theoretical underpinning, and offer novel detection avenues and opportunities. The phenomenology of hidden-sector DM depends primarily on the nature of the force and its force carrier. The most-widely considered cases are (pseudo-)scalar and (axial-)vector mediators. Among the structures for the mediators’ coupling to the visible sector, renormalizable “portals” include the $H^\dagger H$ operator, through Lagrangian terms of the type $(\mu\phi + \lambda\phi^2)H^\dagger H$, coupling to the hypercharge field strength $B^{\mu\nu}$ via kinetic mixing, $\epsilon' B_{\mu\nu} F'^{\mu\nu}$, and the “neutrino” portal, $y_n L H N$, where L is the lepton doublet of any generation, N is a right-handed neutrino, H is the SM Higgs doublet, and y_n the Yukawa coupling. Other possibilities are for instance a vector mediator directly coupled to SM fermions charged under its corresponding symmetry [96], or a Z' associated to U(1) $_{B-L}$. Additional possibilities, arising for instance from vector couplings to anomalous global symmetries of the SM like baryon or lepton number, also exist [95]. The accelerator program necessary to probe hidden-sector DM often involves small-scale colliders and fixed-target experiments, with experiments utilizing missing energy and momentum offering the best sensitivity. Beam-dump experiments can test large ranges of DM-mediator couplings as long as mediators decay or scatter

inside the detector (see e.g. the recent review [97]). Such experiments can also probe dark sectors with light vectors coupled to visible matter besides gauge kinetic mixing: an instance are neutrino trident scattering used to place bounds on e.g. $L_\mu - L_\tau$ Z' gauge bosons. Being virtually unconstrained, the phenomenology of dark sectors can be arbitrarily rich, with possibilities ranging from dark non-Abelian gauge interactions creating non-trivial self-interacting and/or particle number-changing dynamics, to models of “dynamical” DM, with multi-component, unstable DM candidates and a time-variable effective total DM abundance and equation of state [98].

27.6 Laboratory detection of dark matter

Laboratory searches for DM particles can be roughly classified in direct detection experiments, axion searches (see Axions and Other Similar Particles—Sec. 91), and searches at accelerators and colliders.

27.6.1 Searches at Accelerators and Colliders

Various searches for dark matter have been carried out by the CMS and ATLAS collaborations at the LHC in pp collisions [99–103]. In general, these assume that dark matter particles escape the detector without interacting leading to significant amounts of missing energy and momentum.

Searches for DM with the LHC and other colliders have targeted DM models that interact with the SM via Higgs or Z boson exchange, effective field theories with heavy mediators, UV-complete models such as supersymmetry, models with long-lived particles, and models with rich dark sectors. The experimental program correspondingly includes searches for invisible-particle production mediated by a SM boson, generic searches for invisible particles produced via new particle mediators, and specific searches for complete models.

There are a variety of types of signals for DM, as noted by Ref. [99]:

- (a) the imbalance in the transverse momentum in an event due to the presence of DM particles, produced together with one Standard Model particle,
- (b) a bump in the di-jet or di-lepton invariant mass distributions, or
- (c) an excess of events in the di-jet angular distribution, produced by a dark matter mediator. No signal for DM has been observed in the LHC experiments so far. Instead limits are set on masses, couplings, and cross-sections. The latter can be compared with direct detection experiments.

Searches strategies are designed to optimize signal-to-noise by selecting specific search-specific cuts: a model-independent instance is initial-state electromagnetic or strong-interaction radiation plus missing transverse energy. Collider searches for DM inform, and are informed, by DM searches through direct or indirect detection (see below), and, if possible, by the inferred thermal relic DM abundance. The collider searches alone cannot prove that a discovery is of dark matter.

In the latter category, searches for DM with the LHC and other colliders have targeted DM models that interact with the SM via Higgs or Z boson exchange, effective field theories with heavy mediators, UV-complete models such as supersymmetry, models with long-lived particles, and models with rich dark sectors. The experimental program correspondingly includes searches for invisible-particle production mediated by a SM boson, generic searches for invisible particles produced via new particle mediators, and specific searches for complete models. Searches strategies are designed to optimize signal-to-noise by selecting specific search-specific cuts: a model-independent instance is initial-state electromagnetic or strong-interaction radiation plus missing transverse energy.

27.6.2 Direct detection formalism

Direct detection experiments mostly aim to observe elastic or inelastic scatters of Galactic DM particles with atomic nuclei, or with electrons in the detector material. Predicted event rates assume a certain mass and scattering cross section, as well as a set of astrophysical parameters: the local density ρ_0 , the velocity distribution $f(\vec{v})$, and the escape velocity v_{esc} (see Sec. 27.4).

Interactions with atomic nuclei: For DM scattering off nuclei, the differential scattering rate R as a function of nuclear recoil energy E_R is

$$\frac{dR(E_R, t)}{dE_R} = N_T \frac{\rho_0}{m_{\text{DM}}} \int_{v > v_{\min}} v f(\vec{v} + \vec{v}_E(t)) \frac{d\sigma(E_R, v)}{dE_R} d^3v, \quad (27.10)$$

where N_T is the number of target nuclei, m_{DM} is the mass of the DM particles, $v = |\vec{v}|$ is the speed of the particle in the experiment’s rest frame, $f(\vec{v} + \vec{v}_E(t))$ is the velocity distribution in the Earth’s frame, v_{\min} is the minimum speed of the DM particles that can cause a recoil energy E_R and σ is the scattering cross section on the nucleus [29, 121]. For elastic scattering, the minimum velocity is $v_{\min} = (m_N E_R / 2m_r^2)^{1/2}$, with m_N being the mass of the nucleus, and $m_r = (m_N m_{\text{DM}}) / (m_N + m_{\text{DM}})$ the reduced mass of the nucleus-DM system. In case of inelastic scattering, the minimum speed becomes $v_{\min} = (m_N E_R / 2m_r^2)^{1/2} + E^* / (2m_N E_R)^{1/2}$, with the nuclear excitation energy E^* , for part of the kinetic energy of the incoming particle will be spent on exciting the nucleus. The prompt de-excitation energy, if observed in addition to the nuclear recoil energy, will boost the region-of-interest to higher energies [122].

If one assumes the standard, leading order spin-independent (SI) and spin-dependent (SD) interactions, which couple to the charge/mass and spin of the nucleus, respectively, the differential cross section is proportional to the inverse squared speed of the DM particle, $d\sigma/dE_R \propto v^{-2}$, and the dependence on the velocity distribution can be expressed as:

$$g(v_{\min}, t) = \int_{v > v_{\min}} \frac{f(\vec{v} + \vec{v}_E(t))}{v} d^3v. \quad (27.11)$$

This functions allows for the comparison of various experimental results independently of the underlying velocity distribution [123], for a given DM mass. The time-integrated differential cross section is the sum of the SI and SD contributions:

$$\frac{d\sigma(E_R, v)}{dE_R} = \frac{m_N}{2m_r^2 v^2} \left(\sigma_0^{SI} F_{SI}^2(E_R) + \sigma_0^{SD} F_{SD}^2(E_R) \right), \quad (27.12)$$

where $F^2(E_R)$ are the nuclear form factors and σ_0 the cross sections in the limit of zero momentum transfer. Since the incoming particle velocity is $v/c \sim 10^{-3}$, the nuclear recoil energy is at most tens of keV (much smaller than typical nuclear binding energies per nucleon), and the momentum transfer $q = (2m_N E_R)^{1/2} \sim \mathcal{O}(10\text{--}100\text{ MeV})$. This implies that $1/q$ can be of the same order as nuclear radii $R \sim A^{1/3}$ fm, and that nuclei are not point-like from the perspective of a DM particle. The cross sections will thus involve nuclear form factors. These were calculated in [124] and [125] for the SI and SD case, respectively, for specific target nuclei, while the cross sections are often expressed in terms of single-nucleon cross sections and effective couplings of the DM particle to protons and neutrons. In the SI case, all the nucleons in the nucleus contribute coherently to the cross section (under the assumption of iso-spin independence in the DM couplings). Dominant sources of uncertainty are the nucleon sigma terms, especially for Higgs-dominated interactions, where the couplings are proportional to the quark masses. An overview is presented in Ref. [126]. For SD scattering, the nuclear spin contents due to the protons and neutrons must be considered.

The interactions of DM particles with nuclei can be treated in a non-relativistic effective field theory (NR-EFT) approach, which considers more general DM scenarios based on the lowest-order, four-field operators that describe the couplings to nucleons. These operators, which correspond to different types of interactions between the DM and quark fields, can be momentum- and velocity-dependent, and might be leading when momentum-independent interactions are suppressed, or even vanish in the limit of zero momentum [127, 128]. In Ref. [128, 129] all 15 operators (arising from 20 possible bilinear combinations between the DM and nucleon fields) which obey Galilean-invariance, T -symmetry and are Hermitian are written out up to quadratic order in q , and the

Table 27.1: Best constraints from direct detection experiments on the SI (at high >5 GeV and low < 5 GeV masses) and SD DM-nucleon couplings.

Experiment	Target	Fiducial mass [kg]	Cross section [cm ²]	DM mass [GeV]	Ref.
Spin independent high mass (>5 GeV)					
XENON1T	Xe	1042	4.1×10^{-47}	30	[104]
PandaX-II	Xe	364	8.6×10^{-47}	40	[105]
LUX	Xe	118	1.1×10^{-46}	50	[106]
SuperCDMS	Ge	12	1.0×10^{-44}	46	[107]
DarkSide-50	Ar	46	1.14×10^{-44}	100	[108]
DEAP-3600	Ar	2000	3.9×10^{-45}	100	[109]
Spin independent low mass (<5 GeV)					
LUX (Migdal)	Xe	118	6.9×10^{-38}	2	[110]
XENON1T (Migdal)	Xe	1042	3×10^{-40}	2	[111]
XENON1T (ionisation only)	Xe	1042	3.6×10^{-41}	3	[112]
DarkSide-50 (ionisation only)	Ar	20	1×10^{-41}	2	[113]
SuperCDMS (CDMSlite)	Ge	0.6	2×10^{-40}	2	[114]
CRESST	CaWO ₄ - O	0.024	1×10^{-39}	2	[115]
NEWS-G	Ne	0.3	1×10^{-38}	2	[116]
Spin dependent proton					
PICO60	C ₃ F ₈ - F	49	3.2×10^{-41}	25	[117]
Spin dependent neutron					
XENON1T	Xe	1042	6.3×10^{-42}	30	[118]
PandaX-II	Xe	364	1.6×10^{-41}	40	[119]
LUX	Xe	118	1.6×10^{-41}	35	[120]

nuclear response functions evaluated in shell-model calculations for DM targets made of F, Na, Ge, I and Xe isotopes. The connection to particle physics within the context of *simplified DM models* is made in Ref. [130, 131], where the simplified models assume a single DM particle with one mediator which couples it to quarks. More recently the DM-nucleus scattering was also analysed in the framework of chiral effective field theory (Ch-EFT), a low-energy effective theory of QCD, which allows for a consistent derivation of the nuclear responses beyond the leading-order expressions [132, 133]. Ch-EFT preserves the QCD symmetries, and predicts DM couplings to two nucleons (e.g., when the hypothetical particle couples to a virtual pion exchanged between the nucleons). It also provides a power counting that suggests a hierarchy of the various NR-EFT operators, which is however approximate given that the couplings between the DM and the Standard Model fields are not known. The generalised SI structure factors for spin-1/2 and spin-0 DM particles and various isotopes of F, Si, Ar, Ge and Xe employed in direct detection experiments are provided in Ref. [133].

Scattering off bound electrons and absorption: For DM particle masses below the GeV-scale, most searches for DM-nucleus scattering rapidly lose sensitivity, due to energy thresholds around a few 100 eV - few keV. As an example, a light DM particle with a mass of 100 MeV and $v \propto 10^{-3}c$ will induce a nuclear recoil energy of about 0.5 eV in a target made of argon. Another strategy is to search for DM scattering off bound electrons, allowing for all of the kinetic energy (50 eV in the above case) to be transferred to the material [134]. The leading possibilities are ionisation, excitation, and molecular dissociation processes, which typically require energies of (1-10) eV, and thus allow to probe scattering of DM particles with masses down to the $\mathcal{O}(\text{MeV})$ range.

For a bound electron with binding energy E_B DM particle masses of $m_{\text{DM}} \geq 250 \text{ keV} \times E_B/1 \text{ eV}$ can in principle be probed. The signal depends on the material, and can consist of one or more electrons (in semiconductors, noble liquids, graphene), one or more photons (in scintillators) or phonons (in superconductors and superfluids) and quasiparticles (in superconductors). As an example, the differential event rate for ionisation in atoms is given by

$$\frac{dR_{\text{ion}}}{d \ln E_R} = N_T \frac{\rho_0}{m_{\text{DM}}} \frac{d\langle \sigma_{\text{ion}} v \rangle}{d \ln E_R}, \quad (27.13)$$

where E_R is the recoil energy transferred to the electron, $\langle \sigma_{\text{ion}} v \rangle$ is the thermally averaged ionisation cross section and N_T is the number of target atoms per unit mass. The cross section is related

to the non relativistic DM-electron elastic scattering cross section (σ_e):

$$\begin{aligned} \frac{dR_{\text{ion}}}{d \ln E_R} &= \frac{6.2}{A} \left(\frac{\rho_0}{0.4 \text{ GeV cm}^{-3}} \right) \left(\frac{\sigma_e}{10^{-40} \text{ cm}^2} \right) \left(\frac{10 \text{ MeV}}{m_{\text{DM}}} \right) \\ &\times \frac{d\langle \sigma_{\text{ion}} v \rangle / d \ln E_R}{10^{-3} \sigma_e} \frac{\text{events}}{\text{kg d}} \end{aligned} \quad (27.14)$$

Predicted differential rates in various materials (He, Ar, Ge, Xe) and for different particle masses are shown in [134], together with cross section sensitivities as a function of mass and expected background rates from neutrinos.

Two classes of DM candidates, axion-like-particles (ALPs) and dark (or hidden) photons (see Sec. 27.5), can be absorbed in a target material by interactions with bound electrons via the axioelectric effect, which is analogous to the photoelectric effect: a boson is absorbed by a bound electron, which is then ejected from the atom [71, 135, 136]. The dark photon arises in extensions of the SM by a new massive or massless $U(1)'$ field, coupled to the SM $U(1)_Y$ via a kinetic mixing term κ , see Sec. 27.5. The absorption cross section of a massive, NR particle m_V with coupling $e' = e\kappa$ to electrons is (in natural units, and for energies $E_V \ll m_e$)

$$\sigma_{\text{abs}} = \frac{\alpha'}{\alpha} \left(\frac{E_V}{2m_e} \right)^2 \sigma_{pe}, \quad (27.15)$$

where σ_{pe} is the photoelectric cross section, and an analogue to the electromagnetic fine structure constant α is introduced, $\alpha' = (e\kappa)^2/4\pi$. The rate per atom is

$$R \simeq \frac{\rho_0}{m_V} \times \kappa^2 \sigma_{pe}. \quad (27.16)$$

Since the kinetic energy of the dark photon is negligible compared to its rest energy, a mono-energetic peak at its mass is expected in the spectrum of a direct detection experiment. Dark photons with a thermally generated abundance are excluded by direct detection experiments [71], however non-thermal mechanisms (e.g., via perturbations during inflation) could create the relic abundance, see Section 27.3.

Similarly to axions, ALPs arise from the spontaneous breaking of a global symmetry, and are phenomenologically described by a mass m_a and a decay constant f_a . Unlike for QCD axions,

however, there is no strict relation between m_a and f_a . The coupling strength to electrons with mass m_e is parameterised by $g_{ae} = 2m_e/f_a$, and the absorption cross section of a particle with incoming velocity v_a is related to the cross section for the photoelectric effect as

$$\sigma_{abs} v_a \simeq \frac{3E_a^2}{4\pi\alpha f_a^2} \sigma_{pe} = \frac{3g_{ae}^2}{4\pi\alpha} \left(\frac{E_a}{2m_e}\right)^2 \sigma_{pe}. \quad (27.17)$$

As in the case of the dark photon, the signature is a monoenergetic peak at the mass of the particle, broadened by the energy resolution of the detector. Constraints on the couplings of ALPs and dark photons to electrons from direct detection experiments in m_a and m_V mass ranges from $\sim (1 - 10^4)$ eV were derived in Ref. [137, 138], and compared to indirect limits from anomalous energy losses in the Sun, in red-giant and horizontal-branch stars. For a detailed discussion of axion and ALP searches, we refer to the *Axion* review.

27.6.3 Current and future direct detection technologies

Direct detection experiments aim to observe the small (keV-scale and below) and rare (fewer than ~ 1 event/(kg y)) signals which are induced by DM particle scatters in a detector, mostly in the form of ionisation, scintillation or lattice vibrations. A majority of experiments detects more than one signal, which allows to distinguish between scattering off of electrons (electronic recoils, ER) and off of atomic nuclei (nuclear recoils, NR). A 3D position resolution is required to define central detector regions (or fiducial volumes) with low background rates from surrounding materials, and the distinction between single- versus multiple-scatters rejects a significant fraction of backgrounds, given that DM will scatter at most once. We refer to [139] for a recent review of the field.

Specific signatures: For NRs, the shape of the differential recoil spectrum is exponentially falling with recoil energy, and depends on the mass of the particle and on the nuclear mass. Unless $m_{DM} \gg m_N$, m_{DM} can in principle be determined from the measured recoil spectrum, where multiple targets will provide tighter constraints [140]. The Earth's motion through the MW induces a seasonal variation of the total event rate and a forward-backward asymmetry in a directional signal [141, 142]. The annual modulation is due to the Earth's motion in the Galactic rest frame, which is a superposition of the Earth's rotation around the Sun and the Sun's rotation around the Galactic center. Since the Earth's orbital speed is much smaller than the Sun's speed, the expected amplitude of the modulation is $\simeq 5\%$. In the SHM, the period is one year, and the phase is 150 d (June 2), when both speeds add up maximally. This expectation is modified for different DM distributions, e.g. in the case of sub-structures such as clumps and streams [143, 144] and a DM disc [145]. In addition, the modulation changes phase at a specific recoil energy (known as crossing-energy) [146], which depends on the DM and nuclear mass, allowing to in principle determine m_{DM} if low energy thresholds can be achieved. A powerful signature is provided by the ability to detect the axis and direction of the recoiling nucleus. Since the DM flux in the laboratory frame is peaked in the direction of motion of the Sun towards the constellation Cygnus, the recoil spectrum is peaked in the opposite direction. The observation of such a dipole feature would provide a 'smoking-gun' evidence for DM, where the forward-backward rates can differ by a factor of ~ 10 , depending on the energy threshold. Ref. [147] provides a recent review of the theoretical framework and of the discovery reach of directional detectors.

Backgrounds, including neutrinos: Early direct detection experiments employing low-background Ge spectrometers featured background levels around 2 events/(kg d keV), while the current generation of liquid Xe experiments reduced this noise by four orders of magnitude, to 2×10^{-4} events/(kg d keV). Nonetheless, the measured energy spectra are still dominated by interactions due to the radioactivity of detector components, followed by cosmic muons and their secondaries such as fast neutrons. The cosmic and environmental radiation are suppressed by going deep underground and surrounding the experiments with appropriate shielding structures (mainly large water Cherenkov detectors for the current and next-generation detectors). Activation of mate-

rials via cosmic-ray interactions produce long-lived radio-nuclides (e.g., ^{39}Ar , ^{60}Co , ^{68}Ge , ^{32}Si , etc), while long-lived, human-made isotopes (^{85}Kr , ^{137}Cs , etc) can mix with detector materials or generate surface backgrounds. For details, we refer to *Section 36.6* of this *Review*.

The final backgrounds will be due to the irreducible neutrino flux from the Sun, the atmosphere and the diffuse supernovae background [148]. Solar pp-neutrinos will dominate the electronic recoil background due to elastic neutrino-electron scatters, at a level of $\sim (10 - 25)$ events/(t y) below energies of ~ 100 keV, while coherent elastic neutrino-nucleus scatters (CE ν NS) from ^8B solar neutrinos will induce up to $\sim 10^3$ events/(t y) for high-A targets, at nuclear recoil energies below \sim few keV. Nuclear recoils from atmospheric neutrinos and the diffuse supernovae neutrino background will yield event rates in the range $(1 - 5)$ events/(100 t y), depending on the detector material. In general, ^8B and atmospheric neutrinos will impact light (≤ 6 GeV) and heavy (100 GeV and above) DM searches for cross sections on nucleons below $\sim 10^{-45}$ cm 2 and $\sim 10^{-49}$ cm 2 , respectively. The precise cross sections where neutrinos constitute a dominant background depend however on the uncertainties on the flux of each neutrino source, and on the astrophysical parameters that enter in the DM signal models [149]. For very low energy thresholds to nuclear recoils, e.g. 10-30 eV in Ge and Si detectors, CE ν NS due to the ^7Be neutrino flux become relevant for exposures of ~ 50 kg y [150]. For DM searches with electron recoils via DM-electron scattering and dark photon or ALP absorption, solar neutrinos will also limit the sensitivity to DM masses in the range $\sim (1-10^3)$ MeV and $\sim (1-10^3)$ eV, respectively, for large exposures ~ 1 t y, as shown in Ref. [151].

Solid-state cryogenic detectors: Current experiments using the bolometric technique (see *Section 36.5* of this *Review*), together with either charge or light readout, are SuperCDMS (Si, Ge) at Soudan [107], EDELWEISS (Ge) at the Laboratoire Souterrain de Modane (LSM) [152] and CRESST (CaWO $_3$) at the Laboratori Nazionali del Gran Sasso (LNGS) [115]. These experiments are optimised for low-mass DM searches, and can probe masses down to ~ 0.2 GeV. CDMSlite also operates detectors at higher bias voltages to amplify the phonon signals produced by drifting charges and thus have access to light DM around 1.5 GeV [114]. The goal of their future phases is to probe the low-mass region down to cross sections of 10^{-43} - 10^{-44} cm 2 . Much smaller, gram-scale versions of cryogenic detectors can have single-charge resolution and thus probe low-mass DM via inelastic electron recoils. A SuperCDMS single-charge sensitive Si detector placed upper limits on DM interacting with electrons for masses between $(0.5 - 10^4)$ MeV, as well as on dark photon kinetic mixing for dark photon masses in the range $(1.5 - 40)$ eV [153].

Germanium ionisation detectors operated at 77 K can reach sub-keV energy thresholds and low backgrounds, but lack the ability to distinguish electronic from nuclear recoils. The current CDEX-10 experiment [154], located at the China Jinping Underground Laboratory (CJPL), uses p-type, point-contact Ge detectors operated in liquid nitrogen, and probes DM masses down to 3 GeV. The neutrinoless double beta experiment Majorana Demonstrator at SURF has obtained constraints on the couplings of ALPs and dark photons to electrons, with masses between $(6-100)$ keV [155].

Noble liquids: Liquid argon (LAr) and liquid xenon (LXe) are employed as DM targets, while R&D on liquid helium and neon is ongoing. We refer to Ref. [156] for a review of the liquid noble gas detector technology in low-energy physics, as well to *Section 36.4* of this *Review*. At present the best constraints on DM-nucleus interactions come from experiments using xenon: the LUX experiment which was operated at SURF [106], PandaX-II at CJPL [105] and XENON1T at LNGS [104]. These experiments probe particle masses down to ~ 6 GeV (when using both light and charge signals) and the SI DM-nucleon cross section down to 4.1×10^{-47} cm 2 (at 30 GeV). LAr experiments use the powerful pulse shape discrimination (PSD) that allows for distinguishing between ER and NR events, at the expense of higher energy thresholds than in LXe. The DarkSide-50 TPC at LNGS [108] sets a minimum upper limit on the SI, DM-nucleon cross section

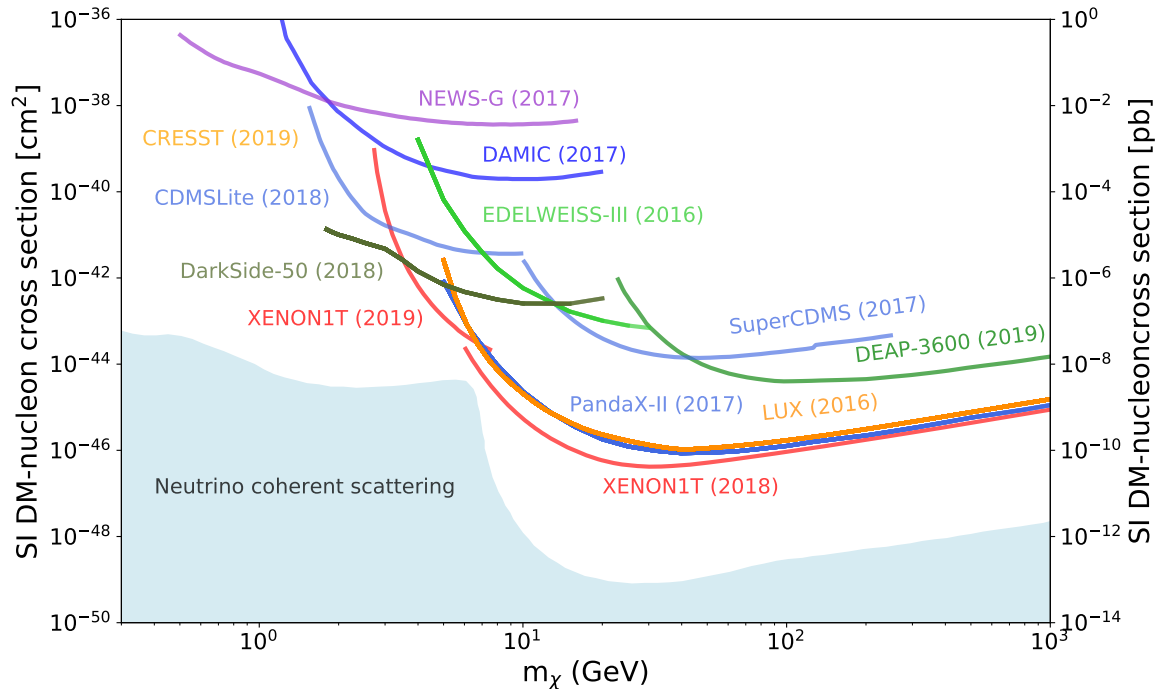


Figure 27.1: Upper limits on the SI DM-nucleon cross section as a function of DM mass.

of $1.09 \times 10^{-44} \text{ cm}^2$ at 126 GeV, while the single-phase experiment DEAP-3600 at SNOLAB [109] constrains the SI cross section to values below $3.9 \times 10^{-45} \text{ cm}^2$ at 100 GeV.

In noble liquids, sub-GeV DM particles can be searched for by observing inelastic, ER processes following a low-energy nuclear recoil: excitation and ionisation of the recoiling atom (the hypothetical Migdal effect) and a bremsstrahlung photon [157]. As an example, LUX and XENON1T constrained DM particle masses between (0.3 – 5) GeV via bremsstrahlung photons and Migdal electrons [110, 111]. Even lower masses are accessible when using the amplified, charge signal only, at the expense of giving up discrimination between ERs and NRs. XENON1T probed particle masses down to 60 MeV [112], while DarkSide-50 published constraints on WIMP masses as low as 1.8 GeV [113]. DM masses at the MeV-scale can also be probed by exploiting the scattering off electrons. The XENON1T experiment recently presented a light DM search with ionisation signals, with a background level of $< 1 \text{ event}/(\text{t d keV})$ above 0.4 keV [112]. LXe TPCs also search for solar axions, Galactic ALPs and dark photons. PandaX-II and LUX set upper limits on the axion-electron coupling of 3.5×10^{-12} in the mass range ($10^{-5} - 1$) eV for solar axions, and probe couplings around 4×10^{-13} in the mass range (1 – 10) keV for Galactic ALPs [158, 159].

The next generation of liquefied noble gas detectors, either in construction (DarkSide-20k [160], LZ [161], PandaX-4T [162], XENONnT [163]) or at the design and R&D stage (DARWIN [164]) will increase the sensitivity to various DM candidates by 1-2 orders of magnitude, with the ultimate goal of exploring the experimentally accessible parameter space, until the backgrounds from neutrinos will start dominating the event rates.

Room temperature scintillators: Several large DM experiments using high-purity NaI(Tl) crystals are acquiring data in various underground laboratories. Of these, DAMA/LIBRA at LNGS has the highest mass, 250 kg, and the largest exposure: 1.33 ty with an energy threshold of 1 keV and 2.46 ty with an energy threshold of 2 keV [165]. It is the only experiment in the field that reported an annually modulated event rate with a statistical significance of 12.9σ C.L. (20 annual cycles), with a modulation amplitude around 0.02 events/(kg d keV) in the energy region (1-4) keV. These findings were interpreted as due to DM interactions via nuclear or electronic recoils. The ANAIS experiment at Canfranc operates 112.5 kg of NaI(Tl) scintilla-

tors with an energy threshold of 1 keV and a background rate of 3.6 events/(kg d keV) in the (1-6) keV region. A first analysis of 1.5 y of data, for an exposure of 157.55 kg y is consistent with an absence of modulation [166], while 5 years of data are required to test the DAMA/LIBRA result at 3σ . The COSINE-100 experiment, located at the Yangyang Underground Laboratory, operates 106 kg of NaI(Tl) crystals in a liquid scintillator, with an energy threshold of 2 keV and a background rate of 2.7 events/(kg d keV). Results from a search based on 1.7 y of data (97.7 kg y exposure) in the (2-6) eV energy range are consistent, at 68.3% C.L., with both the null hypothesis and DAMA/LIBRA's best fit value in the same energy range. A larger exposure and a reduced energy threshold are required to test DAMA/LIBRA for 3σ coverage [167]. The SABRE experiment plans to operate a total of 50 kg of NaI(Tl) crystals, focussing on reaching a background level of 0.1 events/(kg d keV), an order of magnitude below DAMA/LIBRA [168]. Twin detectors will be installed at LNGS and at the Stawell Underground Physics Laboratory in the Southern hemisphere. While a DM-induced signal is expected to have the same phase in both hemispheres, seasonal or site-related effects would show different amplitudes and phases in the twin detectors. The COSINUS R&D project aims to develop a cryogenic scintillating bolometer with undoped NaI crystals with phonon and light readout, the ratio of which allows for particle discrimination. The hope is that it will shed light on the type of interactions responsible for the modulated signal [169].

Room temperature ionisation detectors: Silicon charged-coupled devices (CCDs) are employed for low-mass DM searches, as well as for hidden photon searches in the eV-mass range. Ionisation events induced in bulk silicon of high-resistivity, fully depleted CCDs are observed with charge resolutions around $1-2 e^-$ and extremely low leakage currents, at the level of few $e^- \text{ mm}^{-2} \text{ d}^{-1}$. The position of an energy deposit is reconstructed in 3 dimensions and the particle type (electron, neutron, muon, α -particles, etc) is reconstructed based on the recorded track pattern.

The DAMIC experiment at SNOLAB yielded new constraints on DM-electron scattering, and on the hidden-photon kinetic mixing parameter in the mass range (1-30) eV with an exposure of 7.6 kg d [170]. The SENSEI projects employ the skipper technology demonstrated in [171] to achieve single-electron sensitivity. A run with a prototype detector (0.0947 g) in a shallow

underground site at Fermilab yielded the most stringent direct-detection constraints on DM-electron scattering for masses in the range 500 keV–5 MeV, and on dark photon absorption below 12 eV [172]. The skipper technology will also be employed in the next stage of the DAMIC programme, DAMIC-M at LSM, which plans for a kg-size mass. The goal is to achieve thresholds of 2–3 electrons and to probe the DM-nucleon cross section down to $\text{few} \times 10^{-43} \text{cm}^2$ around 2–3 GeV and the DM-electron cross section down to $2 \times 10^{-41} \text{cm}^2$ at 10 MeV mass.

The NEWS-G collaboration operates spherical proportional counters [173] filled with a noble gas. Advantages of this technology are the low intrinsic electronic noise and a high amplification gain, allowing for low energy thresholds down to single-electron detection, and the possibility to use different light targets (He, Ne, etc.). A 60 cm diameter chamber operated at LSM with a gas mixture of Ne + CH₄ (0.7%) at 3.1 bar, excluded SI, WIMP-nucleon cross sections above $4.4 \times 10^{-37} \text{cm}^2$ at 0.5 GeV after an exposure of 9.6 kg d [116] with an energy threshold $\sim 100 \text{eV}$. The next iteration, a 140 cm sphere detector made of very low radioactivity copper (few $\mu\text{Bq/kg}$ of ²³⁸U and ²³²Th) is under construction and is to start running at SNOLAB in 2019.

Superheated liquid detectors: Investigation of the spin-dependent interaction channel calls for target nuclei with uneven total angular momentum. A particularly favourable candidate is ¹⁹F, the spin of which is carried mostly by the unpaired proton, yielding a cross section which is almost a factor of ten higher than of other employed nuclei with spin (e.g., ²³Na, ⁷³Ge, ¹²⁷I, ¹²⁹Xe, ¹³¹Xe). Fluorine is part of the target of experiments using superheated liquids, such as the ones operated by the PICO [117] and MOSCAB [174] collaborations. A search in the PICO-60 C₃F₆ bubble chamber at SNOLAB with an exposure of 1404 kg d and an energy threshold of 2.45 keV, yielded the most stringent constraint on the DM-proton SD cross section at $3.2 \times 10^{-41} \text{cm}^2$ for a 25 GeV particle mass. In construction is a ton-scale detector (PICO-500) to be deployed in the cube area hall of SNOLAB. MOSCAB successfully built and tested a geyser-concept bubble chamber, the operation of which is based on a continuous process of evaporation and condensation, with the detector recovering its superheated state automatically after each event. After first results in a surface laboratory [174], the detector was moved underground to LNGS for science data taking.

Directional detectors: Detectors capable of measuring the direction of the recoiling nucleus would unequivocally confirm the Galactic origin of a signal and could probe the region below the neutrino floor [175, 176]. Because nuclear recoils have a range which is about 10 times smaller than the one of Compton recoils of the same energy, gaseous detectors have an excellent intrinsic background rejection if they can measure the range of events precisely. Several directional detectors are presently in operation: DRIFT in the Boulby Mine [177], DMTPC at the Waste Isolation Pivot Plant [178], MIMAC at LSM [179] and NEWAGE in the Kamioka laboratory [180]. A 1 m³ detector has a typical mass of a few 100 g, depending on the target gas and its operating pressure, and can measure the sense of an incoming nuclear recoil above a few tens of keV.

A new technique is based on fine-grained nuclear emulsions (solid-state detectors with silver halide crystals uniformly dispersed in a gelatine film, where each crystal works as a sensor for charged particles), as proposed by the NEWSdm collaboration [181]. These act as target and nanometric tracking device, and the expected NR tracks are sub- μm in size. Due to the small crystal size and larger number density, a superior spatial resolution compared to gaseous detectors is obtained. Simulations show that to reach the neutrino floor, exposures of 10 t y and 100 t y are required if a 30 nm and 50 nm threshold for detecting the track length is reached. This requires further R&D, since current emulsions allow for 100 nm tracking and target masses are around 1 kg, with 10 kg y exposures planned. A proposed approach for the directional detection of sub-GeV DM is to use two-dimensional materials such as monolayer graphene [182], from which the DM particle can eject electrons. Their energy and direction, correlated with the direction of the incoming DM, can be measured for instance with the proposed PTOLEMY experiment [183].

New techniques: To probe light (sub-GeV) DM particles, either via scatters off electrons or via couplings to phonons, new techniques beyond the ones discussed above are proposed. The DM particle mass that can be accessed in DM-electron scattering in noble liquids and semiconductors is limited by the minimum ionisation/excitation energy and the size of the band gap, respectively (at the $\sim \text{eV}$ -scale). To reach lower energy thresholds, materials with smaller band gaps for electron excitations ($\sim \text{meV}$), such as superconductors and superfluids, as well as Dirac materials were recently proposed [184–186]. These would in principle allow for the detection of keV-scale DM. Other ideas to detect keV–MeV scale DM are to observe NRs in superfluid He, via collective excitation modes in the fluid [187], or based on the breaking of chemical bonds between atoms [188].

Even lighter DM, with masses in the meV–eV range, could be detected via absorption on a conduction electron in a superconductor, followed by the emission of an athermal phonon [189]. Another proposed target for light DM are polar materials (for example GaAs, sapphire), which are especially sensitive for scattering through an ultralight dark photon, via excitation of single optical phonons [190]. If an anisotropic crystal such as sapphire is employed, a daily modulation interaction rate could be established [191]. A new class of detectors for bosonic DM, based on resonant absorption onto a gas of small polyatomic molecules, is proposed in [192]. The DM would effectively act as a laser that resonantly excites transitions in molecules when its mass closely matches the transition energy. While DM with SI couplings can efficiently excite phonons, it has been shown in [193] that if DM couples to the electron spin, magnon excitations (quanta of collective spin wave excitations) in materials with magnetic dipole order may also offer a promising detection avenue. Yet another approach for sub-GeV DM is to employ superconducting nanowires as both target and sensor, and first bounds on DM-electron interactions were already placed from a 4.3 ng tungsten-silicide prototype with a 0.8 eV energy threshold [194].

The detection of light DM via collective excitations in condensed matter systems and other methods is a rapidly evolving field, and a growing area of research at the interface of DM physics, condensed matter and materials science. We refer to Ref. [95, 195] for discussions of some of these new directions and models. Critical challenges are to detect these very small energy depositions, and to reliably assess the background noise.

Table 27.1 summarises the most stringent constraints on the DM-nucleon SI and SD cross sections, and Figure 27.1 shows the best constraints for SI couplings in the cross section versus DM mass parameter space, above masses of 0.3 GeV.

27.7 Astrophysical detection of dark matter

DM as a microscopic constituent can have measurable, macroscopic effects on astrophysical systems. Indirect DM detection refers to the search for the annihilation or decay debris from DM particles, resulting in detectable species, including especially gamma rays, neutrinos, and antimatter particles. The production rate of such particles depends on (i) the annihilation (or decay) rate (ii) the density of pairs (respectively, of individual particles) in the region of interest, and (iii) the number of final-state particles produced in one annihilation (decay) event. In formulae, the rate for production of a final state particle f per unit volume from DM annihilation can be cast as

$$\Gamma_f^A = c \frac{\rho_{\text{DM}}^2}{m_{\text{DM}}^2} \langle \sigma v \rangle N_f^A, \quad (27.18)$$

where $\langle \sigma v \rangle$ indicates the thermally-averaged cross section for DM annihilation times relative velocity [27], calculated at the appropriate temperature, ρ_{DM} is the physical density of DM, and N_f^A is the number of final state particles f produced in one individual annihilation event. The constant c depends on whether the DM is its own antiparticle, in which case $c = 1/2$, or if there is a mixture of DM particles and antiparticles (in case there is no asymmetry, $c = 1/4$). The analog for decay is

$$\Gamma_f^D = \frac{\rho_{\text{DM}}}{m_{\text{DM}}} \frac{1}{\tau_{\text{DM}}} N_f^D, \quad (27.19)$$

with the same conventions for the symbols, and where τ_{DM} is the DM's lifetime.

Gamma Rays: DM annihilation to virtually any final state produces gamma rays: emission processes include the dominant two-photon decay mode of neutral pions resulting from the hadronization of strongly-interacting final states; final state radiation; and internal bremsstrahlung, the latter two including, possibly, the emission of massive gauge or Higgs bosons subsequently producing photons via their decay products. Similarly, neutrinos are produced from charged pion decay and from radiative processes. The flux of gamma rays and neutrinos is calculated integrating the rate Γ_f per steradian (simply meaning, for isotropic emission, $\Gamma_f/(4\pi)$) along the line of sight within the appropriate angular region (the *differential* flux is obtained in the same way by simply replacing N_f with the differential flux at production, at the appropriate redshift in the case of cosmologically distant sources),

$$\phi_f = \int_{\Delta\Omega} d\Omega \int_{\text{l.o.s.}} dl \frac{\Gamma_f}{4\pi}. \quad (27.20)$$

It is customary to factor out, in the expression for the rate, a *particle physics* factor, depending upon the DM particle mass and its annihilation or decay rate, and an *astrophysical* factor, which only depends on the observational target. The latter is sometimes denoted with $J_{\Delta\Omega}(\psi)$ with ψ indicating the direction of the line of sight. Although different conventions are in use, a common choice is to define

$$J_{\Delta\Omega}(\psi) = \int_{\Delta\Omega} \int_{\text{l.o.s.}(\psi)} \rho_{\text{DM}}^2(l, \Omega) dl d\Omega. \quad (27.21)$$

For a target with uniform density ρ and radius r at a distance $d \gg r$, such that the target is entirely within the solid angle $\Delta\Omega$,

$$J \simeq \frac{4\pi r^3 \rho_{\text{DM}}^2}{3d^2}. \quad (27.22)$$

Searches for gamma-ray emission from DM annihilation have focused on targets chosen based on a variety of considerations, primarily intended to maximize signal to noise. Nearby dwarf spheroidal galaxies contain very small amounts of gas, and do not host any significant astrophysical background at gamma-ray or X-ray frequencies, and are thus an optimal target choice for DM searches. An accurate determination of the DM density profile in these objects results in somewhat large systematics when deriving constraints from the non-observation of emission from DM; future optical surveys will help pinpoint with greater accuracy stellar kinematics and thus reduce such uncertainty; a second target is the inner region of the Milky Way: while nearby and potentially hosting a large density of DM, the Galactic center region is however very bright at almost any wavelength, making the extraction of a signal highly problematic; nearby clusters of galaxies are also known to host significant astrophysical emission, but are potentially ideally suited to constrain DM decay. Finally, putative nearby DM clumps are also a possible source of a bright DM signal (albeit from an unknown direction), as is the annihilation of DM in all halos at all redshifts.

DM annihilation and decay can lead to striking spectral features. Since the process happens typically at very low particle velocities, if the DM pair-annihilates e.g. to two photons or two neutrinos, the final-state particles will be nearly monoenergetic, with an energy close to the DM particle mass and a width proportional to the DM velocity in units of c (if a $\gamma\gamma$ line is present electroweak symmetry also implies a $Z\gamma$ line, if kinematically allowed). No astrophysical processes are known to produce lines at gamma-ray or neutrino energies in the GeV and above (with, perhaps, the possible exception of cold pulsar winds [196]) making this channel virtually background-free. At lower energy, lines are expected from radiative decay modes of candidates such as sterile neutrinos (see Sec. 27.5). DM annihilation or decay can lead to additional spectral features besides lines. These include (one or more) “boxes” [197], produced by boosted final states decaying to monochromatic photons (such as e.g. neutral pions), or combinations thereof. Processes occurring at higher redshift can distort

these spectral features by smearing them to lower energies. Neglecting gamma-ray attenuation, the flux of gamma rays from all redshift can be cast as

$$\frac{dN_\gamma}{dE_\gamma}(E_\gamma) = \frac{c}{8\pi} \int \frac{\langle\sigma v\rangle \rho_{\text{DM}}(z) dz}{H(z)(1+z)^3 m_{\text{DM}}^2} \left(\frac{dN_\gamma}{dE'} \right)_{E'=E_\gamma(1+z)}. \quad (27.23)$$

While the calculation of the differential spectrum of gamma rays from a given final state f , dN_f^i/dE_γ , is carried out using numerical tools, such as PYTHIA [198] that reproduce hadronization and particle decay for masses well above a few GeV, in the sub-GeV range gamma-ray production follows primarily from meson decay and radiative processes well outside the range of applicability of the Altarelli-Parisi splitting function. The MeV gamma-ray range will soon be probed with forthcoming satellites [199]. Recently a code that provides the expected gamma-ray spectrum for sub-GeV DM, **Hazma**, has become available [200].

Observations with the Fermi Large Area Telescope (LAT) and with ground-based facilities such as HESS, VERITAS, MAGIC, and HAWC have provided an unprecedented picture of the gamma-ray sky ideally suited to look for a signal from DM annihilation or decay for DM particles from a few GeV mass up to several TeV. The LAT has provided some of the most stringent constraints to-date on DM pair-annihilation for a variety of annihilation final states, chiefly from stacked observations of nearby satellite dwarf spheroidal galaxies [201]. Excesses of gamma rays over the expected diffuse and point-source background have been claimed, most importantly from the direction of the inner Galaxy, where a signal from DM annihilation might be especially bright [202, 203]. The nature of this excess is quite controversial: while the morphology and spectrum fall within what expected for a standard WIMP with a mass of a few tens of GeV [204], unresolved point sources, including especially an (expected) population of milli-second pulsars (MSPs) have been advocated as a possible plausible counterpart [205]. Statistical methods to discriminate between DM and MSPs have been utilized [206, 207], but recent studies indicate that such results might not be conclusive [208]. Large uncertainties in the Galactic diffuse background emission model are additionally known to exist, and possible plague the morphological and spectral information [209, 210]. Other notable potential gamma-ray excesses include a diffuse emission from the Andromeda galaxy (M31) [211–213], possibly in excess of what expected from cosmic-ray models [214]; and a diffuse emission at 511 keV energy in the inner Galaxy from Integral-SPI observations [215]; such emission has known astrophysical counterparts [216], as well as several proposed DM explanations (e.g. [217]).

While DM annihilation and decay typically occurs at low velocities, the possibility of “boosted” DM has also been considered [218]. In this case, the DM particle might dominantly pair-annihilate to a lighter dark species, which does interact with Standard Model particle, and could be detected with neutrino telescopes or direct detection experiments. Future facilities that promise to widen the reach of gamma-ray searches for DM include especially the Cherenkov Telescope Array (CTA), see fig. 27.2.

Neutrinos: DM can be captured in celestial bodies in significant amounts, depending on the DM scattering cross section off of nucleons, the DM mass, and the DM flux incident on the celestial body of interest. For DM masses at or around the GeV scale, evaporation from the celestial body plays an important role [219]. If enough DM accumulates, DM annihilation inside the celestial body can then lead to the production of Standard Model particles. Such particles can heat up the body, if they lose most of their energy before escaping. Utilizing models for heat production in planets, or stellar interior models in the case of stars, constraints can be put on DM particle properties. Of note are constraints from anomalous warming of cold planets such as Uranus [220], alterations to the stellar structure or the Sun's seismic activity [221], and anomalous Earth heat flow [222]. Alternately, DM annihilation in celestial bodies can result in the production of particles that can escape the body. Within the Standard Model, the only such instance is annihilation to neutrinos, but, similarly to the boosted DM case the DM can annihilate to a (stable or unstable) dark-sector particles, whose decay or interactions can be detected

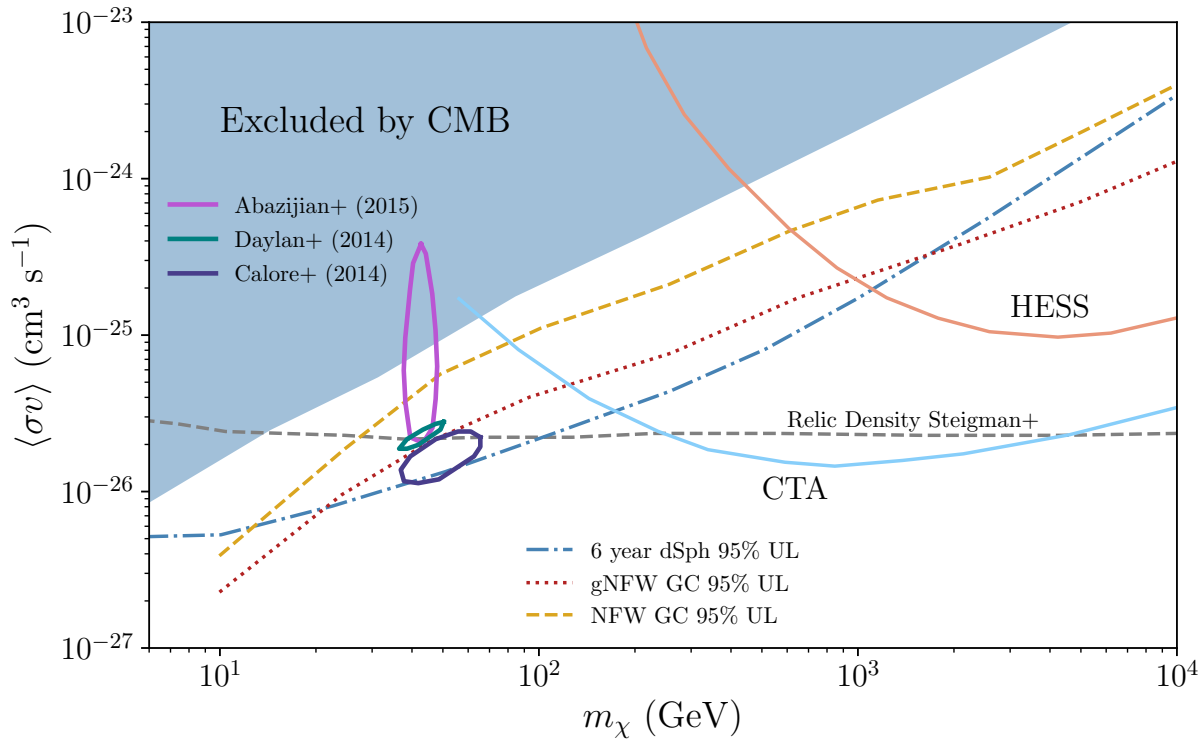


Figure 27.2: Upper limits and projected sensitivity from CTA on the pair-annihilation rate versus the DM mass from gamma-ray and CMB observations (figure courtesy of Logan Morrison).

on Earth [223,224]. For direct annihilation to neutrinos, given the lower limit on the DM mass from evaporation, the typical neutrino energies usually exceed the energy of neutrinos from the Sun, the best target for this type of searches, making this a virtually background-free DM search. Significant neutrino fluxes can only be achieved, however, if near-equilibration is reached between the capture and annihilation rates. In turn, this requires large-enough DM-nucleon scattering cross sections, to-date very close to the limits from direct detection (see sec. 27.6). Only spin-dependent cross section, and capture in the Sun usually provide large-enough neutrino fluxes. IceCube and ANTARES searches for an anomalous flux of high-energy neutrinos from the Sun yielded null results, which can be interpreted as constraints on spin-dependent nucleon-DM interactions under the assumption of equilibration and of specific annihilation final states [225,226]. Lower-threshold detectors, including DeepCore [227] and PINGU [228], can produce interesting limits on lower-mass DM candidates above the evaporation threshold.

Cosmic-ray Antimatter: Stable charged particles produced by decays of products of, or directly from DM annihilation or decay, populate the cosmic radiation and are a prime target for indirect DM searches. To maximize signal to noise, searches focus on relatively rare particle species, such as positrons, antiprotons, and antinuclei. While in certain models the production of particles and antiparticles is not symmetric [229], generally DM annihilation or decay produces as many particles as antiparticles in the final state. Charged particles produced by DM propagate and lose energy prior to reaching detectors. The transport of charged particles is customarily carried out in the context of diffusion models such as the Galactic “leaky box” setup, see e.g. [230]. While progress in constraining the uncertain propagation and energy-loss processes has been steady with improved data from new detectors such as PAMELA [231] and AMS-02 [232], the calculation of the particle flux at Earth from that at production suffers from significant uncertainties [230].

An excess of high-energy positrons over the standard secondary production from inelastic cosmic-ray interactions has been firmly established by several experiments, most recently and with the highest statistics by AMS-02 [233]. The excess has been ascribed

to DM annihilation, although strong constraints from the non-observation of corresponding anomalies in other channels, such as antiprotons and gamma rays, and the peculiar spectral shape, force DM models to be quite convoluted (see e.g. [234]). Alternatively, excess *primary* positrons can be produced in the magnetosphere of nearby pulsars [235,236]. This latter explanation was questioned in [237] in connection with the detection of a TeV halo around two candidate pulsars, leading to the determination of a highly suppressed diffusion coefficient within the pulsar nebula; with such low diffusion coefficient, positrons from the pulsars would not contribute significantly to the flux at Earth; Ref. [238], however, showed that likely the diffusion coefficient is not constant, and that if it increases outside the nebula, as expected from other cosmic-ray measurements, pulsars can still be considered as the counterpart to the positron excess. Other explanations for the excess, albeit somewhat controversial, and increasingly constrained by data, also exist [239,240].

The antiproton spectrum in the cosmic radiation as measured by AMS-02 [232] also exhibits features that might be considered as excess flux between 10 and 20 GeV, and energies above 100 GeV [241], which have been interpreted as possible signal of DM annihilation; more realistically, however, systematic uncertainties in the antiproton production cross section, in cosmic-ray transport, reacceleration at high energy and, at low energy, solar modulation make it extremely difficult to assess the robustness of the excesses [242,243].

Antinuclei such as anti-deuterium and anti-helium could also form as a result of DM annihilation or decay. While baryon number conservation forces the typical kinetic energy of antinuclei produced in inelastic cosmic-ray processes to large values, antinuclei arising from hadronization of DM-initiated jets have low energy, offering optimal signal-to-noise when a low-energy cut on the antinucleus kinetic energy is used [244–248]. Specific detector designs have been developed to single out low-energy cosmic-ray antinuclei (e.g. $E < 0.25$ GeV/nucleon in the case of the General Antiparticle Spectrometer, or GAPS [249]). The detection of even a single antinucleus would have considerable importance as a possible sign of new physics [250].

Multi-wavelength studies: Electrons and positrons from

DM lose energy quite efficiently, radiating at a variety of wavelengths. This *secondary* radiative emission presents spectral and morphological features that might provide an important additional indirect detection channel. The most efficient energy loss mechanisms for high-energy electrons and positrons are inverse Compton (IC) up-scattering of background photons, and synchrotron radiation in the presence of magnetic fields. Depending on the DM mass, the emitted light from synchrotron peaks at MHz-GHz frequencies, while the IC emission at X-ray to gamma-ray frequencies, depending on the energy of the background radiation, typically ranging from CMB photons up to starlight photons [251–253]. The calculation of the secondary emission from DM entails both solving the transport of the electrons and positrons from DM, and for the radiative emission; codes exist that perform these calculations for certain astrophysical environments [254–256], with diffusion playing an increasingly critical role in smaller and smaller structures such as dwarf galaxies [252]. It has been demonstrated that for large magnetic fields and for certain final states, the synchrotron emission is more constraining than the gamma-ray emission [257].

Stellar Physics: Microscopic properties of the DM can meaningfully alter, and thus be constrained by, several astrophysical environments, from planets and stars, up to the universe as a whole. DM particles light enough to be produced in collisional processes inside stars, with typically temperatures in the keV, or supernovae, with energy scales in the MeV, lead to an additional energy-loss mechanism, if capable of escaping the system. If this is the case, the increased needed energy output would also result in an increased neutrino flux, leading to constraints on the masses and couplings of the DM, see e.g. [258] for a comprehensive review. DM annihilation can even have fueled early stages of stellar evolution, perhaps with measurable consequences [259]. DM capture in neutron stars could lead to the collapse of the star into black holes; the existence of neutron stars in DM-rich environments can thus be used to constrain the mass and interaction cross section of DM with nucleons [260] and even relatively light, but stable, primordial black holes [261].

Cosmology: Energy injection from DM processes in the early universe, as well as the contribution of DM to the effective relativistic degrees of freedom, are severely constrained from data on Big Bang Nucleosynthesis (see Sec. 24 in this *Review*) and on the energy and anisotropy power spectrum of the CMB (see Sec. 29). Codes exist that perform the calculation of the constraints on particle DM models [200,262].

PBH Detection: Macroscopic DM candidates can gravitationally perturb structure and compromise the stability of, for instance, globular clusters such as Eridanus II [24], and/or disrupt wide binaries [263]. This constrains the maximal mass of a macroscopic DM candidate to not much more than $5 M_{\odot}$ [263] (see also [24]). In the specific case of primordial black holes, strong constraints also stem from the acceleration of charged particles around and after recombination, with significant effects on the CMB [264], albeit a lively debate exists over the accretion efficiency around such objects at high redshift [265,266]. Whether or not PBH in the solar-mass range can be 100% of the DM is therefore disputed at present. Other effects produced by macroscopic, massive DM candidates are the microlensing of stars [267, 268] and quasars [269], femtolensing of gamma-ray bursts [270], and neutron star capture [261]. It is important to note that recently constraints from both microlensing and femtolensing have been corrected after the realization of important finite-size source and wave effects [268, 271, 272], leaving a substantial window, at PBH masses $10^{17} \lesssim M_{\text{BH}}/g \lesssim 10^{21}$ where PBH can be 100% of the DM. Light black holes, $M_{\text{BH}} \lesssim 10^{17}$ g, are also constrained by the non-detection of products of evaporation [273].

References

- [1] J. D. Simon, arXiv e-prints arXiv:1901.05465 (2019), [arXiv:1901.05465].
- [2] P. Salucci, *Astron. Astrophys. Rev.* **27**, 1, 2 (2019), [arXiv:1811.08843].
- [3] S. W. Allen, A. E. Evrard and A. B. Mantz, *Annual Review of Astronomy and Astrophysics* **49**, 1, 409 (2011),

- [arXiv:1103.4829].
- [4] N. A. Bahcall *et al.*, *ApJ* **541**, 1 (2000).
- [5] S. D. M. White, G. Efstathiou and C. S. Frenk, *Mon. Not. Roy. Astron. Soc.* **262**, 1023 (1993).
- [6] A. J. S. Hamilton and M. Tegmark, *Mon. Not. Roy. Astron. Soc.* **330**, 506 (2002), [arXiv:astro-ph/0008392].
- [7] B. Famaey and S. McGaugh, *Living Rev. Rel.* **15**, 10 (2012), [arXiv:1112.3960].
- [8] S. W. Randall *et al.*, *Astrophys. J.* **679**, 1173 (2008), [arXiv:0704.0261].
- [9] R. H. Sanders, *Int. J. Mod. Phys. D* **27**, 14, 14 (2018), [arXiv:1805.06804].
- [10] S. D. McDermott, H.-B. Yu and K. M. Zurek, *Phys. Rev. D* **83**, 063509 (2011), [arXiv:1011.2907].
- [11] D. A. Buote *et al.*, *Astrophys. J.* **577**, 183 (2002), [arXiv:astro-ph/0205469].
- [12] D. Harvey *et al.*, *Science* **347**, 1462 (2015), [arXiv:1503.07675].
- [13] S. Tulin and H.-B. Yu, *Phys. Rept.* **730**, 1 (2018), [arXiv:1705.02358].
- [14] D. N. Spergel and P. J. Steinhardt, *Phys. Rev. Lett.* **84**, 3760 (2000), [arXiv:astro-ph/9909386].
- [15] S. Tremaine and J. E. Gunn, *Phys. Rev. Lett.* **42**, 407 (1979), [66(1979)].
- [16] L. Randall, J. Scholtz and J. Unwin, *Mon. Not. Roy. Astron. Soc.* **467**, 2, 1515 (2017), [arXiv:1611.04590].
- [17] R. Hlozek *et al.*, *Phys. Rev. D* **91**, 10, 103512 (2015), [arXiv:1410.2896].
- [18] E. Armengaud *et al.*, *Mon. Not. Roy. Astron. Soc.* **471**, 4, 4606 (2017), [arXiv:1703.09126].
- [19] M. Nori *et al.*, *Mon. Not. Roy. Astron. Soc.* **482**, 3, 3227 (2019), [arXiv:1809.09619].
- [20] B. Bozek *et al.*, *Mon. Not. Roy. Astron. Soc.* **450**, 1, 209 (2015), [arXiv:1409.3544].
- [21] H.-Y. Schive *et al.*, *Astrophys. J.* **818**, 1, 89 (2016), [arXiv:1508.04621].
- [22] E. O. Nadler *et al.*, *Astrophys. J.* **878**, 2, L32 (2019), [*Astrophys. J. Lett.* 878,32(2019)], [arXiv:1904.10000].
- [23] M. A. Monroy-Rodríguez and C. Allen, *ApJ* **790**, 2, 159 (2014), [arXiv:1406.5169].
- [24] T. D. Brandt, *Astrophys. J.* **824**, 2, L31 (2016), [arXiv:1605.03665].
- [25] B. Audren *et al.*, *JCAP* **1412**, 12, 028 (2014), [arXiv:1407.2418].
- [26] M. Dutra *et al.*, *JCAP* **1803**, 037 (2018), [arXiv:1801.05447].
- [27] P. Gondolo and G. Gelmini, *Nucl. Phys. B* **360**, 145 (1991).
- [28] J. L. Feng and J. Kumar, *Phys. Rev. Lett.* **101**, 231301 (2008), [arXiv:0803.4196].
- [29] G. Jungman, M. Kamionkowski and K. Griest, *Phys. Rept.* **267**, 195 (1996), [hep-ph/9506380].
- [30] J. Edsjo *et al.*, *JCAP* **0304**, 001 (2003), [hep-ph/0301106].
- [31] G. Servant and T. M. P. Tait, *Nucl. Phys. B* **650**, 391 (2003), [hep-ph/0206071].
- [32] D. Hooper and S. Profumo, *Phys. Rept.* **453**, 29 (2007), [hep-ph/0701197].
- [33] K. Griest and D. Seckel, *Phys. Rev. D* **43**, 3191 (1991).
- [34] R. T. Co *et al.*, *JCAP* **1512**, 12, 024 (2015), [arXiv:1506.07532].
- [35] V. S. Rychkov and A. Strumia, *Phys. Rev. D* **75**, 075011 (2007), [hep-ph/0701104].
- [36] E. D. Carlson, M. E. Machacek and L. J. Hall, *Astrophys. J.* **398**, 43 (1992).

- [37] D. Pappadopulo, J. T. Ruderman and G. Trevisan, *Phys. Rev.* **D94**, 3, 035005 (2016), [arXiv:1602.04219].
- [38] Y. Hochberg *et al.*, *Phys. Rev. Lett.* **113**, 171301 (2014), [arXiv:1402.5143].
- [39] E. Kuflik *et al.*, *Phys. Rev. Lett.* **116**, 22, 221302 (2016), [arXiv:1512.04545].
- [40] W. B. Lin *et al.*, *Phys. Rev. Lett.* **86**, 954 (2001), [arXiv:astro-ph/0009003].
- [41] G. B. Gelmini and P. Gondolo, *Phys. Rev.* **D74**, 023510 (2006), [hep-ph/0602230].
- [42] M. Hindmarsh, R. Kirk and S. M. West, *JCAP* **1403**, 037 (2014), [arXiv:1311.1637].
- [43] T. Moroi and L. Randall, *Nucl. Phys.* **B570**, 455 (2000), [hep-ph/9906527].
- [44] P. Hut and K. A. Olive, *Phys. Lett.* **87B**, 144 (1979).
- [45] S. Nussinov, *Phys. Lett.* **165B**, 55 (1985).
- [46] K. M. Zurek, *Phys. Rept.* **537**, 91 (2014), [arXiv:1308.0338].
- [47] Y. B. Zel'dovich and I. D. Novikov, *Soviet Ast.* **10**, 602 (1967).
- [48] S. Hawking, *Mon. Not. R. Astron. Soc* **152**, 75 (1971).
- [49] B. J. Carr, *ApJ* **201**, 1 (1975).
- [50] J. I. Read, *J. Phys.* **G41**, 063101 (2014), [arXiv:1404.1938].
- [51] J. Buch, S. C. J. Leung and J. Fan, *JCAP* **1904**, 026 (2019), [arXiv:1808.05603].
- [52] J. Bovy *et al.*, *Astrophys. J.* **759**, 131 (2012), [arXiv:1209.0759].
- [53] T. Piffl *et al.*, *Astron. Astrophys.* **562**, A91 (2014), [arXiv:1309.4293].
- [54] A. M. Green, *J. Phys.* **G44**, 8, 084001 (2017), [arXiv:1703.10102].
- [55] M. Vogelsberger *et al.*, *Mon. Not. Roy. Astron. Soc.* **395**, 797 (2009), [arXiv:0812.0362].
- [56] C. Kelso *et al.*, *JCAP* **1608**, 071 (2016), [arXiv:1601.04725].
- [57] N. Bozorgnia *et al.*, *JCAP* **1605**, 05, 024 (2016), [arXiv:1601.04707].
- [58] J. D. Sloane *et al.*, *Astrophys. J.* **831**, 93 (2016), [arXiv:1601.05402].
- [59] A. Helmi *et al.*, *Nature* **7729**, 985 (2018).
- [60] L. Necib, M. Lisanti and V. Belokurov (2018), [arXiv:1807.02519].
- [61] N. W. Evans, C. A. J. O'Hare and C. McCabe, *Phys. Rev.* **D99**, 2, 023012 (2019), [arXiv:1810.11468].
- [62] J. S. Bullock and M. Boylan-Kolchin, *Ann. Rev. Astron. Astrophys.* **55**, 343 (2017), [arXiv:1707.04256].
- [63] J. Zavala and C. S. Frenk (2019), [arXiv:1907.11775].
- [64] J. F. Navarro *et al.*, *Mon. Not. Roy. Astron. Soc.* **402**, 21 (2010), [arXiv:0810.1522].
- [65] M. Boylan-Kolchin, J. S. Bullock and M. Kaplinghat, *Mon. Not. Roy. Astron. Soc.* **415**, L40 (2011), [arXiv:1103.0007].
- [66] K. E. Andrade *et al.* (2019), [arXiv:1901.00507].
- [67] G. Servant, in "Particle dark matter," 164–189 (2010).
- [68] L. Hui *et al.*, *Phys. Rev.* **D95**, 4, 043541 (2017), [arXiv:1610.08297].
- [69] A. Fattahi *et al.* (2016), [arXiv:1607.06479].
- [70] D. J. E. Marsh, *Phys. Rept.* **643**, 1 (2016), [arXiv:1510.07633].
- [71] H. An *et al.*, *Phys. Lett.* **B747**, 331 (2015), [arXiv:1412.8378].
- [72] P. W. Graham and S. Rajendran, *Phys. Rev.* **D88**, 035023 (2013), [arXiv:1306.6088].
- [73] P. W. Graham *et al.*, *Phys. Rev.* **D93**, 7, 075029 (2016), [arXiv:1512.06165].
- [74] A. Arvanitaki *et al.*, *Phys. Rev.* **D97**, 7, 075020 (2018), [arXiv:1606.04541].
- [75] P. W. Graham *et al.*, *Phys. Rev.* **D97**, 5, 055006 (2018), [arXiv:1709.07852].
- [76] I. M. Bloch *et al.* (2019), [arXiv:1907.03767].
- [77] A. Pierce, K. Riles and Y. Zhao, *Phys. Rev. Lett.* **121**, 6, 061102 (2018), [arXiv:1801.10161].
- [78] Y. Kahn, B. R. Safdi and J. Thaler, *Phys. Rev. Lett.* **117**, 14, 141801 (2016), [arXiv:1602.01086].
- [79] R. Henning *et al.* (ABRACADABRA), in "Proceedings, 13th Patras Workshop on Axions, WIMPs and WISPs, (PATRAS 2017): Thessaloniki, Greece, 15 May 2017 - 19, 2017," 28–31 (2018).
- [80] S. Chaudhuri *et al.*, *Phys. Rev.* **D92**, 7, 075012 (2015), [arXiv:1411.7382].
- [81] P. Sikivie, N. Sullivan and D. B. Tanner, *Phys. Rev. Lett.* **112**, 13, 131301 (2014), [arXiv:1310.8545].
- [82] B. M. Brubaker *et al.*, *Phys. Rev.* **D96**, 12, 123008 (2017), [arXiv:1706.08388].
- [83] G. Rybka (ADMX), *Phys. Dark Univ.* **4**, 14 (2014).
- [84] S. Dodelson and L. M. Widrow, *Phys. Rev. Lett.* **72**, 17 (1994), [hep-ph/9303287].
- [85] E. Bulbul *et al.*, *Astrophys. J.* **789**, 13 (2014), [arXiv:1402.2301].
- [86] A. Boyarsky *et al.*, *Phys. Rev. Lett.* **113**, 251301 (2014), [arXiv:1402.4119].
- [87] T. E. Jeltema and S. Profumo, *Mon. Not. Roy. Astron. Soc.* **450**, 2, 2143 (2015), [arXiv:1408.1699].
- [88] M. E. Anderson, E. Churazov and J. N. Bregman, *Mon. Not. Roy. Astron. Soc.* **452**, 4, 3905 (2015), [arXiv:1408.4115].
- [89] D. Malyshev, A. Neronov and D. Eckert, *Phys. Rev.* **D90**, 103506 (2014), [arXiv:1408.3531].
- [90] T. E. Jeltema and S. Profumo, *Mon. Not. Roy. Astron. Soc.* **458**, 4, 3592 (2016), [arXiv:1512.01239].
- [91] F. A. Aharonian *et al.* (Hitomi), *Astrophys. J.* **837**, 1, L15 (2017), [arXiv:1607.07420].
- [92] I. Yu. Kobzarev, L. B. Okun and I. Ya. Pomeranchuk, *Sov. J. Nucl. Phys.* **3**, 6, 837 (1966), [*Yad. Fiz.* 3,1154(1966)].
- [93] M. J. Strassler and K. M. Zurek, *Phys. Lett.* **B651**, 374 (2007), [hep-ph/0604261].
- [94] M. J. Strassler (2006), [hep-ph/0607160].
- [95] M. Battaglieri *et al.*, in "U.S. Cosmic Visions: New Ideas in Dark Matter College Park, MD, USA, March 23–25, 2017," (2017), [arXiv:1707.04591], URL <http://lss.fnal.gov/archive/2017/conf/fermilab-conf-17-282-ae-ppd-t.pdf>.
- [96] Y. Kahn *et al.*, *JHEP* **05**, 002 (2017), [arXiv:1609.09072].
- [97] J. Alexander *et al.* (2016), [arXiv:1608.08632], URL <http://lss.fnal.gov/archive/2016/conf/fermilab-conf-16-421.pdf>.
- [98] K. R. Dienes and B. Thomas, *Phys. Rev.* **D85**, 083523 (2012), [arXiv:1106.4546].
- [99] N. Trevisani (ATLAS, CMS), *Universe* **4**, 11, 131 (2018).
- [100] E. Tolley (ATLAS), *PoS ICHEP2018*, 171 (2019).
- [101] W. C. Kalderon (ATLAS), *PoS DIS2018*, 085 (2018).
- [102] D. Vannerom (CMS), *PoS DIS2019*, 111 (2019).
- [103] G. Gómez-Ceballos (CMS), *PoS EDSU2018*, 014 (2018).
- [104] E. Aprile *et al.* (XENON), *Phys. Rev. Lett.* **121**, 11, 111302 (2018), [arXiv:1805.12562].
- [105] X. Cui *et al.* (PandaX-II), *Phys. Rev. Lett.* **119**, 18, 181302 (2017), [arXiv:1708.06917].
- [106] D. S. Akerib *et al.* (LUX), *Phys. Rev. Lett.* **118**, 2, 021303 (2017), [arXiv:1608.07648].

- [107] R. Agnese *et al.* (SuperCDMS), Phys. Rev. Lett. **120**, 6, 061802 (2018), [arXiv:1708.08869].
- [108] P. Agnes *et al.* (DarkSide), Phys. Rev. **D98**, 10, 102006 (2018), [arXiv:1802.07198].
- [109] R. Ajaj *et al.* (DEAP), Phys. Rev. **D100**, 022004 (2019), [arXiv:1902.04048].
- [110] D. S. Akerib *et al.* (LUX), Phys. Rev. Lett. **122**, 13, 131301 (2019), [arXiv:1811.11241].
- [111] E. Aprile *et al.* (XENON) (2019), [arXiv:1907.12771].
- [112] E. Aprile *et al.* (2019), [arXiv:1907.11485].
- [113] P. Agnes *et al.* (DarkSide), Phys. Rev. Lett. **121**, 8, 081307 (2018), [arXiv:1802.06994].
- [114] R. Agnese *et al.* (SuperCDMS), Phys. Rev. **D99**, 6, 062001 (2019), [arXiv:1808.09098].
- [115] A. H. Abdelhameed *et al.* (CRESST) (2019), [arXiv:1904.00498].
- [116] Q. Arnaud *et al.* (NEWS-G), Astropart. Phys. **97**, 54 (2018), [arXiv:1706.04934].
- [117] C. Amole *et al.* (PICO), Phys. Rev. **D100**, 2, 022001 (2019), [arXiv:1902.04031].
- [118] E. Aprile *et al.* (XENON), Phys. Rev. Lett. **122**, 14, 141301 (2019), [arXiv:1902.03234].
- [119] J. Xia *et al.* (PandaX-II), Phys. Lett. **B792**, 193 (2019), [arXiv:1807.01936].
- [120] D. S. Akerib *et al.* (LUX), Phys. Rev. Lett. **118**, 25, 251302 (2017), [arXiv:1705.03380].
- [121] J. D. Lewin and P. F. Smith, Astropart. Phys. **6**, 87 (1996).
- [122] J. R. Ellis, R. A. Flores and J. D. Lewin, Phys. Lett. **B212**, 375 (1988).
- [123] P. J. Fox, J. Liu and N. Weiner, Phys. Rev. **D83**, 103514 (2011), [arXiv:1011.1915].
- [124] L. Vietze *et al.*, Phys. Rev. **D91**, 4, 043520 (2015), [arXiv:1412.6091].
- [125] P. Klos *et al.*, Phys. Rev. **D88**, 8, 083516 (2013), [Erratum: Phys. Rev. **D89**, no.2, 029901(2014)], [arXiv:1304.7684].
- [126] J. Ellis, N. Nagata and K. A. Olive, Eur. Phys. J. **C78**, 7, 569 (2018), [arXiv:1805.09795].
- [127] J. Fan, M. Reece and L.-T. Wang, JCAP **1011**, 042 (2010), [arXiv:1008.1591].
- [128] A. L. Fitzpatrick *et al.*, JCAP **1302**, 004 (2013), [arXiv:1203.3542].
- [129] N. Anand, A. L. Fitzpatrick and W. C. Haxton, Phys. Rev. **C89**, 6, 065501 (2014), [arXiv:1308.6288].
- [130] M. I. Gresham and K. M. Zurek, Phys. Rev. **D89**, 12, 123521 (2014), [arXiv:1401.3739].
- [131] J. B. Dent *et al.*, Phys. Rev. **D92**, 6, 063515 (2015), [arXiv:1505.03117].
- [132] D. Gazda, R. Catena and C. Forssén, Phys. Rev. **D95**, 10, 103011 (2017), [arXiv:1612.09165].
- [133] M. Hoferichter *et al.*, Phys. Rev. **D99**, 5, 055031 (2019), [arXiv:1812.05617].
- [134] R. Essig, J. Mardon and T. Volansky, Phys. Rev. **D85**, 076007 (2012), [arXiv:1108.5383].
- [135] F. T. Avignone, III *et al.*, Phys. Rev. **D35**, 2752 (1987).
- [136] M. Pospelov, A. Ritz and M. B. Voloshin, Phys. Rev. **D78**, 115012 (2008), [arXiv:0807.3279].
- [137] I. M. Bloch *et al.*, JHEP **06**, 087 (2017), [arXiv:1608.02123].
- [138] Y. Hochberg, T. Lin and K. M. Zurek, Phys. Rev. **D95**, 2, 023013 (2017), [arXiv:1608.01994].
- [139] M. Schumann (2019), [arXiv:1903.03026].
- [140] M. Pato *et al.*, Phys. Rev. **D83**, 083505 (2011), [arXiv:1012.3458].
- [141] A. K. Drukier, K. Freese and D. N. Spergel, Phys. Rev. **D33**, 3495 (1986).
- [142] D. N. Spergel, Phys. Rev. **D37**, 1353 (1988).
- [143] D. Stiff, L. M. Widrow and J. Frieman, Phys. Rev. **D64**, 083516 (2001), [arXiv:astro-ph/0106048].
- [144] K. Freese *et al.*, Phys. Rev. Lett. **92**, 111301 (2004), [arXiv:astro-ph/0310334].
- [145] T. Bruch *et al.*, Astrophys. J. **696**, 920 (2009), [arXiv:0804.2896].
- [146] M. J. Lewis and K. Freese, Phys. Rev. **D70**, 043501 (2004), [arXiv:astro-ph/0307190].
- [147] F. Mayet *et al.*, Phys. Rept. **627**, 1 (2016), [arXiv:1602.03781].
- [148] L. E. Strigari, New J. Phys. **11**, 105011 (2009), [arXiv:0903.3630].
- [149] C. A. J. O'Hare, Phys. Rev. **D94**, 6, 063527 (2016), [arXiv:1604.03858].
- [150] L. E. Strigari, Phys. Rev. **D93**, 10, 103534 (2016), [arXiv:1604.00729].
- [151] R. Essig, M. Sholapurkar and T.-T. Yu, Phys. Rev. **D97**, 9, 095029 (2018), [arXiv:1801.10159].
- [152] Q. Arnaud *et al.* (EDELWEISS), Phys. Rev. **D97**, 2, 022003 (2018), [arXiv:1707.04308].
- [153] R. Agnese *et al.* (SuperCDMS), Phys. Rev. Lett. **121**, 5, 051301 (2018), [Erratum: Phys. Rev. Lett. **122**, no.6, 069901(2019)], [arXiv:1804.10697].
- [154] H. Jiang *et al.* (CDEX), Phys. Rev. Lett. **120**, 24, 241301 (2018), [arXiv:1802.09016].
- [155] N. Abgrall *et al.* (Majorana), Phys. Rev. Lett. **118**, 16, 161801 (2017), [arXiv:1612.00886].
- [156] V. Chepel and H. Araujo, JINST **8**, R04001 (2013), [arXiv:1207.2292].
- [157] M. J. Dolan, F. Kahlhoefer and C. McCabe, Phys. Rev. Lett. **121**, 10, 101801 (2018), [arXiv:1711.09906].
- [158] C. Fu *et al.* (PandaX), Phys. Rev. Lett. **119**, 18, 181806 (2017), [arXiv:1707.07921].
- [159] D. S. Akerib *et al.* (LUX), Phys. Rev. Lett. **118**, 26, 261301 (2017), [arXiv:1704.02297].
- [160] C. E. Aalseth *et al.*, Eur. Phys. J. Plus **133**, 131 (2018), [arXiv:1707.08145].
- [161] D. S. Akerib *et al.* (LUX-ZEPLIN) (2018), [arXiv:1802.06039].
- [162] H. Zhang *et al.* (PandaX), Sci. China Phys. Mech. Astron. **62**, 3, 31011 (2019), [arXiv:1806.02229].
- [163] E. Aprile *et al.* (XENON), JCAP **1604**, 04, 027 (2016), [arXiv:1512.07501].
- [164] J. Aalbers *et al.* (DARWIN), JCAP **1611**, 017 (2016), [arXiv:1606.07001].
- [165] R. Bernabei *et al.*, Universe **4**, 11, 116 (2018), [Nucl. Phys. Atom. Energy **19**, no.4, 307(2018)], [arXiv:1805.10486].
- [166] J. Amaré *et al.*, Phys. Rev. Lett. **123**, 3, 031301 (2019), [arXiv:1903.03973].
- [167] G. Adhikari *et al.* (COSINE-100), Phys. Rev. Lett. **123**, 3, 031302 (2019), [arXiv:1903.10098].
- [168] G. D'Imperio *et al.* (Sabre), PoS **ICHEP2018**, 653 (2019).
- [169] K. Schäffner *et al.*, J. Low. Temp. Phys. **193**, 5-6, 1174 (2018).
- [170] A. Aguilar-Arevalo *et al.* (DAMIC) (2019), [arXiv:1907.12628].
- [171] J. Tiffenberg *et al.* (SENSEI), Phys. Rev. Lett. **119**, 13, 131802 (2017), [arXiv:1706.00028].
- [172] O. Abramoff *et al.* (SENSEI), Phys. Rev. Lett. **122**, 16, 161801 (2019), [arXiv:1901.10478].

- [173] I. Giomataris *et al.*, JINST **3**, P09007 (2008), [arXiv:0807.2802].
- [174] A. Antonicci *et al.* (MOSCAB), Eur. Phys. J. **C77**, 11, 752 (2017), [arXiv:1708.00101].
- [175] P. Grothaus, M. Fairbairn and J. Monroe, Phys. Rev. **D90**, 5, 055018 (2014), [arXiv:1406.5047].
- [176] C. A. J. O'Hare *et al.*, Phys. Rev. **D92**, 6, 063518 (2015), [arXiv:1505.08061].
- [177] J. B. R. Battat *et al.* (DRIFT), Astropart. Phys. **91**, 65 (2017), [arXiv:1701.00171].
- [178] C. Deaconu *et al.*, Phys. Rev. **D95**, 12, 122002 (2017), [arXiv:1705.05965].
- [179] Y. Tao *et al.* (2019), [arXiv:1903.02159].
- [180] T. Hashimoto *et al.*, AIP Conf. Proc. **1921**, 1, 070001 (2018), [arXiv:1707.09744].
- [181] G. De Lellis, EPJ Web Conf. **209**, 01019 (2019).
- [182] Y. Hochberg *et al.*, Phys. Lett. **B772**, 239 (2017), [arXiv:1606.08849].
- [183] E. Baracchini *et al.* (PTOLEMY) (2018), [arXiv:1808.01892].
- [184] Y. Hochberg, Y. Zhao and K. M. Zurek, Phys. Rev. Lett. **116**, 1, 011301 (2016), [arXiv:1504.07237].
- [185] Y. Hochberg *et al.*, JHEP **08**, 057 (2016), [arXiv:1512.04533].
- [186] Y. Hochberg *et al.*, Phys. Rev. **D97**, 1, 015004 (2018), [arXiv:1708.08929].
- [187] S. Knapen, T. Lin and K. M. Zurek, Phys. Rev. **D95**, 5, 056019 (2017), [arXiv:1611.06228].
- [188] R. Essig *et al.*, Phys. Rev. **D95**, 5, 056011 (2017), [arXiv:1608.02940].
- [189] Y. Hochberg, T. Lin and K. M. Zurek, Phys. Rev. **D94**, 1, 015019 (2016), [arXiv:1604.06800].
- [190] S. Knapen *et al.*, Phys. Lett. **B785**, 386 (2018), [arXiv:1712.06598].
- [191] S. Griffin *et al.*, Phys. Rev. **D98**, 11, 115034 (2018), [arXiv:1807.10291].
- [192] A. Arvanitaki, S. Dimopoulos and K. Van Tilburg, Phys. Rev. **X8**, 4, 041001 (2018), [arXiv:1709.05354].
- [193] T. Trickle, Z. Zhang and K. M. Zurek (2019), [arXiv:1905.13744].
- [194] Y. Hochberg *et al.*, Phys. Rev. Lett. **123**, 15, 151802 (2019), [arXiv:1903.05101].
- [195] T. Lin, PoS **333**, 009 (2019), [arXiv:1904.07915].
- [196] F. Aharonian, D. Khangulyan and D. Malyshev, Astron. Astrophys. **547**, A114 (2012), [arXiv:1207.0458].
- [197] K. K. Boddy *et al.*, Phys. Rev. **D94**, 9, 095027 (2016), [arXiv:1606.07440].
- [198] T. Sjöstrand (2019), [arXiv:1907.09874].
- [199] M. Tavani *et al.* (e-ASTROGAM), JHEAp **19**, 1 (2018), [arXiv:1711.01265].
- [200] A. Coogan, L. Morrison and S. Profumo (2019), [arXiv:1907.11846].
- [201] M. Ackermann *et al.* (Fermi-LAT), Phys. Rev. Lett. **115**, 23, 231301 (2015), [arXiv:1503.02641].
- [202] D. Hooper and L. Goodenough, Phys. Lett. **B697**, 412 (2011), [arXiv:1010.2752].
- [203] M. Ackermann *et al.* (Fermi-LAT), Astrophys. J. **840**, 1, 43 (2017), [arXiv:1704.03910].
- [204] F. Calore, I. Cholis and C. Weniger, JCAP **1503**, 038 (2015), [arXiv:1409.0042].
- [205] K. N. Abazajian and M. Kaplinghat, Phys. Rev. **D86**, 083511 (2012), [Erratum: Phys. Rev. **D87**, 129902 (2013)], [arXiv:1207.6047].
- [206] S. K. Lee, M. Lisanti and B. R. Safdi, JCAP **1505**, 05, 056 (2015), [arXiv:1412.6099].
- [207] T. Daylan *et al.*, Phys. Dark Univ. **12**, 1 (2016), [arXiv:1402.6703].
- [208] R. K. Leane and T. R. Slatyer (2019), [arXiv:1904.08430].
- [209] E. Carlson, T. Linden and S. Profumo, Phys. Rev. Lett. **117**, 11, 111101 (2016), [arXiv:1510.04698].
- [210] M. Ajello *et al.* (Fermi-LAT), Astrophys. J. **819**, 1, 44 (2016), [arXiv:1511.02938].
- [211] M. Ackermann *et al.* (Fermi-LAT), Astrophys. J. **836**, 2, 208 (2017), [arXiv:1702.08602].
- [212] A. McDaniel, T. Jeltema and S. Profumo, Phys. Rev. **D97**, 10, 103021 (2018), [arXiv:1802.05258].
- [213] C. Karwin *et al.* (2019), [arXiv:1903.10533].
- [214] A. McDaniel, T. Jeltema and S. Profumo, Phys. Rev. **D100**, 2, 023014 (2019), [arXiv:1903.06833].
- [215] R. L. Kinzer *et al.*, Astrophys. J. **559**, 282 (2001).
- [216] R. M. Bandyopadhyay *et al.*, Mon. Not. Roy. Astron. Soc. **392**, 1115 (2009), [arXiv:0810.3674].
- [217] D. P. Finkbeiner and N. Weiner, Phys. Rev. **D76**, 083519 (2007), [arXiv:astro-ph/0702587].
- [218] K. Agashe *et al.*, JCAP **1410**, 10, 062 (2014), [arXiv:1405.7370].
- [219] T. Damour and L. M. Krauss, Phys. Rev. Lett. **81**, 5726 (1998), [arXiv:astro-ph/9806165].
- [220] S. L. Adler, Phys. Lett. **B671**, 203 (2009), [arXiv:0808.2823].
- [221] J. Casanellas and I. Lopes, Astrophys. J. **765**, L21 (2013), [arXiv:1212.2985].
- [222] G. D. Mack, J. F. Beacom and G. Bertone, Phys. Rev. **D76**, 043523 (2007), [arXiv:0705.4298].
- [223] J. Smolinsky and P. Tanedo, Phys. Rev. **D95**, 7, 075015 (2017), [Erratum: Phys. Rev. **D96**, no.9, 099902 (2017)], [arXiv:1701.03168].
- [224] C. Niblaeus, A. Beniwal and J. Edsjo (2019), [arXiv:1903.11363].
- [225] M. G. Aartsen *et al.* (IceCube), JCAP **1604**, 04, 022 (2016), [arXiv:1601.00653].
- [226] S. Adrian-Martinez *et al.* (ANTARES), Phys. Lett. **B759**, 69 (2016), [arXiv:1603.02228].
- [227] C. R. Das *et al.*, Phys. Lett. **B725**, 297 (2013), [arXiv:1110.5095].
- [228] M. G. Aartsen *et al.* (IceCube), J. Phys. **G44**, 5, 054006 (2017), [arXiv:1607.02671].
- [229] Y. Zhao and K. M. Zurek, JHEP **07**, 017 (2014), [arXiv:1401.7664].
- [230] A. W. Strong, I. V. Moskalenko and V. S. Ptuskin, Ann. Rev. Nucl. Part. Sci. **57**, 285 (2007), [arXiv:astro-ph/0701517].
- [231] O. Adriani *et al.* (PAMELA), Phys. Rev. Lett. **111**, 081102 (2013), [arXiv:1308.0133].
- [232] M. Aguilar *et al.* (AMS), Phys. Rev. Lett. **117**, 9, 091103 (2016).
- [233] M. Aguilar *et al.* (AMS), Phys. Rev. Lett. **110**, 141102 (2013).
- [234] S. Profumo, F. Queiroz and C. Siqueira (2019), [arXiv:1903.07638].
- [235] D. Hooper, P. Blasi and P. D. Serpico, JCAP **0901**, 025 (2009), [arXiv:0810.1527].
- [236] S. Profumo, Central Eur. J. Phys. **10**, 1 (2011), [arXiv:0812.4457].
- [237] A. U. Abeysekara *et al.* (HAWC), Science **358**, 6365, 911 (2017), [arXiv:1711.06223].

- [238] S. Profumo *et al.*, Phys. Rev. **D97**, 12, 123008 (2018), [arXiv:1803.09731].
- [239] R. Cowsik, B. Burch and T. Madziwa-Nussinov, Astrophys. J. **786**, 124 (2014), [arXiv:1305.1242].
- [240] K. Blum, B. Katz and E. Waxman, Phys. Rev. Lett. **111**, 21, 211101 (2013), [arXiv:1305.1324].
- [241] M.-Y. Cui *et al.*, Phys. Rev. Lett. **118**, 19, 191101 (2017), [arXiv:1610.03840].
- [242] A. Reinert and M. W. Winkler, JCAP **1801**, 01, 055 (2018), [arXiv:1712.00002].
- [243] M. W. Winkler, JCAP **1702**, 02, 048 (2017), [arXiv:1701.04866].
- [244] F. Donato, N. Fornengo and P. Salati, Phys. Rev. **D62**, 043003 (2000), [hep-ph/9904481].
- [245] K. Mori *et al.*, Astrophys. J. **566**, 604 (2002), [arXiv:astro-ph/0109463].
- [246] H. Baer and S. Profumo, JCAP **0512**, 008 (2005), [arXiv:astro-ph/0510722].
- [247] E. Carlson *et al.*, Phys. Rev. **D89**, 7, 076005 (2014), [arXiv:1401.2461].
- [248] M. Cirelli *et al.*, JHEP **08**, 009 (2014), [arXiv:1401.4017].
- [249] R. Bird *et al.*, in “36th International Cosmic Ray Conference (ICRC 2019) Madison, Wisconsin, USA, July 24-August 1, 2019,” (2019), [arXiv:1908.03154].
- [250] A. Coogan and S. Profumo, Phys. Rev. **D96**, 8, 083020 (2017), [arXiv:1705.09664].
- [251] S. Colafrancesco, S. Profumo and P. Ullio, Astron. Astrophys. **455**, 21 (2006), [arXiv:astro-ph/0507575].
- [252] S. Colafrancesco, S. Profumo and P. Ullio, Phys. Rev. **D75**, 023513 (2007), [arXiv:astro-ph/0607073].
- [253] S. Profumo and P. Ullio (2010), [arXiv:1001.4086].
- [254] T. E. Jeltema and S. Profumo, JCAP **0811**, 003 (2008), [arXiv:0808.2641].
- [255] M. Cirelli *et al.*, JCAP **1103**, 051 (2011), [Erratum: JCAP1210,E01(2012)], [arXiv:1012.4515].
- [256] A. McDaniel *et al.*, JCAP **1709**, 09, 027 (2017), [arXiv:1705.09384].
- [257] E. Storm *et al.*, Astrophys. J. **768**, 106 (2013), [arXiv:1210.0872].
- [258] G. G. Raffelt, *Stars as laboratories for fundamental physics* (1996), ISBN 9780226702728, URL <http://wwwth.mpp.mpg.de/members/raffelt/mypapers/199613.pdf>.
- [259] D. Spolyar, K. Freese and P. Gondolo, Phys. Rev. Lett. **100**, 051101 (2008), [arXiv:0705.0521].
- [260] S. Dimopoulos, J. Preskill and F. Wilczek, Phys. Lett. **119B**, 320 (1982).
- [261] P. Pani and A. Loeb, JCAP **1406**, 026 (2014), [arXiv:1401.3025].
- [262] H. Liu, G. W. Ridgway and T. R. Slatyer (2019), [arXiv:1904.09296].
- [263] M. A. Monroy-Rodríguez and C. Allen, Astrophys. J. **790**, 2, 159 (2014), [arXiv:1406.5169].
- [264] M. Ricotti, J. P. Ostriker and K. J. Mack, Astrophys. J. **680**, 829 (2008), [arXiv:0709.0524].
- [265] S. Bird *et al.*, Phys. Rev. Lett. **116**, 20, 201301 (2016), [arXiv:1603.00464].
- [266] V. Poulin *et al.*, Phys. Rev. **D96**, 8, 083524 (2017), [arXiv:1707.04206].
- [267] P. Tisserand *et al.* (EROS-2), Astron. Astrophys. **469**, 387 (2007), [arXiv:astro-ph/0607207].
- [268] H. Niikura *et al.*, Nat. Astron. **3**, 6, 524 (2019), [arXiv:1701.02151].
- [269] E. Mediavilla *et al.*, Astrophys. J. **706**, 1451 (2009), [arXiv:0910.3645].
- [270] A. Barnacka, J. F. Glicenstein and R. Moderski, Phys. Rev. **D86**, 043001 (2012), [arXiv:1204.2056].
- [271] A. Katz *et al.*, JCAP **1812**, 005 (2018), [arXiv:1807.11495].
- [272] N. Smyth *et al.* (2019), [arXiv:1910.01285].
- [273] B. J. Carr *et al.*, Phys. Rev. **D81**, 104019 (2010), [arXiv:0912.5297].

28. Dark Energy

Revised August 2019 by D.H. Weinberg (Ohio State U.) and M. White (UC Berkeley; LBNL).

28.1 Repulsive Gravity and Cosmic Acceleration

In the first modern cosmological model, Einstein [1] modified his field equation of General Relativity (GR), introducing a “cosmological term” that enabled a solution with time-independent, spatially homogeneous matter density ρ_m and constant positive space curvature. Although Einstein did not frame it this way, one can view the “cosmological constant” Λ as representing a constant energy density of the vacuum [2], whose repulsive gravitational effect balances the attractive gravity of matter and thereby allows a static solution. After the development of dynamic cosmological models [3, 4] and the discovery of cosmic expansion [5], the cosmological term appeared unnecessary, and Einstein and de Sitter [6] advocated adopting an expanding, homogeneous and isotropic, spatially flat, matter-dominated Universe as the default cosmology until observations dictated otherwise. Such a model has matter density equal to the critical density, $\Omega_m \equiv \rho_m/\rho_c = 1$, and negligible contribution from other energy components [7].

By the mid-1990s, the Einstein-de Sitter model was showing numerous cracks, under the combined onslaught of data from the cosmic microwave background (CMB), large-scale galaxy clustering, and direct estimates of the matter density, the expansion rate (H_0), and the age of the Universe. As noted in a number of papers from this time, introducing a cosmological constant offered a potential resolution of many of these tensions, yielding the most empirically successful version of the inflationary cold dark matter scenario. In the late 1990s, supernova surveys by two independent teams provided direct evidence for accelerating cosmic expansion [8, 9], establishing the cosmological constant model (with $\Omega_m \simeq 0.3$, $\Omega_\Lambda \simeq 0.7$) as the preferred alternative to the $\Omega_m = 1$ scenario. Shortly thereafter, CMB evidence for a spatially flat Universe [10, 11], and thus for $\Omega_{\text{tot}} \simeq 1$, cemented the case for cosmic acceleration by firmly eliminating the free-expansion alternative with $\Omega_m \ll 1$ and $\Omega_\Lambda = 0$. Today, the accelerating Universe is well established by multiple lines of independent evidence from a tight web of precise cosmological measurements.

As discussed in the Big Bang Cosmology article of this *Review* (Sec. 22), the scale factor $R(t)$ of a homogeneous and isotropic Universe governed by GR grows at an accelerating rate if the pressure $p < -\frac{1}{3}\rho$ (in $c = 1$ units). A cosmological constant has $\rho_\Lambda = \text{constant}$ and pressure $p_\Lambda = -\rho_\Lambda$ (see Eq. 22.10), so it will drive acceleration if it dominates the total energy density. However, acceleration could arise from a more general form of “dark energy” that has negative pressure, typically specified in terms of the equation-of-state-parameter $w = p/\rho$ ($= -1$ for a cosmological constant). Furthermore, the conclusion that acceleration requires a new energy component beyond matter and radiation relies on the assumption that GR is the correct description of gravity on cosmological scales. The title of this article follows the common but inexact usage of “dark energy” as a catch-all term for the origin of cosmic acceleration, regardless of whether it arises from a new form of energy or a modification of GR. Our account here draws on the much longer review of cosmic acceleration by Ref. [12], which provides background explanation and extensive literature references for the discussion in Secs. 28.2 and 28.3.

Below we will use the abbreviation Λ CDM to refer to a model with cold dark matter, a cosmological constant, inflationary initial conditions, standard radiation and neutrino content, and a flat Universe with $\Omega_{\text{tot}} = 1$ (though we will sometimes describe this model as “flat Λ CDM” to emphasize this last restriction). We will use w CDM to denote a model with the same assumptions but a free, constant value of w . Models with the prefix “o” (*e.g.*, o w CDM) allow non-zero space curvature.

28.2 Theories of Cosmic Acceleration

28.2.1 Dark Energy or Modified Gravity?

A cosmological constant is the mathematically simplest, and perhaps the physically simplest, theoretical explanation for the accelerating Universe. The problem is explaining its unnaturally small magnitude, as discussed in Sec. 22.4.7 of this *Review*. An alternative (which still requires finding a way to make the cos-

mological constant zero or at least negligibly small) is that the accelerating cosmic expansion is driven by a new form of energy such as a scalar field [13] with potential $V(\phi)$. The energy density and pressure of the field $\phi(\mathbf{x})$ take the same forms as for inflationary scalar fields, given in Eq. (22.52) of the Big Bang Cosmology article. In the limit that $\frac{1}{2}\dot{\phi}^2 \ll |V(\phi)|$, the scalar field acts like a cosmological constant, with $p_\phi \simeq -\rho_\phi$. In this scenario, today’s cosmic acceleration is closely akin to the epoch of inflation, but with radically different energy and timescale.

More generally, the value of $w = p_\phi/\rho_\phi$ in scalar field models evolves with time in a way that depends on $V(\phi)$ and on the initial conditions ($\phi_i, \dot{\phi}_i$); some forms of $V(\phi)$ have attractor solutions in which the late-time behavior is insensitive to initial values. Many forms of time evolution are possible, including ones where w is approximately constant and broad classes where w “freezes” towards or “thaws” away from $w = -1$, with the transition occurring when the field comes to dominate the total energy budget. If ρ_ϕ is even approximately constant, then it becomes dynamically insignificant at high redshift, because the matter density scales as $\rho_m \propto (1+z)^3$. “Early dark energy” models are ones in which ρ_ϕ is a small but not negligible fraction (*e.g.*, a few percent) of the total energy throughout the matter- and radiation-dominated eras, tracking the dominant component before itself coming to dominate at low redshift.

Instead of introducing a new energy component, one can attempt to modify gravity in a way that leads to accelerated expansion [14]. One option is to replace the Ricci scalar \mathcal{R} with a function $\mathcal{R} + f(\mathcal{R})$ in the gravitational action [15]. Other changes can be more radical, such as introducing extra dimensions and allowing gravitons to “leak” off the brane that represents the observable Universe (the “DGP” model [16]). The DGP example has inspired a more general class of “galileon” and massive gravity models. Constructing viable modified gravity models is challenging, in part because it is easy to introduce theoretical inconsistencies (such as “ghost” fields with negative kinetic energy), but above all because GR is a theory with many high-precision empirical successes on solar system scales [17]. Modified gravity models typically invoke screening mechanisms that force model predictions to approach those of GR in regions of high density or strong gravitational potential. Screening offers potentially distinctive signatures, as the strength of gravity (*i.e.*, the effective value of G_N) can vary by order unity in environments with different gravitational potentials.

More generally, one can search for signatures of modified gravity by comparing the history of cosmic structure growth to the history of cosmic expansion. Within GR, these two are linked by a consistency relation, as described below (Eq. (28.2)). Modifying gravity can change the predicted rate of structure growth, and it can make the growth rate dependent on scale or environment. In some circumstances, modifying gravity alters the combinations of potentials responsible for gravitational lensing and the dynamics of non-relativistic tracers (such as galaxies or stars) in different ways (see Sec. 22.4.7 in this *Review*), leading to order unity mismatches between the masses of objects inferred from lensing and those inferred from dynamics in unscreened environments.

At present there are no fully realized and empirically viable modified gravity theories that explain the observed level of cosmic acceleration. The constraints on $f(\mathcal{R})$ models now force them so close to GR that they cannot produce acceleration without introducing a separate dark energy component [18]. The DGP model is empirically ruled out by several tests, including the expansion history, the integrated Sachs-Wolfe effect, and redshift-space distortion measurements of the structure growth rate [19]. The near-simultaneous arrival of gravitational waves and electromagnetic signals from the neutron star merger event GW170817, which shows that gravitational waves travel at almost exactly the speed of light, is a further strong constraint on modified gravity theories [20]. The elimination of models should be considered an important success of the program to empirically test theories of cosmic acceleration. However, it is worth recalling that there was no fully realized gravitational explanation for the precession of Mercury’s orbit prior to the completion of GR in 1915, and the fact that no complete and viable modified gravity theory exists

today does not mean that one will not arise in the future. In the meantime, we can continue empirical investigations that can tighten restrictions on such theories or perhaps point towards the gravitational sector as the origin of accelerating expansion.

28.2.2 Expansion History and Growth of Structure

The main line of empirical attack on dark energy is to measure the history of cosmic expansion and the history of matter clustering with the greatest achievable precision over a wide range of redshift. Within GR, the expansion rate $H(z)$ is governed by the Friedmann equation (see the articles on Big Bang Cosmology and Cosmological Parameters—Secs. 22 and 25.1 in this *Review*). For dark energy with an equation of state $w(z)$, the cosmological constant contribution to the expansion, Ω_Λ , is replaced by a redshift-dependent contribution. The evolution of the dark energy density follows from Eq. (22.10),

$$\begin{aligned} \Omega_{\text{de}} \frac{\rho_{\text{de}}(z)}{\rho_{\text{de}}(z=0)} &= \Omega_{\text{de}} \exp \left[3 \int_0^z [1 + w(z')] \frac{dz'}{1+z'} \right] \\ &= \Omega_{\text{de}} (1+z)^{3(1+w)}, \end{aligned} \quad (28.1)$$

where the second equality holds for constant w . If Ω_m , Ω_r , and the present value of Ω_{tot} are known, then measuring $H(z)$ pins down $w(z)$. (Note that Ω_{de} is the same quantity denoted Ω_v in Sec. 22, but we have adopted the ‘de’ subscript to avoid implying that dark energy is necessarily a vacuum effect.)

While some observations can probe $H(z)$ directly, others measure the distance-redshift relation. The basic relations between angular diameter distance or luminosity distance and $H(z)$ are given in Ch. 22—and these are generally unaltered in time-dependent dark energy or modified gravity models. For convenience, in later sections, we will sometimes refer to the comoving angular distance, $D_{A,c}(z) = (1+z)D_A(z)$.

In GR-based linear perturbation theory, the density contrast $\delta(\mathbf{x}, t) \equiv \rho(\mathbf{x}, t)/\bar{\rho}(t) - 1$ of pressureless matter grows in proportion to the linear growth function $G(t)$ (not to be confused with the gravitational constant G_N), which follows the differential equation

$$\ddot{G} + 2H(z)\dot{G} - \frac{3}{2}\Omega_m H_0^2 (1+z)^3 G = 0. \quad (28.2)$$

To a good approximation, the logarithmic derivative of $G(z)$ is

$$f(z) \equiv -\frac{d \ln G}{d \ln(1+z)} \simeq \left[\Omega_m (1+z)^3 \frac{H_0^2}{H^2(z)} \right]^\gamma, \quad (28.3)$$

where $\gamma \simeq 0.55$ for relevant values of cosmological parameters [21]. In an $\Omega_m = 1$ Universe, $G(z) \propto (1+z)^{-1}$, but growth slows when Ω_m drops significantly below unity. One can integrate Eq. (28.3) to get an approximate integral relation between $G(z)$ and $H(z)$, but the full (numerical) solution to Eq. (28.2) should be used for precision calculations. Even in the non-linear regime, the amplitude of clustering is determined mainly by $G(z)$, so observations of non-linear structure can be used to infer the linear $G(z)$, provided one has good theoretical modeling to relate the two.

In modified gravity models the growth rate of gravitational clustering may differ from the GR prediction. A general strategy to test modified gravity, therefore, is to measure both the expansion history and the growth history to see whether they yield consistent results for $H(z)$ or $w(z)$.

28.2.3 Parameters

Constraining a general history of $w(z)$ is nearly impossible, because the dark energy density, which affects $H(z)$, is given by an integral over $w(z)$, and distances and the growth factor involve a further integration over functions of $H(z)$. Oscillations in $w(z)$ over a range $\Delta z/(1+z) \ll 1$ are therefore extremely difficult to constrain. It has become conventional to phrase constraints or projected constraints on $w(z)$ in terms of a linear evolution model,

$$w(a) = w_0 + w_a(1-a) = w_p + w_a(a_p - a), \quad (28.4)$$

where $a \equiv (1+z)^{-1}$, w_0 is the value of w at $z = 0$, and w_p is the value of w at a ‘pivot’ redshift $z_p \equiv a_p^{-1} - 1$, where it

is best constrained by a given set of experiments. For typical data combinations, $z_p \simeq 0.5$. This simple parameterization can provide a good approximation to the predictions of many physically motivated models for observables measured with percent-level precision. A widely used ‘Figure of Merit’ (FoM) for dark energy experiments [22] is the projected combination of errors $[\sigma(w_p)\sigma(w_a)]^{-1}$. Ambitious future experiments with 0.1–0.3% precision on observables can constrain richer descriptions of $w(z)$, which can be characterized by principal components.

There has been less convergence on a standard parameterization for describing modified gravity theories. Deviations from the GR-predicted growth rate can be described by a deviation $\Delta\gamma$ in the index of Eq. (28.3), together with an overall multiplicative offset relative to the $G(z)$ expected from extrapolating the CMB-measured fluctuation amplitude to low redshift. However, these two parameters may not accurately capture the growth predictions of all physically interesting models. Another important parameter to constrain is the ratio of the gravitational potentials governing space curvature and the acceleration of non-relativistic test particles. The possible phenomenology of modified gravity models is rich, which enables many consistency tests but complicates the task of constructing parameterized descriptions.

The more general set of cosmological parameters is discussed elsewhere in this *Review* (Sec. 25.1), but here we highlight a few that are particularly important to the dark energy discussion.

- The dimensionless Hubble parameter $h \equiv H_0/100 \text{ km s}^{-1} \text{ Mpc}^{-1}$ determines the present day value of the critical density and the overall scaling of distances inferred from redshifts.
- Ω_m and Ω_{tot} affect the expansion history and the distance-redshift relation.
- The sound horizon $r_s = \int_0^{t_{\text{rec}}} c_s(t) dt/a(t)$, the comoving distance that pressure waves can propagate between $t = 0$ and recombination, determines the physical scale of the acoustic peaks in the CMB and the baryon acoustic oscillation (BAO) feature in low-redshift matter clustering [23].
- The amplitude of matter fluctuations, conventionally represented by the quantity $\sigma_8(z)$, scales the overall amplitude of growth measures such as weak lensing or redshift-space distortions (discussed in the next section).

Specifically, $\sigma_8(z)$ refers to the rms fluctuation of the matter overdensity $\rho/\bar{\rho}$ in spheres of radius $8h^{-1}\text{Mpc}$, computed from the linear theory matter power spectrum at redshift z , and σ_8 on its own refers to the value at $z = 0$ (just like our convention for Ω_m).

While discussions of dark energy are frequently phrased in terms of values and errors on quantities like w_p , w_a , $\Delta\gamma$, and Ω_{tot} , parameter precision is the means to an end, not an end in itself. The underlying goal of empirical studies of cosmic acceleration is to address two physically profound questions:

1. Does acceleration arise from a breakdown of GR on cosmological scales or from a new energy component that exerts repulsive gravity within GR?
2. If acceleration is caused by a new energy component, is its energy density constant in space and time, as expected for a fundamental vacuum energy, or does it show variations that indicate a dynamical field?

Substantial progress towards answering these questions, in particular any definitive rejection of the cosmological constant ‘null hypothesis,’ would be a major breakthrough in cosmology and fundamental physics.

28.3 Observational Probes

We briefly summarize the observational probes that play the greatest role in current constraints on dark energy. Further discussion can be found in other articles of this *Review*, in particular Secs. 25.1 (Cosmological Parameters) and 29 (The Cosmic Microwave Background), and in Ref. [12], which provides extensive references to background literature. Recent observational results from these methods are discussed in Sec. 28.4.

28.3.1 Methods, Sensitivity, Systematics

Cosmic Microwave Background Anisotropies: Although CMB anisotropies provide limited information about dark energy on their own, CMB constraints on the geometry, matter content, and radiation content of the Universe play a critical role in dark energy studies when combined with low-redshift probes. In particular, CMB data supply measurements of $\theta_s = r_s/D_{A,c}(z_{\text{rec}})$, the angular size of the sound horizon at recombination, from the angular location of the acoustic peaks, measurements of $\Omega_m h^2$ and $\Omega_b h^2$ from the heights of the peaks, and normalization of the amplitude of matter fluctuations at z_{rec} from the amplitude of the CMB fluctuations themselves. *Planck* data yield a 0.18% determination of r_s , which scales as $(\Omega_m h^2)^{-0.25}$ for cosmologies with standard matter and radiation content. The uncertainty in the matter fluctuation amplitude at the epoch of recombination is 0.5%. Secondary anisotropies, including the integrated Sachs-Wolfe effect, the Sunyaev-Zeldovich (SZ, [24]) effect, and weak lensing of primary anisotropies, provide additional information about dark energy by constraining low-redshift structure growth.

Type Ia Supernovae (SN): Type Ia supernovae, produced by the thermonuclear explosions of white dwarfs, exhibit 10–15% scatter in peak luminosity after correction for light curve duration (the time to rise and fall) and color (which is a diagnostic of dust extinction). Since the peak luminosity is not known *a priori*, supernova surveys constrain ratios of luminosity distances at different redshifts. If one is comparing a high-redshift sample to a local calibrator sample measured with much higher precision (and distances inferred from Hubble’s law), then one essentially measures the luminosity distance in $h^{-1}\text{Mpc}$, constraining the combination $hD_L(z)$. With distance uncertainties of 5–8% per well observed supernova, a sample of around 100 SNe is sufficient to achieve sub-percent statistical precision. The 1–2% systematic uncertainties in current samples are dominated by uncertainties associated with photometric calibration and dust extinction corrections plus the observed dependence of luminosity on host galaxy properties. Another potential systematic is redshift evolution of the supernova population itself, which can be tested by analyzing subsamples grouped by spectral properties or host galaxy properties to confirm that they yield consistent results.

Baryon Acoustic Oscillations (BAO): Pressure waves that propagate in the pre-recombination photon-baryon fluid imprint a characteristic scale in the clustering of matter and galaxies, which appears in the galaxy correlation function as a localized peak at the sound horizon scale r_s , or in the power spectrum as a series of oscillations. Since observed galaxy coordinates consist of angles and redshifts, measuring this “standard ruler” scale in a galaxy redshift survey determines the angular diameter distance $D_A(z)$ and the expansion rate $H(z)$, which convert coordinate separations to comoving distances. Errors on the two quantities are correlated, and in existing galaxy surveys the best determined combination is approximately $D_V(z) = [czD_{A,c}^2(z)/H(z)]^{1/3}$. As an approximate rule of thumb, a survey that fully samples structures at redshift z over a comoving volume V , and is therefore limited by cosmic variance rather than shot noise, measures $D_{A,c}(z)$ with a fractional error of $0.005(V/10\text{Gpc}^3)^{-1/2}$ and $H(z)$ with a fractional error 1.6–1.8 times higher. The most precise BAO measurements to date come from large galaxy redshift surveys probing $z < 0.8$, and these will be extended to higher redshifts by future projects. At redshifts $z > 2$, BAO can also be measured in the Lyman- α forest of intergalactic hydrogen absorption towards background quasars, where the fluctuating absorption pattern provides tens or hundreds of samples of the density field along each quasar sightline. For Lyman- α forest BAO, the best measured parameter combination is more heavily weighted towards $H(z)$ because of strong redshift-space distortions that enhance clustering in the line-of-sight direction. Radio intensity mapping, which maps large-scale structure in redshifted 21-cm hydrogen emission without resolving individual galaxies, offers a potentially promising route to measuring BAO over large volumes at relatively low cost, but the technique is still under development. Photometric redshifts in optical imaging surveys can be used to measure BAO in the angular direction, though the typical distance precision is a factor of 3–4 lower compared to a well sampled spectroscopic survey

of the same area, and angular BAO measurements do not directly constrain $H(z)$. BAO distance measurements complement SN distance measurements by providing absolute rather than relative distances (with precise calibration of r_s from the CMB) and by having greater achievable precision at high redshift thanks to the increasing comoving volume available. Theoretical modeling suggests that BAO measurements from even the largest feasible redshift surveys will be limited by statistical rather than systematic uncertainties.

Weak Gravitational Lensing: Gravitational light bending by a clustered distribution of matter shears the shapes of higher redshift background galaxies in a spatially coherent manner, producing a correlated pattern of apparent ellipticities. By studying the weak lensing signal for source galaxies binned by photometric redshift (estimated from broad-band colors), one can probe the correlation of source ellipticities to deduce the clustering of intervening matter. “Galaxy-galaxy lensing” (GGL) uses the correlation between a shear map and a foreground galaxy sample to measure the average mass profile around the foreground galaxies, which can be combined with galaxy clustering to constrain total matter clustering. For a specified expansion history, the predicted signals scale approximately as $\sigma_8 \Omega_m^\alpha$, with $\alpha \simeq 0.3\text{--}0.5$. The predicted signals also depend on the distance-redshift relation, so weak lensing becomes more powerful in concert with SN or BAO measurements that can pin this relation down independently. The most challenging systematics are shape measurement biases, biases in the distribution of photometric redshifts, and intrinsic alignments of galaxy orientations that could contaminate the lensing-induced signal. Weak lensing of CMB anisotropies is an increasingly powerful tool, in part because it circumvents many of these observational and astrophysical systematics. Predicting the large-scale weak lensing signal is straightforward in principle, but the number of independent modes on large scales is small, and the inferences are therefore dominated by sample variance. Exploiting small-scale measurements, for tighter constraints, requires modeling the effects of complex physical processes such as star formation and feedback on the matter power spectrum. Strong gravitational lensing can also provide constraints on dark energy, either through time delay measurements that probe the absolute distance scale, or through measurements of multiple-redshift lenses that constrain distance ratios. The primary uncertainty for strong lensing constraints is modeling the mass distribution of the lens systems.

Clusters of Galaxies: Like weak lensing, the abundance of massive dark-matter halos probes structure growth by constraining $\sigma_8 \Omega_m^\alpha$, where $\alpha \simeq 0.3\text{--}0.5$. These halos can be identified as dense concentrations of galaxies or through the signatures of hot ($10^7\text{--}10^8\text{K}$) gas in X-ray emission or SZ distortion of the CMB. The critical challenge in cluster cosmology is calibrating the relation $P(M_{\text{halo}}|O)$ between the halo mass as predicted from theory and the observable O used for cluster identification. Measuring the stacked weak lensing signal from clusters has emerged as a promising approach to achieve percent-level accuracy in calibration of the mean relation, which is required for clusters to remain competitive with other growth probes. This method requires accurate modeling of completeness and contamination of cluster catalogs, projection effects on cluster selection and weak lensing measurements, and possible baryonic physics effects on the mass distribution within clusters.

Redshift-Space Distortions (RSD) and the Alcock-Paczynski (AP) Effect: Redshift-space distortions of galaxy clustering, induced by peculiar motions, probe structure growth by constraining the parameter combination $f(z)\sigma_8(z)$, where $f(z)$ is the growth rate defined by Eq. (28.3). Uncertainties in theoretical modeling of non-linear gravitational evolution and the non-linear bias between the galaxy and matter distributions currently limit application of the method to large scales (comoving separations $r \gtrsim 10h^{-1}\text{Mpc}$ or wavenumbers $k \lesssim 0.2h\text{Mpc}^{-1}$). A second source of anisotropy arises if one adopts the wrong cosmological metric to convert angles and redshifts into comoving separations, a phenomenon known as the Alcock-Paczynski effect [26]. Demanding isotropy of clustering at redshift z constrains the parameter combination

Table 28.1: A selection of major dark-energy experiments, based on Ref. [25]. Abbreviations in the “Data” column refer to optical (Opt) or near-infrared (NIR) imaging (I) or spectroscopy (S). For spectroscopic experiments, the “Spec- z ” column lists the primary redshift range for galaxies (gals), quasars (QSOs), or the Lyman- α forest (Ly α F). Abbreviations in the “Methods” column are weak lensing (WL), clusters (CL), supernovae (SN), baryon acoustic oscillations (BAO), and redshift-space distortions (RSD).

Project	Dates	Area/deg ²	Data	Spec- z Range	Methods
BOSS	2008–2014	10,000	Opt-S	0.3–0.7 (gals) 2–3.5 (Ly α F)	BAO/RSD
KiDS	2011–2019	1500	Opt-I	—	WL/CL
DES	2013–2019	5000	Opt-I	—	WL/CL SN/BAO
eBOSS	2014–2018	7500	Opt-S	0.6–2.0 (gal/QSO) 2–3.5 (Ly α F)	BAO/RSD
SuMIRE	2014–2024	1500	Opt-I	—	WL/CL
HETDEX	2017–2023	450	Opt/NIR-S	0.8–2.4 (gals)	BAO/RSD
DESI	2020–2025	14,000	Opt-S	1.9 < z < 3.5 (gals)	BAO/RSD
LSST	2022–2032	20,000	Opt-S	0–1.7 (gals) 2–3.5 (Ly α F)	BAO/RSD
LSST	2022–2032	20,000	Opt-I	—	WL/CL SN/BAO
<i>Euclid</i>	2022–2028	15,000	Opt-I	—	WL/CL
<i>WFIRST</i>	2025–2030	2200	NIR-S	0.7–2.2 (gals)	BAO/RSD
<i>WFIRST</i>	2025–2030	2200	NIR-I	—	WL/CL/SN
<i>WFIRST</i>	2025–2030	2200	NIR-S	1.0–3.0 (gals)	BAO/RSD

$H(z)D_A(z)$. The main challenge for the AP method is correcting for the anisotropy induced by peculiar velocity RSD.

Low Redshift Measurement of H_0 : The value of H_0 sets the current value of the critical density $\rho_c = 3H_0^2/8\pi G_N$, and combination with CMB measurements provides a long lever arm for constraining the evolution of dark energy. The challenge in conventional H_0 measurements is establishing distances to galaxies that are “in the Hubble flow,” *i.e.*, far enough away that their peculiar velocities are small compared to the expansion velocity $v = H_0 d$. This can be done by building a ladder of distance indicators tied to stellar parallax on its lowest rung, or by using gravitational-lens time delays or geometrical measurements of maser data to circumvent this ladder.

28.3.2 Dark Energy Experiments

Most observational applications of these methods now take place in the context of large cosmological surveys, for which constraining dark energy and modified gravity theories is a central objective. Table 28.1 lists a selection of current and planned dark-energy experiments, taken originally from the Snowmass 2013 Dark Energy Facilities review [25], which focused on projects in which the U.S. has either a leading role or significant participation. References and links to further information about these projects can be found in Ref. [25]. We have adjusted some of the dates in this Table relative to those in Ref. [25] and added the European-led KiloDegree Survey (KiDS). Dates in the Table correspond to the duration of survey observations, and the final cosmological results frequently require 1–3 years of analysis and modeling beyond the end of data taking.

Beginning our discussion with imaging surveys, the Dark Energy Survey (DES) has observed 1/8 of the sky to a depth roughly 2 magnitudes deeper than the Sloan Digital Sky Survey (SDSS), enabling weak lensing measurements with much greater statistical precision, cluster measurements calibrated by weak lensing, and angular BAO measurements based on photometric redshifts. With repeat imaging over a smaller area, DES has identified thousands of Type Ia SNe, which together with spectroscopic follow-up data enable significant improvements on the current state-of-the-art for supernova (SN) cosmology. Cosmological results from weak lensing and galaxy clustering analyses of the first year DES data are presented in Ref. [27] and discussed further below, while the first cosmological results from the DES supernova survey are presented in Ref. [28]. The Hyper-Suprime Camera (HSC) on the Subaru 8.2-m telescope is carrying out a similar type of optical imaging survey, probing a smaller area than DES but to greater

depth. First cosmological results from HSC weak lensing are reported in Refs. [29, 30]. The HSC survey is one component of the Subaru Measurement of Images and Redshifts (SuMIRE) project. Beginning in the early 2020s, the dedicated Large Synoptic Survey Telescope (LSST) will scan the southern sky to SDSS-like depth every four nights. LSST imaging co-added over its decade-long primary survey will reach extraordinary depth, enabling weak lensing, cluster, and photometric BAO studies from billions of galaxies. Additionally, LSST time-domain monitoring will identify and measure light curves for thousands of Type Ia SNe per year.

Turning to spectroscopic surveys, the Baryon Oscillation Spectroscopic Survey (BOSS) and its successor eBOSS used fiber-fed optical spectrographs to map the redshift-space distributions of millions of galaxies and quasars. These 3-dimensional maps enable BAO and RSD measurements, and Lyman- α forest spectra of high-redshift quasars extend these measurements to redshifts $z > 2$. As discussed below, the BOSS Collaboration has now published BAO and RSD analyses of its final data sets, and eBOSS has released BAO measurements from quasar clustering at $z = 1$ –2. The Hobby-Eberly Telescope Dark Energy Experiment (HETDEX) uses integral field spectrographs to detect Lyman- α emission-line galaxies at $z \simeq 1.9$ –3.5, probing a small sky area but a substantial comoving volume. The Dark Energy Spectroscopic Instrument (DESI) will follow a strategy similar to BOSS/eBOSS but on a much grander scale, using a larger telescope (4-m vs. 2.5-m) and a much higher fiber multiplex (5000 vs. 1000) to survey an order-of-magnitude more galaxies. A new Prime Focus Spectrograph (PFS) for the Subaru telescope will enable the spectroscopic component of SuMIRE, with the large telescope aperture and wavelength sensitivity that extends to the near-infrared (NIR) allowing it to probe a higher redshift galaxy population than DESI, over a smaller area of sky.

Compared to ground-based observations, space observations afford higher angular resolution and a far lower NIR sky background. The *Euclid* and *WFIRST* (*Wide Field Infrared Survey Telescope*) missions will exploit these advantages, conducting large area imaging surveys for weak lensing and cluster studies and slitless spectroscopic surveys of emission-line galaxies for BAO and RSD studies. *WFIRST* will also incorporate an imaging and spectrophotometric supernova (SN) survey, extending to redshift $z \simeq 1.7$. Survey details are likely to evolve prior to launch, but in the current designs one can roughly characterize the difference between the *Euclid* and *WFIRST* dark-energy experiments as “wide vs. deep,” with planned survey areas of 15,000 deg² and

2200 deg², respectively. For weak lensing shape measurements, *Euclid* will use a single wide optical filter, while *WFIRST* will use three NIR filters. The *Euclid* galaxy redshift survey will cover a large volume at relatively low space density, while the *WFIRST* survey will provide denser sampling of structure in a smaller volume. There are numerous synergies among the LSST, *Euclid*, and *WFIRST* dark energy programs, as discussed in Ref. [31].

28.4 Current Constraints on Expansion, Growth, and Dark Energy

The last decade has seen dramatic progress in measurements of the cosmic expansion history and structure growth, leading to much tighter constraints on the parameters of dark energy models. CMB data from the *WMAP* and *Planck* satellites and from higher resolution ground-based experiments have provided an exquisitely detailed picture of structure at the recombination epoch and the first CMB-based measures of low-redshift structure through lensing and SZ cluster counts. Cosmological supernova samples have increased in size from tens to many hundreds, with continuous coverage from $z = 0$ to $z \simeq 1.4$, alongside major improvements in data quality, analysis methods, and detailed understanding of local populations. BAO measurements have advanced from the first detections to 1–2% precision at multiple redshifts, with increasingly sophisticated methods for testing systematics, fitting models, and evaluating statistical errors. Advances in X-ray, SZ, and weak-lensing observations of large samples of galaxy clusters allow a multi-faceted approach to mass calibration, improving statistical precision but also revealing sources of astrophysical uncertainty. Cluster constraints have been joined by the first precise matter-clustering constraints from cosmic-shear weak lensing and galaxy-galaxy lensing, and by redshift-space distortion measurements that probe different aspects of structure growth at somewhat lower precision. The precision of low-redshift H_0 measurements has sharpened from the roughly 10% error of the *HST* Key Project [32] to 2–4% in recent analyses.

As an illustration of current measurements of the cosmic expansion history, Fig. 28.1 compares distance-redshift measurements from SN and BAO data to the predictions for a flat Universe with a cosmological constant. SN cosmology relies on compilation analyses that try to bring data from different surveys probing distinct redshift ranges to a common scale. Here we use the “joint light curve analysis” (JLA) sample of Ref. [34], who carried out a careful intercalibration of the 3-year Supernova Legacy Survey (SNLS3, [35]) and the full SDSS-II Supernova Survey [3] data in combination with several local supernova samples and high-redshift supernovae from *HST*. Results from the Union2.1 sample [36], which partly overlaps JLA but has different analysis procedures, would be similar. Other state-of-the-art supernova data sets include the Pan-STARRS1 sample incorporated in the PANTHEON compilation [37] and the first sample of spectroscopically confirmed supernovae from DES [28]. For illustration purposes, we have binned the JLA data in redshift and plotted the diagonal elements of the covariance matrix as error bars, and we have converted the SN luminosity distances to an equivalent comoving angular diameter distance. Because the peak luminosity of a fiducial SN Ia is an unknown free parameter, the SN distance measurements could all be shifted up and down by a constant multiplicative factor; cosmological information resides in the relative distances as a function of redshift. The normalization used here corresponds to a Hubble parameter $h = 0.674$.

The $z < 2$ BAO data points come from the 6-degree-Field Galaxy Survey 6dFGS survey [39], the SDSS-II Main Galaxy Sample [40], the final galaxy clustering data set from BOSS [38], and the first BAO measurement from quasar clustering in eBOSS [41]. For the 6dFGS, SDSS-II, and eBOSS data points, values of D_V have been converted to $D_{A,c}$. The BOSS analysis measures $D_{A,c}$ directly; we have taken values from the “BAO only” column of table 7 of Ref. [38]. At $z = 2.34$ we plot $D_{A,c}$ measured from the BAO analysis of the eBOSS Lyman- α forest auto-correlation and cross-correlation with quasars [42]. The BAO measurements are converted to absolute distances using the sound horizon scale $r_s = 147.09$ Mpc from *Planck* 2018 CMB data, whose 0.18% uncertainty is small compared to the current BAO measurement er-

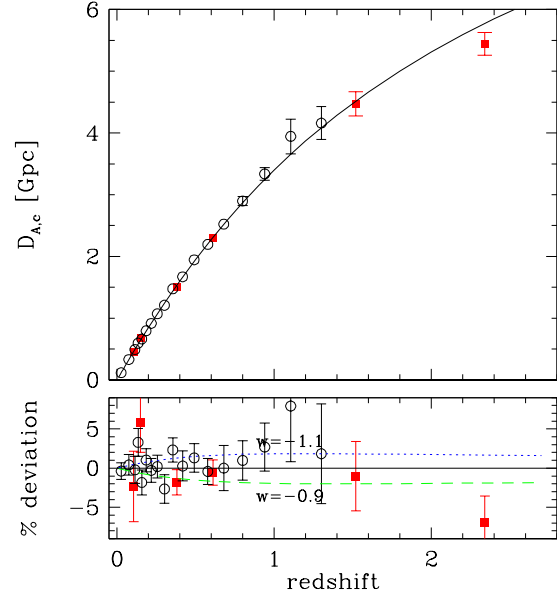


Figure 28.1: Distance-redshift relation measured from Type Ia SNe and BAO compared to the predictions (black curve) of a flat Λ CDM model with $\Omega_m = 0.315$ and $h = 0.674$, the best-fit parameters inferred from *Planck* CMB data [33]. Circles show binned luminosity distances from the JLA SN sample [34], multiplied by $(1+z)^{-1}$ to convert to comoving angular diameter distance. Red squares show BAO distance measurements from the 6dFGS, SDSS-II, BOSS, and eBOSS surveys (see text for details and references). The lower panel plots residuals from the Λ CDM prediction, with dashed and dotted curves that show the effect of changing w by ± 0.1 while all other parameters are held fixed. Note that the SN data points can be shifted up or down by a constant factor to account for freedom in the peak luminosity, while the BAO data points are calibrated to 0.2% precision by the sound horizon scale computed from *Planck* data. The errors on the BAO data points are approximately independent. In the upper panel, error bars are plotted only at $z > 0.7$ to avoid visual confusion.

rors. The BOSS galaxy and eBOSS Lyman- α forest analyses also measure $H(z)$ at the same redshifts, providing further leverage on expansion history that is not captured in Fig. 28.1.

The plotted cosmological model has $\Omega_m = 0.315$ and $h = 0.674$, the best-fit values from *Planck* (TT+TE+EE+lowE+lensing) assuming $w = -1$ and $\Omega_{\text{tot}} = 1$ [33]. The SN, BAO, and CMB data sets, probing a wide range of redshifts with radically different techniques, are for the most part mutually consistent with the predictions of a flat Λ CDM cosmology. The eBOSS Lyman- α forest BAO measurements lie about 1.7σ from the *Planck* Λ CDM prediction [42], notably closer than the 2.3σ difference obtained with earlier BOSS data and discussed in the 2018 edition of this *Review*. Dotted and dashed curves in the lower panel of Fig. 28.1 show the effect of changing w by ± 0.1 with all other parameters held fixed, which leads to significantly worse agreement with the data. However, such a single-parameter comparison does not capture the impact of parameter degeneracies or the ability of complementary data sets to break them, and if one instead forced a match to CMB data by changing h and Ω_m when changing w then the predicted BAO distances would diverge at $z = 0$ rather than converging there.

Figure 28.2, taken from Ref. [38], presents constraints on models that allow a free but constant value of w with non-zero space curvature (ow CDM, left panel) or the evolving equation of state of Eq. (28.4) in a flat Universe (w_0w_a CDM, right panel). Green contours show constraints from the combination of *Planck* 2015 CMB data and the JLA supernova sample. Gray contours show the combination of *Planck* with BAO measurements from BOSS, 6dFGS, and SDSS-II. Red contours adopt a more aggressive anal-

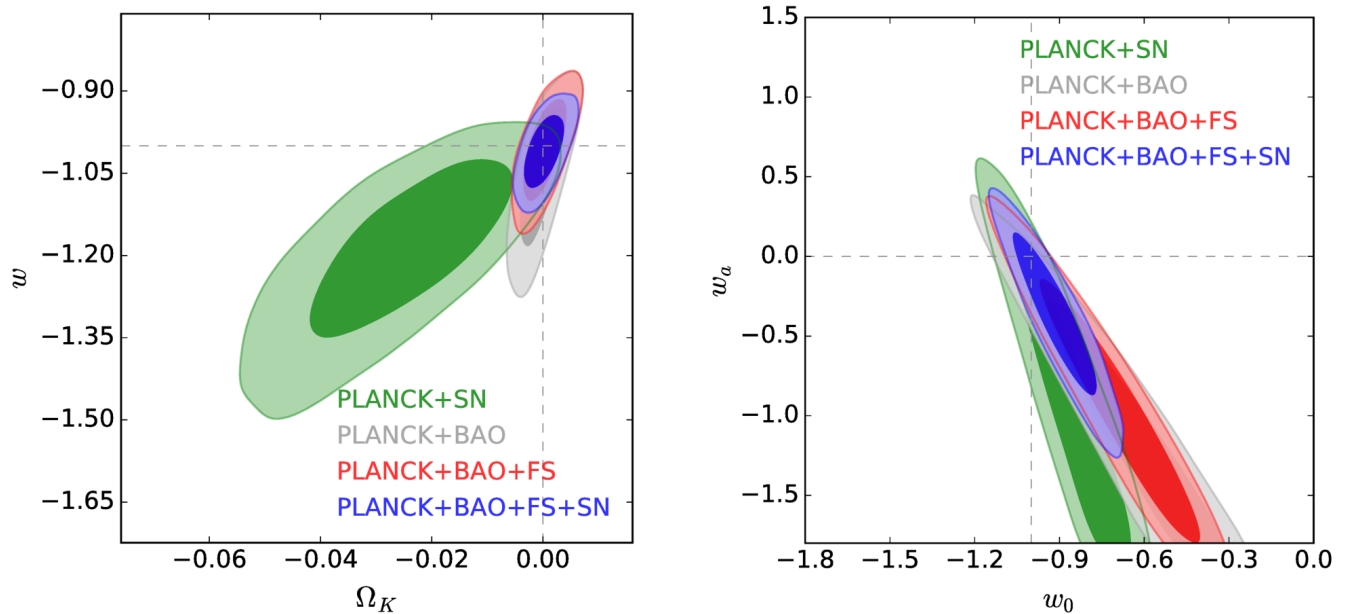


Figure 28.2: Constraints on dark energy model parameters from combinations of CMB, BAO, galaxy clustering, and supernova (SN) data, taken from Ref. [38]. The left panel shows 68% and 95% confidence contours in the ow CDM model, with constant equation-of-state parameter w and non-zero space curvature $\Omega_K \equiv 1 - \Omega_{\text{tot}}$. Green and gray contours show the combination of *Planck* CMB data with SN or BAO data, respectively. Red contours combine CMB, BAO, and the full shape (FS) of redshift-space galaxy clustering. Blue contours add SN data to this combination. The right panel shows confidence contours for the same data combinations in the w_0w_a CDM model, which assumes a flat Universe and an evolving equation of state with $w(a) = w_0 + w_a(1 - a)$.

ysis of the BOSS galaxy data that uses the full shape (FS) of the redshift-space power spectrum and correlation function, modeled via perturbation theory, in addition to the measurement of the BAO scale itself. The full shape analysis improves the constraining power of the data, primarily because measurement of the Alcock-Paczynski effect on sub-BAO scales helps to break the degeneracy between $D_{A,c}(z)$ and $H(z)$. Blue contours show constraints from the full combination of CMB, BAO+FS, and SN data. Supernovae provide fine-grained relative distance measurements with good bin-by-bin precision at $z < 0.7$ (see Fig. 28.1), which is complementary to BAO for constraining redshift evolution of w . In both classes of model, the flat Λ CDM parameters ($w = w_0 = -1$, $\Omega_K = w_a = 0$) lie within the 68% confidence contour.

The precision on dark energy parameters depends, of course, on both the data being considered and the flexibility of the model being assumed. For the ow CDM model and the Planck+BAO+FS+SN data combination, Ref. [38] finds $w = -1.01 \pm 0.04$. Assuming a flat Universe and incorporating *Planck* 2018 data and DES Year 1 weak lensing, in addition to BAO and SN, Ref. [33] finds

$$w = -1.028 \pm 0.031. \quad (28.5)$$

We consider either of these results to be a reasonable characterization of current knowledge about the dark energy equation of state. In the w_0w_a CDM model there is strong degeneracy between w_0 and w_a , as one can see in Fig. 28.2. However, the value of w at the pivot redshift $z_p = 0.29$ is well constrained by the Planck+BAO+FS+SN data combination, with $w_p = -1.05 \pm 0.06$ [38]. The constraint on the evolution parameter, by contrast, remains poor even with this data combination, $w_a = -0.39 \pm 0.34$. For examinations of a wide range of dark energy, dark matter, neutrino content, and modified gravity models, see Refs. [33, 38, 43].

A flat Λ CDM model fit to *Planck* CMB data alone predicts $H_0 = 67.4 \pm 0.5 \text{ km s}^{-1} \text{ Mpc}^{-1}$ (see Chapter 29 of this *Review*). This prediction and its error bar are sensitive to the assumptions of constant dark energy and a flat Universe. However, by adding BAO and supernova data one can construct an “inverse distance ladder” to measure H_0 precisely, even with a general dark energy model and free curvature [44]. Ref. [45] applies this approach to obtain $H_0 = 67.8 \pm 1.3 \text{ km s}^{-1} \text{ Mpc}^{-1}$. As discussed in

Sec. 25.3.1 of this *Review*, recent measurements from low-redshift data yield higher values of H_0 . Figure 28.3 compares the CMB-anchored H_0 estimates cited above to distance-ladder estimates that use Cepheid [46] or tip-of-the-red-giant-branch (TRGB) [47] stars to calibrate SNe Ia luminosities, and to an entirely independent estimate that uses gravitational-lens time delays [48]. The Cepheid and lensing estimates are discrepant with the CMB-anchored estimates at a statistically significant level (Ref. [46] quotes 4.4σ relative to *Planck* Λ CDM), while the TRGB calibration yields an intermediate result that is consistent with either the “high” or “low” values of H_0 .

The tension in H_0 could reflect some combination of statistical flukes and systematic errors in one or more of the data sets employed in these analyses. However, if the resolution lies in new physics rather than measurement errors, then this is probably physics that operates in the *pre-recombination* Universe, rescaling the BAO standard ruler in a way that shifts the Λ CDM and inverse-distance-ladder values upward. Models with extra relativistic degrees of freedom or dark energy that is dynamically significant in the early Universe can achieve this effect by increasing the early expansion rate, but they are tightly constrained by the damping tail of CMB anisotropies. A finely tuned model in which early dark energy decays rapidly after recombination can mitigate the tension between CMB data and local H_0 measurements [49], though it still prefers H_0 values below those of Ref. [46].

The amplitude of CMB anisotropies is proportional to the amplitude of density fluctuations present at recombination, and by assuming GR and a specified dark energy model one can extrapolate the growth of structure forward to the present day to predict σ_8 . Probes of low-redshift structure yield constraints in the (σ_8, Ω_m) plane, which can be summarized in terms of the parameter combination $S_8 \equiv \sigma_8(\Omega_m/0.3)^{0.5}$. As discussed in earlier editions of this *Review*, many but not all weak-lensing and cluster studies to date yield S_8 values lower than those predicted for *Planck*-normalized Λ CDM. The right panel of Fig. 28.3 illustrates the current state-of-play, comparing a selection of recently published S_8 estimates to the *Planck*+ Λ CDM prediction of $S_8 = 0.832 \pm 0.013$.

The first four points show cosmic-shear weak-lensing estimates from the Deep Lens Survey [50], KiDS [51], DES [52], and HSC [29]. All of these estimates lie below the *Planck* central value,

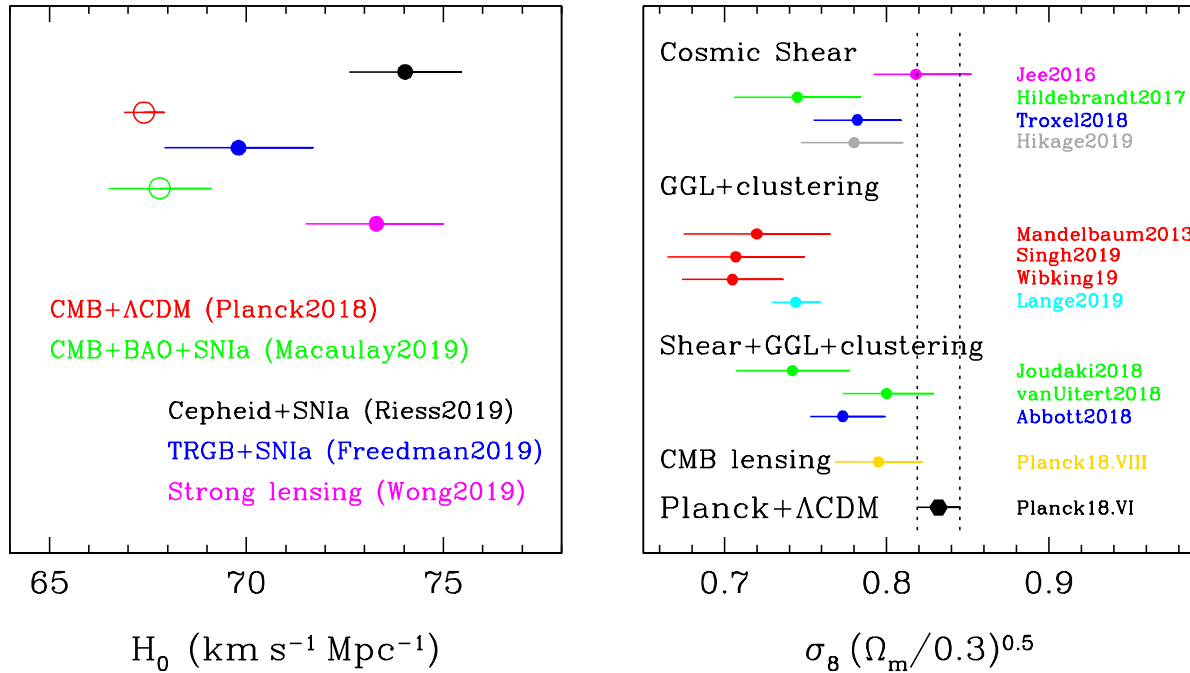


Figure 28.3: Tensions between low-redshift cosmological measurements and the predictions of a CMB-normalized Λ CDM model. All error bars are 1σ ; see text for observational references. (Left) Open circles show values of H_0 for flat Λ CDM with *Planck* parameters or a general dark energy model constrained by a combination of CMB, BAO, and supernova data. Filled circles show distance-ladder estimates based on Cepheid or TRGB calibration or an independent estimate using gravitational-lens time delays. (Right) Matter clustering characterized by the parameter combination $\sigma_8(\Omega_m/0.3)^{0.5}$, as predicted by a *Planck*-normalized Λ CDM model (vertical dotted lines, black hexagon) and estimated from weak gravitational lensing using cosmic shear, galaxy-galaxy lensing and galaxy clustering, or a combination of the two constraints. Points of the same color are based on the same weak-lensing data. The “CMB lensing” point shows the value of σ_8 for $\Omega_m = 0.3$ inferred from *Planck* CMB lensing, a measurement that is independent of the “Planck+ Λ CDM” prediction and weighted to somewhat higher redshift than the other weak-lensing points.

though only the KiDS estimate is discrepant by $\sim 2\sigma$. The next four points use galaxy-galaxy lensing in combination with galaxy clustering. Ref. [53] used weak-lensing data from SDSS imaging and the SDSS main galaxy redshift catalog, restricting the analysis to scales well described by perturbation theory. Refs. [54] and [55] used the same weak-lensing data but the BOSS LOWZ galaxy sample, and they employed two quite different approaches to model the clustering and lensing signals into the strongly non-linear regime ($r \approx 1 h^{-1} \text{Mpc}$) so that they could fully exploit the constraining power of the data. Ref. [56] found a strong discrepancy on these non-linear scales between the predictions of a *Planck*-normalized Λ CDM model and the galaxy-galaxy lensing of BOSS CMASS galaxies, measured from 250 deg^2 of deep imaging from the Canada-France-Hawaii Telescope. Ref. [57], plotted in Figure 28.3, revisited these data with a more general modeling approach and showed that the discrepancy persists over a range of redshift and galaxy stellar mass.

The third set of points in this panel shows S_8 estimates that combine cosmic shear with galaxy-galaxy lensing and galaxy clustering (a.k.a. “ 3×2 ” analyses because they combine three 2-point correlations), restricted to fairly large scales in the perturbative regime. Refs. [58] and [59] use KiDS weak-lensing data but two different galaxy samples; although they are statistically consistent with each other, the difference of their central values illustrates the sensitivity to external data and analysis choices. Ref. [27] presents constraints from the 3×2 analysis of the Year 1 DES data, which yields an S_8 value lower than the *Planck* prediction but consistent at the $\sim 2\sigma$ level.

The “CMB lensing” point shows the matter-clustering amplitude inferred from *Planck* CMB lensing; we have evaluated Eq. (38) of Ref. [60] at $\Omega_m = 0.3$ and adopted the same fractional error. It is important to emphasize that this is a measurement of low-redshift clustering even though the background being lensed is the CMB. The CMB lensing kernels peak at $z \lesssim 1$, with tails to $z \sim 5$, so the effective redshift of the S_8 measurement is somewhat

higher than that of the other weak-lensing data points. The result is consistent with the *Planck*+ Λ CDM prediction at 1σ , and it is also consistent with the lower value corresponding to the mean or median of the optical weak-lensing measurements.

No one of these analyses provides convincing evidence of a conflict with the Λ CDM cosmological model. However, the case for such a conflict has grown stronger as the low inferred clustering amplitude has persisted across multiple statistically independent weak-lensing surveys and multiple analysis methods. One possible explanation is that several of the weak lensing surveys are affected by a common, unrecognized, systematic bias. Another possibility is a true deviation between the clustering growth extrapolated forward from the early Universe and the clustering of matter at late times. The consistency of CMB lensing and Lyman- α forest measurements with Λ CDM clustering predictions suggests that any such deviation sets in mainly at $z < 1$, coinciding with the era of cosmic acceleration. Because the expansion history is well constrained by BAO and supernova data, it is difficult to change low-redshift matter clustering by simply changing the equation of state of dark energy. Instead, a deviation between predicted and observed clustering might point towards modified gravity, decaying dark matter, or coupling between dark matter and dark energy.

The next 2–3 years should see rapid progress on this conundrum. As the KiDS, DES, and HSC data sets grow in size, their statistical uncertainties will shrink, which will in turn enable more stringent internal cross-checks that test for consistent results from different redshift ranges, different scales, and different lens and source populations. Modeling methods that exploit non-linear scales will also be more stringently tested. Clusters of galaxies with weak-lensing mass calibration provide an alternative route to S_8 measurement, with competitive statistical precision. Recent cluster-based S_8 estimates span a wide range, some of them consistent with *Planck*+ Λ CDM and others implying lower matter clustering, and we have not quoted results here because it is diffi-

cult to decide which are most reliable. However, the opportunity to combine multiple cluster samples with multiple weak-lensing surveys may lead to consistent and convincing measurements in the near future. CMB lensing constraints will improve with higher angular resolution data from the South Pole Telescope and the Atacama Cosmology Telescope and their successors. Finally, the DESI survey will soon allow the first RSD-based measurements of structure growth at the 1–2% level, providing an entirely distinct route to probe the clustering tension hinted at in Fig. 28.3.

28.5 Summary and Outlook

Figure 28.2 focuses on model parameter constraints, but to describe the observational situation it is more useful to characterize the precision, redshift range, and systematic uncertainties of the basic expansion and growth measurements. At present, supernova surveys constrain distance ratios at the 1–2% level in redshift bins of width $\Delta z = 0.1$ over the range $0 < z < 0.6$, with larger but still interesting error bars out to $z \simeq 1.3$. These measurements are currently limited by systematics tied to photometric calibration, dust reddening, host-galaxy correlations, and possible evolution of the SN population. BAO surveys have measured the absolute distance scale (calibrated to the sound horizon r_s) to 4% at $z = 0.15$, 1% at $z = 0.38$ and $z = 0.61$, and 2% at $z = 2.3$. Multiple studies have used clusters of galaxies or weak-lensing cosmic shear or galaxy-galaxy lensing to measure a parameter combination $\sigma_8 \Omega_m^\alpha$ with $\alpha \simeq 0.3$ – 0.5 . The estimated errors of the most recent studies, including both statistical contributions and identified systematic uncertainties, are 3–5%. RSD measurements constrain the combination $f(z)\sigma_8(z)$, and recent determinations span the redshift range $0 < z < 0.9$ with typical estimated errors of about 10%. These errors are dominated by statistics, but shrinking them further will require improvements in modeling non-linear effects on small scales. Distance-ladder estimates of H_0 now span a small range, using overlapping data but distinct treatments of key steps; individual studies quote uncertainties of 2–5%, with similar statistical and systematic contributions. *Planck* data and higher resolution ground-based experiments now measure CMB anisotropies with exquisite precision; for example, CMB measurements now constrain the physical size of the BAO sound horizon to 0.2% and the angular scale of the sound horizon to 0.01%.

A flat Λ CDM model with standard radiation and neutrino content can fit the CMB data and the BAO and SN distance measurements to within their estimated uncertainties. The CMB+BAO parameters for this model are in significant tension with some but not all recent measurements of H_0 determined from low-redshift data. The discrepancy could reflect underestimated systematic errors in one or more of the input data sets. If the conflict is real, then it may point to new physics in the pre-recombination Universe that rescales the sound horizon, such as early dark energy or extra relativistic degrees of freedom. Many measurements of low-redshift matter clustering from weak lensing lie below the predictions of a Λ CDM model extrapolated forward from the *Planck* CMB anisotropies. No one analysis presents a convincing conflict, but the difference persists across several independent data sets and analysis methods. If real, this discrepancy could point towards modified gravity, decaying dark matter, or coupling between dark matter and dark energy. However, none of the tensions present in the data yet provides compelling evidence for new physics.

Analyses of the final KiDS and DES weak-lensing data sets and the expanding HSC weak-lensing data set should yield measurements of matter clustering that have sharper statistical precision and more stringent tests of internal consistency. Fully exploiting these data will require further development of accurate models of matter clustering, galaxy clustering, and weak lensing by galaxy clusters into the fully non-linear regime, including robust methods of accounting for uncertainties in the baryonic mass distribution. It will also require further progress on the thorny challenge of photometric redshift calibration so that these uncertainties do not dominate the error budget. Higher signal-to-noise CMB lensing maps cross-correlated with galaxies will provide independent tests that avoid some of the systematic uncertainties of optical weak lensing. H_0 measurements will improve with increasing numbers of Cepheid or TRGB distances to supernova host galaxies, improv-

ing *Gaia* parallaxes of Galactic Cepheids, increasing numbers of strong gravitational-lens time delays, and continued attention to the systematic uncertainties in each method. Improving measurements of the CMB damping tail from ground-based experiments will provide increasingly strong constraints on solutions involving pre-recombination physics.

After beginning operations in early 2020, the DESI galaxy redshift survey will quickly exceed the size of the existing SDSS and BOSS surveys, enabling high precision BAO measurements of expansion history at $z \approx 0.7$ – 1.4 and, for the first time, percent-level measurements of structure growth through RSD. Precise BAO and RSD measurements at higher redshifts will come from DESI Lyman- α forest maps and the HETDEX and Subaru PFS galaxy surveys. The BAO measurements will complement increasingly precise measurements of the relative distance scale at $z < 1$ from the DES photometric supernova sample and from improved local supernova samples ($z < 0.1$) that provide a low-redshift anchor. Large galaxy samples will also enable more powerful applications of the Alcock-Paczynski effect, which can amplify the power of BAO and supernova distance measurements by converting them to constraints on the expansion rate $H(z)$.

The early-to-mid 2020s will see another major leap in observational capabilities with the advent of LSST, *Euclid*, and *WFIRST*. LSST will be the ultimate ground-based optical weak-lensing experiment, measuring several billion galaxy shapes over 20,000 deg² of the southern hemisphere sky, and it will detect and monitor many thousands of SNe per year. *Euclid* and *WFIRST* also have weak lensing as a primary science goal, taking advantage of the high angular resolution and extremely stable image quality achievable from space. Both missions plan large spectroscopic galaxy surveys, which will provide better sampling at high redshifts than DESI or PFS because of the lower infrared sky background above the atmosphere. *WFIRST* is also designed to carry out what should be the ultimate supernova cosmology experiment, with deep, high resolution, near-IR observations and the stable calibration achievable with a space platform. The 2020s will also see dramatic advances in CMB lensing from the Simons Observatory and, potentially, CMB-S4 and/or a space-based probe; cross-correlation with galaxy surveys allows precise tomographic measurements of clustering as a function of redshift.

If the anomalies suggested in Fig. 28.3 are real, then the experiments of the 2020s will map out their redshift, scale, and environment dependence in great detail, providing detailed empirical constraints on dynamical dark energy or modified gravity models. If these tensions dissipate with improved measurements, then the experiments of the 2020s will achieve much more stringent tests of the Λ CDM paradigm, with the potential to reveal deviations that are within the statistical uncertainties of current data. The critical clue to the origin of cosmic acceleration could also come from a surprising direction, such as laboratory or solar-system tests that challenge GR, time variation of fundamental “constants,” or anomalous behavior of gravity in some astronomical environments. Experimental advances along these multiple axes could confirm today’s relatively simple, but frustratingly incomplete, “standard model” of cosmology, or they could force yet another radical revision in our understanding of energy, or gravity, or the spacetime structure of the Universe.

References

- [1] A. Einstein, Sitzungsber. Preuss. Akad. Wiss. Berlin (Math. Phys.), 142 (1917).
- [2] Ya. B. Zel’dovich, A. Krasinski and Ya. B. Zeldovich, Sov. Phys. Usp. **11**, 381 (1968), [Gen. Rel. Grav.40,1557(2008); Usp. Fiz. Nauk95,209(1968)].
- [3] A. Friedman, Z. Phys. **10**, 377 (1922), [Gen. Rel. Grav.31,1991(1999)].
- [4] G. Lemaître, Annales de la Societe Scientifique de Bruxelles **47**, 49 (1927).
- [5] E. Hubble, Proc. Nat. Acad. Sci. **15**, 168 (1929).
- [6] A. Einstein and W. de Sitter, Proc. Nat. Acad. Sci. **18**, 213 (1932).

- [7] For background and definitions, see Big-Bang Cosmology – Sec. 22 of this *Review*.
- [8] A. G. Riess *et al.* (Supernova Search Team), *Astron. J.* **116**, 1009 (1998), [arXiv:astro-ph/9805201].
- [9] S. Perlmutter *et al.* (Supernova Cosmology Project), *Astrophys. J.* **517**, 565 (1999), [arXiv:astro-ph/9812133].
- [10] P. de Bernardis *et al.* (Boomerang), *Nature* **404**, 955 (2000), [arXiv:astro-ph/0004404].
- [11] S. Hanany *et al.*, *Astrophys. J.* **545**, L5 (2000), [arXiv:astro-ph/0005123].
- [12] D. H. Weinberg *et al.*, *Phys. Rept.* **530**, 87 (2013), [arXiv:1201.2434].
- [13] C. Wetterich, *Nucl. Phys.* **B302**, 668 (1988), [arXiv:1711.03844].
- [14] A. Joyce *et al.*, *Phys. Rept.* **568**, 1 (2015), [arXiv:1407.0059].
- [15] S. M. Carroll *et al.*, *Phys. Rev.* **D70**, 043528 (2004), [arXiv:astro-ph/0306438].
- [16] G. R. Dvali, G. Gabadadze and M. Porrati, *Phys. Lett.* **B485**, 208 (2000), [hep-th/0005016].
- [17] C.M. Will, *Living Reviews in Relativity*, **9**, 3 (2006). See also the chapter on Experimental Tests of Gravitational Theory – in this *Review*.
- [18] J. Wang, L. Hui and J. Khoury, *Phys. Rev. Lett.* **109**, 241301 (2012), [arXiv:1208.4612].
- [19] M. Fairbairn and A. Goobar, *Phys. Lett.* **B642**, 432 (2006), [arXiv:astro-ph/0511029]; Y.-S. Song, I. Sawicki and W. Hu, *Phys. Rev.* **D75**, 064003 (2007), [arXiv:astro-ph/0606286]; C. Blake *et al.*, *Mon. Not. Roy. Astron. Soc.* **415**, 2876 (2011), [arXiv:1104.2948].
- [20] T. Baker *et al.*, *Phys. Rev. Lett.* **119**, 25, 251301 (2017), [arXiv:1710.06394].
- [21] E. V. Linder, *Phys. Rev.* **D72**, 043529 (2005), [arXiv:astro-ph/0507263].
- [22] This is essentially the FoM proposed in the Dark Energy Task Force (DETF) report, A. Albrecht *et al.*, [astro-ph/0609591](https://arxiv.org/abs/astro-ph/0609591), though they based their FoM on the area of the 95 in the $w_0 - w_a$ plane.
- [23] For high accuracy, the impact of acoustic oscillations must be computed with a full Boltzmann code, but the simple integral for r_s captures the essential physics and the scaling with cosmological parameters.
- [24] R. A. Sunyaev and Ya. B. Zeldovich, *Astrophys. Space Sci.* **7**, 3 (1970).
- [25] D. Weinberg *et al.* (2013), [arXiv:1309.5380].
- [26] C. Alcock and B. Paczynski, *Nature* **281**, 358 (1979).
- [27] T. M. C. Abbott *et al.* (DES), *Phys. Rev.* **D98**, 4, 043526 (2018), [arXiv:1708.01530].
- [28] T. M. C. Abbott *et al.* (DES), *Astrophys. J.* **872**, 2, L30 (2019), [arXiv:1811.02374].
- [29] C. Hikage *et al.* (HSC), *Publ. Astron. Soc. Jap.* **71**, 2, Publications of the Astronomical Society of Japan, Volume 71, Issue 2, April 2019, 43, <https://doi.org/10.1093/pasj/psz010> (2019), [arXiv:1809.09148].
- [30] T. Hamana *et al.* (2019), [arXiv:1906.06041].
- [31] B. Jain *et al.* (2015), [arXiv:1501.07897].
- [32] W. L. Freedman *et al.* (HST), *Astrophys. J.* **553**, 47 (2001), [arXiv:astro-ph/0012376].
- [33] N. Aghanim *et al.* (Planck) (2018), [arXiv:1807.06209].
- [34] M. Betoule *et al.*, *Astron. & Astrophys.* **568**, 22 (2014).
- [35] M. Sullivan *et al.* (SNLS), *Astrophys. J.* **737**, 102 (2011), [arXiv:1104.1444].
- [36] N. Suzuki *et al.* (Supernova Cosmology Project), *Astrophys. J.* **746**, 85 (2012), [arXiv:1105.3470].
- [37] D. M. Scolnic *et al.*, *Astrophys. J.* **859**, 2, 101 (2018), [arXiv:1710.00845].
- [38] S. Alam *et al.* (BOSS), *Mon. Not. Roy. Astron. Soc.* **470**, 3, 2617 (2017), [arXiv:1607.03155].
- [39] F. Beutler *et al.*, *Mon. Not. Roy. Astron. Soc.* **416**, 3017 (2011), [arXiv:1106.3366].
- [40] A. J. Ross *et al.*, *Mon. Not. Roy. Astron. Soc.* **449**, 1, 835 (2015), [arXiv:1409.3242].
- [41] M. Ata *et al.*, *Mon. Not. Roy. Astron. Soc.* **473**, 4, 4773 (2018), [arXiv:1705.06373].
- [42] M. Blomqvist *et al.*, *Astron. Astrophys.* **629**, A86 (2019), [arXiv:1904.03430].
- [43] Planck Collab. 2015 Results XIV, *Astron. & Astrophys.* **594**, A14 (2016).
- [44] E. Aubourg *et al.*, *Phys. Rev.* **D92**, 12, 123516 (2015), [arXiv:1411.1074].
- [45] E. Macaulay *et al.* (DES), *Mon. Not. Roy. Astron. Soc.* **486**, 2, 2184 (2019), [arXiv:1811.02376].
- [46] A. G. Riess *et al.*, *Astrophys. J.* **876**, 1, 85 (2019), [arXiv:1903.07603].
- [47] W.L. Friedman, *Astron. J.* **882** (2019) 34.
- [48] K. C. Wong *et al.* (2019), [arXiv:1907.04869].
- [49] V. Poulin *et al.*, *Phys. Rev. Lett.* **122**, 22, 221301 (2019), [arXiv:1811.04083].
- [50] M. J. Jee *et al.*, *Astrophys. J.* **824**, 2, 77 (2016), [arXiv:1510.03962].
- [51] H. Hildebrandt *et al.*, *Mon. Not. Roy. Astron. Soc.* **465**, 1454 (2017), [arXiv:1606.05338].
- [52] M. A. Troxel *et al.* (DES), *Phys. Rev.* **D98**, 4, 043528 (2018), [arXiv:1708.01538].
- [53] R. Mandelbaum *et al.*, *Mon. Not. Roy. Astron. Soc.* **432**, 1544 (2013), [arXiv:1207.1120].
- [54] S. Singh *et al.*, *Mon. Not. Roy. Astron. Soc.* **491**, 1, 51 (2020), [arXiv:1811.06499].
- [55] B. D. Wibking *et al.*, *Mon. Not. Roy. Astron. Soc.* **492**, 2, 2872 (2020), [arXiv:1907.06293].
- [56] A. Leauthaud *et al.*, *Mon. Not. Roy. Astron. Soc.* **467**, 3, 3024 (2017), [arXiv:1611.08606].
- [57] J. U. Lange *et al.*, *Mon. Not. Roy. Astron. Soc.* **488**, 4, 5771 (2019), [arXiv:1906.08680].
- [58] S. Joudaki *et al.*, *Mon. Not. Roy. Astron. Soc.* **474**, 4, 4894 (2018), [arXiv:1707.06627].
- [59] E. van Uitert *et al.*, *Mon. Not. Roy. Astron. Soc.* **476**, 4, 4662 (2018), [arXiv:1706.05004].
- [60] N. Aghanim *et al.* (Planck) (2018), [arXiv:1807.06210].

29. Cosmic Microwave Background

Revised August 2019 by D. Scott (U. of British Columbia) and G.F. Smoot (HKUST; Paris U.; UC Berkeley; LBNL).

29.1 Introduction

The energy content in electromagnetic radiation from beyond our Galaxy is dominated by the cosmic microwave background (CMB), discovered in 1965 [1]. The spectrum of the CMB is well described by a blackbody function with $T = 2.7255$ K. This spectral form is a main supporting pillar of the hot Big Bang model for the Universe. The lack of any observed deviations from a blackbody spectrum constrains physical processes over cosmic history at redshifts $z \lesssim 10^7$ (see earlier versions of this review).

Currently the key CMB observable is the angular variation in temperature (or intensity) correlations, and to a growing extent polarization [2–4]. Since the first detection of these anisotropies by the Cosmic Background Explorer (*COBE*) satellite [5], there has been intense activity to map the sky at increasing levels of sensitivity and angular resolution by ground-based and balloon-borne measurements. These were joined in 2003 by the first results from NASA’s Wilkinson Microwave Anisotropy Probe (*WMAP*) [6], which were improved upon by analyses of data added every 2 years, culminating in the 9-year results [7]. In 2013 we had the first results [8] from the third generation CMB satellite, ESA’s *Planck* mission [9, 10], which were enhanced by results from the 2015 *Planck* data release [11, 12], and then the final 2018 *Planck* data release [13, 14]. Additionally, CMB anisotropies have been extended to smaller angular scales by ground-based experiments, particularly the Atacama Cosmology Telescope (ACT) [15] and the South Pole Telescope (SPT) [16]. Together these observations have led to a stunning confirmation of the ‘Standard Model of Cosmology.’ In combination with other astrophysical data, the CMB anisotropy measurements place quite precise constraints on a number of cosmological parameters, and have launched us into an era of precision cosmology. With the study of the CMB now past the half-century mark, the program to map temperature anisotropies is effectively wrapping up, and attention is increasingly focussing on polarization measurements as the future arena in which to test fundamental physics.

29.2 CMB Spectrum

It is well known that the spectrum of the microwave background is very precisely that of blackbody radiation, whose temperature evolves with redshift as $T(z) = T_0(1+z)$ in an expanding universe. As a direct test of its cosmological origin, this relationship has been tested by measuring the strengths of emission and absorption lines in high-redshift systems [17].

Measurements of the spectrum are consistent with a blackbody distribution over more than three decades in frequency (there is a claim by ARCADE [18] of a possible unexpected extragalactic emission signal at low frequency, but the interpretation is debated [19]). All viable cosmological models predict a very nearly Planckian spectrum to within the current observational limits. Because of this, measurements of deviations from a blackbody spectrum have received little attention in recent years, with only a few exceptions. However, that situation will eventually change, since proposed experiments (such as PIXIE [20] and PRISM [21]) have the potential to dramatically improve the constraints on energy release in the early Universe. It now seems feasible to probe spectral distortion mechanisms that are *required* in the standard picture, such as those arising from the damping and dissipation of relatively small primordial perturbations, or the average effect of inverse Compton scattering. A more ambitious goal would be to reach the precision needed to detect the residual lines from the cosmological recombination of hydrogen and helium and hence test whether conditions at $z \gtrsim 1000$ accurately follow those in the standard picture [22].

29.3 Description of CMB Anisotropies

Observations show that the CMB contains temperature anisotropies at the 10^{-5} level and polarization anisotropies at the 10^{-6} (and lower) level, over a wide range of angular scales. These anisotropies are usually expressed using a spherical harmonic expansion

of the CMB sky:

$$T(\theta, \phi) = \sum_{\ell m} a_{\ell m} Y_{\ell m}(\theta, \phi) \quad (29.1)$$

(with the linear polarization pattern written in a similar way using the so-called spin-2 spherical harmonics). Increasing angular resolution requires that the expansion goes to higher multipoles. Because there are only very weak phase correlations seen in the CMB sky and since we notice no preferred direction, the vast majority of the cosmological information is contained in the temperature 2-point function, *i.e.*, the variance as a function only of angular separation. Equivalently, the power per unit $\ln \ell$ is $\ell \sum_m |a_{\ell m}|^2 / 4\pi$.

29.3.1 The Monopole

The CMB has a mean temperature of $T_\gamma = 2.7255 \pm 0.0006$ K (1σ) [23], which can be considered as the monopole component of CMB maps, a_{00} . Since all mapping experiments involve difference measurements, they are insensitive to this average level; monopole measurements can only be made with absolute temperature devices, such as the FIRAS instrument on the *COBE* satellite [24]. The measured kT_γ is equivalent to 0.234 meV or $4.60 \times 10^{-10} m_e c^2$. A blackbody of the measured temperature has a number density $n_\gamma = (2\zeta(3)/\pi^2) T_\gamma^3 \simeq 411 \text{ cm}^{-3}$, energy density $\rho_\gamma = (\pi^2/15) T_\gamma^4 \simeq 4.64 \times 10^{-34} \text{ g cm}^{-3} \simeq 0.260 \text{ eV cm}^{-3}$, and a fraction of the critical density $\Omega_\gamma \simeq 5.38 \times 10^{-5}$.

29.3.2 The Dipole

The largest anisotropy is in the $\ell = 1$ (dipole) first spherical harmonic, with amplitude 3.3621 ± 0.0010 mK [13]. The dipole is interpreted to be the result of the Doppler boosting of the monopole caused by the Solar System motion relative to the nearly isotropic blackbody field, as broadly confirmed by measurements of the radial velocities of local galaxies (*e.g.*, Ref. [25]); the intrinsic part of the signal is expected to be 2 orders of magnitude smaller (and fundamentally difficult to distinguish). The motion of an observer with velocity $\beta \equiv v/c$ relative to an isotropic Planckian radiation field of temperature T_0 produces a Lorentz-boosted temperature pattern

$$T(\theta) = T_0(1 - \beta^2)^{1/2} / (1 - \beta \cos \theta) \\ \simeq T_0 \left[1 + \beta \cos \theta + (\beta^2/2) \cos 2\theta + \mathcal{O}(\beta^3) \right]. \quad (29.2)$$

At every point in the sky, one observes a blackbody spectrum, with temperature $T(\theta)$. The spectrum of the dipole has been confirmed to be the differential of a blackbody spectrum [26]. At higher order there are additional effects arising from aberration and from modulation of the anisotropy pattern, which have also been observed [27].

The implied velocity for the Solar System barycenter is $v = 369.82 \pm 0.11 \text{ km s}^{-1}$, assuming a value $T_0 = T_\gamma$, towards $(l, b) = (264.021^\circ \pm 0.011^\circ, 48.253^\circ \pm 0.005^\circ)$ [13]. Such a Solar System motion implies a velocity for the Galaxy and the Local Group of galaxies relative to the CMB. The derived value is $v_{\text{LG}} = 620 \pm 15 \text{ km s}^{-1}$ towards $(l, b) = (271.9^\circ \pm 2.0^\circ, 29.6^\circ \pm 1.4^\circ)$ [13], where most of the error comes from uncertainty in the velocity of the Solar System relative to the Local Group.

The dipole is a frame-dependent quantity, and one can thus determine the ‘CMB frame’ (in some sense this is a special frame) as that in which the CMB dipole would be zero. Any velocity of the receiver relative to the Earth and the Earth around the Sun is removed for the purposes of CMB anisotropy studies, while our velocity relative to the Local Group of galaxies and the Local Group’s motion relative to the CMB frame are normally removed for cosmological studies. The dipole is now routinely used as a primary calibrator for mapping experiments, either via the time-varying orbital motion of the Earth, or through the cosmological dipole measured by satellite experiments.

29.3.3 Higher-Order Multipoles

The variations in the CMB temperature maps at higher multipoles ($\ell \geq 2$) are interpreted as being mostly the result of per-

turbations in the density of the early Universe, manifesting themselves at the epoch of the last scattering of the CMB photons. In the hot Big Bang picture, the expansion of the Universe cools the plasma so that by a redshift $z \simeq 1100$ (with little dependence on the details of the model), the hydrogen and helium nuclei can bind electrons into neutral atoms, a process usually referred to as recombination [28]. Before this epoch, the CMB photons were tightly coupled to the baryons, while afterwards they could freely stream towards us. By measuring the $a_{\ell m}$ s we are thus learning directly about physical conditions in the early Universe.

A statistically-isotropic sky means that all m s are equivalent, *i.e.*, there is no preferred axis, so that the temperature correlation function between two positions on the sky depends only on angular separation and not orientation. Together with the assumption of Gaussian statistics (*i.e.*, no correlations between the modes), the 2-point function of the temperature field (or equivalently the power spectrum in ℓ) then fully characterizes the anisotropies. The power summed over all m s at each ℓ is $(2\ell+1)C_\ell/(4\pi)$, where $C_\ell \equiv \langle |a_{\ell m}|^2 \rangle$. Thus averages of $a_{\ell m}$ s over m can be used as estimators of the C_ℓ s to constrain their expectation values, which are the quantities predicted by a theoretical model. For an idealized full-sky observation, the variance of each measured C_ℓ (*i.e.*, the variance of the variance) is $[2/(2\ell+1)]C_\ell^2$. This sampling uncertainty (known as ‘cosmic variance’) comes about because each C_ℓ is χ^2 distributed with $(2\ell+1)$ degrees of freedom for our observable volume of the Universe. For fractional sky coverage, f_{sky} , this variance is increased by $1/f_{\text{sky}}$ and the modes become partially correlated.

It is important to understand that theories predict the expectation value of the power spectrum, whereas our sky is a single realization. Hence the cosmic variance is an unavoidable source of uncertainty when constraining models; it dominates the scatter at lower ℓ s, while the effects of instrumental noise and resolution dominate at higher ℓ s [29].

Theoretical models generally predict that the $a_{\ell m}$ modes are Gaussian random fields to high precision, matching the empirical tests, *e.g.*, standard slow-roll inflation’s non-Gaussian contribution is expected to be at least an order of magnitude below current observational limits [30]. Although non-Gaussianity of various forms is possible in early Universe models, tests show that Gaussianity is an extremely good simplifying approximation [31]. The only current indications of any non-Gaussianity or statistical anisotropy are some relatively weak signatures at large scales, seen in both *WMAP* [32] and *Planck* data [33], but not of high enough significance to reject the simplifying assumption. Nevertheless, models that deviate from the inflationary slow-roll conditions can have measurable non-Gaussian signatures. So while the current observational limits make the power spectrum the dominant probe of cosmology, it is worth noting that higher-order correlations are becoming a tool for constraining otherwise viable theories.

29.3.4 Angular Resolution and Binning

There is no one-to-one conversion between multipole ℓ and the angle subtended by a particular spatial scale projected onto the sky. However, a single spherical harmonic $Y_{\ell m}$ corresponds to angular variations of $\theta \sim \pi/\ell$. CMB maps contain anisotropy information from the size of the map (or in practice some fraction of that size) down to the beam-size of the instrument, σ (the standard deviation of the beam, in radians). One can think of the effect of a Gaussian beam as rolling off the power spectrum with the function $e^{-\ell(\ell+1)\sigma^2}$.

For less than full sky coverage, the ℓ modes become correlated. Hence, experimental results are usually quoted as a series of ‘band powers,’ defined as estimators of $\ell(\ell+1)C_\ell/2\pi$ over different ranges of ℓ . Because of the strong foreground signals in the Galactic plane, even ‘all-sky’ surveys, such as *WMAP* and *Planck*, involve a cut sky. The amount of binning required to obtain uncorrelated estimates of power also depends on the map size.

29.4 Cosmological Parameters

The current ‘Standard Model’ of cosmology contains around 10 free parameters, only six of which are required to have non-null values (see The Cosmological Parameters—Sec. 25.1 of this *Re-*

view). The basic framework is the Friedmann-Robertson-Walker (FRW) metric (*i.e.*, a universe that is approximately homogeneous and isotropic on large scales), with density perturbations laid down at early times and evolving into today’s structures (see Big-Bang cosmology—Sec. 22 of this *Review*). The most general possible set of density variations is a linear combination of an adiabatic density perturbation and some isocurvature perturbations. Adiabatic means that there is no change to the entropy per particle for each species, *i.e.*, $\delta\rho/\rho$ for matter is $(3/4)\delta\rho/\rho$ for radiation. Isocurvature means that the set of individual density perturbations adds to zero, for example, matter perturbations compensate radiation perturbations so that the total energy density remains unperturbed, *i.e.*, $\delta\rho$ for matter is $-\delta\rho$ for radiation. These different modes give rise to distinct (temporal) phases during growth, with those of the adiabatic scenario being fully consistent with the data. Models that generate mainly isocurvature type perturbations (such as most topological defect scenarios) are not viable. However, an admixture of the adiabatic mode with up to 1.7% isocurvature contribution (depending on details of the mode) is still allowed [34].

29.4.1 Initial Condition Parameters

Within the adiabatic family of models, there is, in principle, a free function describing the variation of comoving curvature perturbations, $\mathcal{R}(\mathbf{x}, t)$. The great virtue of \mathcal{R} is that, on large scales, it is constant in time on super-horizon scales for a purely adiabatic perturbation. There are physical reasons to anticipate that the variance of these perturbations will be described well by a power law in scale, *i.e.*, in Fourier space $\langle |\mathcal{R}|_k^2 \rangle \propto k^{n_s-4}$, where k is wavenumber and n_s is spectral index as usually defined. So-called ‘scale-invariant’ initial conditions (meaning gravitational potential fluctuations that are independent of k) correspond to $n_s = 1$. In inflationary models [35] (see Inflation—Sec. 23 of this *Review*), perturbations are generated by quantum fluctuations, which are set by the energy scale of inflation, together with the slope and higher derivatives of the inflationary potential. One generally expects that the Taylor series expansion of $\ln \mathcal{R}_k(\ln k)$ has terms of steadily decreasing size. For the simplest models, there are thus two parameters describing the initial conditions for density perturbations, namely the amplitude and slope of the power spectrum. These can be explicitly defined, for example, through

$$\mathcal{P}_{\mathcal{R}}^2 \equiv k^3 \langle |\mathcal{R}|_k^2 \rangle / 2\pi^2 \simeq A_s (k/k_0)^{n_s-1}, \quad (29.3)$$

with $A_s \equiv \mathcal{P}_{\mathcal{R}}^2(k_0)$ and $k_0 = 0.05 \text{ Mpc}^{-1}$, say. There are other equally valid definitions of the amplitude parameter (see also Secs. 22, 23, and 25.1 of this *Review*), and we caution that the relationships between some of them can be cosmology-dependent. In slow-roll inflationary models, this normalization is proportional to the combination $V^3/(V')^2$, for the inflationary potential $V(\phi)$. The slope n_s also involves V'' , and so the combination of A_s and n_s can constrain potentials.

Inflation generates tensor (gravitational wave) modes, as well as scalar (density perturbation) modes. This fact introduces another parameter, measuring the amplitude of a possible tensor component, or equivalently the ratio of the tensor to scalar contributions. The tensor amplitude is $A_t \propto V$, and thus one expects a larger gravitational wave contribution in models where inflation happens at higher energies. The tensor power spectrum also has a slope, often denoted n_t , but since this seems unlikely to be measured in the near future (and there is also a consistency relation with tensor amplitude), it is sufficient for now to focus only on the amplitude of the gravitational wave component. It is most common to define the tensor contribution through r , the ratio of tensor to scalar perturbation spectra at some fixed value of k (*e.g.*, $k = 0.002 \text{ Mpc}^{-1}$, although it was historically defined in terms of the ratio of contributions at $\ell = 2$). Different inflationary potentials will lead to different predictions, *e.g.*, for 50 e-folds $\lambda\phi^4$ inflation gives $r = 0.32$ and $m^2\phi^2$ inflation gives $r = 0.16$ (both now disfavored by the data), while other models can have arbitrarily small values of r . In any case, whatever the specific definition, and whether they come from inflation or something else, the ‘initial conditions’ give rise to a minimum of three parameters, A_s , n_s , and r .

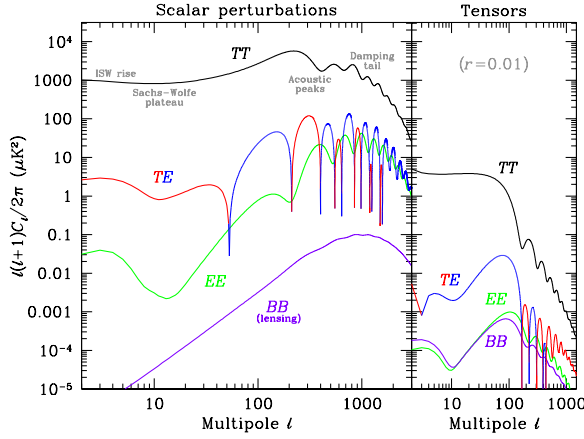


Figure 29.1: Theoretical CMB anisotropy power spectra, using the best-fitting Λ CDM model from *Planck*, calculated using CAMB. The panel on the left shows the theoretical expectation for scalar perturbations, while the panel on the right is for tensor perturbations, with an amplitude set to $r = 0.01$ for illustration. Note that the horizontal axis is logarithmic here. For the well-measured scalar TT spectrum, the regions, each covering roughly a decade in ℓ , are labeled as in the text: the ISW rise; Sachs-Wolfe plateau; acoustic peaks; and damping tail. The TE cross-correlation power spectrum changes sign, and that has been indicated by plotting the absolute value, but switching color for the negative parts.

29.4.2 Background Cosmology Parameters

The FRW cosmology requires an expansion parameter (the Hubble constant, H_0 , often represented through $H_0 = 100 h \text{ km s}^{-1} \text{ Mpc}^{-1}$) and several parameters to describe the matter and energy content of the Universe. These are usually given in terms of the critical density, *i.e.*, for species ‘x,’ $\Omega_x \equiv \rho_x / \rho_{\text{crit}}$, where $\rho_{\text{crit}} \equiv 3H_0^2 / 8\pi G$. Since physical densities $\rho_x \propto \Omega_x h^2 \equiv \omega_x$ are what govern the physics of the CMB anisotropies, it is these ω_s that are best constrained by CMB data. In particular, CMB observations constrain $\Omega_b h^2$ for baryons and $\Omega_c h^2$ for cold dark matter (with $\rho_m = \rho_c + \rho_b$ for the sum).

The contribution of a cosmological constant Λ (or other form of dark energy, see Dark Energy—Sec. 28) is usually included together with a parameter that quantifies the curvature, $\Omega_K \equiv 1 - \Omega_{\text{tot}}$, where $\Omega_{\text{tot}} = \Omega_m + \Omega_\Lambda$. The radiation content, while in principle a free parameter, is precisely enough determined by the measurement of T_γ that it can be considered fixed, and makes a $< 10^{-4}$ contribution to Ω_{tot} today.

Astrophysical processes at relatively low redshift can also affect the C_ℓ s, with a particularly significant effect coming through reionization. The Universe became reionized at some redshift z_i , long after recombination, affecting the CMB through the integrated Thomson scattering optical depth:

$$\tau = \int_0^{z_i} \sigma_T n_e(z) \frac{dt}{dz} dz, \quad (29.4)$$

where σ_T is the Thomson cross-section, $n_e(z)$ is the number density of free electrons (which depends on astrophysics), and dt/dz is fixed by the background cosmology. In principle, τ can be determined from the small-scale matter power spectrum, together with the physics of structure formation and radiative feedback processes; however, this is a sufficiently intricate calculation that in practice τ needs to be considered as a free parameter.

Thus, we have eight basic cosmological parameters: A_s , n_s , r , h , $\Omega_b h^2$, $\Omega_c h^2$, Ω_{tot} , and τ . One can add additional parameters to this list, particularly when using the CMB in combination with other data sets. The next most relevant ones might be: $\Omega_\nu h^2$, the massive neutrino contribution; w ($\equiv p/\rho$), the equation of state parameter for the dark energy; and $dn_s/d \ln k$, measuring deviations from a constant spectral index. To these 11 one could of course add further parameters describing additional physics, such as details of the reionization process, features in the ini-

tial power spectrum, a sub-dominant contribution of isocurvature modes, *etc.*

As well as these underlying parameters, there are other (dependent) quantities that can be obtained from them. Such derived parameters include the actual Ω_s of the various components (*e.g.*, Ω_m), the variance of density perturbations at particular scales (*e.g.*, σ_8), the angular scale of the sound horizon (θ_*), the age of the Universe today (t_0), the age of the Universe at recombination, reionization, *etc.* (see The Cosmological Parameters—Sec. 25.1).

29.5 Physics of Anisotropies

The cosmological parameters affect the anisotropies through the well understood physics of the evolution of linear perturbations within a background FRW cosmology. There are very effective, fast, and publicly-available software codes for computing the CMB temperature, polarization, and matter power spectra, *e.g.*, CMBFAST [36], CAMB [37], and CLASS [38]. These have been tested over a wide range of cosmological parameters and are considered to be accurate to much better than the 1% level [39], so that numerical errors are less than 10% of the parameter uncertainties for *Planck* [8].

For pedagogical purposes, it is easiest to focus on the temperature anisotropies, before moving to the polarization power spectra. A description of the physics underlying the C_ℓ^{TT} s can be separated into four main regions (the first two combined below), as shown in the top left part of Fig. 29.1.

29.5.1 The ISW Rise, $\ell \lesssim 10$, and Sachs-Wolfe Plateau, $10 \lesssim \ell \lesssim 100$

The horizon scale (or more precisely, the angle subtended by the Hubble radius) at last scattering corresponds to $\ell \simeq 100$. Anisotropies at larger scales have not evolved significantly, and hence directly reflect the ‘initial conditions.’ Temperature variations are $\delta T/T = -(1/5)\mathcal{R}(\mathbf{x}_{\text{LSS}}) \simeq (1/3)\delta\phi/c^2$, where $\delta\phi$ is the perturbation to the gravitational potential, evaluated on the last scattering surface (LSS). This is a result of the combination of gravitational redshift and intrinsic temperature fluctuations, and is usually referred to as the Sachs-Wolfe effect [40].

Assuming that a nearly scale-invariant spectrum of curvature and corresponding density perturbations was laid down at early times (*i.e.*, $n_s \simeq 1$, meaning equal power per decade in k), then $\ell(\ell+1)C_\ell \simeq \text{constant}$ at low ℓ s. This effect is hard to see unless the multipole axis is plotted logarithmically (as in Fig. 29.1, and part of Fig. 29.2).

Time variation of the potentials (*i.e.*, time-dependent metric perturbations) at late times leads to an upturn in the C_ℓ s in the lowest several multipoles; any deviation from a total equation of state $w = 0$ has such an effect. So the dominance of the dark energy at low redshift (see Dark Energy—Sec. 28) makes the lowest ℓ s rise above the plateau. This is usually called the integrated Sachs-Wolfe effect (or ISW rise), since it comes from the line integral of $\dot{\phi}$; it has been confirmed through correlations between the large-angle anisotropies and large-scale structure [41, 42]. Specific models can also give additional contributions at low ℓ (*e.g.*, perturbations in the dark-energy component itself [43]), but typically these are buried in the cosmic variance.

In principle, the mechanism that produces primordial perturbations could generate scalar, vector, and tensor modes. However, the vector (vorticity) modes decay with the expansion of the Universe. The tensors (transverse trace-free perturbations to the metric) generate temperature anisotropies through the integrated effect of the locally-anisotropic expansion of space. Since the tensor modes also redshift away after they enter the horizon, they contribute only to angular scales above about 1° (see Fig. 29.1). Hence some fraction of the low- ℓ signal could be due to a gravitational wave contribution, although small amounts of tensors are essentially impossible to discriminate from other effects that might raise the level of the plateau. Nevertheless, the tensors *can* be distinguished using polarization information (see Sec. ??).

29.5.2 The Acoustic Peaks, $100 \lesssim \ell \lesssim 1000$

On sub-degree scales, the rich structure in the anisotropy spectrum is the consequence of gravity-driven acoustic oscillations oc-

curing before the atoms in the Universe became neutral [44]. Perturbations inside the horizon at last scattering have been able to evolve causally and produce anisotropy at the last-scattering epoch, which reflects this evolution. The frozen-in phases of these sound waves imprint a dependence on the cosmological parameters, which gives CMB anisotropies their great constraining power.

The underlying physics can be understood as follows. Before the Universe became neutral, the proton-electron plasma was tightly coupled to the photons, and these components behaved as a single ‘photon-baryon fluid.’ Perturbations in the gravitational potential, dominated by the dark-matter component, were steadily evolving. They drove oscillations in the photon-baryon fluid, with photon pressure providing most of the restoring force and baryons giving some additional inertia. The perturbations were quite small in amplitude, $\mathcal{O}(10^{-5})$, and so evolved linearly. That means each Fourier mode developed independently, and hence can be described as a driven harmonic oscillator, with frequency determined by the sound speed in the fluid. Thus the fluid density underwent oscillations, giving time variations in temperature. These combine with a velocity effect, which is $\pi/2$ out of phase and has its amplitude reduced by the sound speed.

After the Universe recombined, the radiation decoupled from the baryons and could travel freely towards us. At that point, the (temporal) phases of the oscillations were frozen-in, and became projected on the sky as a harmonic series of peaks. The main peak is the mode that went through 1/4 of a period, reaching maximal compression. The even peaks are maximal *under*-densities, which are generally of smaller amplitude because the rebound has to fight against the baryon inertia. The troughs, which do not extend to zero power, are partially filled by the Doppler effect because they are at the velocity maxima.

The physical length scale associated with the peaks is the sound horizon at last scattering, which can be straightforwardly calculated. This length is projected onto the sky, leading to an angular scale that depends on the geometry of space, as well as the distance to last scattering. Hence the angular position of the peaks is a sensitive probe of a particular combination of cosmological parameters. In fact, the angular scale, θ_* , is the most precisely measured observable, and hence is usually treated as an element of the cosmological parameter set.

One additional effect arises from reionization at redshift z_i . A fraction of photons (τ) will be isotropically scattered at $z < z_i$, partially erasing the anisotropies at angular scales smaller than those subtended by the Hubble radius at z_i . This corresponds typically to ℓ s above about 10, depending on the specific reionization model. The acoustic peaks are therefore reduced by a factor $e^{-2\tau}$ relative to the plateau.

These peaks were a clear theoretical prediction going back to about 1970 [45]. One can think of them as a snapshot of stochastic standing waves. Since the physics governing them is simple and their structure rich, one can see how they encode extractable information about the cosmological parameters. Their empirical existence started to become clear around 1994 [46], and the emergence, over the following decade, of a coherent series of acoustic peaks and troughs is a triumph of modern cosmology. This picture has received further confirmation with the detection in the power spectrum of galaxies (at redshifts $z \lesssim 1$) of the imprint of these same acoustic oscillations in the baryon component [47], as well as through detection of the expected oscillations in CMB polarization power spectra (see Sec. 29.7).

29.5.3 The Damping Tail, $\ell \gtrsim 1000$

The recombination process is not instantaneous, which imparts a thickness to the last-scattering surface. This leads to a damping of the anisotropies at the highest ℓ s, corresponding to scales smaller than that subtended by this thickness. One can also think of the photon-baryon fluid as having imperfect coupling, so that there is diffusion between the two components, and hence the amplitudes of the oscillations decrease with time. These effects lead to a damping of the $C_{\ell s}$, sometimes called Silk damping [48], which cuts off the anisotropies at multipoles above about 2000. So, although in principle it is possible to measure to ever smaller scales, this becomes increasingly difficult in practice.

29.5.4 Gravitational Lensing Effects

An extra effect at high ℓ s comes from gravitational lensing, caused structures at low redshift along the line of sight to the last-scattering surface. The $C_{\ell s}$ are convolved with a smoothing function in a calculable way, partially flattening the peaks and troughs, generating a power-law tail at the highest multipoles, and complicating the polarization signal [49]. The expected effects of lensing on the CMB have been definitively detected through the 4-point function, which correlates temperature gradients and small-scale anisotropies (enabling a map of the lensing potential to be constructed [50]), as well as through the smoothing effect on the shape of the $C_{\ell s}$. Lensing is important because it gives an independent estimate of A_s , breaking the parameter combination $A_s e^{-2\tau}$ that is largely degenerate in the temperature anisotropy power spectra.

Lensing is an example of a ‘secondary effect,’ *i.e.*, the processing of anisotropies due to relatively nearby structures (see Sec. 29.8.2). Galaxies and clusters of galaxies give several such effects; all are expected to be of low amplitude, but are increasingly important at the highest ℓ s. Such effects carry additional cosmological information (about evolving gravitational potentials in the low-redshift Universe) and are receiving more attention as experiments push to higher sensitivity and angular resolution. The lensing power spectrum can potentially constrain dark-energy evolution, while future measurements at high ℓ are a particularly sensitive probe of the sum of the neutrino masses [51].

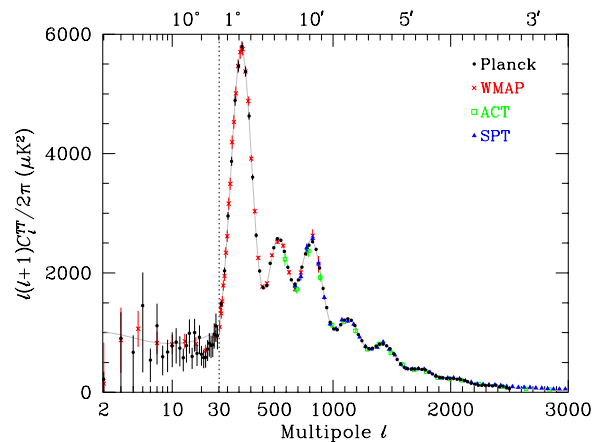


Figure 29.2: CMB temperature anisotropy band-power estimates from the *Planck*, *WMAP*, ACT, and SPT experiments. Note that the widths of the ℓ -bands vary between experiments and have not been plotted. This figure represents only a selection of the most recent available experimental results, and some points with large error bars have been omitted. At the higher multipoles these band-powers involve subtraction of particular foreground models, and so proper analysis requires simultaneous fitting of CMB and foregrounds over multiple frequencies. The horizontal axis here is logarithmic for the lowest multipoles, to show the Sachs-Wolfe plateau, and linear for the other multipoles. The acoustic peaks and damping region are very clearly observed, with no need for a theoretical line to guide the eye; however, the curve plotted is the best-fit *Planck* Λ CDM model.

29.6 Current Temperature Anisotropy Data

There has been a steady improvement in the quality of CMB data that has led to the development of the present-day cosmological model. The most robust constraints currently available come from *Planck* satellite [52] [53] data (together with constraints from non-CMB cosmological data sets), although smaller-scale results from the ACT [54] and SPT [55] experiments are beginning to add useful constraining power. We plot power spectrum estimates from these experiments in Fig. 29.2, along with *WMAP* data [7] to show the consistency (see previous versions of this review for data from earlier experiments). Comparisons among data sets show consistency, both in maps and in derived power spectra (up

to systematic uncertainties in the overall calibration for some experiments). This makes it clear that systematic effects are largely under control.

The band-powers shown in Fig. 29.2 are in very good agreement with a ‘ Λ CDM’ model. As described earlier, several (at least seven) of the peaks and troughs are quite apparent. For details of how these estimates were arrived at, the strength of correlations between band-powers, and other information required to properly interpret them, the original papers should be consulted.

29.7 CMB Polarization

Thomson scattering of an anisotropic radiation field also generates linear polarization and the CMB is predicted to be polarized, at the level of roughly 5% of the temperature anisotropies [56]. Polarization is a spin-2 field on the sky, and the algebra of the modes in ℓ -space is strongly analogous to spin-orbit coupling in quantum mechanics [57]. The linear polarization pattern can be decomposed in a number of ways, with two quantities required for each pixel in a map, often given as the Q and U Stokes parameters. However, the most intuitive and physical decomposition is a geometrical one, splitting the polarization pattern into a part that comes from a divergence (often referred to as the ‘ E mode’) and a part with a curl (called the ‘ B mode’) [58]. More explicitly, the modes are defined in terms of second derivatives of the polarization amplitude, with the Hessian for the E modes having principal axes in the same sense as the polarization, while the B -mode pattern can be thought of as a 45° rotation of the E -mode pattern. Globally one sees that the E modes have $(-1)^\ell$ parity (like the spherical harmonics), while the B modes have $(-1)^{\ell+1}$ parity.

The existence of this linear polarization allows for six different cross-power spectra to be determined from data that measure the full temperature and polarization anisotropy information. Parity considerations make two of these zero, and we are left with four potential observables, C_ℓ^{TT} , C_ℓ^{TE} , C_ℓ^{EE} , and C_ℓ^{BB} (see Fig. 29.1). Because scalar perturbations have no handedness, the B -mode power spectrum can only be sourced by vectors or tensors. Moreover, since inflationary scalar perturbations give only E modes, while tensors generate roughly equal amounts of E and B modes, then the determination of a non-zero B -mode signal is a way to measure the gravitational-wave contribution (and thus potentially derive the energy scale of inflation). However, since the signal is expected to be rather weak, one must first eliminate the foreground contributions and other systematic effects down to very low levels. In addition, CMB lensing creates B modes from E modes, further complicating the extraction of a tensor signal.

Like with temperature, the polarization C_ℓ s exhibit a series of acoustic peaks generated by the oscillating photon-baryon fluid. The main ‘ EE ’ power spectrum has peaks that are out of phase with those in the ‘ TT ’ spectrum because the polarization anisotropies are sourced by the fluid velocity. The ‘ TE ’ part of the polarization and temperature patterns comes from correlations between density and velocity perturbations on the last-scattering surface, which can be both positive and negative, and is of larger amplitude than the EE signal. There is no polarization Sachs-Wolfe effect, and hence no large-angle plateau. However, scattering during a recent period of reionization can create a polarization ‘bump’ at large angular scales.

Because the polarization anisotropies have only a small fraction of the amplitude of the temperature anisotropies, they took longer to detect. The first measurement of a polarization signal came in 2002 from the DASI experiment [59], which provided a convincing detection, confirming the general paradigm, but of low enough significance that it lent no real constraint to models. Despite dramatic progress since then, it is still the case that polarization data mainly support the basic paradigm, while reducing error bars on parameters by only around 20%. However, there are exceptions to this, specifically in the reionization optical depth, and the potential to constrain primordial gravitational waves. Moreover the situation is expected to change dramatically as more of the available polarization modes are measured.

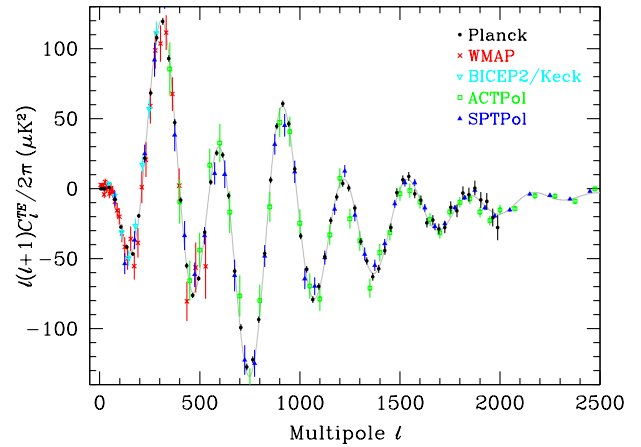


Figure 29.3: Cross-power spectrum band-powers of the temperature anisotropies and E -mode polarization signal from *Planck* (the low multipole data have been binned here), as well as *WMAP*, *BICEP2/Keck*, *ACTPol*, and *SPTPol*. The curve is the best fit to the *Planck* temperature, polarization, and lensing band-powers. Note that each band-power is an average over a range of multipoles, and hence to compare in detail with a model one has to integrate the theoretical curve through the band.

29.7.1 T - E Power Spectrum

Since the T and E skies are correlated, one has to measure the TE power spectrum, as well as TT and EE , in order to extract all the cosmological information. This TE signal has now been mapped out extremely accurately by *Planck* [53], and these band-powers are shown in Fig. 29.3, along with those from *WMAP* [60] and *BICEP2/Keck* [61], with *ACTPol* [62] [63] and *SPTPol* [64] extending to smaller angular scales. The anti-correlation at $\ell \approx 150$ and the peak at $\ell \approx 300$ were the first features to become distinct, but now a whole series of oscillations is clearly seen in this power spectrum (including at least six peaks and troughs [13]). The measured shape of the cross-correlation power spectrum provides supporting evidence for the general cosmological picture, as well as directly constraining the thickness of the last-scattering surface. Since the polarization anisotropies are generated in this scattering surface, the existence of correlations at angles above about a degree demonstrates that there were super-Hubble fluctuations at the recombination epoch. The sign of this correlation also confirms the adiabatic paradigm.

The overall picture of the source of CMB polarization and its oscillations has also been confirmed through tests that average the maps around both temperature hot spots and cold spots [65]. One sees precisely the expected patterns of radial and tangential polarization configurations, as well as the phase shift between polarization and temperature. This leaves no doubt that the oscillation picture is the correct one and that the polarization is coming from Thomson scattering at $z \approx 1100$.

29.7.2 E - E Power Spectrum

Experimental band-powers for C_ℓ^{EE} from *Planck*, *WMAP*, *BICEP2/Keck Array* [61], *ACTPol* [63], and *SPTPol* [64] are shown in Fig. 29.4. Without the benefit of correlating with the temperature anisotropies (i.e., measuring C_ℓ^{TE}), the polarization anisotropies are very weak and challenging to measure. Nevertheless, the oscillatory pattern is now well established and the data closely match the TT -derived theoretical prediction. In Fig. 29.4 one can clearly see the ‘shoulder’ expected at $\ell \approx 140$, the first main peak at $\ell \approx 400$ (corresponding to the first trough in C_ℓ^{TT}), and the series of oscillations that is out of phase with those of the temperature anisotropy power spectrum (including four or five peaks and troughs [13]).

Perhaps the most unique result from the polarization measurements is at the largest angular scales ($\ell < 10$) in C_ℓ^{TE} and C_ℓ^{EE} , where there is evidence for an excess signal (not visible in Fig. 29.4) compared to that expected from the temperature power

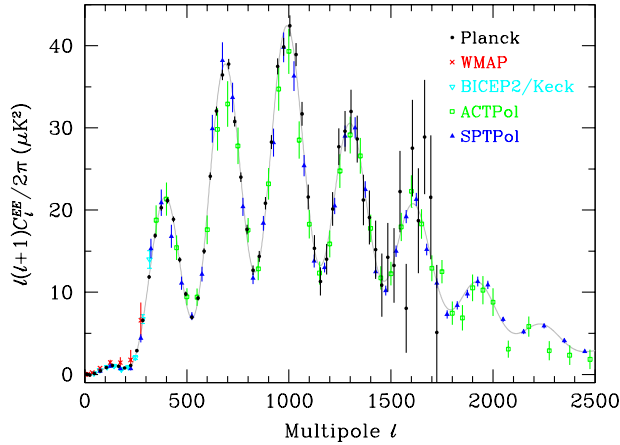


Figure 29.4: Power spectrum of E -mode polarization from *Planck*, together with *WMAP*, BICEP2/Keck, ACTPol, and SPTPol. Note that some band-powers with larger uncertainties have been omitted and that the unbinned *Planck* low- ℓ data have been binned here. Also plotted is the best-fit theoretical model from *Planck* temperature, polarization, and lensing data.

spectrum alone. This is precisely the signal anticipated from an early period of reionization, arising from Doppler shifts during the partial scattering at $z < z_i$. The amplitude of the signal indicates that the first stars, presumably the source of the ionizing radiation, formed around $z \simeq 8$ (although the uncertainty is still quite large). Since this corresponds to scattering optical depth $\tau \simeq 0.06$, then roughly 6% of CMB photons were re-scattered at the reionization epoch, with the other 94% last scattering at $z \simeq 1100$. However, estimates of the amplitude of this reionization excess have come down since the first measurements by *WMAP* (indicating that this is an extremely difficult measurement to make) and the latest *Planck* results have reduced the value further [14].

29.7.3 B - B Power Spectrum

The expected amplitude of C_ℓ^{BB} is very small, and so measurements of this polarization curl-mode are extremely challenging. The first indication of the existence of the BB signal came from the detection of the expected conversion of E modes to B modes by gravitational lensing, through a correlation technique using the lensing potential and polarization measurements from SPT [66]. However, the real promise of B modes lies in the detection of primordial gravitational waves at larger scales. This tensor signature could be seen either in the ‘recombination bump’ at around $\ell = 100$ (caused by an ISW effect as gravitational waves redshift away at the last-scattering epoch) or the ‘reionization bump’ at $\ell \lesssim 10$ (from additional scattering at low redshifts).

Results from the BICEP-2 experiment [67] in 2014 suggested a detection of the primordial B -mode signature around the recombination peak. BICEP-2 mapped a small part of the CMB sky with the best sensitivity level reached at that time (below 100 nK), but at a single frequency. Higher frequency data from *Planck* indicated that much of the BICEP2 signal was due to dust within our Galaxy, and a combined analysis by the BICEP-2, Keck Array, and *Planck* teams [68] indicated that the data are consistent with no primordial B modes. The current constraint from *Planck* data alone is $r < 0.10$ (95% [14]) and this limit is reduced to $r < 0.06$ with the inclusion of Keck Array data at 95 GHz [69].

Several experiments are continuing to push down the sensitivity of B -mode measurements, motivated by the enormous importance of a future detection of this telltale signature of inflation (or other physics at the highest energies). A compilation of experimental results for C_ℓ^{BB} is shown in Fig. 29.5, coming from a combination of direct estimates of the B modes (BICEP2/Keck Array [61], POLARBEAR [70], SPTPol [71], and ACTPol [63]) and indirect determinations of the lensing B modes based on estimating the effect of measured lensing on measured E modes (*Planck* [72], SPT [66], and ACT [73]). Additional band-power estimates are expected from these and other experiments in the near future,

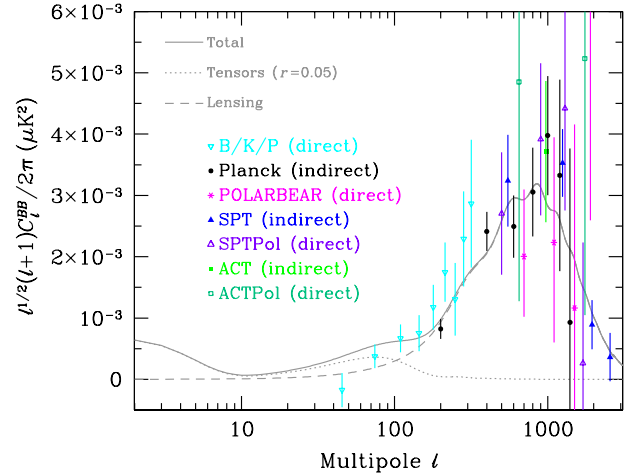


Figure 29.5: Power spectrum of B -mode polarization, including results from the BICEP2/Keck Array/*Planck* combined analysis (B/K/P), *Planck*, POLARBEAR, SPT, and ACT. Note that some of the measurements are direct estimates of B modes on the sky, while others are only sensitive to the lensing signal and come from combining E -mode and lensing potential measurements. Several earlier experiments reported upper limits, which are all off the top of this plot. A logarithmic horizontal axis is adopted here and the y -axis has been divided by a factor of $\sqrt{\ell}$ in order to show all three theoretically expected contributions: the low- ℓ reionization bump; the $\ell \simeq 100$ recombination peak; and the high- ℓ lensing signature. The dotted line is for a tensor (primordial gravitational wave) fraction $r = 0.05$, simply as an example, with all other cosmological parameters set at the best *Planck*-derived values, for which model the expected lensing B modes have also been shown with a dashed line.

with the Simons Observatory [74], the so-called ‘Stage 4’ CMB project [75] and the *LiteBIRD* satellite [76], holding great promise for pushing down to the $r \sim 0.001$ level.

29.7.4 ϕ - ϕ Power Spectrum

One further CMB observable that can be measured is the gravitational lensing deflection, leading to the construction of a map of the lensing potential. The latest *Planck* results [77] give a map that is detected at the 40σ level using a minimum-variance procedure from the 4-point function of temperature and polarization data. From this estimates can be constructed of $C_\ell^{\phi\phi}$, the lensing-potential power spectrum, and this is found to be consistent with predictions from the best-fit temperature and polarization model.

We can think of each sky pixel as possessing three independent quantities that can be measured, namely T , E , and ϕ (and potentially B , if that becomes detectable). Determining the constraining power comes down to counting $Y_{\ell m}$ modes [78], as well as appreciating that some modes help to break particular parameter degeneracies. We have only scratched the surface of CMB lensing so far, and it is expected that future small-scale experiments will lead to dramatically more of the cosmological information being extracted. Further information can also be derived about the lower- z Universe by cross-correlating CMB lensing with other cosmological tracers of large-scale structure. Additionally, small-scale lensing, combined with E -mode measurements, can be used to ‘delens’ CMB B -mode data, which will be important for pushing down into the $r \lesssim 0.01$ regime [79].

29.8 Complications

There are a number of issues that complicate the interpretation of CMB anisotropy data (and are considered to be *signal* by many astrophysicists), some of which we sketch out below.

29.8.1 Foregrounds

The microwave sky contains significant emission from our Galaxy and from extragalactic sources [80]. Fortunately, the frequency dependence of these various sources is in general substan-

tially different from that of the CMB anisotropy signals. The combination of Galactic synchrotron, bremsstrahlung, and dust emission reaches a minimum at a frequency of roughly 100 GHz (or wavelength of about 3 mm). As one moves to greater angular resolution, the minimum moves to slightly higher frequencies, but becomes more sensitive to unresolved (point-like) sources.

At frequencies around 100 GHz, and for portions of the sky away from the Galactic plane, the foregrounds are typically 1 to 10% of the CMB anisotropies. By making observations at multiple frequencies, it is relatively straightforward to separate the various components and determine the CMB signal to the few per cent level. For greater sensitivity, it is necessary to use the spatial information and statistical properties of the foregrounds to separate them from the CMB. Furthermore, at higher ℓ s it is essential to carefully model extragalactic foregrounds, particularly the clustering of infrared-emitting galaxies, which dominate the measured power spectrum as we move into the damping tail.

The foregrounds for CMB polarization follow a similar pattern to those for temperature, but are intrinsically brighter relative to CMB anisotropies. *WMAP* showed that the polarized foregrounds dominate at large angular scales, and that they must be well characterized in order to be discriminated [81]. *Planck* has shown that it is possible to characterize the foreground polarization signals, with synchrotron dominating at low frequencies and dust at high frequencies [82]. On smaller scales there are no strongly-polarized foregrounds, and hence it is in principle easier to measure foreground-free modes at high multipoles in polarization than in temperature. Although foreground contamination will no doubt become more complicated as we push down in sensitivity, and they will make analysis more difficult, for the time being, foreground contamination is not a fundamental limit for CMB experiments.

29.8.2 Secondary Anisotropies

With increasingly precise measurements of the primary anisotropies, there is growing theoretical and observational interest in ‘secondary anisotropies,’ pushing experiments to higher angular resolution and sensitivity. These secondary effects arise from the processing of the CMB due to ionization history and the evolution of structure, including gravitational lensing (which was already discussed) and patchy reionization effects [83]. Additional information can thus be extracted about the Universe at $z \ll 1000$. This tends to be most effectively done through correlating CMB maps with other cosmological probes of structure. Secondary signals are also typically non-Gaussian, unlike the primary CMB anisotropies.

A secondary signal of great current interest is the Sunyaev-Zeldovich (SZ) effect [84], which is Compton scattering ($\gamma e \rightarrow \gamma' e'$) of the CMB photons by hot electron gas. This creates spectral distortions by transferring energy from the electrons to the photons. It is particularly important for clusters of galaxies, through which one observes a partially Comptonized spectrum, resulting in a decrement at radio wavelengths and an increment in the submillimeter.

The imprint on the CMB sky is of the form $\Delta T/T = y f(x)$, with the y -parameter being the integral of Thomson optical depth times $kT_e/m_e c^2$ through the cluster, and $f(x)$ describing the frequency dependence. This is simply $x \coth(x/2) - 4$ for a non-relativistic gas (the electron temperature in a cluster is typically a few keV), where the dimensionless frequency $x \equiv h\nu/kT_\gamma$. As well as this ‘thermal’ SZ effect, there is also a smaller ‘kinetic’ effect due to the bulk motion of the cluster gas, giving $\Delta T/T \sim \tau(v/c)$, with either sign, but having the same spectrum as the primary CMB anisotropies.

A significant advantage in finding galaxy clusters via the SZ effect is that the signal is largely independent of redshift, so in principle clusters can be found to arbitrarily large distances. The SZ effect can be used to find and study individual clusters, and to obtain estimates of the Hubble constant. There is also the potential to constrain cosmological parameters, such as the clustering amplitude σ_8 and the equation of state of the dark energy, through counts of detected clusters as a function of redshift. The promise of the method has been realized through detections of clusters purely through the SZ effect by SPT [85], ACT [86], and

Planck [87]. Results from *Planck* clusters [88] suggest a somewhat lower value of σ_8 than inferred from CMB anisotropies, but there are still systematic uncertainties that might encompass the difference, and a more recent analysis of SPT-detected clusters shows better agreement [89]. Further analysis of scaling relations among cluster properties should enable more robust cosmological constraints to be placed in future, so that we can understand whether this ‘tension’ might be a sign of new physics.

29.8.3 Higher-order Statistics

Although most of the CMB anisotropy information is contained in the power spectra, there will also be weak signals present in higher-order statistics. These can measure any primordial non-Gaussianity in the perturbations, as well as non-linear growth of the fluctuations on small scales and other secondary effects (plus residual foreground contamination of course). There are an infinite variety of ways in which the CMB could be non-Gaussian [30]; however, there is a generic form to consider for the initial conditions, where a quadratic contribution to the curvature perturbations is parameterized through a dimensionless number f_{NL} . This weakly non-linear component can be constrained in several ways, the most popular being through measurements of the bispectrum (or 3-point function).

The constraints depend on the shape of the triangles in harmonic space, and it has become common to distinguish the ‘local’ or ‘squeezed’ configuration (in which one side is much smaller than the other two) from the ‘equilateral’ configuration. Other configurations are also relevant for specific theories, such as ‘orthogonal’ non-Gaussianity, which has positive correlations for $k_1 \simeq 2k_2 \simeq 2k_3$, and negative correlations for the equilateral configuration. The latest results from the *Planck* team [90] are $f_{\text{NL}}^{\text{local}} = 1 \pm 5$, $f_{\text{NL}}^{\text{equil}} = -26 \pm 47$, and $f_{\text{NL}}^{\text{ortho}} = -38 \pm 24$.

These results are consistent with zero, but are at a level that is now interesting for model predictions. The amplitude of f_{NL} expected is small, so that a detection of $f_{\text{NL}} \gg 1$ would rule out all single-field, slow-roll inflationary models. It is still possible to improve upon these *Planck* results, and it certainly seems feasible that a measurement of primordial non-Gaussianity may yet be within reach. *Non*-primordial detections of non-Gaussianity from expected signatures have already been made. For example, the bispectrum and trispectrum contain evidence of gravitational lensing, the ISW effect, and Doppler boosting. For now the primordial signal is elusive, but should it be detected, then detailed measurements of non-Gaussianity will become a unique probe of inflationary-era physics. Because of that, much effort continues to be devoted to honing predictions and measurement techniques, with the expectation that we will need to go beyond the CMB to dramatically improve the constraints.

29.8.4 Anomalies

Several features seen in the *Planck* data [33, 65, 91] confirm those found earlier with *WMAP* [32], showing mild deviations from a simple description of the data; these are often referred to as ‘anomalies.’ One such feature is the lack of power in the multipole range $\ell \simeq 20\text{--}30$ [14] [53]. Other examples involve the breaking of statistical anisotropy, caused by alignment of the lowest multipoles, as well as a somewhat excessive cold spot and a power asymmetry between hemispheres. No such feature is significant at more than the roughly 3σ level, and the importance of ‘a posteriori’ statistics here has been emphasized by many authors. Since these effects are at large angular scales, where cosmic variance dominates, the results will not increase in significance with more data, although there is the potential for more sensitive polarization measurements to provide independent tests.

29.9 Constraints on Cosmological Parameters

The most striking outcome of the last couple of decades of experimental results is that the standard cosmological paradigm continues to be in very good shape. A large amount of high-precision data on the power spectrum is adequately fit with fewer than 10 free parameters (and only six need non-trivial values). The framework is that of FRW models, which have nearly flat geometry, containing dark matter and dark energy, and with adiabatic perturbations having close to scale-invariant initial condi-

tions.

Within this basic picture, the values of the cosmological parameters can be constrained. Of course, more stringent bounds can be placed on models that cover a restricted parameter space, *e.g.*, assuming that $\Omega_{\text{tot}} = 1$ or $r = 0$. More generally, the constraints depend upon the adopted prior probability distributions, even if they are implicit, for example by restricting the parameter freedom or their ranges (particularly where likelihoods peak near the boundaries), or by using different choices of other data in combination with the CMB. As the data become even more precise, these considerations will be less important, but for now we caution that restrictions on model space and choice of non-CMB data sets and priors need to be kept in mind when adopting specific parameter values and uncertainties.

There are some combinations of parameters that fit the CMB anisotropies almost equivalently. For example, there is a nearly exact geometric degeneracy, where any combination of Ω_m and Ω_Λ that provides the same angular-diameter distance to last scattering will give nearly identical C_ℓ s. There are also other less exact degeneracies among the parameters. Such degeneracies can be broken when using the CMB results in combination with other cosmological data sets. Particularly useful are complementary constraints from baryon acoustic oscillations, galaxy clustering, the abundance of galaxy clusters, weak gravitational lensing measurements, and Type Ia supernova distances. For an overview of some of these other cosmological constraints, see The Cosmological Parameters—Sec. 25.1 of this *Review*.

Within the context of a 6-parameter family of models (which fixes $\Omega_{\text{tot}} = 1$, $dn_s/d\ln k = 0$, $r = 0$, and $w = -1$) the *Planck* results for *TT*, together with *TE*, *EE*, and CMB lensing, yield [14]: $\ln(10^{10} A_s) = 3.044 \pm 0.014$; $n_s = 0.965 \pm 0.004$; $\Omega_b h^2 = 0.02237 \pm 0.00015$; $\Omega_c h^2 = 0.1200 \pm 0.0012$; $100\theta_* = 1.04092 \pm 0.00031$; and $\tau = 0.054 \pm 0.007$. Other parameters can be derived from this basic set, including $h = 0.674 \pm 0.005$, $\Omega_\Lambda = 0.685 \pm 0.007 (= 1 - \Omega_m)$ and $\sigma_8 = 0.811 \pm 0.006$. Somewhat different (although consistent) values are obtained using other data combinations, such as including BAO, supernova, H_0 , or weak-lensing constraints (see Sec. 25.1 of this *Review*). However, the results quoted above are currently the best available from CMB data alone.

The standard cosmological model still fits the data well, with the error bars on the parameters continuing to shrink. Improved measurement of higher acoustic peaks has dramatically reduced the uncertainty in the θ_* parameter, which is now detected at $> 3000\sigma$. The evidence for $n_s < 1$ is now at the 8σ level from *Planck* data alone. The value of the reionization optical depth has decreased compared with earlier estimates; it is convincingly detected, but still not at very high significance.

Constraints can also be placed on parameters beyond the basic six, particularly when including other astrophysical data sets. Relaxing the flatness assumption, the constraint on Ω_{tot} is 1.011 ± 0.006 . Note that for h , the CMB data alone provide only a very weak constraint if spatial flatness is not assumed. However, with the addition of other data (particularly powerful in this context being a compilation of BAO measurements; see Sec. 25.1 of this *Review*), the constraints on the Hubble constant and curvature improve considerably, leading to $\Omega_{\text{tot}} = 0.9993 \pm 0.0019$ [14].

For $\Omega_b h^2$ the CMB-derived value is generally consistent with completely independent constraints from Big Bang nucleosynthesis (see Sec. 24 of this *Review*). Related are constraints on additional neutrino-like relativistic degrees of freedom, which lead to $N_{\text{eff}} = 2.99 \pm 0.17$ (including BAO), *i.e.*, no evidence for extra neutrino species.

The best limit on the tensor-to-scalar ratio is $r < 0.06$ (measured at $k = 0.002 \text{ Mpc}^{-1}$) from a combination of *Planck* and BICEP/Keck data. This limit depends on how the slope n_t is restricted and whether $dn_s/d\ln k \neq 0$ is allowed. The joint constraints on n_s and r allow specific inflationary models to be tested [34, 92, 93]. Looking at the (n_s, r) plane, this means that $m^2 \phi^2$ (mass-term quadratic) inflation is now disfavored by the data, as well as $\lambda \phi^4$ (self-coupled) inflation.

The addition of the dark-energy equation of state w adds the partial degeneracy of being able to fit a ridge in (w, h) space,

extending to low values of both parameters. This degeneracy is broken when the CMB is used in combination with other data sets, *e.g.*, adding a compilation of BAO and supernova data gives $w = -1.028 \pm 0.031$. Constraints can also be placed on more general dark energy and modified-gravity models [94]. However, when extending the search space, one needs to be careful not to over-interpret some tensions between data sets as evidence for new physics.

For the reionization optical depth, a reanalysis of *Planck* data in 2016 resulted in a reduction in the value of τ , with the tightest result giving $\tau = 0.055 \pm 0.009$, and the newest analysis gives similar numbers. This corresponds to $z_i = 7.8\text{--}8.8$ (depending on the functional form of the reionization history), with an uncertainty of ± 0.9 [95]. This redshift is only slightly higher than that suggested from studies of absorption lines in high- z quasar spectra [96] and Ly α -emitting galaxies [97], perhaps hinting that the process of reionization was not as complex as previously suspected. The important constraint provided by CMB polarization, in combination with astrophysical measurements, thus allows us to investigate how the first stars formed and brought about the end of the cosmic dark ages.

29.10 Particle Physics Constraints

CMB data place limits on parameters that are directly relevant for particle physics models. For example, there is a limit on the sum of the masses of the neutrinos, $\sum m_\nu < 0.12 \text{ eV}$ (95%) [14] coming from *Planck* together with BAO measurements (although limits are weaker when considering both N_{eff} and $\sum m_\nu$ as free parameters). This assumes the usual number density of fermions, which decoupled when they were relativistic. The limit is tantalizingly only a factor of a few higher than the minimum value coming from neutrino mixing experiments (see Neutrino Mixings—Secs. 14 and 26). As well as being an indirect probe of the neutrino background, *Planck* data also require that the neutrino background has perturbations, *i.e.*, that it possesses a sound speed $c_s^2 \simeq 1/3$, as expected [12].

The current suite of data suggests that $n_s < 1$, with a best-fitting value about 0.035 below unity. This is already quite constraining for inflationary models, particularly along with r limits. There is no current evidence for running of the spectral index, with $dn_s/d\ln k = -0.004 \pm 0.007$ from *Planck* alone [14] (with a similar value when BAO data are included), although this is less of a constraint on models. Similarly, primordial non-Gaussianity is being probed to interesting levels, although tests of simple inflationary models will only come with significant reductions in uncertainty.

The large-angle anomalies, such as the hemispheric modulation of power and the dip in power at $\ell \simeq 20\text{--}30$, have the potential to be hints of new physics. Such effects might be expected in a universe that has a large-scale power cut-off, or anisotropy in the initial power spectrum, or is topologically non-trivial. However, cosmic variance and *a posteriori* statistics limit the significance of these anomalies, absent the existence of a model that naturally yields some of these features (and ideally also predicting other phenomena that can be tested).

Constraints on ‘cosmic birefringence’ (*i.e.*, rotation of the plane of CMB polarization that generates non-zero *TB* and *EB* power) can be used to place limits on theories involving parity violation, Lorentz violation, or axion-photon mixing [98].

It is possible to place limits on additional areas of physics [99], for example annihilating dark matter [12, 12], primordial magnetic fields [100], and time variation of the fine-structure constant [101], as well as the neutrino chemical potential, a contribution of warm dark matter, topological defects, or physics beyond general relativity. Further particle physics constraints will follow as the smaller-scale and polarization measurements continue to improve.

The CMB anisotropy measurements precisely pin down physics at the time of last-scattering, and so any change of physics can be constrained if it affects the relevant energies or timescales. Future, higher sensitivity measurements of the CMB frequency spectrum will push the constraints back to cover energy injection at much earlier times (~ 1 year). Comparison of CMB and BBN observables extend these constraints to timescales of order seconds, and energies in the MeV range. And to the extent that inflation pro-

vides an effective description of the generation of perturbations, the inflationary observables may constrain physics at GUT-type energy scales.

More generally, careful measurement of the CMB power spectra and non-Gaussianity can in principle put constraints on physics at the highest energies, including ideas of string theory, extra dimensions, colliding branes, *etc.* At the moment any calculation of predictions appears to be far from definitive. However, there is a great deal of activity on implications of string theory for the early Universe, and hence a very real chance that there might be observational implications for specific scenarios.

29.11 Fundamental Lessons

More important than the precise values of parameters is what we have learned about the general features that describe our observable Universe. Beyond the basic hot Big Bang picture, the CMB has taught us that:

- the (observable) Universe is very close to isotropic;
- the Universe recombined at $z \sim 1000$ and started to become ionized again at $z \sim 10$;
- the geometry of the Universe is close to flat;
- both dark matter and dark energy are required;
- gravitational instability is sufficient to grow all of the observed large structures in the Universe;
- topological defects were not important for structure formation;
- there were ‘synchronized’ super-Hubble modes generated in the early Universe;
- the initial perturbations were predominantly adiabatic in nature;
- the primordial perturbation spectrum has a slightly red tilt;
- the perturbations had close to Gaussian (*i.e.*, maximally random) initial conditions.

These features form the basis of the cosmological standard model, Λ CDM, for which it is tempting to make an analogy with the Standard Model of particle physics (see earlier Sections of this *Review*). The cosmological model is much further from any underlying ‘fundamental theory,’ which might ultimately provide the values of the parameters from first principles. Nevertheless, any genuinely complete ‘theory of everything’ must include an explanation for the values of these cosmological parameters in addition to the parameters of the Standard Model of particle physics.

29.12 Future Directions

Given the significant progress in measuring the CMB sky, which has been instrumental in tying down the cosmological model, what can we anticipate for the future? There will be a steady improvement in the precision and confidence with which we can determine the appropriate cosmological parameters. Ground-based experiments operating at smaller angular scales will continue to place tighter constraints on the damping tail, lensing, and cross-correlations. New polarization experiments at small scales will probe further into the damping tail, without the limitation of extragalactic foregrounds. And polarization experiments at large angular scales will push down the limits on primordial B modes.

Planck, the third generation CMB satellite mission, was launched in May 2009, and has produced a large number of papers, including a set of cosmological studies based on the first two full surveys of the sky (accompanied by a public release of data products) in 2013, a further series coming from analysis of the full mission data release in 2015 (eight surveys for the Low Frequency Instrument and five surveys for the High Frequency Instrument), and a third series derived from a final analysis of the 2018 data release, including full constraints from polarization data.

A set of cosmological parameters is now known to percent-level accuracy, and that may seem sufficient for many people. However, we should certainly demand more of measurements that describe *the entire observable Universe!* Hence a lot of activity in the coming years will continue to focus on determining those parameters with increasing precision. This necessarily includes testing for consistency among different predictions of the cosmological

Standard Model, and searching for signals that might require additional physics.

A second area of focus will be the smaller-scale anisotropies and ‘secondary effects.’ There is a great deal of information about structure formation at $z \ll 1000$ encoded in the CMB sky. This may involve higher-order statistics and cross-correlations with other large-scale structure tracers, as well as spectral signatures, with many experiments targeting the galaxy cluster SZ effect. The current status of CMB lensing is similar (in terms of total signal-to-noise) to the quality of the first CMB anisotropy measurements by *COBE*, and thus we can expect that experimental probes of lensing will improve dramatically in the coming years. All of these investigations can provide constraints on the dark-energy equation of state, for example, which is a major area of focus for several future cosmological surveys at optical wavelengths. CMB lensing also promises to yield a measurement of the sum of the neutrino masses.

A third direction is increasingly sensitive searches for specific signatures of physics at the highest energies. The most promising of these may be the primordial gravitational wave signals in C_ℓ^{BB} , which could be a probe of the $\sim 10^{16}$ GeV energy range. There are several ground- and balloon-based experiments underway that are designed to search for the polarization B modes. Additionally, non-Gaussianity holds the promise of constraining models beyond single-field slow-roll inflation.

Anisotropies in the CMB have proven to be the premier probe of cosmology and the early Universe. Theoretically the CMB involves well-understood physics in the linear regime, and is under very good calculational control. A substantial and improving set of observational data now exists. Systematics appear to be under control and are not currently a limiting factor. And so for the next several years we can expect an increasing amount of cosmological information to be gleaned from CMB anisotropies, with the prospect also of some genuine surprises.

References

- [1] A. A. Penzias and R. W. Wilson, *Astrophys. J.* **142**, 419 (1965); R. H. Dicke *et al.*, *Astrophys. J.* **142**, 414 (1965).
- [2] M. White, D. Scott and J. Silk, *Ann. Rev. Astron. Astrophys.* **32**, 319 (1994).
- [3] W. Hu and S. Dodelson, *Ann. Rev. Astron. Astrophys.* **40**, 171 (2002).
- [4] A. Challinor and H. Peiris, in M. Novello and S. Perez, editors, “American Institute of Physics Conference Series,” volume 1132, 86–140 (2009), [arXiv:0903.5158].
- [5] G. F. Smoot *et al.*, *Astrophys. J. Lett.* **396**, L1 (1992).
- [6] C. L. Bennett *et al.*, *Astrophys. J. Supp.* **148**, 1 (2003).
- [7] G. Hinshaw *et al.*, *Astrophys. J. Supp.* **208**, 19 (2013), [arXiv:1212.5226].
- [8] Planck Collab. 2013 Results XVI, *Astron. Astrophys.* **571**, A16 (2014), [arXiv:1303.5076].
- [9] J. A. Tauber *et al.*, *Astron. Astrophys.* **520**, A1 (2010).
- [10] Planck Collab. 2013 Results I, *Astron. Astrophys.* **571**, A1 (2014), [arXiv:1303.5062].
- [11] Planck Collab. 2015 Results I, *Astron. Astrophys.* **594**, A1 (2016), [arXiv:1502.01582].
- [12] Planck Collab. 2015 Results XIII, *Astron. Astrophys.* **594**, A13 (2016), [arXiv:1502.01589].
- [13] Planck Collab. 2018 Results I, arXiv e-prints arXiv:1807.06205 (2018), [arXiv:1807.06205].
- [14] Planck Collab. 2018 Results VI, arXiv e-prints arXiv:1807.06209 (2018), [arXiv:1807.06209].
- [15] D. S. Swetz *et al.*, *Astrophys. J. Supp.* **194**, 41 (2011), [arXiv:1007.0290].
- [16] J. E. Carlstrom *et al.*, *Proc. Astron. Soc. Pacific* **123**, 568 (2011), [arXiv:0907.4445].
- [17] P. Noterdaeme *et al.*, *Astron. Astrophys.* **526**, L7 (2011), [arXiv:1012.3164]; S. Muller *et al.*, *Astron. & Astrophys.* **551**, A109 (2013), [arXiv:1212.5456].

- [18] D. J. Fixsen *et al.*, *Astrophys. J.* **734**, 5 (2011), [arXiv:0901.0555].
- [19] J. Singal *et al.*, *Pub. Astron. Soc. Pac.* **130**, 985, 036001 (2018).
- [20] A. Kogut *et al.*, in “Space Telescopes and Instrumentation 2014: Optical, Infrared, and Millimeter Wave,” volume 9143 of *Proc. SPIE*, 91431E (2014).
- [21] P. André *et al.*, *JCAP* **2014**, 2, 006 (2014), [arXiv:1310.1554].
- [22] V. Desjacques *et al.*, *Mon. Not. R. Astron. Soc.* **451**, 4460 (2015), [arXiv:1503.05589].
- [23] D. J. Fixsen, *Astrophys. J.* **707**, 916 (2009), [arXiv:0911.1955].
- [24] J. C. Mather *et al.*, *Astrophys. J.* **512**, 511 (1999).
- [25] Y. Hoffman, H. M. Courtois and R. B. Tully, *Mon. Not. R. Astron. Soc.* **449**, 4494 (2015), [arXiv:1503.05422].
- [26] D. J. Fixsen *et al.*, *Astrophys. J.* **420**, 445 (1994).
- [27] Planck Collab. 2013 Results XXVII, *Astron. Astrophys.* **571**, A27 (2014), [arXiv:1303.5087].
- [28] S. Seager, D. D. Sasselov and D. Scott, *Astrophys. J. Supp.* **128**, 407 (2000).
- [29] L. Knox, *Phys. Rev.* 4307–4318 (1995).
- [30] N. Bartolo *et al.*, *Phys. Rep.* **402**, 103 (2004).
- [31] Planck Collab. 2013 Results XXIV, *Astron. Astrophys.* **571**, A24 (2014), [arXiv:1303.5084].
- [32] C. L. Bennett *et al.*, *Astrophys. J. Supp.* **192**, 17 (2011), [arXiv:1001.4758].
- [33] Planck Collab. 2013 Results XXIII, *Astron. Astrophys.* **571**, A23 (2014), [arXiv:1303.5083].
- [34] Planck Collab. 2018 Results X, arXiv e-prints arXiv:1807.06211 (2018), [arXiv:1807.06211].
- [35] A. R. Liddle and D. H. Lyth, *Cosmological Inflation and Large-Scale Structure* (2000).
- [36] U. Seljak and M. Zaldarriaga, *Astrophys. J.* **469**, 437 (1996).
- [37] A. Lewis, A. Challinor and A. Lasenby, *Astrophys. J.* **538**, 473 (2000).
- [38] D. Blas, J. Lesgourgues and T. Tram, *J. Cosmology Astropart. Phys.* **7**, 034 (2011), [arXiv:1104.2933].
- [39] U. Seljak *et al.*, *Phys. Rev.* , 8, 083507 (2003).
- [40] R. K. Sachs and A. M. Wolfe, *Astrophys. J.* **147**, 73 (1967).
- [41] R. G. Crittenden and N. Turok, *Phys. Rev. Lett.* **76**, 575 (1996).
- [42] Planck Collab. 2015 Results XXI, *Astron. Astrophys.* **594**, A21 (2016), [arXiv:1502.01595].
- [43] W. Hu *et al.*, *Phys. Rev.* **59**, 2, 023512 (1999).
- [44] W. Hu, N. Sugiyama and J. Silk, *Nature* **386**, 37 (1997).
- [45] P. J. E. Peebles and J. T. Yu, *Astrophys. J.* **162**, 815 (1970); R. A. Sunyaev and Y. B. Zeldovich, *Astron. Astrophys. Supp.* **7**, 3 (1970).
- [46] D. Scott, J. Silk and M. White, *Science* **268**, 829 (1995).
- [47] D. J. Eisenstein, *New Astron. Rev.* **49**, 360 (2005).
- [48] J. Silk, *Astrophys. J.* **151**, 459 (1968).
- [49] M. Zaldarriaga and U. Seljak, *Phys. Rev.* , 2, 023003 (1998).
- [50] Planck Collab. 2013 Result XVII, *Astron. Astrophys.* **571**, A17 (2014), [arXiv:1303.5077].
- [51] M. Kaplinghat, L. Knox and Y.-S. Song, *Phys. Rev. Lett.* **91**, 24, 241301 (2003).
- [52] Planck Collab. 2013 Results XV, *Astron. Astrophys.* **571**, A15 (2014), [arXiv:1303.5075].
- [53] Planck Collab. 2018 Results V, arXiv e-prints arXiv:1907.12875 (2019), [arXiv:1907.12875].
- [54] S. Das *et al.*, *J. Cosmology Astropart. Phys.* **4**, 014 (2014), [arXiv:1301.1037].
- [55] K. T. Story *et al.*, *Astrophys. J.* **779**, 86 (2013), [arXiv:1210.7231].
- [56] W. Hu and M. White, *New Astron.* **2**, 323 (1997).
- [57] W. Hu and M. White, *Phys. Rev.* 596–615 (1997).
- [58] M. Zaldarriaga and U. Seljak, *Phys. Rev.* 1830–1840 (1997).
- [59] J. M. Kovac *et al.*, *Nature* **420**, 772 (2002).
- [60] D. Larson *et al.*, *Astrophys. J. Supp.* **192**, 16 (2011), [arXiv:1001.4635].
- [61] Keck Array and BICEP2 Collabs. V, *Astrophys. J.* **811**, 126 (2015), [arXiv:1502.00643].
- [62] S. Naess *et al.*, *J. Cosmology Astropart. Phys.* **10**, 007 (2014), [arXiv:1405.5524].
- [63] T. Louis *et al.*, *J. Cosmology Astropart. Phys.* **6**, 031 (2017), [arXiv:1610.02360].
- [64] A. T. Crites *et al.*, *Astrophys. J.* **805**, 36 (2015), [arXiv:1411.1042].
- [65] Planck Collab. 2018 Results VII, arXiv e-prints arXiv:1906.02552 (2019), [arXiv:1906.02552].
- [66] D. Hanson *et al.*, *Phys. Rev. Lett.* **111**, 14, 141301 (2013), [arXiv:1307.5830].
- [67] BICEP2 Collab., *Phys. Rev. Lett.* **112**, 24, 241101 (2014), [arXiv:1403.3985].
- [68] BICEP2/Keck and Planck Collabs., *Phys. Rev. Lett.* **114**, 10, 101301 (2015), [arXiv:1502.00612].
- [69] BICEP2 Collaboration and Keck Array Collaboration, *Phys. Rev. Lett.* **121**, 22, 221301 (2018).
- [70] POLARBEAR Collab., *Astrophys. J.* **848**, 121 (2017), [arXiv:1705.02907].
- [71] R. Keisler *et al.*, *Astrophys. J.* **807**, 151 (2015), [arXiv:1503.02315].
- [72] Planck Collab. 2015 Results XV, *Astron. Astrophys.* **594**, A15 (2016), [arXiv:1502.01591].
- [73] A. van Engelen *et al.*, *Astrophys. J.* **808**, 7 (2015), [arXiv:1412.0626].
- [74] P. Ade *et al.* (The Simons Observatory collaboration), *JCAP* **2019**, 2, 056 (2019).
- [75] K. N. Abazajian *et al.*, ArXiv e-prints (2016), [arXiv:1610.02743].
- [76] Y. Sekimoto *et al.*, in “Proc. SPIE,” volume 10698 of *Society of Photo-Optical Instrumentation Engineers (SPIE) Conference Series*, 106981Y (2018).
- [77] Planck Collab. 2018 Results VIII, arXiv e-prints arXiv:1807.06210 (2018), [arXiv:1807.06210].
- [78] D. Scott *et al.*, *JCAP* **2016**, 6, 046 (2016), [arXiv:1603.03550].
- [79] L. Knox and Y.-S. Song, *Phys. Rev. Lett.* **89**, 1, 011303 (2002), [arXiv:astro-ph/0202286]; M. Kesden, A. Cooray and M. Kamionkowski, *Phys. Rev. Lett.* **89**, 011304 (2002), [arXiv:astro-ph/0202434]; C. M. Hirata and U. Seljak, *Phys. Rev.* **D68**, 8, 083002 (2003), [arXiv:astro-ph/0306354].
- [80] Planck Collab. 2013 Results XII, *Astron. Astrophys.* **571**, A12 (2014), [arXiv:1303.5072].
- [81] B. Gold *et al.*, *Astrophys. J. Supp.* **192**, 15 (2011), [arXiv:1001.4555].
- [82] Planck Collab. Interm. Results XXX, *Astron. Astrophys.* **586**, A133 (2016), [arXiv:1409.5738].
- [83] M. Millea *et al.*, *Astrophys. J.* **746**, 4 (2012), [arXiv:1102.5195].
- [84] R. A. Sunyaev and I. B. Zeldovich, *Ann. Rev. Astron. Astrophys.* **18**, 537 (1980).
- [85] R. Williamson *et al.*, *Astrophys. J.* **738**, 139 (2011), [arXiv:1101.1290].
- [86] T. A. Marriage *et al.*, *Astrophys. J.* **737**, 61 (2011), [arXiv:1010.1065].

- [87] Planck Collab. Early Results VIII, *Astron. Astrophys.* **536**, A8 (2011), [arXiv:1101.2024].
- [88] Planck Collab. 2013 Results XX, *Astron. Astrophys.* **571**, A20 (2014), [arXiv:1303.5080].
- [89] T. de Haan *et al.*, *Astrophys. J.* **832**, 95 (2016), [arXiv:1603.06522].
- [90] Planck Collab. 2018 Results IX, arXiv e-prints arXiv:1905.05697 (2019), [arXiv:1905.05697].
- [91] Planck Collab. 2015 Results XVI, *Astron. Astrophys.* **594**, A16 (2016), [arXiv:1506.07135].
- [92] Planck Collab. 2013 Results XXII, *Astron. Astrophys.* **571**, A22 (2014), [arXiv:1303.5082].
- [93] Planck Collab. 2015 Results XX, *Astron. Astrophys.* **594**, A20 (2016), [arXiv:1502.02114].
- [94] Planck Collab. 2015 Results XIV, *Astron. Astrophys.* **594**, A14 (2016), [arXiv:1502.01590].
- [95] Planck Collab. Interm. Results XLVI, *Astron. Astrophys.* **596**, A107 (2016), [arXiv:1605.02985].
- [96] X. Fan, C. L. Carilli and B. Keating, *Ann. Rev. Astron. Astrophys.* **44**, 415 (2006).
- [97] T. R. Choudhury *et al.*, *Mon. Not. R. Astron. Soc.* **452**, 261 (2015), [arXiv:1412.4790].
- [98] B. Feng *et al.*, *Phys. Rev. Lett.* **96**, 22, 221302 (2006).
- [99] M. Kamionkowski and A. Kosowsky, *Ann. Rev. Nucl. Part. Sci.* **49**, 77 (1999).
- [100] Planck Collab. 2015 Results XIX, *Astron. Astrophys.* **594**, A19 (2016), [arXiv:1502.01594].
- [101] Planck Collab. Interm. Results XXIV, *Astron. Astrophys.* **580**, A22 (2015), [arXiv:1406.7482].

30. Cosmic Rays

Revised October 2019 by J.J. Beatty (Ohio State U.), J. Matthews (Louisiana State U.) and S.P. Wakely (Chicago U.; Chicago U., Kavli Inst.).

Cosmic rays are a population of energetic elementary particles and nuclei with a steeply falling near-power law spectrum extending from a few MeV to tens of Joules per particle. Primary cosmic rays can be measured directly by experiments in space or on balloons at energies where there is sufficient flux (§30.1). Atmospheric interactions of primary cosmic rays produce fluxes of secondary elementary particles which can be detected in the atmosphere (§30.2), at the Earth's surface (§30.3), and underground (§30.4). At high energies, air showers of particles generated by a single primary can be detected (§30.5). These showers can be reconstructed to determine the energy, direction, and composition of the incident particle. Energetic neutrinos are closely linked to high energy cosmic rays, both through their production at astrophysical sites of particle acceleration and by production during propagation of extremely high energy cosmic rays (§30.6).

30.1 Primary Spectra from Direct Measurements

The cosmic radiation incident at the top of the terrestrial atmosphere includes all stable charged particles and nuclei with lifetimes of order 10^6 years or longer. When discussing the astrophysical origin of cosmic rays, "primary" cosmic rays are those particles accelerated at astrophysical sources and "secondaries" are those particles produced in interaction of the primaries with interstellar gas¹. Thus electrons, protons and helium, as well as carbon, oxygen, iron, and other nuclei synthesized in stars, are primaries. Nuclei such as lithium, beryllium, and boron (which are not abundant end-products of stellar nucleosynthesis) are secondaries. Antiprotons and positrons are also in large part secondary. Whether a small fraction of these particles may be primary is a question of current interest.

Apart from particles associated with solar flares², the cosmic radiation comes from outside the solar system. The incoming charged particles are "modulated" by the solar wind, the expanding magnetized plasma generated by the Sun, which decelerates and partially excludes the lower energy galactic cosmic rays from the inner solar system. There is a significant anticorrelation between solar activity (which has an alternating eleven-year cycle) and the intensity of the cosmic rays with rigidities below about 10 GV. In addition, the lower-energy cosmic rays are affected by the geomagnetic field, which they must penetrate to reach the top of the atmosphere. Thus the intensity of any component of the cosmic radiation in the GeV range depends both on the location and time.

There are four different ways to describe the spectra of the components of the cosmic radiation: (1) By particles per unit rigidity. Propagation (and probably also acceleration) through cosmic magnetic fields depends on gyroradius or *magnetic rigidity*, R , which is gyroradius multiplied by the magnetic field strength:

$$R = \frac{pc}{Ze} = r_L B \quad (30.1)$$

(2) By particles per energy-per-nucleon. Fragmentation of nuclei propagating through the interstellar gas depends on energy per nucleon, since that quantity is approximately conserved when a nucleus breaks up on interaction with the gas. (3) By nucleons per energy-per-nucleon. Production of secondary cosmic rays in the atmosphere depends on the intensity of nucleons per energy-per-nucleon, approximately independently of whether the incident nucleons are free protons or bound in nuclei. (4) By particles per energy-per-nucleus. Air shower experiments that use the atmosphere as a calorimeter generally measure a quantity that is related to total energy per particle.

The units of differential intensity I are $[\text{m}^{-2} \text{s}^{-1} \text{sr}^{-1} \mathcal{E}^{-1}]$, where \mathcal{E} represents the units of one of the four variables listed above.

¹'Primary' and 'secondary' are used in a different but analogous sense when discussing cosmic ray interactions in the atmosphere.

²Energetic particles accelerated by the Sun and at other sites within the heliosphere and at its boundary are outside the scope of this review

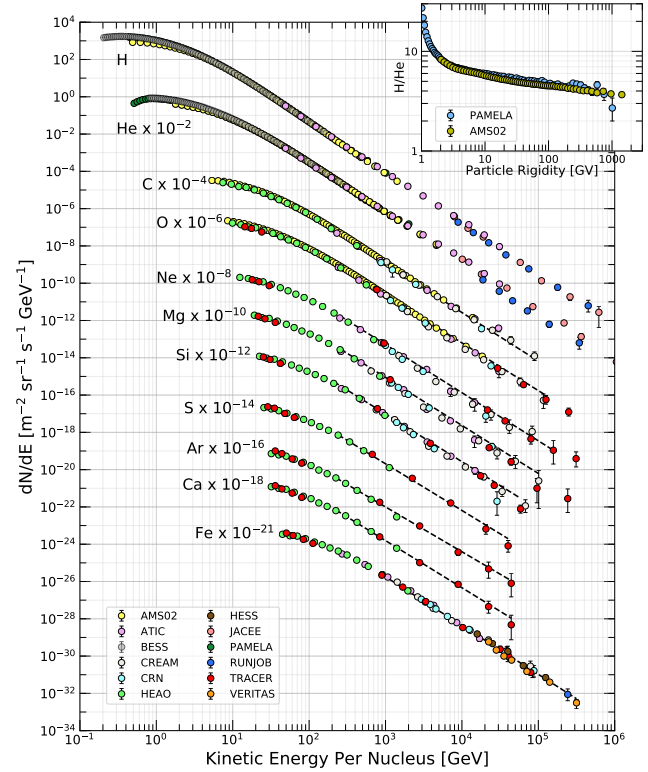


Figure 30.1: Fluxes of nuclei of the primary cosmic radiation in particles per energy-per-nucleus are plotted vs energy-per-nucleus using data from Refs. [1–13]. The inset shows the H/He ratio as a function of rigidity [1, 3].

The intensity of primary nucleons in the energy range from several GeV to somewhat beyond 100 TeV is given approximately by

$$I_N(E) \approx 1.8 \times 10^4 (E/1 \text{ GeV})^{-\alpha} \frac{\text{nucleons}}{\text{m}^2 \text{ s sr GeV}}, \quad (30.2)$$

where E is the energy-per-nucleon (including rest mass energy) and α ($\equiv \gamma + 1$) ≈ 2.7 is the differential spectral index of the cosmic-ray flux and γ is the integral spectral index. About 74% of the primary nucleons are free protons and about 70% of the rest are nucleons bound in helium nuclei. The fractions of the primary nuclei are nearly constant over this energy range (with a few interesting variations, e.g. [1]). Fractions of both primary and secondary incident nuclei are listed in Table 30.1. Figure 30.1 shows the major nuclear components for kinetic energies greater than 0.22 GeV/nucleus. A useful compendium of experimental data for cosmic-ray nuclei and electrons is described in [14].

The composition and energy spectra of nuclei are typically interpreted in the context of propagation models, in which the sources of the primary cosmic radiation are located within the Galaxy [15]. The ratio of secondary to primary nuclei is observed to decrease with increasing energy, a fact often interpreted to mean that the lifetime of cosmic rays in the Galaxy decreases with energy. Measurements of radioactive "clock" isotopes in the low energy cosmic radiation are consistent with a lifetime in the Galaxy of about 15 Myr [16].

Cosmic rays are nearly isotropic at most energies due to diffusive propagation in the galactic magnetic field. Milagro [17], HAWC and IceCube [18], and the Tibet-III air shower array [19] have observed anisotropy at the level of about 10^{-3} for cosmic rays with energy of a few TeV, possibly due the direction of local Galactic magnetic fields, motion of the solar system in the Galaxy, and to the distribution of sources.

The spectrum of electrons and positrons incident at the top of

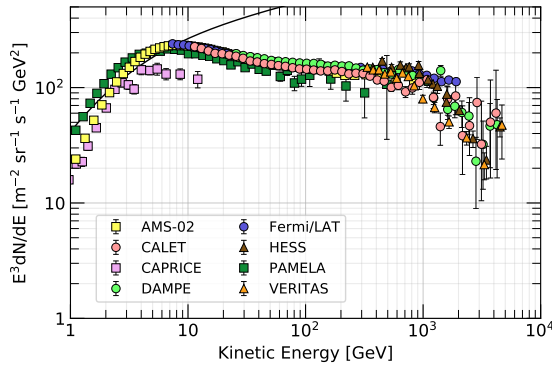


Figure 30.2: Differential spectrum of electrons plus positrons (except PAMELA data, which are electrons only) multiplied by E^3 [20–28]. The line shows the proton spectrum [29] multiplied by 0.01.

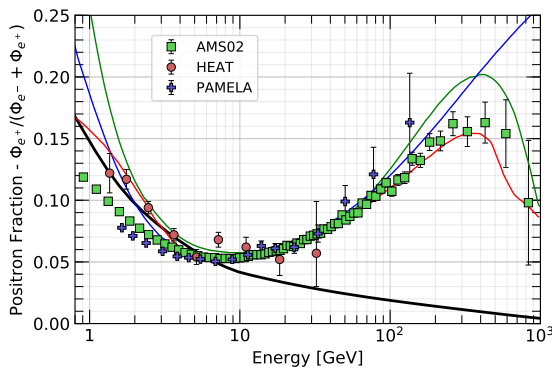


Figure 30.3: The positron fraction (ratio of the flux of e^+ to the total flux of e^+ and e^-) [22, 30–32]. The heavy black line is a model of pure secondary production [33] and the three thin lines show three representative attempts to model the positron excess with different phenomena: green: dark matter decay [34]; blue: propagation physics [35]; red: production in pulsars [36]. The ratio below 10 GeV is dependent on the polarity of the solar magnetic field.

the atmosphere is generally expected to steepen by one power of E above an energy of 5 GeV because of radiative energy loss effects in the Galaxy. Most modern measurements of the combined electron+positron spectrum at high energy, which includes data from spectrometers, calorimeters, and ground-based air Cherenkov telescopes, reveal a relatively smooth spectrum to approximately 1 TeV, where evidence of a cutoff has been reported [24, 26, 28].

The PAMELA [30, 31] and AMS-02 [37, 38] satellite experi-

Table 30.1: Relative abundances F of cosmic-ray nuclei at 10.6 GeV/nucleon normalized to oxygen ($\equiv 1$) [9]. The oxygen flux at kinetic energy of 10.6 GeV/nucleon is $3.29 \times 10^{-2} (\text{m}^2 \text{ s sr GeV/nucleon})^{-1}$. Abundances of hydrogen and helium are from Refs.(citerange) [2–4]. Note that one can not use these values to extend the cosmic-ray flux to high energy because the power law indices for each element may differ slightly.

Z	Element	F	Z	Element	F
1	H	550	13–14	Al-Si	0.19
2	He	34	15–16	P-S	0.03
3–5	Li-B	0.40	17–18	Cl-Ar	0.01
6–8	C-O	2.20	19–20	K-Ca	0.02
9–10	F-Ne	0.30	21–25	Sc-Mn	0.05
11–12	Na-Mg	0.22	26–28	Fe-Ni	0.12

ments measured the positron to electron ratio to increase above 10 GeV instead of the expected decrease [33] at higher energy, confirming earlier hints seen by the HEAT balloon-borne experiment [32]. The structure in the electron spectrum, as well as the increase in the positron fraction, may be related to contributions from individual nearby sources (supernova remnants or pulsars) emerging above a background suppressed at high energy by synchrotron losses [39]. Other explanations have invoked propagation effects [35] or dark matter decay/annihilation processes (see, e.g., [34]). The significant disagreement in the ratio below ~ 10 GeV is attributable to differences in charge-sign dependent solar modulation effects present near Earth at the times of measurement.

The ratio of antiprotons to protons is $\sim 2 \times 10^{-4}$ [40] at around 10–20 GeV, and there is clear evidence [41] for the kinematic suppression at lower energy that is the signature of secondary antiprotons. The \bar{p}/p ratio also shows a strong dependence on the phase and polarity of the solar cycle [42] in the opposite sense to that of the positron fraction. There is at this time no evidence for a significant primary component of antiprotons. No antihelium or antideuteron has been found in the cosmic radiation. The best measured upper limit on the ratio antihelium/helium is currently approximately 1×10^{-7} [43]. The upper limit on the flux of antideuterons around 1 GeV/nucleon is approximately $2 \times 10^{-4} (\text{m}^2 \text{ s sr GeV/nucleon})^{-1}$ [44].

A useful method for calculating the effect of solar modulation including time, charge-sign, and rigidity-dependent effects is given in Ref. [45].

30.2 Cosmic Rays in the Atmosphere

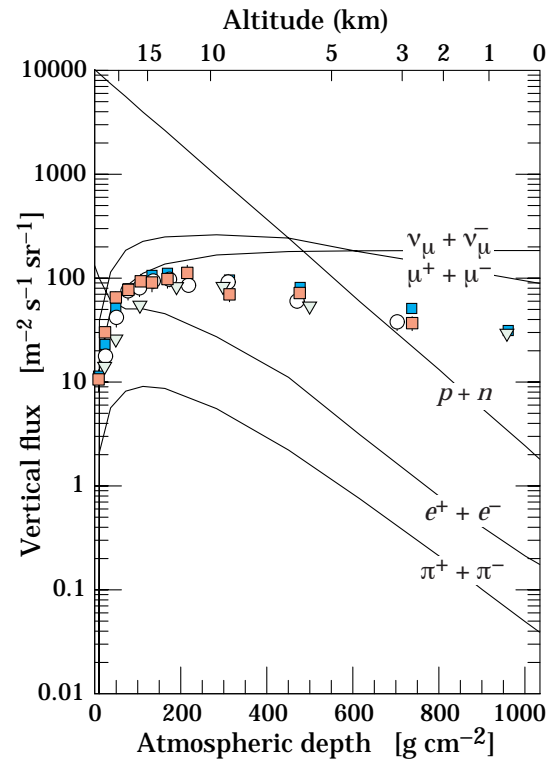


Figure 30.4: Vertical fluxes of cosmic rays in the atmosphere with $E > 1$ GeV estimated from the nucleon flux of Eq. (30.2). The points show measurements of negative muons with $E_\mu > 1$ GeV [46–51].

Figure 30.4 shows the vertical fluxes of the major cosmic-ray components in the atmosphere in the energy region where the particles are most numerous (except for electrons, which are most numerous near their critical energy, which is about 81 MeV in air). Except for protons and electrons near the top of the atmosphere,

all particles are produced in interactions of the primary³ cosmic rays in the air. Muons and neutrinos are products of the decay chain of charged mesons, while electrons and photons originate in decays of neutral mesons.

Most measurements are made at ground level or near the top of the atmosphere, but there are also measurements of muons and electrons from airplanes and balloons. Fig. 30.4 shows measurements of negative muons [46–51]. Since $\mu^+(\mu^-)$ are produced in association with $\nu_\mu(\bar{\nu}_\mu)$, the measurement of muons near the maximum of the intensity curve for the parent pions serves to calibrate the atmospheric ν_μ beam [52]. Because muons typically lose almost 2 GeV in passing through the atmosphere, the comparison near the production altitude is important for the sub-GeV range of $\nu_\mu(\bar{\nu}_\mu)$ energies.

The flux of cosmic rays through the atmosphere is described by a set of coupled cascade equations with boundary conditions at the top of the atmosphere to match the primary spectrum. Numerical or Monte Carlo calculations are needed to account accurately for decay and energy-loss processes, and for the energy-dependences of the cross sections and of the primary spectral index γ . Approximate analytic solutions are, however, useful in limited regions of energy [53, 54]. For example, the vertical intensity of charged pions with energy $E_\pi \ll \epsilon_\pi = 115$ GeV is

$$I_\pi(E_\pi, X) \approx \frac{Z_{N\pi}}{\lambda_N} I_N(E_\pi, 0) e^{-X/\Lambda} \frac{X E_\pi}{\epsilon_\pi} \quad (30.3)$$

where Λ is the characteristic length for exponential attenuation of the parent nucleon flux in the atmosphere. This expression has a maximum at $X = \Lambda \approx 121 \pm 4$ g cm⁻² [55], which corresponds to an altitude of 15 kilometers. The quantity $Z_{N\pi}$ is the spectrum-weighted moment of the inclusive distribution of charged pions in interactions of nucleons with nuclei of the atmosphere. The intensity of low-energy pions is much less than that of nucleons because $Z_{N\pi} \approx 0.079$ is small and because most pions with energy much less than the critical energy ϵ_π decay rather than interact.

30.3 Cosmic rays at the surface

30.3.1 Muons

Muons are the most numerous charged particles at sea level (see Fig. 30.4). Most muons are produced high in the atmosphere (typically 15 km) and lose about 2 GeV to ionization before reaching the ground. Their energy and angular distribution reflect a convolution of the production spectrum, energy loss in the atmosphere, and decay. For example, 2.4 GeV muons have a decay length of 15 km, which is reduced to 8.7 km by energy loss. The mean energy of muons at the ground is ≈ 4 GeV. The energy spectrum is almost flat below 1 GeV, steepens gradually to reflect the primary spectrum in the 10–100 GeV range, and steepens further at higher energies because pions with $E_\pi > \epsilon_\pi$ tend to interact in the atmosphere before they decay. Asymptotically ($E_\mu \gg 1$ TeV), the energy spectrum of atmospheric muons is one power steeper than the primary spectrum. The integral intensity of vertical muons above 1 GeV/c at sea level is ≈ 70 m⁻²s⁻¹sr⁻¹ [56] [57], with recent measurements [51, 58, 59] favoring a lower normalization by 10–15%. Experimentalists are familiar with this number in the form $I \approx 1$ cm⁻² min⁻¹ for horizontal detectors. The overall angular distribution of muons at the ground as a function of zenith angle θ is $\propto \cos^2 \theta$, which is characteristic of muons with $E_\mu \sim 3$ GeV. At lower energy the angular distribution becomes increasingly steep, while at higher energy it flattens, approaching a sec θ distribution for $E_\mu \gg \epsilon_\pi$ and $\theta < 70^\circ$.

Figure 30.5 shows the muon energy spectrum at sea level for two angles. At large angles low energy muons decay before reaching the surface and high energy pions decay before they interact, thus the average muon energy increases. An approximate extrapolation formula valid when muon decay is negligible ($E_\mu > 100/\cos \theta$ GeV) and the curvature of the Earth can be neglected ($\theta < 70^\circ$) is

$$\frac{dN_\mu}{dE_\mu d\Omega} \approx \frac{0.14 E_\mu^{-2.7}}{\text{cm}^2 \text{ s sr GeV}} \times \left\{ \frac{1}{1 + \frac{1.1 E_\mu \cos \theta}{115 \text{ GeV}}} + \frac{0.054}{1 + \frac{1.1 E_\mu \cos \theta}{850 \text{ GeV}}} \right\} \quad (30.4)$$

where the two terms give the contribution of pions and charged kaons. Eq. (30.4) neglects a small contribution from charm and heavier flavors which is negligible except at very high energy [64].

The muon charge ratio reflects the excess of π^+ over π^- and K^+ over K^- in the forward fragmentation region of proton initiated interactions together with the fact that there are more free and bound protons than free and bound neutrons in the primary spectrum. The increase with energy of μ^+/μ^- shown in Fig. 30.6 reflects the increasing importance of kaons in the TeV range [65] and indicates a significant contribution of associated production by cosmic-ray protons ($p \rightarrow \Lambda + K^+$). The same process is even more important for atmospheric neutrinos at high energy.

30.3.2 Electromagnetic component

At the ground, this component consists of electrons, positrons, and photons primarily from cascades initiated by decay of neutral and charged mesons. Muon decay is the dominant source of low-energy electrons at sea level. Decay of neutral pions is more important at high altitude or when the energy threshold is high. Knock-on electrons also make a small contribution at low energy [66]. The integral vertical intensity of electrons plus positrons is very approximately 30, 6, and 0.2 m⁻²s⁻¹sr⁻¹ above 10, 100, and 1000 MeV respectively [57, 67], but the exact numbers depend sensitively on altitude, and the angular dependence is complex because of the different altitude dependence of the different sources of electrons [66, 68]. The ratio of photons to electrons plus positrons is approximately 1.3 above 1 GeV and 1.7 below the critical energy [68].

30.3.3 Nucleons

Nucleons above 1 GeV/c at ground level are degraded remnants of the primary cosmic radiation. The intensity is approximately $I_N(E, 0) \times \exp(-X/\cos \theta \Lambda)$ for $\theta < 70^\circ$. At sea level, about 1/3 of the nucleons in the vertical direction are neutrons (up from $\approx 10\%$ at the top of the atmosphere as the n/p ratio approaches equilib-

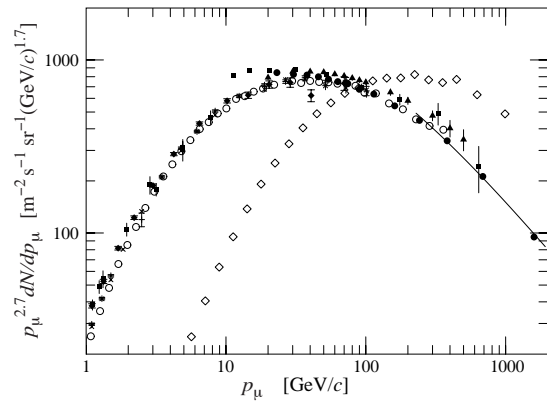


Figure 30.5: Spectrum of muons at $\theta = 0^\circ$ (\diamond [56], \blacksquare [60], \blacktriangledown [61], \blacktriangle [62], \times , $+$ [58], \circ [51], and \bullet [59]) and $\theta = 75^\circ$ \diamond [63]). The line plots the result from Eq. (30.4) for vertical showers.

Table 30.2: Average muon range R and energy loss parameters calculated for standard rock. Range is given in km-water-equivalent, or 10^5 g cm⁻².

E_μ GeV	R km.w.e.	a MeV g ⁻¹ cm ²	b_{brems}	b_{pair}	b_{nucl} 10^{-6} g ⁻¹ cm ²	$\sum b_i$	$\sum b_{\text{ice}}$
10	0.05	2.17	0.70	0.70	0.50	1.90	1.66
100	0.41	2.44	1.10	1.53	0.41	3.04	2.51
1000	2.45	2.68	1.44	2.07	0.41	3.92	3.17
10000	6.09	2.93	1.62	2.27	0.46	4.35	3.78

³When discussing cosmic rays in the atmosphere, ‘primary’ is used to denote the original particle and ‘secondary’ to denote the particles produced in interactions.

rium). The integral intensity of vertical protons above 1 GeV/c at sea level is $\approx 0.9 \text{ m}^{-2}\text{s}^{-1}\text{sr}^{-1}$ [57,69].

30.4 Cosmic Rays Underground

Only muons and neutrinos penetrate to significant depths underground. The muons produce tertiary fluxes of photons, electrons, and hadrons.

30.4.1 Muons

As discussed in Section 34.6 of this *Review*, muons lose energy by ionization and by radiative processes: bremsstrahlung, direct production of e^+e^- pairs, and photonuclear interactions. The total muon energy loss may be expressed as a function of the amount of matter traversed as

$$-\frac{dE_\mu}{dX} = a + bE_\mu \quad (30.5)$$

where a is the ionization loss and b is the fractional energy loss by the three radiation processes. Both are slowly varying functions of energy. The quantity $\epsilon \equiv a/b$ ($\approx 500 \text{ GeV}$ in standard rock) defines a critical energy below which continuous ionization loss is more important than radiative losses. Table 30.2 shows a and b values for standard rock, and b for ice, as a function of muon energy. The second column of Table 30.2 shows the muon range in standard rock ($A = 22$, $Z = 11$, $\rho = 2.65 \text{ g cm}^{-3}$). These parameters are quite sensitive to the chemical composition of the rock, which must be evaluated for each location.

The intensity of muons underground can be estimated from the muon intensity in the atmosphere and their rate of energy loss. To the extent that the mild energy dependence of a and b can be neglected, Eq. (30.5) can be integrated to provide the following relation between the energy $E_{\mu,0}$ of a muon at production in the atmosphere and its average energy E_μ after traversing a thickness X of rock (or ice or water):

$$E_{\mu,0} = (E_\mu + \epsilon)e^{bX} - \epsilon. \quad (30.6)$$

Especially at high energy, however, fluctuations are important and an accurate calculation requires a simulation that accounts for stochastic energy-loss processes [72].

There are two depth regimes for which Eq. (30.6) can be simplified. For $X \ll b^{-1} \approx 2.5 \text{ km}$ water equivalent, $E_{\mu,0} \approx E_\mu(X) + aX$, while for $X \gg b^{-1}$ $E_{\mu,0} \approx (\epsilon + E_\mu(X)) \exp(bX)$. Thus at shallow depths the differential muon energy spectrum is approximately constant for $E_\mu < aX$ and steepens to reflect the surface muon spectrum for $E_\mu > aX$, whereas for $X > 2.5 \text{ km.w.e.}$ the differential spectrum underground is again constant for small muon energies but steepens to reflect the surface muon spectrum

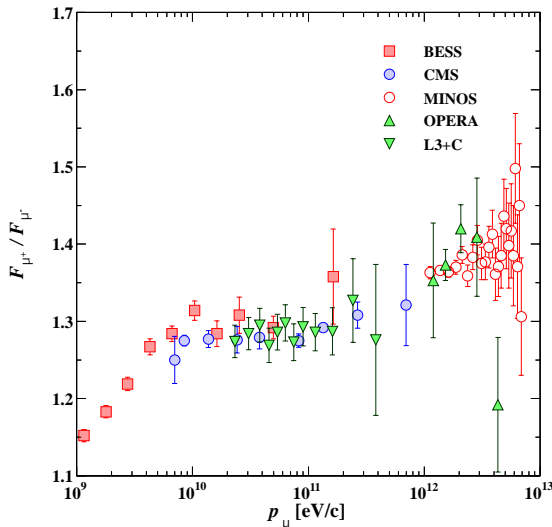


Figure 30.6: Muon charge ratio as a function of the muon momentum from Refs. [51, 59, 65, 70, 71].

for $E_\mu > \epsilon \approx 0.5 \text{ TeV}$. In the deep regime the shape is independent of depth although the intensity decreases exponentially with depth. In general the muon spectrum at slant depth X is

$$\frac{dN_\mu(X)}{dE_\mu} = \frac{dN_\mu}{dE_{\mu,0}} \frac{dE_{\mu,0}}{dE_\mu} = \frac{dN_\mu}{dE_{\mu,0}} e^{bX} \quad (30.7)$$

where $E_{\mu,0}$ is the solution of Eq. (30.6) in the approximation neglecting fluctuations.

Fig. 30.7 shows the vertical muon intensity versus depth. In constructing this “depth-intensity curve,” each group has taken account of the angular distribution of the muons in the atmosphere, the map of the overburden at each detector, and the properties of the local medium in connecting measurements at various slant depths and zenith angles to the vertical intensity. Use of data from a range of angles allows a fixed detector to cover a wide range of depths. The flat portion of the curve is due to muons produced locally by charged-current interactions of ν_μ . The inset shows the vertical intensity curve for water and ice [79–82]. It is not as steep as the one for rock because of the lower muon energy loss in water.

30.4.2 Neutrinos

Because neutrinos have small interaction cross sections, measurements of atmospheric neutrinos require a deep detector to avoid backgrounds. There are two types of measurements: contained (or semi-contained) events, in which the vertex is determined to originate inside the detector, and neutrino-induced muons. The latter are muons that enter the detector from zenith angles so large (*e.g.*, nearly horizontal or upward) that they cannot be muons produced in the atmosphere. In neither case is the neutrino flux measured directly. What is measured is a convolution of the neutrino flux and cross section with the properties

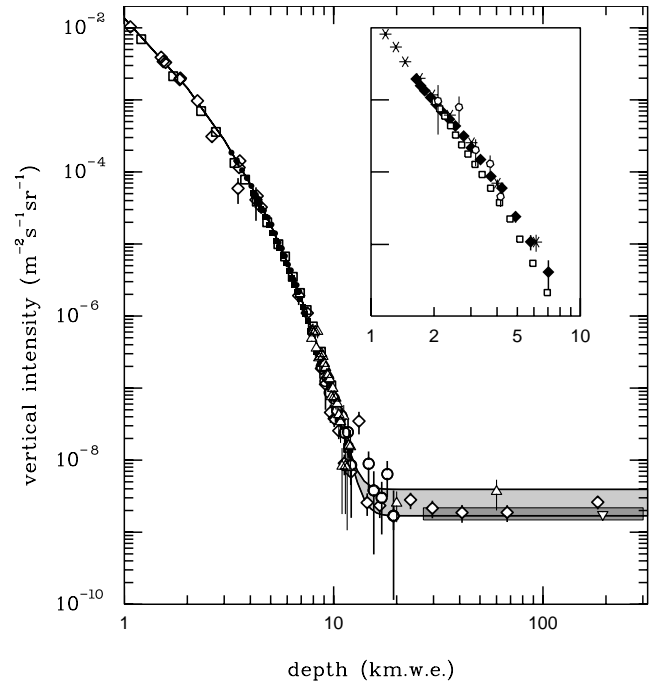


Figure 30.7: Vertical muon intensity vs depth (1 km.w.e. = 10^5 g cm^{-2} of standard rock). The experimental data are from: \diamond : the compilations of Crouch [73], \square : Baksanu [74], \circ : LVD [75], \bullet : MACRO [76], \blacksquare : Frejus [77], and \triangle : SNO [78]. The shaded area at large depths represents neutrino-induced muons of energy above 2 GeV. The upper line is for horizontal neutrino-induced muons, the lower one for vertically upward muons. Darker shading shows the muon flux measured by the SuperKamiokande experiment. The inset shows the vertical intensity curve for water and ice published in Refs. [79–82]. Additional data extending to slant depths of 13 km are available in [83].

Table 30.3: Measured fluxes ($10^{-9} \text{ m}^{-2} \text{ s}^{-1} \text{ sr}^{-1}$) of neutrino-induced muons as a function of the effective minimum muon energy E_μ .

$E_\mu >$	1 GeV	1 GeV	1 GeV	2 GeV	3 GeV	3 GeV
Ref.	CWI [84]	Baksan [85]	MACRO [86, 87]	IMB [88, 89]	Kam [90]	SuperK [91]
F_μ	2.17 ± 0.21	2.77 ± 0.17	2.29 ± 0.15	2.26 ± 0.11	1.94 ± 0.12	1.74 ± 0.07

of the detector (which includes the surrounding medium in the case of entering muons). This section focuses on neutrinos below about 1 TeV. For discussion of atmospheric neutrinos in the TeV–PeV region including a prompt component produced by charmed meson decays, see Ref. [53].

Contained and semi-contained events reflect neutrinos in the sub-GeV to multi-GeV region where the product of increasing cross section and decreasing flux is maximum. In the GeV region the neutrino flux and its angular distribution depend on the geomagnetic location of the detector and, to a lesser extent, on the phase of the solar cycle. Naively, we expect $\nu_\mu/\nu_e = 2$ from counting neutrinos of the two flavors coming from the chain of pion and muon decays. Contrary to expectation, however, the numbers of the two classes of events are similar rather than different by a factor of two. This is now understood to be a consequence of neutrino flavor oscillations [92]. (See the article on neutrino properties in this *Review*.)

Two well-understood properties of atmospheric cosmic rays provide a standard for comparison of the measurements of atmospheric neutrinos to expectation. These are the “sec θ effect” and the “east-west effect” [93]. The former refers originally to the enhancement of the flux of > 10 GeV muons (and neutrinos) at large zenith angles because the parent pions propagate more in the low density upper atmosphere where decay is enhanced relative to interaction. For neutrinos from muon decay, the enhancement near the horizontal becomes important for $E_\nu > 1$ GeV and arises mainly from the increased pathlength through the atmosphere for muon decay in flight. Fig. 14.4 from Ref. [94] shows a comparison between measurement and expectation for the zenith angle dependence of multi-GeV electron-like (mostly ν_e) and muon-like (mostly ν_μ) events separately. The ν_e show an enhancement near the horizontal and approximate equality for nearly upward ($\cos \theta \approx -1$) and nearly downward ($\cos \theta \approx 1$) events. There is, however, a very significant deficit of upward ($\cos \theta < 0$) ν_μ events, which have long pathlengths comparable to the radius of the Earth. This feature is the principal signature for atmospheric neutrino oscillations [92].

Muons that enter the detector from outside after production in charged-current interactions of neutrinos naturally reflect a higher energy portion of the neutrino spectrum than contained events because the muon range increases with energy as well as the cross section. The relevant energy range is $\sim 10 < E_\nu < 1000$ GeV, depending somewhat on angle. Neutrinos in this energy range show a sec θ effect similar to muons (see Eq. (30.4)). This causes the flux of horizontal neutrino-induced muons to be approximately a factor two higher than the vertically upward flux. The upper and lower edges of the horizontal shaded region in Fig. 30.7 correspond to horizontal and vertical intensities of neutrino-induced muons. Table 30.3 gives the measured fluxes of upward-moving neutrino-induced muons averaged over the lower hemisphere. Generally the definition of minimum muon energy depends on where it passes through the detector. The tabulated effective minimum energy estimates the average over various accepted trajectories.

30.5 Air Showers

So far we have discussed inclusive or uncorrelated fluxes of various components of the cosmic radiation. An air shower is caused by a single cosmic ray with energy high enough for its cascade to be detectable at the ground. The shower has a hadronic core, which acts as a collimated source of electromagnetic subshowers, generated mostly from $\pi^0 \rightarrow \gamma\gamma$ decays. The resulting electrons and positrons are the most numerous charged particles in the shower. The number of muons, produced by decays of charged mesons, is an order of magnitude lower. Air showers spread over a large area on the ground, and arrays of detectors operated for long times are useful for studying cosmic rays with primary en-

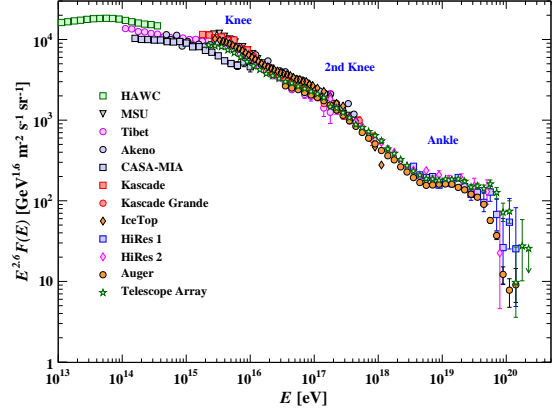


Figure 30.8: The all-particle spectrum as a function of E (energy-per-nucleus) from air shower measurements [95–105]

ergy $E_0 > 100$ TeV, where the low flux makes measurements with small detectors in balloons and satellites difficult.

Greisen [106] gives the following approximate analytic expressions for the numbers and lateral distributions of particles in showers at ground level. The total number of muons N_μ with energies above 1 GeV is

$$N_\mu(> 1\text{GeV}) \approx 0.95 \times 10^5 \left(N_e/10^6 \right)^{3/4}, \quad (30.8)$$

where N_e is the total number of charged particles in the shower (not just e^\pm). The number of muons per square meter, ρ_μ , as a function of the lateral distance r (in meters) from the center of the shower is

$$\rho_\mu = \frac{1.25 N_\mu}{2\pi \Gamma(1.25)} \left(\frac{1}{320} \right)^{1.25} r^{-0.75} \left(1 + \frac{r}{320} \right)^{-2.5}, \quad (30.9)$$

where Γ is the gamma function. The number density of charged particles is

$$\rho_e = C_1(s, d, C_2) x^{(s-2)} (1+x)^{(s-4.5)} (1+C_2 x^d). \quad (30.10)$$

Here s , d , and C_2 are parameters in terms of which the overall normalization constant $C_1(s, d, C_2)$ is given by

$$C_1(s, d, C_2) = \frac{N_e}{2\pi r_1^2} [B(s, 4.5 - 2s) C_2 B(s + d, 4.5 - d - 2s)]^{-1}, \quad (30.11)$$

where $B(m, n)$ is the beta function. The values of the parameters depend on shower size (N_e), depth in the atmosphere, identity of the primary nucleus, etc. For showers with $N_e \approx 10^6$ at sea level, Greisen uses $s = 1.25$, $d = 1$, and $C_2 = 0.088$. Finally, x is r/r_1 , where r_1 is the Molière radius, which depends on the density of the atmosphere and hence on the altitude at which showers are detected. At sea level $r_1 \approx 78$ m. It increases with altitude as the air density decreases. (See the section on electromagnetic cascades in the article on the passage of particles through matter in this *Review*.)

The lateral spread of a shower is determined largely by Coulomb scattering of the many low-energy electrons and is characterized by the Molière radius. The lateral spread of the muons (ρ_μ) is larger and depends on the transverse momenta of the muons at production as well as multiple scattering.

There are large fluctuations in development from shower to shower, even for showers initiated by primaries of the same energy and mass—especially for small showers, which are usually

well past maximum development when observed at the ground. Thus the shower size N_e and primary energy E_0 are only related in an average sense, and even this relation depends on depth in the atmosphere. One estimate of the relation is [98]

$$E_0 \sim 3.9 \times 10^6 \text{ GeV} (N_e/10^6)^{0.9} \quad (30.12)$$

for vertical showers with $10^{14} < E < 10^{17}$ eV at 920 g cm^{-2} (965 m above sea level). As E_0 increases, the shower maximum (on average) moves down into the atmosphere and the relation between N_e and E_0 changes. Moreover, because of fluctuations, N_e as a function of E_0 is not correctly obtained by inverting Eq. (30.12). At the maximum of shower development, there are approximately 2/3 particles per GeV of primary energy.

Cosmic ray shower development is sensitive to hadronic physics in the forward region above energies that can be probed at accelerators. Hadronic interaction models used to interpret air shower measurements now incorporate data from the LHC, reducing the extrapolation required. However, differences between the simulated and observed properties of showers remain. Most notably, the observed muon content of showers near 10^{19} eV exceeds that given by models by 30–60% [107].

There are three common types of air shower detectors: shower arrays that measure a ground parameter related to shower size N_e and muon number N_μ as well as the lateral distribution on the ground, optical Cherenkov and radio detectors that detect forward-beamed emission by the charged particles of the shower, and ‘fluorescence’ detectors that measure nitrogen scintillation excited by the charged particles in the shower. The fluorescence light is emitted isotropically so the showers can be observed from the side. Detection of radiofrequency emission from showers via geomagnetic and Askaryan mechanisms has been successfully employed in recent experiments [108]. Detailed simulations and cross-calibrations between different types of detectors are necessary to establish the primary energy spectrum from air-shower experiments.

Figure 30.8 shows the ‘all-particle’ spectrum. The differential energy spectrum has been multiplied by $E^{2.6}$ in order to display the features of the steep spectrum that are otherwise difficult to discern. The steepening that occurs between 10^{15} and 10^{16} eV is known as the *knee* of the spectrum. Another steepening occurs around 10^{17} eV, known as the *second knee*. The feature around $10^{18.5}$ eV is called the *ankle* of the spectrum.

Air shower experiments typically have uncertain energy scales, dependent on an assumed composition and on the hadronic interaction model used when interpreting the data. Their systematic errors are therefore simplest when plotting $\frac{dN}{d \ln E} = E \frac{dN}{dE}$. When the spectrum is multiplied by a different power of energy, systematic errors in energy scale result in an apparent shift in the normalization of the spectrum; for example, when the spectrum is multiplied by $E^{2.6}$ a systematic shift of 20% in the energy scale results in a 34% change in the normalization of the plotted flux. See Ref. [53], §2.5.2 for further discussion of this issue.

In the energy range above 10^{17} eV, the fluorescence technique [109] is particularly useful because it can establish the primary energy in a nearly model-independent way by observing most of the longitudinal development of each shower, from which E_0 is obtained by integrating the energy deposition in the atmosphere. The result, however, depends strongly on the light absorption in the atmosphere and the calculation of the detector’s aperture.

Assuming the cosmic-ray spectrum below 10^{18} eV is of galactic origin, the knee could indicate that most cosmic accelerators in the Galaxy have reached their maximum energy for acceleration of protons. Some types of expanding supernova remnants, for example, are estimated not to be able to accelerate protons above energies in the range of 10^{15} eV. Effects of propagation and confinement in the Galaxy [110] also need to be considered. A discussion of models of the knee may be found in Ref. [111].

The second knee may have a similar origin to the knee, but corresponding to steepening of the spectrum of heavy nuclei, particularly iron. The Cascade-Grande experiment has reported observation of a second steepening of the spectrum near 8×10^{16} eV, with evidence that this structure is accompanied by a transition to

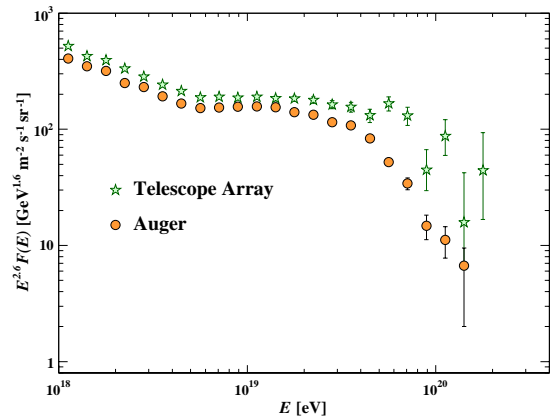


Figure 30.9: Expanded view of the highest energy portion of the cosmic-ray spectrum from data of the Pierre Auger Observatory [104] and the Telescope Array [105].

electron-poor showers resulting from heavy primaries [101]. Cascade Grande has also reported that the spectrum of light nuclei is steeper than the all-particle spectrum below the second knee and flattens in the vicinity of the second knee [112]. IceCube has performed a composition analysis using coincident surface (Ice-Top) and in-ice data, and finds that the mean logarithmic mass increases between 5×10^{15} eV and 10^{17} eV [113]. Together, these data are suggestive that the knee and second knee may result from a *Peters cycle*, with a steepening of the spectrum of each primary element taking place at the same rigidity but different energy per particle [114].

The Auger and Telescope Array (TA) experiments have studied composition using the depth of shower maximum X_{max} , a quantity that correlates strongly with $\ln(E/A)$ and with the interaction cross section of the primary particle. The Auger collaboration [115], using a post-LHC hadronic interaction model, reports a composition becoming light up to 2×10^{18} eV but then becoming heavier above that energy, with the mean mass intermediate between protons and iron at 3×10^{19} eV. The TA collaboration [116], using a different post-LHC model, has interpreted their data as implying a light primary composition (mainly p and He) of ultrahigh-energy cosmic-rays (UHECR) from 1.3×10^{18} to 4×10^{19} eV. Auger and TA have also conducted a thorough joint analysis [117] and state that, at the current level of statistics and understanding of systematics, both data sets are compatible with being drawn from the same parent distribution, and that the TA data is compatible both with a light composition below 10^{19} eV and with the mixed composition above 10^{19} eV as reported by Auger.

Possible contributions to the origin of the ankle include a higher energy population of particles overtaking a lower energy population, for example an extragalactic flux beginning to dominate over the Galactic flux (e.g. Ref. [109]). Another proposed mechanism is that the dip structure in the region of the ankle is due to $p\gamma \rightarrow e^+ + e^-$ energy losses of extragalactic protons on the 2.7 K cosmic microwave radiation (CMB) [118].

If the cosmic-ray flux at the highest energies is extragalactic in origin, there should be a rapid steepening of the spectrum (called the GZK feature) around 5×10^{19} eV, resulting from the onset of inelastic interactions of UHE cosmic rays with the cosmic microwave background [119] [120]. Photo-dissociation of heavy nuclei in the mixed composition model [121] would have a similar effect. UHECR experiments have detected events of energy above 10^{20} eV [109, 122]. The HiRes fluorescence experiment [103, 123] detected evidence of a suppression consistent with the GZK effect, and the Auger observatory [104] has also presented spectra showing this suppression based on surface detector measurements calibrated against fluorescence detectors using events detected in hybrid mode, i.e. with both the surface and the fluorescence detectors. The Telescope Array (TA) [105] has also presented a spectrum showing this suppression. The differential energy spec-

tra measured by the TA and by Auger agree within systematic errors below 10^{19} eV (Fig. 30.9).

Cosmic rays above 5×10^{19} eV are predominantly from nearby sources (< 100 Mpc). Auger has reported the observation of a dipole of amplitude $6.6^{+1.2}_{-0.8}\%$ for cosmic rays with energies above 8×10^{18} eV. The direction of the dipole indicates an extragalactic origin for these particles [124]. There are also hints of structure at smaller angular scales. TA has reported a ‘hot spot’ in the Northern Hemisphere at energies above 5.5×10^{19} eV of radius $\sim 25^\circ$ with a chance probability of this excess with respect to an isotropic distribution of 2.1×10^{-3} [125]. Auger has also reported an excess of events above 3.7×10^{19} eV in a region near the radio-loud active galaxy Centaurus A with a post-trial significance of 3.9σ , and a correlation of the distribution of ultrahigh energy events with several catalogs of nearby astrophysical objects, with starburst galaxies giving the highest significance at 4.5σ [126].

30.6 Neutrinos at High Energies

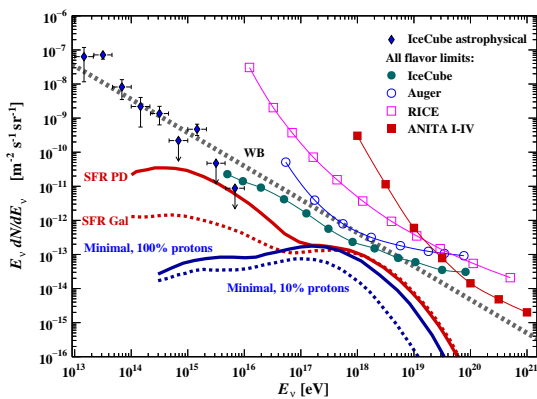


Figure 30.10: The best-fit IceCube *astrophysical* all-flavor neutrino flux [127]. Also shown are differential limits on the flux of *cosmogenic* neutrinos set by four experiments [128–131]. The IceCube limit on cosmogenic neutrinos accounts for a nuisance background of astrophysical neutrinos. The curves show the Waxman-Bahcall benchmark flux (solid grey) [132, 133], cosmogenic models with cosmic ray sources with maximum proton energy of $10^{20.5}$ eV evolving with the star-formation rate in proton dip (solid red) and Galactic composition (dashed red) scenarios [134], and ‘minimal’ cosmogenic models with protons constituting 100% (solid blue) and 10% (dashed red) of the cosmic rays [135].

Neutrinos are expected to be produced in hadronic interactions in a variety of astrophysical objects. IceCube has reported a population of astrophysical neutrino events extending from tens of TeV to beyond ten PeV [127, 136, 137]. Multimessenger observations of the flaring blazar TXS 0506+056 have identified this object as a high-energy neutrino source [138, 139].

There is also expected to be a neutrino flux produced in cosmic ray GZK interactions. Measuring this *cosmogenic*⁴ neutrino flux above 10^{18} eV would help resolve the UHECR uncertainties mentioned above. One half of the energy that UHECR protons lose in photoproduction interactions that cause the GZK effects ends up in neutrinos [140]. Heavier nuclei produce lower energy neutrinos due to the lower energy of their constituent nucleons. The magnitude of the cosmogenic neutrino flux depends strongly on the cosmic-ray spectrum at acceleration, the cosmic-ray composition, the cosmological evolution of the cosmic-ray sources, and the energy of the Galactic-extragalactic transition.

The expected rate of cosmogenic neutrinos is lower than current limits obtained by IceCube [127], the Auger observatory [130], RICE [129, 141], and ANITA [131], which are shown in Fig. 30.10 together with a models for cosmogenic neutrino production [134, 135] and the Waxman-Bahcall benchmark flux of

neutrinos produced in cosmic ray sources [132, 133]. At production, the dominant component of neutrinos comes from π^\pm decays and has flavor content $\nu_e:\nu_\mu:\nu_\tau = 1:2:0$. After oscillations, the arriving cosmogenic neutrinos are expected to be a 1:1:1 mixture of flavors. The sensitivity of each experiment depends on neutrino flavor, and all limits are expressed as three-flavor limits assuming a 1:1:1 mixture.

References

- [1] O. Adriani *et al.* (PAMELA), *Science* **332**, 69 (2011).
- [2] M. Aguilar *et al.* (AMS), *Phys. Rev. Lett.* **114**, 171103 (2015).
- [3] M. Aguilar *et al.* (AMS), *Phys. Rev. Lett.* **115**, 21, 211101 (2015).
- [4] K. Abe *et al.*, *Astrophys. J.* **822**, 2, 65 (2016).
- [5] M. J. Christ *et al.*, *Astrophys. J.* **502**, 278 (1998).
- [6] A.D. Panov *et al.* (ATIC Collab.), *Bull. Russian Acad. of Science, Physics*, **73**, 564 (2009).
- [7] V. A. Derbina *et al.* (RUNJOB), *Astrophys. J.* **628**, L41 (2005).
- [8] H. S. Ahn *et al.*, *Astrophys. J.* **707**, 593 (2009).
- [9] J.J. Engelmann *et al.* (HEAO3-C2 Collab.), *Astron. & Astrophys.* **233**, 96 (1990).
- [10] D. Müller *et al.* (CRN Collab.), *Astrophys. J.* **374**, 356 (1991).
- [11] M. Ave *et al.*, *Astrophys. J.* **678**, 262 (2008).
- [12] F. Aharonian *et al.* (H.E.S.S.), *Phys. Rev.* **D75**, 042004 (2007).
- [13] A. Archer *et al.* (VERITAS), *Phys. Rev.* **D98**, 2, 022009 (2018).
- [14] D. Maurin *et al.*, *Astron. & Astrophys.* **569**, A32 (2014).
- [15] A. W. Strong, I. V. Moskalenko and V. S. Ptuskin, *Ann. Rev. Nucl. Part. Sci.* **57**, 285 (2007).
- [16] R.A. Mewaldt *et al.*, *Space Science Reviews* 99,27(2001).
- [17] A. A. Abdo *et al.*, *Astrophys. J.* **698**, 2121 (2009).
- [18] A. U. Abeysekera *et al.* (HAWC, IceCube), *Astrophys. J.* **871**, 1, 96 (2019).
- [19] M. Amenomori *et al.*, *Astrophys. J.* **711**, 119 (2010).
- [20] O. Adriani *et al.* (PAMELA), *Phys. Rev. Lett.* **106**, 201101 (2011).
- [21] M. Boezio *et al.*, *Astrophys. J.* **532**, 653 (2000).
- [22] M. Aguilar *et al.* (AMS), *Phys. Rev. Lett.* **122**, 10, 101101 (2019).
- [23] S. Abdollahi *et al.* (Fermi-LAT), *Phys. Rev.* **D95**, 8, 082007 (2017).
- [24] G. Ambrosi *et al.* (DAMPE), *Nature* **552**, 63 (2017).
- [25] O. Adriani *et al.* (CALET), *Phys. Rev. Lett.* **122**, 18, 181102 (2019).
- [26] F. Aharonian *et al.* (H.E.S.S.), *Phys. Rev. Lett.* **101**, 261104 (2008).
- [27] F. Aharonian *et al.* (H.E.S.S.), *Astron. Astrophys.* **508**, 561 (2009).
- [28] A. Archer *et al.* (VERITAS), *Phys. Rev.* **D98**, 6, 062004 (2018).
- [29] Y. Shikaze *et al.*, *Astropart. Phys.* **28**, 154 (2007).
- [30] O. Adriani *et al.* (PAMELA), *Nature* **458**, 607 (2009).
- [31] O. Adriani *et al.*, *Phys. Rev. Lett.* **102**, 051101 (2009).
- [32] J.J. Beatty *et al.*, *Phys. Rev. Lett.* **93**, 24112 (2004).
- [33] I. V. Moskalenko and A. W. Strong, *Astrophys. J.* **493**, 694 (1998).
- [34] A. Ibarra, D. Tran and C. Weniger, *Int. J. Mod. Phys.* **A28**, 1330040 (2013).
- [35] D. Gaggero *et al.*, *Phys. Rev. Lett.* **111**, 021102 (2013).

⁴Here we use cosmogenic to denote neutrinos produced by photoproduction during propagation, and astrophysical to denote neutrinos produced by other mechanisms or close to sources.

- [36] P.-F. Yin *et al.*, Phys. Rev. **D88**, 2, 023001 (2013).
- [37] M. Aguilar *et al.* (AMS), Phys. Rev. Lett. **110**, 141102 (2013).
- [38] L. Accardo *et al.* (AMS), Phys. Rev. Lett. **113**, 121101 (2014).
- [39] J. Nishimura *et al.*, Adv. Space Research **19**, 767 (1997).
- [40] A. S. Beach *et al.*, Phys. Rev. Lett. **87**, 271101 (2001).
- [41] A. Yamamoto *et al.*, Adv. Space Research **42**, 443(2008).
- [42] Y. Asaoka *et al.*, Phys. Rev. Lett. **88**, 51101 (2002).
- [43] K. Abe *et al.*, Phys. Rev. Lett. **108**, 131301 (2012).
- [44] H. Fuke *et al.*, Phys. Rev. Lett. **95**, 081101 (2005).
- [45] I. Cholis, D. Hooper and T. Linden, Phys. Rev. **D93**, 4, 043016 (2016).
- [46] R. Bellotti *et al.*, Phys. Rev. **D53**, 35 (1996).
- [47] R. Bellotti *et al.* (WiZard/MAS2), Phys. Rev. **D60**, 052002 (1999).
- [48] M. Boezio *et al.* (WiZard/CAPRICE), Phys. Rev. **D62**, 032007 (2000).
- [49] M. Boezio *et al.*, Phys. Rev. **D67**, 072003 (2003).
- [50] S. Coutu *et al.*, Phys. Rev. **D62**, 032001 (2000).
- [51] S. Haino *et al.*, Phys. Lett. **B594**, 35 (2004).
- [52] T. Sanuki *et al.*, Phys. Rev. **D75**, 043005 (2007).
- [53] T.K. Gaisser, R. Engel, and E. Resconi, *Cosmic Rays and Particle Physics (second edition)*, Cambridge University Press (2016).
- [54] P. Lipari, Astropart. Phys. **1**, 195 (1993).
- [55] E. Mocchiutti *et al.*, in *Proc. 28th Int. Cosmic Ray Conf.*, Tsukuba, 1627 (2003). [<http://adsabs.harvard.edu/abs/2003ICRC...3.1627M>].
- [56] M. P. De Pascale *et al.*, J. Geophys. Res. **98**, A3, 3501 (1993).
- [57] P.K.F. Grieder, *Cosmic Rays at Earth*, Elsevier Science (2001).
- [58] J. Kremer *et al.*, Phys. Rev. Lett. **83**, 4241 (1999).
- [59] P. Achard *et al.* (L3), Phys. Lett. **B598**, 15 (2004).
- [60] O. C. Allkofer, K. Carstensen and D. W. Dau, Phys. Lett. **36B**, 425 (1971).
- [61] B. C. Rastin, J. Phys. **G10**, 1609 (1984).
- [62] C. A. Ayre *et al.*, J. Phys. **G1**, 584 (1975).
- [63] H. Jokisch *et al.*, Phys. Rev. **D19**, 1368 (1979).
- [64] C. G. S. Costa, Astropart. Phys. **16**, 193 (2001).
- [65] P. Adamson *et al.* (MINOS), Phys. Rev. **D76**, 052003 (2007).
- [66] S. Hayakawa, *Cosmic Ray Physics*, Wiley, Interscience, New York (1969).
- [67] R.R. Daniel and S.A. Stephens, Revs. Geophysics & Space Sci. **12**, 233 (1974).
- [68] K.P. Beuermann and G. Wibberenz, Can. J. Phys. **46**, S1034 (1968).
- [69] I. S. Diggory *et al.*, J. Phys. **A7**, 741 (1974).
- [70] V. Khachatryan *et al.* (CMS), Phys. Lett. **B692**, 83 (2010).
- [71] N. Agafonova *et al.* (OPERA), Eur. Phys. J. **C67**, 25 (2010).
- [72] P. Lipari and T. Stanev, Phys. Rev. **D44**, 3543 (1991).
- [73] M. Crouch, in *Proc. 20th Int. Cosmic Ray Conf.*, Moscow, **6**, 165 (1987) [<http://adsabs.harvard.edu/abs/1987ICRC...6..165C>].
- [74] Yu.M. Andreev, V.I. Gurentzov, and I.M. Kogai, in *Proc. 20th Int. Cosmic Ray Conf.*, Moscow, **6**, 200 (1987), [<http://adsabs.harvard.edu/abs/1987ICRC...6..200A>].
- [75] M. Aglietta *et al.* (LVD), Astropart. Phys. **3**, 311 (1995).
- [76] M. Ambrosio *et al.* (MACRO), Phys. Rev. **D52**, 3793 (1995).
- [77] C. Berger *et al.* (FREJUS), Phys. Rev. **D40**, 2163 (1989).
- [78] C. Waltham *et al.*, in *Proc. 27th Int. Cosmic Ray Conf.*, Hamburg, 991 (2001), [<http://adsabs.harvard.edu/abs/2001ICRC...3..991W>].
- [79] I. A. Belolaptikov *et al.* (BAIKAL), Astropart. Phys. **7**, 263 (1997).
- [80] J. Babson *et al.* (DUMAND), Phys. Rev. **D42**, 3613 (1990).
- [81] P. Desiati *et al.*, in *Proc. 28th Int. Cosmic Ray Conf.*, Tsukuba, 1373 (2003) [<http://adsabs.harvard.edu/abs/2003ICRC...3.1373D>].
- [82] T. Pradier (ANTARES), in "Proceedings, 43rd Rencontres de Moriond on Electroweak Interactions and Unified Theories: La Thuile, Italy, March 1-8, 2008," 423-430 (2008).
- [83] S. Aiello *et al.* (NEMO), Astropart. Phys. **66**, 1 (2015).
- [84] F. Reines *et al.*, Phys. Rev. Lett. **15**, 429 (1965).
- [85] M.M. Boliev *et al.*, in *Proc. 3rd Int. Workshop on Neutrino Telescopes* (ed. Milla Baldo Ceolin), 235 (1991).
- [86] M. Ambrosio *et al.* (MACRO), Phys. Lett. **B434**, 451 (1998).
- [87] F. Ronga (MACRO), in "Proceedings, 26th International Cosmic Ray Conference (ICRC), August 17-25, 1999, Salt Lake City: Invited, Rapporteur, and Highlight Papers," volume 2, 172 (1999), URL http://krusty.physics.utah.edu/~icrc1999/root/vol2/h4_1_07.pdf.
- [88] R. Becker-Szendy *et al.*, Phys. Rev. Lett. **69**, 1010 (1992).
- [89] *Proc. 25th Int. Conf. High-Energy Physics*, Singapore (eds. K.K. Phua and Y. Yamaguchi, World Scientific), 662 1991.
- [90] S. Hatakeyama *et al.* (Kamiokande), Phys. Rev. Lett. **81**, 2016 (1998).
- [91] Y. Fukuda *et al.* (Super-Kamiokande), Phys. Rev. Lett. **82**, 2644 (1999).
- [92] Y. Fukuda *et al.* (Super-Kamiokande), Phys. Rev. Lett. **81**, 1562 (1998).
- [93] T. Futagami *et al.* (Super-Kamiokande), Phys. Rev. Lett. **82**, 5194 (1999).
- [94] Y. Ashie *et al.* (Super-Kamiokande), Phys. Rev. **D71**, 112005 (2005).
- [95] R. Alfaro *et al.* (HAWC), Phys. Rev. **D96**, 12, 122001 (2017).
- [96] Yu. A. Fomin *et al.*, *Proc. 22nd Int. Cosmic Ray Conf.*, Dublin, **2**, 85 (1991) [<http://adsabs.harvard.edu/abs/1991ICRC...2..85F>].
- [97] M. Amenomori *et al.*, Astrophys. J. **268**, 1165 (2008).
- [98] M. Nagano *et al.*, J. Phys. **G10**, 1295 (1984).
- [99] M. A. K. Glasmacher *et al.*, Astropart. Phys. **10**, 291 (1999).
- [100] T. Antoni *et al.* (KASCADE), Astropart. Phys. **24**, 1 (2005).
- [101] W. D. Apel *et al.* (KASCADE Grande), Phys. Rev. Lett. **107**, 171104 (2011).
- [102] K. Andeen, M. Plum *et al.*, (IceCube Collab.), *Proceedings of Science (ICRC2019)*, 172 (2019).
- [103] R. U. Abbasi *et al.* (HiRes), Phys. Rev. Lett. **100**, 101101 (2008).
- [104] V. Verzi *et al.*, (Auger Collab.), *Proceedings of Science (ICRC2019)*, 450 (2019).
- [105] D. Ivanov *et al.*, (Telescope Array Collab.), *Proceedings of Science (ICRC2019)*, 298 (2019).
- [106] K. Greisen, Ann. Rev. Nucl. Sci. **10**, 63 (1960).
- [107] A. Aab *et al.* (Pierre Auger), Phys. Rev. Lett. **117**, 19, 192001 (2016).
- [108] T. Huege, Phys. Rept. **620**, 1 (2016).

- [109] D. J. Bird *et al.* (HiRes), *Astrophys. J.* **424**, 491 (1994).
- [110] V.S. Ptuskin *et al.*, *Astron. & Astrophys.* **268**, 726 (1993).
- [111] J. R. Hoerandel, *Astropart. Phys.* **21**, 241 (2004).
- [112] W. D. Apel *et al.*, *Phys. Rev.* **D87**, 081101 (2013), [arXiv:1304.7114].
- [113] M. G. Aartsen *et al.* (IceCube) (2019), [arXiv:1906.04317].
- [114] B. Peters, *Nuovo Cimento* **XXII**, 800 (1961).
- [115] J. Bellido *et al.* (Auger Collab.), *Proceedings of Science(ICRC2017)*, 506 (2017).
- [116] D. Ikeda *et al.* (TA Collab.), *Proceedings of Science(ICRC2017)*, 515 (2017).
- [117] V. de Souza *et al.* (TA and Auger Collabs.), *Proceedings of Science(ICRC2017)*, 522 (2017).
- [118] V. Berezhinsky, A. Z. Gazizov and S. I. Grigorieva, *Phys. Rev.* **D74**, 043005 (2006).
- [119] K. Greisen, *Phys. Rev. Lett.* **16**, 748 (1966).
- [120] G. T. Zatsepin and V. A. Kuzmin, *JETP Lett.* **4**, 78 (1966), [*Pisma Zh. Eksp. Teor. Fiz.*4,114(1966)].
- [121] D. Allard *et al.*, *Astron. & Astrophys.* **443**, L29 (2005).
- [122] M. Takeda *et al.*, *Astropart. Phys.* **19**, 447 (2003).
- [123] R. U. Abbasi *et al.* (HiRes), *Astropart. Phys.* **32**, 53 (2009).
- [124] E. Roulet *et al.*, (Auger Collab.), *Proceedings of Science (ICRC2019)*, 408 (2019).
- [125] K. Kawata *et al.*, (Telescope Array Collab.), *Proceedings of Science (ICRC2019)*, 310 (2019).
- [126] L. Caccianiga *et al.*, (Auger Collab.), *Proceedings of Science (ICRC2019)*, 206 (2019).
- [127] M. G. Aartsen *et al.* (IceCube), *Astrophys. J.* **809**, 1, 98 (2015).
- [128] M. G. Aartsen *et al.* (IceCube), *Phys. Rev.* **D98**, 6, 062003 (2018).
- [129] I. Kravchenko *et al.*, *Phys. Rev.* **D85**, 062004 (2012).
- [130] F. Pedrera *et al.*, (Auger Collab.), *Proceedings of Science (ICRC2019)*, 172 (2019).
- [131] C. Deaconu *et al.*, (ANITA Collab.), *Proceedings of Science (ICRC2019)*, 867 (2019).
- [132] E. Waxman and J. N. Bahcall, *Phys. Rev.* **D59**, 023002 (1999).
- [133] E. Waxman, 33–45 (2017).
- [134] K. Kotera, D. Allard and A. V. Olinto, *JCAP* **1010**, 013 (2010).
- [135] M. Ahlers and F. Halzen, *Phys. Rev.* **D86**, 083010 (2012).
- [136] M. G. Aartsen *et al.* (IceCube), *Science* **342**, 1242856 (2013).
- [137] M. G. Aartsen *et al.* (IceCube), *Phys. Rev. Lett.* **113**, 101101 (2014).
- [138] M. G. Aartsen *et al.* (IceCube, Fermi-LAT, MAGIC, AGILE, ASAS-SN, HAWC, H.E.S.S., INTEGRAL, Kanata, Kiso, Kapteyn, Liverpool Telescope, Subaru, Swift NuSTAR, VERITAS, VLA/17B-403), *Science* **361**, eaat1378 (2018).
- [139] M. G. Aartsen *et al.* (IceCube), *Science* **361**, 6398, 147 (2018).
- [140] V. S. Berezhinsky and G. T. Zatsepin, *Phys. Lett.* **28B**, 423 (1969).
- [141] I. Kravchenko *et al.*, *Phys. Rev.* **D73**, 082002 (2006).

Experimental Methods and Colliders

31. Accelerator physics of colliders (rev.)	521
32. High-energy collider parameters (rev.)	529
33. Neutrino beam lines at high-energy proton synchrotrons (rev.)	534
34. Passage of particles through matter (rev.)	535
35. Particle detectors at accelerators (rev.)	551
36. Particle detectors for non-accelerator phys. (rev.)	589
37. Radioactivity and radiation protection (rev.)	612
38. Commonly used radioactive sources (rev.)	618

31. Accelerator Physics of Colliders

Revised August 2019 by M.J. Syphers (Northern Illinois U.; FNAL) and F. Zimmermann (CERN).

This article provides background for the High-Energy Collider Parameter Tables that follow and some additional information.

31.1 Luminosity

The number of events, N_{exp} , is the product of the cross section of interest, σ_{exp} , and the time integral over the instantaneous luminosity, \mathcal{L} :

$$N_{exp} = \sigma_{exp} \times \int \mathcal{L}(t) dt. \quad (31.1)$$

Today's colliders all employ bunched beams. If two bunches containing n_1 and n_2 particles collide head-on with average collision frequency f_{coll} , a basic expression for the luminosity is

$$\mathcal{L} = f_{coll} \frac{n_1 n_2}{4\pi \sigma_x^* \sigma_y^*} \mathcal{F} \quad (31.2)$$

where σ_x^* and σ_y^* characterize the rms transverse beam sizes in the horizontal (bend) and vertical directions at the interaction point, and \mathcal{F} is a factor of order 1, that takes into account geometric effects such as a crossing angle and finite bunch length, and dynamic effects, such as the mutual focusing of the two beam during the collision. For a circular collider, f_{coll} equals the number of bunches per beam times the revolution frequency. In 31.2, it is assumed that the bunches are identical in transverse profile, that the profiles are Gaussian and independent of position along the bunch, and the particle distributions are not altered during bunch crossing. Nonzero beam crossing angles θ_c in the horizontal plane and long bunches (rms bunch length σ_z) will reduce the luminosity, e.g., by a factor $\mathcal{F} \approx 1/(1 + \phi^2)^{1/2}$, where the parameter $\phi \equiv \theta_c \sigma_z / (2\sigma_x^*)$ is known as the Piwinski angle. Another luminosity reduction for long bunches is due to the "hourglass" effect (see below).

Whatever the distribution at the source, by the time the beam reaches high energy, the normal form is a useful approximation as suggested by the σ -notation. In the case of an electron storage ring, synchrotron radiation leads to a Gaussian distribution in equilibrium, but even in the absence of radiation the central limit theorem of probability and the diminished importance of space charge effects produce a similar result. Beam tails are often modelled by the superposition of a second Gaussian distribution with larger size and much lower intensity.

The luminosity may be obtained directly by measurement of the beam properties in Eq. 31.2. For continuous measurements, an expression similar to Eq. 31.1 with N_{ref} from a known reference cross section, σ_{ref} , may be used to determine σ_{exp} according to $\sigma_{exp} = (N_{exp}/N_{ref})\sigma_{ref}$.

In the Tables, luminosity is stated in units of $\text{cm}^{-2}\text{s}^{-1}$. Integrated luminosity, on the other hand, is usually quoted as the inverse of the standard measures of cross section such as femtobarns and, recently, attobarns. Subsequent sections in this report briefly expand on the dynamics behind collider design, comment on the realization of collider performance in a selection of today's facilities, and end with some remarks on future possibilities.

31.2 Beam Dynamics

The first concern of beam dynamics is stability. While a reference particle proceeds along the design, or reference, trajectory other particles in the bunch are to remain close by. Assume that the reference particle carries a right-handed Cartesian coordinate system, with the z -coordinate pointed in the direction of motion along the reference trajectory. The right-handed coordinate system would indicate the reference particle to travel clockwise around a storage ring. The independent variable is the distance s of the reference particle along this trajectory rather than time, and for simplicity this path is taken to be planar. The transverse coordinates are x and y , where $\{x, z\}$ defines the plane of the reference trajectory.

Several time scales are involved, and the approximations used in writing the equations of motion reflect that circumstance. All of today's high energy colliders are alternating-gradient synchrotrons

or, respectively, storage rings [1,2], and the shortest time scale is that associated with transverse motion, that is described in terms of betatron oscillations, so called because of their analysis for the betatron accelerator species years ago. The linearized equations of motion of a particle displaced from the reference particle are

$$\begin{aligned} x'' + K_x x &= 0, & K_x &\equiv \frac{q}{p} \frac{\partial B}{\partial x} + \frac{1}{\rho^2} \\ y'' + K_y y &= 0, & K_y &\equiv -\frac{q}{p} \frac{\partial B}{\partial x} \\ z' &= -x/\rho \end{aligned} \quad (31.3)$$

where the magnetic field $B(s)$ along the design trajectory is only in the y direction, contains only dipole and quadrupole terms, and is treated as static here. The radius of curvature due to the field on the reference orbit is ρ ; z represents the longitudinal distance from the reference particle; p and q are the particle's momentum and charge, respectively. The prime denotes d/ds . The pair (x, x') describes approximately-canonical variables. For more general cases (e.g. acceleration) one should use (x, p_x) instead, where p_x denotes the transverse momentum in the x -direction.

The equations for x and y are those of harmonic oscillators but with a restoring force periodic in s ; that is, they are instances of Hill's equation. The solution may be written in the form

$$x(s) = A_x \sqrt{\beta_x} \cos \psi_x \quad (31.4)$$

$$x'(s) = -\frac{A_x}{\sqrt{\beta_x}} [\alpha_x \cos \psi_x + \sin \psi_x] \quad (31.5)$$

where A_x is a constant of integration, $\alpha_x \equiv -(1/2)d\beta_x(s)/ds$, and the envelope of the motion is modulated by the *amplitude function*, β_x . A solution of the same form describes the motion in y . The subscripts will be suppressed in the following discussion.

The amplitude function satisfies

$$2\beta\beta'' - \beta'^2 + 4\beta^2 K = 4, \quad (31.6)$$

and in a region free of magnetic field it should be noted that the solution of Eq. 31.6 is a parabola. Expressing A in terms of x , x' yields

$$\begin{aligned} A^2 &= \gamma x^2 + 2\alpha x x' + \beta x'^2 \\ &= \frac{1}{\beta} [x^2 + (\alpha x + \beta x')^2] \end{aligned} \quad (31.7)$$

with $\gamma \equiv (1 + \alpha^2)/\beta$. In a single pass system such as a linac, the *Courant-Snyder parameters* α , β , γ may be selected to match the x , x' distribution of the input beam; in a recursive system, the parameters are usually defined by the structure rather than by the beam.

The relationships between the parameters and the structure may be seen by treatment of a simple *lattice* consisting of equally-spaced thin-lens quadrupoles whose magnetic-field gradients are equal in magnitude but alternating in sign. For this discussion, the weak focusing effects of the bending magnets may be neglected. The propagation of $X \equiv \{x, x'\}$ through a repetition period may be written $X_2 = MX_1$, with the matrix $M = FODO$ composed of the matrices

$$F = \begin{pmatrix} 1 & 0 \\ -1/f & 1 \end{pmatrix}, \quad D = \begin{pmatrix} 1 & 0 \\ 1/f & 1 \end{pmatrix}, \quad O = \begin{pmatrix} 1 & L \\ 0 & 1 \end{pmatrix}, \quad (31.8)$$

where f is the magnitude of the focal length and L the lens spacing. Then

$$M = \begin{pmatrix} 1 + \frac{L}{f} & 2L + \frac{L^2}{f} \\ -\frac{L}{f^2} & 1 - \frac{L}{f} - \frac{L^2}{f^2} \end{pmatrix}. \quad (31.9)$$

The matrix for y is identical in form differing only by a change in sign of the terms linear in $1/f$. An eigenvector-eigenvalue analysis of the matrix M shows that the motion is stable provided $f > L/2$. While that criterion is easily met, in practice instability may be caused by many other factors, including the beam-beam interaction.

Standard focus-drift-defocus-drift, or *FODO*, cells such as characterized in simple form by Eq. 31.9 occupy most of the layout of

a large collider ring and may be used to set the scale of the amplitude function and related phase advance. Conversion of Eq. 31.4 to a matrix form equivalent to Eq. 31.9 (but more generally valid, i.e. for any stable periodic linear motion) gives

$$M = \begin{pmatrix} C + \alpha S & \beta S \\ -\gamma S & C - \alpha S \end{pmatrix} \quad (31.10)$$

where $C \equiv \cos \Delta\psi$, $S \equiv \sin \Delta\psi$, and the relation between structure and amplitude function is specified by setting the values of the latter to be the same at both ends of the cell. By comparison of Eq. 31.9 and Eq. 31.10 one finds $C = 1 - L^2/(2f^2)$, so that the choice $f = L/\sqrt{2}$ would give a phase advance $\Delta\psi$ of 90 degrees for the standard cell. The amplitude function would have a maximum at the focusing quadrupole of magnitude $\hat{\beta} = 2.7L$, illustrating the relationship of alternating gradient focusing amplitudes to relatively local aspects of the design. Other functionalities such as injection, extraction, and HEP experiments are included by lattice sections matched to the standard cell parameters (β , α) at the insertion points.

The phase advances according to $d\psi/ds = 1/\beta$; that is, β also plays the role of a local $\lambda/2\pi$, and the *tune*, ν , is the number of such oscillations per turn about the closed path. In the neighborhood of an interaction point (IP), the beam optics of the ring is configured so as to produce a narrow focus; the value of the amplitude function at this point is designated β^* .

The motion as it develops with s describes an ellipse in $\{x, x' \equiv dx/ds\}$ phase space, the area of which is πA^2 , where A is the constant in Eq. 31.4. If the interior of that ellipse is populated by an ensemble of non-interacting particles, that area, given the name *emittance* and denoted by ε , would change only with energy. More precisely, for a beam with a Gaussian distribution in x, x' , the area containing one standard deviation σ_x , divided by π , is used as the definition of emittance in the Tables:

$$\varepsilon_x \equiv \frac{\sigma_x^2}{\beta_x}, \quad (31.11)$$

with a corresponding expression in the other transverse direction, y . For most of the entries in the Tables the standard deviation is used as the beam radius.

At larger transverse amplitudes, due to the influence of nonlinear magnetic fields, the particle motion does not remain linear. Nonlinear fields arise, e.g., from the sextupole magnets deployed to correct the chromaticity (i.e., the change of focusing with particle momentum), or from persistent-current field errors in the superconducting magnets of hadron synchrotrons. At a certain amplitude the nonlinear particle motion ceases to be stable, and particles are lost after circulating for a possibly large number of turns. This limit of stability is called the “dynamic aperture”.

To complete the coordinates used to describe the particle motion, and to characterize the longitudinal behavior, we take as the variable conjugate to z the fractional momentum deviation $\delta p/p$ from that of the reference particle. Radiofrequency electric fields in the s direction provide a means for longitudinal oscillations, and the frequency determines the bunch length. The frequency of this system appears in the Tables as does the rms value of $\delta p/p$ characterized as “energy spread” of the beam.

For HEP bunch length is a significant quantity for a variety of reasons, but in the present context if the bunch length, or (with nonzero crossing angle) the effective interaction length, becomes larger than β^* the luminosity is adversely affected. This is because β grows parabolically as one proceeds away from the interaction point and so the beam size increases thus lowering the contribution to the luminosity from such locations. This is often called the “hourglass” effect.

In a storage ring, the bunch length tends to increase with higher bunch intensity due to the so-called longitudinal “impedance” or “wake fields”. Similar collective electromagnetic interactions with the beam environment can lead to longitudinal and transverse single- or multi-bunch instabilities [3,4], which may either increase energy spread or beam emittance, and even result in a beam loss.

Another major external electromagnetic field interaction, in the single particle context, is the production of synchrotron radiation

due to centripetal acceleration, given by the Larmor formula multiplied by a relativistic magnification factor of γ^4 [5]. In the case of electron rings this process determines the equilibrium emittance through a balance between radiation damping and excitation of oscillations, and further serves as a barrier to future higher energy versions in this variety of collider. A more comprehensive discussion of betatron oscillations, longitudinal motion, and synchrotron radiation is available in the 2008 version of the PDG review [6].

Synchrotron radiation emitted during the collision in the field of the opposing beam is called beamstrahlung. Beamstrahlung is relevant for both linear colliders, where it may degrade the luminosity spectrum, and for future highest-energy circular colliders, where it may limit the beam lifetime, and also increases the energy spread and bunch length of the stored beam. For both types of colliders the beamstrahlung is mitigated by making the colliding beams as flat as possible at the interaction point ($\sigma_x^* \gg \sigma_y^*$). The photon energy spectrum of the beamstrahlung is characterized by the parameter Upsilon $\Upsilon = (2/3)\hbar\omega_c/E_b$ [7], with $\hbar\omega_c$ denoting the critical photon energy and E_b the beam energy. The spectrum strongly deviates from the classical synchrotron radiation spectrum for Υ approaching 1.

31.3 Road to High Luminosity

Eq. 31.2 can be recast in terms of emittances and amplitude functions as

$$\mathcal{L} = f \frac{n_1 n_2}{4\pi \sqrt{\varepsilon_x \beta_x^* \varepsilon_y \beta_y^*}} \mathcal{F}. \quad (31.12)$$

Under the assumption $\mathcal{F} \approx 1$, to achieve high luminosity, all one has to do is make high population bunches of low emittance collide at high frequency at locations where the beam optics provides as low values of the amplitude functions as possible.

Expressions for the reductions due to crossing angle and other effects can be found elsewhere [8]. While there are no fundamental limits to producing luminosity, there are certainly challenges. Here we have space to mention only a few of these. The beam-beam tune shift appears in the Tables. A bunch in beam 1 presents a (nonlinear) lens to a particle in beam 2 resulting in changes to the particle’s transverse tune with a range characterized by the (vertical) beam-beam parameter [8]

$$\xi_{y,2} = \frac{m_e r_e q_1 q_2 n_1 \beta_{y,2}^*}{2\pi m_{A,2} \gamma_2 \sigma_{y,1}^* (\sigma_{x,1}^* + \sigma_{y,1}^*)} \quad (31.13)$$

where r_e denotes the classical electron radius ($r_e \approx 2.8 \times 10^{-15}$ m), m_e the electron mass, q_1 (q_2) the particle charge of beam 1 (2) in units of the elementary charge, and $m_{A,2}$ the mass of beam-2 particles. The transverse oscillations are susceptible to resonant perturbations from a variety of sources such as imperfections in the magnetic guide field, so that certain values of the tune must be avoided. Accordingly, the tune spread arising from ξ is limited [9–11]. A glance at the Tables shows that electrons are more forgiving than protons thanks to the damping effects of synchrotron radiation; the ξ -values for the former are about an order of magnitude larger than those for protons. In linear colliders, the strength of the collision is measured by the ratio of the rms bunch length σ_z to the approximate (linear, thin-lens) beam-beam focal length. This ratio, called disruption parameter D_y [7], is related to ξ_y via $D_y = 4\pi\sigma_z\xi_y/\beta_y^*$. For hadron colliders, two fundamental luminosity limits are the beam lifetime, determined by burn-off in the collisions, and the radiation from the collision debris, which affects the equipment lifetime.

A subject of present intense interest is the *electron-cloud effect* [12,13]; actually a variety of related processes come under this heading. They typically involve a buildup of electron density in the vacuum chamber due to emission from the chamber walls stimulated by electrons or photons originating from the beam itself. For instance, there is a process closely resembling the multipacting effects familiar from radiofrequency system commissioning. Low energy electrons are ejected from the walls by photons from positron or proton beam-produced synchrotron radiation. These electrons are accelerated toward a beam bunch, but by the time they reach the center of the vacuum chamber the bunch has gone

and so the now-energetic electrons strike the opposite wall to produce more secondaries. These secondaries are now accelerated by a subsequent bunch, and so on. Among the disturbances that this electron accumulation can produce is an enhancement of the tune spread within the bunch; the near-cancellation of bunch-induced electric and magnetic fields is no longer in effect.

If the luminosity of Eq. 31.12 is rewritten in terms of the beam-beam parameter, Eq. 31.13, the emittance itself disappears. However, the emittance must be sufficiently small to realize a desired magnitude of beam-beam parameter, but once ξ_y reaches this limit, further lowering the emittance does not lead to higher luminosity.

For electron synchrotrons and storage rings, radiation damping provides an automatic route to achieve a small emittance. In fact, synchrotron radiation is of key importance in the design and optimization of e^+e^- colliders. While vacuum stability and electron clouds can be of concern in the positron rings, synchrotron radiation along with the restoration of longitudinal momentum by the RF system has the positive effect of generating very small transverse beam sizes and small momentum spread. Further reduction of beam size at the interaction points using standard beam optics techniques and successfully contending with high beam currents has led to record luminosities in these rings. To maximize integrated luminosity the beam can be “topped off” by injecting new particles without removing existing ones – a feature difficult to imitate in hadron colliders.

For hadrons, particularly antiprotons, two inventions have played a prominent role. Stochastic cooling [14] was employed first to prepare beams for the $S\bar{p}pS$ and subsequently in the Tevatron, and to cool the beams at full energy in RHIC [15–17]. Electron cooling [18] was also used in the Tevatron, RHIC and LHC complexes to great advantage. Further innovations are underway driven by the needs of potential future projects; these are noted in the final section. For future energy-frontier hadron colliders, like the proposed FCC-hh and SPPC, also synchrotron radiation damping becomes an important cooling mechanism.

31.4 Recent High Energy Colliders

Collider accelerator physics of course goes far beyond the elements of the preceding sections. In this and the following section elaboration is made on various issues associated with some of the recently operating colliders, particularly factors which impact integrated luminosity. The various colliders utilizing hadrons each have unique characteristics and are, therefore, discussed separately. As space is limited, general references are provided where much further information can be obtained. A more complete list of recent colliders and their parameters can be found in the High-Energy Collider Parameters tables.

31.4.1 Tevatron

The first synchrotron in history using superconducting magnets, the Tevatron [19], was the highest energy collider for 25 years. Its 4.5 T dipole magnets employed superconducting Nb-Ti cable operating at 4.5 K [20], requiring what was then the world’s largest cryogenic system [21]. Tevatron operation was terminated in September 2011, after delivering more than 10 fb^{-1} to the $p\text{-}\bar{p}$ collider experiments CDF and D0. The route to high integrated luminosity in the Tevatron was governed by the antiproton production rate, the turn-around time to produce another store, and the resulting optimization of store time. The antiproton production complex [22] consisted of three 8 GeV \bar{p} accelerators — Accumulator, Debuncher, and Recycler — and employed 25 independent stochastic cooling systems and one high energy electron cooling set-up [23] to accumulate up to record high $25 \times 10^{10} \bar{p}$ per hour. The proton and antiproton beams in the Tevatron circulated in a single vacuum pipe and thus were placed on separated orbits which wrapped around each other in a helical pattern outside of the interaction regions. As the available aperture was limited, the long-range encounters played an important role. Despite these limitations, a total beam-beam tuneshift parameter of $N_{IP}\xi \approx 0.025\text{--}0.03$ was achieved, a record for hadron beams [24], where N_{IP} denotes the number of collision points (2 for the Tevatron). Other notable advances at the Tevatron included the first permanent-magnet-based high energy accelerator

(Recycler), novel longitudinal beam manipulation techniques such as *slip-stacking* and *momentum mining* [25,26], and the first use of electron lenses [27] for beam collimation and for compensation of long-range beam-beam effects. The Tevatron ultimately achieved luminosities a factor of 430 over its original design specification.

31.4.2 HERA

HERA [28], operated between 1992 and 2007, delivered nearly 1 fb^{-1} of integrated luminosity to the electron-proton collider experiments H1 and ZEUS. HERA was the first high-energy lepton-hadron collider, and also the first facility to employ both applications of superconductivity: magnets and accelerating structures. The proton beams of HERA had a maximum energy of 920 GeV. The lepton beams (positrons or electrons) were provided by the existing DESY complex, and were accelerated to 27.5 GeV using conventional magnets. At collision a 4-times higher frequency RF system, compared with the injection RF, was used to generate shorter bunches, thus helping alleviate the hourglass effect at the collision points. The lepton beam naturally would become transversely polarized (within about 40 minutes) and “spin rotators” were implemented on either side of an IP to produce longitudinal polarization at the experiment.

31.4.3 LEP

Installed in a tunnel of 27 km circumference, LEP [29] was the largest circular e^+e^- collider built so far. LEP was operated from 1989 to 2000 with beam energies ranging from 45.6 to 104.5 GeV and a maximum luminosity of $10^{32} \text{ cm}^{-2}\text{s}^{-1}$, at 98 GeV, surpassing all relevant design parameters. Up to about 60 GeV, LEP used resonant depolarization to precisely measure the beam energy [30,31].

31.4.4 SLC

Based on an existing 3-km long S-band linac, the SLC [32] was the first and only linear collider. It was operated from 1987 to 1998 with a constant beam energy of 45.6 GeV, up to about 80% electron-beam polarization, quasi-flat beams, a final-focus optics with local chromatic correction based on four interleaved sextupoles and $\beta_y^* \approx 1 \text{ mm}$. In its last year, SLC achieved a peak luminosity of about $3 \times 10^{30} \text{ cm}^{-2}\text{s}^{-1}$, roughly half of the design value.

31.5 Present Collider Facilities

31.5.1 LHC

The superconducting Large Hadron Collider [33] presently is the world’s highest energy collider. Early operations for HEP were first at 3.5 TeV (in 2011) and then 4 TeV per proton [34] (since 2012), with the beam energy increased to 6.5 TeV in 2015. The current status is best checked at the Web site [35]. In 2017 peak luminosities above $2 \times 10^{34} \text{ cm}^{-2}\text{s}^{-1}$ (more than twice the design value) have been achieved. To meet its luminosity goals the LHC operates with a high beam current of approximately 0.5 A, leading to stored energies of several hundred MJ per beam. Component protection, beam collimation, and controlled energy deposition were given a high priority. Additionally, at energies of 5–7 TeV per particle, synchrotron radiation moves from being a curiosity to a challenge in a hadron accelerator for the first time. At design beam current the cryogenic system must remove roughly 7 kW due to synchrotron radiation, intercepted at a temperature of about 5–20 K. As the photons are emitted their interactions with the vacuum chamber wall can generate free electrons, with consequent “electron cloud” development. Much care was taken to design a special beam screen for the chamber to mitigate this issue. The two proton beams are contained in separate pipes throughout most of the circumference, and are brought together into a single pipe at the interaction points. The large number of bunches, and subsequent short bunch spacing, would lead to approximately 30 head-on collisions through 120 m of common beam pipe at each IP. Thus, a small crossing angle is employed, which reduces the luminosity by about 15%. Still, the bunches moving in one direction experience multiple long-range encounters with the counter-rotating bunches and the resulting perturbations of the particle motion continues to remain a concern. The luminosity scale is absolutely calibrated by the “van der Meer method” as was invented for the ISR [36], and followed by multiple, re-

dundant luminosity monitors (see for example [37] and references therein). The Tables also show the LHC luminosity performance in Pb-Pb collisions, which for the ATLAS and CMS experiments well exceeded the design value, while for the ALICE [38] experiment, the luminosity is “levelled” near the Pb-Pb design value of $10^{27} \text{ cm}^{-2}\text{s}^{-1}$. The LHC can also provide Pb-p collisions as it did in 2013 and 2016, and other ion-ion or ion-proton collisions, at different energies.

In the coming years, an ambitious upgrade program, HL-LHC [39, 40], has as its target an order-of-magnitude increase in integrated luminosity through the utilization of Nb₃Sn superconducting magnets, superconducting compact “crab” cavities and luminosity leveling also for ATLAS and CMS as its key ingredients.

31.5.2 e^+e^- Rings

Asymmetric energies of the two beams have allowed for the enhancement of B -physics research and for interesting interaction region designs. As the bunch spacing can be quite short, the lepton beams sometimes pass through each other at an angle, which may reduce the luminosity — unless the crossing angle can be taken advantage of. KEKB [41] installed high frequency “crab crossing” schemes to fully restore the geometric overlap of the colliding bunches. It attained over 1 fb^{-1} of integrated luminosity in a single day. A different collision approach, called “crab waist”, which relies on special sextupoles together with a large crossing angle, has been successfully implemented at DAΦNE [42]. The crab-waist collision scheme has also been partly realized at the KEKB upgrade, SuperKEKB, and it has indeed become a key ingredient for all proposed future e^+e^- circular colliders. SuperKEKB is aiming for luminosities of $8 \times 10^{35} \text{ cm}^{-2}\text{s}^{-1}$ [43]. Other e^+e^- ring colliders currently in operation are BEPC-II, VEPP-2000 and VEPP-4M [43].

31.5.3 RHIC

The Relativistic Heavy Ion Collider [44] employs superconducting magnets, and collides combinations of fully-stripped ions such as H-H (p-p), p-Al, p-Au, d-Au, h-Au, Cu-Cu, Cu-Au, Zr-Zr, Ru-Ru, Au-Au, and U-U over a wide energy range [45]. The high charge per particle (+79 for gold, for instance) makes intra-beam scattering of particles within the bunch a special concern, even for seemingly moderate bunch intensities. In 2012, 3-D stochastic cooling was successfully implemented in RHIC [17] and is now routinely used. With stochastic cooling, steady increases in the bunch intensity, and numerous other upgrades, RHIC now operates at 44 times the Au-Au design average luminosity. Another special feature of accelerating heavy ions in RHIC is that the beams cross the “transition energy” during acceleration — a point where the derivative with respect to momentum of the revolution period is zero. This is more typical of low-energy accelerators, where the necessary phase jump required of the RF system is implemented rapidly and little time is spent near this condition. In the case of RHIC with heavy ions, the superconducting magnets do not ramp very quickly and the period of time spent crossing transition is long and must be dealt with carefully. For p-p operation the RHIC beams are always above their transition energy and so this condition is completely avoided. A RHIC physics program in search of a critical point in the nuclear matter phase diagram required operation below the nominal injection energy, and in order to reach the integrated luminosity goals the first bunched beam electron cooler was successfully commissioned for the lowest energies [46].

RHIC is also unique in its ability to accelerate and collide polarized proton beams. As proton beam polarization must be maintained from its low-energy source, successful acceleration through the myriad of depolarizing resonance conditions in high energy circular accelerators has taken years to accomplish. An energy of 255 GeV per proton with 55% final polarization per beam has been realized. As part of a scheme to compensate the head-on beam-beam effect, electron lenses operated routinely during the polarized proton operation at 100 GeV in 2015 [47].

Collisions between a RHIC proton beam and an electron beam stored in a new ring (eRHIC) is one of the two proposed configuration of a future US electron-ion collider (EIC) for nuclear physics

[48], the alternative being the addition of figure-8 hadron and electron storage rings to the CEBAF facility at JLAB (JLEIC).

31.6 Future High Energy Colliders and Prospects

Recent accomplishments of particle physics have been obtained through high-energy and high-intensity experiments using hadron-hadron, lepton-lepton, and lepton-proton colliders. Following the discovery of the Higgs particle at the LHC and in view of ongoing searches for “new physics” and rare phenomena, various options are under discussions and development to pursue future particle-physics research at higher energy and with appropriate luminosity. This is the basis for several new projects, ideas, and R&D activities, which can only briefly be summarized here. Specifically, the following projects are noted: an energy upgrade of the LHC based on 16 T dipole magnets (HE-LHC) [49], two approaches to an electron-positron linear collider [50, 51], larger 100-km circular tunnels supporting e^+e^- collisions up to either 240 [52] or 365 GeV [53] in the centre of mass along with a subsequent 70-140 TeV or 100-TeV proton-proton collider, possible future, or far future, muon-ring colliders [54,55], and potential use of plasma acceleration and other advanced schemes. Complementary studies are ongoing of a high-energy lepton-hadron collider bringing into collision a 60-GeV electron beam from an energy-recovery linac with the 7 TeV protons circulating in the LHC (LHeC) [56, 57], or, much later, with the 50(35) TeV protons of the 100(70) TeV collider (FCC-eh, SPPC), and of $\gamma\gamma$ collider Higgs factories based on recirculating electron linacs (e.g. SAPPHiRE [58]). Tentative parameters of some of the colliders discussed, or mentioned, in this section are summarized in Table 31.1 and Table 31.2.

31.6.1 Electron-Positron Linear Colliders

For more than four decades, efforts have been devoted to develop high-gradient technology e^+e^- colliders in order to overcome the synchrotron radiation limitations of circular e^+e^- machines in the TeV energy range.

The primary challenge confronting a high energy, high luminosity single pass collider design is the power requirement, so that measures must be taken to keep the demand within bounds as illustrated in a transformed Eq. 31.2 [60]:

$$\mathcal{L} \approx \frac{137}{8\pi r_e} \frac{P_{\text{wall}}}{E_{\text{cm}}} \frac{\eta}{\sigma_y^*} N_\gamma H_D. \quad (31.14)$$

Here, P_{wall} is the total wall-plug power of the collider, $\eta \equiv P_b/P_{\text{wall}}$ the efficiency of converting wall-plug power into beam power $P_b = f_{\text{coll}} n E_{\text{cm}}$, E_{cm} the cms energy, n ($= n_1 = n_2$) the bunch population, and σ_y^* the vertical rms beam size at the collision point. In formulating Eq. 31.14 the number of beamstrahlung photons emitted per e^\pm , was approximated as $N_\gamma \approx 2\alpha r_e n / \sigma_y^*$, where α denotes the fine-structure constant. The management of P_{wall} leads to an upward push on the bunch population n with an attendant rise in the energy radiated due to the electromagnetic field of one bunch acting on the particles of the other. Keeping a significant fraction of the luminosity close to the nominal energy represents a design goal, which is met if N_γ does not exceed a value of about 1. A consequence is the use of flat beams, where N_γ is managed by the beam width, and luminosity adjusted by the beam height, thus the explicit appearance of the vertical beam size σ_y^* . The final factor in Eq. 31.14, H_D , represents the enhancement of luminosity due to the pinch effect during bunch crossing (the effect of which has been neglected in the expression for N_γ).

The approach designated by the International Linear Collider (ILC) is presented in the Tables, and the contrast with the collision-point parameters of the circular colliders is striking, though reminiscent in direction of those of the SLAC Linear Collider. The ILC *Technical Design Report* [50,61] has a baseline cms energy of 500 GeV with upgrade provision for 1 TeV, and luminosity comparable to the LHC; recent tendencies have been toward a baseline of 250 GeV. The ILC is based on superconducting accelerating structures of the 1.3 GHz TESLA variety. Progress toward higher field gradients and Q values continues to be made, with nitrogen-doping techniques being a recent example [62].

At CERN, a design effort is underway on the Compact Linear

Table 31.1: Tentative parameters of selected future e^+e^- high-energy colliders. Parameters associated with different beam energy scenarios are comma-separated.

	FCC-ee	CEPC	ILC	CLIC
Species	e^+e^-	e^+e^-	e^+e^-	e^+e^-
Beam energy (GeV)	46, 120, 183	46, 120	125, 250	190, 1500
Circumference / Length (km)	97.75	100	20.5, 31	11, 50
Interaction regions	2	2	1	1
Est. integrated luminosity per experiment ($\text{ab}^{-1}/\text{year}$)	26, 0.9, 0.17	4, 0.4	0.2, 0.2	0.2, 0.6
Peak luminosity ($10^{34}/\text{cm}^2/\text{s}$)	230, 8.5, 1.6	32, 3	1.4, 1.8	1.5, 6
Time between collisions (μs)	0.015, 0.75, 8.5	0.025, 0.68	0.55	0.0005
Energy spread (rms, 10^{-3})	1.3, 1.65, 2.0	0.4, 1.0	e^- : 1.9, 1.2 e^+ : 1.5, 0.7	3.5
Bunch length (rms, mm)	12.1, 5.3, 3.8	8.5, 3.3	0.3	0.09, 0.044
IP beam size (μm)	H: 6.3, 14, 38 V: 0.03, 0.04, 0.07	H: 5.9, 21 V: 0.04, 0.07	H: 0.52, 0.47 V: 0.008, 0.006	H: 0.15, 0.04 V: 0.003, 0.001
Injection energy (GeV)	on energy (topping off)	on energy (topping off)	5.0 (linac)	9.0 (linac)
Transv. rms emittance (pm)	H: 270, 630, 1340 V: 1, 1, 3	H: 170, 1210 V: 2, 3	H: 20, 10 V: 0.14, 0.07	H: 2.4, 0.22 V: 0.8, 0.01
β^* at interaction point (cm)	H: 15, 30, 100 V: 0.08, 0.1, 0.16	H: 20, 36 V: 0.1, 0.15	H: 1.3, 2.2 V: 0.041, 0.048	H: 0.8, 0.69 V: 0.01, 0.0068
Full crossing angle (mrad)	30	33	14	20
Crossing scheme	crab waist	crab waist	crab crossing	crab crossing
Piwinski angle $\phi = \sigma_z \theta_c / (2\sigma_x^*)$	28.5, 5.8, 1.5	23.8, 2.6	0	0
Beam-beam param. $\xi_y (10^{-3})$	133, 118, 144	72, 109	n/a	n/a
Disruption parameter D_y	0.9, 1.1, 1.9	0.3, 1.0	34, 25	8, 12
Average Upsilon \mathcal{U}	0.0002, 0.0004, 0.0006	0.0001, 0.0005	0.03, 0.06	0.26, 3.4
RF frequency (MHz)	400, 400, 800	650	1300	11994
Particles per bunch (10^{10})	17, 15, 27	8, 15	2	0.52, 0.37
Bunches per beam	16640, 328, 33	12000, 242	1312 (pulse)	352, 312 (trains at 50 Hz)
Average beam current (mA)	1390, 29, 5.4	19.2	6 (in train)	1660, 1200 (in train)
RF gradient (MV/m)	1.3, 9.8, 19.8	3.6, 19.7	31.5	72, 100
Polarization (%)	≥ 10 , 0, 0	5–10, 0	e^- : 80% e^+ : 30%	e^- : 70% at IP
SR power loss (MW)	100	64	n/a	n/a
Beam power/beam (MW)	n/a	n/a	5.3, 10.5	3, 14
Novel technology	—	—	high grad. SC RF	two-beam accel.

Collider (CLIC), each linac of which is itself a two-beam accelerator, in that a high energy, low current beam is fed by a low energy, high current driver [63]. The CLIC design employs normal conducting 12 GHz accelerating structures at a gradient of 100 MeV/m, some three times the current capability of the superconducting ILC cavities. The design cms energy is 3 TeV, though recent staging options – 0.38, 1.5, and 3 TeV – have been developed [51].

31.6.2 Future Circular Colliders

The discovery, in 2012, of the Higgs boson at the LHC has stimulated interest in constructing a large circular tunnel which could host a variety of energy-frontier machines, including high-energy electron-positron, proton-proton, and lepton-hadron colliders. Such projects are under study by a global collaboration hosted at CERN (FCC) [53, 64, 65] and another one centered in China (CEPC/SPPC) [52], following earlier proposals for a Very Large Hadron Collider (VLHC) [66] and a Very Large Lepton Collider (VLLC) in the US, which would have been housed in the same 230-km long tunnel.

The maximum beam energy of a hadron collider is directly proportional to the magnetic field and to the ring circumference. The LHC magnets, based on Nb-Ti superconductor, achieve a maximum operational field of 8.33 T. The HL-LHC project develops the technology of higher field Nb₃Sn magnets as well as cables made from high-temperature superconductor (HTS). Nb₃Sn dipoles could ultimately reach an operational field around 16 T, and HTS inserts, requiring new engineering materials and substantial dedicated R&D, could boost this further. More cost-effective hybrid magnet designs incorporating Nb-Ti, two types of Nb₃Sn, and an inner layer of HTS providing fields of about

20 T have been examined [67]. However present project efforts are not utilizing this hybrid approach as of yet.

Aside from the magnets, the cryogenic beam vacuum system is another key component of any future hadron collider. A beam screen inside the cold bore of the magnets can intercept the synchrotron radiation at an elevated temperature, allowing a more efficient extraction of the synchrotron-radiation heat load. While the LHC beam screen has a temperature of 5–20 K, future, higher-energy machines are likely to raise this temperature to 50 K or 100 K.

Further substantial increases in collision energy are possible only with a larger tunnel. The FCC hadron collider (FCC-hh) [64, 68, 69], formerly called VHE-LHC, is based on a new tunnel of about 100 km circumference, which would allow exploring energies up to 100 TeV in the centre of mass with proton-proton collisions, using 16 T magnets. This new tunnel could also accommodate a high-luminosity circular e^+e^- Higgs factory (FCC-ee) as well as a lepton-hadron collider (FCC-eh). The SPPC is a 100 km hadron collider based on 12 T (later 24 T) iron-based high-temperature superconducting magnets, which could be installed in the same tunnel as the e^+e^- collider CEPC.

In order to serve as a Higgs factory a new circular e^+e^- collider needs to achieve a cms energy of at least 240 GeV. FCC-ee [53, 68] (formerly TLEP), installed in the ~ 100 km tunnel of the FCC-hh, could reach even higher energies, e.g. 365 GeV cms for $t\bar{t}$ production. At these energies, the luminosity, limited by the synchrotron radiation power, would still be above $10^{34} \text{ cm}^{-2}\text{s}^{-1}$ at each of two or four collision points. At lower energies (Z pole and WW threshold) FCC-ee could deliver two to three orders of magnitude higher luminosities, and also profit from radiative self polarization for

Table 31.2: Tentative parameters of selected future high-energy hadronic colliders. Parameters associated with different beam energy scenarios for a μ collider are comma-separated. Parameters of HL-LHC can be found in the High-Energy Collider Parameters review tables. The listed luminosity for the LHeC refers to parasitic operation in parallel to the HL-LHC pp collisions; it could be significantly increased for dedicated operation [59].

	LHeC	HE-LHC	FFC-hh	SPPC	μ collider
Species	ep	pp	pp	pp	$\mu^+\mu^-$
Beam Energy (TeV)	0.06(e), 7 (p)	13.5	50	37.5	0.063, 3
Circumference (km)	9(e), 26.7 (p)	26.7	97.75	100	0.3, 6
Interaction regions	1	2 (4)	4	2	1, 2
Estimated integrated luminosity per experiment ($\text{ab}^{-1}/\text{year}$)	0.1	0.5	0.2–1.0	0.4	0.001, 1.0
Peak luminosity ($10^{34}/\text{cm}^2/\text{s}$)	0.8	16	5–30	10	2.2, 71
Time between collisions (μs)	0.025	0.025	0.025	0.025	1, 20
Energy spread (rms, 10^{-3})	0.03 (e), 0.1(p)	0.1	0.1	0.2	0.04, 1
Bunch length (rms, mm)	0.06 (e), 75.5(p)	80	80	75.5	63, 2
IP beam size (μm)	4.3 (round)	8.8	6.7–3.5 (init.)	6.8 (init.)	75, 1.5
Injection energy (GeV)	1(e), 450(p)	1300	3300	2100	on energy
Transverse emittance (rms, nm)	0.45(e), 0.27(p)	0.17	0.04 (init.)	0.06 (init.)	335, 0.9
β^* , amplitude fcn. at IP (cm)	5.0(e), 7.0(p)	45	110–30	75	1.7, 0.25
Beam-beam parameter/IP (10^{-3})	–(e), 0.4(p)	12	5–15	7.5	20, 90
RF frequency (MHz)	800(e), 400(p)	400	400	400/200	805
Particles per bunch (10^{10})	0.23(e), 22(p)	22	10	15	400, 200
Bunches per beam	–(e), 2808(p)	2808	10600	10080	1
Average beam current (mA)	15(e), 883(p)	1120	500	730	640, 16 (peak)
Length of standard cell (m)	52.4(e arc), 107(p)	137	213	148	N/A
Phase advance per cell (deg)	310/90(e H/V) 90(p)	90	90	90	N/A
Peak magnetic field (T)	0.264(e), 8.33(p)	16	16	12	10
Polarization (%)	90(e), 0(p)	0	0	0	0
SR power loss/beam (MW)	30(e), 0.01(p)	0.1	2.4	1.1	3×10^{-5} , 0.068
Novel technology	high-energy ERL	16T Nb ₃ Sn magnets	16T Nb ₃ Sn magnets	HTS magnets	muon prod.

precise energy calibration. The short beam lifetime at the high target luminosity, due to radiative Bhabha scattering, requires FCC-ee to be constructed as a double ring, where the collider rings operating at constant energy are complemented by a full-energy injector ring installed in the same tunnel to “top off” the collider current. Beamstrahlung, i.e. synchrotron radiation emitted during the collision in the field of the opposing beam, introduces an additional beam lifetime limitation depending on momentum acceptance (so that achieving sufficient off-momentum dynamic aperture becomes one of the design challenges), as well as some bunch lengthening.

31.6.3 Muon Collider

The muon to electron mass ratio of 210 implies less concern about synchrotron radiation by a factor of about 2×10^9 and its $2.2 \mu\text{s}$ lifetime means that it will last for some $300B$ turns in a ring with an average bending magnets field of B (Tesla). Design effort became serious in the mid 1990s and a collider outline emerged quickly.

Removal of the synchrotron radiation barrier reduces the scale of a muon collider facility to a level compatible with on-site placement at existing accelerator laboratories. The Higgs production cross section in the s-channel is enhanced by a factor of $(m_\mu/m_e)^2$ compared to that in e^+e^- collisions. The obvious advantage in colliding muons rather than protons is that the muon collider center of mass energy \sqrt{s} , is entirely available to produce short-distance reactions rather than being spread among proton constituents and, e.g., a 14 TeV muon collider with sufficient luminosity might be very effective as a direct exploration machine, with a physics potential similar to that of a 100 TeV proton-proton collider [70]. Muon colliders are expected to be more compact, power efficient and significantly less expensive than equivalent energy frontier hadron or e^+e^- machines, and a neutrino factory could

potentially be realized in the course of construction [71].

The challenges to luminosity achievement are clear and amenable to immediate study: targeting, collection, and emittance reduction are paramount, as well as the bunch manipulation required to produce $> 10^{12}$ muons per bunch without emittance degradation. A multi-TeV c.m.e. high luminosity $O(10^{34} \text{ cm}^{-2}\text{s}^{-1})$ muon collider would consist of [72, 73]: (i) a high power proton driver (SRF 8 GeV 2-4 MW H^- linac), (ii) pre-target accumulation and compressor rings, in which high intensity 1-3 ns long proton bunches are formed, (iii) a liquid-mercury target for converting the proton beam into a tertiary muon beam with energy of about 200 MeV, (iv) a multi-stage ionization cooling section that reduces transverse and longitudinal emittances and creates a low emittance beam, (v) a multistage acceleration system, possibly employing recirculating linear accelerators (RLA) to accelerate muons in a modest number of turns up to 2 TeV using superconducting RF technology, and, finally, (vi) a 2–6 km diameter collider ring located some 100 m underground, where counter-propagating muon beams are stored and collide over the roughly 1000–2000 turns corresponding to the muon lifetime.

Collection of muons from the decay of pions produced in proton-nucleus interactions results in a large initial 6D phase volume for the muons, which must be reduced (cooled) by a factor of 10^6 , otherwise, the luminosity reach will not exceed $O(10^{31} \text{ cm}^{-2}\text{s}^{-1})$. The technique of ionization cooling [74, 75] is uniquely applicable to muons because of their minimal interaction with matter [76]; a proof-of-principle was recently demonstrated in the pioneering MICE experiment at RAL [77]. Muon collider R&D has led to a number of remarkable advances in the past decade [78], including a novel concept to generate muon pairs at threshold using the annihilation of 45 GeV positrons with electrons at rest [79, 80], and alternative concepts based on laser-hadron collisions [55, 81, 82], all of which might allow low emittance beams to be obtained directly,

without any cooling.

31.6.4 Plasma Acceleration and Other Advanced Concepts

At the 1956 CERN Symposium, a paper by Veksler, in which he suggested acceleration of protons to the TeV scale using a bunch of electrons, anticipated current interest in plasma acceleration [83]. A half-century later this became more than a suggestion, with the demonstration, as a striking example, of electron energy doubling from 42 to 84 GeV over 85 cm at SLAC [84], the creation of a 1 GeV electron bunch with relatively small energy spread accelerated through a cm-scale plasma [85], and the achievement of proton-driven plasma acceleration of electrons at CERN [86].

Whether plasma acceleration will find application in an HEP facility is not yet clear, given the necessity of staging and phase-locking acceleration in multiple plasma chambers. However, strides continue to be made, as multi-stage coupling of independent laser plasma accelerators have been demonstrated recently [87]. Another critical issue is the power efficiency η for a collider based on plasma acceleration, whose luminosity would still be described by 31.14. Maintaining beam quality and beam position as well as the acceleration of high-repetition bunch trains are also primary feasibility issues, addressed by active R&D. For a recent status report on laser-plasma acceleration and the steps towards a future electron positron collider based on this technology, see [88].

Additional approaches aiming at accelerating gradients higher, or much higher, than those achievable with conventional metal cavities include the use of dielectric materials and, for the long-term future, crystals. Combining several innovative ideas, even a linear crystal muon collider driven by X-ray lasers has been proposed [89], as well as “accelerators on a chip” [90,91]. Not only the achievable accelerating gradient, but also the overall power efficiency, e.g. the attainable luminosity as a function of electrical input power, along with the beam stability [92] will determine the suitability of any novel technology for use in future high-energy accelerators.

References

- [1] E. D. Courant and H. S. Snyder, *Annals Phys.* **3**, 1 (1958), *Annals Phys.* 281,360(2000). This is the classic article on the alternating gradient synchrotron.
- [2] A. W. Chao *et al.*, editors, *Handbook of accelerator physics and engineering*, World Scientific, Hackensack, USA (2013), ISBN 9789814415842, URL <http://www.worldscientific.com/worldscibooks/10.1142/8543>.
- [3] A. W. Chao, *Physics of collective beam instabilities in high energy accelerators*, Wiley, New York, NY (1993), URL <https://cds.cern.ch/record/246480>.
- [4] K. Y. Ng, *Physics of intensity dependent beam instabilities*, World Scientific, Hoboken, NJ (2006), URL <https://cds.cern.ch/record/1012829>.
- [5] H. Wiedemann, in *Handbook of Accelerator Physics and Engineering* [2], *ibid*, Sec. 3.1.
- [6] C. Amsler *et al.* (Particle Data Group), *Phys. Lett.* **B667**, 1 (2008).
- [7] K. Yokoya and P. Chen, *Lect. Notes Phys.* **400**, 415 (1992).
- [8] M.A. Furman and M.S. Zisman, *Handbook of Accelerator Physics and Engineering* [2], *ibid*, Sec. 4.1.
- [9] R. Assmann and K. Cornelis, in “Particle accelerator. Proceedings, 7th European Conference, EPAC 2000, Vienna, Austria, June 26-30, 2000. Vol. 1-3,” 1187–1189 (2000), URL <http://web1lib.cern.ch/abstract?CERN-SL-2000-046-0P>.
- [10] J. Gao, *Nucl. Instrum. Meth.* **A533**, 270 (2004).
- [11] K. Ohmi and F. Zimmermann, *Phys. Rev. ST Accel. Beams* **18**, 12, 121003 (2015).
- [12] M.A. Furman, *Handbook of Accelerator Physics and Engineering* [2], *ibid*, Sec. 2.4.14.
- [13] <http://ab-abp-rlc.web.cern.ch/ab-abp-rlc-ecloud/>. This site contains many references as well as videos of electron cloud simulations.
- [14] D. Mohl *et al.*, *Phys. Rept.* **58**, 73 (1980).
- [15] M. Blaskiewicz and J. M. Brennan, *Phys. Rev. ST Accel. Beams* **10**, 061001 (2007).
- [16] M. Blaskiewicz, J. M. Brennan and F. Severino, *Phys. Rev. Lett.* **100**, 174802 (2008).
- [17] M. Blaskiewicz, J. M. Brennan and K. Mernick, *Phys. Rev. Lett.* **105**, 094801 (2010).
- [18] G. I. Budker, *Sov. Atom. Energ.* **22**, 438 (1967), [*At. Energ.* 22,346(1967)].
- [19] H. T. Edwards, *Ann. Rev. Nucl. Part. Sci.* **35**, 605 (1985).
- [20] A. Tollestrup and E. Todesco, in “Reviews Of Accelerator Science And Technology: Volume 1,” 185–210, World Scientific (2008).
- [21] W. Fowler, *Particle Accelerators* **26**, 179 (1990).
- [22] M. Church and J. Marriner, *Annual Review of Nuclear and Particle Science* **43**, 1, 253 (1993).
- [23] S. Nagaitsev *et al.*, *Physical Review Letters* **96**, 4, 044801 (2006).
- [24] V. Shiltsev *et al.*, *Physical Review Special Topics-Accelerators and Beams* **8**, 10, 101001 (2005).
- [25] K. Koba and J. Steimel, in “AIP Conference Proceedings,” volume 642, 223–225, AIP (2002).
- [26] C. Bhat, *Physics Letters A* **330**, 6, 481 (2004).
- [27] V. D. Shiltsev, *Electron lenses for super-colliders*, Springer (2016).
- [28] Brief history at http://en.wikipedia.org/wiki/Hadron_Elektron_Ring_Anlage.
- [29] R. Assmann, M. Lamont and S. Myers, *Nucl. Phys. Proc. Suppl.* **109B**, 17 (2002), [17(2002)].
- [30] R. Assmann *et al.*, *Eur. Phys. J.* **C6**, 187 (1999).
- [31] R. Assmann *et al.*, in “Proceedings, 1999 Particle Accelerator Conference (PAC’99): New York, New York, March 29-April 2, 1999,” 2999–3001 (1999), URL <http://accelconf.web.cern.ch/AccelConf/p99/PAPERS/THP23.PDF>.
- [32] N. Phinney, eConf **C00082**, MO102 (2000), [1(2000)], [arXiv:physics/0010008].
- [33] L. Evans, *Ann. Rev. Nucl. Part. Sci.* **61**, 435 (2011).
- [34] M. Draper, editor, *Proceedings, LHC Performance Workshop (Chamonix 2014)*, CERN, CERN, Geneva (2015), ISBN 9789290834137.
- [35] Detailed information from the multi-volume design report to present status may be found at <http://lhc.web.cern.ch/lhc/>.
- [36] S. van der Meer (1968).
- [37] G. Aad *et al.* (ATLAS), *Eur. Phys. J.* **C73**, 8, 2518 (2013), [arXiv:1302.4393].
- [38] <http://aliceinfo.cern.ch/Public/Welcome.html>.
- [39] <http://hilumilhc.web.cern.ch>.
- [40] G. Apollinari *et al.*, *CERN Yellow Rep. Monogr.* **4**, 1 (2017).
- [41] S. Kurokawa and E. Kikutani, *Nucl. Instrum. Meth.* **A499**, 1 (2003).
- [42] M. Zobov *et al.*, *Phys. Rev. Lett.* **104**, 174801 (2010).
- [43] An overview of electron-positron colliders past and present may be found in ICFA Beam Dynamics Newsletter No. 46, April 2009, <http://icfa-bd.kek.jp/>. A daily account of the luminosity progress at SuperKEKB may be found at <http://www-linac.kek.jp/skekb/snapshot/dailysnap.html>.
- [44] M. Harrison *et al.*, *Nucl. Instrum. Meth.* **A499**, 1 (2003).
- [45] <http://www.rhichome.bnl.gov/RHIC/Runs/>.
- [46] A. Fedotov, *et al.*, *Proceedings NAPAC 2019* (2019).
- [47] W. Fischer *et al.*, *Phys. Rev. Lett.* **115**, 26, 264801 (2015).
- [48] F. Pilat, in “Proceedings, 9th International Particle Accelerator Conference (IPAC 2018): Vancouver, BC Canada,” TUXGBD3 (2018).

- [49] F. Zimmermann *et al.*, The European Physical Journal Special Topics **228**, 5, 1109 (2019), ISSN 1951-6401, URL <https://doi.org/10.1140/epjst/e2019-900088-6>.
- [50] P. Bambade *et al.* (2019), [arXiv:1903.01629].
- [51] T. K. Charles *et al.* (CLICdp, CLIC), CERN Yellow Rep. Monogr. **1802**, 1 (2018), [arXiv:1812.06018].
- [52] CEPC Study Group (2018), [arXiv:1809.00285].
- [53] M. Benedikt *et al.*, The European Physical Journal Special Topics **228**, 2, 261 (2019).
- [54] D. Neuffer and V. Shiltsev, JINST **13**, 10, T10003 (2018), [arXiv:1811.10694].
- [55] F. Zimmermann MOPMF065 (2018), [J. Phys. Conf. Ser.1067,no.2,022017(2018)].
- [56] J. L. Abelleira Fernandez *et al.* (LHeC Study Group), J. Phys. **G39**, 075001 (2012), [arXiv:1206.2913].
- [57] J. L. Abelleira Fernandez *et al.* (LHeC Study Group) (2012), [arXiv:1211.5102].
- [58] S. A. Bogacz *et al.* (2012), [arXiv:1208.2827].
- [59] F. Bordry *et al.* (2018), [arXiv:1810.13022].
- [60] F. Zimmermann, AIP Conf. Proc. **592**, 1, 494 (2001).
- [61] <http://www.linearcollider.org/ILC/Publications/Technical-Design-Report>.
- [62] A. Grassellino *et al.*, Supercond. Sci. Technol. **26**, 102001 (2013), [arXiv:1306.0288].
- [63] <http://lcd.web.cern.ch/lcd/CDR/CDR.html>.
- [64] M. Benedikt *et al.*, The European Physical Journal Special Topics **228**, 4, 755 (2019), ISSN 1951-6401, URL <https://doi.org/10.1140/epjst/e2019-900087-0>.
- [65] M. Mangano *et al.*, The European Physical Journal C **79**, 6, 474 (2019), ISSN 1434-6052, URL <https://doi.org/10.1140/epjc/s10052-019-6904-3>.
- [66] <http://vlhc.org>.
- [67] E. Todesco and F. Zimmermann, editors, *Proceedings, EuCARD-AccNet-EuroLumi Workshop: The High-Energy Large Hadron Collider (HE-LHC10): Villa Bighi, Malta, Republic of Malta, October 14-16, 2010. EuCARD-AccNet-EuroLumi Workshop: The High-Energy Large Hadron Collider*, CERN, CERN, Geneva (2011), 29 lectures, 156 pages, published as CERN Yellow Report, URL <https://cds.cern.ch/record/1344820>.
- [68] <http://fcc.web.cern.ch>.
- [69] M. Benedikt, D. Schulte and F. Zimmermann, Phys. Rev. ST Accel. Beams **18**, 101002 (2015).
- [70] D. Neuffer and V. Shiltsev, Journal of Instrumentation **13**, 10, T10003 (2018).
- [71] http://en.wikipedia.org/wiki/Neutrino_Factory.
- [72] C. M. Ankenbrandt *et al.*, Physical Review Special Topics Accelerators and Beams **2**, 8, 081001 (1999).
- [73] J.-P. Delahaye *et al.*, in “Proceedings, 2013 Community Summer Study on the Future of U.S. Particle Physics: Snowmass on the Mississippi (CSS2013): Minneapolis, MN, USA, July 29-August 6, 2013,” (2013), [arXiv:1308.0494], URL <http://www.slac.stanford.edu/econf/C1307292/docs/submittedArxivFiles/1308.0494.pdf>.
- [74] A. Skrinsky and V. Parkhomchuk, Sov. J. Part. Nucl **12**, 223, 210 (1981).
- [75] D. Neuffer, Particle Accelerators **14**, 75 (1983).
- [76] R. Palmer, Reviews of Accelerator Science and Technology **7**, 137 (2014).
- [77] M. Bogomilov *et al.*, arXiv preprint arXiv:1907.08562 (2019).
- [78] M. Boscolo, J. P. Delahaye and M. Palmer, Reviews of Accelerator Science and Technology **10**, 189 (2019), arXiv preprint arXiv:1808.01858.
- [79] M. Antonelli *et al.*, Nucl. Instrum. Meth. **A807**, 101 (2016), [arXiv:1509.04454].
- [80] M. Biagini *et al.*, in “Proceedings, 10th International Particle Accelerator Conference (IPAC2019): Melbourne, Australia, May 19-24, 2019,” MOZZPLS2 (2019).
- [81] C. Curatolo, F. Broggi and L. Serafini, Nucl. Instrum. Meth. **A865**, 128 (2017).
- [82] M. W. Krasny (2015), [arXiv:1511.07794].
- [83] V. I. Veksler (1956), URL <http://cds.cern.ch/record/1241563>.
- [84] I. Blumenfeld *et al.*, Nature **445**, 741 (2007).
- [85] W. P. Leemans *et al.*, Nature Phys. **2**, 696 (2006).
- [86] E. Gschwendtner and M. Turner (AWAKE) (2019), [arXiv:1901.04171].
- [87] S. Steinke *et al.*, Nature **530**, 7589, 190 (2016).
- [88] ALEGRO Collab., Towards an Advanced Linear International Collider, arXiv:1901.10370 .
- [89] V. D. Shiltsev, Phys. Usp. **55**, 965 (2012), [arXiv:1205.3087].
- [90] J. Breuer and P. Hommelhoff, Phys. Rev. Lett. **111**, 13, 134803 (2013), [arXiv:1308.0464].
- [91] E. A. Peralta *et al.*, Nature **503**, 91 (2013).
- [92] V. Lebedev, A. Burov and S. Nagaitsev, Phys. Rev. Accel. Beams **20**, 12, 121301 (2017), [Erratum: Phys. Rev. Accel. Beams **21**, 059901 (2018)], [arXiv:1701.01498].

32. High-Energy Collider Parameters

High-Energy Collider Parameters: e^+e^- Colliders (I)

Table 32.1: Updated in March 2020 with numbers received from representatives of the colliders (contact E. Pianori, LBNL). The table shows the parameter values achieved. Quantities are, where appropriate, r.m.s.; unless noted otherwise, energies refer to beam energy; H and V indicate horizontal and vertical directions; s.c. stands for superconducting. Parameters for the defunct SPEAR, DORIS, PETRA, PEP, TRISTAN, and VEPP-2M colliders may be found in our 1996 edition (Phys. Rev. **D54**, 1 July 1996, Part I).

	VEPP-2000 (Novosibirsk)	VEPP-4M (Novosibirsk)	BEPC (China)	BEPC-II (China)	DAΦNE (Frascati)
Physics start date	2010	1994	1989	2008	1999
Physics end date	—	—	2005	—	—
Maximum beam energy (GeV)	1.0	6	2.5	1.89 (2.35 max)	0.510
Delivered integrated luminosity per exp. (fb^{-1})	0.25	0.05	0.11	24.6	≈ 4.7 in 2001-2007 ≈ 2.7 w/crab-waist ≈ 1.8 since Nov 2014
Luminosity ($10^{30} \text{ cm}^{-2} \text{ s}^{-1}$)	50	20	12.6 at 1.843 GeV 5 at 1.55 GeV	1000	453
Time between collisions (μs)	0.04	0.6	0.8	0.008	0.0027
Full crossing angle (μ rad)	0	0	0	2.2×10^4	5×10^4
Energy spread (units 10^{-3})	0.71	1	0.58 at 2.2 GeV	0.52	0.40
Bunch length (cm)	4	5	≈ 5	≈ 1.2	low current: 1 at 15mA: 2
Beam radius (10^{-6} m)	125 (round)	H:1000 V:30	H:890 V:37	H:347 V:4.5	H:260 V:4.8
Free space at interaction point (m)	± 0.5	± 2	± 2.15	± 0.63	± 0.295
Luminosity lifetime (hr)	continuous	2	7-12	1.5	0.2
Turn-around time (min)	continuous	18	32	4 (topping up)	2 (topping up)
Injection energy (GeV)	0.2-1.0	1.8	1.55	1.89	on energy
Transverse emittance (10^{-9} m)	H:150 V:150	H:200 V:20	H:660 V:28	H:121 V:1.56	H:260 V:2.6
β^* , amplitude function at interaction point (m)	H:0.05 - 0.11 V:0.05 - 0.11	H:0.75 V:0.05	H:1.2 V:0.05	H:1.0 V:0.0129	H:0.26 V:0.009
Beam-beam tune shift per crossing (units 10^{-4})	H:850 V:850	500	350	383	440 (crab-waist test)
RF frequency (MHz)	172	180	199.53	499.8	356
Particles per bunch (units 10^{10})	8	15	20 at 2 GeV 11 at 1.55 GeV	3.8	e^- : 3.2 e^+ : 2.1
Bunches per ring per species	1	2	1	119	100 to 105 (120 buckets)
Average beam current per species (mA)	160	80	40 at 2 GeV 22 at 1.55 GeV	851	e^- : 1250 e^+ : 800
Circumference or length (km)	0.024	0.366	0.2404	0.23753	0.098
Interaction regions	2	1	2	1	1
Magnetic length of dipole (m)	1.1	2	1.6	outer ring: 1.6 inner ring: 1.41	outer ring: 1.2 inner ring: 1
Length of standard cell (m)	12	7.2	6.6	outer ring: 6.6 inner ring: 6.2	n/a
Phase advance per cell (deg)	H:745 V:385	65	≈ 60	60-90 non-standard cells	—
Dipoles in ring	8	78	40 + 4 weak	84 + 8 weak	8
Quadrupoles in ring	24 + 4 s.c.	150	68	134+2 s.c.	48
Peak magnetic field (T)	2.4	0.6	0.903 at 2.8 GeV	outer ring: 0.677 inner ring: 0.766	1.2

High-Energy Collider Parameters: e^+e^- Colliders (II)

Table 32.2: Updated in March 2020 with numbers received from representatives of the colliders (contact E. Pianori, LBNL). The table shows the parameter values achieved. Quantities are, where appropriate, r.m.s.; unless noted otherwise, energies refer to beam energy; H and V indicate horizontal and vertical directions; s.c. stands for superconducting. ILC and CLIC parameters are documented in the Accelerator physics of colliders review.

	CESR (Cornell)	CESR-C (Cornell)	LEP (CERN)	SLC (SLAC)
Physics start date	1979	2002	1989	1989
Physics end date	2002	2008	2000	1998
Maximum beam energy (GeV)	6	6	100 - 104.6	50
Delivered integrated luminosity per experiment (fb^{-1})	41.5	2.0	0.221 at Z peak 0.501 at 65 – 100 GeV 0.275 at >100 GeV	0.022
Luminosity ($10^{30} \text{ cm}^{-2}\text{s}^{-1}$)	1280 at 5.3 GeV	76 at 2.08 GeV	24 at Z peak 100 at > 90 GeV	2.5
Time between collisions (μs)	0.014 to 0.22	0.014 to 0.22	22	8300
Full crossing angle (μ rad)	± 2000	± 3300	0	0
Energy spread (units 10^{-3})	0.6 at 5.3 GeV	0.82 at 2.08 GeV	0.7→1.5	1.2
Bunch length (cm)	1.8	1.2	1.0	0.1
Beam radius (μm)	H:460 V:4	H:340 V:6.5	H:200→300 V:2.5→8	H:1.5 V:0.5
Free space at interaction point (m)	± 2.2 (± 0.6 to REC quads)	± 2.2 (± 0.3 to PM quads)	± 3.5	± 2.8
Luminosity lifetime (hr)	2–3	2–3	20 at Z peak 10 at > 90 GeV	—
Turn-around time (min)	5 (topping up)	1.5 (topping up)	50	120 Hz (pulsed)
Injection energy (GeV)	1.8–6	1.5–6	22	45.64
Transverse emittance (10^{-9} m)	210 1	120 3.5	H:20–45 V:0.25→1	H:0.5 V:0.05
β^* , amplitude function at interaction point (m)	1.0 0.018	0.94 0.012	1.5 0.05	0.0025 0.0015
Beam-beam tune shift per crossing (10^{-4}) or disruption	250 620	e^- : 420 (H), 280 (V) e^+ : 410 (H), 270 (V)	830	0.75 (H) 2.0 (V)
RF frequency (MHz)	500	500	352.2	2856
Particles per bunch (units 10^{10})	1.15	4.7	45 in collision 60 in single beam	4.0
Bunches per ring per species	9 trains of 5 bunches	8 trains of 3 bunches	4 trains of 1 or 2	1
Average beam current per species (mA)	340	72	4 at Z peak 4→6 at > 90 GeV	0.0008
Beam polarization (%)	—	—	55 at 45 GeV 5 at 61 GeV	e^- : 80
Circumference or length (km)	0.768	0.768	26.66	1.45 +1.47
Interaction regions	1	1	4	1
Magnetic length of dipole (m)	1.6–6.6	1.6–6.6	11.66/pair	2.5
Length of standard cell (m)	16	16	79	5.2
Phase advance per cell (deg)	45–90 (no standard cell)	45–90 (no standard cell)	102/90	108
Dipoles in ring	86	84	3280 + 24 inj. + 64 weak	460+440
Quadrupoles in ring	101 + 4 s.c.	101 + 4 s.c.	520 + 288 + 8 s.c.	—
Peak magnetic field (T)	0.3 / 0.8 at 8 GeV	0.3 / 0.8 at 8 GeV, 2.1 wigglers at 1.9 GeV	0.135	0.597

High-Energy Collider Parameters: e^+e^- Colliders (III)

Table 32.3: Updated in March 2020 with numbers received from representatives of the colliders (contact E. Pianori, LBNL). The table shows the parameter values achieved. Design parameters for SuperKEKEB may be found in our 2018 edition (Phys. Rev. **D98**, 030001 (2018)) Quantities are, where appropriate, r.m.s.; unless noted otherwise, energies refer to beam energy; H and V indicate horizontal and vertical directions; s.c. stands for superconducting.

	KEKB (KEK)	PEP-II (SLAC)	SuperKEKB (KEK)
Physics start date	1999	1999	2018
Physics end date	2010	2008	—
Maximum beam energy (GeV)	e^- : 8.33 (8.0 nominal) e^+ : 3.64 (3.5 nominal)	e^- : 7–12 (9.0 nominal) e^+ : 2.5–4 (3.1 nominal)	e^- : 7 e^+ : 4
Delivered integrated luminosity per exp. (fb^{-1})	1040	557	10.57
Luminosity ($10^{30} \text{ cm}^{-2}\text{s}^{-1}$)	21083	12069 (design: 3000)	1.88×10^4
Time between collisions (μs)	0.00590 or 0.00786	0.0042	0.0065
Full crossing angle (μ rad)	$\pm 11000^*$	0	± 41500
Energy spread (units 10^{-3})	0.7	e^-/e^+ : 0.61/0.77	e^-/e^+ : 0.64/0.81
Bunch length (cm)	0.65	e^-/e^+ : 1.1/1.0	e^-/e^+ : 0.5/0.6
Beam radius (μm)	H: 124 (e^-), 117 (e^+) V: 1.9	157 4.7	e^- : 16.6 (H), 0.25 (V) e^+ : 12.6 (H), 0.25 (V)
Free space at interaction point (m)	+0.75/−0.58 (+300/−500) mrad cone	± 0.2 , ± 300 mrad cone	e^- : +1.20/−1.28, e^+ : +0.78/−0.73 (+300/−500) mrad cone
Luminosity lifetime (hr)	continuous	continuous	continuous
Turn-around time (min)	continuous	continuous	continuous
Injection energy (GeV)	e^-/e^+ : 8.0/3.5 (nominal)	e^-/e^+ : 9.0/3.1 (nominal)	e^-/e^+ : 7/4
Transverse emittance (10^{-9} m)	e^- : 24 (57^\dagger) (H), 0.61 (V) e^+ : 18 (55^\dagger) (H), 0.56 (V)	e^- : 48 (H), 1.8 (V) e^+ : 24 (H), 1.8 (V)	e^- : 4.7 (H), 0.061 (V) e^+ : 2.0 (H), 0.061 (V)
β^* , amplitude function at interaction point (m)	e^- : 1.2 (0.27^\dagger) (H), 0.0059 (V) e^+ : 1.2 (0.23^\dagger) (H), 0.0059 (V)	e^- : 0.50 (H), 0.012 (V) e^+ : 0.50 (H), 0.012 (V)	e^- : 0.060 (H), 1×10^{-3} (V) e^+ : 0.080 (H), 1×10^{-3} (V)
Beam-beam tune shift per crossing (units 10^{-4})	e^- : 1020 (H), 900 (V) e^+ : 1270 (H), 1290 (V)	e^- : 703 (H), 498 (V) e^+ : 510 (H), 727 (V)	e^- : 12 (H), 270 (V) e^+ : 23 (H), 270 (V)
RF frequency (MHz)	508.887	476	508.887
Particles per bunch (units 10^{10})	e^-/e^+ : 4.7/6.4	e^-/e^+ : 5.2/8.0	e^-/e^+ : 2.76/3.52
Bunches per ring per species	1585	1732	1476
Average beam current per species (mA)	e^-/e^+ : 1188/1637	e^-/e^+ : 1960/3026	e^-/e^+ : 640/819
Beam polarization (%)	—	—	—
Circumference or length (km)	3.016	2.2	3.016
Interaction regions	1	1	1
Magnetic length of dipole (m)	e^-/e^+ : 5.86/0.915	e^-/e^+ : 5.4/0.45	e^-/e^+ : 5.9/4.0
Length of standard cell (m)	e^-/e^+ : 75.7/76.1	15.2	e^-/e^+ : 75.7/76.1
Phase advance per cell (deg)	450	e^-/e^+ : 60/90	450
Dipoles in ring	e^-/e^+ : 116/112	e^-/e^+ : 192/192	e^-/e^+ : 116/112
Quadrupoles in ring	e^-/e^+ : 452/452	e^-/e^+ : 290/326	e^-/e^+ : 466/460
Peak magnetic field (T)	e^-/e^+ : 0.25/0.72	e^-/e^+ : 0.18/0.75	e^-/e^+ : 0.22/0.19

*KEKB was operated with crab crossing from 2007 to 2010.

† With dynamic beam-beam effect.

High-Energy Collider Parameters: ep , $\bar{p}p$, pp Colliders

Table 32.4: Updated in March 2020 with numbers received from representatives of the colliders (contact E. Pianori, LBNL). The table shows the parameter values achieved. Parameters for the defunct $Spp\bar{p}S$ collider may be found in our 2002 edition (Phys. Rev. D66, 010001 (2002)). Quantities are, where appropriate, r.m.s.; unless noted otherwise, energies refer to beam energy; H and V indicate horizontal and vertical directions; s.c. stands for superconducting.

	HERA (DESY)	TEVATRON* (Fermilab)	RHIC Brookhaven	LHC (CERN)		
Physics start date	1992	1987	2001	2009	2015	2026 (HL-LHC)
Physics end date	2007	2011	—	—		
Particles collided	ep	$p\bar{p}$	pp (polarized)	pp		
Maximum beam energy (TeV)	e : 0.030 p : 0.92	0.980	0.255 55% polarization	4.0	6.5	7.0
Max. delivered integrated luminosity per exp. (fb^{-1})	0.8	12	0.38 at 100 GeV 1.3 at 250/255 GeV	23.3 at 4.0 TeV 6.1 at 3.5 TeV	160	250/y
Luminosity ($10^{30} \text{ cm}^{-2} \text{ s}^{-1}$)	75	431	245 (pk) 160 (avg)	7.7×10^3	2.1×10^4	5.0×10^4 (leveled)
Time between collisions (ns)	96	396	107	49.90	24.95	24.95
Full crossing angle (μ rad)	0	0	0	290	$320 \rightarrow 260^\dagger$	500
Energy spread (units 10^{-3})	e : 0.91 p : 0.2	0.14	0.15	0.1445	0.105	0.129
Bunch length (cm)	e : 0.83 p : 8.5	p : 50 \bar{p} : 45	60	9.4	8	9
Beam radius (10^{-6} m)	e : 110 (H), 30 (V) p : 111 (H), 30 (V)	p : 28 \bar{p} : 16	85	18.8	8.5^\ddagger	7^\ddagger
Free space at interaction point (m)	± 2	± 6.5	16	38	38	38
Initial luminosity decay time, $-L/(dL/dt)$ (hr)	10	6 (avg)	7.5	≈ 6	≈ 8	≈ 7.5 (leveled)
Turn-around time (min)	e : 75, p : 135	90	25	180	150	145
Injection energy (TeV)	e : 0.012 p : 0.040	0.15	0.023	0.450	0.450	0.450
Transverse emittance (10^{-9} m)	e : 20 (H), 3.5 (V) p : 5 (H), 5 (V)	p : 3 \bar{p} : 1	11	0.59	0.3	0.33
β^* , ampl. function at interaction point (m)	e : 0.6 (H), 0.26 (V) p : 2.45 (H), 0.18 (V)	0.28	0.65	0.6	$0.3 \rightarrow 0.29^\S$	$0.6 \rightarrow 0.15^\S$
Beam-beam tune shift per crossing (units 10^{-4})	e : 190 (H), 450 (V) p : 12 (H), 9 (V)	p : 120 \bar{p} : 120	73	72	45	86
RF frequency (MHz)	e : 499.7 p : 208.2/52.05	53	accel: 9 store: 28	400.8	400.8	400.8
Particles per bunch (units 10^{10})	e : 3 p : 7	p : 26 \bar{p} : 9	18.5	16	11	22
Bunches per ring per species	e : 189 p : 180	36	111	1380	2556 2544 (i.r. 1/5 ¶)	2760 2748 (i.r. 1/5 ¶)
Average beam current per species (mA)	e : 40 p : 90	p : 70 \bar{p} : 24	257	400	510	1100
Circumference (km)	6.336	6.28	3.834	26.659		
Interaction regions	2 colliding beams 1 fixed target (e beam)	2 high \mathcal{L}	6 total, 2 high \mathcal{L}	4 total, 2 high \mathcal{L}		
Magnetic length of dipole (m)	e : 9.185; p : 8.82	6.12	9.45	14.3		
Length of standard cell (m)	e : 23.5 p : 47	59.5	29.7	106.90		
Phase advance per cell (deg)	e : 60 p : 90	67.8	84	90		
Dipoles in ring	e : 396 p : 416	774	192 per ring + 12 common	1232 main dipoles		
Quadrupoles in ring	e : 580 p : 280	216	246 per ring	482 2-in-1 24 1-in-1		
Magnet types	e : C-shaped p : s.c., col., warm iron	s.c., $\cos\theta$ warm iron	s.c., $\cos\theta$ cold iron	s.c., 2-in-1 cold iron		
Peak magnetic field (T)	e : 0.274; p : 5	4.4	3.5	8.3 $^{\parallel}$		

*Other TEVATRON parameters: \bar{p} source accum. rate: $25 \times 10^{10} \text{ hr}^{-1}$; max. no. of \bar{p} stored: 3.4×10^{12} (Accumulator), 6.1×10^{12} (Recycler).

† Variable crossing angle decreasing during the fill with the reduction in bunch population

‡ Minimum beam radius during levelling

§ β^* levelling

¶ Number of bunches colliding at the interaction regions (i.r.) 1 (ATLAS) and 5 (CMS).

$^{\parallel}$ Value for design beam energy of 7 TeV.

High-Energy Collider Parameters: Heavy Ion Colliders

Table 32.5: Updated in March 2020 with numbers received from representatives of the collider (contact E. Pianori, LBNL) The table shows the parameter values achieved. For the LHC, only maximum values for the ATLAS and CMS experiments are provided (ALICE and LHCb have different requirements for energy and luminosity). Design values for a high-luminosity upgrade are also given. Quantities are, where appropriate, r.m.s.; unless noted otherwise, energies refer to beam energy; s.c. stands for superconducting. pk and avg denote peak and average values.

	RHIC (Brookhaven)			LHC (CERN)			
Physics start date	2000	2012 / 2018 / 2018 / 2012 / 2004 2014 / 2002 / 2015 / 2015		2010	2012	2017	≥ 2021 (high lum.)*
Physics end date	—			—			
Particles collided	Au Au	U U / Zr Zr / Ru Ru / Cu Au Cu Cu / h Au d Au / p Au / p Al		Pb Pb	p Pb	Xe Xe	Pb Pb
Max. beam energy (TeV/n)	0.1	0.1		2.51	p:6.5 Pb:2.56	2.72	2.76
$\sqrt{s_{NN}}$ (TeV)	0.2	0.2		5.02	8.16	5.44	5.5
Max. delivered int. nucleon-pair lumin. per exp. (pb^{-1})	2639 (at 100 GeV/n)	21 / 36 / 36.9 / 167 / 60 43 / 169 / 124 / 63 (all at 100 GeV/n)		77.8	194	0.05	$\approx 121/y$
Luminosity ($10^{27} \text{ cm}^{-2} \text{ s}^{-1}$)	pk: 15.5 avg: 8.7	pk: 0.4 / 4.8 / 3.8 / 12 / 21 170 / 850 / 880 / 7600 avg: 0.6 / 2.2 / 2.1 / 10 / 8 100 / 500 / 450 / 3800		6.1	900	0.4	6.4 (leveled)
Time between collisions (ns)	107	107 / 107 / 107 107/ 107 / 321 107 / 107 / 107 / 107		74.9 / 149.7	99.8 / 149.7	≈ 5500	49.9
Full crossing angle (μ rad)	0	0		320	280	300	340
Energy spread (units 10^{-3})	0.75	0.75		0.11	0.11	0.11	0.11
Bunch length (cm)	30	30		8.0	p / Pb: 9 / 11.5	11	7.9
Beam radius (10^{-6} m)	114 [†]	123 [†] / 87 [†] / 88 [†] / 163 [†] / 145 [†] 136 [†] / 124 [†] / 147 [†] / 128 [†]		21	19	12	17
Free space at inter. point (m)	16	16		38	38	38	38
Initial luminosity decay time, $-L/(dL/dt)$ (hr)	1	$-0.35^{\ddagger} / \infty^{\S} / \infty^{\S} / \infty^{\ddagger} / 1.8$ $0.6 / \infty^{\ddagger} / 0.5 / 0.25$		3.3	≈ 2	≈ 6	∞
Turn-around time (min)	30	60 [¶] / 40 [¶] / 40 [¶] / 160 [¶] / 90 [¶] 45 [¶] / 90 [¶] / 60 [¶] / 50 [¶]		≈ 180	150	180	≈ 200
Injection energy (TeV/n)	0.011	0.011		0.177	p / Pb: 0.45 / 0.177	0.188	0.177
Transverse emittance (10^{-9} m)	19 [†]	22 [†] / 10.7 [†] / 11.2 [†] / 38 [†] / 23 [†] 19 [†] / 22 [†] / 26 [†] / 21 [†]		0.85	0.29	0.3	0.5
β^* , ampl. function at interaction point (m)	0.7	0.7 / 0.7 / 0.7 / 0.7 / 0.9 1.0 / 0.7 / 0.8 / 0.8		0.5	0.5	0.4	0.5
Beam-beam tune shift per crossing (units 10^{-4})	39 [†]	6 [†] / 18 [†] / 21 [†] / 14 [†] , 14 [†] / 30 [†] / 42 [†] , 22 [†] 40 [†] , 27 [†] / 53 [†] , 41 [†] / 80 [†] , 59 [†]		15	15	≈ 10	11
RF frequency (MHz)	accel: 28, store: 197			400.8	400.8	400.8	400.8
Particles per bunch (units 10^{10})	0.20	0.03 / 0.1 / 0.1 / 0.4, 0.13 / 0.45 4.5, 0.13 / 13, 0.20 / 22.5, 0.16 / 24, 1.1		0.022 (r.m.s.)	p:2.6 Pb:0.022	0.027	0.018
Bunches per ring per species	111	111 / 111 / 111 / 111 / 37 111 / 111 / 111 / 111		733	p:540 Pb:684	16	1232
Average beam current per species (mA)	224	38 / 56 / 61 / 160, 138 / 60 / 125, 143 181, 213 / 313, 176 / 334, 199		23.8	p:16 Pb:15	0.54	32
Circumference (km)	3.834			26.659			
Interaction regions	6 total, 2 high \mathcal{L}			4 total, 3 high \mathcal{L}			
Magnetic length of dipole (m)	9.45			14.3			
Length of standard cell (m)	29.7			106.90			
Phase advance per cell (deg)	93	84 / 84 / 84 / 84 / 84 93 / 84(d), 93 / 84(p), 93 / 84(p), 93		90			
Dipoles in ring	192 per ring, + 12 common			1232, main dipoles			
Quadrupoles in ring	246 per ring			482 2-in-1, 24 1-in-1			
Magnet Type	s.c. $\cos\theta$, cold iron			s.c., 2 in 1, cold iron			
Peak magnetic field (T)	3.5			8.3			

*High luminosity upgrade expected ≥ 2021 ; will extend throughout HL-LHC running. Very preliminary, conservative estimates.

[†]Initial value, possibly larger after cooling

[‡]Negative or infinite decay time is effect of cooling.

[§]luminosity leveled to flat after set to target value, with cooling

[¶]measured minimum, not theoretical

33. Neutrino Beam Lines at High-Energy Proton Synchrotrons

Revised August 2019 with numbers verified by representatives of the synchrotrons (contact C.-J. Lin, LBNL). For existing (future) neutrino beam lines the latest achieved (design) values are given.

The main source of neutrinos at proton synchrotrons is from the decay of pions and kaons produced by protons striking a nuclear target. There are different schemes to focus the secondary particles to enhance neutrino flux and/or tune the neutrino energy profile. In wide-band beams (WBB), the neutrino parent mesons are focused over a wide momentum range to obtain maximum neutrino intensity. In narrow-band beams (NBB), the secondary particles are first momentum-selected to produce a monochromatic parent beam. Another approach to generate a narrow-band neutrino spectrum is to select neutrinos that are emitted off-axis relative to the momentum of the parent mesons. For a comprehensive review of the topic, including other historical neutrino beam lines, see the article by S. E. Kopp, "Accelerator-based neutrino beams," Phys. Rept. **439**, 101 (2007).

	PS (CERN)				SPS (CERN)				PS (KEK)	Main Ring (JPARC)
	1963	1969	1972	1983	1977	1977	1995	2006	1999	2017
Date	1963	1969	1972	1983	1977	1977	1995	2006	1999	2017
Proton Kinetic Energy (GeV)	20.6	20.6	26	19	350	350	450	400	12	30 (50)
Protons per Cycle (10^{12})	0.7	0.6	5	5	10	10	36	48	6	240 (330)
Cycle Time (s)	3	2.3	-	-	-	-	14.4	6	2.2	2.48 (3.5)
Beam Power (kW)	0.8	0.9	-	-	-	-	180	510	5	500 (750)
Target	-	-	-	-	-	-	Be	Graphite	Al	Graphite
Target Length (cm)	-	-	-	-	-	-	290	130	66	91
Secondary Focussing	1-horn WBB	3-horn WBB	2-horn WBB	bare target	dichromatic NBB	2-horn WBB	2-horn WBB	2-horn WBB	2-horn WBB	3-horn off-axis
Decay Pipe Length (m)	-	-	-	-	-	-	110	1090	200	96
$\langle E_\nu \rangle$ (GeV)	1.5	1.5	1.5	1	50,150 [†]	20	24.3	17	1.3	0.6
Experiments	HLBC, Spark Ch.	HLBC, Spark Ch.	GGM, Aachen-Padova	CDHS, CHARM	CDHS, CHARM, BEBC	GGM, CDHS, CHARM, BEBC	NOMAD, CHORUS	OPERA, ICARUS	K2K	T2K

	Main Ring (Fermilab)					Booster (Fermilab)	Main Injector (Fermilab)			
	1974	1979	1976	1991	1998	2002, (2020)	2005	2017	(2020)	(2026)
Date	1974	1979	1976	1991	1998	2002, (2020)	2005	2017	(2020)	(2026)
Proton Kinetic Energy (GeV)	300	400	350	800	800	8	120	120	120	(60 – 120)
Protons per Cycle (10^{12})	10	10	13	10	12	4.5	37	54	(65)	(75)
Cycle Time (s)	-	-	-	60	60	0.2	2	1.333	(1.2)	(1.2)
Beam Power (kW)	-	-	-	20	25	29	350	720	(1000)	(1200)
Target	-	-	-	-	BeO	Be	Graphite	Graphite	Graphite	(Graphite)
Target Length (cm)	-	-	-	-	31	71	95	120	120	(150-220)
Secondary Focussing	dichromatic NBB	2-horn WBB	1-horn WBB	quad trip.	SSQT WBB	1-horn WBB	2-horn WBB	2-horn off-axis	2-horn off-axis	(3-horn WBB)
Decay Pipe Length (m)	400	400	400	400	400	50	675	675	675	(220)
$\langle E_\nu \rangle$ (GeV)	50,180 [†]	25	100	90,260	70,180	1	3-20 [‡]	2	2	(2.5)
Experiments	CITF, HPWF, 15' BC	15' BC	HPWF 15' BC	15' BC, CCFRR	NuTeV	MiniBooNE, SciBooNE, MicroBooNE, (SBND, ICARUS)	MINOS, MINERνA	NOνA, MINERνA, MINOS+	NOνA	LBNF/ DUNE

[†]Pion and kaon peaks in the momentum-selected channel.

[‡]Tunable WBB energy spectrum.

34. Passage of Particles Through Matter

Revised August 2019 by D.E. Groom (LBNL) and S.R. Klein (NSD LBLN).

34.1	Notation	535
34.2	Electronic energy loss by heavy particles	535
34.2.1	Moments and cross sections	535
34.2.2	Maximum energy transfer in a single collision	535
34.2.3	Stopping power at intermediate energies	536
34.2.4	Mean excitation energy	538
34.2.5	Density effect	538
34.2.6	Energy loss at low energies	538
34.2.7	Energetic knock-on electrons (δ rays)	538
34.2.8	Restricted energy loss rates for relativistic ionizing particles	539
34.2.9	Fluctuations in energy loss	539
34.2.10	Energy loss in mixtures and compounds	540
34.2.11	Ionization yields	540
34.3	Multiple scattering through small angles	540
34.4	Photon and electron interactions in matter	541
34.4.1	Collision energy losses by e^\pm	541
34.4.2	Radiation length	541
34.4.3	Bremsstrahlung energy loss by e^\pm	542
34.4.4	Critical energy	542
34.4.5	Energy loss by photons	543
34.4.6	Bremsstrahlung and pair production at very high energies	543
34.4.7	Photonuclear and electronuclear interactions at still higher energies	544
34.5	Electromagnetic cascades	545
34.6	Muon energy loss at high energy	546
34.7	Cherenkov and transition radiation	547
34.7.1	Optical Cherenkov radiation	547
34.7.2	Coherent radio Cherenkov radiation	547
34.7.3	Transition radiation	548

This review covers the interactions of photons and electrically charged particles in matter, concentrating on energies of interest for high-energy physics and astrophysics and processes of interest for particle detectors (ionization, Cherenkov radiation, transition radiation). Much of the focus is on particles heavier than electrons (π^\pm , p , etc.). Although the charge number z of the projectile is included in the equations, only $z = 1$ is discussed in detail. Muon radiative losses are discussed, as are photon/electron interactions at high to ultrahigh energies. Neutrons are not discussed.

34.1 Notation

The notation and important numerical values are shown in Table 34.1.

34.2 Electronic energy loss by heavy particles

34.2.1 Moments and cross sections

The electronic interactions of fast charged particles with speed $v = \beta c$ occur in *single collisions with energy losses* W [1], leading to ionization, atomic, or collective excitation. Most frequently the energy losses are small (for 90% of all collisions the energy losses are less than 100 eV). In thin absorbers few collisions will take place and the total energy loss will show a large variance [1]; also see Sec. 34.2.9 below. For particles with charge ze more massive than electrons (“heavy” particles), scattering from free electrons is adequately described by the Rutherford differential cross section [2],

$$\frac{d\sigma_R(W; \beta)}{dW} = \frac{2\pi r_e^2 m_e c^2 z^2}{\beta^2} \frac{(1 - \beta^2 W/W_{\max})}{W^2}, \quad (34.1)$$

where W_{\max} is the maximum energy transfer possible in a single collision. But in matter electrons are not free. W must be finite and depends on atomic and bulk structure. For electrons bound in atoms Bethe [3] used “Born Theorie” to obtain the differential cross section

$$\frac{d\sigma_B(W; \beta)}{dW} = \frac{d\sigma_R(W; \beta)}{dW} B(W). \quad (34.2)$$

Electronic binding is accounted for by the correction factor $B(W)$. Examples of $B(W)$ and $d\sigma_B/dW$ can be seen in Figs. 5 and 6 of Ref. [1].

Table 34.1: Summary of variables used in this section. The kinematic variables β and γ have their usual relativistic meanings.

Symb.	Definition	Value or (usual) units
$m_e c^2$	electron mass $\times c^2$	0.510 998 950 00(15) MeV
r_e	classical electron radius $e^2/4\pi\epsilon_0 m_e c^2$	2.817 940 3262(13) fm
α	fine structure constant $e^2/4\pi\epsilon_0 \hbar c$	1/137.035 999 084(21)
N_A	Avogadro’s number	6.022 140 76 $\times 10^{23}$ mol $^{-1}$
ρ	density	g cm $^{-3}$
x	mass per unit area	g cm $^{-2}$
M	incident particle mass	MeV/ c^2
E	incident part. energy $\gamma M c^2$	MeV
T	kinetic energy, $(\gamma - 1) M c^2$	MeV
W	energy transfer to an electron in a single collision	MeV
W_{\max}	Maximum possible energy transfer to an electron in a single collision	MeV
k	bremsstrahlung photon energy	MeV
z	charge number of incident particle	
Z	atomic number of absorber	
A	atomic mass of absorber	g mol $^{-1}$
K	$4\pi N_A r_e^2 m_e c^2$ (Coefficient for dE/dx)	0.307 075 MeV mol $^{-1}$ cm 2
I	mean excitation energy	eV (<i>Nota bene!</i>)
$\delta(\beta\gamma)$	density effect correction to ionization energy loss	
$\hbar\omega_p$	plasma energy $\sqrt{4\pi N_e r_e^3 m_e c^2}/\alpha$	$\sqrt{\rho(Z/A)} \times 28.816$ eV $\hookrightarrow \rho$ in g cm $^{-3}$
N_e	electron density	(units of r_e) $^{-3}$
w_j	weight fraction of the j th element in a compound or mixt.	
n_j	α number of j th kind of atoms in a compound or mixture	
X_0	radiation length	g cm $^{-2}$
E_c	critical energy for electrons	MeV
$E_{\mu c}$	critical energy for muons	GeV
E_s	scale energy $\sqrt{4\pi/\alpha} m_e c^2$	21.2052 MeV
R_M	Molière radius	g cm $^{-2}$

Bethe’s original theory applies only to energies above which atomic effects are not important. The free-electron cross section (Eq. (34.1)) can be used to extend the cross section to W_{\max} . At high energies σ_B is further modified by polarization of the medium, and this “density effect,” discussed in Sec. 34.2.5, must also be included. Smaller corrections are discussed below.

The mean number of collisions with energy loss between W and $W + dW$ occurring in a distance δx is $N_e \delta x (d\sigma/dW) dW$, where $d\sigma(W; \beta)/dW$ contains all contributions. It is convenient to define the moments

$$M_j(\beta) = N_e \delta x \int W^j \frac{d\sigma(W; \beta)}{dW} dW, \quad (34.3)$$

so that M_0 is the mean number of collisions in δx , M_1 is the mean energy loss in δx , $(M_2 - M_1^2)$ is the variance, etc. The number of collisions is Poisson-distributed with mean M_0 . N_e is either measured in electrons/g ($N_e = N_A Z/A$) or electrons/cm 3 ($N_e = N_A \rho Z/A$). The former is used throughout this chapter, since quantities of interest (dE/dx , X_0 , etc.) vary smoothly with composition when there is no density dependence.

34.2.2 Maximum energy transfer in a single collision

For a particle with mass M ,

$$W_{\max} = \frac{2m_e c^2 \beta^2 \gamma^2}{1 + 2\gamma m_e/M + (m_e/M)^2}. \quad (34.4)$$

In older references [2, 7] the “low-energy” approximation $W_{\max} = 2m_e c^2 \beta^2 \gamma^2$, valid for $2\gamma m_e \ll M$, is often implicit. For

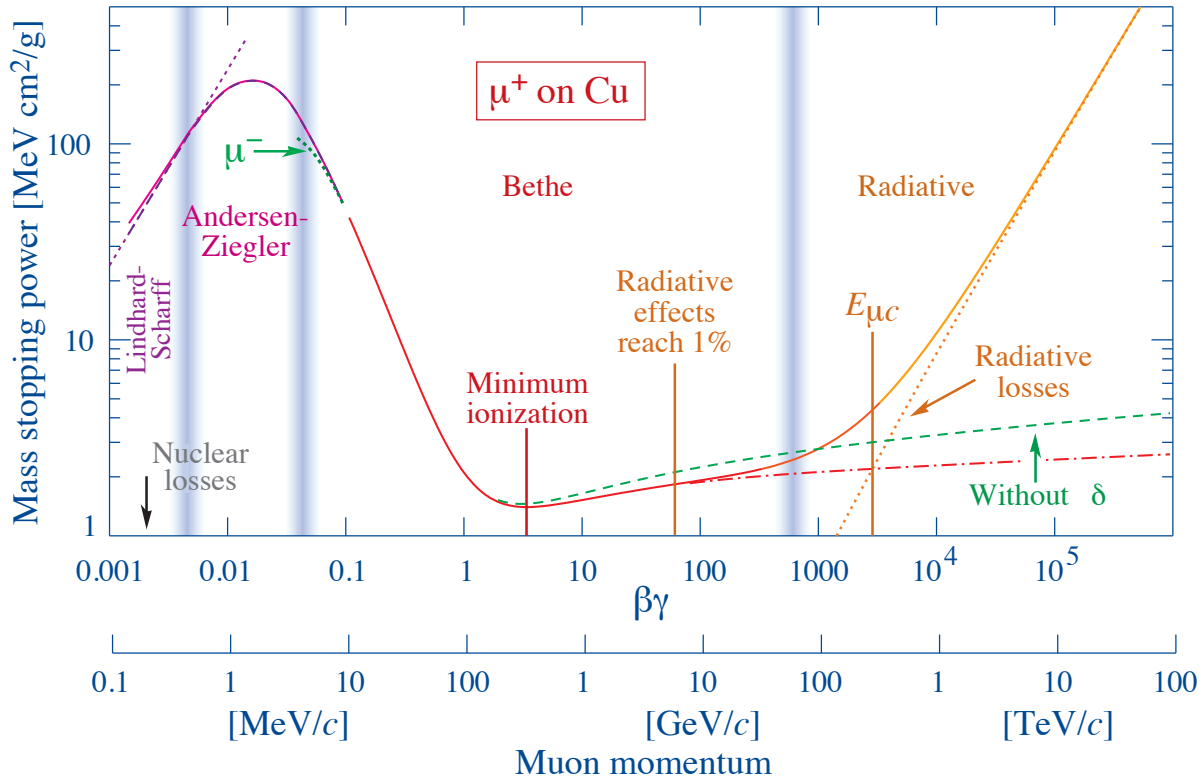


Figure 34.1: Mass stopping power ($= \langle -dE/dx \rangle$) for positive muons in copper as a function of $\beta\gamma = p/Mc$ over nine orders of magnitude in momentum (12 orders of magnitude in kinetic energy). Solid curves indicate the total stopping power. Data below the break at $\beta\gamma \approx 0.1$ are taken from ICRU 49 [4] assuming only β dependence, and data at higher energies are from [5]. Vertical bands indicate boundaries between different approximations discussed in the text. The short dotted lines labeled “ μ^- ” illustrate the “Barkas effect”, the dependence of stopping power on projectile charge at very low energies [6]. dE/dx in the radiative region is not simply a function of β .

a pion in copper, the error thus introduced into dE/dx is greater than 6% at 100 GeV. For $2\gamma m_e \gg M$, $W_{\max} = Mc^2 \beta^2 \gamma$.

At energies of order 100 GeV, the maximum 4-momentum transfer to the electron can exceed 1 GeV/c, where hadronic structure effects modify the cross sections. This problem has been investigated by J.D. Jackson [8], who concluded that for incident hadrons (but not for large nuclei) corrections to dE/dx are negligible below energies where radiative effects dominate. While the cross section for rare hard collisions is modified, the average stopping power, dominated by many softer collisions, is almost unchanged.

34.2.3 Stopping power at intermediate energies

The mean rate of energy loss by moderately relativistic charged heavy particles is well described by the “Bethe equation,”

$$\left\langle -\frac{dE}{dx} \right\rangle = K z^2 \frac{Z}{A} \frac{1}{\beta^2} \left[\frac{1}{2} \ln \frac{2m_e c^2 \beta^2 \gamma^2 W_{\max}}{I^2} - \beta^2 - \frac{\delta(\beta\gamma)}{2} \right]. \quad (34.5)$$

Eq. (34.5) is valid in the region $0.1 \lesssim \beta\gamma \lesssim 1000$ with an accuracy of a few percent. Small corrections are discussed below.

This is the *mass stopping power*; with the symbol definitions and values given in Table 34.1, the units are $\text{MeV g}^{-1}\text{cm}^2$. As can be seen from Fig. 34.2, $\langle dE/dx \rangle$ defined in this way is about the same for most materials, decreasing slowly with Z . The *linear stopping power*, in MeV/cm , is $\rho \langle dE/dx \rangle$, where ρ is the density in g/cm^3 .

At $\beta\gamma \sim 0.1$ the projectile velocity is comparable to atomic electron “velocities” (Sec. 34.2.6), and at $\beta\gamma \sim 1000$ radiative effects begin to be important (Sec. 34.6). Both limits are Z dependent. A minor dependence on M at high energies is introduced through W_{\max} , but for all practical purposes $\langle dE/dx \rangle$ in a given material is a function of β alone.

The stopping power at first falls as $1/\beta^\alpha$ where $\alpha \approx 1.4$ – 1.7 ,

depending slightly on the incident particle’s mass and decreasing somewhat with Z , and reaches a broad minimum at $\beta\gamma = 3.5$ – 3.0 as Z goes from 7 to 100. It then inexorably rises as the argument of the logarithmic term increases. Two independent mechanisms contribute. Two thirds of the rise is produced by the explicit $\beta^2 \gamma^2$ dependence through the relativistic flattening and extension of the particle’s electric field. Rather than producing ionization at greater and greater distances, the field polarizes the medium, cancelling the increase in the logarithmic term at high energies. This is taken into account by the density-effect correction $\delta(\beta\gamma)$. The other third is introduced by the $\beta^2 \gamma$ dependence of W_{\max} , the maximum possible energy transfer to a recoil electron. “Hard collision” events increasingly extend the tail of the energy loss distribution, increasing the mean but with little effect on the position of the maximum, the most probable energy loss.

Few concepts in high-energy physics are as misused as dE/dx , since the mean is weighted by rare events with large single-collision energy losses. Even with samples of hundreds of events in a typical detector, the mean energy loss cannot be obtained dependably. Far better and more easily measured is the most probable energy loss, discussed in Sec. 34.2.9. The most probable energy loss in a typical detector is considerably smaller than the mean given by the Bethe equation. It does not continue to rise with the mean stopping power, but approaches a “Fermi plateau.”

In analysing TPC data (Sec. 35.6.5), the same end is often accomplished by using the mean of 50%–70% of the samples with the smallest signals as the estimator.

Although it must be used with cautions and caveats, $\langle dE/dx \rangle$ as described in Eq. (34.5) still forms the basis of much of our understanding of energy loss by charged particles. Extensive tables are available [4, 5] and pdg.lbl.gov/AtomicNuclearProperties/.

For heavy projectiles, like ions, additional terms are required to account for higher-order photon coupling to the target, and to account for the finite target radius. These can change dE/dx by a

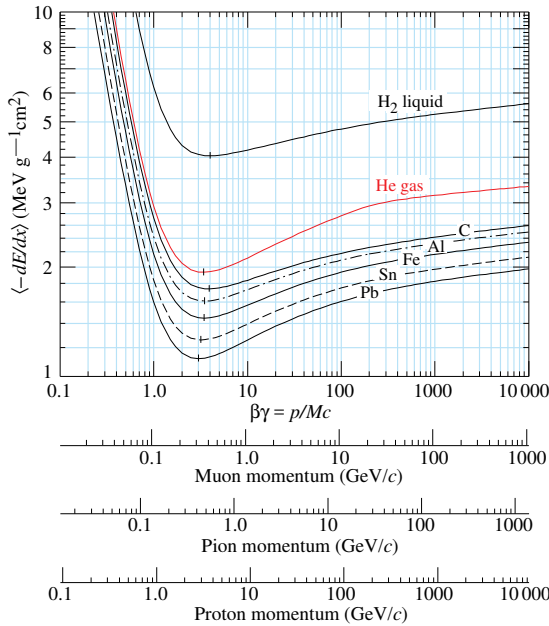


Figure 34.2: Mean energy loss rate in liquid (bubble chamber) hydrogen, gaseous helium, carbon, aluminum, iron, tin, and lead. Radiative effects, relevant for muons and pions, are not included. These become significant for muons in iron for $\beta\gamma \gtrsim 1000$, and at lower momenta for muons in higher- Z absorbers. See Fig. 34.23.

factor of two or more for the heaviest nuclei in certain kinematic regimes [9].

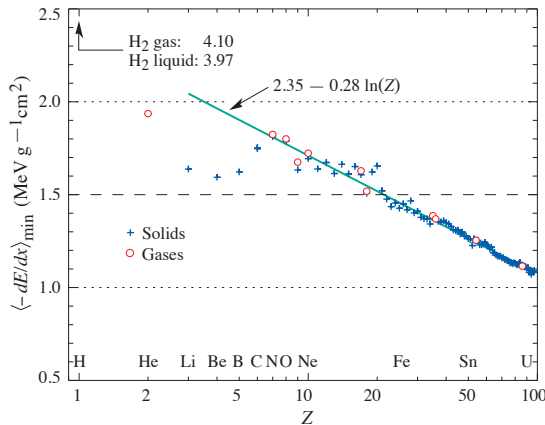


Figure 34.3: Mass stopping power at minimum ionization for the chemical elements. The straight line is fitted for $Z > 6$. A simple functional dependence on Z is not to be expected, since $\langle -dE/dx \rangle$ also depends on other variables.

The function as computed for muons on copper is shown as the “Bethe” region of Fig. 34.1. Mean energy loss behavior below this region is discussed in Sec. 34.2.6, and the radiative effects at high energy are discussed in Sec. 34.6. Only in the Bethe region is it a function of β alone; the mass dependence is more complicated elsewhere. The stopping power in several other materials is shown in Fig. 34.2. Except in hydrogen, particles with the same velocity have similar rates of energy loss in different materials, although there is a slow decrease in the rate of energy loss with increasing Z . The qualitative behavior difference at high energies between a gas (He in the figure) and the other materials shown in the figure is due to the density-effect correction, $\delta(\beta\gamma)$, discussed in Sec. 34.2.5. The stopping power functions are characterized by broad minima whose position drops from $\beta\gamma = 3.5$ to 3.0 as Z goes from 7 to 100. The values of minimum ionization as a function of atomic number are shown in Fig. 34.3.

In practical cases, most relativistic particles (*e.g.*, cosmic-ray muons) have mean energy loss rates close to the minimum; they are “minimum-ionizing particles,” or mip’s.

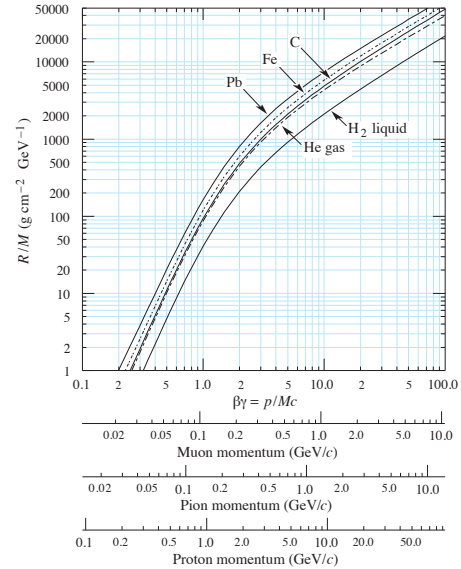


Figure 34.4: Range of heavy charged particles in liquid (bubble chamber) hydrogen, helium gas, carbon, iron, and lead. For example: For a K^+ whose momentum is 700 MeV/ c , $\beta\gamma = 1.42$. For lead we read $R/M \approx 396$, and so the range is 195 g cm⁻² (17 cm).

Eq. (34.5) may be integrated to find the total (or partial) “continuous slowing-down approximation” (CSDA) range R for a particle which loses energy only through ionization and atomic excitation. Since dE/dx depends only on β , R/M is a function of E/M or pc/M . In practice, range is a useful concept only for low-energy hadrons ($R \lesssim \lambda_I$, where λ_I is the nuclear interaction length), and for muons below a few hundred GeV (above which radiative effects dominate). Fig. 34.4 shows R/M as a function of $\beta\gamma$ ($= p/Mc$) for a variety of materials.

The mass scaling of dE/dx and range is valid for the electronic losses described by the Bethe equation, but not for radiative losses.

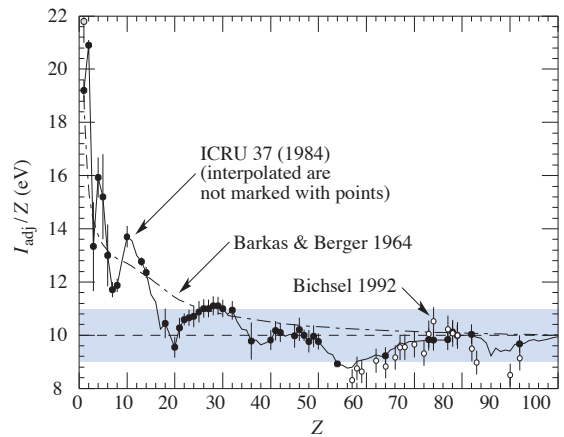


Figure 34.5: Mean excitation energies (divided by Z) as adopted by the ICRU [10]. Those based on experimental measurements are shown by symbols with error flags; the interpolated values are simply joined. The grey point is for liquid H₂; the black point at 19.2 eV is for H₂ gas. The open circles show more recent determinations by Bichsel [11]. The dash-dotted curve is from the approximate formula of Barkas [12] used in early editions of this Review.

34.2.4 Mean excitation energy

“The determination of the mean excitation energy is the principal non-trivial task in the evaluation of the Bethe stopping-power formula” [13]. Recommended values have varied substantially with time. Estimates based on experimental stopping-power measurements for protons, deuterons, and alpha particles and on oscillator-strength distributions and dielectric-response functions were given in ICRU 49 [4]. See also ICRU 37 [10]. These values, shown in Fig. 34.5, have since been widely used. Machine-readable versions can also be found [14].

34.2.5 Density effect

As the particle energy increases, its electric field flattens and extends, so that the distant-collision contribution to the logarithmic term in Eq. (34.5) increases as $\beta^2\gamma^2$. However, real media become polarized, limiting the field extension and effectively truncating this part of the logarithmic rise [2–5,15,16]. At very high energies,

$$\delta(\beta\gamma)/2 \rightarrow \ln(\hbar\omega_p/I) + \ln\beta\gamma - 1/2, \quad (34.6)$$

where $\delta(\beta\gamma)/2$ is the density effect correction introduced in Eq. (34.5) and $\hbar\omega_p$ is the plasma energy defined in Table 34.1. A comparison with Eq. (34.5) shows that $|dE/dx|$ then grows as $\ln T_{\max}$ rather than $\ln\beta^2\gamma^2 T_{\max}$, and that the mean excitation energy I is replaced by the plasma energy $\hbar\omega_p$. An example of the ionization stopping power as calculated with and without the density effect correction is shown in Fig. 34.1. Since the plasma frequency scales as the square root of the electron density, the correction is much larger for a liquid or solid than for a gas, as is illustrated in Fig. 34.2.

The density effect correction is usually computed using Sternheimer’s parameterization [15]:

$$\delta(\beta\gamma) = \begin{cases} 2(\ln 10)x - \bar{C} & \text{if } x \geq x_1; \\ 2(\ln 10)x - \bar{C} + a(x_1 - x)^k & \text{if } x_0 \leq x < x_1; \\ 0 & \text{if } x < x_0 \text{ (nonconductors);} \\ \delta_0 10^{2(x-x_0)} & \text{if } x < x_0 \text{ (conductors)} \end{cases} \quad (34.7)$$

Here $x = \log_{10} \beta\gamma = \log_{10}(p/Mc)$. \bar{C} (the negative of the C used in Ref. [15]) is obtained by equating the high-energy case of Eq. (34.7) with the limit given in Eq. (34.6). The other parameters are adjusted to give a best fit to the results of detailed calculations for momenta below $Mc \exp(x_1)$. For nonconductors the correction is 0 below $\beta\gamma = 10^{x_0}$, corresponding to 100–200 MeV for pions and 1–2 GeV for protons. For conductors it decreases rapidly below this point. Parameters for the elements and nearly 200 compounds and mixtures of interest are published in a variety of places, notably in Ref. [16]. A recipe for finding the coefficients for nontabulated materials is given by Sternheimer and Peierls [17] and is summarized in Ref. [5].

The remaining relativistic rise comes from the $\beta^2\gamma$ growth of W_{\max} , which in turn is due to (rare) large energy transfers to a few electrons. When these events are excluded, the energy deposit in an absorbing layer approaches a constant value, the Fermi plateau (see Sec. 34.2.8 below). At even higher energies (e.g., > 332 GeV for muons in iron, and at a considerably higher energy for protons in iron), radiative effects are more important than ionization losses. These are especially relevant for high-energy muons, as discussed in Sec. 34.6.

34.2.6 Energy loss at low energies

The theory of energy loss by ionization and excitation as given by Bethe is based on a first-order Born approximation. It assumes free electrons, and should be valid when the projectile’s velocity is large compared to that of the atomic electrons. This presents a problem at low energies, where W_{\max} is less than the K shell binding energy. However, Mott showed that the Born approximation can be applied at energies much smaller than atomic binding energies [18]; the incident particle can be treated by classical mechanics since its wavelength is shorter than atomic dimensions. The Born method is actually better justified when its velocity is not large compared to the K electron velocity [19].

Higher-order corrections must still be made to extend the Bethe equation Eq. (34.5) to low energies, e.g. below 10 MeV for protons.

An improved approximation for the terms in the square brackets of Eq. (34.5) at low energies is obtained with

$$L(\beta) = L_a(\beta) - \frac{C(\beta)}{Z} + zL_1(\beta) + z^2L_2(\beta). \quad (34.8)$$

Here L_a is the square-bracketed terms of Eq. (34.5), C/Z is the sum of shell corrections and zL_1 and z^2L_2 are Barkas and Bloch correction terms [4,20]. With these corrections, the Bethe treatment is accurate to about 1% down to $\beta \approx 0.05$, or about 1 MeV for protons.

Shell correction $-C/Z$. As the velocity of the projectile decreases, the contribution to the stopping power from K shell electrons decreases, and at even lower velocities contributions from L and higher shells further reduce it. The correction $(C_K + C_L + \dots)/Z$ is included in the square brackets of Eq. (34.5). It is calculated and tabulated (for a few common materials) in a number of places; Refs. [4,10,20] are especially useful. As an example, the shell correction for a 30 MeV proton traversing aluminum is 0.6%, but increases to 9.9% as the proton’s energy decreases to 0.3 MeV.

Barkas correction zL_1 . Qualitatively, one might imagine an atom’s electron cloud slightly recoiling at the approach of a negative projectile and being attracted toward an approaching positive projectile. Hence the stopping power for negative particles should be slightly smaller than the stopping power for positive particles. In a 1956 paper, Barkas *et al.* noted that negative pions possibly had a longer range than positive pions [6]. The effect has been measured for a number of negative/positive particle pairs, and more recently in detailed studies with antiprotons at the CERN LEAR facility [21]. Since no complete theory exists, an empirical approach is necessary. A 1972 harmonic-oscillator model by Ashley *et al.* [22] is often used; it has two parameters determined by experimental data.

Bloch correction z^2L_2 . Bloch’s extension of Bethe’s theory introduced a low-energy correction that takes account of perturbations of the atomic wave functions. The form obtained by Lindhard and Sørensen [9] is used e.g. in Refs. [4,20].

For the interval $0.01 < \beta < 0.05$ there is no satisfactory theory. For protons, one usually relies on the phenomenological fitting formulae developed by Andersen and Ziegler [4,23]. As tabulated in ICRU 49 [4], the nuclear plus electronic proton stopping power in copper is $113 \text{ MeV cm}^2 \text{ g}^{-1}$ at $T = 10 \text{ keV}$ ($\beta\gamma = 0.005$), rises to a maximum of $210 \text{ MeV cm}^2 \text{ g}^{-1}$ at $T \approx 120 \text{ keV}$ ($\beta\gamma = 0.016$), then falls to $118 \text{ MeV cm}^2 \text{ g}^{-1}$ at $T = 1 \text{ MeV}$ ($\beta\gamma = 0.046$). Above 0.5–1.0 MeV the corrected Bethe theory is adequate.

For particles moving more slowly than $\approx 0.01c$ (more or less the velocity of the outer atomic electrons), Lindhard has been quite successful in describing electronic stopping power, which is proportional to β [24]. Finally, we note that at even lower energies, e.g., for protons of less than several hundred eV, non-ionizing nuclear recoil energy loss dominates the total energy loss [4,24,25].

34.2.7 Energetic knock-on electrons (δ rays)

The distribution of secondary electrons with kinetic energies $T \gg I$ is [2]

$$\frac{d^2N}{dTdx} = \frac{1}{2} K z^2 \frac{Z}{A} \frac{1}{\beta^2} \frac{F(T)}{T^2} \quad (34.9)$$

for $I \ll T \leq W_{\max}$, where W_{\max} is given by Eq. (34.4). Here β is the velocity of the primary particle. The factor F is spin-dependent, but is about unity for $T \ll W_{\max}$. For spin-0 particles $F(T) = (1 - \beta^2 T/W_{\max})$; forms for spins 1/2 and 1 are also given by Rossi [2] (Sec. 2.3, Eqs. 7 and 8). Additional formulae are given in [26]. Equation Eq. (34.9) is inaccurate for T close to I [27].

δ rays of even modest energy are rare. For a $\beta \approx 1$ particle, for example, on average only one collision with $T_e > 10 \text{ keV}$ will occur along a path length of 90 cm of argon gas [1].

A δ ray with kinetic energy T_e and corresponding momentum p_e is produced at an angle θ given by

$$\cos \theta = (T_e/p_e)(p_{\max}/W_{\max}), \quad (34.10)$$

where p_{\max} is the momentum of an electron with the maximum possible energy transfer W_{\max} .

34.2.8 Restricted energy loss rates for relativistic ionizing particles

Further insight can be obtained by examining the mean energy deposit by an ionizing particle when energy transfers are restricted to $T \leq W_{\text{cut}} \leq W_{\text{max}}$. The restricted energy loss rate is

$$-\frac{dE}{dx} \Big|_{T < W_{\text{cut}}} = K z^2 \frac{Z}{A} \frac{1}{\beta^2} \left[\frac{1}{2} \ln \frac{2m_e c^2 \beta^2 \gamma^2 W_{\text{cut}}}{I^2} - \frac{\beta^2}{2} \left(1 + \frac{W_{\text{cut}}}{W_{\text{max}}} \right) - \frac{\delta}{2} \right]. \quad (34.11)$$

This form approaches the normal Bethe function (Eq. (34.5)) as $W_{\text{cut}} \rightarrow W_{\text{max}}$. It can be verified that the difference between Eq. (34.5) and Eq. (34.11) is equal to $\int_{W_{\text{cut}}}^{W_{\text{max}}} T(d^2N/dTdx)dT$, where $d^2N/dTdx$ is given by Eq. (34.9).

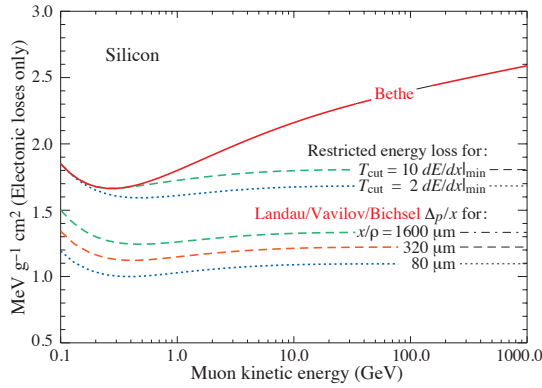


Figure 34.6: Bethe dE/dx , two examples of restricted energy loss, and the Landau most probable energy per unit thickness in silicon. The change of Δ_p/x with thickness x illustrates its $a \ln x + b$ dependence. Minimum ionization ($dE/dx|_{\text{min}}$) is $1.664 \text{ MeV g}^{-1} \text{ cm}^2$. Radiative losses are excluded. The incident particles are muons.

Since W_{cut} replaces W_{max} in the argument of the logarithmic term of Eq. (34.5), the $\beta\gamma$ term producing the relativistic rise in the close-collision part of dE/dx is replaced by a constant, and $|dE/dx|_{T < W_{\text{cut}}}$ approaches the constant “Fermi plateau.” (The density effect correction δ eliminates the explicit $\beta\gamma$ dependence produced by the distant-collision contribution.) This behavior is illustrated in Fig. 34.6, where restricted loss rates for two examples of W_{cut} are shown in comparison with the full Bethe dE/dx and the Landau-Vavilov most probable energy loss (to be discussed in Sec. 34.2.9 below).

“Restricted energy loss” is cut at the total mean energy, not the single-collision energy above W_{cut} . It is of limited use. The most probable energy loss, discussed in the next Section, is far more useful in situations where single-particle energy loss is observed.

34.2.9 Fluctuations in energy loss

For detectors of moderate thickness x (e.g. scintillators or LAr cells),¹ the energy loss probability distribution $f(\Delta; \beta\gamma, x)$ is adequately described by the highly-skewed Landau (or Landau-Vavilov) distribution [28, 29].

The most probable energy loss is [30]²

$$\Delta_p = \xi \left[\ln \frac{2mc^2 \beta^2 \gamma^2}{I} + \ln \frac{\xi}{I} + j - \beta^2 - \delta(\beta\gamma) \right], \quad (34.12)$$

¹“Moderate thickness” means $G \lesssim 0.05-0.1$, where G is given by Rossi Ref. [2], Eq. 2.7(10). It is Vavilov’s κ [28]. G is proportional to the absorber’s thickness, and as such parameterizes the constants describing the Landau distribution. These are fairly insensitive to thickness for $G \lesssim 0.1$, the case for most detectors.

²Practical calculations can be expedited by using the tables of δ and β from the text versions of the muon energy loss tables to be found at pdg.lbl.gov/AtomicNuclearProperties.

where $\xi = (K/2) \langle Z/A \rangle z^2 (x/\beta^2) \text{ MeV}$ for a detector with a thickness x in g cm^{-2} , and $j = 0.200$ [30].³ While dE/dx is independent of thickness, Δ_p/x scales as $a \ln x + b$. The density correction $\delta(\beta\gamma)$ was not included in Landau’s or Vavilov’s work, but it was later included by Bichsel [30]. The high-energy behavior of $\delta(\beta\gamma)$ (Eq. (34.6)) is such that

$$\Delta_p \xrightarrow{\beta\gamma \gtrsim 100} \xi \left[\ln \frac{2mc^2 \xi}{(\hbar\omega_p)^2} + j \right]. \quad (34.13)$$

Thus the Landau-Vavilov most probable energy loss, like the restricted energy loss, reaches a Fermi plateau. The Bethe dE/dx and Landau-Vavilov-Bichsel Δ_p/x in silicon are shown as a function of muon energy in Fig. 34.6. The energy deposit in the $1600 \mu\text{m}$ case is roughly the same as in a 3 mm thick plastic scintillator.

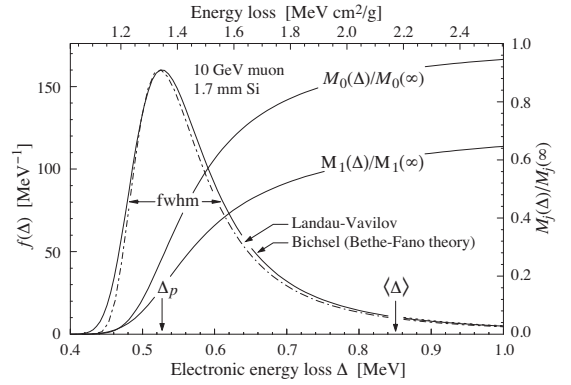


Figure 34.7: Electronic energy deposit distribution for a 10 GeV muon traversing 1.7 mm of silicon, the stopping power equivalent of about 0.3 cm of PVT-based scintillator [1, 11, 32]. The Landau-Vavilov function (dot-dashed) uses a Rutherford cross section without atomic binding corrections but with a kinetic energy transfer limit of W_{max} . The solid curve was calculated using Bethe-Fano theory. $M_0(\Delta)$ and $M_1(\Delta)$ are the cumulative 0th moment (mean number of collisions) and 1st moment (mean energy loss) in crossing the silicon. (See Sec. 34.2.1). The fwhm of the Landau-Vavilov function is about 4ξ for detectors of moderate thickness. Δ_p is the most probable energy loss, and $\langle \Delta \rangle$ divided by the thickness is the Bethe (dE/dx).

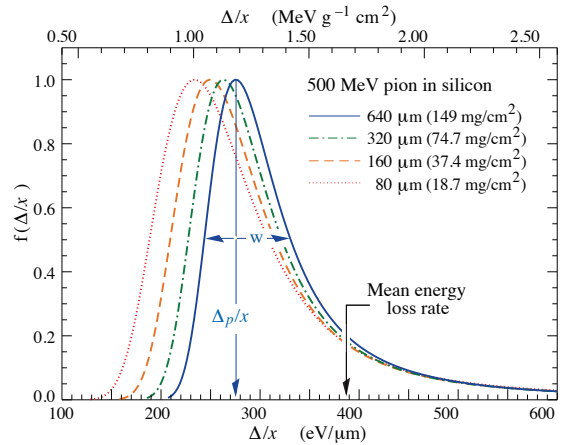


Figure 34.8: Straggling functions in silicon for 500 MeV pions, normalized to unity at the most probable value Δ_p/x . The width w is the full width at half maximum.

The distribution function for the energy deposit by a 10 GeV muon going through a detector of about this thickness is shown

³Rossi [2], Talman [31], and others give somewhat different values for j . The most probable loss is not sensitive to its value.

in Fig. 34.7. In this case the most probable energy loss is 62% of the mean ($M_1(\langle\Delta\rangle)/M_1(\infty)$). Folding in experimental resolution displaces the peak of the distribution, usually toward a higher value. 90% of the collisions ($M_1(\langle\Delta\rangle)/M_1(\infty)$) contribute to energy deposits below the mean. It is the very rare high-energy-transfer collisions, extending to W_{\max} at several GeV, that drives the mean into the tail of the distribution. The large weight of these rare events makes the mean of an experimental distribution consisting of a few hundred events subject to large fluctuations and sensitive to cuts. *The mean of the energy loss given by the Bethe equation, Eq. (34.5), is thus ill-defined experimentally and is not useful for describing energy loss by single particles.*⁴ It rises as $\ln\gamma$ because W_{\max} increases as γ at high energies. *The most probable energy loss should be used.*

A practical example: For muons traversing 0.25 inches (0.64 cm) of PVT (polyvinyltoluene) based plastic scintillator, the ratio of the most probable E loss rate to the mean loss rate via the Bethe equation is [0.69, 0.57, 0.49, 0.42, 0.38] for $T_\mu = [0.01, 0.1, 1, 10, 100]$ GeV. Radiative losses add less than 0.5% to the total mean energy deposit at 10 GeV, but add 7% at 100 GeV. The most probable E loss rate rises slightly beyond the minimum ionization energy, then is essentially constant.

The Landau distribution fails to describe energy loss in thin absorbers such as gas TPC cells [1] and Si detectors [30], as can be seen *e.g.* in Fig. 1 of Ref. [1] for an argon-filled TPC cell. Also see Talman [31]. While Δ_p/x may be calculated adequately with Eq. (34.12), the distributions are significantly wider than the Landau width $w = 4\xi$ Ref. [30], Fig. 15. Examples for 500 MeV pions incident on thin silicon detectors are shown in Fig. 34.8. For very thick absorbers the distribution is less skewed but never approaches a Gaussian.

The most probable energy loss, scaled to the mean loss at minimum ionization, is shown in Fig. 34.9 for several silicon detector thicknesses.

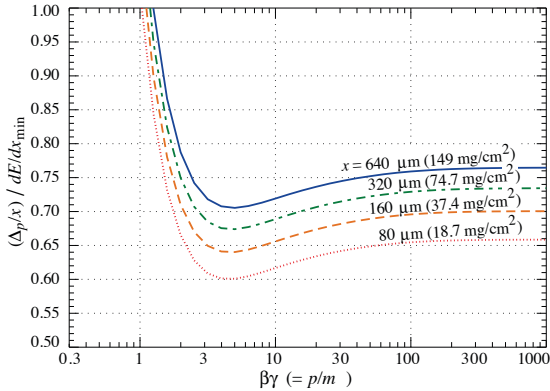


Figure 34.9: Most probable energy loss in silicon, scaled to the mean loss of a minimum ionizing particle, $388 \text{ eV}/\mu\text{m}$ ($1.66 \text{ MeV g}^{-1}\text{cm}^2$).

34.2.10 Energy loss in mixtures and compounds

A mixture or compound can be thought of as made up of thin layers of pure elements in the right proportion (Bragg additivity). In this case,

$$\left\langle \frac{dE}{dx} \right\rangle = \sum w_j \left\langle \frac{dE}{dx} \right\rangle_j, \quad (34.14)$$

where $dE/dx|_j$ is the mean rate of energy loss (in MeV g cm^{-2}) in the j th element. Eq. (34.5) can be inserted into Eq. (34.14) to find expressions for $\langle Z/A \rangle$, $\langle I \rangle$, and $\langle \delta \rangle$; for example, $\langle Z/A \rangle = \sum w_j Z_j/A_j = \sum n_j Z_j / \sum n_j A_j$. However, $\langle I \rangle$ as defined this way is an underestimate, because in a compound electrons are more tightly bound than in the free elements, and $\langle \delta \rangle$ as calculated this way has little relevance, because it is the electron density that matters. If possible, one uses the tables given in

⁴It does find application in dosimetry, where only bulk deposit is relevant.

Refs. [16, 33], or the recipes given in [17] (repeated in Ref. [5]), that include effective excitation energies and interpolation coefficients for calculating the density effect correction for the chemical elements and nearly 200 mixtures and compounds. Otherwise, use the recipe for δ given in Refs. [5, 17], and calculate $\langle I \rangle$ following the discussion in Ref. [13]. (Note the “13%” rule!)

34.2.11 Ionization yields

The Bethe equation describes energy loss via excitation and ionization. Many gaseous detectors (proportional counters or TPCs) or liquid ionization detectors count the number of electrons or positive ions from ionization, rather than the ionization energy. As a further complication, the electron liberated in the initial ionization often has enough energy to ionize other atoms or molecules; this process can happen several times. The number of electron-ion pairs per unit length is typically three or more times the original number. Ion or electron counting is a proxy for a direct dE/dx measurement. Calibrations link the number of observed ions to the traversing particle’s dE/dx .

The details depend on the gases (or liquids) and the particular detector involved. A useful discussion of the physics is provided in Sec.35.6 of this Review.

34.3 Multiple scattering through small angles

A charged particle traversing a medium is deflected by many small-angle scatters. Most of this deflection is due to Coulomb scattering from nuclei as described by the Rutherford cross section. (However, for hadronic projectiles, the strong interactions also contribute to multiple scattering.) For many small-angle scatters the net scattering and displacement distributions are Gaussian via the central limit theorem. Less frequent “hard” scatters produce non-Gaussian tails. These Coulomb scattering distributions are well-represented by the theory of Molière [34]. Accessible discussions are given by Rossi [2] and Jackson [35], and exhaustive reviews have been published by Scott [36] and Motz *et al.* [37]. Experimental measurements have been published by Bichsel [38] (low energy protons) and by Shen *et al.* [39] (relativistic pions, kaons, and protons).⁵

If we define

$$\theta_0 = \theta_{\text{plane}}^{\text{rms}} = \frac{1}{\sqrt{2}} \theta_{\text{space}}^{\text{rms}}, \quad (34.15)$$

then it is sufficient for many applications to use a Gaussian approximation for the central 98% of the projected angular distribution, with an rms width given by Lynch & Dahl [40]:

$$\begin{aligned} \theta_0 &= \frac{13.6 \text{ MeV}}{\beta c p} z \sqrt{\frac{x}{X_0}} \left[1 + 0.088 \log_{10} \left(\frac{x z^2}{X_0 \beta^2} \right) \right] \\ &= \frac{13.6 \text{ MeV}}{\beta c p} z \sqrt{\frac{x}{X_0}} \left[1 + 0.038 \ln \left(\frac{x z^2}{X_0 \beta^2} \right) \right] \end{aligned} \quad (34.16)$$

Here p , βc , and z are the momentum, velocity, and charge number of the incident particle, and x/X_0 is the thickness of the scattering medium in radiation lengths (defined below). This takes into account the p and z dependence quite well at small Z , but for large Z and small x the β -dependence is not well represented. Further improvements are discussed in Ref. [40].

Eq. (34.16) describes scattering from a single material, while the usual problem involves the multiple scattering of a particle traversing many different layers and mixtures. Since it is from a fit to a Molière distribution, it is incorrect to add the individual θ_0 contributions in quadrature; the result is systematically too small. It is much more accurate to apply Eq. (34.16) once, after finding x and X_0 for the combined scatterer.

The nonprojected (space) and projected (plane) angular distributions are given approximately by [34]

$$\frac{1}{2\pi \theta_0^2} \exp \left(-\frac{\theta_{\text{space}}^2}{2\theta_0^2} \right) d\Omega, \quad (34.17)$$

⁵Shen *et al.*’s measurements show that Bethe’s simpler methods of including atomic electron effects agrees better with experiment than does Scott’s treatment.

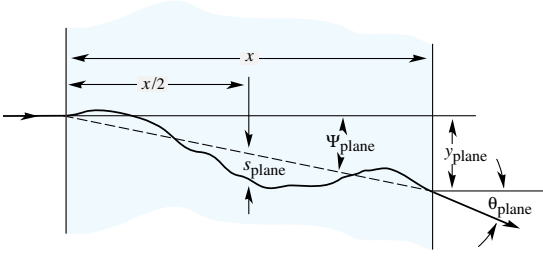


Figure 34.10: Quantities used to describe multiple Coulomb scattering. The particle is incident in the plane of the figure.

$$\frac{1}{\sqrt{2\pi}\theta_0} \exp\left(-\frac{\theta_{\text{plane}}^2}{2\theta_0^2}\right) d\theta_{\text{plane}}, \quad (34.18)$$

where θ is the deflection angle. In this approximation, $\theta_{\text{space}}^2 \approx (\theta_{\text{plane},x}^2 + \theta_{\text{plane},y}^2)$, where the x and y axes are orthogonal to the direction of motion, and $d\Omega \approx d\theta_{\text{plane},x} d\theta_{\text{plane},y}$. Deflections into $\theta_{\text{plane},x}$ and $\theta_{\text{plane},y}$ are independent and identically distributed. Fig. 34.10 shows these and other quantities sometimes used to describe multiple Coulomb scattering. They are

$$\psi_{\text{plane}}^{\text{rms}} = \frac{1}{\sqrt{3}} \theta_{\text{plane}}^{\text{rms}} = \frac{1}{\sqrt{3}} \theta_0, \quad (34.19)$$

$$y_{\text{plane}}^{\text{rms}} = \frac{1}{\sqrt{3}} x \theta_{\text{plane}}^{\text{rms}} = \frac{1}{\sqrt{3}} x \theta_0, \quad (34.20)$$

$$s_{\text{plane}}^{\text{rms}} = \frac{1}{4\sqrt{3}} x \theta_{\text{plane}}^{\text{rms}} = \frac{1}{4\sqrt{3}} x \theta_0. \quad (34.21)$$

All the quantitative estimates in this section apply only in the limit of small $\theta_{\text{plane}}^{\text{rms}}$ and in the absence of large-angle scatters. The random variables s , ψ , y , and θ in a given plane are correlated. Obviously, $y \approx x\psi$. In addition, y and θ have the correlation coefficient $\rho_{y\theta} = \sqrt{3}/2 \approx 0.87$. For Monte Carlo generation of a joint $(y_{\text{plane}}, \theta_{\text{plane}})$ distribution, or for other calculations, it may be most convenient to work with independent Gaussian random variables (z_1, z_2) with mean zero and variance one, and then set

$$y_{\text{plane}} = z_1 x \theta_0 (1 - \rho_{y\theta}^2)^{1/2} / \sqrt{3} + z_2 \rho_{y\theta} x \theta_0 / \sqrt{3} \quad (34.22a)$$

$$= z_1 x \theta_0 / \sqrt{12} + z_2 x \theta_0 / 2; \quad (34.22b)$$

$$\theta_{\text{plane}} = z_2 \theta_0. \quad (34.22c)$$

Note that the second term for y_{plane} equals $x\theta_{\text{plane}}/2$ and represents the displacement that would have occurred had the deflection θ_{plane} all occurred at the single point $x/2$.

For heavy ions the multiple Coulomb scattering has been measured and compared with various theoretical distributions [41].

34.4 Photon and electron interactions in matter

At low energies electrons and positrons primarily lose energy by ionization, although other processes (Møller scattering, Bhabha scattering, e^+ annihilation) contribute, as shown in Fig. 34.11. While ionization loss rates rise logarithmically with energy, bremsstrahlung losses rise nearly linearly (fractional loss is nearly independent of energy), and dominates above the critical energy (Sec. 34.4.4 below), a few tens of MeV in most materials

34.4.1 Collision energy losses by e^\pm

Stopping power differs somewhat for electrons and positrons, and both differ from stopping power for heavy particles because of the kinematics, spin, charge, and the identity of the incident electron with the electrons that it ionizes. Complete discussions and tables can be found in Refs. [10, 13, 33].

For electrons, large energy transfers to atomic electrons (taken as free) are described by the Møller cross section. From Eq. (34.4), the maximum energy transfer in a single collision should be the entire kinetic energy, $W_{\text{max}} = m_e c^2 (\gamma - 1)$, but because the particles are identical, the maximum is half this, $W_{\text{max}}/2$. (The results are the same if the transferred energy is ϵ or if the transferred energy is $W_{\text{max}} - \epsilon$. The stopping power is by convention calculated

for the faster of the two emerging electrons.) The first moment of the Møller cross section [26] (divided by dx) is the stopping power:

$$\left\langle -\frac{dE}{dx} \right\rangle = \frac{1}{2} K \frac{Z}{A} \frac{1}{\beta^2} \left[\ln \frac{m_e c^2 \beta^2 \gamma^2 \{m_e c^2 (\gamma - 1)/2\}}{I^2} + (1 - \beta^2) - \frac{2\gamma - 1}{\gamma^2} \ln 2 + \frac{1}{8} \left(\frac{\gamma - 1}{\gamma} \right)^2 - \delta \right] \quad (34.23)$$

The logarithmic term can be compared with the logarithmic term in the Bethe equation (Eq. (34.2)) by substituting $W_{\text{max}} = m_e c^2 (\gamma - 1)/2$.

Electron-positron scattering is described by the fairly complicated Bhabha cross section [26]. There is no identical particle problem, so $W_{\text{max}} = m_e c^2 (\gamma - 1)$. The first moment of the Bhabha equation yields

$$\left\langle -\frac{dE}{dx} \right\rangle = \frac{1}{2} K \frac{Z}{A} \frac{1}{\beta^2} \left[\ln \frac{m_e c^2 \beta^2 \gamma^2 \{m_e c^2 (\gamma - 1)\}}{2I^2} + 2 \ln 2 - \frac{\beta^2}{12} \left(23 + \frac{14}{\gamma + 1} + \frac{10}{(\gamma + 1)^2} + \frac{4}{(\gamma + 1)^3} \right) - \delta \right]. \quad (34.24)$$

Following ICRU 37 [10], the density effect correction δ has been added to Uehling's equations [26] in both cases.

For heavy particles, shell corrections were developed assuming that the projectile is equivalent to a perturbing potential whose center moves with constant velocity. This assumption has no sound theoretical basis for electrons. The authors of ICRU 37 [10] estimated the possible error in omitting it by assuming the correction was twice as great as for a proton of the same velocity. At $T = 10$ keV, the error was estimated to be $\approx 2\%$ for water, $\approx 9\%$ for Cu, and $\approx 21\%$ for Au.

As shown in Fig. 34.11, stopping powers for e^- , e^+ , and heavy particles are not dramatically different. In silicon, the minimum value for electrons is $1.50 \text{ MeV cm}^2/\text{g}$ (at $\gamma = 3.3$); for positrons, $1.46 \text{ MeV cm}^2/\text{g}$ (at $\gamma = 3.7$), and for muons, $1.66 \text{ MeV cm}^2/\text{g}$ (at $\gamma = 3.58$).

34.4.2 Radiation length

High-energy electrons predominantly lose energy in matter by bremsstrahlung, and high-energy photons by e^+e^- pair production. The characteristic amount of matter traversed for these related interactions is called the radiation length X_0 , usually measured in g cm^{-2} . It is the mean distance over which a high-energy electron loses all but $1/e$ of its energy by bremsstrahlung. It is also the appropriate scale length for describing high-energy electromagnetic cascades. X_0 has been calculated and tabulated by Y.S. Tsai [42]:

$$\frac{1}{X_0} = 4\alpha r_e^2 \frac{N_A}{A} \left\{ Z^2 [L_{\text{rad}} - f(Z)] + Z L'_{\text{rad}} \right\}. \quad (34.25)$$

For $A = 1 \text{ g mol}^{-1}$, $4\alpha r_e^2 N_A/A = (716.408 \text{ g cm}^{-2})^{-1}$. L_{rad} and L'_{rad} are given in Table 34.2. The function $f(Z)$ is an infinite sum, but for elements up to uranium can be represented to 4-place accuracy by

$$f(Z) = a^2 \left[(1 + a^2)^{-1} + 0.20206 - 0.0369 a^2 + 0.0083 a^4 - 0.002 a^6 \right], \quad (34.26)$$

where $a = \alpha Z$ [43].

The radiation length in a mixture or compound may be approximated by

$$1/X_0 = \sum w_j / X_j, \quad (34.27)$$

where w_j and X_j are the fraction by weight and the radiation length for the j th element.

Table 34.2: Tsai’s L_{rad} and L'_{rad} , for use in calculating the radiation length in an element using Eq. (34.25).

Element	Z	L_{rad}	L'_{rad}
H	1	5.31	6.144
He	2	4.79	5.621
Li	3	4.74	5.805
Be	4	4.71	5.924
Others	> 4	$\ln(184.15 Z^{-1/3})$	$\ln(1194 Z^{-2/3})$

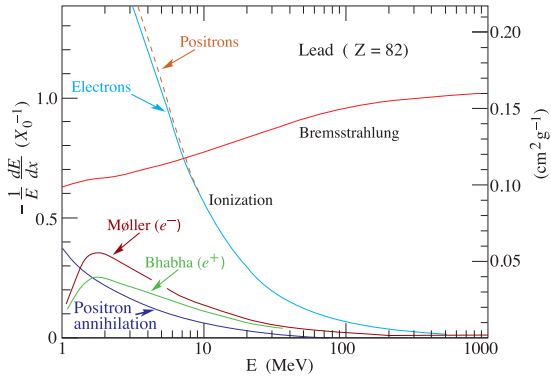


Figure 34.11: Fractional energy loss per radiation length in lead as a function of electron or positron energy. Electron (positron) scattering is considered as ionization when the energy loss per collision is below 0.255 MeV, and as Møller (Bhabha) scattering when it is above. Adapted from Fig. 3.2 from Messel and Crawford, *Electron-Photon Shower Distribution Function Tables for Lead, Copper, and Air Absorbers*, Pergamon Press, 1970. Messel and Crawford use $X_0(\text{Pb}) = 5.82 \text{ g/cm}^2$, but we have modified the figures to reflect the value given in the Table of Atomic and Nuclear Properties of Materials ($X_0(\text{Pb}) = 6.37 \text{ g/cm}^2$).

34.4.3 Bremsstrahlung energy loss by e^\pm

At very high energies and except at the high-energy tip of the bremsstrahlung spectrum, the cross section can be approximated in the “complete screening case” as [42]

$$d\sigma/dk = (1/k)4\alpha r_e^2 \left\{ \left(\frac{4}{3} - \frac{4}{3}y + y^2 \right) [Z^2(L_{\text{rad}} - f(Z)) + Z L'_{\text{rad}}] + \frac{1}{9}(1-y)(Z^2 + Z) \right\}, \tag{34.28}$$

where $y = k/E$ is the fraction of the electron’s energy transferred to the radiated photon. At small y (the “infrared limit”) the term on the second line ranges from 1.7% (low Z) to 2.5% (high Z) of the total. If it is ignored and the first line simplified with the definition of X_0 given in Eq. (34.25), we have

$$\frac{d\sigma}{dk} = \frac{A}{X_0 N_A k} \left(\frac{4}{3} - \frac{4}{3}y + y^2 \right). \tag{34.29}$$

This cross section (times k) is shown by the top curve in Fig. 34.12.

This formula is accurate except near $y = 1$, where screening may become incomplete, and near $y = 0$, where the infrared divergence is removed by the interference of bremsstrahlung amplitudes from nearby scattering centers (the LPM effect) [44, 45] and dielectric suppression [46, 47]. These and other suppression effects in bulk media are discussed in Sec. 34.4.6.

With decreasing energy ($E \lesssim 10 \text{ GeV}$) the high- y cross section drops and the curves become rounded as $y \rightarrow 1$. Curves of this familiar shape can be seen in Rossi [2] (Figs. 2.11.2,3); see also the review by Koch & Motz [48].

Except at these extremes, and still in the complete-screening approximation, the number of photons with energies between k_{min}

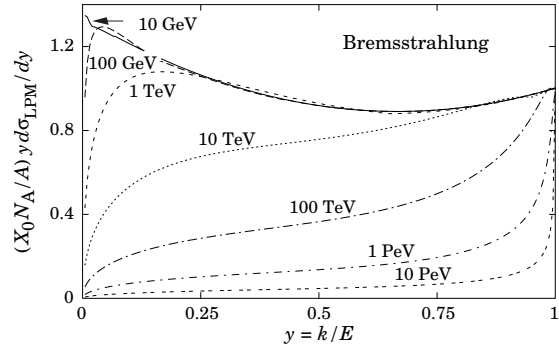


Figure 34.12: The normalized bremsstrahlung cross section $k d\sigma_{LPM}/dk$ in lead versus the fractional photon energy $y = k/E$. The vertical axis has units of photons per radiation length.

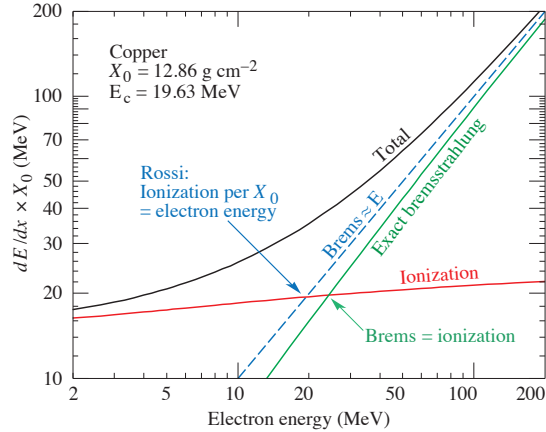


Figure 34.13: Two definitions of the critical energy E_c .

and k_{max} emitted by an electron travelling a distance $d \ll X_0$ is

$$N_\gamma = \frac{d}{X_0} \left[\frac{4}{3} \ln \left(\frac{k_{\text{max}}}{k_{\text{min}}} \right) - \frac{4(k_{\text{max}} - k_{\text{min}})}{3E} + \frac{k_{\text{max}}^2 - k_{\text{min}}^2}{2E^2} \right]. \tag{34.30}$$

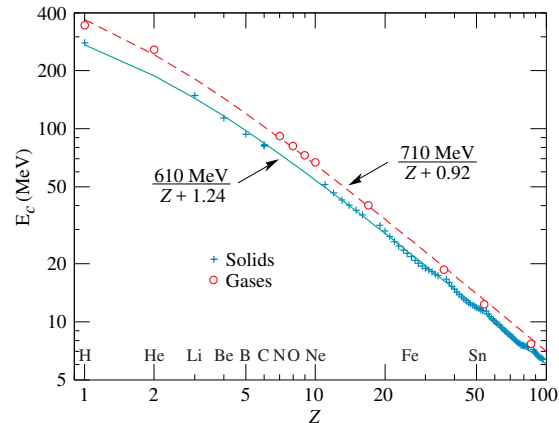


Figure 34.14: Electron critical energy for the chemical elements, using Rossi’s definition [2]. The fits shown are for solids and liquids (solid line) and gases (dashed line). The rms deviation is 2.2% for the solids and 4.0% for the gases.

34.4.4 Critical energy

An electron loses energy by bremsstrahlung at a rate nearly proportional to its energy, while the ionization loss rate varies only logarithmically with the electron energy. The *critical energy* E_c is sometimes defined as the energy at which the two loss rates

are equal [49]. Among alternate definitions is that of Rossi [2], who defines the critical energy as the energy at which the ionization loss per radiation length is equal to the electron energy. Equivalently, it is the same as the first definition with the approximation $|dE/dx|_{\text{brems}} \approx E/X_0$. This form has been found to describe transverse electromagnetic shower development more accurately (see below). These definitions are illustrated in the case of copper in Fig. 34.13.

The accuracy of approximate forms for E_c has been limited by the failure to distinguish between gases and solid or liquids, where there is a substantial difference in ionization at the relevant energy because of the density effect. We distinguish these two cases in Fig. 34.14. Fits were also made with functions of the form $a/(Z+b)^\alpha$, but α was found to be essentially unity. Since E_c also depends on A , I , and other factors, such forms are at best approximate.

Values of E_c for both electrons and positrons in more than 300 materials can be found at pdg.lbl.gov/AtomicNuclearProperties.

34.4.5 Energy loss by photons

Contributions to the photon cross section in a light element (carbon) and a heavy element (lead) are shown in Fig. 34.15. At low energies it is seen that the photoelectric effect dominates, although Compton scattering, Rayleigh scattering, and photonuclear absorption also contribute. The photoelectric cross section is characterized by discontinuities (absorption edges) as thresholds for photoionization of various atomic levels are reached. Photon attenuation lengths for a variety of elements are shown in Fig. 34.16, and data for $30 \text{ eV} < k < 100 \text{ GeV}$ for all elements are available from the web pages given in the caption. Here k is the photon energy.

The increasing domination of pair production as the energy increases is shown in Fig. 34.17. Using approximations similar to those used to obtain Eq. (34.29), Tsai's formula for the differential cross section [42] reduces to

$$\frac{d\sigma}{dx} = \frac{A}{X_0 N_A} \left[1 - \frac{4}{3}x(1-x) \right] \quad (34.31)$$

in the complete-screening limit valid at high energies. Here $x = E/k$ is the fractional energy transfer to the pair-produced electron (or positron), and k is the incident photon energy. The cross section is very closely related to that for bremsstrahlung, since the Feynman diagrams are variants of one another. The cross section is of necessity symmetric between x and $1-x$, as can be seen by the solid curve in Fig. 34.18. See the review by Motz, Olsen, & Koch for a more detailed treatment [54]. Eq. (34.31) may be integrated to find the high-energy limit for the total e^+e^- pair-production cross section:

$$\sigma = \frac{7}{9}(A/X_0 N_A). \quad (34.32)$$

Equation Eq. (34.32) is accurate to within a few percent down to energies as low as 1 GeV, particularly for high- Z materials.

34.4.6 Bremsstrahlung and pair production at very high energies

At ultrahigh energies, Eqns. 34.28–34.32 will fail because of quantum mechanical interference between amplitudes from different scattering centers. Since the longitudinal momentum transfer to a given center is small ($\propto k/E(E-k)$, in the case of bremsstrahlung), the interaction is spread over a comparatively long distance called the formation length ($\propto E(E-k)/k$) via the uncertainty principle. In alternate language, the formation length is the distance over which the highly relativistic electron and the photon “split apart.” The interference is usually destructive. Calculations of the “Landau-Pomeranchuk-Migdal” (LPM) effect may be made semi-classically based on the average multiple scattering, or more rigorously using a quantum transport approach [44, 45].

In amorphous media, bremsstrahlung is suppressed if the pho-

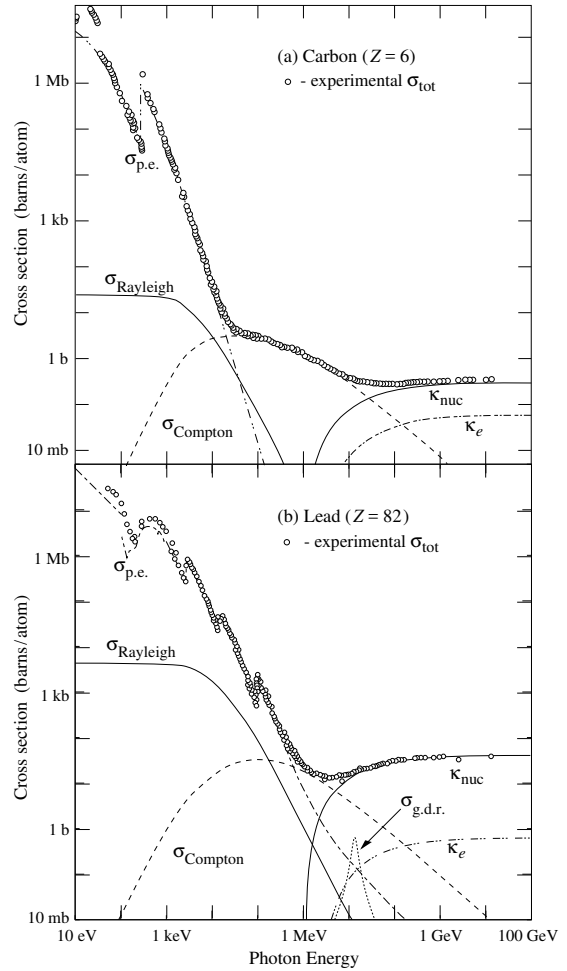


Figure 34.15: Photon total cross sections as a function of energy in carbon and lead, showing the contributions of different processes [50]:

- $\sigma_{\text{p.e.}}$ = Atomic photoelectric effect (electron ejection, photon absorption)
- σ_{Rayleigh} = Rayleigh (coherent) scattering—atom neither ionized nor excited
- σ_{Compton} = Incoherent scattering (Compton scattering off an electron)
- κ_{nuc} = Pair production, nuclear field
- κ_e = Pair production, electron field
- $\sigma_{\text{g.d.r.}}$ = Photonuclear interactions, most notably the Giant Dipole Resonance [51]. In these interactions, the target nucleus is usually broken up.

Original figures through the courtesy of John H. Hubbell (NIST).

ton energy k is less than $E^2/(E + E_{LPM})$ [45], where⁶

$$E_{LPM} = (m_e c^2)^2 \alpha \frac{X_0}{4\pi\hbar c \rho} = (7.7 \text{ TeV/cm}) \times \frac{X_0}{\rho}. \quad (34.33)$$

Since physical distances are involved, X_0/ρ , in cm, appears. The energy-weighted bremsstrahlung spectrum for lead, $k d\sigma_{LPM}/dk$, is shown in Fig. 34.12. With appropriate scaling by X_0/ρ , other materials behave similarly.

For photons, pair production is reduced for $E(k-E) > k E_{LPM}$. The pair-production cross sections for different photon energies are shown in Fig. 34.18.

If $k \ll E$, several additional mechanisms can also produce suppression. When the formation length is long, even weak factors

⁶This definition differs from that of Ref. [55] by a factor of two. E_{LPM} scales as the 4th power of the mass of the incident particle, so that $E_{LPM} = (1.4 \times 10^{10} \text{ TeV/cm}) \times X_0/\rho$ for a muon.

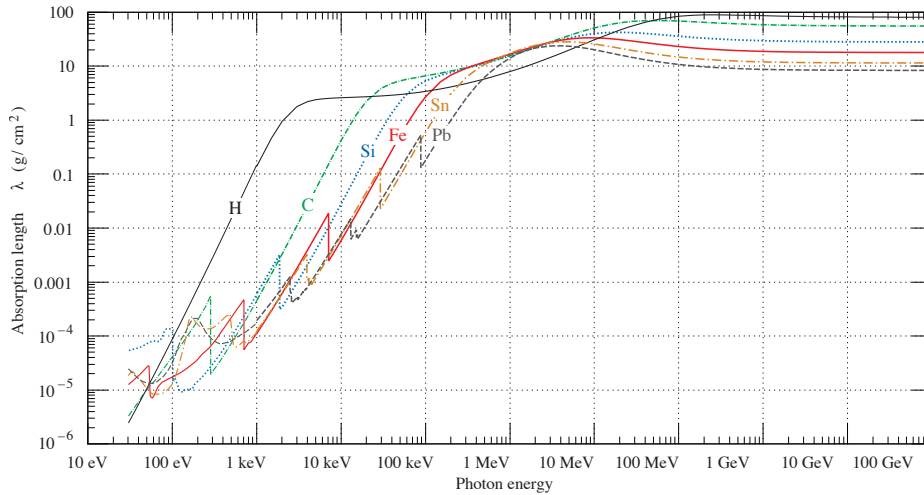


Figure 34.16: The photon mass attenuation length (or mean free path) $\lambda = 1/(\mu/\rho)$ for various elemental absorbers as a function of photon energy. The mass attenuation coefficient is μ/ρ , where ρ is the density. The intensity I remaining after traversal of thickness t (in mass/unit area) is given by $I = I_0 \exp(-t/\lambda)$. The accuracy is a few percent. For a chemical compound or mixture, $1/\lambda_{\text{eff}} \approx \sum_{\text{elements}} w_Z/\lambda_Z$, where w_Z is the proportion by weight of the element with atomic number Z . The processes responsible for attenuation are given in Fig. 34.11. Since coherent processes are included, not all these processes result in energy deposition. The data for $30 \text{ eV} < E < 1 \text{ keV}$ are from Ref. [52], those for $1 \text{ keV} < E < 100 \text{ GeV}$ from Ref. [53].

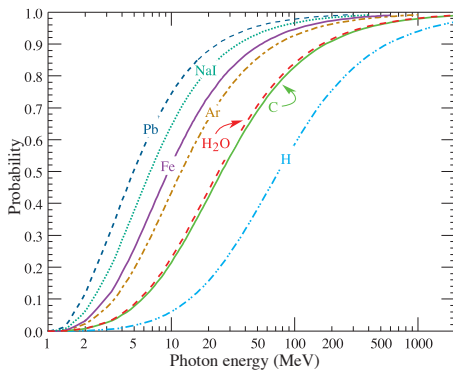


Figure 34.17: Probability P that a photon interaction will result in conversion to an e^+e^- pair. Except for a few-percent contribution from photonuclear absorption around 10 or 20 MeV, essentially all other interactions in this energy range result in Compton scattering off an atomic electron. For a photon attenuation length λ (Fig. 34.16), the probability that a given photon will produce an electron pair (without first Compton scattering) in thickness t of absorber is $P[1 - \exp(-t/\lambda)]$.

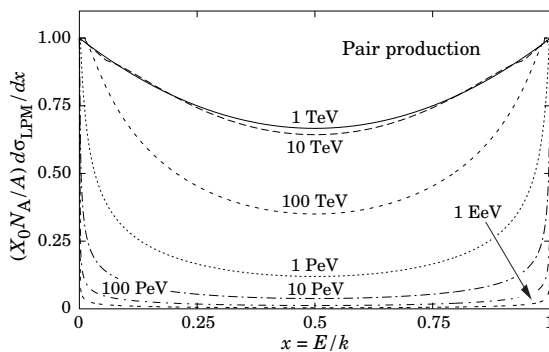


Figure 34.18: The normalized pair production cross section $d\sigma_{LPM}/dx$, versus fractional electron energy $x = E/k$.

can perturb the interaction. For example, the emitted photon can coherently forward scatter off of the electrons in the media. Because of this, for $k < \omega_p E/m_e \sim 10^{-4}$, bremsstrahlung is sup-

pressed by a factor $(km_e/\omega_p E)^2$ [47]. Magnetic fields can also suppress bremsstrahlung.

In crystalline media, the situation is more complicated, with coherent enhancement or suppression possible. The cross section depends on the electron and photon energies and the angles between the particle direction and the crystalline axes [56].

34.4.7 Photonuclear and electronuclear interactions at still higher energies

At still higher photon and electron energies, where the bremsstrahlung and pair production cross-sections are heavily suppressed by the LPM effect, photonuclear and electronuclear interactions predominate over electromagnetic interactions.

At photon energies above about 10^{20} eV, for example, photons usually interact hadronically. The exact cross-over energy depends on the model used for the photonuclear interactions. These processes are illustrated in Fig. 34.19. At still higher energies ($\gtrsim 10^{23}$ eV), photonuclear interactions can become coherent, with the photon interaction spread over multiple nuclei. Essentially, the photon coherently converts to a ρ^0 , in a process that is somewhat similar to kaon regeneration [57].

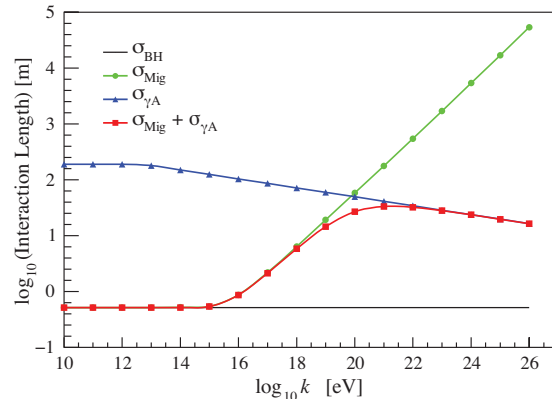


Figure 34.19: Interaction length for a photon in ice as a function of photon energy for the Bethe-Heitler (BH), LPM (Mig) and photonuclear (γA) cross sections [57]. The Bethe-Heitler interaction length is $9X_0/7$, and X_0 is 0.393 m in ice.

Similar processes occur for electrons. As electron energies increase and the LPM effect suppresses bremsstrahlung, electronu-

clear interactions become more important. At energies above 10^{21} eV, these electronuclear interactions dominate electron energy loss [57].

34.5 Electromagnetic cascades

When a high-energy electron or photon is incident on a thick absorber, it initiates an electromagnetic cascade as pair production and bremsstrahlung generate more electrons and photons with lower energy. The longitudinal development is governed by the high-energy part of the cascade, and therefore scales as the radiation length in the material. Electron energies eventually fall below the critical energy, and then dissipate their energy by ionization and excitation rather than by the generation of more shower particles. In describing shower behavior, it is therefore convenient to introduce the scale variables

$$t = x/X_0, \quad y = E/E_c, \quad (34.34)$$

so that distance is measured in units of radiation length and energy in units of critical energy.

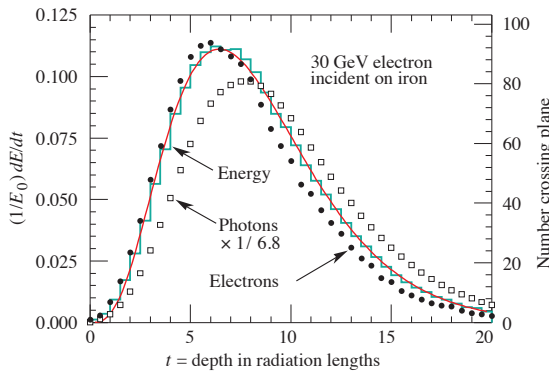


Figure 34.20: An EGS4 simulation of a 30 GeV electron-induced cascade in iron. The histogram shows fractional energy deposition per radiation length, and the curve is a gamma-function fit to the distribution. Circles indicate the number of electrons with total energy greater than 1.5 MeV crossing planes at $X_0/2$ intervals (scale on right) and the squares the number of photons with $E \geq 1.5$ MeV crossing the planes (scaled down to have same area as the electron distribution).

Longitudinal profiles from an EGS4 [58] simulation of a 30 GeV electron-induced cascade in iron are shown in Fig. 34.20. The number of particles crossing a plane (very close to Rossi's Π function [2]) is sensitive to the cutoff energy, here chosen as a total energy of 1.5 MeV for both electrons and photons. The electron number falls off more quickly than energy deposition. This is because, with increasing depth, a larger fraction of the cascade energy is carried by photons. Exactly what a calorimeter measures depends on the device, but it is not likely to be exactly any of the profiles shown. In gas counters it may be very close to the electron number, but in glass Cherenkov detectors and other devices with “thick” sensitive regions it is closer to the energy deposition (total track length). In such detectors the signal is proportional to the “detectable” track length T_d , which is in general less than the total track length T . Practical devices are sensitive to electrons with energy above some detection threshold E_d , and $T_d = T F(E_d/E_c)$. An analytic form for $F(E_d/E_c)$ obtained by Rossi [2] is given by Fabjan in Ref. [59]; see also Amaldi [60].

The mean longitudinal profile of the energy deposition in an electromagnetic cascade is reasonably well described by a gamma distribution [61]:

$$\frac{dE}{dt} = E_0 b \frac{(bt)^{a-1} e^{-bt}}{\Gamma(a)} \quad (34.35)$$

The maximum t_{\max} occurs at $(a-1)/b$. We have made fits to shower profiles in elements ranging from carbon to uranium, at energies from 1 GeV to 100 GeV. The energy deposition profiles

are well described by Eq. (34.35) with

$$t_{\max} = (a-1)/b = 1.0 \times (\ln y + C_j), \quad j = e, \gamma, \quad (34.36)$$

where $C_e = -0.5$ for electron-induced cascades and $C_\gamma = +0.5$ for photon-induced cascades. To use Eq. (34.35), one finds $(a-1)/b$ from Eq. (34.36) and Eq. (34.34), then finds a either by assuming $b \approx 0.5$ or by finding a more accurate value from Fig. 34.21. The results are very similar for the electron number profiles, but there is some dependence on the atomic number of the medium. A similar form for the electron number maximum was obtained by Rossi in the context of his “Approximation B,” [2] (see Fabjan’s review in Ref. [59]), but with $C_e = -1.0$ and $C_\gamma = -0.5$; we regard this as superseded by the EGS4 result.

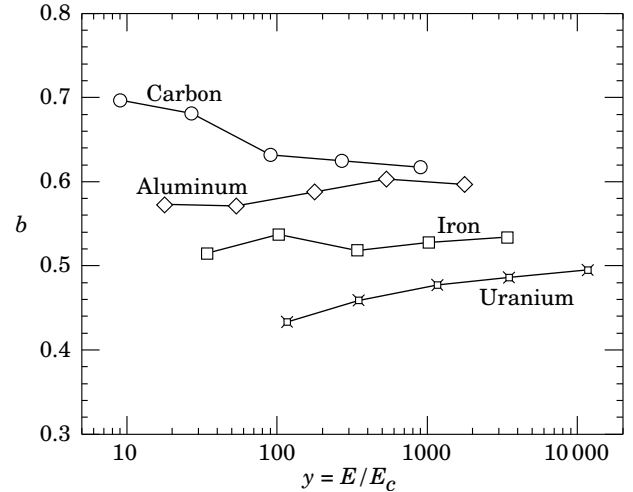


Figure 34.21: Fitted values of the scale factor b for energy deposition profiles obtained with EGS4 for a variety of elements for incident electrons with $1 \leq E_0 \leq 100$ GeV. Values obtained for incident photons are essentially the same.

The “shower length” $X_s = X_0/b$ is less conveniently parameterized, since b depends upon both Z and incident energy, as shown in Fig. 34.21. As a corollary of this Z dependence, the number of electrons crossing a plane near shower maximum is underestimated using Rossi’s approximation for carbon and seriously overestimated for uranium. Essentially the same b values are obtained for incident electrons and photons. For many purposes it is sufficient to take $b \approx 0.5$.

The length of showers initiated by ultra-high energy photons and electrons is somewhat greater than at lower energies since the first or first few interaction lengths are increased via the mechanisms discussed above.

The gamma function distribution is very flat near the origin, while the EGS4 cascade (or a real cascade) increases more rapidly. As a result Eq. (34.35) fails badly for about the first two radiation lengths; it was necessary to exclude this region in making fits.

Because fluctuations are important, Eq. (34.35) should be used only in applications where average behavior is adequate. Grindhammer *et al.* have developed fast simulation algorithms in which the variance and correlation of a and b are obtained by fitting Eq. (34.35) to individually simulated cascades, then generating profiles for cascades using a and b chosen from the correlated distributions [62].

The transverse development of electromagnetic showers in different materials scales fairly accurately with the *Molière radius* R_M , given by [63,64]

$$R_M = X_0 E_s/E_c, \quad (34.37)$$

where $E_s \approx 21$ MeV (Table 34.1), and the Rossi definition of E_c is used.

In a material containing a weight fraction w_j of the element with critical energy E_{c_j} and radiation length X_j , the Molière radius is

given by

$$\frac{1}{R_M} = \frac{1}{E_s} \sum \frac{w_j E_{cj}}{X_j} \quad (34.38)$$

Measurements of the lateral distribution in electromagnetic cascades are shown in Refs. [63,64]. On the average, only 10% of the energy lies outside the cylinder with radius R_M . About 99% is contained inside of $3.5R_M$, but at this radius and beyond composition effects become important and the scaling with R_M fails. The distributions are characterized by a narrow core, and broaden as the shower develops. They are often represented as the sum of two Gaussians.

At high enough energies, the LPM effect (Sec. 34.4.6) reduces the cross sections for bremsstrahlung and pair production, and hence can cause significant elongation of electromagnetic cascades [45].

34.6 Muon energy loss at high energy

At sufficiently high energies, radiative processes become more important than ionization for all charged particles. For muons and pions in materials such as iron, this “critical energy” occurs at several hundred GeV. (There is no simple scaling with particle mass, but for protons the “critical energy” is much, much higher.) Radiative effects dominate the energy loss of energetic muons found in cosmic rays or produced at the newest accelerators. These processes are characterized by small cross sections, hard spectra, large energy fluctuations, and the associated generation of electromagnetic and (in the case of photonuclear interactions) hadronic showers [65–73]. As a consequence, at these energies the treatment of energy loss as a uniform and continuous process is for many purposes inadequate.

It is convenient to write the average rate of muon energy loss as [74]

$$-dE/dx = a(E) + b(E)E. \quad (34.39)$$

Here $a(E)$ is the ionization energy loss given by Eq. (34.5), and $b(E)$ is the sum of e^+e^- pair production, bremsstrahlung, and photonuclear contributions. To the approximation that these slowly-varying functions are constant, the mean range x_0 of a muon with initial energy E_0 is given by

$$x_0 \approx (1/b) \ln(1 + E_0/E_{\mu c}), \quad (34.40)$$

where $E_{\mu c} = a/b$.

Fig. 34.22 shows contributions to $b(E)$ for iron. Since $a(E) \approx 0.002 \text{ GeV g}^{-1} \text{ cm}^2$, $b(E)E$ dominates the energy loss above several hundred GeV, where $b(E)$ is nearly constant. The rates of energy loss for muons in hydrogen, uranium, and iron are shown in Fig. 34.23 [5].

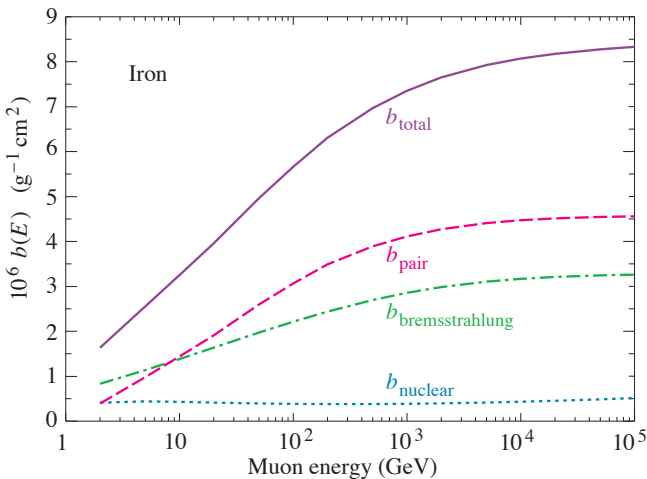


Figure 34.22: Contributions to the fractional energy loss by muons in iron due to e^+e^- pair production, bremsstrahlung, and photonuclear interactions, as obtained from Groom *et al.* [5] except for post-Born corrections to the cross section for direct pair production from atomic electrons.

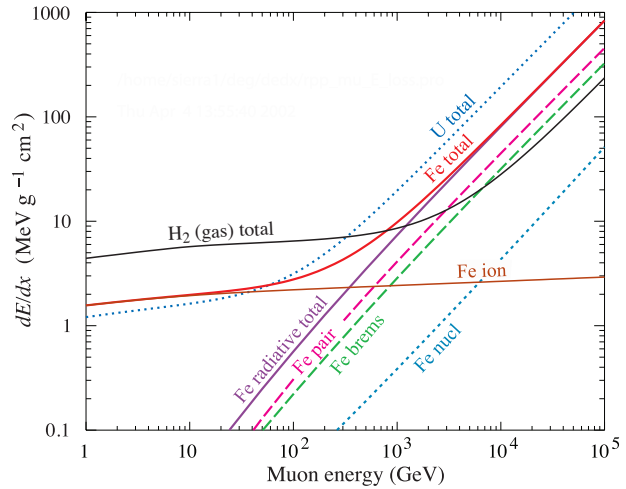


Figure 34.23: The average energy loss of a muon in hydrogen, iron, and uranium as a function of muon energy. Contributions to dE/dx in iron from ionization and pair production, bremsstrahlung and photonuclear interactions are also shown.

The “muon critical energy” $E_{\mu c}$ can be defined more exactly as the energy at which radiative and ionization losses are equal, and can be found by solving $E_{\mu c} = a(E_{\mu c})/b(E_{\mu c})$. This definition corresponds to the solid-line intersection in Fig. 34.13, and is different from the Rossi definition we used for electrons. It serves the same function: below $E_{\mu c}$ ionization losses dominate, and above $E_{\mu c}$ radiative effects dominate. The dependence of $E_{\mu c}$ on atomic number Z is shown in Fig. 34.24.

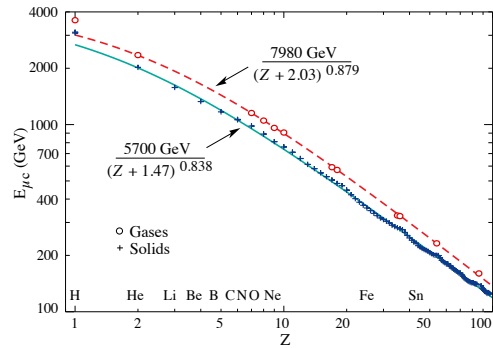


Figure 34.24: Muon critical energy for the chemical elements, defined as the energy at which radiative and ionization energy loss rates are equal [5]. The equality comes at a higher energy for gases than for solids or liquids with the same atomic number because of a smaller density effect reduction of the ionization losses. The fits shown in the figure exclude hydrogen. Alkali metals fall 3–4% above the fitted function, while most other solids are within 2% of the function. Among the gases the worst fit is for radon (2.7% high).

The radiative cross sections are expressed as functions of the fractional energy loss ν . The bremsstrahlung cross section goes roughly as $1/\nu$ over most of the range, while for the pair production case the distribution goes as ν^{-3} to ν^{-2} [75]. “Hard” losses are therefore more probable in bremsstrahlung, and in fact energy losses due to pair production may very nearly be treated as continuous. The simulated momentum distribution of an incident 1 TeV/c muon beam after it crosses 3 m of iron is shown in Fig. 34.25 [5]. The most probable loss is 8 GeV, or 3.4 MeV $\text{g}^{-1} \text{ cm}^2$. The full width at half maximum is 9 GeV/c, or 0.9%. The radiative tail is almost entirely due to bremsstrahlung, although most of the events in which more than 10% of the incident energy lost experienced relatively hard photonuclear interactions. The latter can exceed detector resolution [76], necessitating the

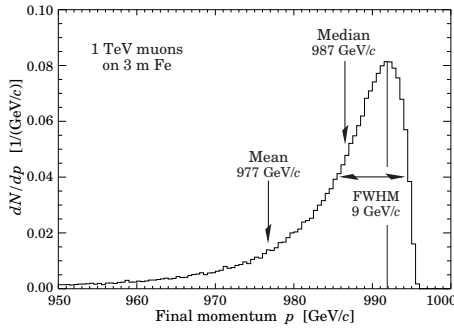


Figure 34.25: The momentum distribution of 1 TeV/c muons after traversing 3 m of iron as calculated by S.I. Striganov [5].

reconstruction of lost energy. Tables in Ref. [5] list the stopping power as $9.82 \text{ MeV g}^{-1}\text{cm}^2$ for a 1 TeV muon, so that the mean loss should be 23 GeV ($\approx 23 \text{ GeV}/c$), for a final momentum of 977 GeV/c, far below the peak. This agrees with the indicated mean calculated from the simulation. Electromagnetic and hadronic cascades in detector materials can obscure muon tracks in detector planes and reduce tracking efficiency [77].

34.7 Cherenkov and transition radiation [35, 78, 79]

A charged particle radiates if its velocity is greater than the local phase velocity of light (Cherenkov radiation) or if it crosses suddenly from one medium to another with different optical properties (transition radiation). Neither process is important for energy loss, but both are used in high-energy and cosmic-ray physics detectors.

34.7.1 Optical Cherenkov radiation

The angle θ_c of Cherenkov radiation, relative to the particle's direction, for a particle with velocity βc in a medium with index of refraction n is

$$\begin{aligned} \cos \theta_c &= (1/n\beta) \\ \text{or } \tan \theta_c &= \sqrt{\beta^2 n^2 - 1} \\ &\approx \sqrt{2(1 - 1/n\beta)} \quad \text{for small } \theta_c, \text{ e.g. in gases.} \end{aligned} \quad (34.41)$$

The threshold velocity β_t is $1/n$, and $\gamma_t = 1/(1 - \beta_t^2)^{1/2}$. Therefore, $\beta_t \gamma_t = 1/(2\delta + \delta^2)^{1/2}$, where $\delta = n - 1$. Values of δ for various commonly used gases are given as a function of pressure and wavelength in Ref. [80]. See its Table 6.1 for values at atmospheric pressure. Data for other commonly used materials are given in Ref. [81].

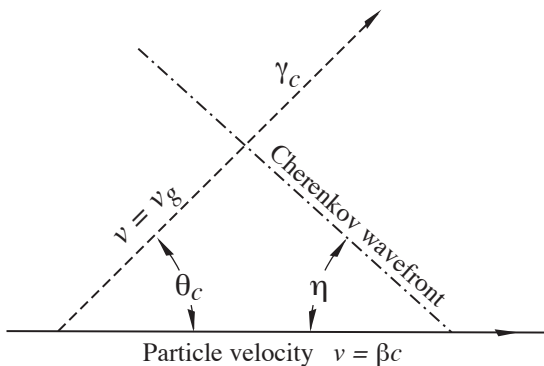


Figure 34.26: Cherenkov light emission and wavefront angles. In a dispersive medium, $\theta_c + \eta \neq 90^\circ$.

Practical Cherenkov radiator materials are dispersive. Let ω be the photon's frequency, and let $k = 2\pi/\lambda$ be its wavenumber. The photons propagate at the group velocity $v_g = d\omega/dk = c/[n(\omega) + \omega(dn/d\omega)]$. In a non-dispersive medium, this simplifies to $v_g = c/n$.

In his classical paper, Tamm [82] showed that for dispersive media the radiation is concentrated in a thin conical shell whose vertex is at the moving charge, and whose opening half-angle η is

$$\begin{aligned} \cot \eta &= \left[\frac{d}{d\omega} (\omega \tan \theta_c) \right]_{\omega_0} \\ &= \left[\tan \theta_c + \beta^2 \omega n(\omega) \frac{dn}{d\omega} \cot \theta_c \right]_{\omega_0}, \end{aligned} \quad (34.42)$$

where ω_0 is the central value of the small frequency range under consideration. (See Fig. 34.26.) This cone has a opening half-angle η , and, unless the medium is non-dispersive ($dn/d\omega = 0$), $\theta_c + \eta \neq 90^\circ$. The Cherenkov wavefront 'sideslips' along with the particle [83]. This effect has timing implications for ring imaging Cherenkov counters [84], but it is probably unimportant for most applications.

The number of photons produced per unit path length of a particle with charge ze and per unit energy interval of the photons is

$$\begin{aligned} \frac{d^2 N}{dE dx} &= \frac{\alpha z^2}{hc} \sin^2 \theta_c = \frac{\alpha^2 z^2}{r_e m_e c^2} \left(1 - \frac{1}{\beta^2 n^2(E)} \right) \\ &\approx 370 \sin^2 \theta_c(E) \text{ eV}^{-1} \text{ cm}^{-1} \quad (z = 1), \end{aligned} \quad (34.43)$$

or, equivalently,

$$\frac{d^2 N}{dx d\lambda} = \frac{2\pi \alpha z^2}{\lambda^2} \left(1 - \frac{1}{\beta^2 n^2(\lambda)} \right). \quad (34.44)$$

The index of refraction n is a function of photon energy $E = \hbar\omega$, as is the sensitivity of the transducer used to detect the light. For practical use, Eq. (34.43) must be multiplied by the the transducer response function and integrated over the region for which $\beta n(\omega) > 1$. Further details are given in the discussion of Cherenkov detectors in the Particle Detectors section (Sec. 35.5 of this Review).

When two particles are close together (lateral separation $\lesssim 1$ wavelength), the electromagnetic fields from the particles may add coherently, affecting the Cherenkov radiation. Because of their opposite charges, the radiation from an e^+e^- pair at close separation is suppressed compared to two independent leptons [85].

34.7.2 Coherent radio Cherenkov radiation

Coherent Cherenkov radiation is produced by many charged particles with a non-zero net charge moving through matter on an approximately common "wavefront"—for example, the electrons and positrons in a high-energy electromagnetic cascade. The signals can be visible for energies above 10^{16} eV; see Sec. 36.3.3.3 for more details. The phenomenon is called the Askaryan effect [86]. Near the end of a shower, when typical particle energies are below E_c (but still relativistic), a charge imbalance develops. Photons can Compton-scatter atomic electrons, and positrons can annihilate with atomic electrons to contribute even more photons which can in turn Compton scatter. These processes result in a roughly 20% excess of electrons over positrons in a shower. The net negative charge leads to coherent radio Cherenkov emission. The radiation includes a component from the decelerating charges (as in bremsstrahlung). Because the emission is coherent, the electric field strength is proportional to the shower energy, and the signal power increases as its square. The electric field strength also increases linearly with frequency, up to a maximum frequency determined by the lateral spread of the shower. This cutoff occurs at about 1 GHz in ice, and scales inversely with the Moliere radius. At low frequencies, the radiation is roughly isotropic, but, as the frequency rises toward the cutoff frequency, the radiation becomes increasingly peaked around the Cherenkov angle. The radiation is linearly polarized in the plane containing the shower axis and the photon direction. A measurement of the signal polarization can be used to help determine the shower direction. The characteristics of this radiation have been nicely demonstrated in a series of experiments at SLAC [87]. A detailed discussion of the radiation can be found in Ref. [88].

34.7.3 Transition radiation

The energy radiated when a particle with charge ze crosses the boundary between vacuum and a medium with plasma frequency ω_p is

$$I = \alpha z^2 \gamma \hbar \omega_p / 3, \quad (34.45)$$

where

$$\hbar \omega_p = \sqrt{4\pi N_e r_e^3} m_e c^2 / \alpha = \sqrt{\rho \text{ (in g/cm}^3\text{)} \langle Z/A \rangle} \times 28.81 \text{ eV}. \quad (34.46)$$

For styrene and similar materials, $\hbar \omega_p \approx 20$ eV; for air it is 0.7 eV.

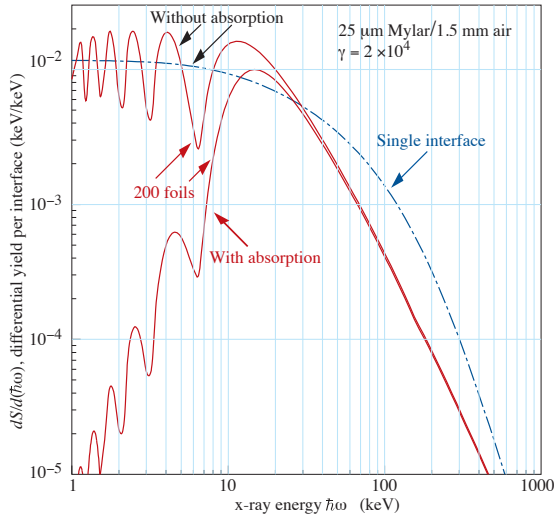


Figure 34.27: X-ray photon energy spectra for a radiator consisting of 200 25 μm thick foils of Mylar with 1.5 mm spacing in air (solid lines) and for a single surface (dashed line). Curves are shown with and without absorption. Adapted from Ref. [89].

The number spectrum $dN_\gamma/d(\hbar\omega)$ diverges logarithmically at low energies and decreases rapidly for $\hbar\omega/\gamma\hbar\omega_p > 1$. About half the energy is emitted in the range $0.1 \leq \hbar\omega/\gamma\hbar\omega_p \leq 1$. Inevitable absorption in a practical detector removes the divergence. For a particle with $\gamma = 10^3$, the radiated photons are in the soft x-ray range 2 to 40 keV. The γ dependence of the emitted energy thus comes from the hardening of the spectrum rather than from an increased quantum yield.

The number of photons with energy $\hbar\omega > \hbar\omega_0$ is given by the answer to problem 13.15 in Ref. [35],

$$N_\gamma(\hbar\omega > \hbar\omega_0) = \frac{\alpha z^2}{\pi} \left[\left(\ln \frac{\gamma \hbar \omega_p}{\hbar \omega_0} - 1 \right)^2 + \frac{\pi^2}{12} \right], \quad (34.47)$$

within corrections of order $(\hbar\omega_0/\gamma\hbar\omega_p)^2$. The number of photons above a fixed energy $\hbar\omega_0 \ll \gamma\hbar\omega_p$ thus grows as $(\ln \gamma)^2$, but the number above a fixed fraction of $\gamma\hbar\omega_p$ (as in the example above) is constant. For example, for $\hbar\omega > \gamma\hbar\omega_p/10$, $N_\gamma = 2.519 \alpha z^2 / \pi = 0.59\% \times z^2$.

The particle stays “in phase” with the x ray over a distance called the formation length, $d(\omega) = (2c/\omega)(1/\gamma^2 + \theta^2 + \omega_p^2/\omega^2)^{-1}$. Most of the radiation is produced in this distance. Here θ is the x-ray emission angle, characteristically $1/\gamma$. For $\theta = 1/\gamma$ the formation length has a maximum at $d(\gamma\omega_p/\sqrt{2}) = \gamma c/\sqrt{2}\omega_p$. In practical situations it is tens of μm .

Since the useful x-ray yield from a single interface is low, in practical detectors it is enhanced by using a stack of N foil radiators—foils L thick, where L is typically several formation lengths—separated by gas-filled gaps. The amplitudes at successive interfaces interfere to cause oscillations about the single-interface spectrum. At increasing frequencies above the position of the last interference maximum ($L/d(\omega) = \pi/2$), the formation zones, which have opposite phase, overlap more and more and the

spectrum saturates, $dI/d\omega$ approaching zero as $L/d(\omega) \rightarrow 0$. This is illustrated in Fig. 34.27 for a realistic detector configuration.

For regular spacing of the layers fairly complicated analytic solutions for the intensity have been obtained [89,90]. Although one might expect the intensity of coherent radiation from the stack of foils to be proportional to N^2 , the angular dependence of the formation length conspires to make the intensity $\propto N$.

References

- [1] H. Bichsel, Nucl. Instrum. Meth. **A562**, 154 (2006).
- [2] B. Rossi, *High Energy Particles*, Prentice-Hall, Inc., Englewood Cliffs, NJ, 1952.
- [3] H.A. Bethe, *Zur Theorie des Durchgangs schneller Korpuskularstrahlen durch Materie*, H. Bethe, Ann. Phys. **5**, 325 (1930).
- [4] “Stopping Powers and Ranges for Protons and Alpha Particles,” ICRU Report No. 49 (1993); Tables and graphs are available at <http://physics.nist.gov/PhysRefData/Star/Text/PSTAR.html> and <http://physics.nist.gov/PhysRefData/Star/Text/ASTAR.html>.
- [5] D.E. Groom, N.V. Mokhov, and S.I. Striganov, “Muon stopping-power and range tables: 10 MeV–100 TeV,” Atomic Data and Nuclear Data Tables **78**, 183–356 (2001). Since submission of this paper it has become likely that post-Born corrections to the direct pair production cross section should be made. Code used to make Figs. 34.22–34.24 included these corrections [D.Yu. Ivanov *et al.*, Phys. Lett. **B442**, 453 (1998)]. The effect is negligible except at high Z . (It is less than 1% for iron.); Extensive printable and machine-readable tables are given at <http://pdg.lbl.gov/AtomicNuclearProperties/>.
- [6] W. H. Barkas, W. Birnbaum and F. M. Smith, Phys. Rev. **101**, 778 (1956).
- [7] U. Fano, Ann. Rev. Nucl. Sci. **13**, 1 (1963).
- [8] J. D. Jackson, Phys. Rev. **D59**, 017301 (1999).
- [9] J. Lindhard and A. H. Sørensen, Phys. Rev. **A53**, 2443 (1996).
- [10] “Stopping Powers for Electrons and Positrons,” ICRU Report No. 37 (1984); Tables and graphs are available at <http://physics.nist.gov/PhysRefData/Star/Text/ESTAR.html>.
- [11] H. Bichsel, Phys. Rev. **A46**, 5761 (1992).
- [12] W.H. Barkas and M.J. Berger, *Tables of Energy Losses and Ranges of Heavy Charged Particles*, NASA-SP-3013 (1964).
- [13] S.M. Seltzer and M.J. Berger, Int. J. of Applied Rad. **33**, 1189 (1982).
- [14] <http://physics.nist.gov/PhysRefData/XrayMassCoef/tab1.html>.
- [15] R. M. Sternheimer, Phys. Rev. **88**, 851 (1952).
- [16] R. M. Sternheimer, M. J. Berger and S. M. Seltzer, Atom. Data Nucl. Data Tabl. **30**, 261 (1984); Minor errors are corrected in Ref. 5. Chemical composition for the tabulated materials is given in Ref. 10.
- [17] R. M. Sternheimer and R. F. Peierls, Phys. Rev. **B3**, 3681 (1971).
- [18] N. F. Mott, Proceedings of the Cambridge Philosophical Society **27**, 553 (1931).
- [19] M. S. Livingston and H. A. Bethe, Rev. Mod. Phys. **9**, 245 (1937).
- [20] H. Bichsel, Phys. Rev. **A65**, 5, 052709 (2002).
- [21] S. P. Møller *et al.*, Phys. Rev. **A56**, 4, 2930 (1997).
- [22] J. C. Ashley, R. H. Ritchie and W. Brandt, Phys. Rev. **B5**, 2393 (1972).
- [23] H.H. Andersen and J.F. Ziegler, *Hydrogen: Stopping Powers and Ranges in All Elements*. Vol. 3 of *The Stopping and Ranges of Ions in Matter* (Pergamon Press 1977).

- [24] J. Lindhard, Kgl. Danske Videnskab. Selskab, Mat.-Fys. Medd. **28**, No. 8 (1954); J. Lindhard, M. Scharff, and H.E. Schiøtt, Kgl. Danske Videnskab. Selskab, Mat.-Fys. Medd. **33**, No. 14 (1963).
- [25] J.F. Ziegler, J.F. Biersac, and U. Littmark, *The Stopping and Range of Ions in Solids*, Pergamon Press 1985.
- [26] E.A. Uehling, Ann. Rev. Nucl. Sci. **4**, 315 (1954) (For heavy particles with unit charge, but e^\pm cross sections and stopping powers are also given).
- [27] N.F. Mott and H.S.W. Massey, *The Theory of Atomic Collisions*, Oxford Press, London, 1965.
- [28] P. V. Vavilov, Sov. Phys. JETP **5**, 749 (1957), [Zh. Eksp. Teor. Fiz.32,920(1957)].
- [29] L.D. Landau, J. Exp. Phys. (USSR) **8**, 201 (1944).
- [30] H. Bichsel, Rev. Mod. Phys. **60**, 663 (1988).
- [31] R. Talman, Nucl. Instrum. Meth. **159**, 189 (1979).
- [32] H. Bichsel, Ch. 87 in the Atomic, Molecular and Optical Physics Handbook, G.W.F. Drake, editor (Am. Inst. Phys. Press, Woodbury NY, 1996).
- [33] S.M. Seltzer and M.J. Berger, Int. J. of Applied Rad. **35**, 665 (1984). This paper corrects and extends the results of Ref. [13].
- [34] H. A. Bethe, Phys. Rev. **89**, 1256 (1953).
- [35] J.D. Jackson, *Classical Electrodynamics*, 3rd edition, (John Wiley and Sons, New York, 1998).
- [36] W. T. Scott, Rev. Mod. Phys. **35**, 231 (1963).
- [37] J. W. Motz, H. Olsen and H. W. Koch, Rev. Mod. Phys. **36**, 881 (1964).
- [38] H. Bichsel, Phys. Rev. **112**, 182 (1958).
- [39] G. Shen *et al.*, Phys. Rev. **D20**, 1584 (1979).
- [40] G. R. Lynch and O. I. Dahl, Nucl. Instrum. Meth. **B58**, 6 (1991).
- [41] M. Wong *et al.*, Med. Phys. **17**, 163 (1990).
- [42] Y.-S. Tsai, Rev. Mod. Phys. **46**, 815 (1974), [Erratum: Rev. Mod. Phys.49,521(1977)].
- [43] H. Davies, H. A. Bethe and L. C. Maximon, Phys. Rev. **93**, 788 (1954).
- [44] L. D. Landau and I. Pomeranchuk, Dokl. Akad. Nauk Ser. Fiz. **92**, 535 (1953); **92**, 735 (1953). These papers are available in English in L. Landau, *The Collected Papers of L.D. Landau*, Pergamon Press, 1965; A. B. Migdal, Phys. Rev. **103**, 1811 (1956).
- [45] S. Klein, Rev. Mod. Phys. **71**, 1501 (1999).
- [46] M.L. Ter-Mikaelian, SSSR **94**, 1033 (1954); M.L. Ter-Mikaelian, *High Energy Electromagnetic Processes in Condensed Media* (John Wiley and Sons, New York, 1972).
- [47] P. L. Anthony *et al.*, Phys. Rev. Lett. **76**, 3550 (1996).
- [48] H. W. Koch and J. W. Motz, Rev. Mod. Phys. **31**, 920 (1959).
- [49] M.J. Berger and S.M. Seltzer, "Tables of Energy Losses and Ranges of Electrons and Positrons," National Aeronautics and Space Administration Report NASA-SP-3012 (Washington DC 1964).
- [50] Curves for these and other elements, compounds, and mixtures may be obtained from <https://www.nist.gov/pml/xcom-photon-cross-sections-database>. The photon total cross section is approximately flat for at least two decades beyond the energy range shown.
- [51] B. L. Berman and S. C. Fultz, Rev. Mod. Phys. **47**, 713 (1975).
- [52] http://www.cxro.lbl.gov/optical_constants/pert_form.html.
- [53] <https://physics.nist.gov/PhysRefData/XrayMassCoef/tab3.html>.
- [54] J. W. Motz, H. A. Olsen and H. W. Koch, Rev. Mod. Phys. **41**, 581 (1969).
- [55] P. L. Anthony *et al.*, Phys. Rev. Lett. **75**, 1949 (1995).
- [56] U. I. Uggerhøj, Rev. Mod. Phys. **77**, 1131 (2005).
- [57] L. Gerhardt and S. R. Klein, Phys. Rev. **D82**, 074017 (2010).
- [58] W.R. Nelson, H. Hirayama, and D.W.O. Rogers, "The EGS4 Code System," SLAC-265, Stanford Linear Accelerator Center (Dec. 1985).
- [59] *Experimental Techniques in High Energy Physics*, ed. T. Ferbel (Addison-Wesley, Menlo Park CA 1987).
- [60] U. Amaldi, Phys. Scripta **23**, 409 (1981).
- [61] E. Longo and I. Sestili, Nucl. Instrum. Meth. **128**, 283 (1975), [Erratum: Nucl. Instrum. Meth.135,587(1976)].
- [62] G. Grindhammer *et al.*, in *Proceedings of the 1988 Summer Study on High Energy Physics in the 1990's*, Snowmass, CO, June 27 – July 15, 1990, edited by F.J. Gilman and S. Jensen, (World Scientific, Teaneck, NJ, 1989) p. 151.
- [63] W. R. Nelson *et al.*, Phys. Rev. **149**, 201 (1966).
- [64] G. Bathow *et al.*, Nucl. Phys. **B20**, 592 (1970).
- [65] H. Bethe and W. Heitler, Proc. Roy. Soc. Lond. **A146**, 83 (1934); H.A. Bethe, *Proc. Cambridge Phil. Soc.* **30**, 542 (1934).
- [66] A.A. Petrukhin and V.V. Shestakov, Can. J. Phys. **46**, S377 (1968).
- [67] V.M. Galitskii and S.R. Kel'ner, Sov. Phys. JETP **25**, 948 (1967).
- [68] S.R. Kel'ner and Yu.D. Kotov, Sov. J. Nucl. Phys. **7**, 237 (1968).
- [69] R.P. Kokoulin and A.A. Petrukhin, in *Proceedings of the International Conference on Cosmic Rays*, Hobart, Australia, August 16–25, 1971, Vol. **4**, p. 2436.
- [70] A. I. Nikishov, Sov. J. Nucl. Phys. **27**, 677 (1978), [Yad. Fiz.27,1281(1978)].
- [71] Yu. M. Andreev, L. B. Bezrukov and E. V. Bugaev, Phys. Atom. Nucl. **57**, 2066 (1994), [Yad. Fiz.57,2146(1994)].
- [72] L. B. Bezrukov and E. V. Bugaev, Yad. Fiz. **33**, 1195 (1981), [Sov. J. Nucl. Phys.33,635(1981)].
- [73] N.V. Mokhov and C.C. James, The MARS Code System User's Guide, Fermilab-FN-1058-APC (2018), <https://mars.fnal.gov/>; N. Mokhov *et al.*, Prog. Nucl. Sci. Tech. **4**, 496 (2014).
- [74] P. H. Barrett *et al.*, Rev. Mod. Phys. **24**, 3, 133 (1952).
- [75] A. Van Ginneken, Nucl. Instrum. Meth. **A251**, 21 (1986).
- [76] U. Becker *et al.*, Nucl. Instrum. Meth. **A253**, 15 (1986).
- [77] J.J. Eastman and S.C. Loken, in *Proceedings of the Workshop on Experiments, Detectors, and Experimental Areas for the Supercollider*, Berkeley, CA, July 7–17, 1987, edited by R. Donaldson and M.G.D. Gilchriese (World Scientific, Singapore, 1988), p. 542.
- [78] *Methods of Experimental Physics*, L.C.L. Yuan and C.-S. Wu, editors, Academic Press, 1961, Vol. 5A, p. 163.
- [79] W.W.M. Allison and P.R.S. Wright, "The Physics of Charged Particle Identification: dE/dx , Cherenkov Radiation, and Transition Radiation," p. 371 in *Experimental Techniques in High Energy Physics*, T. Ferbel, editor, (Addison-Wesley 1987).
- [80] E.R. Hayes, R.A. Schluter, and A. Tamosaitis, "Index and Dispersion of Some Cherenkov Counter Gases," ANL-6916 (1964).
- [81] T. Ypsilantis, in "Proceedings of the Symposium on Particle Identification at High Luminosity Hadron Colliders, Apr 5-7, 1989 Batavia, Ill.," 0661–676 (1989).
- [82] I. Tamm, J. Phys. U.S.S.R., **1**, 439 (1939).
- [83] H. Motz and L.I. Schiff, Am. J. Phys. **21**, 258 (1953).
- [84] B. N. Ratcliff, Nucl. Instrum. Meth. **A502**, 211 (2003).
- [85] S. K. Mandal, S. R. Klein and J. D. Jackson, Phys. Rev. **D72**, 093003 (2005).

- [86] G. A. Askar'yan, Sov. Phys. JETP **14**, 2, 441 (1962), [Zh. Eksp. Teor. Fiz.41,616(1961)].
- [87] P. W. Gorham *et al.*, Phys. Rev. **D72**, 023002 (2005).
- [88] E. Zas, F. Halzen and T. Stanev, Phys. Rev. **D45**, 362 (1992).
- [89] M. L. Cherry *et al.*, Phys. Rev. **D10**, 3594 (1974); M. L. Cherry, Phys. Rev. **D17**, 2245 (1978).
- [90] B. Dolgoshein, Nucl. Instrum. Meth. **A326**, 434 (1993).

35. Particle Detectors at Accelerators

Revised 2019. See the various sections for authors.

35.1	Introduction	551
35.2	Photon detectors	551
35.2.1	Vacuum photodetectors	552
35.2.2	Gaseous photon detectors	553
35.2.3	Solid-state photon detectors	553
35.3	Organic scintillators	554
35.3.1	Scintillation mechanism	554
35.3.2	Caveats and cautions	555
35.3.3	Scintillating and wavelength-shifting fibers	555
35.4	Inorganic scintillators	555
35.5	Cherenkov detectors	558
35.6	Gaseous detectors	560
35.6.1	Energy loss and charge transport in gases	560
35.6.2	Multi-Wire Proportional and Drift Chambers	562
35.6.3	High Rate Effects	563
35.6.4	Micro-Pattern Gas Detectors	563
35.6.5	Time-projection chambers	565
35.6.6	Transition radiation detectors (TRD's)	567
35.6.7	Resistive-plate chambers	568
35.7	Semiconductor detectors	569
35.7.1	Materials Requirements	569
35.7.2	Detector Configurations	570
35.7.3	Signal Formation	570
35.7.4	Radiation Damage	571
35.8	Low-noise electronics	571
35.9	Calorimeters	573
35.9.1	Introduction	573
35.9.2	Electromagnetic calorimeters	574
35.9.3	Hadronic calorimeters	575
35.9.4	Free electron drift velocities in liquid ionization chambers	578
35.10	Accelerator-based neutrino detectors	579
35.10.1	Introduction	579
35.10.2	Signals and Backgrounds	579
35.10.3	Instances of Neutrino Detector Technology	579
35.10.4	Outlook	582
35.11	Superconducting magnets for collider detectors	582
35.11.1	Solenoid Magnets	582
35.11.2	Properties of collider detector magnets	583
35.11.3	Toroidal magnets	584
35.12	Measurement of particle momenta in a uniform magnetic field	584

35.1 Introduction

This review summarizes the detector technologies employed at accelerator particle physics experiments. Several of these detectors are also used in a non-accelerator context and examples of such applications will be provided. The detector techniques which are specific to non-accelerator particle physics experiments are the subject of Chap. 36. More detailed discussions of detectors and their underlying physics can be found in books by Ferbel [1], Kleinknecht [2], Knoll [3], Green [4], Leroy & Rancoita [5], and Grupen [6].

In Table 35.1 are given typical resolutions and deadtimes of common charged particle detectors. The quoted numbers are usually based on typical devices, and should be regarded only as rough approximations for new designs. The spatial resolution refers to the intrinsic detector resolution, i.e. without multiple scattering. We note that analog detector readout can provide better spatial resolution than digital readout by measuring the deposited charge in neighboring channels. Quoted ranges attempt to be representative of both possibilities. The time resolution is defined by how accurately the time at which a particle crossed the detector can be determined. The deadtime is the minimum separation in time between two resolved hits on the same channel. Typical performance of calorimetry and particle identification are provided in the relevant sections below.

Table 35.1: Typical resolutions and deadtimes of common charged particle detectors. Revised November 2011.

Detector Type	Intrinsic Spatial Resolution (rms)	Time Resolution	Dead Time
Resistive plate chamber	$\lesssim 10$ mm	1 ns (50 ps [*])	—
Streamer chamber	$300 \mu\text{m}^\dagger$	$2 \mu\text{s}$	100 ms
Liquid argon drift [7]	$\sim 175\text{--}450 \mu\text{m}$	~ 200 ns	$\sim 2 \mu\text{s}$
Scintillation tracker	$\sim 100 \mu\text{m}$	$100 \text{ps}/n^\ddagger$	10 ns
Bubble chamber	$10\text{--}150 \mu\text{m}$	1 ms	50ms^\S
Proportional chamber	$50\text{--}100 \mu\text{m}^\P$	2 ns	20-200 ns
Drift chamber	$50\text{--}100 \mu\text{m}$	2ns^\parallel	20-100 ns
Micro-pattern gas detect.	$30\text{--}40 \mu\text{m}$	< 10 ns	10-100 ns
Silicon strip	pitch/(3 to 7)**	few ns ^{††}	$\lesssim 50 \text{ns}^{\dagger\dagger}$
Silicon pixel	$\lesssim 10 \mu\text{m}$	few ns ^{††}	$\lesssim 50 \text{ns}^{\dagger\dagger}$
Emulsion	$1 \mu\text{m}$	—	—

*For multiple-gap RPCs.

[†] $300 \mu\text{m}$ is for 1 mm pitch (wirespacing/ $\sqrt{12}$).

[‡] n = index of refraction.

[§]Multiple pulsing time.

[¶]Delay line cathode readout can give $\pm 150 \mu\text{m}$ parallel to anode wire.

^{||}For two chambers

**The highest resolution (“7”) is obtained for small-pitch detectors ($\lesssim 25 \mu\text{m}$) with pulse-height-weighted center finding.

^{††}Limited by the readout electronics [8]

35.2 Photon detectors

Revised August 2011 by D. Chakraborty (Northern Illinois U.) and T. Sumiyoshi (Tokyo Metropolitan U.).

Most detectors in high-energy, nuclear, and astrophysics rely on the detection of photons in or near the visible range, $100 \text{nm} \lesssim \lambda \lesssim 1000 \text{nm}$, or $E \approx$ a few eV. This range covers scintillation and Cherenkov radiation as well as the light detected in many astronomical observations.

Generally, photodetection involves generating a detectable electrical signal proportional to the (usually very small) number of incident photons. The process involves three distinct steps:

1. generation of a primary photoelectron or electron-hole (e - h) pair by an incident photon by the photoelectric or photoconductive effect,
2. amplification of the p.e. signal to detectable levels by one or more multiplicative bombardment steps and/or an avalanche process (usually), and,
3. collection of the secondary electrons to form the electrical signal.

The important characteristics of a photodetector include the following in statistical averages:

1. quantum efficiency (QE or ϵ_Q): the number of primary photoelectrons generated per incident photon ($0 \leq \epsilon_Q \leq 1$; in silicon more than one e - h pair per incident photon can be generated for $\lambda \lesssim 165 \text{nm}$),
2. collection efficiency (CE or ϵ_C): the overall acceptance factor other than the generation of photoelectrons ($0 \leq \epsilon_C \leq 1$),
3. gain (G): the number of electrons collected for each photoelectron generated,
4. dark current or dark noise: the electrical signal when there is no photon,
5. energy resolution: electronic noise (ENC or N_e) and statistical fluctuations in the amplification process compound the Poisson distribution of n_γ photons from a given source:

$$\frac{\sigma(E)}{\langle E \rangle} = \sqrt{\frac{f_N}{n_\gamma \epsilon_Q \epsilon_C} + \left(\frac{N_e}{G n_\gamma \epsilon_Q \epsilon_C} \right)^2}, \quad (35.1)$$

where f_N , or the excess noise factor (ENF), is the contribution to the energy distribution variance due to amplification statistics [9],

6. dynamic range: the maximum signal available from the detector (this is usually expressed in units of the response to noise-equivalent power, or NEP, which is the optical input power that produces a signal-to-noise ratio of 1),
7. time dependence of the response: this includes the transit time, which is the time between the arrival of the photon and the electrical pulse, and the transit time spread, which contributes to the pulse rise time and width, and
8. rate capability: inversely proportional to the time needed, after the arrival of one photon, to get ready to receive the next.

The QE is a strong function of the photon wavelength (λ), and is usually quoted at maximum, together with a range of λ where the QE is comparable to its maximum. Spatial uniformity and linearity with respect to the number of photons are highly desirable in a photodetector's response.

Optimization of these factors involves many trade-offs and vary widely between applications. For example, while a large gain is desirable, attempts to increase the gain for a given device also increases the ENF and after-pulsing ("echos" of the main pulse). In solid-state devices, a higher QE often requires a compromise in the timing properties. In other types, coverage of large areas by focusing increases the transit time spread.

Other important considerations also are highly application-specific. These include the photon flux and wavelength range, the total area to be covered and the efficiency required, the volume available to accommodate the detectors, characteristics of the environment such as chemical composition, temperature, magnetic field, ambient background, as well as ambient radiation of different types and, mode of operation (continuous or triggered), bias (high-voltage) requirements, power consumption, calibration needs, aging, cost, and so on. Several technologies employing different phenomena for the three steps described above, and many variants within each, offer a wide range of solutions to choose from. The salient features of the main technologies and the common variants are described below. Some key characteristics are summarized in Table 35.2.

35.2.1 Vacuum photodetectors

Vacuum photodetectors can be broadly subdivided into three types: photomultiplier tubes, microchannel plates, and hybrid photodetectors.

35.2.1.1 Photomultiplier tubes

A versatile class of photon detectors, vacuum photomultiplier tubes (PMT) has been employed by a vast majority of all particle physics experiments to date [9]. Both "transmission-" and "reflection-type" PMT's are widely used. In the former, the photocathode material is deposited on the inside of a transparent window through which the photons enter, while in the latter, the photocathode material rests on a separate surface that the incident photons strike. The cathode material has a low work function, chosen for the wavelength band of interest. When a photon hits the cathode and liberates an electron (the photoelectric effect), the latter is accelerated and guided by electric fields to impinge on a secondary-emission electrode, or dynode, which then emits a few (~ 5) secondary electrons. The multiplication process is repeated typically 10 times in series to generate a sufficient number of electrons, which are collected at the anode for delivery to the external circuit. The total gain of a PMT depends on the applied high voltage V as $G = AV^{kn}$, where $k \approx 0.7-0.8$ (depending on the dynode material), n is the number of dynodes in the chain, and A a constant (which also depends on n). Typically, G is in the range of 10^5-10^6 . Pulse risetimes are usually in the few nanosecond range. With *e.g.* two-level discrimination the effective time resolution can be much better.

A large variety of PMT's, including many just recently developed, covers a wide span of wavelength ranges from infrared (IR) to extreme ultraviolet (XUV) [10]. They are categorized by the window materials, photocathode materials, dynode struc-

tures, anode configurations, *etc.* Common window materials are borosilicate glass for IR to near-UV, fused quartz and sapphire (Al_2O_3) for UV, and MgF_2 or LiF for XUV. The choice of photocathode materials include a variety of mostly Cs- and/or Sb-based compounds such as CsI, CsTe, bi-alkali (SbRbCs, SbKCs), multi-alkali (SbNa₂KCs), GaAs(Cs), GaAsP, *etc.* Sensitive wavelengths and peak quantum efficiencies for these materials are summarized in Table-35.3. Typical dynode structures used in PMT's are circular cage, line focusing, box and grid, venetian blind, and fine mesh. In some cases, limited spatial resolution can be obtained by using a mosaic of multiple anodes. Fast PMT's with very large windows—measuring up to 508 mm across—have been developed in recent years for detection of Cherenkov radiation in neutrino experiments such as Super-Kamiokande and KamLAND among many others. Specially prepared low-radioactivity glass is used to make these PMT's, and they are also able to withstand the high pressure of the surrounding liquid.

PMT's are vulnerable to magnetic fields—sometimes even the geomagnetic field causes large orientation-dependent gain changes. A high-permeability metal shield is often necessary. However, proximity-focused PMT's, *e.g.* the fine-mesh types, can be used even in a high magnetic field (≥ 1 T) if the electron drift direction is parallel to the field. CMS uses custom-made vacuum phototriodes (VPT) mounted on the back face of projective lead tungstate crystals to detect scintillation light in the endcap sections of its electromagnetic calorimeters, which are inside a 3.8 T superconducting solenoid. A VPT employs a single dynode (thus, $G \approx 10$) placed close to the photocathode, and a mesh anode plane between the two, to help it cope with the strong magnetic field, which is not too unfavorably oriented with respect to the photodetector axis in the endcaps (within 25°), but where the radiation level is too high for Avalanche Photodiodes (APD's) like those used in the barrel section.

35.2.1.2 Microchannel plates

A typical Microchannel plate (MCP) photodetector consists of one or more ~ 2 mm thick glass plates with densely packed $O(10 \mu\text{m})$ -diameter cylindrical holes, or "channels", sitting between the transmission-type photocathode and anode planes, separated by $O(1 \text{ mm})$ gaps. Instead of discrete dynodes, the inner surface of each cylindrical tube serves as a continuous dynode for the entire cascade of multiplicative bombardments initiated by a photoelectron. Gain fluctuations can be minimized by operating in a saturation mode, whence each channel is only capable of a binary output, but the sum of all channel outputs remains proportional to the number of photons received so long as the photon flux is low enough to ensure that the probability of a single channel receiving more than one photon during a single time gate is negligible. MCP's are thin, offer good spatial resolution, have excellent time resolution (~ 20 ps), and can tolerate random magnetic fields up to 0.1 T and axial fields up to ~ 1 T. However, they suffer from relatively long recovery time per channel and short lifetime. MCP's are widely employed as image-intensifiers, although not so much in HEP or astrophysics.

35.2.1.3 Hybrid photon detectors

Hybrid photon detectors (HPD) combine the sensitivity of a vacuum PMT with the excellent spatial and energy resolutions of a Si sensor [11]. A single photoelectron ejected from the photocathode is accelerated through a potential difference of ~ 20 kV before it impinges on the silicon sensor/anode. The gain nearly equals the maximum number of $e-h$ pairs that could be created from the entire kinetic energy of the accelerated electron: $G \approx eV/w$, where e is the electronic charge, V is the applied potential difference, and $w \approx 3.7$ eV is the mean energy required to create an $e-h$ pair in Si at room temperature. Since the gain is achieved in a single step, one might expect to have the excellent resolution of a simple Poisson statistic with large mean, but in fact it is even better, thanks to the Fano effect discussed in Sec. 35.7.

Low-noise electronics must be used to read out HPD's if one intends to take advantage of the low fluctuations in gain, *e.g.* when counting small numbers of photons. HPD's can have the same $\epsilon_Q \epsilon_C$ and window geometries as PMT's and can be segmented down to $\sim 50 \mu\text{m}$. However, they require rather high biases and

Table 35.2: Representative characteristics of some photodetectors commonly used in particle physics. The time resolution of the devices listed here vary in the 10–2000 ps range.

Type	λ (nm)	$\epsilon_Q \epsilon_C$	Gain	Risetime (ns)	Area (mm ²)	1-p.e noise (Hz)	HV (V)	Price (USD)
PMT *	115–1700	0.15–0.25	10^3 – 10^7	0.7–10	10^2 – 10^5	10 – 10^4	500–3000	100–5000
MCP*	100–650	0.01–0.10	10^3 – 10^7	0.15–0.3	10^2 – 10^4	0.1–200	500–3500	10–6000
HPD*	115–850	0.1–0.3	10^3 – 10^4	7	10^2 – 10^5	10 – 10^3	$\sim 2 \times 10^4$	~ 600
GPM*	115–500	0.15–0.3	10^3 – 10^6	$O(0.1)$	$O(10)$	10 – 10^3	300–2000	$O(10)$
APD	300–1700	~ 0.7	10 – 10^8	$O(1)$	10 – 10^3	1 – 10^3	400–1400	$O(100)$
PPD	320–900	0.15–0.3	10^5 – 10^6	~ 1	1–10	$O(10^6)$	30–60	$O(100)$
VLPC	500–600	~ 0.9	$\sim 5 \times 10^4$	~ 10	1	$O(10^4)$	~ 7	~ 1

*These devices often come in multi-anode configurations. In such cases, area, noise, and price are to be considered on a “per readout-channel” basis.

will not function in a magnetic field. The exception is proximity-focused devices (\Rightarrow no (de)magnification) in an axial field. With time resolutions of ~ 10 ps and superior rate capability, proximity-focused HPD’s can be an alternative to MCP’s. Current applications of HPD’s include the CMS hadronic calorimeter and the RICH detector in LHCb. Large-size HPD’s with sophisticated focusing may be suitable for future water Cherenkov experiments.

Hybrid APD’s (HAPD’s) add an avalanche multiplication step following the electron bombardment to boost the gain by a factor of ~ 50 . This affords a higher gain and/or lower electrical bias, but also degrades the signal definition.

Table 35.3: Properties of photocathode and window materials commonly used in vacuum photodetectors.

Photocathode material	λ (nm)	Window material	Peak ϵ_Q (λ/nm)
CsI	115–200	MgF ₂	0.11 (140)
CsTe	115–320	MgF ₂	0.14 (240)
Bi-alkali	300–650	Borosilicate	0.27 (390)
	160–650	Synthetic Silica	0.27 (390)
“Ultra Bi-alkali”	300–650	Borosilicate	0.43 (350)
	160–650	Synthetic Silica	0.43 (350)
Multi-alkali	300–850	Borosilicate	0.20 (360)
	160–850	Synthetic Silica	0.20 (360)
GaAs(Cs)*	160–930	Synthetic Silica	0.23 (280)
GaAsP(Cs)	300–750	Borosilicate	0.50 (500)
InP/InGaAsP [†]	350–1700	Borosilicate	0.01 (1100)

*Reflection type photocathode is used.

[†]Requires cooling to $\sim -80^\circ\text{C}$.

35.2.2 Gaseous photon detectors

In gaseous photomultipliers (GPM) a photoelectron in a suitable gas mixture initiates an avalanche in a high-field region, producing a large number of secondary impact-ionization electrons. In principle the charge multiplication and collection processes are identical to those employed in gaseous tracking detectors such as multiwire proportional chambers, micromesh gaseous detectors (Micromegas), or gas electron multipliers (GEM). These are discussed in Sec. 35.6.4.

The devices can be divided into two types depending on the photocathode material. One type uses solid photocathode materials much in the same way as PMT’s. Since it is resistant to gas mixtures typically used in tracking chambers, CsI is a common choice. In the other type, photoionization occurs on suitable molecules vaporized and mixed in the drift volume. Most gases have photoionization work functions in excess of 10 eV, which would limit their sensitivity to wavelengths far too short. However, vapors of TMAE (tetrakis dimethyl-amine ethylene) or TEA (tri-ethyl-amine), which have smaller work functions (5.3 eV for TMAE and 7.5 eV for TEA), are suited for XUV photon detection [12]. Since devices like GEM’s offer sub-mm spatial resolution, GPM’s are often used as position-sensitive photon detectors.

They can be made into flat panels to cover large areas ($O(1\text{ m}^2)$), can operate in high magnetic fields, and are relatively inexpensive. Many of the ring imaging Cherenkov (RICH) detectors to date have used GPM’s for the detection of Cherenkov light [13–16]. Special care must be taken to suppress the photon-feedback process in GPM’s. It is also important to maintain high purity of the gas as minute traces of O₂ can significantly degrade the detection efficiency.

35.2.3 Solid-state photon detectors

In a phase of rapid development, solid-state photodetectors are competing with vacuum- or gas-based devices for many existing applications and making way for a multitude of new ones. Compared to traditional vacuum- and gaseous photodetectors, solid-state devices are more compact, lightweight, rugged, tolerant to magnetic fields, and often cheaper. They also allow fine pixelization, are easy to integrate into large systems, and can operate at low electric potentials, while matching or exceeding most performance criteria. They are particularly well suited for detection of γ - and X-rays. Except for applications where coverage of very large areas or dynamic range is required, solid-state detectors are proving to be the better choice. Some hybrid devices attempt to combine the best features of different technologies while applications of nanotechnology are opening up exciting new possibilities.

Silicon photodiodes (PD) are widely used in high-energy physics as particle detectors and in a great number of applications (including solar cells!) as light detectors. The structure is discussed in some detail in Sec. 35.7. In its simplest form, the PD is a reverse-biased p - n junction. Photons with energies above the indirect bandgap energy (wavelengths shorter than about 1050 nm, depending on the temperature) can create e - h pairs (the photoconductive effect), which are collected on the p and n sides, respectively. Often, as in the PD’s used for crystal scintillator readout in CLEO, L3, Belle, BaBar, and GLAST, intrinsic silicon is doped to create a p - i - n structure. The reverse bias increases the thickness of the depleted region; in the case of these particular detectors, to full depletion at a depth of about 100 μm . Increasing the depletion depth decreases the capacitance (and hence electronic noise) and extends the red response. Quantum efficiency can exceed 90%, but falls toward the red because of the increasing absorption length of light in silicon. The absorption length reaches 100 μm at 985 nm. However, since $G = 1$, amplification is necessary. Optimal low-noise amplifiers are slow, but, even so, noise limits the minimum detectable signal in room-temperature devices to several hundred photons.

Very large arrays containing $O(10^7)$ of $O(10\ \mu\text{m}^2)$ -sized photodiodes pixelizing a plane are widely used to photograph all sorts of things from everyday subjects at visible wavelengths to crystal structures with X-rays and astronomical objects from infrared to UV. To limit the number of readout channels, these are made into charge-coupled devices (CCD), where pixel-to-pixel signal transfer takes place over thousands of synchronous cycles with sequential output through shift registers [17]. Thus, high spatial resolution is achieved at the expense of speed and timing precision. Custom-made CCD’s have virtually replaced photographic plates and other imagers for astronomy and in spacecraft. Typical QE’s

exceed 90% over much of the visible spectrum, and “thick” CCD’s have useful QE up to $\lambda = 1 \mu\text{m}$. Active Pixel Sensor (APS) arrays with a preamplifier on each pixel and CMOS processing afford higher speeds, but are challenged at longer wavelengths. Much R&D is underway to overcome the limitations of both CCD and CMOS imagers.

In APD’s, an exponential cascade of impact ionizations initiated by the original photogenerated e - h pair under a large reverse-bias voltage leads to an avalanche breakdown [18–21]. As a result, detectable electrical response can be obtained from low-intensity optical signals down to single photons. Excellent junction uniformity is critical, and a guard ring is generally used as a protection against edge breakdown. Well-designed APD’s, such as those used in CMS’ crystal-based electromagnetic calorimeter, have achieved $\epsilon_Q \epsilon_C \approx 0.7$ with sub-ns response time. The sensitive wavelength window and gain depend on the semiconductor used. The gain is typically 10–200 in linear and up to 10^8 in Geiger mode of operation. Stability and close monitoring of the operating temperature are important for linear-mode operation, and substantial cooling is often necessary. Position-sensitive APD’s use time information at multiple anodes to calculate the hit position.

One of the most promising recent developments in the field is that of devices consisting of large arrays ($O(10^3)$) of tiny APD’s packed over a small area ($O(1 \text{ mm}^2)$) and operated in a limited Geiger mode [22–24]. Among different names used for this class of photodetectors, “PPD” (for “Pixelized Photon Detector”) is most widely accepted (formerly “SiPM”). Although each cell only offers a binary output, linearity with respect to the number of photons is achieved by summing the cell outputs in the same way as with a MCP in saturation mode (see above). PPD’s are being adopted as the preferred solution for various purposes including medical imaging, *e.g.* positron emission tomography (PET). These compact, rugged, and economical devices allow auto-calibration through decent separation of photoelectron peaks and offer gains of $O(10^6)$ at a moderate bias voltage ($\sim 50 \text{ V}$). However, the single-photoelectron noise of a PPD, being the logical “or” of $O(10^3)$ Geiger APD’s, is rather large: $O(1 \text{ MHz/mm}^2)$ at room temperature. PPD’s are particularly well-suited for applications where triggered pulses of several photons are expected over a small area, *e.g.* fiber-guided scintillation light. Intense R&D is expected to lower the noise level and improve radiation hardness, resulting in coverage of larger areas and wider applications. Attempts are being made to combine the fabrication of the sensors and the front-end electronics (ASIC) in the same process with the goal of making PPD’s and other finely pixelized solid-state photodetectors extremely easy to use.

Of late, much R&D has been directed to p - i - n diode arrays based on thin polycrystalline diamond films formed by chemical vapor deposition (CVD) on a hot substrate ($\sim 1000 \text{ K}$) from a hydrocarbon-containing gas mixture under low pressure ($\sim 100 \text{ mbar}$). These devices have maximum sensitivity in the extreme- to moderate-UV region [25–27]. Many desirable characteristics, including high tolerance to radiation and temperature fluctuations, low dark noise, blindness to most of the solar radiation spectrum, and relatively low cost make them ideal for space-based UV/XUV astronomy, measurement of synchrotron radiation, and luminosity monitoring at (future) lepton collider(s).

Visible-light photon counters (VLPC) utilize the formation of an impurity band only 50 meV below the conduction band in As-doped Si to generate strong ($G \approx 5 \times 10^4$) yet sharp response to single photons with $\epsilon_Q \approx 0.9$ [28–30]. The smallness of the band gap considerably reduces the gain dispersion. Only a very small bias ($\sim 7 \text{ V}$) is needed, but high sensitivity to infrared photons requires cooling below 10 K. The dark noise increases sharply and exponentially with both temperature and bias. The Run 2 DØ detector used 86000 VLPC’s to read the optical signal from its scintillating-fiber tracker and scintillator-strip preshower detectors.

35.3 Organic scintillators

Revised August 2017 by K.F. Johnson (Florida State U.).

Organic scintillators are broadly classed into three types, crystalline, liquid, and plastic, all of which utilize the ionization produced by charged particles (see Sec. 34.2 of this *Review*) to generate optical photons, usually in the blue to green wavelength regions [31]. Plastic scintillators are by far the most widely used, liquid organic scintillator is finding increased use, and crystal organic scintillators are practically unused in high-energy physics. Plastic scintillator densities range from 1.03 to 1.20 g cm^{-3} . Typical photon yields are about 1 photon per 100 eV of energy deposit [32]. A one-cm-thick scintillator traversed by a minimum-ionizing particle will therefore yield $\approx 2 \times 10^4$ photons. The resulting photoelectron signal will depend on the collection and transport efficiency of the optical package and the quantum efficiency of the photodetector.

Organic scintillator does not respond linearly to the ionization density. Very dense ionization columns emit less light than expected on the basis of dE/dx for minimum-ionizing particles. A widely used semi-empirical model by Birks posits that recombination and quenching effects between the excited molecules reduce the light yield [33]. These effects are more pronounced the greater the density of the excited molecules. Birks’ formula is

$$\frac{d\mathcal{L}}{dx} = \mathcal{L}_0 \frac{dE/dx}{1 + k_B dE/dx}, \quad (35.2)$$

where \mathcal{L} is the luminescence, \mathcal{L}_0 is the luminescence at low specific ionization density, and k_B is Birks’ constant, which must be determined for each scintillator by measurement. Decay times are in the ns range; rise times are much faster.

The high light yield and fast response time allow the possibility of sub-ns timing resolution [34]. The fraction of light emitted during the decay “tail” can depend on the exciting particle. This allows pulse shape discrimination as a technique to carry out particle identification. Because of the hydrogen content (carbon to hydrogen ratio ≈ 1) plastic scintillator is sensitive to proton recoils from neutrons.

Ease of fabrication into desired shapes and low cost has made plastic scintillator a common detector element. In the form of scintillating fiber it has found widespread use in tracking and calorimetry [35].

Demand for large volume detectors has led to increased use of liquid organic scintillator, which has the same scintillation mechanism as plastic scintillator, due to its cost advantage. The containment vessel defines the detector shape; photodetectors or wavelighters may be immersed in the liquid.

35.3.1 Scintillation mechanism

A charged particle traversing matter leaves behind it a wake of excited molecules. Certain types of molecules, however, will release a small fraction ($\approx 3\%$) of this energy as optical photons. This process, scintillation, is especially marked in those organic substances which contain aromatic rings, such as polystyrene (PS) and polyvinyltoluene (PVT). Liquids which scintillate include toluene, xylene and pseudocumene.

In fluorescence, the initial excitation takes place via the absorption of a photon, and de-excitation by emission of a longer wavelength photon. Fluors are used as “wavelighters” to shift scintillation light to a more convenient wavelength. Occurring in complex molecules, the absorption and emission are spread out over a wide band of photon energies, and have some overlap, that is, there is some fraction of the emitted light which can be re-absorbed [36]. This “self-absorption” is undesirable for detector applications because it causes a shortened attenuation length. The wavelength difference between the major absorption and emission peaks is called the Stokes’ shift. It is usually the case that the greater the Stokes’ shift, the smaller the self absorption thus, a large Stokes’ shift is a desirable property for a fluor.

The plastic scintillators used in high-energy physics are binary or ternary solutions of selected fluors in a plastic base containing aromatic rings. (See appendix in Ref. [37] for a comprehensive list of components.) Virtually all plastic scintillators contain as a base either PVT or PS. PVT-based scintillator can be up to 50% brighter.

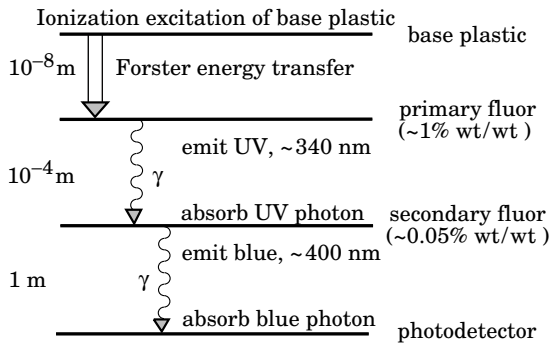


Figure 35.1: Cartoon of scintillation “ladder” depicting the operating mechanism of organic scintillator. Approximate fluor concentrations and energy transfer distances for the separate sub-processes are shown.

Ionization in the plastic base produces UV photons with short attenuation length (several mm). Longer attenuation lengths are obtained by dissolving a “primary” fluor in high concentration (1% by weight) into the base, which is selected to efficiently re-radiate absorbed energy at wavelengths where the base is more transparent (see Fig. 35.1).

The primary fluor has a second important function. The decay time of the scintillator base material can be quite long – in pure polystyrene it is 16 ns, for example. The addition of the primary fluor in high concentration can shorten the decay time by an order of magnitude and increase the total light yield. At the concentrations used (1% and greater), the average distance between a fluor molecule and an excited base unit is around 100 Å, much less than a wavelength of light. At these distances the predominant mode of energy transfer from base to fluor is not the radiation of a photon, but a resonant dipole-dipole interaction, first described by Foerster, which strongly couples the base and fluor [38]. The strong coupling sharply increases the speed and the light yield of the plastic scintillators.

Normally a fluor which fulfills other requirements is not adequate with respect to emission wavelength or attenuation length, so it is necessary to add yet another waveshifter (the “secondary” fluor), at fractional percent levels, and occasionally a third (not shown in Fig. 35.1).

External wavelength shifters are widely used to aid light collection in complex geometries. Scintillation light is captured by a lightpipe comprising a wave-shifting fluor dissolved in a non-scintillating base. The wavelength shifter must be insensitive to ionizing radiation and Cherenkov light. A typical wavelength shifter uses an acrylic base because of its good optical qualities, a single fluor to shift the light emerging from the plastic scintillator to the blue-green, and contains ultra-violet absorbing additives to deaden response to Cherenkov light.

By drastically increasing fluor concentrations beyond those discussed above, scintillators of increased radiation resistance or with special properties such as neutron/gamma discrimination may be made [39].

35.3.2 Caveats and cautions

Plastic scintillators are reliable, robust, and convenient. However, exposure to solvent vapors, high temperatures, mechanical flexing, irradiation, or rough handling will cause degradation. A The surface is particularly fragile region and can “craze” – develop microcracks which degrade transmission of light by total internal reflection. crazing is particularly likely where oils, solvents, or *fingerprints* have contacted the surface.

They have a long-lived luminescence which does not follow a simple exponential decay. Intensities at the 10^{-4} level of the initial fluorescence can persist for hundreds of ns [31] [40].

They can decrease their light yield with increasing partial pressure of oxygen. This can be a 10% effect in an artificial atmosphere [41].

Their light yield may be changed by a magnetic field. Increases of $\approx 3\%$ at 0.45 T have been reported [42].

Irradiation of plastic scintillator creates color centers which absorb light more strongly in the UV and blue than at longer wavelengths. This poorly understood effect appears as a reduction both of light yield and attenuation length. Radiation damage depends not only on the integrated dose, but on the dose rate, atmosphere, and temperature, before, during and after irradiation, as well as the materials properties of the base such as glass transition temperature, polymer chain length, *etc.* Annealing also occurs, accelerated by the diffusion of atmospheric oxygen and elevated temperatures. The phenomena are complex, unpredictable, and not well understood [43]. Since color centers are most disruptive at shorter wavelengths, the most reliable method of mitigating radiation damage is to shift emissions at every step to the longest practical wavelengths, *e.g.*, utilize fluors with large Stokes’ shifts (aka the “Better red than dead” strategy).

35.3.3 Scintillating and wavelength-shifting fibers

The clad optical fiber comprising scintillator and wavelength shifter (WLS) is particularly useful [44]. Since the initial demonstration of the scintillating fiber (SCIFI) calorimeter [45], SCIFI techniques have become mainstream [46]. SCIFI calorimeters are fast, dense, radiation hard, and can have leadglass-like resolution. SCIFI trackers can handle high rates and are radiation tolerant, but the low photon yield at the end of a long fiber (see below) requires use of sensitive photodetectors. WLS-only fiber readout of a calorimeter allows a very high level of hermeticity since the solid angle blocked by the fiber on its way to the photodetector is very small.

The sensitive region of scintillating fibers can be controlled by splicing them onto clear (non-scintillating/non-WLS) fibers.

A typical configuration would be fibers with a core of polystyrene-based scintillator or WLS (index of refraction $n = 1.59$), surrounded by a cladding of PMMA ($n = 1.49$) a few microns thick, or, for added light capture, with another cladding of fluorinated PMMA with $n = 1.42$, for an overall diameter of 0.5 to 1 mm. The fraction of generated light which is transported down the optical fiber is denoted the capture fraction and is about 6% for the single-clad fiber and 10% for the double-clad fiber. A minimum-ionizing particle traversing a high-quality 1 mm diameter fiber perpendicular to its axis will produce fewer than 2000 photons, of which about 200 are captured. Attenuation may eliminate 95% of these photons in a large collider tracker.

A scintillating or WLS fiber is often characterized by its attenuation length, over which the signal is attenuated to $1/e$ of its original value. Factors determining attenuation length include re-absorption of emitted photons by the polymer base or dissolved fluors, the level of crystallinity of the base polymer, variation of photodetector sensitivity to emitted wavelengths, and the quality of the internal surface [47]. Attenuation lengths of several meters are obtained by high quality fibers.

35.4 Inorganic scintillators

Revised August 2019 by C.L. Woody (BNL) and R.-Y. Zhu (HEP California Inst. of Technology).

Inorganic crystals form a class of scintillating materials with much higher densities than organic plastic scintillators (typically $\sim 4\text{--}8\text{ g/cm}^3$) with a variety of different properties for use as scintillation detectors. Due to their high density and high effective atomic number, they can be used in applications where high stopping power or a high conversion efficiency for electrons or photons is required. These include total absorption electromagnetic calorimeters (see Sec. 35.9.2), which consist of a totally active absorber (as opposed to a sampling calorimeter), as well as serving as gamma ray detectors over a wide range of energies. Many of these crystals also have very high light output, and can therefore provide excellent energy resolution down to very low energies (\sim few hundred keV).

Some crystals are intrinsic scintillators in which the luminescence is produced by a part of the crystal lattice itself. However, other crystals require the addition of a dopant, typically fluorescent ions such as thallium (Tl) or cerium (Ce) which is responsible for producing the scintillation light. However, in both cases, the

Table 35.4: Properties of several inorganic crystals. Most of the notation is defined in Sec. 6 of this Review.

Parameter:	ρ	MP	X_0^*	R_M^*	dE/dx^*	λ_I^*	τ_{decay}	λ_{max}	n^\dagger	Relative output [‡]	Hygroscopic [§]	$d(\text{LY})/dT$ %/°C [§]
Units:	g/cm ³	°C	cm	cm	MeV/cm	cm	ns	nm				
NaI(Tl)	3.67	651	2.59	4.13	4.8	42.9	245	410	1.85	100	yes	-0.2
BGO	7.13	1050	1.12	2.23	9.0	22.8	300	480	2.15	21	no	-0.9
BaF ₂	4.89	1280	2.03	3.10	6.5	30.7	650 ^s <0.6 ^f	300 ^s 220 ^f	1.50	36 ^s 4.1 ^f	no	-1.9 ^s 0.1 ^f
CsI(Tl)	4.51	621	1.86	3.57	5.6	39.3	1220	550	1.79	165	slight	0.4
CsI(Na)	4.51	621	1.86	3.57	5.6	39.3	690	420	1.84	88	yes	0.4
CsI(pure)	4.51	621	1.86	3.57	5.6	39.3	30 ^s 6 ^f	310	1.95	3.6 ^s 1.1 ^f	slight	-1.4
PbWO ₄	8.30	1123	0.89	2.00	10.1	20.7	30 ^s 10 ^f	425 ^s 420 ^f	2.20	0.3 ^s 0.077 ^f	no	-2.5
LSO(Ce)	7.40	2050	1.14	2.07	9.6	20.9	40	402	1.82	85	no	-0.2
PbF ₂	7.77	824	0.93	2.21	9.4	21.0	-	-	-	Cherenkov	no	-
CeF ₃	6.16	1460	1.70	2.41	8.42	23.2	30	340	1.62	7.3	no	0
LaBr ₃ (Ce)	5.29	783	1.88	2.85	6.90	30.4	20	356	1.9	180	yes	0.2
CeBr ₃	5.23	722	1.96	2.97	6.65	31.5	17	371	1.9	165	yes	-0.1

* Numerical values calculated using formulae in this review.

† Refractive index at the wavelength of the emission maximum.

‡ Relative light output measured for samples of 1.5 X₀ cube with a Tyvek paper wrapping and a full end face coupled to a photodetector. The quantum efficiencies of the photodetector are taken out.

§ Variation of light yield with temperature evaluated at the room temperature.

^f = fast component, ^s = slow component

scintillation mechanism is the same. Energy is deposited in the crystal by ionization, either directly by charged particles, or by the conversion of photons into electrons or positrons which subsequently produce ionization. This energy is transferred to the luminescent centers which then radiate scintillation photons. The light yield L in terms of the number of scintillation photons produced per MeV of energy deposit in the crystal can be expressed as [48]

$$L = 10^6 S \cdot Q / (\beta \cdot E_g), \quad (35.3)$$

where $\beta \cdot E_g$ is the energy required to create an e-h pair expressed as a multiple of the band gap energy E_g (eV), S is the efficiency of energy transfer to the luminescent center and Q is the quantum efficiency of the luminescent center. The values of β , S and Q are crystal dependent and are the main factors in determining the intrinsic light yield of the scintillator. The decay time of the scintillator is mainly dominated by the decay time of the luminescent center.

Table-35.4 lists the basic properties of some commonly used inorganic crystals. NaI(Tl) is one of the most common and widely used scintillators, with an emission that is well matched to a bialkali photomultiplier tube, but it is highly hygroscopic and difficult to work with, and has a rather low density. CsI(Tl) and CsI(Na) have high light yield, low cost, and are mechanically robust (high plasticity and resistance to cracking). However, they need careful surface treatment and are slightly and highly hygroscopic respectively. Pure CsI has identical mechanical properties as CsI(Tl), but a faster emission at shorter wavelength and a much lower light output.

Undoped BaF₂ has a fast component with a less than 0.6 ns decay time, and is the fastest known scintillator. However, it also has a slow component with a much longer decay time (~ 630 ns). Bismuth germanate (Bi₄Ge₃O₁₂ or BGO) has a high density, and consequently a short radiation length X_0 and Molière radius R_M . Similar to CsI(Tl), BGO's emission is well-matched to the spectral sensitivity of photodiodes, and it is easy to handle and not hygroscopic. Lead tungstate (PbWO₄ or PWO) has a very high density, with a very short X_0 and R_M , but its intrinsic light yield is rather low.

Cerium doped lutetium oxyorthosilicate (Lu₂SiO₅:Ce, or LSO:Ce) [49] and cerium doped lutetium-yttrium oxyorthosilicate (Lu_{2(1-x)}Y_{2x}SiO₅, LYSO:Ce) [50] are dense crystal scintillators which have a high light yield and a fast decay time. Only the properties of LSO:Ce are listed in Table-35.4 since the properties of LYSO:Ce are similar to that of LSO:Ce except a slightly lower density than LSO:Ce depending on the yttrium fraction (typically

5 to 10%) in LYSO:Ce. This material is also featured with excellent radiation hardness [51, 52], so is expected to be used where extraordinary radiation hardness is required.

Also listed in Table-35.4 are other fluoride crystals such as PbF₂ as a Cherenkov material and CeF₃, which have been shown to provide excellent energy resolution in calorimeter applications. Table-35.4 also includes cerium doped lanthanum tri-halides, such as LaBr₃ [53] and CeBr₃ [54], which are brighter and faster than LSO:Ce, but they are highly hygroscopic and have a lower density. The FWHM energy resolution measured for these materials coupled to a PMT with bi-alkali photocathode for 0.662 MeV γ -rays from a ¹³⁷Cs source is about 3%, and has recently been improved to 2% by co-doping with cerium and strontium [55], which is the best among all inorganic crystal scintillators. For this reason, LaBr₃ and CeBr₃ are expected to be used in applications where a good energy resolution for low energy photons are required, such as homeland security.

Beside the crystals listed in Table-35.4, a number of new crystals are being developed that may have potential applications in high energy or nuclear physics. Of particular interest is the family of yttrium and lutetium perovskites and garnet, which include YAP (YAlO₃:Ce), LuAP (LuAlO₃:Ce), YAG (Y₃Al₅O₁₂:Ce) and LuAG (Lu₃Al₅O₁₂:Ce) and their mixed compositions. These have been shown to be linear over a large energy range [56], and have the potential for providing good intrinsic energy resolution.

Aiming at the best jet-mass resolution inorganic scintillators are being investigated for HEP calorimeters with dual readout for both Cherenkov and scintillation light to be used at future linear lepton colliders. These materials may be used for an electromagnetic calorimeter [57] or a homogeneous hadronic calorimetry (HHCAL) detector concept, including both electromagnetic and hadronic parts [58, 59]. Because of the unprecedented volume (70 to 100 m³) foreseen for the HHCAL detector concept the materials must be (1) dense (to minimize the leakage) and (2) cost-effective. It should also be UV transparent (for effective collection of the Cherenkov light) and allow for a clear discrimination between the Cherenkov and scintillation light. The preferred scintillation light is thus at a longer wavelength, and not necessarily bright or fast. Dense crystals, scintillating glasses and ceramics offer a very attractive implementation for this detector concept [60].

The fast scintillation light provides timing information about electromagnetic interactions and showers, which may be used to mitigate pile-up effects and/or for particle identification since the time development of electromagnetic and hadronic showers, as well as minimum ionizing particles, are different. The timing in-

formation is primarily determined by the scintillator rise time and decay time, and the number of photons produced. For fast timing, it is important to have a large number of photons emitted in the initial part of the scintillation pulse, e.g. in the first ns, since one is often measuring the arrival time of the particle in the crystal using the leading edge of the light pulse. A good example of this is BaF_2 , which has $\sim 10\%$ of its light in its fast component with a decay time of less than 0.6 ns. Recent investigation shows that doping with yttrium in BaF_2 reduces its slow component significantly, while keeping its ultrafast scintillation component unchanged [61, 62]. The light propagation can spread out the arrival time of the scintillation photons at the photodetector due to time dispersion [63]. The time response of the photodetector also plays a major role in achieving good time resolution with fast scintillating crystals.

Table-35.4 gives the light output of other crystals relative to $\text{NaI}(\text{Tl})$ and their dependence to the temperature variations measured for 1.5 X_0 cube crystal samples with a Tyvek paper wrapping and a full end face coupled to a photodetector [64]. The quantum efficiency of the photodetector is taken out to facilitate a direct comparison of crystal's light output. However, the useful signal produced by a scintillator is usually quoted in terms of the number of photoelectrons per MeV produced by a given photodetector. The relationship between the light yield (LY) in number of photons/MeV produced ($N_{\text{photons}}/\text{MeV}$) and the light output in number of photoelectrons/MeV detected involves the factors for the light collection efficiency (LC) and the quantum efficiency (QE) of the photodetector:

$$N_{p.e.}/\text{MeV} = LY \cdot LC \cdot QE. \quad (35.4)$$

LC depends on the size and shape of the crystal, and includes effects such as the transmission of scintillation light within the crystal (i.e., the bulk attenuation length of the material), scattering from within the crystal, reflections and scattering from the crystal surfaces, and re-bouncing back into the crystal by wrapping materials. These factors can vary considerably depending on the sample, but can be in the range of $\sim 10\text{--}60\%$. The internal light transmission depends on the intrinsic properties of the material, e.g. the density and type of the scattering centers and defects that can produce internal absorption within the crystal, and can be highly affected by factors such as radiation damage, as discussed below.

The quantum efficiency depends on the type of photodetector used to detect the scintillation light, which is typically $\sim 15\text{--}30\%$ for photomultiplier tubes and $\sim 70\%$ for silicon photodetectors for visible wavelengths. The quantum efficiency of the detector is usually highly wavelength dependent and should be matched to the particular crystal of interest to give the highest quantum yield at the wavelength corresponding to the peak of the scintillation emission. Fig. 35.2 shows the quantum efficiencies of two photodetectors, a Hamamatsu R2059 PMT with bi-alkali cathode and quartz window and a Hamamatsu S8664 avalanche photodiode (APD) as a function of wavelength. Also shown in the figure are emission spectra of three crystal scintillators, BGO, LSO:Ce/LYSO:Ce and $\text{CsI}(\text{Tl})$, and the numerical values of the emission weighted quantum efficiency. The area under each emission spectrum is proportional to crystal's light yield, as shown in Table-35.4, where the quantum efficiencies of the photodetector has been taken out. Results with different photodetectors can be significantly different. For example, the response of $\text{CsI}(\text{Tl})$ relative to $\text{NaI}(\text{Tl})$ with a standard photomultiplier tube with a bi-alkali photo-cathode, e.g. Hamamatsu R2059, would be 45 rather than 165 because of the photomultiplier's low quantum efficiency at longer wavelengths. For scintillators which emit in the UV, a detector with a quartz window should be used.

For very low energy applications (typically below 1 MeV), non-proportionality of the scintillation light yield may be important. It has been known for a long time that the conversion factor between the energy deposited in a crystal scintillator and the number of photons produced is not constant. It is also known that the energy resolution measured by all crystal scintillators for low energy γ -rays is significantly worse than the contribution from photo-electron statistics alone, indicating an intrinsic contribu-

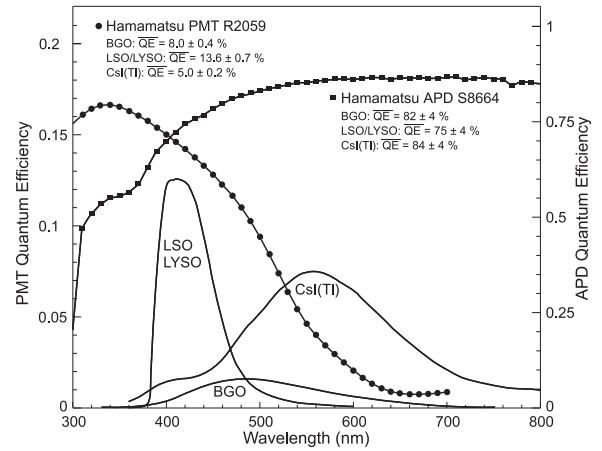


Figure 35.2: The quantum efficiencies of two photodetectors, a Hamamatsu R2059 PMT with bi-alkali cathode and a Hamamatsu S8664 avalanche photodiode (APD), are shown as a function of wavelength. Also shown in the figure are emission spectra of three crystal scintillators, BGO, LSO and $\text{CsI}(\text{Tl})$, and the numerical values of the emission weighted quantum efficiencies. The area under each emission spectrum is proportional to crystal's light yield.

tion from the scintillator itself. Precision measurement using low energy electron beam shows that this non-proportionality is crystal dependent [65]. Recent study on this issue also shows that this effect is also sample dependent even for the same crystal [66]. Further work is therefore needed to fully understand this subject.

One important issue related to the application of a crystal scintillator is its radiation hardness. Stability of its light output, or the ability to track and monitor the variation of its light output in a radiation environment, is required for high resolution and precision calibration [67]. All known crystal scintillators suffer from ionization dose induced radiation damage [68], where a common damage phenomenon is the appearance of radiation induced absorption caused by the formation of color centers originated from the impurities or point defects in the crystal. This radiation induced absorption reduces the light attenuation length in the crystal, and hence its light output. For crystals with high defect density, a severe reduction of light attenuation length may cause a distortion of the light response uniformity, leading to a degradation of the energy resolution. Additional radiation damage effects may include a reduced intrinsic scintillation light yield (damage to the luminescent centers) and an increased phosphorescence (afterglow). For crystals to be used in a high precision calorimeter in a radiation environment, its scintillation mechanism must not be damaged and its light attenuation length in the expected radiation environment must be long enough so that its light response uniformity, and thus its energy resolution, does not change.

While radiation damage induced by ionization dose is well understood [69], investigation is on-going to understand radiation damage caused by hadrons, including both charged hadrons [70] and neutrons [71]. Two additional fundamental processes may cause defects by hadrons: displacement damage and nuclear breakup. While charged hadrons can produce all three types of damage (and it's often difficult to separate them), neutrons can produce only the last two, and electrons and photons only produce ionization damage. Studies on hadron induced radiation damage to lead tungstate [72] show a proton-specific damage component caused by fragments from fission induced in lead and tungsten by particles in the hadronic shower. The fragments cause a severe, local damage to the crystalline lattice due to their extremely high energy loss over a short distance [72]. Recent investigation also sees evidence of neutron-specific damage in various crystals [71].

Most of the crystals listed in Table-35.4 have been used in high energy or nuclear physics experiments when the ultimate energy resolution for electrons and photons is desired. Examples are the Crystal Ball $\text{NaI}(\text{Tl})$ calorimeter at SPEAR, the L3 BGO

calorimeter at LEP, the CLEO CsI(Tl) calorimeter at CESR, the KTeV CsI calorimeter at the Tevatron, and the BaBar, BELLE and BES III CsI(Tl) calorimeters at PEP-II, KEK and BEPC II, respectively. Because of their high density and relative low cost, PWO calorimeters are used by CMS and ALICE at LHC, by CLAS and PrimEx at CEBAF and by PANDA at GSI. Similarly, PbF₂ calorimeters are used by the A4 experiment at MAINZ and by the g-2 experiment at Fermilab. A CsI calorimeter is being built for the Mu2e experiment at Fermilab. An LYSO:Ce calorimeter is being built for the COMET experiment at J-PARC, and an LYSO:Ce crystal-based precision timing layer is being built for the CMS experiment at the HL-LHC.

35.5 Cherenkov detectors

Revised July 2019 by B.N. Ratcliff (SLAC) and J. Schwiening (GSI Darmstadt).

Although devices using Cherenkov radiation are often thought of as only particle identification (PID) detectors, in practice they are used over a much broader range of applications including; (1) fast particle counters; (2) hadronic PID; (3) electromagnetic calorimeters (EMC); and (4) tracking detectors performing complete event reconstruction. Examples of applications from each category include; (1) the BaBar luminosity detector [73] and the Quartic fast timing counter for the ATLAS Forward Proton Detector, designed to measure small angle scatters at the LHC [74]; (2) the hadronic PID detectors at the B factory detectors—DIRC in BaBar [75], and the modern Imaging Aerogel and TOP counters at Belle II [76]; (3) the CMS Hadron Forward calorimeter based on Cherenkov light emitted in quartz fibers embedded in a steel absorber [77]; and (4) large water Cherenkov counters such as Super-Kamiokande [78].

Cherenkov counters contain two main elements; (1) a radiator through which the charged particle passes, and (2) a photodetector. As Cherenkov radiation is a weak source of photons, light collection and detection must be as efficient as possible. The refractive index n and the particle's path length through the radiator L appear in the Cherenkov relations allowing the tuning of these quantities for particular applications. One or more of the properties of Cherenkov radiation discussed in the Passages of Particles through Matter section (Sec. 34 of this *Review*) are utilized in Cherenkov detectors: the prompt emission of a light pulse; the existence of a velocity threshold for radiation; and the dependence of the Cherenkov cone half-angle θ_c and the number of emitted photons on the velocity of the particle v_p and the refractive index n of the medium. The Cherenkov angle can be calculated as

$$\cos \theta_c = \frac{1}{n(E)\beta}, \quad (35.5)$$

where $\beta = v_p/c$ with c being the speed of light, and E the photon energy. The number of photoelectrons ($N_{p.e.}$) detected in a given device with radiator of length L is

$$N_{p.e.} = L \frac{\alpha^2 z^2}{r_e m_e c^2} \int \epsilon(E) \sin^2 \theta_c(E) dE, \quad (35.6)$$

where $\epsilon(E)$ is the efficiency for collecting the Cherenkov light and transducing it into photoelectrons, and $\alpha^2/(r_e m_e c^2) = 370 \text{ cm}^{-1} \text{ eV}^{-1}$. The quantities ϵ and θ_c are functions of the photon energy. As the typical energy dependent variation of the index of refraction is modest, a quantity called the *Cherenkov detector quality factor* N_0 can be defined as

$$N_0 = \frac{\alpha^2 z^2}{r_e m_e c^2} \int \epsilon dE, \quad (35.7)$$

so that, taking the charge number $z = 1$ (the usual case in high-energy physics),

$$N_{p.e.} \approx LN_0(\sin^2 \theta_c). \quad (35.8)$$

This definition of the quality factor N_0 is not universal, nor, indeed, very useful for those common situations where ϵ factorizes as $\epsilon = \epsilon_{\text{coll}}\epsilon_{\text{det}}$ with the geometrical photon collection efficiency (ϵ_{coll}) varying substantially for different tracks while the

photon detector efficiency (ϵ_{det}) remains nearly track independent. In this case, it can be useful to explicitly remove (ϵ_{coll}) from the definition of N_0 . A typical value of N_0 for a photomultiplier (PMT) detection system working in the visible and near UV, and collecting most of the Cherenkov light, is about 100 cm^{-1} . Practical counters, utilizing a variety of different photodetectors, have values ranging between about 30 and 180 cm^{-1} . Radiators can be chosen from a variety of transparent materials (Sec. 34 of this *Review* and Table 6.1). In addition to refractive index, the choice requires consideration of factors such as material density, radiation length and radiation hardness, transmission bandwidth, absorption length, chromatic dispersion, optical workability (for solids), availability, and cost. When the momenta of particles to be identified is high, the refractive index must be set close to one, so that the photon yield per unit length is low and a long particle path in the radiator is required. Recently, the gap in refractive index that has traditionally existed between gases and liquid or solid materials has been partially closed with transparent *silica aerogels* with indices that range between about 1.007 and 1.13.

Cherenkov counters may be classified as either *imaging* or *threshold* types, depending on whether they do or do not make use of Cherenkov angle (θ_c) information. Imaging counters may be used to track particles as well as identify them. The recent development of very fast photodetectors such as micro-channel plate PMTs (MCP PMT) (see 35.2 of this *Review*) also potentially allows very fast Cherenkov based time of flight (TOF) detectors of either class [79]. The track timing resolution of imaging detectors can be extremely good as it scales approximately as $\frac{1}{\sqrt{N_{p.e.}}}$.

Threshold Cherenkov detectors [80], in their simplest form, make a yes/no decision based on whether the particle is above or below the Cherenkov threshold velocity $\beta_t = 1/n$. A straightforward enhancement of such detectors uses the number of observed photoelectrons (or a calibrated pulse height) to discriminate between species or to set probabilities for each particle species [81]. This strategy can increase the momentum range of particle separation by a modest amount (to a momentum some 20% above the threshold momentum of the heavier particle in a typical case).

Careful designs give $\langle \epsilon_{\text{coll}} \rangle \gtrsim 90\%$. For a photomultiplier with a typical alkali cathode, $\int \epsilon_{\text{det}} dE \approx 0.27 \text{ eV}$, so that

$$N_{p.e.}/L \approx 90 \text{ cm}^{-1} (\sin^2 \theta_c) \quad (\text{i.e., } N_0 = 90 \text{ cm}^{-1}). \quad (35.9)$$

Suppose, for example, that n is chosen so that the threshold for species a is p_t ; that is, at this momentum species a has velocity $\beta_a = 1/n$. A second, lighter, species b with the same momentum has velocity β_b , so $\cos \theta_c = \beta_a/\beta_b$, and

$$N_{p.e.}/L \approx 90 \text{ cm}^{-1} \frac{m_a^2 - m_b^2}{p_t^2 + m_a^2}. \quad (35.10)$$

For K/π separation at $p = p_t = 1(5) \text{ GeV}/c$, $N_{p.e.}/L \approx 16(0.8) \text{ cm}^{-1}$ for π 's and (by design) 0 for K 's.

For limited path lengths $N_{p.e.}$ will usually be small. The overall efficiency of the device is controlled by Poisson fluctuations, which can be especially critical for separation of species where one particle type is dominant. Moreover, the effective number of photoelectrons is often less than the average number calculated above due to additional equivalent noise from the photodetector (see the discussion of the excess noise factor in 35.2 of this *Review*). It is common to design for at least 10 photoelectrons for the high velocity particle in order to obtain a robust counter. As rejection of the particle that is below threshold depends on *not* seeing a signal, electronic and other background noise, especially overlapping tracks, can be important. Physics sources of light production for the below threshold particle, such as decay to an above threshold particle, scintillation light, or the production of delta rays in the radiator, often limit the separation attainable, and need to be carefully considered. Well designed, modern multi-channel counters, such as the ACC at Belle [82], can attain adequate particle separation performance over a substantial momentum range.

Imaging counters make the most powerful use of the information available by measuring the ring-correlated angles of emission

of the individual Cherenkov photons. They typically provide positive ID information both for the “wanted” and the “unwanted” particles, thus reducing mis-identification substantially. Since low-energy photon detectors can measure only the position (and, perhaps, a precise detection time) of the individual Cherenkov photons (not the angles directly), the photons must be “imaged” onto a detector so that their angles can be derived [83]. Typically the optics map the Cherenkov cone onto (a portion of) a distorted “circle” at the photodetector. Though the imaging process is directly analogous to familiar imaging techniques used in telescopes and other optical instruments, there is a somewhat bewildering variety of methods used in a wide variety of counter types with different names. Some of the imaging methods used include (1) focusing by a lens or mirror; (2) proximity focusing (i.e., focusing by limiting the emission region of the radiation); and (3) focusing through an aperture (a pinhole). In addition, the prompt Cherenkov emission coupled with the speed of some modern photon detectors allows the use of (4) time imaging, a method which is little used in conventional imaging technology, and may allow some separation with particle TOF. Finally, (5) correlated tracking (and event reconstruction) can be performed in large water counters by combining the individual space position and time of each photon together with the constraint that Cherenkov photons are emitted from each track at the same polar angle (Sec. 36.3.1 of this *Review*).

In a simple model of an imaging PID counter, the fractional error on the particle velocity (δ_β) is given by

$$\delta_\beta = \frac{\sigma_\beta}{\beta} = \tan \theta_c \sigma(\theta_c), \quad (35.11)$$

where

$$\sigma(\theta_c) = \frac{\langle \sigma(\theta_i) \rangle}{\sqrt{N_{p.e.}}} \oplus C, \quad (35.12)$$

and $\langle \sigma(\theta_i) \rangle$ is the average single photoelectron resolution, as defined by the optics, detector resolution and the intrinsic chromaticity spread of the radiator index of refraction averaged over the photon detection bandwidth. C combines a number of other contributions to resolution including, (1) correlated terms such as tracking, alignment, and multiple scattering, (2) hit ambiguities, (3) background hits from random sources, and (4) hits coming from other tracks. The actual separation performance is also limited by physics effects such as decays in flight and particle interactions in the material of the detector. In many practical cases, the performance is limited by these effects.

For a $\beta \approx 1$ particle of momentum (p) well above threshold entering a radiator with index of refraction (n), the number of σ separation (N_σ) between particles of mass m_1 and m_2 is approximately

$$N_\sigma \approx \frac{|m_1^2 - m_2^2|}{2p^2 \sigma(\theta_c) \sqrt{n^2 - 1}}. \quad (35.13)$$

In practical counters, the angular resolution term $\sigma(\theta_c)$ varies between about 0.1 and 5 mrad depending on the size, radiator, and photodetector type of the particular counter. The range of momenta over which a particular counter can separate particle species extends from the point at which the number of photons emitted becomes sufficient for the counter to operate efficiently as a threshold device ($\sim 20\%$ above the threshold for the lighter species) to the value in the imaging region given by the equation above. For example, for $\sigma(\theta_c) = 2$ mrad, a fused silica radiator ($n = 1.474$), or a fluorocarbon gas radiator (C_5F_{12} , $n = 1.0017$), would separate π/K 's from the threshold region starting around 0.15(3) GeV/ c through the imaging region up to about 4.2(18) GeV/ c at better than 3σ .

Many different imaging counters have been built during the last several decades [79]. Among the earliest examples of this class of counters are the very limited acceptance *Differential Cherenkov detectors*, designed for particle selection in high momentum beam lines. These devices use optical focusing and/or geometrical masking to select particles having velocities in a specified region. With careful design, a velocity resolution of $\sigma_\beta/\beta \approx 10^{-4}$ – 10^{-5} can be obtained [80].

Practical multi-track *Ring-Imaging Cherenkov detectors* (generally called RICH counters) are a more recent development. RICH counters are sometimes further classified by ‘generations’ that differ based on historical timing, performance, design, and photodetection techniques.

Prototypical examples of first generation RICH counters are those used in the DELPHI and SLD detectors at the LEP and SLC Z factory e^+e^- colliders [79]. They have both liquid (C_6F_{14} , $n = 1.276$) and gas (C_5F_{12} , $n = 1.0017$) radiators, the former being proximity imaged with the latter using mirrors. The phototransducers are a TPC/wire-chamber combination. They are made sensitive to photons by doping the TPC gas (usually, ethane/methane) with $\sim 0.05\%$ TMAE (tetrakis(dimethylamino)ethylene). Great attention to detail is required, (1) to avoid absorbing the UV photons to which TMAE is sensitive, (2) to avoid absorbing the single photoelectrons as they drift in the long TPC, and (3) to keep the chemically active TMAE vapor from interacting with materials in the system. In spite of their unforgiving operational characteristics, these counters attained good $e/\pi/K/p$ separation over wide momentum ranges (from about 0.25 to 20 GeV/ c) during several years of operation at LEP and SLC. Related but smaller acceptance devices include the OMEGA RICH at the CERN SPS, and the RICH in the balloon-borne CAPRICE detector [79].

Later generation counters [79] generally operate at much higher rates, with more detection channels, than the first generation detectors just described. They also utilize faster, more forgiving photon detectors, covering different photon detection bandwidths. Radiator choices have broadened to include materials such as lithium fluoride, fused silica, and aerogel. Vacuum-based photodetection systems (e.g., single or multi anode PMTs, MCP-PMTs, or hybrid photodiodes (HPD)) have become increasingly common (see 35.2 of this *Review*). They handle high rates, and can be used with a wide choice of radiators. Examples include (1) the SELEX RICH at Fermilab, which mirror focuses the Cherenkov photons from a neon radiator onto a camera array made of ~ 2000 PMTs to separate hadrons over a wide momentum range (to well above 200 GeV/ c for heavy hadrons); (2) the NA62 RICH at CERN, which uses a 17 m long tank filled with neon gas as radiator and spherical mirrors to focus the photons on two arrays of 2000 PMTs to separate pions from muons for momenta between 15 and 35 GeV/ c ; (3) the CBM RICH under construction at FAIR where the Cherenkov photons, produced in about 30 m³ of CO₂ radiator gas, are mirror-focused on arrays of multi-anode PMTs (MaPMTs) with a total of about 55,000 pixels, to identify electrons with momenta up to 10 GeV/ c ; and (4) the LHCb detector now running at the LHC. It uses two separate counters. One volume contains C₄F₁₀ (originally in combination with aerogel, which was removed in 2015) while the second volume contains CF₄. Photons are mirror-focused onto detector arrays of HPDs to cover a π/K separation momentum range between 1 and 150 GeV/ c . Further upgrades, including the replacement of the HPDs by MaPMTs and improved readout electronics, are necessary to deal with increases in luminosity.

Other fast detection systems that use solid cesium iodide (CsI) photocathodes or triethylamine (TEA) doping in proportional chambers are useful with certain radiator types and geometries. Examples include (1) the CLEO-III RICH at CESR that uses a LiF radiator with TEA doped proportional chambers; (2) the ALICE detector at the LHC that uses proximity focused liquid (C_6F_{14} radiators and solid CsI photocathodes (similar photodetectors have been used for several years by the HADES and COMPASS detectors), and the hadron blind detector (HBD) in the PHENIX detector at RHIC that couples a low index CF₄ radiator to a photodetector based on electron multiplier (GEM) chambers with reflective CsI photocathodes [79].

Recent technological advances in the production of aerogel with improved transparency in the UV range and finely tuned refractive indices enable several new RICH designs. The innovative hybrid geometry of the CLAS12 RICH, with complex photon paths that feature multiple passes through the aerogel tiles, is only possible due to the improved scattering length of the aerogel. It minimizes the material inside of the detector acceptance as well as the

cost of the photon sensor array. Beam tests have demonstrated that the counter will be able to provide clean π/K separation up to 8 GeV/c. The forward endcap Aerogel RICH (ARICH) for the Belle II upgrade at KEKB, designed to provide clean π/K separation for momenta up to 3.5 GeV/c, is an example of the so-called focusing aerogel approach [84]. The radiator is a dual-layer aerogel, with a thickness of 20 mm for each layer and increasing refractive indices of $n = 1.045$ and $n = 1.055$ along the particle path. The Cherenkov ring images from the two layers overlap on the array of Hybrid Avalanche Photo Detectors (HAPDs), which provide efficient single photon detection in the 1.5 T magnetic field.

A DIRC (Detection [of] Internally Reflected Cherenkov [light]) is a distinctive, compact RICH subtype first used in the BaBar detector [75]. A DIRC “inverts” the usual RICH principle for use of light from the radiator by collecting and imaging the total internally reflected light rather than the transmitted light. It utilizes the optical material of the radiator in two ways, simultaneously: as a Cherenkov radiator and as a light pipe. The magnitudes of the photon angles are preserved during transport by the flat, rectangular cross section radiators, allowing the photons to be efficiently transported to a detector outside the path of the particle where they may be imaged in up to three independent dimensions (the usual two in space and, due to the long photon paths lengths, one in time). Because the index of refraction in the radiator is large ($n \sim 1.47$ for fused silica), the momentum range with good π/K separation goes up to 4–5 GeV/c. It is plausible, but difficult, to extend it up to about 10 GeV/c with an improved design.

The BaBar experiment at the asymmetric PEP-II e^+e^- collider studied CP violation in $\Upsilon(4S)$ decays. Excellent pion/kaon separation for particle momenta up to 4 GeV/c was required. The BaBar DIRC used 4.9 m long, rectangular bars made from synthetic fused silica as radiator and light guide. The photons were imaged via a “pin-hole” through an expansion region filled with 6 000 liters of purified water onto an array of 10 752 densely packed photomultiplier tubes placed at a distance of about 1.2 m from the bar end. During more than 8 years of operation, the BaBar DIRC achieved π/K separation of 2.5 standard deviations or more up to 4 GeV/c momentum. For a pion identification rate around 85% the DIRC provided a kaon misidentification rate well below 1% up to 3 GeV/c.

The next generation of DIRC detectors takes advantage of the new, very fast, pixelated photodetectors becoming available, such as MaPMTs and MCP-PMTs. They typically utilize either time imaging or lens/mirror-focused optics, or both, leading not only to a precision measurement of the Cherenkov angle, but in some cases, to a precise measurement of the particle time of flight, and/or to correction of the chromatic dispersion in the radiator. Examples [79] include (1) the Belle II Time of Propagation (TOP) counter that emphasizes precision timing for both Cherenkov imaging and TOF to perform π/K separation of at least 3 standard deviations up to 4 GeV/c; (2) the DIRC upgrade of the GlueX experiment at Jefferson Lab that places four decommissioned BaBar DIRC modules, coupled to upgraded optics and readout, perpendicular to the beamline and will be the first application of a DIRC in a detector endcap; (3) the PANDA Barrel DIRC at FAIR, to be installed in 2023, that will be the first DIRC counter to use lens focusing and is expected to provide more than 3 standard deviations π/K separation up to 3.5 GeV/c; and (4) the TORCH proposal being developed for an LHCb upgrade in 2024 which uses DIRC imaging for individual photons with fast photon detectors to provide particle separation via particle TOF with a precision of 10–15 ps per track over a flight path length of 9.5 m.

35.6 Gaseous detectors

35.6.1 Energy loss and charge transport in gases

Revised March 2010 by F. Sauli (CERN) and M. Titov (CEA Saclay, DSM/IRFU/SPP).

Gas-filled detectors localize the ionization produced by charged particles, generally after charge multiplication. The statistics of

ionization processes having asymmetries in the ionization trails, affect the coordinate determination deduced from the measurement of drift time, or of the center of gravity of the collected charge. For thin gas layers, the width of the energy loss distribution can be larger than its average, requiring multiple sample or truncated mean analysis to achieve good particle identification. In the truncated mean method for calculating $\langle dE/dx \rangle$, the ionization measurements along the track length are broken into many samples and then a fixed fraction of high-side (and sometimes also low-side) values are rejected [85].

The energy loss of charged particles and photons in matter is discussed in Sec. 34. Table 35.5 provides values of relevant parameters in some commonly used gases at NTP (normal temperature, 20° C, and pressure, 1 atm) for unit-charge minimum-ionizing particles (MIPs) [86, 87].

Values often differ, depending on the source, so those in the table should be taken only as approximate. For different conditions and for mixtures, and neglecting internal energy transfer processes (*e.g.*, Penning effect), one can scale the density, N_P , and N_T with temperature and pressure assuming a perfect gas law.

Table 35.5: Properties of noble and molecular gases at normal temperature and pressure (NTP: 20° C, one atm). E_X , E_I : first excitation, ionization energy; W_I : average energy per ion pair; $dE/dx|_{\min}$, N_P , N_T : differential energy loss, primary and total number of electron-ion pairs per cm, for unit charge minimum ionizing particles.

Gas	Density, mg cm ⁻³	E_X eV	E_I eV	W_I eV	$dE/dx _{\min}$ keV cm ⁻¹	N_P cm ⁻¹	N_T cm ⁻¹
He	0.179	19.8	24.6	41.3	0.32	3.5	8
Ne	0.839	16.7	21.6	37	1.45	13	40
Ar	1.66	11.6	15.7	26	2.53	25	97
Xe	5.495	8.4	12.1	22	6.87	41	312
CH ₄	0.667	8.8	12.6	30	1.61	28	54
C ₂ H ₆	1.26	8.2	11.5	26	2.91	48	112
iC ₄ H ₁₀	2.49	6.5	10.6	26	5.67	90	220
CO ₂	1.84	7.0	13.8	34	3.35	35	100
CF ₄	3.78	10.0	16.0	54	6.38	63	120

When an ionizing particle passes through the gas it creates electron-ion pairs, but often the ejected electrons have sufficient energy to further ionize the medium. As shown in Table 35.5, the total number of electron-ion pairs (N_T) is usually a few times larger than the number of primaries (N_P).

The probability for a released electron to have an energy E or larger follows an approximate $1/E^2$ dependence (Rutherford law), taking into account the electronic structure of the medium

The probability for a released electron to have an energy E or larger follows an approximate $1/E^2$ dependence (Rutherford law), shown in Fig. 35.3 for Ar/CH₄ at NTP (dotted line, left scale). More detailed estimates taking into account the electronic structure of the medium are shown in the figure, for three values of the particle velocity factor $\beta\gamma$ [88]. The dot-dashed line provides, on the right scale, the practical range of electrons (including scattering) of energy E . As an example, about 0.6% of released electrons have 1 keV or more energy, substantially increasing the ionization loss rate. The practical range of 1 keV electrons in argon (dot-dashed line, right scale) is 70 μ m and this can contribute to the error in the coordinate determination.

The number of electron-ion pairs per primary ionization, or cluster size, has an exponentially decreasing probability; for argon, there is about 1% probability for primary clusters to contain ten or more electron-ion pairs [89].

Once released in the gas, and under the influence of an applied electric field, electrons and ions drift in opposite directions and diffuse towards the electrodes. The drift velocity and diffusion of electrons depend very strongly on the nature of the gas. Large drift velocities are achieved by adding polyatomic gases (usually CH₄, CO₂, or CF₄) having large inelastic cross sections at moderate energies, which results in “cooling” electrons into the energy range of the Ramsauer-Townsend minimum (at ~ 0.5 eV) of the

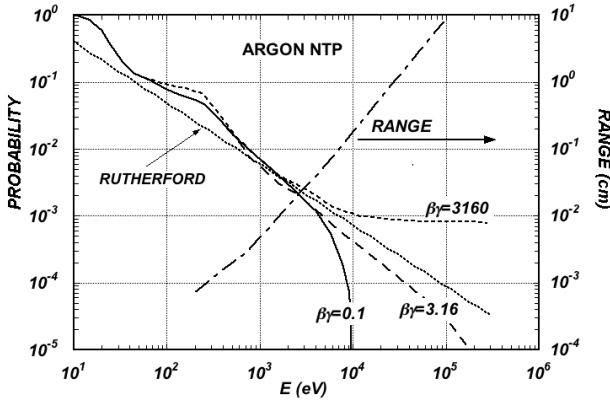


Figure 35.3: Probability of single collisions in which released electrons have an energy E or larger (left scale) and practical range of electrons in Ar/CH₄ (P10) at NTP (dot-dashed curve, right scale) [88].

elastic cross-section of argon. In a simple approximation, gas kinetic theory provides the drift velocity v as a function of the mean collision time τ and the electric field E : $v = eE\tau/m_e$ (Townsend's expression). In the presence of an external magnetic field, the Lorentz force acting on electrons between collisions deflects the drifting electrons and modifies the drift properties.

Once released in the gas, and under the influence of an applied electric field, electrons and ions drift in opposite directions and diffuse towards the electrodes. The scattering cross section is determined by the details of atomic and molecular structure. Therefore, the drift velocity and diffusion of electrons depend very strongly on the nature of the gas, specifically on the inelastic cross-section involving the rotational and vibrational levels of molecules. In noble gases, the inelastic cross section is zero below excitation and ionization thresholds. Large drift velocities are achieved by adding polyatomic gases (usually CH₄, CO₂, or CF₄) having large inelastic cross sections at moderate energies, which results in "cooling" electrons into the energy range of the Ramsauer-Townsend minimum (at ~ 0.5 eV) of the elastic cross-section of argon. The reduction in both the total electron scattering cross-section and the electron energy results in a large increase of electron drift velocity (for a compilation of electron-molecule cross sections see Ref. [90]). Another principal role of the polyatomic gas is to absorb the ultraviolet photons emitted by the excited noble gas atoms. Extensive collections of experimental data [91] and theoretical calculations based on transport theory [92] permit estimates of drift and diffusion properties in pure gases and their mixtures. In a simple approximation, gas kinetic theory provides the drift velocity v as a function of the mean collision time τ and the electric field E : $v = eE\tau/m_e$ (Townsend's expression). Values of drift velocity and diffusion for some commonly used gases at NTP are given in Fig. 35.4 and Fig. 35.5.

These have been computed with the MAGBOLTZ program [87]. For different conditions, the horizontal axis must be scaled inversely with the gas density. Standard deviations for longitudinal (σ_L) and transverse diffusion (σ_T) are given for one cm of drift, and scale with the square root of the drift distance. Since the collection time is inversely proportional to the drift velocity, diffusion is less in gases such as CF₄ that have high drift velocities. In the presence of an external magnetic field, the Lorentz force acting on electrons between collisions deflects the drifting electrons and modifies the drift properties. The electron trajectories, velocities and diffusion parameters can be computed with MAGBOLTZ. A simple theory, the friction force model, provides an expression for the vector drift velocity \mathbf{v} as a function of electric and magnetic field vectors \mathbf{E} and \mathbf{B} , of the Larmor frequency $\omega = eB/m_e$, and of the mean collision time τ :

$$\mathbf{v} = \frac{e}{m_e} \frac{\tau}{1 + \omega^2\tau^2} \left(\mathbf{E} + \frac{\omega\tau}{B} (\mathbf{E} \times \mathbf{B}) + \frac{\omega^2\tau^2}{B^2} (\mathbf{E} \cdot \mathbf{B})\mathbf{B} \right) \quad (35.14)$$

To a good approximation, and for moderate fields, one can as-

sume that the energy of the electrons is not affected by B , and use for τ the values deduced from the drift velocity at $B = 0$ (the Townsend expression). For \mathbf{E} perpendicular to \mathbf{B} , the drift angle to the relative to the electric field vector is $\tan\theta_B = \omega\tau$ and $v = (E/B)(\omega\tau/\sqrt{1 + \omega^2\tau^2})$. For parallel electric and magnetic fields, drift velocity and longitudinal diffusion are not affected, while the transverse diffusion can be strongly reduced: $\sigma_T(B) = \sigma_T(B=0)/\sqrt{1 + \omega^2\tau^2}$. The dotted line in Fig. 35.5 represents σ_T for the classic Ar/CH₄ (90:10) mixture at 4 T. Large values of $\omega\tau \sim 20$ at 5 T are consistent with the measurement of diffusion coefficient in Ar/CF₄/iC₄H₁₀ (95:3:2). This reduction is exploited in time projection chambers (Sec. 35.6.5) to improve spatial resolution.

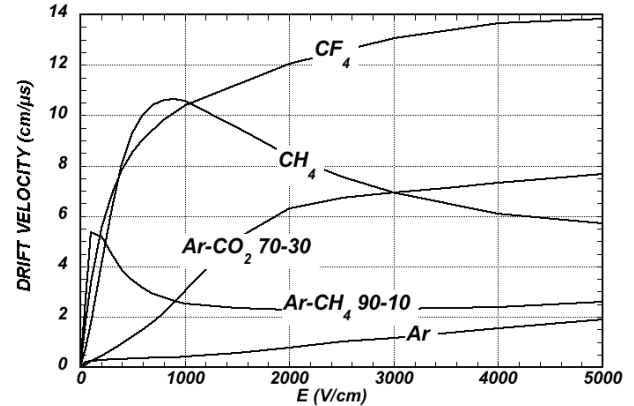


Figure 35.4: Computed electron drift velocity as a function of electric field in several gases at NTP and $B = 0$ [87].

In mixtures containing electronegative molecules, such as O₂ or H₂O, electrons can be captured to form negative ions. Capture cross-sections are strongly energy-dependent, and therefore the capture probability is a function of applied field. For example, the electron is attached to the oxygen molecule at energies below 1 eV. The three-body electron attachment coefficients may differ greatly for the same additive in different mixtures. As an example, at moderate fields (up to 1 kV/cm) the addition of 0.1% of oxygen to an Ar/CO₂ mixture results in an electron capture probability about twenty times larger than the same addition to Ar/CH₄.

Carbon tetrafluoride is not electronegative at low and moderate fields, making its use attractive as drift gas due to its very low diffusion. However, CF₄ has a large electron capture cross section at fields above ~ 8 kV/cm, before reaching avalanche field strengths. Depending on detector geometry, some signal reduction and resolution loss can be expected using this gas.

If the electric field is increased sufficiently, electrons gain enough energy between collisions to ionize molecules. Above a gas-dependent threshold, the mean free path for ionization, λ_i , decreases exponentially with the field; its inverse, $\alpha = 1/\lambda_i$, is the first Townsend coefficient. In wire chambers, most of the increase of avalanche particle density occurs very close to the anode wires, and a simple electrostatic consideration shows that the largest fraction of the detected signal is due to the motion of positive ions receding from the wires. The electron component, although very fast, contributes very little to the signal. This determines the characteristic shape of the detected signals in the proportional mode: a fast rise followed by a gradual increase.

The slow component, the so-called "ion tail" that limits the time resolution of the detector, is usually removed by differentiation of the signal. In uniform fields, N_0 initial electrons multiply over a length x forming an electron avalanche of size $N = N_0 e^{\alpha x}$; N/N_0 is the gain of the detector. Fig. 35.6 shows examples of Townsend coefficients for several gas mixtures, computed with MAGBOLTZ [87].

Positive ions released by the primary ionization or produced in the avalanches drift and diffuse under the influence of the electric field. Negative ions may also be produced by electron attachment to gas molecules. The drift velocity of ions in the fields encoun-

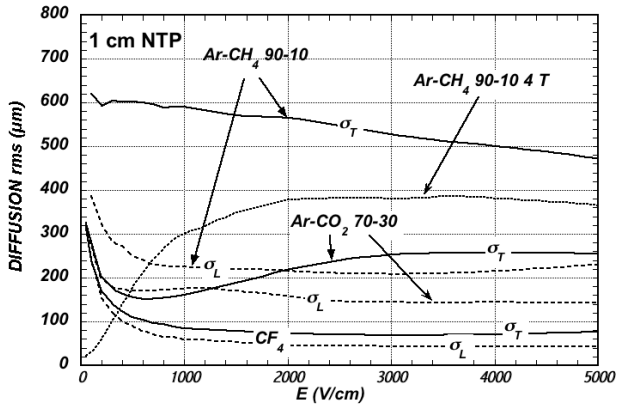


Figure 35.5: Electron longitudinal diffusion (σ_L) (dashed lines) and transverse diffusion (σ_T) (full lines) for 1 cm of drift at NTP and $B = 0$. The dotted line shows σ_T for the P10 mixture at 4 T [87].

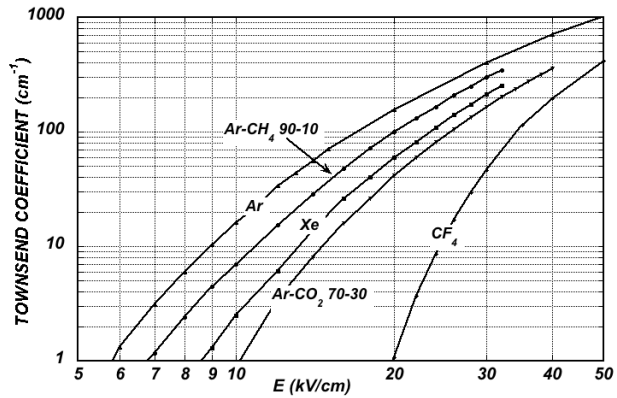


Figure 35.6: Computed first Townsend coefficient α as a function of electric field in several gases at NTP [87].

tered in gaseous detectors (up to few kV/cm) is typically about three orders of magnitude less than for electrons. The ion mobility μ , the ratio of drift velocity to electric field, is constant for a given ion type up to very high fields. Values of mobility at NTP for ions in their own and other gases are given in Table 35.6 [93]. For different temperatures and pressures, the mobility can be scaled inversely with the density assuming an ideal gas law. For mixtures, due to a very effective charge transfer mechanism, only ions with the lowest ionization potential survive after a short path in the gas. Both the lateral and transverse diffusion of ions are proportional to the square root of the drift time, with a coefficient that depends on temperature but not on the ion mass. Accumulation of ions in the gas drift volume may induce field distortions (see Sec. 35.6.5).

Table 35.6: Mobility of ions in gases at NTP [93].

Gas	Ion	Mobility μ ($\text{cm}^2 \text{V}^{-1} \text{s}^{-1}$)
He	He^+	10.4
Ne	Ne^+	4.7
Ar	Ar^+	1.54
Ar/ CH_4	CH_4^+	1.87
Ar/ CO_2	CO_2^+	1.72
CH_4	CH_4^+	2.26
CO_2	CO_2^+	1.09

35.6.2 Multi-Wire Proportional and Drift Chambers

Revised March 2010 by F. Sauli (CERN) and M. Titov (CEA

Saclay, DSM/IRFU/SPP).

Single-wire counters that detect the ionization produced in a gas by a charged particle, followed by charge multiplication and collection around a thin wire have been used for decades. Good energy resolution is obtained in the proportional amplification mode, while very large saturated pulses can be detected in the streamer and Geiger modes [94].

Multiwire proportional chambers (MWPCs) [95,96], introduced in the late '60's, detect, localize and measure energy deposit by charged particles over large areas. A mesh of parallel anode wires at a suitable potential, inserted between two cathodes, acts almost as a set of independent proportional counters (see Fig. 35.7a). Electrons released in the gas volume drift towards the anodes and produce avalanches in the increasing field. Analytic expressions for the electric field can be found in many textbooks. The fields close to the wires $E(r)$, in the drift region E_D , and the capacitance C per unit length of anode wire are approximately given by

$$E(r) = \frac{CV_0}{2\pi\epsilon_0} \frac{1}{r} \quad E_D = \frac{CV_0}{2\epsilon_0 s} \quad C = \frac{2\pi\epsilon_0}{\pi(\ell/s) - \ln(2\pi a/s)}, \quad (35.15)$$

where r is the distance from the center of the anode, s the wire spacing, ℓ and V_0 the distance and potential difference between anode and cathode, and a the anode wire radius.

Because of electrostatic forces, anode wires are in equilibrium only for a perfect geometry. Small deviations result in forces displacing the wires alternatively below and above the symmetry plane, sometimes with catastrophic results. These displacement forces are countered by the mechanical tension of the wire, up to a maximum unsupported stable length, L_M [97], above which the wire deforms:

$$L_M = \frac{s}{CV_0} \sqrt{4\pi\epsilon_0 T_M} \quad (35.16)$$

The maximum tension T_M depends on the wire diameter and modulus of elasticity. Table 35.7 gives approximate values for tungsten and the corresponding maximum stable wire length under reasonable assumptions for the operating voltage ($V_0 = 5 \text{ kV}$) [98]. Internal supports and spacers can be used in the construction of longer detectors to overcome limits on the wire length imposed by Eq. (35.16).

Table 35.7: Maximum tension T_M and stable unsupported length L_M for tungsten wires with spacing s , operated at $V_0 = 5 \text{ kV}$. No safety factor is included.

Wire diameter (μm)	T_M (newton)	s (mm)	L_M (cm)
10	0.16	1	25
20	0.65	2	85

Detection of charge on the wires over a predefined threshold provides the transverse coordinate to the wire with an accuracy comparable to that of the wire spacing. The coordinate along each wire can be obtained by measuring the ratio of collected charge at the two ends of resistive wires. Making use of the charge profile induced on segmented cathodes, the so-called center-of gravity (COG) method, permits localization of tracks to sub-mm accuracy. Due to the statistics of energy loss and asymmetric ionization clusters, the position accuracy is $\sim 50 \mu\text{m}$ rms for tracks perpendicular to the wire plane, but degrades to $\sim 250 \mu\text{m}$ at 30° to the normal [99]. The intrinsic bi-dimensional characteristic of the COG readout has found numerous applications in medical imaging.

Drift chambers, developed in the early '70's, can be used to estimate the longitudinal position of a track by exploiting the arrival time of electrons at the anodes if the time of interaction is known [100]. The distance between anode wires is usually several cm, allowing coverage of large areas at reduced cost. In the original design, a thicker wire (the field wire) at the proper voltage, placed between the anode wires, reduces the field at the mid-point between anodes and improves charge collection (Fig. 35.7b). In some drift chamber designs, and with the help of suitable voltages

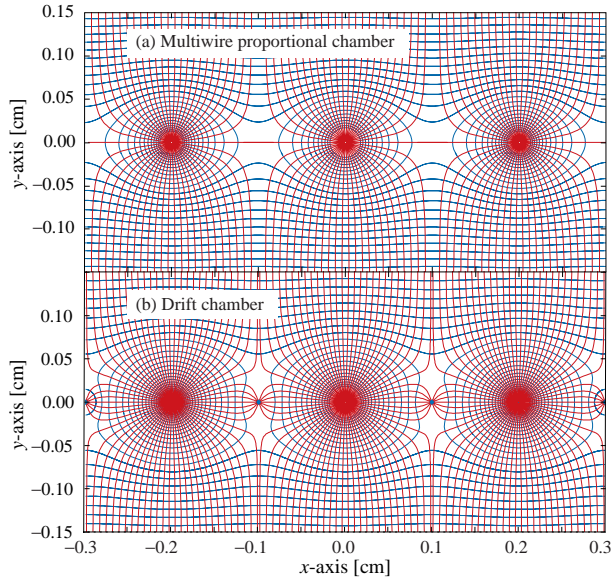


Figure 35.7: Electric field lines and equipotentials in (a) a multiwire proportional chamber and (b) a drift chamber.

applied to field-shaping electrodes, the electric field structure is adjusted to improve the linearity of space-to-drift-time relation, resulting in better spatial resolution [101].

Drift chambers can reach a longitudinal spatial resolution from timing measurement of order $100 \mu\text{m}$ (rms) or better for minimum ionizing particles, depending on the geometry and operating conditions. However, a degradation of resolution is observed [102] due to primary ionization statistics for tracks close to the anode wires, caused by the spread in arrival time of the nearest ionization clusters. The effect can be reduced by operating the detector at higher pressures. Sampling the drift time on rows of anodes led to the concept of multiple arrays such as the multi-drift module [103] and the JET chamber [104]. A measurement of drift time, together with the recording of charge sharing from the two ends of the anode wires provides the coordinates of segments of tracks. The total charge gives information on the differential energy loss and is exploited for particle identification. The time projection chamber (TPC) [105] combines a measurement of drift time and charge induction on cathodes, to obtain excellent tracking for high multiplicity topologies occurring at moderate rates (see Sec. 35.6.5). In all cases, a good knowledge of electron drift velocity and diffusion properties is required. This has to be combined with the knowledge of the electric fields in the structures, computed with commercial or custom-developed software [106, 107]. For an overview of detectors exploiting the drift time for coordinate measurement see Refs. [108] and [97].

Multiwire and drift chambers have been operated with a variety of gas fillings and operating modes, depending on experimental requirements. The so-called “Magic Gas,” a mixture of argon, isobutane and Freon [96], permits very high and saturated gains ($\sim 10^6$). This gas mixture was used in early wire chambers, but was found to be susceptible to severe aging processes. With present-day electronics, proportional gains around 10^4 are sufficient for detection of minimum ionizing particles, and noble gases with moderate amounts of polyatomic gases, such as methane or carbon dioxide, are used.

Although very powerful in terms of performance, multi-wire structures have reliability problems when used in harsh or hard-to-access environments, since a single broken wire can disable the entire detector. Introduced in the '80's, straw and drift tube systems make use of large arrays of wire counters encased in individual enclosures, each acting as an independent wire counter [109]. Techniques for low-cost mass production of these detectors have been developed for large experiments, such as the Transition Radiation Tracker and the Drift Tubes arrays for CERN's LHC ex-

periments [110].

35.6.3 High Rate Effects

Revised March 2010 by F. Sauli (CERN) and M. Titov (CEA Saclay, DSM/IRFU/SPP).

The production of positive ions in the avalanches and their slow drift before neutralization result in a rate-dependent accumulation of positive charge in the detector. This may result in significant field distortion, gain reduction and degradation of spatial resolution. As shown in Fig. 35.8 [111], the proportional gain drops above a charge production rate around 10^9 electrons per second and mm of wire, independently of the avalanche size. For a proportional gain of 10^4 and 100 electrons per track, this corresponds to a particle flux of $10^3 \text{ s}^{-1} \text{ mm}^{-1}$ (1 kHz/mm² for 1 mm wire spacing).

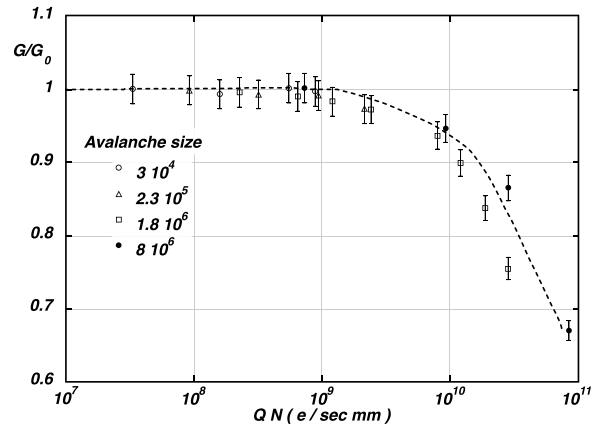


Figure 35.8: Charge rate dependence of normalized gas gain G/G_0 (relative to zero counting rate) in proportional thin-wire detectors [111]. Q is the total charge in single avalanche; N is the particle rate per wire length.

At high radiation fluxes, a fast degradation of detectors due to the formation of polymers deposits (aging) is often observed. The process has been extensively investigated, often with conflicting results. Several causes have been identified, including organic pollutants and silicone oils. Addition of small amounts of water in many (but not all) cases has been shown to extend the lifetime of the detectors. Addition of fluorinated gases (*e.g.*, CF_4) or oxygen may result in an etching action that can overcome polymer formation, or even eliminate already existing deposits. However, the issue of long-term survival of gas detectors with these gases is controversial [112]. Under optimum operating conditions, a total collected charge of a few coulombs per cm of wire can usually be reached before noticeable degradation occurs. This corresponds, for one mm spacing and at a gain of 10^4 , to a total particle flux of $\sim 10^{14}$ MIPs/cm².

35.6.4 Micro-Pattern Gas Detectors

Revised March 2010 by F. Sauli (CERN) and M. Titov (CEA Saclay, DSM/IRFU/SPP).

Despite various improvements, position-sensitive detectors based on wire structures are limited by basic diffusion processes and space charge effects to localization accuracies of 50–100 μm [113]. Modern photolithographic technology led to the development of novel Micro-Pattern Gas Detector (MPGD) concepts [114], revolutionizing cell size limitations for many gas detector applications. By using pitch size of a few hundred μm , an order of magnitude improvement in granularity over wire chambers, these detectors offer intrinsic high rate capability ($> 10^6$ Hz/mm²), excellent spatial resolution ($\sim 30 \mu\text{m}$), multi-particle resolution ($\sim 500 \mu\text{m}$), and single photo-electron time resolution in the ns range.

The Micro-Strip Gas Chamber (MSGC), invented in 1988, was the first of the micro-structure gas chambers [115]. It consists of a set of tiny parallel metal strips laid on a thin resistive support, alternatively connected as anodes and cathodes. Owing to

the small anode-to-cathode distance ($\sim 100 \mu\text{m}$), the fast collection of positive ions reduces space charge build-up, and provides a greatly increased rate capability. Unfortunately, the fragile electrode structure of the MSGC turned out to be easily destroyed by discharges induced by heavily ionizing particles [116]. Nevertheless, detailed studies of their properties, and in particular, on the radiation-induced processes leading to discharge breakdown, led to the development of the more powerful devices: GEM and Micromegas. These have improved reliability and radiation hardness. The absence of space-charge effects in GEM detectors at the highest rates reached so far and the fine granularity of MPGDs improve the maximum rate capability by more than two orders of magnitude (Fig. 35.9) [117] [118]. Even larger rate capability has been reported for Micromegas [119].

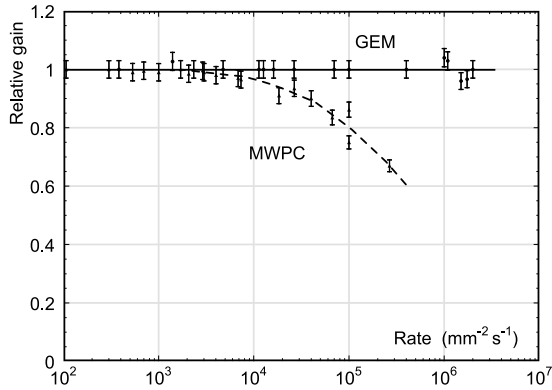


Figure 35.9: Normalized gas gain as a function of particle rate for MWPC [117] and GEM [118].

The Gas Electron Multiplier (GEM) detector consists of a thin-foil copper-insulator-copper sandwich chemically perforated to obtain a high density of holes in which avalanches occur [120]. The hole diameter is typically between $25 \mu\text{m}$ and $150 \mu\text{m}$, while the corresponding distance between holes varies between $50 \mu\text{m}$ and $200 \mu\text{m}$. The central insulator is usually (in the original design) the polymer Kapton, with a thickness of $50 \mu\text{m}$. Application of a potential difference between the two sides of the GEM generates the electric fields indicated in Fig. 35.10. Each hole acts as an independent proportional counter. Electrons released by the primary ionization particle in the upper conversion region (above the GEM foil) drift into the holes, where charge multiplication occurs in the high electric field ($50\text{--}70 \text{ kV/cm}$). Most of avalanche electrons are transferred into the gap below the GEM. Several GEM foils can be cascaded, allowing the multi-layer GEM detectors to operate at overall gas gain above 10^4 in the presence of highly ionizing particles, while strongly reducing the risk of discharges. This is a major advantage of the GEM technology [121]. Localization can then be performed by collecting the charge on a patterned one- or two-dimensional readout board of arbitrary pattern, placed below the last GEM.

The micro-mesh gaseous structure (Micromegas) is a thin parallel-plate avalanche counter, as shown in Fig. 35.11 [122]. It consists of a drift region and a narrow multiplication gap ($25\text{--}150 \mu\text{m}$) between a thin metal grid (micromesh) and the readout electrode (strips or pads of conductor printed on an insulator board). Electrons from the primary ionization drift through the holes of the mesh into the narrow multiplication gap, where they are amplified. The electric field is homogeneous both in the drift (electric field $\sim 1 \text{ kV/cm}$) and amplification ($50\text{--}70 \text{ kV/cm}$) gaps. In the narrow multiplication region, gain variations due to small variations of the amplification gap are approximately compensated by an inverse variation of the amplification coefficient, resulting in a more uniform gain. The small amplification gap produces a narrow avalanche, giving rise to excellent spatial resolution: $12 \mu\text{m}$ accuracy, limited by the micro-mesh pitch, has been achieved for MIPs, as well as very good time resolution and energy resolution ($\sim 12\%$ FWHM with 6 keV x rays) [123].

The performance and robustness of GEM and Micromegas have

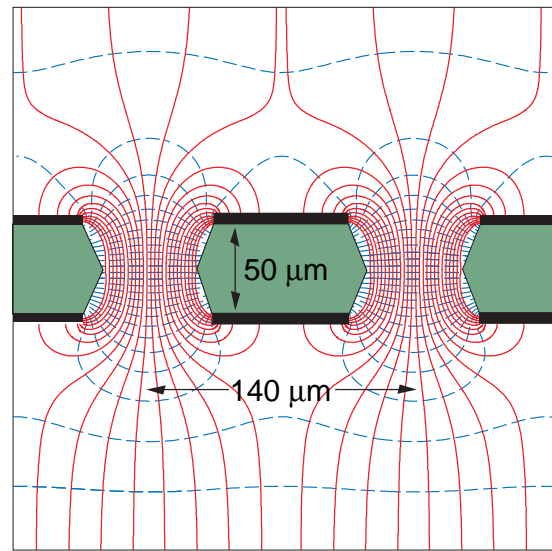


Figure 35.10: Schematic view and typical dimensions of the hole structure in the GEM amplification cell. Electric field lines (solid) and equipotentials (dashed) are shown.

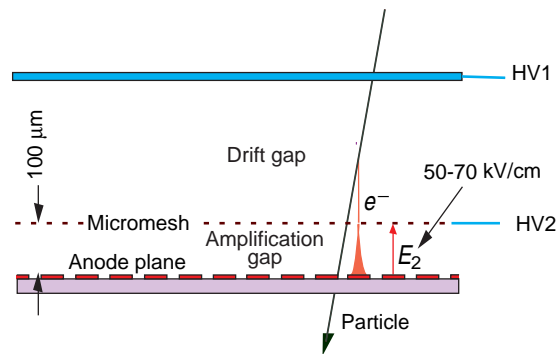


Figure 35.11: Schematic drawing of the Micromegas detector.

encouraged their use in high-energy and nuclear physics, UV and visible photon detection, astroparticle and neutrino physics, neutron detection and medical physics. Most structures were originally optimized for high-rate particle tracking in nuclear and high-energy physics experiments. COMPASS, a high-luminosity experiment at CERN, pioneered the use of large-area ($\sim 40 \times 40 \text{ cm}^2$) GEM and Micromegas detectors close to the beam line with particle rates of 25 kHz/mm^2 . Both technologies achieved a tracking efficiency of close to 100% at gas gains of about 10^4 , a spatial resolution of $70\text{--}100 \mu\text{m}$ and a time resolution of $\sim 10 \text{ ns}$. GEM detectors are also used for triggering in the LHCb Muon System and for tracking in the TOTEM Telescopes. Both GEM and Micromegas devices are foreseen for the upgrade of the LHC experiments and for one of the readout options for the Time Projection Chamber (TPC) at the International Linear Collider (ILC). The development of new fabrication techniques—“bulk” Micromegas technology [124] and single-mask GEMs [125]—is a big step toward industrial production of large-size MPGDs. In some applications requiring very large-area coverage with moderate spatial resolution, coarse macro-patterned detectors, such as Thick GEMs (THGEM) [126] or patterned resistive-plate devices [127] might offer economically interesting solutions.

Sensitive and low-noise electronics enlarge the range of the MPGD applications. Recently, the GEM and Micromegas detectors were read out by high-granularity ($\sim 50 \mu\text{m}$ pitch) CMOS chips assembled directly below the GEM or Micromegas amplification structures [128]. These detectors use the bump-bonding pads of a pixel chip as an integrated charge collecting anode. With this arrangement signals are induced at the input gate of a charge-

sensitive preamplifier (top metal layer of the CMOS chip). Every pixel is then directly connected to the amplification and digitization circuits, integrated in the underlying active layers of the CMOS technology, yielding timing and charge measurements as well as precise spatial information in 3D.

The operation of a MPGD with a Timepix CMOS chip has demonstrated the possibility of reconstructing 3D-space points of individual primary electron clusters with $\sim 30 \mu\text{m}$ spatial resolution and event-time resolution with nanosecond precision. This has become indispensable for tracking and triggering and also for discriminating between ionizing tracks and photon conversions. The GEM, in conjunction with a CMOS ASIC,¹ can directly view the absorption process of a few keV x-ray quanta and simultaneously reconstruct the direction of emission, which is sensitive to the x-ray polarization. Thanks to these developments, a micro-pattern device with finely segmented CMOS readout can serve as a high-precision “electronic bubble chamber.” This may open new opportunities for x-ray polarimeters, detection of weakly interacting massive particles (WIMPs) and axions, Compton telescopes, and 3D imaging of nuclear recoils.

An elegant solution for the construction of the Micromegas with pixel readout is the integration of the amplification grid and CMOS chip by means of an advanced “wafer post-processing” technology [129]. This novel concept is called “Ingrid” (see Fig. 35.12). With this technique, the structure of a thin ($1 \mu\text{m}$) aluminum grid is fabricated on top of an array of insulating pillars, which stands $\sim 50 \mu\text{m}$ above the CMOS chip. The sub- μm precision of the grid dimensions and avalanche gap size results in a uniform gas gain. The grid hole size, pitch and pattern can be easily adapted to match the geometry of any pixel readout chip.

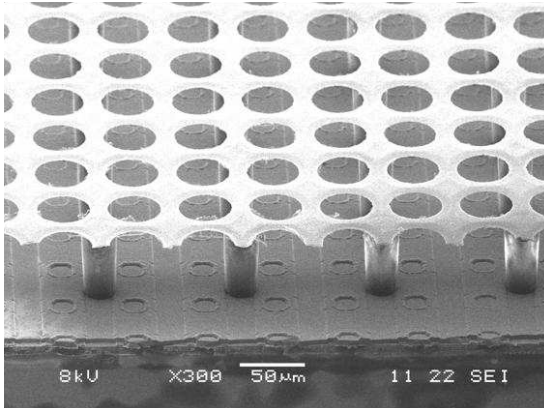


Figure 35.12: Photo of the Micromegas “Ingrid” detector. The grid holes can be accurately aligned with readout pixels of CMOS chip. The insulating pillars are centered between the grid holes, thus avoiding dead regions.

Recent developments in radiation hardness research with state-of-the-art MPGDs are reviewed in Ref. [130]. Earlier aging studies of GEM and Micromegas concepts revealed that they might be even less vulnerable to radiation-induced performance degradation than standard silicon microstrip detectors.

The RD51 collaboration was established in 2008 to further advance technological developments of micro-pattern detectors and associated electronic-readout systems for applications in basic and applied research [131].

35.6.5 Time-projection chambers

Revised August 2019 by C. Lippmann (GSI Darmstadt).

The Time Projection Chamber (TPC) concept was invented by David Nygren in the 1970’s [132]. It consists of a cylindrical or square field cage that is filled with a gaseous (or liquid) detection medium. Charged particles produce tracks of ionization electrons that drift in a uniform electric field towards a position-sensitive amplification stage which provides a 2D projection of the particle

trajectories. The third coordinate can be calculated from the arrival times of the drifted electrons. The start for this drift time measurement is usually derived from an external detector, e.g. a fast interaction trigger detector.

This section focuses on the gas-filled TPCs that are often used in particle or nuclear physics experiments at accelerators on account of their low material budget. For neutrino physics (Sec. 35.10) or for detecting rare events (Sec. 36.4), on the contrary, usually high density and large active mass are required, and a liquid detection medium is favored.

The TPC enables full 3D measurements of charged particle tracks, which gives it a distinct advantage over other tracking detector designs which record information only in two-dimensional detector planes and have less overall segmentation. The track points recorded in a TPC are basically adjacent, which facilitates the track finding enormously. This advantage is often exploited for pattern recognition in events with large numbers of particles, e.g. heavy-ion collisions. Two examples of modern large-volume gaseous TPCs are shown in (Figure 35.13) and (Figure 35.14).

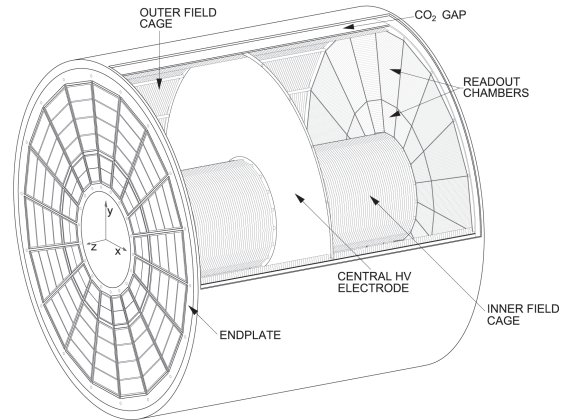


Figure 35.13: Schematic view of the ALICE TPC [133]. The drift volume with 5 m diameter is divided into two halves, each providing 2.5 m drift length.

Identification of the charged particles crossing the TPC is possible by simultaneously measuring their momentum and specific energy deposit through ionisation (dE/dx). The momentum, as well as the charge sign, are calculated from a helix fit to the particle trajectory in the presence of a magnetic field (typically parallel to the drift field). For this application, precise spatial measurements in the plane transverse to the magnetic field are most important. The specific energy deposit is estimated from many charge measurements along the particle trajectory (e.g. one measurement per anode wire or per row of readout pads). As the charge collected per readout segment depends on the track angle and on the ambient conditions, the measured values are corrected for the effective length of the track segments and for variations of the gas temperature and pressure. The most probable value of the corrected signal amplitudes provides the best estimator for the specific energy deposit (see Sec. 34.2.3); it is usually approximated by the truncated mean, i.e. the average of the 50%–70% smallest values. The resulting particle identification performance is illustrated in (Figure 35.15), for the ALICE TPC.

The dependence of the achievable energy resolution on the number of measurements N , on the thickness of the sampling layers t , and on the gas pressure P can be estimated using an empirical formula [135]:

$$\sigma_{dE/dx} = 0.41 N^{-0.43} (tP)^{-0.32}. \quad (35.17)$$

Typical values at nominal pressure are $\sigma_{dE/dx} = 4.5$ to 7.5%, with $t = 0.4$ to 1.5 cm and $N = 40$ up to more than 300. Due to the high gas pressure of 8.5 bar, the resolution achieved with the PEP-4/9 TPC was an unprecedented 3% [136].

The greatest challenges for a large TPC are due to the length of the drift of up to several meters. In particular, it can make

¹Application Specific Integrated Circuit

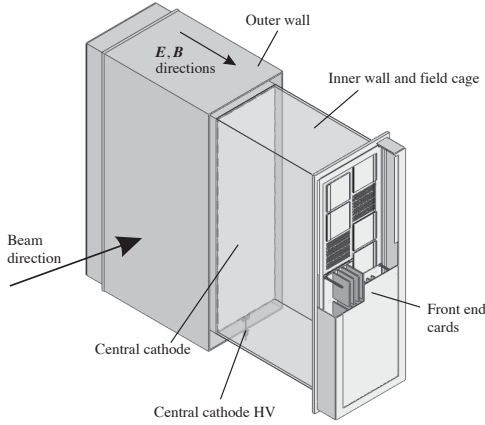


Figure 35.14: One of the 3 TPC modules for the near detector of the T2K experiment [134]. The size is $2 \times 2 \times 0.8 \text{ m}^3$. Micromegas devices are used for gas amplification and readout.

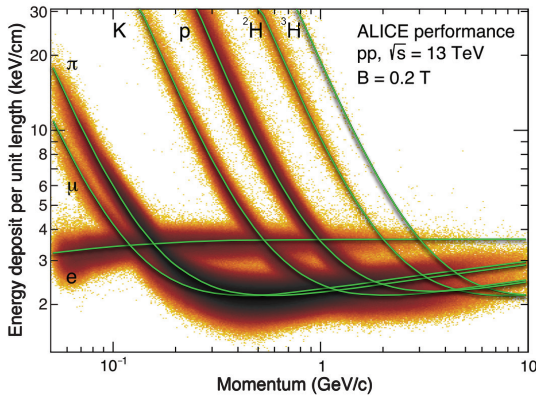


Figure 35.15: Energy deposit versus momentum measured in the ALICE TPC.

the device sensitive to small distortions in the electric field. Such distortions can arise from a number of sources, e.g. imperfections in the field cage construction or the presence of ions in the drift volume. The electron drift in a TPC in the presence of a magnetic field is defined by Eq. (35.14). The $E \times B$ term of Eq. (35.14) vanishes for perfectly aligned electric and magnetic fields, which can however be difficult to achieve in practice. Furthermore, the electron drift depends on the $\omega\tau$ factor, which is defined by the gas mixture and the magnetic field strength. The electrons will tend to follow the magnetic field lines for $\omega\tau > 1$ or the electric field lines for $\omega\tau < 1$. The former mode of operation makes the TPC less sensitive to non-uniformities of the electric field, which is usually desirable.

The drift of the ionization electrons is superposed with a random diffusion motion which degrades their position information. The ultimate resolution of a single position measurement is limited to around

$$\sigma_x = \frac{\sigma_D \sqrt{L}}{\sqrt{n}}, \quad (35.18)$$

where σ_D is the transverse diffusion coefficient for 1 cm drift, L is the drift length in cm and n is the effective number of electrons collected. Without a magnetic field, $\sigma_{D,B=0} \sqrt{L}$ is typically a few mm after a drift of $L = 100 \text{ cm}$. However, in a strong magnetic field parallel to the drift field, a large value of $\omega\tau$ can significantly reduce diffusion:

$$\frac{\sigma_{D,B>0}}{\sigma_{D,B=0}} = \frac{1}{\sqrt{1 + \omega^2 \tau^2}}. \quad (35.19)$$

This factor can reach values of up to 10. In practice, the final resolution limit due to diffusion will typically be around $\sigma_x = 100 \mu\text{m}$.

The drift and diffusion of electrons depend strongly on the gas mixture. The optimal gas mixture varies according to the environment in which the TPC will operate. In all cases, the oxygen concentration must be kept very low (few ten parts per million in a large TPC) in order to avoid electron loss through attachment.

Ideally, the drift velocity should depend only weakly on the electric field at the nominal operating condition. The classic Ar/CH₄ (90:10) mixture, known as P10, has a drift velocity maximum of $5 \text{ cm}/\mu\text{s}$ at an electric field of only $125 \text{ V}/\text{cm}$ (Figure 35.4). In this regime, the electron arrival time is not affected by small variations in the ambient conditions. Moreover, low electric fields simplify the design and operation of the field cage. The mixture has a large transverse diffusion at $B = 0$, but this can be reduced significantly in a strong magnetic field due to the relatively large value of $\omega\tau$.

For some applications organic gases like CH₄ are not desirable since they may cause aging. An alternative is to replace CH₄ with CO₂. An Ar/CO₂ (90:10) mixture features a low transverse diffusion at all magnetic field strengths, but does not provide a saturated drift velocity for the typical electric fields used in TPCs (up to a few $100 \text{ V}/\text{cm}$), so it is quite sensitive to the ambient conditions. Freon admixtures like CF₄ can be an attractive option for a TPC as well, since the resulting gas mixtures provide high drift velocities at low electric fields. However, the use of CF₄ always needs to be thoroughly validated for compatibility with all materials of the detector and the gas system.

Historically, the amplification stages used in gaseous TPCs have been planes of anode wires operated in proportional mode. The performance is limited by effects related to the feature size of a few mm (wire spacing). Since near the wires the electric and magnetic fields are not parallel, the incoming ionisation electrons are displaced in the direction of the wires (“wire $E \times B$ effect”), which degrades the resolution. The smaller feature sizes of Micro-Pattern Gas Detectors (MPGDs) like GEMs and Micromegas lead to many advantages as compared to wire planes (see Sec. 35.6.4). In particular, $E \times B$ effects in the amplification stage are much smaller. Moreover, the signal induction process in MPGDs leads to a very narrow pad response, allowing for a much finer segmentation and improving the separation of two nearby tracks. Combinations of MPGDs with silicon sensors have resulted in the highest granularity readout systems so far (see Sec. 35.6.4). These devices make it possible to count the number of ionization clusters along the length of a track, which can, in principle, improve the particle identification capability. However, the big challenge for such a system is the huge number of readout channels for a TPC of a typical size.

The accumulation of the positive ions created by the ionization from the particle tracks can lead to time-dependent distortions of the drift field. Due to their low drift velocity, ions from many events may coexist in the drift volume. To reduce the effect of such a build-up of space charge, Argon can be replaced by Neon as the main component of the gas mixture. Neon features a lower number of ionisation electrons per unit of track length (see 35.5) and a higher ion mobility (see 35.6).

Of much greater concern are the ions produced in the gas amplification stage. In order to prevent them from entering the drift volume, large TPCs built until now usually have a gating grid. The gating grid can be switched to transparent mode (usually in the presence of an interaction trigger) to allow the ionization electrons to pass into the amplification region. After all electrons have reached the amplification region, it is usually closed such that it is rendered opaque to electrons and ions.

A gating grid implies a principal rate limitation to a few kHz. Different groups are therefore working towards the goal of continuous readout for applications where a triggered operation would lead to unacceptable data loss (e.g. ALICE [137], sPHENIX [138]).

New readout schemes using MPGDs enable continuous readout, as they can be optimised in order to limit the ion back-flow at the same effective gain as MWPCs. Extensive work has been carried out during the 2010's to design such readout structures. In ALICE and sPHENIX ion back-flow values below 1% are achieved with a thorough adjustment of the various fields in a quadruple GEM system. Similar levels of ion back-flow can be reached with Micromegas detectors [139].

On the other hand, combinations of MPGDs and a gating structure may be used for triggered operation.

35.6.6 Transition radiation detectors (TRD's)

Revised August 2019 by P. Nevski (BNL) and A. Romaniouk (MEPhI Moscow).

Transition radiation (TR) x-rays are produced when a highly relativistic particle ($\gamma \gtrsim 10^3$) crosses a refractive index interface, as discussed in Sec. 34.7. Since the TR yield is about 1% per boundary crossing, radiation from multiple surface crossings (e.g., a stack of foils) is used in practical detectors. The x-rays, ranging from a few keV to a few dozen keV or more, are emitted in a forward direction at small angles (within few mrad) to the particle trajectory. The TR intensity for a single boundary crossing always increases with γ , but, for multiple boundary crossings, interference leads to saturation above a Lorentz factor $\gamma_{\text{sat}} = 0.6 \omega_1 \sqrt{\ell_1 \ell_2} / c$ [140], where ω_1 is the radiator material plasma frequency, ℓ_1 is its thickness, and ℓ_2 the spacing between material elements. The probability density function of TR is a fairly complex function of γ , radiator parameters, angle (θ) and photon energy (ω). For well defined radiator parameters a measured two-dimensional energy vs angle distribution is in a very good agreement with the theory predictions [141]. Integration over the angle yields the TR spectrum, which typically features many maxima (see Sec. 34.7). Most of the TR energy is emitted near the last maximum of the spectra determined by radiator material parameters at $\omega_{\text{max}} = \ell_1 \omega_1^2 / 2\pi c$. The effective TR photon emission starts at about $\gamma_{\text{thr}} = \ell_1 \omega_1 / c$. By varying radiator parameters one may optimize the particle separation for a given range of the γ -factor. The angular distribution of TR photons has a few maxima and extends up to $\theta_{\text{max}} = (1/\gamma^2 + \omega_1^2/\omega^2)^{1/2}$ [142]. For a single foil the largest part of the TR energy is emitted around the most probable angle $\theta = (1/\gamma^2 + \omega_2^2/\omega^2)^{1/2}$, where ω_2 is the plasma frequency of the gas surrounding the radiator material elements. However, in case of multiple interfaces, interference effects may significantly change this angle. For instance, for a stack of foils of $15.5 \mu\text{m}$ thickness spaced by $210 \mu\text{m}$ TR produced by 20 GeV electrons is emitted mostly around $\theta \sim 0.9$ mrad [143].

In the simplest concept, a detector module might consist of a low- Z TR radiator followed by a high- Z active layer made of proportional counters filled with a Xe-rich gas mixture. The atomic number considerations follow from the dominant photoelectric absorption cross section per atom going roughly as Z^n/ω^3 , where n varies between 4 and 5 over the region of interest.² To minimize self-absorption, materials such as polypropylene, Mylar, carbon, and (rarely) lithium in the form of foils, fibers or foams are used as radiators. The TR signal in the active regions is in most cases superimposed upon the particle ionization losses, which are proportional to Z . In most of the detectors used in particle physics the radiator parameters are chosen to provide $\gamma_{\text{sat}} \approx 2000$. Those detectors normally work as threshold devices, ensuring the best electron/pion separation in the momentum range $1 \text{ GeV}/c \lesssim p \lesssim 150 \text{ GeV}/c$.

One can distinguish two design concepts—"thick" and "thin" detectors:

In "thick" detectors the radiator, optimized for a minimum total radiation length at maximum TR yield and total TR absorption in the detector, consists of few hundred foils (for instance 300 $20 \mu\text{m}$ thick polypropylene foils). Most of the TR photons are absorbed in the radiator itself. To maximise the number of TR photons reaching the detector, part of the radiator far from the active layers is often made of thicker foils, which shifts the x-ray

spectrum to higher energies. The detector thickness, about 2-4 cm for Xe-filled gas chambers, is optimized to absorb the incoming x-ray spectrum. A classical detector is composed of several similar modules which respond nearly independently. Such detectors were used in the UA2, NA34 and other experiments [144], and are being used in the ALICE experiment [145] [146].

In another TRD concept a fine granular radiator/detector structure exploits the soft part of the TR spectrum more efficiently and thereby may act also as an integral part of the tracking detector providing many points of measurements on the particle track. This can be achieved, for instance, by distributing small-diameter straw-tube detectors uniformly or in thin layers throughout the radiator material. Even with a relatively thin radiator stack, radiation below 4 keV is mostly lost in the radiators themselves. However, for photon energies above this value, the absorption is reduced and the radiation can be registered by several consecutive detector layers, thus creating a strong TR build-up effect. This approach allows to realise a TRD as an integral part of a tracking detector. Descriptions of detectors using this approach in both accelerator and space experiments can be found in [145, 147–150]. For example, in the ATLAS TR tracker (TRT), charged particles on average cross about 35 straw tube layers embedded in the radiator material [147]. The effective thickness of the Xe gas per straw is about 2.5 mm and the average number of foils per straw is about 40 with an effective foil thickness of about $18 \mu\text{m}$. In this approach straw walls also act as radiators and make some contribution to the TR spectrum.

Although the values mentioned above are typical for most of the plastic radiators used with Xe-based detectors, they vary significantly depending on the detector requirements. Careful simulations are usually needed to build a detector optimized for a particular application. For TRD simulations the codes are based on well understood TR emission formulas (see for instance [142]). They are realised as the stand-alone simulation programs [151] and GEANT4 based ones [152] and give both a good agreement of the TR energy spectra with data [141, 143, 153].

The discrimination between electrons and pions can be based on the charge deposition measured in each detection module, on the number of clusters – energy depositions observed above an optimal threshold (usually it is 5–7 keV), or on more sophisticated methods such as analyzing the pulse shape as a function of time. The total energy measurement technique is more suitable for thick gas volumes, which absorb most of the TR radiation and where the ionization loss fluctuations are relatively small. The cluster-counting method works better for detectors with thin gas layers, where the fluctuations of the ionization losses are bigger. Cluster-counting replaces the Landau-Vavilov distribution of background ionization energy losses with the Poisson statistics of δ -electrons, responsible for the distribution tails. The latter distribution is narrower than the Landau-Vavilov distribution. In practice, most of the experiments use a likelihood method, which exploits detailed knowledge of the detector response for different particles and gives the best separation. The more parameters are considered, the better achievable separation power. For example, for the TRD in the AMS experiment the rejection power achieved in the real experiment is better by almost one order of magnitude than that obtained in the beam test if stringent criteria for track selection are applied, see in [150]. Another example is the neural network method used by the ALICE TRD (ALICE point in 35.16) which gives another factor of 2–3 in rejection power with respect to the likelihood method [145].

The major factor in the performance of any TRD is its overall length. This is illustrated in Fig. 35.16, which shows, for a variety of detectors, the pion efficiency at a fixed electron efficiency of 90% as a function of the overall detector length. As TRD performance depends on particle energy, the experimental data in this figure covering a range of particle energies from 1 GeV to 40 GeV, are rescaled to an energy of 10 GeV when possible. Phenomenologically, the rejection power against pions increases as $5 \cdot 10^{L/38}$, where the range of validity is $L \approx 20\text{--}100$ cm. Apart from the beam energy variations, the observed scattering of the points in the plot reflects how effectively the detector space is used and how well the exact response to different particles is taken into account

²Photon absorption coefficients for the elements (via a NIST link), and $dE/dx|_{\text{min}}$ and plasma energies for many materials are given in pdg.lbl.gov/AtomicNuclearProperties.

in the analysis. For instance, the ATLAS TRT was built as a compromise between TR and tracking requirements; that is why the test-beam prototype result (lower point) is better than the real End-Cap TRT performance at the LHC shown in Fig. 35.16 for different regions in the detector (in agreement with MC).

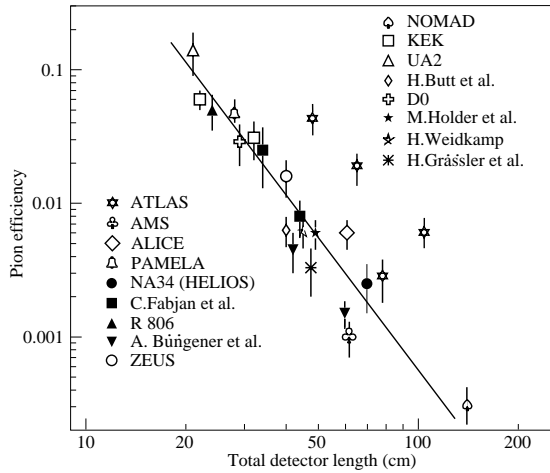


Figure 35.16: Pion efficiency measured (or predicted) for different TRDs as a function of the detector length for a fixed electron efficiency of 90%. The plot is based on the table given in [144]. Results from more recent detectors are added from [145, 148–150, 154].

In most cases, recent TRDs combine particle identification with charged-track measurement in the same detector [145, 149, 155]. This is particularly important for collider experiments, where the available space for the inner detector is very limited. For a modest increase of the radiation length due to the radiator ($\sim 4\% X_0$), a significant enhancement of the electron identification was obtained in the case of the ATLAS TRT. Here, the combination of the two detector functions provides a powerful tool for electron identification even at very high particle densities.

In addition to the enhancement of the electron identification during offline data analysis, TRD signatures are often used in the trigger algorithms at collider experiments. The ALICE experiment [146] is a good example for the use of the TRD in a First Level Trigger. In the ATLAS experiment, the TRT information is used in the High Level Trigger (HLT) algorithms. At increasing luminosities, the electron trigger output rate becomes so high, that a significant increase of the calorimeter energy threshold is required to keep it at an acceptable level. This may affect the trigger efficiency of very important physics channels (e.g. $W \rightarrow e\nu$ inclusive decay). Even a very soft TR cut at the HLT level, which preserves high electron efficiency (98%), allows to suppress a significant part of fake triggers and enhance the purity for physics events with electrons in a final state. The TRT also plays a crucial role in the studies where an electron suppression is required (e.g. hadronic mode of τ -decays). TR information is a completely independent tool for electron identification and allows to study systematic uncertainties of other electron reconstruction methods.

Electron identification is not the only TRD application. Some TRDs for particle astrophysics are designed to directly measure the Lorentz factor of high-energy nuclei by using the quadratic dependence of the TR yield on nuclear charge; see, for instance, in [156]. The radiator configuration (ℓ_1, ℓ_2) is tuned to extend the TR yield rise up to $\gamma \approx 10^5$ using the more energetic part of the TR spectrum (up to 100 keV). High density radiator materials (such as Al) are the best for this purpose. Direct absorption of the TR-photons of these energies with thin detectors becomes problematic and TR detection methods based on Compton scattering have been proposed, see in [156].

The high granularity of the semiconductor pixel or microstrip detectors provides spatial separation of the TR photons and dE/dx losses at relatively modest distances between radiator and detector. These detectors may be the basis for novel devices which

combine precise tracking and PID properties [141, 143]. Use of the TR production angle in addition to its energy can help to improve PID properties of the TRD. The presence of a magnetic field could enhance the separation between TR photons and dE/dx losses [157]. New detector techniques for TRDs are also under consideration. GasPixel detectors allow to reconstruct a track segment with a space point accuracy of $< 30 \mu\text{m}$ and exploit all details of the particle tracks to highlight individual TR clusters in the gas, see in [158]. Thin films of heavy scintillators might be a very attractive option for non-gas based TRD [159].

35.6.7 Resistive-plate chambers

Revised October 2019 by G. Aielli (Rome U. Tor Vergata).

The resistive-plate chamber (RPC) is a gaseous detector developed by R. Santonico and R. Cardarelli in the early 1980's [160]³. Although its original purpose was to provide a competitive alternative to large scintillator counters, the RPC's potential for timing tracker systems was quickly recognized given its high detection efficiency ($>95\%$), excellent temporal and spatial resolutions and ease of constructing large-format single frame detectors. The RPC, as sketched in Fig. 35.17, is a large planar capacitor with two parallel high bulk resistivity electrode plates (10^9 – $10^{13} \Omega\cdot\text{cm}$) separated by a set of insulating spacers. The spacers define a gap in the range from a few millimeters down to 0.1 mm with a precision of a few $\sim \mu\text{m}$. The gap is filled with a suitable atmospheric-pressure gas mixture which serves as a target for ionizing radiation. The gas gap thickness practically determines the time resolution of the RPC, on the other side the limit for reaching full detection efficiency (depending also on the gas density) is typically 1mm. Since the primary ionization for sub-millimeter gas gaps is insufficient, multiple gaps can be combined to ensure high detection efficiency [162]. The electrodes are most commonly made of high pressure phenolic-melaminic laminate (HPL), improperly referred to as "bakelite", or glass. A moderate electrode resistivity

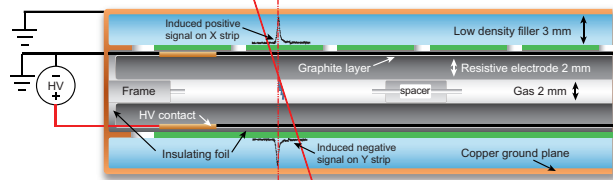


Figure 35.17: Schematic cross section of a generic single gap RPC.

($\sim 10^5 \Omega/\square$) establishes a uniform electric field of several kV/mm across the gap, which initiates an electron avalanche following primary ionization. The above resistivity is low enough to ensure uniformity of the electric field, yet still transparent to fast signal transients from avalanches. Due to the high electrode resistivity in RPCs, the electrode time constant is much longer than discharge processes. Therefore only the locally-stored electrostatic energy contributes to the discharge, which prevents the formation of sparks and leaves the rest of the detector field unaffected. This field configuration and resistive feedback offers, besides the excellent time resolution, an excellent spacial localization of the discharge, without the need of micro-patterned electrodes. The gas-facing surface of HPL electrodes are commonly coated with a few μm -thick layer of polymerized linseed oil. This layer has a similar resistivity as the electrode, and is smooth to aid the uniformity of the electric field. It also protects the electrode from the free radicals generated in the discharge e.g. in presence of hydrocarbons or fluorocarbons. As with other gaseous detectors, the gas mixture is optimized for each specific application. In general it needs to contain a UV photons absorber, to quench the spurious counts and an electronegative component to limit the avalanche growth in presence of very high electric fields [163] [164]. According to a first order approximation, each primary ionization in an RPC is exponentially amplified according to its distance from the anode, due to the uniform field. Therefore RPC signals span a large dynamic range (unlike gaseous detectors where

³The RPC was based on earlier work on a spark counter with one metallic and one high-resistivity plate [161].

ionization and amplification occur in separate regions) following the exponential distribution, having the most probable signals toward the zero. For increasingly stronger fields, the avalanche exponential growth progressively saturates to linear and the signal amplitude distribution peak detaches from zero, making easier to distinguish the signal and the noise, [165], and finally reaches a strongly-saturated "streamer" transition which exhausts all the locally-available energy [166], generating an almost fixed amplitude signal. Any of this operating regimes can be used, in function of the front-end electronics sensitivity, and depending on the operating environment. A set of metallic readout electrodes (e.g. pads or strips) placed behind the resistive electrodes detect the charge pulse induced by the fast movement of the avalanche electrons. The signal is isotropically distributed with respect to the field direction and present with equal but opposite amplitude on the two electrodes. This feature allows for 2D localization of the signal with uniform spatial resolution. The induced charge density projected in 1D can be calculated for a simplified RPC model [167] as: $\sigma(x) = A/\cosh[(x - \bar{x})/\delta]$ where \bar{x} is the center of the avalanche and $\delta = (g+2d)/\pi$ depends on the gap and electrode width (g and d , respectively). The spatial extent of actual signals are generally larger than those given by this model [168] [169]. Conductivity of the graphite layer results in the most prominent broadening. Cross-talk from parasitic coupling of neighboring electrodes can also spread the signal spatially. Although the broadened charge distribution preserves most of the original spatial resolution, it can adversely impact signal clustering, so the detector layout must be calculated according to the expected application requirements. Sensitivity to high-frequency electron avalanche signals over large RPC areas requires a correspondingly adequate Faraday cage and readout structure design. To preserve the excellent timing features of the RPC signal, the front end electronics should have a short rise time (ideally \ll than the signal rise time) and low noise, although these requirements are usually in competition [170].

35.6.7.1 RPC types and applications

RPCs are generally classified in two categories depending on the gas gap structure: single gap RPCs (described above) and multiple gap RPCs (typically referred as mRPCs or timing RPCs). While they are both based on the same principle they have different construction techniques, performance and limitations, making them suitable for different applications. Due to its simplicity and robustness, the single gap RPC is ideal for covering very large surfaces. Typical detector systems can have sensitive surface areas up to $\sim 10^4$ m², with single module areas of a few m², and a space-time resolution down to ~ 0.4 ns \times 100 μ m [171] [172]. Sensible examples are the ATLAS [173] and CMS [174] muon systems or ground and underground based cosmic rays and neutrino arrays [175]. Moreover, single gap RPCs have recently found an application in tracking calorimetry [176]. The mRPC allows for smaller gas gap thicknesses while still maintaining a sufficient gaseous target. The most common version [177] consists of a stack of floating glass electrodes separated by monofilament (i.e. fishing line), sandwiched between two external electrodes which provide the high-voltage bias. The floating glass electrodes assume a potential determined by the avalanche processes occurring between them. mRPCs have been largely used in TOF systems and in applications such as timing PET.

35.6.7.2 Time and space resolution

The RPC field configuration generates an avalanche which is strongly correlated in space and time to the original ionizing event. Space-time uncertainties generally arise from the statistical fluctuations of the ionization and multiplication processes, and from the characteristics of the readout and front-end electronics. The intrinsic signal latency is commonly in a few ns range, making the RPC suitable for applications where a low latency is essential. A higher time resolution and shorter signal duration is correlated with a thinner gas gap, although a higher electric field is required for sufficient avalanche development [177] [178]. Typical timing performances range from around 1 ns with a 2 mm gas gap, down to 20 ps for a stack of several 0.1 mm gaps [179]. The mechanical delicacy of sub-mm-gap structures makes this technique less suitable for very large detector areas. Digital strip

readouts are commonly used, with spatial resolution determined by the strip pitch and the cluster size (~ 0.5 cm). A more precise measurement of the charge in each strip involved in the cluster, and demonstrated recently, through charge centroid techniques that the RPC avalanche space-time localization is better than ~ 50 ps \times 40 μ m [180].

35.6.7.3 Rate capability and ageing

RPC rate capability is limited by the voltage drop on resistive electrodes, $\Delta V = V_a - V_{\text{gas}} = I \cdot R$ [181]. Here V_a is the applied voltage, V_{gas} is the effective voltage on the gas, $R = \rho \cdot d/S$ is the total electrode resistance and I is the working current. Expressing I as the particle flux Φ times an average charge per avalanche $\langle Q \rangle$ gives $\Delta V/\Phi = \rho \cdot d \cdot \langle Q \rangle$. A large I not only limits the rate capability but also affects the long term performance of the detector. Discharges deplete the conductive properties of HPL electrodes [182]. In the presence of fluorocarbons and water, discharges generate hydrofluoric acid (HF) which damages internal detector surfaces, particularly glass electrodes [183]. HF damage can be mitigated by preventing water vapor contamination (for glass electrodes) or by sufficient flushing of the gas gap (for HPL electrodes where water vapor is unavoidable). Operating in the streamer regime puts low requirements on the front end electronics sensitivity, but generally limits the counting rate capability to ~ 100 Hz/cm² and requires stability over a large gain range. Higher-rate operation can be achieved by reducing gas gain in favor of electronic amplification, operating the detector in avalanche mode. Increasing concentrations of electronegative gases, such as C₂H₂F₄ and SF₆ [164], shifts the streamer transition to higher gains. The avalanche signal has a higher dynamic range, a drawback which can be compensated with appropriate electronics. With these techniques, stable performance at high rates (e.g. 10 kHz/cm²) has been achieved for large area single gap RPCs [170]. Complementary strategies rely on the natural redundancy and higher signal yield of multiple micro gap structures [184] and electrodes made with lower resistivity materials [185]. Lowering the electrode resistivity finds a limit in the increasing probability of discharge in presence of high uniform field, thus lowering the average charge per count, i.e. the applied electric field is also a gateway to further lower the electrode resistivity without spoiling the detector stability.

35.7 Semiconductor detectors

Revised November 2013 by H. Spieler (LBNL).

Semiconductor detectors provide a unique combination of energy and position resolution. In collider detectors they are most widely used as position sensing devices and photodetectors (Sec. 35.2).

Integrated circuit technology allows the formation of high-density micron-scale electrodes on large (15–20 cm diameter) wafers, providing excellent position resolution. Furthermore, the density of silicon and its small ionization energy yield adequate signals with active layers only 100–300 μ m thick, so the signals are also fast (typically tens of ns). The high energy resolution is a key parameter in x-ray, gamma, and charged particle spectroscopy, e.g., in neutrinoless double beta decay searches. Silicon and germanium are the most commonly used materials, but gallium-arsenide, CdTe, CdZnTe, and other materials are also useful. CdZnTe provides a higher stopping power and the ratio of Cd to Zn concentrations changes the bandgap. Ge detectors are commonly operated at liquid nitrogen temperature to reduce the bias current, which depends exponentially on temperature. Semiconductor detectors depend crucially on low-noise electronics (see Sec. 35.8), so the detection sensitivity is determined by signal charge and capacitance. For a comprehensive discussion of semiconductor detectors and electronics see [186] or the tutorial website <http://www-physics.lbl.gov/spieler>.

35.7.1 Materials Requirements

Semiconductor detectors are essentially solid state ionization chambers. Absorbed energy forms electron-hole pairs, i.e., negative and positive charge carriers, which under an applied electric field move towards their respective collection electrodes, where

they induce a signal current. The energy required to form an electron-hole pair is proportional to the bandgap. In tracking detectors the energy loss in the detector should be minimal, whereas for energy spectroscopy the stopping power should be maximized, so for gamma rays high- Z materials are desirable.

Measurements on silicon photodiodes [187] show that for photon energies below 4 eV one electron-hole ($e-h$) pair is formed per incident photon. The mean energy E_i required to produce an $e-h$ pair peaks at 4.4 eV for a photon energy around 6 eV. Above ~ 1.5 keV it assumes a constant value, 3.67 eV at room temperature. It is larger than the bandgap energy because momentum conservation requires excitation of lattice vibrations (phonons). For minimum-ionizing particles, the most probable charge deposition in a 300 μm thick silicon detector is about 3.5 fC (22000 electrons). Other typical ionization energies are 2.96 eV in Ge, 4.2 eV in GaAs, and 4.43 eV in CdTe.

Since both electronic and lattice excitations are involved, the variance in the number of charge carriers $N = E/E_i$ produced by an absorbed energy E is reduced by the Fano factor F (about 0.1 in Si and Ge). Thus, $\sigma_N = \sqrt{FN}$ and the energy resolution $\sigma_E/E = \sqrt{FE_i/E}$. However, the measured signal fluctuations are usually dominated by electronic noise or energy loss fluctuations in the detector.

The electronic noise contributions depend on the pulse shaping in the signal processing electronics, so the choice of the shaping time is critical (see Sec. 35.8).

A smaller bandgap would produce a larger signal and improve energy resolution, but the intrinsic resistance of the material is critical. Thermal excitation, given by the Fermi-Dirac distribution, promotes electrons into the conduction band, so the thermally excited carrier concentration increases exponentially with decreasing bandgaps. In pure Si the carrier concentration is $\sim 10^{10} \text{cm}^{-3}$ at 300 K, corresponding to a resistivity $\rho \approx 400 \text{k}\Omega \text{cm}$. In reality, crystal imperfections and minute impurity concentrations limit Si carrier concentrations to $\sim 10^{11} \text{cm}^{-3}$ at 300 K, corresponding to a resistivity $\rho \approx 40 \text{k}\Omega \text{cm}$. In practice, resistivities up to 20 $\text{k}\Omega \text{cm}$ are available, with mass production ranging from 5 to 10 $\text{k}\Omega \text{cm}$. Signal currents at keV scale energies are of order μA . However, for a resistivity of $10^4 \Omega \text{cm}$ a 300 μm thick sensor with 1cm^2 area would have a resistance of 300 Ω , so 30 V would lead to a current flow of 100 mA and a power dissipation of 3 W. On the other hand, high-quality single crystals of Si and Ge can be grown economically with suitably large volumes, so to mitigate the effect of resistivity one resorts to reverse-biased diode structures. Although this reduces the bias current relative to a resistive material, the thermally excited leakage current can still be excessive at room temperature, so Ge diodes are typically operated at liquid nitrogen temperature (77 K).

A major effort is to find high- Z materials with a bandgap that is sufficiently high to allow room-temperature operation while still providing good energy resolution. Compound semiconductors, *e.g.*, CdZnTe, can allow this, but typically suffer from charge collection problems, characterized by the product $\mu\tau$ of mobility and carrier lifetime. In Si and Ge $\mu\tau > 1 \text{cm}^2 \text{V}^{-1}$ for both electrons and holes, whereas in compound semiconductors it is in the range 10^{-3} – 10^{-8} . Since for holes $\mu\tau$ is typically an order of magnitude smaller than for electrons, detector configurations where the electron contribution to the charge signal dominates—*e.g.*, strip or pixel structures—can provide better performance.

35.7.2 Detector Configurations

A $p-n$ junction operated at reverse bias forms a sensitive region depleted of mobile charge and sets up an electric field that sweeps charge liberated by radiation to the electrodes. Detectors typically use an asymmetric structure, *e.g.*, a highly doped p electrode and a lightly doped n region, so that the depletion region extends predominantly into the lightly doped volume.

In a planar device the thickness of the depleted region is

$$W = \sqrt{2\epsilon(V + V_{bi})/Ne} = \sqrt{2\rho\mu\epsilon(V + V_{bi})} \quad (35.20)$$

where V = external bias voltage

V_{bi} = “built-in” voltage (≈ 0.5 V for resistivities typically used in Si detectors)

N = doping concentration

e = electronic charge

ϵ = dielectric constant = $11.9 \epsilon_0 \approx 1 \text{pF/cm}$ in Si

ρ = resistivity (typically 1–10 $\text{k}\Omega \text{cm}$ in Si)

μ = charge carrier mobility

= 1350 $\text{cm}^2 \text{V}^{-1} \text{s}^{-1}$ for electrons in Si

= 450 $\text{cm}^2 \text{V}^{-1} \text{s}^{-1}$ for holes in Si

In Si

$$W = 0.5[\mu\text{m}\sqrt{\Omega\text{-cm}\cdot\text{V}}] \times \sqrt{\rho(V + V_{bi})} \text{ for } n\text{-type Si, and}$$

$$W = 0.3[\mu\text{m}\sqrt{\Omega\text{-cm}\cdot\text{V}}] \times \sqrt{\rho(V + V_{bi})} \text{ for } p\text{-type Si.}$$

The conductive p and n regions together with the depleted volume form a capacitor with the capacitance per unit area

$$C = \epsilon/W \approx 1 [\text{pF/cm}] / W \text{ in Si.} \quad (35.21)$$

In strip and pixel detectors the capacitance is dominated by the fringing capacitance to neighboring electrodes. For example, the strip-to-strip Si fringing capacitance is ~ 1 – 1.5pF cm^{-1} of strip length at a strip pitch of 25–50 μm .

Large volume ($\sim 10^2$ – 10^3cm^3) Ge detectors are commonly configured as coaxial detectors, *e.g.*, a cylindrical n -type crystal with 5–10 cm diameter and 10 cm length with an inner 5–10 mm diameter n^+ electrode and an outer p^+ layer forming the diode junction. Ge can be grown with very low impurity levels, 10^9 – 10^{10}cm^{-3} (HPGe), so these large volumes can be depleted with several kV.

35.7.3 Signal Formation

The signal pulse shape depends on the instantaneous carrier velocity $v(x) = \mu E(x)$ and the electrode geometry, which determines the distribution of induced charge (*e.g.*, see [186], pp. 71–83). Charge collection time decreases with increasing bias voltage, and can be reduced further by operating the detector with “overbias,” *i.e.*, a bias voltage exceeding the value required to fully deplete the device. Note that in partial depletion the electric field goes to zero, whereas going beyond full depletion adds a constantly distributed field. The collection time is limited by velocity saturation at high fields (in Si approaching 10^7cm/s at $E > 10^4 \text{V/cm}$); at an average field of 10^4V/cm the collection time is about 15 ps/ μm for electrons and 30 ps/ μm for holes. In typical fully-depleted detectors 300 μm thick, electrons are collected within about 10 ns, and holes within about 25 ns.

Position resolution is limited by transverse diffusion during charge collection (typically 5 μm for 300 μm thickness) and by knock-on electrons. Resolutions of 2–4 μm (rms) have been obtained in beam tests. In magnetic fields, the Lorentz drift deflects the electron and hole trajectories and the detector must be tilted to reduce spatial spreading (see “Hall effect” in semiconductor textbooks).

Electrodes can be in the form of cm-scale pads, strips, or μm -scale pixels. Various readout structures have been developed for pixels, *e.g.*, CCDs, DEPFETs, monolithic pixel devices that integrate sensor and electronics (MAPS), and hybrid pixel devices that utilize separate sensors and readout ICs connected by two-dimensional arrays of solder bumps. For an overview and further discussion see Ref. [186].

In gamma ray spectroscopy ($E_\gamma > 10^2 \text{keV}$) Compton scattering dominates, so for a significant fraction of events the incident gamma energy is not completely absorbed, *i.e.*, the Compton scattered photon escapes from the detector and the energy deposited by the Compton electron is only a fraction of the total. Distinguishing multi-interaction events, *e.g.*, multiple Compton scatters with a final photoelectric absorption, from single Compton scatters allows background suppression. Since the individual interactions take place in different parts of the detector volume, these events can be distinguished by segmenting the outer electrode of a coaxial detector and analyzing the current pulse shapes. The

different collection times can be made more distinguishable by using “point” electrodes, where most of the signal is induced when charges are close to the electrode, similarly to strip or pixel detectors. Charge clusters arriving from different positions in the detector will arrive at different times and produce current pulses whose major components are separated in time. Point electrodes also reduce the electrode capacitance, which reduces electronic noise, but careful design is necessary to avoid low-field regions in the detector volume.

35.7.4 Radiation Damage

Radiation damage occurs through two basic mechanisms:

1. Bulk damage due to displacement of atoms from their lattice sites. This leads to increased leakage current, carrier trapping, and build-up of space charge that changes the required operating voltage. Displacement damage depends on the nonionizing energy loss and the energy imparted to the recoil atoms, which can initiate a chain of subsequent displacements, *i.e.*, damage clusters. Hence, it is critical to consider both particle type and energy.
2. Surface damage due to charge build-up in surface layers, which leads to increased surface leakage currents. In strip detectors the inter-strip isolation is affected. The effects of charge build-up are strongly dependent on the device structure and on fabrication details. Since the damage is proportional to the absorbed energy (when ionization dominates), the dose can be specified in rad (or Gray) independent of particle type.

The increase in reverse bias current due to bulk damage is $\Delta I_r = \alpha \Phi$ per unit volume, where Φ is the particle fluence and α the damage coefficient ($\alpha \approx 3 \times 10^{-17}$ A/cm for minimum ionizing protons and pions after long-term annealing; $\alpha \approx 2 \times 10^{-17}$ A/cm for 1 MeV neutrons). The reverse bias current depends strongly on temperature

$$\frac{I_R(T_2)}{I_R(T_1)} = \left(\frac{T_2}{T_1}\right)^2 \exp\left[-\frac{E}{2k} \left(\frac{T_1 - T_2}{T_1 T_2}\right)\right] \quad (35.22)$$

where $E = 1.2$ eV, so rather modest cooling can reduce the current substantially (~ 6 -fold current reduction in cooling from room temperature to 0°C).

Displacement damage forms acceptor-like states. These trap electrons, building up a negative space charge, which in turn requires an increase in the applied voltage to sweep signal charge through the detector thickness. This has the same effect as a change in resistivity, *i.e.*, the required voltage drops initially with fluence, until the positive and negative space charge balance and very little voltage is required to collect all signal charge. At larger fluences the negative space charge dominates, and the required operating voltage increases ($V \propto N$). The safe limit on operating voltage ultimately limits the detector lifetime. Strip detectors specifically designed for high voltages have been extensively operated at bias voltages >500 V. Since the effect of radiation damage depends on the electronic activity of defects, various techniques have been applied to neutralize the damage sites. For example, additional doping with oxygen can increase the allowable charged hadron fluence roughly three-fold [188]. Detectors with columnar electrodes normal to the surface can also extend operational lifetime [189]. The increase in leakage current with fluence, on the other hand, appears to be unaffected by resistivity and whether the material is *n* or *p*-type. At fluences beyond 10^{15} cm^{-2} decreased carrier lifetime becomes critical [190] [191].

Strip and pixel detectors have remained functional at fluences beyond 10^{15} cm^{-2} for minimum ionizing protons. At this damage level, charge loss due to recombination and trapping becomes significant and the high signal-to-noise ratio obtainable with low-capacitance pixel structures extends detector lifetime. The higher mobility of electrons makes them less sensitive to carrier lifetime than holes, so detector configurations that emphasize the electron contribution to the charge signal are advantageous, *e.g.*, n^+ strips or pixels on a *p*- or *n*-substrate. The occupancy of the defect charge states is strongly temperature dependent; competing processes can increase or decrease the re-

quired operating voltage. It is critical to choose the operating temperature judiciously (-10 to 0°C in typical collider detectors) and limit warm-up periods during maintenance. For a more detailed summary see [192] and the web-sites of the ROSE and RD50 collaborations at <http://RD48.web.cern.ch/rd48> and <http://RD50.web.cern.ch/rd50>. Materials engineering, *e.g.*, introducing oxygen interstitials, can improve certain aspects and is under investigation. At high fluences diamond is an alternative, but operates as an insulator rather than a reverse-biased diode.

Currently, the lifetime of detector systems is still limited by the detectors; in the electronics use of standard “deep submicron” CMOS fabrication processes with appropriately designed circuitry has increased the radiation resistance to fluences $> 10^{15}$ cm^{-2} of minimum ionizing protons or pions. For a comprehensive discussion of radiation effects see [193].

35.8 Low-noise electronics

Revised November 2013 by H. Spieler (LBNL).

Many detectors rely critically on low-noise electronics, either to improve energy resolution or to allow a low detection threshold. A typical detector front-end is shown in Fig. 35.18.

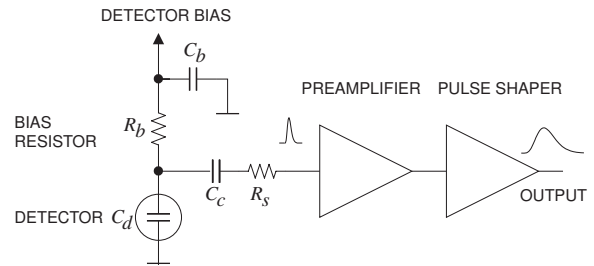


Figure 35.18: Typical detector front-end circuit.

The detector is represented by a capacitance C_d , a relevant model for most detectors. Bias voltage is applied through resistor R_b and the signal is coupled to the preamplifier through a blocking capacitor C_c . The series resistance R_s represents the sum of all resistances present in the input signal path, *e.g.* the electrode resistance, any input protection networks, and parasitic resistances in the input transistor. The preamplifier provides gain and feeds a pulse shaper, which tailors the overall frequency response to optimize signal-to-noise ratio while limiting the duration of the signal pulse to accommodate the signal pulse rate. Even if not explicitly stated, all amplifiers provide some form of pulse shaping due to their limited frequency response.

The equivalent circuit for the noise analysis (Fig. 35.19) includes both current and voltage noise sources. The leakage current of a semiconductor detector, for example, fluctuates due to continuous electron emission statistics. The statistical fluctuations in the charge measurement will scale with the square root of the total number of recorded charges, so this noise contribution increases with the width of the shaped output pulse. This “shot noise” i_{nd} is represented by a current noise generator in parallel with the detector. Resistors exhibit noise due to thermal velocity fluctuations of the charge carriers. This yields a constant noise power density vs. frequency, so increasing the bandwidth of the shaped output pulse, *i.e.* reducing the shaping time, will increase the noise. This noise source can be modeled either as a voltage or current generator. Generally, resistors shunting the input act as noise current sources and resistors in series with the input act as noise voltage sources (which is why some in the detector community refer to current and voltage noise as “parallel” and “series” noise). Since the bias resistor effectively shunts the input, as the capacitor C_b passes current fluctuations to ground, it acts as a current generator i_{nb} and its noise current has the same effect as the shot noise current from the detector. Any other shunt resistances can be incorporated in the same way. Conversely, the series resistor R_s acts as a voltage generator. The electronic noise of the amplifier is described fully by a combination of voltage and current sources at its input, shown as e_{na} and i_{na} .

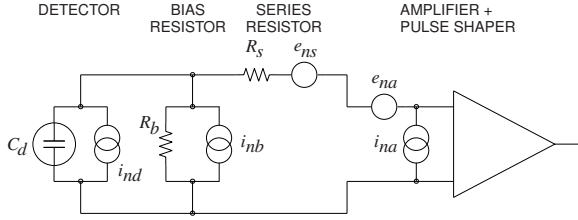


Figure 35.19: Equivalent circuit for noise analysis.

Shot noise and thermal noise have a “white” frequency distribution, *i.e.* the spectral power densities $dP_n/df \propto di_n^2/df \propto de_n^2/df$ are constant with the magnitudes

$$\begin{aligned} i_{nd}^2 &= 2eI_d, \\ i_{nb}^2 &= \frac{4kT}{R_b}, \\ e_{ns}^2 &= 4kTR_s, \end{aligned} \quad (35.23)$$

where e is the electronic charge, I_d the detector bias current, k the Boltzmann constant and T the temperature. Typical amplifier noise parameters e_{na} and i_{na} are of order $nV/\sqrt{\text{Hz}}$ and $pA/\sqrt{\text{Hz}}$. Trapping and detrapping processes in resistors, dielectrics and semiconductors can introduce additional fluctuations whose noise power frequently exhibits a $1/f$ spectrum. The spectral density of the $1/f$ noise voltage is

$$e_{nf}^2 = \frac{A_f}{f}, \quad (35.24)$$

where the noise coefficient A_f is device specific and of order 10^{-10} – 10^{-12} V^2 .

A fraction of the noise current flows through the detector capacitance, resulting in a frequency-dependent noise voltage $i_n/(\omega C_d)$, which is added to the noise voltage in the input circuit. Thus, the current noise contribution increases with lowering frequency, so its contribution increases with shaping pulse width. Since the individual noise contributions are random and uncorrelated, they add in quadrature. The total noise at the output of the pulse shaper is obtained by integrating over the full bandwidth of the system. Superimposed on repetitive detector signal pulses of constant magnitude, purely random noise produces a Gaussian signal distribution.

Since radiation detectors typically convert the deposited energy into charge, the system’s noise level is conveniently expressed as an equivalent noise charge Q_n , which is equal to the detector signal that yields a signal-to-noise ratio of one. The equivalent noise charge is commonly expressed in Coulombs, the corresponding number of electrons, or the equivalent deposited energy (eV). For a capacitive sensor

$$Q_n^2 = i_n^2 F_i T_S + e_n^2 F_v \frac{C^2}{T_S} + F_{vf} A_f C^2, \quad (35.25)$$

where C is the sum of all capacitances shunting the input, F_i , F_v , and F_{vf} depend on the shape of the pulse determined by the shaper and T_S is a characteristic time, for example, the peaking time of a semi-gaussian pulse or the sampling interval in a correlated double sampler. The form factors F_i, F_v are easily calculated

$$F_i = \frac{1}{2T_S} \int_{-\infty}^{\infty} [W(t)]^2 dt, \quad F_v = \frac{T_S}{2} \int_{-\infty}^{\infty} \left[\frac{dW(t)}{dt} \right]^2 dt, \quad (35.26)$$

where for time-invariant pulse-shaping $W(t)$ is simply the system’s impulse response (the output signal seen on an oscilloscope) for a short input pulse with the peak output signal normalized to unity. For more details see Refs. [194, 195] and [196, 197].

A pulse shaper formed by a single differentiator and integrator with equal time constants has $F_i = F_v = 0.9$ and $F_{vf} = 4$, in-

dependent of the shaping time constant. The overall noise bandwidth, however, depends on the time constant, *i.e.* the characteristic time T_S . The contribution from noise currents increases with shaping time, *i.e.* pulse duration, whereas the voltage noise decreases with increasing shaping time, *i.e.* reduced bandwidth. Noise with a $1/f$ spectrum depends only on the ratio of upper to lower cutoff frequencies (integrator to differentiator time constants), so for a given shaper topology the $1/f$ contribution to Q_n is independent of T_S . Furthermore, the contribution of noise voltage sources to Q_n increases with detector capacitance. Pulse shapers can be designed to reduce the effect of current noise, *e.g.*, mitigate radiation damage. Increasing pulse symmetry tends to decrease F_i and increase F_v (*e.g.*, to 0.45 and 1.0 for a shaper with one CR differentiator and four cascaded integrators). For the circuit shown in Fig. 35.19,

$$\begin{aligned} Q_n^2 &= \left(2eI_d + 4kT/R_b + i_{na}^2 \right) F_i T_S \\ &+ \left(4kTR_s + e_{na}^2 \right) F_v C_d^2 / T_S + F_{vf} A_f C_d^2. \end{aligned} \quad (35.27)$$

As the characteristic time T_S is changed, the total noise goes through a minimum, where the current and voltage contributions are equal. Fig. 35.20 shows a typical example. At short shaping times the voltage noise dominates, whereas at long shaping times the current noise takes over. The noise minimum is flattened by the presence of $1/f$ noise. Increasing the detector capacitance will increase the voltage noise and shift the noise minimum to longer shaping times.

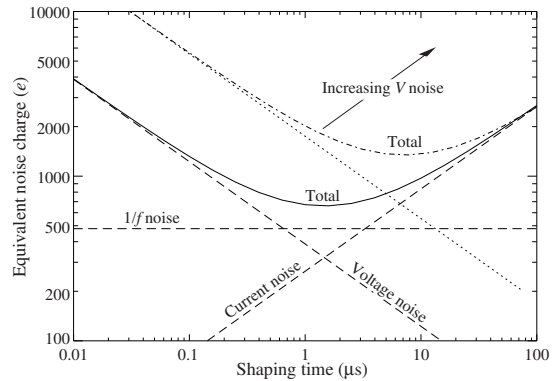


Figure 35.20: Equivalent noise charge *vs* shaping time. Changing the voltage or current noise contribution shifts the noise minimum. Increased voltage noise is shown as an example.

For quick estimates, one can use the following equation, which assumes an FET amplifier (negligible i_{na}) and a simple CR – RC shaper with time constants τ (equal to the peaking time):

$$\begin{aligned} (Q_n/e)^2 &= 12 \left[\frac{1}{\text{nA} \cdot \text{ns}} \right] I_d \tau + 6 \times 10^5 \left[\frac{\text{k}\Omega}{\text{ns}} \right] \frac{\tau}{R_b} \\ &+ 3.6 \times 10^4 \left[\frac{\text{ns}}{(\text{pF})^2 (\text{nV})^2 / \text{Hz}} \right] e_n^2 \frac{C^2}{\tau}. \end{aligned} \quad (35.28)$$

Noise is improved by reducing the detector capacitance and leakage current, judiciously selecting all resistances in the input circuit, and choosing the optimum shaping time constant. Another noise contribution to consider is that noise cross-couples from the neighboring front-ends in strip and pixel detectors through the inter-electrode capacitance.

The noise parameters of the amplifier depend primarily on the input device. In field effect transistors, the noise current contribution is very small, so reducing the detector leakage current and increasing the bias resistance will allow long shaping times with correspondingly lower noise. In bipolar transistors, the base current sets a lower bound on the noise current, so these devices are

best at short shaping times. In special cases where the noise of a transistor scales with geometry, *i.e.*, decreasing noise voltage with increasing input capacitance, the lowest noise is obtained when the input capacitance of the transistor is equal to the detector capacitance, albeit at the expense of power dissipation. Capacitive matching is useful with field-effect transistors, but not bipolar transistors. In bipolar transistors, the minimum obtainable noise is independent of shaping time, but only at the optimum collector current I_C , which does depend on shaping time.

$$Q_{n,\min}^2 = 4kT \frac{C}{\sqrt{\beta_{DC}}} \sqrt{F_i F_v} \quad \text{at} \quad I_c = \frac{kT}{e} C \sqrt{\beta_{DC}} \sqrt{\frac{F_v}{F_i}} \frac{1}{T_S}, \quad (35.29)$$

where β_{DC} is the DC current gain. For a CR - RC shaper and $\beta_{DC} = 100$,

$$Q_{n,\min}/e \approx 250 \sqrt{C/\text{pF}}. \quad (35.30)$$

Practical noise levels range from $\sim 1e$ for CCD's at long shaping times to $\sim 10^4 e$ in high-capacitance liquid argon calorimeters. Silicon strip detectors typically operate at $\sim 10^3$ electrons, whereas pixel detectors with fast readout provide noise of several hundred electrons.

In timing measurements, the slope-to-noise ratio must be optimized, rather than the signal-to-noise ratio alone, so the rise time t_r of the pulse is important. The "jitter" σ_t of the timing distribution is

$$\sigma_t = \frac{\sigma_n}{(dS/dt)_{S_T}} \approx \frac{t_r}{S/N}, \quad (35.31)$$

where σ_n is the rms noise and the derivative of the signal dS/dt is evaluated at the trigger level S_T . To increase dS/dt without incurring excessive noise, the amplifier bandwidth should match the rise-time of the detector signal. The 10 to 90% rise time of an amplifier with bandwidth f_U is $0.35/f_U$. For example, an oscilloscope with 350 MHz bandwidth has a 1 ns rise time. When amplifiers are cascaded, which is invariably necessary, the individual rise times add in quadrature.

$$t_r \approx \sqrt{t_{r1}^2 + t_{r2}^2 + \dots + t_{rn}^2}. \quad (35.32)$$

Increasing signal-to-noise ratio also improves time resolution, so minimizing the total capacitance at the input is also important. At high signal-to-noise ratios, the time jitter can be much smaller than the rise time. The timing distribution may shift with signal level ("walk"), but this can be corrected by various means, either in hardware or software [198].

The basic principles discussed above apply to both analog and digital signal processing. In digital signal processing the pulse shaper shown in Fig. 35.18 is replaced by an analog to digital converter (ADC) followed by a digital processor that determines the pulse shape. Digital signal processing allows great flexibility in implementing filtering functions. The software can be changed readily to adapt to a wide variety of operating conditions and it is possible to implement filters that are impractical or even impossible using analog circuitry. However, this comes at the expense of increased circuit complexity and increased demands on the ADC compared to analog shaping.

If the sampling rate of the ADC is too low, high frequency components will be transferred to lower frequencies ("aliasing"). The sampling rate of the ADC must be high enough to capture the maximum frequency component of the input signal. Apart from missing information on the fast components of the pulse, under-sampling introduces spurious artifacts. If the frequency range of the input signal is much greater, the noise at the higher frequencies will be transferred to lower frequencies and increase the noise level in the frequency range of pulses formed in the subsequent digital shaper. The Nyquist criterion states that the sampling frequency must be at least twice the maximum relevant input frequency. This requires that the bandwidth of the circuitry preceding the ADC must be limited. The most reliable technique is to insert a low-pass filter.

The digitization process also introduces inherent noise, since the voltage range ΔV corresponding to a minimum bit introduces

quasi-random fluctuations relative to the exact amplitude

$$\sigma_n = \frac{\Delta V}{\sqrt{12}}. \quad (35.33)$$

When the Nyquist condition is fulfilled the noise bandwidth Δf_n is spread nearly uniformly and extends to 1/2 the sampling frequency f_S , so the spectral noise density

$$e_n = \frac{\sigma_n}{\sqrt{\Delta f_n}} = \frac{\Delta V}{\sqrt{12}} \cdot \frac{1}{\sqrt{f_S/2}} = \frac{\Delta V}{\sqrt{6f_S}}. \quad (35.34)$$

Sampling at a higher frequency spreads the total noise over a larger frequency range, so oversampling can be used to increase the effective resolution. In practice, this quantization noise is increased by differential nonlinearity. Furthermore, the equivalent input noise of ADCs is often rather high, so the overall gain of the stages preceding the ADC must be sufficiently large for the preamplifier input noise to override.

When implemented properly, digital signal processing provides significant advantages in systems where the shape of detector signal pulses changes greatly, for example in large semiconductor detectors for gamma rays or in gaseous detectors (*e.g.* TPCs) where the duration of the current pulse varies with drift time, which can range over orders of magnitude. Where is analog signal processing best (most efficient)? In systems that require fast time response the high power requirements of high-speed ADCs are prohibitive. Systems that are not sensitive to pulse shape can use fixed shaper constants and rather simple filters, which can be either continuous or sampled. In high density systems that require small circuit area and low power (*e.g.* strip and pixel detectors), analog filtering often yields the required response and tends to be most efficient.

It is important to consider that additional noise is often introduced by external electronics, *e.g.* power supplies and digital systems. External noise can couple to the input. Often the "common grounding" allows additional noise current to couple to the current loop connecting the detector to the preamp. Recognizing additional noise sources and minimizing cross-coupling to the detector current loop is often important. Understanding basic physics and its practical effects is important in forming a broad view of the detector system and recognizing potential problems (*e.g.* modified data), rather than merely following standard recipes.

For a more detailed introduction to detector signal processing and electronics see Ref. [199] or the tutorial website <http://www-physics.lbl.gov/spieler>.

35.9 Calorimeters

35.9.1 Introduction

Revised August 2019 by D.E. Groom (LBNL).

A calorimeter is designed to measure a particle's (or jet's) energy and direction for an (ideally) contained electromagnetic (EM) or hadronic shower. The characteristic interaction distance for an electromagnetic interaction is the radiation length X_0 , which ranges from 13.8 g cm^{-2} in iron to 6.0 g cm^{-2} in uranium.⁴ Similarly, the characteristic nuclear interaction length λ_I varies from 132.1 g cm^{-2} (Fe) to 209 g cm^{-2} (U).⁵ In either case, a calorimeter must be many interaction lengths deep, where "many" is determined by physical size, cost, and other factors. EM calorimeters tend to be 15 – $30 X_0$ deep, while hadronic calorimeters are usually compromised at 5 – $8 \lambda_I$. In real experiments the shower begins in the EM calorimeter and then develops in a succession of different structures.

There is a premium on small λ_I/ρ and X_0/ρ (both with units of length). These quantities are shown for $Z > 20$ for the chemical elements in Fig. 35.21. For the hadronic case, metallic absorbers in the W–Au region are best, followed by U. Elements in the Ru–Pd region are not used since they are too rare and expensive.

⁴ $X_0 = 120 \text{ g cm}^{-2} Z^{-2/3}$ to better than 5% for $Z > 23$.

⁵ $\lambda_I = 37.8 \text{ g cm}^{-2} A^{0.312}$ to within 0.8% for $Z > 15$.
See pdg.lbl.gov/AtomicNuclearProperties for actual values.

Given cost considerations, Fe, Cu, or Pb are generally appropriate. For EM calorimeters high Z is preferred; tungsten and lead are popular choices.

These considerations are for *sampling calorimeters* consisting of metallic absorber sandwiched or (threaded) with an active material which generates signal. The active medium may be a scintillator, an ionizing noble liquid, a gas, silicon, or a Cherenkov radiator. The average interaction length is thus greater than that of the absorber alone, sometimes substantially so.

There are also *homogeneous calorimeters*, in which the entire volume is sensitive, *i.e.*, contributes signal. Homogeneous calorimeters may be built with inorganic heavy (high density, high $\langle Z \rangle$) scintillating crystals or non-scintillating Cherenkov radiators such as lead glass and lead fluoride. Scintillation light and/or ionization in noble liquids can be detected. Nuclear interaction lengths in inorganic crystals range from 17.8 cm (LuAlO₃) to 42.2 cm (NaI). Popular choices have been BGO with $\lambda_I = 22.3$ cm and $X_0 = 1.12$ cm, and PbWO₄ (20.3 cm and 0.89 cm). Properties of these and other commonly used inorganic crystal scintillators can be found in Table-35.4.

Homogeneous calorimeters at accelerators are usually electromagnetic, but in non-accelerator physics experiments the sensitive medium can be water or ice, scintillator, or the atmosphere itself.

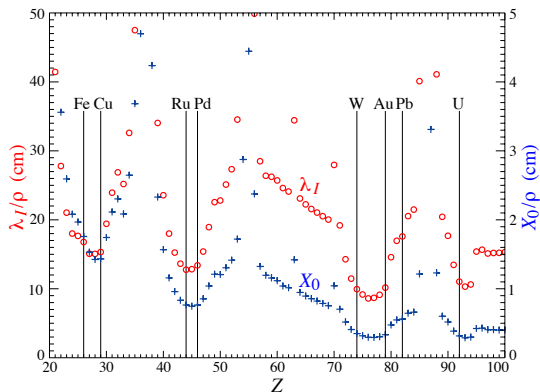


Figure 35.21: Nuclear interaction length λ_I/ρ (circles) and radiation length X_0/ρ (+) in cm for the chemical elements with $Z > 20$ and $\lambda_I < 50$ cm.

Comprehensive tables of particle-physics calorimeters are given as Appendix C in Ref. [200].

35.9.2 Electromagnetic calorimeters

Revised August 2019 by C.L. Woody (BNL) and R.-Y. Zhu (HEP California Inst. of Technology).

The development of electromagnetic showers is discussed in the section on “Passage of Particles Through Matter” (Sec. 34 of this *Review*). Formulae are given which approximately describe average showers, but since the physics of electromagnetic showers is well understood, a detailed and reliable Monte Carlo simulation is possible. EGS4 [201] and GEANT [202] have emerged as the standards.

Electromagnetic calorimeters are devices that are designed to measure the total energy of electrons and photons by total absorption. They come in two general categories: homogeneous and sampling. In a homogeneous calorimeter, all of the particle’s energy is deposited in the active detector volume and is used to produce a measurable signal (either scintillation light, Cherenkov light or charge). Homogeneous electromagnetic calorimeters are typically constructed using high density, high Z inorganic scintillating crystals such as BaF₂, BGO, CsI, CsI(Tl), LYSO, NaI(Tl) and PWO, non-scintillating Cherenkov radiators such as lead glass and lead fluoride (PbF₂), or ionizing noble liquids such as liquid argon, liquid krypton or liquid xenon. The properties of some commonly used inorganic crystal scintillators can be found in Table-35.4. Total absorption homogeneous calorimeters such as those built with heavy crystal scintillators provide the best energy resolution for

measuring electromagnetic showers and are generally used when the best possible performance is required, particularly at lower energies.

A sampling calorimeter consists of an active medium which generates a signal and a passive medium which functions as an absorber. In this case, most of the particle’s energy is deposited in the absorber and only a fraction of the energy is detected in the active medium. The ratio of energy in the sampling medium to the total energy in calorimeter is called the sampling fraction. The active medium may be a scintillator, an ionizing noble liquid, a semiconductor, or a gas ionization detector. The absorber is typically a heavy metal with a high Z such as lead, tungsten, iron, copper, or depleted uranium. The active material is interspersed with the passive absorber in a variety of ways, *e.g.* by using alternating plates of active material and absorber or embedding the active material, such as scintillating fibers, into the absorber. The main difficulty in this approach is extracting the signal from the active material. This can be done using a so-called “spaghetti” design, where scintillating fibers are brought to the front or back of the detector and read out. This can also be done with either wavelength shifting plates or fibers, such as in a so-called “shashlik” design where wavelength shifting fibers run through the stack of alternating scintillator and absorber plates and are read out at one end, or embedding wavelength shifting fibers in the scintillating plates which are then brought out to the edges or back of the detector and read out. For ionization detectors, there is also an “accordion” design where the absorber plates are folded into an accordion shape along with interspersed electrodes to collect the ionization charge [203]. While these readout schemes are generally more complicated than those for homogeneous calorimeters, the sampling calorimeter design allows the construction of large calorimeters at much lower cost than homogeneous calorimeters.

The energy resolution σ_E/E of a calorimeter can be parameterized as $a/\sqrt{E} \oplus b \oplus c/E$, where \oplus represents addition in quadrature and E is in GeV. The stochastic term a represents statistics-related fluctuations such as intrinsic shower fluctuations, photoelectron statistics, dead material at the front of the calorimeter, and sampling fluctuations for minimum ionizing particles. For a fixed number of radiation lengths, the stochastic term a for a sampling calorimeter is expected to be proportional to $\sqrt{t/f}$, where t is plate thickness and f is sampling fraction [204–206]. The stochastic term a is typically on the order of a few percent level for a homogeneous calorimeter, and is generally in the range of 10 to 20% for sampling calorimeters, depending on the sampling fraction.

The main contributions to the systematic, or constant, term b are detector non-uniformity and calibration uncertainties. In the case of hadronic cascades discussed below, non-compensation also contributes deviations from \sqrt{E} scaling. Another important contribution to the energy resolution of calorimeters that are used in high radiation environments such as high luminosity colliders is radiation damage of the active medium. Radiation damage can induce optical absorption in scintillating materials which reduces the measured light output and produces non-uniformities in light collection. This can be mitigated by developing radiation-hard active media [68], by reducing the signal path length [207] and by frequent *in situ* calibration and monitoring [67, 206]. With effort, the constant term b can be reduced to below one percent. The term c is due mainly to electronic noise summed over the readout channels required to measure the shower energy (typically a few Molière radii).

The position resolution depends on the effective Molière radius and the transverse granularity of the calorimeter. Like the energy resolution, it can be factored as $a/\sqrt{E} \oplus b$, where a is the stochastic term, typically on the order a few mm to 20 mm, and b can be as small as a fraction of mm for a dense calorimeter with fine granularity. Electromagnetic calorimeters may also provide directionality measurements for electrons and photons. This is particularly important for photon-related physics when there are uncertainties in the event origin, since photons are not detected by the tracking system of the overall experiment. The typical photon angular resolution is about $45 \text{ mrad}/\sqrt{E}$, which can be achieved by implementing longitudinal segmentation [203] for a

Table 35.8: Resolution of typical electromagnetic calorimeters. E is in GeV.

Technology (Experiment)	Depth	Energy resolution	Date
NaI(Tl) (Crystal Ball)	$20X_0$	$2.7\%/E^{1/4}$	1983
$\text{Bi}_4\text{Ge}_3\text{O}_{12}$ (BGO) (L3)	$22X_0$	$2\%/ \sqrt{E} \oplus 0.7\%$	1993
CsI (KTeV)	$27X_0$	$2\%/ \sqrt{E} \oplus 0.45\%$	1996
CsI(Tl) (BaBar)	$16\text{--}18X_0$	$2.3\%/E^{1/4} \oplus 1.4\%$	1999
CsI(Tl) (BELLE)	$16X_0$	1.7% for $E_\gamma > 3.5$ GeV	1998
CsI(Tl) (BES III)	$15X_0$	2.5% for $E_\gamma = 1$ GeV	2010
PbWO_4 (CMS)	$25X_0$	$3\%/ \sqrt{E} \oplus 0.5\% \oplus 0.2/E$	1997
PbWO_4 (ALICE)	$19X_0$	$3.6\%/ \sqrt{E} \oplus 1.2\%$	2008
Lead glass (OPAL)	$20.5X_0$	$5\%/ \sqrt{E}$	1990
Liquid Kr (NA48)	$27X_0$	$3.2\%/ \sqrt{E} \oplus 0.42\% \oplus 0.09/E$	1998
Scintillator/depleted U (ZEUS)	$20\text{--}30X_0$	$18\%/ \sqrt{E}$	1988
Scintillator/Pb (CDF)	$18X_0$	$13.5\%/ \sqrt{E}$	1988
Scintillator fiber/Pb spaghetti (KLOE)	$15X_0$	$5.7\%/ \sqrt{E} \oplus 0.6\%$	1995
Liquid Ar/Pb (NA31)	$27X_0$	$7.5\%/ \sqrt{E} \oplus 0.5\% \oplus 0.1/E$	1988
Liquid Ar/Pb (SLD)	$21X_0$	$8\%/ \sqrt{E}$	1993
Liquid Ar/Pb (H1)	$20\text{--}30X_0$	$12\%/ \sqrt{E} \oplus 1\%$	1998
Liquid Ar/depl. U (DØ)	$20.5X_0$	$16\%/ \sqrt{E} \oplus 0.3\% \oplus 0.3/E$	1993
Liquid Ar/Pb accordion (ATLAS)	$25X_0$	$10\%/ \sqrt{E} \oplus 0.4\% \oplus 0.3/E$	1996

sampling calorimeter or by adding a preshower detector [208] for a homogeneous calorimeter without longitudinal segmentation.

There have been many electromagnetic calorimeters built and used in particle physics experiments for a variety of applications. Table-35.8 provides a short list of the major ones used in some of the larger experiments. Also listed are calorimeter depths in radiation lengths (X_0) and the achieved energy resolution. Whenever possible, the performance of the calorimeters *in situ* are quoted, which is usually in good agreement with prototype test beam results as well as EGS or GEANT simulations, provided that all systematic effects are properly included. Details about detector design and performance can be found in Appendix C of reference [206] and Proceedings of the International Conference series on Calorimetry in High Energy Physics.

35.9.3 Hadronic calorimeters

Revised August 2019 by D.E. Groom (LBNL).

Hadronic calorimetry [200, 209] is considerably more difficult than electromagnetic (EM) calorimetry due to the large differences in the character of energy deposition processes, the length of shower development, and the lumpy character of the depositions. Nuclear disassociation results in undetectable energy loss. For the same cascade containment fraction discussed in the previous section, the calorimeter would need to be ~ 10 times deeper. Electromagnetic energy deposit from the decay of π^0 's produced in the cascade is usually detected with greater efficiency than are the hadronic parts of the cascade, themselves subject to large fluctuations in neutron production, undetectable energy loss to nuclear disassociation, and other effects [200].

Most large hadron calorimeters are parts of large 4π detectors at colliding beam facilities. These have been sampling calorimeters: plates of absorber (Fe, Pb, U, or occasionally Cu or W) alternating with plastic scintillators (plates, tiles, bars, fibers), crystals, silicon, liquid argon (LAr), or gaseous detectors. The ionization is measured directly, or via scintillation or Cherenkov light observed by conventional photomultipliers (PMT's), photodiodes or silicon photomultipliers (SiPM's). Wavelength-shifting fibers are often used to solve difficult problems of geometry and light collection uniformity. There are as many variants of these schemes as there are calorimeters, including variations in geometry of the absorber and sensors, *e.g.*, scintillating fibers threading an absorber [210], and the "accordion" LAr detector [211]. The latter has zig-zag absorber plates to minimize channeling effects; the calorimeter is hermetic (no cracks), and plates are oriented so that cascades cross the same plate repeatedly. Another departure

from the traditional sandwich structure is the LAr-tube design shown in Fig. 35.22(a) [212].

Ideally the calorimeter is segmented in ϕ and θ (or $\eta = -\ln \tan(\theta/2)$). An example, a wedge of the ATLAS central barrel calorimeter, is shown in Fig. 35.22(b) [213].

Calorimeters based on Cherenkov light detection are more usual in EM calorimeters, since comparatively little Cherenkov radiation is produced by the hadronic fraction of a shower. An important exception is the radiation-hard forward calorimeter in CMS, with iron absorber and quartz fibers read out by PMT's, and Cherenkov light detection is an essential half of dual-readout calorimetry.

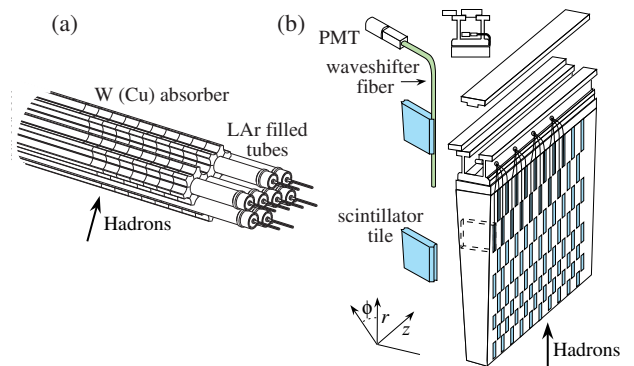


Figure 35.22: (a) ATLAS forward hadronic calorimeter structure (FCal2, 3) [212]. Tubes containing LAr are embedded in a mainly tungsten matrix. (b) ATLAS central calorimeter wedge; iron with plastic scintillator tile with wavelength-shifting fiber read-out [213].

The SICAPO collaboration has demonstrated the possibility of operating hadronic calorimeters using silicon sensors [214]. These satisfy the requirements required by the new generation of experiments, including compactness, high granularity, radiation hardness [215, 216], fast charge collection, and compensation via local hardening effects [217]. They are being studied for ILC detectors, and are part of the CMS HCAL upgrade.

High-granularity calorimeters play an increasingly important role. Greater segmentation has accordingly been an important part of LHC detector upgrades. For some time, the CALICE collaboration has built and tested an increasingly sophisticated

series of “tracking” calorimeters with a highly granular readout [218]. Most are EM (ECAL) and hadronic (HCAL) calorimeters with analog readout (scintillator plates), but digital (Sec. 35.6.7) and semidigital (Sec. 35.6.4) readouts are also explored. A recent example is a SiPM-on-tile readout HCAL with $> 22,000$ channels [219].

Much of the following discussion assumes an idealized calorimeter, with the same structure throughout and without leakage.

In an inelastic hadronic collision a significant fraction f_{em} of the energy is removed from further hadronic interaction by the production of secondary π^0/η 's, whose decay photons generate high-energy electromagnetic showers. Charged secondaries (π^\pm, p, \dots) deposit energy via ionization and excitation, but also interact with nuclei, producing evaporation neutrons, spallation protons and neutrons, and heavier spallation fragments. The charged collision products produce detectable ionization, as do the showering γ -rays from the prompt de-excitation of highly excited nuclei. The recoiling nuclei generate little or no detectable signal. The neutrons lose kinetic energy in elastic collisions, thermalize on a time scale of several μ s, and are captured, with the production of more γ -rays—usually outside the acceptance gate of the electronics. Between endothermic spallation losses, nuclear recoils, and late neutron capture, a significant fraction of the hadronic energy (20%–40%, depending on the absorber and energy of the incident particle) is used to overcome nuclear binding energies and is therefore lost or “invisible.”

In contrast to EM showers, hadronic cascade processes are characterized by the production of relatively few high-energy particles. The lost energy and f_{em} are highly variable from event to event. Unless there is event-by-event knowledge of both the EM fraction and the invisible energy loss, the energy resolution of a hadron calorimeter is significantly worse than that of its EM counterpart.

The efficiency e with which EM deposit is detected varies from event to event, but because of the large multiplicity in EM showers the variation is small. In contrast, because a variable fraction of the hadronic energy deposit is detectable, the efficiency h with which hadronic energy is detected is subject to considerably larger fluctuations. It thus makes sense to consider the ratio h/e as a stochastic variable.

Most energy deposit is by very low-energy electrons and charged hadrons. Because so many generations are involved in a high-energy cascade, the hadron spectra in a given material are essentially independent of energy except for overall normalization [220,221]. For this reason $\langle h/e \rangle$ is a robust concept, independently of hadron energy and species.

If the detection efficiency for the EM sector is e and that for the hadronic sector is h , then the ratio of the mean response to a pion relative to that for an electron is

$$\langle \pi/e \rangle = \langle f_{em} \rangle + \langle f_h \rangle \langle h/e \rangle = 1 - (1 - \langle h/e \rangle) \langle f_h \rangle \quad (35.35)$$

It has been shown by a simple induction argument and verified by simulation and experiment that the decrease in the average value of the hadronic energy fraction $\langle f_h \rangle = 1 - \langle f_{em} \rangle$ as the projectile energy E increases is fairly well described by the power law [220,221]

$$\langle f_h \rangle \approx (E/E_0)^{m-1} \quad (\text{for } E > E_0), \quad (35.36)$$

at least up to a few hundred GeV. The exponent m depends logarithmically on the mean multiplicity and the mean fractional loss to π^0 production in a single interaction. It is in the range 0.80–0.87, depending on the composition of the absorber. The scale factor E_0 , roughly the energy for the onset of inelastic collisions, is 1 GeV or a little less for incident pions [221]. Both m and E_0 must be obtained experimentally for a given calorimeter configuration.

Only the product $(1 - \langle h/e \rangle)E_0^{1-m}$ can be obtained by measuring $\langle \pi/e \rangle$ as a function of energy. Since $1 - m$ is small and $E_0 \approx 1$ GeV for pion-induced cascades, this fact is usually ignored and $\langle h/e \rangle$ or the usual $\langle e/h \rangle$ is reported.

In a hadron-nucleus collision a large fraction of the incident energy is carried by a “leading particle” with the same quark content as the incident hadron. If the projectile is a charged pion, the

leading particle is usually a pion, which can be neutral and hence contributes to the EM sector. This is not true for incident protons. The result is an increased mean hadronic fraction for incident protons: The power m is the same, but $E_0 \approx 2.6$ GeV [221–224]. Data obtained by Akhurin *et al.* [223] with a quartz-fiber calorimeter indicate that proton-induced showers are shorter than pion-induced showers, and the resolution is substantially better. The “leading particle” effect evidently persists as the shower develops.

By definition, $0 \leq f_{em} \leq 1$. With increasing energy $\langle f_{em} \rangle \rightarrow 1$, while its variance, $\sigma_{f_{em}}^2$, decreases slowly [222]. For $\langle h/e \rangle \neq 1$ (*noncompensation*), fluctuations in f_{em} significantly contribute to or even dominate the resolution. Since the f_{em} distribution has a high-energy tail, the calorimeter response is non-Gaussian with a high-energy tail if $\langle h/e \rangle < 1$. Noncompensation thus seriously degrades resolution and produces a nonlinear response. It is clearly desirable to *compensate* the response, *i.e.*, to design the calorimeter such that $\langle h/e \rangle = 1$. *This is possible only with a sampling calorimeter*, where several variables can be chosen or tuned:

1. Decrease the EM sensitivity. EM cross sections increase with Z ,^{||} and most of the energy in an EM shower is deposited by low-energy electrons. A disproportionate fraction of the EM energy is thus deposited in the higher- Z absorber. Lower- Z cladding, such as the steel cladding on ZEUS U plates, preferentially absorbs low-energy γ 's in EM showers and thus also lowers the electronic response. The degree of EM signal suppression can be tuned by varying the sensor/absorber thickness ratio.

Hardening: The SICIPO collaboration has shown that the response of a W (or Pb) plate EM calorimeter is reduced by low- Z absorbers (G10) in contact with the silicon sensors. This is understood to result of the G10 absorbing electrons below the critical energy (E_c) in the W or Pb [225]. They also showed that interspersing low- Z layers (Fe, with large E_c) with high- Z layers (Pb, low E_c) dramatically modified the response of a hadron calorimeter. In either case, ionization energy losses begin to dominate below E_c . The energy spectrum of shower electrons becomes softer when moving from the Pb to the Fe, with the Fe producing the same filtering effect as G10. $\langle e/h \rangle$ ranging from 0.89 to 1.11 was obtained with various combinations of Pb and Fe plates [217].

2. *Software compensation* provides another approach to decreasing the EM sensitivity. It takes advantage of the fact that in heavy absorbers the radiation length is much smaller than the nuclear interaction length. As a result, showers from π^0/η decay are fairly local. Given sufficient segmentation, the contribution of these “hot spots” can be given lower weight in summing the energy deposit, effectively decreasing f_{em} . Software compensation was first exploited in the CDMS detector [226]. Even with its few longitudinal segments, resolution was substantially improved for single particles of known high energy. It was further developed for the H1 [227] and ATLAS [228] detectors. Three-dimensional granularity considerably extends these techniques. For example, a 2007 CERN SPS study with the CALICE analog scintillator-steel hadronic calorimeter (AHCAL, with 7608 scintillator cells) obtained a 12–25% resolution improvement for 10–80 GeV incident π^\pm 's [229,230]. Jets are more problematical, in part because of the nonlinear response to the large fraction of their particles with $E < 10$ GeV.
3. Increase the hadronic sensitivity. The abundant neutrons produced in the cascade have large n - p elastic scattering cross sections, so that low-energy scattered protons are produced in hydrogenous sampling materials such as butane-filled proportional counters or plastic scintillator. The number of spallation neutrons is highly correlated with missing energy. (The maximal fractional energy loss when a neutron scatters from a nucleus with mass number A is $4A/(1+A)^2$.) The down side in the scintillator case is that the signal from a highly-ionizing stopping proton can be reduced by as much as 90%

^{||}The asymptotic pair-production cross section scales roughly as $Z^{0.75}$, and $|dE/dx|$ slowly decreases with increasing Z .

by recombination and quenching (Birks' Law, Eq. (35.2)).

4. Fabjan and Willis proposed that the additional signal generated in the aftermath of fission in ^{238}U absorber plates should compensate nuclear fluctuations [231]. The production of fission fragments due to fast n capture was later observed [232]. However, while a very large amount of energy is released, it is mostly carried by low-velocity, very highly ionizing fission fragments produce very little observable signal because of recombination and quenching. In fact much of the compensation observed with the ZEUS and DØ ^{238}U /scintillator calorimeters was mainly the result of mechanisms 1 and 3 above.

Motivated very much by the work of Brau, Gabriel, Brückmann, and Wigmans in 1985–87 [233–236], several groups explored a variety of compensation mechanisms and built calorimeters which were very nearly compensating. The degree of compensation was sensitive to the acceptance gate width, and so could be somewhat further tuned. Examples are given in Table 35.9.

Another approach to compensation is provided by a *dual-readout calorimeter*, in which the signal is sensed by two readout systems with highly contrasting $\langle h/e \rangle$. The concept, proposed by Mockett in 1983 [246], has been explored by a number of others since. Winn and Worstell, for example, proposed using an “orange” scintillator, observing the ionization contribution through an orange filter and the Cherenkov contribution through a blue filter [247]. The dual-readout technique was implemented by the DREAM collaboration in the late 1990’s [248,249]. The test beam calorimeter consisted of copper tubes, each filled with scintillator and quartz fibers. If the two signals C and S (quartz and scintillator) are both normalized to electron response, then for each event Eq. (35.35)

$$\begin{aligned} C &= E[f_{em} + \langle h/e \rangle_C |C(1 - f_{em})] \\ S &= E[f_{em} + \langle h/e \rangle_S |S(1 - f_{em})] . \end{aligned} \quad (35.37)$$

On a scatter plot of C vs S (or C/E vs S/E), events scatter about a line-segment locus, as shown in Fig. 35.23 [222]. With increasing energy the distribution moves upward along the locus and becomes tighter. Equations 35.37 are linear in $1/E$ and f_{em} , and are easily solved to obtain estimators of the *corrected* energy and f_{em} for each event. Both are subject to resolution effects, but contributions due to fluctuations in f_{em} are eliminated. The solution for the corrected energy is given by [222]:

$$E = \frac{\xi S - C}{\xi - 1} , \text{ where } \xi = \frac{1 - \langle h/e \rangle_C}{1 - \langle h/e \rangle_S} . \quad (35.38)$$

Here ξ is the energy-independent slope of the event locus on a plot of C vs S . It can be found either from the fitted slope or by measuring π/e as a function of E . The slope ξ must be as far from unity as possible to optimize resolution, which in practical terms means that the scintillator readout of the calorimeter must be as compensating as possible [250].

The fractional energy resolution in an ideal calorimeter can be represented by

$$\frac{\sigma}{E} = \frac{a_1(E)}{\sqrt{E}} \oplus [1 - \langle h/e \rangle | \sigma_{f_{em}}] , \quad (35.39)$$

where $\sigma_{f_{em}}^2$ is the variance of f_{em} [222]. The coefficient a_1 is expected to have mild energy dependence for a number of reasons. For example, the sampling variance contribution to a_1 is $(\pi/e)E$ rather than E . $\sigma_{f_{em}}$ slowly decreases with increasing energy, as discussed above. Usually a plot of $(\sigma/E)^2$ vs $1/E$ is well described by a straight line (constant a_1) with a finite intercept—the right term in Eq. (35.39), is called “the constant term.” Precise data show the slight downturn of a_1 [210,222].

Although the usually-dominant contribution of the f_{em} distribution to the resolution can be minimized by compensation or the use of dual calorimetry, there remain significant contributions to the resolution:

1. Incomplete corrections for leakage, differences in light collection efficiency, and electronics calibration.

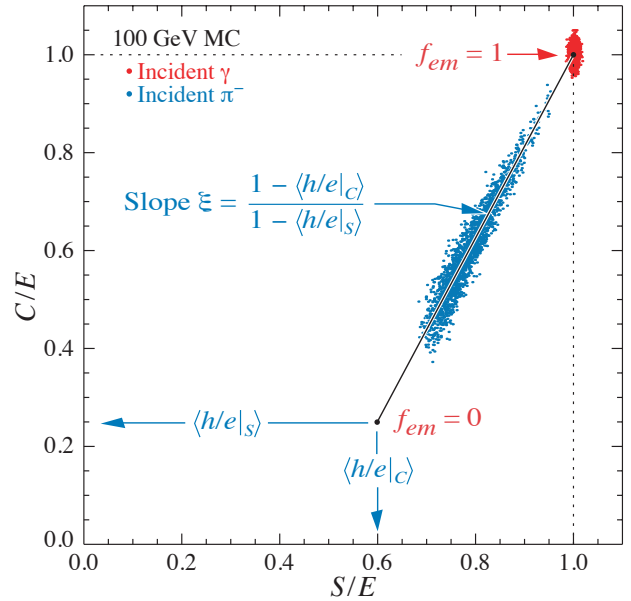


Figure 35.23: Scatter plot of Monte Carlo C/E (Cherenkov) vs S/E (scintillator) signals for individual events in a dual readout calorimeter. Hadronic events are shown in blue, and scatter about the indicated event locus. Electromagnetic events cluster about $(C/E, S/E) = (1,1)$. In this case worse resolution (fewer p.e.’s) was assumed for the Cherenkov events, leading to the “elliptical” distribution.

2. Readout transducer shot noise (usually photoelectron statistics), plus electronic noise.
3. Sampling fluctuations. Only a small part of the energy deposit takes place in the scintillator or other sensor, and that fraction is subject to large fluctuations. It depends on the sensor/absorber ratio, often chosen to achieve compensation. If this is the case, it is small in the scint/Fe and somewhat more forgiving in the scint/U case.
4. Intrinsic fluctuations. The many ways ionization can be produced in a hadronic shower have different detection efficiencies and are subject to stochastic fluctuations. In particular, a very large fraction of the hadronic energy is “invisible.” The lost fraction depends on the readout—it will be greater for a Cherenkov readout, less for an organic scintillator readout.

Except in a sampling calorimeter especially designed for the purpose, sampling and intrinsic resolution contributions cannot be separated. This may have been best studied by Drews *et al.* [240], who used a calorimeter in which even- and odd-numbered scintillators were separately read out. Sums and differences of the variances were used to separate sampling and intrinsic contributions.

The above discussion concerns stand-alone hadron calorimeters that exist only in test beams. In a collider experiment there is a central tracker in a magnetic field, then an EM calorimeter, a sequence of calorimeters, and finally a possible muon detector. Particle flow analysis uses all available information in analyzing the event [251,252]. The tracker supplies the charged particle positions and momenta, the EM calorimeter the γ energy (and some hadronic energy), and the hadron calorimeter the energy deposit from neutral hadrons as well as the most of the energy deposit from the particles observed in the tracker. Good calorimeter granularity is essential. Simulations via GEANT4 [253,254] support the analysis as well as the development of new analysis algorithms.

Despite the central importance of particle flow analysis, further discussion is beyond the scope of this specialized description of hadron calorimeters.

As a last topic, we discuss the mean spatial distribution of

Table 35.9: Examples of near-compensating sampling hadron calorimeters. For our present purposes some calorimeter structure variation and “constant terms” in the fitted resolution have been ignored.

Calorimeter	Passive	Active	Resolution	$\langle e/h \rangle$	Reference
(Akesson <i>et al.</i>)	U, U/Cu (3/5 m)	Scint (2.5mm)	$36\%/\sqrt{E}$	1.11	[237]
HELIOS	U (3 mm)	Scint (2.5 mm)	$34\%/\sqrt{E}$	1.016 ± 0.006	[238]
(Drews <i>et al.</i>)	Pb (10 mm)	Scint (2.5 mm)	$44\%/\sqrt{E}$	1.10 ± 0.01	[239, 240]
(Drews <i>et al.</i>)	U (3.2 mm)	Scint (3.0 mm)	$36\%/\sqrt{E}$	1.02 ± 0.01	[240]
WA80	U (3 mm)	Scint (3 mm)	$67\%/\sqrt{E}$	1.12	[241]
ZEUS FCAL	U (3.0/3.2 mm)	Scint (2,5/3.0 mm)	$35\%/\sqrt{E}$	0.97	[242, 243]
SPACAL	Pb (4× scint vol)	1 mm scint fibers	$30\%/\sqrt{E}$	1.15 ± 0.02	[244]
SICAPO	Fe/Pb	Si		$1.11-0.89^*$	[217]
DØ	U (6 mm) [†]	LAr (2 × 2.3)	$44\%/\sqrt{E}$	1.08	[245]

* SICAPO: Various Fe/Pb configurations, G10 plates next to Si detectors.
[†] DØ: 1 mm G10 between LAr gaps may help compensation.

hadronic cascades. After the first interaction of the incident hadron, the average longitudinal distribution rises to a smooth peak whose position increases slowly with energy. The distribution becomes nearly exponential after several interaction lengths. Examples from the CDHS magnetized iron-scintillator sandwich calorimeter test beam calibration runs [255] and the ATLAS TileCal results [224] are shown in Fig. 35.24. Proton-induced cascades are somewhat shorter and broader than pion-induced cascades [224]. A gamma distribution fairly well describes the longitudinal development of an EM shower, as discussed in Sec. 34.5. Following this logic, Bock *et al.* suggested that the profile of a hadronic cascade could be fitted by the sum of two Γ distributions, one with a characteristic length X_0 and the other with length λ_I [256, 257]. Fits to this 4-parameter function are commonly used, *e.g.*, by the ATLAS TileCal collaboration [224]. If the interaction point is not known (the usual case), the distribution must be convoluted with an exponential in the interaction length of the incident particle. Adragna *et al.* give an analytic form for the convoluted function [224].

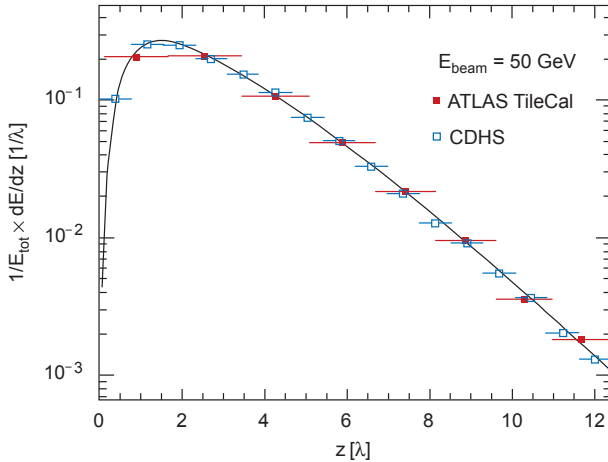


Figure 35.24: Mean profiles of π^+ (mostly) induced cascades in the CDHS neutrino detector [255] and in the ATLAS tile calorimeter [224]. Measurements are front of the calorimeter, and so are convoluted with the first interaction distance.

The transverse energy deposit is characterized by a central core dominated by EM cascades, together with a wide “skirt” produced by wide-angle hadronic interactions [258].

While the average distributions might be useful in designing a calorimeter, they have little meaning for individual events, whose distributions are extremely variable because of the small number of particles involved early in the cascade.

Particle identification, primarily $e-\pi$ discrimination, is accomplished in most calorimeters by observing the depth development. An EM shower is mostly contained in $15X_0$ while a

hadronic shower takes about $4\lambda_I$. In high- A absorbers such as Pb, $X_0/\lambda_I \sim 0.03$. In a fiber calorimeter, such as the RD52 dual-readout calorimeter, $e-\pi$ discrimination is achieved by differences in the Cerenkov and scintillation signals, lateral spread, and timing differences, ultimately achieving about 500:1 discrimination [259].

35.9.4 Free electron drift velocities in liquid ionization chambers

Revised August 2009 by W. Walkowiak (Siegen U.).

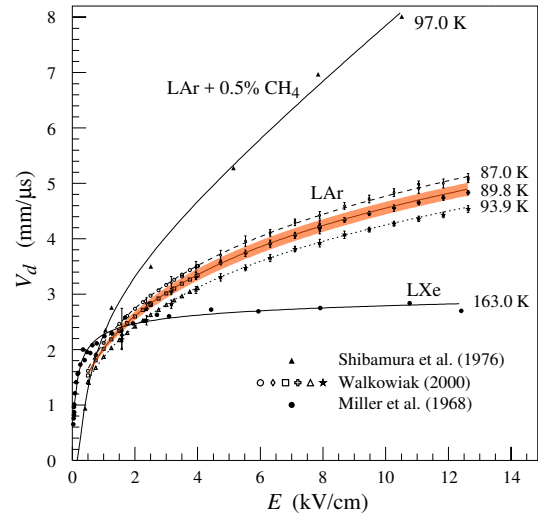


Figure 35.25: Drift velocity of free electrons as a function of electric field strength for LAr [260], LAr + 0.5% CH₄ [261] and LXe [262]. The average temperatures of the liquids are indicated. Results of a fit to an empirical function [263] are superimposed. In case of LAr at 91 K the error band for the global fit [260] including statistical and systematic errors as well as correlations of the data points is given. Only statistical errors are shown for the individual LAr data points.

Drift velocities of free electrons in LAr [260] are given as a function of electric field strength for different temperatures of the medium in Fig. 35.25. The drift velocities in LAr have been measured using a double-gridded drift chamber with electrons produced by a laser pulse on a gold-plated cathode. The average temperature gradient of the drift velocity of the free electrons in LAr is described [260] by

$$\frac{\Delta v_d}{\Delta T v_d} = (-1.72 \pm 0.08) \%/\text{K}. \quad (35.40)$$

Previous measurements [261, 262, 264, 265] range from 13% higher [262] to 18% lower [264] than these measurements. They

used different techniques and show drift velocities for free electrons which cannot be explained by the temperature dependence mentioned above.

Drift velocities of free electrons in LXe [261] as a function of electric field strength are also displayed in Fig. 35.25. The drift velocity saturates for $|E| > 3$ kV/cm, and decreases with increasing temperature for LXe as well as measured e.g. by [266].

The addition of small concentrations of other molecules like N_2 , H_2 and CH_4 in solution to the liquid typically increases the drift velocities of free electrons above the saturation value [261, 264], see example for CH_4 admixture to LAr in Fig. 35.25. Therefore, actual drift velocities are critically dependent on even small additions or contaminations.

35.10 Accelerator-based neutrino detectors

Revised August 2017 by M.O. Wascko (Imperial Coll. London).

35.10.1 Introduction

Accelerator-based neutrino experiments span many orders of magnitude in neutrino energy, from a few MeV to hundreds of GeV. This wide range of neutrino energy is driven by the many physics applications of accelerator-based neutrino beams. Foremost among them is neutrino oscillation, which varies as the ratio L/E_ν , where L is the neutrino baseline (distance traveled), and E_ν is the neutrino energy. But accelerator-based neutrino beams have also been used to study the nature of the weak interaction, to probe nucleon form factors and structure functions, and to study nuclear structure.

The first accelerator-based neutrino experiment used neutrinos from the decays of high energy pions in flight to show that the neutrinos emitted from pion decay are different from the neutrinos emitted by beta decay [267]. The field of accelerator-based neutrino experiments would likely not have expanded beyond this without Simon van der Meer's invention of the magnetic focusing horn [268], which significantly increased the flux of neutrinos aimed toward the detector. In this mini-review, we focus on experiments employing decay-in-flight beams—pions, kaons, charmed mesons, and taus—producing fluxes of neutrinos and antineutrinos from ~ 10 MeV to ~ 100 GeV.

Neutrino interactions with matter proceed only through the weak interaction, making the cross section extremely small and requiring high fluxes of neutrinos and large detector masses in order to achieve satisfactory event rates. Therefore, neutrino detector design is a balancing act taking into account sufficient numbers of nuclear targets (often achieved with inactive detector materials), adequate sampling/segmentation to ensure accurate reconstruction of the tracks and showers produced by neutrino-interaction secondary particles, and practical readout systems to allow timely analysis of data.

35.10.2 Signals and Backgrounds

The neutrino interaction processes available increase with increasing neutrino energy as interaction thresholds are crossed; in general neutrino-interaction cross sections grow with energy; for a detailed discussion of neutrino interactions see [269]. The multiplicity of secondary particles from each interaction process grows in complexity with neutrino energy, while the forward-boost due to increasing E_ν compresses the occupied phase space in the lab frame, impacting detector designs. Because decay-in-flight beams produce neutrinos at well-defined times, leading to very small duty factors, the predominant backgrounds usually stem from unwanted beam-induced neutrino interactions, i.e. neutrinos interacting via other processes than the one being studied. A noteworthy exception is time projection chambers, wherein the long drift times can admit substantially more cosmic backgrounds than most other detection methods. Cosmic backgrounds are more rare at higher energies because the secondary particles produced by neutrino interactions yield detector signals that resemble cosmic backgrounds less and less.

Below, we describe a few of the dominant neutrino interaction processes, with a focus on the final state particle content and topologies.

35.10.2.1 Charged-Current Quasi-Elastic Scattering and Pion Production

Below ~ 2 GeV neutrino energy, the dominant neutrino-nucleus interaction process is quasi-elastic (QE) scattering. In the charged current (CC) mode, the CCQE base neutrino reaction is $\nu_\ell n \rightarrow \ell^- p$, where $\ell = e, \mu, \tau$, and similarly for antineutrinos, $\bar{\nu}_\ell p \rightarrow \ell^+ n$. The final state particles are a charged lepton, and perhaps a recoiling nucleon if it is given enough energy to escape the nucleus. Detectors designed to observe this process should have good single-particle track resolution for muon neutrino interactions, but should have good μ/e separation for electron neutrino interactions. Because the interaction cross section falls sharply with Q^2 , the lepton typically carries away more of the neutrino's kinetic energy than the recoiling nucleon. The fraction of backward-scattered leptons is large, however, so detectors with 4π coverage are desirable. The dominant backgrounds in this channel tend to come from single pion production events in which the pion is not detected.

Near 1 GeV, the quasi-elastic cross section is eclipsed by pion production processes. A typical single pion production ($CC1\pi$) reaction is $\nu_\ell n \rightarrow \ell^- \pi^+ n$, but many more final state particle combinations are possible. Single pion production proceeds through the coherent channel and many incoherent processes, dominated by resonance production. With increasing neutrino energy, higher-order resonances can be excited, leading to multiple pions in the final state. Separating these processes from quasi-elastic scattering, and indeed from each other, requires tagging, and ideally reconstructing, the pions. Since these processes can produce neutral pions, electromagnetic (EM) shower reconstruction is more important here than it is for the quasi-elastic channel. The predominant backgrounds for pion production change with increasing neutrino energy. Detection of pion processes is also complicated because near threshold the quasi-elastic channel creates pion backgrounds through final state interactions of the recoiling nucleon, and at higher energies backgrounds come from migration of multiple pion events in which one or more pions is not detected.

35.10.2.2 Deep Inelastic Scattering

Beyond a few GeV, the neutrino has enough energy to probe the nucleon at the parton scale, leading to deep inelastic scattering (DIS). In the charged-current channel, the DIS neutrino reaction is $\nu_\ell N \rightarrow \ell^- X$, where N is a nucleon and X encompasses the entire recoiling hadronic system. The final state particle reconstruction revolves around accurate reconstruction of the lepton momentum and containment and reconstruction of the hadronic shower energy. Because of the high neutrino energies involved, DIS events are very forward boosted, and can have extremely long particle tracks. For this reason, detectors measuring DIS interactions must be large to contain the hadronic showers in the detector volume.

35.10.2.3 Neutral Currents

Neutrino interactions proceeding through the neutral current (NC) channel are identified by the lack of a charged lepton in the final state. For example, the NC elastic reaction is $\nu_\ell N \rightarrow \nu_\ell N$, and the NC DIS reaction is $\nu_\ell N \rightarrow \nu_\ell X$. NC interactions are suppressed relative to CC interactions by a factor involving the weak mixing angle; the primary backgrounds for NC interactions come from CC interactions in which the charged lepton is misidentified.

35.10.3 Instances of Neutrino Detector Technology

Below we describe many of the actual detectors that have been built and operated for use in accelerator-based neutrino beams.

35.10.3.1 Spark Chambers

In the first accelerator-based neutrino beam experiment, Lederman, Schwartz, and Steinberger [267] used an internally-triggered spark chamber detector, filled with 10 tons of Al planes and surrounded by external scintillator veto planes, to distinguish muon tracks from electron showers, and hence muon neutrinos from electron neutrinos. The inactive Al planes served as the neutrino interaction target and as radiators for EM shower development. The detector successfully showed the presence of muon tracks from neutrino interactions. It was also sensitive to the hadronic show-

Table 35.10: Properties of detectors for accelerator-based neutrino beams.

Name	Type	Target	Mass* (t)	Location	$\langle E_{\nu} \rangle$ (GeV)	Dates
Lederman et al.	Spark	Al	10	BNL	0.2–2	1962
CERN-spark	Spark	Al	20	CERN	1.5	1964
Serpukhov	Spark	Al	20	IHEP	4	1977
Aachen-Padova	Spark	Al	30	CERN	1.5	1976–77
Gargamelle	Bubble	Freon	6	CERN	1.5, 20	1972, 1977
BEBC	Bubble	H, D, Ne-H	2–42	CERN	50, 150 & 20	1977–84
SKAT	Bubble	Freon	8	IHEP	4	1977–1987
ANL-12ft	Bubble	H, D	1–2	ANL	0.5	1970
BNL-7ft	Bubble	H, D	0.4–0.9	BNL	1.3, 3	1976–82
Fermilab-15ft	Bubble	D, Ne	1–20	FNAL	50, 180 & 25, 100	1974–92
CITF	Iron	Fe	92	FNAL	50, 180	1977–83
CDHS	Iron	Fe	750	CERN	50, 150	1977–83
MINOS	Iron	Fe	980, 5.4k	FNAL	4–15	2005–2016
INGRID	Iron	Fe	99	J-PARC	0.7–3	2009–
Super-Kamiokande	Cherenkov	H ₂ O	22,500	Kamioka	0.6	1996–
K2K-1kt	Cherenkov	H ₂ O	25	KEK	0.8	1998–2004
MiniBooNE	Cherenkov	CH ₂	440	FNAL	0.6	2002–12
HWPF	Scintillation	CH ₂	2	FNAL	2	2014–
LSND	Scintillation	CH ₂	130	LANL	0.06	1993–98
NOvA	Scintillation	CH ₂	300, 14k	FNAL/Ash River	2	2013–
SciBar	Scintillation	CH	12	KEK/FNAL	0.8, 0.6	2004, 2007–8
ICARUS	LArTPC	Ar	760	LNGS	20	2006–12
Argoneut	LArTPC	Ar	0.025	FNAL	3	2009–10
MicroBooNE	LArTPC	Ar	170	FNAL	0.8	2014–
FNAL-E-531	Emulsion	Ag, Br	0.009	FNAL	25	1984
CHORUS	Emulsion	Ag, Br	1.6	CERN	20	1995
DONuT	Emulsion	Fe	0.26	FNAL	100	1997
OPERA	Emulsion	Pb	1.3k	LNGS	20	2006–12
NINJA	Emulsion	Fe	0.001	J-PARC	0.6	2016–
CHARM	Hybrid	CaCO ₃	150	CERN	20	1977
CHARM-II	Hybrid	glass	692	CERN	20	1983
BNL-E-734	Hybrid	CH ₂	172	BNL	1.3	1987
BNL-E-776	Hybrid	concrete	240	BNL	3	1990
NOMAD	Hybrid	CH	3	CERN	20	1995–98
CCFR	Hybrid	Fe	690	FNAL	90, 260	1991
NuTeV	Hybrid	Fe	690	FNAL	70, 180	1996–97
MINERvA	Hybrid	CH, H ₂ O, Fe, Pb, C, He	8	FNAL	3, 8	2009–
T2K-ND280	Hybrid	CH, H ₂ O, Pb, Cu	4	J-PARC	0.6	2009–

*Fiducial.

ers induced by NC interactions, which were unknown at the time. In 1963, CERN also built and ran a large (20 ton) Al plane spark chamber in a wideband beam based on the PS accelerator [270]. More than a decade later, the Aachen-Padova [271] experiment at CERN employed a 30 ton Al spark chamber in the PS-WBB.

35.10.3.2 Bubble Chambers

Several large bubble chamber detectors were employed as accelerator neutrino detectors in the 1970s and 80s, performing many of the first studies of the properties of the weak interaction. Bubble chambers provide exquisite granularity in the reconstruction of secondary particles, allowing very accurate separation of interaction processes. However, the extremely slow and labor-intensive acquisition and analysis of the data from photographic film led to them being phased out in favor of electronically read out detectors.

The Gargamelle [272] detector at CERN used Freon and propane gas targets to make the first observation of neutrino-induced NC interactions and more. The BEBC [273] detector at CERN was a bubble chamber that was alternately filled with liquid hydrogen, deuterium, and a neon-hydrogen mixture; BEBC was also outfitted with a track-sensitive detector to improve event tagging, and sometimes used with a small emulsion chamber. The SKAT [274] Freon bubble chamber was exposed to wideband neutrino and antineutrino beams at the Serpukhov laboratory in the former Soviet Union. A series of American bubble chambers in the 1970's and 1980's made measurements on free nucleons that

are still crucial inputs for neutrino-nucleus scattering predictions. The 12-foot bubble chamber at ANL [275] in the USA used both deuterium and hydrogen targets, as did the 7-foot bubble chamber at BNL [276]. Fermilab's 15 foot bubble chamber [277] used deuterium and neon targets.

35.10.3.3 Iron Tracking Calorimeters

Because of the forward boost of high energy interactions, long detectors made of magnetized iron interspersed with active detector layers have been very successfully employed. The long magnetized detectors allow measurements of the momentum of penetrating muons. The iron planes also act as shower-inducing layers, allowing separation of EM and hadronic showers; the large number of iron planes provide enough mass for high statistics and/or shower containment. Magnetized iron spectrometers have been used for studies of the weak interaction, measurements of structure functions, and searches for neutrino oscillation. Non-magnetized iron detectors have also been successfully employed as neutrino monitors for oscillation experiments and also for neutrino-nucleus interaction studies.

The Caltech-Fermilab counter (CITF) [275] combined a 92 ton iron-scintillator target-calorimeter detector with a downstream toroidal magnet to perform early studies of weak interactions—including observations of neutral currents. The CDHS [278] detector used layers of magnetized iron modules interspersed with wire drift chambers, with a fiducial mass of 750 t, to detector neutrinos in the range 30–300 GeV. Within each iron module,

5 cm (or 15 cm) iron plates were interspersed with scintillation counters. The MINOS [279] detectors, a near detector of 980 t at FNAL and a far detector of 5400 t in the Soudan mine, were functionally identical magnetized iron calorimeters, comprised of iron plates interleaved with layers of 4 cm wide plastic scintillator strips in alternating orientations. The T2K [280] on-axis detector, INGRID, consists of 16 non-magnetized iron scintillator sandwich detectors, each with nine 6.5 cm iron plane (7.1 t total) interspersed between layers of 5 cm wide plastic scintillator strips readout out by multi-pixel photon counters (MPPCs) coupled to WLS fibers. Fourteen of the INGRID modules are arranged in a cross-hair configuration centered on the neutrino beam axis.

35.10.3.4 Cherenkov Detectors

Open volume water Cherenkov detectors were originally built to search for proton decay. Large volumes of ultra-pure water were lined with photomultipliers to collect Cherenkov light emitted by the passage of relativistic charged particles. See Sec. 36.3.1 for a detailed discussion of deep liquid detectors for rare processes. The Cherenkov light, which has significant production in the visible range, appears on the walls of the detectors in distinctive ring patterns, and topological characteristics of the rings are employed to separate muon-induced rings from electron-induced with very high accuracy. As neutrino detectors, Cherenkov detectors optimize the design balance since the entire neutrino target is also active detector medium.

When used to detect \sim GeV neutrinos, the detector medium acts as a natural filter for final state particles below the Cherenkov threshold; this feature has been exploited successfully by the K2K, MiniBooNE (using mineral oil instead of water), and T2K neutrino oscillation experiments. This makes event reconstruction simple and robust since electrons and muons have very different signatures, but does require making assumptions when inferring neutrino energy since not all final state particles are observed. At higher energies Cherenkov detectors become less accurate because the overlapping rings from many final state particles become increasingly difficult to resolve.

The second-generation Cherenkov detector in Japan, Super-Kamiokande [78] (Super-K), comprises 22.5 kt of water viewed by 50 cm photomultiplier tubes with 40% photocathode coverage; it is surrounded by an outer detector region viewed by 20 cm photomultipliers. Super-K is the far detector for K2K and T2K, and is described in greater detail elsewhere in this review. The K2K experiment also employed a 1 kt water Cherenkov detector in the suite of near detectors [281], with 40% photocathode coverage. The MiniBooNE detector at FNAL was a 0.8 kt [282] mineral oil Cherenkov detector, with 20 cm photomultipliers giving 10% photocathode coverage, surrounded by a veto detector also with 20 cm photomultipliers.

35.10.3.5 Scintillation Detectors

Liquid and solid scintillator detectors also employ fully (or nearly fully) active detector media. Typically organic scintillators, which emit into the ultraviolet range, are dissolved in mineral oil or plastic and read out by photomultipliers coupled to wavelength shifters (WLS). Open volume scintillation detectors lined with photomultipliers are conceptually similar to Cherenkov detectors, although energy reconstruction is calorimetric in nature as opposed to kinematic (see also Sec. 36.3.1). For higher energies and higher particle multiplicities, it becomes beneficial to use segmented detectors to help distinguish particle tracks and showers from each other.

The HWPf collaboration [283] employed a 2 t liquid scintillator total-absorption hadron calorimeter followed by a magnetic spectrometer to observe neutral current events in the early days of Fermilab. The LSND [284] detector at LANL was a 130 t open volume liquid scintillator detector employed to detect relatively low energy (<300 MeV) neutrinos. The NOvA [285] detectors use segmented volumes of liquid scintillator in which the scintillation light is collected by WLS fibers in the segments that are coupled to avalanche photodiodes (APDs) at the ends of the volumes. The NOvA far detector, located in Ash River, MN, is comprised of 896 layers of 15.6 m long extruded PVC scintillator cells for a total mass of 14 kt; the NOvA near detector is comprised of 214 layers

of 4.1 m scintillator volumes for a total mass of 300 t. Both are placed in the NuMI beamline at 0.8° off-axis. The SciBar (Scintillation Bar) detector was originally built for K2K at KEK in Japan and then re-used for SciBooNE [286] at FNAL. SciBar used plastic scintillator strips with $1.5\text{ cm} \times 2.5\text{ cm}$ rectangular cross section, read out by multianode photomultipliers (MAPMTs) coupled to WLS fibers, arranged in alternating horizontal and vertical layers. Both SciBooNE and K2K employed an EM calorimeter downstream of SciBar and a muon range detector (MRD) downstream of that.

35.10.3.6 Liquid Argon Time Projection Chambers

Liquid argon time projection chambers (LAr-TPCs) were conceived in the 1970s as a way to achieve a fully active detector with sub-centimeter track reconstruction [287]. A massive volume of purified liquid argon is put under a strong electric field (hundreds of V/cm), so that the liberated electrons from the paths of ionizing particles can be drifted to the edge of the volume and read out, directly by collecting charge from wire planes or non-destructively through charge induction in the wire planes. A dual-phase readout method is also being developed, in which the charge is drifted vertically and then passed through an amplification region inside a gas volume above the liquid volume; the bottom of the liquid volume is equipped with a PMT array for detecting scintillation photons from the liquid argon. The first large scale LAr-TPC was the ICARUS T-600 module [288], comprising 760 t of liquid argon with a charge drift length of 1.5 m read out by wires with 3 mm pitch, which operated in LNGS, both standalone and also exposed to the CNGS high energy neutrino beam. The ICARUS detector has been transported to Fermilab and is being installed in an on-axis position in the Booster Neutrino Beamline, where it will also be exposed to off-axis neutrinos from the NuMI beamline. The ArgoNeuT [289] detector at FNAL, with fiducial mass 25 kg of argon read out with 4 mm pitch wires, was exposed to the NuMI neutrino and antineutrino beams. The MicroBooNE [290] detector at FNAL comprises 170 t of liquid Ar, read out with 3 mm wire pitch, which began collecting data in the Booster Neutrino Beam Oct 2015. A LAr-TPC has also been chosen as the detector design for the future DUNE neutrino oscillation experiment, from FNAL to Sanford Underground Research Facility; both single and dual phase modules are planned.

35.10.3.7 Emulsion Detectors

Photographic film emulsions have been employed in particle physics experiments since the 1940s [291]. Thanks to advances in scanning technology and automation [292], they have been successfully employed as neutrino detectors. Emulsions are used for experiments observing CC tau neutrino interactions, where the short lifetime of the tau, $\tau_\tau = 2.90 \times 10^{-13}$ s, leading to the short mean path length, $c \times \tau = 87\ \mu\text{m}$, requires extremely precise track resolution. They are employed in hybrid detectors in which the emulsion bricks are embedded inside fine-grained tracker detectors. In the data analysis, the tracker data are used to select events with characteristics typical of a tau decay in the final state, such as missing energy and unbalanced transverse momentum. The reconstructed tracks are projected back into an emulsion brick and used as the search seed for a neutrino interaction vertex.

E531 [293] at Fermilab tested many of the emulsion-tracker hybrid techniques employed by later neutrino experiments, in a detector with approximately 9 kg of emulsion target. The CHORUS [292] experiment at CERN used 1,600 kg of emulsion, in a hybrid detector with a fiber tracker, high resolution calorimeter, and muon spectrometer, to search for $\nu_\mu \rightarrow \nu_\tau$ oscillation. The DONuT [294] experiment at FNAL used a hybrid detector, with 260 kg of emulsion bricks interspersed with fiber trackers, followed by a magnetic spectrometer, and calorimeter, to make the first direct observation of tau neutrino CC interactions. The OPERA [295] [296] [297] experiment used an automated hybrid emulsion detector, with 1,300 t of emulsion, to make the first direct observation of the appearance of ν_τ in a ν_μ beam. Recently, the NINJA collaboration has developed an emulsion cloud chamber detector to observe neutrinos in the J-PARC neutrino beam [298].

35.10.3.8 Hybrid Detectors

In the previous neutrino detector examples, one can point to a specific detection technology or configuration that defines a category of detectors. In this section we look at detectors that combine multiple elements or techniques, without one facet being specifically dominant or crucial; we call these detectors hybrids.

The CHARM detector [299] at CERN was built to study neutral-current interactions and search for muon neutrino oscillation. It was a fine-grained ionization calorimeter tracker with approximately 150 t of marble as neutrino target, surrounded by a magnetized iron muon system for tagging high angle muons, and followed downstream by a muon spectrometer. The CHARM II detector [300] at CERN comprised a target calorimeter followed by a downstream muon spectrometer. Each target calorimeter module consists of a 4.8 cm thick glass plate followed by a layer of plastic streamer tubes, with spacing 1 cm, instrumented with 2 cm wide pickup strips. Every fifth module is followed by a 3 cm thick scintillator layer. The total mass of the target calorimeter was 692 t.

The Brookhaven E-734 [301] detector was a tracking calorimeter made up of 172 t liquid scintillator modules interspersed with proportional drift tubes, followed by a dense EM calorimeter and a muon spectrometer downstream of that. The detector was exposed to a wideband horn-focused beam with peak neutrino energy near 1 GeV. The Brookhaven E-776 [302] experiment comprised a finely segmented EM calorimeter, with 2.54 cm concrete absorbers interspersed with planes of drift tubes and acrylic scintillation counters, with total mass 240 t, followed by a muon spectrometer.

The FNAL Lab-E neutrino detector was used by the CCFR [303] and NuTeV [304] collaborations to perform a series of experiments in the Fermilab high energy neutrino beam (50 GeV < E_ν < 300 GeV). The detector was comprised of six iron target calorimeter modules, with 690 t total target mass, followed by three muon spectrometer modules, followed by two drift chambers. Each iron target calorimeter module comprised 5.2 cm thick steel plates interspersed with liquid scintillation counters and drift chambers.

The NOMAD [305] detector at CERN consisted of central tracker detector inside a 0.4 T dipole magnet (the magnet was originally used by the UA1 experiment at CERN) followed by a hadronic calorimeter and muon detectors downstream of the magnet. The main neutrino target is 3 t of drift chambers followed downstream by transition radiation detectors which are followed by an EM calorimeter. NOMAD was exposed to the same wideband neutrino beam as was CHORUS.

MINERvA [306] is a hybrid detector based around a central plastic scintillator tracker: 8.3 t of plastic scintillator strips with triangular cross section read out by MAPMTs coupled to WLS fibers. The scintillator tracker is surrounded by electromagnetic and hadronic calorimetry, which is achieved by interleaving thin lead (steel) layers between the scintillator layers for the ECAL (HCAL). MINERvA is situated upstream of the MINOS near detector which acts as a muon spectrometer. Upstream of the scintillator tracker is a nuclear target region containing inactive layers of C (graphite), Pb, Fe (steel), and O (water). MINERvA's physics goals span a wide range of neutrino-nucleus interaction studies, from form factors to nuclear effects.

T2K [280] in Japan employs two near detectors at 280 m from the neutrino beam target, one centered on the axis of the horn-focused J-PARC neutrino beam and one placed 2.5° off-axis. The on-axis detector, INGRID, is described above. The 2.5° off-axis detector, ND280, employs the UA1 magnet (at 0.2 T) previously used by NOMAD. Inside the magnet volume are three separate detector systems: the trackers, the Pi0 Detector (P0D), and several ECAL modules. The tracker detectors comprise two fine-grained scintillator detectors (FGDs), read out by MPPCs coupled to WLS fibers, interleaved between three gas TPCs read out by micromegas planes. The downstream FGD contains inactive water layers in addition to the scintillators. Upstream of the tracker is the P0D, a sampling tracker calorimeter with active detector materials comprising plastic scintillator read out by MPPCs and WLS fibers, and inactive sheets of brass radiators and refillable

water modules. Surrounding the tracker and P0D, but still inside the magnet, are lead-scintillator EM sampling calorimeters.

35.10.4 Outlook

Detectors for accelerator-based neutrino beams have been in use, and constantly evolving, for six decades now. The rich program of neutrino oscillation physics and attendant need for newer and better neutrino-nucleus scattering measurements means that more neutrino detectors with broader capabilities will be needed in the coming decades.

One of the most intriguing prospects is a large volume, high pressure gas time projection chamber (HPTPC). With the prospect of megawatt power accelerator-based neutrino beams, it is entirely feasible to collect high statistics data sets with a gas target. The low momentum thresholds for particle detection, and excellent momentum resolution and particle identification capabilities, of an HPTPC would open a new window into the physics of neutrino-nucleus scattering. Moreover, the ability to change the gas mixtures in the HPTPC would allow measurements in the same detector on multiple nuclear targets, which would, in turn, allow unprecedentedly accurate constraints and tuning of neutrino-nucleus interaction models.

35.11 Superconducting magnets for collider detectors

Revised August 2019 by Y. Makida (KEK).

35.11.1 Solenoid Magnets

In all cases SI unit are assumed, so that the magnetic field, B , is in Tesla, the stored energy, E , is in joules, the dimensions are in meters, and vacuum permeability of $\mu_0 = 4\pi \times 10^{-7}$.

The magnetic field (B) in an simple solenoid with a flux return iron yoke, in which the magnetic field is lower than magnetic saturation of < 2 T, is given by

$$B = \frac{\mu_0 n I}{L} \quad (35.41)$$

where n is the number of turns, I is the current and L is the coil length.

In an air-core solenoid case, the central field is given by

$$B(0, 0) = \mu_0 n I \frac{1}{\sqrt{L^2 + 4R^2}}, \quad (35.42)$$

where R is the coil radius.

In most cases, momentum analysis is made by measuring the circular trajectory of the passing particles according to $p = mv = qrB$, where p is the momentum, m the mass, q the charge, r the bending radius. The sagitta, s , of the trajectory is given by

$$s = q B \ell^2 / 8p, \quad (35.43)$$

where ℓ is the path length in the magnetic field. In a practical momentum measurement in colliding beam detectors, it is more effective to increase the magnetic volume than the field strength, since

$$dp/p \propto p/B \ell^2, \quad (35.44)$$

where ℓ corresponds to the solenoid coil radius R . The energy stored in the magnetic field of any magnet is calculated by integrating B^2 over all space:

$$E = \frac{1}{2\mu_0} \int B^2 dV \quad (35.45)$$

If the coil thin and inside an iron return yoke, (which is the case if it is to superconducting coil), then

$$E \approx (B^2/2\mu_0)\pi R^2 L. \quad (35.46)$$

For a detector in which the calorimetry is outside the aperture of the solenoid, the coil must be transparent in terms of radiation and absorption lengths. This usually means that the superconducting solenoid and its cryostat is of minimum real thickness and is made of a material with long radiation length. There are two major contributors to the thickness of a thin solenoid:

Table 35.11: Progress of superconducting magnets for particle physics detectors.

Experiment	Laboratory	B [T]	Radius [m]	Length [m]	Energy [MJ]	X/X_0	E/M [kJ/kg]
TOPAZ*	KEK	1.2	1.45	5.4	20	0.70	4.3
CDF*	Tsukuba/Fermi	1.5	1.5	5.07	30	0.84	5.4
VENUS*	KEK	0.75	1.75	5.64	12	0.52	2.8
AMY*	KEK	3	1.29	3	40	†	
CLEO-II*	Cornell	1.5	1.55	3.8	25	2.5	3.7
ALEPH*	Saclay/CERN	1.5	2.75	7.0	130	2.0	5.5
DELPHI*	RAL/CERN	1.2	2.8	7.4	109	1.7	4.2
ZEUS*	INFN/DESY	1.8	1.5	2.85	11	0.9	5.5
H1*	RAL/DESY	1.2	2.8	5.75	120	1.8	4.8
BaBar*	INFN/SLAC	1.5	1.5	3.46	27	†	3.6
D0*	Fermi	2.0	0.6	2.73	5.6	0.9	3.7
BELLE*	KEK	1.5	1.8	4	42	†	5.3
BES-III	IHEP	1.0	1.475	3.5	9.5	†	2.6
ATLAS-CS	ATLAS/CERN	2.0	1.25	5.3	38	0.66	7.0
ATLAS-BT	ATLAS/CERN	1	4.7–9.75	26	1080	(Toroid)†	
ATLAS-ET	ATLAS/CERN	1	0.825–5.35	5	2 × 250	(Toroid)†	
CMS	CMS/CERN	4	6	12.5	2600	†	12
SiD**	ILC	5	2.9	5.6	1560	†	12
ILD**	ILC	4	3.8	7.5	2300	†	13
SiD**	CLIC	5	2.8	6.2	2300	†	14
ILD**	CLIC	4	3.8	7.9	2300	†	
FCC**		6	6	23	54000	†	12

* No longer in service
** Conceptual design in future
† EM calorimeter is inside solenoid, so small X/X_0 is not a goal

1. The conductor consisting of the current-carrying superconducting material (usually Nb-Ti/Cu) and the quench protecting stabilizer (usually aluminum) are wound on the inside of a structural support cylinder (usually aluminum also). The coil thickness scales as B^2R , so the thickness in radiation lengths (X_0) is

$$t_{\text{coil}}/X_0 = (R/\sigma_h X_0)(B^2/2\mu_0), \quad (35.47)$$

where t_{coil} is the physical thickness of the coil, X_0 the average radiation length of the coil/stabilizer material, and σ_h is the hoop stress in the coil [307]. $B^2/2\mu_0$ is the magnetic pressure. In large detector solenoids, the aluminum stabilizer and support cylinders dominate the thickness; the superconductor (Nb-Ti/Cu) contributes a smaller fraction. The main coil and support cylinder components typically contribute about 2/3 of the total thickness in radiation lengths.

2. Another contribution to the material comes from the outer cylindrical shell of the vacuum vessel. Since this shell is susceptible to buckling collapse, its thickness is determined by the diameter, length and the modulus of the material of which it is fabricated. The outer vacuum shell represents about 1/3 of the total thickness in radiation length.

35.11.2 Properties of collider detector magnets

The physical dimensions, central field stored energy and thickness in radiation lengths normal to the beam line of the superconducting solenoids associated with the major collider are given in Table 35.11 [308]. Fig. 35.26 shows thickness in radiation lengths as a function of B^2R in various collider detector solenoids.

The ratio of stored energy to cold mass (E/M) is a useful performance measure. It can also be expressed as the ratio of the stress, σ_h , to twice the equivalent density, ρ , in the coil [307]:

$$\frac{E}{M} = \frac{E}{\rho 2\pi t_{\text{coil}} RL} \approx \frac{\sigma_h}{2\rho} \quad (35.48)$$

The E/M ratio in the coil is approximately equivalent to H ,** the enthalpy of the coil, and it determines the average coil temperature rise after energy absorption in a quench:

$$E/M = H(T_2) - H(T_1) \approx H(T_2) \quad (35.49)$$

** The enthalpy, or heat content, is called H in the thermodynamics literature. It is not to be confused with the magnetic field intensity B/μ .

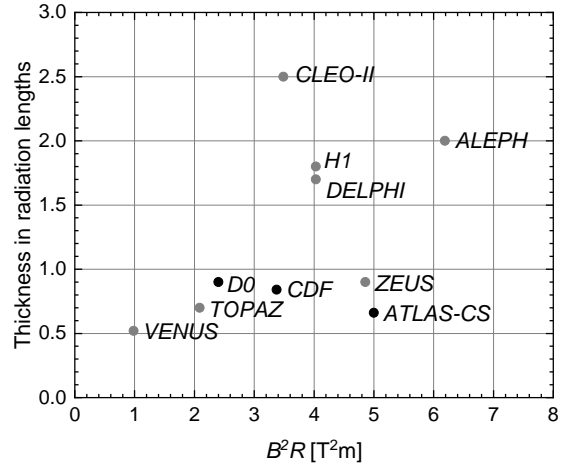


Figure 35.26: Magnet wall thickness in radiation length as a function of B^2R for various detector solenoids. Gray entries are for magnets no longer in use, and entries underlined are not listed in Table 35.11. Open circles are for magnets not designed to be “thin.” The SSC-SDC prototype provided important R&D for LHC magnets.

where T_2 is the average coil temperature after the full energy absorption in a quench, and T_1 is the initial temperature. E/M ratios of 5, 10, and 20 kJ/kg correspond to ~ 65 , ~ 80 , and ~ 100 K, respectively. The E/M ratios of various detector magnets are shown in Fig. 35.27 as a function of total stored energy. One would like the cold mass to be as small as possible to minimize the thickness, but temperature rise during a quench must also be minimized. An E/M ratio as large as 12 kJ/kg is designed into the CMS solenoid, with the possibility that about half of the stored energy can go to an external dump resistor. Thus the coil temperature can be kept below 80 K if the energy extraction system works well. The limit is set by the maximum temperature that the coil design can tolerate during a quench. This maximum local temperature should be <130 K (50 K + 80 K), so that thermal expansion effects, which are remarkable beyond 80 K, in

the coil are manageable less than 50 K.

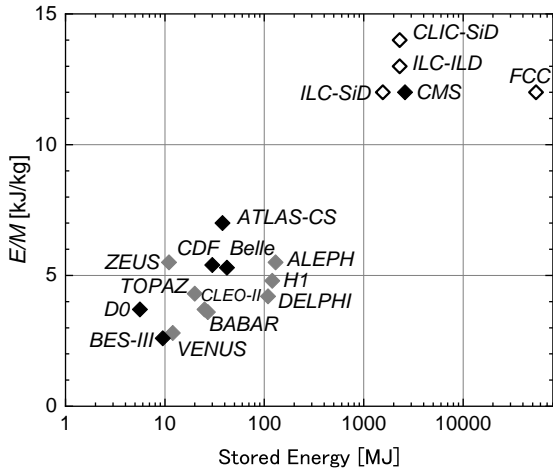


Figure 35.27: Ratio of stored energy to cold mass for major detector solenoids. Gray indicates magnets no longer in operation.

35.11.3 Toroidal magnets

Toroidal coils uniquely provide a closed magnetic field without the necessity of an iron flux-return yoke. Because no field exists at the collision point and along the beam line, there is, in principle, no effect on the beam. On the other hand, the field profile generally has $1/r$ dependence. The particle momentum may be determined by measurements of the deflection angle combined with the sagitta. The deflection (bending) power BL is

$$BL \approx \int_{R_i}^{R_0} \frac{B_i R_i dR}{R \sin \theta} = \frac{B_i R_i}{\sin \theta} \ln(R_0/R_i), \quad (35.50)$$

where R_i is the inner coil radius, R_0 is the outer coil radius, and θ is the angle between the particle trajectory and the beam line axis. The momentum resolution given by the deflection may be expressed as

$$\frac{\Delta p}{p} \propto \frac{p}{BL} \approx \frac{p \sin \theta}{B_i R_i \ln(R_0/R_i)}. \quad (35.51)$$

The momentum resolution is better in the forward/backward (smaller θ) direction. The geometry has been found to be optimal when $R_0/R_i \approx 3-4$. In practical designs, the coil is divided into 6–12 lumped coils in order to have reasonable acceptance and accessibility. This causes the coil design to be much more complex. The mechanical structure needs to sustain the decentering force between adjacent coils, and the peak field in the coil is 3–5 times higher than the useful magnetic field for the momentum analysis [309].

35.12 Measurement of particle momenta in a uniform magnetic field

The trajectory of a particle with momentum p (in GeV/c) and charge ze in a constant magnetic field \vec{B} is a helix, with radius of curvature R and pitch angle λ . The radius of curvature and momentum component perpendicular to \vec{B} are related by

$$p \cos \lambda = 0.3 z B R, \quad (35.52)$$

where B is in tesla and R is in meters.

The distribution of measurements of the curvature $k \equiv 1/R$ is approximately Gaussian. The curvature error for a large number of uniformly spaced measurements on the trajectory of a charged particle in a uniform magnetic field can be approximated by

$$(\delta k)^2 = (\delta k_{\text{res}})^2 + (\delta k_{\text{ms}})^2, \quad (35.53)$$

where δk = curvature error
 δk_{res} = curvature error due to finite measurement resolution
 δk_{ms} = curvature error due to multiple scattering.

If many (≥ 10) uniformly spaced position measurements are made along a trajectory in a uniform medium,

$$\delta k_{\text{res}} = \frac{\epsilon}{L'} \sqrt{\frac{720}{N+4}}, \quad (35.54)$$

where N = number of points measured along track
 L' = the projected length of the track onto the bending plane
 ϵ = measurement error for each point, perpendicular to the trajectory.

If a vertex constraint is applied at the origin of the track, the coefficient under the radical becomes 320.

For arbitrary spacing of coordinates s_i measured along the projected trajectory and with variable measurement errors ϵ_i the curvature error δk_{res} is calculated from:

$$(\delta k_{\text{res}})^2 = \frac{4}{w} \frac{V_{ss}}{V_{ss} V_{s^2 s^2} - (V_{s^2})^2}, \quad (35.55)$$

where V are covariances defined as $V_{s^m s^n} = \langle s^m s^n \rangle - s^m s^n$ with $\rangle s^m = w^{-1} \sum (s_i^m / \epsilon_i^2)$ and $w = \sum \epsilon_i^{-2}$.

The contribution due to multiple Coulomb scattering is approximately

$$\delta k_{\text{ms}} \approx \frac{(0.016)(\text{GeV}/c)z}{Lp\beta \cos^2 \lambda} \sqrt{\frac{L}{X_0}}, \quad (35.56)$$

where p = momentum (GeV/c)
 z = charge of incident particle in units of e
 L = the total track length
 X_0 = radiation length of the scattering medium (in units of length; the X_0 defined elsewhere must be multiplied by density)
 β = the kinematic variable v/c .

More accurate approximations for multiple scattering may be found in the section on Passage of Particles Through Matter (Sec. 34 of this Review). The contribution to the curvature error is given approximately by $\delta k_{\text{ms}} \approx 8s_{\text{plane}}^{\text{rms}}/L^2$, where $s_{\text{plane}}^{\text{rms}}$ is defined there.

References

- [1] T. Ferbel (ed.), *Experimental Techniques in High Energy Physics*, Addison-Wesley, Menlo Park, CA (1987).
- [2] K. Kleinknecht, *Detectors for Particle Radiation*, Cambridge University Press, Cambridge (1998).
- [3] G.F. Knoll, *Radiation Detection and Measurement*, 3rd edition, John Wiley & Sons, New York (1999).
- [4] D.R. Green, *The Physics of Particle Detectors*, Cambridge Monographs on Particle Physics, Nuclear Physics and Cosmology, Cambridge University Press, Cambridge (2000).
- [5] C. Leroy and P.-G. Rancoita, *Principles of Radiation Interaction in Matter and Detection*, World Scientific, Singapore (2004).
- [6] C. Grupen, *Particle Detectors*, Cambridge Monographs on Particle Physics, Nuclear Physics and Cosmology, Cambridge University Press (2008).
- [7] ICARUS Collab., ICARUS-TM/2001-09 [LGNS-EXP 13/89 add.2/01] (2001).
- [8] H. Spieler, *IEEE Trans.* **NS29**, 1142 (1982).
- [9] K. Arisaka, *Nucl. Instrum. Meth.* **A442**, 80 (2000).
- [10] T. Hakamata (ed.), *Photomultiplier Tubes: Basics and Applications*, 3rd edition, Hamamatsu Photonics K.K., Hamamatsu (2006).
- [11] A. Braem *et al.*, *Nucl. Instrum. Meth.* **A518**, 574 (2004).
- [12] R. Arnold *et al.*, *Nucl. Instrum. Meth.* **A314**, 465 (1992).
- [13] P. Mangeot *et al.*, *Nucl. Instrum. Methods* **A216**, 79 (1983).
- [14] R. Apsimon *et al.*, *IEEE Trans.* **NS33**, 112 (1986).
- [15] R. Arnold *et al.*, *Nucl. Instrum. Meth.* **A270**, 255 (1988).
- [16] D. Aston *et al.*, *Nucl. Instrum. Meth.* **A283**, 582 (1989).

- [17] J. Janesick, *Scientific charge-coupled devices*, SPIE Press, Bellingham, WA (2001).
- [18] R. Haitz *et al.*, *J. Appl. Phys.* **36**, 3123 (1965).
- [19] R. McIntyre, *IEEE Trans. Electron Devices* **13**, 164 (1966).
- [20] H. Dautet *et al.*, *Applied Optics*, **32**, 3894 (1993).
- [21] Perkin-Elmer Optoelectronics, *Avalanche Photodiodes: A User's Guide*, (2003).
- [22] P. Buzhan *et al.*, *Nucl. Instrum. Meth.* **A504**, 48 (2003).
- [23] Z. Sadygov *et al.*, *Nucl. Instrum. Methods* **A504**, 301 (2003).
- [24] V. Golovin and V. Savelev, *Nucl. Instrum. Meth.* **A518**, 560 (2004).
- [25] M. Landstrass *et al.*, *Diam. & Rel. Matter*, **2**, 1033 (1993).
- [26] R. McKeag and R. Jackman, *Diam. & Rel. Matter*, **7**, 513 (1998).
- [27] R. Brascia *et al.*, *Phys. Stat. Sol.* **199**, 113 (2003).
- [28] M. Petrov, M. Stapelbroek, and W. Kleinhans, *Appl. Phys. Lett.* **51**, 406 (1987).
- [29] M. Atac and M. Petrov, *IEEE Trans.* **NS36**, 163 (1989).
- [30] M. Atac *et al.*, *Nucl. Instrum. Meth.* **A314**, 56 (1992).
- [31] J.B. Birks, *The Theory and Practice of Scintillation Counting*, Pergamon, London (1964).
- [32] D. Clark, *Nucl. Instrum. Methods* **117**, 295 (1974).
- [33] J. B. Birks, *Proc. Phys. Soc.* **A64**, 874 (1951).
- [34] B. Bengston and M. Moszynski, *Nucl. Instrum. Methods* **117**, 227 (1974); J. Bialkowski *et al.*, *Nucl. Instrum. Methods* **117**, 221 (1974).
- [35] C. P. Achenbach (2004), [arXiv:nucl-ex/0404008].
- [36] I.B. Berlman, *Handbook of Fluorescence Spectra of Aromatic Molecules*, 2nd edition, Academic Press, New York (1971).
- [37] F. Sauli (ed.), *Instrumentation in High Energy Physics*, World Scientific, Singapore (1992), see pp. 218–279 by C. Zorn.
- [38] T. Foerster, *Ann. Phys.* **2**, 55 (1948).
- [39] N. Zaitseva *et al.*, *Nucl. Instrum. Methods* **A668**, 88 (2012).
- [40] J.M. Fluornoy, *Rad. Phys. and Chem.* **41**, 389 (1993).
- [41] D. Horstman and U. Holm, *Rad. Phys. and Chem.* **41**, 395 (1993).
- [42] D. Blomker *et al.*, *Nucl. Instrum. Meth.* **A311**, 505 (1992).
- [43] K.F. Johnson and R.L. Clough (eds.), *Proceedings of the International Conference on Radiation-Tolerant Plastic Scintillators and Detectors*, *Rad. Phys. and Chem.* **41** (1993).
- [44] S.R. Borenstein and R.C. Strand, *IEEE Trans.* **NS31**, 396 (1984).
- [45] P. Sonderegger, *Nucl. Instrum. Meth.* **A257**, 523 (1987).
- [46] P. Achenbach *et al.*, *Nucl. Instrum. Meth.* **A593**, 353 (2008), [arXiv:0802.2830].
- [47] C. M. Hawkes *et al.*, *Nucl. Instrum. Meth.* **A292**, 329 (1990).
- [48] S.E. Derenzo, W.-S. Choong and W.W. Moses, *Phys. Med. Biol.* **59**, 3261 (2014).
- [49] C. Melcher and J. Schweitzer, *Nucl. Instrum. Methods* **A314**, 212 (1992).
- [50] D.W. Cooke *et al.*, *J. Appl. Phys.* **88**, 7360 (2000).
- [51] J.M. Chen *et al.*, *IEEE Trans.* **NS54**, 718 (2007).
- [52] J.M. Chen *et al.*, *IEEE Trans.* **NS54**, 1319 (2007).
- [53] E.V.D. van Loef *et al.*, *Nucl. Instrum. Methods* **A486**, 254 (2002).
- [54] W. Drozdowski *et al.*, *IEEE Trans.* **NS55**, 1391 (2008).
- [55] M.S. Alekhin *et al.*, *Appl. Phys. Lett.* **102**, 161915 (2013).
- [56] C. Kuntner *et al.* (Crystal Clear), *Nucl. Instrum. Meth.* **A493**, 131 (2002).
- [57] N. Akchurin *et al.*, *Nucl. Instrum. Meth.* **A595**, 359 (2008).
- [58] A. Para, FERMILAB-CONF-11-519-CD (2011).
- [59] H. Wenzel *et al.*, FERMILAB-PUB-11-531-CD-E (2011).
- [60] R.H. Mao, L.Y. Zhang and R.Y. Zhu, *IEEE Trans.* **NS59**, 2229 (2012).
- [61] R. Y. Zhu, TIPP 2017, SPPHY 213, 70 (2018).
- [62] C. Hu *et al.*, *IEEE Trans.* **NS66**, DOI: 10.1109/TNS.2019.2918305 (2019).
- [63] W.W. Moses, W.-S. Choong and S.E. Derenzo, *Acta Physica Polonica* **B7**, 725 (2014).
- [64] R.H. Mao, L.Y. Zhang and R.Y. Zhu, *IEEE Trans.* **NS55**, 2425 (2008).
- [65] B.D. Rooney and J.D. Valentine, *IEEE Trans.* **NS44**, 509 (1997).
- [66] W.W. Moses *et al.*, *IEEE Trans.* **NS55**, 1049 (2008).
- [67] G. Gratta, H. Newman and R. Y. Zhu, *Ann. Rev. Nucl. Part. Sci.* **44**, 453 (1994).
- [68] R. Y. Zhu, *Nucl. Instrum. Meth.* **A413**, 297 (1998).
- [69] F. Yang *et al.*, *IEEE Trans.* **NS63**, 612 (2016).
- [70] F. Yang *et al.*, *IEEE Trans.* **NS64**, 665 (2017).
- [71] C. Hu *et al.*, *Journal of Physics: Conference Series (Calor2018)*, **1162** 012020 (2019).
- [72] G. Dissertori *et al.*, *Nucl. Instrum. Methods* **745**, 1 (2014), and references therein.
- [73] S. Ecklund, C. Field and G. Mazaheri, *Nucl. Instr. and Meth. Res. Sect.* **A463**, 68 (2001).
- [74] M. G. Albrow *et al.*, *JINST* **7**, P10027 (2012), [arXiv:1207.7248].
- [75] B. Aubert *et al.* (BaBar), *Nucl. Instr. and Meth. Res. Sect.* **A479**, 1 (2002), [hep-ex/0105044].
- [76] E. Torassa (Belle-II PID Group), *Nucl. Instr. and Meth. Res. Sect.* **A824**, 152 (2016).
- [77] G. Bayatian *et al.* (CMS), *Eur. Phys. J.* **C53**, 139 (2008).
- [78] Y. Fukuda *et al.* (Super-Kamiokande), *Nucl. Instrum. Meth.* **A501**, 418 (2003).
- [79] Proceedings of the International Workshops on Ring Imaging Cherenkov Detectors, *Nucl. Instr. and Meth. Res. Sect.* **A343**, 1 (1993); *Nucl. Instr. and Meth. Res. Sect.* **A371**, 1 (1996); *Nucl. Instr. and Meth. Res. Sect.* **A433**, 1 (1999); *Nucl. Instr. and Meth. Res. Sect.* **A502**, 1 (2003); *Nucl. Instr. and Meth. Res. Sect.* **A553**, 1 (2005); *Nucl. Instr. and Meth. Res. Sect.* **A595**, 1 (2008); *Nucl. Instr. and Meth. Res. Sect.* **A639**, 1 (2011); *Nucl. Instr. and Meth. Res. Sect.* **A766**, 1 (2014); *Nucl. Instr. and Meth. Res. Sect.* **A876**, 1 (2017); *Nucl. Instr. and Meth. Res. Sect.* **A 952**, 1 (2019).
- [80] J. Litt and R. Meunier, *Ann. Rev. Nucl. Part. Sci.* **23**, 1 (1973).
- [81] D. Bartlett *et al.*, *Nucl. Instr. and Meth. Res. Sect.* **A260**, 55 (1987).
- [82] A. Abashian *et al.*, *Nucl. Instr. and Meth. Res. Sect.* **A479**, 117 (2002).
- [83] B. N. Ratcliff, *Nucl. Instr. and Meth. Res. Sect.* **A502**, 211 (2003).
- [84] T. Iijima *et al.*, *Nucl. Instr. and Meth. Res. Sect.* **A548**, 383 (2005), [arXiv:physics/0504220].
- [85] W. Blum, W. Riegler, and L. Rolandi, *Particle Detection with Drift Chambers*, Springer-Verlag, Berlin (2008).
- [86] L.G. Christophorou, *Atomic and Molecular Radiation Physics*, John Wiley & Sons, Hoboken (1971).
- [87] <http://consult.cern.ch/writeup/magboltz/>.
- [88] H. Bichsel, *Nucl. Instrum. Meth.* **A562**, 154 (2006).

- [89] H. Fischle, J. Heintze and B. Schmidt, Nucl. Instrum. Meth. **A301**, 202 (1991).
- [90] <http://rjd.web.cern.ch/rjd/cgi-bin/cross>.
- [91] A. Peisert and F. Sauli (1984).
- [92] S. F. Biagi, Nucl. Instrum. Meth. **A421**, 1-2, 234 (1999).
- [93] E. McDaniel and E. Mason, *The Mobility and Diffusion of Ions in Gases*, John Wiley & Sons, Hoboken (1973); G. Schultz, G. Charpak and F. Sauli, Rev. Phys. Appl. **12**, 1, 67 (1977).
- [94] G.F. Knoll, *Radiation Detection and Measurement*, 3rd edition, John Wiley & Sons, New York (1999).
- [95] G. Charpak *et al.*, Nucl. Instrum. Methods **A62**, 262 (1968).
- [96] G. Charpak and F. Sauli, Ann. Rev. Nucl. Sci. **34**, 285 (1984).
- [97] W. Blum, W. Riegler, and L. Rolandi, *Particle Detection with Drift Chambers*, Springer-Verlag, Berlin (2008).
- [98] T. Ferbel (ed.), *Experimental Techniques in High Energy Physics*, Addison-Wesley, Menlo Park, CA (1987), see "Principles of Operation of Multiwire Proportional and Drift Chambers".
- [99] G. Charpak *et al.*, Nucl. Instrum. Methods **A167**, 455 (1979).
- [100] A.H. Walenta *et al.*, Nucl. Instrum. Methods **A92**, 373 (1971).
- [101] A. Breskin *et al.*, Nucl. Instrum. Methods **A124**, 189 (1975).
- [102] A. Breskin *et al.*, Nucl. Instrum. Methods **A156**, 147 (1978).
- [103] R. Bouclier *et al.*, Nucl. Instrum. Meth. **A265**, 78 (1988), [556(1987)].
- [104] H. Drumm *et al.*, Nucl. Instrum. Methods **A176**, 333 (1980).
- [105] D.R. Nygren and J.N. Marx, Phys. Today **31N10**, 46 (1978).
- [106] <http://consult.cern.ch/writeup/magboltz/>.
- [107] <http://www.ansoft.com>.
- [108] C. Grupen, *Particle Detectors*, Cambridge Monographs on Particle Physics, Nuclear Physics and Cosmology, Cambridge University Press (2008).
- [109] P. S. Baringer *et al.*, Nucl. Instrum. Meth. **A254**, 542 (1987).
- [110] J. Virdee, Phys. Reports **403**, 401 (2004).
- [111] A. H. Walenta, Phys. Scripta **23**, 354 (1981).
- [112] J. Va'vra, ICFA Instrum. Bull. **24**, 1 (2002), [1(2002)].
- [113] M. Aleksa *et al.*, Nucl. Instrum. Meth. **A446**, 435 (2000).
- [114] F. Sauli and A. Sharma, Ann. Rev. Nucl. Part. Sci. **49**, 341 (1999).
- [115] A. Oed, Nucl. Instrum. Meth. **A263**, 351 (1988), [124(1988)].
- [116] Y. Bagaturia *et al.* (HERA-B Inner Tracker), Nucl. Instrum. Meth. **A490**, 223 (2002), [ICFA Instrum. Bull.24,54(2002)], [hep-ex/0204011].
- [117] A. Breskin *et al.*, Nucl. Instrum. Methods **A124**, 189 (1975).
- [118] J. Benlloch *et al.*, IEEE Trans. **NS45**, 234 (1998).
- [119] Y. Giomataris, Nucl. Instrum. Meth. **A419**, 239 (1998).
- [120] F. Sauli, Nucl. Instrum. Meth. **A386**, 531 (1997); A. Bressan *et al.*, Nucl. Instrum. Meth. **A425**, 262 (1999).
- [121] S. Bachmann *et al.*, Nucl. Instrum. Meth. **A479**, 294 (2002); A. Bressan *et al.*, Nucl. Instrum. Meth. **A424**, 321 (1999).
- [122] Y. Giomataris *et al.*, Nucl. Instrum. Meth. **A376**, 29 (1996).
- [123] J. Derre *et al.*, Nucl. Instrum. Meth. **A459**, 523 (2001); G. Charpak *et al.*, Nucl. Instrum. Meth. **A478**, 26 (2002).
- [124] I. Giomataris *et al.*, Nucl. Instrum. Meth. **A560**, 405 (2006), [arXiv:physics/0501003].
- [125] S. Duarte Pinto *et al.*, IEEE NSS Conf. Record **N08-4**, 1426 (2008).
- [126] L. Periale *et al.*, Nucl. Instrum. Meth. **A478**, 377 (2002), [arXiv:physics/0106048]; R. Chechik *et al.*, Nucl. Instrum. Meth. **A535**, 303 (2004), [arXiv:physics/0404119]; A. Breskin *et al.*, Nucl. Instrum. Meth. **A598**, 107 (2009), [arXiv:0807.2026].
- [127] A. Di Mauro *et al.*, Nucl. Instrum. Meth. **A581**, 225 (2007), [arXiv:0706.0102].
- [128] R. Bellazzini *et al.*, Nucl. Instrum. Meth. **A535**, 477 (2004), [arXiv:physics/0403019]; M. Campbell *et al.*, Nucl. Instrum. Meth. **A540**, 295 (2005), [arXiv:physics/0409048]; A. Bamberger *et al.*, Nucl. Instrum. Meth. **A573**, 361 (2007), [arXiv:physics/0611229].
- [129] M. Chefderville *et al.*, Nucl. Instrum. Meth. **A556**, 490 (2006).
- [130] M. P. Titov, ICFA Instrum. Bull. **26**, 002 (2004), [199(2004)], [arXiv:physics/0403055].
- [131] <http://rd51-public.web.cern.ch/RD51-Public>.
- [132] D.R. Nygren and J.N. Marx, Phys. Today **31N10**, 46 (1978).
- [133] J. Alme *et al.*, Nucl. Instrum. Meth. **A622**, 316 (2010), [arXiv:1001.1950].
- [134] N. Abgrall *et al.* (T2K ND280 TPC), Nucl. Instrum. Meth. **A637**, 25 (2011), [arXiv:1012.0865].
- [135] A. H. Walenta *et al.*, Nucl. Instrum. Meth. **161**, 45 (1979).
- [136] H. Aihara *et al.*, IEEE Trans. **NS30**, 63 (1983).
- [137] T. A. collaboration (ALICE) (2014).
- [138] K. Dehmelt (sPHENIX), PoS **MPGD2017**, 044 (2019).
- [139] P. Colas, I. Giomataris and V. Lepeltier, Nucl. Instrum. Meth. **A535**, 226 (2004).
- [140] X. Artru, G. B. Yodh and G. Mennessier, Phys. Rev. **D12**, 1289 (1975).
- [141] E. J. Schioppa *et al.*, Nucl. Instrum. Meth. **A936**, 523 (2019).
- [142] M. L. Cherry *et al.*, Phys. Rev. **D10**, 3594 (1974).
- [143] J. Alozy *et al.*, Nucl. Instrum. Meth. **A927**, 1 (2019), [arXiv:1901.11265].
- [144] B. Dolgoshein, Nucl. Instrum. Meth. **A326**, 434 (1993).
- [145] A. Andronic and J. P. Wessels, Nucl. Instrum. Meth. **A666**, 130 (2012).
- [146] S. Acharya *et al.* (ALICE), Nucl. Instrum. Meth. **A881**, 88 (2018), [arXiv:1709.02743].
- [147] T. Akesson *et al.* (ATLAS TRT), Nucl. Instrum. Meth. **A522**, 131 (2004).
- [148] M. Ambriola *et al.*, Nucl. Instrum. Meth. **A522**, 77 (2004).
- [149] J. Adelman (ATLAS), Nucl. Instrum. Meth. **A706**, 33 (2013).
- [150] T. Kirn (AMS 02 TRD), Nucl. Instrum. Meth. **A706**, 43 (2013).
- [151] P. Nevski, Nucl. Instrum. Meth. **A522**, 116 (2004).
- [152] V. M. Grishin and S. S. Sadilov, Nucl. Instrum. Meth. **A522**, 122 (2004).
- [153] B. Beischer *et al.*, Nucl. Instrum. Meth. **A583**, 485 (2007).
- [154] T. Akesson *et al.* (ATLAS TRT), Nucl. Instrum. Meth. **A412**, 200 (1998).
- [155] M. Petris *et al.*, Nucl. Instrum. Meth. **A714**, 17 (2013).
- [156] M. L. Cherry, Nucl. Instrum. Meth. **A706**, 39 (2013).
- [157] M. Brigida *et al.*, Nucl. Instrum. Meth. **A706**, 69 (2013).

- [158] F. Hartjes *et al.*, Nucl. Instrum. Meth. **A706**, 59 (2013).
- [159] V. V. Berdnikov *et al.*, Nucl. Instrum. Meth. **A706**, 65 (2013).
- [160] R. Santonico and R. Cardarelli, Nucl. Instrum. Methods **A187**, 377 (1981).
- [161] V.V. Parkhomchuck, Yu.N. Pestov, and N.V. Petrovykh, Nucl. Instrum. Methods **93**, 269 (1971).
- [162] E. Cerron Zeballos *et al.*, Nucl. Instrum. Meth. **A374**, 132 (1996).
- [163] R. Cardarelli, A. Di Ciaccio and R. Santonico, Nucl. Instrum. Meth. **A333**, 399 (1993).
- [164] P. Camarri *et al.*, Nucl. Instrum. Meth. **A414**, 317 (1998).
- [165] G. Aielli *et al.*, Nucl. Instrum. Meth. **A508**, 6 (2003).
- [166] R. Cardarelli, R. Santonico and V. Makeev, Nucl. Instrum. Meth. **A382**, 470 (1996).
- [167] I. Crotty *et al.*, Nucl. Instrum. Methods **A505**, 203 (2006).
- [168] R. Santonico, Nucl. Instrum. Meth. **A456**, 1 (2000).
- [169] W. Riegler and D. Burgarth, Nucl. Instrum. Meth. **A481**, 130 (2002).
- [170] R. Cardarelli *et al.*, JINST **8**, P01003 (2013).
- [171] G. Aielli *et al.*, JINST **9**, 09, C09030 (2014).
- [172] R. Santonico, JINST **9**, 11, C11007 (2014).
- [173] G. Aad *et al.* (ATLAS), JINST **3**, S08003 (2008).
- [174] S. Chatrchyan *et al.* (CMS), JINST **3**, S08004 (2008).
- [175] R. Santonico, Nucl. Instrum. Meth. **A661**, S2 (2012).
- [176] M. Bedjidian *et al.*, JINST **6**, P02001 (2011), [arXiv:1011.5969].
- [177] P. Fonte, A. Smirnitsky and M. C. S. Williams (ALICE), Nucl. Instrum. Meth. **A443**, 201 (2000).
- [178] L. Paolozzi *et al.*, PoS **RPC2012**, 065 (2012).
- [179] S. An *et al.*, Nucl. Instrum. Meth. **A594**, 39 (2008).
- [180] C. Iacobaeus *et al.*, Nucl. Instrum. Meth. **A513**, 244 (2003), [arXiv:physics/0210006].
- [181] G. Aielli *et al.*, Nucl. Instrum. Meth. **A456**, 82 (2000).
- [182] G. Aielli *et al.*, IEEE Trans. **NS53**, 567 (2006).
- [183] H. Sakai *et al.*, Nucl. Instrum. Meth. **A484**, 153 (2002).
- [184] R. Santonico, JINST **8**, P04023 (2013).
- [185] L. Lopes *et al.*, Nucl. Instrum. Meth. **A533**, 69 (2004).
- [186] H. Spieler, *Semiconductor Detector Systems*, Oxford Univ. Press, Oxford (2005).
- [187] F. Scholze *et al.*, Nucl. Instrum. Methods **A439**, 208 (2000).
- [188] G. Lindstrom *et al.* (ROSE), Nucl. Instrum. Meth. **A465**, 60 (2000), [280(2000)].
- [189] C. Da Via *et al.*, Nucl. Instrum. Meth. **A509**, 86 (2003).
- [190] G. Kramberger *et al.*, Nucl. Instrum. Meth. **A481**, 297 (2002).
- [191] O. Krasel *et al.*, IEEE Trans. **NS51**, 3055 (2004).
- [192] G. Lindstrom, M. Moll and E. Fretwurst, Nucl. Instrum. Meth. **A426**, 1 (1999).
- [193] A. Holmes-Siedle and L. Adams, *Handbook of Radiation Effects*, 2nd edition, Oxford Univ. Press, Oxford (2002).
- [194] V. Radeka, IEEE Trans. **NS15**, 455 (1968).
- [195] V. Radeka, IEEE Trans. **NS21**, 51 (1974).
- [196] F. S. Goulding, Nucl. Instrum. Meth. **100**, 493 (1972).
- [197] F.S. Goulding and D.A. Landis, IEEE Trans. **NS29**, 1125 (1982).
- [198] H. Spieler, IEEE Trans. **NS29**, 1142 (1982).
- [199] H. Spieler, *Semiconductor Detector Systems*, Oxford Univ. Press, Oxford (2005).
- [200] R. Wigmans, *Calorimetry*, International Series of Monographs on Physics, Oxford University Press (2017).
- [201] W.R. Nelson, H. Hirayama, and D.W.O. Rogers, SLAC-265 (1985).
- [202] R. Brun *et al.*, CERN DD/EE/84-1 (1987).
- [203] ATLAS Collab., CERN/LHCC 96-41 (1996).
- [204] D. Hitlin *et al.*, Nucl. Instrum. Meth. **137**, 225 (1976).
- [205] W. J. Willis and V. Radeka, Nucl. Instrum. Meth. **120**, 221 (1974).
- [206] R. Wigmans, *Calorimetry: Energy Measurement in Particle Physics*, Inter. Series of Monographs on Phys. **107**, Second Edition, Oxford Scholarship Online (2017).
- [207] R.Y. Zhu, Journal of Physics: Conference Series **587**, 012055 (2015).
- [208] CMS Collab., CERN/LHCC 97-33 (1997).
- [209] C. Leroy and P. Rancoita, Rept. Prog. Phys. **63**, 505 (2000).
- [210] N. Akchurin *et al.*, Nucl. Instrum. Meth. **A399**, 202 (1997).
- [211] B. Aubert *et al.*, Nucl. Instrum. Meth. **A321**, 467 (1992).
- [212] A. Artamonov *et al.*, JINST **3**, P02010 (2008).
- [213] F. Ariztizabal *et al.* (RD-34), Nucl. Instrum. Meth. **A349**, 384 (1994).
- [214] E. Borchini *et al.* (SICAPO), Nucl. Instrum. Meth. **A279**, 57 (1989).
- [215] G. Abbiendi, R. G. Kellogg and D. M. Strom, in "Calorimetry in particle physics. Proceedings, 10th International Conference, CALOR 2002, Pasadena, USA, March 25-29, 2002," 287-295 (2002), [hep-ex/0206074].
- [216] S. C. Berridge *et al.*, IEEE Trans. Nucl. Sci. **39**, 1242 (1992).
- [217] E. Borchini *et al.*, IEEE Transactions on Nuclear Science **40**, 508 (1993).
- [218] <https://twiki.cern.ch/twiki/bin/view/CALICE/CaliceDetectors>.
- [219] F. Sefkow and F. Simon (CALICE), J. Phys. Conf. Ser. **1162**, 1, 012012 (2019), [arXiv:1808.09281].
- [220] D. E. Groom, in "ECFA Study Week on Instrumentation Technology for High Luminosity Hadron Colliders Barcelona, Spain, September 14-21, 1989," URL http://lss.fnal.gov/cgi-bin/find_paper.pl?other/ssc/ssc-227.pdf.
- [221] T. A. Gabriel *et al.*, Nucl. Instrum. Meth. **A338**, 336 (1994).
- [222] D. E. Groom, Nucl. Instrum. Meth. **A572**, 633 (2007), erratum: Nucl. Instrum. Meth. **A593**, 628 (2008).
- [223] N. Akchurin *et al.*, Nucl. Instr. Methods **A408**, 380 (1998); An energy-independent analysis of these data is given in [222].
- [224] P. Adragna *et al.*, Nucl. Instrum. Meth. **A615**, 158 (2010).
- [225] F. Lemeilleur *et al.*, Physics Letters B **222**, 3, 518 (1989), ISSN 0370-2693, URL <http://www.sciencedirect.com/science/article/pii/0370269389903560>.
- [226] H. Abramowicz *et al.*, Nucl. Instrum. Meth. **180**, 429 (1981).
- [227] B. Andrieu *et al.* (H1 Calorimeter Group), Nucl. Instrum. Meth. **A336**, 499 (1993).
- [228] C. Cojocaru *et al.* (ATLAS), Nucl. Instrum. Meth. **A531**, 3, 481 (2004).
- [229] C. Adloff *et al.* (CALICE), J. Instr. **7**, 09, P09017 (2012).
- [230] C. Adloff *et al.* (CALICE), JINST **8**, 07005 (2013).
- [231] C. W. Fabjan *et al.*, Phys. Lett. **60B**, 105 (1975).
- [232] C. Leroy, J. Sirois, and R. Wigmans, Nucl. Instrum. Methods **A252**, 4 (1986).
- [233] J. Brau *et al.*, Nucl. Instrum. Meth. **A238**, 489 (1985).
- [234] H. Brückmann and H. Kowalski, ZEUS Int. Note 86/026 DESY, Hamburg (1986).
- [235] R. Wigmans, Nucl. Instrum. Meth. **A259**, 389 (1987).
- [236] R. Wigmans, Nucl. Instrum. Meth. **A265**, 273 (1988).
- [237] T. Akesson *et al.*, Nucl. Instrum. Meth. **A241**, 17 (1985).

- [238] T. Akesson *et al.*, Nucl. Instrum. Meth. **A262**, 243 (1987).
- [239] E. Bernardi *et al.*, Nucl. Instrum. Meth. **A262**, 229 (1987).
- [240] G. Drews *et al.*, Nucl. Instrum. Meth. **A290**, 335 (1990).
- [241] G. R. Young *et al.*, Nucl. Instrum. Meth. **A279**, 503 (1989).
- [242] A. Andresen *et al.* (ZEUS Calorimeter Group, ZEUS), Nucl. Instrum. Meth. **A309**, 101 (1991).
- [243] www-zeus.desy.de/bluebook/ch05/subsection2_4_15_3.html.
- [244] D. Acosta *et al.*, Nucl. Instrum. Meth. **A308**, 481 (1991).
- [245] S. Abachi *et al.* (D0), Nucl. Instrum. Meth. **A338**, 185 (1994).
- [246] P. Mockett, SLAC-267, 335 (1983).
- [247] D.R. Winn and W.A. Worstell, "Compensating Hadron Calorimeters with Cerenkov Light", IEEE TNS, NS-36, 334 (1989).
- [248] R. Wigmans, *Proc. 7th Inter. Conf. on Calorimetry in High Energy Physics*, 182 World Scientific, River Edge, NJ, (1998);.
- [249] S. Lee, M. Livan and R. Wigmans, Rev. Mod. Phys. **90**, 2, 025002 (2018).
- [250] D. E. Groom, Nucl. Instrum. Meth. **A705**, 24 (2013).
- [251] J.-C. Brient, J. Phys. Conf. Ser. **160**, 012025 (2009).
- [252] F. Sefkow *et al.*, Rev. Mod. Phys. **88**, 015003 (2016).
- [253] J. Apostolakis *et al.*, J. Phys. Conf. Ser. **160**, 012073 (2009).
- [254] J. Allison *et al.*, Nucl. Instrum. Meth. **A835**, 186 (2016).
- [255] M. Holder *et al.*, Nucl. Instrum. Meth. **151**, 69 (1978).
- [256] R.K. Bock, T. Hansl-Kozanecka, and T.P. Shah, Nucl. Instrum. Methods **186**, 533 (1981) Y.A. Kulchitsky and V.B. Vinogradov, Nucl. Instrum. Methods **A455**, 499 (2000).
- [257] Y.A. Kulchitsky and V.B. Vinogradov, Nucl. Instrum. Methods **A455**, 499 (2000).
- [258] D. Acosta *et al.*, Nucl. Instrum. Meth. **A316**, 184 (1992).
- [259] N. Akchurin *et al.*, Nucl. Instrum. Meth. **A735**, 120 (2014).
- [260] W. Walkowiak, Nucl. Instrum. Meth. **A449**, 288 (2000).
- [261] E. Shibamura *et al.*, Nucl. Instrum. Methods **A316**, 184 (1975).
- [262] L. S. Miller, S. Howe and W. E. Spear, Phys. Rev. **166**, 871 (1968).
- [263] A.M. Kalinin *et al.*, ATLAS-LARG-NO-058 (1996).
- [264] K. Yoshino, U. Sowada and W. F. Schmidt, Phys. Rev. **A14**, 438 (1976).
- [265] A.O. Allen *et al.*, NSRDS-NBS-58 (1976).
- [266] P. Benetti *et al.*, Nucl. Instrum. Methods **A32**, 361 (1993).
- [267] G. Danby *et al.*, Phys. Rev. Lett. **9**, 36 (1962).
- [268] S. van der Meer (1961).
- [269] J. A. Formaggio and G. P. Zeller, Rev. Mod. Phys. **84**, 1307 (2012), [arXiv:1305.7513].
- [270] H. Faissner, "CERN Spark Chamber Neutrino Experiment", INSPIRE-1377455.
- [271] H. Faissner *et al.*, Phys. Lett. **68B**, 377 (1977).
- [272] F. J. Hasert *et al.* (Gargamelle Neutrino), Nucl. Phys. **B73**, 1 (1974).
- [273] N. Armenise *et al.* (BEBC TST Neutrino), Phys. Lett. **81B**, 385 (1979).
- [274] A.E. Asratien *et al.*, Phys. Lett. **79**, 497 (1978).
- [275] S. J. Barish *et al.*, Phys. Rev. **D16**, 3103 (1977).
- [276] N. J. Baker *et al.*, Phys. Rev. **D23**, 2499 (1981).
- [277] J. W. Chapman *et al.*, Phys. Rev. **D14**, 5 (1976).
- [278] M. Holder *et al.*, Nucl. Instrum. Meth. **148**, 235 (1978).
- [279] I. Ambats *et al.* (MINOS) (1998).
- [280] K. Abe *et al.* (T2K), Nucl. Instrum. Meth. **A659**, 106 (2011), [arXiv:1106.1238].
- [281] M. H. Ahn *et al.* (K2K), Phys. Rev. **D74**, 072003 (2006), [hep-ex/0606032].
- [282] A. A. Aguilar-Arevalo *et al.* (MiniBooNE), Nucl. Instrum. Meth. **A599**, 28 (2009), [arXiv:0806.4201].
- [283] A. C. Benvenuti *et al.*, Nucl. Instrum. Meth. **125**, 447 (1975).
- [284] C. Athanassopoulos *et al.* (LSND), Nucl. Instrum. Meth. **A388**, 149 (1997), [arXiv:nucl-ex/9605002].
- [285] D. S. Ayres *et al.* (NOvA) (2007).
- [286] K. Hiraide *et al.* (SciBooNE), Phys. Rev. **D78**, 112004 (2008), [arXiv:0811.0369].
- [287] C. Rubbia, CERN-EP-INT-77-08 (1977).
- [288] S. Amerio *et al.* (ICARUS), Nucl. Instrum. Meth. **A527**, 329 (2004).
- [289] C. Anderson *et al.*, JINST **7**, 10020 (2012).
- [290] H. Chen *et al.*, FERMILAB-PROPOSAL-0974 (2007).
- [291] D. H. Perkins, Nature **159**, 126 (1947).
- [292] S. Aoki *et al.*, Nucl. Instrum. Meth. **A447**, 361 (2000).
- [293] N. Uhida *et al.*, Nucl. Instrum. Methods **224**, 50 (1984).
- [294] K. Kodama *et al.*, Nucl. Instrum. Meth. **B93**, 340 (1994).
- [295] T. Adam *et al.*, Nucl. Instrum. Meth. **A577**, 523 (2007), [arXiv:physics/0701153].
- [296] D. Di Ferdinando (OPERA), Radiat. Meas. **44**, 840 (2009), [arXiv:0812.0451].
- [297] R. Acquafredda *et al.* (OPERA), New J. Phys. **8**, 303 (2006), [hep-ex/0611023].
- [298] T. Fukuda *et al.*, PTEP **2017**, no. 6, 063C02 (2017).
- [299] A. N. Diddens *et al.* (CERN-Hamburg-Amsterdam-Rome-Moscow), Nucl. Instrum. Meth. **178**, 27 (1980).
- [300] D. Geiregat *et al.* (CHARM-II), Nucl. Instrum. Meth. **A325**, 92 (1993).
- [301] L. A. Ahrens *et al.*, Nucl. Instrum. Meth. **A254**, 515 (1987).
- [302] G. Gidal, LBL-91 Suppl., Rev. (1985).
- [303] W. K. Sakumoto *et al.*, Nucl. Instrum. Meth. **A294**, 179 (1990).
- [304] D. A. Harris *et al.* (NuTeV), Nucl. Instrum. Meth. **A447**, 377 (2000), [hep-ex/9908056].
- [305] J. Altegoer *et al.* (NOMAD), Nucl. Instrum. Meth. **A404**, 96 (1998).
- [306] L. Aliaga *et al.* (MINERvA), Nucl. Instrum. Meth. **A743**, 130 (2014), [arXiv:1305.5199].
- [307] A. Yamamoto, Nucl. Instrum. Meth. **A453**, 445 (2000).
- [308] A. Yamamoto and Y. Makida, Nucl. Instrum. Meth. **A494**, 255 (2002).
- [309] T. M. Taylor, Phys. Scripta **23**, 459 (1981).
- [310] R. L. Gluckstern, Nucl. Instrum. Meth. **24**, 381 (1963).
- [311] V. Karimaki, Nucl. Instrum. Meth. **A410**, 284 (1998).

36. Particle Detectors for Non-Accelerator Physics

36.1	Introduction	589
36.2	High-energy cosmic-ray hadron and gamma-ray detectors	589
36.2.1	Atmospheric fluorescence detectors	589
36.2.2	Atmospheric Cherenkov telescopes for high-energy gamma ray astronomy	591
36.3	Large neutrino detectors	592
36.3.1	Deep liquid detectors for rare processes	592
36.3.2	Neutrino telescopes	594
36.3.3	Radio emission from (ultra-)high energy particle showers	598
36.4	Large time-projection chambers for rare event detection	601
36.4.1	Dark matter and other low energy signals	601
36.4.2	$0\nu\beta\beta$ Decay	603
36.5	Sub-Kelvin detectors	603
36.5.1	Equilibrium thermal detectors	603
36.5.2	Nonequilibrium Detectors	604
36.6	Low-radioactivity background techniques	605
36.6.1	Defining the problem	606
36.6.2	Environmental radioactivity	606
36.6.3	Radioactive impurities in detector and shielding components	606
36.6.4	Radon and its progeny	607
36.6.5	Cosmic rays	608
36.6.6	Neutrons	608

36.1 Introduction

Non-accelerator experiments have become increasingly important in particle physics. These include cosmic ray experiments (with surface, space and underground detectors), neutrino oscillation measurements with solar and atmospheric neutrinos in underground laboratories, searches for neutrino-less double beta decays and dark matter candidates again in underground laboratories, and searches for more exotic phenomena. The detectors are in the majority of the cases different from those used at accelerators. Even when the detectors are based on the same physics (e. g. tracking detectors), they are employed in radically different ways. The methods range from atmospheric scintillation detectors to massive Cherenkov detectors, from large liquid scintillator detectors to dual phase TPCs, from ultrapure ionization calorimeters to cryogenic solid state detectors. With the exception of the cosmic ray detectors, techniques for producing and testing radiologically ultra-pure materials are constantly developed. Progress is linked to pushing forward the ultra-low background frontier. In this section, some important technologies relevant for detectors on the surface and underground are discussed. Space-based detectors also use some unique instrumentation, but these are beyond the present scope of this review.

36.2 High-energy cosmic-ray hadron and gamma-ray detectors

36.2.1 Atmospheric fluorescence detectors

Revised August 2019 by L.R. Wiencke (Colorado School of Mines).

Cosmic-ray fluorescence detectors (FDs) use the atmosphere as a giant calorimeter to measure isotropic scintillation light that traces the development profiles of extensive air showers. An extensive air shower (EAS) is produced by the interactions of ultra high-energy ($E > 10^{17}$ eV) subatomic particles in the stratosphere and upper troposphere. The amount of scintillation light generated by an EAS is proportional to the energy deposited in the atmosphere and nearly independent of the primary species. With energies extending beyond 10^{20} eV these are the highest energy subatomic particles known to exist. In addition to particle arrival directions, energy spectra and primary composition, the astroparticle science investigated with FDs also includes multimessenger studies, searches for high energy photons, neutrinos, monopoles and deeply penetrating forms of dark matter.

Previous experiments with FDs included the pioneering Fly's Eye [1, 2], and the High Resolution Fly's Eye (HiRes and HiRes prototype) [3]. The current generation of experiments include the Telescope Array (TA) [4] in the northern hemisphere, and the much larger Pierre Auger Observatory (Auger) [5] in the southern hemisphere. Both are hybrid observatories. Their FD telescopes overlook sparse arrays of particle detectors on the ground. Select parameters are listed in Table 36.1. TA and Auger have each one FD site populated with additional telescopes that view up to 60° in elevation to measure lower EASs using a combination of scintillation and direct Cherenkov light. The Auger FD also measures UV scintillation that traces the development of atmospheric transient luminous events called "Elves" that are initiated by lightning [6]. At TA a prototype FD telescope, dubbed FAST [7], has observed EASs using wide field of view PMTs and fast timing.

The fluorescence light is emitted primarily between 290 and 430 nm (Figure 36.1) with major lines at 337, 357, and 391 nm, when relativistic charged particles, primarily electrons and positrons, excite nitrogen molecules in air, resulting in transitions of the 1P and 2P systems. Reviews and references for the pioneering and recent laboratory measurements of fluorescence yield, $Y(\lambda, P, T, u)$, including dependence on wavelength (λ), temperature (T), pressure (p), and humidity (u) may be found in Refs. [8–10]. The results of various laboratory experiments have been combined (Figure 36.2) to obtain an absolute average and uncertainty for $Y(337 \text{ nm}, 800 \text{ hPa}, 293 \text{ K}, \text{ dry air})$ of $7.04 \pm 0.24 \text{ ph/MeV}$ after corrections for different electron beam energies and other factors. The units of ph/MeV correspond to the number of fluorescence photons produced per MeV of energy deposited in the atmosphere by the electromagnetic component of an EAS.

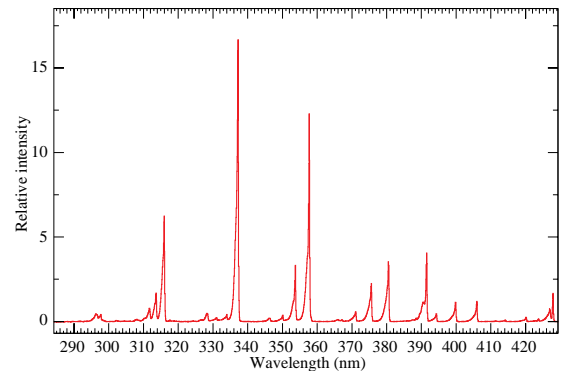


Figure 36.1: Measured fluorescence spectrum excited by 3 MeV electrons in dry air at 800 hPa and 293 K. Airfly experiment. Figure from Ref [11].

An FD element (telescope) consists of a non-tracking spherical mirror of less than astronomical quality, a close-packed “camera” of photomultiplier tubes (PMTs) near the focal plane, and a flash ADC readout system with a pulse and track-finding trigger scheme [5, 13]. The major experiments listed in Table 36.1 all use conventional PMTs (for example, Hamamatsu R9508 or Photonis XP3062) with grounded cathodes and AC coupled readout. Segmented mirrors have been fabricated from slumped or slumped/polished glass with an anodized aluminum coating or fabricated using shaped aluminum that was then chemically anodized with AlMgSiO_5 . A broadband UV filter (custom fabricated or Schott MUG-6) reduces background light such as starlight, air-glow, man-made light pollution, and airplane strobe-lights.

At 10^{20} eV, where the flux drops below 1 EAS/km²century, the aperture for an eye of adjacent FD telescopes that span the horizon can reach $10^4 \text{ km}^2 \text{ sr}$. FD operation requires (nearly) moonless nights and clear atmospheric conditions, which imposes a duty cycle of about 10%. Arrangements of LEDs, calibrated diffuse sources [14], pulsed UV lasers [15], LIDARs¹ and IR detectors

¹LIDAR stands for “Light Detection and Ranging” and refers here to

Table 36.1: Parameters of major fluorescence detectors. Note 1: Year when all FD sites were operational. Note 2: At TA 1 of the 3 FD sites features 24 telescopes from the HiRes experiment. Note 3: A-C for one telescope where A is the full area and C the area obscured by the camera and support structures. Thus A-C is the effective light collecting area. For the modified Schmidt design at Auger, the area of the entrance pupil, A, is listed because the pupil is smaller than the mirror and thus defines the entrance aperture. For the other experiments, the area of the mirror, A, is listed

Observatory	Fly's Eye	HiRes	Telescope Array	Pierre Auger
Location	Dugway UT US	Dugway UT US	Delta UT US	Malargüe AR
Start-End	1981-1992	1996-2006	2008-present	2005-present
Sites (note 1)	2 (1986)	2 (1999)	3 (2008)	4 (2008)
Separation	3.3 km	12.6 km	31-40 km	39-62 km
Telescopes/site	67,18	21,42	12,12,14+10	6, 6, 6, 6+3
Pixel FOV	5.5°	1°	1°	1.5°
Telescope FOV	≈18° × ≈18°	16° × 13.5°	18° × 15° (note 2)	30° × 28.1°
Azi × Elv				
Light collection area (note 3)	1.95 m ² - 0.25 m ²	3.72 m ² - 0.5 m ²	6.8 m ² - 0.85 m ² (for 2 sites)	3.80 m ² - 0.80 m ² (modified schmidt)
Energy Scale	≤40%	≈20%	≈20%	14%
Uncertainty				

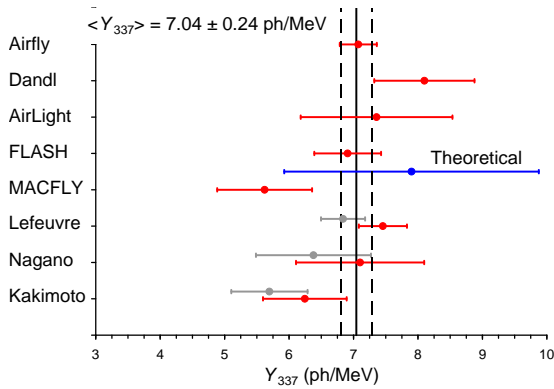


Figure 36.2: Fluorescence yield values and associated uncertainties at 337 nm (Y_{337}) in dry air at 800 hPa and 293 K. The methodology and corrections that were applied to obtain the average and the uncertainty are discussed extensively in this reference. The vertical axis denotes different laboratory experiments that measured FY. The gray bars show three of the original measurements to illustrate the scale of the corrections applied. Figure from Ref [12].

that are sensitive to clouds are used for photometric calibration, atmospheric calibration [16], and determination of exposure [17]. For purposes of optical transmission, the atmosphere is treated as having a dominant molecular component and a secondary aerosol component. The latter is well described [18] by molecular scattering theory and models derived from radiosonde measurements. The aerosol component can include dust, haze and pollution and the aerosol optical depth profile must be measured on site in the UV during FD data taking.

The EAS generates a track consistent with a light source moving at $v = c$ across the FOV. The number of photons (N_γ) as a function of atmospheric depth (X) can be expressed as [9]

$$\frac{dN_\gamma}{dX} = \frac{dE_{\text{dep}}^{\text{tot}}}{dX} \int Y(\lambda, P, T, u) \cdot \tau_{\text{atm}}(\lambda, X) \cdot \varepsilon_{\text{FD}}(\lambda) d\lambda, \quad (36.1)$$

where $\tau_{\text{atm}}(\lambda, X)$ is the atmospheric transmission, including wavelength (λ) dependence, and $\varepsilon_{\text{FD}}(\lambda)$ is the FD efficiency. $\varepsilon_{\text{FD}}(\lambda)$ includes geometric factors and collection efficiency of the optics, quantum efficiency of the PMTs, and other throughput factors. The typical systematic uncertainties, τ_{atm} (10%) and ε_{FD} (photometric calibration 10%), currently dominate the systematic uncertainty the absolute EAS energy scale. FD energy resolu-

systems that measure atmospheric properties from the light scattered backwards from laser pulses directed into the sky.

tion, defined as event-to-event statistical uncertainty, is typically less than 10% for final data samples used for science analysis.

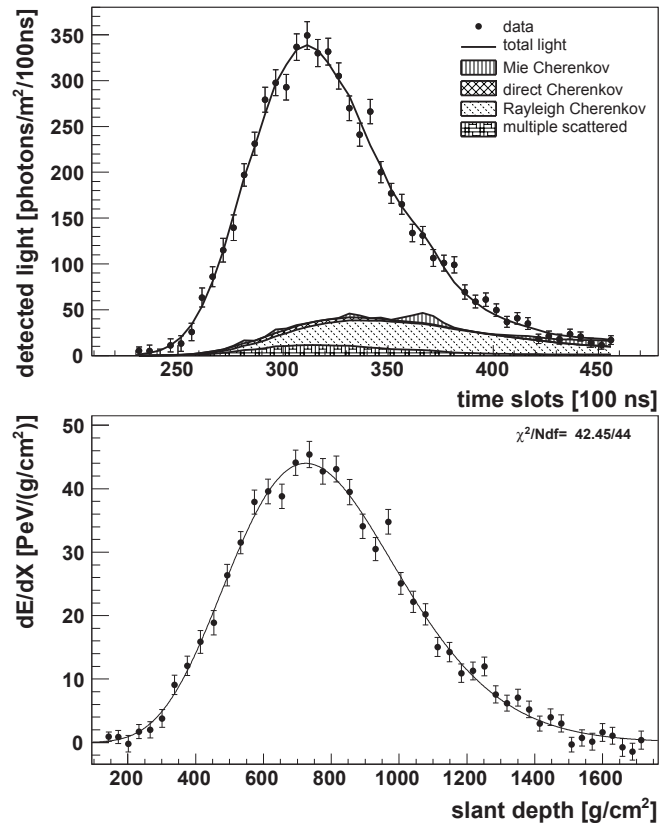


Figure 36.3: Example light profile (left) of one EAS recorded by the Pierre Auger FD and the corresponding profile (right) of energy deposited in the atmosphere vs atmospheric slant depth. The light profiles include the estimated components of Cherenkov light that have been scattered out of the forward beam by the molecular and aerosol (Mie) components of the atmosphere. The reconstructed energy of this EAS was $3.0 \pm 0.2 \times 10^{19}$ eV. Figure from Ref [19].

Analysis methods to reconstruct the EAS profile and deconvolve the contributions of re-scattered scintillation light, and direct and scattered Cherenkov light are described in [1] and more recently in [20]. The EAS energy is typically obtained by integrating over the Gaisser-Hillas function [21]

$$E_{\text{cal}} = \int_0^{\infty} [w_{\text{max}} \left(\frac{X - X_0}{X_{\text{max}} - X_0} \right)^{(X_{\text{max}} - X_0)/\lambda} e^{(X_{\text{max}} - X)/\lambda}] dX, \quad (36.2)$$

where E_{cal} is the energy of electromagnetic energy component of the EAS and X_{max} is the atmospheric slant depth at which the shower reaches its maximum energy deposit rate. This maximum dE/dX is denoted as w_{max} . X_0 and λ are two shape parameters. The energy of the primary cosmic ray is obtained by correcting E_{cal} upward by about 10% to account for the invisible energy carried by particles that do not interact in the atmosphere. Energy resolution, $\Delta E/E$, of 15-20% is achievable, provided the geometric fit of the EAS axis is constrained, typically by multi-eye stereo projection or hybrid observations, and the profile fit of EAS development along the track is constrained by the observed rise and fall about X_{max} . An example of a recorded EAS light profile and its corresponding dE/dX development profile are shown in Fig. 36.3.

The EAS generates a track consistent with a light source moving at $v = c$ across the FOV. The number of photons (N_γ) as a function of atmospheric depth (X) can be expressed as [9]

R&D toward an FD in space is at the design and prototype phase. A proposed space based FD instrument [22] by the JEM-EUSO collaboration would look down on the earth's atmosphere from space to view a much larger area than ground based instruments. Prototypes that have been built and flown include the TUS instrument [23], operated 2016-2018 onboard the Lomonosov satellite, and two FD telescopes flown on stratospheric balloons in 2014 [24] and 2017 [25]. The prototype instrument Mini-EUSO [26] (25 cm diameter aperture), currently at the International Space Station (ISS), will survey terrestrial UV emission by looking down through a UV window from inside the ISS beginning late 2019. The proposed POEMMA twin-satellite space mission [27] would record scintillation and Cherenkov light from EASs the atmosphere to measure UHECRs and PeV scale cosmogenic tau neutrinos.

36.2.2 Atmospheric Cherenkov telescopes for high-energy gamma ray astronomy

Revised August 2019 by J. Holder (Delaware U.; Delaware U., Bartol Inst.).

A wide variety of astrophysical objects are now known to produce high-energy γ -ray photons. Leptonic or hadronic particles, accelerated to relativistic energies in the source, produce γ -rays typically through inverse Compton boosting of ambient photons or through the decay of neutral pions produced in hadronic interactions. At energies below ~ 30 GeV, γ -ray emission can be efficiently detected using satellite or balloon-borne instrumentation, with an effective area approximately equal to the size of the detector (typically < 1 m²). At higher energies, a technique with much larger effective collection area is desirable to measure astrophysical γ -ray fluxes, which decrease rapidly with increasing energy. Atmospheric Cherenkov detectors achieve effective collection areas of $> 10^5$ m² by employing the Earth's atmosphere as an intrinsic part of the detection technique.

As described in Chapter 30, a hadronic cosmic ray or high energy γ -ray incident on the Earth's atmosphere triggers a particle cascade, or air shower. Relativistic charged particles in the cascade generate Cherenkov radiation, which is emitted along the shower direction, resulting in a light pool on the ground with a radius of ~ 130 m. Cherenkov light is produced throughout the cascade development, with the maximum emission occurring when the number of particles in the cascade is largest, at an altitude of ~ 10 km for primary energies of 100 GeV–1 TeV. Following absorption and scattering in the atmosphere, the Cherenkov light at ground level peaks at a wavelength, $\lambda \approx 300$ –350 nm. The photon density is typically ~ 100 photons/m² for a 1 TeV primary, arriving in a brief flash of a few nanoseconds duration. This Cherenkov pulse can be detected from any point within the light pool radius by using large reflecting surfaces to focus the Cherenkov light on to fast photon detectors (Fig. 36.4).

Modern atmospheric Cherenkov telescopes, such as those built and operated by the VERITAS [28], H.E.S.S. [29] and MAGIC [30]

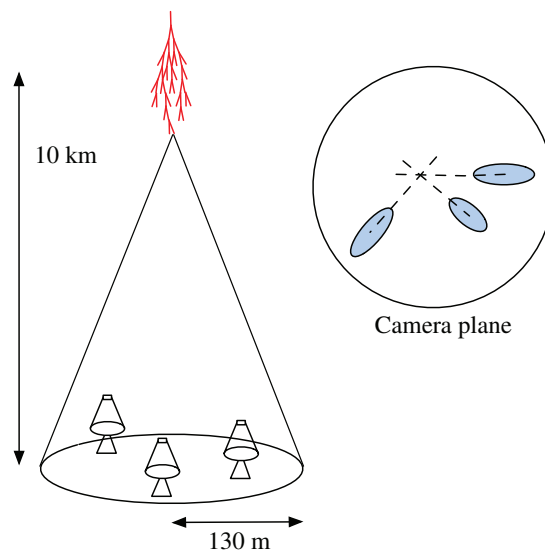


Figure 36.4: A schematic illustration of an imaging atmospheric Cherenkov telescope array. The primary particle initiates an air shower, resulting in a cone of Cherenkov radiation. Telescopes within the Cherenkov light pool record elliptical images; the intersection of the long axes of these images indicates the arrival direction of the primary, and hence the location of a γ -ray source in the sky

collaborations, consist of large (> 100 m²) segmented mirrors on steerable altitude-azimuth mounts. A camera made from an array of photosensors is placed at the focus of each mirror and used to record a Cherenkov image of each air shower. In these imaging atmospheric Cherenkov telescopes, single-anode photomultiplier tubes (PMTs) have traditionally been used (2048, in the case of H.E.S.S. II), but silicon devices now feature in more modern designs. The telescope cameras typically cover a field-of-view of $3 - 10^\circ$ in diameter. Images are recorded at kHz rates, the vast majority of which are due to showers with hadronic cosmic-ray primaries. The shape and orientation of the Cherenkov images are used to discriminate γ -ray photon events from this cosmic-ray background, and to reconstruct the photon energy and arrival direction. γ -ray images result from purely electromagnetic cascades and appear as narrow, elongated ellipses in the camera plane. The long axis of the ellipse corresponds to the vertical extension of the air shower, and points back towards the source position in the field-of-view. If multiple telescopes are used to view the same shower (“stereoscopy”), the source position is simply the intersection point of the various image axes. Cosmic-ray primaries produce secondaries with large transverse momenta, which initiate sub-showers. Their images are consequently wider and less regular than those with γ -ray primaries and, since the original charged particle has been deflected by Galactic magnetic fields before reaching the Earth, the images have no preferred orientation.

The measurable differences in Cherenkov image orientation and morphology provide the background discrimination which makes ground-based γ -ray astronomy possible. For point-like sources, such as distant active galactic nuclei, modern instruments can reject over 99.999% of the triggered cosmic-ray events, while retaining up to 50% of the γ -ray population. In the case of spatially extended sources, such as Galactic supernova remnants, the background rejection is less efficient, but the technique can be used to produce γ -ray maps of the emission from the source. The angular resolution depends upon the number of telescopes which view the image and the energy of the primary γ -ray, but is typically less than 0.1° per event (68% containment radius) at energies above a few hundred GeV.

The total Cherenkov yield from the air shower is proportional to the energy of the primary particle. The image intensity, combined with the reconstructed distance of the shower core from each

telescope, can therefore be used to estimate the primary energy. The energy resolution of this technique, also energy-dependent, is typically 15–20% at energies above a few hundred GeV. Energy spectra of γ -ray sources can be measured over a wide range, depending upon the instrument characteristics, source properties (flux, spectral slope, elevation angle, *etc.*), and exposure time. The effective energy range is typically from 30 GeV to 100 TeV and peak sensitivity lies in the range from 100 GeV to a few TeV.

The first astrophysical source to be convincingly detected using the imaging atmospheric Cherenkov technique was the Crab Nebula [31], with an integral flux of 2.1×10^{-11} photons $\text{cm}^{-2} \text{s}^{-1}$ above 1 TeV [32]. Modern imaging atmospheric Cherenkov telescopes have sensitivity sufficient to detect sources with less than 1% of the Crab Nebula flux in a few tens of hours. The TeV source catalog now consists of over 200 sources (see e.g. Ref. [33]). A large fraction of these were detected by scanning the Galactic plane from the southern hemisphere with the H.E.S.S. telescope array [34]. Recent reviews of the field include [35] and [36], and a historical overview can be found in [37].

Major upgrades of the existing telescope arrays have recently been completed, including the addition of a 28 m diameter central telescope to H.E.S.S. (H.E.S.S. II). Development is also underway for the next generation instrument, the Cherenkov Telescope Array (CTA), which will consist of a northern and a southern hemisphere observatory, with a combined total of more than 100 telescopes [38]. Telescopes of three different sizes are planned, spread over an area of $> 1 \text{ km}^2$, providing wider energy coverage, improved angular and energy resolutions, and an order of magnitude improvement in sensitivity relative to existing imaging atmospheric Cherenkov telescopes. Baseline telescope designs are similar to existing devices, but exploit technological developments such as dual mirror optics and silicon photo-detectors.

36.3 Large neutrino detectors

36.3.1 Deep liquid detectors for rare processes

Revised August 2018 by K. Scholberg (Duke U.) and C.W. Walter (Duke U.).

Deep, large detectors for rare processes tend to be multi-purpose with physics reach that includes not only solar, reactor, supernova and atmospheric neutrinos, but also searches for baryon number violation, searches for exotic particles such as magnetic monopoles, and neutrino and cosmic-ray astrophysics in different energy regimes. The detectors may also serve as targets for long-baseline neutrino beams for neutrino oscillation physics studies. In general, detector design considerations can be divided into high- and low-energy regimes, for which background and event reconstruction issues differ. The high-energy regime, from about 100 MeV to a few hundred GeV, is relevant for proton decay searches, atmospheric neutrinos and high-energy astrophysical neutrinos. The low-energy regime (a few tens of MeV or less) is relevant for supernova, solar, reactor and geological neutrinos.

Large water Cherenkov and scintillator detectors (see Table 36.2) usually consist of a volume of transparent liquid viewed by photomultiplier tubes (PMTs) (see Sec 35.2); the liquid serves as active target. PMT hit charges and times are recorded and digitized, and triggering is usually based on coincidence of PMT hits within a time window comparable to the detector's light-crossing time. Because photosensors lining an inner surface represent a driving cost that scales as surface area, very large volumes can be used for comparatively reasonable cost. Some detectors are segmented into subvolumes individually viewed by PMTs, and may include other detector elements (*e.g.*, tracking detectors). Devices to increase light collection, *e.g.*, reflectors or waveshifter plates, may be employed. A common configuration is to have at least one concentric outer layer of liquid material separated from the inner part of the detector to serve as shielding against ambient background. If optically separated and instrumented with PMTs, an outer layer may also serve as an active veto against entering cosmic rays and other background events. The PMTs for large detectors typically range in size from 20 cm to 51 cm diameter, and typical quantum efficiencies are in the 20–25% range for scintillation and water-Cherenkov photons. PMTs with higher quantum

efficiencies, 35% or higher, have recently become available. The active liquid volume requires purification and there may be continuous recirculation of liquid. For large homogeneous detectors, the event interaction vertex is determined using relative timing of PMT hits, and energy deposition is determined from the number of recorded photoelectrons. A “fiducial volume” is usually defined within the full detector volume, some distance away from the PMT array. Inside the fiducial volume, enough PMTs are illuminated per event that reconstruction is considered reliable, and furthermore, entering background from the enclosing walls is suppressed by a buffer of self-shielding. PMT and detector optical parameters are calibrated using laser, LED, or other light sources. Quality of event reconstruction typically depends on photoelectron yield, pixelization and timing.

Because in most cases one is searching for rare events, large detectors are usually sited underground to reduce cosmic-ray-related background (see Chapter 30). The minimum depth required varies according to the physics goals [39].

36.3.1.1 Liquid scintillator detectors

Past and current large underground detectors based on hydrocarbon scintillators include LVD, MACRO, Baksan, Borexino, KamLAND and SNO+; JUNO is a future detector. Experiments at nuclear reactors include CHOOZ, Double CHOOZ, Daya Bay, and RENO. Organic liquid scintillators (see Section 35.3) for large detectors are chosen for high light yield and attenuation length, good stability, compatibility with other detector materials, high flash point, low toxicity, appropriate density for mechanical stability, and low cost. They may be doped with waveshifters and stabilizing agents. Popular choices are pseudocumene (1,2,4-trimethylbenzene) with a few g/L of the PPO (2,5-diphenyloxazole) fluor, and linear alkylbenzene (LAB). In a typical detector configuration there will be active or passive regions of undoped scintillator, non-scintillating mineral oil or water surrounding the inner neutrino target volume. A thin vessel or balloon made of nylon, acrylic or other material transparent to scintillation light may contain the inner target; if the scintillator is buoyant with respect to its buffer, ropes may hold the balloon in place. For phototube surface coverages in the 20–40% range, yields in the few hundreds of photoelectrons per MeV of energy deposition can be obtained. Typical energy resolution is about $7\%/\sqrt{E(\text{MeV})}$, and typical position reconstruction resolution is a few tens of cm at $\sim 1 \text{ MeV}$, scaling as $\sim N^{-1/2}$, where N is the number of photoelectrons detected.

Shallow detectors for reactor neutrino oscillation experiments require excellent muon veto capabilities. For $\bar{\nu}_e$ detection via inverse beta decay on free protons, $\bar{\nu}_e + p \rightarrow n + e^+$, the neutron is captured by a proton on a $\sim 180 \mu\text{s}$ timescale, resulting in a 2.2 MeV γ ray, observable by Compton scattering and which can be used as a tag in coincidence with the positron signal. The positron annihilation γ rays may also contribute. Inverse beta decay tagging may be improved by addition of Gd at $\sim 0.1\%$ by mass, which for natural isotope abundance has a $\sim 49,000$ barn cross-section for neutron capture (in contrast to the 0.3 barn cross-section for capture on free protons). Gd capture takes $\sim 30 \mu\text{s}$, and is followed by a cascade of γ rays adding up to about 8 MeV. Gadolinium doping of scintillator requires specialized formulation to ensure adequate attenuation length and stability.

Scintillation detectors have an advantage over water Cherenkov detectors in the lack of Cherenkov threshold and the high light yield. However, scintillation light emission is nearly isotropic, and therefore directional capabilities are relatively weak. Liquid scintillator is especially suitable for detection of low-energy events. Radioactive backgrounds are a serious issue, and include long-lived cosmogenics. To go below a few MeV, very careful selection of materials and purification of the scintillator is required (see Section 36.6). Fiducialization and tagging can reduce background. One can also dissolve neutrinoless double beta decay ($0\nu\beta\beta$) isotopes in scintillator. This has been realized by KamLAND-Zen, which deployed a 1.5 m-radius balloon containing enriched Xe dissolved in scintillator inside KamLAND, and ^{130}Te is planned for SNO+. Although for this approach, energy resolution is poor compared to other $0\nu\beta\beta$ search experiments, the quantity of iso-

Table 36.2: Properties of large detectors for rare processes. If total target mass is divided into large submodules, the number of subdetectors is indicated in parentheses. Projects with first data expected in 2021 or later are indicated in italics.

Detector	Mass, kton (modules)	PMTs (diameter, cm)	ξ	p.e./MeV	Dates
Baksan	0.33, scint (3150)	1/module (15)	segmented	40	1980–
MACRO	0.56, scint (476)	2-4/module (20)	segmented	18	1989–2000
LVD	1, scint. (840)	3/module (15)	segmented	15	1992–
KamLAND	0.41*, scint	1325(43)+554(51) [†]	34%	460	2002–
Borexino	0.1*, scint	2212 (20)	30%	500	2007–
SNO+	0.78, scint [‡]	9394 (20)	47%	400–600	2019 (exp.)
CHOOZ	0.005, scint (Gd)	192 (20)	15%	130	1997–1998
Double Chooz	0.017, scint (Gd)(2)	534/module (20)	13%	180	2011–
Daya Bay	0.160, scint (Gd)(8)	192/module (20)	5.6% [§]	100	2011–
RENO	0.032, scint (Gd)(2)	342/module (25)	12.6%	100	2011–
<i>JUNO</i>	20.0*, scint	17613 (51)/25600 (8)	77.9%	1200	2021 (exp.)
IMB-1	3.3*, H ₂ O	2048 (12.5)	1%	0.25	1982–1985
IMB-2	3.3*, H ₂ O	2048 (20)	4.5%	1.1	1987–1990
Kam I	0.88/0.78*, H ₂ O	1000/948 (51)	20%	3.4	1983–1985
Kam II	1.04*, H ₂ O	948 (51)	20%	3.4	1986–1990
Kam III	1.04*, H ₂ O	948 (51)	20% [¶]	4.3	1990–1995
SK I	22.5*, H ₂ O	11146 (51)	40%	6	1996–2001
SK II	22.5*, H ₂ O	5182 (51)	19%	3	2002–2005
SK III-V	22.5*, H ₂ O	11129 (51)	40%	6	2006–
SK-Gd	22.5*, H ₂ O (Gd)	11129 (51)	40%	6	2020 (exp.)
<i>Hyper-K</i>	187*, H ₂ O	40000 (51)	40%	12	2027 (exp.)
SNO	1, D ₂ O/1.7, H ₂ O	9438 (20)	31%**	9	1999–2006

*Indicates typical fiducial mass used for data analysis; this may vary by physics topic.

[†]Measurements made before 2003 only considered data from the 43 cm PMTs.

[‡]SNO+ ran with water fill from May 2017 to July 2019.

[§]The effective Daya Bay coverage is 12% with top and bottom reflectors.

[¶]The effective Kamiokande III coverage was 25% with light collectors.

^{||}A second staged module is planned.

**The effective SNO coverage was 54% with light collectors.

tope can be so large that the kinematic signature of $0\nu\beta\beta$ would be visible as a clear feature in the spectrum.

36.3.1.2 Water Cherenkov detectors

Very large imaging water detectors reconstruct ten-meter-scale Cherenkov rings produced by charged particles (see Section 35.5). The first such large detectors were IMB and Kamiokande. The only currently existing instance of this class of detector, with fiducial mass of 22.5 kton and total mass of 50 kton, is Super-Kamiokande (Super-K, SK). Hyper-Kamiokande (Hyper-K) plans at least one, and possibly two, detectors with 187-kton fiducial mass. For volumes of this scale, absorption and scattering of Cherenkov light are non-negligible, and a wavelength-dependent factor $\exp(-d/L(\lambda))$ (where d is the distance from emission to the sensor and $L(\lambda)$ is the attenuation length of the medium) must be included in the integral of Eq. (35.6) for the photoelectron yield. Attenuation lengths on the order of 100 meters have been achieved.

Cherenkov detectors are excellent electromagnetic calorimeters, and the number of Cherenkov photons produced by an e/γ is nearly proportional to its kinetic energy. For massive particles, the number of photons produced is also related to the energy, but not linearly. For any type of particle, the *visible energy* E_{vis} is defined as the energy of an electron which would produce the same number of Cherenkov photons. The number of collected photoelectrons depends on the scattering and attenuation in the water along with the photo-cathode coverage, quantum efficiency and the optical parameters of any external light collection systems or protective material surrounding them. Event-by-event corrections are made for geometry and attenuation. For a typical case, in water $N_{\text{p.e.}} \sim 15 \xi E_{\text{vis}}(\text{MeV})$, where ξ is the effective fractional photosensor coverage. Cherenkov photoelectron yield per MeV of energy is relatively small compared to that for scintillator, *e.g.*, ~ 6 p.e./MeV for Super-K with a PMT surface coverage of $\sim 40\%$. In spite of light yield and Cherenkov threshold issues, the intrinsic directionality of Cherenkov light allows individual particle tracks to be reconstructed. Vertex and direction fits are performed us-

ing PMT hit charges and times, requiring that the hit pattern be consistent with a Cherenkov ring.

High-energy (~ 100 MeV or more) neutrinos from the atmosphere or beams interact with nucleons; for the nucleons bound inside the ^{16}O nucleus, nuclear effects must be considered both at the interaction and as the particles leave the nucleus. Various event topologies can be distinguished by their timing and fit patterns, and by presence or absence of light in a veto. “Fully-contained” events are those for which the neutrino interaction final state particles do not leave the inner part of the detector; these have their energies relatively well measured. Neutrino interactions for which the lepton is not contained in the inner detector sample have higher-energy parent neutrino energy distributions. For example, in “partially-contained” events, the neutrino interacts inside the inner part of the detector but the lepton (almost always a muon, since only muons are penetrating) exits. “Upward-going muons” can arise from neutrinos which interact in the rock below the detector and create muons which enter the detector and either stop, or go all the way through (entering downward-going muons cannot be distinguished from cosmic rays). At high energies, multi-photoelectron hits are likely and the charge collected by each PMT (rather than the number of PMTs firing) must be used; this degrades the energy resolution to approximately $2\%/\sqrt{\xi E_{\text{vis}}(\text{GeV})}$. The absolute energy scale in this regime can be known to $\sim 2\text{--}3\%$ using cosmic-ray muon energy deposition, Michel electrons and π^0 from atmospheric neutrino interactions. Typical vertex resolutions for GeV energies are a few tens of cm [40]. Angular resolution for determination of the direction of a charged particle track is a few degrees. For a neutrino interaction, because some final-state particles are usually below Cherenkov threshold, knowledge of direction of the incoming neutrino direction itself is generally worse than that of the lepton direction, and dependent on neutrino energy.

Multiple particles in an interaction (so long as they are above Cherenkov threshold) may be reconstructed, allowing for the exclusive reconstruction of final states. In searches for proton decay,

multiple particles can be kinematically reconstructed to form a decaying nucleon. High-quality particle identification is also possible: γ rays and electrons shower, and electrons scatter, which results in fuzzy rings, whereas muons, pions and protons make sharp rings. These patterns can be quantitatively separated with high reliability using maximum likelihood methods [41]. A e/μ misidentification probability of $\sim 0.4\%/\xi$ in the sub-GeV range is consistent with the performance of several experiments for $4\% < \xi < 40\%$. Sources of background for high energy interactions include misidentified cosmic muons and anomalous light patterns when the PMTs sometimes “flash” and emit photons themselves. The latter class of events can be removed using its distinctive PMT signal patterns, which may be repeated. More information about high energy event selection and reconstruction may be found in reference [42].

In spite of the fairly low light yield, large water Cherenkov detectors may be employed for reconstructing low-energy events, down to *e.g.* ~ 4 -5 MeV for Super-K [43]. Low-energy neutrino interactions of solar neutrinos in water are predominantly elastic scattering off atomic electrons; single electron events are then reconstructed. At solar neutrino energies, the visible energy resolution ($\sim 30\%/\sqrt{\xi E_{\text{vis}}(\text{MeV})}$) is about 20% worse than photoelectron counting statistics would imply. Using an electron LINAC and/or nuclear sources, approximately 0.5% determination of the absolute energy scale has been achieved at solar neutrino energies. Angular resolution is limited by multiple scattering in this energy regime (25–30°). At these energies, radioactive backgrounds become a dominant issue. These backgrounds include radon in the water itself or emanated from detector materials, and γ rays from the rock and detector materials. In the few to few tens of MeV range, radioactive products of cosmic-ray-muon-induced spallation are troublesome, and are removed by proximity in time and space to preceding muons, at some cost in dead time. Gadolinium doping using 0.2% $\text{Gd}_2(\text{SO}_4)_3$ is planned for Super-K to improve selection of low-energy $\bar{\nu}_e$ and other events with accompanying neutrons [44].

The Sudbury Neutrino Observatory (SNO) detector [45] is the only instance of a large heavy water detector and deserves mention here. In addition to an outer 1.7 kton of light water, SNO contained 1 kton of D_2O , giving it unique sensitivity to neutrino neutral current ($\nu_x + d \rightarrow \nu_x + p + n$), and charged current ($\nu_e + d \rightarrow p + p + e^-$) deuteron breakup reactions. The neutrons were detected in three ways: In the first phase, via the reaction $n + d \rightarrow t + \gamma + 6.25$ MeV; Cherenkov radiation from electrons Compton-scattered by the γ rays was observed. In the second phase, NaCl was dissolved in the water. ^{35}Cl captures neutrons, $n + ^{35}\text{Cl} \rightarrow ^{36}\text{Cl} + \gamma + 8.6$ MeV. The γ rays were observed via Compton scattering. In a final phase, specialized low-background ^3He counters (“neutral current detectors” or NCDs) were deployed in the detector. These counters detected neutrons via $n + ^3\text{He} \rightarrow p + t + 0.76$ MeV; ionization charge from energy loss of the products was recorded in proportional counters.

36.3.2 Neutrino telescopes

Revised August 2019 by U.F. Katz (Erlangen U.) and C. Spiering (DESY, Zeuten).

The primary goal of neutrino telescopes (NTs) is the detection of astrophysical neutrinos, in particularly those which are expected to accompany the production of high-energy cosmic rays in astrophysical accelerators. NTs in addition address a variety of other fundamental physics issues like indirect search for dark matter, study of neutrino oscillations, search for exotic particles like magnetic monopoles or study of cosmic rays and their interactions [46–48]. Electromagnetic radio frequency detectors for high energy neutrinos are discussed in “Radio emission from (ultra-) high energy particle showers” section 36.3.3.

NTs are large-volume arrays of “optical modules” (OMs) installed in open transparent media like water or ice, at depths that completely block the daylight. The OMs record the Cherenkov light induced by charged secondary particles produced in reactions of high-energy neutrinos in or around the instrumented volume. The neutrino energy, E_ν , and direction can be reconstructed from the hit pattern recorded. NTs typically target an energy

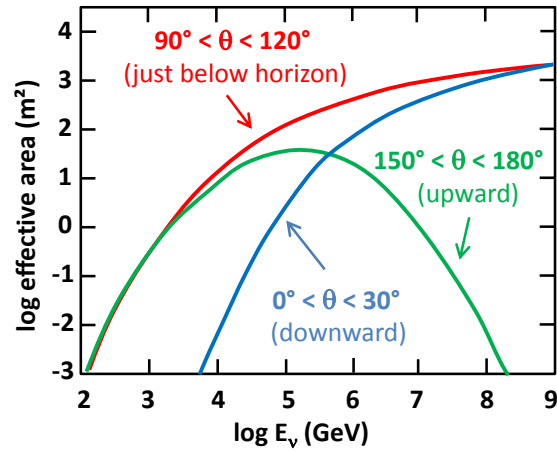


Figure 36.5: Effective $\bar{\nu}_\mu$ area for IceCube as an example of a cubic-kilometre NT, as a function of neutrino energy for three intervals of the zenith angle θ . The values shown here correspond to a specific event selection for point source searches.

range $E_\nu \gtrsim 100$ GeV; sensitivity to lower energies is achieved in dedicated setups with denser instrumentation.

In detecting cosmic neutrinos, three sources of backgrounds have to be considered: (i) *atmospheric neutrinos* from cosmic-ray interactions in the atmosphere, which can be separated from cosmic neutrinos on a statistical basis, or, for down-going neutrinos, by vetoing accompanying muons; (ii) down-going punch-through *atmospheric muons* from cosmic-ray interactions, which are suppressed by several orders of magnitude with respect to the ground level due to the large detector depths. They can be further reduced by selecting upward-going or high-energy neutrinos or by self-veto methods; (iii) random backgrounds due to photomultiplier (PMT) dark counts, ^{40}K decays (mainly in sea water) or bioluminescence (only water), which impact adversely on event recognition and reconstruction. Note that atmospheric neutrinos and muons allow for investigating neutrino oscillations and cosmic ray anisotropies, respectively.

Recently, it has become obvious that a precise measurement of the energy-zenith-distribution of atmospheric neutrinos may allow for determining the neutrino mass hierarchy by exploiting matter-induced oscillation effects in the Earth [49, 50].

Neutrinos can interact with target nucleons N through charged current ($\bar{\nu}_\ell N \rightarrow \ell^\mp X$, CC) or neutral current ($\bar{\nu}_\ell N \rightarrow \bar{\nu}_\ell X$, NC) processes. A CC reaction of a $\bar{\nu}_\mu$ produces a muon track and a hadronic particle cascade, whereas all NC reactions and CC reactions of $\bar{\nu}_\tau$ produce particle cascades only. CC interactions of $\bar{\nu}_\tau$ can have either signature, depending on the τ decay mode. In most astrophysical models, neutrinos are expected to be produced through the $\pi/K \rightarrow \mu \rightarrow e$ decay chain, *i.e.*, with a flavour ratio $\nu_e : \nu_\mu : \nu_\tau \approx 1 : 2 : 0$. For sources outside the solar system, neutrino oscillations turn this ratio to $\nu_e : \nu_\mu : \nu_\tau \approx 1 : 1 : 1$ upon arrival on Earth.

The total neutrino-nucleon cross section is about 10^{-35} cm^2 at $E_\nu = 1$ TeV and rises roughly linearly with E_ν below this energy and as $E_\nu^{0.3-0.5}$ above, flattening out towards high energies. The CC:NC cross-section ratio is about 2:1. At energies above some TeV, neutrino absorption in the Earth becomes noticeable; for vertically upward-moving neutrinos (zenith angle $\theta = 180^\circ$), the survival probability is 74 (27, < 2)% for 10 (100, 1000) TeV. On average, between 50% (65%) and 75% of E_ν is transferred to the final-state lepton in neutrino (antineutrino) reactions between 100 GeV and 10 PeV.

The final-state lepton follows the initial neutrino direction with a RMS mismatch angle $\langle \phi_{\nu\ell} \rangle \approx 1.5^\circ/\sqrt{E_\nu [\text{TeV}]}$, indicating the intrinsic kinematic limit to the angular resolution of NTs. For CC $\bar{\nu}_\mu$ reactions at energies above about 10 TeV, the angular resolution is dominated by the muon reconstruction accuracy of a few times 0.1° at most. For muon energies $E_\mu \gtrsim 1$ TeV, the increasing light emission due to radiative processes allows for re-

constructing E_μ from the measured dE_μ/dx with an accuracy of $\sigma(\log E_\mu) \approx 0.3$; at lower energies, E_μ can be estimated from the length of the muon track if it is contained in the detector. These properties make CC $\bar{\nu}_\mu$ reactions the prime channel for the identification of individual astrophysical neutrino sources.

Hadronic and electromagnetic particle cascades at the relevant energies are 5–20 m long, *i.e.*, short compared to typical OM distances. The total amount of Cherenkov light provides a direct measurement of the cascade energy with an accuracy of about 20% at energies above 10 TeV and 10% beyond 100 TeV for events contained in the instrumented volume. Neutrino flavour and reaction mechanism can, however, hardly be determined and neutrinos from NC reactions or τ decays may carry away significant “invisible” energy. Above 100 TeV, the average directional reconstruction accuracy of cascades is 10–15 degrees in polar ice and better than 2 degrees in water, the difference being due to the inhomogeneity of the ice and stronger light scattering in ice. These features, together with the small background of atmospheric $\bar{\nu}_e$ and $\bar{\nu}_\tau$ events, makes the cascade channel particularly interesting for searches for a diffuse, high-energy excess of extraterrestrial over atmospheric neutrinos. In water, cascade events can also be used for the search for point sources of cosmic neutrinos, albeit the inferior angular accuracy compared to muon tracks leads to a higher background from atmospheric neutrinos.

The detection efficiency of a NT is quantified by its effective area, *e.g.*, the fictitious area for which the full incoming neutrino flux would be recorded (see Figure 36.5). The increase with E_ν is due to the rise of neutrino cross section and muon range, while neutrino absorption in the Earth causes the decrease at large θ . Identification of downward-going neutrinos requires strong cuts

against atmospheric muons, hence the cut-off towards low E_ν . Due to the small cross section, the effective area is many orders of magnitude smaller than the geometrical dimension of the detector; a $\bar{\nu}_\mu$ with 1 TeV can, *e.g.*, be detected with a probability of the order 10^{-6} if the NT is on its path.

Detection of upward-going muons allows for identifying neutrino interactions far outside the instrumented volume. This method, however, is only sensitive to CC $\bar{\nu}_\mu$ interactions and cannot be extended to more than 5–10 degrees above the geometric horizon, where the background of atmospheric muons becomes prohibitive. Alternatively, one can select events that start inside the instrumented volume and thus remove incoming muons that generate early hits in the outer layers of the detector. Such a veto-based event selection is sensitive to neutrinos of all flavours from all directions, albeit with a reduced efficiency since a part of the instrumented volume is sacrificed for the veto. Such a muon veto, or vetoing events with a coincident signal in the surface array, also rejects down-going atmospheric neutrinos that are accompanied by muons from the same air shower and thus reduces the atmospheric-neutrino background. Actually, the breakthrough in detecting high-energy cosmic neutrinos has been achieved with this technique.

Note that the fields of view of NTs at the South Pole and in the Northern hemisphere are complementary for each reaction channel and neutrino energy.

36.3.2.1 The Projects

Table 36.3 lists past, present and future neutrino telescope projects and their main parameters.

Table 36.3: Past, present and future NT projects and their main parameters. The milestone years give the times of project start, of first data taking with partial configurations, of detector completion, and of project termination. Projects with first data expected past 2020 are indicated in italics. The size refers to the largest instrumented volume reached during the project development. See [48] for references to the different projects where unspecified.

Experiment	Milestones	Location	Size (km ³)	Remarks
DUMAND	1978/--/1995	Pacific Ocean		Terminated due to technical/funding problems
NT-200	1980/1993/1998/2015	Lake Baikal	10 ⁻⁴	First proof of principle
GVD [51]	2012/2015/--	Lake Baikal	0.5–1.5	High-energy ν astronomy first 5 clusters installed
NESTOR	1991/--/--	Med. Sea		2004 data taking with prototype
NEMO	1998/--/--	Med. Sea		R&D project, prototype tests
AMANDA	1990/1996/2000/2009	South Pole	0.015	First deep-ice NT
ANTARES	1997/2006/2008/--	Med. Sea	0.010	First deep-sea NT
IceCube	2001/2005/2010/--	South Pole	1.0	First km ³ -sized detector
<i>IceCube-Gen2</i> [52]	2014/--/--	South Pole	5–10	Planned extension of IceCube covering low and high energies, a surface array and radio detection
KM3NeT/ARCA [50]	2013/(2015)/--	Med. Sea	ca. 1	First construction phase started
KM3NeT/ORCA [50]	2014/(2017)/--	Med. Sea	0.003	Low-energy configuration for neutrino mass hierarchy
<i>KM3NeT Phase 3</i>	2013/--/--	Med. Sea	ca. 3	6 ARCA blocks + ORCA

36.3.2.2 Properties of media

The efficiency and quality of event reconstruction depend strongly on the optical properties (absorption and scattering length, intrinsic optical activity) of the medium in the spectral range of alkali photocathodes (300–550 nm). Large absorption lengths result in a better light collection, large scattering lengths in superior angular resolution. Deep-sea sites typically have effective scattering lengths of > 100 m and, at their peak transparency around 450 nm, absorption lengths of 50–65 m. The absorption length for Lake Baikal is 22–24 m. The properties of South Polar ice vary strongly with depth; at the peak transparency wave length (400 nm), the scattering length is between 5 and 75 m and the absorption length between 15 and 250 m, with the best values in the depth region 2200–2450 m and the worst ones in the layer

1950–2100 m.

Noise rates measured by 25 cm PMTs in deep polar ice are about 0.5 kHz per PMT and almost entirely due to radioactivity in the OM components. The corresponding rates in sea water are typically 60 kHz, mostly due to ⁴⁰K decays. Bioluminescence activity can locally cause rates on the MHz scale for seconds; the frequency and intensity of such “bursts” depends strongly on the sea current, the season, the geographic location, and the detector geometry. Experience from ANTARES shows that these backgrounds are manageable without a major loss of efficiency or experimental resolution.

36.3.2.3 Technical realisation

Optical modules (OMs) and PMTs: An OM is a pressure-tight glass sphere housing one or several PMTs with a time resolu-

tion in the nanosecond range, and in most cases also electronics for control, HV generation, operation of calibration LEDs, time synchronisation and signal digitisation.

Hybrid PMTs with 37 cm diameter have been used for NT-200, conventional hemispheric PMTs for AMANDA (20 cm) and for ANTARES, IceCube and Baikal-GVD (25 cm). A novel concept has been chosen for KM3NeT. The OMs (43 cm) are equipped with 31 PMTs (7.5 cm), plus control, calibration and digitisation electronics. The main advantages are that (i) the overall photocathode area exceeds that of a 25 cm PMT by more than a factor of 3; (ii) the individual readout of the PMTs results in a very good separation between one- and two-photoelectron signals which is essential for online data filtering and random background suppression; (iii) the hit pattern on an OM provides directional information; (iv) no mu-metal shielding against the Earth magnetic field is required. Figure 36.6 shows the OM designs of IceCube and KM3NeT.

Readout and data filtering: In current NTs the PMT data are digitised in situ, for ANTARES and Baikal-GVD in special electronics containers close to the OMs, for IceCube and KM3NeT inside the OMs. For IceCube, data are transmitted via electrical cables of up to 3.3 km length, depending on the location of the strings and the depth of the OMs; for ANTARES, KM3NeT and Baikal-GVD optical fibre connections have been chosen (several 10 km for the first two and 4 km for GVD).

The full digitised waveforms of the IceCube OMs are transmitted to the surface for pulses appearing in local coincidences on a string; for other pulses, only time and charge information is provided. For ANTARES (time and charge) and KM3NeT (time over threshold), all PMT signals above an adjustable noise threshold are sent to shore.

The raw data are subsequently processed on online computer farms, where multiplicity and topology-driven filter algorithms are applied to select event candidates. The filter output data rate is about 10 GByte/day for ANTARES and of the order 1 TByte/day for IceCube (100 GByte/day transferred via satellite) and KM3NeT.

Calibration: For efficient event recognition and reconstruction, the OM timing must be synchronised at the few-nanosecond level and the OM positions and orientations must be known to a few 10 cm and a few degrees, respectively. Time calibration is achieved by sending time synchronisation signals to the OM electronics and also by light calibration signals emitted in situ at known times by LED or laser flashers (ANTARES, KM3NeT). Precise position calibration is achieved by measuring the travel time of light calibration signals sent from OM to OM (IceCube) or acoustic signals sent from transducers at the sea floor to receivers on the detector strings (ANTARES, KM3NeT, Baikal-GVD). Absolute pointing and angular resolution can be determined by measuring the “shadow of the moon” (*i.e.*, the directional depletion of muons generated in cosmic-ray interactions). IceCube has shown that both are below 1° , confirming MC calculations which indicate a precision of $\approx 0.5^\circ$ for energies above 10 TeV. For KM3NeT, simulations indicate that sub-degree precision in the absolute pointing can be reached within a few weeks of operation.

Detector configurations: IceCube (see Figure 36.7) consists of 5160 Digital OMs (DOMs) installed on 86 strings at depths of 1450 to 2450 m in the Antarctic ice; except for the DeepCore region, string distances are 125 m and vertical distances between OMs 17 m. 324 further DOMs are installed in IceTop, an array of detector stations on the ice surface above the strings. DeepCore is a high-density sub-array at large depths (*i.e.*, in the best ice layer) at the centre of IceCube.

The NT200 detector in Lake Baikal at a depth of 1100 m consisted of 8 strings attached to an umbrella-like frame, with 12 pairs of OMs per string. The diameter of the instrumented volume was 42 m, its height 70 m. Meanwhile (2019), the Baikal collaboration has installed the first five clusters of a future cubic-kilometre array. A first phase, covering a volume of about 0.4 km^3 , will consist of 9 clusters, each with 288 OMs at 8 strings; its completion is scheduled for 2021. A next stage could comprise about 20 clusters and cover up to 1.5 km^3 .

ANTARES comprises 12 strings with lateral distances of 60–

70 m, each carrying 25 triplets of OMs at vertical distances of 14.5 m. The OMs are located at depths of 2.1–2.4 km, starting 100 m above the sea floor. A further string carries devices for calibration and environmental monitoring. A system to investigate the feasibility of acoustic neutrino detection has also been implemented.

KM3NeT will consist of building blocks of 115 strings each, with 18 OMs per string. Operation of prototypes and the first strings deployed have successfully verified the KM3NeT technology [53]. In the upcoming phase 2.0 of its staged implementation, KM3NeT aims at two building blocks for neutrino astronomy, with vertical distances between OMs of 36 m and a lateral distance between adjacent strings of 90 m (ARCA, for *Astroparticle Research with Cosmics in the Abyss*) and at one block for the measurement of the neutrino mass hierarchy, with vertical distances between OMs of 9 m and a lateral distance between adjacent strings of about 20 m (ORCA, for *Oscillation Research with Cosmics in the Abyss*) [50]. A first installation phase of ARCA near Capo Passero, East of Sicily and of ORCA near Toulon has started in 2015 and comprises 24 (6) ARCA (ORCA) strings to be deployed by 2021 (2019). Completion of the full ARCA (ORCA) arrays is planned for 2026 (2024). The possibility of directing a neutrino beam from the Protvino accelerator to ORCA (P2O) is also under study [54].

36.3.2.4 Results

Atmospheric neutrino fluxes have been precisely measured with AMANDA and ANTARES ($\overline{\nu}_\mu$) and with IceCube ($\overline{\nu}_\mu$, $\overline{\nu}_e$); the results are in agreement with predicted spectra.

In 2013, an excess of track and cascade events between 30 TeV and 1 PeV above background expectations was reported by IceCube; this analysis used the data taken in 2010 and 2011 and for the first time employed containment conditions and an atmospheric muon veto for suppression of down-going atmospheric neutrinos (High-Energy Starting Event analysis, HESE). The observed excess reached a significance of 5.7σ in a subsequent analysis of 3 years of data [56] and increased in significance since then. It cannot be explained by atmospheric neutrinos and misidentified atmospheric muons alone. A consistent observation has also been made by ANTARES [57], albeit with much lower significance. The skymap of HESE and high-energy through-going muon events (see Figure 36.8) does not indicate statistically significant event clusters, nor deviations from an isotropic cosmic neutrino flux. Meanwhile the energy range of the IceCube HESE analysis has been extended down to 1 TeV and the high-energy excess confirmed; also, events with through-going muons showed a corresponding excess of cosmic origin. In [58], the various analyses have been combined. Assuming the cosmic neutrino flux to be isotropic, flavour-symmetric and ν - $\bar{\nu}$ -symmetric at Earth, the all-flavour spectrum is well described by a power law with normalisation $6.7^{+1.1}_{-1.2} \times 10^{-18} \text{ GeV}^{-1} \text{ s}^{-1} \text{ sr}^{-1} \text{ cm}^{-2}$ at 100 TeV and a spectral index -2.50 ± 0.09 for energies between 25 TeV and 2.8 PeV. A spectral index of -2 , an often quoted benchmark value, is disfavoured with a significance of 3.8σ .

Multi-messenger observations triggered by a high-energy IceCube neutrino event in 2017 (see Figure 36.9 for an event display), together with a neutrino excess from the same celestial direction in the 2014/15 archival IceCube data, yielded evidence for a first neutrino signal related to a known astronomical object, the blazar² TXS 0506+056 [59, 60]. Multi-messenger investigations in conjunction with gravitational waves, ultra-high-energy cosmic rays or gamma-ray observations have not revealed further matching neutrino signals to date. Also, no further astrophysical neutrino sources were found in a recent combined IceCube/ANTARES search for steady sources [61].

IceCube has reported an energy-dependent anisotropy of cosmic-ray induced muons and a measurement of the neutrino-nucleon cross section using neutrino absorption in Earth.

No indications for neutrino fluxes from dark matter annihilations or for other exotic phenomena have been found.

²An Active Galactic Nucleus with a relativistic jet outflow pointing to the observer.

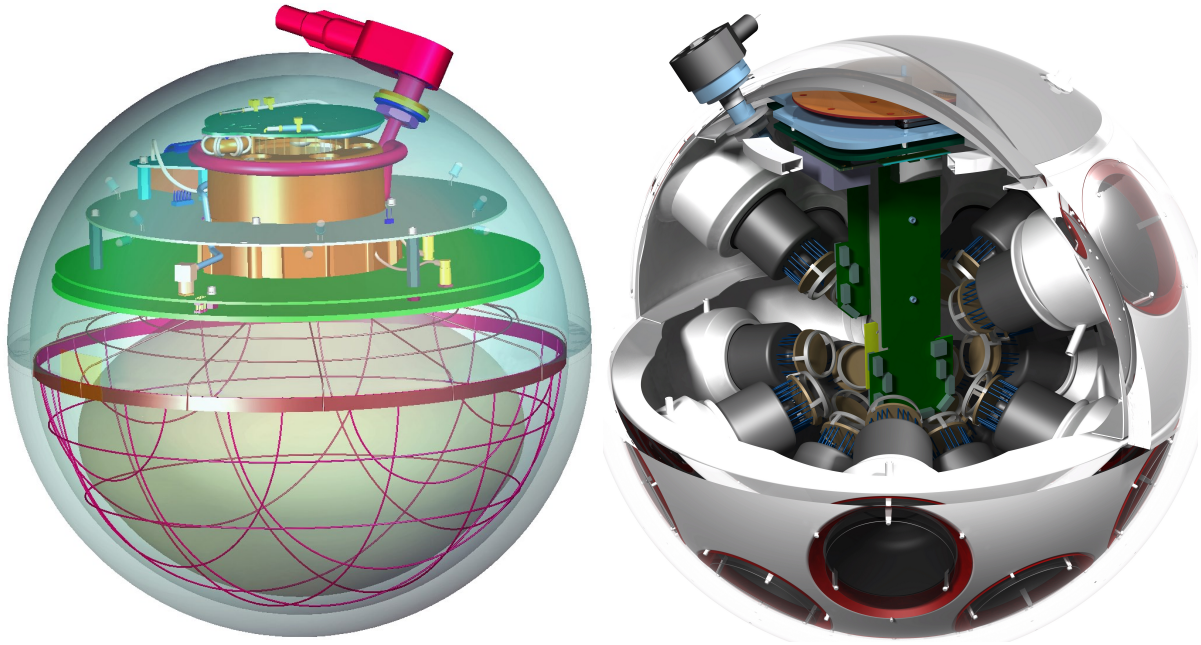


Figure 36.6: Schematic views of the digital OMs of IceCube (left) and KM3NeT (right).

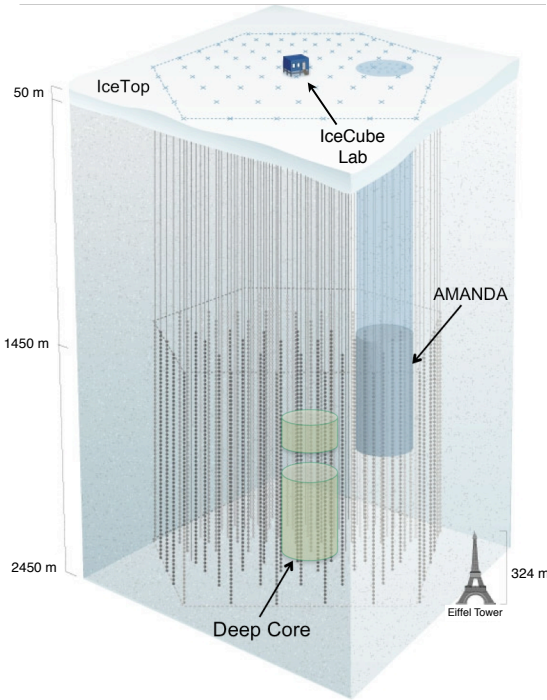


Figure 36.7: Schematic view of the IceCube neutrino observatory comprising the deep-ice detector including its nested dense part DeepCore, and the surface air shower array IceTop. The IceCube Lab houses data acquisition electronics and the computer farm for online processing. Operation of AMANDA was terminated in 2009.

At lower energies, down to 10 GeV, IceCube/DeepCore and ANTARES have identified clear signals of oscillations of atmospheric neutrinos. The closely spaced OMs of DeepCore allow for selecting a very pure sample of low-energy $\bar{\nu}_\mu$ (6–56 GeV) that produce upward moving muons inside the detector. The neutrino energy is determined from the energy of the hadronic shower at the vertex and the muon range. Fits to the energy/zenith-dependent deficit of muon neutrinos provide constraints on the oscillation pa-

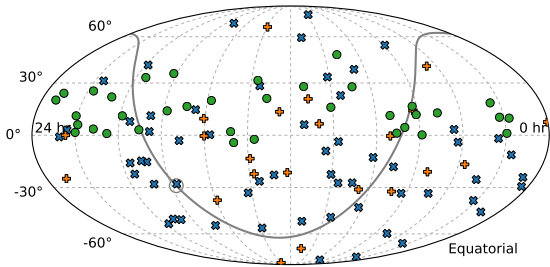


Figure 36.8: Arrival directions of IceCube candidate events for cosmic neutrinos in equatorial coordinates. The plot contains 82 HESE events, with shower-like events marked as blue \times and muon tracks as orange $+$, and in addition 36 through-going muons tracks with an energy deposit exceeding 200 TeV (green circles). Approximately 40% of the events are expected to originate from atmospheric backgrounds. The grey curve denotes the Galactic Plane and the grey circle the Galactic Centre (from [55]).

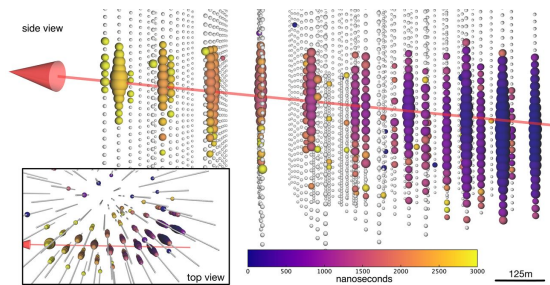


Figure 36.9: Display of the neutrino event IceCube-170922A pointing to the blazar TXS 0506+056. The deposited energy is 24 TeV, the neutrino energy is estimated to be 290 TeV. The colour code indicates the signal timing (blue: early; yellow: late), the size of the coloured circles is a logarithmic measure of the light intensity registered per DOM. The arrow indicates the reconstructed direction, corresponding to a zenith angle of $5.7^{+0.5}_{-0.3}$ degrees below horizon. Figure from [59].

rameters $\sin^2 \theta_{23}$ and Δm_{23}^2 . The analysis of the same dependence for cascade-like events provides a 3σ evidence for ν_τ appearance

– an important measurement to test the unitarity of the PNMS matrix [62].

See [63] and [64] for summaries of recent results of IceCube and ANTARES/KM3NeT, respectively.

36.3.2.5 Plans beyond 2020

Within the future IceCube-Gen2 project, it is planned to extend the sensitivity of IceCube towards both lower and higher energies. A substantially denser instrumentation of a sub-volume of DeepCore would lead to an energy threshold for neutrino detection of a few GeV, aiming primarily at measuring the neutrino mass hierarchy. For higher energies, a large-volume extension, combined with a powerful surface veto, is envisaged [52]. A very first phase with 7 closely spaced strings is in preparation for deployment in 2022/23, aiming to cover part of the low-energy program, to better calibrate the existing IceCube detector and the archival data, and to test new technologies. More information on the future extensions of GVD and KM3NeT are given above, in Table 36.3 and in [50].

36.3.3 Radio emission from (ultra-)high energy particle showers

Revised October 2019 by S.R. Klein (NSD LBNL; UC Berkeley).

Coherent radio-frequency (RF) electromagnetic radiation is an attractive signature to search for particle cascades produced by interactions of high-energy particles. RF signatures have been used to study both cosmic-ray air showers and to search for neutrino-induced showers. The difference in length scale (X_0) between air and the solid materials used for other neutrino searches leads to surprisingly large differences in signal generation. This article will begin with neutrino-induced showers, with air showers covered in subsection 36.3.3.3. At lower energies, incoherent optical Cherenkov radiation is frequently used, as discussed in "Neutrino telescopes" section 36.3.2.

RF detectors can be used to search for energetic neutrinos from three types of sources: astrophysical objects (*i.e.* extending measurements the neutrino energy spectrum observed at TeV to PeV energies upward in energy), searching for cosmogenic neutrinos associated with cosmic-ray-cosmic microwave background radiation interactions, and searching for neutrinos from beyond-standard-model physics. These types are roughly associated with energies below 10^{18} eV, the energy range 10^{18} to 10^{20} eV, and above 10^{20} eV. Cosmogenic neutrinos are produced when ultra-high energy (UHE) protons with energy $E > 4 \times 10^{19}$ eV interact with photons from the cosmic-microwave background radiation, infrared light from old stars, and other extragalactic background light. These protons are excited to a Δ^+ resonance which may decay via $\Delta^+ \rightarrow n\pi^+$, leading to the production of neutrinos with energies above 10^{18} eV [65, 66]. Neutrinos are the only long-range probe of the ultra-high energy cosmos, because protons, heavier nuclei and photons with energies above 5×10^{19} eV are limited to ranges of less than 100 Mpc by interactions with the CMB and early starlight.

The cosmogenic neutrino signal depends heavily on the fraction of UHE cosmic-rays that are protons. For a 100% proton composition (disfavored by most data), observing a cosmogenic neutrino signal of at least a few events per year requires a detector with an active volume of about 100 km^3 , made out of a non-conducting solid (or potentially liquid) medium, with a long absorption length for radio waves. The huge volumes require that this be a common material. A dense medium would reduce the detector volume, but, unfortunately, the available natural media have only moderate density. Optical Cherenkov and acoustical detectors are limited by short (< 300 m) attenuation lengths [67] so would require a prohibitively expensive number of sensors. Radio-detection is the only current approach that can scale to this volume. The two most commonly used media are glacial ice, in Antarctica or Greenland, or the lunar regolith [68].

Electromagnetic and hadronic showers produce radio pulses via the Askaryan effect [69, 70], as discussed in "Passage of Particles Through Matter" review Sec. 34. The shower contains more electrons than positrons. At wavelengths longer than the transverse size of the shower, this leads to coherent Cherenkov emission, where the electric field scales as the square of the net charge ex-

cess. This may also be described more generally as being due to radiation from a time-varying net charge [71]; this latter description also applies to radio emission in cosmic-ray air showers.

High-frequency radiation is concentrated around the Cherenkov angle. Viewed directly on the Cherenkov cone, the electric field strength, ϵ_{Ch} at a frequency f from an electromagnetic shower from a ν_e may be roughly parameterized as [72, 73]

$$\epsilon_{\text{Ch}}(\text{V/mMHz}) = 2.53 \times 10^{-7} \frac{E_\nu}{1\text{TeV}} \frac{f}{f_c} \left[\frac{1}{1 + (f/f_c)^{1.44}} \right]. \quad (36.3)$$

The electric field strength increases linearly with frequency, up to a cut-off frequency f_c , which is set by the transverse size of the shower [74, 75]. The maximum wavelength c/f_c is roughly the Moliere radius divided by $\cos(\theta_C)$ where θ_C is the Cherenkov angle. The cutoff frequencies depend on the density (which affects the Moliere radius). They are about 1 GHz in ice, and about 3 GHz in the lunar regolith. Near f_c , radiation is narrowly concentrated around the Cherenkov angle [74, 75]. At lower frequencies, the limited length of the emitting region leads to a broadening in emission angle around the Cherenkov cone. Away from θ_C , the electric field from Eq. (36.3) is reduced by [72],

$$\frac{\epsilon}{\epsilon_{\text{Ch}}} = \exp \left(-\frac{1}{2} \frac{(\theta - \theta_C)^2}{(2.2^\circ \times [1\text{GHz}/f])^2} \right). \quad (36.4)$$

In both ice and the lunar regolith, the Cherenkov angle is about 56° . At very low frequencies, the distribution is very broad, with $f = 50\text{MHz}$ corresponding to a shower with an angular spread of $\sigma = 45^\circ$.

More accurate calculations of the predicted radio signal from a neutrino require detailed Monte Carlo simulations. These simulations begin with a neutrino induced shower, and then calculate (directly or from a parameterization) the Askaryan signal. The Askaryan signal calculation is tough for two reasons. First, much of the excess charge comes from the lowest energy particles in the shower. Second, it is necessary to keep track of the phase of the signal from each particle, as well as the amplitude and the time (or frequency) dependence. This signal is then propagated through the medium and into an antenna model [73].

Along the Cherenkov cone, the 1 GHz maximum frequency leads to a generated pulse width of ≈ 1 nsec. This pulse broadens by dispersion as it propagates, particularly for signals from the Moon traversing the ionosphere. As long as the dispersion can be compensated for and backgrounds controlled, a large bandwidth detector is the most sensitive. Spectral information can be used to reject background, and to help reconstruct the neutrino direction, because the cutoff frequency depends on the observation angle with respect to the Cherenkov cone.

The electric field is linearly proportional to the neutrino energy, so the power (field strength squared) is proportional to the square of the neutrino energy. Since the signal is a radio wave, the field amplitude decreases as $1/R$, plus absorption in the intervening medium. The detection threshold is determined by the distance to the antenna and the noise characteristics of the detector. For an antenna located in the detection medium, the typical threshold is around 10^{17} eV; for stand-off (remote sensing) detectors, the threshold rises roughly linearly with the distance. These thresholds can be reduced significantly by using directional antennas and/or combining the signals from multiple antennas using beam-forming techniques. Experiments have used both approaches to reduce trigger-level noise, or to reject background at the analysis level. For multi-element arrays, the threshold drops as the square root of number of antennas, since the signal adds in-phase while the backgrounds add with random phases [76].

Some common background sources are anthropogenic noise, antenna/preamp noise, cosmic-ray air showers, charge generated by blowing snow, lightning, and, at low frequencies, radiation from the Milky Way. The need to limit anthropogenic noise has led most experimental groups to select remote locations for their detectors.

Reconstruction of the neutrino arrival direction depends on several aspects of the signal. First, the direction from the antenna

to the interaction site must be determined. This can be done by using the relative timing from separated antennas, or using beam-forming techniques with multi-element arrays. If the radio signal encounters media where the index of refraction vary (like the firm of glacial ice), then it may be necessary to use ray-tracing techniques to follow the signal back to interaction point. The distance (and hence the neutrino energy) can be difficult to determine unless the signal can be triangulated, either using multiple, separated antennas, or observing two pulses with different flight paths (*i. e.* with one including a reflection) in a single antenna.

The neutrino arrival direction can be determined with respect to that direction via two angles, which are determined using very different methods. The first uses the measured frequency spectrum. Equation 36.4 can be used to determine the angular distance between the detector vector and the Cherenkov cone. The second angle can be determined by the polarization of the signal. The radio signal is produced with a linear polarization in the plane containing both the neutrino direction and the photon direction. These two angles can be combined to determine the direction, subject to a (usually) four-fold ambiguity, due to uncertainty as to whether the antenna is inside or outside the Cherenkov cone, and because the neutrino direction can be flipped 180° without affecting the observed signal. Often, some of these solutions can be rejected because they correspond to long path lengths through the Moon or the Earth, where the neutrino would be absorbed.

At energies above 10^{16} eV in ice, the Landau-Pomeranchuk-Migdal effect lengthens electromagnetic showers, by reducing the cross-sections for bremsstrahlung and pair production [77]. The lengthening of the shower leads to a narrowing of the radio emission around the Cherenkov cone, and a reduction in high-frequency emission away from the cone [73]. At higher energies, this leads two separate components of the Askaryan radiation: an un-altered component from the hadronic portion of the shower (on average 20% of the total energy) and a an angularly narrowed component from the LPM-lengthened electromagnetic shower. The angular narrowing scales as $E_\nu^{1/3}$; if these two components can be observed separately, they could, in principle, be combined to determine the inelasticity of the neutrino interaction [78], allowing for improved measurements of parton distributions, and searches for beyond-standard-model interactions.

At still higher energies, above 10^{20} eV, the LPM effect becomes stronger, and the electromagnetic shower splits into multiple sub-showers with significant separation. When this separations become large enough, the subshowers will effectively become independent radiators, with the total emission showing substantial event-by-event variation, depending on the division into subshowers [77]. Because of this, many of the experiments that study higher energy (well above 10^{20} eV) neutrinos focus on the hadronic shower from the struck nucleus. This contains an average of only about 20% of the energy, but with smaller large fluctuations.

Figure 36.10 shows some of the current limits from neutrino searches, including from prototype arrays. Except for LOFAR, which is fully operational, projected limits from future experiments are not shown in the figure.

One variation on the radio-detection approach is to look for radio signals from Earth-skimming ν_τ . Although ν_τ are much less commonly produced than ν_μ and ν_e , as they travel astrophysical distances, oscillations lead to a $\nu_e : \nu_\mu : \nu_\tau$ ratio near 1 : 1 : 1, for almost all non-exotic acceleration and propagation mechanisms [90].

If the ν_τ traverse the Earth and interact while traveling upward, near the surface, the resulting τ^\pm may exit the Earth before decaying. 83% of the time, the decay produces a hadronic or electromagnetic shower in the atmosphere [91]. Experiments have searched for this upgoing shower, and for the resulting optical Cherenkov and coherent RF radiation. The threshold energy dependence for these searches depends on several factors, notably including the average τ^\pm decay length, which increases linearly with energy; the Pierre Auger observatory set limits on the neutrino flux at energies above 10^{17} eV [80]. Radio-detection efforts have similar or slightly higher thresholds. Detection in low-density (compared to rock or ice) air introduces a number of new complications, including the much larger length scale and the effects

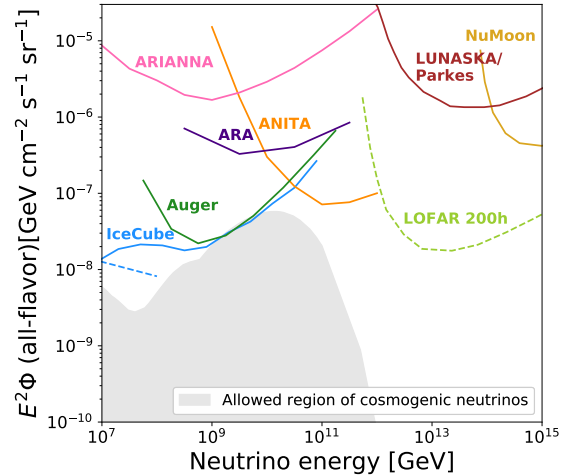


Figure 36.10: Representative 3-flavor (summed, assuming equal fluxes of each flavor) differential (over one decade in energy) limits from different experiments and prototype experiments. Shown are limits from the IceCube ultra-high energy ν search [79], the Auger search for earth-skimming ν_τ [80], the LUNASKA/Parkes [81] and NuMoon lunar searches [82], the ANITA balloon experiment [83], ARA [84] and ARIANNA prototypes [85], along with projections for the LOFAR array [86]. The dashed blue line is the extrapolation of the IceCube through-going ν_μ flux measured at lower energies (few 10s of TeV to 10 PeV), with spectral index $\alpha = -2.28$ [87]. Because of the long extrapolation, this should only be treated as a rough reference. The ARA and ARIANNA limits are from prototype arrays, and indicate the energy range that might be covered, with far higher sensitivity by larger arrays. The shaded area is the allowed region for neutrinos, from a recent global analysis that included the measured cosmic-ray spectrum and composition [88]. Thanks to Anna Nelles (DESY-Zeuthen) for preparing this figure, which is adapted from Ref. [89].

of the Earth's magnetic field. These issues are similar to those inherent in studies of radio signals from cosmic-ray air showers, discussed later.

The ANITA balloon-based radio-detection experiment has even reported two anomalous events [92] which the collaboration has indicated might be from Earth-skimming ν_τ . However, this interpretation is controversial.

A number of prototype ν_τ radio-detection experiments exist. The GRAND Collaboration recently proposed to deploy a 10,000 antenna array, eventually growing to 200,000 antennas spread over 200,000 km^2 [93]. The latter array would be sensitive to cosmogenic neutrinos, unless the UHE cosmic-ray flux is mostly heavier nuclei.

Magnetic monopoles would also emit radio waves, and neutrino experiments have also set monopole flux limits [94].

36.3.3.1 The Moon as a target

Because of its large size and non-conducting regolith, and the availability of large radio-telescopes, the Moon is an attractive target [95]. Conventional radio-telescopes are quite well suited to lunar neutrino searches, with natural beam widths not too dissimilar from the size of the Moon. Still, there are experimental challenges. The attenuation length is typically estimated to be $9m/f(\text{GHz})$, so only near-surface interactions can be studied. The composition of the lunar regolith is not well known, so there are significant uncertainties on this attenuation. And, there is a background from cosmic-ray interactions in the Moon. One big limitation of lunar experiments is that the 240,000 km target-antenna separation leads to neutrino energy thresholds above 10^{20} eV.

The effective volume probed by experiments depends on the geometry, which itself depends on the frequency range used. At high frequencies f , the electric field strength is high, leading to a lower energy threshold, but the sensitive volume is limited because

the Cherenkov cone only points toward the Earth for a narrow range of geometries. Lower frequency radiation is more isotropic, so the effective volume is larger, but, because the electric field is weaker, the energy threshold is higher. The $1/f$ dependence of the attenuation length in the lunar regolith further increases the effective volume at low frequencies. The frequency range affects the energy dependence of the sensitivity. As can be seen in Fig. 36.10, a low-frequency experiment like NuMoon (which covered 115-180 MHz) has good sensitivity, but only above about 10^{14} GeV, while Lunaska/Parkes, which observed in the range 1200-1500 MHz, has a higher flux limit, but is sensitive above about $10^{12.5}$ GeV.

With modern technology, it is increasingly viable to search over very broad frequency ranges [96]. One technical challenge is due to dispersion (frequency dependent time delays) in the ionosphere. Dispersion can be largely removed with a de-dispersion filter, using either analog circuitry or post-collection digital processing.

Lunar experiments use different techniques to reduce the anthropogenic background. Some experiments use multiple antennas, separated by at least hundreds of meters; by requiring a coincidence within a small time window, anthropogenic noise can be rejected. With good enough timing, beam-forming techniques can be used to further reduce the background. An alternative approach is to use beam forming with multiple feed antennas viewing a single reflector, to ensure that the signal points back to the moon.

In the near future, several large radio detector arrays should reach significantly lower limits. The LOFAR array is taking data with 36 detector clusters spread over Northwest Europe [86]. In the longer term, the Square Kilometer Array (SKA) with its 1 km^2 effective area will push thresholds down to near 10^{20} eV [96]. It should be noted that current limits and projected sensitivities are sensitive to many details, and different analyses make different assumptions. A recent review [97] compared different radio-detection experiments using a common framework, and found some significant shifts in sensitivities.

36.3.3.2 Ice-based detectors

Detecting neutrinos with a lower energy threshold requires a smaller antenna-target separation. Natural ice is an attractive medium for this, offering a stable construction platform, with radio attenuation lengths from over 300 m to 1 km. The attenuation length varies with the frequency and ice temperature, with higher attenuation in warmer ice.

Although glacial ice is mostly uniform, the top ≈ 100 m of ice, the 'firn,' exhibits a gradual transition from packed snow at the surface (typical density 0.35 g/cm^3) to solid ice (density 0.92 g/cm^3) below [98]. The thickness of the firn varies with location; it is thicker in central Antarctica than in the coastal ice sheets or in Greenland. The varying density has several implications.

The index of refraction depends linearly on the density, so radio waves curve downward in the firn. This bending reduces the effective volume of surface or aerial antennas. A surface antenna cannot see near-surface interactions at large horizontal distances. The bending also means that the arrival direction of radio waves do not point directly back to the neutrino source. One must use ray tracing to determine the direction of neutrino interactions.

The bending also creates an opportunity to measure the distance from the detector to the neutrino interaction. For some geometries with buried antennas, there may be two paths to the detector: one 'direct' path, with minor bending, and a second where the signal is bent beyond vertical, bouncing off the surface before reaching the antenna. By measuring the time difference between the two paths, the distance to the interaction vertex may be determined; this greatly improves the energy determination [99, 100].

There are also indications that the increase in firn density is non-monotonic [101, 102]. This can lead to a non-monotonic change in index of refraction which may create waveguides which trap a small fraction of the radio energy and propagate it horizontally.

In one type of experiment, antennas mounted on scientific balloons observe the ice from above. Radio signals from in-ice neutrino interactions propagate to the surface, traverse the ice-air

interface, and then travel to the balloon. The surface roughness of the ice can affect signals as they transition from the ice to the atmosphere. The best known example, ANITA, has made four flights around Antarctica, floating at an altitude around 35 km [103]. Its 32/40/48 (depending on the flight) dual-polarization horn antennas scanned the surrounding ice, out to the horizon (650 km away). Because of the small angle of incidence, ANITA could use polarization to separate signals from background; ν signals should be vertically polarized, while most background from cosmic-ray air showers should be horizontally polarized.

Because of the significant source-detector separation, ANITA is most sensitive at energies above 10^{19} eV, above the peak of the cosmogenic neutrino spectrum. As with all radio-detection experiments, ANITA had to contend with anthropogenic backgrounds. The ANITA collaboration uses their multiple antennas as a phased array to achieve good pointing accuracy. They rejected all events that pointed toward known or suspected areas of human habitation. By using the several-meter separation between antennas, they achieved a pointing accuracy of $0.2\text{-}0.4^\circ$ in elevation, and $0.5\text{-}1.1^\circ$ in azimuth. ANITA has set the most stringent flux limits yet on neutrinos with energies above 10^{20} eV [83].

Other ice based experiments use antennas located within the active volume, allowing them to reach thresholds around 10^{17} eV, or lower with phased array antennas. This approach was pioneered by the RICE experiment [104] which buried 18 half-wave dipole antennas in holes drilled for AMANDA at the South Pole, at depths from 100 to 300 m. The hardware was sensitive from 200 MHz to 1 GHz. Each antenna fed an in-situ preamplifier which transmitted the signals to surface digitizing electronics.

Two groups have deployed prototype arrays which have explored different detector concepts. The Askaryan Radio Array (ARA) deployed surface and buried antennas at the South Pole [105], while the Antarctic Ross Iceshelf Antenna Neutrino Array (ARIANNA) installed surface antennas on the Ross Ice Shelf [85], about 110 km north of McMurdo station. ARIANNA offered the possibility of detecting downward-going ν , from the radio waves reflected off the ice-sea water interface on the bottom of the Ross Ice Shelf, while ARA took advantage of the colder ice at the South Pole, with its longer radio attenuation length. ARA buried antennas up to 200 m deep, be able to observe a larger portion of ice, due to the refraction of the signal in the firn. In contrast, ARIANNA deployed antennas just below the surface, allowing them to use high-gain, but large log periodic dipole antennas. Recently, phased-array trigger techniques have been demonstrated that can reduce the energy threshold by a factor of several [76, 106].

Both experiments use stations which operate independently, spaced far enough to maximize sensitivity, but where only a small fraction of neutrino events will be visible in multiple stations. Each station includes multiple antennas, which will include both horizontal and vertical polarization. The collaborations can determine the neutrino arrival direction (modulo a (usually) 4-fold directional ambiguity) by using relative timing to find the direction from the station to the interaction, and the neutrino arrival direction by using the frequency spectrum to find the angular distance from the Cherenkov cone and by measuring the linear polarization of the radio signal. The expected angular resolution is a few degrees.

Looking ahead, the RNO [89] and ARIANNA [107] Collaborations have proposed next-generation experiments combining the best features from ARA and ARIANNA. Both experiments have been proposed for the South Pole, although operation in Greenland may also be considered. Further out, the proposed IceCube Gen2 expansion includes a substantial radio array component [52]

36.3.3.3 Radio-detection of cosmic-ray air showers

The physics of radio-wave generation in air showers is more complex than for neutrino-induced showers [108], although there are enough similarities that some experiments are sensitive to both sources. Particularly in the upper atmosphere, air is much less dense than rock or ice, so the showers develop over much larger distance scales. These larger distance scales lead to significant effects from the Earth's magnetic field.

For cosmic-rays arrival directions that are perpendicular to the magnetic field, the field produces significant charge separation,

as electrons and positrons are bent in different directions as they propagate. This leads to a growing charge dipole (transverse current) [109]. This time-varying transverse current emits radiation, spread over the transverse size of the shower, with a Cherenkov ring around the primary trajectory. Electrons in the shower may also emit synchrotron radiation due to bending in the Earth's field. Since the radiating particles are moving relativistically downward, a ground-based observer sees a Lorentz contracted pulse which can have frequency components reaching the GHz range, limited by the thickness of the particle shower. However, for most geometries, the bulk of the energy is at frequencies below 100 MHz, and most experiments are focused at frequencies below that.

There is still a contribution from coherent radio Cherenkov signals, but it is subdominant. Its most notable effect is to create an azimuthal (around the shower axis) interference pattern, destroying the radial symmetry of the radiation [110].

Since they observe the atmosphere, one of the major issues for radio-detection experiments is anthropogenic noise. Most man-made noise has distinctive characteristics (such as being narrow-band, and coming from near the horizon) which makes it relatively easy to reject during data analysis, via narrow-band filters and other techniques [111]. However, these factors complicate triggering. This is even an issue in Antarctica, where communication radios and passing satellites can mimic showers, at least at the trigger level. For this reason, most experiments have used radio antennas in combination with at least one other detector technology, such as scintillation counters. One exception is ARIANNA, which is located in an uninhabited part of Antarctica, enabling them to self-trigger on air showers [112]. With careful choice of frequency band, it may be possible to reach PeV energies with Antarctic detectors [113]. In more populous areas, the triggering challenges are likely to be bigger.

Radio-detection can be used to determine the shower energy, as done by the Auger and Tunka-Rex experiments [114, 115]. Radio signals can also be used to infer the altitude for shower-maximum, where the shower contains the most particles, as done by the LOPES and Tunka-Rex collaborations [115, 116]. This altitude is sensitive to the cosmic-ray composition. Radio-detection is also useful for energy cross-calibrations between different experiments, and, with improved simulations, may be able to provide an independent energy scale calibration for air shower arrays.

36.4 Large time-projection chambers for rare event detection

Revised October 2019 by T. Shutt (SLAC).

Rare event searches require detectors that combine large target masses and low levels of radioactivity, and that are located deep underground to eliminate cosmic-ray related backgrounds. Past and present efforts include searches for the scattering of particle dark matter, neutrinoless double beta decay, and the measurement of solar neutrinos, while next generation experiments will also probe coherent scattering of solar, atmospheric and diffuse supernova background neutrinos. Large time projection chambers (TPCs) [117], adapted from particle collider experiments, have emerged as a leading technology for these efforts. Events are measured in a central region confined by a field cage and usually filled with a liquid noble element target. Ionization electrons are drifted (in the z direction) to an anode region by use of electrode grids and field shaping rings, where their magnitude and $x - y$ location is measured. In rare event searches (with no external trigger available) scintillation generated at the initial event site is also measured, and the time difference between this prompt signal and the later-arriving charge signal gives the event location in z for a known electron drift speed. Thus, 3D imaging is achieved in a monolithic central volume. The relatively slow readout due to the drift of charges ($\sim 1/2$ ms/m at 1 kV/cm) [118] is not a major pile-up concern in low background experiments. Noble elements have relatively high light yields (comparable to or exceeding the best inorganic scintillators), and the charge signal can be amplified by multiplication or electroluminescence. Radioactive backgrounds are distinguished by event imaging, the separate measurements of charge and light, and scintillation pulse shape. For recent reviews

of noble element detectors, see [119] [120] [121] [122].

Methods for achieving very low radioactive backgrounds are discussed in general in section 35.6. The basic architecture of large TPCs is very favorable for this application because gas or liquid targets can be relatively easily purified, while the generally more radioactive readout and support materials are confined to the periphery. The 3D imaging of the TPC then allows self shielding in the target material, which is quite powerful when the target is large compared to mean scattering lengths of order ~ 10 cm for \sim MeV neutrons and gammas from radioactivity. Most recent experiments have immersed the TPCs in hermetic water shields to eliminate external radioactive backgrounds, and several are also using an active scintillator inner layer to further veto backgrounds from detector materials. While other target fluids are possible, almost all recent efforts have used Xe and Ar. In LHe and LNe the mobility of electrons is $\sim 10^3$ times lower than in the heavier noble elements due to the formation "bubbles" around electrons. [123] [124] It is worth noting that scintillation and electron drift are possible in a number of organic fluids, possibly providing a route to economical large detectors, but with much reduced performance compared to noble elements.

In noble element targets, all non-noble impurities are readily removed (e.g., by chemical reaction in a commercial getter) so that only radioactive noble isotopes are a significant background concern. Xe, Ne and He have no long lived radioactive isotopes (apart from the ^{136}Xe , discussed below, and the very long-lived ^{124}Xe [125]). Kr has ~ 0.3 MBq/kg of the beta emitter ^{85}Kr created by nuclear fuel reprocessing [126], making it unusable as a target, while the ~ 1 Bq/kg level of the beta emitter ^{39}Ar [127] is a nuisance for Ar-based experiments. Both of these can be backgrounds in other target materials, as can Rn emanating from detector components. Relatively low background materials are available for most of the structures surrounding the central target, with the exception of radioactive glasses and ceramics usually present in PMTs, feedthroughs and electrical components. Very low background PMTs with synthetic quartz windows, available over the last 15 years (see, e.g., [128]), have been a key enabling technology for dark matter searches. Radio-clean SiPMTs and related Si-based photon detectors are increasingly being used in cases where their dark rates (which are significantly higher than PMTs) can be tolerated.

An important technical challenge in liquid detectors is achieving the high voltages needed for electron drift and measurement. In general, quench gases which stabilize charge gain and speed electron transport in wire chambers cannot be used, since these absorb and/or quench scintillation light and can trap electrons. It is also important to suppress low-level emission of electrons and associated photons which can otherwise swamp low energy signals. Drift of electrons over meter scales with minimal loss from attachment on trace levels of dissolved impurities (e.g., O_2) has so far required continuous circulating purification.

36.4.1 Dark matter and other low energy signals

A major goal of low background experiments is detection of WIMP (Weakly Interacting Massive Particle) dark matter through scattering on nuclei in a terrestrial detector (for a recent review, see [129]). Energy transfers are generally small, a few tens of keV at most. Liquid noble TPCs distinguish single nuclear recoils (NR) from dark matter from the dominant background of electron recoils (ER) from gamma rays and beta decays by rejecting multiple scatters, and, as described below, based on both the ratio of charge to light and the scintillation pulse shape. Neutrons are a NR background, but are present at much lower rates than gammas and betas, and also undergo significant multiple scattering. To detect small charge signals, a dual phase technique is used wherein electrons from interactions in the liquid target are drifted to the liquid surface and extracted with high field (~ 5 kV/cm) into the gas phase where they create an amplified electroluminescence signal which is usually measured by an array of PMTs located just above the liquid. (While both charge multiplication and electroluminescence are possible in liquid, they require very high fields created by very small electron structures and thus have not seen widespread adoption. For recent progress see [130]) This technique readily measures single electrons with \sim

cm $x - y$ resolution.

The measurement of the initial scintillation signal, by contrast, suffers from loss upon reflection from the TPC walls, and inefficiency in the readout, and usually limits the energy threshold. In LXe, the ~ 178 nm wavelength is just long enough to be transmitted through high purity synthetic quartz PMTs windows, and, remarkably, PTFE immersed in LXe has $\sim 97\%$ reflectivity. [131] The ~ 128 nm scintillation light of LAr requires waveshifting (usually using TPB) both for reflectivity (usually on PTFE) and for efficient measurement. With both liquids, a second sensor array at the bottom of the TPC is used to maximize light collection, and total photon efficiencies have been in the 10-15% range. Typical raw yields for ER are several tens of electrons and photons per keV, and, in LXe, a NR threshold of ~ 5 keV has been achieved [132].

The microscopic processes leading to signals in liquid nobles are complex. Energy deposited by an event generates pairs of free electron and ions, and also atoms in their lowest excited state. The latter rapidly form excimers which de-excite by emitting light. Excimers arise in both triplet and singlet states which have the same energy but different decay times. In an event track, some fraction of electrons recombine with ions, while the rest escape and are measured. Each recombined ion creates an additional excimer, and hence another photon. Finally, some part of the energy is lost as heat - a small fraction for ER but a dominant and energy dependent fraction for NR. The branching into these various modes depends on drift field, energy, and particle type, requiring extensive calibrations. These have largely been carried out for LXe (see, e.g., [133]), and have been incorporated into the NEST Monte Carlo framework. [134]

This complexity also gives rise to discrimination between ER and NR: for the same visible energy, the slower NR create short, denser tracks and generate a higher fraction of initial excitons, leading to a smaller ratio of measured charge to light. NR also generate a higher ratio of short-lived singlet state to long-lived triplet states than ER, so that the scintillation signal itself gives pulse shape discrimination (PSD). Charge/light discrimination has been well mapped in LXe, and, remarkably, is very high ($>99.9\%$) below ~ 10 keV for NR. [132] It has only recently been measured in LAr [135], and has not yet played an important role in LAr based experiments. Qualitatively, PSD is similar in LXe and LAr - strong at high energy and weak at low energy. However it is well mapped only in LAr where it is very high above ~ 50 keV, achieving values above $\sim 10^8$. [136]

This extremely powerful PSD in LAr is sufficient to overcome the ER background from ^{39}Ar , which is roughly 10^7 times higher than the fundamental low energy ER background from p-p solar neutrinos. In a multi-ton detector the event rate from ^{39}Ar poses a significant pile-up challenge, and the DarkSide collaboration is pursuing ^{39}Ar reduction through two methods. One, for which a factor 1400 reduction in ~ 50 kg Ar has been demonstrated, is extracting “aged” Ar from underground (cosmic ray shielded) gas deposits in which the 269 yr half-life ^{39}Ar has decayed. [137] The other method is removal by distillation. The need for ^{39}Ar depleted Ar negates the much lower raw material cost of Ar compared to Xe. Kr must also be removed from both Xe and Ar experiments (and Ar must be from Xe experiments), comparatively easy tasks compared to isotopic separation. This is done through distillation or a chromatographic technique. In current LXe experiments the remaining dominant ER backgrounds is the beta decay of a daughter of ^{222}Rn in the active LXe, where the Rn has emanated from detector materials or external plumbing. Rn will be even more important as experiments scale up in size, but can in principle be reduced by better materials screening and online Rn separation, again by either distillation or chromatography. Neutrons are in general some six orders of magnitude less abundant than gamma rays and betas in U and Th decay chains, but they naturally scatter in the WIMP energy range, and their single scatters cannot be discriminated against. Self shielding is less powerful for neutrons than gamma rays, so that they are an increasingly important background at the current ton scale and future larger experiments, both in Ar and Xe. Active outer shielding layers which tag and veto neutrons are being included in most

next generation experiments.

The WIMP sensitivity is a combination of backgrounds, discrimination, and WIMP scattering rates. The scattering rates are model dependent, but are in general dominated by spin-independent coherent scattering on the full nucleus. This has an A^2 dependence, favoring high mass targets. The energy spectrum is close to a falling exponential, so that the lowest possible energy threshold maximizes sensitivity. Experiments using LXe TPCs have had the leading sensitivity for standard WIMP dark matter for well over a decade, for all but the lowest WIMP masses. The ton-scale XENON1T [138] achieved a WIMP-nucleon sensitivity of $4.1 \times 10^{-47} \text{ cm}^2$ at 30 GeV mass, closely followed by PANDAX-II [139] and LUX [140]. The next generation ~ 7 tonne experiments LZ [141] and XENONnT [142], and ~ 4 tonne PandaX-4T [143] are currently in late stages of construction. The DarkSide program is carrying out WIMP searches with LAr TPCs. The 50 kg DarkSide-50 achieved a sensitivity $\gtrsim 40$ times poorer than XENON1T. A 50 ton scale-up, DarkSide-20 is being pursued which features SiPMs instead of PMTs. [144]. (The best current limit using LAr is not from a TPC, but instead the scintillation-only DEAP-3600 experiment. [136])

LZ and XENONnT project sensitivity to WIMPs about a decade above the “floor” of coherent scattering of astrophysical neutrinos, which, absent a directional measurement (see below), are essentially indistinguishable from WIMPs. DARWIN, a proposed a 50 ton LXe TPC would approach the practical limit set by this floor for WIMP masses above ~ 5 GeV [145], while ARGO a ~ 200 ton LAr detector would achieve similar sensitivity for WIMPs masses well above ~ 50 GeV. [144]

There has been recent interest in models featuring low mass dark matter. These give rise to low energy recoils, and also strongly favor low mass target nuclei (despite the A^2 rate penalty). This has led to renewed focus on events below the scintillation threshold, where the charge signal alone achieves very low threshold due to the gain of the electroluminescence readout. This preserves $x - y$ spatial information, but only very weak depth information based on electron diffusion. Thus it is subject to the high backgrounds at the top and bottom of the active region, and decays of Rn daughters on grids. While the first such results came from XENON10, a recent result in LAr from DarkSide-50 extends to much lower dark matter mass because of the lower mass of Ar. To maximize the sensitivity of such searches in the future, studies have begun to understand and minimize the sources of electron backgrounds from both radioactivity and spurious sources such as field emission from grids. There is also an effort to develop a superfluid He TPC [146] read out with superconducting sensors (similar to the proposed HERON solar neutrino experiment). The rich set of signals in this case - scintillation, rotons, and ionization - potentially offer significant background rejection.

Measurement of NR recoil track direction would provide proof of the galactic origin of a dark matter signal since the prevailing WIMP direction varies on a daily basis as the earth spins. This cannot be achieved for the sub-micron tracks in any existing solid or liquid technology, but the mm-scale tracks in a low pressure gas (typically, $P \sim 50$ Torr) could be imaged with sufficiently dense instrumentation. Directionality can be established with $O(10^2)$ events by measuring just the track direction, while, with finer resolution that distinguishes the diffuse (dense) tail and dense (diffuse) head of NR (ER) tracks, only $O(10)$ events are required. Such imaging requires a high energy threshold, decreasing WIMP sensitivity, but also powerfully rejecting less dense ER background tracks.

A variety of TPC configurations are being pursued to accomplish this, most with a CF_4 target. The longest established effort, DRIFT, avoids diffusion washing out tracks for electron drift distances greater than ~ 20 cm by attaching electrons to CS_2 , which drifts with vastly reduced diffusion. Other efforts drift electrons directly and use a variety of techniques for their measurement: DMTPC (electroluminescence + CCDs), MIMAC (MicroMegs), NEWAGE (GEMs), and D^3 (Si pixels). A related suggestion is that the amount of recombination in a high pressure Xe gas with an electron-cooling additive could be sensitive to the angle between the track and electric field [147], eliminating the need for

track imaging. Directional measurements appear to be the only possibility to push beyond the floor of coherent neutrino scatterers [148], though at the cost of enormous target mass and channel count.

36.4.2 $0\nu\beta\beta$ Decay

Another major class of rare event search is neutrinoless double beta decay ($0\nu\beta\beta$). A limited set of nuclei are unstable against simultaneous beta decay of two neutrons. Fortunately, this includes the Xe isotope ^{136}Xe (Q-value 2458 keV), which can be used as the active material in a detector, and which, as an inert gas, can also be more readily enriched from its natural 8.9% abundance than any other $\beta\beta$ isotope. Observation of the lepton-number violating neutrinoless version of this decay would establish that neutrinos are Majorana particles and provide a direct measure of neutrino mass. For a recent review, see [149] [122]. The signal in $0\nu\beta\beta$ decay is distinctive: the full Q-value energy of the nuclear decay appears as equal energy back-to-back recoil electrons. A large TPC is advantageous for observing this low rate decay for all the reasons described above. The first detector to observe the standard model process two neutrino double beta decay was a gaseous TPC which imaged the two electrons tracks from ^{82}Se embedded in a foil. [150] Modern TPCs use Xe as the detector medium.

The dominant background is gamma rays originating outside the active volume. Most of these undergo multiple Compton-scatters which are efficiently recognized and rejected through sub-cm position resolution, though the few percent of gammas at this energy that photoabsorb are not. Self shielding of gamma rays in the double beta decay energy window is less powerful than in the low energy dark matter window, since in the former case there is some small probability of penetrating to some depth followed by the modestly small probability of photo-absorption. The latter case consists of three small probability processes: penetration to some depth, a very low-energy scatter, and the gamma exiting without a second interaction. Because of this and the fact that background and the signal are both electron recoils (i.e., NR/ER discrimination is of no value), the requirements on radioactivity in all the surrounding materials of a $\beta\beta$ TPC are much more stringent than an otherwise similar dark matter detector, unless other background rejection tools are available. However $\beta\beta$ searches are insensitive to low energy backgrounds (e.g., ^{85}Kr and ^{39}Ar) important for dark matter.

Very good energy resolution is crucial to avoid background from $2\nu\beta\beta$ decays and gammas including the prominent 2615 keV line from ^{208}Tl in the Th chain. Here a combined charge and light measurement largely eliminates the otherwise dominant fluctuations in charge and light. Because of the high energy of the $\beta\beta$ signal, charge can be read out directly, and the scintillation measurement is easily tolerant of the dark rates of SiPMs. These goals have led $\beta\beta$ detectors to have somewhat different optimization than dark matter detectors, although the next generation large Xe dark matter experiments (LZ, XENONnT, DARWIN) have significant $\beta\beta$ reach.

The recently completed EXO-200 experiment used a single-phase LXe TPC with roughly 110 active kg of Xe enriched to 80.7% ^{136}Xe to achieve one of the best $\beta\beta$ search limits [151]. The energy resolution obtained is (FWHM) of 2.71% (at 2458 keV), and lower values in LXe appear possible. A multi-ton successor experiment, nEXO, has been proposed which would fully cover the inverted neutrino mass hierarchy. [152] EXO-200 featured LAAPDs for light readout, and direct charge readout, while nEXO will use SiPMs.

A related but different approach is to use high pressure gaseous Xe TPC. [153] The lower density requires a large apparatus for given target mass, but has two significant advantages. The larger track size allows the two-electron topology of $0\nu\beta\beta$ events to be distinguished from single electrons from photoabsorption of background gammas. In addition, the low recombination fraction in the gas phase suppresses recombination fluctuations, allowing higher energy resolution. Recent progress with a 5 kg prototype by the NEXT collaboration has demonstrated the topology based discrimination, and, notably, 1% (FWHM) energy resolution. A

~ 100 kg detector is now under construction, and ton-scale designs being studied. Finally, a long-standing idea that would provide definitive identification of a $0\nu\beta\beta$ signal is to extract and tag the ionized Ba daughter via atomic physics techniques [154], either in gas or liquid and gas phases. Significant recent progress by both the EXO and NEXT collaborations has now achieved the key milestone of demonstrating single Ba ion sensitivity in test setups. [155] [156] [157]

36.5 Sub-Kelvin detectors

Revised August 2018 by K.D. Irwin (Stanford U.; SLAC).

Many particle physics experiments utilize detectors operated at temperatures below 1 K. These include WIMP searches, beta-decay experiments to measure the absolute mass of the electron neutrino, and searches for neutrinoless-double-beta decay ($0\nu\beta\beta$) to probe the properties of Majorana neutrinos. Sub-Kelvin detectors also provide important cosmological constraints on particle physics through sensitive measurement of the cosmic microwave background (CMB). CMB measurements probe the physics of inflation at $\sim 10^{16}$ GeV, and the absolute mass, hierarchy, and number of neutrino species.

Detectors that operate below 1 K benefit from reduced thermal noise and lower material specific heat and thermal conductivity. At these temperatures, superconducting materials, sensors with high responsivity, and cryogenic preamplifiers and multiplexers are available. We provide a simple overview of the techniques and the experiments using sub-K detectors. A useful review of the broad application of low-temperature detectors is provided in [158], and the proceedings of the International Workshop on Low Temperature Detectors [159] provide an overview of the field.

Sub-Kelvin detectors can be categorized as equilibrium thermal detectors or non-equilibrium detectors. Equilibrium detectors measure a temperature rise in a material when energy is deposited. Non-equilibrium detectors are based on the measurement of prompt, non-equilibrated signals and on the excitation of materials with an energy gap.

36.5.1 Equilibrium thermal detectors

An equilibrium thermal detector consists of a thermometer and absorber with combined heat capacity C coupled to a heat bath through a weak thermal conductance G . The rise time of a thermal detector is limited by the internal equilibration time of the thermometer-absorber system and the electrical time constant of the thermometer. The thermal relaxation time over which heat escapes to the heat bath is $\tau = C/G$. Thermal detectors are often designed so that an energy input to the absorber is thermalized and equilibrated through the absorber and thermometer on timescales shorter than τ , making the operation particularly simple. An equilibrium thermal detector can be operated as either a calorimeter, which measures an incident energy deposition E , or as a bolometer, which measures an incident power P .

In a calorimeter, an energy E deposited by a particle interaction causes a transient change in the temperature $\Delta T = E/C$, where the heat capacity C can be dominated by the phonons in a lattice, the quasiparticle excitations in a superconductor, or the electronic heat capacity of a metal. The thermodynamic energy fluctuations in the absorber and thermometer have variance

$$\Delta E_{\text{rms}}^2 = k_{\text{B}} T^2 C \quad (36.5)$$

when operated near equilibrium, where ΔE_{rms} is the root-mean-square energy fluctuation, k_{B} is the Boltzmann constant and T is the equilibrium temperature. When a sufficiently sensitive thermometer is used, and the energy is thermalized at frequencies large compared to the thermal response frequency ($f_{\text{th}} = 1/2\pi\tau$), the signal-to-noise ratio is nonzero at frequencies higher than f_{th} . In this case, detector energy resolution can be somewhat better than ΔE_{rms} [160]. Deviations from the ideal calorimeter model can cause excess noise and position and energy dependence in the signal shape, leading to degradation in achieved energy resolution.

In a bolometer, a power P deposited by a stream of particles causes a change in the equilibrium temperature $\Delta T = P/G$. The weak thermal conductance G to the heat bath is usually limited by

Table 36.4: Some selected experiments using sub-Kelvin equilibrium bolometers to measure the CMB. These experiments constrain the physics of inflation and the absolute mass, hierarchy, and number of neutrino species. The experiment location determines the part of the sky that is observed. The size of the aperture determines the angular resolution. The table also indicates the type of sensor used, the number of sensors, the frequency range, and the number of frequency bands. The number of sensors and frequency range and bands for ongoing upgrades are provided for some experiments in parentheses.

Sub-K CMB Experiment	Location	Aperture	Sensor type	# Sensors (planned)	Frequency (planned)	Bands (planned)
Ground-based						
Atacama Cosmology Telescope (2007–)	Chile	6 m	TES	1,800 (5,334)	90–150 GHz (28–220 GHz)	2 (5)
BICEP/Keck (2006–)	South Pole	26/68 cm	TES	3,200	95–220 GHz	3
CLASS (2015–)	Chile	60 cm	TES	36 (5,108)	40 GHz (40–220 GHz)	1 (4)
POLARBEAR / Simons (2012–)	Chile	3.5 m	TES	1,274 (22,764)	150 GHz (90–220 GHz)	1 (3)
South Pole Telescope (2007–)	South Pole	10 m	TES	1,536 (16,260)	95–150 GHz (95–220 GHz)	2 (3)
Balloon						
EBEX (2013–)	McMurdo	1.5 m	TES	~1,000	150–410 GHz	3
PIPER (2016–)	New Mexico	2 m	TES	5,120	200–600 GHz	4
SPIDER (2014–)	McMurdo	30 cm	TES	1,959	90–280 GHz	3
Satellite						
Planck HFI (2003–)	L2	1.5 m	NTD	52	100–857 GHz	9

the flow of heat through a phonon or electron system. The thermodynamic power fluctuations in the absorber and thermometer have power spectral density

$$S_P = NEP^2 = 4k_B T^2 G \quad (36.6)$$

when operated near equilibrium, where the units of NEP (noise equivalent power) are W/\sqrt{Hz} .

The minimization of thermodynamic energy and power fluctuations is a primary motivation for the use of sub-Kelvin thermal detectors. These low temperatures also enable the use of materials and structures with extremely low C and G , and the use of superconducting materials and amplifiers.

When very large absorbers are required (e.g. WIMP dark matter searches), dielectric crystals with extremely low specific heat are often used. These materials are operated well below the Debye temperature T_D of a crystal, where the specific heat scales as T^3 . In this low-temperature limit, the dimensionless phononic heat capacity at fixed volume reduces to

$$\frac{C_V}{N k_B} = \frac{12 \pi^4}{5} \left(\frac{T}{T_D} \right)^3, \quad (36.7)$$

where N is the number of atoms in the crystal. Normal metals have higher low-temperature specific heat than dielectric crystals, but they also have superior thermalization properties, making them attractive for some applications in which extreme precision and high energy resolution are required (e.g. beta endpoint experiments to measure neutrino mass using ^{163}Ho). At low temperature, the heat capacity of normal metals is dominated by electrons, and is linear in temperature, with convenient form

$$C = \frac{\rho}{A} \gamma V T, \quad (36.8)$$

where V is the sample volume, γ is the molar specific heat of the material, ρ is the mass density, and A is the atomic weight. Superconducting absorbers are also used. Superconductors combine some of the thermalization advantages of normal metals with the lower specific heats associated with insulators when operated well below T_c , where the electronic heat capacity freezes out, and the material is dominated by phononic heat capacity. At higher temperatures, superconducting materials have more complicated heat capacities, but at their transition temperature T_c , BCS theory predicts that the electronic heat capacity of a superconductor is ~ 2.43 times the normal metal value.

When very low thermal conductances are required for power measurement (e.g. the measurement of the cosmic microwave

background), the weak thermal link is sometimes provided by thin membranes of non-stoichiometric silicon nitride. The thermal conductance of these membranes is:

$$G = 4\sigma A T^3 \xi, \quad (36.9)$$

where σ has a value of $15.7 \text{ mW/cm}^2\text{K}^4$, A is the cross-sectional area perpendicular to the heat flow, and ξ is a numerical factor with a value of one in the case of specular surface scattering but less than one for diffuse surface scattering. The thermal impedance between the electron and phonon systems can also limit the thermal conductance.

The most commonly used sub-Kelvin thermometer is the superconducting transition-edge sensor (TES) [161]. The TES consists of a superconductor biased at the transition temperature T_c , in the region between the superconducting and normal state, where its resistance is a strong function of temperature. The TES is voltage biased. The Joule power provides strong negative electrothermal feedback, which improves linearity, speeds up response to faster than $\tau = C/G$, and provides tolerance for T_c variation between multiple TESs in a large array. The current flowing through a TES is read out by a superconducting quantum interference device (SQUID) amplifier. These amplifiers can be cryogenically multiplexed, allowing a large number of TES devices to be read out with a small number of wires to room temperature.

Neutron-transmutation-doped (NTD) germanium and implanted silicon semiconductors read out by cryogenic FET amplifiers are also used as thermometers [160]. Their electrical resistance is exponentially dependent on $1/T$, and is determined by phonon-assisted hopping conduction between impurity sites. Finally, the temperature dependence of the permeability of a paramagnetic material is used as a thermometer. Detectors using these thermometers are referred to as metallic magnetic calorimeters (MMC) [162]. These detectors operate without dissipation and are inductively readout by SQUIDS.

Equilibrium thermal detectors are simple, and they have important advantages in precision measurements because of their insensitivity to statistical variations in energy down-conversion pathways, as long as the incident energy equilibrates into an equilibrium thermal distribution that can be measured by a thermometer.

36.5.2 Nonequilibrium Detectors

Nonequilibrium detectors use many of the same principles and techniques as equilibrium detectors, but are also sensitive to details of the energy down-conversion before thermalization. Sub-Kelvin nonequilibrium detectors measure athermal phonon sig-

Table 36.5: Selected experiments using sub-Kelvin calorimeters. The table shows only currently operated experiments, and is not exhaustive. WIMP experiments search for dark matter, and beta-decay and neutrinoless double beta decay ($0\nu\beta\beta$) experiments constrain neutrino mass, hierarchy, and Majorana nature. The experiment location determines the characteristics of the radioactive background. The dates of current program phase, detection mode (equilibrium or nonequilibrium phonon measurements, and measurement of ionization or scintillation signals), the absorber and total mass, the sensor type, and the number of sensors and crystals (if different) are given. Many sub-K calorimeter experiments are also in planning and construction phases, including EURECA (dark matter), HOLMES and NuMECs (beta decay), and CUPID-0 ($0\nu\beta\beta$ decay). Many of the existing experiments are being upgraded to larger mass absorbers, different absorber materials, or lower energy threshold.

Sub-K Calorimeter	Location	Detection mode	Absorber Total mass	Sensor type	# Sensor # Crystal
WIMP					
CRESST II (2003–)	Gran Sasso Italy	Noneq. phon. and scint.	CaWO ₄ 5.4 kg	TES	18
EDELWEISS III (2015–)	LSM Modane France	Eq. thermal and ion.	Ge 22 kg	NTD Ge +HEMT	36
SuperCDMS (2012–)	Soudan, USA SNOLAB, Canada	Noneq. phon. and ion.	Ge 9 kg	TES +JFET	120 15
Beta decay					
ECHO (2012–)	Heidelberg Germany	Eq. thermal	Au: ¹⁶³ Ho 0.2μg	MMC	16
$0\nu\beta\beta$ decay					
CUORE (2015–)	Gran Sasso Italy	Eq. thermal	TeO ₂ 741 kg	NTD Ge	988
AMoRe Pilot (2015–)	Yang Yang S. Korea	Noneq. phon. and scint.	CaMoO ₄ 1.5 kg	MMC	5
LUCIFER (2010–)	Gran Sasso Italy	Eq. thermal and scint.	ZnSe 431 g	NTD Ge	1

nals in a dielectric crystal, electron-hole pairs in a semiconductor crystal, athermal quasiparticle excitations in a superconductor, photon emission from a scintillator, or a combination of two of the above to better discriminate recoils from nuclei or electrons. Because the phonons are athermal, sub-Kelvin nonequilibrium detectors can use absorbers with larger heat capacity, and they use information about the details of energy down-conversion pathways in order to better discriminate signal from background.

In WIMP and neutrino experiments using sub-Kelvin dielectric semiconductors, the recoil energy is typically $\gtrsim 0.1$ keV. The majority of the energy is deposited in phonons and a minority in ionization and, in some cases, scintillation. The semiconductor bandgap is typically \sim eV, and $k_B T < 10 \mu\text{eV}$ at $T < 1$ K. Thus, high-energy charge pairs and athermal phonons are initially produced. The charge pairs cascade quickly to the gap edge. The high-energy phonons experience isotopic scattering and anharmonic decay, which downshifts the phonon spectrum until the phonon mean free path approaches the characteristic dimension of the absorber. If the crystal is sufficiently pure, these phonons propagate ballistically, preserving information about the interaction location. They are not thermalized, and thus not affected by an increase in the crystal heat capacity, allowing the use of larger absorbers. Sensors similar to those used in sub-K equilibrium thermal detectors measure the athermal phonons at the crystal surface.

Superconductors can also be used as absorbers in sub-Kelvin detectors when $T \ll T_c$. The superconducting gap is typically \sim meV. Energy absorption breaks Cooper pairs and produces quasiparticles. These particles cascade to the superconducting gap edge, and then recombine after a material-dependent lifetime. During the quasiparticle lifetime, they diffuse through the material. In superconductors with large mean free path, the diffusion length can be more than 1 mm, allowing diffusion to a detector.

In some experiments (e.g. SuperCDMS and CRESST), athermal phonons and quasiparticle diffusion are combined to increase achievable absorber mass. Athermal phonons in a three-dimensional dielectric crystal break Cooper pairs in a two-dimensional superconducting film on the detector surface. The resulting quasiparticles diffuse to thermal sensors (typically a TES) where they are absorbed and detected. While thin superconducting films have diffusion lengths shorter than the diffusion lengths in single crystal superconductors, segmenting the films into small

sections and coupling them to multiple TES sensors allows the instrumentation of large absorber volume. The TES sensors can be wired in parallel to combine their output signal.

The combined measurement of the phonon signal and a secondary signal (ionization or scintillation) can provide a powerful discrimination of signal from background events. Nuclear-recoil events in WIMP searches produce proportionally smaller ionization or scintillation signal than electron-scattering events. Since many of the background events are electron recoils, this discrimination provides a powerful veto. Similarly, beta-decay events produce proportionally smaller scintillation signal than alpha-particle events, allowing rejection of alpha backgrounds in neutrino experiments.

Combined phonon and ionization measurement has been implemented in experiments including CDMS I/II, SuperCDMS, and EDELWEISS I/II/III. These experiments use semiconductor crystal absorbers, in which dark-matter scattering events would produce recoiling particles and generate electron-hole pairs and phonons. The electron-hole pairs are separated and drifted to the surface of the crystal by applying an electric field, where they are measured by a JFET or HEMT using similar techniques to those used in 77 K Ge x-ray spectrometers. However, the field strength must be much lower in sub-K detectors to limit the generation of phonon signals by the Neganov-Luke effect, which can confuse the background discrimination. For detectors with very low threshold, the Neganov-Luke effect can also be used to detect generated charge through the induced phonon signal.

Combined phonon and scintillation measurement has been implemented in CRESST II, ROSEBUD, AMoRE and LUCIFER. For example, the CRESST-II experiment uses CaWO₄ crystal absorbers, and measures both the phonon signal and the scintillation signal with TES calorimeters. A wide variety of scintillating crystals are under consideration, including different tungstates and molybdates, BaF₂, ZnSe, and bismuth germanate (BGO).

36.6 Low-radioactivity background techniques

Revised November 2019 by A. Piepke (Alabama U.).

The physics reach of low-energy rare-event experiments is often limited by background caused by radioactivity. The problems to be addressed span a wide range of energies, particle types, and interactions. Experiments searching for double beta decay, low energy solar neutrinos or neutrino interactions at nuclear reactors

are often concerned about electron recoils and therefore β -decays and γ -ray scattering. The energy scales of interest reach from few keV to few MeV. Dark Matter searches, looking for nuclear recoils, often focus their attention on neutron-induced energy deposits, with electron recoils being of secondary importance. While the energy scales of interest are typically in the keV range, the hadronic physics responsible for the neutron production and interaction spans MeV to GeV. The utilized detector technologies are just as varied, including, among others, large liquid scintillation detectors, solid state calorimeters, gaseous and liquid tracking detectors and crystal scintillators. Except for reactor bound experiments, these searches are typically performed underground to limit the impact of the cosmic radiation. The depth requirements vary depending on the problem and the chosen detector concept. Depending on the chosen detector design, the separation of the physics signal from this unwanted interference can be achieved on an event-by-event basis by active event tagging, utilizing some unique event features, or by reducing the flux of the background-creating radiation by appropriate shielding, material selection and surface cleaning. In all cases, the background rate is proportional to the flux of the interfering radiation. Its reduction is, thus, essential for realizing the full physics potential of the experiment. In this context, “low energy” may be defined as the regime of natural, anthropogenic, or cosmogenic radioactivity; all at energies of up to about 10 MeV. See [163] [164] for in-depth reviews of this subject. Following the classification of [163], sources of background may be categorized into the following classes:

1. environmental radioactivity,
2. radio-impurities in detector or shielding components,
3. radon and its progeny,
4. cosmic rays,
5. neutrons from natural fission, (α, n) reactions and from cosmic-ray muon spallation and capture.

36.6.1 Defining the problem

The application defines the requirements. Background goals can be as demanding as a few low-energy events per year in a ton-size detector. The maximal strength of the physics signal of interest can often be estimated theoretically or from limits derived by earlier experiments. The experiments are then designed for the desired signal-to-background ratio. This requires finding the right balance between “clarity of measurement”, ease of construction, schedule and budget.

It is good practice to use detector simulations to translate the background requirements into limits for the radioactivity content of various detector components, requirements for radiation shielding, and allowable cosmic-ray fluxes. This strategy allows the identification of the most critical components early and facilitates the allocation of analysis and development resources in a rational way. The CERN code GEANT4 [165] is a widely used tool for this purpose. It has incorporated sufficient nuclear physics to allow accurate background estimations. Custom-written event generators, modeling *e.g.*, particle correlations in complex decay schemes, deviations from allowed beta spectra or $\gamma - \gamma$ -angular correlations, are used as well.

36.6.2 Environmental radioactivity

The long-lived, naturally occurring radio-nuclides ^{40}K , ^{232}Th , and ^{238}U have average abundances of 1.6, 11 and 2.7 ppm (corresponding to 412, 45 and 33 Bq/kg, respectively) in the earth’s crust, with large local variations [166]. In most applications, γ radiation emitted in the decay of natural radioactivity and its unstable daughters constitutes the dominant contribution to the local radiation field. Typical low-background applications require levels of natural radioactivity on the order of ppb or ppt in the detector components. Passive or active shielding is used to suppress external γ radiation down to an equivalent level. Fig 36.11 shows the attenuation length $\lambda(E_\gamma)$ as a function of γ -ray energy E_γ for three common shielding materials: water, copper, lead. Assuming exponential damping, the thickness ℓ required to reduce the external flux by a factor $f > 1$, is:

$$\ell = \lambda(E_\gamma) \cdot \ln f. \quad (36.10)$$

At 100 keV, a typical energy scale for dark matter searches (or 2.615 MeV for a typical double-beta decay experiment), attenuation by a factor $f = 10^5$ requires 67(269) cm of H_2O , 2.8(34) cm of Cu, or 0.18(23) cm of Pb. Such estimates allow for an order-of-magnitude determination of the experiment dimensions.

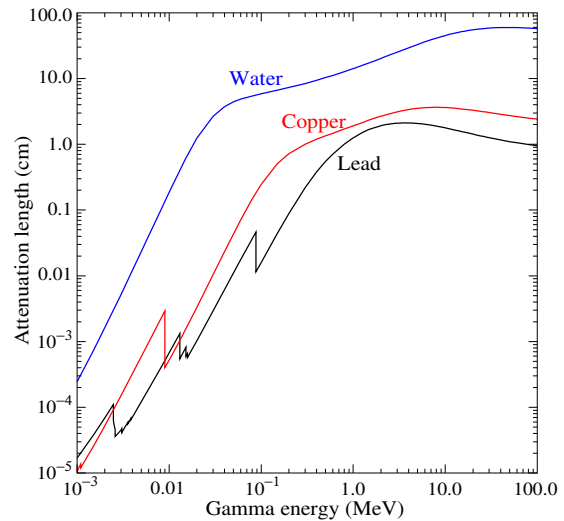


Figure 36.11: γ -ray attenuation lengths in some common shielding materials. The mass attenuation data has been taken from the NIST data base XCOM; see “Atomic Nuclear Properties” at pdg.lbl.gov.

As discussed in the following section, shielding materials contain radioactivity too. Consequently, they are chosen such as to contribute as little as possible to the overall background budget. The shielding materials discussed above, when properly selected, fit that requirement. Th/U concentrations in selected H_2O , Cu and Pb are ≤ 0.1 ppt [167], ≤ 0.5 ppt [168] and ≤ 1 ppt [169], respectively. Although cost effectively available in bulk quantity, steel is often not utilized as it can contain Th/U at concentrations of ≤ 1 ppb.

A precise estimation of the the magnitude of the external gamma-ray background, including scattering and the effect of analysis-energy cuts, requires Monte Carlo simulations based on the knowledge of the radioactivity present in the laboratory. Detailed modeling of the γ -ray flux in a large laboratory, or inside the hermetic shielding, needs to cope with a very small probability of generating any signal in the detector. It is often advantageous to calculate the solid angle of the detector to the background sources and mass attenuation of the radiation shield separately, or to employ importance sampling. The former method can lead to loss of energy-direction correlations while in the latter has to balance CPU-time consumption against the loss of statistical independence. These approaches reduce the computation time required for a statistically meaningful number of detector hits to manageable levels.

Water is commonly used as shielding medium for large detectors. It can be obtained cheaply and purified effectively in large quantity. Water purification technology is commercially available. Ultra-pure water, instrumented with photomultiplier tubes, can serve as active cosmic-ray veto system. Water is also an effective neutron moderator and shield. In more recent underground experiments that involve detectors operating at cryogenic temperature, liquefied gases (*e.g.* argon) are being used for shielding as well.

36.6.3 Radioactive impurities in detector and shielding components

After suppressing the effect of external radioactivity, radioactive impurities, contained in the detector components or attached to their surfaces, become important. Every material contains radioactivity at some level. The activity can be natural, cosmogenic, man-made, or a combination of them. The determination of the

activity content of a specific material or component requires case-by-case analyses, and is rarely obtainable from the manufacturer. However, there are some general rules that can be used to guide the pre-selection. For detectors designed to look for electrons (for example in double-beta decay searches or neutrino detection via inverse beta decay or elastic scattering), intrinsic radioactivity is often the principal source of background. For devices detecting nuclear recoils (for example in dark matter searches), this is often of secondary importance as ionization signals can be actively discriminated on an event-by-event basis. In the latter case radioactive decay-induced nuclear reactions, resulting in the emission of energetic neutrons, become a concern. Scattering of these neutrons on the detector material can lead to nuclear-recoil and, thus, background.

For natural radioactivity, a rule of thumb is that refined materials are more radiopure than their source in nature. Substances with high standard reduction potential tend to be cleaner as the refining process preferentially segregates K, Th, and U from electrodeposited materials. For example, Al is often found to contain considerable amounts of Th and U, while electrolytic Cu is very low in primordial activities. K, Th, and U tend to exist as or form compounds with low vapor pressure. Plastics or liquid hydrocarbons, having been refined by distillation, are often quite radiopure. Zone refining utilizes differences in solubility in the liquid and solid phase of the host material to segregate unwanted impurities. This technique is often used in the production of semiconductor detectors. Depending on the material processing, differences in standard reduction potential, boiling point and vapor pressure (for example for U and Ra) may lead to a breakage of decay chain equilibrium. Tabulated radioassay results for a wide range of materials can be found in Refs. [170], [169], [171] and [168]. Radioassay results from previous experiments are being archived at an online database [167].

The long-lived ^{238}U daughter ^{210}Pb ($T_{1/2}=22.3$ y) is found in all shielding lead. It is a background concern at low energies. This is due to the relatively high endpoint energy ($Q_{\beta}=1.162$ MeV) of its beta-unstable daughter ^{210}Bi . Lead refined from selected low-U ore typically has specific activities of about 5–30 Bq/kg. For applications that require lower specific activity, ancient lead (for example from Roman ships) is sometimes used. Because the ore processing and lead refining removed most of the ^{238}U , the ^{210}Pb decayed during the long waiting time to the level supported by the U-content of the refined lead. Lining the lead with copper to range out the low-energy radiation is another remedy. However, intermediate- Z materials carry additional cosmogenic-activation risks when handled above ground, as will be discussed below. ^{210}Pb is also found in solders, even lead free types.

Man-made radioactivity, released during above-ground nuclear testing and nuclear power production, is a source of background. The fission product ^{137}Cs can often be found attached to the surface of materials. The radioactive noble gas ^{85}Kr , released into the atmosphere by nuclear reactors and nuclear fuel re-processing, is sometimes a background concern, especially due to its high solubility in organic materials. Post-World War II steel typically contains a few tens of mBq/kg of ^{60}Co .

Surface activity is not a material property per se but is added during manufacturing and handling. Surface contamination can be effectively removed by clean machining, solvent washing, etching, leaching with dilute acid or their combination. However, different chemical elements for example the decay chain members Ra, Po and Pb have different attachment characteristics and, therefore may react differently to solvents, leading to incomplete cleaning and chain equilibrium breakage. The assembly of low-background detectors is often performed in controlled enclosures (e.g. clean rooms or glove boxes) to avoid contaminating surfaces with environmental substances, such as dust, containing radioactivity at much higher concentrations than the detector components. Due to the small size of dust particles, a fairly large fraction of ^{226}Ra α -decays results in ^{222}Rn being ejected into the surrounding gas. This fraction can approach 20% for ultra fine dust. Because of its low reactivity, radon can then spread throughout the detector. When not being processed, components are best stored in sealed bags to limit dust deposition on the surface, even inside

clean rooms, and to separate them from radon contained in the air. Nylon bags are also good radon barriers. Storage of parts under vacuum is an alternative solution to limit dust deposition and radon daughter attachment. Surface contamination with environmental dust can be quantified by means of wipe-testing with acid or alcohol wetted Whatman 41 filters. Analysis of acid cleaned paper wipes by means of mass spectroscopy or neutron activation analysis is capable of detecting less than 1 pg/cm² of Th and U.

The most demanding low-rate experiments require screening of *all* components for low levels of radioactivity, which can be a time consuming task. The requirements for activity characterization depend on the experiment, the location and amount of a particular component. Monte Carlo simulations are used to quantify these requirements. Sensitivities of the order $\mu\text{Bq/kg}$ or less are sometimes required for the most critical detector components. At such a level of sensitivity, the characterization becomes a challenging problem in itself. Low-background α , β , and γ -ray counting, mass spectroscopy, and neutron activation analysis are commonly used diagnostic techniques.

36.6.4 Radon and its progeny

The noble gas ^{222}Rn , a pure α -emitter, is a ^{238}U decay product. Due to its relatively long half-life of 3.8 d it is released by surface soil and is found in the atmosphere everywhere. ^{220}Rn (a ^{232}Th decay product) is unimportant for most low-background experiments because of its short half-life of 55.6 s. It has only very little time to escape from its host material before decaying, with its daughters being immobile. The ^{222}Rn activity of air ranges from 10 to 100 mBq/L outdoors and 100 to thousands of mBq/L indoors. The natural radon concentration depends on the weather and shows daily and seasonal variations. Radon levels are lowest above the oceans. For electron detectors, it is not the Rn itself that creates background, but its progeny ^{214}Pb , ^{214}Bi , ^{210}Bi , which emit energetic beta and γ radiation. Thus, not only the detector itself has to be separated from contact with air, but also air-containing internal voids can be a background concern. Radon is soluble in water and even more so in organic solvents. For large liquid scintillation detectors, radon mobility due to convection and diffusion is a concern. To define a scale: typical double-beta-decay searches are restricted to $< \mu\text{Bq/kg}_{\text{detector}}$ (or 1 decay per $\text{kg}_{\text{detector}}$ and per 11.6 days) activities of ^{222}Rn in the active medium. This corresponds to a steady-state population of 0.5 atoms/ $\text{kg}_{\text{detector}}$. The decay of Rn itself is a concern for some recoil type detectors, as nuclear recoil energies in α decays are substantial (100 keV in the case of ^{222}Rn decays).

Low-background detectors are often kept sealed from the air and continuously flushed with boil-off nitrogen, which contains only small amounts of Rn. For the most demanding applications, the nitrogen is purified by multiple distillations, or by using pressure swing adsorption chromatography. Then only the Rn out-gassing of the piping (due to its intrinsic U content) determines the radon concentration. Radon diffuses readily through thin plastic barriers. If the detector is to be isolated from its environment by means of a membrane, the choice of material is important [172].

Prolonged exposure of detector components or raw materials to air leads to the accumulation of the long-lived radon daughter ^{210}Pb on surfaces. Due to its low Q -value of 63.5 keV, ^{210}Pb itself is only a problem when extreme low energy response is important. However, because of its higher Q -value, the lead daughter ^{210}Bi , is a concern up to the MeV scale. The alpha unstable Bi-daughter ^{210}Po ($E_{\alpha} = 5304$ keV) contributes not only to the alpha background but can also induce the emission of energetic neutrons via (α,n) reactions on low- Z materials (such as F, C, Si...etc.). The neutrons, in turn, may capture on other detector components, creating energetic background. The (α,n) reaction yield induced by the α decay of ^{210}Po is typically small (about $6 \cdot 10^{-6}$ n/α in Teflon, for example). This creates a memory effect, the air exposure history impacts the (α,n) background component.

Some data is available on the deposition of radon daughters from air onto materials, see e.g. [173], [174] and [175]. This data indicates a large spread of effective radon daughter collection distances ranging from a few cm to a few m in air. This large spread may indicate dependence on hidden, uncontrolled variables. These considerations limit the allowable air exposure

time but only within a wide range. Many experiments therefore adopt to perform the assembly of detector components in a radon-reduced atmosphere to counter this uncertainty.

In case raw materials (e.g. in the form of granules) were exposed to air at the production site, the bulk (instead of the surface as discussed before) of the finished detector components may be loaded with ^{210}Pb and its daughters. These are difficult to detect as no energetic gamma radiation is emitted in their decays. Careful air-exposure management is the only way to reduce this source of background. This can be achieved by storing the parts under a protective low-radon cover gas or keeping them sealed from radon.

State-of-the-art detectors can detect radon outgassing even at the level of few atoms. Solid state, scintillation, or gas detectors utilize alpha spectroscopy or are exploiting the fast $\beta - \alpha$ decay sequences of ^{214}Bi and ^{214}Po . The efficiency of these devices is sometimes boosted by electrostatic collection of radon ions from a large gas volume onto a small detector. Cryogenic radon collection can also boost the radon sensitivity. Radon outgassing measurement campaigns, similar to the radioactivity measurements discussed above, are conducted by collaborations to assure that the internal radon production stays within its allowance.

36.6.5 Cosmic rays

Cosmic radiation, discussed in detail in Chapter 30, is a source of background for just about any non-accelerator experiment. Primary cosmic rays are about 90% protons, 9% alpha particles, and the rest heavier nuclei (Fig 30.1). They are totally attenuated within the first few hg/cm^2 of atmospheric thickness. At sea level secondary particles ($\pi^\pm : p : e^\pm : n : \mu^\pm$) are observed with relative intensities 1 : 13 : 340 : 480 : 1420 ([176]; also see Fig 30.3).

All but the muon and the neutron components are readily absorbed by overburden such as building ceilings and passive shielding. Only if there is very little overburden ($\lesssim 10 \text{ g}/\text{cm}^2$ [163]) do pions and protons need to be considered when estimating the production rate of cosmogenic radioactivity.

Sensitive experiments are, thus, operated deep underground where essentially only muons can penetrate. As shown in Fig-30.7, the muon intensity falls off rapidly with depth. Active detection systems, capable of tagging events correlated in time with cosmic-ray activity, are needed, depending on the overburden.

The muonic background is related to low-radioactivity techniques insofar as photo-nuclear interactions with atomic nuclei can produce long-lived radioactivity directly or indirectly via the creation of neutrons. This happens at any overburden, however, at strongly depth dependent rates. Muon bremsstrahlung, created in high- Z shielding materials, contributes to the low energy background too. Active muon detection systems are effective in reducing cosmogenic background, but only for activities with sufficiently short half-lives, allowing vetoing with reasonable detector dead time.

Cosmogenic activation of detector components at the surface can be an issue for low-background experiments. Proper management of parts and materials above ground during manufacturing and detector assembly minimizes the accumulation of long-lived activity. Cosmogenic activation is most important for intermediate- Z materials such as Cu and Fe. For the most demanding applications, metals are stored and transported under sufficient shielding to stop the hadronic component of the cosmic rays. Parts can be stored underground for long periods before being used. Underground machine shops are sometimes used to limit the duration of exposure at the surface. Some experiments are even electro-forming copper underground.

36.6.6 Neutrons

Neutrons contribute to the background of low-energy experiments in different ways: directly through nuclear recoil in the detector medium, and indirectly, through the production of radio-nuclides, capture γ s and inelastic scattering inside the detector and its components. The indirect mechanisms allow even remote materials to contribute to the background by means of penetrating γ radiation. Neutrons are thus an important source of low-energy background. They are produced in different ways:

1. At the earth's surface the flux of cosmic-ray secondary neutrons is exceeded only by that of muons;
2. Energetic tertiary neutrons are produced by cosmic-ray muons by nuclear spallation in the detector and laboratory walls;
3. In high- Z materials, often used in radiation shields, nuclear capture of negative muons results in the emission of neutrons;
4. Natural radioactivity has a neutron component through spontaneous fission and (α, n) -reactions.

A calculation with the hadronic simulation code FLUKA [177], using the known energy distribution of secondary neutrons at the earth's surface [178], yields a mass attenuation of $1.5 \text{ hg}/\text{cm}^2$ in concrete for secondary neutrons. In case energy-dependent neutron-capture cross sections are known, such calculations can be used to obtain the production rate of particular radio-nuclides.

At an overburden of only few meters water equivalent, neutron production by muons becomes the dominant mechanism. Neutron production rates are high in high- Z shielding materials. A high- Z radiation shield, discussed earlier as being effective in reducing background due to external radioactivity, thus acts as a source for cosmogenic tertiary high-energy neutrons. Depending on the overburden and the radioactivity content of the laboratory, there is an optimal shielding thickness. Water shields, although bulky, are an attractive alternative due to their low neutron production yield and self-shielding.

Shields made from plastic or water are commonly used to reduce the neutron flux. The shield is sometimes doped with a substance having a high thermal neutron capture cross section (such as boron) to absorb thermal neutrons more quickly. The hydrogen, contained in these shields, serves as a target for elastic scattering, and is effective in reducing the neutron energy. Neutrons from natural radioactivity have relatively low energies and can be effectively suppressed by a neutron shield. Ideally, such a neutron shield should be inside the lead to be effective for tertiary neutrons. However, this is rarely done as it increases the neutron production target (in form of the passive shield), and the costs increase as the cube of the linear dimensions. An active cosmic-ray veto is an effective solution, correlating a neutron with its parent muon. This solution works best if the veto system is as far away from the detector as feasible (outside the radiation shield) in order to correlate as many background-producing muons with neutrons as possible. The vetoed time after a muon hit needs to be sufficiently long to assure muon bremsstrahlung and neutron-induced backgrounds are sufficiently suppressed. An upper limit to the allowable veto period is given by the veto-induced deadtime, which is related to the muon hit rate on the veto detector. This consideration also constitutes the limiting factor for the physical size of the veto system (besides the cost). The background caused by neutron-induced radioactivity with live-times far exceeding the veto time cannot be addressed in this way. Moving the detector deep underground, and thus reducing the muon flux, is the only technique that addresses all sources of cosmogenic the neutron background.

References

- [1] R. M. Baltrusaitis *et al.*, Nucl. Instrum. Meth. **A240**, 410 (1985).
- [2] D. J. Bird *et al.* (HiRes), Astrophys. J. **424**, 491 (1994).
- [3] T. Abu-Zayyad *et al.*, Nucl. Instrum. Meth. **A450**, 253 (2000).
- [4] H. Tokuno *et al.*, Nucl. Instrum. Meth. **A676**, 54 (2012), [arXiv:1201.0002].
- [5] J. Abraham *et al.* (Pierre Auger), Nucl. Instrum. Meth. **A620**, 227 (2010), [arXiv:0907.4282].
- [6] R. Mussa and G. Ciaccio (Pierre Auger), Eur. Phys. J. Plus **127**, 94 (2012).
- [7] T. Fujii *et al.*, Astropart. Phys. **74**, 64 (2016), [arXiv:1504.00692].
- [8] F. Arquerros, J. R. Hoerandel and B. Keilhauer, Nucl. Instrum. Meth. **A597**, 23 (2008), [arXiv:0807.3844].

- [9] F. Arqueros, J. R. Hoerandel and B. Keilhauer, Nucl. Instrum. Meth. **A597**, 1 (2008), [arXiv:0807.3760].
- [10] J. Rosado, F. Blanco and F. Arqueros, Astropart. Phys. **34**, 164 (2010), [arXiv:1004.3971].
- [11] M. Ave *et al.* (AIRFLY), Astropart. Phys. **28**, 41 (2007), [arXiv:astro-ph/0703132].
- [12] J. Rosado, F. Blanco and F. Arqueros, Astropart. Phys. **55**, 51 (2014), [arXiv:1401.4310].
- [13] J. H. Boyer *et al.*, Nucl. Instrum. Meth. **A482**, 457 (2002).
- [14] J. T. Brack *et al.*, Astropart. Phys. **20**, 653 (2004).
- [15] B. Fick *et al.*, JINST **1**, 11, P11003 (2006).
- [16] J. Abraham *et al.* (Pierre Auger), Astropart. Phys. **33**, 108 (2010), [arXiv:1002.0366].
- [17] P. Abreu *et al.* (Pierre Auger), Astropart. Phys. **34**, 368 (2011), [arXiv:1010.6162].
- [18] R. Thalman *et al.* Journal of Quantitative Spectroscopy and Radiative Transfer, **147**, 171 (2014), Erratum-ibid. **189**, 281 (2017).
- [19] J. Abraham *et al.* [Pierre Auger Collab.], Nucl. Instrum. Methods **A789**, 172 (2015).
- [20] M. Unger *et al.*, Nucl. Instrum. Meth. **A588**, 433 (2008), [arXiv:0801.4309].
- [21] T.K. Gaisser and A.M. Hillas, *Proc. 15th Int. Cosmic Ray Conf. Bulgarska Akademia na Naukite, Conf. Papers* **8**, 353 (1978), (archived at <http://adsabs.harvard.edu/abs/1977ICRC....8..353G>).
- [22] A. Huang, G. Medina-Tanco and A. Santangelo, Experimental Astronomy **40**, 1 (2015).
- [23] P. A. Klimov *et al.*, Space Sci. Rev. **212**, 3-4, 1687 (2017), [arXiv:1706.04976].
- [24] G. Abdellaoui *et al.* (JEM-EUSO), Journal of Instrumentation **13**, 5 (2018), ISSN 17480221.
- [25] L. Wiencke and A. Olinto (JEM-EUSO), PoS **ICRC2017**, 1097 (2018).
- [26] F. Capel *et al.*, Advances in Space Research **62**, 2954 (2018).
- [27] A. V. Olinto *et al.*, PoS **ICRC2017**, 542 (2018), [35,542(2017)], [arXiv:1708.07599].
- [28] J. Holder *et al.*, AIP Conf. Proc. **1085**, 657 (2009), [arXiv:0810.0474].
- [29] F. Aharonian *et al.* (H.E.S.S.), Astron. Astrophys. **457**, 899 (2006), [arXiv:astro-ph/0607333].
- [30] J. Albert *et al.* (MAGIC), Astrophys. J. **674**, 1037 (2008), [arXiv:0705.3244].
- [31] T. C. Weekes *et al.*, Astrophys. J. **342**, 379 (1989).
- [32] A. M. Hillas *et al.*, Astrophys. J. **503**, 744 (1998).
- [33] <http://tevcat.uchicago.edu/>.
- [34] F. Aharonian *et al.* (H.E.S.S.), Astrophys. J. **636**, 777 (2006), [arXiv:astro-ph/0510397].
- [35] M. de Naurois and D. Mazin, Comptes Rendus Physique **16**, 610 (2015), [arXiv:1511.00463].
- [36] N. Park, PoS **ICRC2017**, arXiv:1808.10495 (2018), [arXiv:1808.10495].
- [37] A. M. Hillas, Astropart. Phys. **43**, 19 (2013).
- [38] B. S. Acharya *et al.* (CTA Consortium), Astropart. Phys. **43**, 3 (2013).
- [39] A. Bernstein *et al.*, *Report on the Depth Requirements for a Massive Detector at Homestake* (2009), [arXiv:0907.4183].
- [40] Y. Ashie *et al.* (Super-Kamiokande), Phys. Rev. **D71**, 112005 (2005), [hep-ex/0501064].
- [41] S. Kasuga *et al.*, Phys. Lett. **B374**, 238 (1996).
- [42] M. Shiozawa (Super-Kamiokande), Nucl. Instrum. Meth. **A433**, 240 (1999).
- [43] K. Abe *et al.* (Super-Kamiokande), Phys. Rev. **D83**, 052010 (2011), [arXiv:1010.0118].
- [44] J. F. Beacom and M. R. Vagins, Phys. Rev. Lett. **93**, 171101 (2004), [hep-ph/0309300].
- [45] J. Boger *et al.* (SNO), Nucl. Instrum. Meth. **A449**, 172 (2000), [arXiv:nucl-ex/9910016].
- [46] T. K. Gaisser, F. Halzen and T. Stanev, Phys. Rept. **258**, 173 (1995), [Erratum: Phys. Rept.271,355(1996)], [hep-ph/9410384].
- [47] J.G. Learned and K. Mannheim, Ann. Rev. Nucl. and Part. Sci. **50**, 679 (2000).
- [48] U. F. Katz and C. Spiering, Prog. Part. Nucl. Phys. **67**, 651 (2012), [arXiv:1111.0507].
- [49] M. G. Aartsen *et al.* (IceCube), J. Phys. **G44**, 5, 054006 (2017), [arXiv:1607.02671].
- [50] S. Adrián-Martínez *et al.* (KM3NeT), J. Phys. **G43**, 8, 084001 (2016), [arXiv:1601.07459].
- [51] A. D. Avrorin *et al.*, Phys. Part. Nucl. **46**, 2, 211 (2015).
- [52] M. G. Aartsen *et al.* (IceCube) (2014), [arXiv:1412.5106].
- [53] S. Adrián-Martínez *et al.* (KM3NeT), Eur. Phys. J. **C74**, 9, 3056 (2014), [arXiv:1405.0839].
- [54] A. V. Akimov *et al.*, Eur. Phys. J. **C79**, 9, 758 (2019), [arXiv:1902.06083].
- [55] C. Kopper (for the IceCube Collab.), contribution to ICRC2017.
- [56] M. G. Aartsen *et al.* (IceCube), Phys. Rev. Lett. **113**, 101101 (2014), [arXiv:1405.5303].
- [57] A. Albert *et al.* (ANTARES), Astrophys. J. **853**, 1, L7 (2018), [arXiv:1711.07212].
- [58] M. G. Aartsen *et al.* (IceCube), Phys. Rev. **D91**, 7, 072004 (2015), [arXiv:1410.7227].
- [59] M. G. Aartsen *et al.* (IceCube, Fermi-LAT, MAGIC, AGILE, ASAS-SN, HAWC, H.E.S.S., INTEGRAL, Kanata, Kiso, Kapteyn, Liverpool Telescope, Subaru, Swift NuSTAR, VERITAS, VLA/17B-403), Science **361**, 6398, eaat1378 (2018), [arXiv:1807.08816].
- [60] M. G. Aartsen *et al.* (IceCube), Science **361**, 6398, 147 (2018), [arXiv:1807.08794].
- [61] G. Illuminati (for the ANTARES and IceCube Collabs.), contribution to ICRC2019.
- [62] M. G. Aartsen *et al.* (IceCube), Phys. Rev. **D99**, 3, 032007 (2019), [arXiv:1901.05366].
- [63] D. Williams (for the IceCube Collab.), contribution to ICRC2019.
- [64] R. Coniglione (for the ANTARES and KM3NeT Collabs.), contribution to ICRC2019.
- [65] K. Greisen, Phys. Rev. Lett. **16**, 748 (1966).
- [66] G. T. Zatsepin and V. A. Kuzmin, JETP Lett. **4**, 78 (1966), [Pisma Zh. Eksp. Teor. Fiz.4,114(1966)].
- [67] R. Abbasi *et al.* (IceCube), Astropart. Phys. **34**, 382 (2011), [arXiv:1004.1694].
- [68] S. R. Klein, Nucl. Phys. Proc. Supl. **229-232**, 284 (2012), [arXiv:1012.1407].
- [69] G. A. Askar'yan, Sov. Phys. JETP **14**, 2, 441 (1962), [Zh. Eksp. Teor. Fiz.41,616(1961)].
- [70] G.A. Askaryan, Sov. Phys. JETP **21**, 658 (1965).
- [71] C. W. James *et al.*, Phys. Rev. **E84**, 056602 (2011), [arXiv:1007.4146].
- [72] J. Alvarez-Muniz, R. A. Vazquez and E. Zas, Phys. Rev. **D62**, 063001 (2000), [arXiv:astro-ph/0003315].
- [73] C. Glaser *et al.* (2019), [arXiv:1906.01670].
- [74] D. Saltzberg *et al.*, Phys. Rev. Lett. **86**, 2802 (2001), [hep-ex/0011001].
- [75] O. Scholten *et al.*, J. Phys. Conf. Ser. **81**, 012004 (2007).

- [76] A. G. Viereg, K. Bechtol and A. Romero-Wolf, *JCAP* **1602**, 02, 005 (2016), [arXiv:1504.08006].
- [77] L. Gerhardt and S. R. Klein, *Phys. Rev.* **D82**, 074017 (2010), [arXiv:1007.0039].
- [78] J. Alvarez-Muniz, R. A. Vazquez and E. Zas, *Phys. Rev.* **D61**, 023001 (2000), [arXiv:astro-ph/9901278].
- [79] M. G. Aartsen *et al.* (IceCube), *Phys. Rev.* **D98**, 6, 062003 (2018), [arXiv:1807.01820].
- [80] A. Aab *et al.* (Pierre Auger), *JCAP* **1910**, 10, 022 (2019), [arXiv:1906.07422].
- [81] J. D. Bray *et al.*, *Phys. Rev.* **D91**, 6, 063002 (2015), [arXiv:1502.03313].
- [82] O. Scholten *et al.*, *Phys. Rev. Lett.* **103**, 191301 (2009), [arXiv:0910.4745].
- [83] P. W. Gorham *et al.* (ANITA), *Phys. Rev.* **D99**, 12, 122001 (2019), [arXiv:1902.04005].
- [84] P. Allison *et al.* (ARA), in “36th International Cosmic Ray Conference (ICRC 2019) Madison, Wisconsin, USA, July 24-August 1, 2019,” (2019), [arXiv:1907.11125].
- [85] A. Anker *et al.* (2019), [arXiv:1909.00840].
- [86] T. Winchen *et al.*, *J. Phys. Conf. Ser.* **1181**, 1, 012077 (2019), [arXiv:1903.08472].
- [87] J. Stettner (IceCube), in “HAWC Contributions to the 36th International Cosmic Ray Conference (ICRC2019),” (2019), [arXiv:1908.09551].
- [88] A. van Vliet, J. R. Horandel and R. Alves Batista, *PoS ICRC2017*, 562 (2018), [35,562(2017)], [arXiv:1707.04511].
- [89] J. A. Aguilar *et al.* (2019), [arXiv:1907.12526].
- [90] J. G. Learned and S. Pakvasa, *Astropart. Phys.* **3**, 267 (1995), [hep-ph/9405296].
- [91] J. L. Feng *et al.*, *Phys. Rev. Lett.* **88**, 161102 (2002), [hep-ph/0105067].
- [92] P. W. Gorham *et al.* (ANITA), *Phys. Rev. Lett.* **121**, 16, 161102 (2018), [arXiv:1803.05088].
- [93] J. Álvarez Muñiz *et al.* (GRAND), *Sci. China Phys. Mech. Astron.* **63**, 1, 219501 (2020), [arXiv:1810.09994].
- [94] M. Detrixhe *et al.* (ANITA-II), *Phys. Rev.* **D83**, 023513 (2011), [arXiv:1008.1282].
- [95] R.D. Dagkesamanskii and I.M. Zheleznykh, *Sov. Phys. JETP Lett.* **50**, 233 (1989).
- [96] C. W. James *et al.*, *EPJ Web Conf.* **135**, 04001 (2017), [arXiv:1704.05336].
- [97] J. D. Bray, *Astropart. Phys.* **77**, 1 (2016), [arXiv:1601.02980].
- [98] J.A. Dowdeswell and S. Evans, *Rept. on Prog. in Phys.* **67**, 1821 (2004).
- [99] P. Allison *et al.*, *Astropart. Phys.* **108**, 63 (2019), [arXiv:1712.03301].
- [100] A. Anker *et al.*, *JCAP* **1911**, 030 (2019), [arXiv:1909.02677].
- [101] S. W. Barwick *et al.*, *JCAP* **1807**, 07, 055 (2018), [arXiv:1804.10430].
- [102] C. Deaconu *et al.*, *Phys. Rev.* **D98**, 4, 043010 (2018), [arXiv:1805.12576].
- [103] P. W. Gorham *et al.* (ANITA), *Phys. Rev. Lett.* **103**, 051103 (2009), [arXiv:0812.2715].
- [104] I. Kravchenko *et al.*, *Phys. Rev.* **D73**, 082002 (2006), [arXiv:astro-ph/0601148].
- [105] P. Allison *et al.* (ARA), *Phys. Rev.* **D93**, 8, 082003 (2016), [arXiv:1507.08991].
- [106] J. Avva *et al.*, *Nucl. Instrum. Meth.* **A869**, 46 (2017), [arXiv:1605.03525].
- [107] A. Anker *et al.* (ARIANNA), *Adv. Space Res.* **64**, 2595 (2019), [arXiv:1903.01609].
- [108] F. G. Schroder, *Prog. Part. Nucl. Phys.* **93**, 1 (2017), [arXiv:1607.08781].
- [109] T. Huege, *Braz. J. Phys.* **44**, 520 (2014), [1294(2013)], [arXiv:1310.6927].
- [110] S. Buitink *et al.*, *Phys. Rev.* **D90**, 8, 082003 (2014), [arXiv:1408.7001].
- [111] T. Huege, *Phys. Rept.* **620**, 1 (2016), [arXiv:1601.07426].
- [112] S. W. Barwick *et al.*, *Astropart. Phys.* **90**, 50 (2017), [arXiv:1612.04473].
- [113] A. Balagopal V. *et al.*, *Eur. Phys. J.* **C78**, 2, 111 (2018), [erratum: *Eur. Phys. J.* **C78**, 1017 (2018)], [arXiv:1712.09042].
- [114] A. Aab *et al.* (Pierre Auger), *Phys. Rev. Lett.* **116**, 24, 241101 (2016), [arXiv:1605.02564].
- [115] P. A. Bezyazeev *et al.*, *Phys. Rev.* **D97**, 12, 122004 (2018), [arXiv:1803.06862].
- [116] W. D. Apel *et al.* (LOPES), *Phys. Rev.* **D90**, 6, 062001 (2014), [arXiv:1408.2346].
- [117] D. R. Nygren, in “Proceedings, 1975 PEP Summer Study, Berkeley, July 28-August 20, 1975,” 126–133 (1975).
- [118] L. S. Miller, S. Howe and W. E. Spear, *Phys. Rev.* **166**, 871 (1968), URL <https://link.aps.org/doi/10.1103/PhysRev.166.871>.
- [119] E. Aprile and T. Doke, *Rev. Mod. Phys.* **82**, 2053 (2010), [arXiv:0910.4956].
- [120] V. Chepel and H. Araujo, *JINST* **8**, R04001 (2013), [arXiv:1207.2292].
- [121] D. Gonzalez-Diaz, F. Monrabal and S. Murphy, *Nucl. Instrum. Meth.* **A878**, 200 (2018), [arXiv:1710.01018].
- [122] J. J. Gomez-Cadenas, F. Monrabal Capilla and P. Ferrario, *Front.in Phys.* **7**, 51 (2019), [arXiv:1903.02435].
- [123] H. J. Maris, *Journal of the Physical Society of Japan* **77**, 11, 111008 (2008), URL <https://doi.org/10.1143/JPSJ.77.111008>.
- [124] L. Bruschi, G. Mazzi and M. Santini, *Phys. Rev. Lett.* **28**, 1504 (1972), URL <https://link.aps.org/doi/10.1103/PhysRevLett.28.1504>.
- [125] E. Aprile *et al.*, *Nature* **568**, 7753, 532 (2019), URL <https://doi.org/10.1038/s41586-019-1124-4>.
- [126] K. Winger *et al.*, *Journal of Environmental Radioactivity* **80**, 2, 183 (2005), ISSN 0265-931X, URL <http://www.sciencedirect.com/science/article/pii/S0265931X04002887>.
- [127] H. Loosli, *Earth and Planetary Science Letters* **63**, 1, 51 (1983), ISSN 0012-821X, URL <http://www.sciencedirect.com/science/article/pii/0012821X83900213>.
- [128] E. Aprile *et al.* (XENON), *Eur. Phys. J.* **C75**, 11, 546 (2015), [arXiv:1503.07698].
- [129] M. Schumann, *J. Phys.* **G46**, 10, 103003 (2019), [arXiv:1903.03026].
- [130] E. Aprile *et al.*, *JINST* **9**, 11, P11012 (2014), [arXiv:1408.6206].
- [131] F. Neves *et al.*, *JINST* **12**, 01, P01017 (2017), [arXiv:1612.07965].
- [132] D. S. Akerib *et al.* (LUX Collaboration), *Phys. Rev. D* **97**, 102008 (2018), URL <https://link.aps.org/doi/10.1103/PhysRevD.97.102008>.
- [133] D. S. Akerib *et al.* (LUX), *Phys. Rev.* **D95**, 1, 012008 (2017), [arXiv:1610.02076].
- [134] M. Szydagis *et al.*, *Journal of Instrumentation* **6**, 10, P10002 (2011), URL <https://doi.org/10.1088%2F1748-0221%2F6%2F10%2Fp10002>.
- [135] M. Kimura *et al.*, *Phys. Rev.* **D100**, 3, 032002 (2019), [arXiv:1902.01501].
- [136] R. Ajaj *et al.* (DEAP), *Phys. Rev.* **D100**, 2, 022004 (2019), [arXiv:1902.04048].

- [137] P. Agnes *et al.* (DarkSide), Phys. Rev. **D93**, 8, 081101 (2016), [Addendum: Phys. Rev.D95,no.6,069901(2017)], [arXiv:1510.00702].
- [138] E. Aprile *et al.* (XENON), Phys. Rev. Lett. **119**, 18, 181301 (2017), [arXiv:1705.06655].
- [139] X. Cui *et al.* (PandaX-II), Phys. Rev. Lett. **119**, 18, 181302 (2017), [arXiv:1708.06917].
- [140] D. S. Akerib *et al.*, Phys. Rev. Lett. **118**, 25, 251302 (2017).
- [141] D. S. Akerib *et al.* (LUX-ZEPLIN) (2018), [arXiv:1802.06039].
- [142] E. Aprile *et al.* (XENON), JCAP **1604**, 04, 027 (2016), [arXiv:1512.07501].
- [143] H. Zhang *et al.* (PandaX), Sci. China Phys. Mech. Astron. **62**, 3, 31011 (2019), [arXiv:1806.02229].
- [144] C. E. Aalseth *et al.*, Eur. Phys. J. Plus **133**, 131 (2018), [arXiv:1707.08145].
- [145] J. Aalbers *et al.*, Journal of Cosmology and Astroparticle Physics **2016**, 11, 017 (2016), URL <https://doi.org/10.1088%2F1475-7516%2F2016%2F11%2F017>.
- [146] W. Guo and D. N. McKinsey, Phys. Rev. **D87**, 11, 115001 (2013), [arXiv:1302.0534].
- [147] D. R. Nygren, J. Phys. Conf. Ser. **460**, 012006 (2013).
- [148] C. A. J. O'Hare *et al.*, Phys. Rev. **D92**, 6, 063518 (2015), [arXiv:1505.08061].
- [149] S. M. Bilenky and C. Giunti, Mod. Phys. Lett. **A27**, 1230015 (2012), [arXiv:1203.5250].
- [150] S. R. Elliott, A. A. Hahn and M. K. Moe, Phys. Rev. Lett. **59**, 2020 (1987), URL <http://link.aps.org/doi/10.1103/PhysRevLett.59.2020>.
- [151] G. Anton *et al.* (EXO-200), Phys. Rev. Lett. **123**, 16, 161802 (2019), [arXiv:1906.02723].
- [152] S. A. Kharusi *et al.* (nEXO) (2018), [arXiv:1805.11142].
- [153] D. Nygren, Nucl. Instrum. Meth. **A603**, 337 (2009).
- [154] M. K. Moe, Phys. Rev. **C44**, 931 (1991), [1019(1991)].
- [155] A. D. McDonald *et al.*, Phys. Rev. Lett. **120**, 13, 132504 (2018), [arXiv:1711.04782].
- [156] C. Chambers *et al.* (nEXO), Nature **569**, 7755, 203 (2019), [arXiv:1806.10694].
- [157] P. Thapa *et al.* (2019), [arXiv:1904.05901].
- [158] C. Enss, editor, *Cryogenic particle detection*, volume 99 of *Topics in applied physics*, Springer, Berlin, Germany (2005).
- [159] E. Shirokoff (ed.), *Proc. 15th Int. Workshop on Low Temperature Detectors (LTD-15)*, J. Low Temp. Phys. **176**, 131–1108 (2014).
- [160] S.H. Moseley, J.C. Mather, and D. McCammon, J. Appl. Phys. **56**, 1257 (1984).
- [161] K.D. Irwin, Appl. Phys. Lett. **66**, 1998 (1995).
- [162] S.R. Bandler *et al.*, J. Low. Temp. Phys. **93**, 709 (1993).
- [163] G. Heusser, Ann. Rev. Nucl. Part. Sci. **45**, 543 (1995).
- [164] J. A. Formaggio and C. J. Martoff, Ann. Rev. Nucl. Part. Sci. **54**, 361 (2004).
- [165] S. Agostinelli *et al.* (GEANT4), Nucl. Instrum. Meth. **A506**, 250 (2003).
- [166] U. N. S. C. on the Effects of Atomic Radiation, *Sources and Effects of Ionizing Radiation*, p233, United Nations (2010).
- [167] <http://www.radiopurity.org>.
- [168] N. Abgrall *et al.*, Nucl. Instrum. Meth. **A828**, 22 (2016), [arXiv:1601.03779].
- [169] D. S. Leonard *et al.*, Nucl. Instrum. Meth. **A591**, 490 (2008), [arXiv:0709.4524].
- [170] J. Jagam and J. Simpson, Nucl. Instrum. Meth. **A324**, 389 (1993).
- [171] D. S. Leonard *et al.*, Nucl. Instrum. Meth. **A871**, 169 (2017), [arXiv:1703.10799].
- [172] M. Wojcik *et al.*, Nucl. Instrum. Meth. **A449**, 158 (2000).
- [173] V. E. Guiseppe *et al.*, AIP Conf. Proc. **1338**, 95 (2011), [arXiv:1101.0126].
- [174] M. Stein *et al.*, Nucl. Instrum. Meth. **A880**, 92 (2018), [arXiv:1708.09476].
- [175] E. S. Morrison *et al.*, AIP Conf. Proc. **1921**, 1, 090002 (2018), [arXiv:1708.08534].
- [176] National Council on Radiation Protection and Measurement, Report 94, Bethesda, MD (1987).
- [177] T. Boehlen *et al.*, Nuclear Data Sheets **120**, 211 (2014), <http://www.fluka.org/fluka.php>.
- [178] M.S. Gordon *et al.*, IEEE Trans. **NS51**, 3427 (2004).

37. Radioactivity and Radiation Protection

Revised August 2019 by S. Roesler and M. Silari (CERN).

37.1. Definitions [1,2,3]

It would be desirable if legal protection limits could be expressed in directly measurable *physical quantities*. However, this does not allow quantifying biological effects of the exposure of the human body and its detriment to ionizing radiation.

For this reason, protection limits are expressed in terms of so-called *protection quantities* which, although calculable, are not measurable. Protection quantities quantify the extent of exposure of the human body to ionizing radiation from both whole and partial body external irradiation and from intakes of radionuclides.

In order to demonstrate compliance with dose limits, so-called *operational quantities* are typically used, which aim at providing conservative estimates of protection quantities. Often radiation protection detectors used for individual and area monitoring are calibrated in terms of operational quantities and, thus, these quantities become “measurable”.

37.1.1. Physical quantities :

• **Fluence**, Φ (unit: $1/\text{m}^2$): The fluence is the quotient of the sum of the particle track lengths dl in the volume dV

$$\Phi = dl/dV . \quad (37.1)$$

It can also be expressed in terms of number of particles dN incident upon a small sphere of cross-sectional area da

$$\Phi = dN/da .$$

• **Absorbed dose**, D (unit: gray, $1 \text{ Gy}=1 \text{ J/kg}=100 \text{ rad}$): The absorbed dose is the energy imparted by ionizing radiation in a volume element of a specified material divided by the mass of this volume element.

• **Kerma**, K (unit: gray): Kerma is the sum of the initial kinetic energies of all charged particles set in motion by indirectly ionizing radiation in a volume element of the specified material divided by the mass of this volume element.

• **Linear energy transfer, L or LET** (unit: J/m , often given in $\text{keV}/\mu\text{m}$, $1 \text{ keV}/\mu\text{m} \approx 1.602 \times 10^{-10} \text{ J/m}$): The linear energy transfer is the mean energy, dE , lost by a charged particle owing to collisions with electrons in traversing a distance dl in matter. *Low-LET radiation*: X rays and gamma rays (accompanied by charged particles due to interactions with the surrounding medium) or light charged particles such as electrons that produce sparse ionizing events far apart at a molecular scale ($L < 10 \text{ keV}/\mu\text{m}$). *High-LET radiation*: neutrons and heavy charged particles that produce ionizing events densely spaced at a molecular scale ($L > 10 \text{ keV}/\mu\text{m}$). While the above LET definition refers to electronic stopping power only, at low energy nuclear stopping power could be a significant fraction of the total stopping power.

• **Activity**, A (unit: becquerel, $1 \text{ Bq}=1/\text{s}=27 \text{ pCi}$): Activity is the expectation value of the number of nuclear decays occurring in a given quantity of material per unit time.

37.1.2. Protection quantities :

• **Organ absorbed dose**, D_T (unit: gray): The mean absorbed dose in an organ or tissue T of mass m_T is defined as

$$D_T = \frac{1}{m_T} \int_{m_T} D dm .$$

• **Equivalent dose**, H_T (unit: sievert, $1 \text{ Sv}=100 \text{ rem}$): The equivalent dose H_T in an organ or tissue T is equal to the sum of the absorbed doses $D_{T,R}$ in the organ or tissue caused by different radiation types R weighted with so-called radiation weighting factors w_R :

$$H_T = \sum_R w_R \times D_{T,R} . \quad (37.2)$$

Table 37.1: Radiation weighting factors, w_R .

Radiation type	w_R
Photons, electrons and muons	1
Neutrons, $E_n < 1 \text{ MeV}$	$2.5 + 18.2 \times \exp[-(\ln E_n)^2/6]$
$1 \text{ MeV} \leq E_n \leq 50 \text{ MeV}$	$5.0 + 17.0 \times \exp[-(\ln(2E_n))^2/6]$
$E_n > 50 \text{ MeV}$	$2.5 + 3.25 \times \exp[-(\ln(0.04E_n))^2/6]$
Protons and charged pions	2
Alpha particles, fission fragments, heavy ions	20

It expresses long-term risks (primarily cancer and leukemia) from low-level chronic exposure. The values for w_R recommended by ICRP [2] are given in Table 37.1.

• **Effective dose**, E (unit: sievert): The sum of the equivalent doses, weighted by the tissue weighting factors w_T ($\sum_T w_T = 1$) of several organs and tissues T of the body that are considered to be most sensitive [2], is called “effective dose”:

$$E = \sum_T w_T \times H_T . \quad (37.3)$$

37.1.3. Operational quantities :

• **Dose equivalent**, H (unit: sievert): The dose equivalent at a point in tissue is given by

$$H = D \times Q \quad (37.4)$$

where D is the absorbed dose and Q is the quality factor at that point. The quality factor at a point in tissue, is given by:

$$Q = \frac{1}{D} \int_{L=0}^{\infty} Q(L) D_L dL$$

where D_L is the distribution of D in unrestricted linear energy transfer L at the point of interest, and $Q(L)$ is the quality factor as a function of L . The integration is to be performed over D_L , due to all charged particles, excluding their secondary electrons.

• **Ambient dose equivalent**, $H^*(10)$ (unit: sievert): The dose equivalent at a point in a radiation field that would be produced by the corresponding expanded and aligned field in a 30 cm diameter sphere of unit density tissue (ICRU sphere) at a depth of 10 mm on the radius vector opposing the direction of the aligned field. Ambient dose equivalent is the operational quantity for *area monitoring*.

• **Personal dose equivalent**, $H_p(d)$ (unit: sievert): The dose equivalent in ICRU tissue at an appropriate depth, d , below a specified point on the human body. The specified point is normally taken to be where the individual dosimeter is worn. For the assessment of effective dose, $H_p(10)$ with a depth $d = 10 \text{ mm}$ is chosen, and for the assessment of the dose to the skin and to the hands and feet the personal dose equivalent, $H_p(0.07)$, with a depth $d = 0.07 \text{ mm}$, is used. Personal dose equivalent is the operational quantity for *individual monitoring*.

37.1.4. Dose conversion coefficients :

Dose conversion coefficients allow direct calculation of protection or operational quantities from particle fluence and are functions of particle type, energy and irradiation configuration. The most common coefficients are those for effective dose and ambient dose equivalent. The former are based on simulations in which the dose to organs of anthropomorphic phantoms is calculated for approximate actual conditions of exposure, such as irradiation of the front of the body (anterior-posterior irradiation) or isotropic irradiation.

Conversion coefficients from fluence to effective dose are given for anterior-posterior irradiation and various particles in Fig. 37.1 [4]. For example, the effective dose from an anterior-posterior irradiation in a field of 1-MeV neutrons with a fluence of 1 neutron per cm^2 is about 290 pSv. In Monte Carlo simulations such coefficients allow multiplication with fluence at scoring time such that effective dose to a human body at the considered location is directly obtained.

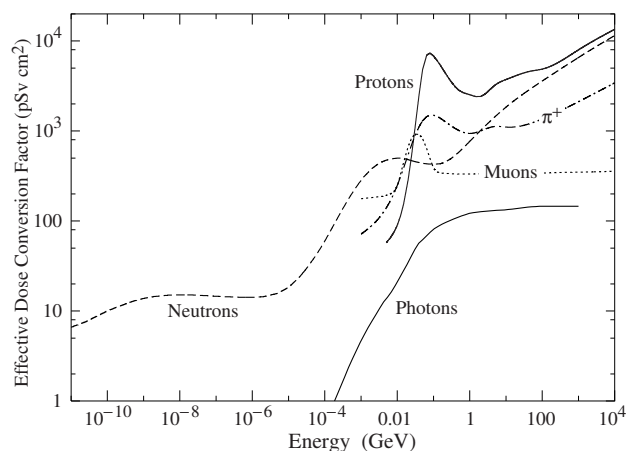


Figure 37.1: Fluence to effective dose conversion coefficients for anterior-posterior irradiation and various particles [4].

37.2. Radiation levels [5]

- **Natural background radiation:** On a worldwide average, the annual whole-body dose equivalent due to all sources of natural background radiation ranges from 1.0 to 13 mSv (0.1–1.3 rem) with an annual average of 2.4 mSv [6]. In certain areas values up to 50 mSv (5 rem) have been measured. A large fraction (typically more than 50%) originates from inhaled natural radioactivity, mostly radon and radon daughters. The latter can vary by more than one order of magnitude: it is 0.1–0.2 mSv in open areas, 2 mSv on average in a house and more than 20 mSv in poorly ventilated mines.
- **Cosmic ray background radiation:** At sea level, the whole-body dose equivalent due to cosmic ray background radiation is dominated by muons; at higher altitudes also nucleons contribute. Dose equivalent rates range from less than 0.1 μ Sv/h at sea level to a few μ Sv/h at aircraft altitudes. Details on cosmic ray fluence levels are given in the Cosmic Rays section (Sec. 30 of this *Review*).

37.3. Health effects of ionizing radiation

Radiation can cause two types of health effects, deterministic and stochastic:

- **Deterministic effects** are tissue reactions which cause injury to a population of cells if a given threshold of absorbed dose is exceeded. The severity of the reaction increases with dose. The quantity in use for tissue reactions is the absorbed dose, D . When particles other than photons and electrons (low-*LET* radiation) are involved, a Relative Biological Effectiveness (*RBE*)-weighted dose may be used. The *RBE* of a given radiation is the reciprocal of the ratio of the absorbed dose of that radiation to the absorbed dose of a reference radiation (usually X rays) required to produce the same degree of biological effect. It is a complex quantity that depends on many factors such as cell type, dose rate, fractionation, etc.
- **Stochastic effects** are malignant diseases and heritable effects for which the probability of an effect occurring, but not its severity, is a function of dose without threshold.
- **Lethal dose:** The whole-body dose from penetrating ionizing radiation resulting in 50% mortality in 30 days (assuming no medical treatment) is 2.5–4.5 Gy (250–450 rad)[†], as measured internally on the body longitudinal center line. The surface dose varies due to variable body attenuation and may be a strong function of energy.
- **Cancer induction:** The cancer induction probability is about 5% per Sv on average for the entire population [3].
- **Recommended effective dose limits:** The International Commission on Radiological Protection (ICRP) recommends a limit for radiation workers of 20 mSv effective dose per year averaged over 5 years, with the provision that the dose should not exceed 50 mSv in any single year [3]. The limit in the EU-countries and Switzerland is

[†] *RBE*-weighted when necessary

20 mSv per year, in the U.S. it is 50 mSv per year (5 rem per year). Many physics laboratories in the U.S. and elsewhere set lower limits. The effective dose limit for general public is typically 1 mSv per year.

37.4. Prompt neutrons at accelerators

Neutrons dominate the radiation environment outside thick shielding (*e.g.*, > 1 m of concrete) for high energy (> a few hundred MeV) electron and hadron accelerators. In addition, for accelerators with energies above about 10 GeV, muons contribute significantly at small angles with regard to the beam, even behind several meters of shielding. Another special case are synchrotron light sources where particular care has to be taken to shield the very intense low-energy photons extracted from the electron synchrotron into the experimental areas. Due to its importance at high energy accelerators this section focuses on prompt neutrons.

37.4.1. Electron accelerators :

At electron accelerators, neutrons are generated via photonuclear reactions from bremsstrahlung photons. Neutron production takes place above a threshold value which varies from 10 to 19 MeV for light nuclei (with important exceptions, such as 2.23 MeV for deuterium and 1.67 MeV for beryllium) and from 4 to 6 MeV for heavy nuclei. It is commonly described by different mechanisms depending on the photon energy: the giant dipole resonance interactions (from threshold up to about 30 MeV, often the dominant process), the quasi-deuteron effect (between 30 MeV and a few hundred MeV), the delta resonance mechanism (between 200 MeV and a few GeV) and the vector meson dominance model at higher energies.

The giant dipole resonance reaction consists in a collective excitation of the nucleus, in which neutrons and protons oscillate in the direction of the photon electric field. The oscillation is damped by friction in a few cycles, with the photon energy being transferred to the nucleus in a process similar to evaporation. Nucleons emitted in the dipolar interaction have an anisotropic angular distribution, with a maximum at 90°, while those leaving the nucleus as a result of evaporation are emitted isotropically with a Maxwellian energy distribution described as [7]:

$$\frac{dN}{dE_n} = \frac{E_n}{T^2} e^{-E_n/T}, \quad (37.5)$$

where T is a nuclear ‘temperature’ (in units of MeV) characteristic of the particular target nucleus and its excitation energy. For heavy nuclei the ‘temperature’ generally lies in the range of $T = 0.5$ –1.0 MeV. Neutron yields from semi-infinite targets per kW of electron beam power are plotted in Fig. 37.2 as a function of the electron beam energy [7].

While for thick targets neutron production is mainly due to photonuclear interactions, for thin targets (thickness of fractions of the radiation length) electronuclear interactions are the dominating process.

Typical neutron energy spectra outside of concrete (80 cm thick, 2.35 g/cm³) and iron (40 cm thick) shields are shown in Fig. 37.3. In order to compare these spectra to those caused by proton beams (see below) the spectra are scaled by a factor of 100, which roughly corresponds to the difference in the high energy hadronic cross sections for photons and hadrons (*e.g.*, the fine structure constant). The shape of these spectra are generally characterized by a low-energy peak at around 1 MeV (evaporation neutrons) and a high-energy shoulder at around 70–80 MeV. In case of concrete shielding, the spectrum also shows a pronounced peak at thermal neutron energies.

37.4.2. Proton accelerators :

At proton accelerators, neutron yields emitted per incident proton by different target materials are roughly independent of proton energy between 20 MeV and 1 GeV, and are given by the ratio C : Al : Cu-Fe : Sn : Ta-Pb = 0.3 : 0.6 : 1.0 : 1.5 : 1.7 [10]. Above about 1 GeV, the neutron yield is proportional to E^m , where $0.80 \leq m \leq 0.85$ [11].

Typical neutron energy spectra outside of concrete and iron shielding are shown in Fig. 37.3. Here, the radiation fields are caused

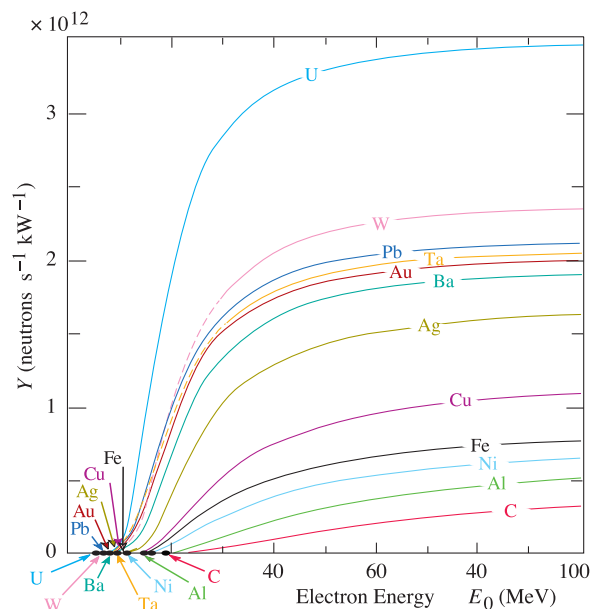


Figure 37.2: Neutron yields from semi-infinite targets per kW of electron beam power, as a function of the electron beam energy, disregarding target self-shielding [7].

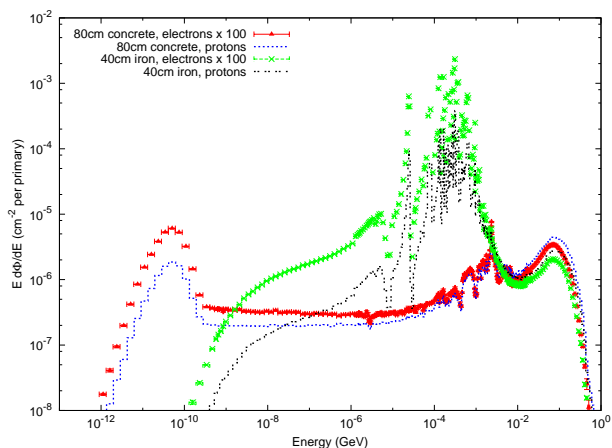


Figure 37.3: Neutron energy spectra calculated with the FLUKA code [8,9] from 25 GeV proton and electron beams on a thick copper target. Spectra are evaluated at 90° to the beam direction behind 80 cm of concrete or 40 cm of iron. All spectra are normalized per beam particle. For better visualization, spectra for electron beam are multiplied by a factor of 100.

by a 25 GeV proton beam interacting with a thick copper target. The comparison of these spectra with those for an electron beam of the same energy reflects the difference in the hadronic cross sections between photons and hadrons above a few 100 MeV. Differences are increasing towards lower energies because of different interaction mechanisms. Furthermore, the slight shift in energy above about 100 MeV follows from the fact that the energies of the interacting photons are lower than 25 GeV. Apart from this the shapes of the two spectra are similar.

The neutron-attenuation length is shown in Fig. 37.4 for concrete and mono-energetic broad-beam conditions. It reaches an asymptotic value of about 117 g/cm^2 above 200 MeV. As the cascade through thick shielding is carried by particles with energies between about 100 MeV and 300 MeV (in this energy range non-elastic cross sections are at minimum and are dominated by quasi-elastic processes leading to low attenuation) this value is equal to the equilibrium attenuation length for particles emitted at 90 degrees in concrete.

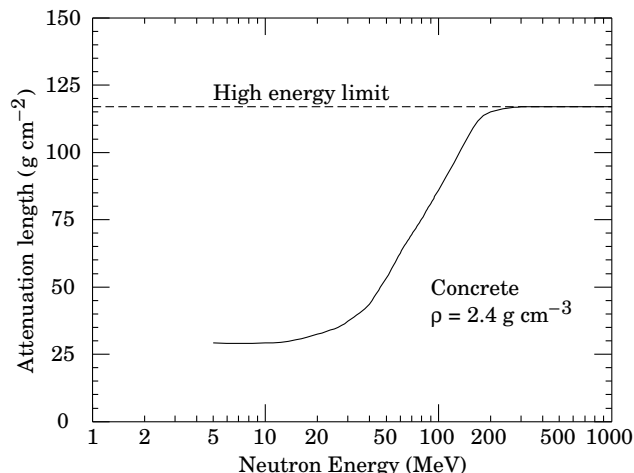


Figure 37.4: The variation of the attenuation length for mono-energetic neutrons in concrete as a function of neutron energy [10].

37.5. Photon sources

The dose equivalent rate in tissue (in mSv/h) from a gamma point source emitting one photon of energy E (in MeV) per second at a distance of 1 m is $4.6 \times 10^{-9} \mu_{en}/\rho E$, where μ_{en}/ρ is the mass energy absorption coefficient. The latter has a value of $0.029 \pm 0.004 \text{ cm}^2/\text{g}$ for photons in tissue over an energy range between 60 keV and 2 MeV (see Ref. 12 for tabulated values).

Similarly, the dose equivalent rate in tissue (in mSv/h) at the surface of a semi-infinite slab of uniformly activated material containing 1 Bq/g of a gamma emitter of energy E (in MeV) is $2.9 \times 10^{-4} R_\mu E$, where R_μ is the ratio of the mass energy absorption coefficients of the photons in tissue and in the material.

37.6. Accelerator-induced radioactivity

Typical medium- and long-lived activation products in metallic components of accelerators are ^{22}Na , ^{46}Sc , ^{48}V , ^{51}Cr , ^{54}Mn , ^{55}Fe , ^{59}Fe , ^{56}Co , ^{57}Co , ^{58}Co , ^{60}Co , ^{63}Ni and ^{65}Zn . Gamma-emitting nuclides dominate doses by external irradiation at longer decay times (more than one day) while at short decay times β^+ emitters are also important (through photons produced by β^+ annihilation). Due to their short range, β^- emitters are relevant, for example, only for dose to the skin and eyes or for doses due to inhalation or ingestion. Fig. 37.5 and Fig. 37.6 show the contributions of gamma and β^+ emitters to the total dose rate at 12.4 cm distance to a copper sample [13]. The sample was activated by the stray radiation field created by a 120 GeV mixed hadron beam dumped in a copper target during about 8 hours at intensities between $10^7 - 10^8$ hadrons per second. Typically, dose rates at a certain decay time are mainly determined by radionuclides having a half-life of the order of the decay time. Extended irradiation periods might be an exception to this general rule as in this case the activity of long-lived nuclides can build up sufficiently so that it dominates that one of short-lived even at short cooling times.

Activation in concrete is dominated by ^{24}Na (short decay time) and ^{22}Na (long decay time). Both nuclides can be produced either by low-energy neutron reactions on the sodium-component in the concrete or by spallation reactions on silicon, calcium and other constituents such as aluminum. At long decay times nuclides of radiological interest in activated concrete can also be ^{60}Co , ^{152}Eu , ^{154}Eu and ^{134}Cs , all of which produced by (n,γ) -reactions with traces of natural cobalt, europium and cesium. Thus, such trace elements might be important even if their content in concrete is only a few parts per million or less by weight.

The explicit simulation of radionuclide production with general-purpose Monte Carlo codes has become the most commonly applied method to calculate induced radioactivity and its radiological consequences [13] (see also Sec. 37.8). They are complemented by

analytical codes based on folding particle fluence spectra with nuclide production cross sections. ActiWiz [14,15] is an example of such a code targeting the domain of radiological characterization and material optimization. It allows for calculating nuclide inventories by convolution of fluence spectra with nuclide production data for 85 chemical elements and arbitrary compounds from threshold to an energy of 100 TeV.

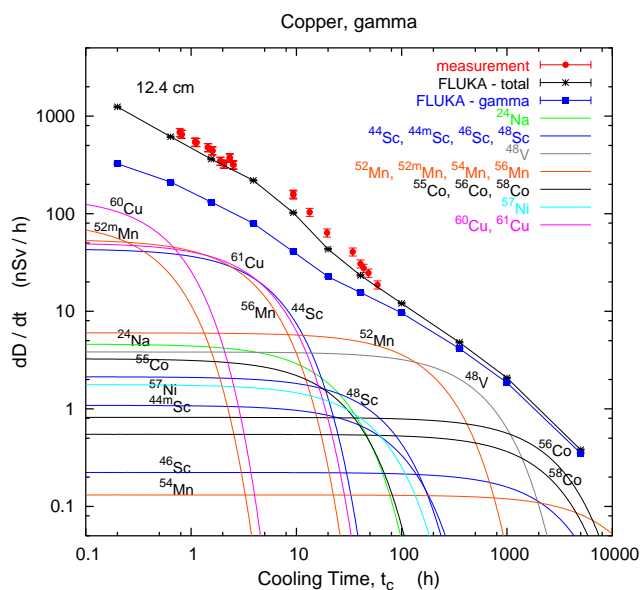


Figure 37.5: Contribution of individual gamma-emitting nuclides to the total dose rate at 12.4 cm distance to an activated copper sample [13].

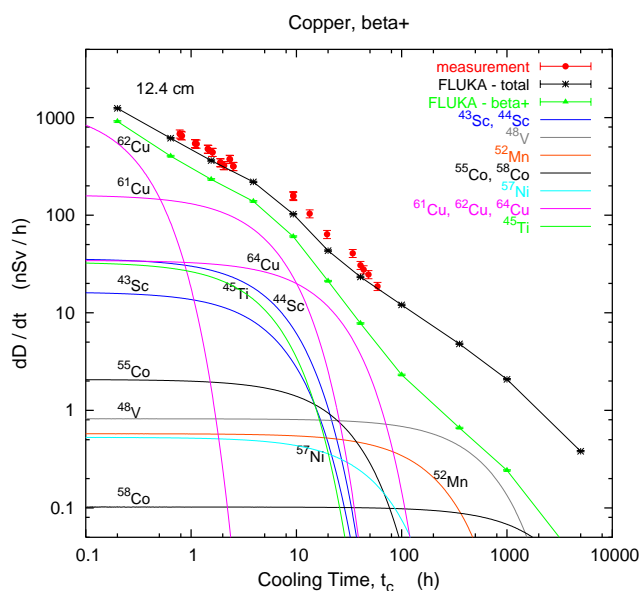


Figure 37.6: Contribution of individual positron-emitting nuclides to the total dose rate at 12.4 cm distance to an activated copper sample [13].

37.7. Radiation protection instrumentation

The capacity to distinguish and measure the high-LET (mostly neutrons) and the low-LET components (photons, electrons, muons) of the radiation field at workplaces is of primary importance to evaluate the exposure of personnel. At proton machines the prompt dose equivalent outside a shield is mainly due to neutrons, with some contribution from photons and, to a minor extent, charged particles. At high-energy electron accelerators the dominant stray radiation during operation consists of high-energy neutrons, because the shielding is normally thick enough to absorb most of the bremsstrahlung photons. Most of the personnel exposure at accelerator facilities is often received during maintenance interventions, and is due to gamma/beta radiation coming from residual radioactivity in accelerator components.

Radiation detectors used both for radiation surveys and area monitoring are normally calibrated in ambient dose equivalent $H^*(10)$.

37.7.1. Neutron detectors :

• **Rem counters:** A rem counter [16] is a portable detector consisting of a thermal neutron counter embedded in a polyethylene moderator, with a response function that approximately follows the curve of the conversion coefficients from neutron fluence to $H^*(10)$ over a wide energy range. Conventional rem counters provide a response to neutrons up to approximately 10-15 MeV, extended-range units are heavier as they include a high-A converter but correctly measure $H^*(10)$ up to several hundred MeV [17].

• **Bonner Sphere Spectrometer (BSS):** A BSS [18] is made up of a thermal neutron detector at the centre of moderating spheres of different diameters made of polyethylene (PE) or a combination of PE and a high-A material to enhance its response to high energy neutrons (similar to rem counters). Each sphere has a different response function versus neutron energy, and the neutron energy, at which the sensitivity peaks, increases with sphere diameter. The energy resolution of the system is rather low but satisfactory for radiation protection purposes. The neutron spectrum is obtained by unfolding the experimental counts of the BSS with its response matrix by a computer code that is often based on an iterative algorithm such as GRAVEL [19] and MAXED [20]. BSS exist in active (using ^3He or BF_3 proportional counters or ^6LiI scintillators) and passive versions (using CR-39 track detectors or LiF), for use *e.g.* in strongly pulsed fields. With ^3He counters the discrimination with respect to gamma rays and noise is excellent.

• **Bubble detectors:** A bubble detector [21] is a dosimeter based on a super-heated emulsion (super-heated droplets suspended in a gel) contained in a vial and acting as a continuously sensitive, miniature bubble chamber. The total number of bubbles evolved from the radiation-induced nucleation of drops gives an integrated measure of the total neutron exposure. Various techniques exist to record and count the bubbles, *e.g.*, visual inspection, automated reading with video cameras or acoustic counting. Bubble detectors are insensitive to low-LET radiation. Super-heated emulsions are used as personal, area and environmental dosimeters, as well as neutron spectrometers.

• **Track etched detectors:** Track etched detectors (TEDs) [22] are based on the preferential dissolution of suitable, mostly insulator, materials along the damage trails of charged particles of sufficiently high-energy deposition density. The detectors are effectively not sensitive to radiation which deposits the energy through the interactions of particles with low LET. These dosimeters are generally able to determine neutron ambient dose equivalent down to around 100 μSv . They are used both as personal dosimeters and for area monitoring, *e.g.*, in BSS.

37.7.2. Photon detectors [23] :

• **GM counters:** Geiger Müller (GM) counters are low cost devices simple to operate. They work in pulse mode and since they only count radiation-induced events, any spectrometric information is lost. In general they are calibrated in terms of air kerma, for instance in a ^{60}Co field. The response of GM counters to photons is constant within 15% for energies up to 2 MeV and shows considerable energy dependence above.

• **Ionization chambers:** Ionization chambers are gas-filled detectors used both as hand-held instruments (*e.g.*, for radiation surveys) and environmental monitors. They are normally operated in current mode although pulse-mode operation is also possible. They possess a relatively flat response to a wide range of X- and gamma ray energies (typically from 10 keV to several MeV), can measure radiation over a wide intensity range and are capable of discriminating between the beta and gamma components of a radiation field (by use of, *e.g.*, a beta window). Pressurized ion chambers (filled, *e.g.*, with Ar or H gas to several tens of bars) are used for environmental monitoring applications. They have good sensitivity to neutrons and charged hadrons in addition to low LET radiation (gammas and muons), with the response function to the former being strongly non-linear with energy.

• **Scintillators:** Scintillation-based detectors are used in radiation protection as hand-held probes and in fixed installations, *e.g.*, portal monitors. A scintillation detector or counter is obtained coupling a scintillator to an electronic light sensor such as a photomultiplier tube (PMT), a photodiode or a silicon photomultiplier (SiPM). There is a wide range of scintillating materials, inorganic (such as CsI and BGO), organic or plastic; they find application in both photon dosimetry and spectrometry.

37.7.3. Operation in pulsed radiation fields :

There are many practical situations with particle accelerators used for scientific, industrial and medical applications where the time structure of the stray radiation limits the use of active monitors or requires specifically designed electronics. Pulsed neutron and gamma fields may be present because of beam losses at, *e.g.*, targets, collimators and beam dumps. The time duration of a single burst can range from a few ns to about 1 ms with a typical repetition rate in the range 0.1–100 Hz. Conventional detectors generally suffer from dead time effects and have strong limitations in the measurements of pulsed fields. Severe under response has been observed, *e.g.*, in commercial rem counters, with tremendous underestimation of the ambient dose equivalent, $H^*(10)$, up to three orders of magnitude. The common techniques used to correct the response of radiation detectors which include dead-time corrections operate properly in a steady-state radiation field, whereas it is much more difficult to cope with dead time losses in a pulsed radiation field of unknown time structure and burst dose. Generally speaking the monitoring instrumentation must be chosen on the basis of the knowledge of the radiation field. Detectors with specifically designed electronics must be employed in pulsed field conditions, such as the recently developed LUPIN [24] in place of conventional rem counters for neutrons. If real-time monitoring is not required, passive detectors or dosimeters such as TEDs mentioned in Sec. 37.7.1 or LiF mentioned in Sec. 37.7.4 can be employed, as they are insensitive to the time structure of the radiation.

37.7.4. Personal dosimeters :

Personal dosimeters, calibrated in $H_p(10)$, are worn by persons exposed to ionizing radiation for professional reasons to record the dose received. They are typically passive detectors, either film, track etched detectors, $^6\text{Li}/^7\text{Li}$ -based dosimeters (*e.g.* LiF), optically stimulated luminescence (OSL) or radiophotoluminescence detectors (RPL) but semi-active dosimeters using miniaturized ion-chambers also exist, like the Direct Ion Storage (DIS) dosimeters in use at CERN.

Electronic personal dosimeters are small active units for on-line monitoring of individual exposure, designed to be worn on the body. They can give an alarm on both the integral dose received or dose rate once a pre-set threshold is exceeded.

37.8. Monte Carlo codes for radiation protection studies

The use of general-purpose particle interaction and transport Monte Carlo codes is often the most accurate and efficient choice for assessing radiation protection quantities at accelerators. Due to the vast spread of such codes to all areas of particle physics and the associated extensive benchmarking with experimental data, the modeling has

reached an unprecedented accuracy. Furthermore, most codes allow the user to simulate all aspects of a high energy particle cascade in one and the same run: from the first interaction of a TeV nucleus over the transport and re-interactions (hadronic and electromagnetic) of the produced secondaries, to detailed nuclear fragmentation, the calculation of radioactive decays and even of the electromagnetic shower caused by the radiation from such decays. A brief account of the codes most widely used for radiation protection studies at high energy accelerators is given in the following.

• **FLUKA [8,9]:** FLUKA is a general-purpose particle interaction and transport code. It comprises all features needed for radiation protection, such as detailed hadronic and nuclear interaction models up to 10 PeV, full coupling between hadronic and electromagnetic processes and numerous variance reduction options. The latter include weight windows, region importance biasing, and leading particle, interaction, and decay length biasing (among others). The capabilities of FLUKA are unique for studies of induced radioactivity, especially with regard to nuclide production, decay, and transport of residual radiation. In particular, particle cascades by prompt and residual radiation are simulated in parallel based on the microscopic models for nuclide production and a solution of the Bateman equations for activity build-up and decay.

• **GEANT4 [25,26,27]:** GEANT4 is an object-oriented toolkit consisting of a kernel that provides the framework for particle transport, including tracking, geometry description, material specifications, management of events and interfaces to external graphics systems. The kernel also provides interfaces to physics processes. It allows the user to freely select the physics models that best serve the particular application needs. Implementations of interaction models exist over an extended range of energies, from optical photons and thermal neutrons to high-energy interactions required for the simulation of accelerator and cosmic ray experiments. To facilitate the use of variance reduction techniques, general-purpose biasing methods such as importance biasing, weight windows, and a weight cut-off method have been introduced directly into the toolkit. Other variance reduction methods, such as leading particle biasing for hadronic processes, come with the respective physics packages.

• **MARS15 [28,29]:** The MARS15 code system is a set of Monte Carlo programs for the simulation of hadronic and electromagnetic cascades. It covers a wide energy range: 1 keV to 100 TeV for muons, charged hadrons, heavy ions and electromagnetic showers; and 0.00215 eV to 100 TeV for neutrons. Hadron-nucleus interactions as well as practically all other strong, weak and electromagnetic interactions in the entire energy range can be simulated either inclusively or exclusively. MARS15 uses ENDFB-VII nuclear data to handle interactions of neutrons with energies below 14 MeV. Several variance reduction techniques, such as weight windows, particle splitting, and Russian roulette, are available. A tagging module allows tagging the origin of a given signal for source term or sensitivity analyses. The geometry module allows either a basic solid body representation option or a ROOT-based powerful engine. Further features of MARS15 include a MAD-MARS merge for a convenient creation of accelerator models and multi-turn tracking and cascade simulation in accelerator and beamline lattices.

• **MCNP6 [30,31]:** MCNP6 is the latest version of the Monte Carlo N-Particle transport (MCNP) family of neutron interaction and transport codes and, therefore, features one of the most comprehensive and detailed descriptions of the related physical processes. It transports 37 different particle types, including ions and electromagnetic particles. The neutron interaction and transport modules use standard evaluated data libraries mixed with physics models where such libraries are not available. The transport is continuous in energy. MCNP6 contains one of the most powerful implementations of variance reduction techniques. Spherical mesh weight windows can be created by a generator in order to focus the simulation time on certain spatial regions of interest. In addition, a more generalized phase space biasing is also possible through energy- and time-dependent weight windows. Other biasing options include pulse-height tallies with variance reduction and criticality source convergence acceleration.

• **PHITS [32,33]**: The Particle and Heavy-Ion Transport code System PHITS was among the first general-purpose codes to simulate the transport and interactions of heavy ions in a wide energy range, from 10 MeV/nucleon to 100 GeV/nucleon. It is based on the high-energy hadron transport code NMTC/JAM that was extended to heavy ions. The transport of low-energy neutrons employs cross sections from evaluated nuclear data libraries such as ENDF and JENDL below 20 MeV. Electromagnetic interactions are simulated based on the ITS code in the energy range between 1 keV and 100 MeV for electrons and positrons and between 1 keV and 100 GeV for photons. Several variance reduction techniques, including weight windows and region importance biasing, are available.

References:

- International Commission on Radiation Units and Measurements, *Fundamental Quantities and Units for Ionizing Radiation*, ICRU Report 60 (1998).
- ICRP, 2010. *Conversion Coefficients for Radiological Protection Quantities for External Radiation Exposures*, ICRP Publication 116, Annals of the ICRP 40(2-5).
- ICRP Publication 103, *The 2007 Recommendations of the International Commission on Radiological Protection*, Annals of the ICRP, Elsevier (2007).
- M. Pelliccioni, *Radiation Protection Dosimetry* **88**, 279 (2000).
- E. Pochin, *Nuclear Radiation: Risks and Benefits*, Clarendon Press, Oxford, 1983.
- United Nations, *Report of the United Nations Scientific Committee on the Effect of Atomic Radiation*, General Assembly, Official Records A/63/46 (2008).
- W.P. Swanson, *Radiological Safety Aspects of the Operation of Electron Linear Accelerators*, IAEA Technical Reports Series No. 188 (1979).
- A. Ferrari, *et al.*, FLUKA: A Multi-particle Transport Code, CERN-2005-010 (2005), <http://www.fluka.org>.
- T.T. Böhlen, *et al.*, The FLUKA code: Developments and Challenges for High Energy and Medical Applications, *Nuclear Data Sheets* **120**, 211 (2014).
- R.H. Thomas and G.R. Stevenson, *Radiological Safety Aspects of the Operation of Proton Accelerators*, IAEA Technical Report Series No. 283 (1988).
- T.A. Gabriel, *et al.*, *Nucl. Instrum. Methods* **A338**, 336 (1994).
- <http://physics.nist.gov/PhysRefData/XrayMassCoef/cover.html>.
- S. Roesler, *et al.*, "Simulation of Remanent Dose Rates and Benchmark Measurements at the CERN-EU High Energy Reference Field Facility," in *Proceedings of the Sixth International Meeting on Nuclear Applications of Accelerator Technology*, San Diego, CA, 1-5 June 2003, 655–662 (2003).
- C. Theis and H. Vincke, "The use of ActiWiz in operational radiation protection," in *Proceedings of the Twelfth Meeting of Task-Force on Shielding Aspects of Accelerators, Targets and Irradiation Facilities of Accelerator Technology, SATIF12 FNAL*, 28-30 April 2014, Nuclear Science Report NEA/NSC/R 3, (2015).
- C. Theis and H. Vincke, "ActiWiz3 an overview of the concepts, architecture and new features," CERN Technical Note CERN-RP-2016-117-REPORTS-TN (2016), <http://actiwiz.web.cern.ch>.
- I.O. Andersson and J. Braun, A neutron rem counter with uniform sensitivity from 0.025 eV to 10 MeV in *Proceedings of the IAEA Symposium on Neutron dosimetry*, IAEA, Vienna, Vol. II, 87–95, (1963).
- C. Birattari, *et al.*, *Radiation Protection Dosimetry* **76**, 135 (1998).
- R.L. Bramblett, R.I. Ewing and T.W. Bonner, *Nucl. Instrum. Methods* **9**, 1 (1960).
- M. Matzke, PTB, Braunschweig PTBN-19, (1994).
- M. Reginatto and P. Goldhagen, *Health Physics* **77**, 579 (1999).
- F. d'Errico, *Nucl. Instrum. Methods* **B184**, 229 (2001).
- K. Becker, Dosimetric applications of track etching, in *Topics in Radiation Dosimetry* Ed. F.H. Attix, Academic Press, London, 79–143, (1972).
- G.F. Knoll, *Radiation detection and measurements*, Wiley (2010).
- M. Caresana, *et al.*, A new version of the LUPIN detector: Improvements and latest experimental verification, *Review of Scientific Instruments* **85**, 065102 (2014).
- S. Agostinelli, *et al.*, *Nucl. Instrum. Methods* **A506**, 250 (2003).
- J. Allison, *et al.*, *IEEE Transactions on Nuclear Science* **53**, 270 (2006).
- J. Allison, *et al.*, *Nucl. Instrum. Methods* **A835**, 186 (2016), <http://geant4.cern.ch>.
- N.V. Mokhov and C.C. James The MARS Code System Users Guide, Fermilab-FN-1058-APC (2018), <https://mars.fnal.gov>.
- N.V. Mokhov, *et al.*, *Prog. Nucl. Sci. Technol.* **4**, 496 (2014).
- D. Pelowitz, *et al.*, Los Alamos National Laboratory report, LA-CP-14-00745 (2014), <https://mcnp.lanl.gov>.
- J.T. Goorley, *et al.*, *Nuclear Technology* **180**, 298 (2012).
- T. Sato, *et al.*, *Journal of Nuclear Science and Technology* **55**, 684 (2018).
- T. Sato, *et al.*, PHITS Particle and Heavy Ion Transport code System, Version 3.10 (2019), <https://phits.jaea.go.jp>.

38. Commonly Used Radioactive Sources

Table 38.1. Revised September 2019 by D.E. Groom (LBNL).

Nuclide	Half-life	Type of decay	Particle		Photon	
			Energy (MeV)	Emission prob.	Energy (MeV)	Emission prob.
$^{22}_{11}\text{Na}$	2.603 y	β^+ , EC	0.546	90%	0.511 1.275	Annih. 100%
$^{51}_{24}\text{Cr}$	27.70 d	EC			0.320 V K x rays	10% 100%
Neutrino calibration source						
$^{54}_{25}\text{Mn}$	0.855 y	EC			0.835 Cr K x rays	100% 26%
$^{55}_{26}\text{Fe}$	2.747 y	EC			Mn K x rays: 0.00590 0.00649	24.4% 2.86%
$^{57}_{27}\text{Co}$	271.8 d	EC			0.014 0.122 0.136	9% 86% 11%
					Fe K x rays	58%
$^{60}_{27}\text{Co}$	5.271 y	β^-	0.317	99.9%	1.173 1.333	99.9% 99.9%
$^{68}_{32}\text{Ge}$	271.0 d	EC			Ga K x rays	42%
$\rightarrow ^{68}_{31}\text{Ga}$	67.8 m	β^+ , EC	1.899	90%	0.511 1.077	Annih. 3%
$^{90}_{38}\text{Sr}$	28.8 y	β^-	0.546	100%		
$\rightarrow ^{90}_{39}\text{Y}$	2.67 d	β^-	2.279	100%		
$^{106}_{44}\text{Ru}$	371.5 d	β^-	0.039	100%		
$\rightarrow ^{106}_{45}\text{Rh}$	30.1 s	β^-	3.546	79%	0.512 0.622	21% 10%
$^{109}_{48}\text{Cd}$	1.265 y	EC	0.063 0.084	e^- 42% e^- 44%	0.088 Ag K x rays	3.7% 100%
$^{113}_{50}\text{Sn}$	115.1 d	EC	0.364 0.388	e^- 28% e^- 6%	0.392 In K x rays	65% 97%
$^{137}_{55}\text{Cs}$	30.0 y	β^-	0.514 1.176	94% 6%	0.662	85%
$^{133}_{56}\text{Ba}$	10.55 y	EC	0.045 0.075	e^- 50% e^- 6%	0.081 0.356	33% 62%
					Cs K x rays	121%
$^{152}_{63}\text{Eu}$	13.537 y	EC β^-		72.1% 27.9%	Many γ 's 0.1218–1.408 MeV	
$^{207}_{83}\text{Bi}$	32.9 y	EC	0.481 0.975 1.047	e^- 2% e^- 7% e^- 2%	0.569 1.063 1.770	98% 75% 7%
					Pb K x rays	78%
$^{228}_{90}\text{Th}$	1.912 y	6 α : 3 β^- :	5.341 to 8.785 0.334 to 2.246		0.239 0.583 2.614	44% 31% 36%
($\rightarrow ^{224}_{88}\text{Ra}$)	($\rightarrow ^{220}_{86}\text{Rn}$)	($\rightarrow ^{216}_{84}\text{Po}$)	($\rightarrow ^{212}_{82}\text{Pb}$)	($\rightarrow ^{212}_{83}\text{Bi}$)	($\rightarrow ^{212}_{84}\text{Po}$)	
(361 d)	(55.8 s)	(0.148 s)	(10.64 h)	(60.54 m)	(300 ns)	
$^{241}_{95}\text{Am}$	432.6 y	α	5.443 5.486	13% 84%	0.060 Np L x rays	36% 38%
$^{241}_{95}\text{Am/Be}$	432.6 y	6×10^{-5} neutrons ($\langle E \rangle = 4$ MeV) and 4×10^{-5} γ 's (4.43 MeV from $^9_4\text{Be}(\alpha, n)$)				
$^{244}_{96}\text{Cm}$	18.11 y	α	5.763 5.805	24% 76%	Pu L x rays	$\sim 9\%$
$^{252}_{98}\text{Cf}$	2.645 y	α (97%)	6.076 6.118	15% 82%		
		Fission (3.1%): Average 7.8 γ 's/fission; $\langle E_\gamma \rangle = 0.88$ MeV ≈ 4 neutrons/fission; $\langle E_n \rangle = 2.14$ MeV				

“Emission probability” is the probability per decay of a given emission; because of cascades these may total more than 100%. Only principal emissions are listed. EC means electron capture, and e^- means monoenergetic internal conversion (Auger) electron. The intensity of 0.511 MeV e^+e^- annihilation photons depends upon the number of stopped positrons. Endpoint β^\pm energies are listed. In some cases when energies are closely spaced, the γ -ray values are approximate weighted averages. Radiation from short-lived daughter isotopes is included where relevant.

Half-lives, energies, and intensities may be found in www-pub.iaea.org/books/IAEABooks/7551/Update-of-X-Ray-and-Gamma-Ray-Decay-Data-Standards-for-Detector-Calibration-and-Other-Applications, IAEA (2007) or Nuclear Data Sheets (www.journals.elsevier.com/nuclear-data-sheets) (2007).

Neutron sources: See *e.g.* “Neutron Calibration Sources in the Daya Bay Experiment,” J. Liu *et al.*, Nuclear Instrum. Methods **A797**, 260 (2005) (arXiv.1504.07911).

^{51}Cr calibration of neutrino detectors is discussed in *e.g.* J.N. Abdurashitov *et al.* [SAGE Collaboration], Phys. Rev. **C59**, 2246 (1999). The use of $^{75}_{34}\text{Se}$ and other isotopes has also been proposed.

Mathematical Tools or Statistics, Monte Carlo, Group Theory

39. Probability (rev.)	621
40. Statistics (rev.)	626
41. Monte Carlo techniques (rev.)	642
42. Monte Carlo event generators	646
43. Monte Carlo neutrino event generators (rev.)	657
44. Monte Carlo particle numbering scheme (rev.)	661
45. Clebsch-Gordan coefficients, spherical harmonics, and d functions	665
46. SU(3) isoscalar factors and representation matrices	666
47. SU(n) multiplets and Young diagrams	667



39. Probability

Revised August 2019 by G. Cowan (RHUL).

39.1 General

[1–8] An abstract definition of probability can be given by considering a set S , called the sample space, and possible subsets A, B, \dots , the interpretation of which is left open. The probability P is a real-valued function defined by the following axioms due to Kolmogorov [9]:

1. For every subset A in S , $P(A) \geq 0$;
2. For disjoint subsets (*i.e.*, $A \cap B = \emptyset$), $P(A \cup B) = P(A) + P(B)$;
3. $P(S) = 1$.

In addition, one defines the conditional probability $P(A|B)$ (read as P of A given B) as

$$P(A|B) = \frac{P(A \cap B)}{P(B)}. \quad (39.1)$$

From this definition and using the fact that $A \cap B$ and $B \cap A$ are the same, one obtains *Bayes' theorem*,

$$P(A|B) = \frac{P(B|A)P(A)}{P(B)}. \quad (39.2)$$

From the three axioms of probability and the definition of conditional probability, one obtains the *law of total probability*,

$$P(B) = \sum_i P(B|A_i)P(A_i), \quad (39.3)$$

for any subset B and for disjoint A_i with $\cup_i A_i = S$. This can be combined with Bayes' theorem (Eq. (39.2)) to give

$$P(A|B) = \frac{P(B|A)P(A)}{\sum_i P(B|A_i)P(A_i)}, \quad (39.4)$$

where the subset A could, for example, be one of the A_i .

The most commonly used interpretation of the elements of the sample space are outcomes of a repeatable experiment. The probability $P(A)$ is assigned a value equal to the limiting frequency of occurrence of A . This interpretation forms the basis of *frequentist statistics*.

The elements of the sample space might also be interpreted as *hypotheses*, *i.e.*, statements that are either true or false, such as ‘The mass of the W boson lies between 80.3 and 80.5 GeV.’ Upon repetition of a measurement, however, such statements are either always true or always false, *i.e.*, the corresponding probabilities in the frequentist interpretation are either 0 or 1. Using *subjective probability*, however, $P(A)$ is interpreted as the degree of belief that the hypothesis A is true. Subjective probability is used in *Bayesian* (as opposed to frequentist) statistics. Bayes' theorem can be written

$$P(\text{theory}|\text{data}) \propto P(\text{data}|\text{theory})P(\text{theory}), \quad (39.5)$$

where ‘theory’ represents some hypothesis and ‘data’ is the outcome of the experiment. Here $P(\text{theory})$ is the *prior* probability for the theory, which reflects the experimenter's degree of belief before carrying out the measurement, and $P(\text{data}|\text{theory})$ is the probability to have gotten the data actually obtained, given the theory, which is also called the *likelihood*.

Bayesian statistics provides no fundamental rule for obtaining the prior probability, which may depend on previous measurements, theoretical prejudices, *etc.* Once this has been specified, however, Eq. (39.5) tells how the probability for the theory must be modified in the light of the new data to give the *posterior* probability, $P(\text{theory}|\text{data})$. As Eq. (39.5) is stated as a proportionality, the probability must be normalized by summing (or integrating) over all possible hypotheses.

39.2 Random variables

A *random variable* is a numerical characteristic assigned to an element of the sample space. In the frequency interpretation of probability, it corresponds to an outcome of a repeatable experiment. Let x be a possible outcome of an observation. If x can take on any value from a continuous range, we write $f(x; \theta)dx$ as the probability that the measurement's outcome lies between x and $x + dx$. The function $f(x; \theta)$ is called the *probability density function* (p.d.f.), which may depend on one or more parameters θ . If x can take on only discrete values (*e.g.*, the non-negative integers), then we use $f(x; \theta)$ to denote the probability to find the value x . In the following the term p.d.f. is often taken to cover both the continuous and discrete cases, although technically the term density should only be used in the continuous case.

The p.d.f. is always normalized to unity. Both x and θ may have multiple components and are then often written as vectors. If θ is unknown, we may wish to estimate its value from a given set of measurements of x ; this is a central topic of *statistics* (see Sec. 40).

The *cumulative distribution function* $F(a)$ is the probability that $x \leq a$:

$$F(a) = \int_{-\infty}^a f(x) dx. \quad (39.6)$$

Here and below, if x is discrete-valued, the integral is replaced by a sum. The endpoint a is expressly included in the integral or sum. Then $0 \leq F(x) \leq 1$, $F(x)$ is nondecreasing, and $P(a < x \leq b) = F(b) - F(a)$. If x is discrete, $F(x)$ is flat except at allowed values of x , where it has discontinuous jumps equal to $f(x)$.

Any function of random variables is itself a random variable, with (in general) a different p.d.f. The *expectation value* of any function $u(x)$ is

$$E[u(x)] = \int_{-\infty}^{\infty} u(x) f(x) dx, \quad (39.7)$$

assuming the integral is finite. The expectation value is linear, *i.e.*, for any two functions u and v of x and constants c_1 and c_2 , $E[c_1 u + c_2 v] = c_1 E[u] + c_2 E[v]$.

The n^{th} moment of a random variable x is

$$\alpha_n \equiv E[x^n] = \int_{-\infty}^{\infty} x^n f(x) dx, \quad (39.8a)$$

and the n^{th} central moment of x (or moment about the mean, α_1) is

$$m_n \equiv E[(x - \alpha_1)^n] = \int_{-\infty}^{\infty} (x - \alpha_1)^n f(x) dx. \quad (39.8b)$$

The most commonly used moments are the mean μ and variance σ^2 :

$$\mu \equiv \alpha_1, \quad (39.9a)$$

$$\sigma^2 \equiv V[x] \equiv m_2 = \alpha_2 - \mu^2. \quad (39.9b)$$

The mean is the location of the ‘center of mass’ of the p.d.f., and the variance is a measure of the square of its width. Note that $V[cx + k] = c^2 V[x]$. It is often convenient to use the *standard deviation* of x , σ , defined as the square root of the variance.

Any odd moment about the mean is a measure of the skewness of the p.d.f. The simplest of these is the dimensionless coefficient of skewness $\gamma_1 = m_3/\sigma^3$.

The fourth central moment m_4 provides a convenient measure of the tails of a distribution. For the Gaussian distribution (see Sec. 39.4), one has $m_4 = 3\sigma^4$. The *kurtosis* is defined as $\gamma_2 = m_4/\sigma^4 - 3$, *i.e.*, it is zero for a Gaussian, positive for a *leptokurtic* distribution with longer tails, and negative for a *platykurtic* distribution with tails that die off more quickly than those of a Gaussian.

The *quantile* x_α is the value of the random variable x at which the cumulative distribution is equal to α . That is, the quantile

is the inverse of the cumulative distribution function, i.e., $x_\alpha = F^{-1}(\alpha)$. An important special case is the *median*, x_{med} , defined by $F(x_{\text{med}}) = 1/2$, i.e., half the probability lies above and half lies below x_{med} . (More rigorously, x_{med} is a median if $P(x \geq x_{\text{med}}) \geq 1/2$ and $P(x \leq x_{\text{med}}) \geq 1/2$. If only one value exists, it is called ‘the median.’)

Under a monotonic change of variable $x \rightarrow y(x)$, the quantiles of a distribution (and hence also the median) obey $y_\alpha = y(x_\alpha)$. In general the expectation value and *mode* (most probable value) of a distribution do not, however, transform in this way.

Let x and y be two random variables with a *joint* p.d.f. $f(x, y)$. The *marginal* p.d.f. of x (the distribution of x with y unobserved) is

$$f_1(x) = \int_{-\infty}^{\infty} f(x, y) dy, \tag{39.10}$$

and similarly for the marginal p.d.f. $f_2(y)$. The *conditional* p.d.f. of y given fixed x (with $f_1(x) \neq 0$) is defined by $f_3(y|x) = f(x, y)/f_1(x)$, and similarly $f_4(x|y) = f(x, y)/f_2(y)$. From these, we immediately obtain Bayes’ theorem (see Eqs. (39.2) and (39.4)),

$$f_4(x|y) = \frac{f_3(y|x)f_1(x)}{f_2(y)} = \frac{f_3(y|x)f_1(x)}{\int f_3(y|x')f_1(x') dx'}. \tag{39.11}$$

The mean of x is

$$\mu_x = \int_{-\infty}^{\infty} \int_{-\infty}^{\infty} x f(x, y) dx dy = \int_{-\infty}^{\infty} x f_1(x) dx, \tag{39.12}$$

and similarly for y . The *covariance* of x and y is

$$\text{cov}[x, y] = E[(x - \mu_x)(y - \mu_y)] = E[xy] - \mu_x \mu_y. \tag{39.13}$$

A dimensionless measure of the covariance of x and y is given by the *correlation coefficient*,

$$\rho_{xy} = \text{cov}[x, y]/\sigma_x \sigma_y, \tag{39.14}$$

where σ_x and σ_y are the standard deviations of x and y . It can be shown that $-1 \leq \rho_{xy} \leq 1$.

Two random variables x and y are *independent* if and only if

$$f(x, y) = f_1(x)f_2(y). \tag{39.15}$$

If x and y are independent, then $\rho_{xy} = 0$; the converse is not necessarily true. If x and y are independent, $E[u(x)v(y)] = E[u(x)]E[v(y)]$, and $V[x+y] = V[x] + V[y]$; otherwise, $V[x+y] = V[x] + V[y] + 2\text{cov}[x, y]$, and $E[uv]$ does not necessarily factorize.

Consider a set of n continuous random variables $\mathbf{x} = (x_1, \dots, x_n)$ with joint p.d.f. $f(\mathbf{x})$, and a set of n new variables $\mathbf{y} = (y_1, \dots, y_n)$, related to \mathbf{x} by means of a function $\mathbf{y}(\mathbf{x})$ that is one-to-one, i.e., the inverse $\mathbf{x}(\mathbf{y})$ exists. The joint p.d.f. for \mathbf{y} is given by

$$g(\mathbf{y}) = f(\mathbf{x}(\mathbf{y}))|J|, \tag{39.16}$$

where $|J|$ is the absolute value of the determinant of the square matrix $J_{ij} = \partial x_i / \partial y_j$ (the Jacobian determinant). If the transformation from \mathbf{x} to \mathbf{y} is not one-to-one, the \mathbf{x} -space must be broken into regions where the function $\mathbf{y}(\mathbf{x})$ can be inverted, and the contributions to $g(\mathbf{y})$ from each region summed.

Given a set of functions $\mathbf{y} = (y_1, \dots, y_m)$ with $m < n$, one can construct $n - m$ additional independent functions, apply the procedure above, then integrate the resulting $g(\mathbf{y})$ over the unwanted y_i to find the marginal distribution of those of interest.

For a one-to-one transformation of discrete random variables, the probability is obtained by simple substitution; no Jacobian is necessary because in this case f is a probability rather than a probability density. If the transformation is not one-to-one, then one must sum the probabilities for all values of the original variable that contribute to a given value of the transformed variable. If f depends on a set of parameters θ , a change to a different parameter set $\eta(\theta)$ is made by simple substitution; no Jacobian is used.

39.3 Characteristic functions

The characteristic function $\phi(u)$ associated with the p.d.f. $f(x)$ is essentially its Fourier transform, or the expectation value of e^{iux} :

$$\phi(u) = E[e^{iux}] = \int_{-\infty}^{\infty} e^{iux} f(x) dx. \tag{39.17}$$

Once $\phi(u)$ is specified, the p.d.f. $f(x)$ is uniquely determined and vice versa; knowing one is equivalent to the other. Characteristic functions are useful in deriving a number of important results about moments and sums of random variables.

It follows from Eqs. (39.8) and (39.17) that the n^{th} moment of a random variable x that follows $f(x)$ is given by

$$i^{-n} \left. \frac{d^n \phi}{du^n} \right|_{u=0} = \int_{-\infty}^{\infty} x^n f(x) dx = \alpha_n. \tag{39.18}$$

Thus it is often easy to calculate all the moments of a distribution defined by $\phi(u)$, even when $f(x)$ cannot be written down explicitly.

If the p.d.f.s $f_1(x)$ and $f_2(y)$ for independent random variables x and y have characteristic functions $\phi_1(u)$ and $\phi_2(u)$, then the characteristic function of the weighted sum $ax + by$ is $\phi_1(au)\phi_2(bu)$. The rules of addition for several important distributions (e.g., that the sum of two Gaussian distributed variables also follows a Gaussian distribution) easily follow from this observation.

Let the (partial) characteristic function corresponding to the conditional p.d.f. $f_2(x|z)$ be $\phi_2(u|z)$, and the p.d.f. of z be $f_1(z)$. The characteristic function after integration over the conditional value is

$$\phi(u) = \int \phi_2(u|z)f_1(z) dz. \tag{39.19}$$

Suppose we can write ϕ_2 in the form

$$\phi_2(u|z) = A(u)e^{ig(u)z}. \tag{39.20}$$

Then

$$\phi(u) = A(u)\phi_1(g(u)). \tag{39.21}$$

The cumulants (semi-invariants) κ_n of a distribution with characteristic function $\phi(u)$ are defined by the relation

$$\phi(u) = \exp \left[\sum_{n=1}^{\infty} \frac{\kappa_n}{n!} (iu)^n \right] = \exp \left(i\kappa_1 u - \frac{1}{2} \kappa_2 u^2 + \dots \right). \tag{39.22}$$

The values κ_n are related to the moments α_n and m_n . The first few relations are

$$\begin{aligned} \kappa_1 &= \alpha_1 (= \mu, \text{ the mean}) \\ \kappa_2 &= m_2 = \alpha_2 - \alpha_1^2 (= \sigma^2, \text{ the variance}) \\ \kappa_3 &= m_3 = \alpha_3 - 3\alpha_1 \alpha_2 + 2\alpha_1^3. \end{aligned} \tag{39.23}$$

39.4 Commonly used probability distributions

Table 39.1 gives a number of common probability density functions and corresponding characteristic functions, means, and variances. Further information may be found in Refs. [1–8] [10], and [11], which has particularly detailed tables. Monte Carlo techniques for generating each of them may be found in our Sec. 41.4 and in Ref. [10]. We comment below on all except the trivial uniform distribution.

39.4.1 Binomial and multinomial distributions

A random process with exactly two possible outcomes which occur with fixed probabilities is called a *Bernoulli* process. If the probability of obtaining a certain outcome (a ‘‘success’’) in an individual trial is p , then the probability of obtaining exactly r successes ($r = 0, 1, 2, \dots, N$) in N independent trials, without regard to the order of the successes and failures, is given by the binomial distribution $f(r; N, p)$ in Table 39.1. If r and s are binomially distributed with parameters (N_r, p) and (N_s, p) , then $t = r + s$ follows a binomial distribution with parameters $(N_r + N_s, p)$. If

there are m possible outcomes for each trial having probabilities p_1, p_2, \dots, p_m , then the joint probability to find r_1, r_2, \dots, r_m of each outcome after a total of N independent trials is given by the multinomial distribution as shown in Table 39.1. We can regard outcome i as “success” and all the rest as “failure”, so individually, any of the r_i follow a binomial distribution for N trials and a success probability p_i .

39.4.2 Poisson distribution

The Poisson distribution $f(n; \nu)$ gives the probability of finding exactly n events in a given interval of x (e.g., space or time) when the events occur independently of one another and of x at an average rate of ν per the given interval. The variance σ^2 equals ν . It is the limiting case $p \rightarrow 0, N \rightarrow \infty, Np = \nu$ of the binomial distribution. The Poisson distribution approaches the Gaussian distribution for large ν .

For example, a large number of radioactive nuclei of a given type will result in a certain number of decays in a fixed time interval. If this interval is small compared to the mean lifetime, then the probability for a given nucleus to decay is small, and thus the number of decays in the time interval is well modeled as a Poisson variable.

39.4.3 Normal or Gaussian distribution

The normal (or Gaussian) probability density function $f(x; \mu, \sigma^2)$ given in Table 39.1 has mean $E[x] = \mu$ and variance $V[x] = \sigma^2$. Comparison of the characteristic function $\phi(u)$ given in Table 39.1 with Eq. (39.22) shows that all cumulants κ_n beyond κ_2 vanish; this is a unique property of the Gaussian distribution. Some other properties are:

$$\begin{aligned} P(x \text{ in range } \mu \pm \sigma) &= 0.6827, \\ P(x \text{ in range } \mu \pm 0.6745\sigma) &= 0.5, \\ E[|x - \mu|] &= \sqrt{2/\pi}\sigma = 0.7979\sigma, \\ \text{half-width at half maximum} &= \sqrt{2 \ln 2}\sigma = 1.177\sigma. \end{aligned}$$

For a Gaussian with $\mu = 0$ and $\sigma^2 = 1$ (the *standard normal*)

$$f(x_1, x_2; \mu_1, \mu_2, \sigma_1, \sigma_2, \rho) = \frac{1}{2\pi\sigma_1\sigma_2\sqrt{1-\rho^2}} \times \exp \left\{ \frac{-1}{2(1-\rho^2)} \left[\frac{(x_1 - \mu_1)^2}{\sigma_1^2} - \frac{2\rho(x_1 - \mu_1)(x_2 - \mu_2)}{\sigma_1\sigma_2} + \frac{(x_2 - \mu_2)^2}{\sigma_2^2} \right] \right\}. \quad (39.26)$$

The characteristic function for the multivariate Gaussian is

$$\phi(\mathbf{u}; \boldsymbol{\mu}, V) = \exp \left[i\boldsymbol{\mu} \cdot \mathbf{u} - \frac{1}{2}\mathbf{u}^T V \mathbf{u} \right]. \quad (39.27)$$

If the components of \mathbf{x} are independent, then Eq. (39.27) is the product of the characteristic functions of n Gaussians.

For an n -dimensional Gaussian distribution for \mathbf{x} with mean $\boldsymbol{\mu}$ and covariance matrix V , the marginal distribution for any single x_i is a one-dimensional Gaussian with mean μ_i and variance V_{ii} . The equation $(\mathbf{x} - \mathbf{a})^T V^{-1}(\mathbf{x} - \mathbf{a}) = C$, where C is any positive number, defines an n -dimensional ellipse centered about \mathbf{a} . If \mathbf{a} is equal to the mean $\boldsymbol{\mu}$, then C is a random variable obeying the χ^2 distribution for n degrees of freedom, which is discussed in the following section. The probability that \mathbf{x} lies outside the ellipsoid for a given value of C is given by $1 - F_{\chi^2}(C; n)$, where F_{χ^2} is the cumulative χ^2 distribution. This may be read from Fig. 40.1. For example, the “ s -standard-deviation ellipsoid” occurs at $C = s^2$. For the two-variable case ($n = 2$), the point \mathbf{x} lies outside the one-standard-deviation ellipsoid with 61% probability. The use of these ellipsoids as indicators of probable error is described in Sec. 40.4.2.2; the validity of those indicators assumes that $\boldsymbol{\mu}$ and V are correct.

39.4.4 Log-normal distribution

If a random variable y follows a Gaussian distribution with mean μ and variance σ^2 , then $x = e^y$ follows a log-normal distribution, as given in Table 39.1. As a consequence of the central limit theorem described in Sec. 39.4.3, the distribution of the product of a large number of positive random variables approaches

the cumulative distribution, often written $\Phi(x)$, is related to the error function erf by

$$F(x; 0, 1) \equiv \Phi(x) = \frac{1}{2} \left[1 + \text{erf}(x/\sqrt{2}) \right]. \quad (39.24)$$

The error function and standard Gaussian are tabulated in many references (e.g., Ref. [11, 12]) and are available in software packages such as ROOT [13]. For a mean μ and variance σ^2 , replace x by $(x - \mu)/\sigma$. The probability of x in a given range can be calculated with Eq. (40.70).

For x and y independent and normally distributed, $z = ax + by$ follows a normal p.d.f. $f(z; a\mu_x + b\mu_y, a^2\sigma_x^2 + b^2\sigma_y^2)$; that is, the weighted means and variances add.

The Gaussian derives its importance in large part from the *central limit theorem*:

If independent random variables x_1, \dots, x_n are distributed according to any p.d.f. with finite mean and variance, then the sum $y = \sum_{i=1}^n x_i$ will have a p.d.f. that approaches a Gaussian for large n . If the p.d.f.s of the x_i are not identical, the theorem still holds under somewhat more restrictive conditions. The mean and variance are given by the sums of corresponding terms from the individual x_i . Therefore, the sum of a large number of fluctuations x_i will be distributed as a Gaussian, even if the x_i themselves are not.

For a set of n Gaussian random variables \mathbf{x} with means $\boldsymbol{\mu}$ and covariances $V_{ij} = \text{cov}[x_i, x_j]$, the p.d.f. for the one-dimensional Gaussian is generalized to

$$f(\mathbf{x}; \boldsymbol{\mu}, V) = \frac{1}{(2\pi)^{n/2} \sqrt{|V|}} \exp \left[-\frac{1}{2}(\mathbf{x} - \boldsymbol{\mu})^T V^{-1}(\mathbf{x} - \boldsymbol{\mu}) \right], \quad (39.25)$$

where the determinant $|V|$ must be greater than 0. For diagonal V (independent variables), $f(\mathbf{x}; \boldsymbol{\mu}, V)$ is the product of the p.d.f.s of n Gaussian distributions.

For $n = 2$, $f(\mathbf{x}; \boldsymbol{\mu}, V)$ is

a log-normal. It is bounded below by zero and is thus well suited for modeling quantities that are intrinsically non-negative such as an efficiency. One can implement a log-normal model for a random variable x by defining $y = \ln x$ so that y follows a Gaussian distribution.

39.4.5 χ^2 distribution

If x_1, \dots, x_n are independent Gaussian random variables, the sum $z = \sum_{i=1}^n (x_i - \mu_i)^2/\sigma_i^2$ follows the χ^2 p.d.f. with n degrees of freedom, which we denote by $\chi^2(n)$. More generally, for n correlated Gaussian variables as components of a vector \mathbf{X} with covariance matrix V , $z = \mathbf{X}^T V^{-1} \mathbf{X}$ follows $\chi^2(n)$ as in the previous section. For a set of z_i , each of which follows $\chi^2(n_i)$, $\sum z_i$ follows $\chi^2(\sum n_i)$. For large n , the χ^2 p.d.f. approaches a Gaussian with a mean and variance given by $\mu = n$ and $\sigma^2 = 2n$, respectively (here the formulae for μ and σ^2 are valid for all n).

The χ^2 p.d.f. is often used in evaluating the level of compatibility between observed data and a hypothesis for the p.d.f. that the data might follow. This is discussed further in Sec. 40.3.2 on significance tests.

39.4.6 Student's t distribution

Suppose that y and x_1, \dots, x_n are independent and Gaussian distributed with mean 0 and variance 1. We then define

$$z = \sum_{i=1}^n x_i^2 \quad \text{and} \quad t = \frac{y}{\sqrt{z/n}}. \quad (39.28)$$

The variable z thus follows a $\chi^2(n)$ distribution. Then t is distributed according to Student's t distribution with n degrees of

Table 39.1: Some common probability density functions, with corresponding characteristic functions and means and variances. In the Table, $\Gamma(k)$ is the gamma function, equal to $(k - 1)!$ when k is an integer; ${}_1F_1$ is the confluent hypergeometric function of the 1st kind [11].

Distribution	Probability density function f (variable; parameters)	Characteristic function $\phi(u)$	Mean	Variance
Uniform	$f(x; a, b) = \begin{cases} 1/(b-a) & a \leq x \leq b \\ 0 & \text{otherwise} \end{cases}$	$\frac{e^{ibu} - e^{iau}}{(b-a)iu}$	$\frac{a+b}{2}$	$\frac{(b-a)^2}{12}$
Binomial	$f(r; N, p) = \frac{N!}{r!(N-r)!} p^r q^{N-r}$ $r = 0, 1, 2, \dots, N; \quad 0 \leq p \leq 1; \quad q = 1 - p$	$(q + pe^{iu})^N$	Np	Npq
Multinomial	$f(r_1, \dots, r_m; N, p_1, \dots, p_m) = \frac{N!}{r_1! \dots r_m!} p_1^{r_1} \dots p_m^{r_m}$	$(\sum_{k=1}^m p_k e^{iu_k})^N$	$E[r_i] = Np_i$	$\text{cov}[r_i, r_j] = Np_i(\delta_{ij} - p_j)$
Poisson	$f(n; \nu) = \frac{\nu^n e^{-\nu}}{n!}; \quad n = 0, 1, 2, \dots; \quad \nu > 0$	$\exp[\nu(e^{iu} - 1)]$	ν	ν
Normal (Gaussian)	$f(x; \mu, \sigma^2) = \frac{1}{\sigma\sqrt{2\pi}} \exp(-(x - \mu)^2/2\sigma^2)$	$\exp(i\mu u - \frac{1}{2}\sigma^2 u^2)$	μ	σ^2
Multivariate Gaussian	$f(\mathbf{x}; \boldsymbol{\mu}, \mathbf{V}) = \frac{1}{(2\pi)^{n/2} \sqrt{ \mathbf{V} }} \times \exp[-\frac{1}{2}(\mathbf{x} - \boldsymbol{\mu})^T \mathbf{V}^{-1}(\mathbf{x} - \boldsymbol{\mu})]$ $-\infty < x_j < \infty; \quad -\infty < \mu_j < \infty; \quad \mathbf{V} > 0$	$\exp[i\boldsymbol{\mu} \cdot \mathbf{u} - \frac{1}{2}\mathbf{u}^T \mathbf{V} \mathbf{u}]$	\mathbf{u}	V_{jk}
Log-normal	$f(x; \mu, \sigma^2) = \frac{1}{\sigma\sqrt{2\pi}} \frac{1}{x} \exp(-(\ln x - \mu)^2/2\sigma^2)$ $0 < x < \infty; \quad -\infty < \mu < \infty; \quad \sigma > 0$	—	$\exp(\mu + \sigma^2/2)$	$\exp(2\mu + \sigma^2) \times [\exp(\sigma^2) - 1]$
χ^2	$f(z; n) = \frac{z^{n/2-1} e^{-z/2}}{2^{n/2} \Gamma(n/2)}; \quad z \geq 0$	$(1 - 2iu)^{-n/2}$	n	$2n$
Student's t	$f(t; n) = \frac{1}{\sqrt{n\pi}} \frac{\Gamma[(n+1)/2]}{\Gamma(n/2)} \left(1 + \frac{t^2}{n}\right)^{-(n+1)/2}$ $-\infty < t < \infty; \quad n \text{ not required to be integer}$	—	0 for $n > 1$	$n/(n-2)$ for $n > 2$
Gamma	$f(x; \lambda, k) = \frac{x^{k-1} \lambda^k e^{-\lambda x}}{\Gamma(k)}; \quad 0 \leq x < \infty; \quad k \text{ not required to be integer}$	$(1 - iu/\lambda)^{-k}$	k/λ	k/λ^2
Beta	$f(x; \alpha, \beta) = \frac{\Gamma(\alpha+\beta)}{\Gamma(\alpha)\Gamma(\beta)} x^{\alpha-1} (1-x)^{\beta-1}$ $0 \leq x \leq 1$	${}_1F_1(\alpha; \alpha + \beta; iu)$	$\frac{\alpha}{\alpha+\beta}$	$\frac{\alpha\beta}{(\alpha+\beta)^2(\alpha+\beta+1)}$

freedom, $f(t; n)$, given in Table 39.1.

If defined through gamma functions as in Table 39.1, the parameter n is not required to be an integer. As $n \rightarrow \infty$, the distribution approaches a Gaussian, and for $n = 1$ it is a *Cauchy* or *Breit-Wigner* distribution.

As an example, consider the *sample mean* $\bar{x} = \sum x_i/n$ and the *sample variance* $s^2 = \sum (x_i - \bar{x})^2/(n-1)$ for normally distributed x_i with unknown mean μ and variance σ^2 . The sample mean has a Gaussian distribution with a variance σ^2/n , so the variable $(\bar{x} - \mu)/\sqrt{\sigma^2/n}$ is normal with mean 0 and variance 1. The quantity $(n-1)s^2/\sigma^2$ is independent of this and follows $\chi^2(n-1)$. The ratio

$$t = \frac{(\bar{x} - \mu)/\sqrt{\sigma^2/n}}{\sqrt{(n-1)s^2/\sigma^2(n-1)}} = \frac{\bar{x} - \mu}{\sqrt{s^2/n}} \tag{39.29}$$

is distributed as $f(t; n-1)$. The unknown variance σ^2 cancels, and t can be used to test the hypothesis that the true mean is some particular value μ .

39.4.7 Gamma distribution

For a process that generates events as a function of x (e.g., space or time) according to a Poisson distribution, the distance in x from an arbitrary starting point (which may be some particular event) to the k^{th} event follows a *gamma* distribution, $f(x; \lambda, k)$. The Poisson parameter μ is λ per unit x . The special case $k = 1$ (i.e., $f(x; \lambda, 1) = \lambda e^{-\lambda x}$) is called the *exponential* distribution. A sum of k' exponential random variables x_i is distributed as $f(\sum x_i; \lambda, k')$.

The parameter k is not required to be an integer. For $\lambda = 1/2$ and $k = n/2$, the gamma distribution reduces to the $\chi^2(n)$ distribution.

39.4.8 Beta distribution

The beta distribution describes a continuous random variable x in the interval $[0, 1]$. By scaling and translation one can easily

generalize it to have arbitrary endpoints. In Bayesian inference about the parameter p of a binomial process, if the prior p.d.f. is a beta distribution $f(p; \alpha, \beta)$ then the observation of r successes out of N trials gives a posterior beta distribution $f(p; r + \alpha, N - r + \beta)$ (Bayesian methods are discussed further in Sec. 40). The uniform distribution is a beta distribution with $\alpha = \beta = 1$.

References

- [1] H. Cramér, *Mathematical Methods of Statistics*, (Princeton Univ. Press, New Jersey, 1958).
- [2] A. Stuart and J.K. Ord, *Kendall's Advanced Theory of Statistics*, Vol. 1 *Distribution Theory* 6th Ed., (Halsted Press, New York, 1994), and earlier editions by Kendall and Stuart.
- [3] F.E. James, *Statistical Methods in Experimental Physics*, 2nd Ed., (World Scientific, Singapore, 2006).
- [4] L. Lyons, *Statistics for Nuclear and Particle Physicists*, (Cambridge University Press, New York, 1986).
- [5] B.R. Roe, *Probability and Statistics in Experimental Physics*, 2nd Ed., (Springer, New York, 2001).
- [6] R.J. Barlow, *Statistics: A Guide to the Use of Statistical Methods in the Physical Sciences*, (John Wiley, New York, 1989).
- [7] S. Brandt, *Data Analysis*, 3rd Ed., (Springer, New York, 1999).
- [8] G. Cowan, *Statistical Data Analysis*, (Oxford University Press, Oxford, 1998).
- [9] A.N. Kolmogorov, *Grundbegriffe der Wahrscheinlichkeitstheorie*, (Springer, Berlin, 1933); *Foundations of the Theory of Probability*, 2nd Ed., (Chelsea, New York 1956).
- [10] Ch. Walck, *Hand-book on Statistical Distributions for Experimentalists*, University of Stockholm Internal Report SUP-PFY/96-01, available from www.physto.se/~walck.
- [11] M. Abramowitz and I. Stegun, eds., *Handbook of Mathematical Functions*, (Dover, New York, 1972).

- [12] F.W.J. Olver *et al.*, eds., NIST Handbook of Mathematical Functions, (Cambridge University Press, 2010); A companion Digital Library of Mathematical Functions is available at dlmf.nist.gov.
- [13] R. Brun and F. Rademakers, Nucl. Instrum. Meth. **A389**, 81 (1997); See also root.cern.ch.

40. Statistics

Revised October 2019 by G. Cowan (RHUL).

This chapter gives an overview of statistical methods used in high-energy physics. In statistics, we are interested in using a given sample of data to make inferences about a probabilistic model, *e.g.*, to assess the model's validity or to determine the values of its parameters. There are two main approaches to statistical inference, which we may call frequentist and Bayesian.

In frequentist statistics, probability is interpreted as the frequency of the outcome of a repeatable experiment. The most important tools in this framework are parameter estimation, covered in Section 40.2, statistical tests, discussed in Section 40.3, and confidence intervals, which are constructed so as to cover the true value of a parameter with a specified probability, as described in Section 40.4.2. Note that in frequentist statistics one does not define a probability for a hypothesis or for the value of a parameter.

In Bayesian statistics, the interpretation of probability is more general and includes *degree of belief* (called subjective probability). One can then speak of a probability density function (p.d.f.) for a parameter, which expresses one's state of knowledge about where its true value lies. Bayesian methods provide a natural means to include additional information, which in general may be subjective; in fact they *require* prior probabilities for the hypotheses (or parameters) in question, *i.e.*, the degree of belief about the parameters' values, before carrying out the measurement. Using Bayes' theorem (Eq. (39.4)), the prior degree of belief is updated by the data from the experiment. Bayesian methods for interval estimation are discussed in Sections 40.4.1 and 40.4.2.4.

For many inference problems, the frequentist and Bayesian approaches give similar numerical values, even though they answer different questions and are based on fundamentally different interpretations of probability. In some important cases, however, the two approaches may yield very different results. For a discussion of Bayesian vs. non-Bayesian methods, see references written by a statistician [1], by a physicist [2], or the detailed comparison in Ref. [3].

40.1 Fundamental concepts

Consider an experiment whose outcome is characterized by one or more data values, which we can write as a vector \mathbf{x} . A *hypothesis* H is a statement about the probability for the data, often written $P(\mathbf{x}|H)$. (We will usually use a capital letter for a probability and lower case for a probability density. Often the term p.d.f. is used loosely to refer to either a probability or a probability density.) This could, for example, define completely the p.d.f. for the data (a *simple* hypothesis), or it could specify only the functional form of the p.d.f., with the values of one or more parameters not determined (a *composite* hypothesis).

If the probability $P(\mathbf{x}|H)$ for data \mathbf{x} is regarded as a function of the hypothesis H , then it is called the *likelihood* of H , usually written $L(H)$. Often the hypothesis is characterized by one or more parameters θ , in which case $L(\theta) = P(\mathbf{x}|\theta)$ is called the likelihood function.

In some cases one can obtain at least approximate frequentist results using the likelihood evaluated only with the data obtained. In general, however, the frequentist approach requires a full specification of the probability model $P(\mathbf{x}|H)$ both as a function of the data \mathbf{x} and hypothesis H .

In the Bayesian approach, inference is based on the posterior probability for H given the data \mathbf{x} , which represents one's degree of belief that H is true given the data. This is obtained from Bayes' theorem (39.4), which can be written

$$P(H|\mathbf{x}) = \frac{P(\mathbf{x}|H)\pi(H)}{\int P(\mathbf{x}|H')\pi(H')dH'} \quad (40.1)$$

Here $P(\mathbf{x}|H)$ is the likelihood for H , which depends only on the data actually obtained. The quantity $\pi(H)$ is the prior probability for H , which represents one's degree of belief for H before carrying out the measurement. The integral in the denominator (or sum, for discrete hypotheses) serves as a normalization factor. If H is characterized by a continuous parameter θ then the posterior

probability is a p.d.f. $p(\theta|\mathbf{x})$. Note that the likelihood function itself is not a p.d.f. for θ .

40.2 Parameter estimation

Here we review *point estimation* of parameters, first with an overview of the frequentist approach and its two most important methods, maximum likelihood and least squares, treated in Sections 40.2.2 and 40.2.3. The Bayesian approach is outlined in Sec. 40.2.5.

An *estimator* $\hat{\theta}$ (written with a hat) is a function of the data used to estimate the value of the parameter θ . Sometimes the word 'estimate' is used to denote the value of the estimator when evaluated with given data. There is no fundamental rule dictating how an estimator must be constructed. One tries, therefore, to choose that estimator which has the best properties. The most important of these are (a) *consistency*, (b) *bias*, (c) *efficiency*, and (d) *robustness*.

(a) An estimator is said to be *consistent* if the estimate $\hat{\theta}$ converges in probability (see Ref. [3]) to the true value θ as the amount of data increases. This property is so important that it is possessed by all commonly used estimators.

(b) The *bias*, $b = E[\hat{\theta}] - \theta$, is the difference between the expectation value of the estimator and the true value of the parameter. The expectation value is taken over a hypothetical set of similar experiments in which $\hat{\theta}$ is constructed in the same way. When $b = 0$, the estimator is said to be unbiased. The bias depends on the chosen metric, *i.e.*, if $\hat{\theta}$ is an unbiased estimator of θ , then $\hat{\theta}^2$ is not in general an unbiased estimator for θ^2 .

(c) *Efficiency* is the ratio of the minimum possible variance for any estimator of θ to the variance $V[\hat{\theta}]$ of the estimator $\hat{\theta}$. For the case of a single parameter, under rather general conditions the minimum variance is given by the Rao-Cramér-Fr chet bound,

$$\sigma_{\min}^2 = \left(1 + \frac{\partial b}{\partial \theta}\right)^2 / I(\theta), \quad (40.2)$$

where

$$I(\theta) = E \left[\left(\frac{\partial \ln L}{\partial \theta} \right)^2 \right] = -E \left[\frac{\partial^2 \ln L}{\partial \theta^2} \right] \quad (40.3)$$

is the *Fisher information*, L is the likelihood, and the operator $E[\]$ in (40.3) is the expectation value with respect to the data. For the final equality to hold, the range of allowed data values must not depend on θ .

The *mean-squared error*,

$$\text{MSE} = E[(\hat{\theta} - \theta)^2] = V[\hat{\theta}] + b^2, \quad (40.4)$$

is a measure of an estimator's quality which combines bias and variance.

(d) *Robustness* is the property of being insensitive to departures from assumptions in the p.d.f., *e.g.*, owing to uncertainties in the distribution's tails.

It is not in general possible to optimize simultaneously for all the measures of estimator quality described above. For some common estimators, the properties above are known exactly. More generally, it is possible to evaluate them by Monte Carlo simulation. Note that they will in general depend on the unknown θ .

40.2.1 Estimators for mean, variance, and median

Suppose we have a set of n independent measurements, x_1, \dots, x_n , each assumed to follow a p.d.f. with unknown mean μ and unknown variance σ^2 (the measurements do not necessarily have to follow a Gaussian distribution). Then

$$\hat{\mu} = \frac{1}{n} \sum_{i=1}^n x_i \quad (40.5)$$

$$\hat{\sigma}^2 = \frac{1}{n-1} \sum_{i=1}^n (x_i - \hat{\mu})^2 \quad (40.6)$$

are unbiased estimators of μ and σ^2 . The variance of $\hat{\mu}$ is σ^2/n and the variance of $\hat{\sigma}^2$ is

$$V[\hat{\sigma}^2] = \frac{1}{n} \left(m_4 - \frac{n-3}{n-1} \sigma^4 \right), \quad (40.7)$$

where m_4 is the 4th central moment of x (see Eq. (39.8)). For Gaussian distributed x_i , this becomes $2\sigma^4/(n-1)$ for any $n \geq 2$, and for large n the standard deviation of $\hat{\sigma}$ is $\sigma/\sqrt{2n}$. For any n and Gaussian x_i , $\hat{\mu}$ is an efficient estimator for μ , and the estimators $\hat{\mu}$ and $\hat{\sigma}^2$ are uncorrelated. Otherwise the arithmetic mean (40.5) is not necessarily the most efficient estimator; this is discussed further in Sec. 8.7 of Ref. [4].

If σ^2 is known, it does not improve the estimate $\hat{\mu}$, as can be seen from Eq. (40.5); however, if μ is known, one can substitute it for $\hat{\mu}$ in Eq. (40.6) and replace $n-1$ by n to obtain an estimator of σ^2 still with zero bias but smaller variance. If the x_i have different, known variances σ_i^2 , then the weighted average

$$\hat{\mu} = \frac{1}{w} \sum_{i=1}^n w_i x_i, \quad (40.8)$$

where $w_i = 1/\sigma_i^2$ and $w = \sum_i w_i$, is an unbiased estimator for μ with a smaller variance than an unweighted average. The standard deviation of $\hat{\mu}$ is $1/\sqrt{w}$.

As an estimator for the median x_{med} , one can use the value \hat{x}_{med} such that half the x_i are below and half above (the sample median). If there are an even number of observations and the sample median lies between two observed values, the estimator is set by convention to their arithmetic average. If the p.d.f. of x has the form $f(x-\mu)$ and μ is both mean and median, then for large n the variance of the sample median approaches $1/[4nf^2(0)]$, provided $f(0) > 0$. Although estimating the median can often be more difficult computationally than the mean, the resulting estimator is generally more robust, as it is insensitive to the exact shape of the tails of a distribution.

40.2.2 The method of maximum likelihood

Suppose we have a set of measured quantities \mathbf{x} and the likelihood $L(\boldsymbol{\theta}) = P(\mathbf{x}|\boldsymbol{\theta})$ for a set of parameters $\boldsymbol{\theta} = (\theta_1, \dots, \theta_N)$. The *maximum likelihood* (ML) estimators for $\boldsymbol{\theta}$ are defined as the values that give the maximum of L . Because of the properties of the logarithm, it is usually easier to work with $\ln L$, and since both are maximized for the same parameter values $\boldsymbol{\theta}$, the ML estimators can be found by solving the *likelihood equations*,

$$\frac{\partial \ln L}{\partial \theta_i} = 0, \quad i = 1, \dots, N. \quad (40.9)$$

Often the solution must be found numerically. Maximum likelihood estimators are important because they are asymptotically (*i.e.*, for large data samples) unbiased, efficient and have a Gaussian sampling distribution under quite general conditions, and the method has a wide range of applicability.

In general the likelihood function is obtained from the probability of the data under assumption of the parameters. An important special case is when the data consist of *i.i.d.* (independent and identically distributed) values. Here one has a set of n statistically independent quantities $\mathbf{x} = (x_1, \dots, x_n)$, where each component follows the same p.d.f. $f(x; \boldsymbol{\theta})$. In this case the joint p.d.f. of the data sample factorizes and the likelihood function is

$$L(\boldsymbol{\theta}) = \prod_{i=1}^n f(x_i; \boldsymbol{\theta}). \quad (40.10)$$

In this case the number of events n is regarded as fixed. If however the probability to observe n events itself depends on the parameters $\boldsymbol{\theta}$, then this dependence should be included in the likelihood. For example, if n follows a Poisson distribution with mean μ and the independent x values all follow $f(x; \boldsymbol{\theta})$, then the likelihood becomes

$$L(\boldsymbol{\theta}) = \frac{\mu^n}{n!} e^{-\mu} \prod_{i=1}^n f(x_i; \boldsymbol{\theta}). \quad (40.11)$$

Equation (40.11) is often called the *extended likelihood* (see, *e.g.*, Refs. [5–7]). If μ is given as a function of $\boldsymbol{\theta}$, then including the probability for n given $\boldsymbol{\theta}$ in the likelihood provides additional information about the parameters. This therefore leads to a reduction in their statistical uncertainties and in general changes their estimated values.

In evaluating the likelihood function, it is important that any normalization factors in the p.d.f. that involve $\boldsymbol{\theta}$ be included. However, we will only be interested in the maximum of L and in ratios of L at different values of the parameters; hence any multiplicative factors that do not involve the parameters that we want to estimate may be dropped, including factors that depend on the data but not on $\boldsymbol{\theta}$.

Under a one-to-one change of parameters from $\boldsymbol{\theta}$ to $\boldsymbol{\eta}$, the ML estimators $\hat{\boldsymbol{\theta}}$ transform to $\boldsymbol{\eta}(\hat{\boldsymbol{\theta}})$. That is, the ML solution is invariant under change of parameter. However, other properties of ML estimators, in particular the bias, are not invariant under change of parameter.

The inverse V^{-1} of the covariance matrix $V_{ij} = \text{cov}[\hat{\theta}_i, \hat{\theta}_j]$ for a set of ML estimators can be estimated by using

$$(\hat{V}^{-1})_{ij} = - \left. \frac{\partial^2 \ln L}{\partial \theta_i \partial \theta_j} \right|_{\hat{\boldsymbol{\theta}}}. \quad (40.12)$$

For finite samples, however, Eq. (40.12) can result in a misestimation of the variances. In the large sample limit (or in a linear model with Gaussian data), L has a Gaussian form and $\ln L$ is (hyper)parabolic. In this case, s times the standard deviations σ_i of the estimators for the parameters can be obtained from the hypersurface defined by the $\boldsymbol{\theta}$ such that

$$\ln L(\boldsymbol{\theta}) = \ln L_{\text{max}} - s^2/2, \quad (40.13)$$

where $\ln L_{\text{max}}$ is the value of $\ln L$ at the solution point (compare with Eq. (40.73)). The minimum and maximum values of θ_i on the hypersurface then give an approximate s -standard deviation confidence interval for θ_i (see Section 40.4.2.2).

40.2.2.1 ML with binned data

If the total number of data values x_i , ($i = 1, \dots, n_{\text{tot}}$), is small, the unbinned maximum likelihood method, *i.e.*, use of Equation (40.10) (or (40.11) for extended ML), is preferred since binning can only result in a loss of information, and hence larger statistical errors for the parameter estimates. If the sample is large, it can be convenient to bin the values in a histogram with N bins, so that one obtains a vector of data $\mathbf{n} = (n_1, \dots, n_N)$ with expectation values $\boldsymbol{\mu} = E[\mathbf{n}]$ and probabilities $f(\mathbf{n}; \boldsymbol{\mu})$. Suppose the mean values $\boldsymbol{\mu}$ can be determined as a function of a set of parameters $\boldsymbol{\theta}$. Then one may maximize the likelihood function based on the contents of the bins.

As mentioned in Sec. 40.2.2, the total number of events $n_{\text{tot}} = \sum_i n_i$ can be regarded either as fixed or as a random variable. If it is fixed, the histogram follows a multinomial distribution,

$$f_M(\mathbf{n}; \boldsymbol{\theta}) = \frac{n_{\text{tot}}!}{n_1! \dots n_N!} p_1^{n_1} \dots p_N^{n_N}, \quad (40.14)$$

where we assume the probabilities p_i are given functions of the parameters $\boldsymbol{\theta}$. The distribution can be written equivalently in terms of the expected number of events in each bin, $\mu_i = n_{\text{tot}} p_i$. If the n_i are regarded as independent and Poisson distributed, then the data are instead described by a product of Poisson probabilities,

$$f_P(\mathbf{n}; \boldsymbol{\theta}) = \prod_{i=1}^N \frac{\mu_i^{n_i}}{n_i!} e^{-\mu_i}, \quad (40.15)$$

where the mean values μ_i are given functions of $\boldsymbol{\theta}$. The total number of events n_{tot} thus follows a Poisson distribution with mean $\mu_{\text{tot}} = \sum_i \mu_i$.

When using maximum likelihood with binned data, one can find the ML estimators and at the same time obtain a statistic usable for a test of goodness-of-fit (see Sec. 40.3.2). Maximizing the likelihood $L(\boldsymbol{\theta}) = f_{M/P}(\mathbf{n}; \boldsymbol{\theta})$ is equivalent to maximizing

the likelihood ratio $\lambda(\theta) = f_{M/P}(n; \theta) / f(n; \hat{\mu})$, where in the denominator $f(n; \mu)$ is a model with an adjustable parameter for each bin, $\mu = (\mu_1, \dots, \mu_N)$, and the corresponding estimators are $\hat{\mu} = (n_1, \dots, n_N)$ (called the “saturated model”). Equivalently one often minimizes the quantity $-2 \ln \lambda(\theta)$. For independent Poisson distributed n_i this is [8]

$$-2 \ln \lambda(\theta) = 2 \sum_{i=1}^N \left[\mu_i(\theta) - n_i + n_i \ln \frac{n_i}{\mu_i(\theta)} \right], \quad (40.16)$$

where for bins with $n_i = 0$, the last term in (40.16) is zero. The expression (40.16) without the terms $\mu_i - n_i$ also gives $-2 \ln \lambda(\theta)$ for multinomially distributed n_i , *i.e.*, when the total number of entries is regarded as fixed. In the limit of zero bin width, minimizing (40.16) is equivalent to maximizing the unbinned extended likelihood function (40.11); in the corresponding multinomial case without the $\mu_i - n_i$ terms one obtains Eq. (40.10).

A smaller value of $-2 \ln \lambda(\hat{\theta})$ corresponds to better agreement between the data and the hypothesized form of $\mu(\theta)$. The value of $-2 \ln \lambda(\hat{\theta})$ can thus be translated into a *p*-value as a measure of goodness-of-fit, as described in Sec. 40.3.2. Assuming the model is correct, then according to Wilks’ theorem [9], for sufficiently large μ_i and provided certain regularity conditions are met, the minimum of $-2 \ln \lambda$ as defined by Eq. (40.16) follows a χ^2 distribution (see, *e.g.*, Ref. [8]). If there are N bins and m fitted parameters, then the number of degrees of freedom for the χ^2 distribution is $N - m$ if the data are treated as Poisson-distributed, and $N - m - 1$ if the n_i are multinomially distributed.

Suppose the n_i are Poisson-distributed and the overall normalization $\mu_{\text{tot}} = \sum_i \mu_i$ is taken as an adjustable parameter, so that $\mu_i = \mu_{\text{tot}} p_i(\theta)$, where the probability to be in the *i*th bin, $p_i(\theta)$, does not depend on μ_{tot} . Then by minimizing Eq. (40.16), one obtains that the area under the fitted function is equal to the sum of the histogram contents, *i.e.*, $\sum_i \hat{\mu}_i = \sum_i n_i$. This is a property not possessed by the estimators from the method of least squares (see, *e.g.*, Sec. 40.2.3 and Ref. [7]).

40.2.2.2 *Frequentist treatment of nuisance parameters*

Suppose we want to determine the values of parameters θ using a set of measurements x described by a probability model $P_x(x|\theta)$. In general the model is not perfect, which is to say it cannot provide an accurate description of the data even at the most optimal point of its parameter space. As a result, the estimated parameters can have a systematic bias.

One can improve the model by including in it additional parameters. That is, $P_x(x|\theta)$ is replaced by a more general model $P_x(x|\theta, \nu)$, which depends on parameters of interest θ and *nuisance parameters* ν . The additional parameters are not of intrinsic interest but must be included for the model to be accurate for some point in the enlarged parameter space.

Although including additional parameters may eliminate or at least reduce the effect of systematic uncertainties, their presence will result in increased statistical uncertainties for the parameters of interest. This occurs because the estimators for the nuisance parameters and those of interest will in general be correlated, which results in an enlargement of the contour defined by Eq. (40.13).

To reduce the impact of the nuisance parameters one often tries to constrain their values by means of control or calibration measurements, say, having data y . For example, some components of y could represent estimates of the nuisance parameters, often from separate experiments. Suppose the measurements y are statistically independent from x and are described by a model $P_y(y|\nu)$. The joint model for both x and y is in this case therefore the product of the probabilities for x and y , and thus the likelihood function for the full set of parameters is

$$L(\theta, \nu) = P_x(x|\theta, \nu) P_y(y|\nu). \quad (40.17)$$

Note that in this case if one wants to simulate the experiment by means of Monte Carlo, both the primary and control measurements, x and y , must be generated for each repetition under assumption of fixed values for the parameters θ and ν .

Using all of the parameters (θ, ν) in Eq. (40.13) to find the statistical errors in the parameters of interest θ is equivalent to using the *profile likelihood*, which depends only on θ . It is defined as

$$L_p(\theta) = L(\theta, \hat{\hat{\nu}}(\theta)), \quad (40.18)$$

where the double-hat notation indicates the profiled values of the parameters ν , defined as the values that maximize L for the specified θ . The profile likelihood is discussed further in Section 40.3.2.1 in connection with hypothesis tests.

40.2.3 *The method of least squares*

The *method of least squares* (LS) coincides with the method of maximum likelihood in the following special case. Consider a set of N independent measurements y_i at known points x_i . The measurement y_i is assumed to be Gaussian distributed with mean $\mu(x_i; \theta)$ and known variance σ_i^2 . The goal is to construct estimators for the unknown parameters θ . The log-likelihood function contains the sum of squares

$$\chi^2(\theta) = -2 \ln L(\theta) + \text{constant} = \sum_{i=1}^N \frac{(y_i - \mu(x_i; \theta))^2}{\sigma_i^2}. \quad (40.19)$$

The parameter values that maximize L are the same as those which minimize χ^2 .

The minimum of the chi-square function in Equation (40.19) defines the least-squares estimators $\hat{\theta}$ for the more general case where the y_i are not Gaussian distributed as long as they are independent. If they are not independent but rather have a covariance matrix $V_{ij} = \text{cov}[y_i, y_j]$, then the LS estimators are determined by the minimum of

$$\chi^2(\theta) = (\mathbf{y} - \boldsymbol{\mu}(\theta))^T V^{-1} (\mathbf{y} - \boldsymbol{\mu}(\theta)), \quad (40.20)$$

where $\mathbf{y} = (y_1, \dots, y_N)$ is the (column) vector of measurements, $\boldsymbol{\mu}(\theta)$ is the corresponding vector of predicted values, and the superscript T denotes the transpose. If the y_i are not Gaussian distributed, then the LS and ML estimators will not in general coincide.

Often one further restricts the problem to the case where $\mu(x_i; \theta)$ is a linear function of the parameters, *i.e.*,

$$\mu(x_i; \theta) = \sum_{j=1}^m \theta_j h_j(x_i). \quad (40.21)$$

Here the $h_j(x)$ are m linearly independent functions, *e.g.*, $1, x, x^2, \dots, x^{m-1}$ or Legendre polynomials. We require $m < N$ and at least m of the x_i must be distinct.

Minimizing χ^2 in this case with m parameters reduces to solving a system of m linear equations. Defining $H_{ij} = h_j(x_i)$ and minimizing χ^2 by setting its derivatives with respect to the θ_i equal to zero gives the LS estimators,

$$\hat{\theta} = (H^T V^{-1} H)^{-1} H^T V^{-1} \mathbf{y} \equiv D \mathbf{y}. \quad (40.22)$$

The covariance matrix for the estimators $U_{ij} = \text{cov}[\hat{\theta}_i, \hat{\theta}_j]$ is given by

$$U = D V D^T = (H^T V^{-1} H)^{-1}, \quad (40.23)$$

or equivalently, its inverse U^{-1} can be found from

$$(U^{-1})_{ij} = \frac{1}{2} \frac{\partial^2 \chi^2}{\partial \theta_i \partial \theta_j} \Big|_{\theta = \hat{\theta}} = \sum_{k,l=1}^m h_i(x_k) (V^{-1})_{kl} h_j(x_l). \quad (40.24)$$

The LS estimators can also be found from the expression

$$\hat{\theta} = U \mathbf{g}, \quad (40.25)$$

where the vector \mathbf{g} is defined by

$$\mathbf{g}_i = \sum_{j,k=1}^m y_j h_i(x_k) (V^{-1})_{jk}. \quad (40.26)$$

For the case of uncorrelated y_i , for example, one can use (40.25) with

$$(U^{-1})_{ij} = \sum_{k=1}^N \frac{h_i(x_k)h_j(x_k)}{\sigma_k^2}, \quad (40.27)$$

$$g_i = \sum_{k=1}^N \frac{y_k h_i(x_k)}{\sigma_k^2}. \quad (40.28)$$

Expanding $\chi^2(\boldsymbol{\theta})$ about $\hat{\boldsymbol{\theta}}$, one finds that the contour in parameter space defined by

$$\chi^2(\boldsymbol{\theta}) = \chi^2(\hat{\boldsymbol{\theta}}) + 1 = \chi_{\min}^2 + 1 \quad (40.29)$$

has tangent planes located at plus-or-minus-one standard deviation $\sigma_{\hat{\boldsymbol{\theta}}}$ from the LS estimates $\hat{\boldsymbol{\theta}}$ (the relation is approximate if the fit function $\mu(x; \boldsymbol{\theta})$ is nonlinear in the parameters).

In constructing the quantity $\chi^2(\boldsymbol{\theta})$ one requires the variances or, in the case of correlated measurements, the covariance matrix. Often these quantities are not known *a priori* and must be estimated from the data. In this case the least-squares and maximum-likelihood methods are no longer exactly equivalent even for Gaussian distributed measurements. An important example is where the measured value y_i represents the event count in a histogram bin. If, for example, y_i represents a Poisson variable, for which the variance is equal to the mean, then one can either estimate the variance from the predicted value, $\mu(x_i; \boldsymbol{\theta})$, or from the observed number itself, y_i . In the first option, the variances become functions of the parameters, and as a result the estimators may need to be found numerically. The second option can be undefined if y_i is zero, and for small y_i , the variance will be poorly estimated. In either case, one should constrain the normalization of the fitted curve to the correct value, *i.e.*, one should determine the area under the fitted curve directly from the number of entries in the histogram (see Ref. [7], Section 7.4). As noted in Sec. 40.2.2.1, this issue is avoided when using the method of extended maximum likelihood with binned data by minimizing Eq. (40.16). In that case if the expected number of events μ_{tot} does not depend on the other fitted parameters $\boldsymbol{\theta}$, then its extended ML estimator is equal to the observed total number of events.

As the minimum value of the χ^2 represents the level of agreement between the measurements and the fitted function, it can be used for assessing the goodness-of-fit; this is discussed further in Section 40.3.2.

40.2.4 Parameter estimation with constraints

In some applications one is interested in using a set of measured quantities $\mathbf{y} = (y_1, \dots, y_N)$ to estimate a set of parameters $\boldsymbol{\theta} = (\theta_1, \dots, \theta_M)$ subject to a number of constraints. For example, one may have measured coordinates from two tracks, and one wishes to estimate their momentum vectors subject to the constraint that the tracks have a common vertex. The parameters can also include momenta of undetected particles such as neutrinos, as long as the constraints from conservation of energy and momentum and from known masses of particles involved in the reaction chain provide enough information for these quantities to be inferred.

A set of K constraints can be given in the form of equations

$$c_k(\boldsymbol{\theta}) = 0, \quad k = 1, \dots, K. \quad (40.30)$$

In some problems it may be possible to define a new set of parameters $\boldsymbol{\eta} = (\eta_1, \dots, \eta_L)$ with $L = M - K$ such that every point in $\boldsymbol{\eta}$ -space automatically satisfies the constraints. If this is possible then the problem reduces to one of estimating $\boldsymbol{\eta}$ with, *e.g.*, maximum likelihood or least squares and then transforming the estimators back into $\boldsymbol{\theta}$ -space.

In many cases it may be difficult or impossible to find an appropriate transformation $\boldsymbol{\eta}(\boldsymbol{\theta})$. Suppose that the parameters are determined through minimizing an objective function such as $\chi^2(\boldsymbol{\theta})$ in the method of least squares. Here one may enforce the con-

straints by finding the stationary points of the *Lagrange function*

$$\mathcal{L}(\boldsymbol{\theta}, \boldsymbol{\lambda}, \mathbf{y}) = \chi^2(\boldsymbol{\theta}, \mathbf{y}) + \sum_{k=1}^K \lambda_k c_k(\boldsymbol{\theta}) \quad (40.31)$$

with respect to both the parameters $\boldsymbol{\theta}$ and a set of *Lagrange multipliers* $\boldsymbol{\lambda} = (\lambda_1, \dots, \lambda_K)$. Combining the parameters and Lagrange multipliers into an $(M + K)$ -component vector $\boldsymbol{\gamma} = (\theta_1, \dots, \theta_M, \lambda_1, \dots, \lambda_K)$, the solutions for $\boldsymbol{\gamma}$, *i.e.*, the estimators $\hat{\boldsymbol{\gamma}}$, are found (*e.g.*, numerically) from the system of equations

$$F_i(\boldsymbol{\gamma}, \mathbf{y}) \equiv \frac{\partial \mathcal{L}}{\partial \gamma_i} = 0, \quad i = 1, \dots, M + K. \quad (40.32)$$

To obtain the covariance matrix of the estimated parameters one can find solutions $\hat{\boldsymbol{\gamma}}$ corresponding to the expectation values of the data $\langle \mathbf{y} \rangle$ and expand $F_i(\hat{\boldsymbol{\gamma}}, \mathbf{y})$ to first order about these values. This gives (see, *e.g.*, Sec. 11.6 of Ref. [7]) linearized approximations for the estimators, $\hat{\boldsymbol{\gamma}}(\mathbf{y}) \approx \hat{\boldsymbol{\gamma}} + C(\mathbf{y} - \langle \mathbf{y} \rangle)$, where the matrix $C = -A^{-1}B$, and A and B are given by

$$A_{ij} = \left[\frac{\partial F_i}{\partial \gamma_j} \right]_{\hat{\boldsymbol{\gamma}}, \langle \mathbf{y} \rangle} \quad \text{and} \quad B_{ij} = \left[\frac{\partial F_i}{\partial y_j} \right]_{\hat{\boldsymbol{\gamma}}, \langle \mathbf{y} \rangle}. \quad (40.33)$$

In practice the values $\langle \mathbf{y} \rangle$ and corresponding solutions $\hat{\boldsymbol{\gamma}}$ are estimated using the data from the actual measurement. Using this approximation for $\hat{\boldsymbol{\gamma}}(\mathbf{y})$, one can find the covariance matrix $U_{ij} = \text{cov}[\hat{\gamma}_i, \hat{\gamma}_j]$ of the the estimators for the γ_i in terms of that of the data $V_{ij} = \text{cov}[y_i, y_j]$ using error propagation (*cf.* Eqs. (40.42) and (40.43)),

$$U = CVC^T. \quad (40.34)$$

The upper-left $M \times M$ block of the matrix U gives the covariance matrix for the estimated parameters $\text{cov}[\hat{\theta}_i, \hat{\theta}_j]$. One can show for linear constraints that $\text{cov}[\hat{\theta}_i, \hat{\theta}_j]$ is also given by the upper-left $M \times M$ block of $2A^{-1}$. If the parameters are estimated using the method of least squares, then the number of degrees of freedom for the distribution of the minimized χ^2 is increased by the number of constraints, *i.e.*, it becomes $N - M + K$. Further details can be found in, *e.g.*, Ch. 8 of Ref. [4] and Ch. 7 of Ref. [10].

40.2.5 The Bayesian approach

In the frequentist methods discussed above, probability is associated only with data, not with the value of a parameter. This is no longer the case in Bayesian statistics, however, which we introduce in this section. For general introductions to Bayesian statistics see, *e.g.*, Refs. [11–14].

Suppose the outcome of an experiment is characterized by a vector of data \mathbf{x} , whose probability distribution depends on an unknown parameter (or parameters) $\boldsymbol{\theta}$ that we wish to determine. In Bayesian statistics, all knowledge about $\boldsymbol{\theta}$ is summarized by the posterior p.d.f. $p(\boldsymbol{\theta}|\mathbf{x})$, whose integral over any given region gives the degree of belief for $\boldsymbol{\theta}$ to take on values in that region, given the data \mathbf{x} . It is obtained by using Bayes' theorem,

$$p(\boldsymbol{\theta}|\mathbf{x}) = \frac{P(\mathbf{x}|\boldsymbol{\theta})\pi(\boldsymbol{\theta})}{\int P(\mathbf{x}|\boldsymbol{\theta}')\pi(\boldsymbol{\theta}') d\boldsymbol{\theta}'}, \quad (40.35)$$

where $P(\mathbf{x}|\boldsymbol{\theta})$ is the likelihood function, *i.e.*, the joint p.d.f. for the data viewed as a function of $\boldsymbol{\theta}$, evaluated with the data actually obtained in the experiment, and $\pi(\boldsymbol{\theta})$ is the prior p.d.f. for $\boldsymbol{\theta}$. Note that the denominator in Eq. (40.35) serves to normalize the posterior p.d.f. to unity.

As it can be difficult to report the full posterior p.d.f. $p(\boldsymbol{\theta}|\mathbf{x})$, one would usually summarize it with statistics such as the mean (or median) value, and covariance matrix. In addition one may construct intervals with a given probability content, as is discussed in Sec. 40.4.1 on Bayesian interval estimation.

40.2.5.1 Priors

Bayesian statistics supplies no unique rule for determining the prior $\pi(\boldsymbol{\theta})$; this reflects the analyst's subjective degree of belief (or state of knowledge) about $\boldsymbol{\theta}$ before the measurement was carried out. For the result to be of value to the broader community,

whose members may not share these beliefs, it is important to carry out a *sensitivity analysis*, that is, to show how the result changes under a reasonable variation of the prior probabilities.

One might like to construct $\pi(\theta)$ to represent complete ignorance about the parameters by setting it equal to a constant. A problem here is that if the prior p.d.f. is flat in θ , then it is not flat for a nonlinear function of θ , and so a different parametrization of the problem would lead in general to a non-equivalent posterior p.d.f.

For the special case of a constant prior, one can see from Bayes' theorem (40.35) that the posterior is proportional to the likelihood, and therefore the mode (peak position) of the posterior is equal to the ML estimator. The posterior mode, however, will change in general upon a transformation of parameter. One may use as the Bayesian estimator a summary statistic other than the mode, such as the median, which is invariant under parameter transformation. But this will not in general coincide with the ML estimator.

The difficult and subjective nature of encoding personal knowledge into priors has led to what is called *objective Bayesian statistics*, where prior probabilities are based not on an actual degree of belief but rather derived from formal rules. These give, for example, priors which are invariant under a transformation of parameters, or ones which result in a maximum gain in information for a given set of measurements. For an extensive review see, e.g., [15].

Objective priors do not in general reflect degree of belief, but they could in some cases be taken as possible, although perhaps extreme, subjective priors. The posterior probabilities as well therefore do not necessarily reflect a degree of belief. However one may regard investigating a variety of objective priors to be an important part of the sensitivity analysis. Furthermore, use of objective priors with Bayes' theorem can be viewed as a recipe for producing estimators or intervals which have desirable frequentist properties.

An important procedure for deriving objective priors is due to Jeffreys. According to *Jeffreys' rule* one takes the prior as

$$\pi(\theta) \propto \sqrt{\det(I(\theta))}, \tag{40.36}$$

where

$$I_{ij}(\theta) = -E \left[\frac{\partial^2 \ln P(x|\theta)}{\partial \theta_i \partial \theta_j} \right] \tag{40.37}$$

is the *Fisher information matrix*. One can show that the Jeffreys prior leads to inference that is invariant under a transformation of parameters. One should note that the Jeffreys prior does not in general correspond to one's degree of belief about the value of a parameter. As examples, the Jeffreys prior for the mean μ of a Gaussian distribution is a constant, and for the mean of a Poisson distribution one finds $\pi(\mu) \propto 1/\sqrt{\mu}$.

Neither the constant nor $1/\sqrt{\mu}$ priors can be normalized to unit area and are therefore said to be *improper*. This can be allowed because the prior always appears multiplied by the likelihood function, and if the likelihood falls to zero sufficiently quickly then one may have a normalizable posterior density.

An important type of objective prior is the reference prior due to Bernardo and Berger [16]. To find the reference prior for a given problem one considers the Kullback-Leibler divergence $D_n[\pi, p]$ of the posterior $p(\theta|x)$ relative to a prior $\pi(\theta)$, obtained from a set of i.i.d. data $\mathbf{x} = (x_1, \dots, x_n)$:

$$D_n[\pi, p] = \int p(\theta|x) \ln \frac{p(\theta|x)}{\pi(\theta)} d\theta. \tag{40.38}$$

This is effectively a measure of the gain in information provided by the data. The reference prior is chosen so that the expectation value of this information gain is maximized for the limiting case of $n \rightarrow \infty$, where the expectation is computed with respect to the marginal distribution of the data,

$$p(\mathbf{x}) = \int p(\mathbf{x}|\theta)\pi(\theta) d\theta. \tag{40.39}$$

For a single, continuous parameter the reference prior is usually identical to the Jeffreys prior. In the multiparameter case an iterative algorithm exists, which requires sorting the parameters by order of inferential importance. Often the result does not depend on this order, but when it does, this can be part of a sensitivity analysis. Further discussion and applications to particle physics problems can be found in Ref. [17].

40.2.5.2 Bayesian treatment of nuisance parameters

As discussed in Sec. 40.2.2, a model may depend on parameters of interest θ as well as on nuisance parameters ν , which must be included for an accurate description of the data. Knowledge about the values of ν may be supplied by control measurements, theoretical insights, physical constraints, etc. Suppose, for example, one has data \mathbf{y} from a control measurement which is characterized by a probability $P_{\mathbf{y}}(\mathbf{y}|\nu)$. Suppose further that before carrying out the control measurement one's state of knowledge about ν is described by an initial prior $\pi_0(\nu)$, which in practice is often taken to be a constant or in any case very broad. By using Bayes' theorem (40.1) one obtains the updated prior $\pi(\nu)$ (i.e., now $\pi(\nu) = \pi(\nu|\mathbf{y})$, the probability for ν given \mathbf{y}),

$$\pi(\nu|\mathbf{y}) \propto P(\mathbf{y}|\nu)\pi_0(\nu). \tag{40.40}$$

In the absence of a model for $P(\mathbf{y}|\nu)$ one may make some reasonable but *ad hoc* choices. For a single nuisance parameter ν , for example, one might characterize the uncertainty by a p.d.f. $\pi(\nu)$ centered about its nominal value with a certain standard deviation σ_ν . Often a Gaussian p.d.f. provides a reasonable model for one's degree of belief about a nuisance parameter; in other cases, more complicated shapes may be appropriate. If, for example, the parameter represents a non-negative quantity then a log-normal or gamma p.d.f. can be a more natural choice than a Gaussian truncated at zero. Note also that truncation of the prior of a nuisance parameter ν at zero will in general make $\pi(\nu)$ nonzero at $\nu = 0$, which can lead to an unnormalizable posterior for a parameter of interest that appears multiplied by ν .

The likelihood function, prior, and posterior p.d.f.s all depend on both θ and ν , and are related by Bayes' theorem, as usual. Note that the likelihood here only refers to the primary measurement \mathbf{x} . Once any control measurements \mathbf{y} are used to find the updated prior $\pi(\nu)$ for the nuisance parameters, this information is fully encapsulated in $\pi(\nu)$ and the control measurements do not appear further.

One can obtain the posterior p.d.f. for θ alone by integrating over the nuisance parameters, i.e.,

$$p(\theta|x) = \int p(\theta, \nu|x) d\nu. \tag{40.41}$$

Such integrals can often not be carried out in closed form, and if the number of nuisance parameters is large, then they can be difficult to compute with standard Monte Carlo methods. *Markov Chain Monte Carlo* (MCMC) techniques are often used for computing integrals of this type (see Sec. 41.5).

40.2.6 Propagation of errors

Consider a set of n quantities $\theta = (\theta_1, \dots, \theta_n)$ and a set of m functions $\eta(\theta) = (\eta_1(\theta), \dots, \eta_m(\theta))$. Suppose we have estimated $\hat{\theta} = (\hat{\theta}_1, \dots, \hat{\theta}_n)$, using, say, maximum-likelihood or least-squares, and we also know or have estimated the covariance matrix $V_{ij} = \text{cov}[\hat{\theta}_i, \hat{\theta}_j]$. The goal of *error propagation* is to determine the covariance matrix for the functions, $U_{ij} = \text{cov}[\hat{\eta}_i, \hat{\eta}_j]$, where $\hat{\eta} = \eta(\hat{\theta})$. In particular, the diagonal elements $U_{ii} = V[\hat{\eta}_i]$ give the variances. The new covariance matrix can be found by expanding the functions $\eta(\theta)$ about the estimates $\hat{\theta}$ to first order in a Taylor series. Using this one finds

$$U_{ij} \approx \sum_{k,l} \frac{\partial \eta_i}{\partial \theta_k} \frac{\partial \eta_j}{\partial \theta_l} \Big|_{\hat{\theta}} V_{kl}. \tag{40.42}$$

This can be written in matrix notation as $U \approx AVA^T$ where the matrix of derivatives A is

$$A_{ij} = \frac{\partial \eta_i}{\partial \theta_j} \bigg|_{\hat{\theta}}, \quad (40.43)$$

and A^T is its transpose. The approximation is exact if $\boldsymbol{\eta}(\boldsymbol{\theta})$ is linear (it holds, for example, in Equation (40.23)). If this is not the case, the approximation can break down if, for example, $\boldsymbol{\eta}(\boldsymbol{\theta})$ is significantly nonlinear close to $\hat{\boldsymbol{\theta}}$ in a region of a size comparable to the standard deviations of $\hat{\boldsymbol{\theta}}$.

40.3 Statistical tests

In addition to estimating parameters, one often wants to assess the validity of certain statements concerning the data's underlying distribution. Frequentist *hypothesis tests*, described in Sec. 40.3.1, provide a rule for accepting or rejecting hypotheses depending on the outcome of a measurement. In *significance tests*, covered in Sec. 40.3.2, one gives the probability to obtain a level of incompatibility with a certain hypothesis that is greater than or equal to the level observed with the actual data. In the Bayesian approach, the corresponding procedure is based fundamentally on the posterior probabilities of the competing hypotheses. In Sec. 40.3.3 we describe a related construct called the Bayes factor, which can be used to quantify the degree to which the data prefer one or another hypothesis.

40.3.1 Hypothesis tests

A frequentist *test* of a hypothesis (often called the null hypothesis, H_0) is a rule that states for which data values \boldsymbol{x} the hypothesis is rejected. A region of \boldsymbol{x} -space called the critical region, w , is specified such that there is no more than a given probability under H_0 , α , called the *size* or *significance level* of the test, to find $\boldsymbol{x} \in w$. If the data are discrete, it may not be possible to find a critical region with exact probability content α , and thus we require $P(\boldsymbol{x} \in w|H_0) \leq \alpha$. If the data are observed in the critical region, H_0 is rejected.

The data \boldsymbol{x} used to construct a test could be, for example, a set of values that characterizes an individual event. In this case the test corresponds to classification as, *e.g.*, signal or background. Alternatively the data could represent a set of values from a collection of events. Often one is interested in knowing whether all of the events are of a certain type (background), or whether the sample contains at least some events of a new type (signal). Here the background-only hypothesis plays the role of H_0 , and in the alternative H_1 both signal and background are present. Rejecting H_0 is, from the standpoint of frequentist statistics, the required step to establish discovery of the signal process.

The critical region is not unique. Its choice should take into account the probabilities for the data predicted by some alternative hypothesis (or set of alternatives) H_1 . Rejecting H_0 if it is true is called a *type-I error*, and occurs by construction with probability no greater than α . Not rejecting H_0 if an alternative H_1 is true is called a *type-II error*, and for a given test this will have a certain probability $\beta = P(\boldsymbol{x} \notin w|H_1)$. The quantity $1 - \beta$ is called the *power* of the test of H_0 with respect to the alternative H_1 . A strategy for defining the critical region can therefore be to maximize the power with respect to some alternative (or alternatives) given a fixed size α .

To maximize the power of a test of H_0 with respect to the alternative H_1 , the *Neyman-Pearson lemma* states that the critical region w should be chosen such that for all data values \boldsymbol{x} inside w , the likelihood ratio

$$\lambda(\boldsymbol{x}) = \frac{f(\boldsymbol{x}|H_1)}{f(\boldsymbol{x}|H_0)} \quad (40.44)$$

is greater than or equal to a given constant c_α , and everywhere outside the critical region one has $\lambda(\boldsymbol{x}) < c_\alpha$, where the value of c_α is determined by the size of the test α . Here H_0 and H_1 must be simple hypotheses, *i.e.*, they should not contain undetermined parameters.

It is convenient to define the test using a scalar function of the data \boldsymbol{x} called a *test statistic*, $t(\boldsymbol{x})$, such that the boundary

of the critical region is given by a surface of constant $t(\boldsymbol{x})$. The Neyman-Pearson lemma is equivalent to the statement that the likelihood ratio (40.44) represents the optimal test statistic. It can be difficult in practice, however, to determine $\lambda(\boldsymbol{x})$, since this requires knowledge of the joint p.d.f.s $f(\boldsymbol{x}|H_0)$ and $f(\boldsymbol{x}|H_1)$. Often one does not have explicit formulae for these, but rather Monte Carlo models that allow one to generate instances of \boldsymbol{x} that follow the p.d.f.s.

In the case where the likelihood ratio (40.44) cannot be used explicitly, there exist a variety of other multivariate methods for constructing a test statistic that may approach its performance. These are based on machine-learning algorithms that use samples of *training data* corresponding to the hypotheses in question, often generated from Monte Carlo models. Methods often used in HEP include *Fisher Discriminants*, *Neural Networks*, *Boosted Decision Trees* and *Support Vector Machines*. Descriptions of these and other methods can be found in Refs. [18–21], in *Proceedings of the PHYSTAT* conference series [22], and in the HEP Community White Paper [23]. Software for HEP includes the *TMVA* [24] and *scikit-learn* [25] packages.

An important issue in constructing a test is the choice of variables that enter into the data vector \boldsymbol{x} . For purposes of classification one may choose, for example, to form certain functions of particle momenta such as, *e.g.*, invariant masses that are felt to be physically meaningful in the context of a particular event type. It may be difficult to know, however, whether there may exist further features that would help distinguish between signal and background. Recently, so-called *Deep Neural Networks* containing several or more hidden layers have been applied in HEP [26, 27]; these allow one to use directly as inputs the elements of the data vector \boldsymbol{x} (features) that represent lower-level quantities such as individual particle momenta, rather than needing to first construct “by hand” higher level features. Each hidden layer then allows the network to construct significant high-level features in an automatic way.

The multivariate algorithms designed to classify events into signal and background types also form the basis of tests of the hypothesis that a sample of events consists of background only. Such a test can be constructed using the distributions of the test statistic $t(\boldsymbol{x})$ for event classification obtained from a multivariate algorithm such as a Neural Network output. The distributions $p(t|s)$ and $p(t|b)$ for signal and background events, respectively, are used to construct the likelihood ratio of the signal-plus-background hypothesis relative to that of background only. To the extent that the test statistic $t(\boldsymbol{x})$ approximates the likelihood ratio (or a monotonic function thereof) for individual events given by (40.44), the resulting test of the background-only hypothesis for the event sample will have maximum power with respect to the signal-plus-background alternative (see Ref. [28]).

40.3.2 Tests of significance (goodness-of-fit)

Often one wants to quantify the level of agreement between the data and a hypothesis without explicit reference to alternative hypotheses. This can be done by defining a statistic t whose value reflects in some way the level of agreement between the data and the hypothesis. The analyst must decide what values of the statistic correspond to better or worse levels of agreement with the hypothesis in question; the choice will in general depend on the relevant alternative hypotheses.

The hypothesis in question, H_0 , will determine the p.d.f. $f(t|H_0)$ for the statistic. The significance of a discrepancy between the data and what one expects under the assumption of H_0 is quantified by giving the *p-value*, defined as the probability to find t in the region of equal or lesser compatibility with H_0 than the level of compatibility observed with the actual data. For example, if t is defined such that large values correspond to poor agreement with the hypothesis, then the *p-value* would be

$$p = \int_{t_{\text{obs}}}^{\infty} f(t|H_0) dt, \quad (40.45)$$

where t_{obs} is the value of the statistic obtained in the actual experiment.

The p -value is a function of the data, and is therefore itself a random variable. If the hypothesis used to compute the p -value is true, then for continuous data p will be uniformly distributed between zero and one. Note that the p -value is not the probability for the hypothesis; in frequentist statistics, this is not defined.

The p -value should not be confused with the size (significance level) of a test, or the confidence level of a confidence interval (Section 40.4), both of which are pre-specified constants. We may formulate a hypothesis test, however, by defining the critical region to correspond to the data outcomes that give the lowest p -values, so that finding $p \leq \alpha$ implies that the data outcome was in the critical region. When constructing a p -value, one generally chooses the region of data space deemed to have lower compatibility with the model being tested as one having higher compatibility with a given alternative, such that the corresponding test will have a high power with respect to this alternative.

When searching for a new phenomenon, one tries to reject the hypothesis H_0 that the data are consistent with known (*e.g.*, Standard Model) processes. If the p -value of H_0 is sufficiently low, then one is willing to accept that some alternative hypothesis is true. Often one converts the p -value into an equivalent significance Z , defined so that a Z standard deviation upward fluctuation of a Gaussian random variable would have an upper tail area equal to p , *i.e.*,

$$Z = \Phi^{-1}(1 - p). \quad (40.46)$$

Here Φ is the cumulative distribution of the standard Gaussian, and Φ^{-1} is its inverse (quantile) function. Often in HEP the level of significance where an effect is said to qualify as a discovery is $Z = 5$, *i.e.*, a 5σ effect, corresponding to a p -value of 2.87×10^{-7} . One's actual degree of belief that a new process is present, however, will depend in general on other factors as well, such as the plausibility of the new signal hypothesis and the degree to which it can describe the data, one's confidence in the model that led to the observed p -value, and possible corrections for multiple observations out of which one focuses on the smallest p -value obtained (the "look-elsewhere effect", discussed in Section 40.3.2.2).

40.3.2.1 Treatment of nuisance parameters for frequentist tests

Suppose one wants to test hypothetical values of parameters θ , but the model also contains nuisance parameters ν . To find a p -value for θ we can construct a test statistic q_θ such that larger values constitute increasing incompatibility between the data and the hypothesis. Then for an observed value of the statistic $q_{\theta, \text{obs}}$, the p -value of θ is

$$p_\theta(\nu) = \int_{q_{\theta, \text{obs}}}^{\infty} f(q_\theta | \theta, \nu) dq_\theta, \quad (40.47)$$

which depends in general on the nuisance parameters ν . In the strict frequentist approach, θ is rejected only if the p -value is less than α for all possible values of the nuisance parameters.

The difficulty described above is effectively solved if we can define the test statistic q_θ in such a way that its distribution $f(q_\theta | \theta)$ is independent of the nuisance parameters. Although exact independence is only found in special cases, it can be achieved approximately by use of the *profile likelihood ratio*. This is given by the profile likelihood from Eq.(40.18) divided by the value of the likelihood at its maximum, *i.e.*, when evaluated with the ML estimators $\hat{\theta}$ and $\hat{\nu}$:

$$\lambda_p(\theta) = \frac{L(\theta, \hat{\nu}(\theta))}{L(\hat{\theta}, \hat{\nu})}. \quad (40.48)$$

Wilks' theorem [9] states that, providing certain general conditions are satisfied, the distribution of $-2 \ln \lambda_p(\theta)$, under assumption of θ , approaches a χ^2 distribution in the limit where the data sample is very large, independent of the values of the nuisance parameters ν . Here the number of degrees of freedom is equal to the number of components of θ . More details on use of the profile likelihood are given in Refs. [29, 30] and in contributions to the PHYSTAT conferences [22]; explicit formulae for special cases can be found in Ref. [31]. Further discussion on how to incorporate systematic uncertainties into p -values can be found in Ref. [32].

Even with use of the profile likelihood ratio, for a finite data sample the p -value of hypothesized parameters θ will retain in general some dependence on the nuisance parameters ν . Ideally one would find the maximum of $p_\theta(\nu)$ from Eq. (40.47) explicitly, but that is often impractical. An approximate and computationally feasible technique is to use $p_\theta(\hat{\nu}(\theta))$, where $\hat{\nu}(\theta)$ are the profiled values of the nuisance parameters as defined in Section 40.2.2.2. The resulting p -value is correct if the true values of the nuisance parameters are equal to the profiled values used; otherwise it could be either too high or too low. This is discussed further in Section 40.4.2 on confidence intervals.

One may also treat model uncertainties in a Bayesian manner but then use the resulting model in a frequentist test. Suppose the uncertainty in a set of nuisance parameters ν is characterized by a Bayesian prior p.d.f. $\pi(\nu)$. This can be used to construct the marginal (also called the prior predictive) model for the data x and parameters of interest θ ,

$$P_m(x|\theta) = \int P(x|\theta, \nu)\pi(\nu) d\nu. \quad (40.49)$$

The marginal model does not represent the probability of data that would be generated if one were really to repeat the experiment, as in that case one would assume that the nuisance parameters do not vary. Rather, the marginal model represents a situation in which every repetition of the experiment is carried out with new values of ν , randomly sampled from $\pi(\nu)$. It is in effect an average of models each with a given ν , where the average is carried out with respect to the prior p.d.f. $\pi(\nu)$.

The marginal model for the data x can be used to determine the distribution of a test statistic Q , which can be written

$$P_m(Q|\theta) = \int P(Q|\theta, \nu)\pi(\nu) d\nu. \quad (40.50)$$

In a search for a new signal process, the test statistic can be based on the ratio of likelihoods corresponding to the experiments where signal and background events are both present, L_{s+b} , to that of background only, L_b . Often the likelihoods are evaluated with the profiled values of the nuisance parameters, which may give improved performance. It is important to note, however, that it is through use of the marginal model for the distribution of Q that the uncertainties related to the nuisance parameters are incorporated into the result of the test. Different choices for the test statistic itself only result in variations of the power of the test with respect to different alternatives.

40.3.2.2 The look-elsewhere effect

The "look-elsewhere effect" relates to multiple measurements used to test a single hypothesis. The classic example is when one searches in a distribution for a peak whose position is not predicted in advance. Here the no-peak hypothesis is tested using data in a given range of the distribution. In the frequentist approach the correct p -value of the no-peak hypothesis is the probability, assuming background only, to find a signal as significant as the one found or more so anywhere in the search region. This can be substantially higher than the probability to find a peak of equal or greater significance in the particular place where it appeared. There is in general some ambiguity as to what constitutes the relevant search region or even the broader set of relevant measurements. Although the desired p -value is well defined once the search region has been fixed, an exact treatment can require extensive computation.

The "brute-force" solution to this problem by Monte Carlo involves generating data under the background-only hypothesis and for each data set, fitting a peak of unknown position and recording a measure of its significance. To establish a discovery one often requires a p -value smaller than 2.87×10^{-7} , corresponding to a 5σ or larger effect. Determining this with Monte Carlo thus requires generating and fitting a very large number of experiments, perhaps several times 10^7 . In contrast, if the position of the peak is fixed, then the fit to the distribution is much easier, and furthermore one can in many cases use formulae valid for sufficiently large samples that bypass completely the need for Monte Carlo

(see, e.g., [31]). However, this fixed-position or “local” p -value would not be correct in general, as it assumes the position of the peak was known in advance.

A method that allows one to modify the local p -value computed under assumption of a fixed position to obtain an approximation to the correct “global” value using a relatively simple calculation is described in Ref. [33]. Suppose a test statistic q_0 , defined so that larger values indicate increasing disagreement with the data, is observed to have a value u . Furthermore suppose the model contains a nuisance parameter θ (such as the peak position) which is only defined under the signal model (there is no peak in the background-only model). An approximation for the global p -value is found to be

$$p_{\text{global}} \approx p_{\text{local}} + \langle N_u \rangle, \quad (40.51)$$

where $\langle N_u \rangle$, which is much smaller than one in cases of interest, is the mean number of “upcrossings” of the statistic q_0 above the level u in the range of the nuisance parameter considered (e.g., the mass range).

The value of $\langle N_u \rangle$ can be estimated from the number of upcrossings $\langle N_{u_0} \rangle$ above some much lower value, u_0 , by using a relation due to Davis [34],

$$\langle N_u \rangle \approx \langle N_{u_0} \rangle e^{-(u-u_0)/2}. \quad (40.52)$$

By choosing u_0 sufficiently low, the value of $\langle N_u \rangle$ can be estimated by simulating only a very small number of experiments, or even from the observed data, rather than the 10^7 needed if one is dealing with a 5σ effect.

40.3.2.3 Goodness-of-fit with the method of least squares

When estimating parameters using the method of least squares, one obtains the minimum value of the quantity χ^2 (40.19). This statistic can be used to test the *goodness-of-fit*, i.e., the test provides a measure of the significance of a discrepancy between the data and the hypothesized functional form used in the fit. It may also happen that no parameters are estimated from the data, but that one simply wants to compare a histogram, e.g., a vector of Poisson distributed numbers $\mathbf{n} = (n_1, \dots, n_N)$, with a hypothesis for their expectation values $\mu_i = E[n_i]$. As the distribution is Poisson with variances $\sigma_i^2 = \mu_i$, the χ^2 (40.19) becomes *Pearson’s χ^2 statistic*,

$$\chi^2 = \sum_{i=1}^N \frac{(n_i - \mu_i)^2}{\mu_i}. \quad (40.53)$$

If the hypothesis $\boldsymbol{\mu} = (\mu_1, \dots, \mu_N)$ is correct, and if the expected values μ_i in (40.53) are sufficiently large (or equivalently, if the measurements n_i can be treated as following a Gaussian distribution), then the χ^2 statistic will follow the χ^2 p.d.f. with the number of degrees of freedom equal to the number of measurements N minus the number of fitted parameters.

Alternatively, one may fit parameters and evaluate goodness-of-fit by minimizing $-2 \ln \lambda$ from Eq. (40.16). One finds that the distribution of this statistic approaches the asymptotic limit faster than does Pearson’s χ^2 . Therefore if one uses the asymptotic χ^2 p.d.f. as the statistic’s approximate sampling distribution to compute a p -value, one obtains in general a more accurate result from $-2 \ln \lambda$ than from Pearson’s χ^2 (see Ref. [8] and references therein).

Assuming the goodness-of-fit statistic follows a χ^2 p.d.f., the p -value for the hypothesis is then

$$p = \int_{\chi^2}^{\infty} f(z; n_d) dz, \quad (40.54)$$

where $f(z; n_d)$ is the χ^2 p.d.f. and n_d is the appropriate number of degrees of freedom. Values are shown in Fig. 40.1 or obtained from the ROOT function `TMath::Prob`. If the conditions for using the χ^2 p.d.f. do not hold, the statistic can still be defined as before, but its p.d.f. must be determined by other means in order to obtain the p -value, e.g., using a Monte Carlo calculation.

Since the mean of the χ^2 distribution is equal to n_d , one expects in a “reasonable” experiment to obtain $\chi^2 \approx n_d$. Hence the quantity χ^2/n_d is sometimes reported. Since the p.d.f. of χ^2/n_d

depends on n_d , however, one must report n_d as well if one wishes to determine the p -value. The p -values obtained for different values of χ^2/n_d are shown in Fig. 40.2.

If the minimized χ^2 value indicates a low level of agreement between data and hypothesis, one may be tempted to expect a high degree of uncertainty for any fitted parameters. Poor goodness-of-fit, however, does not mean that one will have large statistical errors for parameter estimates. If, for example, the error bars (or covariance matrix) used in constructing the χ^2 are underestimated, then this will lead to underestimated statistical errors for the fitted parameters. The standard deviations of estimators that one finds from, say, Eq. (40.13) reflect how widely the estimates would be distributed if one were to repeat the measurement many times, assuming that the hypothesis and measurement errors used in the χ^2 are also correct. They do not include the systematic error which may result from an incorrect hypothesis or incorrectly estimated measurement errors in the χ^2 .

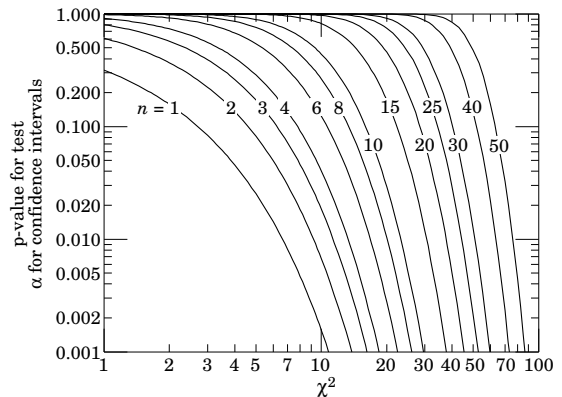


Figure 40.1: One minus the χ^2 cumulative distribution, $1 - F(\chi^2; n)$, for n degrees of freedom. This gives the p -value for the χ^2 goodness-of-fit test as well as one minus the coverage probability for confidence intervals (see Sec. 40.4.2.2).

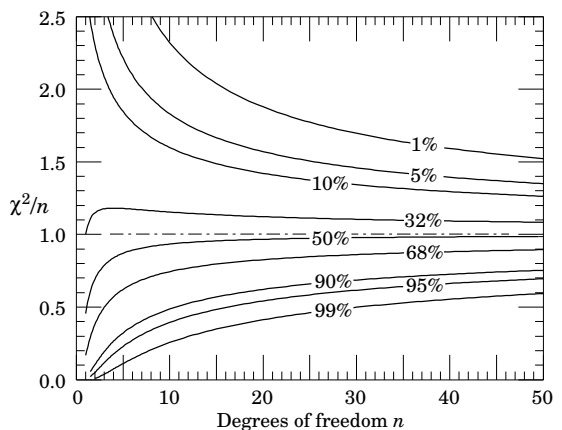


Figure 40.2: The ‘reduced’ χ^2 , equal to χ^2/n , for n degrees of freedom. The curves show as a function of n the χ^2/n that corresponds to a given p -value.

40.3.3 Bayes factors

In Bayesian statistics, all of one’s knowledge about a model is contained in its posterior probability, which one obtains using Bayes’ theorem (Eq. (40.35)). Thus one could reject a hypothesis H if its posterior probability $P(H|\mathbf{x})$ is sufficiently small. The difficulty here is that $P(H|\mathbf{x})$ is proportional to the prior probability $P(H)$, and there will not be a consensus about the prior probabilities for the existence of new phenomena. Nevertheless one can construct a quantity called the Bayes factor (described below), which can be used to quantify the degree to which the

data prefer one hypothesis over another, and is independent of their prior probabilities.

Consider two models (hypotheses), H_i and H_j , described by vectors of parameters θ_i and θ_j , respectively. Some of the components will be common to both models and others may be distinct. The full prior probability for each model can be written in the form

$$\pi(H_i, \theta_i) = P(H_i)\pi(\theta_i|H_i). \quad (40.55)$$

Here $P(H_i)$ is the overall prior probability for H_i , and $\pi(\theta_i|H_i)$ is the normalized p.d.f. of its parameters. For each model, the posterior probability is found using Bayes' theorem,

$$P(H_i|\mathbf{x}) = \frac{\int P(\mathbf{x}|\theta_i, H_i)P(H_i)\pi(\theta_i|H_i) d\theta_i}{P(\mathbf{x})}, \quad (40.56)$$

where the integration is carried out over the internal parameters θ_i of the model. The ratio of posterior probabilities for the models is therefore

$$\frac{P(H_i|\mathbf{x})}{P(H_j|\mathbf{x})} = \frac{\int P(\mathbf{x}|\theta_i, H_i)\pi(\theta_i|H_i) d\theta_i}{\int P(\mathbf{x}|\theta_j, H_j)\pi(\theta_j|H_j) d\theta_j} \frac{P(H_i)}{P(H_j)}. \quad (40.57)$$

The *Bayes factor* is defined as

$$B_{ij} = \frac{\int P(\mathbf{x}|\theta_i, H_i)\pi(\theta_i|H_i) d\theta_i}{\int P(\mathbf{x}|\theta_j, H_j)\pi(\theta_j|H_j) d\theta_j}. \quad (40.58)$$

This gives what the ratio of posterior probabilities for models i and j would be if the overall prior probabilities for the two models were equal. If the models have no nuisance parameters, *i.e.*, no internal parameters described by priors, then the Bayes factor is simply the likelihood ratio. The Bayes factor therefore shows by how much the probability ratio of model i to model j changes in the light of the data, and thus can be viewed as a numerical measure of evidence supplied by the data in favour of one hypothesis over the other.

Although the Bayes factor is by construction independent of the overall prior probabilities $P(H_i)$ and $P(H_j)$, it does require priors for all internal parameters of a model, *i.e.*, one needs the functions $\pi(\theta_i|H_i)$ and $\pi(\theta_j|H_j)$. In a Bayesian analysis where one is only interested in the posterior p.d.f. of a parameter, it may be acceptable to take an unnormalizable function for the prior (an improper prior) as long as the product of likelihood and prior can be normalized. But improper priors are only defined up to an arbitrary multiplicative constant, and so the Bayes factor would depend on this constant. Furthermore, although the range of a constant normalized prior is unimportant for parameter determination (provided it is wider than the likelihood), this is not so for the Bayes factor when such a prior is used for only one of the hypotheses. So to compute a Bayes factor, all internal parameters must be described by normalized priors that represent meaningful probabilities over the entire range where they are defined.

An exception to this rule may be considered when the identical parameter appears in the models for both numerator and denominator of the Bayes factor. In this case one can argue that the arbitrary constants would cancel. One must exercise some caution, however, as parameters with the same name and physical meaning may still play different roles in the two models.

Both integrals in Equation (40.58) are of the form

$$m = \int P(\mathbf{x}|\theta)\pi(\theta) d\theta, \quad (40.59)$$

which is the marginal likelihood seen previously in Eq. (40.49) (in some fields this quantity is called the *evidence*). Computing marginal likelihoods can be difficult; in many cases it can be done with the nested sampling algorithm [35] as implemented, *e.g.*, in the program `MultiNest` [36]. A review of Bayes factors can be found in Ref. [37].

40.4 Intervals and limits

When the goal of an experiment is to determine a parameter θ , the result is usually expressed by quoting, in addition to the point estimate, some sort of interval which reflects the statistical precision of the measurement. In the simplest case, this can be given by the parameter's estimated value $\hat{\theta}$ plus or minus an estimate of the standard deviation of $\hat{\theta}$, $\hat{\sigma}_{\hat{\theta}}$. If, however, the p.d.f. of the estimator is not Gaussian or if there are physical boundaries on the possible values of the parameter, then one usually quotes instead an interval according to one of the procedures described below.

In reporting an interval or limit, the experimenter may wish to

- communicate as objectively as possible the result of the experiment;
- provide an interval that is constructed to cover on average the true value of the parameter with a specified probability;
- provide the information needed by the consumer of the result to draw conclusions about the parameter or to make a particular decision;
- draw conclusions about the parameter that incorporate stated prior beliefs.

With a sufficiently large data sample, the point estimate and standard deviation (or for the multiparameter case, the parameter estimates and covariance matrix) satisfy essentially all of these goals. For finite data samples, no single method for quoting an interval will achieve all of them.

In addition to the goals listed above, the choice of method may be influenced by practical considerations such as ease of producing an interval from the results of several measurements. Of course the experimenter is not restricted to quoting a single interval or limit; one may choose, for example, first to communicate the result with a confidence interval having certain frequentist properties, and then in addition to draw conclusions about a parameter using a judiciously chosen subjective Bayesian prior. It is recommended, however, that there be a clear separation between these two aspects of reporting a result. In the remainder of this section, we assess the extent to which various types of intervals achieve the goals stated here.

40.4.1 Bayesian intervals

As described in Sec. 40.2.5, a Bayesian posterior probability may be used to determine regions that will have a given probability of containing the true value of a parameter. In the single parameter case, for example, an interval (called a Bayesian or credible interval) $[\theta_{\text{lo}}, \theta_{\text{up}}]$ can be determined which contains a given fraction $1 - \alpha$ of the posterior probability, *i.e.*,

$$1 - \alpha = \int_{\theta_{\text{lo}}}^{\theta_{\text{up}}} p(\theta|\mathbf{x}) d\theta. \quad (40.60)$$

Sometimes an upper or lower limit is desired, *i.e.*, θ_{lo} or θ_{up} can be set to a physical boundary or to plus or minus infinity. In other cases, one might be interested in the set of θ values for which $p(\theta|\mathbf{x})$ is higher than for any θ not belonging to the set, which may constitute a single interval or a set of disjoint regions; these are called highest posterior density (HPD) intervals. Note that HPD intervals are not invariant under a nonlinear transformation of the parameter.

If a parameter is constrained to be non-negative, then the prior p.d.f. can simply be set to zero for negative values. An important example is the case of a Poisson variable n , which counts signal events with unknown mean s , as well as background with mean b , assumed known. For the signal mean s , one often uses the prior

$$\pi(s) = \begin{cases} 0 & s < 0 \\ 1 & s \geq 0 \end{cases}. \quad (40.61)$$

This prior may be regarded as providing an interval whose frequentist properties can be studied, rather than as representing a degree of belief. For example, to obtain an upper limit on s , one may proceed as follows. The likelihood for s is given by the Poisson distribution for n with mean $s + b$,

$$P(n|s) = \frac{(s+b)^n}{n!} e^{-(s+b)}, \quad (40.62)$$

along with the prior (40.61) in (40.35) gives the posterior density for s . An upper limit s_{up} at confidence level (or here, rather, *credibility* level) $1 - \alpha$ can be obtained by requiring

$$1 - \alpha = \int_{-\infty}^{s_{\text{up}}} p(s|n) ds = \frac{\int_{-\infty}^{s_{\text{up}}} P(n|s) \pi(s) ds}{\int_{-\infty}^{\infty} P(n|s) \pi(s) ds}, \quad (40.63)$$

where the lower limit of integration is effectively zero because of the cut-off in $\pi(s)$. By relating the integrals in Eq. (40.63) to incomplete gamma functions, the solution for the upper limit is found to be

$$s_{\text{up}} = \frac{1}{2} F_{\chi^2}^{-1} [p, 2(n+1)] - b, \quad (40.64)$$

where $F_{\chi^2}^{-1}$ is the quantile of the χ^2 distribution (inverse of the cumulative distribution). Here the quantity p is

$$p = 1 - \alpha \left(1 - F_{\chi^2} [2b, 2(n+1)] \right), \quad (40.65)$$

where F_{χ^2} is the cumulative χ^2 distribution. For both F_{χ^2} and $F_{\chi^2}^{-1}$ above, the argument $2(n+1)$ gives the number of degrees of freedom. For the special case of $b = 0$, the limit reduces to

$$s_{\text{up}} = \frac{1}{2} F_{\chi^2}^{-1} (1 - \alpha; 2(n+1)). \quad (40.66)$$

It happens that for the case of $b = 0$, the upper limit from Eq. (40.66) coincides numerically with the frequentist upper limit discussed in Section 40.4.2.3. Values for $1 - \alpha = 0.9$ and 0.95 are given by the values μ_{up} in Table 40.3. The frequentist properties of confidence intervals for the Poisson mean found in this way are discussed in Refs. [2] and [38].

As in any Bayesian analysis, it is important to show how the result changes under assumption of different prior probabilities. For example, one could consider the Jeffreys prior as described in Sec. 40.2.5. For this problem one finds the Jeffreys prior $\pi(s) \propto 1/\sqrt{s+b}$ for $s \geq 0$ and zero otherwise. As with the constant prior, one would not regard this as representing one's prior beliefs about s , both because it is improper and also as it depends on b . Rather it is used with Bayes' theorem to produce an interval whose frequentist properties can be studied.

If the model contains nuisance parameters then these are eliminated by marginalizing, as in Eq. (40.41), to obtain the p.d.f. for the parameters of interest. For example, if the parameter b in the Poisson counting problem above were to be characterized by a prior p.d.f. $\pi(b)$, then one would first use Bayes' theorem to find $p(s, b|n)$. This is then marginalized to find $p(s|n) = \int p(s, b|n) \pi(b) db$, from which one may determine an interval for s . One may not be certain whether to extend a model by including more nuisance parameters. In this case, a Bayes factor may be used to determine to what extent the data prefer a model with additional parameters, as described in Section 40.3.3.

40.4.2 Frequentist confidence intervals

The unqualified phrase "confidence intervals" refers to frequentist intervals obtained with a procedure due to Neyman [39], described below. The boundary of the interval (or in the multiparameter case, region) is given by a specific function of the data, which would fluctuate if one were to repeat the experiment many times. The *coverage probability* refers to the fraction of intervals in such an ensemble that contain the true parameter value. Confidence intervals are constructed so as to have a coverage probability greater than or equal to a given *confidence level*, regardless of the true parameter's value. It is important to note that in the frequentist approach, such a probability is not meaningful for a fixed interval. In this section we discuss several techniques for producing intervals that have, at least approximately, this property of coverage.

40.4.2.1 The Neyman construction for confidence intervals

Consider a p.d.f. $f(x; \theta)$ where x represents the outcome of the experiment and θ is the unknown parameter for which we want to construct a confidence interval. The variable x could (and often does) represent an estimator for θ . Using $f(x; \theta)$, we can find using a pre-defined rule and probability $1 - \alpha$ for every value of θ , a set of values $x_1(\theta, \alpha)$ and $x_2(\theta, \alpha)$ such that

$$P(x_1 < x < x_2; \theta) = \int_{x_1}^{x_2} f(x; \theta) dx \geq 1 - \alpha. \quad (40.67)$$

If x is discrete, the integral is replaced by the corresponding sum. In that case there may not exist a range of x values whose summed probability is exactly equal to a given value of $1 - \alpha$, and one requires by convention $P(x_1 < x < x_2; \theta) \geq 1 - \alpha$.

This is illustrated for continuous x in Fig. 40.3: a horizontal line segment $[x_1(\theta, \alpha), x_2(\theta, \alpha)]$ is drawn for representative values of θ . The union of such intervals for all values of θ , designated in the figure as $D(\alpha)$, is known as a *confidence belt*. Typically the curves $x_1(\theta, \alpha)$ and $x_2(\theta, \alpha)$ are monotonic functions of θ , which we assume for this discussion.

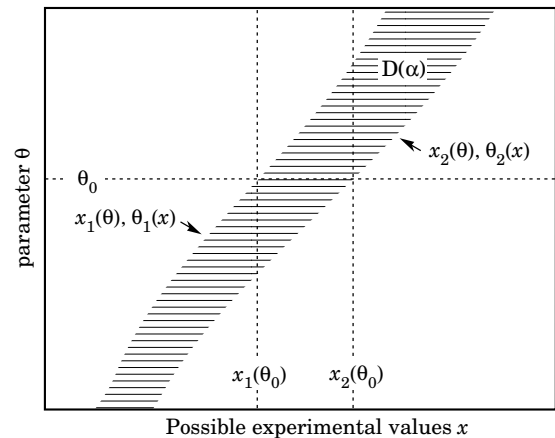


Figure 40.3: Construction of the confidence belt (see text).

Upon performing an experiment to measure x and obtaining a value x_0 , one draws a vertical line through x_0 . The confidence interval for θ is the set of all values of θ for which the corresponding line segment $[x_1(\theta, \alpha), x_2(\theta, \alpha)]$ is intercepted by this vertical line. Such confidence intervals are said to have a *confidence level* (CL) equal to $1 - \alpha$.

Now suppose that the true value of θ is θ_0 , indicated in the figure. We see from the figure that θ_0 lies between $\theta_1(x)$ and $\theta_2(x)$ if and only if x lies between $x_1(\theta_0)$ and $x_2(\theta_0)$. The two events thus have the same probability, and since this is true for any value θ_0 , we can drop the subscript 0 and obtain

$$1 - \alpha = P(x_1(\theta) < x < x_2(\theta)) = P(\theta_2(x) < \theta < \theta_1(x)). \quad (40.68)$$

In this probability statement, $\theta_1(x)$ and $\theta_2(x)$, *i.e.*, the endpoints of the interval, are the random variables and θ is an unknown constant. If the experiment were to be repeated a large number of times, the interval $[\theta_1, \theta_2]$ would vary, covering the fixed value θ in a fraction $1 - \alpha$ of the experiments.

The condition of coverage in Eq. (40.67) does not determine x_1 and x_2 uniquely, and additional criteria are needed. One possibility is to choose *central intervals* such that the probabilities to find x below x_1 and above x_2 are each $\alpha/2$. In other cases, one may want to report only an upper or lower limit, in which case one of $P(x \leq x_1)$ or $P(x \geq x_2)$ can be set to α and the other to zero. Another principle based on *likelihood ratio ordering* for determining which values of x should be included in the confidence belt is discussed below.

When the observed random variable x is continuous, the coverage probability obtained with the Neyman construction is $1 - \alpha$, regardless of the true value of the parameter. Because of the requirement $P(x_1 < x < x_2) \geq 1 - \alpha$ when x is discrete, one obtains

in that case confidence intervals that include the true parameter with a probability greater than or equal to $1 - \alpha$.

An equivalent method of constructing confidence intervals is to consider a test (see Sec. 40.3) of the hypothesis that the parameter's true value is θ (assume one constructs a test for all physical values of θ). One then excludes all values of θ where the hypothesis would be rejected in a test of size α or less. The remaining values constitute the confidence interval at confidence level $1 - \alpha$. If the critical region of the test is characterized by having a p -value $p_\theta \leq \alpha$, then the endpoints of the confidence interval are found in practice by solving $p_\theta = \alpha$ for θ .

In the procedure outlined above, one is still free to choose the test to be used; this corresponds to the freedom in the Neyman construction as to which values of the data are included in the confidence belt. One possibility is to use a test statistic based on the *likelihood ratio*,

$$\lambda(\theta) = \frac{f(x; \theta)}{f(x; \hat{\theta})}, \quad (40.69)$$

where $\hat{\theta}$ is the value of the parameter which, out of all allowed values, maximizes $f(x; \theta)$. This results in the intervals described in Ref. [40] by Feldman and Cousins. The same intervals can be obtained from the Neyman construction described above by including in the confidence belt those values of x which give the greatest values of $\lambda(\theta)$.

If the model contains nuisance parameters ν , then these can be incorporated into the test (or the p -values) used to determine the limit by profiling as discussed in Section 40.3.2.1. As mentioned there, the strict frequentist approach is to regard the parameter of interest θ as excluded only if it is rejected for all possible values of ν . The resulting interval for θ will then cover the true value with a probability greater than or equal to the nominal confidence level for all points in ν -space.

If the p -value is based on the profiled values of the nuisance parameters, *i.e.*, with $\nu = \hat{\nu}(\theta)$ used in Eq. (40.47), then the resulting interval for the parameter of interest will have the correct coverage if the true values of ν are equal to the profiled values. Otherwise the coverage probability may be too high or too low. This procedure has been called *profile construction* in HEP [41] (see also [32]).

40.4.2.2 Gaussian distributed measurements

An important example of constructing a confidence interval is when the data consists of a single random variable x that follows a Gaussian distribution; this is often the case when x represents an estimator for a parameter and one has a sufficiently large data sample. If there is more than one parameter being estimated, the multivariate Gaussian is used. For the univariate case with known σ , the probability that the measured value x will fall within $\pm\delta$ of the true value μ is

$$1 - \alpha = \frac{1}{\sqrt{2\pi}\sigma} \int_{\mu-\delta}^{\mu+\delta} e^{-(x-\mu)^2/2\sigma^2} dx = \text{erf}\left(\frac{\delta}{\sqrt{2}\sigma}\right) = 2\Phi\left(\frac{\delta}{\sigma}\right) - 1, \quad (40.70)$$

where erf is the Gaussian error function, which is rewritten in the final equality using Φ , the Gaussian cumulative distribution. Fig. 40.4 shows a $\delta = 1.64\sigma$ confidence interval unshaded. The choice $\delta = \sigma$ gives an interval called the *standard error* which has $1 - \alpha = 68.27\%$ if σ is known. Values of α for other frequently used choices of δ are given in Table 40.1.

We can set a one-sided (upper or lower) limit by excluding above $x + \delta$ (or below $x - \delta$). The values of α for such limits are half the values in Table 40.1.

The relation (40.70) can be re-expressed using the cumulative distribution function for the χ^2 distribution as

$$\alpha = 1 - F(\chi^2; n), \quad (40.71)$$

for $\chi^2 = (\delta/\sigma)^2$ and $n = 1$ degree of freedom. This can be seen as the $n = 1$ curve in Fig. 40.1 or obtained by using the ROOT function `TMath::Prob`. For multivariate measurements of, say, n parameter estimates $\hat{\theta} = (\hat{\theta}_1, \dots, \hat{\theta}_n)$, construction of the confidence

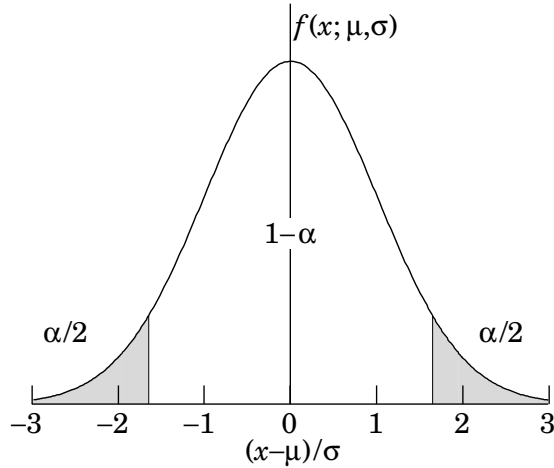


Figure 40.4: Illustration of a symmetric 90% confidence interval (unshaded) for a Gaussian-distributed measurement of a single quantity. Integrated probabilities, defined by $\alpha = 0.1$, are as shown.

Table 40.1: Area of the tails α outside $\pm\delta$ from the mean of a Gaussian distribution.

α	δ	α	δ
0.3173	1σ	0.2	1.28σ
4.55×10^{-2}	2σ	0.1	1.64σ
2.7×10^{-3}	3σ	0.05	1.96σ
6.3×10^{-5}	4σ	0.01	2.58σ
5.7×10^{-7}	5σ	0.001	3.29σ
2.0×10^{-9}	6σ	10^{-4}	3.89σ

region requires the full covariance matrix $V_{ij} = \text{cov}[\hat{\theta}_i, \hat{\theta}_j]$, which can be estimated as described in Sections 40.2.2 and 40.2.3. Under fairly general conditions with the methods of maximum-likelihood or least-squares in the large sample limit, the estimators will be distributed according to a multivariate Gaussian centered about the true (unknown) values θ , and furthermore, the likelihood function itself will take on a Gaussian shape.

The standard error ellipse for the pair $(\hat{\theta}_i, \hat{\theta}_j)$ is shown in Fig. 40.5, corresponding to a contour $\chi^2 = \chi^2_{\text{min}} + 1$ or $\ln L = \ln L_{\text{max}} - 1/2$. The ellipse is centered about the estimated values $\hat{\theta}_i$, and the tangents to the ellipse give the standard deviations of the estimators, σ_i and σ_j . The angle of the major axis of the ellipse is given by

$$\tan 2\phi = \frac{2\rho_{ij}\sigma_i\sigma_j}{\sigma_j^2 - \sigma_i^2}, \quad (40.72)$$

where $\rho_{ij} = \text{cov}[\hat{\theta}_i, \hat{\theta}_j]/\sigma_i\sigma_j$ is the correlation coefficient.

The correlation coefficient can be visualized as the fraction of the distance σ_i from the ellipse's horizontal center-line at which the ellipse becomes tangent to vertical, *i.e.*, at the distance $\rho_{ij}\sigma_i$ below the center-line as shown. As ρ_{ij} goes to $+1$ or -1 , the ellipse thins to a diagonal line.

It could happen that one of the parameters, say, θ_j , is known from previous measurements to a precision much better than σ_j , so that the current measurement contributes almost nothing to the knowledge of θ_j . However, the current measurement of θ_i and its dependence on θ_j may still be important. In this case, instead of quoting both parameter estimates and their correlation, one sometimes reports the value of θ_i , which minimizes χ^2 at a fixed value of θ_j , such as the PDG best value. This θ_i value lies along the dotted line between the points where the ellipse becomes tangent to vertical, and has statistical error σ_{inner} as shown on the figure, where $\sigma_{\text{inner}} = (1 - \rho_{ij}^2)^{1/2}\sigma_i$. Instead of the correlation ρ_{ij} , one reports the dependency $d\hat{\theta}_i/d\theta_j$, which is the slope of the dotted line. This slope is related to the correlation coefficient by

$$d\hat{\theta}_i/d\theta_j = \rho_{ij} \times \frac{\sigma_i}{\sigma_j}.$$

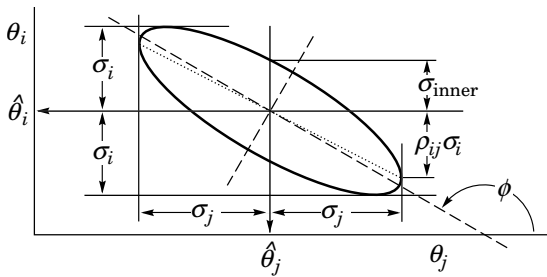


Figure 40.5: Standard error ellipse for the estimators $\hat{\theta}_i$ and $\hat{\theta}_j$. In the case shown the correlation is negative.

As in the single-variable case, because of the symmetry of the Gaussian function between θ and $\hat{\theta}$, one finds that contours of constant $\ln L$ or χ^2 cover the true values with a certain, fixed probability. That is, the confidence region is determined by

$$\ln L(\theta) \geq \ln L_{\max} - \Delta \ln L, \quad (40.73)$$

or where a χ^2 has been defined for use with the method of least-squares,

$$\chi^2(\theta) \leq \chi^2_{\min} + \Delta \chi^2. \quad (40.74)$$

Values of $\Delta \chi^2$ or $2\Delta \ln L$ are given in Table 40.2 for several values of the coverage probability $1 - \alpha$ and number of fitted parameters m . For Gaussian distributed data, these are related by $\Delta \chi^2 = 2\Delta \ln L = F_{\chi_m^2}^{-1}(1 - \alpha)$, where $F_{\chi_m^2}^{-1}$ is the chi-square quantile (inverse of the cumulative distribution) for m degrees of freedom.

Table 40.2: Values of $\Delta \chi^2$ or $2\Delta \ln L$ corresponding to a coverage probability $1 - \alpha$ in the large data sample limit, for joint estimation of m parameters.

$(1 - \alpha)$ (%)	$m = 1$	$m = 2$	$m = 3$
68.27	1.00	2.30	3.53
90.	2.71	4.61	6.25
95.	3.84	5.99	7.82
95.45	4.00	6.18	8.03
99.	6.63	9.21	11.34
99.73	9.00	11.83	14.16

For non-Gaussian data samples, the probability for the regions determined by Equations (40.73) or (40.74) to cover the true value of θ becomes independent of θ only in the large-sample limit. So for a finite data sample these are not exact confidence regions according to our previous definition. Nevertheless, they can still have a coverage probability only weakly dependent on the true parameter, and approximately as given in Table 40.2. In any case, the coverage probability of the intervals or regions obtained according to this procedure can in principle be determined as a function of the true parameter(s), for example, using a Monte Carlo calculation.

One of the practical advantages of intervals that can be constructed from the log-likelihood function or χ^2 is that it is relatively simple to produce the interval for the combination of several experiments. If N independent measurements result in log-likelihood functions $\ln L_i(\theta)$, then the combined log-likelihood function is simply the sum,

$$\ln L(\theta) = \sum_{i=1}^N \ln L_i(\theta). \quad (40.75)$$

This can then be used to determine an approximate confidence interval or region with Eq. (40.73), just as with a single experiment.

40.4.2.3 Poisson or binomial data

Another important class of measurements consists of counting a certain number of events, n . In this section, we will assume these are all events of the desired type, *i.e.*, there is no background. If n represents the number of events produced in a reaction with cross section σ , say, in a fixed integrated luminosity \mathcal{L} , then it follows a Poisson distribution with mean $\mu = \sigma \mathcal{L}$. If, on the other hand, one has selected a larger sample of N events and found n of them to have a particular property, then n follows a binomial distribution where the parameter p gives the probability for the event to possess the property in question. This is appropriate, *e.g.*, for estimates of branching ratios or selection efficiencies based on a given total number of events.

For the case of Poisson distributed n , limits on the mean value μ can be found from the Neyman procedure as discussed in Section 40.4.2.1 with n used directly as the statistic x . The upper and lower limits are found to be

$$\mu_{lo} = \frac{1}{2} F_{\chi^2}^{-1}(\alpha_{lo}; 2n), \quad (40.76a)$$

$$\mu_{up} = \frac{1}{2} F_{\chi^2}^{-1}(1 - \alpha_{up}; 2(n + 1)), \quad (40.76b)$$

where confidence levels of $1 - \alpha_{lo}$ and $1 - \alpha_{up}$ refer separately to the corresponding intervals $\mu \geq \mu_{lo}$ and $\mu \leq \mu_{up}$, and $F_{\chi^2}^{-1}$ is the quantile of the χ^2 distribution (inverse of the cumulative distribution). For central confidence intervals at confidence level $1 - \alpha$, set $\alpha_{lo} = \alpha_{up} = \alpha/2$.

Table 40.3: Lower and upper (one-sided) limits for the mean μ of a Poisson variable given n observed events in the absence of background, for confidence levels of 90% and 95%.

n	$1 - \alpha = 90\%$		$1 - \alpha = 95\%$	
	μ_{lo}	μ_{up}	μ_{lo}	μ_{up}
0	–	2.30	–	3.00
1	0.105	3.89	0.051	4.74
2	0.532	5.32	0.355	6.30
3	1.10	6.68	0.818	7.75
4	1.74	7.99	1.37	9.15
5	2.43	9.27	1.97	10.51
6	3.15	10.53	2.61	11.84
7	3.89	11.77	3.29	13.15
8	4.66	12.99	3.98	14.43
9	5.43	14.21	4.70	15.71
10	6.22	15.41	5.43	16.96

It happens that the upper limit from Eq. (40.76b) coincides numerically with the Bayesian upper limit for a Poisson parameter, using a uniform prior p.d.f. for μ . Values for confidence levels of 90% and 95% are shown in Table 40.3. For the case of binomially distributed n successes out of N trials with probability of success p , the upper and lower limits on p are found to be

$$p_{lo} = \frac{n F_F^{-1}[\alpha_{lo}; 2n, 2(N - n + 1)]}{N - n + 1 + n F_F^{-1}[\alpha_{lo}; 2n, 2(N - n + 1)]}, \quad (40.77a)$$

$$p_{up} = \frac{(n + 1) F_F^{-1}[1 - \alpha_{up}; 2(n + 1), 2(N - n)]}{(N - n) + (n + 1) F_F^{-1}[1 - \alpha_{up}; 2(n + 1), 2(N - n)]}. \quad (40.77b)$$

Here F_F^{-1} is the quantile of the F distribution (also called the Fisher-Snedecor distribution; see Ref. [4]).

40.4.2.4 Parameter exclusion in cases of low sensitivity

An important example of a statistical test arises in the search for a new signal process. Suppose the parameter μ is defined such that it is proportional to the signal cross section. A statistical test may be carried out for hypothesized values of μ , which may be done by computing a p -value, p_μ , for all μ . Those values not rejected in a test of size α , *i.e.*, for which one does not find $p_\mu \leq \alpha$, constitute a confidence interval with confidence level $1 - \alpha$.

In general one will find that for some regions in the parameter space of the signal model, the predictions for data are almost indistinguishable from those of the background-only model. This corresponds to the case where μ is very small, as would occur, *e.g.*, in a search for a new particle with a mass so high that its production rate in a given experiment is negligible. That is, one has essentially no experimental sensitivity to such a model.

One would prefer that if the sensitivity to a model (or a point in a model's parameter space) is very low, then it should not be excluded. Even if the outcomes predicted with or without signal are identical, however, the probability to reject the signal model will equal α , the type-I error rate. As one often takes α to be 5%, this would mean that in a large number of searches covering a broad range of a signal model's parameter space, there would inevitably be excluded regions in which the experimental sensitivity is very small, and thus one may question whether it is justified to regard such parameter values as disfavored.

Exclusion of models to which one has little or no sensitivity occurs, for example, if the data fluctuate very low relative to the expectation of the background-only hypothesis. In this case the resulting upper limit on μ may be anomalously low. As a means of controlling this effect one often determines the mean or median limit under assumption of the background-only hypothesis, as discussed in Sec. 40.5.

One way to mitigate the problem of excluding models to which one is not sensitive is the CL_s method, where the measure used to test a parameter is increased for decreasing sensitivity [42, 43]. The procedure is based on a statistic called CL_s , which is defined as

$$CL_s = \frac{p_\mu}{1 - p_b}, \quad (40.78)$$

where p_b is the p -value of the background-only hypothesis. In the usual formulation of the method, both p_μ and p_b are defined using a single test statistic, and the definition of CL_s above assumes this statistic is continuous; more details can be found in Refs. [42, 43].

A point in a model's parameter space is regarded as excluded if one finds $CL_s \leq \alpha$. As the denominator in Eq. (40.78) is always less than or equal to unity, the exclusion criterion based on CL_s is more stringent than the usual requirement $p_\mu \leq \alpha$. In this sense the CL_s procedure is conservative, and the coverage probability of the corresponding intervals will exceed the nominal confidence level $1 - \alpha$. If the experimental sensitivity to a given value of μ is very low, then one finds that as p_μ decreases, so does the denominator $1 - p_b$, and thus the condition $CL_s \leq \alpha$ is effectively prevented from being satisfied. In this way the exclusion of parameters in the case of low sensitivity is suppressed.

The CL_s procedure has the attractive feature that the resulting intervals coincide with those obtained from the Bayesian method in two important cases: the mean value of a Poisson or Gaussian distributed measurement with a constant prior. The CL_s intervals overcover for all values of the parameter μ , however, by an amount that depends on μ .

The problem of excluding parameter values to which one has little sensitivity is particularly acute when one wants to set a one-sided limit, *e.g.*, an upper limit on a cross section. Here one tests a value of a rate parameter μ against the alternative of a lower rate, and therefore the critical region of the test is taken to correspond to data outcomes with a low event yield. If the number of events found in the search region fluctuates low enough, however, it can happen that all physically meaningful signal parameter values, including those to which one has very little sensitivity, are rejected by the test.

Another solution to this problem, therefore, is to replace the one-sided test by one based on the likelihood ratio, where the critical region is not restricted to low rates. This is the approach followed in the Feldman-Cousins procedure described in Section 40.4.2.1. The critical region for the test of a given value of μ contains data values characteristic of both higher and lower rates. As a result, for a given observed rate one can in general obtain a two-sided interval. If, however, the parameter estimate $\hat{\mu}$ is sufficiently close to the lower limit of zero, then only high values of μ are rejected, and the lower edge of the confidence interval is at zero. Note, however, that the coverage property of

$1 - \alpha$ pertains to the entire interval, not to the probability for the upper edge μ_{up} to be greater than the true value μ . For parameter estimates increasingly far away from the boundary, *i.e.*, for increasing signal significance, the point $\mu = 0$ is excluded and the interval has nonzero upper and lower edges.

An additional difficulty arises when a parameter estimate is not significantly far away from the boundary, in which case it is natural to report a one-sided confidence interval (often an upper limit). It is straightforward to force the Neyman prescription to produce only an upper limit by setting $x_2 = \infty$ in Eq. (40.67). Then x_1 is uniquely determined and the upper limit can be obtained. If, however, the data come out such that the parameter estimate is not so close to the boundary, one might wish to report a central confidence interval (*i.e.*, an interval based on a two-sided test with equal upper and lower tail areas). As pointed out by Feldman and Cousins [40], if the decision to report an upper limit or two-sided interval is made by looking at the data ("flip-flopping"), then in general there will be parameter values for which the resulting intervals have a coverage probability less than $1 - \alpha$. With the confidence intervals suggested in [40], the prescription determines whether the interval is one- or two-sided in a way which preserves the coverage probability (and are thus said to be *unified*).

The intervals according to this method for the mean of Poisson variable in the absence of background are given in Table 40.4. (Note that α in Ref. [40] is defined following Neyman [39] as the coverage probability; this is opposite the modern convention used here in which the coverage probability is $1 - \alpha$.) The values of $1 - \alpha$ given here refer to the coverage of the true parameter by the whole interval $[\mu_1, \mu_2]$. In Table 40.3 for the one-sided upper limit, however, $1 - \alpha$ refers to the probability to have $\mu_{\text{up}} \geq \mu$ (or $\mu_{\text{lo}} \leq \mu$ for lower limits).

Table 40.4: Unified confidence intervals $[\mu_1, \mu_2]$ for a the mean of a Poisson variable given n observed events in the absence of background, for confidence levels of 90% and 95%.

n	$1 - \alpha = 90\%$		$1 - \alpha = 95\%$	
	μ_1	μ_2	μ_1	μ_2
0	0.00	2.44	0.00	3.09
1	0.11	4.36	0.05	5.14
2	0.53	5.91	0.36	6.72
3	1.10	7.42	0.82	8.25
4	1.47	8.60	1.37	9.76
5	1.84	9.99	1.84	11.26
6	2.21	11.47	2.21	12.75
7	3.56	12.53	2.58	13.81
8	3.96	13.99	2.94	15.29
9	4.36	15.30	4.36	16.77
10	5.50	16.50	4.75	17.82

A potential difficulty with unified intervals arises if, for example, one constructs such an interval for a Poisson parameter s of some yet to be discovered signal process with, say, $1 - \alpha = 0.9$. If the true signal parameter is zero, or in any case much less than the expected background, one will usually obtain a one-sided upper limit on s . In a certain fraction of the experiments, however, a two-sided interval for s will result. Since, however, one typically chooses $1 - \alpha$ to be only 0.9 or 0.95 when setting limits, the value $s = 0$ may be found below the lower edge of the interval before the existence of the effect is well established. It must then be communicated carefully that in excluding $s = 0$ at, say, 90% or 95% confidence level from the interval, one is not necessarily claiming to have discovered the effect, for which one would usually require a higher level of significance (*e.g.*, 5σ).

Another possibility is to construct a Bayesian interval as described in Section 40.4.1. The presence of the boundary can be incorporated simply by setting the prior density to zero in the unphysical region. More specifically, the prior may be chosen using formal rules such as the reference prior or Jeffreys prior mentioned in Sec. 40.2.5.

In HEP a widely used prior for the mean μ of a Poisson distributed measurement has been the uniform distribution for

$\mu \geq 0$. This prior does not follow from any fundamental rule nor can it be regarded as reflecting a reasonable degree of belief, since the prior probability for μ to lie between any two finite values is zero. The procedure above can be more appropriately regarded as a way for obtaining intervals with frequentist properties that can be investigated. The resulting upper limits have a coverage probability that depends on the true value of the Poisson parameter, and is nowhere smaller than the stated probability content. Lower limits and two-sided intervals for the Poisson mean based on flat priors undercover, however, for some values of the parameter, although to an extent that in practical cases may not be too severe [2, 38].

In any case, it is important to always report sufficient information so that the result can be combined with other measurements. Often this means giving an unbiased estimator and its standard deviation, even if the estimated value is in the unphysical region.

It can also be useful with a frequentist interval to calculate its subjective probability content using the posterior p.d.f. based on one or several reasonable guesses for the prior p.d.f. If it turns out to be significantly less than the stated confidence level, this warns that it would be particularly misleading to draw conclusions about the parameter's value from the interval alone.

40.5 Experimental sensitivity

In this section we describe methods for characterizing the sensitivity of a search for a new physics signal. As discussed in Sec. 40.3, an experimental analysis can often be formulated as a test of hypothetical model parameters. Therefore we may quantify the sensitivity by giving the results that we expect from such a test under specific assumptions about the signal process.

Here to be concrete we will consider a parameter μ proportional to the rate of a signal process, although the concepts described in this section may be easily generalized to other parameters. One may wish to establish discovery of the signal process by testing and rejecting the hypothesis that $\mu = 0$, and in addition one often wants to test nonzero values of μ to construct a confidence interval (e.g., limits) as described in Sec. 40.4. In the frequentist framework, the result of each tested value of μ is the p -value p_μ or equivalently the significance $Z_\mu = \Phi^{-1}(1 - p_\mu)$, where as usual Φ is the standard Gaussian cumulative distribution and its inverse Φ^{-1} is the standard Gaussian quantile.

Prior to carrying out the experiment, one generally wants to quantify what significance Z_μ is expected under given assumptions for the presence or absence of the signal process. Specifically, for the significance of a test of $\mu = 0$ (the discovery significance) one usually quotes the Z_0 one would expect if the signal is present at a given nominal rate, which we can define in general to correspond to $\mu = 1$. For limits, one often gives the expected limit under assumption of the background-only ($\mu = 0$) model. These quantities are used to optimize the analysis and to quantify the experimental sensitivity, that is, to characterize how likely it is to make a discovery if the signal is present, and to say what values of μ one may be able to exclude if the signal is in fact absent.

First we clarify the notion of *expected significance*. Because the significance Z_μ is a function of the data, it is itself a random quantity characterized by a certain sampling distribution. This distribution depends on the assumed value of μ , which is not necessarily the same as the hypothesized value of μ being tested. We may therefore consider the distribution $f(Z_\mu|\mu')$, i.e., the distribution of Z_μ that would be obtained by considering data samples generated under assumption of μ' . In a similar way one can talk about the sampling distribution of an upper limit for μ , $f(\mu_{\text{up}}|\mu')$.

One can identify the expected significance or limit with either the mean or median of these distributions, but the median may be preferred since it is invariant under monotonic transformations. For example, the monotonic relation between p -value and significance, $p = 1 - \Phi(Z)$, then gives $\text{med}[p_\mu|\mu'] = 1 - \Phi(\text{med}[Z_\mu|\mu'])$, whereas the corresponding relation does not hold in general for the mean.

In some cases one may be able to write down approximate formulae for the distributions of Z_μ and for limits, but more generally they must be determined from Monte Carlo calculations. In many

cases of interest, the significance Z_μ and the limits on μ will have approximate Gaussian distributions.

As an example, consider a Poisson counting experiment, where the result consists of an observed number n of events, modeled as a Poisson distributed variable with a mean of $\mu s + b$. Here s and b , the expected numbers of events from signal and background processes, are taken to be known. If we are interested in discovering the signal process we test and try to reject the hypothesis $\mu = 0$. To characterize the experimental sensitivity, we want to give the discovery significance expected under the assumption of $\mu = 1$.

In the limit where its mean value is large, the Poisson variable n can be approximated as an almost continuous Gaussian variable with mean $\mu s + b$ and standard deviation $\sigma = \sqrt{\mu s + b}$. In the usual case where a physical signal model corresponds to $\mu > 0$, the p -value of $\mu = 0$ is the probability to find n greater than or equal to the value observed,

$$p_0 = \Phi\left(\frac{n-b}{\sqrt{b}}\right), \quad (40.79)$$

and the corresponding significance is $Z_0 = \Phi^{-1}(1 - p_0) = (n - b)/\sqrt{b}$. The median (here equal to the mean) of n assuming $\mu = 1$ is $s + b$, and therefore the median discovery significance is

$$\text{med}[Z_0|\mu = 1] = \frac{s}{\sqrt{b}}. \quad (40.80)$$

The figure of merit “ s/\sqrt{b} ” has been widely used in HEP as a measure of expected discovery significance. A better approximation for the Poisson counting experiment, however, may be obtained by testing $\mu = 0$ using the likelihood ratio (40.48) $\lambda(0) = L(0)/L(\hat{\mu})$, where

$$L(\mu) = \frac{(\mu s + b)^n}{n!} e^{-(\mu s + b)} \quad (40.81)$$

is the likelihood function, $\hat{\mu} = (n - b)/s$ is the ML estimator. In this example there are no nuisance parameters, as s and b are taken to be known. For the case where the relevant signal models correspond to positive μ , one may test the $\mu = 0$ hypothesis with the statistic $q_0 = -2 \ln \lambda(0)$ when $\hat{\mu} > 0$, i.e., an excess is observed, and $q_0 = 0$ otherwise. One can show (see, e.g., [31]) that in the large-sample limit, the discovery significance is then $Z_0 = \sqrt{q_0}$, for which one finds

$$Z_0 = \sqrt{2 \left(n \ln \frac{n}{b} + b - n \right)} \quad (40.82)$$

for $n > b$ and $Z_0 = 0$ otherwise. To approximate the expected discovery significance assuming $\mu = 1$, one may simply replace n with the expected value $E[n|\mu = 1] = s + b$ (the so-called “Asimov data set”), giving

$$\text{med}[Z_0|\mu = 1] = \sqrt{2 \left((s + b) \ln \left(1 + \frac{s}{b} \right) - s \right)}. \quad (40.83)$$

This has been shown in Ref. [31] to provide a good approximation to the median discovery significance for values of s of several and for b well below unity. The right-hand side of Eq. (40.83) reduces to s/\sqrt{b} in the limit $s \ll b$.

Beyond the simple Poisson counting experiment, in general one may test values of a parameter μ with more complicated functions of the measured data to obtain a p -value p_μ , and from this one can quote the equivalent significance Z_μ or find, e.g., an upper limit μ_{up} . In this case as well one may quantify the experimental sensitivity by giving the significance Z_μ expected if the data are generated with a different value of the parameter μ' . In some problems, finding the sampling distribution of the significance or limits may be possible using large-sample formulae as described, e.g., in Ref. [31]. In other cases a Monte Carlo study may be needed. Using whatever method of calculation is most appropriate, one usually quotes the expected (mean or, preferably, median) significance or limit as the primary measures of experimental sensitivity.

Even if the true signal is present at its nominal rate, the actual discovery significance Z_0 obtained from the real data is subject to statistical fluctuations and will not in general be equal to its expected value. In an analogous way, the observed limit will differ from the expected limit even if the signal is absent. Upon observing such a difference one would like to know how large this is compared to expected statistical fluctuations. Therefore, in addition to the observed significance and limits it is useful to communicate not only their expected values but also a measure of the width of their distributions.

As the distributions of significance and limits are often well approximated by a Gaussian, one may indicate the intervals corresponding to plus-or-minus one and/or two standard deviations. If the distributions are significantly non-Gaussian, one may use instead the quantiles that give the same probability content, *i.e.*, [0.1587, 0.8413] for $\pm 1\sigma$, [0.02275, 0.97725] for $\pm 2\sigma$. An upper limit found significantly below the background-only expectation may indicate a strong downward fluctuation of the data, or perhaps as well an incorrect estimate of the background rate.

The procedures described above pertain to frequentist hypothesis tests and limits. Bayesian limits, just like those found from a frequentist procedure, are functions of the data and one may therefore find, usually with approximations or Monte Carlo studies, their sampling distribution and corresponding mean (or, preferably, median) and standard deviation.

When trying to establish discovery of a signal process, the Bayesian approach may employ a Bayes factor as described in Sec. 40.3.3. In the case of the Poisson counting experiment with the likelihood from Eq. (40.81), the log of the Bayes factor that compares $\mu = 1$ to $\mu = 0$ is $\ln B_{10} = \ln(L(1)/L(0)) = n \ln(1 + s/b) - s$. That is, the expectation value, assuming $\mu = 1$, of $\ln B_{10}$ for this problem is

$$E[\ln B_{10} | \mu = 1] = (s + b) \ln \left(1 + \frac{s}{b} \right) - s. \quad (40.84)$$

Comparing this to Eq. (40.83), one finds $\text{med}[Z_0 | 1] = \sqrt{2E[\ln B_{10} | 1]}$. Thus for this particular problem the frequentist median discovery significance can be related to the corresponding Bayes factor in a simple way.

In some analyses, the goal may not be to establish discovery of a signal process but rather to measure, as accurately as possible, the signal rate. If we consider again the Poisson counting experiment described by the likelihood function of Eq. (40.81), the ML estimator $\hat{\mu} = (n - b)/s$ has a variance, assuming $\mu = 1$, of

$$V[\hat{\mu}] = V \left[\frac{n - b}{s} \right] = \frac{1}{s^2} V[n] = \frac{s + b}{s^2}, \quad (40.85)$$

so that the standard deviation of $\hat{\mu}$ is $\sigma_{\hat{\mu}} = \sqrt{s + b}/s$. One may therefore use $s/\sqrt{s + b}$ as a figure of merit to be maximized in order to obtain the best measurement accuracy of a rate parameter. The quantity $s/\sqrt{s + b}$ is also the expected significance with which one rejects s assuming the signal is absent, and thus can be used to optimize the expected upper limit on s .

References

- [1] B. Efron, *Am. Stat.* **40**, 11 (1986).
- [2] R. D. Cousins, *Am. J. Phys.* **63**, 398 (1995).
- [3] A. Stuart, J.K. Ord, and S. Arnold, *Kendall's Advanced Theory of Statistics*, Vol. 2A: *Classical Inference and the Linear Model*, 6th ed., Oxford Univ. Press (1999), and earlier editions by Kendall and Stuart. The likelihood-ratio ordering principle is described at the beginning of Ch. 23. Chapter 26 compares different schools of statistical inference.
- [4] F. James, *Statistical methods in experimental physics* (2006), ISBN 9789812567956.
- [5] L. Lyons, *Statistics for Nuclear and Particle Physicists* (1986), ISBN 9780521379342, URL <http://www.cambridge.org/uk/catalogue/catalogue.asp?isbn=0521255406>.
- [6] R. J. Barlow, *Nucl. Instrum. Meth.* **A297**, 496 (1990).
- [7] G. Cowan, *Statistical data analysis* (1998), ISBN 9780198501565.
- [8] S. Baker and R. D. Cousins, *Nucl. Instrum. Meth.* **221**, 437 (1984).
- [9] S. S. Wilks, *Annals Math. Statist.* **9**, 1, 60 (1938).
- [10] O. Behnke *et al.*, editors, *Data analysis in high energy physics*, Wiley-VCH, Weinheim, Germany (2013), ISBN 9783527410583, 9783527653447, 9783527653430, URL <http://www.wiley-vch.de/publish/dt/books/ISBN3-527-41058-9>.
- [11] A. O'Hagan and J.J. Forster, *Bayesian Inference*, (2nd edition, volume 2B of *Kendall's Advanced Theory of Statistics*, Arnold, London, 2004).
- [12] D. Sivia and J. Skilling, *Data Analysis: A Bayesian Tutorial*, (Oxford University Press, 2006).
- [13] P.C. Gregory, *Bayesian Logical Data Analysis for the Physical Sciences*, (Cambridge University Press, 2005).
- [14] J.M. Bernardo and A.F.M. Smith, *Bayesian Theory*, (Wiley, 2000).
- [15] Robert E. Kass and Larry Wasserman, *J. Am. Stat. Assoc.* **91**, 1343 (1996).
- [16] J.M. Bernardo, *J. R. Statist. Soc.* **B41**, 113 (1979); J.M. Bernardo and J.O. Berger, *J. Am. Stat. Assoc.* **84**, 200 (1989). See also J.M. Bernardo, *Reference Analysis*, in *Handbook of Statistics*, 25 (D.K. Dey and C.R. Rao, eds.), 17-90, Elsevier (2005) and references therein.
- [17] L. Demortier, S. Jain and H. B. Prosper, *Phys. Rev.* **D82**, 034002 (2010), [arXiv:1002.1111].
- [18] Christopher M. Bishop, *Pattern Recognition and Machine Learning*, (Springer, New York, 2006).
- [19] T. Hastie, R. Tibshirani, and J. Friedman, *The Elements of Statistical Learning*, (2nd edition, Springer, New York, 2009).
- [20] A. Webb, *Statistical Pattern Recognition*, 2nd ed., (Wiley, New York, 2002).
- [21] L.I. Kuncheva, *Combining Pattern Classifiers*, (Wiley, New York, 2004).
- [22] Links to the *Proceedings of the PHYSTAT* conference series (Durham 2002, Stanford 2003, Oxford 2005, and Geneva 2007, 2011) can be found at phystat.org.
- [23] K. Albertsson *et al.* (2018), [arXiv:1807.02876].
- [24] A. Hocker *et al.* (2007), [arXiv:physics/0703039]; Software available from tmva.sourceforge.net.
- [25] F. Pedregosa *et al.*, *J. Machine Learning Res.* **12**, 2825 (2011), [arXiv:1201.0490].
- [26] P. Baldi, P. Sadowski and D. Whiteson, *Nature Commun.* **5**, 4308 (2014), [arXiv:1402.4735].
- [27] D. Guest, K. Cranmer and D. Whiteson, *Ann. Rev. Nucl. Part. Sci.* **68**, 161 (2018), [arXiv:1806.11484].
- [28] K. Cranmer, J. Pavez and G. Louppe (2015), [arXiv:1506.02169].
- [29] N. Reid, *Likelihood Inference in the Presence of Nuisance Parameters*, *Proceedings of PHYSTAT2003*, L. Lyons, R. Mount, and R. Reitmeyer, eds., eConf C030908, Stanford, 2003.
- [30] W. A. Rolke, A. M. Lopez and J. Conrad, *Nucl. Instrum. Meth.* **A551**, 493 (2005), [arXiv:physics/0403059].
- [31] G. Cowan *et al.*, *Eur. Phys. J.* **C71**, 1554 (2011), [Erratum: *Eur. Phys. J.* **C73**, 2501 (2013)], [arXiv:1007.1727].
- [32] L. Demortier, *P-Values and Nuisance Parameters*, *Proceedings of PHYSTAT 2007*, CERN-2008-001, p. 23.
- [33] E. Gross and O. Vitells, *Eur. Phys. J.* **C70**, 525 (2010), [arXiv:1005.1891].
- [34] R. B. Davies, *Biometrika* **74**, 33 (1987).
- [35] J. Skilling, *Nested Sampling*, *AIP Conference Proceedings*, **735**, 395-405 (2004).
- [36] F. Feroz, M. P. Hobson and M. Bridges, *Mon. Not. Roy. Astron. Soc.* **398**, 1601 (2009), [arXiv:0809.3437].

- [37] R. E. Kass and A. E. Raftery, *J. Am. Statist. Assoc.* **90**, 430, 773 (1995).
- [38] B. P. Roe and M. B. Woodroffe, *Phys. Rev.* **D63**, 013009 (2001), [hep-ex/0007048].
- [39] J. Neyman, *Phil. Trans. Roy. Soc. Lond.* **A236**, 767, 333 (1937); Reprinted in *A Selection of Early Statistical Papers on J. Neyman*, (University of California Press, Berkeley, 1967).
- [40] G. J. Feldman and R. D. Cousins, *Phys. Rev.* **D57**, 3873 (1998), [arXiv:physics/9711021]; This paper does not specify what to do if the ordering principle gives equal rank to some values of x . Eq. 21.6 of Ref. [3] gives the rule: all such points are included in the acceptance region (the domain $D(\alpha)$)/ Some authors have assumed the contrary, and shown that one can then obtain null intervals.
- [41] K. Cranmer, in “Statistical Problems in Particle Physics, Astrophysics and Cosmology (PHYSTAT 05): Proceedings, Oxford, UK, September 12-15, 2005,” 112–123 (2005), [arXiv:physics/0511028], URL http://www.physics.ox.ac.uk/phystat05/proceedings/files//Cranmer_LHCStatisticalChallenges.ps.
- [42] A. L. Read, in “Workshop on confidence limits, CERN, Geneva, Switzerland, 17-18 Jan 2000: Proceedings,” 81–101 (2000), URL <http://weblib.cern.ch/abstract?CERN-OPEN-2000-205>.
- [43] T. Junk, *Nucl. Instrum. Meth.* **A434**, 435 (1999), [hep-ex/9902006].

41. Monte Carlo Techniques

Revised August 2019 by G. Cowan (RHUL).

Monte Carlo techniques are often the only practical way to evaluate difficult integrals or to sample random variables governed by complicated probability density functions. Here we describe an assortment of methods for sampling some commonly occurring probability density functions.

41.1 Sampling the uniform distribution

Most Monte Carlo sampling or integration techniques assume a “random number generator,” which generates uniform statistically independent values on the half open interval $[0, 1)$; for reviews see, *e.g.*, Refs. [1, 2].

Uniform random number generators are available in software libraries such as CLHEP [3], and ROOT [4]. For example, in addition to a basic congruential generator TRandom (see below), ROOT provides three more sophisticated routines: TRandom1 implements the RANLUX generator [5] based on the method by Lüscher, and allows the user to select different quality levels, trading off quality with speed; TRandom2 is based on the maximally equidistributed combined Tausworthe generator by L’Ecuyer [6]; the TRandom3 generator implements the Mersenne twister algorithm of Matsumoto and Nishimura [7]. All of the algorithms produce a periodic sequence of numbers, and to obtain effectively random values, one must not use more than a small subset of a single period. The Mersenne twister algorithm has an extremely long period of $2^{19937} - 1$.

The performance of the generators can be investigated with tests such as DIEHARD [8] or TestU01 [9]. Many commonly available congruential generators fail these tests and often have sequences (typically with periods less than 2^{32}), which can be easily exhausted on modern computers. A short period is a problem for the TRandom generator in ROOT, which, however, has the advantage that its state is stored in a single 32-bit word. The generators TRandom1, TRandom2, or TRandom3 have much longer periods, with TRandom3 being recommended by the ROOT authors as providing the best combination of speed and good random properties. For further information see, *e.g.*, Ref. [10].

41.2 Inverse transform method

If the desired probability density function is $f(x)$ on the range $-\infty < x < \infty$, its cumulative distribution function (expressing the probability that $x \leq a$) is given by Eq. (39.6). If a is chosen with probability density $f(a)$, then the integrated probability up to point a , $F(a)$, is itself a random variable which will occur with uniform probability density on $[0, 1]$. Suppose u is generated according to a uniformly distributed in $(0, 1)$. If x can take on any value, and ignoring the endpoints, we can then find a unique x chosen from the p.d.f. $f(x)$ for a given u if we set

$$u = F(x), \tag{41.1}$$

provided we can find an inverse of F , defined by

$$x = F^{-1}(u). \tag{41.2}$$

This method is shown in Fig. 41.1a. It is most convenient when one can calculate by hand the inverse function of the indefinite integral of f . This is the case for some common functions $f(x)$ such as $\exp(x)$, $(1 - x)^n$, and $1/(1 + x^2)$ (Cauchy or Breit-Wigner), although it does not necessarily produce the fastest generator. Standard libraries contain software to implement this method numerically, working from functions or histograms in one or more dimensions, *e.g.*, the UNU.RAN package [11], available in ROOT. For a discrete distribution, $F(x)$ will have a discontinuous jump of size $f(x_k)$ at each allowed $x_k, k = 1, 2, \dots$. Choose u from a uniform distribution on $(0, 1)$ as before. Find x_k such that

$$F(x_{k-1}) < u \leq F(x_k) \equiv \text{Prob}(x \leq x_k) = \sum_{i=1}^k f(x_i); \tag{41.3}$$

then x_k is the value we seek (note: $F(x_0) \equiv 0$). This algorithm is illustrated in Fig. 41.1b.

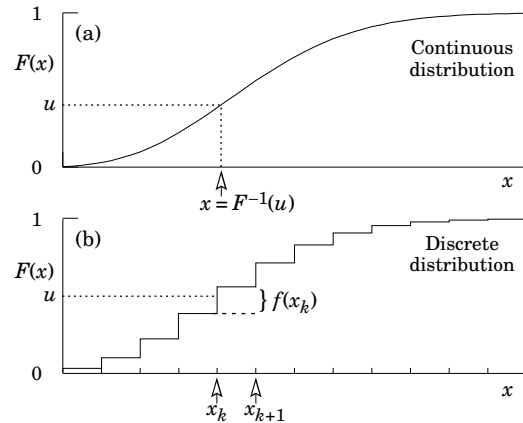


Figure 41.1: Use of a random number u chosen from a uniform distribution $(0, 1)$ to find a random number x from a distribution with cumulative distribution function $F(x)$.

41.3 Acceptance-rejection method (Von Neumann)

Very commonly an analytic form for $F(x)$ is unknown or too complex to work with, so that obtaining an inverse as in Eq. (41.2) is impractical. We suppose that for any given value of x , the probability density function $f(x)$ can be computed, and further that enough is known about $f(x)$ that we can enclose it entirely inside a shape which is C times an easily generated distribution $h(x)$, as illustrated in Fig. 41.2. That is, $Ch(x) \geq f(x)$ must hold for all x . Frequently $h(x)$ is uniform or is a normalized

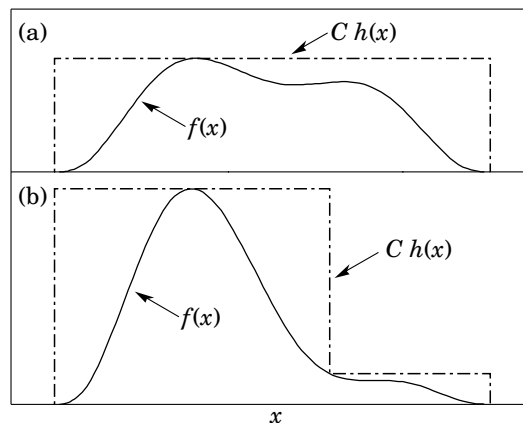


Figure 41.2: Illustration of the acceptance-rejection method. Random points are chosen inside the upper bounding figure, and rejected if the ordinate exceeds $f(x)$. The lower figure illustrates a method to increase the efficiency (see text).

sum of uniform distributions. Note that both $f(x)$ and $h(x)$ must be normalized to unit area, and therefore, the proportionality constant $C > 1$. To generate $f(x)$, first generate a candidate x according to $h(x)$. Calculate $f(x)$ and the height of the envelope $Ch(x)$; generate u and test if $uCh(x) \leq f(x)$. If so, accept x ; if not reject x and try again. If we regard x and $uCh(x)$ as the abscissa and ordinate of a point in a two-dimensional plot, these points will populate the entire area $Ch(x)$ in a smooth manner; then we accept those which fall under $f(x)$. The efficiency is the ratio of areas, which must equal $1/C$; therefore we must keep C as close as possible to 1.0. Therefore, we try to choose $Ch(x)$ to be as close to $f(x)$ as convenience dictates, as in the lower part of Fig. 41.2.

41.4 Algorithms

Algorithms for generating random numbers belonging to many different distributions are given for example by Press [12], Ahrens and Dieter [13], Rubinstein [14], Devroye [15], Walck [16] and Gentle [17]. For many distributions, alternative algorithms exist, varying in complexity, speed, and accuracy. For time-critical applications, these algorithms may be coded in-line to remove the significant overhead often encountered in making function calls.

In the examples given below, we use the notation for the variables and parameters given in Table 39.1. Variables named “ u ” are assumed to be independent and uniform on $[0,1]$. Denominators must be verified to be non-zero where relevant.

41.4.1 Exponential decay

This is a common application of the inverse transform method, and uses the fact that if u is uniformly distributed in $[0, 1]$, then $(1 - u)$ is as well. Consider an exponential p.d.f. $f(t) = (1/\tau) \exp(-t/\tau)$ that is truncated so as to lie between two values, a and b , and renormalized to unit area. To generate decay times t according to this p.d.f., first let $\alpha = \exp(-a/\tau)$ and $\beta = \exp(-b/\tau)$; then generate u and let

$$t = -\tau \ln(\beta + u(\alpha - \beta)). \tag{41.4}$$

For $(a, b) = (0, \infty)$, we have simply $t = -\tau \ln u$. (See also Sec. 41.4.6.)

41.4.2 Isotropic direction in 3D

Isotropy means the density is proportional to solid angle, the differential element of which is $d\Omega = d(\cos \theta)d\phi$. Hence $\cos \theta$ is uniform $(2u_1 - 1)$ and ϕ is uniform $(2\pi u_2)$. For alternative generation of $\sin \phi$ and $\cos \phi$, see the next subsection.

41.4.3 Sine and cosine of random angle in 2D

Generate u_1 and u_2 . Then $v_1 = 2u_1 - 1$ is uniform on $(-1,1)$, and $v_2 = u_2$ is uniform on $(0,1)$. Calculate $r^2 = v_1^2 + v_2^2$. If $r^2 > 1$, start over. Otherwise, the sine (S) and cosine (C) of a random angle (*i.e.*, uniformly distributed between zero and 2π) are given by

$$S = 2v_1v_2/r^2 \quad \text{and} \quad C = (v_1^2 - v_2^2)/r^2. \tag{41.5}$$

41.4.4 Gaussian distribution

If u_1 and u_2 are uniform on $(0,1)$, then

$$z_1 = \sin(2\pi u_1)\sqrt{-2 \ln u_2} \quad \text{and} \quad z_2 = \cos(2\pi u_1)\sqrt{-2 \ln u_2} \tag{41.6}$$

are independent and Gaussian distributed with mean 0 and $\sigma = 1$.

There are many variants of this basic algorithm, which may be faster. For example, construct $v_1 = 2u_1 - 1$ and $v_2 = 2u_2 - 1$, which are uniform on $(-1,1)$. Calculate $r^2 = v_1^2 + v_2^2$, and if $r^2 > 1$ start over. If $r^2 < 1$, it is uniform on $(0,1)$. Then

$$z_1 = v_1 \sqrt{\frac{-2 \ln r^2}{r^2}} \quad \text{and} \quad z_2 = v_2 \sqrt{\frac{-2 \ln r^2}{r^2}} \tag{41.7}$$

are independent numbers chosen from a normal distribution with mean 0 and variance 1. $z'_i = \mu + \sigma z_i$ distributes with mean μ and variance σ^2 .

For a multivariate Gaussian with an $n \times n$ covariance matrix V , one can start by generating n independent Gaussian variables, $\{\eta_j\}$, with mean 0 and variance 1 as above. Then the new set $\{x_i\}$ is obtained as $x_i = \mu_i + \sum_j L_{ij}\eta_j$, where μ_i is the mean of x_i , and L_{ij} are the components of L , the unique lower triangular matrix that fulfils $V = LL^T$. The matrix L can be easily computed by the following recursive relation (Cholesky’s method):

$$L_{jj} = \left(V_{jj} - \sum_{k=1}^{j-1} L_{jk}^2 \right)^{1/2}, \tag{41.8a}$$

$$L_{ij} = \frac{V_{ij} - \sum_{k=1}^{j-1} L_{ik}L_{jk}}{L_{jj}}, \quad j = 1, \dots, n; \quad i = j + 1, \dots, n, \tag{41.8b}$$

where $V_{ij} = \rho_{ij}\sigma_i\sigma_j$ are the components of V . For $n = 2$ one has

$$L = \begin{pmatrix} \sigma_1 & 0 \\ \rho\sigma_2 & \sqrt{1 - \rho^2}\sigma_2 \end{pmatrix}, \tag{41.9}$$

and therefore the correlated Gaussian variables are generated as $x_1 = \mu_1 + \sigma_1\eta_1$, $x_2 = \mu_2 + \rho\sigma_2\eta_1 + \sqrt{1 - \rho^2}\sigma_2\eta_2$.

41.4.5 $\chi^2(n)$ distribution

To generate a variable following the χ^2 distribution for n degrees of freedom, use the Gamma distribution with $k = n/2$ and $\lambda = 1/2$ using the method of Sec. 41.4.6.

41.4.6 Gamma distribution

All of the following algorithms are given for $\lambda = 1$. For $\lambda \neq 1$, divide the resulting random number x by λ .

- If $k = 1$ (the exponential distribution), accept $x = -\ln u$. (See also Sec. 41.4.1.)
- If $0 < k < 1$, initialize with $v_1 = (e+k)/e$ (with $e = 2.71828\dots$ being the natural log base). Generate u_1, u_2 . Define $v_2 = v_1 u_1$.

Case 1: $v_2 \leq 1$. Define $x = v_2^{1/k}$. If $u_2 \leq e^{-x}$, accept x and stop, else restart by generating new u_1, u_2 .

Case 2: $v_2 > 1$. Define $x = -\ln([v_1 - v_2]/k)$. If $u_2 \leq x^{k-1}$, accept x and stop, else restart by generating new u_1, u_2 . Note that, for $k < 1$, the probability density has a pole at $x = 0$, so that return values of zero due to underflow must be accepted or otherwise dealt with.

- Otherwise, if $k > 1$, initialize with $c = 3k - 0.75$. Generate u_1 and compute $v_1 = u_1(1 - u_1)$ and $v_2 = (u_1 - 0.5)\sqrt{c/v_1}$. If $x = k + v_2 - 1 \leq 0$, go back and generate new u_1 ; otherwise generate u_2 and compute $v_3 = 64v_1^3u_2^2$. If $v_3 \leq 1 - 2v_2^2/x$ or if $\ln v_3 \leq 2\{[k - 1] \ln[x/(k - 1)] - v_2\}$, accept x and stop; otherwise go back and generate new u_1 .

41.4.7 Binomial distribution

Begin with $k = 0$ and generate u uniform in $[0, 1)$. Compute $P_k = (1 - p)^n$ and store P_k into B . If $u \leq B$ accept $r_k = k$ and stop. Otherwise, increment k by one; compute the next P_k as $P_k \cdot (p/(1 - p)) \cdot (n - k)/(k + 1)$; add this to B . Again, if $u \leq B$, accept $r_k = k$ and stop, otherwise iterate until a value is accepted. If $p > 1/2$, it will be more efficient to generate r from $f(r; n, q)$, *i.e.*, with p and q interchanged, and then set $r_k = n - r$.

41.4.8 Poisson distribution

Iterate until a successful choice is made: Begin with $k = 1$ and set $A = 1$ to start. Generate u . Replace A with uA ; if now $A < \exp(-\mu)$, where μ is the Poisson parameter, accept $n_k = k - 1$ and stop. Otherwise increment k by 1, generate a new u and repeat, always starting with the value of A left from the previous try.

Note that the Poisson generator used in ROOT’s **TRandom** classes before version 5.12 (including the derived classes **TRandom1**, **TRandom2**, **TRandom3**) uses a Gaussian approximation when μ exceeds a given threshold. This may be satisfactory (and much faster) for some applications. To do this, generate z from a Gaussian with zero mean and unit standard deviation; then use $x = \max(0, [\mu + z\sqrt{\mu} + 0.5])$ where $[\]$ signifies the greatest integer \leq the expression. The routines from Numerical Recipes [12] and CLHEP’s routine **RandPoisson** do not make this approximation (see, *e.g.*, Ref. [10]).

41.4.9 Student’s t distribution

Generate u_1 and u_2 uniform in $(0,1)$; then $t = \sin(2\pi u_1)[n(u_2^{-2/n} - 1)]^{1/2}$ follows the Student’s t distribution for $n > 0$ degrees of freedom (n not necessarily an integer).

Alternatively, generate x from a Gaussian with mean 0 and $\sigma^2 = 1$ according to the method of 41.4.4. Next generate y ,

an independent gamma random variate, according to 41.4.6 with $\lambda = 1/2$ and $k = n/2$. Then $z = x/\sqrt{y/n}$ is distributed as a t with n degrees of freedom.

For the special case $n = 1$, the Breit-Wigner distribution, generate u_1 and u_2 ; set $v_1 = 2u_1 - 1$ and $v_2 = 2u_2 - 1$. If $v_1^2 + v_2^2 \leq 1$ accept $z = v_1/v_2$ as a Breit-Wigner distribution with unit area, center at 0.0, and FWHM 2.0. Otherwise start over. For center M_0 and FWHM Γ , use $W = z\Gamma/2 + M_0$.

41.4.10 Beta distribution

The choice of an appropriate algorithm for generation of beta distributed random numbers depends on the values of the parameters α and β . For, e.g., $\alpha = 1$, one can use the transformation method to find $x = 1 - u^{1/\beta}$, and similarly if $\beta = 1$ one has $x = u^{1/\alpha}$. For more general cases see, e.g., Refs. [16, 17] and references therein.

41.5 Markov Chain Monte Carlo

In applications involving generation of random numbers following a multivariate distribution with a high number of dimensions, the transformation method may not be possible and the acceptance-rejection technique may have too low of an efficiency to be practical. If it is not required to have independent random values, but only that they follow a certain distribution, then Markov Chain Monte Carlo (MCMC) methods can be used. In depth treatments of MCMC can be found, e.g., in the texts by Robert and Casella [18], Liu [19], and the review by Neal [20]. HEP-oriented software for MCMC is available from the Bayesian Analysis Toolkit (BAT) [21].

MCMC is particularly useful in connection with Bayesian statistics, where a p.d.f. $p(\theta)$ for an n -dimensional vector of parameters $\theta = (\theta_1, \dots, \theta_n)$ is obtained, and one needs the marginal distribution of a subset of the components. Here one samples θ from $p(\theta)$ and simply records the marginal distribution for the components of interest.

A simple and broadly applicable MCMC method is the Metropolis-Hastings algorithm, which allows one to generate multidimensional points θ distributed according to a target p.d.f. that is proportional to a given function $p(\theta)$. It is not necessary to have $p(\theta)$ normalized to unit area, which is useful in Bayesian statistics, as posterior probability densities are often determined only up to an unknown normalization constant.

To generate points that follow $p(\theta)$, one first needs a proposal p.d.f. $q(\theta; \theta_0)$, which can be (almost) any p.d.f. from which independent random values θ can be generated, and which contains as a parameter another point in the same space θ_0 . For example, a multivariate Gaussian centered about θ_0 can be used. Beginning at an arbitrary starting point θ_0 , the Hastings algorithm iterates the following steps:

1. Generate a value θ using the proposal density $q(\theta; \theta_0)$;
2. Form the Hastings test ratio, $\alpha = \min\left[1, \frac{p(\theta)q(\theta_0; \theta)}{p(\theta_0)q(\theta; \theta_0)}\right]$;
3. Generate a value u uniformly distributed in $[0, 1]$;
4. If $u \leq \alpha$, take $\theta_1 = \theta$. Otherwise, repeat the old point, i.e., $\theta_1 = \theta_0$.
5. Set $\theta_0 = \theta_1$ and return to step 1.

If one takes the proposal density to be symmetric in θ and θ_0 , then this is the *Metropolis-Hastings* algorithm, and the test ratio becomes $\alpha = \min[1, p(\theta)/p(\theta_0)]$. That is, if the proposed θ is at a value of probability higher than θ_0 , the step is taken. If the proposed step is rejected, the old point is repeated.

Methods for assessing and optimizing the performance of the algorithm are discussed in, e.g., Refs. [18–20]. One can, for example, examine the autocorrelation as a function of the lag k , i.e., the correlation of a sampled point with that k steps removed. This should decrease as quickly as possible for increasing k .

Generally one chooses the proposal density so as to optimize some quality measure such as the autocorrelation. For certain problems it has been shown that one achieves optimal performance

when the acceptance fraction, that is, the fraction of points with $u \leq \alpha$, is around 40%. This can be adjusted by varying the width of the proposal density. For example, one can use for the proposal p.d.f. a multivariate Gaussian with the same covariance matrix as that of the target p.d.f., but scaled by a constant.

41.6 Generative Adversarial Networks

Recent developments in Machine Learning have led to new types of Monte Carlo methods based on generative models. The goal is to generate events each consisting of a vector of quantities \mathbf{x} , which could represent the set of pixels in an image or energy deposits in the cells of a calorimeter. Suppose, however, that we do not have direct access to the underlying probability density $f(\mathbf{x})$, but rather we only have an implicit model (e.g., a computer program able to simulate the complexities of the physical system), which can provide a set of events usable as training data. In the case of a calorimeter, for example, this could represent real events from a control measurement or simply the output from a detailed simulation.

Generative models such as Variational Autoencoders (VAEs) [22, 23] and Generative Adversarial Networks (GANs) [24] are algorithms for generating events that mimic the training data. Recently GANs have been investigated in HEP for simulation of energy deposits in calorimeters, so far in a simplified setting. They are able to generate events that capture detailed properties of those from a detailed Monte Carlo simulation but require far less computing time (for a recent example see, e.g., Ref. [25]).

Here we sketch the main ideas behind GANs used to simulate a random vector \mathbf{x} . This follows some distribution $f(\mathbf{x})$ which itself is not known, but we have a set of instances (events) $\mathbf{x}_1, \dots, \mathbf{x}_N$ as training data, here regarded as representative of the true distribution. We seek a function (the generator) $G(\mathbf{z})$ which takes as input a vector of random numbers \mathbf{z} and produces directly as output an event vector, i.e., $\mathbf{x} = G(\mathbf{z})$. The method is in this sense similar to the transformation method described in 41.2, but here both the function G and the input of random values \mathbf{z} are multidimensional. As a prototypical example we can take the components of \mathbf{z} as independent and Gaussian distributed about zero with unit variance.

The GAN makes use of two functions, the generator $G(\mathbf{z})$ and a discriminator $D(\mathbf{x})$. The generator tries to produce events \mathbf{x} that mimic the (real) training data and thus look as if they were sampled from the unknown distribution $f(\mathbf{x})$. Simultaneously, the discriminator is trained to do its best to distinguish the generated events from the real ones.

To find the function $G(\mathbf{z})$ that generates events that are as similar as possible to the training data, one may use a Deep Neural Network (DNN), i.e., a neural network with a sufficiently large number of hidden layers, and thus having a large set of parameters θ_g . This is needed so that network is capable of modelling accurately the potentially complex density $f(\mathbf{x})$. The input layer corresponds to the components of the random vector \mathbf{z} and the multidimensional output layer to \mathbf{x} . The goal is thus reduced to finding optimal values of the parameters θ_g using the training data.

The discriminator function $D(\mathbf{x}; \theta_d)$ can also be a DNN containing parameters θ_d . It takes as input an event (an instance in \mathbf{x} -space) and provides a single scalar output in $[0, 1]$, which should be as close as possible to zero for generated and one for real events.

The parameters of the generator and discriminator are chosen such that the function

$$V(\theta_g, \theta_d) = E_{\mathbf{x}}[\log(D(\mathbf{x}; \theta_d))] + E_{\mathbf{z}}[\log(1 - D(G(\mathbf{z}; \theta_g); \theta_d))] \quad (41.10)$$

is minimized with respect to θ_g and simultaneously maximized with respect to θ_d . For the expectation value in the first term, \mathbf{x} is sampled from the (real) training data; for the second term \mathbf{z} follows its given distribution, e.g., a multivariate standard Gaussian. That is, the discriminator is adjusted to maximize the probability that it will correctly identify an event as real or generated, and simultaneously the generator is tuned such that it produces

events which appear as real as possible when evaluated by the discriminator.

Challenges with GANs such as difficulty training the networks are an active area of research in Machine Learning. Once an optimal set of parameters is found, the transformation $\mathbf{x} = G(\mathbf{z}; \theta_g)$ can be used to generate events in \mathbf{x} -space that capture detailed properties of the training data. Further information on applications, network architecture and training procedures can be found in, e.g., Ref. [25] and references therein.

References

- [1] F. James, *Comput. Phys. Commun.* **60**, 329 (1990).
- [2] P. L'Ecuyer, *Proc. 1997 Winter Simulation Conference*, IEEE Press, Dec. 1997, 127–134.
- [3] L. Lonnblad, *Comput. Phys. Commun.* **84**, 307 (1994).
- [4] R. Brun and F. Rademakers, *Nucl. Instrum. Meth.* **A389**, 81 (1997); See also `root.cern.ch`.
- [5] F. James, *Comput. Phys. Commun.* **79**, 111 (1994), [Erratum: *Comput. Phys. Commun.* 97,357(1996)]; M. Luscher, *Comput. Phys. Commun.* **79**, 100 (1994), [hep-lat/9309020].
- [6] P. L'Ecuyer, *Mathematics of Computation*, **65**, 213 (1996) and **65**, 225 (1999).
- [7] M. Matsumoto and T. Nishimura, *ACM Transactions on Modeling and Computer Simulation*, Vol. 8, No. 1, January 1998, 3–30.
- [8] Much of DIEHARD is described in: G. Marsaglia, *A Current View of Random Number Generators*, keynote address, *Computer Science and Statistics: 16th Symposium on the Interface*, Elsevier (1985).
- [9] P. L'Ecuyer and R. Simard, *ACM Transactions on Mathematical Software* 33, 4, Article 1, December 2007.
- [10] J. Heinrich, CDF Note CDF/MEMO/STATISTICS/PUBLIC/8032, 2006.
- [11] UNU.RAN is described at `statmath.wu.ac.at/software/unuran`; See also W. Hörmann, J. Leydold, and G. Derflinger, *Automatic Nonuniform Random Variate Generation*, (Springer, New York, 2004).
- [12] W.H. Press *et al.*, *Numerical Recipes*, 3rd edition, (Cambridge University Press, New York, 2007).
- [13] J.H. Ahrens and U. Dieter, *Computing* **12**, 223 (1974).
- [14] R.Y. Rubinstein, *Simulation and the Monte Carlo Method*, (John Wiley and Sons, Inc., New York, 1981).
- [15] L. Devroye, *Non-Uniform Random Variate Generation*, (Springer-Verlag, New York, 1986); Available online at `luc.devroye.org/rnbookindex.html`.
- [16] C. Walck, *Handbook on Statistical Distributions for Experimentalists*, University of Stockholm Report SUF-PFY/96-01, available from `www.fysik.su.se/~walck`.
- [17] J.E. Gentle, *Random Number Generation and Monte Carlo Methods*, 2nd ed., (Springer, New York, 2003).
- [18] C.P. Robert and G. Casella, *Monte Carlo Statistical Methods*, 2nd ed., (Springer, New York, 2004).
- [19] J.S. Liu, *Monte Carlo Strategies in Scientific Computing*, (Springer, New York, 2001).
- [20] R.M. Neal, *Probabilistic Inference Using Markov Chain Monte Carlo Methods*, Technical Report CRG-TR-93-1, Dept. of Computer Science, University of Toronto, available from `www.cs.toronto.edu/~radford/res-mcmc.html`.
- [21] A. Caldwell, D. Kollar, K. Kröninger, *Comput. Phys. Commun.* **180** (2009) pages 2197-2209.
- [22] D.P. Kingma and M. Welling, *Auto-Encoding Variational Bayes*, Int. Conf. on Learning Representations, ICLR, 2014; E-print: arXiv:1312.6114 [stat.ML].
- [23] D.J. Rezende, S. Mohamed and D. Wierstra, *Stochastic Backpropagation and Approximate Inference in Deep Generative Models*, Proc. 31st Int. Conf. on Machine Learning, Beijing, 2014. JMLR: W&CP vol. 32; E-print: arXiv:1401.4082 [stat.ML].
- [24] I.J. Goodfellow *et al.*, *Generative Adversarial Nets*, Proceedings of Advances in Neural Information Processing Systems 27 (Z. Ghahramani *et al.*, eds., NIPS 2014) pages 2672–2680; E-print: arXiv:1406.2661 [stat.ML].
- [25] M. Paganini, L. de Oliveira and B. Nachman, *Phys. Rev. Lett.* **120**, 4, 042003 (2018), [arXiv:1705.02355].

42. Monte Carlo Event Generators

Revised September 2017 by P. Nason (INFN, Milan) and P.Z. Skands (Monash University).

General-purpose Monte Carlo (GPMC) generators like HERWIG [1,2,3], PYTHIA [4,5], and SHERPA [6], provide detailed simulations of high-energy collisions. They play an essential role in QCD modeling (in particular for aspects beyond fixed-order perturbative QCD) and in data analysis and the planning of new experiments, where they are used together with detector simulation to estimate signals and backgrounds in high-energy processes. They are built from several components, that describe the physics starting from very short distance scales, up to the typical scale of hadron formation and decay. Since QCD is weakly interacting at short distances (below a femtometer), the components of the GPMC dealing with short-distance physics are based upon perturbation theory. At larger distances, all soft hadronic phenomena, like hadronization and the formation of the underlying event in hadron collisions, cannot be computed from first principles at present, and one must rely upon QCD-inspired models.

The purpose of this review is to illustrate the main components of these generators. It is divided into four sections. The first one deals with short-distance, perturbative phenomena. The basic concepts leading to the simulations of the dominant QCD processes are illustrated here. In the second section, the nonperturbative transition from partons to hadrons (“hadronization”) is treated. The two most popular hadronization models, the string and cluster models, are illustrated. The basics of the implementation of decay chains of unstable “primary” hadrons into stable “secondaries” is also illustrated here. In the third section, models for soft hadron physics are discussed. These include models for the underlying event and for minimum-bias interactions. Issues of Bose-Einstein and color-reconnection effects are also discussed here. The fourth section briefly introduces the challenges of MC uncertainty estimates and tuning.

We use natural units throughout, such that $c = 1$ and $\hbar = 1$, with energy, momenta and masses measured in GeV, and time and distances measured in GeV^{-1} .

42.1. Short-distance physics in GPMC generators

The short-distance components of a GPMC generator deal with the computation of the primary process at hand, with decays of short-lived particles, and with the generation of QCD and QED radiation. QCD radiation is computable in perturbation theory as long as the time scales involved are well below $1/\Lambda$, where Λ is a typical hadronic scale of few hundred MeV. Because of the presence of logarithmic enhancements due to both collinear and soft emissions, this description involves an indefinite number of final-state particles that are emitted at time scales below $1/\Lambda$. In e^+e^- annihilation into hadrons, for example, the time scale of the primary process is of the order of the inverse of the annihilation energy Q . Collinear and soft emissions take place at all time scales between $1/Q$ and $1/\Lambda$. Technically, the computation of the dominant collinear and soft radiation is carried out by the so called shower algorithms. Historically, such algorithms were first developed for resummation of collinear singularities, leading to the so called “Parton Shower” algorithms. We will briefly describe this approach in this section. We stress, however, that many modern generators adopt approaches that focus initially upon soft singularities, leading to the so called “Dipole Showers” discussed in Sec. 42.1.3.

Collinear singularities arise when the angle between two emitted light partons becomes small. For example, in a process in which a quark and a gluon are emitted, if the angle θ among them is very small (and is smaller than the angles among all other pairs of light partons in the process) the squared amplitude factorizes as follows

$$|M_{qg}|^2 d\Phi_{qg} \approx |M_q|^2 d\Phi_q \frac{\alpha_s}{2\pi} P_{q,gg}(z) dz \frac{d\phi}{2\pi} \frac{d\theta^2}{\theta^2} \quad (42.1)$$

where M_{qg} , $d\Phi_{qg}$ are the amplitude and phase space when both the gluon and the quark are emitted; M_q , $d\Phi_q$ are the amplitude and phase space when only the quark is emitted; $z = E_q/(E_q + E_g)$ is the fraction of energy carried by the quark; ϕ is the azimuth of the splitting plane, and $P_{q,gg}(z) = C_F(1+z^2)/(1-z)$ is the Altarelli-Parisi

splitting kernel for gluon emission from a quark line, with color factor $C_F = 4/3$. The factorized form of Eq. (42.1) is due to the fact that for small angle the process is dominated by a single amplitude in which the splitting quark is almost on shell and hence propagates for long distances. We define the energy scale corresponding to the inverse of this distance as the *hardness* of the splitting process, so that larger hardness corresponds to shorter distance. We can define the hardness t as the product $E^2\theta^2$, or as the virtuality of the splitting parton p^2 , or as a measure of the relative transverse momentum in the splitting such as the k_t of an emitted parton relative to its parent, defined by $p^2 = 2E^2z(1-z)(1-\cos\theta) \approx z(1-z)E^2\theta^2$, $k_T^2 = z^2(1-z)^2E^2\theta^2$. (42.2)

If the region of small values of z and $1-z$ was not important, these definitions would be equivalent. In QCD we also have soft divergences, arising when soft gluons are emitted. In Eq. (42.1) they appear as $z \rightarrow 1$, because of the $1/(1-z)$ singularity of $P_{q,gg}(z)$. Thus, we expect that the choice of the appropriate ordering variable will be relevant when dealing with soft divergences (see Sec. 42.3). The $d\theta^2/\theta^2$ factor in Eq. (42.1) can be equivalently written in terms of the hardness dt/t . After integration it gives rise to a logarithmic factor $\log(Q^2/\Lambda^2)$. We can have many subsequent splittings, that we can describe by applying Eq. (42.1) recursively, as long as the splittings are strongly ordered in decreasing hardness. This means that, from a typical final-state configuration, by clustering together final-state parton pairs with the smallest hardness recursively, we can reconstruct a branching tree, that may be viewed as the splitting history of the event. We stress that all hardness values between the hardness of the primary process and the cutoff scale Λ are equally involved here. The collinear approximation is applied recursively to splitting processes that have much smaller hardness with respect to all previous ones.

By integrating over the phase space, a process with n collinear splittings will be of order $(\alpha_s(Q^2) \log(Q^2/\Lambda^2))^n$ with respect to the primary process. Since $\alpha_s(Q^2) \propto 1/\log(Q^2/\Lambda^2)$ [7], these corrections are not small. The so-called KLN theorem [8,9] guarantees that large logarithmic enhancements arising from final-state collinear splitting cancel against the virtual corrections in inclusive cross sections, order by order in perturbation theory. Furthermore, the factorization theorem guarantees that initial-state collinear singularities can be factorized into the parton density functions (PDFs) [7]. Therefore, the cross section for the basic process remains accurate up to corrections of higher orders in $\alpha_s(Q)$, provided it is interpreted as an inclusive cross section, rather than as a bare partonic cross section. For example, the leading order (LO) cross section for $e^+e^- \rightarrow q\bar{q}$ is a good LO estimate of the e^+e^- cross section for the production of a pair of quarks accompanied by an arbitrary number of collinear and soft gluons, but is not a good estimate of the cross section for the production of a $q\bar{q}$ pair with no extra radiation. In summary, perturbation theory at fixed order can yield increasingly accurate predictions for inclusive observables, but cannot be used to describe the indefinite sequence of collinear and soft radiations that accompany the hard partons.

Parton-Shower algorithms are used to compute the cross section for generic hard processes including all dominant collinear radiation. These algorithms begin with the generation of the kinematics of the basic process, performed with a probability proportional to its LO partonic cross section. This is interpreted physically as the inclusive cross section for the basic process, followed by an arbitrary sequence of shower splittings. The algorithm then assigns a probability to each splitting sequence, so that the initial LO cross section is partitioned into the cross sections for a multitude of final states of arbitrary multiplicity, with their sum equal to the cross section of the primary process. This property of the GPMCs reflects the KLN cancellation mentioned earlier, and it is often called “unitarity of the shower process”, a name that reminds us that the KLN cancellation itself is a consequence of unitarity. The fact that a quantum mechanical process can be described in terms of composition of probabilities, rather than amplitudes, follows from the collinear approximation. In fact, because of strong ordering, a radiated parton cannot be collinear to more than one parton in the amplitude, and this suppresses interference effects.

We now illustrate the basic parton-shower algorithm, as first introduced in Ref. 11. (For more pedagogical introductions see Ref. 18

and references therein.) For simplicity, we consider the example of e^+e^- annihilation into $q\bar{q}$ pairs, where we only have to deal with final state radiation (FSR). We consider all final states that can be built by dressing the q and \bar{q} partons with an indefinite number of splitting processes. By recursively clustering together final state parton pairs with the smallest relative hardness, from each final state configuration we can construct two trees rooted at the q and \bar{q} partons. The momenta of all intermediate lines of the tree diagrams are then uniquely determined from the final-state momenta. Hardnesses in the trees are ordered. One assigns to each splitting vertex the hardness t , the energy fractions z and $1-z$ of the two generated partons, and the azimuth ϕ of the splitting process with respect to the momentum of the incoming parton. For definiteness, we assume that z and ϕ are defined in the center-of-mass (CM) frame of the e^+e^- collision. The differential cross section for a given final state is given by the product of the differential cross section for the initial $e^+e^- \rightarrow q\bar{q}$ process, multiplied by a factor

$$\Delta_i(t_m, t_n) \frac{\alpha_S(t)}{2\pi} P_{i,jk}(z) \frac{dt_m}{t_m} dz \frac{d\phi}{2\pi} \quad (42.3)$$

for each intermediate line arising from the n^{th} and ending in the m^{th} splitting vertex. $\Delta(t_m, t_n)$ is the so-called Sudakov form factor

$$\Delta_i(t_m, t_n) = \exp \left[- \int_{t_m}^{t_n} \frac{dq^2}{q^2} \frac{\alpha_S(q^2)}{2\pi} \sum_{jk} P_{i,jk}(z) dz \frac{d\phi}{2\pi} \right]. \quad (42.4)$$

The suffixes i and jk represent the parton species of the incoming and final partons, respectively, and $P_{i,jk}(z)$ are the Altarelli-Parisi [12] splitting kernels. Notice that the endpoints on the z integration depend upon the definition of hardness. For example, in case of virtuality or transverse momentum ordering, the z integration is automatically cut-off near the extremes, see eq. (1.2). When this is not the case (as, for example, for angular ordering) an explicit cut-off on z must be introduced, corresponding to the requirement that an emission must have some minimum energy to be distinguishable from no emission. For lines originating at the primary vertex, the scale t_n is replaced by the typical scale of the primary process and for lines ending without any further splitting the scale t_m is replaced by t_0 , an infrared cutoff defined by the shower hadronization scale (at which the charges are screened by hadronization) or, for an unstable particle, its width (a source cannot emit radiation with a period exceeding its lifetime).

Eq. (42.3) can be obtained by iterating formula Eq. (42.1) recursively, with two important corrections: a) the strong coupling is evaluated at a scale corresponding to the hardness of the splitting process; b) the presence of the Sudakov form factor. Both these modifications arise from the inclusion of all collinear-dominant virtual corrections.

Notice that the Sudakov form factor for a small hardness interval $\Delta_i(t, t + \delta t)$ is equal to one minus the integrated emission probability of Eq. (42.3), i.e. it can be interpreted as the probability of no emission in the interval $t, t + \delta t$. From this, it immediately follows that $\Delta_i(t_m, t_n)$ can be interpreted as the no-emission probability in the full t_m, t_n interval. This interpretation allows to formulate the shower process as a probabilistic algorithm. We first notice that $0 < \Delta_i(t_m, t_n) \leq 1$, where the upper extreme is reached for $t_m = t_n$, and the lower extreme is approached for $t_m = t_0$. Starting from each of the partons in the primary process (e.g., $e^+e^- \rightarrow q\bar{q}$), event generation then proceeds recursively as follows. Given a parton exiting a vertex with hardness t_n , (taken to be of order the annihilation scale Q^2 for the first branching) one seeks a solution of the equation $r = \Delta_i(t_m, t_n)$, with $r \in [0, 1]$ a uniform random number, and solves it for the hardness of the next branching t_m . If $t_m \leq t_0$, no splitting is generated and the line is interpreted as a final parton. If $t_m > t_0$, a branching is generated at the scale t_m . Its z value and the final parton species jk are generated with a probability proportional to $P_{i,jk}(z)$. The azimuth is generated uniformly, neglecting angular correlations (see Sec. 42.1.1). This procedure is started with each of the primary process partons, and is applied recursively to all generated partons. It

may generate an arbitrary number of partons, and it stops when no final-state partons undergo further splitting.

The four-momenta of the final-state partons are reconstructed from the momenta of the initial ones, and from the whole sequence of splitting variables, subject to overall momentum conservation. Different algorithms employ different strategies to treat recoil effects due to momentum conservation, which may be applied either locally for each splitting, or globally for the entire set of partons (a procedure called *momentum reshuffling*.) This has a subleading effect with respect to the collinear approximation.

We emphasize that the shower cross sections described above can be derived from perturbative QCD by keeping only the collinear-dominant real and virtual contributions to the cross section. As such it is unproductive for large-angle radiation. It is thus unsafe to rely upon Parton Shower Monte Carlo alone to compute backgrounds to new physics signals that are characterized by several widely separated jets.

A Shower Monte Carlo builds its final state as if it developed from an iterative process, often with each intermediate stage made available to the user. It should be remarked that the meaning of these intermediate stages is only relevant within the approximation adopted by the generator, and could also differ in different implementations.

42.1.1. Angular correlations :

In gluon-splitting processes ($g \rightarrow q\bar{q}$, $g \rightarrow gg$) in the collinear approximation, the distribution of the split pair is not uniform in azimuth, and the Altarelli-Parisi splitting functions are recovered only after azimuthal averaging. This dependence is due to the interference of positive and negative helicity states for the gluon that undergoes splitting. Spin correlations propagate through the splitting process, and determine acasual correlations of the EPR kind [13]. A method to partially account for these effects was introduced in Ref. 14, in which the azimuthal correlation between two successive splittings is computed by averaging over polarizations. This can then be applied at each branching step. Acasual correlations are argued to be small, and are discarded with this method, that is still used in PYTHIA [4]. A method that fully includes spin correlation effects was later proposed [15], and has been implemented in HERWIG [16,3].

42.1.2. Initial-state radiation :

Initial-state radiation (ISR) arises because incoming particles may undergo collinear radiation before entering the hard-scattering process. In doing so, they acquire a non-vanishing transverse momentum, and their virtuality becomes negative (spacelike). It turns out to be convenient to develop the ISR shower starting with the highest hardness (i.e. with the hard process) and ending with the smallest (i.e. with the incoming parton in the hadron). Unlike the case of FSR, however, hardness ordering is opposite to time ordering in the ISR case. A corresponding backwards-evolution algorithm was formulated by Sjöstrand [17], and was basically adopted in all shower models. It can be illustrated by considering a primary interaction initiated by a quark where no collinear emission of hardness $\geq t$ have taken place, and the same process where the quark also emits a collinear gluon of hardness t . The respective cross sections are proportional to

$$|M_q(x)|^2 dx f_q(x, t), \text{ and } |M_q(x)|^2 dx \frac{\alpha_S(t)}{2\pi} f_q(x/z, t) P_{q,gg}(z) dz \frac{d\phi}{2\pi} \frac{dt}{t}. \quad (42.5)$$

Here f_q is the quark PDF in the incoming hadron, x is the fraction of momentum of the incoming quark that enters the basic process, while x/z is the fraction of momentum of the incoming quark *before* it emits the collinear gluon. The elementary *emission probability* is the ratio of the second over the first expression in Eq. (42.5). In analogy with the final state radiation case, this ratio will appear in the exponent of the Sudakov form factor, that (after the inclusion of all splitting subprocesses) is given by

$$\Delta_i^{\text{ISR}}(t, t') = \exp \left[- \int_{t'}^t \frac{dt''}{t''} \frac{\alpha_S(t'')}{2\pi} \int_x^1 \frac{dz}{z} \sum_{jk} P_{j,ik}(z) \frac{f_j(t'', x/z)}{f_i(t'', x)} \right]. \quad (42.6)$$

Notice that there are two uses of the PDFs: they are used to compute the cross section for the basic hard process, and they control

ISR via backward evolution. Since the evolution is generated with leading-logarithmic accuracy, it is acceptable to use two different PDF sets for these two tasks, provided they agree at the LO level.

In the context of GPMC evolution, each ISR emission generates a finite amount of transverse momentum. Details on how the recoils generated by these transverse “kicks” are distributed among other partons in the event, in particular the ones involved in the hard process, constitute one of the main areas of difference between existing algorithms, see Ref. 18. An additional $\mathcal{O}(1 \text{ GeV})$ of “primordial k_T ” is typically added, to represent the sum of unresolved and/or non-perturbative motion below the shower cutoff scale.

42.1.3. Soft emissions and QCD coherence :

Soft singularities arise in QCD due to the real or virtual emission of soft gluons. For example, the cross section for the emission of a soft gluon in e^+e^- annihilation into hadrons is given by

$$\begin{aligned} d\sigma_{q\bar{q}g} &\approx d\sigma_{q\bar{q}} \frac{4}{3} (4\pi\alpha_s) \left[\frac{2 p_q \cdot p_{\bar{q}}}{p_q \cdot l p_{\bar{q}} \cdot l} \right] \frac{d^3l}{2l^0(2\pi)^3} \\ &= d\sigma_{q\bar{q}} \frac{\alpha_s}{2\pi} \frac{4}{3} \frac{d\phi}{l^0} \frac{d\cos\theta}{2\pi} \frac{1}{1-\cos^2\theta}, \end{aligned} \quad (42.7)$$

where p_q , $p_{\bar{q}}$ and l are the quark, antiquark and gluon momentum, and θ and ϕ are the polar and azimuthal angle of the gluon momentum with respect to the quark direction. Since the gluon is soft, we may assume that p_q and $p_{\bar{q}}$ are unaffected by the gluon emission. The soft singularity is manifest in the $d\phi^0/l^0$ factor. Notice that also collinear singularities are present at the same time when $\theta \rightarrow 0$ and $\theta \rightarrow \pi$, corresponding to the gluon becoming collinear to either the quark or the antiquark. It is easy to check that in the collinear limits Eq. (42.7) becomes equivalent to Eq. (42.1) with $P_{q,gg}(z) = (4/3)2/(1-z)$, i.e. the limiting form of $P_{q,gg}(z)$ when z approaches 1. Thus, soft singularities coexist with collinear ones, so that two potentially large logarithms can arise simultaneously due to gluon emission.

Unlike the case of collinear emission, soft emission is not tied to a single emitting particle. The amplitude for the emission of a soft gluon from an external (incoming or outgoing) line with momentum p is proportional to $p \cdot \epsilon/p \cdot l$. When squaring the amplitude, products like the one appearing in the square bracket of Eq. (42.1) arise for all pairs of external particles, with the product of a single emission amplitude with itself appearing only if $p^2 > 0$, i.e. for massive coloured particles. Thus interference plays here a crucial role. This is unlike the case of collinear singularities, where because of strong ordering a radiated parton cannot be collinear to more than one other parton.

It was shown in a set of publications (see Ref. 19) that, within the conventional parton-shower formalism based on collinear factorization, the region of collinear and soft emissions can be correctly described by using the angle of the emissions as the ordering variable, rather than the virtuality, and by setting the argument of α_s at the splitting vertex equal to the relative parton transverse momentum after the splitting. Physically, the ordering in angle approximates the coherent interference arising from large-angle soft emission from a bunch of collinear partons. Without this effect, the particle multiplicity would grow too rapidly with energy, in conflict with e^+e^- data. For this reason, angular ordering is used as the default evolution variable in all versions of HERWIG (see Ref. 20). To partially account for soft interference effects, an angular veto is imposed on the virtuality-ordered evolution in PYTHIA 6 [21].

A radical alternative formulation of QCD cascades first proposed in Ref. 22 focuses upon soft emission, rather than collinear emission, as the basic splitting mechanism. It then becomes natural to consider a branching process where it is a parton pair (i.e. a dipole) rather than a single parton, that emits a soft parton. Adding a suitable correction for non-soft, collinear partons, one can simultaneously achieve the correct logarithmic structure for both the collinear and soft emissions in the so called leading color approximation, i.e. when terms suppressed by a power of the number of colors are neglected. The ARIADNE [23] and VINCIA [25] programs are based on this approach. Dipole-type showers [26] are also used by default in SHERPA [27] and exist as an option in HERWIG [28]. An alternative dipole-based model is available in PYTHIA and SHERPA via the DIRE [29]

plugin. The p_{\perp} -ordered showers in PYTHIA 6 and 8 represent a hybrid, combining collinear splitting kernels with dipole kinematics [30].

42.1.4. Resummation :

It is notoriously difficult to assess the accuracy of shower Monte Carlos in comparison with QCD resummation calculations [7]. The latter start from the definition of a specific infrared-safe observable, which develops towers of large logarithms in certain regions of phase space. A dedicated resummation calculation must in general be performed for each new observable. The predictions of shower MCs, on the other hand, are cast in terms of complete sets of final-state momenta, on which one can evaluate any observable; i.e., the shower algorithm itself is normally independent of the specific observable(s) under study.

Generally, shower MCs perform much better than strict LL resummations; this is related to their inclusion of several universal but formally subleading aspects. But there are no guarantees. A shower MC may do well for some specific observables, and not for others. At present, it is difficult to make more precise and general statements than that. Instead, it is common to specify what kind of corrections are included. Typically, collinear emissions are accounted for, although not always including angular correlations. Soft emissions are dealt with to some extent via angular ordering or dipole approaches. The most important and ubiquitous aspects beyond the strict LL approximation are momentum conservation and optimised scale choices. The former is obviously physical, hence including it should yield better results than not doing so (indeed, momentum conservation does become an aspect of QCD resummation calculations beyond LL), although the precise way of how the resulting recoil effects are handled in the shower is ambiguous. The latter can be tied, e.g., to reaching NLL accuracy for soft emissions for observables such as the transverse momentum of Drell-Yan pairs [101].

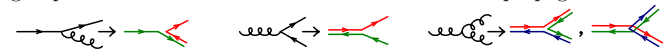
42.1.5. Massive quarks :

Quark masses act as a cut-off on collinear singularities. If the mass of a quark is below, or of the order of Λ , its effect in the shower is small. For larger quark masses, like in c , b , or t production, it is the mass, rather than the typical hadronic scale, that cuts off collinear radiation. For a quark with energy E and mass m_Q , the divergent behavior $d\theta/\theta$ of the collinear splitting process is regulated for $\theta \leq \theta_0 = m_Q/E$. We thus expect less collinear activity for heavy quarks than for light ones, which in turn is the reason why heavy quarks carry a larger fraction of the momentum acquired in the hard production process.

This feature can be implemented with different levels of sophistication. Using the fact that soft emission exhibits a zero at zero emission angle, older parton shower algorithms simply limited the shower emission to be not smaller than the angle θ_0 . More modern approaches are used in both PYTHIA, where mass effects are included using a kind of matrix-element correction method [31], and in HERWIG++ and SHERPA, where a generalization of the Altarelli-Parisi splitting kernel is used for massive quarks [32].

42.1.6. Color information :

In event generators, quarks and antiquarks are represented by color lines, with arrows indicating the direction of color flow. In the limit of infinitely many colors (called the leading color approximation), each such line can be associated with a unique label; the probability for two quarks (or antiquarks) to have the same color (anticolor) vanishes. Moreover, in the same limit gluons can be represented by a pair of color lines with opposite arrows, as can be realised e.g. from the SU(3) group relation $8 = 3 \otimes \bar{3} \ominus 1$. The rules for color propagation are:



During the shower development, partons are connected by color lines. We can have a quark directly connected by a color line to an antiquark, or via an arbitrary number of intermediate gluons, as shown in Fig. 42.1. It is also possible for a set of gluons to be connected cyclically in color, as e.g. in the decay $\Upsilon \rightarrow ggg$.

The color information is used in angular-ordered showers, where the angle of color-connected partons (i.e. partons connected by the same color line) determines the initial angle for the shower development, and in dipole showers, where dipoles are always color-connected partons. It is also used in hadronization models, where the initial strings or

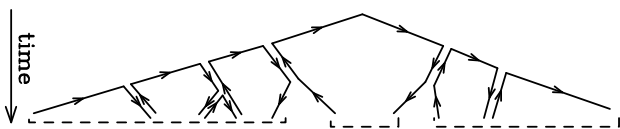


Figure 42.1: Color development of a shower in e^+e^- annihilation. Color-neutral clusters of partons are indicated by the dashed under-brackets.

clusters used for hadronization are formed by color-neutral clusters of partons.

42.1.7. Electromagnetic corrections :

The physics of photon emission from light charged particles can also be treated with a shower MC algorithm. High-energy electrons and quarks, for example, are accompanied by bremsstrahlung photons. Also here, similarly to the QCD case, electromagnetic corrections are of order $\alpha_{\text{em}} \ln(Q/m)$, where m is the mass of the radiating particle, or even of order $\alpha_{\text{em}} \ln(Q/m) \ln(E_\gamma/E)$ in the region where soft photon emission is important, so that, especially for the case of electrons, their inclusion in the simulation process is mandatory. This is done in most of the GPMC's (for a recent comparative study see [33]). The specialized generator PHOTOS [34] is sometimes used as an afterburner for an improved treatment of QED radiation in non-hadronic resonance decays.

For photon emissions off leptons, the shower can be continued down to virtualities arbitrarily close to the lepton mass shell (unlike the case in QCD). In practice, an infrared cutoff is still required for the shower algorithm to terminate. Therefore, there is always an energy cut-off for emitted photons that depends upon the implementations [33]. In the case of electrons, this energy is typically of the order of its mass. Electromagnetic radiation below this scale is not enhanced by collinear singularities, and is thus bound to be soft, so that the electron momentum is not affected by it.

For photons emitted from quarks, we have instead the obvious limitation that the photon wavelength cannot exceed the typical hadronic size. Longer-wavelength photons are in fact emitted by hadrons, rather than quarks. This last effect is in practice never modeled by existing shower MC implementations. Thus, electromagnetic radiation from quarks is cut off at a typical hadronic scale. Finally, hadron (and τ) decays involving charged particles can produce additional soft bremsstrahlung. This is implemented in a general way in HERWIG++/HERWIG 7 [35] and SHERPA [36].

42.1.8. Beyond-the-Standard-Model Physics :

The inclusion of processes for physics beyond the Standard Model (BSM) in event generators is to some extent only a matter of implementing the relevant hard processes and (chains of) decays, with the level of difficulty depending on the complexity of the model and the degree of automation [37,38]. Notable exceptions are long-lived colored particles [39], particles in exotic color representations, and particles showering under new gauge symmetries, with a growing set of implementations documented in the individual GPMC manuals. Further complications that may be relevant are finite-width effects (discussed in Sec. 42.1.9) and the assumed threshold behavior.

In addition to code-specific implementations [18], there are a few commonly adopted standards that are useful for transferring information and events between codes. Currently, the most important of these is the Les Houches Event File (LHEF) standard [40], normally used to transfer parton-level events from a hard-process generator to a shower generator. Another important standard is the Supersymmetry Les Houches Accord (SLHA) format [41], originally used to transfer information on supersymmetric particle spectra and couplings, but by now extended to apply also to more general BSM frameworks and incorporated within the LHEF standard [42].

42.1.9. Decay Chains and Particle Widths :

In most BSM processes and some SM ones, an important aspect of the event simulation is how decays of short-lived particles, such as top quarks, EW and Higgs bosons, and new BSM resonances, are

handled. We here briefly summarize the spectrum of possibilities, but emphasize that there is no universal standard. Users are advised to check whether the treatment of a given code is adequate for the physics study at hand.

The appearance of an unstable resonance as a physical particle at an intermediate stage of the event generation implies that its production and decay processes are treated as being factorized. This is valid up to corrections of order Γ/m_0 , with Γ the width and m_0 the pole mass. States whose widths are a substantial fraction of their mass should instead be treated as intrinsically off-shell internal propagator lines.

For states treated as physical particles, two aspects are relevant: the mass distribution of the decaying particle itself and the distributions of its decay products. For the former, matrix-element generators often use a simple δ function at m_0 . The next level up, typically used in GPMCs, is to use a Breit-Wigner distribution (relativistic or non-relativistic), which formally resums higher-order virtual corrections to the mass distribution. Note, however, that this still only generates an improved picture for moderate fluctuations away from m_0 . Similarly to above, particles that are significantly off-shell (in units of Γ) should not be treated as resonant, but rather as internal off-shell propagator lines. In most GPMCs, further refinements are included, for instance by letting Γ be a function of m (“running widths”) and by limiting the magnitude of the allowed fluctuations away from m_0 . We finally point out that recently NLO+PS generators have appeared that can deal with resonances including off-shell effects, non-resonance contributions and interference of radiation generated in resonance decay and production, see [24] and references therein.

For the distributions of the decay products, the simplest treatment is again to assign them their respective m_0 values, with a uniform phase-space distribution. A more sophisticated treatment distributes the decay products according to the differential decay matrix elements, capturing at least the internal dynamics and helicity structure of the decay process, including EPR-like correlations. Further refinements include polarizations of the external states [43] and assigning the decay products their own Breit-Wigner distributions, the latter of which opens the possibility to include also intrinsically off-shell decay channels, like $H \rightarrow WW^*$.

GPMC manuals often give instructions on how to include new decay modes, at varying levels of sophistication ranging from simple uniform phase-space sampling (which the user can reweight a posteriori) and step-function thresholds, to fully matrix-element weighted decay implementations including potential off-shell / threshold effects.

During subsequent showering of the decay products, most parton-shower models will preserve the total invariant mass of the decayed resonance, so as not to skew the original resonance shape. In the context of passing externally generated LHEF files [40] to a GPMC for showering, note that this is only possible if the intermediate resonances are present (with status code 2) in the LHEF event record [44].

42.1.10. Matching with Matrix Elements :

Shower algorithms are based upon a combination of the collinear (small-angle) and soft (small-energy) approximations and are thus normally inaccurate for hard, wide-angle emissions (i.e., additional well-resolved jets). They also contain only the leading singular pieces of next-to-leading order (NLO) and higher corrections to the basic process.

Traditional GPMCs, like HERWIG and PYTHIA, have included for a long time the so called Matrix Element Corrections (MEC), first formulated in Ref. 45 with later developments summarized in Ref. 18. They are typically available for $2 \rightarrow 1$ or $1 \rightarrow 2$ processes, like DIS, vector boson and Higgs production and decays, and top decays. The MEC corrects the emission of the hardest jet at large angles, so that it becomes exact at LO. A generalization of the method to multiple emissions was formulated recently [46].

Aside from MECs implemented directly in the GPMCs, the improvements on the parton-shower description of hard collisions have been made in two main directions: the so called Matrix Elements and Parton Shower matching (ME+PS from now on), and the matching of NLO calculations and Parton Showers (NLO+PS). We now discuss

each of these, and then briefly summarise techniques becoming available for combining them.

The ME+PS method allows one to use tree-level matrix elements for hard, large-angle emissions. It was first formulated in the so-called CKKW paper [47], and several variants have appeared, including the CKKW-L, MLM, and pseudoshower methods, see Refs. 48, 18 for summaries. So called “Truncated Showers” are required [49] to maintain color coherence when interfacing to angular-ordered parton showers, and care must be taken to use consistent α_S choices for the real (ME-driven) and virtual (PS-driven) corrections [50].

In the ME+PS method one typically starts by generating LO matrix elements for the production of the basic process plus a certain number $\leq n$ of other partons. A minimum separation is imposed on the produced partons, requiring, for example, that the relative transverse momentum in any pair of partons is above a given cut Q_{cut} . One then reweights these amplitudes in such a way that, in the strongly ordered region, the virtual effects that are included in the shower algorithm (i.e. running couplings and Sudakov form factors) are also accounted for. At this stage, before parton showers are added, the generated configurations are tree-level accurate at large angle, and at small angle they match the results of the shower algorithm, except that there are no emissions below the scale Q_{cut} , and no final states with more than n partons. These kinematic configurations are thus fed into a GPMC, that must generate all splittings with relative transverse momentum below the scale Q_{cut} , for initial events with less than n partons, or below the scale of the smallest pair transverse momentum, for events with n partons. The matching parameter Q_{cut} must be chosen to be large enough for fixed-order perturbation theory to hold, but small enough so that the shower is accurate for emissions below it. Notice that the accuracy achieved with MEC is equivalent to that of ME+PS with $n = 1$, where MEC has the advantage of not having a matching parameter Q_{cut} .

The popularity of the ME+PS method is due to the fact that processes with many jets appear often as backgrounds to new-physics searches. These jets are typically required to be well separated, and to have large transverse momenta. These kinematical configurations are exactly those for which pure shower algorithms are unreliable, hence it is mandatory to describe them using at least LO matrix elements.

Several ME+PS implementations use existing LO generators, like ALPGEN [51], MADGRAPH [52], and others summarized in Ref. 48, for the calculation of the matrix elements, and feed the partonic events to a GPMC like PYTHIA or HERWIG using the Les Houches Interface for User Processes (LHI/LHEF) [44,40]. SHERPA and HERWIG 7 also include their own matrix-element generators.

The NLO+PS methods promote the accuracy of the generation of the basic process from LO to NLO in QCD. They must thus include the radiation of one extra parton with tree-level accuracy, since this radiation constitutes a NLO correction to the basic process. They must also include NLO virtual corrections. They can be viewed as an extension of the MEC methods with the inclusion of NLO virtual corrections. They are however more general, since they are applicable to processes of arbitrary complexity. Two of these methods are now widely used: MC@NLO [53] and POWHEG [49,54], with several alternative methods now also being pursued, see Ref. 18 and references therein.

NLO+PS generators produce NLO accurate distributions for inclusive quantities, and generate the hardest jet with tree-level accuracy. It should be recalled, though, that in $2 \rightarrow 1$ processes like Z/W production, GPMCs including MEC and weighted by a constant K factor may perform nearly as well, and, if suitably tuned, may even yield a better description of data. In this context, note also that the optimal tuning of an NLO+PS generator may well be different from that of the pure PS.

Several NLO+PS processes are implemented in the MC@NLO program [53], together with the new AMC@NLO development [55], and in the POWHEG BOX framework [54]. HERWIG 7 supports now its own variants of POWHEG and MC@NLO for several processes. SHERPA instead implements a variant of the MC@NLO method.

For applications that require an accurate description of more than one hard, large-angle jet associated with the primary process, ME+PS schemes are still superior to NLO+PS ones. Ideally, one

would like to improve NLO generators in such a way that also the production of associated jets achieves NLO accuracy. The FFX [57], UNLOPS [58], MiNLO [59] and MEPS@NLO [60] methods address this problem. In turn, its solution is a prerequisite for the construction of NNLO+PS generators, that in fact have already appeared for the $gg \rightarrow H$ and Drell-Yan processes (see ref. [61] and references therein).

42.2. Hadronization Models

In the context of GPMCs, *hadronization* denotes the process by which a set of colored partons (*after* showering) is transformed into a set of “primary hadrons”, which may then subsequently decay further (to “secondary hadrons”). This non-perturbative transition takes place at the *hadronization scale* Q_{had} , which by construction is equal to the infrared cutoff of the parton shower. In the absence of a first-principles solution to the relevant dynamics, GPMCs use QCD-inspired phenomenological models to describe this transition.

An important result in “quenched” lattice QCD (see Chap. 17 of PDG book) is that the potential energy between two partons with opposite color charges grows linearly with their separation, at distances greater than about a femtometer. This is known as “linear confinement”, and it forms the starting point for the *string model of hadronization*, discussed below in Sec. 42.2.1. Alternatively, a property of perturbative QCD called “preconfinement” is the basis of the *cluster model of hadronization*, discussed in Sec. 42.2.2.

A key difference between MC hadronization models and the fragmentation-function (FF) formalism used to describe inclusive hadron spectra in perturbative QCD (see Chap. 9 and Chap. 19 of PDG book) is that FFs can be defined at an arbitrary perturbative scale Q while MC hadronization models are intrinsically defined at the scale Q_{had} . Direct comparisons are therefore only meaningful if the perturbative evolution between Q and Q_{had} is taken into account. FFs are calculable in pQCD, given a non-perturbative initial condition obtained by fits to hadron spectra. In the MC context, one can prove that the correct QCD evolution of the FFs arises from the shower formalism, with the hadronization model providing an explicit parameterization of the non-perturbative component. However, the MC modeling of shower and hadronization includes much more information on the final state since it is fully exclusive (i.e., it addresses all particles in the final state explicitly), while FFs only describe inclusive spectra. This exclusivity also enables MC models to make use of the color-flow information coming from the perturbative shower evolution (see Sec. 42.1.6) to determine between which partons confining potentials should arise. E.g., in the string picture, the nonperturbative limit of a QCD dipole is a string piece [62].

Given an exact hadronization model, its dependence on the scale Q_{had} should in principle be compensated by the corresponding scale dependence of the shower algorithm, which stops generating branchings at the scale Q_{had} . However, due to their complicated and fully exclusive nature, it is generally not possible to enforce this compensation automatically in MC models. One must therefore be aware that the nonperturbative model parameters must be “retuned” by hand if the infrared cutoff is modified. Any other changes to the perturbative part of the calculation, such as matching to further (fixed-order or resummed) coefficients, may also necessitate a retuning. Tuning is discussed briefly in Sec. 42.4.

Finally, it should be emphasized that the so-called “parton level” that can be obtained by switching off hadronization in a GPMC, is not a universal concept, since each model defines Q_{had} differently (e.g. via a cutoff in p_{\perp} , invariant mass, etc., with different tunes using different values for the cutoff). Comparisons to distributions at this level may therefore be used to provide an idea of the overall impact of hadronization corrections within a given model, but should be avoided in the context of physical observables.

42.2.1. The String Model :

Starting from early concepts [63], several hadronization models based on strings have been proposed [18]. Of these, the most widely used today is the so-called Lund model [64,65], implemented in PYTHIA [4,5]. We concentrate on that particular model here, though many of the overall concepts would be shared by any string-inspired method.

Consider a color-connected quark-antiquark pair emerging from the parton shower (like the $\bar{q}q$ pair in the center of Fig. 42.1). As the charges move apart, linear confinement implies that a potential $V(r) = \kappa r$ is reached for large distances r . (At short distances, there is a Coulomb term $\propto 1/r$ as well, but this is neglected in the Lund string.) This potential describes a string with tension $\kappa \sim 1 \text{ GeV/fm} \sim 0.2 \text{ GeV}^2$. The physical picture is that of a color flux tube being stretched between the q and the \bar{q} .

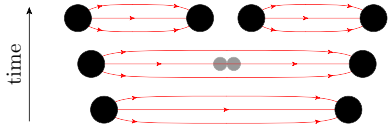


Figure 42.2: Illustration of string breaking by quark pair-creation in the string field.

As the string grows, the nonperturbative creation of quark-antiquark pairs can break the string, via the process illustrated in Fig. 42.2. The model is Lorentz invariant, so considerations involving boosted string systems are straightforward, involving the usual Lorentz effects. More complicated configurations involving intermediate gluons are treated by representing gluons as transverse “kinks”, illustrated in Fig. 42.3, and considerations involving boosted string systems are subject to the usual Lorentz effects. In the leading-color approximation, the order of these kinks follows directly from the color ordering produced by the parton shower, cf. the $\bar{q}gggq$ and $\bar{q}gq$ systems on the left and right part of Fig. 42.1. (Modifications to this order, by possible color reconnection/rearrangement effects, are discussed in Sec. 42.3.3.)

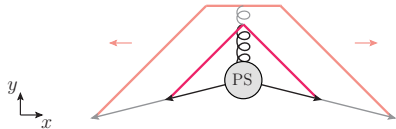


Figure 42.3: Schematic illustration of an $e^+e^- \rightarrow q\bar{q}$ configuration emerging from the parton shower (PS). Snapshots of string positions are shown at two different times (full and shaded lines respectively). The gluon forms a transverse kink which grows in the y direction until all the gluon’s kinetic energy has been used up.

Thus gluons effectively build up a transverse structure in the originally one-dimensional object, with infinitely soft ones smoothly absorbed into the string. Note: cyclic topologies made entirely of gluons (closed strings) are also possible, e.g. in decays such as $H \rightarrow gg$ or $\Upsilon \rightarrow ggg$. The space-time evolution is more involved when kinks are taken into account [65], but no additional free parameters need to be introduced. The main difference between quark and gluon hadronization stems from the fact that gluons are connected to two string pieces (one on either side), while quarks are only connected to a single string piece. Hence, the relative rate of energy loss per unit invariant time — and consequently also the rate of hadron production — is larger by a factor of 2 for gluons (similar to the ratio of color Casimirs $C_A/C_F = 2.25$).

To convert a set of partons to hadrons, the first step is thus to map color-connected pairs of partons to string pieces, with quarks as endpoints and gluons as kinks. Next, the strings evolve, with a constant probability density for string breaks to occur per unit string space-time area. In this context, it is important to note that the individual string breaks are causally disconnected [65], hence they do not have to be generated in any particular time-ordered sequence. This is exploited in the Lund model to allow to consider the formation of a single on-shell hadron at a time, in an order that corresponds to decreasing average absolute rapidity (along the string). Selecting randomly between the left and right sides of the string, the first hadron to be generated is thus the “outermost” one, formed by combining

the original hadronizing endpoint quark (or antiquark) q_0 with an antiquark (or quark) \bar{q}_1 produced by a breakup. The new leftover quark (or antiquark) q_1 becomes the string endpoint for the next iteration, in a Markov chain which continues, alternating randomly between the left and right ends of the string, until finally a small last bit of string is decayed directly to two hadrons, with no energy left over.

For each breakup vertex, quantum mechanical tunneling is assumed to control the masses and p_\perp kicks (transverse to the string axis, in a frame in which the string itself has no transverse motion) that can be produced, leading to a Gaussian suppression

$$\text{Prob}(m_q^2, p_{\perp q}^2) \propto \exp\left(\frac{-\pi m_q^2}{\kappa}\right) \exp\left(\frac{-\pi p_{\perp q}^2}{\kappa}\right), \quad (42.8)$$

where m_q is the mass of the produced quark flavor and p_\perp is the nonperturbative transverse momentum imparted to it by the breakup process, with a universal average value of $\langle p_{\perp q}^2 \rangle = \kappa/\pi \sim (250 \text{ MeV})^2$. The antiquark has the same mass and opposite p_\perp .

In an MC model with a fixed shower cutoff t_0 , the effective amount of p_\perp in string breaks may be larger than the purely nonperturbative κ/π above, to account for effects of additional (unresolved) radiation below t_0 .

From the mass term in Eq. (42.8), one concludes that charm and bottom quarks are too heavy to be produced in string breaks, while strange quarks will be suppressed relative to up and down ones. Lacking unambiguous and precise mass definitions for light quarks, however, the effective amount of strangeness suppression is normally extracted from experimental data, using observables such as K/π and K^*/ρ ratios.

Baryon production can also be incorporated, by allowing string breaks to produce pairs of *diquarks*, loosely bound states of two quarks in an overall $\bar{3}$ representation. Again, since diquark masses are difficult to define, the relative rate of diquark to quark production is extracted, e.g. from the p/π ratio. Since the perturbative shower splittings do not produce diquarks, the optimal value for this parameter is mildly correlated with the amount of $g \rightarrow q\bar{q}$ splittings produced by the shower. More advanced scenarios for baryon production have also been proposed, see Ref. 65. Within the PYTHIA framework, a hadronization model including baryon string junctions [66] is also available.

The next step of the algorithm is the assignment of the produced quarks within hadron multiplets. Using a nonrelativistic classification of spin states, the hadronizing q may combine with the \bar{q}' from a newly created breakup to produce a meson — or baryon, if diquarks are involved — of a given spin S and angular momentum L . The lowest-lying pseudoscalar and vector meson multiplets, and spin-1/2 and -3/2 baryons, are assumed to dominate in a string framework¹, but individual rates are not predicted by the model. This is therefore the sector that contains the largest amount of free parameters. The ratio V/P of vectors to pseudoscalars is expected to be 3, but in practice it is only in the B meson sector that this is approximately true. For lighter flavors, the difference in phase space caused by the $V-P$ mass splittings implies a suppression of vector production. When extracting the corresponding parameters from data, it is advisable to begin with the heaviest states, since so-called feed-down from the decays of higher-lying hadron states complicates the extraction for lighter particles, see Sec. 42.2.3. For baryons, additional parameters control the relative rates of spin-1 diquarks vs. spin-0 ones.

With p_\perp^2 and m^2 now fixed, the final step is to select the longitudinal momentum component of the created hadron along the string axis. This is parameterized by a nonperturbative *fragmentation function*, $f(z)$, which governs the probability for a hadron to take a fraction $z \in [0, 1]$ of the total available momentum. In a string framework, the requirement that the hadronization be independent of

¹ PYTHIA includes the lightest pseudoscalar and vector mesons, with the four $L = 1$ multiplets (scalar, tensor, and 2 pseudovectors) available but disabled by default, largely because several states are poorly known and thus may result in a worse overall description when included. For baryons, the lightest spin-1/2 and -3/2 multiplets are included.

the sequence in which breakups are considered (causality) imposes a “left-right symmetry” which strongly constrains the functional form of $f(z)$, with the solution

$$f(z) \propto \frac{1}{z} (1-z)^a \exp\left(-\frac{b(m_h^2 + p_{\perp h}^2)}{z}\right). \quad (42.9)$$

This is known as the Lund symmetric fragmentation function (normalized to unit integral). The dimensionless parameter a dampens the hard tail of the fragmentation function, towards $z \rightarrow 1$, and may in principle be flavor-dependent, while b , with dimension GeV^{-2} , is a universal constant related to the string tension [65] which determines the behavior in the soft limit, $z \rightarrow 0$. Note that the dependence on the hadron mass, m_h , in $f(z)$ implies that heavier hadrons have higher $\langle z \rangle$.

As a by-product, the probability distribution in invariant time τ of $q'\bar{q}$ breakup vertices, or equivalently $\Gamma = (\kappa\tau)^2$, is also obtained, with $dP/d\Gamma \propto \Gamma^a \exp(-b\Gamma)$ implying an area law for the color flux, and the average breakup time lying along a hyperbola of constant invariant time $\tau_0 \sim 10^{-23}\text{s}$ [65].

For massive endpoints (e.g. c and b quarks), which do not move along straight lightcone sections, the exponential suppression with string area leads to modifications of the form $f(z) \rightarrow f(z)/z^{bm_Q^2}$, with m_Q the mass of the heavy quark [67]. Although different forms, such as the Peterson formula [68], can also be used to describe inclusive heavy-meson spectra (see Sec 19.8 of PDG book), such choices are not strictly consistent with causality in the string framework.

42.2.2. The Cluster Model :

The cluster hadronization model is based on *preconfinement*, i.e., on the observation [69,70] that the color structure of a perturbative QCD shower evolution at any scale Q_0 is such that color-singlet subsystems of partons (labeled “clusters”) occur with a universal invariant mass distribution which is power suppressed at large masses. For any starting scale $Q \gg Q_0 \gg \Lambda_{\text{QCD}}$, only the number of such clusters depends on Q , while the shape of their mass distribution only depends on Q_0 and on Λ_{QCD} .

Following early models based on this universality [11,71], the cluster model developed by Webber [72] has for many years been a hallmark of the HERWIG generators, with an alternative implementation [73] now available in the SHERPA generator. The key idea, in addition to preconfinement, is to force “by hand” all gluons to split into quark-antiquark pairs at the end of the parton shower. Compared with the string description, this effectively amounts to viewing gluons as “seeds” for string breaks, rather than as kinks in a continuous object. After the splittings, a new set of low-mass color-singlet clusters is obtained, formed only by quark-antiquark pairs. These can be decayed to on-shell hadrons in a simple manner, with the relative yields of different hadron species mainly governed by their masses and the size of the phase space.

The algorithm starts by generating the forced $g \rightarrow q\bar{q}$ breakups, and by assigning flavors and momenta to the produced quark pairs. For a typical shower cutoff corresponding to a gluon virtuality of $Q_{\text{had}} \sim 1\text{GeV}$, the p_{\perp} generated by the splittings can be neglected. The constituent light-quark masses, $m_{u,d} \sim 300\text{MeV}$ and $m_s \sim 450\text{MeV}$, imply a suppression (typically even an absence) of strangeness production. In principle, the model also allows for diquarks to be produced at this stage, but due to the larger constituent masses this would only become relevant for shower cutoffs larger than 1GeV .

If a cluster formed in this way has an invariant mass above some cutoff value, typically 3–4 GeV, it is forced to undergo sequential $1 \rightarrow 2$ cluster breakups, along an axis defined by the constituent partons of the original cluster, until all sub-cluster masses fall below the cutoff value. Due to the preservation of the original axis in these breakups, this treatment has some resemblance to the string-like picture, though the nonperturbative p_{\perp} kicks generated in this way are generally larger, up to half the allowed cluster mass.

Next, on the low-mass side of the spectrum, some clusters are allowed to decay directly to a single hadron, with nearby clusters

absorbing any excess momentum. This improves the description of the high- z part of the spectrum — where the hadron carries almost all the momentum of its parent jet — at the cost of introducing one additional parameter, controlling the probability for single-hadron cluster decay.

Having obtained a final distribution of small-mass clusters, now with a strict cutoff at 3–4 GeV and with the component destined to decay to single hadrons already removed, the remaining clusters are interpreted as a smoothed-out spectrum of excited mesons, each of which decays isotropically to two hadrons, with relative probabilities proportional to the available phase space for each possible two-hadron combination that is consistent with the cluster’s internal flavors, including spin degeneracy. It is important that all the light members (containing only uds) of each hadron multiplet be included, as the absence of members can lead to unphysical isospin or SU(3) flavor violation. Typically, the lightest pseudoscalar, vector, scalar, even and odd charge conjugation pseudovector, and tensor multiplets of light mesons are included. In addition, some excited vector multiplets of light mesons may be available. For baryons, usually only the lightest flavor-octet, -decuplet and -singlet baryons are present, although both the HERWIG++ and SHERPA implementations now include some heavier baryon multiplets as well.

Differently from the string model, the mechanism of phase-space suppression employed here leads to a natural enhancement of the lighter pseudoscalars, and no parameters beyond the spectrum of hadron masses need to be introduced at this point. The phase space also limits the transverse momenta of the produced hadrons relative to the jet axis.

Note that, since the masses and decays of excited heavy-flavor hadrons in particular are not well known, there is some freedom in the model to adjust these, which in turn will affect their relative phase-space populations.

42.2.3. Hadron and τ Decays :

Of the so-called primary hadrons, originating directly from string breaks and/or cluster decays (see above), many are unstable and so decay further, until a set of particles is obtained that can be considered stable on time scales relevant to the given measurement. (A typical hadron-collider definition of a “stable particle” $c\tau \geq 10\text{mm}$ includes weakly-decaying strange hadrons K , Λ , Σ^{\pm} , $\bar{\Sigma}^{\pm}$, Ξ , Ω .) The decay modeling can therefore have a significant impact on final particle yields and spectra, especially for the lowest-lying hadronic states, which receive the largest relative contributions from decays (feed-down). This interplay also implies that hadronization parameters may need to be retuned if significant changes to the decay treatment are made.

Particle summary tables, such as those given elsewhere in this *Review*, represent a condensed summary of the available experimental measurements and hence may be incomplete and/or exhibit inconsistencies within the experimental precision. In an MC decay package, on the other hand, all information must be quantified and consistent, with all branching ratios summing to unity. When adapting particle summary information for use in a decay package, a number of choices must therefore be made. The amount of ambiguity increases as more excited hadron multiplets are added to the simulation, about which less and less is known from experiment, with each GPMC making its own choices.

A related choice is how to distribute the decay products differentially in phase space, in particular which matrix elements to use. Historically, MC generators contained matrix elements only for selected (generator-specific) classes of hadron and τ decays, coupled with a Breit-Wigner smearing of the masses, truncated at the edges of the physical decay phase space (the treatment of decay thresholds can be important for certain modes [18]). A more sophisticated treatment can then be obtained by reweighting the generated events using the obtained particle four-momenta and/or by using specialized external packages such as EVTGEN [74] for hadron decays and TAUOLA [75] for τ decays.

More recently, HERWIG++ and SHERPA include helicity-dependence in τ decays [76,6], with a more limited treatment available in PYTHIA 8 [5]. The HERWIG++ and SHERPA generators have also included significantly improved internal simulations of hadronic

decays, which include spin correlations between those decays for which matrix elements are used. Photon-bremstrahlung effects are discussed in Sec. 42.1.7.

HERWIG++ and PYTHIA include the probability for B mesons to oscillate into \bar{B} ones before decay. SHERPA and EVTGEN also include CP-violating effects and, for common decay modes of the neutral meson and its antiparticle, the interference between the direct decay and oscillation followed by decay.

We end on a note of warning on double counting. This may occur if a particle can decay via an intermediate on-shell resonance. An example is $a_1 \rightarrow \pi\pi\pi$ which may proceed via $a_1 \rightarrow \rho\pi$, $\rho \rightarrow \pi\pi$. If these decay channels of the a_1 are both included, each with their full partial width, a double counting of the on-shell $a_1 \rightarrow \rho\pi$ contribution would result. Such cases are normally dealt with consistently in the default MC generator packages, so this warning is mostly for users that wish to edit decay tables on their own.

42.3. Models for Soft Hadron-Hadron Physics

42.3.1. Minimum-Bias and Diffraction :

The term “minimum bias” (MB) originates from the experimental requirement of a minimal number of tracks (or hits) in a given instrumented region. In order to make MC predictions for such observables, all possible contributions to the relevant phase-space region must be accounted for. There are essentially four types of physics processes, which together make up the total hadron-hadron (hh) cross section: 1) elastic scattering²: $hh \rightarrow hh$, 2) single diffractive dissociation: $hh \rightarrow h + \text{gap} + X$, with X denoting anything that is not the original beam particle, and “gap” denoting a rapidity region devoid of observed activity; 3) double diffractive dissociation: $hh \rightarrow X + \text{gap} + X$, and 4) inelastic non-diffractive scattering: everything else. A fifth class may also be defined, called central diffraction ($hh \rightarrow h + \text{gap} + X + \text{gap} + h$). Note that different terminologies exist [77]: in experimental settings, diffraction is typically defined by an observable gap, of some minimal size in rapidity, while in the MC context, each diffractive physics process produces a whole spectrum of gaps, with small ones suppressed but not excluded.

The inelastic non-diffractive part of the cross section is typically modeled either by smoothly regulating and extending the perturbative QCD scattering cross sections all the way to zero p_\perp [78] (PYTHIA and SHERPA), or by regulating the QCD cross sections with a sharp cutoff [79] and adding a separate class of nonperturbative scatterings below that scale [80] (HERWIG). See also Sec. 42.3.2. In all cases, the most important ingredients are: 1) the IR regularization of the perturbative scattering cross sections, including their PDF dependence, 2) the assumed matter distribution of the colliding hadrons, possibly including multi-parton correlations [66] and/or x dependence [81], and 3) additional soft-QCD effects such as color reconnections, discussed in Sec. 42.3.3.

Currently, there are essentially three methods for simulating diffraction in the main MC models: 1) in PYTHIA 6, one picks a diffractive mass according to parameterized cross sections $\propto dM^2/M^2$ [82]. This mass is represented as a string, which is hadronized as described in Sec. 42.2.1, though differences in the effective scale of the hadronization may necessitate a (re)tuning of the hadronization parameters for diffraction; 2) in PYTHIA 8, the high-mass tail beyond $M \sim 10$ GeV is augmented by a partonic description in terms of pomeron PDFs [83], allowing diffractive jet production including showers and underlying event [84]; 3) the PHOJET and DPMJET programs also include central diffraction and rely directly on a formulation in terms of pomerons (color-singlet multi-gluon states) [85–87]. . Cut pomerons correspond to exchanges of soft gluons while uncut ones give elastic and diffractive topologies as well as virtual corrections that help preserve unitarity. So-called “hard pomerons” provide a transition to the perturbative regime. Hadronization is still handled using the Lund string model, so there is some overlap with the above models at the hadronization stage.

² The QED elastic cross section diverges and is normally a non-default option.

In addition, a pomeron-based package exists for HERWIG [88], and an effort is underway to construct an MC implementation of the “KMR” model [89] within the SHERPA generator. Color reconnections (Sec. 42.3.3) may also play a role in creating rapidity gaps and the underlying event (Sec. 42.3.2) in filling them.

42.3.2. Underlying Event and Jet Pedestals :

In the GPMC context, “underlying event” (UE) denotes any additional activity *beyond* the basic process and its associated ISR and FSR activity. The UE is thus only defined in the context of events selected with a “hard” (i.e., high- p_\perp) trigger which defines the basic process at hand. (This is distinct from the MB selection which does not require any hard perturbative activity.) The dominant contribution to the UE is believed to come from additional color exchanges between the colliding hadronic states. These multiple exchanges can be modeled either as additional perturbative (mainly t -channel gluon) exchanges, called multiple parton-parton interactions (MPI), or nonperturbatively using so-called cut pomerons (roughly equivalent to exchange of gluons with $p_\perp \rightarrow 0$). The experimental observation that events with a hard trigger are accompanied by a higher-than-average level of associated activity (UE particle densities and related quantities are greater than those of MB events at the same CM energy) is called the “jet pedestal” effect.

The most clearly identifiable consequence of MPI is arguably the possibility of observing several hard parton-parton interactions in one and the same hadron-hadron event. Typically, these are QCD $2 \rightarrow 2$ interactions, which produce additional back-to-back jet pairs, with each pair having a small value of $\text{sum}(\vec{p}_\perp)$. The fraction of MPI that give rise to additional reconstructible jets is, however, small. Soft interactions, that exchange color and a small amount of momentum without giving rise to observable jets, are much more plentiful, and can give significant corrections to the color flow and total scattered energy of the event. This affects the final-state activity in a more global way, increasing hadron-multiplicity and summed E_T distributions, and contributing to the break-up of the beam remnants in the forward direction.

The first detailed Monte Carlo model for perturbative MPI was proposed in Ref. 78, and with some variation this still forms the basis for most modern implementations. Some useful additional references can be found in Ref. 18. The first crucial observation is that the t -channel propagators appearing in perturbative QCD $2 \rightarrow 2$ scattering almost go on shell at low p_\perp , causing the differential cross sections to behave roughly as

$$d\sigma_{2 \rightarrow 2} \propto \frac{dt}{t^2} \sim \frac{dp_\perp^2}{p_\perp^4} . \quad (42.10)$$

This cross section represents the inclusive scattering of partons against partons in perturbative QCD, summed over all partons. Thus, if a single hadron-hadron scattering contains *two* parton-parton interactions, that event will contribute twice to the parton-parton cross section $\sigma_{2 \rightarrow 2}$ but only once to the hadron-hadron one σ_{tot} , and so on. In the limit that all the parton-parton interactions are independent and equivalent, one has

$$\sigma_{2 \rightarrow 2} = \langle n \rangle \sigma_{\text{tot}} , \quad (42.11)$$

with $\langle n \rangle$ the average number of parton-parton interactions, typically defined with some minimal $p_\perp > p_{\perp \text{min}}$ to render the parton-parton cross section finite. The probability for n parton-parton scatterings then follows a Poisson distribution,

$$\mathcal{P}_n = \langle n \rangle^n \frac{\exp(-\langle n \rangle)}{n!} . \quad (42.12)$$

This simple argument expresses unitarity; instead of the total hadron-hadron interaction cross section diverging as the parton-parton $p_\perp \rightarrow 0$ (which would violate unitarity), we have restated the problem so that it is now the *number of parton-parton interactions per hadron-hadron collision* that diverges, with the total hadron-hadron cross section remaining finite. At LHC energies, the parton-parton scattering cross sections computed using the LO QCD cross section folded with modern PDFs become larger than the total pp one for $p_{\perp \text{min}}$ values of

order 4–5 GeV (see e.g. [90,91]). One therefore expects the average number of perturbative MPI to exceed unity at around that scale.

Two ingredients remain to fully regulate the remaining divergence. Firstly, the interactions cannot use up more momentum than is available in the parent hadron. This suppresses the large- n tail of the estimate above. In PYTHIA-based models, the MPI are ordered in p_{\perp} , and the parton densities for each successive interaction are explicitly constructed so that the sum of x fractions can never be greater than unity. In the HERWIG models, the Poisson estimate of $\langle n \rangle$ above is used as an initial guess, but the generation of actual MPI is stopped once the energy-momentum conservation limit is reached. Both of these approaches generate momentum (conservation) correlations among the MPI.

The second ingredient invoked to suppress the number of interactions, at low p_{\perp} and x , is color screening; if the wavelength $\sim 1/p_{\perp}$ of an exchanged colored parton becomes larger than a typical color-anticolor separation distance, it will only see an *average* color charge that vanishes in the limit $p_{\perp} \rightarrow 0$. This provides an infrared cutoff for MPI similar to that provided by the hadronization scale for parton showers. A first estimate of the color-screening cutoff would be the proton size, $p_{\perp\text{min}} \approx \hbar/r_p \approx 0.3 \text{ GeV} \approx \Lambda_{\text{QCD}}$, but empirically this appears to be far too low. In current models, one replaces the proton radius r_p in the above formula by a “typical color screening distance,” i.e., an average size of a region within which the net compensation of a given color charge occurs. This number is not known from first principles [89] and is perceived of simply as an effective cutoff parameter. The simplest choice is to introduce a step function $\Theta(p_{\perp} - p_{\perp\text{min}})$. Alternatively, one may note that the jet cross section is divergent like $\alpha_S^2(p_{\perp}^2)/p_{\perp}^4$, cf. Eq. (42.10), and that therefore a factor

$$\frac{\alpha_S^2(p_{\perp 0}^2 + p_{\perp}^2)}{\alpha_S^2(p_{\perp}^2)} \frac{p_{\perp 0}^4}{(p_{\perp 0}^2 + p_{\perp}^2)^2} \quad (42.13)$$

would smoothly regulate the divergences, now with $p_{\perp 0}$ as the free parameter. Regardless of whether it is imposed as a smooth (PYTHIA and SHERPA) or steep (HERWIG++) function, this is effectively the main “tuning” parameter in such models.

Note that the numerical value obtained for the cross section depends upon the PDF set used, and therefore the optimal value to use for the cutoff will also depend on this choice. Note also that the cutoff does not have to be energy-independent. Higher energies imply that parton densities can be probed at smaller x values, where the number of partons rapidly increases. Partons then become closer packed and the color screening distance d decreases. The uncertainty on the energy and/or x scaling of the cutoff is a major concern when extrapolating between different collider energies [92].

We now turn to the origin of the observational fact that hard jets appear to sit on top of a higher “pedestal” of underlying activity than events with no hard jets. This is interpreted as a consequence of impact-parameter-dependence: in peripheral collisions, only a small fraction of events contain any high- p_{\perp} activity, whereas central collisions are more likely to contain at least one hard scattering; a high- p_{\perp} triggered sample will therefore be biased towards small impact parameters, b . The ability of a model to describe the shape of the pedestal (e.g. to describe both MB and UE distributions simultaneously) therefore depends upon its modeling of the b -dependence, and correspondingly the impact-parameter shape constitutes another main tuning parameter.

For each impact parameter b , the number of interactions $\tilde{n}(b)$ can still be assumed to be distributed according to Eq. (42.12), again modulo momentum conservation, but now with the mean value of the Poisson distribution depending on impact parameter, $\langle \tilde{n}(b) \rangle$. This causes the final n -distribution (integrated over b) to be wider than a Poissonian.

Finally, there are two perturbative modeling aspects which go beyond the introduction of MPI themselves: 1) parton showers off the MPI, and 2) perturbative parton-rescattering effects. Without showers, MPI models would generate very sharp peaks for back-to-back MPI jets, caused by unshowered partons passed directly to

the hadronization model. However, with the exception of the oldest PYTHIA6 model, all GPMC models do include such showers [18], and hence should exhibit more realistic (i.e., broader and more decorrelated) MPI jets. On the initial-state side, the main questions are whether and how correlated multi-parton densities are taken into account and, as discussed previously, how the showers are regulated at low p_{\perp} and/or low x . Although none of the MC models currently impose a rigorous correlated multi-parton evolution, all of them include some elementary aspects. The most significant for parton-level results is arguably momentum conservation, which is enforced explicitly in all the models. The so-called “interleaved” models [30] attempt to go a step further, generating an explicitly correlated multi-parton evolution in which flavor sum rules are imposed to conserve, e.g. the total numbers of valence and sea quarks [66].

Perturbative rescattering in the final state can occur if partons are allowed to undergo several distinct interactions, with showering activity possibly taking place in-between. This has so far not been studied extensively, but a first exploratory model is available [93]. In the initial state, parton rescattering/recombination effects have so far not been included in any of the GPMC models.

42.3.3. Bose-Einstein and Color-Reconnection Effects :

In the context of e^+e^- collisions, Bose-Einstein (BE) correlations have mostly been discussed as a source of uncertainty on high-precision W mass determinations at LEP [94]. In hadron-hadron (and nucleus-nucleus) collisions, however, BE correlations are used extensively to study the space-time structure of hadronizing matter (“femtoscopy”).

In MC models of hadronization, each string break or particle/cluster decay is normally factorized from all other ones. This reduces the number of variables that must be considered in each step, but also makes it intrinsically difficult to introduce correlations among particles from different breaks/decays. In GPMCs, a few semi-classical models are available within the PYTHIA 6 and 8 generators [95], in which the BE effect is mimicked by an attractive interaction between pairs of identical particles in the final state, with no higher correlations included. Variants of this model differ mainly by the assumed shape of the correlation function and how overall momentum conservation is handled.

As discussed in Sec. 42.2, leading-color (“planar”) color flows are used to set up the hadronizing systems (clusters or strings) at the hadronization stage. If the systems do not overlap significantly in space and time, subleading-color ambiguities and/or nonperturbative reconections are expected to be small. However, if the density of displaced color charges is sufficiently high that several systems can overlap significantly, full-color and/or reconnection effects should become progressively larger.

In the specific context of MPI, a crucial question is how color is neutralized *between* different MPI systems, including the remnants. The large rapidity differences involved imply large invariant masses (though normally low p_{\perp}), and hence large amounts of (soft) particle production. Indeed, in the context of soft-inclusive physics, it is these “inter-system” strings/clusters that furnish the dominant particle-production mechanism, and hence their modeling is an essential part of the soft-physics description, affecting topics such as MB/UE multiplicity and p_{\perp} distributions, rapidity gaps, and precision mass measurements. Reviews of color-reconnection effects can be found in Refs. 18,96.

42.4. Uncertainties and Tuning

The accuracy that can be achieved by a GPMC model depends on the sophistication of the theory models it incorporates, on the available constraints on its free parameters, and on the nature of the observable(s) under study. Using existing data (or more accurate theory calculations) to constrain the model parameters is referred to as generator tuning. Although tuned models do tend to yield improved results also for observables that they have not been tuned to, the question of evaluating the remaining uncertainties reliably is still far from solved. It is worth noting, however, that all of the GPMCs now provide options for automatic evaluation of perturbative shower uncertainties (e.g., via renormalization-scale variations), in the form

of vectors of alternative event weights [97,98,99] although significant weight fluctuations can be a problem for processes with many or large shower phase spaces. One must be aware that these variations are not necessarily exhaustive and care must be taken in their interpretation. Nonperturbative uncertainties must normally still be evaluated by varying salient model parameters by hand. A general method called eigentunes [100] is also available, based on global fits to data.

Typically, the overall event properties are determined by only a few, very important parameters, such as the value of α_S , for perturbative corrections, and the shape of the fragmentation functions, for nonperturbative ones. More parameters may then be introduced to describe successively more detailed aspects (e.g., the rates and decays of individual hadron species), but these should have progressively less impact on the overall modeling. One may therefore take a factorized approach, first constraining the perturbative parameters and thereafter the nonperturbative ones, in order of decreasing significance to the overall modeling. Furthermore, by identifying which measurements are most sensitive to each parameter, this ordering can be reflected in the way that data is selected and applied to constrain the models. Thus, measurements sensitive to global event properties would typically be applied first, to constrain the most inclusive parameters, and so on for progressively more exclusive aspects.

At LO \times LL, perturbation theory is doing well if it agrees with an IR safe measurement within $\sim 10\%$. It would therefore not make much sense to tune a GPMC beyond roughly 5% (it might even be dangerous, due to overfitting). The advent of NLO Monte Carlos may reduce this number slightly, but only for quantities for which one expects NLO precision. For quantities governed by nonperturbative physics, uncertainties are larger. For some quantities, e.g. ones for which the underlying modeling is known to be poor, an order-of-magnitude agreement or worse may have to be accepted. Note further that the unitarity of shower and hadronization models implies that the Born-level cross-section normalization is not tunable, hence in tuning contexts one tends to focus on the shapes of distributions rather than their normalizations.

In the context of LO \times LL GPMC tuning, subleading aspects of coupling-constant and PDF choices are relevant. In particular, one should be aware that the choice of QCD Λ parameter $\Lambda_{\overline{\text{MS}}} = 1.569\Lambda_{\overline{\text{MS}}}$ (for 5 active flavors) improves the predictions of coherent shower algorithms at the NLL level for a class of relevant observables [101], and hence this scheme is often considered the baseline for shower tuning. The question of LO vs. NLO PDFs is more involved [18], but it should be emphasized that the gluon PDF at (very) low x is important for determining the level of the underlying event in MPI models (Sec. 42.3.2), and hence the MB/UE tuning (and energy scaling [92]) is linked to the choice of PDF in such models. Further issues and an example of a specific recipe that could be followed in a realistic set-up can be found in Ref. 90. A useful online resource can be found at the mcplots.cern.ch web site [102], based on the RIVET tool [103].

Recent years have seen the emergence of automated tools to reduce the amount of both computer and manpower required for tuning [100]. Automating the human expert input is more difficult. In the tools currently on the market, this is addressed by a combination of input solicited from the GPMC authors (e.g., which parameters and ranges to consider, which observables constitute a complete set, etc) and a set of weights determining the relative priority given to each bin in each distribution. The final result is therefore still subjective but at least reproducible. When backed by careful demonstrations of sensitivities, correlations, and uncertainties, the quality of the resulting tunes is by now competitive. The field is still burgeoning, with future sophistications to be expected.

References:

1. G. Corcella *et al.*, JHEP **0101**, 010 (2001), hep-ph/0011363.
2. M.Bähr *et al.*, Eur. Phys. J. **C58**, 639 (2008), arXiv:0803.0883.
3. J. Bellm *et al.*, Eur. Phys. J. **C76**, 196 (2016), arXiv:1512.01178.
4. T. Sjöstrand, S. Mrenna, and P. Z. Skands, JHEP **05**, 026 (2006), hep-ph/0603175.
5. T. Sjöstrand *et al.*, Comp. Phys. Comm. **191**, 159 (2015), arXiv:1410.3012.
6. T. Gleisberg *et al.*, JHEP **0902**, 007 (2009), arXiv:0811.4622.
7. QCD summary, PDG..
8. T. Kinoshita, J. Math. Phys. **3**, 650 (1962).
9. T. Lee and M. Nauenberg, Phys. Rev. **133**, 1549 (1964).
10. A. Buckley *et al.*, arXiv:1101.2599, and references therein..
11. G.C. Fox and S. Wolfram, Nucl. Phys. **B168**, 285 (1980).
12. G. Altarelli and G. Parisi, Nucl. Phys. **B126**, 298 (1977).
13. A. Einstein, B. Podolsky, and N. Rosen, Phys. Rev. **47**, 777 (1935).
14. B.R. Webber, Phys. Lett. **B193**, 91 (1987).
15. J.C. Collins, Nucl. Phys. **B304**, 794 (1988).
16. I.G. Knowles, Comp. Phys. Comm. **58**, 271 (1990).
17. T. Sjöstrand, Phys. Lett. **B157**, 321 (1985).
18. A. Buckley *et al.*, Phys. Reports **504**, 145 (2011), arXiv:1101.2599.
19. G. Marchesini and B.R. Webber, Nucl. Phys. **B310**, 461 (1988).
20. S. Gieseke, P. Stephens, and B. Webber, JHEP **0312**, 045 (2003), hep-ph/0310083.
21. M. Bengtsson and T. Sjöstrand, Nucl. Phys. **B289**, 810 (1987).
22. G. Gustafson and U. Pettersson, Nucl. Phys. **B306**, 746 (1988).
23. L. Lönnblad, Comp. Phys. Comm. **71**, 15 (1992).
24. T. Ježo *et al.*, Eur. Phys. J. **C76**, 691 (2016), arXiv:1607.04538.
25. W.T. Giele, D.A. Kosower, and P.Z. Skands, Phys. Rev. **D78**, 014026 (2008), arXiv:0707.3652.
26. Z. Nagy and D.E. Soper, JHEP **0510**, 024 (2005), hep-ph/0503053.
27. S. Schumann and F. Krauss, JHEP **0803**, 038 (2008), arXiv:0709.1027.
28. S. Plätzer and S. Gieseke, Eur. Phys. J. **C72**, 2187 (2012), arXiv:1109.6256.
29. S. Höche and S. Prestel, Eur. Phys. J. **C75**, 461 (2015), arXiv:1506.05057.
30. T. Sjöstrand and P.Z. Skands, Eur. Phys. J. **C39**, 129 (2005), hep-ph/0408302.
31. E. Norrbin and T. Sjöstrand, Nucl. Phys. **B603**, 297 (2001), hep-ph/0010012.
32. S. Catani *et al.*, Nucl. Phys. **B627**, 189 (2002), hep-ph/0201036.
33. J. Cambranos *et al.*, (2013), arXiv:1305.2124.
34. N. Davidson, T. Przedzinski, and Z. Was, (2010), arXiv:1011.0937.
35. K. Hamilton and P. Richardson, JHEP **0607**, 010 (2006), hep-ph/0603034.
36. M. Schönherr and F. Krauss, JHEP **0812**, 018 (2008), arXiv:0810.5071.
37. A. Semenov, Comp. Phys. Comm. **180**, 431 (2009), arXiv:0805.0555.
38. N.D. Christensen and C. Duhr, Comp. Phys. Comm. **180**, 1614 (2009), arXiv:0806.4194.
39. M. Fairbairn *et al.*, Phys. Reports **438**, 1 (2007), hep-ph/0611040.
40. J. Alwall *et al.*, Comp. Phys. Comm. **176**, 300 (2007), hep-ph/0609017.
41. P.Z. Skands *et al.*, JHEP **0407**, 036 (2004), hep-ph/0311123.
42. J. Alwall *et al.*, (2007), arXiv:0712.3311.
43. P. Richardson, JHEP **0111**, 029 (2001), hep-ph/0110108.
44. E. Boos *et al.*, (2007), hep-ph/0109068.
45. M. Bengtsson and T. Sjöstrand, Phys. Lett. **B185**, 435 (1987).
46. W. T. Giele, D. A. Kosower and P. Z. Skands, Phys. Rev. **D84**, 054003 (2011), arXiv:1102.2126.
47. S. Catani *et al.*, JHEP **11**, 063 (2001), hep-ph/0109231.
48. J. Alwall *et al.*, Eur. Phys. J. **C53**, 473 (2008), arXiv:0706.2569.
49. P. Nason, JHEP **11**, 040 (2004), hep-ph/0409146.
50. B. Cooper *et al.*, Eur. Phys. J. **C72**, 2078 (2012), arXiv:1109.5295.
51. M.L. Mangano *et al.*, JHEP **0307**, 001 (2003), hep-ph/0206293.
52. J. Alwall *et al.*, JHEP **1106**, 128 (2011), arXiv:1106.0522.

53. S. Frixione and B.R. Webber, JHEP **06**, 029 (2002), [hep-ph/0204244](#).
54. S. Alioli *et al.*, JHEP **1006**, 043 (2010), [arXiv:1002.2581](#).
55. J. Alwall *et al.*, JHEP **07**, 079 (2014), [arXiv:1405.0301](#).
56. S. Alioli, K. Hamilton, and E. Re, JHEP **09**, 104 (2011), [arXiv:1108.0909](#).
57. R. Frederix and S. Frixione, JHEP **12**, 061 (2012), [arXiv:1209.6215](#).
58. L. Lönnblad and S. Prestel, JHEP **03**, 166 (2013), [arXiv:1211.7278](#).
59. K. Hamilton, P. Nason and G. Zanderighi, JHEP **10**, 155 (2012), [arXiv:1206.3572](#).
60. S. Höche *et al.*, JHEP **04**, 027 (2013), [arXiv:1207.5030](#).
61. K. Hamilton, P. Nason and G. Zanderighi, JHEP **05**, 140 (2015), [arXiv:1501.04637](#).
62. G. Gustafson, Phys. Lett. **B175**, 453 (1986).
63. X. Artru and G. Mennessier, Nucl. Phys. **B70**, 93 (1974).
64. B. Andersson *et al.*, Phys. Reports **97**, 31 (1983).
65. B. Andersson, Camb. Monogr. Part. Phys. Nucl. Phys. Cosmol. **7** (1997).
66. T. Sjöstrand and P.Z. Skands, JHEP **0403**, 053 (2004), [hep-ph/0402078](#).
67. M. Bowler, Z. Phys. **C11**, 169 (1981).
68. C. Peterson *et al.*, Phys. Rev. **D27**, 105 (1983).
69. D. Amati and G. Veneziano, Phys. Lett. **B83**, 87 (1979).
70. A. Bassetto, M. Ciafaloni, and G. Marchesini, Phys. Lett. **B83**, 207 (1979).
71. R.D. Field and S. Wolfram, Nucl. Phys. **B213**, 65 (1983).
72. B.R. Webber, Nucl. Phys. **B238**, 492 (1984).
73. J.-C. Winter, F. Krauss, and G. Soff, Eur. Phys. J. **C36**, 381 (2004), [hep-ph/0311085](#).
74. D. Lange, Nucl. Instrum. Methods **A462**, 152 (2001).
75. S. Jadach *et al.*, Comp. Phys. Comm. **76**, 361 (1993).
76. D. Grellscheid and P. Richardson, (2007), [arXiv:0710.1951](#).
77. V. Khoze *et al.*, Eur. Phys. J. **C69**, 85 (2010), [arXiv:1005.4839](#).
78. T. Sjöstrand and M. van Zijl, Phys. Rev. **D36**, 2019 (1987).
79. J.M. Butterworth, J.R. Forshaw, and M.H. Seymour, Z. Phys. **C72**, 637 (1996), [hep-ph/9601371](#).
80. M. Bähr *et al.*, (2009), [arXiv:0905.4671](#).
81. R. Corke and T. Sjöstrand, JHEP **1105**, 009 (2011), [1101.5953](#).
82. G.A. Schuler and T. Sjöstrand, Phys. Rev. **D49**, 2257 (1994).
83. G. Ingelman and P. Schlein, Phys. Lett. **B152**, 256 (1985).
84. S. Navin, (2010), [arXiv:1005.3894](#).
85. P. Aurenche *et al.*, Comp. Phys. Comm. **83**, 107 (1994), [hep-ph/9402351](#).
86. F.W. Bopp, R. Engel, and J. Ranft, (1998), [hep-ph/9803437](#).
87. S. Roesler, R. Engel, and J. Ranft, p. 1033 (2000), [hep-ph/0012252](#).
88. B.E. Cox and J.R. Forshaw, Comp. Phys. Comm. **144**, 104 (2002), [hep-ph/0010303](#).
89. M. Ryskin, A. Martin, and V. Khoze, Eur. Phys. J. **C71**, 1617 (2011), [arXiv:1102.2844](#).
90. P. Skands, S. Carrazza and J. Rojo, Eur. Phys. J. **C74**, 3024 (2014), [arXiv:1404.5630](#).
91. M. Bähr, J.M. Butterworth, and M.H. Seymour, JHEP **01**, 065 (2009), [arXiv:0806.2949](#).
92. H. Schulz and P.Z. Skands, Eur. Phys. J. **C71**, 1644 (2011), [arXiv:1103.3649](#).
93. R. Corke and T. Sjöstrand, JHEP **01**, 035 (2009), [arXiv:0911.1901](#).
94. LEP Electroweak Working Group, (2005), [hep-ex/0511027](#).
95. L. Lönnblad and T. Sjöstrand, Eur. Phys. J. **C2**, 165 (1998), [hep-ph/9711460](#).
96. J. R. Christiansen and P. Z. Skands, JHEP **08**, 003 (2015), [arXiv:1505.01681](#).
97. J. Bellm *et al.*, Phys. Rev. **D94**, 034028 (2016), [arXiv:1605.08256](#).
98. S. Mrenna and P. Skands, Phys. Rev. **D94**, 074005 (2016), [arXiv:1605.08352](#).
99. E. Bothmann, M. Schnherr and S. Schumann, Eur. Phys. J. **C76**, 590 (2016), [arXiv:1606.08753](#).
100. A. Buckley *et al.*, Eur. Phys. J. **C65**, 331 (2010), [arXiv:0907.2973](#).
101. S. Catani, B. R. Webber, and G. Marchesini, Nucl. Phys. **B349**, 635 (1991).
102. A. Karneyeu *et al.*, Eur. Phys. J. **C74**, 2714 (2013), [arXiv:1306.3436](#).
103. A. Buckley *et al.*, Comp. Phys. Comm. **184**, 2803 (2010), [arXiv:1003.0694](#).

43. Monte Carlo Neutrino Generators

Revised August 2019 by H. Gallagher (Tufts U.) and Y. Hayato (Kamioka Observatory, ICRR, UTokyo).

Monte Carlo neutrino generators are programs or libraries which simulate neutrino interactions with electrons, nucleons and nuclei. In this capacity their usual task is to take an input neutrino and nucleus and produce a set of 4-vectors for particles emerging from the interaction, which are then input to full detector simulations. Since these generators have to simulate not only the initial interaction of neutrinos with target particles, but re-interactions of the generated particles in the nucleus, they contain a wide range of elementary particle and nuclear physics. Viewed more broadly, they are the access point for neutrino experimentalists to the theory inputs needed for analysis. Examples include cross section libraries for event rate calculations and parameter uncertainties and reweighting tools for systematic error evaluation.

Neutrino experiments typically operate in neutrino beams that are neither completely pure nor mono-energetic. Generators are a crucial component in the convolution of beam flux, neutrino interaction physics, and detector response that is necessary to make predictions about observable quantities. Similarly they are used to relate reconstructed quantities back to true quantities. In these various capacities they are used from the detector design stage through the extraction of physics measurements from reconstructed observables. Monte Carlo neutrino generators play unique and important roles in the experimental study of neutrino interactions and oscillations.

There are several neutrino event generators available, such as ANIS [1], GENIE [2], GiBUU [3, 4], MARLEY [5], NEGN [6], NEUT [7], NUANCE [8], the FLUKA routines NUNDIS/NUNRES [9] [10], and NuWro [11], as well as tools to facilitate cross-generator comparisons [12]. Historically, experiments would develop their own generators. This was often because they were focused on a particular measurement, energy range, or target, and wanted to ensure that the best physics was included for it. These ‘home-grown’ generators were often tuned primarily or exclusively to the neutrino data most similar to the data that the experiment would be collecting. A major advance in the field was the introduction of conference series devoted to the topic of neutrino interaction physics, NuINT (<https://nuint2017.physics.utoronto.ca>) and NuFACT (<https://indico.uu.se/event/324/>) in particular. Event generator comparisons have been a regular staple of the NuINT conference series from its inception, and a great deal of information on this topic can be found in the Proceedings of these meetings. These meetings have facilitated experiment-theory discussions leading to the first generator developed by a theory group (NuWro) [11], the extension of established nuclear interaction codes (FLUKA and GiBUU) to include neutrino-nuclear processes [3] [4] [9] [10], and inclusion of theorists in existing generator development teams.

These activities have led to more careful scrutiny of the crucial nuclear theory inputs to these generators, which is evaluated in particular through comparisons to electron-scattering data. At this point in time all simulation codes face challenges in describing the full extent of the lepton scattering data, and the tension between incorporating the best available theory versus obtaining the best agreement with the data plays out in a variety of ways within the field. For the field to make progress, inclusion of state of the art theory needs to be coupled to global analyses that correctly incorporate correlations between measurements. Given the rapid pace of new data and the complexity of analyses, this is a significant challenge for the field in the coming years.

There are many neutrino experiments which use various sources of neutrinos, from reactors, accelerators, the atmosphere, and astrophysical sources, thereby covering a range of energies from MeV to TeV. Much of the emphasis has been on the few-GeV region in the generators, as this is the relevant energy range for short- and long-baseline neutrino oscillation experiments. These generators use the impulse approximation, which treats the nucleus as a collection of independent nucleons and the primary interaction occurs between the probe and a single nucleon, for most

of the initial interaction, and subsequently simulates the interactions of secondary particles in the nucleus in semi-classical ways. Semi-classical hadron transport approaches are commonly used as they are able to simulate a variety of nuclei in a single model, and for practical considerations as these approaches are fast. However, there are several challenges facing these simulations coming mainly from the complexity of the nuclear physics, and avoiding double counting in combining perturbative and non-perturbative models for the neutrino-nucleon scattering processes. The overall validity of this impulse approximation-based scheme, and in particular the importance of scattering channels that involve more than one nucleon, is a crucial question that is the topic of much current work. While generators share many common ingredients, differences in implementation, parameter values, and approaches to avoid double counting can yield dramatically different predictions [13]. In the following sections, interaction models and their implementations including the interactions of generated particles in the nuclei are described.

In order to assure its validity, neutrino event generators are tuned and validated against a wide variety of data, including data from photon, charged lepton, neutrino, and hadron probes. The results from these external data tuning exercises are important for experiments as they quantify the uncertainty on model parameters, needed by experiments in the evaluation of generator-related systematic errors. Electron scattering data plays an important role in determining the vector contribution to the form-factors and structure functions, as well as in evaluating specific aspects of the nuclear model [14]. Hadron scattering data is used in validating the nuclear model, in particular of interactions between hadrons produced in the primary interaction and the residual target nucleus (final state interactions). Tuning of neutrino-nucleon scattering and hadronization models relies heavily on the previous generation of high energy neutrino scattering and hydrogen and deuterium bubble chamber experiments, and more recent data from the K2K, MiniBooNE, NOMAD, SciBooNE, MINOS, T2K, ArgoNEUT, MINERvA, NOvA, MicroBooNE, and SBND experiments either has been, or will be, used for this purpose.

43.1 Neutrino-Nucleon Scattering

Event generators typically begin with free-nucleon cross sections which are then embedded into a nuclear physics model. The most important processes are quasi-elastic (elastic for neutral current (NC)) scattering, resonance production, and non-resonant inelastic scattering, which make comparable contributions for few-GeV interactions. The neutrino cross sections in this energy range can be seen in Figures 51.1 through 51.3 of this *Review*.

43.1.1 Quasi-Elastic Scattering

The cross section for the neutrino nucleon charged current quasi-elastic scattering is described in terms of the leptonic and hadronic weak currents, where dominant contributions to the hadronic current come from the vector (V) and axial-vector (A) form factors. Contributions from the pseudo-scalar form factor (P) are typically small for muon and electron neutrinos and are related to the axial form factor (A) assuming partially conserved axial currents (PCAC). The vector form factors are related via the conserved vector current (CVC) hypothesis to those measured by precise electron scattering experiments, which are known to have some deviation from the simple dipole form [15]. Therefore, most of the generators use parametrizations of this form factor taken directly from the data. For the axial form factor there is no such precise experiment, and most of the generators use a dipole form [16]. Generally, the value of axial form factor at $q^2 = 0$ (q is the four-momentum transfer) is extracted from the polarized nucleon beta decay experiment. However, the selection of the axial vector mass parameter depends on each generator, with values typically around $1.00 \text{ GeV}/c^2$. Recently, there are several attempts to use the other functions for the axial form factors [17, 18] and some generators have already implemented these form factors [19].

43.1.2 Resonance Production

Most generators use the prescriptions of Rein-Sehgal [20] to simulate neutrino-induced single pion production. To obtain the

cross section for a particular channel, they calculate the amplitude for the production of each resonance multiplied by the probability for the decay of that resonance into that particular channel. Implementation differences include the number of resonances included, whether the amplitudes are added coherently or incoherently, the invariant mass range over which the model is used, how non-resonant backgrounds are included, inclusion of lepton mass terms, and the model parameter values (in particular the axial mass). In this model it is also possible to calculate the cross-sections of single photon, kaon and η productions by changing the decay probability of the resonances, which are included in some of the programs. However, it is known that discrepancies exist between the recent pion electro/photoproduction data and the results from the simulation data with the same framework, i.e. vector part of this model. There are several attempts to overcome this issue [21] and some of the generators started using more appropriate form factors. Recently, there is another attempt to further improve the model itself and make it possible to reproduce both electron and neutrino scatterings [22]. This work is expected to be implemented in the generators soon. GiBUU and NuWro generators do not use the Rein-Sehgal model, and instead rely directly on electro-production data for the vector contribution and fit bubble chamber data to determine the remaining parameters for the axial contribution [23–25]. The dynamical coupled-channel model, which has been developed to simulate various electro- and photo-meson productions, was extended to simulate the neutrino single pion production [26]. This model is also being implemented and expected to be available in some of the generators in future.

43.1.3 Deep and Shallow Inelastic Scattering

For this process the fundamental target shifts from the nucleon to its quark constituents. Therefore, the generators use the standard expression for the constructions for the nucleon structure functions F_2 and xF_3 from parton distributions for high Q^2 (the DIS regime: $W > 2 \text{ GeV}/c^2$ and $Q^2 > 1 \text{ GeV}^2$) to calculate direction and momentum of lepton. The first challenge is in extending this picture to the lower values of Q^2 and W that dominate the available phase space for few-GeV interactions (the so-called ‘shallow inelastic scattering’, or SIS regime). GRV98LO parton distribution functions [27] with the corrections proposed in [28] are widely used, while others [9] implement their own modifications to the parton distributions at low Q^2 . Both DIS and SIS generates hadrons but their production depends on each generator’s implementation of a hadronization model as described in the next section. There are various difficulties not only in the actual hadronization but the relation with the single meson production. It is necessary to avoid double counting between the resonance and SIS/DIS models, and all generators are different in this regard. The scheme chosen can have a significant impact on the results of simulations at a few-GeV neutrino energies.

43.2 Hadronization Models

For hadrons produced via baryonic resonances, the underlying model amplitudes and resonance branching fractions can be used to fully characterize the hadronic system. For non-resonant production, a hadronization model is required. Most generators use PYTHIA [29] for this purpose, although some with modified parameters. In addition some implement their own models to handle invariant masses that are too low for PYTHIA, typically somewhere around $2.0 \text{ GeV}/c^2$. Such models rely heavily on measurements of neutrino hadro-production in high-resolution devices, such as bubble chambers and the CHORUS [30] and NOMAD experiments [31], to construct empirical parametrizations that reproduce the key features of the data [32, 33]. The basic ingredients are the empirical observations that average charged particle multiplicities increase logarithmically with the invariant mass of the hadronic system, and that the distribution of charged particle multiplicities about this average are described by a single function (an observation known as KNO scaling [34]). Neutral particles are assumed to be produced with an average multiplicity that is 50% of the charged particle multiplicity. Simple parametrizations to more accurately reproduce differences observed in the forward/backward hemispheres of hadronic systems are included in GENIE, NEUT, and NuWro.

43.3 Nuclear Physics

The nuclear physics relevant to neutrino-nucleus scattering at few-GeV energies is complicated, involving Fermi motion, nuclear binding, Pauli blocking, in-medium modifications of form factors and hadronization, intranuclear rescattering of hadrons, and many-body scattering mechanisms including long- and short-range nucleon-nucleon correlations.

43.3.1 Treatments of scattering kinematics in nucleus

In order to obtain the cross-section off nucleons in the nucleus, it is necessary to take into account various in-medium effects. Most of the models used for neutrino-nuclear scattering kinematics were developed in the context of few-GeV inclusive electron scattering, by experiments going back nearly 50 years. The basic models employed in event generators rely on impulse approximation schemes, the most simple of which is the Relativistic Fermi Gas Model. The most common implementations have been the Smith-Moniz [35] and Bodek-Ritchie [36] models. However, the results from neutrino-nucleus scattering experiments in 2000 and afterwards, such as K2K, MiniBooNE have shown large discrepancies from the naive expectation from the models. Most striking differences are a suppression of forward going muons (low Q^2), a high Q^2 enhancement in the event rate, and an overall larger than expected number of observed events. In order to reproduce the data, the quasi-elastic axial mass was used as the effective parameter and increased by roughly 20% from the nominal values obtained by an earlier generation of bubble chamber experiments using hydrogen or deuterium [16]. These inconsistency between nucleon and nucleus targets suggests that the simple nuclear model is not appropriate in describing the data. Moreover, these simple Fermi-Gas models are not expected to describe the kinematical distributions of final state nucleons. Actually, recent hadronic energy measurements by MINERvA have shown that the simple global Fermi-gas model is not appropriate to reproduce the small energy deposit. Therefore, several generators have to implement better models, such as local Fermi-Gas model or more sophisticated models. Within the electron scattering community, the analogous calculations have for decades relied on spectral functions, which incorporate information about nucleon momenta and binding energies in the impulse approximation scheme. Therefore, most of the generators have implemented the spectral functions in their latest releases.

Actually, the discrepancies in small q^2 could not be solved alone by just introducing the local Fermi-gas model nor spectral function models. This implies that the additional medium correction effects are needed to be taken into account. One of the implemented solutions is the local Fermi-Gas model with medium correction calculated using the random phase approximation, which is known to give large suppression in small q^2 . Although, the fundamental parts of the models are same, actual implementations are quite different between the generators. Especially, the constructions of the final state hadron kinematics are quite different. Especially for the quasi-elastic scattering case, treatment of the nucleon masses in the nucleus, the binding and the separation energies are sometimes quite different. Recently, Super-Scaling model with relativistic mean field theory effects (SuSAv2) [37] was also implemented.

The cause of the discrepancy of small q^2 seems to be identified but the issue of the observed interaction rates are not solved. This implies that there must be some interaction channels which are missing and not considered in the generators.

These led to a revisit of the role played by scattering from multi-particle/hole states in the nucleus, and the experimental search for evidence of these scattering channels is an area of intense experimental interest [38]. The contribution of these scattering processes is an extremely active area of theoretical research as well, with significant implications for generators and analyses [39]. Several approaches, ranging from strictly phenomenological descriptions to full theoretical calculations, have recently been incorporated into generators [40–42]. One example of a phenomenological approach utilizes an Effective Spectral Function [43] and a Transverse Enhancement Model [44], which together encapsulate information derived from electron scattering experiments at relevant kinematics. The microscopic model of Nieves and collab-

orators is now available in GENIE and NEUT [45, 46]. SuSAv2 model also has capability to simulate this multi-nucleon quasi-elastic like interaction and is also implemented in GENIE.

One of the challenges in incorporating full theoretical models of these processes is that they are typically slow, so generators have developed new approaches whereby much of the computation is done offline, and the generators simply read in the hadronic tensor components. This allows for a full prediction of the lepton kinematics, however the ability to simulate the hadronic component of these multinucleon states then relies on separate models. The other challenges is that the theoretical models are not designed to describe exclusive final states. Precisely speaking, some of the neutrino interactions could not be separated each other because of the interference between those channels. Also, there are limitation of the model itself to describe some of the kinematic regions. However, the generators need to simulate final all the state particles and thus, several assumptions are made by authors of the generators from time to time.

Also, it is known from photo and electro-nuclear scattering that the Delta width is affected by Pauli blocking and collisional broadening. These effects are included in some, but not all generators.

When scattering from a nucleus, coherent scattering of various kinds is possible. Most simulations incorporate, at least, neutral and charged coherent single pion production. While the interaction rate for these interactions is typically around a percent of the total yield, the unique kinematic features of these events can make them potential backgrounds for oscillation searches. Implemented in Monte Carlo are several PCAC-based methods [47, 48], and microscopic models [49, 50], valid at lower neutrino energies, have also been implemented in several generators. One of the commonly used model by Rein and Sehgal [47] predicts much larger charged current cross-section compared to the recent measurements of MINER ν A and T2K gives a few times smaller cross-section for the charged current coherent pion production. However, the cross-section is sensitive to the pion cross-section used in the model as parameters and improved models with lepton mass correction [48] give better agreement with the recent data. This improved model is implemented in most of the generators.

43.3.2 Hadron Production in Nuclei

Neutrino pion production is one of the dominant interactions in a few-GeV region and the interaction cross sections of pions in nucleus from those interactions are quite large. Therefore, the interactions of pions in nucleus changes the kinematics of the pions and can have large effects on the results of simulations at these energies. Most generators implement this physics through an intranuclear cascade simulation. In generators which utilize cascade models, a hadron, which has been formed in the nucleus, is moved step by step until it interacts with the other nucleon or escapes from the nucleus. The probabilities of each interaction in nucleus are usually given as the mean free paths and used to determine whether the hadron is interacted or not. If the hadron is found to be interacted, appropriate interactions are selected and simulated. Usually, absorption, elastic, charge exchange, and inelastic scatterings including particle productions are simulated as intranuclear interactions. The determination method of the kinematics for the final state particles heavily depends on the generators but most of them use experimentally validated models to simulate hadron interactions in nucleus. No two interanuclear cascade simulations implemented in neutrino event generators are the same. In all cases hadrons propagate from an interaction vertex chosen based on the density distribution of the target nucleus. In determining the generated position of the hadrons in nucleus, the concept of the formation length is sometimes employed. Based on this idea, the hadronization process is not instantaneous and it takes some time before generating the hadrons [11]. The basis for formation times are measurements at relatively high energy and Q^2 , and most generators that employ the concept do not apply them to resonance interactions.

GiBUU does not employ an intranuclear cascade simulation, instead, it utilizes a semi-classical transport model in coupled channels that describes the space-time evolution of a many body system in the presence of potentials and a collision term [3]. This approach assures consistency between nuclear effects in the initial

state, such as Fermi motion, Pauli blocking, hadron self-energies, and modified cross sections, and the final state, such as particle re-interactions, since the two are derived from the same model. This model has been previously used to describe a wide variety of nuclear interaction data. Similarly, the hadronic simulation of the NUNDIS/NUNRES programs are handled by the well-established FLUKA hadronic simulation package [9].

References

- [1] A. Gazizov and M. P. Kowalski, *Comput. Phys. Commun.* **172**, 203 (2005), [arXiv:astro-ph/0406439].
- [2] C. Andreopoulos *et al.*, *Nucl. Instrum. Meth.* **A614**, 87 (2010), [arXiv:0905.2517].
- [3] O. Buss *et al.*, *Phys. Rept.* **512**, 1 (2012), [arXiv:1106.1344].
- [4] K. Gallmeister, U. Mosel and J. Weil, *Phys. Rev.* **C94**, 3, 035502 (2016), [arXiv:1605.09391].
- [5] S. Gardiner, C. Grant, E. Panic, and R. Svoboda, <http://www.marleygen.org>.
- [6] D. Autiero, *Nucl. Phys. Proc. Suppl.* **139**, 253 (2005).
- [7] Y. Hayato, *Nucl. Phys. Proc. Suppl.* **112**, 171 (2002).
- [8] D. Casper, *Nucl. Phys. Proc. Suppl.* **112**, 161 (2002), [hep-ph/0208030].
- [9] G. Battistoni *et al.*, *Acta Phys. Polon.* **B40**, 2491 (2009).
- [10] T. T. Böhlen *et al.*, *Nucl. Data Sheets* **120**, 211 (2014).
- [11] T. Golan, C. Juszczak and J. T. Sobczyk, *Phys. Rev.* **C86**, 015505 (2012), [arXiv:1202.4197].
- [12] P. Stowell *et al.*, *JINST* **12**, 01, P01016 (2017), [arXiv:1612.07393].
- [13] S. Boyd *et al.*, *AIP Conf. Proc.* **1189**, 1, 60 (2009).
- [14] O. Benhar, D. day and I. Sick, *Rev. Mod. Phys.* **80**, 189 (2008), [arXiv:nucl-ex/0603029].
- [15] A. Bodek *et al.*, *Eur. Phys. J.* **C53**, 349 (2008), [arXiv:0708.1946].
- [16] H. Gallagher, G. Garvey and G. P. Zeller, *Ann. Rev. Nucl. Part. Sci.* **61**, 355 (2011).
- [17] E. Tomasi-Gustafsson, G. I. Gakh and C. Adamuscin, *Phys. Rev.* **C73**, 045204 (2006), [arXiv:nucl-th/0512039].
- [18] B. Bhattacharya, R. J. Hill and G. Paz, *Phys. Rev.* **D84**, 073006 (2011), [arXiv:1108.0423].
- [19] A. S. Meyer *et al.*, *Phys. Rev.* **D93**, 11, 113015 (2016), [arXiv:1603.03048].
- [20] D. Rein and L. M. Sehgal, *Annals Phys.* **133**, 79 (1981).
- [21] K. M. Graczyk and J. T. Sobczyk, *Phys. Rev.* **D77**, 053001 (2008), [Erratum: *Phys. Rev.* **D79**, 079903 (2009)], [arXiv:0707.3561].
- [22] M. Kabirnezhad, *Phys. Rev.* **D97**, 1, 013002 (2018), [arXiv:1711.02403].
- [23] O. Lalakulich and E. A. Paschos, *Phys. Rev.* **D71**, 074003 (2005), [hep-ph/0501109].
- [24] J. A. Nowak, *Phys. Scripta* **T127**, 70 (2006), [hep-ph/0607081].
- [25] L. Alvarez-Ruso, S. K. Singh and M. J. Vicente Vacas, *Phys. Rev.* **C57**, 2693 (1998), [arXiv:nucl-th/9712058].
- [26] S. X. Nakamura, H. Kamano and T. Sato, *Phys. Rev.* **D92**, 7, 074024 (2015), [arXiv:1506.03403].
- [27] M. Glück, E. Reya and A. Vogt, *Eur. Phys. J.* **C5**, 461 (1998), [hep-ph/9806404].
- [28] A. Bodek and U. K. Yang, *J. Phys.* **G29**, 1899 (2003), [hep-ex/0210024].
- [29] T. Sjostrand, S. Mrenna and P. Z. Skands, *JHEP* **05**, 026 (2006), [hep-ph/0603175].
- [30] A. Kayis-Topaksu *et al.* (CHORUS), *Eur. Phys. J.* **C51**, 775 (2007), [arXiv:0707.1586].
- [31] J. Altegoer *et al.* (NOMAD), *Phys. Lett.* **B445**, 439 (1999).

- [32] T. Yang *et al.*, Eur. Phys. J. **C63**, 1 (2009), [arXiv:0904.4043].
- [33] J. A. Nowak and J. T. Sobczyk, Acta Phys. Polon. **B37**, 2371 (2006), [hep-ph/0608108].
- [34] Z. Koba, H. B. Nielsen and P. Olesen, Nucl. Phys. **B40**, 317 (1972).
- [35] R. A. Smith and E. J. Moniz, Nucl. Phys. **B43**, 605 (1972), [Erratum: Nucl. Phys.B101,547(1975)].
- [36] A. Bodek and J. L. Ritchie, Phys. Rev. **D24**, 1400 (1981).
- [37] J. A. Caballero *et al.*, Phys. Lett. **B653**, 366 (2007), [arXiv:0705.1429].
- [38] P. A. Rodrigues *et al.* (MINERvA), Phys. Rev. Lett. **116**, 071802 (2016), [Addendum: Phys. Rev. Lett.121,no.20,209902(2018)], [arXiv:1511.05944].
- [39] L. Alvarez-Ruso *et al.*, Prog. Part. Nucl. Phys. **100**, 1 (2018), [arXiv:1706.03621].
- [40] T. Katori, AIP Conf. Proc. **1663**, 1, 030001 (2015), [arXiv:1304.6014].
- [41] M. Alam *et al.* (2015), [arXiv:1512.06882].
- [42] C. Wilkinson *et al.*, Phys. Rev. **D93**, 7, 072010 (2016), [arXiv:1601.05592].
- [43] A. Bodek, M. E. Christy and B. Coopersmith, Eur. Phys. J. **C74**, 10, 3091 (2014), [arXiv:1405.0583].
- [44] A. Bodek, H. S. Budd and M. E. Christy, Eur. Phys. J. **C71**, 1726 (2011), [arXiv:1106.0340].
- [45] J. Nieves, I. Ruiz Simo and M. J. Vicente Vacas, Phys. Rev. **C83**, 045501 (2011), [arXiv:1102.2777].
- [46] R. Gran *et al.*, Phys. Rev. **D88**, 11, 113007 (2013), [arXiv:1307.8105].
- [47] D. Rein and L. M. Sehgal, Nucl. Phys. **B223**, 29 (1983).
- [48] C. Berger and L. M. Sehgal, Phys. Rev. **D79**, 053003 (2009), [arXiv:0812.2653].
- [49] L. Alvarez-Ruso *et al.*, Phys. Rev. **C75**, 055501 (2007), [Erratum: Phys. Rev.C80,019906(2009)], [arXiv:nucl-th/0701098].
- [50] L. Alvarez-Ruso, L. S. Geng and M. J. Vicente Vacas, Phys. Rev. **C76**, 068501 (2007), [Erratum: Phys. Rev.C80,029904(2009)], [arXiv:0707.2172].

44. Monte Carlo Particle Numbering Scheme

Revised August 2019 by F. Krauss (Durham U.), S. Navas (Dp.de Fisica. U. de Granada), P. Richardson (Durham U.) and T. Sjöstrand (Lund U.).

The Monte Carlo particle numbering scheme presented here is intended to facilitate interfacing between event generators, detector simulators, and analysis packages used in particle physics. The numbering scheme was introduced in 1988 [1] and a revised version [2, 3] was adopted in 1998 in order to allow systematic inclusion of quark model states which are as yet undiscovered and hypothetical particles such as SUSY particles. The numbering scheme is used in several event generators, *e.g.* HERWIG, PYTHIA, and SHERPA, and interfaces, *e.g.* /HEPEVT/ and HepMC.

The general form is a 7-digit number:

$$\pm n \ n_r \ n_L \ n_{q_1} \ n_{q_2} \ n_{q_3} \ n_J .$$

This encodes information about the particle's spin, flavor content, and internal quantum numbers. The details are as follows:

1. Particles are given positive numbers, antiparticles negative numbers. The PDG convention for mesons is used, so that K^+ and B^+ are particles.
2. Quarks and leptons are numbered consecutively starting from 1 and 11 respectively; to do this they are first ordered by family and within families by weak isospin.
3. In composite quark systems (diquarks, mesons, and baryons) $n_{q_{1-3}}$ are quark numbers used to specify the quark content, while the rightmost digit $n_J = 2J + 1$ gives the system's spin (except for the K_S^0 and K_L^0). The scheme does not cover particles of spin $J > 4$.
4. Diquarks have 4-digit numbers with $n_{q_1} \geq n_{q_2}$ and $n_{q_3} = 0$.
5. The numbering of mesons is guided by the nonrelativistic (L - S decoupled) quark model, as listed in Tables 15.2, 15.3, and 15.4.
 - (a) The numbers specifying the meson's quark content conform to the convention $n_{q_1} = 0$ and $n_{q_2} \geq n_{q_3}$. The special case K_L^0 is the sole exception to this rule.
 - (b) The quark numbers of flavorless, light (u, d, s) mesons are: 11 for the member of the isotriplet (π^0, ρ^0, \dots), 22 for the lighter isosinglet (η, ω, \dots), and 33 for the heavier isosinglet (η', ϕ, \dots). Since isosinglet mesons are often large mixtures of $u\bar{u} + d\bar{d}$ and $s\bar{s}$ states, 22 and 33 are assigned by mass and do not necessarily specify the dominant quark composition.
 - (c) The special numbers 310 and 130 are given to the K_S^0 and K_L^0 respectively.
 - (d) The fifth digit n_L is reserved to distinguish mesons of the same total (J) but different spin (S) and orbital (L) angular momentum quantum numbers. For $J > 0$ the numbers are: (L, S) = ($J - 1, 1$) $n_L = 0$, ($J, 0$) $n_L = 1$, ($J, 1$) $n_L = 2$ and ($J + 1, 1$) $n_L = 3$. For the exceptional case $J = 0$ the numbers are ($0, 0$) $n_L = 0$ and ($1, 1$) $n_L = 1$ (*i.e.* $n_L = L$). See Table 44.1.
 - (e) If a set of physical mesons correspond to a (non-negligible) mixture of basis states, differing in their internal quantum numbers, then the lightest physical state gets the smallest basis state number. For example the $K_1(1270)$ is numbered 10313 ($1^1P_1 K_{1B}$) and the $K_1(1400)$ is numbered 20313 ($1^3P_1 K_{1A}$).
 - (f) The sixth digit n_r is used to label mesons radially excited above the ground state.
 - (g) Numbers have been assigned for complete $n_r = 0$ S - and P -wave multiplets, even where states remain to be identified.
 - (h) In some instances assignments within the $q\bar{q}$ meson model are only tentative; here best guess assignments are made.
 - (i) Many states appearing in the Meson Listings are not yet assigned within the $q\bar{q}$ model. Here $n_{q_{2-3}}$ and n_J

Table 44.1: Meson numbering logic. Here qq stands for $n_{q_2} n_{q_3}$.

J	$L = J - 1, S = 1$			$L = J, S = 0$			$L = J, S = 1$			$L = J + 1, S = 1$		
	code	J^{PC}	L	code	J^{PC}	L	code	J^{PC}	L	code	J^{PC}	L
0	—	—	—	00qq1	0 ⁻⁺	0	—	—	—	10qq1	0 ⁺⁺	1
1	00qq3	1 ⁻⁻	0	10qq3	1 ⁺⁻	1	20qq3	1 ⁺⁺	1	30qq3	1 ⁻⁻	2
2	00qq5	2 ⁺⁺	1	10qq5	2 ⁻⁺	2	20qq5	2 ⁻⁻	2	30qq5	2 ⁺⁺	3
3	00qq7	3 ⁻	2	10qq7	3 ⁺⁻	3	20qq7	3 ⁺⁺	3	30qq7	3 ⁻	4
4	00qq9	4 ⁺⁺	3	10qq9	4 ⁻⁺	4	20qq9	4 ⁻⁻	4	30qq9	4 ⁺⁺	5

are assigned according to the state's likely flavors and spin; all such unassigned light isoscalar states are given the flavor code 22. Within these groups $n_L = 0, 1, 2, \dots$ is used to distinguish states of increasing mass. These states are flagged using $n = 9$. It is to be expected that these numbers will evolve as the nature of the states are elucidated. Codes are assigned to all mesons which are listed in the one-page table at the end of the Meson Summary Table as long as they have a preferred or established spin. Additional heavy meson states expected from heavy quark spectroscopy are also assigned codes.

6. The numbering of baryons is again guided by the nonrelativistic quark model, see Table 15.7. This numbering scheme is illustrated through a few examples in Table 44.2.
 - (a) The numbers specifying a baryon's quark content are such that in general $n_{q_1} \geq n_{q_2} \geq n_{q_3}$.
 - (b) Two states exist for $J = 1/2$ baryons containing 3 different types of quarks. In the lighter baryon ($\Lambda, \Xi, \Omega, \dots$) the light quarks are in an antisymmetric ($J = 0$) state while for the heavier baryon ($\Sigma^0, \Xi', \Omega', \dots$) they are in a symmetric ($J = 1$) state. In this situation n_{q_2} and n_{q_3} are reversed for the lighter state, so that the smaller number corresponds to the lighter baryon.
 - (c) For excited baryons a scheme is adopted, where the n_r label is used to denote the excitation bands in the harmonic oscillator model, see Sec. 15.4. Using the notation employed there, n_r is given by the N -index of the D_N band identifier.
 - (d) Further degeneracies of excited hadron multiplets with the same excitation number n_r and spin J are lifted by labelling such multiplets with the n_L index according to their mass, as given by its N or Δ -equivalent.
 - (e) In such excited multiplets extra singlets may occur, the $\Lambda(1520)$ being a prominent example. In such cases the ordering is reversed such that the heaviest quark label is pushed to the last position: $n_{q_3} > n_{q_1} > n_{q_2}$.
 - (f) For pentaquark states $n = 9$, $n_r n_L n_{q_1} n_{q_2}$ gives the four quark numbers in order $n_r \geq n_L \geq n_{q_1} \geq n_{q_2}$, n_{q_3} gives the antiquark number, and $n_J = 2J + 1$, with the assumption that $J = 1/2$ for the states currently reported.
7. The gluon, when considered as a gauge boson, has official number 21. In codes for glueballs, however, 9 is used to allow a notation in close analogy with that of hadrons.
8. The pomeron and odderon trajectories and a generic reggeon trajectory of states in QCD are assigned codes 990, 9990, and 110 respectively, where the final 0 indicates the indeterminate nature of the spin, and the other digits reflect the expected "valence" flavor content. We do not attempt a complete classification of all reggeon trajectories, since there is currently no need to distinguish a specific such trajectory from its lowest-lying member.
9. Two-digit numbers in the range 21–30 are provided for the Standard Model gauge bosons and Higgs.
10. Codes 81–100 are reserved for generator-specific pseudoparticles and concepts. Codes 901–930, 1901–1930, 2901–2930, and 3901–3930 are for additional components of Standard Model parton distribution functions, where the latter three

Table 44.2: Some examples of octet (top) and decuplet (bottom) members for the numbering scheme for excited baryons. Here qqq stands for $n_{q_1}n_{q_2}n_{q_3}$. See the text for the definition of the notation. The numbers in parenthesis correspond to the mass of the baryons. The states marked as (?) are not experimentally confirmed.

J^P	(D, L_N^P)	$n_r n_L n_{q_1} n_{q_2} n_{q_3} n_J$	N	Λ_8	Σ	Ξ	Λ_1
Octet							
1/2 ⁺	(56, 0 ₀ ⁺)	00qqq2	(939)	(1116)	(1193)	(1318)	—
1/2 ⁺	(56, 0 ₂ ⁺)	20qqq2	(1440)	(1600)	(1660)	(1690)	—
1/2 ⁺	(70, 0 ₂ ⁺)	21qqq2	(1710)	(1810)	(1880)	(?)	(?)
1/2 ⁻	(70, 1 ₁ ⁻)	10qqq2	(1535)	(1670)	(1620)	(1750)	(1405)
J^P	(D, L_N^P)	$n_r n_L n_{q_1} n_{q_2} n_{q_3} n_J$	Δ	Σ	Ξ	Ω	
Decuplet							
3/2 ⁺	(56, 0 ₀ ⁺)	00qqq4	(1232)	(1385)	(1530)	(333)	—
3/2 ⁺	(56, 0 ₂ ⁺)	20qqq4	(1600)	(1690)	(?)	(?)	—
1/2 ⁻	(70, 1 ₁ ⁻)	11qqq2	(1620)	(1750)	(?)	(?)	—
3/2 ⁻	(70, 1 ₁ ⁻)	12qqq4	(1700)	(?)	(?)	(?)	—

ranges are intended to distinguish left/ right/ longitudinal components. Codes 998 and 999 are reserved for GEANT tracking purposes.

11. The search for physics beyond the Standard Model is an active area, so these codes are also standardized as far as possible.
 - (a) A standard fourth generation of fermions is included by analogy with the first three.
 - (b) The graviton and the boson content of a two-Higgs-doublet scenario and of additional SU(2)×U(1) groups are found in the range 31–40.
 - (c) “One-of-a-kind” exotic particles are assigned numbers in the range 41–80. The subrange 61–80 can be used for new heavier fermions in generic models, where partners to the SM fermions would have codes offset by 60. If required, however, other assignments could be made.
 - (d) Fundamental supersymmetric particles are identified by adding a nonzero n to the particle number. The superpartner of a boson or a left-handed fermion has $n = 1$ while the superpartner of a right-handed fermion has $n = 2$. When mixing occurs, such as between the winos and charged Higgsinos to give charginos, or between left and right sfermions, the lighter physical state is given the smaller basis state number.
 - (e) Technicolor states have $n = 3$, with technifermions treated like ordinary fermions. States which are ordinary color singlets have $n_r = 0$. Color octets have $n_r = 1$. If a state has non-trivial quantum numbers under the topcolor groups SU(3)₁ × SU(3)₂, the quantum numbers are specified by tech, ij , where i and j are 1 or 2. n_L is then $2i + j$. The colon, V_8 , is a heavy gluon color octet and thus is 3100021.
 - (f) Excited (composite) quarks and leptons are identified by setting $n = 4$ and $n_r = 0$.
 - (g) Within several scenarios of new physics, it is possible to have colored particles sufficiently long-lived for color-singlet hadronic states to form around them. In the context of supersymmetric scenarios, these states are called R -hadrons, since they carry odd R -parity. R -hadron codes, defined here, should be viewed as templates for corresponding codes also in other scenarios, for any long-lived particle that is either an unflavored color octet or a flavored color triplet. The R -hadron code is obtained by combining the SUSY particle code with a code for the light degrees of freedom, with as many intermediate zeros removed from the former as required to make place for the latter at the end. (To exemplify, a sparticle $n00000n_{\bar{q}}$ combined with quarks q_1 and q_2 obtains code $n00n_{\bar{q}}n_{q_1}n_{q_2}n_J$.) Specifically, the new-particle spin decouples in the limit of large masses, so that the final n_J digit is defined by the spin state of the light-quark system alone. An appropriate number of n_q digits is used to define the ordinary-quark content. As usual, 9

rather than 21 is used to denote a gluon/gluino in composite states. The sign of the hadron agrees with that of the constituent new particle (a color triplet) where there is a distinct new antiparticle, and else is defined as for normal hadrons. Particle names are R with the flavor content as lower index.

- (h) A black hole in models with extra dimensions has code 5000040. Kaluza-Klein excitations in models with extra dimensions have $n = 5$ or $n = 6$, to distinguish excitations of left- or right-handed fermions or, in case of mixing, the lighter or heavier state (cf. 11d). The nonzero n_r digit gives the radial excitation number, in scenarios where the level spacing allow these to be distinguished. Should the model also contain supersymmetry, excited SUSY states would be denoted by an $n_r > 0$, with $n = 1$ or 2 as usual. Should some colored states be long-lived enough that hadrons would form around them, the coding strategy of 11g applies, with the initial two nn_r digits preserved in the combined code.
 - (i) Magnetic monopoles and dyons are assumed to have one unit of Dirac monopole charge and a variable integer number $n_{q_1}n_{q_2}n_{q_3}$ units of electric charge. Codes $411n_{q_1}n_{q_2}n_{q_3}0$ are then used when the magnetic and electrical charge sign agree and $412n_{q_1}n_{q_2}n_{q_3}0$ when they disagree, with the overall sign of the particle set by the magnetic charge. For now no spin information is provided.
 - (j) The nature of Dark Matter (DM) is not known, and therefore a definitive classification is too early. Candidates within specific scenarios are classified therein, such as 1000022 for the lightest neutralino. Generic fundamental states can be given temporary codes in the range 51 - 60, with 51, 52 and 53 reserved for spin 0, 1/2 and 1 ones (this could also be an axion state). Generic mediators of s-channel DM pair creation or annihilation can be given codes 54 and 55 for spin 0 or 1 ones. Separate antiparticles, with negative codes, may or may not exist. More elaborate new scenarios should be constructed with $n = 5$ and $n_r = 9$.
 - (k) Hidden Valley particles have $n = 4$ and $n_r = 9$, and trailing numbers in agreement with their nearest-analog standard particles, as far as possible. Thus 4900021 is the gauge boson g_v of a confining gauge field, 490000 n_{q_v} and 490001 n_{ℓ_v} fundamental constituents charged or not under this, 4900022 is the γ_v of a non-confining field, and 4900 $n_{q_{v1}}n_{q_{v2}}n_J$ a Hidden Valley meson.
12. Occasionally program authors add their own states. To avoid confusion, these should be flagged by setting $nn_r = 99$.
 13. Concerning the non-99 numbers, it may be noted that only quarks, excited quarks, squarks, and diquarks have $n_{q_3} = 0$; only diquarks, baryons (including pentaquarks), and the odderon have $n_{q_1} \neq 0$; and only mesons, the reggeon, and the pomeron have $n_{q_1} = 0$ and $n_{q_2} \neq 0$. Concerning mesons

(not antimesons), if n_{q1} is odd then it labels a quark and an antiquark if even.

14. Nuclear codes are given as 10-digit numbers $\pm 10LZZZAAAI$. For a (hyper)nucleus consisting of n_p protons, n_n neutrons and n_A A 's, $A = n_p + n_n + n_A$ gives the total baryon number, $Z = n_p$ the total charge and $L = n_A$ the total number of strange quarks. I gives

the isomer level, with $I = 0$ corresponding to the ground state and $I > 0$ to excitations, see [4], where states denoted m, n, p, q translate to $I = 1-4$. As examples, the deuteron is 1000010020 and ^{235}U is 1000922350. To avoid ambiguities, nuclear codes should not be applied to a single hadron, like p, n or A^0 , where quark-contents-based codes already exist.

QUARKS		DIQUARKS		LIGHT I = 1 MESONS		LIGHT I = 0 MESONS ($u\bar{u}, d\bar{d}, s\bar{s}$ admixtures)		STRANGE MESONS	
d	1	$(dd)_1$	1103	π^0	111	η	221	K^0	130
u	2	$(ud)_0$	2101	π^+	211	$\eta'(958)$	331	K^+_0	310
s	3	$(ud)_1$	2103	$a_0(980)^+$	9000111	$f_0(500)$	9000221	$K^+_0(700)^0$	9000311
c	4	$(uu)_1$	2203	$\pi(1300)^0$	100111	$f_0(980)$	9010221	$K^*_0(700)^+$	9000321
b	5	$(sd)_0$	3101	$\pi(1300)^+$	100211	$\eta(1295)$	100221	$K^*_0(1430)^0$	10311
t	6	$(sd)_1$	3103	$a_0(1450)^0$	10111	$f_0(1370)$	10221	$K^*_0(1430)^+$	10321
b'	7	$(su)_0$	3201	$a_0(1450)^+$	10211	$\eta(1405)$	9020221	$K(1460)^0$	100311
t'	8	$(su)_1$	3203	$\pi(1800)^0$	9010111	$\eta(1475)$	100331	$K(1460)^+$	100321
		$(ss)_1$	3303	$\rho(1770)^0$	113	$f_0(1500)$	9030221	$K(1830)^0$	9010311
		$(cd)_0$	4101	$\rho(770)^+$	213	$f_0(1710)$	10331	$K(1830)^+$	9010321
		$(cd)_1$	4103	$b_1(1235)^0$	10113	$\eta(1760)$	9040221	$K^*_0(1950)^0$	9020311
		$(cu)_0$	4201	$b_1(1235)^+$	10213	$f_0(2020)$	9050221	$K^*_0(1950)^+$	9020321
		$(cu)_1$	4203	$a_1(1260)^0$	20113	$f_0(2100)$	9060221	$K^*(892)^0$	313
		$(cs)_0$	4301	$a_1(1260)^+$	20213	$f_0(2200)$	9070221	$K^*(892)^+$	323
		$(cs)_1$	4303	$\pi_1(1400)^0$	9000113	$\eta(2225)$	9080221	$K_1(1270)^0$	10313
		$(cc)_1$	4403	$\pi_1(1400)^+$	9000213	$\omega(782)$	223	$K_1(1270)^+$	10323
		$(bd)_0$	5101	$\rho(1450)^0$	100113	$\phi(1020)$	333	$K_1(1400)^0$	20313
		$(bd)_1$	5103	$\rho(1450)^+$	100213	$h_1(1170)$	10223	$K_1(1400)^+$	20323
		$(bu)_0$	5201	$\pi_1(1600)^0$	9010113	$f_1(1285)$	20223	$K^*(1410)^0$	100313
		$(bu)_1$	5203	$\pi_1(1600)^+$	9010213	$h_1(1380)$	10333	$K^*(1410)^+$	100323
		$(bs)_0$	5301	$a_1(1640)^0$	9020113	$f_1(1420)$	20333	$K_1(1650)^0$	9000313
		$(bs)_1$	5303	$a_1(1640)^+$	9020213	$\omega(1420)$	1000223	$K_1(1650)^+$	9000323
		$(bc)_0$	5401	$\rho(1700)^0$	30113	$f_1(1510)$	9000223	$K^*(1680)^0$	30313
		$(bc)_1$	5403	$\rho(1700)^+$	30213	$h_1(1595)$	9010223	$K^*(1680)^+$	30323
		$(bb)_1$	5503	$\rho(1900)^0$	9030113	$\omega(1650)$	30223	$K^*_2(1430)^0$	315
				$\rho(1900)^+$	9030213	$\phi(1680)$	100333	$K^*_2(1430)^+$	325
				$\rho(2150)^0$	9040113	$f_2(1270)$	225	$K_2(1580)^0$	9000315
				$\rho(2150)^+$	9040213	$f_2(1430)$	9000225	$K_2(1580)^+$	9000325
				$a_2(1320)^0$	115	$f'_2(1525)$	335	$K_2(1770)^0$	10315
				$a_2(1320)^+$	215	$f_2(1565)$	9010225	$K_2(1770)^+$	10325
				$\pi_2(1670)^0$	10115	$f_2(1640)$	9020225	$K_2(1820)^0$	20315
				$\pi_2(1670)^+$	10215	$\eta_2(1645)$	10225	$K_2(1820)^+$	20325
				$a_2(1700)^0$	9000115	$f_2(1810)$	9030225	$K^*_2(1980)^0$	9010315
				$a_2(1700)^+$	9000215	$\eta_2(1870)$	10335	$K^*_2(1980)^+$	9010325
				$\pi_2(2100)^0$	9010115	$f_2(1910)$	9040225	$K_2(2250)^0$	9020315
				$\pi_2(2100)^+$	9010215	$f_2(1950)$	9050225	$K_2(2250)^+$	9020325
				$\rho_3(1690)^0$	117	$f_2(2010)$	9060225	$K^*_3(1780)^0$	317
				$\rho_3(1690)^+$	217	$f_2(2150)$	9070225	$K^*_3(1780)^+$	327
				$\rho_3(1990)^0$	9000117	$f_2(2300)$	9080225	$K_3(2320)^0$	9010317
				$\rho_3(1990)^+$	9000217	$f_2(2340)$	9090225	$K_3(2320)^+$	9010327
				$\rho_3(2250)^0$	9010117	$\omega_3(1670)$	227	$K^*_4(2045)^0$	319
				$\rho_3(2250)^+$	9010217	$\phi_3(1850)$	337	$K^*_4(2045)^+$	329
				$a_4(2040)^0$	119	$f_4(2050)$	229	$K_4(2500)^0$	9000319
				$a_4(2040)^+$	219	$f_{fJ}(2220)$	9000229	$K_4(2500)^+$	9000329
						$f_4(2300)$	9010229		
LEPTONS		SUSY PARTICLES							
e^-	11	\tilde{d}_L	1000001						
ν_e	12	\tilde{u}_L	1000002						
μ^-	13	\tilde{s}_L	1000003						
ν_μ	14	\tilde{c}_L	1000004						
τ^-	15	\tilde{b}_1	1000005 ^a						
ν_τ	16	\tilde{t}_1	1000006 ^a						
τ'^-	17	\tilde{e}_L	1000011						
$\nu_{\tau'}$	18	$\tilde{\nu}_eL$	1000012						
GAUGE AND HIGGS BOSONS		$\tilde{\mu}_L$	1000013						
g	(9) 21	$\tilde{\nu}_\mu L$	1000014						
γ	22	$\tilde{\tau}_1^-$	1000015 ^a						
Z^0	23	$\tilde{\nu}_{\tau}L$	1000016						
W^+	24	\tilde{d}_R	2000001						
h^0/H^0_1	25	\tilde{u}_R	2000002						
Z'/Z^0_2	32	\tilde{s}_R	2000002						
Z''/Z^0_3	33	\tilde{c}_R	2000003						
W'/W^+_2	34	\tilde{b}_2	2000005 ^a						
H^0/H^0_2	35	\tilde{t}_2	2000006 ^a						
A^0/H^0_3	36	\tilde{e}_R	2000011						
H^+	37	$\tilde{\nu}_eL$	1000012						
H^{++}	38*	$\tilde{\mu}_L$	1000013						
a^0/H^0_4	40*	$\tilde{\nu}_\mu L$	1000014						
		$\tilde{\tau}_1^-$	1000015 ^a						
		$\tilde{\nu}_{\tau}L$	1000016						
SPECIAL PARTICLES		\tilde{d}_R	2000001						
G (graviton)	39	\tilde{u}_R	2000002						
R^0	41	\tilde{s}_R	2000003						
LQ^c	42	\tilde{b}_2	2000005 ^a						
$DM (S=0)$	51	\tilde{t}_2	2000006 ^a						
$DM (S=\frac{1}{2})$	52	\tilde{e}_R	2000011						
$DM (S=1)$	53	$\tilde{\mu}_R$	2000013						
<i>reggeon</i>	110	$\tilde{\tau}_2^-$	2000015 ^a						
<i>pomeron</i>	990	g	1000021						
<i>odderon</i>	9990	$\tilde{\chi}^0_1$	1000022 ^b						
for MC internal use		$\tilde{\chi}^0_2$	1000023 ^b						
81-100,		$\tilde{\chi}^0_3$	1000025 ^b						
901-930, 998-999*		$\tilde{\chi}^+_1$	1000024 ^b						
1901-1930,		$\tilde{\chi}^+_2$	1000026 ^b						
2901-2930, and		$\tilde{\chi}^0_3$	1000025 ^b						
3901-3930		$\tilde{\chi}^0_4$	1000035 ^b						
		$\tilde{\chi}^+_2$	1000037 ^b						
		G	1000039						

CHARMED MESONS		B_c^{*+}	10541	$\Upsilon(11020)$	9010553	CHARMED BARYONS		BOTTOM BARYONS	
D^+	411	B_c^{*+}	543	$\chi_{b2}(1P)$	555	Λ_c^+	4122	Λ_b^0	5122
D^0	421	$B_{c1}(L)^+$	10543	$\eta_{b2}(1D)$	10555	Σ_c^{*+}	4222	Σ_b^-	5112
$D_0^*(2400)^+$	10411	$B_{c1}(H)^+$	20543	$\Upsilon_2(1D)$	20555	Σ_c^+	4212	Σ_b^0	5212
$D_0^*(2400)^0$	10421	B_{c2}^{*+}	545	$\chi_{b2}(2P)$	100555	Σ_c^0	4112	Σ_b^+	5222
$D^*(2010)^+$	413			$\eta_{b2}(2D)$	110555	Σ_c^{*0}	4224	Σ_b^{*-}	5114
$D^*(2007)^0$	423			$\Upsilon_2(2D)$	120555	Σ_c^+	4214	Σ_b^{*0}	5214
$D_1(2430)^+$	10413			$\chi_{b2}(3P)$	200555	Σ_c^{*0}	4114	Σ_b^{*+}	5224
$D_1(2420)^0$	10423			$\Upsilon_3(1D)$	557	Ξ_c^+	4232	Ξ_b^-	5132
$D_1(H)^+$	20413			$\Upsilon_3(2D)$	100557	Ξ_c^0	4132	Ξ_b^0	5232
$D_1(2430)^0$	20423					Ξ_c^+	4322	Ξ_b^+	5312
$D_2^*(2460)^+$	415					Ξ_c^0	4312	Ξ_b^0	5322
$D_2^*(2460)^0$	425					Ξ_c^{*+}	4324	Ξ_b^+	5314
D_s^+	431					Ξ_c^{*0}	4314	Ξ_b^{*0}	5324
$D_{s0}^*(2317)^+$	10431					Ω_c^0	4332	Ω_b^-	5332
D_s^{*+}	433					Ω_c^{*0}	4334	Ω_b^{*-}	5334
$D_{s1}(2536)^+$	10433					Ξ_{cc}^+	4412	Ξ_{bc}^0	5142
$D_{s1}(2460)^+$	20433					Ξ_{cc}^{*+}	4422	Ξ_{bc}^{*0}	5242
$D_{s2}^*(2573)^+$	435					Ξ_{cc}^{*0}	4414	Ξ_{bc}^{*+}	5412
						Ξ_{cc}^{*+}	4424	Ξ_{bc}^{*0}	5422
						Ω_{cc}^+	4432	Ξ_{bc}^{*+}	5414
						Ω_{cc}^{*+}	4434	Ξ_{bc}^{*0}	5424
						Ω_{ccc}^+	4444	Ξ_{bc}^{*+}	5342
								Ω_{bc}^0	5432
								Ω_{bc}^{*0}	5434
								Ω_{bc}^{*+}	5442
								Ω_{bc}^{*+}	5444
								Ξ_{bb}^-	5512
								Ξ_{bb}^0	5522
								Ξ_{bb}^{*0}	5514
								Ξ_{bb}^{*+}	5524
								Ω_{bb}^-	5532
								Ω_{bb}^0	5542
								Ω_{bb}^{*0}	5544
								Ω_{bbb}	5554
								PENTAQUARKS	
								Θ^+	9221132
								Φ^{--}	9331122

Footnotes to the Tables:

*) Numbers or names in bold face are new or have changed since the 2018 *Review*.

a) Particular in the third generation, the left and right fermion states may mix, as shown. The lighter mixed state is given the smaller number.

b) The physical $\tilde{\chi}$ states are admixtures of the pure $\tilde{\gamma}$, \tilde{Z}^0 , \tilde{W}^+ , \tilde{H}_1^0 , \tilde{H}_2^0 , and \tilde{H}^+ states.

c) Σ^* and Ξ^* are alternate names for $\Sigma(1385)$ and $\Xi(1530)$.

This text and full lists of particle numbers can be found on-

line [5].

References

[1] G. P. Yost *et al.* (Particle Data Group), Phys. Lett. **B204**, 1 (1988).
 [2] I.G.Knowles *et al.*, CERN 96-01, p. 103.
 [3] C. Caso *et al.* (Particle Data Group), Eur. Phys. J. **C3**, 1 (1998).
 [4] G. Audi *et al.*, Nucl. Phys. **A729**, 3 (2003).
 [5] <http://pdg.lbl.gov/current/mc-particle-id>.

45. Clebsch-Gordan Coefficients, Spherical Harmonics, and d Functions

Note: A square-root sign is to be understood over every coefficient, e.g., for $-8/15$ read $-\sqrt{8/15}$.

Notation: $\begin{matrix} J & J & \dots \\ M & M & \dots \end{matrix}$

$$1/2 \times 1/2 \begin{array}{|c|c|c|} \hline 1 & & \\ \hline +1 & 1 & 0 \\ \hline +1/2 & -1/2 & 1/2 & 1/2 \\ \hline -1/2 & +1/2 & 1/2 & -1/2 \\ \hline -1/2 & -1/2 & 1 & \\ \hline \end{array}$$

$$Y_1^0 = \sqrt{\frac{3}{4\pi}} \cos \theta$$

$$Y_1^1 = -\sqrt{\frac{3}{8\pi}} \sin \theta e^{i\phi}$$

$$Y_2^0 = \sqrt{\frac{5}{4\pi}} \left(\frac{3}{2} \cos^2 \theta - \frac{1}{2} \right)$$

$$Y_2^1 = -\sqrt{\frac{15}{8\pi}} \sin \theta \cos \theta e^{i\phi}$$

$$Y_2^2 = \frac{1}{4} \sqrt{\frac{15}{2\pi}} \sin^2 \theta e^{2i\phi}$$

m_1	m_2	Coefficients
m_1	m_2	
\vdots	\vdots	
\vdots	\vdots	

$$1 \times 1/2 \begin{array}{|c|c|c|} \hline 3/2 & & \\ \hline +3/2 & 3/2 & 1/2 \\ \hline +1 & +1/2 & +1/2 \\ \hline +1 & -1/2 & 1/3 & 2/3 & 3/2 & 1/2 \\ \hline 0 & +1/2 & 2/3 & -1/3 & -1/2 & -1/2 \\ \hline \end{array}$$

$$3/2 \times 1 \begin{array}{|c|c|c|} \hline 5/2 & & \\ \hline +5/2 & 5/2 & 3/2 \\ \hline +3/2 & +1 & +3/2 & +3/2 \\ \hline +3/2 & 0 & 2/5 & 3/5 & 5/2 & 3/2 & 1/2 \\ \hline +1/2 & +1 & 3/5 & -2/5 & +1/2 & +1/2 & +1/2 \\ \hline \end{array}$$

$$3/2 \times 1/2 \begin{array}{|c|c|c|} \hline 2 & & \\ \hline +2 & 2 & 1 \\ \hline +3/2 & +1/2 & 1 & +1 & +1 \\ \hline +3/2 & -1/2 & 1/4 & 3/4 & 2 & 1 \\ \hline +1/2 & +1/2 & 3/4 & -1/4 & 0 & 0 \\ \hline \end{array}$$

$$2 \times 1 \begin{array}{|c|c|c|} \hline 3 & & \\ \hline +3 & 3 & 2 \\ \hline +2 & +1 & +2 & +2 \\ \hline +2 & 0 & 1/3 & 2/3 & 3 & 2 & 1 \\ \hline +1 & +1 & 2/3 & -1/3 & +1 & +1 & +1 \\ \hline \end{array}$$

$$1 \times 1 \begin{array}{|c|c|c|} \hline 2 & & \\ \hline +2 & 2 & 1 \\ \hline +1 & +1 & +1 & +1 \\ \hline +1 & 0 & 1/2 & 1/2 & 2 & 1 & 0 \\ \hline 0 & +1 & 1/2 & -1/2 & 0 & 0 & 0 \\ \hline \end{array}$$

$$d_{\ell}^{\ell} = (-1)^m Y_{\ell}^m e^{-im\phi}$$

$$d_{\ell}^{\ell} = \sqrt{\frac{4\pi}{2\ell+1}} Y_{\ell}^m e^{-im\phi}$$

$$\langle j_1 j_2 m_1 m_2 | j_1 j_2 J M \rangle = (-1)^{J-j_1-j_2} \langle j_2 j_1 m_2 m_1 | j_2 j_1 J M \rangle$$

$$d_{m',m}^j = (-1)^{m-m'} d_{-m,-m'}^j = d_{-m,-m'}^j$$

$$3/2 \times 3/2 \begin{array}{|c|c|c|} \hline 3 & & \\ \hline +3/2 & +3/2 & 3 & 2 \\ \hline +1/2 & +3/2 & 1/2 & 1/2 & +1 & +1 & +1 \\ \hline +3/2 & -1/2 & 1/5 & 1/2 & 3/10 & 3 & 2 & 1 \\ \hline +1/2 & +1/2 & 3/5 & 0 & -2/5 & -1 & -1 & -1 \\ \hline -1/2 & +3/2 & 1/5 & -1/2 & 3/10 & -1 & -1 & -1 \\ \hline \end{array}$$

$$d_{0,0}^1 = \cos \theta \quad d_{1/2,1/2}^{1/2} = \cos \frac{\theta}{2} \quad d_{1,1}^1 = \frac{1 + \cos \theta}{2}$$

$$d_{1/2,-1/2}^{1/2} = -\sin \frac{\theta}{2} \quad d_{1,0}^1 = -\frac{\sin \theta}{\sqrt{2}}$$

$$d_{1,-1}^1 = \frac{1 - \cos \theta}{2}$$

$$2 \times 3/2 \begin{array}{|c|c|c|} \hline 7/2 & & \\ \hline +7/2 & 7/2 & 5/2 \\ \hline +2 & +3/2 & 1 & +5/2 & +5/2 \\ \hline +2 & +1/2 & 3/7 & 4/7 & 7/2 & 5/2 & 3/2 \\ \hline +1 & +3/2 & 4/7 & -3/7 & +3/2 & +3/2 & +3/2 \\ \hline \end{array}$$

$$2 \times 2 \begin{array}{|c|c|c|} \hline 4 & & \\ \hline +4 & 4 & 3 \\ \hline +2 & +2 & 1 & +3 & +3 \\ \hline +2 & +1 & 1/2 & 1/2 & 4 & 3 & 2 \\ \hline +1 & +2 & 1/2 & -1/2 & +2 & +2 & +2 \\ \hline \end{array}$$

$$d_{3/2,3/2}^{3/2} = \frac{1 + \cos \theta}{2} \cos \frac{\theta}{2}$$

$$d_{3/2,1/2}^{3/2} = -\sqrt{3} \frac{1 + \cos \theta}{2} \sin \frac{\theta}{2}$$

$$d_{3/2,-1/2}^{3/2} = \sqrt{3} \frac{1 - \cos \theta}{2} \cos \frac{\theta}{2}$$

$$d_{3/2,-3/2}^{3/2} = -\frac{1 - \cos \theta}{2} \sin \frac{\theta}{2}$$

$$d_{1/2,1/2}^{3/2} = \frac{3 \cos \theta - 1}{2} \cos \frac{\theta}{2}$$

$$d_{1/2,-1/2}^{3/2} = -\frac{3 \cos \theta + 1}{2} \sin \frac{\theta}{2}$$

$$d_{2,2}^2 = \left(\frac{1 + \cos \theta}{2} \right)^2$$

$$d_{2,1}^2 = -\frac{1 + \cos \theta}{2} \sin \theta$$

$$d_{2,0}^2 = \frac{\sqrt{6}}{4} \sin^2 \theta$$

$$d_{2,-1}^2 = -\frac{1 - \cos \theta}{2} \sin \theta$$

$$d_{2,-2}^2 = \left(\frac{1 - \cos \theta}{2} \right)^2$$

$$d_{1,1}^2 = \frac{1 + \cos \theta}{2} (2 \cos \theta - 1)$$

$$d_{1,0}^2 = -\sqrt{\frac{3}{2}} \sin \theta \cos \theta$$

$$d_{1,-1}^2 = \frac{1 - \cos \theta}{2} (2 \cos \theta + 1)$$

$$d_{0,0}^2 = \left(\frac{3}{2} \cos^2 \theta - \frac{1}{2} \right)$$

46. SU(3) isoscalar factors and representation matrices

Written by R.L. Kelly (LBNL).

The most commonly used SU(3) isoscalar factors, corresponding to the singlet, octet, and decuplet content of $8 \otimes 8$ and $10 \otimes 8$, are shown at the right. The notation uses particle names to identify the coefficients, so that the pattern of relative couplings may be seen at a glance. We illustrate the use of the coefficients below. See J.J de Swart, Rev. Mod. Phys. **35**, 916 (1963) for detailed explanations and phase conventions.

A $\sqrt{}$ is to be understood over every integer in the matrices; the exponent 1/2 on each matrix is a reminder of this. For example, the $\Xi \rightarrow \Omega K$ element of the $10 \rightarrow 10 \otimes 8$ matrix is $-\sqrt{6}/\sqrt{24} = -1/2$.

Intramultiplet relative decay strengths may be read directly from the matrices. For example, in decuplet \rightarrow octet + octet decays, the ratio of $\Omega^* \rightarrow \Xi \bar{K}$ and $\Delta \rightarrow N \pi$ partial widths is, from the $10 \rightarrow 8 \times 8$ matrix,

$$\frac{\Gamma(\Omega^* \rightarrow \Xi \bar{K})}{\Gamma(\Delta \rightarrow N \pi)} = \frac{12}{6} \times (\text{phase space factors}). \quad (46.1)$$

Including isospin Clebsch-Gordan coefficients, we obtain, e.g.,

$$\frac{\Gamma(\Omega^{*-} \rightarrow \Xi^0 K^-)}{\Gamma(\Delta^+ \rightarrow p \pi^0)} = \frac{1/2}{2/3} \times \frac{12}{6} \times p.s.f. = \frac{3}{2} \times p.s.f. \quad (46.2)$$

Partial widths for $8 \rightarrow 8 \otimes 8$ involve a linear superposition of 8_1 (symmetric) and 8_2 (antisymmetric) couplings. For example,

$$\Gamma(\Xi^* \rightarrow \Xi \pi) \sim \left(-\sqrt{\frac{9}{20}} g_1 + \sqrt{\frac{3}{12}} g_2 \right)^2. \quad (46.3)$$

The relations between g_1 and g_2 (with de Swart's normalization) and the standard D and F couplings that appear in the interaction Lagrangian,

$$\mathcal{L} = -\sqrt{2} D Tr(\{\bar{B}, B\}M) + \sqrt{2} F Tr([\bar{B}, B]M), \quad (46.4)$$

where $[\bar{B}, B] \equiv \bar{B}B - B\bar{B}$ and $\{\bar{B}, B\} \equiv \bar{B}B + B\bar{B}$, are

$$D = \frac{\sqrt{30}}{40} g_1, \quad F = \frac{\sqrt{6}}{24} g_2. \quad (46.5)$$

Thus, for example,

$$\Gamma(\Xi^* \rightarrow \Xi \pi) \sim (F - D)^2 \sim (1 - 2\alpha)^2, \quad (46.6)$$

where $\alpha \equiv F/(D + F)$. (This definition of α is de Swart's. The alternative $D/(D + F)$, due to Gell-Mann, is also used.)

The generators of SU(3) transformations, λ_a ($a = 1, 8$), are 3×3 matrices that obey the following commutation and anticommutation relationships:

$$[\lambda_a, \lambda_b] \equiv \lambda_a \lambda_b - \lambda_b \lambda_a = 2i f_{abc} \lambda_c \quad (46.7)$$

$$\{\lambda_a, \lambda_b\} \equiv \lambda_a \lambda_b + \lambda_b \lambda_a = \frac{4}{3} \delta_{ab} I + 2d_{abc} \lambda_c, \quad (46.8)$$

where I is the 3×3 identity matrix, and δ_{ab} is the Kronecker delta symbol. The f_{abc} are odd under the permutation of any pair of indices, while the d_{abc} are even. The nonzero values are

$1 \rightarrow 8 \otimes 8$

$$(\Lambda) \rightarrow (N \bar{K} \Sigma \pi \Lambda \eta \Xi K) = \frac{1}{\sqrt{8}} (2 \ 3 \ -1 \ -2)^{1/2}$$

$8_1 \rightarrow 8 \otimes 8$

$$\begin{pmatrix} N \\ \Sigma \\ \Lambda \\ \Xi \end{pmatrix} \rightarrow \begin{pmatrix} N\pi & N\eta & \Sigma K & \Lambda K \\ N\bar{K} & \Sigma\pi & \Lambda\pi & \Sigma\eta & \Xi K \\ N\bar{K} & \Sigma\pi & \Lambda\eta & \Xi K \\ \Sigma\bar{K} & \Lambda\bar{K} & \Xi\pi & \Xi\eta \end{pmatrix} = \frac{1}{\sqrt{20}} \begin{pmatrix} 9 & -1 & -9 & -1 \\ -6 & 0 & 4 & 4 & -6 \\ 2 & -12 & -4 & -2 \\ 9 & -1 & -9 & -1 \end{pmatrix}^{1/2}$$

$8_2 \rightarrow 8 \otimes 8$

$$\begin{pmatrix} N \\ \Sigma \\ \Lambda \\ \Xi \end{pmatrix} \rightarrow \begin{pmatrix} N\pi & N\eta & \Sigma K & \Lambda K \\ N\bar{K} & \Sigma\pi & \Lambda\pi & \Sigma\eta & \Xi K \\ N\bar{K} & \Sigma\pi & \Lambda\eta & \Xi K \\ \Sigma\bar{K} & \Lambda\bar{K} & \Xi\pi & \Xi\eta \end{pmatrix} = \frac{1}{\sqrt{12}} \begin{pmatrix} 3 & 3 & 3 & -3 \\ 2 & 8 & 0 & 0 & -2 \\ 6 & 0 & 0 & 6 \\ 3 & 3 & 3 & -3 \end{pmatrix}^{1/2}$$

$10 \rightarrow 8 \otimes 8$

$$\begin{pmatrix} \Delta \\ \Sigma \\ \Xi \\ \Omega \end{pmatrix} \rightarrow \begin{pmatrix} N\pi & \Sigma K \\ N\bar{K} & \Sigma\pi & \Lambda\pi & \Sigma\eta & \Xi K \\ \Sigma\bar{K} & \Lambda\bar{K} & \Xi\pi & \Xi\eta \\ \Xi\bar{K} \end{pmatrix} = \frac{1}{\sqrt{12}} \begin{pmatrix} -6 & 6 \\ -2 & 2 & -3 & 3 & 2 \\ 3 & -3 & 3 & 3 \\ 12 \end{pmatrix}^{1/2}$$

$8 \rightarrow 10 \otimes 8$

$$\begin{pmatrix} N \\ \Sigma \\ \Lambda \\ \Xi \end{pmatrix} \rightarrow \begin{pmatrix} \Delta\pi & \Sigma K \\ \Delta\bar{K} & \Sigma\pi & \Sigma\eta & \Xi K \\ \Sigma\bar{K} & \Sigma\pi & \Xi K \\ \Xi\bar{K} & \Xi\pi & \Xi\eta & \Omega K \end{pmatrix} = \frac{1}{\sqrt{15}} \begin{pmatrix} -12 & 3 \\ 8 & -2 & -3 & 2 \\ -9 & 6 \\ 3 & -3 & -3 & 6 \end{pmatrix}^{1/2}$$

$10 \rightarrow 10 \otimes 8$

$$\begin{pmatrix} \Delta \\ \Sigma \\ \Xi \\ \Omega \end{pmatrix} \rightarrow \begin{pmatrix} \Delta\pi & \Delta\eta & \Sigma K \\ \Delta\bar{K} & \Sigma\pi & \Sigma\eta & \Xi K \\ \Sigma\bar{K} & \Xi\pi & \Xi\eta & \Omega K \\ \Xi\bar{K} & \Omega\eta \end{pmatrix} = \frac{1}{\sqrt{24}} \begin{pmatrix} 15 & 3 & -6 \\ 8 & 8 & 0 & -8 \\ 12 & 3 & -3 & -6 \\ 12 & -12 \end{pmatrix}^{1/2}$$

abc	f_{abc}	abc	d_{abc}	abc	d_{abc}
123	1	118	$1/\sqrt{3}$	355	1/2
147	1/2	146	1/2	366	-1/2
156	-1/2	157	1/2	377	-1/2
246	1/2	228	$1/\sqrt{3}$	448	$-1/(2\sqrt{3})$
257	1/2	247	-1/2	558	$-1/(2\sqrt{3})$
345	1/2	256	1/2	668	$-1/(2\sqrt{3})$
367	-1/2	338	$1/\sqrt{3}$	778	$-1/(2\sqrt{3})$
458	$\sqrt{3}/2$	344	1/2	888	$-1/\sqrt{3}$
678	$\sqrt{3}/2$				

The λ_a 's are

$$\lambda_1 = \begin{pmatrix} 0 & 1 & 0 \\ 1 & 0 & 0 \\ 0 & 0 & 0 \end{pmatrix} \quad \lambda_2 = \begin{pmatrix} 0 & -i & 0 \\ i & 0 & 0 \\ 0 & 0 & 0 \end{pmatrix} \quad \lambda_3 = \begin{pmatrix} 1 & 0 & 0 \\ 0 & -1 & 0 \\ 0 & 0 & 0 \end{pmatrix}$$

$$\lambda_4 = \begin{pmatrix} 0 & 0 & 1 \\ 0 & 0 & 0 \\ 1 & 0 & 0 \end{pmatrix} \quad \lambda_5 = \begin{pmatrix} 0 & 0 & -i \\ 0 & 0 & 0 \\ i & 0 & 0 \end{pmatrix} \quad \lambda_6 = \begin{pmatrix} 0 & 0 & 0 \\ 0 & 0 & 1 \\ 0 & 1 & 0 \end{pmatrix}$$

$$\lambda_7 = \begin{pmatrix} 0 & 0 & 0 \\ 0 & 0 & -i \\ 0 & i & 0 \end{pmatrix} \quad \lambda_8 = \frac{1}{\sqrt{3}} \begin{pmatrix} 1 & 0 & 0 \\ 0 & 1 & 0 \\ 0 & 0 & -2 \end{pmatrix}$$

Equation (46.7) defines the Lie algebra of SU(3). A general d -dimensional representation is given by a set of $d \times d$ matrices satisfying Eq. (46.7) with the f_{abc} given above. Equation (46.8) is specific to the defining 3-dimensional representation.

47. *SU(n) Multiplets and Young Diagrams*

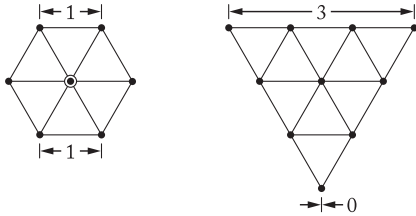
Written by C.G. Wohl (LBNL).

This note tells (1) how *SU(n)* particle multiplets are identified or labeled, (2) how to find the number of particles in a multiplet from its label, (3) how to draw the Young diagram for a multiplet, and (4) how to use Young diagrams to determine the overall multiplet structure of a composite system, such as a 3-quark or a meson-baryon system.

In much of the literature, the word “representation” is used where we use “multiplet,” and “tableau” is used where we use “diagram.”

47.1. Multiplet labels

An *SU(n)* multiplet is uniquely identified by a string of $(n-1)$ nonnegative integers: $(\alpha, \beta, \gamma, \dots)$. Any such set of integers specifies a multiplet. For an *SU(2)* multiplet such as an isospin multiplet, the single integer α is the number of *steps* from one end of the multiplet to the other (*i.e.*, it is one fewer than the number of particles in the multiplet). In *SU(3)*, the two integers α and β are the numbers of steps across the top and bottom levels of the multiplet diagram. Thus the labels for the *SU(3)* octet and decuplet



are (1,1) and (3,0). For larger n , the interpretation of the integers in terms of the geometry of the multiplets, which exist in an $(n-1)$ -dimensional space, is not so readily apparent.

The label for the *SU(n)* singlet is $(0, 0, \dots, 0)$. In a flavor *SU(n)*, the n quarks together form a $(1, 0, \dots, 0)$ multiplet, and the n antiquarks belong to a $(0, \dots, 0, 1)$ multiplet. These two multiplets are *conjugate* to one another, which means their labels are related by $(\alpha, \beta, \dots) \leftrightarrow (\dots, \beta, \alpha)$.

47.2. Number of particles

The number of particles in a multiplet, $N = N(\alpha, \beta, \dots)$, is given as follows (note the pattern of the equations).

In *SU(2)*, $N = N(\alpha)$ is

$$N = \frac{(\alpha + 1)}{1} \tag{47.1}$$

In *SU(3)*, $N = N(\alpha, \beta)$ is

$$N = \frac{(\alpha + 1)}{1} \cdot \frac{(\beta + 1)}{1} \cdot \frac{(\alpha + \beta + 2)}{2} \tag{47.2}$$

In *SU(4)*, $N = N(\alpha, \beta, \gamma)$ is

$$N = \frac{(\alpha+1)}{1} \cdot \frac{(\beta+1)}{1} \cdot \frac{(\gamma+1)}{1} \cdot \frac{(\alpha+\beta+2)}{2} \cdot \frac{(\beta+\gamma+2)}{2} \cdot \frac{(\alpha+\beta+\gamma+3)}{3} \tag{47.3}$$

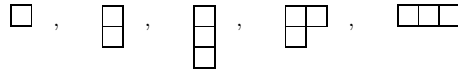
Note that in Eq. (47.3) there is no factor with $(\alpha + \gamma + 2)$: only a *consecutive* sequence of the label integers appears in any factor. One more example should make the pattern clear for any *SU(n)*. In *SU(5)*, $N = N(\alpha, \beta, \gamma, \delta)$ is

$$N = \frac{(\alpha+1)}{1} \cdot \frac{(\beta+1)}{1} \cdot \frac{(\gamma+1)}{1} \cdot \frac{(\delta+1)}{1} \cdot \frac{(\alpha+\beta+2)}{2} \cdot \frac{(\beta+\gamma+2)}{2} \cdot \frac{(\gamma+\delta+2)}{2} \cdot \frac{(\alpha+\beta+\gamma+3)}{3} \cdot \frac{(\beta+\gamma+\delta+3)}{3} \cdot \frac{(\alpha+\beta+\gamma+\delta+4)}{4} \tag{47.4}$$

From the symmetry of these equations, it is clear that multiplets that are conjugate to one another have the same number of particles, but so can other multiplets. For example, the *SU(4)* multiplets (3,0,0) and (1,1,0) each have 20 particles. Try the equations and see.

47.3. Young diagrams

A Young diagram consists of an array of boxes (or some other symbol) arranged in one or more *left-justified* rows, with each row being *at least as long* as the row beneath. The correspondence between a diagram and a multiplet label is: The top row juts out α boxes to the right past the end of the second row, the second row juts out β boxes to the right past the end of the third row, *etc.* A diagram in *SU(n)* has at most n rows. There can be any number of “completed” columns of n boxes buttressing the left of a diagram; these don’t affect the label. Thus in *SU(3)* the diagrams



represent the multiplets (1,0), (0,1), (0,0), (1,1), and (3,0). In any *SU(n)*, the quark multiplet is represented by a single box, the antiquark multiplet by a column of $(n-1)$ boxes, and a singlet by a completed column of n boxes.

47.4. Coupling multiplets together

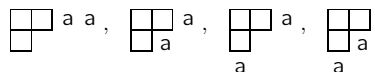
The following recipe tells how to find the multiplets that occur in coupling two multiplets together. To couple together more than two multiplets, first couple two, then couple a third with each of the multiplets obtained from the first two, *etc.*

First a definition: A sequence of the letters a, b, c, \dots is *admissible* if at any point in the sequence at least as many a ’s have occurred as b ’s, at least as many b ’s have occurred as c ’s, *etc.* Thus $abcd$ and $aabc$ are admissible sequences and abb and acb are not. Now the recipe:

(a) Draw the Young diagrams for the two multiplets, but in one of the diagrams replace the boxes in the first row with a ’s, the boxes in the second row with b ’s, *etc.* Thus, to couple two *SU(3)* octets (such as the π -meson octet and the baryon octet), we start with $\begin{smallmatrix} \square \\ \square \end{smallmatrix}$ and

$\begin{smallmatrix} a & a \\ b \end{smallmatrix}$. The *unlettered* diagram forms the *upper left-hand corner* of all the enlarged diagrams constructed below.

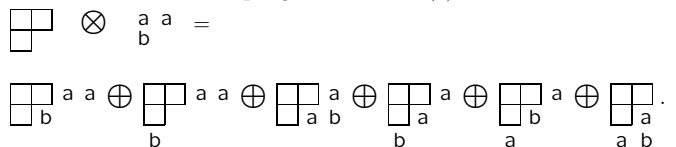
(b) Add the a ’s from the lettered diagram to the right-hand ends of the rows of the unlettered diagram to form all possible legitimate Young diagrams that have no more than one a per column. In general, there will be several distinct diagrams, and all the a ’s appear in each diagram. At this stage, for the coupling of the two *SU(3)* octets, we have:



(c) Use the b ’s to further enlarge the diagrams already obtained, subject to the same rules. Then throw away any diagram in which the full sequence of letters formed by reading *right to left* in the first row, then the second row, *etc.*, is not admissible.

(d) Proceed as in (c) with the c ’s (if any), *etc.*

The final result of the coupling of the two *SU(3)* octets is:



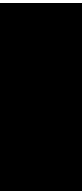
Here only the diagrams with admissible sequences of a ’s and b ’s and with fewer than four rows (since $n = 3$) have been kept. In terms of multiplet labels, the above may be written

$$(1, 1) \otimes (1, 1) = (2, 2) \oplus (3, 0) \oplus (0, 3) \oplus (1, 1) \oplus (1, 1) \oplus (0, 0) .$$

In terms of numbers of particles, it may be written

$$8 \otimes 8 = 27 \oplus 10 \oplus \overline{10} \oplus 8 \oplus 8 \oplus 1 .$$

The product of the numbers on the left here is equal to the sum on the right, a useful check. (See also Sec. 15 on the Quark Model.)



Kinematics, Cross-Section Formulae, and Plots

48. Kinematics (rev.)	671
49. Resonances (rev.)	675
50. Cross-section formulae for specific processes (rev.)	682
51. Neutrino cross section measurements (rev.)	691
52. Plots of cross sections and related quantities (rev.)	696

48. Kinematics

Reviewed August 2019 by D. Miller (Glasgow), D.R. Tovey (Sheffield) and January 2000 by J.D. Jackson (LBNL).

Throughout this section units are used in which $\hbar = c = 1$. The following conversions are useful: $\hbar c = 197.3$ MeV fm, $(\hbar c)^2 = 0.3894$ (GeV)² mb.

48.1 Lorentz transformations

The energy E and 3-momentum \mathbf{p} of a particle of mass m form a 4-vector $p = (E, \mathbf{p})$ whose square $p^2 \equiv E^2 - |\mathbf{p}|^2 = m^2$. The velocity of the particle is $\beta = \mathbf{p}/E$. The energy and momentum (E^*, \mathbf{p}^*) viewed from a frame moving with velocity β_f are given by

$$\begin{pmatrix} E^* \\ p_{\parallel}^* \end{pmatrix} = \begin{pmatrix} \gamma_f & -\gamma_f \beta_f \\ -\gamma_f \beta_f & \gamma_f \end{pmatrix} \begin{pmatrix} E \\ p_{\parallel} \end{pmatrix}, \quad p_T^* = p_T, \quad (48.1)$$

where $\gamma_f = (1 - \beta_f^2)^{-1/2}$ and p_T (p_{\parallel}) are the components of \mathbf{p} perpendicular (parallel) to β_f . Other 4-vectors, such as the space-time coordinates of events, of course transform in the same way. The scalar product of two 4-momenta $p_1 \cdot p_2 = E_1 E_2 - \mathbf{p}_1 \cdot \mathbf{p}_2$ is invariant (frame independent).

48.2 Center-of-mass energy and momentum

In the collision of two particles of masses m_1 and m_2 the total center-of-mass energy can be expressed in the Lorentz-invariant form

$$\begin{aligned} E_{\text{cm}} &= [(E_1 + E_2)^2 - (\mathbf{p}_1 + \mathbf{p}_2)^2]^{1/2}, \\ &= [m_1^2 + m_2^2 + 2E_1 E_2 (1 - \beta_1 \beta_2 \cos \theta)]^{1/2}, \end{aligned} \quad (48.2)$$

where θ is the angle between the particles. In the frame where one particle (of mass m_2) is at rest (lab frame),

$$E_{\text{cm}} = (m_1^2 + m_2^2 + 2E_{1\text{lab}} m_2)^{1/2}. \quad (48.3)$$

The velocity of the center-of-mass in the lab frame is

$$\beta_{\text{cm}} = \mathbf{p}_{\text{lab}} / (E_{1\text{lab}} + m_2), \quad (48.4)$$

where $\mathbf{p}_{\text{lab}} \equiv \mathbf{p}_{1\text{lab}}$ and

$$\gamma_{\text{cm}} = (E_{1\text{lab}} + m_2) / E_{\text{cm}}. \quad (48.5)$$

The c.m. momenta of particles 1 and 2 are of magnitude

$$p_{\text{cm}} = p_{\text{lab}} \frac{m_2}{E_{\text{cm}}}. \quad (48.6)$$

For example, if a 0.80 GeV/c kaon beam is incident on a proton target, the center of mass energy is 1.699 GeV and the center of mass momentum of either particle is 0.442 GeV/c. It is also useful to note that

$$E_{\text{cm}} dE_{\text{cm}} = m_2 dE_{1\text{lab}} = m_2 \beta_{1\text{lab}} dp_{1\text{lab}}. \quad (48.7)$$

48.3 Lorentz-invariant amplitudes

The matrix elements for a scattering or decay process are written in terms of an invariant amplitude $-i\mathcal{M}$. As an example, the S -matrix for $2 \rightarrow 2$ scattering is related to \mathcal{M} by

$$\begin{aligned} \langle p'_1 p'_2 | S | p_1 p_2 \rangle &= I - i(2\pi)^4 \delta^4(p_1 + p_2 - p'_1 - p'_2) \\ &\times \frac{\mathcal{M}(p_1, p_2; p'_1, p'_2)}{(2E_1)^{1/2} (2E_2)^{1/2} (2E'_1)^{1/2} (2E'_2)^{1/2}}. \end{aligned} \quad (48.8)$$

The state normalization is such that

$$\langle p' | p \rangle = (2\pi)^3 \delta^3(\mathbf{p} - \mathbf{p}'). \quad (48.9)$$

For a $2 \rightarrow 2$ scattering process producing unstable particles $1'$ and $2'$ decaying via $1' \rightarrow 3'4'$ and $2' \rightarrow 5'6'$ the matrix element

for the complete process can be written in the narrow width approximation as:

$$\begin{aligned} \mathcal{M}(12 \rightarrow 3'4'5'6') &= \\ \sum_{h_{1'}, h_{2'}} &\frac{\mathcal{M}(12 \rightarrow 1'2') \mathcal{M}(1' \rightarrow 3'4') \mathcal{M}(2' \rightarrow 5'6')}{(m_{3'4'}^2 - m_{1'}^2 + im_{1'} \Gamma_{1'}) (m_{5'6'}^2 - m_{2'}^2 + im_{2'} \Gamma_{2'})}. \end{aligned} \quad (48.10)$$

Here, m_{ij} is the invariant mass of particles i and j , m_k and Γ_k are the mass and total width of particle k , and the sum runs over the helicities of the intermediate particles. This enables the cross section for such a process to be written as the product of the cross section for the initial $2 \rightarrow 2$ scattering process with the branching ratios (relative partial decay rates) of the subsequent decays.

48.4 Particle decays

The partial decay rate of a particle of mass M into n bodies in its rest frame is given in terms of the Lorentz-invariant matrix element \mathcal{M} by

$$d\Gamma = \frac{(2\pi)^4}{2M} |\mathcal{M}|^2 d\Phi_n(P; p_1, \dots, p_n), \quad (48.11)$$

where $d\Phi_n$ is an element of n -body phase space given by

$$d\Phi_n(P; p_1, \dots, p_n) = \delta^4(P - \sum_{i=1}^n p_i) \prod_{i=1}^n \frac{d^3 p_i}{(2\pi)^3 2E_i}. \quad (48.12)$$

This phase space can be generated recursively, viz.

$$\begin{aligned} d\Phi_n(P; p_1, \dots, p_n) &= d\Phi_j(q; p_1, \dots, p_j) \\ &\times d\Phi_{n-j+1}(P; q, p_{j+1}, \dots, p_n) (2\pi)^3 dq^2, \end{aligned} \quad (48.13)$$

where $q^2 = (\sum_{i=1}^j E_i)^2 - |\sum_{i=1}^j \mathbf{p}_i|^2$. This form is particularly useful in the case where a particle decays into another particle that subsequently decays.

48.4.1 Survival probability

If a particle of mass M has mean proper lifetime $\tau (= 1/\Gamma)$ and has momentum (E, \mathbf{p}) , then the probability that it lives for a time t_0 or greater before decaying is given by

$$P(t_0) = e^{-t_0 \Gamma/\gamma} = e^{-M t_0 \Gamma/E}, \quad (48.14)$$

and the probability that it travels a distance x_0 or greater is

$$P(x_0) = e^{-M x_0 \Gamma/|\mathbf{p}|}. \quad (48.15)$$

48.4.2 Two-body decays

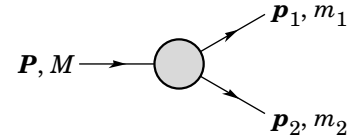


Figure 48.1: Definitions of variables for two-body decays.

In the rest frame of a particle of mass M , decaying into 2 particles labeled 1 and 2,

$$E_1 = \frac{M^2 - m_2^2 + m_1^2}{2M}, \quad (48.16)$$

$$\begin{aligned} |\mathbf{p}_1| &= |\mathbf{p}_2| \\ &= \frac{[(M^2 - (m_1 + m_2)^2)(M^2 - (m_1 - m_2)^2)]^{1/2}}{2M}, \end{aligned} \quad (48.17)$$

and

$$d\Gamma = \frac{1}{32\pi^2} |\mathcal{M}|^2 \frac{|\mathbf{p}_1|}{M^2} d\Omega, \quad (48.18)$$

where $d\Omega = d\phi_1 d(\cos\theta_1)$ is the solid angle of particle 1. The invariant mass M can be determined from the energies and momenta using Eq. (48.2) with $M = E_{\text{cm}}$.

48.4.3 Three-body decays

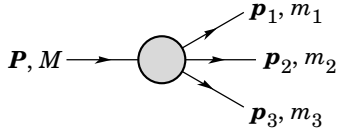


Figure 48.2: Definitions of variables for three-body decays.

Defining $p_{ij} = p_i + p_j$ and $m_{ij}^2 = p_{ij}^2$, then $m_{12}^2 + m_{23}^2 + m_{13}^2 = M^2 + m_1^2 + m_2^2 + m_3^2$ and $m_{12}^2 = (P - p_3)^2 = M^2 + m_3^2 - 2ME_3$, where E_3 is the energy of particle 3 in the rest frame of M . In that frame, the momenta of the three decay particles lie in a plane. The relative orientation of these three momenta is fixed if their energies are known. The momenta can therefore be specified in space by giving three Euler angles (α, β, γ) that specify the orientation of the final system relative to the initial particle. The direction of any one of the particles relative to the frame in which the initial particle is described can be specified in space by two angles (α, β) while a third angle, γ , can be set as the azimuthal angle of a second particle around the first [1]. Then

$$d\Gamma = \frac{1}{(2\pi)^5} \frac{1}{16M} |\mathcal{M}|^2 dE_1 dE_3 d\alpha d(\cos\beta) d\gamma. \quad (48.19)$$

Alternatively

$$d\Gamma = \frac{1}{(2\pi)^5} \frac{1}{16M^2} |\mathcal{M}|^2 |\mathbf{p}_1^*| |\mathbf{p}_3| dm_{12} d\Omega_1^* d\Omega_3, \quad (48.20)$$

where $(|\mathbf{p}_1^*|, \Omega_1^*)$ is the momentum of particle 1 in the rest frame of 1 and 2, and Ω_3 is the angle of particle 3 in the rest frame of the decaying particle. $|\mathbf{p}_1^*|$ and $|\mathbf{p}_3|$ are given by

$$|\mathbf{p}_1^*| = \frac{[(m_{12}^2 - (m_1 + m_2)^2)(m_{12}^2 - (m_1 - m_2)^2)]^{1/2}}{2m_{12}}, \quad (48.21a)$$

and

$$|\mathbf{p}_3| = \frac{[(M^2 - (m_{12} + m_3)^2)(M^2 - (m_{12} - m_3)^2)]^{1/2}}{2M}. \quad (48.21b)$$

[Compare with Eq. (48.17).]

If the decaying particle is a scalar or we average over its spin states, then integration over the angles in Eq. (48.19) gives

$$\begin{aligned} d\Gamma &= \frac{1}{(2\pi)^3} \frac{1}{8M} |\overline{\mathcal{M}}|^2 dE_1 dE_3 \\ &= \frac{1}{(2\pi)^3} \frac{1}{32M^3} |\overline{\mathcal{M}}|^2 dm_{12}^2 dm_{23}^2. \end{aligned} \quad (48.22)$$

This is the standard form for the Dalitz plot.

48.4.3.1 Dalitz plot

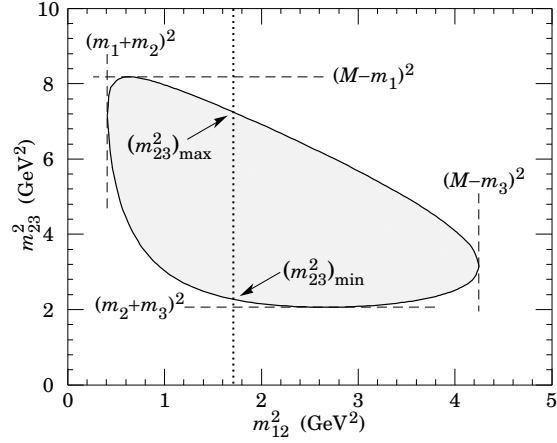
For a given value of m_{12}^2 , the range of m_{23}^2 is determined by its values when \mathbf{p}_2 is parallel or antiparallel to \mathbf{p}_3 :

$$(m_{23}^2)_{\max} = (E_2^* + E_3^*)^2 - \left(\sqrt{E_2^{*2} - m_2^2} - \sqrt{E_3^{*2} - m_3^2} \right)^2, \quad (48.23a)$$

$$(m_{23}^2)_{\min} = (E_2^* + E_3^*)^2 - \left(\sqrt{E_2^{*2} - m_2^2} + \sqrt{E_3^{*2} - m_3^2} \right)^2. \quad (48.23b)$$

Here $E_2^* = (m_{12}^2 - m_1^2 + m_2^2)/2m_{12}$ and $E_3^* = (M^2 - m_{12}^2 - m_3^2)/2m_{12}$ are the energies of particles 2 and 3 in the m_{12} rest frame. The scatter plot in m_{12}^2 and m_{23}^2 is called a Dalitz plot. If $|\overline{\mathcal{M}}|^2$ is constant, the allowed region of the plot will be uniformly populated with events [see Eq. (48.22)]. A nonuniformity

in the plot gives immediate information on $|\mathcal{M}|^2$. For example, in the case of $D \rightarrow K\pi\pi$, bands appear when $m_{(K\pi)} = m_{K^*(892)}$, reflecting the appearance of the decay chain $D \rightarrow K^*(892)\pi \rightarrow K\pi\pi$.

Figure 48.3: Dalitz plot for a three-body final state. In this example, the state is $\pi^+ \bar{K}^0 p$ at 3 GeV. Four-momentum conservation restricts events to the shaded region.

48.4.4 Kinematic limits

48.4.4.1 Three-body decays

In a three-body decay (Fig. 48.2) the maximum of $|\mathbf{p}_3|$, [given by Eq. (48.21)], is achieved when $m_{12} = m_1 + m_2$, *i.e.*, particles 1 and 2 have the same vector velocity in the rest frame of the decaying particle. If, in addition, $m_3 > m_1, m_2$, then $|\mathbf{p}_3|_{\max} > |\mathbf{p}_1|_{\max}, |\mathbf{p}_2|_{\max}$. The distribution of m_{12} values possesses an end-point or maximum value at $m_{12} = M - m_3$. This can be used to constrain the mass difference of a parent particle and one invisible decay product.

48.4.4.2 Sequential two-body decays

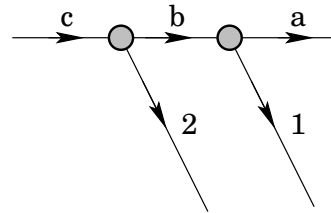


Figure 48.4: Particles participating in sequential two-body decay chain. Particles labeled 1 and 2 are visible while the particle terminating the chain (a) is invisible.

When a heavy particle initiates a sequential chain of two-body decays terminating in an invisible particle, constraints on the masses of the states participating in the chain can be obtained from end-points and thresholds in invariant mass distributions of the aggregated decay products. For the two-step decay chain depicted in Fig. 48.4 the invariant mass distribution of the two visible particles possesses an end-point given by:

$$(m_{12}^{\max})^2 = \frac{(m_c^2 - m_b^2)(m_b^2 - m_a^2)}{m_b^2}, \quad (48.24)$$

provided particles 1 and 2 are massless. If visible particle 1 has non-zero mass m_1 then Eq. (48.24) is replaced by

$$(m_{12}^{\max})^2 = m_1^2 + \frac{(m_c^2 - m_b^2)}{2m_b^2} \times \left(m_1^2 + m_b^2 - m_a^2 + \sqrt{(-m_1^2 + m_b^2 - m_a^2)^2 - 4m_1^2 m_a^2} \right) \quad (48.25)$$

See Refs. [2] and [3] for other cases.

48.4.5 Multibody decays

The above results may be generalized to final states containing any number of particles by combining some of the particles into “effective particles” and treating the final states as 2 or 3 “effective particle” states. Thus, if $p_{ijk\dots} = p_i + p_j + p_k + \dots$, then

$$m_{ijk\dots} = \sqrt{p_{ijk\dots}^2}, \quad (48.26)$$

and $m_{ijk\dots}$ may be used in place of *e.g.*, m_{12} in the relations in Sec. 48.4.3 or Sec. 48.4.4 above.

48.5 Cross sections

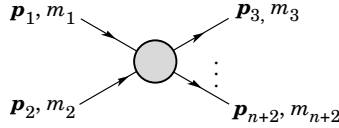


Figure 48.5: Definitions of variables for production of an n -body final state.

The differential cross section is given by

$$d\sigma = \frac{(2\pi)^4 |\mathcal{M}|^2}{4\sqrt{(p_1 \cdot p_2)^2 - m_1^2 m_2^2}} \times d\Phi_n(p_1 + p_2; p_3, \dots, p_{n+2}). \quad (48.27)$$

[See Eq. (48.12).] In the rest frame of m_2 (lab),

$$\sqrt{(p_1 \cdot p_2)^2 - m_1^2 m_2^2} = m_2 p_{1\text{lab}}; \quad (48.28a)$$

while in the center-of-mass frame

$$\sqrt{(p_1 \cdot p_2)^2 - m_1^2 m_2^2} = p_{1\text{cm}} \sqrt{s}. \quad (48.28b)$$

48.5.1 Two-body reactions

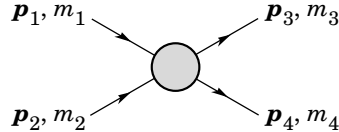


Figure 48.6: Definitions of variables for a two-body final state.

Two particles of momenta p_1 and p_2 and masses m_1 and m_2 scatter to particles of momenta p_3 and p_4 and masses m_3 and m_4 ; the Lorentz-invariant Mandelstam variables are defined by

$$s = (p_1 + p_2)^2 = (p_3 + p_4)^2 = m_1^2 + 2E_1 E_2 - 2\mathbf{p}_1 \cdot \mathbf{p}_2 + m_2^2, \quad (48.29)$$

$$t = (p_1 - p_3)^2 = (p_2 - p_4)^2 = m_1^2 - 2E_1 E_3 + 2\mathbf{p}_1 \cdot \mathbf{p}_3 + m_3^2, \quad (48.30)$$

$$u = (p_1 - p_4)^2 = (p_2 - p_3)^2 = m_1^2 - 2E_1 E_4 + 2\mathbf{p}_1 \cdot \mathbf{p}_4 + m_4^2, \quad (48.31)$$

and they satisfy

$$s + t + u = m_1^2 + m_2^2 + m_3^2 + m_4^2. \quad (48.32)$$

The two-body cross section may be written as

$$\frac{d\sigma}{dt} = \frac{1}{64\pi s} \frac{1}{|\mathbf{p}_{1\text{cm}}|^2} |\mathcal{M}|^2. \quad (48.33)$$

In the center-of-mass frame

$$\begin{aligned} t &= (E_{1\text{cm}} - E_{3\text{cm}})^2 - (p_{1\text{cm}} - p_{3\text{cm}})^2 \\ &\quad - 4p_{1\text{cm}} p_{3\text{cm}} \sin^2(\theta_{\text{cm}}/2) \\ &= t_0 - 4p_{1\text{cm}} p_{3\text{cm}} \sin^2(\theta_{\text{cm}}/2), \end{aligned} \quad (48.34)$$

where θ_{cm} is the angle between particle 1 and 3. The limiting values t_0 ($\theta_{\text{cm}} = 0$) and t_1 ($\theta_{\text{cm}} = \pi$) for $2 \rightarrow 2$ scattering are

$$t_0(t_1) = \left[\frac{m_1^2 - m_3^2 - m_2^2 + m_4^2}{2\sqrt{s}} \right]^2 - (p_{1\text{cm}} \mp p_{3\text{cm}})^2. \quad (48.35)$$

In the literature the notation t_{min} (t_{max}) for t_0 (t_1) is sometimes used, which should be discouraged since $t_0 > t_1$. The center-of-mass energies and momenta of the incoming particles are

$$E_{1\text{cm}} = \frac{s + m_1^2 - m_2^2}{2\sqrt{s}}, \quad E_{2\text{cm}} = \frac{s + m_2^2 - m_1^2}{2\sqrt{s}}, \quad (48.36)$$

For $E_{3\text{cm}}$ and $E_{4\text{cm}}$, change m_1 to m_3 and m_2 to m_4 . Then

$$p_{i\text{cm}} = \sqrt{E_{i\text{cm}}^2 - m_i^2} \text{ and } p_{1\text{cm}} = \frac{p_{1\text{lab}} m_2}{\sqrt{s}}. \quad (48.37)$$

Here the subscript lab refers to the frame where particle 2 is at rest. [For other relations see Eqs. (48.2)–(48.4).]

48.5.2 Inclusive reactions

Choose some direction (usually the beam direction) for the z -axis; then the energy and momentum of a particle can be written as

$$E = m_T \cosh y, \quad p_x, p_y, p_z = m_T \sinh y, \quad (48.38)$$

where m_T , conventionally called the ‘transverse mass’, is given by

$$m_T^2 = m^2 + p_x^2 + p_y^2. \quad (48.39)$$

and the rapidity y is defined by

$$\begin{aligned} y &= \frac{1}{2} \ln \left(\frac{E + p_z}{E - p_z} \right) \\ &= \ln \left(\frac{E + p_z}{m_T} \right) = \tanh^{-1} \left(\frac{p_z}{E} \right). \end{aligned} \quad (48.40)$$

Note that the definition of the transverse mass in Eq. (48.39) differs from that used by experimentalists at hadron colliders (see Sec. 48.6.1 below). Under a boost in the z -direction to a frame with velocity β , $y \rightarrow y - \tanh^{-1} \beta$. Hence the shape of the rapidity distribution dN/dy is invariant, as are differences in rapidity. The invariant cross section may also be rewritten

$$E \frac{d^3\sigma}{d^3p} = \frac{d^3\sigma}{d\phi dy p_T dp_T} \implies \frac{d^2\sigma}{\pi dy d(p_T^2)}. \quad (48.41)$$

The second form is obtained using the identity $dy/dp_z = 1/E$, and the third form represents the average over ϕ .

Feynman’s x variable is given by

$$x = \frac{p_z}{p_{z\text{max}}} \approx \frac{E + p_z}{(E + p_z)_{\text{max}}} \quad (p_T \ll |p_z|). \quad (48.42)$$

In the c.m. frame,

$$x \approx \frac{2p_{z\text{cm}}}{\sqrt{s}} = \frac{2m_T \sinh y_{\text{cm}}}{\sqrt{s}} \quad (48.43)$$

and

$$= (y_{\text{cm}})_{\text{max}} = \ln(\sqrt{s}/m). \quad (48.44)$$

The invariant mass M of the two-particle system described in Sec. 48.4.2 can be written in terms of these variables as

$$M^2 = m_1^2 + m_2^2 + 2[E_T(1)E_T(2) \cosh \Delta y - \mathbf{p}_T(1) \cdot \mathbf{p}_T(2)], \quad (48.45)$$

where

$$E_T(i) = \sqrt{|\mathbf{p}_T(i)|^2 + m_i^2}, \quad (48.46)$$

and $\mathbf{p}_T(i)$ denotes the transverse momentum vector of particle i .

For $p \gg m$, the rapidity [Eq. (48.40)] may be expanded to obtain

$$y = \frac{1}{2} \ln \frac{\cos^2(\theta/2) + m^2/4p^2 + \dots}{\sin^2(\theta/2) + m^2/4p^2 + \dots} \approx -\ln \tan(\theta/2) \equiv \eta \quad (48.47)$$

where $\cos \theta = p_z/p$. The pseudorapidity η defined by the second line is approximately equal to the rapidity y for $p \gg m$ and $\theta \gg 1/\gamma$, and in any case can be measured when the mass and momentum of the particle are unknown. From the definition one can obtain the identities

$$\sinh \eta = \cot \theta, \quad \cosh \eta = 1/\sin \theta, \quad \tanh \eta = \cos \theta. \quad (48.48)$$

48.6 Transverse variables

At hadron colliders, a significant and unknown proportion of the energy of the incoming hadrons in each event escapes down the beam-pipe. Consequently if invisible particles are created in the final state, their net momentum can only be constrained in the plane transverse to the beam direction. Defining the z -axis as the beam direction, this net momentum is equal to the missing transverse energy vector

$$\mathbf{E}_T^{\text{miss}} = -\sum_i \mathbf{p}_T(i), \quad (48.49)$$

where the sum runs over the transverse momenta of all visible final state particles.

48.6.1 Single production with semi-invisible final state

Consider a single heavy particle of mass M produced in association with visible particles which decays as in Fig. 48.1 to two particles, of which one (labeled particle 1) is invisible. The mass of the parent particle can be constrained with the quantity M_T defined by

$$M_T^2 \equiv [E_T(1) + E_T(2)]^2 - [\mathbf{p}_T(1) + \mathbf{p}_T(2)]^2 = m_1^2 + m_2^2 + 2[E_T(1)E_T(2) - \mathbf{p}_T(1) \cdot \mathbf{p}_T(2)], \quad (48.50)$$

where

$$\mathbf{p}_T(1) = \mathbf{E}_T^{\text{miss}}. \quad (48.51)$$

This quantity is called the ‘transverse mass’ by hadron collider experimentalists but it should be noted that it is quite different from that used in the description of inclusive reactions [Eq. (48.39)]. The distribution of event M_T values possesses an end-point at $M_T^{\text{max}} = M$. If $m_1 = m_2 = 0$ then

$$M_T^2 = 2|\mathbf{p}_T(1)||\mathbf{p}_T(2)|(1 - \cos \phi_{12}), \quad (48.52)$$

where ϕ_{ij} is defined as the angle between particles i and j in the transverse plane.

48.6.2 Pair production with semi-invisible final states

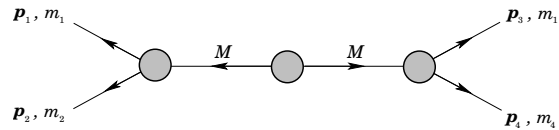


Figure 48.7: Definitions of variables for pair production of semi-invisible final states. Particles 1 and 3 are invisible while particles 2 and 4 are visible.

Consider two identical heavy particles of mass M produced such that their combined center-of-mass is at rest in the transverse plane (Fig. 48.7). Each particle decays to a final state consisting of an invisible particle of fixed mass m_1 together with an additional visible particle. M and m_1 can be constrained with the variables M_{T2} and M_{CT} which are defined in Refs. [4] and [5].

References

- [1] J.D. Jackson in *High Energy Physics, Les Houches 1965 Summer School*, GORDON AND BREACH Science Publishers (1965), p. 348.
- [2] I. Hinchliffe *et al.*, Phys. Rev. **D55**, 5520 (1997), [hep-ph/9610544].
- [3] B. C. Allanach *et al.*, JHEP **09**, 004 (2000), [hep-ph/0007009].
- [4] C. G. Lester and D. J. Summers, Phys. Lett. **B463**, 99 (1999), [hep-ph/9906349].
- [5] D. R. Tovey, JHEP **04**, 034 (2008), [arXiv:0802.2879].

49. Resonances

Revised August 2019 by D.M. Asner (BNL), C. Hanhart (Jülich) and E. Klempt (Bonn U.).

49.1 General Considerations

Perturbative methods can be applied to systems of quarks and gluons only for large momentum transfers (see review on ‘Quantum Chromodynamics’) and, under certain conditions, to some properties of systems that contain heavy quarks or very large momentum scales (see review on ‘Heavy-Quark and Soft-Collinear Effective Theory’). Dealing with Quantum Chromodynamics (QCD) in the low momentum transfer region is a very complicated, non-perturbative problem. The physical states appear as poles of the S -matrix either on physical sheet (bound states) or on the unphysical sheets (resonances) and manifest themselves as structures in experimental observables.

Resonances can show up either in so-called formation experiments, typically of the kind

$$A + B \rightarrow \mathbf{R} \rightarrow C_1 + \dots + C_n,$$

where they become visible in an energy scan (a perfect example of this being the R -function measured in e^+e^- annihilations — *cf.* the corresponding plots in the review on ‘Plots of Cross Sections and Related Quantities’), or together with a spectator particle S in production experiments of the kind

$$\begin{aligned} A + B &\rightarrow \mathbf{R} + S \rightarrow [C_1 + \dots + C_n] + S, \\ Z &\rightarrow \mathbf{R} + S \rightarrow [C_1 + \dots + C_n] + S. \end{aligned}$$

where the first reaction corresponds to an associated production, the second is a decay (see ‘Review of Multibody Charm Analyses’). In the latter case the resonance properties are commonly extracted from a Dalitz plot analysis (see review on ‘Kinematics’) or projections thereof.

Resonance phenomena are very rich: while typical hadronic widths are of the order of 100 MeV (*e.g.*, for the meson resonances $\rho(770)$ or $\psi(4040)$ or the baryon resonance $\Delta(1232)$) corresponding to a lifetime of 10^{-23} s, the widths can also be as small as a few MeV (*e.g.* of $\phi(1020)$ or J/ψ) or as large as several hundred

MeV (*e.g.* of the meson resonances $f_0(500)$ or $D_1(2430)$ or the baryon resonance $N(2190)$).

Typically, a resonance appears as a peak in the total cross section. If the structure is narrow and if there are no relevant thresholds or other resonances nearby, the resonance properties may be extracted employing a standard Breit-Wigner parameterization, if necessary improved by using an energy-dependent width (*cf.* Sec. 49.3.1 of this review). However, in general, unitarity and analyticity call for the use of more refined tools. When there are overlapping resonances with the same quantum numbers, the resonance terms should not simply be added but combined in a non-trivial way either in a K -matrix approximation (*cf.* Sec. 49.3.2 of this review) or using other advanced methods (*cf.* Sec. 49.3.6 of this review). Additional constraints from the S -matrix allow one to build more reliable amplitudes and in turn to reduce the systematic uncertainties of the resonance parameters: pole locations and residues. In addition, for broad resonances there is no direct relation anymore between pole location and the total width/lifetime — then the pole residues need to be used in order to quantify the decay properties.

For simplicity, throughout this review the formulas are given for distinguishable, scalar particles. The additional complications that appear in the presence of spins can be controlled in the helicity framework developed by Jacob and Wick [1], or in a non-covariant [2] or covariant [3] tensor operator formalism. Within these approaches, sequential (cascade) decays are commonly treated as a coherent sum of two-body interactions. Most of the expressions below are given for two-body kinematics.

49.1.1 Properties of the S -matrix

The unitary operator that connects asymptotic *in* and *out* states is called the S -matrix. The scattering amplitude is defined as the interacting part of the S matrix. For the case of two interacting particles, it reads: (*cf.* Eq. (8) of the review on ‘Kinematics’ but note: we here use a different sign convention as well as a different normalisation of the fields to be consistent with most books on field theory)

$$i(2\pi)^4 \delta^4(p_1 + p_2 - p'_1 - p'_2) \mathcal{M}(p_1, p_2; p_1, p'_2)_{ba} = {}_{\text{out}} \langle p'_1 p'_2, b | S - 1 | p_1 p_2, a \rangle_{\text{in}} \quad (49.1)$$

where $|p_1 p_2, a\rangle$ and $|p'_1 p'_2, b\rangle$ are asymptotic states of two non-interacting particles with momentum p_1, p_2 and p'_1, p'_2 . The channel labels a and b are multi-indices specifying all additional properties of the channel. In general, \mathcal{M} is a matrix in channel space. For single particle states we employ the common relativistic normalization,

$$\langle p' | p \rangle = (2\pi)^3 2E_p \delta^3(\vec{p}' - \vec{p}), \quad (49.2)$$

with $E_p = \sqrt{\vec{p}^2 + m^2}$. The scattering amplitude an analytic function of the Mandelstam variables s, t and u up to poles and kinematic singularities. Branch points appear whenever there is a channel opening — at each two-particle threshold the number of Riemann sheets doubles. Triangle topologies can induce logarithmic singularities on the unphysical sheets often called triangle singularities (TS) [4–6]. Analyticity and unitarity principles of the S -matrix put strong constraints to the function $\mathcal{M}(s, t)$. Poles refer either to bound states or to resonances. The former poles are located on the physical sheet, the latter are located on unphysical sheets. Naturally those located on the unphysical sheet closest to the physical one, often called the second sheet, have usually the largest impact on observables. Moreover, as follows from analyticity, if there is a pole at some complex value of s , there must be another pole at its complex conjugate value, s^* . The pole with a negative imaginary part is closer to the physical axis and thus influences the observables in the vicinity of the resonance region more strongly (see Fig. 49.1). However, at the threshold both poles are always equally important. If there are

resonances in subsystems of multi-particle states, branch points appear in the complex plane of the unphysical sheet(s) [6]. Any of these singularities can lead to some structure in the observables (see also Ref. [7]). If certain kinematical constraints are met, especially the TS can mimic resonance signals, as claimed in Refs. [8–13] or could in certain channels lead to significant shifts of resonance signals [14]. For a partial-wave-projected amplitude (see Sec. 49.1.3) additional singularities not related to resonance physics may emerge as a result of the partial-wave projection [15].

Further constraints come, *e.g.*, from crossing symmetry and duality [16]. Approaches based on analyticity and crossing symmetry, implemented via dispersion theory, like the Roy equations [17] or variants thereof, were developed and applied to $\pi\pi \rightarrow \pi\pi$ scattering [18–20], πK scattering [21], $\gamma\gamma \rightarrow \pi\pi$ [22] as well as pion-nucleon scattering [23].

49.1.2 Consequences from unitarity

In what follows, scattering amplitudes \mathcal{M} and production amplitudes \mathcal{A} will be distinguished, since unitarity puts different constraints on these. For the production amplitudes we require that the initial state is weakly coupled and, hence, the probability of the time-reversed reaction is negligibly small compared to the other coupled channels.

The discontinuity of the scattering amplitude over the unitarity

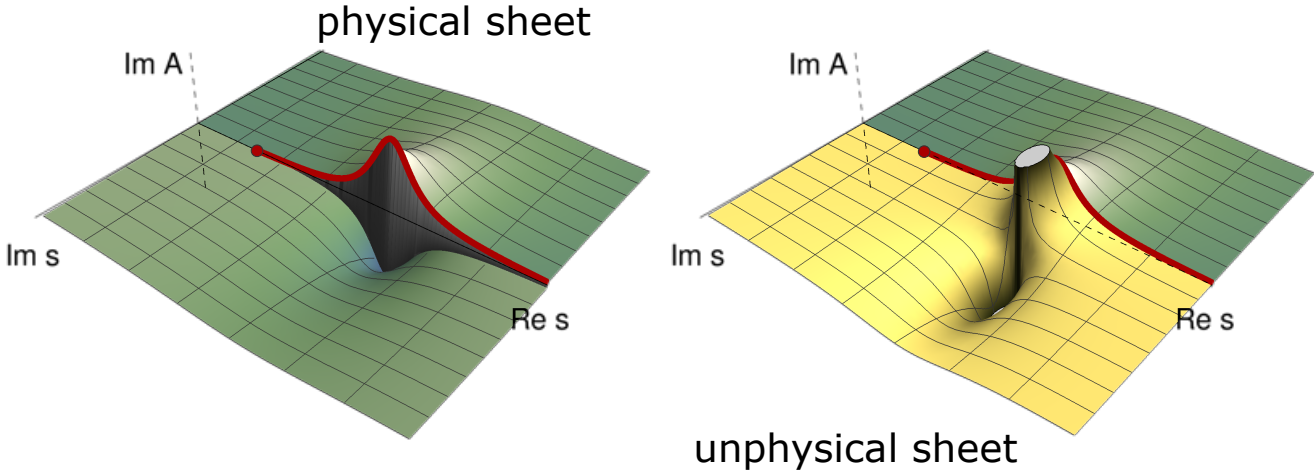


Figure 49.1: Imaginary part of a typical single-channel scattering amplitude with an isolated resonance. The solid red line shows the physical range of the Mandelstam variable s : It is real valued and starts from threshold shown by the red dot. The left plot shows the imaginary part of the amplitude in the complex S -plane that corresponds to the first physical sheet (green surface). The right plot shows analytic continuation of the same amplitude to the lower plane of the unphysical sheet (yellow surface). The latter contains the resonance pole. The two sheets are connected smoothly along the real axis above the threshold.

cut is constrained by unitarity [24] to

$$\text{Disc } \mathcal{M}_{ba} = [\mathcal{M}_{ba} - \mathcal{M}_{ab}^*] = i(2\pi)^4 \sum_c \int d\Phi_c \mathcal{M}_{cb}^* \mathcal{M}_{ca}, \quad (49.3)$$

with Φ_c being the invariant phase space for channel c . The sum includes only open channels, *i.e.* those for which the production threshold is below the energy of the scattered system. Using time-reversal symmetry, and $\text{Disc } \mathcal{M}(s, t) = 2i \text{Im}(\mathcal{M}(s + i\epsilon, t))$ for the s -channel, the optical theorem follows

$$\text{Im } \mathcal{M}_{aa}(s, 0) = 2q_a \sqrt{s} \sigma_{\text{tot}}(a \rightarrow \text{anything}), \quad (49.4)$$

where q_a denotes the relative momentum of the particles of channel a (see Eq. (17) of the review on “Kinematics”). The value $t = 0$ in Eq. (49.4) corresponds to forward scattering.

The unitarity relation for a production amplitude for a channel a is given by

$$[\mathcal{A}_a - \mathcal{A}_a^*] = i(2\pi)^4 \sum_c \int d\Phi_c \mathcal{M}_{ca}^* \mathcal{A}_c. \quad (49.5)$$

One application of the two-body-unitarity constraint from Eq. (49.5) is studies of the three-body decays in the Khuri-Treiman framework [25]. The standard procedure here is to derive the equations for the production amplitude for small values of the mass of the decaying particle in the scattering domain and relate it to the decay kinematics by an analytic continuation in the decay mass. Note that in this kinematics the connection between imaginary part and discontinuity employed to derive Eq. (49.4) no longer holds. The method was successfully applied to various decays of light mesons, $\eta \rightarrow 3\pi$ in Refs. [26–28], $\phi/\omega \rightarrow 3\pi$ in Ref. [29,30], $\eta' \rightarrow \eta\pi\pi$ in Ref. [31], as well as to the charm-mesons decays $D^+ \rightarrow K^0/\pi^0/\pi^+$ [32,33].

49.1.3 Partial-wave decomposition

It is often convenient to expand the scattering amplitude in partial waves. Since resonances have a well-defined spin, in the s -channel they appear only in the corresponding partial waves. For scalar particles only one may write

$$\mathcal{M}_{ba}(s, t) = \sum_{j=0}^{\infty} (2j+1) \mathcal{M}_{ba}^j(s) P_j(\cos(\theta)), \quad (49.6)$$

where j denotes the total angular momentum. For scalar particles it coincides with the orbital angular momentum of the particle

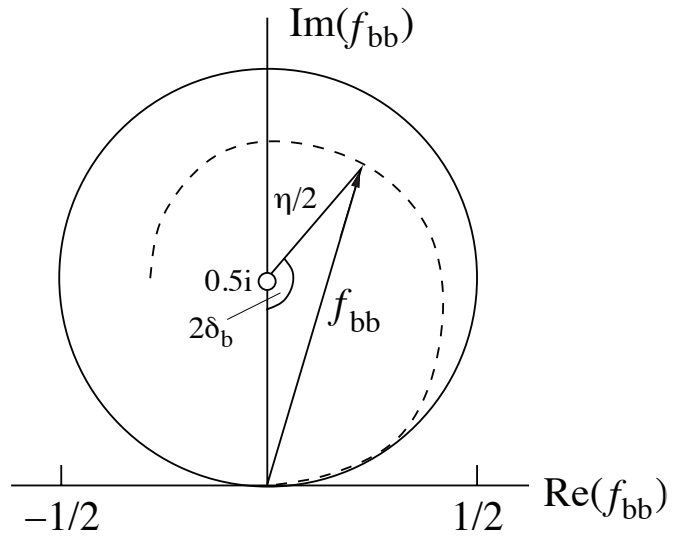


Figure 49.2: Argand plot showing a diagonal element of a partial-wave amplitude, a_{bb} , as a function of energy. The amplitude leaves the unitary circle (solid line) as soon as inelasticity sets in, $\eta < 1$ (dashed line).

pairs in the initial and the final state. To simplify notations we will drop the label j for the single-argument function $\mathcal{M}_{ba}(s)$. The unitarity constraint for $\mathcal{M}_{ba}(s)$ reads,

$$\text{Im } \mathcal{M}_{ba} = \sum_c \mathcal{M}_{cb}^* \rho_c \mathcal{M}_{ca} \quad (49.7)$$

with ρ_c being a factor that is related to the two-body phase space in Eq. (12) of the review on “Kinematics”,

$$\rho_c(s) = \frac{(2\pi)^4}{2} \int d\Phi_2 = \frac{1}{16\pi} \frac{2|\vec{q}_c|}{\sqrt{s}}. \quad (49.8)$$

The partial-wave amplitudes $f_{ba}(s)$ are connected to $\mathcal{M}_{ba}(s)$ via

$$f_{ba}(s) = \sqrt{\rho_b} \mathcal{M}_{ba}(s) \sqrt{\rho_a}. \quad (49.9)$$

From this definition it follows for the unitarity condition that $\text{Im } f_{ba}^{-1} = -\delta_{ba}$. Moreover, $\mathbb{I} + 2if$ is a unitary matrix. Hence, it

can be parameterized as,

$$f_{bb} = (\eta_b \exp(2i\delta_b) - 1)/2i, \quad (49.10)$$

where δ_b denotes the phase shift for the scattering from channel b to channel b , η_b is elasticity parameter — also called inelasticity. One has $0 \leq \eta_b \leq 1$, where $\eta_b = 1$ refers to purely elastic scattering. The evolution with energy of a partial-wave amplitude f_{bb} can be displayed as a trajectory in an Argand plot, as shown in Fig. 49.2. In case of a two-channel problem, $\eta_b = \eta_a = \eta$, and the off-diagonal element is $f_{ba} = \sqrt{1 - \eta^2}/2 \exp(i(\delta_b + \delta_a))$.

The partial-wave-projected production amplitude $\mathcal{A}(s)$ (the label j is dropped for consistency) is also constrained by unitarity. From Eq. (49.5) follows,

$$\text{Im } \mathcal{A}_a = \sum_b \mathcal{M}_{ab}^* \rho_b \mathcal{A}_b, \quad (49.11)$$

where the sum runs over all open channels. For purely elastic scattering, where the sum collapses to just the channel a , the Watson theorem, stating that the phase of \mathcal{A}_a agrees with that of \mathcal{M}_{aa} , follows straightforwardly, since the left-hand side of Eq. (49.11) is a real number.

49.2 Properties of resonances

The main characteristics of a resonance is its pole position, s_R , in the complex s -plane that is independent of the reaction studied. The more traditional parameters mass M_R and total width Γ_R may be introduced via the pole parameters

$$\sqrt{s_R} = M_R - i\Gamma_R/2. \quad (49.12)$$

Note that the standard Breit-Wigner parameters M_{BW} and Γ_{BW} , also introduced below, in general deviate from the pole parameters, *e.g.*, due to finite width effects and the influence of thresholds.

In addition to the pole location a resonance is characterized also by its residues that quantify its couplings to the various channels and allow one to define branching ratios. In the Meson Particle Listings the two-photon width of $f_0(500)$ is defined in terms of the corresponding residue. The Baryon Particle Listings give the elastic pole residues and normalized transition residues. However, different conventions are used in the two sectors, which are shortly outlined here.

In the close vicinity of the resonance pole the scattering matrix \mathcal{M} can be written as

$$\lim_{s \rightarrow s_R} (s - s_R) \mathcal{M}_{ba} = -\mathcal{R}_{ba}. \quad (49.13)$$

The residues may be calculated via an integration along a closed contour around the pole using

$$\mathcal{R}_{ba} = -\frac{1}{2\pi i} \oint ds \mathcal{M}_{ba}. \quad (49.14)$$

The factorization of the residue $(\mathcal{R}_{ba})^2 = \mathcal{R}_{aa} \times \mathcal{R}_{bb}$ allows one to introduce pole couplings according to

$$\tilde{g}_a = \mathcal{R}_{ba} / \sqrt{\mathcal{R}_{bb}}. \quad (49.15)$$

The pole couplings are the only quantities that characterize the transition strength of a given resonance to some channel a independently of how the particular resonance was produced. One may define a partial width and a branching fraction even for a broad resonance via

$$\Gamma_{R \rightarrow a} = \frac{|\tilde{g}_a|^2}{M_R} \rho_a(M_R^2) \quad \text{and} \quad \text{Br}_a = \Gamma_{R \rightarrow a} / \Gamma_R, \quad (49.16)$$

where M_R and Γ_R were introduced in Eq. (49.12). This expression was used to define a two-photon width for the broad $f_0(500)$ (also called σ) [34, 35]. Eq. (49.16) defines a partial-decay width independent of the reaction used to extract the parameters. For a narrow resonance it maps smoothly onto the other common definition of the branching fraction, discussed in Eq. (49.22).

In the baryon sector it is common to define the residue with respect to the partial-wave amplitudes $f_{ba}(s)$ defined in Eq. (49.9) and with respect to \sqrt{s} instead of s . Accordingly in the baryon listings the elastic pole residue, which refers to $\pi N \rightarrow \pi N$ scattering, is related to the residues introduced above via

$$r_{\pi N, \pi N} = \frac{\rho_{\pi N}(s_R)}{\sqrt{4s_R}} \mathcal{R}_{\pi N, \pi N}, \quad (49.17)$$

where the phase-space factor is to be evaluated at the pole.

49.3 Common parameterizations

Up to a few exceptions where sophisticated dispersive methods can be used or one restricts oneself to a very small energy range, there is in general no universal model-independent recipe to build the scattering amplitude. The resonance parameters extracted should not depend on the approach used, however, assuming that the amplitude fits relevant data of sufficient quality well. Deviations of resonance parameters obtained in different models which equally-well describe the data must be attributed to the systematic theory uncertainties.

49.3.1 The Breit-Wigner parameterization

First we focus on the most common case of resonances that appear in production reactions and consider the simplest approximation that is only appropriate for a narrow resonance located far from all relevant thresholds. In this case, one may use the constant-width Breit-Wigner parameterization,

$$\mathcal{A}(s) = \frac{\tilde{\alpha}}{M_{BW}^2 - s - i\sqrt{s}\Gamma_{BW}} \approx \frac{\tilde{\alpha}}{M_{BW}^2 - s - iM_{BW}\Gamma_{BW}}, \quad (49.18)$$

where $\tilde{\alpha}$ contains the resonance coupling to the source as well as to the final state. It is common to replace \sqrt{s} by M_{BW} as done in the right expression.

To use a constant partial width for a resonance coupling to some channel a in an analysis is justified only, if $2(M_R - \sqrt{s_{\text{thr}_a}})/\Gamma_R \gg 1$, where $\sqrt{s_{\text{thr}_a}}$ denotes the location of the threshold for channel a . Otherwise, it is important to build in the appropriate threshold behavior and use the energy-dependent expression for the denominator.

$$\mathcal{A}_a(s) = \frac{\alpha g_a n_a(s)}{M_{BW}^2 - s - i \sum_b g_b^2 \rho_b(s) n_b^2(s)}, \quad (49.19)$$

where the sum in the denominator is taken over all open channels, n_a combines the threshold and barrier factors, $n_a = (q_a/q_0)^{l_a} F_{l_a}(q_a, q_0)$, with l_a being the orbital angular momentum in channel a , q_a is given by Eq. (17) of the review on ‘‘Kinematics’’, and q_0 denotes a momentum scale. The factor $(q_a)^{l_a}$ guarantees the correct threshold behavior. The rapid growth of this factor for angular momenta $l > 0$ is commonly compensated at higher energies by a phenomenological form factor, here denoted by $F_{l_a}(q_a, q_0)$. Often the Blatt-Weisskopf form factors are used [36–38], where $F_j(q, q_0) = F_j(q/q_0)$ and, *e.g.* $F_0^2(z) = 1$, $F_1^2(z) = 1/(1+z)$ and $F_2^2(z) = 1/(9+3z+z^2)$. The denominator can be written as $M_{BW}^2 - s - iM_{BW}\Gamma_{\text{tot}}(s)$, with

$$\Gamma_{\text{tot}}(s) = \sum_b \Gamma_b(s) \quad (49.20)$$

for the energy-dependent total width. An often used parameterization for the partial width $\Gamma_a(s)$ trades the coupling for the resonance width:

$$\Gamma_a(s) = \Gamma_{BW a} \frac{\rho_a(s)}{\rho_a(M_{BW}^2)} \left(\frac{q_a}{q_{aR}} \right)^{2l_a} \frac{F_{l_a}^2(q_a, q_0)}{F_{l_a}^2(q_{aR}, q_0)}. \quad (49.21)$$

Here q_{aR} are the values of the break-up momentum evaluated at $s = M_{BW}^2$. The Breit-Wigner parameters M_{BW} and Γ_{BW} in Eq. (49.18) as well as the coupling g_a in Eq. (49.19) allow for an effective description of resonance phenomena but in general do not have strict physical meaning. The mass and width agree with the pole parameters only if the resonance is narrow in the sense

defined above. Otherwise, the Breit-Wigner parameters deviate from the pole parameters and are in general reaction dependent.

Branching fractions for individual, isolated resonances may be

$$\text{Br}'_a = \frac{\int_{s_{\text{thr},a}}^{\infty} ds \frac{|g_a|^2 n_a^2 \rho_a(s)}{|M_{\text{BW}}^2 - s - iM_{\text{BW}}\Gamma_{\text{tot}}(s)|^2}}{\sum_c \int_{s_{\text{thr},c}}^{\infty} ds \frac{|g_c|^2 n_c^2 \rho_c(s)}{|M_{\text{BW}}^2 - s - iM_{\text{BW}}\Gamma_{\text{tot}}(s)|^2}}, \quad (49.23)$$

is also often used.

If there is more than one resonance in one partial wave that significantly couples to the same channel, it is in general incorrect to use a sum of Breit-Wigner functions, for this usually leads to violation of unitarity constraints. Then, more refined methods should be used, like the K -matrix approximation described in the next section.

49.3.2 K -matrix approximation and Flatté parameterizations

The K -matrix method is a general construction for coupled-channel scattering amplitudes \mathcal{M}_{ba} that guarantees two-particle unitarity, but does not allow for the inclusion of left-hand cuts [39]. The amplitude reads,

$$n_b \mathcal{M}_{ba}^{-1} n_a = \mathcal{K}_{ba}^{-1} - i\delta_{ba} \rho_a n_a^2, \quad (49.24)$$

where \mathcal{K}_{ba} is an arbitrary real function. The factor n_a becomes important for the waves with non-zero angular momentum. As mentioned before $n_a = q_a^{l_a}$ or $n_a = (q_a/q_0)^{l_a} F_{l_a}(q_a, q_0)$.

As there is no unique rigorous recipe to build \mathcal{K} , various parameterizations thereof have to be studied, in order to get access to the theoretical systematic uncertainty. One possible choice for the K -matrix is

$$\mathcal{K}_{ba}(s) = \sum_R \frac{g_b^R g_a^R}{M_R^2 - s} + \sum_{i=0}^{N_{\text{b.g.}}} b_{ba}^{(i)} s^i, \quad (49.25)$$

where M_R is referred to as the bare mass of the resonance R , g_a^R is the bare coupling of the resonance R to the channel a and the $b_{ba}^{(i)}$ are matrices parameterizing the non-pole parts of the K -matrix. As long as all parameters appearing in Eq. (49.25) are real the amplitude is unitary. From the ansatz given above the scattering amplitude \mathcal{M} can be calculated directly using the matrix form,

$$\mathcal{M} = n[1 - \mathcal{K} i \rho n^2]^{-1} \mathcal{K} n. \quad (49.26)$$

This solution also applies in those cases in which the inverse of \mathcal{K} does not exist.

As an alternative to Eq. (49.25), the same functional form as on the right side of Eq. (49.25) can be used to parameterize the inverse K -matrix, called by authors of Ref. [40] the M -matrix. The K -matrix framework is extensively used to parameterize the scattering amplitudes needed to analyse the data from lattice QCD calculations [41–43]

One notices that the evaluation of the K -matrix amplitude for the multichannel problem requires an analytic continuation already on the real axis. For a given closed channel c (the channel c is called closed, if $s < s_{\text{thr},c}$), the factor $q_c(s)$ that enters ρ_c and n_c has to be calculated below the corresponding threshold, *i.e.* in the unphysical region of the particular channel c . This is done using analytic continuation as described *e.g.* in Refs. [44, 45]:

$$q_c = i\sqrt{-q_c^2} \quad \text{for} \quad q_c^2 < 0. \quad (49.27)$$

The resulting line shape above and below the threshold of channel c is called the Flatté parameterization [44]. The continuation given

introduced based on the parameters introduced above:

$$\text{Br}'_a = \frac{\Gamma_{\text{BW}a}}{\Gamma_{\text{BW,tot}}} \quad (49.22)$$

where $\Gamma_{\text{BW,tot}} = \sum_a \Gamma_{\text{BW}a}$ denotes the total width evaluated at the Breit-Wigner mass.

The branching fraction definition based on a probability of the decay to a certain channel,

above stays on the physical sheet. To reach the unphysical sheet the negative square root needs to be chosen. If the coupling of a resonance to the channel opening nearby is very strong, the Flatté parameterization shows a scaling invariance and does not allow for an extraction of individual partial decay widths, but only of ratios [46]. The position of the resonance poles can be determined by a study of the zeros of the analytic function $\det[1 - \mathcal{K} i \rho n^2]$. Due to the ρ factor, this determinant has a complicated multisheet structure, however, the closest unphysical sheet is always the one which is determined by the heaviest threshold below the studied point s .

49.3.3 Scattering-length approximation

A scattering length, a , is introduced as the first term in an expansion of the scattering phase shift introduced in Eq. (49.10). For S -waves one finds

$$q \cot \delta = 1/a + O(q^2), \quad (49.28)$$

where q is a break-up momentum of the scattering system. In this approximation, the scattering amplitude reads

$$\mathcal{M}(s) = \frac{8\pi\sqrt{s}}{1/a - iq(s)}. \quad (49.29)$$

The scattering length is proportional to the value of the amplitude at threshold. The sign of the scattering length is a matter of convention — notably in nuclear physics a sign convention different from Eq. (49.28) is common. A scattering length approximation is applicable only in a very limited energy range, however, might well be appropriate to analyse the recently discovered narrow near-threshold states [47, 48] from this point of view, *e.g.*, in Refs. [49–51]. Moreover, it is possible to introduce the effect of a weakly coupled lower channel. To see this one might start from

$$\mathcal{K} = \begin{pmatrix} \gamma & \beta \\ \beta & 0 \end{pmatrix}, \quad (49.30)$$

with β, γ being real numbers. It leads to

$$\mathcal{M}_{\text{el.}}(s) = \frac{1}{1/(\gamma + i\beta^2 \rho_{\text{inel.}}(s)) - i\rho(s)}, \quad (49.31)$$

with $\rho_{\text{inel.}}(s)$ being the phase-space factor of the inelastic channel. The scattering length for the amplitude in Eq. (49.31) obtains an imaginary part due to the coupling to the lower channel,

$$a = \frac{1}{8\pi\sqrt{s_{\text{thr}}}} (\gamma + i\beta^2 \rho_{\text{inel.}}(s_{\text{thr}})). \quad (49.32)$$

If the function $\beta^2 \rho_{\text{inel.}}(s)$ does not vary significantly in the energy range studied, the scattering length approximation with a complex value is justified. For large values of a the amplitude of Eq. (49.31) develops a near threshold pole located on the physical or unphysical sheet for negative or positive values of γ , respectively. While easy to use, it is important to stress, however, that the approximation in Eq. (49.30) is a specific choice of the dynamic function that produces a single pole near the physical

region pointing at a hadronic molecule nature of the state studied [51–53]. For practical analyses, various modifications of the parameterization have to be tested.

49.3.4 Two methods to build the production amplitude

When the unitary scattering amplitude is fixed, it can be used to build the production amplitude in a way that it is consistent with unitarity [38, 54].

1. The Q -vector approach is discussed in Ref. [38, 40, 55]. It reads,

$$A_a(s) = \sum_c \mathcal{M}_{ac}(s) Q_c(s) / n_c, \quad Q_c(s) = \sum_i Q_c^{(i)} s^i. \quad (49.33)$$

The unitarity condition of Eq. (49.11) is satisfied when $Q_c(s)$ is a real function and in particular does not have singularities above the lowest threshold for all channels c . Besides these conditions $Q_c(s)$ is arbitrary. Note that in the Q -vector approach the left hand cuts of the scattering matrix $\mathcal{M}_{ac}(s)$ get imported to the production amplitude which might generate a wrong analytic structure. If this problem is relevant needs to be investigated on a case-by-case basis. In a study of $\gamma\gamma \rightarrow \pi\pi$, cf. Ref. [34, 35] a low-order polynomial is claimed to be sufficient to parametrize the energy dependence of the function $Q_c(s)$. The Q -vector method is convenient, if the full matrix \mathcal{M} is known, cf. Ref. [40].

2. The P -vector is a parameterization that exploits the K -matrix of the scattering amplitude [39, 54]. It contains two components: the background term B_c that is coupled to the K -matrix via an intermediate loop represented by the $i\rho$ factor, and the “direct” resonance production term with couplings α_c^R :

$$A_a(s) = n_a \sum_c \left[1 - \mathcal{K} i\rho n^2 \right]_{ac}^{-1} P_c, \quad P_c = \sum_R \frac{\alpha_c^R g_c^R}{M_R^2 - s} + B_c. \quad (49.34)$$

Again, unitarity requires the parameters B_c and α_c^R to be real. Importantly, the masses M_R need to agree with those in \mathcal{K} in Eq. (49.25).

An important difference between the methods is to be noticed [54]: When the two-particle scattering amplitude goes to zero, the production amplitude in the Q -vector method vanishes for finite values of Q_c , while it stays finite in the P -vector approach. An advanced version of the P -vector approach that exploits analytic properties of production amplitude [54, 56, 57] is widely used, e.g. in the dispersive Khuri-Treiman framework [25, 58] for construction of three-body-decay amplitude.

49.3.5 Further improvements: Chew-Mandelstam function

The K -matrix described above usually allows one to get a proper fit of physical amplitudes and it is easy to deal with, however, it also has an important deficit: it violates constraints from analyticity — e.g., ρ_a , given by Eq. (49.8), is ill-defined at $s = 0$, and for unequal masses it develops an unphysical cut (see Fig. 49.3). A method to improve the analytic properties was suggested in Refs. [59–63]. It replaces the phase-space factor $i\rho_a(s)$ in Eq. (49.24) by the analytic function $\Sigma_a(s)$ that produces the identical imaginary part on the right-hand cut. This function is called the Chew-Mandelstam function and for S -waves it reads [56, 61]:

$$\Sigma_a(s) = \frac{1}{16\pi^2} \left[\frac{2q_a}{\sqrt{s}} \log \frac{m_1^2 + m_2^2 - s + 2\sqrt{s}q_a}{2m_1 m_2} \right. \quad (49.35)$$

$$\left. - (m_1^2 - m_2^2) \left(\frac{1}{s} - \frac{1}{(m_1 + m_2)^2} \right) \log \frac{m_1}{m_2} \right], \quad (49.36)$$

where m_1 and m_2 are masses of the final-state particles in channel a , $s_{\text{thr}_a} = (m_1 + m_2)^2$. The function along the real axis is plotted on the right pane of Fig. 49.1. For channels with $j > 0$, the threshold behavior has to be incorporated properly. This can be

done, e.g., by computing the dispersion integral

$$\Sigma_a(s + i0) = \frac{s - s_{\text{thr}_a}}{\pi} \int_{s_{\text{thr}_a}}^{\infty} \frac{\rho_a(s') n_a^2(s')}{(s' - s_{\text{thr}_a})(s' - s - i0)} ds'. \quad (49.37)$$

A further discussion of the calculation of the Chew-Mandelstam function can be found in Ref. [64].

If there is only a single resonance in a given channel, it is possible to feed the imaginary part of the Breit-Wigner function, Eq. (49.19) with an energy-dependent width, directly into a dispersion integral to get a resonance propagator with the correct analytic structure [65, 66].

49.3.6 Two-potential decomposition

The other advanced technique to construct the scattering amplitude which is widely used in the literature [67–71] is based on the two-potential formalism [72]. The method is usually formulated for the full unprojected amplitude $\mathcal{M}_{ba}(s, t)$, however, in order to simplify the discussion we present the equations in the partial-wave-projected form.

The scattering amplitude \mathcal{M} is decomposed into a pole part and a non-pole part, often called background (b.g.)

$$\mathcal{M}(s) = \mathcal{M}^{\text{b.g.}}(s) + \mathcal{M}^{\text{pole}}(s). \quad (49.38)$$

The splitting given in Eq. (49.38) is not unique and model-dependent (see, e.g., the discussions in Refs. [73, 74]). The background scattering matrix is assumed to be unitary by itself. One option is to parameterize it, e.g. at low energies directly in terms of phase shifts and inelasticities — see, e.g., Refs. [71, 75]. In this case the vertex functions $\Omega(s)_{ab}$ introduced below can be written in terms of an Omnes matrix [75], which reduces to the well known Omnes function in the single channel case [57]. Alternatively, it can be computed based on some potential, $V^{\text{b.g.}}$, fed into a proper scattering equation.

The complete amplitude \mathcal{M} of Eq. (49.38) is unitary if the pole part is chosen as

$$\mathcal{M}^{\text{pole}}(s) = \Omega(s) [1 - V^{\text{R}}(s) \Sigma^u(s)]^{-1} V^{\text{R}}(s) \Omega^T(s). \quad (49.39)$$

where the resonance potential reads in channel space

$$V_{ab}^{\text{R}}(s) = \sum_R \frac{g_a^R g_b^R}{M_R^2 - s}, \quad (49.40)$$

Σ_{ab}^u denotes the self-energy matrix, and g_a^R and M_R denote the bare coupling of the resonance R to channel a and its bare mass, respectively. A relation analogous to Eq. (49.5) holds for the normalized vertex functions, however, with the final state interaction provided by $\mathcal{M}^{\text{b.g.}}$.

$$\text{Disc } \Omega_{ab}(s) = 2i \sum_c \mathcal{M}_{ca}^{\text{b.g.}*}(s) \rho_c(s) \Omega_{cb}(s). \quad (49.41)$$

The discontinuity of the self-energy matrix $\Sigma^u(s)$ is

$$\text{Disc } \Sigma_{ab}^u(s) = 2i \sum_c \Omega_{ca}^*(s) \rho_c(s) \Omega_{cb}(s). \quad (49.42)$$

The real part of Σ^u can be calculated from Eq. (49.42) via a properly subtracted dispersion integral. If $\mathcal{M}^{\text{b.g.}}$ is unitary, the use of Eq. (49.39) leads to a unitary full amplitude, cf. Eq. (49.38). However, the pole term alone is unitary only for a vanishing background amplitude. In this situation the amplitude just described reduces to the analytically improved K -matrix of Sec. 49.3.5. While the omission of non-pole terms is a bad approximation for, e.g., scalar-isoscalar $\pi\pi$ interactions at low energies [76], it typically works well for higher partial waves.

The algebra of the two potential splitting presented in Eq. (49.38) is found to be very practical in various other cases, beyond the pole-background separation. It was employed in Refs. [71, 75] to treat the pion vector and scalar form factor, respectively, over a sizable energy range including inelasticities. A

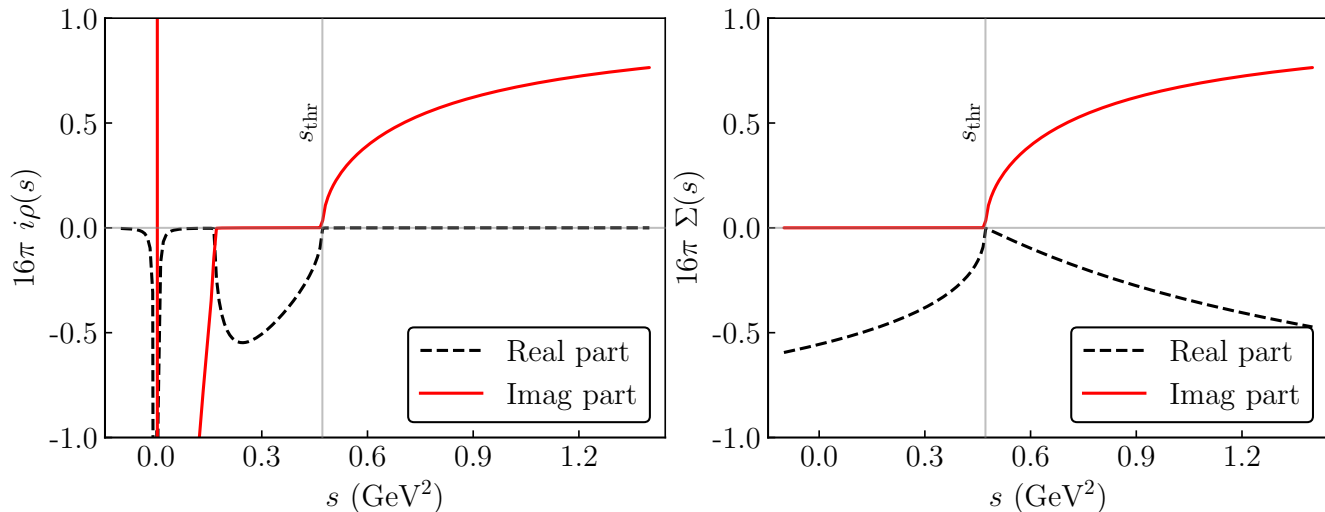


Figure 49.3: Comparison of the $i\rho$ function (left plot) to the Chew-Mandelstam function from Eq. (49.36) (right plot), evaluated for the case of S -wave $\eta\pi$ scattering. The values of s are taken slightly above the real axis, $s + i0$. The solid red line shows the imaginary part that is the same for both functions above threshold. The dashed black line presents the real part. One finds indications of the unphysical left-hand singularities of the function $i\rho$ on the left plot, while the Chew-Mandelstam function is analytic below the two-particle threshold.

similar decomposition applied to the $3 \rightarrow 3$ scattering problem provided a way to isolate the non-separable one-particle exchange singularity from the short-range resonance interaction [77].

Acknowledgement

We are very grateful to Mikhail Mikhasenko, who gave vital input to improve this review.

References

- [1] M. Jacob and G. C. Wick, *Annals Phys.* **7**, 404 (1959), [*Annals Phys.*281,774(2000)].
- [2] C. Zemach, *Phys. Rev.* **140B**, 97, 109 (1965).
- [3] A. V. Anisovich *et al.*, *J. Phys.* **G28**, 15 (2002), [*hep-ph/0105330*].
- [4] L. Landau, *Nucl. Phys.* **13**, 181 (1959).
- [5] R. Cutkosky, *J. Math. Phys.* **1**, 429 (1960).
- [6] V. N. Gribov, Y. L. Dokshitzer and J. Nyiri, *Strong Interactions of Hadrons at High Energies – Gribov Lectures on Theoretical Physics*, Cambridge University Press, Cambridge (2009).
- [7] A rapid change in an amplitude is not an unambiguous signal of a singularity of the S -matrix [78], however, for realistic interactions this connection holds.
- [8] S. Coleman and R. E. Norton, *Nuovo Cim.* **38**, 438 (1965).
- [9] C. Schmid, *Phys. Rev.* **154**, 5, 1363 (1967).
- [10] I. J. R. Aitchison and C. Kacser, *Il Nuovo Cimento A* (1965-1970) **40**, 2, 576 (1965), ISSN 1826-9869, URL <https://doi.org/10.1007/BF02721045>.
- [11] M. Mikhasenko, B. Ketzner and A. Sarantsev, *Phys. Rev.* **D91**, 9, 094015 (2015), [*arXiv:1501.07023*].
- [12] M. Bayar *et al.*, *Phys. Rev.* **D94**, 7, 074039 (2016), [*arXiv:1609.04133*].
- [13] F. Aceti, L. R. Dai and E. Oset, *Phys. Rev.* **D94**, 9, 096015 (2016), [*arXiv:1606.06893*].
- [14] J.-J. Wu *et al.*, *Phys. Rev. Lett.* **108**, 081803 (2012), [*arXiv:1108.3772*].
- [15] G. Höhler, *Pion-Nucleon Scattering – Methods and Results of Phenomenological Analyses*, Springer-Verlag Berlin, Heidelberg, New York, 1983.
- [16] M. Fukugita and K. Igi, *Phys. Rept.* **31**, 237 (1977).
- [17] S. M. Roy, *Phys. Lett.* **36B**, 353 (1971).
- [18] B. Ananthanarayan *et al.*, *Phys. Rept.* **353**, 207 (2001), [*hep-ph/0005297*].
- [19] G. Colangelo, J. Gasser and H. Leutwyler, *Nucl. Phys.* **B603**, 125 (2001), [*hep-ph/0103088*].
- [20] R. Garcia-Martin *et al.*, *Phys. Rev.* **D83**, 074004 (2011), [*arXiv:1102.2183*].
- [21] P. Buettiker, S. Descotes-Genon and B. Moussallam, *Eur. Phys. J.* **C33**, 409 (2004), [*hep-ph/0310283*].
- [22] M. Hoferichter, D. R. Phillips and C. Schat, *Eur. Phys. J.* **C71**, 1743 (2011), [*arXiv:1106.4147*].
- [23] M. Hoferichter *et al.*, *Phys. Rept.* **625**, 1 (2016), [*arXiv:1510.06039*].
- [24] M. P. Peskin and D. V. Schroeder, *An Introduction to Quantum Field Theory*, Westview Press, 1995.
- [25] N. N. Khuri and S. B. Treiman, *Phys. Rev.* **119**, 1115 (1960).
- [26] P. Guo *et al.*, *Phys. Lett.* **B771**, 497 (2017), [*arXiv:1608.01447*].
- [27] M. Albaladejo and B. Moussallam, *Eur. Phys. J.* **C77**, 8, 508 (2017), [*arXiv:1702.04931*].
- [28] G. Colangelo *et al.*, *Eur. Phys. J.* **C78**, 11, 947 (2018), [*arXiv:1807.11937*].
- [29] F. Niecknig, B. Kubis and S. P. Schneider, *Eur. Phys. J.* **C72**, 2014 (2012), [*arXiv:1203.2501*].
- [30] I. V. Danilkin *et al.*, *Phys. Rev.* **D91**, 9, 094029 (2015), [*arXiv:1409.7708*].
- [31] T. Isken *et al.*, *Eur. Phys. J.* **C77**, 7, 489 (2017), [*arXiv:1705.04339*].
- [32] F. Niecknig and B. Kubis, *JHEP* **10**, 142 (2015), [*arXiv:1509.03188*].
- [33] F. Niecknig and B. Kubis, *Phys. Lett.* **B780**, 471 (2018), [*arXiv:1708.00446*].
- [34] D. Morgan and M. R. Pennington, *Z. Phys.* **C37**, 431 (1988), [Erratum: *Z. Phys.*C39,590(1988)].
- [35] D. Morgan and M. R. Pennington, *Z. Phys.* **C48**, 623 (1990).
- [36] J. M. Blatt and V. F. Weisskopf, *Theoretical nuclear physics*, Springer, New York (1952), ISBN 9780471080190.
- [37] F. Von Hippel and C. Quigg, *Phys. Rev.* **D5**, 624 (1972).
- [38] S. U. Chung *et al.*, *Annalen Phys.* **4**, 404 (1995).
- [39] I. J. R. Aitchison, *Nucl. Phys.* **A189**, 417 (1972).

- [40] K. L. Au, D. Morgan and M. R. Pennington, *Phys. Rev.* **D35**, 1633 (1987).
- [41] J. J. Dudek, R. G. Edwards and D. J. Wilson (Hadron Spectrum), *Phys. Rev.* **D93**, 9, 094506 (2016), [arXiv:1602.05122].
- [42] R. A. Briceno *et al.*, *Phys. Rev.* **D97**, 5, 054513 (2018), [arXiv:1708.06667].
- [43] A. J. Woss *et al.* (2019), [arXiv:1904.04136].
- [44] S. M. Flatte, *Phys. Lett.* **63B**, 224 (1976).
- [45] V. V. Anisovich and A. V. Sarantsev, *Eur. Phys. J.* **A16**, 229 (2003), [hep-ph/0204328].
- [46] V. Baru *et al.*, *Eur. Phys. J.* **A23**, 523 (2005), [arXiv:nucl-th/0410099].
- [47] S. K. Choi *et al.* (Belle), *Phys. Rev. Lett.* **91**, 262001 (2003), [hep-ex/0309032].
- [48] R. Aaij *et al.* (LHCb), *Phys. Rev. Lett.* **122**, 22, 222001 (2019), [arXiv:1904.03947].
- [49] E. Braaten and J. Stapleton, *Phys. Rev.* **D81**, 014019 (2010), [arXiv:0907.3167].
- [50] V. Baru *et al.*, *Eur. Phys. J.* **A44**, 93 (2010), [arXiv:1001.0369].
- [51] C. Fernández-Ramírez *et al.* (JPAC), *Phys. Rev. Lett.* **123**, 9, 092001 (2019), [arXiv:1904.10021].
- [52] D. Morgan, *Nucl. Phys.* **A543**, 632 (1992).
- [53] V. Baru *et al.*, *Phys. Lett.* **B586**, 53 (2004), [hep-ph/0308129].
- [54] I. J. R. Aitchison (2015), [arXiv:1507.02697].
- [55] R. N. Cahn and P. V. Landshoff, *Nucl. Phys.* **B266**, 451 (1986).
- [56] J. L. Basdevant and E. L. Berger, *Phys. Rev.* **D16**, 657 (1977).
- [57] R. Omnes, *Nuovo Cim.* **8**, 316 (1958).
- [58] I. J. R. Aitchison and R. Pasquier, *Phys. Rev.* **152**, 4, 1274 (1966).
- [59] G. J. Gounaris and J. J. Sakurai, *Phys. Rev. Lett.* **21**, 244 (1968).
- [60] M. R. Pennington *et al.*, *Eur. Phys. J.* **C56**, 1 (2008), [arXiv:0803.3389].
- [61] J. A. Oller and E. Oset, *Phys. Rev.* **D60**, 074023 (1999), [hep-ph/9809337].
- [62] N. N. Achasov and A. V. Kiselev, *Phys. Rev.* **D83**, 054008 (2011), [arXiv:1011.4446].
- [63] A. V. Anisovich *et al.*, *Phys. Rev.* **D84**, 076001 (2011).
- [64] J. H. Reid and N. N. Trofimennoff, *J. Math. Phys.* **25**, 3540 (1984).
- [65] E. L. Lomon and S. Pacetti, *Phys. Rev.* **D85**, 113004 (2012), [Erratum: *Phys. Rev.* **D86**, 039901(2012)], [arXiv:1201.6126].
- [66] B. Moussallam, *Eur. Phys. J.* **C73**, 2539 (2013), [arXiv:1305.3143].
- [67] I. R. Afnan and B. Blankleider, *Phys. Rev.* **C22**, 1638 (1980).
- [68] A. D. Lahiff and I. R. Afnan, *Phys. Rev.* **C60**, 024608 (1999), [arXiv:nucl-th/9903058].
- [69] A. Matsuyama, T. Sato and T. S. H. Lee, *Phys. Rept.* **439**, 193 (2007), [arXiv:nucl-th/0608051].
- [70] D. Ronchen *et al.*, *Eur. Phys. J.* **A49**, 44 (2013), [arXiv:1211.6998].
- [71] C. Hanhart, *Phys. Lett.* **B715**, 170 (2012), [arXiv:1203.6839].
- [72] K. Nakano, *Phys. Rev.* **C26**, 1123 (1982).
- [73] D. Djukanovic, J. Gegelia and S. Scherer, *Phys. Rev.* **D76**, 037501 (2007), [arXiv:0707.2030].
- [74] M. Doring *et al.*, *Phys. Lett.* **B681**, 26 (2009), [arXiv:0903.1781].
- [75] S. Ropertz, C. Hanhart and B. Kubis, *Eur. Phys. J.* **C78**, 12, 1000 (2018), [arXiv:1809.06867].
- [76] J. Gasser and U. G. Meissner, *Nucl. Phys.* **B357**, 90 (1991).
- [77] M. Mikhasenko *et al.*, *JHEP* **08**, 080 (2019), [arXiv:1904.11894].
- [78] G. Calucci, L. Fonda and G. C. Ghirardi, *Phys. Rev.* **166**, 1719 (1968).

50. Cross-Section Formulae for Specific Processes

Revised August 2019 by H. Baer (Oklahoma U.) and R.N. Cahn (LBNL).

PART I: STANDARD MODEL PROCESSES

Setting aside leptonproduction (for which, see Sec. 16 of this *Review*), the cross sections of primary interest are those with light incident particles, e^+e^- , $\gamma\gamma$, $q\bar{q}$, gq , gg , etc., where g and q represent gluons and light quarks. The produced particles include both light particles and heavy ones - t , W , Z , and the Higgs boson H . We provide the production cross sections calculated within the Standard Model for several such processes.

50.1 Resonance Formation

Resonant cross sections are generally described by the Breit-Wigner formula (Sec. 18 of this *Review*).

$$\sigma(E) = \frac{2J+1}{(2S_1+1)(2S_2+1)} \frac{4\pi}{k^2} \left[\frac{\Gamma^2/4}{(E-E_0)^2 + \Gamma^2/4} \right] B_{in} B_{out}, \quad (50.1)$$

where E is the c.m. energy, J is the spin of the resonance, and the number of polarization states of the two incident particles are $2S_1+1$ and $2S_2+1$. The c.m. momentum in the initial state is k , E_0 is the c.m. energy at the resonance, and Γ is the full width at half maximum height of the resonance. The branching fraction for the resonance into the initial-state channel is B_{in} and into the final-state channel is B_{out} . For a narrow resonance, the factor in square brackets may be replaced by $\pi\Gamma\delta(E-E_0)/2$.

50.2 Production of light particles

The production of point-like, spin-1/2 fermions in e^+e^- annihilation through a virtual photon, $e^+e^- \rightarrow \gamma^* \rightarrow f\bar{f}$, at c.m. energy squared s is given by

$$\frac{d\sigma}{d\Omega} = N_c \frac{\alpha^2}{4s} \beta [1 + \cos^2\theta + (1-\beta^2)\sin^2\theta] Q_f^2, \quad (50.2)$$

where β is v/c for the produced fermions in the c.m., θ is the c.m. scattering angle, and Q_f is the charge of the fermion. The factor N_c is 1 for charged leptons and 3 for quarks. In the ultrarelativistic limit, $\beta \rightarrow 1$,

$$\sigma = N_c Q_f^2 \frac{4\pi\alpha^2}{3s} = N_c Q_f^2 \frac{86.8 \text{ nb}}{s(\text{GeV}^2)}. \quad (50.3)$$

The cross section for the annihilation of a $q\bar{q}$ pair into a distinct pair $q'\bar{q}'$ through a gluon is completely analogous up to color factors, with the replacement $\alpha \rightarrow \alpha_s$. Treating all quarks as massless, averaging over the colors of the initial quarks and defining $t = -s \sin^2(\theta/2)$, $u = -s \cos^2(\theta/2)$, one finds [1]

$$\frac{d\sigma}{d\Omega}(q\bar{q} \rightarrow q'\bar{q}') = \frac{\alpha_s^2}{9s} \frac{t^2 + u^2}{s^2}. \quad (50.4)$$

Crossing symmetry gives

$$\frac{d\sigma}{d\Omega}(qq' \rightarrow qq') = \frac{\alpha_s^2}{9s} \frac{s^2 + u^2}{t^2}. \quad (50.5)$$

If the quarks q and q' are identical, we have

$$\frac{d\sigma}{d\Omega}(q\bar{q} \rightarrow q\bar{q}) = \frac{\alpha_s^2}{9s} \left[\frac{t^2 + u^2}{s^2} + \frac{s^2 + u^2}{t^2} - \frac{2u^2}{3st} \right], \quad (50.6)$$

and by crossing

$$\frac{d\sigma}{d\Omega}(qq \rightarrow qq) = \frac{\alpha_s^2}{9s} \left[\frac{t^2 + s^2}{u^2} + \frac{s^2 + u^2}{t^2} - \frac{2s^2}{3ut} \right]. \quad (50.7)$$

Annihilation of e^+e^- into $\gamma\gamma$ has the cross section

$$\frac{d\sigma}{d\Omega}(e^+e^- \rightarrow \gamma\gamma) = \frac{\alpha^2}{2s} \frac{u^2 + t^2}{tu}. \quad (50.8)$$

The related QCD process also has a triple-gluon coupling. The cross section is

$$\frac{d\sigma}{d\Omega}(q\bar{q} \rightarrow gg) = \frac{8\alpha_s^2}{27s} (t^2 + u^2) \left(\frac{1}{tu} - \frac{9}{4s^2} \right). \quad (50.9)$$

The crossed reactions are

$$\frac{d\sigma}{d\Omega}(qg \rightarrow qg) = \frac{\alpha_s^2}{9s} (s^2 + u^2) \left(-\frac{1}{su} + \frac{9}{4t^2} \right) \quad (50.10)$$

and

$$\frac{d\sigma}{d\Omega}(gg \rightarrow q\bar{q}) = \frac{\alpha_s^2}{24s} (t^2 + u^2) \left(\frac{1}{tu} - \frac{9}{4s^2} \right). \quad (50.11)$$

Finally,

$$\frac{d\sigma}{d\Omega}(gg \rightarrow gg) = \frac{9\alpha_s^2}{8s} \left(3 - \frac{ut}{s^2} - \frac{su}{t^2} - \frac{st}{u^2} \right). \quad (50.12)$$

Lepton-quark scattering is analogous (neglecting Z exchange)

$$\frac{d\sigma}{d\Omega}(eq \rightarrow eq) = \frac{\alpha^2}{2s} e_q^2 \frac{s^2 + u^2}{t^2}. \quad (50.13)$$

where e_q is the charge of the quark. For neutrino scattering with the four-Fermi interaction

$$\frac{d\sigma}{d\Omega}(\nu d \rightarrow \ell^- u) = \frac{G_F^2 s}{4\pi^2}, \quad (50.14)$$

where the Cabibbo angle suppression is ignored. Similarly

$$\frac{d\sigma}{d\Omega}(\nu \bar{u} \rightarrow \ell^- \bar{d}) = \frac{G_F^2 s}{4\pi^2} \frac{(1 + \cos\theta)^2}{4}. \quad (50.15)$$

To obtain the formulae for deep inelastic scattering (presented in more detail in Section 18) we consider quarks of type i carrying a fraction $x = Q^2/(2M\nu)$ of the nucleon's energy, where $\nu = E - E'$ is the energy lost by the lepton in the nucleon rest frame. With $y = \nu/E$ we have the correspondences

$$1 + \cos\theta \rightarrow 2(1-y),$$

$$d\Omega_{cm} \rightarrow 4\pi f_i(x) dx dy, \quad (50.16)$$

where the latter incorporates the quark distribution, $f_i(x)$. In this way we find

$$\begin{aligned} \frac{d\sigma}{dx dy}(eN \rightarrow eX) &= \frac{4\pi\alpha^2 x s}{Q^4} \frac{1}{2} [1 + (1-y)^2] \\ &\times \left[\frac{4}{9}(u(x) + \bar{u}(x) + \dots) + \frac{1}{9}(d(x) + \bar{d}(x) + \dots) \right] \end{aligned} \quad (50.17)$$

where now $s = 2ME$ is the cm energy squared for the electron-nucleon collision and we have suppressed contributions from higher mass quarks.

Similarly,

$$\frac{d\sigma}{dx dy}(\nu N \rightarrow \ell^- X) = \frac{G_F^2 x s}{\pi} [(d(x) + \dots) + (1-y)^2(\bar{u}(x) + \dots)] \quad (50.18)$$

and

$$\frac{d\sigma}{dx dy}(\bar{\nu} N \rightarrow \ell^+ X) = \frac{G_F^2 x s}{\pi} [(\bar{d}(x) + \dots) + (1-y)^2(u(x) + \dots)]. \quad (50.19)$$

Quasi-elastic neutrino scattering ($\nu_\mu n \rightarrow \mu^- p$, $\bar{\nu}_\mu p \rightarrow \mu^+ n$) is directly related to the crossed reaction, neutron decay. The formula for the differential cross section is presented, for example, in N.J. Baker *et al.*, Phys. Rev. **D23**, 2499 (1981).

50.3 Hadroproduction of heavy quarks

For hadroproduction of heavy quarks $Q = c, b, t$, it is important to include mass effects in the formulae. For $q\bar{q} \rightarrow Q\bar{Q}$, one has

$$\frac{d\sigma}{d\Omega}(q\bar{q} \rightarrow Q\bar{Q}) = \frac{\alpha_s^2}{9s^3} \sqrt{1 - \frac{4m_Q^2}{s}} \left[(m_Q^2 - t)^2 + (m_Q^2 - u)^2 + 2m_Q^2 s \right], \quad (50.20)$$

while for $gg \rightarrow Q\bar{Q}$ one has

$$\begin{aligned} \frac{d\sigma}{d\Omega}(gg \rightarrow Q\bar{Q}) = & \frac{\alpha_s^2}{32s} \sqrt{1 - \frac{4m_Q^2}{s}} \left[\frac{6}{s^2} (m_Q^2 - t)(m_Q^2 - u) - \right. \\ & - \frac{m_Q^2 (s - 4m_Q^2)}{3(m_Q^2 - t)(m_Q^2 - u)} + \\ & + \frac{4}{3} \frac{(m_Q^2 - t)(m_Q^2 - u) - 2m_Q^2 (m_Q^2 + t)}{(m_Q^2 - t)^2} \\ & + \frac{4}{3} \frac{(m_Q^2 - t)(m_Q^2 - u) - 2m_Q^2 (m_Q^2 + u)}{(m_Q^2 - u)^2} \\ & - 3 \frac{(m_Q^2 - t)(m_Q^2 - u) + m_Q^2 (u - t)}{s(m_Q^2 - t)} \\ & \left. - 3 \frac{(m_Q^2 - t)(m_Q^2 - u) + m_Q^2 (t - u)}{s(m_Q^2 - u)} \right]. \quad (50.21) \end{aligned}$$

50.4 Production of Weak Gauge Bosons

50.4.1 W and Z resonant production

Resonant production of a single W or Z is governed by the partial widths

$$\Gamma(W \rightarrow \ell_i \bar{\nu}_i) = \frac{\sqrt{2} G_F m_W^3}{12\pi} \quad (50.22)$$

$$\Gamma(W \rightarrow q_i \bar{q}_j) = 3 \frac{\sqrt{2} G_F |V_{ij}|^2 m_W^3}{12\pi} \quad (50.23)$$

$$\begin{aligned} \Gamma(Z \rightarrow f\bar{f}) = & N_c \frac{\sqrt{2} G_F m_Z^3}{6\pi} \\ & \times \left[(T_3 - Q_f \sin^2 \theta_W)^2 + (Q_f \sin^2 \theta_W)^2 \right]. \quad (50.24) \end{aligned}$$

The weak mixing angle is θ_W . The CKM matrix elements are indicated by V_{ij} and N_c is 3 for $q\bar{q}$ final states and 1 for leptonic final states.

The full differential cross section for $f_i \bar{f}_j \rightarrow (W, Z) \rightarrow f_i' \bar{f}_j'$ is given by

$$\begin{aligned} \frac{d\sigma}{d\Omega} = & \frac{N_c^f}{N_c^i} \cdot \frac{1}{256\pi^2 s} \cdot \frac{s^2}{(s - M^2)^2 + s\Gamma^2} \\ & \times \left[(L^2 + R^2)(L'^2 + R'^2)(1 + \cos^2 \theta) \right. \\ & \left. + (L^2 - R^2)(L'^2 - R'^2) 2 \cos \theta \right] \quad (50.25) \end{aligned}$$

where M is the mass of the W or Z . The couplings for the W are $L = (8G_F m_W^2 / \sqrt{2})^{1/2} V_{ij} / \sqrt{2}$; $R = 0$ where V_{ij} is the corresponding CKM matrix element, with an analogous expression for L' and R' . For Z , the couplings are $L = (8G_F m_Z^2 / \sqrt{2})^{1/2} (T_3 -$

$\sin^2 \theta_W Q)$; $R = -(8G_F m_Z^2 / \sqrt{2})^{1/2} \sin^2 \theta_W Q$, where T_3 is the weak isospin of the initial left-handed fermion and Q is the initial fermion's electric charge. The expressions for L' and R' are analogous. The color factors $N_c^{i,f}$ are 3 for initial or final quarks and 1 for initial or final leptons.

50.4.2 Production of pairs of weak gauge bosons

The cross section for $f\bar{f} \rightarrow W^+ W^-$ is given in term of the couplings of the left-handed and right-handed fermion f , $\ell = 2(T_3 - Qx_W)$, $r = -2Qx_W$, where T_3 is the third component of weak isospin for the left-handed f , Q is its electric charge (in units of the proton charge), and $x_W = \sin^2 \theta_W$:

$$\begin{aligned} \frac{d\sigma}{dt} = & \frac{2\pi\alpha^2}{N_c s^2} \left\{ \left[\left(Q + \frac{\ell + r}{4x_W} \frac{s}{s - m_Z^2} \right)^2 \right. \right. \\ & \left. \left. + \left(\frac{\ell - r}{4x_W} \frac{s}{s - m_Z^2} \right)^2 \right] A(s, t, u) \right. \\ & \left. + \frac{1}{2x_W} \left(Q + \frac{\ell}{2x_W} \frac{s}{s - m_Z^2} \right) \right. \\ & \left. (\Theta(-Q)I(s, t, u) - \Theta(Q)I(s, u, t)) \right. \\ & \left. + \frac{1}{8x_W^2} (\Theta(-Q)E(s, t, u) + \Theta(Q)E(s, u, t)) \right\}, \quad (50.26) \end{aligned}$$

where $\Theta(x)$ is 1 for $x > 0$ and 0 for $x < 0$, and where

$$\begin{aligned} A(s, t, u) = & \left(\frac{tu}{m_W^4} - 1 \right) \left(\frac{1}{4} - \frac{m_W^2}{s} + 3 \frac{m_W^4}{s^2} \right) + \frac{s}{m_W^2} - 4, \\ I(s, t, u) = & \left(\frac{tu}{m_W^4} - 1 \right) \left(\frac{1}{4} - \frac{m_W^2}{2s} - \frac{m_W^4}{st} \right) + \frac{s}{m_W^2} - 2 + 2 \frac{m_W^2}{t}, \\ E(s, t, u) = & \left(\frac{tu}{m_W^4} - 1 \right) \left(\frac{1}{4} + \frac{m_W^4}{t^2} \right) + \frac{s}{m_W^2}, \quad (50.27) \end{aligned}$$

and s, t, u are the usual Mandelstam variables with $s = (p_f + p_{\bar{f}})^2$, $t = (p_f - p_{W^-})^2$, $u = (p_f - p_{W^+})^2$. The factor N_c is 3 for quarks and 1 for leptons.

The analogous cross-section for $q_i \bar{q}_j \rightarrow W^\pm Z^0$ is

$$\begin{aligned} \frac{d\sigma}{dt} = & \frac{\pi\alpha^2 |V_{ij}|^2}{6s^2 x_W^2} \left\{ \left(\frac{1}{s - m_W^2} \right)^2 \left[\left(\frac{9 - 8x_W}{4} \right) (ut - m_W^2 m_Z^2) \right. \right. \\ & \left. \left. + (8x_W - 6) s (m_W^2 + m_Z^2) \right] \right. \\ & \left. + \left[\frac{ut - m_W^2 m_Z^2 - s(m_W^2 + m_Z^2)}{s - m_W^2} \right] \left[\frac{\ell_j}{t} - \frac{\ell_i}{u} \right] \right. \\ & \left. + \frac{ut - m_W^2 m_Z^2}{4(1 - x_W)} \left[\frac{\ell_j^2}{t^2} + \frac{\ell_i^2}{u^2} \right] + \frac{s(m_W^2 + m_Z^2)}{2(1 - x_W)} \frac{\ell_i \ell_j}{tu} \right\}, \quad (50.28) \end{aligned}$$

where ℓ_i and ℓ_j are the couplings of the left-handed q_i and q_j as defined above. The CKM matrix element between q_i and q_j is V_{ij} .

The cross section for $q_i \bar{q}_i \rightarrow Z^0 Z^0$ is

$$\frac{d\sigma}{dt} = \frac{\pi\alpha^2}{96} \frac{\ell_i^4 + r_i^4}{x_W^2 (1 - x_W^2)^2 s^2} \left[\frac{t}{u} + \frac{u}{t} + \frac{4m_Z^2 s}{tu} - m_Z^4 \left(\frac{1}{t^2} + \frac{1}{u^2} \right) \right]. \quad (50.29)$$

50.5 Production of Higgs Bosons

50.5.1 Resonant Production

The Higgs boson of the Standard Model can be produced resonantly in the collisions of quarks, leptons, W or Z bosons, gluons, or photons. The production cross section is thus controlled by the partial width of the Higgs boson into the entrance channel and its total width. The branching fractions for the Standard Model Higgs boson are shown in Fig. 1 of the ‘‘Searches for Higgs bosons’’ review in the Particle Listings section, as a function of the Higgs boson mass. The partial widths are given by the relations

$$\Gamma(H \rightarrow f\bar{f}) = \frac{G_F m_f^2 m_H N_c}{4\pi\sqrt{2}} \left(1 - 4m_f^2/m_H^2\right)^{3/2}, \quad (50.30)$$

$$\Gamma(H \rightarrow W^+W^-) = \frac{G_F m_H^3 \beta_W}{32\pi\sqrt{2}} \left(4 - 4a_W + 3a_W^2\right), \quad (50.31)$$

$$\Gamma(H \rightarrow ZZ) = \frac{G_F m_H^3 \beta_Z}{64\pi\sqrt{2}} \left(4 - 4a_Z + 3a_Z^2\right), \quad (50.32)$$

where N_c is 3 for quarks and 1 for leptons and where $a_W = 1 - \beta_W^2 = 4m_W^2/m_H^2$ and $a_Z = 1 - \beta_Z^2 = 4m_Z^2/m_H^2$. The decay to two gluons proceeds through quark loops, with the t quark dominating [2]. Explicitly,

$$\Gamma(H \rightarrow gg) = \frac{\alpha_s^2 G_F m_H^3}{36\pi^3 \sqrt{2}} \left| \sum_q I(m_q^2/m_H^2) \right|^2, \quad (50.33)$$

where $I(z)$ is complex for $z < 1/4$. For $z < 2 \times 10^{-3}$, $|I(z)|$ is small so the light quarks contribute negligibly. For $m_H < 2m_t$, $z > 1/4$ and

$$I(z) = 3 \left[2z + 2z(1-4z) \left(\sin^{-1} \frac{1}{2\sqrt{z}} \right)^2 \right], \quad (50.34)$$

which has the limit $I(z) \rightarrow 1$ as $z \rightarrow \infty$.

50.5.2 Higgs Boson Production in W^* and Z^* decay

The Standard Model Higgs boson can be produced in the decay of a virtual W or Z (‘‘Higgstrahlung’’) [3, 4]: In particular, if k is the c.m. momentum of the Higgs boson,

$$\sigma(q_i \bar{q}_j \rightarrow WH) = \frac{\pi\alpha^2 |V_{ij}|^2}{36 \sin^4 \theta_W} \frac{2k}{\sqrt{s}} \frac{k^2 + 3m_W^2}{(s - m_W^2)^2} \quad (50.35)$$

$$\sigma(f\bar{f} \rightarrow ZH) = \frac{2\pi\alpha^2 (\ell_f^2 + r_f^2)}{48N_c \sin^4 \theta_W \cos^4 \theta_W} \frac{2k}{\sqrt{s}} \frac{k^2 + 3m_Z^2}{(s - m_Z^2)^2}, \quad (50.36)$$

where ℓ and r are defined as above.

50.5.3 W and Z Fusion

Just as high-energy electrons can be regarded as sources of virtual photon beams, at very high energies they are sources of virtual W and Z beams. For Higgs boson production, it is the longitudinal components of the W s and Z s that are important [5]. The distribution of longitudinal W s carrying a fraction y of the electron’s energy is [6]

$$f(y) = \frac{g^2}{16\pi^2} \frac{1-y}{y}, \quad (50.37)$$

where $g = e/\sin\theta_W$. In the limit $s \gg m_H \gg m_W$, the partial decay rate is $\Gamma(H \rightarrow W_L W_L) = (g^2/64\pi)(m_H^3/m_W^2)$ and in the equivalent W approximation [7]

$$\sigma(e^+e^- \rightarrow \bar{\nu}_e \nu_e H) = \frac{1}{16m_W^2} \left(\frac{\alpha}{\sin^2 \theta_W} \right)^3 \times \left[\left(1 + \frac{m_H^2}{s} \right) \log \frac{s}{m_H^2} - 2 + 2 \frac{m_H^2}{s} \right]. \quad (50.38)$$

There are significant corrections to this relation when m_H is not large compared to m_W [8]. For $m_H = 150$ GeV, the estimate is too high by 51% for $\sqrt{s} = 1000$ GeV, 32% too high at $\sqrt{s} = 2000$ GeV, and 22% too high at $\sqrt{s} = 4000$ GeV. Fusion of ZZ to make a Higgs boson can be treated similarly. Identical formulae apply for Higgs production in the collisions of quarks whose charges permit the emission of a W^+ and a W^- , except that QCD corrections and CKM matrix elements are required. Even in the absence of QCD corrections, the fine-structure constant ought to be evaluated at the scale of the collision, say m_W . All quarks contribute to the ZZ fusion process.

50.6 Inclusive hadronic reactions

One-particle inclusive cross sections $E d^3\sigma/d^3p$ for the production of a particle of momentum p are conveniently expressed in terms of rapidity y (see above) and the momentum p_T transverse to the beam direction (in the c.m.):

$$E \frac{d^3\sigma}{d^3p} = \frac{d^3\sigma}{d\phi dy p_T dp_T}. \quad (50.39)$$

In appropriate circumstances, the cross section may be decomposed as a partonic cross section multiplied by the probabilities of finding partons of the prescribed momenta:

$$\sigma_{\text{hadronic}} = \sum_{ij} \int dx_1 dx_2 f_i(x_1) f_j(x_2) d\hat{\sigma}_{\text{partonic}}, \quad (50.40)$$

The probability that a parton of type i carries a fraction of the incident particle’s that lies between x_1 and $x_1 + dx_1$ is $f_i(x_1)dx_1$ and similarly for partons in the other incident particle. The partonic collision is specified by its c.m. energy squared $\hat{s} = x_1 x_2 s$ and the momentum transfer squared \hat{t} . The final hadronic state is more conveniently specified by the rapidities y_1, y_2 of the two jets resulting from the collision and the transverse momentum p_T . The connection between the differentials is

$$dx_1 dx_2 d\hat{t} = dy_1 dy_2 \frac{\hat{s}}{s} dp_T^2, \quad (50.41)$$

so that

$$\frac{d^3\sigma}{dy_1 dy_2 dp_T^2} = \frac{\hat{s}}{s} \left[f_i(x_1) f_j(x_2) \frac{d\hat{\sigma}}{d\hat{t}}(\hat{s}, \hat{t}, \hat{u}) + f_i(x_2) f_j(x_1) \frac{d\hat{\sigma}}{d\hat{t}}(\hat{s}, \hat{u}, \hat{t}) \right], \quad (50.42)$$

where we have taken into account the possibility that the incident parton types might arise from either incident particle. The second term should be dropped if the types are identical: $i = j$.

50.7 Two-photon processes

In the Weizsäcker-Williams picture, a high-energy electron beam is accompanied by a spectrum of virtual photons of energies ω and invariant-mass squared $q^2 = -Q^2$, for which the photon number density is

$$dn = \frac{\alpha}{\pi} \left[1 - \frac{\omega}{E} + \frac{\omega^2}{E^2} - \frac{m_e^2 \omega^2}{Q^2 E^2} \right] \frac{d\omega}{\omega} \frac{dQ^2}{Q^2}, \quad (50.43)$$

where E is the energy of the electron beam. The cross section for $e^+e^- \rightarrow e^+e^- X$ is then [9]

$$d\sigma_{e^+e^- \rightarrow e^+e^- X}(s) = dn_1 dn_2 d\sigma_{\gamma\gamma \rightarrow X}(W^2), \quad (50.44)$$

where $W^2 = m_X^2$. Integrating from the lower limit $Q^2 = m_e^2 \frac{\omega_i^2}{E_i(E_i - \omega_i)}$ to a maximum Q^2 gives

$$\sigma_{e^+e^- \rightarrow e^+e^- X}(s) = \frac{\alpha^2}{\pi^2} \int_{z_{th}}^1 \frac{dz}{z} \times \left[\left(\ln \frac{Q_{max}^2}{zm_e^2} - 1 \right)^2 f(z) + \frac{1}{3} (\ln z)^3 \right] \sigma_{\gamma\gamma \rightarrow X}(zs), \quad (50.45)$$

where

$$f(z) = \left(1 + \frac{1}{2}z\right)^2 \ln(1/z) - \frac{1}{2}(1-z)(3+z). \quad (50.46)$$

The appropriate value of Q_{max}^2 depends on the properties of the produced system X . For production of hadronic systems, $Q_{max}^2 \approx m_\rho^2$, while for lepton-pair production, $Q^2 \approx W^2$. For production of a resonance with spin $J \neq 1$, we have

$$\sigma_{e^+e^- \rightarrow e^+e^- R}(s) = (2J+1) \frac{8\alpha^2 \Gamma_{R \rightarrow \gamma\gamma}}{m_R^3} \times \left[f(m_R^2/s) \left(\ln \frac{m_V^2 s}{m_e^2 m_R^2} - 1 \right)^2 - \frac{1}{3} \left(\ln \frac{s}{M_R^2} \right)^3 \right], \quad (50.47)$$

where m_V is the mass that enters into the form factor for the $\gamma\gamma \rightarrow R$ transition, typically m_ρ .

PART II: PROCESSES BEYOND THE STANDARD MODEL

50.8 Production of supersymmetric particles

In supersymmetric (SUSY) theories (see Supersymmetric Particle Searches in this *Review*), every boson has a fermionic superpartner, and every fermion has a bosonic superpartner. The minimal supersymmetric Standard Model (MSSM) is a direct supersymmetrization of the Standard Model (SM), although a second Higgs doublet is needed to avoid triangle anomalies [10]. Under *soft* SUSY breaking, superpartner masses are lifted above the SM particle masses. In weak scale SUSY, the superpartners are invoked to stabilize the weak scale under radiative corrections, so the superpartners are expected to have masses of order the TeV scale.

50.8.1 Gluino and squark production

The superpartners of gluons are the color octet, spin- $\frac{1}{2}$ gluinos (\tilde{g}), while each helicity component of quark flavor has a spin-0 squark partner, *e.g.* \tilde{q}_L and \tilde{q}_R . Third generation left- and right- squarks are expected to have large mixing, resulting in mass eigenstates \tilde{q}_1 and \tilde{q}_2 , with $m_{\tilde{q}_1} < m_{\tilde{q}_2}$ (here, q denotes any of the SM flavors of quarks and \tilde{q}_i the corresponding flavor and type ($i = L, R$ or 1, 2) of squark). Gluino pair production ($\tilde{g}\tilde{g}$) takes place via either glue-gluon or quark-antiquark annihilation [11].

The subprocess cross sections are usually presented as differential distributions in the Mandelstam variables s , t and u . Note that for a $2 \rightarrow 2$ scattering subprocess $ab \rightarrow cd$, the Mandelstam variable $s = (p_a + p_b)^2 = (p_c + p_d)^2$, where p_a is the 4-momentum of particle a , and so forth. The variable $t = (p_c - p_a)^2$, where c and a are taken conventionally to be the most similar particles in the subprocess. The variable u would then be equal to $(p_d - p_a)^2$. Note that since s , t and u are squares of 4-vectors, they are invariants in any inertial reference frame.

Gluino pair production at hadron colliders is described by:

$$\frac{d\sigma}{dt}(gg \rightarrow \tilde{g}\tilde{g}) = \frac{9\pi\alpha_s^2}{4s^2} \left\{ \frac{2(m_g^2 - t)(m_g^2 - u)}{s^2} + \frac{(m_g^2 - t)(m_g^2 - u) - 2m_g^2(m_g^2 + t)}{(m_g^2 - t)^2} + \frac{(m_g^2 - t)(m_g^2 - u) - 2m_g^2(m_g^2 + u)}{(m_g^2 - u)^2} + \frac{m_g^2(s - 4m_g^2)}{(m_g^2 - t)(m_g^2 - u)} \right\},$$

$$\left. \frac{(m_g^2 - t)(m_g^2 - u) + m_g^2(u - t)}{s(m_g^2 - t)} - \frac{(m_g^2 - t)(m_g^2 - u) + m_g^2(t - u)}{s(m_g^2 - u)} \right\}, \quad (50.48)$$

where α_s is the strong fine structure constant. Also,

$$\frac{d\sigma}{dt}(q\bar{q} \rightarrow \tilde{g}\tilde{g}) = \frac{8\pi\alpha_s^2}{9s^2} \left\{ \frac{4}{3} \left(\frac{m_g^2 - t}{m_q^2 - t} \right)^2 + \frac{4}{3} \left(\frac{m_g^2 - u}{m_q^2 - u} \right)^2 + \frac{3}{s^2} [(m_g^2 - t)^2 + (m_g^2 - u)^2 + 2m_g^2 s] - 3 \frac{[(m_g^2 - t)^2 + m_g^2 s]}{s(m_q^2 - t)} - 3 \frac{[(m_g^2 - u)^2 + m_g^2 s]}{s(m_q^2 - u)} + \frac{1}{3} \frac{m_g^2 s}{(m_q^2 - t)(m_q^2 - u)} \right\}. \quad (50.49)$$

Gluinos can also be produced in association with squarks: $\tilde{g}\tilde{q}_i$ production, where \tilde{q}_i represents any of the various types (left, right- or mixed) and flavors of squarks. The subprocess cross section is independent of whether the squark is the right-, left- or mixed type:

$$\frac{d\sigma}{dt}(gq \rightarrow \tilde{g}\tilde{q}_i) = \frac{\pi\alpha_s^2}{24s^2} \left\{ \frac{16}{3}(s^2 + (m_{\tilde{q}_i}^2 - u)^2) + \frac{4}{3}s(m_{\tilde{q}_i}^2 - u) \right\} \times \left((m_g^2 - u)^2 + (m_{\tilde{q}_i}^2 - m_g^2)^2 + \frac{2sm_g^2(m_{\tilde{q}_i}^2 - m_g^2)}{(m_g^2 - t)} \right). \quad (50.50)$$

There are many different subprocesses for production of squark pairs. Since left- and right- squarks generally have different masses and different decay patterns, we present the differential cross section for each subprocess of \tilde{q}_i ($i = L, R$ or 1, 2) separately. (In early literature, the following formulae were often combined into a single equation which didn't differentiate the various squark types.) The result for $gg \rightarrow \tilde{q}_i\tilde{q}_i$ is:

$$\frac{d\sigma}{dt}(gg \rightarrow \tilde{q}_i\tilde{q}_i) = \frac{\pi\alpha_s^2}{4s^2} \left\{ \frac{1}{3} \left(\frac{m_q^2 + t}{m_q^2 - t} \right)^2 + \frac{1}{3} \left(\frac{m_q^2 + u}{m_q^2 - u} \right)^2 + \frac{3}{32s^2} (8s(4m_q^2 - s) + 4(u - t)^2) + \frac{7}{12} - \frac{1}{48} \frac{(4m_q^2 - s)^2}{(m_q^2 - t)(m_q^2 - u)} + \frac{3}{32} \frac{[(t - u)(4m_q^2 + 4t - s) - 2(m_q^2 - u)(6m_q^2 + 2t - s)]}{s(m_q^2 - t)} + \frac{3}{32} \frac{[(u - t)(4m_q^2 + 4u - s) - 2(m_q^2 - t)(6m_q^2 + 2u - s)]}{s(m_q^2 - u)} + \frac{7}{96} \frac{[4m_q^2 + 4t - s]}{m_q^2 - t} + \frac{7}{96} \frac{[4m_q^2 + 4u - s]}{m_q^2 - u} \right\}, \quad (50.51)$$

which has an obvious $u \leftrightarrow t$ symmetry.

For $q\bar{q} \rightarrow \tilde{q}_i\tilde{q}_i$ with the same initial and final state flavors, we have

$$\frac{d\sigma}{dt}(q\bar{q} \rightarrow \tilde{q}_i\tilde{q}_i) = \frac{2\pi\alpha_s^2}{9s^2} \left\{ \frac{1}{(t - m_{\tilde{q}_i}^2)^2} + \frac{2}{s^2} - \frac{2/3}{s(t - m_{\tilde{q}_i}^2)} \right\} \times [-st - (t - m_{\tilde{q}_i}^2)^2], \quad (50.52)$$

while if initial and final state flavors are different ($q\bar{q} \rightarrow \tilde{q}'_i\tilde{q}'_i$) we instead have

$$\frac{d\sigma}{dt}(q\bar{q} \rightarrow \tilde{q}'_i\tilde{q}'_i) = \frac{4\pi\alpha_s^2}{9s^4} \left[-st - (t - m_{\tilde{q}'_i}^2)^2 \right]. \quad (50.53)$$

If the two initial state quarks are of different flavors, then we have

$$\frac{d\sigma}{dt}(q\bar{q}' \rightarrow \tilde{q}_i\tilde{q}'_i) = \frac{2\pi\alpha_s^2}{9s^2} \frac{-st - (t - m_{\tilde{q}_i}^2)^2}{(t - m_{\tilde{q}'_i}^2)^2}. \quad (50.54)$$

If the initial quarks are of different flavor and final state squarks are of different type ($i \neq j$) then

$$\frac{d\sigma}{dt}(q\bar{q}' \rightarrow \tilde{q}_i\tilde{q}'_j) = \frac{2\pi\alpha_s^2}{9s^2} \frac{m_{\tilde{g}}^2 s}{(t - m_{\tilde{g}}^2)^2}. \quad (50.55)$$

For same-flavor initial state quarks, but final state unlike-type squarks, we also have

$$\frac{d\sigma}{dt}(q\bar{q} \rightarrow \tilde{q}_i\tilde{q}_j) = \frac{2\pi\alpha_s^2}{9s^2} \frac{m_{\tilde{g}}^2 s}{(t - m_{\tilde{g}}^2)^2}. \quad (50.56)$$

There also exist cross sections for quark-quark annihilation to squark pairs. For same flavor quark-quark annihilation to same flavor/same type final state squarks,

$$\begin{aligned} \frac{d\sigma}{dt}(qq \rightarrow \tilde{q}_i\tilde{q}_i) &= \\ &= \frac{\pi\alpha_s^2}{9s^2} m_{\tilde{g}}^2 s \left\{ \frac{1}{(t - m_{\tilde{g}}^2)^2} + \frac{1}{(u - m_{\tilde{g}}^2)^2} - \frac{2/3}{(t - m_{\tilde{g}}^2)(u - m_{\tilde{g}}^2)} \right\}, \end{aligned} \quad (50.57)$$

while if the final type squarks are different ($i \neq j$), we have

$$\begin{aligned} \frac{d\sigma}{dt}(qq \rightarrow \tilde{q}_i\tilde{q}_j) &= \\ &= \frac{2\pi\alpha_s^2}{9s^2} \times \\ &\left\{ \frac{[-st - (t - m_{\tilde{q}_i}^2)(t - m_{\tilde{q}_j}^2)]}{(t - m_{\tilde{g}}^2)} + \frac{[-su - (u - m_{\tilde{q}_i}^2)(u - m_{\tilde{q}_j}^2)]}{(u - m_{\tilde{g}}^2)} \right\}. \end{aligned} \quad (50.58)$$

If initial/final state flavors are different, but final state squark types are the same, then

$$\frac{d\sigma}{dt}(q\bar{q}' \rightarrow \tilde{q}_i\tilde{q}'_i) = \frac{2\pi\alpha_s^2}{9s^2} \frac{m_{\tilde{g}}^2 s}{(t - m_{\tilde{g}}^2)^2}. \quad (50.59)$$

If initial quark flavors are different and final squark types are different, then

$$\frac{d\sigma}{dt}(q\bar{q}' \rightarrow \tilde{q}_i\tilde{q}'_j) = \frac{2\pi\alpha_s^2}{9s^2} \frac{-st - (t - m_{\tilde{q}_i}^2)(t - m_{\tilde{q}_j}^2)}{(t - m_{\tilde{g}}^2)^2}. \quad (50.60)$$

50.8.2 Gluino and squark associated production

In the MSSM, the charged spin- $\frac{1}{2}$ winos and higgsinos mix to make chargino states $\chi_{1,2}^{\pm}$ and χ_2^{\pm} , with $m_{\chi_1^{\pm}} < m_{\chi_2^{\pm}}$. The spin- $\frac{1}{2}$ neutral bino, wino and higgsino fields mix to give four neutralino mass eigenstates $\chi_{1,2,3,4}^0$ ordered according to mass. We sometimes denote the charginos and neutralinos collectively as -inos for notational simplicity

For gluino and squark production in association with charginos and neutralinos [12], the quark-squark-neutralino couplings¹ are

¹The couplings $A_{\tilde{\chi}_i^0}^f$ and $B_{\tilde{\chi}_i^0}^f$ are given explicitly in Ref. [13] in Eq. (8.87). Also, the couplings $A_{\tilde{\chi}_i^-}^d$ and $A_{\tilde{\chi}_i^-}^u$ are given in Eq. (8.93). The couplings X_i^j and Y_i^j are given by Eq. (8.103), while the x_i and y_i couplings are given in Eq. (8.100). Finally, the couplings W_{ij} are given in Eq. (8.101).

defined by the interaction Lagrangian terms

$$\mathcal{L}_{\tilde{f}f\tilde{\chi}_i^0} = \left[iA_{\tilde{\chi}_i^0}^f \tilde{f}_L^{\dagger} \tilde{\chi}_i^0 P_L f + iB_{\tilde{\chi}_i^0}^f \tilde{f}_R^{\dagger} \tilde{\chi}_i^0 P_R f + \text{h.c.} \right]$$

, where $A_{\tilde{\chi}_i^0}^f$ and $B_{\tilde{\chi}_i^0}^f$ are coupling constants involving gauge couplings, neutralino mixing elements and in the case of third generation fermions, Yukawa couplings. Their form depends on the conventions used for setting up the MSSM Lagrangian, and can be found in various reviews [14] and textbooks [13,15]. P_L and P_R are the usual left- and right- spinor projection operators and f denotes any of the SM fermions u, d, e, ν_e, \dots . The fermion-sfermion- chargino couplings have the form $\mathcal{L} = \left[iA_{\tilde{\chi}_i^-}^d \tilde{u}_L^{\dagger} \tilde{\chi}_i^- P_L d + iA_{\tilde{\chi}_i^-}^u \tilde{d}_L^{\dagger} \tilde{\chi}_i^- P_L u + \text{h.c.} \right]$ for u and d quarks, where the $A_{\tilde{\chi}_i^-}^d$ and $A_{\tilde{\chi}_i^-}^u$ couplings are again convention-dependent, and can be found in textbooks. The superscript c denotes ‘‘charge conjugate spinor’’, defined by $\psi^c \equiv C\bar{\psi}^T$.

The subprocess cross sections for chargino-squark associated production occur via squark exchange and are given by

$$\frac{d\sigma}{dt}(\bar{u}g \rightarrow \tilde{\chi}_i^- \bar{d}_L) = \frac{\alpha_s}{24s^2} |A_{\tilde{\chi}_i^-}^u|^2 \psi(m_{\tilde{d}_L}, m_{\tilde{\chi}_i^-}, t), \quad (50.61)$$

$$\frac{d\sigma}{dt}(dg \rightarrow \tilde{\chi}_i^- \bar{u}_L) = \frac{\alpha_s}{24s^2} |A_{\tilde{\chi}_i^-}^d|^2 \psi(m_{\tilde{u}_L}, m_{\tilde{\chi}_i^-}, t), \quad (50.62)$$

while neutralino-squark production is given by

$$\frac{d\sigma}{dt}(qg \rightarrow \tilde{\chi}_i^0 \tilde{q}) = \frac{\alpha_s}{24s^2} \left(|A_{\tilde{\chi}_i^0}^q|^2 + |B_{\tilde{\chi}_i^0}^q|^2 \right) \psi(m_{\tilde{q}}, m_{\tilde{\chi}_i^0}, t), \quad (50.63)$$

where

$$\begin{aligned} \psi(m_1, m_2, t) &= \frac{s + t - m_1^2}{2s} - \frac{m_1^2(m_2^2 - t)}{(m_1^2 - t)^2} \\ &+ \frac{t(m_2^2 - m_1^2) + m_2^2(s - m_2^2 + m_1^2)}{s(m_1^2 - t)}. \end{aligned} \quad (50.64)$$

Here, the variable t is given by the square of ‘‘squark-minus-quark’’ four-momentum. The neutralino-gluino associated production cross section also occurs via squark exchange and is given by

$$\begin{aligned} \frac{d\sigma}{dt}(q\bar{q} \rightarrow \tilde{\chi}_i^0 \tilde{g}) &= \frac{\alpha_s}{18s^2} \left(|A_{\tilde{\chi}_i^0}^q|^2 + |B_{\tilde{\chi}_i^0}^q|^2 \right) \left[\frac{(m_{\tilde{\chi}_i^0}^2 - t)(m_{\tilde{g}}^2 - t)}{(m_{\tilde{q}}^2 - t)^2} \right. \\ &+ \left. \frac{(m_{\tilde{\chi}_i^0}^2 - u)(m_{\tilde{g}}^2 - u)}{(m_{\tilde{q}}^2 - u)^2} - \frac{2\eta_i \eta_{\tilde{g}} m_{\tilde{g}} m_{\tilde{\chi}_i^0} s}{(m_{\tilde{q}}^2 - t)(m_{\tilde{q}}^2 - u)} \right], \end{aligned} \quad (50.65)$$

where η_i is the sign of the neutralino mass eigenvalue and $\eta_{\tilde{g}}$ is the sign of the gluino mass eigenvalue. We also have chargino-gluino associated production:

$$\begin{aligned} \frac{d\sigma}{dt}(\bar{u}d \rightarrow \tilde{\chi}_i^- \tilde{g}) &= \frac{\alpha_s}{18s^2} \left[|A_{\tilde{\chi}_i^-}^u|^2 \frac{(m_{\tilde{\chi}_i^-}^2 - t)(m_{\tilde{g}}^2 - t)}{(m_{\tilde{d}_L}^2 - t)^2} \right. \\ &+ \left. |A_{\tilde{\chi}_i^-}^d|^2 \frac{(m_{\tilde{\chi}_i^-}^2 - u)(m_{\tilde{g}}^2 - u)}{(m_{\tilde{u}_L}^2 - u)^2} + \frac{2\eta_{\tilde{g}} \text{Re}(A_{\tilde{\chi}_i^-}^u A_{\tilde{\chi}_i^-}^d)}{(m_{\tilde{d}_L}^2 - t)(m_{\tilde{u}_L}^2 - u)} m_{\tilde{g}} m_{\tilde{\chi}_i^-} s \right], \end{aligned} \quad (50.66)$$

where $\hat{t} = (\tilde{g} - d)^2$ and in the third term one must take the real part of the in general complex coupling constant product.

50.8.3 Slepton and sneutrino production

The subprocess cross section for $\tilde{\ell}_L \bar{\nu}_{\ell L}$ production ($\ell = e$ or μ) occurs via s -channel W exchange and is given by

$$\frac{d\sigma}{dt}(d\bar{u} \rightarrow \tilde{\ell}_L \bar{\nu}_{\ell L}) = \frac{g^4 |D_W(s)|^2}{192\pi s^2} \left(tu - m_{\tilde{\ell}_L}^2 m_{\tilde{\nu}_{\ell L}}^2 \right), \quad (50.67)$$

where $D_W(s) = 1/(s - M_W^2 + iM_W\Gamma_W)$ is the W -boson propagator denominator. The production of $\tilde{\tau}_1 \bar{\nu}_\tau$ is given as above, but replacing $m_{\tilde{\ell}_L} \rightarrow m_{\tilde{\tau}_1}$, $m_{\tilde{\nu}_{\ell L}} \rightarrow m_{\tilde{\nu}_\tau}$ and multiplying by an overall factor of $\cos^2 \theta_\tau$ (where θ_τ is the tau-slepton mixing angle). Similar substitutions hold for $\tilde{\tau}_2 \bar{\nu}_\tau$ production, except the overall factor is $\sin^2 \theta_\tau$.

Table 50.1: The constants α_f and β_f that appear in in the SM neutral current Lagrangian. Here $t \equiv \tan \theta_W$ and $c \equiv \cot \theta_W$.

f	q_f	α_f	β_f
ℓ	-1	$\frac{1}{4}(3t - c)$	$\frac{1}{4}(t + c)$
ν_ℓ	0	$\frac{1}{4}(t + c)$	$-\frac{1}{4}(t + c)$
u	$\frac{2}{3}$	$-\frac{5}{12}t + \frac{1}{4}c$	$-\frac{1}{4}(t + c)$
d	$-\frac{1}{3}$	$\frac{1}{12}t - \frac{1}{4}c$	$\frac{1}{4}(t + c)$

The subprocess cross section for $\tilde{\ell}_L \bar{\ell}_L$ production occurs via s -channel γ and Z exchange, and depends on the neutral current interaction, with fermion couplings to γ and Z^0 given by $\mathcal{L}_{\text{neutral}} = -eq_f \bar{f} \gamma^\mu f A_\mu + e \bar{f} \gamma^\mu (\alpha_f + \beta_f \gamma_5) f Z_\mu$ (with values of q_f , α_f , and β_f given in Table-50.1).

The subprocess cross section is given by

$$\begin{aligned} \frac{d\sigma}{dt}(q\bar{q} \rightarrow \tilde{\ell}_L \bar{\ell}_L) &= \frac{e^4}{24\pi s^2} \left(tu - m_{\tilde{\ell}_L}^4 \right) \times \\ &\left\{ \frac{q_\ell^2 q_q^2}{s^2} + (\alpha_\ell - \beta_\ell)^2 (\alpha_q^2 + \beta_q^2) |D_Z(s)|^2 \right. \\ &\left. + \frac{2q_\ell q_q \alpha_q (\alpha_\ell - \beta_\ell) (s - M_Z^2)}{s} |D_Z(s)|^2 \right\}, \quad (50.68) \end{aligned}$$

where $D_Z(s) = 1/(s - M_Z^2 + iM_Z\Gamma_Z)$. The cross section for sneutrino production is given by the same formula, but with α_ℓ , β_ℓ , q_ℓ and $m_{\tilde{\ell}_L}$ replaced by α_ν , β_ν , 0 and $m_{\tilde{\nu}_L}$, respectively. The cross section for $\tilde{\tau}_1 \bar{\tau}_1$ production is obtained by replacing $m_{\tilde{\ell}_L} \rightarrow m_{\tilde{\tau}_1}$ and $\beta_\ell \rightarrow \beta_\ell \cos 2\theta_\tau$. The cross section for $\tilde{\ell}_R \bar{\ell}_R$ production is given by substituting $\alpha_\ell - \beta_\ell \rightarrow \alpha_\ell + \beta_\ell$ and $m_{\tilde{\ell}_L} \rightarrow m_{\tilde{\ell}_R}$ in the equation above. The cross section for $\tilde{\tau}_2 \bar{\tau}_2$ production is obtained from the formula for $\tilde{\ell}_R \bar{\ell}_R$ production by replacing $m_{\tilde{\ell}_R} \rightarrow m_{\tilde{\tau}_2}$ and $\beta_\ell \rightarrow \beta_\ell \cos 2\theta_\tau$.

Finally, the cross section for $\tilde{\tau}_1 \bar{\tau}_2$ production occurs only via Z exchange, and is given by

$$\begin{aligned} \frac{d\sigma}{dt}(q\bar{q} \rightarrow \tilde{\tau}_1 \bar{\tau}_2) &= \frac{d\sigma}{dt}(q\bar{q} \rightarrow \tilde{\tau}_1 \bar{\tau}_2) = \\ &\frac{e^4}{24\pi s^2} (\alpha_q^2 + \beta_q^2) \beta_\ell^2 \sin^2 2\theta_\tau |D_Z(s)|^2 (ut - m_{\tilde{\tau}_1}^2 m_{\tilde{\tau}_2}^2). \quad (50.69) \end{aligned}$$

50.8.4 Chargino and neutralino pair production

50.8.4.1 $\tilde{\chi}_i^- \tilde{\chi}_j^0$ production

The subprocess cross section for $d\bar{u} \rightarrow \tilde{\chi}_i^- \tilde{\chi}_j^0$ depends on Lagrangian couplings

$$\mathcal{L}_{W\bar{u}d} = -\frac{g}{\sqrt{2}} \bar{u} \gamma_\mu P_L d W^{+\mu} + \text{h.c.}$$

$$\mathcal{L}_{W\tilde{\chi}_i^- \tilde{\chi}_j^0} = -g(-i)^{\theta_j} \bar{\tilde{\chi}}_i^- [X_i^j + Y_i^j \gamma_5] \gamma_\mu \tilde{\chi}_j^0 W^{-\mu} + \text{h.c.}$$

$$\mathcal{L}_{q\bar{q}\tilde{\chi}_i^-} = iA_{\tilde{\chi}_i^-}^d \bar{u}_L^\dagger \tilde{\chi}_i^- P_L d + iA_{\tilde{\chi}_i^-}^u \bar{d}_L^\dagger \tilde{\chi}_i^- P_L u + \text{h.c.}$$

and

$$\mathcal{L}_{q\bar{q}\tilde{\chi}_j^0} = iA_{\tilde{\chi}_j^0}^q \bar{q}_L^\dagger \tilde{\chi}_j^0 P_L q + \text{h.c.}$$

Contributing diagrams include W exchange and also \tilde{d}_L and \tilde{u}_L squark exchange. The X_i^j and Y_i^j couplings are new, and again convention-dependent: the cross section formulae works if the interaction Lagrangian is written in the above form, so that the couplings can be suitably extracted. The term $\theta_j = 0$ (1) if $m_{\tilde{\chi}_j^0} > 0$ (< 0); it comes about because the neutralino field must be re-defined by a $-i\gamma_5$ transformation if its mass eigenvalue is negative [13]. The subprocess cross section is given in terms of dot products of four momenta, where particle labels are used to denote their four-momenta; note that all mass terms in the cross section formulae are positive definite, so that the signs of mass eigenstates have been absorbed into the Lagrangian couplings, as for instance in Ref. [13]. We then have

$$\frac{d\sigma}{dt}(d\bar{u} \rightarrow \tilde{\chi}_i^- \tilde{\chi}_j^0) = \frac{1}{192\pi s^2}$$

$$\left[T_W + T_{\tilde{d}_L} + T_{\tilde{u}_L} + T_{W\tilde{d}_L} + T_{W\tilde{u}_L} + T_{\tilde{d}_L\tilde{u}_L} \right] \quad (50.70)$$

where

$$\begin{aligned} T_W &= 8g^4 |D_W(s)|^2 \left\{ [X_i^{j2} + Y_i^{j2}] (\tilde{\chi}_j^0 \cdot d\tilde{\chi}_i^- \cdot \bar{u} + \tilde{\chi}_j^0 \cdot \bar{u}\tilde{\chi}_i^- \cdot d) \right. \\ &+ 2(X_i^j Y_i^j) (\tilde{\chi}_j^0 \cdot d\tilde{\chi}_i^- \cdot \bar{u} - \tilde{\chi}_j^0 \cdot \bar{u}\tilde{\chi}_i^- \cdot d) \\ &\left. + [X_i^{j2} - Y_i^{j2}] m_{\tilde{\chi}_i^-} m_{\tilde{\chi}_j^0} d \cdot \bar{u} \right\}, \quad (50.71) \end{aligned}$$

$$T_{\tilde{d}_L} = \frac{4|A_{\tilde{\chi}_i^-}^u|^2 |A_{\tilde{\chi}_j^0}^d|^2}{[(\tilde{\chi}_i^- - \bar{u})^2 - m_{\tilde{d}_L}^2]^2} d \cdot \tilde{\chi}_j^0 \tilde{\chi}_i^- \cdot \bar{u}, \quad (50.72)$$

$$T_{\tilde{u}_L} = \frac{4|A_{\tilde{\chi}_i^-}^d|^2 |A_{\tilde{\chi}_j^0}^u|^2}{[(\tilde{\chi}_j^0 - \bar{u})^2 - m_{\tilde{u}_L}^2]^2} \bar{u} \cdot \tilde{\chi}_j^0 \tilde{\chi}_i^- \cdot d \quad (50.73)$$

$$\begin{aligned} T_{W\tilde{d}_L} &= \frac{-\sqrt{2}g^2 \text{Re}[A_{\tilde{\chi}_j^0}^{d*} A_{\tilde{\chi}_i^-}^u (-i)^{\theta_j}](s - M_W^2) |D_W(s)|^2}{(\tilde{\chi}_i^- - \bar{u})^2 - m_{\tilde{d}_L}^2} \\ &\times \left\{ 8(X_i^j + Y_i^j) \tilde{\chi}_j^0 \cdot d\bar{u} \cdot \tilde{\chi}_i^- + 4(X_i^j - Y_i^j) m_{\tilde{\chi}_i^-} m_{\tilde{\chi}_j^0} d \cdot \bar{u} \right\} \quad (50.74) \end{aligned}$$

$$\begin{aligned} T_{W\tilde{u}_L} &= \frac{\sqrt{2}g^2 \text{Re}[A_{\tilde{\chi}_i^-}^{d*} A_{\tilde{\chi}_j^0}^u (-i)^{\theta_j}](s - M_W^2) |D_W(s)|^2}{(\tilde{\chi}_j^0 - \bar{u})^2 - m_{\tilde{u}_L}^2} \\ &\times \left\{ 8(X_i^j - Y_i^j) \tilde{\chi}_j^0 \cdot \bar{u}d \cdot \tilde{\chi}_i^- + 4(X_i^j + Y_i^j) m_{\tilde{\chi}_i^-} m_{\tilde{\chi}_j^0} d \cdot \bar{u} \right\} \quad (50.75) \end{aligned}$$

and

$$T_{\tilde{d}_L\tilde{u}_L} = -\frac{4\text{Re}[A_{\tilde{\chi}_j^0}^d A_{\tilde{\chi}_i^-}^{u*} A_{\tilde{\chi}_i^-}^{d*} A_{\tilde{\chi}_j^0}^u] m_{\tilde{\chi}_i^-} m_{\tilde{\chi}_j^0} d \cdot \bar{u}}{[(\tilde{\chi}_i^- - \bar{u})^2 - m_{\tilde{d}_L}^2][(\tilde{\chi}_j^0 - \bar{u})^2 - m_{\tilde{u}_L}^2]}. \quad (50.76)$$

50.8.4.2 Chargino pair production

The subprocess cross section for $d\bar{d} \rightarrow \tilde{\chi}_i^- \tilde{\chi}_i^+$ ($i = 1, 2$) depends on Lagrangian couplings $\mathcal{L} = e\tilde{\chi}_i^- \gamma_\mu \tilde{\chi}_i^- A^\mu - e \cot \theta_W \tilde{\chi}_i^- \gamma_\mu (x_i - y_i \gamma_5) \tilde{\chi}_i^- Z^\mu$ and also $\mathcal{L} \ni iA_{\tilde{\chi}_i^-}^d \tilde{u}_L^\dagger \tilde{\chi}_i^- P_L d + iA_{\tilde{\chi}_i^-}^u \tilde{d}_L^\dagger \tilde{\chi}_i^- P_L u + \text{h.c.}$

Contributing diagrams include s -channel γ , Z^0 exchange and t -channel \tilde{u}_L exchange [16, 17]. The couplings x_i and y_i are again new and as usual convention-dependent.

The subprocess cross section is given by

$$\frac{d\sigma}{dt}(d\bar{d} \rightarrow \tilde{\chi}_i^- \tilde{\chi}_i^+) = \frac{1}{192\pi s^2} [T_\gamma + T_Z + T_{\tilde{u}_L} + T_{\gamma Z} + T_{\gamma \tilde{u}_L} + T_{Z\tilde{u}_L}] \quad (50.77)$$

where

$$T_\gamma = \frac{32e^4 q_d^2}{s^2} \left[d \cdot \tilde{\chi}_i^+ \bar{d} \cdot \tilde{\chi}_i^- + d \cdot \tilde{\chi}_i^- \bar{d} \cdot \tilde{\chi}_i^+ + m_{\tilde{\chi}_i^-}^2 d \cdot \bar{d} \right] \quad (50.78)$$

$$T_Z = 32e^4 \cot^2 \theta_W |D_Z(s)|^2$$

$$\left\{ (\alpha_d^2 + \beta_d^2)(x_i^2 + y_i^2) \left[d \cdot \tilde{\chi}_i^+ \bar{d} \cdot \tilde{\chi}_i^- + d \cdot \tilde{\chi}_i^- \bar{d} \cdot \tilde{\chi}_i^+ + m_{\tilde{\chi}_i^-}^2 d \cdot \bar{d} \right] \right. \\ \left. \mp 4\alpha_d \beta_d x_i y_i \left[d \cdot \tilde{\chi}_i^+ \bar{d} \cdot \tilde{\chi}_i^- - d \cdot \tilde{\chi}_i^- \bar{d} \cdot \tilde{\chi}_i^+ \right] - 2y_i^2 (\alpha_d^2 + \beta_d^2) m_{\tilde{\chi}_i^-}^2 d \cdot \bar{d} \right\} \quad (50.79)$$

$$T_{\tilde{u}_L} = \frac{4|A_{\tilde{\chi}_i^-}^d|^4}{[(d - \tilde{\chi}_i^-)^2 - m_{\tilde{u}_L}^2]^2} d \cdot \tilde{\chi}_i^- \bar{d} \cdot \tilde{\chi}_i^+ \quad (50.80)$$

$$T_{\gamma Z} = \frac{64e^4 \cot \theta_W q_d (s - M_Z^2) |D_Z(s)|^2}{s} \times \\ \left\{ \alpha_d x_i \left(d \cdot \tilde{\chi}_i^+ \bar{d} \cdot \tilde{\chi}_i^- + d \cdot \tilde{\chi}_i^- \bar{d} \cdot \tilde{\chi}_i^+ + m_{\tilde{\chi}_i^-}^2 d \cdot \bar{d} \right) \right. \\ \left. \pm \beta_d y_i \left(d \cdot \tilde{\chi}_i^- \bar{d} \cdot \tilde{\chi}_i^+ - d \cdot \tilde{\chi}_i^+ \bar{d} \cdot \tilde{\chi}_i^- \right) \right\} \quad (50.81)$$

$$T_{\gamma \tilde{u}_L} = \mp \frac{8e^2 q_d}{s} \frac{|A_{\tilde{\chi}_i^-}^d|^2}{[(d - \tilde{\chi}_i^-)^2 - m_{\tilde{u}_L}^2]} \left\{ 2\bar{d} \cdot \tilde{\chi}_i^+ d \cdot \tilde{\chi}_i^- + m_{\tilde{\chi}_i^-}^2 d \cdot \bar{d} \right\} \quad (50.82)$$

and

$$T_{Z\tilde{u}_L} = \mp 8e^2 \cot \theta_W |D_Z(s)|^2 \frac{|A_{\tilde{\chi}_i^-}^d|^2 (s - M_Z^2)}{[(d - \tilde{\chi}_i^-)^2 - m_{\tilde{u}_L}^2]} (\alpha_d - \beta_d) \\ \times \left\{ 2(x_i \mp y_i) d \cdot \tilde{\chi}_i^- \bar{d} \cdot \tilde{\chi}_i^+ + m_{\tilde{\chi}_i^-}^2 (x_i \pm y_i) d \cdot \bar{d} \right\} \quad (50.83)$$

using the upper of the sign choices.

The cross section for $u\bar{u} \rightarrow \tilde{\chi}_i^+ \tilde{\chi}_i^-$ can be obtained from the above by replacing $\alpha_d \rightarrow \alpha_u$, $\beta_d \rightarrow \beta_u$, $q_d \rightarrow q_u$, $\tilde{u}_L \rightarrow \tilde{d}_L$, $A_{\tilde{\chi}_i^-}^d \rightarrow A_{\tilde{\chi}_i^-}^u$, $d \rightarrow \bar{u}$, $\bar{d} \rightarrow u$ and adopting the lower of the sign choices everywhere.

The cross section for $q\bar{q} \rightarrow \tilde{\chi}_1^- \tilde{\chi}_2^+$, $\tilde{\chi}_1^+ \tilde{\chi}_2^-$ can occur via Z and \tilde{q}_L exchange. It is usually much smaller than $\tilde{\chi}_{1,2}^- \tilde{\chi}_{1,2}^+$ production, so the cross section will not be presented here. It can be found in Appendix A of Ref. [13].

50.8.4.3 Neutralino pair production

Neutralino pair production via $q\bar{q}$ fusion takes place via s -channel Z exchange plus t - and u -channel left- and right- squark exchange (5 diagrams) [17, 18]. The Lagrangian couplings (see previous footnote*) needed include terms given above plus terms of the form $\mathcal{L} = W_{ij} \tilde{\chi}_i^- \gamma_\mu (\gamma_5)^{\theta_i + \theta_j + 1} \tilde{\chi}_j^0 Z^\mu$. The couplings W_{ij}

depend only on the *higgsino* components of the neutralinos i and j . The subprocess cross section is given by:

$$\frac{d\sigma}{dt}(q\bar{q} \rightarrow \tilde{\chi}_i^0 \tilde{\chi}_j^0) = \frac{1}{192\pi s^2} [T_Z + T_{\tilde{q}_L} + T_{\tilde{q}_R} + T_{Z\tilde{q}_L} + T_{Z\tilde{q}_R}] \quad (50.84)$$

where

$$T_Z = 128e^2 |W_{ij}|^2 (\alpha_q^2 + \beta_q^2) |D_Z(s)|^2$$

$$\left[q \cdot \tilde{\chi}_i^0 \bar{q} \cdot \tilde{\chi}_j^0 + q \cdot \tilde{\chi}_j^0 \bar{q} \cdot \tilde{\chi}_i^0 - \eta_i \eta_j m_{\tilde{\chi}_i^0} m_{\tilde{\chi}_j^0} q \cdot \bar{q} \right], \quad (50.85)$$

$$T_{\tilde{q}_L} = 4|A_{\tilde{\chi}_i^0}^q|^2 |A_{\tilde{\chi}_j^0}^q|^2 \left\{ \frac{q \cdot \tilde{\chi}_i^0 \bar{q} \cdot \tilde{\chi}_j^0}{[(\tilde{\chi}_i^0 - q)^2 - m_{\tilde{q}_L}^2]^2} + \frac{q \cdot \tilde{\chi}_j^0 \bar{q} \cdot \tilde{\chi}_i^0}{[(\tilde{\chi}_j^0 - q)^2 - m_{\tilde{q}_L}^2]^2} \right. \\ \left. - \eta_i \eta_j \frac{m_{\tilde{\chi}_i^0} m_{\tilde{\chi}_j^0} q \cdot \bar{q}}{[(\tilde{\chi}_i^0 - q)^2 - m_{\tilde{q}_L}^2][(\tilde{\chi}_j^0 - q)^2 - m_{\tilde{q}_L}^2]} \right\} \quad (50.86)$$

$$T_{\tilde{q}_R} = 4|B_{\tilde{\chi}_i^0}^q|^2 |B_{\tilde{\chi}_j^0}^q|^2 \left\{ \frac{q \cdot \tilde{\chi}_i^0 \bar{q} \cdot \tilde{\chi}_j^0}{[(\tilde{\chi}_i^0 - q)^2 - m_{\tilde{q}_R}^2]^2} + \frac{q \cdot \tilde{\chi}_j^0 \bar{q} \cdot \tilde{\chi}_i^0}{[(\tilde{\chi}_j^0 - q)^2 - m_{\tilde{q}_R}^2]^2} \right. \\ \left. - \eta_i \eta_j \frac{m_{\tilde{\chi}_i^0} m_{\tilde{\chi}_j^0} q \cdot \bar{q}}{[(\tilde{\chi}_i^0 - q)^2 - m_{\tilde{q}_R}^2][(\tilde{\chi}_j^0 - q)^2 - m_{\tilde{q}_R}^2]} \right\} \quad (50.87)$$

$$T_{Z\tilde{q}_L} = 16e(\alpha_q - \beta_q)(s - M_Z^2) |D_Z(s)|^2$$

$$\left\{ \frac{Re(W_{ij} A_{\tilde{\chi}_i^0}^{q*} A_{\tilde{\chi}_j^0}^q)}{[(\tilde{\chi}_i^0 - q)^2 - m_{\tilde{q}_L}^2]} \left[2q \cdot \tilde{\chi}_i^0 \bar{q} \cdot \tilde{\chi}_j^0 - \eta_i \eta_j m_{\tilde{\chi}_i^0} m_{\tilde{\chi}_j^0} q \cdot \bar{q} \right] \right. \\ \left. + \eta_i \eta_j \frac{Re(W_{ij} A_{\tilde{\chi}_i^0}^q A_{\tilde{\chi}_j^0}^{q*})}{[(\tilde{\chi}_j^0 - q)^2 - m_{\tilde{q}_L}^2]} \left[2q \cdot \tilde{\chi}_j^0 \bar{q} \cdot \tilde{\chi}_i^0 - \eta_i \eta_j m_{\tilde{\chi}_i^0} m_{\tilde{\chi}_j^0} q \cdot \bar{q} \right] \right\} \quad (50.88)$$

$$T_{Z\tilde{q}_R} = 16e(\alpha_q + \beta_q)(s - M_Z^2) |D_Z(s)|^2$$

$$\left\{ \frac{Re(W_{ij} B_{\tilde{\chi}_i^0}^{q*} B_{\tilde{\chi}_j^0}^q)}{[(\tilde{\chi}_i^0 - q)^2 - m_{\tilde{q}_R}^2]} \left[2q \cdot \tilde{\chi}_i^0 \bar{q} \cdot \tilde{\chi}_j^0 - \eta_i \eta_j m_{\tilde{\chi}_i^0} m_{\tilde{\chi}_j^0} q \cdot \bar{q} \right] \right. \\ \left. - \frac{Re(W_{ij} B_{\tilde{\chi}_i^0}^q B_{\tilde{\chi}_j^0}^{q*})}{[(\tilde{\chi}_j^0 - q)^2 - m_{\tilde{q}_R}^2]} \left[2q \cdot \tilde{\chi}_j^0 \bar{q} \cdot \tilde{\chi}_i^0 - \eta_i \eta_j m_{\tilde{\chi}_i^0} m_{\tilde{\chi}_j^0} q \cdot \bar{q} \right] \right\}. \quad (50.89)$$

As before, $\eta_i = \pm 1$ corresponding to whether the neutralino mass eigenvalue is positive or negative. When $i = j$ in the above formula, one must remember to integrate over just 2π steradians of solid angle to avoid double counting in the total cross section.

50.9 Universal extra dimensions

In the Universal Extra Dimension (UED) model of Ref. [19] (see Ref. [20] for a review of models with extra spacetime dimensions), the Standard Model is embedded in a five dimensional theory, where the fifth dimension is compactified on an S_1/Z_2 orbifold. Each SM chirality state is then the zero mode of an infinite tower of Kaluza-Klein excitations labelled by $n = 0 - \infty$. A KK parity is usually assumed to hold, where each state is assigned KK-parity $P = (-1)^n$. If the compactification scale is around a TeV, then the $n = 1$ (or even higher) KK modes may be accessible to collider searches.

Of interest for hadron colliders are the production of massive $n \geq 1$ quark or gluon pairs. These production cross sections have been calculated in Ref. [21, 22]. We list here results for the $n = 1$ case only with $M_1 = 1/R$ (R is the compactification radius) and s , t and u are the usual Mandelstam variables; more general formulae can be found in Ref. [22]. The superscript * stands for any KK excited state, while \bullet stands for left chirality states and \circ stands for right chirality states.

$$\frac{d\sigma}{dt} = \frac{1}{16\pi s^2} T \quad (50.90)$$

where

$$T(q\bar{q} \rightarrow g^* g^*) = \frac{2g_s^4}{27} \left[M_1^2 \left(-\frac{4s^3}{t'^2 u'^2} + \frac{57s}{t'u'} - \frac{108}{s} \right) + \frac{20s^2}{t'u'} - 93 + \frac{108t'u'}{s^2} \right] \quad (50.91)$$

and

$$T(gg \rightarrow g^* g^*) = \frac{9g_s^4}{27} \left[3M_1^4 \frac{s^2 + t'^2 + u'^2}{t'^2 u'^2} - 3M_1^2 \frac{s^2 + t'^2 + u'^2}{st'u'} + 1 + \frac{(s^2 + t'^2 + u'^2)^3}{4s^2 t'^2 u'^2} - \frac{t'u'}{s^2} \right] \quad (50.92)$$

where $t' = t - M_1^2$ and $u' = u - M_1^2$.

Also,

$$T(q\bar{q} \rightarrow q_1^* \bar{q}_1^*) = \frac{4g_s^4}{9} \left[\frac{2M_1^2}{s} + \frac{t'^2 + u'^2}{s^2} \right],$$

$$T(q\bar{q} \rightarrow q_1^* \bar{q}_1^*) = \frac{g_s^4}{9} \left[2M_1^2 \left(\frac{4}{s} + \frac{s}{t'^2} - \frac{1}{t'} \right) + \frac{23}{6} + \frac{2s^2}{t'^2} + \frac{8s}{3t'} + \frac{6t'}{s} + \frac{8t'^2}{s^2} \right],$$

$$T(qq \rightarrow q_1^* \bar{q}_1^*) = \frac{g_s^4}{27} \left[M_1^2 \left(6 \frac{t'}{u'^2} + 6 \frac{u'}{t'^2} - \frac{s}{t'u'} \right) + 2 \left(3 \frac{t'^2}{u'^2} + 3 \frac{u'^2}{t'^2} + 4 \frac{s^2}{t'u'} - 5 \right) \right],$$

$$T(gg \rightarrow q_1^* \bar{q}_1^*) = g_s^4 \left[M_1^4 \frac{-4}{t'u'} \left(\frac{s^2}{6t'u'} - \frac{3}{8} \right) + M_1^2 \frac{4}{s} \left(\frac{s^2}{6t'u'} - \frac{3}{8} \right) + \frac{s^2}{6t'u'} - \frac{17}{24} + \frac{3t'u'}{4s^2} \right],$$

$$T(gq \rightarrow g^* q_1^*) = \frac{-g_s^4}{3} \left[\frac{5s^2}{12t'^2} + \frac{s^3}{t'^2 u'} + \frac{11su'}{6t'^2} + \frac{5u'^2}{12t'^2} + \frac{u'^3}{st'^2} \right],$$

$$T(q\bar{q}' \rightarrow q_1^* \bar{q}_1^*) = \frac{g_s^4}{18} \left[4M_1^4 \frac{s}{t'^2} + 5 + 4 \frac{s^2}{t'^2} + 8 \frac{s}{t'} \right],$$

$$T(qq' \rightarrow q_1^* q_1^*) = \frac{2g_s^4}{9} \left[-M_1^2 \frac{s}{t'^2} + \frac{1}{4} + \frac{s^2}{t'^2} \right],$$

$$T(qq \rightarrow q_1^* q_1^{\circ}) =$$

$$\frac{g_s^4}{9} \left[M_1^2 \left(\frac{2s^3}{t'^2 u'^2} - \frac{4s}{t'u'} \right) + 2 \frac{s^4}{t'^2 u'^2} - 8 \frac{s^2}{t'u'} + 5 \right],$$

$$T(q\bar{q}' \rightarrow q_1^* \bar{q}_1^{\circ}) = \frac{g_s^4}{9} \left[2M_1^2 \left(\frac{1}{t'} + \frac{u'}{t'^2} \right) + \frac{5}{2} + \frac{4u'}{t'} + \frac{2u'^2}{t'^2} \right],$$

and

$$T(qq' \rightarrow q_1^* q_1^{\circ}) = \frac{g_s^4}{9} \left[-2M_1^2 \left(\frac{1}{t'} + \frac{u'}{t'^2} \right) + \frac{1}{2} + \frac{2u'^2}{t'^2} \right].$$

50.10 Large extra dimensions

In the ADD theory [23] with large extra dimensions (LED), the SM particles are confined to a 3-brane, while gravity propagates in the bulk. It is assumed that the n extra dimensions are compactified on an n -dimensional torus of volume $(2\pi r)^n$, so that the fundamental $4+n$ dimensional Planck scale M_* is related to the usual 4-dimensional Planck scale M_{Pl} by $M_{Pl}^2 = M_*^{n+2} (2\pi r)^n$. If $M_* \sim 1$ TeV, then the $M_W - M_{Pl}$ hierarchy problem is just due to gravity propagating in the large extra dimensions.

In these theories, the KK-excited graviton states $G_{\mu\nu}^n$, for $n = 1 - \infty$ can be produced at collider experiments. The graviton couplings to matter are suppressed by $1/M_{Pl}$, so that graviton emission cross sections $d\sigma/dt \sim 1/M_{Pl}^2$. However, the mass splittings between the excited graviton states can be tiny, so the graviton eigenstates are usually approximated by a continuum distribution. A summation (integration) over all allowed graviton emissions ends up cancelling the $1/M_{Pl}^2$ factor, so that observable cross section rates can be attained. Some of the fundamental production formulae for a KK graviton (denoted G) of mass m at hadron colliders include the subprocesses

$$\frac{d\sigma_m}{dt}(f\bar{f} \rightarrow \gamma G) = \frac{\alpha Q_f^2}{16N_f} \frac{1}{sM_{Pl}^2} F_1\left(\frac{t}{s}, \frac{m^2}{s}\right), \quad (50.93)$$

where Q_f is the charge of fermion f and N_f is the number of QCD colors of f . Also,

$$\frac{d\sigma_m}{dt}(q\bar{q} \rightarrow gG) = \frac{\alpha_s}{36} \frac{1}{sM_{Pl}^2} F_1\left(\frac{t}{s}, \frac{m^2}{s}\right), \quad (50.94)$$

$$\frac{d\sigma_m}{dt}(qg \rightarrow qG) = \frac{\alpha_s}{96} \frac{1}{sM_{Pl}^2} F_2\left(\frac{t}{s}, \frac{m^2}{s}\right), \quad (50.95)$$

$$\frac{d\sigma_m}{dt}(gg \rightarrow gG) = \frac{3\alpha_s}{16} \frac{1}{sM_{Pl}^2} F_3\left(\frac{t}{s}, \frac{m^2}{s}\right), \quad (50.96)$$

where

$$F_1(x, y) = \frac{1}{x(y-1-x)} \left[-4x(1+x)(1+2x+2x^2) + y(1+6x+18x^2+16x^3) - 6y^2x(1+2x) + y^3(1+4x) \right] \quad (50.97)$$

$$F_2(x, y) = -(y-1-x)F_1\left(\frac{x}{y-1-x}, \frac{y}{y-1-x}\right) \quad (50.98)$$

and

$$F_3(x, y) = \frac{1}{x(y-1-x)} \left[1 + 2x + 3x^2 + 2x^3 + x^4 - 2y(1+x^3) + 3y^2(1+x^2) - 2y^3(1+x) + y^4 \right] \quad (50.99)$$

These formulae must then be multiplied by the graviton density of states formula $dN = S_{n-1} \frac{M_{Pl}^2}{M_*^{n+2}} m^{n-1} dm$ to gain the cross section

$$\frac{d^2\sigma}{dtdm} = S_{n-1} \frac{M_{Pl}^2}{M_*^{n+2}} m^{n-1} \frac{d\sigma_m}{dt} \quad (50.100)$$

where $S_n = \frac{(2\pi)^{n/2}}{\Gamma(n/2)}$ is the surface area of an n -dimensional sphere of unit radius.

Virtual graviton processes can also be searched for at colliders. For instance, in Ref. [24] the cross section for Drell-Yan production of lepton pairs via gluon fusion was calculated, where it is found that, in the center-of-mass system

$$\frac{d\sigma}{dz}(gg \rightarrow \ell^+ \ell^-) = \frac{\lambda^2 s^3}{64\pi M_*^8} (1-z^2)(1+z^2) \quad (50.101)$$

where $z = \cos\theta$ and λ is a model-dependent coupling constant ~ 1 . Formulae for Drell-Yan production via $q\bar{q}$ fusion can also be found in Refs. [24, 25].

50.11 Warped extra dimensions

In the Randall-Sundrum model [26] of warped extra dimensions, the arena for physics is a 5-d anti-deSitter (AdS_5) spacetime, for which a non-factorizable metric exists with a metric warp factor $e^{-2\sigma(\phi)}$. It is assumed that two opposite tension 3-branes exist within AdS_5 at the two ends of an S_1/Z_2 orbifold parametrized by co-ordinate ϕ which runs from $0-\pi$. The 4-D solution of the Einstein equations yields $\sigma(\phi) = kr_c|\phi|$, where r_c is the compactification radius of the extra dimension and $k \sim M_{Pl}$. The 4-D effective action allows one to identify $\overline{M}_{Pl}^2 = \frac{M^3}{k}(1 - e^{-2kr_c\pi})$, where M is the 5-D Planck scale. Physical particles on the TeV scale (SM) brane have mass $m = e^{-kr_c\pi}m_0$, where m_0 is a fundamental mass of order the Planck scale. Thus, the weak scale-Planck scale hierarchy occurs due to the existence of the exponential warp factor if $kr_c \sim 12$.

In the simplest versions of the RS model, the TeV-scale brane contains only SM particles plus a tower of KK gravitons. The RS gravitons have mass $m_n = kx_n e^{-kr_c\pi}$, where the x_i are roots of Bessel functions $J_1(x_n) = 0$, with $x_1 \simeq 3.83$, $x_2 \simeq 7.02$ etc. While the RS zero-mode graviton couplings suppressed by $1/\overline{M}_{Pl}$ and are thus inconsequential for collider searches, the $n = 1$ and higher modes have couplings suppressed instead by $A_\pi = e^{-kr_c\pi}\overline{M}_{Pl} \sim TeV$. The $n = 1$ RS graviton should have width $\Gamma_1 = \rho m_1 x_1^2 (k/\overline{M}_{Pl})^2$, where ρ is a constant depending on how many decay modes are open. The formulae for dilepton production via virtual RS graviton exchange can be gained from the above formulae for the ADD scenario via the replacement [27]

$$\frac{\lambda}{M_*^4} \rightarrow \frac{i^2}{8\Lambda_\pi^2} \sum_{n=1}^{\infty} \frac{1}{s - m_n^2 + im_n\Gamma_n}. \quad (50.102)$$

References

- [1] J. F. Owens, E. Reya and M. Gluck, Phys. Rev. **D18**, 1501 (1978).
- [2] F. Wilczek, Phys. Rev. Lett. **39**, 1304 (1977).
- [3] B. L. Ioffe and V. A. Khoze, Sov. J. Part. Nucl. **9**, 50 (1978), [Fiz. Elem. Chast. Atom. Yadra9,118(1978)].
- [4] J. R. Ellis, M. K. Gaillard and D. V. Nanopoulos, Nucl. Phys. **B106**, 292 (1976).
- [5] R. N. Cahn and S. Dawson, Phys. Lett. **136B**, 196 (1984), [Erratum: Phys. Lett.138B,464(1984)].
- [6] S. Dawson, Nucl. Phys. **B249**, 42 (1985).
- [7] M. S. Chanowitz and M. K. Gaillard, Phys. Lett. **142B**, 85 (1984).
- [8] R. N. Cahn, Nucl. Phys. **B255**, 341 (1985), [Erratum: Nucl. Phys.B262,744(1985)].
- [9] V. M. Budnev *et al.*, Phys. Rept. **15**, 181 (1975), see for an exhaustive treatment.
- [10] See *e.g.* H.Haber, *Supersymmetry, Part I (Theory)*, this Review.
- [11] P. R. Harrison and C. H. Llewellyn Smith, Nucl. Phys. **B213**, 223 (1983), [Erratum: Nucl. Phys.B223,542(1983)]; S. Dawson, E. Eichten and C. Quigg, Phys. Rev. **D31**, 1581 (1985); V. D. Barger *et al.*, Phys. Rev. **D31**, 528 (1985); H. Baer and X. Tata, Phys. Lett. **160B**, 159 (1985).
- [12] H. Baer, D. D. Karatas and X. Tata, Phys. Rev. **D42**, 2259 (1990).
- [13] Weak Scale Supersymmetry: From Superfields to Scattering Events, H. Baer and X. Tata (Cambridge University Press) 2006.
- [14] H. E. Haber and G. L. Kane, Phys. Rept. **117**, 75 (1985).
- [15] Theory and Phenomenology of Sparticles, M. Drees, R. Godbole, and P. Roy (World Scientific) 2005.
- [16] A. Bartl, H. Fraas and W. Majerotto, Z. Phys. **C30**, 441 (1986).
- [17] H. Baer *et al.*, Int. J. Mod. Phys. **A4**, 4111 (1989).
- [18] A. Bartl, H. Fraas and W. Majerotto, Nucl. Phys. **B278**, 1 (1986).
- [19] T. Appelquist, H.-C. Cheng and B. A. Dobrescu, Phys. Rev. **D64**, 035002 (2001), [hep-ph/0012100].
- [20] For a review of models with extra spacetime dimensions, see G. Giudice and J. Wells, *Extra Dimensions, this Review*.
- [21] J. M. Smillie and B. R. Webber, JHEP **10**, 069 (2005), [hep-ph/0507170].
- [22] C. Macesanu, C. D. McMullen and S. Nandi, Phys. Rev. **D66**, 015009 (2002), [hep-ph/0201300].
- [23] N. Arkani-Hamed, S. Dimopoulos and G. R. Dvali, Phys. Lett. **B429**, 263 (1998), [hep-ph/9803315]; N. Arkani-Hamed, S. Dimopoulos and G. R. Dvali, Phys. Rev. **D59**, 086004 (1999), [hep-ph/9807344].
- [24] J. L. Hewett, Phys. Rev. Lett. **82**, 4765 (1999), [hep-ph/9811356].
- [25] G. F. Giudice, R. Rattazzi and J. D. Wells, Nucl. Phys. **B544**, 3 (1999), [hep-ph/9811291]; E. A. Mirabelli, M. Perelstein and M. E. Peskin, Phys. Rev. Lett. **82**, 2236 (1999), [hep-ph/9811337]; T. Han, J. D. Lykken and R.-J. Zhang, Phys. Rev. **D59**, 105006 (1999), [hep-ph/9811350].
- [26] L. Randall and R. Sundrum, Phys. Rev. Lett. **83**, 3370 (1999), [hep-ph/9905221].
- [27] H. Davoudiasl, J. L. Hewett and T. G. Rizzo, Phys. Rev. Lett. **84**, 2080 (2000), [hep-ph/9909255].

51. Neutrino Cross Section Measurements

Revised August 2019 by G.P. Zeller (FNAL).

Neutrino cross sections are an essential ingredient in all neutrino experiments. Interest in neutrino scattering has recently increased due to the need for such information in the interpretation of neutrino oscillation data [1]. Historically, neutrino scattering results on both charged current (CC) and neutral current (NC) channels have been collected over many decades using a variety of targets, analysis techniques, and detector technologies. With the advent of intense neutrino sources constructed for neutrino oscillation investigations, experiments are now remeasuring these cross sections with a renewed appreciation for nuclear effects¹ and the importance of improved neutrino flux estimations. This work summarizes accelerator-based neutrino cross section measurements performed in the $\sim 0.1 - 300$ GeV range with an emphasis on inclusive, quasi-elastic (pionless), and pion production processes, areas where we have the most experimental input at present (Table 51.1). For a more comprehensive discussion of neutrino cross sections, including neutrino-electron elastic scattering and lower energy neutrino measurements, the reader is directed to a review of this subject [2]. Here, we survey existing experimental data on neutrino interactions and do not attempt to provide a census of the associated theoretical calculations [3], which are both critical and plentiful, or the important constraints being gleaned from electron-nucleus scattering as input to neutrino event generators.

Table 51.1: List of beam properties, nuclear targets, and run durations for modern accelerator-based neutrino experiments studying neutrino scattering.

Experiment	beam	$\langle E_\nu \rangle, \langle E_{\bar{\nu}} \rangle$ GeV	neutrino target(s)	run period
ArgoNeuT	$\nu, \bar{\nu}$	4.3, 3.6	Ar	2009 – 2010
ICARUS (at CNGS)	ν	20.0	Ar	2010 – 2012
K2K	ν	1.3	CH, H ₂ O	2003 – 2004
MicroBooNE	ν	0.8	Ar	2015 –
MINERvA	$\nu, \bar{\nu}$	3.5 (LE), 5.5 (ME)	He, C, CH, H ₂ O, Fe, Pb	2009 – 2019
MiniBooNE	$\nu, \bar{\nu}$	0.8, 0.7	CH ₂	2002 – 2019
MINOS	$\nu, \bar{\nu}$	3.5, 6.1	Fe	2004 – 2016
NOMAD	$\nu, \bar{\nu}$	23.4, 19.7	C-based	1995 – 1998
NOvA	$\nu, \bar{\nu}$	2.0, 2.0	CH ₂	2010 –
SciBooNE	$\nu, \bar{\nu}$	0.8, 0.7	CH	2007 – 2008
T2K	$\nu, \bar{\nu}$	0.6, 0.6	CH, H ₂ O, Fe	2010 –

51.1 Inclusive Scattering

Over the years, many experiments have measured the total inclusive charged current cross section for neutrino ($\nu_\mu N \rightarrow \mu^- X$) and antineutrino ($\bar{\nu}_\mu N \rightarrow \mu^+ X$) scattering off nucleons covering a broad range of neutrino energies. As can be seen in Fig. 51.1, the inclusive cross section approaches a linear dependence on neutrino energy. This behavior is expected for point-like scattering of neutrinos from quarks, an assumption which breaks down at lower energies. Modern measurements of such inclusive scattering cross sections and their target nuclei are summarized in Table 51.2.

To provide a more complete picture, single and double differential cross sections for such inclusive scattering processes have been reported – these include measurements on iron from NuTeV [4] and, more recently, on a variety of nuclear targets from ArgoNeuT [5, 6], MicroBooNE [7], MINERvA [8], and T2K [9, 10]. More recently, MicroBooNE has measured the multiplicity of charged tracks emanating from neutrino scattering on argon [11] and T2K has reported detailed ratios of CC cross sections on hydrocarbon, water, and iron [12]. T2K has also provided the first measurement of the antineutrino CC inclusive cross section at low energy [13]

¹Nuclear effects refer to kinematic and final state effects which impact neutrino scattering off nuclei. Such effects can be significant and are particularly relevant given that modern neutrino experiments make use of nuclear targets to increase their event yields.

²In the case of deuterium, many experiments additionally observed the spectator proton.

(Fig. 51.1). At high energy, the inclusive cross section is dominated by deep inelastic scattering (DIS). Several neutrino experiments have measured DIS cross sections for specific targets and final states, for example, MINERvA has measured ratios of muon neutrino inclusive and DIS cross sections on a variety of nuclear targets including lead, iron, and carbon [14, 15]. Other experiments have measured opposite-sign dimuon production, the most recent being from CHORUS [16], NOMAD [17], and NuTeV [18]. At lower neutrino energies, the inclusive cross section is an additionally complex combination of quasi-elastic scattering and pion production processes, two areas we discuss next.

Table 51.2: Published measurements of neutrino and antineutrino CC inclusive cross sections from modern accelerator-based neutrino experiments.

experiment	measurement	target
ArgoNeuT	ν_μ [5, 6], $\bar{\nu}_\mu$ [6]	Ar
MicroBooNE	ν_μ [7]	Ar
MINERvA	ν_μ [8, 14, 15, 19], $\bar{\nu}_\mu$ [19], $\bar{\nu}_\mu/\nu_\mu$ [20]	CH, C/CH, Fe/CH, Pb/CH
MINOS	ν_μ [21], $\bar{\nu}_\mu$ [21]	Fe
NOMAD	ν_μ [22]	C
SciBooNE	ν_μ [23]	CH
T2K	ν_μ [9, 10, 12, 24, 25], ν_e [26, 27], $\bar{\nu}_\mu/\nu_\mu$ [13]	CH, H ₂ O, Fe

51.2 Quasi-elastic scattering

Quasi-elastic (QE) scattering is the dominant neutrino interaction for neutrino energies less than ~ 1 GeV and represents a large fraction of the signal samples in many neutrino oscillation experiments, which is why this process has received considerable attention in recent years. Historically, neutrino (antineutrino) quasi-elastic scattering refers to the process, $\nu_\mu n \rightarrow \mu^- p$ ($\bar{\nu}_\mu p \rightarrow \mu^+ n$), where a charged lepton and single nucleon are ejected in the elastic interaction of a neutrino (or antineutrino) with a nucleon in the target material. This is the final state one would strictly observe, for example, in scattering off of a *free* nucleon target. There were many early measurements of neutrino QE scattering that span back to the 1970's [2]. In many of these initial measurements, bubble chamber experiments employed light targets (hydrogen or deuterium) and required both the detection of the final state muon and single nucleon²; thus the final state was clear and elastic kinematic conditions could be verified. The situation is more complicated, of course, for heavier nuclear targets used in modern neutrino experiments. In this case, nuclear effects can impact the size and shape of the cross section as well as the final state composition, kinematics, and topology. Due to intranuclear hadron rescattering and the effects of correlations between target nucleons, additional particles may be ejected in the final state; hence, a QE interaction on a nuclear target does not necessarily imply the ejection of a lepton and a *single* nucleon. One therefore needs to take care in defining what one means by neutrino QE scattering when scattering off targets heavier than hydrogen or deuterium. Because of this, modern experiments tend to instead report cross sections for processes involving pionless (e.g., nucleon-only) final states, often referred to as CC 0π or QE-like reactions in recent literature. Such measurements are summarized in Table 51.3. Many modern experiments have also recently opted to report nucleon-only cross sections as a function of final state particle kinematics [28–36]. Such distributions can be more difficult to directly compare between experiments but are much less model-dependent and provide more stringent tests of the theory than historical cross sections as a function of neutrino energy (E_ν) or 4-momentum transfer (Q^2). Recent work has been done to develop a means to directly compare experimental measurements produced in these less model-dependent forms [37].

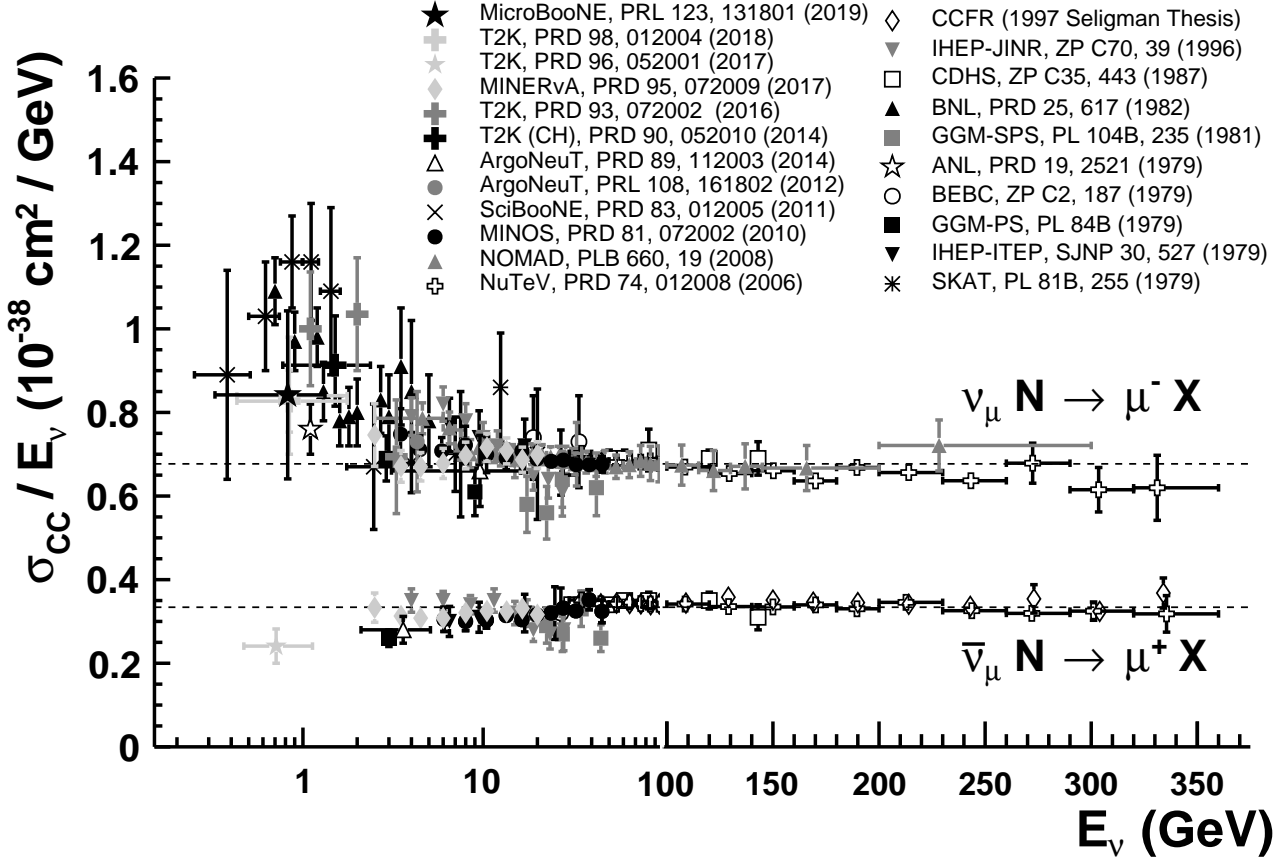


Figure 51.1: Measurements of per nucleon ν_μ and $\bar{\nu}_\mu$ CC inclusive scattering cross sections divided by neutrino energy as a function of neutrino energy. Note the transition between logarithmic and linear scales occurring at 100 GeV. Neutrino cross sections are typically twice as large as their corresponding antineutrino counterparts, although this difference can be larger at lower energies. NC cross sections (not shown) are generally smaller compared to the CC case.

Table 51.3: Published measurements of CC and NC scattering cross sections with nucleon-only final states from modern neutrino experiments.

experiment	measurement	target
ArgoNeuT	2p [38]	Ar
K2K	M_A [39]	H ₂ O
MINERvA	$\frac{d\sigma}{dQ^2}$ [40–42], 1p [43], ν_e [44], $\frac{d^2\sigma}{dp_T dp_{ }}$ [28, 29], $\frac{d\sigma}{dp_n} \frac{d\sigma}{d\delta\alpha_T}$ [30], $\frac{d^2\sigma}{dE_{avail} dq_3}$ [45]	CH, Fe, Pb
MiniBooNE	$\frac{d^2\sigma}{dT_\mu d\theta_\mu}$ [31, 32], M_A [46], NC [47, 48]	CH ₂
MINOS	M_A [49]	Fe
NOMAD	M_A , $\sigma(E_\nu)$ [50]	C
Super-K	NC [51]	H ₂ O
T2K	$\frac{d^2\sigma}{dT_\mu d\theta_\mu}$ [33–35], $\sigma(E_\nu)$ [52], M_A [53], NC [54], $\frac{d\sigma}{d\delta p_T} \frac{d\sigma}{d\delta\alpha_T}$ [36]	CH, H ₂ O

The topic of neutrino QE scattering began drawing increased attention following the first double differential cross section measurements of this process that revealed a significantly larger cross section than originally anticipated, predominantly in the backwards muon scattering region [31, 32]. Such an enhancement was observed many years prior in transverse electron-nucleus scattering [55] and was attributed to the presence of correlations between target nucleons in the nucleus. As a result, the impact of such nuclear effects on neutrino QE scattering has recently become the subject of intense experimental and theoretical scrutiny with implications on event rates, nucleon emission, neutrino energy reconstruction, and neutrino versus antineutrino cross sections. The reader is referred to reviews of the situation in [3, 56, 57]. To help drive further progress in understanding the underlying nuclear contributions, pionless (e.g., nucleon-only)

cross sections have been reported for the first time in the form of double-differential distributions by MiniBooNE [31, 32], MINERvA [28, 29, 45], and T2K [33–35]. Such double-differential cross sections in terms of final state particle kinematics reduce some of the model-dependence of the reported data, provide the most robust measurements available, and allow a more rigorous two-dimensional test of the underlying nuclear theory. MINERvA and T2K have been especially prolific in recent years in probing this interaction process (Table 51.3). Neutrino experiments have also launched dedicated studies of the hadronic side of these interactions, including ArgoNeuT [38, 58], MINERvA [43], and T2K [36]. MINERvA has been the first modern experiment to measure neutron emission in antineutrino interactions [59]. In addition, the exploration of transverse kinematic variables in neutrino scattering is allowing better constraints on the various contributions to the

cross section, including recent evaluations from MINERvA [28–30] and T2K [36]. With the MiniBooNE results having first revealed these additional complexities in neutrino-nucleus QE scattering, measurements from multiple neutrino experiments, on other targets, and using additional kinematics are crucial for getting a better handle on the underlying nuclear physics impacting neutrino-nucleus interactions. What we once thought was “simple” QE scattering is in fact not so simple.

In addition to such charged current investigations, measurements of the neutral current counterpart of this channel have also been performed. The most recent NC elastic scattering cross section measurements include those from BNL E734 [60], MiniBooNE [47, 48], Super-K [51], and T2K [54]. A number of measurements of the Cabibbo-suppressed antineutrino QE hyperon production cross section have additionally been reported [61, 62], although not in recent years.

51.3 Pion Production

In addition to such elastic scattering processes, neutrinos can also inelastically scatter producing a nucleon excited state (Δ , N^*). Such baryonic resonances quickly decay, most often to a nucleon and single-pion final state. Historically, experiments have measured various exclusive final states associated with these reactions, the majority of which have been on hydrogen and deuterium targets [2]. There have been several recent re-analyses of this data to better understand the consistency between data sets [63], nucleon form factors [64], and non-resonant contributions [65]. Also, modern measurements of neutrino-induced pion production have since been performed on a variety of nuclear targets (Table 51.4).

Table 51.4: Summary of modern measurements of NC and CC scattering cross sections involving a pion (or pions) in the final state.

experiment	π^\pm	π^0	target
	measurement	measurement	
ArgoNeuT	CC [66]	NC [67]	Ar
K2K	CC [68, 69]	CC [70], NC [71]	CH, H ₂ O
MicroBooNE	–	CC [72]	Ar
MINERvA	CC [73–77]	CC [74, 78, 79], NC [80]	CH
MiniBooNE	CC [81, 82]	CC [83], NC [84, 85]	CH ₂
MINOS	–	NC [86]	Fe
NOMAD	–	NC [87]	C
NOvA	–	NC [88]	C
SciBooNE	CC [89]	NC [90, 91]	CH
T2K	CC [92, 93]	–	CH, H ₂ O

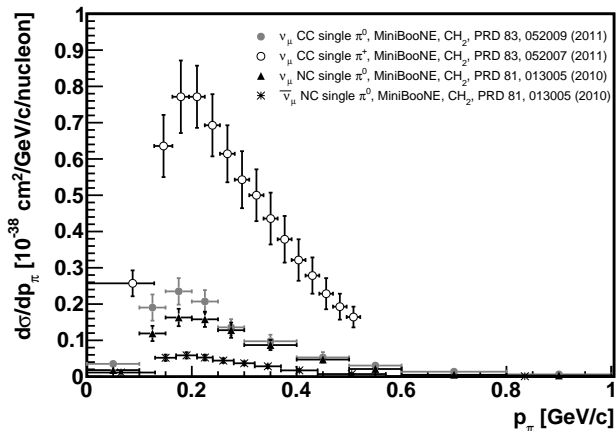


Figure 51.2: Differential cross sections for CC and NC pion production from MiniBooNE at a mean neutrino energy of 0.8 GeV. Shown here are the measurements as a function of the momentum of the outgoing pion in the interaction, a kinematic that is particularly sensitive to final state interactions. Other distributions are also available in the publications listed in the legend.

In addition to resonance production processes, neutrinos can also coherently scatter off of the entire nucleus and produce a distinctly forward-scattered single pion final state. Both CC ($\nu_\mu A \rightarrow \mu^- A\pi^+$, $\bar{\nu}_\mu A \rightarrow \mu^+ A\pi^-$) and NC ($\nu_\mu A \rightarrow \nu_\mu A\pi^0$, $\bar{\nu}_\mu A \rightarrow \bar{\nu}_\mu A\pi^0$) processes are possible in this case. Even though the level of coherent pion production is small compared to their resonant counterpart, observations exist across a broad energy range and on multiple nuclear targets [94]. More recently, several modern neutrino experiments have either measured or set limits on coherent pion production cross sections including ArgoNeuT [66], K2K [69], MINERvA [75, 77], MiniBooNE [85], MINOS [86], NOMAD [87], NOvA [88], SciBooNE [89, 91], and T2K [69].

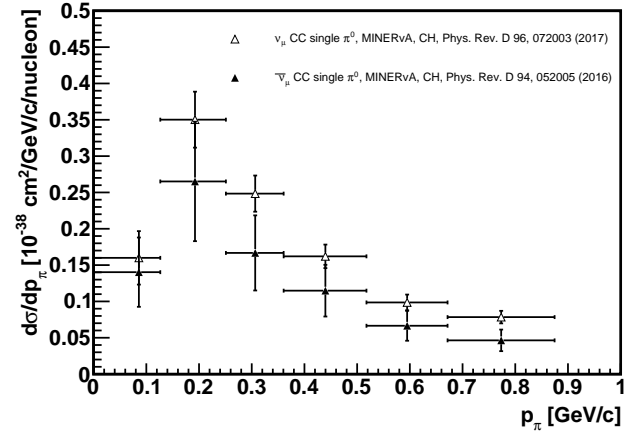


Figure 51.3: Differential cross sections for neutrino ($W < 1.4$ GeV) and antineutrino ($W < 1.8$ GeV) CC π^0 production from MINERvA at a mean neutrino energy of 3.3 GeV. Shown here are the measurements as a function of the momentum of the outgoing pion in the interaction, a kinematic that is particularly sensitive to final state interactions. Other distributions are available in the publications listed in the legend as well as for charged pion production [74].

As with QE scattering, a new appreciation for the significance of nuclear effects has surfaced in pion production channels, again due to the use of heavy nuclear targets in modern neutrino experiments. Many experiments have been careful to report cross sections for various detected final states, thereby not correcting for large and uncertain nuclear effects (e.g., pion rescattering, charge exchange, and absorption) which can introduce significant sources of uncertainty and model dependence. Providing the most comprehensive survey of neutrino single-pion production to date, MiniBooNE has published a total of 16 single- and double-differential cross sections for both the final state muon (in the case of CC scattering) and pions in these interactions; thus, providing the first measurements of these distributions (Fig. 51.2) [81–84]. MINERvA has recently produced similar kinematic measurements at higher neutrino energies (Fig. 51.3) [74, 76, 79] and T2K at lower energies [92]. Importantly, MINERvA has been working towards an improved nuclear model that can describe all of the pion reaction channels simultaneously, an issue that many experiments have struggled with up until now [74]. ArgoNeuT [67] and MicroBooNE [72] have been adding new information on single pion production in argon. Regardless of the interaction channel or target material, differential cross section measurements in terms of observed final state particle kinematics are preferred for their reduced model dependence and for the additional kinematic information they provide. Such a new direction has been the focus of modern measurements as opposed to the reporting of more model-dependent, historical cross sections as a function of E_ν or Q^2 . Together with similar results for other interaction channels, a better understanding and modeling of nuclear effects will be possible moving forward. MINERvA [95] has already taken a large step in this direction by explicitly tuning the physics in existing neutrino event generators to best fit the experimental data on pion production.

It should be noted that baryonic resonances can also decay to multi-pion, other mesonic (K , η , ρ , etc.), and even photon final states. Experimental results for these channels are typically sparse or non-existent [2]; however, photon production processes can be an important background for $\nu_\mu \rightarrow \nu_e$ appearance searches and thus have become the focus of recent experimental investigations, most notably in NOMAD [96] and T2K [97]. There have also been several recent measurements of kaon final states produced in neutrino NC and CC scattering in MINERvA [98–100] that are providing needed background constraints for certain nucleon decay searches.

51.4 Outlook

Currently operating experiments will continue to produce additional neutrino cross section measurements as they accumulate additional statistics, while a few new experiments will soon be coming online. Analysis of a broad energy range of data from MINERvA is providing some of the most detailed analysis of nuclear effects in neutrino interactions by examining multiple nuclei in a single experiment. Data from ArgoNeuT, ICARUS, Micro-BooNE, and SBND will probe deeper into complex neutrino final states using the superior capabilities of liquid argon time projection chambers, while the T2K and NOvA near detectors will continue to collect high statistics samples in intense neutrino beams. Together with dedicated discussions between the experiments on how best to report neutrino cross section measurements [101] and accompanying improvements in nuclear model calculations [3], these investigations are crucial for significantly advancing our understanding of neutrino-nucleus scattering.

51.5 Acknowledgments

The author thanks Anne Schukraft (Fermilab) for her help in preparing the plots and content of this review.

References

- [1] O. Benhar *et al.*, Phys. Rept. **700**, 1 (2017), [arXiv:1501.06448].
- [2] J. A. Formaggio and G. P. Zeller, Rev. Mod. Phys. **84**, 1307 (2012), [arXiv:1305.7513].
- [3] L. Alvarez-Ruso *et al.*, Prog. Part. Nucl. Phys. **100**, 1 (2018), [arXiv:1706.03621].
- [4] M. Tzanov *et al.* (NuTeV), Phys. Rev. **D74**, 012008 (2006), [hep-ex/0509010].
- [5] C. Anderson *et al.* (ArgoNeuT), Phys. Rev. Lett. **108**, 161802 (2012), [arXiv:1111.0103].
- [6] R. Acciarri *et al.* (ArgoNeuT), Phys. Rev. **D89**, 11, 112003 (2014), [arXiv:1404.4809].
- [7] P. Abratenko *et al.* (MicroBooNE), Phys. Rev. Lett. **123**, 13, 131801 (2019), [arXiv:1905.09694].
- [8] P. A. Rodrigues *et al.* (MINERvA), Phys. Rev. Lett. **116**, 071802 (2016), [Addendum: Phys. Rev. Lett.121,no.20,209902(2018)], [arXiv:1511.05944].
- [9] K. Abe *et al.* (T2K), Phys. Rev. **D87**, 9, 092003 (2013), [arXiv:1302.4908].
- [10] K. Abe *et al.* (T2K), Phys. Rev. **D98**, 012004 (2018), [arXiv:1801.05148].
- [11] C. Adams *et al.* (MicroBooNE), Eur. Phys. J. **C79**, 3, 248 (2019), [arXiv:1805.06887].
- [12] K. Abe *et al.* (T2K) (2019), [arXiv:1904.09611].
- [13] K. Abe *et al.* (T2K), Phys. Rev. **D96**, 5, 052001 (2017), [arXiv:1706.04257].
- [14] B. G. Tice *et al.* (MINERvA), Phys. Rev. Lett. **112**, 23, 231801 (2014), [arXiv:1403.2103].
- [15] J. Mousseau *et al.* (MINERvA), Phys. Rev. **D93**, 7, 071101 (2016), [arXiv:1601.06313].
- [16] A. Kayis-Topaksu *et al.* (CHORUS), Nucl. Phys. **B798**, 1 (2008), [arXiv:0804.1869].
- [17] O. Samoylov *et al.* (NOMAD), Nucl. Phys. **B876**, 339 (2013), [arXiv:1308.4750].
- [18] D. Mason *et al.* (NuTeV), Phys. Rev. Lett. **99**, 192001 (2007).
- [19] J. Devan *et al.* (MINERvA), Phys. Rev. **D94**, 11, 112007 (2016), [arXiv:1610.04746].
- [20] L. Ren *et al.* (MINERvA), Phys. Rev. **D95**, 7, 072009 (2017), [Addendum: Phys. Rev.D97,no.1,019902(2018)], [arXiv:1701.04857].
- [21] P. Adamson *et al.* (MINOS), Phys. Rev. **D81**, 072002 (2010), [arXiv:0910.2201].
- [22] Q. Wu *et al.* (NOMAD), Phys. Lett. **B660**, 19 (2008), [arXiv:0711.1183].
- [23] Y. Nakajima *et al.* (SciBooNE), Phys. Rev. **D83**, 012005 (2011), [arXiv:1011.2131].
- [24] K. Abe *et al.* (T2K), Phys. Rev. **D90**, 5, 052010 (2014), [arXiv:1407.4256].
- [25] K. Abe *et al.* (T2K), Phys. Rev. **D93**, 7, 072002 (2016), [arXiv:1509.06940].
- [26] K. Abe *et al.* (T2K), Phys. Rev. Lett. **113**, 24, 241803 (2014), [arXiv:1407.7389].
- [27] K. Abe *et al.* (T2K), Phys. Rev. **D91**, 112010 (2015), [arXiv:1503.08815].
- [28] D. Ruterbories *et al.* (MINERvA), Phys. Rev. **D99**, 1, 012004 (2019), [arXiv:1811.02774].
- [29] C. E. Patrick *et al.* (MINERvA), Phys. Rev. **D97**, 5, 052002 (2018), [arXiv:1801.01197].
- [30] X. G. Lu *et al.* (MINERvA), Phys. Rev. Lett. **121**, 2, 022504 (2018), [arXiv:1805.05486].
- [31] A. A. Aguilar-Arevalo *et al.* (MiniBooNE), Phys. Rev. **D81**, 092005 (2010), [arXiv:1002.2680].
- [32] A. A. Aguilar-Arevalo *et al.* (MiniBooNE), Phys. Rev. **D88**, 3, 032001 (2013), [arXiv:1301.7067].
- [33] K. Abe *et al.* (T2K), Phys. Rev. **D93**, 11, 112012 (2016), [arXiv:1602.03652].
- [34] K. Abe *et al.* (T2K), Phys. Rev. **D97**, 1, 012001 (2018), [arXiv:1708.06771].
- [35] K. Abe *et al.* (2019), [arXiv:1908.10249].
- [36] K. Abe *et al.* (T2K), Phys. Rev. **D98**, 3, 032003 (2018), [arXiv:1802.05078].
- [37] K. Mahn, C. Marshall and C. Wilkinson, Ann. Rev. Nucl. Part. Sci. **68**, 105 (2018), [arXiv:1803.08848].
- [38] R. Acciarri *et al.* (ArgoNeuT), Phys. Rev. **D90**, 1, 012008 (2014), [arXiv:1405.4261].
- [39] R. Gran *et al.* (K2K), Phys. Rev. **D74**, 052002 (2006), [hep-ex/0603034].
- [40] G. A. Fiorentini *et al.* (MINERvA), Phys. Rev. Lett. **111**, 022502 (2013), [arXiv:1305.2243].
- [41] L. Fields *et al.* (MINERvA), Phys. Rev. Lett. **111**, 2, 022501 (2013), [arXiv:1305.2234].
- [42] M. Betancourt *et al.* (MINERvA), Phys. Rev. Lett. **119**, 8, 082001 (2017), [arXiv:1705.03791].
- [43] T. Walton *et al.* (MINERvA), Phys. Rev. **D91**, 7, 071301 (2015), [arXiv:1409.4497].
- [44] J. Wolcott *et al.* (MINERvA), Phys. Rev. Lett. **116**, 8, 081802 (2016), [arXiv:1509.05729].
- [45] R. Gran *et al.* (MINERvA), Phys. Rev. Lett. **120**, 22, 221805 (2018), [arXiv:1803.09377].
- [46] A. A. Aguilar-Arevalo *et al.* (MiniBooNE), Phys. Rev. Lett. **100**, 032301 (2008), [arXiv:0706.0926].
- [47] A. A. Aguilar-Arevalo *et al.* (MiniBooNE), Phys. Rev. **D82**, 092005 (2010), [arXiv:1007.4730].
- [48] A. A. Aguilar-Arevalo *et al.* (MiniBooNE), Phys. Rev. **D91**, 1, 012004 (2015), [arXiv:1309.7257].
- [49] P. Adamson *et al.* (MINOS), Phys. Rev. **D91**, 1, 012005 (2015), [arXiv:1410.8613].

- [50] V. Lyubushkin *et al.* (NOMAD), *Eur. Phys. J.* **C63**, 355 (2009), [arXiv:0812.4543].
- [51] L. Wan *et al.* (Super-Kamiokande), *Phys. Rev.* **D99**, 3, 032005 (2019), [arXiv:1901.05281].
- [52] K. Abe *et al.* (T2K), *Phys. Rev.* **D91**, 11, 112002 (2015), [arXiv:1503.07452].
- [53] K. Abe *et al.* (T2K), *Phys. Rev.* **D92**, 11, 112003 (2015), [arXiv:1411.6264].
- [54] K. Abe *et al.* (T2K), *Phys. Rev.* **D90**, 7, 072012 (2014), [arXiv:1403.3140].
- [55] J. Carlson *et al.*, *Phys. Rev.* **C65**, 024002 (2002), [arXiv:nucl-th/0106047].
- [56] H. Gallagher, G. Garvey and G. P. Zeller, *Ann. Rev. Nucl. Part. Sci.* **61**, 355 (2011).
- [57] G. T. Garvey *et al.*, *Phys. Rept.* **580**, 1 (2015), [arXiv:1412.4294].
- [58] O. Palamara (ArgoNeuT), *JPS Conf. Proc.* **12**, 010017 (2016).
- [59] M. Elkins *et al.* (MINERvA), *Phys. Rev.* **D100**, 5, 052002 (2019), [arXiv:1901.04892].
- [60] L. A. Ahrens *et al.*, *Phys. Rev.* **D35**, 785 (1987).
- [61] J. Brunner *et al.* (SKAT), *Z. Phys.* **C45**, 551 (1990).
- [62] V. V. Ammosov *et al.*, *Z. Phys.* **C36**, 377 (1987); O. Erriquez *et al.*, *Phys. Lett.* **70B**, 383 (1977); T. Eichten *et al.*, *Phys. Lett.* **40B**, 593 (1972).
- [63] C. Wilkinson *et al.*, *Phys. Rev.* **D90**, 11, 112017 (2014), [arXiv:1411.4482].
- [64] A. S. Meyer *et al.*, *Phys. Rev.* **D93**, 11, 113015 (2016), [arXiv:1603.03048].
- [65] P. Rodrigues, C. Wilkinson and K. McFarland, *Eur. Phys. J.* **C76**, 8, 474 (2016), [arXiv:1601.01888].
- [66] R. Acciarri *et al.* (ArgoNeuT), *Phys. Rev. Lett.* **113**, 26, 261801 (2014), [erratum: *Phys. Rev. Lett.* 114, no. 3, 039901 (2015)], [arXiv:1408.0598].
- [67] R. Acciarri *et al.* (ArgoNeuT), *Phys. Rev.* **D96**, 1, 012006 (2017), [arXiv:1511.00941].
- [68] A. Rodriguez *et al.* (K2K), *Phys. Rev.* **D78**, 032003 (2008), [arXiv:0805.0186].
- [69] M. Hasegawa *et al.* (K2K), *Phys. Rev. Lett.* **95**, 252301 (2005), [hep-ex/0506008].
- [70] C. Mariani *et al.* (K2K), *Phys. Rev.* **D83**, 054023 (2011), [arXiv:1012.1794].
- [71] S. Nakayama *et al.* (K2K), *Phys. Lett.* **B619**, 255 (2005), [hep-ex/0408134].
- [72] C. Adams *et al.* (MicroBooNE), *Phys. Rev.* **D99**, 9, 091102 (2019), [arXiv:1811.02700].
- [73] B. Eberly *et al.* (MINERvA), *Phys. Rev.* **D92**, 9, 092008 (2015), [arXiv:1406.6415].
- [74] C. L. McGivern *et al.* (MINERvA), *Phys. Rev.* **D94**, 5, 052005 (2016), [arXiv:1606.07127].
- [75] A. Higuera *et al.* (MINERvA), *Phys. Rev. Lett.* **113**, 26, 261802 (2014), [arXiv:1409.3835].
- [76] T. Le *et al.* (MINERvA), *Phys. Rev.* **D100**, 5, 052008 (2019), [arXiv:1906.08300].
- [77] A. Mislivec *et al.* (MINERvA), *Phys. Rev.* **D97**, 3, 032014 (2018), [arXiv:1711.01178].
- [78] T. Le *et al.* (MINERvA), *Phys. Lett.* **B749**, 130 (2015), [arXiv:1503.02107].
- [79] O. Altinok *et al.* (MINERvA), *Phys. Rev.* **D96**, 7, 072003 (2017), [arXiv:1708.03723].
- [80] J. Wolcott *et al.* (MINERvA), *Phys. Rev. Lett.* **117**, 11, 111801 (2016), [arXiv:1604.01728].
- [81] A. A. Aguilar-Arevalo *et al.* (MiniBooNE), *Phys. Rev.* **D83**, 052007 (2011), [arXiv:1011.3572].
- [82] A. A. Aguilar-Arevalo *et al.* (MiniBooNE), *Phys. Rev. Lett.* **103**, 081801 (2009), [arXiv:0904.3159].
- [83] A. A. Aguilar-Arevalo *et al.* (MiniBooNE), *Phys. Rev.* **D83**, 052009 (2011), [arXiv:1010.3264].
- [84] A. A. Aguilar-Arevalo *et al.* (MiniBooNE), *Phys. Rev.* **D81**, 013005 (2010), [arXiv:0911.2063].
- [85] A. A. Aguilar-Arevalo *et al.* (MiniBooNE), *Phys. Lett.* **B664**, 41 (2008), [arXiv:0803.3423].
- [86] P. Adamson *et al.* (MINOS), *Phys. Rev.* **D94**, 7, 072006 (2016), [arXiv:1608.05702].
- [87] C. T. Kullenberg *et al.* (NOMAD), *Phys. Lett.* **B682**, 177 (2009), [arXiv:0910.0062].
- [88] M. A. Acero *et al.* (NOvA) (2019), [arXiv:1902.00558].
- [89] K. Hiraida *et al.* (SciBooNE), *Phys. Rev.* **D78**, 112004 (2008), [arXiv:0811.0369].
- [90] Y. Kurimoto *et al.* (SciBooNE), *Phys. Rev.* **D81**, 033004 (2010), [arXiv:0910.5768].
- [91] Y. Kurimoto *et al.* (SciBooNE), *Phys. Rev.* **D81**, 111102 (2010), [arXiv:1005.0059].
- [92] K. Abe *et al.* (T2K), *Phys. Rev.* **D95**, 1, 012010 (2017), [arXiv:1605.07964].
- [93] K. Abe *et al.* (T2K), *Phys. Rev. Lett.* **117**, 19, 192501 (2016), [arXiv:1604.04406].
- [94] P. Vilain *et al.* (CHARM-II), *Phys. Lett.* **B313**, 267 (1993); A compilation of historical coherent pion production data.
- [95] P. Stowell *et al.* (MINERvA), *Phys. Rev.* **D100**, 7, 072005 (2019), [arXiv:1903.01558].
- [96] C. T. Kullenberg *et al.* (NOMAD), *Phys. Lett.* **B706**, 268 (2012), [arXiv:1111.3713].
- [97] K. Abe *et al.* (T2K), *J. Phys.* **G46**, 8, 08LT01 (2019), [arXiv:1902.03848].
- [98] C. M. Marshall *et al.* (MINERvA), *Phys. Rev.* **D94**, 1, 012002 (2016), [arXiv:1604.03920].
- [99] C. M. Marshall *et al.* (MINERvA), *Phys. Rev. Lett.* **119**, 1, 011802 (2017), [arXiv:1611.02224].
- [100] Z. Wang *et al.* (MINERvA), *Phys. Rev. Lett.* **117**, 6, 061802 (2016), [arXiv:1606.08890].
- [101] M. Betancourt *et al.*, *Phys. Rept.* **773-774**, 1 (2018), [arXiv:1805.07378].

52. Plots of Cross Sections and Related Quantities

Updated in 2019. See various sections for details.

52.1	Pseudorapidity Distributions in pp and $\bar{p}p$ Interactions	696
52.2	Average Hadron Multiplicities in Hadronic e^+e^- Annihilation Events	697
52.3	σ and R in e^+e^- Collisions	699
52.4	Annihilation Cross Section Near M_Z	701
52.5	Total Hadronic Cross Sections	702

52.1 Pseudorapidity Distributions in pp and $\bar{p}p$ Interactions

Revised August 2013 by D.R. Ward (Cavendish Lab.).

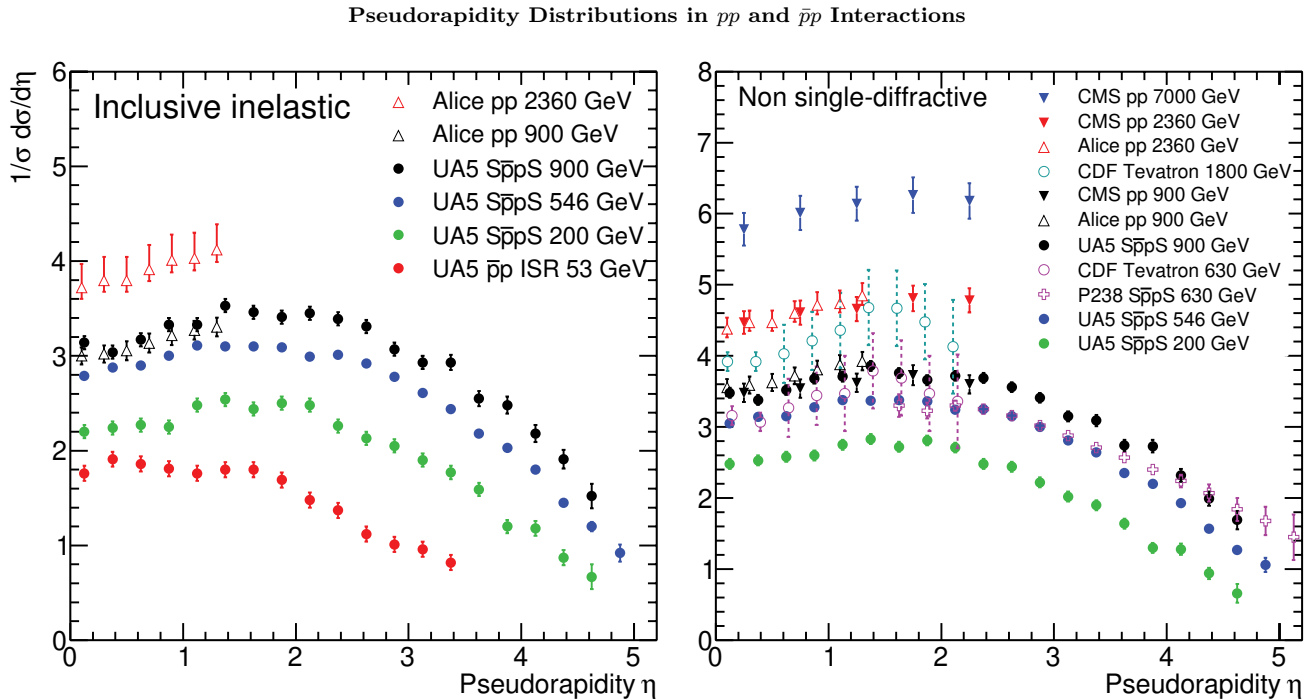


Figure 52.1: Charged particle pseudorapidity distributions in $\bar{p}p$ collisions for $53 \text{ GeV} \leq \sqrt{s} \leq 1800 \text{ GeV}$. UA5 data from the $S\bar{p}\bar{p}S$ are taken from [1], and from the ISR from [2]. The UA5 data are shown for both the full inelastic cross-section and with singly diffractive events excluded. Additional non single-diffractive measurements are available from CDF at the Tevatron [3] and from P238 at the $S\bar{p}\bar{p}S$ [4]. These may be compared with both inclusive and non single-diffractive measurements in pp collisions at the LHC from ALICE [5] and for non single-diffractive interactions from CMS [6, 7]. (Courtesy of D.R. Ward, Cambridge Univ., 2013)

52.2 Average Hadron Multiplicities in Hadronic e^+e^- Annihilation Events

Revised August 2019 by O. Biebel (Ludwig-Maximilians U.).

Table 52.1: Average hadron multiplicities per hadronic e^+e^- annihilation event at $\sqrt{s} \approx 10, 29\text{--}35, 91,$ and $130\text{--}200$ GeV. The rates given include decay products from resonances with $c\tau < 10$ cm, and include the corresponding anti-particle state. Correlations of the systematic uncertainties were considered for the calculation of the averages. Quoted errors are not increased by scale factor S .

Particle	$\sqrt{s} \approx 10$ GeV	$\sqrt{s} = 29\text{--}35$ GeV	$\sqrt{s} = 91$ GeV	$\sqrt{s} = 130\text{--}200$ GeV	References
Pseudoscalar mesons:					
π^+	6.52 ± 0.11	3 ± 0.4	17.02 ± 0.19	21.24 ± 0.39	[8–17]
π^0	3.2 ± 0.35	83 ± 0.28	9.42 ± 0.32		[12, 18–23]
K^+	0.953 ± 0.018	1.48 ± 0.09	2.228 ± 0.059	2.82 ± 0.19	[9–17, 24, 25]
K^0	0.91 ± 0.05	1.48 ± 0.07	2.049 ± 0.026	2.10 ± 0.12	[12, 17, 20, 26–36]
η	0.20 ± 0.04	0.61 ± 0.07	1.049 ± 0.080		[12, 18, 19, 22, 23, 37–40]
$\eta'(958)$	0.03 ± 0.01	0.26 ± 0.10	0.152 ± 0.020		[20, 39, 41–43]
D^+	$0.194 \pm 0.019^{(a)}$	0.17 ± 0.03	0.175 ± 0.016		[12, 44–47]
D^0	$0.446 \pm 0.032^{(a)}$	0.45 ± 0.07	0.454 ± 0.030		[12, 44–47]
D_s^+	$0.063 \pm 0.014^{(a)}$	$0.45 \pm 0.20^{(b)}$	0.131 ± 0.021		[8, 39, 44, 47–49]
$B^{(c)}$	—	—	$0.134 \pm 0.016^{(d)}$		[46, 50]
B^+	—	—	$0.141 \pm 0.004^{(d)}$		[51]
B_s^0	—	—	$0.054 \pm 0.011^{(d)}$		[52, 53]
Scalar mesons:					
$f_0(980)$	0.024 ± 0.006	$0.05 \pm 0.02^{(e)}$	0.146 ± 0.012		[41, 54–56]
$a_0(980)^\pm$	—	—	$0.27 \pm 0.11^{(f)}$		[43]
Vector mesons:					
$\rho(770)^0$	0.35 ± 0.04	0.81 ± 0.08	1.231 ± 0.098		[9, 12, 55, 57, 58]
$\rho(770)^\pm$	—	—	$2.40 \pm 0.43^{(f)}$		[43]
$\omega(782)$	0.30 ± 0.08	—	1.016 ± 0.065		[40, 42, 43, 57]
$K^*(892)^+$	0.27 ± 0.03	0.64 ± 0.05	0.714 ± 0.055		[9, 12, 33, 57, 59, 60]
$K^*(892)^0$	0.29 ± 0.03	0.56 ± 0.06	0.738 ± 0.024		[9, 12, 36, 57, 58, 61, 62]
$\phi(1020)$	0.044 ± 0.003	0.085 ± 0.011	0.0963 ± 0.0032		[12, 36, 56–58, 61]
$D^*(2010)^+$	$0.177 \pm 0.022^{(a)}$	0.43 ± 0.07	$0.1937 \pm 0.0057^{(g)}$		[12, 44–46, 63, 64]
$D^*(2007)^0$	$0.168 \pm 0.019^{(a)}$	0.27 ± 0.11	—		[12, 44, 45]
$D_s^*(2112)^+$	$0.048 \pm 0.014^{(a)}$	—	$0.101 \pm 0.048^{(h)}$		[48, 65]
$B^{*(i)}$	—	—	0.288 ± 0.026		[66, 67]
$J/\psi(1S)$	$0.00050 \pm 0.00005^{(a)}$	—	$0.0052 \pm 0.0004^{(j)}$		[68–73]
$\psi(2S)$	—	—	$0.0023 \pm 0.0004^{(j)}$		[71, 73, 74]
$\Upsilon(1S)$	—	—	$0.00014 \pm 0.00007^{(j)}$		[75]
Pseudovector mesons:					
$f_1(1285)$	—	—	0.165 ± 0.051		[76]
$f_1(1420)$	—	—	0.056 ± 0.012		[76]
$\chi_{c1}(3510)$	—	—	$0.0041 \pm 0.0011^{(j)}$		[71, 74]
Tensor mesons:					
$f_2(1270)$	0.09 ± 0.02	0.14 ± 0.04	0.166 ± 0.020		[54–56, 77]
$f_2'(1525)$	—	—	0.012 ± 0.006		[55]
$K_2^*(1430)^+$	—	0.09 ± 0.03	—		[55, 78]
$K_2^*(1430)^0$	—	0.12 ± 0.06	0.084 ± 0.022		[54, 55, 79]
$B^{** (k)}$	—	—	0.118 ± 0.024		[80]
D_{s1}^\pm	—	—	$0.0052 \pm 0.0011^{(l)}$		[81]
D_{s2}^\pm	—	—	$0.0083 \pm 0.0031^{(l)}$		[81]
Baryons:					
p	0.266 ± 0.008	0.640 ± 0.050	1.050 ± 0.032	1.41 ± 0.18	[10, 13–17, 24, 25, 77]
Λ	$0.093 \pm 0.006^{(a)}$	0.205 ± 0.010	0.3915 ± 0.0065	0.39 ± 0.03	[17, 20, 34, 36, 77, 82–85]
Σ^0	$0.0221 \pm 0.0018^{(a)}$	—	0.078 ± 0.010		[10, 59, 82, 86–88]
Σ^-	—	—	0.081 ± 0.010		[88, 89]
Σ^+	—	—	0.107 ± 0.011		[87, 88]
Σ^\pm	—	—	0.174 ± 0.009		[84, 88]
Ξ^-	$0.0055 \pm 0.0004^{(a)}$	0.0176 ± 0.0027	0.0262 ± 0.0009		[9, 59, 77, 82–85]
$\Delta(1232)^{++}$	0.040 ± 0.010	—	0.085 ± 0.014		[90–92]
$\Sigma(1385)^-$	0.006 ± 0.002	0.017 ± 0.004	0.0240 ± 0.0017		[59, 82, 84, 85, 93]
$\Sigma(1385)^+$	$0.0062 \pm 0.0011^{(a)}$	0.017 ± 0.004	0.0239 ± 0.0015		[59, 82–85, 93]

Particle	$\sqrt{s} \approx 10$ GeV	$\sqrt{s} = 29\text{--}35$ GeV	$\sqrt{s} = 91$ GeV	$\sqrt{s} = 130\text{--}200$ GeV
$\Sigma(1385)^\pm$	0.0106 ± 0.0020	0.033 ± 0.008	0.0472 ± 0.0027	[59, 82, 84, 85, 93]
$\Xi(1530)^0$	$0.00130 \pm 0.00010^{(a)}$	—	0.00694 ± 0.00049	[59, 82, 83, 85, 94]
Ω^-	$0.00060 \pm 0.00033^{(a)}$	0.014 ± 0.007	0.00124 ± 0.00018	[59, 77, 82, 83, 85, 86]
Λ_c^+	$0.0479 \pm 0.0038^{(a,m)}$	0.110 ± 0.050	0.078 ± 0.017	[47, 49, 77, 83, 95]
Λ_b^0	—	—	0.031 ± 0.016	[96]
Σ_c^0	$0.0025 \pm 0.0004^{(a)}$	—	—	[83]
$\Lambda(1520)$	$0.0046 \pm 0.0004^{(a)}$	—	0.0222 ± 0.0027	[83, 85, 89, 97]

- (a) $\sigma_{\text{had}} = 3.33 \pm 0.05 \pm 0.21$ nb (CLEO: [98]) has been used in converting the measured cross sections to average hadron multiplicities.
- (b) $B(D_s \rightarrow \eta\pi, \eta'\pi)$ was used (RPP 1994).
- (c) Comprises both charged and neutral B meson states.
- (d) The Standard Model $B(Z \rightarrow b\bar{b}) = 0.217$ was used.
- (e) $x_p = p/p_{\text{beam}} > 0.1$ only.
- (f) Both charge states.
- (g) $B(D^*(2010)^+ \rightarrow D^0\pi^+) \times B(D^0 \rightarrow K^-\pi^+)$ has been used (RPP 2000).
- (h) $B(D_s^* \rightarrow D_s^+\gamma)$, $B(D_s^+ \rightarrow \phi\pi^+)$, $B(\phi \rightarrow K^+K^-)$ have been used (RPP 1998).
- (i) Any charge state (*i.e.*, B_d^* , B_u^* , or B_s^*).
- (j) $B(Z \rightarrow \text{hadrons}) = 0.699$ was used (RPP 1994).
- (k) Any charge state (*i.e.*, B_d^{**} , B_u^{**} , or B_s^{**}).
- (l) Assumes $B(D_{s1}^+ \rightarrow D^{*+}K^0 + D^{*0}K^+) = 100\%$ and $B(D_{s2}^+ \rightarrow D^0K^+) = 45\%$.
- (m) The value was derived from the cross section of $\Lambda_c^+ \rightarrow p\pi K$ using (a) and assuming the branching fraction to be $(5.0 \pm 1.3)\%$ (RPP 2004).

References grouped by collaboration for Table-52.1:

- RPP: [12]
- ALEPH: [13, 20, 40, 58, 59, 63, 70, 81],
- ARGUS: [8, 24, 37, 41, 57, 82, 90, 97],
- BaBar: [10, 48, 68, 95],
- Belle: [44, 69, 83],
- CELLO: [19, 26],
- CLEO: [9, 45, 49, 98],
- Crystal Ball: [38],
- DELPHI: [14, 17, 21, 25, 33, 46, 50–52, 55, 61, 66, 71, 76, 80, 84, 86, 89, 91, 94],
- HRS: [27, 54, 78, 93],
- L3: [22, 34, 42, 67, 72, 74, 87]
- MARK II: [29, 39],
- JADE: [18, 28],
- OPAL: [15, 23, 35, 43, 47, 53, 56, 60, 62, 64, 65, 73, 75, 79, 85, 88, 92, 96],
- PLUTO: [30]
- SLD: [16, 36],
- TASSO: [31]
- TPC: [32].

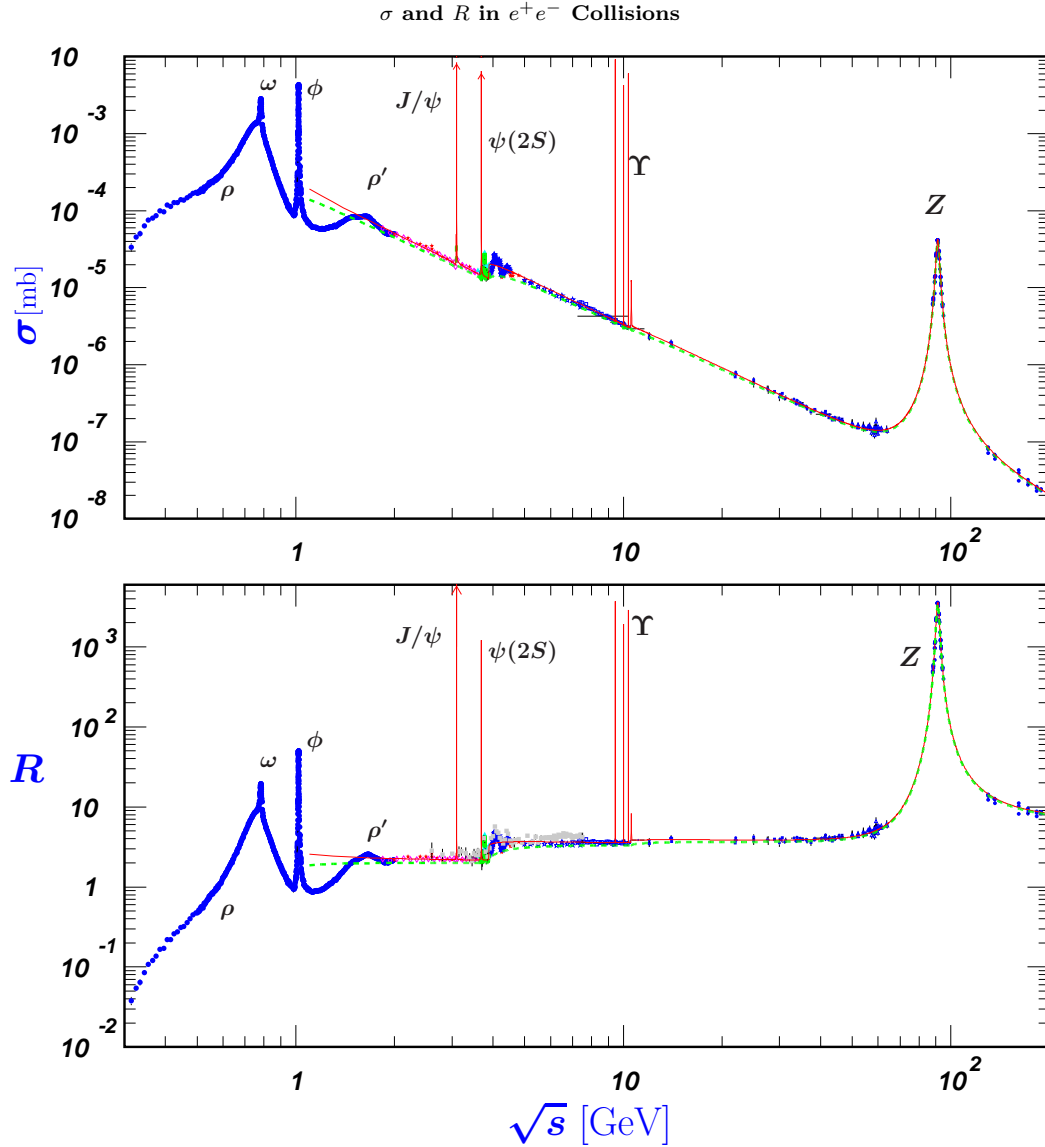
52.3 σ and R in e^+e^- Collisions

Figure 52.2: World data on the total cross section of $e^+e^- \rightarrow \text{hadrons}$ and the ratio $R(s) = \sigma(e^+e^- \rightarrow \text{hadrons}, s) / \sigma(e^+e^- \rightarrow \mu^+\mu^-, s)$. $\sigma(e^+e^- \rightarrow \text{hadrons}, s)$ is the experimental cross section corrected for initial state radiation and electron-positron vertex loops, $\sigma(e^+e^- \rightarrow \mu^+\mu^-, s) = 4\pi\alpha^2(s)/3s$. Data errors are total below 2 GeV and statistical above 2 GeV. The curves are an educative guide: the broken one (green) is a naive quark-parton model prediction, and the solid one (red) is 3-loop pQCD prediction (see “Quantum Chromodynamics” section of this *Review*, Eq. (9.7) or, for more details [99], Breit-Wigner parameterizations of J/ψ , $\psi(2S)$, and $\Upsilon(nS)$, $n = 1, 2, 3, 4$ are also shown. The full list of references to the original data and the details of the R ratio extraction from them can be found in [100]. Corresponding computer-readable data files are available at <http://pdg.lbl.gov/current/xsect/>. (Courtesy of the COMPAS (Protvino) and HEPDATA (Durham) Groups, August 2019. Corrections by P. Janot (CERN) and M. Schmitt (Northwestern U.))

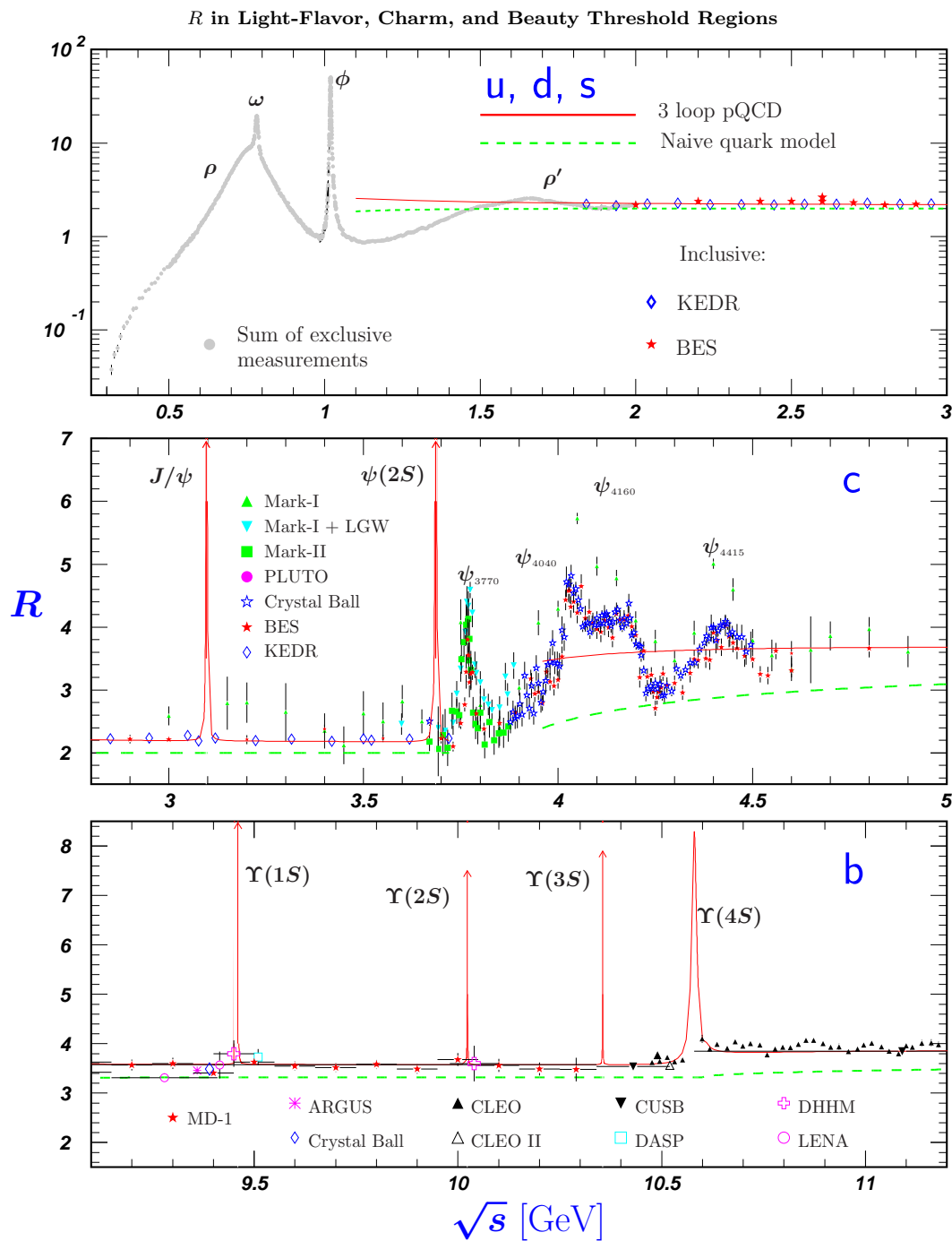


Figure 52.3: R in the light-flavor, charm, and beauty threshold regions. Data errors are total below 2 GeV and statistical above 2 GeV. The curves are the same as in Fig. 52.2. **Note:** CLEO data above $\Upsilon(4S)$ were not fully corrected for radiative effects, and we retain them on the plot only for illustrative purposes with a normalization factor of 0.8. The full list of references to the original data and the details of the R ratio extraction from them can be found in [100]. The computer-readable data are available at <http://pdg.lbl.gov/current/xsect/>. (Courtesy of the COMPAS (Protvino) and HEPDATA (Durham) Groups, August 2019.)

52.4 Annihilation Cross Section Near M_Z

Courtesy of M. Grünewald and the LEP Electroweak Working Group, 2007.

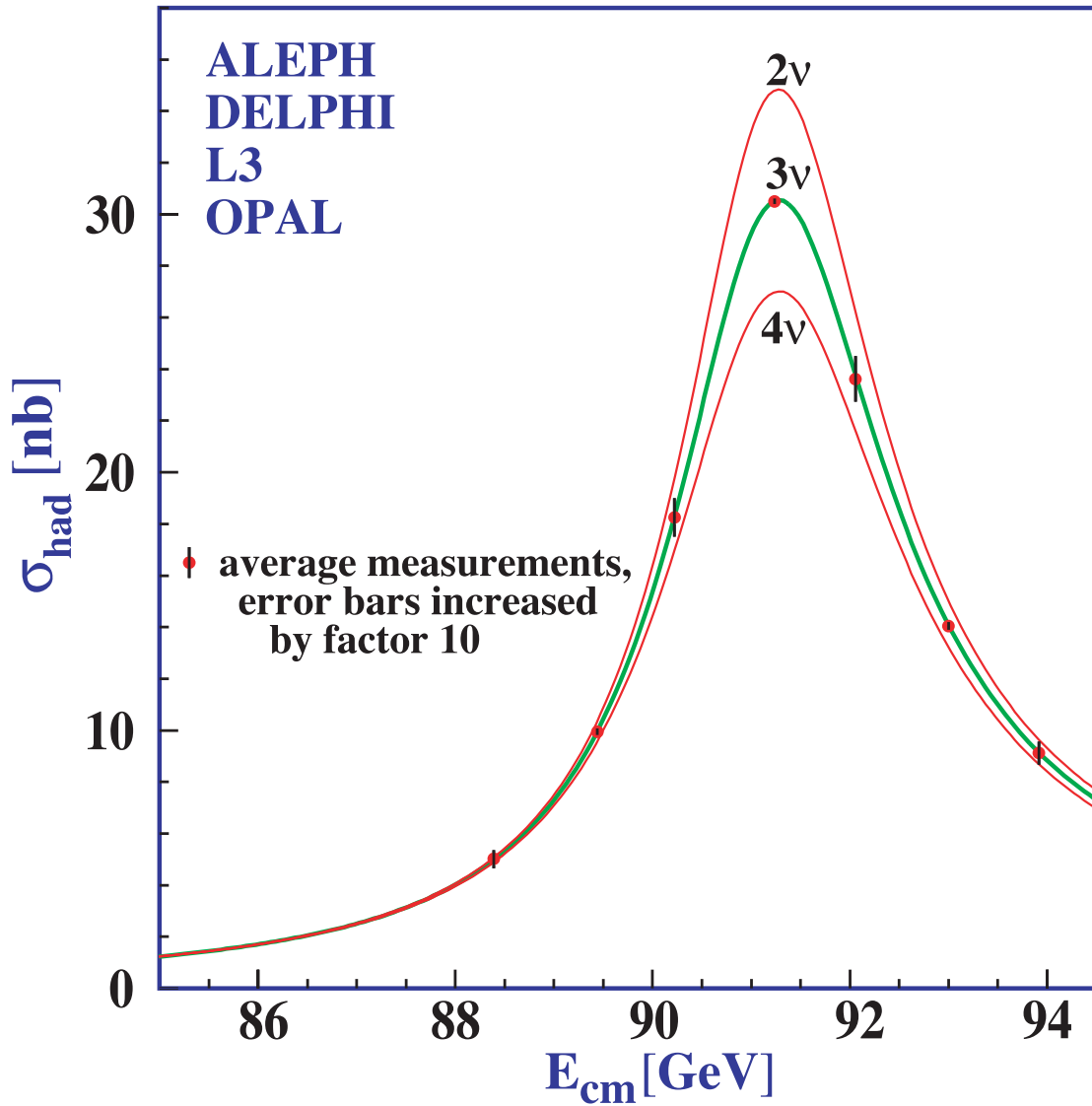


Figure 52.4: Combined data from the ALEPH, DELPHI, L3, and OPAL Collaborations for the cross section in e^+e^- annihilation into hadronic final states as a function of the center-of-mass energy near the Z pole. The curves show the predictions of the Standard Model with two, three, and four species of light neutrinos. The asymmetry of the curve is produced by initial-state radiation. Note that the error bars have been increased by a factor ten for display purposes. References: ALEPH [101], DELPHI [102], L3 [103], OPAL [104], Combination [105],

52.5 Total Hadronic Cross Sections

Revised August 2019 by COMPAS Group (NRC KI – IHEP, Protvino).

In this section, plots of total cross section for various processes are presented. The plots include data from hadronic collisions such as pp and $\bar{p}p$, as well as γp , γd , and $\gamma\gamma$ processes. The cross section data provide crucial inputs to the study of QCD physics. In particular, to probe the non-perturbative part of QCD processes which are described by a number of diffractive models. We begin by introducing some models of diffractive scatterings and listing references for further reading.

Diffractive scattering here means scattering of hadrons at small angles and exhibiting typical diffraction pattern in angular distribution of scattered particles. Beyond purely elastic scattering diffraction phenomena include inelastic processes with large rapidity gaps: those of single and double diffractive dissociation and “central diffractive” events. In distinction from the most of other processes considered in the SM diffraction processes (DP) are related to large spatio-temporal scales growing with energy of collision. Being caused by strong interactions DP are a subject of the fundamental strong interaction theory, QCD, and hereby a part of the longstanding problem of QCD at large distances.

One of the most important basic notions and tools in general theoretical framework related to the diffractive processes is the notion of the Regge poles, or Reggeons, generalizing the simple one-particle exchange (of Yukawa type) by virtual particles of fixed spin to exchanges by states with “running spin” dependent on the transferred momenta [106,107]. The simplest case of the one-Reggeon exchange amplitude is given by the amplitude (at high c.m. energy \sqrt{s} and fixed (small) transferred momentum squared, t): $T(s, t) = \beta(t)s^{\alpha(t)}$ which qualitatively exhibits many typical features of generic diffractive processes (e.g. the growth of the interaction radius with energy). In practice the single-pole Reggeon model is insufficient for many diffractive processes but still serves a building block for more sophisticated schemes. Up to now no firm results concerning Regge trajectories $\alpha(t)$ and Regge residues $\beta(t)$ were obtained from the first principles of QCD. General principles imply that both $\alpha(t)$ and $\beta(t)$ are analytic functions with right cuts from some $t_0 > 0$ to positive infinity.

The theoretical requisite for analyzing diffractive phenomena is therefore represented by various model approaches. The more commonly discussed models in the literatures are:

- **Regge -Eikonal approach** [108–115]: this approach automatically satisfy the s -channel unitarity condition and generalizes the impact parameter approximation to the relativistic case.
- **Regge pole models with minimal corrections due to two-Reggeon exchanges** [116–118]: in this model, contribution of the leading trajectory is supplemented by a two-Reggeon exchange with arbitrary coefficient chosen from the fitting details.
- **U -matrix (or resonance) approach** [119,120]: the unitarity respecting approach with the scattering amplitude defined by a reaction matrix.
- **Direct functional modelling of the amplitudes without Regge trajectories** [121,122]: this approach appeals to only very general properties of the amplitudes leaving aside all dynamical assumptions and mostly aiming at the best phenomenological description of the data.
- **Quasi-classical approach** [123–126]: based on the observation that diffractive processes deal with high quantum numbers, in particular with large number of virtual quanta.

For readers who are interested in examples of both total and elastic cross section parametrizations and fits, see previous edition of the *Plots of Cross Sections and Related Quantities* review [127]. For the cross section plots shown in the following pages, the example fits are using parametrizations as described in [127] with the fit range starting at about $\sqrt{s} = 5$ GeV.

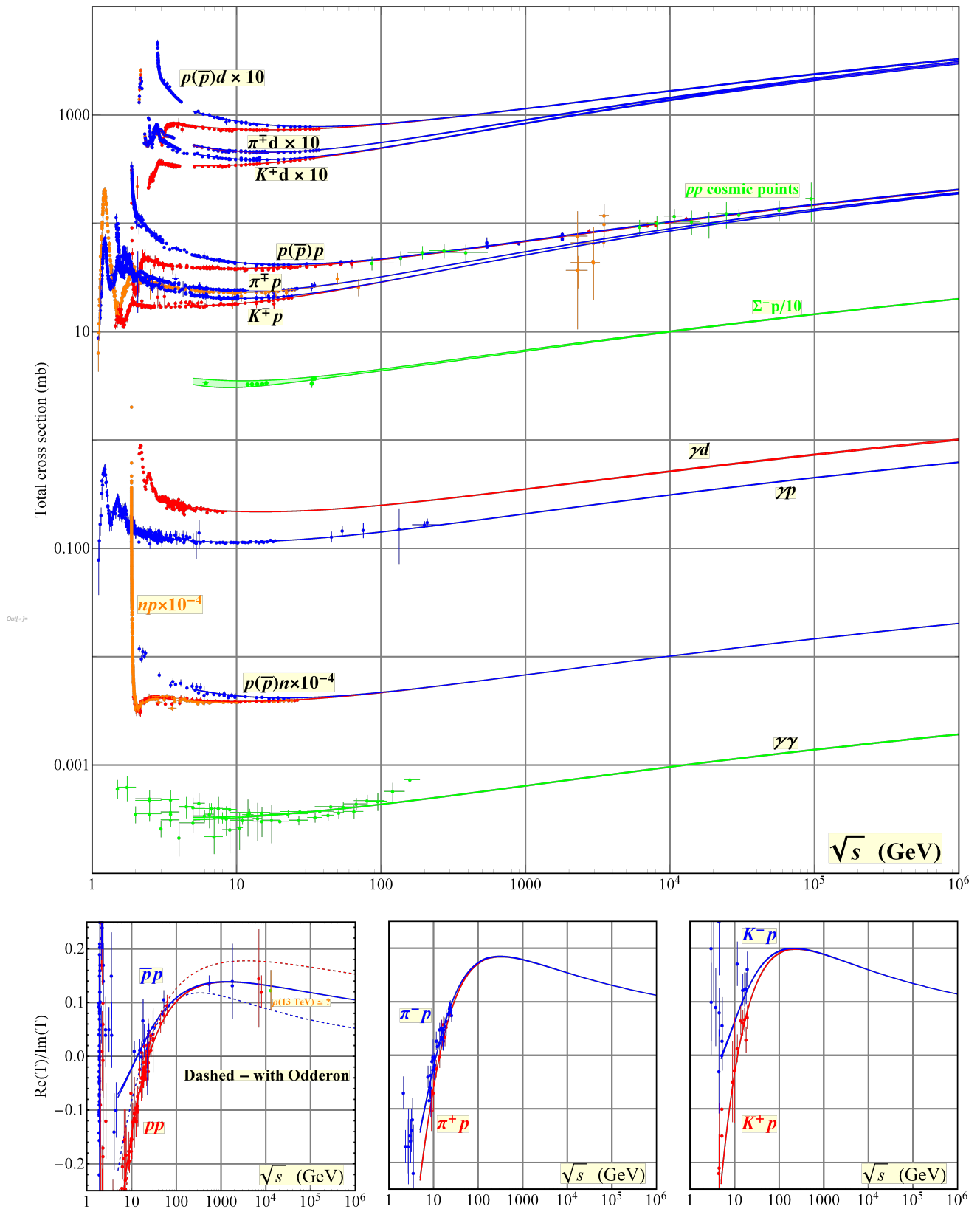


Figure 52.5: Summary of hadronic, γp , γd , and $\gamma\gamma$ total cross sections, and ratio of the real to imaginary parts of the forward hadronic amplitudes. Corresponding computer-readable data files may be found at <http://pdg.lbl.gov/current/xsect/>. (Courtesy of the COMPAS group, NRC KI – IHEP, Protvino, August 2019.)

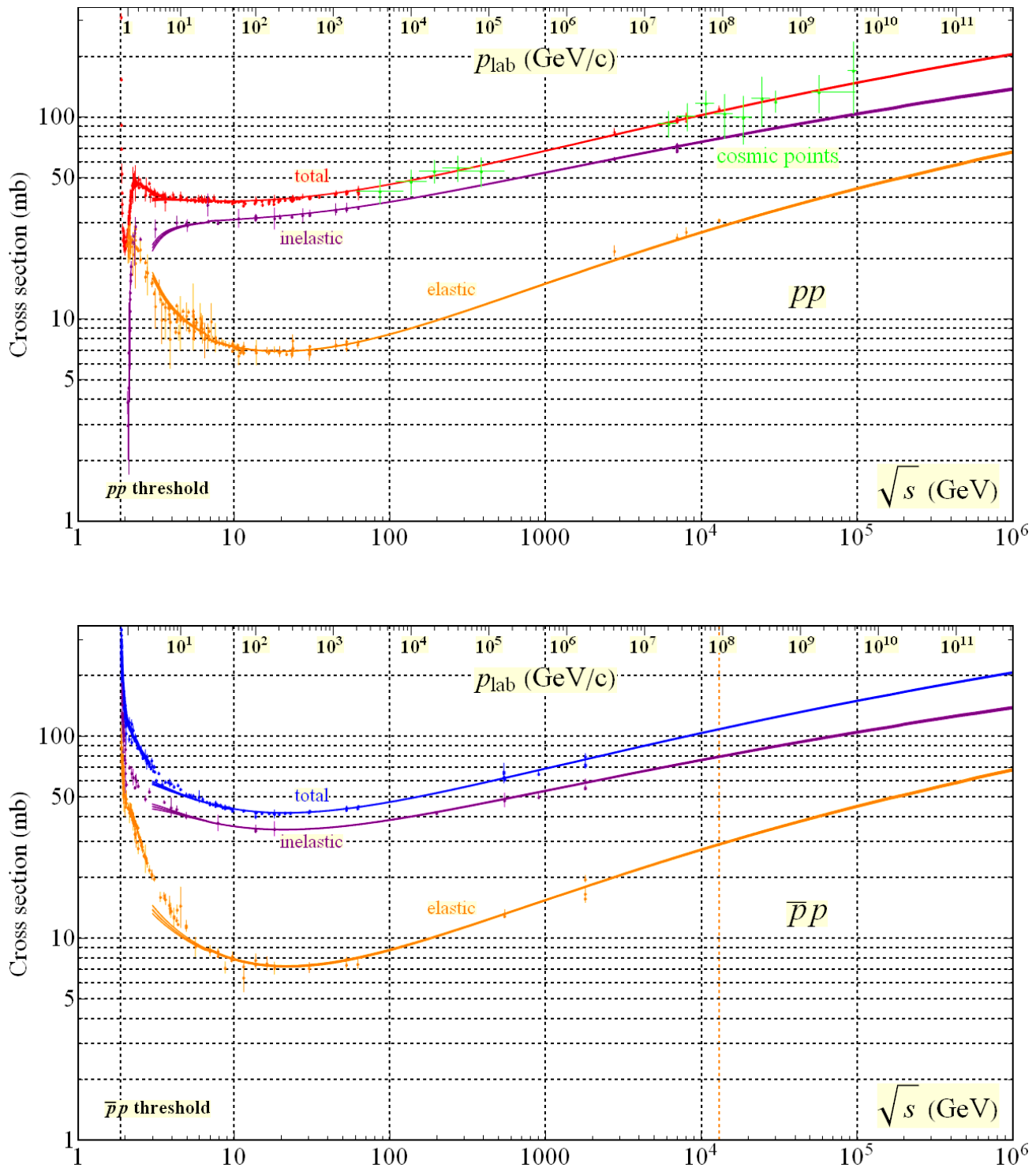


Figure 52.6: Total and elastic cross sections for pp and $\bar{p}p$ collisions as a function of laboratory beam momentum and total center-of-mass energy. σ_{el} is computed using the nuclear part of the elastic scattering amplitude [126]. Corresponding computer-readable data files may be found at <http://pdg.lbl.gov/current/xsect/>. (Courtesy of the COMPAS group, NRC KI – IHEP, Protvino, August 2019.)

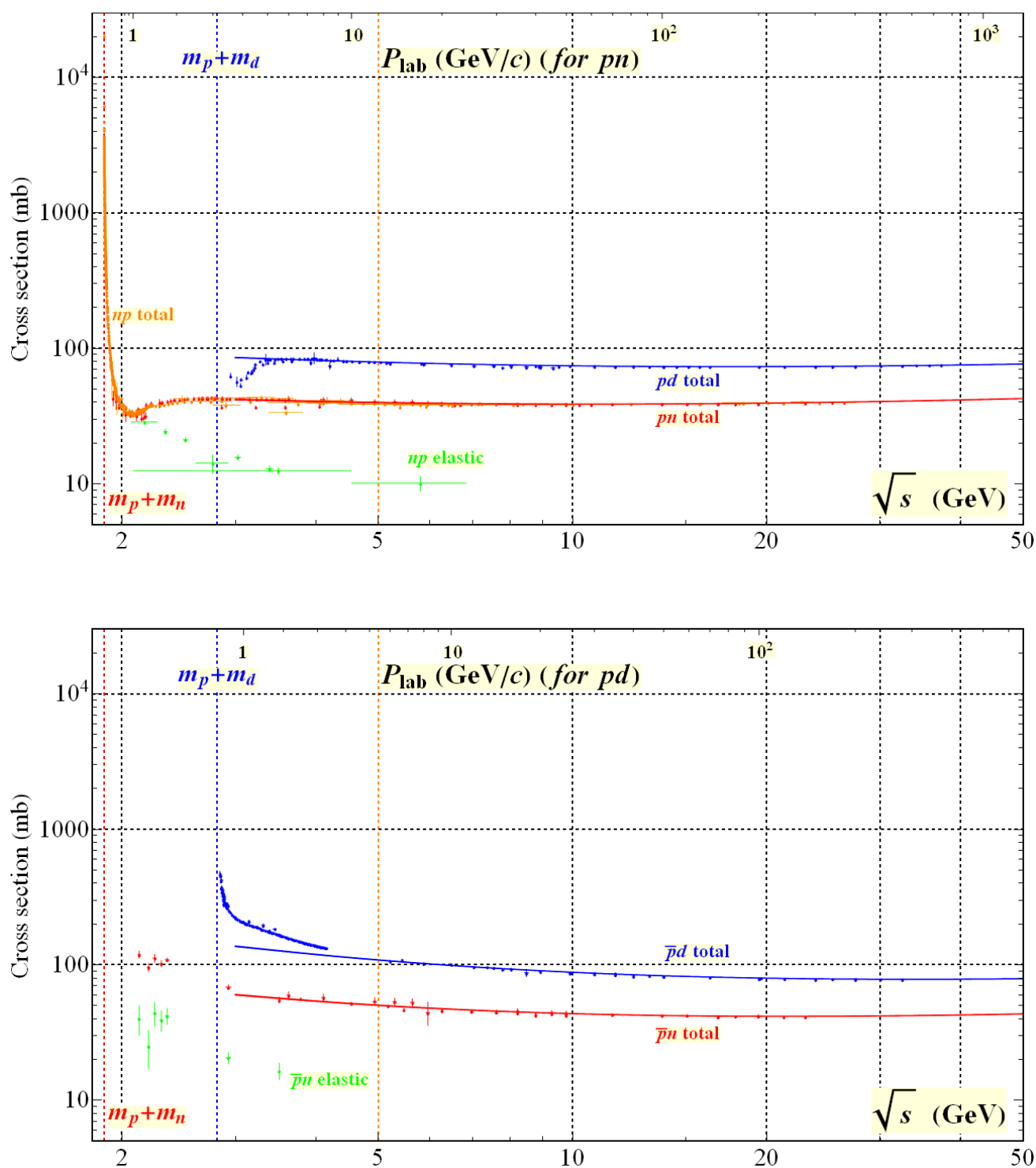


Figure 52.7: Total and elastic cross sections for pd (total only), np , $\bar{p}d$ (total only), and $\bar{p}n$ collisions as a function of laboratory beam momentum and total center-of-mass energy. Corresponding computer-readable data files may be found at <http://pdg.lbl.gov/current/xsect/>. (Courtesy of the COMPAS Group, NRC KI – IHEP, Protvino, August 2019.)

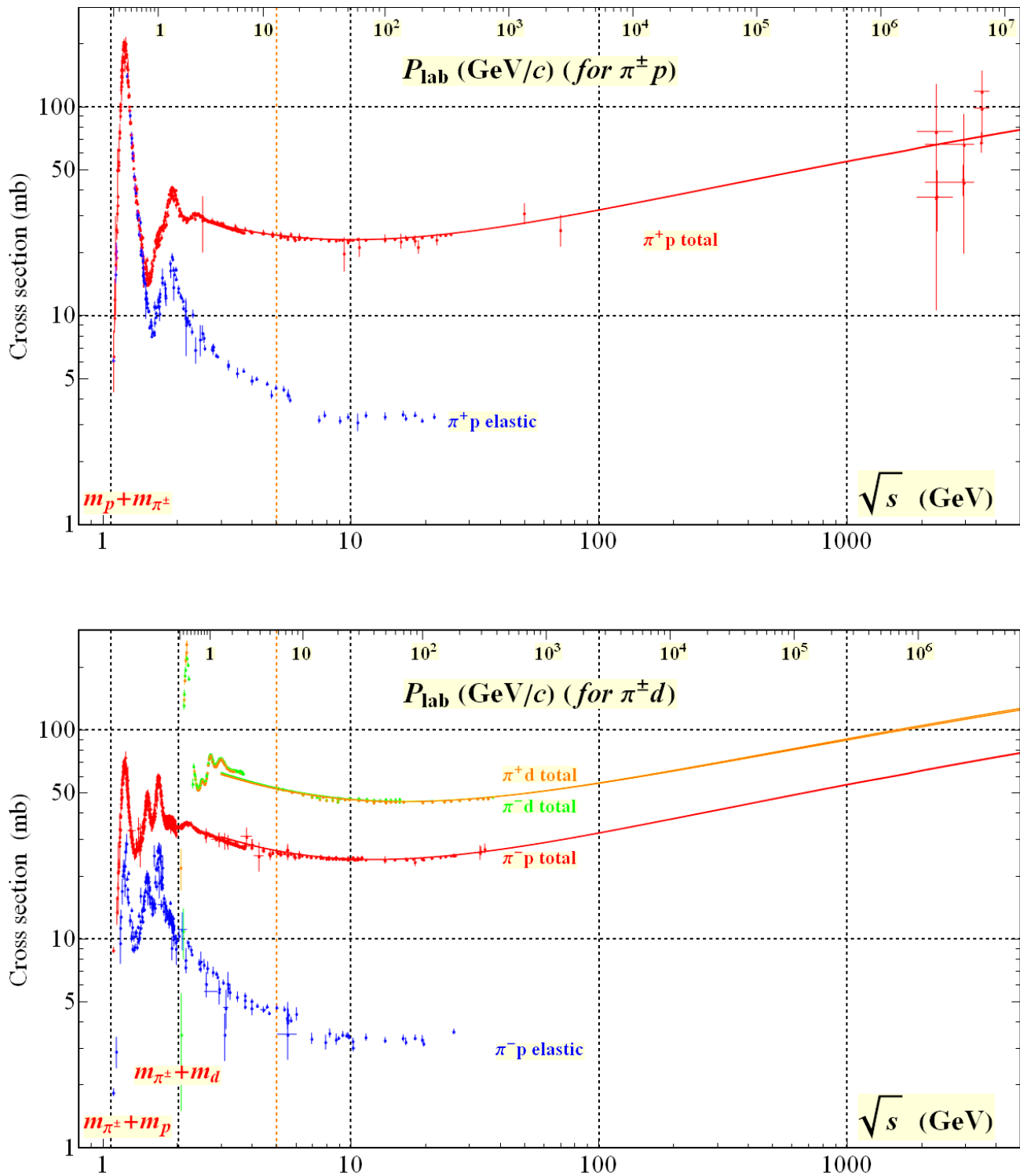


Figure 52.8: Total and elastic cross sections for $\pi^\pm p$ and $\pi^\pm d$ (total only) collisions as a function of laboratory beam momentum and total center-of-mass energy. Corresponding computer-readable data files may be found at <http://pdg.lbl.gov/current/xsect/>. (Courtesy of the COMPAS Group, NRC KI – IHEP, Protvino, August 2019.)

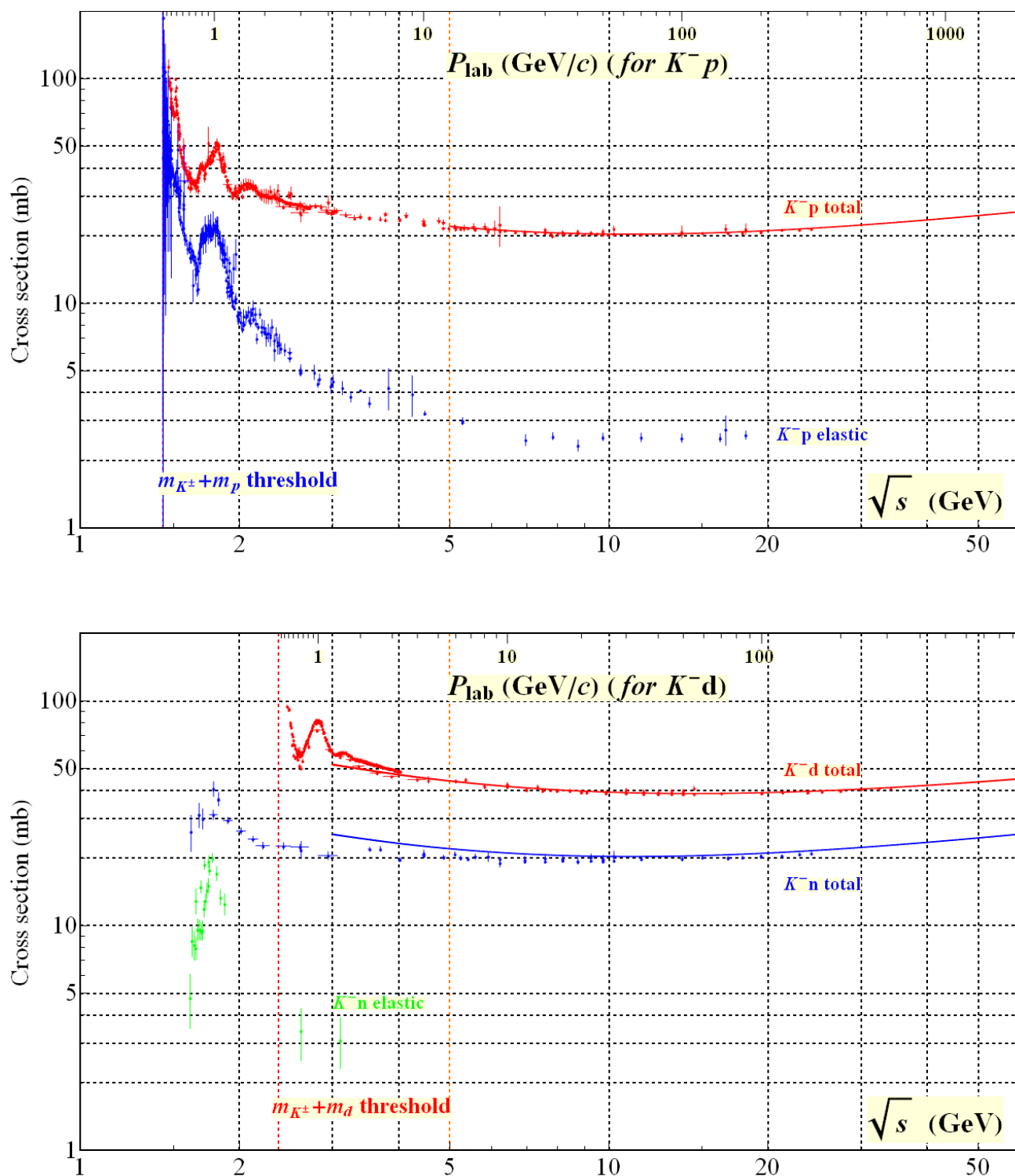


Figure 52.9: Total and elastic cross sections for $K^- p$ and $K^- d$ (total only), and $K^- n$ collisions as a function of laboratory beam momentum and total center-of-mass energy. Corresponding computer-readable data files may be found at <http://pdg.lbl.gov/current/xsect/>. (Courtesy of the COMPAS Group, NRC KI – IHEP, Protvino, August 2019.)

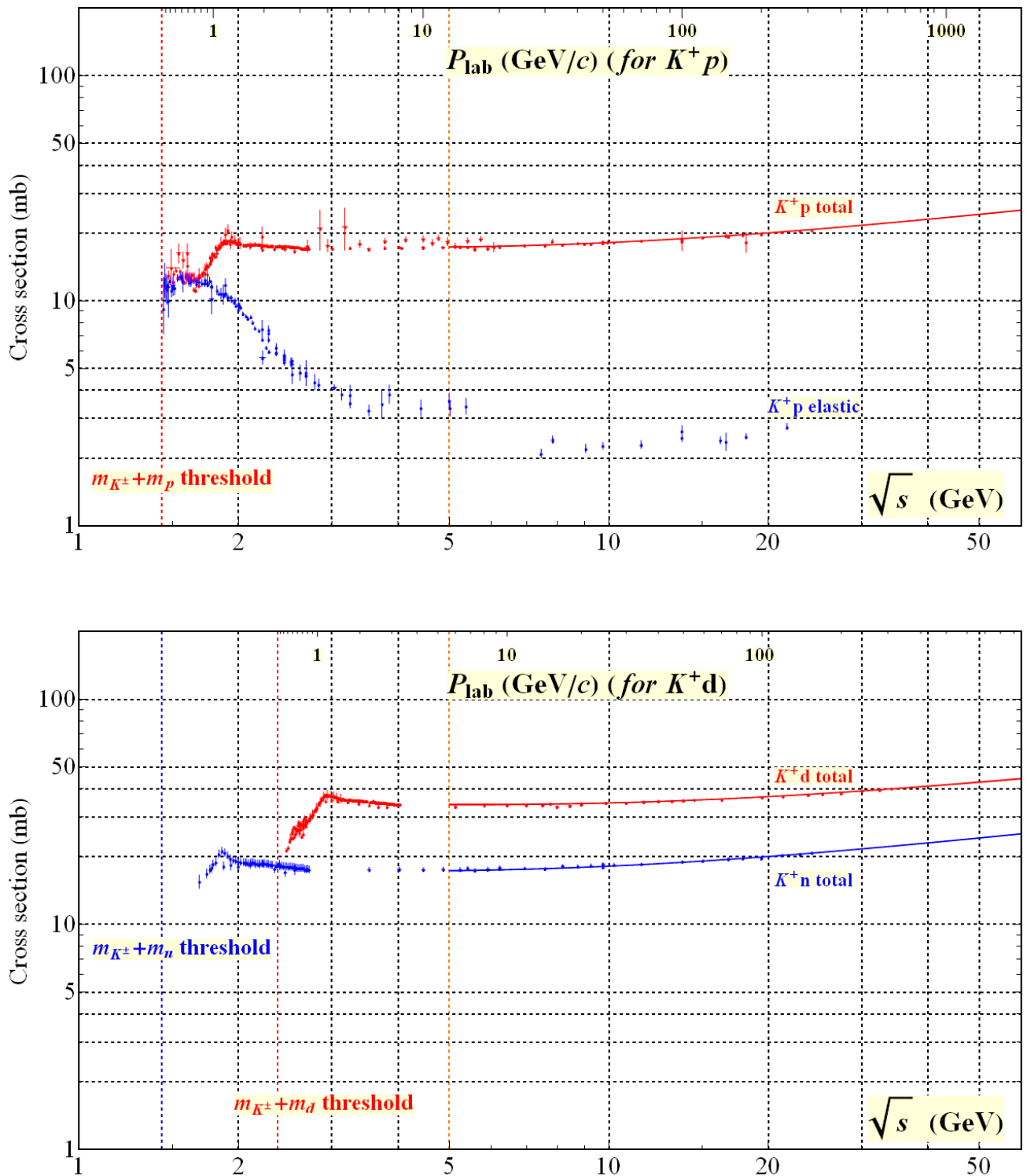


Figure 52.10: Total and elastic cross sections for K^+p and total cross sections for K^+d and K^+n collisions as a function of laboratory beam momentum and total center-of-mass energy. Corresponding computer-readable data files may be found at <http://pdg.lbl.gov/current/xsect/>. (Courtesy of the COMPAS Group, NRC KI – IHEP, Protvino, August 2019.)

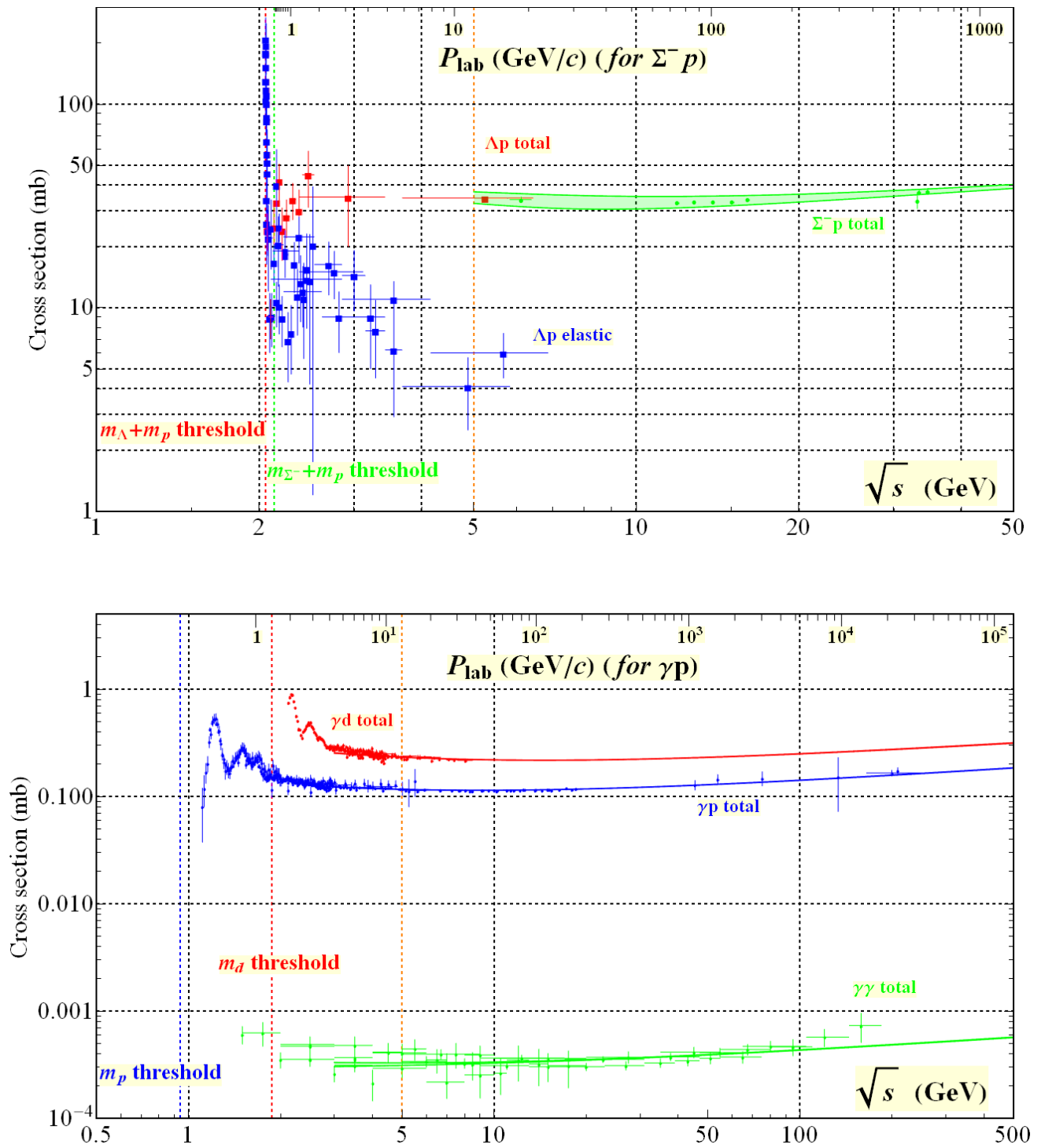


Figure 52.11: Total and elastic cross sections for Δp , total cross section for $\Sigma^- p$, and total hadronic cross sections for γd , γp , and $\gamma\gamma$ collisions as a function of laboratory beam momentum and the total center-of-mass energy. Corresponding computer-readable data files may be found at <http://pdg.lbl.gov/current/xsect/>. (Courtesy of the COMPAS group, NRC KI – IHEP, Protvino, August 2019.)

References

- [1] G. J. Alner *et al.* (UA5), *Z. Phys.* **C33**, 1 (1986).
- [2] K. Alpgard *et al.* (UA5), *Phys. Lett.* **112B**, 183 (1982).
- [3] F. Abe *et al.* (CDF), *Phys. Rev.* **D41**, 2330 (1990), [119(1989)].
- [4] R. Harr *et al.*, *Phys. Lett.* **B401**, 176 (1997), [hep-ex/9703002].
- [5] K. Aamodt *et al.* (ALICE), *Eur. Phys. J.* **C68**, 89 (2010), [arXiv:1004.3034].
- [6] V. Khachatryan *et al.* (CMS), *JHEP* **02**, 041 (2010), [arXiv:1002.0621].
- [7] V. Khachatryan *et al.* (CMS), *Phys. Rev. Lett.* **105**, 022002 (2010), [arXiv:1005.3299].
- [8] H. Albrecht *et al.* (ARGUS), *Z. Phys.* **C54**, 1 (1992).
- [9] S. Behrends *et al.* (CLEO), *Phys. Rev.* **D31**, 2161 (1985).
- [10] J. P. Lees *et al.* (BaBar), *Phys. Rev.* **D88**, 032011 (2013), [arXiv:1306.2895].
- [11] H. Albrecht *et al.*, *Phys. Lett.* **102B**, 291 (1981).
- [12] K. Hikasa *et al.* (Particle Data Group), *Phys. Rev.* **D45**, S1 (1992), [Erratum: *Phys. Rev.*D46,5210(1992)].
- [13] R. Barate *et al.* (ALEPH), *Eur. Phys. J.* **C5**, 205 (1998).
- [14] P. Abreu *et al.* (DELPHI), *Eur. Phys. J.* **C5**, 585 (1998).
- [15] R. Akers *et al.* (OPAL), *Z. Phys.* **C63**, 181 (1994).
- [16] K. Abe *et al.* (SLD), *Phys. Rev.* **D69**, 072003 (2004), [hep-ex/0310017].
- [17] P. Abreu *et al.* (DELPHI), *Eur. Phys. J.* **C18**, 203 (2000), [Erratum: *Eur. Phys. J.*C25,493(2002)], [hep-ex/0103031].
- [18] D. D. Pitzl *et al.* (JADE), *Z. Phys.* **C46**, 1 (1990), [Erratum: *Z. Phys.*C47,676(1990)].
- [19] H. J. Behrend *et al.* (CELLO), *Z. Phys.* **C47**, 1 (1990).
- [20] R. Barate *et al.* (ALEPH), *Eur. Phys. J.* **C16**, 613 (2000).
- [21] W. Adam *et al.* (DELPHI), *Z. Phys.* **C69**, 561 (1996).
- [22] M. Acciarri *et al.* (L3), *Phys. Lett.* **B371**, 126 (1996).
- [23] G. Abbiendi *et al.* (OPAL), *Eur. Phys. J.* **C17**, 373 (2000), [hep-ex/0007017].
- [24] H. Albrecht *et al.* (ARGUS), *Z. Phys.* **C44**, 547 (1989).
- [25] P. Abreu *et al.* (DELPHI), *Nucl. Phys.* **B444**, 3 (1995).
- [26] H. J. Behrend *et al.* (CELLO), *Z. Phys.* **C46**, 397 (1990).
- [27] M. Derrick *et al.*, *Phys. Rev.* **D35**, 2639 (1987).
- [28] W. Bartel *et al.* (JADE), *Z. Phys.* **C20**, 187 (1983).
- [29] H. Schellman *et al.*, *Phys. Rev.* **D31**, 3013 (1985).
- [30] C. Berger *et al.* (PLUTO), *Phys. Lett.* **104B**, 79 (1981).
- [31] M. Althoff *et al.* (TASSO), *Z. Phys.* **C27**, 27 (1985).
- [32] H. Aihara *et al.* (TPC/Two Gamma), *Phys. Rev. Lett.* **53**, 2378 (1984).
- [33] P. Abreu *et al.* (DELPHI), *Z. Phys.* **C65**, 587 (1995).
- [34] M. Acciarri *et al.* (L3), *Phys. Lett.* **B407**, 389 (1997), [Erratum: *Phys. Lett.*B427,409(1998)].
- [35] R. Akers *et al.* (OPAL), *Z. Phys.* **C67**, 389 (1995).
- [36] K. Abe *et al.* (SLD), *Phys. Rev.* **D59**, 052001 (1999), [hep-ex/9805029].
- [37] H. Albrecht *et al.* (ARGUS), *Z. Phys.* **C46**, 15 (1990).
- [38] C. Bieler *et al.* (Crystal Ball), *Z. Phys.* **C49**, 225 (1991).
- [39] G. Wormser *et al.*, *Phys. Rev. Lett.* **61**, 1057 (1988).
- [40] A. Heister *et al.* (ALEPH), *Phys. Lett.* **B528**, 19 (2002), [hep-ex/0201012].
- [41] H. Albrecht *et al.* (ARGUS), *Z. Phys.* **C58**, 199 (1993).
- [42] M. Acciarri *et al.* (L3), *Phys. Lett.* **B393**, 465 (1997).
- [43] K. Ackerstaff *et al.* (OPAL), *Eur. Phys. J.* **C5**, 411 (1998), [hep-ex/9805011].
- [44] R. Seuster *et al.* (Belle), *Phys. Rev.* **D73**, 032002 (2006), [hep-ex/0506068].
- [45] M. Artuso *et al.* (CLEO), *Phys. Rev.* **D70**, 112001 (2004), [hep-ex/0402040].
- [46] P. Abreu *et al.* (DELPHI), *Z. Phys.* **C59**, 533 (1993), [Erratum: *Z. Phys.*C65,709(1995)].
- [47] G. Alexander *et al.* (OPAL), *Z. Phys.* **C72**, 1 (1996).
- [48] B. Aubert *et al.* (BaBar), *Phys. Rev.* **D65**, 091104 (2002), [hep-ex/0201041].
- [49] D. Bortoletto *et al.* (CLEO), *Phys. Rev.* **D37**, 1719 (1988), [Erratum: *Phys. Rev.*D39,1471(1989)].
- [50] P. Abreu *et al.* (DELPHI), *Z. Phys.* **C57**, 181 (1993).
- [51] J. Abdallah *et al.* (DELPHI), *Phys. Lett.* **B576**, 29 (2003), [hep-ex/0311005].
- [52] P. Abreu *et al.* (DELPHI), *Z. Phys.* **C61**, 407 (1994).
- [53] R. Akers *et al.* (OPAL), *Z. Phys.* **C66**, 555 (1995).
- [54] S. Abachi *et al.*, *Phys. Rev. Lett.* **57**, 1990 (1986).
- [55] P. Abreu *et al.* (DELPHI), *Phys. Lett.* **B449**, 364 (1999).
- [56] K. Ackerstaff *et al.* (OPAL), *Eur. Phys. J.* **C4**, 19 (1998), [hep-ex/9802013].
- [57] H. Albrecht *et al.* (ARGUS), *Z. Phys.* **C61**, 1 (1994).
- [58] D. Buskulic *et al.* (ALEPH), *Z. Phys.* **C69**, 379 (1996).
- [59] R. Barate *et al.* (ALEPH), *Phys. Rept.* **294**, 1 (1998).
- [60] P. D. Acton *et al.* (OPAL), *Phys. Lett.* **B305**, 407 (1993).
- [61] P. Abreu *et al.* (DELPHI), *Z. Phys.* **C73**, 61 (1996).
- [62] K. Ackerstaff *et al.* (OPAL), *Phys. Lett.* **B412**, 210 (1997), [hep-ex/9708022].
- [63] R. Barate *et al.* (ALEPH), *Eur. Phys. J.* **C16**, 597 (2000), [hep-ex/9909032].
- [64] K. Ackerstaff *et al.* (OPAL), *Eur. Phys. J.* **C1**, 439 (1998), [hep-ex/9708021].
- [65] K. Ackerstaff *et al.* (OPAL), *Eur. Phys. J.* **C5**, 1 (1998), [hep-ex/9802008].
- [66] P. Abreu *et al.* (DELPHI), *Z. Phys.* **C68**, 353 (1995).
- [67] M. Acciarri *et al.* (L3), *Phys. Lett.* **B345**, 589 (1995).
- [68] B. Aubert *et al.* (BaBar), *Phys. Rev. Lett.* **87**, 162002 (2001), [hep-ex/0106044].
- [69] K. Abe *et al.* (Belle), *Phys. Rev. Lett.* **88**, 052001 (2002), [hep-ex/0110012].
- [70] D. Buskulic *et al.* (ALEPH), *Phys. Lett.* **B295**, 396 (1992).
- [71] P. Abreu *et al.* (DELPHI), *Phys. Lett.* **B341**, 109 (1994).
- [72] M. Acciarri *et al.* (L3), *Phys. Lett.* **B453**, 94 (1999).
- [73] G. Alexander *et al.* (OPAL), *Z. Phys.* **C70**, 197 (1996).
- [74] M. Acciarri *et al.* (L3), *Phys. Lett.* **B407**, 351 (1997).
- [75] G. Alexander *et al.* (OPAL), *Phys. Lett.* **B370**, 185 (1996).
- [76] J. Abdallah *et al.* (DELPHI), *Phys. Lett.* **B569**, 129 (2003), [hep-ex/0309057].
- [77] A. De Angelis, *J. Phys.* **G19**, 1233 (1993).
- [78] S. Abachi *et al.*, *Phys. Lett.* **B199**, 151 (1987).
- [79] R. Akers *et al.* (OPAL), *Z. Phys.* **C68**, 1 (1995).
- [80] P. Abreu *et al.* (DELPHI), *Phys. Lett.* **B345**, 598 (1995).
- [81] A. Heister *et al.* (ALEPH), *Phys. Lett.* **B526**, 34 (2002), [hep-ex/0112010].
- [82] H. Albrecht *et al.* (ARGUS), *Z. Phys.* **C39**, 177 (1988).
- [83] M. Niiyama *et al.* (Belle), *Phys. Rev.* **D97**, 7, 072005 (2018), [arXiv:1706.06791].
- [84] P. Abreu *et al.* (DELPHI), *Z. Phys.* **C67**, 543 (1995).
- [85] G. Alexander *et al.* (OPAL), *Z. Phys.* **C73**, 569 (1997).
- [86] W. Adam *et al.* (DELPHI), *Z. Phys.* **C70**, 371 (1996).
- [87] M. Acciarri *et al.* (L3), *Phys. Lett.* **B479**, 79 (2000), [hep-ex/0002066].

- [88] G. Alexander *et al.* (OPAL), *Z. Phys.* **C73**, 587 (1997).
- [89] P. Abreu *et al.* (DELPHI), *Phys. Lett.* **B475**, 429 (2000), [hep-ex/0103020].
- [90] H. Albrecht *et al.* (ARGUS), *Phys. Lett.* **B230**, 169 (1989).
- [91] P. Abreu *et al.* (DELPHI), *Phys. Lett.* **B361**, 207 (1995).
- [92] G. Alexander *et al.* (OPAL), *Phys. Lett.* **B358**, 162 (1995).
- [93] S. Abachi *et al.*, *Phys. Rev. Lett.* **58**, 2627 (1987), [Erratum: *Phys. Rev. Lett.*59,2388(1987)].
- [94] J. Abdallah *et al.* (DELPHI), *Eur. Phys. J.* **C44**, 299 (2005), [hep-ex/0510023].
- [95] B. Aubert *et al.* (BaBar), *Phys. Rev.* **D75**, 012003 (2007), [hep-ex/0609004].
- [96] P. D. Acton *et al.* (OPAL), *Phys. Lett.* **B281**, 394 (1992).
- [97] H. Albrecht *et al.* (ARGUS), *Phys. Rept.* **276**, 223 (1996).
- [98] R. Giles *et al.* (CLEO), *Phys. Rev.* **D29**, 1285 (1984).
- [99] K. G. Chetyrkin, R. V. Harlander and J. H. Kuhn, *Nucl. Phys.* **B586**, 56 (2000), [Erratum: *Nucl. Phys.*B634,413(2002)], [hep-ph/0005139].
- [100] V. V. Ezhela, S. B. Lugovsky and O. V. Zenin (2003), [hep-ph/0312114].
- [101] R. Barate *et al.* (ALEPH), *Eur. Phys. J.* **C14**, 1 (2000).
- [102] P. Abreu *et al.* (DELPHI), *Eur. Phys. J.* **C16**, 371 (2000).
- [103] M. Acciarri *et al.* (L3), *Eur. Phys. J.* **C16**, 1 (2000), [hep-ex/0002046].
- [104] G. Abbiendi *et al.* (OPAL), *Eur. Phys. J.* **C19**, 587 (2001), [hep-ex/0012018].
- [105] S. Schael *et al.* (ALEPH, DELPHI, L3, OPAL, SLD, LEP Electroweak Working Group, SLD Electroweak Group, SLD Heavy Flavour Group), *Phys. Rept.* **427**, 257 (2006), [hep-ex/0509008].
- [106] P. Collins, *An Introduction to Regge Theory and High-Energy Physics*, Cambridge Monographs on Mathematical Physics, Cambridge Univ. Press, Cambridge, UK (2009), ISBN 9780521110358.
- [107] G. Pancheri and Y. N. Srivastava, *Eur. Phys. J.* **C77**, 3, 150 (2017), [arXiv:1610.10038].
- [108] L. A. Harland-Lang, V. A. Khoze and M. G. Ryskin, *Int. J. Mod. Phys.* **A30**, 1542013 (2015).
- [109] V. A. Petrov and A. Prokudin, *Phys. Rev.* **D87**, 3, 036003 (2013), [arXiv:1212.1924].
- [110] C. Bourrely, J. Soffer and T. T. Wu, *Eur. Phys. J.* **C28**, 97 (2003), [hep-ph/0210264].
- [111] M. M. Block *et al.*, *Phys. Rev.* **D92**, 1, 014030 (2015), [arXiv:1505.04842].
- [112] O. V. Selyugin, *Phys. Rev.* **D91**, 11, 113003 (2015), [Erratum: *Phys. Rev.*D92,no.9,099901(2015)], [arXiv:1505.02426].
- [113] L. G. Dakhno and V. A. Nikonov, *Eur. Phys. J.* **A5**, 209 (1999), [hep-ph/9902320].
- [114] A. A. Godizov, *Phys. Lett.* **B735**, 57 (2014), [arXiv:1404.2851].
- [115] E. Gotsman, E. M. Levin and U. Maor, *Phys. Rev.* **D49**, R4321 (1994), [hep-ph/9310257].
- [116] A. Donnachie and P. V. Landshoff, *Phys. Lett.* **B727**, 500 (2013), [Erratum: *Phys. Lett.*B750,669(2015)], [arXiv:1309.1292].
- [117] E. Martynov, *Phys. Rev.* **D87**, 11, 114018 (2013), [arXiv:1305.3093].
- [118] L. Jenkovszky, *Nuovo Cim.* **C037**, 02, 99 (2014).
- [119] S. M. Troshin and N. E. Tyurin, *Int. J. Mod. Phys.* **A32**, 17, 1750103 (2017), [arXiv:1704.00443].
- [120] V. V. Anisovich, *Phys. Usp.* **58**, 10, 963 (2015).
- [121] D. A. Fagundes, M. J. Menon and P. V. R. G. Silva, *Nucl. Phys.* **A946**, 194 (2016), [arXiv:1509.04108].
- [122] E. Martynov and B. Nicolescu, *Eur. Phys. J.* **C56**, 57 (2008), [arXiv:0712.1685].
- [123] W. Heisenberg, *Z. Phys.* **133**, 65 (1952).
- [124] J. R. Cudell *et al.*, *Phys. Rev.* **D65**, 074024 (2002), [hep-ph/0107219].
- [125] H. Nastase and J. Sonnenschein, *Phys. Rev.* **D92**, 105028 (2015), [arXiv:1504.01328].
- [126] V. I. Belousov *et al.*, *Phys. Atom. Nucl.* **79**, 1, 113 (2016), [*Yad. Fiz.*79,no.1,55(2016)].
- [127] C. Patrignani *et al.* (Particle Data Group), *Chin. Phys.* **C40**, 10, 100001 (2016).



Particle Properties

Gauge Bosons

53. Mass and width of the W boson (rev.)	715
54. Z boson	717

Charged Leptons

55. Muon anomalous magnetic moment (rev.)	722
56. Muon decay parameters (rev.)	725
57. τ branching fractions (rev.)	728
58. τ -lepton decay parameters	731

Quarks

59. Quark masses (rev.)	733
60. Top quark (rev.)	741

Mesons

61. Form factors for rad. pion & kaon decays (rev.)	762
62. Scalar mesons below 2 GeV (rev.)	764
63. Pseudoscalar and pseudovector mesons in the 1400 MeV region (rev.)	771
64. Rare kaon decays (rev.)	774
65. CPT invariance tests in neutral kaon decay (rev.)	779
66. V_{ud} , V_{us} , Cabibbo angle, and CKM unitarity (rev.)	781
67. CP -violation in K_L decays	784
68. Review of multibody charm analyses (rev.)	788
69. $D^0-\bar{D}^0$ mixing (rev.)	792
70. D_s^+ branching fractions (rev.)	801
71. Leptonic decays of charged pseudoscalar mesons (rev.)	803
72. Production and decay of b -flavored hadrons (rev.)	814
73. Polarization in B decays (rev.)	824
74. $B^0-\bar{B}^0$ mixing (rev.)	828
75. Semileptonic B decays, V_{cb} and V_{ub} (rev.)	835
76. CKM angles from B hadrons, Determination of (new)	849
77. Spectroscopy of mesons containing two heavy quarks (rev.)	854
78. Non- $q\bar{q}$ mesons (rev.)	861

Baryons

79. Baryon decay parameters	868
80. N and Δ resonances (rev.)	869
81. Baryon magnetic moments	874
82. Λ and Σ resonances (rev.)	875
83. Pole structure of the $\Lambda(1405)$ region (rev.)	878
84. Charmed baryons (rev.)	879
85. Pentaquarks (rev.)	881

Notes in Volume 2

Extraction of triple gauge couplings (TGC's)	1017
Anomalous $ZZ\gamma$, $Z\gamma\gamma$, and ZZV couplings	1042
Anomalous W/Z quartic couplings	1043
Neutrino properties (rev.)	1135
Sum of neutrino masses (rev.)	1138
Number of light neutrino types from collider experiments	1143
Neutrinoless double- β decay (rev.)	1145
Three-neutrino mixing parameters (rev.)	1155
$\rho(770)$ (rev.)	1221
$\rho(1450)$ and the $\rho(1700)$ (rev.)	1302
Charged kaon mass	1337
Dalitz plot parameters for $K \rightarrow 3\pi$ decays	1345
$K_{\ell 3}^{\pm}$ and $K_{\ell 3}^0$ form factors	1347
CP -violation in $K_S \rightarrow 3\pi$	1357
Heavy Flavor Averaging Group (rev.)	1465
Charmonium system (rev.)	1668
Branching ratios of $\psi(2S)$ and $\chi_{c0,1,2}$ (rev.)	1698
Bottomonium system (rev.)	1782
Width determination of the Υ states	1782
$\Sigma(1670)$ region	1938
Radiative hyperon decays	1960
Ξ resonances	1964

53. Mass and Width of the W Boson

Revised June 2019 by M.W. Grünewald (U. College Dublin) and A. Gurtu (Kyung Hee U.).

Precision determination of the W-mass is of great importance in testing the internal consistency of the Standard Model. From the time of its discovery in 1983, the W-boson has been studied and its mass determined in $p\bar{p}$ and e^+e^- interactions; it is currently studied in pp interactions at the LHC. The W mass and width definition used here corresponds to a Breit-Wigner with mass-dependent width.

Production of on-shell W bosons at hadron colliders is tagged by the high p_T charged lepton from its decay. Owing to the unknown parton-parton effective energy and missing energy in the longitudinal direction, the collider experiments reconstruct the transverse mass of the W, and derive the W mass from comparing the transverse mass distribution with Monte Carlo predictions as a function of M_W . These analyses use the electron and muon decay modes of the W boson.

In the e^+e^- collider (LEP) a precise knowledge of the beam energy enables one to determine the $e^+e^- \rightarrow W^+W^-$ cross section as a function of center of mass energy, as well as to reconstruct the W mass precisely from its decay products, even if one of them decays leptonically. Close to the W^+W^- threshold (161 GeV), the dependence of the W-pair production cross section on M_W is large, and this was used to determine M_W . At higher energies (172 to 209 GeV) this dependence is much weaker and W-bosons were directly reconstructed and the mass determined as the invariant mass of its decay products, improving the resolution with a kinematic fit.

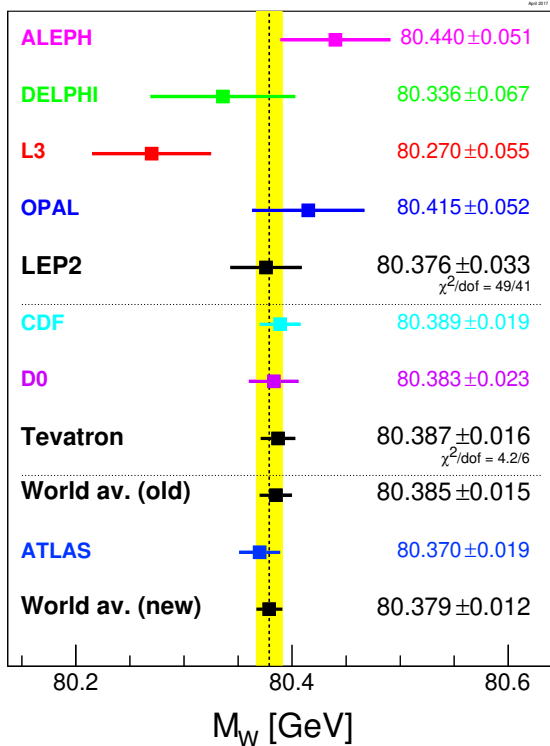


Figure 53.1: Measurements of the W-boson mass by the LEP, Tevatron and LHC experiments.

In order to compute the LEP average W mass, each experiment provided its measured W mass for the $q\bar{q}q\bar{q}$ and $q\bar{q}l\bar{\nu}_\ell$, $\ell = e, \mu, \tau$ channels at each center-of-mass energy, along with a detailed break-up of errors: statistical, uncorrelated, partially correlated and fully correlated systematics [1]. These have been combined to obtain a LEP W mass of $M_W = 80.376 \pm 0.033$ GeV. Errors due to uncertainties in LEP energy (9 MeV), and possible effect of color reconnection (CR) and Bose-Einstein correlations (BEC) between quarks from different W's (8 MeV) are included. The mass difference between $q\bar{q}q\bar{q}$ and

$q\bar{q}l\bar{\nu}_\ell$ final states (due to possible CR and BEC effects) is -12 ± 45 MeV. In a similar manner, the width results obtained at LEP have been combined, resulting in $\Gamma_W = 2.195 \pm 0.083$ GeV [1].

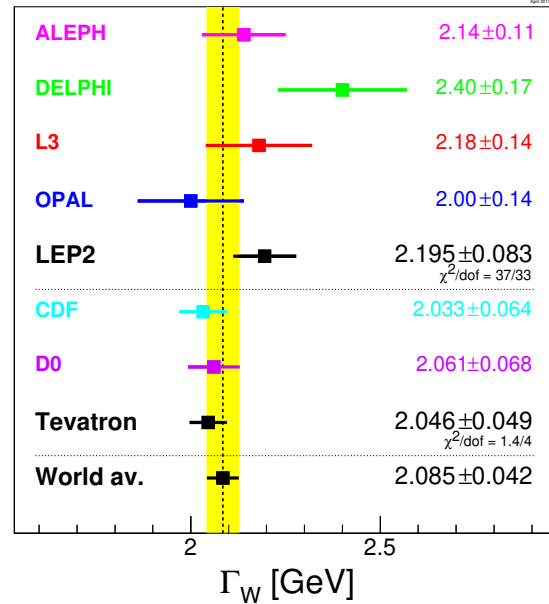


Figure 53.2: Measurements of the W-boson width by the LEP and Tevatron experiments.

The two Tevatron experiments have also identified common systematic errors. Between the two experiments, uncertainties due to the parton distribution functions, radiative corrections, and choice of mass (width) in the width (mass) measurements are treated as correlated. An average W width of $\Gamma_W = 2.046 \pm 0.049$ GeV [2] is obtained. Errors of 20 MeV and 7 MeV accounting for PDF and radiative correction uncertainties in this width combination dominate the correlated uncertainties. At the 2011/12 winter conferences, the CDF and D0 experiments have presented new results for the mass of the W boson based on $2 - 4 \text{ fb}^{-1}$ of Run-II data, 80.387 ± 0.019 GeV [3] and 80.375 ± 0.023 GeV [4], respectively. The W-mass determination from the Tevatron experiments has thus become very precise. Combining all Tevatron results from Run-I and Run-II using an improved treatment of correlations, a new average of 80.387 ± 0.016 GeV is obtained [5], with common uncertainties of 10 MeV (PDF) and 4 MeV (radiative corrections).

Good agreement between the LEP and Tevatron results is observed. Combining these results, assuming no common systematic uncertainties between the LEP and the Tevatron measurements, yields an average W mass of $M_W = 80.385 \pm 0.015$ GeV and a W width of $\Gamma_W = 2.085 \pm 0.042$ GeV.

At the 2016/17 winter conferences, the ATLAS collaboration presented a measurement of the mass of the W boson in pp collisions at $\sqrt{s} = 7$ TeV, $M_W = 80.370 \pm 0.019$ GeV, since then published [6], which is compatible with the above world average and of similar precision to the best measurements of CDF and D0. Assuming a Tevatron/LHC common PDF uncertainty of 7 MeV [7], this results in a new world average of $M_W = 80.379 \pm 0.012$ GeV.

The LEP, Tevatron and LHC results on mass and width, which are based on all results available, are compared in Fig. 53.1 and Fig. 53.2. The Standard Model prediction from the electroweak fit, including Z-pole data and m_{top} and M_H measurements, gives a W-boson mass of $M_W = 80.354 \pm 0.007$ GeV and a W-boson width of $\Gamma_W = 2.091 \pm 0.001$ GeV [8].

References:

1. The LEP Collaborations: ALEPH, DELPHI, L3, OPAL, the LEP Electroweak Working Group, CERN-PH-EP/2013-022, [arXiv:1302.3415 \[hep-ex\]](https://arxiv.org/abs/1302.3415), Phys.Rept. 532 (2013) 119-244.
2. The Tevatron Electroweak Working Group, for the CDF and D0 Collaborations: *Combination of CDF and D0 Results on the Width of the W Boson*, March 2010, [arXiv:1003.2826 \[hep-ex\]](https://arxiv.org/abs/1003.2826).
3. The CDF Collaboration, *Precise measurement of the W-boson mass with the CDF II detector*, [arXiv:1203.0275 \[hep-ex\]](https://arxiv.org/abs/1203.0275), Phys. Rev. Lett. **108**, 151803 (2012).
4. The D0 Collaboration, *Measurement of the W Boson Mass with the D0 Detector*, [arXiv:1203.0293 \[hep-ex\]](https://arxiv.org/abs/1203.0293), Phys. Rev. Lett. **108**, 151804 (2012).
5. The CDF and D0 Collabs: *Combination of CDF and D0 W-Boson Mass Measurements*, July 2013, [arXiv:1307.7627 \[hep-ex\]](https://arxiv.org/abs/1307.7627), Phys. Rev. **D88**, 052018 (2013).
6. The ATLAS Collaboration, *Measurement of the W-boson mass in pp collisions at $\sqrt{s} = 7$ TeV with the ATLAS detector*, January 2017, [arXiv:1701.07240 \[hep-ex\]](https://arxiv.org/abs/1701.07240), Eur.Phys.J. C78 (2018) no.2, 110.
7. Jens Erler, *Precision in EW measurements at Run 2 and beyond*, Talk presented at the 52nd Rencontres de Moriond EW, March 2017.
8. J. Haller et al., *Update of the global electroweak fit and constraints on two-Higgs-doublet models*, Eur. Phys. J. C78, 675 (2018).

54. Z Boson

Revised September 2013 by M.W. Gr unewald (U. College Dublin and U. Ghent) and A. Gurtu (Formerly Tata Inst.).

Precision measurements at the Z -boson resonance using electron–positron colliding beams began in 1989 at the SLC and at LEP. During 1989–95, the four LEP experiments (ALEPH, DELPHI, L3, OPAL) made high-statistics studies of the production and decay properties of the Z . Although the SLD experiment at the SLC collected much lower statistics, it was able to match the precision of LEP experiments in determining the effective electroweak mixing angle $\sin^2\bar{\theta}_W$ and the rates of Z decay to b - and c -quarks, owing to availability of polarized electron beams, small beam size, and stable beam spot.

The Z -boson properties reported in this section may broadly be categorized as:

- The standard ‘lineshape’ parameters of the Z consisting of its mass, M_Z , its total width, Γ_Z , and its partial decay widths, $\Gamma(\text{hadrons})$, and $\Gamma(\ell\bar{\ell})$ where $\ell = e, \mu, \tau, \nu$;
- Z asymmetries in leptonic decays and extraction of Z couplings to charged and neutral leptons;
- The b - and c -quark-related partial widths and charge asymmetries which require special techniques;
- Determination of Z decay modes and the search for modes that violate known conservation laws;
- Average particle multiplicities in hadronic Z decay;
- Z anomalous couplings.

The effective vector and axial-vector coupling constants describing the Z -to-fermion coupling are also measured in $p\bar{p}$ and ep collisions at the Tevatron and at HERA. The corresponding cross-section formulae are given in Section 39 (Cross-section formulae for specific processes) and Section 16 (Structure Functions) in this *Review*. In this minireview, we concentrate on the measurements in e^+e^- collisions at LEP and SLC.

The standard ‘lineshape’ parameters of the Z are determined from an analysis of the production cross sections of these final states in e^+e^- collisions. The $Z \rightarrow \nu\bar{\nu}(\gamma)$ state is identified directly by detecting single photon production and indirectly by subtracting the visible partial widths from the total width. Inclusion in this analysis of the forward-backward asymmetry of charged leptons, $A_{FB}^{(0,\ell)}$, of the τ polarization, $P(\tau)$, and its forward-backward asymmetry, $P(\tau)^{fb}$, enables the separate determination of the effective vector (\bar{g}_V) and axial vector (\bar{g}_A) couplings of the Z to these leptons and the ratio (\bar{g}_V/\bar{g}_A), which is related to the effective electroweak mixing angle $\sin^2\bar{\theta}_W$ (see the ‘‘Electroweak Model and Constraints on New Physics’’ review).

Determination of the b - and c -quark-related partial widths and charge asymmetries involves tagging the b and c quarks for which various methods are employed: requiring the presence of a high momentum prompt lepton in the event with high transverse momentum with respect to the accompanying jet; impact parameter and lifetime tagging using precision vertex measurement with high-resolution detectors; application of neural-network techniques to classify events as b or non- b on a statistical basis using event–shape variables; and using the presence of a charmed meson (D/D^*) or a kaon as a tag.

54.1. Z -parameter determination

LEP was run at energy points on and around the Z mass (88–94 GeV) constituting an energy ‘scan.’ The shape of the cross-section variation around the Z peak can be described by a Breit-Wigner ansatz with an energy-dependent total width [1–3]. The **three** main properties of this distribution, viz., the **position** of the peak, the **width** of the distribution, and the **height** of the peak, determine respectively the values of M_Z , Γ_Z , and $\Gamma(e^+e^-) \times \Gamma(f\bar{f})$, where $\Gamma(e^+e^-)$ and $\Gamma(f\bar{f})$ are the electron and fermion partial widths of the Z . The quantitative determination of these parameters is done by writing analytic expressions for these cross sections in terms of the parameters, and fitting the calculated cross sections to the measured ones by varying these parameters, taking properly into account all the

errors. Single-photon exchange (σ_γ^0) and γ - Z interference ($\sigma_{\gamma Z}^0$) are included, and the large ($\sim 25\%$) initial-state radiation (ISR) effects are taken into account by convoluting the analytic expressions over a ‘Radiator Function’ [1–5] $H(s, s')$. Thus for the process $e^+e^- \rightarrow f\bar{f}$:

$$\sigma_f(s) = \int H(s, s') \sigma_f^0(s') ds' \quad (54.1)$$

$$\sigma_f^0(s) = \sigma_Z^0 + \sigma_\gamma^0 + \sigma_{\gamma Z}^0 \quad (54.2)$$

$$\sigma_Z^0 = \frac{12\pi}{M_Z^2} \frac{\Gamma(e^+e^-)\Gamma(f\bar{f})}{\Gamma_Z^2} \frac{s \Gamma_Z^2}{(s - M_Z^2)^2 + s^2\Gamma_Z^2/M_Z^2} \quad (54.3)$$

$$\sigma_\gamma^0 = \frac{4\pi\alpha^2(s)}{3s} Q_f^2 N_c^f \quad (54.4)$$

$$\begin{aligned} \sigma_{\gamma Z}^0 = & -\frac{2\sqrt{2}\alpha(s)}{3} (Q_f G_F N_c^f \mathcal{G}_V^f \mathcal{G}_V^f) \\ & \times \frac{(s - M_Z^2)M_Z^2}{(s - M_Z^2)^2 + s^2\Gamma_Z^2/M_Z^2} \end{aligned} \quad (54.5)$$

where Q_f is the charge of the fermion, $N_c^f = 3$ for quarks and 1 for leptons, and \mathcal{G}_V^f is the vector coupling of the Z to the fermion-antifermion pair $f\bar{f}$.

Since $\sigma_{\gamma Z}^0$ is expected to be much less than σ_Z^0 , the LEP Collaborations have generally calculated the interference term in the framework of the Standard Model. This fixing of $\sigma_{\gamma Z}^0$ leads to a tighter constraint on M_Z , and consequently a smaller error on its fitted value. It is possible to relax this constraint and carry out the fit within the S-matrix framework, which is briefly described in the next section.

In the above framework, the QED radiative corrections have been explicitly taken into account by convoluting over the ISR and allowing the electromagnetic coupling constant to run [6]: $\alpha(s) = \alpha/(1 - \Delta\alpha)$. On the other hand, weak radiative corrections that depend upon the assumptions of the electroweak theory and on the values of M_{top} and M_{Higgs} are accounted for by **absorbing them into the couplings**, which are then called the *effective* couplings \mathcal{G}_V and \mathcal{G}_A (or alternatively the effective parameters of the $*$ scheme of Kennedy and Lynn [7].)

\mathcal{G}_V^f and \mathcal{G}_A^f are complex numbers with small imaginary parts. As experimental data does not allow simultaneous extraction of both real and imaginary parts of the effective couplings, the convention $g_A^f = \text{Re}(\mathcal{G}_A^f)$ and $g_V^f = \text{Re}(\mathcal{G}_V^f)$ is used and the imaginary parts are added in the fitting code [4].

Defining

$$A_f = 2 \frac{g_V^f \cdot g_A^f}{(g_V^f)^2 + (g_A^f)^2} \quad (54.6)$$

the lowest-order expressions for the various lepton-related asymmetries on the Z pole are [8–10] $A_{FB}^{(0,\ell)} = (3/4)A_e A_f$, $P(\tau) = -A_\tau$, $P(\tau)^{fb} = -(3/4)A_e$, $A_{LR} = A_e$. The full analysis takes into account the energy-dependence of the asymmetries. Experimentally A_{LR} is defined as $(\sigma_L - \sigma_R)/(\sigma_L + \sigma_R)$, where $\sigma_{L(R)}$ are the $e^+e^- \rightarrow Z$ production cross sections with left- (right)-handed electrons.

The definition of the partial decay width of the Z to $f\bar{f}$ includes the effects of QED and QCD final-state corrections, as well as the contribution due to the imaginary parts of the couplings:

$$\Gamma(f\bar{f}) = \frac{G_F M_Z^3}{6\sqrt{2}\pi} N_c^f (|\mathcal{G}_A^f|^2 R_A^f + |\mathcal{G}_V^f|^2 R_V^f) + \Delta_{ew/\text{QCD}} \quad (54.7)$$

where R_V^f and R_A^f are radiator factors to account for final state QED and QCD corrections, as well as effects due to nonzero fermion masses, and $\Delta_{ew/\text{QCD}}$ represents the non-factorizable electroweak/QCD corrections.

54.2. S-matrix approach to the Z

While most experimental analyses of LEP/SLC data have followed the ‘Breit-Wigner’ approach, an alternative S-matrix-based analysis is also possible. The Z, like all unstable particles, is associated with a complex pole in the S matrix. The pole position is process-independent and gauge-invariant. The mass, \overline{M}_Z , and width, $\overline{\Gamma}_Z$, can be defined in terms of the pole in the energy plane via [11–14]

$$\overline{s} = \overline{M}_Z^2 - i\overline{M}_Z\overline{\Gamma}_Z \quad (54.8)$$

leading to the relations

$$\begin{aligned} \overline{M}_Z &= M_Z / \sqrt{1 + \Gamma_Z^2 / M_Z^2} \\ &\approx M_Z - 34.1 \text{ MeV} \end{aligned} \quad (54.9)$$

$$\begin{aligned} \overline{\Gamma}_Z &= \Gamma_Z / \sqrt{1 + \Gamma_Z^2 / M_Z^2} \\ &\approx \Gamma_Z - 0.9 \text{ MeV} . \end{aligned} \quad (54.10)$$

The LEP collaborations [15] have analyzed their data using the S-matrix approach as defined in Eq. (54.8), in addition to the conventional one. They observe a downward shift in the Z mass as expected.

54.3. Handling the large-angle e^+e^- final state

Unlike other $f\overline{f}$ decay final states of the Z, the e^+e^- final state has a contribution not only from the s-channel but also from the t-channel and s-t interference. The full amplitude is not amenable to fast calculation, which is essential if one has to carry out minimization fits within reasonable computer time. The usual procedure is to calculate the non-s channel part of the cross section separately using the Standard Model programs ALIBABA [16] or TOPAZ0 [17], with the measured value of M_{top} , and $M_{\text{Higgs}} = 150 \text{ GeV}$, and add it to the s-channel cross section calculated as for other channels. This leads to two additional sources of error in the analysis: firstly, the theoretical calculation in ALIBABA itself is known to be accurate to $\sim 0.5\%$, and secondly, there is uncertainty due to the error on M_{top} and the unknown value of M_{Higgs} (100–1000 GeV). These errors are propagated into the analysis by including them in the systematic error on the e^+e^- final state. As these errors are common to the four LEP experiments, this is taken into account when performing the LEP average.

54.4. Errors due to uncertainty in LEP energy determination

The systematic errors related to the LEP energy measurement, see Refs. 18–23, can be classified as:

- The absolute energy scale error;
- Energy-point-to-energy-point errors due to the nonlinear response of the magnets to the exciting currents;
- Energy-point-to-energy-point errors due to possible higher-order effects in the relationship between the dipole field and beam energy;
- Energy reproducibility errors due to various unknown uncertainties in temperatures, tidal effects, corrector settings, RF status, etc.

Precise energy calibration was done outside normal data-taking using the resonant depolarization technique. Run-time energies were determined every 10 minutes by measuring the relevant machine parameters and using a model which takes into account all the known effects, including leakage currents produced by trains in the Geneva area and the tidal effects due to gravitational forces of the Sun and the Moon. The LEP Energy Working Group has provided a covariance matrix from the determination of LEP energies for the different running periods during 1993–1995 [18].

54.5. Choice of fit parameters

The LEP Collaborations have chosen the following primary set of parameters for fitting: M_Z , Γ_Z , σ_{hadron}^0 , $R(\text{lepton})$, $A_{FB}^{(0,\ell)}$, where $R(\text{lepton}) = \Gamma(\text{hadrons})/\Gamma(\text{lepton})$, $\sigma_{\text{hadron}}^0 = 12\pi\Gamma(e^+e^-)\Gamma(\text{hadrons})/M_Z^2\Gamma_Z^2$. With a knowledge of these fitted parameters and their covariance matrix, any other parameter can be derived. The main advantage of these parameters is that they form a physics motivated set of parameters with much reduced correlations.

Thus, the most general fit carried out to cross section and asymmetry data determines the **nine parameters**: M_Z , Γ_Z , σ_{hadron}^0 , $R(e)$, $R(\mu)$, $R(\tau)$, $A_{FB}^{(0,e)}$, $A_{FB}^{(0,\mu)}$, $A_{FB}^{(0,\tau)}$. Assumption of lepton universality leads to a **five-parameter fit** determining M_Z , Γ_Z , σ_{hadron}^0 , $R(\text{lepton})$, $A_{FB}^{(0,\ell)}$.

54.6. Combining results from LEP and SLC experiments

With a steady increase in statistics over the years and improved understanding of the common systematic errors between LEP experiments, the procedures for combining results have evolved continuously [24]. The Line Shape Sub-group of the LEP Electroweak Working Group investigated the effects of these common errors, and devised a combination procedure for the precise determination of the Z parameters from LEP experiments. Using these procedures, this note also gives the results after combining the final parameter sets from the four experiments, and these are the results quoted as the fit results in the Z listings below. Transformation of variables leads to values of derived parameters like partial decay widths and branching ratios to hadrons and leptons. Finally, transforming the LEP combined nine parameter set to $(M_Z, \Gamma_Z, \sigma_{\text{hadron}}^0, g_A^f, g_V^f, f = e, \mu, \tau)$ using the average values of lepton asymmetry parameters (A_e, A_μ, A_τ) as constraints, leads to the best fitted values of the vector and axial-vector couplings (g_V, g_A) of the charged leptons to the Z.

Brief remarks on the handling of common errors and their magnitudes are given below. The identified common errors are those coming from

- LEP energy-calibration uncertainties, and
- the theoretical uncertainties in (i) the luminosity determination using small angle Bhabha scattering, (ii) estimating the non-s channel contribution to large angle Bhabha scattering, (iii) the calculation of QED radiative effects, and (iv) the parametrization of the cross section in terms of the parameter set used.

54.7. Common LEP energy errors

All the collaborations incorporate in their fit the full LEP energy error matrix as provided by the LEP energy group for their intersection region [18]. The effect of these errors is separated out from that of other errors by carrying out fits with energy errors scaled up and down by $\sim 10\%$ and redoing the fits. From the observed changes in the overall error matrix, the covariance matrix of the common energy errors is determined. Common LEP energy errors lead to uncertainties on M_Z , Γ_Z , and σ_{hadron}^0 of 1.7, 1.2 MeV, and 0.011 nb, respectively.

54.8. Common luminosity errors

BHLUMI 4.04 [25] is used by all LEP collaborations for small-angle Bhabha scattering leading to a common uncertainty in their measured cross sections of 0.061% [26]. BHLUMI does not include a correction for production of light fermion pairs. OPAL explicitly corrects for this effect and reduces their luminosity uncertainty to 0.054%, which is taken fully correlated with the other experiments. The other three experiments among themselves have a common uncertainty of 0.061%.

54.9. Common non-*s* channel uncertainties

The same standard model programs ALIBABA [16] and TOPAZ0 [17] are used to calculate the non-*s* channel contribution to the large angle Bhabha scattering [27]. As this contribution is a function of the *Z* mass, which itself is a variable in the fit, it is parametrized as a function of M_Z by each collaboration to properly track this contribution as M_Z varies in the fit. The common errors on R_e and $A_{FB}^{(0,e)}$ are 0.024 and 0.0014 respectively, and are correlated between them.

54.10. Common theoretical uncertainties: QED

There are large initial-state photon and fermion pair radiation effects near the *Z* resonance, for which the best currently available evaluations include contributions up to $\mathcal{O}(\alpha^3)$. To estimate the remaining uncertainties, different schemes are incorporated in the standard model programs ZFITTER [5], TOPAZ0 [17], and MIZA [28]. Comparing the different options leads to error estimates of 0.3 and 0.2 MeV on M_Z and Γ_Z respectively, and of 0.02% on $\sigma_{\text{hadron}}^\circ$.

54.11. Common theoretical uncertainties: parametrization of lineshape and asymmetries

To estimate uncertainties arising from ambiguities in the model-independent parametrization of the differential cross-section near the *Z* resonance, results from TOPAZ0 and ZFITTER were compared by using ZFITTER to fit the cross sections and asymmetries calculated using TOPAZ0. The resulting uncertainties on M_Z , Γ_Z , $\sigma_{\text{hadron}}^\circ$, $R(\text{lepton})$, and $A_{FB}^{(0,\ell)}$ are 0.1 MeV, 0.1 MeV, 0.001 nb, 0.004, and 0.0001 respectively.

Thus, the overall theoretical errors on M_Z , Γ_Z , $\sigma_{\text{hadron}}^\circ$ are 0.3 MeV, 0.2 MeV, and 0.008 nb respectively; on each $R(\text{lepton})$ is 0.004 and on each $A_{FB}^{(0,\ell)}$ is 0.0001. Within the set of three $R(\text{lepton})$'s and the set of three $A_{FB}^{(0,\ell)}$'s, the respective errors are fully correlated.

All the theory-related errors mentioned above utilize Standard Model programs which need the Higgs mass and running electromagnetic coupling constant as inputs; uncertainties on these inputs will also lead to common errors. All LEP collaborations used the same set of inputs for Standard Model calculations: $M_Z = 91.187$ GeV, the Fermi constant $G_F = (1.16637 \pm 0.00001) \times 10^{-5}$ GeV⁻² [29], $\alpha^{(5)}(M_Z) = 1/128.877 \pm 0.090$ [30], $\alpha_s(M_Z) = 0.119$ [31], $M_{\text{top}} = 174.3 \pm 5.1$ GeV [31] and $M_{\text{Higgs}} = 150$ GeV. The only observable effect, on M_Z , is due to the variation of M_{Higgs} between 100–1000 GeV (due to the variation of the γ/Z interference term which is taken from the Standard Model): M_Z changes by +0.23 MeV per unit change in $\log_{10} M_{\text{Higgs}}/\text{GeV}$, which is not an error but a correction to be applied once M_{Higgs} is determined. The effect is much smaller than the error on M_Z (± 2.1 MeV).

54.12. Methodology of combining the LEP experimental results

The LEP experimental results actually used for combination are slightly modified from those published by the experiments (which are given in the Listings below). This has been done in order to facilitate the procedure by making the inputs more consistent. These modified results are given explicitly in [24]. The main differences compared to the published results are (a) consistent use of ZFITTER 6.23 and TOPAZ0 (the published ALEPH results used ZFITTER 6.10); (b) use of the combined energy-error matrix, which makes a difference of 0.1 MeV on the M_Z and Γ_Z for L3 only as at that intersection the RF modeling uncertainties are the largest.

Thus, nine-parameter sets from all four experiments with their covariance matrices are used together with all the common errors correlations. A grand covariance matrix, V , is constructed and a combined nine-parameter set is obtained by minimizing $\chi^2 = \Delta^T V^{-1} \Delta$, where Δ is the vector of residuals of the combined parameter set to the results of individual experiments. Imposing

lepton universality in the combination results in the combined five parameter set.

54.13. Study of $Z \rightarrow b\bar{b}$ and $Z \rightarrow c\bar{c}$

In the sector of *c*- and *b*-physics, the LEP experiments have measured the ratios of partial widths $R_b = \Gamma(Z \rightarrow b\bar{b})/\Gamma(Z \rightarrow \text{hadrons})$, and $R_c = \Gamma(Z \rightarrow c\bar{c})/\Gamma(Z \rightarrow \text{hadrons})$, and the forward-backward (charge) asymmetries $A_{FB}^{b\bar{b}}$ and $A_{FB}^{c\bar{c}}$. The SLD experiment at SLC has measured the ratios R_c and R_b and, utilizing the polarization of the electron beam, was able to obtain the final state coupling parameters A_b and A_c from a measurement of the left-right forward-backward asymmetry of *b*- and *c*-quarks. The high precision measurement of R_c at SLD was made possible owing to the small beam size and very stable beam spot at SLC, coupled with a highly precise CCD pixel detector. Several of the analyses have also determined other quantities, in particular the semileptonic branching ratios, $B(b \rightarrow \ell^-)$, $B(b \rightarrow c \rightarrow \ell^+)$, and $B(c \rightarrow \ell^+)$, the average time-integrated $B^0\bar{B}^0$ mixing parameter $\bar{\chi}$ and the probabilities for a *c*-quark to fragment into a D^+ , a D_s , a D^{*+} , or a charmed baryon. The latter measurements do not concern properties of the *Z* boson, and hence they do not appear in the Listing below. However, for completeness, we will report at the end of this minireview their values as obtained fitting the data contained in the *Z* section. All these quantities are correlated with the electroweak parameters, and since the mixture of *b* hadrons is different from the one at the $\Upsilon(4S)$, their values might differ from those measured at the $\Upsilon(4S)$.

All the above quantities are correlated to each other since:

- Several analyses (for example the lepton fits) determine more than one parameter simultaneously;
- Some of the electroweak parameters depend explicitly on the values of other parameters (for example R_b depends on R_c);
- Common tagging and analysis techniques produce common systematic uncertainties.

The LEP Electroweak Heavy Flavour Working Group has developed [32] a procedure for combining the measurements taking into account known sources of correlation. The combining procedure determines fourteen parameters: the six parameters of interest in the electroweak sector, R_b , R_c , $A_{FB}^{b\bar{b}}$, $A_{FB}^{c\bar{c}}$, A_b and A_c and, in addition, $B(b \rightarrow \ell^-)$, $B(b \rightarrow c \rightarrow \ell^+)$, $B(c \rightarrow \ell^+)$, $\bar{\chi}$, $f(D^+)$, $f(D_s)$, $f(c_{\text{baryon}})$ and $P(c \rightarrow D^{*+}) \times B(D^{*+} \rightarrow \pi^+ D^0)$, to take into account their correlations with the electroweak parameters. Before the fit both the peak and off-peak asymmetries are translated to the common energy $\sqrt{s} = 91.26$ GeV using the predicted energy-dependence from ZFITTER [5].

54.14. Summary of the measurements and of the various kinds of analysis

The measurements of R_b and R_c fall into two classes. In the first, named single-tag measurement, a method for selecting *b* and *c* events is applied and the number of tagged events is counted. A second technique, named double-tag measurement, has the advantage that the tagging efficiency is directly derived from the data thereby reducing the systematic error on the measurement.

The measurements in the *b*- and *c*-sector can be essentially grouped in the following categories:

- Lifetime (and lepton) double-tagging measurements of R_b . These are the most precise measurements of R_b and obviously dominate the combined result. The main sources of systematics come from the charm contamination and from estimating the hemisphere *b*-tagging efficiency correlation;
- Analyses with $D/D^{*\pm}$ to measure R_c . These measurements make use of several different tagging techniques (inclusive/exclusive double tag, exclusive double tag, reconstruction of all weakly decaying charmed states) and no assumptions are made on the energy-dependence of charm fragmentation;
- A measurement of R_c using single leptons and assuming $B(b \rightarrow c \rightarrow \ell^+)$;

- Lepton fits which use hadronic events with one or more leptons in the final state to measure the asymmetries $A_{FB}^{b\bar{b}}$ and $A_{FB}^{c\bar{c}}$. Each analysis usually gives several other electroweak parameters. The dominant sources of systematics are due to lepton identification, to other semileptonic branching ratios and to the modeling of the semileptonic decay;
- Measurements of $A_{FB}^{b\bar{b}}$ using lifetime tagged events with a hemisphere charge measurement. These measurements dominate the combined result;
- Analyses with $D/D^{*\pm}$ to measure $A_{FB}^{c\bar{c}}$ or simultaneously $A_{FB}^{b\bar{b}}$ and $A_{FB}^{c\bar{c}}$;
- Measurements of A_b and A_c from SLD, using several tagging methods (lepton, kaon, D/D^* , and vertex mass). These quantities are directly extracted from a measurement of the left–right forward–backward asymmetry in $c\bar{c}$ and $b\bar{b}$ production using a polarized electron beam.

54.15. Averaging procedure

All the measurements are provided by the LEP and SLD Collaborations in the form of tables with a detailed breakdown of the systematic errors of each measurement and its dependence on other electroweak parameters.

The averaging proceeds via the following steps:

- Define and propagate a consistent set of external inputs such as branching ratios, hadron lifetimes, fragmentation models *etc.* All the measurements are checked to ensure that all use a common set of assumptions (for instance, since the QCD corrections for the forward–backward asymmetries are strongly dependent on the experimental conditions, the data are corrected before combining);
- Form the full (statistical and systematic) covariance matrix of the measurements. The systematic correlations between different analyses are calculated from the detailed error breakdown in the measurement tables. The correlations relating several measurements made by the same analysis are also used;
- Take into account any explicit dependence of a measurement on the other electroweak parameters. As an example of this dependence, we illustrate the case of the double-tag measurement of R_b , where c -quarks constitute the main background. The normalization of the charm contribution is not usually fixed by the data and the measurement of R_b depends on the assumed value of R_c , which can be written as:

$$R_b = R_b^{\text{meas}} + a(R_c) \frac{(R_c - R_c^{\text{used}})}{R_c}, \quad (54.11)$$

where R_b^{meas} is the result of the analysis which assumed a value of $R_c = R_c^{\text{used}}$ and $a(R_c)$ is the constant which gives the dependence on R_c ;

- Perform a χ^2 minimization with respect to the combined electroweak parameters.

After the fit the average peak asymmetries $A_{FB}^{c\bar{c}}$ and $A_{FB}^{b\bar{b}}$ are corrected for the energy shift from 91.26 GeV to M_Z and for QED (initial state radiation), γ exchange, and γZ interference effects, to obtain the corresponding pole asymmetries $A_{FB}^{0,c}$ and $A_{FB}^{0,b}$.

This averaging procedure, using the fourteen parameters described above, and applied to the data contained in the Z particle listing below, gives the following results (where the last 8 parameters do not depend directly on the Z):

$$\begin{aligned} R_b^0 &= 0.21629 \pm 0.00066 \\ R_c^0 &= 0.1721 \pm 0.0030 \\ A_{FB}^{0,b} &= 0.0992 \pm 0.0016 \\ A_{FB}^{0,c} &= 0.0707 \pm 0.0035 \end{aligned}$$

$$A_b = 0.923 \pm 0.020$$

$$A_c = 0.670 \pm 0.027$$

$$B(b \rightarrow \ell^-) = 0.1071 \pm 0.0022$$

$$B(b \rightarrow c \rightarrow \ell^+) = 0.0801 \pm 0.0018$$

$$B(c \rightarrow \ell^+) = 0.0969 \pm 0.0031$$

$$\bar{\chi} = 0.1250 \pm 0.0039$$

$$f(D^+) = 0.235 \pm 0.016$$

$$f(D_s) = 0.126 \pm 0.026$$

$$f(c_{\text{baryon}}) = 0.093 \pm 0.022$$

$$P(c \rightarrow D^{*+}) \times B(D^{*+} \rightarrow \pi^+ D^0) = 0.1622 \pm 0.0048$$

Among the non–electroweak observables, the B semileptonic branching fraction $B(b \rightarrow \ell^-)$ is of special interest, since the dominant error source on this quantity is the dependence on the semileptonic decay model for $b \rightarrow \ell^-$, with $\Delta B(b \rightarrow \ell^-)_{b \rightarrow \ell^- \text{-model}} = 0.0012$. Extensive studies have been made to understand the size of this error. Among the electroweak quantities, the quark asymmetries with leptons depend also on the semileptonic decay model, while the asymmetries using other methods usually do not. The fit implicitly requires that the different methods give consistent results and this effectively constrains the decay model, and thus reduces in principle the error from this source in the fit result.

To obtain a conservative estimate of the modelling error, the above fit has been repeated removing all asymmetry measurements. The results of the fit on B–decay related observables are [24]: $B(b \rightarrow \ell^-) = 0.1069 \pm 0.0022$, with $\Delta B(b \rightarrow \ell^-)_{b \rightarrow \ell^- \text{-model}} = 0.0013$, $B(b \rightarrow c \rightarrow \ell^+) = 0.0802 \pm 0.0019$ and $\bar{\chi} = 0.1259 \pm 0.0042$.

References:

1. R.N. Cahn, Phys. Rev. **D36**, 2666 (1987).
2. F.A. Berends *et al.*, “Z Physics at LEP 1,” CERN Report 89-08 (1989), Vol. 1, eds. G. Altarelli, R. Kleiss, and C. Verzegnassi, p. 89.
3. A. Borrelli *et al.*, Nucl. Phys. **B333**, 357 (1990).
4. D. Bardin and G. Passarino, “Upgrading of Precision Calculations for Electroweak Observables,” hep-ph/9803425; D. Bardin, G. Passarino, and M. Grünewald, “Precision Calculation Project Report,” hep-ph/9902452.
5. D. Bardin *et al.*, Z. Phys. **C44**, 493 (1989); Comp. Phys. Comm. **59**, 303 (1990); D. Bardin *et al.*, Nucl. Phys. **B351**, 1 (1991); Phys. Lett. **B255**, 290 (1991), and CERN-TH/6443/92 (1992); Comp. Phys. Comm. **133**, 229 (2001).
6. G. Burgers *et al.*, “Z Physics at LEP 1,” CERN Report 89-08 (1989), Vol. 1, eds. G. Altarelli, R. Kleiss, and C. Verzegnassi, p. 55.
7. D.C. Kennedy and B.W. Lynn, Nucl. Phys. **B322**, 1 (1989).
8. M. Consoli *et al.*, “Z Physics at LEP 1,” CERN Report 89-08 (1989), Vol. 1, eds. G. Altarelli, R. Kleiss, and C. Verzegnassi, p. 7.
9. M. Böhm *et al.*, *ibid.*, p. 203.
10. S. Jadach *et al.*, *ibid.*, p. 235.
11. R. Stuart, Phys. Lett. **B262**, 113 (1991).
12. A. Sirlin, Phys. Rev. Lett. **67**, 2127 (1991).
13. A. Leike, T. Riemann, and J. Rose, Phys. Lett. **B273**, 513 (1991).
14. See also D. Bardin *et al.*, Phys. Lett. **B206**, 539 (1988).
15. The LEP Collaborations: ALEPH, DELPHI, L3, OPAL, the LEP Electroweak Working Group, CERN-PH-EP/2013-022, arXiv:1302.3415 [hep-ex], Phys.Rept. 532 (2013) 119-244.
16. W. Beenakker, F.A. Berends, and S.C. van der Marck, Nucl. Phys. **B349**, 323 (1991).

17. G. Montagna *et al.*, Nucl. Phys. **B401**, 3 (1993); Comp. Phys. Comm. **76**, 328 (1993); Comp. Phys. Comm. **93**, 120 (1996); G. Montagna *et al.*, Comp. Phys. Comm. **117**, 278 (1999).
18. R. Assmann *et al.*, (Working Group on LEP Energy), Eur. Phys. J. **C6**, 187 (1999).
19. R. Assmann *et al.*, (Working Group on LEP Energy), Z. Phys. **C66**, 567 (1995).
20. L. Arnaudon *et al.*, (Working Group on LEP Energy and LEP Collabs.), Phys. Lett. **B307**, 187 (1993).
21. L. Arnaudon *et al.*, (Working Group on LEP Energy), CERN-PPE/92-125 (1992).
22. L. Arnaudon *et al.*, Phys. Lett. **B284**, 431 (1992).
23. R. Bailey *et al.*, 'LEP Energy Calibration' CERN-SL-90-95-AP, *Proceedings of the "2nd European Particle Accelerator Conference*, Nice, France, 12–16 June 1990, pp. 1765-1767.
24. The LEP Collabs.: ALEPH, DELPHI, L3, OPAL, the LEP Electroweak Working Group, and the SLD Heavy Flavour Group: Phys. Reports **427**, 257 (2006).
25. S. Jadach *et al.*, BHLUMI 4.04, Comp. Phys. Comm. **102**, 229 (1997); S. Jadach and O. Nicosini, Event generators for Bhabha scattering, in Physics at LEP2, CERN-96-01 Vol. 2, February 1996.
26. B.F.L. Ward *et al.*, Phys. Lett. **B450**, 262 (1999).
27. W. Beenakker and G. Passarino, Phys. Lett. **B425**, 199 (1998).
28. M. Martinez *et al.*, Z. Phys. **C49**, 645 (1991); M. Martinez and F. Teubert, Z. Phys. **C65**, 267 (1995), updated with results summarized in S. Jadach, B. Pietrzyk, and M. Skrzypek, Phys. Lett. **B456**, 77 (1999) and Reports of the working group on precision calculations for the *Z* resonance, CERN 95-03, ed. D. Bardin, W. Hollik, and G. Passarino, and references therein.
29. T. van Ritbergen and R. Stuart, Phys. Lett. **B437**, 201 (1998); Phys. Rev. Lett. **82**, 488 (1999).
30. S. Eidelman and F. Jegerlehner, Z. Phys. **C67**, 585 (1995); M. Steinhauser, Phys. Lett. **B429**, 158 (1998).
31. Particle Data Group (D.E. Groom *et al.*), Eur. Phys. J. **C15**, 1 (2000).
32. The LEP Experiments: ALEPH, DELPHI, L3, and OPAL Nucl. Instrum. Methods **A378**, 101 (1996).

55. Muon Anomalous Magnetic Moment

Updated August 2019 by A. Hoecker (CERN) and W.J. Marciano (BNL).

The Dirac equation predicts a muon magnetic moment, $\vec{M} = g\mu \frac{e}{2m_\mu} \vec{S}$, with gyromagnetic ratio $g_\mu = 2$. Quantum loop effects lead to a small calculable deviation from $g_\mu = 2$, parameterized by the anomalous magnetic moment

$$a_\mu \equiv \frac{g_\mu - 2}{2}. \quad (55.1)$$

That quantity can be accurately measured and, within the Standard Model (SM) framework, precisely predicted. Hence, comparison of experiment and theory tests the SM at its quantum loop level. A deviation in a_μ^{exp} from the SM expectation would signal effects of new physics, with current sensitivity reaching up to mass scales of $\mathcal{O}(\text{TeV})$ [1,2]. For recent thorough muon $g - 2$ reviews, see e.g. Refs. [3–5].

The E821 experiment at Brookhaven National Lab (BNL) studied the precession of μ^+ and μ^- in a constant external magnetic field as they circulated in a confining storage ring. It found¹ [6]

$$\begin{aligned} a_{\mu^+}^{\text{exp}} &= 11\,659\,204(6)(5) \times 10^{-10}, \\ a_{\mu^-}^{\text{exp}} &= 11\,659\,215(8)(3) \times 10^{-10}, \end{aligned} \quad (55.2)$$

where the first errors are statistical and the second systematic. Assuming CPT invariance and taking into account correlations between systematic uncertainties, one finds for their average [6,7]

$$a_\mu^{\text{exp}} = 11\,659\,209.1(5.4)(3.3) \times 10^{-10}. \quad (55.3)$$

These results represent about a factor of 14 improvement over the classic CERN experiments of the 1970's [8]. Improvement of the measurement by a factor of four by setting up the E821 storage ring at Fermilab, and utilizing a cleaner and more intense muon beam and improved detectors [9] is in progress with the commissioning of the experiment having started in 2017. First results are expected in 2019. Another muon $g - 2$ experiment with similar sensitivity but using an alternative zero-electric-field technique with a low-emittance and low-momentum muon beam is currently under construction at J-PARC in Japan [10].

The SM prediction for a_μ^{SM} is generally divided into three parts (see Fig. 55.1 for representative Feynman diagrams)

$$a_\mu^{\text{SM}} = a_\mu^{\text{QED}} + a_\mu^{\text{EW}} + a_\mu^{\text{Had}}. \quad (55.4)$$

The QED part includes all photonic and leptonic (e, μ, τ) loops starting with the classic $\alpha/2\pi$ Schwinger contribution. It has been computed through 5 loops [11]

$$\begin{aligned} a_\mu^{\text{QED}} &= \frac{\alpha}{2\pi} + 0.765\,857\,425(17) \left(\frac{\alpha}{\pi}\right)^2 + 24.050\,509\,96(32) \left(\frac{\alpha}{\pi}\right)^3 \\ &\quad + 130.879\,6(6\,3) \left(\frac{\alpha}{\pi}\right)^4 + 752.2(1.0) \left(\frac{\alpha}{\pi}\right)^5 + \dots \end{aligned} \quad (55.5)$$

with little change in the coefficients since our last update of this review. Employing $\alpha^{-1} = 137.035\,999\,046(27)$, obtained from the precise measurements of h/m_{Cs} [12], the Rydberg constant, and m_{Cs}/m_e leads to [11]

$$a_\mu^{\text{QED}} = 116\,584\,718.92(0.03) \times 10^{-11}, \quad (55.6)$$

where the small error results mainly from the uncertainty in α .

¹ The results reported by the experiment have been updated in Eqs. (55.2) and (55.3) to the newest value for the absolute muon-to-proton magnetic ratio $\lambda = 3.183\,345\,107(84)$ [7]. The change induced in a_μ^{exp} with respect to the value of $\lambda = 3.183\,345\,39(10)$ used in Ref. 6 amounts to $+1.12 \times 10^{-10}$.

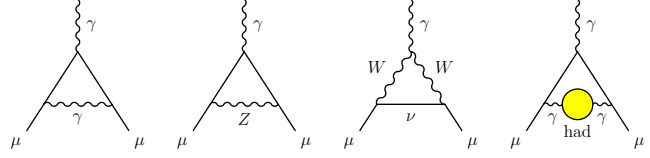


Figure 55.1: Representative diagrams contributing to a_μ^{SM} . From left to right: first order QED (Schwinger term), lowest-order weak, lowest-order hadronic.

Loop contributions involving heavy W^\pm, Z or Higgs particles are collectively labeled as a_μ^{EW} . They are suppressed by at least a factor of $(\alpha/\pi) \cdot (m_\mu^2/m_W^2) \simeq 4 \times 10^{-9}$. At 1-loop order [13]

$$\begin{aligned} a_\mu^{\text{EW}}[\text{1-loop}] &= \frac{G_\mu m_\mu^2}{8\sqrt{2}\pi^2} \left[\frac{5}{3} + \frac{1}{3} (1 - 4\sin^2\theta_W)^2 \right] + \mathcal{O}\left(\frac{m_\mu^2}{M_W^2}\right) + \mathcal{O}\left(\frac{m_\mu^2}{m_H^2}\right) \\ &= 194.8 \times 10^{-11}, \end{aligned} \quad (55.7)$$

for $\sin^2\theta_W \equiv 1 - M_W^2/M_Z^2 \simeq 0.223$, and where $G_\mu \simeq 1.166 \times 10^{-5} \text{ GeV}^{-2}$ is the Fermi coupling constant. Two-loop corrections are relatively large and negative [14]. For a Higgs boson mass of 125 GeV it amounts to $a_\mu^{\text{EW}}[\text{2-loop}] = -41.2(1.0) \times 10^{-11}$ [14], where the uncertainty stems from quark triangle loops. The 3-loop leading logarithms are negligible, $\mathcal{O}(10^{-12})$ [14,15]. A recent full 2-loop numerical evaluation of the electroweak correction [16] reproduces the total 1+2-loop contribution when adjusted for appropriate light quark masses

$$a_\mu^{\text{EW}} = 153.6(1.0) \times 10^{-11}. \quad (55.8)$$

Hadronic (quark and gluon) loop contributions to a_μ^{SM} give rise to its main theoretical uncertainties. At present, those effects are not precisely calculable from first principles, but such an approach, at least partially, may become possible as lattice QCD matures [17]. Instead, one currently relies on a dispersion relation approach to evaluate the lowest-order $\mathcal{O}(\alpha^2)$ hadronic vacuum polarization contribution $a_\mu^{\text{Had}}[\text{LO}]$ from corresponding cross section measurements [18]

$$a_\mu^{\text{Had}}[\text{LO}] = \frac{1}{3} \left(\frac{\alpha}{\pi}\right)^2 \int_{m_\pi^2}^{\infty} ds \frac{K(s)}{s} R^{(0)}(s), \quad (55.9)$$

where $K(s)$ is a QED kernel function [19], and where $R^{(0)}(s)$ denotes the ratio of the bare² cross section for e^+e^- annihilation into hadrons to the pointlike muon-pair cross section at center-of-mass energy \sqrt{s} . The function $K(s) \sim 1/s$ in Eq. (55.9) emphasizes the low-energy part of the integral so that $a_\mu^{\text{Had}}[\text{LO}]$ is dominated by the $\rho(770) \rightarrow \pi^+\pi^-$ resonance.

The analysis of Eq. (55.9) results in the representative value [20]

$$a_\mu^{\text{Had}}[\text{LO}] = 6939(39)(7) \times 10^{-11}, \quad (55.10)$$

where the first error is experimental, dominated by systematic uncertainties in the $e^+e^- \rightarrow$ hadrons cross-section data, and the second due to perturbative QCD, which is used at intermediate and large energies in the dispersion integral to predict the contribution from the quark-antiquark continuum. The experimental precision is currently limited by a discrepancy between the most precise $\pi^+\pi^-$ data from the BABAR and KLOE experiments [20]. Other recent evaluations [31,32] of $a_\mu^{\text{Had}}[\text{LO}]$ find consistent results with Eq. (55.10).

Alternatively, one can use precise vector spectral functions from $\tau \rightarrow \nu_\tau +$ hadrons decays [21] that can be related to isovector $e^+e^- \rightarrow$ hadrons cross sections by isospin symmetry. Analyses replaced e^+e^- data in the two-pion and four-pion channels by

² The bare cross section is defined as the measured cross section corrected for initial-state radiation, electron-vertex loop contributions and vacuum-polarization effects in the photon propagator. However, QED effects in the hadron vertex and final state, as photon radiation, are included.

the corresponding isospin-transformed τ data, and applied isospin-violating corrections [22]. Owing to the progress in the precision of the e^+e^- data, the τ data are now less precise and less reliable due to additional theoretical uncertainties, so that recent $a_\mu^{\text{Had}}[\text{LO}]$ evaluations ignored them.

Higher order hadronic contributions are obtained from dispersion relations using the same $e^+e^- \rightarrow$ hadrons data [23], giving $a_\mu^{\text{Had,Disp}}[\text{NLO}] = (-98.7 \pm 0.9) \times 10^{-11}$ and $a_\mu^{\text{Had,Disp}}[\text{NNLO}] = (12.4 \pm 0.1) \times 10^{-11}$ [24], along with model-dependent estimates of the hadronic light-by-light scattering contribution, $a_\mu^{\text{Had,LBL}}[\text{NLO}]$, motivated by large- N_C QCD [25–30].³ Following [29], one finds for the sum of the three terms

$$a_\mu^{\text{Had}}[\text{N(N)LO}] = 19(26) \times 10^{-11}, \quad (55.11)$$

where the error is dominated by hadronic light-by-light uncertainty.

Adding Eqs. (55.6), (55.8), (55.10) and (55.11) gives the representative SM prediction

$$a_\mu^{\text{SM}} = 116\,591\,830(1)(40)(26) \times 10^{-11}, \quad (55.12)$$

where the errors are due to the electroweak, lowest-order hadronic, and higher-order hadronic contributions, respectively. The difference between experiment and theory

$$\Delta a_\mu = a_\mu^{\text{exp}} - a_\mu^{\text{SM}} = 261(63)(48) \times 10^{-11}, \quad (55.13)$$

where the errors are from experiment and theory prediction (with all errors combined in quadrature), respectively, represents an interesting but not conclusive discrepancy of 3.3 times the combined 1σ error. All the recent estimates for the hadronic contribution compiled in Fig. 55.2 exhibit similar discrepancies.

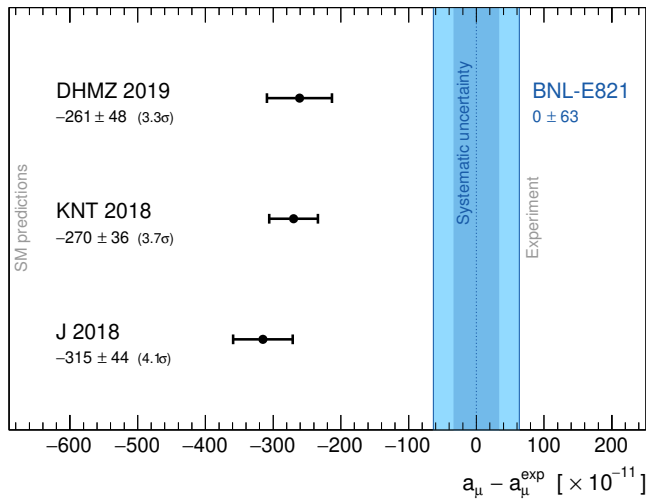


Figure 55.2: Compilation of recent results for a_μ (in units of 10^{-11}), subtracted by the central value of the experimental average (55.3). The shaded (dark shaded) vertical band indicates the total (systematic) experimental uncertainty. The SM predictions are taken from: DHMZ 2019 [20], KNT 2018 [31], and J 2017 [32]. Note that the quoted errors in the figure do not include the uncertainty on the subtracted experimental value. To obtain for each theory calculation a result equivalent to Eq. (55.13), the errors from theory and experiment must be added in quadrature.

³ Some representative recent estimates of the hadronic light-by-light scattering contribution, $a_\mu^{\text{Had,LBL}}[\text{NLO}]$ are: $105(26) \times 10^{-11}$ [29], $110(40) \times 10^{-11}$ [25], $136(25) \times 10^{-11}$ [26]. An approach based on dispersion relations is proposed in [28].

An exciting interpretation is that Δa_μ may be a new physics signal with supersymmetric particle loops as the leading candidate explanation. Such a scenario is quite natural, since generically, supersymmetric models predict [1] an additional contribution to a_μ^{SM}

$$a_\mu^{\text{SUSY}} \simeq \pm 130 \times 10^{-11} \cdot \left(\frac{100 \text{ GeV}}{m_{\text{SUSY}}} \right)^2 \tan\beta, \quad (55.14)$$

where m_{SUSY} is a representative supersymmetric mass scale, $\tan\beta \simeq 3\text{--}40$ a potential enhancement factor, and ± 1 corresponds to the sign of the μ term in the supersymmetric Lagrangian. Supersymmetric particles in the mass range 100–500 GeV could be the source of the deviation Δa_μ . If so, those particles should be directly observable at the Large Hadron Collider at CERN. So far, there is however no direct evidence in support of the supersymmetry interpretation.

New physics effects [1] other than supersymmetry could also explain a non-vanishing Δa_μ . A popular scenario involves the “dark photon”, a relatively light hypothetical vector boson from the dark matter sector that couples to our world of particle physics through mixing with the ordinary photon [33–35]. As a result, it couples to ordinary charged particles with strength $\varepsilon \cdot e$ and gives rise to an additional muon anomalous magnetic moment contribution

$$a_\mu^{\text{dark photon}} = \frac{\alpha}{2\pi} \varepsilon^2 F(m_V/m_\mu), \quad (55.15)$$

where $F(x) = \int_0^1 2z(1-z)^2 / [(1-z)^2 + x^2z] dz$. For values of $\varepsilon \sim 1\text{--}2 \times 10^{-3}$ and $m_V \sim 10\text{--}100$ MeV, the dark photon, which was originally motivated by cosmology, can provide a viable solution to the muon $g-2$ discrepancy. However, recent experimental constraints disfavor such a scenario [36] under the assumption that the dark photon decays primarily into charged lepton pairs. Direct searches for the dark photon continue to be well motivated [37], but with primary guidance coming from phenomena outside the muon anomalous magnetic moment discrepancy. More recent popular solutions to the muon anomaly discrepancy have focused on loop contributions coming from relatively light new scalar or pseudoscalar particle appendages from physics beyond the SM.

References:

1. A. Czarnecki and W.J. Marciano, Phys. Rev. **D64**, 013014 (2001).
2. M. Davier and W.J. Marciano, Ann. Rev. Nucl. and Part. Sci. **54**, 115 (2004).
3. J. Miller, E. de Rafael, and B. Lee Roberts, Rept. Prog. Phys. **70**, 795 (2007).
4. F. Jegerlehner and A. Nyffeler, Phys. Reports **477**, 1 (2009).
5. J.P. Miller *et al.*, Ann. Rev. Nucl. and Part. Sci. **62**, 237 (2012).
6. G.W. Bennett *et al.*, Phys. Rev. Lett. **89**, 101804 (2002); Erratum *ibid.* Phys. Rev. Lett. **89**, 129903 (2002); G.W. Bennett *et al.*, Phys. Rev. Lett. **92**, 161802 (2004); G.W. Bennett *et al.*, Phys. Rev. **D73**, 072003 (2006).
7. P.J. Mohr, B.N. Taylor, and D.B. Newell, CODATA Group, Rev. Mod. Phys. **84**, 1527 (2012).
8. J. Bailey *et al.*, Nucl. Phys. **B150**, 1 (1979).
9. J. Grange *et al.*, FERMILAB-DESIGN-2014-02, arXiv:1501.06858 (2015).
10. M. Abe *et al.*, Prog. Theor. Exp. Phys. 053C02 (2019), arXiv:1901.03047.
11. T. Aoyama *et al.*, Phys. Rev. Lett. **109**, 111808 (2012); T. Aoyama *et al.*, Phys. Rev. Lett. **109**, 111807 (2012); T. Kinoshita and M. Nio, Phys. Rev. **D73**, 013003 (2006); T. Aoyama *et al.*, Phys. Rev. Lett. **99**, 110406 (2007); T. Kinoshita and M. Nio, Phys. Rev. **D70**, 113001 (2004); T. Kinoshita, Nucl. Phys. **B144**, 206 (2005)(Proc. Supp.); T. Kinoshita and M. Nio, Phys. Rev. **D73**, 053007 (2006); S. Laporta, Phys. Lett. **B772**, 232 (2017); A. Kurz *et al.*, Phys. Rev. **D93**, 053017 (2016); A.L. Kataev, arXiv:hep-ph/0602098 (2006); M. Passera, J. Phys. **G31**, 75 (2005).
12. R.H. Parker *et al.*, Science **Vol. 360**, Issue 6385, 191 (2018).

13. R. Jackiw and S. Weinberg, Phys. Rev. **D5**, 2396 (1972);
G. Altarelli *et al.*, Phys. Lett. **B40**, 415 (1972);
I. Bars and M. Yoshimura, Phys. Rev. **D6**, 374 (1972);
K. Fujikawa, B.W. Lee, and A.I. Sanda, Phys. Rev. **D6**, 2923 (1972).
14. C. Gnendiger, D. Stöckinger, H. Stöckinger-Kim, Phys. Rev. **D88**, 053005 (2013);
A. Czarnecki *et al.*, Phys. Rev. **D67**, 073006 (2003);
Erratum *ibid.* Phys. Rev. **D73**, 119901 (2006);
S. Heinemeyer, D. Stockinger, and G. Weiglein, Nucl. Phys. **B699**, 103 (2004);
T. Gribouk and A. Czarnecki, Phys. Rev. **D72**, 053016 (2005);
A. Czarnecki, B. Krause, and W.J. Marciano, Phys. Rev. Lett. **76**, 3267 (1996);
A. Czarnecki, B. Krause, and W.J. Marciano, Phys. Rev. **D52**, 2619, (1995);
S. Peris, M. Perrottet, and E. de Rafael, Phys. Lett. **B355**, 523 (1995);
T. Kukhto *et al.*, Nucl. Phys. **B371**, 567 (1992).
15. G. Degrossi and G.F. Giudice, Phys. Rev. **D58**, 053007 (1998).
16. T. Ishikawa, N. Nakazawa, and Y. Yasui, Phys. Rev. **D99**, 073004 (2019).
17. BMW Collaboration, Phys. Rev. Lett. **121**, 022002 (2018);
HPQCD Collaboration, [arXiv:1902.04223](https://arxiv.org/abs/1902.04223) (2019);
RBC and UKQCD Collaborations, Phys. Rev. Lett. **121**, 022003 (2018);
A. Gérardin *et al.*, Phys. Rev. **D100**, 014510 (2019);
D. Giusti, F. Sanfilippo, and S. Simula, Phys. Rev. **D98**, 114504 (2018);
B. Chakraborty *et al.*, Phys. Rev. **D96**, 034516 (2017);
T. Blum *et al.*, Phys. Rev. **D96**, 034515 (2017);
T. Blum, Phys. Rev. Lett. **118**, 022005 (2017);
B. Chakraborty *et al.*, Phys. Rev. **D93**, 074509 (2016);
C. Lehner, [arXiv:1710.06874](https://arxiv.org/abs/1710.06874) (2017).
18. C. Bouchiat and L. Michel, J. Phys. Radium **22**, 121 (1961);
M. Gourdin and E. de Rafael, Nucl. Phys. **B10**, 667 (1969).
19. S.J. Brodsky and E. de Rafael, Phys. Rev. **168**, 1620 (1968).
20. M. Davier *et al.*, [arXiv:1908.00921](https://arxiv.org/abs/1908.00921) (2019).
21. R. Alemany *et al.*, Eur. Phys. J. **C2**, 123 (1998).
22. M. Davier *et al.*, Eur. Phys. J. **C71**, 1515 (2011).
23. B. Krause, Phys. Lett. **B390**, 392 (1997).
24. A. Kurz *et al.*, Phys. Lett. **B734**, 144 (2014).
25. J. Bijnens and J. Prades, Mod. Phys. Lett. **A22**, 767 (2007).
26. K. Melnikov and A. Vainshtein, Phys. Rev. **D70**, 113006 (2004).
27. M. Knecht and A. Nyffeler, Phys. Rev. **D65**, 073034 (2002);
M. Knecht *et al.*, Phys. Rev. Lett. **88**, 071802 (2002).
28. G. Colangelo *et al.*, JHEP **1409**, 091 (2014).
29. J. Prades, E. de Rafael, and A. Vainshtein, Advanced series on directions in high energy physics 20, Editors B.L. Roberts and W. Marciano, [arXiv:0901.0306](https://arxiv.org/abs/0901.0306) (2009).
30. E. de Rafael, Phys. Lett. **B322**, 239 (1994).
31. A. Keshavarzi, D. Nomura, and T. Teubner, Phys. Rev. **D97**, 114025 (2018).
32. F. Jegerlehner, EPJ Web of Conferences **166**, 00022 (2018).
33. P. Fayet, Phys. Rev. **D75**, 115017 (2007).
34. M. Pospelov, Phys. Rev. **D80**, 095002 (2009).
35. D. Tucker-Smith and I. Yavin, Phys. Rev. **D83**, 101702 (R)(2011).
36. NA48/2 Collaboration (J.R. Batley *et al.*), Phys. Lett. **B746**, 178 (2015).
37. J. Alexander *et al.*, Dark Sectors 2016 Workshop: Community Report, [arXiv:1608.08632](https://arxiv.org/abs/1608.08632) (2017).

56. Muon Decay Parameters

Revised March 2019 by W. Fetscher (ETH Zurich) and H.-J. Gerber (ETH Zurich).

56.1 Introduction:

All measurements in direct muon decay, $\mu^- \rightarrow e^- + 2$ neutrals, and its inverse, $\nu_\mu + e^- \rightarrow \mu^- + \text{neutral}$, are successfully described by the “ V - A interaction,” which is a particular case of a local, derivative-free, lepton-number-conserving, four-fermion interaction [1]. As shown below, within this framework, the Standard Model assumptions, such as the V - A form and the nature of the neutrals (ν_μ and $\bar{\nu}_e$), and hence the doublet assignments $(\nu_e e^-)_L$ and $(\nu_\mu \mu^-)_L$, have been determined from experiments [2, 3]. All considerations on muon decay are valid for the leptonic tau decays $\tau^- \rightarrow \ell^- + \nu_\tau + \bar{\nu}_\ell$ with the replacements $m_\mu \rightarrow m_\tau$, $m_e \rightarrow m_{\ell}$, $\ell^- = e^-, \mu^-$.

56.2 Parameters:

The differential decay probability to obtain an e^\pm with (reduced) energy between x and $x + dx$, emitted in the direction $\hat{\mathbf{x}}_3$ at an angle between ϑ and $\vartheta + d\vartheta$ with respect to the muon polarization vector \mathbf{P}_μ , and with its spin parallel to the arbitrary direction $\hat{\boldsymbol{\zeta}}$, neglecting radiative corrections, is given by

$$\begin{aligned} \frac{d^2\Gamma}{dx d\cos\vartheta} &= \frac{m_\mu}{4\pi^3} W_{e\mu}^4 G_F^2 \sqrt{x^2 - x_0^2} \\ &\times (F_{\text{IS}}(x) \pm P_\mu \cos\vartheta F_{\text{AS}}(x)) \\ &\times [1 + \hat{\boldsymbol{\zeta}} \cdot \mathbf{P}_e(x, \vartheta)]. \end{aligned} \quad (56.1)$$

Here, $W_{e\mu} = \max(E_e) = (m_\mu^2 + m_e^2)/2m_\mu$ is the maximum e^\pm energy, $x = E_e/W_{e\mu}$ is the reduced energy, $x_0 = m_e/W_{e\mu} = 9.67 \times 10^{-3}$, and $P_\mu = |\mathbf{P}_\mu|$ is the degree of muon polarization. $\hat{\boldsymbol{\zeta}}$ is the direction in which a perfect polarization-sensitive electron detector is most sensitive. The isotropic part of the spectrum, $F_{\text{IS}}(x)$, the anisotropic part $F_{\text{AS}}(x)$, and the electron polarization, $\mathbf{P}_e(x, \vartheta)$, may be parametrized by the Michel parameter ρ [1], by η [4], by ξ and δ [5, 6], *etc.* These are bilinear combinations of the coupling constants $g_{e\mu}^\gamma$, which occur in the matrix element (given below).

If the masses of the neutrinos as well as x_0^2 are neglected, the energy and angular distribution of the electron in the rest frame of a muon (μ^\pm) measured by a polarization insensitive detector, is given by

$$\begin{aligned} \frac{d^2\Gamma}{dx d\cos\vartheta} &\sim x^2 \cdot \left\{ 3(1-x) + \frac{2\rho}{3}(4x-3) + 3\eta x_0(1-x)/x \right. \\ &\left. \pm P_\mu \cdot \boldsymbol{\xi} \cdot \cos\vartheta \left[1-x + \frac{2\delta}{3}(4x-3) \right] \right\}. \end{aligned} \quad (56.2)$$

Here, ϑ is the angle between the electron momentum and the muon spin, and $x \equiv 2E_e/m_\mu$. For the Standard Model coupling, we obtain $\rho = \xi\delta = 3/4$, $\xi = 1$, $\eta = 0$ and the differential decay rate is

$$\frac{d^2\Gamma}{dx d\cos\vartheta} = \frac{G_F^2 m_\mu^5}{192\pi^3} [3 - 2x \pm P_\mu \cos\vartheta(2x-1)] \cdot x^2. \quad (56.3)$$

The coefficient in front of the square bracket is the total decay rate.

If only the neutrino masses are neglected, and if the e^\pm polarization is detected, then the functions in Eq. (56.1) become

$$F_{\text{IS}}(x) = x(1-x) + \frac{2}{3}\rho(4x^2 - 3x - x_0^2) + \eta \cdot x_0(1-x) \quad (56.4a)$$

$$\begin{aligned} F_{\text{AS}}(x) &= \frac{1}{3}\xi \sqrt{x^2 - x_0^2} \\ &\times \left[(1-x) + \frac{2}{3}\delta \left\{ (4x-3) + \left(\sqrt{1-x_0^2} - 1 \right) \right\} \right] \end{aligned} \quad (56.4b)$$

$$\mathbf{P}_e(x, \vartheta) = P_{T_1} \cdot \hat{\mathbf{x}}_1 + P_{T_2} \cdot \hat{\mathbf{x}}_2 + P_L \cdot \hat{\mathbf{x}}_3 \quad (56.4c)$$

Here $\hat{\mathbf{x}}_1$, $\hat{\mathbf{x}}_2$, and $\hat{\mathbf{x}}_3$ are orthogonal unit vectors defined as follows:

$$\begin{aligned} \hat{\mathbf{x}}_3 &\text{ is along the } e \text{ momentum } \mathbf{p}_e \\ \frac{\hat{\mathbf{x}}_3 \times \mathbf{P}_\mu}{|\hat{\mathbf{x}}_3 \times \mathbf{P}_\mu|} &= \hat{\mathbf{x}}_2 \text{ is transverse to } \mathbf{p}_e \text{ and perpendicular to} \\ &\text{“the decay plane”} \\ \hat{\mathbf{x}}_2 \times \hat{\mathbf{x}}_3 &= \hat{\mathbf{x}}_1 \text{ is transverse to } \mathbf{p}_e \text{ and in the decay plane} \end{aligned}$$

The components of \mathbf{P}_e then are given by

$$P_{T_1}(x, \vartheta) = P_\mu \sin\vartheta \cdot F_{T_1}(x) / \{F_{\text{IS}}(x) \pm P_\mu \cos\vartheta \cdot F_{\text{AS}}(x)\} \quad (56.5a)$$

$$P_{T_2}(x, \vartheta) = P_\mu \sin\vartheta \cdot F_{T_2}(x) / \{F_{\text{IS}}(x) \pm P_\mu \cos\vartheta \cdot F_{\text{AS}}(x)\} \quad (56.5b)$$

$$P_L(x, \vartheta) = \frac{\pm F_{\text{IP}}(x) + P_\mu \cos\vartheta \cdot F_{\text{AP}}(x)}{F_{\text{IS}}(x) \pm P_\mu \cos\vartheta \cdot F_{\text{AS}}(x)}, \quad (56.5c)$$

where

$$F_{T_1}(x) = \frac{1}{12} \left\{ -2 \left[\xi'' + 12 \left(\rho - \frac{3}{4} \right) \right] (1-x)x_0 - 3\eta(x^2 - x_0^2) + \eta''(-3x^2 + 4x - x_0^2) \right\} \quad (56.6a)$$

$$F_{T_2}(x) = \frac{1}{3} \sqrt{x^2 - x_0^2} \cdot \left\{ 3 \frac{\alpha'}{A} (1-x) + 2 \frac{\beta'}{A} \sqrt{1-x_0^2} \right\} \quad (56.6b)$$

$$F_{\text{IP}}(x) = \frac{1}{54} \sqrt{x^2 - x_0^2} \cdot \left\{ 9\xi' \left(-2x + 2 + \sqrt{1-x_0^2} \right) + 4\xi \left(\delta - \frac{3}{4} \right) 4x - 4 + \sqrt{1-x_0^2} \right\} \quad (56.6c)$$

$$F_{\text{AP}}(x) = \frac{1}{6} \left\{ \xi'' (2x^2 - x - x_0^2) + 4 \left(\rho - \frac{3}{4} \right) (4x^2 - 3x - x_0^2) + 2\eta''(1-x)x_0 \right\}. \quad (56.6d)$$

For the experimental values of the parameters ρ , ξ , ξ' , ξ'' , δ , η , η'' , α/A , β/A , α'/A , β'/A , which are not all independent, see the Data Listings below. Experiments in the past have also been analyzed using the parameters a , b , c , a' , b' , c' , α/A , β/A , α'/A , β'/A (and $\eta = (\alpha - 2\beta)/2A$), as defined by Kinoshita and Sirlin [5] [6]. They serve as a model-independent summary of all possible measurements on the decay electron (see Listings below). The relations between the two sets of parameters are

$$\rho - \frac{3}{4} = \frac{3}{4}(-a + 2c)/A \quad (56.7a)$$

$$\eta = (\alpha - 2\beta)/A \quad (56.7b)$$

$$\eta'' = (3\alpha + 2\beta)/A \quad (56.7c)$$

$$\delta - \frac{3}{4} = \frac{9}{4} \cdot \frac{(a' - 2c')/A}{1 - [a + 3a' + 4(b + b') + 6c - 14c']/A} \quad (56.7d)$$

$$1 - \xi \frac{\delta}{\rho} = 4 \frac{[(b + b') + 2(c - c')]/A}{1 - (a - 2c)/A} \quad (56.7e)$$

$$1 - \xi = \left[(a + a') + 4(b + b') + 6(c + c') \right] / A \quad (56.7f)$$

$$1 - \xi'' = (-2a + 20c)/A \quad (56.7g)$$

$$\text{with } A = a + 4b + 6c \quad (56.7h)$$

The differential decay probability to obtain a *left-handed* ν_e with (reduced) energy between y and $y + dy$, neglecting radiative corrections as well as the masses of the electron and of the neutrinos, is given by [7]

$$\frac{d\Gamma}{dy} = \frac{m_\mu^5 G_F^2}{16\pi^3} \cdot Q_L^{\nu_e} \cdot y^2 \left\{ (1-y) - \omega_L \cdot \left(y - \frac{3}{4} \right) \right\}. \quad (56.8)$$

Here, $y = 2 E_{\nu_e}/m_\mu$. $Q_L^{\nu_e}$ and ω_L are parameters. ω_L is the neutrino analog of the spectral shape parameter ρ of Michel. Since in the Standard Model, $Q_L^{\nu_e} = 1$, $\omega_L = 0$, the measurement of $d\Gamma/dy$ has allowed a null-test of the Standard Model (see Listings below).

Table 56.1: Coupling constants $g_{\varepsilon\mu}^\gamma$ and some combinations of them. Ninety-percent confidence level experimental limits. The limits on $|g_{LL}^S|$ and $|g_{LL}^V|$ are from [8–10], and the others from a general analysis of muon decay measurements. Top three rows: [11], fourth row: [12], next three rows: [13], last row: [14]. The experimental uncertainty on the muon polarization in pion decay is included. Note that, by definition, $|g_{\varepsilon\mu}^S| \leq 2$, $|g_{\varepsilon\mu}^V| \leq 1$ and $|g_{\varepsilon\mu}^T| \leq 1/\sqrt{3}$.

$ g_{RR}^S < 0.035$	$ g_{RR}^V < 0.017$	$ g_{RR}^T \equiv 0$
$ g_{LR}^S < 0.050$	$ g_{LR}^V < 0.023$	$ g_{LR}^T < 0.015$
$ g_{RL}^S < 0.420$	$ g_{RL}^V < 0.105$	$ g_{RL}^T < 0.105$
$ g_{LL}^S < 0.550$	$ g_{LL}^V > 0.960$	$ g_{LL}^T \equiv 0$
$ g_{LR}^S + 6g_{LR}^T < 0.143$	$ g_{RL}^S + 6g_{RL}^T < 0.418$	
$ g_{LR}^S + 2g_{LR}^T < 0.108$	$ g_{RL}^S + 2g_{RL}^T < 0.417$	
$ g_{LR}^S - 2g_{LR}^T < 0.070$	$ g_{RL}^S - 2g_{RL}^T < 0.418$	
$Q_{RR} + Q_{LR} < 8.2 \times 10^{-4}$		

56.3 Matrix element:

All results in direct muon decay (energy spectra of the electron and of the neutrinos, polarizations, and angular distributions), and in inverse muon decay (the reaction cross section) at energies well below $m_W c^2$, may be parametrized in terms of amplitudes $g_{\varepsilon\mu}^\gamma$ and the Fermi coupling constant G_F , using the matrix element

$$\frac{4G_F}{\sqrt{2}} \sum_{\substack{\gamma=S,V,T \\ \varepsilon,\mu=R,L}} g_{\varepsilon\mu}^\gamma \langle \bar{e}_\varepsilon | \Gamma^\gamma | (\nu_e)_n \rangle \langle \bar{\nu}_\mu \rangle_m | \Gamma_\gamma | \mu_\mu \rangle \quad (56.9)$$

We use the notation of Fetscher *et al.* [2], who in turn use the sign conventions and definitions of Scheck [15]. Here, $\gamma = S, V, T$ indicates a scalar, vector, or tensor interaction; and $\varepsilon, \mu = R, L$ indicate a right- or left-handed chirality of the electron or muon. The chiralities n and m of the ν_e and $\bar{\nu}_\mu$ are then determined by the values of γ, ε , and μ . The particles are represented by fields of definite chirality [16].

As shown by Langacker and London [17], explicit lepton-number nonconservation still leads to a matrix element equivalent to Eq. (56.9). They conclude that it is not possible, even in principle, to test lepton-number conservation in (leptonic) muon decay if the final neutrinos are massless and are not observed.

The ten complex amplitudes $g_{\varepsilon\mu}^\gamma$ (g_{RR}^T and g_{LL}^T are identically zero) and G_F constitute 19 independent (real) parameters to be determined by experiment. The Standard Model interaction corresponds to one single amplitude g_{LL}^V being unity and all the others being zero.

The (direct) muon decay experiments are compatible with an arbitrary mix of the scalar and vector amplitudes g_{LL}^S and g_{LL}^V – in the extreme even with purely scalar $g_{LL}^S = 2$, $g_{LL}^V = 0$. The decision in favour of the Standard Model comes from the quantitative observation of inverse muon decay, which would be forbidden for pure g_{LL}^S [2].

56.4 Experimental determination of $V-A$:

In order to determine the amplitudes $g_{\varepsilon\mu}^\gamma$ uniquely from experiment, the following set of equations, where the left-hand sides

represent experimental results, has to be solved.

$$a = 16 \left(|g_{RL}^V|^2 + |g_{LR}^V|^2 \right) + |g_{RL}^S + 6g_{RL}^T|^2 + |g_{LR}^S + 6g_{LR}^T|^2 \quad (56.10a)$$

$$a' = 16 \left(|g_{RL}^V|^2 - |g_{LR}^V|^2 \right) + |g_{RL}^S + 6g_{RL}^T|^2 - |g_{LR}^S + 6g_{LR}^T|^2 \quad (56.10b)$$

$$\alpha = 8 \operatorname{Re} \left\{ g_{RL}^V \left(g_{LR}^{S*} + 6g_{LR}^{T*} \right) + g_{LR}^V \left(g_{RL}^{S*} + 6g_{RL}^{T*} \right) \right\} \quad (56.10c)$$

$$a' = 8 \operatorname{Im} \left\{ g_{RL}^V \left(g_{LR}^{S*} + 6g_{LR}^{T*} \right) - g_{LR}^V \left(g_{RL}^{S*} + 6g_{RL}^{T*} \right) \right\} \quad (56.10d)$$

$$b = 4 \left(|g_{RR}^V|^2 + |g_{LL}^V|^2 \right) + |g_{RR}^S|^2 + |g_{LL}^S|^2 \quad (56.10e)$$

$$b' = 4 \left(|g_{RR}^V|^2 - |g_{LL}^V|^2 \right) + |g_{RR}^S|^2 - |g_{LL}^S|^2 \quad (56.10f)$$

$$c = \frac{1}{2} \left\{ |g_{RL}^S|^2 - 2|g_{RL}^T|^2 + |g_{LR}^S|^2 - 2|g_{LR}^T|^2 \right\} \quad (56.10g)$$

$$c' = \frac{1}{2} \left\{ |g_{RL}^S|^2 - 2|g_{RL}^T|^2 - |g_{LR}^S|^2 + 2|g_{LR}^T|^2 \right\} \quad (56.10h)$$

and

$$Q_L^{\nu_e} = 1 - \left\{ \frac{1}{4} |g_{LR}^S|^2 + \frac{1}{4} |g_{LL}^S|^2 + |g_{RR}^V|^2 + |g_{RL}^V|^2 + 3|g_{LR}^T|^2 \right\} \quad (56.10i)$$

$$\omega_L = \frac{3}{4} \frac{|g_{RR}^S|^2 + 4|g_{LR}^V|^2 + |g_{RL}^S|^2 + 2|g_{LR}^T|^2}{|g_{RL}^S|^2 + |g_{RR}^S|^2 + 4|g_{LL}^V|^2 + 4|g_{LR}^V|^2 + 12|g_{RL}^T|^2} \quad (56.10j)$$

It has been noted earlier by C. Jarlskog [18], that certain experiments observing the decay electron are especially informative if they yield the $V-A$ values. The complete solution is now found as follows. Fetscher *et al.* [2] introduced four probabilities $Q_{\varepsilon\mu}(\varepsilon, \mu = R, L)$ for the decay of a μ -handed muon into an ε -handed electron, and showed that there exist upper bounds on Q_{RR} , Q_{LR} , and Q_{RL} , and a lower bound on Q_{LL} . These probabilities are given in terms of the $g_{\varepsilon\mu}^\gamma$'s by

$$Q_{\varepsilon\mu} = \frac{1}{4} |g_{\varepsilon\mu}^S|^2 + |g_{\varepsilon\mu}^V|^2 + 3(1 - \delta_{\varepsilon\mu}) |g_{\varepsilon\mu}^T|^2 \quad (56.11)$$

where $\delta_{\varepsilon\mu} = 1$ for $\varepsilon = \mu$, and $\delta_{\varepsilon\mu} = 0$ for $\varepsilon \neq \mu$. They are related to the parameters a , b , c , a' , b' , and c' by

$$Q_{RR} = 2(b + b')/A \quad (56.12a)$$

$$Q_{LR} = [(a - a') + 6(c - c')]/2A \quad (56.12b)$$

$$Q_{RL} = [(a + a') + 6(c + c')]/2A \quad (56.12c)$$

$$Q_{LL} = 2(b - b')/A \quad (56.12d)$$

with $A = 16$. In the Standard Model, $Q_{LL} = 1$ and the others are zero.

Since the upper bounds on Q_{RR} , Q_{LR} , and Q_{RL} are found to be small, and since the helicity of the ν_μ in pion decay is known from experiment [19, 20] to very high precision to be -1 [21], the cross section S of *inverse* muon decay, normalized to the $V-A$ value, yields [2]

$$|g_{LL}^S|^2 \leq 4(1 - S) \quad (56.13a)$$

and

$$|g_{LL}^V|^2 = S. \quad (56.13b)$$

Thus the Standard Model assumption of a pure $V-A$ leptonic charged weak interaction of e and μ is derived (within errors)

from experiments at energies far below the mass of the W^\pm : Eq. (56.13 b) gives a lower limit for $V-A$, and Eqs. (56.12 a, b, c) and (56.13 a) give upper limits for the other four-fermion interactions. The existence of such upper limits may also be seen from $Q_{RR} + Q_{RL} = (1 - \xi')/2$ (e^+ longitudinal polarization) and $Q_{RR} + Q_{LR} = \frac{1}{2}(1 + \xi/3 - 16\xi\delta/9)$ (decay asymmetry). Table 56.1 gives the current experimental limits on the magnitudes of the $g_{\bar{e}\mu}^\gamma$'s. More stringent limits on the six coupling constants $g_{LR}^S, g_{LR}^V, g_{LR}^T, g_{RL}^S, g_{RL}^V,$ and g_{RL}^T have been derived from upper limits on the neutrino mass [22]. Limits on the "charge retention" coordinates, as used in the older literature (*e.g.*, Ref. [23]), are given by Burkard *et al.* [24].

References

- [1] L. Michel, Proc. Phys. Soc. **A63**, 514 (1950).
- [2] W. Fetscher, H. J. Gerber and K. F. Johnson, Phys. Lett. **B173**, 102 (1986).
- [3] P. Langacker, Comments Nucl. Part. Phys. **19**, 1, 1 (1989).
- [4] C. Bouchiat and L. Michel, Phys. Rev. **106**, 170 (1957).
- [5] T. Kinoshita and A. Sirlin, Phys. Rev. **107**, 593 (1957).
- [6] T. Kinoshita and A. Sirlin, Phys. Rev. **108**, 844 (1957).
- [7] W. Fetscher, Phys. Rev. **D49**, 5945 (1994).
- [8] S. R. Mishra *et al.*, Phys. Lett. **B252**, 170 (1990).
- [9] S. R. Mishra, private communication.
- [10] P. Vilain *et al.* (CHARM-II), Phys. Lett. **B364**, 121 (1995).
- [11] A. Hillairet *et al.* (TWIST), Phys. Rev. **D85**, 092013 (2012), [arXiv:1112.3606].
- [12] R. P. MacDonald *et al.* (TWIST), Phys. Rev. **D78**, 032010 (2008), [arXiv:0807.1125].
- [13] C. A. Gagliardi, R. E. Tribble and N. J. Williams, Phys. Rev. **D72**, 073002 (2005), [hep-ph/0509069].
- [14] R. Bayes *et al.* (TWIST), Phys. Rev. Lett. **106**, 041804 (2011).
- [15] F. Scheck, in *Electroweak and Strong Interactions* (Springer Verlag, 1996).
- [16] K. Mursula and F. Scheck, Nucl. Phys. **B253**, 189 (1985).
- [17] P. Langacker and D. London, Phys. Rev. **D39**, 266 (1989).
- [18] C. Jarlskog, Nucl. Phys. **75**, 659 (1966).
- [19] A. Jodidio *et al.*, Phys. Rev. **D34**, 1967 (1986), [Erratum: Phys. Rev.D37,237(1988)].
- [20] L. P. Roesch *et al.*, Helv. Phys. Acta **55**, 74 (1982).
- [21] W. Fetscher, Phys. Lett. **140B**, 117 (1984).
- [22] G. Prezeau and A. Kurylov, Phys. Rev. Lett. **95**, 101802 (2005), [hep-ph/0409193].
- [23] S. E. Derenzo, Phys. Rev. **181**, 1854 (1969).
- [24] H. Burkard *et al.*, Phys. Lett. **160B**, 343 (1985).

57. τ Branching Fractions

Revised May 2019 by Sw. Banerjee (Louisville U.) and A. Lusiani (SNS, Pisa; INFN, Pisa).

57.1 τ Branching Fractions

The τ Listings contains 244 entries that correspond to either a τ partial decay fraction into a specific decay mode (branching fraction) or a ratio of two τ partial decay fractions (branching ratio). Experimental information provides values for 147 of these quantities, upper limits for 61 branching fractions to Lepton Family number, Lepton number, or Baryon number violating modes, and 36 additional upper limits for other modes. A total of 170 measurements of τ branching fraction and branching ratio measurements is used for a global fit that determines 129 quantities.

57.2 The constrained fit to τ branching fractions

The τ branching fractions fit uses the reported values, uncertainties and statistical correlations of the τ branching fractions and branching ratios measurements. Asymmetric uncertainties are symmetrized as $\sigma_{\text{symm}}^2 = (\sigma_+^2 + \sigma_-^2)/2$. Additionally, the most precise experimental inputs are treated according to how they depend on external parameters on the basis of their documentation [1]. The τ measurements may depend on parameters such as the τ pair production cross-section in e^+e^- annihilations at the $\Upsilon(4S)$ peak. In some cases, measurements reported in different papers by the same collaboration may depend on common parameters like the estimate of the integrated luminosity or of particle identification efficiencies. For all the significant detected dependencies, the τ measurements and their uncertainties are updated to account for the updated values of the external parameters. The dependencies on common systematic effects are also determined in size and sign, and all the common systematic dependencies of different measurements are used together with the published statistical and systematic uncertainties and correlations in order to compute a single all-inclusive variance and covariance matrix of the experimental inputs of the fit.

The fit procedure parameters correspond to τ quantities that are fit to the experimental measurements while respecting relations described by a series of constraint equations. All the experimental inputs and all the constraint equations are reported in the τ Listings section that follows this review. With respect to the 2016, 2017 and 2018 editions, the fit uses one more experimental measurement, published by the BaBar collaboration in 2018, on $\mathcal{B}(\tau \rightarrow K^- K^0 \nu_\tau)$ [2]. If only a few measurements are correlated, the correlation coefficients are listed in the footnote for each measurement (see for example $\Gamma(\text{particle}^- \geq 0 \text{ neutrals} \geq 0 K^0 \nu_\tau \text{ ("1-prong")})/\Gamma_{\text{total}}$). If a large number of measurements are correlated, then the full correlation matrix is listed in the footnote to the measurement that first appears in the τ Listings. Footnotes to the other measurements refer to the first one. For example, the large correlation matrices for the branching fraction or ratio measurements contained in Refs. [3] [4] are listed in Footnotes to the $\Gamma(e^- \bar{\nu}_e \nu_\tau)/\Gamma_{\text{total}}$ and $\Gamma(h^- \nu_\tau)/\Gamma_{\text{total}}$ measurements respectively. The constraints between the τ branching fractions and ratios include coefficients that correspond to physical quantities, like for instance the branching fractions of the η and ω mesons. All quantities are taken from the 2018 edition of the Review of Particle Physics. Their uncertainties are neglected in the fit.

We obtain the branching fraction of $\tau \rightarrow a_1^- (\rightarrow \pi^- \gamma) \nu_\tau$ using the ALEPH estimate for $\mathcal{B}(a_1^- \rightarrow \pi^- \gamma)$ [3], which uses the measurement of $\Gamma(a_1^- \rightarrow \pi^- \gamma)$ [5]. In the fit, we assume that $\mathcal{B}(\tau^- \rightarrow a_1^- \nu_\tau)$ is equal to $\mathcal{B}(\tau \rightarrow \pi^- \pi^- \pi^+ \nu_\tau \text{ (ex. } K^0, \omega)) + \mathcal{B}(\tau \rightarrow \pi^- 2\pi^0 \nu_\tau \text{ (ex. } K^0))$, neglecting the observed but negligible branching fractions to other modes, including $\mathcal{B}(a_1^- \rightarrow \pi^- \gamma)$.

In some cases, constraints describe approximate relations that nevertheless hold within the present experimental precision. For instance, the constraint $\mathcal{B}(\tau \rightarrow K^- K^- K^+ \nu_\tau) = \mathcal{B}(\tau \rightarrow K^- \phi \nu_\tau) \times \mathcal{B}(\phi \rightarrow K^+ K^-)$ is justified within the current experimental evidence.

In the fit, scale factors are applied to the published uncertainties of measurements only if significant inconsistency between different measurements remain after accounting for all relevant uncertainties and correlations. After examining the data and the fit pulls,

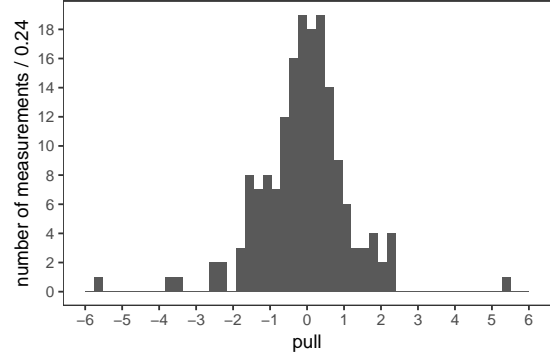


Figure 57.1: Pulls of individual measurements against the respective fitted quantity. No scale factor is used.

it has been decided to apply just one scale factor of 5.4 on the measurements of $\mathcal{B}(\tau \rightarrow K^- K^- K^+ \nu_\tau)$. The scale factor has been computed and applied according to the standard PDG procedure. Without the scale factor applied, the χ^2 probability of the fit is about 2%. On a per-measurement basis, the pull distribution in figure 57.1 indicates that just a few measurements have more than 3σ pulls. (The uncertainties to obtain the pulls are computed using the measurements variance matrix and the variance matrix of the result, accounting for the fact that the variance matrix of the result is obtained from the measurement variance with the fit.) The pull probability distribution in figure 57.2 is reasonably flat. With many measurements some entries on the tails of the normal distribution must be expected. There are 170 pulls, one per measurement. They are partially correlated, and the effective number of independent pulls is equal to the number of degrees of freedom of the fit, 125. Only the $\tau \rightarrow K^- K^- K^+ \nu_\tau$ decay mode has a pull that is inconsistent at the level of more than 3σ even if considered as the largest pull in a set of 125. This confirms the choice of adopting just that one scale factor.

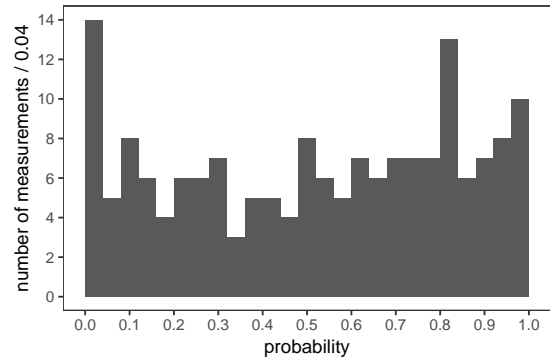


Figure 57.2: Probability of individual measurement pulls against the respective fitted quantity. No scale factor is used.

After scaling the error, the constrained fit has a χ^2 of 135 for 125 degrees of freedom, corresponding to a χ^2 probability of 26%. We use 170 measurements and 84 constraints on the branching fractions and ratios to determine 129 quantities, consisting of 112 branching fractions and 17 branching ratios. A total of 85 quantities have at least one measurement in the fit. The constraints include the unitarity constraint on the sum of all the exclusive τ decay modes, $\mathcal{B}_{\text{all}} = 1$. If the unitarity constraint is released, the fit result for \mathcal{B}_{all} is consistent with unitarity with $1 - \mathcal{B}_{\text{all}} = (0.00 \pm 0.10)\%$.

For the convenience of summarizing the fit results, we list in the following the values and uncertainties for a set of 46 “basis” decay modes, from which all remaining branching fractions and ratios can be obtained using the constraints. The basis decay modes are not intended to sum up to 1. Since some basis quantities represent multiple branching fractions that are related by constraint

equations, they are properly weighted and the unitarity constraint corresponds to a linear combination whose coefficients are listed in the following. The correlation matrix between the basis modes is reported in the τ Listings.

decay mode	fit result (%)	coefficient
$\mu^- \bar{\nu}_\mu \nu_\tau$	17.3937 ± 0.0384	1.0000
$e^- \bar{\nu}_e \nu_\tau$	17.8175 ± 0.0399	1.0000
$\pi^- \nu_\tau$	10.8164 ± 0.0512	1.0000
$K^- \nu_\tau$	0.6964 ± 0.0096	1.0000
$\pi^- \pi^0 \nu_\tau$	25.4941 ± 0.0893	1.0000
$K^- \pi^0 \nu_\tau$	0.4328 ± 0.0148	1.0000
$\pi^- 2\pi^0 \nu_\tau$ (ex. K^0)	9.2595 ± 0.0964	1.0021
$K^- 2\pi^0 \nu_\tau$ (ex. K^0)	0.0647 ± 0.0218	1.0000
$\pi^- 3\pi^0 \nu_\tau$ (ex. K^0)	1.0429 ± 0.0707	1.0000
$K^- 3\pi^0 \nu_\tau$ (ex. K^0, η)	0.0478 ± 0.0212	1.0000
$h^- 4\pi^0 \nu_\tau$ (ex. K^0, η)	0.1118 ± 0.0391	1.0000
$\pi^- \bar{K}^0 \nu_\tau$	0.8384 ± 0.0138	1.0000
$K^- K^0 \nu_\tau$	0.1486 ± 0.0034	1.0000
$\pi^- \bar{K}^0 \pi^0 \nu_\tau$	0.3817 ± 0.0129	1.0000
$K^- \pi^0 K^0 \nu_\tau$	0.1500 ± 0.0070	1.0000
$\pi^- \bar{K}^0 2\pi^0 \nu_\tau$ (ex. K^0)	0.0263 ± 0.0226	1.0000
$\pi^- K_S^0 K_S^0 \nu_\tau$	0.0235 ± 0.0006	2.0000
$\pi^- K_S^0 K_L^0 \nu_\tau$	0.1081 ± 0.0241	1.0000
$\pi^- \pi^0 K_S^0 K_S^0 \nu_\tau$	0.0018 ± 0.0002	2.0000
$\pi^- \pi^0 K_S^0 K_L^0 \nu_\tau$	0.0325 ± 0.0119	1.0000
$\bar{K}^0 h^- h^- h^+ \nu_\tau$	0.0247 ± 0.0199	1.0000
$\pi^- \pi^- \pi^+ \nu_\tau$ (ex. K^0, ω)	8.9868 ± 0.0513	1.0021
$\pi^- \pi^- \pi^+ \pi^0 \nu_\tau$ (ex. K^0, ω)	2.7404 ± 0.0710	1.0000
$h^- h^- h^+ 2\pi^0 \nu_\tau$ (ex. K^0, ω, η)	0.0981 ± 0.0356	1.0000
$\pi^- K^- K^+ \nu_\tau$	0.1435 ± 0.0027	1.0000
$\pi^- K^- K^+ \pi^0 \nu_\tau$	0.0061 ± 0.0018	1.0000
$K^- \pi^0 \eta \nu_\tau$	0.1389 ± 0.0072	1.0000
$K^- \eta \nu_\tau$	0.0155 ± 0.0008	1.0000
$K^- \pi^0 \eta \nu_\tau$	0.0048 ± 0.0012	1.0000
$\pi^- \bar{K}^0 \eta \nu_\tau$	0.0094 ± 0.0015	1.0000
$\pi^- \pi^+ \pi^- \eta \nu_\tau$ (ex. K^0)	0.0220 ± 0.0013	1.0000
$K^- \omega \nu_\tau$	0.0410 ± 0.0092	1.0000
$h^- \pi^0 \omega \nu_\tau$	0.4085 ± 0.0419	1.0000
$K^- \phi \nu_\tau$	0.0044 ± 0.0016	0.8320
$\pi^- \omega \nu_\tau$	1.9494 ± 0.0645	1.0000
$K^- \pi^- \pi^+ \nu_\tau$ (ex. K^0, ω)	0.2927 ± 0.0068	1.0000
$K^- \pi^- \pi^+ \pi^0 \nu_\tau$ (ex. K^0, ω, η)	0.0394 ± 0.0142	1.0000
$\pi^- 2\pi^0 \omega \nu_\tau$ (ex. K^0)	0.0072 ± 0.0016	1.0000
$2\pi^- \pi^+ 3\pi^0 \nu_\tau$ (ex. K^0, η, ω, f_1)	0.0014 ± 0.0027	1.0000
$3\pi^- 2\pi^+ \nu_\tau$ (ex. K^0, ω, f_1)	0.0775 ± 0.0030	1.0000
$K^- 2\pi^- 2\pi^+ \nu_\tau$ (ex. K^0)	0.0001 ± 0.0001	1.0000
$2\pi^- \pi^+ \omega \nu_\tau$ (ex. K^0)	0.0084 ± 0.0006	1.0000
$3\pi^- 2\pi^+ \pi^0 \nu_\tau$ (ex. K^0, η, ω, f_1)	0.0038 ± 0.0009	1.0000
$K^- 2\pi^- 2\pi^+ \pi^0 \nu_\tau$ (ex. K^0)	0.0001 ± 0.0001	1.0000
$\pi^- f_1 \nu_\tau$ ($f_1 \rightarrow 2\pi^- 2\pi^+$)	0.0052 ± 0.0004	1.0000
$\pi^- 2\pi^0 \eta \nu_\tau$	0.0195 ± 0.0038	1.0000

In defining the fit constraints and in selecting the modes that sum up to one we made some assumptions and choices. We assume that some channels, like $\tau^- \rightarrow \pi^- K^+ \pi^- \geq 0\pi^0 \nu_\tau$ and $\tau^- \rightarrow \pi^+ K^- K^- \geq 0\pi^0 \nu_\tau$, have negligible branching fractions as expected from the Standard Model, even if the experimental limits for these branching fractions are not very stringent. The 95% confidence level upper limits are $\mathcal{B}(\tau^- \rightarrow \pi^- K^+ \pi^- \geq 0\pi^0 \nu_\tau) < 0.25\%$ and $\mathcal{B}(\tau^- \rightarrow \pi^+ K^- K^- \geq 0\pi^0 \nu_\tau) < 0.09\%$, values not so different from measured branching fractions for allowed 3-prong modes containing charged kaons. For decays to final states containing one neutral kaon we assume that the branching fraction with the K_L^0 are the same as the corresponding one with a K_S^0 . On decays with two neutral kaons we assume that the branching fractions with $K_L^0 K_L^0$ are the same as the ones with $K_S^0 K_S^0$.

57.3 BaBar and Belle measure on average lower branching fractions and ratios.

We compare the BaBar and Belle measurements with the results of a fit where all their measurements have been excluded. We find that that BaBar and Belle measure on average lower τ branching

fractions and ratios than the other experiments. Figures 57.3 and 57.4 show histograms of the 28 normalized differences between the B -factory measurements and the respective non- B -factory fit results. The normalization is the uncertainty on the difference. The average normalized difference between the two sets of measurements is -0.8σ (-0.7σ for the 16 Belle measurements and -0.8σ for the 12 BaBar measurements).

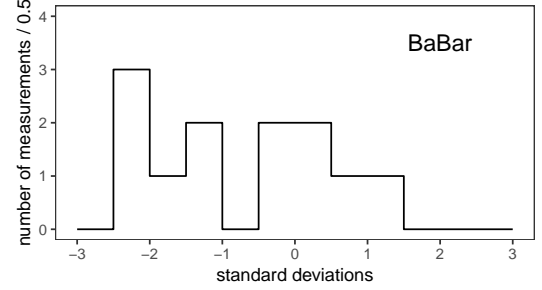


Figure 57.3: Distribution of the normalized difference between 12 measurements of branching fractions and ratios published by the BaBar collaboration and the respective averages computed using only non- B -factory measurements.

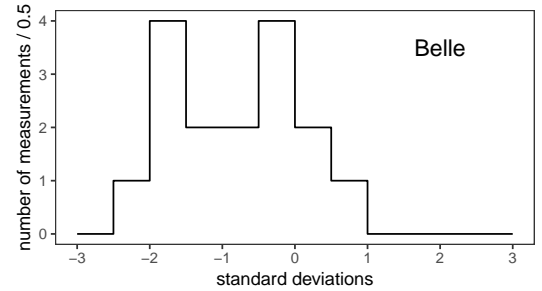


Figure 57.4: Distribution of the normalized difference between 16 measurements of branching fractions and ratios published by the Belle collaboration and the respective averages computed using only non- B -factory measurements.

57.4 Overconsistency of Leptonic Branching Fraction Measurements.

As observed in the previous editions of this review, measurements of the leptonic branching fractions are more consistent with each other than expected from the quoted errors on the individual measurements. The χ^2 is 0.34 for \mathcal{B}_e and 0.08 for \mathcal{B}_μ . Assuming normal errors, the probability of a smaller χ^2 is 1.3% for \mathcal{B}_e and 0.08% for \mathcal{B}_μ .

57.5 Technical implementation of the fit

The fit computes a set of quantities denoted with q_i by minimizing a χ^2 while respecting a series of equality constraints on the q_i . The χ^2 is computed using the measurements m_i and their covariance matrix E_{ij} as $\chi^2 = (m_i - A_{ik} q_k)^t E_{ij}^{-1} (m_j - A_{jl} q_l)$, where the model matrix A_{ij} is used to get the vector of the predicted measurements m'_i from the vector of the fit parameters q_j as $m'_i = A_{ij} q_j$. In this particular implementation the measurements are grouped by the quantity that they measure, and all quantities with at least one measurement correspond to a fit parameter. Therefore, the matrix A_{ij} has one row per measurement m_i and one column per fitted quantity q_j , with unity coefficients for the rows and column that identify a measurement m_i of the quantity q_j , respectively. The constraints are equations involving the fit parameters. The fit does not impose limitations on the functional form of the constraints. In summary, the fit requires:

$$\min [\chi^2(q_k)] = \min [(m_i - A_{ik} q_k)^t E_{ij}^{-1} (m_j - A_{jl} q_l)] \quad (57.1)$$

$$\text{subjected to } f_r(q_s) - c_r = 0, \quad (57.2)$$

where the left term of Eq. 57.2 defines the constraint expressions. Using the method of Lagrange multipliers, a set of equations is

obtained by taking the derivatives with respect to the fitted quantities q_k and the Lagrange multipliers λ_r of the sum of the χ^2 and the constraint expressions multiplied by the Lagrange multipliers λ_r , one for each constraint:

$$\begin{aligned} \min \left[(A_{ik}q_k - m_i)^t E_{ij}^{-1} (A_{jl}q_l - m_j) + 2\lambda_r (f_r(q_s) - c_r) \right] = \\ = \min \left[\tilde{\chi}^2(q_k, \lambda_r) \right] , \\ (\partial/\partial q_k, \partial/\partial \lambda_r) \left[\tilde{\chi}^2(q_k, \lambda_r) \right] = 0 . \end{aligned} \quad (57.3)$$

Eq. 57.3 defines a set of equations for the vector of the unknowns (q_k, λ_r) , some of which may be non-linear, in case of non-linear constraints. An iterative minimization procedure approximates at each step the non-linear constraint expressions by their first order Taylor expansion around the current values of the fitted quantities, \bar{q}_s :

$$f_r(q_s) - c_r = f_r(\bar{q}_s) + \left. \frac{\partial f_r(q_s)}{\partial q_s} \right|_{\bar{q}_s} (q_s - \bar{q}_s) - c_r ,$$

which can be written as

$$B_{rs}q_s - c'_r ,$$

where c'_r are the resulting constant known terms, independent of q_s at first order. After linearization, the differentiation by q_k and λ_r is trivial and leads to a set of linear equations

$$A_{ki}^t E_{ij}^{-1} A_{jl}q_l + B_{kr}^t \lambda_r = A_{ki}^t E_{ij}^{-1} m_j , \quad (57.4)$$

$$B_{rs}q_s = c'_r , \quad (57.5)$$

which can be expressed as

$$F_{ij}u_j = v_i , \quad (57.6)$$

where $u_j = (q_k, \lambda_r)$ and v_i is the vector of the known constant terms running over the index k and then r in the right terms of Eq. 57.4 and Eq. 57.5, respectively. Solving the equation set in Eq. 57.6 by matrix inversion gives the the fitted quantities and their variance and covariance matrix, using the measurements and their variance and covariance matrix. The fit procedure starts by computing the linear approximation of the non-linear constraint expressions around the quantities seed values. With an iterative procedure, the unknowns are updated at each step by solving the equations and the equations are then linearized around the updated values, until the variation of the fitted unknowns is reduced below a numerically small threshold.

References

- [1] D. Asner *et al.* (Heavy Flavor Averaging Group) (2010), [arXiv:1010.1589].
- [2] J. P. Lees *et al.* (BaBar), Phys. Rev. **D98**, 3, 032010 (2018), [arXiv:1806.10280].
- [3] S. Schael *et al.* (ALEPH), Phys. Rept. **421**, 191 (2005), [hep-ex/0506072].
- [4] J. Abdallah *et al.* (DELPHI), Eur. Phys. J. **C46**, 1 (2006), [hep-ex/0603044].
- [5] M. Zielinski *et al.*, Phys. Rev. Lett. **52**, 1195 (1984).

58. τ -Lepton Decay Parameters

Updated August 2011 by A. Stahl (RWTH Aachen).

The purpose of the measurements of the decay parameters (also known as Michel parameters) of the τ is to determine the structure (spin and chirality) of the current mediating its decays.

58.1. Leptonic Decays:

The Michel parameters are extracted from the energy spectrum of the charged daughter lepton $\ell = e, \mu$ in the decays $\tau \rightarrow \ell \nu_\ell \nu_\tau$. Ignoring radiative corrections, neglecting terms of order $(m_\ell/m_\tau)^2$ and $(m_\tau/\sqrt{s})^2$, and setting the neutrino masses to zero, the spectrum in the laboratory frame reads

$$\frac{d\Gamma}{dx} = \frac{G_{\tau\ell}^2 m_\tau^5}{192 \pi^3} \times \left\{ f_0(x) + \rho f_1(x) + \eta \frac{m_\ell}{m_\tau} f_2(x) - P_\tau [\xi g_1(x) + \xi \delta g_2(x)] \right\}, \quad (58.1)$$

with

$$\begin{aligned} f_0(x) &= 2 - 6x^2 + 4x^3 \\ f_1(x) &= -\frac{4}{9} + 4x^2 - \frac{32}{9}x^3 & g_1(x) &= -\frac{2}{3} + 4x - 6x^2 + \frac{8}{3}x^3 \\ f_2(x) &= 12(1-x)^2 & g_2(x) &= \frac{4}{9} - \frac{16}{3}x + 12x^2 - \frac{64}{9}x^3. \end{aligned}$$

The quantity x is the fractional energy of the daughter lepton ℓ , *i.e.*, $x = E_\ell/E_{\ell,max} \approx E_\ell/(\sqrt{s}/2)$ and P_τ is the polarization of the tau leptons. The integrated decay width is given by

$$\Gamma = \frac{G_{\tau\ell}^2 m_\tau^5}{192 \pi^3} \left(1 + 4\eta \frac{m_\ell}{m_\tau} \right). \quad (58.2)$$

The situation is similar to muon decays $\mu \rightarrow e \nu_e \nu_\mu$. The generalized matrix element with the couplings $g_{\ell\mu}^\gamma$ and their relations to the Michel parameters ρ, η, ξ , and δ have been described in the ‘‘Note on Muon Decay Parameters.’’ The Standard Model expectations are 3/4, 0, 1, and 3/4, respectively. For more details, see Ref. 1.

58.2. Hadronic Decays:

In the case of hadronic decays $\tau \rightarrow h \nu_\tau$, with $h = \pi, \rho$, or a_1 , the ansatz is restricted to purely vectorial currents. The matrix element is

$$\frac{G_{\tau h}}{\sqrt{2}} \sum_{\lambda=R,L} g_\lambda \langle \bar{\Psi}_\omega(\nu_\tau) | \gamma^\mu | \Psi_\lambda(\tau) \rangle J_\mu^h \quad (58.3)$$

with the hadronic current J_μ^h . The neutrino chirality ω is uniquely determined from λ . The spectrum depends only on a single parameter ξ_h

$$\frac{d^n \Gamma}{dx_1 dx_2 \dots dx_n} = f(\vec{x}) + \xi_h P_\tau g(\vec{x}), \quad (58.4)$$

with f and g being channel-dependent functions of the n observables $\vec{x} = (x_1, x_2, \dots, x_n)$ (see Ref. 2). The parameter ξ_h is related to the couplings through

$$\xi_h = |g_L|^2 - |g_R|^2. \quad (58.5)$$

ξ_h is the negative of the chirality of the τ neutrino in these decays. In the Standard Model, $\xi_h = 1$. Also included in the Data Listings for ξ_h are measurements of the neutrino helicity which coincide with ξ_h , if the neutrino is massless (ASNER 00 [3], ACKERSTAFF 97R [4], AKERS 95P [5], ALBRECHT 93C [6], and ALBRECHT 90I [7]).

58.3. Combination of Measurements:

The individual measurements are combined, taking into account the correlations between the parameters. In a first fit, universality between the two leptonic decays, and between all hadronic decays, is assumed. A second fit is made without these assumptions. The results of the two fits are provided as OUR FIT in the Data Listings below in the tables whose title includes ‘‘(e or mu)’’ or ‘‘(all hadronic modes)’’, and ‘‘(e),’’ ‘‘(mu)’’ *etc.*, respectively. The measurements show good agreement with the Standard Model. The χ^2 values with respect to the Standard model predictions are 24.1 for 41 degrees of freedom and 26.8 for 56 degrees of freedom, respectively. The correlations are reduced through this combination to less than 20%, with the exception of ρ and η which are correlated by +23%, for the fit with universality and by +70% for $\tau \rightarrow \mu \nu_\mu \nu_\tau$.

58.4. Model-independent Analysis:

From the Michel parameters, limits can be derived on the couplings $g_{\varepsilon\lambda}^\kappa$ without further model assumptions. In the Standard model $g_{LL}^V = 1$ (leptonic decays), and $g_L = 1$ (hadronic decays) and all other couplings vanish. First, the partial decay widths have to be compared to the Standard Model predictions to derive limits on the normalization of the couplings $A_x = G_{\tau x}^2/G_F^2$ with Fermi’s constant G_F :

$$\begin{aligned} A_e &= 1.0029 \pm 0.0046, \\ A_\mu &= 0.981 \pm 0.018, \\ A_\pi &= 1.0020 \pm 0.0073. \end{aligned} \quad (58.6)$$

Then limits on the couplings (95% CL) can be extracted (see Ref. 8 and Ref. 9). Without the assumption of universality, the limits given in Table 58.1 are derived.

Table 58.1: Coupling constants $g_{\varepsilon\mu}^\gamma$. 95% confidence level experimental limits. The limits include the quoted values of A_e, A_μ , and A_π and assume $A_\rho = A_{a_1} = 1$.

$\tau \rightarrow e \nu_e \nu_\tau$		
$ g_{RR}^S < 0.70$	$ g_{RR}^V < 0.17$	$ g_{RR}^T \equiv 0$
$ g_{LR}^S < 0.99$	$ g_{LR}^V < 0.13$	$ g_{LR}^T < 0.082$
$ g_{RL}^S < 2.01$	$ g_{RL}^V < 0.52$	$ g_{RL}^T < 0.51$
$ g_{LL}^S < 2.01$	$ g_{LL}^V < 1.005$	$ g_{LL}^T \equiv 0$
$\tau \rightarrow \mu \nu_\mu \nu_\tau$		
$ g_{RR}^S < 0.72$	$ g_{RR}^V < 0.18$	$ g_{RR}^T \equiv 0$
$ g_{LR}^S < 0.95$	$ g_{LR}^V < 0.12$	$ g_{LR}^T < 0.079$
$ g_{RL}^S < 2.01$	$ g_{RL}^V < 0.52$	$ g_{RL}^T < 0.51$
$ g_{LL}^S < 2.01$	$ g_{LL}^V < 1.005$	$ g_{LL}^T \equiv 0$
$\tau \rightarrow \pi \nu_\tau$		
$ g_R^V < 0.15$	$ g_L^V > 0.992$	
$\tau \rightarrow \rho \nu_\tau$		
$ g_R^V < 0.10$	$ g_L^V > 0.995$	
$\tau \rightarrow a_1 \nu_\tau$		
$ g_R^V < 0.16$	$ g_L^V > 0.987$	

58.5. Model-dependent Interpretation:

More stringent limits can be derived assuming specific models. For example, in the framework of a two Higgs doublet model, the measurements correspond to a limit of $m_{H^\pm} > 1.9 \text{ GeV} \times \tan \beta$ on the mass of the charged Higgs boson, or a limit of 253 GeV on the mass of the second W boson in left-right symmetric models for arbitrary mixing (both 95% CL). See Ref. 9 and Ref. 10.

References:

1. F. Scheck, Phys. Reports **44**, 187 (1978);
W. Fetscher and H.J. Gerber in *Precision Tests of the Standard Model*, edited by P. Langacker, World Scientific, 1993;
A. Stahl, *Physics with τ Leptons*, Springer Tracts in Modern Physics.
2. M. Davier *et al.*, Phys. Lett. **B306**, 411 (1993).

3. CLEO Collab., D.M. Asner *et al.*, Phys. Rev. **D61**, 012002 (2000).
4. OPAL Collab., K. Ackerstaff *et al.*, Z. Phys. **C75**, 593 (1997).
5. OPAL Collab., R. Akers *et al.*, Z. Phys. **C67**, 45 (1995).
6. ARGUS Collab., H. Albrecht *et al.*, Z. Phys. **C58**, 61 (1993).
7. ARGUS Collab., H. Albrecht *et al.*, Phys. Lett. **B250**, 164 (1990).
8. OPAL Collab., K. Ackerstaff *et al.*, Eur. Phys. J. **C8**, 3 (1999).
9. A. Stahl, Nucl. Phys. (Proc. Supp.) **B76**, 173 (1999).
10. M.-T. Dova *et al.*, Phys. Rev. **D58**, 015005 (1998);
T. Hebbeker and W. Lohmann, Z. Phys. **C74**, 399 (1997);
A. Pich and J.P. Silva, Phys. Rev. **D52**, 4006 (1995).

59. Quark Masses

Updated August 2019 by A.V. Manohar (UC, San Diego), L.P. Lellouch (CNRS & Aix-Marseille U.), and R.M. Barnett (LBNL).

59.1. Introduction

This note discusses some of the theoretical issues relevant for the determination of quark masses, which are fundamental parameters of the Standard Model of particle physics. Unlike the leptons, quarks are confined inside hadrons and are not observed as physical particles. Quark masses therefore cannot be measured directly, but must be determined indirectly through their influence on hadronic properties. Although one often speaks loosely of quark masses as one would of the mass of the electron or muon, any quantitative statement about the value of a quark mass must make careful reference to the particular theoretical framework that is used to define it. It is important to keep this *scheme dependence* in mind when using the quark mass values tabulated in the data listings.

Historically, the first determinations of quark masses were performed using quark models. These are usually called constituent quark masses and are of order 350 MeV for the u and d quarks. Constituent quark masses model the effects of dynamical chiral symmetry breaking discussed below, and are not directly related to the quark mass parameters m_q of the QCD Lagrangian of Eq. (59.1). The resulting masses only make sense in the limited context of a particular quark model, and cannot be related to the quark mass parameters, m_q , of the Standard Model. In order to discuss quark masses at a fundamental level, definitions based on quantum field theory must be used, and the purpose of this note is to discuss these definitions and the corresponding determinations of the values of the masses.

59.2. Mass parameters and the QCD Lagrangian

The QCD [1] Lagrangian is

$$\mathcal{L} = \sum_{q=u,d,s,\dots,t} \bar{q} (i\not{D} - m_q) q - \frac{1}{2} \text{tr} G_{\mu\nu} G^{\mu\nu}, \quad (59.1)$$

where the sum runs over the quark flavors u, d, s, c, b and t . $\not{D} = (\partial_\mu - iqA_\mu)\gamma^\mu$ is the gauge covariant derivative, A_μ is the $su(3)$ -valued gluon field, $G_{\mu\nu} = \frac{i}{g}[D_\mu, D_\nu]$ is the gluon field strength, m_q is the mass parameter of quark flavor q , and q is the quark Dirac field. After renormalization, the QCD Lagrangian Eq. (59.1) gives finite values for physical quantities, such as scattering amplitudes. Renormalization is a procedure that invokes a subtraction scheme to render the amplitudes finite, and requires the introduction of a dimensionful scale parameter μ . The mass parameters in the QCD Lagrangian Eq. (59.1) depend on the renormalization scheme used to define the theory, and also on the scale parameter μ . The most commonly used renormalization scheme for QCD perturbation theory is the $\overline{\text{MS}}$ scheme.

The QCD Lagrangian has a chiral symmetry in the limit that the quark masses vanish. This symmetry is spontaneously broken by dynamical chiral symmetry breaking, and explicitly broken by the quark masses. The non-perturbative scale of dynamical chiral symmetry breaking, Λ_χ , is around 1 GeV [2]. It is conventional to call quarks heavy if $m_q > \Lambda_\chi$, so that explicit chiral symmetry breaking dominates (c, b , and t quarks are heavy), and light if $m_q < \Lambda_\chi$, so that spontaneous chiral symmetry breaking dominates (the u and d are light and the s is considered to be light when using $SU(3)_L \times SU(3)_R$ chiral perturbation theory). The determination of light- and heavy-quark masses is considered separately in Sec. 59.4 and Sec. 59.5 below.

At high energies or short distances, non-perturbative effects, such as chiral symmetry breaking, become small and one can, in principle, determine quark masses by analyzing mass-dependent effects using QCD perturbation theory. Such computations are conventionally performed using the $\overline{\text{MS}}$ scheme at a scale $\mu \gg \Lambda_\chi$, and give the $\overline{\text{MS}}$ “running” mass $\overline{m}(\mu)$. We use the $\overline{\text{MS}}$ scheme when reporting quark masses; one can readily convert these values into other schemes using perturbation theory.

The μ dependence of $\overline{m}(\mu)$ at short distances can be calculated using the renormalization group (RG) equation,

$$\mu^2 \frac{d\overline{m}(\mu)}{d\mu^2} = -\gamma(\overline{\alpha}_s(\mu)) \overline{m}(\mu), \quad (59.2)$$

where γ is the anomalous dimension which is now known to four-loop order in perturbation theory [3,4]. $\overline{\alpha}_s$ is the coupling constant [1] in the $\overline{\text{MS}}$ scheme. Defining the expansion coefficients γ_r by

$$\gamma(\overline{\alpha}_s) \equiv \sum_{r=1}^{\infty} \gamma_r \left(\frac{\overline{\alpha}_s}{4\pi} \right)^r,$$

the first four coefficients are given by

$$\begin{aligned} \gamma_1 &= 4, \\ \gamma_2 &= \frac{202}{3} - \frac{20N_L}{9}, \\ \gamma_3 &= 1249 + \left(-\frac{2216}{27} - \frac{160}{3}\zeta(3) \right) N_L - \frac{140}{81} N_L^2, \\ \gamma_4 &= \frac{4603055}{162} + \frac{135680}{27} \zeta(3) - 8800\zeta(5) \\ &\quad + \left(-\frac{91723}{27} - \frac{34192}{9}\zeta(3) + 880\zeta(4) + \frac{18400}{9}\zeta(5) \right) N_L \\ &\quad + \left(\frac{5242}{243} + \frac{800}{9}\zeta(3) - \frac{160}{3}\zeta(4) \right) N_L^2 \\ &\quad + \left(-\frac{332}{243} + \frac{64}{27}\zeta(3) \right) N_L^3, \end{aligned}$$

where N_L is the number of active light quark flavors at the scale μ , i.e. flavors with masses $< \mu$, and ζ is the Riemann zeta function ($\zeta(3) \simeq 1.2020569$, $\zeta(4) \simeq 1.0823232$, and $\zeta(5) \simeq 1.0369278$). Eq. (59.2) must be solved in conjunction with the RG equation for $\overline{\alpha}_s(\mu)$ given in [1]. In addition, as the renormalization scale crosses quark mass thresholds one needs to match the scale dependence of \overline{m} below and above the threshold. There are finite threshold corrections; the necessary formulae can be found in Ref. [5].

59.3. Lattice QCD

The use of lattice QCD calculations for *ab initio* determinations of the fundamental parameters of QCD, including the coupling constant and quark masses (except for the top-quark mass) is a very active area of research (see the review on Lattice Quantum Chromodynamics in this *Review*). Here we only briefly recall those features which are required for the determination of quark masses. In order to determine the lattice spacing (a , i.e. the distance between neighboring points of the lattice) and quark masses, one computes a convenient and appropriate set of physical quantities (frequently chosen to be a set of hadronic masses) for a variety of input values of the quark masses in units of the lattice spacing. These input quark masses are then tuned to their true (physical) values by requiring that the calculation correctly reproduces the set of physical quantities being used for the calibration.

The resulting values of the quark masses are bare quark masses, corresponding to a particular discretization of QCD and with the lattice spacing as the ultraviolet cut-off. In order for these results to be useful in phenomenological applications, it is necessary to relate them to renormalized masses defined in some standard renormalization scheme such as $\overline{\text{MS}}$. Provided that both the ultraviolet cut-off a^{-1} and the renormalization scale μ are much greater than Λ_{QCD} , the bare and renormalized masses can be related in perturbation theory. However, in order to avoid uncertainties due to the unknown higher-order coefficients in lattice perturbation theory, most results obtained recently use *non-perturbative renormalization* to relate the bare masses to those defined in renormalization schemes which can be realized directly in lattice QCD (e.g. those obtained from quark and gluon Green functions at specified momenta in the Landau gauge [6]

or those defined using finite-volume techniques and the Schrödinger functional [7], but not $\overline{\text{MS}}$ that is only defined for dimensional regularization). These methods require $\mu \gg \Lambda_{\text{QCD}}$ so that unwanted (non-perturbative) corrections proportional to inverse powers of μ , which appear in some approaches, remain small corrections that can be identified and removed. This condition is also necessary so that matching to other schemes can be performed reliably in perturbation theory. Moreover, these methods require $a^{-1} \gg \mu$ so that cutoff effects are small enough to be extrapolated away. Thus, the calculations are repeated for finer and finer lattices spacings and the continuum limit, $a \rightarrow 0$, of these non-perturbatively renormalized masses is taken to eliminate all cutoff effects. The conversion to the $\overline{\text{MS}}$ scheme is then performed using continuum perturbation theory, which is more readily obtained to higher orders and is usually better behaved than its lattice counterpart.

It is important to note that the issues surrounding the renormalization of quark masses disappear when considering pairwise ratios of these masses (up to electromagnetic effects for quarks of different charge, which are negligible compared to other uncertainties at present). Indeed, if the same scheme and scale are implemented, QCD renormalization factors are identical for all quark flavors, and these factors therefore cancel exactly in quark-mass ratios. In particular, this means that these ratios are scheme and scale independent. Moreover, these ratios suffer little from the uncertainties in the determination of the lattice scale because they are dimensionless. Thus, quark-mass ratios are typically determined with significantly higher precision using lattice QCD than are the individual masses.

The determination of quark masses using lattice simulations is well established and the current emphasis is on the reduction and control of the systematic uncertainties. With improved algorithms and access to more powerful computing resources, the precision of the results has improved immensely in recent years. Vacuum polarization effects are included with $N_f = 2$, $2 + 1$ or $N_f = 2 + 1 + 1$ flavors of sea quarks. The number 2 here indicates that the up and down quarks are degenerate. Simulations with $2 + 1$ and $2 + 1 + 1$ flavors represent controlled approximations to physical QCD at the low energies considered for quark mass determinations, up to corrections of $O((\Lambda_{\text{QCD}}/m_c)^2/N_c)$ and $O((\Lambda_{\text{QCD}}/m_b)^2/N_c)$, respectively. This is not the case for simulations with $N_f = 2$ or in which vacuum polarization effects are completely neglected (this is the so-called *quenched* approximation) and results obtained in such frameworks will not enter the discussion here.

Particularly pleasing is the observation that different formulations of lattice QCD, with different systematic uncertainties, yield results which are largely consistent with each other. This gives us broad confidence in the estimates of the systematic errors. As the precision of the results approaches (or even exceeds in some cases) 1%, isospin breaking effects, including electromagnetic corrections need to be included and this is beginning to be done as will be discussed below. In particular, a reliable estimate of these effects is required for determining the individual u and d quark masses.

Members of the lattice QCD community have organized a Flavour Lattice Averaging Group (FLAG) which critically reviews quantities computed in lattice QCD relevant to flavor physics, including the determination of quark masses, against stated quality criteria and presents its view of the current status of the results. The latest edition reviews lattice results published before September 30th 2018 [8]. Since that deadline, only a single lattice determination of quark masses has appeared [9]. It is a computation of m_c and m_b in $N_f = 2 + 1$ QCD, based on the method of Euclidean-time moments of pseudoscalar, two-point functions of $c\bar{c}$ quark-bilinear operators described below. Its results are fully consistent with the lattice averages quoted later.

59.4. Light quarks

In this section we review the determination of the masses of the light quarks u , d and s from lattice simulations and then discuss the consequences of the approximate chiral symmetry.

59.4.1. Lattice QCD results :

The most reliable determinations of the strange quark mass m_s and of the average of the up and down quark masses $m_{ud} = (m_u + m_d)/2$ are obtained from lattice simulations. As explained in Sec. 59.3 above, the simulations are generally performed with degenerate up and down quarks ($m_u = m_d$) and so it is the average which is obtained directly from the computations. Below we discuss the derivation of m_u and m_d separately, but we start by briefly presenting our estimate of the current status of the latest lattice results in the isospin symmetric limit. The FLAG Review [8] bases its summary numbers for these quark masses largely on references [10–15] for $N_f = 2 + 1$ and references [16–19] for $N_f = 2 + 1 + 1$ flavors of sea quarks, which its authors consider to have the most reliable estimates of the systematic uncertainties. For $N_f = 2 + 1$ flavors, they quote $\overline{m}_{ud} = (3.364 \pm 0.041)$ MeV, $\overline{m}_s = (92.03 \pm 0.88)$ MeV and $(\overline{m}_s/\overline{m}_{ud}) = 27.42 \pm 0.12$. These numbers are $\overline{m}_{ud} = (3.410 \pm 0.043)$ MeV, $\overline{m}_s = (93.44 \pm 0.68)$ MeV and $(\overline{m}_s/\overline{m}_{ud}) = 27.23 \pm 0.10$ for $N_f = 2 + 1 + 1$ simulations. The masses are given in the $\overline{\text{MS}}$ scheme at a renormalization scale of 2 GeV. Because of the systematic errors, these results are not simply the combinations of all the results in quadrature, but include a judgement of the remaining uncertainties. Since the different collaborations use different formulations of lattice QCD, the (relatively small) variations of the results between the groups provides important information about the reliability of the estimates.

Despite being reported in the $\overline{\text{MS}}$ scheme at a renormalization scale of 2 GeV, the results for \overline{m}_{ud} and \overline{m}_s in the two frameworks differ in their renormalization schemes, since $N_f = 2 + 1$ results are renormalized with $N_L = 3$ and $N_f = 2 + 1 + 1$ ones with $N_L = 4$. Thus, for a comparison, in principle one should convert the results to the same scheme. This is not the case for $(\overline{m}_s/\overline{m}_{ud})$, where renormalization factors cancel. The conversion of the $N_f = 2 + 1$ results to the $N_L = 4$ scheme can be performed, for instance, by running them down to the charm threshold in the $N_L = 3$ theory, matching the results to the $N_L = 4$ theory and running them back up to 2 GeV in that theory. Such a conversion, however, leads to shifts in the values of the quark masses that are well within the quoted errors. Thus, we choose simply to average the results from the two frameworks, yielding as a final lattice QCD estimate in the $\overline{\text{MS}}$ scheme at $\mu = 2$ GeV in the $N_L = 4$ theory:

$$\overline{m}_{ud} = (3.39 \pm 0.04) \text{ MeV} \quad (59.3)$$

$$\overline{m}_s = (92.9 \pm 0.7) \text{ MeV}, \quad (59.4)$$

and

$$\frac{\overline{m}_s}{\overline{m}_{ud}} = 27.37 \pm 0.10. \quad (59.5)$$

where the error bars encompass statistical and systematic errors combined in quadrature. In performing these averages, the only slight tension found is in \overline{m}_s where the weighted average carries a $\chi^2/dof = 1.6$, used to increase the error by the usual $\sqrt{\chi^2/dof}$ scale factor. Note also that we do not allow the errors to become smaller than those on the individual averages because of possible common systematics.

To obtain the individual values of \overline{m}_u and \overline{m}_d requires the introduction of isospin breaking effects, including electromagnetism. This is now being done completely using lattice field theory, albeit neglecting electromagnetic effects in the sea in most cases (see the computation of the neutron-proton mass splitting [20] for an exception). The effect of this neglect on the u and d quark masses has been estimated in [21], to induce a contribution to the uncertainty that ranges from about 3% in $\overline{m}_u/\overline{m}_d$ to less than 1% in \overline{m}_d . FLAG has reviewed these quantities in [8]. Again, they separate results obtained from $N_f = 2 + 1$ and $N_f = 2 + 1 + 1$ simulations. For the former, their final averages are the results of [21], and for the latter, those of [22]. Thus, for $N_f = 2 + 1$ they quote $\overline{m}_u = 2.27(9)$ MeV, $\overline{m}_d = 4.67(9)$ MeV, $(\overline{m}_u/\overline{m}_d) = 0.485(19)$ and, for $N_f = 2 + 1 + 1$, $\overline{m}_u = 2.50(17)$ MeV, $\overline{m}_d = 4.88(20)$ MeV, $(\overline{m}_u/\overline{m}_d) = 0.513(31)$. As for the light quark masses in the isospin limit, we average the results obtained with different numbers of sea-quark flavors. Here, only the \overline{m}_u average has a $\chi^2/dof = 1.4 > 1$, and its error is thus appropriately

scaled. Again, we do not allow the errors to become smaller than those on the individual averages because of possible common systematics. Thus, we give as a final lattice QCD estimate in the $\overline{\text{MS}}$ scheme at $\mu = 2 \text{ GeV}$ in the $N_L = 4$ theory:

$$\overline{m}_u = 2.32(10) \text{ MeV}, \quad \overline{m}_d = 4.71(9) \text{ MeV}, \quad \frac{\overline{m}_u}{\overline{m}_d} = 0.493(19). \quad (59.6)$$

Of particular importance is the fact that $m_u \neq 0$ to more than 20 standard deviations, since there would have been no strong CP problem had m_u been equal to zero.

The results for the light quark masses given in the listings are dominated by the lattice values, since most continuum extractions have larger uncertainties.

59.4.2. Chiral Perturbation Theory :

For light quarks, one can use the techniques of chiral perturbation theory [23–25] to extract quark mass ratios. The mass term for light quarks in the QCD Lagrangian is

$$\overline{\Psi} M \Psi = \overline{\Psi}_L M \Psi_R + \overline{\Psi}_R M^\dagger \Psi_L, \quad (59.7)$$

where M is the light quark mass matrix,

$$M = \begin{pmatrix} m_u & 0 & 0 \\ 0 & m_d & 0 \\ 0 & 0 & m_s \end{pmatrix}, \quad (59.8)$$

$\Psi = (u, d, s)$, and L and R are the left- and right-chiral components of Ψ given by $\Psi_{L,R} = P_{L,R} \Psi$, $P_L = (1 - \gamma_5)/2$, $P_R = (1 + \gamma_5)/2$. The mass term is the only term in the QCD Lagrangian that mixes left- and right-handed quarks. In the limit $M \rightarrow 0$, there is an independent $\text{SU}(3) \times \text{U}(1)$ flavor symmetry for the left- and right-handed quarks. The vector $\text{U}(1)$ symmetry is baryon number; the axial $\text{U}(1)$ symmetry of the classical theory is broken in the quantum theory due to the anomaly. The remaining $G_\chi = \text{SU}(3)_L \times \text{SU}(3)_R$ chiral symmetry of the QCD Lagrangian is spontaneously broken to $\text{SU}(3)_V$, which, in the limit $M \rightarrow 0$, leads to eight massless Goldstone bosons, the π 's, K 's, and η .

The symmetry G_χ is only an approximate symmetry, since it is explicitly broken by the quark mass matrix M . The Goldstone bosons acquire masses which can be computed in a systematic expansion in M , in terms of low-energy constants, which are unknown non-perturbative parameters of the effective theory, and are not fixed by the symmetries. One treats the quark mass matrix M as an external field that transforms under G_χ as $M \rightarrow L M R^\dagger$, where $\Psi_L \rightarrow L \Psi_L$ and $\Psi_R \rightarrow R \Psi_R$ are the $\text{SU}(3)_L$ and $\text{SU}(3)_R$ transformations, and writes down the most general Lagrangian invariant under G_χ . Then one sets M to its given constant value Eq. (59.8), which implements the symmetry breaking. To first order in M one finds that [26]

$$\begin{aligned} m_{\pi^0}^2 &= B(m_u + m_d), \\ m_{\pi^\pm}^2 &= B(m_u + m_d) + \Delta_{\text{em}}, \\ m_{K^0}^2 &= m_{\overline{K}^0}^2 = B(m_d + m_s), \\ m_{K^\pm}^2 &= B(m_u + m_s) + \Delta_{\text{em}}, \\ m_\eta^2 &= \frac{1}{3} B(m_u + m_d + 4m_s), \end{aligned} \quad (59.9)$$

with two unknown constants B and Δ_{em} , the electromagnetic mass difference. From Eq. (59.9), one can determine the quark mass ratios [26]

$$\begin{aligned} \frac{m_u}{m_d} &= \frac{2m_{\pi^0}^2 - m_{\pi^+}^2 + m_{K^+}^2 - m_{\overline{K}^0}^2}{m_{K^0}^2 - m_{K^+}^2 + m_{\pi^+}^2} = 0.56, \\ \frac{m_s}{m_d} &= \frac{m_{K^0}^2 + m_{K^+}^2 - m_{\pi^+}^2}{m_{K^0}^2 + m_{\pi^+}^2 - m_{K^+}^2} = 20.2, \end{aligned} \quad (59.10)$$

to lowest order in chiral perturbation theory, with an error which will be estimated below. Since the mass ratios extracted using chiral perturbation theory use the symmetry transformation property of M under the chiral symmetry G_χ , it is important to use a renormalization scheme for QCD that does not change this transformation law. Any mass independent subtraction scheme such as $\overline{\text{MS}}$ is suitable. The ratios of quark masses are scale independent in such a scheme (up to electromagnetic corrections), and Eq. (59.10) can be taken to be the ratio of $\overline{\text{MS}}$ masses. Chiral perturbation theory cannot determine the overall scale of the quark masses, since it uses only the symmetry properties of M , and any multiple of M has the same G_χ transformation law as M .

Chiral perturbation theory is a systematic expansion in powers of the light quark masses. The typical expansion parameter is $m_K^2/\Lambda_\chi^2 \sim 0.25$ if one uses $\text{SU}(3)$ chiral symmetry, and $m_\pi^2/\Lambda_\chi^2 \sim 0.02$ if instead one uses $\text{SU}(2)$ chiral symmetry. Electromagnetic effects at the few percent level also break $\text{SU}(2)$ and $\text{SU}(3)$ symmetry. The mass formulæ Eq. (59.9) were derived using $\text{SU}(3)$ chiral symmetry, and are expected to have approximately a 25% uncertainty due to second order corrections. This estimate of the uncertainty is consistent with the lattice results summarized in Eq. (59.4)–Eq. (59.5).

There is a subtlety which arises when one tries to determine quark mass ratios at second order in chiral perturbation theory. The second order quark mass term [27]

$$\left(M^\dagger\right)^{-1} \det M^\dagger \quad (59.11)$$

(which can be generated by instantons) transforms in the same way under G_χ as M . Chiral perturbation theory cannot distinguish between M and $(M^\dagger)^{-1} \det M^\dagger$; one can make the replacement $M \rightarrow M(\lambda) = M + \lambda M (M^\dagger M)^{-1} \det M^\dagger$ in the chiral Lagrangian,

$$\begin{aligned} M(\lambda) &= \text{diag}(m_u(\lambda), m_d(\lambda), m_s(\lambda)) \\ &= \text{diag}(m_u + \lambda m_d m_s, m_d + \lambda m_u m_s, m_s + \lambda m_u m_d), \end{aligned} \quad (59.12)$$

and leave all observables unchanged.

The combination

$$\left(\frac{m_u}{m_d}\right)^2 + \frac{1}{Q^2} \left(\frac{m_s}{m_d}\right)^2 = 1 \quad (59.13)$$

where

$$Q^2 = \frac{m_s^2 - m_{ud}^2}{m_d^2 - m_u^2}, \quad m_{ud} = \frac{1}{2}(m_u + m_d),$$

is insensitive to the transformation in Eq. (59.12). Eq. (59.13) gives an ellipse in the $m_u/m_d - m_s/m_d$ plane. The ellipse is well-determined by chiral perturbation theory, but the exact location on the ellipse, and the absolute normalization of the quark masses, has larger uncertainties. Q is determined to be 22.1(7) from $\eta \rightarrow 3\pi$ decay and the electromagnetic contribution to the $K^+ - K^0$ and $\pi^+ - \pi^0$ mass differences [28]. Lattice QCD collaborations have also reported determinations of Q . Using $N_f = 2 + 1$ simulations, [21] obtains $Q = 23.4(6)$ and [22] determines $Q = 23.8(1.1)$ with $N_f = 2 + 1 + 1$ simulations, which are fully compatible. The $N_f = 2 + 1$ result is about 2 standard deviations larger than the one from phenomenology given above [28]. These values can also be compared to the leading-order result for Q in $\text{SU}(3)$ chiral perturbation theory, that can be derived using Eq. (59.9) and the values for the relevant meson masses given in this review. This result also holds to next-to-leading order, thus: $Q^{\text{NLO}} = 24.3$.

The absolute normalization of the quark masses cannot be determined using chiral perturbation theory. Other methods, such as lattice simulations discussed above, or spectral function sum rules [29,30] for hadronic correlation functions reviewed next, are necessary.

59.4.3. Sum rules :

Sum rule methods have been used extensively to determine quark masses and for illustration we briefly discuss here their application to hadronic τ decays [31]. Other applications involve very similar techniques.

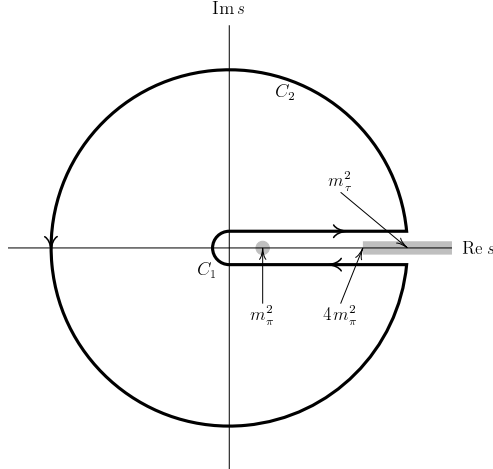


Figure 59.1: The analytic structure of $\Pi(s)$ in the complex s -plane. The contours C_1 and C_2 are the integration contours discussed in the text, and the integral over the closed contour $C_1 + C_2$ vanishes. m_τ^2 has not been drawn to scale; $m_\tau^2 \sim 40(4m_\pi^2)$.

The experimentally measured quantity is R_τ ,

$$\frac{dR_\tau}{ds} = \frac{d\Gamma/ds(\tau^- \rightarrow \text{hadrons} + \nu_\tau(\gamma))}{\Gamma(\tau^- \rightarrow e^- \bar{\nu}_e \nu_\tau(\gamma))} \quad (59.14)$$

the hadronic invariant mass spectrum in semihadronic τ decay, normalized to the leptonic τ decay rate. It is useful to define q as the total momentum of the hadronic final state, so $s = q^2$ is the hadronic invariant mass. The total hadronic τ decay rate R_τ is then given by integrating dR_τ/ds over the kinematically allowed range $0 \leq s \leq M_\tau^2$.

R_τ can be written as

$$R_\tau = 12\pi \int_0^{M_\tau^2} \frac{ds}{M_\tau^2} \left(1 - \frac{s}{M_\tau^2}\right)^2 \times \left[\left(1 + 2\frac{s}{M_\tau^2}\right) \text{Im} \Pi^T(s) + \text{Im} \Pi^L(s) \right] \quad (59.15)$$

where the hadronic spectral functions $\Pi^{L,T}$ are defined from the time-ordered correlation function of two weak currents ($j^\mu(x)$ and $j^\nu(0)$) by

$$\Pi^{\mu\nu}(q) = i \int d^4x e^{iq \cdot x} \langle 0 | T(j^\mu(x) j^\nu(0)^\dagger) | 0 \rangle, \quad (59.16)$$

$$\Pi^{\mu\nu}(q) = (-g^{\mu\nu} + q^\mu q^\nu) \Pi^T(s) + q^\mu q^\nu \Pi^L(s), \quad (59.17)$$

and the decomposition Eq. (59.17) is the most general possible structure consistent with Lorentz invariance.

By the optical theorem, the imaginary part of $\Pi^{\mu\nu}$ is proportional to the total cross-section for the current to produce all possible states. A detailed analysis including the phase space factors leads to Eq. (59.15). The spectral functions $\Pi^{L,T}(s)$ are analytic in the complex s plane, with singularities along the real axis. There is an isolated pole at $s = m_\pi^2$, and single- and multi-particle singularities for $s \geq 4m_\pi^2$, the two-particle threshold. The discontinuity along the real axis is $\Pi^{L,T}(s+i0^+) - \Pi^{L,T}(s-i0^+) = 2i \text{Im} \Pi^{L,T}(s)$. As a result, Eq. (59.15) can be rewritten with the replacement $\text{Im} \Pi^{L,T}(s) \rightarrow -i \Pi^{L,T}(s)/2$, and the integration being over the contour C_1 . Finally, the contour

C_1 can be deformed to $-C_2$ without crossing any singularities, and so leaving the integral unchanged, i.e. the integral over the closed contour $C_1 + C_2$ vanishes. One can derive a series of sum rules analogous to Eq. (59.15) by weighting the differential τ hadronic decay rate by different powers of the hadronic invariant mass [32],

$$R_\tau^{kl} = \int_0^{M_\tau^2} ds \left(1 - \frac{s}{M_\tau^2}\right)^k \left(\frac{s}{M_\tau^2}\right)^l \frac{dR_\tau}{ds} \quad (59.18)$$

where dR_τ/ds is the hadronic invariant mass distribution in τ decay normalized to the leptonic decay rate. This leads to the final form of the sum rule(s),

$$R_\tau^{kl} = -6\pi i \int_{C_2} \frac{ds}{M_\tau^2} \left(1 - \frac{s}{M_\tau^2}\right)^{2+k} \left(\frac{s}{M_\tau^2}\right)^l \times \left[\left(1 + 2\frac{s}{M_\tau^2}\right) \Pi^T(s) + \Pi^L(s) \right]. \quad (59.19)$$

The manipulations so far are completely rigorous and exact, relying only on the general analytic structure of quantum field theory. The left-hand side of the sum rule Eq. (59.19) is obtained from experiment. The right hand-side can be computed for s far away from any physical cuts using the operator product expansion (OPE) for the time-ordered product of currents in Eq. (59.16), and QCD perturbation theory. The OPE is an expansion for the time-ordered product Eq. (59.16) in a series of local operators, and is an expansion about the $q \rightarrow \infty$ limit. It gives $\Pi^{L,T}(s)$ as an expansion in powers of $\alpha_s(s)$ and Λ_{QCD}^2/s , and is valid when s is far (in units of Λ_{QCD}^2) from any singularities in the complex s -plane.

The OPE gives $\Pi^{L,T}(s)$ as a series in α_s , quark masses, and various non-perturbative vacuum matrix elements. By computing $\Pi^{L,T}(s)$ theoretically, and comparing with the experimental values of R_τ^{kl} , one determines various parameters such as α_s and the quark masses. The theoretical uncertainties in using Eq. (59.19) arise from neglected higher order corrections (both perturbative and non-perturbative), and because the OPE is no longer valid near the real axis, where $\Pi^{L,T}$ have singularities. The contribution of neglected higher order corrections can be estimated as for any other perturbative computation. The error due to the failure of the OPE is more difficult to estimate. In Eq. (59.19), the OPE fails on the endpoints of C_2 that touch the real axis at $s = M_\tau^2$. The weight factor $(1 - s/M_\tau^2)$ in Eq. (59.19) vanishes at this point, so the importance of the endpoint can be reduced by choosing larger values of k .

Light quark masses are often determined using QCD sum rules [30], which are similar to the τ sum rules. One takes the correlator of two light-quark-bilinear operators (e.g. an axial vector current), as in Eq. (59.16), and computes their Laplace transforms or moments

$$\mathcal{L}_n(\tau) = \int_0^\infty ds s^n e^{-\tau s} \text{Im} \Pi(s), \quad \mathcal{M}_n(Q^2) = \int_0^\infty \frac{ds}{(s+Q^2)^n} \text{Im} \Pi(s)$$

to get Laplace or moment sum rules, respectively. The quark masses are extracted by comparing the theoretical and experimental values of $\mathcal{L}_n(\tau)$ and $\mathcal{M}_n(Q^2)$. Considerable theoretical effort has gone into optimizing n and Q^2 to improve the precision of the resulting light quark masses.

59.5. Heavy quarks

59.5.1. Continuum approaches and results :

For heavy quark physics one can exploit the fact that $m_Q \gg \Lambda_{\text{QCD}}$ to construct effective theories (m_Q is the mass of the heavy quark Q). The masses and decay rates of hadrons containing a single heavy quark, such as the B and D mesons can be determined using the heavy quark effective theory (HQET) [33]. The theoretical calculations involve radiative corrections computed in perturbation theory with an expansion in $\alpha_s(m_Q)$ and non-perturbative corrections with an expansion in powers of Λ_{QCD}/m_Q . Due to the asymptotic nature of the QCD perturbation series, the two kinds of corrections are intimately related; an example of this are renormalon effects in the

perturbative expansion which are associated with non-perturbative corrections.

Systems containing two heavy quarks such as the Υ or J/Ψ are treated using non-relativistic QCD (NRQCD) [34]. The typical momentum and energy transfers in these systems are $\alpha_s m_Q$, and $\alpha_s^2 m_Q$, respectively, so these bound states are sensitive to scales much smaller than m_Q . However, smeared observables, such as the cross-section for $e^+e^- \rightarrow \bar{b}b$ averaged over some range of s that includes several bound state energy levels, are better behaved and only sensitive to scales near m_Q . For this reason, most determinations of the c, b quark masses using perturbative calculations compare smeared observables with experiment [35–37]. The method is similar to that outlined for τ decays. The current correlator in Eq. (59.16) is the electromagnetic current, and the experimental data is the value of $R(s)$ in the threshold region for $e^+e^- \rightarrow Q\bar{Q}$. The theoretical values for the moments are computed using renormalization group improved calculations in non-relativistic QCD.

There are many continuum extractions of the c and b quark masses, some with quoted errors of 10 MeV or smaller. There are systematic effects of comparable size, which are typically not included in these error estimates. Reference [38], for example, shows that even though the error estimate of m_c using the rapid convergence of the α_s perturbation series is only a few MeV, the central value of m_c can differ by a much larger amount depending on which algorithm (all of which are formally equally good) is used to determine m_c from the data. This leads to a systematic error from perturbation theory of around 20 MeV for the c quark and 25 MeV for the b quark. Electromagnetic effects, which also are important at this precision, are often not included. For this reason, we inflate the errors on the continuum extractions of m_c and m_b . The average values of m_c and m_b from continuum determinations are (see Sec. G for the 1S scheme)

$$\begin{aligned} \overline{m}_c(\overline{m}_c) &= (1.280 \pm 0.025) \text{ GeV}, \\ \overline{m}_b(\overline{m}_b) &= (4.18 \pm 0.03) \text{ GeV}, \quad m_b^{1S} = (4.65 \pm 0.03) \text{ GeV}. \end{aligned}$$

59.5.2. Lattice approaches and results :

Lattice simulations of QCD lead to discretization errors which are powers of am_Q (modulated by logarithms); the power depends on the formulation of lattice QCD being used and in most cases is quadratic. Clearly these errors can be reduced by performing simulations at smaller lattice spacings, but also by using *improved* discretizations of the theory. Recently, with more powerful computing resources, better algorithms and techniques, it has become possible to perform simulations in the charm quark region and beyond, also decreasing the extrapolation which has to be performed to reach the b -quark.

Traditionally the charm quark mass is obtained by tuning its bare, simulation value to reproduce the physical mass of charmonium mesons or of the D, D_s mesons (requiring a more precise tuning of the light quark masses). This mass can then be renormalized to the $\overline{\text{MS}}$ scheme using the methods discussed for the light quarks.

An alternative approach for obtaining the $\overline{\text{MS}}$ mass from the tuned bare quark mass was proposed in [39]. Euclidean-time moments of pseudoscalar, two-point functions of $c\bar{c}$ quark-bilinear operators can readily be computed on the lattice and extrapolated to the continuum limit where they can be compared to perturbative calculations of the same quantities at 4-loop order. In this way, both the strong coupling constant and the charm quark mass can be determined with remarkably small errors. As this approach uses the same perturbative expressions for two-point correlators as the continuum determinations discussed above, it suffers from similar perturbation-theory, systematic errors. FLAG [8] has reviewed lattice determinations of the charm quark mass obtained using both approaches. The most advanced calculations are performed with $N_f = 2 + 1 + 1$ simulations. For these, the quoted average is

$$\overline{m}_c(\overline{m}_c) = 1.280(13) \text{ GeV},$$

based on the calculations performed in [17,16,40,18,19], in good agreement with the continuum result quoted above, but with a smaller

error. It is worth noting that while three [17,18,19] of the four calculations entering this average agree, the fourth [16,40] is about two standard deviations larger, and this is taken into account in the error bar. It should also be remembered that these results were obtained in QCD with exact isospin symmetry, though isospin breaking corrections to the physical inputs, including electromagnetism, are accounted for using phenomenology.

Historically, the main approach to controlling the discretization errors in lattice studies of b quark physics was to perform simulations of effective theories such as HQET and NRQCD. This remains an important technique, both in its own right and in providing additional information for extrapolations from lower masses to the bottom region. Using effective theories, m_b is obtained from what is essentially a computation of the difference of $M_{H_b} - m_b$, where M_{H_b} is the mass of a hadron H_b containing a b -quark. The relative error on m_b is therefore much smaller than that for $M_{H_b} - m_b$. The principal systematic errors are the matching of the effective theories to QCD and the presence of power divergences in a^{-1} in the $1/m_b$ corrections which have to be subtracted numerically. A procedure for performing these subtractions fully non-perturbatively was proposed and implemented for the first time in [41].

The most recent lattice QCD determinations of the b quark mass rely on a variety of approaches, including Euclidean-time moments of correlation functions with [42] or without NRQCD [17] and HQET based interpolations [43,44] or extrapolations [18] from above the charm to the b region. The overall agreement of the results obtained using these very different approaches, which have different systematic errors, is a confirmation that the various groups control these uncertainties. As the range of heavy-quark masses which can be used in numerical simulations increases, results obtained by extrapolating the results to b -physics are becoming ever more reliable (see e.g. [18]) . FLAG's compilation [8] of the above $N_f = 2 + 1 + 1$ results yields

$$\overline{m}_b(\overline{m}_b) = 4.198(12) \text{ GeV}.$$

Again, this result is compatible with the average value of continuum results, but with a significantly smaller uncertainty.

As explained in Sec. 59.3, ratios of quark masses can have significantly smaller errors than the individual masses if they are computed in the same lattice QCD framework and in the same renormalization scheme at identical scales. This led HPQCD to leverage their precise determination of m_c [39] to determine m_s and m_{ud} [57], through a precise computation of m_c/m_s [57] and of m_s/m_{ud} [58]. This $N_f = 2 + 1$ calculation was updated using $N_f = 2 + 1 + 1$ simulations in [17]. The ratio m_s/m_c was also computed in [15,59] with $N_f = 2 + 1$ simulations and in [16,18] with $N_f = 2 + 1 + 1$ ones. Based on [57,59], FLAG quotes [8] $m_c/m_s = 11.82(16)$ for $N_f = 2 + 1$, and $m_c/m_s = 11.768(33)$ for $N_f = 2 + 1 + 1$, based on [16,17,18], where a 50% stretch of the combined error was applied due to a tension between the results of [16] and [17]. As a final lattice number we give the $N_f = 2 + 1 + 1$ average

$$m_c/m_s = 11.768(33),$$

which is renormalization scheme and scale independent.

The ratio m_b/m_c has also been computed on the lattice. The most advanced calculations have been performed with $N_f = 2 + 1 + 1$ simulations [17,43,18]. Averaging these results using the FLAG [8] procedure yields

$$m_b/m_c = 4.576(11),$$

where a scale factor of $\sqrt{\chi^2/dof} = 1.45$ has been applied to the error bar. Indeed, [43] contributes 3.3 to the total χ^2 .

59.5.3. Warnings concerning the use of the pole mass :

For an observable particle such as the electron, the position of the pole in the propagator is the definition of its mass. In QCD this definition of the quark mass is known as the pole mass. It is known that the on-shell quark propagator has no infrared divergences in perturbation theory [45,46], so this provides a perturbative definition of the quark mass. However, the pole mass cannot be used to arbitrarily high accuracy because of non-perturbative infrared effects

in QCD. In fact the full quark propagator has no pole because the quarks are confined, so that the pole mass cannot be defined outside of perturbation theory. The relation between the pole mass m_Q and the $\overline{\text{MS}}$ mass \overline{m}_Q , used throughout this review, is known to three loops [47–50]

$$m_Q = \overline{m}_Q(\overline{m}_Q) \left\{ 1 + \frac{4\overline{\alpha}_s(\overline{m}_Q)}{3\pi} + \left[-1.0414 \sum_q \left(1 - \frac{4}{3} \frac{\overline{m}_q}{\overline{m}_Q} \right) + 13.4434 \right] \left[\frac{\overline{\alpha}_s(\overline{m}_Q)}{\pi} \right]^2 + \left[0.6527 N_L^2 - 26.655 N_L + 190.595 \right] \left[\frac{\overline{\alpha}_s(\overline{m}_Q)}{\pi} \right]^3 \right\}, \quad (59.20)$$

where $\overline{\alpha}_s(\mu)$ is the strong interaction coupling constants in the $\overline{\text{MS}}$ scheme, and the sum over q extends over the N_L flavors lighter than Q . The complete mass dependence of the α_s^2 term can be found in [47]; the mass dependence of the α_s^3 term is not known. For the b -quark, Eq. (59.20) reads

$$m_b = \overline{m}_b(\overline{m}_b) [1 + 0.10 + 0.05 + 0.03], \quad (59.21)$$

where the contributions from the different orders in α_s are shown explicitly. The two and three loop corrections are comparable in size and have the same sign as the one loop term. This is a signal of the asymptotic nature of the perturbation series (there is a renormalon in the pole mass [51]). Such a badly behaved perturbation expansion can be avoided by directly extracting, from data, the mass defined in the $\overline{\text{MS}}$ (used in this review) or other short-distance schemes (see below), without invoking the pole mass as an intermediate step.

59.6. Numerical values and caveats

The quark masses in the particle data listings have been obtained by using a wide variety of methods. Each method involves its own set of approximations and uncertainties. In most cases, the errors are an estimate of the size of neglected higher-order corrections or other uncertainties. The expansion parameters for some of the approximations are not very small (for example, they are $m_K^2/\Lambda_\chi^2 \sim 0.25$ for the SU(3) chiral expansion and $\Lambda_{\text{QCD}}/m_b \sim 0.1$ for the heavy-quark expansion), so an unexpectedly large coefficient in a neglected higher-order term could significantly alter the results. Thus, before using a particular result, it is important to understand the possible limitations of the approach used to obtain it. It is also important to note that the quark mass values can be significantly different in the different schemes.

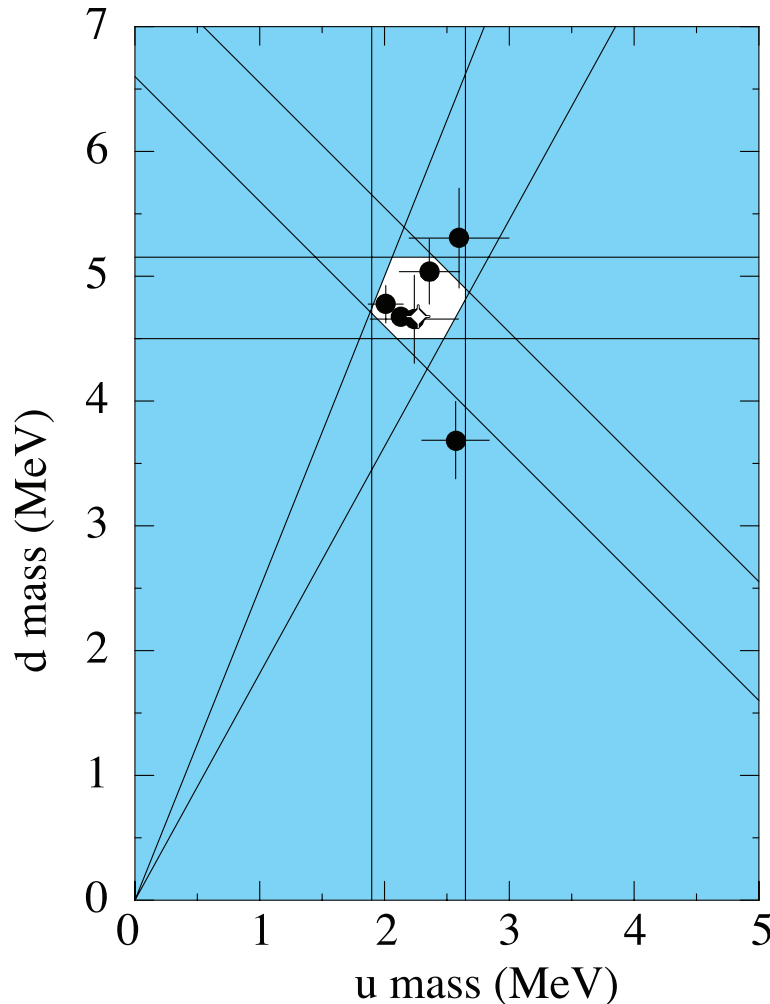


Figure 59.2: The allowed region (shown in white) for up quark and down quark masses renormalized in the $\overline{\text{MS}}$ scheme at 2 GeV. This region was determined in part from papers reporting values for m_u and m_d (data points shown) and in part from an analysis of the allowed ranges of other mass parameters (see Fig. 59.3). The parameter $(m_u + m_d)/2$ yields the two downward-sloping lines, while m_u/m_d yields the two rising lines originating at (0,0). There are two overlapping data points, so one of them is shown as a white diamond (it has very small error bars).

We have specified all masses in the $\overline{\text{MS}}$ scheme. For light quarks, the renormalization scale has been chosen to be $\mu = 2 \text{ GeV}$. Quoting these masses at smaller values of μ , where perturbative corrections become significantly larger, would introduce unnecessary uncertainties in the results. In fact, as lattice calculations, performed on finer and finer lattices, allow to determine quark masses, fully non-perturbatively, at larger and larger values of μ , it may become advantageous to quote quark mass results at renormalization scales above 2 GeV , where perturbative uncertainties are smaller.

Given the small size of the charm quark mass, in the future it may become advantageous to quote its value at larger values of μ so as not to introduce unnecessary perturbative uncertainties (see discussion above). Analyses of inclusive B meson decays have shown that other mass definitions lead to a better behaved perturbation series than for the $\overline{\text{MS}}$ mass, and hence to more accurate mass values [52,53,54,56]. Thus, we have chosen to also give values for one of these, the b quark mass in the $1S$ -scheme [52,53]. Other schemes that have been proposed are the PS -scheme [54], the kinetic scheme [55] and, most

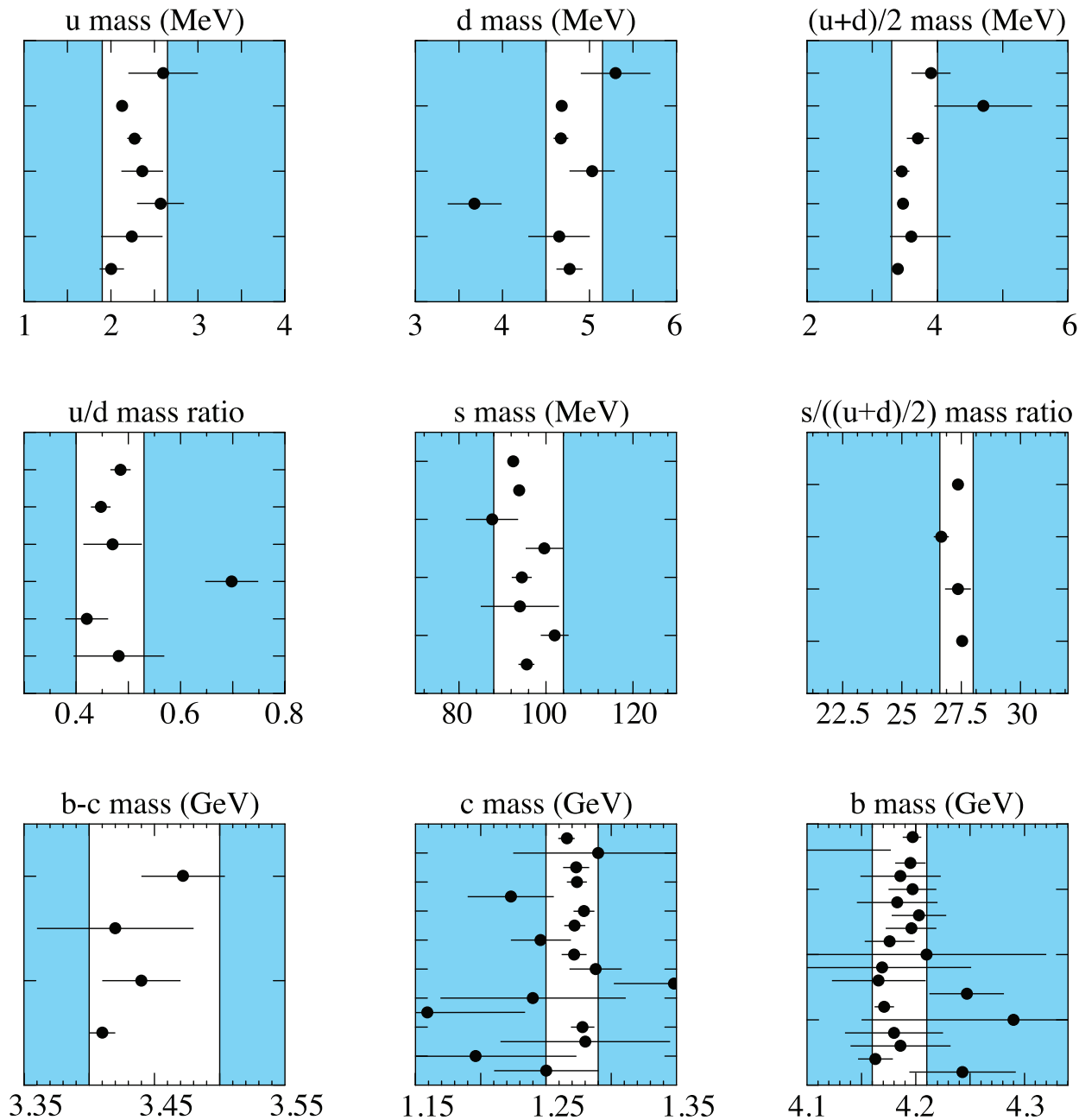


Figure 59.3: The values of each quark mass parameter taken from the Data Listings. The points are in chronological order with the more recent measurements at the top. The shaded regions indicate values excluded by our evaluations; some regions were determined in part through examination of Fig. 59.2.

The heavy quark masses obtained using HQET, QCD sum rules, or lattice gauge theory are consistent with each other if they are all converted into the same scheme and scale. For these quarks it is conventional to choose the renormalization scale equal to the quark mass, so we have quoted $\overline{m}_Q(\mu)$ at $\mu = \overline{m}_Q$ for the c and b quarks.

recently, the minimal renormalon-subtracted mass (MRS) [56] used in the lattice calculation [18].

If necessary, we have converted values in the original papers to our chosen scheme using two-loop formulae. It is important to realize that our conversions introduce significant additional errors. In converting to the $\overline{\text{MS}}$ b -quark mass, for example, the three-loop

conversions from the 1S and pole masses give values about 35 MeV and 135 MeV lower than the two-loop conversions. The uncertainty in $\alpha_s(M_Z) = 0.1179 \pm 0.0010$ [1] gives an uncertainty of ± 9 MeV and ± 21 MeV respectively in the same conversions. We have not added these additional errors when we do our conversions. The α_s value in the conversion is correlated with the α_s value used in determining the quark mass, so the conversion error is not a simple additional error on the quark mass.

References:

1. See the review of QCD in this volume..
2. A.V. Manohar and H. Georgi, Nucl. Phys. **B234**, 189 (1984).
3. K.G. Chetyrkin, Phys. Lett. **B404**, 161 (1997).
4. J.A.M. Vermaseren, S.A. Larin, and T. van Ritbergen, Phys. Lett. **B405**, 327 (1997).
5. K.G. Chetyrkin, B.A. Kniehl, and M. Steinhauser, Nucl. Phys. **B510**, 61 (1998).
6. G. Martinelli *et al.*, Nucl. Phys. **B445**, 81 (1995).
7. K. Jansen *et al.*, Phys. Lett. **B372**, 275 (1996).
8. S. Aoki *et al.* [Flavour Lattice Averaging Group], [arXiv:1902.08191 [hep-lat]].
9. P. Petreczky and J. H. Weber, arXiv:1901.06424 [hep-lat].
10. A. Bazavov *et al.* [MILC collaboration], PoS **CD09** (2009) 007.
11. A. Bazavov *et al.*, PoS **LATTICE2010** (2010) 083.
12. S. Durr *et al.*, Phys. Lett. **B701**, 265 (2011).
13. S. Durr *et al.*, JHEP **1108**, 148 (2011).
14. T. Blum *et al.* [RBC and UKQCD collaborations], Phys. Rev. **D93**, 074505 (2016).
15. Y. Maetzawa and P. Petreczky, Phys. Rev. **D94**, 034507 (2016).
16. N. Carrasco *et al.* [ETM collaboration], Nucl. Phys. **B887**, 19 (2014).
17. B. Chakraborty *et al.* [HPQCD collaboration], Phys. Rev. **D91**, 054508 (2015).
18. A. Bazavov *et al.* [Fermilab Lattice and MILC and TUMQCD collaborations], Phys. Rev. **D98**, 054517 (2018).
19. A. T. Lytle *et al.* [HPQCD collaboration], Phys. Rev. **D98**, 014513 (2018).
20. S. Borsanyi *et al.* [BMW collaboration], Science **347**, 1452 (2015).
21. Z. Fodor *et al.* [BMW collaboration], Phys. Rev. Lett. **117**, 082001 (2016).
22. D. Giusti, V. Lubicz, C. Tarantino, G. Martinelli, S. Sanfilippo, S. Simula and N. Tantalo [RM123 collaboration], Phys. Rev. **D95**, 114504 (2017).
23. S. Weinberg, Physica **96A**, 327 (1979).
24. J. Gasser and H. Leutwyler, Ann. Phys. **158**, 142 (1984).
25. For a review, see A. Pich, Rept. on Prog. in Phys. **58**, 563 (1995).
26. S. Weinberg, Trans. N.Y. Acad. Sci. **38**, 185 (1977).
27. D.B. Kaplan and A.V. Manohar, Phys. Rev. Lett. **56**, 2004 (1986).
28. G. Colangelo, S. Lanz, H. Leutwyler and E. Passemar, Eur. Phys. J. C **78**, no. 11, 947 (2018).
29. S. Weinberg, Phys. Rev. Lett. **18**, 507 (1967).
30. M.A. Shifman, A.I. Vainshtein, and V.I. Zakharov, Nucl. Phys. **B147**, 385 (1979).
31. E. Braaten, S. Narison, and A. Pich, Nucl. Phys. **B373**, 581 (1992).
32. F. Le Diberder and A. Pich, Phys. Lett. **B286**, 147 (1992) doi:10.1016/0370-2693(92)90172-Z.
33. N. Isgur and M.B. Wise, Phys. Lett. **B232**, 113 (1989), *ibid*, **B237**, 527 (1990).
34. G.T. Bodwin, E. Braaten, and G.P. Lepage, Phys. Rev. **D51**, 1125 (1995).
35. A.H. Hoang, Phys. Rev. **D61**, 034005 (2000).
36. K. Melnikov and A. Yelkhovsky, Phys. Rev. **D59**, 114009 (1999).
37. M. Beneke and A. Signer, Phys. Lett. **B471**, 233 (1999).
38. B. Dehnadi, A. H. Hoang, V. Mateu and S. M. Zebarjad, JHEP **1309**, 103 (2013).
39. I. Allison *et al.* [HPQCD collaboration], Phys. Rev. **D78**, 054513 (2008).
40. C. Alexandrou, V. Drach, K. Jansen, C. Kallidonis and G. Koutsou, Phys. Rev. D **90**, no. 7, 074501 (2014).
41. J. Heitger *et al.* [ALPHA collaboration], JHEP **0402**, 022 (2004).
42. B. Colquhoun, R. J. Dowdall, C. T. H. Davies, K. Hornbostel and G. P. Lepage [HPQCD collaboration], Phys. Rev. D **91**, no. 7, 074514 (2015).
43. A. Bussone *et al.* [ETM collaboration], Phys. Rev. D **93**, no. 11, 114505 (2016).
44. P. Gambino, A. Melis and S. Simula, Phys. Rev. D **96**, no. 1, 014511 (2017).
45. R. Tarrach, Nucl. Phys. **B183**, 384 (1981).
46. A. Kronfeld, Phys. Rev. **D58**, 051501 (1998).
47. N. Gray *et al.*, Z. Phys. **C48**, 673 (1990).
48. D.J. Broadhurst, N. Gray, and K. Schilcher, Z. Phys. **C52**, 111 (1991).
49. K.G. Chetyrkin and M. Steinhauser, Phys. Rev. Lett. **83**, 4001 (1999).
50. K. Melnikov and T. van Ritbergen, Phys. Lett. **B482**, 99 (2000).
51. M. Beneke and V. M. Braun, Nucl. Phys. B **426**, 301 (1994).
52. A.H. Hoang, Z. Ligeti, A.V. Manohar, Phys. Rev. Lett. **82**, 277 (1999).
53. A.H. Hoang, Z. Ligeti, A.V. Manohar, Phys. Rev. **D59**, 074017 (1999).
54. M. Beneke, Phys. Lett. **B434**, 115 (1998).
55. P. Gambino and N. Uraltsev, Eur. Phys. J. **C34**, 181 (2004).
56. N. Brambilla *et al.* [TUMQCD collaboration], Phys. Rev. D **97**, no. 3, 034503 (2018).
57. C.T.H. Davies *et al.* [HPQCD collaboration], Phys. Rev. Lett. **104**, 132003 (2010).
58. A. Bazavov *et al.* [MILC Collaboration], Rev. Mod. Phys. **82**, 1349 (2010).
59. Y. B. Yang *et al.* [χ QCD collaboration], Phys. Rev. D **92**, no. 3, 034517 (2015).

60. Top Quark

Revised August 2019 by T.M. Liss (City Coll. of New York), F. Maltoni (CP3 U. catholique de Louvain; Bologna U.) and A. Quadt (Göttingen U.).

60.1 Introduction

In the Standard Model (SM), the left-handed top quark is the $Q = 2/3, T_3 = +1/2$ member of the weak-isospin doublet containing the bottom quark, while the right-handed top is an $SU(2)_L$ singlet (see, e.g., the review “Electroweak Model and Constraints on New Physics”). Its phenomenology is driven by its large mass. Being heavier than a W boson, it is the only quark that decays semi-weakly, i.e., into a real W boson and a b quark. Therefore, it has a very short lifetime and decays before hadronization can occur. In addition, it is the only quark whose Yukawa coupling to the Higgs boson is of order unity. For these reasons, the top quark plays a special role in the Standard Model and in many extensions thereof. Top quark physics provides a unique laboratory where our understanding of the strong interactions, both in the perturbative and non-perturbative regimes, can be tested. An accurate knowledge of its properties (mass, couplings, production cross sections, decay branching ratios, *etc.*) can bring key information on fundamental interactions at the electroweak symmetry-breaking scale and beyond. This review provides a concise discussion of the experimental and theoretical issues involved in the determination of the top-quark properties.

60.2 Top-quark production at the Tevatron and LHC

In hadron collisions, top quarks are produced dominantly in pairs through the processes $q\bar{q} \rightarrow t\bar{t}$ and $gg \rightarrow t\bar{t}$, at leading order in QCD. Approximately 85% of the production cross section at the Tevatron ($p\bar{p}$ at 1.96 TeV) is from $q\bar{q}$ annihilation, with the remainder from gluon-gluon fusion, while at LHC (pp) energies about 90% of the production is from the latter process at $\sqrt{s} = 14$ TeV ($\approx 80\%$ at $\sqrt{s} = 7$ TeV).

Predictions for the top-quark production total cross sections are available at next-to-next-to leading order (NNLO) [1, 2], also including next-to-next-to-leading-log (NNLL) soft gluon resummation. Assuming a top-quark mass of 173.3 GeV/ c^2 , close to the Tevatron + LHC average [3], the resulting theoretical prediction of the top-quark pair cross-section at NNLO+NNLL accuracy at the Tevatron at $\sqrt{s} = 1.96$ TeV is $\sigma_{t\bar{t}} = 7.16^{+0.11+0.17}_{-0.20-0.12}$ pb where the first uncertainty is from scale dependence and the second from parton distribution functions. At the LHC, assuming a top-quark mass of 172.5 GeV/ c^2 the cross sections are: $\sigma_{t\bar{t}} = 177.3^{+4.6+9.0}_{-6.0-9.0}$ pb at $\sqrt{s} = 7$ TeV, $\sigma_{t\bar{t}} = 252.9^{+6.4+11.5}_{-8.6-11.5}$ pb at $\sqrt{s} = 8$ TeV, $\sigma_{t\bar{t}} = 831.8^{+19.8+35.1}_{-29.2-35.1}$ pb at $\sqrt{s} = 13$ TeV, and $\sigma_{t\bar{t}} = 984.5^{+23.2+41.3}_{-34.7-41.3}$ pb at $\sqrt{s} = 14$ TeV [1].

Electroweak single top-quark production mechanisms, namely from $q\bar{q}' \rightarrow t\bar{b}$ [4], $qb \rightarrow q't$ [5], mediated by virtual s -channel and t -channel W -bosons, and Wt -associated production, through $bg \rightarrow W^-t$, lead to somewhat smaller cross sections. For example, t -channel production, while suppressed by the weak coupling with respect to the strong pair production, is kinematically enhanced, resulting in a sizeable cross section both at Tevatron and LHC energies. At the Tevatron, the t - and s -channel cross sections for top quarks are identical to those for antitop quarks, while at the LHC they are not, due to the charge-asymmetric initial state. Approximate NNLO cross sections for t -channel single top-quark production ($t + \bar{t}$) are calculated for $m_t = 173.3$ GeV/ c^2 to be $2.06^{+0.13}_{-0.13}$ pb in $p\bar{p}$ collisions at $\sqrt{s} = 1.96$ TeV (scale and parton distribution functions uncertainties are combined in quadrature) [6]. Recently, calculations at NNLO accuracy for the t -channel cross section at the LHC have appeared [7, 8], predicting ($m_t = 172.5$ GeV/ c^2): $\sigma_{t+\bar{t}} = 64.0^{+0.77}_{-0.38}$ pb at $\sqrt{s} = 7$ TeV, $\sigma_{t+\bar{t}} = 84.6^{+1.0}_{-0.51}$ pb at $\sqrt{s} = 8$ TeV, $\sigma_{t+\bar{t}} = 215^{+2.1}_{-1.3}$ pb at $\sqrt{s} = 13$ TeV, and $\sigma_{t+\bar{t}} = 245^{+2.7}_{-1.3}$ pb at $\sqrt{s} = 14$ TeV, where the quoted uncertainties are from scale variation only. For the s -channel, NNLO approximated calculations yield $1.03^{+0.05}_{-0.05}$ pb for the Tevatron, and $4.5^{+0.2}_{-0.2}(5.5^{+0.2}_{-0.2})$ pb for $\sqrt{s} = 7$ (8) TeV at the LHC, with 69% (31%) of top (anti-top) quarks [9]. While negligible at the Tevatron, at LHC energies the Wt -associated

production becomes relevant. At $\sqrt{s} = 7$ (8) TeV, an approximate NNLO calculation gives $15.5^{+1.2}_{-1.2}(22.1^{+1.5}_{-1.5})$ pb ($t + \bar{t}$), with an equal proportion of top and anti-top quarks [10].

Assuming $|V_{tb}| \gg |V_{td}|, |V_{ts}|$ (see the review “The CKM Quark-Mixing Matrix” for more information), the cross sections for single top production are proportional to $|V_{tb}|^2$, and no extra hypothesis is needed on the number of quark families or on the unitarity of the CKM matrix in extracting $|V_{tb}|$. Separate measurements of the s - and t -channel processes provide sensitivity to physics beyond the Standard Model [11].

With a mass above the Wb threshold, and $|V_{tb}| \gg |V_{td}|, |V_{ts}|$, the decay width of the top quark is expected to be dominated by the two-body channel $t \rightarrow Wb$. Neglecting terms of order m_b^2/m_t^2 , α_s^2 , and $(\alpha_s/\pi)M_W^2/m_t^2$, the width predicted in the SM at NLO is [12]:

$$\Gamma_t = \frac{G_F m_t^3}{8\pi\sqrt{2}} \left(1 - \frac{M_W^2}{m_t^2}\right)^2 \left(1 + 2\frac{M_W^2}{m_t^2}\right) \left[1 - \frac{2\alpha_s}{3\pi} \left(\frac{2\pi^2}{3} - \frac{5}{2}\right)\right], \quad (60.1)$$

where m_t refers to the top-quark pole mass. The width for a value of $m_t = 173.3$ GeV/ c^2 is 1.35 GeV/ c^2 (we use $\alpha_s(M_Z) = 0.118$) and increases with mass. With its correspondingly short lifetime of $\approx 0.5 \times 10^{-24}$ s, the top quark is expected to decay before top-flavored hadrons or $t\bar{t}$ -quarkonium-bound states can form [13]. In fact, since the decay time is close to the would-be-resonance binding time, a peak will be visible in e^+e^- scattering at the $t\bar{t}$ threshold [14] and it is in principle present (yet very difficult to measure) in hadron collisions, too [15]. The order α_s^2 QCD corrections to Γ_t are also available [16], thereby improving the overall theoretical accuracy to better than 1%.

The final states for the leading pair-production process can be divided into three classes:

- A. $t\bar{t} \rightarrow W^+ b W^- \bar{b} \rightarrow q\bar{q}' b q'' \bar{q}''' \bar{b}$, (45.7%)
- B. $t\bar{t} \rightarrow W^+ b W^- \bar{b} \rightarrow q\bar{q}' b \ell^- \bar{\nu}_\ell \bar{b} + \ell^+ \nu_\ell b q'' \bar{q}''' \bar{b}$, (43.8%)
- C. $t\bar{t} \rightarrow W^+ b W^- \bar{b} \rightarrow \ell^+ \nu_\ell b \ell'^- \bar{\nu}_{\ell'}$. (10.5%)

The quarks in the final state evolve into jets of hadrons. A, B, and C are referred to as the all-hadronic, lepton+jets (ℓ +jets), and dilepton ($\ell\ell$) channels, respectively. Their relative contributions, including hadronic corrections, are given in parentheses assuming lepton universality. While ℓ in the above processes refers to e , μ , or τ , most of the analyses distinguish the e and μ from the τ channel, which is more difficult to reconstruct. Therefore, in what follows, we will use ℓ to refer to e or μ , unless otherwise noted. Here, typically leptonic decays of τ are included. In addition to the quarks resulting from the top-quark decays, extra QCD radiation (quarks and gluons) from the colored particles in the event can lead to extra jets.

The number of jets reconstructed in the detectors depends on the decay kinematics, as well as on the algorithm for reconstructing jets used by the analysis. Information on the transverse momenta of neutrinos is obtained from the imbalance in transverse momentum measured in each event (missing p_T , which is here also called missing E_T).

The identification of top quarks in the electroweak single top channel is much more difficult than in the QCD $t\bar{t}$ channel, due to a less distinctive signature and significantly larger backgrounds, mostly due to $t\bar{t}$ and W +jets production.

Fully exclusive predictions via Monte Carlo generators for the $t\bar{t}$ and single top production processes at NLO accuracy in QCD, including top-quark decays and possibly off-shell effects are available [17, 18] through the MC@NLO [19] and POWHEG [20] methods.

Besides fully inclusive QCD or EW top-quark production, more exclusive final states can be accessed at hadron colliders, whose cross sections are typically much smaller, yet can provide key information on the properties of the top quark. For all relevant final states (e.g., $t\bar{t}V$, $t\bar{t}VV$ with $V = \gamma, W, Z$, $t\bar{t}H$, $t\bar{t}$ +jets, $t\bar{t}b\bar{b}$, $t\bar{t}t\bar{t}$) automatic or semi-automatic predictions at NLO accuracy in QCD also in the form of event generators, i.e., interfaced

to parton-shower programs, are available (see the review “Monte Carlo event generators” for more information).

60.3 Top-quark measurements

Since the discovery of the top quark, direct measurements of $t\bar{t}$ production have been made at six center-of-mass energies in pp or $p\bar{p}$ and one in pPb collisions, providing stringent tests of QCD. The first measurements were made in Run I at the Tevatron at $\sqrt{s} = 1.8$ TeV. In Run II at the Tevatron relatively precise measurements were made at $\sqrt{s} = 1.96$ TeV. Finally, beginning in 2010, measurements have been made at the LHC at $\sqrt{s} = 7$ TeV, $\sqrt{s} = 8$ TeV, and $\sqrt{s} = 13$ TeV, and recently also in a dedicated low energy run at $\sqrt{s} = 5.02$ TeV and at 8.16 TeV in pPb collisions.

Production of single top quarks through electroweak interactions has now been measured with good precision at the Tevatron at $\sqrt{s} = 1.96$ TeV, and at the LHC at $\sqrt{s} = 7$ TeV, $\sqrt{s} = 8$ TeV, and also at $\sqrt{s} = 13$ TeV. Measurements at the Tevatron have managed to separate the s - and t -channel production cross sections, and at the LHC, the tW mechanism as well, though the t -channel is measured with best precision to date. The measurements allow an extraction of the CKM matrix element V_{tb} . Also more exclusive production modes and top-quark properties have been measured in single-top production.

With approximately 10 fb⁻¹ of Tevatron data, and almost 5 fb⁻¹ at 7 TeV, 20 fb⁻¹ at 8 TeV and 139 fb⁻¹ at 13 TeV at the LHC, many properties of the top quark have been measured with high precision. These include properties related to the production mechanism, such as $t\bar{t}$ spin correlations, forward-backward or charge asymmetries, and differential production cross sections, as well as properties related to the tWb decay vertex, such as the helicity of the W -bosons from the top-quark decay. Also studies of the $t\bar{t}\gamma$, $t\bar{t}Z$ vertices as well as contact $t\bar{t}b\bar{b}$, and $t\bar{t}t\bar{t}$ interactions have been made. In addition, many searches for physics beyond the Standard Model or $t\bar{t}h$ or th production are being performed with increasing reach in both production and decay channels.

In the following sections we review the current status of measurements of the characteristics of the top quark.

60.3.1 Top-quark production

60.3.1.1 $t\bar{t}$ production

Fig. 60.1 summarizes the $t\bar{t}$ production cross-section measurements from both the Tevatron and LHC. Please note that some cross section measurements at the LHC have luminosity-related uncertainties which have improved in the meantime [21]. The most recent measurement from DØ [22] ($p\bar{p}$ at $\sqrt{s} = 1.96$ TeV), combining the measurements from the dilepton and lepton plus jets final states in 9.7 fb⁻¹, is $7.26 \pm 0.13^{+0.57}_{-0.50}$ pb.

From CDF the most precise measurement made recently [23] is in 8.8 fb⁻¹ in the dilepton channel requiring at least one b -tag, yielding 7.09 ± 0.84 pb. Both of these measurements assume a top-quark mass of 172.5 GeV/ c^2 . The dependence of the cross-section measurements on the value chosen for the mass is less than that of the theory calculations because it only affects the determination of the acceptance. In some analyses also the shape of topological variables might be modified.

Combining the recent cross section measurements with older ones in other channels yields $\sigma_{t\bar{t}} = 7.63 \pm 0.50$ pb (6.6%) for CDF, $\sigma_{t\bar{t}} = 7.56 \pm 0.59$ pb (7.8%) for DØ and $\sigma_{t\bar{t}} = 7.60 \pm 0.41$ pb (5.4%) for the Tevatron combination [24] in good agreement with the SM expectation of $7.35^{+0.28}_{-0.33}$ pb at NNLO+NNLL in perturbative QCD [1] for a top mass of 172.5 GeV. The contributions to the uncertainty are 0.20 pb from statistical sources, 0.29 pb from systematic sources, and 0.21 pb from the uncertainty on the integrated luminosity.

CDF has measured the $t\bar{t}$ production cross section in the dilepton channel with one hadronically decaying tau in 9.0 fb⁻¹, yielding $\sigma_{t\bar{t}} = 8.1 \pm 2.1$ pb. By separately identifying the single-tau and the ditau components, they measure the branching fraction of the top quark into the tau lepton, tau neutrino, and bottom quark to be $(9.6 \pm 2.8)\%$ [25]. CDF also performs measurements of the $t\bar{t}$ production cross section normalized to the Z production cross section in order to reduce the impact of the luminosity uncertainty [26].

DØ has performed a measurement of differential $t\bar{t}$ cross sections in 9.7 fb⁻¹ of lepton+jets data as a function of the transverse momentum and absolute value of the rapidity of the top quarks as well as of the invariant mass of the $t\bar{t}$ pair [27]. Observed differential cross sections are consistent with SM predictions.

The LHC experiments ATLAS and CMS use similar techniques to measure the $t\bar{t}$ cross section in pp collisions. The most precise measurements come from the dilepton channel, and in particular the $e\mu$ channel. At $\sqrt{s} = 7$ TeV, ATLAS uses 4.6 fb⁻¹ of $e\mu$ events in which they select an extremely clean sample and determine the $t\bar{t}$ cross section simultaneously with the efficiency to reconstruct and tag b -jets, yielding $\sigma_{t\bar{t}} = 182.9 \pm 7.1$ pb, corresponding to 3.9% precision [28]. Other measurements by ATLAS at $\sqrt{s} = 7$ TeV, include a measurement in 0.7 fb⁻¹ in the lepton+jets channel [29], in the dilepton channel [30], and in 1.02 fb⁻¹ in the all-hadronic channel [31], which together yield a combined value of $\sigma_{t\bar{t}} = 177 \pm 3(stat.)^{+8}_{-7}(syst.) \pm 7(lumi.)$ pb (6.2%) assuming $m_t = 172.5$ GeV/ c^2 [32]. In 4.7 fb⁻¹ of all-hadronic events, they obtain $\sigma_{t\bar{t}} = 168 \pm 62$ pb [33]. Further analyses in the hadronic τ plus jets channel in 1.67 fb⁻¹ [34] and the hadronic τ + lepton channel in 2.05 fb⁻¹ [35], and the all-hadronic channel in 4.7 fb⁻¹ [33] yield consistent albeit less precise results. Another simultaneous measurement of the $t\bar{t}, W^+W^-$, and $Z/\gamma^* \rightarrow \tau\tau$ cross section using the full 7 TeV dataset with 4.6 fb⁻¹ yields $\sigma_{t\bar{t}} = 181 \pm 11$ pb, corresponding to a 6% precision [36]. The most precise measurement from CMS at $\sqrt{s} = 7$ TeV is also obtained in the dilepton channel, where they measure $\sigma_{t\bar{t}} = 162 \pm 2(stat.) \pm 5(syst.) \pm 4(lumi.)$ pb, corresponding to a 4.2% precision [37]. Other measurements at $\sqrt{s} = 7$ TeV from CMS include measurements with 2.3 fb⁻¹ in the e/μ +jets channel [38], with 3.5 fb⁻¹ in the all-hadronic channel [39], with 2.2 fb⁻¹ in the lepton+ τ channel [40], and with 3.9 fb⁻¹ in the τ +jets channel [41]. ATLAS and CMS also provide a combined cross section at $\sqrt{s} = 7$ TeV of $173.3 \pm 2.3(stat.) \pm 7.6(syst.) \pm 6.3(lumi.)$ pb using slightly older results based on 0.7 – 1.1 fb⁻¹ [42].

At $\sqrt{s} = 8$ TeV, ATLAS measures the $t\bar{t}$ cross section with 20.3 fb⁻¹ using $e\mu$ dilepton events, with a simultaneous measurement of the b -tagging efficiency, yielding $\sigma_{t\bar{t}} = 242.4 \pm 1.7(stat.) \pm 5.5(syst.) \pm 7.5(lumi.) \pm 4.2(beam\ energy)$ pb [43] assuming $m_t = 172.5$ GeV/ c^2 , which corresponds to a 4.7% precision. In the lepton+jets channel, they measure $\sigma_{t\bar{t}} = 260 \pm 1(stat.)^{+20}_{-23}(syst.) \pm 8(lumi.) \pm 4(beam\ energy)$ pb [29] in 20.3 fb⁻¹ using a likelihood discriminant fit and b -jet identification. Subsequently, ATLAS performed a new analysis in 20.2 fb⁻¹ lepton+jets events. They model the W +jets background using Z +jets data and employ neural networks in three jet-multiplicity and b -jet multiplicity regions for the signal and background separation, yielding $\sigma_{t\bar{t}} = 248.3 \pm 0.7(stat.) \pm 13.4(syst.) \pm 4.7(lumi.)$ pb [44]. ATLAS also performed a cross section measurement in the hadronic τ +jets channel yielding consistent, albeit less precise results [45]. CMS performs a template fit to the $M_{b\bar{b}}$ mass distribution using 19.6 fb⁻¹ in the lepton+jets channel yielding $\sigma_{t\bar{t}} = 228.5 \pm 3.8(stat.) \pm 13.7(syst.) \pm 6(lumi.)$ pb [46, 47]. These 8 TeV measurements are in agreement with QCD predictions up to NLO accuracy. In the $e\mu$ channel, initially using 5.3 fb⁻¹ [47] and then using 19.7 fb⁻¹, the cross sections are extracted using a binned likelihood fit to multi-differential final state distributions related to identified b quark and other jets in the event, yielding $\sigma_{t\bar{t}} = 244.9 \pm 1.4(stat.)^{+6.3}_{-5.5}(syst.) \pm 6.4(lumi.)$ pb [48]. The cross section and its ratio between 7 TeV and 8 TeV measurements are found to be consistent with pQCD calculations. The cross section is also measured in the hadronic τ +jets channel, yielding $\sigma_{t\bar{t}} = 257 \pm 3(stat.) \pm 24(syst.) \pm 7(lumi.)$ pb [49] and in the all-hadronic final state giving $\sigma_{t\bar{t}} = 275.6 \pm 6.1(stat.) \pm 37.8(syst.) \pm 7.2(lumi.)$ pb [50]. In combination of the most precise $e\mu$ measurements in 5.3 – 20.3 fb⁻¹, ATLAS and CMS together yield at 8 TeV $\sigma_{t\bar{t}} = 241.5 \pm 1.4(stat.) \pm 5.7(syst.) \pm 6.2(lumi.)$ pb [51], which corresponds to a 3.5% precision, challenging the precision of the corresponding theoretical predictions. The LHCb collaboration presented the first observation of top-quark production in the forward region in pp -collisions. The $W+b$ final state with $W \rightarrow \mu\nu$ is reconstructed using muons with a transverse momentum, $p_{T\mu}$, larger than 25 GeV in the pseudorapidity range $2.0 < \eta < 4.5$.

The b -jets are required to have $50 \text{ GeV} < p_T < 100 \text{ GeV}$ and $2.2 < \eta < 4.2$, while the transverse component of the sum of the muon and b -jet momenta must satisfy $p_T > 20 \text{ GeV}$. The results are based on data corresponding to integrated luminosities of 1.0 and 2.0 fb^{-1} collected at center-of-mass energies of 7 and 8 TeV by LHCb. The inclusive top quark production cross sections in the fiducial region are $\sigma_{t\bar{t}} = 239 \pm 53(\text{stat.}) \pm 38(\text{syst.}) \text{ pb}$ at 7 TeV, and $\sigma_{t\bar{t}} = 289 \pm 43(\text{stat.}) \pm 46(\text{syst.}) \text{ pb}$ at 8 TeV [52].

ATLAS and CMS have also measured the $t\bar{t}$ production cross section with Run-II data at $\sqrt{s} = 13 \text{ TeV}$. In the $e\mu$ events with at least one b -tag, ATLAS uses 78 pb^{-1} and obtains $\sigma_{t\bar{t}} = 825 \pm 114 \text{ pb}$ [53]. This measurement is updated with lepton identification and trigger efficiencies to give $\sigma_{t\bar{t}} = 829 \pm 50(\text{stat.}) \pm 56(\text{syst.}) \pm 83(\text{lumi.}) \text{ pb}$ [54]. In this note, ATLAS also presents a $t\bar{t}$ cross section measurement in the ee and $\mu\mu$ dilepton channel with one and two b -tags using a counting approach, yielding $\sigma_{t\bar{t}} = 749 \pm 57(\text{stat.}) \pm 79(\text{syst.}) \pm 74(\text{lumi.}) \text{ pb}$. In the lepton-plus-jets channel, using 85 pb^{-1} , the cross-section is extracted by counting the number of events with exactly one electron or muon and at least four jets, at least one of which is identified as originating from a b -quark, yielding $\sigma_{t\bar{t}} = 817 \pm 13(\text{stat.}) \pm 103(\text{syst.}) \pm 88(\text{lumi.}) \text{ pb}$, both assuming $m_t = 172.5 \text{ GeV}$ [54]. The cross section measurement in the $e\mu$ channel counting events with one or with two b -tags is also repeated using 3.2 pb^{-1} and yields $\sigma_{t\bar{t}} = 818 \pm 8(\text{stat.}) \pm 27(\text{syst.}) \pm 19(\text{lumi.}) \pm 12(\text{beam.}) \text{ pb}$ [55], consistent with theoretical QCD calculations at NNLO. Very recently, ATLAS measures the inclusive $t\bar{t}$ cross section in 139 fb^{-1} in the lepton-plus-jets channel through a profile-likelihood fit to be $\sigma_{t\bar{t}} = 830.4 \pm 0.4(\text{stat.})^{+38.2}_{-37.0}(\text{syst.}) \text{ pb}$, with a relative uncertainty of 4.6% [56]. The result is consistent with the theoretical calculations at NLO order in QCD perturbation theory. In 36.1 fb^{-1} of $e\mu$ data with one or two b -tags, ATLAS measures the $t\bar{t}$ cross section to $\sigma_{t\bar{t}} = 826.4 \pm 3.6(\text{stat.}) \pm 11.5(\text{syst.}) \pm 15.7(\text{lumi.}) \pm 1.9(\text{beam.}) \text{ pb}$, giving a total of 2.4%. This measurement is also used to determine the top quark pole mass and to derive ratios and double ratios of $t\bar{t}$ and Z cross-sections at different energies as well as absolute and normalised differential cross-sections as functions of single lepton and dilepton kinematic variables [57]. CMS uses 43 pb^{-1} in the $e\mu$ channel to measure $\sigma_{t\bar{t}} = 746 \pm 58(\text{stat.}) \pm 53(\text{syst.}) \pm 36(\text{lumi.}) \text{ pb}$, in agreement with the expectation from the standard model [58]. Using 2.2 fb^{-1} in the $e\mu$ channel with at least one b -jet, CMS measures $\sigma_{t\bar{t}} = 815 \pm 9(\text{stat.}) \pm 38(\text{syst.}) \pm 19(\text{lumi.}) \text{ pb}$, in agreement with the expectation from the Standard Model [59]. A first measurement of the total inclusive and the normalized differential cross section in the lepton-plus-jets channel is made in 42 pb^{-1} yielding $\sigma_{t\bar{t}} = 836 \pm 27(\text{stat.}) \pm 88(\text{syst.}) \pm 100(\text{lumi.}) \text{ pb}$ [60]. In 2.2 fb^{-1} , lepton-plus-jets events are categorized according to the accompanying jet multiplicity. From a likelihood fit to the invariant mass distribution of the isolated lepton and a b -jet, the cross section is measured to be $\sigma_{t\bar{t}} = 888 \pm 2(\text{stat.})^{+26}_{-28}(\text{syst.}) \pm 20(\text{lumi.}) \text{ pb}$, in agreement with the SM prediction [61]. This result is also used to extract the top-quark mass. Using 35.9 fb^{-1} of dilepton data, CMS measures the $t\bar{t}$ cross section using a likelihood fit $\sigma_{t\bar{t}} = 803 \pm 2(\text{stat.}) \pm 25(\text{syst.}) \pm 20(\text{lumi.}) \text{ pb}$, in agreement with the expectation from the SM calculation at NLO order. This result is also used to extract the top quark mass and the strong coupling constant [62]. Very recently, using the same dataset in the dilepton channel with a hadronically decaying τ , they measure $\sigma_{t\bar{t}} = 781 \pm 7(\text{stat.}) \pm 62(\text{syst.}) \pm 20(\text{lumi.}) \text{ pb}$ [63]. In the all-hadronic channel, CMS uses 2.53 fb^{-1} of data, yielding a cross section of $\sigma_{t\bar{t}} = 834 \pm 25(\text{stat.}) \pm 23(\text{lumi.}) \text{ pb}$ [64]. Also differential cross sections as a function of the leading top quark transverse momentum are measured. As general feature found across channels, it is found that measured top quark p_T spectrum is significantly softer than the theory predictions.

In addition, CMS has also measured the top-quark pair production cross section in a special LHC run with $\sqrt{s} = 5.02 \text{ TeV}$, accumulating 27.4 pb^{-1} . The measurement is performed by analyzing events with at least one charged lepton. The measured cross section is $\sigma_{t\bar{t}} = 69.5 \pm 8.4 \text{ pb}$ [65], in agreement with the expectation from the Standard Model. In order to test consistency of the cross-section measurements with some systematic uncertain-

ties cancelling out while testing pQCD and PDFs, cross-section ratios between measurements at 7 TeV and at 8 TeV are performed and cited in several cases. In other cases, the cross-section ratio between $t\bar{t}$ - and Z -production is determined as that is independent of luminosity uncertainties, but keeps its sensitivity to the ratio of gluon versus quark PDFs. These experimental results should be compared to the theoretical calculations at NNLO+NNLL that yield $7.16^{+0.20}_{-0.23} \text{ pb}$ for top-quark mass of $173.3 \text{ GeV}/c^2$ [1] at $\sqrt{s} = 1.96 \text{ TeV}$, and for top-quark mass of $173.2 \text{ GeV}/c^2$ $\sigma_{t\bar{t}} = 173.6^{+4.5+8.9}_{-5.9-8.9} \text{ pb}$ at $\sqrt{s} = 7 \text{ TeV}$, $\sigma_{t\bar{t}} = 247.7^{+6.3+11.5}_{-8.5-11.5} \text{ pb}$ at $\sqrt{s} = 8 \text{ TeV}$, and $\sigma_{t\bar{t}} = 816.0^{+19.4+34.4}_{-28.6-34.4} \text{ pb}$ at $\sqrt{s} = 13 \text{ TeV}$, at the LHC [1]. CMS also performed a measurement of top-quark pair production in pPb heavy ion collisions at $\sqrt{s} = 8.16 \text{ TeV}$ in 174 nb^{-1} of lepton+jets events. They measure a cross section of $\sigma_{t\bar{t}} = 45 \pm 8 \text{ pb}$, which is consistent with pQCD calculations and with the scaled pp data [66].

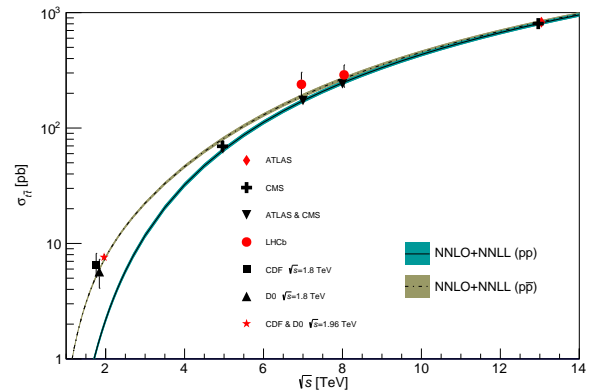


Figure 60.1: Measured and predicted $t\bar{t}$ production cross sections from Tevatron energies in $p\bar{p}$ collisions to LHC energies in pp collisions. Tevatron data points at $\sqrt{s} = 1.8 \text{ TeV}$ are from Refs. [67, 68]. Those at $\sqrt{s} = 1.96 \text{ TeV}$ are from Refs. [22–24]. The ATLAS, CMS, and LHCb data points are from Refs. [28, 37, 42, 47, 51, 52, 55, 62], and [65], respectively. Theory curves and uncertainties are generated using [1] for $m_t = 172.5 \text{ GeV}/c^2$, the m_t value assumed in the cross-section measurements. Figure adapted from Ref. [69].

In Fig. 60.1, one sees the importance of $p\bar{p}$ at Tevatron energies where the valence antiquarks in the antiprotons contribute to the dominant $q\bar{q}$ production mechanism. At LHC energies, the dominant production mode is gluon-gluon fusion and the pp - $p\bar{p}$ difference nearly disappears. The excellent agreement of these measurements with the theory calculations is a strong validation of QCD and the soft-gluon resummation techniques employed in the calculations. The measurements reach high precision and provide stringent tests of pQCD calculations at NNLO+NNLL level including their respective PDF uncertainties.

Most of these measurements assume a $t \rightarrow Wb$ branching ratio of 100%. CDF and D0 have made direct measurements of the $t \rightarrow Wb$ branching ratio [70]. Comparing the number of events with 0, 1 and 2 tagged b jets in the lepton+jets channel, and also in the dilepton channel, using the known b -tagging efficiency, the ratio $R = B(t \rightarrow Wb) / \sum_{q=d,s,b} B(t \rightarrow Wq)$ can be extracted. In 5.4 fb^{-1} of data, D0 measures $R = 0.90 \pm 0.04$, 2.5σ from unity. The currently most precise measurement was made by CMS in 19.7 fb^{-1} at $\sqrt{s} = 8 \text{ TeV}$. They find $R = 1.014 \pm 0.003(\text{stat.}) \pm 0.032(\text{syst.})$ and $R > 0.955$ at 95% C.L. [71]. A significant deviation of R from unity would imply either non-SM top-quark decay (for example a flavor-changing neutral-current decay), or a fourth generation of quarks.

Thanks to the large available event samples, the Tevatron and the LHC experiments also performed differential cross-section measurements in $t\bar{t}$ production. Such measurements are crucial, as they allow even more stringent tests of perturbative QCD as description of the production mechanism, allow the extraction or the use of PDF fits, and enhance the sensitivity to possible

new physics contributions, especially now that NNLO predictions for the main differential observables in $t\bar{t}$ prediction have become available [72] and recently confirmed [2]. Furthermore, such measurements reduce the uncertainty in the description of $t\bar{t}$ production as background in Higgs physics and searches for rare processes or beyond Standard Model physics. Differential cross sections are typically measured by a selection of candidate events, their kinematic reconstruction and subsequent unfolding of the obtained event counts in bins of kinematic distributions in order to correct for detector resolution effects, acceptance and migration effects. In some cases a bin-by-bin unfolding is used, while other analyses use more sophisticated techniques.

Experiments at Tevatron and LHC measure the differential cross section with respect to the $t\bar{t}$ invariant mass, $d\sigma/dM_{t\bar{t}}$. The spectra are fully corrected for detector efficiency and resolution effects and are compared to several Monte Carlo simulations as well as selected theoretical calculations.

Using 9.45 fb^{-1} , CDF measured $d\sigma/dM_{t\bar{t}}$, in the lepton+jets channel providing sensitivity to a variety of exotic particles decaying into $t\bar{t}$ pairs [73]. In 9.7 fb^{-1} of lepton+jets data, DØ measured the differential $t\bar{t}$ production cross section with respect to the transverse momentum and absolute rapidity of the top quarks as well as of the invariant mass of the $t\bar{t}$ pair [27], which are all found to be in good agreement with the SM predictions.

ATLAS measured the differential $t\bar{t}$ production cross section with respect to the top-quark transverse momentum, and of the mass, transverse momentum and rapidity of the top quark, the antitop quark as well as the $t\bar{t}$ system in 4.6 fb^{-1} at $\sqrt{s} = 7 \text{ TeV}$ in the lepton+jets channel [74–76]. It is found that data is softer than all predictions for higher values of the mass of the $t\bar{t}$ system as well as in the tail of the top-quark p_T spectrum beginning at 200 GeV, particularly in the case of the **Alpgen+Herwig** generator. The $M_{t\bar{t}}$ spectrum is not well described by NLO+NNLL calculations and there are also disagreements between the measured rapidity of the $t\bar{t}$ system spectrum and the **MC@NLO+Herwig** and **POWHEG+Herwig** generators, both evaluated with the CT10 PDF set. All distributions show a preference for HERAPDF1.5 when used for the NLO QCD predictions. In 5.0 fb^{-1} of $\sqrt{s} = 7 \text{ TeV}$ data in the lepton+jets and the dilepton channels, CMS measured normalised differential $t\bar{t}$ cross sections with respect to kinematic properties of the final-state charged leptons and jets associated to b -quarks, as well as those of the top quarks and the $t\bar{t}$ system. The data are compared with several predictions from perturbative QCD calculations and found to be consistent [77]. ATLAS uses 4.6 fb^{-1} of data at 7 TeV and 20.2 fb^{-1} at 8 TeV to measure the differential $t\bar{t}$ cross section in the dilepton final state as a function of the mass, the transverse momentum and the rapidity of the $t\bar{t}$ system [78]. The results are compared with different Monte Carlo generators and theoretical calculations of $t\bar{t}$ production and found to be consistent with the majority of predictions in a wide kinematic range. Using 20.3 fb^{-1} of $t\bar{t}$ events in the lepton+jets channel, ATLAS measures the normalized differential cross sections of $t\bar{t}$ production as a function of the top-quark, $t\bar{t}$ system and event-level kinematic observables [79]. The observables have been chosen to emphasize the $t\bar{t}$ production process and to be sensitive to effects of initial- and final-state radiation, to the different parton distribution functions, and to non-resonant processes and higher-order corrections. The results are in fair agreement with the predictions over a wide kinematic range. Nevertheless, most generators predict a harder top-quark transverse momentum distribution at high values than what is observed in the data. Predictions beyond NLO accuracy improve the agreement with data at high top-quark transverse momenta. Using the current settings in the Monte Carlo programs and parton distribution functions, the rapidity distributions are not well modelled by any generator under consideration. However, the level of agreement is improved when more recent sets of parton distribution functions are used. Using 20.3 fb^{-1} of 8 TeV data, ATLAS performed a dedicated differential $t\bar{t}$ cross-section measurement of highly boosted top quarks in the lepton+jets channel, where the hadronically decaying top quark has a transverse momentum above 300 GeV [80]. Jet substructure techniques are employed to identify top quarks, which are reconstructed with an anti- k_t jet with a radius param-

eters $R = 1.0$. The predictions of NLO and LO matrix element plus parton shower Monte Carlo generators are found to generally overestimate the measured cross sections.

Using 5.0 fb^{-1} of data at 7 TeV and 19.7 fb^{-1} at 8 TeV in the lepton+jets channel, CMS reports measurements of normalized differential cross sections for $t\bar{t}$ production with respect to four kinematic event variables: the missing transverse energy; the scalar sum of the jet transverse momentum (p_T); the scalar sum of the p_T of all objects in the event; and the p_T of leptonically decaying W bosons from top quark decays [81]. No significant deviations from the predictions of several SM event generators are observed. Using the full 19.7 fb^{-1} data in the $e\mu$ channel, CMS measures normalized double-differential cross sections for $t\bar{t}$ production as a function of various pairs of observables characterizing the kinematics of the top quark and $t\bar{t}$ system [82]. The data are compared to calculations using perturbative QCD at NLO and approximate NNLO orders. They are also compared to predictions of Monte Carlo event generators that complement fixed-order computations with parton showers, hadronization, and multiple-parton interactions. Overall agreement is observed with the predictions, which is improved when the latest global sets (as determined here by CMS) of proton parton distribution functions are used. The inclusion of the measured $t\bar{t}$ cross sections in a fit of parametrized parton distribution functions is shown to have significant impact on the gluon distribution [82]. Another analysis at high transverse momentum regime for the top quarks, is performed by the CMS collaboration in 19.7 fb^{-1} at $\sqrt{s} = 8 \text{ TeV}$ [83]. The measurement is performed for events in electron/muon plus jets final states where the hadronically decaying top quark is reconstructed as a single large-radius jet and identified as a top candidate using jet substructure techniques. The integrated cross section is measured at particle-level within a fiducial region resembling the detector-level selection as well as at parton-level. At particle-level, the fiducial cross section is measured to be $\sigma_{t\bar{t}} = 1.28 \pm 0.09(\text{stat.} + \text{syst.}) \pm 0.10(\text{pdf}) \pm 0.09(\text{scales}) \pm 0.03(\text{lumi.})$ pb for $p_T > 400 \text{ GeV}$. At parton-level, it translates to $\sigma_{t\bar{t}} = 1.44 \pm 0.10(\text{stat.} + \text{syst.}) \pm 0.13(\text{pdf}) \pm 0.15(\text{scales}) \pm 0.04(\text{lumi.})$ pb.

At parton-level, interactions between incoming partons (quarks or gluons) are considered via a gauge interaction yielding final state partons. While such interactions can be well described theoretically, partons are not visible in the detector. At the particle-level, visible and measurable hadrons, i.e. bound states of quarks and anti-quarks, are considered to form jets. The hadronisation process takes us from one level to the other.

In 19.7 fb^{-1} at $\sqrt{s} = 8 \text{ TeV}$, CMS repeated those measurements in the lepton+jets and in the dilepton channels [84]. While the overall precision is improved, no significant deviations from the Standard Model are found, yet a softer spectrum for the top quark at high p_T with respect to theoretical available predictions has been observed. This behaviour has been also observed in the all-hadronic final state [85], where also a total cross measurement is performed, yielding $\sigma_{t\bar{t}} = 275.6 \pm 6.1(\text{stat}) \pm 37.8(\text{syst}) \pm 7.2(\text{lumi})$ pb is obtained. In 3.2 fb^{-1} at $\sqrt{s} = 13 \text{ TeV}$, ATLAS measured the differential $t\bar{t}$ cross section as a function of the transverse momentum and absolute rapidity of the top quark, and of the transverse momentum, absolute rapidity and invariant mass of the $t\bar{t}$ system [86,87]. The measured differential cross sections are compared to predictions of NLO generators matched to parton showers and the measurements are found to be consistent with all models within the experimental uncertainties with the exception of the Powheg-Box+ Herwig++ predictions, which differ significantly from the data in both the transverse momentum of the top quark and the mass of the $t\bar{t}$ system. Using 3.2 fb^{-1} of data in the lepton+jets channel, ATLAS measured the differential cross sections of $t\bar{t}$ production in fiducial phase-spaces as a function of top-quark and $t\bar{t}$ system kinematic observables [88]. Two separate selections are applied that each focus on different top-quark momentum regions, referred to as resolved and boosted topologies of the $t\bar{t}$ final state. The measured spectra are corrected for detector effects and are compared to several Monte Carlo simulations by means of calculated χ^2 and p -values. At a center-of-mass energy of 13 TeV, ATLAS presents a measurement of the boosted top quark

differential cross section in the all-hadronic decay mode [89]. They require two top-quark candidates, one with $p_T > 500$ GeV and a second with $p_T > 350$ GeV, with each candidate reconstructed as an anti- k_T jet with radius parameter $R = 1.0$. The top-quark candidates are separated from the multijet background using the jet substructure and the presence of a b -quark tag in each jet. The observed kinematic distributions are unfolded to recover the differential cross sections in a limited phase-space region and compared with SM predictions, showing agreement. In addition, ATLAS measures the differential $t\bar{t}$ cross section of highly boosted top-quarks decaying to all-hadronic final states in 36.1 fb^{-1} using jet substructure information [90]. In 36 fb^{-1} , ATLAS measures the single- and double-differential $t\bar{t}$ cross-section in the lepton + jets channel at particle and parton level. Two topologies, resolved and boosted, are considered and the results are presented as a function of several kinematic variables characterising the top and $t\bar{t}$ system and jet multiplicities. Overall, there is good agreement between the theoretical predictions and the data [91]. In 2.1 fb^{-1} at $\sqrt{s} = 13$ TeV, CMS measures the normalized differential cross sections for $t\bar{t}$ production in the dilepton channels as a function of the kinematic properties of the leptons, jets from bottom quark hadronization, top quarks, and top quark pairs at the particle and parton levels [92]. The results are compared to several Monte Carlo generators that implement calculations up to NLO in perturbative QCD interfaced with parton showering, and also to fixed-order theoretical calculations of top quark pair production up to NNLO, showing agreement. In 2.3 fb^{-1} of events in the lepton+jets channel, CMS measures the differential and double-differential cross sections for the $t\bar{t}$ production as a function of jet multiplicity and of kinematic variables of the top quarks and the $t\bar{t}$ system [93]. The differential cross sections are presented at particle level, within a phase space close to the experimental acceptance, and at parton level in the full phase space. The results are compared to several SM predictions. Using 35.9 fb^{-1} , CMS measures the differential $t\bar{t}$ cross section in the single-lepton decay channel, as a function of a number of kinematic event variables. The data are compared to a variety of state-of-the-art LO and NLO simulations [94]. In 35.8 fb^{-1} , CMS measures the differential and double-differential $t\bar{t}$ cross sections in the lepton-plus-jets channel as a function of kinematic variables of the top quarks and the top quark-antiquark ($t\bar{t}$) system. In addition, kinematic variables and multiplicities of jets associated with the $t\bar{t}$ production are measured. The kinematic variables of the top quarks and the $t\bar{t}$ system are reasonably described in general, though none predict all the measured distributions. In particular, the transverse momentum distribution of the top quarks is more steeply falling than predicted. The kinematic distributions and multiplicities of jets are adequately modeled by certain combinations of NLO calculations and parton shower models [95]. In the dilepton channel, CMS measures differential $t\bar{t}$ cross sections in 35.9 fb^{-1} as functions of kinematic observables of the top quarks and their decay products, the $t\bar{t}$ system, and the total number of jets in the event. All results are compared with SM predictions from Monte Carlo simulations with NLO accuracy in QCD at matrix-element level interfaced to parton-shower simulations. Where possible, parton-level results are compared to calculations with beyond-NLO precision in QCD. Significant disagreement is observed between data and all predictions for several observables. The measurements are used to constrain the top quark chromomagnetic dipole moment in an effective field theory framework at NLO in QCD and to extract $t\bar{t}$ and leptonic charge asymmetries [96]. In 35.9 fb^{-1} of dilepton events, CMS measures normalised multi-differential $t\bar{t}$ cross sections as a function of the kinematic properties of the top quark and of the $t\bar{t}$ system at parton level in the full phase space. A triple-differential measurement is performed as a function of the invariant mass and rapidity of the $t\bar{t}$ system and the multiplicity of additional jets at particle level. The data are compared to predictions of Monte Carlo event generators that complement NLO QCD calculations with parton showers. The measurement is used to extract the strong coupling constant and the top-quark pole mass and parton distribution functions [97]. Further cross-section measurements are performed by ATLAS for $t\bar{t}$ +heavy flavour [98] and $t\bar{t}$ +jets production as well as the differential measurement of

the jet multiplicity in $t\bar{t}$ events [99, 100]. Here, MC@NLO+Herwig MC is found to predict too few events at higher jet multiplicities. In addition, CMS measured the cross-section ratio $\sigma_{t\bar{t}b\bar{b}}/\sigma_{t\bar{t}j\bar{j}}$ using 19.6 fb^{-1} of 8 TeV data [101]. This is of high relevance for top quark production as background to searches, for example for measurements of $t\bar{t}h$ production and ongoing searches for 4-top quark production. Later, ATLAS also measured the $t\bar{t}$ production cross section along with as the branching ratios into channels with leptons and quarks using 4.6 fb^{-1} of 7 TeV data [102]. They find agreement with the standard model at the level of a few percent. In 36.1 fb^{-1} , ATLAS measures the $t\bar{t}b\bar{b}$ cross section in the dilepton and the lepton-plus-jet channels. Results are presented at particle level in the form of inclusive cross-sections of $t\bar{t}$ final states with three and four b -jets as well as differential cross-sections as a function of global event properties and properties of b -jet pairs. The measured inclusive fiducial cross-sections generally exceed the $t\bar{t}b\bar{b}$ predictions from various NLO matrix element calculations matched to a parton shower, but are compatible within the total uncertainties [103]. In 2.3 fb^{-1} , CMS measures the $t\bar{t}b\bar{b}$ cross section in the dilepton channel [104]. They also determine the cross section ratio $\sigma_{t\bar{t}b\bar{b}}/\sigma_{t\bar{t}j\bar{j}}$. In 35.9 fb^{-1} , CMS recently measured the cross section $t\bar{t}b\bar{b}$ as well as the cross section ratio $\sigma_{t\bar{t}b\bar{b}}/\sigma_{t\bar{t}j\bar{j}}$ in the dilepton and the lepton+jets channel [105]. They fit the distribution of the b tagging discriminant variable of the two jets that do not belong to the $t\bar{t}$ decay. In the same dataset, CMS measures the $t\bar{t}b\bar{b}$ cross section in the all-jet channel by selecting events containing at least eight jets, of which at least two are identified as b -jets. A combination of multivariate analysis techniques is used to reduce the large background from multijet events not containing a top quark pair, and to help discriminate between jets originating from top quark decays and other additional jets. The measured cross sections are found to be larger than theoretical predictions by a factor of 1.5-2.4, corresponding to 1-2 standard deviations [106].

60.3.1.2 Single-top production

Single-top quark production was first observed in 2009 by $D\bar{0}$ [107] and CDF [108, 109] at the Tevatron. The production cross section at the Tevatron is roughly half that of the $t\bar{t}$ cross section, but the final state with a single W -boson and typically two jets is less distinct than that for $t\bar{t}$ and much more difficult to distinguish from the background of W +jets and other sources. A comprehensive review of the first observation and the techniques used to extract the signal from the backgrounds can be found in [110].

The dominant production at the Tevatron is through s -channel and t -channel W -boson exchange. Associated production with a W -boson (tW production) has a cross section that is too small to observe at the Tevatron. The t -channel process is $qb \rightarrow q't$, while the s -channel process is $q\bar{q}' \rightarrow t\bar{b}$. The s - and t -channel productions can be separated kinematically. This is of particular interest because potential physics beyond the Standard Model, such as fourth-generation quarks, heavy W and Z bosons, flavor-changing-neutral-currents [11], or a charged Higgs boson, would affect the s - and t -channels differently. However, the separation is difficult and initial observations and measurements at the Tevatron by both experiments were of combined $s + t$ -channel production. The two experiments combined their measurements for maximum precision with a resulting $s+t$ -channel production cross section of $2.76_{-0.47}^{+0.58}$ pb [111]. The measured value assumes a top-quark mass of $170 \text{ GeV}/c^2$. The mass dependence of the result comes both from the acceptance dependence and from the $t\bar{t}$ background evaluation. Also the shape of discriminating topological variables is sensitive to m_t . The dependence on m_T is therefore not necessarily a simple linear dependence but amounts to only a few tenths of picobarns over the range $170 - 175 \text{ GeV}/c^2$. The measured value agrees well with the theoretical calculation at $m_t = 173 \text{ GeV}/c^2$ of $\sigma_{s+t} = 3.12$ pb (including both top and anti-top production) [6, 9].

Using the full Run-II data set of up to 9.7 fb^{-1} , CDF and $D\bar{0}$ have measured the t -channel single-top quark production to be $\sigma_{t+\bar{t}} = 2.25_{-0.31}^{+0.29}$ pb [112, 113]. In the same publication, they also present the simultaneously measured s - and t -channel cross

sections and the $s+t$ combined cross section measurement resulting in $\sigma_{s+t} = 3.30_{-0.40}^{+0.52}$ pb, without assuming the SM ratio of σ_s/σ_t . The modulus of the CKM matrix element obtained from the $s+t$ -channel measurement is $|V_{tb}| = 1.02_{-0.05}^{+0.06}$ and its value is used to set a lower limit of $|V_{tb}| > 0.92$ at 95% C.L. Those results are in good agreement with the theoretical value at the mass $172.5 \text{ GeV}/c^2$ of $\sigma_t = 2.08 \pm 0.13$ pb [6]. It should be noted that the theory citations here list cross sections for t or \bar{t} alone, whereas the experiments measure the sum. At the Tevatron, these cross sections are equal. The theory values quoted here already include this factor of two.

Using datasets of 9.7 fb^{-1} each, CDF and DØ combine their analyses and report the first observation of single-top-quark production in the s -channel, yielding $\sigma_s = 1.29_{-0.24}^{+0.26}$ pb [114]. The probability of observing a statistical fluctuation of the background of the given size is 1.8×10^{-10} , corresponding to a significance of 6.3 standard deviations.

At the LHC, the t -channel cross section is expected to be more than three times as large as s -channel and tW production, combined. Both ATLAS and CMS have measured single top production cross sections at $\sqrt{s} = 7 \text{ TeV}$ in pp collisions (assuming $m_t = 172.5 \text{ GeV}/c^2$ unless noted otherwise).

Using 4.59 fb^{-1} of data at $\sqrt{s} = 7 \text{ TeV}$, ATLAS measures the t -channel single-top quark cross section in the lepton plus 2 or 3 jets channel with one b -tag by fitting the distribution of a multivariate discriminant constructed with a neural network, yielding $\sigma_t = 46 \pm 6$ pb, $\sigma_{\bar{t}} = 23 \pm 4$ pb with a ratio $R_t = \sigma_t/\sigma_{\bar{t}} = 2.04 \pm 0.18$ and $\sigma_{t+\bar{t}} = 68 \pm 8$ pb, consistent with SM expectations [115,116]. CMS follows two approaches in 1.6 fb^{-1} of lepton plus jets events. The first approach exploits the distributions of the pseudorapidity of the recoil jet and reconstructed top-quark mass using background estimates determined from control samples in data. The second approach is based on multivariate analysis techniques that probe the compatibility of the candidate events with the signal. They find $\sigma_{t+\bar{t}}^{t\text{-channel}} = 67.2 \pm 6.1$ pb, and $|V_{tb}| = 1.020 \pm 0.046(\text{exp.}) \pm 0.017(\text{th.})$ [117].

At $\sqrt{s} = 8 \text{ TeV}$, both experiments repeat and refine their measurements. ATLAS uses 20.2 fb^{-1} of data. Total, fiducial and differential cross-sections are measured for both top-quark and top-antiquark production [118]. An artificial neural network is employed to separate signal from background. The fiducial cross-section is measured with a precision of 5.8% (top quark) and 7.8% (top antiquark), respectively. The total cross-sections are measured to be $\sigma_t^{t\text{-channel}}(tq) = 56.7_{-3.8}^{+4.3}$ pb for top-quark production and $\sigma_{\bar{t}}^{t\text{-channel}}(\bar{t}q) = 32.9_{-2.7}^{+3.0}$ pb for top-antiquark production, in agreement with the SM prediction. In addition, the ratio of top-quark to top-antiquark production cross-sections is determined to be $R_t = 1.72 \pm 0.09$. The total cross-section is used to extract the Wtb coupling: $f_{LV} \cdot |V_{tb}| = 1.029 \pm 0.048$, which corresponds to $|V_{tb}| > 0.92$ at the 95% confidence level, when assuming $f_{LV} = 1$ and restricting the range of $|V_{tb}|$ to the interval $[0, 1]$. The differential cross-sections as a function of the transverse momentum and rapidity of both the top quark and the top antiquark are measured at both the parton and particle levels. The transverse momentum and rapidity differential cross-sections of the accompanying jet from the t -channel scattering are measured at particle level. All measurements are compared to various Monte Carlo predictions as well as to fixed-order QCD calculations where available. The SM predictions provide good descriptions of the data. Using the same dataset, ATLAS probes the Wtb vertex structure from polarisation observables in t -channel single-top quark events. The polarisation observables are extracted from asymmetries in angular distributions measured with respect to spin quantisation axes appropriately chosen for the top quark and the W -boson. The asymmetry measurements are performed at parton level by correcting the observed angular distributions for detector effects and hadronisation after subtracting the background contributions. The measured top-quark and W -boson polarisation values are in agreement with the Standard Model predictions [119]. CMS uses 19.7 fb^{-1} in the electron or muon plus jets channel, exploiting the pseudorapidity distribution of the recoil jet. They find

$\sigma_t = 53.8 \pm 1.5(\text{stat.}) \pm 4.4(\text{syst.})$ pb and $\sigma_{\bar{t}} = 27.6 \pm 1.3(\text{stat.}) \pm 3.7(\text{syst.})$ pb, resulting in an inclusive t -channel cross section of $\sigma_{t+\bar{t}} = 83.6 \pm 2.3(\text{stat.}) \pm 7.4(\text{syst.})$ [120]. They measure a cross section ratio of $R_t = \sigma_t/\sigma_{\bar{t}} = 1.95 \pm 0.10(\text{stat.}) \pm 0.19(\text{syst.})$, in agreement with the SM. The CKM matrix element V_{tb} is extracted to be $|V_{tb}| = 0.998 \pm 0.038(\text{exp.}) \pm 0.016(\text{th.})$. Later, CMS has also provided a fiducial cross section measurement for t -channel single top at $\sqrt{s} = 8 \text{ TeV}$ with 19.7 fb^{-1} of data in signal events with exactly one muon or electron and two jets, one of which is associated with a b -hadron [121]. The definition of the fiducial phase space follows closely the constraints imposed by event-selection criteria and detector acceptance. The total fiducial cross section is measured using different generators at next-to-leading order plus parton-shower accuracy. Using as reference the aMC@NLO MC predictions in the four-flavour scheme a $\sigma_t^{\text{fid}} = 3.38 \pm 0.25(\text{exp.}) \pm 0.20(\text{th.})$ pb is obtained, in good agreement with the theory predictions. At 13 TeV, ATLAS uses 3.2 fb^{-1} to measurement the t -channel cross section. Using a binned maximum-likelihood fit to the discriminant distribution of a neural network, the cross-sections are determined to be $\sigma_t(tq) = 156 \pm 5(\text{stat.}) \pm 27(\text{syst.}) \pm 3(\text{lumi.})$ pb and $\sigma(\bar{t}q) = 91 \pm 4(\text{stat.}) \pm 18(\text{syst.}) \pm 2(\text{lumi.})$ pb [122]. The cross-section ratio is measured to be $R_t = \sigma_t/\sigma_{\bar{t}} = 1.72 \pm 0.09(\text{stat.}) \pm 0.18(\text{syst.})$. All results are in agreement with SM predictions. A measurement of the t -channel single top-quark cross section is also available at 13 TeV with the CMS detector, corresponding to an integrated luminosity of 2.2 fb^{-1} . Fits to the transverse W -mass and the output of an artificial neural network allow the determination of the background and the signal contribution. The measured cross-section is $\sigma_t = 238 \pm 13 \pm 29$ pb [123]. The CKM matrix is determined to $|V_{tb}| = 1.05 \pm 0.07(\text{exp.}) \pm 0.02(\text{th.})$. Using 35.9 fb^{-1} of data, CMS performs measurements of the t -channel cross sections of single top quarks and antiquarks in the t channel, and their ratio. Events with one muon or electron are selected, and different categories of jet and b -jet multiplicity and multivariate discriminators are applied to separate the signal from the background, resulting in $\sigma_t(tq) = 136 \pm 1(\text{stat}) \pm 22(\text{syst})$ pb and $\sigma_{\bar{t}}(\bar{t}q) = 82 \pm 1(\text{stat}) \pm 14(\text{syst})$ pb, respectively, and their ratio is $1.66 \pm 0.02(\text{stat}) \pm 0.05(\text{syst})$. The results are in agreement with the predictions from the Standard Model [124].

The predicted cross section for tW process at the LHC $\sqrt{s} = 7 \text{ TeV}$ is 15.6 ± 1.2 pb [10]. This is of interest because it probes the Wtb vertex in a different kinematic region than s - and t -channel production, and because of its similarity to the associated production of a charged-Higgs boson and a top quark. The signal is difficult to extract because of its similarity to the $t\bar{t}$ signature. Furthermore, it is difficult to uniquely define because at NLO a subset of diagrams have the same final state as $t\bar{t}$ and the two interfere [125]. The cross section is calculated using the *diagram removal* technique [126] to define the signal process. In the diagram removal technique the interfering diagrams are removed, at the amplitude level, from the signal definition (an alternative technique, *diagram subtraction* removes these diagrams at the cross-section level and yields similar results [126]). These techniques work provided the selection cuts are defined such that the interference effects are small, which is usually the case.

Both, ATLAS and CMS, also provide evidence for the associate tW production at $\sqrt{s} = 7 \text{ TeV}$ [127, 128]. ATLAS uses 2.05 fb^{-1} in the dilepton plus missing E_T plus jets channel, where a template fit to the final classifier distributions resulting from boosted decision trees as signal to background separation is performed. The result is incompatible with the background-only hypothesis at the 3.3σ (3.4σ expected) level, yielding $\sigma_{tW} = 16.8 \pm 2.9(\text{stat.}) \pm 4.9(\text{syst.})$ pb and $|V_{tb}| = 1.03_{-0.19}^{+0.16}$ [127]. CMS uses 4.9 fb^{-1} in the dilepton plus jets channel with at least one b -tag. A multivariate analysis based on kinematic properties is utilized to separate the $t\bar{t}$ background from the signal. The observed signal has a significance of 4.0σ and corresponds to a cross section of $\sigma_{tW} = 16_{-4}^{+5}$ pb [128].

Both experiments repeated their tW -analyses at $\sqrt{s} = 8 \text{ TeV}$. ATLAS uses 20.3 fb^{-1} to select events with two leptons and one central b -jet. The tW signal is separated from the backgrounds using boosted decision trees, each of which combines a number

of discriminating variables into one classifier. Production of tW events is observed with a significance of 7.7σ . The cross section is extracted in a profile likelihood fit to the classifier output distributions. The tW cross section, inclusive of decay modes, is measured to be $\sigma_{tW} = 23.0 \pm 1.3(\text{stat.})_{-3.5}^{+3.2}(\text{syst.}) \pm 1.1(\text{lumi.})$ pb, yielding a value for the CKM matrix element $|V_{tb}| = 1.01 \pm 0.10$ and a lower limit of 0.80 at the 95% C.L. [129]. A fiducial cross section is also measured. CMS uses 12.2 fb^{-1} in events with two leptons and a jet originated from a b quark. A multivariate analysis based on kinematic properties is utilized to separate the signal and background. The tW associate production signal is observed at the level of 6.1σ , yielding $\sigma_{tW} = 23.4 \pm 5.4$ pb and $|V_{tb}| = 1.03 \pm 0.12(\text{exp.}) \pm 0.04(\text{th.})$ [130]. ATLAS and CMS also combine their measurements and obtain $\sigma_{tW} = 25.0 \pm 1.4(\text{stat.}) \pm 4.4(\text{syst.}) \pm 0.7(\text{lumi.})$ pb = 25.0 ± 4.7 pb [131], in agreement with the NLO+NNLL expectation. They extract a 95% C.L. lower limit on the CKM matrix element of $|V_{tb}| > 0.79$.

At 13 TeV in the tW -channel, ATLAS uses 3.2 fb^{-1} of events with two opposite sign isolated leptons and at least one jet; they are separated into signal and control regions based on their jet multiplicity and the number of jets with b -tags. Signal is separated from background in two regions using boosted decision trees. The cross section is extracted by fitting templates to the data distributions, and is measured to be $\sigma_{tW} = 94 \pm 10(\text{stat.})_{-22}^{+28}(\text{syst.}) \pm 2(\text{lumi.})$ pb [132]. The measurement is in agreement with the SM prediction. CMS uses 36 fb^{-1} of events with two opposite sign isolated leptons, one tight and one loose jet and one b -tag. Signal and background is separated in categories depending on the number of jets and the subset of b -tagged jets using a boosted decision tree. A maximum likelihood fits yields $\sigma_{tW} = 63.1 \pm 6.6$ pb [133].

The s -channel production cross section is expected to be 4.6 ± 0.3 pb for $m_t = 173 \text{ GeV}/c^2$ at $\sqrt{s} = 7 \text{ TeV}$ [9]. At ATLAS, a search for s -channel single top quark production is performed in 0.7 fb^{-1} at 7 TeV using events containing one lepton, missing transverse energy and two b -jets. Using a cut-based analysis, an observed (expected) upper limit at 95% C.L. on the s -channel cross-section of $\sigma_s < 26.5$ (20.5) pb is obtained [134]. At 8 TeV, ATLAS uses 20.3 fb^{-1} of data with one lepton, large missing transverse momentum and exactly two b -tagged jets. They perform a maximum-likelihood fit of a discriminant based on a Matrix Element Method and optimized in order to separate single top-quark s -channel events from the main background contributions which are top-quark pair production and W boson production in association with heavy flavour jets. They find $\sigma_s = 4.8 \pm 0.8(\text{stat.})_{-1.3}^{+1.6}(\text{syst.})$ pb with a signal significance of 3.2 standard deviations [135], which provides first evidence for s -channel single-top production at 8 TeV. The signal is extracted through a maximum-likelihood fit to the distribution of a multivariate discriminant defined using boosted decision trees to separate the expected signal contribution from background processes. At 7 TeV and 8 TeV, CMS uses 5.1 fb^{-1} and 19.3 fb^{-1} , respectively, and analyses leptonic decay modes by performing a maximum likelihood fit to a multivariate discriminant defined using a Boosted Decision Tree, yielding cross sections of $\sigma_s = 7.1 \pm 8.1$ pb and $\sigma_s = 13.4 \pm 7.3$ pb, respectively, and a best fit value of 2.0 ± 0.9 for the combined ratio of the measured σ_s values and the ones expected in the Standard Model [136]. The signal significance is 2.5 standard deviations. ATLAS and CMS present the combinations of their single-top-quark production cross-section measurements, using Run-I data corresponding to integrated luminosities of 1.17 to 5.1 fb^{-1} at $\sqrt{s} = 7 \text{ TeV}$ and 12.2 to 20.3 fb^{-1} at $\sqrt{s} = 8 \text{ TeV}$. These combinations are performed per centre-of-mass energy and for each production mode: t -channel, tW , and s -channel. The combined t -channel cross-sections are 67.5 ± 5.7 pb and 87.7 ± 5.8 pb at $\sqrt{s} = 7$ and 8 TeV, respectively. The combined tW cross-sections are 16.3 ± 4.1 pb and 23.1 ± 3.6 pb at $\sqrt{s} = 7$ and 8 TeV, respectively. For the s -channel cross-section, the combination yields 4.9 ± 1.4 pb at $\sqrt{s} = 8 \text{ TeV}$. The square of the magnitude of the CKM matrix element V_{tb} multiplied by a form factor f_{LV} is determined for each production mode and centre-of-mass energy, using the ratio of the measured cross-section to its theoretical prediction. All combined measurements are consistent with their corresponding SM pre-

dictions [137]. Both, ATLAS and CMS, also measured the electroweak production of single top-quarks in association with a Z -boson, see section C.2.4 of this review.

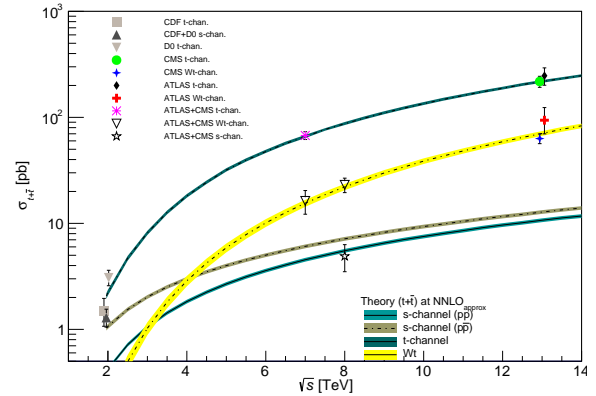


Figure 60.2: Measured and predicted single top production cross sections from Tevatron energies in $p\bar{p}$ collisions to LHC energies in pp collisions. Tevatron data points at $\sqrt{s} = 1.96 \text{ TeV}$ are from Refs. [113, 114]. The ATLAS and CMS data points at $\sqrt{s} = 7 \text{ TeV}$ are from Refs. [115, 117, 127, 128, 134, 136]. The ones at $\sqrt{s} = 8 \text{ TeV}$ are from Refs. [118, 120, 129, 130, 135, 136]. The ones at $\sqrt{s} = 13 \text{ TeV}$ are from Refs. [122, 123]. Theory curves are generated using [6, 9, 10].

Fig. 60.2 provides a summary of all single top cross-section measurements at the Tevatron and the LHC as a function of the center-of-mass energy. All cross-section measurements are very well described by the theory calculation within their uncertainty.

Thanks to the large statistics now available at the LHC, both CMS and ATLAS experiments also performed differential cross-section measurements in single-top t -channel production [115], [138]. Such measurements are extremely useful as they test our understanding of both QCD and EW top-quark interactions. The CMS collaboration has measured differential single top quark t -channel production cross sections as functions of the transverse momentum and the absolute value of the rapidity of the top quark. The analysis is performed in the leptonic decay channels of the top quark, with either a muon or an electron in the final state, using data collected with the CMS experiment at the LHC at $\sqrt{s} = 8 \text{ TeV}$ and corresponding to an integrated luminosity of 19.7 fb^{-1} . Neural networks are used to discriminate the signal process from the various background contributions. The results are found to agree with predictions from Monte Carlo generators [138]. Using the same data set and under the assumption that the spin analyzing power of a charged lepton is 100% as predicted in the SM, they are also able to measure the polarization of the top quark $P_t = 0.82 \pm 0.12(\text{stat.}) \pm 0.32(\text{syst.})$ [139]. At 13 TeV, using 35.9 fb^{-1} , CMS measures the differential t -channel cross sections, for the first time in single-top production, and charge ratios for t -channel single top quark production [140]. The results are found to be in agreement with SM predictions using various NLO event generators and sets of parton distribution functions. Additionally, the spin asymmetry, sensitive to the top quark polarisation, is determined from the differential distribution of the polarisation angle at parton level to be 0.439 ± 0.062 , in agreement with the SM prediction. This disfavors the results obtained at 8 TeV.

ATLAS has measured the differential tW cross section in 36.1 fb^{-1} at 13 TeV with respect to the energy of the b -jet, the energy of the system of the two leptons and b -jet, and the transverse mass or mass of combinations of leptons, the b -jet and neutrinos [141].

In 35.9 fb^{-1} , CMS managed to establish the first evidence for the production of a single top quark in association with a photon [142]. A multivariate discriminant based on topological and kinematic event properties is employed to separate signal from background processes. An excess above the background-only hypothesis is observed, with a significance of 4.4 standard deviations.

60.3.1.3 Top-Quark Forward-Backward & Charge Asymmetry

A forward-backward asymmetry in $t\bar{t}$ production at a $p\bar{p}$ collider arises starting at order α_S^3 in QCD from the interference between the Born amplitude $q\bar{q} \rightarrow t\bar{t}$ with 1-loop box production diagrams and between diagrams with initial- and final-state gluon radiation. The asymmetry, A_{FB} , is defined by

$$A_{FB} = \frac{N(\Delta y > 0) - N(\Delta y < 0)}{N(\Delta y > 0) + N(\Delta y < 0)}, \quad (60.2)$$

where $\Delta y = y_t - y_{\bar{t}}$ is the rapidity difference between the top- and the anti-top quark. Calculations at α_S^3 predict a measurable A_{FB} at the Tevatron. The most recent calculations up to order α_S^4 , including electromagnetic and electroweak corrections, yield a predicted asymmetry of $\approx (9.5 \pm 0.7)\%$ [143]. This is about 10% higher than the previous calculation at NLO [144, 145], and improves the agreement with experiment.

Both CDF and DØ measured asymmetry values in excess of the SM prediction, fueling speculation about exotic production mechanisms (see, for example, [146] and references therein). The first measurement of this asymmetry by DØ in 0.9 fb^{-1} [147] found an asymmetry at the detector level of $(12 \pm 8)\%$. The first CDF measurement in 1.9 fb^{-1} [148] yielded $(24 \pm 14)\%$ at parton level. Both values were higher, though statistically consistent with the SM expectation. With the addition of more data, the uncertainties have been reduced, and the central values, if somewhat smaller, have remained consistent with the first measurements. At the same time, the improved calculations from theory have increased the predicted asymmetry values to the point where the discrepancy is no longer statistically significant.

CDF and DØ have now combined results using the full Tevatron dataset at $\sqrt{s} = 1.96 \text{ TeV}$ [149]. Three combined asymmetries are reported: $A_{FB}^{t\bar{t}}$ as defined in Eq. 2 for fully-reconstructed $t\bar{t}$ events, a single-lepton asymmetry, A_{FB}^{ℓ} defined as in Eq. 2 but with Δy replaced by the product of the lepton charge and pseudo-rapidity, and a dilepton asymmetry, $A_{FB}^{\ell\ell}$, defined as in Eq. 2 but with Δy replaced by $\Delta\eta$ between the two leptons. The combined results are $A_{FB}^{t\bar{t}} = 0.128 \pm 0.021 \pm 0.014$, $A_{FB}^{\ell} = 0.073 \pm 0.016 \pm 0.012$, and $A_{FB}^{\ell\ell} = 0.108 \pm 0.043 \pm 0.016$, where the first uncertainty is statistical and the second systematic. These are to be compared to SM predictions at NNLO QCD and NLO electroweak of $A_{FB}^{t\bar{t}} = 0.095 \pm 0.007$ [143], $A_{FB}^{\ell} = 0.038 \pm 0.003$, and $A_{FB}^{\ell\ell} = 0.048 \pm 0.004$ [145], respectively. Both experiments have also measured differential asymmetries, in bins of $M_{t\bar{t}}$, Δy , $q_\ell \times \eta_\ell$, and $\Delta\eta_{\ell\ell}$, with consistent results, though the growth of $A_{FB}^{t\bar{t}}$ with increasing $M_{t\bar{t}}$ and Δy appears somewhat more rapid than the SM prediction [149].

At the LHC, where the dominant $t\bar{t}$ production mechanism is the charge-symmetric gluon-gluon fusion, the measurement is more difficult. For the sub-dominant $q\bar{q}$ production mechanism, the symmetric pp collision does not define a forward and backward direction. Instead, the charge asymmetry, A_C , is defined in terms of a positive versus a negative $t - \bar{t}$ rapidity difference, Δy

$$A_C^{t\bar{t}} = \frac{N(\Delta|y| > 0) - N(\Delta|y| < 0)}{N(\Delta|y| > 0) + N(\Delta|y| < 0)}. \quad (60.3)$$

Both CMS and ATLAS have measured A_C in the LHC dataset. Using lepton+jets events in 4.7 fb^{-1} of data at $\sqrt{s} = 7 \text{ TeV}$, ATLAS measures $A_C^{t\bar{t}} = (0.6 \pm 1.0)\%$ [150]. ATLAS has reported on the same measurement performed at $\sqrt{s} = 8 \text{ TeV}$ with 20.3 fb^{-1} of data, with a result of $A_C^{t\bar{t}} = (0.009 \pm 0.005)\%$ [151]. In the dilepton channel at $\sqrt{s} = 8 \text{ TeV}$, ATLAS measures [152] $A_C^{t\bar{t}} = 0.021 \pm 0.016$, and $A_C^{\ell\ell} = 0.008 \pm 0.006$ (defined in terms of the $\Delta\eta$ of the two leptons) in agreement with the SM predictions of $(1.11 \pm 0.04)\%$ and $(0.64 \pm 0.03)\%$, respectively [145]. Using lepton+jets events CMS has measured A_C at both $\sqrt{s} = 7$ and 8 TeV . They measure $A_C^{t\bar{t}} = (0.4 \pm 1.5)\%$ and $A_C^{\ell\ell} = (0.33 \pm 0.26(\text{stat.}) \pm 0.33(\text{sys.}))\%$ in 5.0 fb^{-1} at $\sqrt{s} = 7 \text{ TeV}$ and in 19.7 fb^{-1} at $\sqrt{s} = 8 \text{ TeV}$, respectively [153, 154]. Both measurements are consistent with the SM expectations of

$A_C^{t\bar{t}} = 1.23 \pm 0.05\%$ at $\sqrt{s} = 7 \text{ TeV}$ and $1.11 \pm 0.04\%$ at $\sqrt{s} = 8 \text{ TeV}$ [145], although the uncertainties are still too large for a precision test. In 19.5 fb^{-1} of dilepton events at $\sqrt{s} = 8 \text{ TeV}$, CMS measures $A_C^{t\bar{t}} = 0.011 \pm .013$ and $A_C^{\ell\ell} = 0.003 \pm 0.007$ [155], consistent with SM expectations [156].

In their 7 and 8 TeV analyses ATLAS and CMS also provide differential measurements as a function of $M_{t\bar{t}}$ and the transverse momentum p_T and rapidity y of the $t\bar{t}$ system. To reduce model-dependence, the CMS Collaboration has performed a measurement in a reduced fiducial phase space [157], with a result of $A_C = -0.0035 \pm 0.0072(\text{stat.}) \pm 0.0031(\text{sys.})$, in agreement with SM expectations.

To specifically address the dependence of the asymmetry on $M_{t\bar{t}}$, ATLAS has performed a measurement in boosted $t\bar{t}$ events [158]. In 20.3 fb^{-1} of data at $\sqrt{s} = 8 \text{ TeV}$, in events with $M_{t\bar{t}} > 0.75 \text{ TeV}$, and $|\Delta|y| < 2$, ATLAS measures $A_C^{t\bar{t}} = (4.2 \pm 3.2)\%$ compared to a NLO SM prediction of $(1.60 \pm 0.04)\%$. The measurement is also presented in three bins of $M_{t\bar{t}}$, each in agreement, though with large uncertainties, with the SM expectations.

Both ATLAS and CMS have measured asymmetries in the distribution of leptons from $t\bar{t}$ decays. ATLAS, in 4.6 fb^{-1} of $\sqrt{s} = 7 \text{ TeV}$ data, has measured $A^{\ell\ell} = (2.4 \pm 1.5(\text{stat.}) \pm 0.9(\text{sys.}))\%$ in dilepton events [159]. Using a neutrino weighting technique in the same dataset to reconstruct the top quarks, ATLAS measures $A_C = (2.1 \pm 2.5(\text{stat.}) \pm 1.7(\text{sys.}))\%$. CMS, in 5.0 fb^{-1} of $\sqrt{s} = 7 \text{ TeV}$ data, uses dilepton events to measure $A_C = (1.0 \pm 1.5(\text{stat.}) \pm 0.6(\text{sys.}))\%$, where a matrix weighting technique is used to reconstruct the top quarks, and $A^{\ell\ell} = (0.9 \pm 1.0(\text{stat.}) \pm 0.6(\text{sys.}))\%$ [160]. An earlier result using lepton+jets events from the same CMS dataset found $A_C = (0.4 \pm 1.0 \pm 1.1)\%$ [153]. Combined results from ATLAS and CMS have recently been released [161]. At $\sqrt{s} = 7 \text{ TeV}$ the combined result is $A_C = (0.5 \pm 0.7(\text{stat.}) \pm 0.6(\text{sys.}))\%$, and at $\sqrt{s} = 8 \text{ TeV}$ it is $A_C = (0.55 \pm 0.23 \pm 0.25)\%$. These results are all consistent, within their large uncertainties, with the SM expectations of $A^{\ell\ell} = (0.70 \pm 0.03)\%$ and $A_C = (1.23 \pm 0.05)\%$ [145].

A model-independent comparison of the Tevatron and LHC results is made difficult by the differing $t\bar{t}$ production mechanisms at work at the two accelerators and by the symmetric nature of the pp collisions at the LHC. A recent result from the CMS Collaboration [162] in 35.9 fb^{-1} of lepton plus jets events at $\sqrt{s} = 13 \text{ TeV}$, uses a likelihood analysis in to separate the $q\bar{q}$ process from production via gluon-gluon and gluon-quark interactions and extract $A_{FB} = 0.048_{-0.084}^{+0.088}(\text{stat.}) \pm 0.028(\text{sys.})$. In addition, given a particular model of BSM physics, a comparison can be obtained through the resulting asymmetry predicted by the model at the two machines, see for example [158].

60.3.2 Top-Quark Properties

60.3.2.1 Top-Quark Mass Measurements

The most precisely studied property of the top quark is its mass. The top-quark mass has been measured in the lepton+jets, the dilepton, and the all-jets channel by all four Tevatron and LHC experiments. The latest and/or most precise results are summarized in Table 60.1. The lepton+jets channel yields the most precise single measurements because of good signal to background ratio (in particular after b -tagging) and the presence of only a single neutrino in the final state. The momentum of a single neutrino can be reconstructed (up to a quadratic ambiguity) via the missing E_T measurement and the constraint that the lepton and neutrino momenta reconstruct to the known W boson mass. In the large data samples available at the LHC, measurements in the dilepton channel can be competitive and certainly complementary to those in the lepton+jets final state.

A large number of techniques have now been applied to measuring the top-quark mass. The original ‘template method’ [163], in which Monte Carlo templates of reconstructed mass distributions are fit to data, has evolved into a precision tool in the lepton+jets channel, where the systematic uncertainty due to the jet energy scale (JES) uncertainty is controlled by a simultaneous, *in situ* fit to the $W \rightarrow jj$ hypothesis [164]. All the latest measurements in the lepton+jets and the all-jets channels use this technique in one way or another. In 20.2 fb^{-1} of data at $\sqrt{s} = 8 \text{ TeV}$ in the lep-

ton+jets channel, ATLAS achieves a total uncertainty of 0.53% with a statistical component of 0.23% [165]. The measurement is based on a 3-dimensional template fit, determining the top-quark mass, the global jet energy scale and a b -to-light jet energy scale factor. The most precise CMS result in the lepton+jets channel uses an ideogram method and comes from a so-called ‘hybrid’ approach in which the prior knowledge about the jet energy scale is incorporated as a Gaussian constraint, with a width determined by the uncertainty on the jet energy corrections. In 19.7 fb^{-1} of $\sqrt{s} = 8 \text{ TeV}$ data, CMS achieves a total uncertainty of 0.30% with a statistical component of 0.09% with the hybrid approach [166]. Using this same method, CMS has recently released the first top-mass measurement from $\sqrt{s} = 13 \text{ TeV}$ data. Using 35.9 fb^{-1} of lepton+jets events they measure the top mass with a precision of 0.36%, with a statistical component of 0.05% [167]. The measurements at $\sqrt{s} = 13 \text{ TeV}$ include, for the first time, an uncertainty due to ‘color reconnection’ [168,169]. In this same dataset, CMS has extracted a top mass from highly boosted top-quark decays by selecting events in which the hadronic-side top decay is reconstructed as a single jet with $P_T > 400 \text{ GeV}$. The cross section as a function of jet mass is unfolded at the particle level to extract a top mass with a precision of 1.4% [170].

The template method is complemented by the ‘matrix element’ method. This method was first applied by the DØ Collaboration [171], and is similar to a technique originally suggested by Kondo *et al.* [172] and Dalitz and Goldstein [173]. In the matrix element method a probability for each event is calculated as a function of the top-quark mass, using a LO matrix element for the production and decay of $t\bar{t}$ pairs. The *in situ* calibration of dijet pairs to the $W \rightarrow jj$ hypothesis is now also used with the matrix element technique to constrain the jet energy scale uncertainty. In the lepton+jets channel, DØ uses the full Tevatron dataset of 9.7 fb^{-1} and yields an uncertainty of about 0.43% [174].

In the dilepton channel, the signal to background is typically very good, but reconstruction of the mass is non-trivial because there are two neutrinos in the final state, yielding a kinematically unconstrained system. A variety of techniques have been developed to handle this. An analytic solution to the problem has been proposed [175], but this has not yet been used in the mass measurement. One of the most precise measurements in the dilepton channel comes from using the invariant mass of the charged lepton and b -quark system ($M_{\ell b}$), which is sensitive to the top-quark mass and avoids the kinematic difficulties of the two-neutrino final state. In 4.6 fb^{-1} of $\sqrt{s} = 7 \text{ TeV}$ data, ATLAS has measured the top-quark mass in the dilepton channel to a precision of 0.53% using a template fit to the $M_{\ell b}$ distribution [176]. Using 19.7 fb^{-1} of data at $\sqrt{s} = 8 \text{ TeV}$, CMS has released [177] a mass measurement in the dilepton channel based on a simultaneous fit to $M_{\ell b}$ and a transverse-mass-like variable M_{T2} [178]. The most precise result in this analysis, which comes from a linear combination of fits with the jet energy scale fixed at its nominal value and one that simultaneously determines the top mass and jet energy scale, has a total uncertainty of 0.54%. At the LHC, because of their precision, these techniques have largely displaced a number of earlier techniques in the dilepton channel, though these techniques are still included, and described, in the combined results from CMS, reported in Ref. [166].

In the neutrino weighting technique, used by CDF to analyze the full Run 2 dilepton dataset of 9.1 fb^{-1} , a weight is assigned by assuming a top-quark mass value and applying energy-momentum conservation to the top-quark decay, resulting in up to four possible pairs of solutions for the neutrino and anti-neutrino momenta. The missing E_T calculated in this way is then compared to the observed missing E_T to assign a weight [182]. The CDF result achieves a precision of 1.8% using a combination of neutrino weighting and an ‘alternative mass’, which is insensitive to the jet energy scale [183]. The alternative mass depends on the angles between the leptons and the leading jets and the lepton four-momenta.

In the all-jets channel there is no ambiguity due to neutrino momenta, but the signal to background is significantly poorer due to the severe QCD multijets background. The emphasis therefore has been on background modeling, and reduction through event

selection. The most recent measurement in the all-jets channel, by CMS in 35.9 fb^{-1} of $\sqrt{s} = 13 \text{ TeV}$ data [179], uses an ideogram method and a 2-dimensional simultaneous fit for m_t and the jet energy scale to extract the top-quark mass and achieves a precision of 0.36%. A recent measurement from ATLAS [180] uses a template fit to the ratio of three-jet (m_t) to two-jet (M_W) mass in the all-hadronic channel, the two-jet denominator provides an *in situ* fit to the $W \rightarrow jj$ hypothesis. In 20.2 fb^{-1} of data at $\sqrt{s} = 8 \text{ TeV}$, the result has a precision of 0.65%. A measurement from CDF in 9.3 fb^{-1} uses a two-dimensional template fit and achieves a precision of 1.1% [184].

The CMS Collaboration has, for the first time, extracted a top-quark mass measurement from single-top events [185], something not previously done because of the poor signal to background ratio. The mass is extracted from the invariant mass of the muon, bottom quark, and missing transverse energy. In 19.7 fb^{-1} of data at $\sqrt{s} = 8 \text{ TeV}$, a precision of 0.71% is achieved.

A dominant systematic uncertainty in these methods is the understanding of the jet energy scale, and so several techniques have been developed that have little sensitivity to the jet energy scale uncertainty. In addition to Reference [183] mentioned above, these include the measurement of the top-quark mass using the following techniques: Fitting of the lepton p_T spectrum of candidate events [186]; fitting of the transverse decay length of the b -jet (L_{xy}) [187]; fitting the invariant mass of a lepton from the W -decay and a muon from the semileptonic b decay [188], kinematic properties of secondary vertices from b -quark fragmentation [189], the invariant mass of the $J/\psi + \ell$ system in events in which a b -quark fragments to a J/ψ particle [190], fitting the b -jet energy peak [191], and dilepton kinematics in $e\mu$ events [192].

Several measurements have now been made in which the top-quark mass is extracted from the measured $t\bar{t}$ cross section using the theoretical relationship between the mass and the production cross section. These determinations make use of predictions calculated at higher orders, where the top mass enters as an input parameter defined in a given scheme. At variance with the usual methods, which involve the kinematic properties of the final states and therefore the pole mass, this approach can also directly determine a short-distance mass, such as the $\overline{\text{MS}}$ mass [193]. With an alternative method ATLAS recently extracted the top-quark pole mass using $t\bar{t}$ events with at least one additional jet, basing the measurement on the relationship between the differential rate of gluon radiation and the mass of the quark [194]. A similar analysis by CMS used the differential cross section as a function of the invariant mass of the $t\bar{t}$ system and the leading jet not associated with the top decays [195].

Each of the experiments has produced a measurement combining its various results. The combined measurement from CMS with up to 19.7 fb^{-1} of data achieves statistical and systematic uncertainties of 0.08% and 0.27%, respectively [166]. The combined measurement from ATLAS, with up to 20.3 fb^{-1} yields statistical and systematic uncertainties of 0.14% and 0.24%, respectively [165]. CDF has combined measurements with up to 9.3 fb^{-1} [196] and achieves a statistical precision of 0.33% and a systematic uncertainty of 0.43%. DØ achieves a 0.33% statistical+JES and a 0.28% systematic uncertainty by combining results in 9.7 fb^{-1} [197].

Combined measurements from the Tevatron experiments and from the LHC experiments take into account the correlations between different measurements from a single experiment and between measurements from different experiments. The Tevatron average [181], using up to 9.7 fb^{-1} of data, now has a precision of 0.37%. The LHC combination, using up to 4.9 fb^{-1} of data, has a precision of 0.56% [198], where more work on systematic uncertainties is required. A Tevatron-LHC combination has been released, combining the results of all four experiments, using the full Tevatron dataset and the $\sqrt{s} = 7 \text{ TeV}$ LHC data, with a resulting precision of 0.44% [3].

The direct measurements of the top-quark mass, such as those shown in Table 60.1, correspond to the parameter used in the Monte Carlo generators, which is generally agreed to be the pole mass. The relation between the pole mass and short-distance

Table 60.1: Measurements of top-quark mass from Tevatron and LHC. $\int \mathcal{L}dt$ is given in fb^{-1} . The results are a selection of both published and preliminary (not yet submitted for publication as of September 2019) measurements. For a complete set of published results see the Listings. Statistical uncertainties are listed first, followed by systematic uncertainties.

m_t (GeV/ c^2)	Source	$\int \mathcal{L}dt$	Ref.	Channel
$172.08 \pm 0.25 \pm 0.41$	ATLAS	20.2	[165]	ℓ +jets+ $\ell\ell$ +All jets
$172.44 \pm 0.13 \pm 0.47$	CMS	19.7	[166]	ℓ +jets+ $\ell\ell$ +All jets
$172.35 \pm 0.16 \pm 0.48$	CMS	19.7	[166]	ℓ +jets
$172.34 \pm 0.20 \pm 0.70$	CMS	35.9	[179]	$\ell\ell$
$173.72 \pm 0.55 \pm 1.01$	ATLAS	20.2	[180]	All jets
$172.25 \pm 0.08 \pm 0.62$	CMS	35.9	[167]	ℓ +jets
$174.30 \pm 0.35 \pm 0.54$	CDF,DØ (I+II)	≤ 9.7	[181]	publ. or prelim.
$173.34 \pm 0.27 \pm 0.71$	Tevatron+LHC	$\leq 8.7 + \leq 4.9$	[3]	publ. or prelim.

masses, such as $\overline{M\overline{S}}$, is affected by non-perturbative effects. Recent calculations evaluate the size of this ambiguity to be below 250 MeV and therefore still smaller than the current measurement uncertainty [199, 200].

As a result of renormalization at higher-orders in perturbation theory, the top quark mass depends on the scale at which it is evaluated. The CMS collaboration has made the first measurement of the so-called running of the top-quark mass in the $\overline{M\overline{S}}$ scheme [201]. The running mass is extracted from a measurement of the differential cross section as a function of the $t\bar{t}$ invariant mass, unfolded back to the parton level, in $e\mu$ final states. The running mass varies by about 15% from $M_{t\bar{t}} = 400$ GeV to $M_{t\bar{t}} \approx 1$ TeV, in good agreement with the renormalization group calculation at one-loop level. Compared to the hypothesis of no running, the significance of the measured running is 2.6σ .

With the discovery of a Higgs boson at the LHC with a mass of about 125 GeV/ c^2 [202, 203], the precision measurement of the top-quark mass takes a central role in the question of the stability of the electroweak vacuum because top-quark radiative corrections tend to drive the Higgs quartic coupling, λ , negative, potentially leading to an unstable vacuum. A recent calculation at NNLO [204] leads to the conclusion of vacuum stability for a Higgs mass satisfying $M_H \geq 129.4 \pm 5.6$ GeV/ c^2 [205]. Given the uncertainty, a Higgs mass of 125 GeV/ c^2 satisfies the limit, but the central values of the Higgs and top-quark masses put the electroweak vacuum squarely in the metastable region. The uncertainty is dominated by the precision of the top-quark mass measurement and its interpretation as the pole mass. For more details, see the Higgs boson review in this volume.

As a test of the CPT-symmetry, the mass difference of top- and antitop-quarks $\Delta m_t = m_t - m_{\bar{t}}$, which is expected to be zero, can be measured. CDF measures the mass difference in 8.7 fb^{-1} of 1.96 TeV data in the lepton+jets channel using a template method to find $\Delta m_t = -1.95 \pm 1.11(\text{stat.}) \pm 0.59(\text{syst.})$ GeV/ c^2 [206] while DØ uses 3.6 fb^{-1} of lepton+jets events and the matrix element method with at least one b -tag. They find $\Delta m_t = 0.8 \pm 1.8(\text{stat.}) \pm 0.5(\text{syst.})$ GeV/ c^2 [207]. In 4.7 fb^{-1} of 7 TeV data, ATLAS measures the mass difference in lepton+jets events with a double b -tag requirement and hence very low background to find $\Delta m_t = 0.67 \pm 0.61(\text{stat.}) \pm 0.41(\text{syst.})$ GeV/ c^2 [208]. CMS measures the top-quark mass difference in 5 fb^{-1} of 7 TeV data in the lepton+jets channel and finds $\Delta m_t = -0.44 \pm 0.46(\text{stat.}) \pm 0.27(\text{syst.})$ GeV/ c^2 [209]. They repeat this measurement with 19.6 fb^{-1} of 8 TeV data to find $\Delta m_t = -0.15 \pm 0.19(\text{stat.}) \pm 0.09(\text{syst.})$ GeV/ c^2 [210]. All measurements are consistent with the SM expectation.

60.3.2.2 Top-Quark Spin Correlations, Polarization, and Width

One of the unique features of the top quark is that it decays before its spin can be flipped by the strong interaction. Thus the top-quark polarization is directly observable via the angular distribution of its decay products and it is possible to define and measure observables sensitive to the top-quark spin and its production mechanism. Although the top- and antitop-quarks produced by strong interactions in hadron collisions are essentially unpolarized, the spins of t and \bar{t} are correlated. For QCD production at threshold, the $t\bar{t}$ system is produced in a 3S_1 state with parallel spins for $q\bar{q}$ annihilation or in a 1S_0 state with antiparal-

lel spins for gluon-gluon fusion. The situations at the Tevatron, where the production is primarily from $q\bar{q}$ annihilation, and at the LHC, where the production is primarily from gluon-gluon fusion, are therefore somewhat complementary. However, at the LHC production of $t\bar{t}$ pairs at large invariant mass occurs primarily via fusion of gluons with opposite helicities, and the $t\bar{t}$ pairs so produced have parallel spins as in production at the Tevatron via $q\bar{q}$ annihilation. The direction of the top-quark spin is 100% correlated to the angular distributions of the down-type fermion (charged leptons or d -type quarks) in the decay. The joint angular distribution [211–213]

$$\frac{1}{\sigma} \frac{d^2\sigma}{d(\cos\theta_+)d(\cos\theta_-)} = \frac{1}{4}(1 + B_+ \cos\theta_+ + B_- \cos\theta_- + \kappa \cdot \cos\theta_+ \cdot \cos\theta_-), \quad (60.4)$$

where θ_+ and θ_- are the angles of the daughters in the top-quark rest frame with respect to a particular spin quantization axis (assumed here to be the same for θ_+ and θ_-), is a very sensitive observable. The maximum value for κ , 0.782 at NLO at the Tevatron [214], is found in the off-diagonal basis [211], while at the LHC the value at NLO is 0.326 in the helicity basis [214]. The coefficients B_+ and B_- are near zero in the SM because the top quarks are unpolarized in $t\bar{t}$ production. In place of κ , $A\alpha_+\alpha_-$ is often used, where α_i is the spin analyzing power, and A is the spin correlation coefficient, defined as

$$A = \frac{N(\uparrow\uparrow) + N(\downarrow\downarrow) - N(\uparrow\downarrow) - N(\downarrow\uparrow)}{N(\uparrow\uparrow) + N(\downarrow\downarrow) + N(\uparrow\downarrow) + N(\downarrow\uparrow)}, \quad (60.5)$$

where the first arrow represents the direction of the top-quark spin along a chosen quantization axis, and the second arrow represents the same for the antitop-quark. The spin analyzing power α_i is +0.998 for positively charged leptons, -0.966 for down-type quarks from W decays, and -0.393 for bottom quarks [215]. The sign of α flips for the respective antiparticles. The spin correlation could be modified by a new $t\bar{t}$ production mechanism such as through a Z' boson, Kaluza-Klein gluons, a dark-matter mediator, or a Higgs boson.

The experiments typically use a Monte Carlo to provide templates for the measured distributions, or alternatively a matrix-element technique, and fit a parameter f , representing the fraction of events with the expected Standard Model correlation, with $(1-f)$ the fraction with no correlation. The correlation coefficient is extracted via $A_{\text{meas}} = f \cdot A_{\text{SM}}$. A ‘fraction’ $f > 1$ means that the measured correlation coefficient is larger than the Standard Model expectation.

CDF used 5.1 fb^{-1} in the dilepton channel to measure the correlation coefficient in the beam axis [216]. The measurement was made using the expected distributions of $(\cos\theta_+, \cos\theta_-)$ and $(\cos\theta_b, \cos\theta_{\bar{b}})$ of the charged leptons or the b -quarks in the $t\bar{t}$ signal and background templates to calculate a likelihood of observed reconstructed distributions as a function of assumed κ . They determined the 68% confidence interval for the correlation coefficient κ as $-0.52 < \kappa < 0.61$ or $\kappa = 0.04 \pm 0.56$ assuming $m_t = 172.5$ GeV/ c^2 .

CDF also analyzed lepton+jets events in 5.3 fb^{-1} [217] assuming $m_t = 172.5$ GeV/ c^2 . They form three separate tem-

plates - the same-spin template, the opposite-spin template, and the background template for the 2-dimensional distributions in $\cos(\theta_l)\cos(\theta_d)$ vs. $\cos(\theta_l)\cos(\theta_b)$. The fit to the data in the helicity basis returns an opposite helicity fraction of $F_{OH} = 0.74 \pm 0.24(stat.) \pm 0.11(syst.)$. Converting this to the spin correlation coefficient yields $\kappa_{helicity} = 0.48 \pm 0.48(stat.) \pm 0.22(syst.)$. In the beamline basis, they find an opposite spin fraction of $F_{OS} = 0.86 \pm 0.32(stat.) \pm 0.13(syst.)$ which can be converted into a correlation coefficient of $\kappa_{beam} = 0.72 \pm 0.64(stat.) \pm 0.26(syst.)$.

$D\bar{O}$ performed a measurement of the ratio f of events with correlated t and \bar{t} spins to the total number of $t\bar{t}$ events. Combining dilepton and lepton plus jets events, and using a matrix-element technique in 9.7 fb^{-1} of Tevatron data, $D\bar{O}$ measures $f = 1.16 \pm 0.21$, corresponding to $A_{exp.} = 0.89 \pm 0.22(stat. + syst.)$ in the off-diagonal basis [218].

In Ref. [219] $D\bar{O}$ presents a measurement of top-quark polarization in $t\bar{t}$ production at the Tevatron. In 9.7 fb^{-1} of $p\bar{p}$ collisions, $D\bar{O}$ uses lepton angular distributions in lepton+jets events to measure polarization in the beam, helicity, and transverse bases. The measurements are, respectively, 0.081 ± 0.048 , -0.102 ± 0.061 and, 0.040 ± 0.035 , where the beam-basis result is a combination with an earlier $D\bar{O}$ result in dilepton events [220]. These results are all consistent near-zero polarization, as predicted in the SM.

Spin correlations have been conclusively measured at the LHC by both the ATLAS and CMS collaborations. In the dominant gluon fusion production mode for $t\bar{t}$ pairs at the LHC, the angular distribution between the two leptons in $t\bar{t}$ decays to dileptons is sensitive to the degree of spin correlation [221].

Measurements have been made at 7, 8, and now 13 TeV. While there is some interest in the \sqrt{s} dependence of the correlations as a test of the production mechanism ($q\bar{q}$ vs gluon-gluon and possible sensitivity to new physics) the earlier measurements at 7 and 8 TeV [222–227] had relatively large uncertainties and have now been overtaken by the high-statistics 13 TeV measurements, which we review here.

The most recent result from ATLAS, in 36.1 fb^{-1} at $\sqrt{s} = 13 \text{ TeV}$, uses $\Delta\phi$, the azimuthal angle between the two charged leptons in $e\mu$ events in an analysis that also measures the differential cross sections in $\Delta\phi$ and $\Delta\eta$ between the two leptons [228]. The result, measured by comparison with NLO Monte Carlo generators, is $f = 1.249 \pm 0.024 \pm 0.061 \pm 0.040$, where the uncertainties are statistical, systematic, and theoretical, is again greater than 1.0. Whereas the previous results were statistically consistent with the Standard Model expectation of 1.0, this result is inconsistent at the level of 3.2σ . The NLO generators are NLO in QCD only (and only at the production level). Including electroweak couplings produces an expected Standard Model distribution consistent with the data, but results in a large scale uncertainty, giving $f = 1.03 \pm 0.13$.

In 35.9 fb^{-1} of data at $\sqrt{s} = 13 \text{ TeV}$, CMS has measured spin correlations in dilepton events using $\Delta\phi$ and found $f = 1.05 \pm 0.03 \pm 0.08^{+0.09}_{-0.12}$ [229], where the uncertainties are statistical, systematic, and theoretical. The correlation is also measured using the coefficient κ in Eq. 60.4 (called $-C_{ij}$ in Reference [229]) using three orthogonal spin quantization axes defined in Ref. [230]. All results are consistent with $f = 1$. Measurements of the coefficients B_i in Eq. 60.4 in this analysis, which are expected to be nearly zero in the SM, yield $B_+ = 0.005 \pm 0.023$ and $B_- = 0.007 \pm 0.023$, consistent with the SM predictions at NLO of $0.0040^{+0.0017}_{-0.0012}$ [230]. These results are part of a complete study of the top-quark spin density matrix at $\sqrt{s} = 13 \text{ TeV}$, through the measurement of the coefficients of Eq. 60.4.

In a similar ATLAS measurement at $\sqrt{s} = 8 \text{ TeV}$ [231], the spin-correlation coefficient κ is measured in the helicity basis to be $\kappa = 0.296 \pm 0.093$ in good agreement with the SM expectation of 0.318 (corresponding to a central value of f of 0.931). The polarization coefficients, B , in Eq. 60.4 are measured, also in the helicity basis, to be $B_+ = -0.044 \pm 0.038$ and $B_- = -0.064 \pm 0.040$, consistent with the SM predictions of 0.0030 ± 0.0010 and 0.0034 ± 0.00104 , respectively.

Observation of top-quark spin correlations requires a top-quark lifetime less than the spin decorrelation timescale [232]. The top-quark width, inversely proportional to its lifetime, is expected

to be of order $1 \text{ GeV}/c^2$ (Eq. 1). Early measurements made at CDF [233] and CMS [234] established confidence-level intervals for the width, but did not have the sensitivity to make a direct measurement.

The first direct measurement comes from an ATLAS analysis that directly fits reconstructed lepton+jets events in 20.2 fb^{-1} of data at $\sqrt{s} = 8 \text{ TeV}$. They find $\Gamma_t = 1.76 \pm 0.33^{+0.79}_{-0.68} \text{ GeV}/c^2$ [235]. A more recent measurement from ATLAS with 139 fb^{-1} of data at $\sqrt{s} = 13 \text{ TeV}$ [236], uses a template fit to the lepton- b -quark invariant mass in dilepton final states. The result, $\Gamma_t = (1.9 \pm 0.5) \text{ GeV}/c^2$, is the most precise measurement to date.

The total width of the top-quark can also be determined from the partial decay width $\Gamma(t \rightarrow Wb)$ and the branching fraction $B(t \rightarrow Wb)$. $D\bar{O}$ obtains $\Gamma(t \rightarrow Wb)$ from the measured t -channel cross section for single top-quark production in 5.4 fb^{-1} , and $B(t \rightarrow Wb)$ is extracted from a measurement of the ratio $R = B(t \rightarrow Wb)/B(t \rightarrow Wq)$ in $t\bar{t}$ events in lepton+jets channels with 0, 1 and 2 b -tags. Assuming $B(t \rightarrow Wq) = 1$, where q includes any kinematically accessible quark, the result is: $\Gamma_t = 2.00^{+0.47}_{-0.43} \text{ GeV}/c^2$ which translates to a top-quark lifetime of $\tau_t = (3.29^{+0.90}_{-0.63}) \times 10^{-25} \text{ s}$. Assuming a high mass fourth generation b' quark and unitarity of the four-generation quark-mixing matrix, they set the first upper limit on $|V_{tb'}| < 0.59$ at 95% C.L. [237]. A similar analysis has been performed by CMS in 19.7 fb^{-1} of $\sqrt{s} = 8 \text{ TeV}$ data. It provides a better determination of the total width with respect to the measurement by $D\bar{O}$ giving $\Gamma_t = 1.36 \pm 0.02(stat.)^{+0.14}_{-0.11}(syst.) \text{ GeV}/c^2$ [71].

60.3.2.3 W -Boson Helicity in Top-Quark Decay

The Standard Model dictates that the top quark has the same vector-minus-axial-vector ($V - A$) charged-current weak interactions $\left(-i\frac{g}{\sqrt{2}}V_{tb}\gamma^\mu\frac{1}{2}(1 - \gamma_5)\right)$ as all the other fermions. In the SM, the fraction of top-quark decays to longitudinally polarized W bosons is proportional to its Yukawa coupling and hence enhanced with respect to the weak coupling. It is expected to be [238] $\mathcal{F}_0^{\text{SM}} \approx x/(1+x)$, $x = m_t^2/2M_W^2$ ($\mathcal{F}_0^{\text{SM}} \sim 70\%$ for $m_t = 175 \text{ GeV}/c^2$). Fractions of left-handed, right-handed, or longitudinal W bosons are denoted as \mathcal{F}_- , \mathcal{F}_+ , and \mathcal{F}_0 respectively. In the SM, \mathcal{F}_- is expected to be $\approx 30\%$ and $\mathcal{F}_+ \approx 0\%$. Predictions for the W polarization fractions at NNLO in QCD are available [239].

The Tevatron and the LHC experiments use various techniques to measure the helicity of the W boson in top-quark decays, in both the lepton+jets and in dilepton channels in $t\bar{t}$ production.

The first method uses a kinematic fit, similar to that used in the lepton+jets mass analyses, but with the top-quark mass constrained to a fixed value, to improve the reconstruction of final-state observables, and render the under-constrained dilepton channel solvable. Alternatively, in the dilepton channel the final-state momenta can also be obtained through an algebraic solution of the kinematics. The distribution of the helicity angle ($\cos\theta^*$) between the lepton and the b quark in the W rest frame provides the most direct measure of the W helicity. In a simplified version of this approach, the $\cos\theta^*$ distribution is reduced to a forward-backward asymmetry.

The second method (p_T^{ℓ}) uses the different lepton p_T spectra from longitudinally or transversely polarized W -decays to determine the relative contributions.

A third method uses the invariant mass of the lepton and the b -quark in top-quark decays ($M_{\ell b}^2$) as an observable, which is directly related to $\cos\theta^*$.

At the LHC, top-quark pairs in the dilepton channels are reconstructed by solving a set of six independent kinematic equations in the missing transverse energy in x - and in y -direction, two W -masses, and the two top/antitop-quark masses. In addition, the two jets with the largest p_T in the event are interpreted as b -jets. The pairing of the jets to the charged leptons is based on the minimization of the sum of invariant masses M_{min} . Simulations show that this criterion gives the correct pairing in 68% of the events.

Finally, the Matrix Element Method (MEM) has also been used [172], in which a likelihood is formed from a product of event probabilities calculated from the MEM for a given set of measured

kinematic variables and assumed W -helicity fractions.

The results of recent CDF, $D\bar{O}$, ATLAS, and CMS analyses are summarized in Table 60.2. The datasets are now large enough to allow for a simultaneous fit of \mathcal{F}_0 , \mathcal{F}_- and \mathcal{F}_+ , which we denote by ‘3-param’ or \mathcal{F}_0 and \mathcal{F}_+ , which we denote by ‘2-param’ in the table. Results with either \mathcal{F}_0 or \mathcal{F}_+ fixed at its SM value are denoted ‘1-param’. For the simultaneous fits, the correlation coefficient between the two values is about -0.8 . A complete set of published results can be found in the Listings. All results are in agreement with the SM expectation.

CDF and $D\bar{O}$ combined their results based on $2.7 - 5.4 \text{ fb}^{-1}$ [240] for a top-quark mass of $172.5 \text{ GeV}/c^2$. ATLAS presents results from 1.04 fb^{-1} of $\sqrt{s} = 7 \text{ TeV}$ data using a template method for the $\cos\theta^*$ distribution and angular asymmetries from the unfolded $\cos\theta^*$ distribution in the lepton+jets and the dilepton channel [241]. CMS performs a similar measurement based on template fits to the $\cos\theta^*$ distribution with 5.0 fb^{-1} of 7 TeV data in the lepton+jets final state [242]. As the polarization of the W bosons in top-quark decays is sensitive to the Wtb vertex Lorentz structure and anomalous couplings, both experiments also derive limits on anomalous contributions to the Wtb couplings. Recently, both experiments also combined their results from 7 TeV data to obtain values on the helicity fractions as well as limits on anomalous couplings [243].

At 8 TeV , ATLAS came out with a measurement of the W -helicity fractions in 20.2 fb^{-1} in lepton+jets events with at least one b -tag [244]. Using 19.8 fb^{-1} of 8 TeV data, CMS measured the W -helicity in lepton + 4 jet events with two b -tags [245]. In $t\bar{t}$ events with two opposite-sign leptons (electron or muon) in the final state in this dataset, CMS applied six kinematic constraints on the kinematics of the produced particles [246]. Also, using the same dataset a first measurement of the W -boson helicity in top-quark decays was made in electroweak single top production [247], yielding similarly precise and consistent results.

60.3.2.4 Top-Quark Electroweak Charges and Couplings

The top quark is the only quark whose electric charge has not been measured through production at threshold in e^+e^- collisions. Furthermore, it is the only quark whose electromagnetic coupling has not been observed and studied until recently. Since the CDF and $D\bar{O}$ analyses on top-quark production did not associate the b , \bar{b} , and W^\pm uniquely to the top or antitop, decays such as $t \rightarrow W^+\bar{b}, \bar{t} \rightarrow W^-b$ were not excluded. A charge $4/3$ quark of this kind is consistent with current electroweak precision data. The $Z \rightarrow \ell^+\ell^-$ and $Z \rightarrow b\bar{b}$ data, in particular the discrepancy between A_{LR} from SLC at SLAC and $A_{FB}^{0,b}$ of b -quarks and $A_{FB}^{0,\ell}$ of leptons from LEP at CERN, can be fitted with a top quark of mass $m_t = 270 \text{ GeV}/c^2$, provided that the right-handed b quark mixes with the isospin $+1/2$ component of an exotic doublet of charge $-1/3$ and $-4/3$ quarks, $(Q_1, Q_4)_R$ [249, 250]. Also the third component of the top quark’s weak isospin has not been measured so far.

$D\bar{O}$ studied the top-quark charge in double-tagged lepton+jets events, CDF did it in single tagged lepton+jets and dilepton events. Assuming the top- and antitop-quarks have equal but opposite electric charge, then reconstructing the charge of the b -quark through jet charge discrimination techniques, the $|Q_{top}| = 4/3$ and $|Q_{top}| = 2/3$ scenarios can be differentiated. For the exotic model of Chang *et al.* [250] with a top-quark charge $|Q_{top}| = 4/3$, CDF excluded the model at 99% C.L. [251] in 5.6 fb^{-1} , while $D\bar{O}$ excluded the model at a significance greater than 5 standard deviations using 5.3 fb^{-1} and set an upper limit of 0.46 on the fraction of such quarks in the selected sample [252]. These results indicate that the observed particle is indeed consistent with being a SM $|Q| = 2/3$ quark.

In 2.05 fb^{-1} at $\sqrt{s} = 7 \text{ TeV}$, ATLAS performed a similar analysis, reconstructing the b -quark charge either via a jet-charge technique or via the lepton charge in soft muon decays in combination with a kinematic likelihood fit. They measure the top-quark charge to be $0.64 \pm 0.02(stat.) \pm 0.08(sys.)$ from the charges of the top-quark decay products in single lepton $t\bar{t}$ events, and hence exclude the exotic scenario with charge $-4/3$ at more than 8σ [253].

In 4.6 fb^{-1} at $\sqrt{s} = 7 \text{ TeV}$, CMS discriminates between the SM

and the exotic top-quark charge scenario in the muon+jets final states in $t\bar{t}$ events. They exploit the charge correlation between high- p_t muons from W -boson decays and soft muons from B -hadron decays in b -jets. Using an asymmetry technique, where $A = -1$ represent the exotic $Q = -4/3$ scenario and $A = +1$ the SM $Q = +2/3$ scenario, they find $A_{meas} = 0.97 \pm 0.12(stat.) \pm 0.31(sys.)$, which agrees with the Standard Model expectation and excludes the exotic scenario at 99.9% C.L. [254].

The electromagnetic or the weak coupling of the top quark can be probed directly by investigating $t\bar{t}$ events with an additional gauge boson, such as $t\bar{t}\gamma$, $t\bar{t}W$, and $t\bar{t}Z$ events. The corresponding coupling can be extracted from the corresponding cross section or extracted from effective field theory (EFT) fits to various measured distributions and differential cross sections.

CDF performed a search for events containing a lepton, a photon, significant missing transverse momentum, and a jet identified as containing a b -quark and at least three jets and large total transverse energy in 6.0 fb^{-1} . They reported evidence for the observation of $t\bar{t}\gamma$ production with a cross section $\sigma_{t\bar{t}\gamma} = 0.18 \pm 0.08 \text{ pb}$ and a ratio of $\sigma_{t\bar{t}\gamma}/\sigma_{t\bar{t}} = 0.024 \pm 0.009$ [255].

ATLAS performed a first measurement of the $t\bar{t}\gamma$ cross section in pp collisions at $\sqrt{s} = 7 \text{ TeV}$ using 4.6 fb^{-1} of data. Events are selected that contain a large transverse momentum electron or muon and a large transverse momentum photon, yielding 140 and 222 events in the electron and muon samples, respectively. The production of $t\bar{t}\gamma$ events was observed with a significance of 5.3 standard deviations. The resulting cross section times branching ratio into the single lepton channel for $t\bar{t}\gamma$ production with a photon with transverse momentum above 20 GeV is $\sigma^{fid.}(t\bar{t}\gamma) \times BR = 63 \pm 8(stat.)_{-13}^{+17}(sys.) \pm 1(lumi.) \text{ pb}$ per lepton flavour [256], which is consistent with leading-order theoretical calculations.

At 8 TeV , ATLAS has used 20.2 fb^{-1} of data to measure the $t\bar{t}\gamma$ cross section with a photon above 15 GeV and $|\eta| < 2.37$. The fiducial cross section is measured to be $139 \pm 18 \text{ fb}$ [257], in good agreement with the NLO prediction [258]. Using 19.7 fb^{-1} of data at 8 TeV , CMS performed a similar measurement of the $t\bar{t}\gamma$ production cross section in the lepton+jets decay mode with a photon transverse momentum above 25 GeV and $|\eta| < 1.44$. They obtain a normalized cross section $\mathcal{R} = \sigma_{t\bar{t}\gamma}/\sigma_{t\bar{t}} = (5.7 \pm 1.8) \times 10^{-4}$ in e -jets and $(4.7 \pm 1.3) \times 10^{-4}$ in μ -jets. The fiducial $t\bar{t}\gamma$ cross section is obtained by multiplying by the measured $t\bar{t}$ fiducial cross section of $244.9 \pm 1.4(stat.)_{-5.5}^{+6.3}(sys.) \pm 6.4(lumi.) \text{ pb}$. Extrapolating to the full phase space, the result is $\sigma_{t\bar{t}\gamma} \times BR = (515 \pm 108) \text{ fb}$, per lepton+jets final state [259], in good agreement with the theoretical prediction.

At $\sqrt{s} = 13 \text{ TeV}$, using 36.1 fb^{-1} of single-lepton and dilepton events with exactly one photon, ATLAS measures the $t\bar{t}\gamma$ cross section. They employ neural network algorithms to separate the signal from the backgrounds. The fiducial cross-sections are measured to be $521 \pm 9(stat.) \pm 41(sys.) \text{ fb}$ and $69 \pm 3(stat.) \pm 4(sys.) \text{ fb}$ for the single-lepton and dilepton channels, respectively. The differential cross-sections are measured as a function of photon transverse momentum, photon absolute pseudorapidity, and angular distance between the photon and its closest lepton in both channels, as well as azimuthal opening angle and absolute pseudorapidity difference between the two leptons in the dilepton channel. All measurements are in agreement with the theoretical predictions [260]. Very recently, ATLAS uses 139 fb^{-1} of $\sqrt{s} = 13 \text{ TeV}$ $e\mu + \gamma$ events with at least two jets, out of which at least one is b -tagged, to measure the inclusive and differential cross-sections for the production of a top-quark pair in association with a photon. The fiducial cross-section is measured to be $44.2 \pm 2.6 \text{ fb}$. Differential cross-sections as functions of several observables are compared to state-of-the-art Monte Carlo simulations and next-to-leading order theoretical calculations. These include cross-sections as functions of the photon transverse momentum and absolute pseudorapidity and angular variables related to the photon and the leptons and between the two leptons in the event. All measurements are in agreement with the predictions [261]. In 35.9 fb^{-1} of lepton-plus-photon-plus-jets events, CMS manages to establish the first evidence for the associated production of a single-top quark and a photon at $\sqrt{s} = 13 \text{ TeV}$. They employ

Table 60.2: Measurement and 95% C.L. upper limits of the W helicity in top-quark decays. The table includes both preliminary, as of October 2019, and published results. A full set of published results is given in the Listings.

W Helicity	Source	$\int \mathcal{L} dt$ (fb^{-1})	Ref.	Method
$\mathcal{F}_0 = 0.722 \pm 0.081$	CDF+DØ Run II	2.7-5.4	[240]	$\cos \theta^*$ 2-param
$\mathcal{F}_0 = 0.682 \pm 0.057$	CDF+DØ Run II	2.7-5.4	[240]	$\cos \theta^*$ 1-param
$\mathcal{F}_0 = 0.726 \pm 0.094$	CDF Run II	8.7	[248]	ME 2-param
$\mathcal{F}_0 = 0.67 \pm 0.07$	ATLAS (7 TeV)	1.0	[241]	$\cos \theta^*$ 3-param
$\mathcal{F}_0 = 0.682 \pm 0.045$	CMS (7 TeV)	5.0	[242]	$\cos \theta^*$ 3-param
$\mathcal{F}_0 = 0.626 \pm 0.059$	ATLAS+CMS (7 TeV)	2.2	[243]	$\cos \theta^*$ 3-param
$\mathcal{F}_0 = 0.709 \pm 0.019$	ATLAS (8 TeV)	20.2	[244]	$\cos \theta^*$ 3-param
$\mathcal{F}_0 = 0.681 \pm 0.026$	CMS (8 TeV)	19.8	[245]	$\cos \theta^*$ 3-param
$\mathcal{F}_0 = 0.653 \pm 0.029$	CMS (8 TeV)	19.7	[246]	$\cos \theta^*$ 3-param
$\mathcal{F}_0 = 0.720 \pm 0.054$	CMS (8 TeV)	19.7	[247]	$\cos \theta^*$ 3-param
$\mathcal{F}_+ = -0.033 \pm 0.046$	CDF+DØ Run II	2.7-5.4	[240]	$\cos \theta^*$ 2-param
$\mathcal{F}_+ = -0.015 \pm 0.035$	CDF+DØ Run II	2.7-5.4	[240]	$\cos \theta^*$ 1-param
$\mathcal{F}_+ = -0.045 \pm 0.073$	CDF Run II	8.7	[248]	ME 2-param
$\mathcal{F}_+ = 0.01 \pm 0.05$	ATLAS (7 TeV)	1.0	[241]	$\cos \theta^*$ 3-param
$\mathcal{F}_+ = 0.008 \pm 0.018$	CMS (7 TeV)	5.0	[242]	$\cos \theta^*$ 3-param
$\mathcal{F}_+ = 0.015 \pm 0.034$	ATLAS+CMS (7 TeV)	2.2	[243]	$\cos \theta^*$ 3-param
$\mathcal{F}_+ = -0.008 \pm 0.014$	ATLAS (8 TeV)	20.2	[244]	$\cos \theta^*$ 3-param
$\mathcal{F}_+ = -0.004 \pm 0.015$	CMS (8 TeV)	19.8	[245]	$\cos \theta^*$ 3-param
$\mathcal{F}_+ = 0.018 \pm 0.027$	CMS (8 TeV)	19.7	[246]	$\cos \theta^*$ 3-param
$\mathcal{F}_+ = -0.018 \pm 0.022$	CMS (8 TeV)	19.7	[247]	$\cos \theta^*$ 3-param

a multivariate discriminant based on topological and kinematic event properties to separate signal from background processes. An excess above the background-only hypothesis is observed, with a significance of 4.4 standard deviations. A fiducial cross section is measured for isolated photons with transverse momentum greater than 25 GeV in the central region of the detector. The measured product of the cross section and branching fraction is $\sigma(pp \rightarrow t\gamma j)B(t \rightarrow \mu\gamma b) = 115 \pm 17(stat) \pm 30(syst)$ fb, which is consistent with the SM prediction [262]. A precision test of the vector and axial vector couplings in $t\bar{t}\gamma$ events or searches for possible tensor couplings of top-quarks to photons will only be feasible with an integrated luminosity of several hundred fb^{-1} in the future [263].

ATLAS and CMS have also studied the associate production of top-antitop quark pairs along with an electroweak gauge boson, where in the Standard Model the W -boson is expected to be produced via initial state radiation, while the Z -boson can also be radiated from a final-state top-quark and hence provides sensitivity to the top-quark neutral current weak gauge coupling, which implies a sensitivity to the third component of the top-quark's weak isospin, which has not been measured so far.

CMS performed measurements of the $t\bar{t}W$ and $t\bar{t}Z$ production cross section at $\sqrt{s} = 7$ TeV with 5 fb^{-1} , yielding $\sigma_{t\bar{t}V} = 0.43_{-0.15}^{+0.17}(stat.)_{-0.07}^{+0.09}(syst.)$ pb ($V = Z, W$) and $\sigma_{t\bar{t}Z} = 0.28_{-0.11}^{+0.14}(stat.)_{-0.03}^{+0.06}(syst.)$ fb, at about 3 standard deviations significance [264] and compatible with the SM expectations of $0.306_{-0.053}^{+0.031}$ pb and $0.137_{-0.016}^{+0.012}$ pb, respectively [265, 266]. ATLAS performed a similar analysis with 4.7 fb^{-1} in the three-lepton channel and set an upper limit of 0.71 pb at 95% C.L. [267].

Using 20.3 fb^{-1} of 8 TeV data, ATLAS performs a simultaneous measurement of the $t\bar{t}W$ and $t\bar{t}Z$ cross section. They observe the $t\bar{t}W$ and $t\bar{t}Z$ production at the 5.0σ and 4.2σ level, respectively, yielding $\sigma_{t\bar{t}W} = 369_{-91}^{+100}$ fb and $\sigma_{t\bar{t}Z} = 176_{-52}^{+58}$ fb [268]. CMS performs an analysis where signal events are identified by matching reconstructed objects in the detector to specific final state particles from $t\bar{t}W$ and $t\bar{t}Z$ decays using 19.5 fb^{-1} of 8 TeV data. They obtain $\sigma_{t\bar{t}W} = 382_{-102}^{+117}$ fb and $\sigma_{t\bar{t}Z} = 242_{-55}^{+65}$ fb, yielding a significance of 4.8 and 6.4 standard, respectively [269]. These measurements are used to set bounds on five anomalous dimension-six operators that would affect the $t\bar{t}W$ and $t\bar{t}Z$ cross sections.

The most recent measurements in these channels are made at 13 TeV from ATLAS and CMS in multilepton final states. ATLAS made a measurement using 36.1 fb^{-1} of events with two, three or four leptons. In multiple regions, the $t\bar{t}Z$ and $t\bar{t}W$ cross

sections are simultaneously measured using a combined fit to all regions, yielding $\sigma_{t\bar{t}Z} = 0.95 \pm 0.08(stat) \pm 0.10(syst)$ pb and $\sigma_{t\bar{t}W} = 0.87 \pm 0.13(stat) \pm 0.14(syst)$ pb [270] to be compared with the NLO+NLL (QCD) and NLO (EW) SM predictions, $\sigma_{t\bar{t}W} = 579_{-9\%}^{+14\%}$ fb and $\sigma_{t\bar{t}Z} = 811_{-10\%}^{+11\%}$ fb [271].

CMS uses 35.9 fb^{-1} of data to measure $t\bar{t}W$ and $t\bar{t}Z$ production cross sections of $0.77_{-0.11}^{+0.12}$ pb and $0.99_{-0.08}^{+0.09}$ pb, and significances over the background-only hypotheses of 5.5σ and 9.5σ , respectively [272], firmly establishing the observation of these processes. Very recently, CMS measured the inclusive $t\bar{t}Z$ cross section in 77.5 fb^{-1} of events with three or four charged leptons, and the Z boson is detected through its decay to an oppositely charged lepton pair. The production cross section is measured to be $\sigma(t\bar{t}Z) = 0.95 \pm 0.05(stat) \pm 0.06(syst)$ pb. This measurement includes differential cross sections as functions of the transverse momentum of the Z boson and the angular distribution of the negatively charged lepton from the Z boson decay as well as stringent direct limits on the anomalous tZ couplings [273].

The electroweak couplings can also be probed in single-top production in association with a Z boson. The $pp \rightarrow tZq$ process at the LHC probes both the WWZ coupling in the case where the Z emerges from the t -channel W in single-top production and, in the case where the Z is radiated from the top quark, the tZ coupling. A CMS search at 8 TeV produced a hint of a tZq signal in tri-lepton events, with a significance compared to the background-only hypothesis of 2.4σ [274]. At 13 TeV the signal has begun to emerge. In 35.9 fb^{-1} of events with three leptons, the tZq production cross section is measured to be $\sigma_{tZq} = 123_{-31}^{+33}(stat)_{-23}^{+29}(syst)$ fb, where l also includes tau leptons, with observed and expected significances of 3.7 and 3.1 standard deviations, respectively [262].

Searches for and now also measurements of the associate production of a top-antitop quark pair along with a Higgs boson, $t\bar{t}h$, with various subsequent decays provide sensitivity to the top-Higgs Yukawa coupling. For further details, see the review on "Higgs".

60.3.3 Searches for Physics Beyond the Standard Model

The top quark plays a special role in the SM. Being the only quark with a coupling to the Higgs boson of order one, it provides the most important contributions to the quadratic radiative corrections to the Higgs mass exposing the issue of the naturalness of the SM. It is therefore very common for models where the naturalness problem is addressed to have new physics associated with the top quark. In SUSY, for instance, naturalness predicts the scalar top partners to be the lightest among the squarks and to

be accessible at the LHC energies (see the review ‘‘Supersymmetry: Theory’’). In models where the Higgs is a pseudo-Goldstone boson, such as Little Higgs models, naturalness predicts the existence of partners of the top quarks with the same spin and color, but with different electroweak couplings, the so-called vectorial t' . Stops and t' 's are expected to have sizeable branching ratios to top quarks. Another intriguing prediction of SUSY models with universal couplings at the unification scale is that for a top-quark mass close to the measured value, the running of the Yukawa coupling down to 1 TeV naturally leads to the radiative breaking of the electroweak symmetry [275]. In fact, the top quark plays a role in the dynamics of electroweak symmetry breaking in many models [276]. One example is topcolor [277], where a large top-quark mass can be generated through the formation of a dynamic $t\bar{t}$ condensate, X , which is formed by a new strong gauge force coupling preferentially to the third generation. Another example is topcolor-assisted technicolor [278], predicting the existence of a heavy Z' boson that couples preferentially to the third generation of quarks. If light enough such a state might be directly accessible at the present hadron collider energies, or if too heavy, lead to four-top interactions possibly visible in the $t\bar{t}t\bar{t}$ final state. This final state has been recently observed by CMS [279] and limits are provided by ATLAS [280].

Current strategies to search for new physics in top-quark events at hadron colliders are either tailored to the discovery of specific models or model independent. They can be broadly divided in two classes. In the first class new resonant states are looked for through decay processes involving the top quarks. Current searches for bosonic resonances in $t\bar{t}$ final states, or for direct stop and t' production, or for a charged Higgs in $H^+ \rightarrow t\bar{b}$ fall in the category. On the other hand, if new states are too heavy to be directly produced, they might still give rise to deviations from the SM predictions for the strength and Lorentz form of the top-quark couplings to other SM particles. Accurate SM predictions and measurements are therefore needed and the results be efficiently interpreted in the framework of an effective field theory [281,282] as done for example in recent analyses sensitive to the strength and structure of the top quark couplings [270,279]. Global effective field theory interpretations based on publicly available measurements in the top quark sector have also appeared [283–285].

60.3.3.1 New Physics in Top Quark Production

Theoretical [286,287] and experimental efforts have been devoted to the searches of $t\bar{t}$ resonances.

At the Tevatron, both the CDF and DØ collaborations have searched for resonant production of $t\bar{t}$ pairs in the lepton+jets channel [288,289]. In both analyses, the data indicate no evidence of resonant production of $t\bar{t}$ pairs. They place upper limits on the production cross section times branching fraction to $t\bar{t}$ in comparison to the prediction for a narrow ($\Gamma_{Z'} = 0.012M_{Z'}$) leptophobic topcolor Z' boson. Within this model, they exclude Z' bosons with masses below 915 (CDF-full data set) and 835 (DØ, 5 fb⁻¹) GeV/c² at the 95% C.L. These limits turn out to be independent of couplings of the $t\bar{t}$ resonance (pure vector, pure axial-vector, or SM-like Z'). A similar analysis has been performed by CDF in the all-hadronic channel using 2.8 fb⁻¹ of data [290].

At the LHC, both the CMS and ATLAS collaborations have searched for resonant production of $t\bar{t}$ pairs, employing different techniques and final-state signatures (all-hadronic, lepton+jets, dilepton) at $\sqrt{s} = 7, 8$ and 13 TeV. In the low mass range, from the $t\bar{t}$ threshold to about one TeV/c², standard techniques based on the reconstruction of each of the decay objects (lepton, jets and b -jets, missing E_T) are used to identify the top quarks, while at higher invariant mass, the top quarks are boosted and the decay products more collimated and can appear as large-radius jets with substructure. Dedicated reconstruction techniques have been developed in recent years for boosted top quarks [291] that are currently employed at the LHC. Most of the analyses are model-independent (i.e., no assumption on the quantum numbers of the resonance is made) yet they assume a small width and no signal-background interference.

Using lepton+jets and fully hadronic channels in a data set corresponding to an integrated luminosity of 35.9 fb⁻¹ at 13 TeV, the CMS collaboration finds no significant deviations from the SM

background [292]. In particular, the existence of a leptophobic topcolor particle Z' is excluded at the 95% confidence level for resonances in the mass range $0.6 < M_{Z'} < 3.8$ TeV/c², $0.5 < M_{Z'} < 5.25$ TeV/c², and $0.5 < M_{Z'} < 6.65$ TeV/c² for $\Gamma_{Z'} = 1\%, 10\%, 30\%M_{Z'}$, respectively [293]. Kaluza-Klein excitations of a gluon with $M_{G_{KK}} < 4.55$ TeV/c² (at 95% confidence level) in the Randall-Sundrum model are also excluded.

The ATLAS collaboration has performed a search for resonant $t\bar{t}$ production in the lepton+jets channel using 36.1 fb⁻¹ of proton-proton (pp) collision data collected at a center-of-mass energy $\sqrt{s} = 13$ TeV [294]. A search for local excesses in the number of data events compared to the Standard Model expectation in the $t\bar{t}$ invariant mass spectrum is performed. No evidence for a $t\bar{t}$ resonance is found and 95% confidence-level limits on the production rate are determined for massive states predicted in several benchmark models. For instance, a narrow leptophobic topcolor Z' boson with a mass below 3.0 TeV/c² is excluded. A Kaluza-Klein excitation of the graviton is excluded for masses in the range 0.45 TeV/c² $< m_G < 0.65$ TeV/c². A Kaluza-Klein excitation of the gluon in a Randall-Sundrum model is excluded for masses below 3.8 TeV/c².

ATLAS has also conducted a search for resonances in the all-jet final state at 13 TeV corresponding to an integrated luminosity of 36.1 fb⁻¹ [295]. The $t\bar{t}$ events are reconstructed by selecting two top quarks in their fully hadronic decay modes. The invariant mass distribution of the two reconstructed top-quark candidates is examined for resonant production of new particles with various spins and decay widths. No significant deviation from the Standard Model prediction is observed and limits are set on the production cross-section times branching fraction for new hypothetical Z' bosons, dark-matter mediators, Kaluza-Klein gravitons and Kaluza-Klein gluons. For example, the Z' in the topcolor-assisted-technicolor model is excluded for masses up to 3.1–3.6 TeV, the dark-matter mediators in a simplified framework are excluded in the mass ranges from 0.8 to 0.9 TeV/c² and from 2.0 to 2.2 TeV/c², and the Kaluza-Klein gluon is excluded for masses up to 3.4 TeV/c², depending on the decay widths of the particles.

Heavy charged bosons, such as W' or H^+ , can also be searched for in $t\bar{b}, t\bar{j}$ final states (for more information see the review ‘‘ W' -boson searches’’ and ‘‘Higgs Bosons: theory and searches’’), while heavy fermion resonances, such as vectorial or excited quarks, in final states such as tZ, tH, tW, bW .

CMS has performed several searches in this context, the most stringent limits coming from those at $\sqrt{s} = 13$ TeV [296–302]. For instance, a $W' \rightarrow t\bar{b}$ has been searched for in lepton+jets in 35.9 fb⁻¹. No evidence has been found for a right-handed W' boson and masses below 3.6 TeV/c² are excluded at 95% confidence level providing the most stringent limits for right-handed W' bosons in the top and bottom quark decay channel to date [296].

Single production of a vector-like quark decaying to a W boson and a top quark, with one lepton in the final state, also been searched in the same data set. No significant deviation from the standard model background expectation is observed. Exclusion limits at 95% confidence level are set on the product of the production cross section and branching fraction as a function of the vector-like quark mass, which range from 0.3 to 0.03 pb for vector-like quark masses of 700 to 2000 GeV/c². Mass exclusion limits up to 1660 GeV/c² are obtained, depending on the vector-like quark type, coupling, and decay width. These represent the most stringent exclusion limits for the single production of vector-like quarks in this channel. [303]

In the same data set, searches for pair production of vector-like T or B quarks in fully hadronic final states have been performed based on two different techniques. A first cut-based analysis targets the bW decay mode of the T quark, while a second analysis, a multi-classification algorithm is deployed to label candidate jets as originating from top quarks, and $W, Z,$ and H . Both analyses probe all possible branching fraction combinations of the T and B quarks and set limits at 95% confidence level on their masses, ranging from 740 to 1370 GeV/c² [304].

ATLAS has performed searches for heavy bosons and fermions decaying to one top quark at $\sqrt{s} = 7, 8$ and 13 TeV. A $W' \rightarrow t\bar{b}$

has been searched for at 13 TeV in lepton+jets in 36.1 fb^{-1} . No evidence has been found for a right-handed W' boson with a mass below $3.25 \text{ TeV}/c^2$ are excluded at 95% [305]. ATLAS has conducted a search for the single and pair production of a new charge $+2/3$ quark (T) decaying via $T \rightarrow Zt$ (and also $-1/3$ quark (B) decaying via $B \rightarrow Zb$) in a dataset corresponding to 36.1 fb^{-1} luminosity at $\sqrt{s} = 13 \text{ TeV}$ [306]. The final state used is characterized by the presence of b-tagged jets, as well as a Z boson with high transverse momentum, which is reconstructed from a pair of opposite-sign same-flavor leptons. No significant excess of events above the SM expectation is observed, and upper limits are derived for vector-like quarks of various masses in a two-dimensional plane of branching ratios. Under branching ratio assumptions corresponding to a weak-isospin singlet scenario, a T quark with mass lower than $1030 \text{ GeV}/c^2$ ($1010 \text{ GeV}/c^2$ for a B quark) is excluded at the 95% confidence level. Under branching ratio assumptions corresponding to a particular weak-isospin doublet scenario, a T quark with mass lower than $1210 \text{ GeV}/c^2$ ($1140 \text{ GeV}/c^2$ for a B quark) is excluded at the 95% confidence level.

In the same dataset, ATLAS combines the searches for pair-produced vector-like partners of the top and bottom quarks in various decay channels ($T \rightarrow Zt/Wb/Ht, B \rightarrow Zb/Wt/Hb$). The observed data are found to be in good agreement with the Standard Model background prediction in all individual searches. Therefore, combined 95% confidence-level upper limits are set on the production cross-section for a range of vector-like quark scenarios, significantly improving upon the reach of the individual searches. Model-independent limits are set assuming the vector-like quarks decay to Standard Model particles. A singlet T is excluded for masses below $1.31 \text{ TeV}/c^2$ and a singlet B is excluded for masses below $1.22 \text{ TeV}/c^2$. Assuming a weak isospin (T, B) doublet and $|V_{Tb}| \ll |V_{tB}|$, T and B masses below $1.37 \text{ TeV GeV}/c^2$ are excluded [307].

In many models top-quark partners preferably decay to top quarks and weakly interacting neutral stable particles, i.e., possibly dark matter candidates, that are not detected. An observable especially sensitive to new physics effects in $t\bar{t}$ production is therefore the missing transverse momentum.

CMS has presented a differential cross section measurement of top-quark pair and single production with missing transverse energy and corresponding interpretations in the context of dark matter (effective and simplified) models at 8 and 13 TeV [308–311]. The results obtained so far are consistent with the SM expectations. In particular the search performed at 13 TeV [311] is based on 35.9 fb^{-1} of integrated luminosity. Upper limits are derived on the production cross section and interpreted in terms of a simplified model with a scalar/pseudoscalar mediator. Scalar and pseudoscalar mediator particles with masses below 290 and $300 \text{ GeV}/c^2$, respectively, are excluded at 95% confidence level, assuming a dark matter particle mass of $1 \text{ GeV}/c^2$ and mediator couplings to fermions and dark matter particles equal to unity.

A search for top squarks at a center-of-mass energy of 13 TeV in 36 fb^{-1} of data has been performed by ATLAS [312] in final states with one isolated electron or muon, several energetic jets, and missing transverse momentum. The analysis also targets spin-0 mediator models, where the mediator decays into a pair of dark-matter particles and is produced in association with a pair of top quarks. No significant excess over the Standard Model prediction is observed. For pair-produced top-squarks decaying into top quarks, top-squark masses up to $940 \text{ GeV}/c^2$ are excluded. Stringent exclusion limits are also derived for all other considered top-squark decay scenarios. For the spin-0 mediator models, upper limits are set on the visible cross-section.

Flavor-changing-neutral-currents (FCNC) are hugely suppressed in the SM as non zero contributions only arise at one-loop and are proportional to the splitting between the quark masses. In the case of the top quark $B(t \rightarrow Bq)$ with $B = g, \gamma, Z, H$ and $q = u, c$ are predicted to be order of 10^{-12} ($t \rightarrow cg$) or much smaller [313]. Several observables are accessible at colliders to test and constrain such couplings.

CMS has performed several studies on the search for FCNC in top-quark production. They have considered single-top quark production in the t -channel in 5 fb^{-1} integrated luminosity at 7 TeV

and 19.7 fb^{-1} integrated luminosity at 8 TeV [314]. Events with the top quark decaying into a muon, neutrino and two or three jets are selected. The upper limits on effective coupling strength can be translated to the 95% upper limits on the corresponding branching ratios $B(t \rightarrow gu) \leq 2.0 \cdot 10^{-5}$, $B(t \rightarrow gc) \leq 4.1 \cdot 10^{-4}$. They have performed a search for a single top quark produced in association with a photon in 19.1 fb^{-1} integrated luminosity at 8 TeV [315]. The event selection requires the presence of one isolated muon and jets in the final state. The upper limits on effective coupling strength can be translated to the 95% upper limits on the corresponding branching ratios $B(t \rightarrow \gamma u) \leq 0.0161\%$, $B(t \rightarrow \gamma c) \leq 0.182\%$.

Recently, a search for flavor-changing neutral currents in associated production of a top quark with a Higgs boson decaying into $b\bar{b}$ has also been presented by CMS, corresponding to an integrated luminosity of 35.9 fb^{-1} at 13 TeV. Two complementary channels are considered: top quark pair production, with FCNC decay of the top quark or antiquark, and single top associated production. A final state with one isolated lepton and at least three reconstructed jets, among which at least two are identified as b quark jets, is considered. No significant deviation is observed from predicted background and upper limits at 95% confidence level are set on the branching ratios of top quark decays, $B(t \rightarrow uH) < 0.47\%$ and $B(t \rightarrow cH) < 0.47\%$ [316], which are similar to the combined limits on all decay channels obtained with the full data set at 8 TeV [317].

ATLAS has presented results on the search for single top-quark production via FCNC's in strong interactions using data collected at $\sqrt{s}=8 \text{ TeV}$ and corresponding to an integrated luminosity of 20.3 fb^{-1} . Flavor-changing-neutral-current events are searched for in which a light quark (u or c) interacts with a gluon to produce a single top quark, either with or without the associated production of another light quark or gluon. Candidate events of top quarks decaying into leptons and jets are selected and classified into signal- and background-like events using a neural network. The observed 95% C.L. limit is $\sigma_{qq \rightarrow t} \times B(t \rightarrow Wb) < 3.4 \text{ pb}$ that can be interpreted as limits on the branching ratios, $B(t \rightarrow ug) < 4 \cdot 10^{-5}$ and $B(t \rightarrow cg) < 1.7 \cdot 10^{-4}$ [318].

ATLAS has set limits on the coupling of a top quark, a photon, and an up or charm quark using 81 fb^{-1} of data 13 TeV. Events with a photon, an electron or muon, a b-tagged jet, and missing transverse momentum are selected. The data are consistent with the background-only hypothesis, and limits are set on the strength of the $tq\gamma$ coupling in an effective field theory. These are also interpreted as 95% CL upper limits on $t \rightarrow u\gamma$ branching ratio via a left-handed (right-handed) interaction of 2.8×10^{-5} (6.1×10^{-5}) and on the $t \rightarrow c\gamma$ branching ratio for of 22×10^{-5} (18×10^{-5}) [319].

Constraints on FCNC couplings of the top quark can also be obtained from searches for anomalous single top-quark production in e^+e^- collisions, via the process $e^+e^- \rightarrow \gamma, Z^* \rightarrow t\bar{q}$ and its charge-conjugate ($q = u, c$), or in $e^\pm p$ collisions, via the process $e^\pm u \rightarrow e^\pm t$. For a leptonic W decay, the topology is at least a high- p_T lepton, a high- p_T jet and missing E_T , while for a hadronic W -decay, the topology is three high- p_T jets. Limits on the cross section for this reaction have been obtained by the LEP collaborations [320] in e^+e^- collisions, and by H1 [321] and ZEUS [322] in $e^\pm p$ collisions. When interpreted in terms of branching ratios in top decay [323,324], the LEP limits lead to typical 95% C.L. upper bounds of $B(t \rightarrow qZ) < 0.137$. Assuming no coupling to the Z boson, the 95% C.L. limits on the anomalous FCNC coupling $\kappa_\gamma < 0.13$ and < 0.27 by ZEUS and H1, respectively, are stronger than the CDF limit of $\kappa_\gamma < 0.42$, and improve over LEP sensitivity in that domain. The H1 limit is slightly weaker than the ZEUS limit due to an observed excess of five-candidate events over an expected background of 3.2 ± 0.4 . If this excess is attributed to FCNC top-quark production, this leads to a total cross section of $\sigma(ep \rightarrow e + t + X, \sqrt{s} = 319 \text{ GeV}) < 0.25 \text{ pb}$ [321,325].

60.3.3.2 New Physics in Top-Quark decays

The large sample of top quarks produced at the Tevatron and the LHC allows to measure or set stringent limits on the branching ratios of rare top-quark decays. For example, the existence of a light H^+ can be constrained by looking for $t \rightarrow H^+b$ decay, in

particular with tau-leptons in the final state (for more information see the review “Higgs Bosons: theory and searches”).

A first class of searches for new physics focuses on the structure of the Wtb vertex. Using up to 2.7 fb^{-1} of data, $D\bar{O}$ has measured the Wtb coupling form factors by combining information from the W -boson helicity in top-quark decays in $t\bar{t}$ events and single top-quark production, allowing to place limits on the left-handed and right-handed vector and tensor couplings [326–328].

ATLAS has published the results of a search for CP -violation in the decay of single top quarks produced in the t -channel where the top quarks are predicted to be highly polarized, using the lepton+jets final state [329]. The data analyzed are from pp collisions at $\sqrt{s} = 7 \text{ TeV}$ and correspond to an integrated luminosity of 4.7 fb^{-1} . In the Standard Model, the couplings at the Wtb vertex are left-handed, right-handed couplings being absent. A forward-backward asymmetry with respect to the normal to the plane defined by the W -momentum and the top-quark polarization has been used to probe the complex phase of a possibly non-zero value of the right-handed coupling, signaling a source of CP -violation beyond the SM. The measured value of the asymmetry is $0.031 \pm 0.065(\text{stat.})_{-0.031}^{+0.029}(\text{syst.})$ in good agreement with the Standard Model.

A second class of searches focuses on FCNC's in the top-quark decays. Both, CDF and $D\bar{O}$, have provided the first limits for FCNC's in Run I and II. The most recent results from CDF give $B(t \rightarrow qZ) < 3.7\%$ and $B(t \rightarrow q\gamma) < 3.2\%$ at the 95% C.L. [330] while $D\bar{O}$ [331, 332] sets $B(t \rightarrow qZ) (q = u, c \text{ quarks}) < 3.2\%$ at 95% C.L., $B(t \rightarrow gu) < 2.0 \cdot 10^{-4}$, and $B(t \rightarrow gc) < 3.9 \cdot 10^{-3}$ at the 95% C.L. At the LHC, CMS has used a sample at a center-of-mass energy of 8 TeV corresponding to 19.7 fb^{-1} of integrated luminosity to perform a search for flavor changing neutral current top-quark decay $t \rightarrow Zq$. Events with a topology compatible with the decay chain $t\bar{t} \rightarrow Wb + Zq \rightarrow \ell\nu b + \ell\ell q$ are searched for. There is no excess seen in the observed number of events relative to the SM prediction; thus no evidence for flavor changing neutral current in top-quark decays is found. A combination with a previous search at 7 TeV excludes a $t \rightarrow Zq$ branching fraction greater than 0.05% at the 95% confidence level [333]. CMS has also performed a search for the production of a single top quark in association with a Z boson in the same data set at 8 TeV. Final states with three leptons (electrons or muons) and at least one jet are investigated. Exclusion limits at 95% confidence level on the branching fractions are found to be $B(t \rightarrow uZ) < 0.022\%$ and $B(t \rightarrow cZ) < 0.049\%$ [334].

The ATLAS collaboration has also searched for FCNC processes in 31.1 fb^{-1} of $t\bar{t}$ events at a center-of-mass energy of 13 TeV, with one top quark decaying through FCNC ($t \rightarrow qZ$) and the other through the SM dominant mode ($t \rightarrow bW$). Only the decays of the Z boson to charged leptons and leptonic W boson decays were considered as signal, leading to a final state topology characterized by the presence of three isolated leptons, at least two jets and missing transverse energy from the undetected neutrino. No evidence for an FCNC signal was found. An upper limit on the $t \rightarrow qZ$ branching ratio of $B(t \rightarrow Zu(c)) < 1.7(2.4) \times 10^{-4}$ is set at the 95% confidence level [335].

Another search for FCNCs is the interactions of a top-quark to a Higgs boson and a light parton, tqH , $q = u, c$. The CMS collaboration has performed a search using a sample at a center-of-mass energy of 13 TeV corresponding to 35.9 fb^{-1} of integrated luminosity, [336], combining single top quark FCNC production in association with the Higgs boson ($pp \rightarrow tH$), and top quark pair production with FCNC decay of the top quark ($t \rightarrow qH$). The combined analysis sets an upper limit on the $t \rightarrow u/cH$ branching ratios of $B(t \rightarrow u/cH) < 0.47\%$ at 95% confidence level. The ATLAS collaboration considers $t \rightarrow qH$, $q = u, c$ with 36.1 fb^{-1} of $t\bar{t}$ events at $\sqrt{s} = 13 \text{ TeV}$. A combined measurement including $H \rightarrow b\bar{b}$ and $H \rightarrow \tau\tau$ modes yields a 95% C.L. upper limit of 0.11% and 0.12% on the branching ratios of $B(t \rightarrow cH)$ and $B(t \rightarrow uH)$, respectively [337].

60.4 Outlook

Top-quark physics at hadron colliders has developed into precision physics. Various properties of the top quark have been measured with high precision, where the LHC has by now surpassed

the Tevatron precision and reach in the majority of relevant observables. Several \sqrt{s} -dependent physics quantities, such as the production cross-section, have been measured at several energies at the Tevatron and the LHC. Up to now, all measurements are consistent with the SM predictions and allow stringent tests of the underlying production mechanisms by strong and weak interactions. Given the very large event samples available at the LHC, top-quark properties will be further determined in $t\bar{t}$ as well as in electroweak single top-quark production. At the Tevatron, the t - and s -channels for electroweak single top-quark production have been measured separately. At the LHC, quick progress has been achieved in the last years making all three relevant channels measured with more than 5 sigma significance. Furthermore, $t\bar{t}\gamma$, $t\bar{t}Z$, and $t\bar{t}W$ together with $t\bar{t}H$ associated production have started to provide key information on the top-quark electroweak couplings. At the same time various models of physics beyond the SM involving top-quark production are being constrained. With the first results from LHC Run-II at a higher center-of-mass energy and much higher luminosity starting to be released, top-quark physics has the potential to shed light on open questions and new aspects of physics at the TeV scale.

CDF note references can be retrieved from

<https://www-cdf.fnal.gov/physics/new/top/top.html>,
and $D\bar{O}$ note references from

<https://www-d0.fnal.gov/Run2Physics/WWW/documents/Run2Results.htm>,

and ATLAS note references from

<https://twiki.cern.ch/twiki/bin/view/AtlasPublic/TopPublicResults>,

and CMS note references from

<https://twiki.cern.ch/twiki/bin/view/CMSPublic/PhysicsResultsTOP>.

References

- [1] M. Czakon, P. Fiedler and A. Mitov, Phys. Rev. Lett. **110**, 252004 (2013), [arXiv:1303.6254].
- [2] S. Catani *et al.*, JHEP **07**, 100 (2019), [arXiv:1906.06535].
- [3] ATLAS, CMS, CDF, & D0 Collab, Phys. Rev. Lett. , **110**, 25204 (2013); [arXiv:403,4427].
- [4] S. Cortese and R. Petronzio, Phys. Lett. **B253**, 494 (1991).
- [5] S. S. D. Willenbrock and D. A. Dicus, Phys. Rev. **D34**, 155 (1986).
- [6] N. Kidonakis, Phys. Rev. **D83**, 091503 (2011), [arXiv:1103.2792].
- [7] M. Brucherseifer, F. Caola and K. Melnikov, Phys. Lett. **B736**, 58 (2014), [arXiv:1404.7116].
- [8] E. L. Berger, J. Gao and H. X. Zhu, JHEP **11**, 158 (2017), [arXiv:1708.09405].
- [9] N. Kidonakis, Phys. Rev. **D81**, 054028 (2010), [arXiv:1001.5034].
- [10] N. Kidonakis, Phys. Rev. **D82**, 054018 (2010), [arXiv:1005.4451].
- [11] T. M. P. Tait and C. P. Yuan, Phys. Rev. **D63**, 014018 (2000), [hep-ph/0007298].
- [12] M. Jezabek and J. H. Kuhn, Nucl. Phys. **B314**, 1 (1989).
- [13] I. I. Y. Bigi *et al.*, Phys. Lett. **B181**, 157 (1986).
- [14] A. H. Hoang *et al.*, Phys. Rev. **D65**, 014014 (2002), [hep-ph/0107144].
- [15] K. Hagiwara, Y. Sumino and H. Yokoya, Phys. Lett. **B666**, 71 (2008), [arXiv:0804.1014].
- [16] A. Czarnecki and K. Melnikov, Nucl. Phys. **B544**, 520 (1999), [hep-ph/9806244]; K. G. Chetyrkin *et al.*, Phys. Rev. **D60**, 114015 (1999), [hep-ph/9906273].
- [17] S. Frixione, P. Nason and B. R. Webber, JHEP **08**, 007 (2003), [hep-ph/0305252]; W. Kim and H. Shin, JHEP **07**, 070 (2007), [arXiv:0706.3563]; S. Frixione, P. Nason and G. Ridolfi, JHEP **09**, 126 (2007), [arXiv:0707.3088]; J. M. Campbell *et al.*, JHEP **04**, 114 (2015), [arXiv:1412.1828]; T. Ježo *et al.*, Eur. Phys. J. **C76**, 12, 691 (2016), [arXiv:1607.04538].

- [18] S. Frixione *et al.*, JHEP **03**, 092 (2006), [hep-ph/0512250]; V. Marotta and A. Naddeo, JHEP **08**, 029 (2008), [arXiv:0810.4759]; S. Alioli *et al.*, JHEP **09**, 111 (2009), [Erratum: JHEP02,011(2010)], [arXiv:0907.4076]; E. Re, Eur. Phys. J. **C71**, 1547 (2011), [arXiv:1009.2450]; R. Frederix, E. Re and P. Torrielli, JHEP **09**, 130 (2012), [arXiv:1207.5391]; R. Frederix *et al.*, JHEP **06**, 027 (2016), [arXiv:1603.01178].
- [19] S. Frixione and B. R. Webber, JHEP **06**, 029 (2002), [hep-ph/0204244].
- [20] P. Nason, JHEP **11**, 040 (2004), [hep-ph/0409146].
- [21] E. Todesco and J. Wenninger, Phys. Rev. Accel. Beams **20**, 8, 081003 (2017).
- [22] V. M. Abazov *et al.* (D0), Phys. Rev. **D94**, 092004 (2016), [arXiv:1605.06168].
- [23] T. Aaltonen *et al.* (CDF), Phys. Rev. **D88**, 091103 (2013), [arXiv:1304.7961].
- [24] T. A. Aaltonen *et al.* (CDF, D0), Phys. Rev. **D89**, 7, 072001 (2014), [arXiv:1309.7570].
- [25] T. A. Aaltonen *et al.* (CDF), Phys. Rev. **D89**, 9, 091101 (2014), [arXiv:1402.6728].
- [26] T. Aaltonen *et al.* (CDF), Phys. Rev. Lett. **105**, 012001 (2010), [arXiv:1004.3224].
- [27] V. M. Abazov *et al.* (D0), Phys. Rev. **D90**, 9, 092006 (2014), [arXiv:1401.5785].
- [28] G. Aad *et al.* (ATLAS), Eur. Phys. J. **C74**, 10, 3109 (2014), [Addendum: Eur. Phys. J.C76,no.11,642(2016)], [arXiv:1406.5375].
- [29] G. Aad *et al.* (ATLAS), Phys. Rev. **D91**, 11, 112013 (2015), [arXiv:1504.04251].
- [30] G. Aad *et al.* (ATLAS), JHEP **05**, 059 (2012), [arXiv:1202.4892].
- [31] ATLAS Collab., ATLAS-CONF-2011-140.
- [32] ATLAS Collab., ATLAS-CONF-2012-024.
- [33] ATLAS Collab., ATLAS-CONF-2012-031.
- [34] G. Aad *et al.* (ATLAS), Eur. Phys. J. **C73**, 3, 2328 (2013), [arXiv:1211.7205].
- [35] G. Aad *et al.* (ATLAS), Phys. Lett. **B717**, 89 (2012), [arXiv:1205.2067].
- [36] G. Aad *et al.* (ATLAS), Phys. Rev. **D91**, 5, 052005 (2015), [arXiv:1407.0573].
- [37] S. Chatrchyan *et al.* (CMS), JHEP **11**, 067 (2012), [arXiv:1208.2671].
- [38] S. Chatrchyan *et al.* (CMS), Phys. Lett. **B720**, 83 (2013), [arXiv:1212.6682].
- [39] S. Chatrchyan *et al.* (CMS), JHEP **05**, 065 (2013), [arXiv:1302.0508].
- [40] S. Chatrchyan *et al.* (CMS), Phys. Rev. **D85**, 112007 (2012), [arXiv:1203.6810].
- [41] S. Chatrchyan *et al.* (CMS), Eur. Phys. J. **C73**, 4, 2386 (2013), [arXiv:1301.5755].
- [42] ATLAS & CMS Collab., ATLAS-CONF-2012-134, CMS-PAS-TOP-12-003.
- [43] G. Aad *et al.* (ATLAS), Eur. Phys. J. **C74**, 10, 3109 (2014), [Addendum: Eur. Phys. J.C76,no.11,642(2016)], [arXiv:1406.5375].
- [44] M. Aaboud *et al.* (ATLAS), Eur. Phys. J. **C78**, 487 (2018), [arXiv:1712.06857].
- [45] M. Aaboud *et al.* (ATLAS), Phys. Rev. **D95**, 7, 072003 (2017), [arXiv:1702.08839].
- [46] V. Khachatryan *et al.* (CMS), Eur. Phys. J. **C77**, 1, 15 (2017), [arXiv:1602.09024].
- [47] S. Chatrchyan *et al.* (CMS), JHEP **02**, 024 (2014), [Erratum: JHEP02,102(2014)], [arXiv:1312.7582].
- [48] V. Khachatryan *et al.* (CMS), JHEP **08**, 029 (2016), [arXiv:1603.02303].
- [49] V. Khachatryan *et al.* (CMS), Phys. Lett. **B739**, 23 (2014), [arXiv:1407.6643].
- [50] V. Khachatryan *et al.* (CMS), Eur. Phys. J. **C76**, 3, 128 (2016), [arXiv:1509.06076].
- [51] ATLAS Collab., ATLAS-CONF-2014-053, CMS Collab., CMS-PAS-TOP-14-016.
- [52] R. Aaij *et al.* (LHCb), Phys. Rev. Lett. **115**, 11, 112001 (2015), [arXiv:1506.00903].
- [53] ATLAS Collab., ATLAS-CONF-2015-033.
- [54] ATLAS collab., ATLAS-CONF-2015-049.
- [55] M. Aaboud *et al.* (ATLAS), Phys. Lett. **B761**, 136 (2016), [Erratum: Phys. Lett.B772,879(2017)], [arXiv:1606.02699].
- [56] ATLAS Collab., ATLAS-CONF-2019-044.
- [57] ATLAS Collab., ATLAS-CONF-2019-041 (2019).
- [58] V. Khachatryan *et al.* (CMS), Phys. Rev. Lett. **116**, 5, 052002 (2016), [arXiv:1510.05302].
- [59] V. Khachatryan *et al.* (CMS), Eur. Phys. J. **C77**, 172 (2017), [arXiv:1611.04040].
- [60] CMS Collab., CMS-PAS-TOP-15-005.
- [61] A. M. Sirunyan *et al.* (CMS), JHEP **09**, 051 (2017), [arXiv:1701.06228].
- [62] A. M. Sirunyan *et al.* (CMS), Eur. Phys. J. **C79**, 5, 368 (2019), [arXiv:1812.10505].
- [63] CMS Collab., CMS-PAS-TOP-18-005.
- [64] CMS Collab., CMS-PAS-TOP-16-013.
- [65] A. M. Sirunyan *et al.* (CMS), JHEP **03**, 115 (2018), [arXiv:1711.03143].
- [66] A. M. Sirunyan *et al.* (CMS), Phys. Rev. Lett. **119**, 24, 242001 (2017), [arXiv:1709.07411].
- [67] V. M. Abazov *et al.* (D0), Phys. Rev. **D67**, 012004 (2003), [hep-ex/0205019].
- [68] T. Affolder *et al.* (CDF), Phys. Rev. **D64**, 032002 (2001), [Erratum: Phys. Rev.D67,119901(2003)], [hep-ex/0101036].
- [69] ATLAS Collab., ATLAS-CONF-2011-108.
- [70] V. M. Abazov *et al.* (D0), Phys. Rev. Lett. **107**, 121802 (2011), [arXiv:1106.5436]; D. Acosta *et al.* (CDF), Phys. Rev. Lett. **95**, 102002 (2005), [hep-ex/0505091].
- [71] V. Khachatryan *et al.* (CMS), Phys. Lett. **B736**, 33 (2014), [arXiv:1404.2292].
- [72] M. Czakon, D. Heymes and A. Mitov, Phys. Rev. Lett. **116**, 8, 082003 (2016), [arXiv:1511.00549].
- [73] T. Aaltonen *et al.* (CDF), Phys. Rev. Lett. **110**, 12, 121802 (2013), [arXiv:1211.5363].
- [74] G. Aad *et al.* (ATLAS), Eur. Phys. J. **C73**, 1, 2261 (2013), [arXiv:1207.5644].
- [75] G. Aad *et al.* (ATLAS), Phys. Rev. **D90**, 7, 072004 (2014), [arXiv:1407.0371].
- [76] G. Aad *et al.* (ATLAS), JHEP **06**, 100 (2015), [arXiv:1502.05923].
- [77] S. Chatrchyan *et al.* (CMS), Eur. Phys. J. **C73**, 3, 2339 (2013), [arXiv:1211.2220].
- [78] M. Aaboud *et al.* (ATLAS), Phys. Rev. **D94**, 9, 092003 (2016), [arXiv:1607.07281].
- [79] G. Aad *et al.* (ATLAS), Eur. Phys. J. **C76**, 10, 538 (2016), [arXiv:1511.04716].
- [80] G. Aad *et al.* (ATLAS), Phys. Rev. **D93**, 3, 032009 (2016), [arXiv:1510.03818].
- [81] V. Khachatryan *et al.* (CMS), Phys. Rev. **D94**, 5, 052006 (2016), [arXiv:1607.00837].
- [82] A. M. Sirunyan *et al.* (CMS), Eur. Phys. J. **C77**, 7, 459 (2017), [arXiv:1703.01630].

- [83] V. Khachatryan *et al.* (CMS), Phys. Rev. **D94**, 7, 072002 (2016), [arXiv:1605.00116].
- [84] V. Khachatryan *et al.* (CMS), Eur. Phys. J. **C75**, 11, 542 (2015), [arXiv:1505.04480].
- [85] V. Khachatryan *et al.* (CMS), Eur. Phys. J. **C76**, 3, 128 (2016), [arXiv:1509.06076].
- [86] M. Aaboud *et al.* (ATLAS), Eur. Phys. J. **C77**, 5, 292 (2017), [arXiv:1612.05220].
- [87] CMS Collab., CMS-PAS-TOP-15-010.
- [88] M. Aaboud *et al.* (ATLAS), JHEP **11**, 191 (2017), [arXiv:1708.00727].
- [89] ATLAS collab., ATLAS-CONF-2016-100.
- [90] M. Aaboud *et al.* (ATLAS), Phys. Rev. **D98**, 1, 012003 (2018), [arXiv:1801.02052].
- [91] G. Aad *et al.* (ATLAS) (2019), [arXiv:1908.07305].
- [92] A. M. Sirunyan *et al.* (CMS), JHEP **04**, 060 (2018), [arXiv:1708.07638].
- [93] V. Khachatryan *et al.* (CMS), Phys. Rev. **D95**, 9, 092001 (2017), [arXiv:1610.04191].
- [94] A. M. Sirunyan *et al.* (CMS), JHEP **06**, 002 (2018), [arXiv:1803.03991].
- [95] A. M. Sirunyan *et al.* (CMS), Phys. Rev. **D97**, 11, 112003 (2018), [arXiv:1803.08856].
- [96] A. M. Sirunyan *et al.* (CMS), JHEP **02**, 149 (2019), [arXiv:1811.06625].
- [97] A. M. Sirunyan *et al.* (CMS), Submitted to: Eur. Phys. J. (2019), [arXiv:1904.05237].
- [98] G. Aad *et al.* (ATLAS), Eur. Phys. J. **C76**, 1, 11 (2016), [arXiv:1508.06868].
- [99] G. Aad *et al.* (ATLAS), JHEP **01**, 020 (2015), [arXiv:1407.0891].
- [100] S. Chatrchyan *et al.* (CMS), Eur. Phys. J. **C74**, 3014 (2015), [Erratum: Eur. Phys. J. **C75**, no.5, 216(2015)], [arXiv:1404.3171].
- [101] V. Khachatryan *et al.* (CMS), Phys. Lett. **B746**, 132 (2015), [arXiv:1411.5621].
- [102] G. Aad *et al.* (ATLAS), Phys. Rev. **D92**, 7, 072005 (2015), [arXiv:1506.05074].
- [103] M. Aaboud *et al.* (ATLAS), JHEP **04**, 046 (2019), [arXiv:1811.12113].
- [104] A. M. Sirunyan *et al.* (CMS), Phys. Lett. **B776**, 355 (2018), [arXiv:1705.10141].
- [105] CMS Collab., CMS-PAS-TOP-18-002.
- [106] A. M. Sirunyan *et al.* (CMS) (2019), [arXiv:1909.05306].
- [107] V. M. Abazov *et al.* (D0), Phys. Rev. Lett. **103**, 092001 (2009), [arXiv:0903.0850]; V. M. Abazov *et al.* (D0), Phys. Rev. **D78**, 012005 (2008), [arXiv:0803.0739]; V. M. Abazov *et al.* (D0), Phys. Rev. Lett. **98**, 181802 (2007), [hep-ex/0612052].
- [108] T. Aaltonen *et al.* (CDF), Phys. Rev. Lett. **103**, 092002 (2009), [arXiv:0903.0885]; T. Aaltonen *et al.* (CDF), Phys. Rev. **D81**, 072003 (2010), [arXiv:1001.4577].
- [109] T. Aaltonen *et al.* (CDF), Phys. Rev. **D82**, 112005 (2010), [arXiv:1004.1181].
- [110] A. Heinson and T. R. Junk, Ann. Rev. Nucl. Part. Sci. **61**, 171 (2011), [arXiv:1101.1275].
- [111] Tevatron Electroweak Working Group, (2009), [arXiv:0908.2171].
- [112] CDF Collab., CDF conference note 11113 (2014), DØ Collab., DØ conference note 6448 (2014).
- [113] T. A. Aaltonen *et al.* (CDF, D0), Phys. Rev. Lett. **115**, 15, 152003 (2015), [arXiv:1503.05027].
- [114] T. A. Aaltonen *et al.* (CDF, D0), Phys. Rev. Lett. **112**, 231803 (2014), [arXiv:1402.5126].
- [115] G. Aad *et al.* (ATLAS), Phys. Rev. **D90**, 11, 112006 (2014), [arXiv:1406.7844].
- [116] G. Aad *et al.* (ATLAS), Phys. Lett. **B717**, 330 (2012), [arXiv:1205.3130].
- [117] S. Chatrchyan *et al.* (CMS), JHEP **12**, 035 (2012), [arXiv:1209.4533].
- [118] M. Aaboud *et al.* (ATLAS), Eur. Phys. J. **C77**, 8, 531 (2017), [arXiv:1702.02859].
- [119] M. Aaboud *et al.* (ATLAS), JHEP **04**, 124 (2017), [arXiv:1702.08309].
- [120] V. Khachatryan *et al.* (CMS), JHEP **06**, 090 (2014), [arXiv:1403.7366].
- [121] CMS Collab., CMS-PAS-TOP-15-007.
- [122] M. Aaboud *et al.* (ATLAS), JHEP **04**, 086 (2017), [arXiv:1609.03920].
- [123] A. M. Sirunyan *et al.* (CMS), Phys. Lett. **B772**, 752 (2017), [arXiv:1610.00678].
- [124] A. M. Sirunyan *et al.* (CMS) (2018), [arXiv:1812.10514].
- [125] C. D. White *et al.*, JHEP **11**, 074 (2009), [arXiv:0908.0631].
- [126] S. Frixione *et al.*, JHEP **07**, 029 (2008), [arXiv:0805.3067].
- [127] G. Aad *et al.* (ATLAS), Phys. Lett. **B716**, 142 (2012), [arXiv:1205.5764].
- [128] S. Chatrchyan *et al.* (CMS), Phys. Rev. Lett. **110**, 022003 (2013), [arXiv:1209.3489].
- [129] G. Aad *et al.* (ATLAS), JHEP **01**, 064 (2016), [arXiv:1510.03752].
- [130] S. Chatrchyan *et al.* (CMS), Phys. Rev. Lett. **112**, 23, 231802 (2014), [arXiv:1401.2942].
- [131] ATLAS Collab., ATLAS-CONF-2014-052, CMS Collab., CMS-PAS-TOP-14-009.
- [132] M. Aaboud *et al.* (ATLAS), JHEP **01**, 063 (2018), [arXiv:1612.07231].
- [133] A. M. Sirunyan *et al.* (CMS), JHEP **10**, 117 (2018), [arXiv:1805.07399].
- [134] ATLAS Collab., ATLAS-CONF-2011-118.
- [135] G. Aad *et al.* (ATLAS), Phys. Lett. **B756**, 228 (2016), [arXiv:1511.05980].
- [136] V. Khachatryan *et al.* (CMS), JHEP **09**, 027 (2016), [arXiv:1603.02555].
- [137] M. Aaboud *et al.* (ATLAS, CMS), JHEP **05**, 088 (2019), [arXiv:1902.07158].
- [138] CMS Collab., CMS-PAS-TOP-14-004.
- [139] CMS Collab., CMS-PAS-TOP-13-001.
- [140] A. M. Sirunyan *et al.* (CMS) (2019), [arXiv:1907.08330].
- [141] ATLAS collab., ATLAS-CONF-2016-012.
- [142] A. M. Sirunyan *et al.* (CMS), Phys. Rev. Lett. **121**, 22, 221802 (2018), [arXiv:1808.02913].
- [143] M. Czakon, P. Fiedler and A. Mitov, Phys. Rev. Lett. **115**, 5, 052001 (2015), [arXiv:1411.3007].
- [144] W. Hollik and D. Pagani, Phys. Rev. **D84**, 093003 (2011), [arXiv:1107.2606].
- [145] W. Bernreuther and Z.-G. Si, Phys. Rev. **D86**, 034026 (2012), [arXiv:1205.6580].
- [146] S. Jung *et al.*, Phys. Rev. **D81**, 015004 (2010), [arXiv:0907.4112].
- [147] V. M. Abazov *et al.* (D0), Phys. Rev. Lett. **100**, 142002 (2008), [arXiv:0712.0851].
- [148] T. Aaltonen *et al.* (CDF), Phys. Rev. Lett. **101**, 202001 (2008), [arXiv:0806.2472].
- [149] T. A. Aaltonen *et al.* (CDF, D0), Phys. Rev. Lett. **120**, 4, 042001 (2018), [arXiv:1709.04894].
- [150] G. Aad *et al.* (ATLAS), JHEP **02**, 107 (2014), [arXiv:1311.6724].

- [151] G. Aad *et al.* (ATLAS), *Eur. Phys. J.* **C76**, 2, 87 (2016), [Erratum: *Eur. Phys. J.* **C77**, 564(2017)], [arXiv:1509.02358].
- [152] G. Aad *et al.* (ATLAS), *Phys. Rev.* **D94**, 3, 032006 (2016), [arXiv:1604.05538].
- [153] S. Chatrchyan *et al.* (CMS), *Phys. Lett.* **B717**, 129 (2012), [arXiv:1207.0065].
- [154] V. Khachatryan *et al.* (CMS), *Phys. Rev.* **D93**, 3, 034014 (2016), [arXiv:1508.03862].
- [155] V. Khachatryan *et al.* (CMS), *Phys. Lett.* **B760**, 365 (2016), [arXiv:1603.06221].
- [156] M. Czakon *et al.*, *Phys. Rev.* **D98**, 1, 014003 (2018), [arXiv:1711.03945].
- [157] V. Khachatryan *et al.* (CMS), *Phys. Lett.* **B757**, 154 (2016), [arXiv:1507.03119].
- [158] G. Aad *et al.* (ATLAS), *Phys. Lett.* **B756**, 52 (2016), [arXiv:1512.06092].
- [159] G. Aad *et al.* (ATLAS), *JHEP* **05**, 061 (2015), [arXiv:1501.07383].
- [160] S. Chatrchyan *et al.* (CMS), *JHEP* **04**, 191 (2014), [arXiv:1402.3803].
- [161] M. Aaboud *et al.* (ATLAS, CMS), *JHEP* **04**, 033 (2018), [arXiv:1709.05327].
- [162] C. Collaboration (CMS) (2019).
- [163] F. Abe *et al.* (CDF), *Phys. Rev.* **D50**, 2966 (1994).
- [164] A. Abulencia *et al.* (CDF), *Phys. Rev.* **D73**, 032003 (2006), [hep-ex/0510048].
- [165] M. Aaboud *et al.* (ATLAS), *Eur. Phys. J.* **C79**, 4, 290 (2019), [arXiv:1810.01772].
- [166] V. Khachatryan *et al.* (CMS), *Phys. Rev.* **D93**, 7, 072004 (2016), [arXiv:1509.04044].
- [167] A. M. Sirunyan *et al.* (CMS), *Eur. Phys. J.* **C78**, 11, 891 (2018), [arXiv:1805.01428].
- [168] S. Argyropoulos and T. Sjöstrand, *JHEP* **11**, 043 (2014), [arXiv:1407.6653].
- [169] J. R. Christiansen and P. Z. Skands, *JHEP* **08**, 003 (2015), [arXiv:1505.01681].
- [170] C. Collaboration (CMS) (2019).
- [171] V. M. Abazov *et al.* (D0), *Nature* **429**, 638 (2004), [hep-ex/0406031].
- [172] K. Kondo, T. Chikamatsu and S. H. Kim, *J. Phys. Soc. Jap.* **62**, 1177 (1993).
- [173] R. H. Dalitz and G. R. Goldstein, *Phys. Rev.* **D45**, 1531 (1992); R. H. Dalitz and G. R. Goldstein, *Phys. Lett.* **B287**, 225 (1992).
- [174] V. M. Abazov *et al.* (D0), *Phys. Rev. Lett.* **113**, 032002 (2014), [arXiv:1405.1756].
- [175] L. Sonnenschein, *Phys. Rev.* **D73**, 054015 (2006), [Erratum: *Phys. Rev.* **D78**, 079902(2008)], [hep-ph/0603011].
- [176] G. Aad *et al.* (ATLAS), *Eur. Phys. J.* **C75**, 7, 330 (2015), [arXiv:1503.05427].
- [177] A. M. Sirunyan *et al.* (CMS), *Phys. Rev.* **D96**, 3, 032002 (2017), [arXiv:1704.06142].
- [178] C. G. Lester and D. J. Summers, *Phys. Lett.* **B463**, 99 (1999), [hep-ph/9906349].
- [179] A. M. Sirunyan *et al.* (CMS), *Eur. Phys. J.* **C79**, 4, 313 (2019), [arXiv:1812.10534].
- [180] M. Aaboud *et al.* (ATLAS), *JHEP* **09**, 118 (2017), [arXiv:1702.07546].
- [181] The Tevatron Electroweak Working Group and Aaltonen, T., For the CDF and D0 Collab., arXiv:1608.01881, FERMI-LAB-CONF-16-298-E.
- [182] B. Abbott *et al.* (D0), *Phys. Rev.* **D60**, 052001 (1999), [hep-ex/9808029]; F. Abe *et al.* (CDF), *Phys. Rev. Lett.* **82**, 271 (1999), [Erratum: *Phys. Rev. Lett.* **82**, 2808(1999)], [hep-ex/9810029].
- [183] T. Aaltonen *et al.* (CDF), *Phys. Rev.* **D92**, 3, 032003 (2015), [arXiv:1505.00500].
- [184] T. A. Aaltonen *et al.* (CDF), *Phys. Rev.* **D90**, 9, 091101 (2014), [arXiv:1409.4906].
- [185] A. M. Sirunyan *et al.* (CMS), *Eur. Phys. J.* **C77**, 5, 354 (2017), [arXiv:1703.02530].
- [186] T. Aaltonen *et al.* (CDF), *Phys. Lett.* **B698**, 371 (2011), [arXiv:1101.4926].
- [187] CMS Collab., CMS-PAS-TOP-12-030.
- [188] T. Aaltonen *et al.* (CDF), *Phys. Rev.* **D80**, 051104 (2009), [arXiv:0906.5371].
- [189] V. Khachatryan *et al.* (CMS), *Phys. Rev.* **D93**, 9, 092006 (2016), [arXiv:1603.06536].
- [190] V. Khachatryan *et al.* (CMS), *JHEP* **12**, 123 (2016), [arXiv:1608.03560].
- [191] CMS Collab., CMS-PAS-TOP-15-002.
- [192] CMS Collab., CMS-PAS-TOP-16-002.
- [193] V. M. Abazov *et al.* (D0), *Phys. Rev. Lett.* **100**, 192004 (2008), [arXiv:0803.2779]; S. Chatrchyan *et al.* (CMS), *Phys. Lett.* **B728**, 496 (2014), [Erratum: *Phys. Lett.* **B738**, 526(2014)], [arXiv:1307.1907]; V. M. Abazov *et al.* (D0), *Phys. Lett.* **B703**, 422 (2011), [arXiv:1104.2887]; ATLAS Collab., ATLAS-CONF-2019-041; U. Langenfeld, S. Moch and P. Uwer, *Phys. Rev.* **D80**, 054009 (2009), [arXiv:0906.5273].
- [194] G. Aad *et al.* (ATLAS) (2019), [arXiv:1905.02302].
- [195] CMS Collab., CMS-PAS-TOP-13-006 (2016).
- [196] CDF Collab., CDF conference note 11080 (2014).
- [197] V. M. Abazov *et al.* (D0), *Phys. Rev.* **D91**, 11, 112003 (2015), [arXiv:1501.07912].
- [198] CMS Collab., CMS-PAS-TOP-13-005.
- [199] M. Beneke *et al.*, *Phys. Lett.* **B775**, 63 (2017), [arXiv:1605.03609].
- [200] A. H. Hoang, C. Lepenik and M. Preisser, *JHEP* **09**, 099 (2017), [arXiv:1706.08526].
- [201] C. Collaboration (CMS) (2019), [arXiv:1909.09193].
- [202] G. Aad *et al.* (ATLAS), *Phys. Lett.* **B716**, 1 (2012), [arXiv:1207.7214].
- [203] S. Chatrchyan *et al.* (CMS), *Phys. Lett.* **B716**, 30 (2012), [arXiv:1207.7235].
- [204] G. Degrossi *et al.*, *JHEP* **08**, 098 (2012), [arXiv:1205.6497].
- [205] S. Alekhin, A. Djouadi and S. Moch, *Phys. Lett.* **B716**, 214 (2012), [arXiv:1207.0980].
- [206] T. Aaltonen *et al.* (CDF), *Phys. Rev.* **D87**, 5, 052013 (2013), [arXiv:1210.6131].
- [207] V. M. Abazov *et al.* (D0), *Phys. Rev.* **D84**, 052005 (2011), [arXiv:1106.2063].
- [208] G. Aad *et al.* (ATLAS), *Phys. Lett.* **B728**, 363 (2014), [arXiv:1310.6527].
- [209] S. Chatrchyan *et al.* (CMS), *JHEP* **06**, 109 (2012), [arXiv:1204.2807].
- [210] S. Chatrchyan *et al.* (CMS), *Phys. Lett.* **B770**, 50 (2017), [arXiv:1610.09551].
- [211] G. Mahlon and S. J. Parke, *Phys. Rev.* **D53**, 4886 (1996), [hep-ph/9512264]; G. Mahlon and S. J. Parke, *Phys. Lett.* **B411**, 173 (1997), [hep-ph/9706304].
- [212] G.R. Goldstein, in *Spin 96: Proceedings of the 12th International Symposium on High Energy Spin Physics*, Amsterdam, 1996, ed. C.W. Jager (World Scientific, Singapore, 1997), p. 328.
- [213] T. Stelzer and S. Willenbrock, *Phys. Lett.* **B374**, 169 (1996), [hep-ph/9512292].
- [214] W. Bernreuther *et al.*, *Nucl. Phys.* **B690**, 81 (2004), [hep-ph/0403035].

- [215] A. Brandenburg, Z. G. Si and P. Uwer, Phys. Lett. **B539**, 235 (2002), [hep-ph/0205023].
- [216] CDF Collab., CDF conference note 10719 (2011).
- [217] CDF Collab., CDF conference note 10211 (2010).
- [218] V. M. Abazov *et al.* (D0), Phys. Lett. **B757**, 199 (2016), [arXiv:1512.08818].
- [219] V. M. Abazov *et al.* (D0), Phys. Rev. **D95**, 1, 011101 (2017), [arXiv:1607.07627].
- [220] V. M. Abazov *et al.* (D0), Phys. Rev. **D92**, 052007 (2015), [arXiv:1507.05666].
- [221] G. Mahlon and S. J. Parke, Phys. Rev. **D81**, 074024 (2010), [arXiv:1001.3422].
- [222] G. Aad *et al.* (ATLAS), Phys. Rev. **D90**, 11, 112016 (2014), [arXiv:1407.4314].
- [223] G. Aad *et al.* (ATLAS), Phys. Rev. Lett. **114**, 14, 142001 (2015), [arXiv:1412.4742].
- [224] G. Aad *et al.* (ATLAS), Phys. Rev. **D93**, 1, 012002 (2016), [arXiv:1510.07478].
- [225] S. Chatrchyan *et al.* (CMS), Phys. Rev. Lett. **112**, 18, 182001 (2014), [arXiv:1311.3924].
- [226] V. Khachatryan *et al.* (CMS), Phys. Lett. **B758**, 321 (2016), [arXiv:1511.06170].
- [227] V. Khachatryan *et al.* (CMS), Phys. Rev. **D93**, 5, 052007 (2016), [arXiv:1601.01107].
- [228] M. Aaboud *et al.* (ATLAS), Submitted to: Eur. Phys. J. (2019), [arXiv:1903.07570].
- [229] A. M. Sirunyan *et al.* (CMS), Phys. Rev. **D100**, 7, 072002 (2019), [arXiv:1907.03729].
- [230] W. Bernreuther, D. Heisler and Z.-G. Si, JHEP **12**, 026 (2015), [arXiv:1508.05271].
- [231] M. Aaboud *et al.* (ATLAS), JHEP **03**, 113 (2017), [arXiv:1612.07004].
- [232] A. F. Falk and M. E. Peskin, Phys. Rev. **D49**, 3320 (1994), [hep-ph/9308241].
- [233] T. A. Aaltonen *et al.* (CDF), Phys. Rev. Lett. **111**, 20, 202001 (2013), [arXiv:1308.4050].
- [234] CMS Collab., CMS-PAS-TOP-16-019.
- [235] M. Aaboud *et al.* (ATLAS), Eur. Phys. J. **C78**, 2, 129 (2018), [arXiv:1709.04207].
- [236] ATLAS-CONF-2019-038.
- [237] V. M. Abazov *et al.* (D0), Phys. Rev. **D85**, 091104 (2012), [arXiv:1201.4156].
- [238] G. L. Kane, G. A. Ladinsky and C. P. Yuan, Phys. Rev. **D45**, 124 (1992).
- [239] A. Czarnecki, J. G. Korner and J. H. Piclum, Phys. Rev. **D81**, 111503 (2010), [arXiv:1005.2625].
- [240] T. Aaltonen *et al.* (CDF, D0), Phys. Rev. **D85**, 071106 (2012), [arXiv:1202.5272].
- [241] G. Aad *et al.* (ATLAS), JHEP **06**, 088 (2012), [arXiv:1205.2484].
- [242] S. Chatrchyan *et al.* (CMS), JHEP **10**, 167 (2013), [arXiv:1308.3879].
- [243] ATLAS and CMS Collab., ATLAS-CONF-2013-033, CMS-PAS-TOP-11-025.
- [244] M. Aaboud *et al.* (ATLAS), Eur. Phys. J. **C77**, 4, 264 (2017), [Erratum: Eur. Phys. J. C79, no.1, 19(2019)], [arXiv:1612.02577].
- [245] V. Khachatryan *et al.* (CMS), Phys. Lett. **B762**, 512 (2016), [arXiv:1605.09047].
- [246] CMS Collab., CMS-PAS-TOP-14-017.
- [247] V. Khachatryan *et al.* (CMS), JHEP **01**, 053 (2015), [arXiv:1410.1154].
- [248] T. Aaltonen *et al.* (CDF), Phys. Rev. **D87**, 3, 031104 (2013), [arXiv:1211.4523].
- [249] D. Choudhury, T. M. P. Tait and C. E. M. Wagner, Phys. Rev. **D65**, 053002 (2002), [hep-ph/0109097].
- [250] D. Chang, W.-F. Chang and E. Ma, Phys. Rev. **D59**, 091503 (1999), [hep-ph/9810531]; D. Chang, W.-F. Chang and E. Ma, Phys. Rev. **D61**, 037301 (2000), [hep-ph/9909537].
- [251] T. Aaltonen *et al.* (CDF), Phys. Rev. **D88**, 3, 032003 (2013), [arXiv:1304.4141].
- [252] V. M. Abazov *et al.* (D0), Phys. Rev. **D90**, 5, 051101 (2014), [Erratum: Phys. Rev. D90, no.7, 079904(2014)], [arXiv:1407.4837].
- [253] G. Aad *et al.* (ATLAS), JHEP **11**, 031 (2011).
- [254] CMS Collab., CMS-PAS-TOP-11-031.
- [255] T. Aaltonen *et al.* (CDF), Phys. Rev. **D84**, 031104 (2011), [arXiv:1106.3970].
- [256] G. Aad *et al.* (ATLAS), Phys. Rev. **D91**, 7, 072007 (2015), [arXiv:1502.00586].
- [257] M. Aaboud *et al.* (ATLAS), JHEP **11**, 086 (2017), [arXiv:1706.03046].
- [258] K. Melnikov, M. Schulze and A. Scharf, Phys. Rev. **D83**, 074013 (2011), [arXiv:1102.1967].
- [259] A. M. Sirunyan *et al.* (CMS), JHEP **10**, 006 (2017), [arXiv:1706.08128].
- [260] M. Aaboud *et al.* (ATLAS), Eur. Phys. J. **C79**, 5, 382 (2019), [arXiv:1812.01697].
- [261] ATLAS Collab., ATLAS-CONF-2019-042.
- [262] A. M. Sirunyan *et al.* (CMS), Phys. Lett. **B779**, 358 (2018), [arXiv:1712.02825].
- [263] M. Cepeda *et al.* (HL/HE WG2 group) (2019), [arXiv:1902.00134].
- [264] S. Chatrchyan *et al.* (CMS), Phys. Rev. Lett. **110**, 172002 (2013), [arXiv:1303.3239].
- [265] J. M. Campbell and R. K. Ellis, JHEP **07**, 052 (2012), [arXiv:1204.5678].
- [266] M. V. Garzelli *et al.*, JHEP **11**, 056 (2012), [arXiv:1208.2665].
- [267] ATLAS Collab., ATLAS-CONF-2012-126.
- [268] G. Aad *et al.* (ATLAS), JHEP **11**, 172 (2015), [arXiv:1509.05276].
- [269] V. Khachatryan *et al.* (CMS), JHEP **01**, 096 (2016), [arXiv:1510.01131].
- [270] M. Aaboud *et al.* (ATLAS), Phys. Rev. **D99**, 7, 072009 (2019), [arXiv:1901.03584].
- [271] A. Broggio *et al.*, JHEP **08**, 039 (2019), [arXiv:1907.04343].
- [272] A. M. Sirunyan *et al.* (CMS), JHEP **08**, 011 (2018), [arXiv:1711.02547].
- [273] (2019), [arXiv:1907.11270].
- [274] A. M. Sirunyan *et al.* (CMS), JHEP **07**, 003 (2017), [arXiv:1702.01404].
- [275] S. P. Martin 1–98 (1997), [Adv. Ser. Direct. High Energy Phys.18,1(1998)], [hep-ph/9709356].
- [276] C. T. Hill and E. H. Simmons, Phys. Rept. **381**, 235 (2003), [Erratum: Phys. Rept.390,553(2004)], [hep-ph/0203079].
- [277] C. T. Hill, Phys. Lett. **B266**, 419 (1991).
- [278] C. T. Hill, Phys. Lett. **B345**, 483 (1995), [hep-ph/9411426].
- [279] A. M. Sirunyan *et al.* (CMS) (2019), [arXiv:1908.06463].
- [280] M. Aaboud *et al.* (ATLAS), Phys. Rev. **D99**, 5, 052009 (2019), [arXiv:1811.02305].
- [281] C. Zhang and S. Willenbrock, Phys. Rev. **D83**, 034006 (2011), [arXiv:1008.3869].
- [282] J. A. Aguilar-Saavedra, Nucl. Phys. **B843**, 638 (2011), [Erratum: Nucl. Phys. B851,443(2011)], [arXiv:1008.3562].
- [283] A. Buckley *et al.*, JHEP **04**, 015 (2016), [arXiv:1512.03360].

- [284] N. P. Hartland *et al.*, JHEP **04**, 100 (2019), [arXiv:1901.05965].
- [285] I. Brivio *et al.* (2019), [arXiv:1910.03606].
- [286] V. Barger, T. Han and D. G. E. Walker, Phys. Rev. Lett. **100**, 031801 (2008), [hep-ph/0612016].
- [287] R. Frederix and F. Maltoni, JHEP **01**, 047 (2009), [arXiv:0712.2355].
- [288] T. Aaltonen *et al.* (CDF), Phys. Rev. Lett. **110**, 12, 121802 (2013), [arXiv:1211.5363].
- [289] D. Acosta *et al.* (CDF), Phys. Rev. Lett. **94**, 211801 (2005), [hep-ex/0501050].
- [290] T. Aaltonen *et al.* (CDF), Phys. Rev. **D84**, 072003 (2011), [arXiv:1108.4755].
- [291] A. Altheimer *et al.*, J. Phys. **G39**, 063001 (2012), [arXiv:1201.0008].
- [292] A. M. Sirunyan *et al.* (CMS), JHEP **04**, 031 (2019), [arXiv:1810.05905].
- [293] A. M. Sirunyan *et al.* (CMS), JHEP **07**, 001 (2017), [arXiv:1704.03366].
- [294] M. Aaboud *et al.* (ATLAS), Eur. Phys. J. **C78**, 7, 565 (2018), [arXiv:1804.10823].
- [295] M. Aaboud *et al.* (ATLAS), Phys. Rev. **D99**, 9, 092004 (2019), [arXiv:1902.10077].
- [296] A. M. Sirunyan *et al.* (CMS), Phys. Lett. **B777**, 39 (2018), [arXiv:1708.08539].
- [297] A. M. Sirunyan *et al.* (CMS), Phys. Lett. **B781**, 574 (2018), [arXiv:1708.01062].
- [298] A. M. Sirunyan *et al.* (CMS), JHEP **08**, 073 (2017), [arXiv:1705.10967].
- [299] A. M. Sirunyan *et al.* (CMS), Phys. Lett. **B772**, 634 (2017), [arXiv:1701.08328].
- [300] V. Khachatryan *et al.* (CMS), Phys. Lett. **B771**, 80 (2017), [arXiv:1612.00999].
- [301] A. M. Sirunyan *et al.* (CMS), JHEP **04**, 136 (2017), [arXiv:1612.05336].
- [302] A. M. Sirunyan *et al.* (CMS), JHEP **05**, 029 (2017), [arXiv:1701.07409].
- [303] A. M. Sirunyan *et al.* (CMS), Eur. Phys. J. **C79**, 90 (2019), [arXiv:1809.08597].
- [304] A. M. Sirunyan *et al.* (CMS), Phys. Rev. **D100**, 7, 072001 (2019), [arXiv:1906.11903].
- [305] M. Aaboud *et al.* (ATLAS), Phys. Lett. **B788**, 347 (2019), [arXiv:1807.10473].
- [306] M. Aaboud *et al.* (ATLAS), Phys. Rev. **D98**, 11, 112010 (2018), [arXiv:1806.10555].
- [307] M. Aaboud *et al.* (ATLAS), Phys. Rev. Lett. **121**, 21, 211801 (2018), [arXiv:1808.02343].
- [308] CMS Collab. CMS-PAS-TOP-12-042 (2013).
- [309] V. Khachatryan *et al.* (CMS), JHEP **06**, 121 (2015), [arXiv:1504.03198].
- [310] A. M. Sirunyan *et al.* (CMS), Eur. Phys. J. **C77**, 12, 845 (2017), [arXiv:1706.02581].
- [311] A. M. Sirunyan *et al.* (CMS), JHEP **03**, 141 (2019), [arXiv:1901.01553].
- [312] M. Aaboud *et al.* (ATLAS), JHEP **06**, 108 (2018), [arXiv:1711.11520].
- [313] J. A. Aguilar-Saavedra, Acta Phys. Polon. **B35**, 2695 (2004), [hep-ph/0409342].
- [314] V. Khachatryan *et al.* (CMS), JHEP **02**, 028 (2017), [arXiv:1610.03545].
- [315] CMS Collab., CMS-PAS-TOP-14-003.
- [316] CMS Collab., CMS-PAS-TOP-17-003.
- [317] V. Khachatryan *et al.* (CMS), JHEP **02**, 079 (2017), [arXiv:1610.04857].
- [318] G. Aad *et al.* (ATLAS), Eur. Phys. J. **C76**, 2, 55 (2016), [arXiv:1509.00294].
- [319] G. Aad *et al.* (ATLAS), Phys. Lett. **B800**, 135082 (2020), [arXiv:1908.08461].
- [320] A. Heister *et al.* (ALEPH), Phys. Lett. **B543**, 173 (2002), [hep-ex/0206070]; J. Abdallah *et al.* (DELPHI), Phys. Lett. **B590**, 21 (2004), [hep-ex/0404014]; P. Achard *et al.* (L3), Phys. Lett. **B549**, 290 (2002), [hep-ex/0210041]; G. Abbiendi *et al.* (OPAL), Phys. Lett. **B521**, 181 (2001), [hep-ex/0110009].
- [321] F. D. Aaron *et al.* (H1), Phys. Lett. **B678**, 450 (2009), [arXiv:0904.3876].
- [322] H. Abramowicz *et al.* (ZEUS), Phys. Lett. **B708**, 27 (2012), [arXiv:1111.3901].
- [323] M. Beneke *et al.*, in “1999 CERN Workshop on standard model physics (and more) at the LHC, CERN, Geneva, Switzerland, 25-26 May: Proceedings,” 419–529 (2000), [hep-ph/0003033], URL <http://weblib.cern.ch/abstract?CERN-TH-2000-100>.
- [324] V. F. Obraztsov, S. R. Slabospitsky and O. P. Yushchenko, Phys. Lett. **B426**, 393 (1998), [hep-ph/9712394].
- [325] T. Carli, D. Dannheim and L. Bellagamba, Mod. Phys. Lett. **A19**, 1881 (2004), [hep-ph/0402012].
- [326] V. M. Abazov *et al.* (D0), Phys. Rev. Lett. **102**, 092002 (2009), [arXiv:0901.0151].
- [327] V. M. Abazov *et al.* (DØ Collab.), DØ conference note 5838 (2009).
- [328] V. M. Abazov *et al.* (D0), Phys. Lett. **B708**, 21 (2012), [arXiv:1110.4592].
- [329] ATLAS Collab., ATLAS-CONF-2013-032.
- [330] T. Aaltonen *et al.* (CDF), Phys. Rev. Lett. **101**, 192002 (2008), [arXiv:0805.2109].
- [331] V. M. Abazov *et al.* (D0), Phys. Lett. **B701**, 313 (2011), [arXiv:1103.4574].
- [332] V. M. Abazov *et al.* (D0), Phys. Lett. **B693**, 81 (2010), [arXiv:1006.3575].
- [333] S. Chatrchyan *et al.* (CMS), Phys. Rev. Lett. **112**, 17, 171802 (2014), [arXiv:1312.4194].
- [334] A. M. Sirunyan *et al.* (CMS), JHEP **07**, 003 (2017), [arXiv:1702.01404].
- [335] M. Aaboud *et al.* (ATLAS), JHEP **07**, 176 (2018), [arXiv:1803.09923].
- [336] A. M. Sirunyan *et al.* (CMS), JHEP **06**, 102 (2018), [arXiv:1712.02399].
- [337] M. Aaboud *et al.* (ATLAS), JHEP **05**, 123 (2019), [arXiv:1812.11568].

61. Form Factors for Radiative Pion and Kaon Decays

Revised August 2019 by M.A. Bychkov (Virginia U.) and G. D'Ambrosio (INFN, Napoli).

The radiative decays, $\pi^\pm \rightarrow l^\pm \nu \gamma$ and $K^\pm \rightarrow l^\pm \nu \gamma$, with l standing for an e or a μ , and γ for a real or virtual photon (e^+e^- pair), provide a powerful tool to investigate the hadronic structure of pions and kaons. The structure-dependent part SD_i of the amplitude describes the emission of photons from virtual hadronic states, and is parametrized in terms of form factors V, A , (vector, axial vector), in the standard description [1–4]. Note that in the Listings and some literature, equivalent nomenclature F_V and F_A for the vector and axial form factors is often used. Exotic, non-standard contributions like $i = T, S$ (tensor, scalar) have also been considered. Apart from the SD terms, there is also the Inner Bremsstrahlung amplitude, IB, corresponding to photon radiation from external charged particles and described by Low theorem in terms of the physical decay $\pi^\pm(K^\pm) \rightarrow l^\pm \nu$. Experiments try to optimize their kinematics so as to minimize the IB part of the amplitude.

The SD amplitude in its standard form is given as

$$M(SD_V) = \frac{-eG_F U_{qq'}}{\sqrt{2}m_P} \epsilon^\mu l^\nu V^P \epsilon_{\mu\nu\sigma\tau} k^\sigma q^\tau \quad (61.1)$$

$$M(SD_A) = \frac{-ieG_F U_{qq'}}{\sqrt{2}m_P} \epsilon^\mu l^\nu \{A^P [(qk - k^2)g_{\mu\nu} - q_\mu k_\nu] + R^P k^2 g_{\mu\nu}\}, \quad (61.2)$$

which contains an additional axial form factor R^P which only can be accessed if the photon remains virtual. $U_{qq'}$ is the Cabibbo-Kobayashi-Maskawa mixing-matrix element; ϵ^μ is the polarization vector of the photon (or the effective vertex, $\epsilon^\mu = (e/k^2)\bar{u}(p_-)\gamma^\mu v(p_+)$, of the e^+e^- pair); $\ell^\nu = \bar{u}(p_\nu)\gamma^\nu(1 - \gamma_5)v(p_\ell)$ is the lepton-neutrino current; q and k are the meson and photon four-momenta ($k = p_+ + p_-$ for virtual photons); and P stands for π or K .

For decay processes where the photon is real, the partial decay width can be written in analytical form as a sum of IB, SD, and IB/SD interference terms INT [1,4]:

$$\frac{d^2\Gamma_{P \rightarrow \ell\nu\gamma}}{dx dy} = \frac{d^2(\Gamma_{IB} + \Gamma_{SD} + \Gamma_{INT})}{dx dy}$$

$$= \frac{\alpha}{2\pi} \Gamma_{P \rightarrow \ell\nu} \frac{1}{(1-r)^2} \left\{ \text{IB}(x, y) + \frac{1}{r} \left(\frac{m_P}{2f_P} \right)^2 \left[(V+A)^2 \text{SD}^+(x, y) + (V-A)^2 \text{SD}^-(x, y) \right] + \epsilon_P \frac{m_P}{f_P} \left[(V+A) S_{INT}^+(x, y) + (V-A) S_{INT}^-(x, y) \right] \right\}. \quad (61.3)$$

Here

$$\text{IB}(x, y) = \left[\frac{1-y+r}{x^2(x+y-1-r)} \right]$$

$$\left[x^2 + 2(1-x)(1-r) - \frac{2xr(1-r)}{x+y-1-r} \right]$$

$$\text{SD}^+(x, y) = (x+y-1-r) \left[(x+y-1)(1-x) - r \right]$$

$$\text{SD}^-(x, y) = (1-y+r) \left[(1-x)(1-y) + r \right]$$

$$S_{INT}^+(x, y) = \left[\frac{1-y+r}{x(x+y-1-r)} \right] \left[(1-x)(1-x-y) + r \right]$$

$$S_{INT}^-(x, y) = \left[\frac{1-y+r}{x(x+y-1-r)} \right] \left[x^2 - (1-x)(1-x-y) - r \right] \quad (61.4)$$

where $x = 2E_\gamma/m_P$, $y = 2E_\ell/m_P$, $r = (m_\ell/m_P)^2$, f_P is the meson decay constant, and ϵ_P is +1 for pions and -1 for kaons. The

structure dependent terms SD^+ and SD^- are shown in Fig. 1. The SD^- term is maximized in the same kinematic region where overwhelming IB term dominates (along $x+y=1$ diagonal). Thus experimental yields with less background are dominated by SD^+ contribution and proportional to $A^P + V^P$ making simultaneous precise determination of the form factors difficult.

Recently, formulas 61.3 and 61.4 have been extended to describe polarized distributions in radiative meson and muon decays [5].

The ‘‘helicity’’ factor r is responsible for the enhancement of the SD over the IB amplitude in the decays $\pi^\pm \rightarrow e^\pm \nu \gamma$, while $\pi^\pm \rightarrow \mu^\pm \nu \gamma$ is dominated by IB. Interference terms are important for the decay $K^\pm \rightarrow \mu^\pm \nu \gamma$ [6], but contribute only a few percent correction to pion decays. However, they provide the basis for determining the signs of V and A . Radiative corrections to the decay $\pi^+ \rightarrow e^+ \nu \gamma$ have to be taken into account in the analysis of the precision experiments. They make up to 4% corrections in the total decay rate [7]. In $\pi^\pm \rightarrow e^\pm \nu e^+ e^-$ and $K^\pm \rightarrow \ell^\pm \nu e^+ e^-$ decays, all three form factors, V^P , A^P , and R^P , can be determined [8,9].

Theoretically, the first non-trivial χPT contributions to A^P and V^P appear at $\mathcal{O}(p^4)$ [4], respectively from Gasser-Leutwyler coefficients, L_i 's, and the anomalous lagrangian:

$$A^P = \frac{4\sqrt{2}M_P}{F_\pi} (L_9^r + L_{10}^r), \quad V^P = \frac{\sqrt{2}M_P}{8\pi^2 F_\pi}. \quad (61.5)$$

In case of the kaon $A^K = 0.042$ and $V^K = 0.096$. $\mathcal{O}(p^6)$ contributions to A^K can be predicted accurately: they are flat in the momentum dependence and shift the $\mathcal{O}(p^4)$ value to 0.034. $\mathcal{O}(p^6)$ contributions to V^K are model dependent and can be approximated by a form factor linearly dependent on momentum. For example, when looking at the spread of results obtained within two different models, the constant piece of this linear form factor is shifted to 0.078 ± 0.005 [1,2,4].

We give the experimental π^\pm form factors V^π , A^π , and R^π in the Listings. In the K^\pm Listings, we give the extracted sum $A^K + V^K$ and difference $A^K - V^K$, as well as V^K , A^K and R^K . In particular KLOE has measured for the constant piece of the form factor $A^K + V^K = 0.125 \pm 0.007 \pm 0.001$ [10] while ISTRA+, $V^K - A^K = 0.21 \pm 0.04 \pm 0.04$ [11].

The pion vector form factor, V^π , is related via CVC (Conserved Vector Current) to the $\pi^0 \rightarrow \gamma\gamma$ decay width. The constant term is given by $|V^\pi(0)| = (1/\alpha)\sqrt{2}\Gamma_{\pi^0 \rightarrow \gamma\gamma}/\pi m_{\pi^0}$ [3]. The resulting value, $V^\pi(0) = 0.0259(9)$, has been confirmed by calculations based on chiral perturbation theory (χPT) [4], and by two experiments given in the Listings. A recent experiment by the PIBETA collaboration [12] obtained a $V^\pi(0)$ that is in excellent agreement with the CVC hypothesis. It also measured the slope parameter a in $V^\pi(s) = V^\pi(0)(1 + a \cdot s)$, where $s = (1 - 2E_\gamma/m_\pi)^2$, and E_γ is the gamma energy in the pion rest frame: $a = 0.095 \pm 0.058$. A functional dependence on s is expected for all form factors. It becomes non-negligible in the case of $V^\pi(s)$ when a wide range of photon momenta is recorded; proper treatment in the analysis of K decays is mandatory.

The form factor, R^P , can be related to the electromagnetic radius, r_P , of the meson [2]: $R^P = \frac{1}{3}m_P f_P (r_P^2)$ using PCAC (Partial Conserved Axial vector Current).

In lowest order χPT , the ratio A^π/V^π is related to the pion electric polarizability $\alpha_E = [\alpha/(8\pi^2 m_\pi f_\pi^2)] \times A^\pi/V^\pi$ [13]. Direct experimental and theoretical status of pion polarizability studies currently is not settled. Most recent theoretical predictions from χPT [14] and experimental results from COMPASS collaboration [15] favor a small value of pion polarizability $\alpha_\pi \sim (2 \div 3) \times 10^{-4} \text{ fm}^3$. Dispersive analysis of $\gamma\gamma \rightarrow \pi^+\pi^-$ crosssection [16] and experimental results from MAMI collaboration [17] report a much larger value of $\alpha_\pi \sim 6 \times 10^{-4} \text{ fm}^3$. Precise measurement of the pion form factors by PIBETA collaboration favors smaller values of polarizability $\alpha_\pi = 2.7_{-0.5}^{+0.6} \times 10^{-4} \text{ fm}^3$.

Several searches for the exotic form factors F_T^π , F_T^K (tensor), and F_S^K (scalar) have been pursued in the past. In particular, F_T^π has been brought into focus by experimental as well as theoretical work [18]. New high-statistics data from the PIBETA collabora-

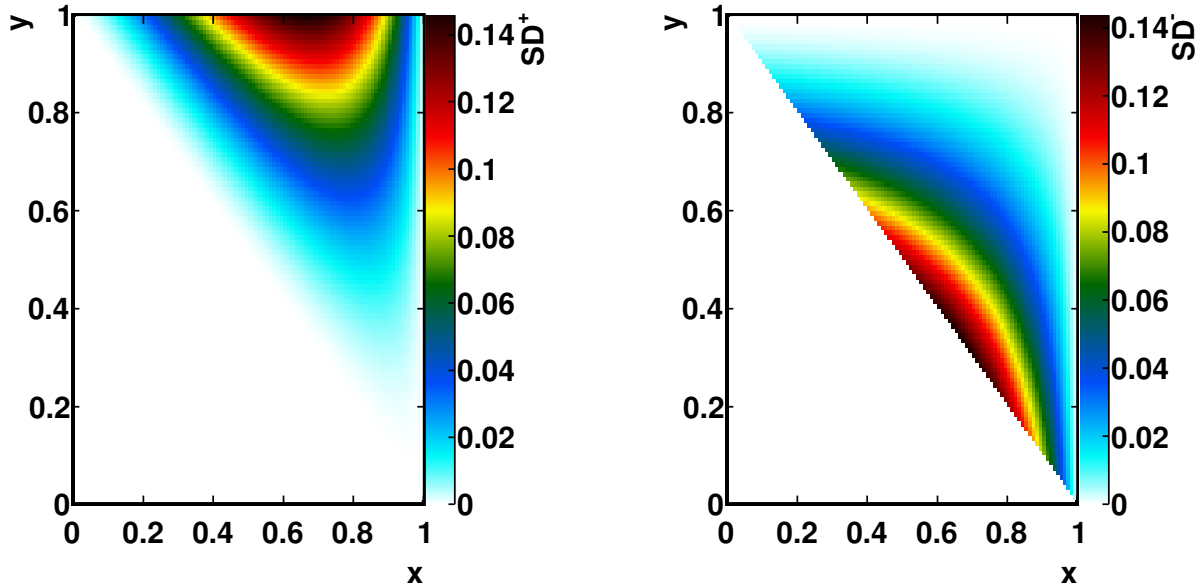


Figure 61.1: Components of the structure dependent terms of the decay width. Left: SD^+ , right: SD^-

tion have been re-analyzed together with an additional data set optimized for low backgrounds in the radiative pion decay. In particular, lower beam rates have been used in order to reduce the accidental background, thereby making the treatment of systematic uncertainties easier and more reliable. The PIBETA analysis now restricts F_T^π to the range $-5.2 \times 10^{-4} < F_T^\pi < 4.0 \times 10^{-4}$ at a 90% confidence limit [12]. This result is in excellent agreement with the most recent theoretical work [4].

Precision measurements of radiative pion and kaon decays are effective tools to study QCD in the non-perturbative region and are of interest beyond the scope of radiative decays. Meanwhile other processes such as $\pi^+ \rightarrow e^+\nu$ that seem to be better suited to search for new physics at the precision frontier are currently studied. The advantages of such process are the very accurate and reliable theoretical predictions and the more straightforward experimental analysis.

References

- [1] D. A. Bryman, P. Depommier and C. Leroy, Phys. Rept. **88**, 151 (1982), see our note on “Decay Constants of Charged Pseudoscalar Mesons” elsewhere in this *Review*; S. G. Brown and S. A. Bludman, Phys. Rev. **136**, B1160 (1964); P. DeBaenst and J. Pestieau, Nuovo Cimento **A53**, 137 (1968).
- [2] W. T. Chu, T. Ebata and D. M. Scott, Phys. Rev. **166**, 1577 (1968); D. Yu. Bardin and E. A. Ivanov, Sov. J. Part. Nucl. **7**, 286 (1976), [Fiz. Elem. Chast. Atom. Yadra7,726(1976)]; A. Kersch and F. Scheck, Nucl. Phys. **B263**, 475 (1986).
- [3] V.G. Vaks and B.L. Ioffe, Nuovo Cimento **10**, 342 (1958); V.F. Muller, Z. Phys. **173**, 438 (1963).
- [4] C. Q. Geng, I.-L. Ho and T. H. Wu, Nucl. Phys. **B684**, 281 (2004), [hep-ph/0306165]; J. Bijnens and P. Talavera, Nucl. Phys. **B489**, 387 (1997), [hep-ph/9610269]; V. Mateu and J. Portoles, Eur. Phys. J. **C52**, 325 (2007), [arXiv:0706.1039]; R. Unterdorfer and H. Pichl, Eur. Phys. J. **C55**, 273 (2008), [arXiv:0801.2482]; V. Cirigliano *et al.*, Rev. Mod. Phys. **84**, 399 (2012), [arXiv:1107.6001].
- [5] E. Gabrielli and L. Trentadue, Nucl. Phys. **B792**, 48 (2008), [hep-ph/0507191].
- [6] S. Adler *et al.* (E787), Phys. Rev. Lett. **85**, 2256 (2000), [hep-ex/0003019].
- [7] E. A. Kuraev, Yu. M. Bystritsky and E. P. Velicheva, Phys. Rev. **D69**, 114004 (2004), [hep-ph/0310275]; R. Unterdorfer and H. Pichl have treated radiative corrections of the structure terms to lowest order within χPT for the first time. See the reference under [4].
- [8] S. Egli *et al.* (SINDRUM), Phys. Lett. **B175**, 97 (1986).
- [9] A. A. Poblaguev *et al.*, Phys. Rev. Lett. **89**, 061803 (2002), [hep-ex/0204006].
- [10] F. Ambrosino *et al.* (KLOE), Eur. Phys. J. **C64**, 627 (2009), [Erratum: Eur. Phys. J.65,703(2010)], [arXiv:0907.3594].
- [11] V. A. Duk *et al.* (ISTRA+), Phys. Lett. **B695**, 59 (2011), [arXiv:1005.3517].
- [12] D. Pocanic *et al.*, Phys. Rev. Lett. **93**, 181803 (2004), [hep-ex/0312030]; E. Frlez *et al.*, Phys. Rev. Lett. **93**, 181804 (2004), [hep-ex/0312029]; M. Bychkov *et al.*, Phys. Rev. Lett. **103**, 051802 (2009), [arXiv:0804.1815].
- [13] J. F. Donoghue and B. R. Holstein, Phys. Rev. **D40**, 2378 (1989).
- [14] J. Gasser, M. A. Ivanov and M. E. Sainio, Nucl. Phys. **B745**, 84 (2006), [hep-ph/0602234].
- [15] C. Adolph *et al.* (COMPASS), Phys. Rev. Lett. **114**, 062002 (2015), [arXiv:1405.6377].
- [16] L. V. Fil’kov and V. L. Kashevarov, Phys. Rev. **C73**, 035210 (2006), [arXiv:nucl-th/0512047].
- [17] J. Ahrens *et al.*, Eur. Phys. J. **A23**, 113 (2005), [arXiv:nucl-ex/0407011].
- [18] A. A. Poblaguev, Phys. Lett. **B238**, 108 (1990); V. N. Bolotov *et al.*, Phys. Lett. **B243**, 308 (1990); V. M. Belyaev and I. I. Kogan, Phys. Lett. **B280**, 238 (1992); A. V. Chernyshev *et al.*, Mod. Phys. Lett. **A12**, 1669 (1997); A. A. Poblaguev, Phys. Rev. **D68**, 054020 (2003), [hep-ph/0307166]; M. V. Chizhov, Phys. Part. Nucl. Lett. **2**, 193 (2005), [Pisma Fiz. Elem. Chast. Atom. Yadra2005,no.4,7(2005)], [hep-ph/0402105].

62. Scalar Mesons below 2 GeV

Revised August 2019 by C. Amsler (Stefan Meyer Inst.), S. Eidelman (Budker Inst., Novosibirsk; Novosibirsk U.), T. Gutsche (Tübingen U.), C. Hanhart (Jülich) and S. Spanier (Tennessee U.).

62.1 Introduction

In contrast to the vector and tensor mesons, the identification of the scalar mesons is a long-standing puzzle. Scalar resonances are difficult to resolve because some of them have large decay widths which cause a strong overlap between resonances and background. In addition, several decay channels sometimes open up within a short mass interval (*e.g.* at the $K\bar{K}$ and $\eta\eta$ thresholds), producing cusps in the line shapes of the near-by resonances. Furthermore, one expects non- $q\bar{q}$ scalar objects, such as glueballs and multi-quark states in the mass range below 2 GeV (for reviews see, *e.g.*, Refs. [1–5] and the mini-review on *non- $q\bar{q}$ states* in this Review of Particle Physics (RPP)).

Light scalars are produced, for example, in πN scattering on polarized/unpolarized targets, $p\bar{p}$ annihilation, central hadronic production, J/ψ , B -, D - and K -meson decays, $\gamma\gamma$ formation, and ϕ radiative decays. Especially for the lightest scalar mesons simple parameterizations fail and more advanced theory tools are necessary to extract the resonance parameters from data. In the analyses available in the literature fundamental properties of the amplitudes such as unitarity, analyticity, Lorentz invariance, chiral and flavor symmetry are implemented at different levels of rigor. Especially, chiral symmetry implies the appearance of zeros close to the threshold in elastic S -wave scattering amplitudes involving soft pions [6,7], which may be shifted or removed in associated production processes [8]. The methods employed are the K -matrix formalism, the N/D -method, the Dalitz–Tuan ansatz, unitarized quark models with coupled channels, effective chiral field theories and the linear sigma model, *etc.* Dynamics near the lowest two-body thresholds in some analyses are described by crossed channel (t , u) meson exchange or with an effective range parameterization instead of, or in addition to, resonant features in the s -channel. Dispersion theoretical approaches are applied to pin down the location of resonance poles for the low-lying states [9–12].

The mass and width of a resonance are found from the position of the nearest pole in the process amplitude (T -matrix or S -matrix) at an unphysical sheet of the complex energy plane, traditionally labeled as

$$\sqrt{s_{\text{Pole}}} = M - i\Gamma/2. \quad (62.1)$$

It is important to note that the pole of a Breit-Wigner parameterization agrees with this pole position only for narrow and well-separated resonances, far away from the opening of decay channels. For a detailed discussion of this issue we refer to the review on *Resonances* in this RPP.

In this note, we discuss the light scalars below 2 GeV organized in the listings under the entries ($I = 1/2$) $K_0^*(700)$ (or κ), $K_0^*(1430)$, ($I = 1$) $a_0(980)$, $a_0(1450)$, and ($I = 0$) $f_0(500)$ (or σ), $f_0(980)$, $f_0(1370)$, $f_0(1500)$, and $f_0(1710)$. This list is minimal and does not necessarily exhaust the list of actual resonances. The ($I = 2$) $\pi\pi$ and ($I = 3/2$) $K\pi$ phase shifts do not exhibit any resonant behavior.

62.2 The $I = 1/2$ States

The $K_0^*(1430)$ [13] is perhaps the least controversial of the light scalar mesons. The $K\pi$ S -wave scattering has two possible isospin channels, $I=1/2$ and $I=3/2$. The $I=3/2$ wave is elastic and repulsive up to 1.7 GeV [14] and contains no known resonances. The $I=1/2$ $K\pi$ phase shift, measured from about 100 MeV above threshold in Kp production, rises smoothly, passes 90° at 1350 MeV, and continues to rise to about 170° at 1600 MeV. The first important inelastic threshold is $K\eta'(958)$. In the inelastic region the continuation of the amplitude is uncertain since the partial-wave decomposition has several solutions. The data are extrapolated towards the $K\pi$ threshold using effective range type formulas [13,15] or chiral perturbation predictions [16,17]. From analyses using unitarized amplitudes there is agreement on the presence of a resonance pole around 1410 MeV having a width of

about 300 MeV. With reduced model dependence, Ref. [18] finds a larger width of 500 MeV.

Similar to the situation for the $f_0(500)$, discussed in the next section, the presence and properties of the light $K_0^*(700)$ (or κ) meson in the 700–900 MeV region are difficult to establish since it appears to have a very large width ($\Gamma \approx 500$ MeV) and resides close to the $K\pi$ threshold. Hadronic D - and B -meson decays provide additional data points in the vicinity of the $K\pi$ threshold and are discussed in detail in the *Review on Multibody Charm Analyses* in this RPP. Precision information from semileptonic D decays avoiding the theoretically more demanding final states with three strongly interacting particles is not available. BES II [19] (re-analyzed in [20]) finds a $K_0^*(700)$ -like structure in J/ψ decays to $\bar{K}^{*0}(892)K^+\pi^-$ where $K_0^*(700)$ recoils against the $K^*(892)$. Also clean with respect to final-state interaction is the decay $\tau^- \rightarrow K_S^0\pi^-\nu_\tau$ studied by Belle [21], with $K_0^*(700)$ parameters fixed to those of Ref. [19].

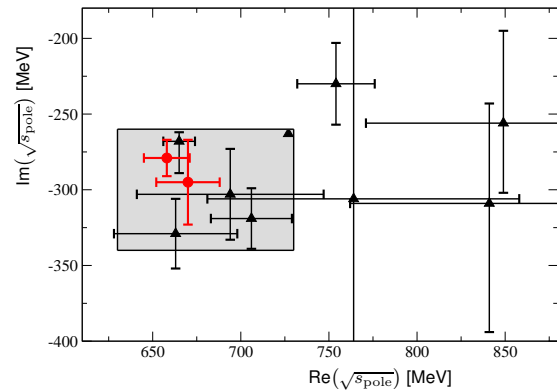


Figure 62.1: Location of the $K_0^*(700)$ (or κ) poles in the complex energy plane. Circles denote the results of the most refined analyses based on dispersion relations, while all other analyses quoted in the listings are denoted by triangles. The corresponding references are given in the listing.

Some authors find a $K_0^*(700)$ pole in their phenomenological analysis (see, *e.g.*, [22–33]), while others do not need to include it in their fits (see, *e.g.*, [17,34–37]). Similarly to the case of the $f_0(500)$ discussed below, all works including constraints from chiral symmetry at low energies naturally seem to find a light $K_0^*(700)$ below 800 MeV, see, *e.g.*, [38–42]. In these works the $K_0^*(700)$, $f_0(500)$, $f_0(980)$ and $a_0(980)$ appear to form a nonet [39,40]. Additional evidence for this assignment is presented in Ref. [12], where the couplings of the nine states to $q\bar{q}$ sources were compared. The same low-lying scalar nonet was also found earlier in the unitarized quark model of Ref. [41]. The analysis of Ref. [43] is based on the Roy-Steiner equations, which include analyticity and crossing symmetry. Ref. [44] uses the Padé method to extract pole parameters after refitting scattering data constrained to satisfy forward dispersion relations. Both arrive at compatible pole positions for the $K_0^*(700)$ that are consistent with the pole parameters deduced either from other theoretical methods or Breit-Wigner fits. This is illustrated in Fig. 62.1. The compilation in this figure is used as justification for the range of pole parameters of the $K_0^*(700)$ we quote as "our estimate", namely

$$\sqrt{s_{\text{Pole}}^{\kappa}} = (630 - 730) - i(260 - 340) \text{ MeV}. \quad (62.2)$$

62.3 The $I = 1$ States

Two isovector scalar states are known below 2 GeV, the $a_0(980)$ and the $a_0(1450)$. Independent of any model, the $K\bar{K}$ component in the $a_0(980)$ wave function must be large: it lies just below the opening of the $K\bar{K}$ channel to which it strongly couples [15,45]. This generates an important cusp-like behavior in the resonant amplitude. Hence, its mass and width parameters are strongly distorted. To reveal its true coupling constants, a coupled-channel model with energy-dependent widths and mass

shift contributions is necessary. All listed $a_0(980)$ measurements agree on a mass position value near 980 MeV, but the width takes values between 50 and 100 MeV, mostly due to the different models. For example, the analysis of the $p\bar{p}$ -annihilation data [15] using a unitary K -matrix description finds a width as determined from the T -matrix pole of 92 ± 8 MeV, while the observed width of the peak in the $\pi\eta$ mass spectrum is about 45 MeV.

The relative coupling $K\bar{K}/\pi\eta$ is determined indirectly from $f_1(1285)$ [46–48] or $\eta(1410)$ decays [49–51], from the line shape observed in the $\pi\eta$ decay mode [52–55], or from the coupled-channel analysis of the $\pi\pi\eta$ and $K\bar{K}\pi$ final states of $p\bar{p}$ annihilation at rest [15].

The $a_0(1450)$ is seen in $p\bar{p}$ annihilation experiments with stopped and higher momenta antiprotons, with a mass of about 1450 MeV or close to the $a_2(1320)$ meson which is typically a dominant feature. A contribution from $a_0(1450)$ is also found in the analysis of the $D^\pm \rightarrow K^+K^-\pi^\pm$ [56] and $D^0 \rightarrow K_S^0K^\pm\pi^\mp$ [57] decay.

62.4 The $I = 0$ States

The $I = 0$, $J^{PC} = 0^{++}$ sector is the most complex one, both experimentally and theoretically. The data have been obtained from the $\pi\pi$, $K\bar{K}$, $\eta\eta$, 4π , and $\eta\eta'(958)$ systems produced in S -wave. Analyses based on several different production processes conclude that probably four poles are needed in the mass range from $\pi\pi$ threshold to about 1600 MeV. The claimed isoscalar resonances are found under separate entries $f_0(500)$ (or σ), $f_0(980)$, $f_0(1370)$, and $f_0(1500)$.

For discussions of the $\pi\pi$ S wave below the $K\bar{K}$ threshold and on the long history of the $f_0(500)$, which was suggested in linear sigma models more than 50 years ago, see our reviews in previous editions and the review [5].

Information on the $\pi\pi$ S -wave phase shift $\delta_I^I = \delta_0^0$ was already extracted many years ago from πN scattering [58–60], and near threshold from the K_{e4} -decay [61]. The kaon decays were later revisited leading to consistent data, however, with very much improved statistics [62, 63]. The reported $\pi\pi \rightarrow K\bar{K}$ cross sections [64–67] have large uncertainties. The πN data have been analyzed in combination with high-statistics data (see entries labeled as RVUE for re-analyses of the data). The $2\pi^0$ invariant mass spectra of the $p\bar{p}$ annihilation at rest [68–70] and the central collision [71] do not show a distinct resonance structure below 900 MeV, but these data are consistently described with the standard solution for πN data [59, 72], which allows for the existence of the broad $f_0(500)$. An enhancement is observed in the $\pi^+\pi^-$ invariant mass near threshold in the decays $D^+ \rightarrow \pi^+\pi^-\pi^+$ [73–75] and $J/\psi \rightarrow \omega\pi^+\pi^-$ [76, 77], and in $\psi(2S) \rightarrow J/\psi\pi^+\pi^-$ with very limited phase space [78, 79].

The precise $f_0(500)$ (or σ) pole is difficult to establish because of its large width, and because it can certainly not be modeled by a naive Breit-Wigner resonance. The $\pi\pi$ scattering amplitude shows an unusual energy dependence due to the presence of a zero in the unphysical regime close to the threshold [6, 7], required by chiral symmetry, and possibly due to crossed channel exchanges, the $f_0(1370)$, and other dynamical features. However, most of the analyses listed under $f_0(500)$ agree on a pole position near $(500 - i250)$ MeV. In particular, analyses of $\pi\pi$ data that include unitarity, $\pi\pi$ threshold behavior, strongly constrained by the K_{e4} data, and the chiral symmetry constraints from Adler zeroes and/or scattering lengths find a light $f_0(500)$, see, e.g., [80, 81].

Precise pole positions with an uncertainty of less than 20 MeV (see our table for the T -matrix pole) were extracted by use of Roy equations, which are twice subtracted dispersion relations derived from crossing symmetry and analyticity. In Ref. [10] the subtraction constants were fixed to the S -wave scattering lengths a_0^0 and a_2^0 derived from matching Roy equations and two-loop chiral perturbation theory [9]. The only additional relevant input to fix the $f_0(500)$ pole turned out to be the $\pi\pi$ -wave phase shifts at 800 MeV. The analysis was improved further in Ref. [12]. Alternatively, in Ref. [11] only data were used as input inside Roy equations. In that reference also once-subtracted Roy-like equations, called GKPY equations, were used, since the extrapolation

into the complex plane based on the twice subtracted equations leads to larger uncertainties mainly due to the limited experimental information on the isospin-2 $\pi\pi$ scattering length. Ref. [82] uses Padé approximants for the analytic continuation. All these extractions find consistent results. Using analyticity and unitarity only to describe data from $K_{2\pi}$ and K_{e4} decays, Ref. [83] finds consistent values for the pole position and the scattering length a_0^0 . The importance of the $\pi\pi$ scattering data for fixing the $f_0(500)$ pole is nicely illustrated by comparing analyses of $p\bar{p} \rightarrow 3\pi^0$ omitting [68, 84] or including [69, 85] information on $\pi\pi$ scattering: while the former analyses find an extremely broad structure above 1 GeV, the latter find $f_0(500)$ masses of the order of 400 MeV.

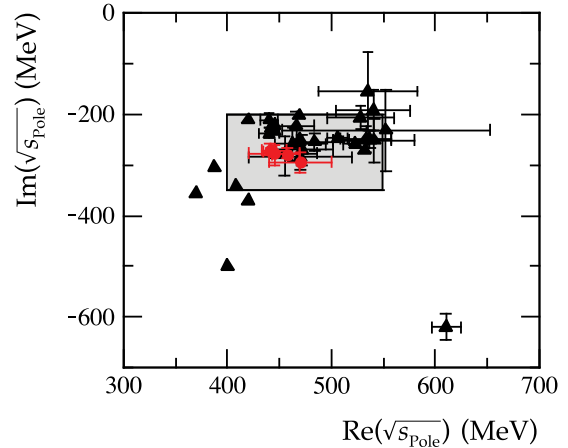


Figure 62.2: Location of the $f_0(500)$ (or σ) poles in the complex energy plane. Circles denote the recent analyses based on Roy(-like) dispersion relations, while all other analyses are denoted by triangles. The corresponding references are given in the listing.

As a result of the sensitivity of the extracted $f_0(500)$ pole position on the high accuracy low energy $\pi\pi$ scattering data [62, 63], the currently quoted range of pole positions for the $f_0(500)$, namely

$$\sqrt{s_{\text{Pole}}} = (400 - 550) - i(200 - 350) \text{ MeV}, \quad (62.3)$$

in the listing was fixed including only those analyses consistent with these data, Refs. [26] [29] [39] [41] [42] [54] [69] [78–81, 83] [75, 86–99] as well as the advanced dispersion analyses [9–12, 82]. The pole positions from those references are compared to the range of pole positions quoted above in Fig. 62.2. Note that this range is labeled as 'our estimate' — it is not an average over the quoted analyses but is chosen to include the bulk of the analyses consistent with the mentioned criteria. An averaging procedure is not justified, since the analyses use overlapping or identical data sets.

If one uses just the most advanced dispersive analyses of Refs. [9–12] shown as solid dots in Fig. 62.2 to determine the pole location of the $f_0(500)$ the range narrows down to [5]

$$\sqrt{s_{\text{Pole}}} = (449_{-16}^{+22}) - i(275 \pm 12) \text{ MeV}, \quad (62.4)$$

which is labeled as 'conservative dispersive estimate' in this reference.

Due to the large strong width of the $f_0(500)$ an extraction of its two-photon width directly from data is not possible. Thus, the values for $\Gamma(\gamma\gamma)$ quoted in the literature as well as the listing are based on the expression in the narrow width approximation [100] $\Gamma(\gamma\gamma) \simeq \alpha^2 |g_\gamma|^2 / (4\text{Re}(\sqrt{s_{\text{Pole}}}))$ where g_γ is derived from the residue at the $f_0(500)$ pole to two photons and α denotes the electromagnetic fine structure constant. The explicit form of the expression may vary between different authors due to different definitions of the coupling constant, however, the expression given for $\Gamma(\gamma\gamma)$ is free of ambiguities. According to Refs. [101, 102], the data for $f_0(500) \rightarrow \gamma\gamma$ are consistent with what is expected for a

two-step process of $\gamma\gamma \rightarrow \pi^+\pi^-$ via pion exchange in the t - and u -channel, followed by a final state interaction $\pi^+\pi^- \rightarrow \pi^0\pi^0$. The same conclusion is drawn in Ref. [103] where the bulk part of the $f_0(500) \rightarrow \gamma\gamma$ decay width is dominated by re-scattering. Therefore, it might be difficult to learn anything new about the nature of the $f_0(500)$ from its $\gamma\gamma$ coupling. For the most recent work on $\gamma\gamma \rightarrow \pi\pi$, see [83–106]. There are theoretical indications (e.g., [107–137]) that the $f_0(500)$ pole behaves differently from a $q\bar{q}$ -state – see next section and the mini-review on *non $q\bar{q}$ -states* in this RPP for details.

The $f_0(980)$ overlaps strongly with the background represented mainly by the $f_0(500)$ and the $f_0(1370)$. This can lead to a dip in the $\pi\pi$ spectrum at the $K\bar{K}$ threshold. It changes from a dip into a peak structure in the $\pi^0\pi^0$ invariant mass spectrum of the reaction $\pi^-p \rightarrow \pi^0\pi^0n$ [111], with increasing four-momentum transfer to the $\pi^0\pi^0$ system, which means increasing the a_1 -exchange contribution in the amplitude, while the π -exchange decreases. The $f_0(500)$ and the $f_0(980)$ are also observed in data for radiative decays ($\phi \rightarrow f_0\gamma$) from SND [112,113], CMD2 [114], and KLOE [115,116]. A dispersive analysis was used to simultaneously pin down the pole parameters of both the $f_0(500)$ and the $f_0(980)$ [11]; the uncertainty in the pole position quoted for the latter state is of the order of 10 MeV, only. We now quote for the mass

$$M_{f_0(980)} = 990 \pm 20 \text{ MeV} . \quad (62.5)$$

which is a range not an average, but is labeled as 'our estimate'.

Analyses of $\gamma\gamma \rightarrow \pi\pi$ data [117–119] underline the importance of the $K\bar{K}$ coupling of $f_0(980)$, while the resulting two-photon width of the $f_0(980)$ cannot be determined precisely [120]. The prominent appearance of the $f_0(980)$ in the semileptonic D_s decays and decays of B and B_s -mesons implies a dominant ($\bar{s}s$) component: those decays occur via weak transitions that alternatively result in $\phi(1020)$ production. Ratios of decay rates of B and/or B_s mesons into J/ψ plus $f_0(980)$ or $f_0(500)$ were proposed to allow for an extraction of the flavor mixing angle and to probe the tetraquark nature of those mesons within a certain model [121] [122]. The phenomenological fits of the LHCb collaboration using the isobar model do neither allow for a contribution of the $f_0(980)$ in the $B \rightarrow J/\psi\pi\pi$ [123] nor for an $f_0(500)$ in $B_s \rightarrow J/\psi\pi\pi$ decays [124]. From the former analysis the authors conclude that their data is incompatible with a model where $f_0(500)$ and $f_0(980)$ are formed from two quarks and two antiquarks (tetraquarks) at the eight standard deviation level. In addition, they extract an upper limit for the mixing angle of 17° at 90% C.L. between the $f_0(980)$ and the $f_0(500)$ that would correspond to a substantial ($\bar{s}s$) content in $f_0(980)$ [123]. However, in a dispersive analysis of the same data that allows for a model-independent inclusion of the hadronic final state interactions in Ref. [125] a substantial $f_0(980)$ contribution is also found in the B -decays putting into question the conclusions of Ref. [123].

Let us now deal with the f_0 's above 1 GeV. A meson resonance that is very well studied experimentally, is the $f_0(1500)$ seen by the Crystal Barrel experiment in five decay modes: $\pi\pi$, $K\bar{K}$, $\eta\eta$, $\eta\eta'(958)$, and 4π [15,69,70]. Due to its interference with the $f_0(1370)$ (and $f_0(1710)$), the peak attributed to the $f_0(1500)$ can appear shifted in invariant mass spectra. Therefore, the application of simple Breit-Wigner forms arrives at slightly different resonance masses for $f_0(1500)$. Analyses of central-production data of the likewise five decay modes Refs. [126,127] agree on the description of the S -wave with the one above. The $p\bar{p}$, $p\bar{n}/n\bar{p}$ measurements [70,128–130] show a single enhancement at 1400 MeV in the invariant 4π mass spectra, which is resolved into $f_0(1370)$ and $f_0(1500)$ [131] [132]. The data on 4π from central production [133] require both resonances, too, but disagree on the relative content of $\rho\rho$ and $f_0(500)f_0(500)$ in 4π . All investigations agree that the 4π decay mode represents about half of the $f_0(1500)$ decay width and is dominant for $f_0(1370)$.

The determination of the $\pi\pi$ coupling of $f_0(1370)$ is aggravated by the strong overlap with the broad $f_0(500)$ and $f_0(1500)$. Since it does not show up prominently in the 2π spectra, its mass and width are difficult to determine. Multichannel analyses of hadronically produced two- and three-body final states agree on

a mass between 1300 MeV and 1400 MeV and a narrow $f_0(1500)$, but arrive at a somewhat smaller width for $f_0(1370)$.

The existence of the $f_0(1370)$ is questioned in the analysis of the $\pi^-p \rightarrow \pi^-\pi^-\pi^+p$ data from COMPASS [138]. However, $D^0 \rightarrow \pi^+\pi^-\pi^+\pi^-$ data from CLEO-c require a contribution from $f_0(500)f_0(1370) \rightarrow 4\pi$ [139].

62.5 Interpretation of the scalars below 1 GeV

In the literature, many suggestions are discussed, such as conventional $q\bar{q}$ mesons, compact (qq)($\bar{q}\bar{q}$) structures (tetraquarks) or meson-meson bound states. In addition, one expects a scalar glueball in this mass range. In reality, there can be superpositions of these components, and one often depends on models to determine the dominant one. Although we have seen progress in recent years, this question remains open. Here, we mention some of the present conclusions.

The $f_0(980)$ and $a_0(980)$ are often interpreted as compact tetraquark states [134–137,140] or $K\bar{K}$ bound states [141]. The insight into their internal structure using two-photon widths [113] [142–148] is not conclusive. The $f_0(980)$ appears as a peak structure in $J/\psi \rightarrow \phi\pi^+\pi^-$ and in D_s decays without $f_0(500)$ background, while being nearly invisible in $J/\psi \rightarrow \omega\pi^+\pi^-$. Based on that observation it is suggested that $f_0(980)$ has a large $s\bar{s}$ component, which according to Ref. [149] is surrounded by a virtual $K\bar{K}$ cloud (see also Ref. [150]). Data on radiative decays ($\phi \rightarrow f_0\gamma$ and $\phi \rightarrow a_0\gamma$) from SND, CMD2, and KLOE (see above) are consistent with a prominent role of kaon loops. This observation is interpreted as evidence for a compact four-quark [151] or a molecular [152,153] nature of these states. Details of this controversy are given in the comments [154,155]; see also Ref. [156]. It remains quite possible that the states $f_0(980)$ and $a_0(980)$, together with the $f_0(500)$ and the $K_0^*(700)$, form a new low-mass state nonet of predominantly four-quark states, where at larger distances the quarks recombine into a pair of pseudoscalar mesons creating a meson cloud (see, e.g., Ref. [157]). Different QCD sum rule studies [158–162] do not agree on a tetraquark configuration for the same particle group.

Models that start directly from chiral Lagrangians, either in non-linear [25,42,80,152] or in linear [163–169] realization, predict the existence of the $f_0(500)$ meson near 500 MeV. Here the $f_0(500)$, $a_0(980)$, $f_0(980)$, and $K_0^*(700)$ (in some models the $K_0^*(1430)$) would form a nonet (not necessarily $q\bar{q}$). In the linear sigma models the lightest pseudoscalars appear as their chiral partners. In these models the light $f_0(500)$ is often referred to as the "Higgs boson of strong interactions", since here the $f_0(500)$ plays a role similar to the Higgs particle in electro-weak symmetry breaking: within the linear sigma models it is important for the mechanism of chiral symmetry breaking, which generates most of the proton mass, and what is referred to as the constituent quark mass.

In the non-linear approaches of Refs. [25] and [80] the above resonances together with the low lying vector states are generated starting from chiral perturbation theory predictions near the first open channel, and then by extending the predictions to the resonance regions using unitarity and analyticity.

Ref. [163] uses a framework with explicit resonances that are unitarized and coupled to the light pseudoscalars in a chirally invariant way. Evidence for a non- $\bar{q}q$ nature of the lightest scalar resonances is derived from their mixing scheme. In Ref. [164] the scheme is extended and applied to the decay $\eta' \rightarrow \eta\pi\pi$, which lead to the same conclusions. To identify the nature of the resonances generated from scattering equations, in Ref. [170] the large N_c behavior of the poles was studied, with the conclusion that, while the light vector states behave consistent with what is predicted for $\bar{q}q$ states, the light scalars behave very differently. This finding provides strong support for a non- $\bar{q}q$ nature of the light scalar resonances. Note, the more refined study of Ref. [107] found, in case of the $f_0(500)$, in addition to a dominant non- $\bar{q}q$ nature, indications for a subdominant $\bar{q}q$ component located around 1 GeV. Additional support for the non- $\bar{q}q$ nature of the $f_0(500)$ is given in Ref. [171], where the connection between the pole of resonances and their Regge trajectories is analyzed.

A model-independent method to identify hadronic molecules goes back to a proposal by Weinberg [172], shown to be equiva-

lent to the pole counting arguments of [173–182] in Ref. [176]. The formalism allows one to extract the amount of molecular component in the wave function from the effective coupling constant of a physical state to a nearby continuum channel. It can be applied to near threshold states only and provided strong evidence that the $f_0(980)$ is a $\bar{K}K$ molecule, while the situation turned out to be less clear for the $a_0(980)$ (see also Refs. [146, 148]) Further insights into $a_0(980)$ and $f_0(980)$ are expected from their mixing [177]. The corresponding signal predicted in Refs. [178, 179] was recently observed at BES III [180]. It turned out that in order to get a quantitative understanding of those data in addition to the mixing mechanism itself, some detailed understanding of the production mechanism seems necessary [181].

In the unitarized quark model with coupled $q\bar{q}$ and meson-meson channels, the light scalars can be understood as additional manifestations of bare $q\bar{q}$ confinement states, strongly mass shifted from the 1.3 - 1.5 GeV region and very distorted due to the strong 3P_0 coupling to S -wave two-meson decay channels [182, 183]. Thus, in these models the light scalar nonet comprising the $f_0(500)$, $f_0(980)$, $K_0^*(700)$, and $a_0(980)$, as well as the nonet consisting of the $f_0(1370)$, $f_0(1500)$ (or $f_0(1710)$), $K_0^*(1430)$, and $a_0(1450)$, respectively, are two manifestations of the same bare input states (see also Ref. [184]).

Other models with different groupings of the observed resonances exist and may, *e.g.*, be found in earlier versions of this review.

62.6 Interpretation of the f_0 's above 1 GeV

The $f_0(1370)$ and $f_0(1500)$ decay mostly into pions (2π and 4π) while the $f_0(1710)$ decays mainly into the $K\bar{K}$ final states. The $K\bar{K}$ decay branching ratio of the $f_0(1500)$ is small [126] [185].

If one uses the naive quark model, it is natural to assume that the $f_0(1370)$, $a_0(1450)$, and the $K_0^*(1430)$ are in the same SU(3) flavor nonet, being the $(u\bar{u} + d\bar{d})$, $u\bar{d}$ and $u\bar{s}$ states, probably mixing with the light scalars [186], while the $f_0(1710)$ is the $s\bar{s}$ state. Indeed, the production of $f_0(1710)$ (and $f_2'(1525)$) is observed in $p\bar{p}$ annihilation [187] but the rate is suppressed compared to $f_0(1500)$ (respectively, $f_2(1270)$), as would be expected from the OZI rule for $s\bar{s}$ states. The $f_0(1500)$ would also qualify as a $(u\bar{u} + d\bar{d})$ state, although it is very narrow compared to the other states and too light to be the first radial excitation.

However, in $\gamma\gamma$ collisions leading to $K_S^0 K_S^0$ [188] a spin-0 signal is observed at the $f_0(1710)$ mass (together with a dominant spin-2 component), while the $f_0(1500)$ is not observed in $\gamma\gamma \rightarrow K\bar{K}$ nor $\pi^+\pi^-$ [189]. In $\gamma\gamma$ collisions leading to $\pi^0\pi^0$ Ref. [190] reports the observation of a scalar around 1470 MeV albeit with large uncertainties on the mass and $\gamma\gamma$ couplings. This state could be the $f_0(1370)$ or the $f_0(1500)$. The upper limit from $\pi^+\pi^-$ [189] excludes a large $n\bar{n}$ (here n stands for the two lightest quarks) content for the $f_0(1500)$ and hence points to a mainly $s\bar{s}$ state [191]. This appears to contradict the small $K\bar{K}$ decay branching ratio of the $f_0(1500)$ and makes a $q\bar{q}$ assignment difficult for this state. Hence the $f_0(1500)$ could be mainly glue due the absence of a 2γ -coupling, while the $f_0(1710)$ coupling to 2γ would be compatible with an $s\bar{s}$ state. This is in accord with the recent high-statistics Belle data in $\gamma\gamma \rightarrow K_S^0 K_S^0$ [192] in which the $f_0(1500)$ is absent, while a prominent peak at 1710 MeV is observed with quantum numbers 0^{++} , compatible with the formation of an $s\bar{s}$ state. However, the 2γ -couplings are sensitive to glue mixing with $q\bar{q}$ [193].

Note that an isovector scalar, possibly the $a_0(1450)$ (albeit at a lower mass of 1317 MeV) is observed in $\gamma\gamma$ collisions leading to $\eta\pi^0$ [194]. The state interferes destructively with the non-resonant background, but its $\gamma\gamma$ coupling is comparable to that of the $a_2(1320)$, in accord with simple predictions (see, *e.g.*, Ref. [191]).

The small width of $f_0(1500)$, and its enhanced production at low transverse momentum transfer in central collisions [195–197] also favor $f_0(1500)$ to be non- $q\bar{q}$. In the mixing scheme of Ref. [193], which uses central production data from WA102 and the recent hadronic J/ψ decay data from BES [198, 199], glue is shared between $f_0(1370)$, $f_0(1500)$ and $f_0(1710)$. The $f_0(1370)$ is mainly $n\bar{n}$, the $f_0(1500)$ mainly glue and the $f_0(1710)$ dominantly $s\bar{s}$. This agrees with previous analyses [200, 201].

However, alternative schemes have been proposed (*e.g.*, in [202–208], for detailed reviews see, *e.g.*, Ref. [1] and the mini-review on *non- $q\bar{q}$ states* in this Review of Particle Physics (RPP)). In Ref. [208], a large K^+K^- scalar signal reported by Belle in B decays into $KK\bar{K}$ [209], compatible with the $f_0(1500)$, is explained as due to constructive interference with a broad glueball background. However, the Belle data are inconsistent with the BaBar measurements which show instead a broad scalar at this mass for B decays into both $K^\pm K^\pm K^\mp$ [210] and $K^+K^-\pi^0$ [211].

The $f_0(1500)$ has also been proposed as a tetraquarks state [212]. Whether the $f_0(1500)$ is observed in 'gluon rich' radiative J/ψ decays is debatable [213] because of the limited amount of data - more data for this and the $\gamma\gamma$ mode are needed. In Ref. [214], further refined in Ref. [215], $f_0(1370)$ and $f_0(1710)$ (together with $f_2(1270)$ and $f_2'(1525)$) were interpreted as bound systems of two vector mesons. This picture could be tested in radiative J/ψ decays [216] as well as radiative decays of the states themselves [217]. The vector-vector component of the $f_0(1710)$ might also be the origin of the enhancement seen in $J/\psi \rightarrow \gamma\phi\omega$ near threshold [218] observed at BES [219]. Note that the results of Refs. [214] [215] were challenged in Ref. [220] where in a covariant formalism, *e.g.*, the $f_2(1270)$ did not emerge as a $\rho\rho$ -bound state.

References

- [1] C. Amsler and N. A. Tornqvist, Phys. Rept. **389**, 61 (2004).
- [2] D. V. Bugg, Phys. Rept. **397**, 257 (2004), [hep-ex/0412045].
- [3] F. E. Close and N. A. Tornqvist, J. Phys. **G28**, R249 (2002), [hep-ph/0204205].
- [4] E. Klempt and A. Zaitsev, Phys. Rept. **454**, 1 (2007), [arXiv:0708.4016].
- [5] J. R. Pelaez, Phys. Rept. **658**, 1 (2016), [arXiv:1510.00653].
- [6] S. L. Adler, Phys. Rev. **137**, B1022 (1965), [140(1964)].
- [7] S. L. Adler, Phys. Rev. **139**, B1638 (1965), [152(1965)].
- [8] J. A. Oller, Phys. Rev. **D71**, 054030 (2005), [hep-ph/0411105].
- [9] G. Colangelo, J. Gasser and H. Leutwyler, Nucl. Phys. **B603**, 125 (2001), [hep-ph/0103088].
- [10] I. Caprini, G. Colangelo, and H. Leutwyler, Phys. Rev. Lett. **96**, 132001 (2006).
- [11] R. Garcia-Martin *et al.*, Phys. Rev. Lett. **107**, 072001 (2011), [arXiv:1107.1635].
- [12] B. Moussallam, Eur. Phys. J. **C71**, 1814 (2011), [arXiv:1110.6074].
- [13] D. Aston *et al.*, Nucl. Phys. **B296**, 493 (1988).
- [14] P. Estabrooks *et al.*, Nucl. Phys. **B133**, 490 (1978).
- [15] A. Abele *et al.*, Phys. Rev. **D57**, 3860 (1998).
- [16] V. Bernard, N. Kaiser and U. G. Meissner, Phys. Rev. **D43**, 2757 (1991).
- [17] S. N. Cherry and M. R. Pennington, Nucl. Phys. **A688**, 823 (2001), [hep-ph/0005208].
- [18] J. M. Link *et al.* (FOCUS), Phys. Lett. **B648**, 156 (2007), [hep-ex/0612032].
- [19] M. Ablikim *et al.* (BES), Phys. Lett. **B633**, 681 (2006), [hep-ex/0506055].
- [20] F.-K. Guo *et al.*, Nucl. Phys. **A773**, 78 (2006), [hep-ph/0509050].
- [21] D. Epifanov *et al.* (Belle), Phys. Lett. **B654**, 65 (2007), [arXiv:0706.2231].
- [22] C. Cawlfild *et al.* (CLEO), Phys. Rev. **D74**, 031108 (2006), [hep-ex/0606045].
- [23] A. V. Anisovich and A. V. Sarantsev, Phys. Lett. **B413**, 137 (1997), [hep-ph/9705401].
- [24] R. Delbourgo and M. D. Scadron, Int. J. Mod. Phys. **A13**, 657 (1998), [hep-ph/9807504].

- [25] J. A. Oller, E. Oset and J. R. Pelaez, Phys. Rev. **D59**, 074001 (1999), [Erratum: Phys. Rev.D75,099903(2007)], [hep-ph/9804209].
- [26] J. A. Oller and E. Oset, Phys. Rev. **D60**, 074023 (1999), [hep-ph/9809337].
- [27] C. M. Shakin and H. Wang, Phys. Rev. **D63**, 014019 (2001).
- [28] M. D. Scadron *et al.*, Nucl. Phys. **A724**, 391 (2003), [hep-ph/0211275].
- [29] D. V. Bugg, Phys. Lett. **B572**, 1 (2003), [Erratum: Phys. Lett.B595,556(2004)].
- [30] M. Ishida, Prog. Theor. Phys. Suppl. **149**, 190 (2003), [hep-ph/0212383].
- [31] H. Q. Zheng *et al.*, Nucl. Phys. **A733**, 235 (2004), [hep-ph/0310293].
- [32] Z. Y. Zhou and H. Q. Zheng, Nucl. Phys. **A775**, 212 (2006), [hep-ph/0603062].
- [33] J. M. Link *et al.* (FOCUS), Phys. Lett. **B653**, 1 (2007), [arXiv:0705.2248].
- [34] B. Aubert *et al.* (BaBar), Phys. Rev. **D76**, 011102 (2007), [arXiv:0704.3593].
- [35] S. Kopp *et al.* (CLEO), Phys. Rev. **D63**, 092001 (2001), [hep-ex/0011065].
- [36] J. M. Link *et al.* (FOCUS), Phys. Lett. **B535**, 43 (2002), [hep-ex/0203031].
- [37] J. M. Link *et al.* (FOCUS), Phys. Lett. **B621**, 72 (2005), [hep-ex/0503043].
- [38] M. Jamin, J. A. Oller and A. Pich, Nucl. Phys. **B587**, 331 (2000), [hep-ph/0006045].
- [39] D. Black *et al.*, Phys. Rev. **D64**, 014031 (2001), [hep-ph/0012278].
- [40] J. A. Oller, Nucl. Phys. **A727**, 353 (2003), [hep-ph/0306031].
- [41] E. van Beveren *et al.*, Z. Phys. **C30**, 615 (1986), [arXiv:0710.4067].
- [42] J. R. Pelaez, Mod. Phys. Lett. **A19**, 2879 (2004), [hep-ph/0411107].
- [43] S. Descotes-Genon and B. Moussallam, Eur. Phys. J. **C48**, 553 (2006), [hep-ph/0607133].
- [44] J. R. Peláez, A. Rodas and J. Ruiz de Elvira, Eur. Phys. J. **C77**, 2, 91 (2017), [arXiv:1612.07966].
- [45] M. Bargiotti *et al.* (OBELIX), Eur. Phys. J. **C26**, 371 (2003).
- [46] D. Barberis *et al.* (WA102), Phys. Lett. **B440**, 225 (1998), [hep-ex/9810003].
- [47] M. J. Corden *et al.*, Nucl. Phys. **B144**, 253 (1978).
- [48] C. Defoix *et al.*, Nucl. Phys. **B44**, 125 (1972).
- [49] Z. Bai *et al.* (MARK-III), Phys. Rev. Lett. **65**, 2507 (1990).
- [50] T. Bolton *et al.*, Phys. Rev. Lett. **69**, 1328 (1992).
- [51] C. Amsler *et al.* (Crystal Barrel), Phys. Lett. **B353**, 571 (1995).
- [52] S. M. Flatte, Phys. Lett. **63B**, 224 (1976).
- [53] C. Amsler *et al.* (Crystal Barrel), Phys. Lett. **B333**, 277 (1994).
- [54] G. Janssen *et al.*, Phys. Rev. **D52**, 2690 (1995), [arXiv:nucl-th/9411021].
- [55] D. V. Bugg, Phys. Rev. **D78**, 074023 (2008), [arXiv:0808.2706].
- [56] P. Rubin *et al.* (CLEO), Phys. Rev. **D78**, 072003 (2008), [arXiv:0807.4545].
- [57] R. Aaij *et al.* (LHCb), Phys. Rev. **D93**, 5, 052018 (2016), [arXiv:1509.06628].
- [58] S. D. Protopopescu *et al.*, Phys. Rev. **D7**, 1279 (1973).
- [59] G. Grayer *et al.*, Nucl. Phys. **B75**, 189 (1974).
- [60] H. Becker *et al.* (CERN-Cracow-Munich), Nucl. Phys. **B151**, 46 (1979).
- [61] L. Rosselet *et al.*, Phys. Rev. **D15**, 574 (1977).
- [62] S. Pislak *et al.* (BNL-E865), Phys. Rev. Lett. **87**, 221801 (2001), [Erratum: Phys. Rev. Lett.105,019901(2010)], [hep-ex/0106071].
- [63] J. R. Batley *et al.* (NA48-2), Eur. Phys. J. **C70**, 635 (2010).
- [64] W. Wetzel *et al.*, Nucl. Phys. **B115**, 208 (1976).
- [65] V. A. Polychronakos *et al.*, Phys. Rev. **D19**, 1317 (1979).
- [66] D. H. Cohen *et al.*, Phys. Rev. **D22**, 2595 (1980).
- [67] A. Etkin *et al.*, Phys. Rev. **D25**, 1786 (1982).
- [68] C. Amsler *et al.*, Phys. Lett. **B342**, 433 (1995).
- [69] C. Amsler *et al.* (Crystal Barrel), Phys. Lett. **B355**, 425 (1995).
- [70] A. Abele *et al.* (Crystal Barrel), Phys. Lett. **B380**, 453 (1996).
- [71] D.M. Alde *et al.*, Phys. Lett. **B397**, 250 (1997).
- [72] R. Kaminski, L. Lesniak and K. Rybicki, Z. Phys. **C74**, 79 (1997), [hep-ph/9606362].
- [73] E. M. Aitala *et al.* (E791), Phys. Rev. Lett. **86**, 770 (2001), [hep-ex/0007028].
- [74] J. M. Link *et al.* (FOCUS), Phys. Lett. **B585**, 200 (2004), [hep-ex/0312040].
- [75] G. Bonvicini *et al.* (CLEO), Phys. Rev. **D76**, 012001 (2007), [arXiv:0704.3954].
- [76] J. E. Augustin *et al.* (DM2), Nucl. Phys. **B320**, 1 (1989).
- [77] M. Ablikim *et al.* (BES), Phys. Lett. **B598**, 149 (2004), [hep-ex/0406038].
- [78] A. Gallegos, J. L. Lucio M. and J. Pestieau, Phys. Rev. **D69**, 074033 (2004), [hep-ph/0311133].
- [79] M. Ablikim *et al.* (BES), Phys. Lett. **B645**, 19 (2007), [hep-ex/0610023].
- [80] A. Dobado and J. R. Pelaez, Phys. Rev. **D56**, 3057 (1997), [hep-ph/9604416].
- [81] I. Caprini, Phys. Rev. **D77**, 114019 (2008), [arXiv:0804.3504].
- [82] P. Masjuan, J. Ruiz de Elvira, J.J. Sanz-Cillero, Phys. Rev. **D90**, 097901 (2014).
- [83] F. J. Yndurain, R. Garcia-Martin and J. R. Pelaez, Phys. Rev. **D76**, 074034 (2007), [hep-ph/0701025].
- [84] V.V. Anisovich *et al.*, Sov. Phys. Usp. **41**, 419 (1998).
- [85] V. V. Anisovich, Int. J. Mod. Phys. **A21**, 3615 (2006), [hep-ph/0510409].
- [86] B. S. Zou and D. V. Bugg, Phys. Rev. **D48**, R3948 (1993).
- [87] N. A. Tornqvist and M. Roos, Phys. Rev. Lett. **76**, 1575 (1996), [hep-ph/9511210].
- [88] R. Kaminski, L. Lesniak and J. P. Maillet, Phys. Rev. **D50**, 3145 (1994), [hep-ph/9403264].
- [89] N. N. Achasov and G. N. Shestakov, Phys. Rev. **D49**, 5779 (1994).
- [90] M. P. Locher, V. E. Markushin and H. Q. Zheng, Eur. Phys. J. **C4**, 317 (1998), [hep-ph/9705230].
- [91] J. A. Oller and E. Oset, Nucl. Phys. **A620**, 438 (1997), [Erratum: Nucl. Phys.A652,407(1999)], [hep-ph/9702314].
- [92] T. Hannah, Phys. Rev. **D60**, 017502 (1999), [hep-ph/9905236].
- [93] R. Kaminski, L. Lesniak and B. Loiseau, Phys. Lett. **B413**, 130 (1997), [hep-ph/9707377].
- [94] R. Kaminski, L. Lesniak and B. Loiseau, Eur. Phys. J. **C9**, 141 (1999), [hep-ph/9810386].
- [95] M. Ishida *et al.*, Prog. Theor. Phys. **104**, 203 (2000), [hep-ph/0005251].
- [96] Y.S. Surovtsev *et al.*, Phys. Rev. **D61**, 054024 (2001).

- [97] M. Ishida *et al.*, Phys. Lett. **B518**, 47 (2001).
- [98] Z. Y. Zhou *et al.*, JHEP **02**, 043 (2005), [hep-ph/0406271].
- [99] D. V. Bugg, J. Phys. **G34**, 151 (2007), [hep-ph/0608081].
- [100] D. Morgan and M. R. Pennington, Z. Phys. **C48**, 623 (1990).
- [101] M. R. Pennington, Phys. Rev. Lett. **97**, 011601 (2006).
- [102] M. R. Pennington, Mod. Phys. Lett. **A22**, 1439 (2007), [arXiv:0705.3314].
- [103] G. Mennessier, S. Narison and W. Ochs, Phys. Lett. **B665**, 205 (2008), [arXiv:0804.4452].
- [104] R. Garcia-Martin and B. Moussallam, Eur. Phys. J. **C70**, 155 (2010), [arXiv:1006.5373].
- [105] M. Hoferichter, D. R. Phillips and C. Schat, Eur. Phys. J. **C71**, 1743 (2011), [arXiv:1106.4147].
- [106] L.-Y. Dai and M. R. Pennington, Phys. Rev. **D90**, 3, 036004 (2014), [arXiv:1404.7524].
- [107] J. R. Pelaez and G. Rios, Phys. Rev. Lett. **97**, 242002 (2006), [hep-ph/0610397].
- [108] H.-X. Chen, A. Hosaka and S.-L. Zhu, Phys. Lett. **B650**, 369 (2007), [hep-ph/0609163].
- [109] F. Giacosa, Phys. Rev. **D75**, 054007 (2007), [hep-ph/0611388].
- [110] L. Maiani *et al.*, Eur. Phys. J. **C50**, 609 (2007), [hep-ph/0604018].
- [111] N. N. Achasov and G. N. Shestakov, Phys. Rev. **D58**, 054011 (1998), [hep-ph/9802286].
- [112] M. N. Achasov *et al.*, Phys. Lett. **B479**, 53 (2000), [hep-ex/0003031].
- [113] M. N. Achasov *et al.*, Phys. Lett. **B485**, 349 (2000), [hep-ex/0005017].
- [114] R. R. Akhmetshin *et al.* (CMD-2), Phys. Lett. **B462**, 371 (1999), [hep-ex/9907005].
- [115] A. Aloisio *et al.* (KLOE), Phys. Lett. **B536**, 209 (2002), [hep-ex/0204012].
- [116] F. Ambrosino *et al.* (KLOE), Eur. Phys. J. **C49**, 473 (2007), [hep-ex/0609009].
- [117] M. Boglione and M. R. Pennington, Eur. Phys. J. **C9**, 11 (1999), [hep-ph/9812258].
- [118] T. Mori *et al.* (Belle), Phys. Rev. **D75**, 051101 (2007), [hep-ex/0610038].
- [119] N. N. Achasov and G. N. Shestakov, Phys. Rev. **D77**, 074020 (2008), [arXiv:0712.0885].
- [120] M. R. Pennington *et al.*, Eur. Phys. J. **C56**, 1 (2008), [arXiv:0803.3389].
- [121] R. Fleischer, R. Knegjens and G. Ricciardi, Eur. Phys. J. **C71**, 1832 (2011), [arXiv:1109.1112].
- [122] S. Stone and L. Zhang, Phys. Rev. Lett. **111**, 6, 062001 (2013), [arXiv:1305.6554].
- [123] R. Aaij *et al.* (LHCb), Phys. Rev. **D90**, 1, 012003 (2014), [arXiv:1404.5673].
- [124] R. Aaij *et al.* (LHCb), Phys. Rev. **D89**, 9, 092006 (2014), [arXiv:1402.6248].
- [125] J. T. Daub, C. Hanhart and B. Kubis, JHEP **02**, 009 (2016), [arXiv:1508.06841].
- [126] D. Barberis *et al.* (WA102), Phys. Lett. **B462**, 462 (1999), [hep-ex/9907055].
- [127] D. Barberis *et al.* (WA102), Phys. Lett. **B479**, 59 (2000), [hep-ex/0003033].
- [128] M. Gaspero, Nucl. Phys. **A562**, 407 (1993).
- [129] A. Adamo *et al.*, Nucl. Phys. **A558**, 13C (1993).
- [130] C. Amsler *et al.* (Crystal Barrel), Phys. Lett. **B322**, 431 (1994).
- [131] A. Abele *et al.* (Crystal Barrel), Eur. Phys. J. **C19**, 667 (2001).
- [132] A. Abele *et al.* (CRYSTAL BARREL), Eur. Phys. J. **C21**, 261 (2001).
- [133] D. Barberis *et al.* (WA102), Phys. Lett. **B471**, 440 (2000), [hep-ex/9912005].
- [134] R. L. Jaffe, Phys. Rev. **D15**, 267 (1977).
- [135] M. G. Alford and R. L. Jaffe, Nucl. Phys. **B578**, 367 (2000), [hep-lat/0001023].
- [136] L. Maiani *et al.*, Phys. Rev. Lett. **93**, 212002 (2004), [hep-ph/0407017].
- [137] L. Maiani, A. D. Polosa and V. Riquer, Phys. Lett. **B651**, 129 (2007), [hep-ph/0703272].
- [138] C. Adolph *et al.* (COMPASS), Phys. Rev. **D95**, 3, 032004 (2017), [arXiv:1509.00992].
- [139] P. d'Argent *et al.*, JHEP **05**, 143 (2017), [arXiv:1703.08505].
- [140] G. 't Hooft *et al.*, Phys. Lett. **B662**, 424 (2008), [arXiv:0801.2288].
- [141] J. D. Weinstein and N. Isgur, Phys. Rev. **D41**, 2236 (1990).
- [142] T. Barnes, Phys. Lett. **165B**, 434 (1985).
- [143] Z. P. Li, F. E. Close and T. Barnes, Phys. Rev. **D43**, 2161 (1991).
- [144] R. Delbourgo, D.-s. Liu and M. D. Scadron, Phys. Lett. **B446**, 332 (1999), [hep-ph/9811474].
- [145] J. L. Lucio Martinez and M. Napsuciale, Phys. Lett. **B454**, 365 (1999), [hep-ph/9903234].
- [146] C. Hanhart *et al.*, Phys. Rev. **D75**, 074015 (2007), [hep-ph/0701214].
- [147] R. H. Lemmer, Phys. Lett. **B650**, 152 (2007), [hep-ph/0701027].
- [148] T. Branz, T. Gutsche and V. E. Lyubovitskij, Eur. Phys. J. **A37**, 303 (2008), [arXiv:0712.0354].
- [149] A. Deandrea *et al.*, Phys. Lett. **B502**, 79 (2001), [hep-ph/0012120].
- [150] K. M. Ecklund *et al.* (CLEO), Phys. Rev. **D80**, 052009 (2009), [arXiv:0907.3201].
- [151] N. N. Achasov and V. N. Ivanchenko, Nucl. Phys. **B315**, 465 (1989).
- [152] J. A. Oller, Nucl. Phys. **A714**, 161 (2003), [hep-ph/0205121].
- [153] Yu. S. Kalashnikova *et al.*, Eur. Phys. J. **A24**, 437 (2005), [hep-ph/0412340].
- [154] Yu. S. Kalashnikova *et al.*, Phys. Rev. **D78**, 058501 (2008), [arXiv:0711.2902].
- [155] N. N. Achasov and A. V. Kiselev, Phys. Rev. **D78**, 058502 (2008), [arXiv:0806.2993].
- [156] M. Boglione and M. R. Pennington, Eur. Phys. J. **C30**, 503 (2003), [hep-ph/0303200].
- [157] F. Giacosa and G. Pagliara, Phys. Rev. **C76**, 065204 (2007), [arXiv:0707.3594].
- [158] S. Narison, Nucl. Phys. **B96**, 244 (2001).
- [159] H.-J. Lee, Eur. Phys. J. **A30**, 423 (2006), [hep-ph/0512212].
- [160] H.-X. Chen, A. Hosaka and S.-L. Zhu, Phys. Rev. **D76**, 094025 (2007), [arXiv:0707.4586].
- [161] J. Sugiyama *et al.*, Phys. Rev. **D76**, 114010 (2007), [arXiv:0707.2533].
- [162] T. Kojo and D. Jido, Phys. Rev. **D78**, 114005 (2008), [arXiv:0802.2372].
- [163] D. Black *et al.*, Phys. Rev. **D59**, 074026 (1999), [hep-ph/9808415].
- [164] A. H. Fariborz *et al.*, Phys. Rev. **D90**, 3, 033009 (2014), [arXiv:1407.3870].

- [165] M. D. Scadron, *Eur. Phys. J.* **C6**, 141 (1999), [hep-ph/9710317].
- [166] M. Ishida, *Prog. Theor. Phys.* **101**, 661 (1999), [hep-ph/9902260].
- [167] N. A. Tornqvist, *Eur. Phys. J.* **C11**, 359 (1999), [hep-ph/9905282].
- [168] M. Napsuciale and S. Rodriguez, *Phys. Lett.* **B603**, 195 (2004), [hep-ph/0403072].
- [169] M. Napsuciale and S. Rodriguez, *Phys. Rev.* **D70**, 094043 (2004), [hep-ph/0407037].
- [170] J. R. Pelaez, *Phys. Rev. Lett.* **92**, 102001 (2004), [hep-ph/0309292].
- [171] J. T. Londergan *et al.*, *Phys. Lett.* **B729**, 9 (2014), [arXiv:1311.7552].
- [172] S. Weinberg, *Phys. Rev.* **130**, 776 (1963).
- [173] D. Morgan and M. R. Pennington, *Phys. Lett.* **B258**, 444 (1991), [Erratum: *Phys. Lett.* **B269**, 477 (1991)].
- [174] D. Morgan, *Nucl. Phys.* **A543**, 632 (1992).
- [175] N. A. Tornqvist, *Phys. Rev.* **D51**, 5312 (1995), [hep-ph/9403234].
- [176] V. Baru *et al.*, *Phys. Lett.* **B586**, 53 (2004), [hep-ph/0308129].
- [177] N. N. Achasov, S. A. Devyanin and G. N. Shestakov, *Phys. Lett.* **88B**, 367 (1979).
- [178] J.-J. Wu, Q. Zhao and B. S. Zou, *Phys. Rev.* **D75**, 114012 (2007), [arXiv:0704.3652].
- [179] C. Hanhart, B. Kubis and J. R. Pelaez, *Phys. Rev.* **D76**, 074028 (2007), [arXiv:0707.0262].
- [180] M. Ablikim *et al.* (BESIII), *Phys. Rev.* **D83**, 032003 (2011), [arXiv:1012.5131].
- [181] L. Roca, *Phys. Rev.* **D88**, 014045 (2013), [arXiv:1210.4742].
- [182] N. A. Tornqvist, *Z. Phys.* **C68**, 647 (1995), [hep-ph/9504372].
- [183] E. van Beveren and G. Rupp, *Eur. Phys. J.* **C22**, 493 (2001), [hep-ex/0106077].
- [184] M. Boglione and M. R. Pennington, *Phys. Rev.* **D65**, 114010 (2002), [hep-ph/0203149].
- [185] A. Abele *et al.* (Crystal Barrel), *Phys. Lett.* **B385**, 425 (1996).
- [186] D. Black, A. H. Fariborz and J. Schechter, *Phys. Rev.* **D61**, 074001 (2000), [hep-ph/9907516].
- [187] C. Amsler *et al.* (Crystal Barrel), *Phys. Lett.* **B639**, 165 (2006).
- [188] M. Acciarri *et al.* (L3), *Phys. Lett.* **B501**, 173 (2001), [hep-ex/0011037].
- [189] R. Barate *et al.* (ALEPH), *Phys. Lett.* **B472**, 189 (2000), [hep-ex/9911022].
- [190] S. Uehara *et al.* (Belle), *Phys. Rev.* **D78**, 052004 (2008), [arXiv:0805.3387].
- [191] C. Amsler, *Phys. Lett.* **B541**, 22 (2002), [hep-ph/0206104].
- [192] S. Uehara, *et al.*, *Prog. Theor. Exp. Phys.* **2013**, 123C01 (2013).
- [193] F. E. Close and Q. Zhao, *Phys. Rev.* **D71**, 094022 (2005), [hep-ph/0504043].
- [194] S. Uehara *et al.* (Belle), *Phys. Rev.* **D80**, 032001 (2009), [arXiv:0906.1464].
- [195] F. E. Close and A. Kirk, *Phys. Lett.* **B397**, 333 (1997), [hep-ph/9701222].
- [196] F. E. Close, *Phys. Lett.* **B419**, 387 (1998), [hep-ph/9710450].
- [197] A. Kirk, *Phys. Lett.* **B489**, 29 (2000), [hep-ph/0008053].
- [198] M. Ablikim *et al.* (BES), *Phys. Lett.* **B603**, 138 (2004), [hep-ex/0409007].
- [199] M. Ablikim *et al.* (BES), *Phys. Lett.* **B607**, 243 (2005), [hep-ex/0411001].
- [200] C. Amsler and F. E. Close, *Phys. Rev.* **D53**, 295 (1996), [hep-ph/9507326].
- [201] F. E. Close and A. Kirk, *Eur. Phys. J.* **C21**, 531 (2001), [hep-ph/0103173].
- [202] P. Minkowski and W. Ochs, *Eur. Phys. J.* **C9**, 283 (1999), [hep-ph/9811518].
- [203] W.-J. Lee and D. Weingarten, *Phys. Rev.* **D61**, 014015 (2000), [hep-lat/9910008].
- [204] M. Chanowitz, *Phys. Rev. Lett.* **95**, 172001 (2005), [hep-ph/0506125].
- [205] F. Brünner and A. Rebhan, *Phys. Rev. Lett.* **115**, 13, 131601 (2015), [arXiv:1504.05815].
- [206] S. Janowski, F. Giacosa and D. H. Rischke, *Phys. Rev.* **D90**, 11, 114005 (2014), [arXiv:1408.4921].
- [207] M. Albaladejo and J. A. Oller, *Phys. Rev. Lett.* **101**, 252002 (2008), [arXiv:0801.4929].
- [208] P. Minkowski and W. Ochs, *Eur. Phys. J.* **C39**, 71 (2005), [hep-ph/0404194].
- [209] A. Garmash *et al.* (Belle), *Phys. Rev.* **D71**, 092003 (2005), [hep-ex/0412066].
- [210] B. Aubert *et al.* (BaBar), *Phys. Rev.* **D74**, 032003 (2006), [hep-ex/0605003].
- [211] B. Aubert *et al.* (BaBar), *Phys. Rev. Lett.* **99**, 161802 (2007), [arXiv:0706.3885].
- [212] L. Zou *et al.*, *Phys. Rev.* **D99**, 114024 (2019).
- [213] M. Ablikim *et al.*, *Phys. Lett.* **B642**, 441 (2006), [hep-ex/0603048].
- [214] R. Molina, D. Nicmorus and E. Oset, *Phys. Rev.* **D78**, 114018 (2008), [arXiv:0809.2233].
- [215] C. García-Recio *et al.*, *Phys. Rev.* **D87**, 9, 096006 (2013), [arXiv:1304.1021].
- [216] L. S. Geng *et al.*, *Eur. Phys. J.* **A44**, 305 (2010), [arXiv:0910.5192].
- [217] T. Branz, L. S. Geng and E. Oset, *Phys. Rev.* **D81**, 054037 (2010), [arXiv:0911.0206].
- [218] A. Martínez Torres *et al.*, *Phys. Lett.* **B719**, 388 (2013), [arXiv:1210.6392].
- [219] M. Ablikim *et al.* (BES), *Phys. Rev. Lett.* **96**, 162002 (2006), [hep-ex/0602031].
- [220] D. Gülmez, U. G. Meißner and J. A. Oller, *Eur. Phys. J.* **C77**, 7, 460 (2017), [arXiv:1611.00168].

63. Pseudoscalar and Pseudovector Mesons in the 1400 MeV Region

Revised August 2019 by C. Amsler (Stefan Meyer Inst.) and A. Masoni (INFN, Cagliari).

This minireview deals with some of the 0^{-+} and 1^{++} mesons reported in the 1200–1500 MeV region, namely the $\eta(1295)$, $\eta(1405)$, $\eta(1475)$, $f_1(1285)$, $f_1(1420)$, $a_1(1420)$ and $f_1(1510)$. The first observation of a pseudoscalar resonance around 1400 MeV – the $\eta(1440)$ – was made in $p\bar{p}$ annihilation at rest into $\eta(1440)\pi^+\pi^-$, $\eta(1440) \rightarrow K\bar{K}\pi$ [1]. This state was reported to decay into $a_0(980)\pi$ and $K^*(892)\bar{K}$ with roughly equal contributions. The $\eta(1440)$ was also observed in radiative $J/\psi(1S)$ decay into $K\bar{K}\pi$ [2–4] and $\gamma\rho$ [5] and was in the eighties considered as a glueball candidate

However, two pseudoscalars are now observed in this mass region, the $\eta(1405)$ and $\eta(1475)$. The former decays mainly through $a_0(980)\pi$ (or direct $K\bar{K}\pi$) and the latter mainly to $K^*(892)\bar{K}$. The simultaneous observation of two pseudoscalars is reported in three production mechanisms: π^-p [6, 7]; radiative $J/\psi(1S)$ decay [8, 9]; and $p\bar{p}$ annihilation at rest [10–13]. All of them give values for the masses, widths, and decay modes that are in reasonable agreement. (However, Ref. [9] favors a state decaying into $K^*(892)\bar{K}$ at a lower mass than the state decaying into $a_0(980)\pi$.) In $J/\psi(1S)$ radiative decay, the $\eta(1405)$ decays into $K\bar{K}\pi$ through $a_0(980)\pi$, and hence a signal is also expected in the $\eta\pi\pi$ mass spectrum. This was indeed observed by MARK III in $\eta\pi^+\pi^-$ [14], which reported a mass of 1400 MeV, in line with the existence of the $\eta(1405)$ decaying into $a_0(980)\pi$.

BESII [15] observes an enhancement in $K^+K^-\pi^0$ around 1.44 GeV in $J/\psi(1S)$ decay, recoiling against an ω (but not a ϕ) without resolving the presence of two states nor performing a spin-parity analysis, due to low statistics. This state could also be the $f_1(1420)$ (see below). On the other hand, BESII observes $\eta(1405) \rightarrow \eta\pi\pi$ in $J/\psi(1S)$ decay, recoiling against an ω [16]. A single unresolved broad peak is also observed by BESIII in the decay $\psi(2S) \rightarrow \omega K^*K$ which could be due to $\eta(1405)$, $\eta(1475)$ and $f_1(1420)$ [17]. The $\eta(1405)$ is also observed in $p\bar{p}$ annihilation at rest into $\eta\pi^+\pi^-\pi^0\pi^0$, where it decays into $\eta\pi\pi$ [18]. The intermediate $a_0(980)\pi$ accounts for roughly half of the $\eta\pi\pi$ signal, in agreement with MARK III [14] and DM2 [4].

Whether one or two pseudoscalar mesons exist in this mass region is still an open issue. According to Ref. [19] the splitting of a single state is due to nodes in the decay amplitudes which differ in $\eta\pi\pi$ and $K^*(892)\bar{K}$. Based on the isospin violating decay $J/\psi(1S) \rightarrow \gamma 3\pi$ observed by BESIII [20] the splitting could also be due to a triangular singularity mixing $\eta\pi\pi$ and $K^*(892)\bar{K}$ [21, 22]. In a further paper [23], using the approach of [21], the authors conclude that the BESIII results can be reproduced either with the $\eta(1405)$ or the $\eta(1475)$, or by a mixture of these two states.

The $\eta(1295)$ has been observed by four π^-p experiments [7, 24–26], and evidence is reported in $p\bar{p}$ annihilation [27–29]. In $J/\psi(1S)$ radiative decay, the $\eta(1295)$ signal is evident in the 0^{-+} $\eta\pi\pi$ wave of the DM2 data [9]. Also BaBar [30] reports evidence for a signal around 1295 MeV in B decays into $\eta\pi\pi K$. Nonetheless, the existence of the $\eta(1295)$ is questioned in Refs. [19] and [31] in which the authors also claim the existence of a single pseudoscalar meson at 1440 MeV, the first radial excitation of the η . This conclusion is mainly based on a PhD thesis of the annihilation channel $p\bar{p} \rightarrow 4\pi\eta$ with Crystal Barrel data [32].

Since the $\eta(1295)$ has been reported by several experiments, using different production mechanisms, let us assume this state to be established. The $\eta(1475)$ could then be the first radial excitation of the η' , with the $\eta(1295)$ being the first radial excitation of the η . Ideal mixing, suggested by the $\eta(1295)$ and $\pi(1300)$ mass degeneracy, would then imply that the second isoscalar in the nonet is mainly $s\bar{s}$, and hence couples to $K^*\bar{K}$, in agreement with properties of the $\eta(1475)$. Also, its width matches the expected width for the radially excited $s\bar{s}$ state [33, 34]. A study of radial excitations of pseudoscalar mesons [35] favors the $s\bar{s}$ interpretation of the $\eta(1475)$. However, due to the strong kinematical suppression the data are not sufficient to exclude a sizeable $s\bar{s}$ admixture also in the $\eta(1405)$.

The $K\bar{K}\pi$ and $\eta\pi\pi$ channels were studied in $\gamma\gamma$ collisions by

L3 [36]. The analysis led to a clear $\eta(1475)$ signal in $K\bar{K}\pi$, decaying into $K^*\bar{K}$, very well identified in the untagged data sample, where contamination from spin 1 resonances is not allowed. At the same time, L3 [36] did not observe the $\eta(1405)$, neither in $K\bar{K}\pi$ nor in $\eta\pi\pi$. The observation of the $\eta(1475)$, combined with the absence of an $\eta(1405)$ signal, strengthens the two-resonances hypothesis. Since gluonium production is presumably suppressed in $\gamma\gamma$ collisions, the L3 results [36] suggest that $\eta(1405)$ has a large gluonic content (see also Refs. [37] and [38]). The L3 result is somewhat in disagreement with that of CLEO-II, which did not observe any pseudoscalar signal in $\gamma\gamma \rightarrow \eta(1475) \rightarrow K_S^0 K^\pm \pi^\mp$ [39]. However, more data are required. Moreover, after the CLEO-II result, L3 performed a further analysis with full statistics [40], confirming their previous evidence for the $\eta(1475)$. The CLEO upper limit [39] for $\Gamma_{\gamma\gamma}(\eta(1475))$, and the L3 results [40], are consistent with the world average for the $\eta(1475)$ width.

BaBar [30] also reports the $\eta(1475)$ in B decays into $K\bar{K}^*$ recoiling against a K , but upper limits only are given for the $\eta(1405)$. As mentioned above, in B decays into $\eta\pi\pi K$ the $\eta(1295) \rightarrow \eta\pi\pi$ is observed while only upper limits are given for the $\eta(1405)$. The $f_1(1420)$ (and $f_1(1285)$) are not seen.

Under the assumption that two pseudoscalars exist in the 1400 MeV region, the $\eta(1405)$ could be a glueball, but this interpretation for the $\eta(1405)$ is not favored by lattice gauge theories which predict the 0^{-+} state above 2 GeV [41, 42] (see also the article on the “Quark model” in this issue of the Review). However, the $\eta(1405)$ is an excellent candidate for the 0^{-+} glueball in the flux-tube model [43]. In this model, the 0^{++} $f_0(1500)$ glueball is also naturally related to a 0^{-+} glueball with mass degeneracy broken in QCD. Also, Ref. [44] shows that the pseudoscalar glueball could lie at a lower mass than predicted from lattice calculation. In this model the $\eta(1405)$ appears as the natural glueball candidate, see also Refs. [45–47]. A detailed review of the experimental situation is available in Ref. [48].

Let us now deal with the 1^{++} mesons. The pseudovector nonet is believed to consist of the isovector $a_1(1260)$, the isoscalars $f_1(1285)$ and $f_1(1420)$, and the K_{1A} , which is a superposition with mixing angle $\sim 34^\circ$ of $K_1(1270)$ and $K_1(1400)$ [49]. The $f_1(1285)$ could also be a $K^*\bar{K}$ molecule [50] or as a tetraquark state [51] and the $f_1(1420)$ a $K^*\bar{K}$ molecule, due to the proximity of the $K^*\bar{K}$ threshold [52]. LHCb has analyzed the decays \bar{B}^0 and $\bar{B}_s^0 \rightarrow J/\psi(1S)f_1(1285)$ and determined the nonet mixing angle to be consistent with a mostly $u\bar{u} + d\bar{d}$ structure [53] without specifying the identity of its isoscalar partner. This is consistent with earlier determinations assuming the $f_1(1420)$ as the isoscalar partner [54] and the ratio of \bar{B}^0/\bar{B}_s^0 decay rates excludes the tetraquark interpretation of this state [53].

The $f_1(1420)$, decaying into $K^*\bar{K}$, was first reported in π^-p reactions at 4 GeV/c [55]. However, later analyses found that the 1400–1500 MeV region was far more complex [56–58]. A reanalysis of the MARK III data in radiative $J/\psi(1S)$ decay into $K\bar{K}\pi$ [8] shows the $f_1(1420)$ decaying into $K^*\bar{K}$. A $C=+1$ state is also seen in tagged $\gamma\gamma$ collisions (*e.g.*, Ref. [59]).

In $\pi^-p \rightarrow \eta\pi\pi n$ charge-exchange reactions at 8–9 GeV/c the $\eta\pi\pi$ mass spectrum is dominated by the $\eta(1440)$ and $\eta(1295)$ [24, 60], and at 100 GeV/c Ref. [25] reports the $\eta(1295)$ and $\eta(1440)$ decaying into $\eta\pi^0\pi^0$ with a weak $f_1(1285)$ signal, and no evidence for the $f_1(1420)$.

Axial (1^{++}) mesons are not observed in $p\bar{p}$ annihilation at rest in liquid hydrogen, which proceeds dominantly through S -wave annihilation. However, in gaseous hydrogen, P -wave annihilation is enhanced and, indeed, Ref. [11] reports $f_1(1420)$ decaying into $K^*\bar{K}$. The $f_1(1420)$, decaying into $K\bar{K}\pi$, is also seen in pp central production, together with the $f_1(1285)$. The latter decays via $a_0(980)\pi$, and the former only via $K^*\bar{K}$, while the $\eta(1440)$ is absent [61, 62]. The $K_S^0 K_S^0 \pi^0$ decay mode of the $f_1(1420)$ establishes unambiguously $C=+1$. On the other hand, there is no evidence for any state decaying into $\eta\pi\pi$ around 1400 MeV, and hence the $\eta\pi\pi$ mode of the $f_1(1420)$ must be suppressed [63].

The COMPASS Collaboration has recently reported an isovector state at 1411 MeV, the $a_1(1420)$ [64] [65]. This relatively

narrow state (161 MeV) is produced by diffractive dissociation with 190 GeV pions in $\pi N \rightarrow 3\pi N$, decays into $f_0(980)\pi \rightarrow 3\pi$ (P-wave) and has therefore the quantum numbers $(I^G)J^{PC} = (1^-)1^{++}$. The pseudovector nonet already contains the established $a_1(1260)$ as the $I = 1$ state. As mentioned above, the $f_1(1420)$ has been interpreted as a $K^*\bar{K}$ molecule [52]. The new $a_1(1420)$ could be its isovector partner. Arguments favoring the $f_1(1420)$ being a hybrid $q\bar{q}g$ meson [66] or a four-quark state [67] were also put forward. The $q\bar{q}$ state would then remain to be identified, with the $f_1(1510)$ (see below) as a candidate. However, alternative explanations are suggested: A single 1^{++} isovector around 1400 MeV, can lead to two peaks in the 3π mass spectrum, depending on the production mechanism, $\rho\pi$ [68] or $K^*\bar{K} \rightarrow K\bar{K}\pi \rightarrow f_0(980)\pi$ [69] for the $a_1(1260)$ and $f_0(980)\pi$ for the $a_1(1420)$.

A similar mechanism is invoked for the $f_1(1420)$, which is claimed to result from the $K^*\bar{K}$ and $a_0(980)\pi$ decay modes of the $f_1(1285)$ [70]. The absence of $f_1(1420)$ in K^-p [71] indeed argues against the $f_1(1420)$ being the $s\bar{s}$ member of the 1^{++} nonet. However, the $f_1(1420)$ was reported in K^-p but not in π^-p [72], while two experiments do not observe the $f_1(1510)$ in K^-p [72,73]. The latter is also not seen in central collisions [62], nor $\gamma\gamma$ collisions [74], although, surprisingly for an $s\bar{s}$ state, a signal is reported in 4π decays [75].

We now turn to the experimental evidence for the $f_1(1510)$ which competes with the $f_1(1420)$ to be the $s\bar{s}$ 1^{++} meson. The $f_1(1510)$ was seen in $K^-p \rightarrow \Lambda K\bar{K}\pi$ at 4 GeV/c [76], and at 11 GeV/c [71]. Evidence is also reported in π^-p at 8 GeV/c, based on the phase motion of the 1^{++} $K^*\bar{K}$ wave [58]. A somewhat broader 1^{++} signal is also observed in $J/\psi(1S) \rightarrow \gamma\eta\pi^+\pi^-$ [77] as well as a small signal in $J/\psi(1S) \rightarrow \gamma\eta'\pi^+\pi^-$, attributed to the $f_1(1510)$ [78]. The $f_1(1510)$ is not well established [79].

Summarizing, there is evidence for two isovector 1^{++} states in the 1400 MeV region, the $a_1(1260)$ and $a_1(1420)$, which cannot be both $q\bar{q}$ states. These two states could stem from the same pole, or the latter be exotic (tetraquark or hybrid) or a molecular state. The $f_1(1285)$ and the $f_1(1420)$ are well known but their nature ($q\bar{q}$, tetraquark or molecular) remains to be established. In the 0^{-+} sector there is evidence for two pseudoscalars in the 1400 MeV region, the $\eta(1405)$ and $\eta(1475)$, decaying into $a_0(980)\pi$ and $K^*\bar{K}$, respectively. These two structures could originate from a single pole. Doubts have been expressed on the existence of the $\eta(1295)$. The $f_1(1510)$ remains to be firmly established.

References

- [1] P. H. Baillon *et al.*, Nuovo Cim. **A50**, 393 (1967).
- [2] D. L. Scharre *et al.*, Phys. Lett. **97B**, 329 (1980).
- [3] C. Edwards *et al.*, Phys. Rev. Lett. **49**, 259 (1982), [Erratum: Phys. Rev. Lett.50,219(1983)].
- [4] J. E. Augustin *et al.* (DM2), Phys. Rev. **D42**, 10 (1990).
- [5] J. Z. Bai *et al.* (BES), Phys. Lett. **B594**, 47 (2004), [hep-ex/0403008].
- [6] M. G. Rath *et al.*, Phys. Rev. **D40**, 693 (1989).
- [7] G. S. Adams *et al.* (E852), Phys. Lett. **B516**, 264 (2001), [hep-ex/0107042].
- [8] Z. Bai *et al.* (MARK-III), Phys. Rev. Lett. **65**, 2507 (1990).
- [9] J. E. Augustin *et al.* (DM2), Phys. Rev. **D46**, 1951 (1992).
- [10] A. Bertin *et al.* (OBELIX), Phys. Lett. **B361**, 187 (1995).
- [11] A. Bertin *et al.* (OBELIX), Phys. Lett. **B400**, 226 (1997).
- [12] C. Cicalo *et al.* (OBELIX), Phys. Lett. **B462**, 453 (1999).
- [13] F. Nichitiu *et al.* (OBELIX), Phys. Lett. **B545**, 261 (2002).
- [14] T. Bolton *et al.*, Phys. Rev. Lett. **69**, 1328 (1992).
- [15] M. Ablikim *et al.* (BES), Phys. Rev. **D77**, 032005 (2008), [arXiv:0712.1411].
- [16] M. Ablikim *et al.* (BESIII), Phys. Rev. Lett. **107**, 182001 (2011), [arXiv:1107.1806].
- [17] M. Ablikim *et al.* (BESIII), Phys. Rev. **D87**, 092006 (2013), [arXiv:1303.6360].
- [18] C. Amsler *et al.* (Crystal Barrel), Phys. Lett. **B358**, 389 (1995).
- [19] E. Klempt and A. Zaitsev, Phys. Rept. **454**, 1 (2007), [arXiv:0708.4016].
- [20] M. Ablikim *et al.* (BESIII), Phys. Rev. Lett. **108**, 182001 (2012), [arXiv:1201.2737].
- [21] J.-J. Wu *et al.*, Phys. Rev. Lett. **108**, 081803 (2012), [arXiv:1108.3772].
- [22] X.-G. Wu *et al.*, Phys. Rev. **D87**, 1, 014023 (2013), [arXiv:1211.2148].
- [23] F. Aceti *et al.*, Phys. Rev. **D86**, 114007 (2012), [arXiv:1209.6507].
- [24] S. Fukui *et al.*, Phys. Lett. **B267**, 293 (1991), [,293(1991)].
- [25] D. Alde *et al.* (GAMS), Phys. Atom. Nucl. **60**, 386 (1997), [Yad. Fiz.60,458(1997)].
- [26] J. J. Manak *et al.* (E852), Phys. Rev. **D62**, 012003 (2000), [hep-ex/0001051].
- [27] A. V. Anisovich *et al.*, Nucl. Phys. **A690**, 567 (2001).
- [28] A. Abele *et al.*, Phys. Rev. **D57**, 3860 (1998).
- [29] C. Amsler *et al.*, Eur. Phys. J. **C33**, 23 (2004).
- [30] B. Aubert *et al.* (BaBar), Phys. Rev. Lett. **101**, 091801 (2008), [arXiv:0804.0411].
- [31] E. Klempt, Int. J. Mod. Phys. **A21**, 739 (2006).
- [32] J. Reinhardt, PhD Thesis, University of Bonn (2003), unpublished.
- [33] F. E. Close and A. Kirk, Phys. Lett. **B397**, 333 (1997), [hep-ph/9701222].
- [34] T. Barnes *et al.*, Phys. Rev. **D55**, 4157 (1997), [hep-ph/9609339].
- [35] T. Gutsche, V. E. Lyubovitskij and M. C. Tichy, Phys. Rev. **D79**, 014036 (2009), [arXiv:0811.0668].
- [36] M. Acciarri *et al.* (L3), Phys. Lett. **B501**, 1 (2001), [hep-ex/0011035].
- [37] F. E. Close, G. R. Farrar and Z.-p. Li, Phys. Rev. **D55**, 5749 (1997), [hep-ph/9610280].
- [38] D. M. Li, H. Yu and S. S. Fang, Eur. Phys. J. **C28**, 335 (2003).
- [39] R. Ahohe *et al.* (CLEO), Phys. Rev. **D71**, 072001 (2005), [hep-ex/0501026].
- [40] P. Achard *et al.* (L3), JHEP **03**, 018 (2007).
- [41] G. S. Bali *et al.* (UKQCD), Phys. Lett. **B309**, 378 (1993), [hep-lat/9304012].
- [42] C. J. Morningstar and M. J. Peardon, Phys. Rev. **D60**, 034509 (1999), [hep-lat/9901004].
- [43] L. Faddeev, A. J. Niemi and U. Wiedner, Phys. Rev. **D70**, 114033 (2004), [hep-ph/0308240].
- [44] H.-Y. Cheng, H.-n. Li and K.-F. Liu, Phys. Rev. **D79**, 014024 (2009), [arXiv:0811.2577].
- [45] G. Li, Q. Zhao and C.-H. Chang, J. Phys. **G35**, 055002 (2008), [hep-ph/0701020].
- [46] T. Gutsche, V. E. Lyubovitskij and M. C. Tichy, Phys. Rev. **D80**, 014014 (2009), [arXiv:0904.3414].
- [47] B. A. Li, Phys. Rev. **D81**, 114002 (2010), [arXiv:0912.2323].
- [48] A. Masoni, C. Cicalo and G. L. Usai, J. Phys. **G32**, R293 (2006).
- [49] H.-Y. Cheng, Phys. Lett. **B707**, 116 (2012), [arXiv:1110.2249].
- [50] F. Aceti, J.-J. Xie and E. Oset, Phys. Lett. **B750**, 609 (2015), [arXiv:1505.06134].
- [51] S. Stone and L. Zhang, Phys. Rev. Lett. **111**, 6, 062001 (2013), [arXiv:1305.6554].
- [52] R. S. Longacre, Phys. Rev. **D42**, 874 (1990).

- [53] R. Aaij *et al.* (LHCb), Phys. Rev. Lett. **112**, 9, 091802 (2014), [arXiv:1310.2145].
- [54] G. Gidal *et al.*, Phys. Rev. Lett. **59**, 2012 (1987).
- [55] C. Dionisi *et al.* (CERN-College de France-Madrid-Stockholm), Nucl. Phys. **B169**, 1 (1980).
- [56] S. U. Chung *et al.*, Phys. Rev. Lett. **55**, 779 (1985), [Erratum: Phys. Rev. Lett.55,2093(1985)].
- [57] D. F. Reeves *et al.*, Phys. Rev. **D34**, 1960 (1986).
- [58] A. Birman *et al.*, Phys. Rev. Lett. **61**, 1557 (1988), [Erratum: Phys. Rev. Lett.62,1577(1989)].
- [59] H. J. Behrend *et al.* (CELLO), Z. Phys. **C42**, 367 (1989).
- [60] A. Ando *et al.*, Phys. Rev. Lett. **57**, 1296 (1986).
- [61] T. A. Armstrong *et al.* (WA76), Phys. Lett. **B221**, 216 (1989).
- [62] D. Barberis *et al.* (WA102), Phys. Lett. **B413**, 225 (1997), [hep-ex/9707022].
- [63] T. A. Armstrong *et al.* (WA76, Athens-Bari-Birmingham-CERN-College de France), Z. Phys. **C52**, 389 (1991).
- [64] C. Adolph *et al.* (COMPASS), Phys. Rev. Lett. **115**, 8, 082001 (2015), [arXiv:1501.05732].
- [65] M. Aghasyan *et al.* (COMPASS), Phys. Rev. **D98**, 9, 092003 (2018), [arXiv:1802.05913].
- [66] S. Ishida *et al.*, Prog. Theor. Phys. **82**, 119 (1989).
- [67] D.O. Caldwell, *Hadron 89 Conf., Ajaccio, Corsica*, p. 127.
- [68] J.-L. Basdevant and E. L. Berger, Phys. Rev. Lett. **114**, 19, 192001 (2015), [arXiv:1504.05955].
- [69] M. Mikhasenko, B. Ketzer and A. Sarantsev, Phys. Rev. **D91**, 9, 094015 (2015), [arXiv:1501.07023].
- [70] V. R. Debastiani *et al.*, Phys. Rev. **D95**, 3, 034015 (2017), [arXiv:1611.05383].
- [71] D. Aston *et al.*, Phys. Lett. **B201**, 573 (1988).
- [72] P. F. Ermolov *et al.*, Sov. J. Nucl. Phys. **39**, 738 (1984), [Yad. Fiz.39,1170(1984)].
- [73] J. Dowd *et al.*, Nucl. Phys. Proc. Suppl. **21**, 11 (1991).
- [74] H. Aihara *et al.* (TPC/Two Gamma), Phys. Rev. **D38**, 1 (1988).
- [75] D. A. Bauer *et al.* (TPC/Two Gamma), Phys. Rev. **D48**, 3976 (1993).
- [76] P. Gavillet *et al.*, Z. Phys. **C16**, 119 (1982).
- [77] J. Z. Bai *et al.* (BES), Phys. Lett. **B446**, 356 (1999).
- [78] M. Ablikim *et al.* (BESIII), Phys. Rev. Lett. **106**, 072002 (2011), [arXiv:1012.3510].
- [79] F. E. Close and A. Kirk, Z. Phys. **C76**, 469 (1997), [hep-ph/9706543].

64. Rare Kaon Decays

Revised August 2019 by L. Littenberg (BNL) and G. Valencia (Monash U.).

64.1 Introduction

There are several useful reviews on rare kaon decays and related topics [1–12]. Activity in rare kaon decays can be divided roughly into four categories:

1. Searches for explicit violations of the Standard Model (SM)
2. The golden modes: $K \rightarrow \pi\nu\bar{\nu}$
3. Other constraints on SM parameters
4. Studies of strong interactions at low energy.

The paradigm of Category 1 is the lepton flavor violating decay $K_L \rightarrow \mu e$. Category 2 includes the two modes that can be calculated with negligible theoretical uncertainty, $K^+ \rightarrow \pi^+\nu\bar{\nu}$ and $K_L \rightarrow \pi^0\nu\bar{\nu}$. These modes can lead to precision determinations of CKM parameters or, in combination with other measurements of these parameters, they can constrain new interactions. They constitute the main focus of the current experimental kaon program. Category 3 is focused on decays with charged leptons, such as $K_L \rightarrow \pi^0\ell^+\ell^-$ or $K_L \rightarrow \ell^+\ell^-$ where $\ell \equiv e, \mu$. These modes are sensitive to CKM parameters but they suffer from multiple hadronic uncertainties that can be addressed, at least in part, through a systematic study of the peripheral modes indicated in Fig. 64.1. The interplay between Categories 3-4 and their complementarity to Category 2 is illustrated in the figure. Category 4 includes reactions like $K^+ \rightarrow \pi^+\ell^+\ell^-$ where long distance contributions are dominant and which constitute a testing ground for the ideas of chiral perturbation theory. Other decays in this category are $K_L \rightarrow \pi^0\gamma\gamma$ and $K_L \rightarrow \ell^+\ell^-\gamma$. The former is important in understanding a CP -conserving contribution to $K_L \rightarrow \pi^0\ell^+\ell^-$, whereas the latter could shed light on long distance contributions to $K_L \rightarrow \mu^+\mu^-$.

64.2 Explicit violations of the Standard Model

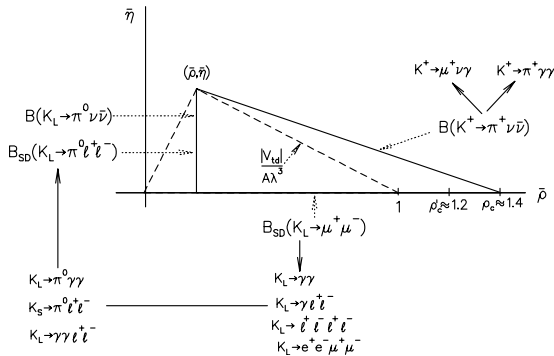


Figure 64.1: Role of rare kaon decays in determining the unitarity triangle. The solid arrows point to auxiliary modes needed to interpret the main results, or potential backgrounds to them.

Much activity has focussed on searches for lepton flavor violation (LFV). This is motivated by the fact that many extensions of the minimal Standard Model violate lepton flavor and by the potential to access very high energy scales. For example, the tree-level exchange of a LFV vector boson of mass M_X that couples to left-handed fermions with electroweak strength and without mixing angles yields $B(K_L \rightarrow \mu e) = 4.7 \times 10^{-12} (148 \text{ TeV}/M_X)^4$ [2]. This simple dimensional analysis may be used to read from Table 64.1 that the reaction $K_L \rightarrow \mu e$ is already probing scales of over 100 TeV. Table 64.1 summarizes the present experimental situation vis-à-vis LFV. The decays $K_L \rightarrow \mu^\pm e^\mp$ and $K^+ \rightarrow \pi^+ e^\mp \mu^\pm$ (or $K_L \rightarrow \pi^0 e^\mp \mu^\pm$) provide complementary information on potential family number violating interactions, since the former is sensitive to parity-odd couplings and the latter is sensitive to parity-even couplings.

Limits on certain lepton-number violating (LNV) kaon decays also have been obtained, with recent interest arising from their role in constraining possible extensions of the neutrino sector [13,

14], and we list those in the table as well. Related searches in μ and τ processes are discussed in our section “Tests of Conservation Laws.”

Table 64.1: Searches for lepton flavor and lepton number violation in K decay

LFV mode	90% CL upper limit	Experiment	Yr./Ref.	Type
$K^+ \rightarrow \pi^+ e^- \mu^+$	1.3×10^{-11}	BNL-865	2005/ [15]	LFV
$K^+ \rightarrow \pi^+ e^+ \mu^-$	5.2×10^{-10}	BNL-865	2000/ [16]	LFV
$K_L \rightarrow \mu e$	4.7×10^{-12}	BNL-871	1998/ [17]	LFV
$K_L \rightarrow \pi^0 e \mu$	7.6×10^{-11}	KTeV	2008/ [18]	LFV
$K_L \rightarrow \pi^0 \pi^0 e \mu$	1.7×10^{-10}	KTeV	2008/ [18]	LFV
$K^+ \rightarrow \pi^- e^+ e^+$	2.2×10^{-10}	NA-62	2019/ [19]	LNV
$K^+ \rightarrow \pi^- \mu^+ \mu^+$	4.2×10^{-11}	NA-62	2019/ [19]	LNV
$K^\pm \rightarrow \pi^\mp \mu^\pm \mu^\pm$	8.6×10^{-11}	NA48/2	2017/ [20]	LNV
$K_L \rightarrow e^\pm e^\pm \mu^\mp \mu^\mp$	4.12×10^{-11}	KTeV	2003/ [21]	LNV
$K^+ \rightarrow \pi^- \mu^+ e^+$	5.0×10^{-10}	BNL-865	2000/ [16]	LNVF

Physics beyond the SM is also pursued through the search for $K^+ \rightarrow \pi^+ X^0$, where X^0 is a new light particle. The searches cover both long-lived particles (*e.g.*, hyperphoton, axion, familon, *etc.*), and short-lived ones that decay to muon, electron or photon pairs. The 90% CL upper limit on $K^+ \rightarrow \pi^+ X^0$ is 7.3×10^{-11} [22] for the case of massless X^0 ; additional results as a function of the X^0 mass can be found in [23]. Recently these limits have been reinterpreted in connection with a dark photon [24] or dark Z [25]. Such vectors have also been sought in their e^+e^- decay mode by NA48/2 [26]. Additional bounds for a short lived pseudoscalar X^0 decaying to muons or photons are $B(K_L \rightarrow \pi^0 \pi^0 \mu^+ \mu^-) < 1 \times 10^{-10}$ [27] and $B(K_L \rightarrow \pi^0 \pi^0 \gamma \gamma) < 2.4 \times 10^{-7}$ [28].

64.3 The golden modes: $K \rightarrow \pi\nu\bar{\nu}$

In the SM, the decay $K^+ \rightarrow \pi^+\nu\bar{\nu}$ is dominated by one-loop diagrams with top-quark intermediate states while long-distance contributions are known to be quite small [29–31]. This permits a precise calculation of this rate in terms of SM parameters. Studies of this process are thus motivated by the possibility of detecting non-SM physics when comparing with the results of global fits [32, 33].

The branching ratio can be written in a compact form that exhibits the different ingredients that go into the calculation [34],

$$B(K^+ \rightarrow \pi^+\nu\bar{\nu}(\gamma)) = \kappa_+(1 + \Delta_{\text{EM}}) \left[\left(\frac{\text{Im}(V_{ts}^* V_{td})}{\lambda^5} X_t \right)^2 + \left(\frac{\text{Re}(V_{cs}^* V_{cd})}{\lambda} (P_c + \delta P_{c,u}) + \frac{\text{Re}(V_{ts}^* V_{td})}{\lambda^5} X_t \right)^2 \right]. \quad (64.1)$$

The parameters in Eq. 64.1 incorporate the *a priori* unknown hadronic matrix element in terms of the very well-measured K_{e3} rate [29] in κ_+ ; long distance QED corrections in Δ_{EM} [35]; the Inami-Lim function for the short distance top-quark contribution [36] including NLO QCD corrections [37, 38] and the two-loop electroweak correction [34], all in X_t ; and the charm-quark contributions due to short distance effects including NNLO QCD corrections [39, 40] and NLO electroweak corrections via P_c [41], as well as certain long distance effects via $\delta P_{c,u}$ [31, 42]. An interesting approximate way to cast this result in terms of the CKM parameters λ , V_{cb} , $\bar{\rho}$ and $\bar{\eta}$ (see our Section on “The Cabibbo-Kobayashi-Maskawa mixing matrix”) [43] is:

$$B(K^+ \rightarrow \pi^+\nu\bar{\nu}) \approx 1.6 \times 10^{-5} |V_{cb}|^4 [\sigma \bar{\eta}^2 + (\rho_c - \bar{\rho})^2], \quad (64.2)$$

where $\rho_c \approx 1.45$ and $\sigma \equiv \frac{1}{(1 - \frac{1}{2}\lambda^2)^2}$. Thus, $B(K^+ \rightarrow \pi^+\nu\bar{\nu})$ determines an ellipse in the $\bar{\rho}$, $\bar{\eta}$ plane with center $(\rho_c, 0)$ and semiaxes $\approx \frac{1}{|V_{cb}|^2} \sqrt{\frac{B(K^+ \rightarrow \pi^+\nu\bar{\nu})}{1.6 \times 10^{-5}}}$ and $\frac{1}{\sigma |V_{cb}|^2} \sqrt{\frac{B(K^+ \rightarrow \pi^+\nu\bar{\nu})}{1.6 \times 10^{-5}}}$.

BNL-787 observed two candidate events [44, 45] in the clean high π^+ momentum and one event [46] in the low-momentum region. The successor experiment BNL-949 observed one more

in the high-momentum region [22] and three more in the low-momentum region [47], yielding a branching ratio of $(1.73_{-1.05}^{+1.15}) \times 10^{-10}$ [23].

The NA62 experiment, performed with in-flight decays at CERN, aims to reach a sensitivity of $\sim 10^{-12}$ /event. NA62 was commissioned in 2015 and has taken data in 2016, 2017 and 2018. The short 2016 run resulted in the observation of one event over an expected background of 0.152 events, which allowed a 95% C.L. limit of 14×10^{-10} to be set [48]. Very recently, preliminary results from the 2017 run have been announced. Two additional events were observed, over an expected background of 1.5 events. Combining this data with that of 2016, they obtain a 90% C.L. limit of 1.85×10^{-10} [49].

Using the latest CKMfitter input [32], we estimate $B(K^+ \rightarrow \pi^+ \nu \bar{\nu}) = (8.5 \pm 0.5) \times 10^{-11}$, near the lower end of the measurement of BNL-787 and 949. However, current parametric uncertainty in the CKM angles can result in numbers with central values differing from this one by up to 10% [50].

The second golden mode is the neutral counterpart to our preceding discussion: $K_L \rightarrow \pi^0 \nu \bar{\nu}$. It is dominantly CP -violating and free of hadronic uncertainties [29, 51, 52]. In the Standard Model, this mode is dominated by an intermediate top-quark state and does not suffer from the small uncertainty associated with the charm-quark intermediate state that affects $K^+ \rightarrow \pi^+ \nu \bar{\nu}$. The branching ratio is given by Ref. [43]:

$$B(K_L \rightarrow \pi^0 \nu \bar{\nu}) = \kappa_L \left(\frac{\text{Im}(V_{ts}^* V_{td})}{\lambda^5} X_t \right)^2 \approx 7.6 \times 10^{-5} |V_{cb}|^4 \bar{\eta}^2. \quad (64.3)$$

As with the charged mode, the hadronic matrix element can be related to that measured in $K_{\ell 3}$ decay and is parameterized in κ_L .

Our estimate for the branching ratio, using the latest CKMfitter input [32], is $(3.0 \pm 0.2) \times 10^{-11}$. But similarly to the charged kaon case, parametric uncertainty in the CKM angles can result in a central value that differs from this one by up to almost 20% [50].

Grossman and Nir (GN) [53] pointed out that, in a nearly model-independent manner, the two golden modes satisfy the relation $B(K_L \rightarrow \pi^0 \nu \bar{\nu}) \lesssim 4.4 B(K^+ \rightarrow \pi^+ \nu \bar{\nu})$. Using the BNL 787/949 90% CL bound on $K^+ \rightarrow \pi^+ \nu \bar{\nu}$, GN then predict $B(K_L \rightarrow \pi^0 \nu \bar{\nu}) < 1.46 \times 10^{-9}$. Using instead the latest NA62 result, the GN upper bound becomes $B(K_L \rightarrow \pi^0 \nu \bar{\nu}) < 8.14 \times 10^{-10}$ as can be seen in Figure 64.2.

The KOTO experiment at J-PARC, whose initial goal is to observe this decay, has been running since 2013 and in 2018 published a 90% CL upper limit of 3.0×10^{-9} [54], based on their 2015 data. They have run every year since, making incremental upgrades to the experimental configuration between runs.

It was pointed out in a recent paper that the GN bound obtained from the BNL result applies to the three body decay $K_L \rightarrow \pi^0 \nu \bar{\nu}$ and not necessarily to two body modes such as $K_L \rightarrow \pi^0 X^0$. In this case KOTO can provide interesting constraints on new physics even at the current sensitivity level [55]. Using the 2015 data, they have established a 90% CL upper limit of 2.4×10^{-9} on $K_L \rightarrow \pi^0 X^0$ for $m_{X^0} \approx m_{\pi^0}$ [54].

Much theoretical work has explored beyond the SM scenarios that can populate this window as well as their correlations with other rare processes outside kaon physics. Although it would be relatively straight forward to establish the existence of new physics by observing deviations from their SM values in the $K \rightarrow \pi \nu \bar{\nu}$ modes, it would take much more extensive global fits to pinpoint the origin of any such deviation. Partial summaries with references can be found in Refs. [9, 56–58]. There has also been a recent classification of the different possibilities in terms of the neutrino couplings [59], and several studies on the effect of neutrinos with different lepton flavor. [60–62].

The current theoretical and experimental situation for the golden modes is summarized in Fig. 64.2. The red area corresponds to the 1σ SM prediction we obtain with the latest input available from CKMfitter (summer 2018) [32]. The yellow region shows the result established by the combined BNL-787 and BNL-949 results, whereas the green region marks the new 90% CL upper bound from NA62 for $K^+ \rightarrow \pi^+ \nu \bar{\nu}$. The black shaded region

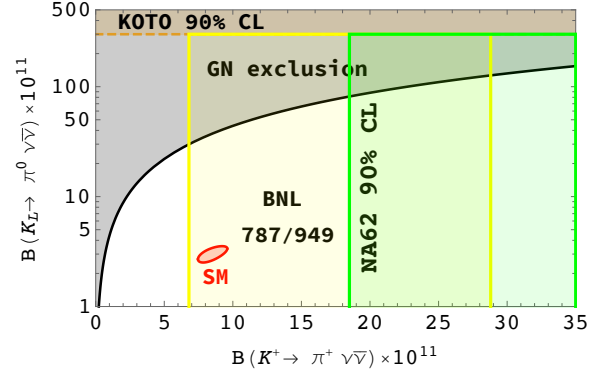


Figure 64.2: Summary of current situation for the golden modes $K \rightarrow \pi \nu \bar{\nu}$. The red ellipse shows the 1σ SM prediction with input from CKMfitter; the yellow region corresponds to the BNL 1σ measurement; the vertical green line marks the 90% CL upper bound from NA62, with the corresponding exclusion region shaded green; and the dashed orange line marks the 90% CL KOTO upper bound. The black shaded region shows the GN exclusion.

marks the GN exclusion, which lies significantly above the SM expectation leaving a large window for discovery of new physics contributions by experiments seeking to measure $B(K_L \rightarrow \pi^0 \nu \bar{\nu})$. The 90% CL upper bound on this mode from KOTO is shown as a dashed orange line, and is seen to still lie in the GN excluded zone.

Related modes with one extra pion, $K \rightarrow \pi \pi \nu \bar{\nu}$, are similarly dominated by short distance contributions [63–65]. However, they occur at much lower rates with branching ratios of order 10^{-13} . The current best bound comes from KEK-391a, it is $B(K_L \rightarrow \pi^0 \pi^0 \nu \bar{\nu}) < 8.1 \times 10^{-7}$ at 90% CL [66]. There is also a bound $B(K^+ \rightarrow \pi^+ \pi^0 \nu \bar{\nu}) < 4.3 \times 10^{-5}$ at 90% CL [67] from BNL-787.

64.4 Other constraints on Standard Model parameters

The decay $K_L \rightarrow \mu^+ \mu^-$ has a short distance contribution sensitive to the CKM parameter $\bar{\rho}$, given by [43]:

$$B_{SD}(K_L \rightarrow \mu^+ \mu^-) \approx 2.7 \times 10^{-4} |V_{cb}|^4 (\rho'_c - \bar{\rho})^2 \quad (64.4)$$

where ρ'_c depends on the charm quark mass and is approximately 1.2. This decay, however, is dominated by a long-distance contribution from a two-photon intermediate state. The absorptive (imaginary) part of the long-distance component is determined by the measured rate for $K_L \rightarrow \gamma \gamma$ to be $B_{\text{abs}}(K_L \rightarrow \mu^+ \mu^-) = (6.64 \pm 0.07) \times 10^{-9}$; and it almost completely saturates the observed rate $B(K_L \rightarrow \mu^+ \mu^-) = (6.84 \pm 0.11) \times 10^{-9}$ [68]. The difference between the observed rate and the absorptive component can be attributed to the (coherent) sum of the short-distance amplitude and the real part of the long-distance amplitude. The latter cannot be derived directly from experiment [69], but can be estimated with certain assumptions [70, 71].

By contrast, the decay $K_L \rightarrow e^+ e^-$ is completely dominated by long distance physics and is easier to estimate. The result, $B(K_L \rightarrow e^+ e^-) \sim 9 \times 10^{-12}$ [69, 72], is in good agreement with the BNL-871 measurement, $(8.7_{-4.1}^{+5.7}) \times 10^{-12}$ [73].

The mode $K_S \rightarrow \mu^+ \mu^-$ similarly has a short distance contribution proportional to the square of the CKM parameter $\bar{\eta}$ entering at the 10^{-13} level [10]. It also has long distance contributions arising from the two photon intermediate state which result in a rate $B(K_S \rightarrow \mu^+ \mu^-)_{LD} = 5.1 \times 10^{-12}$ [10]. A 90% CL limit $B(K_S \rightarrow \mu^+ \mu^-) < 2.1 \times 10^{-10}$ was recently obtained by LHCb [74, 75]. The interplay between $K_L \rightarrow \mu^+ \mu^-$ and $K_S \rightarrow \mu^+ \mu^-$ has been the subject of [76, 77].

The decay $K_L \rightarrow \pi^0 e^+ e^-$ is sensitive to the CKM parameter η through its CP -violating component. There are both direct and indirect CP -violating amplitudes that can interfere. The direct CP -violating amplitude is short distance dominated and has been calculated in detail within the SM [5]. The indirect CP -violating

amplitude can be inferred from a measurement of $K_S \rightarrow \pi^0 e^+ e^-$. The complete CP -violating contribution to the rate can be written as [78–80]:

$$B_{CPV} \approx 10^{-12} \left[15.7 |a_S|^2 \pm 1.4 \left(\frac{|V_{cb}|^2 \bar{\eta}}{10^{-4}} \right) |a_S| + 0.12 \left(\frac{|V_{cb}|^2 \bar{\eta}}{10^{-4}} \right)^2 \right] \quad (64.5)$$

where the three terms correspond to the indirect CP violation, the interference, and the direct CP violation, respectively. The parameter a_S has been extracted by NA48/1 from a measurement of $K_S \rightarrow \pi^0 e^+ e^-$ with the result $|a_S| = 1.06_{-0.21}^{+0.26} \pm 0.07$ [81], as well as from a measurement of $K_S \rightarrow \pi^0 \mu^+ \mu^-$ with the result $|a_S| = 1.54_{-0.32}^{+0.40} \pm 0.06$ [82]. With current constraints on the CKM parameters, and assuming a positive sign for the interference term [80, 83], this implies that $B_{CPV}(K_L \rightarrow \pi^0 e^+ e^-) \approx (3.1 \pm 0.9) \times 10^{-11}$, where the three contributions to the central value from indirect, interference and direct CP violation are $(1.76, 0.9, 0.45) \times 10^{-11}$ respectively. It should be noted that more recent studies suggest a much larger uncertainty in the value of a_S [84]. The complete CP violating amplitude for the related mode $K_L \rightarrow \pi^0 \mu^+ \mu^-$ is predicted to be $B_{CPV}(K_L \rightarrow \pi^0 \mu^+ \mu^-) \approx (1.4 \pm 0.5) \times 10^{-11}$ [10, 85].

$K_L \rightarrow \pi^0 e^+ e^-$ also has a CP -conserving component dominated by a two-photon intermediate state. This component can be decomposed into an absorptive and a dispersive part. The absorptive part can be extracted from the measurement of the low $m_{\gamma\gamma}$ region of the $K_L \rightarrow \pi^0 \gamma\gamma$ spectrum. The rate and the shape of the distribution $d\Gamma/dm_{\gamma\gamma}$ in $K_L \rightarrow \pi^0 \gamma\gamma$ are well described in chiral perturbation theory in terms of three (*a priori*) unknown parameters [86–89].

Both KTeV and NA48 have studied the mode $K_L \rightarrow \pi^0 \gamma\gamma$, reporting similar results. KTeV finds $B(K_L \rightarrow \pi^0 \gamma\gamma) = (1.29 \pm 0.03_{\text{stat}} \pm 0.05_{\text{sys}}) \times 10^{-6}$ [90], while NA48 finds $B(K_L \rightarrow \pi^0 \gamma\gamma) = (1.36 \pm 0.03_{\text{stat}} \pm 0.03_{\text{sys}} \pm 0.03_{\text{norm}}) \times 10^{-6}$ [91]. Both experiments are consistent with a negligible rate in the low $m_{\gamma\gamma}$ region, suggesting a very small CP -conserving component $B_{CP}(K_L \rightarrow \pi^0 e^+ e^-) \sim \mathcal{O}(10^{-13})$ [80, 89, 91]. There remains some model dependence in the estimate of the dispersive part of the CP -conserving $K_L \rightarrow \pi^0 e^+ e^-$ [80].

The related process, $K_L \rightarrow \pi^0 \gamma e^+ e^-$, is potentially an additional background to $K_L \rightarrow \pi^0 e^+ e^-$ in some region of phase space [92]. This process has been observed with a branching ratio of $(1.62 \pm 0.14_{\text{stat}} \pm 0.09_{\text{sys}}) \times 10^{-8}$ [93].

The decay $K_L \rightarrow \gamma \gamma e^+ e^-$ constitutes the dominant background to $K_L \rightarrow \pi^0 e^+ e^-$. It was first observed by BNL-845 [94], and subsequently confirmed with a much larger sample by KTeV [95]. It has been estimated that this background will enter at about the 10^{-10} level [96, 97], comparable to or larger than the signal level. Because of this, the observation of $K_L \rightarrow \pi^0 e^+ e^-$ at the SM level will depend on background subtraction with good statistics. Possible alternative strategies are discussed in Ref. [80] and references cited therein.

The 90% CL upper bound for the process $K_L \rightarrow \pi^0 e^+ e^-$ is 2.8×10^{-10} [97]. For the closely related muonic process, the published upper bound is $B(K_L \rightarrow \pi^0 \mu^+ \mu^-) \leq 3.8 \times 10^{-10}$ [98], compared with the SM prediction of $(1.5 \pm 0.3) \times 10^{-11}$ [85] (assuming positive interference between the direct- and indirect- CP violating components).

A study of $K_L \rightarrow \pi^0 \mu^+ \mu^-$ has indicated that it might be possible to extract the direct CP -violating contribution by a joint study of the Dalitz plot variables and the components of the μ^+ polarization [99]. The latter tends to be quite substantial so that large statistics may not be necessary.

Combined information from $K_L \rightarrow \pi^0 \ell^+ \ell^-$ as well as $K_L \rightarrow \mu^+ \mu^-$ complements the $K \rightarrow \pi \nu \bar{\nu}$ measurements in constraining physics beyond the SM [100].

64.5 Other long distance dominated modes

The decays $K^+ \rightarrow \pi^+ \ell^+ \ell^-$ ($\ell = e$ or μ) have received considerable attention. The rate and spectrum have been measured for both the electron and muon modes [101–106]. The theoretical status of these modes has been summarized recently [84, 107].

The measurements have been used to exclude new physics such as a dark photon [24]. Ref. [78, 79] has proposed a parameterization inspired by chiral perturbation theory, which provides a successful description of data but indicates the presence of large corrections beyond leading order. More work is needed to fully understand the origin of these large corrections. The mode $K^+ \rightarrow \pi^+ \pi^0 e^+ e^-$, recently analyzed by NA48/2 [108], is also dominated by long distance physics but it has been argued that measuring asymmetries can provide information on the short distance components [109]. The related mode $K_S \rightarrow \pi^+ \pi^- e^+ e^-$, which was measured by NA48/1 [110], has received new interest by LHCb [111] as an important background to other rare decays. An update of the theory for these modes can be found in [112].

The decay $K^+ \rightarrow \pi^+ \gamma\gamma$ can be predicted in terms of one unknown parameter to leading order in χ PT resulting in a correlation between the rate and the diphoton mass spectrum [113]. Certain important corrections at the next order are also known [114]. The rate was first measured by E787 [115], and more recently NA48/2 [116] has obtained a more precise result with a 6% error, as well as the corresponding spectrum fits. The most recent, and precise, result is from NA62 based on a sample of 232 events [117] but is still insufficient to distinguish between the leading order and next order χ PT parameterizations.

Much information has been recorded by KTeV and NA48 on the rates and spectrum for the Dalitz pair conversion modes $K_L \rightarrow \ell^+ \ell^- \gamma$ [118, 119], and $K_L \rightarrow \ell^+ \ell^- \ell'^+ \ell'^-$ for $\ell, \ell' = e$ or μ [21, 120]. More recently, LHCb has performed preliminary studies of $K_S \rightarrow \ell^+ \ell^- \ell'^+ \ell'^-$ [111]. All these results are used to test hadronic models and should eventually help unravel the underlying physics in $K_L \rightarrow \mu^+ \mu^-$ [71, 76, 121].

References

- [1] L. Littenberg and G. Valencia, *Ann. Rev. Nucl. Part. Sci.* **43**, 729 (1993), [hep-ph/9303225].
- [2] J. L. Ritchie and S. G. Wojcicki, *Rev. Mod. Phys.* **65**, 1149 (1993).
- [3] B. Winstein and L. Wolfenstein, *Rev. Mod. Phys.* **65**, 1113 (1993).
- [4] A. Pich, *Rept. Prog. Phys.* **58**, 563 (1995), [hep-ph/9502366].
- [5] G. Buchalla, A. J. Buras and M. E. Lautenbacher, *Rev. Mod. Phys.* **68**, 1125 (1996), [hep-ph/9512380].
- [6] G. D'Ambrosio and G. Isidori, *Int. J. Mod. Phys. A* **13**, 1 (1998), [hep-ph/9611284].
- [7] P. Buchholz and B. Renk, *Prog. Part. Nucl. Phys.* **39**, 253 (1997).
- [8] A. R. Barker and S. H. Kettell, *Ann. Rev. Nucl. Part. Sci.* **50**, 249 (2000), [hep-ex/0009024].
- [9] A. J. Buras, F. Schwab and S. Uhlig, *Rev. Mod. Phys.* **80**, 965 (2008), [hep-ph/0405132].
- [10] V. Cirigliano *et al.*, *Rev. Mod. Phys.* **84**, 399 (2012), [arXiv:1107.6001].
- [11] D. Bryman *et al.*, *Ann. Rev. Nucl. Part. Sci.* **61**, 331 (2011).
- [12] T. K. Komatsubara, *Prog. Part. Nucl. Phys.* **67**, 995 (2012), [arXiv:1203.6437].
- [13] A. Atre *et al.*, *JHEP* **05**, 030 (2009), [arXiv:0901.3589].
- [14] L. S. Littenberg and R. Shrock, *Phys. Lett.* **B491**, 285 (2000), [hep-ph/0005285].
- [15] A. Sher *et al.*, *Phys. Rev.* **D72**, 012005 (2005), [hep-ex/0502020].
- [16] R. Appel *et al.*, *Phys. Rev. Lett.* **85**, 2877 (2000), [hep-ex/0006003].
- [17] D. Ambrose *et al.* (BNL), *Phys. Rev. Lett.* **81**, 5734 (1998), [hep-ex/9811038].

- [18] E. Abouzaid *et al.* (KTeV), Phys. Rev. Lett. **100**, 131803 (2008), [arXiv:0711.3472].
- [19] E. Cortina Gil *et al.* (NA62), Phys. Lett. **B797**, 134794 (2019), [arXiv:1905.07770].
- [20] J. R. Batley *et al.* (NA48/2), Phys. Lett. **B769**, 67 (2017), [arXiv:1612.04723].
- [21] A. Alavi-Harati *et al.* (KTeV), Phys. Rev. Lett. **90**, 141801 (2003), [hep-ex/0212002].
- [22] V. V. Anisimovsky *et al.* (E949), Phys. Rev. Lett. **93**, 031801 (2004), [hep-ex/0403036].
- [23] A. V. Artamonov *et al.* (BNL-E949), Phys. Rev. **D79**, 092004 (2009), [arXiv:0903.0030].
- [24] M. Pospelov, Phys. Rev. **D80**, 095002 (2009), [arXiv:0811.1030].
- [25] H. Davoudiasl, H.-S. Lee and W. J. Marciano, Phys. Rev. **D89**, 9, 095006 (2014), [arXiv:1402.3620].
- [26] J. R. Batley *et al.* (NA48/2), Phys. Lett. **B746**, 178 (2015), [arXiv:1504.00607].
- [27] E. Abouzaid *et al.* (KTeV), Phys. Rev. Lett. **107**, 201803 (2011), [arXiv:1105.4800].
- [28] Y. C. Tung *et al.* (E391a), Phys. Rev. Lett. **102**, 051802 (2009), [arXiv:0810.4222].
- [29] J. S. Hagelin and L. S. Littenberg, Prog. Part. Nucl. Phys. **23**, 1 (1989).
- [30] M. Lu and M. B. Wise, Phys. Lett. **B324**, 461 (1994), [hep-ph/9401204].
- [31] A. F. Falk, A. Lewandowski and A. A. Petrov, Phys. Lett. **B505**, 107 (2001), [hep-ph/0012099].
- [32] J. Charles *et al.*, Phys. Rev. **D84**, 033005 (2011), [arXiv:1106.4041].
- [33] M. Bona *et al.* (UTfit), JHEP **03**, 049 (2008), [arXiv:0707.0636].
- [34] J. Brod, M. Gorbahn and E. Stamou, Phys. Rev. **D83**, 034030 (2011), [arXiv:1009.0947].
- [35] F. Mescia and C. Smith, Phys. Rev. **D76**, 034017 (2007), [arXiv:0705.2025].
- [36] T. Inami and C. S. Lim, Prog. Theor. Phys. **65**, 297 (1981), [Erratum: Prog. Theor. Phys.65,1772(1981)].
- [37] G. Buchalla and A. J. Buras, Nucl. Phys. **B548**, 309 (1999), [hep-ph/9901288].
- [38] M. Misiak and J. Urban, Phys. Lett. **B451**, 161 (1999), [hep-ph/9901278].
- [39] A. J. Buras *et al.*, Phys. Rev. Lett. **95**, 261805 (2005), [hep-ph/0508165].
- [40] A. J. Buras *et al.*, JHEP **11**, 002 (2006), [Erratum: JHEP11,167(2012)], [hep-ph/0603079].
- [41] J. Brod and M. Gorbahn, Phys. Rev. **D78**, 034006 (2008), [arXiv:0805.4119].
- [42] G. Isidori, F. Mescia and C. Smith, Nucl. Phys. **B718**, 319 (2005), [hep-ph/0503107].
- [43] A. J. Buras and R. Fleischer, Adv. Ser. Direct. High Energy Phys. **15**, 65 (1998), [65(1997)], [hep-ph/9704376].
- [44] S. Adler *et al.* (E787), Phys. Rev. Lett. **88**, 041803 (2002), [hep-ex/0111091].
- [45] S. Adler *et al.* (E787), Phys. Rev. Lett. **84**, 3768 (2000), [hep-ex/0002015].
- [46] S. S. Adler *et al.* (E787), Phys. Lett. **B537**, 211 (2002), [hep-ex/0201037].
- [47] A. V. Artamonov *et al.* (E949), Phys. Rev. Lett. **101**, 191802 (2008), [arXiv:0808.2459].
- [48] E. Cortina Gil *et al.* (NA62), Phys. Lett. **B791**, 156 (2019), [arXiv:1811.08508].
- [49] G. Ruggiero, NA62 collaboration “Latest measurement of $K^+ \rightarrow \pi^+ \nu \bar{\nu}$ with the NA62 experiment at CERN”, talk at KAON 2019, [https://indico.cern.ch/event/769729/].
- [50] A. J. Buras *et al.*, JHEP **11**, 033 (2015), [arXiv:1503.02693].
- [51] L. S. Littenberg, Phys. Rev. **D39**, 3322 (1989).
- [52] G. Buchalla and G. Isidori, Phys. Lett. **B440**, 170 (1998), [hep-ph/9806501].
- [53] Y. Grossman and Y. Nir, Phys. Lett. **B398**, 163 (1997), [hep-ph/9701313].
- [54] J. K. Ahn *et al.* (KOTO), Phys. Rev. Lett. **122**, 2, 021802 (2019), [arXiv:1810.09655].
- [55] K. Fuyuto, W.-S. Hou and M. Kohda, Phys. Rev. Lett. **114**, 171802 (2015), [arXiv:1412.4397].
- [56] G. D’Ambrosio and G. Isidori, Phys. Lett. **B530**, 108 (2002), [hep-ph/0112135].
- [57] D. Bryman *et al.*, Int. J. Mod. Phys. **A21**, 487 (2006), [hep-ph/0505171].
- [58] A. J. Buras, D. Buttazzo and R. Knegjens, JHEP **11**, 166 (2015), [arXiv:1507.08672].
- [59] X.-G. He, G. Valencia and K. Wong, Eur. Phys. J. **C78**, 6, 472 (2018), [arXiv:1804.07449].
- [60] M. Bordone *et al.*, Eur. Phys. J. **C77**, 9, 618 (2017), [arXiv:1705.10729].
- [61] X.-G. He, J. Tandean and G. Valencia, JHEP **07**, 022 (2019), [arXiv:1903.01242].
- [62] X.-G. He, J. Tandean and G. Valencia, Phys. Lett. **B797**, 134842 (2019), [arXiv:1904.04043].
- [63] L. S. Littenberg and G. Valencia, Phys. Lett. **B385**, 379 (1996), [hep-ph/9512413].
- [64] C.-W. Chiang and F. J. Gilman, Phys. Rev. **D62**, 094026 (2000), [hep-ph/0007063].
- [65] C. Q. Geng, I. J. Hsu and Y. C. Lin, Phys. Rev. **D50**, 5744 (1994), [hep-ph/9406313].
- [66] R. Ogata *et al.* (E391a), Phys. Rev. **D84**, 052009 (2011), [arXiv:1106.3404].
- [67] S. Adler *et al.* (E787), Phys. Rev. **D63**, 032004 (2001), [hep-ex/0009055].
- [68] D. Ambrose *et al.* (E871), Phys. Rev. Lett. **84**, 1389 (2000).
- [69] G. Valencia, Nucl. Phys. **B517**, 339 (1998), [hep-ph/9711377].
- [70] G. D’Ambrosio, G. Isidori and J. Portoles, Phys. Lett. **B423**, 385 (1998), [hep-ph/9708326].
- [71] G. Isidori and R. Unterdorfer, JHEP **01**, 009 (2004), [hep-ph/0311084].
- [72] D. Gomez Dumm and A. Pich, Phys. Rev. Lett. **80**, 4633 (1998), [hep-ph/9801298].
- [73] D. Ambrose *et al.* (BNL E871), Phys. Rev. Lett. **81**, 4309 (1998), [hep-ex/9810007].
- [74] R. Aaij *et al.* (LHCb), Eur. Phys. J. **C77**, 10, 678 (2017), [arXiv:1706.00758].
- [75] Miguel Ramos Pernas, LHCb collaboration “Search for $K_S \rightarrow \mu^+ \mu^-$ at LHCb”, talk at KAON 2019, [https://indico.cern.ch/event/769729/].
- [76] G. D’Ambrosio and T. Kitahara, Phys. Rev. Lett. **119**, 20, 201802 (2017), [arXiv:1707.06999].
- [77] V. Chobanova *et al.*, JHEP **05**, 024 (2018), [arXiv:1711.11030].
- [78] G. D’Ambrosio *et al.*, JHEP **08**, 004 (1998), [hep-ph/9808289].
- [79] C. Dib, I. Dunietz and F. J. Gilman, Phys. Rev. **D39**, 2639 (1989).
- [80] G. Buchalla, G. D’Ambrosio and G. Isidori, Nucl. Phys. **B672**, 387 (2003), [hep-ph/0308008].
- [81] J. R. Batley *et al.* (NA48/1), Phys. Lett. **B576**, 43 (2003), [hep-ex/0309075].
- [82] J. R. Batley *et al.* (NA48/1), Phys. Lett. **B599**, 197 (2004), [hep-ex/0409011].

- [83] S. Friot, D. Greynat and E. De Rafael, Phys. Lett. **B595**, 301 (2004), [hep-ph/0404136].
- [84] G. D'Ambrosio, D. Greynat and M. Knecht, JHEP **02**, 049 (2019), [arXiv:1812.00735].
- [85] G. Isidori, C. Smith and R. Unterdorfer, Eur. Phys. J. **C36**, 57 (2004), [hep-ph/0404127].
- [86] G. Ecker, A. Pich and E. de Rafael, Phys. Lett. **B237**, 481 (1990).
- [87] L. Cappiello, G. D'Ambrosio and M. Miragliuolo, Phys. Lett. **B298**, 423 (1993).
- [88] A. G. Cohen, G. Ecker and A. Pich, Phys. Lett. **B304**, 347 (1993).
- [89] F. Gabbiani and G. Valencia, Phys. Rev. **D66**, 074006 (2002), [hep-ph/0207189].
- [90] E. Abouzaid *et al.* (KTeV), Phys. Rev. **D77**, 112004 (2008), [arXiv:0805.0031].
- [91] A. Lai *et al.* (NA48), Phys. Lett. **B536**, 229 (2002), [hep-ex/0205010].
- [92] J. F. Donoghue and F. Gabbiani, Phys. Rev. **D56**, 1605 (1997), [hep-ph/9702278].
- [93] E. Abouzaid *et al.* (KTeV), Phys. Rev. **D76**, 052001 (2007), [arXiv:0706.4074].
- [94] W. M. Morse *et al.*, Phys. Rev. **D45**, 36 (1992).
- [95] A. Alavi-Harati *et al.* (KTeV), Phys. Rev. **D64**, 012003 (2001), [hep-ex/0010059].
- [96] H. B. Greenlee, Phys. Rev. **D42**, 3724 (1990).
- [97] A. Alavi-Harati *et al.* (KTeV), Phys. Rev. Lett. **93**, 021805 (2004), [hep-ex/0309072].
- [98] A. Alavi-Harati *et al.* (KTeV), Phys. Rev. Lett. **84**, 5279 (2000), [hep-ex/0001006].
- [99] M. V. Diwan, H. Ma and T. L. Trueman, Phys. Rev. **D65**, 054020 (2002), [hep-ph/0112350].
- [100] F. Mescia, C. Smith and S. Trine, JHEP **08**, 088 (2006), [hep-ph/0606081].
- [101] R. Appel *et al.* (E865), Phys. Rev. Lett. **83**, 4482 (1999), [hep-ex/9907045].
- [102] J. R. Batley *et al.* (NA48/2), Phys. Lett. **B677**, 246 (2009), [arXiv:0903.3130].
- [103] S. Adler *et al.* (E787), Phys. Rev. Lett. **79**, 4756 (1997), [hep-ex/9708012].
- [104] H. Ma *et al.* (e865), Phys. Rev. Lett. **84**, 2580 (2000), [hep-ex/9910047].
- [105] H. K. Park *et al.* (HyperCP), Phys. Rev. Lett. **88**, 111801 (2002), [hep-ex/0110033].
- [106] J. R. Batley *et al.* (NA48/2), Phys. Lett. **B697**, 107 (2011), [arXiv:1011.4817].
- [107] G. D'Ambrosio, D. Greynat and M. Knecht, Phys. Lett. (2019), [arXiv:1906.03046].
- [108] J. R. Batley *et al.* (NA48/2), Phys. Lett. **B788**, 552 (2019), [arXiv:1809.02873].
- [109] L. Cappiello *et al.*, Eur. Phys. J. **C72**, 1872 (2012), [Erratum: Eur. Phys. J. **C72**, 2208(2012)], [arXiv:1112.5184].
- [110] J. R. Batley *et al.* (NA48/1), Phys. Lett. **B694**, 301 (2011).
- [111] C. Marin Benito (LHCb), J. Phys. Conf. Ser. **800**, 1, 012031 (2017).
- [112] L. Cappiello, O. Catà and G. D'Ambrosio, Eur. Phys. J. **C78**, 3, 265 (2018), [arXiv:1712.10270].
- [113] G. Ecker, A. Pich and E. de Rafael, Nucl. Phys. **B303**, 665 (1988).
- [114] G. D'Ambrosio and J. Portoles, Phys. Lett. **B386**, 403 (1996), [Erratum: Phys. Lett. **B395**, 389(1997)], [hep-ph/9606213].
- [115] P. Kitching *et al.* (E787), Phys. Rev. Lett. **79**, 4079 (1997), [hep-ex/9708011].
- [116] J. R. Batley *et al.* (NA48/2), Phys. Lett. **B730**, 141 (2014), [arXiv:1310.5499].
- [117] C. Lazzeroni *et al.* (NA62), Phys. Lett. **B732**, 65 (2014), [arXiv:1402.4334].
- [118] A. Alavi-Harati *et al.* (KTeV), Phys. Rev. Lett. **87**, 071801 (2001).
- [119] E. Abouzaid *et al.* (KTeV), Phys. Rev. Lett. **99**, 051804 (2007), [hep-ex/0702039].
- [120] V. Fanti *et al.* (NA48), Phys. Lett. **B458**, 553 (1999).
- [121] G. D'Ambrosio, D. Greynat and G. Vulvert, Eur. Phys. J. **C73**, 12, 2678 (2013), [arXiv:1309.5736].

65. CPT Invariance Tests in Neutral Kaon Decay

Revised August 2019 by M. Antonelli (INFN, Frascati), G. D'Ambrosio (INFN, Napoli) and M.S. Sozzi (Pisa U.).

CPT theorem is based on three assumptions: quantum field theory, locality, and Lorentz invariance, and thus it is a fundamental probe of our basic understanding of particle physics. Strangeness oscillation in $K^0 - \bar{K}^0$ system, described by the equation

$$i \frac{d}{dt} \begin{bmatrix} K^0 \\ \bar{K}^0 \end{bmatrix} = [M - i\Gamma/2] \begin{bmatrix} K^0 \\ \bar{K}^0 \end{bmatrix},$$

where M and Γ are hermitian matrices (see PDG review [1], references [2,3], and KLOE paper [4] for notations and previous literature), allows a very accurate test of *CPT* symmetry; indeed since *CPT* requires $M_{11} = M_{22}$ and $\Gamma_{11} = \Gamma_{22}$, the mass and width eigenstates, $K_{S,L}$, have a *CPT*-violating piece, δ , in addition to the usual *CPT*-conserving parameter ϵ :

$$K_{S,L} = \frac{1}{\sqrt{2(1+|\epsilon_{S,L}|^2)}} \left[(1+\epsilon_{S,L}) K^0 \pm (1-\epsilon_{S,L}) \bar{K}^0 \right]$$

$$\epsilon_{S,L} = \frac{-i\Im(M_{12}) - \frac{1}{2}\Im(\Gamma_{12}) \mp \frac{1}{2} [M_{11} - M_{22} - \frac{i}{2}(\Gamma_{11} - \Gamma_{22})]}{m_L - m_S + i(\Gamma_S - \Gamma_L)/2}$$

$$\equiv \epsilon \pm \delta. \quad (65.1)$$

Using the phase convention $\Im(\Gamma_{12}) = 0$, we determine the phase of ϵ to be $\varphi_{SW} \equiv \arctan \frac{2(m_L - m_S)}{\Gamma_S - \Gamma_L}$. Imposing unitarity to an arbitrary combination of K^0 and \bar{K}^0 wave functions, we obtain the Bell-Steinberger relation [5] connecting *CP* and *CPT* violation in the mass matrix to *CP* and *CPT* violation in the decay; in fact, neglecting $\mathcal{O}(\epsilon)$ corrections to the coefficient of the *CPT*-violating parameter, δ , we can write [4]

$$\left[\frac{\Gamma_S + \Gamma_L}{\Gamma_S - \Gamma_L} + i \tan \phi_{SW} \right] \left[\frac{\Re(\epsilon)}{1+|\epsilon|^2} - i\Im(\delta) \right] = \frac{1}{\Gamma_S - \Gamma_L} \sum_f A_L(f) A_S^*(f), \quad (65.2)$$

where $A_{L,S}(f) \equiv A(K_{L,S} \rightarrow f)$. We stress that this relation is phase-convention-independent. The advantage of the neutral kaon system is that only a few decay modes give significant contributions to the r.h.s. in Eq. (65.2); in fact, defining for the hadronic modes

$$\alpha_i \equiv \frac{1}{\Gamma_S} \langle A_L(i) A_S^*(i) \rangle = \eta_i \mathcal{B}(K_S \rightarrow i),$$

$$i = \pi^0 \pi^0, \pi^+ \pi^- (\gamma), 3\pi^0, \pi^0 \pi^+ \pi^- (\gamma), \quad (65.3)$$

the recent data from CPLEAR, KLOE, KTeV, and NA48 have led to the following determinations (the analysis described in Ref. [4] has been updated by using the recent measurements of K_L branching ratios from KTeV [6, 7], NA48 [8, 9], the results described in the *CP* violation in K_L decays minireview, and the KLOE result [10])

$$\alpha_{\pi^+ \pi^-} = ((1.121 \pm 0.010) + i(1.061 \pm 0.010)) \times 10^{-3},$$

$$\alpha_{\pi^0 \pi^0} = ((0.493 \pm 0.005) + i(0.471 \pm 0.005)) \times 10^{-3},$$

$$\alpha_{\pi^+ \pi^- \pi^0} = ((0 \pm 2) + i(0 \pm 2)) \times 10^{-6},$$

$$|\alpha_{\pi^0 \pi^0 \pi^0}| < 1.5 \times 10^{-6} \text{ at 95\% CL.} \quad (65.4)$$

The semileptonic contribution to the right-handed side of Eq. (65.2) requires the determination of several observables: we

define [2, 3]

$$\begin{aligned} \mathcal{A}(K^0 \rightarrow \pi^- l^+ \nu) &= \mathcal{A}_0(1 - y), \\ \mathcal{A}(K^0 \rightarrow \pi^+ l^- \nu) &= \mathcal{A}_0^*(1 + y^*)(x_+ - x_-)^*, \\ \mathcal{A}(\bar{K}^0 \rightarrow \pi^+ l^- \nu) &= \mathcal{A}_0^*(1 + y^*), \\ \mathcal{A}(\bar{K}^0 \rightarrow \pi^- l^+ \nu) &= \mathcal{A}_0(1 - y)(x_+ + x_-), \end{aligned} \quad (65.5)$$

where x_+ (x_-) describes the violation of the $\Delta S = \Delta Q$ rule in *CPT*-conserving (violating) decay amplitudes, and y parametrizes *CPT* violation for $\Delta S = \Delta Q$ transitions. Taking advantage of their tagged $K^0(\bar{K}^0)$ beams, CPLEAR has measured $\Im(x_+)$, $\Re(x_-)$, $\Im(\delta)$, and $\Re(\delta)$ [11]. These determinations have been improved in Ref. [4] by including the information $A_S - A_L = 4[\Re(\delta) + \Re(x_-)]$ (valid at first order in the small parameters), where $A_{L,S}$ are the K_L and K_S semileptonic charge asymmetries, respectively, from the PDG [12] and the new KLOE semileptonic measurement [13]. Here we are also including the *T*-violating asymmetry measurement from CPLEAR [14] with a finer binning than appearing in the published article.

Table 65.1: Values, errors, and correlation coefficients for $\Re(\delta)$, $\Im(\delta)$, $\Re(x_-)$, $\Im(x_+)$, and $A_S + A_L$ obtained from a combined fit, including KLOE [4, 13] and CPLEAR [14].

	value	Correlations coefficients			
$\Re(\delta)$	$(4.3 \pm 2.7) \times 10^{-4}$	1			
$\Im(\delta)$	$(-0.9 \pm 0.6) \times 10^{-2}$	-0.40	1		
$\Re(x_-)$	$(-0.22 \pm 0.10) \times 10^{-2}$	-0.14	-0.30	1	
$\Im(x_+)$	$(0.06 \pm 0.19) \times 10^{-2}$	-0.12	-0.02	0.34	1
$A_S + A_L$	$(-0.23 \pm 0.38) \times 10^{-2}$	-0.12	-0.29	0.94	0.18

The value $A_S + A_L$ in Table 65.1 can be directly included in the semileptonic contributions to the Bell Steinberger relations in Eq. (65.2)

$$\begin{aligned} \sum_{\pi l \nu} \langle A_L(\pi l \nu) A_S^*(\pi l \nu) \rangle \\ = 2\Gamma(K_L \rightarrow \pi l \nu) (\Re(\epsilon) - \Re(y) - i(\Im(x_+) + \Im(\delta))) \\ = 2\Gamma(K_L \rightarrow \pi l \nu) ((A_S + A_L)/4 - i(\Im(x_+) + \Im(\delta))). \end{aligned} \quad (65.6)$$

Defining

$$\alpha_{\pi l \nu} \equiv \frac{1}{\Gamma_S} \sum_{\pi l \nu} \langle A_L(\pi l \nu) A_S^*(\pi l \nu) \rangle + 2i \frac{\tau_{K_S}}{\tau_{K_L}} \mathcal{B}(K_L \rightarrow \pi l \nu) \Im(\delta), \quad (65.7)$$

we find:

$$\alpha_{\pi l \nu} = ((-0.1 \pm 0.2) + i(-0.1 \pm 0.5)) \times 10^{-5}. \quad (65.8)$$

Table 65.2: Summary of results: values, errors, and correlation coefficients for $\Re(\epsilon)$, $\Im(\delta)$, $\Re(\delta)$, and $\Re(x_-)$.

	value	Correlations coefficients			
$\Re(\epsilon)$	$(161.2 \pm 0.5) \times 10^{-5}$	+1			
$\Im(\delta)$	$(-0.3 \pm 1.4) \times 10^{-5}$	+0.08	1		
$\Re(\delta)$	$(2.6 \pm 2.5) \times 10^{-4}$	+0.00	-0.05	1	
$\Re(x_-)$	$(-2.7 \pm 1.0) \times 10^{-3}$	+0.05	0.13	-0.30	1

Inserting the values of the α parameters into Eq. (65.2), we find

$$\begin{aligned} \Re(\epsilon) &= (161.2 \pm 0.5) \times 10^{-5}, \\ \Im(\delta) &= (-0.3 \pm 1.4) \times 10^{-5}. \end{aligned} \quad (65.9)$$

The complete information on Eq. (65.9) is given in Table 65.2.

Now the agreement with *CPT* conservation, $\Im(\delta) = \Re(\delta) = \Re(x_-) = 0$, is at 18% C.L.

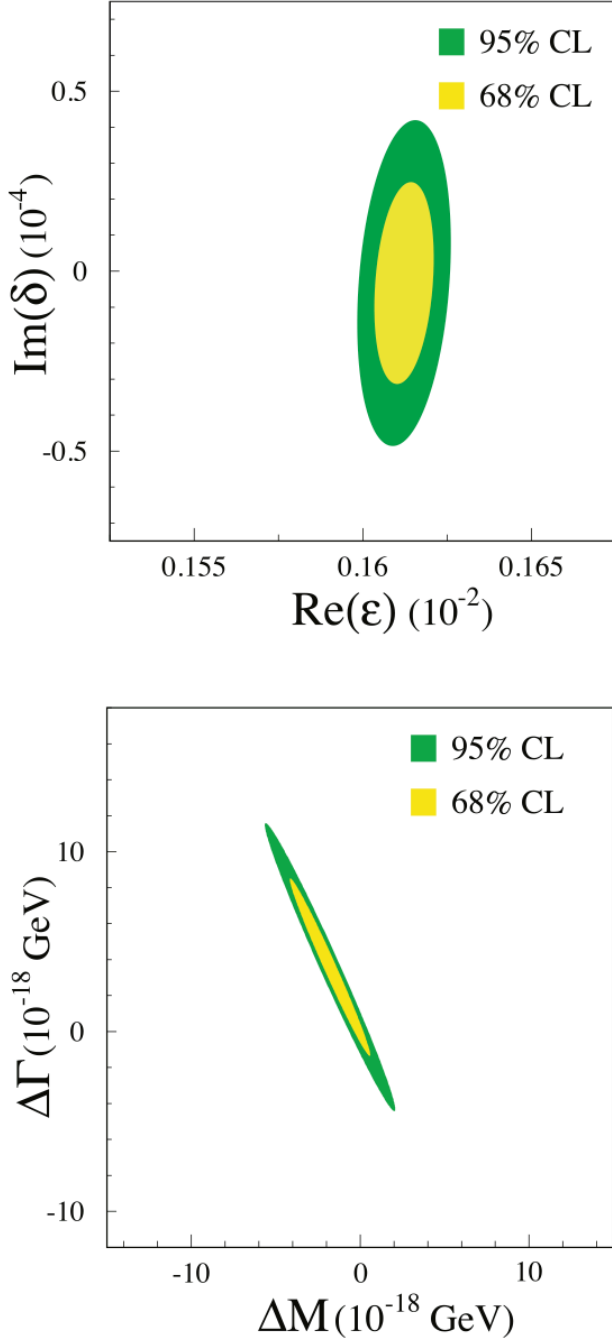


Figure 65.1: Top: allowed region at 68% and 95% C.L. in the $\Re(\epsilon)$, $\Im(\delta)$ plane. Bottom: allowed region at 68% and 95% C.L. in the ΔM , $\Delta\Gamma$ plane.

The allowed region in the $\Re(\epsilon) - \Im(\delta)$ plane at 68% CL and 95% C.L. is shown in the top panel of Fig. 65.1.

The process giving the largest contribution to the size of the allowed region is $K_L \rightarrow \pi^+\pi^-$, through the uncertainty on ϕ_{+-} .

The limits on $\Im(\delta)$ and $\Re(\delta)$ can be used to constrain the $K^0 - \bar{K}^0$ mass and width difference

$$\delta = \frac{i(m_{K^0} - m_{\bar{K}^0}) + \frac{1}{2}(\Gamma_{K^0} - \Gamma_{\bar{K}^0})}{\Gamma_S - \Gamma_L} \cos\phi_{SW} e^{i\phi_{SW}} [1 + \mathcal{O}(\epsilon)].$$

The allowed region in the $\Delta M = (m_{K^0} - m_{\bar{K}^0})$, $\Delta\Gamma = (\Gamma_{K^0} - \Gamma_{\bar{K}^0})$ plane is shown in the bottom panel of Fig. 65.1. As a result, we improve on the previous limits (see for instance, P. Bloch in Ref. [12]) and in the limit $\Gamma_{K^0} - \Gamma_{\bar{K}^0} = 0$ we obtain

$$-4.0 \times 10^{-19} \text{ GeV} < m_{K^0} - m_{\bar{K}^0} < 4.0 \times 10^{-19} \text{ GeV} \quad \text{at 95 \% C.L.}$$

References

- [1] See the “CP Violation in Meson Decays,” in this *Review*.
- [2] L. Maiani, “CP And CPT Violation in Neutral Kaon Decays,” L. Maiani, G. Pancheri, and N. Paver, *The Second DAΦNE Physics Handbook*, Vol. 1,2.
- [3] G. D’Ambrosio, G. Isidori and A. Pugliese, in “2nd DAΦNE Physics Handbook:63-96,” 63–96 (1994), [hep-ph/9411389], URL <http://preprints.cern.ch/cgi-bin/setlink?base=preprint&categ=cern&id=th-7504-94>.
- [4] G. D’Ambrosio and G. Isidori (KLOE), *JHEP* **12**, 011 (2006), [hep-ex/0610034].
- [5] J. S. Bell and J. Steinberger, in “Wolfenstein, L. (ed.): CP violation, 42-57. (In Oxford International Symposium Conference on Elementary Particles),” 195–208, 221–222 (1966), (See Book Index).
- [6] T. Alexopoulos *et al.* (KTeV), *Phys. Rev.* **D70**, 092006 (2004), [hep-ex/0406002].
- [7] E. Abouzaid *et al.* (KTeV), *Phys. Rev.* **D83**, 092001 (2011), [arXiv:1011.0127].
- [8] A. Lai *et al.* (NA48), *Phys. Lett.* **B645**, 26 (2007), [hep-ex/0611052]; A. Lai *et al.* (NA48), *Phys. Lett.* **B602**, 41 (2004), [hep-ex/0410059].
- [9] We thanks G. Isidori and M. Palutan for their contribution to the original analysis [4] performed with KLOE data.
- [10] D. Babusci *et al.* (KLOE), *Phys. Lett.* **B723**, 54 (2013), [arXiv:1301.7623].
- [11] A. Angelopoulos *et al.* (CPLEAR), *Phys. Lett.* **B444**, 52 (1998).
- [12] W. M. Yao *et al.* (Particle Data Group), *J. Phys.* **G33**, 1 (2006).
- [13] A. Anastasi *et al.* (KLOE-2), *JHEP* **09**, 021 (2018), [arXiv:1806.08654].
- [14] P. Bloch, M. Fidecaro, private communication of the data in a finer binning format; A. Angelopoulos *et al.* (CPLEAR), *Phys. Lett.* **B444**, 43 (1998).

66. V_{ud} , V_{us} , the Cabibbo Angle, and CKM Unitarity

Updated November 2019 by E. Blucher (Univ. of Chicago) and W.J. Marciano (BNL)

The Cabibbo-Kobayashi-Maskawa (CKM) [1,2] three-generation quark mixing matrix written in terms of the Wolfenstein parameters (λ, A, ρ, η) [3] nicely illustrates the orthonormality constraint of unitarity as well as central role played by λ .

$$V_{\text{CKM}} = \begin{pmatrix} V_{ud} & V_{us} & V_{ub} \\ V_{cd} & V_{cs} & V_{cb} \\ V_{td} & V_{ts} & V_{tb} \end{pmatrix} = \begin{pmatrix} 1 - \lambda^2/2 & \lambda & A\lambda^3(\rho - i\eta) \\ -\lambda & 1 - \lambda^2/2 & A\lambda^2 \\ A\lambda^3(1 - \rho - i\eta) & -A\lambda^2 & 1 \end{pmatrix} + \mathcal{O}(\lambda^4). \quad (66.1)$$

That cornerstone is a carryover from the two-generation Cabibbo angle, $\lambda = \sin(\theta_{\text{Cabibbo}}) = V_{us}$. Its value is an important component in tests of CKM unitarity.

For some time, the precise value of λ was controversial, with kaon decays suggesting [4] $\lambda \simeq 0.220$, while indirect determinations via V_{ud} obtained from nuclear β -decays implied a somewhat larger $\lambda \simeq 0.225 - 0.230$. This difference resulted in a 2 – 2.5 sigma deviation from the first row unitarity requirement

$$|V_{ud}|^2 + |V_{us}|^2 + |V_{ub}|^2 = 1, \quad (66.2)$$

a potential signal [5] for new physics effects. Below, we describe the current status of V_{ud} , V_{us} , and their associated unitarity test in Eq. (66.2). (Since $|V_{ub}|^2 \simeq 1.7 \times 10^{-5}$ is negligibly small, it is ignored in this discussion.) Eq. (66.2) is currently the most stringent test of unitarity in the CKM matrix. However, as we shall see, it is again showing signs of 2 to 3 sigma inconsistency.

66.1. V_{ud}

Precise values of V_{ud} have been obtained from superallowed nuclear, neutron and pion beta decays. Currently, the best determination of V_{ud} comes from analysis of a set of 14 measured superallowed nuclear beta-decays [5] ($0^+ \rightarrow 0^+$ transitions). Measuring their half-lives, t , and Q values gives the decay rate factors, f , which lead to a precise determination of V_{ud} via [6–10]. . . Based on those studies, one finds the average [11]

$$|V_{ud}|^2 = 0.97148(20)/(1 + \Delta_R^V), \quad (66.3)$$

where Δ_R^V denotes the so-called inner or universal electroweak radiative corrections (RC) to superallowed nuclear beta decays. A dispersion relation (DR) calculational approach [12] to quantum loop corrections, specifically the gamma-W box diagram, gives $\Delta_R^V = 0.02467(22)$. Because of its small uncertainty and more rigorous theoretical footing, we use that value below. A somewhat different approach [13] found $\Delta_R^V = 0.02426(32)$. These recent values are roughly consistent. Both are larger than the 2018 PDG value of $0.02361(38)$. Implications and possible nuclear physics modifications of those studies are still under scrutiny [14]. Nevertheless, currently the 14 most precisely measured superallowed transitions [11] lead to the DR based weighted average of

$$V_{ud} = 0.97370(10)_{\text{exp.,nucl.}}(10)_{\text{RC}} \text{ (superallowed)}, \quad (66.4)$$

which, assuming unitarity, corresponds to the relatively large $\lambda = 0.2278(6)$. This recent determination of V_{ud} has shifted significantly down compared to the 2018 value [11] of $0.97420(21)$. Taken at face value, that reduced V_{ud} would seem to violate the first row unitarity requirement and thus suggest the presence of “new physics”.

Measurements of the neutron lifetime, τ_n , the ratio of axial-vector/vector couplings, $g_A \equiv G_A/G_V$, via neutron decay asymmetries combined with the inner radiative corrections can also be used to determine V_{ud} :

$$|V_{ud}|^2 = \frac{5024.7 \text{ s}}{\tau_n(1 + 3g_A^2)(1 + \Delta_R^V)}, \quad (66.5)$$

where Δ_R^V represents the same inner electroweak radiative corrections [7,8] as discussed above.

Using the current world averages

$$\begin{aligned} \tau_n^{\text{ave}} &= 879.4(6) \text{ s} \quad (1.5 \text{ PDG scale factor}) \\ g_A^{\text{ave}} &= 1.2762(5) \end{aligned} \quad (66.6)$$

leads to

$$|V_{ud}| = 0.9733(3)_{\tau_n(3)} g_A(1)_{\text{RC}}, \quad (66.7)$$

for an inner radiative correction of $0.02467(22)$ while for $0.02426(32)$ it increases to $0.9735(5)$. Those values are both low, compared with CKM unitarity expectations and the superallowed nuclear beta decay result reported above. Reconciliation suggests a shorter neutron lifetime near 878 s or a somewhat smaller g_A . Future neutron studies [15] are expected to resolve any current inconsistencies and significantly reduce the uncertainties in g_A and τ_n .

The PIBETA experiment at PSI measured the very small ($\mathcal{O}(10^{-8})$) branching ratio for $\pi^+ \rightarrow \pi^0 e^+ \nu_e$ with about $\pm 0.6\%$ precision. Its result gives [16]

$$|V_{ud}| = 0.9739(27) \left[\frac{BR(\pi^+ \rightarrow e^+ \nu_e(\gamma))}{1.2325 \times 10^{-4}} \right]^{\frac{1}{2}} \quad (66.8)$$

which is normalized using the very precisely measured $BR(\pi^+ \rightarrow e^+ \nu_e(\gamma)) = 1.2325(23) \times 10^{-4}$ [6], rather than the theoretical branching ratio of $1.2350(2) \times 10^{-4}$ which if used, would increase $|V_{ud}|$ to $0.9749(27)$. Theoretical uncertainties in pion beta decay are very small and would allow for a factor of 2 to 3 improvement of its small branching ratio. However, it would be difficult to have it compete with superallowed beta decays or future neutron decay efforts at direct $|V_{ud}|$ determination.

66.2. V_{us}

$|V_{us}|$ may be directly obtained from kaon decays, hyperon decays, and tau decays. Early determinations most often used $K\ell 3$ decays:

$$\Gamma_{K\ell 3} = \frac{G_F^2 M_K^5}{192\pi^3} S_{EW}(1 + \delta_K^\ell + \delta_{SU2}) C^2 |V_{us}|^2 f_+^2(0) I_K^\ell. \quad (66.9)$$

Here, ℓ refers to either e or μ , G_F is the Fermi constant, M_K is the kaon mass, S_{EW} is the short-distance radiative correction, δ_K^ℓ is the mode-dependent long-distance radiative correction, $f_+(0)$ is the calculated form factor at zero momentum transfer for the $\ell\nu$ system, and I_K^ℓ is the phase-space integral, which depends on measured semileptonic form factors. For charged kaon decays, δ_{SU2} is the deviation from one of the ratio of $f_+(0)$ for the charged to neutral kaon decay; it is zero for the neutral kaon. C^2 is 1 (1/2) for neutral (charged) kaon decays. Most early determinations of $|V_{us}|$ were based solely on $K \rightarrow \pi e \nu$ decays; $K \rightarrow \pi \mu \nu$ decays were not used because of large uncertainties in I_K^μ . The experimental measurements are the semileptonic decay widths (based on the semileptonic branching fractions and lifetime) and form factors (allowing calculation of the phase space integrals). Theory is needed for S_{EW} , δ_K^ℓ , δ_{SU2} , and $f_+(0)$.

Many measurements during the last 15 years have resulted in a shift in $|V_{us}|$. Most importantly, the $K \rightarrow \pi e \nu$ branching fractions are significantly different than earlier PDG averages, probably as a result of inadequate treatment of radiation in older experiments. This effect was first observed by BNL E865 [17] in the charged kaon system and then by KTeV [18,19] in the neutral kaon system; subsequent measurements were made by KLOE [20–23], NA48 [24–26], and ISTRA+ [27]. Current averages (*e.g.*, by the PDG [28] or Flavianet [29]) of the semileptonic branching fractions are based only on recent, high-statistics experiments where the treatment of radiation is clear. In addition to measurements of branching fractions, new measurements of lifetimes [30] and form factors [31–35], have resulted in improved precision for all of the experimental inputs to $|V_{us}|$. Precise measurements of form factors for $K_{\mu 3}$ decay make it possible to use both semileptonic decay modes to extract V_{us} .

Following the analysis of Moulson [36], the Flavianet group [29], and more recent updates [37], one finds, after including the isospin violating effect, δ_{SU2} , the values of $|V_{us}|f_+(0)$ in Table 66.1. The average of these measurements, including correlation effects [36], gives

$$f_+(0)|V_{us}| = 0.2165(4). \quad (66.10)$$

Lattice QCD calculations of $f_+(0)$ have been carried out for 2, 2+1, and 2+1+1 quark flavors and range from about 0.96 to 0.97. Here, we use recent FLAG averages [38] for 2+1 and 2+1+1 flavors:

$$\begin{aligned} f_+(0) &= 0.9677(27) \quad N_f = 2 + 1 \\ f_+(0) &= 0.9706(27) \quad N_f = 2 + 1 + 1 \end{aligned} \quad (66.11)$$

One finds from Eq. (66.10) and Eq. (66.11),

$$\begin{aligned} |V_{us}| &= 0.2237(4)_{\text{exp+RC}}(6)_{\text{lattice}} \quad (N_f = 2 + 1, K_{\ell 3} \text{ decays}) \\ &= 0.2231(4)_{\text{exp+RC}}(6)_{\text{lattice}} \quad (N_f = 2 + 1 + 1, K_{\ell 3} \text{ decays}) \end{aligned} \quad (66.12)$$

Table 66.1: $|V_{us}|f_+(0)$ from $K\ell 3$.

Decay Mode	$ V_{us} f_+(0)$
$K^\pm e 3$	0.2169 ± 0.0008
$K^\pm \mu 3$	0.2167 ± 0.0011
$K_L e 3$	0.2164 ± 0.0006
$K_L \mu 3$	0.2167 ± 0.0006
$K_S e 3$	0.2156 ± 0.0013
Average (including correlation effects [36])	0.2165 ± 0.0004

A value of V_{us} can also be obtained from a comparison of the radiative inclusive decay rates for $K \rightarrow \mu\nu(\gamma)$ and $\pi \rightarrow \mu\nu(\gamma)$ combined with a lattice gauge theory calculation of f_{K^+}/f_{π^+} via

$$\frac{|V_{us}|f_{K^+}}{|V_{ud}|f_{\pi^+}} = 0.23871(20) \left[\frac{\Gamma(K \rightarrow \mu\nu(\gamma))}{\Gamma(\pi \rightarrow \mu\nu(\gamma))} \right]^{\frac{1}{2}} \quad (66.13)$$

with the small error coming from electroweak radiative corrections [39]. Employing

$$\frac{\Gamma(K \rightarrow \mu\nu(\gamma))}{\Gamma(\pi \rightarrow \mu\nu(\gamma))} = 1.3367(28), \quad (66.14)$$

which includes $\Gamma(K \rightarrow \mu\nu(\gamma)) = 5.134(11) \times 10^7 \text{s}^{-1}$ [36,40], leads to

$$\frac{|V_{us}|f_{K^+}}{|V_{ud}|f_{\pi^+}} = 0.27600(37). \quad (66.15)$$

Employing the FLAG [38] lattice QCD averages for the isospin broken decay constants

$$\begin{aligned} \frac{f_{K^+}}{f_{\pi^+}} &= 1.1917(37) \quad N_f = 2 + 1 \\ &= 1.1932(19) \quad N_f = 2 + 1 + 1. \end{aligned} \quad (66.16)$$

along with the value of $|V_{ud}|$ in Eq. (66.4) leads to

$$\begin{aligned} |V_{us}| &= 0.2255(8) \quad (N_f = 2 + 1, K_{\mu 2} \text{ decays}) \\ &= 0.2252(5) \quad (N_f = 2 + 1 + 1, K_{\mu 2} \text{ decays}) \end{aligned} \quad (66.17)$$

Together, weighted averages of the $K\ell 3$ (Eq. (66.12)) and $K_{\mu 2}$ (Eq. (66.17)) values give similar results for $N_f = 2 + 1$ and $2 + 1 + 1$ flavors:

$$\begin{aligned} |V_{us}| &= 0.2245(5) \quad N_f = 2 + 1 \\ |V_{us}| &= 0.2245(4) \quad N_f = 2 + 1 + 1. \end{aligned} \quad (66.18)$$

Note that the differences between $K\ell 3$ and $K_{\mu 2}$ values for V_{us} differ by 2 and 3 sigma, respectively, for $N_f = 2 + 1$ and $2 + 1 + 1$ flavors. One should, therefore, scale the uncertainties in Eq. (66.18) accordingly. For that reason, we employ an error scale factor of 2 in the uncertainty, $|V_{us}| = 0.2245(8)$, when we consider the first row test of CKM unitarity.

It should be mentioned that hyperon decay fits suggest [41]

$$|V_{us}| = 0.2250(27) \quad (\text{Hyperon Decays}) \quad (66.19)$$

modulo SU(3) breaking effects that could shift that value up or down. We note that a representative effort [42] that incorporates SU(3) breaking found $V_{us} = 0.226(5)$. Strangeness changing tau decays, averaging both inclusive and exclusive measurements, give [43]

$$|V_{us}| = 0.2221(13) \quad (\text{Tau Decays}), \quad (66.20)$$

which differs by about 2 sigma from the kaon determination discussed above, and would, if combined with V_{ud} from super-allowed beta decays, lead to a 4 sigma deviation from unitarity. This discrepancy results mainly from the inclusive tau decay results that rely on Finite Energy Sum Rule techniques and assumptions, as well as experimental uncertainties. Recent investigation of that approach suggests a larger value for V_{us} , which is more in accord with other determinations [44].

Employing the values of V_{ud} and V_{us} with an error scale factor of 2 from Eq. (66.4) and Eq. (66.18), respectively, leads to the unitarity consistency check

$$|V_{ud}|^2 + |V_{us}|^2 + |V_{ub}|^2 = 0.9985(3)(4). \quad (66.21)$$

where the first error is the uncertainty from $|V_{ud}|^2$ and the second error is the uncertainty from $|V_{us}|^2$ for both $N_f = 2 + 1 + 1$. One finds an overall 3 sigma deviation from unitarity. That deviation could be due a problem with $|V_{ud}|$ theory (RC or NP), the lattice determination of $f_+(0)$ or new physics.

66.3. CKM Unitarity Constraints

The current 3 sigma experimental disagreement with unitarity, $|V_{ud}|^2 + |V_{us}|^2 + |V_{ub}|^2 = 0.9985(5)$, still provides strong confirmation of Standard Model radiative corrections (which range between 3-4% depending on the nucleus used) at a high significance level [45]. In addition, it implies constraints on ‘‘New Physics’’ effects at both the tree and quantum loop levels. Those effects could be in the form of contributions to nuclear beta decays, K decays and/or muon decays, with the last of these providing normalization via the muon lifetime [46], which is used to obtain the Fermi constant, $G_\mu = 1.1663787(6) \times 10^{-5} \text{GeV}^{-2}$.

In the following examples, we illustrate the implications of CKM unitarity for (1) exotic muon decays [47] (beyond ordinary muon decay $\mu^+ \rightarrow e^+ \nu_e \bar{\nu}_\mu$) and (2) new heavy quark mixing V_{uD} [48]. Other examples in the literature [49,50] include Z_χ boson quantum loop effects, supersymmetry, leptoquarks, compositeness etc.

Exotic Muon Decays

If additional lepton flavor violating decays such as $\mu^+ \rightarrow e^+ \bar{\nu}_e \nu_\mu$ (wrong neutrinos) occur, they would cause confusion in searches for neutrino oscillations at, for example, muon storage rings/neutrino factories or other neutrino sources from muon decays. Calling the rate for all such decays $\Gamma(\text{exotic } \mu \text{ decays})$, they should be subtracted before the extraction of G_μ and normalization of the CKM matrix. Since that is not done and unitarity works, one has (at one-sided 95% CL)

$$|V_{ud}|^2 + |V_{us}|^2 + |V_{ub}|^2 = 1 - BR(\text{exotic } \mu \text{ decays}) \geq 0.9977 \quad (66.22)$$

or

$$BR(\text{exotic } \mu \text{ decays}) \leq 0.0023. \quad (66.23)$$

This bound is a factor of 10 better than the direct experimental bound on $\mu^+ \rightarrow e^+ \bar{\nu}_e \nu_\mu$.

New Heavy Quark Mixing

Heavy D quarks naturally occur in fourth quark generation models and some heavy quark “new physics” scenarios such as E_6 grand unification. Their mixing with ordinary quarks gives rise to V_{uD} , which is constrained by unitarity (one sided 95% CL)

$$\begin{aligned} |V_{ud}|^2 + |V_{us}|^2 + |V_{ub}|^2 &= 1 - |V_{uD}|^2 \geq 0.9977 \\ |V_{uD}| &\leq 0.05. \end{aligned} \quad (66.24)$$

A similar constraint applies to heavy neutrino mixing and the couplings $V_{\mu N}$ and V_{eN} .

References:

1. N. Cabibbo, Phys. Rev. Lett. **10**, 531 (1963).
2. M. Kobayashi and T. Maskawa, Prog. Theor. Phys. **49**, 652 (1973).
3. L. Wolfenstein, Phys. Rev. Lett. **51**, 1945 (1983).
4. S. Eidelman *et al.* [Particle Data Group], Phys. Lett. **B592**, 1 (2004).
5. I.S. Towner and J.C. Hardy Rep. Prog. Phys. **73**, 046301 (2010).
6. W.J. Marciano and A. Sirlin, Phys. Rev. Lett. **71**, 3629 (1993).
7. A. Czarnecki, W.J. Marciano, and A. Sirlin, Phys. Rev. **D70**, 093006 (2004) [hep-ph/0406324].
8. W.J. Marciano and A. Sirlin, Phys. Rev. Lett. **96**, 032002 (2006) [hep-ph/0510099].
9. I.S. Towner and J.C. Hardy, Phys. Rev. **C77**, 025501 (2008).
10. J.C. Hardy and I.S. Towner, Phys. Rev. **C79**, 055502 (2009).
11. J.C. Hardy and I.S. Towner, Phys. Rev. **C91**, 0255012 (2015); PoS **CKM 2016**, 028 (2016).
12. C. Y. Seng, M. Gorchtein, H. H. Patel, and M. J. Ramsey-Musolf, Phys. Rev. Lett. **121**, 241804 (2018).
13. A.Czarnecki, W. J. Marciano, and A. Sirlin, Phys. Rev. **D100**, 073008 (2019).
14. C. Y. Seng, M. Gorchtein, and M. J. Ramsey-Musolf, Phys. Rev. **D100**, 013001 (2019); M. Gorchtein, Phys. Rev. **D123**, 042503 (2019).
15. H. Abele, Prog. in Part. Nucl. Phys. **60**, 1 (2008).
16. D. Poganic *et al.*, Phys. Rev. Lett. **93**, 181803 (2004) [hep-ex/0312030]; A. Czarnecki, W. J. Marciano and A. Sirlin, arXiv:1911.04685 [hep-ph].
17. A. Sher *et al.*, Phys. Rev. Lett. **91**, 261802 (2003).
18. T. Alexopoulos *et al.* [KTeV Collab.], Phys. Rev. Lett. **93**, 181802 (2004) [hep-ex/0406001].
19. T. Alexopoulos *et al.* [KTeV Collab.], Phys. Rev. **D70**, 092006 (2004) [hep-ex/0406002].
20. F. Ambrosino *et al.* [KLOE Collab.], Phys. Lett. **B632**, 43 (2006) [hep-ex/0508027].
21. F. Ambrosino *et al.* [KLOE Collab.], Phys. Lett. **B638**, 140 (2006) [hep-ex/0603041].
22. F. Ambrosino *et al.* [KLOE Collab.], Phys. Lett. **B636**, 173 (2006) [hep-ex/0601026].
23. F. Ambrosino *et al.* [KLOE Collab.], PoS **HEP2005**, 287 (2006) [hep-ex/0510028].
24. A. Lai *et al.* [NA48 Collab.], Phys. Lett. **B602**, 41 (2004) [hep-ex/0410059].
25. A. Lai *et al.* [NA48 Collab.], Phys. Lett. **B645**, 26 (2007) [hep-ex/0611052].
26. J.R. Batley *et al.* [NA48/2 Collab.], Eur. Phys. J. **C50**, 329 (2007) [hep-ex/0702015].
27. V.I. Romanovsky *et al.*, [hep-ex/0704.2052].
28. K.A. Olive *et al.* [Particle Data Group], Chin. Phys. C **38**, 090001 (2014).
29. Flavianet Working Group on Precise SM Tests in K Decays, M. Antonelli *et al.*, Eur. Phys. J. **C69**, 399 (2010). For a detailed review, see M. Antonelli *et al.*, [hep-ph/0907.5386].
30. F. Ambrosino *et al.* [KLOE Collab.], Phys. Lett. **B626**, 15 (2005) [hep-ex/0507088].
31. T. Alexopoulos *et al.* [KTeV Collab.], Phys. Rev. **D70**, 092007 (2004) [hep-ex/0406003].
32. E. Abouzaid *et al.* [KTeV Collab.], Phys. Rev. **D74**, 097101 (2006) [hep-ex/0608058].
33. F. Ambrosino *et al.* [KLOE Collab.], Phys. Lett. **B636**, 166 (2006) [hep-ex/0601038].
34. A. Lai *et al.* [NA48 Collab.], Phys. Lett. **B604**, 1 (2004) [hep-ex/0410065].
35. O.P. Yushchenko *et al.*, Phys. Lett. **B589**, 111 (2004) [hep-ex/0404030].
36. M. Moulson, [hep-ex/1704.04104]; PoS **CKM 2016**, 033 (2017).
37. E. Passemar, talk at CKM2018, <https://zenodo.org/record/2565480>.
38. S. Aoki *et al.* [Flavour Lattice Averaging Group], arXiv:1902.08191 [hep-lat] based on A. Bazavov *et al.*, Phys. Rev. Lett. **112**, 112001 (2014) [arXiv:1312.1228 [hep-ph]]; N. Carrasco, P. Lami, V. Lubich, L. Riggio, S. Simula and C. Tarantino, Phys. Rev. **D93**, 114512 (2016) [arXiv:1602.04113 [hep-lat]]; A. Bazavov *et al.*, Phys. Rev. **D87**, 073012 (2013) [arXiv:1212.4993 [hep-lat]]; P. A. Boyle *et al.* [RBC/UKQCD Collaboration], JHEP **1506**, 164 (2015) [arXiv:1504.01692 [hep-lat]] A. Bazavov *et al.*, Phys. Rev. **D98**, 074512 (2018) [arXiv:1712.09262 [hep-lat]]; T. Blum *et al.* [RBC and UKQCD Collaborations], Phys. Rev. **D93**, 074505 (2016) [arXiv:1411.7017 [hep-lat]]; R. J. Dowdall, C. T. H. Davies, G. P. Lepage and C. McNeile, Phys. Rev. **D88**, 074504 (2013) [arXiv:1303.1670 [hep-lat]]; N. Carrasco *et al.*, Phys. Rev. **D91**, 054507 (2015) [arXiv:1411.7908 [hep-lat]]; E. Follana *et al.* [HPQCD and UKQCD Collaborations], Phys. Rev. Lett. **100**, 062002 (2008) [arXiv:0706.1726 [hep-lat]]; A. Bazavov *et al.* [MILC Collaboration], PoS **LATTICE 2010**, 074 (2010) [arXiv:1012.0868 [hep-lat]]; S. Durr *et al.*, Phys. Rev. **D81**, 054507 (2010) [arXiv:1001.4692 [hep-lat]]; S. Durr *et al.*, Phys. Rev. **D95**, 054513 (2017) [arXiv:1601.05998 [hep-lat]] V. G. Bornyakov *et al.* [QCDSF-UKQCD Collaboration], Phys. Lett. **B767**, 366 (2017) [arXiv:1612.04798 [hep-lat]].
39. V. Cirigliano and H. Neufeld, Phys. Lett. **B700**, 7 (2011); W.J. Marciano, Phys. Rev. Lett. **93**, 231803 (2004) [hep-ph/0402299].
40. D. Babusci *et al.* [KLOE Collab.], Phys. Lett. **B738**, 128 (2014) [arXiv:1407.2028].
41. N. Cabibbo, E.C. Swallow, and R. Winston, Phys. Rev. Lett. **92**, 251803 (2004) [hep-ph/0307214].
42. V. Mateu and A. Pich, JHEP **0510**, 041 (2005).
43. Y. S. Amhis *et al.* [HFLAV Collaboration], arXiv:1909.12524 [hep-ex].
44. R. J. Hudspith, R. Lewis, K. Maltman and J. Zanotti, Phys. Lett. **B781**, 206 (2018) [arXiv:1702.01767 [hep-ph]]; P. Boyle *et al.* [RBC and UKQCD Collaborations], Phys. Rev. Lett. **121**, 202003 (2018) [arXiv:1803.07228 [hep-lat]].
45. A. Sirlin, Rev. Mod. Phys. **50**, 573 (1978).
46. D. Webber *et al.* [MuLan Collab.], Phys. Rev. Lett. **106**, 041803 (2011); V. Tishchenko *et al.* [MuLan Collab.], Phys. Rev. **D87**, 052003 (2013).
47. K.S. Babu and S. Pakvasa, hep-ph/0204236.
48. W. Marciano and A. Sirlin, Phys. Rev. Lett. **56**, 22 (1986); P. Langacker and D. London, Phys. Rev. **D38**, 886 (1988).
49. W. Marciano and A. Sirlin, Phys. Rev. **D35**, 1672 (1987).
50. R. Barbieri *et al.*, Phys. Lett. **156B**, 348 (1985); K. Hagiwara *et al.*, Phys. Rev. Lett. **75**, 3605 (1995); A. Kurylov and M. Ramsey-Musolf, Phys. Rev. Lett. **88**, 071804 (2000); S. Bauman, J. Erler, and M. Ramsey-Musolf, Phys. Rev. **D87**, 035012 (2013).

67. CP Violation in K_L Decays

Updated April 2016 by L. Wolfenstein (Carnegie-Mellon University), C.-J. Lin (LBNL), and T.G. Trippe (LBNL).

The symmetries C (particle-antiparticle interchange) and P (space inversion) hold for strong and electromagnetic interactions. After the discovery of large C and P violation in the weak interactions, it appeared that the product CP was a good symmetry. In 1964 CP violation was observed in K^0 decays at a level given by the parameter $\epsilon \approx 2.3 \times 10^{-3}$.

A unified treatment of CP violation in K , D , B , and B_s mesons is given in “ CP Violation in Meson Decays” by D. Kirkby and Y. Nir in this *Review*. A more detailed review including a thorough discussion of the experimental techniques used to determine CP violation parameters is given in a book by K. Kleinknecht [1]. Here we give a concise summary of the formalism needed to define the parameters of CP violation in K_L decays, and a description of our fits for the best values of these parameters.

67.1. Formalism for CP violation in Kaon decay

CP violation has been observed in the semi-leptonic decays $K_L^0 \rightarrow \pi^\pm \ell^\pm \nu$, and in the nonleptonic decay $K_L^0 \rightarrow 2\pi$. The experimental numbers that have been measured are

$$A_L = \frac{\Gamma(K_L^0 \rightarrow \pi^- \ell^+ \nu) - \Gamma(K_L^0 \rightarrow \pi^+ \ell^- \nu)}{\Gamma(K_L^0 \rightarrow \pi^- \ell^+ \nu) + \Gamma(K_L^0 \rightarrow \pi^+ \ell^- \nu)} \quad (67.1a)$$

$$\begin{aligned} \eta_{+-} &= A(K_L^0 \rightarrow \pi^+ \pi^-) / A(K_S^0 \rightarrow \pi^+ \pi^-) \\ &= |\eta_{+-}| e^{i\phi_{+-}} \end{aligned} \quad (67.1b)$$

$$\begin{aligned} \eta_{00} &= A(K_L^0 \rightarrow \pi^0 \pi^0) / A(K_S^0 \rightarrow \pi^0 \pi^0) \\ &= |\eta_{00}| e^{i\phi_{00}}. \end{aligned} \quad (67.1c)$$

CP violation can occur either in the $K^0 - \bar{K}^0$ mixing or in the decay amplitudes. Assuming CPT invariance, the mass eigenstates of the $K^0 - \bar{K}^0$ system can be written

$$|K_S\rangle = p|K^0\rangle + q|\bar{K}^0\rangle, \quad |K_L\rangle = p|K^0\rangle - q|\bar{K}^0\rangle. \quad (67.2)$$

If CP invariance held, we would have $q = p$ so that K_S would be CP -even and K_L CP -odd. (We define $|\bar{K}^0\rangle$ as $CP|K^0\rangle$.) CP violation in $K^0 - \bar{K}^0$ mixing is then given by the parameter $\tilde{\epsilon}$ where

$$\frac{p}{q} = \frac{(1 + \tilde{\epsilon})}{(1 - \tilde{\epsilon})}. \quad (67.3)$$

CP violation can also occur in the decay amplitudes

$$A(K^0 \rightarrow \pi\pi(I)) = A_I e^{i\delta_I}, \quad A(\bar{K}^0 \rightarrow \pi\pi(I)) = A_I^* e^{i\delta_I}, \quad (67.4)$$

where I is the isospin of $\pi\pi$, δ_I is the final-state phase shift, and A_I would be real if CP invariance held. The CP -violating observables are usually expressed in terms of ϵ and ϵ' defined by

$$\eta_{+-} = \epsilon + \epsilon', \quad \eta_{00} = \epsilon - 2\epsilon'. \quad (67.5a)$$

One can then show [2]

$$\epsilon = \tilde{\epsilon} + i (\text{Im } A_0 / \text{Re } A_0), \quad (67.5b)$$

$$\sqrt{2}\epsilon' = i e^{i(\delta_2 - \delta_0)} (\text{Re } A_2 / \text{Re } A_0) (\text{Im } A_2 / \text{Re } A_2 - \text{Im } A_0 / \text{Re } A_0), \quad (67.5c)$$

$$A_L = 2\text{Re } \epsilon / (1 + |\epsilon|^2) \approx 2\text{Re } \epsilon. \quad (67.5d)$$

In Eqs. (67.5a), small corrections [3] of order $\epsilon' \times \text{Re}(A_2/A_0)$ are neglected, and Eq. (67.5d) assumes the $\Delta S = \Delta Q$ rule.

The quantities $\text{Im } A_0$, $\text{Im } A_2$, and $\text{Im } \tilde{\epsilon}$ depend on the choice of phase convention, since one can change the phases of K^0 and \bar{K}^0 by a transformation of the strange quark state $|s\rangle \rightarrow |s\rangle e^{i\alpha}$; of course, observables are unchanged. It is possible by a choice of phase convention to set $\text{Im } A_0$ or $\text{Im } A_2$ or $\text{Im } \tilde{\epsilon}$ to zero, but none of these is zero with the usual phase conventions in the Standard Model. The choice $\text{Im } A_0 = 0$ is called the Wu-Yang phase convention [4], in which

case $\epsilon = \tilde{\epsilon}$. The value of ϵ' is independent of phase convention, and a nonzero value demonstrates CP violation in the decay amplitudes, referred to as direct CP violation. The possibility that direct CP violation is essentially zero, and that CP violation occurs only in the mixing matrix, was referred to as the superweak theory [5].

By applying CPT invariance and unitarity the phase of ϵ is given approximately by

$$\phi_\epsilon \approx \tan^{-1} \frac{2(m_{K_L} - m_{K_S})}{\Gamma_{K_S} - \Gamma_{K_L}} \approx 43.52 \pm 0.05^\circ, \quad (67.6a)$$

while Eq. (67.5c) gives the phase of ϵ' to be

$$\phi_{\epsilon'} = \delta_2 - \delta_0 + \frac{\pi}{2} \approx 42.3 \pm 1.5^\circ, \quad (67.6b)$$

where the numerical value is based on an analysis of $\pi - \pi$ scattering using chiral perturbation theory [6]. The approximation in Eq. (67.6a) depends on the assumption that direct CP violation is very small in all K^0 decays. This is expected to be good to a few tenths of a degree, as indicated by the small value of ϵ' and of η_{+-} and η_{00} , the CP -violation parameters in the decays $K_S \rightarrow \pi^+ \pi^- \pi^0$ [7], and $K_S \rightarrow \pi^0 \pi^0 \pi^0$ [8]. The relation in Eq. (67.6a) is exact in the superweak theory, so this is sometimes called the superweak-phase ϕ_{SW} . An important point for the analysis is that $\cos(\phi_{\epsilon'} - \phi_\epsilon) \simeq 1$. The consequence is that only two real quantities need be measured, the magnitude of ϵ and the value of (ϵ'/ϵ) , including its sign. The measured quantity $|\eta_{00}/\eta_{+-}|^2$ is very close to unity so that we can write

$$|\eta_{00}/\eta_{+-}|^2 \approx 1 - 6\text{Re}(\epsilon'/\epsilon) \approx 1 - 6\epsilon'/\epsilon, \quad (67.7a)$$

$$\text{Re}(\epsilon'/\epsilon) \approx \frac{1}{3}(1 - |\eta_{00}/\eta_{+-}|). \quad (67.7b)$$

From the experimental measurements in this edition of the *Review*, and the fits discussed in the next section, one finds

$$|\epsilon| = (2.228 \pm 0.011) \times 10^{-3}, \quad (67.8a)$$

$$\phi_\epsilon = (43.5 \pm 0.5)^\circ, \quad (67.8b)$$

$$\text{Re}(\epsilon'/\epsilon) \approx \epsilon'/\epsilon = (1.66 \pm 0.23) \times 10^{-3}, \quad (67.8c)$$

$$\phi_{+-} = (43.4 \pm 0.5)^\circ, \quad (67.8d)$$

$$\phi_{00} - \phi_{+-} = (0.34 \pm 0.32)^\circ, \quad (67.8e)$$

$$A_L = (3.32 \pm 0.06) \times 10^{-3}. \quad (67.8f)$$

Direct CP violation, as indicated by ϵ'/ϵ , is expected in the Standard Model. However, the numerical value cannot be reliably predicted because of theoretical uncertainties [9]. The value of A_L agrees with Eq. (67.5d). The values of ϕ_{+-} and $\phi_{00} - \phi_{+-}$ are used to set limits on CPT violation [see “Tests of Conservation Laws”].

67.2. Fits for K_L^0 CP -violation parameters

In recent years, K_L^0 CP -violation experiments have improved our knowledge of CP -violation parameters, and their consistency with the expectations of CPT invariance and unitarity. To determine the best values of the CP -violation parameters in $K_L^0 \rightarrow \pi^+ \pi^-$ and $\pi^0 \pi^0$ decay, we make two types of fits, one for the phases ϕ_{+-} and ϕ_{00} jointly with Δm and τ_S , and the other for the amplitudes $|\eta_{+-}|$ and $|\eta_{00}|$ jointly with the $K_L^0 \rightarrow \pi\pi$ branching fractions.

67.2.1. Fits to ϕ_{+-} , ϕ_{00} , $\Delta\phi$, Δm , and τ_S data :

These are joint fits to the data on ϕ_{+-} , ϕ_{00} , the phase difference $\Delta\phi = \phi_{00} - \phi_{+-}$, the $K_L^0 - K_S^0$ mass difference Δm , and the K_S^0 mean life τ_S , including the effects of correlations.

Measurements of ϕ_{+-} and ϕ_{00} are highly correlated with Δm and τ_S . Some measurements of τ_S are correlated with Δm . The correlations are given in the footnotes of the ϕ_{+-} and ϕ_{00} sections of the K_L^0 Listings, and the τ_S section of the K_S^0 Listings.

In most cases, the correlations are quoted as 100%, *i.e.*, with the value and error of ϕ_{+-} or ϕ_{00} given at a fixed value of Δm and τ_S , with additional terms specifying the dependence of the value on Δm and τ_S . These cases lead to diagonal bands in Figs. 67.1 and 67.2. The KTeV experiment [10] quotes its results as values of Δm , τ_S , ϕ_ϵ , $\text{Re}(\epsilon'/\epsilon)$, and $\text{Im}(\epsilon'/\epsilon)$ with correlations, leading to the ellipses labeled “b.” The correlations for the KTeV measurements are given in the $\text{Im}(\epsilon'/\epsilon)$ section of the K_L^0 Listings. For small $|\epsilon'/\epsilon|$, $\phi_{+-} \approx \phi_\epsilon + \text{Im}(\epsilon'/\epsilon)$.

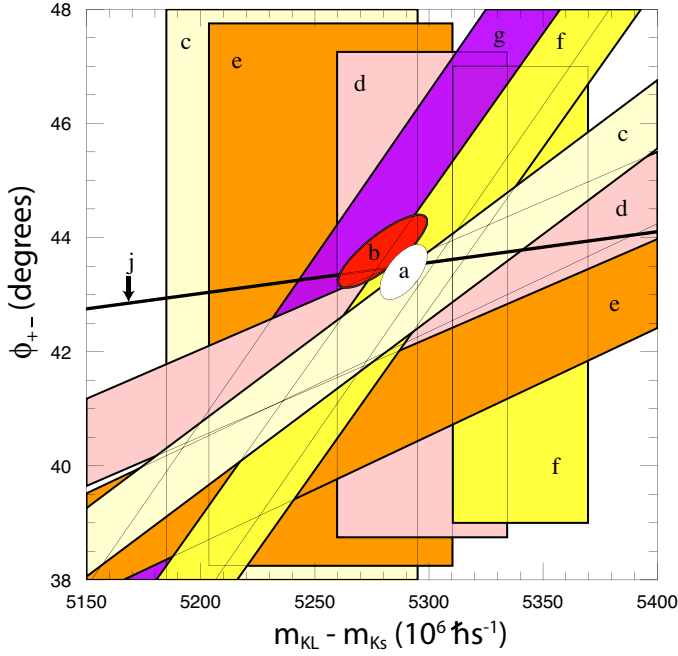


Figure 67.1: ϕ_{+-} vs Δm for experiments which do not assume CPT invariance. Δm measurements appear as vertical bands spanning $\Delta m \pm 1\sigma$, cut near the top and bottom to aid the eye. Most ϕ_{+-} measurements appear as diagonal bands spanning $\phi_{+-} \pm \sigma_\phi$. Data are labeled by letters: “b”–FNAL KTeV, “c”–CERN CPLEAR, “d”–FNAL E773, “e”–FNAL E731, “f”–CERN, “g”–CERN NA31, and are cited in Table 67.1. The narrow band “j” shows ϕ_{SW} . The ellipse “a” shows the $\chi^2 = 1$ contour of the fit result.

Table 67.1: References, Document ID’s, and sources corresponding to the letter labels in the figures. The data are given in the ϕ_{+-} and Δm sections of the K_L Listings, and the τ_S section of the K_S Listings.

Label	Source	PDG Document ID	Ref.
a	this Review	OUR FIT	
b	FNAL KTeV	ABOUZAID 11	[10]
c	CERN CPLEAR	APOSTOLAKIS 99C	[11]
d	FNAL E773	SCHWINGENHEUER 95	[12]
e	FNAL E731	GIBBONS 93,93C	[13,14]
f	CERN	GEWENIGER 74B,74C	[15,16]
g	CERN NA31	CAROSI 90	[17]
h	CERN NA48	LAI 02C	[18]
i	CERN NA31	BERTANZA 97	[19]
j	this Review	SUPERWEAK 16	

The data on τ_S , Δm , and ϕ_{+-} shown in Figs. 67.1 and 67.2 are combined with data on ϕ_{00} and $\phi_{00} - \phi_{+-}$ in two fits, one without assuming CPT , and the other with this assumption. The results without assuming CPT are shown as ellipses labeled “a.” These ellipses are seen to be in good agreement with the superweak phase

$$\phi_{SW} = \tan^{-1} \left(\frac{2\Delta m}{\Delta\Gamma} \right) = \tan^{-1} \left(\frac{2\Delta m \tau_S \tau_L}{\hbar(\tau_L - \tau_S)} \right). \quad (67.9)$$

In Figs. 67.1 and 67.2, ϕ_{SW} is shown as narrow bands labeled “j.”

Table 67.2 column 2, “Fit w/o CPT ,” gives the resulting fitted parameters, while Table 67.3 gives the correlation matrix for this fit. The white ellipses labeled “a” in Fig. 67.1 and Fig. 67.2 are the $\chi^2 = 1$ contours for this fit.

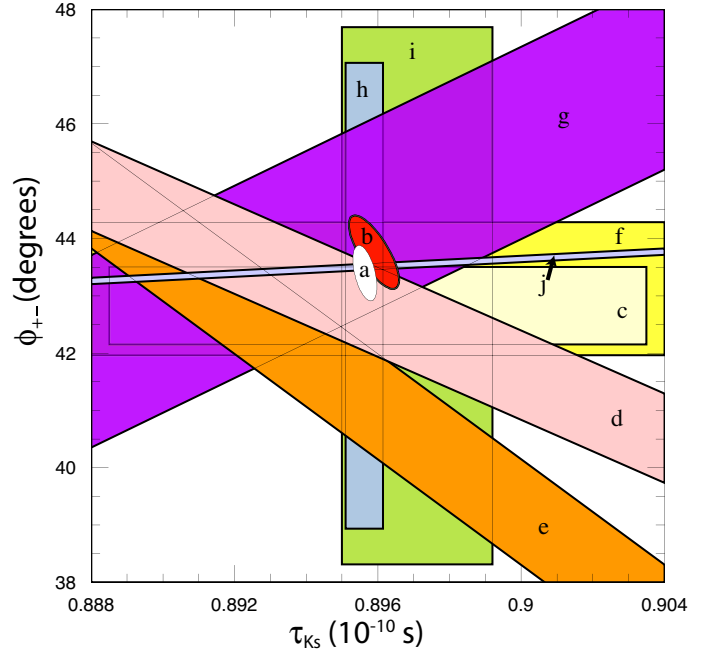


Figure 67.2: ϕ_{+-} vs τ_S . τ_S measurements appear as vertical bands spanning $\tau_S \pm 1\sigma$, some of which are cut near the top and bottom to aid the eye. Most ϕ_{+-} measurements appear as diagonal or horizontal bands spanning $\phi_{+-} \pm \sigma_\phi$. Data are labeled by letters: “b”–FNAL KTeV, “c”–CERN CPLEAR, “d”–FNAL E773, “e”–FNAL E731, “f”–CERN, “g”–CERN NA31, “h”–CERN NA48, “i”–CERN NA31, and are cited in Table 67.1. The narrow band “j” shows ϕ_{SW} . The ellipse “a” shows the fit result’s $\chi^2 = 1$ contour.

For experiments which have dependencies on unseen fit parameters, that is, parameters other than those shown on the x or y axis of the figure, their band positions are evaluated using the fit results and their band widths include the fitted uncertainty in the unseen parameters. This is also true for the ϕ_{SW} bands.

If CPT invariance and unitarity are assumed, then by Eq. (67.6a), the phase of ϵ is constrained to be approximately equal to

$$\phi_{SW} = (43.50258 \pm 0.00021)^\circ + 54.1(\Delta m - 0.5289)^\circ + 32.0(\tau_S - 0.89564) \quad (67.10)$$

where we have linearized the Δm and τ_S dependence of Eq. (67.9). The error ± 0.00021 is due to the uncertainty in τ_L . Here Δm has units $10^{10} \text{ hbar s}^{-1}$ and τ_S has units 10^{-10} s .

If in addition we use the observation that $\text{Re}(\epsilon'/\epsilon) \ll 1$ and $\cos(\phi_{\epsilon'} - \phi_\epsilon) \simeq 1$, as well as the numerical value of $\phi_{\epsilon'}$ given in Eq. (67.6b), then Eqs. (67.5a), which are sketched in Fig. 67.3, lead to the constraint

$$\begin{aligned} \phi_{00} - \phi_{+-} &\approx -3 \text{Im} \left(\frac{\epsilon'}{\epsilon} \right) \\ &\approx -3 \text{Re} \left(\frac{\epsilon'}{\epsilon} \right) \tan(\phi_{\epsilon'} - \phi_\epsilon) \\ &\approx 0.006^\circ \pm 0.008^\circ, \end{aligned} \quad (67.11)$$

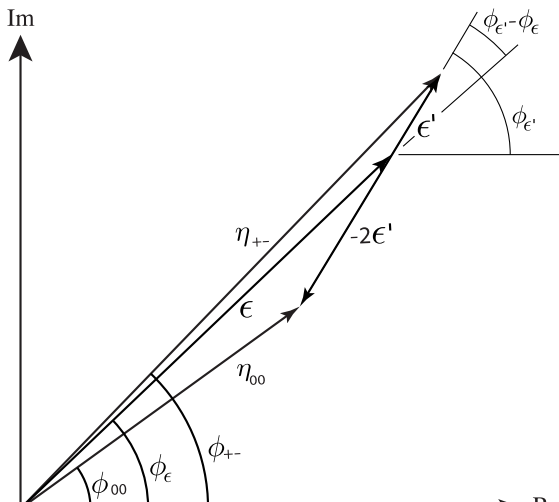
so that $\phi_{+-} \approx \phi_{00} \approx \phi_\epsilon \approx \phi_{SW}$.

In the fit assuming CPT , we constrain $\phi_\epsilon = \phi_{SW}$ using the linear expression in Eq. (67.10), and constrain $\phi_{00} - \phi_{+-}$ using Eq. (67.11). These constraints are inserted into the Listings with the Document ID of SUPERWEAK 16. Some additional data for which the authors assumed CPT are added to this fit or substitute for other less precise data for which the authors did not make this assumption. See the Listings for details.

The results of this fit are shown in Table 67.2, column 3, “Fit w/ CPT ,” and the correlation matrix is shown in Table 67.4. The Δm precision is improved by the CPT assumption.

Table 67.2: Fit results for ϕ_{+-} , Δm , τ_S , ϕ_{00} , $\Delta\phi = \phi_{00} - \phi_{+-}$, and ϕ_ϵ without and with the CPT assumption.

Quantity(units)	Fit w/o CPT	Fit w/ CPT
$\phi_{+-}(\circ)$	43.4 ± 0.5 (S=1.2)	43.51 ± 0.05 (S=1.2)
$\Delta m(10^{10} \hbar s^{-1})$	0.5289 ± 0.0010	0.5293 ± 0.0009 (S=1.3)
$\tau_S(10^{-10} s)$	0.89564 ± 0.00033	0.8954 ± 0.0004 (S=1.1)
$\phi_{00}(\circ)$	43.7 ± 0.6 (S=1.2)	43.52 ± 0.05 (S=1.3)
$\Delta\phi(\circ)$	0.34 ± 0.32	0.006 ± 0.014 (S=1.7)
$\phi_\epsilon(\circ)$	43.5 ± 0.5 (S=1.3)	43.52 ± 0.05 (S=1.2)
χ^2	16.4	20.0
# Deg. Free.	14	16

**Figure 67.3:** Sketch of Eqs. (67.5a). Not to scale.**Table 67.3:** Correlation matrix for the results of the fit without the CPT assumption

	ϕ_{+-}	Δm	τ_S	ϕ_{00}	$\Delta\phi$	ϕ_ϵ
ϕ_{+-}	1.000	0.596	-0.488	0.827	-0.040	0.976
Δm	0.596	1.000	-0.572	0.487	-0.035	0.580
τ_S	-0.488	-0.572	1.000	-0.423	-0.014	-0.484
ϕ_{00}	0.827	0.487	-0.423	1.000	0.529	0.929
$\Delta\phi$	-0.040	-0.035	-0.014	0.529	1.000	0.178
ϕ_ϵ	0.976	0.580	-0.484	0.929	0.178	1.000

Table 67.4: Correlation matrix for the results of the fit with the CPT assumption

	ϕ_{+-}	Δm	τ_S	ϕ_{00}	$\Delta\phi$	ϕ_ϵ
ϕ_{+-}	1.000	0.972	-0.311	0.957	-0.105	0.995
Δm	0.972	1.000	-0.509	0.958	-0.007	0.977
τ_S	-0.311	-0.509	1.000	-0.306	0.004	-0.312
ϕ_{00}	0.957	0.958	-0.306	1.000	0.189	0.981
$\Delta\phi$	-0.105	-0.007	0.004	0.189	1.000	-0.006
ϕ_ϵ	0.995	0.977	-0.312	0.981	-0.006	1.000

67.2.2. Fits for ϵ'/ϵ , $|\eta_{+-}|$, $|\eta_{00}|$, and $B(K_L \rightarrow \pi\pi)$:

We list measurements of $|\eta_{+-}|$, $|\eta_{00}|$, $|\eta_{00}/\eta_{+-}|$, and ϵ'/ϵ . Independent information on $|\eta_{+-}|$ and $|\eta_{00}|$ can be obtained from measurements of the K_L^0 and K_S^0 lifetimes (τ_L , τ_S), and branching ratios (B) to $\pi\pi$, using the relations

$$|\eta_{+-}| = \left[\frac{B(K_L^0 \rightarrow \pi^+\pi^-)}{\tau_L} \frac{\tau_S}{B(K_S^0 \rightarrow \pi^+\pi^-)} \right]^{1/2}, \quad (67.12a)$$

$$|\eta_{00}| = \left[\frac{B(K_L^0 \rightarrow \pi^0\pi^0)}{\tau_L} \frac{\tau_S}{B(K_S^0 \rightarrow \pi^0\pi^0)} \right]^{1/2}. \quad (67.12b)$$

For historical reasons, the branching ratio fits and the CP -violation fits are done separately, but we want to include the influence of $|\eta_{+-}|$, $|\eta_{00}|$, $|\eta_{00}/\eta_{+-}|$, and ϵ'/ϵ measurements on $B(K_L^0 \rightarrow \pi^+\pi^-)$ and $B(K_L^0 \rightarrow \pi^0\pi^0)$ and vice versa. We approximate a global fit to all of these measurements by first performing two independent fits: 1) BRFIT, a fit to the K_L^0 branching ratios, rates, and mean life, and 2) ETAFIT, a fit to the $|\eta_{+-}|$, $|\eta_{00}|$, $|\eta_{+-}/\eta_{00}|$, and ϵ'/ϵ measurements. The results from fit 1, along with the K_S^0 values from this edition, are used to compute values of $|\eta_{+-}|$ and $|\eta_{00}|$, which are included as measurements in the $|\eta_{00}|$ and $|\eta_{+-}|$ sections with a document ID of BRFIT 16. Thus, the fit values of $|\eta_{+-}|$ and $|\eta_{00}|$ given in this edition include both the direct measurements and the results from the branching ratio fit.

The process is reversed in order to include the direct $|\eta|$ measurements in the branching ratio fit. The results from fit 2 above (before including BRFIT 16 values) are used along with the K_L^0 and K_S^0 mean lives and the $K_S^0 \rightarrow \pi\pi$ branching fractions to compute the K_L^0 branching ratio $\Gamma(K_L^0 \rightarrow \pi^0\pi^0)/\Gamma(K_L^0 \rightarrow \pi^+\pi^-)$. This branching ratio value is included as a measurement in the branching ratio section with a document ID of ETAFIT 16. Thus, the K_L^0 branching ratio fit values in this edition include the results of the direct measurement of $|\eta_{00}/\eta_{+-}|$ and ϵ'/ϵ . Most individual measurements of $|\eta_{+-}|$ and $|\eta_{00}|$ enter our fits directly via the corresponding measurements of $\Gamma(K_L^0 \rightarrow \pi^+\pi^-)/\Gamma(\text{total})$ and $\Gamma(K_L^0 \rightarrow \pi^0\pi^0)/\Gamma(\text{total})$, and those that do not have too large errors to have any influence on the fitted values of these branching ratios. A more detailed discussion of these fits is given in the 1990 edition of this *Review* [20].

References:

1. K. Kleinknecht, "Uncovering CP violation: experimental clarification in the neutral K meson and B meson systems," *Springer Tracts in Modern Physics*, vol. 195 (Springer Verlag 2003).
2. B. Winstein and L. Wolfenstein, *Rev. Mod. Phys.* **65**, 1113 (1993).
3. M.S. Sozzi, *Eur. Phys. J.* **C36**, 37 (2004).
4. T.T. Wu and C.N. Yang, *Phys. Rev. Lett.* **13**, 380 (1964).
5. L. Wolfenstein, *Phys. Rev. Lett.* **13**, 562 (1964); L. Wolfenstein, *Comm. Nucl. Part. Phys.* **21**, 275 (1994).
6. G. Colangelo, J. Gasser, and H. Leutwyler, *Nucl. Phys.* **B603**, 125 (2001).
7. R. Adler *et al.*, (CLEAR Collab.), *Phys. Lett.* **B407**, 193 (1997); P. Bloch, *Proceedings of Workshop on K Physics* (Orsay 1996), ed. L. Ikonomidou-Fayard, Edition Frontieres, Gif-sur-Yvette, France (1997) p. 307.
8. A. Lai *et al.*, *Phys. Lett.* **B610**, 165 (2005).
9. G. Buchalla, A.J. Buras, and M.E. Lautenbacher, *Rev. Mod. Phys.* **68**, 1125 (1996); S. Bosch *et al.*, *Nucl. Phys.* **B565**, 3 (2000); S. Bertolini, M. Fabrichesi, and J.O. Egg, *Rev. Mod. Phys.* **72**, 65 (2000).
10. E. Abouzaid *et al.*, *Phys. Rev.* **D83**, 092001 (2011).
11. A. Apostolakis *et al.*, *Phys. Lett.* **B458**, 545 (1999).
12. B. Schwingerheuer *et al.*, *Phys. Rev. Lett.* **74**, 4376 (1995).
13. L.K. Gibbons *et al.*, *Phys. Rev. Lett.* **70**, 1199 (1993) and footnote in Ref. 12.
14. L.K. Gibbons, Thesis, RX-1487, Univ. of Chicago, 1993.
15. C. Geweniger *et al.*, *Phys. Lett.* **48B**, 487 (1974).

16. C. Geweniger *et al.*, Phys. Lett. **52B**, 108 (1974).
17. R. Carosi *et al.*, Phys. Lett. **B237**, 303 (1990).
18. A. Lai *et al.*, Phys. Lett. **B537**, 28 (2002).
19. L. Bertanza *et al.*, Z. Phys. **C73**, 629 (1997).
20. J.J. Hernandez *et al.*, Particle Data Group, Phys. Lett. **B239**, 1 (1990).

68. Review of Multibody Charm Analyses

Revised 2019 by D. M. Asner (Brookhaven National Laboratory) and J. Rademacker (University of Bristol)

68.1. Kinematics & Models

The differential decay rate to a point $\mathbf{s} = (s_1, \dots, s_n)$ in n dimensional phase space can be expressed as

$$d\Gamma = |\mathcal{M}(\mathbf{s})|^2 \left| \frac{\partial^n \phi}{\partial (s_1 \dots s_n)} \right| d^n s \quad (68.1)$$

where $|\partial^n \phi / \partial (s_1 \dots s_n)|$ represents the density of states at \mathbf{s} , and \mathcal{M} the matrix element for the decay at that point in phase space, which is 2, 5, 8, ... dimensional for D decays to 3, 4, 5, ... spinless particles. Additional parameters are required to fully describe decays involving particles with non-zero spin in the initial or final state.

For the important case of D decays to 3 pseudoscalars, the decay kinematics can be represented in a two dimensional Dalitz plot [1]. This is usually parametrized in terms of $s_{12} \equiv (p_1 + p_2)^2$ and $s_{23} \equiv (p_2 + p_3)^2$, where p_1, p_2, p_3 are the four-momenta of the final state particles. In terms of these variables, phase-space density is constant across the kinematically allowed region, so that any structure seen in the Dalitz plot is a direct consequence of the dynamics encoded in $|\mathcal{M}|^2$. Note that here, because the 3-momenta of the decay products are confined to a plane, no parity violating kinematic observables can be constructed (unless they also violate rotational invariance). This is not the case for decays to four or more particles. These can therefore not be unambiguously described in terms of analogously-defined variables s_{ij}, s_{ijk} , which are parity-even. The use of parity-odd observables in four body decays is discussed below.

In the widely-used isobar approach, the matrix element \mathcal{M} is modeled as a sum of interfering decay amplitudes, each proceeding through resonant two-body decays [2]. See Refs. 2–4 for a review of resonance phenomenology. In most analyses, each resonance is described by a Breit-Wigner [5] or Flatté [6] lineshape, and the model includes a non-resonant term with a constant phase and magnitude. This approach has well-known theoretical limitations, such as the violation of unitarity and analyticity, which can break the relationship between magnitude and phase across phase space. This motivates the use of more sophisticated descriptions, especially for broad, overlapping resonances (frequently found in S-wave components) where these limitations are particularly problematic. In charm analyses, these approaches have included the K-matrix approach [5–8] which respects two-body unitarity; the use of LASS scattering data [9]; dispersive methods [10–13]; methods based on chiral symmetry [14–16], QCD factorisation (although this seems better suited to B decays) [17–19]; and quasi model-independent parametrizations which use generic lineshapes, with minimal theory input and many free parameters, for a subset of resonances [20–23]. An important example, with a rich resonance structure, is $D^0 \rightarrow K_S \pi^+ \pi^-$, which is a key channel in Charge-Parity (CP) violation and charm mixing analyses. The first analysis by CLEO [24] described the Dalitz plot with 5k signal events with 10 resonant components. This and later analyses by Belle [25] and CDF [26] model the Dalitz plot as a sum of Breit Wigner and Flatté line shapes, and a non-resonant component. BaBar [27] on the other hand use a K-matrix description for the $\pi\pi$ S-wave based on [28] and input from LASS scattering data for the $K - \pi$ S-wave, with no need to add a non-resonant component to describe the data. This approach is also followed in the latest analysis of this channel, published jointly by BaBar and Belle [29]. In total 18 resonant components, including four doubly Cabibbo suppressed ones, are required to describe the Dalitz plot with 1.1M $D^0 \rightarrow K_S \pi^+ \pi^-$ events. Belle's and BaBar's data have been re-analyzed by [17] in a QCD factorization framework, using line-shape parametrizations for the S [30,31] and P wave [11] contributions that preserve 2-body unitarity and analyticity. The measurements give compatible results for the components they share.

The field of amplitude analyses remains very active. Publications since the last update of this review two years ago include Dalitz plot analyses of $D_s^+ \rightarrow \pi^+ \pi^0 \eta$ by BES III [32]; $D^+ \rightarrow K^+ K^- K^+$ by LHCb [33]; $D^0 \rightarrow \pi^+ \pi^- \pi^0$ by BaBar [34]; BaBar and Belle's joint

analysis of $D^0 \rightarrow K_S \pi^+ \pi^-$ [29]; and a re-analysis of $D^+ \rightarrow K_S \pi^0 \pi^+$ and $D^+ \rightarrow K^- \pi^+ \pi^+$ data from FOCUS, CLEO and BES III by Niecknig and Kubis [13]. Ahn, Yang and Nam developed amplitude models for $\Lambda_c^+ \rightarrow K^- p \pi^+$ and $\Lambda_c^+ \rightarrow K_S p \pi^0$ [35] based on BELLE data [36]. There has also been significant progress in four body amplitude analyses: $D^0 \rightarrow K^+ K^- \pi^+ \pi^-$ and $D^0 \rightarrow \pi^+ \pi^- \pi^+ \pi^-$ using CLEO data [22]; $D^+ \rightarrow K_S \pi^+ \pi^+ \pi^-$, $D^0 \rightarrow K^- \pi^+ \pi^- \pi^+$ and $D^0 \rightarrow K^- \pi^+ \pi^0 \pi^0$ by BES III [37–39]; and $D^0 \rightarrow K^+ K^- \pi^+ \pi^-$, $D^0 \rightarrow K^\mp \pi^\pm \pi^\mp \pi^\pm$ [23,40] by LHCb. Noteworthy is the increasing sophistication of recent amplitude analyses, most of which go substantially beyond the isobar model with Breit Wigner and Flatté lineshapes. However, with the notable exception of [13] and [33], they remain within the isobar framework which describes the decay as a series of 2-body processes; even if these are modeled with increasing sophistication, the approach ignores long-range hadronic effects such as re-scattering and does not respect 3 (or 4)-body unitarity and analyticity.

Several groups work on improved models. Dispersive techniques, which respect 3-body unitarity and analyticity, have been successfully applied to regions of the $D^+ \rightarrow K^- \pi^+ \pi^+$ and $D^+ \rightarrow K_S \pi^0 \pi^+$ Dalitz plots below the η/K threshold [12,13], where they provide a good description of the data with fewer fit parameters than the isobar approach. Ref. [41] uses a unitary coupled channel approach to describe $D^+ \rightarrow K^- \pi^+ \pi^+$, which has no restrictions on the kinematic range, but requires additional parameters to describe the Dalitz plot above the η/K threshold. Using an effective chiral Lagrangian, the authors of Ref. [16] provide a description of the annihilation contribution to the decay amplitude which respects 3-body unitarity. This approach provides a good description of LHCb $D^+ \rightarrow K^+ K^- K^+$ data, with fewer parameters than an equivalent isobar model [33].

Limitations in the theoretical description of interfering resonances are the leading source of systematic uncertainty in many analyses. This is set to become increasingly problematic given the statistical precision achievable with the vast, clean charm samples available at the B factories, LHCb, and their upgrades. In some cases, the model uncertainty can be removed through model-independent methods, often relying on input from the charm threshold, as discussed below. Ref. 42 expand the scope and applicability of the quasi model-independent approach in amplitude fits. At the same time, increasingly sophisticated models are being developed, and applied to data.

68.2. Applications of multibody charm analyses

Amplitude analyses provide sensitivity to both relative magnitudes and phases of the interfering decay amplitudes. It is especially this sensitivity to phases that makes amplitude analyses such a uniquely powerful tool for studying a wide range of phenomena. Here we concentrate on their use for CP violation and mixing measurements in charm, and charm inputs to CP violation analyses in B meson decays (see also [43,44]). The properties of light-meson resonances determined in D amplitude analyses are reported in the light-unflavored-meson section of this Review.

68.2.1. Time-integrated searches for CP violation in charm :

Comparing the results of amplitude fits for CP -conjugate decay modes provides a measure of CP violation. Recent CP violation searches using this method include amplitude analyses of $D^0 \rightarrow K_S^0 K^\pm \pi^\mp$ and $D^0 \rightarrow K^+ K^- \pi^+ \pi^-$ by LHCb [45,40], and $D^0 \rightarrow K^+ K^- \pi^+ \pi^-$, $D^0 \rightarrow \pi^+ \pi^- \pi^+ \pi^-$ [46,22] using CLEO data.

A widely-used amplitude model-independent technique to search for local CP violation is based on performing a χ^2 comparison of CP -conjugate phase-space distributions. This method was pioneered by BaBar [47] and developed further in [48–50], with recent results reported by BaBar [51] and LHCb in $D^\pm \rightarrow K^+ K^- \pi^\pm$ [52,53], CDF in $D^0 \rightarrow K_S \pi^+ \pi^-$ [26], and LHCb in $D^+ \rightarrow \pi^- \pi^+ \pi^+$ [55], $D^0 \rightarrow K^+ K^- \pi^+ \pi^-$ and $D^0 \rightarrow \pi^+ \pi^- \pi^+ \pi^-$ [50]. Un-binned methods can increase the sensitivity [54] and have been applied by LHCb to $D^+ \rightarrow \pi^- \pi^+ \pi^+$, $D^0 \rightarrow \pi^+ \pi^- \pi^0$ and $D^0 \rightarrow \pi^+ \pi^- \pi^+ \pi^-$ [55,56,73].

An alternative model-independent approach is based on constructing observables in four body decays that are odd under motion reversal

(“naive T”) [58–66], which is equivalent to P for scalar particles [66]. One such observable is $C_T = \vec{p}_2 \cdot (\vec{p}_3 \times \vec{p}_4) = (1/m_D)\epsilon_{\alpha\beta\gamma\delta} p_1^\alpha p_2^\beta p_3^\gamma p_4^\delta$, where \vec{p}_i are the decay products’ three momenta in the decay’s restframe, and p_i are their four-momenta. Identical particles (as in $D^0 \rightarrow K^+\pi^-\pi^+\pi^-$) are ordered by momentum magnitude. Comparing the P violating asymmetry $A_T \equiv \frac{\Gamma(C_T>0) - \Gamma(C_T<0)}{\Gamma(C_T>0) + \Gamma(C_T<0)}$ with its C -conjugate in \bar{D}^0 decays, provides sensitivity to CP violation. Searches for CP violation in this manner have been carried out for $D^0 \rightarrow K^+K^-\pi^+\pi^-$ by FOCUS, BaBar, LHCb and Belle [67,68,69,70], where LHCb increase the sensitivity of the method by analysing the data in bins of phase space, and Belle’s analysis considers several new, hitherto unused P -odd variables; $D^+ \rightarrow K^+K_S\pi^+\pi^-$ and $D_s^+ \rightarrow K^+K_S\pi^+\pi^-$ by BaBar [71]; and $D^0 \rightarrow K_S\pi^+\pi^-\pi^0$ by Belle [72]. LHCb’s unbinned comparison of kinematic distributions in $D^0, \bar{D}^0 \rightarrow \pi^+\pi^-\pi^+\pi^-$ is sensitive to CP violation in both P even and P -odd kinematic variables [73].

The results of all measurements described in this section are compatible with CP conservation in charm. Given the recent discovery of CP violation in $D^0 \rightarrow K^+K^-$, $D^0 \rightarrow \pi^+\pi^-$ decays, and in view of the vast data samples about to be collected, one might expect this to change in the foreseeable future.

68.2.2. Charm Mixing and CP violation : Time-dependent amplitude analyses in decays to final states that are accessible to both D^0 and \bar{D}^0 have unique sensitivity to mixing parameters. A Dalitz plot analysis of a self-conjugate final state, such as $K_S\pi^+\pi^-$ and $K_S K^+K^-$, allows the measurement of the phase difference between the relevant D^0 and \bar{D}^0 decay amplitudes, and thus a direct measurement of x and y , the normalised mass and width difference of the $D^0 - \bar{D}^0$ system’s mass eigenstates. This is in contrast to decays like $D^0 \rightarrow K\pi$ [74] which only provide access to the decay-specific parameters x'^2, y' . Multibody charm analyses are also sensitive to CP violation in mixing and in the interference between mixing and decay; these results are summarised in [43,44].

68.2.3. CP violation in decays of Beauty to Charm : Neutral D mesons originating from $B^- \rightarrow DK^-$ (here denoted as D_{B^-}) are a superposition of D^0 and \bar{D}^0 with a relative phase that depends on the CKM unitarity triangle parameter γ/ϕ_3 ,

$$D_{B^-} \propto D^0 + r_B e^{i(\delta_B - \gamma)} \bar{D}^0,$$

where δ_B is a CP conserving strong phase, and $r_B \sim 0.1$. In the corresponding CP -conjugate expression, γ/ϕ_3 changes sign. An amplitude analysis of the subsequent decay of the D_{B^\pm} to a state accessible to both D^0 and \bar{D}^0 allows the measurement of γ/ϕ_3 [75–79]. The method generalizes to similar B hadron decays, such as $B^0 \rightarrow DK^{*0}$. Measurements based on this technique have been reported by BaBar [80,81], Belle [25,82] and LHCb [83–92]. The most precise individual results come from the study of $D_{B^-} \rightarrow K_S\pi^+\pi^-$ and $D_{B^-} \rightarrow K_S K^+K^-$ with an uncertainty of $\sim 10^\circ$ [25,80,82,86,92]; combining measurements in multiple decay modes leads to a current uncertainty on γ/ϕ_3 of less than 6° .

The interference between mixing and decay in $B^0 \rightarrow D^0 h^0$ with $h^0 = \pi^0, \eta, \omega$ provides sensitivity to β , which can be extracted from the Dalitz plot of the subsequent $D^0 \rightarrow K_S\pi^+\pi^-$ decay [29,93–96]. The combined BaBar/Belle analysis based on this technique resolved the ambiguity in β present in other measurements, such as $B^0 \rightarrow J/\psi K_S$, in favour of the solution compatible with other unitarity triangle constraints [29].

68.3. Model Independent Methods and the Charm Threshold

The precision measurement of mixing or CP violation parameters such γ/ϕ_3 from multibody charm decays requires as input the phase-differences between the D^0 and \bar{D}^0 amplitudes across phase space, as well as their magnitudes, for each final state of interest. While the magnitudes are fairly easily measured, the phase information requires either amplitude models with reliable phase motion, or model-independent approaches.

Model-independent measurements of the relevant phase differences rely on interference effects in the decays of well-defined coherent superpositions of D^0 and \bar{D}^0 . These are accessible at the charm threshold, where CLEO-c and BES III operate [43,97–104]. Charm mixing also results in a (time-dependent) $D^0 - \bar{D}^0$ superposition, that can be used to measure the relevant phase information as input to γ/ϕ_3 measurements. This method is particularly powerful in doubly Cabibbo-suppressed decays such as $D^0 \rightarrow K^+\pi^-\pi^+\pi^-$, and when used in combination with threshold data [105,106]. Under some circumstances, with large data sets, the relevant strong phases and γ/ϕ_3 can be extracted simultaneously without external input, for example in simultaneous analysis of the $B^0 \rightarrow DK^+\pi^-$ Dalitz plot and that of the subsequent $D \rightarrow K_S\pi^+\pi^-$ decay [115]. However, the global effort to achieve a measurement of γ/ϕ_3 to sub-degree precision will continue to rely critically on input from the charm threshold.

The model-independent phase information is provided either integrated over the entire phase space of the decay, or in sub-regions/bins. The results can be expressed in terms of one complex parameter $\mathcal{Z} = R e^{-i\delta} = c + is$ per pair of CP -conjugate bins, with magnitude $R \leq 1$. Larger R values lead to higher sensitivity to γ/ϕ_3 . Amplitude models can be used to optimise the binning for sensitivity to γ/ϕ_3 , without introducing a model-dependent bias in the result.

CLEO-c data have been analyzed to provide binned \mathcal{Z} for the self-conjugate decays $D^0 \rightarrow K_S\pi^+\pi^-$, $D^0 \rightarrow K_S K^+K^-$, $D^0 \rightarrow \pi^+\pi^-\pi^+\pi^-$, and $D^0 \rightarrow K_S\pi^-\pi^+\pi^0$ [107–110]; and phase space-integrated values for $D^0, \bar{D}^0 \rightarrow K_S K^+\pi^-$, $K^+\pi^-\pi^0$ and $K^+\pi^-\pi^+\pi^-$ [111,112]. Adding input from LHCb’s charm mixing analysis significantly improves the constraints on \mathcal{Z} for $D^0, \bar{D}^0 \rightarrow K^+\pi^-\pi^+\pi^-$ [112,113]. A recent study based on LHCb’s $D^0, \bar{D}^0 \rightarrow K^+\pi^-\pi^+\pi^-$ amplitude models [23] and CLEO-c data indicates that a binned analysis of $D^0, \bar{D}^0 \rightarrow K^+\pi^-\pi^+\pi^-$ could lead to the most precise individual measurement of γ/ϕ_3 [114]. For self-conjugate decays such as $D^0 \rightarrow \pi^+\pi^-\pi^0$, analysed with a single pair of bins, \mathcal{Z} is real-valued, and usually expressed in terms of the CP -even fraction $F_+ \equiv \frac{1}{2}(\text{Re}(\mathcal{Z}) + 1)$, defined such that a CP -even eigenstate has $F_+ = 1$, while a CP -odd eigenstate has $F_+ = 0$ [102]. Recent analyses of CLEO-c data reveal that $D^0 \rightarrow \pi^+\pi^-\pi^0$ is compatible with being completely CP -even with $F_+ = 0.973 \pm 0.017$, while $D^0 \rightarrow K^+K^-\pi^0$ has $F_+ = 0.732 \pm 0.055$, $D^0 \rightarrow \pi^+\pi^-\pi^+\pi^-$ has $F_+ = 0.769 \pm 0.023$ and $D^0 \rightarrow K_S\pi^+\pi^-\pi^0$ has 0.238 ± 0.020 [103,109,110].

It is interesting to compare these values with those obtained from amplitude models as a cross check of the models’ phase-motion. $F_+^{4\pi \text{ model}} = 0.729 \pm 0.020$ calculated from Ref. 22’s $D^0 \rightarrow \pi^+\pi^-\pi^+\pi^-$ model, compares well to the measured value given above, as does $\mathcal{Z}^{K3\pi \text{ model}} = 0.459 \pm 0.025$ [23] to $\mathcal{Z}^{K3\pi \text{ meas}} = (0.32_{-0.13}^{+0.17}) \exp(-i(128_{-17}^{+28}^\circ))$ [112,113]. Binwise comparisons for $D^0 \rightarrow K_S\pi^+\pi^-$, $D^0 \rightarrow K_S K^+K^-$, $D^0 \rightarrow \pi^+\pi^-\pi^+\pi^-$, and $D^0, \bar{D}^0 \rightarrow K^+\pi^-\pi^+\pi^-$ can be found in [107–109,114].

68.4. Summary

Multibody charm decays offer a rich phenomenology, including unique sensitivity to CP violation and charm mixing. This is a highly dynamic field with many new results (some of which we presented here) and rapidly increasing, high quality datasets. These datasets constitute a huge opportunity, but also a challenge to improve the theoretical descriptions of soft hadronic effects in multibody decays. For some measurements, model-independent methods, many relying on input from the charm threshold, provide a way of removing model-induced uncertainties. At the same time, substantial progress in the theoretical description of multibody decays is being made.

References:

1. R.H. Dalitz, *Phil. Mag.* **44**, 1068 (1953).
2. M. Bauer, B. Stech, and M. Wirbel, *Z. Phys.* **C4**, 103 (1987); P. Bedaque, A. Das, and V.S. Mathur, *Phys. Rev.* **D49**, 269 (1994); L.-L. Chau and H.-Y. Cheng, *Phys. Rev.* **D36**, 137 (1987); K. Terasaki, *Int. J. Mod. Phys.* **A10**, 3207 (1995); F. Buccella, M. Lusignoli, and A. Pugliese, *Phys. Lett.* **B379**, 249 (1996).

3. J.D. Jackson, *Nuovo Cimento* **34**, 1644 (1964).
4. See the note on Resonances in this *Review*.
5. E.P. Wigner, *Phys. Rev.* **70**, 15 (1946).
6. S. M. Flatté, *Phys. Lett.* **63B**, 224 (1976) *Phys. Lett.* **63B**, 224 (1976).
7. S.U. Chung *et al.*, *Ann. Phys.* **4**, 404 (1995).
8. I.J.R. Aitchison, *Nucl. Phys.* **A189**, 417 (1972).
9. D. Aston *et al.* (LASS Collab.), *Nucl. Phys.* **B296**, 493 (1988).
10. R. Omnes, *Nuovo Cimento* **8**, 316 (1958).
11. C. Hanhart, *Phys. Lett.* **B715**, 170 (2012).
12. F. Niecknig and B. Kubis, *JHEP* **1510**, 142 (2015).
13. F. Niecknig and B. Kubis, *Phys. Lett.* **B780**, 471 (2018).
14. P. C. Magalhães and M. R. Robilotta, *Phys. Rev. D* **92**, 9,094005(2015).
15. P. C. Magalhães *et al.*, *Phys. Rev. D* **84**, 094001(2011).
16. R. T. Aoude, P. C. Magalhães, A. C. Dos Reis and M. R. Robilotta, *Phys. Rev.* **D97**, 5,056021 (2018).
17. J.P. Dedonder *et al.* *Phys. Rev.* **D89**, 094018 (2014).
18. D. Boito, J.-P. Dedonder, B. El-Bennich, R. Escribano, R. Kaminski, L. Lesniak and B. Loiseau, *Phys. Rev.* **D96**, 11,113003 (2017).
19. R. Klein, T. Mannel, J. Virto and K. K. Vos, *JHEP* **1710**, 117 (2017).
20. E.M. Aitala *et al.* (E791 Collab.), *Phys. Rev.* **D73**, 032004 (2006) [*Phys. Rev.* **D74**, 059901 (E)(2006)].
21. G. Bonvicini *et al.* (CLEO Collab.), *Phys. Rev.* **D78**, 052001 (2008).
22. P. d'Argent *et al.*, *JHEP* **1705**, 142 (2017).
23. R. Aaij *et al.* [LHCb Collaboration], *Eur. Phys. J.* **C78**, 6,443 (2018).
24. H. Muramatsu *et al.* (CLEO Collab.), *Phys. Rev. Lett.* **89**, 251802 (2002).
25. A. Poluektov *et al.* (Belle Collab.), *Phys. Rev.* **D81**, 112002 (2010).
26. T. Aaltonen *et al.* (CDF Collab.), *Phys. Rev.* **D86**, 032007 (2012).
27. P. del Amo Sanchez *et al.* (BaBar Collab.), *Phys. Rev. Lett.* **105**, 081803 (2010).
28. V. V. Anisovich and A. V. Sarantsev, *Eur. Phys. J.* **A16**, 229 (2018).
29. I. Adachi *et al.* [BaBar and Belle Collaborations], *Phys. Rev. Lett.* **121**, 26,261801 (2018) *Phys. Rev.* **D98**, 11,112012 (2018).
30. B. El-Bennich *et al.* *Phys. Rev.* **D79**, 094005 (2009) [*Phys. Rev.* **D83**, 039903(E) (2011)].
31. J.P. Dedonder *et al.* *Acta Phys. Polon. B* **42** (2011) 2013.
32. M. Ablikim *et al.* [BESIII Collaboration], arXiv:1903.04118 [hep-ex]. (remove if still unpublished by end of review, otherwise update).
33. R. Aaij *et al.* [LHCb Collaboration], *JHEP* **1904**, 063 (2019).
34. J. P. Lees *et al.* [BaBar Collaboration], *Phys. Rev. D* **93**, 11,112014(2016).
35. J. K. Ahn, S. Yang and S. I. Nam, *Phys. Rev. D* **100**, 3,034027(2019).
36. analysing data published in S. B. Yang *et al.* [Belle Collaboration], *Phys. Rev. Lett.* **117**, 1,011801 (2016).
37. M. Ablikim *et al.* [BESIII Collaboration], arXiv:1901.05936 [hep-ex]. (remove if still unpublished by end of the review, otherwise update).
38. M. Ablikim *et al.* [BESIII Collaboration], *Phys. Rev. D* **95**, 7,072010(2017).
39. M. Ablikim *et al.* [BESIII Collaboration], *Phys. Rev.* **D99**, 9,092008 (2019).
40. R. Aaij *et al.* [LHCb Collaboration], *JHEP* **1902**, 126 (2019).
41. S. X. Nakamura, *Phys. Rev. D* **93**, 1,014005(2016).
42. F. Krinner, D. Greenwald, D. Ryabchikov, B. Grube and S. Paul, *Phys. Rev. D* **97**, 11,114008(2018).
43. See the note on $D^0-\bar{D}^0$ Mixing in this *Review*.
44. See the note CP violation in the quark sector in this *Review*.
45. R. Aaij *et al.* [LHCb Collaboration], *Phys. Rev.* **D93**, 052018 (2016).
46. M. Artuso *et al.* (CLEO Collab.), *Phys. Rev.* **D85**, 122002 (2012).
47. B. Aubert *et al.* (BABAR Collab.), *Phys. Rev.* **D78**, 051102 (2008).
48. I. Bediaga *et al.*, *Phys. Rev.* **D80**, 096006 (2009).
49. I. Bediaga *et al.*, *Phys. Rev.* **D86**, 036005 (2012).
50. R. Aaij *et al.* (LHCb Collab.), *Phys. Lett.* **B726**, 623 (2013).
51. J.P. Lees *et al.* (BaBar Collab.), *Phys. Rev.* **D87**, 052010 (2013).
52. R. Aaij *et al.* (LHCb Collab.), *Phys. Rev.* **D84**, 112008 (2011).
53. R. Aaij *et al.* (LHCb Collab.), *JHEP* **1306**, 112 (2013).
54. M. Williams, *Phys. Rev.* **D84**, 054015 (2011).
55. R. Aaij *et al.* (LHCb Collab.), *Phys. Lett.* **B728**, 585 (2014).
56. R. Aaij *et al.* (LHCb Collab.), *Phys. Lett.* **B740**, 158 (2015).
57. R. Aaij *et al.* [LHCb Collaboration], *Phys. Lett.* **B769**, 345 (2017).
58. E. Golowich and G. Valencia, *Phys. Rev.* **D40**, 112, (1989).
59. G. Valencia, *Phys. Rev.* **D39**, 3339 (1989).
60. W. Bensalem and D. London, *Phys. Rev.* **D64**, 116003 (2001).
61. I.I.Y. Bigi, hep-ph/0107102.
62. W. Bensalem, A. Datta, and D. London, *Phys. Rev.* **D66**, 094004 (2002).
63. W. Bensalem, A. Datta, and D. London, *Phys. Lett.* **B538**, 309 (2002).
64. A. Datta and D. London, *Int. J. Mod. Phys.* **A19**, 2505 (2004).
65. M. Gronau and J.L. Rosner, *Phys. Rev.* **D84**, 096013 (2011).
66. G. Durieux and Y. Grossman, *Phys. Rev.* **D92**, 076013 (2015).
67. J.M. Link *et al.* (FOCUS Collab.), *Phys. Lett.* **B622**, 239 (2005).
68. P. del Amo Sanchez *et al.* (BaBar Collab.), *Phys. Rev.* **D81**, 111103 (2010).
69. R. Aaij *et al.* (LHCb Collab.), *JHEP* **1410**, 005 (2014).
70. J. B. Kim *et al.* [Belle Collaboration], *Phys. Rev.* **D99**, 1,011104 (2019).
71. J.P. Lees *et al.* (BaBar Collab.), *Phys. Rev.* **D84**, 031103 (2011).
72. K. Prasanth *et al.* [Belle Collaboration], *Phys. Rev.* **D95**, 9,091101 (2017).
73. R. Aaij *et al.* [LHCb Collaboration], *Phys. Lett.* **B769**, 345 (2017).
74. D.M. Asner *et al.* (CLEO Collab.), *Phys. Rev.* **D72**, 012001 (2005).
75. M. Gronau and D. Wyler, *Phys. Lett.* **B265**, 172 (1991).
76. M. Gronau and D. London, *Phys. Lett.* **B253**, 483 (1991).
77. D. Atwood *et al.*, *Phys. Rev. Lett.* **78**, 17, 3257 (1997).
78. A. Poluektov *et al.* (Belle Collab.), *Phys. Rev.* **D70**, 7, 072003 (2004).
79. J. Rademacker and G. Wilkinson, *Phys. Lett.* **B647**, 400 (2007).
80. P. del Amo Sanchez *et al.* (BaBar Collab.), *Phys. Rev. Lett.* **105**, 121801 (2010).
81. J.P. Lees *et al.* (BaBar Collab.), *Phys. Rev.* **D84**, 012002 (2011).
82. H. Aihara *et al.* (Belle Collab.), *Phys. Rev.* **D85**, 112014 (2012).
83. R. Aaij *et al.* (LHCb Collab.), *Phys. Lett.* **B726**, 151 (2013).
84. R. Aaij *et al.* (LHCb Collab.), *Phys. Lett.* **B723**, 44 (2013).
85. R. Aaij *et al.* (LHCb Collab.), *Phys. Lett.* **B718**, 43 (2012).
86. R. Aaij *et al.* (LHCb Collab.), *JHEP* **1410**, 97 (2014).
87. R. Aaij *et al.* (LHCb Collab.), *Phys. Lett.* **B733**, 36 (2014).
88. R. Aaij *et al.* (LHCb Collab.), *Nucl. Phys.* **B888**, 169 (2014).
89. R. Aaij *et al.* (LHCb Collab.), *Phys. Rev.* **D91**, 112014 (2015).
90. R. Aaij *et al.* [LHCb Collaboration], *JHEP* **1606**, 131 (2016).
91. R. Aaij *et al.* [LHCb Collaboration], *JHEP* **1612**, 087 (2016).
92. R. Aaij *et al.* [LHCb Collaboration], *JHEP* **1808**, 176 (2018), Erratum: *JHEP* **1810**, 107 (2018).
93. A. Bondar, T. Gershon and P. Krokovny, *Phys. Lett.* **B624**, 1 (2005).
94. P. Krokovny *et al.* [Belle Collaboration], *Phys. Rev. Lett.* **97**, 1,081801 (2006).
95. B. Aubert *et al.* [BaBar Collaboration], *Phys. Rev. Lett.* **99**, 231802 (2007).

96. V. Vorobyev *et al.* [Belle Collaboration], Phys. Rev. **D94**, 5,052004 (2016).
97. A. Giri *et al.*, Phys. Rev. **D68**, 5, 054018 (2003).
98. D. Atwood and A. Soni, Phys. Rev. **D68**, 033003 (2003).
99. S. Malde and G. Wilkinson, Phys. Lett. **B701**, 353 (2011).
100. A. Bondar *et al.*, Phys. Rev. **D82**, 034033 (2010).
101. C. Thomas and G. Wilkinson, JHEP **1210**, 184 (2012).
102. M. Nayak *et al.* Phys. Lett. **B740**, 1 (2015).
103. S. Malde *et al.* Phys. Lett. **B747**, 9 (2015).
104. S. Malde, C. Thomas, and G. Wilkinson, Phys. Rev. **D91**, 094032 (2015).
105. S. Harnew and J. Rademacker, Phys. Lett. **B728**, 296 (2014).
106. S. Harnew and J. Rademacker, JHEP **1503**, 169 (2015).
107. J. Libby *et al.* (CLEO Collab.), Phys. Rev. **D82**, 112006 (2010).
108. R.A. Briere *et al.* (CLEO Collab.), Phys. Rev. **D80**, 032002 (2009).
109. S. Harnew *et al.*, JHEP **1801**, 144 (2018).
110. P.K. Resmi *et al.*, JHEP **1801**, 082 (2018).
111. J. Insler *et al.* (CLEO Collab.), Phys. Rev. **D85**, 092016 (2012) erratum Phys. Rev. D 94,9,09905(2016).
112. T. Evans *et al.*, Phys. Lett. **B757**, 520 (2017), erratum Phys. Lett. **B765**, 402, (2017).
113. R. Aaij *et al.* [LHCb Collaboration], Phys. Rev. Lett. **117**, 24,241801 (2016).
114. T. Evans *et al.*, arXiv:1909.10196 [hep-ex].
115. D. Craik, T. Gershon and A. Poluektov, Phys. Rev. **D97**, 5,056002 (2018).

69. D^0 - \bar{D}^0 Mixing

Revised August 2019 by D.M. Asner (BNL) and A.J. Schwartz (Cincinnati U.).

The formalism for D^0 - \bar{D}^0 mixing is closely related to that for CP violation, which is also presented in the note “ CP Violation in the Quark Sector” in this *Review*. The time evolution of the D^0 - \bar{D}^0 system is described by the Schrödinger equation

$$i \frac{\partial}{\partial t} \begin{pmatrix} D^0(t) \\ \bar{D}^0(t) \end{pmatrix} = \left(\mathbf{M} - \frac{i}{2} \mathbf{\Gamma} \right) \begin{pmatrix} D^0(t) \\ \bar{D}^0(t) \end{pmatrix}, \quad (69.1)$$

where the \mathbf{M} and $\mathbf{\Gamma}$ matrices are Hermitian, and CPT invariance requires that $M_{11} = M_{22} \equiv M$ and $\Gamma_{11} = \Gamma_{22} \equiv \Gamma$. The off-diagonal elements of \mathbf{M} and $\mathbf{\Gamma}$ are referred to as the dispersive and absorptive parts, respectively, of the mixing. The mass eigenstates D_1 and D_2 of the Hamiltonian $\mathbf{M} - i\mathbf{\Gamma}/2$ are defined as

$$|D_{1,2}\rangle \equiv p|D^0\rangle \pm q|\bar{D}^0\rangle, \quad (69.2)$$

where normalization imposes $|p|^2 + |q|^2 = 1$. If $p = q$, then the mass eigenstates are CP eigenstates and CP is conserved. Our phase convention is $CP|D^0\rangle = -|\bar{D}^0\rangle$, which implies that, in the absence of CP violation, D_2 is CP -even and D_1 is CP -odd.

The eigenvalues of $\mathbf{M} - i\mathbf{\Gamma}/2$ are

$$\omega_{1,2} = \left(M - \frac{i}{2} \Gamma \right) \pm \frac{q}{p} \left(M_{12} - \frac{i}{2} \Gamma_{12} \right) \equiv m_{1,2} - \frac{i}{2} \Gamma_{1,2}, \quad (69.3)$$

where $m_{1,2}$ and $\Gamma_{1,2}$ are real and correspond to the masses and decay widths, respectively, of the $D_{1,2}$ mass eigenstates. As the trace $\Gamma_{11} + \Gamma_{22} = 2\Gamma$ is unchanged by diagonalizing $\mathbf{\Gamma}$, $\Gamma = (\Gamma_1 + \Gamma_2)/2$, i.e., the mean decay width. Solving for the eigenstates of the eigenvalues yields

$$\left(\frac{q}{p} \right)^2 = \frac{M_{12}^* - \frac{i}{2} \Gamma_{12}^*}{M_{12} - \frac{i}{2} \Gamma_{12}}. \quad (69.4)$$

If CP is conserved, $(q/p) = 1$ and thus M_{12} and Γ_{12} must be real. In this case the difference in eigenvalues is $\Delta m \equiv m_2 - m_1 = 2M_{12}$ and $\Delta\Gamma \equiv \Gamma_2 - \Gamma_1 = 2\Gamma_{12}$. The signs of Δm and $\Delta\Gamma$ are difficult to predict from theory and thus must be determined experimentally.

We define dimensionless mixing parameters x and y as

$$x \equiv \frac{\Delta m}{\Gamma} \quad (69.5)$$

$$y \equiv \frac{\Delta\Gamma}{2\Gamma}. \quad (69.6)$$

These parameters are measured in several ways. The most precise values are obtained using the time dependence of D^0 decays. For all methods, the initial flavor of the D^0 or \bar{D}^0 (at the production point) must be determined. The most common method used for this is to reconstruct $D^{*+} \rightarrow D^0\pi^+$ or $D^{*-} \rightarrow \bar{D}^0\pi^-$ decays; the charge of the accompanying pion (which has low momentum in the lab frame and is often referred to as the “soft” pion) determines the flavor of the neutral D . BaBar and LHCb have also identified the flavor of the neutral D by reconstructing semileptonic $B^+ \rightarrow \bar{D}^0\ell^+\nu$, $B^0 \rightarrow D^{*-}\ell^+\nu$, $B^- \rightarrow D^0\ell^-\nu$, and $\bar{B}^0 \rightarrow D^{*+}\ell^-\nu$ decays; in this case the charge of the accompanying lepton determines the D flavor. At e^+e^- collider experiments such as Belle, BaBar, and BESIII, the D flavor can also be determined by fully reconstructing a D decay on the “opposite side” of an event, i.e., recoiling against the signal-side D decay.

At BESIII, where DD pairs are produced near their threshold via $e^+e^- \rightarrow \psi(3770) \rightarrow D^0\bar{D}^0$, there is relatively little background and the purity of opposite-side tagging is equivalent to that achieved using $D^{*\pm}$ decays. However, BESIII operates at a symmetric e^+e^- collider, and the DD pairs are produced almost at rest in the lab frame. As a consequence, the D 's do not travel any appreciable distance before decaying, and time-dependent analyses are not possible. To overcome this, measurements of mixing at BESIII utilize the quantum coherence of the initial $\psi(3770) \rightarrow D^0\bar{D}^0$ state and time-integrated measurements [1–5].

69.1 Time-Dependent Analyses

We extend the formalism of this *Review*'s note on “ CP Violation in Meson Decays.” Our notation is as follows: Cabibbo-favored (“right-sign”) decay amplitudes are denoted $\bar{A}_f \equiv \langle f|H|\bar{D}^0\rangle$ and $A_{\bar{f}} \equiv \langle \bar{f}|H|D^0\rangle$; i.e., the final state is $f = K^+\ell^-\nu$, $K^+\pi^-$, $K^+\pi^-\pi^0$, etc. Doubly-Cabibbo-suppressed (“wrong-sign”) decay amplitudes are denoted $A_f \equiv \langle f|H|D^0\rangle$ and $\bar{A}_{\bar{f}} \equiv \langle \bar{f}|H|\bar{D}^0\rangle$.

Starting from a pure $|D^0\rangle$ or $|\bar{D}^0\rangle$ state at $t = 0$, the time-dependent decay rates to wrong-sign final states are

$$r(t) \equiv |\langle f|H|D^0(t)\rangle|^2 = |\bar{A}_f|^2 \left| \frac{q}{p} \right|^2 |g_+(t)\lambda_f^{-1} + g_-(t)|^2 \quad (69.7)$$

$$\bar{r}(t) \equiv |\langle \bar{f}|H|\bar{D}^0(t)\rangle|^2 = |A_{\bar{f}}|^2 \left| \frac{p}{q} \right|^2 |g_+(t)\lambda_{\bar{f}} + g_-(t)|^2, \quad (69.8)$$

where

$$\lambda_f \equiv \frac{q\bar{A}_f}{pA_f}, \quad \lambda_{\bar{f}} \equiv \frac{q\bar{A}_{\bar{f}}}{pA_{\bar{f}}}, \quad (69.9)$$

and

$$g_{\pm}(t) = \frac{1}{2} (e^{-i\omega_1 t} \pm e^{-i\omega_2 t}). \quad (69.10)$$

A change in convention for the relative phase of D^0 and \bar{D}^0 would cancel between q/p and \bar{A}_f/A_f (or $\bar{A}_{\bar{f}}/A_{\bar{f}}$), leaving λ_f (or $\lambda_{\bar{f}}$) unchanged. For multibody final states, these equations apply separately to each point in phase-space. Integrating over regions of phase-space can lead to enhanced sensitivity to CP violation; see the discussion below on multibody decays and the “Review of Multibody Charm Analyses” in this *Review* [6]. As the mixing parameters x and y are very small, $r(t)$ and $\bar{r}(t)$ are usually expanded to second order in x and y .

69.2 Semileptonic decays

Consider the final state $f = K^+\ell^-\bar{\nu}_\ell$, where $A_f = \bar{A}_{\bar{f}} = 0$ is an excellent approximation in the Standard Model. The final state f is accessible from a D^0 only via mixing,¹ and the decay rate is

$$r(t) = |\bar{A}_f|^2 \left| \frac{q}{p} \right|^2 |g_-(t)|^2 \approx |\bar{A}_f|^2 \left| \frac{q}{p} \right|^2 \left(\frac{x^2 + y^2}{4} \right) (\Gamma t)^2 e^{-\Gamma t}. \quad (69.11)$$

For $\bar{r}(t)$, q/p is replaced by p/q . In the Standard Model, CP violation in charm mixing is small and $|q/p| \approx 1$. In the limit of CP conservation, $r(t) = \bar{r}(t)$, and the time-integrated mixing rate relative to the time-integrated right-sign decay rate for semileptonic decays is

$$\frac{\int_0^\infty r(t) dt}{\int_0^\infty |\bar{A}_f|^2 e^{-\Gamma t} dt} = \frac{x^2 + y^2}{2} \equiv R_M. \quad (69.12)$$

Table 69.1 summarizes results for R_M from semileptonic decays; the world average from the Heavy Flavor Averaging Group (HFLAV) [7] is $R_M = (1.30 \pm 2.69) \times 10^{-4}$.

69.3 Wrong-sign decays to hadronic non- CP eigenstates

Consider the final state $f = K^+\pi^-$, i.e., A_f and $\bar{A}_{\bar{f}}$ are doubly Cabibbo-suppressed. Allowing for CP violation, the ratio of decay amplitudes can be parameterized as

$$\frac{A_f}{\bar{A}_f} = -\sqrt{R_D^+} e^{-i\delta_f}, \quad \frac{\bar{A}_{\bar{f}}}{A_{\bar{f}}} = -\sqrt{R_D^-} e^{-i\delta_f}, \quad (69.13)$$

where δ_f is the strong phase difference. The minus sign orig-

¹There exists a doubly Cabibbo-suppressed amplitude in which the c and \bar{u} quarks exchange a W , and then the resulting d quark (from c) decays semileptonically. We neglect this second-order process.

Table 69.1: Results for R_M in D^0 semileptonic decays. The HFLAV average assumes reported statistical and systematic uncertainties are uncorrelated. When a single uncertainty is listed, that corresponds to statistical and systematic uncertainties combined. The measurements with an asterisk (*) have been superseded and thus are not included in the HFLAV average.

Year	Experiment	Final state(s)	$R_M (\times 10^{-3})$	90% C.L. ($\times 10^{-3}$)
2008	Belle (492 fb^{-1}) [8]	$K^{(*)+}e^{-}\bar{\nu}_e$	$0.13 \pm 0.22 \pm 0.20$	< 0.61
2007	BaBar (344 fb^{-1}) [9]	$K^{(*)+}e^{-}\bar{\nu}_e$	$0.04^{+0.70}_{-0.60}$	$(-1.3, 1.2)$
2005	CLEO (9.0 fb^{-1}) [10]	$K^{(*)+}e^{-}\bar{\nu}_e$	$1.6 \pm 2.9 \pm 2.9$	< 7.8
1996	E791 (2×10^{10} evts) [11]	$K^+\ell^{-}\bar{\nu}_\ell$	$1.1^{+3.0}_{-2.7}{}^{+0.0}_{-0.1}$	< 5.0
HFLAV Average [7]			0.130 ± 0.269	
2005*	Belle (253 fb^{-1}) [12]	$K^{(*)+}e^{-}\bar{\nu}_e$	$0.02 \pm 0.47 \pm 0.14$	< 1.0
2004*	BaBar (87 fb^{-1}) [13]	$K^{(*)+}e^{-}\bar{\nu}_e$	$2.3 \pm 1.2 \pm 0.4$	< 4.2

Table 69.2: Results for R , R_D , and A_D as measured using $D^0 \rightarrow K^\pm \pi^\mp$ decays. When a single uncertainty is listed, that corresponds to statistical and systematic uncertainties combined. The measurements with an asterisk (*) have been superseded and thus are not included in the HFLAV average. The measurements with a dagger (†) are not included in the HFLAV average due to poorer precision.

Year	Experiment	$R (\times 10^{-3})$	$R_D (\times 10^{-3})$	$A_D (\%)$
2018	LHCb ($5.0 \text{ fb}^{-1} D^*$ tag) [14]	—	3.454 ± 0.031	-0.01 ± 0.91
2017	LHCb ($3.0 \text{ fb}^{-1} B$ tag) [15]	—	3.48 ± 0.10	—
2014	Belle (976 fb^{-1}) [16]	3.86 ± 0.06	3.53 ± 0.13	—
2013	CDF (9.6 fb^{-1}) [17]	4.30 ± 0.05	3.51 ± 0.35	—
2007	BaBar (384 fb^{-1}) [18]	$3.53 \pm 0.08 \pm 0.04$	$3.03 \pm 0.16 \pm 0.10$	$-2.1 \pm 5.2 \pm 1.5$
HFLAV Average [7]			3.435 ± 0.022	$-0.55^{+0.49}_{-0.51}$
2013b*	LHCb ($3.0 \text{ fb}^{-1} D^*$ tag) [19]	—	3.568 ± 0.066	-0.7 ± 1.9
2013a*	LHCb (1.0 fb^{-1}) [20]	4.25 ± 0.04	3.52 ± 0.15	—
2008*	CDF (1.5 fb^{-1}) [21]	4.15 ± 0.10	3.04 ± 0.55	—
2006*	Belle (400 fb^{-1}) [22]	$3.77 \pm 0.08 \pm 0.05$	3.64 ± 0.18	2.3 ± 4.7
2005†	FOCUS (234 evts) [23]	$4.29^{+0.63}_{-0.61} \pm 0.27$	$5.17^{+1.47}_{-1.58} \pm 0.76$	$13^{+33}_{-25} \pm 10$
2000†	CLEO (9.0 fb^{-1}) [24]	$3.32^{+0.63}_{-0.65} \pm 0.40$	$4.8 \pm 1.2 \pm 0.4$	$-1^{+16}_{-17} \pm 1$
1998†	E791 (5643 evts) [25]	$6.8^{+3.4}_{-3.3} \pm 0.7$	—	—

inates from the weak phase difference between the amplitudes, specifically, the relative signs of V_{us} and V_{cd} . The parameters R_D^+ and R_D^- are the ratios of the doubly Cabibbo-suppressed (DCS) decay rate to the Cabibbo-favored (CF) decay rate. From the relevant CKM matrix elements, one estimates $R_D^+, R_D^- \sim \tan^4 \theta_c$, where θ_c is the Cabibbo angle. With this parameterization, Eq. (69.9) becomes

$$\lambda_f^{-1} = \frac{p}{q} \frac{A_f}{\bar{A}_f} = -\sqrt{R_D^+} \left| \frac{p}{q} \right| e^{-i(\delta_f + \phi)} \quad (69.14)$$

$$\lambda_{\bar{f}} = \frac{q}{p} \frac{\bar{A}_{\bar{f}}}{A_{\bar{f}}} = -\sqrt{R_D^-} \left| \frac{q}{p} \right| e^{-i(\delta_f - \phi)}, \quad (69.15)$$

where ϕ is a weak phase difference. In the Standard Model, the weak phase of A_f/\bar{A}_f or $\bar{A}_{\bar{f}}/A_{\bar{f}}$ is, to excellent approximation, -1 , which is already factored out, and thus $\phi = \text{Arg}(q/p)$. As ϕ is essentially independent of the final state, it is referred to as “universal.” CP violation in mixing is characterized by $|q/p| \neq |p/q| \neq 1$. CP violation in the decay amplitudes $A_f, \bar{A}_f, A_{\bar{f}}, \bar{A}_{\bar{f}}$ is referred to as *direct* CP violation and is parameterized by $A_D \equiv (R_D^+ - R_D^-)/(R_D^+ + R_D^-)$. The mean value is denoted $R_D \equiv (R_D^+ + R_D^-)/2$.

With these definitions, we expand the decay rates Eqs. (69.7) and (69.8) to second order in the small mixing parameters x and y to obtain [26, 27]:

$$r(t) = \left| \bar{A}_f \right|^2 e^{-\Gamma t} \times [R_D(1 + A_D) + \sqrt{R_D(1 + A_D)} \left| \frac{q}{p} \right| y'_+(\Gamma t) + \left| \frac{q}{p} \right|^2 \frac{(x'_+{}^2 + y'_+{}^2)}{4} (\Gamma t)^2]$$

and

$$\bar{r}(t) = \left| A_{\bar{f}} \right|^2 e^{-\Gamma t} \times [R_D(1 - A_D) + \sqrt{R_D(1 - A_D)} \left| \frac{p}{q} \right| y'_-(\Gamma t) + \left| \frac{p}{q} \right|^2 \frac{(x'_-{}^2 + y'_-{}^2)}{4} (\Gamma t)^2],$$

where

$$\begin{aligned} x'_\pm &= x \cos(\delta_f \pm \phi) + y \sin(\delta_f \pm \phi) \\ &\equiv x' \cos \phi \pm y' \sin \phi, \end{aligned} \quad (69.16)$$

$$\begin{aligned} y'_\pm &= y \cos(\delta_f \pm \phi) - x \sin(\delta_f \pm \phi) \\ &\equiv y' \cos \phi \mp x' \sin \phi, \end{aligned} \quad (69.17)$$

and

$$x' = x \cos \delta_f + y \sin \delta_f \quad (69.18)$$

$$y' = y \cos \delta_f - x \sin \delta_f. \quad (69.19)$$

In Eqs. (69.16) and (69.16), a fourth term $R_D(1 \pm A_D)(x'_\pm{}^2 - y'_\pm{}^2)/4 \times (\Gamma t)^2$ has been dropped, as, for the range of decay times measured by experiments, it is negligible relative to the other terms.

The parameters (x', y') are the mixing parameters (x, y) rotated by the strong phase δ_f . The parameters (x'_\pm, y'_\pm) are the parameters (x', y') rotated by the weak phase $\pm \phi$. Note that $x'_+{}^2 + y'_+{}^2 = x'_-{}^2 + y'_-{}^2 = x'^2 + y'^2 = x^2 + y^2$. Comparing Eqs. (69.16) and (69.16), one sees that $r(t) \neq \bar{r}(t)$ (CP is violated) if either $A_D \neq 0$, $|q/p| \neq 1$, or $\phi \neq 0$. These three inequalities correspond, respectively, to the three types of CP violation: in the (doubly Cabibbo-suppressed) decay amplitudes; in the mixing; and due to interference between a mixed amplitude and an unmixed decay amplitude. Whereas CP violation in the decay amplitudes is parameterized by A_D , CP violation in the mixing is parameterized by $A_M \equiv (|q/p| - |p/q|)/(|q/p| + |p/q|)$.

Table 69.3: Results for x'^2 and y' , as measured using $D^0 \rightarrow K^\pm \pi^\mp$ decays. When a single uncertainty is listed, that corresponds to statistical and systematic uncertainties combined. The measurements with an asterisk (*) have been superseded and thus are not included in the HFLAV global fit. The measurements with a dagger (\dagger) are not included in the HFLAV global fit due to poorer precision. All confidence limits and intervals correspond to 95% C.L. The Belle 2006 results restrict x'^2 to the physical region. The BaBar confidence intervals are obtained from the fit, whereas Belle uses a Feldman-Cousins method, and CDF uses a Bayesian method.

Year	Experiment	No CP violation		Allowing for CP violation	
		$x'^2 (\times 10^{-3})$	$y' (\%)$	$x'^2 (\times 10^{-3})$	$y' (\%)$
2018	LHCb (5.0 fb^{-1} D^* tag) [14]	0.039 ± 0.027	0.528 ± 0.052	$\begin{cases} D^0: 0.061 \pm 0.037 \\ \bar{D}^0: 0.016 \pm 0.039 \end{cases}$	$\begin{cases} 0.501 \pm 0.074 \\ 0.554 \pm 0.074 \end{cases}$
2017	LHCb (3.0 fb^{-1} B tag) [15]	0.028 ± 0.310	0.46 ± 0.37	$\begin{cases} D^0: -0.019 \pm 0.447 \\ \bar{D}^0: 0.079 \pm 0.433 \end{cases}$	$\begin{cases} 0.581 \pm 0.526 \\ 0.332 \pm 0.523 \end{cases}$
2014	Belle (976 fb^{-1}) [16]	0.09 ± 0.22	0.46 ± 0.34	—	—
2013	CDF (9.6 fb^{-1}) [17]	0.08 ± 0.18	0.43 ± 0.43	—	—
2007	BaBar (384 fb^{-1}) [18]	-0.22 ± 0.37	0.97 ± 0.54	$\begin{cases} D^0: -0.24 \pm 0.52 \\ \bar{D}^0: -0.20 \pm 0.50 \end{cases}$	$\begin{cases} 0.98 \pm 0.78 \\ 0.96 \pm 0.75 \end{cases}$
2006	Belle (400 fb^{-1}) [22]	$(0.18^{+0.21}_{-0.23})^*$	$(0.06^{+0.40}_{-0.39})^*$	< 0.72	$-2.8 < y' < 2.1$
2013b*	LHCb (3.0 fb^{-1} D^* tag) [19]	0.055 ± 0.049	0.48 ± 0.10	$\begin{cases} D^0: 0.049 \pm 0.070 \\ \bar{D}^0: 0.060 \pm 0.068 \end{cases}$	$\begin{cases} 0.51 \pm 0.14 \\ 0.45 \pm 0.14 \end{cases}$
2013a*	LHCb (1.0 fb^{-1}) [20]	-0.09 ± 0.13	0.72 ± 0.24	—	—
2008*	CDF (1.5 fb^{-1}) [21]	-0.12 ± 0.35	0.85 ± 0.76	—	—
2005 \dagger	FOCUS (234 evts) [23]	< 8.3	$-7.2 < y' < 4.1$	< 8.0	$-11.2 < y' < 6.7$
2000 \dagger	CLEO (9.0 fb^{-1}) [24]	0.00 ± 0.23	$-2.3^{+1.3}_{-1.4}$	0.00 ± 0.23	$-2.5^{+1.4}_{-1.6}$
1998 \dagger	E791 (5643 evts) [25]	< 17	< 13	—	—

Table 69.4: Results from time-dependent multibody analyses. The errors are statistical, systematic, and, when a third error is listed, due to the decay-model, respectively. The measurement with an asterisk (*) has been superseded and thus is not included in the HFLAV global fit. The measurement with a dagger (\dagger) is not included in the HFLAV global fit due to poorer precision. The 2019 LHCb result utilizes strong-phase measurements from CLEO-c [28] and thus is decay-model independent. This fit determines CP -violating parameters Δx and Δy ; the translation of these parameters to $|q/p|$ and ϕ is given in Ref. [29].

No CP Violation				
Year	Experiment	Final State(s)	$x (\times 10^{-3})$	$y (\times 10^{-3})$
2019	LHCb (3.0 fb^{-1} B tag) [30]	$K_S^0 \pi^+ \pi^-$	$2.7 \pm 1.6 \pm 0.4$	$7.4 \pm 3.6 \pm 1.1$
2016	LHCb (1.0 fb^{-1} D^* tag) [31]	$K_S^0 \pi^+ \pi^-$	$-8.6 \pm 5.3 \pm 1.7$	$0.3 \pm 4.6 \pm 1.3$
2016	BaBar (468 fb^{-1}) [32]	$\pi^+ \pi^- \pi^0$	$15 \pm 12 \pm 6$	$2 \pm 9 \pm 5$
2014	Belle (921 fb^{-1}) [33]	$K_S^0 \pi^+ \pi^-$	$5.6 \pm 1.9^{+0.3+0.6}_{-0.9-0.9}$	$3.0 \pm 1.5^{+0.4+0.3}_{-0.5-0.6}$
2010	BaBar (469 fb^{-1}) [34]	$\begin{cases} K_S^0 \pi^+ \pi^- \\ K_S^0 K^+ K^- \end{cases}$	$1.6 \pm 2.3 \pm 1.2 \pm 0.8$	$5.7 \pm 2.0 \pm 1.3 \pm 0.7$
2007*	Belle (540 fb^{-1}) [35]	$K_S^0 \pi^+ \pi^-$	$8.0 \pm 2.9^{+0.9+1.0}_{-0.7-1.4}$	$3.3 \pm 2.4^{+0.8+0.6}_{-1.2-0.8}$
2005 \dagger	CLEO (9.0 fb^{-1}) [36]	$K_S^0 \pi^+ \pi^-$	$19^{+32}_{-33} \pm 4 \pm 4$	$-14 \pm 24 \pm 8 \pm 4$

With CP Violation				
Year	Experiment	Final State(s)	$ q/p $	ϕ
2019	LHCb (3.0 fb^{-1}) [30]	$K_S^0 \pi^+ \pi^-$	$\begin{cases} 1.05^{+0.22}_{-0.17} \\ \Delta x \times 10^{-3} = \\ -0.53 \pm 0.70 \pm 0.22 \end{cases}$	$\begin{cases} (-5.2^{+6.3}_{-9.2})^\circ \\ \Delta y \times 10^{-3} = \\ 0.6 \pm 1.6 \pm 0.3 \end{cases}$
2014	Belle (921 fb^{-1}) [33]	$K_S^0 \pi^+ \pi^-$	$0.90^{+0.16+0.05+0.06}_{-0.15-0.04-0.05}$	$(-6 \pm 11 \pm 3^{+3}_{-4})^\circ$
2007* \ddagger	Belle (540 fb^{-1}) [35]	$K_S^0 \pi^+ \pi^-$	$0.86^{+0.30+0.06}_{-0.29-0.03} \pm 0.08$	$(-14^{+16+5+2}_{-18-3-4})^\circ$

\ddagger This result allows for all CP violations and is superseded by Ref. [33], which assumes no direct CP violation in doubly Cabibbo-suppressed decays.

In the limit of CP conservation, $A_D = 0$, $|q/p| = 1$, and $\phi = 0$. In this case

$$r(t) = \bar{r}(t) = \left| A_{\bar{f}} \right|^2 e^{-\Gamma t} \left[R_D + \sqrt{R_D} y'(\Gamma t) + \frac{x'^2 + y'^2}{4} (\Gamma t)^2 \right], \quad (69.20)$$

and the number of wrong-sign decays divided by the number of right-sign decays is

$$R = \frac{\int_0^\infty r(t) dt}{\int_0^\infty \left| A_{\bar{f}} \right|^2 e^{-\Gamma t} dt} = R_D + \sqrt{R_D} y' + \frac{x'^2 + y'^2}{2}. \quad (69.21)$$

The ratio R is straightforward to measure, as there is no time-dependence. In Table 69.2 we report measurements of R , R_D , and A_D in $D^0 \rightarrow K^+ \pi^-$ decays, and HFLAV world averages [7] obtained from a global fit that allows for both mixing and CP violation. Typically, the experimental fitted parameters are R_D , x'^2 , and y' ; the results for x'^2 and y' are summarized in Table 69.3. Allowing for CP violation, the parameters (R_D^+, x'^2, y'_+) and (R_D^-, x'^2, y'_-) [or equivalently (R_D, A_D) instead of (R_D^+, R_D^-)] are obtained by separately fitting $D^0 \rightarrow K^+ \pi^-$ and $\bar{D}^0 \rightarrow K^- \pi^+$ event samples.

Extraction of the mixing parameters x and y from measurements of x' and y' requires knowledge of the strong phase difference $\delta_{K\pi}$. This can be determined from the decay rates of $D_\pm \rightarrow K^+ \pi^-$, where D_+ (D_-) denotes the CP -even (CP -odd)

Table 69.5: Results for y_{CP} and A_Γ from $D^0 \rightarrow K^+K^-$ and $D^0 \rightarrow \pi^+\pi^-$ decays. When a single uncertainty is listed, that corresponds to statistical and systematic uncertainties combined. The measurements with an asterisk (*) have been superseded and thus are not included in the HFLAV average. Results from LHCb labeled “ B tag” have the D^0 or \bar{D}^0 flavor identified via $B^\pm \rightarrow D\mu^\pm\nu_\mu X$ decays.

Year	Experiment	final state(s)	y_{CP} (%)	$A_\Gamma (\times 10^{-3})$
2020	LHCb (8.4 fb $^{-1}$ $B+D^*$ tags) [37]	$K^+K^- + \pi^+\pi^-$	—	$-0.29 \pm 0.20 \pm 0.06$
2020	LHCb (5.4 fb $^{-1}$ B tag) [37]	K^+K^-	—	$-0.43 \pm 0.36 \pm 0.05$
2020	LHCb (5.4 fb $^{-1}$ B tag) [37]	$\pi^+\pi^-$	—	$0.22 \pm 0.70 \pm 0.08$
2019	LHCb (3 fb $^{-1}$ B tag) [38]	$K^+K^- + \pi^+\pi^-$	$0.57 \pm 0.13 \pm 0.09$	—
2017	LHCb (3 fb $^{-1}$ D^* tag) [39]	$K^+K^- + \pi^+\pi^-$	—	$-0.13 \pm 0.28 \pm 0.10$
2017	LHCb (3 fb $^{-1}$ D^* tag) [39]	K^+K^-	—	$-0.30 \pm 0.32 \pm 0.10$
2017	LHCb (3 fb $^{-1}$ D^* tag) [39]	$\pi^+\pi^-$	—	$0.46 \pm 0.58 \pm 0.12$
2016	Belle (976 fb $^{-1}$) [40]	$K^+K^- + \pi^+\pi^-$	$1.11 \pm 0.22 \pm 0.09$	$-0.3 \pm 2.0 \pm 0.7$
2015	LHCb (3 fb $^{-1}$ B tag) [41]	$K^+K^- + \pi^+\pi^-$	—	-1.25 ± 0.73
2015	LHCb (3 fb $^{-1}$ B tag) [41]	K^+K^-	—	$-1.34 \pm 0.77^{+0.26}_{-0.34}$
2015	LHCb (3 fb $^{-1}$ B tag) [41]	$\pi^+\pi^-$	—	$-0.92 \pm 1.45^{+0.25}_{-0.33}$
2015	BES III (2.9 fb $^{-1}$) [42]	$\left\{ \begin{array}{l} K^+K^-, \pi^+\pi^- \\ K_S^0\pi^0, K_S^0\pi^0\pi^0 \\ K_S^0\eta, K_S^0\omega \end{array} \right.$	$-2.0 \pm 1.3 \pm 0.7$	—
2014	CDF (9.7 fb $^{-1}$) [43]	$K^+K^- + \pi^+\pi^-$	—	-1.2 ± 1.2
2014	CDF (9.7 fb $^{-1}$) [43]	K^+K^-	—	$-1.9 \pm 1.5 \pm 0.4$
2014	CDF (9.7 fb $^{-1}$) [43]	$\pi^+\pi^-$	—	$-0.1 \pm 1.8 \pm 0.3$
2012	BaBar (468 fb $^{-1}$) [44]	$K^+K^- + \pi^+\pi^-$	$0.72 \pm 0.18 \pm 0.12$	$0.9 \pm 2.6 \pm 0.6$
2009	Belle (673 fb $^{-1}$) [45]	$K_S^0 K^+K^-$	$0.11 \pm 0.61 \pm 0.52$	—
2002	CLEO (9.0 fb $^{-1}$) [46]	$K^+K^- + \pi^+\pi^-$	$-1.2 \pm 2.5 \pm 1.4$	—
2000	FOCUS (1×10^6 evts) [47]	K^+K^-	$3.42 \pm 1.39 \pm 0.74$	—
1999	E791 (2×10^{10} evts) [48]	K^+K^-	$0.73 \pm 2.89 \pm 1.03$	—
HFLAV Average [7]			0.715 \pm 0.111	-0.32 \pm 0.26
2013*	LHCb (1.0 fb $^{-1}$ D^* tag) [49]	K^+K^-	—	$-0.35 \pm 0.62 \pm 0.12$
2013*	LHCb (1.0 fb $^{-1}$ D^* tag) [49]	$\pi^+\pi^-$	—	$0.33 \pm 1.06 \pm 0.14$
2011* \ddagger	LHCb (29 pb $^{-1}$ D^* tag) [50]	K^+K^-	$0.55 \pm 0.63 \pm 0.41$	$-5.9 \pm 5.9 \pm 2.1$
2009*	BaBar (384 fb $^{-1}$) [51]	K^+K^-	$1.16 \pm 0.22 \pm 0.18$	—
2008*	BaBar (384 fb $^{-1}$) [52]	$K^+K^- + \pi^+\pi^-$	$1.03 \pm 0.33 \pm 0.19$	$2.6 \pm 3.6 \pm 0.8$
2007*	Belle (540 fb $^{-1}$) [53]	$K^+K^- + \pi^+\pi^-$	$1.31 \pm 0.32 \pm 0.25$	$0.1 \pm 3.0 \pm 1.5$
2003*	BaBar (91 fb $^{-1}$) [54]	$K^+K^- + \pi^+\pi^-$	$0.8 \pm 0.4^{+0.5}_{-0.4}$	—
2001*	Belle (23.4 fb $^{-1}$) [55]	K^+K^-	$-0.5 \pm 1.0^{+0.7}_{-0.8}$	—

\ddagger This result for y_{CP} is not superseded but is not included in the HFLAV average due to having some correlations with, and much poorer precision than, the result of Ref. [38].

eigenstate. Since $|D_\pm\rangle = (|D^0\rangle \mp |\bar{D}^0\rangle)/\sqrt{2}$,

$$\sqrt{2}A(D_\pm \rightarrow K^+\pi^-) = A(D^0 \rightarrow K^+\pi^-) \mp A(\bar{D}^0 \rightarrow K^+\pi^-). \quad (69.22)$$

Squaring this amplitude and using Eq. (69.13) yields the relation

$$\cos\delta_{K\pi} = \frac{|A(D_+ \rightarrow K^+\pi^-)|^2 - |A(D_- \rightarrow K^+\pi^-)|^2}{2|A(D^0 \rightarrow K^+\pi^-)||A(\bar{D}^0 \rightarrow K^+\pi^-)|}. \quad (69.23)$$

Measuring the right-hand side is possible only if one can identify pure D_+ , D_- , D^0 , and \bar{D}^0 initial states. This is accomplished at CLEOc and BESIII utilizing the processes $e^+e^- \rightarrow \psi(3770) \rightarrow \bar{D}^0 D^0 \rightarrow (f_{CP})(K^+\pi^-)$, or $\psi(3770) \rightarrow \bar{D}^0 D^0 \rightarrow (f_{\bar{D}^0})(K^+\pi^-)$. In the first case, quantum coherence and CP symmetry insures that the $K^+\pi^-$ state originates from a neutral D with CP opposite that of f_{CP} . In the second case, at the time when the \bar{D}^0 decays, the opposite side is D^0 . However, it can potentially mix to \bar{D}^0 before decaying to $K^+\pi^-$, and this introduces some dependence on the mixing parameters x and y . This dependence is seen explicitly in the observable

$$A_{K\pi}^{CP} \equiv \frac{|A(D_- \rightarrow K^-\pi^+)|^2 - |A(D_+ \rightarrow K^-\pi^+)|^2}{|A(D_- \rightarrow K^-\pi^+)|^2 + |A(D_+ \rightarrow K^-\pi^+)|^2}. \quad (69.24)$$

To lowest order in the mixing parameters [56],

$$A_{K\pi}^{CP} = \frac{2\sqrt{R_D} \cos\delta_{K\pi} + y}{1 + R}, \quad (69.25)$$

where R is defined in Eq. (69.21).

69.3.1 Wrong-sign decays to multibody final states

For multibody final states, Eqs. (69.13)-(69.21) apply essentially to each point in phase-space. Although x and y do not vary across phase-space, knowledge of the resonant substructure is needed to extrapolate the strong phase difference δ from point to point to determine x and y . Alternatively, model-independent methods to determine x and y require knowledge of the relative phases of D^0 and \bar{D}^0 decay amplitudes across the phase-space distribution [6]. This required phase information can be measured at the charm threshold, where CLEO-c and BESIII took data.

A time-dependent analysis of $D^0 \rightarrow K^+\pi^-\pi^0$ decays at BaBar [66,67] determined the *relative* strong phase variation across the Dalitz plot and reported $x'' = (2.61^{+0.57}_{-0.68} \pm 0.39)\%$ and $y'' = (-0.06^{+0.55}_{-0.64} \pm 0.34)\%$. These mixing parameters are defined as

$$\begin{aligned} x'' &= x \cos\delta_{K\pi\pi^0} + y \sin\delta_{K\pi\pi^0} \\ y'' &= y \cos\delta_{K\pi\pi^0} - x \sin\delta_{K\pi\pi^0}, \end{aligned} \quad (69.26)$$

in analogy with x' , y' , and $\delta_{K\pi}$ of Eqs. (69.18) and (69.19). Here, $\delta_{K\pi\pi^0}$ is the strong phase difference between the amplitudes $A(D^0 \rightarrow K^+\pi^-\pi^0)$ and $A(\bar{D}^0 \rightarrow K^+\pi^-\pi^0)$ at a “reference point” of the Dalitz plot. In this case the reference point chosen is $m_{\pi^-\pi^0} = m_{\rho^-}$. The strong phase difference $\delta_{K\pi\pi^0}$ can be determined in a manner similar to that for $\delta_{K\pi}$: by using Eq. (69.23) and quantum-correlated measurements of the branching fractions $B(D_+ \rightarrow K^+\rho^-)$, $B(D_- \rightarrow K^+\rho^-)$, $B(D^0 \rightarrow K^+\rho^-)$, and $B(\bar{D}^0 \rightarrow K^+\rho^-)$ in $e^+e^- \rightarrow \psi(3770)$ events.

For the decay modes D^0 and $\bar{D}^0 \rightarrow K^+\pi^-\pi^+\pi^-$, Belle measured $R = (0.324 \pm 0.008 \pm 0.007)\%$ [68]. Subsequently, a phase-space-integrated analysis from LHCb [69] measured the product of a coherence factor $R_D^{K^3\pi}$ and the strong-phase-rotated mixing

Table 69.6: Results for the difference in time-integrated CP asymmetries ΔA_{CP} between $D^0 \rightarrow K^+K^-$ and $D^0 \rightarrow \pi^+\pi^-$ decays. When a single uncertainty is listed, that corresponds to statistical and systematic uncertainties combined. The measurements with an asterisk (*) have been either superseded or combined with subsequent results and thus are not included in the HFLAV global fit.

Year	Experiment	$\Delta A_{CP} (\times 10^{-3})$
2019	LHCb (8.9 fb $^{-1}$ $B+D^*$ tags) [57]	-1.54 ± 0.29
2013	CDF (9.7 fb $^{-1}$ D^* tag) [58]	$-6.2 \pm 2.1 \pm 1.0$
2008	BaBar (386 fb $^{-1}$) [59]	$2.4 \pm 6.2 \pm 2.6$
2008	Belle (540 fb $^{-1}$) [60]	$-8.6 \pm 6.0 \pm 0.7$
2016*	LHCb (3.0 fb $^{-1}$ D^* tag) [61]	$-1.0 \pm 0.8 \pm 0.3$
2014*	LHCb (3.0 fb $^{-1}$ B tag) [62]	$1.4 \pm 1.6 \pm 0.8$
2013*	LHCb (1.0 fb $^{-1}$ B tag) [63]	$4.9 \pm 3.0 \pm 1.4$
2012*	LHCb (0.62 fb $^{-1}$ D^* tag) [64]	$-8.2 \pm 2.1 \pm 1.1$
2012 ‡	Belle (976 fb $^{-1}$) [65]	$-8.7 \pm 4.1 \pm 0.6$

‡ This preliminary result was not published and thus is not included in the HFLAV global fit.

Table 69.7: HFLAV global fit results (see text) [7].

Parameter	No CP Violation	No CP Violation in DCS Decays	All CP Violation Allowed	95% C.L. Interval CPV Allowed
x (%)	$0.50^{+0.13}_{-0.14}$	$0.43^{+0.10}_{-0.11}$	$0.39^{+0.11}_{-0.12}$	[0.16, 0.61]
y (%)	0.62 ± 0.07	0.63 ± 0.06	$0.651^{+0.063}_{-0.069}$	[0.51, 0.77]
$\delta_{K\pi}$ ($^\circ$)	$8.9^{+8.2}_{-8.9}$	$9.3^{+8.3}_{-9.2}$	$12.1^{+8.6}_{-10.2}$	[-10.4, 28.2]
R_D (%)	0.344 ± 0.002	0.344 ± 0.002	0.344 ± 0.002	[0.339, 0.348]
A_D (%)	—	—	$-0.55^{+0.49}_{-0.51}$	[-1.5, 0.4]
$ q/p $	—	0.998 ± 0.008	$0.969^{+0.050}_{-0.045}$	[0.89, 1.07]
ϕ ($^\circ$)	—	0.08 ± 0.31	$-3.9^{+4.5}_{-4.6}$	[-13.2, 5.1]
$\delta_{K\pi\pi}$ ($^\circ$)	$18.5^{+22.7}_{-23.4}$	$22.1^{+22.6}_{-23.4}$	$25.8^{+23.0}_{-23.8}$	[-21.3, 70.3]
$A_{CP}^{\pi\pi}$ (%)	—	0.05 ± 0.16	0.06 ± 0.16	[-0.25, 0.38]
A_{CP}^{KK} (%)	—	-0.11 ± 0.16	-0.09 ± 0.16	[-0.40, 0.22]
x_{12} (%)	—	$0.43^{+0.10}_{-0.11}$	—	[0.22, 0.63]
y_{12} (%)	—	0.63 ± 0.06	—	[0.50, 0.75]
ϕ_{12} ($^\circ$)	—	$-0.25^{+0.96}_{-0.99}$	—	[-2.5, 1.8]

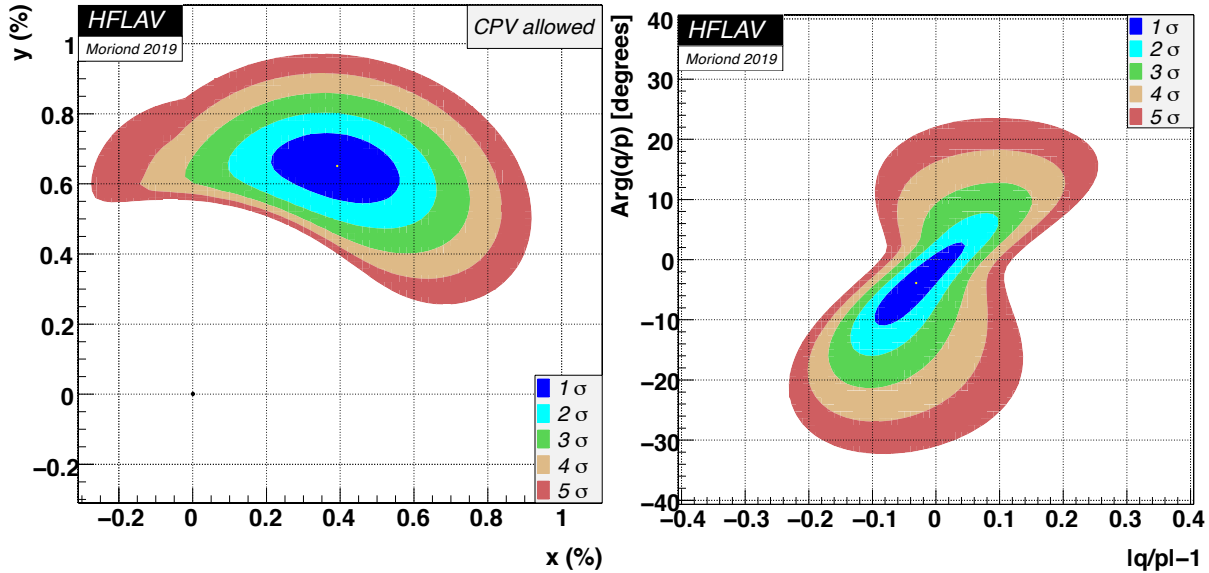


Figure 69.1: Two-dimensional 1σ - 5σ contours for (x, y) (left) and for $(|q/p|, \text{Arg}(q/p))$ (right) as obtained by HFLAV [7], from measurements of $D^0 \rightarrow K^{(*)}\ell\nu$, h^+h^- , $K^+\pi^-$, $K^+\pi^-\pi^0$, $K^+\pi^-\pi^+\pi^-$, $K_S^0\pi^+\pi^-$, $K_S^0K^+K^-$, and $\pi^+\pi^-\pi^0$ decays, and double-tagged branching fractions measured at the $\psi(3770)$ resonance.

parameter $y''_{K3\pi}$. This measurement resulted in an observation of charm mixing with 8.2σ significance.

Both the sign and magnitude of x and y without strong phases entering or sign ambiguity can be measured using the time-dependent resonant substructure of multibody D^0 decays [35, 36]. In $D^0 \rightarrow K_S^0\pi^+\pi^-$, the DCS and CF decay amplitudes populate the same Dalitz plot, which allows for di-

rect measurement of the relative strong phases. Belle [33, 35], BaBar [34], and CLEO [70] have measured the relative strong phase between $D^0 \rightarrow K^*(892)^-\pi^+$ and $D^0 \rightarrow K^*(892)^+\pi^-$ to be $(173.9 \pm 0.7 \text{ (stat. only)})^\circ$, $(177.6 \pm 1.1 \text{ (stat. only)})^\circ$, and $(189 \pm 10 \pm 3^{+15}_{-5})^\circ$, respectively. These results are close to the 180° expected from Cabibbo factors and a small strong phase. Two LHCb measurements [30, 31] of x, y are decay-model inde-

pendent, i.e., the model of resonances in the intermediate state is replaced by strong-phase measurements from CLEO-c [28]. Table 69.4 summarizes mixing results from time-dependent multi-body analyses. World average values for the measurements listed are given later, as a result of the HFLAV global fit.

In addition, Belle [33,35] has measured the relative strong phase (statistical errors only) and the ratio R (central values only) of the DCS fit fraction relative to the CF fit fraction for five excited K states: $K^*(892)^+\pi^-$, $K_0^*(1430)^+\pi^-$, $K_2^*(1430)^+\pi^-$, $K^*(1410)^+\pi^-$, and $K^*(1680)^+\pi^-$. Similarly, BaBar [34, 71, 72] has reported central values of R for $K^*(892)^+\pi^-$, $K_0^*(1430)^+\pi^-$, and $K_2^*(1430)^+\pi^-$. The systematic uncertainties on R are not evaluated. Large differences in R are observed among these final states, which indicates interesting hadronic effects.

69.4 Decays to CP Eigenstates

When the final state f is a CP eigenstate, there is no distinction between f and \bar{f} . Thus $A_f = A_{\bar{f}}$ and $\bar{A}_{\bar{f}} = \bar{A}_f$. We denote final states with CP eigenvalues ± 1 by f_{\pm} and write λ_{\pm} for $\lambda_{f_{\pm}}$.

The quantity y may be measured by comparing the rate for D^0 decays to CP eigenstates such as K^+K^- with the rate to non- CP states such as $K^-\pi^+$ [27]. If decays to K^+K^- have a shorter effective lifetime than those to $K^-\pi^+$, then $\Gamma_+ > \Gamma_-$, or, since CP violation is very small, $\Gamma_2 > \Gamma_1$ and y is positive.

In the limit of small mixing ($x, y \ll 1$) and the absence of direct CP violation in DCS decays ($A_D = 0$), one can write

$$\lambda_{\pm} = \left| \frac{q}{p} \right| e^{\pm i\phi}. \quad (69.27)$$

In this scenario, to a good approximation, the decay rates for states that are initially D^0 and \bar{D}^0 to a CP eigenstate have exponential time dependence:

$$r_{\pm}(t) \propto \exp(-\Gamma_{\pm} t) \quad (69.28)$$

$$\bar{r}_{\pm}(t) \propto \exp(-\bar{\Gamma}_{\pm} t). \quad (69.29)$$

The effective decay widths are given by

$$\Gamma_{\pm} = 1 \pm \left| \frac{q}{p} \right| (y \cos \phi - x \sin \phi), \quad (69.30)$$

$$\bar{\Gamma}_{\pm} = 1 \pm \left| \frac{p}{q} \right| (y \cos \phi + x \sin \phi). \quad (69.31)$$

Thus the effective decay rate to a CP eigenstate combining both D^0 and \bar{D}^0 decays is

$$r_{\pm}(t) + \bar{r}_{\pm}(t) \propto e^{-(1 \pm y_{CP})t}, \quad (69.32)$$

where

$$y_{CP} = \frac{1}{2} \left(\left| \frac{q}{p} \right| + \left| \frac{p}{q} \right| \right) y \cos \phi - \frac{1}{2} \left(\left| \frac{q}{p} \right| - \left| \frac{p}{q} \right| \right) x \sin \phi \quad (69.33)$$

$$\approx y \cos \phi - A_M x \sin \phi. \quad (69.34)$$

If CP is conserved, $y_{CP} = y$. Almost all measurements of y_{CP} are relative to the $D^0 \rightarrow K^-\pi^+$ decay rate. Belle [45] has reported y_{CP} also for the final state $K_S^0 K^+K^-$, which is dominated by the CP -odd final state $K_S^0 \phi$. Table 69.5 summarizes the current status of measurements.

In addition to y_{CP} , Belle [40], BaBar [44], LHCb [50], and CDF [43] have reported measurements of the decay-rate asymmetry for CP -even final states

$$A_{\Gamma} \equiv \frac{\Gamma_+ - \bar{\Gamma}_+}{\Gamma_+ + \bar{\Gamma}_+} = \frac{(1/\tau_+) - (1/\bar{\tau}_+)}{(1/\tau_+) + (1/\bar{\tau}_+)} = \frac{\bar{\tau}_+ - \tau_+}{\bar{\tau}_+ + \tau_+} \quad (69.35)$$

$$\approx \frac{1}{2} \left(\left| \frac{q}{p} \right| - \left| \frac{p}{q} \right| \right) y \cos \phi - \frac{1}{2} \left(\left| \frac{q}{p} \right| + \left| \frac{p}{q} \right| \right) x \sin \phi \quad (69.36)$$

$$\approx A_M y \cos \phi - x \sin \phi. \quad (69.37)$$

If CP is conserved, $A_{\Gamma} = 0$.

The asymmetry A_{Γ} relates to the full decay width. An asymmetry in partial widths is referred to as A_{CP} and is final-state dependent:

$$A_{CP} \equiv \frac{\Gamma(D^0 \rightarrow f) - \Gamma(\bar{D}^0 \rightarrow \bar{f})}{\Gamma(D^0 \rightarrow f) + \Gamma(\bar{D}^0 \rightarrow \bar{f})}. \quad (69.38)$$

Unlike A_{Γ} , A_{CP} is a time-integrated quantity, i.e., it does not require measuring decay times. For neutral D decays, A_{CP} receives contributions from both direct (in the decay amplitudes) and indirect (due to mixing) processes: $A_{CP}(D^0 \rightarrow f) = A_{CP}^f + A_{CP}^{\text{indirect}}$. The latter indirect contribution depends on the mixing parameters x and y :

$$\begin{aligned} A_{CP}^{\text{indirect}} &= \frac{1}{2} \left(\left| \frac{q}{p} \right| + \left| \frac{p}{q} \right| \right) x \sin \phi - \frac{1}{2} \left(\left| \frac{q}{p} \right| - \left| \frac{p}{q} \right| \right) y \cos \phi \\ &= -A_{\Gamma}. \end{aligned} \quad (69.39)$$

Numerous measurements of A_{CP} for decays to CP eigenstates are listed in this *Review* [73]. Table 69.6 summarizes the current status of measurements of the difference in A_{CP} for $D^0 \rightarrow K^+K^-$ and $D^0 \rightarrow \pi^+\pi^-$ decays: $\Delta A_{CP} \equiv A_{CP}(K^+K^-) - A_{CP}(\pi^+\pi^-)$. Measuring the difference is advantageous, as numerous systematic uncertainties cancel. As A_{CP}^{indirect} is universal (independent of final state), it subtracts out of the difference ΔA_{CP} . However, at hadron experiments such as LHCb, there are differences in efficiencies between K^+K^- and $\pi^+\pi^-$ final states, and a small contribution to ΔA_{CP} remains. The most recent result from LHCb [57], based on 8.9 fb^{-1} of data, differs from zero with a statistical significance of 5.3σ . Thus, this measurement constitutes the first observation of CP violation in charm meson or charm baryon decays. These CP asymmetries are included in HFLAV's global fit for charm mixing parameters discussed below; the fit shows that the CP violation observed is due to the direct contributions A_{CP}^{KK} and $A_{CP}^{\pi\pi}$.

69.5 Quantum-correlated $D^0\bar{D}^0$ Analyses

Measurements of R_D , $\cos \delta_{K\pi}$, $\sin \delta_{K\pi}$, x , and y can be obtained from a combined fit to time-integrated yields of single-tagged (ST) and double-tagged (DT) $D^0\bar{D}^0$ events produced at the $\psi(3770)$ resonance [74,75]. Single-tagged events are those in which either the D^0 or \bar{D}^0 decay is reconstructed (identified), and the other neutral D decays generically. Double-tagged events are those in which both D^0 and \bar{D}^0 decays are identified. Due to quantum correlations, the decay of a D^0, \bar{D}^0, D_+ , or D_- projects the other neutral D into a state \bar{D}^0, D^0, D_- , and D_+ , respectively. The CP -specific D_- and D_+ decays (or, neglecting CP violation, D_1 and D_2 decays) include interference between D^0 and \bar{D}^0 amplitudes, and this provides sensitivity to R_D and $\cos \delta_{K\pi}$. The flavor-specific D^0 and \bar{D}^0 decays include interference between D_1 and D_2 amplitudes, and this provides sensitivity to x and y . For details of this method, see Refs. [1–5].

BESIII has reported results using 2.92 fb^{-1} of $e^+e^- \rightarrow \psi(3770)$ data, where the quantum-correlated $D^0\bar{D}^0$ pairs are produced in a $C = -1$ state. They measure $y_{CP} = (-2.0 \pm 1.3 \pm 0.7)\%$ [42] from DT yields using a CP eigenstate tag for one D and a semileptonic tag for the other; and they measure $A_{K\pi}^{CP} = (12.7 \pm 1.3 \pm 0.7)\%$ [56] from DT yields using a CP tag for one D and a $K^{\pm}\pi^{\mp}$ tag for the other. For y_{CP} , the CP eigenstates used are K^-K^+ (f_+), $\pi^+\pi^-$ (f_+), $K_S^0\pi^0\pi^0$ (f_+), $K_S^0\pi^0$ (f_-), $K_S^0\eta$ (f_-), and $K_S^0\omega$ (f_-). For $A_{K\pi}^{CP}$, additional CP eigenstates included are $\pi^0\pi^0$ (f_+) and $\rho^0\pi^0$ (f_+). Using external inputs for R_D and y from HFLAV [76], and R from the PDG [77] (see Eq. (69.25)), BESIII obtains $\cos \delta_{K\pi} = 1.02 \pm 0.11 \pm 0.06 \pm 0.01$ [56], where the third uncertainty is due to the external inputs.

CLEO-c has reported results using 0.82 fb^{-1} of $e^+e^- \rightarrow \psi(3770)$ data [78–80]. The values of y , R_M , $\cos \delta_{K\pi}$, and $\sin \delta_{K\pi}$ are determined from a combined fit to the ST (hadronic only) and DT yields. The DT yields include events in which one D is reconstructed in a hadronic mode and the other D is partially reconstructed in either $D \rightarrow K^{\mp}e^{\pm}\nu$ or $D \rightarrow K^{\mp}\mu^{\pm}\nu$.

The CLEO-c analysis obtains $\cos \delta_{K\pi} = 0.81^{+0.22+0.07}_{-0.18-0.05}$ and $\sin \delta_{K\pi} = -0.01 \pm 0.41 \pm 0.04$. These fits allow $\cos \delta_{K\pi}$, $\sin \delta_{K\pi}$, and x^2 to be unphysical. Constraining $\cos \delta_{K\pi}$ and $\sin \delta_{K\pi}$ to the physical range $[-1, +1]$ (i.e., interpreting $\delta_{K\pi}$ as an angle) and also using external inputs for x , y and y_{CP} from HFLAV [81], CLEO-c obtains $\delta_{K\pi} = (18^{+11}_{-17})^\circ$ [80].

69.6 Summary of Experimental Results

Several recent results indicate that charm mixing is at the upper end of the range of Standard Model predictions. For $D^0 \rightarrow K^+\pi^-$, LHCb [19, 20], CDF [17], and Belle [16] each exclude the no-mixing hypothesis by more than 5 standard deviations. For y_{CP} in $D^0 \rightarrow K^+K^-$ and $\pi^+\pi^-$, BaBar [44], Belle [40], and LHCb [38] measure 3.3σ , 4.7σ , and 3.6σ effects, respectively. The most sensitive measurements of x and y are from $D^0 \rightarrow K_S^0\pi^+\pi^-$ decays at Belle [33] and LHCb [30]. In a similar analysis using $D^0 \rightarrow K_S^0\pi^+\pi^-$ and $D^0 \rightarrow K_S^0K^+K^-$ decays, BaBar [34] finds the no-mixing solution excluded at 1.9σ . LHCb [69] has reported the observation of charm mixing in $D^0 \rightarrow K^+\pi^-\pi^+\pi^-$ with 8.2σ significance. However, the strong phase difference for this decay is not known, and thus x and y cannot be extracted. The current situation would benefit from better knowledge of the strong phase difference $\delta_{K\pi}$ than provided by the current CLEO-c [80] and BESIII [56] results, and knowledge of the strong phase difference $\delta_{K\pi\pi\pi}$. Such knowledge would allow one to extract x and y from $D^0 \rightarrow K^+\pi^-$ measurements of (x', y') , and from $D^0 \rightarrow K^+\pi^-\pi^+\pi^-$ measurements of (x'', y'') . In fact, the most precise knowledge of $\delta_{K\pi}$ comes from combining measurements of y' (Table 69.3) with measurements of y (Table 69.4) and y_{CP} (Table 69.5), as done in the HFLAV global fit described below.

The experimental data consistently indicate that the D^0 and \bar{D}^0 mesons mix. The mixing is presumably dominated by long-range processes. Under the assumption that the observed mixing is due entirely to non-Standard Model processes, significant constraints on New Physics models can be obtained [82]. A serious limitation to the interpretation of charm mixing in terms of New Physics is the theoretical uncertainty on the Standard Model predictions [83, 84].

69.7 HFLAV Global Fit for Charm Mixing Parameters

The Heavy Flavor Averaging Group (HFLAV) performs a global fit to all relevant mixing measurements to obtain world average values for 10 fitted parameters: x , y , $\delta_{K\pi}$, $\delta_{K\pi\pi^0}$, $R_D(K^+\pi^-)$, $A_D(K^+\pi^-)$, $|q/p|$, $\text{Arg}(q/p) \equiv \phi$, and the direct CP -violating asymmetries $A_{CP}^{K^+K^-}$ and $A_{CP}^{\pi^+\pi^-}$. Correlations among observables are taken into account by using the error matrices provided by the experiments. Measurements of $D^0 \rightarrow K^{(*)+\ell^-\bar{\nu}}$, K^+K^- , $\pi^+\pi^-$, $K^+\pi^-$, $K^+\pi^-\pi^0$, $K^+\pi^-\pi^+\pi^-$, $K_S^0\pi^+\pi^-$, $K_S^0K^+K^-$, and $\pi^+\pi^-\pi^0$ decays are used, as well as CLEO-c and BESIII results for double-tagged branching fractions measured at the $\psi(3770)$. There are three observables input to the fit that are themselves world average values calculated by HFLAV: R_M from $D^0 \rightarrow K^{(*)+\ell^-\bar{\nu}}$ decays (Table 69.1), and y_{CP} and A_Γ from $D^0 \rightarrow f_{CP}$ decays (Table 69.5). A measurement by LHCb of R_M using $D^0 \rightarrow K^+\pi^-\pi^+\pi^-$ decays is input separately. Details of the fitting procedure are given in Ref. [7].

The results of the fit as of March 2019 are listed in Table 69.7. Three separate fits are performed: (a) assuming no CP violation; (b) assuming no CP violation in doubly Cabibbo-suppressed decays; and (c) allowing all CP violation. The second fit (b) corresponds to the theory expectation [85, 86]; in this case four fitted parameters are reduced to three using the relationship $\tan \phi = (x/y) \cdot (1 - |q/p|^2)/(1 + |q/p|^2)$ [85–87]. Alternatively, one can fit for the three parameters $x_{12} \equiv 2|M_{12}|/\Gamma$, $y_{12} \equiv |F_{12}|/\Gamma$, and $\phi_{12} \equiv \text{Arg}(M_{12}/F_{12})$, from which x , y , $|q/p|$, and ϕ can be derived.

Confidence contours in the two dimensions (x, y) and $(|q/p|, \phi)$ from the fit are plotted in Fig. 69.1. These contours are obtained by letting, for any point in the two-dimensional plane, all other fit parameters take their preferred values. The 1σ – 5σ boundaries drawn are the loci of points in which the χ^2 has risen above the minimum by 2.30, 6.18, 11.83, 19.33, and 28.67 units. The fit

excludes the no-mixing point $x=y=0$ at more than 11.5σ , when CP violation is allowed. The fit is consistent with no CP violation ($|q/p|=1$, $\phi=0$) at the 63% confidence level.

One-dimensional likelihood functions for parameters are obtained by allowing, for any value of the parameter, all other fit parameters to take their preferred values. The resulting likelihood functions give central values, 68.3% C.L. intervals, and 95% C.L. intervals as listed in Table 69.7. The parameter ranges $x \leq 0$ and $y \leq 0$ are excluded at 3.1σ and $>11.4\sigma$ significance, respectively. The χ^2 of the fit is 60.7 for $49 - 10 = 39$ degrees of freedom, indicating some disagreement among the measurements.

From the results of the HFLAV averaging, the following can be concluded: (1) Since CP violation is small and y_{CP} is positive, the CP -even state is shorter-lived, as in the $K^0\bar{K}^0$ system. (2) However, since x appears to be positive, the CP -even state is heavier, unlike in the $K^0\bar{K}^0$ system. (3) The strong phase difference $\delta_{K\pi}$ is consistent with the $SU(3)$ expectation of zero, and large values are unlikely (its magnitude is $< 30^\circ$ at 95% C.L.) (4) While direct CP violation has now been observed in D decays, there is no evidence for indirect CP violation, i.e., $|q/p| \neq 1$ or $\phi \neq 0$. Observing such CP violation at the current level of sensitivity would indicate new physics.

69.8 Future Data

Current results are based primarily upon CLEO-c (0.82 fb^{-1} of $e^+e^- \rightarrow \psi(3770)$ data), Belle and BaBar ($\sim 1.4 \text{ ab}^{-1}$ of $e^+e^- \rightarrow Y(4S)$ data), and LHCb Runs 1 and 2 ($3.0 \text{ fb}^{-1} + 5.9 \text{ fb}^{-1}$ of pp collision data at $\sqrt{s} = 7, 8, 13 \text{ TeV}$).

BESIII has accumulated 2.9 fb^{-1} of $e^+e^- \rightarrow \psi(3770)$ data and plans to collect up to 20 fb^{-1} in the next few years. These data should provide strong phase measurements that enable improved model-independent determinations of mixing parameters from Belle II and LHCb. In 2019, Belle II began accumulating 50 ab^{-1} of $e^+e^- \rightarrow Y(4S)$ data [88], which is expected to take approximately ten years to collect. At LHCb, Run 2 was completed in 2018, Run 3 is planned for 2021–23, and Run 4 is planned for 2026–29 [89]. The goal for Runs 3+4 is to accumulate an additional 50 fb^{-1} of pp data at $\sqrt{s} = 14 \text{ TeV}$. These data, along with the large e^+e^- dataset from Belle II, should provide significantly greater sensitivity to D^0 - \bar{D}^0 mixing and direct and indirect CP violation in D^0 decays.

References

- [1] D. M. Asner and W. M. Sun, Phys. Rev. **D73**, 034024 (2006), [Erratum: Phys. Rev. **D77**, 019901 (2008)], [hep-ph/0507238].
- [2] D. Atwood and A. A. Petrov, Phys. Rev. **D71**, 054032 (2005), [hep-ph/0207165].
- [3] M. Gronau, Y. Grossman and J. L. Rosner, Phys. Lett. **B508**, 37 (2001), [hep-ph/0103110].
- [4] Z.-z. Xing, Phys. Rev. **D55**, 196 (1997), [hep-ph/9606422].
- [5] M. Goldhaber and J. L. Rosner, Phys. Rev. **D15**, 1254 (1977).
- [6] See “Review of Multibody Charm Analyses” in this *Review*.
- [7] Y. Amhis *et al.* (Heavy Flavor Averaging Group) (2019), [arXiv:1909.12524].
- [8] U. Bitenc *et al.* (Belle), Phys. Rev. **D77**, 112003 (2008), [arXiv:0802.2952].
- [9] B. Aubert *et al.* (BaBar), Phys. Rev. **D76**, 014018 (2007), [arXiv:0705.0704].
- [10] C. Cawthfield *et al.* (CLEO), Phys. Rev. **D71**, 077101 (2005), [hep-ex/0502012].
- [11] E. M. Aitala *et al.* (E791), Phys. Rev. Lett. **77**, 2384 (1996), [hep-ex/9606016].
- [12] U. Bitenc *et al.* (Belle), Phys. Rev. **D72**, 071101 (2005), [hep-ex/0507020].
- [13] B. Aubert *et al.* (BaBar), Phys. Rev. **D70**, 091102 (2004), [hep-ex/0408066].
- [14] R. Aaij *et al.* (LHCb), Phys. Rev. **D97**, 3, 031101 (2018), [arXiv:1712.03220].

- [15] R. Aaij *et al.* (LHCb), Phys. Rev. **D95**, 5, 052004 (2017), [Erratum: Phys. Rev. **D96**, 099907 (2017)], [arXiv:1611.06143].
- [16] B. R. Ko *et al.* (Belle), Phys. Rev. Lett. **112**, 11, 111801 (2014), [Addendum: Phys. Rev. Lett. **112**, 139903 (2014)], [arXiv:1401.3402].
- [17] T. A. Aaltonen *et al.* (CDF), Phys. Rev. Lett. **111**, 23, 231802 (2013), [arXiv:1309.4078].
- [18] B. Aubert *et al.* (BaBar), Phys. Rev. Lett. **98**, 211802 (2007), [hep-ex/0703020].
- [19] R. Aaij *et al.* (LHCb), Phys. Rev. Lett. **111**, 25, 251801 (2013), [arXiv:1309.6534].
- [20] R. Aaij *et al.* (LHCb), Phys. Rev. Lett. **110**, 10, 101802 (2013), [arXiv:1211.1230].
- [21] T. Aaltonen *et al.* (CDF), Phys. Rev. Lett. **100**, 121802 (2008), [arXiv:0712.1567].
- [22] L. M. Zhang *et al.* (Belle), Phys. Rev. Lett. **96**, 151801 (2006), [hep-ex/0601029].
- [23] J. M. Link *et al.* (FOCUS), Phys. Lett. **B618**, 23 (2005), [hep-ex/0412034].
- [24] R. Godang *et al.* (CLEO), Phys. Rev. Lett. **84**, 5038 (2000), [hep-ex/0001060].
- [25] E. M. Aitala *et al.* (E791), Phys. Rev. **D57**, 13 (1998), [hep-ex/9608018].
- [26] Y. Nir, Lectures given at 27th SLAC Summer Institute on Particle Physics: “ CP Violation in and Beyond the Standard Model (SSI 99),” Stanford, California, 7-16 July 1999. Published in Trieste 1999, *Particle Physics*, pp. 165-243.
- [27] S. Bergmann *et al.*, Phys. Lett. **B486**, 418 (2000), [hep-ph/0005181].
- [28] J. Libby *et al.* (CLEO), Phys. Rev. **D82**, 112006 (2010), [arXiv:1010.2817].
- [29] A. Di Canto *et al.*, Phys. Rev. **D99**, 1, 012007 (2019), [arXiv:1811.01032].
- [30] R. Aaij *et al.* (LHCb), Phys. Rev. Lett. **122**, 23, 231802 (2019), [arXiv:1903.03074].
- [31] R. Aaij *et al.* (LHCb), JHEP **04**, 033 (2016), [arXiv:1510.01664].
- [32] J. P. Lees *et al.* (BaBar), Phys. Rev. **D93**, 11, 112014 (2016), [arXiv:1604.00857].
- [33] T. Peng *et al.* (Belle), Phys. Rev. **D89**, 9, 091103 (2014), [arXiv:1404.2412].
- [34] P. del Amo Sanchez *et al.* (BaBar), Phys. Rev. Lett. **105**, 081803 (2010), [arXiv:1004.5053].
- [35] K. Abe *et al.* (Belle), Phys. Rev. Lett. **99**, 131803 (2007), [arXiv:0704.1000].
- [36] D. M. Asner *et al.* (CLEO), Phys. Rev. **D72**, 012001 (2005), [hep-ex/0503045].
- [37] R. Aaij *et al.* (LHCb), Phys. Rev. **D101**, 1, 012005 (2020), [arXiv:1911.01114].
- [38] R. Aaij *et al.* (LHCb), Phys. Rev. Lett. **122**, 1, 011802 (2019), [arXiv:1810.06874].
- [39] R. Aaij *et al.* (LHCb), Phys. Rev. Lett. **118**, 26, 261803 (2017), [arXiv:1702.06490].
- [40] M. Starič *et al.* (Belle), Phys. Lett. **B753**, 412 (2016), [arXiv:1509.08266].
- [41] R. Aaij *et al.* (LHCb), JHEP **04**, 043 (2015), [arXiv:1501.06777].
- [42] M. Ablikim *et al.* (BESIII), Phys. Lett. **B744**, 339 (2015), [arXiv:1501.01378].
- [43] T. A. Aaltonen *et al.* (CDF), Phys. Rev. **D90**, 11, 111103 (2014), [arXiv:1410.5435].
- [44] J. P. Lees *et al.* (BaBar), Phys. Rev. **D87**, 1, 012004 (2013), [arXiv:1209.3896].
- [45] A. Zupanc *et al.* (Belle), Phys. Rev. **D80**, 052006 (2009), [arXiv:0905.4185].
- [46] S. E. Csorna *et al.* (CLEO), Phys. Rev. **D65**, 092001 (2002), [hep-ex/0111024].
- [47] J. M. Link *et al.* (FOCUS), Phys. Lett. **B485**, 62 (2000), [hep-ex/0004034].
- [48] E. M. Aitala *et al.* (E791), Phys. Rev. Lett. **83**, 32 (1999), [hep-ex/9903012].
- [49] R. Aaij *et al.* (LHCb), Phys. Rev. Lett. **112**, 4, 041801 (2014), [arXiv:1310.7201].
- [50] R. Aaij *et al.* (LHCb), JHEP **04**, 129 (2012), [arXiv:1112.4698].
- [51] B. Aubert *et al.* (BaBar), Phys. Rev. **D80**, 071103 (2009), [arXiv:0908.0761].
- [52] B. Aubert *et al.* (BaBar), Phys. Rev. **D78**, 011105 (2008), [arXiv:0712.2249].
- [53] M. Staric *et al.* (BELLE), Phys. Rev. Lett. **98**, 211803 (2007), [65(2007)], [hep-ex/0703036].
- [54] B. Aubert *et al.* (BaBar), Phys. Rev. Lett. **91**, 121801 (2003), [hep-ex/0306003].
- [55] K. Abe *et al.* (Belle), Phys. Rev. Lett. **88**, 162001 (2002), [hep-ex/0111026].
- [56] M. Ablikim *et al.* (BESIII), Phys. Lett. **B734**, 227 (2014), [arXiv:1404.4691].
- [57] R. Aaij *et al.* (LHCb), Phys. Rev. Lett. **122**, 21, 211803 (2019), [arXiv:1903.08726].
- [58] T. Aaltonen *et al.* (CDF), Phys. Rev. Lett. **109**, 111801 (2012), [arXiv:1207.2158].
- [59] B. Aubert *et al.* (BaBar), Phys. Rev. Lett. **100**, 061803 (2008), [arXiv:0709.2715].
- [60] M. Staric *et al.* (Belle), Phys. Lett. **B670**, 190 (2008), [arXiv:0807.0148].
- [61] R. Aaij *et al.* (LHCb), Phys. Rev. Lett. **116**, 19, 191601 (2016), [arXiv:1602.03160].
- [62] R. Aaij *et al.* (LHCb), JHEP **07**, 041 (2014), [arXiv:1405.2797].
- [63] R. Aaij *et al.* (LHCb), Phys. Lett. **B723**, 33 (2013), [arXiv:1303.2614].
- [64] R. Aaij *et al.* (LHCb), Phys. Rev. Lett. **108**, 111602 (2012), [arXiv:1112.0938].
- [65] B. R. Ko (Belle), in “7th International Workshop on the CKM Unitarity Triangle (CKM 2012) Cincinnati, Ohio, USA, September 28-October 2, 2012,” (2012), [arXiv:1212.5320].
- [66] B. Aubert *et al.* (BaBar), Phys. Rev. Lett. **97**, 221803 (2006), [hep-ex/0608006].
- [67] B. Aubert *et al.* (BaBar), Phys. Rev. Lett. **103**, 211801 (2009), [arXiv:0807.4544].
- [68] E. White *et al.* (Belle), Phys. Rev. **D88**, 5, 051101 (2013), [arXiv:1307.5935].
- [69] R. Aaij *et al.* (LHCb), Phys. Rev. Lett. **116**, 24, 241801 (2016), [arXiv:1602.07224].
- [70] H. Muramatsu *et al.* (CLEO), Phys. Rev. Lett. **89**, 251802 (2002), [Erratum: Phys. Rev. Lett. **90**, 059901 (2003)], [hep-ex/0207067].
- [71] B. Aubert *et al.* (BaBar), Phys. Rev. Lett. **95**, 121802 (2005), [hep-ex/0504039].
- [72] B. Aubert *et al.* (BaBar), Phys. Rev. **D78**, 034023 (2008), [arXiv:0804.2089].
- [73] See the tabulation of A_{CP} results in the D^0 and D^+ Listings in this *Review*.
- [74] R.A. Briere *et al.*, (CLEO Collab.), CLNS 01-1742, (2001).
- [75] D. M. Asner *et al.*, (BES-III Collab.), Int. J. Mod. Phys. **A**, 24 (2009).
- [76] Heavy Flavor Averaging Group, https://hflav-eos.web.cern.ch/hflav-eos/charm/CHARM13/results_mix_cpv.html.

- [77] J. Beringer *et al.* (Particle Data Group), Phys. Rev. **D86**, 010001 (2012).
- [78] J. L. Rosner *et al.* (CLEO), Phys. Rev. Lett. **100**, 221801 (2008), [arXiv:0802.2264].
- [79] D. M. Asner *et al.* (CLEO), Phys. Rev. **D78**, 012001 (2008), [arXiv:0802.2268].
- [80] D. M. Asner *et al.* (CLEO), Phys. Rev. **D86**, 112001 (2012), [arXiv:1210.0939].
- [81] Heavy Flavor Averaging Group, https://hflav-eos.web.cern.ch/hflav-eos/charm/March12/results_mix_cpv.html.
- [82] E. Golowich *et al.*, Phys. Rev. **D76**, 095009 (2007), [arXiv:0705.3650].
- [83] G. Isidori *et al.*, Phys. Lett. **B711**, 46 (2012), [arXiv:1111.4987].
- [84] E. Franco, S. Mishima and L. Silvestrini, JHEP **05**, 140 (2012), [arXiv:1203.3131].
- [85] Y. Grossman, Y. Nir and G. Perez, Phys. Rev. Lett. **103**, 071602 (2009), [arXiv:0904.0305].
- [86] A. L. Kagan and M. D. Sokoloff, Phys. Rev. **D80**, 076008 (2009), [arXiv:0907.3917].
- [87] M. Ciuchini *et al.*, Phys. Lett. **B655**, 162 (2007), [hep-ph/0703204].
- [88] E. Kou *et al.* (Belle-II) (2018), [arXiv:1808.10567].
- [89] R. Aaij *et al.* (LHCb) (2018), [arXiv:1808.08865].

70. D_s^+ Branching Fractions

Updated September 2019 by J.L. Rosner (University of Chicago) and C.G. Wohl (LBNL).

Figure 70.1 shows a partial breakdown of the D_s^+ branching fractions. The rest of this note is about how the figure was constructed. The values shown make heavy use of CLEO measurements of inclusive branching fractions [1]. For references to other data cited in the following, see the Listings.

70.1. Modes with leptons

The bottom (18.0 ± 1.0)% of Fig. 70.1 shows the fractions for the modes that include leptons. The measured $K^0 e^+ \nu_e$ and $K^{*0} e^+ \nu_e$ fractions have been doubled to take account of the corresponding $\mu^+ \nu_\mu$ fractions. The sum of the exclusive $X e^+ \nu_e$ fractions is (6.0 ± 0.3)%, consistent with an inclusive semileptonic measurement of (6.5 ± 0.4)%. There seems to be little missing here.

70.2. Inclusive hadronic $K\bar{K}$ fractions

The Cabibbo-favored $c \rightarrow s$ decay in D_s^+ decay produces a final state with both an s and an \bar{s} ; and thus modes with a $K\bar{K}$ pair or with an η , ω , η' , or ϕ predominate (as may already be seen in Fig. 70.1 in the semileptonic fractions). We consider the $K\bar{K}$ modes first. A complete picture of the exclusive $K\bar{K}$ charge modes is not yet possible, because branching fractions for many of those modes have not yet been measured. However, CLEO has measured the inclusive K^+ , K^- , K_S^0 , $K^+ K^-$, $K^+ K_S^0$, $K^- K_S^0$, and $2K_S^0$ fractions (these include modes with leptons) [1]. And each of these inclusive fractions with a K_S^0 is equal to the corresponding fraction with a K_L^0 : $f(K^+ K_L^0) = f(K^+ K_S^0)$, $f(2K_L^0) = f(2K_S^0)$, etc. Therefore, of all inclusive fractions pairing a K^+ , K_S^0 , or K_L^0 with a K^- , K_S^0 , or K_L^0 , we know all but $f(K_S^0 K_L^0)$.

We can get that fraction. The total K_S^0 fraction is

$$f(K_S^0) = f(K^+ K_S^0) + f(K^- K_S^0) + 2f(2K_S^0) + f(K_S^0 K_L^0) + f(\text{single } K_S^0),$$

where $f(\text{single } K_S^0)$ is the sum of the branching fractions for modes such as $K_S^0 \pi^+ 2\pi^0$ with a K_S^0 and no second K . The $K_S^0 \pi^+ 2\pi^0$ mode is in fact the only unmeasured single- K_S^0 mode (throughout, we shall assume that fractions for modes with a K or $K\bar{K}$ and more than three pions are negligible), and we shall take its fraction to be the same as for the $K_S^0 2\pi^+ \pi^-$ mode, (0.30 ± 0.11)%. Any reasonable deviation from this value would be too small to matter much in the following. Adding the several small single- K_S^0 branching fractions, including those from semileptonic modes, we get $f(\text{single } K_S^0) = (1.7 \pm 0.2)\%$.

Using this, we have:

$$\begin{aligned} f(K_S^0 K_L^0) &= f(K_S^0) - f(K^+ K_S^0) - f(K^- K_S^0) \\ &\quad - 2f(2K_S^0) - f(\text{single } K_S^0) \\ &= (19.0 \pm 1.1) - (5.8 \pm 0.5) - (1.9 \pm 0.4) \\ &\quad - 2 \times (1.7 \pm 0.3) - (1.7 \pm 0.2) \\ &= (6.2 \pm 1.4)\% . \end{aligned}$$

Here and below we treat the errors as uncorrelated, although often they are not. However, our main aim is to get numbers for Fig. 70.1; errors are secondary.

There is a check on our result: The ϕ inclusive branching fraction is (15.7 ± 1.0)%, of which 34%, or (5.34 ± 0.34)% of D_s^+ decays, produces a $K_S^0 K_L^0$. Our $f(K_S^0 K_L^0) = (6.2 \pm 1.4)\%$ has to be at least this large—and it is, within the sizable error.

We now have all the inclusive $K\bar{K}$ fractions. We use $f(K^+ K\bar{K}^0) = 2 f(K^+ K_S^0)$, and likewise for $f(K^- K\bar{K}^0)$. For $K^+ K^-$ and $K_S^0 K_L^0$, we subtract off the contributions from $\phi l^+ \nu$ decay to get the purely

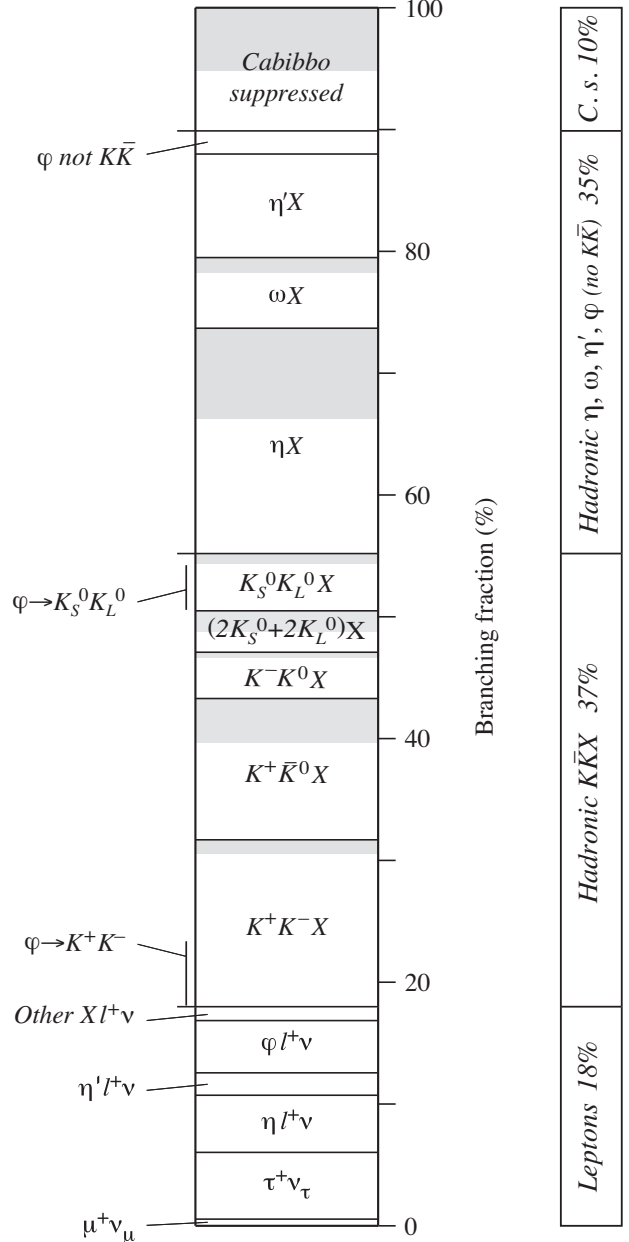


Figure 70.1: A partial breakdown of D_s^+ branching fractions. The hadronic bins in the left column show inclusive fractions. Shading within a bin shows how much of the inclusive fraction is not yet accounted for by adding up all the relevant exclusive fractions. The inclusive hadronic ϕ fraction is spread over three bins, in proportion to its decay fractions into $K^+ K^-$, $K_S^0 K_L^0$, and no- $K\bar{K}$ modes.

hadronic $K\bar{K}$ inclusive fractions:

$$\begin{aligned} f(K^+ K^-, \text{hadronic}) &= (15.8 \pm 0.7) - (2.1 \pm 0.3) \\ &= (13.7 \pm 0.8)\% \\ f(K^+ \bar{K}^0, \text{hadronic}) &= (11.6 \pm 1.0)\% \\ f(K^- K^0, \text{hadronic}) &= (3.8 \pm 0.8)\% \\ f(2K_S^0 + 2K_L^0, \text{hadronic}) &= (3.4 \pm 0.6)\% \\ f(K_S^0 K_L^0, \text{hadronic}) &= (6.2 \pm 1.4) - (1.5 \pm 0.2) \\ &= (4.7 \pm 1.4)\% . \end{aligned}$$

The fractions are shown in Fig. 70.1. They total (37.2 ± 2.2)% of D_s^+ decays.

We can add more information to the figure by summing up measured branching fractions for exclusive modes within each bin:

K^+K^- modes—The sum of measured $K^+K^-\pi^+$, $K^+K^-\pi^+\pi^0$, and $K^+K^-\pi^+\pi^-\pi^0$ branching fractions is $(12.6 \pm 0.6)\%$. That leaves $(1.1 \pm 1.0)\%$ for the $K^+K^-\pi^+\pi^0$ mode, which is the only other K^+K^- mode with three or fewer pions. In Fig. 70.1, this unmeasured part of the K^+K^- bin is shaded.

$K^+\bar{K}^0$ modes—Two times the sum of the measured $K^+K_S^0$, $K^+K_L^0\pi^0$, and $K^+K_S^0\pi^+\pi^-$ branching fractions is $(8.0 \pm 0.5)\%$. This leaves $(3.6 \pm 1.1)\%$ for the unmeasured $K^+\bar{K}^0$ modes (there are three such modes with three or fewer pions). This is shaded in the figure.

K^-K^0 modes—Twice the $K^-K_S^0\pi^+\pi^-$ fraction is $(3.4 \pm 0.2)\%$, which leaves about $(0.4 \pm 0.8)\%$ for $K^-K^0\pi^+\pi^0$, the only other K^-K^0 mode with three or fewer pions.

$2K_S^0 + 2K_L^0$ modes—The $2K_S^0\pi^+$ and $2K_S^0\pi^+\pi^-$ fractions sum to $(0.86 \pm 0.07)\%$; this times two (for the corresponding $2K_L^0$ modes) is $(1.72 \pm 0.14)\%$. This leaves about $(1.7 \pm 0.7)\%$ for other $2K_S^0 + 2K_L^0$ modes.

$K_S^0K_L^0$ modes—Most of the $K_S^0K_L^0$ fraction is accounted for by ϕ decays (see below).

70.3. Inclusive hadronic η , ω , η' , and ϕ fractions

These are easier. We start with the inclusive branching fractions, and then, to avoid double counting, subtract: (1) fractions for modes with leptons; (2) η mesons that are included in the inclusive η' fraction; and (3) K^+K^- and $K_S^0K_L^0$ from ϕ decays:

$$f(\eta \text{ hadronic}) = f(\eta \text{ inclusive}) - 0.65 f(\eta' \text{ inclusive})$$

$$-f(\eta\ell^+\nu) = (18.5 \pm 3.0)\%$$

$$f(\omega \text{ hadronic}) = f(\omega \text{ inclusive}) - 0.026 f(\eta' \text{ inclusive}) \\ = (5.8 \pm 1.4)\%$$

$$f(\eta' \text{ hadronic}) = f(\eta' \text{ inclusive}) - f(\eta'\ell^+\nu) \\ = (8.5 \pm 1.5)\%$$

$$f(\phi \text{ hadronic, } \not\rightarrow K\bar{K}) = 0.17 [f(\phi \text{ inclusive}) - f(\phi\ell^+\nu)] \\ = (1.9 \pm 0.2)\% .$$

The factors 0.65, 0.026, and 0.17 are the $\eta' \rightarrow \eta$, $\eta' \rightarrow \omega$, and $\phi \rightarrow K\bar{K}$ branching fractions. Figure 70.1 shows the results; the sum is $(34.7 \pm 3.6)\%$, which is about equal to the hadronic $K\bar{K}$ total.

Note that the bin marked ϕ near the top of Fig. 70.1 includes neither the $\phi\ell^+\nu$ decays nor the 83% of other ϕ decays that produce a $K\bar{K}$ pair. There is twice as much ϕ in the $K_S^0K_L^0$ bin, and nearly three times as much in the K^+K^- bin. These contributions are indicated in those bins.

Again, we can show how much of each bin is accounted for by measured exclusive branching fractions:

η modes—The sum of $\eta\pi^+$, $\eta\pi^+\pi^0$ (nearly all $\eta\rho^+$), and ηK^+ branching fractions is $(11.1 \pm 1.2)\%$, which leaves a good part of the inclusive hadronic η fraction, $(18.5 \pm 3.0)\%$, to be accounted for. This is shaded in the figure.

ω modes—The sum of $\omega\pi^+$, $\omega\pi^+\pi^0$, and $\omega 2\pi^+\pi^-$ fractions is $(4.6 \pm 0.9)\%$, which is nearly as large as the inclusive hadronic ω fraction, $(5.8 \pm 1.4)\%$.

η' modes—The sum of $\eta'\pi^+$, $\eta'\rho^+$, and $\eta'K^+$ fractions is $(9.9 \pm 1.5)\%$, which is larger than but not in serious disagreement with the inclusive hadronic η' fraction, $(8.5 \pm 1.5)\%$.

70.4. Cabibbo-suppressed modes

The sum of the fractions for modes with a $K\bar{K}$, η , ω , η' , or leptons is $(89.9 \pm 4.4)\%$. The remaining $(10.1 \pm 4.4)\%$ is to Cabibbo-suppressed modes, mainly single- K pions and multiple-pion modes (see below). However, it should be noted that some small parts of the modes already discussed are Cabibbo-suppressed. For example, the $(1.1 \pm 0.2)\%$ of D_s^+ decays to $K^0\ell\nu$ or $K^{*0}\ell\nu$ is already in the $X\ell\nu$ bin in Fig. 70.1. And the inclusive measurements of η , ω , and η' fractions do not distinguish between (and therefore include both) Cabibbo-allowed and -suppressed modes. We shall not try to make a separation here.

$K^0 + \text{pions}$ —Above, we found that $f(\text{single } K_S^0) = (1.7 \pm 0.2)\%$. Subtracting semileptonic fractions with a K_S^0 leaves $(1.3 \pm 0.2)\%$. The hadronic single- K^0 fraction is twice this, about $(2.6 \pm 0.4)\%$. The sum of measured $K^0\pi^+$, $K^0\pi^+\pi^0$, and $K^0\pi^+\pi^-\pi^0$ fractions is $(1.8 \pm 0.3)\%$, about two-thirds as much.

$K^+ + \text{pions}$ —The $K^+\pi^0$ and $K^+\pi^+\pi^-$ fractions sum to $(0.72 \pm 0.05)\%$. The total K^+ fraction wanted here is probably in the 1-to-2% range.

Multi-pions —The $2\pi^+\pi^-$, $\pi^+2\pi^0$, and $3\pi^+2\pi^-$ fractions total $(2.5 \pm 0.2)\%$. Modes not measured might double this.

The sum of the actually measured fractions is, including the semileptonics, $(4.9 \pm 0.3)\%$. The error on our Cabibbo-suppressed total, $(10.1 \pm 4.4)\%$ is too large to know how much we might be missing.

References:

1. S. Dobbs *et al.*, Phys. Rev. **D79**, 112008 (2009).

71. Leptonic Decays of Charged Pseudoscalar Mesons

Revised September 2019 by J.L. Rosner (Chicago U.), S.L. Stone (Syracuse U.) and R. Van de Water (FNAL).

71.1 Introduction

Charged mesons formed from a quark and antiquark can decay to a lepton-neutrino pair when these objects annihilate via a virtual W boson. Fig. 71.1 illustrates this process for the purely leptonic decay of a D^+ meson.

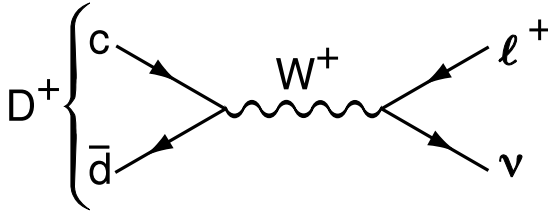


Figure 71.1: The annihilation process for pure D^+ leptonic decays in the standard model.

Similar quark-antiquark annihilations via a virtual W^+ to the $\ell^+\nu$ final states occur for the π^+ , K^+ , D_s^+ , and B^+ mesons. (Whenever pseudoscalar-meson charges are specified in this article, use of the charge-conjugate particles and corresponding decays are also implied.) Let P be any of these pseudoscalar mesons. To lowest order, the decay width is

$$\Gamma^{(0)}(P \rightarrow \ell\nu) = \frac{G_F^2}{8\pi} f_P^2 m_\ell^2 M_P \left(1 - \frac{m_\ell^2}{M_P^2}\right)^2 |V_{q_1 q_2}|^2. \quad (71.1)$$

Here M_P is the P mass, m_ℓ is the ℓ mass, $V_{q_1 q_2}$ is the Cabibbo-Kobayashi-Maskawa (CKM) matrix element between the quarks $q_1 q_2$ in P , and G_F is the Fermi coupling constant. The decay constant f_P is proportional to the matrix element of the axial current between the one- P -meson state and the vacuum:

$$\langle 0 | \bar{q}_1 \gamma_\mu \gamma_5 q_2 | P(p) \rangle = i p_\mu f_P, \quad (71.2)$$

and can be thought of as the “wavefunction overlap” of the quark and antiquark. In this article we use the convention in which $f_\pi \approx 130$ MeV. For brevity, we will often denote the purely leptonic decay width in Eq. (71.1) by $\Gamma^{(0)}$.

The decay of P^\pm starts with a spin-0 meson, and ends up with a left-handed neutrino or right-handed antineutrino. By angular momentum conservation, the ℓ^\pm must then also be left-handed or right-handed, respectively. In the $m_\ell = 0$ limit, the decay is forbidden, and can only occur as a result of the finite ℓ mass. This helicity suppression is the origin of the m_ℓ^2 dependence of the decay width.

Experimentally, it is difficult to isolate events in which there are *only* a lepton and neutrino in the final state from those with a lepton, neutrino, and soft photon. Thus, radiative contributions must be removed from the experimental measurements *a posteriori* to obtain $\Gamma^{(0)}$. The radiative contributions can be broken into three pieces: the short-distance contribution to leptonic and semileptonic decays mediated by a W^\pm boson that accounts for electroweak corrections not included in the definition of G_F , the long-distance internal bremsstrahlung (IB) contribution, and the contribution from photon emission that depends upon the hadron’s structure. The universal electroweak correction was calculated at $\mathcal{O}(\alpha)$ by Sirlin [1], and increases the purely leptonic decay rate by ~ 1.8 – 2.2% depending on the decaying meson. The $\mathcal{O}(\alpha)$ IB contribution was calculated by Kinoshita [2], and again is universal for all leptonic decays at this order. Numerically, the universal long-distance contribution lowers the purely leptonic decay rate by ~ 0.4 – 2.4% , where the correction is smallest for pions and largest for $D_{(s)}$ mesons. The structure-dependent contributions have been estimated within various effective theories to increase the purely leptonic rate by one to a few percent [3–8].

In this review we treat the radiative corrections differently for the light, charm, and bottom meson systems for several reasons. First, the experimental uncertainties on the decay widths vary

substantially. Thus, while the inclusion of radiative corrections is essential for the pion, kaon, and D -meson decay widths, which have been measured to (sub)-percent precision, radiative corrections can be neglected (for now) for $B \rightarrow \tau\nu$ decay. Second, the photons are treated differently on the experimental side for the different decay processes. For pions and kaons, the experimental measurements of $\Gamma_{P\ell 2[\gamma]}$ are fully inclusive, while for D mesons, the experiments impose cuts on the energy of any neutral cluster deposited in the calorimeter, which reduce the soft-photon background substantially. Some experiments also remove the QED bremsstrahlung in the leading-logarithmic approximation using the PHOTOS Monte-Carlo generator [9]. Third, the theoretical knowledge of the structure-dependent corrections varies for each meson system.

Once radiative corrections have been accounted for, measurements of purely leptonic decay branching fractions and lifetimes allow an experimental determination of the product $|V_{q_1 q_2}| f_P$. If the decay constant f_P is known to sufficient precision from theory, one can obtain the corresponding CKM element within the standard model. If, on the other hand, one takes the value of $|V_{q_1 q_2}|$ assuming CKM unitarity, one can infer an “experimental measurement” of the decay constant that can then be compared with theory.

The importance of measuring $\Gamma(P \rightarrow \ell\nu)$ depends on the particle being considered. Leptonic decays of charged pseudoscalar mesons occur at tree level within the standard model. Thus one does not expect large new-physics contributions to measurements of $\Gamma(P \rightarrow \ell\nu)$ for the lighter mesons $P = \pi^+, K^+$, and these processes in principle provide clean standard-model determinations of $|V_{ud}|$ and $|V_{us}|$. The situation is different for leptonic decays of charm and bottom mesons. The presence of new heavy particles such as charged Higgs bosons or leptoquarks could lead to observable effects in $\Gamma(P \rightarrow \ell\nu)$ for $P = D_{(s)}^+, B^+$ [10–14]. Thus the determination of $|V_{ub}|$ from $B^+ \rightarrow \tau\nu$ decay, in particular, should be considered a probe of new physics. More generally, the ratio of leptonic decays to $\tau\nu$ over $\mu\nu$ final states probes lepton universality [10, 15].

The determinations of CKM elements from leptonic decays of charged pseudoscalar mesons provide complementary information to those from other decay processes. The decay $P \rightarrow \ell\nu$ proceeds in the standard model via the axial-vector current $\bar{q}_1 \gamma_\mu \gamma_5 q_2$, whereas semileptonic pseudoscalar meson decays $P_1 \rightarrow P_2 \ell\nu$ proceed via the vector current $\bar{q}_1 \gamma_\mu q_2$. Thus the comparison of determinations of $|V_{q_1 q_2}|$ from leptonic and semileptonic decays tests the $V - A$ structure of the standard-model electroweak charged-current interaction. More generally, a small right-handed admixture to the standard-model weak current would lead to discrepancies between $|V_{q_1 q_2}|$ obtained from leptonic pseudoscalar-meson decays, exclusive semileptonic pseudoscalar-meson decays, exclusive semileptonic baryon decays, and inclusive semileptonic decays [16, 17].

Both measurements of the decay rates $\Gamma(P \rightarrow \ell\nu)$ and theoretical calculations of the decay constants f_P for $P = \pi^+, K^+, D_{(s)}^+$ from numerical lattice-QCD simulations are now quite precise. As a result, the elements of the first row of the CKM matrix $|V_{ud}|$ and $|V_{us}|$ can be obtained to sub-percent precision from $\pi^+ \rightarrow \ell\nu$ and $K^+ \rightarrow \ell\nu$, where the limiting error is from theory. The elements of the second row of the CKM matrix $|V_{cd(s)}|$ can be obtained from leptonic decays of charged pseudoscalar mesons to few-percent precision, where here the limiting error is from experiment. These enable stringent tests of the unitarity of the first and second rows of the CKM matrix.

This review is organized as follows. Because the experimental and theoretical issues associated with measurements of pions and kaons, charmed mesons, and bottom mesons differ, we discuss each one separately. We begin with the pion and kaon system in Sec. 71.2. First, in Sec. 71.2.1 we review current measurements of the experimental decay rates. We provide tables of branching-ratio measurements and determinations of the product $|V_{ud(s)}| f_{\pi^+(K^+)}$, as well as average values for these quantities including correlations and other effects needed to combine results.

Then, in Sec. 71.2.2 we summarize the status of theoretical calculations of the decay constants. We provide tables of recent lattice-QCD results for f_{π^+} , f_{K^+} , and their ratio from simulations including dynamical u , d , s , and (in some cases c) quarks, along with averages including correlations and strong SU(2)-isospin breaking corrections as needed. We next discuss the charmed meson system in Sec. 71.3, again reviewing current experimental rate measurements in Sec. 71.3.1 and theoretical decay-constant calculations in Sec. 71.3.2. Last, we discuss the bottom meson system in Sec. 71.4, following the same organization as the two previous sections. For almost all of the decay constants presented in Secs. 71.2.2, 71.3.2, and 71.4.2, we take as our preferred values the four-flavor averages from 2019 Flavor Lattice Averaging Group (FLAG) review [18], which incorporate all lattice-QCD results that appeared before 30 September 2018. There have not been any new decay-constant results that would qualify for the FLAG average since then.

After having established the status of both experimental measurements and theoretical calculations of leptonic charged pseudoscalar-meson decays, we discuss some implications for phenomenology in Sec. 71.5. For each process discussed in Secs. 71.2–71.4, we combine the average $\mathcal{B}(P \rightarrow \ell\nu)$ with the decay constant f_P to infer the associated CKM matrix element. We then compare these results with determinations of the same CKM elements from other processes. We also use the CKM elements obtained from leptonic decays to test the unitarity of the first and second rows of the CKM matrix. Further, as in previous reviews, we combine the experimental $\mathcal{B}(P \rightarrow \ell\nu)$ s with the associated CKM elements obtained from CKM unitarity to infer “experimental” values for the decay constants. The comparison of these values with theory provides a test of lattice and other QCD approaches, assuming that new-physics contributions to these processes are not significant.

71.2 Pions and kaons

71.2.1 Experimental rate measurements

Experimental rate measurements of pion and kaon leptonic decays are fully radiation inclusive. Following Refs. [19, 20], and references therein, we combine the $\mathcal{O}(\alpha)$ radiative corrections to the purely leptonic rate as follows:

$$\Gamma(P \rightarrow \ell\nu[\gamma]) = \Gamma(P \rightarrow \ell\nu) \left[1 + \frac{\alpha}{\pi} C_P \right], \quad (71.3)$$

where $P = \pi, K$. The full expressions for C_π and C_K are given in Eq. (114) of Ref. [5]. In addition to the universal short- [1] and long-distance [2] corrections, C_π and C_K include hadronic-structure dependent contributions [3] through $\mathcal{O}(\alpha p^4)$ in chiral perturbation theory (χ Pt), where p is the pion or kaon momentum. The inclusion of radiative corrections to the purely leptonic rates is numerically important given the level of precision achieved on the experimental measurements of the $\pi^\pm \rightarrow \mu^\pm \nu$ and $K^\pm \rightarrow \mu^\pm \nu$ decay widths.

We evaluate $\delta_P \equiv (\alpha/\pi)C_P$ using the latest experimentally-measured meson and lepton masses and coupling constants from the Particle Data group [21], and taking the low-energy constants (LECs) that parameterize the hadronic contributions from Refs. [5, 22, 23]. Because the finite non-logarithmic parts of the LECs were estimated within the large- N_C approximation assuming that contributions from the lowest-lying resonances dominate, we conservatively assign a 100% uncertainty to the LECs, which leads to a ± 0.9 error in $C_{\pi,K}$.¹ We obtain the following correction factors to the individual charged pion and kaon decay widths:

$$\delta_\pi = 0.0176(21) \quad \text{and} \quad \delta_K = 0.0107(21). \quad (71.4)$$

The error on the ratio of kaon-to-pion leptonic decay widths is under better theoretical control because the hadronic contributions

¹This uncertainty on $C_{\pi,K}$ is smaller than the error estimated by Marciano and Sirlin in Ref. [24], which predates the calculations of the hadronic-structure contributions in Refs. [3, 5, 22, 23]. The hadronic LECs incorporate the large short-distance electroweak logarithm discussed in Ref. [24], and their dependence on the chiral renormalization scale cancels the scale-dependence induced by chiral loops, thereby removing the dominant scale uncertainty of the Marciano–Sirlin analysis [24].

from low-energy constants estimated within the large- N_C framework cancel at lowest order in the chiral expansion. For the ratio, we use the correction factor

$$\delta_{K/\pi} = -0.0069(17), \quad (71.5)$$

where we take the estimated error due to higher-order corrections in the chiral expansion from Ref. [25].

There have been no new measurements of the pion leptonic decay rate since our previous review [26]. The sum of branching fractions for $\pi^- \rightarrow \mu^- \bar{\nu}$ and $\pi^- \rightarrow \mu^- \bar{\nu} \gamma$ is 99.98770(4)% [21]. Together with the lifetime 26.033(5) ns [21] this implies $\Gamma(\pi^- \rightarrow \mu^- \bar{\nu}[\gamma]) = 3.8408(7) \times 10^7 \text{ s}^{-1}$. We then subtract the estimated radiative correction factor δ_π in Eq. (71.4) to obtain the purely leptonic rate $\Gamma^{(0)}(\pi^- \rightarrow \mu^- \bar{\nu})$. Using this rate and the masses from the 2014 PDG review [21] in Eq. (71.1) gives

$$f_{\pi^-} |V_{ud}| = (127.13 \pm 0.02 \pm 0.13) \text{ MeV}, \quad (71.6)$$

where the errors are from the experimental rate measurement and the radiative correction factor, respectively.

The uncertainty on $f_{\pi^-} |V_{ud}|$ is dominated by that from the theoretical estimate of the hadronic structure-dependent radiative corrections. Recently the first direct lattice-QCD calculation of the radiative corrections to the pion and kaon leptonic decay rates was performed by the RM123-Soton Collaboration [8]. The results for both $\delta_\pi = 0.0153(19)$ and $\delta_K = 0.0088(9)$, which are given in the Gasser-Rusetsky-Scimemi scheme [27], are compatible with our chiral-perturbation-theory estimates above and have smaller quoted uncertainties, especially for δ_K . While independent confirmation of these results is needed, they demonstrate a promising approach for reducing the theoretical uncertainties on the pion and kaon leptonic decay rates in the future.

The world average for the $K \rightarrow \mu\nu$ decay rate is obtained from a global fit of several kaon-decay branching ratios and lifetime measurements, and was last updated by the FlaviaNet Working Group on Kaon Decays in 2014 [37]. Thus, the radiation-inclusive branching ratio $\mathcal{B}(K^- \rightarrow \mu^- \bar{\nu}[\gamma]) = 63.58(11)\%$ and lifetime $\tau_{K^\pm} = 12.384(15)$ ns are unchanged from our previous review. These measurements imply $\Gamma(K^- \rightarrow \mu^- \bar{\nu}[\gamma]) = 5.134(11) \times 10^7 \text{ s}^{-1}$. As before, we subtract δ_K in Eq. (71.4) from the radiation-inclusive decay width to obtain $\Gamma^{(0)}(K^- \rightarrow \mu^- \bar{\nu})$. We then use Eq. (71.1) to obtain

$$f_{K^+} |V_{us}| = (35.09 \pm 0.04 \pm 0.04) \text{ MeV}, \quad (71.7)$$

where the errors are from the experimental rate measurement and the radiative correction factor, respectively.

Short-distance radiative corrections cancel in the ratio of pion-to-kaon decay rates [38]:

$$\frac{\Gamma_{K\ell 2[\gamma]}}{\Gamma_{\pi\ell 2[\gamma]}} = \frac{|V_{us}|^2 f_{K^-}^2}{|V_{ud}|^2 f_{\pi^-}^2} \frac{m_K(1 - m_\ell^2/m_K^2)^2}{m_\pi(1 - m_\ell^2/m_\pi^2)^2} (1 + \delta_{K/\pi}), \quad (71.8)$$

where $\delta_{K/\pi}$ is given in Eq. (71.5). The left-hand side of Eq. (71.8) is 1.3367(28), which implies

$$\frac{|V_{us}| f_{K^-}}{|V_{ud}| f_{\pi^-}} = 0.27599 \pm 0.00029 \pm 0.00024, \quad (71.9)$$

where the first uncertainty is from the branching fractions and the second is from $\delta_{K/\pi}$. Here, the estimated error on the hadronic structure-dependent radiative corrections is commensurate with the experimental error.

In summary, the main experimental results pertaining to charged pion and kaon leptonic decays are

$$|V_{ud}| f_{\pi^-} = (127.13 \pm 0.02 \pm 0.13) \text{ MeV}, \quad (71.10)$$

$$|V_{us}| f_{K^+} = (35.09 \pm 0.04 \pm 0.04) \text{ MeV}, \quad (71.11)$$

$$\frac{|V_{us}| f_{K^+}}{|V_{ud}| f_{\pi^-}} = 0.27599 \pm 0.00029 \pm 0.00024, \quad (71.12)$$

where the errors are from the experimental uncertainties in the branching fractions and the theoretical uncertainties in the radiative correction factors δ_P , respectively. All of these values are the same as in our previous review [26].

Table 71.1: Recent published lattice-QCD results for f_{π^+} , f_{K^+} , and their ratio. The upper and lower panels show $(2+1+1)$ -flavor and $(2+1)$ -flavor determinations, respectively. When two errors are shown, they are statistical and systematic, respectively. Results for f_{π} and f_K in the isospin-symmetric limit $m_u = m_d$ are noted with an “ \ddagger ”; they are corrected for isospin breaking via Eq. (71.13) before computing the averages.

Reference	N_f	f_{π^+} (MeV)	f_{K^+} (MeV)	f_{K^+}/f_{π^+}
Fermilab/MILC 17 [28] *	2+1+1	–	–	1.1950(15) $^{(+6)}_{(-18)}$
ETM 14 [29] *	2+1+1	–	154.4(1.5)(1.3)	1.184(12)(11)
Fermilab/MILC 14 [7] *	2+1+1	–	155.92(13) $^{(+42)}_{(-34)}$	1.1956(10) $^{(+26)}_{(-18)}$ †
HPQCD 13 [30] *	2+1+1	–	155.37(20)(28)	1.1916(15)(16)
FLAG 19 average [18]	2+1+1	–	155.7(3)	1.1932(19)
QCDSF/UKQCD 16 [31]	2+1	–	–	1.190(10)(13)
BMW 16 [32]	2+1	–	–	1.178(10)(26)
RBC/UKQCD 14 [33] ‡	2+1	130.19(89)	155.51(83)	1.1945(45)
MILC 10 [34]	2+1	129.2(0.4)(1.4)	156.1(4) $^{(+6)}_{(-9)}$	1.197(2) $^{(+3)}_{(-7)}$
BMW 10 [35] ‡	2+1	–	–	1.192(7)(6)
HPQCD/UKQCD 07 [36] ‡	2+1	132(2)	157(2)	1.189(2)(7)
FLAG 19 average [18]	2+1	130.2(8)	155.7(7)	1.1917(37)

*PDG 2014 value of $f_{\pi^+} = 130.41(21)$ MeV used to set absolute lattice scale.

†Superseded by f_{K^+}/f_{π^+} from Fermilab/MILC 17.

71.2.2 Theoretical decay-constant calculations

Table 71.1 presents recent published results for the charged pion and kaon decay constants and their ratio from numerical lattice-QCD simulations with three ($N_f = 2 + 1$) or four flavors ($N_f = 2 + 1 + 1$) of dynamical quarks. The uncertainties on both the individual decay constants and their ratio are at the sub-percent level. The $SU(3)$ -breaking ratio f_{K^+}/f_{π^+} can be obtained with especially small errors because statistical errors associated with the Monte Carlo simulations are correlated between the numerator and denominator, as are some systematics. The results in Table 71.1 were obtained using several independent sets of gauge-field configurations, and a variety of lattice fermion actions that are sensitive to different systematic uncertainties.² Thus, the good agreement between them indicates that the lattice-QCD uncertainties are controlled and the associated error estimates are reliable.³

Table 71.1 also shows the three- and four-flavor averages for the pion and kaon decay constants and their ratio from the 2019 Flavour Lattice Averaging Group (FLAG) review [18] in the lines labeled “FLAG 19 average.” There is no four-flavor average for the pion decay constant in Table 71.1 because all of the four-flavor calculations use the quantity f_{π^+} as an input to fix the absolute lattice scale needed to convert from lattice-spacing units to GeV [7, 29, 30].

All of the results in Table 71.1 were obtained using isospin-symmetric gauge-field configurations, *i.e.*, the dynamical up and down quarks have the same mass. Fortunately, however, the dominant effect of strong-isospin breaking is easily included in lattice-QCD calculations as follows. Because the up-down mass difference $\Delta m_{ud} \equiv (m_u - m_d) \sim -2.5$ MeV [18, 49] is much less than typical hadronic scales, the strong-isospin breaking corrections to physical observables can systematically be expanded in the small parameter $\delta m_{ud} \equiv \Delta m_{ud}/\Lambda_{\text{QCD}}$. The leading strong-isospin-breaking corrections to pseudoscalar-meson decay constants arise from the light *valence* quarks in the initial- and final-state hadrons. (See, *e.g.*, the discussion in Ref. [50], for a detailed discussion of isospin-breaking effects in pion and kaon observables.) Thus, to include the effect of nondegenerate up- and down-quark masses, most recent lattice-QCD calculations of f_{π^+} and f_{K^+} evaluate the masses of the valence quarks in the pion at the physical m_u and m_d , and the mass of the valence light quark in the kaon at the physical m_u .

This procedure yields a correction to the kaon decay constant below 0.5%. Consequently, strong-isospin breaking corrections from the light sea-quark masses – which are suppressed by an additional power of δm_{ud} – can be neglected given present uncertainties.

Some earlier lattice-QCD calculations, however, only provide the decay constants and their ratio in the $SU(2)$ isospin-symmetric limit [33, 35, 36]. The Flavour Lattice Averaging Group corrects these results for strong-isospin breaking using chiral perturbation theory before including them in the averages. The leading strong-isospin-breaking corrections to the pion and kaon decay constants in χ PT can be parameterized as [25, 51]

$$f_{\pi^+} = f_{\pi}, \quad f_{K^+} = f_K \sqrt{1 + \delta_{SU(2)}}, \quad (71.13)$$

where f_{π} and f_K denote the values of the decay constants in the isospin-symmetric limit. The pion decay constant does not receive corrections linear in $m_u - m_d$ because of the G -parity symmetry of the pion triplet, so at first order the δm_{ud} expansion, strong-isospin breaking corrections are characterized by a single parameter, $\delta_{SU(2)}$. Next-to-leading order χ PT yields numerical values for $\delta_{SU(2)}$ of approximately -0.004 . Recent direct lattice-QCD calculations of $\delta_{SU(2)}$ give larger values of around -0.005 to -0.008 [8, 28–30, 50, 52], but further studies are needed. Thus, to be conservative, FLAG includes an uncertainty of 100% on the χ PT estimate for $\delta_{SU(2)}$ when correcting those decay-constant values that are quoted in the isospin-symmetric limit.

The errors on the decay-constant results in Table 71.1 obtained from $(2+1)$ -flavor lattice-QCD simulations do not include an estimate of the systematic uncertainty from the omission of charm sea quarks in the simulation. Consequently, when the uncertainty on the $(2+1+1)$ -flavor FLAG average is comparable to or better than that on the $(2+1)$ -flavor FLAG average, we simply use the four-flavor average as our preferred value. This is not possible, however, for the pion decay constant. To account for this, we first estimate the systematic uncertainty on pseudoscalar-meson decay constants associated with the omission of charm sea quarks. We then add this estimate in quadrature to the quoted error on the $(2+1)$ -flavor FLAG average for f_{π^+} to obtain our preferred value.

The error introduced by omitting charm sea quarks can be roughly estimated by expanding the charm-quark determinant in powers of $1/m_c$ [53]; the resulting leading contribution is of order $\alpha_s (\Lambda_{\text{QCD}}/2m_c)^2$ [54]. Taking the $\overline{\text{MS}}$ values $\overline{m}_c(\overline{m}_c) = 1.275$ GeV, $\overline{\Lambda}_{\text{QCD}} \sim 340$ MeV from FLAG [40], and $\overline{\alpha}(\overline{m}_c) \sim 0.4$, leads to an estimate of about 0.7% for the contribution to the decay constants from charm sea quarks. We can compare this power-counting estimate of charm sea-quark contributions with

²See the PDG mini-review on “Lattice Quantum Chromodynamics” [39] for a general review of numerical lattice-QCD simulations. Details on the different methods used in modern lattice-QCD calculations are provided in Appendix A of the FLAG “Review[s] of lattice results concerning low energy particle physics” [18, 40, 41].

³See the review by Kronfeld [42] for a summary of the large body of evidence validating the methods employed in modern lattice-QCD simulations.

Table 71.2: Experimental results for $\mathcal{B}(D^+ \rightarrow \mu^+\nu[\gamma])$, $\mathcal{B}(D^+ \rightarrow \tau^+\nu[\gamma])$, and $|V_{cd}|f_{D^+}$. The systematic errors on the inferred values of $|V_{cd}|f_{D^+}$ include those from the D^+ lifetime and mass. The error from radiative corrections is only included in the entries labeled “our average.”

Experiment	Mode	\mathcal{B}	$ V_{cd} f_{D^+}$ (MeV)
CLEO-c [43, 44]	$\mu^+\nu$	$(3.93 \pm 0.35 \pm 0.09) \times 10^{-4}$	$46.70 \pm 2.10 \pm 0.55$
CLEO-c [43, 44]	$\mu^+\nu + \tau^+\nu$	$(3.82 \pm 0.32 \pm 0.09) \times 10^{-4}$	$46.00 \pm 1.91 \pm 0.56$
BES III [45]	$\mu^+\nu$	$(3.71 \pm 0.19 \pm 0.06) \times 10^{-4}$	$45.33 \pm 1.17 \pm 0.38$
Our average	Lines 2+3	$(3.74 \pm 0.17) \times 10^{-4}$	45.50 ± 1.22
CLEO-c [46, 47]	$\tau^+\nu$ ($\pi^+\bar{\nu}$)	$< 1.2 \times 10^{-3}$	
BES III [48]	$\tau^+\nu$ ($\pi^+\bar{\nu}$)	$(1.20 \pm 0.24 \pm 0.12) \times 10^{-3}$	49.95 ± 2.48
Our average	$\mu^+\nu + \tau^+\nu$		46.17 ± 1.16

the observed differences between the (2+1)- and (2+1+1)-flavor lattice-QCD averages for kaon, $D_{(s)}$ -meson, and $B_{(s)}$ -decay constants in Tables 71.1, 71.4, and 71.6. Looking at Table 71.1, the three- and four-flavor averages for f_{K^+} agree to much better than our simple power-counting estimate. Inspection of Tables 71.4 and 71.6 shows, however, that charm sea-quark effects of this size are still allowed for both $D_{(s)}$ -meson and $B_{(s)}$ -meson decay constants.

Our final preferred theoretical values for the charged pion and kaon decay constants are

$$f_{\pi^+} = 130.2(1.2) \text{ MeV}, \quad f_{K^+} = 155.7(3) \text{ MeV}, \quad \frac{f_{K^+}}{f_{\pi^+}} = 1.193(2), \quad (71.14)$$

where f_{K^+} and f_{K^+}/f_{π^+} are simply the four-flavor FLAG 2019 averages [18], and f_{π^+} is the three-flavor FLAG 2019 average with the error increased by the estimated 0.7% charm sea-quark contribution. The errors on all three quantities in Eq. (71.14) have decreased since our previous review [26, 55].

71.3 Charmed mesons

71.3.1 Experimental rate measurements

Measurements have been made of the branching fractions for D^+ and D_s^+ mesons decaying to both $\mu^+\nu$ and $\tau^+\nu$ final states. The CLEO-c, BES, and BES III experiments have made measurements of D^+ decays using e^+e^- collisions at the $\psi(3770)$ resonant energy where D^-D^+ pairs are copiously produced. They fully reconstruct one of the D^+ s; for concreteness, we will take this to be the D^- . Counting the number of these events provides the normalization for the branching fraction measurement. The experimental analyses then proceed by identifying a candidate μ^+ and forming the missing-mass squared, $MM^2 = (E_{\text{CM}} - E_{D^-})^2 - (\vec{p}_{\text{CM}} - \vec{p}_{D^-} - \vec{p}_{\mu^+})^2$, where E_{CM} and p_{CM} are the center-of-mass energy (which is known) and momentum (which equals zero in e^+e^- collisions). A peak at zero MM^2 implies the existence of a missing neutrino, and hence the $\mu^+\nu$ decay of the D^+ . CLEO-c does not explicitly identify the muon, so their data consists of a combination of $\mu^+\nu$ and $\tau^+\nu$, $\tau^+ \rightarrow \pi^+\nu$ events. This permits them to do two fits: in one they fit for the individual components, and in the other they fix the ratio of $\tau^+\nu/\mu^+\nu$ events to be that given by the standard-model expectation. Thus, the former measurement should be used for new-physics searches, and the latter for standard-model predictions. Our average uses the fixed-ratio value.

Table 71.2 shows the available measurements of $D^+ \rightarrow \mu^+\nu$, as an upper limit on $D^+ \rightarrow \tau^+\nu$ from CLEO-c and the first measurement of this decay from BES III. To extract the values of $|V_{cd}|f_{D^+}$ via Eq. (71.1), we use values of $m_{D^+} = 1.86961$ GeV and the well-measured D^+ lifetime of 1.040(7) ps [64], and apply radiative corrections as described below. For calculating the average $\mu^+\nu$ number, we use the CLEO-c result from $\mu^+\nu + \tau^+\nu$.

To obtain the purely leptonic rates $\Gamma^{(0)}(D^+ \rightarrow \mu^+(\tau^+)\nu)$, we subtract the radiative contributions as in Sec. 71.2.1, but use numerical values for the corrections appropriate for D mesons. First, we reduce both the $\mu^+\nu$ and $\tau^+\nu$ branching fractions in Table 71.2 by 1.8%, which is the universal short-distance electroweak contribution of Sirlin [1] evaluated using the D -meson mass for the factorization scale. We do not adjust the experimental rates

by the universal long-distance correction [2]. This is because QED bremsstrahlung contributions have already been subtracted at leading-log order from the measurements in Table 71.2 using Monte-Carlo estimates computed with PHOTOS [9]. The $\mu^+\nu$ rates should also be reduced by the 1% estimate of the structure-dependent contributions from Dobrescu and Kronfeld [14]. This correction accounts for tree-level radiative processes in which the D meson decays into a real photon and an off-shell vector meson, which subsequently decays weakly to a charged lepton and neutrino. It is estimated using Eq. (12) of Burdman *et al.* [4] with the CLEO-c cut on the photon energy from Ref. [65], which is typical of all the measurements. We do not need to apply the structure-dependent correction to the $\mu^+\nu$ branching fractions in Table 71.2, however, because the experiments have already included it in their quoted results. Therefore, in summary, we reduce both the $D^+ \rightarrow \mu^+\nu$ and the $D^+ \rightarrow \tau^+\nu$ rates by 1.8% to account for radiative corrections. It is worth noting, however, that the universal long-distance electromagnetic contribution estimated for point-like charged mesons by Kinoshita [2], which we are not including because IB contributions are already subtracted from the measurements via PHOTOS, would *increase* both rates by about 2.5%.

We now discuss the D_s^+ decay process. Measurements of the leptonic decay rate have been made by several groups and are listed in Table 71.3. We exclude older values obtained by normalizing to D_s^+ decay modes that are not well defined. Many measurements, for example, used the $\phi\pi^+$ mode. This decay is a subset of the $D_s^+ \rightarrow K^+K^-\pi^+$ channel which has interferences from other modes populating the K^+K^- mass region near the ϕ , the most prominent of which is the $f_0(980)$. Thus, the extraction of the effective $\phi\pi^+$ rate is sensitive to the mass resolution of the experiment and the cuts used to define the ϕ mass region [66].⁴

To find D_s decays in the $\mu^+\nu$ signal channels, the experiments rely on fully reconstructing all of the final state particles except for the neutrino and using a missing-mass technique to infer the existence of the neutrino. CLEO and BES III use $e^+e^- \rightarrow D_s D_s^*$ collisions at 4170 MeV, while Babar and Belle use $e^+e^- \rightarrow DK n \pi D_s^*$ collisions at energies near the $\Upsilon(4S)$. CLEO and BES III do a similar analysis as was done for the D^+ above. Babar and Belle do a similar MM^2 calculation by using the reconstructed hadrons, the photon from the D_s^{*+} decay and a detected μ^+ . To get the normalization they do a MM^2 fit without the μ^+ and use the signal at the D_s^+ mass squared to determine the total D_s^+ yield.

When selecting the $\tau^+ \rightarrow \pi^+\bar{\nu}$ and $\tau^+ \rightarrow \rho^+\bar{\nu}$ decay modes, CLEO uses both the calculation of the missing-mass and the fact that there should be no extra energy in the event beyond that deposited by the measured tagged D_s^- and the τ^+ decay products. The $\tau^+ \rightarrow e^+\nu\bar{\nu}$ mode, however, uses only extra energy. Babar and Belle also use the extra energy to discriminate signal from background in their $\tau^+\nu$ measurements. BES III uses $\tau^+ \rightarrow \pi^+\bar{\nu}$ decays, where they calculate the MM^2 and discriminate against μ^+ from $D_s^+ \rightarrow \mu^+\nu$ decays.

When extracting $|V_{cs}|f_{D_s^+}$ via Eq. (71.1), we first apply the -1.8% universal electroweak correction [1] to all of the $\mu^+\nu$ and

⁴We have not included the BaBar result for $\mathcal{B}(D_s^+ \rightarrow \mu^+\nu)$ reported in Ref. [67] because this measurement determined the ratio of the leptonic decay rate to the hadronic decay rate $\Gamma(D_s^+ \rightarrow \ell^+\nu)/\Gamma(D_s^+ \rightarrow \phi\pi^+)$.

Table 71.3: Experimental results for $\mathcal{B}(D_s^+ \rightarrow \mu^+\nu[\gamma])$, $\mathcal{B}(D_s^+ \rightarrow \tau^+\nu[\gamma])$, and $|V_{cs}|f_{D_s^+}$. The systematic errors on the inferred values of $|V_{cs}|f_{D_s^+}$ include those from the D^+ lifetime and mass. The entries labeled “our average” take into account correlations between systematic errors common to the experiments, and also include errors from radiative corrections.

Experiment	Mode	$\mathcal{B}(\%)$	$ V_{cs} f_{D_s^+}$ (MeV)
CLEO-c [46, 47]	$\mu^+\nu$	$(0.565 \pm 0.045 \pm 0.017)$	$247.6 \pm 9.9 \pm 4.1$
BaBar* [57]	$\mu^+\nu$	$(0.602 \pm 0.038 \pm 0.034)$	$254.3 \pm 8.0 \pm 7.4$
Belle [58]	$\mu^+\nu$	$(0.531 \pm 0.028 \pm 0.020)$	$238.8 \pm 6.3 \pm 4.8$
BES III [59]	$\mu^+\nu$	$(0.549 \pm 0.016 \pm 0.015)$	$244.9 \pm 3.6 \pm 3.7$
Our average	$\mu^+\nu$	(0.552 ± 0.016)	244.0 ± 5.2
CLEO-c [46, 47]	$\tau^+\nu$ ($\pi^+\bar{\nu}$)	$(6.42 \pm 0.81 \pm 0.18)$	$267.3 \pm 16.9 \pm 4.2$
CLEO-c [60]	$\tau^+\nu$ ($\rho^+\bar{\nu}$)	$(5.52 \pm 0.57 \pm 0.21)$	$247.9 \pm 12.8 \pm 5.0$
CLEO-c [61, 62]	$\tau^+\nu$ ($e^+\nu\bar{\nu}$)	$(5.30 \pm 0.47 \pm 0.22)$	$242.9 \pm 10.8 \pm 5.3$
BaBar [57]	$\tau^+\nu$ ($e^+(\mu^+)\nu\bar{\nu}$)	$(5.00 \pm 0.35 \pm 0.49)$	$236.9 \pm 8.3 \pm 11.7$
Belle [58]	$\tau^+\nu$ ($\pi^+\bar{\nu}$)	$(6.04 \pm 0.43^{+0.46}_{-0.40})$	$260.3 \pm 9.3^{+10.1}_{-8.8}$
Belle [58]	$\tau^+\nu$ ($e^+\nu\bar{\nu}$)	$(5.37 \pm 0.33^{+0.35}_{-0.31})$	$244.5 \pm 7.5^{+8.2}_{-7.4}$
Belle [58]	$\tau^+\nu$ ($\mu^+\nu\bar{\nu}$)	$(5.86 \pm 0.37^{+0.34}_{-0.59})$	$255.4 \pm 8.0^{+7.6}_{-13.1}$
BES III [63]	$\tau^+\nu$ ($\pi^+\bar{\nu}$)	$(0.483 \pm 0.65 \pm 0.26)$	$231.9 \pm 15.7 \pm 6.5$
Our average	$\tau^+\nu$	(5.51 ± 0.20)	248.3 ± 6.1
Our average	$\mu^+\nu + \tau^+\nu$		245.7 ± 4.6

*We do not use a previous unpublished BaBar result from a subsample of data that uses a different technique for obtaining the branching fraction normalization [56].

$\tau^+\nu$ branching fractions in Table 71.3; this is the same as for D^+ mesons. We also decrease the Babar and Belle $\mu^+\nu$ branching fractions by the 1% structure-dependent correction [14]. This correction was already included in CLEO and BES results for the $\mu^+\nu$ branching fractions in Table 71.3. We use the masses and lifetimes $m_{D_s^+} = 1.96834(7)$ GeV, $m_{\tau^+} = 1.7686(12)$ GeV, and $\tau_{D_s^+} = 0.504(4)$ ps [64]. The inferred values for $f_{D_s^+}|V_{cs}|$ are in good agreement for the $\mu^+\nu$ and $\tau^+\nu$ decay modes.

It is clear from the discussion of radiative corrections in this section that they are less well understood theoretically for D^+ and D_s^+ meson decays than for pions and kaons. We therefore assign a 2.8% systematic uncertainty to the purely leptonic decay rates, which is the full size of the applied radiative corrections. This translates to a 1.4% error on the products of the decay constant times CKM matrix element. Putting everything together, the main experimental pertaining charmed meson leptonic decays are (see the bottom lines of Tables 71.2 and 71.3):

$$|V_{cd}|f_{D^+} = 46.2 \pm 1.0 \pm 0.6 \text{ MeV}, \quad (71.15)$$

$$|V_{cs}|f_{D_s^+} = 245.7 \pm 3.1 \pm 3.4 \text{ MeV}, \quad (71.16)$$

where the errors are from the measured branching fractions and the applied radiative corrections, respectively.

71.3.2 Theoretical decay-constant calculations

Table 71.4 presents recent theoretical calculations of charmed heavy-light meson decay constants and their ratio in the isospin-symmetric limit $m_u = m_d$. (As in Sec. 71.2.2, we denote the physical D^+ -meson decay constant by f_{D^+} , and use f_D for the isospin-symmetric value.) The upper two panels show results from lattice-QCD simulations with three ($N_f = 2 + 1$) or four flavors ($N_f = 2 + 1 + 1$) of dynamical quarks. Although there are fewer available results than for the pion and kaon sector, both f_D and f_{D_s} have been obtained using multiple sets of gauge-field configurations with different lattice fermion actions, providing independent confirmation. For comparison, the bottom panel of Table 71.4 shows QCD-model calculations of the D - and D_s -meson decay constants for which uncertainty estimates are provided. The lattice and non-lattice results agree, but numerical lattice-QCD simulations have now reached significantly greater precision than other approaches.

The lattice-QCD decay-constant results in Table 71.4 were all obtained using isospin-symmetric gauge-field configurations. As discussed in Sec. 71.2.2, however, the leading strong-isospin breaking corrections to heavy-light pseudoscalar-meson decay constants can be accounted for by using the physical down (or up) quark in

the D (or B) meson. Strong-isospin breaking corrections to heavy-strange meson decay constants are roughly an order-of-magnitude smaller because there are no light valence quarks involved. Recently, the Fermilab Lattice and MILC Collaborations used this approach to calculate directly the dominant strong-isospin breaking corrections to both f_D and f_B , finding [28]

$$f_{D^+} - f_D = 0.58(1)(7) \text{ MeV}, \quad f_{B^+} - f_B = -0.53(5)(7) \text{ MeV}. \quad (71.17)$$

These results agree with independent estimates of the strong-isospin-breaking corrections to heavy-light meson decay constants from Borelized sum rules [80]. Combined with the determinations of f_D and f_B from the same work, Eq. (71.17) implies that the corrections to the SU(3)-flavor breaking ratios are

$$\frac{f_{D_s}}{f_{D^+}} = \frac{f_{D_s}}{f_D} (1 - 0.0027(3)), \quad \frac{f_{B_s}}{f_{B^+}} = \frac{f_{B_s}}{f_B} (1 + 0.0028(5)). \quad (71.18)$$

These estimated strong-isospin-breaking corrections to f_D and f_{D_s}/f_D above are commensurate with the uncertainties on the (2+1+1)-flavor FLAG averages in Table 71.4. Consequently, it is important to account isospin-breaking effects before combining the theoretical decay constants with the corresponding experimental decay rates.

To obtain the charged D^+ -meson decay constant, we apply the correction in Eq. (71.17) to the (2+1+1)-flavor 2019 FLAG average for the D -meson decay constant in the isospin-symmetric limit. Similarly we use Eq. (71.18) to correct the (2+1+1)-flavor 2019 FLAG average for f_{D_s}/f_D . We take the four-flavor FLAG 2019 average for f_{D_s} directly. Our final preferred theoretical values for the charmed pseudoscalar-meson decay constants are

$$\begin{aligned} f_{D^+} &= 212.6(7) \text{ MeV}, \\ f_{D_s} &= 249.9(5) \text{ MeV}, \\ \frac{f_{D_s}}{f_{D^+}} &= 1.175(2). \end{aligned} \quad (71.19)$$

For all three quantities in Eq. (71.19), the uncertainties are roughly half the size of those in our previous review [26, 55].

Table 71.4: Recent theoretical determinations of f_D , f_{D_s} , and their ratio in the isospin-symmetric limit. The upper panels show results from lattice-QCD simulations with $(2 + 1 + 1)$ and $(2 + 1)$ dynamical quark flavors, respectively. Statistical and systematic errors are quoted separately. The bottom panel shows estimates from QCD sum rules (QCD SR) and the light-front quark model (LFQM). These are not used to obtain our preferred decay-constant values.

Reference	Method	N_f	f_D (MeV)	f_{D_s} (MeV)	f_{D_s}/f_D
Fermilab/MILC 17 [28]	LQCD	2+1+1	212.1(0.3)(0.5)	249.9(0.3)(0.3)	1.1782(06)(15) [*]
ETM 14 [29]	LQCD	2+1+1	207.4(3.7)(0.9)	247.2(3.9)(1.4)	1.192(19)(11)
FLAG 19 average [18]	LQCD	2+1+1	212.0(0.7)	249.9(0.5)	1.1783(16)
RBC/UKQCD 18 [68] [†]	LQCD	2+1	–	–	1.1652(35)(⁺¹²⁰ ₋₅₇)
RBC/UKQCD 17 [69]	LQCD	2+1	208.7(2.8)(^{+2.1} _{-1.8})	246.4(1.3)(^{+1.3} _{-1.9})	1.1667(77)(⁺⁵² ₋₄₃)
χ QCD 14 [70]	LQCD	2+1	–	254(2)(4)	–
HPQCD 12 [71]	LQCD	2+1	208.3(1.0)(3.3)	–	1.187(4)(12)
Fermilab/MILC 11 [72]	LQCD	2+1	218.9(9.2)(6.6)	260.1(8.9)(6.1)	1.188(14)(21)
HPQCD 10 [73]	LQCD	2+1	–	248.0(1.4)(2.1)	–
FLAG 19 average [18]	LQCD	2+1	209.0(2.4)	248.0(1.6)	1.174(7)
Wang 15 [74] [‡]	QCD SR		208(10)	240(10)	1.15(6)
Gelhausen 13 [75]	QCD SR		201(⁺¹² ₋₁₃)	238(⁺¹³ ₋₂₃)	1.15(^{+0.04} _{-0.05})
Narison 12 [76]	QCD SR		204(6)	246(6)	1.21(4)
Lucha 11 [77]	QCD SR		206.2(8.9)	245.3(16.3)	1.193(26)
Hwang 09 [78]	LFQM		–	264.5(17.5) [§]	1.29(7)

^{*}Ref. [28] provides values for f_D and f_{D_s} in the isospin-symmetric limit, but not for their ratio. Here we infer the central value from those of the individual decay constants, and take the statistical and systematic errors to be the same as for the physical ratio f_{D_s}/f_D .

[†]Preprint submitted to the arXiv and JHEP after the deadline for inclusion in the 2019 FLAG review.

[‡]Obtained using m_c^{MS} ; results using m_c^{pole} are also given in the paper.

[§]Obtained by combining PDG value $f_D = 205.8(8.9)$ MeV [79] with f_{D_s}/f_D from this work.

71.4 Bottom mesons

71.4.1 Experimental rate measurements

The Belle and BaBar collaborations have found evidence for $B^- \rightarrow \tau^- \bar{\nu}$ decay in $e^+e^- \rightarrow B^- B^+$ collisions at the $\Upsilon(4S)$ energy. The analysis relies on reconstructing a hadronic or semileptonic B decay tag, finding a τ candidate in the remaining track and photon candidates, and examining the extra energy in the event which should be close to zero for a real τ^- decay to $e^- \nu \bar{\nu}$ or $\mu^- \nu \bar{\nu}$ opposite a B^+ tag. While the BaBar results have remained unchanged, Belle reanalyzed both samples of their data. The branching fraction using hadronic tags changed from $1.79^{+0.56+0.46}_{-0.49-0.51} \times 10^{-4}$ [81] to $0.72^{+0.27}_{-0.25} \pm 0.11 \times 10^{-4}$ [82], while the corresponding change using semileptonic tags was from $1.54^{+0.38+0.29}_{-0.37-0.31}$ to $1.25 \pm 0.28 \pm 0.27$. These changes demonstrate the difficulty of the analysis. The results are listed in Table 71.5.

Table 71.5: Experimental results for $\mathcal{B}(B^- \rightarrow \tau^- \bar{\nu})$ and $|V_{ub}|f_{B^+}$. To extract the values of $|V_{ub}|f_{B^+}$ via Eq. (71.1), we use the PDG 2018 value of the B^+ lifetime of 1.638 ± 0.004 ps, and the τ^+ and B^+ masses of 1.77686 and 5.27933 GeV, respectively.

Experiment	Tag	\mathcal{B} (units of 10^{-4})	$ V_{ub} f_{B^+}$ (MeV)
Belle [82]	Hadronic	$0.72^{+0.27}_{-0.25} \pm 0.11$	
Belle [83]	Semileptonic	$1.25 \pm 0.28 \pm 0.27$	
Belle [83]	Average	0.91 ± 0.22	0.72 ± 0.09
BaBar [84]	Hadronic	$1.83^{+0.53}_{-0.49} \pm 0.24$	
BaBar [85]	Semileptonic	$1.7 \pm 0.8 \pm 0.2$	
BaBar [84]	Average	1.79 ± 0.48	1.01 ± 0.14
Our average		1.06 ± 0.20	0.77 ± 0.07

Because there are large backgrounds under the signals for these measurements, as well as substantial systematic errors, the significances of the individual results are still below the 5σ discovery threshold. Belle quotes 4.6σ for their combined hadronic and semileptonic tags, while BaBar quotes 3.3σ and 2.3σ , for hadronic and semileptonic tags. Greater precision is necessary to determine if any effects beyond the Standard Model are present.

We do not correct the measured branching ratios in Table 71.5 for radiative corrections because the experimental uncertainties are so large. The radiative corrections are expected to be bigger, however, for $B \rightarrow \mu\nu$ leptonic decays because the corrections are

no longer helicity suppressed [6], and may be a significant fraction of the purely leptonic rate. More theoretical work is needed to understand radiative corrections to leptonic B decays in anticipation of future measurements with greater precision, and of new decay channels.

71.4.2 Theoretical decay-constant calculations

Table 71.6 presents recent theoretical calculations of bottom heavy-light meson decay constants and their ratio in the isospin-symmetric limit $m_u = m_d$. The upper two panels show results from lattice-QCD simulations with three ($N_f = 2 + 1$) or four flavors ($N_f = 2 + 1 + 1$) of dynamical quarks. For all decay constants, calculations using different gauge-field configurations, light-quark actions, and b -quark actions provide independent confirmation. For comparison, the bottom panel of Table 71.6 shows QCD-model calculations of the B^- and B_s^- -meson decay constants for which uncertainty estimates are provided. These are consistent with the lattice values, but with much larger uncertainties.

The lattice-QCD decay-constant results in Table 71.6 were all obtained using isospin-symmetric gauge-field configurations. Some calculations, however, account for the dominant effect of strong-isospin-breaking by using the correct value for the valence light-quark mass in the B meson (m_u for f_{B^+} and m_d for f_{B^0}). Early estimates of the strong-isospin-breaking correction obtained $f_{B^+} - f_B \sim 2$ MeV [88, 90], which would significant given the present lattice-QCD uncertainties. It turns out, however, that these calculations inadvertently introduced a spurious sea-quark contribution, and therefore overestimated the size of the effect. A more recent calculation by the Fermilab/MILC Collaboration finds very little evidence for isospin violation ($f_{B^+} - f_B \sim 0.5$ MeV) [28], which is more than two times smaller than the total uncertainties on present lattice-QCD calculations. For this reason, we quote isospin averages in the current review.

Our preferred theoretical values for the bottom pseudoscalar-meson decay constants are

$$\begin{aligned}
 f_B &= 190.0(1.3) \text{ MeV}, \\
 f_{B_s} &= 230.0(1.3) \text{ MeV}, \\
 \frac{f_{B_s}}{f_B} &= 1.209(5),
 \end{aligned} \tag{71.20}$$

which are simply the $N_f = 2 + 1 + 1$ FLAG 2019 averages [18]. Because the uncertainties on the three-flavor results in Table 71.6

Table 71.6: Recent theoretical determinations of f_B , f_{B_s} , and their ratio in the isospin-symmetric limit. The upper panels show results from lattice-QCD simulations with $(2+1+1)$ and $(2+1)$ dynamical quark flavors, respectively. When available, statistical and systematic errors are quoted separately. The bottom panel shows estimates from the relativistic potential model (RPM), QCD sum rules, and the light-front quark model, which are not used to obtain our preferred decay-constant values.

Reference	Method	N_f	f_B (MeV)	f_{B_s} (MeV)	f_{B_s}/f_B
FNAL/MILC 17 [28]	LQCD	2+1+1	189.9(1.4)	230.7(1.2)	1.2180(49)
HPQCD 17 [86]*	LQCD	2+1+1	196(6)	236(7)	1.207(7)
ETM 16 [87]	LQCD	2+1+1	193(6)	229(5)	1.184(25)
HPQCD 13 [88]	LQCD	2+1+1	186(4)	224(5)	1.217(8)
FLAG 19 average [18]	LQCD	2+1+1	190.0(1.3)	230.3(1.3)	1.209(5)
Aoki 14 [89] [†]	LQCD	2+1	218.8(6.5)(30.8)	263.5(4.8)(36.7)	1.193(20)(44)
RBC/UKQCD 14 [90] [‡]	LQCD	2+1	195.6(6.4)(13.3)	235.4(5.2)(11.1)	1.223(14)(70)
HPQCD 12 [91]	LQCD	2+1	191(1)(8)	228(3)(10)	1.188(12)(13)
HPQCD 12 [91]	LQCD	2+1	189(3)(3)*	–	–
HPQCD 11 [92]	LQCD	2+1	–	225(3)(3)	–
Fermilab/MILC 11 [72]	LQCD	2+1	196.9(5.5)(7.0)	242.0(5.1)(8.0)	1.229(13)(23)
FLAG 19 average [18]	LQCD	2+1	192.0(4.3)	228.4(3.7)	1.201(16)
Sun 16 [93] [§]	RPM		219(15)	266(19)	1.21(9)
Wang 15 [74] [§]	QCD SR		194(15)	231(16)	1.19(10)
Baker 13 [94]	QCD SR		186(14)	222(12)	1.19(4)
Lucha 13 [95]	QCD SR		192.0(14.6)	228.0(19.8)	1.184(24)
Gelhausen 13 [75]	QCD SR		207 ⁽⁺¹⁷⁾ ₍₋₉₎	242 ⁽⁺¹⁷⁾ ₍₋₁₂₎	1.17 ⁽⁺³⁾ ₍₋₄₎
Narison 12 [76]	QCD SR		206(7)	234(5)	1.14(3)
Hwang 09 [78]	LFQM		–	270.0(42.8) [¶]	1.32(8)

*Re-analysis of data from HPQCD 13.

[†]Obtained with static b quarks (*i.e.* $m_b \rightarrow \infty$).

[‡]Ref. [90] does not provide results in the isospin-symmetric limit, so we show f_{B^+} and f_{B^0}/f_{B^+} for this work. dsdecaycons:foot:ddag3

[§]Obtained using $m_b^{\overline{\text{MS}}}$; results using m_b^{pole} are also given in the paper.

[¶]Obtained by combining PDG value $f_B = 204(31)$ MeV [79] with f_{B_s}/f_B from this work. dsdecaycons:foot:mpar3

are substantially larger than those on the four-flavor results, including them in the average leaves the central values unchanged, and decreases the errors only slightly.

71.5 Phenomenological implications

71.5.1 $|V_{ud}|$, $|V_{us}|$, and status of first-row unitarity

Using the average values for $f_{\pi^+}|V_{ud}|$, $f_{K^+}|V_{us}|$, and their ratio from Eqs. (71.10)–(71.12) and for f_{π^+} , f_{K^+} , and their ratio from Eq. (71.14), we obtain the following determinations of the CKM matrix elements $|V_{ud}|$, $|V_{us}|$, and their ratio from leptonic decays within the standard model:

$$|V_{ud}| = 0.9764(2)(90)(10), \quad |V_{us}| = 0.2254(3)(4)(3),$$

$$\frac{|V_{us}|}{|V_{ud}|} = 0.2313(2)4(2), \quad (71.21)$$

where the errors are from the experimental branching fraction(s), the pseudoscalar decay constant(s), and radiative corrections, respectively. These results enable a precise test of the unitarity of the first row of the CKM matrix from leptonic decays alone (the contribution from $|V_{ub}|$ is negligible). Using the values of $|V_{ud}|$ and $|V_{us}|$ from Eq. (71.21), we find

$$|V_{ud}|^2 + |V_{us}|^2 + |V_{ub}|^2 - 1 = 0.004(18), \quad (71.22)$$

which is consistent with three-generation unitarity at the few-percent level.

The determinations of $|V_{ud}|$ and $|V_{us}|$ from leptonic decays in Eq. (71.21) can be compared to those obtained from other processes. The result above for $|V_{ud}|$ agrees with the determination from superallowed β -decay, $|V_{ud}| = 0.97420(21)$ [96], but has an error about forty times larger that is primarily due to the uncertainty in the theoretical determination of f_{π^+} . The CKM element $|V_{us}|$ can be determined from semileptonic $K^+ \rightarrow \pi^0 \ell^+ \nu$ decay. Here experimental measurements provide a value for the product $f_+^{K\pi}(0)|V_{us}|$, where $f_+^{K\pi}(0)$ is the form-factor at zero four-momentum transfer between the initial state kaon and the final state pion. Taking the most recent experimental determination

of $|V_{us}|f_+^{K\pi}(0) = 0.2165(4)$ from Moulson [37]⁵ and the 2019 $(2+1+1)$ -flavor FLAG average for $f_+(0)^{K\pi} = 0.9706(27)$ [18] based on the calculations of ETM [100] and Fermilab/MILC [101] gives $|V_{us}| = 0.2231(6)_{\text{LQCD}}(4)_{\text{exp}}$ from $K_{\ell 3}$ decay. The determinations of $|V_{us}|$ from leptonic and semileptonic kaon decays are both quite precise (with the error from leptonic decay being about 25% smaller), but the central values differ by 2.5σ . (This difference would be reduced to 1.8σ , but not eliminated, using the $(2+1)$ -flavor FLAG average for $f_+(0)^{K\pi} = 0.9677(27)$ instead.) Finally, the combination of the ratio $|V_{us}|/|V_{ud}|$ from leptonic decays [Eq. (71.21)] with $|V_{ud}|$ from β decay implies an alternative determination of $|V_{us}| = 0.2254(5)$ which agrees with the value from leptonic kaon decay, but disagrees with the $K_{\ell 3}$ -decay result at the 1.8σ level.

Given the roughly 2σ tension between $|V_{us}|$ from leptonic and semileptonic kaon decays, it is important to scrutinize the uncertainties on the theoretical and experimental inputs to $|V_{us}|$ and other elements of the first row of the CKM matrix. Recently, Seng *et al.* introduced a new approach for calculating radiative corrections to neutron and nuclear beta decays using dispersion relations [102–105]. These calculations imply a lower value of $|V_{ud}| = 0.97395(23)$ than the Hardy and Towner analysis [106] by almost 1σ . An independent calculation of the radiative corrections by Czarnecki and Marciano using QCD sum rules yields similar results [107]. Using this value of $|V_{ud}|$ with the determination of $|V_{us}|$ from leptonic kaon decays in Eq. (71.21), we obtain $|V_{ud}|^2 + |V_{us}|^2 + |V_{ub}|^2 - 1 = -0.0006(5)$, again (roughly) consistent with first-row unitarity.

Last, we combine the experimental measurement of $f_{\pi^+}|V_{ud}|$ in Eq. (71.10) with $|V_{ud}|$ from superallowed β -decay [96] to infer an “experimental” value for the pion decay constant:

$$f_{\pi^-}^{\text{“exp”}} = 130.50(2)(3)(13) \text{ MeV}, \quad (71.23)$$

⁵This is an update of the 2010 Flavianet review [38] that includes new measurements of the K_S lifetime [97, 98], $\text{Re}(\epsilon'/\epsilon)$ [98], and $\mathcal{B}(K^\pm \rightarrow \pi^\pm \pi^+ \pi^-)$ [99]. The latter measurement is the primary source of the reduced error on $\mathcal{B}(K_{\ell 3})$, via the constraint that the sum of all branching ratios must equal unity.

where the uncertainties are from the errors on Γ , $|V_{ud}|$, and higher-order corrections, respectively. Many recent (2+1+1)-flavor lattice-QCD calculations use this quantity to set the overall physical scale in their simulations, *e.g.*, Refs. [7, 28–30]. Conversely, comparing $f_{\pi^-}^{\text{exp}}$ with the 2019 FLAG (2+1)-flavor average $f_{\pi^+} = 130.2(8)$ MeV, which only includes lattice-QCD results that employ observables to set the scale [31–36], provides a test of lattice-QCD methods. The values are in good agreement within present uncertainties. We do not quote an “experimental” value for the kaon decay constant because the value of $|V_{us}|$ is less clear given the $\sim 2\sigma$ tension between the values of $|V_{us}|$ obtained from leptonic and semileptonic kaon decays.

71.5.2 $|V_{cd}|$, $|V_{cs}|$, and status of second-row unitarity

Using the average values for $|V_{cd}|f_{D^+}$ and $|V_{cs}|f_{D_s^+}$ from Eqs. (71.15) and (71.16), and for f_{D^+} and $f_{D_s^+}$ from Eq. (71.19), we obtain the following determinations of the CKM matrix elements $|V_{cd}|$ and $|V_{cs}|$ from leptonic decays within the standard model:

$$|V_{cd}| = 0.217(5)(3)(1) \quad \text{and} \quad |V_{cs}| = 0.983(13)(14)(2), \quad (71.24)$$

where the errors are from the measured branching fractions, radiative corrections, and decay constants, respectively. These results enable a test of the unitarity of the second row of the CKM matrix. We obtain

$$|V_{cd}|^2 + |V_{cs}|^2 + |V_{cb}|^2 - 1 = 0.016(37), \quad (71.25)$$

in agreement with three-generation unitarity.

The uncertainty on $|V_{cd}|$ in Eq. (71.24) is limited by the measurement error on the $D^+ \rightarrow \mu^+\nu$ decay rate. For $|V_{cs}|$, however, the experimental and radiative-correction errors are commensurate. It is worth noting that the value of $|V_{cs}|$ from leptonic D_s decays has decreased substantially from the value of 1.007(17) in the previous version of this review [26, 55], and is now below unity as expected in the three-generation CKM framework. This change is due to our new, more consistent treatment of the radiative corrections, which lower the purely leptonic decay rates for the $\mu^+\nu$ and $\tau^+\nu$ channels by 2.8% and 1%, respectively. We emphasize, however, that we have taken a generous 100% uncertainty on these estimates, and that more theoretical work is needed to really pin down the sizes of the radiative corrections to $D_{(s)}$ -meson leptonic decays.

The CKM matrix elements $|V_{cd}|$ and $|V_{cs}|$ can also be obtained from semileptonic $D^+ \rightarrow \pi^0\ell^+\nu$ and $D_s^+ \rightarrow K^0\ell^+\nu$ decays, respectively. Here experimental measurements determine the product of the form factor times the CKM element, and theory provides the value for the form factor at zero four-momentum transfer between the initial $D_{(s)}$ meson and the final pion or kaon. The latest experimental averages from the Heavy Flavor Averaging Group (HFLAV) are $f_+^{D\pi}(0)|V_{cd}| = 0.1426(19)$ and $f_+^{D_s K}(0)|V_{cs}| = 0.7226(34)$ [108]. There are not enough published lattice-QCD calculations of the zero-momentum $D_{(s)}$ -meson semileptonic form factors with $N_f \geq 3$ to permit an average by the FLAG Collaboration. Taking the most precise three-flavor form-factor results $f_+^{D\pi}(0) = 0.666(29)$ and $f_+^{D_s K}(0) = 0.747(19)$ from the HPQCD Collaboration [109, 110] gives for the CKM matrix elements $|V_{cd}| = 0.2141(97)$ and $|V_{cs}| = 0.967(25)$, in agreement with those from leptonic decays in Eq. (71.24). A newer, four-flavor calculation of the form factors by the ETM Collaboration, however, yields a smaller value of $f_+^{D\pi}(0) = 0.612(35)$ by 1.2σ and a larger $f_+^{D_s K}(0) = 0.765(31)$ by 0.5σ . These imply $|V_{cd}| = 0.233(14)$ and $|V_{cs}| = 0.945(39)$, which are about 1σ above and below the values from leptonic decays in Eq. (71.24), respectively. Independent lattice-QCD calculations of the $D^+ \rightarrow \pi^0\ell^+\nu$ and $D_s^+ \rightarrow K^0\ell^+\nu$ form factors now in progress [111, 112] may help clarify the picture.

We can combine the experimental measurements of $f_{D^+}|V_{cd}|$ and $f_{D_s^+}|V_{cs}|$ from Tables 71.2 and 71.3 with $|V_{cd}| = 0.22438(44)$ and $|V_{cs}| = 0.97359(10)$ from the PDG 2018 global unitarity-triangle analysis [64] to infer “experimental” values for the decay

constants within the standard model. We take the CKM elements from the global fit because they are based on many input quantities, thereby reducing the sensitivity to any one outlying measurement or calculation. We obtain for the decay constants

$$\begin{aligned} f_{D^+}^{\text{exp}} &= 205.8(4.5)(0.4)(2.7) \text{ MeV}, \\ f_{D_s^+}^{\text{exp}} &= 252.4(3.2)(0.03)(3.5) \text{ MeV}, \\ \left(\frac{f_{D_s^+}}{f_{D^+}}\right)^{\text{exp}} &= 1.226(31)(2)(3). \end{aligned} \quad (71.26)$$

where the uncertainties are from the errors on $\Gamma^{(0)}$, CKM matrix elements, and radiative corrections, respectively. For the decay-constant ratio, we expect most of the radiative corrections to cancel, and therefore multiply the 1.4% error from Sec. 71.3.1 by the SU(3)-breaking factor $(m_s - m_d)/\Lambda_{\text{QCD}} \sim 1/5$. The “experimental” values f_{D^+} ($f_{D_s^+}/f_{D^+}$) are about 1.3σ lower (1.6σ higher) than the (2+1+1)-flavor lattice-QCD averages in Eq. (71.19). The CKM matrix element $|V_{cd}|$ is, however, proportional to $|V_{us}|$ within the Wolfenstein parameterization [113, 114]. Thus, resolving the inconsistencies between determinations of $|V_{us}|$ from leptonic and semileptonic decays discussed in Sec. 71.5.1 may also reduce the mild tensions observed here.

Last, we can test lepton-flavor universality in charm meson decays by checking the following relationship derived from Eq. (71.1):

$$\frac{\Gamma(D_s^+ \rightarrow \tau^+\nu)}{\Gamma(D_s^+ \rightarrow \mu^+\nu)} = \frac{m_\tau^2 (1 - m_\tau^2/M_{D_s}^2)^2}{m_\mu^2 (1 - m_\mu^2/M_{D_s}^2)^2} = 9.75, \quad (71.27)$$

where the uncertainties from the masses are negligible to the number of digits quoted. The measured ratio of $\tau^+\nu$ to $\mu^+\nu$ rates is 9.98 ± 0.46 , consistent with the standard-model expectation.

71.5.3 $|V_{ub}|$ and other applications

Using the average value for $|V_{ub}|f_{B^+}$ from Table 71.5, and for f_{B^+} from Eq. (71.20), we obtain the following determination of the CKM matrix element $|V_{ub}|$ from leptonic decays within the standard model:

$$|V_{ub}| = 4.05(37)(3) \times 10^{-3}, \quad (71.28)$$

where the errors are from experiment and theory, respectively. One should bear in mind when interpreting Eq. (71.28) that none of the experimental measurements that enter the average for $|V_{ub}|f_{B^+}$ have individually reached the 5σ discovery level (see Sec. 71.4.1). Further, decays involving the third generation of quarks and leptons may be particularly sensitive to new physics associated with electroweak symmetry breaking due to their larger masses [10, 12], so Eq. (71.28) is more likely to be influenced by new physics than the determinations of the elements of the first and second rows of the CKM matrix in the previous sections.

The CKM element $|V_{ub}|$ can also be obtained from semileptonic B -meson decays. For more than a decade, there has remained a persistent 2-3 σ tension between the determinations of $|V_{ub}|$ from exclusive $B \rightarrow \pi\ell\nu$ decay and from inclusive $B \rightarrow X_u\ell\nu$ decay, where X_u denotes all hadrons which contain a constituent up quark [21, 108, 115–118]. The currently most precise determination of $|V_{ub}|^{\text{excl}} = 3.73(14) \times 10^{-3}$ is obtained from a joint z -fit by FLAG [18] of the vector and scalar form factors $f_+^{B\pi}(q^2)$ and $f_0^{B\pi}(q^2)$ calculated in (2+1)-flavor lattice QCD [119–121] and experimental measurements of the differential decay rate from BaBar [122, 123] and Belle [124, 125]. On the other hand, the PDG 2018 inclusive determination obtained using the theoretical frameworks in Refs. [126–128] is $|V_{ub}|^{\text{incl}} = 4.49(28) \times 10^{-3}$ [64, 129]. The value of $|V_{ub}|$ from leptonic $B \rightarrow \tau\nu$ decay in Eq. (71.28) splits the difference between the inclusive and exclusive determinations, and is compatible (within large uncertainties) with both.

Given the large uncertainties on the experimental measurements of $\mathcal{B}(B^- \rightarrow \tau^-\bar{\nu})$, and the more than 2σ disagreement between $|V_{ub}|$ obtained from inclusive and exclusive semileptonic B decays, we do not present an “experimental” value of the decay constant f_{B^+} .

Acknowledgements

We thank V. Cirigliano, C. Davies, A. El Khadra, A. Khodjamirian, A. Kronfeld, J. Laiho, W. Marciano, M. Moulson, S. Narison, S. Sharpe, and Z.-G. Wang for useful discussions on this and previous versions of the review. We thank M. Della Morte and S. Simula for valuable feedback on the manuscript, and for providing information on the 2019 FLAG lattice averages. We gratefully acknowledge support of the U. S. National Science Foundation and the U. S. Department of Energy through Grant No. DE-FG02-13ER41598. The work of J. L. R. was performed in part at the Aspen Center for Physics, which is supported by National Science Foundation grant PHY-1066293. Fermilab is operated by the Fermi Research Alliance, LLC, under Contract No. DE-AC02-07CH11359 with the U.S. Department of Energy, Office of Science, Office of High Energy Physics.

References

- [1] A. Sirlin, Nucl. Phys. **B196**, 83 (1982).
- [2] T. Kinoshita, Phys. Rev. Lett. **2**, 477 (1959).
- [3] M. Knecht *et al.*, Eur. Phys. J. **C12**, 469 (2000), [hep-ph/9909284].
- [4] G. Burdman, J. T. Goldman and D. Wyler, Phys. Rev. **D51**, 111 (1995), [hep-ph/9405425].
- [5] V. Cirigliano and I. Rosell, JHEP **10**, 005 (2007), [arXiv:0707.4464].
- [6] D. Becirevic, B. Haas and E. Kou, Phys. Lett. **B681**, 257 (2009), [arXiv:0907.1845].
- [7] A. Bazavov *et al.* (Fermilab Lattice and MILC), Phys. Rev. **D90**, 074509 (2014), [arXiv:1407.3772].
- [8] M. Di Carlo *et al.*, Phys. Rev. **D100**, 034514 (2019), [arXiv:1904.08731].
- [9] E. Barberio and Z. Was, Comput. Phys. Commun. **79**, 291 (1994).
- [10] W.-S. Hou, Phys. Rev. **D48**, 2342 (1993).
- [11] A. G. Akeroyd and S. Recksiegel, Phys. Lett. **B554**, 38 (2003), [hep-ph/0210376].
- [12] A. G. Akeroyd and S. Recksiegel, J. Phys. **G29**, 2311 (2003), [hep-ph/0306037].
- [13] A. G. Akeroyd, Prog. Theor. Phys. **111**, 295 (2004), [hep-ph/0308260].
- [14] B. A. Dobrescu and A. S. Kronfeld, Phys. Rev. Lett. **100**, 241802 (2008), [arXiv:0803.0512].
- [15] J. L. Hewett, in “Heavy flavor physics. Proceedings, LISHEP 95, LAFEX International School on High-Energy Physics, session C, cbt Workshop, Rio de Janeiro, Brazil, February 21-23, 1995,” 171–187 (1995), [hep-ph/9505246], URL <http://www-public.slac.stanford.edu/sciDoc/docMeta.aspx?slacPubNumber=SLAC-PUB-6821>.
- [16] A. Crivellin, Phys. Rev. **D81**, 031301 (2010), [arXiv:0907.2461].
- [17] F. U. Bernlochner, Z. Ligeti and S. Turczyk, Phys. Rev. **D90**, 094003 (2014), [arXiv:1408.2516].
- [18] S. Aoki *et al.* (Flavour Lattice Averaging Group) (2019), [arXiv:1902.08191].
- [19] W. J. Marciano, Phys. Rev. Lett. **93**, 231803 (2004), [hep-ph/0402299].
- [20] V. Cirigliano *et al.*, Rev. Mod. Phys. **84**, 399 (2012), [arXiv:1107.6001].
- [21] K. A. Olive *et al.* (Particle Data Group), Chin. Phys. **C38**, 090001 (2014).
- [22] B. Ananthanarayan and B. Moussallam, JHEP **06**, 047 (2004), [hep-ph/0405206].
- [23] S. Descotes-Genon and B. Moussallam, Eur. Phys. J. **C42**, 403 (2005), [hep-ph/0505077].
- [24] W. J. Marciano and A. Sirlin, Phys. Rev. Lett. **71**, 3629 (1993).
- [25] V. Cirigliano and H. Neufeld, Phys. Lett. **B700**, 7 (2011), [arXiv:1102.0563].
- [26] J. L. Rosner, S. Stone and R. S. Van de Water (2015), review prepared for PDG 2015 edition, [arXiv:1509.02220].
- [27] J. Gasser, A. Rusetsky and I. Scimemi, Eur. Phys. J. **C32**, 97 (2003), [hep-ph/0305260].
- [28] A. Bazavov *et al.*, Phys. Rev. **D98**, 7, 074512 (2018), [arXiv:1712.09262].
- [29] N. Carrasco *et al.* (ETM), Phys. Rev. **D91**, 054507 (2015), [arXiv:1411.7908].
- [30] R. Dowdall *et al.* (HPQCD), Phys. Rev. **D88**, 074504 (2013), [arXiv:1303.1670].
- [31] V. G. Bornyakov *et al.* (QCDSF-UKQCD), Phys. Lett. **B767**, 366 (2017), [arXiv:1612.04798].
- [32] S. Durr *et al.*, Phys. Rev. **D95**, 5, 054513 (2017), [arXiv:1601.05998].
- [33] T. Blum *et al.* (RBC, UKQCD), Phys. Rev. **D93**, 074505 (2016), [arXiv:1411.7017].
- [34] A. Bazavov *et al.* (MILC), PoS **LATTICE2010**, 074 (2010), [arXiv:1012.0868].
- [35] S. Durr *et al.* (BMW), Phys. Rev. **D81**, 054507 (2010), [arXiv:1001.4692].
- [36] E. Follana *et al.* (HPQCD, UKQCD), Phys. Rev. Lett. **100**, 062002 (2008), [arXiv:0706.1726].
- [37] M. Moulson, in “8th International Workshop on the CKM Unitarity Triangle (CKM2014) Vienna, Austria, September 8-12, 2014,” (2014), [arXiv:1411.5252].
- [38] M. Antonelli *et al.* (FlaviaNet Working Group on Kaon Decays), Eur. Phys. J. **C69**, 399 (2010), [arXiv:1005.2323].
- [39] S. Hashimoto, J. Laiho and S. R. Sharpe, “Lattice Quantum Chromodynamics,” <http://pdg.lbl.gov/2019/reviews/rpp2018-rev-lattice-qcd.pdf> (2017), review prepared for PDG 2018 edition.
- [40] S. Aoki *et al.* (Flavour Lattice Averaging Group), Eur. Phys. J. **C74**, 2890 (2014), [arXiv:1310.8555].
- [41] S. Aoki *et al.*, Eur. Phys. J. **C77**, 2, 112 (2017), [arXiv:1607.00299].
- [42] A. S. Kronfeld, Ann. Rev. Nucl. Part. Sci. **62**, 265 (2012), [arXiv:1203.1204].
- [43] M. Artuso *et al.* (CLEO), Phys. Rev. Lett. **95**, 251801 (2005), [hep-ex/0508057].
- [44] B. I. Eisenstein *et al.* (CLEO), Phys. Rev. **D78**, 052003 (2008), [arXiv:0806.2112].
- [45] M. Ablikim *et al.* (BESIII), Phys. Rev. **D89**, 051104 (2014), [arXiv:1312.0374].
- [46] M. Artuso *et al.* (CLEO), Phys. Rev. Lett. **99**, 071802 (2007), [arXiv:0704.0629].
- [47] J. P. Alexander *et al.* (CLEO), Phys. Rev. **D79**, 052001 (2009), [arXiv:0901.1216].
- [48] M. Ablikim *et al.* (BESIII) (2019), [arXiv:1908.08877].
- [49] A. V. Manohar, C. T. Sachrajda and R. M. Barnett, “Quark Masses,” <http://pdg.lbl.gov/2019/reviews/rpp2018-rev-quark-masses.pdf> (2018), review prepared for PDG 2018 update.
- [50] G. M. de Divitiis *et al.*, JHEP **04**, 124 (2012), [arXiv:1110.6294].
- [51] J. Gasser and H. Leutwyler, Nucl. Phys. **B250**, 465 (1985).
- [52] G. M. de Divitiis *et al.* (RM123), Phys. Rev. **D87**, 11, 114505 (2013), [arXiv:1303.4896].
- [53] M. Nobes (2005), [hep-lat/0501009].
- [54] A. Bazavov *et al.* (Fermilab Lattice, MILC), Phys. Rev. **D93**, 11, 113016 (2016), [arXiv:1602.03560].
- [55] C. Patrignani *et al.* (Particle Data Group), Chin. Phys. **C40**, 10, 100001 (2016).

- [56] J. P. Lees *et al.* (BaBar) (2010), [arXiv:1003.3063].
- [57] P. del Amo Sanchez *et al.* (BaBar), Phys. Rev. **D82**, 091103 (2010), [Erratum: Phys. Rev.D91,no.1,019901(2015)], [arXiv:1008.4080].
- [58] A. Zupanc *et al.* (Belle), JHEP **1309**, 139 (2013), [arXiv:1307.6240].
- [59] M. Ablikim *et al.* (BESIII), Phys. Rev. Lett. **122**, 071802 (2019), [arXiv:1811.10890].
- [60] P. Naik *et al.* (CLEO), Phys. Rev. **D80**, 112004 (2009), [arXiv:0910.3602].
- [61] K. M. Ecklund *et al.* (CLEO), Phys. Rev. Lett. **100**, 161801 (2008), [arXiv:0712.1175].
- [62] P. U. E. Onyisi *et al.* (CLEO), Phys. Rev. **D79**, 052002 (2009), [arXiv:0901.1147].
- [63] M. Ablikim *et al.* (BESIII), Phys. Rev. **D94**, 072004 (2016), [arXiv:1608.06732].
- [64] M. Tanabashi *et al.* (Particle Data Group), Phys. Rev. **D98**, 3, 030001 (2018).
- [65] T. K. Pedlar *et al.* (CLEO), Phys. Rev. **D76**, 072002 (2007), [arXiv:0704.0437].
- [66] J. P. Alexander *et al.* (CLEO), Phys. Rev. Lett. **100**, 161804 (2008), [arXiv:0801.0680].
- [67] B. Aubert *et al.* (BaBar), Phys. Rev. Lett. **98**, 141801 (2007), [hep-ex/0607094].
- [68] P. A. Boyle *et al.* (RBC/UKQCD) (2018), [arXiv:1812.08791].
- [69] P. A. Boyle *et al.*, JHEP **12**, 008 (2017), [arXiv:1701.02644].
- [70] Y.-B. Yang *et al.* (χ QCD), Phys. Rev. **D92**, 034517 (2015), [arXiv:1410.3343].
- [71] H. Na *et al.* (HPQCD), Phys. Rev. **D86**, 054510 (2012), [arXiv:1206.4936].
- [72] A. Bazavov *et al.* (Fermilab Lattice and MILC), Phys. Rev. **D85**, 114506 (2012), [arXiv:1112.3051].
- [73] C. T. H. Davies *et al.* (HPQCD), Phys. Rev. **D82**, 114504 (2010), [arXiv:1008.4018].
- [74] Z.-G. Wang, Eur. Phys. J. **C75**, 427 (2015), [arXiv:1506.01993].
- [75] P. Gelhausen *et al.*, Phys.Rev. **D88**, 014015 (2013), [arXiv:1305.5432].
- [76] S. Narison, Phys. Lett. **B718**, 1321 (2013), [arXiv:1209.2023].
- [77] W. Lucha, D. Melikhov and S. Simula, Phys. Lett. **B701**, 82 (2011), [arXiv:1101.5986].
- [78] C.-W. Hwang, Phys. Rev. **D81**, 054022 (2010), [arXiv:0910.0145].
- [79] C. Amsler *et al.* (Particle Data Group), Phys. Lett. **B667**, 1 (2008), and 2009 partial update for the 2010 edition.
- [80] W. Lucha, D. Melikhov and S. Simula, Eur. Phys. J. **C78**, 2, 168 (2018), [Erratum: Eur. Phys. J.C78,no.11,936(2018)], [arXiv:1702.07537].
- [81] K. Ikado *et al.* (Belle), Phys. Rev. Lett. **97**, 251802 (2006), [hep-ex/0604018].
- [82] I. Adachi *et al.* (Belle), Phys. Rev. Lett. **110**, 131801 (2013), [arXiv:1208.4678].
- [83] B. Kronenbitter *et al.* (Belle), Phys. Rev. **D92**, 051102 (2015), [arXiv:1503.05613].
- [84] J. P. Lees *et al.* (BaBar), Phys. Rev. **D88**, 031102 (2013), [arXiv:1207.0698].
- [85] B. Aubert *et al.* (BaBar), Phys. Rev. **D81**, 051101 (2010), [arXiv:0912.2453].
- [86] C. Hughes, C. T. H. Davies and C. J. Monahan, Phys. Rev. **D97**, 5, 054509 (2018), [arXiv:1711.09981].
- [87] A. Bussone *et al.* (ETM), Phys. Rev. **D93**, 11, 114505 (2016), [arXiv:1603.04306].
- [88] R. Dowdall *et al.* (HPQCD), Phys. Rev. Lett. **110**, 222003 (2013), [arXiv:1302.2644].
- [89] Y. Aoki *et al.*, Phys. Rev. **D91**, 114505 (2015), [arXiv:1406.6192].
- [90] N. H. Christ *et al.* (RBC/UKQCD), Phys. Rev. **D91**, 054502 (2015), [arXiv:1404.4670].
- [91] H. Na *et al.* (HPQCD), Phys. Rev. **D86**, 034506 (2012), [arXiv:1202.4914].
- [92] C. McNeile *et al.* (HPQCD), Phys. Rev. **D85**, 031503 (2012), [arXiv:1110.4510].
- [93] H.-K. Sun and M.-Z. Yang, Phys. Rev. **D95**, 11, 113001 (2017), [arXiv:1609.08958].
- [94] M. J. Baker *et al.*, JHEP **07**, 032 (2014), [arXiv:1310.0941].
- [95] W. Lucha, D. Melikhov and S. Simula, Phys.Rev. **D88**, 056011 (2013), [arXiv:1305.7099].
- [96] J. Hardy and I. S. Towner, PoS **CKM2016**, 028 (2016).
- [97] F. Ambrosino *et al.* (KLOE), Eur. Phys. J. **C71**, 1604 (2011), [arXiv:1011.2668].
- [98] E. Abouzaid *et al.* (KTeV), Phys. Rev. **D83**, 092001 (2011), [arXiv:1011.0127].
- [99] D. Babusci *et al.* (KLOE KLOE-2), Phys. Lett. **B738**, 128 (2014), [arXiv:1407.2028].
- [100] N. Carrasco *et al.*, Phys. Rev. **D93**, 11, 114512 (2016), [arXiv:1602.04113].
- [101] A. Bazavov *et al.* (Fermilab Lattice and MILC), Phys. Rev. Lett. **112**, 112001 (2014), [arXiv:1312.1228].
- [102] C.-Y. Seng *et al.*, Phys. Rev. Lett. **121**, 241804 (2018), [arXiv:1807.10197].
- [103] C. Y. Seng, M. Gorchtein and M. J. Ramsey-Musolf, Phys. Rev. **D100**, 013001 (2019), [arXiv:1812.03352].
- [104] M. Gorchtein, Phys. Rev. Lett. **123**, 042503 (2019), [arXiv:1812.04229].
- [105] C.-Y. Seng and U.-G. Meißner, Phys. Rev. Lett. **122**, 211802 (2019), [arXiv:1903.07969].
- [106] J. C. Hardy and I. S. Towner, Phys. Rev. **C91**, 025501 (2015), [arXiv:1411.5987].
- [107] A. Czarnecki, W. J. Marciano and A. Sirlin (2019), [arXiv:1907.06737].
- [108] Y. Amhis *et al.* (HFLAV), Eur. Phys. J. **C77**, 12, 895 (2017), [arXiv:1612.07233].
- [109] H. Na *et al.* (HPQCD), Phys. Rev. **D82**, 114506 (2010), [arXiv:1008.4562].
- [110] H. Na *et al.* (HPQCD), Phys. Rev. **D84**, 114505 (2011), [arXiv:1109.1501].
- [111] B. Chakraborty *et al.*, EPJ Web Conf. **175**, 13027 (2018), [arXiv:1710.07334].
- [112] R. Li *et al.* (Fermilab Lattice, MILC), PoS **LAT-TICE2018**, 269 (2019), [arXiv:1901.08989].
- [113] L. Wolfenstein, Phys. Rev. Lett. **51**, 1945 (1983).
- [114] J. Charles *et al.* (CKMfitter Group), Eur. Phys. J. **C41**, 1 (2005), updated results and plots available at: <http://ckmfitter.in2p3.fr>, [hep-ph/0406184].
- [115] M. Antonelli *et al.*, Phys. Rept. **494**, 197 (2010), [arXiv:0907.5386].
- [116] J. N. Butler *et al.* (Quark Flavor Physics Working Group), in “Community Summer Study 2013: Snowmass on the Mississippi (CSS2013) Minneapolis, MN, USA, July 29-August 6, 2013,” (2013), [arXiv:1311.1076], URL <http://www.slac.stanford.edu/econf/C1307292/docs/IntensityFrontier/QuarkF1-15.pdf>.
- [117] Y. Amhis *et al.* (Heavy Flavor Averaging Group) (2014), [arXiv:1412.7515].
- [118] A. J. Bevan *et al.* (Belle, BaBar), Eur. Phys. J. **C74**, 3026 (2014), [arXiv:1406.6311].

- [119] E. Dalgic *et al.*, Phys. Rev. **D73**, 074502 (2006), [Erratum: Phys. Rev.D75,119906(2007)], [hep-lat/0601021].
- [120] J. M. Flynn *et al.* (RBC/UKQCD), Phys. Rev. **D91**, 074510 (2015), [arXiv:1501.05373].
- [121] J. A. Bailey *et al.* (Fermilab Lattice, MILC), Phys. Rev. **D92**, 014024 (2015), [arXiv:1503.07839].
- [122] P. del Amo Sanchez *et al.* (BaBar), Phys. Rev. **D83**, 032007 (2011), [arXiv:1005.3288].
- [123] J. P. Lees *et al.* (BaBar), Phys. Rev. **D86**, 092004 (2012), [arXiv:1208.1253].
- [124] H. Ha *et al.* (Belle), Phys. Rev. **D83**, 071101 (2011), [arXiv:1012.0090].
- [125] A. Sibidanov *et al.* (Belle), Phys.Rev. **D88**, 032005 (2013), [arXiv:1306.2781].
- [126] S. W. Bosch *et al.*, Phys. Rev. Lett. **93**, 221801 (2004), [hep-ph/0403223].
- [127] J. R. Andersen and E. Gardi, JHEP **01**, 097 (2006), [hep-ph/0509360].
- [128] P. Gambino *et al.*, JHEP **10**, 058 (2007), [arXiv:0707.2493].
- [129] R. Kowalewski and T. Mannel, “Semileptonic b -Hadron Decays, Determination of V_{cb} , V_{ub} ,” <http://pdg.lbl.gov/2019/reviews/rpp2018-rev-vcb-vub.pdf> (2017), review prepared for PDG 2018 update.

72. Production and Decay of b -flavored Hadrons

Revised April 2020 by P. Eerola (Helsinki U.), M. Kreps (Warwick U.) and Y. Kwon (Yonsei U., Seoul).

The b quark belongs to the third generation of quarks and is the weak-doublet partner of the t quark. The existence of the third-generation quark doublet was proposed in 1973 by Kobayashi and Maskawa [1] in their model of the quark mixing matrix (“CKM” matrix), and confirmed four years later by the first observation of a $b\bar{b}$ meson [2]. In the KM model, CP violation is explained within the Standard Model (SM) by an irreducible phase of the 3×3 unitary matrix. The regular pattern of the three lepton and quark families is one of the most intriguing puzzles in particle physics. The existence of families gives rise to many of the free parameters in the SM, including the fermion masses, and the elements of the CKM matrix.

Since the b quark is the lighter element of the third-generation quark doublet, the decays of b -flavored hadrons occur via generation-changing processes through CKM matrix. Because of this, and the fact that the CKM matrix is close to a 3×3 unit matrix, many interesting features such as loop and box diagrams, flavor oscillations, as well as large CP asymmetries, can be observed in the weak decays of b -flavored hadrons.

The CKM matrix is parameterized by three real parameters and one complex phase. This complex phase can become a source of CP violation in B meson decays. A crucial milestone was the first observation of CP violation in the B meson system in 2001, by the BaBar [3] and Belle [4] collaborations. They measured a large value for the parameter $\sin 2\beta$ ($= \sin 2\phi_1$) [5], almost four decades after the discovery of a small CP asymmetry in neutral kaons. A more detailed discussion of the CKM matrix and CP violation can be found elsewhere in this Review [6, 7].

The structure of this mini-review is organized as follows. After a discussion of b -quark production and current results on spectroscopy, we discuss lifetimes of b -flavored hadrons. We then discuss some basic properties of B -meson decays, followed by summaries of hadronic, rare, and electroweak penguin decays of B -mesons. There are separate mini-reviews for B^0 - \bar{B}^0 mixing [8] and the extraction of the CKM matrix elements V_{cb} and V_{ub} from B -meson decays [9] in this Review.

72.1 Production and spectroscopy

The bound states of a \bar{b} antiquark and a u , d , s , or c quark are referred to as the B_u (B^+), B_d (B^0), B_s (B_s^0), and B_c (B_c^+) mesons, respectively. The B_c^+ is the heaviest of the ground-state b -flavored mesons, and the most difficult to produce: it was observed for the first time in the semileptonic mode by CDF in 1998 [10], but its mass was accurately determined only in 2006, from the fully reconstructed mode $B_c^+ \rightarrow J/\psi\pi^+$ [11]. Many exclusive decay channels can now be used for the accurate mass measurements, given the large statistics available at the LHC. Currently the most precise measurement is made by LHCb using the $B_c^+ \rightarrow J/\psi D^0 K^+$ decay, yielding $m(B_c^+) = 6274.28 \pm 1.40 \pm 0.32$ MeV/ c^2 [12].

The first excited meson is called the B^* meson, while B^{**} is the generic name for the four orbitally excited ($L = 1$) B -meson states that correspond to the P -wave mesons in the charm system, D^{**} . Excited states of the B_s^0 meson are similarly named B_s^* and B_s^{**} . Of the possible bound $b\bar{b}$ states, the $\Upsilon(nS)$ and $\chi_{b,J}(nP)$ states are well studied.

The pseudoscalar ground state η_b has been observed for the first time by BaBar [13] indirectly through the decay $\Upsilon(3S) \rightarrow \gamma\eta_b$, and then confirmed by Babar in $\Upsilon(2S)$ decays [14] and CLEO in $\Upsilon(3S)$ decays [15]. The most accurate mass and width measurements come now from Belle, using decays $\Upsilon(5S) \rightarrow h_b(1P)\pi^+\pi^-$, $h_b(1P) \rightarrow \gamma\eta_b(1S)$ [16] and $\Upsilon(4S) \rightarrow \eta h_b(1P)$, $h_b(1P) \rightarrow \gamma\eta_b(1S)$ [17]. Belle has also reported first evidence for the $\eta_b(2S)$ in the $h_b(2P) \rightarrow \eta_b(2S)\gamma$ transition [16]. See Ref. [18] for classification and naming of these and other states.

Experimental studies of b decays have been performed in e^+e^- collisions at the $\Upsilon(4S)$ (ARGUS, CLEO, Belle, BaBar) and $\Upsilon(5S)$ (CLEO, Belle) resonances. The full data samples of BaBar and Belle are 560 fb^{-1} and 1020 fb^{-1} , respectively, of which 433 fb^{-1} and 710 fb^{-1} are at the $\Upsilon(4S)$ resonance. The Belle II experiment at SuperKEKB has started recording data in 2019, and the

experiment has so far collected about 12.4 fb^{-1} of data (March 2020). The $e^+e^- \rightarrow b\bar{b}$ production cross-section at the $\Upsilon(4S)$ ($\Upsilon(5S)$) resonance is about 1.1 nb (0.3 nb). At the Z resonance (SLC, LEP) all species of b -flavored hadrons could be studied for the first time. The $e^+e^- \rightarrow b\bar{b}$ production cross-section at the Z resonance is about 6.6 nb .

High-energy $p\bar{p}$ (Tevatron) and pp collisions (LHC) produce b -flavored hadrons of all species with large cross-sections. At the Tevatron ($\sqrt{s} = 1.96 \text{ TeV}$) the visible cross section $\sigma(p\bar{p} \rightarrow bX, |\eta| < 1)$ is about $30 \mu\text{b}$. CDF and D0 experiments at the Tevatron have accumulated by the end of their running about 10 fb^{-1} each.

At the LHC pp collider at $\sqrt{s} = 7 - 13 \text{ TeV}$, the visible b -hadron cross section at the LHCb experiment with pseudorapidity acceptance $2 < \eta < 5$ has been measured to be $\sim 72 \mu\text{b}$ at 7 TeV and $\sim 144 \mu\text{b}$ at 13 TeV [19] (cross section at 13 TeV corrected in Erratum). LHCb has collected about 1 fb^{-1} at 7 TeV , 2 fb^{-1} at 8 TeV , and close to 5.9 fb^{-1} at 13 TeV during LHC Runs 1 and 2. CMS and ATLAS have collected each about 5 fb^{-1} of data at $\sqrt{s} = 7$, 20 fb^{-1} at 8 TeV and about 150 fb^{-1} at 13 TeV during LHC Runs 1 and 2. The LHCb experiment is undergoing currently major upgrade. The LHC operation is planned to resume in 2021.

In hadron collisions, production happens as $b\bar{b}$ pairs via leading order flavor creation or higher order processes such as gluon-splitting. Single b -quarks can be produced by flavor excitation. The total b -production cross section is an interesting test of our understanding of leading and higher order QCD processes. With a wealth of measurements at LHC and at Tevatron (see Ref. [19] and references therein), and improved calculations [20], there is a reasonable agreement between measurements and predictions.

Each quark of a $b\bar{b}$ pair produced in hadron collisions hadronizes separately and incoherently from the other, but it is still possible to obtain a statistical indication of the charge of a produced b/\bar{b} quark (“flavor tag” or “charge tag”) from the accompanying particles produced in the hadronization process, or from the decay products of the other quark. The momentum spectrum of produced b -quarks typically peaks near the b -quark mass, and extends to much higher momenta, dropping by about a decade for every ten GeV. Typical decay lengths are of the order of a centimeter at 13 TeV pp collisions; the resolution for the decay vertex must be more precise than this to resolve the fast oscillations of B_s^0 mesons.

In e^+e^- colliders, since the B mesons are very slow in the $\Upsilon(4S)$ rest frame, asymmetric beam energies are used to boost the decay products to allow time-dependent measurements that are crucial for the study of CP violation. At KEKB, the boost was $\beta\gamma = 0.43$, while PEP-II used a slightly larger boost, $\beta\gamma = 0.55$. The typical B -meson decay length is dilated from $\approx 20 \mu\text{m}$ to $\approx 200 \mu\text{m}$. At SuperKEKB the boost is lower, $\beta\gamma = 0.28$, which puts more demanding requirements on the track reconstruction precision at Belle II to reach a resolution in decay time measurements similar to Belle. The two B mesons produced in $\Upsilon(4S)$ decay are in a coherent quantum state, which makes it easier than in hadron collisions to infer the charge state of one B meson from observation of the other; however, the coherence also requires determination of the decay time of both mesons, rather than just one, in order to perform time-dependent CP -violation measurements. For B_s^0 , which can be produced at $\Upsilon(5S)$ the situation is less favourable, as boost is not high enough to provide sufficient time resolution to resolve the fast B_s^0 oscillations.

For the measurement of branching fractions, the initial composition of the data sample must be known. The $\Upsilon(4S)$ resonance decays predominantly to $B^0\bar{B}^0$ and B^+B^- ; the current experimental upper limit for non- $B\bar{B}$ decays of the $\Upsilon(4S)$ is less than 4% at the 95% confidence level (CL) [21]. The observed modes of this category are decays to lower Υ states and a pion pair, η , or η' , measured branching fractions being of order $10^{-4} - 10^{-5}$ [22], and decays to $h_b(1P)\eta$ with branching fraction of order 10^{-3} [17].

The ratio f_+/f_0 of the fractions of charged to neutral B productions from $\Upsilon(4S)$ decays has been measured by CLEO, BaBar, and Belle in various ways. They typically use pairs of isospin-related decays of B^+ and B^0 , such that it can be assumed that

$\Gamma(B^+ \rightarrow x^+) = \Gamma(B^0 \rightarrow x^0)$. In this way, the ratio of the number of events observed in these modes is proportional to $(f_+ \tau_+)/ (f_0 \tau_0)$ [23, 24]. BaBar has also performed an independent measurement of f_0 with a different method that does not require isospin symmetry or the value of the lifetime ratio, based on the number of events with one or two reconstructed $B^0 \rightarrow D^{*-} \ell^+ \nu$ decays [25]. The combined result, from the current average of τ_+/τ_0 , is $f_+/f_0 = 1.058 \pm 0.024$ [26]. The result is consistent within 2.4σ with equal production of B^+B^- and $B^0\bar{B}^0$ pairs, and we assume $f_+/f_0 = 1$ in this mini-review except where explicitly stated otherwise. This assumption is also supported by the near equality of the B^+ and B^0 masses: our fit yields $m(B^0) = 5279.65 \pm 0.12$ MeV/ c^2 , $m(B^+) = 5279.34 \pm 0.12$ MeV/ c^2 , and $m(B^0) - m(B^+) = 0.31 \pm 0.05$ MeV/ c^2 .

Data collected at the $\Upsilon(5S)$ resonance gave CLEO, Belle and BaBar access to B_s^0 decays. In $\Upsilon(5S)$ decays there are seven possible final states including a pair of non-strange B mesons and 0, 1 or 2 pions, and three with a pair of strange B mesons ($B_s^* \bar{B}_s^{*0}$, $B_s^* \bar{B}_s^0$, and $B_s^0 \bar{B}_s^0$). The fraction of events with a pair of B_s^0 mesons over the total number of events with a pair of b -flavored hadrons has been measured to be $f_s[\Upsilon(5S)] = 0.199^{+0.030}_{-0.029}$ [27], of which 88% is $B_s^* \bar{B}_s^0$ events. However, the small boost of B_s^0 mesons produced in this way prevents resolution of their fast oscillations for time-dependent measurements; these are only accessible in hadron collisions (or at the Z peak).

In high-energy collisions, the produced b or \bar{b} quarks can hadronize with different probabilities into the full spectrum of b -hadrons, either in their ground or excited states. The hadronization does not have to be identical in $p\bar{p}$ or pp collisions and in Z decay, because of the different momentum distributions of the b -quark in these processes; the sample used in the $p\bar{p}$ measurements has momenta close to the b mass, rather than $m_Z/2$. The available data from Tevatron and LHC show that the production fractions f_d , f_u , f_s , and f_{baryon} of B^0 , B^+ , B_s^0 , and b baryons, respectively, of weakly decaying b hadrons depend on the kinematics of the produced b hadron. The production fractions of b hadrons are discussed in more detail in the $B^0 - \bar{B}^0$ mixing section in this Review [8].

Excited B -meson states have been thoroughly studied by CLEO, LEP, CUSB, D0 and CDF (an admixture of B mesons) and LHCb (B^{*+} -meson). The current world average of the $B^* - B$ mass difference is 45.21 ± 0.21 MeV/ c^2 . Excited B_s^* -meson states have been observed in $\Upsilon(5S)$ decays by CUSB, CLEO and Belle.

For orbitally excited B meson states, with relative angular momentum $L=1$ of the two quarks, there exist four states $(J, j_q) = (0, 1/2), (1, 1/2), (1, 3/2), (2, 3/2)$, where j_q is the total angular momentum of the light u , d or s quark and J is the total angular momentum of the B meson. These states are collectively called as $B_{(s)}^{**}$ mesons. The $j_q = 1/2$ states are named $B_{(s)0}^*$ ($J = 0$) and $B_{(s)1}$ ($J = 1$) mesons, while the states with $j_q = 3/2$ are named $B_{(s)1}$ ($J = 1$) and $B_{(s)2}^*$ ($J = 2$) mesons. The states with $j_q = 1/2$ can decay through an S -wave transition and are expected to have a large width, but the $j_q = 3/2$ states are narrow D -wave decays. Evidence for B^{**} production has been initially obtained at LEP as a broad $B\pi$ resonance [28] or a B^+K^- enhancement [29]. Detailed results have been obtained for the narrow states $B_1(5721)^{0,+}$ and $B_2(5747)^{0,+}$ at the Tevatron and by LHCb, and clear enhancements compatible with the higher mass states $B_J(5840)^{0,+}$ and $B_J(5970)^{0,+}$ have been observed [30, 31]. Also the narrow B_s^{**} states $B_{s1}(5830)^0$ and $B_{s2}(5840)^0$ have been measured at the CDF [30], LHCb [32], and CMS [33].

Excited states of B_c^+ mesons will provide important information about the strong potential. A $B_c^+ \pi^+ \pi^-$ resonance has been observed for the first time by ATLAS [34]. The mass of the resonance has been measured precisely by CMS and LHCb as 6871.6 ± 1.1 MeV/ c^2 [35, 36]. The resonance may be interpreted as the second S -wave state of the B_c^+ meson, $B_c^+(2S)$, but the quantum numbers are to be confirmed.

Baryon states containing a b quark are labeled according to the same scheme used for non- b baryons, with the addition of a b subscript [18]. The first observed b baryon was the Λ_b^0 (quark composition udb). Thanks to the large samples accumulated at

the Tevatron and specially at the LHC many new b baryons have been found. The masses of all these new baryons have been measured to a precision of a few MeV/ c^2 , and found to be in agreement with predictions from Heavy Quark Effective Theory (HQET).

Clear signals of four strongly-decaying baryon states, Σ_b^+ , Σ_b^{*+} (uub), Σ_b^- , Σ_b^{*-} (ddb) have been obtained by CDF [37] and LHCb [38]. LHCb has also observed two new mass peaks in the $\Lambda_b^0 \pi^\pm$ systems, consistent with single resonances and named as $\Sigma_b^\pm(6097)$ [38]. The nature of these resonances is, however, not yet clear. The isodoublet of strange b baryons Ξ_b^0 (usb) and Ξ_b^\pm (dsb) has been observed by CDF and D0 [39]. Masses, lifetimes, and branching ratios have been accurately measured by LHCb [40] and CDF [41]. LHCb has also measured several parameters sensitive to P and CP violation [42]. Other observed Ξ_b baryons are spin-3/2 states $\Xi_b(5945)^0$ (Ξ_b^{*0}) [43, 44] and $\Xi_b(5955)^{*-}$ [45], a spin-1/2 state $\Xi_b'(5935)^-$ [45], and a resonance state $\Xi_b^-(6227)$ [46]. The doubly-strange bottom baryon Ω_b^- has been observed first by D0 and CDF [47]. Mass and mean life have been measured precisely by LHCb [48] and CDF [41].

The so-called exotic states have raised a lot of interest recently. While many exotic states were seen in the charm sector, in bottom sector there are fewer seen. The D0 Collaboration claimed a narrow state $X(5568)$ decaying into a $B_s^0 \pi^\pm$ final state [49]. While this would be an interesting addition to the observed states as the first exotic state with constituent quarks with four different flavours (b , s , u , d), analysis by LHCb yields negative result [50]. Also CMS finds no such a state [51].

72.2 Lifetimes

Precise lifetimes are key in extracting the weak parameters that are important for understanding the role of the CKM matrix in CP violation, such as the determination of V_{cb} and $B_s^0 \bar{B}_s^0$ mixing parameters. In the naive spectator model, the heavy quark can decay only via the external spectator mechanism, and thus, the lifetimes of all mesons and baryons containing b quarks would be equal. Non-spectator effects, such as the interference between contributing amplitudes, modify this simple picture and give rise to a lifetime hierarchy for b -flavored hadrons similar to the one in the charm sector. However, since the lifetime differences are expected to scale as $1/m_Q^2$, where m_Q is the mass of the heavy quark, the variations in the b system are expected to be only 10% or less [52, 53]. We expect:

$$\tau(B^+) \geq \tau(B^0) \approx \tau(B_s^0) > \tau(\Lambda_b^0) \gg \tau(B_c^+) . \quad (72.1)$$

For the B_c^+ , both quarks decay weakly, so the lifetime is much shorter.

Measurements of the lifetimes of the different b -flavored hadrons thus provide a means to determine the importance of non-spectator mechanisms in the b sector. Availability of large samples of fully-reconstructed decays of different b -hadron species has resulted in precise measurements with small statistical and systematic uncertainties ($\sim 1\%$). The world averages given in Table 72.1 have been determined by the Heavy Flavor Averaging Group (HFLAV) [27].

Table 72.1: Summary of i world-average b -hadron lifetime measurements. For the B_s^0 lifetimes, see text below.

Particle	Lifetime [ps]
B^+	1.638 ± 0.004
B^0	1.519 ± 0.004
B_s^0	1.515 ± 0.004
B_s^0	1.423 ± 0.005
B_s^{0L}	1.620 ± 0.007
B_c^+	0.510 ± 0.009
Λ_b^0	1.471 ± 0.009
Ξ_b^-	1.572 ± 0.040
Ξ_b^0	1.480 ± 0.030
Ω_b^-	$1.64^{+0.18}_{-0.17}$

The B_s^0 lifetime in Table 72.1 is defined as $1/\Gamma_s$, where Γ_s is the average width of the light (L) and heavy (H) mass eigenstates, $(\Gamma_L + \Gamma_H)/2$. In the absence of CP violation, the light (heavy) B_s^0 mass eigenstate is the CP -even (CP -odd) eigenstate. Thus, the lifetime of the light (heavy) mass eigenstate can be measured from CP -even (odd) final states. The lifetimes can also be obtained from time-dependent angular analysis of $B_s^0 \rightarrow J/\psi\phi$ decays.

The short B_c^+ lifetime is in good agreement with predictions [54]. With large samples of B_c^+ mesons at the LHC precision on the lifetimes can still improve. The measurement using semileptonic decays gives $\tau_{B_c^+} = 0.509 \pm 0.008 \pm 0.012$ ps [55] while using decays $B_c^+ \rightarrow J/\psi\pi^+$ yields $\tau_{B_c^+} = 0.5134 \pm 0.0110 \pm 0.0057$ ps [56]. Each of these is more precise than the combination of all previous experiments.

The recent A_b^0 lifetime measurements from LHC experiments and CDF are precise and favour lifetime close to the lifetime of B^0 meson, in agreement with theory.

For precision comparisons with theory, lifetime ratios are more sensitive. Experimentally it is found [27]:

$$\frac{\tau_{B^+}}{\tau_{B^0}} = 1.076 \pm 0.004, \quad \frac{\tau_{B_s^0}}{\tau_{B^0}} = 0.998 \pm 0.004,$$

$$\frac{\tau_{A_b^0}}{\tau_{B^0}} = 0.969 \pm 0.006,$$

while recent Heavy Quark Expansion (HQE) predictions give [53]:

$$\frac{\tau_{B^+}}{\tau_{B^0}} = 1.04_{-0.01}^{+0.05} \pm 0.02 \pm 0.01, \quad \frac{\tau_{B_s^0}}{\tau_{B^0}} = 1.001 \pm 0.002,$$

$$\frac{\tau_{A_b^0}}{\tau_{B^0}} = 0.935 \pm 0.054.$$

The ratio of B^+ to B^0 lifetimes has a precision of better than 1%, and is significantly different from 1.0, in agreement with predictions [52]. The ratio of B_s^0 to B^0 lifetimes is expected to be very close to 1.0.

For a detailed discussion on neutral B^0 and B_s^0 oscillation and relevant CP violation measurements see Ref. [8].

72.3 Features of decays

The ground states of *b*-flavored hadrons decay via weak interactions. In most decays of the *b*-flavored hadrons, where the *b*-quark is accompanied by lighter partner quarks (*d*, *u*, *s*, or *c*), the decay modes are well described by the decay of the *b* quark (spectator model) [57]. The dominant decay mode of a *b* quark is $b \rightarrow cW^{*-}$ (referred to as a “tree” or “spectator” decay), where the virtual *W* materializes either into a pair of leptons $l\bar{\nu}$ (“semileptonic decay”), or into a pair of quarks which then hadronizes. The transition $b \rightarrow u$ is suppressed by $|V_{ub}/V_{cb}|^2 \sim (0.1)^2$ relative to $b \rightarrow c$ transitions. The decays in which the spectator quark combines with one of the quarks from W^* to form one of the final state hadrons are suppressed by a factor $\sim (1/3)^2$, because the colors of the two quarks from different sources must match (“color-suppression”).

Semileptonic *B* decays $B \rightarrow X_c l \nu$ and $B \rightarrow X_u l \nu$ provide an excellent way to measure the magnitude of the CKM elements $|V_{cb}|$ and $|V_{ub}|$ respectively, because the strong interaction effects are much simplified due to the two leptons in the final state. Both exclusive and inclusive decays can be used with dominant uncertainties being complementary. For exclusive decay analysis, knowledge of the form factors for the exclusive hadronic system $X_{c(u)}$ is required. For inclusive analysis, it is usually necessary to restrict the available phase-space of the decay products to suppress backgrounds; subsequently uncertainties are introduced in the extrapolation to the full phase-space. Moreover, restriction to a small corner of the phase-space may result in breakdown of the operator-product expansion scheme, thus making theoretical calculations unreliable. One of the recent unexpected results was determination of $|V_{ub}|$ using $A_b^0 \rightarrow p\mu^-\bar{\nu}_\mu$ decays by LHCb [58]. Besides, there have been measurements of inclusive semileptonic decays rates of B_s^0 [59] and B_c^+ [60] mesons. A more detailed discussion of *B* semileptonic decays and the extraction of $|V_{cb}|$ and $|V_{ub}|$ is given elsewhere in this *Review* [9].

On the other hand, hadronic *B* decays are complicated because of strong interaction effects caused by the surrounding cloud of light quarks and gluons. While this complicates the extraction of CKM matrix elements, it also provides a great opportunity to study perturbative and non-perturbative QCD, hadronization, and Final State Interaction (FSI) effects.

Many aspects of *B* decays can be understood through the Heavy Quark Effective Theory (HQET) [61]. This has been particularly successful for semileptonic decays. For further discussion of HQET, see for instance Ref. [62]. For hadronic decays, one typically uses effective Hamiltonian calculations that rely on a perturbative expansion with Wilson coefficients. In addition, some form of the factorization hypothesis is commonly used, where, in analogy with semileptonic decays, two-body hadronic decays of *B* mesons are expressed as the product of two independent hadronic currents, one describing the formation of a charm meson (in case of the dominant $b \rightarrow cW^{*-}$ decays), and the other the hadronization of the remaining $\bar{u}d$ (or $\bar{c}s$) system from the virtual W^- . Qualitatively, for *B* decays with a large energy release, e.g. $b \rightarrow uW^{*-}$ transitions, the $\bar{u}d$ pair (produced as a color singlet) travels fast enough to leave the interaction region without influencing the charm meson. This is known to work well for the dominant spectator decays [63]. There are several common implementations of these ideas for hadronic *B* decays, the most common of which are QCD factorization (QCDF) [64–67], perturbative QCD (pQCD) [68–72], and soft collinear effective theory (SCET) [73–75].

The transitions $b \rightarrow s$ and $b \rightarrow d$ are flavor-changing neutral-current (FCNC) processes. Although they are not allowed in the SM as a tree-process, they can occur via more complicated loop diagrams (denoted “penguin” decays). The rates for $b \rightarrow s$ penguin decays are comparable to the CKM-suppressed $b \rightarrow u$ tree processes. Pure-penguin decays were first established by the observation of $B \rightarrow K^*(892)\gamma$ [76]. Penguin processes involving $b \rightarrow d$ transitions are further suppressed by CKM, and have been observed for $B \rightarrow (\rho/\omega)\gamma$ decays [77, 78]. LHCb has observed a $b \rightarrow d$ penguin transition in the $B^+ \rightarrow \pi^+\mu^+\mu^-$ mode and measured its branching fraction to be $(1.83 \pm 0.24 \pm 0.05) \times 10^{-8}$ [79].

Other decay processes discussed in this *Review* include *W*-exchange (a *W* is exchanged between initial-state quarks), penguin annihilation (the gluon from a penguin loop attaches to the spectator quark, similar to an exchange diagram), and pure-annihilation (the initial quarks annihilate to a virtual *W*, which then decays). Some observed decay modes such as $B^0 \rightarrow D_s^- K^+$, may be interpreted as evidence of a *W*-exchange process [80]. The evidence for the purely leptonic decay $B^+ \rightarrow \tau^+\nu$ from Belle [81] and BaBar [82] is the first sign of a pure annihilation decay. The average branching fraction is $(1.09 \pm 0.24) \times 10^{-4}$, which is somewhat larger than, though consistent with, the value expected in the SM. A substantial region of parameter space of charged Higgs mass vs. $\tan\beta$ is excluded by the measurements of this mode. A dedicated discussion of purely leptonic decays of charged pseudoscalar mesons is given elsewhere in this *Review* [83].

72.4 Dominant hadronic decays

Most of the hadronic *B* decays involve $b \rightarrow c$ transition at the quark level, resulting in a charmed hadron or charmonium in the final state. Other types of hadronic decays are very rare and will be discussed separately in the next section. The experimental results on hadronic *B* decays have steadily improved over the years, and the measurements have reached sufficient precision to challenge our understanding of the dynamics of these decays. With good particle detection and hadron identification capabilities of *B*-factory detectors, a substantial fraction (roughly on the order of a few per mill) of hadronic *B* decay events can be fully reconstructed. In particular, good performances for detecting π^0 and other neutral particles helped Belle and BaBar to make comprehensive measurements of the decays $\bar{B}^0 \rightarrow D^{(*)0}h^0$ [84], where h^0 stands for light neutral mesons such as $\pi^0, \eta^{(\prime)}, \rho^0, \omega$. The measurements are being complemented by LHCb, in decays like $B^0 \rightarrow D^0\pi^+\pi^-$ [85], where no neutral particles reconstruction is needed. These decays proceed through color-suppressed diagrams, hence they provide useful tests on the factorization models.

Because of the kinematic constraint of $\Upsilon(4S) \rightarrow B\bar{B}$, the energy sum of the final-state particles of a B meson decay is always equal to one half of the total energy in the center of mass frame. As a result, the two variables, ΔE (energy difference) and M_B (B candidate mass with a beam-energy constraint) are very effective for reducing combinatorial background both from $\Upsilon(4S)$ and $e^+e^- \rightarrow q\bar{q}$ continuum events. In particular, the energy-constraint in M_B improves the signal resolution by almost an order of magnitude.

The kinematically clean environment of B meson decays provides an excellent opportunity to search for new states. For instance, quark-level $b \rightarrow c\bar{c}s$ decays have been used to search for new charmonium and charm-strange mesons and study their properties in detail. While narrow charm-strange states $D_{s0}^*(2317)$ [86] and $D_{s1}(2460)$ [87] were discovered by BaBar and CLEO, respectively, the properties of these new states were revealed by studying the B meson decays, $B \rightarrow DD_{s0}^*(2317)$ and $B \rightarrow DD_{s1}(2460)$ by Belle [88] and BaBar [89]. Another example is Dalitz plot analysis of decay $B_s^0 \rightarrow \bar{D}^0 K^- \pi^+$ in which the decay to spin-3 resonance was observed for the first time [90].

Information on B_s^0 , B_c^+ and Λ_b^0 decays have been remarkably improved with recent studies of large samples from LHCb. Noticeable additions in B_s include decay modes to $D_s^{(*)+} D_s^{(*)-}$, $\bar{D}^0 \bar{K}^0$, and $J/\psi \bar{K}^*(892)^0$. The $B_s^0 \rightarrow D_s^{(*)+} D_s^{(*)-}$ decays were first observed by CDF [91], followed by Belle [92]. LHCb has improved the precision with $\mathcal{B}(B_s^0 \rightarrow D_s^{(*)+} D_s^{(*)-}) = (3.07 \pm 0.22 \pm 0.33)\%$ [93], which suggests that $B_s^0 \rightarrow D_s^{(*)+} D_s^{(*)-}$ decays do not saturate the CP -even modes of the B_s decays. The $B_s^0 \rightarrow \bar{D}^0 \bar{K}^0$ decay occurs mostly via a color-suppressed tree diagram, and has a small theoretical uncertainty in the SM, thus this mode can significantly improve the determination of the CP -violation angle ϕ_s . LHCb has observed this decay and the branching fraction is $(4.3 \pm 0.5 \pm 0.7) \times 10^{-4}$ [94]. The $B_s^0 \rightarrow J/\psi \bar{K}^*(892)^0$ decay can be used to constrain the penguin pollution in determining ϕ_s . LHCb has updated the branching fraction and measured the CP asymmetries of this decay, thereby constraining the penguin pollution in ϕ_s [95], although a much more stringent constraint on penguin pollution can come from $B^0 \rightarrow J/\psi \rho^0$ which has been observed by BaBar [96] and LHCb [97]. The $B_c^+ \rightarrow B_s^0 \pi^+$ decay is unique as the only observed mode of b -flavored hadron decays where the partner quark decays (c in this case) while the b quark remains a spectator. LHCb has observed this mode and measured $[\sigma(B_c^+)/\sigma(B_s^0)] \times \mathcal{B}(B_c^+ \rightarrow B_s^0 \pi^+) = (2.37 \pm 0.31 \pm 0.11_{-0.13}^{+0.17}) \times 10^{-3}$ [98]. In addition, LHCb [99] and ATLAS [100] have measured $B_c^+ \rightarrow J/\psi D_s^{(*)+}$, which, by comparing with $B_c^+ \rightarrow B_s^0 \pi^+$, provides a ratio of exclusive $b \rightarrow c$ and $c \rightarrow s$ decays of B_c^+ . For $\Lambda_b^0 \rightarrow \Lambda_c^+ \pi^+ \pi^- \pi^-$ [101], not only the total rate is measured, but also structure involving decays through excited Λ_c and Σ_c baryons.

In addition, a variety of exotic particles that do not fit the conventional meson spectroscopy have been discovered in B decays. Belle found the $X(3872)$ state by studying $B^+ \rightarrow J/\psi \pi^+ \pi^- K^+$ [102], which was confirmed by CDF [103], D0 [104] and BaBar [105]. Production of $X(3872)$ has been studied by the LHC experiments, LHCb [106], CMS [107] and ATLAS [108].

A charged charmonium-like state $X(4430)^\pm$ that decays to $\psi(2S)\pi^\pm$ was observed by Belle in $B \rightarrow \psi(2S)K\pi^\pm$ [109]. Since it is charged, it could not be an ordinary charmonium state. A high-statistics study by LHCb confirmed the existence of the $X(4430)^\pm$ in decays $B \rightarrow \psi(2S)K\pi^\pm$ [110], demonstrated its resonance character by studying the phase motion, unambiguously determined its spin-parity, and saw evidence for another state. In a Dalitz plot analysis of $\bar{B}^0 \rightarrow J/\psi K^- \pi^+$ [111], Belle has found another state, labelled as $X(4200)^+$ in this Review, adding to the list of exotic charged charmonium-like states. In an amplitude analysis of the decay $\Lambda_b^0 \rightarrow J/\psi p K^-$, LHCb observed exotic structures, labelled as $P_c(4380)^+$ and $P_c(4450)^+$ in this Review, in the $J/\psi p$ channel [112]. The subsequent analysis with significantly increased statistics observed additional state and resolved the peak at 4450 MeV/ c^2 as being due to the two states close in the mass [113]. They are referred to as charmonium-pentaquark states. More detailed discussions of exotic meson-like states and pentaquarks are

given elsewhere in this Review [114].

72.5 Rare hadronic decays

All B -meson decays that do not occur through the $b \rightarrow c$ transition are usually called rare B decays. These include both semileptonic and hadronic $b \rightarrow u$ decays that are suppressed at leading order by the small CKM matrix element V_{ub} , as well as higher-order $b \rightarrow s(d)$ processes such as electroweak and gluonic penguin decays. In this section, we review hadronic rare B decays, while electroweak penguin decays and others are discussed in the next.

Charmless B meson decays into two-body hadronic final states such as $B \rightarrow \pi\pi$ and $K\pi$ are experimentally clean, and provide good opportunities to probe new physics and search for indirect and direct CP violations. Since the final state particles in these decays tend to have larger momenta than average B decay products, the event environment is cleaner than for $b \rightarrow c$ decays. Branching fractions are typically around 10^{-5} . Over the past decade, many such modes have been observed not only by e^+e^- collider experiments such as BaBar and Belle, but also by hadron collider experiments such as CDF ($p\bar{p}$) and LHCb (pp). In the latter cases, huge data samples of the modes with all charged final-state particles have been reconstructed by triggering on the impact parameter of the charged tracks. This has also allowed observation of charmless decays of the B_s , in final states such as $\phi\phi$ [115, 116], K^+K^- [117, 118], and $K^- \pi^+$ [118, 119], and of charmless decays of the Λ_b^0 baryon [119]. The large samples available at LHCb experiment allow to perform also time-dependent CP violation measurements [120, 121]. Charmless B_s modes are related to corresponding B^0 modes by U -spin symmetry, and are determined by similar amplitudes. Combining the observables from B_s^0 and B^0 modes is a further way of eliminating hadronic uncertainties and extracting relevant CKM information [122].

Because of relatively high-momenta for final state particles, the dominant source of background in e^+e^- collisions is $q\bar{q}$ continuum events; sophisticated background suppression techniques exploiting event shape variables are essential for these analyses. In hadron collisions, the dominant background comes from QCD or partially reconstructed heavy flavors, and is similarly suppressed by a combination of kinematic and isolation requirements. The results are in general consistent among the experiments.

Most rare decay modes including $B^0 \rightarrow K^+ \pi^-$ have contributions from both $b \rightarrow u$ tree and $b \rightarrow sg$ penguin processes. If the size of the two contributions are comparable, the interference between them may result in direct CP violation, seen experimentally as a charge asymmetry in the decay rate measurement. BaBar [123], Belle [124], CDF [117], and LHCb [120] have measured the direct CP violating asymmetry in $B^0 \rightarrow K^+ \pi^-$ decays. Direct CP violation has been observed in this decay with a significance of more than 5σ . The world average value of the asymmetry is now rather precise, $A_{CP}(K^+ \pi^-) = -0.083 \pm 0.004$. The CP asymmetry in $B^+ \rightarrow K^+ \pi^0$ mode has been measured by BaBar [125] and Belle [124] with the average value $A_{CP}(K^+ \pi^0) = 0.037 \pm 0.021$. These two asymmetries differ by more than 5σ significance, in contrast to a naive expectation based on simplified picture in the SM. For more detailed tests, there are sum rules [126] that relate the decay rates and decay-rate asymmetries between the four $K\pi$ charge states. With the future improvements via Belle II and upgraded LHCb, the measurements are expected to become precise enough to test these sum rules. The CP asymmetry in the $\pi^+ K^-$ mode has also been measured in B_s^0 decays, by CDF [117] and LHCb [120]. The combined value is $A_{CP}(B_s^0 \rightarrow \pi^+ K^-) = 0.221 \pm 0.015$.

In addition to $B_{(s)} \rightarrow K\pi$ modes, significant ($> 3\sigma$) non-zero CP asymmetries have been measured in several other rare decay modes: $A_{CP}(B^+ \rightarrow \rho^0 K^+) = 0.37 \pm 0.10$ [127], $A_{CP}(B^+ \rightarrow \eta K^+) = -0.37 \pm 0.08$ [128], $A_{CP}(B^0 \rightarrow \eta K^{*0}) = 0.19 \pm 0.05$ [129], and $A_{CP}(B^+ \rightarrow f_2(1270)K^+) = -0.68_{-0.17}^{+0.19}$ [127]. In at least the first two cases, a large direct CP violation might be expected since the penguin amplitude is suppressed so the tree and penguin amplitudes may have comparable magnitudes. There are also measurements by LHCb of CP asymmetries in several 3-body modes: $A_{CP}(B^+ \rightarrow \pi^+ \pi^- \pi^+) = 0.057 \pm 0.013$, $A_{CP}(B^+ \rightarrow K^+ \pi^- \pi^+) = 0.027 \pm 0.008$, $A_{CP}(B^+ \rightarrow K^+ K^- \pi^+) = -0.122 \pm 0.0021$, and $A_{CP}(B^+ \rightarrow K^+ K^- K^+) = -0.033 \pm 0.008$ [130, 131].

Many of these analyses now include Dalitz plot treatments with many intermediate resonances.

BaBar [132] and Belle [124, 133] have observed the decays $B^+ \rightarrow \bar{K}^0 K^+$ and $B^0 \rightarrow K^0 \bar{K}^0$. The world-average branching fractions are $\mathcal{B}(B^0 \rightarrow K^0 \bar{K}^0) = (1.21 \pm 0.16) \times 10^{-6}$ and $\mathcal{B}(B^+ \rightarrow \bar{K}^0 K^+) = (1.31 \pm 0.17) \times 10^{-6}$. These are the first observations of hadronic $b \rightarrow d$ transitions, with significance bigger than 5σ for all four measurements. CP asymmetries have been measured for these modes, but with large errors. LHCb has observed $B^0 \rightarrow K^+ K^-$ mode which occurs via a weak-annihilation process and is the rarest hadronic B -meson decay thus far observed, with $\mathcal{B}(B^0 \rightarrow K^+ K^-) = (7.80 \pm 1.52) \times 10^{-8}$ [134]. $B_s^0 \rightarrow K^+ K^-$ decay mode, which occurs mostly via $b \rightarrow s$ penguin process, has been observed by Belle [135], CDF [136] and LHCb [118]. The average branching fraction is $\mathcal{B}(B_s^0 \rightarrow K^+ K^-) = (25.4 \pm 1.6) \times 10^{-6}$. Belle has also observed $B_s^0 \rightarrow K^0 \bar{K}^0$ which also occurs via $b \rightarrow s$ penguin transition in the SM. The branching fraction is $(1.96_{-0.56}^{+0.62}) \times 10^{-5}$ [137].

The decay $B^0 \rightarrow \pi^+ \pi^-$ can be used to extract the CKM angle α (for details see elsewhere in this *Review* [138]). This is complicated by the presence of significant contributions from penguin diagrams. An isospin analysis [139] can be used to untangle the penguin complications. The decay $B^0 \rightarrow \pi^0 \pi^0$ is crucial in this analysis. Both BaBar and Belle have observed $B^0 \rightarrow \pi^0 \pi^0$, with a mild tension in the measured branching fractions: $(1.83 \pm 0.25) \times 10^{-6}$ for BaBar [123] and $(1.31 \pm 0.26) \times 10^{-6}$ for Belle [140]. It turns out that the amount of penguin pollution in the $B \rightarrow \pi\pi$ system is rather large. In the past few years, measurements in the $B^0 \rightarrow \rho\rho$ system have produced more precise values of α , since penguin amplitudes are generally smaller for decays with vector mesons. An important ingredient in the analysis is the $B^0 \rightarrow \rho^0 \rho^0$ branching fraction. The average of measurements from BaBar [141] and Belle [142] yields a branching fraction of $(0.96 \pm 0.15) \times 10^{-6}$. This is only 3% of the $\rho^+ \rho^-$ branching fraction, much smaller than the corresponding ratio ($\gtrsim 20\%$) in the $\pi\pi$ system.

Since $B \rightarrow \rho\rho$ has two vector mesons in the final state, the CP eigenvalue of the final state depends on the longitudinal polarization fraction f_L for the decay. Therefore, a measurement of f_L is needed to extract the CKM angle α . Both BaBar and Belle have measured f_L for the decays $\rho^+ \rho^-$ [143] and $\rho^+ \rho^0$ [144] and in both cases the measurements show $f_L > 0.9$, making a complete angular analysis unnecessary. In $B^0 \rightarrow \rho^0 \rho^0$, f_L is measured by BaBar [141], Belle [142] and LHCb [145], with the average value being $0.71_{-0.09}^{+0.08}$.

By analyzing the angular distributions of the B decays to two vector mesons, we can learn a lot about both weak- and strong-interaction dynamics in B decays. Decays that are penguin-dominated surprisingly have values of f_L near 0.5. The list of such decays has now grown to include $B \rightarrow \phi K^*(892)$, $B \rightarrow \rho K^*(892)$, and $B \rightarrow \omega K^*(892)$. The reasons for this "polarization puzzle" are not fully understood. A detailed description of the angular analysis of B decays to two vector mesons can be found in a separate mini-review [146] in this *Review*.

72.6 Electroweak penguin decays

Electroweak decays are one-loop FCNC decays proceeding through penguin or box Feynman diagrams with final state including real photon or pair of leptons. Such decays were first observed by CLEO experiment when it observed decay $B \rightarrow K^*(892)\gamma$ [76]. Since then significant amount of experimental information was obtained. Branching fractions for these decays are 10^{-5} or less, which makes them excellent candidates for searches for new physics beyond SM. Often several observables are available, which allows for stringent tests of the SM.

Starting with radiative decays, experimentally easiest to study are exclusive decays with a fully reconstructed final state. The best studied decay in this class is $B \rightarrow K^*(892)\gamma$ seen by CLEO, Belle, BaBar experiments [147–149] with world average branching fraction $\mathcal{B}(B^0 \rightarrow K^*(892)^0 \gamma) = (41.8 \pm 2.5) \times 10^{-6}$. Decays through several other kaon resonances such as $B \rightarrow K_1(1270)\gamma$, $K_2^*(1430)\gamma$, etc. were studied at B-factories [150–153]. It is worth to mention decay $B^+ \rightarrow K^+ \pi^+ \pi^- \gamma$ for which besides measure-

ments of the branching fraction [151, 154, 155] one can also use the angular distribution to access photon polarisation. Such a measurement was done by the LHCb experiment, which was able to clearly demonstrate that the photon in $B^+ \rightarrow K^+ \pi^+ \pi^- \gamma$ decay is polarised [156]. Unfortunately given non-trivial hadronic structure, more work is needed before turning this into test of the SM. The latest addition to the observed exclusive radiative decays is $B_s^0 \rightarrow \phi\gamma$, seen by the Belle and LHCb experiments [157, 158] with an average branching fraction of $(3.4 \pm 0.4) \times 10^{-5}$.

Compared to $b \rightarrow s\gamma$, the $b \rightarrow d\gamma$ transitions such as $B \rightarrow \rho\gamma$, are suppressed by the CKM elements ratio $|V_{td}/V_{ts}|^2$. Both Belle and BaBar have observed these decays [77, 78]. The world average $\mathcal{B}(B \rightarrow (\rho, \omega)\gamma) = (1.30 \pm 0.23) \times 10^{-6}$. This can be used to calculate $|V_{td}/V_{ts}|$ [159]; the measured values are $0.195_{-0.024}^{+0.025}$ from Belle [77] and $0.233_{-0.032}^{+0.033}$ from BaBar [78].

The observed radiative penguin branching fractions can constrain a large class of SM extensions [160]. However, due to the uncertainties in the hadronization, only the inclusive $b \rightarrow s\gamma$ rate can be reliably compared with theoretical calculations. This rate can be measured from the endpoint of the inclusive photon spectrum in B decay. By combining the measurements of $B \rightarrow X_s \gamma$ from the CLEO, BaBar, and Belle experiments [161–163], HFLAV obtains the new average: $\mathcal{B}(B \rightarrow X_s \gamma) = (3.32 \pm 0.15) \times 10^{-4}$ [27] for $E_\gamma \geq 1.6$ GeV, averaging over B^+ and B^0 . Consistent but less precise results have been reported by ALEPH for inclusive b -hadrons produced at the Z , which includes also contribution from B_s^0 and A_b^0 hadrons. Using the sum of seven exclusive final states, the BaBar experiment measured the branching fraction of inclusive $b \rightarrow d\gamma$ decays to be $(9.2 \pm 2.0 \pm 2.3) \times 10^{-6}$ [164]. The measured branching fraction can be compared to theoretical calculations. Recent calculations of $\mathcal{B}(b \rightarrow s\gamma)$ at NNLO level predict for the $E_\gamma \geq 1.6$ GeV values of $(3.36 \pm 0.23) \times 10^{-4}$ for $b \rightarrow s\gamma$ and $(1.73_{-0.22}^{+0.12}) \times 10^{-5}$ for $b \rightarrow d\gamma$ decays [165].

The CP asymmetry in $b \rightarrow s\gamma$ is extensively studied theoretically both in the SM and beyond [166]. According to the SM, the CP asymmetry in $b \rightarrow s\gamma$ is smaller than 1%, but some non-SM models allow significantly larger CP asymmetry ($\sim 10\%$) without altering the branching fraction. The current world average is $A_{CP} = 0.015 \pm 0.011$, again dominated by BaBar and Belle [167]. In addition to the CP asymmetry, BaBar and Belle also measured the isospin asymmetry $\Delta_{0-} = -0.006 \pm 0.020$ in $b \rightarrow s\gamma$ measured using sum of exclusive decays [167, 168]. An alternative measurement using full reconstruction of the companion B in the hadronic decay modes yields a consistent, but less precise result [169]. Both Belle and BaBar experiments measured the isospin asymmetry in exclusive $B \rightarrow K^*(892)\gamma$ decay with average of $6.3 \pm 1.7\%$ [148, 149] and therefore providing evidence for the non-zero isospin asymmetry.

In addition, experiments have measured the inclusive photon energy spectrum for $b \rightarrow s\gamma$, and by analyzing the shape of the spectrum they obtain the first and second moments for photon energies. Belle has measured these moments covering the widest range in the photon energy ($1.7 < E_\gamma < 2.8$ GeV) [163]. The measurement by BaBar has slightly smaller range with lower limit at 1.8 GeV [170]. These results can be used to extract non-perturbative HQET parameters that are needed for precise determination of the CKM matrix element V_{ub} .

Additional information on FCNC processes can be obtained from $b \rightarrow s\ell^+ \ell^-$ decays. These processes are studied as a function of dilepton invariant mass squared, q^2 . Different q^2 regions are sensitive to different physics. Starting at the very low q^2 decays exhibit sensitivity to the same physics as the radiative decays. Then for the q^2 in region 1.1 to 6.0 GeV²/c⁴ the SM and new physics have best chance to compete. At the high q^2 above the $\psi(2S)$ mass, the interference of SM and new physics is to some extent complementary to that in lower q^2 . Regions around J/ψ and $\psi(2S)$ is normally excluded from measurements as these are dominated by the $b \rightarrow c$ transitions to charmonia. For exclusive decays, theory predictions require calculations of hadronic form factors. With current theory predictions, the most useful are measurements within the q^2 regions 1.1 to 6.0 GeV²/c⁴ and from 16.0 GeV²/c⁴ up to the kinematic limit. From this reason in the listing we provide results mainly in those two regions.

Similar as for radiative decays, also for the $b \rightarrow s\ell^+\ell^-$ decays the inclusive measurements provide some benefits. Both Belle and BaBar performed such measurement without reconstructing hadronic part exclusively and measure a branching fraction of $(5.8 \pm 1.3) \times 10^{-6}$ [171]. Unfortunately this measurement is not trivially possible at hadron colliders and also does not easily allow the angular distributions of the decay products to be exploited. One alternative is to extract information on the inclusive decay as sum of exclusive decays. Such a measurement was performed by Belle [172], but in this case the difficulty lies in extrapolation for the missing hadronic states.

Turning to the exclusive decays, the initial measurements performed by B-factories typically averaged between charged and neutral B mesons as well as between e^+e^- and $\mu^+\mu^-$ final states. The experiments CDF, LHCb, ATLAS and CMS are much better suited for the $\mu^+\mu^-$ final states compared to the e^+e^- final states. As such most measurements at hadron colliders are done only with $\mu^+\mu^-$ decays and by separating charged and neutral B mesons. The best studied decays are $B^+ \rightarrow K^+\ell^+\ell^-$ and $B^0 \rightarrow K^*(892)^0\ell^+\ell^-$. At hadron colliders other b hadrons are produced and as such CDF and LHCb experiments did observe also $B_s^0 \rightarrow \phi\mu^+\mu^-$ [173, 174], $A_b^0 \rightarrow \Lambda\mu^+\mu^-$ [173, 175] and $A_b^0 \rightarrow pK^-\mu^+\mu^-$ decays [176]. The total branching fractions integrated over whole q^2 regions are $(5.5 \pm 0.7) \times 10^{-7}$ for $B^+ \rightarrow K^+e^+e^-$, $(4.41 \pm 0.23) \times 10^{-7}$ for $B^+ \rightarrow K^+\mu^+\mu^-$, $(1.03_{-0.17}^{+0.19}) \times 10^{-6}$ for $B^0 \rightarrow K^*(892)^0e^+e^-$ and $(0.94 \pm 0.05) \times 10^{-6}$ for $B^0 \rightarrow K^*(892)^0\mu^+\mu^-$ decays [177–180]. The total branching fractions for $B_s^0 \rightarrow \phi\mu^+\mu^-$ and $A_b^0 \rightarrow \Lambda\mu^+\mu^-$ decays are $(8.2 \pm 1.2) \times 10^{-7}$ [173, 174] and $(1.08 \pm 0.28) \times 10^{-6}$ [173, 175] respectively. With increased precision of $B^0 \rightarrow K^*(892)^0\ell^+\ell^-$ decay, there is a question on what fraction of the seen branching fraction is due to the $K^*(892)^0$ resonance and what fraction is due to the $K\pi$ in s -wave. This has been studied by LHCb which found that the $K\pi$ in s -wave fraction varies between 1% and about 10% depending on the q^2 region [180]. It should be noted, that for all relevant B meson decays the branching fractions so far studied are consistently below the SM expectation.

In the $b \rightarrow s\ell^+\ell^-$ decays angular distributions offer rich source of information. For the decays $B^+ \rightarrow K^+\ell^+\ell^-$ and $B^0 \rightarrow K^*(892)^0\ell^+\ell^-$ full angular analysis was already performed [181–186], while for other decays only partial angular analyses are available [174, 187]. Recently a lot of progress was done by constructing observables, which have reduced theory uncertainties and measurements of these are done. Most notably the observable called P'_5 [188] shows a discrepancy with the SM in the q^2 region which is highly sensitive to new physics [185, 186]. Measurements of the CP asymmetries [176, 178, 189], the isospin asymmetry [177–179] were also performed. All these measurements are well consistent with the small ACP and small isospin asymmetry expected in the SM [190]. With statistics available at the LHC, the measurement of phase difference between long- and short-distance contribution in $B^+ \rightarrow K^+\mu^+\mu^-$ decays became possible [191].

With the data samples available at LHC, the lepton universality in $b \rightarrow s\ell^+\ell^-$ can be tested. While in the SM decays to electron-positron and muon pairs are expected to be same up to small corrections due to the different masses of leptons, in extensions of the SM this does not have to hold. The angular analysis of $B^0 \rightarrow K^*(892)^0e^+e^-$ decays was performed by LHCb at low dilepton invariant masses [192] and Belle in several regions over whole q^2 range [186]. The most notable result on lepton universality test is the ratio of branching fractions between $B^+ \rightarrow K^+\mu^+\mu^-$ and $B^+ \rightarrow K^+e^+e^-$ and between $B^0 \rightarrow K^*(892)^0\mu^+\mu^-$ and $B^0 \rightarrow K^*(892)^0e^+e^-$ decays. In both cases, the measurements by LHCb show similar discrepancy from the SM, each being in the region of 2.1 – 2.6σ [193, 194]. Recently, LHCb experiment performed similar test with $A_b^0 \rightarrow pK^-\ell^+\ell^-$ decays [195].

While $b \rightarrow d\ell^+\ell^-$ decays are further suppressed, they recently became accessible. Signals were observed for $B^+ \rightarrow \pi^+\mu^+\mu^-$ [79], $B^0 \rightarrow \pi^+\pi^-\mu^+\mu^-$ [196] and $A_b^0 \rightarrow p\pi^-\mu^+\mu^-$ [197] decays. The total branching fractions are only quantities measured and these are about 2×10^{-8} for the meson decays and about 7×10^{-8} for the A_b^0 decay.

Finally the decays $B_{(s)}^0 \rightarrow e^+e^-$ and $\mu^+\mu^-$ are interesting since they only proceed at second order in weak interactions in the SM, but may have large contributions from supersymmetric loops, proportional to $(\tan\beta)^6$. First limits were published 30 years ago and since then experiments at Tevatron, B -factories and LHC gradually improved those and effectively excluded whole models of new physics and significantly constrained allowed parameter space of others. For the decays to $\mu^+\mu^-$, Tevatron experiments pushed the limits down to roughly factor of 5–10 above the SM expectation [198, 199]. The long journey in the search for these decays culminated in 2012, when first evidence for $B_s^0 \rightarrow \mu^+\mu^-$ decay was seen [200]. Subsequently, LHC experiments ATLAS [201], CMS [202] and LHCb [203] observed statistically significant signal for $B_s^0 \rightarrow \mu^+\mu^-$ decay. The average branching fraction is found to be $(3.0 \pm 0.4) \times 10^{-9}$. In experiments at hadron colliders searches for $B^0 \rightarrow \mu^+\mu^-$ decays are performed at the same time. The best limit on $B(B^0 \rightarrow \mu^+\mu^-) < 3.4 \times 10^{-10}$ at 95% C.L. [203]. The limits for the e^+e^- modes are: $< 2.8 \times 10^{-7}$ and $< 8.3 \times 10^{-8}$, respectively, for B_s^0 and B^0 [204]. The searches for decays to $\tau^+\tau^-$ are more challenging with current best limits of $B(B^0 \rightarrow \tau^+\tau^-) < 2.1 \times 10^{-3}$ and $B(B_s^0 \rightarrow \tau^+\tau^-) < 6.8 \times 10^{-3}$ at 95% C.L. [205]. All existing measurements of B^0 and B_s^0 decays to same flavour dilepton pair is consistent with SM expectation [206]. With $B_s^0 \rightarrow \mu^+\mu^-$ decay observed, it was suggested that the effective lifetime is useful further test of the decay [207]. Attempt was made by LHCb experiment, but its precision is not yet sufficient to provide test of the SM [203]. It will take couple of years until interesting precision is reached. The searches were also performed for lepton flavour violating decays to two leptons with best limits in $e^\pm\mu^\mp$ channel, where limits are $< 3.7 \times 10^{-9}$ for B^0 and $< 1.4 \times 10^{-8}$ for B_s^0 , at 95% confidence level [208].

Several theory groups performed global analysis of electroweak decays concluding that significant tension between data and SM is present [209]. The tension can be relieved by new physics beyond SM. For more detailed reviews see e.g. Ref. [210].

72.7 Summary and Outlook

The study of B mesons continues to be one of the most productive fields in particle physics. With the two asymmetric B -factory experiments Belle and BaBar, we now have a combined data sample of well over 1 ab^{-1} . CP violation has been firmly established in many decays of B mesons. Evidence for direct CP violation has been observed. Many rare decays resulting from hadronic $b \rightarrow u$ transitions and $b \rightarrow s(d)$ penguin decays have been observed, and the emerging pattern is still full of surprises. Despite the remarkable successes of the B -factory experiments, many fundamental questions in the flavor sector remain unanswered.

At Fermilab, CDF and D0 each has accumulated about 10 fb^{-1} , which is the equivalent of about 10^{12} b -hadrons produced. In spite of the low trigger efficiency of hadronic experiments, a selection of modes have been reconstructed in large quantities, giving a start to a program of studies on B_s and b -flavored baryons, in which a first major step has been the determination of the B_s oscillation frequency.

As Tevatron and B -factories finished their taking data, the new experiments at the LHC have become very active. LHCb has collected about 1 fb^{-1} at 7 TeV, 2 fb^{-1} at 8 TeV, and close to 5.9 fb^{-1} at 13 TeV during LHC Runs 1 and 2. CMS and ATLAS have collected each about 5 fb^{-1} of data at $\sqrt{s} = 7 \text{ TeV}$, 20 fb^{-1} at 8 TeV and about 150 fb^{-1} at 13 TeV during LHC Runs 1 and 2. LHCb, which is dedicated to the studies of b - and c -hadrons, has a data sample that is for many decays larger than the sum of all previous experiments. With it, we are entering to regime of precision physics even for many rare decays, which allows much more detailed measurements.

The Belle II experiment at the SuperKEKB has started recording data in 2019 and has so far collected about 12.4 fb^{-1} of data (March 2020). The aim to increase sample to $\sim 50 \text{ ab}^{-1}$ will make it possible to explore the indirect evidence of new physics beyond the SM in the heavy-flavor particles (b , c , and τ), in a way that is complementary to the LHC. In the same time period, LHCb Collaboration is working on the upgrade of its detector,

installation of which is ongoing. The aim of the upgrade is to increase flexibility of the trigger, which will allow about a factor of five increase in instantaneous luminosity and of about a factor of two in efficiencies on triggering on purely hadronic decays. The plan is to integrate about 50 fb^{-1} of data starting from 2021.

These experiments promise a rich spectrum of rare and precise measurements that have the potential to fundamentally affecting our understanding of the SM and CP -violating phenomena.

References

- [1] M. Kobayashi and T. Maskawa, *Prog. Theor. Phys.* **49**, 652 (1973).
- [2] S. W. Herb *et al.*, *Phys. Rev. Lett.* **39**, 252 (1977).
- [3] B. Aubert *et al.* (BaBar), *Phys. Rev. Lett.* **87**, 091801 (2001), [hep-ex/0107013].
- [4] K. Abe *et al.* (Belle), *Phys. Rev. Lett.* **87**, 091802 (2001), [hep-ex/0107061].
- [5] Currently two different notations (ϕ_1, ϕ_2, ϕ_3) and (α, β, γ) are used in the literature for CKM unitarity angles. In this mini-review, we use the latter notation following the other mini-reviews in this *Review*. The two notations are related by $\phi_1 = \beta$, $\phi_2 = \alpha$ and $\phi_3 = \gamma$.
- [6] See the “ CP Violation in Meson Decays” by D. Kirkby and Y. Nir in this *Review*.
- [7] See the “CKM Quark Mixing Matrix,” by A. Cecucci, Z. Ligeti, and Y. Sakai, in this *Review*.
- [8] See the note on “ $B^0 - \bar{B}^0$ mixing,” by O. Schneider in this *Review*.
- [9] See the “Determination of $|V_{cb}|$ and $|V_{ub}|$,” by R. Kowalewski and T. Mannel in this *Review*.
- [10] F. Abe *et al.* (CDF), *Phys. Rev. Lett.* **81**, 2432 (1998), [hep-ex/9805034]; F. Abe *et al.* (CDF), *Phys. Rev.* **D58**, 112004 (1998), [hep-ex/9804014].
- [11] A. Abulencia *et al.* (CDF), *Phys. Rev. Lett.* **96**, 082002 (2006), [hep-ex/0505076].
- [12] R. Aaij *et al.* (LHCb), *Phys. Rev.* **D95**, 3, 032005 (2017), [arXiv:1612.07421].
- [13] B. Aubert *et al.* (BaBar), *Phys. Rev. Lett.* **101**, 071801 (2008), [Erratum: *Phys. Rev. Lett.* 102,029901(2009)], [arXiv:0807.1086].
- [14] B. Aubert *et al.* (BaBar), *Phys. Rev. Lett.* **103**, 161801 (2009), [arXiv:0903.1124].
- [15] G. Bonvicini *et al.* (CLEO), *Phys. Rev.* **D81**, 031104 (2010), [arXiv:0909.5474].
- [16] R. Mizuk *et al.* (Belle), *Phys. Rev. Lett.* **109**, 232002 (2012), [arXiv:1205.6351].
- [17] U. Tamponi *et al.* (Belle), *Phys. Rev. Lett.* **115**, 14, 142001 (2015), [arXiv:1506.08914].
- [18] See the note on “Naming scheme for hadrons,” by M. Roos and C.G. Wohl in this *Review*.
- [19] R. Aaij *et al.* (LHCb), *Phys. Rev. Lett.* **118**, 5, 052002 (2017), [Erratum: *Phys. Rev. Lett.* 119,no.16,169901(2017)], [arXiv:1612.05140].
- [20] M. Cacciari *et al.*, *JHEP* **10**, 137 (2012), [arXiv:1205.6344]; B. A. Kniehl *et al.*, *Phys. Rev.* **D84**, 094026 (2011), [arXiv:1109.2472]; M. Cacciari, M. L. Mangano and P. Nason, *Eur. Phys. J.* **C75**, 12, 610 (2015), [arXiv:1507.06197].
- [21] B. Barish *et al.* (CLEO), *Phys. Rev. Lett.* **76**, 1570 (1996).
- [22] E. Guido *et al.* (Belle), *Phys. Rev. Lett.* **121**, 062001 (2018), [arXiv:1803.10303]; E. Guido *et al.* (Belle), *Phys. Rev.* **D96**, 052005 (2017), [arXiv:1707.04973]; A. Sokolov *et al.* (Belle), *Phys. Rev.* **D79**, 051103 (2009), [arXiv:0901.1431]; B. Aubert *et al.* (BaBar), *Phys. Rev.* **D78**, 112002 (2008), [arXiv:0807.2014].
- [23] J. P. Alexander *et al.* (CLEO), *Phys. Rev. Lett.* **86**, 2737 (2001), [hep-ex/0006002]; S. B. Athar *et al.* (CLEO), *Phys. Rev.* **D66**, 052003 (2002), [hep-ex/0202033].
- [24] N. C. Hastings *et al.* (Belle), *Phys. Rev.* **D67**, 052004 (2003), [hep-ex/0212033].
- [25] B. Aubert *et al.* (BaBar), *Phys. Rev. Lett.* **95**, 042001 (2005), [hep-ex/0504001].
- [26] Y. Amhis *et al.* (HFLAV), *Eur. Phys. J.* **C77**, 12, 895 (2017), [arXiv:1612.07233].
- [27] Y. S. Amhis *et al.* (HFLAV) (2019), and online update at <https://hflav.web.cern.ch/content/lifetimes-and-oscillation-parameters>, [arXiv:1909.12524].
- [28] P. Abreu *et al.* (DELPHI), *Phys. Lett.* **B345**, 598 (1995).
- [29] R. Akers *et al.* (OPAL), *Z. Phys.* **C66**, 19 (1995).
- [30] T. A. Aaltonen *et al.* (CDF), *Phys. Rev.* **D90**, 1, 012013 (2014), [arXiv:1309.5961].
- [31] R. Aaij *et al.* (LHCb), *JHEP* **04**, 024 (2015), [arXiv:1502.02638].
- [32] R. Aaij *et al.* (LHCb), *Phys. Rev. Lett.* **110**, 15, 151803 (2013), [arXiv:1211.5994].
- [33] A. M. Sirunyan *et al.* (CMS), *Eur. Phys. J.* **C78**, 939 (2018), [arXiv:1809.03578].
- [34] G. Aad *et al.* (ATLAS), *Phys. Rev. Lett.* **113**, 21, 212004 (2014), [arXiv:1407.1032].
- [35] A. Sirunyan *et al.* (CMS), *Phys. Rev. Lett.* **122**, 132001 (2019), [arXiv:1902.00571].
- [36] R. Aaij *et al.* (LHCb), *Phys. Rev. Lett.* **122**, 232001 (2019), [arXiv:1904.00081].
- [37] T. Aaltonen *et al.* (CDF), *Phys. Rev. Lett.* **99**, 202001 (2007), [arXiv:0706.3868]; T. Aaltonen *et al.* (CDF), *Phys. Rev.* **D85**, 092011 (2012), [arXiv:1112.2808].
- [38] R. Aaij *et al.* (LHCb), *Phys. Rev. Lett.* **122**, 012001 (2019), [arXiv:1809.07752].
- [39] V. M. Abazov *et al.* (D0), *Phys. Rev. Lett.* **99**, 052001 (2007), [arXiv:0706.1690]; T. Aaltonen *et al.* (CDF), *Phys. Rev. Lett.* **99**, 052002 (2007), [arXiv:0707.0589].
- [40] R. Aaij *et al.* (LHCb), *Phys. Rev. Lett.* **113**, 032001 (2014), [arXiv:1405.7223]; R. Aaij *et al.* (LHCb), *Phys. Lett.* **B736**, 154 (2014), [arXiv:1405.1543]; R. Aaij *et al.* (LHCb), *Phys. Rev.* **D89**, 3, 032001 (2014), [arXiv:1311.4823]; R. Aaij *et al.* (LHCb), *Phys. Rev. Lett.* **113**, 24, 242002 (2014), [arXiv:1409.8568]; R. Aaij *et al.* (LHCb), *Phys. Rev. Lett.* **115**, 24, 241801 (2015), [arXiv:1510.03829]; R. Aaij *et al.* (LHCb), *Phys. Rev. Lett.* **118**, 7, 071801 (2017), [arXiv:1612.02244]; R. Aaij *et al.* (LHCb), *Phys. Lett.* **B722**, 265 (2017), [arXiv:1701.05274]; R. Aaij *et al.* (LHCb), *Phys. Rev. Lett.* **118**, 071801 (2017), [arXiv:1612.02244]; R. Aaij *et al.* (LHCb), *JHEP* **02**, 98 (2018), [arXiv:1711.05490]; R. Aaij *et al.* (LHCb), *Phys. Rev.* **D99**, 052006 (2019), [arXiv:1901.07075].
- [41] T. A. Aaltonen *et al.* (CDF), *Phys. Rev.* **D89**, 7, 072014 (2014), [arXiv:1403.8126].
- [42] R. Aaij *et al.* (LHCb), *JHEP* **08**, 039 (2018), [arXiv:1805.03941].
- [43] S. Chatrchyan *et al.* (CMS), *Phys. Rev. Lett.* **108**, 252002 (2012), [arXiv:1204.5955].
- [44] R. Aaij *et al.* (LHCb), *JHEP* **1605**, 161 (2016), [arXiv:1604.03896].
- [45] R. Aaij *et al.* (LHCb), *Phys. Rev. Lett.* **114**, 062004 (2015), [arXiv:1411.4849].
- [46] R. Aaij *et al.* (LHCb), *Phys. Rev. Lett.* **121**, 072002 (2018), [arXiv:1805.09418].
- [47] V. M. Abazov *et al.* (D0), *Phys. Rev. Lett.* **101**, 232002 (2008), [arXiv:0808.4142]; T. Aaltonen *et al.* (CDF), *Phys. Rev.* **D80**, 072003 (2009), [arXiv:0905.3123].
- [48] R. Aaij *et al.* (LHCb), *Phys. Rev. Lett.* **110**, 18, 182001 (2013), [arXiv:1302.1072]; R. Aaij *et al.* (LHCb), *Phys. Lett.* **B736**, 154 (2014), [arXiv:1405.1543]; R. Aaij *et al.* (LHCb), *Phys. Rev.* **D93**, 9, 092007 (2016), [arXiv:1604.01412].

- [49] V. M. Abazov *et al.* (D0), Phys. Rev. Lett. **117**, 2, 022003 (2016), [arXiv:1602.07588]; V. M. Abazov *et al.* (D0), Phys. Rev. **D97**, 092004 (2018), [arXiv:1712.10176].
- [50] R. Aaij *et al.* (LHCb), Phys. Rev. Lett. **117**, 15, 152003 (2016), [Addendum: Phys. Rev. Lett.118,no.10,109904(2017)], [arXiv:1608.00435].
- [51] A. Sirunyan *et al.* (CMS), Phys. Rev. Lett. **120**, 202005 (2018), [arXiv:1712.06144].
- [52] C. Tarantino, Eur. Phys. J. **C33**, S895 (2004), [hep-ph/0310241]; F. Gabbiani, A. I. Onishchenko and A. A. Petrov, Phys. Rev. **D70**, 094031 (2004), [hep-ph/0407004]; F. Gabbiani, A. I. Onishchenko and A. A. Petrov, Phys. Rev. **D68**, 114006 (2003), [hep-ph/0303235].
- [53] A. Lenz, Int. J. Mod. Phys. **A30**, 10, 1543005 (2015), [arXiv:1405.3601].
- [54] C.-H. Chang *et al.*, Phys. Rev. **D64**, 014003 (2001), [hep-ph/0007162]; V. V. Kiselev, A. E. Kovalsky and A. K. Likhoded, Nucl. Phys. **B585**, 353 (2000), [hep-ph/0002127]; A. Yu. Anisimov *et al.*, Phys. Lett. **B452**, 129 (1999), [hep-ph/9812514]; M. Beneke and G. Buchalla, Phys. Rev. **D53**, 4991 (1996), [hep-ph/9601249].
- [55] R. Aaij *et al.* (LHCb), Eur. Phys. J. **C74**, 5, 2839 (2014), [arXiv:1401.6932].
- [56] R. Aaij *et al.* (LHCb), Phys. Lett. **B742**, 29 (2015), [arXiv:1411.6899].
- [57] The B_c is a special case, where a weak decay of the c quark is also possible, but the spectator model still applies.
- [58] R. Aaij *et al.* (LHCb), Nature Phys. **11**, 743 (2015), [arXiv:1504.01568].
- [59] J. P. Lees *et al.* (BaBar), Phys. Rev. **D85**, 011101 (2012), [arXiv:1110.5600]; C. Oswald *et al.* (Belle), Phys. Rev. **D87**, 7, 072008 (2013), [Erratum: Phys. Rev.D90,no.11,119901(2014)], [arXiv:1212.6400]; C. Oswald *et al.* (Belle), Phys. Rev. **D92**, 7, 072013 (2015), [arXiv:1504.02004].
- [60] T. A. Aaltonen *et al.* (CDF), Phys. Rev. **D93**, 5, 052001 (2016), [arXiv:1601.03819].
- [61] B. Grinstein, Nucl. Phys. **B339**, 253 (1990); H. Georgi, Phys. Lett. **B240**, 447 (1990); A. F. Falk *et al.*, Nucl. Phys. **B343**, 1 (1990); E. Eichten and B. R. Hill, Phys. Lett. **B234**, 511 (1990).
- [62] "Heavy-Quark and Soft-Collinear Effective Theory" by C.W. Bauer and M. Neubert in this *Review*.
- [63] M. Neubert, "Aspects of QCD Factorization," hep-ph/0110093, *Proceedings of HF9*, Pasadena (2001) and references therein; Z. Ligeti, M. E. Luke and M. B. Wise, Phys. Lett. **B507**, 142 (2001), [hep-ph/0103020].
- [64] M. Beneke *et al.*, Phys. Rev. Lett. **83**, 1914 (1999), [hep-ph/9905312].
- [65] M. Beneke *et al.*, Nucl. Phys. **B591**, 313 (2000), [hep-ph/0006124].
- [66] M. Beneke *et al.*, Nucl. Phys. **B606**, 245 (2001), [hep-ph/0104110].
- [67] M. Beneke and M. Neubert, Nucl. Phys. **B675**, 333 (2003), [hep-ph/0308039].
- [68] Y.-Y. Keum, H.-n. Li and A. I. Sanda, Phys. Lett. **B504**, 6 (2001), [hep-ph/0004004].
- [69] Y. Y. Keum, H.-N. Li and A. I. Sanda, Phys. Rev. **D63**, 054008 (2001), [hep-ph/0004173].
- [70] Y.-Y. Keum and H.-n. Li, Phys. Rev. **D63**, 074006 (2001), [hep-ph/0006001].
- [71] C.-D. Lu, K. Ukai and M.-Z. Yang, Phys. Rev. **D63**, 074009 (2001), [hep-ph/0004213].
- [72] C.-D. Lu and M.-Z. Yang, Eur. Phys. J. **C23**, 275 (2002), [hep-ph/0011238].
- [73] C. W. Bauer, S. Fleming and M. E. Luke, Phys. Rev. **D63**, 014006 (2000), [hep-ph/0005275].
- [74] C. W. Bauer *et al.*, Phys. Rev. **D63**, 114020 (2001), [hep-ph/0011336].
- [75] C. W. Bauer and I. W. Stewart, Phys. Lett. **B516**, 134 (2001), [hep-ph/0107001].
- [76] R. Ammar *et al.* (CLEO), Phys. Rev. Lett. **71**, 674 (1993).
- [77] N. Taniguchi *et al.* (Belle), Phys. Rev. Lett. **101**, 111801 (2008), [Erratum: Phys. Rev. Lett.101,129904(2008)], [arXiv:0804.4770].
- [78] B. Aubert *et al.* (BaBar), Phys. Rev. **D78**, 112001 (2008), [arXiv:0808.1379].
- [79] R. Aaij *et al.* (LHCb), JHEP **10**, 034 (2015), [arXiv:1509.00414].
- [80] P. Krokovny *et al.* (Belle), Phys. Rev. Lett. **89**, 231804 (2002), [hep-ex/0207077]; B. Aubert *et al.* (BaBar), Phys. Rev. Lett. **98**, 081801 (2007), [hep-ex/0604012].
- [81] B. Kronenbitter *et al.* (Belle), Phys. Rev. **D92**, 5, 051102 (2015), [arXiv:1503.05613]; I. Adachi *et al.* (Belle), Phys. Rev. Lett. **110**, 13, 131801 (2013), [arXiv:1208.4678].
- [82] J. P. Lees *et al.* (BaBar), Phys. Rev. **D88**, 3, 031102 (2013), [arXiv:1207.0698]; B. Aubert *et al.* (BaBar), Phys. Rev. **D81**, 051101 (2010), [arXiv:0912.2453].
- [83] See the "Leptonic decays of charged pseudoscalar mesons," by J. Rosner, S. Stone, and R. Van de Water, in this *Review*.
- [84] J. P. Lees *et al.* (BaBar), Phys. Rev. **D84**, 112007 (2011), [Erratum: Phys. Rev.D87,no.3,039901(2013)], [arXiv:1107.5751]; S. Blyth *et al.* (Belle), Phys. Rev. **D74**, 092002 (2006), [hep-ex/0607029].
- [85] R. Aaij *et al.* (LHCb), Phys. Rev. D **92**, 3, 032002 (2015), [arXiv:1505.01710].
- [86] B. Aubert *et al.* (BaBar), Phys. Rev. Lett. **90**, 242001 (2003), [hep-ex/0304021].
- [87] D. Besson *et al.* (CLEO), Phys. Rev. **D68**, 032002 (2003), [Erratum: Phys. Rev.D75,119908(2007)], [hep-ex/0305100].
- [88] P. Krokovny *et al.* (Belle), Phys. Rev. Lett. **91**, 262002 (2003), [hep-ex/0308019]; Y. Mikami *et al.* (Belle), Phys. Rev. Lett. **92**, 012002 (2004), [hep-ex/0307052].
- [89] B. Aubert *et al.* (BaBar), Phys. Rev. Lett. **93**, 181801 (2004), [hep-ex/0408041].
- [90] R. Aaij *et al.* (LHCb), Phys. Rev. Lett. **113**, 162001 (2014), [arXiv:1407.7574].
- [91] T. Aaltonen *et al.* (CDF), Phys. Rev. Lett. **108**, 201801 (2012), [arXiv:1204.0536].
- [92] S. Esen *et al.* (Belle), Phys. Rev. **D87**, 3, 031101 (2013), [arXiv:1208.0323].
- [93] R. Aaij *et al.* (LHCb), Phys. Rev. **D93**, 9, 092008 (2016), [arXiv:1602.07543].
- [94] R. Aaij *et al.* (LHCb), Phys. Rev. Lett. **116**, 16, 161802 (2016), [arXiv:1603.02408].
- [95] R. Aaij *et al.* (LHCb), JHEP **11**, 082 (2015), [arXiv:1509.00400].
- [96] B. Aubert *et al.* (BaBar), Phys. Rev. **D76**, 031101 (2007), [arXiv:0704.1266].
- [97] R. Aaij *et al.* (LHCb), Phys. Rev. **D90**, 1, 012003 (2014), [arXiv:1404.5673].
- [98] R. Aaij *et al.* (LHCb), Phys. Rev. Lett. **111**, 18, 181801 (2013), [arXiv:1308.4544].
- [99] R. Aaij *et al.* (LHCb), Phys. Rev. **D87**, 11, 112012 (2013), [Addendum: Phys. Rev.D89,no.1,019901(2014)], [arXiv:1304.4530].
- [100] G. Aad *et al.* (ATLAS), Eur. Phys. J. **C76**, 1, 4 (2016), [arXiv:1507.07099].
- [101] R. Aaij *et al.* (LHCb), Phys. Rev. **D84**, 092001 (2011), [Erratum: Phys. Rev.D85,039904(2012)], [arXiv:1109.6831]; T. Aaltonen *et al.* (CDF), Phys. Rev. **D85**, 032003 (2012), [arXiv:1112.3334].

- [102] S. K. Choi *et al.* (Belle), Phys. Rev. Lett. **91**, 262001 (2003), [hep-ex/0309032].
- [103] D. Acosta *et al.* (CDF), Phys. Rev. Lett. **93**, 072001 (2004), [hep-ex/0312021].
- [104] V. M. Abazov *et al.* (D0), Phys. Rev. Lett. **93**, 162002 (2004), [hep-ex/0405004].
- [105] B. Aubert *et al.* (BaBar), Phys. Rev. **D71**, 071103 (2005), [hep-ex/0406022].
- [106] R. Aaij *et al.* (LHCb), Eur. Phys. J. **C72**, 1972 (2012), [arXiv:1112.5310].
- [107] S. Chatrchyan *et al.* (CMS), JHEP **04**, 154 (2013), [arXiv:1302.3968].
- [108] M. Aaboud *et al.* (ATLAS), JHEP **01**, 117 (2017), [arXiv:1610.09303].
- [109] S. K. Choi *et al.* (Belle), Phys. Rev. Lett. **100**, 142001 (2008), [arXiv:0708.1790]; R. Mizuk *et al.* (Belle), Phys. Rev. **D80**, 031104 (2009), [arXiv:0905.2869].
- [110] R. Aaij *et al.* (LHCb), Phys. Rev. Lett. **112**, 22, 222002 (2014), [arXiv:1404.1903]; R. Aaij *et al.* (LHCb), Phys. Rev. **D92**, 11, 112009 (2015), [arXiv:1510.01951].
- [111] K. Chilikin *et al.* (Belle), Phys. Rev. **D90**, 11, 112009 (2014), [arXiv:1408.6457].
- [112] R. Aaij *et al.* (LHCb), Phys. Rev. Lett. **115**, 072001 (2015), [arXiv:1507.03414].
- [113] R. Aaij *et al.* (LHCb), Phys. Rev. Lett. **122**, 22, 222001 (2019), [arXiv:1904.03947].
- [114] See the “Non- $q\bar{q}$ mesons,” by C. Amsler and C. Hanhart, and “Pentaquarks,” by M. Karliner and T. Skwarnicki, in this *Review*.
- [115] T. Aaltonen *et al.* (CDF), Phys. Rev. Lett. **107**, 261802 (2011), [arXiv:1107.4999].
- [116] R. Aaij *et al.* (LHCb), JHEP **10**, 053 (2015), [arXiv:1508.00788].
- [117] T. A. Aaltonen *et al.* (CDF), Phys. Rev. Lett. **113**, 24, 242001 (2014), [arXiv:1403.5586].
- [118] R. Aaij *et al.* (LHCb), JHEP **10**, 037 (2012), [arXiv:1206.2794].
- [119] T. Aaltonen *et al.* (CDF), Phys. Rev. Lett. **103**, 031801 (2009), [arXiv:0812.4271].
- [120] R. Aaij *et al.* (LHCb), Phys. Rev. D **98**, 3, 032004 (2018), [arXiv:1805.06759].
- [121] R. Aaij *et al.* (LHCb), JHEP **12**, 155 (2019), [arXiv:1907.10003].
- [122] R. Fleischer, Phys. Lett. **B459**, 306 (1999), [hep-ph/9903456]; D. London and J. Matias, Phys. Rev. **D70**, 031502 (2004), [hep-ph/0404009].
- [123] J. P. Lees *et al.* (BaBar), Phys. Rev. **D87**, 5, 052009 (2013), [arXiv:1206.3525].
- [124] Y. T. Duh *et al.* (Belle), Phys. Rev. **D87**, 3, 031103 (2013), [arXiv:1210.1348].
- [125] B. Aubert *et al.* (BaBar), Phys. Rev. **D76**, 091102 (2007), [arXiv:0707.2798].
- [126] M. Gronau and J. L. Rosner, Phys. Rev. **D71**, 074019 (2005), [hep-ph/0503131]; M. Gronau, Phys. Lett. **B627**, 82 (2005), [hep-ph/0508047].
- [127] B. Aubert *et al.* (BaBar), Phys. Rev. **D78**, 012004 (2008), [arXiv:0803.4451]; A. Garmash *et al.* (Belle), Phys. Rev. Lett. **96**, 251803 (2006), [hep-ex/0512066].
- [128] C. T. Hoi *et al.* (Belle), Phys. Rev. Lett. **108**, 031801 (2012), [arXiv:1110.2000]; B. Aubert *et al.* (BaBar), Phys. Rev. **D80**, 112002 (2009), [arXiv:0907.1743].
- [129] B. Aubert *et al.* (BaBar), Phys. Rev. Lett. **97**, 201802 (2006), [hep-ex/0608005]; C. H. Wang *et al.* (Belle), Phys. Rev. **D75**, 092005 (2007), [hep-ex/0701057].
- [130] R. Aaij *et al.* (LHCb), Phys. Rev. **D90**, 11, 112004 (2014), [arXiv:1408.5373].
- [131] C.-L. Hsu *et al.* (Belle), Phys. Rev. D **96**, 3, 031101 (2017), [arXiv:1705.02640].
- [132] B. Aubert *et al.* (BaBar), Phys. Rev. Lett. **97**, 171805 (2006), [hep-ex/0608036].
- [133] K. Abe *et al.* (Belle), Phys. Rev. Lett. **98**, 181804 (2007), [hep-ex/0608049].
- [134] R. Aaij *et al.* (LHCb), Phys. Rev. Lett. **118**, 8, 081801 (2017), [arXiv:1610.08288].
- [135] C. C. Peng *et al.* (Belle), Phys. Rev. **D82**, 072007 (2010), [arXiv:1006.5115].
- [136] T. Aaltonen *et al.* (CDF), Phys. Rev. Lett. **106**, 181802 (2011), [arXiv:1103.5762].
- [137] B. Pal *et al.* (Belle), Phys. Rev. Lett. **116**, 16, 161801 (2016), [arXiv:1512.02145].
- [138] See the “Determination of CKM angles from B hadrons,” by T. Gershon, M. Kenzie, and K. Trabelsi, in this *Review*.
- [139] M. Gronau and D. London, Phys. Rev. Lett. **65**, 3381 (1990).
- [140] T. Julius *et al.* (Belle), Phys. Rev. **D96**, 3, 032007 (2017), [arXiv:1705.02083].
- [141] B. Aubert *et al.* (BaBar), Phys. Rev. **D78**, 071104 (2008), [arXiv:0807.4977].
- [142] P. Vanhoefer *et al.* (Belle), Phys. Rev. **D89**, 072008 (2014), [Addendum: Phys. Rev. D89,119903(2014)], [arXiv:1212.4015].
- [143] B. Aubert *et al.* (BaBar), Phys. Rev. **D76**, 052007 (2007), [arXiv:0705.2157]; A. Somov *et al.* (Belle), Phys. Rev. Lett. **96**, 171801 (2006), [hep-ex/0601024].
- [144] B. Aubert *et al.* (BaBar), Phys. Rev. Lett. **102**, 141802 (2009), [arXiv:0901.3522]; J. Zhang *et al.* (Belle), Phys. Rev. Lett. **91**, 221801 (2003), [hep-ex/0306007].
- [145] R. Aaij *et al.* (LHCb), Phys. Lett. **B747**, 468 (2015), [arXiv:1503.07770].
- [146] See the “Polarization in B Decays,” by A. Gritsan in this *Review*.
- [147] T. E. Coan *et al.* (CLEO), Phys. Rev. Lett. **84**, 5283 (2000), [hep-ex/9912057].
- [148] T. Horiguchi *et al.* (Belle), Phys. Rev. Lett. **119**, 19, 191802 (2017), [arXiv:1707.00394].
- [149] B. Aubert *et al.* (BaBar), Phys. Rev. Lett. **103**, 211802 (2009), [arXiv:0906.2177].
- [150] B. Aubert *et al.* (BaBar), Phys. Rev. **D70**, 091105 (2004), [hep-ex/0409035].
- [151] H. Yang *et al.* (Belle), Phys. Rev. Lett. **94**, 111802 (2005), [hep-ex/0412039].
- [152] S. Nishida *et al.* (Belle), Phys. Lett. **B610**, 23 (2005), [hep-ex/0411065].
- [153] B. Aubert *et al.* (BaBar), Phys. Rev. **D74**, 031102 (2006), [hep-ex/0603054].
- [154] B. Aubert *et al.* (BaBar), Phys. Rev. Lett. **98**, 211804 (2007), [Erratum: Phys. Rev. Lett.100,199905(2008)], [hep-ex/0507031].
- [155] P. del Amo Sanchez *et al.* (BaBar), Phys. Rev. **D93**, 5, 052013 (2016), [arXiv:1512.03579].
- [156] R. Aaij *et al.* (LHCb), Phys. Rev. Lett. **112**, 16, 161801 (2014), [arXiv:1402.6852].
- [157] J. Wicht *et al.* (Belle), Phys. Rev. Lett. **100**, 121801 (2008), [arXiv:0712.2659]; D. Dutta *et al.* (Belle), Phys. Rev. **D91**, 1, 011101 (2015), [arXiv:1411.7771].
- [158] R. Aaij *et al.* (LHCb), Nucl. Phys. **B867**, 1 (2013), [arXiv:1209.0313].

- [159] A. Ali, E. Lunghi and A. Ya. Parkhomenko, Phys. Lett. **B595**, 323 (2004), [hep-ph/0405075]; P. Ball, G. W. Jones and R. Zwicky, Phys. Rev. **D75**, 054004 (2007), [hep-ph/0612081].
- [160] J. L. Hewett, Phys. Rev. Lett. **70**, 1045 (1993), [hep-ph/9211256].
- [161] S. Chen *et al.* (CLEO), Phys. Rev. Lett. **87**, 251807 (2001), [hep-ex/0108032].
- [162] J. P. Lees *et al.* (BaBar), Phys. Rev. **D86**, 112008 (2012), [arXiv:1207.5772].
- [163] A. Limosani *et al.* (Belle), Phys. Rev. Lett. **103**, 241801 (2009), [arXiv:0907.1384]; T. Saito *et al.* (Belle), Phys. Rev. **D91**, 5, 052004 (2015), [arXiv:1411.7198].
- [164] P. del Amo Sanchez *et al.* (BaBar), Phys. Rev. **D82**, 051101 (2010), [arXiv:1005.4087].
- [165] M. Misiak *et al.*, Phys. Rev. Lett. **114**, 22, 221801 (2015), [arXiv:1503.01789]; M. Czakon *et al.*, JHEP **04**, 168 (2015), [arXiv:1503.01791].
- [166] L. Wolfenstein and Y. L. Wu, Phys. Rev. Lett. **73**, 2809 (1994), [hep-ph/9410253]; G. M. Asatrian and A. Ioannian, Phys. Rev. **D54**, 5642 (1996), [hep-ph/9603318]; M. Ciuchini, E. Gabrielli and G. F. Giudice, Phys. Lett. **B388**, 353 (1996), [Erratum: Phys. Lett. **B393**, 489 (1997)], [hep-ph/9604438]; S. Baek and P. Ko, Phys. Rev. Lett. **83**, 488 (1999), [hep-ph/9812229]; A. L. Kagan and M. Neubert, Phys. Rev. **D58**, 094012 (1998), [hep-ph/9803368]; K. Kiers, A. Soni and G.-H. Wu, Phys. Rev. **D62**, 116004 (2000), [hep-ph/0006280].
- [167] S. Watanuki *et al.* (Belle), Phys. Rev. D **99**, 3, 032012 (2019), [arXiv:1807.04236]; J. P. Lees *et al.* (BaBar), Phys. Rev. **D90**, 9, 092001 (2014), [arXiv:1406.0534].
- [168] B. Aubert *et al.* (BaBar), Phys. Rev. **D72**, 052004 (2005), [hep-ex/0508004].
- [169] B. Aubert *et al.* (BaBar), Phys. Rev. **D77**, 051103 (2008), [arXiv:0711.4889].
- [170] J. P. Lees *et al.* (BaBar), Phys. Rev. Lett. **109**, 191801 (2012), [arXiv:1207.2690].
- [171] M. Iwasaki *et al.* (Belle), Phys. Rev. **D72**, 092005 (2005), [hep-ex/0503044]; J. P. Lees *et al.* (BaBar), Phys. Rev. Lett. **112**, 211802 (2014), [arXiv:1312.5364].
- [172] Y. Sato *et al.* (Belle), Phys. Rev. **D93**, 3, 032008 (2016), [Addendum: Phys. Rev. **D93**, no.5, 059901 (2016)], [arXiv:1402.7134].
- [173] T. Aaltonen *et al.* (CDF), Phys. Rev. Lett. **107**, 201802 (2011), [arXiv:1107.3753].
- [174] R. Aaij *et al.* (LHCb), JHEP **07**, 084 (2013), [arXiv:1305.2168]; R. Aaij *et al.* (LHCb), JHEP **09**, 179 (2015), [arXiv:1506.08777].
- [175] R. Aaij *et al.* (LHCb), Phys. Lett. **B725**, 25 (2013), [arXiv:1306.2577].
- [176] R. Aaij *et al.* (LHCb), JHEP **06**, 108 (2017), [arXiv:1703.00256].
- [177] J. T. Wei *et al.* (Belle), Phys. Rev. Lett. **103**, 171801 (2009), [arXiv:0904.0770].
- [178] J. P. Lees *et al.* (BaBar), Phys. Rev. **D86**, 032012 (2012), [arXiv:1204.3933].
- [179] R. Aaij *et al.* (LHCb), JHEP **06**, 133 (2014), [arXiv:1403.8044].
- [180] R. Aaij *et al.* (LHCb), JHEP **11**, 047 (2016), [Erratum: JHEP **04**, 142 (2017)], [arXiv:1606.04731].
- [181] T. Aaltonen *et al.* (CDF), Phys. Rev. Lett. **108**, 081807 (2012), [arXiv:1108.0695].
- [182] R. Aaij *et al.* (LHCb), JHEP **05**, 082 (2014), [arXiv:1403.8045].
- [183] S. Chatrchyan *et al.* (CMS), Phys. Lett. **B727**, 77 (2013), [arXiv:1308.3409].
- [184] V. Khachatryan *et al.* (CMS), Phys. Lett. **B753**, 424 (2016), [arXiv:1507.08126].
- [185] R. Aaij *et al.* (LHCb), JHEP **02**, 104 (2016), [arXiv:1512.04442].
- [186] S. Wehle *et al.* (Belle), Phys. Rev. Lett. **118**, 11, 111801 (2017), [arXiv:1612.05014].
- [187] R. Aaij *et al.* (LHCb), JHEP **06**, 115 (2015), [Erratum: JHEP **09**, 145 (2018)], [arXiv:1503.07138].
- [188] S. Descotes-Genon *et al.*, JHEP **01**, 048 (2013), [arXiv:1207.2753].
- [189] R. Aaij *et al.* (LHCb), JHEP **09**, 177 (2014), [arXiv:1408.0978].
- [190] J. Lyon and R. Zwicky, Phys. Rev. **D88**, 9, 094004 (2013), [arXiv:1305.4797].
- [191] R. Aaij *et al.* (LHCb), Eur. Phys. J. **C77**, 3, 161 (2017), [arXiv:1612.06764].
- [192] R. Aaij *et al.* (LHCb), JHEP **04**, 064 (2015), [arXiv:1501.03038].
- [193] R. Aaij *et al.* (LHCb), Phys. Rev. Lett. **122**, 19, 191801 (2019), [arXiv:1903.09252].
- [194] R. Aaij *et al.* (LHCb), JHEP **08**, 055 (2017), [arXiv:1705.05802].
- [195] R. Aaij *et al.* (LHCb) (2019), [arXiv:1912.08139].
- [196] R. Aaij *et al.* (LHCb), Phys. Lett. **B743**, 46 (2015), [arXiv:1412.6433].
- [197] R. Aaij *et al.* (LHCb), JHEP **04**, 029 (2017), [arXiv:1701.08705].
- [198] T. Aaltonen *et al.* (CDF), Phys. Rev. Lett. **107**, 191801 (2011), [Addendum: Phys. Rev. Lett. **107**, no.23, 239903 (2011)], [arXiv:1107.2304].
- [199] V. M. Abazov *et al.* (D0), Phys. Rev. **D87**, 7, 072006 (2013), [arXiv:1301.4507].
- [200] R. Aaij *et al.* (LHCb), Phys. Rev. Lett. **110**, 2, 021801 (2013), [arXiv:1211.2674].
- [201] M. Aaboud *et al.* (ATLAS), JHEP **04**, 098 (2019), [arXiv:1812.03017].
- [202] S. Chatrchyan *et al.* (CMS), Phys. Rev. Lett. **111**, 101804 (2013), [arXiv:1307.5025].
- [203] R. Aaij *et al.* (LHCb), Phys. Rev. Lett. **118**, 19, 191801 (2017), [arXiv:1703.05747].
- [204] T. Aaltonen *et al.* (CDF), Phys. Rev. Lett. **102**, 201801 (2009), [arXiv:0901.3803].
- [205] R. Aaij *et al.* (LHCb), Phys. Rev. Lett. **118**, 25, 251802 (2017), [arXiv:1703.02508].
- [206] C. Bobeth *et al.*, Phys. Rev. Lett. **112**, 101801 (2014), [arXiv:1311.0903].
- [207] K. De Bruyn *et al.*, Phys. Rev. Lett. **109**, 041801 (2012), [arXiv:1204.1737]; A. J. Buras *et al.*, JHEP **07**, 77 (2013), [arXiv:1303.3820].
- [208] R. Aaij *et al.* (LHCb), Phys. Rev. Lett. **111**, 141801 (2013), [arXiv:1307.4889].
- [209] J. Aebischer *et al.*, Eur. Phys. J. C **80**, 3, 252 (2020), [arXiv:1903.10434]; F. Beaujean, C. Bobeth and D. van Dyk, Eur. Phys. J. **C74**, 2897 (2014), [Erratum: Eur. Phys. J. **C74**, 3179 (2014)], [arXiv:1310.2478]; M. Algueró *et al.*, JHEP **07**, 096 (2019), [arXiv:1902.04900]; A. Arbey *et al.*, Phys. Rev. D **100**, 1, 015045 (2019), [arXiv:1904.08399].
- [210] T. Blake, G. Lanfranchi and D. M. Straub, Prog. Part. Nucl. Phys. **92**, 50 (2017), [arXiv:1606.00916]; J. Albrecht, S. Reichert and D. van Dyk, Int. J. Mod. Phys. A **33**, 18n19, 1830016 (2018), [arXiv:1806.05010].

73. Polarization in B Decays

Revised August 2019 by A. V. Gritsan (Johns Hopkins University).

We review the notation used in polarization measurements in particle production and decay, with a particular emphasis on the B decays and the CP -violating observables in polarization measurements. We look at several examples of vector-vector and vector-tensor B meson decays, while more details about the theory and experimental results in B decays can be found in a separate mini-review [1] in this Review.

Figure 73.1 illustrates angular observables in an example of the sequential process $ab \rightarrow X \rightarrow P_1 P_2 \rightarrow (p_{11} p_{12})(p_{21} p_{22})$ [2]. The angular distributions are of particular interest because they are sensitive to spin correlations and reveal properties of particles and their interactions, such as quantum numbers and couplings. In the case of a spin-zero particle X , such as B meson or a Higgs boson, there are no spin correlations in the production mechanism and the decay chain is to be analyzed. The angular distribution of decay products can be expressed as a function of three helicity angles which describe the alignment of the particles in the decay chain. The analyzer of the B -daughter polarization is normally chosen for two-body decays, as the direction of the daughters in the center-of-mass of the parent (*e.g.*, $\rho \rightarrow 2\pi$) [3], and for three-body decays as the normal to the decay plane (*e.g.*, $\omega \rightarrow 3\pi$) [4]. An equivalent set of transversity angles is sometimes used in polarization analyses [5]. The differential decay width depends on complex amplitudes $A_{\lambda_1 \lambda_2}$, corresponding to the X -daughter helicity states λ_i .

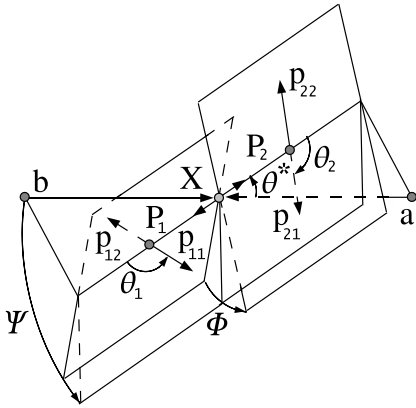


Figure 73.1: Definition of the production and helicity angles in the sequential process $ab \rightarrow X \rightarrow P_1 P_2 \rightarrow (p_{11} p_{12})(p_{21} p_{22})$. The three helicity angles include θ_1 and θ_2 , defined in the rest frame of the two daughters P_1 and P_2 , and Φ , defined in the X frame as the angle between the two decay planes. The two production angles θ^* and Ψ are defined in the X frame, where Ψ is the angle between the production plane and the average of the two decay planes.

In the case of a spin-zero B -meson decay, its daughter helicities are constrained to $\lambda_1 = \lambda_2 = \lambda$. Therefore we simplify amplitude notation as A_λ . Moreover, most B -decay polarization analyses are limited to the case when the spin of one of the B -meson daughters is 1. In that case, there are only three independent amplitudes corresponding to $\lambda = 0$ or ± 1 [6], where the last two can be expressed in terms of parity-even and parity-odd amplitudes $A_{\parallel, \perp} = (A_{+1} \pm A_{-1})/\sqrt{2}$. The overall decay amplitude involves three complex terms proportional to the above amplitudes and the Wigner d functions of helicity angles. The exact angular dependence would depend on the quantum numbers of the B -meson daughters and of their decay products, and can be found in the literature [6,7]. When both B -meson daughters are tensor mesons and the smaller of the two daughter spins is $J_1 > 1$, this formalism can be easily extended by introducing the parity-even and parity-odd amplitudes of higher order $A_{\parallel n, \perp n} = (A_{+n} \pm A_{-n})/\sqrt{2}$, with $1 < n \leq J_1$, while the general angular parameterization may be found in Ref. 7. However, we limit the following discussion to

$J_1 = 1$. The differential decay rate would involve six real quantities α_i , including interference terms,

$$\frac{d\Gamma}{\Gamma d \cos \theta_1 d \cos \theta_2 d\Phi} = \sum_i \alpha_i f_i(\cos \theta_1, \cos \theta_2, \Phi), \quad (73.1)$$

where each $f_i(\cos \theta_1, \cos \theta_2, \Phi)$ has unique angular dependence specific to particle quantum numbers, and the α_i parameters are defined as:

$$\alpha_1 = \frac{|A_0|^2}{\sum |A_\lambda|^2} = f_L, \quad (73.2)$$

$$\alpha_2 = \frac{|A_{\parallel}|^2 + |A_{\perp}|^2}{\sum |A_\lambda|^2} = (1 - f_L), \quad (73.3)$$

$$\alpha_3 = \frac{|A_{\parallel}|^2 - |A_{\perp}|^2}{\sum |A_\lambda|^2} = (1 - f_L - 2f_{\perp}), \quad (73.4)$$

$$\alpha_4 = \frac{\Im m(A_{\perp} A_{\parallel}^*)}{\sum |A_\lambda|^2} = \sqrt{f_{\perp}(1 - f_L - f_{\perp})} \sin(\phi_{\perp} - \phi_{\parallel}), \quad (73.5)$$

$$\alpha_5 = \frac{\Re e(A_{\parallel} A_0^*)}{\sum |A_\lambda|^2} = \sqrt{f_L(1 - f_L - f_{\perp})} \cos(\phi_{\parallel}), \quad (73.6)$$

$$\alpha_6 = \frac{\Im m(A_{\perp} A_0^*)}{\sum |A_\lambda|^2} = \sqrt{f_{\perp} f_L} \sin(\phi_{\perp}), \quad (73.7)$$

where the amplitudes have been expressed with the help of polarization parameters f_L , f_{\perp} , ϕ_{\parallel} , and ϕ_{\perp} defined in Table 73.1. Note that the terms proportional to $\Re e(A_{\perp} A_{\parallel}^*)$, $\Im m(A_{\parallel} A_0^*)$, and $\Re e(A_{\perp} A_0^*)$ are absent in Eqs. (2-7). However, these terms may appear for some three-body decays of a B -meson daughter, see Ref. 7.

Table 73.1: Rate, polarization, and CP -asymmetry parameters defined for the B -meson decays to mesons with non-zero spin. Numerical examples are shown for the average of the $B^0 \rightarrow \varphi K^*(892)^0$ decay measurements obtained from BABAR [8], Belle [9], and LHCb [10]. The first six parameters are defined under the assumption of no CP violation in decay, while they are averaged between the \bar{B} and B parameters in general. The last six parameters involve differences between the \bar{B} and B meson decay parameters. The phase convention δ_0 is chosen with respect to a single A_{00} amplitude from a reference B decay mode, which is $B^0 \rightarrow \varphi K_0^*(1430)^0$ for numerical results.

parameter	definition	average
\mathcal{B}	$\Gamma/\Gamma_{\text{total}}$	$(10.1^{+0.6}_{-0.5}) \times 10^{-6}$
f_L	$ A_0 ^2/\sum A_\lambda ^2$	0.497 ± 0.017
f_{\perp}	$ A_{\perp} ^2/\sum A_\lambda ^2$	0.225 ± 0.015
$\phi_{\parallel} - \pi$	$\arg(A_{\parallel}/A_0) - \pi$	-0.712 ± 0.058
$\phi_{\perp} - \pi$	$\arg(A_{\perp}/A_0) - \pi$	-0.615 ± 0.056
$\delta_0 - \pi$	$\arg(A_{00}/A_0) - \pi$	-0.26 ± 0.10
A_{CP}	$(\bar{\Gamma} - \Gamma)/(\bar{\Gamma} + \Gamma)$	-0.003 ± 0.038
A_{CP}^0	$(\bar{f}_L - f_L)/(\bar{f}_L + f_L)$	-0.007 ± 0.030
A_{CP}^{\perp}	$(\bar{f}_{\perp} - f_{\perp})/(\bar{f}_{\perp} + f_{\perp})$	-0.014 ± 0.057
$\Delta\phi_{\parallel}$	$(\bar{\phi}_{\parallel} - \phi_{\parallel})/2$	$+0.051 \pm 0.053$
$\Delta\phi_{\perp}$	$(\bar{\phi}_{\perp} - \phi_{\perp} - \pi)/2$	$+0.075 \pm 0.050$
$\Delta\delta_0$	$(\bar{\delta}_0 - \delta_0)/2$	$+0.13 \pm 0.08$

Overall, six real parameters describe three complex amplitudes A_0 , A_{\parallel} , and A_{\perp} . These could be chosen to be the four polarization parameters f_L , f_{\perp} , ϕ_{\parallel} , and ϕ_{\perp} , one overall size normalization, such as decay rate Γ , or branching fraction \mathcal{B} , and one overall phase δ_0 . The phase convention is arbitrary for an isolated B decay mode. However, for several B decays, the relative phase could produce meaningful and observable effects through interference with other B decays with the same final states, such as for $B \rightarrow VK_J^*$ with $J = 0, 1, 2, 3, 4, \dots$. The phase could be referenced to the single $B \rightarrow VK_0^*$ amplitude A_{00} in

such a case, as shown in Table 73.1. Here V stands for any spin-one vector meson.

Moreover, CP violation can be tested in the angular distribution of the decay as the difference between the B and \bar{B} . Each of the six real parameters describing the three complex amplitudes would have a counterpart CP -asymmetry term, corresponding to three direct- CP asymmetries in three amplitudes, and three CP -violating phase differences, equivalent to the phase measurements from the mixing-induced CP asymmetries in the time evolution of B -decays [1]. In Table 73.1 and Ref. 11, these are chosen to be the direct- CP asymmetries in the overall decay rate \mathcal{A}_{CP} , in the f_L fraction \mathcal{A}_{CP}^0 , and in the f_\perp fraction \mathcal{A}_{CP}^\perp , and three weak phase differences:

$$\Delta\phi_{\parallel} = \frac{1}{2}\arg(\bar{A}_{\parallel}A_0/A_{\parallel}\bar{A}_0), \quad (73.8)$$

$$\Delta\phi_{\perp} = \frac{1}{2}\arg(\bar{A}_{\perp}A_0/A_{\perp}\bar{A}_0) - \frac{\pi}{2}, \quad (73.9)$$

$$\Delta\delta_0 = \frac{1}{2}\arg(\bar{A}_{00}A_0/A_{00}\bar{A}_0). \quad (73.10)$$

The $\frac{\pi}{2}$ term in Eq. (73.9) reflects the fact that A_{\perp} and \bar{A}_{\perp} differ in phase by π if CP is conserved. The two parameters $\Delta\phi_{\parallel}$ and $\Delta\phi_{\perp}$ are equivalent to triple-product asymmetries constructed from the vectors describing the decay angular distribution [12]. The CP -violating phase difference in the reference decay mode [11] is, in the Wolfenstein CKM quark-mixing phase convention,

$$\Delta\phi_{00} = \frac{1}{2}\arg(A_{00}/\bar{A}_{00}). \quad (73.11)$$

This can be measured only together with the mixing-induced phase difference for some of the neutral B -meson decays similar to other mixing-induced CP asymmetry measurements [1].

It may not always be possible to have a phase-reference decay mode which would define δ_0 and $\Delta\delta_0$ parameters. In that case, it may be possible to define the phase difference directly similarly to Eq. (73.11):

$$\Delta\phi_0 = \frac{1}{2}\arg(A_0/\bar{A}_0). \quad (73.12)$$

One can measure the angles of the CKM unitarity triangle, assuming Standard Model contributions to the $\Delta\phi_0$ and B -mixing phases. Examples include measurements of $\beta = \phi_1$ with $B \rightarrow J/\psi K^*$ and $\alpha = \phi_2$ with $B \rightarrow \rho\rho$.

Most of the B decays that arise from tree-level $b \rightarrow c$ transitions have the amplitude hierarchy $|A_0| > |A_+| > |A_-|$ which is expected from analyses based on quark-helicity conservation [13]. The larger the mass of the vector-meson daughters, the weaker the inequality. The B meson decays to heavy vector particles with charm, such as $B \rightarrow J/\psi K^*$, $\psi(2S)K^*$, $\chi_{c1}K^*$, $D^*\rho$, D^*K^* , D^*D^* , and $D^*D_s^*$, show a substantial fraction of the amplitudes corresponding to transverse polarization of the vector mesons ($A_{\pm 1}$), in agreement with the factorization prediction. The detailed amplitude analysis of the $B \rightarrow J/\psi K^*$ decays has been performed by the BABAR [14], Belle [15], CDF [16], CLEO [17], D0 [18], and LHCb [19] collaborations. Most analyses are performed under the assumption of the absence of direct CP violation. The parameter values are given in the particle listing of this *Review*. The difference between the strong phases ϕ_{\parallel} and ϕ_{\perp} deviates significantly from zero. The measurements [14,15] of CP -violating terms similar to those in $B \rightarrow \varphi K^*$ [11] shown in Table 73.1 are consistent with zero.

In addition, the mixing-induced CP -violating asymmetry is measured in the $B^0 \rightarrow J/\psi K^{*0}$ decay [1,14,15] where angular analysis allows one to separate CP -eigenstate amplitudes. This allows one to resolve the sign ambiguity of the $\cos 2\beta$ ($\cos 2\phi_1$) term that appears in the time-dependent angular distribution due to interference of parity-even and parity-odd terms. This analysis relies on the knowledge of discrete ambiguities in the strong phases ϕ_{\parallel} and ϕ_{\perp} , as discussed below. The BABAR experiment used a method based on the dependence on the $K\pi$ invariant mass of the interference between the S - and P -waves to resolve the discrete ambiguity in the determination of the strong phases ($\phi_{\parallel}, \phi_{\perp}$) in $B \rightarrow J/\psi K^*$ decays [14]. The result

is in agreement with the amplitude hierarchy expectation [13]. The CDF [20], D0 [21], and LHCb [22] experiments have studied the $B_s^0 \rightarrow J/\psi(K^+K^-)$, $J/\psi(\pi^+\pi^-)$, $\psi(K^+\pi^-)$ decays and provided the lifetime, polarization, and phase measurements.

The amplitude hierarchy $|A_0| \gg |A_+| \gg |A_-|$ was expected in B decays to light vector particles in both penguin transitions [23,24] and tree-level transitions [13]. There is confirmation by the BABAR and Belle experiments of predominantly longitudinal polarization in the tree-level $b \rightarrow u$ transition, such as $B^0 \rightarrow \rho^+\rho^-$ [25], $B^+ \rightarrow \rho^0\rho^+$ [26], and $B^+ \rightarrow \omega\rho^+$ [27]; this is consistent with the analysis of the quark helicity conservation [13]. Because the longitudinal amplitude dominates the decay, a detailed amplitude analysis is not possible with current B samples, and limits on the transverse amplitude fraction are obtained. The small branching fractions of $B^0 \rightarrow \rho^0\rho^0, \omega\rho^0, \omega\omega$ [29–31,27] indicate that $b \rightarrow d$ penguin pollution is small in the charmless, strangeless vector-vector B decays. There is a measurement of large longitudinal polarization in $B^0 \rightarrow \rho^0\rho^0$ [29–31] decays. The fraction of transverse polarization is large in decays to heavier mesons such as $B^0 \rightarrow a_1(1260)^+a_1(1260)^-$ [28].

The interest in the polarization and CP -asymmetry measurements in penguin transition, such as $b \rightarrow s$ decays $B \rightarrow \varphi K^*$, ρK^* , ωK^* , or $B_s^0 \rightarrow \varphi\varphi$, K^*K^* , and $b \rightarrow d$ decay $B \rightarrow K^*\bar{K}^*$, is motivated by their potential sensitivity to physics beyond the Standard Model. The decay amplitudes for $B \rightarrow \varphi K^*$ have been measured by the BABAR, Belle, and LHCb experiments [11,9,32,33,10]. The fractions of longitudinal polarization are $f_L = 0.50 \pm 0.05$ for the $B^+ \rightarrow \varphi K^{*+}$ decay and $f_L = 0.497 \pm 0.017$ for the $B^0 \rightarrow \varphi K^{*0}$ decay. These indicate significant departure from the naive expectation of predominant longitudinal polarization, suggesting other contributions to the decay amplitude, previously neglected, either within the Standard Model, such as penguin annihilation [34] or QCD rescattering [35], or from physics beyond the Standard Model [36]. The complete set of twelve amplitude parameters measured in the $B^0 \rightarrow \varphi K^{*0}$ decay is given in Table 73.1. Several other parameters could be constructed from the above twelve parameters, as suggested in Ref. 37.

The discrete ambiguity in the phase ($\phi_{\parallel}, \phi_{\perp}, \Delta\phi_{\parallel}, \Delta\phi_{\perp}$) measurements has been resolved by BABAR in favor of $|A_+| \gg |A_-|$ through interference between the S - and P -waves of $K\pi$. The search for vector-tensor and vector-axialvector $B \rightarrow \varphi K_J^{(*)}$ decays with $J = 1, 2, 3, 4$ revealed a large fraction of longitudinal polarization in the decay $B \rightarrow \varphi K_2^*(1430)$ with $f_L = 0.90_{-0.07}^{+0.06}$ [11,38], but large contribution of transverse amplitude in $B \rightarrow \varphi K_1(1270)$ with $f_L = 0.46_{-0.15}^{+0.13}$ [39].

Like $B \rightarrow \varphi K^*$, the decays $B \rightarrow \rho K^*$ and $B \rightarrow \omega K^*$ may be sensitive to New Physics. Measurements of the longitudinal polarization fraction in $B \rightarrow \rho K^*$ [40] and in both vector-vector and vector-tensor final states of $B \rightarrow \omega K_J^*$ [27] by BABAR and Belle reveal a large fraction of transverse polarization, indicating an anomaly similar to $B \rightarrow \varphi K^*$ except for a different pattern in vector-tensor final states. An angular analysis of the $B^0 \rightarrow \rho^0 K^{*0}$ decay mode by LHCb [41] provides much higher precision and indicates remarkably small longitudinal polarization fraction and a significant direct CP asymmetry observed in angular distributions of $B \rightarrow VV$ decays for the first time. A large transverse polarization is also observed in the $B_s^0 \rightarrow \varphi\varphi$ decay by CDF [42] and LHCb [43], $B_s^0 \rightarrow K^{*0}\bar{K}^{*0}$ decays by LHCb [44], and $B_s^0 \rightarrow \varphi K^{*0}$ decays by LHCb [45]. At the same time, measurement of the polarization in the $b \rightarrow d$ penguin decays $B \rightarrow K^*\bar{K}^*$ indicates a large fraction of longitudinal polarization [44,46]. The LHCb experiment has also provided the very first polarization results on the tensor-tensor, as well as vector-tensor, decays of the B_s^0 meson in the $(K\pi)(K\pi)$ final state [44]. The polarization pattern in penguin-dominated B -meson decays is not fully understood [34–36].

The three-body semileptonic B -meson decays, such as $B \rightarrow V\ell_1\ell_2$, share many features with the two-body $B \rightarrow VV$ decays. Their differential decay width can be parameterized with the two helicity angles defined in the V and $(\ell_1\ell_2)$ frames and with the azimuthal angle, as defined in Fig. 73.1. However, since the $(\ell_1\ell_2)$ pair does not come from an on-shell particle, the angular distribution is unique to each point in the dilepton mass $m_{\ell\ell}$ spectrum. The polarization

measurements as a function of $m_{\ell\ell}$ provide complementary information on physics beyond the Standard Model, as discussed for $B \rightarrow K^*\ell^+\ell^-$ and $B_s \rightarrow \phi\ell^+\ell^-$ decays in Ref. 47. The data in these modes have been analyzed by the BABAR, Belle, CDF, CMS, and LHCb experiments [48–53].

The examples of the angular distributions and observables in $B \rightarrow K^*\ell^+\ell^-$ are discussed in Ref. 47. Two angular observables have been measured in this decay in certain ranges of the dilepton mass $m_{\ell\ell}$. One parameter is the fraction of longitudinal polarization F_L , which is determined by the K^* angular distribution and is similar to f_L defined for exclusive two-body decays. The other parameter is the forward-backward asymmetry of the lepton pair A_{FB} , which is the asymmetry of the decay rate with positive and negative values of $\cos\theta_1$. A complete set of observables and angular terms has been adopted by the LHCb collaboration [52] following Ref. 47 with the F_L , A_{FB} , and $S_3 - S_9$ coefficients in the angular distributions. Additional set of optimized observables $P_i^{(\prime)}$ is derived from those, for example $P_2 = 2A_{FB}/(3 - 3F_L)$ and $P_5' = S_5/\sqrt{F_L(1 - F_L)}$. These observables have the advantage that the leading form-factor uncertainties cancel. There have been hints of deviations from SM in the measurement of P_5' and lepton flavor universality [48–53].

In summary, there has been considerable interest in the polarization measurements of B -meson decays because they reveal both weak- and strong-interaction dynamics [34–36] [54]. New measurements will further elucidate the pattern of spin alignment measurements in rare B decays, and further test the Standard Model and strong interaction dynamics, including the non-factorizable contributions to the B -decay amplitudes.

References:

1. M. Kreps, Y. Kwon, and P. Eerola, “Production and Decay of b -Flavored Hadrons,” mini-review in this *Review*.
2. For an example and further references see Y.Y. Gao *et al.*, Phys. Rev. **D81**, 075022 (2010).
3. M. Jacob and G. C. Wick, Ann. Phys. **7**, 404 (1959).
4. S. M. Berman and M. Jacob, Phys. Rev. **139**, 1023 (1965).
5. I. Dunietz *et al.*, Phys. Rev. **D43**, 2193 (1991).
6. G. Kramer and W.F. Palmer, Phys. Rev. **D45**, 193 (1992).
7. A. Datta *et al.*, Phys. Rev. **D77**, 114025 (2008).
8. BABAR Collab., B. Aubert *et al.*, Phys. Rev. **D78**, 092008 (2008).
9. Belle Collab., M. Prim *et al.*, Phys. Rev. **D88**, 072004 (2013).
10. LHCb Collab., R. Aaij *et al.*, JHEP **05**, 069 (2014).
11. BABAR Collab., B. Aubert *et al.*, Phys. Rev. Lett. **93**, 231804 (2004); Phys. Rev. Lett. **98**, 051801 (2007); Phys. Rev. **D78**, 092008 (2008).
12. G. Valencia, Phys. Rev. **D39**, 3339 (1998); A. Datta and D. London, Int. J. Mod. Phys. **A19**, 2505 (2004).
13. A. Ali *et al.*, Z. Phys. **C1**, 269 (1979); M. Suzuki, Phys. Rev. **D64**, 117503 (2001).
14. BABAR Collab., B. Aubert *et al.*, Phys. Rev. **D71**, 032005 (2005); Phys. Rev. **D76**, 031102 (2007).
15. Belle Collab., R. Itoh *et al.*, Phys. Rev. Lett. **95**, 091601 (2005) Phys. Rev. **D88**, 072004 (2013).
16. CDF Collab., T. Affolder *et al.*, Phys. Rev. Lett. **85**, 4668 (2000); CDF Collab., D. Acosta *et al.*, Phys. Rev. Lett. **94**, 101803 (2005).
17. CLEO Collab., C. P. Jessop, Phys. Rev. Lett. **79**, 4533 (1997).
18. D0 Collab., V. M. Abazov *et al.*, Phys. Rev. Lett. **102**, 032001 (2009).
19. LHCb Collab., R. Aaij *et al.*, Phys. Rev. **D88**, 052002 (2013).
20. CDF Collab., T. Aaltonen *et al.*, Phys. Rev. Lett. **100**, 121803 (2008); Phys. Rev. **D85**, 072002 (2012).
21. D0 Collab., V. M. Abazov *et al.*, Phys. Rev. Lett. **98**, 121801 (2007); Phys. Rev. **D85**, 032006 (2012).
22. LHCb Collab., R. Aaij *et al.*, Phys. Rev. Lett. **108**, 101803 (2012); Phys. Rev. Lett. **114**, 041801 (2015); Phys. Lett. **B747**, 484 (2015); JHEP **1511**, 082 (2015); JHEP **1708**, 037 (2017).
23. H.Y. Cheng and K.C. Yang, Phys. Lett. **B511**, 40 (2001); C.H. Chen, Y.Y. Keum, and H.n. Li, Phys. Rev. **D66**, 054013 (2002).
24. A.L.Kagan, Phys. Lett. **B601**, 151 (2004); Y. Grossman, Int. J. Mod. Phys. **A19**, 907 (2004).
25. BABAR Collab., B. Aubert *et al.*, Phys. Rev. **D76**, 052007 (2007); Belle Collab., A. Somov *et al.*, Phys. Rev. **D93**, 032010 (2016).
26. Belle Collab., J. Zhang *et al.*, Phys. Rev. Lett. **91**, 221801 (2003); BABAR Collab., B. Aubert *et al.*, Phys. Rev. Lett. **102**, 141802 (2009).
27. BABAR Collab., B. Aubert *et al.*, Phys. Rev. **D74**, 051102 (2006); Phys. Rev. **D79**, 052005 (2009).
28. BABAR Collab., B. Aubert *et al.*, Phys. Rev. **D80**, 092007 (2009).
29. BABAR Collab., B. Aubert *et al.*, Phys. Rev. **D78**, 071104 (2008).
30. Belle Collab., I. Adachi *et al.*, Phys. Rev. **D89**, 072008 (2014).
31. LHCb Collab., R. Aaij *et al.*, Phys. Lett. **B747**, 468 (2015).
32. Belle Collab., K.F. Chen *et al.*, Phys. Rev. Lett. **94**, 221804 (2005).
33. BABAR Collab., B. Aubert *et al.*, Phys. Rev. Lett. **99**, 201802 (2007).
34. A.L. Kagan, Phys. Lett. **B601**, 151 (2004); H.n. Li and S. Mishima, Phys. Rev. **D71**, 054025 (2005); C.-H. Chen *et al.*, Phys. Rev. **D72**, 054011 (2005); M. Beneke *et al.*, Phys. Rev. Lett. **96**, 141801 (2006); C.-H. Chen and C.-Q. Geng, Phys. Rev. **D75**, 054010 (2007); A. Datta *et al.*, Phys. Rev. **D76**, 034015 (2007); M. Beneke, J. Rohrer, and D. Yang, Nucl. Phys. **B774**, 64 (2007); H.-Y. Cheng and K.-C. Yang, Phys. Rev. **D78**, 094001 (2008).
35. C. W. Bauer *et al.*, Phys. Rev. **D70**, 054015 (2004); P. Colangelo *et al.*, Phys. Lett. **B597**, 291 (2004); M. Ladisa *et al.*, Phys. Rev. **D70**, 114025 (2004); H. Y. Cheng *et al.*, Phys. Rev. **D71**, 014030 (2005); H. Y. Cheng and K. C. Yang, Phys. Rev. **D83**, 034001 (2011).
36. Y. Grossman, Int. J. Mod. Phys. **A19**, 907 (2004); E. Alvarez *et al.*, Phys. Rev. **D70**, 115014 (2004); P.K. Das and K.C. Yang, Phys. Rev. **D71**, 094002 (2005); C.H. Chen and C.Q. Geng, Phys. Rev. **D71**, 115004 (2005); Y.D. Yang *et al.*, Phys. Rev. **D72**, 015009 (2005); K.C. Yang, Phys. Rev. **72**, 034009 (2005); S. Baek, Phys. Rev. **D72**, 094008 (2005); C.S. Huang *et al.*, Phys. Rev. **D73**, 034026 (2006); C.H. Chen and H. Hatanaka, Phys. Rev. **D73**, 075003 (2006); A. Faessler *et al.*, Phys. Rev. **D75**, 074029 (2007).
37. D. London, N. Sinha, and R. Sinha, Phys. Rev. **D69**, 11401 (2004).
38. BABAR Collab., B. Aubert *et al.*, Phys. Rev. **D76**, 051103 (2007).
39. BABAR Collab., B. Aubert *et al.*, Phys. Rev. Lett. **101**, 161801 (2008).
40. Belle Collab., J. Zhang *et al.*, Phys. Rev. Lett. **95**, 141801 (2005); BABAR Collab., B. Aubert *et al.*, Phys. Rev. Lett. **97**, 201801 (2006); Phys. Rev. **D83**, 051101 (2011); Phys. Rev. **D85**, 072005 (2012).
41. LHCb Collab., R. Aaij *et al.*, JHEP **05**, 026 (2019).
42. CDF Collab., T. Aaltonen *et al.*, Phys. Rev. Lett. **107**, 261802 (2011).
43. LHCb Collab., R. Aaij *et al.*, Phys. Lett. **B713**, 369 (2012); Phys. Rev. **D90**, 052011 (2014); arXiv:1907.10003 [hep-ex].
44. LHCb Collab., R. Aaij *et al.*, Phys. Lett. **B709**, 50 (2012); JHEP **1507**, 166 (2015); JHEP **03**, 140 (2018); JHEP **07**, 032 (2019).
45. LHCb Collab., R. Aaij *et al.*, JHEP **1311**, 092 (2013).
46. BABAR Collab., B. Aubert *et al.*, Phys. Rev. Lett. **100**, 081801 (2008); Phys. Rev. **D79**, 051102 (2009).
47. G. Burdman, Phys. Rev. **D52**, 6400 (1995); F. Kruger and J. Matias, Phys. Rev. **D71**, 094009 (2005); E. Lunghi and J. Matias, JHEP **0704**, 058 (2007); W. Altmannshofer *et al.*, JHEP **0901**, 019 (2009); J. Matias *et al.*, JHEP **1204**, 104 (2012); S. Descotes-Genon *et al.*, JHEP **1301**, 048 (2013).
48. BABAR Collab., B. Aubert *et al.*, Phys. Rev. **D79**, 031102 (2009); J. P. Lees *et al.*, Phys. Rev. **D93**, 052015 (2016).
49. Belle Collab., J.-T. Wei *et al.*, Phys. Rev. Lett. **103**, 171801 (2009); S. Wehle *et al.*, Phys. Rev. Lett. **118**, 111801 (2017).

-
50. CDF Collab., T. Aaltonen *et al.*, Phys. Rev. Lett. **108**, 081807 (2012).
51. CMS Collab., S. Chatrchyan *et al.*, Phys. Lett. **B727**, 77 (2013); V. Khachatryan *et al.*, Phys. Lett. **B753**, 424 (2016); A. M. Sirunyan *et al.*, Phys. Lett. **B781**, 517 (2018).
52. LHCb Collab., R. Aaij *et al.*, JHEP **1308**, 131 (2013); JHEP **1504**, 064 (2015); JHEP **1602**, 104 (2016); JHEP **1611**, 047 (2016); JHEP **1612**, 065 (2016); JHEP **1708**, 055 (2017).
53. LHCb Collab., R. Aaij *et al.*, JHEP **1509**, 179 (2015).
54. C.H. Chen and H.n. Li, Phys. Rev. **D71**, 114008 (2005).

74. $B^0-\bar{B}^0$ Mixing

Revised March 2020 by O. Schneider (EPFL).

There are two neutral $B^0-\bar{B}^0$ meson systems, $B_d^0-\bar{B}_d^0$ and $B_s^0-\bar{B}_s^0$ (generically denoted $B_q^0-\bar{B}_q^0$, $q = s, d$), which exhibit particle-antiparticle mixing [1]. This mixing phenomenon is described in Ref. [2]. In the following, we adopt the notation introduced in Ref. [2], and assume CPT conservation throughout. In each system, the light (L) and heavy (H) mass eigenstates,

$$|B_{L,H}\rangle = p|B_q^0\rangle \pm q|\bar{B}_q^0\rangle, \quad (74.1)$$

have a mass difference $\Delta m_q = m_H - m_L > 0$, a total decay width difference $\Delta\Gamma_q = \Gamma_L - \Gamma_H$ and an average decay width $\Gamma_q = (\Gamma_L + \Gamma_H)/2$. In the absence of CP violation in the mixing, $|q/p| = 1$, the differences are given by $\Delta m_q = 2|M_{12}|$ and $|\Delta\Gamma_q| = 2|I_{12}|$, where M_{12} and I_{12} are the off-diagonal elements of the mass and decay matrices [2]. The evolution of a pure $|B_q^0\rangle$ or $|\bar{B}_q^0\rangle$ state at $t = 0$ is given by

$$|B_q^0(t)\rangle = g_+(t)|B_q^0\rangle + \frac{q}{p}g_-(t)|\bar{B}_q^0\rangle, \quad (74.2)$$

$$|\bar{B}_q^0(t)\rangle = g_+(t)|\bar{B}_q^0\rangle + \frac{p}{q}g_-(t)|B_q^0\rangle, \quad (74.3)$$

which means that the flavor states remain unchanged (+) or oscillate into each other (-) with time-dependent probabilities proportional to

$$|g_{\pm}(t)|^2 = \frac{e^{-\Gamma_q t}}{2} \left[\cosh\left(\frac{\Delta\Gamma_q}{2}t\right) \pm \cos(\Delta m_q t) \right]. \quad (74.4)$$

In the absence of CP violation, the time-integrated mixing probability $\int |g_-(t)|^2 dt / (\int |g_-(t)|^2 dt + \int |g_+(t)|^2 dt)$ is given by

$$\chi_q = \frac{x_q^2 + y_q^2}{2(x_q^2 + 1)}, \quad \text{where } x_q = \frac{\Delta m_q}{\Gamma_q}, \quad y_q = \frac{\Delta\Gamma_q}{2\Gamma_q}. \quad (74.5)$$

74.1 Standard Model predictions and phenomenology

In the Standard Model, the transitions $B_q^0 \rightarrow \bar{B}_q^0$ and $\bar{B}_q^0 \rightarrow B_q^0$ are due to the weak interaction. They are described, at the lowest order, by box diagrams involving two W bosons and two up-type quarks (see Fig. 74.1), as is the case for $K^0 - \bar{K}^0$ mixing. However, the long range interactions arising from intermediate virtual states are negligible for the neutral B meson systems, because the large B mass is off the region of hadronic resonances. The calculation of the dispersive and absorptive parts of the box diagrams yields the following predictions for the off-diagonal element of the mass and decay matrices [3],

$$M_{12} = -\frac{G_F^2 m_W^2 \eta_B m_{B_q} B_{B_q} f_{B_q}^2}{12\pi^2} S_0(m_t^2/m_W^2) (V_{tq}^* V_{tb})^2, \quad (74.6)$$

$$\begin{aligned} \Gamma_{12} = & \frac{G_F^2 m_b^2 \eta'_B m_{B_q} B_{B_q} f_{B_q}^2}{8\pi} \\ & \times \left[(V_{tq}^* V_{tb})^2 + V_{tq}^* V_{tb} V_{cq}^* V_{cb} \mathcal{O}\left(\frac{m_c^2}{m_b^2}\right) \right. \\ & \left. + (V_{cq}^* V_{cb})^2 \mathcal{O}\left(\frac{m_c^4}{m_b^4}\right) \right], \quad (74.7) \end{aligned}$$

where G_F is the Fermi constant, m_W the W boson mass, and m_i the mass of quark i ; m_{B_q} , f_{B_q} and B_{B_q} are the B_q^0 mass, weak decay constant and bag parameter, respectively. The known function $S_0(x_t)$ can be approximated very well by $0.784 x_t^{0.76}$ [4], and V_{ij} are the elements of the CKM matrix [5]. The QCD corrections η_B and η'_B are of order unity. The only non-negligible contributions to M_{12} are from box diagrams involving two top quarks. The phases of M_{12} and Γ_{12} satisfy

$$\phi_M - \phi_\Gamma = \pi + \mathcal{O}\left(\frac{m_c^2}{m_b^2}\right), \quad (74.8)$$

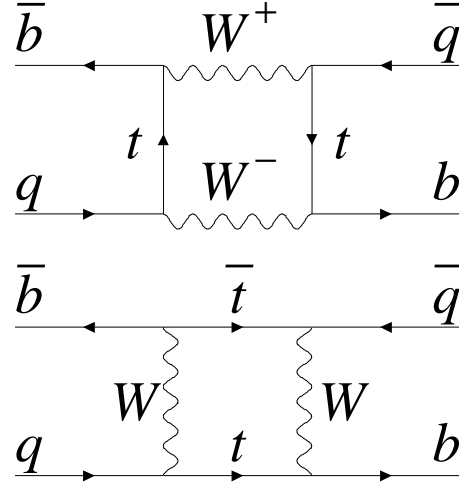


Figure 74.1: Dominant box diagrams for the $B_q^0 \rightarrow \bar{B}_q^0$ transitions ($q = d$ or s). Similar diagrams exist where one or both t quarks are replaced with c or u quarks.

implying that the mass eigenstates have mass and width differences of opposite signs. This means that, like in the $K^0-\bar{K}^0$ system, the heavy state is expected to have a smaller decay width than that of the light state: $\Gamma_H < \Gamma_L$. Hence, $\Delta\Gamma_q = \Gamma_L - \Gamma_H$ is expected to be positive in the Standard Model.

Furthermore, the quantity

$$\left| \frac{\Gamma_{12}}{M_{12}} \right| \simeq \frac{3\pi}{2} \frac{m_b^2}{m_W^2} \frac{1}{S_0(m_t^2/m_W^2)} \sim \mathcal{O}\left(\frac{m_b^2}{m_t^2}\right) \quad (74.9)$$

is small, and a power expansion of $|q/p|^2$ yields

$$\left| \frac{q}{p} \right|^2 = 1 + \left| \frac{\Gamma_{12}}{M_{12}} \right| \sin(\phi_M - \phi_\Gamma) + \mathcal{O}\left(\left| \frac{\Gamma_{12}}{M_{12}} \right|^2\right). \quad (74.10)$$

Therefore, considering both Eqs. (74.8) and (74.9), the CP -violating parameter

$$1 - \left| \frac{q}{p} \right|^2 \simeq \text{Im}\left(\frac{\Gamma_{12}}{M_{12}}\right) \quad (74.11)$$

is expected to be very small: $\sim \mathcal{O}(10^{-3})$ for the $B_d^0-\bar{B}_d^0$ system and $\lesssim \mathcal{O}(10^{-4})$ for the $B_s^0-\bar{B}_s^0$ system [6].

In the approximation of negligible CP violation in mixing, the ratio $\Delta\Gamma_q/\Delta m_q$ is equal to the small quantity $|\Gamma_{12}/M_{12}|$ of Eq. (74.9); it is hence independent of CKM matrix elements, *i.e.*, the same for the $B_d^0-\bar{B}_d^0$ and $B_s^0-\bar{B}_s^0$ systems. Calculations [7] yield $\sim 5 \times 10^{-3}$ with a $\sim 20\%$ uncertainty. Given the published experimental knowledge [8] on the mixing parameter x_q

$$\begin{cases} x_d = 0.769 \pm 0.004 & (B_d^0-\bar{B}_d^0 \text{ system}) \\ x_s = 26.89 \pm 0.07 & (B_s^0-\bar{B}_s^0 \text{ system}) \end{cases}, \quad (74.12)$$

the Standard Model thus predicts that $\Delta\Gamma_d/\Gamma_d$ is very small (below 1%), but $\Delta\Gamma_s/\Gamma_s$ considerably larger ($\sim 10\%$). These width differences are caused by the existence of final states to which both the B_q^0 and \bar{B}_q^0 mesons can decay. Such decays involve $b \rightarrow c\bar{c}q$ quark-level transitions, which are Cabibbo-suppressed if $q = d$ and Cabibbo-allowed if $q = s$.

A complete set of Standard Model predictions for all mixing parameters in both the $B_d^0-\bar{B}_d^0$ and $B_s^0-\bar{B}_s^0$ systems can be found in Ref. [9].

74.2 Experimental issues and methods for oscillation analyses

Time-integrated measurements of B^0 - \bar{B}^0 mixing were published for the first time in 1987 by UA1 [10] and ARGUS [11], and since then by many other experiments. These measurements are typically based on counting same-sign and opposite-sign lepton pairs from the semileptonic decay of the produced $b\bar{b}$ pairs. Such analyses cannot easily separate the contributions from the different b -hadron species, therefore, the clean environment of $\Upsilon(4S)$ machines (where only B_d^0 and charged B_u mesons are produced) is in principle best suited to measure χ_d .

However, better sensitivity is obtained from time-dependent analyses aiming at the direct measurement of the oscillation frequencies Δm_d and Δm_s , from the proper time distributions of B_d^0 or B_s^0 candidates identified through their decay in (mostly) flavor-specific modes, and suitably tagged as mixed or unmixed. This is particularly true for the B_s^0 - \bar{B}_s^0 system, where the large value of x_s implies maximal mixing, *i.e.*, $\chi_s \simeq 1/2$. In such analyses, the B_d^0 or B_s^0 mesons are either fully reconstructed, partially reconstructed from a charm meson, selected from a lepton with the characteristics of a $b \rightarrow \ell^-$ decay, or selected from a reconstructed displaced vertex. At high-energy colliders (LEP, SLC, Tevatron, LHC), the proper time $t = \frac{m_B}{p}L$ is measured from the distance L between the production vertex and the B decay vertex, and from an estimate of the B momentum p . At asymmetric B factories (KEKB, PEP-II), producing $e^+e^- \rightarrow \Upsilon(4S) \rightarrow B_d^0 \bar{B}_d^0$ events with a boost $\beta\gamma$ ($= 0.425, 0.55$), the proper time difference between the two B candidates is estimated as $\Delta t \simeq \frac{\Delta z}{\beta\gamma c}$, where Δz is the spatial separation between the two B decay vertices along the boost direction. In all cases, the good resolution needed on the vertex positions is obtained with silicon detectors.

The average statistical significance \mathcal{S} of a B_q^0 oscillation signal can be approximated as [12]

$$\mathcal{S} \approx \sqrt{N/2} f_{\text{sig}} (1 - 2\eta) e^{-(\Delta m_q \sigma_t)^2/2}, \quad (74.13)$$

where N is the number of selected and tagged candidates, f_{sig} is the fraction of signal in that sample, η is the total mistag probability, and σ_t is the resolution on proper time (or proper time difference). The quantity \mathcal{S} decreases very quickly as Δm_q increases; this dependence is controlled by σ_t , which is therefore a critical parameter for Δm_s analyses. At high-energy colliders, the proper time resolution $\sigma_t \sim \frac{m_B}{(p)} \sigma_L \oplus t \frac{\sigma_p}{p}$ includes a constant contribution due to the decay length resolution σ_L (typically 0.04–0.3 ps), and a term due to the relative momentum resolution σ_p/p (typically 10–20% for partially reconstructed decays), which increases with proper time. At B factories, the boost of the B mesons is estimated from the known beam energies, and the term due to the spatial resolution dominates (typically 1–1.5 ps because of the much smaller B boost).

In order to tag a B_q^0 candidate as mixed or unmixed, it is necessary to determine its flavor both in the initial state and in the final state. The initial and final state mistag probabilities, η_i and η_f , degrade \mathcal{S} by a total factor $(1 - 2\eta) = (1 - 2\eta_i)(1 - 2\eta_f)$. In lepton-based analyses, the final state is tagged by the charge of the lepton from $b \rightarrow \ell^-$ decays; the largest contribution to η_f is then due to $\bar{b} \rightarrow \bar{c} \rightarrow \ell^-$ decays. Alternatively, the charge of a reconstructed charm meson (D^{*-} from B_d^0 or D_s^- from B_s^0), or that of a kaon hypothesized to come from a $b \rightarrow c \rightarrow s$ decay [13], can be used. For fully-inclusive analyses based on topological vertexing, final-state tagging techniques include jet-charge [14] and charge-dipole [15, 16] methods. At high-energy colliders, the methods to tag the initial state (*i.e.*, the state at production), can be divided into two groups: the ones that tag the initial charge of the \bar{b} quark contained in the B_q^0 candidate itself (same-side tag), and the ones that tag the initial charge of the other b quark produced in the event (opposite-side tag). On the same side, the sign of a charged pion, kaon or proton from the primary vertex is correlated with the production state of the B_q^0 meson if that particle is a decay product of a B^{**} state or the first in the fragmentation chain [17, 18]. Jet- and vertex-charge techniques work on both sides and on the opposite side, respec-

tively. Finally, the charge of a lepton from $b \rightarrow \ell^-$, of a kaon from $b \rightarrow c \rightarrow s$ or of a charm hadron from $b \rightarrow c$ [19] can be used as an opposite-side tag, keeping in mind that its performance is degraded due to integrated mixing. At SLC, the beam polarization produced a sizeable forward-backward asymmetry in the $Z \rightarrow b\bar{b}$ decays, and provided another very interesting and effective initial state tag based on the polar angle of the B_q^0 candidate [15]. Initial state tags have also been combined to reach $\eta_i \sim 26\%$ at LEP [18, 20] or 22% at SLD [15] with full efficiency. In the case $\eta_f = 0$, this corresponds to an effective tagging efficiency $Q = \epsilon D^2 = \epsilon(1 - 2\eta)^2$, where ϵ is the tagging efficiency, in the range 23–31%. The equivalent figure achieved by CDF during Tevatron Run I was $\sim 3.5\%$ (see tagging summary on page 160 of Ref. [21]), reflecting the fact that tagging is more difficult at hadron colliders. The CDF and DØ analyses of Tevatron Run II data reached $\epsilon D^2 = (1.8 \pm 0.1)\%$ [22] and $(2.5 \pm 0.2)\%$ [23] for opposite-side tagging, while same-side kaon tagging (for B_s^0 analyses) contributed an additional 3.7–4.8% at CDF [22], and pushed the combined performance to $(4.7 \pm 0.5)\%$ at DØ [24]. LHCb, operating in the forward region at the LHC where the environment is different in terms of track multiplicity and b -hadron production kinematics, has reported $\epsilon D^2 = (2.10 \pm 0.25)\%$ [25] for opposite-side tagging, $(1.80 \pm 0.26)\%$ [26] for same-side kaon tagging, and $(2.11 \pm 0.11)\%$ [27] for same-side pion and proton tagging; the combined figure ranges typically between $(3.73 \pm 0.15)\%$ [28] and $(5.33 \pm 0.25)\%$ [29] depending on the mode in which the tagged B_s^0 meson is reconstructed, and reaches up to $(8.1 \pm 0.6)\%$ [30] for hadronic B_d^0 modes.

At B factories, the flavor of a B_d^0 meson at production cannot be determined, since the two neutral B mesons produced in a $\Upsilon(4S)$ decay evolve in a coherent P -wave state where they keep opposite flavors at any time. However, as soon as one of them decays, the other follows a time-evolution given by Eqs. (74.2) or (74.3), where t is replaced with Δt (which will take negative values half of the time). Hence, the “initial state” tag of a B can be taken as the final-state tag of the other B . Effective tagging efficiencies of 30% are achieved by BaBar and Belle [31], using different techniques including $b \rightarrow \ell^-$ and $b \rightarrow c \rightarrow s$ tags. It is worth noting that, in this case, mixing of the other B (*i.e.*, the coherent mixing occurring before the first B decay) does not contribute to the mistag probability.

Before the experimental observation of a decay-width difference, oscillation analyses typically neglected $\Delta\Gamma_q$ in Eq. (74.4), and described the time dependence with the functions $\Gamma_q e^{-\Gamma_q t} (1 \pm \cos(\Delta m_q t))/2$ (high-energy colliders) or $\Gamma_d e^{-\Gamma_d |\Delta t|} (1 \pm \cos(\Delta m_d \Delta t))/4$ (asymmetric $\Upsilon(4S)$ machines). As can be seen from Eq. (74.4), a non-zero value of $\Delta\Gamma_q$ would effectively reduce the oscillation amplitude with a small time-dependent factor that would be very difficult to distinguish from time resolution effects. Measurements of Δm_q are usually extracted from the data using a maximum likelihood fit.

74.3 Δm_d and $\Delta\Gamma_d$ measurements

Many B_d^0 - \bar{B}_d^0 oscillations analyses have been published [32] by the ALEPH [33], DELPHI [16, 34], L3 [35], OPAL [36, 37], BaBar [38], Belle [39], CDF [17], DØ [23], and LHCb [40–43] collaborations. Although a variety of different techniques have been used, the individual Δm_d results obtained at LEP and Tevatron have remarkably similar precision. Their average is compatible with the recent and more precise measurements at the asymmetric B factories and the LHC. The systematic uncertainties are not negligible; they are often dominated by sample composition, mistag probability, or b -hadron lifetime contributions. Before being combined, the measurements are adjusted on the basis of a common set of input values, including the b -hadron lifetimes and fractions published in this *Review*. Some measurements are statistically correlated. Systematic correlations arise both from common physics sources (fragmentation fractions, lifetimes, branching ratios of b hadrons), and from purely experimental or algorithmic effects (efficiency, resolution, tagging, background description). Combining all measurements [16, 17, 23, 33–43] and accounting for all identified correlations yields $\Delta m_d = 0.5065 \pm 0.0016(\text{stat}) \pm 0.0011(\text{syst}) \text{ ps}^{-1}$ [8], a result dominated by the latest LHCb measurement with

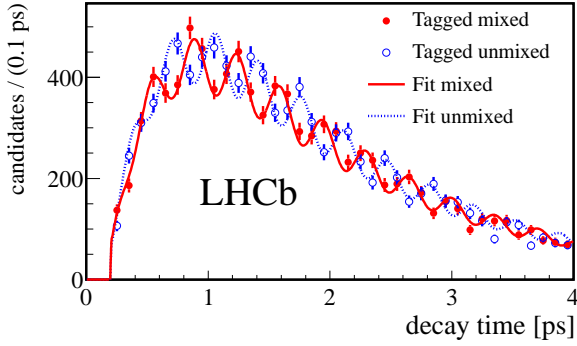


Figure 74.2: Proper time distribution of $B_s^0 \rightarrow D_s^- \pi^+$ candidates tagged as mixed (red) or unmixed (blue) in the LHCb experiment, displaying $B_s^0-\bar{B}_s^0$ oscillations (from Ref. [54]).

$B^0 \rightarrow D^{(*)-} \mu^+ \nu_\mu X$ decays [43].

On the other hand, ARGUS and CLEO have published time-integrated measurements [44–46], which average to $\chi_d = 0.182 \pm 0.015$. Following Ref. [46], the width difference $\Delta\Gamma_d$ could in principle be extracted from the measured value of Γ_d and the above averages for Δm_d and χ_d (see Eq. (74.5)), provided that $\Delta\Gamma_d$ has a negligible impact on the Δm_d measurements. However, direct time-dependent studies published by DELPHI [16], BaBar [47], Belle [48], LHCb [49], ATLAS [50] and CMS [51] provide stronger constraints, which can be combined to yield [8]

$$\Delta\Gamma_d/\Gamma_d = +0.001 \pm 0.010. \quad (74.14)$$

Assuming $\Delta\Gamma_d = 0$ and no CP violation in mixing, and using the B_d^0 lifetime average of 1.519 ± 0.004 ps [8], the Δm_d and χ_d results are combined to yield the world average

$$\Delta m_d = 0.5065 \pm 0.0019 \text{ ps}^{-1} \quad (74.15)$$

or, equivalently,

$$\chi_d = 0.1858 \pm 0.0011. \quad (74.16)$$

This Δm_d value provides an estimate of $2|M_{12}|$, and can be used with Eq. (74.6) to extract $|V_{td}|$ within the Standard Model [52]. The main experimental uncertainties on the result come from m_t and Δm_d , but are still completely negligible with respect to the uncertainty due to the hadronic matrix element $f_{B_d} \sqrt{B_{B_d}} = 225 \pm 9$ MeV [53] obtained from three-flavor lattice QCD calculations.

74.4 Δm_s and $\Delta\Gamma_s$ measurements

After many years of intense search at LEP and SLC, $B_s^0-\bar{B}_s^0$ oscillations were first observed in 2006 by CDF using 1 fb^{-1} of Tevatron Run II data [22]. More recently LHCb observed $B_s^0-\bar{B}_s^0$ oscillations independently with $B_s^0 \rightarrow D_s^- \pi^+$ [40, 54], $B_s^0 \rightarrow D_s^- \mu^+ \nu X$ [42] and even $B_s^0 \rightarrow J/\psi K^+ K^-$ [28] decays, using between 1 and 4.9 fb^{-1} of data collected at the LHC until 2016. Taking systematic correlations into account, the average of all published measurements of Δm_s [22, 28, 40, 42, 54] is

$$\Delta m_s = 17.749 \pm 0.019(\text{stat}) \pm 0.007(\text{syst}) \text{ ps}^{-1}, \quad (74.17)$$

dominated by LHCb (see Fig. 74.2) and still statistically limited.

The information on $|V_{ts}|$ obtained in the framework of the Standard Model is hampered by the hadronic uncertainty, as in the B_d^0 case. However, several uncertainties cancel in the frequency ratio

$$\frac{\Delta m_s}{\Delta m_d} = \frac{m_{B_s}}{m_{B_d}} \xi^2 \left| \frac{V_{ts}}{V_{td}} \right|^2, \quad (74.18)$$

where the SU(3) flavor-symmetry breaking factor $\xi = (f_{B_s} \sqrt{B_{B_s}})/(f_{B_d} \sqrt{B_{B_d}}) = 1.206 \pm 0.017$ is obtained from a

combination of three-flavor lattice QCD calculations [53] dominated by the results of Ref. [55]. Using the measurements of Eqs. (74.15) and (74.17), one can extract

$$\left| \frac{V_{td}}{V_{ts}} \right| = 0.2054 \pm 0.0004(\text{exp}) \pm 0.0029(\text{lattice}), \quad (74.19)$$

in good agreement with (but much more precise than) the value obtained from the ratio of the $b \rightarrow d\gamma$ and $b \rightarrow s\gamma$ transition rates observed at the B factories [52].

The CKM matrix can be constrained using experimental results on observables such as Δm_d , Δm_s , $|V_{ub}/V_{cb}|$, ϵ_K , and $\sin(2\beta)$ together with theoretical inputs and unitarity conditions [52, 56, 57]. The constraint from our knowledge on the ratio $\Delta m_s/\Delta m_d$ is more effective in limiting the position of the apex of the CKM unitarity triangle than the one obtained from the Δm_d measurements alone, due to the reduced hadronic uncertainty in Eq. (74.18). We also note that the measured value of Δm_s is consistent with the Standard Model prediction obtained from CKM fits where no experimental information on Δm_s is used, *e.g.*, $17.25 \pm 0.85 \text{ ps}^{-1}$ [56] or $16.70_{-0.45}^{+0.73} \text{ ps}^{-1}$ [57].

Information on $\Delta\Gamma_s$ can be obtained from the study of the proper time distribution of untagged B_s^0 samples [58]. In the case of an inclusive B_s^0 selection [59], or a flavor-specific (semileptonic or hadronic) B_s^0 decay selection [20, 60–62], both the short- and long-lived components are present, and the proper time distribution is a superposition of two exponentials with decay constants $\Gamma_{L,H} = \Gamma_s \pm \Delta\Gamma_s/2$. In principle, this provides sensitivity to both Γ_s and $(\Delta\Gamma_s/\Gamma_s)^2$. Ignoring $\Delta\Gamma_s$ and fitting for a single exponential leads to an estimate of $1/\Gamma_s$ (called effective lifetime) with a relative bias proportional to $(\Delta\Gamma_s/\Gamma_s)^2$. An alternative approach, sensitive to first order in $\Delta\Gamma_s/\Gamma_s$, is to determine the effective lifetime of untagged B_s^0 decays to pure CP eigenstates; measurements exist for $B_s^0 \rightarrow D_s^+ D_s^-$ [61], $B_s^0 \rightarrow K^+ K^-$ [62, 63], $B_s^0 \rightarrow J/\psi\eta$ [64], $B_s^0 \rightarrow J/\psi f_0(980)$ [65], $B_s^0 \rightarrow J/\psi\pi^+\pi^-$ [51, 66], $B_s^0 \rightarrow J/\psi K_S^0$ [67], and $B_s^0 \rightarrow \mu^+\mu^-$ [68]. The extraction of $1/\Gamma_s$ and $\Delta\Gamma_s$ from such measurements, discussed in detail in Ref. [69], requires additional information in the form of theoretical assumptions or external inputs on weak phases and hadronic parameters. In what follows, we only use the effective lifetimes of decays to CP -even ($D_s^+ D_s^-$, $J/\psi\eta$) and CP -odd ($J/\psi f_0(980)$, $J/\psi\pi^+\pi^-$) final states where CP conservation can be assumed.

The best sensitivity to $1/\Gamma_s$ and $\Delta\Gamma_s$ is achieved by the time-dependent measurements of the $B_s^0 \rightarrow J/\psi K^+ K^-$ (including $B_s^0 \rightarrow J/\psi\phi$) and $B_s^0 \rightarrow \psi(2S)\phi$ decay rates performed at CDF [70], DØ [71], ATLAS [72, 73], CMS [74] and LHCb [28, 75, 76], where the CP -even and CP -odd amplitudes are separated statistically through a full angular analysis. The LHCb collaboration analyzes the $B_s^0 \rightarrow J/\psi K^+ K^-$ decay considering that the $K^+ K^-$ system can be in a P-wave or S-wave state, and measures the dependence of the strong phase difference between the P-wave and S-wave amplitudes as a function of the $K^+ K^-$ invariant mass [28, 77]; this allows the unambiguous determination of the sign of $\Delta\Gamma_s$, which is found to be positive. All these studies use both untagged and tagged B_s^0 candidates and are optimized for the measurement of the CP -violating phase $\phi_s^{c\bar{c}s}$, defined as the weak phase difference between the $B_s^0-\bar{B}_s^0$ mixing amplitude and the $b \rightarrow c\bar{c}s$ decay amplitude. As reported below in Eq. (74.28), the current experimental average of $\phi_s^{c\bar{c}s}$ is consistent with zero. Assuming no CP violation (*i.e.*, $\phi_s^{c\bar{c}s} = 0$) a combination [8] of the published $B_s^0 \rightarrow J/\psi K^+ K^-$, $J/\psi\phi$ and $\psi(2S)\phi$ analyses [28, 70–72, 74–76] and of effective lifetime measurements with flavor-specific [20, 60–62] and pure CP [51, 61, 64–66] final states yields

$$\Delta\Gamma_s = +0.085 \pm 0.004 \text{ ps}^{-1} \text{ and } 1/\Gamma_s = 1.515 \pm 0.004 \text{ ps}, \quad (74.20)$$

or, equivalently,

$$1/\Gamma_L = 1.423 \pm 0.005 \text{ ps} \text{ and } 1/\Gamma_H = 1.620 \pm 0.007 \text{ ps}, \quad (74.21)$$

in good agreement with the Standard Model prediction $\Delta\Gamma_s = 0.088 \pm 0.020 \text{ ps}^{-1}$ [9].

Estimates of $\Delta\Gamma_s/\Gamma_s$ obtained from measurements of the $B_s^0 \rightarrow D_s^{(*)+} D_s^{(*)-}$ branching fractions are not included in the average,

Table 74.1: $\bar{\chi}$ and b -hadron fractions (see text).

	in Z decays [8]	at Tevatron [8]	at LHC [89–91]
$\bar{\chi}$	0.1259 ± 0.0042	0.147 ± 0.011	
$f_u = f_d$	0.408 ± 0.007	0.344 ± 0.021	
f_s	0.100 ± 0.008	0.115 ± 0.013	
f_{baryon}	0.084 ± 0.011	0.198 ± 0.046	
f_s/f_d	0.246 ± 0.023	0.333 ± 0.040	0.247 ± 0.009

since they are based on the questionable [7] assumption that these decays account for all CP -even final states.

74.5 Average b -hadron mixing probability and b -hadron production fractions at high energy

Mixing measurements can significantly improve our knowledge on the fractions f_u , f_d , f_s , and f_{baryon} , defined as the fractions of B_u , B_d^0 , B_s^0 , and b -baryons in an unbiased sample of weakly-decaying b hadrons produced in high-energy collisions. Indeed, time-integrated mixing analyses using lepton pairs from $b\bar{b}$ events at high energy measure the quantity

$$\bar{\chi} = f'_d \chi_d + f'_s \chi_s, \quad (74.22)$$

where f'_q ($q = s, d$) is the B_q^0 fraction in a sample of semileptonic b -hadron decays. Assuming that all b hadrons have the same semileptonic decay width implies $f'_q = f_q/(\Gamma_q \tau_b)$, where τ_b is the average b -hadron lifetime. Hence $\bar{\chi}$ measurements performed at LEP [78] and Tevatron [79, 80], together with χ_d given in Eq. (74.16) and the very good approximation $\chi_s = 1/2$ (in fact $\chi_s = 0.499312 \pm 0.000004$ from Eqs. (74.5), (74.17) and (74.20)), provide constraints on f_d and f_s .

The LEP experiments have measured $\mathcal{B}(\bar{b} \rightarrow B_s^0) \times \mathcal{B}(B_s^0 \rightarrow D_s^- \ell^+ \nu_\ell X)$ [81], $\mathcal{B}(b \rightarrow A_b^0) \times \mathcal{B}(A_b^0 \rightarrow A_c^+ \ell^- \bar{\nu}_\ell X)$ [82], and $\mathcal{B}(b \rightarrow \Xi_b^-) \times \mathcal{B}(\Xi_b^- \rightarrow \Xi^- \ell^- \bar{\nu}_\ell X)$ [83] from partially reconstructed final states including a lepton, f_{baryon} from protons identified in b events [84], and the production rate of charged b hadrons [85]. The b -hadron fraction ratios measured at CDF are based on double semileptonic $K^* \mu \mu$ and $\phi \mu \mu$ final states [86] and lepton-charm final states [87]; in addition CDF and DØ have both measured strange b -baryon production [88]. On the other hand, fraction ratios have been studied by LHCb using fully reconstructed hadronic B_s^0 and B_d^0 decays [89], as well as semileptonic decays of A_b^0 , B_s^0 , B_d^0 and B_u [90]. ATLAS has measured f_s/f_d using $B_s^0 \rightarrow J/\psi \phi$ and $B^0 \rightarrow J/\psi K^{*0}$ decays [91]. Both CDF and LHCb observe that the ratio $f_{A_b^0}/(f_u + f_d)$ decreases with the transverse momentum of the lepton+charm system, indicating that the b -hadron fractions are not the same in different environments. A combination of the available information from LEP and Tevatron yields, under the constraints $f_u = f_d$, $f_u + f_d + f_s + f_{\text{baryon}} = 1$ and Eq. (74.22), the averages of the first two columns of Table 74.1, while the third column shows the average of LHC measurements of $f_s/f_u = f_s/f_d$, which are all compatible. The B_c^+ fraction, neglected in the above constraints, has been measured for the first time by LHCb to be $(0.26 \pm 0.06)\%$ [92].

74.6 CP -violation studies

Evidence for CP violation in B_q^0 - \bar{B}_q^0 mixing has been searched for, both with flavor-specific and inclusive B_q^0 decays, in samples where the initial flavor state is tagged, usually with a lepton from the other b -hadron in the event. In the case of semileptonic (or other flavor-specific) decays, where the final-state tag is also available, the following asymmetry [2]

$$\mathcal{A}_{\text{SL}}^q = \frac{N(\bar{B}_q^0(t) \rightarrow \ell^+ \nu_\ell X) - N(B_q^0(t) \rightarrow \ell^- \bar{\nu}_\ell X)}{N(\bar{B}_q^0(t) \rightarrow \ell^+ \nu_\ell X) + N(B_q^0(t) \rightarrow \ell^- \bar{\nu}_\ell X)} \simeq 1 - |q/p|^2 \quad (74.23)$$

has been measured either in time-integrated analyses at CLEO [46, 93], BaBar [94], CDF [95], DØ [96–98] and LHCb [99], or in time-dependent analyses at LEP [37, 100], BaBar [47, 101] and

Belle [102]. In the inclusive case, also investigated at LEP [100, 103], no final-state tag is used, and the asymmetry [104]

$$\begin{aligned} & \frac{N(\bar{B}_q^0(t) \rightarrow \text{all}) - N(B_q^0(t) \rightarrow \text{all})}{N(\bar{B}_q^0(t) \rightarrow \text{all}) + N(B_q^0(t) \rightarrow \text{all})} \\ & \simeq \mathcal{A}_{\text{SL}}^q \left[\sin^2 \left(\frac{\Delta m_q t}{2} \right) - \frac{x_q}{2} \sin(\Delta m_q t) \right] \end{aligned} \quad (74.24)$$

must be measured as a function of the proper time to extract information on CP violation. In addition LHCb has studied the time dependence of the charge asymmetry of $B^0 \rightarrow D^{(*)-} \mu^+ \nu_\mu X$ decays without tagging the initial state [105], which would be equal to

$$\frac{N(D^{(*)-} \mu^+ \nu_\mu X) - N(D^{(*)+} \mu^- \bar{\nu}_\mu X)}{N(D^{(*)-} \mu^+ \nu_\mu X) + N(D^{(*)+} \mu^- \bar{\nu}_\mu X)} = \mathcal{A}_{\text{SL}}^d \frac{1 - \cos(\Delta m_d t)}{2} \quad (74.25)$$

in absence of detection and production asymmetries.

The DØ collaboration measured a like-sign dimuon charge asymmetry in semileptonic b decays that deviates by 2.8σ from the tiny Standard Model prediction and concluded, from a more refined analysis in bins of muon impact parameters, that the overall discrepancy is at the level of 3.6σ [96]. In all other cases, asymmetries compatible with zero (and the Standard Model [9]) have been found, with a precision limited by the available statistics. Several of the analyses at high energy don't disentangle the B_d^0 and B_s^0 contributions, and either quote a mean asymmetry or a measurement of $\mathcal{A}_{\text{SL}}^d$ assuming $\mathcal{A}_{\text{SL}}^s = 0$: we no longer include these in the average. An exception is the dimuon DØ analysis [96], which separates the two contributions by exploiting their dependence on the muon impact parameter cut. The resulting measurements of $\mathcal{A}_{\text{SL}}^d$ and $\mathcal{A}_{\text{SL}}^s$ are then both compatible with the Standard Model. They are also correlated. We therefore perform a two-dimensional average of the measurements of Refs. [46, 47, 93, 94, 96–99, 101, 102, 105] and obtain [8]

$$\mathcal{A}_{\text{SL}}^d = -0.0021 \pm 0.0017_{\text{stat}}/p|_d = 1.0010 \pm 0.0008, \quad (74.26)$$

$$\mathcal{A}_{\text{SL}}^s = -0.0006 \pm 0.0023_{\text{stat}}/p|_s = 1.0003 \pm 0.0014, \quad (74.27)$$

with a correlation coefficient of -0.054 between $\mathcal{A}_{\text{SL}}^d$ and $\mathcal{A}_{\text{SL}}^s$. These results show no evidence of CP violation and don't constrain yet the Standard Model.

CP violation induced by B_s^0 - \bar{B}_s^0 mixing in $b \rightarrow c\bar{c}s$ decays has been a field of very active study in the past decade. In addition to the previously mentioned $B_s^0 \rightarrow J/\psi K^+ K^-$ (including $B_s^0 \rightarrow J/\psi \phi$) and $B_s^0 \rightarrow \psi(2S)\phi$ studies, the decay modes $B_s^0 \rightarrow J/\psi \pi^+ \pi^-$ (including $B_s^0 \rightarrow J/\psi f_0(980)$) [106] and $B_s^0 \rightarrow D_s^+ D_s^-$ [29] have also been analyzed by LHCb to measure $\phi_s^{c\bar{c}s}$, without the need for an angular analysis. The $J/\psi \pi^+ \pi^-$ final state has been shown indeed to be (very close to) a pure CP -odd state [107]. A two-dimensional fit [8] of all published results [28, 29, 70–72, 74–76, 106] in the $(\phi_s^{c\bar{c}s}, \Delta\Gamma_s)$ plane yields

$$\phi_s^{c\bar{c}s} = -0.051 \pm 0.023. \quad (74.28)$$

Adding to this fit the new ATLAS results recently submitted for publication [73] leads to the preliminary average $\phi_s^{c\bar{c}s} = -0.057 \pm 0.021$, with the overall situation shown on Fig. 74.3. This experimental value is consistent with the Standard Model prediction for $\phi_s^{c\bar{c}s}$, which is equal to $-2\beta_s = -2 \arg(-V_{ts} V_{tb}^*)/(V_{cs} V_{cb}^*) = -0.0370^{+0.0007}_{-0.0008}$ [57] assuming negligible Penguin pollution.

74.7 Summary

B^0 - \bar{B}^0 mixing has been and still is a field of intense study. The mass differences in the B_d^0 - \bar{B}_d^0 and B_s^0 - \bar{B}_s^0 systems are known to relative precisions of 0.38% and 0.11%, respectively. The non-zero decay width difference in the B_s^0 - \bar{B}_s^0 system is well established, with a relative difference of $\Delta\Gamma_s/\Gamma_s = (12.9 \pm 0.6)\%$, meaning that the heavy state of the B_s^0 - \bar{B}_s^0 system lives $\sim 14\%$ longer than the light state. In contrast, the relative decay width difference in the B_d^0 - \bar{B}_d^0 system, $\Delta\Gamma_d/\Gamma_d = (0.1 \pm 1.0)\%$, is still consistent with

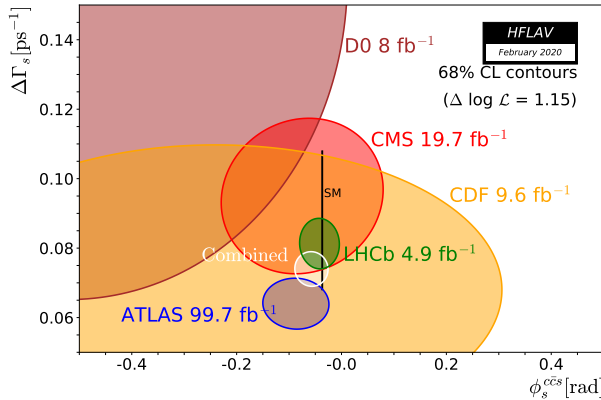


Figure 74.3: 68% CL contours in the $(\phi_s^{c\bar{c}s}, \Delta\Gamma_s)$ plane, showing all measurements from CDF [70], DØ [71], ATLAS [72, 73], CMS [74] and LHCb [28, 29, 75, 76, 106], with their preliminary average [8]. The very thin black rectangle represents the Standard Model predictions of $\phi_s^{c\bar{c}s}$ [57] and $\Delta\Gamma_s$ [9].

zero. CP violation in $B_d^0-\bar{B}_d^0$ or $B_s^0-\bar{B}_s^0$ mixing has not been observed yet, with precisions on the semileptonic asymmetries below 0.3%. CP violation induced by $B_s^0-\bar{B}_s^0$ mixing in $b \rightarrow c\bar{c}s$ transitions has not yet been observed either, with an uncertainty on the $\phi_s^{c\bar{c}s}$ phase of 23 mrad. Despite the recent improvements, all observations remain consistent with the Standard Model expectations.

However, the measurements where New Physics might show up are still statistically limited. More results are awaited from the LHC experiments and Belle II, with promising prospects for the investigation of the CP -violating phase $\arg(-M_{12}/\Gamma_{12})$ and an improved determination of $\phi_s^{c\bar{c}s}$.

Mixing studies have clearly reached the stage of precision measurements, where much effort is needed, both on the experimental and theoretical sides, in particular to further reduce the hadronic uncertainties of lattice QCD calculations. In the long term, a stringent check of the consistency of the B_d^0 and B_s^0 mixing amplitudes (magnitudes and phases) with all other measured flavor-physics observables will be possible within the Standard Model, leading to very tight limits on (or otherwise a long-awaited surprise about) New Physics.

References

- [1] T. D. Lee and C. S. Wu, *Ann. Rev. Nucl. Part. Sci.* **16**, 511 (1966); I. I. Bigi and A. I. Sanda, *Camb. Monogr. Part. Phys. Nucl. Phys. Cosmol.* **9**, 1 (2009), second edition, first published in 2000; G. C. Branco, L. Lavoura and J. P. Silva, *Int. Ser. Monogr. Phys.* **103**, 1 (1999).
- [2] See the review on CP violation in the quark sector by T. Gershon and Y. Nir in this publication.
- [3] A. J. Buras, W. Slominski and H. Steger, *Nucl. Phys.* **B245**, 369 (1984).
- [4] T. Inami and C. S. Lim, *Prog. Theor. Phys.* **65**, 297 (1981), erratum *ibid.* **65**, 1772 (1981); for the power-like approximation, see A. J. Buras and R. Fleischer, page 91 in “Heavy Flavours II,” eds. A. J. Buras and M. Lindner, Singapore World Scientific (1998).
- [5] M. Kobayashi and T. Maskawa, *Prog. Theor. Phys.* **49**, 652 (1973).
- [6] I. I. Bigi *et al.*, in “ CP violation,” ed. C. Jarlskog, Singapore World Scientific (1989).
- [7] A. Lenz and U. Nierste (2011), [arXiv:1102.4274]; A. Lenz and U. Nierste, *JHEP* **06**, 072 (2007), [hep-ph/0612167].
- [8] Y. Amhis *et al.* (HFLAV) (2019), [arXiv:1909.12524]; the combined results on b -hadron fractions, lifetimes and mixing parameters published in this *Review* have been obtained by the B oscillations working group of the Heavy Flavor Averaging (HFLAV) group, using the methods and procedures described in Chapter 4 of the above paper, after updating the list of inputs; for more information, see <https://hflav.web.cern.ch/>.
- [9] T. Jubb *et al.*, *Nucl. Phys.* **B915**, 431 (2017), [arXiv:1603.07770]; M. Artuso, G. Borissov and A. Lenz, *Rev. Mod. Phys.* **88**, 045002 (2016), [arXiv:1511.09466].
- [10] C. Albajar *et al.* (UA1), *Phys. Lett.* **B186**, 247 (1987), erratum *ibid.* **B197**, 565 (1987).
- [11] H. Albrecht *et al.* (ARGUS), *Phys. Lett.* **B192**, 245 (1987).
- [12] H. G. Moser and A. Roussarie, *Nucl. Instrum. Meth.* **A384**, 491 (1997).
- [13] SLD collab., SLAC-PUB-7228, SLAC-PUB-7229, and SLAC-PUB-7230, *28th Int. Conf. on High Energy Physics*, Warsaw (1996); J. L. Wittlin, *A measurement of the time dependence of $B_d^0-\bar{B}_d^0$ mixing with kaon tagging*, Ph.D. thesis, Massachusetts U., Amherst (2001), URL <http://www.lib.umi.com/dissertations/fullcit?p3027272>.
- [14] ALEPH collab., contrib. 596 to *Int. Europhysics Conf. on High Energy Physics*, Jerusalem (1997).
- [15] K. Abe *et al.* (SLD), *Phys. Rev.* **D67**, 012006 (2003), [hep-ex/0209002].
- [16] J. Abdallah *et al.* (DELPHI), *Eur. Phys. J.* **C28**, 155 (2003), [hep-ex/0303032].
- [17] F. Abe *et al.* (CDF), *Phys. Rev. Lett.* **80**, 2057 (1998), [hep-ex/9712004]; F. Abe *et al.* (CDF), *Phys. Rev.* **D59**, 032001 (1999), [hep-ex/9806026]; F. Abe *et al.* (CDF), *Phys. Rev.* **D60**, 051101 (1999); F. Abe *et al.* (CDF), *Phys. Rev.* **D60**, 072003 (1999), [hep-ex/9903011]; T. Affolder *et al.* (CDF), *Phys. Rev.* **D60**, 112004 (1999), [hep-ex/9907053].
- [18] R. Barate *et al.* (ALEPH), *Eur. Phys. J.* **C4**, 367 (1998); R. Barate *et al.* (ALEPH), *Eur. Phys. J.* **C7**, 553 (1999), [hep-ex/9811018].
- [19] R. Aaij *et al.* (LHCb), *JINST* **10**, P10005 (2015), [arXiv:1507.07892].
- [20] P. Abreu *et al.* (DELPHI), *Eur. Phys. J.* **C16**, 555 (2000), [hep-ex/0107077].
- [21] K. Anikeev *et al.* (2002), [hep-ph/0201071].
- [22] A. Abulencia *et al.* (CDF), *Phys. Rev. Lett.* **97**, 242003 (2006), [hep-ex/0609040].
- [23] V. M. Abazov *et al.* (DØ), *Phys. Rev.* **D74**, 112002 (2006), [hep-ex/0609034].
- [24] V. M. Abazov *et al.* (DØ), *Phys. Rev. Lett.* **101**, 241801 (2008), [arXiv:0802.2255].
- [25] R. Aaij *et al.* (LHCb), *Eur. Phys. J.* **C72**, 2022 (2012), [arXiv:1202.4979].
- [26] R. Aaij *et al.* (LHCb), *JINST* **11**, P05010 (2016), [arXiv:1602.07252].
- [27] R. Aaij *et al.* (LHCb), *Eur. Phys. J.* **C77**, 238 (2017), [arXiv:1610.06019].
- [28] R. Aaij *et al.* (LHCb), *Phys. Rev. Lett.* **114**, 041801 (2015), [arXiv:1411.3104]; R. Aaij *et al.* (LHCb), *Eur. Phys. J.* **C79**, 706 (2019), erratum to appear, [arXiv:1906.08356].
- [29] R. Aaij *et al.* (LHCb), *Phys. Rev. Lett.* **113**, 211801 (2014), [arXiv:1409.4619].
- [30] R. Aaij *et al.* (LHCb), *Phys. Rev. Lett.* **117**, 261801 (2016), [arXiv:1608.06620].
- [31] B. Aubert *et al.* (BaBar), *Phys. Rev. Lett.* **94**, 161803 (2005), [hep-ex/0408127]; K. F. Chen *et al.* (Belle), *Phys. Rev.* **D72**, 012004 (2005), [hep-ex/0504023].
- [32] Throughout this document we omit references of results that have been replaced by new published measurements.
- [33] D. Buskulic *et al.* (ALEPH), *Z. Phys.* **C75**, 397 (1997).
- [34] P. Abreu *et al.* (DELPHI), *Z. Phys.* **C76**, 579 (1997).
- [35] M. Acciarri *et al.* (L3), *Eur. Phys. J.* **C5**, 195 (1998).

- [36] G. Alexander *et al.* (OPAL), *Z. Phys.* **C72**, 377 (1996); K. Ackerstaff *et al.* (OPAL), *Z. Phys.* **C76**, 417 (1997), [hep-ex/9707010]; G. Abbiendi *et al.* (OPAL), *Phys. Lett.* **B493**, 266 (2000), [hep-ex/0010013].
- [37] K. Ackerstaff *et al.* (OPAL), *Z. Phys.* **C76**, 401 (1997), [hep-ex/9707009].
- [38] B. Aubert *et al.* (BaBar), *Phys. Rev. Lett.* **88**, 221802 (2002), [hep-ex/0112044]; B. Aubert *et al.* (BaBar), *Phys. Rev.* **D66**, 032003 (2002), [hep-ex/0201020]; B. Aubert *et al.* (BaBar), *Phys. Rev. Lett.* **88**, 221803 (2002), [hep-ex/0112045]; B. Aubert *et al.* (BaBar), *Phys. Rev.* **D67**, 072002 (2003), [hep-ex/0212017]; B. Aubert *et al.* (BaBar), *Phys. Rev.* **D73**, 012004 (2006), [hep-ex/0507054].
- [39] N. C. Hastings *et al.* (Belle), *Phys. Rev.* **D67**, 052004 (2003), [hep-ex/0212033]; Y. Zheng *et al.* (Belle), *Phys. Rev.* **D67**, 092004 (2003), [hep-ex/0211065]; K. Abe *et al.* (Belle), *Phys. Rev.* **D71**, 072003 (2005), erratum *ibid.* **D71**, 079903 (2005), [hep-ex/0408111].
- [40] R. Aaij *et al.* (LHCb), *Phys. Lett.* **B709**, 177 (2012), [arXiv:1112.4311].
- [41] R. Aaij *et al.* (LHCb), *Phys. Lett.* **B719**, 318 (2013), [arXiv:1210.6750].
- [42] R. Aaij *et al.* (LHCb), *Eur. Phys. J.* **C73**, 2655 (2013), [arXiv:1308.1302].
- [43] P. Huang *et al.*, *Eur. Phys. J.* **C76**, 422 (2016), [arXiv:1505.03672].
- [44] H. Albrecht *et al.* (ARGUS), *Z. Phys.* **C55**, 357 (1992); H. Albrecht *et al.* (ARGUS), *Phys. Lett.* **B324**, 249 (1994).
- [45] J. E. Bartelt *et al.* (CLEO), *Phys. Rev. Lett.* **71**, 1680 (1993).
- [46] B. H. Behrens *et al.* (CLEO), *Phys. Lett.* **B490**, 36 (2000), [hep-ex/0005013].
- [47] B. Aubert *et al.* (BaBar), *Phys. Rev. Lett.* **92**, 181801 (2004), [hep-ex/0311037]; B. Aubert *et al.* (BaBar), *Phys. Rev.* **D70**, 012007 (2004), [hep-ex/0403002].
- [48] T. Higuchi *et al.*, *Phys. Rev.* **D85**, 071105 (2012), [arXiv:1203.0930].
- [49] R. Aaij *et al.* (LHCb), *JHEP* **04**, 114 (2014), [arXiv:1402.2554].
- [50] M. Aaboud *et al.* (ATLAS), *JHEP* **06**, 081 (2016), [arXiv:1605.07485].
- [51] A. M. Sirunyan *et al.* (CMS), *Eur. Phys. J.* **C78**, 457 (2018), erratum *ibid.* **C78**, 561 (2018), [arXiv:1710.08949].
- [52] See the review on the CKM quark-mixing matrix by A. Cecucci, Z. Ligeti, and Y. Sakai in this publication.
- [53] S. Aoki *et al.* (Flavour Lattice Averaging Group) (2019), [arXiv:1902.08191].
- [54] R. Aaij *et al.* (LHCb), *New J. Phys.* **15**, 053021 (2013), [arXiv:1304.4741].
- [55] A. Bazavov *et al.* (Fermilab Lattice and MILC), *Phys. Rev.* **D93**, 113016 (2016), [arXiv:1602.03560].
- [56] M. Bona *et al.* (UTfit), *JHEP* **10**, 081 (2006), [hep-ph/0606167]; updated results at <http://www.utfit.org/>.
- [57] J. Charles *et al.*, *Phys. Rev.* **D91**, 073007 (2015), [arXiv:1501.05013]; updated results at <http://ckmfitter.in2p3.fr/>.
- [58] K. Hartkorn and H. G. Moser, *Eur. Phys. J.* **C8**, 381 (1999).
- [59] M. Acciarri *et al.* (L3), *Phys. Lett.* **B438**, 417 (1998).
- [60] D. Buskulic *et al.* (ALEPH), *Phys. Lett.* **B377**, 205 (1996); K. Ackerstaff *et al.* (OPAL), *Phys. Lett.* **B426**, 161 (1998), [hep-ex/9802002]; F. Abe *et al.* (CDF), *Phys. Rev.* **D59**, 032004 (1999), [hep-ex/9808003]; V. M. Abazov *et al.* (DØ), *Phys. Rev. Lett.* **114**, 062001 (2015), [arXiv:1410.1568]; T. Aaltonen *et al.* (CDF), *Phys. Rev. Lett.* **107**, 272001 (2011), [arXiv:1103.1864]; R. Aaij *et al.* (LHCb), *Phys. Rev. Lett.* **113**, 172001 (2014), [arXiv:1407.5873]; R. Aaij *et al.* (LHCb), *Phys. Rev. Lett.* **119**, 101801 (2017), [arXiv:1705.03475].
- [61] R. Aaij *et al.* (LHCb), *Phys. Rev. Lett.* **112**, 111802 (2014), [arXiv:1312.1217].
- [62] R. Aaij *et al.* (LHCb), *Phys. Lett.* **B736**, 446 (2014), [arXiv:1406.7204].
- [63] R. Aaij *et al.* (LHCb), *Phys. Lett.* **B707**, 349 (2012), [arXiv:1111.0521].
- [64] R. Aaij *et al.* (LHCb), *Phys. Lett.* **B762**, 484 (2016), [arXiv:1607.06314].
- [65] T. Aaltonen *et al.* (CDF), *Phys. Rev.* **D84**, 052012 (2011), [arXiv:1106.3682]; V. M. Abazov *et al.* (DØ), *Phys. Rev.* **D94**, 012001 (2016), [arXiv:1603.01302].
- [66] R. Aaij *et al.* (LHCb), *Phys. Rev.* **D87**, 112010 (2013), [arXiv:1304.2600].
- [67] R. Aaij *et al.* (LHCb), *Nucl. Phys.* **B873**, 275 (2013), [arXiv:1304.4500].
- [68] R. Aaij *et al.* (LHCb), *Phys. Rev. Lett.* **118**, 191801 (2017), [arXiv:1703.05747].
- [69] R. Fleischer and R. Knegjens, *Eur. Phys. J.* **C71**, 1789 (2011), [arXiv:1109.5115].
- [70] T. Aaltonen *et al.* (CDF), *Phys. Rev. Lett.* **109**, 171802 (2012), [arXiv:1208.2967].
- [71] V. M. Abazov *et al.* (DØ), *Phys. Rev.* **D85**, 032006 (2012), [arXiv:1109.3166].
- [72] G. Aad *et al.* (ATLAS), *Phys. Rev.* **D90**, 052007 (2014), [arXiv:1407.1796]; G. Aad *et al.* (ATLAS), *JHEP* **08**, 147 (2016), [arXiv:1601.03297].
- [73] G. Aad *et al.* (ATLAS) (2020), [arXiv:2001.07115].
- [74] V. Khachatryan *et al.* (CMS), *Phys. Lett.* **B757**, 97 (2016), [arXiv:1507.07527].
- [75] R. Aaij *et al.* (LHCb), *JHEP* **08**, 037 (2017), [arXiv:1704.08217].
- [76] R. Aaij *et al.* (LHCb), *Phys. Lett.* **B762**, 253 (2016), [arXiv:1608.04855].
- [77] R. Aaij *et al.* (LHCb), *Phys. Rev. Lett.* **108**, 241801 (2012), [arXiv:1202.4717].
- [78] S. Schael *et al.* (ALEPH, DELPHI, L3, OPAL, SLD, LEP Electroweak Working Group, SLD Electroweak Group, SLD Heavy Flavour Group), *Phys. Rept.* **427**, 257 (2006), [hep-ex/0509008]; we use the $\bar{\chi}$ average given in Eq. (5.39).
- [79] D. Acosta *et al.* (CDF), *Phys. Rev.* **D69**, 012002 (2004), [hep-ex/0309030].
- [80] V. M. Abazov *et al.* (DØ), *Phys. Rev.* **D74**, 092001 (2006), [hep-ex/0609014].
- [81] P. Abreu *et al.* (DELPHI), *Phys. Lett.* **B289**, 199 (1992); P. D. Acton *et al.* (OPAL), *Phys. Lett.* **B295**, 357 (1992); D. Buskulic *et al.* (ALEPH), *Phys. Lett.* **B361**, 221 (1995).
- [82] P. Abreu *et al.* (DELPHI), *Z. Phys.* **C68**, 375 (1995); R. Barate *et al.* (ALEPH), *Eur. Phys. J.* **C2**, 197 (1998).
- [83] D. Buskulic *et al.* (ALEPH), *Phys. Lett.* **B384**, 449 (1996); J. Abdallah *et al.* (DELPHI), *Eur. Phys. J.* **C44**, 299 (2005), [hep-ex/0510023].
- [84] R. Barate *et al.* (ALEPH), *Eur. Phys. J.* **C5**, 205 (1998).
- [85] J. Abdallah *et al.* (DELPHI), *Phys. Lett.* **B576**, 29 (2003), [hep-ex/0311005].
- [86] F. Abe *et al.* (CDF), *Phys. Rev.* **D60**, 092005 (1999).
- [87] T. Aaltonen *et al.* (CDF), *Phys. Rev.* **D77**, 072003 (2008), [arXiv:0801.4375]; T. Affolder *et al.* (CDF), *Phys. Rev. Lett.* **84**, 1663 (2000), [hep-ex/9909011]; the measurement of f_{baryon}/f_d in the latter paper has been updated based on; T. Aaltonen *et al.* (CDF), *Phys. Rev.* **D79**, 032001 (2009), [arXiv:0810.3213].
- [88] V. M. Abazov *et al.* (DØ), *Phys. Rev. Lett.* **99**, 052001 (2007), [arXiv:0706.1690]; V. M. Abazov *et al.* (DØ), *Phys. Rev. Lett.* **101**, 232002 (2008), [arXiv:0808.4142]; T. Aaltonen *et al.* (CDF), *Phys. Rev.* **D80**, 072003 (2009), [arXiv:0905.3123].

- [89] R. Aaij *et al.* (LHCb), JHEP **04**, 001 (2013), [arXiv:1301.5286]; the LHCb average of f_s/f_d has been updated in LHCb collab., LHCb-CONF-2013-011 (2013).
- [90] R. Aaij *et al.* (LHCb), Phys. Rev. **D85**, 032008 (2012), [arXiv:1111.2357]; R. Aaij *et al.* (LHCb), Phys. Rev. **D100**, 031102 (2019), [arXiv:1902.06794].
- [91] G. Aad *et al.* (ATLAS), Phys. Rev. Lett. **115**, 262001 (2015), [arXiv:1507.08925].
- [92] R. Aaij *et al.* (LHCb), Phys. Rev. **D100**, 112006 (2019), [arXiv:1910.13404].
- [93] D. E. Jaffe *et al.* (CLEO), Phys. Rev. Lett. **86**, 5000 (2001), [hep-ex/0101006].
- [94] J. P. Lees *et al.* (BaBar), Phys. Rev. Lett. **114**, 081801 (2015), [arXiv:1411.1842].
- [95] F. Abe *et al.* (CDF), Phys. Rev. **D55**, 2546 (1997).
- [96] V. M. Abazov *et al.* (DØ), Phys. Rev. **D89**, 012002 (2014), [arXiv:1310.0447].
- [97] V. M. Abazov *et al.* (DØ), Phys. Rev. **D86**, 072009 (2012), [arXiv:1208.5813].
- [98] V. M. Abazov *et al.* (DØ), Phys. Rev. Lett. **110**, 011801 (2013), [arXiv:1207.1769].
- [99] R. Aaij *et al.* (LHCb), Phys. Rev. Lett. **117**, 061803 (2016), erratum *ibid.* **118**, 129903 (2017), [arXiv:1605.09768].
- [100] R. Barate *et al.* (ALEPH), Eur. Phys. J. **C20**, 431 (2001).
- [101] J. P. Lees *et al.* (BaBar), Phys. Rev. Lett. **111**, 101802 (2013), erratum *ibid.* **111**, 159901 (2013), [arXiv:1305.1575].
- [102] E. Nakano *et al.* (Belle), Phys. Rev. **D73**, 112002 (2006), [hep-ex/0505017].
- [103] G. Abbiendi *et al.* (OPAL), Eur. Phys. J. **C12**, 609 (2000), [hep-ex/9901017].
- [104] M. Beneke, G. Buchalla and I. Dunietz, Phys. Lett. **B393**, 132 (1997), [hep-ph/9609357]; I. Dunietz, Eur. Phys. J. **C7**, 197 (1999), [hep-ph/9806521].
- [105] R. Aaij *et al.* (LHCb), Phys. Rev. Lett. **114**, 041601 (2015), [arXiv:1409.8586].
- [106] R. Aaij *et al.* (LHCb), Phys. Lett. **B736**, 186 (2014), [arXiv:1405.4140]; R. Aaij *et al.* (LHCb), Phys. Lett. **B797**, 134789 (2019), [arXiv:1903.05530].
- [107] R. Aaij *et al.* (LHCb), Phys. Rev. **D86**, 052006 (2012), [arXiv:1204.5643].

75. Semileptonic b -Hadron Decays, Determination of V_{cb} , V_{ub}

Revised August 2019 by T. Mannel (Siegen U.) and P. Urquijo (School of Phys. U. of Melbourne).

75.1 Introduction

Precision determinations of $|V_{ub}|$ and $|V_{cb}|$ are central to testing the CKM sector of the Standard Model, and complement the measurements of CP asymmetries in B decays. The length of the side of the unitarity triangle opposite the well-measured angle β is proportional to the ratio $|V_{ub}|/|V_{cb}|$; its precise determination is a high priority of the heavy-flavor physics program.

The transitions $b \rightarrow c\ell\bar{\nu}_\ell$ and $b \rightarrow u\ell\bar{\nu}_\ell$ (where ℓ refers to an electron or muon) each provide two avenues for determining these CKM matrix elements, namely through inclusive (i.e. the sum over all possible hadronic states) and exclusive final states (decays involving a specific meson, $X = D, D^*, \pi, \rho$ etc.). While the purely leptonic final states in the decays $B_c^- \rightarrow \tau\bar{\nu}$, $B^- \rightarrow \tau\bar{\nu}$, and $B^- \rightarrow \mu\bar{\nu}$ are theoretically very simple, we do not use this information at present since none of the measurements has reached a competitive level of precision and thus the focus is on exclusive and inclusive semileptonic decays. This article and the values quoted here update the previous review [1].

The theory underlying the different determinations of $|V_{qb}|$ is mature, in particular for $|V_{cb}|$. Most of the theoretical approaches use the fact that the masses m_b and m_c of the b and the c quark are large compared to the scale Λ_{QCD} that determines low-energy hadronic physics. Thus the basis for precise calculations is a systematic expansion in powers of Λ/m_b , where $\Lambda \sim 500 - 700$ MeV is a hadronic scale of the order of Λ_{QCD} . Such an expansion can be formulated in the framework of an effective field theory which is described in a separate RPP mini-review [2].

Aside from this there has been significant progress over the last decade in lattice simulations of QCD which is a first-principles method for non-perturbative QCD calculations. Increased computer power as well as improved theoretical methods allow us to include also heavy quarks in this calculations, and thus the results from lattice QCD play an essential role in many of the determinations discussed here. We do not need to describe lattice methods here, they are discussed in a separate RPP mini-review [3].

The measurements discussed in this review are of branching fractions, ratios of branching fractions, and decay kinematic distributions. The determinations of $|V_{cb}|$ and $|V_{ub}|$ also require a measurement of the total decay widths of the corresponding b hadrons, determined from lifetimes, which is the subject of a separate RPP mini-review [4]. The measurements of inclusive semileptonic decays relevant to this review come primarily from $e^+e^- B$ factories operating at the $\Upsilon(4S)$ resonance, while the measurements of exclusive semileptonic decays come from both the $e^+e^- B$ factories and from the LHCb experiment at CERN.

Semileptonic B meson decay amplitudes to electrons and muons are well measured and consistent with the SM, and thus are dominated by the Standard-Model W boson exchange, which is expected to be largely free from any impact of non-Standard Model physics. The decays $\bar{B} \rightarrow D^{(*)}\tau\bar{\nu}_\tau$, however, may become sensitive to effects beyond the Standard Model due to the large mass of the τ lepton. For example, modifications in the Higgs sector such as a charged Higgs boson, may couple to the mass of the leptons, breaking lepton universality beyond the Standard Model. The currently observed anomalies in these decay could be an indication of new physics.

Many of the numerical results quoted in this review have been provided by the Heavy Flavor Averaging Group (HFLAV) [5].

75.2 Determination of $|V_{cb}|$

Summary: The determination of $|V_{cb}|$ from inclusive decays has a relative uncertainty of about 2%; the limitations arise mainly from our ignorance of higher-order perturbative and non-perturbative corrections. Exclusive $\bar{B} \rightarrow D^*\ell\bar{\nu}_\ell$ decays provide a determination of $|V_{cb}|$ with a relative precision of about 2%, with comparable contributions from theory and experiment; the value determined from $\bar{B} \rightarrow D\ell\bar{\nu}_\ell$ decays is consistent and has an uncertainty of 3%. However, as discussed below, recent work has

raised questions about these determinations. We choose to quote a less constraining value from exclusive decays.

The values obtained from the inclusive and exclusive determinations discussed below are:

$$|V_{cb}| = (42.2 \pm 0.8) \times 10^{-3} \quad (\text{inclusive}) \quad (75.1)$$

$$|V_{cb}| = (39.5 \pm 0.9) \times 10^{-3} \quad (\text{exclusive}). \quad (75.2)$$

An average of these determinations has $p(\chi^2) = 2\%$, so we scale the error by $\sqrt{\chi^2/1} = 2.4$ to find

$$|V_{cb}| = (41.0 \pm 1.4) \times 10^{-3} \quad (\text{average}). \quad (75.3)$$

Given the only marginal consistency this average should be treated with caution.

75.2.1 $|V_{cb}|$ from exclusive decays

Exclusive determinations of $|V_{cb}|$ make use of semileptonic B decays into the ground state charmed mesons D and D^* . Based on Lorentz-invariance these decays are collectively described in terms of six independent form factors, which depend on the variable $w \equiv v \cdot v'$, where v and v' are the four velocities of the initial and final-state hadrons. In the rest frame of the decay this variable corresponds to the Lorentz factor of the final state $D^{(*)}$ meson. Heavy Quark Symmetry (HQS) [6] [7] predicts that in the infinite mass limit the six form factors collapse into a single one, which is normalized at the ‘‘zero recoil point’’ $w = 1$, the point of maximum momentum transfer to the leptons.

The determination of $|V_{cb}|$ requires a calculation of the form factors. One possibility is to use the normalization of the form factor at $w = 1$, however, a precise determination requires to include corrections to the HQS prediction for the normalization as well as some information on the shape of the form factors near the point $w = 1$. These calculations utilize Heavy Quark Effective Theory, which is discussed in a separate RPP mini-review [2]. Some of the form factors are normalized at $w = 1$ due to HQS, and this normalization is protected against linear corrections [8], and thus the leading corrections to the normalization are of order $\Lambda_{\text{QCD}}^2/m_c^2$. For the form factors that vanish in the infinite mass limit the corrections are in general linear in Λ_{QCD}/m_c .

In addition to these corrections, there are perturbatively calculable corrections from hard gluons as well as QED radiative corrections, which will be discussed in the relevant sections.

75.2.2 $\bar{B} \rightarrow D^*\ell\bar{\nu}_\ell$

The decay rate for $\bar{B} \rightarrow D^*\ell\bar{\nu}_\ell$ is given by

$$\frac{d\Gamma}{dw}(\bar{B} \rightarrow D^*\ell\bar{\nu}_\ell) = \frac{G_F^2 m_B^5}{48\pi^3} |V_{cb}|^2 (w^2 - 1)^{1/2} P(w) (\eta_{\text{ew}} \mathcal{F}(w))^2, \quad (75.4)$$

where $P(w)$ is a phase space factor,

$$P(w) = r^3 (1 - r)^2 (w + 1)^2 \left(1 + \frac{4w}{w + 1} \frac{1 - 2rw + r^2}{(1 - r)^2} \right). \quad (75.5)$$

with $r = m_{D^*}/m_B$. The form factor $\mathcal{F}(w)$ can be expressed in terms of the vector and axial vector form factors

$$\begin{aligned} \frac{\langle D^*(v', \epsilon) | \bar{e} \gamma^\mu b | B(v) \rangle}{\sqrt{m_B m_{D^*}}} &= h_V(w) \epsilon^{\mu\nu\rho\sigma} v_{B,\nu} v_{D^*,\rho} \epsilon_\sigma^*, \\ \frac{\langle D^*(v', \epsilon) | \bar{e} \gamma^\mu \gamma^5 b | B(v) \rangle}{\sqrt{m_B m_{D^*}}} &= i h_{A_1}(w) (1 + w) \epsilon^{*\mu} \\ &\quad - i [h_{A_2}(w) v_B^\mu + h_{A_3}(w) v_{D^*}^\mu] \epsilon^* \cdot v_B \end{aligned}$$

as

$$P(w) |\mathcal{F}(w)|^2 = |h_{A_1}(w)|^2 \left\{ 2 \frac{r^2 - 2rw + 1}{(1 - r)^2} \left[1 + \frac{w - 1}{w + 1} R_1^2(w) \right] + \left[1 + \frac{w - 1}{1 - r} (1 - R_2(w)) \right]^2 \right\},$$

where the ratios R_1 and R_2 are given by

$$R_1(w) = \frac{h_V(w)}{h_{A_1}(w)}, \quad R_2(w) = \frac{h_{A_3}(w) + r h_{A_2}(w)}{h_{A_1}(w)}. \quad (75.6)$$

Note that \mathcal{F} at $w = 1$ is unity by HQS in the infinite-mass limit [9–12]. Usually the decay rate formulae for semileptonic B decays assume massless leptons. The effect is typically very small, but for the muon case can be non-negligible in fits to data at high hadronic recoil.

The factor $\eta_{ew} = 1.0066 \pm 0.0050$ accounts for the leading electroweak corrections to the four-fermion operator mediating the semileptonic decay [13], and includes an estimated uncertainty for missing long-distance QED radiative corrections [14].

The determination of V_{cb} using the normalization at $w = 1$ involves an extrapolation to the zero-recoil point, for which a parametrization of the shape of $\mathcal{F}(w)$ is needed. Convenient parametrizations make use of analyticity and unitarity constraints on the form factors and are expressed in terms of the variable

$$z = \frac{\sqrt{w+1} - \sqrt{2}}{\sqrt{w+1} + \sqrt{2}}, \quad (75.7)$$

originating from a conformal transformation. In terms of this variable the form factors (generically denoted as F) may be written as [15–17]

$$F(z) = \frac{1}{P_F(z)\phi_F(z)} \sum_{n=0}^{\infty} a_n z^n \quad (75.8)$$

where the sum is bounded, $\sum |a_n|^2 < 1$. Furthermore, the function $P_F(z)$ takes into account the resonances in the $(\bar{c}b)$ system below the $\bar{D}B$ threshold, and the weighting functions $\phi_F(z)$ are derived from the unitarity constraint on the corresponding form factor. The values of z relevant to the decay are $0 \leq z \leq 0.06$, hence only very few terms are needed in the series in z . Eq. (75.8) will be referred to as the ‘‘BGL’’ expansion.

A frequently used parametrization proposed in Ref. [18] is a simple one-parameter form

$$h_{A_1}(w) = h_{A_1}(1) [1 - 8\rho^2 z + (53\rho^2 - 15)z^2 + (231\rho^2 - 91)z^3] \quad (75.9)$$

which has the slope ρ and of the form factor and the value $h_{A_1}(1)$ as the only parameters. Furthermore, the ratios $R_1(w)$ and $R_1(w)$ are expanded in $w - 1$. However, this simple CLN parametrization is inconsistent in subleading orders of the $1/m_{c/b}$ expansion [17, 19–22], and thus the recent fits are based on the BGL expansion. Typical fits include up to three parameters a_n in (75.8) for the different form factors.

The theoretical analysis of $F(w)$ requires, aside from the perturbative calculation of QCD short-distance radiative correction [23], the treatment of non-perturbative aspects. The state-of-the-art input comes from lattice QCD calculations which include a realistic description of the sea quarks using $2 + 1$ or $2 + 1 + 1$ flavors and finite b and c masses.

Currently available are lattice results only for the value $\mathcal{F}(1)$ at the non-recoil point [14, 24] with a total uncertainty at the (1–2)% level. The main contributions to this uncertainty in case of the Fermilab/MILC calculation are from the chiral extrapolation from the light quark masses used in the numerical lattice computation to realistic up and down quark masses, and from discretization errors. In the HPQCD calculation, the dominant source of uncertainty is the perturbative matching calculation for the heavy-light currents. These sources of uncertainty will be reduced with larger lattice sizes and smaller lattice spacings. The average of the two lattice predictions [25] is

$$\mathcal{F}(1) = 0.904 \pm 0.012, \quad (75.10)$$

Lattice calculations for values of $F(w)$ for $w \neq 1$ are underway, but not yet available.

Non-lattice estimates based on zero-recoil sum rules for the form factor tend to yield lower central values for $\mathcal{F}(1)$ [26–28]. Omitting the contributions from excited states, the sum rules indicate that $\mathcal{F}(1) < 0.93$. Including an estimate for the contribution of the excited states yields $\mathcal{F}(1) = 0.86 \pm 0.01 \pm 0.02$ [28, 29] where the second uncertainty accounts for the excited states.

Many experiments [30–40] have measured the differential decay rate as a function of w , employing a variety of methods: using

either B^+ or B^0 decays, with or without B -tagging, and with or without explicit reconstruction of the transition pion from $D^* \rightarrow D$ decays. These measurements are input to a four-dimensional fit [5] for $\eta_{ew}\mathcal{F}(1)|V_{cb}|$, $\rho_{A_1}^2$ and the form-factor ratios $R_1 \propto A_2/A_1$ and $R_2 \propto V/A_1$. The fit has a p -value of 0.8%, so we scale the uncertainty by a factor $\sqrt{\chi^2/23}$ to give $\eta_{ew}\mathcal{F}(1)|V_{cb}| = (35.27 \pm 0.52) \times 10^{-3}$ (CLN).

The leading sources of uncertainty on $\eta_{ew}\mathcal{F}(1)|V_{cb}|$ are due to detection efficiencies and $D^{(*)}$ decay branching fractions. Note that the $\bar{B} \rightarrow D^*\ell\bar{\nu}_\ell$ form factor in the fit is parameterized using the CLN form, which has the drawbacks discussed previously.

Using the value from Eq. 75.10 for $\mathcal{F}(1)$ and accounting for the electroweak correction gives

$$|V_{cb}| = (38.8 \pm 0.6 \pm 0.6) \times 10^{-3} (\bar{B} \rightarrow D^*\ell\bar{\nu}_\ell, \text{ LQCD, CLN}). \quad (75.11)$$

Not yet included in the average is the most recent measurement from Babar [41], which finds consistent results using the CLN form.

A safer approach is to use the more general BGL form-factor parameterization [17, 19]. Two experiments have recently published analyses with BGL based parametrizations at a given order in the expansion [40, 41]. The Belle analysis [40] is based on an untagged approach in the mode $\bar{B}^0 \rightarrow D^{*+}\ell\bar{\nu}_\ell$ and measures 1- d projections in bins of the hadronic recoil w , and angular variables $\cos\theta_\ell$, $\cos\theta_V$, and χ . The Babar analysis [41] is based on a hadronic tagged sample, and performs a full 4- d unbinned analysis of neutral and charged B decay modes. Only the BGL form factors are fit in this analysis, not the normalisation, which based on the world average $\bar{B} \rightarrow D^*\ell\bar{\nu}_\ell$ branching fraction.

At present only Ref. [40] publishes the fully-differential decay rate data and associated covariance matrix. An earlier preliminary measurement by Belle [39] also provided fully-differential decay rate data, used in a number of phenomenology analyses [17, 19], but was not published.

The BGL fit results from Ref. [40], $|V_{cb}| = (38.4 \pm 1.0) \times 10^{-3}$, and Ref. [41], $|V_{cb}| = (38.4 \pm 0.9) \times 10^{-3}$, are consistent with result from the fit with the CLN parametrization, Eq. 75.11. Both studies report fit results at low order in the three BGL expansion terms, ranging from zero-order to second-order in the Belle analysis, and first order for all terms in the Babar analysis. Studies of the impact of higher order expansions based on the Belle published decay rate data have been reported in Refs. [20, 21], where it is shown that the fit uncertainty on $|V_{cb}|$ increases by approximately 50% with respect to the results reported at lower order. This is due to larger number of degrees of freedom allowed in the higher order expansions, however beyond second order there is very little information gain with the current measurements. Form-factor ratios are found to be consistent with HQET predictions based on fits to the published measurements. Without a combination of the two results at this stage, we choose to quote the arithmetic average of the results from Ref. [40, 41], where the central values are the same. The nominal result for $|V_{cb}|$ is therefore

$$|V_{cb}| = (38.4 \pm 0.7 \pm 0.5 \pm 1.0) \times 10^{-3} (\bar{B} \rightarrow D^*\ell\bar{\nu}_\ell, \text{ LQCD, BGL}), \quad (75.12)$$

where the first uncertainty is experimental, the second is from LQCD, and the third is an additional uncertainty added by the authors to compensate for higher order expansion terms in the fit. Lattice QCD results for form factors away from zero recoil will be essential to control higher order terms in the BGL fit.

75.2.3 $\bar{B} \rightarrow D\ell\bar{\nu}_\ell$

The differential rate for $\bar{B} \rightarrow D\ell\bar{\nu}_\ell$ is given by

$$\begin{aligned} \frac{d\Gamma}{dw}(\bar{B} \rightarrow D\ell\bar{\nu}_\ell) = \\ \frac{G_F^2}{48\pi^3} |V_{cb}|^2 (m_B + m_D)^2 m_D^3 (w^2 - 1)^{3/2} (\eta_{ew}\mathcal{G}(w))^2. \end{aligned} \quad (75.13)$$

The form factor is defined in terms of

$$\frac{\langle D(v') | \bar{c} \gamma^\mu b | B(v) \rangle}{\sqrt{m_B m_D}} = h_+(w) (v_B + v_D)^\mu + h_-(w) (v_B - v_D)^\mu \quad (75.14)$$

and reads

$$\mathcal{G}(w) = h_+(w) - \frac{m_B - m_D}{m_B + m_D} h_-(w), \quad (75.15)$$

where h_+ is normalized to unity due to HQS and h_- vanishes in the infinite-mass limit. Thus

$$\mathcal{G}(1) = 1 + \mathcal{O} \left(\left(\frac{m_B - m_D}{m_B + m_D} \right)^2 \frac{\Lambda_{\text{QCD}}}{m_c} \right) \quad (75.16)$$

and the corrections to the HQET predictions are of order $1/m$ in contrast to the case of $F(1)$.

The normalization, $\mathcal{G}(1)$, is obtained from QCD lattice calculations with realistic sea quarks and finite b and c masses. The most recent value for $\mathcal{G}(1)$ is derived in Ref. [42] and is

$$\mathcal{G}(1) = 1.054 \pm 0.004 \pm 0.008 \quad (75.17)$$

Based on a parametrization of the shape of $\mathcal{G}(w)$ a value of $|V_{cb}|$ can be extracted. However, $w \sim 1$ is a region with poor experimental precision given the low decay rate in this kinematic corner.

In fact, lattice calculations for the form factor $\mathcal{G}(w)$ (including sea quarks and finite b and c masses) are now available for values $w \neq 1$, thus providing information over a range of z values (see Eq. (75.7)) [42, 43]. This lattice input can be used in a simultaneous fit, along with the differential branching fraction, in a form-factor expansion in z [15–17, 44].

The most precise measurements of $\bar{B} \rightarrow D \ell \bar{\nu}_\ell$ [37, 45, 46] dominate the CLN average [5] value, $\eta_{\text{ew}} \mathcal{G}(1) |V_{cb}| = (42.00 \pm 1.00) \times 10^{-3}$. Note that this average corresponds to measurements that are fit to the CLN form factor parameterization; the same concerns expressed above for $\bar{B} \rightarrow D^* \ell \bar{\nu}_\ell$ apply here. Using the value from Eq. (75.17) for $\mathcal{G}(1)$ and accounting for the electroweak correction as above gives

$$|V_{cb}| = (39.6 \pm 0.9 \pm 0.3) \times 10^{-3} \quad (\bar{B} \rightarrow D \ell \bar{\nu}_\ell, \text{ LQCD, CLN}), \quad (75.18)$$

where the first uncertainty is from experiment, and the second is from lattice QCD, as well as the electroweak corrections.

Studies have also been conducted using the general BCL form-factor parametrization (z -expansion from Ref. Ref. [44]), combining binned measurements from Belle [46] and Babar [45] with lattice QCD determinations of the form factors as a function of the recoil parameter in the lowest third of the kinematically allowed region [25]. Only Ref. [46] published the full measurement covariance matrix, while Ref. [45] provides the statistical uncertainty covariance. Nevertheless, Ref. [46] is more precise and dominates the average [25], giving

$$|V_{cb}| = (40.1 \pm 1.0) \times 10^{-3} \quad (\bar{B} \rightarrow D \ell \bar{\nu}_\ell, \text{ LQCD, BCL}). \quad (75.19)$$

This result is consistent with the value reported in Ref. [47].

The $|V_{cb}|$ averages from $\bar{B} \rightarrow D^* \ell \bar{\nu}_\ell$ and $\bar{B} \rightarrow D \ell \bar{\nu}_\ell$ decays using the BGL and BCL forms, respectively, are reasonably consistent. The correlations between the lattice uncertainties for $\bar{B} \rightarrow D^* \ell \bar{\nu}_\ell$ and $\bar{B} \rightarrow D \ell \bar{\nu}_\ell$ are discussed in Ref. [25], and considered to be 100% for the statistical uncertainty component. We assume an experimental uncertainty correlation of order 20% and combine the results, giving

$$|V_{cb}| = (39.5 \pm 0.9) \times 10^{-3} \quad (\text{exclusive}). \quad (75.20)$$

75.2.4 $|V_{cb}|$ from inclusive decays

Measurements of the total semileptonic branching decay rate, along with moments of the lepton energy and hadronic invariant mass spectra in inclusive semileptonic $b \rightarrow c$ transitions, can be used for a precision determination of $|V_{cb}|$. The total semileptonic decay rate can be calculated quite reliably in terms of non-perturbative parameters that can be extracted from the information contained in the moments.

75.2.5 Inclusive semileptonic rate

The theoretical foundation for the calculation of the total semileptonic rate is the Operator Product Expansion (OPE) which yields the Heavy Quark Expansion (HQE) [48, 49]. Details can be found in the RPP mini-review on Effective Theories [2].

The OPE result for the total rate can be written schematically (details can be found, *e.g.*, in Ref. [50]) as

$$\begin{aligned} \Gamma = & |V_{cb}|^2 \frac{G_F^2 m_b^5(\mu)}{192\pi^3} \eta_{\text{ew}} \times \\ & \left[z_0^{(0)}(r) + \frac{\alpha_s(\mu)}{\pi} z_0^{(1)}(r) + \left(\frac{\alpha_s(\mu)}{\pi} \right)^2 z_0^{(2)}(r) + \dots \right. \\ & + \frac{\mu_\pi^2}{m_b^2} \left(z_2^{(0)}(r) + \frac{\alpha_s(\mu)}{\pi} z_2^{(1)}(r) + \dots \right) \\ & + \frac{\mu_G^2}{m_b^2} \left(y_2^{(0)}(r) + \frac{\alpha_s(\mu)}{\pi} y_2^{(1)}(r) + \dots \right) \\ & + \frac{\rho_D^3}{m_b^3} \left(z_3^{(0)}(r) + \frac{\alpha_s(\mu)}{\pi} z_3^{(1)}(r) + \dots \right) \\ & \left. + \frac{\rho_{LS}^3}{m_b^3} \left(y_3^{(0)}(r) + \frac{\alpha_s(\mu)}{\pi} y_3^{(1)}(r) + \dots \right) + \dots \right] \quad (75.21) \end{aligned}$$

where r is the ratio m_c/m_b and the y_i and z_i are perturbatively calculable Wilson coefficients functions that appear at different orders of the heavy mass expansion.

The parameters μ_π , μ_G , ρ_D and ρ_{LS} constitute the non-perturbative input into the heavy quark expansion; they correspond to certain matrix elements to be discussed below. In the same way the HQE can be set up for the moments of distributions of charged-lepton energy, hadronic invariant mass and hadronic energy, *e.g.*

$$\langle E_e^n \rangle_{E_e > E_{\text{cut}}} = \int_{E_{\text{cut}}}^{E_{\text{max}}} \frac{d\Gamma}{dE_e} E_e^n dE_e \bigg/ \int_{E_{\text{cut}}}^{E_{\text{max}}} \frac{d\Gamma}{dE_e} dE_e. \quad (75.22)$$

The coefficients of the HQE are known up to order $1/m_b^5$ at tree level [51–54]. The leading term $z_0^{(i)}$ is the parton model, and is known completely to order α_s and α_s^2 [55–57]. The terms of order $\alpha_s^{n+1} \beta_0^n$ (where β_0 is the first coefficient of the QCD β function, $\beta_0 = (33 - 2n_f)/3$) have been included by the usual BLM procedure [50, 58, 59]. Corrections of order $\alpha_s \mu_\pi^2/m_b^2$ have been computed in Ref. [60] and Ref. [61], while the $\alpha_s \mu_G^2/m_b^2$ terms have been calculated in Ref. [62] and Ref. [63].

Starting at order $1/m_b^3$ contributions with an infrared sensitivity to the charm mass, m_c , appear [51, 53, 64, 65]. At order $1/m_b^3$ this “intrinsic charm” contribution manifests as a $\log(m_c)$ in the coefficient of the Darwin term ρ_D^3 . At higher orders, terms such as $1/m_b^3 \times 1/m_c^2$ and $\alpha_s(m_c) 1/m_b^3 \times 1/m_c$ appear, which are comparable in size to the contributions of order $1/m_b^4$.

The HQE parameters are given in terms of forward matrix elements of local operators; the parameters entering the expansion for orders up to $1/m_b^3$ are $(D_\perp^\mu = (g_{\mu\nu} - v_\mu v_\nu) D^\nu, \text{ where } v = p_B/M_B \text{ is the four-velocity of the } B \text{ meson})$

$$\begin{aligned} \bar{\Lambda} &= M_B - m_b, \\ \mu_\pi^2 &= -\langle B | \bar{b} (iD_\perp)^2 b | B \rangle, \\ \mu_G^2 &= \langle B | \bar{b} (iD_\perp^\mu) (iD_\perp^\nu) \sigma_{\mu\nu} b | B \rangle, \\ \rho_D^3 &= \langle B | \bar{b} (iD_{\perp\mu}) (ivD) (iD_\perp^\nu) b | B \rangle, \\ \rho_{LS}^3 &= \langle B | \bar{b} (iD_\perp^\mu) (ivD) (iD_\perp^\nu) \sigma_{\mu\nu} b | B \rangle. \end{aligned} \quad (75.23)$$

These parameters still depend on the heavy quark mass. Sometimes the infinite mass limits of these parameters $\bar{\Lambda} \rightarrow \bar{\Lambda}_{\text{HQET}}$, $\mu_\pi^2 \rightarrow -\lambda_1$, $\mu_G^2 \rightarrow 3\lambda_2$, $\rho_D^3 \rightarrow \rho_1$ and $\rho_{LS}^3 \rightarrow 3\rho_2$, are used instead. Beyond $1/m^3$ the number of independent HQE parameters starts to proliferate [66]. In general, there are 13 parameters (at tree level) up to order $1/m^4$ and 31 (at tree level) up to order $1/m^5$, not including $\bar{\Lambda}$. The HQE parameters of the orders $1/m^4$

and $1/m_b^5$ have been estimated in Ref. [54, 67], their impact on the $|V_{cb}|$ determination has been studied in Ref. [68]. However, it has been pointed out recently that one may reduce the number of independent parameters in the HQE by exploiting reparametrization invariance, which is a symmetry of the HQE stemming from Lorentz invariance of QCD [69]. For a subset of observables this allows us to reduce the number of parameters to three up to order $1/m^3$ (ρ_{LS} can be absorbed into μ_G^2 by a re-definition) and to 8 up to order $1/m^4$ [70].

The rates and the spectra depend strongly on the definition m_b (or equivalently of $\bar{\Lambda}$). This makes the discussion of renormalization issues mandatory, since the size of QCD corrections is strongly correlated with the definitions used for the quark masses. For example, it is well known (see eg. [71]) that using the pole mass definition for heavy quark masses leads to a perturbative series for the decay rates that does not converge very well.

This motivates the use of “short-distance” mass definitions, such as the kinetic scheme [26] or the 1S scheme [72–74]. Both schemes are well suited for the HQE, since they allow the choice of the renormalization scale $\mu \leq m_b$. Furthermore, they both can be extracted from other observables to a sufficient precision, such that a precise determination of $|V_{cb}|$ becomes possible, despite of the strong quark-mass dependence of the total rate.

The 1S scheme eliminates the b quark pole mass by relating it to the perturbative expression for the mass of the 1S state of the Υ system. The b quark mass in the 1S scheme is is half of the perturbatively calculated mass of the 1S state of the Υ system. The best determination of the b quark mass in the 1S scheme is obtained from sum rules for $e^+e^- \rightarrow b\bar{b}$ [75].

A second alternative is the so-called “kinetic mass” $m_b^{\text{kin}}(\mu)$, which is the mass entering the non-relativistic expression for the kinetic energy of a heavy quark, and which is defined using heavy-quark sum rules [26].

75.2.6 Determination of HQE Parameters and $|V_{cb}|$

Several experiments have measured moments in $\bar{B} \rightarrow X_c \ell \bar{\nu}_\ell$ decays [76–84] as a function of the minimum lepton momentum. The measurements of the moments of the electron energy spectrum (0th-3rd) and of the squared hadronic mass spectrum (0th-2nd) have statistical uncertainties that are roughly equal to their systematic uncertainties. The 3rd order hadronic mass spectrum moments have also been measured by some experiments, with relatively large statistical uncertainty. The sets of moments measured within each experiment have strong correlations; their use in a global fit requires fully specified statistical and systematic covariance matrices. Measurements of photon energy moments (0th-2nd) in $B \rightarrow X_s \gamma$ decays [85–89] as a function of the minimum accepted photon energy are also used in some fits; the dominant uncertainties on these measurements are statistical.

Global fits [84, 86, 90–95] to the full set of moments have been performed in the 1S and kinetic schemes. The semileptonic moments alone determine a linear combination of m_b and m_c very accurately but leave the orthogonal combination poorly determined (See e.g. [96]); additional input is required to allow a precise determination of m_b . This additional information can come from the radiative $B \rightarrow X_s \gamma$ moments (with the caveat that the OPE for $b \rightarrow s \gamma$ breaks down beyond leading order in Λ_{QCD}/m_b), which provide complementary information on m_b and μ_π^2 , or from precise determinations of the charm quark mass [97, 98]. The values obtained in the kinetic scheme fits [5, 94, 95] with these two constraints are consistent. Based on the charm quark mass constraint $m_c^{\overline{\text{MS}}}(3 \text{ GeV}) = 0.986 \pm 0.013 \text{ GeV}$ [99], a fit in the kinetic scheme [5] obtains

$$|V_{cb}| = (42.19 \pm 0.78) \times 10^{-3} \quad (75.24)$$

$$m_b^{\text{kin}} = 4.554 \pm 0.018 \text{ GeV} \quad (75.25)$$

$$\mu_\pi^2(\text{kin}) = 0.464 \pm 0.076 \text{ GeV}^2, \quad (75.26)$$

where the errors include experimental and theoretical uncertainties. Theoretical uncertainties from higher orders in $1/m$ as well as in α_s are estimated and included in performing the fits. Similar values for the parameters are obtained with a variety of assumptions about the theoretical uncertainties and their correlations.

The χ^2/dof is well below unity in all fits, which could suggest that the theoretical uncertainties may be overestimated. However, while one could obtain a satisfactory fit with smaller uncertainties, this would result in unrealistically small uncertainties on the extracted HQE parameters, which are used as input to other calculations (e.g. the determination of $|V_{ub}|$). The mass in the $\overline{\text{MS}}$ scheme corresponding to Eq. (75.25) is $m_b^{\overline{\text{MS}}} = 4.19 \pm 0.04 \text{ GeV}$, where the uncertainty includes a contribution from the translation between mass schemes; this can be compared with a value obtained using relativistic sum rules [99], $m_b^{\overline{\text{MS}}} = 4.163 \pm 0.016 \text{ GeV}$, which provides a non-trivial cross-check.

A fit to the measured moments in the 1S scheme [5, 86, 93] gives

$$|V_{cb}| = (41.98 \pm 0.45) \times 10^{-3} \quad (75.27)$$

$$m_b^{1\text{S}} = 4.691 \pm 0.037 \text{ GeV} \quad (75.28)$$

$$\lambda_1(1\text{S}) = -0.362 \pm 0.067 \text{ GeV}^2, \quad (75.29)$$

This fit uses moments measurements from semileptonic and radiative decays and constrains the chromomagnetic operator using the B^*-B and D^*-D mass differences, but does not include the constraint on m_c nor the full NNLO corrections.

The fits in the two renormalization schemes give consistent results for $|V_{cb}|$ and, after translation to a common renormalization scheme, for m_b and μ_π^2 . We take the fit in the kinetic scheme [95], which includes higher-order corrections and results in a more conservative uncertainty, as the inclusive determination of $|V_{cb}|$:

$$|V_{cb}| = (42.2 \pm 0.8) \times 10^{-3} \text{ (inclusive)}. \quad (75.30)$$

The precision of the global fit results can be further improved by calculating higher-order perturbative corrections to the coefficients of the HQE parameters. The inclusion of still-higher-order moments, if they can be measured with the required precision, may improve the sensitivity of the fits to higher-order terms in the HQE.

75.3 Determination of $|V_{ub}|$

Summary: Currently the best determinations of $|V_{ub}|$ are from $\bar{B} \rightarrow \pi \ell \bar{\nu}_\ell$ decays, where combined fits to theory and experimental data as a function of q^2 provide a precision of about 4%; the uncertainties from experiment and theory are comparable in size. Determinations based on inclusive semileptonic decays are based on different observables and use different strategies to suppress the $b \rightarrow c$ background. Most of the determinations are consistent and provide a precision of about 7%, with comparable contributions to the uncertainty from experiment and theory. The exception is the most recent Babar analysis, which observes significant model dependence.

The values obtained from inclusive and exclusive determinations are

$$|V_{ub}| = (4.25 \pm 0.12 \pm_{0.14}^{0.15} \pm 0.23) \times 10^{-3} \text{ (inclusive)}, \quad (75.31)$$

$$|V_{ub}| = (3.70 \pm 0.10 \pm 0.12) \times 10^{-3} \text{ (exclusive)}, \quad (75.32)$$

where the last uncertainty on the inclusive result was added by the authors of this review and is discussed below.

The exclusive and inclusive determinations are independent, and the dominant uncertainties are on multiplicative factors.

To combine these values, the inclusive and exclusive values are weighted by their relative errors and the uncertainties are treated as normally distributed. The resulting average has $p(\chi^2) = 10\%$, so we scale the error by $\sqrt{\chi^2/1} = 1.6$ to find

$$|V_{ub}| = (3.82 \pm 0.24) \times 10^{-3} \text{ (average)}. \quad (75.33)$$

Given the somewhat poor consistency between the two determinations, this average should be treated with caution.

75.3.1 $|V_{ub}|$ from inclusive decays

The theoretical description of inclusive $\bar{B} \rightarrow X_u \ell \bar{\nu}_\ell$ decays is based on the Heavy Quark Expansion and leads to a predicted total decay rate with uncertainties below 5% [73, 100]. However,

the total decay rate is hard to measure due to the large background from CKM-favored $\bar{B} \rightarrow X_c \ell \bar{\nu}_\ell$ transitions, and hence the theoretical methods differ from the $\bar{B} \rightarrow X_c \ell \bar{\nu}_\ell$ case. For a calculation of the partial decay rate in regions of phase space where $\bar{B} \rightarrow X_c \ell \bar{\nu}_\ell$ decays are suppressed one cannot use the HQE as for $b \rightarrow c$, rather the one needs to introduce non-perturbative distribution functions, the “shape functions” (SF) [101,102]. Their exact form is not known, but its moments can be related to the HQE parameters known e.g from the $b \rightarrow c$ case.

The shape functions become important when the light-cone momentum component $P_+ \equiv E_X - |P_X|$ is not large compared to Λ_{QCD} , as is the case near the endpoint of the $\bar{B} \rightarrow X_u \ell \bar{\nu}_\ell$ lepton spectrum. Partial rates for $\bar{B} \rightarrow X_u \ell \bar{\nu}_\ell$ are predicted and measured in a variety of kinematic regions that differ in their sensitivity to shape-function effects.

At leading order in $1/m_b$ only a single shape function (SF) appears, which is universal for all heavy-to-light transitions [101, 102] and can be extracted in $\bar{B} \rightarrow X_s \gamma$ decays. At subleading order in $1/m_b$, several shape functions appear [103], along with “resolved photon contributions” specific for $\bar{B} \rightarrow X_s \gamma$ [104,105], and thus the prescriptions that relate directly the partial rates for $\bar{B} \rightarrow X_s \gamma$ and $\bar{B} \rightarrow X_u \ell \bar{\nu}_\ell$ decays [106–114] are limited to leading order in $1/m_b$.

Existing approaches use parametrizations of the leading SF that respect constraints on the normalization and on the first and second moments, which are given in terms of the HQE parameters $\bar{\Lambda} = M_B - m_b$ and μ_π^2 , respectively. The relations between SF moments and the HQE parameters are known to second order in α_s [115]; as a result, measurements of HQE parameters from global fits to $\bar{B} \rightarrow X_c \ell \bar{\nu}_\ell$ and $\bar{B} \rightarrow X_s \gamma$ moments can be used to constrain the SF moments, as well as to provide accurate values of m_b and other parameters for use in determining $|V_{ub}|$. Flexible parametrizations of the SF using orthogonal basis functions [116] or artificial neural networks [117] would allow global fits to inclusive B meson decay data that incorporate the known short-distance contributions and renormalization properties of the SF.

HFLAV performs fits on the basis of several approaches, with varying degrees of model dependence. We will consider here the approaches documented in Ref. [118] (BLNP), Ref. [119] (GGOU) and Ref. [120] (DGE).

The triple differential rate in the variables

$$P_\ell = M_B - 2E_\ell, \quad P_- = E_X + |\vec{P}_X|, \quad P_+ = E_X - |\vec{P}_X| \quad (75.34)$$

is

$$\frac{d^3\Gamma}{dP_+ dP_- dP_\ell} = \frac{G_F^2 |V_{ub}|^2}{16\pi^2} (M_B - P_+) \quad (75.35)$$

$$\left\{ (P_- - P_\ell)(M_B - P_- + P_\ell - P_+) \mathcal{F}_1 \right.$$

$$\left. + (M_B - P_-)(P_- - P_+) \mathcal{F}_2 + (P_- - P_\ell)(P_\ell - P_+) \mathcal{F}_3 \right\}.$$

The “structure functions”, \mathcal{F}_i , can be calculated using factorization theorems that have been proven to subleading order in the $1/m_b$ expansion [121].

The BLNP [118] calculation uses these factorization theorems to write the \mathcal{F}_i terms as functions of perturbatively calculable hard coefficients H and jet functions J , which are convolved with the (soft) light-cone distribution functions S , which is the shape functions of the B meson. The calculation of $\mathcal{O}(\alpha_s^2)$ contributions [122,123] is not yet complete and is not included in the $|V_{ub}|$ determination given below.

The leading order term in the $1/m_b$ expansion of the \mathcal{F}_i terms contains a single non-perturbative function and is calculated to subleading order in α_s , while at subleading order in the $1/m_b$ expansion there are several independent non-perturbative functions that have been calculated only at tree level in the α_s expansion.

A distinct approach (GGOU) [119] uses a hard, Wilsonian cut-off that matches the definition of the kinetic mass. The non-perturbative input is similar to what is used in BLNP, but the shape functions are defined differently. In particular, they are defined at finite m_b and depend on the light-cone component k_+ of the b quark momentum and on the momentum transfer q^2 to the

leptons. These functions include subleading effects to all orders; as a result they are non-universal, with one shape function corresponding to each structure function in Eq. (75.35). Their k_+ moments can be computed in the OPE and related to observables and to the shape functions defined in Ref. [118].

Going to subleading order in α_s requires the definition of a renormalization scheme for the HQE parameters and for the SF. The relation between the moments of the SF and the forward matrix elements of local operators appearing the HQE is plagued by ultraviolet problems and requires additional renormalization. A scheme for improving this behavior was suggested in Ref. [118] and Ref. [124], which introduce a definition of the quark mass (the so-called shape-function scheme) based on the first moment of the measured $\bar{B} \rightarrow X_s \gamma$ photon energy spectrum. Likewise, the HQE parameters can be defined from measured moments of spectra, corresponding to moments of the SF.

There are various ideas to model the SF, but this requires additional assumptions. One approach (DGE) is the so-called “dressed gluon exponentiation” [120], where the perturbative result is continued into the infrared regime using the renormalon structure obtained in the large β_0 limit, where β_0 has been defined following Eq. (75.21). Other approaches make even stronger assumptions, such as in Ref. [125], which assumes an analytic behavior for the strong coupling in the infrared to perform an extrapolation of perturbation theory.

In order to reduce sensitivity to SF uncertainties, measurements that use a combination of cuts on the leptonic momentum transfer q^2 and the hadronic invariant mass m_X , as suggested in Ref. [126,127], have been made. In general, efforts to extend the experimental measurements of $\bar{B} \rightarrow X_u \ell \bar{\nu}_\ell$ into charm-dominated regions (in order to reduce SF uncertainties) lead to an increased experimental sensitivity to the modeling of $\bar{B} \rightarrow X_u \ell \bar{\nu}_\ell$ decays, resulting in measured partial rates with an undesirable level of model dependence. The measurements quoted below have used a variety of functional forms to parametrize the leading SF; a specific error budget for one determination is quoted in the next section. In no case is the parametrization uncertainty estimated to be more than a 2% on $|V_{ub}|$.

Weak Annihilation [119, 128, 129] (WA) can in principle contribute significantly in the high- q^2 region of $\bar{B} \rightarrow X_u \ell \bar{\nu}_\ell$ decays. Estimates based on semileptonic D_s decays [65,126,127,129] lead to a $\sim 2\%$ uncertainty on the total $\bar{B} \rightarrow X_u \ell \bar{\nu}_\ell$ rate from the $\mathcal{T}(4S)$. The q^2 spectrum of the WA contribution is not well known, but from the OPE it is expected to contribute predominantly at high q^2 . More recent theoretical investigations [65,130,131] and a direct search [132] indicate that WA is a small effect, but may become a significant source of uncertainty for $|V_{ub}|$ measurements that accept only a small fraction of the full $\bar{B} \rightarrow X_u \ell \bar{\nu}_\ell$ phase space.

75.3.2 Measurements

We summarize the measurements used in the determination of $|V_{ub}|$ below. Given the improved precision and more rigorous theoretical interpretation of more recent measurements, determinations [133–136] done with LEP data are not considered in this review.

Inclusive electron momentum measurements [137–139] reconstruct a single charged electron to determine a partial decay rate for $\bar{B} \rightarrow X_u \ell \bar{\nu}_\ell$ near the kinematic endpoint. This results in a selection efficiency of order 50% and only modest sensitivity to the modeling of detector response. The inclusive electron momentum spectrum from $B\bar{B}$ events, after subtraction of the $e^+e^- \rightarrow q\bar{q}$ continuum background, is fitted to a model $\bar{B} \rightarrow X_u \ell \bar{\nu}_\ell$ spectrum and several components ($D\ell\bar{\nu}_\ell$, $D^*\ell\bar{\nu}_\ell$, ...) of the $\bar{B} \rightarrow X_c \ell \bar{\nu}_\ell$ background; the dominant uncertainties are related to this subtraction and modelling. The decay rate can be cleanly extracted for $E_e > 2.3$ GeV, but this is deep in the SF region, where theoretical uncertainties are large. More recent measurements have increased the accessed phase phase. The resulting $|V_{ub}|$ values for various E_e cuts are given in Table 75.1.

The most recent measurement [140] from BABAR is based on the inclusive electron spectrum and determines the partial branching fraction and $|V_{ub}|$ for $E_e > 0.8$ GeV. The analysis shows that the partial branching fraction measurements can have sig-

nal model dependence when the kinematic acceptance includes regions dominated by $\bar{B} \rightarrow X_c \ell \bar{\nu}_\ell$ background. The model dependence enters primarily through the partial branching fractions, and arises because the signal yield fit has sensitivity to $\bar{B} \rightarrow X_u \ell \bar{\nu}_\ell$ decays only in regions with good signal to noise.

An untagged “neutrino reconstruction” measurement [141] from BABAR uses a combination [142] of a high-energy electron with a measurement of the missing momentum vector. This allows $S/B \sim 0.7$ for $E_e > 2.0$ GeV and a $\approx 5\%$ selection efficiency, but at the cost of a smaller accepted phase space for $\bar{B} \rightarrow X_u \ell \bar{\nu}_\ell$ decays and uncertainties associated with the determination of the missing momentum. The corresponding values for $|V_{ub}|$ are given in Table 75.1.

The large samples accumulated at the B factories allow studies in which one B meson is fully reconstructed and the recoiling B decays semileptonically [143–146]. The experiments can fully reconstruct a “tag” B candidate in about 0.5% (0.3%) of $B^+ B^-$ ($B^0 \bar{B}^0$) events. An electron or muon with center-of-mass momentum above 1.0 GeV is required amongst the charged tracks not assigned to the tag B and the remaining particles are assigned to the X_u system. The full set of kinematic properties (E_ℓ , m_X , q^2 , etc.) are available for studying the semileptonically decaying B , making possible selections that accept up to 90% of the full $\bar{B} \rightarrow X_u \ell \bar{\nu}_\ell$ rate; however, the sensitivity to $\bar{B} \rightarrow X_u \ell \bar{\nu}_\ell$ decays is still driven by the regions where $\bar{B} \rightarrow X_c \ell \bar{\nu}_\ell$ decays are suppressed. Despite requirements (e.g. on the square of the missing mass) aimed at rejecting events with additional missing particles, undetected or mis-measured particles from $\bar{B} \rightarrow X_c \ell \bar{\nu}_\ell$ decay (e.g., K_L^0 and additional neutrinos) remain an important source of uncertainty.

BABAR [143] and Belle [144, 145] have measured partial rates with cuts on m_X , m_X and q^2 , P_+ and E_ℓ using the recoil method. In each case the experimental systematics have significant contributions from the modeling of $\bar{B} \rightarrow X_u \ell \bar{\nu}_\ell$ and $\bar{B} \rightarrow X_c \ell \bar{\nu}_\ell$ decays and from the detector response to charged particles, photons and neutral hadrons. The corresponding $|V_{ub}|$ values are given in Table 75.1.

75.3.3 $|V_{ub}|$ from inclusive partial rates

The measured partial rates and theoretical calculations from BLNP, GGOU and DGE described previously are used to determine $|V_{ub}|$ from all measured partial $\bar{B} \rightarrow X_u \ell \bar{\nu}_\ell$ rates [5]; selected values are given in Table 75.1. The correlations amongst the multiple BABAR recoil-based measurements [143] are fully accounted for in the average. The statistical correlations amongst the other measurements used in the average are small (due to small overlaps among signal events and large differences in S/B ratios) and have been ignored. Correlated systematic and theoretical errors are taken into account, both within an experiment and between experiments. As an illustration of the relative sizes of the uncertainties entering $|V_{ub}|$ we give the error breakdown for the GGOU average: statistical—1.6%; experimental—1.6%; $\bar{B} \rightarrow X_c \ell \bar{\nu}_\ell$ modeling—0.9%; $\bar{B} \rightarrow X_u \ell \bar{\nu}_\ell$ modeling—1.5%; HQE parameters (m_b)—1.9%; higher-order corrections—1.5%; q^2 modeling—1.3%; Weak Annihilation— $^{+0.0}_{-1.1}\%$; SF parametrization—0.1%.

The averages quoted here are based on the following m_b values: $m_b^{SF} = 4.582 \pm 0.023 \pm 0.018$ GeV for BLNP, $m_b^{\text{kin}} = 4.554 \pm 0.018$ GeV for GGOU, and $m_b^{\overline{MS}} = 4.188 \pm 0.043$ GeV for DGE. The m_b^{kin} value is determined in a global fit to moments in the kinetic scheme; this value is translated into m_b^{SF} and $m_b^{\overline{MS}}$ at fixed order in α_s . The second uncertainty quoted on m_b arises from the scheme translation.

Hadronization uncertainties also impact the $|V_{ub}|$ determination. The theoretical expressions are valid at the parton level and do not incorporate any resonant structure (e.g. $\bar{B} \rightarrow \pi \ell \bar{\nu}_\ell$); this must be added to the simulated $\bar{B} \rightarrow X_u \ell \bar{\nu}_\ell$ event samples, since the detailed final state multiplicity and structure impacts the estimates of experimental acceptance and efficiency. The experiments have adopted procedures to input resonant structure while preserving the appropriate behavior in the kinematic variables (q^2 , E_ℓ , m_X) averaged over the sample, but these prescriptions are *ad hoc* and ultimately require *in situ* calibration. The resulting uncertainties have been estimated to be ~ 1 -2% on $|V_{ub}|$.

All calculations yield compatible $|V_{ub}|$ values and similar error estimates. The arithmetic mean of the values and errors is $|V_{ub}| = (4.25 \pm 0.12_{\text{exp}} \pm 0.15_{\text{theo}}) \times 10^{-3}$, although there is a spread of approximately 10% in the evaluations with the three theoretical models. For reasons discussed below, we assign an additional uncertainty due to model dependence that is not reflected in the HFLAV averages. As highlighted in the BABAR analysis [140], model dependence entering measurement procedures can be sizeable, and is not consistently treated across analyses. Many of the analyses shown in Table 75.1 were based on partial branching fraction measurements determined in a single model (i.e. the one used by that analysis when simulating $\bar{B} \rightarrow X_u \ell \bar{\nu}_\ell$ decays), although in some cases simulated events were weighted to match the expected spectra in other models and the differences introduced as systematic uncertainties, e.g. Ref. [145]. The $|V_{ub}|$ value quoted by HFLAV for each model are, typically, derived from this unique partial branching fraction combined with another model-specific partial rate calculation. This translation from a single partial branching fraction into $|V_{ub}|$ values in different models suffers, in principle, from the difficulties made explicit in the recent BABAR measurement. The model dependence in the partial branching fraction is sensitive to how the model predictions compare in the restricted region with good signal-to-noise, not by how they compare when integrated over the full kinematic range used in the fit. This effect needs to be accounted for by the experiments; the published results are insufficient to determine it. To account for the range in results using the different theoretical models, we take half of the spread of the averages as an additional systematic uncertainty, denoted ΔBF . With this addition, the inclusive $|V_{ub}|$ average is

$$|V_{ub}| = (4.25 \pm 0.12_{\text{exp}} \pm 0.15_{\text{theo}} \pm 0.23_{\Delta\text{BF}}) \times 10^{-3} \quad (\text{inclusive}), \quad (75.36)$$

75.3.4 $|V_{ub}|$ from exclusive decays

Exclusive charmless semileptonic decays offer a complementary means of determining $|V_{ub}|$. For the experiments, the specification of the final state provides better background rejection, but the branching fraction to a specific final state is typically only a few percent of that for inclusive decays. For theory, the calculation of the form factors for $\bar{B} \rightarrow X_u \ell \bar{\nu}_\ell$ decays is challenging, but brings in a different set of uncertainties from those encountered in inclusive decays. In this review we focus on $\bar{B} \rightarrow \pi \ell \bar{\nu}_\ell$, as it is the most promising decay mode for both experiment and theory. Measurements of other exclusive $\bar{B} \rightarrow X_u \ell \bar{\nu}_\ell$ decays can be found in Refs. [147–160].

75.3.5 $\bar{B} \rightarrow \pi \ell \bar{\nu}_\ell$ form factor calculations

The relevant form factors for the decay $\bar{B} \rightarrow \pi \ell \bar{\nu}_\ell$ are usually defined as

$$\langle \pi(p_\pi) | V^\mu | B(p_B) \rangle = f_+(q^2) \left[p_B^\mu + p_\pi^\mu - \frac{m_B^2 - m_\pi^2}{q^2} q^\mu \right] + f_0(q^2) \frac{m_B^2 - m_\pi^2}{q^2} q^\mu \quad (75.37)$$

in terms of which the rate becomes (in the limit $m_\ell \rightarrow 0$)

$$\frac{d\Gamma}{dq^2} = \frac{G_F^2 |V_{ub}|^2}{24\pi^3} |p_\pi|^3 |f_+(q^2)|^2, \quad (75.38)$$

where p_π is the pion momentum in the B meson rest frame.

Currently available non-perturbative methods for the calculation of the form factors include lattice QCD (LQCD) and light-cone sum rules (LCSR). The two methods are complementary in phase space, since the lattice calculation is restricted to the kinematical range of high momentum transfer, q^2 , to the leptons, while light-cone sum rules provide information near $q^2 = 0$. Interpolations between these two regions can be constrained by unitarity and analyticity.

Lattice simulations for $B \rightarrow \pi \ell \bar{\nu}$ and $B_s \rightarrow K \ell \bar{\nu}$ transitions, where quark loop effects are fully incorporated, have been performed by the Fermilab/MILC [161, 162], HPQCD [163, 164] and RBC/UKQCD [165] collaborations. The calculations differ in the

Table 75.1: $|V_{ub}|$ (in units of 10^{-5}) from inclusive $\bar{B} \rightarrow X_u \ell \bar{\nu}_\ell$ measurements. The first uncertainty on $|V_{ub}|$ is experimental, while the second includes both theoretical and HQE parameter uncertainties. The values are generally listed in order of increasing kinematic acceptance, f_u (0.19 to 0.90), except for the BABAR $E_e > 0.8$ GeV measurement; those below the horizontal bar are based on recoil methods.

Ref.	cut (GeV)	BLNP	GGOU	DGE
CLEO [137]	$E_e > 2.1$	422 ± 49	423 ± 49	386 ± 45
BABAR [141]	$E_e - q^2$	471 ± 32	not available	435 ± 29
BABAR [139]	$E_e > 2.0$	452 ± 26	452 ± 26	430 ± 24
Belle [138]	$E_e > 1.9$	493 ± 46	495 ± 46	482 ± 45
BABAR [140]	$E_e > 0.8$	441 ± 12	396 ± 10	385 ± 11
BABAR [143]	$q^2 > 8$ $m_X < 1.7$	432 ± 23	433 ± 23	424 ± 22
BABAR [143]	$P_+ < 0.66$	409 ± 25	425 ± 26	417 ± 25
BABAR [143]	$m_X < 1.7$	403 ± 22	410 ± 23	422 ± 23
BABAR [143]	$E_\ell > 1$	433 ± 24	444 ± 24	445 ± 24
Belle [145]	$E_\ell > 1$	450 ± 27	462 ± 28	462 ± 28
HFLAV [5]	Combination	444^{+13+21}_{-14-22}	432 ± 12	399 ± 10

way the b quark is simulated. While HPQCD is using nonrelativistic QCD, Fermilab/MILC and RBC/UKQCD are using relativistic b quarks with the Fermilab and Columbia heavy-quark formulations. The results agree within the quoted errors. The form factor f_+ evaluated at $q^2 = 20 \text{ GeV}^2$ has an estimated uncertainty of 3.4%, where the leading contribution is due to the chiral-continuum extrapolation fit, which includes statistical and heavy-quark discretization errors. However, the lattice simulations are restricted to the region of large q^2 , i.e. the region $q_{\text{max}}^2 > q^2 \gtrsim 15 \text{ GeV}^2$.

The extrapolation to small values of q^2 is performed using guidance from analyticity and unitarity. Making use of the heavy-quark limit, stringent constraints on the shape of the form factor can be derived [166], and the conformal mapping of the kinematical variables onto the complex unit disc yields a rapidly converging series in the variable

$$z = \frac{\sqrt{t_+ - t_-} - \sqrt{t_+ - q^2}}{\sqrt{t_+ - t_-} + \sqrt{t_+ - q^2}}, \quad (75.39)$$

where $t_\pm = (M_B \pm m_\pi)^2$. The use of lattice data in combination with experimental measurements of the differential decay rate provides a stringent constraint on the shape of the form factor in addition to precise determination of $|V_{ub}|$ [167].

Another established non-perturbative approach to obtain the form factors is through Light-Cone QCD Sum Rules (LCSR), which, however, are not at the same footing as LQCD. LCSR provide an estimate for the product $f_B f_+(q^2)$, valid in the region $0 < q^2 \lesssim 12 \text{ GeV}^2$. The determination of $f_+(q^2)$ itself requires knowledge of the decay constant f_B , which is usually obtained by replacing f_B by its two-point QCD (SVZ) sum rule [168] in terms of perturbative and condensate contributions. The advantage of this procedure is the approximate cancellation of various theoretical uncertainties in the ratio $(f_B f_+)/f_B$.

The LCSR for $f_B f_+$ is based on the light-cone OPE of the relevant vacuum-to-pion correlation function, calculated in full QCD at finite b -quark mass. The resulting expressions comprise a triple expansion: in the twist t of the operators near the light-cone, in α_s , and in the deviation of the pion distribution amplitudes from their asymptotic form, which is fixed from conformal symmetry. The state-of-the-art calculations include the leading twists two, three and four with full one-loop α_s corrections [169, 170] and partial two-loop corrections [171]. Higher-twist contributions have been investigated in Ref. [172], which turn out to be small. Nevertheless, estimates based on LCSR are always affected by an systematic uncertainty, which is hard to quantify.

A detailed statistical analysis including the various correlations has been performed in Ref. [173], also including unitarity bounds on the form factor. The results obtained are fully compatible with the lattice QCD calculations of the form factor. For a de-

termination of V_{ub} one may use the partial rate expressed by the integral

$$\begin{aligned} \Delta\zeta(0, q_{\text{max}}^2) &= \frac{G_F^2}{24\pi^3} \int_0^{q_{\text{max}}^2} dq^2 p^3 |f_+(q^2)|^2 \\ &= \frac{1}{|V_{ub}|^2 \tau_{B_0}} \int_0^{q_{\text{max}}^2} dq^2 \frac{d\mathcal{B}(B \rightarrow \pi \ell \nu)}{dq^2}, \quad (75.40) \end{aligned}$$

for which the light-cone sum rule gives [173]

$$\Delta\zeta(0, 12 \text{ GeV}^2) = 5.25^{+0.68}_{-0.54} \text{ ps}^{-1}. \quad (75.41)$$

The uncertainty in this integral is about ten percent, which translates to a theoretical uncertainty of about five percent for the determination of V_{ub} with this method.

75.3.6 $\bar{B} \rightarrow \pi \ell \bar{\nu}_\ell$ measurements

The $\bar{B} \rightarrow \pi \ell \bar{\nu}_\ell$ measurements fall into two broad classes: untagged, in which case the reconstruction of the missing momentum of the event serves as an estimator for the unseen neutrino, and tagged, in which the second B meson in the event is fully reconstructed in either a hadronic or semileptonic decay mode. The tagged measurements have better q^2 resolution, high and uniform acceptance and S/B as high as 10, but lower statistical power. The untagged measurements have somewhat higher background ($S/B < 1$) and make slightly more restrictive kinematic cuts, but still provide statistical power precision on the q^2 dependence of the form factor.

CLEO has analyzed $\bar{B} \rightarrow \pi \ell \bar{\nu}_\ell$ and $\bar{B} \rightarrow \rho \ell \bar{\nu}_\ell$ using an untagged analysis [154–156]. Similar analyses have been done at BABAR [157–160] and Belle [174]. The leading systematic uncertainties in the untagged $\bar{B} \rightarrow \pi \ell \bar{\nu}_\ell$ analyses are associated with modeling the missing momentum reconstruction, with background from $\bar{B} \rightarrow X_u \ell \bar{\nu}_\ell$ decays and $e^+e^- \rightarrow q\bar{q}$ continuum events, and with varying the form factor used to model $\bar{B} \rightarrow \rho \ell \bar{\nu}_\ell$ decays.

Analyses [149, 175] based on reconstructing a B in the $\bar{D}^{(*)\ell^+\nu_\ell}$ decay mode and looking for a $\bar{B} \rightarrow \pi \ell \bar{\nu}_\ell$ or $\bar{B} \rightarrow \rho \ell \bar{\nu}_\ell$ decay amongst the remaining particles in the event make use of the fact that the B and \bar{B} are back-to-back in the $\Upsilon(4S)$ frame to construct a discriminant variable that provides a signal-to-noise ratio above unity for all q^2 bins. A related technique was discussed in Ref. [176]. BABAR [175] and Belle [147] have also used their samples of B mesons reconstructed in hadronic decay modes to measure exclusive charmless semileptonic decays, resulting in very clean but smaller samples. The dominant systematic uncertainties in the tagged analyses arise from tag calibration.

$|V_{ub}|$ can be obtained from the average $\bar{B} \rightarrow \pi \ell \bar{\nu}_\ell$ branching fraction and the measured q^2 spectrum. Fits to the q^2 spectrum using a theoretically motivated parametrization (e.g. "BCL" from Ref. [44]) remove most of the model dependence from theoretical uncertainties in the shape of the spectrum. The most sensitive method for determining $|V_{ub}|$ from $\bar{B} \rightarrow \pi \ell \bar{\nu}_\ell$ decays employs a simultaneous fit [5, 161, 166, 167, 177, 178] to measured experimental partial rates and lattice points versus q^2 (or z) to determine $|V_{ub}|$ and the first few coefficients of the expansion of the form factor in z . We quote the result from Ref. [5], which uses as experimental input an average of the measurements in Refs. [147, 157, 160, 174] and an average [179] of the LQCD input from Ref. [161] and Ref. [165]. The probability of the q^2 measurement average is 6%. The average for the total $B^0 \rightarrow \pi^- \ell^+ \nu_\ell$ branching fraction is obtained by summing up the partial branching fractions:

$$\mathcal{B}(B^0 \rightarrow \pi^- \ell^+ \nu_\ell) = (1.50 \pm 0.02_{\text{stat}} \pm 0.06_{\text{syst}}) \times 10^{-4} \quad (75.42)$$

The corresponding value of $|V_{ub}|$ with this approach is found to be

$$|V_{ub}| = (3.70 \pm 0.10 \pm 0.12) \times 10^{-3} \quad (\text{exclusive}), \quad (75.43)$$

where the first uncertainty is experimental and the second is from theory. Adding an additional constraint using input [171] from LCSR gives [5] $|V_{ub}| = (3.67 \pm 0.09 \pm 0.12) \times 10^{-3}$ (exclusive, LQCD+LCSR). Consistent results for $|V_{ub}|$ were found in a fit reported in Ref. [25].

75.4 Semileptonic b -baryon decays and determination of $|V_{ub}|/|V_{cb}|$

Summary: A significant sample of Λ_b^0 baryons is available at the LHCb experiment, and methods have been developed to study their semileptonic decays. Both $\Lambda_b^0 \rightarrow p \mu \bar{\nu}$ and $\Lambda_b^0 \rightarrow \Lambda_c^+ \mu \bar{\nu}$ decays have been measured at LHCb, and the ratio of branching fractions to these two decay modes is used to determine the ratio $|V_{ub}|/|V_{cb}|$. Averaging the LHCb determination with those obtained from inclusive and exclusive B meson decays, we find

$$|V_{ub}|/|V_{cb}| = 0.092 \pm 0.008 \quad (\text{average}) \quad (75.44)$$

where the average has $p(\chi^2) = 0.9\%$ and the uncertainty has been scaled by a factor $\sqrt{\chi^2/2} = 2.2$. In light of the poor consistency of the three determinations considered, the average should be treated with caution.

75.4.1 $\Lambda_b^0 \rightarrow \Lambda_c^+ \mu \bar{\nu}$ and $\Lambda_b^0 \rightarrow p \mu \bar{\nu}$

The $\Lambda_b^0 \rightarrow \Lambda_c^+$ and $\Lambda_b^0 \rightarrow p$ semileptonic transitions are described in terms of six form factors each. The three form factors corresponding to the vector current can be defined as [180]

$$\begin{aligned} \langle F(p', s') | \bar{q} \gamma_\mu b | \Lambda_b^0(p, s) \rangle &= \bar{u}_F(p', s') \left\{ f_0(q^2) (M_{\Lambda_b^0} - m_F) \frac{q_\mu}{q^2} \right. \\ &+ f_+(q^2) \frac{M_{\Lambda_b^0} + m_F}{s_+} \left(p_\mu + p'_\mu - \frac{q_\mu}{q^2} (M_{\Lambda_b^0}^2 - m_F^2) \right) \\ &\left. + f_\perp(q^2) \left(\gamma_\mu - \frac{2m_F}{s_+} p_\mu - \frac{2M_{\Lambda_b^0}}{s_+} p'_\mu \right) \right\} u_{\Lambda_b^0}(p, s), \end{aligned} \quad (75.45)$$

where $F = p$ or Λ_c^+ and where we define $s_\pm = (M_{\Lambda_b^0} \pm m_F)^2 - q^2$. At vanishing momentum transfer, $q^2 \rightarrow 0$, the kinematic constraint $f_0(0) = f_+(0)$ holds. The form factors are defined in such a way that they correspond to time-like (scalar), longitudinal and transverse polarization with respect to the momentum-transfer q^μ for f_0 , f_+ and f_\perp , respectively. Furthermore we have chosen the normalization in such a way that for $f_0, f_+, f_\perp \rightarrow 1$ one recovers the expression for point-like baryons.

Likewise, the expression for the axial-vector current is

$$\begin{aligned} \langle F(p', s') | \bar{q} \gamma_\mu \gamma_5 b | \Lambda_b^0(p, s) \rangle &= \\ &- \bar{u}_F(p', s') \gamma_5 \left\{ g_0(q^2) (M_{\Lambda_b^0} + m_F) \frac{q_\mu}{q^2} \right. \\ &+ g_+(q^2) \frac{M_{\Lambda_b^0} - m_F}{s_-} \left(p_\mu + p'_\mu - \frac{q_\mu}{q^2} (M_{\Lambda_b^0}^2 - m_F^2) \right) \\ &\left. + g_\perp(q^2) \left(\gamma_\mu + \frac{2m_F}{s_-} p_\mu - \frac{2M_{\Lambda_b^0}}{s_-} p'_\mu \right) \right\} u_{\Lambda_b^0}(p, s), \end{aligned} \quad (75.46)$$

with the kinematic constraint $g_0(0) = g_+(0)$ at $q^2 \rightarrow 0$.

The form factors have been discussed in the heavy quark limit; assuming both b and c as heavy, all the form factors f_i and g_i for the case $\Lambda_b^0 \rightarrow \Lambda_c^+ \mu \nu$ turn out to be identical [180]

$$f_0 = f_+ = f_\perp = g_0 = g_+ = g_\perp = \xi_B \quad (75.47)$$

and equal to the Isgur Wise function ξ_B for baryons. In the limit of a light baryon in the final state, the number of independent form factors is still reduced to two through the heavy quark symmetries of the Λ_b^0 . It should be noted that the $\Lambda_b^0 \rightarrow (p/\Lambda_c^+) \mu \nu$ decay rates peak at high q^2 , which facilitates both lattice QCD calculations and experimental measurements.

The form factors for Λ_b^0 decays have been studied with lattice QCD [181]. Based on these results the differential rates for both $\Lambda_b^0 \rightarrow \Lambda_c^+ \mu \bar{\nu}$ as well as for $\Lambda_b^0 \rightarrow p \mu \bar{\nu}$ can be predicted in the full phase space. In particular, for the experimentally interesting region they find the ratio of decay rates to be [181]

$$\frac{\mathcal{B}(\Lambda_b^0 \rightarrow p \mu \bar{\nu})_{q^2 > 15 \text{ GeV}^2}}{\mathcal{B}(\Lambda_b^0 \rightarrow \Lambda_c^+ \mu \bar{\nu})_{q^2 > 7 \text{ GeV}^2}} = (1.471 \pm 0.095 \pm 0.109) \left| \frac{V_{ub}}{V_{cb}} \right|^2 \quad (75.48)$$

where the first uncertainty is statistical and the second, systematic.

75.4.2 Measurements at LHCb

The LHCb experiment has measured the branching fractions of the semileptonic decays $\Lambda_b^0 \rightarrow \Lambda_c^+ \mu \bar{\nu}$ and $\Lambda_b^0 \rightarrow p \mu \bar{\nu}$, from which they determine $|V_{ub}|/|V_{cb}|$. This is the first such determination at a hadron collider, the first to use a b baryon decay, and the first observation of $\Lambda_b^0 \rightarrow p \mu \bar{\nu}$. Excellent vertex resolution allows the calculation of the transverse momentum p_\perp of the $p\mu$ pair relative to the Λ_b^0 flight direction. The corrected mass, $m_{\text{corr}} = \sqrt{p_\perp^2 + m_{p\mu}^2} + p_\perp$, peaks at the Λ_b^0 mass for signal decays and provides good discrimination against background combinations. The topologically similar decay $\Lambda_b^0 \rightarrow \Lambda_c^+ \mu \bar{\nu}$ is also measured, which eliminates the need to know the production cross-section or absolute efficiencies. Using vertex and Λ_b^0 mass constraints, q^2 can be determined up to a two-fold ambiguity. The LHCb analysis requires both solutions to be in the high q^2 region to minimise contamination from the low q^2 region. Their result [182], rescaled [5] to take into account the recent branching fraction measurement [183] $\mathcal{B}(\Lambda_c^+ \rightarrow p K^- \pi^+) = (6.28 \pm 0.32)\%$, is

$$\frac{\mathcal{B}(\Lambda_b^0 \rightarrow p \mu \bar{\nu})_{q^2 > 15 \text{ GeV}^2}}{\mathcal{B}(\Lambda_b^0 \rightarrow \Lambda_c^+ \mu \bar{\nu})_{q^2 > 7 \text{ GeV}^2}} = (0.92 \pm 0.04 \pm 0.07) \times 10^{-2} \quad (75.49)$$

The largest systematic uncertainty is from the measured $\mathcal{B}(\Lambda_c^+ \rightarrow p K^- \pi^+)$; uncertainties due to trigger, tracking and the Λ_c^+ selection efficiency are each about 3%.

A recent LHCb analysis [184] measures the normalized q^2 spectrum and finds good agreement with the shape calculated with lattice QCD [181].

75.4.3 The ratio $|V_{ub}|/|V_{cb}|$

The ratio of matrix elements, $|V_{ub}|/|V_{cb}|$, is often required when testing the compatibility of a set of measurements with theoretical predictions. It can be determined from the ratio of branching

fractions measured by the LHCb experiment, quoted in the previous section. It can also be calculated based on the $|V_{ub}|$ and $|V_{cb}|$ values quoted earlier in this review.

As previously noted, the decay rate for $\Lambda_b^0 \rightarrow p\mu\bar{\nu}$ peaks at high q^2 where the calculation of the associated form factors using lattice QCD is under good control. Using the measured ratio from Eq. (75.49) along with the calculations of Ref. [181] results in [5]

$$|V_{ub}|/|V_{cb}| = 0.079 \pm 0.004 \pm 0.004 \quad (\text{LHCb}). \quad (75.50)$$

where the first uncertainty is experimental and the second is from the LQCD calculation.

Given the similarities in the theoretical frameworks used for charmed and charmless decays, we choose to quote the ratio $|V_{ub}|/|V_{cb}|$ separately for inclusive and exclusive B decays, as discussed earlier:

$$|V_{ub}|/|V_{cb}| = 0.101 \pm 0.007 \quad (\text{inclusive}), \quad (75.51)$$

$$|V_{ub}|/|V_{cb}| = 0.094 \pm 0.005 \quad (\text{exclusive}). \quad (75.52)$$

The respective determinations of $|V_{ub}|$ and $|V_{cb}|$ are taken to be uncorrelated in the ratio, although there could be some small cancellations of the uncertainties in both the experimental and theoretical input. We average the mesonic decay values, along with the baryonic result in Eq. (75.50), weighting by relative errors. The average has $p(\chi^2) = 4\%$, so we scale the uncertainty by a factor $\sqrt{\chi^2/2} = 1.8$ to find

$$|V_{ub}|/|V_{cb}| = 0.091 \pm 0.006 \quad (\text{average}). \quad (75.53)$$

75.5 Semitaucic decays

Summary: Semileptonic decays to third-generation leptons provide sensitivity to non-Standard Model amplitudes, such as from a charged Higgs boson [185–188] and from leptoquarks [189–195]. The ratios of branching fractions of semileptonic decays involving tau leptons to those involving $\ell = e/\mu$, $R(D^{(*)}) \equiv \mathcal{B}(\bar{B} \rightarrow D^{(*)}\tau\bar{\nu}_\tau)/\mathcal{B}(\bar{B} \rightarrow D^{(*)}\ell\bar{\nu}_\ell)$, are predicted with good precision in the Standard Model [42, 43, 47, 196, 197]. For $R(D)$ and $R(D^*)$ we use the values obtained in [198]

$$\begin{aligned} R(D)^{\text{SM}} &= 0.297 \pm 0.003, \\ R(D^*)^{\text{SM}} &= 0.252 \pm 0.003. \end{aligned} \quad (75.54)$$

Measurements [199–207] of these ratios yield higher values; averaging B -tagged measurements of $R(D)$ and $R(D^*)$ at the $\Upsilon(4S)$ and the LHCb measurements of $R(D^*)$ yields [208]

$$\begin{aligned} R(D)^{\text{meas}} &= 0.340 \pm 0.027 \pm 0.013, \\ R(D^*)^{\text{meas}} &= 0.295 \pm 0.011 \pm 0.008, \end{aligned} \quad (75.55)$$

with a linear correlation of -0.38 . These values exceed Standard Model predictions by 1.4σ and 2.5σ , respectively. A variety of new physics models have been proposed, see eg. [185–195] to explain this excess. Most models proposed to explain the semitaucic decay excesses tend to, but not always have very little impact on semileptonic decays involving muons or electrons, so they do not significantly modify the $|V_{ub}|$ or $|V_{cb}|$ determinations discussed previously in this review. Lepton flavour universality in the ratio of electron and muon modes has been confirmed in a direct ratio measurement, $\mathcal{B}(\bar{B} \rightarrow D^{(*)}e\bar{\nu}_e)/\mathcal{B}(\bar{B} \rightarrow D^{(*)}e\bar{\nu}_\mu) = 1.01 \pm 0.03$, from Belle [40]. The uncertainty is dominated by lepton identification uncertainties that do not cancel in the ratio.

75.5.1 Sensitivity of $\bar{B} \rightarrow D^{(*)}\tau\bar{\nu}_\tau$ to additional amplitudes

In addition to the helicity amplitudes present for decays to $e\bar{\nu}_e$ and $\mu\bar{\nu}_\mu$, decays proceeding through $\tau\bar{\nu}_\tau$ include a scalar amplitude H_s . The differential decay rate is given by [209]

$$\begin{aligned} \frac{d\Gamma}{dq^2} &= \frac{G_F^2 |V_{cb}|^2 |\mathbf{p}_{D^{(*)}}^*|^2}{96\pi^3 m_B^2} \left(1 - \frac{m_\tau^2}{q^2} \right)^2 \\ &\left[(|H_+|^2 + |H_-|^2 + |H_0|^2) \left(1 + \frac{m_\tau^2}{2q^2} \right) + \frac{3m_\tau^2}{2q^2} |H_s|^2 \right], \end{aligned} \quad (75.56)$$

where $|\mathbf{p}_{D^{(*)}}^*|$ is the 3-momentum of the $D^{(*)}$ in the \bar{B} rest frame and the helicity amplitudes H depend on the four-momentum transfer q^2 . All four helicity amplitudes contribute to $\bar{B} \rightarrow D^*\tau\bar{\nu}_\tau$, while only H_0 and H_s contribute to $\bar{B} \rightarrow D\tau\bar{\nu}_\tau$; as a result, new physics contributions can produce larger effects in the latter mode. Semi-leptonic B decays into a τ lepton provide a stringent test of the two-Higgs doublet model of type II (2HDM-II), i.e. where the two Higgs doublets couple separately to up- and down-type quarks. The distinct feature of the 2HDM-II is that the contributions of the charged Higgs scalars scale as $m_\tau^2/m_{H^\pm}^2$, since the couplings to the charged Higgs particles are proportional to the mass of the lepton. As a consequence, one may expect visible effects in decays into a τ , but only small effects for decays into e and μ . The present data rule out the 2HDM-II, see below.

75.5.2 Measurement of $R(D^{(*)})$

$\bar{B} \rightarrow D^{(*)}\tau\bar{\nu}_\tau$ decays have been studied at the $\Upsilon(4S)$ resonance and in pp collisions. At the $\Upsilon(4S)$, the majority of experimental measurements are based on signatures that consist of a D or D^* meson, an electron or muon (denoted here by ℓ) from the decay $\tau \rightarrow \ell\nu_\tau\bar{\nu}_\ell$, a fully-reconstructed decay of the second B meson in the event, and multiple missing neutrinos. One analysis reconstructs the τ in a hadronic mode. The analyses that use hadronic B tags separate signal decays from $\bar{B} \rightarrow D^{(*)}\ell\bar{\nu}_\ell$ decays using the lepton momentum and the measured missing mass squared; decays with only a single missing neutrino peak sharply at zero in this variable, while the signal is spread out to positive values. When a semileptonic B tag is used, the discrimination between signal and $\bar{B} \rightarrow D^{(*)}\ell\bar{\nu}_\ell$ decays comes from the calorimeter energy that is unassociated with any particle used in the reconstruction of the B meson candidates, the measured missing mass squared and the cosine of the angle between the $D^*\ell$ system and its parent B meson, which is calculated under the assumption that only one particle (a neutrino) is missing. In both these approaches, background from $\bar{B} \rightarrow D^{**}\ell\bar{\nu}_\ell$ decays with one or more unreconstructed particles is challenging to separate from signal, as is background from $\bar{B} \rightarrow D^{(*)}H_c X$ (where H_c is a hadron containing a \bar{c} quark) decays. The leading sources of systematic uncertainty are due to the limited size of simulation samples used in constructing the PDFs, the composition of the D^{**} states, efficiency corrections, and cross-feed (swapping soft particles between the signal and tag B).

The most recent measurement from Belle [205] uses semileptonic B tags and leptonic τ decays to simultaneously measure $R(D^*)$ and $R(D)$. The measurement provides the single most precise determination of these ratios, combining results from charged and neutral B decays, and is compatible with the standard model expectation within 1σ .

In addition to the ratio measurements, the Belle experiment has recently performed polarization measurements of the τ [204] and D^* [210] respectively. The τ polarization measurement uses hadronic B tags and τ^- decays to $\pi^- \nu_\tau$ or $\rho^- \nu_\tau$. The main discriminant variables are the measured missing mass squared and the unassociated calorimeter energy. This measurement provides the first determination of the τ polarization in the $\bar{B} \rightarrow D^*\tau\bar{\nu}_\tau$ decay, $\mathcal{P}(D^*) = -0.38 \pm 0.51_{-0.16}^{+0.21}$, compatible with the standard model expectation [20], $-0.476_{-0.034}^{+0.037}$.

The main uncertainties on the $R(D^*)$ measurement come from the composition of the hadronic B background and from modeling of semileptonic B decays and mis-reconstructed D^* mesons. The D^* polarization measurement uses an inclusive tag approach based on Refs. [211, 212], and reconstructs the τ decays in $\ell\nu_\tau\bar{\nu}_\ell$ and $\pi^+\bar{\nu}_\tau$ channels. The main discriminant variables are X_{miss} , a quantity that approximates missing mass but does not depend on tag B reconstruction, the visible energy of the event, and the beam-energy constrained mass, M_{bc} , of the inclusively reconstructed tag side B . This measurement provides the first determination of the D^* longitudinal polarization fraction in the $\bar{B} \rightarrow D^*\tau\bar{\nu}_\tau$ decay, $\mathcal{F}_L(D^*) = -0.38 \pm 0.60_{-0.04}^{+0.08}$, compatible with the standard model expectation [213] within 1.7σ .

The LHCb experiment has studied the decay $\bar{B} \rightarrow D^{*+}\tau\bar{\nu}_\tau$ with $D^{*+} \rightarrow D^0\pi^+$, $D^0 \rightarrow K^-\pi^+$ and $\tau \rightarrow \mu\nu_\tau\bar{\nu}_\mu$ in pp collisions. Their analysis [206] takes advantage of the measurable

flight lengths of b and c hadrons and τ leptons. A multivariate discriminant is used to select decays where no additional charged particles are consistent with coming from the signal decay vertices. The separation between the primary and B decay vertices is used to calculate the momentum of the B decay products transverse to the B flight direction. The longitudinal component of the B momentum can be estimated based on the visible decay products; this allows a determination of the B rest frame, with modest resolution, and enables the calculation of the same discrimination variables available at the $e^+e^- B$ factories. The (rest frame) muon energy, missing mass-squared and q^2 are used in a 3- d fit. The most recent LHCb result [214] on $R(D^*)$ uses three-prong τ decays that take advantage of their excellent vertex resolution to isolate the τ decay from hadronic background. A 3- d fit is performed to determine the signal yield, based on the $\tau\nu_\tau$ pair q^2 , the τ lifetime, as well as a boosted decision tree classifier based on isolation, invariant mass and flight distance information. The leading sources of systematic uncertainty are due to the size of the simulation sample used in constructing the fit templates, uncertainties in modelling the background from hadronic $\bar{B} \rightarrow D^{(*)}H_c X$ decays, as well as reconstruction and trigger effects. The result is normalized to $B^0 \rightarrow D^{*-}\pi^+\pi^-\pi^+$ and found to be 1σ from the standard model expectation (using the expectation value quoted here). An analogous measurement of $B_c \rightarrow J/\psi\tau\bar{\nu}_\tau$ was performed by the LHCb measurement [215], in leptonic τ decays. The result, $R(J/\psi) = 0.71 \pm 0.17 \pm 0.18$, while relatively high is compatible within 2σ of the standard model. Systematic uncertainties are dominated by form factors, as B_c decays are relatively unexplored.

Measurements from BABAR [199–201], Belle [202–205] and LHCb [206, 214] result in values for $R(D)$ and $R(D^*)$ that exceed Standard Model predictions. Table 75.2 lists these values and their average. The simultaneous measurements of $R(D)$ and $R(D^*)$ have linear correlation coefficients of -0.27 (BABAR [200, 201]), -0.49 (Belle hadronic tag [202]) and -0.51 (Belle semileptonic tag [205]); the $R(D)$ and $R(D^*)$ averages have a correlation of -0.38 . Two early untagged Belle measurements [211, 212] are subject to larger systematic uncertainties, with a breakdown of the respective contributions that is inconsistent with the more recent determinations, hence they cannot be reliably combined in the average. All three experiments assume the Standard Model kinematic distributions for $\bar{B} \rightarrow D^{(*)}\tau\bar{\nu}_\tau$ in their determinations of the branching fraction ratios.

Table 75.2: Measurements of $R(D)$ and $R(D^*)$, their correlations, ρ , and the combined averages [208].

	$R(D) \times 10^2$	$R(D^*) \times 10^2$	ρ
BABAR [200, 201]	B^0, B^+ $44.0 \pm 5.8 \pm 4.2$	$33.2 \pm 2.4 \pm 1.8$	-0.27
Belle [202]	B^0, B^+ $37.5 \pm 6.4 \pm 2.6$	$29.3 \pm 3.8 \pm 1.5$	-0.49
Belle [204, 216]	B^0, B^+	27.0 ± 3.5	$^{+2.8}_{-2.5}$
Belle [205]	B^0, B^+ $30.7 \pm 3.7 \pm 1.6$	$28.3 \pm 1.8 \pm 1.4$	-0.51
LHCb [206]	B^0	$33.6 \pm 2.7 \pm 3.0$	
LHCb [214]	B^0	$28.0 \pm 1.8 \pm 2.9$	
Average	B^0, B^+ $34.0 \pm 2.7 \pm 1.3$	$29.5 \pm 1.1 \pm 0.8$	-0.38

The measurement combination in the $R(D) - R(D^*)$ plane is shown in Fig. 75.1, compared with an arithmetic average of predictions from Refs. [47, 217, 218]. The figure is taken from Ref. [5]. The tension between the SM prediction and the measurements is at the level of 1.4σ ($R(D)$) and 2.5σ ($R(D^*)$); if one considers these deviations together the significance rises to 3.1σ . This motivates speculation on possible new physics contributions, although this discrepancy has reduced with respect to previous editions of the RPP due to the results reported in Refs. [205, 214, 216]. There is some tension in the combination coming from the BABAR measurement, the only measurement to claim a deviation from the SM of more than 3σ , although the p -value of the full combination is an acceptable 27%.

The current discussion of $R(D)$ and $R(D^*)$ may be embedded in the theoretical analysis of the other anomalies that have been

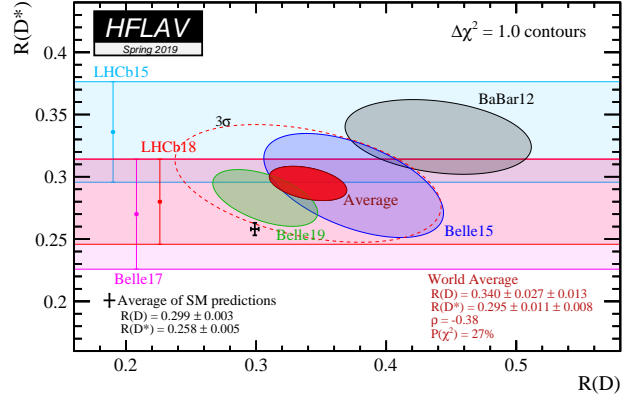


Figure 75.1: Measurements of $R(D)$ and $R(D^*)$ and their two-dimensional average compared with the average predictions for $R(D)$ and $R(D^*)$. Contours correspond to $\Delta\chi^2 = 1$ i.e., 68% CL for the bands and 39% CL for the ellipses. The prediction and the experimental average deviate from each other by 3.08σ . The dashed ellipse corresponds to a 3σ contour (99.73% CL).

observed in semileptonic FCNC ($b \rightarrow s\ell\ell$) transitions. More sophisticated approaches fit the data to a general effective Hamiltonian. Matching this effective Hamiltonian to simplified models, the current situation of the anomalies seems to be compatible with scenarios with an additional Z' or a leptoquark scenario, see eg. [189–195].

75.6 Conclusion

The study of semileptonic B meson decays continues to be an active area for both theory and experiment. The application of HQE calculations to inclusive decays is mature, and fits to moments of $\bar{B} \rightarrow X_c\ell\bar{\nu}_\ell$ decays provide precise values for $|V_{cb}|$ and, in conjunction with input on m_c or from $B \rightarrow X_s\gamma$ decays, provide precise and consistent values for m_b .

The determination of $|V_{ub}|$ from inclusive $\bar{B} \rightarrow X_u\ell\bar{\nu}_\ell$ decays is based on multiple calculational approaches and independent measurements over a variety of kinematic regions, all of which provide consistent results. Further progress in this area is possible, but will require better theoretical control over higher-order terms, improved experimental knowledge of the $\bar{B} \rightarrow X_c\ell\bar{\nu}_\ell$ background and improvements to the modeling of the $\bar{B} \rightarrow X_u\ell\bar{\nu}_\ell$ signal distributions.

In both $b \rightarrow u$ and $b \rightarrow c$ exclusive channels there has been significant recent progress in lattice-QCD calculations, resulting in improved precision on both $|V_{ub}|$ and $|V_{cb}|$. These calculations now provide information on the form factors well away from the high q^2 region, allowing better use of experimental data. For $|V_{cb}|$ recent measurements have provided binned data for fitting form factors with reduced model dependence.

The values from the inclusive and exclusive determinations of $|V_{cb}|$ and $|V_{ub}|$ are only marginally consistent. This is a long-standing puzzle, and the measurement of $|V_{ub}|/|V_{cb}|$ from LHCb based on A_b^0 decays does not simplify the picture.

Both $|V_{cb}|$ and $|V_{ub}|$ are indispensable inputs into unitarity triangle fits. In particular, knowing $|V_{ub}|$ with good precision allows a test of CKM unitarity in a most direct way, by comparing the length of the $|V_{ub}|$ side of the unitarity triangle with the measurement of $\sin(2\beta)$. This comparison of a “tree” process ($b \rightarrow u$) with a “loop-induced” process ($B^0 - \bar{B}^0$ mixing) provides sensitivity to possible contributions from new physics.

The observation of semileptonic decays into τ leptons has opened a new window to the physics of the third generation. The measurements indicate a tension between the data and the Standard Model prediction, which could be a hint for new physics, manifesting itself as a violation of lepton universality beyond the standard-model couplings to the Higgs. It should be noted that none of the most recent measurements alone claim evidence for a deviation from the Standard Model. Combining the data of the semitaonic decays with the anomalies observed in the FCNC

$b \rightarrow s\ell\ell$ transitions allows an interpretation in terms of additional Z' or in terms of additional leptoquarks, but the current data does not allow us to draw a definite conclusion.

The authors would like to acknowledge helpful input from C. Bozzi, M. Rotondo, and C. Schwanda, P. Gambino, Z. Ligeti, F. Bernlochner, S. Stone, S. Meinel, G. Wormser, and D. Robinson.

References

- [1] C. Patrignani *et al.* (Particle Data Group), *Chin. Phys.* **C40**, 10, 100001 (2016).
- [2] See “Heavy-Quark and Soft-Collinear Effective Theory” by C.W. Bauer and M. Neubert in this *Review*.
- [3] See “Lattice Quantum Chromodynamics” by S. Hashimoto, J. Laiho, and S.R. Sharpe in this *Review*.
- [4] See “Production and Decay of b -Flavored Hadrons” by P. Eerola, M. Kreps and Y. Kwon in this *Review*.
- [5] Y. S. Amhis *et al.* (HFLAV) (2019), [arXiv:1909.12524].
- [6] N. Isgur and M. B. Wise, *Phys. Lett.* **B232**, 113 (1989); N. Isgur and M. B. Wise, *Phys. Lett.* **B237**, 527 (1990).
- [7] M. A. Shifman and M. B. Voloshin, *Sov. J. Nucl. Phys.* **47**, 511 (1988), [*Yad. Fiz.*47,801(1988)].
- [8] M. E. Luke, *Phys. Lett.* **B252**, 447 (1990).
- [9] A. V. Manohar and M. B. Wise, *Camb. Monogr. Part. Phys. Nucl. Phys. Cosmol.* **10**, 1 (2000).
- [10] H. Georgi, *Phys. Lett.* **B240**, 447 (1990).
- [11] A. F. Falk *et al.*, *Nucl. Phys.* **B343**, 1 (1990).
- [12] E. Eichten and B. R. Hill, *Phys. Lett.* **B234**, 511 (1990).
- [13] A. Sirlin, *Nucl. Phys.* **B196**, 83 (1982).
- [14] J. A. Bailey *et al.* (Fermilab Lattice, MILC), *Phys. Rev.* **D89**, 11, 114504 (2014), [arXiv:1403.0635].
- [15] C. G. Boyd, B. Grinstein and R. F. Lebed, *Phys. Rev. Lett.* **74**, 4603 (1995), [hep-ph/9412324].
- [16] C. G. Boyd, B. Grinstein and R. F. Lebed, *Phys. Rev.* **D56**, 6895 (1997), [hep-ph/9705252].
- [17] B. Grinstein and A. Kobach, *Phys. Lett.* **B771**, 359 (2017), [arXiv:1703.08170].
- [18] I. Caprini, L. Lellouch and M. Neubert, *Nucl. Phys.* **B530**, 153 (1998), [hep-ph/9712417].
- [19] D. Bigi, P. Gambino and S. Schacht, *Phys. Lett.* **B769**, 441 (2017), [arXiv:1703.06124].
- [20] P. Gambino, M. Jung and S. Schacht, *Phys. Lett.* **B795**, 386 (2019), [arXiv:1905.08209].
- [21] F. U. Bernlochner, Z. Ligeti and D. J. Robinson, *Phys. Rev.* **D100**, 1, 013005 (2019), [arXiv:1902.09553].
- [22] F. U. Bernlochner *et al.*, *Phys. Rev.* **D96**, 9, 091503 (2017), [arXiv:1708.07134].
- [23] A. Czarnecki and K. Melnikov, *Nucl. Phys.* **B505**, 65 (1997), [hep-ph/9703277].
- [24] J. Harrison, C. Davies and M. Wingate (HPQCD), *Phys. Rev.* **D97**, 5, 054502 (2018), [arXiv:1711.11013].
- [25] S. Aoki *et al.* (Flavour Lattice Averaging Group) (2019), [arXiv:1902.08191].
- [26] I. I. Y. Bigi *et al.*, *Phys. Rev.* **D52**, 196 (1995), [hep-ph/9405410].
- [27] A. Kapustin *et al.*, *Phys. Lett.* **B375**, 327 (1996), [hep-ph/9602262].
- [28] P. Gambino, T. Mannel and N. Uraltsev, *Phys. Rev.* **D81**, 113002 (2010), [arXiv:1004.2859].
- [29] P. Gambino, T. Mannel and N. Uraltsev, *JHEP* **10**, 169 (2012), [arXiv:1206.2296].
- [30] D. Buskulic *et al.* (ALEPH), *Phys. Lett.* **B395**, 373 (1997).
- [31] G. Abbiendi *et al.* (OPAL), *Phys. Lett.* **B482**, 15 (2000), [hep-ex/0003013].
- [32] P. Abreu *et al.* (DELPHI), *Phys. Lett.* **B510**, 55 (2001), [hep-ex/0104026].
- [33] J. Abdallah *et al.* (DELPHI), *Eur. Phys. J.* **C33**, 213 (2004), [hep-ex/0401023].
- [34] N. E. Adam *et al.* (CLEO), *Phys. Rev.* **D67**, 032001 (2003), [hep-ex/0210040].
- [35] B. Aubert *et al.* (BaBar), *Phys. Rev.* **D77**, 032002 (2008), [arXiv:0705.4008].
- [36] B. Aubert *et al.* (BaBar), *Phys. Rev. Lett.* **100**, 231803 (2008), [arXiv:0712.3493].
- [37] B. Aubert *et al.* (BaBar), *Phys. Rev.* **D79**, 012002 (2009), [arXiv:0809.0828].
- [38] W. Dungen *et al.* (Belle), *Phys. Rev.* **D82**, 112007 (2010), [arXiv:1010.5620].
- [39] A. Abdesselam *et al.* (Belle) (2017), [arXiv:1702.01521].
- [40] A. Abdesselam *et al.* (Belle) (2018), [arXiv:1809.03290].
- [41] J. P. Lees *et al.* (BaBar), *Phys. Rev. Lett.* **123**, 091801 (2019), [arXiv:1903.10002].
- [42] J. A. Bailey *et al.* (MILC), *Phys. Rev.* **D92**, 3, 034506 (2015), [arXiv:1503.07237].
- [43] H. Na *et al.* (HPQCD), *Phys. Rev.* **D92**, 5, 054510 (2015), [Erratum: *Phys. Rev.*D93,no.11,119906(2016)], [arXiv:1505.03925].
- [44] C. Bourrely, I. Caprini and L. Lellouch, *Phys. Rev.* **D79**, 013008 (2009), [Erratum: *Phys. Rev.*D82,099902(2010)], [arXiv:0807.2722].
- [45] B. Aubert *et al.* (BaBar), *Phys. Rev. Lett.* **104**, 011802 (2010), [arXiv:0904.4063].
- [46] R. Glattauer *et al.* (Belle), *Phys. Rev.* **D93**, 3, 032006 (2016), [arXiv:1510.03657].
- [47] D. Bigi and P. Gambino, *Phys. Rev.* **D94**, 9, 094008 (2016), [arXiv:1606.08030].
- [48] A. V. Manohar and M. B. Wise, *Phys. Rev.* **D49**, 1310 (1994), [hep-ph/9308246].
- [49] I. I. Y. Bigi *et al.*, *Phys. Rev. Lett.* **71**, 496 (1993), [201(1993)], [hep-ph/9304225]; I. I. Y. Bigi *et al.*, *Phys. Lett.* **B323**, 408 (1994), [hep-ph/9311339].
- [50] D. Benson *et al.*, *Nucl. Phys.* **B665**, 367 (2003), [hep-ph/0302262].
- [51] M. Gremm and A. Kapustin, *Phys. Rev.* **D55**, 6924 (1997), [hep-ph/9603448].
- [52] B. M. Dassinger, T. Mannel and S. Turczyk, *JHEP* **03**, 087 (2007), [hep-ph/0611168].
- [53] I. I. Bigi, N. Uraltsev and R. Zwicky, *Eur. Phys. J.* **C50**, 539 (2007), [hep-ph/0511158].
- [54] T. Mannel, S. Turczyk and N. Uraltsev, *JHEP* **11**, 109 (2010), [arXiv:1009.4622].
- [55] A. Pak and A. Czarnecki, *Phys. Rev.* **D78**, 114015 (2008), [arXiv:0808.3509].
- [56] S. Biswas and K. Melnikov, *JHEP* **02**, 089 (2010), [arXiv:0911.4142].
- [57] P. Gambino, *JHEP* **09**, 055 (2011), [arXiv:1107.3100].
- [58] P. Gambino and N. Uraltsev, *Eur. Phys. J.* **C34**, 181 (2004), [hep-ph/0401063].
- [59] V. Aquila *et al.*, *Nucl. Phys.* **B719**, 77 (2005), [hep-ph/0503083].
- [60] T. Becher, H. Boos and E. Lunghi, *JHEP* **12**, 062 (2007), [arXiv:0708.0855].
- [61] A. Alberti *et al.*, *Nucl. Phys.* **B870**, 16 (2013), [arXiv:1212.5082].
- [62] A. Alberti, P. Gambino and S. Nandi, *JHEP* **01**, 147 (2014), [arXiv:1311.7381].
- [63] T. Mannel, A. A. Pivovarov and D. Rosenthal, *Phys. Rev.* **D92**, 5, 054025 (2015), [arXiv:1506.08167].

- [64] C. Breidenbach *et al.*, Phys. Rev. **D78**, 014022 (2008), [arXiv:0805.0971].
- [65] I. Bigi *et al.*, JHEP **04**, 073 (2010), [arXiv:0911.3322].
- [66] A. Kobach and S. Pal, Phys. Lett. **B772**, 225 (2017), [arXiv:1704.00008].
- [67] J. Heinonen and T. Mannel, Nucl. Phys. **B889**, 46 (2014), [arXiv:1407.4384].
- [68] P. Gambino, K. J. Healey and S. Turczyk, Phys. Lett. **B763**, 60 (2016), [arXiv:1606.06174].
- [69] T. Mannel and K. K. Vos, JHEP **06**, 115 (2018), [arXiv:1802.09409].
- [70] M. Fael, T. Mannel and K. Keri Vos, JHEP **02**, 177 (2019), [arXiv:1812.07472].
- [71] I. I. Y. Bigi *et al.*, Phys. Rev. **D50**, 2234 (1994), [hep-ph/9402360].
- [72] A. H. Hoang, Z. Ligeti and A. V. Manohar, Phys. Rev. Lett. **82**, 277 (1999), [hep-ph/9809423].
- [73] A. H. Hoang, Z. Ligeti and A. V. Manohar, Phys. Rev. **D59**, 074017 (1999), [hep-ph/9811239].
- [74] A. H. Hoang and T. Teubner, Phys. Rev. **D60**, 114027 (1999), [hep-ph/9904468].
- [75] A. H. Hoang, Phys. Rev. **D61**, 034005 (2000), [hep-ph/9905550].
- [76] S. E. Csorna *et al.* (CLEO), Phys. Rev. **D70**, 032002 (2004), [hep-ex/0403052].
- [77] A. H. Mahmood *et al.* (CLEO), Phys. Rev. **D70**, 032003 (2004), [hep-ex/0403053].
- [78] B. Aubert *et al.* (BaBar), Phys. Rev. **D69**, 111103 (2004), [hep-ex/0403031].
- [79] B. Aubert *et al.* (BaBar), Phys. Rev. **D69**, 111104 (2004), [hep-ex/0403030].
- [80] C. Schwanda *et al.* (Belle), Phys. Rev. **D75**, 032005 (2007), [hep-ex/0611044].
- [81] P. Urquijo *et al.* (Belle), Phys. Rev. **D75**, 032001 (2007), [hep-ex/0610012].
- [82] J. Abdallah *et al.* (DELPHI), Eur. Phys. J. **C45**, 35 (2006), [hep-ex/0510024].
- [83] D. Acosta *et al.* (CDF), Phys. Rev. **D71**, 051103 (2005), [hep-ex/0502003].
- [84] B. Aubert *et al.* (BaBar), Phys. Rev. **D81**, 032003 (2010), [arXiv:0908.0415].
- [85] A. Limosani *et al.* (Belle), Phys. Rev. Lett. **103**, 241801 (2009), [arXiv:0907.1384].
- [86] C. Schwanda *et al.* (Belle), Phys. Rev. **D78**, 032016 (2008), [arXiv:0803.2158].
- [87] B. Aubert *et al.* (BaBar), Phys. Rev. **D72**, 052004 (2005), [hep-ex/0508004].
- [88] B. Aubert *et al.* (BaBar), Phys. Rev. Lett. **97**, 171803 (2006), [hep-ex/0607071].
- [89] S. Chen *et al.* (CLEO), Phys. Rev. Lett. **87**, 251807 (2001), [hep-ex/0108032].
- [90] M. Battaglia *et al.*, eConf **C0304052**, WG102 (2003), [Phys. Lett. **B556**, 41 (2003)], [hep-ph/0210319].
- [91] B. Aubert *et al.* (BaBar), Phys. Rev. Lett. **93**, 011803 (2004), [hep-ex/0404017].
- [92] O. Buchmüller and H. Flächer, hep-ph/0507253 updated in Ref. [219].
- [93] C. W. Bauer *et al.*, Phys. Rev. **D70**, 094017 (2004), updated in Ref. [219], [hep-ph/0408002].
- [94] P. Gambino and C. Schwanda, Phys. Rev. **D89**, 1, 014022 (2014), [arXiv:1307.4551].
- [95] A. Alberti *et al.*, Phys. Rev. Lett. **114**, 6, 061802 (2015), [arXiv:1411.6560].
- [96] M. Antonelli *et al.*, Phys. Rept. **494**, 197 (2010), see section 5.4.2, [arXiv:0907.5386].
- [97] B. Dehnadi *et al.*, JHEP **09**, 103 (2013), [arXiv:1102.2264].
- [98] I. Allison *et al.* (HPQCD), Phys. Rev. **D78**, 054513 (2008), [arXiv:0805.2999].
- [99] K. G. Chetyrkin *et al.*, Phys. Rev. **D80**, 074010 (2009), [arXiv:0907.2110].
- [100] N. Uraltsev, Int. J. Mod. Phys. **A14**, 4641 (1999), [hep-ph/9905520].
- [101] M. Neubert, Phys. Rev. **D49**, 4623 (1994), [hep-ph/9312311]; M. Neubert, Phys. Rev. **D49**, 3392 (1994), [hep-ph/9311325].
- [102] I. I. Y. Bigi *et al.*, Int. J. Mod. Phys. **A9**, 2467 (1994), [hep-ph/9312359].
- [103] C. W. Bauer, M. E. Luke and T. Mannel, Phys. Rev. **D68**, 094001 (2003), [hep-ph/0102089].
- [104] M. Benzke *et al.*, Phys. Rev. Lett. **106**, 141801 (2011), [arXiv:1012.3167].
- [105] A. Gunawardana and G. Paz (2019), [arXiv:1908.02812].
- [106] M. Neubert, Phys. Lett. **B513**, 88 (2001), [hep-ph/0104280].
- [107] M. Neubert, Phys. Lett. **B543**, 269 (2002), [hep-ph/0207002].
- [108] A. K. Leibovich, I. Low and I. Z. Rothstein, Phys. Rev. **D61**, 053006 (2000), [hep-ph/9909404].
- [109] A. K. Leibovich, I. Low and I. Z. Rothstein, Phys. Rev. **D62**, 014010 (2000), [hep-ph/0001028].
- [110] A. K. Leibovich, I. Low and I. Z. Rothstein, Phys. Lett. **B486**, 86 (2000), [hep-ph/0005124].
- [111] A. K. Leibovich, I. Low and I. Z. Rothstein, Phys. Lett. **B513**, 83 (2001), [hep-ph/0105066].
- [112] A. H. Hoang, Z. Ligeti and M. Luke, Phys. Rev. **D71**, 093007 (2005), [hep-ph/0502134].
- [113] B. O. Lange, M. Neubert and G. Paz, JHEP **10**, 084 (2005), [hep-ph/0508178].
- [114] B. O. Lange, JHEP **01**, 104 (2006), [hep-ph/0511098].
- [115] M. Neubert, Phys. Lett. **B612**, 13 (2005), [hep-ph/0412241].
- [116] Z. Ligeti, I. W. Stewart and F. J. Tackmann, Phys. Rev. **D78**, 114014 (2008), [arXiv:0807.1926].
- [117] P. Gambino, K. J. Healey and C. Mondino, Phys. Rev. **D94**, 1, 014031 (2016), [arXiv:1604.07598].
- [118] B. O. Lange, M. Neubert and G. Paz, Phys. Rev. **D72**, 073006 (2005), [hep-ph/0504071].
- [119] P. Gambino *et al.*, JHEP **10**, 058 (2007), [arXiv:0707.2493].
- [120] J. R. Andersen and E. Gardi, JHEP **01**, 097 (2006), [hep-ph/0509360].
- [121] M. Beneke *et al.*, JHEP **06**, 071 (2005), [hep-ph/0411395].
- [122] C. Greub, M. Neubert and B. D. Pecjak, Eur. Phys. J. **C65**, 501 (2010), [arXiv:0909.1609].
- [123] M. Brucherseifer, F. Caola and K. Melnikov, Phys. Lett. **B721**, 107 (2013), [arXiv:1302.0444].
- [124] T. Mannel and S. Recksiegel, Phys. Rev. **D60**, 114040 (1999), [hep-ph/9904475].
- [125] U. Aglietti *et al.*, Eur. Phys. J. **C59**, 831 (2009), [arXiv:0711.0860].
- [126] C. W. Bauer, Z. Ligeti and M. E. Luke, Phys. Rev. **D64**, 113004 (2001), [hep-ph/0107074].
- [127] C. W. Bauer, Z. Ligeti and M. E. Luke, Phys. Lett. **B479**, 395 (2000), [hep-ph/0002161].
- [128] I. I. Y. Bigi and N. G. Uraltsev, Nucl. Phys. **B423**, 33 (1994), [hep-ph/9310285].
- [129] M. B. Voloshin, Phys. Lett. **B515**, 74 (2001), [hep-ph/0106040].

- [130] Z. Ligeti, M. Luke and A. V. Manohar, Phys. Rev. **D82**, 033003 (2010), [arXiv:1003.1351].
- [131] P. Gambino and J. F. Kamenik, Nucl. Phys. **B840**, 424 (2010), [arXiv:1004.0114].
- [132] J. L. Rosner *et al.* (CLEO), Phys. Rev. Lett. **96**, 121801 (2006), [hep-ex/0601027].
- [133] R. Barate *et al.* (ALEPH), Eur. Phys. J. **C6**, 555 (1999).
- [134] M. Acciarri *et al.* (L3), Phys. Lett. **B436**, 174 (1998).
- [135] G. Abbiendi *et al.* (OPAL), Eur. Phys. J. **C21**, 399 (2001), [hep-ex/0107016].
- [136] P. Abreu *et al.* (DELPHI), Phys. Lett. **B478**, 14 (2000), [hep-ex/0105054].
- [137] A. Bornheim *et al.* (CLEO), Phys. Rev. Lett. **88**, 231803 (2002), [hep-ex/0202019].
- [138] A. Limosani *et al.* (Belle), Phys. Lett. **B621**, 28 (2005), [hep-ex/0504046].
- [139] B. Aubert *et al.* (BaBar), Phys. Rev. **D73**, 012006 (2006), [hep-ex/0509040].
- [140] J. P. Lees *et al.* (BaBar), Phys. Rev. **D95**, 7, 072001 (2017), [arXiv:1611.05624].
- [141] B. Aubert *et al.* (BaBar), Phys. Rev. Lett. **95**, 111801 (2005), [Erratum: Phys. Rev. Lett.97,019903(2006)], [hep-ex/0506036].
- [142] R. V. Kowalewski and S. Menke, Phys. Lett. **B541**, 29 (2002), [hep-ex/0205038].
- [143] J. P. Lees *et al.* (BaBar), Phys. Rev. **D86**, 032004 (2012), [arXiv:1112.0702].
- [144] I. Bizjak *et al.* (Belle), Phys. Rev. Lett. **95**, 241801 (2005), [hep-ex/0505088].
- [145] P. Urquijo *et al.* (Belle), Phys. Rev. Lett. **104**, 021801 (2010), [arXiv:0907.0379].
- [146] B. Aubert *et al.* (BaBar), Phys. Rev. Lett. **96**, 221801 (2006), [hep-ex/0601046].
- [147] A. Sibidanov *et al.* (Belle), Phys. Rev. **D88**, 3, 032005 (2013), [arXiv:1306.2781].
- [148] B. Aubert *et al.* (BaBar), Phys. Rev. Lett. **90**, 181801 (2003), [eConfC0304052,WG117(2003)], [hep-ex/0301001].
- [149] T. Hokuue *et al.* (Belle), Phys. Lett. **B648**, 139 (2007), [hep-ex/0604024].
- [150] B. Aubert *et al.* (BaBar), Phys. Rev. **D79**, 052011 (2009), [arXiv:0808.3524].
- [151] J. P. Lees *et al.* (BaBar), Phys. Rev. **D88**, 7, 072006 (2013), [arXiv:1308.2589].
- [152] J. P. Lees *et al.* (BaBar), Phys. Rev. **D87**, 3, 032004 (2013), [Erratum: Phys. Rev.D87,no.9,099904(2013)], [arXiv:1205.6245].
- [153] C. Schwanda *et al.* (Belle), Phys. Rev. Lett. **93**, 131803 (2004), [hep-ex/0402023].
- [154] N. E. Adam *et al.* (CLEO), Phys. Rev. Lett. **99**, 041802 (2007), [hep-ex/0703041].
- [155] S. B. Athar *et al.* (CLEO), Phys. Rev. **D68**, 072003 (2003), superceded by Ref. [156], [hep-ex/0304019].
- [156] R. Gray *et al.* (CLEO), Phys. Rev. **D76**, 012007 (2007), [Addendum: Phys. Rev.D76,no.3,039901(2007)], [hep-ex/0703042].
- [157] P. del Amo Sanchez *et al.* (BaBar), Phys. Rev. **D83**, 032007 (2011), supercedes Ref. [158], [arXiv:1005.3288].
- [158] B. Aubert *et al.* (BaBar), Phys. Rev. **D72**, 051102 (2005), [hep-ex/0507003].
- [159] P. del Amo Sanchez *et al.* (BaBar), Phys. Rev. **D83**, 052011 (2011), updated in Ref. [160], [arXiv:1010.0987].
- [160] J. P. Lees *et al.* (BaBar), Phys. Rev. **D86**, 092004 (2012), [arXiv:1208.1253].
- [161] J. A. Bailey *et al.* (Fermilab Lattice, MILC), Phys. Rev. **D92**, 1, 014024 (2015), [arXiv:1503.07839].
- [162] A. Bazavov *et al.* (Fermilab Lattice, MILC), Phys. Rev. **D100**, 3, 034501 (2019), [arXiv:1901.02561].
- [163] C. M. Bouchard *et al.*, Phys. Rev. **D90**, 054506 (2014), [arXiv:1406.2279].
- [164] B. Colquhoun *et al.*, Phys. Rev. **D93**, 3, 034502 (2016), [arXiv:1510.07446].
- [165] J. M. Flynn *et al.*, Phys. Rev. **D91**, 7, 074510 (2015), [arXiv:1501.05373].
- [166] T. Becher and R. J. Hill, Phys. Lett. **B633**, 61 (2006), [hep-ph/0509090].
- [167] M. C. Arnesen *et al.*, Phys. Rev. Lett. **95**, 071802 (2005), [hep-ph/0504209].
- [168] M. A. Shifman, A. I. Vainshtein and V. I. Zakharov, Nucl. Phys. **B147**, 385 (1979); M. A. Shifman, A. I. Vainshtein and V. I. Zakharov, Nucl. Phys. **B147**, 448 (1979).
- [169] P. Ball and R. Zwicky, Phys. Rev. **D71**, 014015 (2005), [hep-ph/0406232].
- [170] G. Duplancic *et al.*, JHEP **04**, 014 (2008), [arXiv:0801.1796].
- [171] A. Bharucha, JHEP **05**, 092 (2012), [arXiv:1203.1359].
- [172] A. V. Rusov, Eur. Phys. J. **C77**, 7, 442 (2017), [arXiv:1705.01929].
- [173] I. Sentitemsu Imsong *et al.*, JHEP **02**, 126 (2015), [arXiv:1409.7816].
- [174] H. Ha *et al.* (Belle), Phys. Rev. **D83**, 071101 (2011), [arXiv:1012.0090].
- [175] B. Aubert *et al.* (BaBar), Phys. Rev. Lett. **101**, 081801 (2008), [arXiv:0805.2408].
- [176] W. S. Brower and H. P. Paar, Nucl. Instrum. Meth. **A421**, 411 (1999), [hep-ex/9710029].
- [177] P. Ball, eConf **C070512**, 016 (2007), [arXiv:0705.2290].
- [178] J. M. Flynn and J. Nieves, Phys. Lett. **B649**, 269 (2007), [hep-ph/0703284].
- [179] S. Aoki *et al.*, Eur. Phys. J. **C77**, 2, 112 (2017), [arXiv:1607.00299].
- [180] T. Feldmann and M. W. Y. Yip, Phys. Rev. **D85**, 014035 (2012), [Erratum: Phys. Rev.D86,079901(2012)], [arXiv:1111.1844].
- [181] W. Detmold, C. Lehner and S. Meinel, Phys. Rev. **D92**, 3, 034503 (2015), [arXiv:1503.01421].
- [182] R. Aaij *et al.* (LHCb), Nature Phys. **11**, 743 (2015), [arXiv:1504.01568].
- [183] M. Ablikim *et al.* (BESIII), Phys. Rev. Lett. **116**, 5, 052001 (2016), [arXiv:1511.08380].
- [184] R. Aaij *et al.* (LHCb), Phys. Rev. **D96**, 11, 112005 (2017), [arXiv:1709.01920].
- [185] M. Tanaka, Z. Phys. **C67**, 321 (1995), [hep-ph/9411405].
- [186] H. Itoh, S. Komine and Y. Okada, Prog. Theor. Phys. **114**, 179 (2005), [hep-ph/0409228].
- [187] U. Nierste, S. Trine and S. Westhoff, Phys. Rev. **D78**, 015006 (2008), [arXiv:0801.4938].
- [188] M. Tanaka and R. Watanabe, Phys. Rev. **D82**, 034027 (2010), [arXiv:1005.4306].
- [189] A. Datta, M. Duraisamy and D. Ghosh, Phys. Rev. **D86**, 034027 (2012), [arXiv:1206.3760].
- [190] D. Bečirević, N. Košnik and A. Tayduganov, Phys. Lett. **B716**, 208 (2012), [arXiv:1206.4977].
- [191] S. Fajfer *et al.*, Phys. Rev. Lett. **109**, 161801 (2012), [arXiv:1206.1872].
- [192] A. Crivellin, C. Greub and A. Kokulu, Phys. Rev. **D86**, 054014 (2012), [arXiv:1206.2634].

- [193] M. Bauer and M. Neubert, Phys. Rev. Lett. **116**, 14, 141802 (2016), [arXiv:1511.01900].
- [194] I. Doršner *et al.*, Phys. Rept. **641**, 1 (2016), [arXiv:1603.04993].
- [195] A. Celis *et al.*, Phys. Lett. **B771**, 168 (2017), [arXiv:1612.07757].
- [196] J. F. Kamenik and F. Mescia, Phys. Rev. **D78**, 014003 (2008), [arXiv:0802.3790].
- [197] S. Fajfer, J. F. Kamenik and I. Nisandzic, Phys. Rev. **D85**, 094025 (2012), [arXiv:1203.2654].
- [198] M. Bordone, M. Jung and D. van Dyk (2019), [arXiv:1908.09398].
- [199] B. Aubert *et al.* (BaBar), Phys. Rev. Lett. **100**, 021801 (2008), [arXiv:0709.1698].
- [200] J. P. Lees *et al.* (BaBar), Phys. Rev. Lett. **109**, 101802 (2012), [arXiv:1205.5442].
- [201] J. P. Lees *et al.* (BaBar), Phys. Rev. **D88**, 7, 072012 (2013), [arXiv:1303.0571].
- [202] M. Huschle *et al.* (Belle), Phys. Rev. **D92**, 7, 072014 (2015), [arXiv:1507.03233].
- [203] Y. Sato *et al.* (Belle), Phys. Rev. **D94**, 7, 072007 (2016), [arXiv:1607.07923].
- [204] S. Hirose *et al.* (Belle), Phys. Rev. Lett. **118**, 21, 211801 (2017), [arXiv:1612.00529].
- [205] G. Caria *et al.* (Belle) (2019), [arXiv:1910.05864].
- [206] R. Aaij *et al.* (LHCb), Phys. Rev. Lett. **115**, 11, 111803 (2015), [Erratum: Phys. Rev. Lett.115,no.15,159901(2015)], [arXiv:1506.08614].
- [207] R. Aaij *et al.* (LHCb), Phys. Rev. Lett. **120**, 17, 171802 (2018), [arXiv:1708.08856].
- [208] <http://www.slac.stanford.edu/xorg/hfag/semi/fpcp17/RDRDs.html>.
- [209] J. G. Korner and G. A. Schuler, Z. Phys. **C46**, 93 (1990).
- [210] A. Abdesselam *et al.* (Belle), in “10th International Workshop on the CKM Unitarity Triangle (CKM 2018) Heidelberg, Germany, September 17-21, 2018,” (2019), [arXiv:1903.03102].
- [211] A. Matyja *et al.* (Belle), Phys. Rev. Lett. **99**, 191807 (2007), [arXiv:0706.4429].
- [212] A. Bozek *et al.* (Belle), Phys. Rev. **D82**, 072005 (2010), [arXiv:1005.2302].
- [213] M. Tanaka and R. Watanabe, Phys. Rev. **D87**, 3, 034028 (2013), [arXiv:1212.1878].
- [214] R. Aaij *et al.* (LHCb), Phys. Rev. **D97**, 7, 072013 (2018), [arXiv:1711.02505].
- [215] R. Aaij *et al.* (LHCb), Phys. Rev. Lett. **120**, 12, 121801 (2018), [arXiv:1711.05623].
- [216] S. Hirose *et al.* (Belle), Phys. Rev. **D97**, 1, 012004 (2018), [arXiv:1709.00129].
- [217] F. U. Bernlochner *et al.*, Phys. Rev. **D95**, 11, 115008 (2017), [erratum: Phys. Rev.D97,no.5,059902(2018)], [arXiv:1703.05330].
- [218] S. Jaiswal, S. Nandi and S. K. Patra, JHEP **12**, 060 (2017), [arXiv:1707.09977].
- [219] Y. Amhis *et al.* (HFLAV), Eur. Phys. J. **C77**, 12, 895 (2017), [arXiv:1612.07233].

76. Determination of CKM angles from B hadrons

Written August 2019 by T. Gershon (Warwick U.), M. Kenzie (Warwick U.) and K. Trabelsi (U. Paris-Saclay, IJCLab).

76.1 Introduction

The Cabibbo–Kobayashi–Maskawa (CKM) description of quark mixing [1, 2] leads to a number of triangle relations between pairs of CKM matrix elements. One of these,

$$V_{ud}V_{ub}^* + V_{cd}V_{cb}^* + V_{td}V_{tb}^* = 0, \quad (76.1)$$

is of particular interest since (i) all its terms are of comparable magnitude, and (ii) its properties can be measured through studies of oscillations and decays of B mesons. As the area of this unitary triangle is a measure of the amount of CP violation in the Standard Model [3], it is of particular interest to determine the values of its angles and to test the consistency of the CKM paradigm with the experimental measurements. The angles are defined as

$$\begin{aligned} \alpha &= \arg \left[-\frac{V_{td}V_{tb}^*}{V_{ud}V_{ub}^*} \right], & \beta &= \arg \left[-\frac{V_{cd}V_{cb}^*}{V_{td}V_{tb}^*} \right], \\ \gamma &= \arg \left[-\frac{V_{ud}V_{ub}^*}{V_{cd}V_{cb}^*} \right], \end{aligned} \quad (76.2)$$

with an alternative notation $(\phi_2, \phi_1, \phi_3) \equiv (\alpha, \beta, \gamma)$ also widely used in the literature.

In this mini-review, the most precise methods to determine the CKM angles are described, with a particular focus on nontrivial aspects of the combination of results. More detailed discussions of these points can be found in Ref. [4]. A similar mini-review on the side of the unitarity triangle adjacent to the angle γ can be found in Ref. [5]. A detailed overview of the CKM quark-mixing matrix is given in Ref. [6] while CP violation in the quark sector is discussed in Ref. [7].

76.2 β

The relative weak (*i.e.* CP -violating) phase between the amplitude for any CKM-favoured B^0 meson decay to a CP eigenstate and that for the decay following B^0 – \bar{B}^0 oscillation is twice the angle β . The decay-time-dependent CP asymmetry can be expressed as

$$\begin{aligned} A_{f_{CP}}(t) &\equiv \frac{d\Gamma/dt[\bar{B}_{\text{phys}}^0(t) \rightarrow f_{CP}] - d\Gamma/dt[B_{\text{phys}}^0(t) \rightarrow f_{CP}]}{d\Gamma/dt[\bar{B}_{\text{phys}}^0(t) \rightarrow f_{CP}] + d\Gamma/dt[B_{\text{phys}}^0(t) \rightarrow f_{CP}]}, \\ &= S_f \sin(\Delta m t) - C_f \cos(\Delta m t), \end{aligned} \quad (76.3a)$$

$$(76.3b)$$

where the notation $B_{\text{phys}}^0(t)$ ($\bar{B}_{\text{phys}}^0(t)$) denotes a neutral B meson that decays at time t into the final state f_{CP} , and is known (“tagged”) at time $t = 0$ to have flavour content corresponding to B^0 (\bar{B}^0). In Eq. (76.3b), Δm denotes the mass difference between the two physical eigenstates of the B^0 – \bar{B}^0 system, while the corresponding decay-width difference is assumed to be negligible [8]; moreover CPT symmetry and the absence of CP violation in B^0 – \bar{B}^0 mixing is assumed throughout this mini-review.

In the general case, one can write

$$S_f \equiv \frac{2\mathcal{I}m(\lambda_f)}{1 + |\lambda_f|^2} \quad \text{and} \quad C_f \equiv \frac{1 - |\lambda_f|^2}{1 + |\lambda_f|^2}, \quad (76.4)$$

where the parameter $\lambda_f = \frac{\bar{A}_f}{p A_f}$ is defined in terms of p and q , which define the flavour content of the mass eigenstates of the B^0 – \bar{B}^0 system [8], and the amplitudes \bar{A}_f (A_f) for a \bar{B}^0 (B^0) decay to the final state f_{CP} . In the limit that the decay amplitude is dominated by a CKM-favoured transition, as is the case for $B^0 \rightarrow J/\psi K_S^0$ decays, one obtains simple relations: $S_f = -\eta_{CP} \sin(2\beta)$ and $C_f = 0$, where η_{CP} is the CP eigenvalue of the final state [9, 10]. This method has been pursued intensively by experiments. The current world averages, combining results for

several charmonium-kaon final states but dominated by results on $B^0 \rightarrow J/\psi K_S^0$ (CP odd) and $B^0 \rightarrow J/\psi K_L^0$ (CP even), are [4]

$$-\eta_{CP} S_f = 0.699 \pm 0.017, \quad C_f = -0.005 \pm 0.015. \quad (76.5)$$

Despite the large number of signal events in the data, the dominant uncertainties are still statistical. One important source of potential systematic correlation between results from different experiments is that due to “tag-side interference” [11], which is common to measurements exploiting production through the $e^+e^- \rightarrow \Upsilon(4S) \rightarrow B^0\bar{B}^0$ process, including the latest results from BaBar [12] and Belle [13]. It does not, however, affect the results from LHCb [14] that have comparable statistical sensitivity. Another common source of systematic uncertainty is due to knowledge of the value of Δm , but since this quantity has been measured precisely [8] the effect remains small.

The interpretation of the value of $-\eta_{CP} S_f$ from Eq. (76.5) as $\sin(2\beta)$ assumes negligible contributions from subleading amplitudes with a different weak phase to that of the tree diagram (*i.e.* to that of the CKM matrix elements $V_{cb}V_{cs}^*$). This potential additional contribution is often referred to as “penguin pollution”. All existing data, including the value of C_f in Eq. (76.5), as well as several explicit calculations [15–18], are consistent with penguin pollution in B^0 meson decays to charmonium-kaon decays being negligible at the current level of precision. Therefore, the value of $-\eta_{CP} S_f$ is generally converted to $\sin(2\beta)$ without any correction or additional uncertainty being assigned due to this assumption. This gives [4]

$$\beta = (22.2 \pm 0.7)^\circ, \quad (76.6)$$

where only the solution consistent with the Standard Model is reported (methods to resolve the trigonometric ambiguity in the result are discussed below). It is also possible to use data-driven methods, typically based on flavour symmetries plus some additional assumptions, to constrain the effects of penguin pollution [19–21]. In this case it is necessary to consider each charmonium-kaon final state separately, since the penguin pollution to each may differ. The most common approach [19], which relies on experimental information on $B^0 \rightarrow J/\psi\pi^0$ decays, currently gives an additional uncertainty on $\sin(2\beta)$ from $B^0 \rightarrow J/\psi K_S^0$ of around 0.01.

It is possible to avoid the issue of penguin pollution in the measurement of β by using B^0 meson decays to a charm- and light-meson final state, such as $D_{CP}\pi^0$ (where D_{CP} represents a D^0 meson decaying into a CP eigenstate), instead of the charmonium-kaon final states. These decays do have a CKM-suppressed contribution ($V_{ub}V_{cd}^*$ instead of $V_{cb}V_{ud}^*$), which can in principle bias the determination of $\sin(2\beta)$ from S_f , but this can be calculated and is known to be negligible at current precision. The requirement that the neutral D meson decays to a final state that is common to both D^0 and \bar{D}^0 , such as the CP -even eigenstate K^+K^- , reduces the sample size that is available for analysis. Consequently, the world average [4], $\sin(2\beta) = 0.71 \pm 0.09$, with these channels is not as precise as that from the charmonium-kaon states.

Converting experimental results on $\sin(2\beta)$ into constraints on β leads to a trigonometric ambiguity in the range $[0^\circ, 180^\circ]$. This can be resolved with experimental measurements of $\cos(2\beta)$, which can be obtained from decay-time-dependent analyses of B^0 meson decays to multibody (non- CP -eigenstate) final states. Among the charmonium-kaon decays, study of $B^0 \rightarrow J/\psi K^*(892)^0$ with $K^*(892)^0 \rightarrow K_S^0\pi^0$ is the most promising approach, but due to the limited sample size that has been analysed to date the precision is not sufficient to resolve the ambiguity conclusively. The charm- and light-meson channels such as $B^0 \rightarrow D\pi^0$ with $D \rightarrow K_S^0\pi^+\pi^-$ have been shown to provide good statistical power for this purpose, with a joint analysis of BaBar and Belle data giving $\cos(2\beta) = 0.91 \pm 0.25$ [22, 23], sufficient to rule out the alternative solution for β .

76.3 α

In the limit that only tree amplitudes contribute to B^0 meson decays to light mesons, such as $B^0 \rightarrow \pi^+\pi^-$, then the observables of the decay-time-dependent CP asymmetry of Eq. (76.3) would allow a straight-forward determination of 2α : $S_f = +\eta_{CP} \sin(2\alpha)$

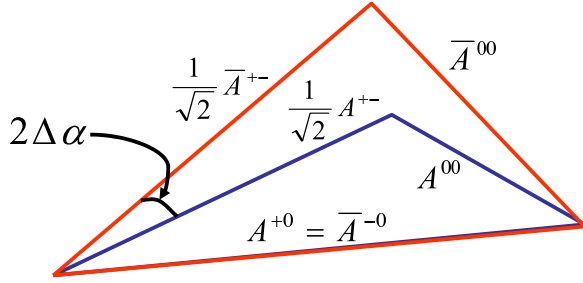


Figure 76.1: Isospin triangles for $B \rightarrow \pi\pi$ decays, reproduced from Ref. [24]. Here, the relative phase between A^{+0} and \bar{A}^{-0} has been rotated away to simplify the picture. The total relative phase probed by $S_{\pi^+\pi^-}$ is $\arg\left(\frac{q}{p}\frac{\bar{A}^{+-}}{A^{+-}}\right) = 2\alpha - 2\Delta\alpha$, including contributions from $B^0\text{--}\bar{B}^0$ mixing, the tree-level amplitudes and the correction $\Delta\alpha$, and exploiting the unitarity requirement $\alpha + \beta + \gamma = 180^\circ$.

and $C_f = 0$. In general, however, the determination of α is complicated by the presence of contributions from $b \rightarrow d(u\bar{u})$ neutral-current penguin transitions, which have a similar level of CKM-suppression as the $b \rightarrow u(\bar{u}d)$ charged-current tree amplitudes but have a different weak phase. Consequently one obtains instead for $B^0 \rightarrow \pi^+\pi^-$

$$S_{\pi^+\pi^-} = \sqrt{1 - C_{\pi^+\pi^-}^2} \sin(2\alpha - 2\Delta\alpha), \quad (76.7)$$

where $\Delta\alpha$ is the *a priori* unknown penguin contribution.

This contribution from the penguin amplitude can be accounted for in an analysis relating the amplitudes for isospin partner decays, *e.g.* A^{+-} for $B^0 \rightarrow \pi^+\pi^-$, A^{+0} for $B^+ \rightarrow \pi^+\pi^0$, A^{00} for $B^0 \rightarrow \pi^0\pi^0$ decays and $(\bar{A}^{+-}, \bar{A}^{-0}, \bar{A}^{00})$ for their charge conjugates. The isospin analysis relies on the fact that there is no penguin contribution to A^{+0} and \bar{A}^{-0} , because $\pi^\pm\pi^0$ is a pure isospin-2 state, and the ($\Delta I = \frac{1}{2}$) QCD-penguin amplitudes only contribute to the isospin-0 final state. One therefore obtains the following isospin triangle relations [25]

$$A^{+0} = \frac{1}{\sqrt{2}}A^{+-} + A^{00} \quad \text{and} \quad \bar{A}^{-0} = \frac{1}{\sqrt{2}}\bar{A}^{+-} + \bar{A}^{00}, \quad (76.8)$$

from which it is possible to determine $\Delta\alpha$, as shown in Fig. 76.1.

Since the determination of $\Delta\alpha$ and thus also α requires construction of amplitude-level relations, it is not appropriate to simply average results of α from different experiments. Instead, measurements of each of the observable quantities needed to determine α are input into a combination. For the $B \rightarrow \pi\pi$ system, the inputs are the branching fractions of $B^0 \rightarrow \pi^+\pi^-$, $B^+ \rightarrow \pi^+\pi^0$ and $B^0 \rightarrow \pi^0\pi^0$ decays, the lifetimes of the B^+ and B^0 mesons (which relate the branching fractions to amplitude-level quantities), and the $S_{\pi^+\pi^-}$, $C_{\pi^+\pi^-}$ and $C_{\pi^0\pi^0}$ observables. Potential sources of correlation must be taken into account, but these are predominantly systematic in origin and thus have a small effect on the combination, since the measurements are statistically limited. An exception is that the LHCb measurements of $(S_{\pi^+\pi^-}, C_{\pi^+\pi^-})$ [26] have a significant statistical correlation due to the fact that the time variable of Eq. (76.3) is the difference between production and decay, and hence is in the range $[0, \infty]$. This correlation is largely absent for measurements from BaBar [27] and Belle [28], where the difference between the signal and tagging B meson decay times is measured, and hence $t \in [-\infty, \infty]$. The combination itself can be performed with different statistical approaches; the procedure described in detail in Ref. [29], based on a frequentist treatment, is used here. The knowledge of $C_{\pi^0\pi^0}$ [27, 30] is currently the limiting factor in the precision on α from the $B \rightarrow \pi\pi$ system, and is likely to remain so for some time due to the difficulty to reconstruct this final state.

In general, the isospin triangle construction gives a four-fold ambiguity on $2\Delta\alpha$ (each triangle can face either up or down), leading to an eight-fold ambiguity on α in the range $[0^\circ, 180^\circ]$.

This is reduced if either or both of the triangles are flat, or if the two triangles have sides of identical length. The ambiguities can also be reduced if measurement of the $S_{\pi^0\pi^0}$ (or equivalent) observable is available, since this can be combined with the corresponding $\Delta\alpha$ parameter from the right-hand corner of the triangle in Fig. 76.1 to provide an additional constraint. None of these possibilities are realised in the $B \rightarrow \pi\pi$ system; in particular a decay-time-dependent analysis of $B^0 \rightarrow \pi^0\pi^0$ is extremely challenging experimentally due to the absence of any charged particle originating from the B decay position. Nonetheless, solutions consistent with $\alpha = 0$ can be rejected on physical grounds [24].

The isospin analysis can also be performed with the $B \rightarrow \rho\rho$ system, which contains two vector particles in the final state and so does not have a fixed CP eigenvalue. In principle the analysis can be performed separately for each $\rho\rho$ polarisation state, but in practise it is found that the longitudinal polarisation fraction, f_L , is close to unity, and hence the final state is approximately CP -even. Compared to $B^0 \rightarrow \pi\pi$, the $\rho\rho$ modes benefit experimentally from a higher branching fraction and smaller penguin contributions, so that the isospin triangles are flatter, reducing the ambiguities. (The value of $\Delta\alpha$ in the $B \rightarrow \rho\rho$ system, obtained from the isospin analysis, has a single solution in $[0, \pi]$ at $(3 \pm 5)^\circ$, while for $B \rightarrow \pi\pi$ there are two solutions at 13° and 27° with $\Delta\alpha \in [7, 33]^\circ$ at 68.3% confidence level (CL). The isospin analysis with either final state has an ambiguity under $\Delta\alpha \leftrightarrow -\Delta\alpha$.) For the BaBar [31] and Belle [32] experiments, the high branching fraction and smaller penguin contribution compensate for the increased difficulty to reconstruct the $\rho\rho$ final state relative to $\pi\pi$. Moreover, in contrast to $S_{\pi^0\pi^0}$, measurement of $S_{\rho^0\rho^0}$ is possible due to the four charged pion final state (following $\rho^0 \rightarrow \pi^+\pi^-$ decay), as has been demonstrated by BaBar [33].

In the $B \rightarrow \rho\pi$ system there are more amplitudes to consider, so that the isospin relation corresponds to a pentagon rather than a triangle and Eq. (76.8) is modified to become

$$\begin{aligned} \sqrt{2}(A^{+0} + A^{0+}) &= A^{+-} + A^{-+} + 2A^{00} \quad \text{and} \\ \sqrt{2}(\bar{A}^{-0} + \bar{A}^{0-}) &= \bar{A}^{+-} + \bar{A}^{-+} + 2\bar{A}^{00}. \end{aligned} \quad (76.9)$$

As in Eq. (76.8), the left-hand sides of these expressions correspond to a pure isospin-2 final state, and therefore the ratio of the right-hand sides gives a pure phase term that, accounting for the $B^0\text{--}\bar{B}^0$ mixing phase that also contributes to the measured quantities, is 2α . The relative amplitudes for B^0 and \bar{B}^0 decays to $\rho^+\pi^-$, $\rho^-\pi^+$ and $\rho^0\pi^0$ can all be determined from a decay-time-dependent analysis of the $\pi^+\pi^-\pi^0$ Dalitz plot, so that study of this channel alone allows determination of α [34]. This analysis in principle leads to a single solution for α in $[0^\circ, 180^\circ]$, but the precision of current measurements [35–37] is limited.

The isospin analysis used to determine α is believed to be valid to high precision, and theoretical uncertainties in the procedure are usually neglected. Nonetheless, it should be noted that the analysis assumes the absence of electroweak penguin amplitudes, which can contribute to $\Delta I = \frac{3}{2}$ transitions with a different weak phase from that of the tree amplitudes [38, 39]. Moreover, isospin-breaking effects such as (π^0, η, η') mixing would impact on the relations of Eq. (76.8). A further complication in the $B \rightarrow \rho\rho$ system is the effect of the non-zero ρ meson width [40]. Estimates of the size of these effects on the determined value of α are typically at the 1° level or less [29]. By contrast, methods to determine α using SU(3) or other flavour symmetries are generally considered to have larger theoretical uncertainties and are not included here.

The world average obtained for the angle α from isospin analysis of $B \rightarrow \pi\pi$, $\rho\pi$ and $\rho\rho$ decays is [4]

$$\alpha = (84.9_{-4.5}^{+5.1})^\circ, \quad (76.10)$$

where the quoted uncertainty is at the 68.3% CL and does not include effects due to isospin-breaking. This world average, together with results split by decay mode, is shown in Fig. 76.2. The combination has a total of 51 experimental inputs from which 24 parameters are determined, and an overall χ^2 of 16.4, which corresponds to a p-value of 94%. Thus, there is excellent overall consistency between the inputs, despite the tension apparent in

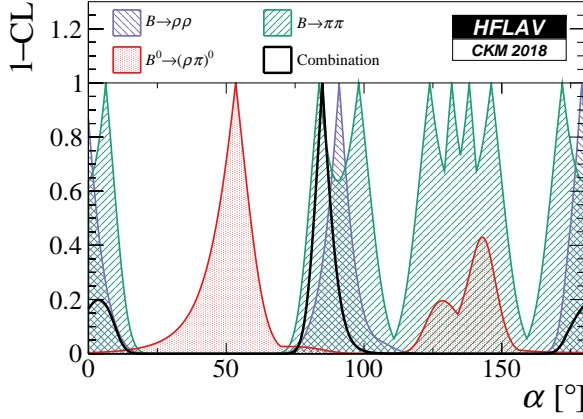


Figure 76.2: World average of α , as well as contributions from individual modes, in terms of 1-CL.

Fig. 76.2 between the results from $B^0 \rightarrow (\rho\pi)^0$ and the others. The combination gives a single best-fit for α in $[0^\circ, 180^\circ]$, but an ambiguous solution exists at $\alpha \Leftrightarrow \alpha + 180^\circ$. A secondary minimum close to zero is disfavoured [29].

76.4 γ

The angle γ is the weak phase between Cabibbo-favoured $b \rightarrow c$ and suppressed $b \rightarrow u$ quark transitions and can be determined by exploiting interference between them. Explicitly, the ratio of suppressed to favoured amplitudes is parametrised by

$$r_B e^{i(\delta_B \pm \gamma)} = \frac{A_{\text{sup}}}{A_{\text{fav}}}, \quad (76.11)$$

where r_B is the ratio of amplitude magnitudes, δ_B the strong phase difference and the + or - sign depends on whether the transition involves a \bar{b} or b quark, respectively. Measurement of γ in this way has negligible theoretical uncertainty in the Standard Model [41], and therefore this approach provides a benchmark against which determinations from other methods, typically involving loop diagrams, can be compared.

Interference between these amplitudes is realised in $B^+ \rightarrow DK^+$ decays, where D represents an admixture of D^0 and \bar{D}^0 mesons. The simplest case is that of D decays to CP -eigenstates (GLW method [42, 43]), either CP -even such as K^+K^- ($CP+$) or CP -odd such as $K_S^0\pi^0$ ($CP-$). The normalised decay rate and CP asymmetry are given by

$$R_{CP\pm} = \frac{\Gamma(B^- \rightarrow D_{CP\pm}K^-) + \Gamma(B^+ \rightarrow D_{CP\pm}K^+)}{\Gamma(B^- \rightarrow D^0K^-) + \Gamma(B^+ \rightarrow \bar{D}^0K^+)} \\ = 1 + r_B^2 \pm 2r_B \cos(\delta_B) \cos(\gamma), \quad (76.12a)$$

$$A_{CP\pm} = \frac{\Gamma(B^- \rightarrow D_{CP\pm}K^-) - \Gamma(B^+ \rightarrow D_{CP\pm}K^+)}{\Gamma(B^- \rightarrow D_{CP\pm}K^-) + \Gamma(B^+ \rightarrow D_{CP\pm}K^+)} \\ = \frac{\pm 2r_B \sin(\delta_B) \sin(\gamma)}{1 + r_B^2 \pm 2r_B \cos(\delta_B) \cos(\gamma)}. \quad (76.12b)$$

These relations assume the absence of direct CP violation in the charm system; experimentally allowed deviations from this assumption are too small to cause a significant bias on γ [7, 44]. It is convenient to determine the $R_{CP\pm}$ quantities through a double ratio, normalising to $B^+ \rightarrow D\pi^+$ decays involving the same final states, since this cancels potential sources of systematic uncertainty due to the branching fractions of the D decays that are used; small possible effects of CP violation in $B^+ \rightarrow D\pi^+$ decays are a source of systematic uncertainty in this procedure. The GLW method can be extended to include final states that are almost CP -eigenstates [45], as is the case in $D \rightarrow \pi^+\pi^-\pi^0$ and $D \rightarrow K^+K^-\pi^0$ decays, via inclusion of a factor encoding the fraction of CP -even (or CP -odd) content, F_{\pm} , which dilutes the sensitivity to γ by reducing the size of the interference terms (the terms linear with r_B) in Eq. (76.12).

For other D decays, the ratio of amplitudes for the D^0 and \bar{D}^0 decays to the final state of interest has to be accounted for in the formalism. The ADS method [46, 47] uses D decays to final states such as $K^\mp\pi^\pm$, which involve interference between Cabibbo-favoured (CF) and doubly-Cabibbo-suppressed (DCS) transitions. The observables in this case are

$$A_{\text{ADS}} = \frac{\Gamma(B^- \rightarrow [K^+\pi^-]_D K^-) - \Gamma(B^+ \rightarrow [K^-\pi^+]_D K^+)}{\Gamma(B^- \rightarrow [K^+\pi^-]_D K^-) + \Gamma(B^+ \rightarrow [K^-\pi^+]_D K^+)} \\ = \frac{2r_B r_D \sin(\delta_B + \delta_D) \sin(\gamma)}{r_B^2 + r_D^2 + 2r_B r_D \cos(\delta_B + \delta_D) \cos(\gamma)}, \quad (76.13a)$$

$$R_{\text{ADS}} = \frac{\Gamma(B^- \rightarrow [K^+\pi^-]_D K^-) + \Gamma(B^+ \rightarrow [K^-\pi^+]_D K^+)}{\Gamma(B^- \rightarrow [K^-\pi^+]_D K^-) + \Gamma(B^+ \rightarrow [K^+\pi^-]_D K^+)} \\ = r_B^2 + r_D^2 + 2r_B r_D \cos(\delta_B + \delta_D) \cos(\gamma), \quad (76.13b)$$

where r_D and δ_D are the amplitude magnitude ratio and strong phase difference between the CF and DCS D decay. An alternative pair of observables, (R_-, R_+) , is also sometimes used, where R_- (R_+) is the ratio of decay rates between the suppressed and favoured transitions for B^- (B^+) decays. The R_- and R_+ observables are statistically independent, while A_{ADS} and R_{ADS} are not (in particular, the uncertainty on A_{ADS} depends on the central value of R_{ADS}). However, the pair (R_-, R_+) has more correlated sources of systematic uncertainty compared to $(A_{\text{ADS}}, R_{\text{ADS}})$. The observables of Eq. (76.13) are therefore usually preferred once a significant signal is established. The ADS method can also be extended to include decays to multibody final states, such as $D \rightarrow K^\pm\pi^\mp\pi^0$ and $D \rightarrow K^\pm\pi^\mp\pi^+\pi^-$, by addition of a coherence factor [48] which appears in the interference terms of Eq. (76.13) and accounts for dilution of the sensitivity due to variation of the decay amplitude across the phase space of the final state. A similar method can be used for singly Cabibbo-suppressed D decays to non- CP eigenstates such as K^*K [49].

For D decays to multibody self-conjugate final states (BPGGSZ method [50, 51]), such as $D \rightarrow K_S^0\pi^+\pi^-$, one can write the partial decay rate as a function of the position in the phase space in terms of the ‘‘Cartesian parameters’’ $x_{\pm} + iy_{\pm} = r_B e^{i(\delta_B \pm \gamma)}$:

$$d\Gamma(B^\pm \rightarrow [K_S^0\pi^+\pi^-]_D K^\pm) = A_{(\mp, \pm)}^2 + r_B^2 A_{(\pm, \mp)}^2 \\ + 2A_{(\pm, \mp)} A_{(\mp, \pm)} [x_{\pm} c_{D(\pm, \mp)} + y_{\pm} s_{D(\pm, \mp)}], \quad (76.14)$$

where the notation $(+, -)$ is shorthand for the dependence on the Dalitz position - the squared invariant masses of $K_S^0\pi^+$ and $K_S^0\pi^-$ combinations, respectively. The quantities $A_{(+, -)}$ and $A_{(-, +)}$ represent the magnitudes of the D^0 and \bar{D}^0 decay amplitudes at the Dalitz point $(+, -)$ and are interchangeable with their CP conjugate amplitudes because CP conservation is assumed in the D decay (*i.e.* $A_{(-, +)} = \bar{A}_{(+, -)}$). The quantities $c_{D(\pm, \mp)}$ and $s_{D(\pm, \mp)}$ are the cosine and sine of the strong phase difference, $\delta_{D(+, -)} = \arg(\bar{A}_{(+, -)}) - \arg(A_{(+, -)})$, between the \bar{D}^0 and D^0 amplitudes. These quantities can be determined from an amplitude model, although this leads to a hard-to-quantify systematic uncertainty associated to the composition of the model. An alternative, ‘‘model-independent’’, approach involves dividing the phase space into appropriate bins. In this case, the analysis benefits from external input on the values of c_D and s_D integrated over each bin. Measurements of these external parameters have been performed for the $D \rightarrow K_S^0\pi^+\pi^-$ decay by the CLEO-c collaboration [52, 53] and will be further improved upon by BES-III. The use of common input values for these parameters in model-independent determinations of γ with the BPGGSZ method by different experiments is a source of correlation between experiments that is currently negligible but will become more significant as the available B meson data samples increase in size.

The discussion above refers to $B^+ \rightarrow DK^+$ decays, but analogous measurements can be made also for additional channels such as $B^+ \rightarrow D^*K^+$ (with $D^* \rightarrow D\pi^0, D\gamma$) and $B^+ \rightarrow DK^{*+}$ (with $K^{*+} \rightarrow K_S^0\pi^+, K^+\pi^0$). In the limit that these can be treated purely as two-body decays, the expressions for $B^+ \rightarrow DK^+$ are modified only by ensuring the r_B and δ_B parameters are specific to each B decay. Moreover, for $B^+ \rightarrow D^*K^+$ decays an

effective shift of the strong phase by π between $D^* \rightarrow D\pi^0$ and $D\gamma$ decays [54] has to be taken into account. In case the finite width of the decaying resonance is non-negligible, as is the case for the $K^*(892)$ state, the sensitivity is diluted by relevant coherence factors, κ_B . For the $B^0 \rightarrow DK^{*0}$ decay, full amplitude analysis of the $B^0 \rightarrow DK^+\pi^-$ Dalitz plot provides additional sensitivity compared to the quasi-two-body approach [55, 56].

It is also possible to measure γ using decay-time-dependent analysis of the B_s^0 meson [57]. The weak phase arising in the interference between direct decay of $B_s^0 \rightarrow D_s^\mp K^\pm$ and decay via mixing is $(\gamma - 2\beta_s)$, where β_s is the angle associated with $B_s^0 \rightarrow J/\psi\phi$ decays in a similar way to the relation between β and $B^0 \rightarrow J/\psi K_S^0$ decays described in Sec. 76.2. Sufficient information can be obtained from the tagged, decay-time-dependent rates of $B_s^0 \rightarrow D_s^\mp K^\pm$ decays that this weak phase can be determined, up to an ambiguity, together with the strong phase difference between, and the ratio of the magnitudes of, the suppressed and favoured amplitudes. Since β_s is known to good precision [8], measurements of the decay-time-dependent CP -asymmetry observables in $B_s^0 \rightarrow D_s^\mp K^\pm$ decays can be used to infer constraints on γ . Alternatively, if effects of penguin pollution in $B_s^0 \rightarrow J/\psi\phi$ decays [17, 18] are a concern, as they will become in the future, results from the $B_s^0 \rightarrow D_s^\mp K^\pm$ mode can be combined with an independent precise measurement of γ to provide a penguin-free determination of β_s .

The average for γ requires a non-trivial combination due the complicated relations between the observables and the physics parameters of interest, such as in Eqs. (76.12), (76.13) and (76.14). Moreover, hadronic parameters such as r_B and δ_B defined in Eq. (76.11) are common to all different D decay modes (but differ for each B decay mode). Thus, it is not correct to simply average results for γ obtained by different experiments or in different channels. Instead, measurements of rate asymmetries, rate ratios and the Cartesian parameters are taken as inputs to the combination, from which results are obtained not only for γ but also for the hadronic parameters. The precision to which γ can be measured with a particular B decay is approximately inversely proportional to the value of r_B . Thus, results from channels with smaller yields but larger values of r_B , such as $B^0 \rightarrow DK^{*0}$ and $B_s^0 \rightarrow D_s^\mp K^\pm$ ($r_B \approx 0.3-0.4$), can have a significant impact on the world average and are included in the combination. By contrast the $B^+ \rightarrow D\pi^+$ mode, for which large samples are available but $r_B \approx 0.005$, has little impact and is also more sensitive to potential systematic biases; hence it is not included. The sensitivity of the world average at present is dominated by results from $B^+ \rightarrow DK^+$, where $r_B \approx 0.1$, in particular results with the GLW [58], ADS [59] and BPGGSZ [60–62] methods.

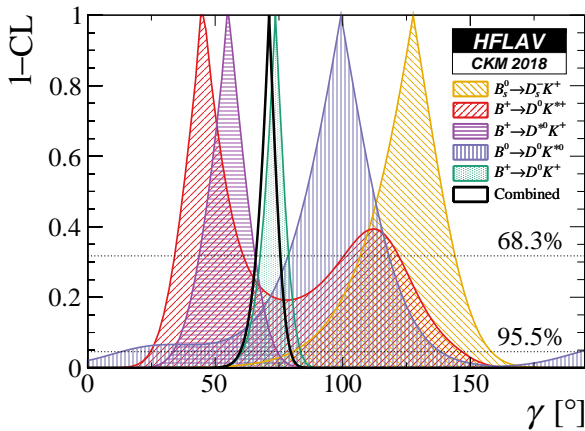


Figure 76.3: World average of $\gamma \equiv \phi_3$, as well as contributions from individual modes, in terms of $1-CL$.

The world average obtained for the angle γ , obtained by combining results from $B^+ \rightarrow DK^+$, D^*K^+ , DK^{*+} , $DK^+\pi^+\pi^-$, $B^0 \rightarrow DK^+\pi^-$ and $B_s^0 \rightarrow D_s^\mp K^\pm$ decays, is [4]

$$\gamma = (72.1_{-4.5}^{+4.1})^\circ, \quad (76.15)$$

where the quoted uncertainty is at the 68.3% CL.

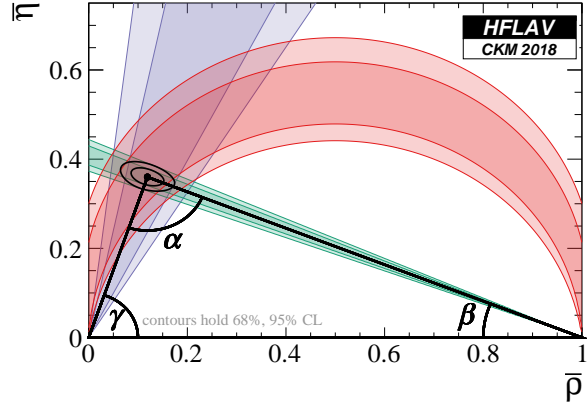


Figure 76.4: Constraints from the measurements of the angles of the CKM unitarity triangle in the $(\bar{\rho}, \bar{\eta})$ plane.

Effects related to charm and kaon mixing and CP violation are generally negligible at the current level of precision, in particular for modes with $r_B \gtrsim 0.1$. An exception is that a dependence of the selection efficiency on the charm decay time can induce a dependence of the observables on charm mixing parameters [63]. Such effects can be important at hadron collider experiments such as LHCb, but can be corrected for. Interactions of neutral kaons with detector material can also cause a bias in determination of γ from modes with low values of r_B [64], such as the BPGGSZ method applied to $B^+ \rightarrow D\pi^+$, but are negligible in modes with larger r_B values.

Effects from correlated uncertainties between amplitude models and strong phase differences in charm decays are negligible and are not explicitly accounted for in the combination, nor are effects related to charm and kaon mixing and CP violation. This world average, together with results split by decay mode, is shown in Fig. 76.3. The combination has a total of 136 experimental inputs from which 29 parameters are determined, an overall χ^2 of 123.4, which corresponds to a p-value of 13% indicating acceptable agreement between the inputs. The combination gives a single solution for γ in $[0^\circ, 180^\circ]$, but an ambiguous solution exists at $\gamma \Leftrightarrow \gamma + 180^\circ$.

76.5 Summary

Experimental progress has resulted in all three angles of the CKM unitarity triangle being measured with good accuracy, with β known to subdegree precision and both α and γ known to about 5° . The constraints from these three measurements in the $(\bar{\rho}, \bar{\eta})$ plane are shown in Fig. 76.4; further discussion and comparison with constraints from independent measurements can be found in Ref. [6]. The determinations of all three angles remain statistically limited, but it will be a challenge for experiments to ensure that this remains the case as the precision improves. Consequently, the correct treatment of sources of correlation between the measurements that go into the world average combinations is becoming increasingly important.

References

- [1] N. Cabibbo, Phys. Rev. Lett. **10**, 531 (1963).
- [2] M. Kobayashi and T. Maskawa, Prog. Theor. Phys. **49**, 652 (1973).
- [3] C. Jarlskog, Phys. Rev. Lett. **55**, 1039 (1985).
- [4] Y. Amhis *et al.* (HFLAV), Eur. Phys. J. **C77**, 895 (2017), [arXiv:1612.07233].
- [5] See the review on “Semileptonic b -Hadron Decays, Determination of V_{cb} , V_{ub} ” in this Review.
- [6] See the review on “Cabibbo-Kobayashi-Maskawa Mixing Matrix,” in this Review.
- [7] See the review on “ CP Violation in the Quark Sector,” in this Review.

- [8] See the review on “ $B^0-\bar{B}^0$ Mixing” in this *Review*.
- [9] A. Carter and A. Sanda, Phys. Rev. **D23**, 1567 (1981).
- [10] I. Bigi and A. Sanda, Nucl. Phys. **B193**, 85 (1981).
- [11] O. Long *et al.*, Phys. Rev. **D68**, 034010 (2003), [hep-ex/0303030].
- [12] B. Aubert *et al.* (BaBar), Phys. Rev. **D79**, 072009 (2009), [arXiv:0902.1708].
- [13] I. Adachi *et al.*, Phys. Rev. Lett. **108**, 171802 (2012), [arXiv:1201.4643].
- [14] R. Aaij *et al.* (LHCb), Phys. Rev. Lett. **115**, 031601 (2015), [arXiv:1503.07089].
- [15] H.-n. Li and S. Mishima, JHEP **03**, 009 (2007), [hep-ph/0610120].
- [16] M. Jung, Phys. Rev. **D86**, 053008 (2012), [arXiv:1206.2050].
- [17] K. De Bruyn and R. Fleischer, JHEP **1503**, 145 (2015), [arXiv:1412.6834].
- [18] P. Frings, U. Nierste and M. Wiebusch, Phys. Rev. Lett. **115**, 6, 061802 (2015), [arXiv:1503.00859].
- [19] M. Ciuchini, M. Pierini and L. Silvestrini, Phys. Rev. Lett. **95**, 221804 (2005), [hep-ph/0507290].
- [20] S. Faller *et al.*, Phys. Rev. **D79**, 014030 (2009), [arXiv:0809.0842].
- [21] Z. Ligeti and D. Robinson, Phys. Rev. Lett. **115**, 251801 (2015), [arXiv:1507.06671].
- [22] I. Adachi *et al.* (BaBar, Belle), Phys. Rev. Lett. **121**, 261801 (2018), [arXiv:1804.06152].
- [23] I. Adachi *et al.* (BaBar, Belle), Phys. Rev. **D98**, 112012 (2018), [arXiv:1804.06153].
- [24] M. Antonelli *et al.*, Phys. Rept. **494**, 197 (2010), [arXiv:0907.5386].
- [25] M. Gronau and D. London, Phys. Rev. Lett. **65**, 3381 (1990).
- [26] R. Aaij *et al.* (LHCb), Phys. Rev. **D98**, 032004 (2018), [arXiv:1805.06759].
- [27] J. P. Lees *et al.* (BaBar), Phys. Rev. **D87**, 052009 (2013), [arXiv:1206.3525].
- [28] I. Adachi *et al.* (Belle), Phys. Rev. **D88**, 092003 (2013), [arXiv:1302.0551].
- [29] J. Charles *et al.*, Eur. Phys. J. **C77**, 574 (2017), [arXiv:1705.02981].
- [30] T. Julius *et al.* (Belle), Phys. Rev. **D96**, 032007 (2017), [arXiv:1705.02083].
- [31] B. Aubert *et al.* (BaBar), Phys. Rev. **D76**, 052007 (2007), [arXiv:0705.2157].
- [32] P. Vanhoefer *et al.* (Belle), Phys. Rev. **D93**, 032010 (2016), [Addendum *ibid.* **D94** 099903 (2016)], [arXiv:1510.01245].
- [33] B. Aubert *et al.* (BaBar), Phys. Rev. **D78**, 071104 (2008), [arXiv:0807.4977].
- [34] A. E. Snyder and H. R. Quinn, Phys. Rev. **D48**, 2139 (1993).
- [35] J. P. Lees *et al.* (BaBar), Phys. Rev. **D88**, 012003 (2013), [arXiv:1304.3503].
- [36] A. Kusaka *et al.* (Belle), Phys. Rev. Lett. **98**, 221602 (2007), [hep-ex/0701015].
- [37] A. Kusaka *et al.* (Belle), Phys. Rev. **D77**, 072001 (2008), [arXiv:0710.4974].
- [38] M. Gronau and J. Zupan, Phys. Rev. **D71**, 074017 (2005), [hep-ph/0502139].
- [39] S. Gardner, Phys. Rev. **D72**, 034015 (2005), [hep-ph/0505071].
- [40] A. Falk *et al.*, Phys. Rev. **D69**, 011502 (2004), [hep-ph/0310242].
- [41] J. Brod and J. Zupan, JHEP **01**, 051 (2014), [arXiv:1308.5663].
- [42] M. Gronau and D. London, Phys. Lett. **B253**, 483 (1991).
- [43] M. Gronau and D. Wyler, Phys. Lett. **B265**, 172 (1991).
- [44] See the review on “ $D^0-\bar{D}^0$ Mixing” in this *Review*.
- [45] M. Nayak *et al.*, Phys. Lett. **B740**, 1 (2015), [arXiv:1410.3964].
- [46] D. Atwood, I. Dunietz and A. Soni, Phys. Rev. Lett. **78**, 3257 (1997), [hep-ph/9612433].
- [47] D. Atwood, I. Dunietz and A. Soni, Phys. Rev. **D63**, 036005 (2001), [hep-ph/0008090].
- [48] D. Atwood and A. Soni, Phys. Rev. **D68**, 033003 (2003), [hep-ph/0304085].
- [49] Y. Grossman, Z. Ligeti and A. Soffer, Phys. Rev. **D67**, 071301 (2003), [hep-ph/0210433].
- [50] A. Giri *et al.*, Phys. Rev. **D68**, 054018 (2003), [hep-ph/0303187].
- [51] A. Bondar, *Proceedings of BINP special analysis meeting on Dalitz analysis*, 24-26 Sep. 2002, unpublished.
- [52] R. Briere *et al.* (CLEO), Phys. Rev. **D80**, 032002 (2009), [arXiv:0903.1681].
- [53] J. Libby *et al.* (CLEO), Phys. Rev. **D82**, 112006 (2010), [arXiv:1010.2817].
- [54] A. Bondar and T. Gershon, Phys. Rev. **D70**, 091503 (2004), [hep-ph/0409281].
- [55] T. Gershon, Phys. Rev. **D79**, 051301 (2009), [arXiv:0810.2706].
- [56] T. Gershon and M. Williams, Phys. Rev. **D80**, 092002 (2009), [arXiv:0909.1495].
- [57] R. Aleksan, I. Dunietz and B. Kayser, Z. Phys. **C54**, 653 (1992).
- [58] R. Aaij *et al.* (LHCb), Phys. Lett. **B777**, 16 (2018), [arXiv:1708.06370].
- [59] R. Aaij *et al.* (LHCb), Phys. Lett. **B760**, 117 (2016), [arXiv:1603.08993].
- [60] P. del Amo Sanchez *et al.* (BaBar), Phys. Rev. Lett. **105**, 121801 (2010), [arXiv:1005.1096].
- [61] A. Poluektov *et al.* (Belle), Phys. Rev. **D81**, 112002 (2010), [arXiv:1003.3360].
- [62] R. Aaij *et al.* (LHCb), JHEP **08**, 176 (2018), [Erratum *ibid.* **10**, 107 (2018)], [arXiv:1806.01202].
- [63] M. Rama, Phys. Rev. **D89**, 014021 (2014), [arXiv:1307.4384].
- [64] M. Bjørn and S. Malde, JHEP **07**, 106 (2019), [arXiv:1904.01129].

77. Spectroscopy of Mesons Containing Two Heavy Quarks

Revised March 2020 by S. Eidelman (Budker Inst., Novosibirsk; Novosibirsk U.), C. Hanhart (Jülich), J. J. Hernández-Rey (IFIC, Valencia), R.E. Mitchell (Indiana U.), S. Navas (Dp.de Fisica. U. de Granada) and C. Patrignani (Bologna U.).

A golden age for heavy quarkonium physics dawned at the turn of this century, initiated by the confluence of exciting advances in quantum chromodynamics (QCD) and an explosion of related experimental activity. The subsequent broad spectrum of breakthroughs, surprises, and continuing puzzles had not been anticipated. Since that time CLEO-c, BESIII and the B-factories, recently joined by ATLAS, CMS and LHCb, have continued to make groundbreaking observations. For an extensive presentation of the status of heavy quarkonium physics, the reader is referred to several reviews [1–6]. This note focuses on experimental developments in heavy quarkonium spectroscopy with very few theoretical comments. Possible theoretical interpretations of the states not predicted by the quark model are presented in the minireview on non- $q\bar{q}$ states. Note that in this review we follow the new naming scheme for hadrons (see the review “Naming scheme for hadrons” in the current edition).

This minireview covers the newly discovered states, where “newly” refers to the period since 2002. In earlier versions of this write-up the particles were sorted according to an assumed *conventional* or *unconventional* nature with respect to the quark model. However, since this classification is not always unambiguous, we here follow Ref. [8] and sort the states into three groups, namely states below (*cf.* Table 77.1), near (*cf.* Table 77.2) and above (*cf.* Table 77.3) the lowest open-flavor thresholds.

Table 77.1 lists properties of newly observed heavy quarkonium states located below the lowest open-flavor thresholds. Those are expected to be (at least prominently) conventional quarkonia. The $h_c(1P)$ is the 1P_1 state of charmonium, singlet partner of the long-known χ_{cJ} triplet 3P_J . The $\eta_c(2S)$ is the first excited state of the pseudoscalar ground state $\eta_c(1S)$, lying just below the mass of its vector counterpart, $\psi(2S)$.

Although $\eta_c(2S)$ measurements began to converge towards a mass and a width some time ago, refinements are still in progress. In particular, Belle [9] has revisited its analysis of $B \rightarrow K\eta_c(2S)$, $\eta_c(2S) \rightarrow K\bar{K}\pi$ decays with more data and methods that account for interference between the above decay chain, an equivalent one with the $\eta_c(1S)$ instead, and one with no intermediate resonance. The net effect of this interference is far from trivial; it shifts the apparent mass by $\sim +10$ MeV and inflates the apparent width by a factor of six. The updated $\eta_c(2S)$ mass and width are in better accordance with other measurements than the previous treatment [10], which did not include interference. Complementing this measurement in B -decay, BaBar [11] updated their previous [12] $\eta_c(2S)$ mass and width measurements in two-photon production, where interference effects, judging from studies of $\eta_c(1S)$, appear to be small. In combination, precision on the $\eta_c(2S)$ mass has improved dramatically. The currently most accurate individual mass measurement is from LHCb using $B^+ \rightarrow K^+\bar{p}p$ [13].

Belle reported an observation of the $\psi_2(1D)$ decaying to $\gamma\chi_{c1}$ with J^{PC} presumed to be 2^{--} [14]. This state is listed in Table 77.1 as $\psi_2(3823)$. Its existence was confirmed with high significance by BESIII [15]. While the negative C-parity is indeed established by its observed decay channel, the assignment of $J = 2$ was done by matching to the closest quark model state. This assignment therefore requires experimental confirmation.

The 1^1D_2 state, or the $\eta_{c2}(1D)$, with a mass expected near 3820 MeV, has not been observed yet. Recently Belle performed its search in $B \rightarrow \eta_{c2}(1D)K(\pi)$ decays in the mass range 3795–3845 MeV and found no signal [16]. Thus, the $\eta_{c2}(1D)$ remains the only unobserved conventional charmonium state that does not have open-charm decays.

A new $c\bar{b}$ state was discovered by the ATLAS Collaboration [17]. Its properties are consistent with expectations for the first excited state of the B_c^\pm meson, the $B_c^\pm(2S)$. The real picture appears to be more complicated. The ATLAS state was observed at 6842 ± 6 MeV. Five years later, the CMS collaboration investigated the $B_c^\pm \pi^+ \pi^-$ invariant mass spectrum and observed two close signals consistent with the $B_c^{*+}(2S)$ and $B_c^+(2S)$ states [18]. The two

peaks are well resolved (a significance of 6.5 standard deviations), with a measured mass difference of $\Delta M = 29.1 \pm 1.5(\text{stat}) \pm 0.7(\text{syst})$ MeV. The mass of the right peak, $B_c^+(2S)$, is measured to be $6871.0 \pm 1.2(\text{stat}) \pm 0.8(\text{syst}) \pm 0.8(B_c^+)$ MeV, where the last term is the uncertainty in the world-average B_c^+ mass. Since the low-energy photon emitted in the $B_c^{*+} \rightarrow B_c^+ + \gamma$ radiative decay is not reconstructed, the observed $B_c^{*+}(2S)$ peak has a mass lower than the true value, which remains unknown. Therefore the $B_c^{*+}(2S)$ does not yet appear in the listings. LHCb confirmed the CMS results and measured masses with higher precision [19]. Their signal corresponding to the $B_c^{*+}(2S)$ is observed at $6841.2 \pm 0.6(\text{stat}) \pm 0.1(\text{syst}) \pm 0.8(B_c^+)$ MeV with a significance of 6.3 standard deviations. Also here the low energy photon was not observed. The data also show a hint (2.2σ) for a second structure consistent with the $B_c^+(2S)$ with a mass $31.0 \pm 1.4(\text{stat}) \pm 0.0(\text{syst})$ higher.

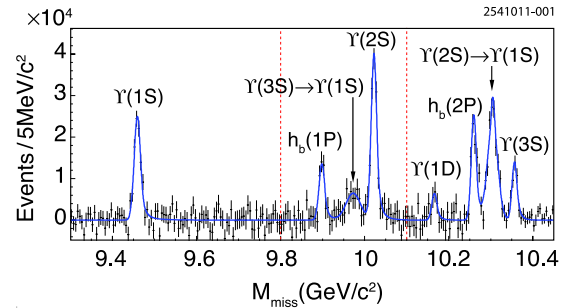


Figure 77.1: From Belle [20], the mass recoiling against $\pi^+\pi^-$ pairs, M_{miss} , in e^+e^- collision data taken near the peak of the $\Upsilon(10860)$ (points with error bars). The smooth combinatorial and $K_S^0 \rightarrow \pi^+\pi^-$ background contributions have been subtracted. The fit to the various labeled signal contributions is overlaid (curve). Adapted from [20] with kind permission, copyright (2011) The American Physical Society.

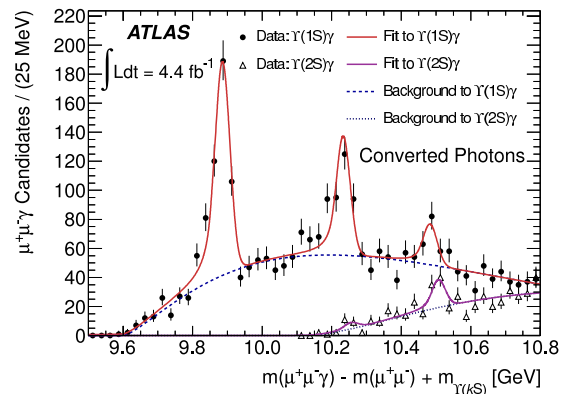


Figure 77.2: From ATLAS [21] pp collision data (points with error bars) taken at $\sqrt{s} = 7$ TeV, the effective mass of $\chi_{bJ}(1P, 2P, 3P) \rightarrow \gamma\Upsilon(1S, 2S)$ candidates in which $\Upsilon(1S, 2S) \rightarrow \mu^+\mu^-$ and the photon is reconstructed as an e^+e^- conversion in the tracking system. Fits (smooth curves) show significant signals for each triplet (J -merged) on top of a smooth background. From [21] with kind permission, copyright (2012) The American Physical Society.

The ground state of bottomonium, $\eta_b(1S)$, was confirmed with a second observation of more than 5σ significance at Belle. In addition, the same experiment collected strong evidence for the $\eta_b(2S)$ [22], but it still needs experimental confirmation at the 5σ level.

Using dipion transitions from the $\Upsilon(10860)$ (Fig. 77.1), Belle simultaneously discovered the $h_b(1P)$, the bottomonium counterpart of the $h_c(1P)$, and the next excited state, the $h_b(2P)$ [20].

Table 77.1: New states below the open-flavor thresholds in the $c\bar{c}$, $b\bar{c}$, and $b\bar{b}$ regions, ordered by mass. Masses m and widths Γ represent the PDG20 weighted averages with statistical and systematic uncertainties added in quadrature. In the Production column, the state is always denoted by X . Ellipses (...) indicate inclusively selected event topologies, *i.e.*, additional particles not directly detected by experiment. A question mark (?) indicates an unmeasured value. The Discovery Year column gives the date of the first measurement cited. The Summary Table column indicates whether or not the state appears in the summary tables, usually requiring at least two independent experiments with significance of $>5\sigma$. Refer to the particle listings for references and further information.

PDG Name	Former Name(s)	m (MeV)	Γ (MeV)	$I^G(J^{PC})$	Production	Decay	Discovery Year	Summary Table
$h_c(1P)$		3525.38 ± 0.11	0.7 ± 0.35	$0^-(1^{+-})$	$\psi(2S) \rightarrow \pi^0 X$ $p\bar{p} \rightarrow X$	$\gamma\eta_c(1S)$ hadrons	2004	YES
$\eta_c(2S)$		3639.2 ± 1.2	$11.3^{+3.2}_{-2.9}$	$0^+(0^{-+})$	$e^+e^- \rightarrow \pi\pi X$ $B \rightarrow KX$	(see listings) $K_S^0 K^- \pi^+$ $\bar{p}p$ hadrons	2002	YES
$\psi_2(3823)$	$X(3823)$	3822.2 ± 1.2	< 16	$0^-(2^{--})$	$e^+e^- \rightarrow e^+e^-X$ $e^+e^- \rightarrow J/\psi X$ $B \rightarrow KX$ $e^+e^- \rightarrow \pi^+\pi^-X$	(see listings) $\gamma\chi_{c1}(1P)$	2013	YES
B_c^+		6274.9 ± 0.8	?	$0(0^-)$	$\bar{p}p \rightarrow X...$ $pp \rightarrow X...$	$\pi^+ J/\psi$ (see listings)	2007	YES
$B_c^+(2S)$		6842 ± 6	?	$0(0^-)$	$pp \rightarrow X...$	$B_c^+ \pi^+ \pi^-$	2014	NO
$\eta_b(1S)$		9399.0 ± 1.3	10^{+5}_{-4}	$0^+(0^{-+})$	$\Upsilon(2S, 3S) \rightarrow \gamma X$ $h_b(1P, 2P) \rightarrow \gamma X$		2008	YES
$h_b(1P)$		9899.3 ± 0.8	?	$0^-(1^{+-})$	$\Upsilon(10860) \rightarrow \pi^+\pi^-X$ $\Upsilon(3S) \rightarrow \pi^0 X$	$\gamma\eta_b(1S)$	2011	YES
$\eta_b(2S)$		$9999.0^{+4.5}_{-4.0}$	< 24	$0^+(0^{-+})$	$h_b(2P) \rightarrow \gamma X$	hadrons	2012	NO
$\Upsilon_2(1D)$		10163.7 ± 1.4	?	$0^-(2^{--})$	$\Upsilon(3S) \rightarrow \gamma\gamma X$ $\Upsilon(10860) \rightarrow \pi^+\pi^-X$	$\gamma\gamma\Upsilon(1S)$ $\pi^+\pi^-\Upsilon(1S)$	2004	YES
$h_b(2P)$		10259.8 ± 1.2	?	$0^-(1^{+-})$	$\Upsilon(10860) \rightarrow \pi^+\pi^-X$	$\gamma\eta_b(1S, 2S)$	2011	NO
$\chi_{b1}(3P)$		10512.1 ± 2.3	?	$0^+(1^{++})$	$pp \rightarrow X...$	$\gamma\mu^+\mu^-$	2011	YES

Table 77.2: As in Table 77.1, but for new states near the first open-flavor thresholds in the $c\bar{c}$ and $b\bar{b}$ regions, ordered by mass. Updated from [7] with kind permission, copyright (2011), Springer, and [8] with kind permission from the authors.

PDG Name	Former Name(s)	m (MeV)	Γ (MeV)	$I^G(J^{PC})$	Production	Decay	Discovery Year	Summary Table
$\chi_{c1}(3872)$	$X(3872)$	3871.69 ± 0.17	< 1.2	$0^+(1^{++})$	$B \rightarrow KX$ $p\bar{p} \rightarrow X...$ $pp \rightarrow X...$ $e^+e^- \rightarrow \gamma X$	$\pi^+\pi^- J/\psi$ $3\pi J/\psi$ $D^{*0}\bar{D}^0$ $\gamma J/\psi$ $\gamma\psi(2S)$ $\pi^0\chi_{c1}(1P)$	2003	YES
$Z_c(3900)$		3886.6 ± 2.4	28.2 ± 2.6	$1^+(1^{+-})$	$\psi(4260) \rightarrow \pi^- X$ $\psi(4260) \rightarrow \pi^0 X$	$\pi^+ J/\psi$ $\pi^0 J/\psi$ $(D\bar{D}^*)^+$ $(D\bar{D}^*)^0$	2013	YES
$X(4020)$	$Z_c(4020)$	4024.1 ± 1.9	13 ± 5	$1^+(?^{?})$	$\psi(4260, 4360) \rightarrow \pi^- X$ $\psi(4260, 4360) \rightarrow \pi^0 X$	$\pi^+ h_c$ $\pi^0 h_c$ $(D^*\bar{D}^*)^+$ $(D^*\bar{D}^*)^0$	2013	YES
$Z_b(10610)$		10607.2 ± 2.0	18.4 ± 2.4	$1^+(1^{+-})$	$\Upsilon(10860) \rightarrow \pi^- X$ $\Upsilon(10860) \rightarrow \pi^0 X$	$\pi^+\Upsilon(1S, 2S, 3S)$ $\pi^0\Upsilon(1S, 2S, 3S)$ $\pi^+ h_b(1P, 2P)$ $(B\bar{B}^*)^+$	2011	YES
$Z_b(10650)$		10652.2 ± 1.5	11.5 ± 2.2	$1^+(1^{+-})$	$\Upsilon(10860) \rightarrow \pi^- X$	$\pi^+\Upsilon(1S, 2S, 3S)$ $\pi^+ h_b(1P, 2P)$ $(B^*\bar{B}^*)^+$	2011	YES

Table 77.3: As in Table 77.1, but for new states above the first open-flavor thresholds in the $c\bar{c}$ and $b\bar{b}$ regions, ordered by mass.

PDG Name	Former Name(s)	m (MeV)	Γ (MeV)	$I^G(J^{PC})$	Production	Decay	Discovery Year	Summary Table
$\psi_3(3842)$		3842.7 ± 0.2	2.79 ± 0.6	$0^+(3^{--})^*$	$pp \rightarrow X\dots$	$D\bar{D}$	2019	NO
$\chi_{c0}(3860)$		3862_{-35}^{+48}	201_{-106}^{+177}	$0^+(0^{++})$	$e^+e^- \rightarrow J/\psi X$	$D\bar{D}$	2017	NO
$X(3915)$	$\chi_{c0}(3915)$, $Y(3940)$	3918.4 ± 1.9	20 ± 5	$0^+(0/2^{++})$	$B \rightarrow KX$	$\omega J/\psi$	2004	YES
$\chi_{c2}(3930)$	$\chi_{c2}(2P)$, $Z(3930)$	3927.2 ± 2.6	24 ± 6	$0^+(2^{++})$	$e^+e^- \rightarrow e^+e^-X$	$D\bar{D}$	2005	YES
$X(3940)$		3942_{-8}^{+9}	37_{-17}^{+27}	$??(???)$	$e^+e^- \rightarrow J/\psi X$	$D\bar{D}^*$	2007	NO
$X(4050)^\pm$	$Z_1(4050)$	4051_{-43}^{+24}	82_{-28}^{+51}	$1^-(???)$	$B \rightarrow KX$	$\pi^+\chi_{c1}(1P)$	2008	NO
$X(4055)^\pm$	$Z_c(4055)$	4054 ± 3	45 ± 13	$1^+(???)$	$e^+e^- \rightarrow \pi^-X$	$\pi^+\psi(2S)$	2017	NO
$\chi_{c1}(4140)$	$Y(4140)$	4146.8 ± 2.4	22_{-7}^{+8}	$0^+(1^{++})$	$B^+ \rightarrow K^+X$	$\phi J/\psi$	2009	YES
					$e^+e^- \rightarrow e^+e^-X$			
$X(4160)$		4156_{-25}^{+29}	139_{-65}^{+113}	$??(???)$	$e^+e^- \rightarrow J/\psi X$	$D\bar{D}^*$	2007	NO
$Z_c(4200)$		4196_{-32}^{+35}	370_{-149}^{+99}	$1^+(1^{+-})$	$\bar{B}^0 \rightarrow K^-X$	$J/\psi\pi^+$	2014	NO
$\psi(4230)$	$Y(4230)$	4218_{-4}^{+5}	59_{-10}^{+12}	$0^-(1^{--})$	$e^+e^- \rightarrow X$	$\omega\chi_{c0}(1P)$ $\pi^+\pi^-\psi(2S)$ $\pi^+\pi^-h_c(1P)$	2015	YES
$R_{c0}(4240)$	$Z_c(4240)$	4239_{-21}^{+48}	220_{-88}^{+118}	$1^+(0^{--})$	$\bar{B}^0 \rightarrow K^-X$	$\pi^+\psi(2S)$	2014	NO
$X(4250)^\pm$	$Z_2(4250)$	4248_{-45}^{+185}	177_{-72}^{+321}	$1^-(???)$	$B \rightarrow KX$	$\pi^+\chi_{c1}(1P)$	2008	NO
$\psi(4260)$	$Y(4260)$	4230 ± 8	55 ± 19	$0^-(1^{--})$	$e^+e^- \rightarrow X$	$\pi\pi J/\psi$	2005	NO
						$\gamma\chi_{c0}(3872)$		
$\chi_{c1}(4274)$	$Y(4274)$	4274_{-6}^{+8}	49 ± 12	$0^+(1^{++})$	$B^+ \rightarrow K^+X$	$\phi J/\psi$	2011	NO
$X(4350)$		$4350.6_{-5.1}^{+4.6}$	$13.3_{-10.0}^{+18.4}$	$0^+(???)$	$e^+e^- \rightarrow e^+e^-X$	$\phi J/\psi$	2009	NO
$\psi(4360)$	$Y(4360)$	4368 ± 13	96 ± 7	$0^-(1^{--})$	$e^+e^- \rightarrow X$	$\pi^+\pi^-\psi(2S)$	2007	YES
$\psi(4390)$	$Y(4390)$	$4391.5_{-6.9}^{+6.4}$	$139.5_{-20.6}^{+16.2}$	$0^-(1^{--})$	$e^+e^- \rightarrow X$	$\pi^+\pi^-h_c(1P)$	2017	NO
$Z_c(4430)$		4478_{-18}^{+15}	181 ± 31	$1^+(1^{+-})$	$\bar{B}^0 \rightarrow K^-X$	$\pi^+\psi(2S)$ π^+J/ψ	2007	YES
$\chi_{c0}(4500)$	$X(4500)$	4506_{-19}^{+16}	92_{-29}^{+30}	$0^+(0^{++})$	$B^+ \rightarrow K^+X$	$\phi J/\psi$	2017	NO
$\psi(4660)$	$Y(4660)$, $X(4630)$	4643 ± 9	72 ± 11	$0^-(1^{--})$	$e^+e^- \rightarrow X$	$\pi^+\pi^-\psi(2S)$ $A_c^+A_c^-$ $D_s^+D_{s1}(2536)$	2007	YES
$\chi_{c0}(4700)$	$X(4700)$	4704_{-26}^{+17}	120_{-45}^{+52}	$0^+(0^{++})$	$B^+ \rightarrow K^+X$	$\phi J/\psi$	2017	NO
$\Upsilon(10753)$		10752.7 ± 5.9	$35.5_{-11.8}^{+18.0}$	$0^-(1^{--})$	$e^+e^- \rightarrow X$	$\pi\pi\Upsilon(1S, 2S, 3S)$	2019	NO
$\Upsilon(10860)$	$\Upsilon(5S)$	$10889.9_{-2.6}^{+3.2}$	51_{-7}^{+6}	$0^-(1^{--})$	$e^+e^- \rightarrow X$	$B_{(s)}^{(*)}\bar{B}_{(s)}^{(*)}(\pi)$ $\pi\pi\Upsilon(1S, 2S, 3S)$ $\pi^+\pi^-h_b(1P, 2P)$ $\eta\Upsilon(1S, 2S)$ $\pi^+\pi^-\Upsilon(1D)$	1985	YES
$\Upsilon(11020)$	$\Upsilon(6S)$	$10992.9_{-3.1}^{+10.0}$	49_{-15}^{+9}	$0^-(1^{--})$	$e^+e^- \rightarrow X$	$B_{(s)}^{(*)}\bar{B}_{(s)}^{(*)}(\pi)$ $\pi\pi\Upsilon(1S, 2S, 3S)$ $\pi^+\pi^-h_b(1P, 2P)$	1985	YES

*Quantum numbers fixed from the quark model and need confirmation.

The same analysis also showed the $\Upsilon_2(1D)$, the lowest-lying D -wave triplet of the $b\bar{b}$ system. The search for the $h_b(1P)$ was directly inspired by a CLEO result [23], which found a surprisingly copious production of $e^+e^- \rightarrow \pi^+\pi^-h_c(1P)$ as well as an indication that $\psi(4230) \rightarrow \pi^+\pi^-h_c(1P)$ occurs at a comparable rate with the signature mode, $\psi(4230) \rightarrow \pi^+\pi^-J/\psi$. The presence of $\Upsilon(nS)$ peaks in Fig. 77.1 at rates two orders of magnitude larger than expected, along with separate studies with exclusive decays $\Upsilon(nS) \rightarrow \mu^+\mu^-$, allow precise calibration of the $\pi^+\pi^-$ recoil mass spectrum and very accurate measurements of $h_b(1P)$ and $h_b(2P)$ masses. Both corresponding hyperfine splittings are consistent with zero within an uncertainty of about 1.5 MeV (lowered to ± 1.1 MeV for $h_b(1P)$ in Ref. [24]).

We no longer mention a hypothetical $Y_b(10888)$ state since a new analysis of the $\Upsilon(10860)$ energy range does not show evidence for an additional state with a mass different from the mass of the $\Upsilon(10860)$ [25]. After the mass of the $\eta_b(1S)$ was shifted upwards by about 10 MeV based on the new Belle measurements [22] [26], all of the bottomonium states mentioned above fit into their respective spectroscopies roughly where expected. An independent experimental confirmation of the shifted masses came from the Belle observation of $\Upsilon(4S) \rightarrow \eta h_b(1P)$ [26].

The $\chi_{bJ}(nP)$ states have been observed at the LHC by ATLAS [21] and confirmed by D0 [27] for $n = 1, 2, 3$, although in each case the three J states are not distinguished from one another. Events are sought which have both a photon and an $\Upsilon(1S, 2S) \rightarrow \mu^+\mu^-$ candidate which together form a mass in the χ_b region. All three J -merged peaks are observed with a significance in excess of 6σ for both unconverted and converted photons. The mass plot for converted photons, which provide better mass resolution, is shown in Fig. 77.2. This marks the first observation of the $\chi_{bJ}(3P)$ triplet, quite near the expected mass. A precise confirmation of this result came from LHCb [28].

A large number of states was discovered recently both near and above the lowest open-flavor thresholds. They are displayed in Table 77.2 and Table 77.3, respectively. With the exception of the tensor state located at 3930 MeV, now called $\chi_{c2}(3930)$, which has properties consistent with those expected for the $\chi_{c2}(2P)$, none of these states can easily be assigned a place in the quark model spectrum of charmonia or bottomonia. At the same time, these states have no universally accepted unconventional interpretation either. The $\chi_{c1}(3872)$, also known as $X(3872)$, is widely studied and seen in many transitions — *c.f.* Table 77.2. Yet its interpretation demands additional experimental attention: after the quantum numbers were fixed at LHCb [29, 30], the next experimental challenge will be a measurement of its lineshape.

LHCb observed in prompt proton-proton collisions a new narrow charmonium state, the $X(3842)$ resonance, in the decay modes $X(3842) \rightarrow D^0\bar{D}^0$ and $X(3842) \rightarrow D^+D^-$ [31]. The mass and width of this state are measured to be $(3842.71 \pm 0.16 \pm 0.12)$ MeV and $(2.79 \pm 0.51 \pm 0.35)$ MeV, respectively. The observed mass and narrow width is consistent with the interpretation of the new state as the unobserved spin-3 $\psi_3(1^3D_3)$ charmonium state. Accordingly the state got the name $\psi_3(3842)$ in the listings with the remark that the quantum numbers were fixed from the quark model and need to be confirmed.

Another state (referred to here as the $X(3915)$), was discovered at 3915 MeV [32] and from a subsequent measurement its quantum numbers were determined to be $J^{PC} = 0^{++}$ [33]. This suggests it may be the $\chi_{c0}(2P)$ quark model state, but this interpretation is not generally accepted [34, 35]. In addition, it was pointed out in Ref. [36] that if the assumption of helicity-2 dominance is abandoned and instead one allows for a sizable helicity-0 component, a $J^{PC} = 2^{++}$ assignment is possible. This could imply that the state at 3930 MeV (referred to here as the $\chi_{c2}(3930)$) is actually identical to the one at 3915 MeV—but to explain the large helicity-0 component a sizable portion of non- $q\bar{q}$ is necessary [36]. Because of this analysis, the name of the state was changed from $\chi_{c0}(3915)$ back to $X(3915)$. An alternative candidate for the $\chi_{c0}(2P)$ (referred to here as the $\chi_{c0}(3860)$) was reported in Ref. [37] with properties more consistent with expectation: its mass is close to the potential model expectations, it decays to $D\bar{D}$, and the preferred quantum numbers are $J^{PC} = 0^{++}$ (this hypothesis is

favored over the 2^{++} one with a 2.5σ significance).

The $\psi(4260)$, also known as $Y(4260)$, and the $\psi(4360)$, also known as $Y(4360)$, are vector states decaying to $\pi^+\pi^-J/\psi$ and $\pi^+\pi^-\psi(2S)$, respectively, yet, unlike most conventional vector charmonia, they do not correspond to enhancements in the e^+e^- hadronic cross section nor decay to $D\bar{D}$. Recently BESIII produced a high-accuracy data set for $e^+e^- \rightarrow \pi^+\pi^-J/\psi$ [38], demonstrating that the lineshape in this mass range is highly non-trivial. The latter observation was interpreted by the authors as the presence of two states. However, this lineshape is also consistent with other possible interpretations, such as one assuming a molecular structure for the $\psi(4260)$ [39]. The data of Ref. [38] also called for a significant downward shift of the mass of $\psi(4260)$ no longer justifying a distinction between $\psi(4260)$ and $\psi(4230)$. The latter was discovered earlier in various decay modes, amongst others $h_c(1P)\pi\pi$ [40]. The original mass parameter for the $\psi(4260)$ was the result of a fit to the $\pi^+\pi^-J/\psi$ cross section using a symmetric Breit-Wigner line shape [41]. Therefore, starting from the 2020 Edition of the Review of Particle Physics, we list the measurement of Ref. [38] under the node $\psi(4230)$ and promoted the $\psi(4230)$ to the summary tables to replace the $\psi(4260)$. BESIII also observed the $\chi_{c1}(3872)$, also known as $X(3872)$, in $e^+e^- \rightarrow \gamma\chi_{c1}(3872)$ in the $\psi(4230)$ mass range [42], which could allow for additional insight into the structure of both the $\psi(4230)$ as well as the $\chi_{c1}(3872)$ (*c.f.* the minireview on non- $q\bar{q}$ states). BESIII also performed a recent study of the process $e^+e^- \rightarrow \pi^+\pi^-\psi(2S)$ and found evidence for a lower mass state, possibly the $\psi(4230)$, in addition to the more dominant $\psi(4360)$ [43].

Note that the data of Ref. [38] does not show any indication of the $Y(4008)$ reported by Belle — the data in this region can either be fit with a non-resonant background component or a much wider resonance at lower mass. Also see the analysis of the $Y(4008)$ region in Ref. [44], where a wide resonance is also extracted.

Another interesting question is whether a heavier $\pi^+\pi^-\psi(2S)$ state, the $\psi(4660)$, discovered by Belle [45, 46] and confirmed by BaBar [47], is identical to the $\Lambda_c^+\Lambda_c^-$ state observed by Belle with a nearby mass and width [48]. Most probably it is, with $\Lambda_c^+\Lambda_c^-$ just being one more decay mode of the $\psi(4660)$ (*c.f.* the minireview on non- $q\bar{q}$ states for more detail). Note that this is the interpretation adopted in the particle listings.

Belle reported the first observation of a vector charmoniumlike state decaying to $D_s^+D_{s1}(2536)$ with a significance of 5.9σ [49]. Its measured mass and width are $(4625.9_{-6.0}^{+6.2} \pm 0.4)$ MeV and $(49.8_{-11.5}^{+13.9} \pm 4.0)$ MeV, respectively, consistent with those of $\psi(4660)$. Therefore these new data appear now as additional decay mode of $\psi(4660)$ in the listings.

Based on a full amplitude analysis of $B^0 \rightarrow K^+\pi^-\psi(2S)$ decays, Belle determined the spin-parity of the $Z_c(4430)$ to be $J^P = 1^+$ [50]. From their study of $B^0 \rightarrow K^+\pi^-J/\psi$ decays, Belle also found evidence for the decay mode $Z_c(4430) \rightarrow \pi J/\psi$ [51], which has an order of magnitude lower branching fraction than the discovery mode $Z_c(4430) \rightarrow \pi\psi(2S)$. In the same analysis, Belle also reported evidence for one more charged state, dubbed $Z_c(4200)$, decaying to $\pi J/\psi$. The existence of the $Z_c(4430)$ in $\pi\psi(2S)$ as well as its quantum number assignments were confirmed at LHCb [52] with much higher statistics. Improved values for the mass and width of the $Z_c(4430)$ from LHCb are consistent with earlier measurements; the experiment even reports a resonant behavior of the $Z_c(4430)$ amplitude. The $Z_c(4430)$ was not confirmed (or excluded) by BaBar [53].

Belle also reported an observation of two charged states decaying to $\pi\chi_{c1}$ in an analysis of $B^0 \rightarrow K^+\pi^-\chi_{c1}$ decays [54]. These were originally called the $Z_1(4050)^\pm$ and the $Z_2(4250)^\pm$, but are referred to in Table 77.3 as $X(4050)^\pm$ and $X(4250)^\pm$. These states were also not confirmed by BaBar [55]. Belle observes signals with 5.0σ significance for both the $Z_1(4050)^\pm$ and $Z_2(4250)^\pm$, whereas BABAR reports 1.1σ and 2.0σ effects, respectively, setting upper limits on product branching fractions that are not inconsistent with Belle's measured rates. The situation remains unresolved.

In addition to the Z_c states discussed above, in 2013 a state named $Z_c(3900)$ was unearthed in the charmonium region at BESIII [56] and Belle [41]. The corresponding spectrum from BESIII

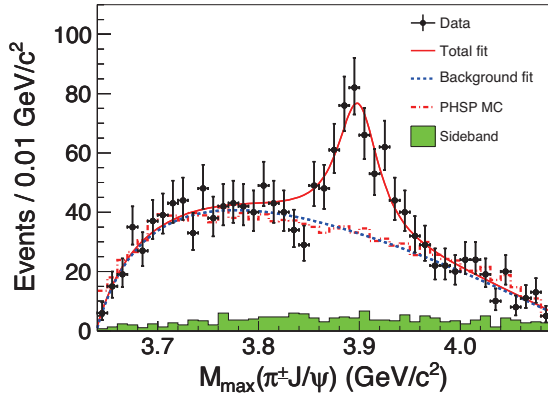


Figure 77.3: $J/\psi\pi$ invariant mass distributions from BES-III [56] e^+e^- collision data taken near the peak of the $Y(4260)$. Adapted from [56] with kind permission, copyright (2013) The American Physical Society.

is shown in Fig. 77.3. Ref. [57] confirmed this finding and also provided evidence for a neutral partner. A nearby signal was also seen in the $D\bar{D}^*$ channel [58] whose quantum numbers were fixed to 1^{+-} . BESIII reported its neutral partner in both $J/\psi\pi^0$ [59] and $D\bar{D}^*$ [60] decay modes. The masses extracted from these experiments in different decay modes have differences reaching up to 2σ . However, since the extraction of the mass and width parameters did not allow for an interference with the background and used Breit-Wigner line shapes, which is not justified near thresholds, there might be some additional systematic uncertainty in the mass values. Therefore in the RPP listings as well as Table 77.2, both structures appear under the name $Z_c(3900)$. BESIII also reported an observation of another charged state, the $X(4020)^\pm$ (originally called $Z_c(4020)^\pm$), in two decay modes — $h_c\pi^\pm$ [61] and $(D^*\bar{D}^*)^\pm$ [62]. The neutral partners have also been observed by BESIII in the $h_c\pi^0$ [63] and $(D^*\bar{D}^*)^0$ [64] final states. The Z_c states show some remarkable similarities to the Z_b states (discussed below), e.g. they decay dominantly to $D^{(*)}\bar{D}^*$ channels. However, current analyses suggest that the mass of the $Z_c(3900)$ might be somewhat above the $D\bar{D}^*$ threshold. If confirmed, this feature would clearly challenge a possible $D\bar{D}^*$ -molecular interpretation. Finally, 3.5σ evidence for one more charged charmoniumlike state at 4055 MeV decaying into $\psi(2S)\pi^\pm$ was reported by Belle in their analysis of the process $e^+e^- \rightarrow \psi(2S)\pi^+\pi^-$ [46]. This state was confirmed by BESIII, although there appears to be complications in the Dalitz plot requiring further investigation [43].

The $Y(4140)$ observed in 2008 by CDF [65] [66] was confirmed at D0 and CMS [67] [68]. However, a second structure, the $Y(4274)$, could not be established unambiguously. Neither of the two states was seen in B decays at Belle [69], LHCb [70] and BaBar [71] or in $\gamma\gamma$ collisions at Belle [72]. The real breakthrough happened recently when LHCb performed a full amplitude analysis of $B^+ \rightarrow J/\psi\phi K^+$ with $J/\psi \rightarrow \mu^+\mu^-$, $\phi \rightarrow K^+K^-$ decays and showed that the data cannot be described in a model that contains only excited kaon states decaying into ϕK^+ [73] [74]. They observe two 1^{++} states with masses close to those originally reported by CDF (the $\chi_{c1}(4140)$ and $\chi_{c1}(4274)$), but the width of the one at 4140 MeV is much larger. In addition, they find two significant 0^{++} structures at 4500 and 4700 MeV (the $\chi_{c0}(4500)$ and $\chi_{c0}(4700)$).

New results on the η_b , h_b , and Z_b mostly come from Belle [20, 22], [24–26], [75–81], all from analyses of 121.4 fb^{-1} of e^+e^- collision data collected near the peak of the $Y(10860)$ resonance as well as from an additional 25 fb^{-1} of data collected during the scans of the c.m. energy range 10.63–11.05 GeV. The η_b , h_b , and Z_b appear in the decay chains: $Y(10860) \rightarrow \pi^- Z_b^+$, $Z_b^+ \rightarrow \pi^+(b\bar{b})$, and, when the $b\bar{b}$ forms an $h_b(1P)$, frequently decaying as $h_b(1P) \rightarrow \gamma\eta_b$.

Belle soon noticed that, for events in the peaks of Fig. 77.1, there seemed to be two intermediate charged states. For exam-

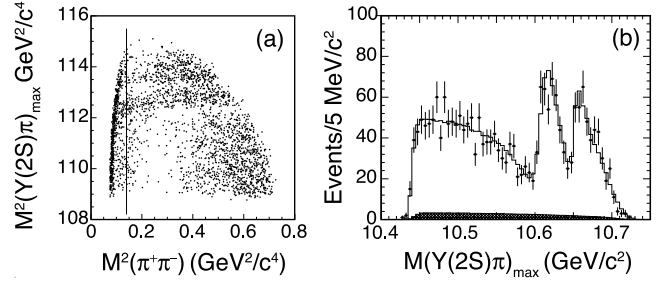


Figure 77.4: From Belle [75] e^+e^- collision data taken near the peak of the $Y(10860)$ for events with a $\pi^+\pi^-$ -missing mass consistent with an $Y(2S) \rightarrow \mu^+\mu^-$, (a) the maximum of the two possible single π^\pm -missing-mass-squared combinations vs. the $\pi^+\pi^-$ -mass-squared; and (b) projection of the maximum of the two possible single π^\pm -missing-mass combinations (*points with error bars*) overlaid with a fit (*curve*). Events to the left of the vertical line in (a) are excluded from amplitude analysis. The hatched histogram in (b) corresponds to the combinatorial background. The two horizontal stripes in (a) and two peaks in (b) correspond to the two Z_b states. Adapted from [75] with kind permission, copyright (2011) The American Physical Society.

ple, Fig. 77.4 shows a Dalitz plot for events restricted to the $Y(2S)$ region of $\pi^+\pi^-$ recoil mass, with $Y(2S) \rightarrow \mu^+\mu^-$ [75]. The two bands observed in the maximum of the two $M[\pi^\pm Y(2S)]^2$ values also appear for $Y(1S)$, $Y(3S)$, $h_b(1P)$, and $h_b(2P)$ samples. Belle fits all subsamples to resonant plus non-resonant amplitudes, allowing for interference (notably, between $\pi^- Z_b^+$ and $\pi^+ Z_b^-$), and finds consistent pairs of Z_b masses for all bottomonium transitions, and comparable strengths of the two states. A recent angular analysis assigned $J^P = 1^+$ for both Z_b states [76], which must also have negative G -parity. Transitions through Z_b to the $h_b(nP)$ saturate the observed $\pi^+\pi^- h_b(nP)$ cross sections. While the two masses of the Z_b states as extracted from Breit-Wigner fits for the various channels are just a few MeV above the $B^*\bar{B}$ and $B^*\bar{B}^*$ thresholds, respectively, more refined analyses find pole locations right below the corresponding thresholds either on the physical [82] or the unphysical sheet [83]. Regardless of their proximity to the corresponding thresholds, both states predominantly decay into these open-flavor channels [78] [84] with branching fractions that exceed 80% and 70%, respectively, at 90% CL. This feature provides strong evidence for their molecular nature.

Belle reported a new measurement of the $e^+e^- \rightarrow Y(nS)\pi^+\pi^-$ ($n = 1, 2, 3$) cross sections at energies from 10.52 to 11.02 GeV [85]. They observed with a 5.2σ significance a new structure in the energy dependence of the cross sections. If described by a Breit-Wigner function, its mass and width are found to be $(10752.7 \pm 5.9^{+0.7}_{-1.1}) \text{ MeV}$ and $(35.5^{+17.6+3.9}_{-11.3-3.3}) \text{ MeV}$. The new structure could have a resonant origin and correspond to a signal for the not yet observed $Y(3D)$ state provided $S-D$ mixing is enhanced, or an exotic state, e.g., a compact tetraquark or hadrobottomonium. It could also be a non-resonant effect due to some complicated rescattering.

References

- [1] R. F. Lebed, R. E. Mitchell and E. S. Swanson, Prog. Part. Nucl. Phys. **93**, 143 (2017), [arXiv:1610.04528].
- [2] A. Ali, J. S. Lange and S. Stone, Prog. Part. Nucl. Phys. **97**, 123 (2017), [arXiv:1706.00610].
- [3] F.-K. Guo *et al.*, Rev. Mod. Phys. **90**, 1, 015004 (2018), [arXiv:1705.00141].
- [4] S. L. Olsen, T. Skwarnicki and D. Zieminska, Rev. Mod. Phys. **90**, 1, 015003 (2018), [arXiv:1708.04012].
- [5] Y.-R. Liu *et al.*, Prog. Part. Nucl. Phys. **107**, 237 (2019), [arXiv:1903.11976].
- [6] N. Brambilla *et al.* (2019), [arXiv:1907.07583].
- [7] N. Brambilla *et al.*, Eur. Phys. J. **C71**, 1534 (2011), [arXiv:1010.5827].

- [8] N. Brambilla *et al.*, Eur. Phys. J. **C74**, 10, 2981 (2014), [arXiv:1404.3723].
- [9] A. Vinokurova *et al.* (Belle), Phys. Lett. **B706**, 139 (2011), [arXiv:1105.0978].
- [10] S. K. Choi *et al.* (Belle), Phys. Rev. Lett. **89**, 102001 (2002), [Erratum: Phys. Rev. Lett.89,129901(2002)], [hep-ex/0206002].
- [11] P. del Amo Sanchez *et al.* (BaBar), Phys. Rev. **D84**, 012004 (2011), [arXiv:1103.3971].
- [12] B. Aubert *et al.* (BaBar), Phys. Rev. Lett. **92**, 142002 (2004), [hep-ex/0311038].
- [13] R. Aaij *et al.* (LHCb), Phys. Lett. **B769**, 305 (2017), [arXiv:1607.06446].
- [14] V. Bhardwaj *et al.* (Belle), Phys. Rev. Lett. **111**, 3, 032001 (2013), [arXiv:1304.3975].
- [15] M. Ablikim *et al.* (BESIII), Phys. Rev. Lett. **115**, 1, 011803 (2015), [arXiv:1503.08203].
- [16] K. Chilikin *et al.* (Belle) (2020), [arXiv:2003.08335].
- [17] G. Aad *et al.* (ATLAS), Phys. Rev. Lett. **113**, 21, 212004 (2014), [arXiv:1407.1032].
- [18] A. M. Sirunyan *et al.* (CMS), Phys. Rev. Lett. **122**, 13, 132001 (2019), [arXiv:1902.00571].
- [19] R. Aaij *et al.* (LHCb), Phys. Rev. Lett. **122**, 23, 232001 (2019), [arXiv:1904.00081].
- [20] I. Adachi *et al.* (Belle), Phys. Rev. Lett. **108**, 032001 (2012), [arXiv:1103.3419].
- [21] G. Aad *et al.* (ATLAS), Phys. Rev. Lett. **108**, 152001 (2012), [arXiv:1112.5154].
- [22] R. Mizuk *et al.* (Belle), Phys. Rev. Lett. **109**, 232002 (2012), [arXiv:1205.6351].
- [23] T. K. Pedlar *et al.* (CLEO), Phys. Rev. Lett. **107**, 041803 (2011), [arXiv:1104.2025].
- [24] I. Adachi (Belle), in "8th International Workshop On Heavy Quarkonium (QWG2011) Darmstadt, Germany, October 3-7, 2011," (2011), [arXiv:1110.3934].
- [25] D. Santel *et al.* (Belle), Phys. Rev. **D93**, 1, 011101 (2016), [arXiv:1501.01137].
- [26] U. Tamponi *et al.* (Belle), Phys. Rev. Lett. **115**, 14, 142001 (2015), [arXiv:1506.08914].
- [27] V. M. Abazov *et al.* (D0), Phys. Rev. **D86**, 031103 (2012), [arXiv:1203.6034].
- [28] R. Aaij *et al.* (LHCb), JHEP **10**, 088 (2014), [arXiv:1409.1408].
- [29] R. Aaij *et al.* (LHCb), Phys. Rev. Lett. **110**, 222001 (2013), [arXiv:1302.6269].
- [30] R. Aaij *et al.* (LHCb), Phys. Rev. **D92**, 1, 011102 (2015), [arXiv:1504.06339].
- [31] R. Aaij *et al.* (LHCb), JHEP **07**, 035 (2019), [arXiv:1903.12240].
- [32] K. Abe *et al.* (Belle), Phys. Rev. Lett. **94**, 182002 (2005), [hep-ex/0408126].
- [33] J. P. Lees *et al.* (BaBar), Phys. Rev. **D86**, 072002 (2012), [arXiv:1207.2651].
- [34] F.-K. Guo and U.-G. Meissner, Phys. Rev. **D86**, 091501 (2012), [arXiv:1208.1134].
- [35] S. L. Olsen, Phys. Rev. **D91**, 5, 057501 (2015), [arXiv:1410.6534].
- [36] Z.-Y. Zhou, Z. Xiao and H.-Q. Zhou, Phys. Rev. Lett. **115**, 2, 022001 (2015), [arXiv:1501.00879].
- [37] K. Chilikin *et al.* (Belle), Phys. Rev. **D95**, 112003 (2017), [arXiv:1704.01872].
- [38] M. Ablikim *et al.* (BESIII), Phys. Rev. Lett. **118**, 9, 092001 (2017), [arXiv:1611.01317].
- [39] M. Cleven *et al.*, Phys. Rev. **D90**, 7, 074039 (2014), [arXiv:1310.2190].
- [40] M. Ablikim *et al.* (BESIII), Phys. Rev. Lett. **118**, 9, 092002 (2017), [arXiv:1610.07044].
- [41] Z. Q. Liu *et al.* (Belle), Phys. Rev. Lett. **110**, 252002 (2013), [arXiv:1304.0121].
- [42] M. Ablikim *et al.* (BESIII), Phys. Rev. Lett. **112**, 9, 092001 (2014), [arXiv:1310.4101].
- [43] M. Ablikim *et al.* (BESIII), Phys. Rev. **D96**, 3, 032004 (2017), [erratum: Phys. Rev.D99,no.1,019903(2019)], [arXiv:1703.08787].
- [44] X. Y. Gao, C. P. Shen and C. Z. Yuan, Phys. Rev. **D95**, 9, 092007 (2017), [arXiv:1703.10351].
- [45] X. L. Wang *et al.* (Belle), Phys. Rev. Lett. **99**, 142002 (2007), [arXiv:0707.3699].
- [46] X. L. Wang *et al.* (Belle), Phys. Rev. **D91**, 112007 (2015), [arXiv:1410.7641].
- [47] J. P. Lees *et al.* (BaBar), Phys. Rev. **D89**, 11, 111103 (2014), [arXiv:1211.6271].
- [48] G. Pakhlova *et al.* (Belle), Phys. Rev. Lett. **101**, 172001 (2008), [arXiv:0807.4458].
- [49] S. Jia *et al.* (Belle), Phys. Rev. **D100**, 11, 111103 (2019), [arXiv:1911.00671].
- [50] K. Chilikin *et al.* (Belle), Phys. Rev. **D88**, 7, 074026 (2013), [arXiv:1306.4894].
- [51] K. Chilikin *et al.* (Belle), Phys. Rev. **D90**, 11, 112009 (2014), [arXiv:1408.6457].
- [52] R. Aaij *et al.* (LHCb), Phys. Rev. Lett. **112**, 22, 222002 (2014), [arXiv:1404.1903].
- [53] B. Aubert *et al.* (BaBar), Phys. Rev. **D79**, 112001 (2009), [arXiv:0811.0564].
- [54] R. Mizuk *et al.* (Belle), Phys. Rev. **D78**, 072004 (2008), [arXiv:0806.4098].
- [55] J. P. Lees *et al.* (BaBar), Phys. Rev. **D85**, 052003 (2012), [arXiv:1111.5919].
- [56] M. Ablikim *et al.* (BESIII), Phys. Rev. Lett. **110**, 252001 (2013), [arXiv:1303.5949].
- [57] T. Xiao *et al.*, Phys. Lett. **B727**, 366 (2013), [arXiv:1304.3036].
- [58] M. Ablikim *et al.* (BESIII), Phys. Rev. Lett. **112**, 2, 022001 (2014), [arXiv:1310.1163].
- [59] M. Ablikim *et al.* (BESIII), Phys. Rev. Lett. **115**, 11, 112003 (2015), [arXiv:1506.06018].
- [60] M. Ablikim *et al.* (BESIII), Phys. Rev. Lett. **115**, 22, 222002 (2015), [arXiv:1509.05620].
- [61] M. Ablikim *et al.* (BESIII), Phys. Rev. Lett. **111**, 24, 242001 (2013), [arXiv:1309.1896].
- [62] M. Ablikim *et al.* (BESIII), Phys. Rev. Lett. **112**, 13, 132001 (2014), [arXiv:1308.2760].
- [63] M. Ablikim *et al.* (BESIII), Phys. Rev. Lett. **113**, 21, 212002 (2014), [arXiv:1409.6577].
- [64] M. Ablikim *et al.* (BESIII), Phys. Rev. Lett. **115**, 18, 182002 (2015), [arXiv:1507.02404].
- [65] T. Aaltonen *et al.* (CDF), Phys. Rev. Lett. **102**, 242002 (2009), [arXiv:0903.2229].
- [66] T. Aaltonen *et al.* (CDF), Mod. Phys. Lett. **A32**, 26, 1750139 (2017), [arXiv:1101.6058].
- [67] V. M. Abazov *et al.* (D0), Phys. Rev. **D89**, 1, 012004 (2014), [arXiv:1309.6580].
- [68] S. Chatrchyan *et al.* (CMS), Phys. Lett. **B734**, 261 (2014), [arXiv:1309.6920].
- [69] J. Brodzicka, Conf. Proc. **C0908171**, 299 (2009), [299(2009)].

- [70] R. Aaij *et al.* (LHCb), Phys. Rev. **D85**, 091103 (2012), [arXiv:1202.5087].
- [71] J. P. Lees *et al.* (BaBar), Phys. Rev. **D91**, 1, 012003 (2015), [arXiv:1407.7244].
- [72] C. P. Shen *et al.* (Belle), Phys. Rev. Lett. **104**, 112004 (2010), [arXiv:0912.2383].
- [73] R. Aaij *et al.* (LHCb), Phys. Rev. **D95**, 1, 012002 (2017), [arXiv:1606.07898].
- [74] R. Aaij *et al.* (LHCb), Phys. Rev. Lett. **118**, 2, 022003 (2017), [arXiv:1606.07895].
- [75] A. Bondar *et al.* (Belle), Phys. Rev. Lett. **108**, 122001 (2012), [arXiv:1110.2251].
- [76] A. Garmash *et al.* (Belle), Phys. Rev. **D91**, 7, 072003 (2015), [arXiv:1403.0992].
- [77] P. Krokovny *et al.* (Belle), Phys. Rev. **D88**, 5, 052016 (2013), [arXiv:1308.2646].
- [78] I. Adachi *et al.* (Belle) (2012), [arXiv:1209.6450].
- [79] K. F. Chen *et al.* (Belle), Phys. Rev. Lett. **100**, 112001 (2008), [arXiv:0710.2577].
- [80] P. Krokovny (Belle Collab.), talk given at Les Rencontres de Physique de la Vallee d'Aoste, La Thuile, Aosta Valley, Italy, 2012.
- [81] A. Abdesselam *et al.* (Belle), Phys. Rev. Lett. **117**, 14, 142001 (2016), [arXiv:1508.06562].
- [82] M. Cleven *et al.*, Eur. Phys. J. **A47**, 120 (2011), [arXiv:1107.0254].
- [83] F. K. Guo *et al.*, Phys. Rev. **D93**, 7, 074031 (2016), [arXiv:1602.00940].
- [84] A. Garmash *et al.* (Belle), Phys. Rev. Lett. **116**, 21, 212001 (2016), [arXiv:1512.07419].
- [85] R. Mizuk *et al.* (Belle), JHEP **10**, 220 (2019), [arXiv:1905.05521].

78. Non- $q\bar{q}$ Mesons

Revised August 2019 by C. Amsler (Stefan Meyer Inst.) and C. Hanhart (Jülich).

The constituent quark model describes the observed meson spectrum as bound $q\bar{q}$ states grouped into SU(N) flavor multiplets (see the ‘Quark Model’ in this issue of the *Review of Particle Physics*). However, the self coupling of gluons in QCD suggests that additional mesons made of bound gluons (glueballs), or $q\bar{q}$ -pairs with an excited gluon (hybrids), may exist. Furthermore, multi-quark color singlet states such as $qq\bar{q}\bar{q}$ (tetraquarks as compact diquark-antidiquark systems and ‘molecular’ bound states of two mesons) or $qqq\bar{q}\bar{q}$ (six-quark and ‘baryonium’ states of two baryons) have also been predicted.

In recent years experimental evidence for states beyond the quark model has accumulated in the heavy quark sector and elsewhere. We therefore split our review into three parts discussing separately light systems, heavy–light systems and heavy–heavy systems. For a more detailed discussion on exotic mesons we refer to [1] for the light meson sector and [2, 3] for the heavy meson sector. Reviews with main focus on tetraquarks and molecular states are presented in [4] and [5], respectively. For an experimental status with focus on the heavy quark sector see [6].

78.1 Light systems

78.1.1 Glueball candidates

Among the signatures naively expected for glueballs are (i) isoscalar states that do not fit into $q\bar{q}$ nonets, (ii) enhanced production in gluon-rich channels such as central production and radiative $J/\psi(1S)$ decay, (iii) decay branching fractions incompatible with SU(N) predictions for $q\bar{q}$ states, and (iv) reduced $\gamma\gamma$ couplings. However, mixing effects with isoscalar $q\bar{q}$ mesons [7–15] and decay form factors [16] can obscure these simple signatures.

Lattice calculations, QCD sum rules, flux tube, and constituent glue models agree that the lightest glueballs have quantum numbers $J^{PC} = 0^{++}$ and 2^{++} . Lattice calculations predict for the ground state (0^{++}) a mass around 1600 – 1700 MeV [12, 17–19] with an uncertainty of about 100 MeV, while the first excited state (2^{++}) has a mass of about 2300 MeV. Hence, the light glueballs lie in the same mass region as ordinary isoscalar $q\bar{q}$ states, in the mass range of the $1^3P_0(0^{++})$, $2^3P_2(2^{++})$, $3^3P_2(2^{++})$, and $1^3F_2(2^{++})$ $q\bar{q}$ states. Heavier glueballs with quantum numbers 0^{-+} , 2^{-+} , 1^{+-} , ... are predicted above 2500 MeV (in holographic QCD the 0^{+-} being very broad [20] and the 1^{+-} at least as broad as its width [21]), and the lowest exotic ones (with non- $q\bar{q}$ quantum numbers such as 0^{+-} and 2^{+-}) are expected above 4000 MeV [19]. The lattice calculations were performed so far in the quenched approximation. Thus neither quark loops nor mixing with conventional mesons were included, although quenching effects seem to be small [22]. (For a recent comparison between quenched and unquenched lattice studies see [23].) The mixing of glueballs with nearby $q\bar{q}$ states of the same quantum numbers should lead to a supernumerary isoscalar state in the SU(3) classification of $q\bar{q}$ mesons. A lattice study in full QCD (performed at unphysical quark masses corresponding to a pion mass of 400 MeV) did not identify states with sizeable overlap with pure gluonic sources [24, 25].

In the following we focus on glueball candidates in the scalar sector. For the 2^{++} sector we refer to the section on non- $q\bar{q}$ mesons in the 2006 issue of the *Review* [26], and for the 0^{-+} glueball to the note on ‘The Pseudoscalar and Pseudovector Mesons in the 1400 MeV Region’ in the *Meson Listings* of the *Review*.

Five isoscalar resonances are established: the very broad $f_0(500)$ (or σ), the $f_0(980)$, the broad $f_0(1370)$, and the comparatively narrow $f_0(1500)$ and $f_0(1710)$, see the note on ‘Scalar Mesons below 2 GeV’ in the *Meson Listings*, and also [27]. Their isospin $\frac{1}{2}$ and isovector partners are the $K_0^*(700)$ (or κ), the $K_0^*(1430)$, the $a_0(980)$ and the $a_0(1450)$. However, none of the proposed $q\bar{q}$ ordering schemes in scalar multiplets is entirely satisfactory. The $f_0(1370)$ and $f_0(1500)$ decay mostly into pions (2π and 4π) while the $f_0(1710)$ decays mainly into $K\bar{K}$ final states. Naively, this suggests an $n\bar{n}$ ($= u\bar{u} + d\bar{d}$) structure for the $f_0(1370)$ and $f_0(1500)$, and $s\bar{s}$ for the $f_0(1710)$. The last state is not observed in $p\bar{p}$ annihilation [28], as expected from the OZI suppress-

sion for an $s\bar{s}$ state.

In $\gamma\gamma$ collisions leading to $K_S K_S$ [29] and $K^+ K^-$ [30] a spin-0 signal is observed at the $f_0(1710)$ mass (together with a dominant spin-2 component), while the $f_0(1500)$ is not observed in $\gamma\gamma \rightarrow K\bar{K}$ nor $\pi^+ \pi^-$ [31]. The $f_0(1500)$ is also not observed by Belle in $\gamma\gamma \rightarrow \pi^0 \pi^0$, although a shoulder is seen which could also be due to the $f_0(1370)$ [32]. The absence of a signal in the $\pi\pi$ channel in $\gamma\gamma$ collisions does not favor an $n\bar{n}$ interpretation for the $f_0(1500)$. The upper limit from $\pi^+ \pi^-$ excludes a large $n\bar{n}$ content, and hence points to a mainly $s\bar{s}$ content [33]. This is in contradiction with the small $K\bar{K}$ decay branching ratio of the $f_0(1500)$ [34–36]. This state could be mainly glue due its absence of $\gamma\gamma$ coupling, while the $f_0(1710)$ coupling to $\gamma\gamma$ would be compatible with an $s\bar{s}$ state. Indeed, Belle finds that in $\gamma\gamma \rightarrow K_S K_S$ collisions the 1500 MeV region is dominated by the $f_2'(1525)$. The $f_0(1710)$ is also observed but its production \times decay rate is too large for a glueball [37]. However, the $\gamma\gamma$ couplings are sensitive to glue mixing with $q\bar{q}$ [38].

Since the $f_0(1370)$ does not couple strongly to $s\bar{s}$ [36], the $f_0(1370)$ or $f_0(1500)$ appear to be supernumerary. The narrow width of the $f_0(1500)$, and its enhanced production at low transverse momentum transfer in central collisions [39–41] also favor the $f_0(1500)$ to be non- $q\bar{q}$. In [7] the ground state scalar nonet is made of the $a_0(1450)$, $f_0(1370)$, $K_0^*(1430)$, and $f_0(1710)$. The isoscalars $f_0(1370)$ and $f_0(1710)$ contain a small fraction of glue, while the $f_0(1500)$ is mostly gluonic (see also [13]). The light scalars $f_0(500)$, $f_0(980)$, $a_0(980)$, and $K_0^*(700)$ are four-quark states or two-meson resonances, see [1] for a review and [42] which focuses on the $f_0(500)$. In the mixing scheme of Ref. [38], which uses central production data from WA102 and the hadronic J/ψ decay data from BES [43, 44], glue is shared between the $f_0(1370)$, $f_0(1500)$ and $f_0(1710)$. The $f_0(1370)$ is mainly $n\bar{n}$, the $f_0(1500)$ mainly glue and the $f_0(1710)$ dominantly $s\bar{s}$. This agrees with previous analyses [7, 13], but, as already pointed out, alternative schemes have been proposed [7–15], in particular with the $f_0(1710)$ as the glueball [45, 46] or the $f_0(1500)$ as a tetraquark [47].

For a scalar glueball the two-gluon coupling to $n\bar{n}$ appears to be suppressed by chiral symmetry [48] and therefore $K\bar{K}$ decay could be enhanced. However, $K\bar{K}$ is naturally enhanced also in the extended linear sigma model with a dilaton as glueball [45] and in the holographic model of [46]. It was argued that chiral symmetry constraints in a multichannel analysis imply that the $f_0(1710)$ is an unmixed scalar glueball [49], a view that is challenged in [50].

Different mixing options have been studied in [15]. In the preferred solution the ground state scalar nonet consists of the $f_0(980)$, $a_0(980)$, $K_0^*(1430)$, $f_0(1500)$ and $f_0(1710)$. The $f_0(980)$ and $f_0(1500)$ mix similarly to the η and η' in the pseudoscalar nonet, while the $f_0(1500)$ mixes with a glueball in the 500 – 1000 MeV mass range, which is identified with the $f_0(500)$ (σ). A reanalysis of the CERN-Munich data shows no signal for the $f_0(1370)$ decaying into $\pi\pi$, in contrast to [51]. However, in this scheme the $K_0^*(700)$ (κ) and the $a_0(1450)$ are left out (see also our note on ‘Scalar Mesons below 2 GeV’ in the *Meson Listings*). The $a_0(1450)$ has recently been confirmed by LHCb data in $D^0 \rightarrow K_S^0 K^\pm \pi^\mp$ [52].

The $f_0(1370)$ is also not needed in the COMPASS $\pi^- p \rightarrow \pi^- \pi^- \pi^+ p$ data [53], which questions its mere existence. However, a recent analysis from CLEO-c on $D^0 \rightarrow \pi^+ \pi^- \pi^+ \pi^-$ decay requires a contribution from $f_0(500) f_0(1370) \rightarrow 4\pi$ [54].

The Dalitz plots of $B^\pm \rightarrow \pi^\pm \pi^\pm \pi^\mp$ have been studied by BaBar [55]. A broad 2π signal is observed around 1400 MeV which is attributed to the $f_0(1370)$, but could also be due to the $f_0(1500)$. LHCb has analyzed \bar{B}^0 decay into $J/\psi \pi^+ \pi^-$ [56]. The fit to the $\pi\pi$ mass spectrum above ~ 1.2 GeV does not show any significant scalar component. However, the data analysis has been challenged [57]. For $\bar{B}_s^0 \rightarrow J/\psi \pi^+ \pi^-$ a strong scalar contribution from the $f_0(1370)$ is found [58]. Following the suggestion in Ref. [15], new data for the same reaction were analyzed by introducing instead the $f_0(500)$ and $f_0(1500)$ without any need for the $f_0(1370)$ [59]. This conclusion does not change when improved theoretical tools, as well as the data from [60] on $\bar{B}_s^0 \rightarrow J/\psi K\bar{K}$,

are employed in the analysis [61].

In $B^\pm \rightarrow K^\pm K^\pm K^\mp$ both BaBar [62] and Belle [63] observe a strong spin-0 activity in $K\bar{K}$ around 1550 MeV. The decay $B \rightarrow J/\psi X$ filters out the $d\bar{d}$ content of X while $B_s^0 \rightarrow J/\psi X$ selects its $s\bar{s}$ component. These decays may therefore be ideal environments to determine the flavor contents of neutral mesons [64].

The contribution of $f_0(1500)$ production in (the supposedly gluon rich) radiative J/ψ decay is not well known. The $f_0(1500)$ is observed by BESII in $J/\psi \rightarrow \gamma\pi\pi$ [65] and by BESIII in $J/\psi \rightarrow \gamma\eta\eta$ [66] with a much smaller rate than for the $f_0(1710)$, which speaks against a glueball interpretation for the former. However, the $f_0(1500)$ mass found by BES is significantly lower than the expected value. The overlap with the $f_0(1370)$ and $f_2'(1525)$, and the statistically limited data sample, prevent a proper K -matrix analysis to be performed. Hence more data are needed in radiative J/ψ decay and in $\gamma\gamma$ collisions to clarify the spectrum of scalar mesons.

78.1.2 Tetraquark candidates and molecular bound states

The existence of multi-quark states was suggested a long time ago based on duality arguments [67], see also [68]. The $a_0(980)$ and $f_0(980)$ could be tetraquark states [69–71] or $K\bar{K}$ molecular states [72–74] due to their large branching ratios into $K\bar{K}$, in spite of their masses being very close to threshold, leaving very little phase space. For $q\bar{q}$ states, the expected $\gamma\gamma$ widths [75, 76] are not significantly larger than for molecular states [75, 77], both predictions being consistent with data. Radiative decays of the $\phi(1020)$ into $a_0(980)$ and $f_0(980)$ were claimed to enable disentangling compact from molecular structures. Interpreting the data from DAΦNE [78, 79] and VEPP-2M [80, 81] along the lines of [82, 83] seems to favor these mesons to be tetraquark states. In Ref. [84] they are made of a four-quark core and a virtual $K\bar{K}$ cloud at the periphery. This is challenged in [85] which shows that ϕ radiative decay data are consistent with molecular structures of the light scalars. The $f_0(980)$ is strongly produced in D_s^+ decay [86], which points to a large $s\bar{s}$ component, assuming Cabibbo-favored $c \rightarrow s$ decay. However, the mainly $n\bar{n}$ $f_0(1370)$ is also strongly produced in D_s^+ decay, indicating that other graphs must contribute [87].

Ratios of decay rates of B and/or B_s mesons into $J/\psi f_0(980)$ or $J/\psi f_0(500)$ were proposed to extract the flavor mixing angle and to probe the tetraquark nature of those mesons within certain models [88, 89]. The phenomenological fits of LHCb, based on an isobar model, do neither allow for a contribution of the $f_0(980)$ in the $B \rightarrow J/\psi\pi\pi$ [56] nor for an $f_0(500)$ in $B_s \rightarrow J/\psi\pi\pi$ decays [59]. Hence the authors conclude that their data are incompatible at the eight standard deviation level with a model in which the $f_0(500)$ and $f_0(980)$ are tetraquarks. They also extract an upper limit for the mixing angle of 17° between the $f_0(980)$ and the $f_0(500)$ that would correspond to a substantial $s\bar{s}$ content in the $f_0(980)$ [59]. However, in a dispersive analysis [90] of the same data that allows for a model independent inclusion of the hadronic final state interactions, a substantial $f_0(980)$ contribution is also found in the B -decays, thus putting into question the conclusions in [59].

COMPASS reports a new 1^{++} isovector meson decaying into $f_0(980)\pi$, the $a_1(1420)$ [91, 92]. The resonance is observed in diffractive dissociation $\pi^-p \rightarrow \pi^-(\pi^+\pi^-)p$. Traditionally, the 1^{++} ground state nonet is believed to contain the $a_1(1260)$, $f_1(1285)$ and $f_1(1420)$ (see ‘The Pseudoscalar and Pseudovector Mesons in the 1400 MeV Region’ in the *Meson Listings*). A molecular $K\bar{K}\pi$ structure has been proposed for the $f_1(1420)$ [93] in view of the proximity of the $K^*\bar{K}$ threshold. The new $a_1(1420)$ could also be a molecular state, the isovector partner of the $f_1(1420)$. However, according to [94], the $f_1(1420)$ may not exist, being a manifestation of the $f_1(1285)$ due to a triangle singularity. Ref. [95] also explains the $a_1(1420)$ as the signature of the $a_1(1260)$ distorted by a triangle singularity.

78.1.3 Baryonia

Bound states of a baryon and an antibaryon have been predicted in the past [96, 97], but have remained elusive. The $f_2(1565)$ which is only observed in $\bar{p}p$ annihilation [98, 99] is a good candidate for a 2^{++} $\bar{p}p$ bound state. Enhancements close to the $\bar{p}p$ thresh-

old have been reported in $B^+ \rightarrow K^+\bar{p}p$, $B^0 \rightarrow K_S^0\bar{p}p$ [100, 101], $\bar{B}^0 \rightarrow D^0\bar{p}p$ [102], $e^+e^- \rightarrow \bar{p}p$ [103, 104], $\bar{p}p \rightarrow \pi^+\pi^-$ and $\bar{p}p \rightarrow e^+e^-$ [105]. The spectacular signal seen in $J/\psi \rightarrow \gamma\bar{p}p$ [106–108] could be due to a 0^{-+} baryonium [109]. Such a pole is not necessarily a compact $qqq\bar{q}\bar{q}$ state, but might be generated via non-perturbative nucleon-antinucleon final state interactions [110–113]. Also the structures visible in various data sets for $e^+e^- \rightarrow n\pi$ [114, 115] near the $\bar{p}p$ threshold appear to be largely explained by the same nucleon-antinucleon final state interactions [116]. However, other explanations have also been proposed to explain e.g. the signals in $B \rightarrow \bar{p}pK$, such as the dynamics of the fragmentation mechanism [101].

The pronounced signal observed by Belle in $e^+e^- \rightarrow A_c^+ A_c^-$ around $\sqrt{s} = 4.63$ GeV [117] was argued to be a strong evidence in favor of an interpretation of $Y(4660)$ as charmed baryonium [118]. However, this picture was challenged in Refs. [119, 120].

78.1.4 Hybrid mesons

Hybrids may be viewed as $q\bar{q}$ mesons with a vibrating gluon flux tube. In contrast to glueballs, they can have isospin 0 or 1. The mass spectrum of hybrids with exotic (non- $q\bar{q}$) quantum numbers was predicted in [121], while [122] also deals with non-exotic quantum numbers. The ground-state hybrids with quantum numbers (0^{-+} , 1^{-+} , 1^{--} , and 2^{-+}) are expected around 1.7 to 1.9 GeV. Lattice calculations predict that the hybrid with exotic quantum numbers 1^{-+} lies at a mass of 1.9 ± 0.2 GeV [123, 124]. Most hybrids are expected to be rather broad, but some can be as narrow as 100 MeV [125]. They prefer to decay into a pair of S - and P -wave mesons. The lattice study in [24, 126], based on full QCD with pion masses around 400 MeV, finds that several of the high-lying states observed in their spectrum show significant overlap with gluon rich source terms interpreted as hybrid states. For a recent experimental and theoretical review on hybrid mesons see [127].

A $J^{PC} = 1^{-+}$ exotic meson, the $\pi_1(1400)$, was reported in $\pi^-p \rightarrow \eta\pi^-p$ [128, 129] and in $\pi^-p \rightarrow \eta\pi^0 n$ [130]. It was observed as an interference between the angular momentum $L = 1$ and $L = 2$ $\eta\pi$ amplitudes, leading to a forward/backward asymmetry in the $\eta\pi$ angular distribution. This state had been reported earlier in π^-p reactions [131], but ambiguous solutions in the partial wave analysis were pointed out [132, 133]. A resonating 1^{-+} contribution to the $\eta\pi$ P -wave is also required in the Dalitz plot analysis of $\bar{p}n$ annihilation into $\pi^-\pi^0\eta$ [134], and in $\bar{p}p$ annihilation into $\pi^0\pi^0\eta$ [135]. Mass and width are consistent with the results of [128].

Another 1^{-+} state, the $\pi_1(1600)$ decaying into $\rho\pi$, was reported by COMPASS with 190 GeV pions hitting a lead target [136]. It was observed earlier in π^-p interactions in the decay modes $\eta'\pi$ [137], $f_1(1285)\pi$ [138], and $\omega\pi\pi$ [139], $b_1(1235)\pi$, but not $\eta\pi$ [140]. A strong enhancement in the 1^{-+} $\eta'\pi$ wave, compared to $\eta\pi$, was reported at this mass in [141]. Ref. [142] suggested that a Deck-generated $\eta\pi$ background from final state rescattering in $\pi_1(1600)$ decay could mimic $\pi_1(1400)$. However, this mechanism is absent in $\bar{p}p$ annihilation. The $\eta\pi\pi$ data require $\pi_1(1400)$ and cannot accommodate a state at 1600 MeV [143]. A coupled channel analysis of the COMPASS data leads to a single pole at 1564 MeV [144].

The flux tube model and the lattice concur to predict a hybrid mass of about 1.9 GeV while the $\pi_1(1400)$ and $\pi_1(1600)$ are lighter. As isovectors, $\pi_1(1400)$ and $\pi_1(1600)$ cannot be glueballs. The coupling to $\eta\pi$ of the former points to a four-quark state [145], while the strong $\eta'\pi$ coupling of the latter is favored for hybrid states [146, 147]. The mass of $\pi_1(1600)$ is also not far below the lattice prediction.

Evidence for a $\pi_1(2015)$ has also been reported [138, 139]. Hybrid candidates with $J^{PC} = 0^{-+}$, 1^{--} , and 2^{-+} have also been reported. The $\pi(1800)$ decays mostly to a pair of S - and P -wave mesons [136, 148], in line with expectations for 0^{-+} hybrid mesons. This meson is also somewhat narrow if interpreted as the second radial excitation of the pion. The evidence for 1^{--} hybrids required in e^+e^- annihilation and in τ decays has been discussed in [149]. A candidate for the 2^{-+} hybrid, the $\eta_2(1870)$, was reported in $\gamma\gamma$ interactions [150], in $\bar{p}p$ annihilation [151], and in central production [152]. The near degeneracy of $\eta_2(1645)$ and

$\pi_2(1670)$ suggests ideal mixing in the 2^{-+} $q\bar{q}$ nonet, and hence, the second isoscalar should be mainly $s\bar{s}$. However, $\eta_2(1870)$ decays mainly to $a_2(1320)\pi$ and $f_2(1270)\pi$ [151], with a relative rate compatible with a hybrid state [122].

78.2 Heavy-light systems

Two very narrow states, $D_{s0}^*(2317)^\pm$ and $D_{s1}(2460)^\pm$, were observed at B factories [153, 154]. They lie far below the predicted masses for the two expected broad P -wave $c\bar{s}$ mesons. These states have hence been interpreted as four-quark states [155–158] or DK (DK^*) molecules [159–163]. However, strong cusp effects, due to the nearby DK (DK^*) thresholds, could shift their masses downwards and quench the observed widths, an effect similar to that claimed for the $a_0(980)$ and $f_0(980)$ mesons, which lie just below $K\bar{K}$ threshold. A hadronic width of typically 100 keV would be the unequivocal signature for a prominent molecular nature of $D_{s0}^*(2317)^\pm$ [161–163]. More compact structures typically produce widths below 10 keV [164, 165]. The currently measured upper bound for the width is 3.8 MeV.

It should be stressed that – akin to $q\bar{q}$ mesons – multi-quark states also appear in multiplets. For example, recent studies [166–168] show that, if $D_{s0}(2317)$ were of molecular nature, the lowest non-strange scalar D -state, the $D_0^*(2300)$, would also be molecular in nature, with a two-pole structure (the lower one at 2105 MeV and the upper one at 2451 MeV, on different physical sheets, however, see Ref. [166] for details) similar to the $A(1405)$, see ‘Pole structure of the $A(1405)$ region’ in the *Review*. In [167] this assignment is demonstrated to be consistent with recent data from LHCb on $B^- \rightarrow D^+\pi^-\pi^-$ [169]. Two poles in the non-strange scalar sector are also generated in the tetraquark picture of Ref. [158], but in this work the real parts of the poles are located at 2308 MeV and 2666 MeV, which should be testable experimentally.

78.3 Heavy-heavy systems

Several unexpected states have been observed in both charmonium and bottomonium regions. With the discovery of the $X(3872)$ in $B^\pm \rightarrow K^\pm X$ ($X \rightarrow J/\psi \pi^+\pi^-$) by Belle [170] in 2003, soon confirmed by BaBar [171], many searches for states beyond the standard quark model were initiated in the charm and in the bottom sectors. For an updated collection of the currently available experimental information on multi-quark states we refer to ‘Spectroscopy of mesons containing two heavy quarks’ in the *Review*. Moreover, in the decay $A_b^0 \rightarrow J/\psi K^- p$ the LHCb collaboration has recently reported the observation of two new baryons decaying into $J/\psi p$, which are candidates for heavy pentaquark states [172]. They are discussed in some depth in ‘Pentaquarks’ in the *Review*.

When restricting ourselves to confirmed states we are faced with several ones that do not seem to fit into the most simple quark models. This is clear for the six established charged states ($Z_c(3900)^\pm$, $Z_c(4020)^\pm$ ¹, $Z_c(4200)^\pm$ and $Z_c(4430)^\pm$ in the charmonium sector, and $Z_b(10610)^\pm$ and $Z_b(10650)^\pm$ in the bottomonium sector). The neutral ones ($\chi_{c1}(3872)$ aka $X(3872)$, $\psi(4260)$ aka $Y(4260)$, $\psi(4360)$ aka $Y(4360)$, $\psi(4660)$ aka $Y(4660)$)² also challenge the quark models since their masses and decay properties are in conflict with expectations.

The quantum numbers of the $X(3872)$ have been determined by LHCb to be $J^{PC} = 1^{++}$, first by assuming the angular momentum zero between the J/ψ and the dipion [173] and then by relaxing this constraint [174]. The $X(3872)$ can hardly be identified with the 2^3P_1 χ'_{c1} since the latter is predicted to lie about 100 MeV higher in mass [175]. Instead, the $X(3940)$ reported by Belle in $e^+e^- \rightarrow J/\psi X$, decaying into $D^*\bar{D}$ but not into $D\bar{D}$ [176], and also observed in $B \rightarrow K(X \rightarrow \omega J/\psi)$ [177] could be the χ'_{c1} . The 2^3P_2 tensor partner (χ'_{c2}) was reported by Belle at 3931 MeV in $\gamma\gamma$ interactions [178].

¹While the $J^P = 1^+$ quantum numbers are plausible for this state, they are not yet established experimentally. This is why this state appears as $X(4020)$ in both listings and summary tables.

²According to the PDG naming scheme the prime name for these states is the quark model name, here listed first for each state, since it expresses the quantum numbers. However, in what follows we use the names mostly used in the literature to ease notations and to avoid confusion.

The $X(3872)$ lies within 200 keV of the $D^0\bar{D}^{*0}$ threshold and therefore the most natural explanation for this state is a 1^{++} DD^* molecule [179], for which strong isospin breaking is predicted [179, 180], since the distance of the pole of the $X(3872)$ to the $D^0\bar{D}^{*0}$ threshold is significantly smaller than to the D^+D^{*-} threshold. Indeed, the comparable rates for $\omega J/\psi$ and $\rho^0 J/\psi$ are consistent with an interpretation of $X(3872)$ as an isoscalar DD^* molecule when the different widths of the ρ and ω are taken into account [181]. A four-quark state $c\bar{q}c\bar{q}'$ is also possible [157] but unlikely, since the charged partner of the $X(3872)$ has not been observed (e.g. not in $B^- \rightarrow \bar{K}^0 X^-$ nor in $B^0 \rightarrow K^+ X^-$, where $X^- \rightarrow J/\psi \pi^-\pi^0$ [182]) – see [183] for a possible explanation of this non-observation within the tetraquark approach. The claim that $X(3872)$ must be a compact (tetraquark) state, since it is also produced at very high p_T in $\bar{p}p$ collisions [184], was challenged in [185], which stresses the importance of rescattering, see also [186, 187].

A broad structure, $Y(4260)$, decaying into $J/\psi \pi^+\pi^-$ was reported by BaBar in initial state radiation $e^+e^- \rightarrow \gamma(e^+e^- \rightarrow Y(4260))$ [188]. A measurement with significantly improved statistics was recently reported by BESIII [189]. The Breit-Wigner fit of these data leads to a mass reduction of 40 MeV, but also requires a second state at 4320 MeV. However, the $D_1\bar{D}$ molecular model for the $Y(4260)$ [190] is capable to describe the same data with just one single pole [191].

There are no charmonium states expected in this mass region with quantum numbers 1^{--} from quark models using the Cornell type of interaction, although this might not be true for some screened versions thereof – for a recent discussion we refer to Ref. [192]. In addition, a charmonium at this mass should have a significant coupling to $\bar{D}D$, a decay channel that is not observed for the $Y(4260)$. This state could be a hybrid charmonium with a spin-1 $\bar{c}c$ [193, 194] or a spin-0 [195, 196] core. However, provided that the observation of $Y(4260)$ decay into $h_c(1P)\pi\pi$ by BESIII [197] is confirmed, the hybrid hypothesis would be under pressure, since the spin of the heavy quarks (coupled to zero in the $h_c(1P)$) should be conserved in leading order in the expansion in $(\Lambda_{\text{QCD}}/m_c)$. (The individual conservation of the heavy quark spin and the total angular momentum of the light quark cloud is a consequence of the heavy-quark spin symmetry, see ‘Heavy-Quark and Soft-Collinear Effective Theory’ in this issue of the *Review*.)

The same criticism applies to the hadrocharmonium interpretation of the $Y(4260)$, which describes this state as spin-1 quarkonium surrounded by a light quark cloud [198]. To circumvent the spin-symmetry argument Ref. [199] argues that $Y(4260)$ and $Y(4360)$ could be mixtures of two hadrocharmonia with spin-triplet and spin-singlet heavy quark pairs. The same kind of mixing could also operate for a hybrid.

A dominant $D_1\bar{D}$ component in the $Y(4260)$ [200] explains naturally why $Z_c(3900)^\pm$ (interpreted by the authors as a $\bar{D}D^*$ bound state) is seen in $Y(4260) \rightarrow \pi^\mp Z_c(3900)^\pm$. Furthermore, a copious production of $X(3872)$ in $Y(4260)$ radiative decays was predicted from the prominent $D_1\bar{D}$ component of the $Y(4260)$ [201], which was confirmed by BESIII [202]. The $Y(4360)$ as a $D_1\bar{D}^*$ bound state could be the spin partner of the $Y(4260)$ [203, 204], but a detailed microscopic calculation is still lacking.

The tetraquark picture explains the observed Y states [205] and is also capable – when including a tailor-made spin-spin interaction [206] – to describe the $X(3872)$, both $Z_c(3900)^\pm$ ⁰ and $Z_c(4020)^\pm$ and even the $Z(4430)^\pm$ confirmed by Belle [207] and LHCb [208]. The latter reference also determined the quantum numbers of this state to $J^P = 1^+$. However, the model predicts many additional charged and neutral states which have not yet been discovered. A possible explanation can be found in [183].

Ref. [209] found a sizeable SU(3) flavor octet contribution when analysing the $\pi\pi$ final state from $Y(4260) \rightarrow J/\psi \pi^+\pi^-$, which is consistent with both a molecular and a tetraquark interpretation of $Y(4260)$, but at odds with a hybrid or a $\bar{c}c$ interpretation.

The charged states $Z_c(3900)^\pm$, first observed by BESIII [210] and the $Z_c(4020)^\pm$ [211] decay predominantly into $\bar{D}D^*$ and \bar{D}^*D^* , respectively, while $Z_b(10610)^\pm$ ⁰ and $Z_b(10650)^\pm$ [212, 213] decay predominantly into $\bar{B}B^*$ and \bar{B}^*B^* [214], respectively, although all of them were discovered in the decay mode heavy

quarkonium plus pion. This suggests that these states are close relatives and their interactions are connected via heavy quark flavor symmetry. A molecular interpretation for the bottomonium states was proposed shortly after the discovery of the Z_b^\pm states [215] and also shortly after that of the $Z_c(3900)^\pm$ [200]. However, some of their properties also appear to be consistent with tetraquark structures [216]. If the molecular picture were correct for the Z_b states, spin symmetry would lead to the existence of spin partner states [217–219], which are still to be found. In Ref. [220] it was shown that the actual pole locations of those partner states would be good probes of the role of the one-pion exchange in the molecular potential, which makes the experimental search for those states even more interesting.

The heaviest confirmed charged state in the charmonium sector is the $Z(4430)^\pm$ observed by Belle [207]. It is interpreted as hadrocharmonium [198], $\bar{D}_1 D^*$ molecule [221] as well as tetraquark [206]. Alternatively, in [222, 223] the $Z(4430)^\pm$ is explained as a cross-channel effect enhanced by a triangle singularity from open charm states. These works were criticised in Ref. [224] where an alternative triangle consisting of a K^* , a π and the $Y(4260)$ is proposed to generate the $Z_c(4430)$. The Argand diagram shows an anticlockwise circle, in line with the experimental analysis [208], while the one of Ref. [223] shows a clockwise motion. By replacing the $Y(4260)$ by the $\psi(3770)$ and changing the K^* one can also interpret the $Z_c(4200)$ as a kinematic effect [224].

It should be stressed that the various scenarios, while describing the data, also make decisive predictions, e.g. yet unobserved quantum numbers [205, 225]. The forthcoming data on heavy meson spectroscopy from various facilities should provide a much deeper understanding on how QCD forms matter out of quarks and gluons.

References

- [1] C. Amsler and N. A. Tornqvist, Phys. Rept. **389**, 61 (2004).
- [2] N. Brambilla *et al.*, Eur. Phys. J. **C71**, 1534 (2011), [arXiv:1010.5827].
- [3] N. Brambilla *et al.* (2019), [arXiv:1907.07583].
- [4] A. Esposito, A. Pilloni and A. D. Polosa, Phys. Rept. **668**, 1 (2017), [arXiv:1611.07920].
- [5] F.-K. Guo *et al.*, Rev. Mod. Phys. **90**, 1, 015004 (2018), [arXiv:1705.00141].
- [6] S. L. Olsen, T. Skwarnicki and D. Zieminska, Rev. Mod. Phys. **90**, 1, 015003 (2018), [arXiv:1708.04012].
- [7] C. Amsler and F. E. Close, Phys. Rev. **D53**, 295 (1996), [hep-ph/9507326].
- [8] N. A. Tornqvist and M. Roos, Phys. Rev. Lett. **76**, 1575 (1996), [hep-ph/9511210].
- [9] A. V. Anisovich, V. V. Anisovich and A. V. Sarantsev, Phys. Lett. **B395**, 123 (1997), [hep-ph/9611333].
- [10] M. Boglione and M. R. Pennington, Phys. Rev. Lett. **79**, 1998 (1997), [hep-ph/9703257].
- [11] P. Minkowski and W. Ochs, Eur. Phys. J. **C9**, 283 (1999), [hep-ph/9811518].
- [12] W.-J. Lee and D. Weingarten, Phys. Rev. **D61**, 014015 (2000), [hep-lat/9910008].
- [13] F. E. Close and A. Kirk, Eur. Phys. J. **C21**, 531 (2001), [hep-ph/0103173].
- [14] H.-Y. Cheng, C.-K. Chua and K.-F. Liu, Phys. Rev. **D74**, 094005 (2006), [hep-ph/0607206].
- [15] W. Ochs, J. Phys. **G40**, 043001 (2013), [arXiv:1301.5183].
- [16] T. Barnes *et al.*, Phys. Rev. **D55**, 4157 (1997), [hep-ph/9609339].
- [17] G. S. Bali *et al.* (UKQCD), Phys. Lett. **B309**, 378 (1993), [hep-lat/9304012].
- [18] C. J. Morningstar and M. J. Peardon, Phys. Rev. **D56**, 4043 (1997), [hep-lat/9704011].
- [19] Y. Chen *et al.*, Phys. Rev. **D73**, 014516 (2006), [hep-lat/0510074].
- [20] J. Leutgeb and A. Rebhan, Phys. Rev. **D101**, 1, 014006 (2020), [arXiv:1909.12352].
- [21] F. Br unner, J. Leutgeb, A. Rebhan, Phys. Lett. **B788**, 431 (2019).
- [22] C. M. Richards *et al.* (UKQCD), Phys. Rev. **D82**, 034501 (2010), [arXiv:1005.2473].
- [23] E. Gregory *et al.*, JHEP **10**, 170 (2012), [arXiv:1208.1858].
- [24] J. J. Dudek *et al.*, Phys. Rev. **D83**, 111502 (2011), [arXiv:1102.4299].
- [25] W. Sun *et al.*, EPJ Web Conf. **175**, 05016 (2018), [arXiv:1711.00711].
- [26] W. M. Yao *et al.* (Particle Data Group), J. Phys. **G33**, 1 (2006).
- [27] C. Amsler, Rev. Mod. Phys. **70**, 1293 (1998), [hep-ex/9708025].
- [28] C. Amsler *et al.* (Crystal Barrel), Eur. Phys. J. **C23**, 29 (2002).
- [29] M. Acciarri *et al.* (L3), Phys. Lett. **B501**, 173 (2001), [hep-ex/0011037].
- [30] K. Abe *et al.* (Belle), Eur. Phys. J. **C32**, 323 (2003), [hep-ex/0309077].
- [31] R. Barate *et al.* (ALEPH), Phys. Lett. **B472**, 189 (2000), [hep-ex/9911022].
- [32] S. Uehara *et al.* (Belle), Phys. Rev. **D78**, 052004 (2008), [arXiv:0805.3387].
- [33] C. Amsler, Phys. Lett. **B541**, 22 (2002), [hep-ph/0206104].
- [34] A. Abele *et al.* (Crystal Barrel), Phys. Lett. **B385**, 425 (1996).
- [35] A. Abele *et al.*, Phys. Rev. **D57**, 3860 (1998).
- [36] D. Barberis *et al.* (WA102), Phys. Lett. **B462**, 462 (1999), [hep-ex/9907055].
- [37] S. Uehara *et al.* (Belle), PTEP **2013**, 12, 123C01 (2013), [arXiv:1307.7457].
- [38] F. E. Close and Q. Zhao, Phys. Rev. **D71**, 094022 (2005), [hep-ph/0504043].
- [39] F. E. Close and A. Kirk, Phys. Lett. **B397**, 333 (1997), [hep-ph/9701222].
- [40] F. E. Close, Phys. Lett. **B419**, 387 (1998), [hep-ph/9710450].
- [41] A. Kirk, Phys. Lett. **B489**, 29 (2000), [hep-ph/0008053].
- [42] J. R. Pelaez, Phys. Rept. **658**, 1 (2016), [arXiv:1510.00653].
- [43] M. Ablikim *et al.* (BES), Phys. Lett. **B603**, 138 (2004), [hep-ex/0409007].
- [44] M. Ablikim *et al.* (BES), Phys. Lett. **B607**, 243 (2005), [hep-ex/0411001].
- [45] S. Janowski, F. Giacosa and D. H. Rischke, Phys. Rev. **D90**, 11, 114005 (2014), [arXiv:1408.4921].
- [46] F. Br enner and A. Rebhan, Phys. Rev. Lett. **115**, 13, 131601 (2015), [arXiv:1504.05815].
- [47] L. Zou *et al.*, Phys. Rev. **D99**, 114024 (2019).
- [48] M. Chanowitz, Phys. Rev. Lett. **95**, 172001 (2005), [hep-ph/0506125].
- [49] M. Albaladejo and J. A. Oller, Phys. Rev. Lett. **101**, 252002 (2008), [arXiv:0801.4929].
- [50] L. S. Geng and E. Oset, Phys. Rev. **D79**, 074009 (2009), [arXiv:0812.1199].
- [51] D. V. Bugg, B. S. Zou and A. V. Sarantsev, Nucl. Phys. **B471**, 59 (1996).
- [52] R. Aaij *et al.* (LHCb), Phys. Rev. **D93**, 5, 052018 (2016), [arXiv:1509.06628].
- [53] C. Adolph *et al.* (COMPASS), Phys. Rev. **D95**, 3, 032004 (2017), [arXiv:1509.00992].
- [54] P. d'Argent *et al.*, JHEP **05**, 143 (2017), [arXiv:1703.08505].

- [55] B. Aubert *et al.* (BaBar), Phys. Rev. **D79**, 072006 (2009), [arXiv:0902.2051].
- [56] R. Aaij *et al.* (LHCb), Phys. Rev. **D90**, 1, 012003 (2014), [arXiv:1404.5673].
- [57] F. E. Close and A. Kirk, Phys. Rev. **D91**, 11, 114015 (2015), [arXiv:1503.06942].
- [58] R. Aaij *et al.* (LHCb), Phys. Rev. **D86**, 052006 (2012), [arXiv:1204.5643].
- [59] R. Aaij *et al.* (LHCb), Phys. Rev. **D89**, 9, 092006 (2014), [arXiv:1402.6248].
- [60] R. Aaij *et al.* (LHCb), JHEP **08**, 037 (2017), [arXiv:1704.08217].
- [61] S. Ropertz, C. Hanhart and B. Kubis, Eur. Phys. J. **C78**, 12, 1000 (2018), [arXiv:1809.06867].
- [62] B. Aubert *et al.* (BaBar), Phys. Rev. **D74**, 032003 (2006), [hep-ex/0605003].
- [63] A. Garmash *et al.* (Belle), Phys. Rev. **D71**, 092003 (2005), [hep-ex/0412066].
- [64] C.-D. Lu *et al.*, Eur. Phys. J. **A49**, 58 (2013), [arXiv:1301.0225].
- [65] M. Ablikim *et al.*, Phys. Lett. **B642**, 441 (2006), [hep-ex/0603048].
- [66] M. Ablikim *et al.* (BESIII), Phys. Rev. **D87**, 9, 092009 (2013), [Erratum: Phys. Rev.D87,no.11,119901(2013)], [arXiv:1301.0053].
- [67] J. L. Rosner, Phys. Rev. Lett. **21**, 950 (1968).
- [68] G. C. Rossi and G. Veneziano, Nucl. Phys. **B123**, 507 (1977).
- [69] R. L. Jaffe, Phys. Rev. **D15**, 281 (1977).
- [70] M. G. Alford and R. L. Jaffe, Nucl. Phys. **B578**, 367 (2000), [hep-lat/0001023].
- [71] G. 't Hooft *et al.*, Phys. Lett. **B662**, 424 (2008), [arXiv:0801.2288].
- [72] J. D. Weinstein and N. Isgur, Phys. Rev. **D41**, 2236 (1990).
- [73] G. Janssen *et al.*, Phys. Rev. **D52**, 2690 (1995), [arXiv:nucl-th/9411021].
- [74] M. P. Locher, V. E. Markushin and H. Q. Zheng, Eur. Phys. J. **C4**, 317 (1998), [hep-ph/9705230].
- [75] J. A. Oller and E. Oset, AIP Conf. Proc. **432**, 1, 413 (1998), [hep-ph/9710557].
- [76] R. Delbourgo, D.-s. Liu and M. D. Scadron, Phys. Lett. **B446**, 332 (1999), [hep-ph/9811474].
- [77] C. Hanhart *et al.*, Phys. Rev. **D75**, 074015 (2007), [hep-ph/0701214].
- [78] A. Aloisio *et al.* (KLOE), Phys. Lett. **B536**, 209 (2002), [hep-ex/0204012].
- [79] A. Aloisio *et al.* (KLOE), Phys. Lett. **B537**, 21 (2002), [hep-ex/0204013].
- [80] R. R. Akhmetshin *et al.* (CMD-2), Phys. Lett. **B462**, 371 (1999), [hep-ex/9907005].
- [81] M. N. Achasov *et al.*, Phys. Lett. **B479**, 53 (2000), [hep-ex/0003031].
- [82] F. E. Close, N. Isgur and S. Kumano, Nucl. Phys. **B389**, 513 (1993), [hep-ph/9301253].
- [83] N. N. Achasov, V. V. Gubin and V. I. Shevchenko, Phys. Rev. **D56**, 203 (1997), [hep-ph/9605245].
- [84] F. E. Close and N. A. Tornqvist, J. Phys. **G28**, R249 (2002), [hep-ph/0204205].
- [85] Yu. S. Kalashnikova *et al.*, Eur. Phys. J. **A24**, 437 (2005), [hep-ph/0412340].
- [86] E. M. Aitala *et al.* (E791), Phys. Rev. Lett. **86**, 765 (2001), [hep-ex/0007027].
- [87] H.-Y. Cheng, Phys. Rev. **D67**, 054021 (2003), [hep-ph/0212361].
- [88] R. Fleischer, R. Knegjens and G. Ricciardi, Eur. Phys. J. **C71**, 1832 (2011), [arXiv:1109.1112].
- [89] S. Stone and L. Zhang, Phys. Rev. Lett. **111**, 6, 062001 (2013), [arXiv:1305.6554].
- [90] J. T. Daub, C. Hanhart and B. Kubis, JHEP **02**, 009 (2016), [arXiv:1508.06841].
- [91] C. Adolph *et al.* (COMPASS), Phys. Rev. Lett. **115**, 8, 082001 (2015), [arXiv:1501.05732].
- [92] M. Aghasyan *et al.* (COMPASS), Phys. Rev. **D98**, 092003 (2018).
- [93] R. S. Longacre, Phys. Rev. **D42**, 874 (1990).
- [94] V. R. Debastiani *et al.*, Phys. Rev. **D 95**, 034015 (2017).
- [95] M. Mikhasenko, B. Ketzner and A. Sarantsev, Phys. Rev. **D91**, 9, 094015 (2015), [arXiv:1501.07023].
- [96] G. C. Rossi and G. Veneziano, Phys. Rep. **63**, 153 (1980).
- [97] L. Montanet, Phys. Rep. **63**, 201 (1980).
- [98] B. May *et al.* (ASTERIX), Z. Phys. **C46**, 203 (1990).
- [99] A. Bertin *et al.* (OBELIX), Phys. Rev. **D57**, 55 (1998).
- [100] K. Abe *et al.* (Belle), Phys. Rev. Lett. **88**, 181803 (2002), [hep-ex/0202017].
- [101] M. Z. Wang *et al.* (Belle), Phys. Lett. **B617**, 141 (2005), [hep-ex/0503047].
- [102] K. Abe *et al.* (Belle), Phys. Rev. Lett. **89**, 151802 (2002), [hep-ex/0205083].
- [103] J. P. Lees *et al.* (BaBar), Phys. Rev. **D87**, 9, 092005 (2013), [arXiv:1302.0055].
- [104] E. P. Solodov *et al.*, EPJ Web Conf. **212**, 07002 (2019).
- [105] G. Bardin *et al.*, Nucl. Phys. **B411**, 3 (1994).
- [106] J. Z. Bai *et al.* (BES), Phys. Rev. Lett. **91**, 022001 (2003), [hep-ex/0303006].
- [107] J. P. Alexander *et al.* (CLEO), Phys. Rev. **D82**, 092002 (2010), [arXiv:1007.2886].
- [108] M. Ablikim *et al.* (BESIII), Phys. Rev. Lett. **108**, 112003 (2012), [arXiv:1112.0942].
- [109] G.-J. Ding and M.-L. Yan, Phys. Rev. **C72**, 015208 (2005), [hep-ph/0502127].
- [110] B. Loiseau and S. Wycech, Phys. Rev. **C72**, 011001 (2005), [hep-ph/0501112].
- [111] A. Sibirtsev *et al.*, Phys. Rev. **D71**, 054010 (2005), [hep-ph/0411386].
- [112] X.-W. Kang, J. Haidenbauer and U.-G. Meissner, JHEP **02**, 113 (2014), [arXiv:1311.1658].
- [113] X.-W. Kang, J. Haidenbauer and U.-G. Meissner, Phys. Rev. **D91**, 7, 074003 (2015), [arXiv:1502.00880].
- [114] B. Aubert *et al.* (BaBar), Phys. Rev. **D76**, 092005 (2007), [Erratum: Phys. Rev.D77,119902(2008)], [arXiv:0708.2461].
- [115] R. R. Akhmetshin *et al.* (CMD-3), Phys. Lett. **B723**, 82 (2013), [arXiv:1302.0053].
- [116] J. Haidenbauer, X. W. Kang and U. G. Meissner, Nucl. Phys. **A929**, 102 (2014), [arXiv:1405.1628].
- [117] G. Pakhlova *et al.* (Belle), Phys. Rev. Lett. **101**, 172001 (2008), [arXiv:0807.4458].
- [118] G. Cotugno *et al.*, Phys. Rev. Lett. **104**, 132005 (2010), [arXiv:0911.2178].
- [119] F.-K. Guo *et al.*, Phys. Rev. **D82**, 094008 (2010), [arXiv:1005.2055].
- [120] L.-Y. Dai, J. Haidenbauer and U. G. Meissner, Phys. Rev. **D96**, 11, 116001 (2017), [arXiv:1710.03142].
- [121] N. Isgur, R. Kokoski and J. Paton, Phys. Rev. Lett. **54**, 869 (1985), [AIP Conf. Proc.132,242(1985)].
- [122] F. E. Close and P. R. Page, Nucl. Phys. **B443**, 233 (1995), [hep-ph/9411301].

- [123] P. Lacock *et al.* (UKQCD), Phys. Lett. **B401**, 308 (1997), [hep-lat/9611011].
- [124] C. W. Bernard *et al.* (MILC), Phys. Rev. **D56**, 7039 (1997), [hep-lat/9707008].
- [125] P. R. Page, E. S. Swanson and A. P. Szczepaniak, Phys. Rev. **D59**, 034016 (1999), [hep-ph/9808346].
- [126] J. J. Dudek *et al.* (Hadron Spectrum), Phys. Rev. **D88**, 9, 094505 (2013), [arXiv:1309.2608].
- [127] C. A. Meyer and E. S. Swanson, Prog. Part. Nucl. Phys. **82**, 21 (2015), [arXiv:1502.07276].
- [128] D. R. Thompson *et al.* (E852), Phys. Rev. Lett. **79**, 1630 (1997), [hep-ex/9705011].
- [129] S. U. Chung *et al.* (E852), Phys. Rev. **D60**, 092001 (1999), [hep-ex/9902003].
- [130] G. S. Adams *et al.* (E862), Phys. Lett. **B657**, 27 (2007), [hep-ex/0612062].
- [131] D. Alde *et al.* (IHEP-Brussels-Los Alamos-Annecy(LAPP)), Phys. Lett. **B205**, 397 (1988).
- [132] Yu. D. Prokoshkin and S. A. Sadovsky, Phys. Atom. Nucl. **58**, 606 (1995), [Yad. Fiz.58N4,662(1995)].
- [133] Yu. D. Prokoshkin and S. A. Sadovsky, Phys. Atom. Nucl. **58**, 853 (1995), [Yad. Fiz.58,921(1995)].
- [134] A. Abele *et al.* (Crystal Barrel), Phys. Lett. **B423**, 175 (1998).
- [135] A. Abele *et al.* (Crystal Barrel), Phys. Lett. **B446**, 349 (1999).
- [136] M. Alekseev *et al.* (COMPASS), Phys. Rev. Lett. **104**, 241803 (2010), [arXiv:0910.5842].
- [137] E. I. Ivanov *et al.* (E852), Phys. Rev. Lett. **86**, 3977 (2001), [hep-ex/0101058].
- [138] J. Kuhn *et al.* (E852), Phys. Lett. **B595**, 109 (2004), [hep-ex/0401004].
- [139] M. Lu *et al.* (E852), Phys. Rev. Lett. **94**, 032002 (2005), [hep-ex/0405044].
- [140] Yu.P. Gouz *et al.*, Proc. XXVI Int. Conf. on HEP, Dallas (1992).
- [141] G. M. Beladidze *et al.* (VES), Phys. Lett. **B313**, 276 (1993).
- [142] A. Donnachie and P. R. Page, Phys. Rev. **D58**, 114012 (1998), [hep-ph/9808225].
- [143] W. Dunnweber (Crystal Barrel), Nucl. Phys. **A663**, 592 (2000).
- [144] A. Rodas *et al.*, Phys. Rev. Lett. **122**, 042002 (2019).
- [145] S. U. Chung, E. Klempt and J. G. Korner, Eur. Phys. J. **A15**, 539 (2002), [hep-ph/0211100].
- [146] F. E. Close and H. J. Lipkin, Phys. Lett. **B196**, 245 (1987).
- [147] F. Iddir and A. S. Safir, Phys. Lett. **B507**, 183 (2001), [hep-ph/0010121].
- [148] D. V. Amelin *et al.* (VES), Phys. Lett. **B356**, 595 (1995).
- [149] A. Donnachie and Yu. S. Kalashnikova, Phys. Rev. **D60**, 114011 (1999), [hep-ph/9901334].
- [150] K. Karch *et al.* (Crystal Ball), Z. Phys. **C54**, 33 (1992).
- [151] J. Adomeit *et al.* (Crystal Barrel), Z. Phys. **C71**, 227 (1996).
- [152] D. Barberis *et al.* (WA102), Phys. Lett. **B413**, 217 (1997), [hep-ex/9707021].
- [153] B. Aubert *et al.* (BaBar), Phys. Rev. Lett. **90**, 242001 (2003), [hep-ex/0304021].
- [154] D. Besson *et al.* (CLEO), Phys. Rev. **D68**, 032002 (2003), [Erratum: Phys. Rev. D75,119908(2007)], [hep-ex/0305100].
- [155] H.-Y. Cheng and W.-S. Hou, Phys. Lett. **B566**, 193 (2003), [hep-ph/0305038].
- [156] K. Terasaki, Phys. Rev. **D68**, 011501 (2003), [hep-ph/0305213].
- [157] L. Maiani *et al.*, Phys. Rev. **D71**, 014028 (2005), [hep-ph/0412098].
- [158] V. Dmitrasinovic, Phys. Rev. Lett. **94**, 162002 (2005).
- [159] T. Barnes, F. E. Close and H. J. Lipkin, Phys. Rev. **D68**, 054006 (2003), [hep-ph/0305025].
- [160] E. E. Kolomeitsev and M. F. M. Lutz, Phys. Lett. **B582**, 39 (2004), [hep-ph/0307133].
- [161] A. Faessler *et al.*, Phys. Rev. **D76**, 014005 (2007), [arXiv:0705.0254].
- [162] M. F. M. Lutz and M. Soyeur, Nucl. Phys. **A813**, 14 (2008), [arXiv:0710.1545].
- [163] L. Liu *et al.*, Phys. Rev. **D87**, 1, 014508 (2013), [arXiv:1208.4535].
- [164] S. Godfrey, Phys. Lett. **B568**, 254 (2003), [hep-ph/0305122].
- [165] P. Colangelo and F. De Fazio, Phys. Lett. **B570**, 180 (2003), [hep-ph/0305140].
- [166] M. Albaladejo *et al.*, Phys. Lett. **B767**, 465 (2017), [arXiv:1610.06727].
- [167] M.-L. Du *et al.*, Phys. Rev. **D98**, 9, 094018 (2018), [arXiv:1712.07957].
- [168] X.-Y. Guo, Y. Heo and M. F. M. Lutz, Phys. Rev. **D98**, 1, 014510 (2018), [arXiv:1801.10122].
- [169] R. Aaij *et al.* (LHCb), Phys. Rev. **D94**, 7, 072001 (2016), [arXiv:1608.01289].
- [170] S. K. Choi *et al.* (Belle), Phys. Rev. Lett. **91**, 262001 (2003), [hep-ex/0309032].
- [171] B. Aubert *et al.* (BaBar), Phys. Rev. **D71**, 071103 (2005), [hep-ex/0406022].
- [172] R. Aaij *et al.* (LHCb), Phys. Rev. Lett. **115**, 072001 (2015), [arXiv:1507.03414].
- [173] R. Aaij *et al.* (LHCb), Phys. Rev. Lett. **110**, 222001 (2013), [arXiv:1302.6269].
- [174] R. Aaij *et al.* (LHCb), Phys. Rev. **D92**, 1, 011102 (2015), [arXiv:1504.06339].
- [175] T. Barnes and S. Godfrey, Phys. Rev. **D69**, 054008 (2004), [hep-ph/0311162].
- [176] K. Abe *et al.* (Belle), Phys. Rev. Lett. **98**, 082001 (2007), [hep-ex/0507019].
- [177] K. Abe *et al.* (Belle), Phys. Rev. Lett. **94**, 182002 (2005), [hep-ex/0408126].
- [178] S. Uehara *et al.* (Belle), Phys. Rev. Lett. **96**, 082003 (2006), [hep-ex/0512035].
- [179] N. A. Tornqvist, Phys. Lett. **B590**, 209 (2004), [hep-ph/0402237].
- [180] E. S. Swanson, Phys. Lett. **B588**, 189 (2004), [hep-ph/0311229].
- [181] D. Gamermann and E. Oset, Phys. Rev. **D80**, 014003 (2009), [arXiv:0905.0402].
- [182] B. Aubert *et al.* (BaBar), Phys. Rev. **D71**, 031501 (2005), [hep-ex/0412051].
- [183] L. Maiani, A. D. Polosa and V. Riquer, Phys. Lett. **B778**, 247 (2018), [arXiv:1712.05296].
- [184] C. Bignamini *et al.*, Phys. Rev. Lett. **103**, 162001 (2009), [arXiv:0906.0882].
- [185] P. Artoisenet and E. Braaten, Phys. Rev. **D81**, 114018 (2010), [arXiv:0911.2016].
- [186] F.-K. Guo *et al.*, JHEP **05**, 138 (2014), [arXiv:1403.4032].
- [187] M. Albaladejo *et al.*, Chin. Phys. **C41**, 12, 121001 (2017), [arXiv:1709.09101].
- [188] B. Aubert *et al.* (BaBar), Phys. Rev. Lett. **95**, 142001 (2005), [hep-ex/0506081].
- [189] M. Ablikim *et al.* (BESIII), Phys. Rev. Lett. **118**, 9, 092001 (2017), [arXiv:1611.01317].

- [190] M. Cleven *et al.*, Phys. Rev. **D90**, 7, 074039 (2014), [arXiv:1310.2190].
- [191] C. Hanhart, Int. J. Mod. Phys. Conf. Ser. **46**, 1860004 (2018), [arXiv:1712.01136].
- [192] C. Hanhart and E. Klempt (2019), [arXiv:1906.11971].
- [193] F. E. Close and P. R. Page, Phys. Lett. **B628**, 215 (2005), [hep-ph/0507199].
- [194] M. Berwein *et al.*, Phys. Rev. **D92**, 11, 114019 (2015), [arXiv:1510.04299].
- [195] E. Kou and O. Pene, Phys. Lett. **B631**, 164 (2005), [hep-ph/0507119].
- [196] Yu. S. Kalashnikova and A. V. Nefediev, Phys. Rev. **D77**, 054025 (2008), [arXiv:0801.2036].
- [197] M. Ablikim *et al.* (BESIII), Phys. Rev. Lett. **111**, 24, 242001 (2013), [arXiv:1309.1896].
- [198] M. B. Voloshin, Prog. Part. Nucl. Phys. **61**, 455 (2008), [arXiv:0711.4556].
- [199] X. Li and M. B. Voloshin, Mod. Phys. Lett. **A29**, 12, 1450060 (2014), [arXiv:1309.1681].
- [200] Q. Wang, C. Hanhart and Q. Zhao, Phys. Rev. Lett. **111**, 13, 132003 (2013), [arXiv:1303.6355].
- [201] F.-K. Guo *et al.*, Phys. Lett. **B725**, 127 (2013), [arXiv:1306.3096].
- [202] M. Ablikim *et al.* (BESIII), Phys. Rev. Lett. **112**, 9, 092001 (2014), [arXiv:1310.4101].
- [203] Q. Wang *et al.*, Phys. Rev. **D89**, 3, 034001 (2014), [arXiv:1309.4303].
- [204] V. Baru *et al.*, Phys. Rev. **D91**, 3, 034002 (2015), [arXiv:1501.02924].
- [205] A. Ali *et al.*, Eur. Phys. J. **C78**, 1, 29 (2018), [arXiv:1708.04650].
- [206] L. Maiani *et al.*, Phys. Rev. **D89**, 114010 (2014), [arXiv:1405.1551].
- [207] K. Chilikin *et al.* (Belle), Phys. Rev. **D88**, 7, 074026 (2013), [arXiv:1306.4894].
- [208] R. Aaij *et al.* (LHCb), Phys. Rev. Lett. **112**, 22, 222002 (2014), [arXiv:1404.1903].
- [209] Y.-H. Chen *et al.*, Phys. Rev. **D99**, 7, 074016 (2019), [arXiv:1902.10957].
- [210] M. Ablikim *et al.* (BESIII), Phys. Rev. Lett. **110**, 252001 (2013), [arXiv:1303.5949].
- [211] M. Ablikim *et al.* (BESIII), Phys. Rev. Lett. **112**, 2, 022001 (2014), [arXiv:1310.1163].
- [212] P. Krokovny *et al.* (Belle), Phys. Rev. **D88**, 5, 052016 (2013), [arXiv:1308.2646].
- [213] A. Bondar *et al.* (Belle), Phys. Rev. Lett. **108**, 122001 (2012), [arXiv:1110.2251].
- [214] A. Garmash *et al.* (Belle), Phys. Rev. Lett. **116**, 21, 212001 (2016), [arXiv:1512.07419].
- [215] A. E. Bondar *et al.*, Phys. Rev. **D84**, 054010 (2011), [arXiv:1105.4473].
- [216] A. Ali *et al.*, Phys. Rev. **D91**, 1, 017502 (2015), [arXiv:1412.2049].
- [217] M. B. Voloshin, Phys. Rev. **D84**, 031502 (2011), [arXiv:1105.5829].
- [218] T. Mehen and J. W. Powell, Phys. Rev. **D84**, 114013 (2011), [arXiv:1109.3479].
- [219] V. Baru *et al.*, JHEP **06**, 158 (2017), [arXiv:1704.07332].
- [220] V. Baru *et al.*, Phys. Rev. **D99**, 9, 094013 (2019), [arXiv:1901.10319].
- [221] T. Branz, T. Gutsche and V. E. Lyubovitskij, Phys. Rev. **D82**, 054025 (2010), [arXiv:1005.3168].
- [222] P. Pakhlov, Phys. Lett. **B702**, 139 (2011), [arXiv:1105.2945].
- [223] P. Pakhlov and T. Uglov, Phys. Lett. **B748**, 183 (2015), [arXiv:1408.5295].
- [224] S. X. Nakamura and K. Tsushima, Phys. Rev. **D100**, 5, 051502 (2019), [arXiv:1901.07385].
- [225] M. Cleven *et al.*, Phys. Rev. **D92**, 1, 014005 (2015), [arXiv:1505.01771].

79. Baryon Decay Parameters

Written 1996 by E.D. Commins (University of California, Berkeley).

79.1. Baryon semileptonic decays

The typical spin-1/2 baryon semileptonic decay is described by a matrix element, the hadronic part of which may be written as:

$$\bar{B}_f \left[f_1(q^2)\gamma_\lambda + i f_2(q^2)\sigma_{\lambda\mu}q^\mu + g_1(q^2)\gamma_\lambda\gamma_5 + g_3(q^2)\gamma_5q_\lambda \right] B_i. \quad (79.1)$$

Here B_i and \bar{B}_f are spinors describing the initial and final baryons, and $q = p_i - p_f$, while the terms in f_1 , f_2 , g_1 , and g_3 account for vector, induced tensor (“weak magnetism”), axial vector, and induced pseudoscalar contributions [1]. Second-class current contributions are ignored here. In the limit of zero momentum transfer, f_1 reduces to the vector coupling constant g_V , and g_1 reduces to the axial-vector coupling constant g_A . The latter coefficients are related by Cabibbo’s theory [2], generalized to six quarks (and three mixing angles) by Kobayashi and Maskawa [3]. The g_3 term is negligible for transitions in which an e^\pm is emitted, and gives a very small correction, which can be estimated by PCAC [4], for μ^\pm modes. Recoil effects include weak magnetism, and are taken into account adequately by considering terms of first order in

$$\delta = \frac{m_i - m_f}{m_i + m_f}, \quad (79.2)$$

where m_i and m_f are the masses of the initial and final baryons.

The experimental quantities of interest are the total decay rate, the lepton-neutrino angular correlation, the asymmetry coefficients in the decay of a polarized initial baryon, and the polarization of the decay baryon in its own rest frame for an unpolarized initial baryon. Formulae for these quantities are derived by standard means [5] and are analogous to formulae for nuclear beta decay [6]. We use the notation of Ref. 6 in the Listings for neutron beta decay. For comparison with experiments at higher q^2 , it is necessary to modify the form factors at $q^2 = 0$ by a “dipole” q^2 dependence, and for high-precision comparisons to apply appropriate radiative corrections [7].

The ratio g_A/g_V may be written as

$$g_A/g_V = |g_A/g_V| e^{i\phi_{AV}}. \quad (79.3)$$

The presence of a “triple correlation” term in the transition probability, proportional to $\text{Im}(g_A/g_V)$ and of the form

$$\sigma_i \cdot (\mathbf{p}_\ell \times \mathbf{p}_\nu) \quad (79.4)$$

for initial baryon polarization or

$$\sigma_f \cdot (\mathbf{p}_\ell \times \mathbf{p}_\nu) \quad (79.5)$$

for final baryon polarization, would indicate failure of time-reversal invariance. The phase angle ϕ has been measured precisely only in neutron decay (and in ^{19}Ne nuclear beta decay), and the results are consistent with T invariance.

79.2. Hyperon nonleptonic decays

The amplitude for a spin-1/2 hyperon decaying into a spin-1/2 baryon and a spin-0 meson may be written in the form

$$M = G_F m_\pi^2 \cdot \bar{B}_f (A - B\gamma_5) B_i, \quad (79.6)$$

where A and B are constants [1]. The transition rate is proportional to

$$R = 1 + \gamma \hat{\omega}_f \cdot \hat{\omega}_i + (1 - \gamma)(\hat{\omega}_f \cdot \hat{\mathbf{n}})(\hat{\omega}_i \cdot \hat{\mathbf{n}}) + \alpha(\hat{\omega}_f \cdot \hat{\mathbf{n}} + \hat{\omega}_i \cdot \hat{\mathbf{n}}) + \beta \hat{\mathbf{n}} \cdot (\hat{\omega}_f \times \hat{\omega}_i), \quad (79.7)$$

where $\hat{\mathbf{n}}$ is a unit vector in the direction of the final baryon momentum, and $\hat{\omega}_i$ and $\hat{\omega}_f$ are unit vectors in the directions of the initial and final baryon spins. (The sign of the last term in the above equation

was incorrect in our 1988 and 1990 editions.) The parameters α , β , and γ are defined as

$$\begin{aligned} \alpha &= 2 \text{Re}(s^*p)/(|s|^2 + |p|^2), \\ \beta &= 2 \text{Im}(s^*p)/(|s|^2 + |p|^2), \\ \gamma &= (|s|^2 - |p|^2)/(|s|^2 + |p|^2), \end{aligned} \quad (79.8)$$

where $s = A$ and $p = |\mathbf{p}_f| B/(E_f + m_f)$; here E_f and \mathbf{p}_f are the energy and momentum of the final baryon. The parameters α , β , and γ satisfy

$$\alpha^2 + \beta^2 + \gamma^2 = 1. \quad (79.9)$$

If the hyperon polarization is \mathbf{P}_Y , the polarization \mathbf{P}_B of the decay baryons is

$$\mathbf{P}_B = \frac{(\alpha + \mathbf{P}_Y \cdot \hat{\mathbf{n}})\hat{\mathbf{n}} + \beta(\mathbf{P}_Y \times \hat{\mathbf{n}}) + \gamma\hat{\mathbf{n}} \times (\mathbf{P}_Y \times \hat{\mathbf{n}})}{1 + \alpha\mathbf{P}_Y \cdot \hat{\mathbf{n}}}. \quad (79.10)$$

Here \mathbf{P}_B is defined in the rest system of the baryon, obtained by a Lorentz transformation along $\hat{\mathbf{n}}$ from the hyperon rest frame, in which $\hat{\mathbf{n}}$ and \mathbf{P}_Y are defined.

An additional useful parameter ϕ is defined by

$$\beta = (1 - \alpha^2)^{1/2} \sin\phi. \quad (79.11)$$

In the Listings, we compile α and ϕ for each decay, since these quantities are most closely related to experiment and are essentially uncorrelated. When necessary, we have changed the signs of reported values to agree with our sign conventions. In the Baryon Summary Table, we give α , ϕ , and Δ (defined below) with errors, and also give the value of γ without error.

Time-reversal invariance requires, in the absence of final-state interactions, that s and p be relatively real, and therefore that $\beta = 0$. However, for the decays discussed here, the final-state interaction is strong. Thus

$$s = |s| e^{i\delta_s} \text{ and } p = |p| e^{i\delta_p}, \quad (79.12)$$

where δ_s and δ_p are the pion-baryon s - and p -wave strong interaction phase shifts. We then have

$$\beta = \frac{-2|s||p|}{|s|^2 + |p|^2} \sin(\delta_s - \delta_p). \quad (79.13)$$

One also defines $\Delta = -\tan^{-1}(\beta/\alpha)$. If T invariance holds, $\Delta = \delta_s - \delta_p$. For $\Lambda \rightarrow p\pi^-$ decay, the value of Δ may be compared with the s - and p -wave phase shifts in low-energy π^-p scattering, and the results are consistent with T invariance.

See also the note on “Radiative Hyperon Decays” in this *Review*.

References:

1. E.D. Commins and P.H. Bucksbaum, *Weak Interactions of Leptons and Quarks* (Cambridge University Press, Cambridge, England, 1983).
2. N. Cabibbo, Phys. Rev. Lett. **10**, 531 (1963).
3. M. Kobayashi and T. Maskawa, Prog. Theor. Phys. **49**, 652 (1973).
4. M.L. Goldberger and S.B. Treiman, Phys. Rev. **111**, 354 (1958).
5. P.H. Frampton and W.K. Tung, Phys. Rev. **D3**, 1114 (1971).
6. J.D. Jackson, S.B. Treiman, and H.W. Wyld, Jr., Phys. Rev. **106**, 517 (1957), and Nucl. Phys. **4**, 206 (1957).
7. Y. Yokoo, S. Suzuki, and M. Morita, Prog. Theor. Phys. **50**, 1894 (1973).

80. *N* and Δ Resonances

Revised July 2019 by V. Burkert (Jefferson Lab), E. Klempt (University of Bonn), U. Thoma (University of Bonn), L. Tiator (University of Mainz), and R.L. Workman (George Washington University).

80.1. Introduction

The excited states of the nucleon have been studied in a large number of formation and production experiments. Until recently, the Breit-Wigner masses and widths, the pole positions, and the elasticities of the *N* and Δ resonances in the Baryon Summary Table came largely from partial-wave analyses of πN total, elastic, and charge-exchange scattering data. The most comprehensive analyses were carried out by the Karlsruhe-Helsinki (KH80) [1], Carnegie Mellon-Berkeley (CMB80) [2], and George Washington U (GWU) [3] groups. Partial-wave analyses have also been performed on much smaller πN reaction data sets to get ηN , $K\Lambda$, and $K\Sigma$ branching fractions (see the Listings for references). Other branching fractions come from analyses of $\pi N \rightarrow \pi\pi N$ data.

In recent years, a large amount of data on photoproduction of many final states has been accumulated, and these data are beginning to tell us much about the properties of baryon resonances. A survey of data on photoproduction can be found in the proceedings of recent conferences [4] and workshops [5], and in recent reviews [6,7].

80.2. Naming scheme for baryon resonances

In the past, when nearly all resonance information came from elastic πN scattering, it was common to label resonances with the incoming partial wave $L_{2I,2J}$, as in $\Delta(1232)P_{33}$ and $N(1680)F_{15}$. However, most recent information has come from γN experiments. Therefore, we have replaced $L_{2I,2J}$ with the spin-parity J^P of the state, as in $\Delta(1232)3/2^+$ and $N(1680)5/2^+$; this name gives intrinsic properties of the resonance that are independent of the specific particles and reactions used to study them. This applies equally to all baryons, including Ξ resonances and charm baryons that are not produced in formation experiments. We do not, however, attach the mass or spin-parity to the names of the ground-state (“stable”) baryons $N, \Lambda, \Sigma, \Xi, \Omega, \Lambda_c, \dots$.

80.3. Using the *N* and Δ listings

Tables 80.1 and 80.2 list all the *N* and Δ entries in the Baryon Listings and give our evaluation of the overall status and the status channel by channel. Only the established resonances (overall status 3 or 4 stars) are promoted to the Baryon Summary Table. We long ago omitted from the Listings information from old analyses, prior to KH80 and CMB80, which can be found in earlier editions. A rather complete survey of older results was given in our 1982 edition [8].

As a rule, we award an overall status **** or *** only to those resonances which are derived from analyses of data sets that include precision differential cross sections and polarization observables, and are confirmed by independent analyses. All other signals are given ** or * status. New results that are not accompanied by proper error evaluation are less valuable for evaluating star ratings. The following criteria are guidelines for future error analysis.

1. Uncertainties in resonance parameters: The publication should have a detailed discussion on how the uncertainties of parameters were estimated. This requires that the error estimates go beyond the simple fit error as e.g. given by MINUIT, and the robustness of the results should be demonstrated.

2. Fit quality: Concrete measures for the fit quality should be provided. The reduced global χ^2 value of the fit, while useful, is insufficient. Other possibilities include quoting variations of local χ^2 values in kinematic regions where evidence for new resonances, or significantly improved information on resonance parameters, is claimed.

3. Weight factors in observables: Analyses sometimes use weight factors for certain data sets to either increase or reduce their impact on the results. This has been particularly important when polarization observables are involved, which often are sensitive to

resonance amplitudes through interferences, but usually have much poorer statistics than differential cross section data. To evaluate sensitivities, the resulting resonance parameters should be checked against variations of the specific weight factors.

Claims of evidence for new baryon states must be based on a sufficiently complete set of partial waves in the fit. The robustness of signals must be demonstrated, e.g. by examining the effect of higher partial waves in the fit.

80.4. Properties of resonances

Resonances are defined by poles of the *S*-matrix, whether in scattering, production or decay matrix elements. These are poles in the complex plane in *s*, as discussed in the new review on *Resonances*. As is traditional, we quote here the pole positions in the complex energy $w = \sqrt{s}$ plane. Crucially, the position of the pole of the *S*-matrix is independent of the process, and the production and decay properties factorize. This is the rationale for listing the pole position first for each resonance. These key properties of the *S*-matrix pole are in contrast to other quantities related to resonance phenomena, such as Breit-Wigner parameters or any *K*-matrix pole. Breit-Wigner parameters depend on the formalism used, such as angular-momentum barrier factors, or cut-off parameters, and the assumed or modeled background. However, the accurate determination of pole parameters from the analysis of data on the real energy axis is not necessarily simple, or even straightforward. It requires the implementation of the correct analytic structure of the relevant (often coupled) channels.

In principle, there are two ways to extract pole parameters from experimental data: (i) analytic continuation of theoretical single- or multi-channel models into the complex energy plane or (ii) local expansions of the partial-wave *T*-matrix amplitudes in the complex energy plane in the vicinity of a pole.

At present, poles are usually extracted using the first method [9–14], but considerable effort has been put into the development of alternate approaches, such as the speed plot [15], time delay [16], N/D method [17], regularization procedure [18], or Padé approximation [19].

Methods of the second type are based on the idea to use first or higher-order derivatives in energy to reduce the importance of, or totally eliminate, the background contribution. One either has to model the background contribution and introduce model dependence, or one is faced with numerical derivatives of single-energy data. In both cases, one reaches almost unsurmountable difficulties.

An alternate way to extract pole parameters from partial waves has been proposed by introducing a Laurent+Pietarinen (L+P) expansion [20–22]

$$T(W) = \sum_{i=1}^N \frac{Res_i}{W - W_i} + \sum_{j=1}^M \sum_{n=0}^{n_{max}} c_n^j \left(\frac{\alpha_j - \sqrt{x_j - W}}{\alpha_j + \sqrt{x_j - W}} \right)^n, \quad (1)$$

where $T(W)$ is a given partial wave amplitude, W_i and Res_i are the *N* complex pole positions and residues. The background is parameterized with *M* Pietarinen functions, where α_j are positive range parameters and x_j are real or complex branch points; c_n^j are real expansion coefficients.

The main idea of this procedure is to find the simplest analytic function, with well-defined poles and cuts, regardless of whether they are generated by a theoretical model or some energy-independent procedure. Instead of searching for the function which reproduces the input amplitudes over the complete complex energy plane, on all Riemann sheets, a representation is searched only in a limited complex energy range, near the real axis, which is defined by the radius of

Table 80.1. The status of the *N* resonances and their decays. Sub-threshold decay modes are omitted. Only resonances with an overall status of *** or **** are included in the main Baryon Summary Table.

Particle J^P	overall	Status as seen in									
		$N\gamma$	$N\pi$	$\Delta\pi$	$N\sigma$	$N\eta$	ΛK	ΣK	$N\rho$	$N\omega$	$N\eta'$
<i>N</i> 1/2 ⁺ ****											
<i>N</i> (1440)1/2 ⁺ ****	****	*****									
<i>N</i> (1520)3/2 ⁻ ****	****	*****				****					
<i>N</i> (1535)1/2 ⁻ ****	****	*****	*			****					
<i>N</i> (1650)1/2 ⁻ ****	****	*****	*			****					
<i>N</i> (1675)5/2 ⁻ ****	****	*****	*	*	*						
<i>N</i> (1680)5/2 ⁺ ****	****	*****	*	*	*						
<i>N</i> (1700)3/2 ⁻ ***	**	***	***	*	*				*		
<i>N</i> (1710)1/2 ⁺ ****	****	*****				***	**	*	*	*	
<i>N</i> (1720)3/2 ⁺ ****	****	*****	*	*	*	****	*	*	*	*	
<i>N</i> (1860)5/2 ⁺ **	*	**	*	*	*						
<i>N</i> (1875)3/2 ⁻ ***	**	**	*	**	*	*	*	*	*	*	
<i>N</i> (1880)1/2 ⁺ ***	**	*	**	*	*	**	**			**	
<i>N</i> (1895)1/2 ⁻ ****	****	*	*	*	*****	**	*	*	*	****	
<i>N</i> (1900)3/2 ⁺ ****	****	**	**	*	*	**	**	*	*	**	
<i>N</i> (1990)7/2 ⁺ **	**	**			*	*	*				
<i>N</i> (2000)5/2 ⁺ **	**	*	**	*	*				*		
<i>N</i> (2040)3/2 ⁺ *		*									
<i>N</i> (2060)5/2 ⁻ ***	***	**	*	*	*	*	*	*	*	*	
<i>N</i> (2100)1/2 ⁺ ***	**	***	**	**	*	*		*	*	**	
<i>N</i> (2120)3/2 ⁻ ***	***	**	**	**	*	**	*	*	*	*	
<i>N</i> (2190)7/2 ⁻ ****	****	*****	*	*	*	**	*	*	*	*	
<i>N</i> (2220)9/2 ⁺ ****	**	****			*	*	*				
<i>N</i> (2250)9/2 ⁻ ****	**	****			*	*	*				
<i>N</i> (2300)1/2 ⁺ **		**									
<i>N</i> (2570)5/2 ⁻ **		**									
<i>N</i> (2600)11/2 ⁻ ***		***									
<i>N</i> (2700)13/2 ⁺ **		**									

**** Existence is certain.
 *** Existence is very likely.
 ** Evidence of existence is fair.
 * Evidence of existence is poor.

convergence of the Laurent decomposition, and which contains the input amplitudes. All details are found in Ref. [21]. Applications of the method can be found in [20–27].

80.5. Photoproduction

A new approach to the nucleon excitation spectrum is provided by dedicated facilities at the Universities of Bonn, Grenoble, and Mainz, and at the national laboratories Jefferson Lab in the US and SPring-8 in Japan. High-precision cross sections and polarization observables for the photoproduction of pseudoscalar mesons provide a data set that is approaching a “complete experiment,” one that fully constrains the four complex amplitudes describing the spin-structure of the reaction [28]. A large number of photoproduction reactions has been studied.

In pseudoscalar meson photoproduction, the four independent helicity amplitudes can be expressed in terms of the four CGLN [29] amplitudes allowed by Lorentz and gauge invariance. These amplitudes can be expanded in a series of electric and magnetic multipoles. Except for $J = 1/2$, one electric and one magnetic multipole contributes to each J^P combination.

Table 80.2. The status of the Δ resonances and their decays. Sub-threshold decay modes are omitted. Only resonances with an overall status of *** or **** are included in the main Baryon Summary Table.

Particle J^P	overall	Status as seen in						
		$N\gamma$	$N\pi$	$\Delta\pi$	ΣK	$N\rho$	$\Delta\eta$	
Δ (1232)3/2 ⁺ ****	****	****	****					
Δ (1600)3/2 ⁺ ****	****	****	***	****				
Δ (1620)1/2 ⁻ ****	****	****	****	****				
Δ (1700)3/2 ⁻ ****	****	****	****	****	*			
Δ (1750)1/2 ⁺ *	*	*	*		*			
Δ (1900)1/2 ⁻ ***	***	***	***	*	**	*		
Δ (1905)5/2 ⁺ ****	****	****	****	**	*	*	**	
Δ (1910)1/2 ⁺ ****	****	***	****	**	**		*	
Δ (1920)3/2 ⁺ ***	***	***	***	***	**		**	
Δ (1930)5/2 ⁻ ***	***	*	***	*	*			
Δ (1940)3/2 ⁻ **	**	*	**	*			*	
Δ (1950)7/2 ⁺ ****	****	****	****	**	***			
Δ (2000)5/2 ⁺ **	**	*	**	*		*		
Δ (2150)1/2 ⁻ *	*		*					
Δ (2200)7/2 ⁻ ***	***	***	**	***	**			
Δ (2300)9/2 ⁺ **	**		**					
Δ (2350)5/2 ⁻ *	*		*					
Δ (2390)7/2 ⁺ *	*		*					
Δ (2400)9/2 ⁻ **	**	**	**					
Δ (2420)11/2 ⁺ ****	****	*	****					
Δ (2750)13/2 ⁻ **	**		**					
Δ (2950)15/2 ⁺ **	**		**					

**** Existence is certain.
 *** Existence is very likely.
 ** Evidence of existence is fair.
 * Evidence of existence is poor.

For a given state, these two amplitudes determine the resonance photo-decay helicity amplitudes $A_{1/2}$ and $A_{3/2}$. As described below, this resonance extraction has been carried out either assuming a Breit-Wigner resonance or at the pole.

If a Breit-Wigner parametrization is used, the $N\gamma$ partial width, Γ_γ , is given in terms of the helicity amplitudes $A_{1/2}$ and $A_{3/2}$ by

$$\Gamma_\gamma = \frac{k_{\text{BW}}^2}{\pi} \frac{2m_N}{(2J+1)m_{\text{BW}}} \left(|A_{1/2}|^2 + |A_{3/2}|^2 \right). \quad (2)$$

Here m_N and m_{BW} are the nucleon and resonance masses, J is the resonance spin, and k_{BW} is the photon c.m. decay momentum. Most earlier analyses have provided these real quantities $A_{1/2}$ and $A_{3/2}$.

More recent studies have quoted related complex quantities, evaluated at the T-matrix pole. These complex helicity amplitudes, $\tilde{A}_{1/2}$ and $\tilde{A}_{3/2}$, can be cast onto the form

$$\tilde{A}_h = \sqrt{\frac{\pi(2J+1)w_{\text{pole}}}{m_N k_{\text{pole}}^2}} \frac{\text{Res}(T_h(\gamma N \rightarrow N b))}{\sqrt{\text{Res}(T(N b \rightarrow N b))}} \quad (3)$$

where the residues (*Res*) are evaluated at the pole position, w_{pole} , and $k_{\text{pole}}^2 = (w_{\text{pole}}^2 - m_N^2)^2 / 4w_{\text{pole}}^2$ [30]. For Breit-Wigner amplitudes, $w_{\text{pole}} = m_{\text{BW}}$ and $\tilde{A}_h = A_h$. Similar relations for the photo and electro couplings at the pole position can be found in [31,32].

The determination of eight real numbers from four complex amplitudes (with one overall phase undetermined) requires at least seven independent measurements. At least one further measurement is required to resolve discrete ambiguities that result from the fact that data are proportional to squared amplitudes. Photon beams and

nucleon targets can be polarized (with linear or circular polarization P_{\perp} , P_{\odot} and \vec{T} , respectively); the recoil polarization of the outgoing baryon \vec{R} can be measured. The experiments can be divided into three classes: (1) the beam and target are polarized (BT); (2) the beam is polarized and the recoil baryon polarization is measured (BR); (3) the target is polarized and the recoil polarization is measured (TR). Different sign conventions are used in the literature, as summarized in [33].

One of the best studied reactions is $\gamma p \rightarrow \Lambda K^+$. Published data include differential cross sections, the beam asymmetry Σ , the target asymmetry T , the recoil polarization P , and the BR double-polarization variables $C_{x'}$, $C_{z'}$, $O_{x'}$, and $O_{z'}$. For the photoproduction of pions and etas, off proton and neutron targets, differential cross sections, single- and double-polarization asymmetries have been measured, mainly for pions.

80.6. Electroproduction

Electroproduction of mesons provides information on the internal structure of resonances. The helicity amplitudes are functions of the (squared) momentum transfer $Q^2 = -(e - e')^2$, where e and e' are the 4-momenta of the incident and scattered electron, and a third amplitude, $S_{1/2}$, measures the resonance response to the longitudinal component of the virtual photon. Most data stem from the reactions $e^- p \rightarrow e^- n \pi^+$ and $e^- p \rightarrow e^- p \pi^0$ but also the reactions $e^- p \rightarrow e^- p \eta$, $e^- p \rightarrow e^- p \pi^+ \pi^-$, and $e^- p \rightarrow e^- \Lambda(\Sigma^0) K^+$ have been studied. The data and their interpretation are reviewed in Refs. [34,35].

The transition to the $\Delta(1232)3/2^+$ is often quantified in terms of the magnetic dipole transition moment M_{1+} (or the magnetic transition form factor $G_{M,Ash}^*(Q^2)$) [36], and the electric and scalar quadrupole transition moments E_{1+} and S_{1+} . Figure 80.1 shows the strength of the $p \rightarrow \Delta^+$ transition plotted versus the photon virtuality Q^2 . At $Q^2 = 0$, M_{1+} dominates the resonance transition strength. The two amplitudes E_{1+} and S_{1+} imply a quadrupole deformation of the transition to the lowest excited state. The magnitude of $R_{EM} = E_{1+}/M_{1+}$ remains nearly constant, while the magnitude of $R_{SM} = S_{1+}/M_{1+}$ increases rapidly up to 25% at the highest Q^2 value.

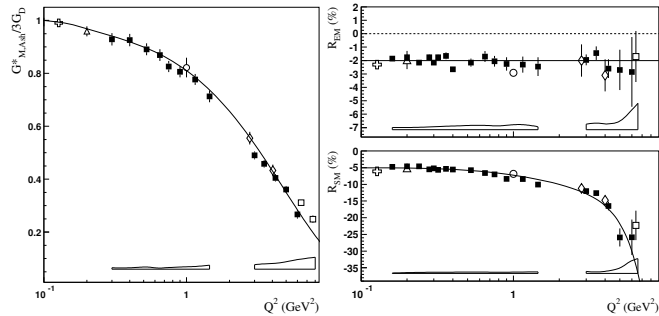


Figure 80.1: Left: The magnetic transition form factor for the $\gamma^* p \rightarrow \Delta^+(1232)$ transition versus the photon virtuality Q^2 . Right: The electric and scalar quadrupole ratios R_{EM} and R_{SM} . The different symbols are results from different experiments at JLab (squares, diamonds, circle) and MAMI (triangle, cross). The boxes near the horizontal axis indicate model uncertainties of the squares. Curves to guide the eyes.

Figure 80.2 shows the transverse and scalar helicity amplitudes for the $N(1440)1/2^+$, $N(1520)3/2^-$, and $N(1535)1/2^-$ resonances from JLab [34]. Similar results have been achieved at Mainz [35]. For the states $N(1440)1/2^+$ and $N(1520)3/2^-$, helicity amplitudes and $\pi\Delta$ and ρp decays were determined at JLab in an analysis of $\pi^+ \pi^- p$ electroproduction [37]. The data show distinctly different Q^2 dependencies that indicate different internal structures.

The $N(1520)3/2^-$ helicity amplitudes reveal the dominance of its three-quark nature: the $A_{3/2}$ amplitude is large at the photon point and decreases rapidly $\sim Q^{-5}$ with increasing Q^2 ; $A_{1/2}$ is small at the

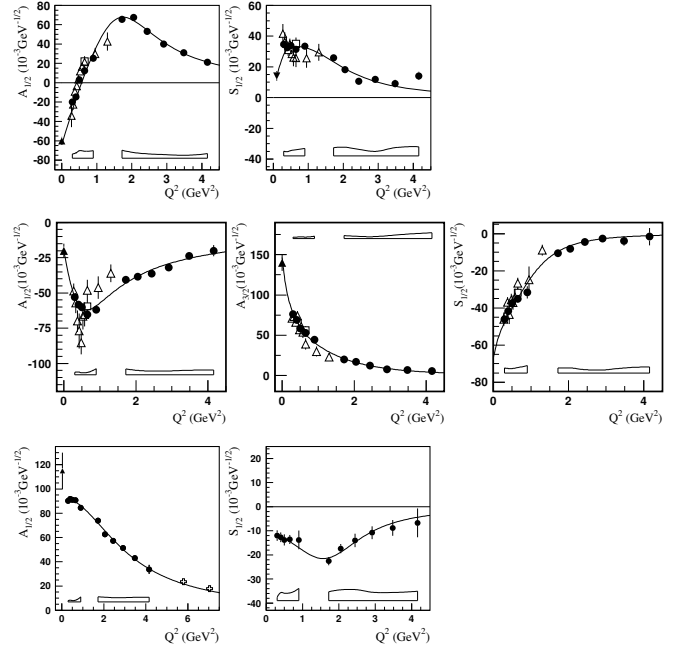


Figure 80.2: Transverse and scalar (longitudinal) helicity amplitudes for $\gamma p \rightarrow N(1440)1/2^+$ (top), $\gamma p \rightarrow N(1520)3/2^-$ (center), and $\gamma p \rightarrow N(1535)1/2^-$ (bottom) as extracted from the JLab/CLAS data in $n\pi^+$ production (full circles), MAMI/A1 data in $p\pi^0$ production (full down triangle), in $p\pi^+\pi^-$ (open triangles), and combined single and double pion production (open squares). The solid triangle is the PDG 2014 value at $Q^2 = 0$. The open boxes are the model uncertainties of the full circles.

photon point, increases rapidly with Q^2 and then falls off with $\sim Q^{-3}$. Quantitative agreement with the data is, however, achieved only when meson cloud effects are included.

At high Q^2 , both amplitudes for $N(1440)1/2^+$ are qualitatively described by light front quark models [38]: at short distances the resonance behaves as expected from a radial excitation of the nucleon. On the other hand, $A_{1/2}$ changes sign at about 0.6GeV^2 . This remarkable behavior has not been observed before for any nucleon form factor or transition amplitude. Obviously, an important change in the structure occurs when the resonance is probed as a function of Q^2 .

The Q^2 dependence of $A_{1/2}$ of the $N(1535)1/2^-$ resonance exhibits the expected Q^{-3} dependence, except for small Q^2 values where meson cloud effects set in.

Figure 80.3 shows the transverse and scalar amplitudes for three states in the 3rd nucleon resonance region, the $\Delta(1620)1/2^-$, the $N(1675)5/2^-$ and $N(1680)5/2^+$. The latter two states have nearly degenerate masses and are parity partners. In the quark model picture, the transverse amplitudes for $N(1675)5/2^-$ on the proton are suppressed due to the Moorhouse selection rule, allowing for a quantitative evaluation of the meson-baryon contributions. The data show significant meson-baryon strength in the $A_{1/2}$ amplitude even at quite high Q^2 , while $A_{3/2}$ drops much faster with Q^2 . $N(1680)5/2^+$ shows qualitatively the features predicted in constituent quark models, a dominant $A_{3/2}$ at the real photon point that drops rapidly with increasing Q^2 , while $A_{1/2}$ becomes the dominant contribution at high Q^2 , indicating a switch of the helicity structure in the resonance transition at short distances.

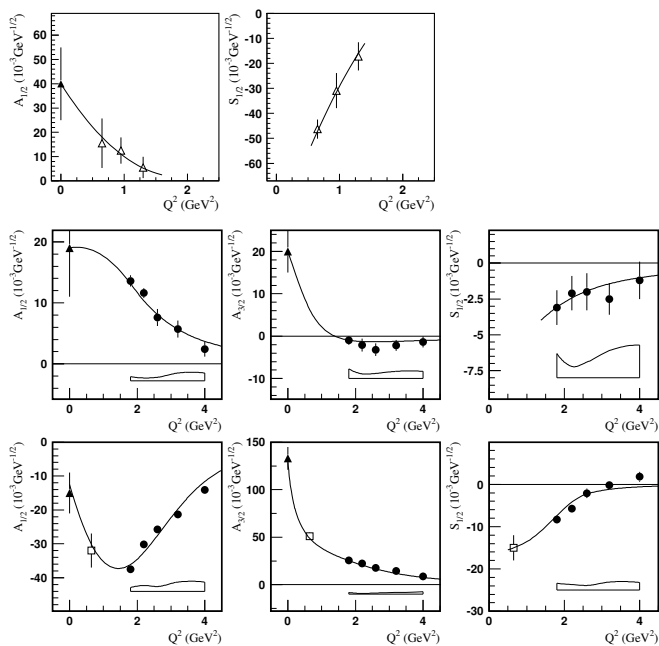


Figure 80.3: Transverse and scalar helicity amplitudes for $\gamma p \rightarrow \Delta(1620)1/2^-$ (top), $\gamma p \rightarrow N(1675)5/2^-$ (center), and $\gamma p \rightarrow N(1680)5/2^+$ (bottom) as extracted from the JLab/CLAS data in $n\pi^+$ production (full circles), $p\pi^+\pi^-$ (open triangles), combined single and double pion production (open square). The solid triangle is the 2014 PDG value at $Q^2 = 0$. The open boxes are the model uncertainties of the full circles. The curves are to guide the eye.

80.7. Partial wave analyses

Several PWA groups are now actively involved in the analysis of the new data. The GWU group maintains a nearly complete database covering reactions from πN and KN elastic scattering to $\gamma N \rightarrow N\pi$, $N\eta$, and $N\eta'$. It is presently the only group determining πN elastic amplitudes from scattering data in sliced energy bins. Given the high-precision of photoproduction data already or soon to be collected, the spectrum of N and Δ resonances will in the near future be better known.

Fits to the data are performed by various groups with the aim to understand the reaction dynamics and to identify N and Δ resonances. For practical reasons, approximations have to be made. We mention several analyses here: (1) The Mainz unitary isobar model [39] focuses on the correct treatment of the low-energy domain. Resonances are added to the unitary amplitude as a sum of Breit-Wigner amplitudes. This model also obtains resonance transition form factors and helicity amplitudes from electroproduction [35]. (2) For $N\pi$ electroproduction, the Yerevan/JLab group uses both the unitary isobar model and the dispersion relation approach developed in [38]. A phenomenological model was developed to extract resonance couplings and partial decay widths from exclusive $\pi^+\pi^-p$ electroproduction [37]. (3) Multichannel analyses using K-matrix parameterizations derive background terms from a chiral Lagrangian - providing a microscopical description of the background - (Giessen [40,41] or from phenomenology (KSU [42,43], Bonn-Gatchina [44]). (4) Several groups (EBAC-Jlab [45,46], ANL-Osaka [47], Dubna-Mainz-Taipeh [48], Bonn-Jülich [49,50,51], Valencia [52]) use dynamical reaction models, driven by chiral Lagrangians, which take dispersive parts of intermediate states into account. Several other groups have made important contributions. The Giessen group pioneered multichannel analyses of large data sets on pion- and photo-induced reactions [40,41]. The Bonn-Gatchina group included recent high-statistics data and reported systematic searches for new baryon resonances in all relevant partial waves. A summary of their results can be found in [44].

References:

- G. Höhler, Pion-Nucleon Scattering, Landolt-Börnstein Vol. I/9b2 (1983), ed. H. Schopper, Springer Verlag.
- R.E. Cutkosky *et al.*, Baryon 1980, *IV International Conference on Baryon Resonances*, Toronto, ed. N. Isgur, p. 19.
- R.A. Arndt *et al.*, Phys. Rev. **C74**, 045205 (2006).
- “Hadron 2011: 14th International Conference on Hadron Spectroscopy”, München, Germany, June, 13 - 17, 2011, published in eConf.
- “NSTAR 2013: 9th International Workshop on the Physics of Excited Nucleons”, 27-30 May 2013, Peñíscola, Spain.
- E. Klempt and J.M. Richard, Rev. Mod. Phys. **82**, 1095 (2010).
- V. Credé and W. Roberts, Rept. on Prog. in Phys. **76**, 076301 (2013).
- M. Roos *et al.*, Phys. Lett. **B111**, 1 (1982).
- M. Döring, C. Hanhart, F. Huang, S. Krewald, and U.-G. Meissner, Nucl. Phys. **A829**, 170 (2009), and references therein.
- N. Suzuki, B. Juliá-Díaz, H. Kamano, T.-S. H. Lee, A. Matsuyama, and T. Sato, Phys. Rev. Lett. **104**, 042302 (2010); H. Kamano, T.-S. H. Lee, A. Matsuyama, T. Sato, N. Suzuki, Phys. Rev. **C80**, 025207 (2009), and references therein.
- R. E. Cutkosky, C. P. Forsyth, R. E. Hendrick, and R. L. Kelly, Phys. Rev. **D20**, 2839 (1979).
- R. A. Arndt, W. J. Briscoe, I. I. Strakovsky, R. L. Workman, and M. M. Pavan, Phys. Rev. **C69**, 035213 (2004)..
- M. Batinić, I. Šlaus, A. Švarc, and B. M. K. Nefkens, Phys. Rev. **C51**, 2310 (1995); M. Batinić *et al.*, Phys. Scr. **58**, 15 (1998).
- A. V. Anisovich, R. Beck, E. Klempt, V. A. Nikonov, A. V. Sarantsev, U. Thoma, Eur. Phys. J. **A48**, 15 (2012), and references therein.
- G. Höhler, πN Newsletter **9**, 1 (1993).
- N. G. Kelkar, M. Nowakowski, Phys. Rev. **A78**, 012709 (2008), and references therein.
- G. F. Chew and S. Mandelstam, Phys. Rev. **119**, 467 (1960).
- S. Ceci, J. Stahov, A. Švarc, S. Watson, and B. Zauner, Phys. Rev. **D77**, 116007 (2008).
- P. Masjuan, J. J. Sanz-Cillero, Eur. Phys. J. **C73**, 2594 (2013).
- A. Švarc, M. Hadžimehmedović, H. Osmanović, J. Stahov, L. Tiator, and R. L. Workman, Phys. Rev. **C88**, 035206 (2013).
- A. Švarc, M. Hadžimehmedović, R. Omerović, H. Osmanović, and J. Stahov, Phys. Rev. **C89**, 045205 (2014).
- A. Švarc, M. Hadžimehmedović, H. Osmanović, J. Stahov, L. Tiator, and R. L. Workman, Phys. Lett. **B 755**, 452 (2016).
- A. Švarc, M. Hadžimehmedović, H. Osmanović, J. Stahov, L. Tiator, and R. L. Workman, Phys. Rev. **C89**, 065208 (2014).
- A. Švarc, M. Hadžimehmedović, H. Osmanović, J. Stahov, and R. L. Workman, Phys. Rev. **C91**, 015207 (2015).
- L. Tiator, M. Döring, R. L. Workman, M. Hadžimehmedović, R. Omerović, H. Osmanović, J. Stahov, and A. Švarc, Phys. Rev. **C94**, 065204 (2016).
- A. V. Anisovich *et al.*, Eur. Phys. J. **A53**, 242 (2017).
- A. V. Anisovich *et al.*, Phys. Rev. Lett. **119**, 062004 (2017).
- C. G. Fasano *et al.*, Phys. Rev. **C46**, 2430 (1992).
- G.F. Chew *et al.*, Phys. Rev. **106**, 1345 (1957).
- R.L. Workman, L. Tiator, and A. Sarantsev, Phys. Rev. **C87**, 068201 (2013).
- N. Suzuki, T. Sato, and T.-S.H. Lee, Phys. Rev. **C82**, 045206 (2010).
- H. Kamano, Phys. Rev. **C88**, 045203 (2013).
- A.M. Sandorfi *et al.*, AIP Conf. Proc. **1432**, 219 (2012).
- I. G. Aznauryan and V. D. Burkert, Prog. in Part. Nucl. Phys. **67**, 1 (2012).
- L. Tiator *et al.*, Eur. Phys. J. ST **198**, 141 (2011); S. Štajner *et al.*, Phys. Rev. Lett. **119**, 022001 (2017).
- W.W. Ash, Phys. Lett. **B24**, 165 (1967).
- V.I. Moiseev *et al.* [CLAS Collab.], Phys. Rev. **C86**, 035203 (2012).
- I.G. Aznauryan, Phys. Rev. **C67**, 015209 (2003).
- D. Drechsel, S.S. Kamalov, and L. Tiator, Eur. Phys. J. **A34**, 69 (2007).
- G. Penner and U. Mosel, Phys. Rev. **C66**, 055211 (2002).

41. G. Penner and U. Mosel, Phys. Rev. **C66**, 055212 (2002).
42. D.M. Manley and E.M. Saleski, Phys. Rev. **D45**, 4002 (1992).
43. M. Shrestha and D.M. Manley, Phys. Rev. **C86**, 055203 (2012).
44. A.V. Anisovich *et al.*, Eur. Phys. J. **A48**, 15 (2012).
45. A. Matsuyama, T. Sato, and T.-S.H. Lee, Phys. Reports **439**, 193 (2007).
46. T. Sato and T.-S.H. Lee, J. Phys. **G36**, 073001 (2009).
47. H. Kamano *et al.*, Phys. Rev. **C88**, 035209 (2013).
48. G.Y. Chen *et al.*, Phys. Rev. **C76**, 035206 (2007).
49. M. Döring *et al.*, Phys. Lett. **B681**, 26 (2009).
50. M. Döring *et al.*, Nucl. Phys. **A829**, 170 (2009).
51. D. Rönchen *et al.*, Eur. Phys. J. **A49**, 44 (2013).
52. S. Sarkar, E. Oset, and M.J. Vicente Vacas, Nucl. Phys. **A750**, 294 (2005) [Erratum-ibid. **A780**, 78 (2006)].

81. Baryon Magnetic Moments

Written 1994 by C.G. Wohl (LBNL).

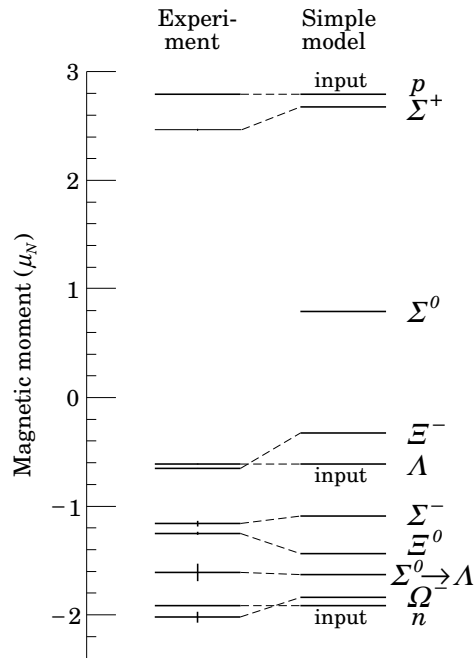
The figure below shows the measured magnetic moments of the stable baryons. It also shows the predictions of the simplest quark model, using the measured p , n , and Λ moments as input. In this model, the moments are [1]

$$\begin{aligned} \mu_p &= (4\mu_u - \mu_d)/3 & \mu_n &= (4\mu_d - \mu_u)/3 \\ \mu_{\Sigma^+} &= (4\mu_u - \mu_s)/3 & \mu_{\Sigma^-} &= (4\mu_d - \mu_s)/3 \\ \mu_{\Xi^0} &= (4\mu_s - \mu_u)/3 & \mu_{\Xi^-} &= (4\mu_s - \mu_d)/3 \\ \mu_\Lambda &= \mu_s & \mu_{\Sigma^0} &= (2\mu_u + 2\mu_d - \mu_s)/3 \\ & & \mu_{\Omega^-} &= 3\mu_s \end{aligned}$$

and the $\Sigma^0 \rightarrow \Lambda$ transition moment is

$$\mu_{\Sigma^0\Lambda} = (\mu_d - \mu_u)/\sqrt{3}.$$

The quark moments that result from this model are $\mu_u = +1.852\mu_N$, $\mu_d = -0.972\mu_N$, and $\mu_s = -0.613\mu_N$. The corresponding effective quark masses, taking the quarks to be Dirac point particles, where $\mu = q\hbar/2m$, are 338, 322, and 510 MeV. As the figure shows, the model gives a good first approximation to the experimental moments. For efforts to make a better model, we refer to the literature [2].



References:

1. See, for example, D.H. Perkins, *Introduction to High Energy Physics* (Addison-Wesley, Reading, MA, 1987), or D. Griffiths, *Introduction to Elementary Particles* (Harper & Row, New York, 1987).
2. See, for example, J. Franklin, Phys. Rev. **D29**, 2648 (1984); H.J. Lipkin, Nucl. Phys. **B241**, 477 (1984); K. Suzuki, H. Kumagai, and Y. Tanaka, Europhys. Lett. **2**, 109 (1986); S.K. Gupta and S.B. Khadkikar, Phys. Rev. **D36**, 307 (1987); M.I. Krivoruchenko, Sov. J. Nucl. Phys. **45**, 109 (1987); L. Brekke and J.L. Rosner, Comm. Nucl. Part. Phys. **18**, 83 (1988); K.-T. Chao, Phys. Rev. **D41**, 920 (1990) and references cited therein; Also, see references cited in discussions of results in the experimental papers..

82. Λ and Σ Resonances

Written December 2019 by V. Burkert (Jefferson Lab), E. Klempt (Bonn U.), U. Thoma (Bonn U.), L. Tiator (KPH, JGU Mainz) and R.L. Workman (George Washington U.).

82.1 Introduction

For several decades, there has been very little new experimental data bearing on the properties of Λ and Σ resonances. An exception was the study at JLab of the reactions $\gamma p \rightarrow K^+ \Sigma^\pm \pi^\mp$ and $\gamma p \rightarrow K^+ \Sigma^0 \pi^0$ [1], which established

the spin and parity of the $\Lambda(1405)$ [2]. There was also from BNL new data on the very low energy region of K^-p scattering [3–7]. Otherwise, the field is starved for data. Recent analyses (see below) have improved what we know about the *properties* of the known Λ and Σ resonances, but the *established* resonances are exactly the same ones that were in our 1984 edition [8]. The 1990 Review [9] gave a full report of the status then, and included Argand plots from the partial-wave analyses. The 2018 Review [10] has a short survey of the 1670 MeV region, which may in fact include three or four states – the well-established $J^P = \Sigma(1670)3/2^-$, the probable $\Sigma(1660)1/2^+$, and “bumps” at 1670 and 1690 MeV.

In the last few years, four groups have re-analyzed K^-p reactions using fuller collections of the old data. These analyses make an update of the status of the Λ and Σ resonances appropriate. Although they have not established any new resonances, they have provided at least some evidence for new states and have given a better understanding of the old ones.

Table I is our evaluation of the status, both over-all and channel by channel, of each Λ and Σ resonance in the Particle Listings. In making these evaluations, we considered, in addition to the four analyses just discussed, the ratings that predated them. The ratings use a 1- to 4-star system. The main Summary Table includes only established states with an overall status of 3 or 4 stars; as has already been noted, they are the same thirteen Λ and eight Σ resonances (above $\Sigma(1385)3/2^+$) that have long been in the Table. In addition, there are four 1-star and four 2-star Λ 's, and four 1-star and six 2-star Σ 's in the Particle Listings.

82.2 New analyses

The new analysis progress was pioneered by the Kent group which collected a large fraction of the available data and performed a comprehensive partial wave analysis [11, 12]. K^-p scattering into a pseudoscalar meson and an octet baryon is governed by two complex amplitudes; hence four quantities need to be measured to construct fully the amplitudes (up to an arbitrary phase per energy and angular bin). Discussions of complete experiments also generally assume perfect data (no experimental errors); realistic errors further complicate the task of amplitude extraction. Here, the available data are limited to the differential cross section and the target or hyperon recoil polarization P and partial-wave amplitudes are required. The authors of Ref. [11] overcame this difficulty by using start values for the partial wave amplitudes determined in [13] and/or from an energy-dependent fit and by freezing or releasing sets of amplitudes. The resulting amplitudes were fitted with a unitary multichannel parameterization [12].

The JPAC group presented a coupled-channel fit to the $\bar{K}N$ partial waves derived by the Kent group [14]. The JPAC approach was based on the K -matrix formalism. Special attention was paid to the analytical properties of the amplitudes determined by the square-root unitary branch points and the continuation to the complex angular momentum plane. The fit described the Kent partial waves reasonably well. However, when observables were calculated from their partial-wave amplitudes, significant discrepancies became apparent. The results were therefore not included in the RPP.

The ANL-Osaka group derived the energy-dependent amplitudes in fits to a large subset of the data collected in Ref. [11] and further data sets described in Ref. [15]. Their fits were based on a phenomenological SU(3) Lagrangian [15]. The two models agree on the leading contributions but differ significantly in cases with weaker candidates [16].

Table 82.1: The status of the Λ resonances. Only those with an overall status of *** or **** are included in the main Baryon Summary Table.

Particle	J^P	Overall status	Status as seen in –		
			$N\bar{K}$	$\Sigma\pi$	Other channels
$\Lambda(1116)$	$1/2^+$	****			$N\pi$ (weakly)
$\Lambda(1380)$	$1/2^-$	**	**	**	
$\Lambda(1405)$	$1/2^-$	****	****	****	
$\Lambda(1520)$	$3/2^-$	****	****	****	$\Lambda\pi\pi, \Lambda\gamma$
$\Lambda(1600)$	$1/2^+$	***	***	***	$\Lambda\pi\pi, \Sigma(1385)\pi$
$\Lambda(1670)$	$1/2^-$	****	****	****	$\Lambda\eta$
$\Lambda(1690)$	$3/2^-$	****	****	***	$\Lambda\pi\pi, \Sigma(1385)\pi$
$\Lambda(1710)$	$1/2^+$	**	**	*	
$\Lambda(1800)$	$1/2^-$	****	**	**	$\Lambda\pi\pi, \Sigma(1385)\pi, N\bar{K}^*$
$\Lambda(1810)$	$1/2^+$	**	**	**	$N\bar{K}_2^*$
$\Lambda(1820)$	$5/2^+$	****	****	****	$\Sigma(1385)\pi$
$\Lambda(1830)$	$5/2^-$	****	****	****	$\Sigma(1385)\pi$
$\Lambda(1890)$	$3/2^+$	****	****	**	$\Sigma(1385)\pi, N\bar{K}^*$
$\Lambda(2000)$	$1/2^-$	*	*	*	
$\Lambda(2050)$	$3/2^-$	*	*	*	$\Sigma(1385)\pi$
$\Lambda(2070)$	$3/2^+$	**	*	*	$\Sigma(1385)\pi$
$\Lambda(2080)$	$5/2^-$	**	**	*	$\Sigma(1385)\pi$
$\Lambda(2085)$	$7/2^+$	*	*	*	$\Sigma(1385)\pi$
$\Lambda(2100)$	$7/2^-$	****	****	**	$\Sigma(1385)\pi$
$\Lambda(2110)$	$5/2^+$	***	***	**	$\Lambda\omega, N\bar{K}^*$
$\Lambda(2325)$	$3/2^-$	*	*	*	$\Lambda\omega$
$\Lambda(2350)$	$9/2^+$	***	***	*	

Table 82.2: The status of the Σ resonances. Only those with an overall status of *** or **** are included in the main Baryon Summary Table.

Particle	J^P	Overall status	Status as seen in –		
			$N\bar{K}$	$\Lambda\pi$	$\Sigma\pi$
$\Sigma(1193)$	$1/2^+$	****			$N\pi$ (weakly)
$\Sigma(1385)$	$3/2^+$	****		****	****
$\Sigma(1620)$	$1/2^-$	**	**	*	**
$\Sigma(1660)$	$1/2^+$	***	***	***	***
$\Sigma(1670)$	$3/2^-$	****	****	****	****
$\Sigma(1730)$	$3/2^+$	*	*	*	*
$\Sigma(1750)$	$1/2^-$	***	***	**	***
$\Sigma(1775)$	$5/2^-$	****	****	****	**
$\Sigma(1880)$	$1/2^+$	**	**	*	
$\Sigma(1950)$	$1/2^-$	**	***	*	**
$\Sigma(1915)$	$5/2^+$	****	***	***	***
$\Sigma(1920)$	$3/2^-$	***	*	**	***
$\Sigma(1940)$	$3/2^+$	**	**	*	
$\Sigma(2010)$	$3/2^-$	*	*	*	
$\Sigma(2030)$	$7/2^+$	****	****	****	**
$\Sigma(2070)$	$5/2^+$	*	*	*	
$\Sigma(2080)$	$3/2^+$	**	**	**	
$\Sigma(2100)$	$7/2^-$	*	*	*	
$\Sigma(2110)$	$1/2^-$	**	***	***	**
$\Sigma(2160)$	$1/2^-$	*	*	*	*
$\Sigma(2230)$	$3/2^+$	**	**	*	*
$\Sigma(2250)$		***	***	*	*

The Bonn-Gatchina (BnGa) group added further (old) data to those analyzed in Ref. [11]. The data set was fitted in a modified K -matrix approach and the resulting amplitudes were compared with those from Refs. [11, 15]. New resonances were found; all resonances were tested for their statistical significance. Additional states with any set of quantum numbers were tested and were found to produce only small improvements in the fit [17]. In Ref. [18], properties of the full set of contributing hyperons were reported.

The star ratings of Λ and Σ resonances given in our earlier editions, and the new results from the Kent, ANL-Osaka and BnGa groups were used to update the star rating of the hyperon resonances. In [18], the overall star rating is directly estimated, for [12] we estimate the overall star rating from the branching-ratio errors. In [16], two solutions are given but no uncertainties for branching ratios. We call a resonance *seen* when it is seen in both solutions with similar properties.

We decided to remove the twelve so-called *bumps*, one 2-star resonance, $\Sigma(1580)3/2^-$, and three 1-star resonances $\Sigma(1770)1/2^+$, $\Sigma(1840)3/2^+$ and $\Sigma(2000)1/2^-$, which were not confirmed in any of the four modern analyses. Apart from $\Lambda(1380)1/2^-$, four further new resonances were included in the Listings: $\Lambda(2070)3/2^+$ and $\Lambda(2080)5/2^-$ with two stars, $\Sigma(2010)3/2^-$ and $\Sigma(2160)1/2^-$ with one star.

82.3 Sign conventions for resonance couplings

In terms of the isospin-0 and isospin-1 elastic scattering amplitudes A_0 and A_1 , the amplitude for $K^-p \rightarrow \bar{K}^0 n$ scattering is $\pm(A_1 - A_0)/2$, where the sign depends on conventions used in conjunction with the Clebsch-Gordan coefficients (such as, is the baryon or the meson the “first” particle). If this reaction is partial-wave analyzed and if the overall phase is chosen so that, say, the $\Sigma(1775)D_{15}$ amplitude at resonance points along the positive imaginary axis (points “up”), then any Σ at resonance will point “up” and any Λ at resonance will point “down” (along the negative imaginary axis). Thus the phase at resonance determines the isospin. The above ignores background amplitudes in the resonating partial waves.

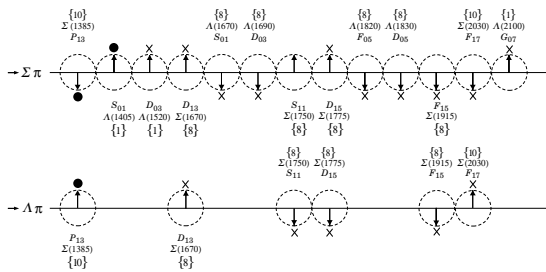


Figure 82.1: The signs of the imaginary parts of resonating amplitudes in the $\bar{K}N \rightarrow \Lambda\pi$ and $\Sigma\pi$ channels. The signs of the $\Sigma(1385)$ and $\Lambda(1405)$, marked with a \bullet , are set by convention, and then the others are determined relative to them. The signs required by the SU(3) assignments of the resonances are shown with an arrow, and the experimentally determined signs are shown with an \times .

That is the basic idea. In a similar but somewhat more complicated way, the phases of the $\bar{K}N \rightarrow \Lambda\pi$ and $\bar{K}N \rightarrow \Sigma\pi$ amplitudes for a resonating wave help determine the SU(3) multiplet to which the resonance belongs. Again, a convention has to be adopted for some overall arbitrary phases: which way is “up”? Our convention is that of Levi-Setti [19] and is shown in Fig. 82.1, which also compares experimental results with theoretical predictions for the signs of several resonances. In the Listings, a + or – sign in front of a measurement of an inelastic resonance coupling indicates the sign (the *absence* of a sign means that the sign is not determined, *not* that it is positive). Also other decay modes can be used to assign a hyperon to a SU(3) multiplet [20, 21]. Modern analyses determine properties of resonances at the pole position. In these analyses, the + or – sign is replaced by a phase. Background amplitudes can lead to significant phase shifts, and an additional phase shift due to rescattering is admitted in some analyses. Three Λ spin doublets can be identified as belonging to SU(3) singlets: the well-known ($\Lambda(1405)1/2^-$, $\Lambda(1520)3/2^-$), the ($\Lambda(2080)5/2^-$, $\Lambda(2100)7/2^-$), and ($\Lambda(2070)3/2^+$, $\Lambda(2110)5/2^+$).

82.4 The $\Lambda(1405)$

In coupled-channels calculations based on the chiral SU(3) effective field theory, the strongly attractive forces between $N\bar{K}$

and $\Sigma\pi$ generate five poles, one SU(3) singlet pole, two Λ octet poles and two octet Σ poles (see Section 100). At least three of them are seen in the 1300 to 1500 MeV mass range. The appearance of two Λ poles in this mass range, a narrow SU(3) octet at ~ 1420 MeV and a wider SU(3) singlet at ~ 1380 MeV, was unexpected. This approach has been pursued by a number of groups; for a summary of the results see our Review 100, “Pole Structure of the $\Lambda(1405)$ Region”. In the Listings, we have introduced the $\Lambda(1380)$ as a new candidate resonance (with two stars), named in accordance with its approximate pole position. The second SU(3) octet Λ state is the well-known $\Lambda(1670)$. The masses of the two associated Σ states are uncertain so far, and no new entries are introduced in the Listings.

In traditional approaches only one resonance was seen, the narrow state at 1405 MeV. It was reported to be the SU(3) singlet state a long time ago in Ref. [22], in contrast to the findings based on coupled-channels calculations within chiral SU(3) effective field theories and in agreement with the quark-model expectations. A recent analysis using a modified K -matrix approach found only one resonance, with a pole at (1422 ± 3) MeV [23]. Its SU(3) structure was found to be consistent with a singlet state. In the Listings, the $\Lambda(1405)$ has been retained with its traditional name. In quark models, this state is identified with the SU(3) singlet state, the two Λ octet states with $\Lambda(1670)$ and $\Lambda(1800)$, and the two Σ states with $\Sigma(1620)$ and $\Sigma(1750)$.

82.5 Errors on masses and widths

The errors quoted on resonance parameters from partial-wave analyses are often only statistical, and the parameters can change by more than these errors when a different parametrization of the waves is used. Furthermore, the different analyses use more or less the same data, so it is not really appropriate to treat the different determinations of the resonance parameters as independent or to average them together. In any case, the spread of the masses, widths, and branching fractions from the different analyses is certainly a better indication of the uncertainties than are the quoted errors. In the Listings, we usually give a range reflecting the spread of the values rather than a particular value with error.

82.6 Production experiments

Partial-wave analyses of course separate partial waves, whereas a peak in a cross section or an invariant mass distribution usually cannot be disentangled from background and analyzed for its quantum numbers; and more than one resonance may be contributing to the peak. The $\Sigma(1385)$ and $\Lambda(1405)$ lie below the $\bar{K}N$ threshold and nearly everything about $\Sigma(1385)$ is learned from production experiments. Our knowledge on $\Lambda(1405)$ benefits greatly from photoproduction of the three $\Sigma\pi$ charge states [1, 2] and from the precise measurement of the energy shift and width of the kaonic hydrogen atom [24].

Production and formation experiments agree quite well in the case of $\Lambda(1520)$ and results have been combined. Above this mass, no new results on peak hunting have been reported for about 40 years. For these early results, we refer the reader to our earlier editions. In photoproduction with energetic photons [25, 26] or at LHCb [27], hyperons are produced abundantly. So far, no attempt has been made to extract hyperon properties from these data. New data on hyperon spectroscopy can be expected from J-PARC [28], JLAB [29], and the forthcoming PANDA experiment [30].

References

- [1] K. Moriya *et al.* (CLAS), Phys. Rev. **C87**, 3, 035206 (2013), [arXiv:1301.5000].
- [2] K. Moriya *et al.* (CLAS), Phys. Rev. Lett. **112**, 8, 082004 (2014), [arXiv:1402.2296].
- [3] A. Starostin *et al.* (Crystal Ball), Phys. Rev. **C64**, 055205 (2001).
- [4] S. Prakhov *et al.*, Phys. Rev. **C69**, 042202 (2004).
- [5] S. Prakhov *et al.* (Crystal Ball), Phys. Rev. **C70**, 034605 (2004).

- [6] R. Manweiler *et al.*, Phys. Rev. **C77**, 015205 (2008).
- [7] S. Prakhov *et al.*, Phys. Rev. **C80**, 025204 (2009), [arXiv:0812.1888].
- [8] C. G. Wohl *et al.* (Particle Data Group), Rev. Mod. Phys. **56**, S1 (1984).
- [9] J. J. Hernandez *et al.* (Particle Data Group), Phys. Lett. **B239**, 1 (1990), [Erratum: Phys. Lett.B253,524(1991)].
- [10] M. Tanabashi *et al.* (Particle Data Group), Phys. Rev. **D98**, 3, 030001 (2018).
- [11] H. Zhang *et al.*, Phys. Rev. **C88**, 3, 035204 (2013), [arXiv:1305.3598].
- [12] H. Zhang *et al.*, Phys. Rev. **C88**, 3, 035205 (2013), [arXiv:1305.4575].
- [13] J. Tulpan, Kent State University, 3, 035205 (2008), [arXiv:1305.4575].
- [14] C. Fernandez-Ramirez *et al.*, Phys. Rev. **D93**, 3, 034029 (2016), [arXiv:1510.07065].
- [15] H. Kamano *et al.*, Phys. Rev. **C90**, 6, 065204 (2014), [arXiv:1407.6839].
- [16] H. Kamano *et al.*, Phys. Rev. **C92**, 2, 025205 (2015), [Erratum: Phys. Rev.C95,no.4,049903(2017)], [arXiv:1506.01768].
- [17] M. Matveev *et al.*, Eur. Phys. J. **A55**, 10, 179 (2019), [arXiv:1907.03645].
- [18] A. V. Sarantsev *et al.*, Eur. Phys. J. **A55**, 10, 180 (2019), [arXiv:1907.13387].
- [19] R. Levi Setti, Conf. Proc. **C690625**, 339 (1969).
- [20] V. Guzey and M. V. Polyakov, Annalen Phys. **13**, 673 (2004).
- [21] V. Guzey and M. V. Polyakov (2005), [hep-ph/0512355].
- [22] R. D. Tripp *et al.*, Phys. Rev. Lett. **21**, 1721 (1968).
- [23] A. V. Anisovich *et al.* (2019), [arXiv:1905.05456].
- [24] M. Bazzi *et al.* (SIDDHARTA), Phys. Lett. **B704**, 113 (2011), [arXiv:1105.3090].
- [25] K. Moriya *et al.* (CLAS), Phys. Rev. **C88**, 045201 (2013), [Addendum: Phys. Rev.C88,no.4,049902(2013)], [arXiv:1305.6776].
- [26] B. Dey *et al.* (CLAS), Phys. Rev. **C89**, 5, 055208 (2014), [Addendum: Phys. Rev.C90,no.1,019901(2014)], [arXiv:1403.2110].
- [27] R. Aaij *et al.* (LHCb), Phys. Rev. Lett. **115**, 072001 (2015), [arXiv:1507.03414].
- [28] K. Hicks and H. Sako (Crystall Ball), Proposal for J-PARC E45 **C70**, 034605 (2013).
- [29] S. Adhikari *et al.* (Crystall Ball), Proposal for JLAB PAC47 **C70**, 034605 (2019).
- [30] F. Iazzi (PANDA), AIP Conf. Proc. **1743**, 1, 050006 (2016).

83. Pole Structure of the $\Lambda(1405)$ Region

Written August 2019 by Ulf-G. Meißner (Bonn Univ. / FZ Jülich) and Tetsuo Hyodo (Tokyo Metropolitan Univ.).

The $\Lambda(1405)$ resonance emerges in the meson-baryon scattering amplitude with the strangeness $S = -1$ and isospin $I = 0$. It is the archetype of what is called a dynamically generated resonance, as pioneered by Dalitz and Tuan [1]. The most powerful and systematic approach for the low-energy regime of the strong interactions is chiral perturbation theory (ChPT), see e.g. Ref. 2. A perturbative calculation is, however, not applicable to this sector because of the existence of the $\Lambda(1405)$ just below the $\bar{K}N$ threshold. In this case, ChPT has to be combined with a non-perturbative resummation technique, just as in the case of the nuclear forces. By solving the Lippmann-Schwinger equation with the interaction kernel determined by ChPT and using a particular regularization, in Ref. 3 a successful description of the low-energy K^-p scattering data as well as the mass distribution of the $\Lambda(1405)$ was achieved (for further developments, see Ref. 4 and references therein).

The study of the pole structure was initiated by Ref. 5, which finds two poles of the scattering amplitude in the complex energy plane between the $\bar{K}N$ and $\pi\Sigma$ thresholds. The spectrum in experiments exhibits one effective resonance shape, while the existence of two poles results in the reaction-dependent lineshape [6]. The origin of this two-pole structure is attributed to the two attractive channels of the leading order interaction in the SU(3) basis (singlet and octet) [6] and in the isospin basis ($\bar{K}N$ and $\pi\Sigma$) [7]. It is remarkable that the sign and the strength of the leading order interaction is determined by a low-energy theorem of chiral symmetry, i.e. the so-called Weinberg-Tomozawa term. The two-pole nature of the $\Lambda(1405)$ is qualitatively different from the case of the N(1440) resonance. Two poles of the N(1440) appear on different Riemann sheets of the complex energy plane separated by the $\pi\Delta$ branch point. These poles reflect a single state, with a nearby pole and a more distant shadow pole. In contrast, the two poles in the $\Lambda(1405)$ region on the same Riemann sheet (where $\pi\Sigma$ channels are unphysical and all other channels physical, correspondingly to the one, connected to the real axis between the $\pi\Sigma$ and $\bar{K}N$ thresholds) are generated from two attractive forces mentioned above [6,7].

Recently, various new experimental results on the $\Lambda(1405)$ have become available [4]. Among these, the most striking measurement is the precise determination of the energy shift and width of kaonic hydrogen by the SIDDHARTA collaboration [8,9], which provides a quantitative and stringent constraint on the K^-p amplitude at threshold through the improved Deser formula [10]. Systematic studies with error analyses based on the next-to-leading order ChPT interaction including the SIDDHARTA constraint have been performed by various groups [11–15]. All these studies confirm that the new kaonic hydrogen data are compatible with the scattering data above threshold.

The results of the pole positions of $\Lambda(1405)$ in the various approaches are summarized in Table 83.1. We may regard the difference among the calculations as a systematic error, which stems from the various approximations of the Bethe-Salpeter equation, the fitting procedure, and also the inclusion of SU(3) breaking effects such as the choice of the various meson decay constants, and so on. A detailed comparison of the various approaches that enter the table is given in Ref. 16. A recent analysis including also the $J^P = 1/2^+$ P-wave contribution (and also an explicit $\Sigma(1385)$ $3/2^+$ state) gives results consistent with the findings reported above, with the pole positions at $(1364 - i43)$ MeV and $(1430 - i15)$ MeV, respectively [17].

The main component for the $\Lambda(1405)$ is the pole 1, whose position converges within a relatively small region near the $\bar{K}N$ threshold. On the other hand, the position of the pole 2 shows a sizeable scatter. Detailed studies of the $\pi\Sigma$ spectrum in various reaction processes, together with the precise experimental lineshape (see e.g. the recent precise photoproduction data from the LEPS collaboration [18] and from the CLAS collaboration [19,20], electroproduction data from the CLAS collaboration [21], and proton-proton collision data from COSY [22] and the HADES collaboration [23]), will shed light on the position of the second pole. The $\pi\Sigma$ spectra from the CLAS data are analyzed in Ref. 24 and Ref. 15. It was shown in Ref. 15 that

several solutions, which agree with the scattering data, are ruled out if confronted with the recent CLAS data. The remaining solutions are collected as solution #2 and solution #4 in Table 83.1. The HADES data are analyzed in Ref. 25 and Ref. 26. Although the result of the pole found in Ref. 25 is not compatible with other results, the authors of Ref. 26 invoke the anomalous triangle singularity mechanism to argue that the invariant mass distribution of the $\pi\Sigma$ system is found at lower masses than in other reactions. It is thus desirable to perform more comprehensive analyses of $\pi\Sigma$ spectra together with the systematic error analysis of the scattering data.

Table 83.1: Comparison of the pole positions of $\Lambda(1405)$ in the complex energy plane from next-to-leading order chiral unitary coupled-channel approaches including the SIDDHARTA constraint. The lower two results also include the CLAS photoproduction data.

approach	pole 1 [MeV]	pole 2 [MeV]
Refs. 11,12, NLO	$1424^{+7}_{-23} - i 26^{+3}_{-14}$	$1381^{+18}_{-6} - i 81^{+19}_{-8}$
Ref. 14, Fit II	$1421^{+3}_{-2} - i 19^{+8}_{-5}$	$1388^{+9}_{-9} - i 114^{+24}_{-25}$
Ref. 15, solution #2	$1434^{+2}_{-2} - i 10^{+2}_{-1}$	$1330^{+4}_{-5} - i 56^{+17}_{-11}$
Ref. 15, solution #4	$1429^{+8}_{-7} - i 12^{+2}_{-3}$	$1325^{+15}_{-15} - i 90^{+12}_{-18}$

References:

1. R.H. Dalitz, S.F. Tuan Phys. Rev. Lett. **2**, 425 (1959).
2. V. Bernard *et al.*, Int. J. Mod. Phys. **E4**, 193 (1995).
3. N. Kaiser *et al.*, Nucl. Phys. **A594**, 325 (1995).
4. T. Hyodo, D. Jido, Prog. in Part. Nucl. Phys. **67**, 55 (2012).
5. J.A. Oller, U.-G. Meißner, Phys. Lett. **B500**, 263 (2001).
6. D. Jido *et al.*, Nucl. Phys. **A725**, 181 (2003).
7. T. Hyodo, W. Weise, Phys. Rev. **C77**, 035204 (2008).
8. M. Bazzi *et al.*, Phys. Lett. **B704**, 113 (2011).
9. M. Bazzi *et al.*, Nucl. Phys. **A881**, 88 (2012).
10. U.-G. Meißner *et al.*, Eur. Phys. J. **C35**, 349 (2004).
11. Y. Ikeda *et al.*, Phys. Lett. **B706**, 63 (2011).
12. Y. Ikeda *et al.*, Nucl. Phys. **A881**, 98 (2012).
13. M. Mai, U.-G. Meißner, Nucl. Phys. **A900**, 51 (2013).
14. Z.-H. Guo, J. Oller, Phys. Rev. **C87**, 035202 (2013).
15. M. Mai, U.-G. Meißner, Eur. Phys. J. **A51**, 30 (2015).
16. A. Cieply *et al.*, Nucl. Phys. **A954**, 17 (2016).
17. D. Sadasivan *et al.*, Phys. Lett. **B789**, 329 (2019).
18. M. Niiyama *et al.*, Phys. Rev. **C78**, 035202 (2008).
19. K. Moriya *et al.*, Phys. Rev. **C87**, 035206 (2013).
20. K. Moriya *et al.*, Phys. Rev. Lett. **112**, 082004 (2014).
21. H.Y. Lu *et al.*, Phys. Rev. **C88**, 045202 (2013).
22. I. Zychor *et al.*, Phys. Lett. **B660**, 167 (2008).
23. G. Agakishiev *et al.*, Phys. Rev. **C87**, 025201 (2013).
24. L. Roca, E. Oset, Phys. Rev. **C87**, 055201 (2013).
25. M. Hassanvand *et al.*, Phys. Rev. **C87**, 055202 (2013).
26. M. Bayar *et al.*, Phys. Rev. **C97**, 035203 (2018).

84. Charmed Baryons

Revised in part June 2020 by D.J. Robinson (LBNL).

84.1 Spectrum

Similar to the light baryons, the naming convention for charmed baryon base symbols is determined by their isospin, I , and charm-strangeness, $C+S$, quantum numbers: In particular, Λ_c , Σ_c , Ξ_c , Ω_c and $\Omega_{c,cc,ccc}$ with $I(C+S) = 0(1), 1(1), 1/2(2)$ and $0(3)$, respectively. While this review considers only the charmed baryons, approximate heavy quark flavor symmetry implies the spectroscopy of the bottom baryons is expected to be similar, up to corrections

of order $\Lambda_{\text{QCD}}/m_{c,b}$.

Figure 84.1(a) shows the spectrum of the singly-charmed baryons: There are now 36 such established states. In the quark model picture (see the *Quark Model* review), states consistent with all singly-charmed ground-state (zero angular momentum, or S -wave, state) baryons have been discovered, along with many excited states. The $\Lambda_c(2860)$ and the five heaviest Ω_c^0 's are recent, intriguing discoveries. The spin-parity quantum numbers of the latter are currently unknown, but one may speculate they correspond to the five ssc excited baryons in a P -wave state, although other interpretations are also possible and plausible.

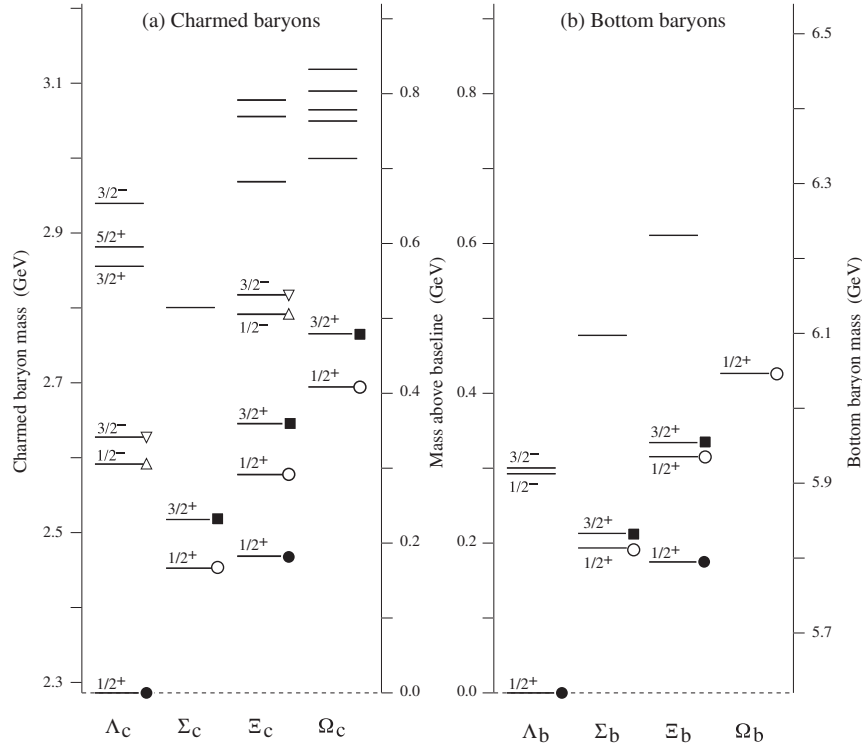


Figure 84.1: (a) The spectrum of established singly-charmed baryons, with their J^P assignments (where known). In accordance with their isospin, the Σ_c (Ξ_c) lines each correspond to three (two) charged or neutral states that are nearly degenerate, with the exception of the upper two Ξ_c lines for which only the charged state has been found. Unique flavor $SU(3)$ representations are shown by various filled and open symbols: The three $J^P = 3/2^+$ ($J^P = 1/2^+$) lines marked with a filled square (open circle) fill a ground-state $\mathbf{6}$ of flavor $SU(3)$; the two $J^P = 1/2^+$ ($1/2^-$ and $3/2^-$) lines marked by a filled circle (open triangles) fill a ground-state (excited-state) $\mathbf{\bar{3}}$. Fig 84.1(b) shows a similar spectrum for several known bottom baryons.

84.2 Flavor symmetry

Just as for the light mesons and baryons, approximate flavor $SU(3)$ symmetry of the light quarks – the u , d , and s – is expected to relate matrix elements of charmed baryons belonging to the same multiplet, up to corrections of order $(m_s - m_d)/\Lambda_{\text{QCD}} \sim 20\%$. (Similarly, isospin relations should hold to the percent level.) This includes Gell-Mann-Okubo mass relations – a set of linear combinations of masses that must vanish up to higher-order $SU(3)$ -breaking corrections – as well as similar relations between matrix elements for charmed baryon multibody decays. These relations may be constructed order-by-order in the appropriate symmetry-breaking parameters.

For singly-charmed baryons with valence quarks $q_1 q_2 c$, the flavor $SU(3)$ tensor product of the two light quarks $\mathbf{3} \times \mathbf{3} = \mathbf{6} + \mathbf{\bar{3}}$. For ground-state baryons, the overall antisymmetry of baryon wavefunction requires the light diquark to either form a spin-0 color antitriplet, antisymmetric under the interchange of the two light quark flavors – i.e. the $\mathbf{\bar{3}}$ – or a spin-1 color antitriplet that is symmetric under this interchange – i.e. the $\mathbf{6}$. The spin-0 $\mathbf{\bar{3}}$ can only combine with the charm quark to form $J^P = 1/2^+$ states, while the spin-1 $\mathbf{6}$ can combine to form states either $J^P = 1/2^+$ or $J^P = 3/2^+$. States consistent with the corresponding $\mathbf{\bar{3}}$ and

two $\mathbf{6}$ $SU(3)$ representations are denoted in Figure 84.1 by filled circles, open circles and filled squares, respectively. In Fig. 84.2 we show the explicit contents of the $\mathbf{\bar{3}}$ and $\mathbf{6}$ ground-state representations. The singly-charmed baryons within each multiplet obey isospin and $SU(3)$ mass relations at the expected orders.

Excited singly-charmed baryon states may arise as higher orbital angular momentum states. For instance, for such a baryon in a P -wave state, the allowed spin-flavor representations for the light diquark are either a spin-1 $\mathbf{\bar{3}}$ or a spin-0 $\mathbf{6}$. Combined with the charm quark, the $\mathbf{\bar{3}}$ can then generate $J^P = 1/2^-, 3/2^-$ or $5/2^-$ states: States consistent with the $1/2^-$ and $3/2^-$ $\mathbf{\bar{3}}$ representations are indicated in Figure 84.1 by open triangles. (One might speculate that the $J^P = 5/2^-$ $\mathbf{\bar{3}}$ could be composed of the claimed $\Lambda_c(2765)$ – not shown in the figure – and the $\Xi_c(2930)$.) Note that excited states might also arise from hadronic ‘molecule’ or pentaquark type states, $\sim qq\bar{q}c$, which may generate baryons in higher $SU(3)$ representations.

To extend this discussion to doubly or triply charmed baryons, or charmless baryons, it is convenient to embed the baryons into flavor $SU(4)$, in which u , d , s and c transform as a $\mathbf{4}$. Flavor $SU(4)$ is heavily broken, and is not a good approximate symmetry of QCD. However, under the decomposition $SU(4) \rightarrow SU(3) \times$

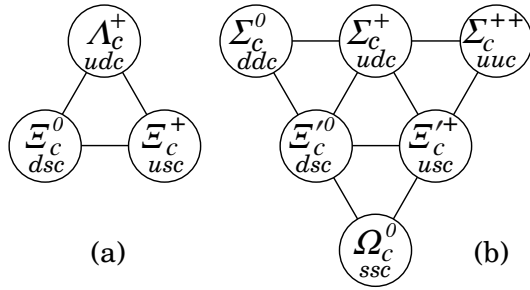


Figure 84.2: The $SU(3)$ $\bar{\mathbf{3}}$ (a) and $\mathbf{6}$ (b) ground-state $J^P = 1/2^+$ representations. The $\mathbf{6}$ ground-state with $J^P = 3/2^+$ is identical in structure to the right-hand figure.

$U(1)_{\text{charm}}$, it does provide a useful bookkeeping scheme for the various flavor $SU(3)$ multiplets with different numbers of valence charm quarks.

For instance, for charmed baryons with three quarks, the tensor product $\mathbf{4} \times \mathbf{4} \times \mathbf{4} = \mathbf{20}_S + \mathbf{20}_M + \mathbf{20}_M + \bar{\mathbf{4}}$.¹ The spin-flavor representation of a ground-state baryon must be fully symmetric, so that ground-state baryons may belong to the $\mathbf{20}_S$ and a single combination of the two $\mathbf{20}_M$'s, with spin and parity $J^P = 3/2^+$ and $J^P = 1/2^+$, respectively. The $\bar{\mathbf{4}}$, however, is fully antisymmetric in flavor indices, and one cannot form the required fully antisymmetrized spin state from three quarks each with two possible spin configurations. This can be also understood directly in terms of the $SU(8)$ contracted spin-flavor group: The only fully symmetric irreducible representation contained in $\mathbf{8} \times \mathbf{8} \times \mathbf{8}$ is the $\mathbf{120}$, which contains a $(\mathbf{20}_S, \mathbf{4})$ and a $(\mathbf{20}_M, \mathbf{2})$ with respect to $SU(4) \times SU(2)_{\text{spin}}$.

The decompositions $\mathbf{20}_S \rightarrow \mathbf{10}_0 + \mathbf{6}_1 + \bar{\mathbf{3}}_2 + \mathbf{1}_3$ and $\mathbf{20}_M \rightarrow \mathbf{8}_0 + \mathbf{6}_1 + \bar{\mathbf{3}}_1 + \mathbf{3}_2$, where the subscript indicates charm number, indicates the expected flavor $SU(3)$ multiplets for each value of charm number in the ground-state baryons. Fig. 84.3(a) shows the $\mathbf{20}_S$ representation, in which each charm number layer in the decomposition to $SU(3) \times U(1)_{\text{charm}}$ is shaded in yellow. The bot-

tom $c = 0$ level is the $J^P = 3/2^+$ flavor $SU(3)$ baryon decuplet containing the $\Delta(1232)$. Fig. 84.3(b) shows the $\mathbf{20}_M$ representation, whose bottom $c = 0$ level is the $1/2^+$ $SU(3)$ light baryon octet, containing the nucleons.

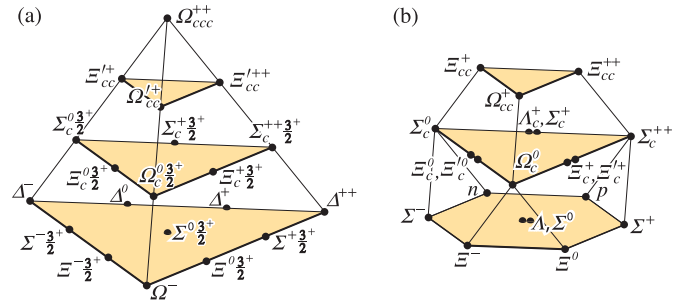


Figure 84.3: (a) The $J^P = 3/2^+$ flavor $SU(4)$ ground-state charmed baryons in the $\mathbf{20}_S$, with the flavor $SU(3)$ baryon decuplet on the lowest level. (b) The $J^P = 1/2^+$ ground-state charmed baryons in the $\mathbf{20}_M$ -plet with the flavor $SU(3)$ baryon octet on the lowest level. In some conventions, the states with a “ $\frac{3}{2}^+$ ” label are instead denoted with a * superscript to distinguish them from the $J^P = 1/2^+$ states.

Of the doubly charmed baryons, only the Ξ_{cc}^{++} has been discovered, though its spin-parity is unknown. For excited baryons in, e.g., a P -wave state, the same contracted spin-flavor analysis implies that there are excited baryon states in, e.g., a $\mathbf{20}_M$ with $J^P = 1/2^-$ or a $\bar{\mathbf{4}}$ with $J^P = 3/2^-$, which together fill the fully antisymmetric $\mathbf{56}$ of $SU(8)$. The $\bar{\mathbf{4}}$ decomposes into $\bar{\mathbf{3}}_1 + \mathbf{1}_0$, consistent with the $3/2^-$ singly-charmed $\bar{\mathbf{3}}$'s denoted by open triangles in Fig. 84.1(a). Just as for flavor $SU(3)$, excited state $\mathbf{20}_{S,M}$ and $\bar{\mathbf{4}}$ representations may also arise with other spin-parity assignments, and higher representations may also be present.

References

[1] R. Slansky, Phys. Rept. **79**, 1 (1981).

¹ More generally, for $SU(N)$, $N \times N \times N = [N(N+1)(N+2)/6] + 2 \times [N(N^2-1)/3] + [N(N-1)(N-2)/6]$. The $\mathbf{20}_S$, $\mathbf{20}_M$ and $\bar{\mathbf{4}}$ correspond to the representations with Dynkin labels $(3, 0, 0)$, $(1, 1, 0)$ and $(0, 0, 1)$, respectively. See Ref. [1] for a review.

85. Pentaquarks

Revised September 2019 by M. Karliner (Tel Aviv U.) and T. Skwarnicki (Syracuse U.).

Experimental searches for pentaquark hadrons comprised of light flavors have a long and vivid history. No undisputed candidates have been found in 50 years. The first wave of observations of pentaquark candidates containing a strange antiquark occurred in the early seventies, see e.g. a review in the 1976 edition of Particle Data Group listings for $Z_0(1780)$, $Z_0(1865)$ and $Z_1(1900)$ [1]. The last mention of these candidates can be found in the 1992 edition [2] with the perhaps prophetic comment “the results permit no definite conclusion - the same story for 20 years. [...] The skepticism about baryons not made of three quarks, and lack of any experimental activity in this area, make it likely that another 20 years will pass before the issue is decided.” A decade later, a second wave of observations occurred, possibly motivated by specific theoretical predictions for their existence [3–5]. The evidence for pentaquarks was based on observations of peaks in the invariant mass distributions of their decay products. More data, or more sensitive experiments did not confirm these claims [6]. In the last mention of the best known candidate from that period, $\Theta(1540)^+$, the 2006 Particle Data Group listing [7] included a statement: “The conclusion that pentaquarks in general, and that Θ^+ , in particular, do not exist, appears compelling.” which well reflected the prevailing mood in the particle physics community until a study of $\Lambda_b^0 \rightarrow J/\psi p K^-$ ($J/\psi \rightarrow \mu^+ \mu^-$) decays by LHCb [8] (charge conjugate modes are implied). From an analysis of 3 fb $^{-1}$ Run 1 data at 7 and 8 TeV at the LHC, the LHCb collaboration reported a significant $J/\psi p$ structure in $\Lambda_b^0 \rightarrow J/\psi p K^-$ decays [8]. The exotic character of this structure, with the minimal quark content of $uudc\bar{c}$, was demonstrated in a nearly model-independent way in Ref. [9], where it was shown that the $J/\psi p$ mass ($m_{J/\psi p}$) peak near 4450 MeV was too narrow to be accounted for by $\Lambda^* \rightarrow p K^-$ reflections (Λ^* denotes a generic Λ excitation), reinforcing the results from the earlier model-dependent six-dimensional amplitude analysis of invariant masses and decay angles describing the Λ_b^0 decay in the same data [8]. Even though not apparent from the $m_{J/\psi p}$ distribution, the amplitude analysis also required a second broad $J/\psi p$ state to obtain a good description of the data, which peaked at $4380 \pm 8 \pm 29$ MeV with a width of $205 \pm 18 \pm 86$ MeV and a fit fraction of $(8.4 \pm 0.7 \pm 4.2)\%$.

The LHCb 6 fb $^{-1}$ Run 2 LHC data at 13 TeV, together with the improvements in the data selection for both runs, resulted in a nine-fold increase in the number of reconstructed $\Lambda_b^0 \rightarrow J/\psi p K^-$ decays [10]. When fit with the same six-dimensional amplitude model, the enlarged data sample gives consistent results for the $P_c(4450)^+$ and $P_c(4380)^+$ parameters, corroborating the compatibility of the data samples. However, the two-state interpretation of the data is contradicted by the observation of new narrow $J/\psi p$ structures which are too faint to have been significant in the Run 1 data analysis. Second horizontal band is observed in the Dalitz plot (Fig. 85.1) near 4312 MeV in the $J/\psi p$ mass. The 4450 MeV structure also appears to consist of two narrower peaks at 4440 and 4457 MeV. Performing a rigorous six-dimensional amplitude analysis of these faint $J/\psi p$ structures is challenging and has not been accomplished yet. Fortunately, the newly observed peaks are so narrow that it is not necessary to construct an amplitude model to prove that these states are not artifacts of interfering Λ^* resonances, as was previously demonstrated in Ref. [9]. Their masses and widths have been characterized by the LHCb (see Table 85.1) from one-dimensional fits to $J/\psi p$ mass distributions, with different levels of suppression of the Λ^* contributions, which peak at the lower $p K^-$ masses (Fig. 85.1). Such analysis is not sensitive to any broad $J/\psi p$ contributions like $P_c(4380)^+$. The histograms analyzed by the LHCb are available in tabular form at <https://www.hepdata.net/record/89271>.

The fit chosen by the LHCb for the central mass and width values is displayed in Fig. 85.2. The $P_c(4312)^+$ state peaks right below the $\Sigma_c^+ \bar{D}^0$ threshold and has statistical significance over 7.6σ . The $P_c(4457)^+$ state peaks right below the $\Sigma_c^+ \bar{D}^{*0}$ threshold, while the $P_c(4440)^+$ state peaks about 20 MeV below it. The significance of the two-peak versus one-peak hypothesis for the 4450 MeV structure is over 5.4σ , rendering the single peak in-

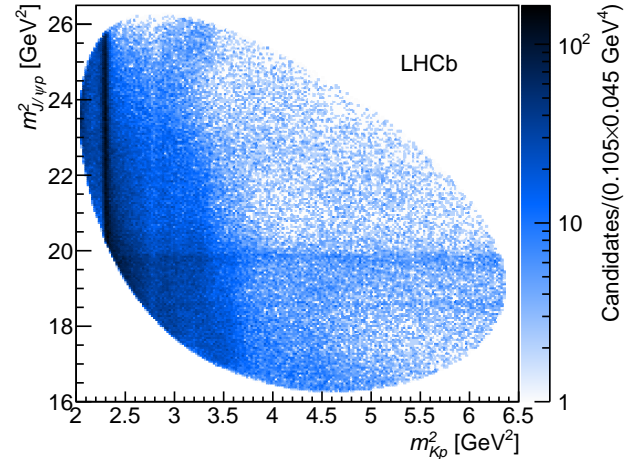


Figure 85.1: Dalitz plot distributions for $\Lambda_b^0 \rightarrow J/\psi p K^-$ decays as observed by LHCb.

terpretation of this region obsolete. The six-dimensional amplitude analysis reported in Ref. [8], which provided evidence for the $P_c(4380)^+$ state, is obsolete since it used the single $P_c(4450)^+$ state and it lacked the $P_c(4312)^+$ state. Therefore, the previously reported evidence for the $P_c(4380)^+$ state is weakened, but not contradicted, since the new one-dimensional analysis by LHCb is not sensitive to wide P_c^+ states. Even if this state exists, any preferences for its quantum numbers [8], which were reported without statistical or systematic significances, are even more uncertain now. An in-depth discussion of the relevant issues is provided in Supplemental Material of Ref. [10]. The LHCb results from the six-dimensional amplitude analysis of the Cabibbo suppressed channel $\Lambda_b^0 \rightarrow J/\psi p \pi^-$ [11], which contain a statistically marginal evidence for the sum of the P_c^+ and the $Z_c(4200)^-$ contributions, took extensive input from Ref. [8], and should be treated with caution until the both amplitude analyses are completed on the enlarged data sets.

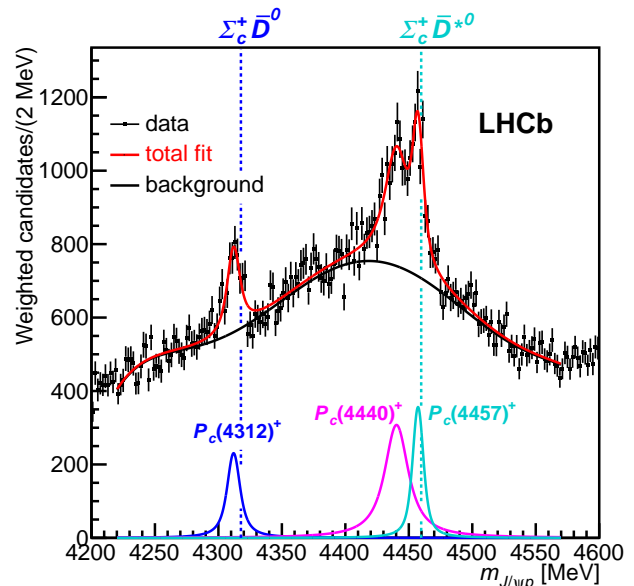


Figure 85.2: Fit to the $J/\psi p$ mass distribution, in which events were weighted to suppress $\Lambda^* \rightarrow p K^-$ backgrounds, of three Breit-Wigner functions and a sixth-order polynomial background. This fit was used to determine the central values of the masses and widths of the P_c^+ states reported by LHCb. The mass thresholds for the $\Sigma_c^+ \bar{D}^0$ and $\Sigma_c^+ \bar{D}^{*0}$ final states are superimposed.

While $\Sigma_c \bar{D}^{(*)}$ states had been predicted [12–15] before the first

Table 85.1: Summary of the narrow P_c^+ properties, interpreted as Breit-Wigner resonances. The central values are based on the fit displayed in Fig. 85.2.

State	M [MeV]	Γ [MeV] (95% CL)	\mathcal{R} [%]
$P_c(4312)^+$	$4311.9 \pm 0.7^{+6.8}_{-0.6}$	$9.8 \pm 2.7^{+3.7}_{-4.5}$ (< 27)	$0.30 \pm 0.07^{+0.34}_{-0.09}$
$P_c(4440)^+$	$4440.3 \pm 1.3^{+4.1}_{-4.7}$	$20.6 \pm 4.9^{+8.7}_{-10.1}$ (< 49)	$1.11 \pm 0.33^{+0.22}_{-0.10}$
$P_c(4457)^+$	$4457.3 \pm 0.6^{+4.1}_{-1.7}$	$6.4 \pm 2.0^{+5.7}_{-1.9}$ (< 20)	$0.53 \pm 0.16^{+0.15}_{-0.13}$

LHCb results [8], after these results became known, many theoretical groups interpreted the $P_c(4450)^+$ and $P_c(4380)^+$ states in terms of diquarks and triquarks as building blocks of a compact pentaquark [16–22], or even of states below the lowest threshold for spontaneous dissociation [23]. In the first implementation of this approach [16], the pentaquark mass splitting was generated mostly by the change of angular momentum between the sub-components (L) from zero to one, which would also make the heavier state narrower and of opposite parity. Explicit modeling of multi-quark systems [24] questions if centrifugal barrier factor provides enough width suppression via spatial separation of c and \bar{c} quarks at these masses, as the phase space for $J/\psi p$ decay is very large (more than 400 MeV). Also, the observed mass splitting was too small to be only due to the mechanism proposed in Ref. [16] and required fine-tuning of such models. A variation of this model, in which the heavy (cu) diquark couples with heavy \bar{c} to form colored triquark attracting the light diquark (ud), has been re-implemented for the narrow P_c^+ states [25]. In this model, the $P_c(4440)^+$ and $P_c(4457)^+$ states are accommodated via spin-orbit interactions for the $L = 1$ states, while the $P_c(4312)^+$ is one of the $L = 0$ states. However, the mass prediction for the latter is off by (-72 ± 29) MeV [25]. This work has recently been extended to $SU(3)_F$ [26]. The width dilemma becomes more severe in view of the narrow widths of the newly observed states (Table 85.1), especially for the $L = 0$ $P_c(4312)^+$ state, and requires a different origin of potential barrier between c and \bar{c} than angular momentum [25, 27], which remains a subject of theoretical controversy.

More effective width suppression mechanism is offered by a loosely bound charmed baryon-anticharmed meson molecular model, in which c and \bar{c} can be separated by much larger distances, resulting in a smaller probability of them getting close enough to each other in order to make a J/ψ . Since molecular binding energy cannot be large, such molecules are in S -wave and their masses must be near the sum of the baryon and meson masses [15]. The mass coincidence of the $P_c(4312)^+$ and of $P_c(4457)^+$ states, with the two related thresholds, $\Sigma_c^+ \bar{D}^0$ and $\Sigma_c^+ \bar{D}^{*0}$, provides very strong experimental evidence in favor of this interpretation. Given how close $P_c(4312)^+$ is to the $\Sigma_c^+ \bar{D}^0$ threshold, it might be a virtual rather than a bound state [28]. It is worth stressing that other baryon-meson combinations, $\Lambda_c^{(*)+} \bar{D}^{(*)0}$ and $\chi_{cJ} p$ are not expected to bind [12, 29]. Since the spins of Σ_c^+ and of \bar{D}^{*0} can be combined in two different ways, the third narrow $P_c(4440)^+$ peak also finds natural explanation in this model, and cannot be a virtual state since it is sufficiently below the $\Sigma_c^+ \bar{D}^{*0}$ threshold. Additional states at, or below, the $\Sigma_c^{*+} \bar{D}$ and $\Sigma_c^{*+} \bar{D}^*$ thresholds, are expected [30–32]. Since Σ_c^{*+} width is likely around 15 MeV [33], more than the width of either $P_c(4312)^+$ or $P_c(4457)^+$, it is important to keep in mind that a molecule's width cannot be smaller than the sum of its constituents' widths [34–36]. For a recent review on hadronic molecules, see [37].

It is useful to consider the $P_c(4312)^+$, $P_c(4440)^+$ and $P_c(4457)^+$ narrow pentaquarks together with several analogous exotic states with hidden charm and bottom in the meson sector. This provides additional significant motivation for the molecular model. At least five exotic mesons are close to thresholds of two heavy-light mesons: $X(3872)$ [38–41], $Z_b(10610)$ and $Z_b(10650)$ in the bottomonium sector [42–46] and $Z_c(3900)$ [47–51] and $Z_c(4020/4025)$ [52–54] in the charmonium sector (see Table II in Ref. [55]; for reviews of experimental information see Ref. [56, 57], as well as *Spectroscopy of Mesons Containing Two Heavy Quarks and Non- $q\bar{q}$ Mesons* in Ref. [33]). These states share several important features: a) their masses are near thresholds and their

spin and parity correspond to S -wave combination of the two mesons; b) they are very narrow, despite very large phase space for decay into quarkonium + pion(s); c) the branching fractions for “fall apart” mode into two mesons are much larger than branching fractions for decay into quarkonium and pion(s). So far, there is no experimental evidence for states at two pseudoscalar thresholds ($D\bar{D}$ and $B\bar{B}$), implying that pseudoscalar exchange is essential for binding in meson-meson systems.

The above provide a strong hint that these states are deuteron-like loosely bound states of two heavy mesons [58–66]. It is then natural to conjecture that similar bound states might exist of two heavy baryons [67, 68], or a meson and a baryon or a baryon and an antibaryon, leading to a rather accurate prediction of the $P_c(4457)^+$ mass as $3/2^- \Sigma_c \bar{D}^*$ molecule (the mass threshold is 4462.4 MeV) [15, 55], following similar predictions obtained in a wider framework of doubly heavy baryon-meson hadronic molecules, which might include mixtures of various two-hadron states [12–14, 29]. However, single pion exchange is not possible in $\Sigma_c^+ \bar{D}^0$ system, thus the existence of $P_c(4312)^+$ points to importance of vector or two-pion exchanges in baryon-meson molecules. Two-pion exchange in $D\bar{D}$ system is highly suppressed, because the intermediate state is $D^* \bar{D}^*$, which is 282 MeV heavier than $D\bar{D}$. On the other hand, there is little suppression in the $\Sigma_c \bar{D}$ system, because the dominant intermediate state is $\Lambda_c \bar{D}^*$ which is just 25 MeV lighter than $\Sigma_c \bar{D}$ [69]. In a generic hadronic molecule it is essential that the two hadrons are heavy, in order to minimize the repulsive kinetic energy [67, 68, 70].

Following the initial LHCb discovery [8], several groups carried out a detailed analysis of the P_c^+ states as hadronic molecules [71–80] followed by further analysis [32, 81–105] after the updated LHCb results [10]. Very recently partial widths of all the allowed decay channels for the P_c states have been estimated within the molecular picture [106]. The most striking result is that $P_c(4312)$ decays are totally dominated by the $\bar{D}^* \Lambda_c$ channel. This channel is also expected to be very prominent in decays of $P_c(4440)$ and $P_c(4457)$.

The P_c states have also been interpreted as so called hadro-charmonium [107], a bound state of relatively compact charmonium states with light hadronic matter. It was proposed that $P_c(4440)^+$ and $P_c(4457)^+$ are spin-split $\psi(2S)p$ bound states with $J^P = \frac{1}{2}^-$ and $\frac{3}{2}^-$, while $P_c(4312)^+$ is a $\chi_{c0} p$ bound state with $J^P = \frac{1}{2}^+$ [108]. While very interesting from theoretical point of view, it is not at all clear why the binding energies between charmonia and the nucleon should conspire to produce states so close to the $\Sigma_c \bar{D}$ and $\Sigma_c \bar{D}^*$ thresholds. Moreover, the predicted widths of $P_c(4440)^+$ and $P_c(4457)^+$ are too big by a factor ~ 2 -3. One should also keep in mind that the molecular and hadro-charmonium pictures provide opposite predictions for the parity of $P_c(4312)^+$. In principle LHCb can check the spin and parity through partial wave analysis, but at present it is not known if systematic uncertainties can be sufficiently reduced to make such an analysis conclusive.

Shortly after the initial experimental discovery it was conjectured that the $P_c(4450)^+$ could be due to coincidence with the $\chi_{c1} p$ threshold, at which peaking can be induced via so called triangle singularity [109–112]. These explanations are no longer popular, since the $P_c(4440)^+$ mass is not at any threshold and the $P_c(4312)^+$ and $P_c(4457)^+$ peak slightly below the $\Sigma_c^+ \bar{D}^0$ and $\Sigma_c^+ \bar{D}^{*0}$ thresholds. The $P_c(4457)^+$ mass is exactly at $\Lambda_c^{*+} \bar{D}^0$ thresholds, but the LHCb has demonstrated that the observed peaking is narrower in the data than expected from the triangle-diagram when a realistic width of the excited D_s^- state exchanged

in the triangle is used (Supplemental Material in Ref. [10]).

More extensive pre-2019 reviews of some of the theoretical issues can be found in Refs. [113,114]. Two recent relevant reviews are Refs. [115,116].

So far the P_c^+ states have been observed by only one experiment in only one channel. It is essential to explore other possible experimental channels, such as $P_c \rightarrow \Lambda_c \bar{D}^{(*)}$, $\eta_c p$. These channels are however much more experimentally challenging than $P_c \rightarrow J/\psi p$. Proposals have also been made to search for heavy pentaquarks in photo-production [117–124]. Ref. [125] discusses photoproduction within the string-junction physical picture of the pentaquarks. Photoproduction is also related to recent work on $J/\psi(\eta_c)N$ scattering on the lattice [126] and on computation of $J/\psi(\eta_c)N$ and $\Upsilon(\eta_b)N$ cross sections [127]. In addition, pentaquark production has been discussed in the context of antiproton-deuteron collisions [128], of heavy ion collisions at LHC [129], in pA collisions [130] and in pion-induced processes [131–133]. Recently, the GlueX Collaboration reported negative search results for the P_c^+ states in photo-production at JLAB [134]. Within the large experimental errors and considerable theoretical model dependence these results do not contradict the molecular interpretations of the narrow P_c^+ states. It was recently suggested to determine the pentaquark photo-couplings and branching ratios by measuring the polarization transfer between the incident photon and the outgoing proton in the exclusive photo-production of J/ψ near threshold [135].

References

- [1] T. G. Trippe *et al.* (Particle Data Group), *Rev. Mod. Phys.* **48**, S1 (1976), [Erratum: *Rev. Mod. Phys.* **48**, 497 (1976)].
- [2] K. Hikasa *et al.* (Particle Data Group), *Phys. Rev.* **D45**, S1 (1992), [Erratum: *Phys. Rev.* **D46**, 5210 (1992)].
- [3] M. Praszalowicz, *Skyrmions and Anomalies, p.112*, M. Jezabek Ed., World Scientific Publishing (1987), ISBN 9971503506.
- [4] D. Diakonov, V. Petrov and M. V. Polyakov, *Z. Phys.* **A359**, 305 (1997), [hep-ph/9703373].
- [5] H. Weigel, *Eur. Phys. J.* **A2**, 391 (1998), [hep-ph/9804260].
- [6] K. H. Hicks, *Eur. Phys. J.* **H37**, 1 (2012).
- [7] W. M. Yao *et al.* (Particle Data Group), *J. Phys.* **G33**, 1 (2006).
- [8] R. Aaij *et al.* (LHCb), *Phys. Rev. Lett.* **115**, 072001 (2015), [arXiv:1507.03414].
- [9] R. Aaij *et al.* (LHCb), *Phys. Rev. Lett.* **117**, 8, 082002 (2016), [arXiv:1604.05708].
- [10] R. Aaij *et al.* (LHCb), *Phys. Rev. Lett.* **122**, 22, 222001 (2019), [arXiv:1904.03947].
- [11] R. Aaij *et al.* (LHCb), *Phys. Rev. Lett.* **117**, 8, 082003 (2016), [Addendum: *Phys. Rev. Lett.* **118**, 119901 (2017)], [arXiv:1606.06999].
- [12] Z.-C. Yang *et al.*, *Chin. Phys.* **C36**, 6 (2012), [arXiv:1105.2901].
- [13] J.-J. Wu *et al.*, *Phys. Rev. Lett.* **105**, 232001 (2010), [arXiv:1007.0573].
- [14] J.-J. Wu, T. S. H. Lee and B. S. Zou, *Phys. Rev.* **C85**, 044002 (2012), [arXiv:1202.1036].
- [15] M. Karliner and J. L. Rosner, *Phys. Rev. Lett.* **115**, 12, 122001 (2015), [arXiv:1506.06386].
- [16] L. Maiani, A. D. Polosa and V. Riquer, *Phys. Lett.* **B749**, 289 (2015), [arXiv:1507.04980].
- [17] R. F. Lebed, *Phys. Lett.* **B749**, 454 (2015), [arXiv:1507.05867].
- [18] V. V. Anisovich *et al.* (2015), [arXiv:1507.07652].
- [19] G.-N. Li, X.-G. He and M. He, *JHEP* **12**, 128 (2015), [arXiv:1507.08252].
- [20] R. Ghosh, A. Bhattacharya and B. Chakrabarti (2015), [arXiv:1508.00356].
- [21] Z.-G. Wang, *Eur. Phys. J.* **C76**, 2, 70 (2016), [arXiv:1508.01468].
- [22] R. Zhu and C.-F. Qiao, *Phys. Lett.* **B756**, 259 (2016), [arXiv:1510.08693].
- [23] J. M. Richard, A. Valcarce and J. Vijande, *Phys. Lett.* **B774**, 710 (2017), [arXiv:1710.08239].
- [24] E. Hiyama *et al.*, *Phys. Rev.* **C98**, 4, 045208 (2018), [arXiv:1803.11369].
- [25] A. Ali and A. Y. Parkhomenko, *Phys. Lett.* **B793**, 365 (2019), [arXiv:1904.00446].
- [26] A. Ali *et al.* (2019), [arXiv:1907.06507].
- [27] L. Maiani, A. D. Polosa and V. Riquer, *Phys. Lett.* **B778**, 247 (2018), [arXiv:1712.05296].
- [28] C. Fernandez-Ramirez *et al.* (JPAC), *Phys. Rev. Lett.* **123**, 9, 092001 (2019), [arXiv:1904.10021].
- [29] W. L. Wang *et al.*, *Phys. Rev.* **C84**, 015203 (2011), [arXiv:1101.0453].
- [30] C. W. Xiao, J. Nieves and E. Oset, *Phys. Rev.* **D88**, 056012 (2013), [arXiv:1304.5368].
- [31] C. W. Xiao, J. Nieves and E. Oset, *Phys. Rev.* **D100**, 1, 014021 (2019), [arXiv:1904.01296].
- [32] M.-Z. Liu *et al.*, *Phys. Rev. Lett.* **122**, 24, 242001 (2019), [arXiv:1903.11560].
- [33] M. Tanabashi *et al.* (Particle Data Group), *Phys. Rev.* **D98**, 3, 030001 (2018).
- [34] C. Hanhart, Yu. S. Kalashnikova and A. V. Nefediev, *Phys. Rev.* **D81**, 094028 (2010), [arXiv:1002.4097].
- [35] A. A. Filin *et al.*, *Phys. Rev. Lett.* **105**, 019101 (2010), [arXiv:1004.4789].
- [36] F.-K. Guo and U.-G. Meissner, *Phys. Rev.* **D84**, 014013 (2011), [arXiv:1102.3536].
- [37] F.-K. Guo *et al.*, *Rev. Mod. Phys.* **90**, 1, 015004 (2018), [arXiv:1705.00141].
- [38] S. K. Choi *et al.* (Belle), *Phys. Rev. Lett.* **91**, 262001 (2003), [hep-ex/0309032].
- [39] D. Acosta *et al.* (CDF), *Phys. Rev. Lett.* **93**, 072001 (2004), [hep-ex/0312021].
- [40] B. Aubert *et al.* (BaBar), *Phys. Rev.* **D71**, 071103 (2005), [hep-ex/0406022].
- [41] V. M. Abazov *et al.* (D0), *Phys. Rev. Lett.* **93**, 162002 (2004), [hep-ex/0405004].
- [42] M. Karliner and H. J. Lipkin (2008), [arXiv:0802.0649].
- [43] K. F. Chen *et al.* (Belle), *Phys. Rev. Lett.* **100**, 112001 (2008), [arXiv:0710.2577].
- [44] A. Bondar *et al.* (Belle), *Phys. Rev. Lett.* **108**, 122001 (2012), [arXiv:1110.2251].
- [45] P. Krokovny *et al.* (Belle), *Phys. Rev.* **D88**, 5, 052016 (2013), [arXiv:1308.2646].
- [46] A. Garmash *et al.* (Belle), *Phys. Rev.* **D91**, 7, 072003 (2015), [arXiv:1403.0992].
- [47] M. Ablikim *et al.* (BESIII), *Phys. Rev. Lett.* **110**, 252001 (2013), [arXiv:1303.5949].
- [48] Z. Q. Liu *et al.* (Belle), *Phys. Rev. Lett.* **110**, 252002 (2013), [arXiv:1304.0121].
- [49] T. Xiao *et al.*, *Phys. Lett.* **B727**, 366 (2013), [arXiv:1304.3036].
- [50] M. Ablikim *et al.* (BESIII), *Phys. Rev. Lett.* **112**, 2, 022001 (2014), [arXiv:1310.1163].
- [51] M. Ablikim *et al.* (BESIII), *Phys. Rev. Lett.* **115**, 11, 112003 (2015), [arXiv:1506.06018].
- [52] M. Ablikim *et al.* (BESIII), *Phys. Rev. Lett.* **111**, 24, 242001 (2013), [arXiv:1309.1896].
- [53] M. Ablikim *et al.* (BESIII), *Phys. Rev. Lett.* **113**, 21, 212002 (2014), [arXiv:1409.6577].

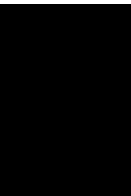
- [54] M. Ablikim *et al.* (BESIII), Phys. Rev. Lett. **112**, 13, 132001 (2014), [arXiv:1308.2760].
- [55] M. Karliner, Acta Phys. Polon. **B47**, 117 (2016).
- [56] M. Karliner, J. L. Rosner and T. Skwarnicki, Ann. Rev. Nucl. Part. Sci. **68**, 17 (2018), [arXiv:1711.10626].
- [57] S. L. Olsen, T. Skwarnicki and D. Zieminska, Rev. Mod. Phys. **90**, 1, 015003 (2018), [arXiv:1708.04012].
- [58] M. B. Voloshin and L. B. Okun, JETP Lett. **23**, 333 (1976), [Pisma Zh. Eksp. Teor. Fiz.23,369(1976)].
- [59] A. De Rujula, H. Georgi and S. Glashow, Phys. Rev. Lett. **38**, 317 (1977).
- [60] N. A. Tornqvist, Phys. Rev. Lett. **67**, 556 (1991).
- [61] N. A. Tornqvist, Z. Phys. **C61**, 525 (1994), [hep-ph/9310247].
- [62] N. A. Tornqvist, Phys. Lett. **B590**, 209 (2004), [hep-ph/0402237].
- [63] C. E. Thomas and F. E. Close, Phys. Rev. **D78**, 034007 (2008), [arXiv:0805.3653].
- [64] M. Suzuki, Phys. Rev. **D72**, 114013 (2005), [hep-ph/0508258].
- [65] S. Fleming *et al.*, Phys. Rev. **D76**, 034006 (2007), [hep-ph/0703168].
- [66] T. E. O. Ericson and G. Karl, Phys. Lett. **B309**, 426 (1993).
- [67] M. Karliner, H. J. Lipkin and N. A. Tornqvist, in "Proceedings, 14th International Conference on Hadron spectroscopy (Hadron 2011)," (2011), [arXiv:1109.3472], URL <http://inspirehep.net/record/927616/files/arXiv:1109.3472.pdf>.
- [68] M. Karliner, H. J. Lipkin and N. A. Tornqvist, Nucl. Phys. Proc. Suppl. **225-227**, 102 (2012).
- [69] M. Karliner, "Open Questions in Heavy Exotics," invited talk at *Bled 2019* Mini-Workshop, Bled, Slovenia, July 15-19, 2019, http://www-f1.ijs.si/Bled2019/Karliner_Bled2019.pdf ; M. Karliner and J. L. Rosner, in preparation.
- [70] X.-Q. Li and X. Liu, Eur. Phys. J. **C74**, 12, 3198 (2014), [arXiv:1409.3332].
- [71] R. Chen *et al.*, Phys. Rev. Lett. **115**, 13, 132002 (2015), [arXiv:1507.03704].
- [72] H.-X. Chen *et al.*, Phys. Rev. Lett. **115**, 17, 172001 (2015), [arXiv:1507.03717].
- [73] L. Roca, J. Nieves and E. Oset, Phys. Rev. **D92**, 9, 094003 (2015), [arXiv:1507.04249].
- [74] J. He, Phys. Lett. **B753**, 547 (2016), [arXiv:1507.05200].
- [75] H. Huang *et al.*, Eur. Phys. J. **C76**, 11, 624 (2016), [arXiv:1510.04648].
- [76] L. Roca and E. Oset, Eur. Phys. J. **C76**, 11, 591 (2016), [arXiv:1602.06791].
- [77] Q.-F. Lü and Y.-B. Dong, Phys. Rev. **D93**, 7, 074020 (2016), [arXiv:1603.00559].
- [78] Y. Shimizu, D. Suenaga and M. Harada, Phys. Rev. **D93**, 11, 114003 (2016), [arXiv:1603.02376].
- [79] C.-W. Shen *et al.*, Nucl. Phys. **A954**, 393 (2016), [arXiv:1603.04672].
- [80] Y. Yamaguchi *et al.*, Phys. Rev. **D96**, 11, 114031 (2017), [arXiv:1709.00819].
- [81] J. F. Giron, R. F. Lebed and C. T. Peterson, JHEP **05**, 061 (2019), [arXiv:1903.04551].
- [82] R. Chen *et al.*, Phys. Rev. **D100**, 1, 011502 (2019), [arXiv:1903.11013].
- [83] F.-K. Guo *et al.*, Phys. Rev. **D99**, 9, 091501 (2019), [arXiv:1903.11503].
- [84] J. He, Eur. Phys. J. **C79**, 5, 393 (2019), [arXiv:1903.11872].
- [85] H. Huang, J. He and J. Ping (2019), [arXiv:1904.00221].
- [86] Y. Shimizu, Y. Yamaguchi and M. Harada (2019), [arXiv:1904.00587].
- [87] Z.-H. Guo and J. A. Oller, Phys. Lett. **B793**, 144 (2019), [arXiv:1904.00851].
- [88] C.-J. Xiao *et al.*, Phys. Rev. **D100**, 1, 014022 (2019), [arXiv:1904.00872].
- [89] Z.-G. Wang (2019), [arXiv:1905.02892].
- [90] L. Meng *et al.*, Phys. Rev. **D100**, 1, 014031 (2019), [arXiv:1905.04113].
- [91] F. Giannuzzi, Phys. Rev. **D99**, 9, 094006 (2019), [arXiv:1903.04430].
- [92] Q. Wu and D.-Y. Chen (2019), [arXiv:1906.02480].
- [93] C.-W. Shen, J.-J. Wu and B.-S. Zou, Phys. Rev. **D100**, 5, 056006 (2019), [arXiv:1906.03896].
- [94] F. Stancu (2019), [arXiv:1902.07101].
- [95] C. W. Xiao, J. Nieves and E. Oset (2019), [arXiv:1906.09010].
- [96] M. B. Voloshin, Phys. Rev. **D100**, 3, 034020 (2019), [arXiv:1907.01476].
- [97] S. Sakai, H.-J. Jing and F.-K. Guo (2019), [arXiv:1907.03414].
- [98] Z.-G. Wang and X. Wang (2019), [arXiv:1907.04582].
- [99] Y. Yamaguchi *et al.* (2019), [arXiv:1907.04684].
- [100] Y.-J. Xu *et al.* (2019), [arXiv:1907.05097].
- [101] M. Pavon Valderrama (2019), [arXiv:1907.05294].
- [102] F.-Z. Peng *et al.* (2019), [arXiv:1907.05322].
- [103] M.-Z. Liu *et al.* (2019), [arXiv:1907.06093].
- [104] Y.-W. Pan *et al.* (2019), [arXiv:1907.11220].
- [105] T. J. Burns and E. S. Swanson (2019), [arXiv:1908.03528].
- [106] Y.-H. Lin and B.-S. Zou, Phys. Rev. **D100**, 5, 056005 (2019), [arXiv:1908.05309].
- [107] S. Dubynskiy and M. B. Voloshin, Phys. Lett. **B666**, 344 (2008), [arXiv:0803.2224].
- [108] M. I. Eides, V. Y. Petrov and M. V. Polyakov (2019), [arXiv:1904.11616].
- [109] F.-K. Guo *et al.*, Phys. Rev. **D92**, 7, 071502 (2015), [arXiv:1507.04950].
- [110] U.-G. Meissner and J. A. Oller, Phys. Lett. **B751**, 59 (2015), [arXiv:1507.07478].
- [111] X.-H. Liu, Q. Wang and Q. Zhao, Phys. Lett. **B757**, 231 (2016), [arXiv:1507.05359].
- [112] M. Mikhasenko (2015), [arXiv:1507.06552].
- [113] T. J. Burns, Eur. Phys. J. **A51**, 11, 152 (2015), [arXiv:1509.02460].
- [114] H.-X. Chen *et al.*, Phys. Rept. **639**, 1 (2016), [arXiv:1601.02092].
- [115] Y.-R. Liu *et al.*, Prog. Part. Nucl. Phys. **107**, 237 (2019), [arXiv:1903.11976].
- [116] N. Brambilla *et al.* (2019), [arXiv:1907.07583].
- [117] Y. Huang *et al.*, J. Phys. **G41**, 11, 115004 (2014), [arXiv:1305.4434].
- [118] Q. Wang, X.-H. Liu and Q. Zhao, Phys. Rev. **D92**, 034022 (2015), [arXiv:1508.00339].
- [119] V. Kubarovsky and M. B. Voloshin, Phys. Rev. **D92**, 3, 031502 (2015), [arXiv:1508.00888].
- [120] M. Karliner and J. L. Rosner, Phys. Lett. **B752**, 329 (2016), [arXiv:1508.01496].
- [121] A. N. Hiller Blin *et al.*, Phys. Rev. **D94**, 3, 034002 (2016), [arXiv:1606.08912].
- [122] X. Cao and J.-p. Dai, Phys. Rev. **D100**, 5, 054033 (2019), [arXiv:1904.06015].

- [123] X.-Y. Wang, X.-R. Chen and J. He, Phys. Rev. **D99**, 11, 114007 (2019), [arXiv:1904.11706].
- [124] J.-J. Wu, T. S. H. Lee and B.-S. Zou, Phys. Rev. **C100**, 3, 035206 (2019), [arXiv:1906.05375].
- [125] G. C. Rossi and G. Veneziano (2019), [arXiv:1909.01753].
- [126] U. Skerbis and S. Prelovsek, Phys. Rev. **D99**, 9, 094505 (2019), [arXiv:1811.02285].
- [127] C. W. Xiao and U. G. Meissner, Phys. Rev. **D92**, 11, 114002 (2015), [arXiv:1508.00924].
- [128] M. B. Voloshin, Phys. Rev. **D99**, 9, 093003 (2019), [arXiv:1903.04422].
- [129] R.-Q. Wang *et al.*, Phys. Rev. **C94**, 4, 044913 (2016), [arXiv:1601.02835].
- [130] I. Schmidt and M. Siddikov, Phys. Rev. **D93**, 9, 094005 (2016), [arXiv:1601.05621].
- [131] Q.-F. Lü *et al.*, Phys. Rev. **D93**, 3, 034009 (2016), [arXiv:1510.06271].
- [132] X.-H. Liu and M. Oka, Nucl. Phys. **A954**, 352 (2016), [arXiv:1602.07069].
- [133] X.-Y. Wang *et al.*, Phys. Lett. **B797**, 134862 (2019), [arXiv:1906.04044].
- [134] A. Ali *et al.* (GlueX), Phys. Rev. Lett. **123**, 7, 072001 (2019), [arXiv:1905.10811].
- [135] D. Winney *et al.* (JPAC), Phys. Rev. **D100**, 3, 034019 (2019), [arXiv:1907.09393].



Hypothetical Particles and Concepts

86. Extra dimensions (rev.)	889
87. W' -boson searches (rev.)	897
88. Z' -boson searches (rev.)	900
89. Supersymmetry: theory (rev.)	905
90. Supersymmetry: experiment (rev.)	923
91. Axions and other similar particles (rev.)	939
92. Quark and lepton compositeness, searches for (rev.)	953
93. Dynamical electroweak symmetry breaking: implications of the $H(0)$ (rev.)	958
94. Grand unified theories (rev.)	971
95. Leptoquarks (rev.)	986
96. Magnetic monopoles (rev.)	989



86. Extra Dimensions

Revised August 2019 by Y. Gershtein (Rutgers U.) and A. Pomarol (U. Autònoma de Barcelona; IFAE).

86.1 Introduction

Proposals for a spacetime with more than three spatial dimensions date back to the 1920s, mainly through the work of Kaluza and Klein, in an attempt to unify the forces of nature [1]. Although their initial idea failed, the formalism that they and others developed is still useful nowadays. Around 1980, string theory proposed again to enlarge the number of space dimensions, this time as a requirement for describing a consistent theory of quantum gravity. The extra dimensions were supposed to be compactified at a scale close to the Planck scale, and thus not testable experimentally in the near future.

A different approach was given by Arkani-Hamed, Dimopoulos, and Dvali (ADD) in their seminal paper in 1998 [2], where they showed that the weakness of gravity could be explained by postulating two or more extra dimensions in which only gravity could propagate. The size of these extra dimensions should range between roughly a millimeter and $\sim 1/\text{TeV}$, leading to possible observable consequences in current and future experiments. A year later, Randall and Sundrum (RS) [3] found a new possibility using a warped geometry, postulating a five-dimensional Anti-de Sitter (AdS) spacetime with a compactification scale of order $1/\text{TeV}$. The origin of the smallness of the electroweak scale versus the Planck scale was explained by the gravitational redshift factor present in the warped AdS metric. As in the ADD model, originally only gravity was assumed to propagate in the extra dimensions, although it was soon clear that this was not necessary in warped extra-dimensions and also the SM gauge fields [4, 5] and SM fermions [6, 7] could propagate in the five-dimensional spacetime.

The physics of warped extra-dimensional models has an alternative interpretation by means of the AdS/CFT correspondence [8–10]. Models with warped extra dimensions are related to four-dimensional strongly-interacting theories, allowing an understanding of the properties of five-dimensional fields as those of four-dimensional composite states [11]. This approach has opened new directions for tackling outstanding questions in particle physics, such as the flavor problem, grand unification, and the origin of electroweak symmetry breaking or supersymmetry breaking.

86.1.1 Experimental Constraints

Constraints on extra-dimensional models arise from astrophysical and cosmological considerations, tabletop experiments exploring gravity at sub-mm distances, and collider experiments. Collider limits on extra-dimensional models are dominated by LHC results, which can be found on the public WWW pages of ATLAS [12] and CMS [13]. This review includes the most recent limits, most of which are published results based on 36 fb^{-1} LHC data collected in 2015–16 at a center-of-mass energy of 13 TeV and legacy results from 20 fb^{-1} of 8 TeV data collected in Run 1. In addition, there are a few published and preliminary results based on the full Run 2 datasets. For most of the models, Run 2 results surpass the sensitivity of Run 1, even in the cases when the integrated luminosity is smaller.

86.1.2 Kaluza-Klein Theories

Field theories with compact extra dimensions can be written as theories in ordinary four dimensions (4D) by performing a Kaluza-Klein (KK) reduction. As an illustration, consider a simple example, namely a field theory of a complex scalar in flat five-dimensional (5D) spacetime. The action will be given by ¹

$$S_5 = - \int d^4x dy M_5 \left[|\partial_\mu \phi|^2 + |\partial_y \phi|^2 + \lambda_5 |\phi|^4 \right], \quad (86.1)$$

where y refers to the extra (fifth) dimension. A universal scale M_5 has been extracted in front of the action in order to keep the

5D field with the same mass-dimension as in 4D. This theory is perturbative for energies $E \lesssim \ell_5 M_5 / \lambda_5$ where $\ell_5 = 24\pi^3$ [14].

Let us now consider that the fifth dimension is compact with the topology of a circle S^1 of radius R , which corresponds to the identification of y with $y + 2\pi R$. In such a case, the 5D complex scalar field can be expanded in a Fourier series:

$$\phi(x, y) = \frac{1}{\sqrt{2\pi R M_5}} \sum_{n=-\infty}^{\infty} e^{iny/R} \phi^{(n)}(x), \quad (86.2)$$

that, inserted in Eq. (86.1) and integrating over y , gives

$$S_5 = S_4^{(0)} + S_4^{(n)}, \quad (86.3)$$

where

$$S_4^{(0)} = - \int d^4x \left[|\partial_\mu \phi^{(0)}|^2 + \lambda_4 |\phi^{(0)}|^4 \right], \quad (86.4)$$

and,

$$S_4^{(n)} = - \int d^4x \sum_{n \neq 0} \left[|\partial_\mu \phi^{(n)}|^2 + \left(\frac{n}{R}\right)^2 |\phi^{(n)}|^2 \right] + \text{quartic interactions}. \quad (86.5)$$

The $n = 0$ mode self-coupling is given by

$$\lambda_4 = \frac{\lambda_5}{2\pi R M_5}. \quad (86.6)$$

The above action corresponds to a 4D theory with a massless scalar $\phi^{(0)}$, referred to as the zero mode, and an infinite tower of massive modes $\phi^{(n)}$ with $n > 0$, known as KK modes. The KK reduction thus allows a treatment of 5D theories as 4D field theories with an infinite number of fields. At energies smaller than $1/R$, the KK modes can be neglected, leaving the zero-mode action of Eq. (86.4). The strength of the interaction of the zero-mode, given by Eq. (86.6), decreases as R increases. Thus, for a large extra dimension $R \gg 1/M_5$, the massless scalar is very weakly coupled.

86.2 Large Extra Dimensions for Gravity

86.2.1 The ADD Scenario

The ADD scenario [2, 15] (for a review see, for example, [16]) assumes a $D = 4 + \delta$ dimensional spacetime, with δ compactified spatial dimensions. The apparent weakness of gravity arises since it propagates in the higher-dimensional space. The SM is assumed to be localized in a 4D subspace, a 3-brane, as can be found in certain string theory constructions [17, 18]. Gravity is described by the Einstein-Hilbert action in $D = 4 + \delta$ spacetime dimensions

$$S_D = - \frac{\bar{M}_D^{2+\delta}}{2} \int d^4x d^\delta y \sqrt{-g} \mathcal{R} + \int d^4x \sqrt{-g_{\text{ind}}} \mathcal{L}_{\text{SM}}, \quad (86.7)$$

where x labels the ordinary four coordinates, y the δ extra coordinates, g refers to the determinant of the D -dimensional metric whose Ricci scalar is defined by \mathcal{R} , and \bar{M}_D is called the reduced Planck scale of the D -dimensional theory. In the second term of Eq. (86.7), which gives the gravitational interactions of SM fields, the D -dimensional metric reduces to the induced metric on the 3-brane where the SM fields propagate. The extra dimensions are assumed to be flat and compactified in a volume V_δ . As an example, consider a toroidal compactification of equal radii R and volume $V_\delta = (2\pi R)^\delta$. After a KK reduction, one finds that the fields that couple to the SM are the spin-2 gravitational field $G_{\mu\nu}(x, y)$ and a tower of spin-1 KK graviscalars [19]. The graviscalars, however, only couple to SM fields through the trace of the energy-momentum tensor, resulting in weaker couplings to the SM fields. The Fourier expansion of the spin-2 field is given by

$$G_{\mu\nu}(x, y) = G_{\mu\nu}^{(0)}(x) + \frac{1}{\sqrt{V_\delta}} \sum_{\vec{n} \neq 0} e^{i\vec{n} \cdot \vec{y}/R} G_{\mu\nu}^{(\vec{n})}(x), \quad (86.8)$$

¹Our convention for the metric is $\eta_{MN} = \text{Diag}(-1, 1, 1, 1, 1)$.

where $\vec{y} = (y_1, y_2, \dots, y_\delta)$ are the extra-dimensional coordinates and $\vec{n} = (n_1, n_2, \dots, n_\delta)$. Eq. (86.8) contains a massless state, the 4D graviton $G_{\mu\nu}^{(0)}$, and its KK tower $G_{\mu\nu}^{(\vec{n})}$ with masses $m_{\vec{n}}^2 = |\vec{n}|^2/R^2$. At energies below $1/R$ the action is that of the zero mode

$$S_4^{(0)} = -\frac{\bar{M}_D^{2+\delta}}{2} \int d^4x V_\delta \sqrt{-g^{(0)}} \mathcal{R}^{(0)} + \int d^4x \sqrt{-g_{\text{ind}}^{(0)}} \mathcal{L}_{\text{SM}}, \tag{86.9}$$

where we can identify the 4D reduced Planck mass, $M_P \equiv 1/\sqrt{8\pi G_N} \simeq 2.4 \times 10^{18}$ GeV, as a function of the D -dimensional parameters:

$$M_P^2 = V^\delta \bar{M}_D^{2+\delta} \equiv R^\delta M_D^{2+\delta}. \tag{86.10}$$

Fixing M_D at around the electroweak scale $M_D \sim \text{TeV}$ to avoid introducing a new mass scale in the model, Eq. (86.10) gives a prediction for R :

$$\delta = 1, 2, \dots, 6 \rightarrow R \sim 10^9 \text{ km}, 0.5 \text{ mm}, \dots, 0.1 \text{ MeV}^{-1}. \tag{86.11}$$

The option $\delta = 1$ is clearly ruled out, as it leads to modifications of Newton’s law at solar system distances. However this is not the case for $\delta \geq 2$, and possible observable consequences can be sought in present and future experiments.

Consistency of the model requires a stabilization mechanism for the radii of the extra dimensions, to the values shown in Eq. (86.11). The fact that we need $R \gg 1/M_D$ leads to a new hierarchy problem, the solution of which might require imposing supersymmetry in the extra-dimensional bulk (for the case of two extra dimensions see for example [20]).

86.2.2 Tests of the Gravitational Force Law at Sub-mm Distances

The KK modes of the graviton give rise to deviations from Newton’s law of gravitation for distances $\lesssim R$. Such deviations are usually parametrized by a modified Newtonian potential of the form

$$V(r) = -G_N \frac{m_1 m_2}{r} [1 + \alpha e^{-r/\lambda}]. \tag{86.12}$$

For a 2-torus compactification, $\alpha = 16/3$ and $\lambda = R$. Searches for deviations from Newton’s law of gravitation have been performed in several experiments. Refs. [21–23] give the present constraints: $R < 37\mu\text{m}$ at 95% CL for $\delta = 2$, corresponding to $M_D > 3.6$ TeV.

86.2.3 Astrophysical and Cosmological Constraints

The light KK gravitons could be copiously produced in stars, carrying away energy. Ensuring that the graviton luminosity is low enough to preserve the agreement of stellar models with observations provides powerful bounds on the scale M_D . The most stringent bound arises from supernova SN1987A, giving $M_D > 27$ (2.4) TeV for $\delta = 2$ (3) [24]. After a supernova explosion, most of the KK gravitons stay gravitationally trapped in the remnant neutron star. The requirement that neutron stars are not excessively heated by KK decays into photons leads to $M_D > 1700$ (76) TeV for $\delta = 2$ (3) [25].

Cosmological constraints are also quite stringent [26]. To avoid overclosure of the universe by relic gravitons one needs $M_D > 7$ TeV for $\delta = 2$. Relic KK gravitons decaying into photons contribute to the cosmic diffuse gamma radiation, from which one can derive the bound $M_D > 100$ TeV for $\delta = 2$.

We must mention however that bounds coming from the decays of KK gravitons into photons can be reduced if we assume that KK gravitons decay mainly into other non-SM states. This could happen, for example, if there were other 3-branes with hidden sectors residing on them [15].

86.2.4 Collider Signals

86.2.4.1 Graviton and Other Particle Production

Although each KK graviton has a purely gravitational coupling, suppressed by $1/M_P$, inclusive processes in which one sums over the almost continuous spectrum of available gravitons have cross sections suppressed only by powers of M_D . Processes involving gravitons are therefore detectable in collider experiments if $M_D \sim \text{TeV}$. A number of experimental searches for evidence of large extra dimensions have been performed at colliders, and interpreted in the context of the ADD model.

One signature arises from direct graviton emission. By making a derivative expansion of Einstein gravity, one can construct an effective theory, valid for energies much lower than M_D , and use it to make predictions for graviton-emission processes at colliders [19, 27, 28]. Gravitons produced in the final state would escape detection, giving rise to missing transverse energy (\cancel{E}_T). The results quoted below are 95% CL lower limits on M_D for a range of values of δ between 2 and 6, with more stringent limits corresponding to lower δ values.

At hadron colliders, experimentally sensitive channels include the jet (j) + \cancel{E}_T and γ + \cancel{E}_T final states. CMS (ATLAS) j + \cancel{E}_T results with 36 fb^{-1} of 13 TeV data provide limits of $M_D > 5.3$ – 9.9 TeV [29] ($M_D > 4.8$ – 7.7 TeV [30]). For these analyses, both experiments are assuming leading order (LO) cross sections. Since the effective theory is only valid for energies much less than M_D , the results are quoted for the full space, and include the information that suppressing the graviton cross section by a factor M_D^4/\hat{s}^2 for $\sqrt{\hat{s}} > M_D$, where $\sqrt{\hat{s}}$ is the parton-level center-of-mass energy of the hard collision, weakens the limits on M_D by a negligible amount for $\delta = 2$ ($\sim 3\%$ for $\delta = 6$). Less stringent limits are obtained by CMS [31] from analysis of 36 fb^{-1} of 13 TeV data in the γ + \cancel{E}_T final state. The analogous ATLAS search [32] has comparable sensitivity but does not quote ADD interpretation of the results.

In models in which the ADD scenario is embedded in a string theory at the TeV scale [18], we expect the string scale M_s to be smaller than M_D , and therefore expect production of string resonances at the LHC [33]. A Run 2 result from CMS analyzing the dijet invariant mass distribution for 36 fb^{-1} of 13 TeV data excludes string resonances that decay predominantly to $q+g$ with masses below 7.7 TeV [34]. ATLAS dijet analysis [35] provides their results in the context of model-independent limits on the cross section times acceptance for generic resonances of a variety of possible widths.

86.2.4.2 Virtual graviton effects

One can also search for virtual graviton effects, the calculation of which however depends on the ultraviolet cut-off of the theory and is therefore very model dependent. In the literature, several different formulations exist [19, 28, 36] for the dimension-eight operator for gravity exchange at tree level:

$$\mathcal{L}_8 = \pm \frac{4}{M_{TT}^4} \left(T_{\mu\nu} T^{\mu\nu} - \frac{1}{\delta + 2} T_\mu^\mu T_\nu^\nu \right), \tag{86.13}$$

where $T_{\mu\nu}$ is the energy-momentum tensor and M_{TT} is related to M_D by some model-dependent coefficient [37]. The relations with the parametrizations of Refs. [36] and [19] are, respectively, $M_{TT} = M_S$ and $M_{TT} = (2/\pi)^{1/4} A_T$. The experimental results below are given as 95% CL lower limits on M_{TT} , including in some cases the possibility of both constructive or destructive interference, depending on the sign chosen in Eq. (9).

The most stringent limits arise from LHC analyses of the dijet angular distribution. Using 35.9 fb^{-1} of 13 TeV data, CMS [38] obtains results that correspond to an approximate limit of $M_{TT} > 9.1$ TeV.

The next most restrictive results come from the analyses of diphoton ($M_{TT} > 6.1$ TeV from ATLAS [39] and $M_{TT} > 7.0$ TeV from CMS [40]) and dilepton mass spectra ($M_{TT} > 6.1$ TeV from CMS [41]). The complete Run 2 (139 fb^{-1}) analysis of ATLAS di-lepton data [42] does not quote the limits on ADD.

At the one-loop level, gravitons can also generate dimension-six operators with coefficients that are also model dependent. Experimental bounds on these operators can also give stringent constraints on M_D [37].

86.2.4.3 Black Hole Production

The physics at energies $\sqrt{s} \sim M_D$ is sensitive to the details of the unknown quantum theory of gravity. Nevertheless, in the transplanckian regime, $\sqrt{s} \gg M_D$, one can rely on a semiclassical description of gravity to obtain predictions. An interesting feature of transplanckian physics is the creation of black holes [43, 44] (for a review see, for example, [45]). A black hole is expected to be formed in a collision in which the impact parameter is smaller

than the Schwarzschild radius [46]:

$$R_S = \frac{1}{M_D} \left[\frac{2^\delta \pi^{(\delta-3)/2}}{\delta+2} \Gamma\left(\frac{\delta+3}{2}\right) \frac{M_{BH}}{M_D} \right]^{1/(\delta+1)}, \quad (86.14)$$

where M_{BH} is the mass of the black hole, which would roughly correspond to the total energy in the collision. The cross section for black hole production can be estimated to be of the same order as the geometric area $\sigma \sim \pi R_S^2$. For $M_D \sim \text{TeV}$, this gives a production of $\sim 10^7$ black holes at the $\sqrt{s} = 14$ TeV LHC with an integrated luminosity of 30 fb^{-1} [43, 44]. A black hole would provide a striking experimental signature since it is expected to thermally radiate with a Hawking temperature $T_H = (\delta+1)/(4\pi R_S)$, and therefore would evaporate democratically into all SM states. Nevertheless, given the present constraints on M_D , the LHC will not be able to reach energies much above M_D . This implies that predictions based on the semiclassical approximation could receive sizable modifications from model-dependent quantum-gravity effects.

The most stringent limits on microscopic black holes arise from LHC searches which observed no excesses above the SM background in high-multiplicity final states. The results are usually quoted as model-independent limits on the cross section for new physics in the final state and kinematic region analyzed. These results can then be used to provide constraints of models of low-scale gravity and weakly-coupled string theory. In addition, limits are sometimes quoted on particular implementations of models, which are used as benchmarks to illustrate the sensitivity.

A CMS analysis [47] of multi-object final states using 36 fb^{-1} of 13 TeV data, excludes semiclassical black holes below masses of up to 10.1 TeV for $M_D = 2$ TeV and $\delta = 6$. Analogous Run 2 ATLAS analysis [48], using 3.0 fb^{-1} of 13 TeV data, excludes black hole masses up to 9.0–9.7 TeV, depending on M_D , for $\delta = 6$. Another ATLAS search [49] for an excess of events with multiple high transverse momentum objects, including charged leptons and jets, using 3.2 fb^{-1} of 13 TeV data, excludes semiclassical black holes below masses of ~ 8.7 TeV for $M_D = 2$ TeV and $\delta = 6$.

A complementary approach is to look for jet extinction at high transverse momenta, as we expect hard short distance scattering processes to be highly suppressed at energies above M_D [50]. The CMS analysis [51] of inclusive jet p_T spectrum in 10.7 fb^{-1} of 8 TeV data set a lower limit of 3.3 TeV on the extinction mass scale.

For black hole masses near M_D , the semi-classical approximation is not valid, and one could instead expect quantum black holes (QBH) that decay primarily into two-body final states [52]. LHC Run 2 results at 13 TeV provide lower limits on QBH masses of order 2.3–9.0 TeV, depending on the details of the model. Searches that consider interpretations in terms of QBH limits include the CMS multi-object analysis [53], ATLAS dijet analysis [35], and different flavor di-lepton analyses at CMS ($e\mu$, 36 fb^{-1} at 13 TeV [54]) and ATLAS ($e\mu$, $e\tau$, $\mu\tau$, 36.1 fb^{-1} at 13 TeV [55]).

In weakly-coupled string models the semiclassical description of gravity fails in the energy range between M_s and M_s/g_s^2 where stringy effects are important. In this regime one expects, instead of black holes, the formation of string balls, made of highly excited long strings, that could be copiously produced at the LHC for $M_s \sim \text{TeV}$ [56], and would evaporate thermally at the Hagedorn temperature giving rise to high-multiplicity events. The same analyses used to search for black holes can be interpreted in the context of string balls. For example, for the case of $\delta = 6$ with $M_s = M_D/1.26 = 3$ TeV, the ATLAS multiple high transverse momentum object analysis [48] excludes string balls with masses below 6.5 to 9.0 TeV for values of $0.2 < g_s < 0.8$. The CMS multi-object analysis [47] studies string ball production in two scenarios, both assuming $\delta = 6$. For the constant $g_s = 0.2$ and $1 < M_s < 3.5$ TeV the string ball masses below 7.2 to 9.4 TeV are excluded, while at constant $M_s = 3.6$ TeV and $0.2 < g_s < 0.4$ masses below 7.2 to 8.1 TeV are excluded.

86.3 TeV-Scale Extra Dimensions

86.3.1 Warped Extra Dimensions

The RS model [3] is the most attractive setup of warped extra dimensions at the TeV scale, since it provides an alternative solution to the hierarchy problem. The RS model is based on a 5D theory with the extra dimension compactified in an orbifold, S^1/Z_2 , a circle S^1 with the extra identification of y with $-y$. This corresponds to the segment $y \in [0, \pi R]$, a manifold with boundaries at $y = 0$ and $y = \pi R$. Let us now assume that this 5D theory has a cosmological constant in the bulk Λ , and on the two boundaries Λ_0 and $\Lambda_{\pi R}$:

$$S_5 = - \int d^4x dy \left\{ \sqrt{-g} \left[\frac{1}{2} M_5^3 \mathcal{R} + \Lambda \right] + \sqrt{-g_0} \delta(y) \Lambda_0 + \sqrt{-g_{\pi R}} \delta(y - \pi R) \Lambda_{\pi R} \right\}, \quad (86.15)$$

where g_0 and $g_{\pi R}$ are the values of the determinant of the induced metric on the two respective boundaries. Einstein's equations can be solved, giving in this case the metric

$$ds^2 = a(y)^2 dx^\mu dx^\nu \eta_{\mu\nu} + dy^2, \quad a(y) = e^{-ky}, \quad (86.16)$$

where $k = \sqrt{-\Lambda/6M_5^3}$. Consistency of the solution requires $\Lambda_0 = -\Lambda_{\pi R} = -\Lambda/k$. The metric in Eq. (86.16) corresponds to a 5D AdS space. The factor $a(y)$ is called the ‘‘warp’’ factor and determines how 4D scales change as a function of the position in the extra dimension. In particular, this implies that energy scales for 4D fields localized at the boundary at $y = \pi R$ are redshifted by a factor $e^{-k\pi R}$ with respect to those localized at $y = 0$. For this reason, the boundaries at $y = 0$ and $y = \pi R$ are usually referred to as the ultraviolet (UV) and infrared (IR) boundaries, respectively.

As in the ADD case, we can perform a KK reduction and obtain the low-energy effective theory of the 4D massless graviton. In this case we obtain

$$M_P^2 = \int_0^{\pi R} dy e^{-2ky} M_5^3 = \frac{M_5^3}{2k} (1 - e^{-2k\pi R}). \quad (86.17)$$

Taking $M_5 \sim k \sim M_P$, we can generate an IR-boundary scale of order $ke^{-k\pi R} \sim \text{TeV}$ for an extra dimension of radius $R \simeq 11/k$. Mechanisms to stabilize R to this value have been proposed [57, 58] that, contrary to the ADD case, do not require introducing any new small or large parameter. Therefore a natural solution to the hierarchy problem can be achieved in this framework if the Higgs field, whose vacuum expectation value (VEV) is responsible for electroweak symmetry breaking, is localized at the IR-boundary where the effective mass scales are of order TeV. The radion field is generically heavy in models with a stabilized R . Nevertheless, it has been recently discussed that under some conditions a naturally light radion can arise [59–62]. In these cases the radion is identified with the dilaton, the Goldstone boson associated to the spontaneous breaking of scale invariance, and its mass can be naturally below $ke^{-k\pi R} \sim \text{TeV}$. Collider bounds on the radion mass and couplings can be found in [63–65].

In the RS model [3], all the SM fields were assumed to be localized on the IR-boundary. Nevertheless, for the hierarchy problem, only the Higgs field has to be localized there. SM gauge bosons and fermions can propagate in the 5D bulk [4–7] (for a review see, for example, [66, 67]). By performing a KK reduction from the 5D action of a gauge boson, we find [4, 5]

$$\frac{1}{g_4^2} = \int_0^{\pi R} dy \frac{1}{g_5^2} = \frac{\pi R}{g_5^2}, \quad (86.18)$$

where g_D ($D = 4, 5$) is the gauge coupling in D -dimensions. Therefore the 4D gauge couplings can be of order one, as is the case of the SM, if one demands $g_5^2 \sim \pi R$. Using $kR \sim 10$ and $g_4 \sim 0.5$, one obtains the 5D gauge coupling

$$g_5 \sim 4/\sqrt{k}. \quad (86.19)$$

Boundary kinetic terms for the gauge bosons can modify this relation, allowing for larger values of $g_5\sqrt{k}$.

Fermions propagating in a warped extra dimension have 4D massless zero-modes with wavefunctions which vary as $f_0 \sim \exp[(1/2 - c_f)ky]$, where $c_f k$ is their 5D mass [7,68]. Depending on the free parameter $c_f k$, fermions can be localized either towards the UV-boundary ($c_f > 1/2$) or IR-boundary ($c_f < 1/2$). Since the Higgs boson is localized on the IR-boundary, one can generate exponentially suppressed Yukawa couplings by having the fermion zero-modes localized towards the UV-boundary, generating naturally the light SM fermion spectrum [7]. A large overlap with the wavefunction of the Higgs is needed for the top quark, in order to generate its large mass, thus requiring it to be localized towards the IR-boundary. In conclusion, the large mass hierarchies present in the SM fermion spectrum can be easily obtained in warped models via suitable choices of the order-one parameters c_f [69]. In these scenarios, deviations in flavor physics from the SM predictions are expected to arise from flavor-changing KK gluon couplings [70], putting certain constraints on the parameters of the models and predicting new physics effects to be observed in B -physics processes (see, for example, [71,72]).

The masses of the KK states can also be calculated. One finds [7]

$$m_n \simeq \left(n + \frac{\alpha}{2} - \frac{1}{4} \right) \pi k e^{-\pi k R}, \quad (86.20)$$

where $n = 1, 2, \dots$ and $\alpha = \{c_f - 1/2, 0, 1\}$ for KK fermions, KK gauge bosons and KK gravitons, respectively. Their masses are of order $ke^{-\pi k R} \sim \text{TeV}$ (for this reason we refer to these scenarios as TeV-scale extra dimensions). The first KK state of the gauge bosons would be the lightest, while gravitons are expected to be the heaviest.

86.3.1.1 Models of Electroweak Symmetry Breaking

Theories in warped extra dimensions can be used to implement symmetry breaking at low energies by boundary conditions (for a review see, for example, [73]). For example, for a $U(1)$ gauge symmetry in the 5D bulk, this can be easily achieved by imposing a Dirichlet boundary condition on the IR-boundary for the gauge-boson field, $A_\mu|_{y=\pi R} = 0$. This makes the zero-mode gauge boson get a mass, given by $m_A = g_4 \sqrt{2k/g_5^2} e^{-\pi k R}$. A very different situation occurs if the Dirichlet boundary condition is imposed on the UV-boundary, $A_\mu|_{y=0} = 0$. In this case the zero-mode gauge boson disappears from the spectrum. Finally, if a Dirichlet boundary condition is imposed on the two boundaries, one obtains a massless 4D scalar corresponding to the fifth component of the 5D gauge boson, A_5 . Thus, different scenarios can be implemented by appropriately choosing the 5D bulk gauge symmetry, \mathcal{G}_5 , and the symmetries to which it reduces on the UV and IR-boundary, \mathcal{H}_{UV} and \mathcal{H}_{IR} , respectively. In all cases the KK spectrum comes in representations of the group \mathcal{G}_5 .

Among the most interesting scenarios are those called gauge-Higgs unified models, where the Higgs boson appears as the fifth component of a 5D gauge boson, A_5 . The Higgs mass is protected by the 5D gauge invariance and can only get a nonzero value from non-local one-loop effects [74]. To guarantee the relation $M_W^2 \simeq M_Z^2 \cos^2 \theta_W$, a custodial $SU(2)_V$ symmetry is needed in the bulk and IR-boundary [75]. The simplest realization [76,77] has

$$\begin{aligned} \mathcal{G}_5 &= SU(3)_c \times SO(5) \times U(1)_X, \\ \mathcal{H}_{IR} &= SU(3)_c \times SO(4) \times U(1)_X, \\ \mathcal{H}_{UV} &= G_{SM}. \end{aligned}$$

The Higgs boson gets a potential at the one-loop level that triggers a VEV, breaking the electroweak symmetry. In these models there is a light Higgs boson whose mass can be around 125 GeV, as required by the discovered Higgs boson [78]. This state, as will be explained in Sec. 86.3.2, behaves as a composite pseudo-Goldstone boson with couplings that deviate from the SM Higgs [79]. The present experimental determination of the Higgs couplings at the LHC, that agrees with the SM predictions, put important constraints on these scenarios [78]. The lightest KK modes of the model are color fermions with charges $Q = -1/3, 2/3$ and $5/3$ [80].

86.3.1.2 Constraints from Electroweak Precision Tests

Models in which the SM gauge bosons propagate in 1/TeV-sized extra dimensions give generically large corrections to electroweak observables. When the SM fermions are confined on a boundary these corrections are universal and can be parametrized by four quantities: \widehat{S} , \widehat{T} , W and Y , as defined in Ref. [81]. For warped models, where the 5D gauge coupling of Eq. (86.19) is large, the most relevant parameter is \widehat{T} , which gives the bound $m_{KK} \gtrsim 10 \text{ TeV}$ [66]. When a custodial symmetry is imposed [75], the main constraint comes from the \widehat{S} parameter, requiring $m_{KK} \gtrsim 3 \text{ TeV}$, independent of the value of g_5 . Corrections to the $Zb_L\bar{b}_L$ coupling can also be important [66], especially in warped models for electroweak symmetry breaking as the ones described above.

86.3.1.3 Kaluza-Klein Searches

The main prediction of 1/TeV-sized extra dimensions is the presence of a discretized KK spectrum, with masses around the TeV scale, associated with the SM fields that propagate in the extra dimension.

In the RS model [3], only gravity propagates in the 5D bulk. Experimental searches have been performed for the lightest KK graviton through its decay to a variety of SM particle-antiparticle pairs. The results are usually interpreted in the plane of the dimensionless coupling k/M_P versus m_1 , where M_P is the reduced Planck mass defined previously and m_1 is the mass of the lightest KK excitation of the graviton. Since the AdS curvature $\sim k$ cannot exceed the cut-off scale of the model, which is estimated to be $\ell_5^{1/3} M_5$ [37], one must demand $k \ll \sqrt{2\ell_5} M_P$.

The most stringent limits currently arise from LHC searches for resonances in the dilepton and diphoton final states, using 13 TeV collisions. Best sensitivities are obtained in the $\gamma\gamma$ final state, which is quite powerful since it has a branching fraction twice that of any individual lepton flavor. The CMS analysis [40] of 36 fb $^{-1}$ of 13 TeV data excludes KK gravitons below 2.3 to 4.6 TeV, depending on the value of the coupling k/M_P , which is varied between 0.01 and 0.2, while ATLAS [39] provides a lower limit on the KK graviton mass of 4.1 TeV for the coupling parameter 0.1. The CMS [82] dilepton analyses, combining results from the ee and $\mu\mu$ channels, exclude KK gravitons with masses below 4.25 TeV for coupling parameter 0.1. The ATLAS [42] analysis of 139fb $^{-1}$ of Run 2 data does not include a RS KK graviton interpretation of the results. Less stringent limits on the KK graviton mass come from analyses of the dijet [34], HH [83,84], and VV [85,86] final states, where V can represent either a W or Z boson.

In warped extra-dimensional models in which the SM fields propagate in the 5D bulk, the couplings of the KK graviton to $ee/\mu\mu/\gamma\gamma$ are suppressed [87], and the above bounds do not apply. Furthermore, the KK graviton is the heaviest KK state (see Eq. (86.20)), and therefore experimental searches for KK gauge bosons and fermions are more appropriate discovery channels in these scenarios. For the scenarios discussed above in which only the Higgs boson and the top quark are localized close to the IR-boundary, the KK gauge bosons mainly decay into top quarks, longitudinal W/Z bosons, and Higgs bosons. Couplings to light SM fermions are suppressed by a factor $g/\sqrt{g_5^2 k} \sim 0.2$ [7] for the value of Eq. (86.19) that is considered from now on. Searches have been made for evidence of the lightest KK excitation of the gluon, through its decay to $t\bar{t}$ pairs. The searches take into account the natural KK gluon width, which is typically $\sim 15\%$ of its mass. The decay of a heavy particle to $t\bar{t}$ would tend to produce highly boosted top (anti-)quarks in the final state. Products of the subsequent top decays would therefore tend to be close to each other in the detector. In the case of $t \rightarrow Wb \rightarrow jjb$ decays, the three jets could overlap one another and not be individually reconstructed with the standard jet algorithms, while $t \rightarrow Wb \rightarrow \ell\nu b$ decays could result in the lepton failing standard isolation requirements due to its proximity to the b -jet; in both cases, the efficiency for properly reconstructing the final state would fall as the mass of the original particle increases. To avoid the loss in sensitivity which would result, a number of techniques, known generally as “top quark tagging”, have been developed to reconstruct and identify highly boosted top quarks, for example by using a single “wide” jet to contain all the decay products of a hadronic top decay. The

large backgrounds from QCD jets can then be reduced by requiring the “jet mass” be consistent with that of a top quark, and also by examining the substructure of the wide jet for indication that it resulted from the hadronic decay of a top quark. These techniques are key to extending to very high masses the range of accessible resonances decaying to $t\bar{t}$ pairs. The CMS analysis [88] of 36 fb^{-1} of 13 TeV data combines di-lepton, lepton-plus-jet, and all-hadronic $t\bar{t}$ decays and excludes KK gluons with masses below 4.55 TeV. ATLAS uses all-hadronic [89] and lepton-plus-jet [90] final states to exclude KK gluons up to 3.4 and 3.8 TeV respectively with 36 fb^{-1} of 13 TeV data. The results are not directly comparable between the two LHC experiments, since they employ in their respective analyses different implementations of the theoretical model. For masses between 3 and 5 TeV, the cross-section limits are around 20 fb for CMS and 30 fb for ATLAS.

A gauge boson KK excitation could be also sought through its decay to longitudinal W/Z bosons. Recent analyses from 36 fb^{-1} of 13 TeV data by ATLAS [91] and CMS [92] searching for heavy vector resonances decaying to a W or Z boson and a Higgs in the $q\bar{q}b\bar{b}$ final state have set a lower limit on the mass of these KK of ~ 2.5 TeV (warped models are equivalent to the Model B considered in the analyses with $g_V \sim g_5\sqrt{k}$). The decay to a pair of intermediate vector bosons has also been exploited to search for KK gravitons in models in which the SM fields propagate in the 5D bulk. The analyses typically reconstruct hadronic W/Z decays using variants of the boosted techniques mentioned previously. An ATLAS analysis [85] combines leptonic and hadronic final states from the KK graviton decay $G^* \rightarrow VV$, where V can represent either a W or Z boson, exclude KK gravitons with masses below 2.3 TeV, for a value of $k/M_P = 1$. CMS VV analysis [93] also provides cross section limits in the context of bulk gravitons; however, a maximum value of $k/M_P = 0.5$ is presented, for which no mass exclusion is possible using the 36 fb^{-1} of 13 TeV data.

The lightest KK states are, in certain models, the partners of the top quark. For example, in 5D composite Higgs models these are colored states with charges $Q = -1/3, 2/3$ and $5/3$ (arising from $SU(2)_L$ doublets with $Y = 7/6, 1/6$), and masses expected to be below the TeV [80]. They can be either singly or pair-produced, and mainly decay into a combination of W/Z with top/bottom quarks [94–97]. An exhaustive review of these searches can be found in Ref. [98]. Of particular note, the $Q = 5/3$ state decays mainly into $W^+t \rightarrow W^+W^+b$, giving a pair of same-sign leptons in the final state. An analysis by ATLAS [99] searching in the lepton-plus-jets final state for evidence of pair production of the $Q = 5/3$ state provides a lower mass limit of 1.25 TeV. A CMS analysis [100] searching for pair production of the $Q = 5/3$ state using both lepton-plus-jets and same sign lepton final states excludes masses below 1.3 TeV. Both LHC experiments have searched for pair production of vector-like quarks T and B of charges $Q = 2/3$ and $-1/3$ respectively, assuming the allowable decays are $T \rightarrow Wb/Zt/Ht$ and $B \rightarrow Wt/Zb/Hb$. In each case, it is assumed the branching fractions of the three decay modes sum to unity, but the individual branching fractions, which are model-dependent, are allowed to vary within this constraint. Both ATLAS [101] and CMS [102–104] obtain lower limits on the mass of the T and B vector-like quark up to 1.3 TeV.

Recent analyses from ATLAS [105] and CMS [106] also search for a single top partner production, the cross section for which is model-dependent [107] but does not carry the kinematic penalty for producing two heavy objects.

86.3.2 Connection with Strongly Coupled Models via the AdS/CFT Correspondence

The AdS/CFT correspondence [8] provides a connection between warped extra-dimensional models and strongly-coupled theories in ordinary 4D. Although the exact connection is only known for certain cases, the AdS/CFT techniques have been very useful to obtain, at the qualitative level, a 4D holographic description of the various phenomena in warped extra-dimensional models [11].

The connection goes as follows. The physics of the bulk AdS₅ models can be interpreted as that of a 4D conformal field theory (CFT) which is strongly coupled. The extra-dimensional coordinate y plays the role of the renormalization scale μ of the CFT by means of the identification $\mu \equiv ke^{-ky}$. Therefore the

UV-boundary corresponds in the CFT to a UV cut-off scale at $A_{UV} = k \sim M_P$, breaking explicitly conformal invariance, while the IR-boundary can be interpreted as a spontaneous breaking of the conformal symmetry at energies $ke^{-k\pi R} \sim \text{TeV}$. Fields localized on the UV-boundary are elementary fields external to the CFT, while fields localized on the IR-boundary and KK states correspond to composite resonances of the CFT. Furthermore, local gauge symmetries in the 5D models, \mathcal{G}_5 , correspond to global symmetries of the CFT, while the UV-boundary symmetry can be interpreted as a gauging of the subgroup \mathcal{H}_{UV} of \mathcal{G}_5 in the CFT. Breaking gauge symmetries by IR-boundary conditions corresponds to the spontaneous breaking $\mathcal{G}_5 \rightarrow \mathcal{H}_{IR}$ in the CFT at energies $\sim ke^{-k\pi R}$. Using this correspondence one can easily derive the 4D massless spectrum of the compactified AdS₅ models. One also has the identification $k^3/M_5^3 \approx 16\pi^2/N^2$ and $g_5^2k \approx 16\pi^2/N^r$ ($r = 1$ or 2 for CFT fields in the fundamental or adjoint representation of the gauge group), where N plays the role of the number of colors of the CFT. Therefore the weak-coupling limit in AdS₅ corresponds to a large- N expansion in the CFT.

Following the above AdS/CFT dictionary one can understand the RS solution to the hierarchy problem from a 4D viewpoint. The equivalent 4D model is a CFT with a TeV mass gap and a Higgs boson emerging as a composite state. In the particular case where the Higgs is the fifth-component of the gauge-boson, A_5 [108], this corresponds to models, similar to those proposed in Ref. [109,110], where the Higgs is a composite pseudo-Goldstone boson arising from the spontaneous breaking $\mathcal{G}_5 \rightarrow \mathcal{H}_{IR}$ in the CFT. The AdS/CFT dictionary tells us that KK states must behave as composite resonances. For example, if the SM gauge bosons propagate in the 5D bulk, the lowest KK $SU(2)_L$ -gauge boson must have properties similar to those of the Techni-rho ρ_T [98] with a coupling to longitudinal W/Z bosons given by $g_5\sqrt{k} \approx g_{\rho T}$, while the coupling to elementary fermions is $g^2/\sqrt{g_5^2k} \approx g^2F_{\rho T}/M_{\rho T}$.

Fermions in compactified AdS₅ also have a simple 4D holographic interpretation. The 4D massless mode described in Sec. 86.3.1 corresponds to an external fermion ψ_i linearly coupled to a fermionic CFT operator \mathcal{O}_i : $\mathcal{L}_{\text{int}} = \lambda_i\bar{\psi}_i\mathcal{O}_i + h.c.$. The dimension of the operator \mathcal{O}_i is related to the 5D fermion mass according to $\text{Dim}[\mathcal{O}_i] = |c_f + 1/2| - 1$. Therefore, by varying c_f one varies $\text{Dim}[\mathcal{O}_i]$, making the coupling λ_i irrelevant ($c_f > 1/2$), marginal ($c_f = 1/2$) or relevant ($c_f < 1/2$). When irrelevant, the coupling is exponentially suppressed at low energies, and then the coupling of ψ_i to the CFT (and eventually to the composite Higgs) is very small. When relevant, the coupling grows in the IR and become as large as g_5 (in units of k), meaning that the fermion is as strongly coupled as the CFT states [76]. In this latter case ψ_i behaves as a composite fermion.

86.3.3 Flat Extra Dimensions

Models with quantum gravity at the TeV scale, as in the ADD scenario, can have extra (flat) dimensions of $1/\text{TeV}$ size, as happens in string scenarios (see, for example, [111]). All SM fields may propagate in these extra dimensions, leading to the possibility of observing their corresponding KK states.

A simple example is to assume that the SM gauge bosons propagate in a flat five-dimensional orbifold S^1/Z_2 of radius R , with the fermions localized on a 4D boundary. The KK gauge bosons behave as sequential SM gauge bosons with a coupling to fermions enhanced by a factor $\sqrt{2}$ [111]. The experimental limits on such sequential gauge bosons could therefore be recast as limits on KK gauge bosons. Such an interpretation of the ATLAS 7 TeV dilepton analysis [112] yielded the bound $1/R > 4.16$ TeV, while a CMS 8 TeV search with a lepton and missing transverse energy in the final state [113] give $1/R > 3.4$ TeV. Indirect bounds from LEP2 require however $1/R \gtrsim 6$ TeV [81,114], a bound that can considerably improve in the future by high-energy measurements of the dilepton invariant mass spectrum from Drell-Yan processes at the LHC [115]. More recent LHC limits on leptonically decaying gauge bosons [42, 82, 116, 117] are not interpreted as bounds on $1/R$ by the collaborations, but the published results allow for independent derivation of such bound.

An alternative scenario, known as Universal Extra Dimensions

(UED) [118] (for a review see, for example, [119]), assumes that all SM fields propagate universally in a flat orbifold S^1/Z_2 with an extra Z_2 parity, called KK-parity, that interchanges the two boundaries. In this case, the lowest KK state is stable and is a Dark Matter candidate. At colliders, the KK particles would have to be created in pairs, and would then cascade decay to the lightest KK particle, which would be stable and escape detection. The UED mass-spectrum depends not only on the extra-dimensional radius R , but also on the cut-off of the 5D theory Λ , since quantum corrections sensitive to ΛR induce mass-splittings between the KK states. Experimental signatures, such as jets or leptons and \cancel{E}_T , would be similar to those of typical R -parity conserving SUSY searches. An interpretation of the recent LHC experimental SUSY searches for UED models has been presented in Refs. [120,121]. A lower bound $1/R > 1.4\text{--}1.5$ TeV was derived for $\Lambda R \sim 5\text{--}35$ [120].

Finally, realistic models of electroweak symmetry breaking can also be constructed with flat extra spatial dimensions, similarly to those in the warped case, requiring, however, the presence of sizeable boundary kinetic terms [122]. There is also the possibility of breaking supersymmetry by boundary conditions [123]. Models of this type could explain naturally the presence of a Higgs boson lighter than $M_D \sim \text{TeV}$ (see, for example, [124–126]).

References

- [1] For a comprehensive collection of the original papers see, “Modern Kaluza-Klein Theories”, edited by T. Appelquist *et al.*, Addison-Wesley (1987).
- [2] N. Arkani-Hamed, S. Dimopoulos and G. Dvali, Phys. Lett. **B429**, 263 (1998), [hep-ph/9803315].
- [3] L. Randall and R. Sundrum, Phys. Rev. Lett. **83**, 3370 (1999), [hep-ph/9905221].
- [4] H. Davoudiasl, J. L. Hewett and T. G. Rizzo, Phys. Lett. **B473**, 43 (2000), [hep-ph/9911262].
- [5] A. Pomarol, Phys. Lett. **B486**, 153 (2000), [hep-ph/9911294].
- [6] S. Chang *et al.*, Phys. Rev. **D62**, 084025 (2000), [hep-ph/9912498].
- [7] T. Gherghetta and A. Pomarol, Nucl. Phys. **B586**, 141 (2000), [hep-ph/0003129].
- [8] J. M. Maldacena, Int. J. Theor. Phys. **38**, 1113 (1999), [Adv. Theor. Math. Phys.2,231(1998)], [hep-th/9711200].
- [9] E. Witten, Adv. Theor. Math. Phys. **2**, 253 (1998), [hep-th/9802150].
- [10] S. S. Gubser, I. R. Klebanov and A. M. Polyakov, Phys. Lett. **B428**, 105 (1998), [hep-th/9802109].
- [11] N. Arkani-Hamed, M. Porrati and L. Randall, JHEP **08**, 017 (2001), [hep-th/0012148].
- [12] ATLAS public results are available on WWW at <https://twiki.cern.ch/twiki/bin/view/AtlasPublic>.
- [13] CMS public results are available on WWW at <https://cms-results.web.cern.ch/cms-results/public-results/publications>.
- [14] Z. Chacko, M. A. Luty and E. Ponton, JHEP **07**, 036 (2000), [hep-ph/9909248].
- [15] N. Arkani-Hamed, S. Dimopoulos and G. R. Dvali, Phys. Rev. **D59**, 086004 (1999), [hep-ph/9807344].
- [16] R. Rattazzi, hep-ph/0607055 (2006); I. Antoniadis, Yellow report CERN-2002-002 (2002).
- [17] J. D. Lykken, Phys. Rev. **D54**, R3693 (1996), [hep-th/9603133].
- [18] I. Antoniadis *et al.*, Phys. Lett. **B436**, 257 (1998), [hep-ph/9804398].
- [19] G. F. Giudice, R. Rattazzi and J. D. Wells, Nucl. Phys. **B544**, 3 (1999), [hep-ph/9811291].
- [20] N. Arkani-Hamed *et al.*, Phys. Rev. **D62**, 105002 (2000), [hep-ph/9912453].
- [21] E. G. Adelberger *et al.*, Prog. Part. Nucl. Phys. **62**, 102 (2009).
- [22] J. Murata and S. Tanaka, Class. Quant. Grav. **32**, 3, 033001 (2015), [arXiv:1408.3588].
- [23] W.-H. Tan *et al.*, Phys. Rev. Lett. **116**, 13, 131101 (2016).
- [24] C. Hanhart *et al.*, Phys. Lett. **B509**, 1 (2001), [arXiv:astro-ph/0102063].
- [25] S. Hannestad and G. G. Raffelt, Phys. Rev. **D67**, 125008 (2003), [Erratum: Phys. Rev.D69,029901(2004)], [hep-ph/0304029].
- [26] L. J. Hall and D. Tucker-Smith, Phys. Rev. **D60**, 085008 (1999), [hep-ph/9904267].
- [27] E. A. Mirabelli, M. Perelstein and M. E. Peskin, Phys. Rev. Lett. **82**, 2236 (1999), [hep-ph/9811337].
- [28] T. Han, J. D. Lykken and R.-J. Zhang, Phys. Rev. **D59**, 105006 (1999), [hep-ph/9811350].
- [29] A. M. Sirunyan *et al.* (CMS), Phys. Rev. **D97**, 9, 092005 (2018), [arXiv:1712.02345].
- [30] M. Aaboud *et al.* (ATLAS), JHEP **01**, 126 (2018), [arXiv:1711.03301].
- [31] A. M. Sirunyan *et al.* (CMS), JHEP **02**, 074 (2019), [arXiv:1810.00196].
- [32] M. Aaboud *et al.* (ATLAS), Eur. Phys. J. **C77**, 6, 393 (2017), [arXiv:1704.03848].
- [33] S. Cullen, M. Perelstein and M. E. Peskin, Phys. Rev. **D62**, 055012 (2000), [hep-ph/0001166].
- [34] A. M. Sirunyan *et al.* (CMS), JHEP **08**, 130 (2018), [arXiv:1806.00843].
- [35] M. Aaboud *et al.* (ATLAS), Phys. Rev. **D96**, 5, 052004 (2017), [arXiv:1703.09127].
- [36] J. L. Hewett, Phys. Rev. Lett. **82**, 4765 (1999), [hep-ph/9811356].
- [37] G. F. Giudice and A. Strumia, Nucl. Phys. **B663**, 377 (2003), [hep-ph/0301232].
- [38] A. M. Sirunyan *et al.* (CMS), Eur. Phys. J. **C78**, 9, 789 (2018), [arXiv:1803.08030].
- [39] M. Aaboud *et al.* (ATLAS), Phys. Lett. **B775**, 105 (2017), [arXiv:1707.04147].
- [40] A. M. Sirunyan *et al.* (CMS), Phys. Rev. **D98**, 9, 092001 (2018), [arXiv:1809.00327].
- [41] A. M. Sirunyan *et al.* (CMS), JHEP **04**, 114 (2019), [arXiv:1812.10443].
- [42] G. Aad *et al.* (ATLAS), Phys. Lett. **B796**, 68 (2019), [arXiv:1903.06248].
- [43] S. B. Giddings and S. D. Thomas, Phys. Rev. **D65**, 056010 (2002), [hep-ph/0106219].
- [44] S. Dimopoulos and G. L. Landsberg, Phys. Rev. Lett. **87**, 161602 (2001), [hep-ph/0106295].
- [45] P. Kanti, Int. J. Mod. Phys. **A19**, 4899 (2004), [hep-ph/0402168].
- [46] R. C. Myers and M. J. Perry, Annals Phys. **172**, 304 (1986).
- [47] A. M. Sirunyan *et al.* (CMS), JHEP **11**, 042 (2018), [arXiv:1805.06013].
- [48] G. Aad *et al.* (ATLAS), JHEP **03**, 026 (2016), [arXiv:1512.02586].
- [49] M. Aaboud *et al.* (ATLAS), Phys. Lett. **B760**, 520 (2016), [arXiv:1606.02265].
- [50] C. Kilic *et al.*, Phys. Rev. **D89**, 1, 016003 (2014), [arXiv:1207.3525].
- [51] V. Khachatryan *et al.* (CMS), Phys. Rev. **D90**, 3, 032005 (2014), [arXiv:1405.7653].
- [52] P. Meade and L. Randall, JHEP **05**, 003 (2008), [arXiv:0708.3017].
- [53] A. M. Sirunyan *et al.* (CMS), Phys. Lett. **B774**, 279 (2017), [arXiv:1705.01403].

- [54] A. M. Sirunyan *et al.* (CMS), JHEP **04**, 073 (2018), [arXiv:1802.01122].
- [55] M. Aaboud *et al.* (ATLAS), Phys. Rev. **D98**, 9, 092008 (2018), [arXiv:1807.06573].
- [56] S. Dimopoulos and R. Emparan, Phys. Lett. **B526**, 393 (2002), [hep-ph/0108060].
- [57] W. D. Goldberger and M. B. Wise, Phys. Rev. Lett. **83**, 4922 (1999), [hep-ph/9907447].
- [58] J. Garriga and A. Pomarol, Phys. Lett. **B560**, 91 (2003), [hep-th/0212227].
- [59] See talk by R. Rattazzi at Planck 2010, CERN.
- [60] B. Bellazzini *et al.*, Eur. Phys. J. **C74**, 2790 (2014), [arXiv:1305.3919].
- [61] F. Coradeschi *et al.*, JHEP **11**, 057 (2013), [arXiv:1306.4601].
- [62] E. Megias and O. Pujolas, JHEP **08**, 081 (2014), [arXiv:1401.4998].
- [63] K. Blum *et al.*, JHEP **03**, 099 (2015), [arXiv:1410.1873].
- [64] A. Efrati *et al.*, Phys. Rev. **D91**, 5, 055034 (2015), [arXiv:1410.2225].
- [65] F. Abu-Ajamieh, J. S. Lee and J. Terning, JHEP **10**, 050 (2018), [arXiv:1711.02697].
- [66] E. P. H. Davoudiasl, S. Gopalakrishna and J. Santiago, New J. Phys. **12**, 075011 (2010), [arXiv:0908.1968].
- [67] T. Gherghetta, in “Physics of the large and the small, TASI 09, proceedings of the Theoretical Advanced Study Institute in Elementary Particle Physics, Boulder, Colorado, USA, 1-26 June 2009,” 165–232 (2011), [arXiv:1008.2570].
- [68] Y. Grossman and M. Neubert, Phys. Lett. **B474**, 361 (2000), [hep-ph/9912408].
- [69] S. J. Huber and Q. Shafi, Phys. Lett. **B498**, 256 (2001), [hep-ph/0010195].
- [70] A. Delgado, A. Pomarol and M. Quiros, JHEP **01**, 030 (2000), [hep-ph/9911252].
- [71] K. Agashe, G. Perez and A. Soni, Phys. Rev. **D71**, 016002 (2005), [hep-ph/0408134].
- [72] M. Bauer *et al.*, JHEP **09**, 017 (2010), [arXiv:0912.1625].
- [73] A. Pomarol, Int. J. Mod. Phys. **A24**, 61 (2009), [In *Kane, Gordon (ed.) et al.: Perspectives on LHC physics*, 259(2008)].
- [74] Y. Hosotani, Phys. Lett. **126B**, 309 (1983).
- [75] K. Agashe *et al.*, JHEP **08**, 050 (2003), [hep-ph/0308036].
- [76] K. Agashe, R. Contino and A. Pomarol, Nucl. Phys. **B719**, 165 (2005), [hep-ph/0412089].
- [77] For a review see, for example, R. Contino, arXiv:1005.4269.
- [78] See, for example, PDG review of Higgs boson in this *Review*.
- [79] G. F. Giudice *et al.*, JHEP **06**, 045 (2007), [hep-ph/0703164].
- [80] R. Contino, L. Da Rold and A. Pomarol, Phys. Rev. **D75**, 055014 (2007), [hep-ph/0612048].
- [81] R. Barbieri *et al.*, Nucl. Phys. **B703**, 127 (2004), [hep-ph/0405040].
- [82] A. M. Sirunyan *et al.* (CMS), JHEP **06**, 120 (2018), [arXiv:1803.06292].
- [83] A. M. Sirunyan *et al.* (CMS), Phys. Rev. Lett. **122**, 12, 121803 (2019), [arXiv:1811.09689].
- [84] M. Aaboud *et al.* (ATLAS), JHEP **01**, 030 (2019), [arXiv:1804.06174].
- [85] M. Aaboud *et al.* (ATLAS), Phys. Rev. **D98**, 5, 052008 (2018), [arXiv:1808.02380].
- [86] A. M. Sirunyan *et al.* (CMS) (2019), [arXiv:1906.05977].
- [87] K. Agashe *et al.*, Phys. Rev. **D76**, 036006 (2007), [hep-ph/0701186].
- [88] A. M. Sirunyan *et al.* (CMS), JHEP **04**, 031 (2019), [arXiv:1810.05905].
- [89] M. Aaboud *et al.* (ATLAS), Phys. Rev. **D99**, 9, 092004 (2019), [arXiv:1902.10077].
- [90] M. Aaboud *et al.* (ATLAS), Eur. Phys. J. **C78**, 7, 565 (2018), [arXiv:1804.10823].
- [91] M. Aaboud *et al.* (ATLAS), Phys. Lett. **B774**, 494 (2017), [arXiv:1707.06958].
- [92] A. M. Sirunyan *et al.* (CMS), Eur. Phys. J. **C77**, 9, 636 (2017), [arXiv:1707.01303].
- [93] A. M. Sirunyan *et al.* (CMS) (2019), [arXiv:1906.00057].
- [94] R. Contino and G. Servant, JHEP **06**, 026 (2008), [arXiv:0801.1679].
- [95] J. A. Aguilar-Saavedra, JHEP **11**, 030 (2009), [arXiv:0907.3155].
- [96] J. Mrazek and A. Wulzer, Phys. Rev. **D81**, 075006 (2010), [arXiv:0909.3977].
- [97] G. Dissertori *et al.*, JHEP **09**, 019 (2010), [arXiv:1005.4414].
- [98] See, for example, PDG review of Technicolor searches in this volume.
- [99] M. Aaboud *et al.* (ATLAS), JHEP **10**, 141 (2017), [arXiv:1707.03347].
- [100] A. M. Sirunyan *et al.* (CMS), JHEP **03**, 082 (2019), [arXiv:1810.03188].
- [101] M. Aaboud *et al.* (ATLAS), Phys. Rev. Lett. **121**, 21, 211801 (2018), [arXiv:1808.02343].
- [102] A. M. Sirunyan *et al.* (CMS), Phys. Lett. **B779**, 82 (2018), [arXiv:1710.01539].
- [103] A. M. Sirunyan *et al.* (CMS), JHEP **08**, 177 (2018), [arXiv:1805.04758].
- [104] A. M. Sirunyan *et al.* (CMS), Eur. Phys. J. **C79**, 4, 364 (2019), [arXiv:1812.09768].
- [105] M. Aaboud *et al.* (ATLAS), JHEP **05**, 164 (2019), [arXiv:1812.07343].
- [106] A. M. Sirunyan *et al.* (CMS), Phys. Lett. **B781**, 574 (2018), [arXiv:1708.01062].
- [107] A. De Simone *et al.*, JHEP **04**, 004 (2013), [arXiv:1211.5663].
- [108] R. Contino, Y. Nomura and A. Pomarol, Nucl. Phys. **B671**, 148 (2003), [hep-ph/0306259].
- [109] H. Georgi, D. B. Kaplan and P. Galison, Phys. Lett. **143B**, 152 (1984).
- [110] D. B. Kaplan and H. Georgi, Phys. Lett. **136B**, 183 (1984).
- [111] I. Antoniadis and K. Benakli, Int. J. Mod. Phys. **A15**, 4237 (2000), [hep-ph/0007226].
- [112] G. Aad *et al.* (ATLAS), JHEP **11**, 138 (2012), [arXiv:1209.2535].
- [113] V. Khachatryan *et al.* (CMS), Phys. Rev. **D91**, 9, 092005 (2015), [arXiv:1408.2745].
- [114] K. Cheung and G. L. Landsberg, Phys. Rev. **D65**, 076003 (2002), [hep-ph/0110346].
- [115] M. Farina *et al.*, Phys. Lett. **B772**, 210 (2017), [arXiv:1609.08157].
- [116] G. Aad *et al.* (ATLAS) (2019), [arXiv:1906.05609].
- [117] A. M. Sirunyan *et al.* (CMS), JHEP **06**, 128 (2018), [arXiv:1803.11133].
- [118] T. Appelquist, H.-C. Cheng and B. A. Dobrescu, Phys. Rev. **D64**, 035002 (2001), [hep-ph/0012100].
- [119] A. Datta, K. Kong and K. T. Matchev, New J. Phys. **12**, 075017 (2010), [arXiv:1002.4624].
- [120] N. Deutschmann, T. Flacke and J. S. Kim, Phys. Lett. **B771**, 515 (2017), [arXiv:1702.00410].
- [121] J. Beuria *et al.*, Comput. Phys. Commun. **226**, 187 (2018), [arXiv:1702.00413].

- [122] G. Panico, M. Safari and M. Serone, JHEP **02**, 103 (2011), [arXiv:1012.2875].
- [123] J. Scherk and J. H. Schwarz, Phys. Lett. **82B**, 60 (1979).
- [124] A. Pomarol and M. Quiros, Phys. Lett. **B438**, 255 (1998), [hep-ph/9806263].
- [125] I. Antoniadis *et al.*, Nucl. Phys. **B544**, 503 (1999), [hep-ph/9810410].
- [126] R. Barbieri, L. J. Hall and Y. Nomura, Phys. Rev. **D63**, 105007 (2001), [hep-ph/0011311].

87. W' -Boson Searches

Revised November, 2019 by B.A. Dobrescu (Fermilab) and S. Willocq (U. Massachusetts).

The W' boson is a massive hypothetical particle of spin 1 and electric charge ± 1 , which is a color singlet and is predicted in various extensions of the Standard Model (SM).

87.1 W' couplings to quarks and leptons

The Lagrangian terms describing the couplings of a W'^+ boson to fermions are given by

$$\frac{W'^+_\mu}{\sqrt{2}} \left[\bar{u}_i (C_{q_{ij}}^R P_R + C_{q_{ij}}^L P_L) \gamma^\mu d_j + \bar{\nu}_i (C_{\ell_{ij}}^R P_R + C_{\ell_{ij}}^L P_L) \gamma^\mu e_j \right]. \quad (87.1)$$

Here, u, d, ν , and e are the SM fermions in the mass eigenstate basis, $i, j = 1, 2, 3$ label the fermion generation, and $P_{R,L} = (1 \pm \gamma_5)/2$. The coefficients $C_{q_{ij}}^L, C_{q_{ij}}^R, C_{\ell_{ij}}^L$, and $C_{\ell_{ij}}^R$ are complex dimensionless parameters. If $C_{\ell_{ij}}^R \neq 0$, then the i th generation includes a right-handed neutrino. Using this notation, the SM W couplings are $C_q^L = g V_{\text{CKM}}, C_\ell^L = g \approx 0.63$ and $C_q^R = C_\ell^R = 0$.

Unitarity considerations imply that the W' boson is associated with a spontaneously-broken gauge symmetry. This is true even when it is a composite particle (e.g. ρ^\pm -like bound states [1]) if its mass is much smaller than the compositeness scale, or a Kaluza-Klein mode in theories where the W boson propagates in extra dimensions [2]. The simplest extension of the electroweak gauge group that includes a W' boson is $SU(2)_1 \times SU(2)_2 \times U(1)$, but larger groups are encountered in some theories. A generic property of these gauge theories is that they also include a Z' boson [3]; the W' -to- Z' mass ratio is often a free parameter.

A tree-level mass mixing may be induced between the electrically-charged gauge bosons. Upon diagonalization of their mass matrix, the W -to- Z mass ratio and the couplings of the observed W boson are shifted from the SM values. Their measurements imply that the mixing angle, θ_+ , between the gauge eigenstates must be smaller than about 10^{-2} . In certain theories the mixing is negligible (e.g., due to a new parity [4]), even when the W' mass is near the electroweak scale. Note that $SU(2)$ gauge invariance suppresses the kinetic mixing between the W and W' bosons (in contrast to the case of a Z' boson [3]).

The W' coupling to WZ is fixed by Lorentz and gauge invariances, and to leading order in θ_+ is given by [5]

$$\frac{g \theta_+ i}{\cos \theta_W} \left[W'^+_\mu (W^-_\nu Z^{\nu\mu} + Z_\nu W^{-\mu\nu}) + Z^\nu W^{-\mu} W'^+_{\nu\mu} \right] + \text{H.c.}, \quad (87.2)$$

where $W^{\mu\nu} \equiv \partial^\mu W^\nu - \partial^\nu W^\mu$, etc. The θ_W dependence shown here corrects the one given in Ref. [6], which has been referred to as the Extended Gauge Model by the experimental collaborations. The W' coupling to Wh^0 , where h^0 is the SM Higgs boson, is

$$-\xi_h g_{W'} M_W W'^+_\mu W^{\mu-} h^0 + \text{H.c.}, \quad (87.3)$$

where $g_{W'}$ is the gauge coupling of the W' boson, and the coefficient ξ_h satisfies $\xi_h \leq 1$ in simple Higgs sectors [5].

In models based on the “left-right symmetric” gauge group [7], $SU(2)_L \times SU(2)_R \times U(1)_{B-L}$, the SM fermions that couple to the W boson transform as doublets under $SU(2)_L$ while the other fermions transform as doublets under $SU(2)_R$. Consequently, the W' boson couples primarily to right-handed fermions; its coupling to left-handed fermions arises due to the θ_+ mixing, so that C_q^L is proportional to the CKM matrix and its elements are much smaller than the diagonal elements of C_q^R . Generically, C_q^R does not need to be proportional to V_{CKM} .

There are many other models based on the $SU(2)_1 \times SU(2)_2 \times U(1)$ gauge symmetry. In the “alternate left-right” model [8], all the couplings shown in Eq. (87.1) vanish, but there are some new fermions such that the W' boson couples to pairs involving a SM fermion and a new fermion. In the “unified SM” [9], the left-handed quarks are doublets under one $SU(2)$, and the left-handed leptons are doublets under a different $SU(2)$, leading to a mostly leptophobic W' boson: $C_{\ell_{ij}}^L \ll C_{q_{ij}}^L$ and $C_{\ell_{ij}}^R = C_{q_{ij}}^R = 0$. Fermions of different generations may also transform

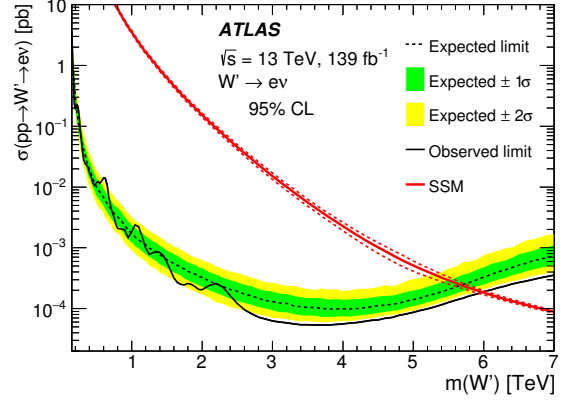


Figure 87.1: Upper limit on $\sigma(pp \rightarrow W'X) B(W' \rightarrow e\nu)$ from ATLAS [12]. The red line shows the theoretical prediction in the Sequential SM.

as doublets under different $SU(2)$ gauge groups [10]. In particular, the couplings to third generation quarks may be enhanced [11].

It is also possible that the W' couplings to SM fermions are highly suppressed. For example, if the quarks and leptons are singlets under one $SU(2)$ [13], then the couplings are proportional to the tiny mixing angle θ_+ . Similar suppressions may arise if some vectorlike fermions mix with the SM fermions [14].

Gauge groups that embed the electroweak symmetry, such as $SU(3)_W \times U(1)$ or $SU(4)_W \times U(1)$, also include one or more W' bosons [15].

87.2 Collider searches

At LEP-II, W' bosons could have been produced in pairs via their photon and Z couplings. The production cross section is large enough to rule out $M_{W'} < \sqrt{s}/2 \approx 105$ GeV for most patterns of decay modes.

At hadron colliders, W' bosons can be detected through resonant pair production of fermions (f and f') or electroweak bosons with a net electric charge equal to ± 1 . When W' has a width much smaller than its mass ($M_{W'}/\Gamma_{W'} \lesssim 7\%$), the contribution of the s -channel W' exchange to the total rate for $pp \rightarrow f f' X$, where X is any final state, may be approximated by the branching fraction $B(W' \rightarrow f f')$ times the production cross section

$$\sigma(pp \rightarrow W'X) \simeq \frac{\pi}{6s} \sum_{i,j} [(C_{q_{ij}}^L)^2 + (C_{q_{ij}}^R)^2] w_{ij} (M_{W'}^2/s, M_{W'}). \quad (87.4)$$

The functions w_{ij} include the information about proton structure, and are given to leading order in α_s by

$$w_{ij}(z, \mu) = \int_z^1 \frac{dx}{x} \left[u_i(x, \mu) \bar{d}_j\left(\frac{z}{x}, \mu\right) + \bar{u}_i(x, \mu) d_j\left(\frac{z}{x}, \mu\right) \right], \quad (87.5)$$

where $u_i(x, \mu)$ and $d_i(x, \mu)$ are the parton distributions inside the proton at the factorization scale μ and parton momentum fraction x for the up- and down-type quarks of the i th generation, respectively. QCD corrections to W' production are sizable (they also include quark-gluon initial states), but preserve the above factorization of couplings at next-to-leading order [16].

The most commonly studied W' signal consists of a high-momentum electron or muon and large missing transverse momentum. The signal transverse mass distribution forms a Jacobian peak with its endpoint at $M_{W'}$ (see Fig. 1 (top) of Ref. [12]). Given that the branching fractions for $W' \rightarrow e\nu$ and $W' \rightarrow \mu\nu$ could be very different, the results in these channels should be presented separately. Searches in these channels often implicitly assume that the left-handed couplings vanish (no interference between W and W'), and that the right-handed neutrino is light compared to the W' boson and escapes the detector. An example of parameter values that satisfy these assumptions is $C_q^R = g V_{\text{CKM}}, C_\ell^R = g, C_q^L = C_\ell^L = 0$, which define a model that

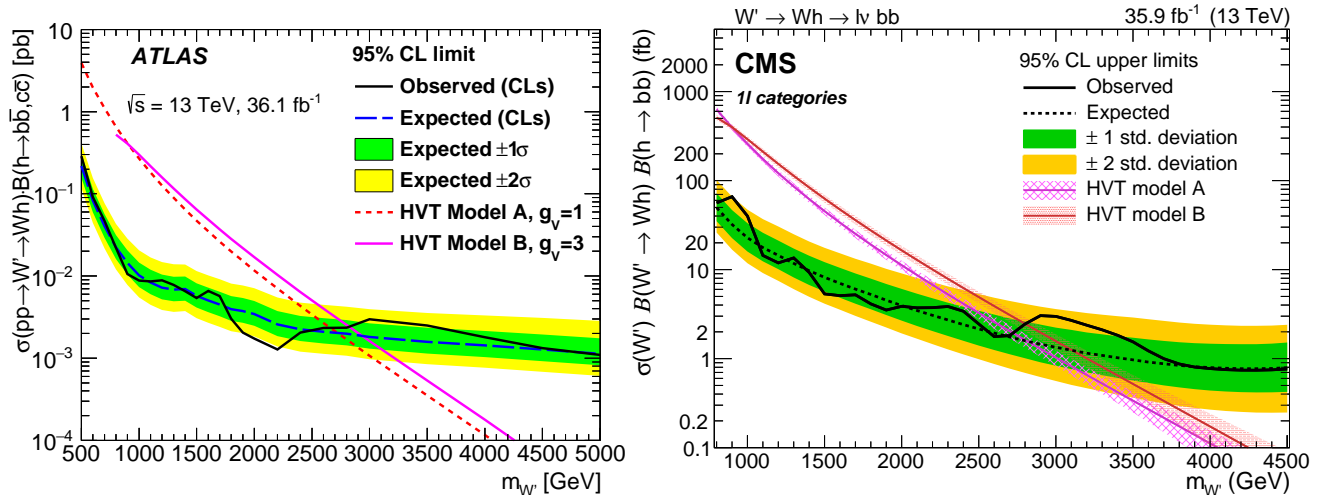


Figure 87.2: Upper limits on W' production cross section times branching fraction into a W and a SM Higgs boson decaying into heavy-flavor quarks, from ATLAS [17] (left) and CMS [18] (right).

preserves lepton universality and predicts the same total cross section as the Sequential SM used in many W' searches. However, if a W' boson were discovered and the final state fermions have left-handed helicity, then the effects of $W - W'$ interference could be observed [19], providing information about the W' couplings. The effects of the W' width on interference are discussed in [20].

In the $e\nu$ channel, the ATLAS and CMS collaborations set limits on the W' production cross section times branching fraction (and thus indirectly on the W' couplings). These limits are set for $M_{W'}$ in the 0.15 – 7 TeV range and are based on 36–139 fb^{-1} at $\sqrt{s} = 13$ TeV [12, 21], as shown in Fig. 87.1 for the most stringent limits. ATLAS sets the strongest mass limit $M_{W'} > 6.0$ TeV in the Sequential SM (all limits in this mini-review are at the 95% CL). The coupling limits are much weaker for $M_{W'} < 150$ GeV, a range last explored with the Tevatron at $\sqrt{s} = 1.8$ TeV [22].

In the $\mu\nu$ channel, ATLAS and CMS set rate limits for $M_{W'}$ in the 0.15–7 TeV range from the same analyses as mentioned above, with the strongest mass lower limit of 5.1 TeV in the Sequential SM set by ATLAS [12] using 139 fb^{-1} of $\sqrt{s} = 13$ TeV data. When combined with the $e\nu$ channel assuming lepton universality, the upper limit on the $\sqrt{s} = 13$ TeV cross section times branching fraction to $\ell\nu$ varies between 0.05 and 2.1 fb for $M_{W'}$ values in the range between 1 and 6 TeV [12]. Only weak limits on $W' \rightarrow \mu\nu$ exist for $M_{W'} < 150$ GeV [23]. Note that masses of the order of the electroweak scale are interesting from a theory point of view, while lepton universality does not necessarily apply to a W' boson.

Dedicated searches for $W' \rightarrow \tau\nu$ have been performed by CMS at 8 TeV [24] and both ATLAS and CMS with 36 fb^{-1} at 13 TeV [25, 26]. Limits are set on $\sigma \cdot B$ for $M_{W'}$ between 0.4 and 4 TeV for the former and between 0.4 and 5.6 TeV for the latter. A mass lower limit of 4.0 TeV is set in the Sequential SM and the upper limit on the cross section times branching fraction to $\tau\nu$ at 13 TeV varies between 1.7 and 12 fb for $M_{W'}$ values in the range between 1 and 5 TeV [26].

The W' decay into a charged lepton and a right-handed neutrino, ν_R , may also be followed by the ν_R decay through a virtual W' boson into a charged lepton and two quark jets. The CMS [27] and ATLAS [28] searches in the $eejj$ and $\mu\mu jj$ channels have set limits on the cross section times branching fraction as a function of the ν_R mass or of $M_{W'}$. No requirement is placed on the charge of the lepton pair. A related W' search in the $\tau\tau jj$ channel with hadronic τ decays was also performed by CMS [29].

The $t\bar{b}$ channel is particularly important because a W' boson that couples only to right-handed fermions cannot decay to leptons when the right-handed neutrinos are heavier than $M_{W'}$. Additional motivations are provided by a W' boson with enhanced couplings to the third generation [11], and by a leptophobic W' boson. The usual signature consists of a leptonically-decaying W boson and two b -jets. Recent studies have also incorporated

the fully hadronic decay channel for $M_{W'} \gg m_t$ with the use of jet substructure techniques to tag highly boosted top-jets. For a detailed discussion of this channel, see Ref. [30].

Searches for dijet resonances may be used to set limits on $W' \rightarrow q\bar{q}'$. ATLAS [31] and CMS [32] provide similar coverage in the $\sim 1.5 - 8.0$ TeV mass range with 139 and 137 fb^{-1} of data, respectively, collected at $\sqrt{s} = 13$ TeV. Interpretation in terms of W' decays with 139 fb^{-1} of 13 TeV data yields a W' mass lower limit of 4.0 TeV in the Sequential SM [31]. For masses in the range $\sim 0.5 - 1.5$ TeV, analyses based on jets reconstructed on-line provide the best sensitivity because they circumvent trigger bandwidth limitations [33, 34]. For W' masses below ~ 0.5 TeV, the best limits are set in novel analyses exploiting boosted technologies and initial state radiation [35–38]. Cross-section limits for W' masses below ~ 1.5 TeV can be derived from the dijet limits on Z' bosons summarized in Ref. [3].

In some theories [4] the W' couplings to SM fermions are suppressed by discrete symmetries. W' production then occurs in pairs, through a photon or Z boson. The decay modes are model-dependent and often involve other new particles. The ensuing collider signals arise from cascade decays and typically include missing transverse momentum.

Searches for WZ resonances at the LHC [30] have focused on the process $pp \rightarrow W' \rightarrow WZ$ with the production mainly from $u\bar{d} \rightarrow W'$ assuming SM-like couplings to quarks. ATLAS and CMS have set the upper limits on the $W'WZ$ coupling for $M_{W'}$ in the 0.2 – 5.0 TeV range with a combination of fully leptonic, semi-leptonic and fully hadronic channels with $\sim 36 \text{fb}^{-1}$ at 13 TeV [39, 40] (see also Ref. [30]). The strongest lower limits on the W' mass are set by ATLAS [41] and CMS [42] at 13 TeV with 139 fb^{-1} and 77 fb^{-1} , respectively, in the $WZ \rightarrow (jj)(jj)$ final state, where the parentheses represent a resonance. The lower limit on $M_{W'}$ is 3.4 TeV in the context of the Heavy Vector Triplet (HVT) weakly-coupled scenario A [43]. A fermiophobic W' boson that couples to WZ may be produced at hadron colliders in association with a Z boson, or via WZ fusion. This would give rise to $(WZ)Z$ and $(WZ)jj$ final states [44].

W' bosons have also been searched for in final states with a W boson and a SM Higgs boson in the channels $W \rightarrow \ell\nu$ or $W \rightarrow q\bar{q}'$ and $h^0 \rightarrow b\bar{b}$ by ATLAS [17, 45] and CMS [18, 46] with 36 fb^{-1} at $\sqrt{s} = 13$ TeV. Cross-section limits are set for W' masses in the range between 0.5 and 5.0 TeV. The ATLAS and CMS 13 TeV analyses both set the most stringent lower limit on the mass: $M_{W'} > 2.7$ TeV for the HVT weakly-coupled scenario A, as shown in Fig. 87.2.

87.3 Low-energy constraints

The properties of W' bosons are also constrained by measurements of processes at energies much below $M_{W'}$. The bounds on

$W - W'$ mixing [47] are mostly due to the change in W properties compared to the SM. Limits on deviations in the ZWW couplings provide a leading constraint for fermiophobic W' bosons [14].

Constraints arising from low-energy effects of W' exchange are strongly model-dependent. If the W' couplings to quarks are not suppressed, then box diagrams involving a W and a W' boson contribute to neutral meson-mixing. In the case of W' couplings to right-handed quarks as in the left-right symmetric model, the limit from $K_L - K_S$ mixing is severe: $M_{W'} > 2.9$ TeV for $C_q^R = gV_{CKM}$ [48]. However, if no correlation between the W' and W couplings is assumed, then the limit on $M_{W'}$ may be significantly relaxed [49].

W' exchange also contributes at tree level to various low-energy processes. In particular, it would impact the measurement of the Fermi constant G_F in muon decay, which in turn would change the predictions of many other electroweak processes. A recent test of parity violation in polarized muon decay [50] has set limits of about 600 GeV on $M_{W'}$, assuming W' couplings to right-handed leptons as in left-right symmetric models and a light ν_R . There are also W' contributions to the neutron electric dipole moment, β decays, and other processes [47].

If right-handed neutrinos have Majorana masses, then there are tree-level contributions to neutrinoless double-beta decay, and a limit on $M_{W'}$ versus the ν_R mass may be derived [51]. For ν_R masses below a few GeV, the W' boson contributes to leptonic and semileptonic B meson decays, so that limits may be placed on various combinations of W' parameters [49]. For ν_R masses below ~ 30 MeV, the most stringent constraints on $M_{W'}$ are due to the limits on ν_R emission from supernovae.

References

- [1] M. Bando, T. Kugo and K. Yamawaki, Phys. Rept. **164**, 217 (1988).
- [2] H.-C. Cheng *et al.*, Phys. Rev. **D64**, 065007 (2001), [hep-th/0104179].
- [3] See the Section on “ Z' -boson searches” in this *Review*.
- [4] H.-C. Cheng and I. Low, JHEP **09**, 051 (2003), [hep-ph/0308199].
- [5] B. A. Dobrescu and Z. Liu, JHEP **10**, 118 (2015), [arXiv:1507.01923].
- [6] G. Altarelli, B. Mele and M. Ruiz-Altaba, Z. Phys. **C45**, 109 (1989), [Erratum: Z. Phys. **C47**, 676 (1990)].
- [7] R. N. Mohapatra and J. C. Pati, Phys. Rev. **D11**, 566 (1975).
- [8] K. S. Babu, X.-G. He and E. Ma, Phys. Rev. **D36**, 878 (1987).
- [9] H. Georgi, E. E. Jenkins and E. H. Simmons, Nucl. Phys. **B331**, 541 (1990).
- [10] X.-y. Li and E. Ma, J. Phys. **G19**, 1265 (1993), [hep-ph/9208210].
- [11] D. J. Muller and S. Nandi, Phys. Lett. **B383**, 345 (1996), [hep-ph/9602390].
- [12] G. Aad *et al.* (ATLAS), Phys. Rev. **D100**, 052013 (2019), [arXiv:1906.05609].
- [13] A. Donini *et al.*, Nucl. Phys. **B507**, 51 (1997), [hep-ph/9705450].
- [14] R. S. Chivukula *et al.*, Phys. Rev. **D74**, 075011 (2006), [hep-ph/0607124].
- [15] F. Pisano and V. Pleitez, Phys. Rev. **D46**, 410 (1992), [hep-ph/9206242].
- [16] Z. Sullivan, Phys. Rev. **D66**, 075011 (2002), [hep-ph/0207290].
- [17] M. Aaboud *et al.* (ATLAS), JHEP **03**, 174 (2018), [Erratum: JHEP **11**, 051 (2018)], [arXiv:1712.06518].
- [18] A. M. Sirunyan *et al.* (CMS), JHEP **11**, 172 (2018), [arXiv:1807.02826].
- [19] T. G. Rizzo, JHEP **05**, 037 (2007), [arXiv:0704.0235].
- [20] E. Accomando *et al.*, Phys. Rev. **D85**, 115017 (2012), [arXiv:1110.0713].
- [21] A. M. Sirunyan *et al.* (CMS), JHEP **06**, 128 (2018), [arXiv:1803.11133].
- [22] F. Abe *et al.* (CDF), Phys. Rev. Lett. **74**, 2900 (1995).
- [23] F. Abe *et al.* (CDF), Phys. Rev. Lett. **67**, 2609 (1991).
- [24] V. Khachatryan *et al.* (CMS), Phys. Lett. **B755**, 196 (2016), [arXiv:1508.04308].
- [25] M. Aaboud *et al.* (ATLAS), Phys. Rev. Lett. **120**, 161802 (2018), [arXiv:1801.06992].
- [26] A. M. Sirunyan *et al.* (CMS), Phys. Lett. **B792**, 107 (2019), [arXiv:1807.11421].
- [27] A. M. Sirunyan *et al.* (CMS), JHEP **05**, 148 (2018), [arXiv:1803.11116].
- [28] M. Aaboud *et al.* (ATLAS), Submitted to: Phys. Lett. (2019), [arXiv:1904.12679].
- [29] A. M. Sirunyan *et al.* (CMS), JHEP **03**, 170 (2019), [arXiv:1811.00806].
- [30] K.M. Black *et al.*, “Dynamical electroweak symmetry breaking” in this *Review*.
- [31] G. Aad *et al.* (ATLAS) (2019), [arXiv:1910.08447].
- [32] CMS Collab., CMS PAS EXO-19-012, Jul. 2019.
- [33] M. Aaboud *et al.* (ATLAS), Phys. Rev. Lett. **121**, 081801 (2018), [arXiv:1804.03496].
- [34] A. M. Sirunyan *et al.* (CMS), JHEP **08**, 130 (2018), [arXiv:1806.00843].
- [35] M. Aaboud *et al.* (ATLAS), Phys. Lett. **B788**, 316 (2019), [arXiv:1801.08769].
- [36] M. Aaboud *et al.* (ATLAS), Phys. Lett. **B795**, 56 (2019), [arXiv:1901.10917].
- [37] A. M. Sirunyan *et al.* (CMS) (2019), [arXiv:1909.04114].
- [38] A. M. Sirunyan *et al.* (CMS) (2019), [arXiv:1905.10331].
- [39] M. Aaboud *et al.* (ATLAS), Phys. Rev. **D98**, 052008 (2018), [arXiv:1808.02380].
- [40] A. M. Sirunyan *et al.* (CMS), Phys. Lett. **B798**, 134952 (2019), [arXiv:1906.00057].
- [41] G. Aad *et al.* (ATLAS), JHEP **09**, 091 (2019), [arXiv:1906.08589].
- [42] A. M. Sirunyan *et al.* (CMS) (2019), [arXiv:1906.05977].
- [43] D. Pappadopulo *et al.*, JHEP **09**, 060 (2014), [arXiv:1402.4431].
- [44] H.-J. He *et al.*, Phys. Rev. **D78**, 031701 (2008), [arXiv:0708.2588].
- [45] M. Aaboud *et al.* (ATLAS), Phys. Lett. **B774**, 494 (2017), [arXiv:1707.06958].
- [46] A. M. Sirunyan *et al.* (CMS), Eur. Phys. J. **C77**, 636 (2017), [arXiv:1707.01303].
- [47] See the particle listings for W' in this *Review*.
- [48] Y. Zhang *et al.*, Phys. Rev. **D76**, 091301 (2007), [arXiv:0704.1662].
- [49] P. Langacker and S. U. Sankar, Phys. Rev. **D40**, 1569 (1989).
- [50] J. F. Bueno *et al.* (TWIST), Phys. Rev. **D84**, 032005 (2011), [arXiv:1104.3632].
- [51] See Fig. 5 of G. Prezeau, M. Ramsey-Musolf, and P. Vogel, Phys. Rev. D **68**, 034016 (2003).

88. Z' -Boson Searches

Revised October, 2019 by B.A. Dobrescu (Fermilab) and S. Willocq (U. Massachusetts).

The Z' boson is a massive, electrically-neutral and color-singlet hypothetical particle of spin 1. This particle is predicted in many extensions of the Standard Model (SM) and has been the object of extensive phenomenological studies [1].

88.1 Z' boson couplings

The couplings of a Z' boson to the first-generation fermions are given by

$$Z'_\mu \left(g_u^L \bar{u}_L \gamma^\mu u_L + g_d^L \bar{d}_L \gamma^\mu d_L + g_u^R \bar{u}_R \gamma^\mu u_R + g_d^R \bar{d}_R \gamma^\mu d_R + g_\nu^L \bar{\nu}_L \gamma^\mu \nu_L + g_e^L \bar{e}_L \gamma^\mu e_L + g_e^R \bar{e}_R \gamma^\mu e_R \right), \quad (88.1)$$

where u, d, ν, e are the quark and lepton fields in the mass eigenstate basis, and the coefficients $g_u^L, g_d^L, g_u^R, g_d^R, g_\nu^L, g_e^L, g_e^R$ are real dimensionless parameters. If the Z' couplings to quarks and leptons are generation-independent, then these seven parameters describe the couplings of the Z' boson to all SM fermions. More generally, however, the Z' couplings to fermions are generation-dependent, in which case Eq. (88.1) may be written with generation indices $i, j = 1, 2, 3$ labeling the quark and lepton fields, and with the seven coefficients promoted to 3×3 Hermitian matrices (e.g., $g_{ij}^L \bar{e}_i^L \gamma^\mu e_j^L$, where e_L^2 is the left-handed muon, etc.).

The parameters describing the Z' boson interactions with quarks and leptons are subject to some theoretical constraints. Quantum field theories that include a heavy spin-1 particle are well behaved at high energies only if that particle is a gauge boson associated with a spontaneously broken gauge symmetry. Quantum effects preserve the gauge symmetry only if the couplings of the gauge boson to fermions satisfy the anomaly equations [2]. Furthermore, the fermion charges under the new gauge symmetry are constrained by the requirement that the quarks and leptons get masses from gauge-invariant interactions with the Higgs fields.

The relation between the couplings displayed in Eq. (88.1) and the gauge charges z_f^L and z_f^R of the fermions $f = u, d, \nu, e$ involves the unitary 3×3 matrices V_f^L and V_f^R that transform the gauge eigenstate fermions f_L^i and f_R^i , respectively, into the mass eigenstates. The Z' couplings also depend on the mixings of the new gauge boson in the gauge eigenstate basis (\tilde{Z}'_μ). The main ones are a kinetic mixing $(-\chi/2)B^{\mu\nu}\tilde{Z}'_{\mu\nu}$ with the hypercharge gauge boson B^μ (χ is a dimensionless parameter), and a mass mixing $\delta M^2 \tilde{Z}'^\mu \tilde{Z}'_\mu$ with the linear combination (\tilde{Z}_μ) of neutral bosons that couples as the SM Z boson [3]. Since both the kinetic and mass mixings shift the mass and couplings of the Z boson, electroweak measurements impose upper limits on χ and $\delta M^2/(M_{Z'}^2 - M_Z^2)$ of the order of 10^{-3} [4]. Keeping only linear terms in these two small quantities, the couplings of the mass-eigenstate Z' boson are given by

$$g_{f_{ij}}^L = g_z V_{f_{ii}'}^L z_{f_{i'j}'}^L (V_f^L)_{i'j}^\dagger + \frac{e}{c_W} \left(\frac{s_W \chi M_{Z'}^2 + \delta M^2}{2s_W (M_{Z'}^2 - M_Z^2)} \sigma_f^3 - \epsilon Q_f \right), \quad (88.2)$$

$$g_{f_{ij}}^R = g_z V_{f_{ii}'}^R z_{f_{i'j}'}^R (V_f^R)_{i'j}^\dagger - \frac{e}{c_W} \epsilon Q_f, \quad (88.3)$$

where g_z is the new gauge coupling, Q_f is the electric charge of f , e is the electromagnetic gauge coupling, s_W and c_W are the sine and cosine of the weak mixing angle, $\sigma_f^3 = +1$ for $f = u, \nu$ and $\sigma_f^3 = -1$ for $f = d, e$, and

$$\epsilon = \frac{\chi (M_{Z'}^2 - c_W^2 M_Z^2) + s_W \delta M^2}{M_{Z'}^2 - M_Z^2}. \quad (88.4)$$

The interaction of the Z' boson with a pair of W bosons has

the form

$$\begin{aligned} & [i (W_\mu^- Z'_\nu - W_\nu^- Z'_\mu) \partial^\mu W^{+\nu} + \text{H.c.}] \\ & + i (W_\mu^+ W_\nu^- - W_\nu^+ W_\mu^-) \partial^\mu Z'^\nu \end{aligned} \quad (88.5)$$

with a coefficient of order $M_W^2/M_{Z'}^2$, [5]. The Z' also couples to one SM Higgs boson and one Z boson, $Z'_\mu Z^\mu h^0$, with a coefficient of order M_Z .

88.2 Z' models

A simple origin of a Z' boson is a new $U(1)'$ gauge symmetry. In that case, the matricial equalities $z_u^L = z_d^L$ and $z_\nu^L = z_e^L$ are required by the SM $SU(2)_W$ gauge symmetry. Given that the $U(1)'$ interaction is not asymptotically free, the theory may be well-behaved at high energies (e.g., by embedding $U(1)'$ in a non-Abelian gauge group) only if the charges are commensurate numbers, i.e. any ratio of charges is a rational number. Satisfying the anomaly equations with rational numbers is highly nontrivial, and typically new fermions charged under $U(1)'$ are necessary.

If the couplings are generation-independent ($V_f^{L,R}$ are then unit matrices in Eq. (88.2)) and the mixings of \tilde{Z}' are negligible, then there are five commensurate couplings: $g_u^R, g_d^R, g_e^R, g_q^L$ ($q = u$ or d), g_l^L ($l = \nu$ or e). Four sets of charges are displayed in Table 88.1, each of them spanned by a free parameter x [6]. The first set, labelled $B - xL$, has charges proportional to the baryon number minus x times the lepton number. These charges allow all SM Yukawa couplings to a Higgs doublet which is neutral under $U(1)_{B-xL}$, so that there is no tree-level $\tilde{Z} - \tilde{Z}'$ mixing. For $x = 1$ one recovers the $U(1)_{B-L}$ group, which is non-anomalous in the presence of one “right-handed neutrino” (a chiral fermion that is a singlet under the SM gauge group) per generation. For $x \neq 1$, it is necessary to include some fermions that are vectorlike (i.e. their mass terms are gauge invariant) with respect to the electroweak gauge group and chiral with respect to $U(1)_{B-xL}$. In the particular cases $x = 0$ or $x \gg 1$, the Z' is leptophobic or quark-phobic, respectively.

The second set, $U(1)_{10+x5}$, has charges that commute with the representations of the $SU(5)$ grand unified group. Here x is related to the mixing angle between the two $U(1)$ bosons encountered in the $E_6 \rightarrow SU(5) \times U(1) \times U(1)$ symmetry breaking patterns of grand unified theories [1, 9]. With these charges, two Higgs doublets are typically required to generate masses for both up- and down- type fermions. This set leads to $\tilde{Z} - \tilde{Z}'$ mass mixing at tree level, such that for a Z' mass close to the electroweak scale, the measurements at the Z -pole require some fine tuning between the charges and VEVs of the two Higgs doublets. Vectorlike fermions charged under the electroweak gauge group and also carrying color are required (except for $x = -3$) to make this set anomaly free. The particular cases $x = -3, 1, -1/2$ are usually labelled $U(1)_\chi, U(1)_\psi$, and $U(1)_\eta$, respectively. Under the third set, $U(1)_{d-xu}$, the weak-doublet quarks are neutral, and the ratio of u_R and d_R charges is $-x$. For $x = 1$, this is the “right-handed” group $U(1)_R$. For $x = 0$, the charges are those of the E_6 -inspired $U(1)_I$ group, which requires new quarks and leptons. Other generation-independent sets of $U(1)'$ charges are given in [10].

In the absence of new fermions charged under the SM group, the most general generation-independent charge assignment is $U(1)_{q+xu}$, which is a linear combination of hypercharge and $B-L$. Many other anomaly-free solutions exist if generation-dependent charges are allowed. An example is $B - xL_e - yL_\mu + (y-3)L_\tau$, with x, y free parameters. This allows all fermion masses to be generated by Yukawa couplings to a single Higgs doublet, without inducing tree-level flavor-changing neutral current (FCNC) processes. There are also lepton-flavor dependent charges that allow neutrino masses to arise only from operators of high dimensionality [11].

If the $SU(2)_W$ -doublet quarks have generation-dependent $U(1)'$ charges, then the mass eigenstate quarks have flavor off-diagonal couplings to the Z' boson (see Eq. (88.1), and note that $V_u^L (V_d^L)^\dagger$

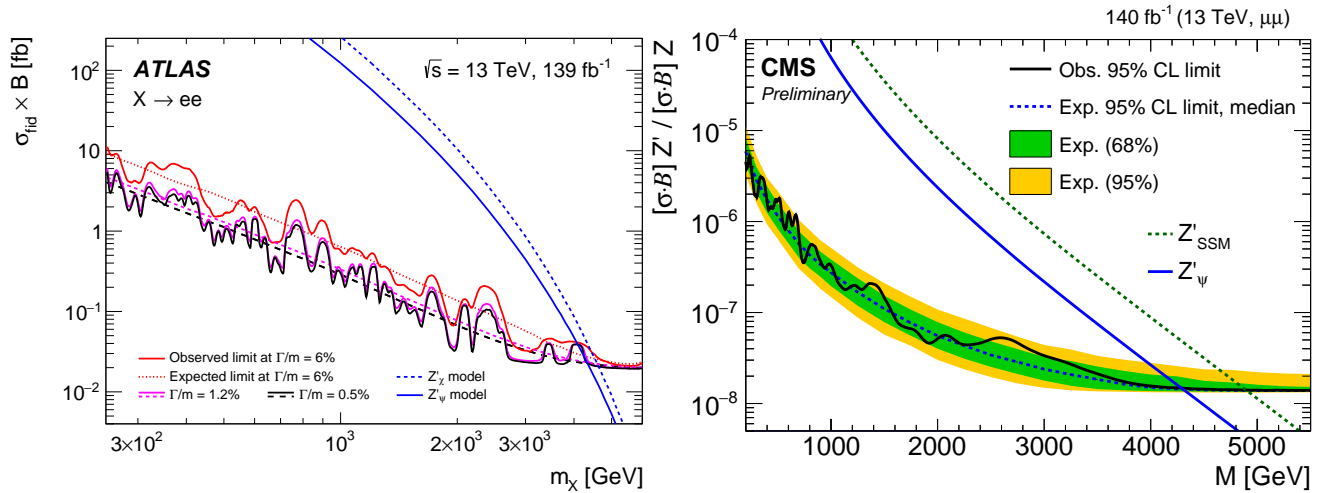


Figure 88.1: Upper limits on the cross section for Z' production times the branching fraction for $Z' \rightarrow e^+e^-$ (left panel, set by ATLAS [7]) or $Z' \rightarrow \mu^+\mu^-$ (right panel, set by CMS [8]) as a function of $M_{Z'}$. The lines labelled by Z'_ψ and Z'_χ are theoretical predictions for the $U(1)_{10+x5}$ models in Table 88.1 with $x = -3$ and $x = +1$, respectively, for g_z fixed by an E_6 unification condition. The Z'_{SSM} line corresponds to Z' couplings equal to those of the Z boson.

Table 88.1: Examples of generation-independent $U(1)'$ charges for quarks and leptons. The parameter x is an arbitrary rational number. Gauge anomaly cancellation requires certain new fermions [6].

fermion	$U(1)_{B-xL}$	$U(1)_{10+x5}$	$U(1)_{d-xu}$	$U(1)_{q+xu}$
(u_L, d_L)	1/3	1/3	0	1/3
u_R	1/3	-1/3	$-x/3$	$x/3$
d_R	1/3	$-x/3$	1/3	$(2-x)/3$
(ν_L, e_L)	$-x$	$x/3$	$(-1+x)/3$	-1
e_R	$-x$	-1/3	$x/3$	$-(2+x)/3$

is the CKM matrix). These are severely constrained by measurements of FCNC processes, which in this case are mediated at tree-level by Z' boson exchange [12]. The constraints are relaxed if the first and second generation charges are the same, although they are increasingly tightened by the measurements of B meson properties [13]. If only the $SU(2)_W$ -singlet quarks have generation-dependent $U(1)'$ charges, there is more freedom in adjusting the flavor off-diagonal couplings because the $V_{u,d}^R$ matrices are not observable in the SM.

The anomaly equations for $U(1)'$ could be circumvented only if there is an axion with certain dimension-5 couplings to the gauge bosons. However, such a scenario violates unitarity unless the quantum field theory description breaks down at a scale near $M_{Z'}$ [14].

Z' bosons may also arise from larger gauge groups. These may extend the electroweak group, as in $SU(2) \times SU(2) \times U(1)$, or may embed the electroweak group, as in $SU(3)_W \times U(1)$ [15]. If the larger group is spontaneously broken down to $SU(2)_W \times U(1)_Y \times U(1)'$ at a scale $v_* \gg M_{Z'}/g_z$, then the above discussion applies up to corrections of order $M_{Z'}^2/(g_z v_*)^2$. For $v_* \sim M_{Z'}/g_z$, additional gauge bosons have masses comparable to $M_{Z'}$, including at least a W' boson [15]. If the larger gauge group breaks together with the electroweak symmetry directly to the electromagnetic $U(1)_{\text{em}}$, then the left-handed fermion charges are no longer correlated ($z_u^L \neq z_d^L$, $z_\nu^L \neq z_e^L$) and a $Z'W^+W^-$ coupling is induced.

If the electroweak gauge bosons propagate in extra dimensions, then their Kaluza-Klein (KK) excitations include a series of Z' boson pairs. Each of these pairs can be associated with a different $SU(2) \times U(1)$ gauge group in four dimensions. The properties of the KK particles depend strongly on the extra-dimensional theory [16]. For example, in universal extra dimensions there is a parity

that forces all couplings of Eq. (88.1) to vanish in the case of the lightest KK bosons, while allowing couplings to pairs of fermions involving a SM and a heavy vectorlike fermion. There are also 4-dimensional gauge theories (*e.g.* little Higgs with T parity) with Z' bosons exhibiting similar properties. By contrast, in a warped extra dimension, the couplings of Eq. (88.1) may be sizable even when SM fields propagate along the extra dimension.

Z' bosons may also be composite particles. For example, in confining gauge theories [17], the ρ -like bound state is a spin-1 boson that may be interpreted as arising from a spontaneously broken gauge symmetry [18].

88.3 Non-resonant Z' signatures at colliders

In the presence of the couplings shown in Eq. (88.1), the Z' boson may be produced in the s -channel at colliders, and would decay to pairs of fermions. The decay width into a pair of electrons is given by

$$\Gamma(Z' \rightarrow e^+e^-) \simeq \left[(g_e^L)^2 + (g_e^R)^2 \right] \frac{M_{Z'}}{24\pi}, \quad (88.6)$$

where small corrections from electroweak loops are not included. The decay width into $q\bar{q}$ is similar, except for an additional color factor of 3, QCD radiative corrections, and fermion mass corrections. Thus, one may compute the Z' branching fractions in terms of the couplings of Eq. (88.1). However, other decay channels, such as WW or a pair of new particles, could have large widths and need to be added to the total decay width.

As mentioned above, there are theories in which the Z' couplings are controlled by a discrete symmetry that forbids decays into a pair of SM particles. Typically, such theories involve several new particles, which may be produced only in pairs and undergo cascade decays through Z' bosons, leading to signals involving missing (transverse) momentum. Given that the cascade decays depend on the properties of new particles other than the Z' boson, this case is not discussed further here.

The Z' contribution to the cross sections for $e^+e^- \rightarrow f\bar{f}$ proceeds through an s -channel Z' exchange (when $f = e$, there are also t - and u -channel exchanges). For $M_{Z'} < \sqrt{s}$, the Z' appears as an $f\bar{f}$ resonance in the radiative return process where photon emission tunes the effective center-of-mass energy to $M_{Z'}$. The agreement between the LEP-II measurements and the SM predictions implies that either the Z' couplings are smaller than or of order 10^{-2} , or else $M_{Z'}$ is above 209 GeV, the maximum energy of LEP-II. In the latter case, the Z' exchange may be approximated

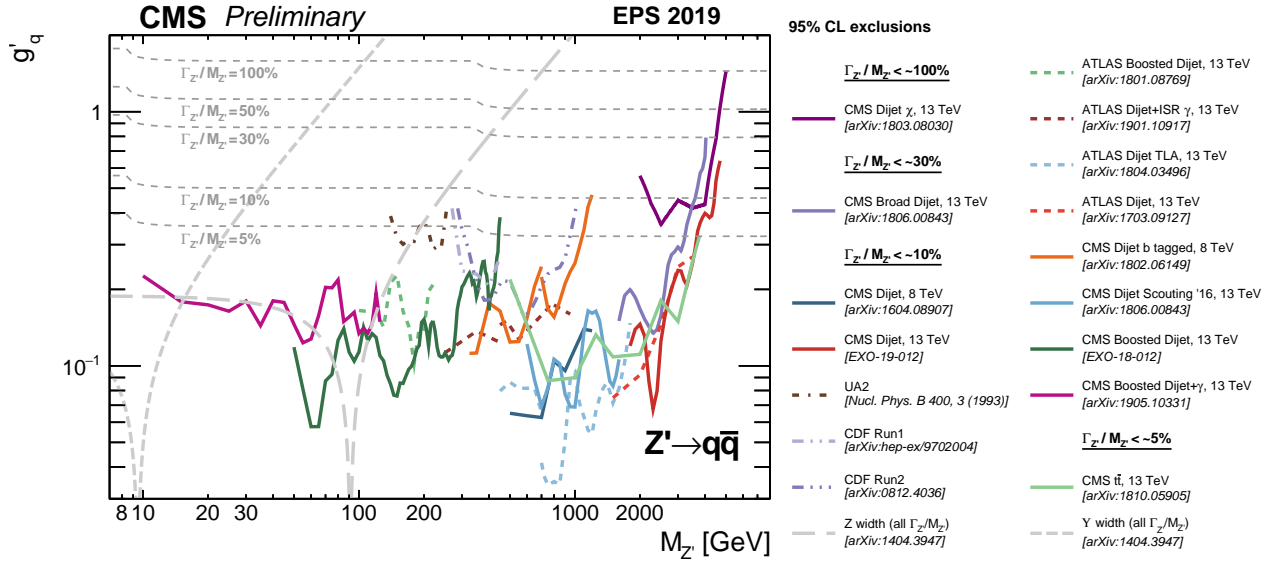


Figure 88.2: Upper limits on the Z' coupling to quarks as a function of $M_{Z'}$ based on various searches performed by the ATLAS, CMS, CDF, and UA2 experiments [19].

up to corrections of order $s/M_{Z'}^2$, by the contact interactions

$$\frac{g_z^2}{M_{Z'}^2 - s} \left[\bar{e} \gamma^\mu (z_e^L P_L + z_e^R P_R) e \right] \left[\bar{f} \gamma^\mu (z_f^L P_L + z_f^R P_R) f \right], \quad (88.7)$$

where $P_{L,R}$ are chirality projection operators, and the relation between Z' couplings and charges (see Eq. (88.2) in the limit where the mass and kinetic mixings are neglected) is used, assuming generation-independent charges. The four LEP collaborations have set limits on the coefficients of such operators for all possible chiral structures and for various combinations of fermions [20]. Thus, one may derive bounds on $(M_{Z'}/g_z) |z_e^L z_f^L|^{-1/2}$ and the analogous combinations of LR , RL and RR charges, which are typically on the order of a few TeV. LEP-II limits were derived [6] on the four sets of charges shown in Table 88.1.

Somewhat stronger bounds can be set on $M_{Z'}/g_z$ for specific sets of Z' couplings if the effects of several operators (88.7) are combined. Dedicated analyses by the LEP collaborations have set limits on Z' bosons for particular values of the gauge coupling (see section 3.5 of Ref. [20]). For example, $M_{Z_{\text{SSM}}} > 1.76$ TeV for a “sequential” Z' of same couplings as the SM Z boson, while $M_{Z_\chi} > 0.785$ TeV for the Z' associated with $U(1)_\chi$ assuming a unification condition for the gauge coupling.

88.4 Searches at hadron colliders

Z' bosons with couplings to quarks (see Eq. (88.1)) may be produced at hadron colliders in the s -channel and would show up as resonances in the invariant mass distribution of the decay products. The cross section for producing a Z' boson at the LHC, which then decays to some $f\bar{f}$ final state, takes the form [21]

$$\sigma(pp \rightarrow Z' X \rightarrow f\bar{f} X) \simeq \frac{\pi}{6s} \sum_q c_q^f w_q(s, M_{Z'}^2) \quad (88.8)$$

for flavor-diagonal couplings to quarks. Here, we have neglected the interference with the SM contribution to $f\bar{f}$ production, which is a good approximation for a narrow Z' resonance (deviations from the narrow width approximation are discussed in Ref. [22]). The coefficients

$$c_q^f = \left[(g_q^L)^2 + (g_q^R)^2 \right] B(Z' \rightarrow f\bar{f}) \quad (88.9)$$

contain all the dependence on the Z' couplings, while the functions w_q include all the information about parton distributions and QCD corrections [6, 10]. This factorization holds exactly to

NLO and the deviations from it induced at NNLO are very small. Note that the w_u and w_d functions are substantially larger than the w_q functions for the other quarks. Eq. (88.8) also applies to the Tevatron, except for changing the pp initial state to $p\bar{p}$, which implies that the $w_q(s, M_{Z'}^2)$ functions are replaced by some other functions $\bar{w}_q((1.96 \text{ TeV})^2, M_{Z'}^2)$.

It is common to present results of Z' searches as limits on the cross section versus $M_{Z'}$ (see for example Fig. 88.1).

An alternative is to plot exclusion curves for fixed $M_{Z'}$ values in the $c_u^f - c_d^f$ planes, allowing a simple derivation of the mass limit within any Z' model. CMS upper limits in the $c_u^\ell - c_d^\ell$ plane ($\ell = e$ or μ) for different $M_{Z'}$ are shown in Ref. [23] (for Tevatron limits, see Refs. [10, 24]).

The discovery of a dilepton resonance at the LHC would determine the Z' mass and width. A measurement of the total cross section would define a band in the $c_u^\ell - c_d^\ell$ plane. Angular distributions can be used to measure several combinations of Z' parameters (angular distributions were used in Ref. [25] to improve the Tevatron sensitivity). Even though the original quark direction in a pp collider is unknown, the leptonic forward-backward asymmetry A_{FB}^ℓ can be extracted from the kinematics of the dilepton system, and is sensitive to parity-violating couplings. A fit to the Z' rapidity distribution can distinguish between the couplings to up and down quarks. These measurements, combined with off-peak observables, have the potential to differentiate among various Z' models [26]. In some cases, A_{FB}^ℓ may provide discovery sensitivity that is competitive with the mass distribution [27]. The spin of the Z' boson may be determined from angular distributions [28].

Searches for Z' decays into e^+e^- and $\mu^+\mu^-$ by the ATLAS and CMS collaborations [7, 8] have set 95% C.L. upper cross-section limits as low as 0.02 fb (see Fig. 88.1), with the mass lower limits in specific models as high as 4.9 TeV in a single channel. Cross section limits in the dimuon channel for low mass regions, below 200 GeV but not near the Z mass, have been set at the LHC by CMS [29] and LHCb [30] (and also in e^+e^- collisions by BaBar [31], assuming a dark photon, *i.e.*, a Z' boson whose couplings arise only from the kinetic mixing with the hypercharge gauge boson).

In the case of final states with tau-leptons, the mass lower limits obtained at 13 TeV are as high as ~ 2.4 TeV for the $\tau^+\tau^-$ [32] decay in the case of a sequential Z' . Limits in the flavor-violating leptonic final states have also been reported by ATLAS [33] and CMS [34] at 13 TeV, for resonances in the $e^\pm\mu^\mp$, $e^\pm\tau^\mp$ and $\mu^\pm\tau^\mp$ channels.

Final states with higher background, $t\bar{t}$, $b\bar{b}$ and jj , are also important as they probe various combinations of Z' couplings to

quarks, see Ref. [35] for further discussion. Besides the improved sensitivity at masses of several TeV, the LHC searches in the dijet channel have been also extended to masses as low as 10 GeV, through the use of new techniques involving boosted topologies and initial state radiation [36]. Limits from such Z' searches in hadronic final states are summarized in Fig. 88.2.

Z' decays to Zh^0 with $Z \rightarrow \ell^+\ell^-$, $\nu\bar{\nu}$ or $q\bar{q}$ and $h^0 \rightarrow b\bar{b}$ have been studied by ATLAS [37, 38] and CMS [39, 40] using 13 TeV data. The most stringent constraint is set in the fully hadronic channel, with a mass lower limit of 2.65 TeV in the context of the Heavy Vector Triplet (HVT) model weakly-coupled scenario A [41].

Searches for a Z' boson lighter than the SM Z and which couples to leptons have been performed in the 4-lepton final state. CMS [42] focused on the Z decays into a muon pair followed by the radiation of a Z' boson which decays itself into a muon pair. ATLAS [43] considered the $h^0 \rightarrow ZZ'$ and $h^0 \rightarrow Z'Z'$ processes followed by the leptonic decays of both Z and Z' .

The $pp \rightarrow Z'X \rightarrow W^+W^-X$ process has also been searched for at the LHC. The channel where the Z' boson is produced through its couplings to quarks, and the W bosons decay hadronically, has been explored using boosted techniques to analyze the 13 TeV data [44, 45] with a mass lower limit of 2.9 TeV in the HVT model A. The Z' boson may also be produced through its couplings to W bosons [46], which has been explored by ATLAS with the use of forward jets consistent with a vector boson fusion event topology.

At the Tevatron, the CDF and DØ collaborations have searched for Z' bosons in the e^+e^- [47], $\mu^+\mu^-$ [48], $e^\pm\mu^\mp$ [49], $\tau^+\tau^-$ [50], $t\bar{t}$ [51], jj [52] and W^+W^- [53] final states. These limits have been mostly superseded by the LHC results.

88.5 Low-energy constraints

Z' boson properties are also constrained by a variety of low-energy experiments [54]. Polarized electron-nucleon scattering and atomic parity violation are sensitive to electron-quark contact interactions, which get contributions from Z' exchange that can be expressed in terms of the couplings introduced in Eq. (88.1) and $M'_{Z'}$. Further corrections to the electron-quark contact interactions are induced in the presence of $\tilde{Z}-\tilde{Z}'$ mixing because of the shifts in the Z couplings to quarks and leptons [3]. Deep-inelastic neutrino-nucleon scattering is similarly affected by Z' bosons. Other low-energy observables are discussed in [4]. Viable models with Z' bosons much lighter than the Z boson have been constructed, despite many additional experimental constraints [55].

In some models, the lower limits on $M_{Z'}$ set by low-energy data are above 1 TeV. For example, $M_{Z'_\chi} > 1.1$ TeV and $M_{Z'_\eta} > 0.43$ TeV assuming that the Higgs sectors consist of electroweak doublets and singlets only [4], while the gauge coupling is fixed by an $SO(10)$ unification condition for $U(1)_\chi$ and $U(1)_\eta$. For more general models, see [1, 6, 56]. The mass bounds from direct searches at the LHC [7, 8] exceed the electroweak constraints by a factor of three or more for the models mentioned here. This conclusion could change if the collider bounds are weakened by exotic decay channels [57].

Although the LHC data are most constraining for many Z' models, one should be careful in assessing the relative reach of various experiments given the freedom in Z' couplings. For example, a Z' coupled to $B-yL_\mu+(y-3)L_\tau$ has implications for the muon $g-2$, neutrino oscillations or τ decays, and would be hard to see in processes involving first-generation fermions. Moreover, the combination of LHC searches and low-energy measurements could allow a precise determination of the Z' parameters [58].

References

[1] A. Leike, Phys. Rept. **317**, 143 (1999), [hep-ph/9805494].
 [2] T. P. Cheng and L. F. Li, *Gauge Theory of Elementary Particle Physics* (1984), ISBN 9780198519614.
 [3] K. S. Babu, C. F. Kolda and J. March-Russell, Phys. Rev. **D57**, 6788 (1998), [hep-ph/9710441].
 [4] J. Erler *et al.*, JHEP **08**, 017 (2009), [arXiv:0906.2435].
 [5] B. A. Dobrescu and P. J. Fox, JHEP **05**, 047 (2016), [arXiv:1511.02148].

[6] M. Carena *et al.*, Phys. Rev. **D70**, 093009 (2004), [hep-ph/0408098].
 [7] G. Aad *et al.* (ATLAS), Phys. Lett. **B796**, 68 (2019), [arXiv:1903.06248].
 [8] CMS Collab., PAS EXO-19-019, Aug. 2019.
 [9] F. Del Aguila, M. Cvetič and P. Langacker, Phys. Rev. **D52**, 37 (1995), [hep-ph/9501390].
 [10] E. Accomando *et al.*, Phys. Rev. **D83**, 075012 (2011), [arXiv:1010.6058].
 [11] M.-C. Chen, A. de Gouvea and B. A. Dobrescu, Phys. Rev. **D75**, 055009 (2007), [hep-ph/0612017].
 [12] P. Langacker and M. Plumacher, Phys. Rev. **D62**, 013006 (2000), [hep-ph/0001204].
 [13] A. J. Buras, F. De Fazio and J. Girrbach, JHEP **02**, 116 (2013), [arXiv:1211.1896].
 [14] L. E. Ibanez and G. G. Ross, Phys. Lett. **B332**, 100 (1994), [hep-ph/9403338].
 [15] See the Section on “ W' searches” in this *Review*.
 [16] J. Parsons and A. Pomarol, “Extra dimensions” in this *Review*.
 [17] K.M. Black *et al.*, “Dynamical electroweak symmetry breaking” in this *Review*.
 [18] M. Bando, T. Kugo and K. Yamawaki, Phys. Rept. **164**, 217 (1988).
 [19] CMS Collab., <https://twiki.cern.ch/twiki/bin/view/CMSPublic/SummaryPlotsEXO13TeV>.
 [20] S. Schael *et al.* (ALEPH, DELPHI, L3, OPAL, LEP Electroweak), Phys. Rept. **532**, 119 (2013), [arXiv:1302.3415].
 [21] G. Paz and J. Roy, Phys. Rev. **D97**, 075025 (2018), [arXiv:1711.02655].
 [22] E. Accomando *et al.*, JHEP **10**, 153 (2013), [arXiv:1304.6700].
 [23] V. Khachatryan *et al.* (CMS), JHEP **04**, 025 (2015), [arXiv:1412.6302].
 [24] A. Abulencia *et al.* (CDF), Phys. Rev. Lett. **95**, 252001 (2005), [hep-ex/0507104].
 [25] A. Abulencia *et al.* (CDF), Phys. Rev. Lett. **96**, 211801 (2006), [hep-ex/0602045].
 [26] F. Petriello and S. Quackenbush, Phys. Rev. **D77**, 115004 (2008), [arXiv:0801.4389].
 [27] E. Accomando *et al.*, JHEP **01**, 127 (2016), [arXiv:1503.02672].
 [28] P. Osland *et al.*, Phys. Rev. **D79**, 115021 (2009), [arXiv:0904.4857].
 [29] CMS Collab., PAS EXO-19-018, Aug. 2019.
 [30] R. Aaij *et al.* (LHCb), Phys. Rev. Lett. **120**, 061801 (2018), [arXiv:1710.02867].
 [31] J. P. Lees *et al.* (BaBar), Phys. Rev. Lett. **113**, 201801 (2014), [arXiv:1406.2980].
 [32] M. Aaboud *et al.* (ATLAS), JHEP **01**, 055 (2018), [arXiv:1709.07242].
 [33] M. Aaboud *et al.* (ATLAS), Phys. Rev. **D98**, 092008 (2018), [arXiv:1807.06573].
 [34] A. M. Sirunyan *et al.* (CMS), JHEP **04**, 073 (2018), [arXiv:1802.01122].
 [35] See the Section on “Dynamical Electroweak Symmetry Breaking” in this *Review*.
 [36] A. M. Sirunyan *et al.* (CMS) (2019), [arXiv:1905.10331].
 [37] M. Aaboud *et al.* (ATLAS), Phys. Lett. **B774**, 494 (2017), [arXiv:1707.06958].
 [38] M. Aaboud *et al.* (ATLAS), JHEP **03**, 174 (2018), [Erratum: JHEP **11**, 051 (2018)], [arXiv:1712.06518].
 [39] A. M. Sirunyan *et al.* (CMS), JHEP **11**, 172 (2018), [arXiv:1807.02826].

- [40] A. M. Sirunyan *et al.* (CMS), Eur. Phys. J. **C77**, 636 (2017), [arXiv:1707.01303].
- [41] D. Pappadopulo *et al.*, JHEP **09**, 060 (2014), [arXiv:1402.4431].
- [42] A. M. Sirunyan *et al.* (CMS), Phys. Lett. **B792**, 345 (2019), [arXiv:1808.03684].
- [43] M. Aaboud *et al.* (ATLAS), JHEP **06**, 166 (2018), [arXiv:1802.03388].
- [44] G. Aad *et al.* (ATLAS), JHEP **09**, 091 (2019), [arXiv:1906.08589].
- [45] A. M. Sirunyan *et al.* (CMS) (2019), [arXiv:1906.05977].
- [46] H.-J. He *et al.*, Phys. Rev. **D78**, 031701 (2008), [arXiv:0708.2588].
- [47] V. M. Abazov *et al.* (D0), Phys. Lett. **B695**, 88 (2011), [arXiv:1008.2023].
- [48] T. Aaltonen *et al.* (CDF), Phys. Rev. Lett. **106**, 121801 (2011), [arXiv:1101.4578].
- [49] A. Abulencia *et al.* (CDF), Phys. Rev. Lett. **96**, 211802 (2006), [hep-ex/0603006].
- [50] D. Acosta *et al.* (CDF), Phys. Rev. Lett. **95**, 131801 (2005), [hep-ex/0506034].
- [51] T. Aaltonen *et al.* (CDF), Phys. Rev. **D84**, 072004 (2011), [arXiv:1107.5063].
- [52] T. Aaltonen *et al.* (CDF), Phys. Rev. **D79**, 112002 (2009), [arXiv:0812.4036].
- [53] T. Aaltonen *et al.* (CDF), Phys. Rev. Lett. **104**, 241801 (2010), [arXiv:1004.4946].
- [54] V. D. Barger *et al.*, Phys. Rev. **D57**, 391 (1998), [hep-ph/9707412].
- [55] R. Harnik, J. Kopp and P. A. N. Machado, JCAP **1207**, 026 (2012), [arXiv:1202.6073].
- [56] E. Rojas and J. Erler, JHEP **10**, 063 (2015), [arXiv:1505.03208].
- [57] J. Kang and P. Langacker, Phys. Rev. **D71**, 035014 (2005), [hep-ph/0412190].
- [58] Y. Li, F. Petriello and S. Quackenbush, Phys. Rev. **D80**, 055018 (2009), [arXiv:0906.4132].

89. Supersymmetry, Part I (Theory)

Revised August 2019 by B.C. Allanach (DAMTP, Cambridge U.) and H.E. Haber (UC Santa Cruz).

89.1	Introduction	905
89.2	Structure of the MSSM	905
89.2.1	R-parity and the lightest supersymmetric particle	906
89.2.2	The goldstino and gravitino	906
89.2.3	Hidden sectors and the structure of SUSY breaking	907
89.2.4	SUSY and extra dimensions	907
89.2.5	Split-SUSY	907
89.3	Parameters of the MSSM	908
89.3.1	The SUSY-conserving parameters	908
89.3.2	The SUSY-breaking parameters	908
89.3.3	MSSM-124	908
89.4	The supersymmetric-particle spectrum	908
89.4.1	The charginos and neutralinos	909
89.4.2	The squarks and sleptons	909
89.5	The supersymmetric Higgs sector	910
89.5.1	The tree-level Higgs sector	910
89.5.2	The radiatively-corrected Higgs sector	910
89.6	Restricting the MSSM parameter freedom	911
89.6.1	Gaugino mass relations	911
89.6.2	Constrained versions of the MSSM: mSUGRA, CMSSM, etc.	911
89.6.3	Gauge-mediated SUSY breaking	912
89.6.4	The phenomenological MSSM	913
89.6.5	Simplified models	913
89.7	Experimental data confronts the MSSM	913
89.7.1	Naturalness constraints and the little hierarchy	913
89.7.2	Constraints from virtual exchange of supersymmetric particles	914
89.8	Massive neutrinos in weak-scale SUSY	915
89.8.1	The supersymmetric seesaw	915
89.8.2	R-parity-violating SUSY	915
89.9	Extensions beyond the MSSM	916

89.1 Introduction

Supersymmetry (SUSY) is a generalization of the space-time symmetries of quantum field theory that transforms fermions into bosons and vice versa [1]. The existence of such a non-trivial extension of the Poincaré symmetry of ordinary quantum field theory was initially surprising, and its form is highly constrained by theoretical principles [2]. SUSY also provides a framework for the unification of particle physics and gravity [3–6] at the Planck energy scale, $M_P \sim 10^{19}$ GeV, where the gravitational interactions become comparable in strength to the gauge interactions. Moreover, supersymmetry can stabilize the hierarchy between the energy scale that characterizes electroweak symmetry breaking, $M_{EW} \sim 100$ GeV, and the Planck scale [7–10] against large radiative corrections. The stability of this large gauge hierarchy with respect to radiative quantum corrections is not possible to maintain in the Standard Model (SM) without an unnatural fine-tuning of the parameters of the fundamental theory at the Planck scale. In contrast, in a supersymmetric extension of the SM, it is possible to maintain the gauge hierarchy while providing a natural framework for elementary scalar fields.

If supersymmetry were an exact symmetry of nature, then particles and their superpartners, which differ in spin by half a unit, would be degenerate in mass. Since superpartners have not (yet) been observed, supersymmetry must be a broken symmetry. Nevertheless, the stability of the gauge hierarchy can still be maintained if the SUSY breaking is soft [11, 12], and the corresponding SUSY-breaking mass parameters are no larger than a few TeV. Whether this is still plausible in light of recent SUSY searches at the LHC (see Sec. 90) will be discussed in Sec. 89.7.

In particular, soft-SUSY-breaking terms of the Lagrangian involve combinations of fields with total mass dimension of three or

less, with some restrictions on the dimension-three terms as elucidated in Ref. [11]. The impact of the soft terms becomes negligible at energy scales much larger than the size of the SUSY-breaking masses. Thus, a theory of weak-scale supersymmetry, where the effective scale of supersymmetry breaking is tied to the scale of electroweak symmetry breaking, provides a natural framework for the origin and the stability of the gauge hierarchy [7–10].

At present, there is no unambiguous experimental evidence for the breakdown of the SM at or below the TeV scale. The expectations for new TeV-scale physics beyond the SM are based primarily on three theoretical arguments. First, in a theory with an elementary scalar field of mass m and interaction strength λ (e.g., a quartic scalar self-coupling, the square of a gauge coupling or the square of a Yukawa coupling), the stability with respect to quantum corrections requires the existence of an energy cutoff roughly of order $(16\pi^2/\lambda)^{1/2}m$, beyond which new physics must enter [13]. A significantly larger energy cutoff would require an unnatural fine-tuning of parameters that govern the effective low-energy theory. Applying this argument to the SM leads to an expectation of new physics at the TeV scale [10].

Second, the unification of the three SM gauge couplings at a very high energy close to the Planck scale is possible if new physics beyond the SM (which modifies the running of the gauge couplings above the electroweak scale) is present. The minimal supersymmetric extension of the SM, where superpartner masses lie below a few TeV, provides an example of successful gauge coupling unification [14].

Third, the existence of dark matter that makes up approximately one quarter of the energy density of the universe, cannot be explained within the SM of particle physics [15]. Remarkably, a stable weakly-interacting massive particle (WIMP) whose mass and interaction rate are governed by new physics associated with the TeV-scale can be consistent with the observed density of dark matter (this is the so-called WIMP miracle, which is reviewed in Ref. [16]). The lightest supersymmetric particle, if stable, is a promising (although not the unique) candidate for the dark matter [17–21]. Further aspects of dark matter can be found in Sec. 27.

89.2 Structure of the MSSM

The minimal supersymmetric extension of the SM (MSSM) consists of the fields of the two-Higgs-doublet extension of the SM and the corresponding superpartners [22, 23]. A particle and its superpartner together form a supermultiplet. The corresponding field content of the supermultiplets of the MSSM and their gauge quantum numbers are shown in Table 89.1. The electric charge $Q = T_3 + \frac{1}{2}Y$ is determined in terms of the third component of the weak isospin (T_3) and the U(1) weak hypercharge (Y).

The gauge supermultiplets consist of the gluons and their gluino fermionic superpartners and the SU(2)×U(1) gauge bosons and their gaugino fermionic superpartners. The matter supermultiplets consist of three generations of left-handed quarks and leptons and their scalar superpartners (squarks and sleptons, collectively referred to as sfermions), and the corresponding antiparticles. The Higgs supermultiplets consist of two complex Higgs doublets, their higgsino fermionic superpartners, and the corresponding antiparticles. The enlarged Higgs sector of the MSSM constitutes the minimal structure needed to guarantee the cancellation of gauge anomalies [25] generated by the higgsino superpartners that can appear as internal lines in triangle diagrams with three external electroweak gauge bosons. Moreover, without a second Higgs doublet, one cannot generate mass for both “up”-type and “down”-type quarks (and charged leptons) in a way consistent with the underlying SUSY [26–28].

In the most elegant treatment of SUSY, spacetime is extended to superspace which consists of the spacetime coordinates and new anticommuting fermionic coordinates θ and θ^\dagger [29, 30]. Each supermultiplet is represented by a superfield that is a function of the superspace coordinates. The fields of a given supermultiplet (which are functions of the spacetime coordinates) are coefficients of the θ and θ^\dagger expansion of the corresponding superfield.

Vector superfields contain the gauge boson fields and their gaugino partners. Chiral superfields contain the spin-0 and spin-1/2

Table 89.1: The fields of the MSSM and their $SU(3)\times SU(2)\times U(1)$ quantum numbers are listed. For simplicity, only one generation of quarks and leptons is exhibited. For each lepton, quark, and Higgs supermultiplet (each denoted by a hatted upper-case letter), there is a corresponding antiparticle multiplet of charge-conjugated fermions and their associated scalar partners [24].

Field Content of the MSSM						
Super-multiplets	Super-field	Bosonic fields	Fermionic partners	SU(3)	SU(2)	U(1)
gluon/gluino	\hat{V}_8	g	\tilde{g}	8	1	0
gauge boson/ gaugino	\hat{V} \hat{V}'	W^\pm, W^0 B	$\tilde{W}^\pm, \tilde{W}^0$ \tilde{B}	1 1	3 1	0 0
slepton/ lepton	\hat{L} \hat{E}^c	$(\tilde{\nu}_L, \tilde{e}_L)$ \tilde{e}_R^+	$(\nu, e^-)_L$ e_L^c	1 1	2 1	-1 2
squark/ quark	\hat{Q} \hat{U}^c \hat{D}^c	$(\tilde{u}_L, \tilde{d}_L)$ \tilde{u}_R^* \tilde{d}_R^*	$(u, d)_L$ u_L^c d_L^c	3 $\bar{3}$ $\bar{3}$	2 1 1	1/3 -4/3 2/3
Higgs/ higgsino	\hat{H}_d \hat{H}_u	(H_d^0, H_d^-) (H_u^+, H_u^0)	$(\tilde{H}_d^0, \tilde{H}_d^-)$ $(\tilde{H}_u^+, \tilde{H}_u^0)$	1 1	2 2	-1 1

fields of the matter or Higgs supermultiplets. A general supersymmetric Lagrangian is determined by three functions of the chiral superfields [4]: the superpotential, the Kähler potential, and the gauge kinetic function (which can be appropriately generalized to accommodate higher derivative terms [31]). Minimal forms for the Kähler potential and gauge kinetic function, which generate canonical kinetic energy terms for all the fields, are required for renormalizable globally supersymmetric theories. A renormalizable superpotential, which is at most cubic in the chiral superfields, yields supersymmetric Yukawa couplings and mass terms. A combination of gauge invariance and SUSY produces couplings of gaugino fields to matter (or Higgs) fields and their corresponding superpartners. The (renormalizable) MSSM Lagrangian is then constructed by including all possible supersymmetric interaction terms (of dimension four or less) that satisfy $SU(3)\times SU(2)\times U(1)$ gauge invariance and $B-L$ conservation (where B = baryon number and L = lepton number). Finally, the most general soft-supersymmetry-breaking terms consistent with these symmetries are added [11, 12, 32].

Although the MSSM is the focus of much of this review, there is some motivation for considering non-minimal supersymmetric extensions of the SM. For example, extra structure is needed to generate non-zero neutrino masses as discussed in Sec. 89.8. In addition, in order to address some theoretical issues and tensions associated with the MSSM, it has been fruitful to introduce one additional singlet Higgs superfield. The resulting next-to-minimal supersymmetric extension of the Standard Model (NMSSM) [33] is considered further in Sec. 89.4–89.7 and 89.9. Finally, one is always free to add additional fields to the SM along with the corresponding superpartners. However, only certain choices for the new fields (e.g., the addition of complete $SU(5)$ multiplets) will preserve the successful gauge coupling unification of the MSSM. Some examples will be briefly mentioned in Sec. 89.9.

89.2.1 R-parity and the lightest supersymmetric particle

The (renormalizable) SM Lagrangian possesses an accidental global $B-L$ symmetry due to the fact that B and L -violating operators composed of SM fields must have dimension $d = 5$ or larger [34]. Consequently, B and L -violating effects are suppressed by $(M_{EW}/M)^{d-4}$, where M is the characteristic mass scale of the physics that generates the corresponding higher dimensional operators. Indeed, values of M of order the grand unification scale or larger yield the observed (approximate) stability of the proton and suppression of neutrino masses. Unfortunately, these results are not guaranteed in a generic supersymmetric extension of the SM. For example, it is possible to construct gauge invariant supersymmetric dimension-four B and L -violating operators made up of fields of SM particles and their superpartners. Such operators, if present in the theory, could yield a proton decay rate many orders of magnitude larger than the current experimental bound. It is for this reason that $B-L$ conservation is imposed on the supersymmetric Lagrangian when defining the MSSM, which

is sufficient for eliminating all B and L -violating operators of dimension $d \leq 4$.

As a consequence of the $B-L$ symmetry, the MSSM possesses a multiplicative R-parity invariance, where $R = (-1)^{3(B-L)+2S}$ for a particle of spin S [35]. This implies that all the particles of the SM have even R-parity, whereas the corresponding superpartners have odd R-parity. The conservation of R-parity in scattering and decay processes has a critical impact on supersymmetric phenomenology. For example, any initial state in a scattering experiment will involve ordinary (R-even) particles. Consequently, it follows that supersymmetric particles must be produced in pairs. In general, these particles are highly unstable and decay into lighter states. Moreover, R-parity invariance also implies that the lightest supersymmetric particle (LSP) is absolutely stable, and must eventually be produced at the end of a decay chain initiated by the decay of a heavy unstable supersymmetric particle.

In order to be consistent with cosmological constraints, a stable LSP is almost certainly electrically and color neutral [19]. Consequently, the LSP in an R-parity-conserving theory is weakly interacting with ordinary matter, i.e., it behaves like a stable heavy neutrino and will escape collider detectors without being directly observed. Thus, the canonical signature for conventional R-parity-conserving supersymmetric theories is missing (transverse) momentum, due to the escape of the LSP. Moreover, as noted in Sec. 89.1 and reviewed in Refs. [20] and [21], the stability of the LSP in R-parity-conserving SUSY makes it a promising candidate for dark matter.

The possibility of relaxing the R-parity invariance of the MSSM (which would generate new B and/or L -violating interactions) will be addressed in Sec. 89.8.2.

89.2.2 The goldstino and gravitino

In the MSSM, SUSY breaking is accomplished by including the most general renormalizable soft-SUSY-breaking terms consistent with the $SU(3)\times SU(2)\times U(1)$ gauge symmetry and R-parity invariance. These terms parameterize our ignorance of the fundamental mechanism of supersymmetry breaking. If supersymmetry breaking occurs spontaneously, then a massless Goldstone fermion called the goldstino ($\tilde{G}_{1/2}$) must exist. The goldstino would then be the LSP, and could play an important role in supersymmetric phenomenology [36].

However, the goldstino degrees of freedom are physical only in models of spontaneously-broken global SUSY. If SUSY is a local symmetry, then the theory must incorporate gravity; the resulting theory is called supergravity [5, 37]. In models of spontaneously-broken supergravity, the goldstino is “absorbed” by the gravitino (\tilde{G}), the spin-3/2 superpartner of the graviton, via the super-Higgs mechanism [38]. Consequently, the goldstino is removed from the physical spectrum and the gravitino acquires a mass (denoted by $m_{3/2}$). If $m_{3/2}$ is smaller than the mass of the lightest superpartner of the SM particles, then the gravitino is the LSP.

In processes with center-of-mass energy $E \gg m_{3/2}$, one can

employ the goldstino–gravitino equivalence theorem [39], which implies that the interactions of the helicity $\pm\frac{1}{2}$ gravitino (whose properties approximate those of the goldstino) dominate those of the helicity $\pm\frac{3}{2}$ gravitino. The interactions of gravitinos with other light fields can be described by a low-energy effective Lagrangian that is determined by fundamental principles [40].

89.2.3 Hidden sectors and the structure of SUSY breaking

It is very difficult (perhaps impossible) to construct a realistic model of spontaneously-broken weak-scale supersymmetry where the supersymmetry breaking arises solely as a consequence of the interactions of the particles of the MSSM. A more successful scheme posits a theory with at least two distinct sectors: a visible sector consisting of the particles of the MSSM [32] and a sector where SUSY breaking is generated. It is often (but not always) assumed that particles of the hidden sector are neutral with respect to the SM gauge group. The effects of the hidden sector supersymmetry breaking are then transmitted to the MSSM by some mechanism (often involving the mediation by particles that comprise an additional messenger sector). Two theoretical scenarios that exhibit this structure are gravity-mediated and gauge-mediated SUSY breaking.

Supergravity models provide a natural mechanism for transmitting the SUSY breaking of the hidden sector to the particle spectrum of the MSSM. In models of gravity-mediated supersymmetry breaking, gravity is the messenger of supersymmetry breaking [41–45]. More precisely, supersymmetry breaking is mediated by effects of gravitational strength (suppressed by inverse powers of the Planck mass). The soft-SUSY-breaking parameters with dimensions of mass arise as model-dependent multiples of the gravitino mass $m_{3/2}$. In this scenario, $m_{3/2}$ is of order the electroweak-symmetry-breaking scale, while the gravitino couplings are roughly gravitational in strength [3, 46]. However, such a gravitino typically plays no direct role in supersymmetric phenomenology at colliders (except perhaps indirectly in the case where the gravitino is the LSP [47]).

Under certain theoretical assumptions on the structure of the Kähler potential (the so-called sequestered form introduced in Ref. [48]), SUSY breaking is due entirely to the super-conformal (super-Weyl) anomaly, which is common to all supergravity models [48]. In particular, gaugino masses are radiatively generated at one-loop, and squark and slepton squared-mass matrices are flavor-diagonal. In sequestered scenarios, sfermion squared-masses arise at two-loops, which implies that gluino and sfermion masses are of the same order of magnitude. This approach is called anomaly-mediated SUSY breaking (AMSB). Indeed, anomaly mediation is more generic than originally conceived, and provides a ubiquitous source of SUSY breaking [49]. However in the simplest formulation of AMSB as applied to the MSSM, the squared-masses of the sleptons are negative (known as the tachyonic slepton problem). It may be possible to cure this otherwise fatal flaw in non-minimal extensions of the MSSM [50]. Alternatively, one can assert that anomaly mediation is not the sole source of SUSY breaking in the sfermion sector. In non-sequestered scenarios, sfermion squared-masses can arise at tree-level, in which case squark masses would be parametrically larger than the loop-suppressed gaugino masses [51].

In gauge-mediated supersymmetry breaking (GMSB), gauge forces transmit the supersymmetry breaking to the MSSM. A typical structure of such models involves a hidden sector where SUSY is broken, a messenger sector consisting of particles (messengers) with nontrivial $SU(3)\times SU(2)\times U(1)$ quantum numbers, and the visible sector consisting of the fields of the MSSM [52–55]. The direct coupling of the messengers to the hidden sector generates a supersymmetry-breaking spectrum in the messenger sector. Supersymmetry breaking is then transmitted to the MSSM via the virtual exchange of the messenger fields. In models of direct gauge mediation, there is no separate hidden sector. In particular, the sector in which the SUSY breaking originates includes fields that carry nontrivial SM quantum numbers, which allows for the direct transmission of SUSY breaking to the MSSM [56].

In models of gauge-mediated SUSY breaking, the gravitino is the LSP [17], as its mass can range from a few eV (in the case of low SUSY breaking scales) up to a few GeV (in the case of high

SUSY breaking scales). In particular, the gravitino is a potential dark matter candidate (for a review and guide to the literature, see Ref. [21]). Big bang nucleosynthesis (see Section 24) also provides some interesting constraints on the gravitino and the properties of the next-to-lightest supersymmetric particle that decays into the gravitino LSP [57]. The couplings of the helicity $\pm\frac{1}{2}$ components of \tilde{G} to the particles of the MSSM (which approximate those of the goldstino as previously noted in Sec. 89.2.2) are significantly stronger than gravitational strength and amenable to experimental collider analyses.

The concept of a hidden sector is more general than SUSY. Hidden valley models [58] posit the existence of a hidden sector of new particles and interactions that are very weakly coupled to particles of the SM. The impact of a hidden valley on supersymmetric phenomenology at colliders can be significant if the LSP lies in the hidden sector [59].

89.2.4 SUSY and extra dimensions

Approaches to SUSY breaking have also been developed in the context of theories in which the number of spatial dimensions is greater than three. In particular, a number of SUSY-breaking mechanisms have been proposed that are inherently extra-dimensional [60]. The size of the extra dimensions can be significantly larger than M_{P}^{-1} ; in some cases of order $(\text{TeV})^{-1}$ or even larger (see, e.g., Sec. 86 or Ref. [61]).

For example, in one approach the fields of the MSSM live on some brane (a lower-dimensional manifold embedded in a higher-dimensional spacetime), while the sector of the theory that breaks SUSY lives on a second spatially-separated brane. Two examples of this approach are AMSB [48] and gaugino-mediated SUSY breaking [62]. In both cases, SUSY breaking is transmitted through fields that live in the bulk (the higher-dimensional space between the two branes). This setup has some features in common with both gravity-mediated and gauge-mediated SUSY breaking (e.g., a hidden and visible sector and messengers).

Since a higher dimensional theory must be compactified to four spacetime dimensions, one can also generate a source of SUSY breaking by employing boundary conditions on the compactified space that distinguish between fermions and bosons. This is the so-called Scherk-Schwarz mechanism [63]. The phenomenology of such models can be strikingly different from that of the usual MSSM [64].

89.2.5 Split-SUSY

If SUSY is not connected with the origin of the electroweak scale, it may still be possible that some remnant of the superparticle spectrum survives down to the TeV-scale or below. This is the idea of split-SUSY [65, 66], in which scalar superpartners of the quarks and leptons are significantly heavier (perhaps by many orders of magnitude) than 1 TeV, whereas the fermionic superpartners of the gauge and Higgs bosons have masses on the order of 1 TeV or below. With the exception of a single light neutral scalar whose properties are practically indistinguishable from those of the SM Higgs boson, all other Higgs bosons are also assumed to be very heavy. Among the supersymmetric particles, only the fermionic superpartners may be kinematically accessible at the LHC.

In models of split SUSY, the top squark masses cannot be arbitrarily large, as these parameters enter in the radiative corrections to the mass of the observed Higgs boson [67, 68]. In the MSSM, a Higgs boson mass of 125 GeV (see Sec. 11) implies an upper bound on the top squark mass scale in the range of 10 to 10^8 TeV [69–71], depending on the value of the ratio of the two neutral Higgs field vacuum expectation values, although this mass range can be somewhat extended by varying other relevant MSSM parameters. In some approaches, gaugino masses are one-loop suppressed relative to the sfermion masses, corresponding to the so-called mini-split SUSY spectrum [68, 72]. The higgsino mass scale may or may not be likewise suppressed depending on the details of the model [73].

The SUSY breaking required to produce such a split-SUSY spectrum would destabilize the gauge hierarchy, and thus would not provide an explanation for the scale of electroweak symmetry breaking. Nevertheless, models of split-SUSY can account for the dark matter (which is assumed to be the LSP gaugino or higgsino)

and gauge coupling unification, thereby preserving two of the desirable features of weak-scale SUSY. Finally, as a consequence of the very large squark and slepton masses, neutral flavor changing and CP-violating effects, which can be problematic in models with TeV-scale SUSY-breaking masses, are sufficiently reduced to avoid conflict with experimental observations.

89.3 Parameters of the MSSM

The parameters of the MSSM are conveniently described by considering separately the supersymmetry-conserving and the supersymmetry-breaking sectors. A careful discussion of the conventions used here in defining the tree-level MSSM parameters can be found in Refs. [74, 75]. For simplicity, consider first the case of one generation of quarks, leptons, and their scalar superpartners.

89.3.1 The SUSY-conserving parameters

The parameters of the supersymmetry-conserving sector consist of: (i) gauge couplings, g_s , g , and g' , corresponding to the SM gauge group $SU(3) \times SU(2) \times U(1)$ respectively; (ii) a supersymmetry-conserving higgsino mass parameter μ ; and (iii) Higgs-fermion Yukawa couplings, λ_u , λ_d , and λ_e , of one generation of left- and right-handed quarks and leptons, and their superpartners to the Higgs bosons and higgsinos. Because there is no right-handed neutrino/sneutrino in the MSSM as defined here, a Yukawa coupling λ_ν is not included. The complex μ parameter and Yukawa couplings enter via the most general renormalizable R-parity-conserving superpotential,

$$W = \lambda_d \hat{H}_d \hat{Q} \hat{D}^c - \lambda_u \hat{H}_u \hat{Q} \hat{U}^c + \lambda_e \hat{H}_d \hat{L} \hat{E}^c + \mu \hat{H}_u \hat{H}_d, \quad (89.1)$$

where the superfields are defined in Table 1 and the gauge group indices are suppressed.

89.3.2 The SUSY-breaking parameters

The supersymmetry-breaking sector contains the following sets of parameters: (i) three complex gaugino Majorana mass parameters, M_3 , M_2 , and M_1 , associated with the $SU(3)$, $SU(2)$, and $U(1)$ subgroups of the SM; (ii) five sfermion squared-mass parameters, M_Q^2 , M_U^2 , M_D^2 , M_L^2 , and M_E^2 , corresponding to the five electroweak gauge multiplets, *i.e.*, superpartners of the left-handed fields $(u, d)_L$, u_L^c , d_L^c , $(\nu, e^-)_L$, and e_L^c , where the superscript c indicates a charge-conjugated fermion field [24]; and (iii) three Higgs-squark-squark and Higgs-slepton-slepton trilinear interaction terms, with complex coefficients $T_U \equiv \lambda_u A_U$, $T_D \equiv \lambda_d A_D$, and $T_E \equiv \lambda_e A_E$ (which define the “ A -parameters”). The notation T_U , T_D and T_E is employed in Ref. [75]. It is conventional to separate out the factors of the Yukawa couplings in defining the A -parameters (originally motivated by a simple class of gravity-mediated SUSY-breaking models [3, 6]). If the A -parameters are parametrically of the same order (or smaller) relative to other SUSY-breaking mass parameters, then only the third generation A -parameters are phenomenologically relevant.

Finally, we have (iv) two real squared-mass parameters, m_1^2 and m_2^2 (also called $m_{H_d}^2$ and $m_{H_u}^2$, respectively, in the literature), and one complex squared-mass parameter, $m_{12}^2 \equiv \mu B$ (the latter defines the “ B -parameter”), which appear in the MSSM tree-level scalar Higgs potential [28],

$$V = (m_1^2 + |\mu|^2) H_d^\dagger H_d + (m_2^2 + |\mu|^2) H_u^\dagger H_u + (m_{12}^2 H_u H_d + \text{h.c.}) + \frac{1}{8} (g^2 + g'^2) (H_d^\dagger H_d - H_u^\dagger H_u)^2 + \frac{1}{2} g^2 |H_d^\dagger H_u|^2, \quad (89.2)$$

where the $SU(2)$ -invariant combination, $H_u H_d \equiv H_u^+ H_d^- - H_u^0 H_d^0$. Note that the quartic Higgs couplings are related to the gauge couplings g and g' as a consequence of SUSY. The breaking of the $SU(2) \times U(1)$ electroweak symmetry group to $U(1)_{EM}$ is only possible after incorporating the SUSY-breaking Higgs squared-mass parameters m_1^2 , m_2^2 (which can be negative) and m_{12}^2 . After minimizing the Higgs scalar potential, these three squared-mass parameters can be re-expressed in terms of the two Higgs vacuum expectation values, $\langle H_d^0 \rangle \equiv v_d/\sqrt{2}$ and $\langle H_u^0 \rangle \equiv v_u/\sqrt{2}$, and the CP-odd Higgs mass m_A [cf. Eqs. (89.4) and (89.5) below]. One is always free to re-phase the Higgs doublet fields such that v_d and

v_u (also called v_1 and v_2 , respectively, in the literature) are both real and positive.

The quantity, $v_d^2 + v_u^2 = 4m_W^2/g^2 = (2G_F^2)^{-1/2} \simeq (246 \text{ GeV})^2$, is fixed by the Fermi constant, G_F , whereas the ratio

$$\tan \beta = v_u/v_d \quad (89.3)$$

is a free parameter such that $0 < \beta < \pi/2$. By employing the tree-level conditions resulting from the minimization of the scalar potential, one can eliminate the diagonal and off-diagonal Higgs squared-masses in favor of $m_Z^2 = \frac{1}{4}(g^2 + g'^2)(v_d^2 + v_u^2)$, the CP-odd Higgs mass m_A and the parameter $\tan \beta$,

$$\sin 2\beta = \frac{2m_{12}^2}{m_1^2 + m_2^2 + 2|\mu|^2} = \frac{2m_{12}^2}{m_A^2}, \quad (89.4)$$

$$\frac{1}{2} m_Z^2 = -|\mu|^2 + \frac{m_1^2 - m_2^2 \tan^2 \beta}{\tan^2 \beta - 1}. \quad (89.5)$$

One must also guard against the existence of charge and/or color breaking global minima due to non-zero vacuum expectation values for the squark and charged slepton fields. This possibility can be avoided if the A -parameters are not unduly large [42, 76, 77]. Additional constraints must also be respected to avoid the possibility of directions in scalar field space in which the full tree-level scalar potential can become unbounded from below [77].

Note that SUSY-breaking mass terms for the fermionic superpartners of scalar fields and non-holomorphic trilinear scalar interactions (*i.e.*, interactions that mix scalar fields and their complex conjugates) have not been included above in the soft-SUSY-breaking sector. These terms can potentially destabilize the gauge hierarchy [11] in models with a gauge-singlet superfield. The latter is not present in the MSSM; hence as noted in Ref. [12], these so-called non-standard soft-SUSY-breaking terms are benign. The phenomenological impact of non-holomorphic soft SUSY-breaking terms has been reconsidered in Refs. [78–80]. However, in the most common approaches to constructing a fundamental theory of SUSY-breaking, the coefficients of these terms (which have dimensions of mass) are significantly suppressed compared to the TeV-scale [81]. Consequently, we follow the usual approach and omit these terms from further consideration.

89.3.3 MSSM-124

The total number of independent physical parameters that define the MSSM (in its most general form) is quite large, primarily due to the soft-supersymmetry-breaking sector. In particular, in the case of three generations of quarks, leptons, and their superpartners, M_Q^2 , M_U^2 , M_D^2 , M_L^2 , and M_E^2 are hermitian 3×3 matrices, and A_U , A_D , and A_E are complex 3×3 matrices. In addition, M_1 , M_2 , M_3 , B , and μ are in general complex parameters. Finally, as in the SM, the Higgs-fermion Yukawa couplings, λ_f ($f = u, d$, and e), are complex 3×3 matrices that are related to the quark and lepton mass matrices via: $M_f = \lambda_f v_f/\sqrt{2}$, where $v_e \equiv v_d$ [with v_u and v_d as defined above Eq. (89.3)].

However, not all these parameters are physical. Some of the MSSM parameters can be eliminated by expressing interaction eigenstates in terms of the mass eigenstates, with an appropriate redefinition of the MSSM fields to remove unphysical degrees of freedom. The analysis of Ref. [82] shows that the MSSM possesses 124 independent real degrees of freedom. Of these, 18 correspond to SM parameters (including the QCD vacuum angle θ_{QCD}), one corresponds to a Higgs sector parameter (the analogue of the SM Higgs mass), and 105 are genuinely new parameters of the model. The latter include: five real parameters and three CP-violating phases in the gaugino/higgsino sector, 21 squark and slepton (sfermion) masses, 36 real mixing angles to define the sfermion mass eigenstates, and 40 CP-violating phases that can appear in sfermion interactions. The most general R-parity-conserving minimal supersymmetric extension of the SM (without additional theoretical assumptions) will be denoted henceforth as MSSM-124 [83].

89.4 The supersymmetric-particle spectrum

The supersymmetric particles (sparticles) differ in spin by half a unit from their SM partners. The superpartners of the gauge and

Higgs bosons are fermions, whose names are obtained by appending “ino” to the end of the corresponding SM particle name. The gluino is the color-octet Majorana fermion partner of the gluon with mass $M_{\tilde{g}} = |M_3|$. The superpartners of the electroweak gauge and Higgs bosons (the gauginos and higgsinos) can mix due to $SU(2) \times U(1)$ breaking effects. As a result, the physical states of definite mass are model-dependent linear combinations of the charged or neutral gauginos and higgsinos, called charginos and neutralinos, respectively (sometimes collectively called electroweakinos). The neutralinos are Majorana fermions, which can lead to some distinctive phenomenological signatures [84,85]. The superpartners of the quarks and leptons are spin-zero bosons: the squarks, charged sleptons, and sneutrinos, respectively. A complete set of Feynman rules for the sparticles of the MSSM can be found in Ref. [86]. The MSSM Feynman rules also are implicitly contained in a number of amplitude generation and Feynman diagram software packages (see *e.g.*, Refs. [87–89]).

It should be noted that all mass formulae quoted below in this Section are tree-level results. Radiative loop corrections will modify these results and must be included in any precision study of supersymmetric phenomenology [90]. Beyond tree level, the definition of the supersymmetric parameters becomes convention-dependent. For example, one can define physical couplings or running couplings, which differ beyond the tree level. This provides a challenge to any effort that attempts to extract supersymmetric parameters from data. The SUSY Les Houches Accord (SLHA) [75,91] has been adopted, which establishes a set of conventions for specifying generic file structures for supersymmetric model specifications and input parameters, supersymmetric mass and coupling spectra, and decay tables. These provide a universal interface between spectrum calculation programs, decay packages, and high energy physics event generators.

89.4.1 The charginos and neutralinos

The mixing of the charged gauginos (\tilde{W}^\pm) and charged higgsinos (\tilde{H}_u^\pm and \tilde{H}_d^\pm) is described (at tree-level) by a 2×2 complex mass matrix [92,93],

$$M_C \equiv \begin{pmatrix} M_2 & \frac{1}{\sqrt{2}} g v_u \\ \frac{1}{\sqrt{2}} g v_d & \mu \end{pmatrix}. \quad (89.6)$$

To determine the physical chargino states and their masses, one must perform a singular value decomposition [94,95] of the complex matrix M_C :

$$U^* M_C V^{-1} = \text{diag}(M_{\tilde{\chi}_1^\pm}, M_{\tilde{\chi}_2^\pm}), \quad (89.7)$$

where U and V are unitary matrices, and the right-hand side of Eq. (89.7) is the diagonal matrix of (real non-negative) chargino masses. The physical chargino states are denoted by $\tilde{\chi}_1^\pm$ and $\tilde{\chi}_2^\pm$. These are linear combinations of the charged gaugino and higgsino states determined by the matrix elements of U and V [92,93]. The chargino masses correspond to the singular values [94] of M_C , *i.e.*, the positive square roots of the eigenvalues of $M_C^\dagger M_C$:

$$M_{\tilde{\chi}_1^\pm, \tilde{\chi}_2^\pm}^2 = \frac{1}{2} \left\{ |\mu|^2 + |M_2|^2 + 2m_W^2 \mp \sqrt{(|\mu|^2 + |M_2|^2 + 2m_W^2)^2 - 4|\mu M_2 - m_W^2 \sin 2\beta|^2} \right\}, \quad (89.8)$$

where the states are ordered such that $M_{\tilde{\chi}_1^\pm} \leq M_{\tilde{\chi}_2^\pm}$. The relative phase of μ and M_2 is physical and potentially observable. The mixing of the neutral gauginos (\tilde{B} and \tilde{W}^0) and neutral higgsinos (\tilde{H}_d^0 and \tilde{H}_u^0) is described (at tree-level) by a 4×4 complex symmetric mass matrix [92,93],

$$M_N \equiv \begin{pmatrix} M_1 & 0 & -\frac{1}{2} g' v_d & \frac{1}{2} g' v_u \\ 0 & M_2 & \frac{1}{2} g v_d & -\frac{1}{2} g v_u \\ -\frac{1}{2} g' v_d & \frac{1}{2} g v_d & 0 & -\mu \\ \frac{1}{2} g' v_u & -\frac{1}{2} g v_u & -\mu & 0 \end{pmatrix}. \quad (89.9)$$

To determine the physical neutralino states and their masses, one must perform an Autonne-Takagi factorization [94,96] (also called Takagi diagonalization [95,97]) of the complex symmetric matrix M_N :

$$W^T M_N W = \text{diag}(M_{\tilde{\chi}_1^0}, M_{\tilde{\chi}_2^0}, M_{\tilde{\chi}_3^0}, M_{\tilde{\chi}_4^0}), \quad (89.10)$$

where W is a unitary matrix and the right-hand side of Eq. (89.10) is the diagonal matrix of (real non-negative) neutralino masses. The physical neutralino states are denoted by $\tilde{\chi}_i^0$ ($i = 1, \dots, 4$), where the states are ordered such that $M_{\tilde{\chi}_1^0} \leq M_{\tilde{\chi}_2^0} \leq M_{\tilde{\chi}_3^0} \leq M_{\tilde{\chi}_4^0}$. The $\tilde{\chi}_i^0$ are the linear combinations of the neutral gaugino and higgsino states determined by the matrix elements of W (which is denoted by N^{-1} in Ref. [92]). The neutralino masses correspond to the singular values of M_N , *i.e.*, the positive square roots of the eigenvalues of $M_N^\dagger M_N$. Exact formulae for these masses can be found in Refs. [98] and [99]. A numerical algorithm for determining the mixing matrix W has been given in Ref. [100].

If a chargino or neutralino state approximates a particular gaugino or higgsino state, it is convenient to employ the corresponding nomenclature. Specifically, if $|M_1|$ and $|M_2|$ are small compared to m_Z and $|\mu|$, then the lightest neutralino $\tilde{\chi}_1^0$ would be nearly a pure photino, $\tilde{\gamma}$, the superpartner of the photon. If $|M_1|$ and m_Z are small compared to $|M_2|$ and $|\mu|$, then the lightest neutralino would be nearly a pure bino, \tilde{B} , the superpartner of the weak hypercharge gauge boson. If $|M_2|$ and m_Z are small compared to $|M_1|$ and $|\mu|$, then the lightest chargino pair and neutralino would constitute a triplet of roughly mass-degenerate pure winos, \tilde{W}^\pm , and \tilde{W}^0 , the superpartners of the weak $SU(2)$ gauge bosons. Finally, if $|\mu|$ and m_Z are small compared to $|M_1|$ and $|M_2|$, then the lightest chargino pair and neutralino would be nearly pure higgsino states, the superpartners of the Higgs bosons. Each of the above cases leads to a strikingly different phenomenology.

In the NMSSM, an additional Higgs singlet superfield is added to the MSSM. This superfield comprises two real Higgs scalar degrees of freedom and an associated neutral higgsino degree of freedom. Consequently, there are five neutralino mass eigenstates that are obtained by a Takagi-diagonalization of the 5×5 neutralino mass matrix. In many cases, the fifth neutralino state is dominated by its $SU(2) \times U(1)$ singlet component, and thus is very weakly coupled to the SM particles and their superpartners.

89.4.2 The squarks and sleptons

For a given Dirac fermion f , there are two superpartners, \tilde{f}_L and \tilde{f}_R , where the L and R subscripts simply identify the scalar partners that are related by SUSY to the left-handed and right-handed fermions, $f_{L,R} \equiv \frac{1}{2}(1 \mp \gamma_5)f$, respectively. (There is no $\tilde{\nu}_R$ in the MSSM.) However, \tilde{f}_L - \tilde{f}_R mixing is possible, in which case \tilde{f}_L and \tilde{f}_R are not mass eigenstates. For three generations of squarks, one must diagonalize 6×6 matrices corresponding to the basis $(\tilde{q}_{iL}, \tilde{q}_{iR})$, where $i = 1, 2, 3$ are the generation labels. For simplicity, only the one-generation case is illustrated in detail below. (The effects of second and third generation squark mixing can be significant and are treated in Ref. [101].)

Using the notation of the third family, the one-generation tree-level squark squared-mass matrix is given by [102],

$$\mathcal{M}^2 = \begin{pmatrix} M_Q^2 + m_q^2 + L_q & m_q X_q^* \\ m_q X_q & M_R^2 + m_q^2 + R_q \end{pmatrix}, \quad (89.11)$$

where

$$X_q \equiv A_q - \mu^* (\cot \beta)^{2T_{3q}}, \quad (89.12)$$

and $T_{3q} = \frac{1}{2} [-\frac{1}{2}]$ for $q = t$ [b]. The diagonal squared-masses are governed by soft-SUSY-breaking squared-masses M_Q^2 and $M_R^2 \equiv M_D^2$ [M_U^2] for $q = t$ [b], the corresponding quark masses m_t [m_b] and the electroweak correction terms:

$$\begin{aligned} L_q &\equiv (T_{3q} - e_q \sin^2 \theta_W) m_Z^2 \cos 2\beta, \\ R_q &\equiv e_q \sin^2 \theta_W m_Z^2 \cos 2\beta, \end{aligned} \quad (89.13)$$

where $\epsilon_q = \frac{2}{3} [-\frac{1}{3}]$ for $q = t [b]$. The off-diagonal squark squared-masses are proportional to the corresponding quark masses and depend on $\tan\beta$, the soft-SUSY-breaking A -parameters and the higgsino mass parameter μ . Assuming that the A -parameters are parametrically of the same order (or smaller) relative to other SUSY-breaking mass parameters, it then follows that the first and second generation $\tilde{q}_L\text{-}\tilde{q}_R$ mixing is smaller than that of the third generation where mixing can be enhanced by factors of m_t and $m_b \tan\beta$.

In the case of third generation $\tilde{q}_L\text{-}\tilde{q}_R$ mixing, the mass eigenstates (usually denoted by \tilde{q}_1 and \tilde{q}_2 , with $m_{\tilde{q}_1} < m_{\tilde{q}_2}$) are determined by diagonalizing the 2×2 matrix \mathcal{M}^2 given by Eq. (89.11). The corresponding squared-masses and mixing angle are given by [102]:

$$m_{\tilde{q}_{1,2}}^2 = \frac{1}{2} \left[\text{Tr} \mathcal{M}^2 \mp \sqrt{(\text{Tr} \mathcal{M}^2)^2 - 4 \det \mathcal{M}^2} \right],$$

$$\sin 2\theta_{\tilde{q}} = \frac{2m_q |X_q|}{m_{\tilde{q}_2}^2 - m_{\tilde{q}_1}^2}.$$
(89.14)

The one-generation results above also apply to the charged sleptons, with the obvious substitutions: $q \rightarrow \ell$ with $T_{3\ell} = -\frac{1}{2}$ and $\epsilon_\ell = -1$, and the replacement of the SUSY-breaking parameters: $M_Q^2 \rightarrow M_L^2$, $M_D^2 \rightarrow M_E^2$, and $A_q \rightarrow A_\tau$. For the neutral sleptons, $\tilde{\nu}_R$ does not exist in the MSSM, so $\tilde{\nu}_L$ is a mass eigenstate.

In the case of three generations, the SUSY-breaking scalar-squared masses [M_Q^2 , M_U^2 , M_D^2 , M_L^2 , and M_E^2] and the A -parameters [A_U , A_D , and A_E] are now 3×3 matrices as noted in Sec. 89.3.3. The diagonalization of the 6×6 squark mass matrices yields $\tilde{f}_{iL}\text{-}\tilde{f}_{jR}$ mixing. In practice, since the $\tilde{f}_L\text{-}\tilde{f}_R$ mixing is appreciable only for the third generation, this additional complication can often be neglected (although see Ref. [101] for examples in which the mixing between the second and third generation squarks is relevant).

89.5 The supersymmetric Higgs sector

Consider first the MSSM Higgs sector [27, 28, 103]. Despite the large number of potential CP -violating phases among the MSSM-124 parameters, the tree-level MSSM Higgs potential given by Eq. (89.2) is automatically CP -conserving. This follows from the fact that the only potentially complex parameter (m_{12}^2) of the MSSM Higgs potential can be chosen real and positive by rephasing the Higgs fields, in which case $\tan\beta$ is a real positive parameter. Consequently, the physical neutral Higgs scalars are CP -eigenstates (at tree-level). The MSSM Higgs sector contains five physical spin-zero particles: a charged Higgs boson pair (H^\pm), two CP -even neutral Higgs bosons (denoted by h^0 and H^0 where $m_h < m_H$), and one CP -odd neutral Higgs boson (A^0). The discovery of a SM-like Higgs boson at the LHC with a mass of 125 GeV (see Sec. 11) strongly suggests that this state should be identified with h^0 , although the possibility that the 125 GeV state should be identified with H^0 cannot yet be completely ruled out [104].

In the NMSSM [33], the scalar component of the singlet Higgs superfield adds two additional neutral states to the Higgs sector. In this model, the tree-level Higgs sector can exhibit explicit CP -violation. If CP is conserved, then the two extra neutral scalar states are CP -even and CP -odd, respectively. These states can potentially mix with the neutral Higgs states of the MSSM. If scalar states exist that are dominantly singlet, then they are weakly coupled to SM gauge bosons and fermions through their small mixing with the MSSM Higgs scalars. Consequently, it is possible that one (or both) of the singlet-dominated states is considerably lighter than the Higgs boson that was observed at the LHC.

89.5.1 The tree-level Higgs sector

The tree-level properties of the Higgs sector are determined by the Higgs potential given by Eq. (89.2). The quartic interaction terms are manifestly supersymmetric (although these are modified by SUSY-breaking effects at the loop level). In general, the quartic couplings arise from two sources: (i) the supersymmetric generalization of the scalar potential (the so-called “ F -terms”), and

(ii) interaction terms related by SUSY to the coupling of the scalar fields and the gauge fields, whose coefficients are proportional to the corresponding gauge couplings (the so-called “ D -terms”).

In the MSSM, F -term contributions to the quartic Higgs self-couplings are absent. As a result, the strengths of the MSSM quartic Higgs interactions are fixed in terms of the gauge couplings, as noted below Eq. (89.2). Consequently, all the tree-level MSSM Higgs-sector parameters depend only on two quantities: $\tan\beta$ [defined in Eq. (89.3)] and one Higgs mass usually taken to be m_A . From these two quantities, one can predict the values of the remaining Higgs boson masses, an angle α that measures the mixture of the hypercharge ± 1 scalar fields, H_u^0 and H_d^0 , in the physical CP -even neutral scalars, and the Higgs boson self-couplings. Moreover, the tree-level mass of the lighter CP -even Higgs boson is bounded, $m_h \leq m_Z |\cos 2\beta| \leq m_Z$ [27, 28]. This bound can be substantially modified when radiative corrections are included, as discussed in Sec. 89.5.2.

In the NMSSM, the superpotential contains a trilinear term that couples the two $Y = \pm 1$ Higgs doublet superfields and the singlet Higgs superfield. The coefficient of this term is denoted by λ . Consequently, the tree-level bound for the mass of the lightest CP -even MSSM Higgs boson is modified [105],

$$m_h^2 \leq m_Z^2 \cos^2 2\beta + \frac{1}{2} \lambda^2 v^2 \sin^2 2\beta,$$
(89.15)

where $v \equiv (v_u^2 + v_d^2)^{1/2} = 246$ GeV. If one demands that λ should stay finite after renormalization-group evolution up to the Planck scale, then λ is constrained to lie below about 0.7–0.8 at the electroweak scale [33] (although larger values of λ have also been considered [106]).

The tree-level Higgs-quark and Higgs-lepton interactions of the MSSM are governed by the Yukawa couplings defined by the superpotential given in Eq. (89.1). In particular, the Higgs sector of the MSSM is a Type-II two-Higgs doublet model [107], in which one Higgs doublet (H_d) couples exclusively to the right-handed down-type quark (or lepton) fields and the second Higgs doublet (H_u) couples exclusively to the right-handed up-type quark fields. Consequently, the diagonalization of the fermion mass matrices simultaneously diagonalizes the matrix Yukawa couplings, resulting in flavor-diagonal tree-level couplings of the neutral Higgs bosons h^0 , H^0 and A^0 to quark and lepton pairs.

89.5.2 The radiatively-corrected Higgs sector

When radiative corrections are incorporated, additional parameters of the supersymmetric model enter via virtual supersymmetric particles that appear in loops. The impact of these corrections can be significant [108]. The qualitative behavior of these radiative corrections can be most easily seen in the large top-squark mass limit, where in addition, both the splitting of the two diagonal entries and the off-diagonal entries of the top-squark squared-mass matrix [Eq. (89.11)] are small in comparison to the geometric mean of the two top-squark squared-masses, $M_S^2 \equiv M_{t_1} M_{t_2}$. In this case (assuming $m_A > m_Z$), the predicted upper bound for m_h is approximately given by

$$m_h^2 \lesssim m_Z^2 \cos^2 2\beta + \frac{3g^2 m_t^4}{8\pi^2 m_W^2} \left[\ln \left(\frac{M_S^2}{m_t^2} \right) + \frac{X_t^2}{M_S^2} \left(1 - \frac{X_t^2}{12M_S^2} \right) \right],$$
(89.16)

where $X_t \equiv A_t - \mu \cot\beta$ [cf. Eq. (89.12)] is proportional to the off-diagonal entry of the top-squark squared-mass matrix (where for simplicity, A_t and μ are taken to be real). The Higgs mass upper limit specified by Eq. (89.16) is saturated when $\tan\beta$ is large (*i.e.*, $\cos^2 2\beta \sim 1$) and $X_t = \sqrt{6} M_S$, which defines the so-called maximal mixing scenario.

A more complete treatment of the radiative corrections shows that Eq. (89.16) somewhat overestimates the true upper bound of m_h . These more refined computations, which incorporate renormalization group improvement, the two loop and the leading three-loop contributions, yield $m_h \lesssim 135$ GeV in the region of large $\tan\beta$ (with an accuracy of a few GeV) for $m_t = 175$ GeV and $M_S \lesssim 2$ TeV [109].

In addition, one-loop radiative corrections can introduce CP -violating effects in the Higgs sector that depend on some of

the CP -violating phases among the MSSM-124 parameters [110]. This phenomenon is most easily understood in a scenario where $m_A \ll M_S$ (i.e., all five physical Higgs states are significantly lighter than the SUSY breaking scale). In this case, one can integrate out the heavy superpartners to obtain a low-energy effective theory with two Higgs doublets. The resulting effective two-Higgs doublet model will now contain all possible Higgs self-interaction terms (both CP -conserving and CP -violating) and Higgs-fermion interactions (beyond those of Type-II) that are consistent with electroweak gauge invariance [111].

In the NMSSM, the dominant radiative correction to Eq. (89.15) is the same as the one given in Eq. (89.16). However, in contrast to the MSSM, one does not need as large a boost from the radiative corrections to achieve a Higgs mass of 125 GeV in certain regimes of the NMSSM parameter space (e.g., $\tan\beta \sim 2$ and $\lambda \sim 0.7$ [112]).

89.6 Restricting the MSSM parameter freedom

In Sections 89.4 and 89.5, we surveyed the parameters that comprise the MSSM-124. However, without additional restrictions on the choice of parameters, a generic parameter set within the MSSM-124 framework is not phenomenologically viable. In particular, a generic point of the MSSM-124 parameter space exhibits: (i) no conservation of the separate lepton numbers $L_e, L_\mu,$ and L_τ ; (ii) unsuppressed flavor-changing neutral currents (FCNCs); and (iii) new sources of CP violation that are inconsistent with the experimental bounds.

For example, the MSSM contains many new sources of CP violation [113]. Indeed, for TeV-scale sfermion and gaugino masses, some combinations of the complex phases of the gaugino-mass parameters, the A -parameters, and μ must be less than about 10^{-2} – 10^{-3} to avoid generating electric dipole moments for the neutron, electron, and atoms [114–116] in conflict with observed data [117]. The rarity of FCNCs [118–120] places additional constraints on the off-diagonal matrix elements of the squark and slepton soft-SUSY-breaking squared-masses and A -parameters (see Sec. 89.3.3).

The MSSM-124 is also theoretically incomplete as it provides no explanation for the fundamental origin of the supersymmetry-breaking parameters. The successful unification of the SM gauge couplings at very high energies close to the Planck scale [8, 66, 121–123] suggests that the high-energy structure of the theory may be considerably simpler than its low-energy realization. In a top-down approach, the dynamics that governs the more fundamental theory at high energies is used to derive the effective broken-supersymmetric theory at the TeV scale. A suitable choice for the high energy dynamics is one that yields a TeV-scale theory that satisfies all relevant phenomenological constraints.

In this Section, we examine a number of theoretical frameworks that potentially yield phenomenologically viable regions of the MSSM-124 parameter space. The resulting supersymmetric particle spectrum is then a function of a relatively small number of input parameters. This is accomplished by imposing a simple structure on the soft SUSY-breaking parameters at a common high-energy scale M_X (typically chosen to be the Planck scale, M_P , the grand unification scale, M_{GUT} , or the messenger scale, M_{mess}). These serve as initial conditions for the MSSM renormalization group equations (RGEs), which are given in the two-loop approximation in Ref. [124] (an automated program to compute RGEs for the MSSM and other models of new physics beyond the SM has been developed in Ref. [125]). Solving these equations numerically, one can then derive the low-energy MSSM parameters relevant for phenomenology. A number of software packages exist that numerically calculate the spectrum of supersymmetric particles, consistent with theoretical conditions on SUSY breaking at high energies and some experimental data at low energies [126].

Examples of this scenario are provided by models of gravity-mediated, anomaly mediated and gauge-mediated SUSY breaking, to be discussed in more detail below. In some of these approaches, one of the diagonal Higgs squared-mass parameters is driven negative by renormalization group evolution [127]. In such models, electroweak symmetry breaking is generated radiatively, and the resulting electroweak symmetry-breaking scale is intimately tied to the scale of low-energy SUSY breaking.

89.6.1 Gaugino mass relations

One prediction of many supersymmetric grand unified models is the unification of the (tree-level) gaugino mass parameters at some high-energy scale, M_X ,

$$M_1(M_X) = M_2(M_X) = M_3(M_X) = m_{1/2}. \quad (89.17)$$

Due to renormalization group running, in the one-loop approximation the effective low-energy gaugino mass parameters (at the electroweak scale) are related,

$$M_3 = (g_s^2/g^2)M_2 \simeq 3.5M_2, \quad M_1 = (5g'^2/3g^2)M_2 \simeq 0.5M_2. \quad (89.18)$$

Eq. (89.18) can arise more generally in gauge-mediated SUSY-breaking models where the gaugino masses are generated at the messenger scale M_{mess} (which typically lies significantly below the unification scale where the gauge couplings unify). In this case, the gaugino mass parameters are proportional to the corresponding squared gauge couplings at the messenger scale.

When Eq. (89.18) is satisfied, the chargino and neutralino masses and mixing angles depend only on three unknown parameters: the gluino mass, μ , and $\tan\beta$. It then follows that the lightest neutralino must be heavier than 46 GeV due to the non-observation of charginos at LEP [128]. If in addition $|\mu| \gg |M_1| \gtrsim m_Z$, then the lightest neutralino is nearly a pure bino, an assumption often made in supersymmetric particle searches at colliders. Although Eq. (89.18) is often assumed in many phenomenological studies, a truly model-independent approach would take the gaugino mass parameters, M_i , to be independent parameters to be determined by experiment. Indeed, an approximately massless neutralino *cannot* be ruled out at present by a model-independent analysis [129].

It is possible that the tree-level masses for the gauginos are zero. In this case, the gaugino mass parameters arise at one-loop and do not satisfy Eq. (89.18). For example, the gaugino masses in AMSB models arise entirely from a model-independent contribution derived from the super-conformal anomaly [48, 130]. In this case, Eq. (89.18) is replaced (in the one-loop approximation) by:

$$M_i \simeq \frac{b_i g_i^2}{16\pi^2} m_{3/2}, \quad (89.19)$$

where $m_{3/2}$ is the gravitino mass and the b_i are the coefficients of the MSSM gauge beta-functions corresponding to the corresponding $U(1)$, $SU(2)$, and $SU(3)$ gauge groups, $(b_1, b_2, b_3) = (\frac{33}{5}, 1, -3)$. Eq. (89.19) yields $M_1 \simeq 2.8M_2$ and $M_3 \simeq -8.3M_2$, which implies that the lightest chargino pair and neutralino comprise a nearly mass-degenerate triplet of winos, $\tilde{W}^\pm, \tilde{W}^0$ (cf. Table 1), over most of the MSSM parameter space. For example, if $|\mu| \gg m_Z, |M_2|$, then Eq. (89.19) implies that $M_{\tilde{\chi}^\pm} \simeq M_{\tilde{\chi}_1^0} \simeq M_2$ [131]. Alternatively, one can construct an AMSB model where $|\mu|, m_Z \ll M_2$, which yields an LSP that is an approximate higgsino state [132]. In both cases, the corresponding supersymmetric phenomenology differs significantly from the standard phenomenology based on Eq. (89.18) [133, 134].

Finally, it should be noted that the unification of gaugino masses (and scalar masses) can be accidental. In particular, the energy scale where unification takes place may not be directly related to any physical scale. One version of this phenomenon has been called mirage unification and can occur in certain theories of fundamental SUSY breaking [135].

89.6.2 Constrained versions of the MSSM: $mSUGRA$, $CMSSM$, etc.

In the minimal supergravity ($mSUGRA$) framework [3–6, 41–43], a form of the Kähler potential is employed that yields minimal kinetic energy terms for the MSSM fields [45]. As a result, the soft supersymmetry-breaking parameters at the high-energy scale M_X take a particularly simple form in which the scalar squared-masses

and the A -parameters are flavor-diagonal and universal [43]:

$$\begin{aligned} M_Q^2(M_X) &= M_U^2(M_X) = M_D^2(M_X) = m_0^2 \mathbf{1}, \\ M_L^2(M_X) &= M_E^2(M_X) = m_0^2 \mathbf{1}, \\ m_1^2(M_X) &= m_2^2(M_X) = m_0^2, \\ A_U(M_X) &= A_D(M_X) = A_E(M_X) = A_0 \mathbf{1}, \end{aligned} \quad (89.20)$$

where $\mathbf{1}$ is a 3×3 identity matrix in generation space. As in the SM, this approach exhibits minimal flavor violation [136, 137], whose unique source is the nontrivial flavor structure of the Higgs-fermion Yukawa couplings. The gaugino masses are also unified according to Eq. (89.17).

Renormalization group evolution is then used to derive the values of the supersymmetric parameters at the low-energy (electroweak) scale. For example, to compute squark masses, one should use the low-energy values for M_Q^2 , M_U^2 , and M_D^2 in Eq. (89.11). Through the renormalization group running with boundary conditions specified in Eq. (89.18) and Eq. (89.20), one can show that the low-energy values of M_Q^2 , M_U^2 , and M_D^2 depend primarily on m_0^2 and $m_{1/2}^2$. A number of useful approximate analytic expressions for superpartner masses in terms of the mSUGRA parameters can be found in Ref. [138].

In the mSUGRA approach, four flavors of squarks (with two squark eigenstates per flavor) are nearly mass-degenerate. If $\tan \beta$ is not very large, \tilde{b}_R is also approximately degenerate in mass with the first two generations of squarks. The \tilde{b}_L mass and the diagonal t_L and t_R masses are typically reduced relative to the common squark mass of the first two generations. In addition, there are six flavors of nearly mass-degenerate sleptons (with two slepton eigenstates per flavor for the charged sleptons and one per flavor for the sneutrinos); the sleptons are expected to be somewhat lighter than the mass-degenerate squarks. As noted below Eq. (89.11), third-generation squark masses and tau-slepton masses are sensitive to the strength of the respective \tilde{f}_L - \tilde{f}_R mixing. The LSP is typically the lightest neutralino, $\tilde{\chi}_1^0$, which is dominated by its bino component. Regions of the mSUGRA parameter space in which the LSP is electrically charged do exist but are not phenomenologically viable [19].

One can count the number of independent parameters in the mSUGRA framework. In addition to 18 SM parameters (excluding the Higgs mass), one must specify m_0 , $m_{1/2}$, A_0 , the Planck-scale values for μ and B -parameters (denoted by μ_0 and B_0), and the gravitino mass $m_{3/2}$. Without additional model assumptions, $m_{3/2}$ is independent of the parameters that govern the mass spectrum of the superpartners of the SM [43]. In principle, A_0 , B_0 , μ_0 , and $m_{3/2}$ can be complex, although in the mSUGRA approach, these parameters are taken (arbitrarily) to be real.

As previously noted, renormalization group evolution is used to compute the low-energy values of the mSUGRA parameters, which then fixes all the parameters of the low-energy MSSM. In particular, the two Higgs vacuum expectation values (or equivalently, m_Z and $\tan \beta$) can be expressed as a function of the Planck-scale supergravity parameters. The most common procedure is to remove μ_0 and B_0 in favor of m_Z and $\tan \beta$ [the sign of μ_0 , denoted $\text{sgn}(\mu_0)$ below, is not fixed in this process]. In this case, the MSSM spectrum and its interaction strengths are determined by five parameters:

$$m_0, A_0, m_{1/2}, \tan \beta, \text{ and } \text{sgn}(\mu_0), \quad (89.21)$$

and an independent gravitino mass $m_{3/2}$ (in addition to the 18 parameters of the SM). In Ref. [139], this framework was dubbed the constrained minimal supersymmetric extension of the SM (CMSSM).

In the early literature, additional conditions were obtained by assuming a simplified form for the hidden sector that provides the fundamental source of SUSY breaking. Two additional relations emerged among the mSUGRA parameters [41, 45]: $B_0 = A_0 - m_0$ and $m_{3/2} = m_0$. These relations characterize a theory that was called minimal supergravity when first proposed. In the subsequent literature, it has been more common to omit these extra

conditions in defining the mSUGRA model (in which case the mSUGRA model and the CMSSM are synonymous). The authors of Ref. [140] advocate restoring the original nomenclature in which the mSUGRA model is defined with the extra conditions as originally proposed. Additional mSUGRA variations can also be considered where different relations among the CMSSM parameters are imposed.

One can also relax the universality of scalar masses by decoupling the squared-masses of the Higgs bosons and the squarks/sleptons. This leads to the non-universal Higgs mass models (NUHMs), thereby adding one or two new parameters to the CMSSM depending on whether the diagonal Higgs scalar squared-mass parameters (m_1^2 and m_2^2) are set equal (NUHM1 [141]) or taken to be independent (NUHM2 [142]) at the high energy scale M_X^2 . Clearly, this modification preserves the minimal flavor violation of the mSUGRA approach. Nevertheless, the mSUGRA approach and its NUHM generalizations are probably too simplistic. Theoretical considerations suggest that the universality of Planck-scale soft SUSY-breaking parameters is not generic [143]. In particular, effective operators at the Planck scale exist that do not respect flavor universality, and it is difficult to find a theoretical principle that would forbid them.

In the framework of supergravity, if anomaly mediation is the sole source of SUSY breaking, then the gaugino mass parameters, diagonal scalar squared-mass parameters, and the SUSY-breaking trilinear scalar interaction terms (proportional to $\lambda_f A_F$) are determined in terms of the beta functions of the gauge and Yukawa couplings and the anomalous dimensions of the squark and slepton fields [48, 130, 134]. As noted in Sec. 89.2.3, this approach yields tachyonic sleptons in the MSSM unless additional sources of SUSY breaking are present. In the minimal AMSB (mAMSB) scenario, a universal squared-mass parameter, m_0^2 , is added to the AMSB expressions for the diagonal scalar squared-masses [134]. Thus, the mAMSB spectrum and its interaction strengths are determined by four parameters, m_0^2 , $m_{3/2}$, $\tan \beta$ and $\text{sgn}(\mu_0)$.

The mAMSB scenario appears to be ruled out based on the observed value of the Higgs boson mass, assuming an upper limit on M_S of a few TeV, since the mAMSB constraint on A_F implies that the maximal mixing scenario cannot be achieved [cf. Eq. (89.16)]. Indeed, under the stated assumptions, the mAMSB Higgs mass upper bound lies below the observed Higgs mass value [144]. Thus within the AMSB scenario, either an additional SUSY-breaking contribution to $\lambda_f A_F$ and/or new ingredients beyond the MSSM are required.

89.6.3 Gauge-mediated SUSY breaking

In contrast to models of gravity-mediated SUSY breaking, the flavor universality of the fundamental soft SUSY-breaking squark and slepton squared-mass parameters is guaranteed in gauge-mediated SUSY breaking (GMSB) because the supersymmetry breaking is communicated to the sector of MSSM fields via gauge interactions [53, 55]. In GMSB models, the mass scale of the messenger sector (or its equivalent) is sufficiently below the Planck scale such that the additional SUSY-breaking effects mediated by supergravity can be neglected.

In the minimal GMSB approach, there is one effective mass scale, Λ , that determines all low-energy scalar and gaugino mass parameters through loop effects, while the resulting A -parameters are suppressed. In order that the resulting superpartner masses be of order 1 TeV, one must have $\Lambda \sim \mathcal{O}(100 \text{ TeV})$. The origin of the μ and B -parameters is model-dependent, and lies somewhat outside the ansatz of gauge-mediated SUSY breaking [145].

The simplest GMSB models appear to be ruled out based on the observed value of the Higgs boson mass. Due to suppressed A parameters, it is difficult to boost the contributions of the radiative corrections in Eq. (89.16) to obtain a Higgs mass as large as 125 GeV. However, this conflict can be alleviated in more complicated GMSB models [146]. To analyze these generalized GMSB models, it has been especially fruitful to develop model-independent techniques that encompass all known GMSB models [147]. These techniques are well-suited for a comprehensive analysis [148] of the phenomenological profile of gauge-mediated SUSY breaking.

The gravitino is the LSP in GMSB models, as noted in Sec. 89.2.3. As a result, the next-to-lightest supersymmetric par-

title (NLSP) now plays a crucial role in the phenomenology of supersymmetric particle production and decays. Note that unlike the LSP, the NLSP can be charged. In GMSB models, the most likely candidates for the NLSP are $\tilde{\chi}_1^0$ and $\tilde{\tau}_R^\pm$. The NLSP will decay into its superpartner plus a gravitino (*e.g.*, $\tilde{\chi}_1^0 \rightarrow \gamma\tilde{G}$, $\tilde{\chi}_1^0 \rightarrow Z\tilde{G}$, $\tilde{\chi}_1^0 \rightarrow h^0\tilde{G}$ or $\tilde{\tau}_1^\pm \rightarrow \tau^\pm\tilde{G}$), with lifetimes and branching ratios that depend on the model parameters. There are also GMSB scenarios in which there are several nearly degenerate co-NLSP's, any one of which can be produced at the penultimate step of a supersymmetric decay chain [149]. For example, in the slepton co-NLSP case, all three right-handed sleptons are close enough in mass and thus can each play the role of the NLSP.

Different choices for the identity of the NLSP and its decay rate lead to a variety of distinctive supersymmetric phenomenologies [55,150]. For example, a long-lived $\tilde{\chi}_1^0$ -NLSP that decays outside collider detectors leads to supersymmetric decay chains with missing energy in association with leptons and/or hadronic jets (this case is indistinguishable from the standard phenomenology of the $\tilde{\chi}_1^0$ -LSP). On the other hand, if $\tilde{\chi}_1^0 \rightarrow \gamma\tilde{G}$ is the dominant decay mode, and the decay occurs inside the detector, then nearly *all* supersymmetric particle decay chains would contain a photon. In contrast, in the case of a $\tilde{\tau}_1^\pm$ -NLSP, the $\tilde{\tau}_1^\pm$ would either be long-lived or would decay inside the detector into a τ -lepton plus missing energy.

A number of attempts have been made to address the origins of the μ and B -parameters in GMSB models based on the field content of the MSSM (see, *e.g.*, Refs. [145,151]). An alternative approach is to consider GMSB models based on the NMSSM [152]. The vacuum expectation value of the additional singlet Higgs superfield can be used to generate effective μ and B -parameters [153]. Such models provide an alternative GMSB framework for achieving a Higgs mass of 125 GeV, while still being consistent with LHC bounds on supersymmetric particle masses [154].

89.6.4 The phenomenological MSSM

Of course, any of the theoretical assumptions described in the previous three subsections must be tested experimentally and could turn out to be wrong. To facilitate the exploration of MSSM phenomena in a more model-independent way while respecting the constraints noted at the beginning of this Section, the phenomenological MSSM (pMSSM) has been introduced [155].

The pMSSM is governed by 19 independent real supersymmetric parameters: the three gaugino mass parameters M_1 , M_2 and M_3 , the Higgs sector parameters m_A and $\tan\beta$, the Higgsino mass parameter μ , five sfermion squared-mass parameters for the degenerate first and second generations ($M_{\tilde{Q}}^2$, $M_{\tilde{U}}^2$, $M_{\tilde{D}}^2$, $M_{\tilde{L}}^2$ and $M_{\tilde{E}}^2$), the five corresponding sfermion squared-mass parameters for the third generation, and three third-generation A -parameters (A_t , A_b and A_τ). The first and second generation A -parameters are typically neglected in pMSSM studies, as their phenomenological consequences are negligible in most applications (one counterexample is the A_μ dependence of the anomalous magnetic moment of the muon, which can be as significant as other contributions due to superpartner mediated radiative corrections [156]). Since its initial proposal, the pMSSM approach has been extended to include CP-violating SUSY-breaking parameters in Ref. [157].

A comprehensive study of the 19-parameter pMSSM is computationally expensive. This is somewhat ameliorated in Ref. [158], where the number of pMSSM parameters is reduced to ten by assuming one common squark squared-mass parameter for the first two generations, a second common squark squared-mass parameter for the third generation, a common slepton squared-mass parameter and a common third generation A parameter. Applications of the pMSSM approach to supersymmetric particle searches, and a discussion of the implications for past and future LHC and dark matter studies can be found in Refs. [158–160].

89.6.5 Simplified models

As Sec. 90 demonstrates, experiments present their searches for supersymmetric particles primarily in terms of simplified models. Simplified models for supersymmetric searches [161] are defined mostly by the empirical objects and kinematic variables involved

in the search. Their interpretation by the experimental collaboration usually involves only a small number of supersymmetric particles (often two or three). Other supersymmetric particles are assumed to play no role (this may happen by virtue of them being too heavy to be produced). Experimental bounds from non-observation of a signal are usually presented in terms of the physical masses of the supersymmetric particles involved. Bounds may be presented on the relevant supersymmetric particle masses assuming a 100% branching ratio for a certain decay, or as an upper bound on signal production cross-section times branching ratio as a function of the relevant supersymmetric particle masses.

For example, consider a search for hadronic jets plus missing transverse momentum. One can match such a search to the simplified model of squark pair production followed by the subsequent decay of each squark into a quark (which appears as a jet) and a neutralino LSP that produces the missing transverse momentum, *i.e.* $\tilde{q}\tilde{q} \rightarrow (q\tilde{\chi}_1^0)(q\tilde{\chi}_1^0)$. Excluded regions resulting from the non-observation of a signal may be exhibited in the squark mass versus LSP mass plane.

Simplified models have the advantage that one makes fewer assumptions, compared to more complete supersymmetric models, where the larger number of free parameters makes it difficult to present excluded regions in any generality. It is hoped that simplified models may be a reasonable approximation over sizeable regions of parameter space of more complete models, within which the simplified model is embedded. On the other hand, as stressed in Sec. 90, simplified models have the disadvantage that the presentation of negative search limits tends to be overly strong when compared to the more complete models, particularly if 100% branching ratios are assumed. A contrast between supersymmetric particle search limits in the context of simplified models and the corresponding constraints obtained in the more complete pMSSM is provided in Ref. [162]. As long as one is able to dispel undue pessimism, simplified models remain an efficient vehicle for organizing and presenting the results of supersymmetric particle searches.

89.7 Experimental data confronts the MSSM

At present, there is no direct evidence for weak-scale SUSY from the data analyzed by the LHC experiments. Recent LHC data have been effectively employed in ruling out the existence of colored supersymmetric particles (primarily the gluino and the first generation of squarks) with masses below about 2 TeV (see Sec. 90). The precise mass limits are model dependent. For example, as Sec. 90 demonstrates, regions of the pMSSM parameter space can be identified in which lighter squarks and gluinos below 1 TeV cannot be definitely ruled out. Additional constraints arise from limits on the contributions of virtual supersymmetric particle exchange to a variety of SM processes [118–120].

In light of these negative results, one must confront the tension that exists between the theoretical expectations for the magnitude of the SUSY-breaking parameters and the non-observation of supersymmetric phenomena at colliders.

89.7.1 Naturalness constraints and the little hierarchy

In Sec. 89.1, weak-scale SUSY was motivated as a natural solution to the hierarchy problem, which could provide an understanding of the origin of the electroweak symmetry-breaking scale without a significant fine-tuning of the fundamental parameters that govern the MSSM. In this context, the weak scale soft supersymmetry-breaking masses must be generally of the order of 1 TeV or below [163]. This requirement is most easily seen in the determination of m_Z by the scalar potential minimum condition. In light of Eq. (89.5), to avoid the fine-tuning of MSSM parameters, the soft SUSY-breaking squared-masses m_1^2 and m_2^2 and the higgsino squared-mass $|\mu|^2$ should all be roughly of $\mathcal{O}(m_Z^2)$. Many authors have proposed quantitative measures of fine-tuning [163–167]. One of the simplest measures is the one advocated by Barbieri and Giudice [163] (which was also introduced previously in Ref. [164]),

$$\Delta_i \equiv \left| \frac{\partial \ln m_Z^2}{\partial \ln p_i} \right|, \quad \Delta \equiv \max \Delta_i, \quad (89.22)$$

where the p_i are the MSSM parameters at the high-energy scale M_X , which are set by the fundamental SUSY-breaking dynamics. The theory is more fine-tuned as Δ becomes larger. However, different measures of fine-tuning yield quantitatively different results; in particular, calculating minimal fine-tuning based on the high-scale parameters [as defined in Eq. (89.22)] yields a difference by a factor ~ 10 to fine-tuning based on TeV-scale parameters [168, 169].

One can apply the fine-tuning measure to any explicit model of SUSY breaking. For example, in the approaches discussed in Sec. 89.6, the p_i are parameters of the model at the energy scale M_X where the soft SUSY-breaking operators are generated by the dynamics of SUSY breaking. Renormalization group evolution then determines the values of the parameters appearing in Eq. (89.5) at the electroweak scale. In this way, Δ is sensitive to all the SUSY-breaking parameters of the model (see e.g. Ref. [170]). It should be noted that the computation of Δ is often based on Eq. (89.5), which is a tree-level condition. For example, an analysis in Ref. [80] shows that the fine tuning measure can be reduced by as much as a factor of two when loop corrections are included [171].

As anticipated, there is a tension between the present experimental lower limits on the masses of colored supersymmetric particles [172, 173] and the expectation that supersymmetry-breaking is associated with the electroweak symmetry-breaking scale. Moreover, this tension is exacerbated [174] by the observed value of the Higgs mass ($m_h \simeq 125$ GeV), which is not far from the MSSM upper bound ($m_h \lesssim 135$ GeV) [which depends on the top-squark mass and mixing as noted in Sec. 89.5.2]. If M_{SUSY} characterizes the scale of supersymmetric particle masses, then one would crudely expect $\Delta \sim M_{\text{SUSY}}^2/m_Z^2$. For example, if $M_{\text{SUSY}} \sim 1$ TeV then one expects a $\Delta^{-1} \sim 1\%$ fine-tuning of the MSSM parameters to achieve the observed value of m_Z . This separation of the electroweak symmetry-breaking and SUSY-breaking scales is an example of the little hierarchy problem [175, 176].

The fine-tuning parameter Δ can depend quite sensitively on the structure of the SUSY-breaking dynamics, such as the value of M_X and relations among SUSY-breaking parameters in the fundamental high energy theory [177]. For example, in so-called focus point SUSY models [166, 178], all squark masses can be as heavy as 5 TeV *without* significant fine-tuning. This can be attributed to a focusing behavior of the renormalization group evolution when certain relations hold among the high-energy values of the scalar squared-mass SUSY-breaking parameters. Although the focus point region of the CMSSM still yields an uncomfortably high value of Δ due to the observed Higgs mass of 125 GeV, one can achieve moderate values of Δ in models with NUHM2 boundary conditions for the scalar masses [174].

Among the colored superpartners, the third generation squarks typically have the most significant impact on the naturalness constraints [179], while their masses are the least constrained by the LHC data. Hence, in the absence of any relation between third generation squarks and those of the first two generations, the naturalness constraints due to present LHC data can be considerably weaker than those obtained in the CMSSM. Indeed, models with first and second generation squark masses in the multi-TeV range do not necessarily require significant fine tuning. Such models have the added benefit that undesirable FCNCs mediated by squark exchange are naturally suppressed [180]. Other MSSM mass spectra that are compatible with moderate fine tuning have been considered in Refs. [177] and [181].

The lower bounds on squark and gluino masses may not be as large as suggested by the experimental analyses based on the CMSSM or simplified models. For example, mass bounds for the gluino and the first and second generation squarks based on the CMSSM can often be evaded in alternative or extended MSSM models, e.g., compressed SUSY [182] and stealth SUSY [183]. Moreover, the experimental upper limits for the third generation squark masses (which have a more direct impact on the fine-tuning measure) are weaker than the corresponding mass limits for other colored supersymmetric states.

Among the uncolored superpartners, the higgsinos are typically the most impacted by the naturalness constraints. Eq. (89.5) sug-

gests that the masses of the two neutral higgsinos and charged higgsino pair (which are governed by $|\mu|$) should not be significantly larger than m_Z to avoid an unnatural fine-tuning of the supersymmetric parameters, which would imply the existence of light higgsinos (whose masses are not well constrained, as they are difficult to detect directly at the LHC due to their soft decay products). Nevertheless, it may be possible to avoid the conclusion that $\mu \sim \mathcal{O}(m_Z)$ if additional correlations among the SUSY breaking mass parameters and μ are present. Such a scenario can be realized in models in which the boundary conditions for SUSY breaking are generated by approximately conformal strong dynamics. For example, in the so-called scalar-sequestering model of Ref. [184], values of $|\mu| > 1$ TeV can be achieved while naturally maintaining the observed value of m_Z .

Finally, one can also consider extensions of the MSSM in which the degree of fine-tuning is relaxed. For example, it has already been noted in Sec. 89.5 that it is possible to accommodate the observed Higgs mass more easily in the NMSSM due to contributions to m_h^2 proportional to the parameter λ^2 . This means that we do not have to rely on a large contribution from the radiative corrections to boost the Higgs mass sufficiently above its tree-level bound. This allows for smaller top squark masses, which are more consistent with the demands of naturalness. The reduction of the fine-tuning in various NMSSM models was initially advocated in Ref. [185], and subsequently treated in more detail in Refs. [106, 186]. Naturalness can also be relaxed in extended supersymmetric models with vector-like quarks [187] and in gauge extensions of the MSSM [188].

The experimental absence of any new physics beyond the Standard Model at the LHC suggests that the principle of naturalness is presently under significant stress [189]. Nevertheless, one must be very cautious when drawing conclusions about the viability of weak-scale SUSY to explain the origin of electroweak symmetry breaking, since different measures of fine-tuning noted above can lead to different assessments [168, 169]. Moreover, the maximal value of Δ that determines whether weak-scale SUSY is a fine-tuned model (should it be $\Delta \sim 10^?$ $100^?$ $1000^?$) is ultimately subjective. Thus, it is premature to conclude that weak-scale SUSY is on the verge of exclusion. However, it might be possible to sharpen the upper bounds on superpartner masses based on naturalness arguments, which ultimately will either confirm or refute the weak scale SUSY hypothesis [190]. Of course, if evidence for supersymmetric phenomena in the multi-TeV regime were to be established at a future collider facility (with an energy reach beyond the LHC [191]), it would be viewed as a spectacularly successful explanation of the large gauge hierarchy between the (multi-)TeV scale and Planck scale. In this case, the remaining little hierarchy, characterized by the somewhat large value of the fine-tuning parameter Δ discussed above, would be regarded as a less pressing issue.

89.7.2 Constraints from virtual exchange of supersymmetric particles

There are a number of low-energy measurements that are sensitive to the effects of new physics through indirect searches via supersymmetric loop effects. For example, the virtual exchange of supersymmetric particles can contribute to the muon anomalous magnetic moment, $a_\mu \equiv \frac{1}{2}(g-2)_\mu$, as reviewed in Ref. [192]. The SM prediction for a_μ exhibits a deviation in the range of $3-4\sigma$ from the experimentally observed value [193]. This discrepancy is difficult to accommodate in the constrained SUSY models of Sec. 89.6.2 and 89.6.3 given the present sparticle mass bounds [173]. Nevertheless, there are regions of the more general pMSSM parameter space that are consistent with the observed value of a_μ [194]. An updated value of the fine structure constant has resulted in a new SM prediction [195] for the electron anomalous magnetic moment a_e which is 2.4σ above the measurement [196]. Indeed, it is possible within the pMSSM to find allowed parameter space regions where the observed values of a_μ and a_e are simultaneously accommodated [197].

The rare inclusive decay $b \rightarrow s\gamma$ also provides a sensitive probe to the virtual effects of new physics beyond the SM. The experimental measurements of $B \rightarrow X_s + \gamma$ [198] are in agreement with the theoretical SM predictions of Ref. [199]. Since supersymmet-

ric loop corrections can contribute an observable shift from the SM predictions, the absence of any significant deviation places useful constraints on the MSSM parameter space [200].

The rare decays $B_s \rightarrow \mu^+ \mu^-$ and $B_d \rightarrow \mu^+ \mu^-$ are especially sensitive to supersymmetric loop effects, with some loop contributions scaling as $\tan^6 \beta$ when $\tan \beta \gg 1$ [201]. At present, a combination of the measurements of these rare decay modes [202] are in slight tension at the 2σ level [203] with the predicted SM rates [204]. Such a tension can be resolved by the aforementioned supersymmetric loop effects [201].

The decays $B^\pm \rightarrow \tau^\pm \nu_\tau$ and $B \rightarrow D^{(*)} \tau^- \bar{\nu}_\tau$ are noteworthy, since in models with extended Higgs sectors such as the MSSM, these processes possess tree-level charged Higgs exchange contributions that can compete with the dominant W -exchange. As Section 71 shows, experimental measurements of $B^\pm \rightarrow \tau^\pm \nu_\tau$ are currently consistent with SM expectations [205]. The BaBar Collaboration measured values of the rates for $\bar{B} \rightarrow D \tau^- \bar{\nu}_\tau$ and $\bar{B} \rightarrow D^* \tau^- \bar{\nu}_\tau$ [206] that showed a combined 3.4σ discrepancy from the SM predictions, which was also not compatible with the Type-II Higgs Yukawa couplings employed by the MSSM. Some subsequent measurements of the LHCb and Belle Collaborations [207] were consistent with the BaBar measurements, although more recent Belle measurements using a semi-leptonic tag are more consistent with SM expectations [208]. The combined difference between the measured and expected values of the $\bar{B} \rightarrow D \tau^- \bar{\nu}_\tau$ and $\bar{B} \rightarrow D^* \tau^- \bar{\nu}_\tau$ decay rates relative to the corresponding SM values has a significance of about three standard deviations [209]. There are a number of additional anomalies in B decay data that have recently attracted some attention, although at present the observed deviations from SM expectations are mostly at the level of about two to three standard deviations (see, *e.g.*, Ref. [203]).

In summary, although there are a few hints of possible deviations from the SM in B decays, none of the discrepancies by themselves are significant enough to conclusively imply the existence of new physics beyond the SM. The absence of definitive evidence for deviations in various B -physics observables from their SM predictions places useful constraints on the MSSM parameter space [120,172,210]. In contrast, if one or more of the B anomalies referred to above were to be experimentally confirmed, it would require significant modifications to the supersymmetric models treated in this review.

Finally, we note that the constraints from precision electroweak observables (see Sec. 10) and measurements of the e'/ϵ anomaly [211], if it persists [212], in the Kaon system are easily accommodated in models of TeV-scale SUSY [213,214]. Thus, robust regions of the MSSM parameter space, compatible with the results of direct and indirect searches for SUSY, remain viable.

89.8 Massive neutrinos in weak-scale SUSY

In the minimal SM and its supersymmetric extension, there are no right-handed neutrinos, and Majorana mass terms for the left-handed neutrinos are absent. However, given the overwhelming evidence for neutrino masses and mixing (see Sec. 14 and Ref. [215]), any viable model of fundamental particles must provide a mechanism for generating neutrino masses [216]. In extended supersymmetric models, various mechanisms exist for producing massive neutrinos [217]. Although one can devise models for generating massive Dirac neutrinos [218], the most common approaches for incorporating neutrino masses are based on L -violating supersymmetric extensions of the MSSM, which generate massive Majorana neutrinos. Two classes of L -violating supersymmetric models will now be considered.

89.8.1 The supersymmetric seesaw

Neutrino masses can be incorporated into the SM by introducing $SU(3) \times SU(2) \times U(1)$ singlet right-handed neutrinos (ν_R) whose mass parameters are very large, typically near the grand unification scale. In addition, one must also include a standard Yukawa couplings between the lepton doublets, the Higgs doublet, and ν_R . The Higgs vacuum expectation value then induces an off-diagonal $\nu_L - \nu_R$ mass on the order of the electroweak scale. Diagonalizing the neutrino mass matrix (in the three-generation model) yields three superheavy neutrino states, and three very

light neutrino states that are identified with the light neutrinos observed in nature. This is the seesaw mechanism [219].

It is straightforward to construct a supersymmetric generalization of the seesaw model of neutrino masses [220,221] by promoting the right-handed neutrino field to a superfield $\hat{N}^c = (\tilde{\nu}_R; \nu_R)$. Integrating out the heavy right-handed neutrino supermultiplet yields a new term in the superpotential [cf. Eq. (89.1)] of the form

$$W_{\text{seesaw}} = \frac{f}{M_R} (\hat{H}_U \hat{L}) (\hat{H}_U \hat{L}), \quad (89.23)$$

where M_R is the mass scale of the right-handed neutrino sector and f is a dimensionless constant. Note that lepton number is broken by two units, which implies that R-parity is conserved. The supersymmetric analogue of the Majorana neutrino mass term in the sneutrino sector leads to sneutrino-antisneutrino mixing phenomena [221,222].

The SUSY Les Houches Accords [75,91], mentioned at the end of the introduction to Sec. 89.4, have been extended to the supersymmetric seesaw (and other extensions of the MSSM) in Ref. [223].

89.8.2 R-parity-violating SUSY

It is possible to incorporate massive neutrinos in renormalizable supersymmetric models while retaining the minimal particle content of the MSSM by relaxing the assumption of R-parity invariance. The most general R-parity-violating (RPV) model involving the MSSM spectrum introduces many new parameters to both the SUSY-conserving and the SUSY-breaking sectors [75,224]. Each new interaction term violates either B or L conservation. For example, starting from the MSSM superpotential given in Eq. (89.1) [suitably generalized to three generations of quarks, leptons and their superpartners], consider the effect of adding the following new terms:

$$W_{\text{RPV}} = (\lambda_L)_{pmn} \hat{L}_p \hat{L}_m \hat{E}_n^c + (\lambda'_L)_{pmn} \hat{L}_p \hat{Q}_m \hat{D}_n^c + (\lambda_B)_{pmn} \hat{U}_p^c \hat{D}_m^c \hat{D}_n^c + (\mu_L)_p \hat{H}_u \hat{L}_p, \quad (89.24)$$

where p , m , and n are generation indices, and gauge group indices are suppressed. Eq. (89.24) yields new scalar-fermion Yukawa couplings consisting of all possible combinations involving two SM fermions and one scalar superpartner.

Note that the term in Eq. (89.24) proportional to λ_B violates B , while the other three terms violate L . The L -violating term in Eq. (89.24) proportional to μ_L is the RPV generalization of the $\mu \hat{H}_u \hat{H}_d$ term of the MSSM superpotential, in which the $Y = -1$ Higgs/higgsino supermultiplet \hat{H}_d is replaced by the slepton/lepton supermultiplet \hat{L}_p .

Phenomenological constraints derived from data on various low-energy B - and L -violating processes can be used to establish limits on each of the coefficients $(\lambda_L)_{pmn}$, $(\lambda'_L)_{pmn}$, and $(\lambda_B)_{pmn}$ taken one at a time [224,225]. If more than one coefficient is simultaneously non-zero, then the limits are in general more complicated [226]. All possible RPV terms cannot be simultaneously present and unsuppressed; otherwise the proton decay rate would be many orders of magnitude larger than the present experimental bound. One way to avoid proton decay is to impose B or L invariance (either one alone would suffice). Otherwise, one must accept the requirement that certain RPV coefficients must be extremely suppressed.

One particularly interesting class of RPV models is one in which B is conserved, but L is violated. It is possible to enforce baryon number conservation (and the stability of the proton), while allowing for lepton-number-violating interactions by imposing a discrete \mathbf{Z}_3 baryon triality symmetry on the low-energy theory [227], in place of the standard \mathbf{Z}_2 R-parity. Since the distinction between the Higgs and matter supermultiplets is lost in RPV models where L is violated, the mixing of sleptons and Higgs bosons, the mixing of neutrinos and neutralinos, and the mixing of charged leptons and charginos are now possible, leading to more complicated mass matrices and mass eigenstates than in the MSSM. The treatment of neutrino masses and mixing in this framework can be found, *e.g.*, in Ref. [228].

Alternatively, one can consider imposing a lepton parity such that all lepton superfields are odd [227, 229]. In this case, only the B -violating term in Eq. (89.24) survives, and L is conserved. Models of this type have been considered in Ref. [230]. Since L is conserved in these models, the mixing of the lepton and Higgs superfields is forbidden. Moreover, neutrino masses (and mixing) are not generated if lepton parity is an exact symmetry. However, one expects that lepton parity cannot be exact due to quantum gravity effects. Remarkably, the standard \mathbf{Z}_2 R-parity and the \mathbf{Z}_3 baryon triality are stable with respect to quantum gravity effects, as they can be identified as residual discrete symmetries that arise from spontaneously broken non-anomalous gauge symmetries [227].

The symmetries employed above to either remove or suppress R-parity violating operators were flavour independent. In contrast, there exist a number of motivated scenarios based on flavor symmetries that can also yield the suppression as required by the experimental data (e.g., see Ref. [231]).

The supersymmetric phenomenology of the RPV models exhibits features that are distinct from that of the MSSM [224]. The LSP is no longer stable, which implies that not all supersymmetric decay chains must yield missing-energy events at colliders. A comprehensive examination of the phenomenology of the MSSM extended by a single R-parity violating coupling at the unification scale and its implications for LHC searches has been given in Ref. [232]. As an example, the sparticle mass bounds obtained in searches for R-parity-conserving SUSY can be considerably relaxed in certain RPV models due to the absence of large missing transverse momentum signatures [233]. This can alleviate some of the tension with naturalness discussed in Sec. 89.7.1.

Nevertheless, the loss of the missing-energy signature is often compensated by other striking signals (which depend on which R-parity-violating parameters are dominant). For example, supersymmetric particles in RPV models can be singly produced (in contrast to R-parity-conserving models where supersymmetric particles must be produced in pairs). The phenomenology of pair-produced supersymmetric particles is also modified in RPV models due to new decay chains not present in R-parity-conserving SUSY models [224].

In RPV models with lepton number violation (these include weak-scale SUSY models with baryon triality mentioned above), both $\Delta L = 1$ and $\Delta L = 2$ phenomena are allowed, leading to neutrino masses and mixing [234], neutrinoless double-beta decay [235], sneutrino-antisneutrino mixing [236], and resonant s -channel production of sneutrinos in e^+e^- collisions [237] and charged sleptons in $p\bar{p}$ and pp collisions [238].

89.9 Extensions beyond the MSSM

Extensions of the MSSM have been proposed to solve a variety of theoretical problems. One such problem involves the μ parameter of the MSSM. Although μ is a SUSY-preserving parameter, it must be of order the effective SUSY-breaking scale of the MSSM to yield a consistent supersymmetric phenomenology [239]. Any natural solution to the so-called μ -problem must incorporate a symmetry that enforces $\mu = 0$ and a small symmetry-breaking parameter that generates a value of μ that is not parametrically larger than the effective SUSY-breaking scale [240]. A number of proposed mechanisms in the literature (e.g., see Refs. [239–241]) provide concrete examples of a natural solution to the μ -problem of the MSSM.

In extensions of the MSSM, new compelling solutions to the μ -problem are possible. For example, one can replace μ by the vacuum expectation value of a new $SU(3) \times SU(2) \times U(1)$ singlet scalar field. This is the NMSSM, which yields phenomena that were briefly discussed in Sections 89.4–89.7. The NMSSM superpotential consists only of trilinear terms whose coefficients are dimensionless. There are some advantages to extending the NMSSM further to the USSM [97] by adding a new broken $U(1)$ gauge symmetry [242], under which the singlet field is charged.

Alternatively, one can consider a generalized version of the NMSSM (called the GNMSSM in Ref. [186]), where all possible renormalizable terms in the superpotential are allowed, which yields new supersymmetric mass terms (analogous to the μ term of the MSSM). A discussion of the parameters of the GNMSSM

can be found in Ref. [75]. Although the GNMSSM does not solve the μ -problem, it does exhibit regions of parameter space in which the degree of fine-tuning is relaxed, as discussed in Sec. 89.7.1.

The generation of the μ term may be connected with the solution to the strong CP problem [243]. Models of this type, which include new gauge singlet fields that are charged under the Peccei-Quinn (PQ) symmetry [244], were first proposed in Ref. [239]. The breaking of the PQ symmetry is thus intimately tied to SUSY breaking, while naturally yielding a value of μ that is of order the electroweak symmetry breaking scale [245].

It is also possible to add higher dimensional Higgs multiplets, such as Higgs triplet superfields [246], provided a custodial-symmetric model (in which the ρ -parameter of precision electroweak physics is close to 1, see Sec. 10) can be formulated. Such models can provide a rich phenomenology of new signals for future LHC studies.

All supersymmetric models discussed so far in this review possess self-conjugate fermions—the Majorana gluinos and neutralinos. However, it is possible to add additional chiral superfields in the adjoint representation. The spin-1/2 components of these new superfields can pair up with the gauginos to form Dirac gauginos [247, 248]. Such states appear in models of so-called supersoft SUSY breaking [249], in some generalized GMSB models [250] and in R-symmetric SUSY [251, 252]. Such approaches often lead to improved naturalness and/or significantly relaxed flavor constraints. The implications of models of Dirac gauginos on the observed Higgs boson mass and its properties are addressed in Ref. [253].

For completeness, we briefly note other MSSM extensions considered in the literature. These include an enlarged electroweak gauge group beyond $SU(2) \times U(1)$ [254]; and/or the addition of new (possibly exotic) matter supermultiplets such as vector-like fermions and their superpartners [187, 255].

References

- [1] *The Supersymmetric World—The Beginnings of the Theory*, World Scientific, Singapore (2000), edited by G. Kane and M. Shifman, contains an early history of supersymmetry and a guide to the original literature.
- [2] R. Haag, J. T. Lopuszanski and M. Sohnius, Nucl. Phys. **B88**, 257 (1975); S. R. Coleman and J. Mandula, Phys. Rev. **159**, 1251 (1967).
- [3] H. P. Nilles, Phys. Rept. **110**, 1 (1984).
- [4] S. Weinberg, *The Quantum Theory of Fields, Volume III: Supersymmetry* (Cambridge University Press, Cambridge, UK, 2000).
- [5] P. Nath, *Supersymmetry, Supergravity, and Unification* (Cambridge University Press, Cambridge, UK, 2017).
- [6] S. P. Martin *A Supersymmetry Primer*, [hep-ph/9709356].
- [7] E. Witten, Nucl. Phys. **B188**, 513 (1981).
- [8] S. Dimopoulos and H. Georgi, Nucl. Phys. **B193**, 150 (1981).
- [9] N. Sakai, Z. Phys. **C11**, 153 (1981).
- [10] L. Susskind, Phys. Rept. **104**, 181 (1984).
- [11] L. Girardello and M. T. Grisaru, Nucl. Phys. **B194**, 65 (1982).
- [12] L. J. Hall and L. Randall, Phys. Rev. Lett. **65**, 2939 (1990); I. Jack and D. R. T. Jones, Phys. Lett. **B457**, 101 (1999), [hep-ph/9903365].
- [13] V. F. Weisskopf, Phys. Rev. **56**, 72 (1939).
- [14] See e.g., N. Polonsky, *Supersymmetry: Structure and phenomena. Extensions of the standard model*, Lect. Notes Phys. **M68**, 1 (2001).
- [15] G. Bertone, D. Hooper and J. Silk, Phys. Rept. **405**, 279 (2005), [hep-ph/0404175].
- [16] D. Hooper, “TASI 2008 Lectures on Dark Matter,” in *The Dawn of the LHC Era, Proceedings of the 2008 Theoretical and Advanced Study Institute in Elementary Particle Physics*, Boulder, Colorado, 2–27 June 2008, edited by Tao Han (World Scientific, Singapore, 2009).

- [17] H. Pagels and J. R. Primack, *Phys. Rev. Lett.* **48**, 223 (1982).
- [18] H. Goldberg, *Phys. Rev. Lett.* **50**, 1419 (1983).
- [19] J. R. Ellis *et al.*, *Nucl. Phys.* **B238**, 453 (1984).
- [20] G. Jungman, M. Kamionkowski, and K. Griest, *Phys. Reports* **267**, 195 (1996).
- [21] F. D. Steffen, *Eur. Phys. J.* **C59**, 557 (2009), [arXiv:0811.3347].
- [22] H. E. Haber and G. L. Kane, *Phys. Rept.* **117**, 75 (1985).
- [23] M. Drees, R. Godbole, and P. Roy, *Theory and Phenomenology of Sparticles* (World Scientific, Singapore, 2005); H. Baer and X. Tata, *Weak Scale Supersymmetry: from Superfields to Scattering Events* (Cambridge University Press, Cambridge, UK, 2006); I.J.R. Aitchison, *Supersymmetry in Particle Physics: an elementary introduction* (Cambridge University Press, Cambridge, UK, 2007).
- [24] Our notation for the charge-conjugated fields follows the notation of P. Langacker, *The Standard Model and Beyond*, 2nd edition (CRC Press, Boca Raton, FL, 2017).
- [25] H. Georgi and S. L. Glashow, *Phys. Rev.* **D6**, 429 (1972).
- [26] P. Fayet, *Nucl. Phys.* **B90**, 104 (1975).
- [27] K. Inoue *et al.*, *Prog. Theor. Phys.* **67**, 1889 (1982).
- [28] J. F. Gunion and H. E. Haber, *Nucl. Phys.* **B272**, 1 (1986), [Erratum: **B402**, 567 (1993)].
- [29] A. Salam and J. A. Strathdee, *Nucl. Phys.* **B76**, 477 (1974).
- [30] J. Wess and J. Bagger, *Supersymmetry and Supergravity* (Princeton University Press, Princeton, NJ, 1992).
- [31] I. L. Buchbinder, S. Kuzenko and Z. Yarevskaya, *Nucl. Phys.* **B411**, 665 (1994); I. Antoniadis, E. Dudas and D. M. Ghilencea, *JHEP* **03**, 045 (2008), [arXiv:0708.0383].
- [32] D. J. H. Chung *et al.*, *Phys. Rept.* **407**, 1 (2005), [hep-ph/0312378].
- [33] J. R. Ellis *et al.*, *Phys. Rev.* **D39**, 844 (1989); U. Ellwanger and C. Hugonie, *Eur. Phys. J.* **C25**, 297 (2002), [hep-ph/9909260]; U. Ellwanger, C. Hugonie and A. M. Teixeira, *Phys. Rept.* **496**, 1 (2010), [arXiv:0910.1785]; M. Maniatis, *Int. J. Mod. Phys.* **A25**, 3505 (2010), [arXiv:0906.0777].
- [34] S. Weinberg, *Phys. Rev. Lett.* **43**, 1566 (1979); S. Weinberg, *Phys. Rev.* **D22**, 1694 (1980); F. Wilczek and A. Zee, *Phys. Rev. Lett.* **43**, 1571 (1979); H. A. Weldon and A. Zee, *Nucl. Phys.* **B173**, 269 (1980).
- [35] P. Fayet, *Phys. Lett.* **69B**, 489 (1977); G. R. Farrar and P. Fayet, *Phys. Lett.* **76B**, 575 (1978).
- [36] P. Fayet, *Phys. Lett.* **84B**, 421 (1979); P. Fayet, *Phys. Lett.* **86B**, 272 (1979).
- [37] D.Z. Freedman and A. Van Proeyen, *Supergravity* (Cambridge University Press, Cambridge, UK, 2012); M. Rausch de Traubenberg and M. Valenzuela, *A Supergravity Primer* (World Scientific, Singapore, 2020).
- [38] S. Deser and B. Zumino, *Phys. Rev. Lett.* **38**, 1433 (1977); E. Cremmer *et al.*, *Phys. Lett.* **79B**, 231 (1978).
- [39] R. Casalbuoni *et al.*, *Phys. Lett.* **B215**, 313 (1988); R. Casalbuoni *et al.*, *Phys. Rev.* **D39**, 2281 (1989); A. L. Maroto and J. R. Pelaez, *Phys. Rev.* **D62**, 023518 (2000), [hep-ph/9912212].
- [40] Z. Komargodski and N. Seiberg, *JHEP* **09**, 066 (2009), [arXiv:0907.2441]; I. Antoniadis *et al.*, *Theor. Math. Phys.* **170**, 26 (2012), [*Teor. Mat. Fiz.* **170**, 34 (2012)].
- [41] A.H. Chamseddine, R. Arnowitt, and P. Nath, *Phys. Rev. Lett.* **49**, 970 (1982); R. Barbieri, S. Ferrara and C. A. Savoy, *Phys. Lett.* **119B**, 343 (1982); L. E. Ibanez, *Nucl. Phys.* **B218**, 514 (1983); H. P. Nilles, M. Srednicki and D. Wyler, *Phys. Lett.* **120B**, 346 (1983); H. P. Nilles, M. Srednicki and D. Wyler, *Phys. Lett.* **124B**, 337 (1983); E. Cremmer, P. Fayet and L. Girardello, *Phys. Lett.* **122B**, 41 (1983); N. Ohta, *Prog. Theor. Phys.* **70**, 542 (1983).
- [42] L. Alvarez-Gaumé, J. Polchinski, and M.B. Wise, *Nucl. Phys.* **B221**, 495 (1983).
- [43] L. J. Hall, J. D. Lykken and S. Weinberg, *Phys. Rev.* **D27**, 2359 (1983).
- [44] S. K. Soni and H. A. Weldon, *Phys. Lett.* **126B**, 215 (1983); Y. Kawamura, H. Murayama and M. Yamaguchi, *Phys. Rev.* **D51**, 1337 (1995), [hep-ph/9406245].
- [45] See, *e.g.*, A. Brignole, L.E. Ibáñez, and C. Muñoz, in *Perspectives on Supersymmetry II*, edited by G.L. Kane (World Scientific, Singapore, 2010) pp. 244–268.
- [46] A. B. Lahanas and D. V. Nanopoulos, *Phys. Rept.* **145**, 1 (1987).
- [47] J. L. Feng, A. Rajaraman and F. Takayama, *Phys. Rev. Lett.* **91**, 011302 (2003), [hep-ph/0302215]; J. L. Feng, A. Rajaraman and F. Takayama, *Phys. Rev.* **D68**, 063504 (2003), [hep-ph/0306024]; J. L. Feng, A. Rajaraman and F. Takayama, *Int. J. Mod. Phys.* **D13**, 2355 (2004), [hep-th/0405248].
- [48] L. Randall and R. Sundrum, *Nucl. Phys.* **B557**, 79 (1999), [hep-th/9810155].
- [49] F. D’Eramo, J. Thaler and Z. Thomas, *JHEP* **06**, 151 (2012), [arXiv:1202.1280]; F. D’Eramo, J. Thaler and Z. Thomas, *JHEP* **09**, 125 (2013), [arXiv:1307.3251]; S. P. de Alwis, *Phys. Rev.* **D77**, 105020 (2008), [arXiv:0801.0578]; S. P. de Alwis, *JHEP* **01**, 006 (2013), [arXiv:1206.6775]; K. Harigaya and M. Ibe, *Phys. Rev.* **D90**, 085028 (2014), [arXiv:1409.5029].
- [50] I. Jack, D. R. T. Jones and R. Wild, *Phys. Lett.* **B535**, 193 (2002), [hep-ph/0202101]; B. Murakami and J. D. Wells, *Phys. Rev.* **D68**, 035006 (2003), [hep-ph/0302209]; R. Kitano, G. D. Kribs and H. Murayama, *Phys. Rev.* **D70**, 035001 (2004), [hep-ph/0402215]; R. Hodgson *et al.*, *Nucl. Phys.* **B728**, 192 (2005), [hep-ph/0507193]; D. R. T. Jones and G. G. Ross, *Phys. Lett.* **B642**, 540 (2006), [hep-ph/0609210].
- [51] S. Asai *et al.*, *Phys. Lett.* **B653**, 81 (2007), [arXiv:0705.3086].
- [52] M. Dine, W. Fischler and M. Srednicki, *Nucl. Phys.* **B189**, 575 (1981); S. Dimopoulos and S. Raby, *Nucl. Phys.* **B192**, 353 (1981); S. Dimopoulos and S. Raby, *Nucl. Phys.* **B219**, 479 (1983); M. Dine and W. Fischler, *Phys. Lett.* **110B**, 227 (1982); C. R. Nappi and B. A. Ovrut, *Phys. Lett.* **113B**, 175 (1982); L. Alvarez-Gaume, M. Claudson and M. B. Wise, *Nucl. Phys.* **B207**, 96 (1982).
- [53] M. Dine and A. E. Nelson, *Phys. Rev.* **D48**, 1277 (1993), [hep-ph/9303230]; M. Dine, A. E. Nelson and Y. Shirman, *Phys. Rev.* **D51**, 1362 (1995), [hep-ph/9408384].
- [54] M. Dine *et al.*, *Phys. Rev.* **D53**, 2658 (1996), [hep-ph/9507378].
- [55] G. F. Giudice and R. Rattazzi, *Phys. Rept.* **322**, 419 (1999), [hep-ph/9801271].
- [56] E. Poppitz and S. P. Trivedi, *Phys. Rev.* **D55**, 5508 (1997), [hep-ph/9609529]; H. Murayama, *Phys. Rev. Lett.* **79**, 18 (1997), [hep-ph/9705271]; M. A. Luty and J. Terning, *Phys. Rev.* **D57**, 6799 (1998), [hep-ph/9709306]; K. Agashe, *Phys. Lett.* **B435**, 83 (1998), [hep-ph/9804450]; N. Arkani-Hamed, J. March-Russell and H. Murayama, *Nucl. Phys.* **B509**, 3 (1998), [hep-ph/9701286]; C. Csaki, Y. Shirman and J. Terning, *JHEP* **05**, 099 (2007), [hep-ph/0612241]; M. Ibe and R. Kitano, *Phys. Rev.* **D77**, 075003 (2008), [arXiv:0711.0416].
- [57] M. Kawasaki *et al.*, *Phys. Rev.* **D78**, 065011 (2008), [arXiv:0804.3745].
- [58] M. J. Strassler and K. M. Zurek, *Phys. Lett.* **B651**, 374 (2007), [hep-ph/0604261]; T. Han *et al.*, *JHEP* **07**, 008 (2008), [arXiv:0712.2041].
- [59] M. J. Strassler [hep-ph/0607160]; K. M. Zurek, *Phys. Rev.* **D79**, 115002 (2009), [arXiv:0811.4429].

- [60] See *e.g.*, M. Quiros, in *Particle Physics and Cosmology: The Quest for Physics Beyond the Standard Model(s), Proceedings of the 2002 Theoretical Advanced Study Institute in Elementary Particle Physics (TASI 2002)*, edited by H.E. Haber and A.E. Nelson (World Scientific, Singapore, 2004) pp. 549–601; C. Csaki, in *ibid.*, pp. 605–698.
- [61] V.A. Rubakov, *Sov. Phys. Usp.* **44**, 871 (2001); J. L. Hewett and M. Spiropulu, *Ann. Rev. Nucl. Part. Sci.* **52**, 397 (2002), [hep-ph/0205106].
- [62] Z. Chacko, M. A. Luty and E. Ponton, *JHEP* **07**, 036 (2000), [hep-ph/9909248]; D. E. Kaplan, G. D. Kribs and M. Schmaltz, *Phys. Rev.* **D62**, 035010 (2000), [hep-ph/9911293]; Z. Chacko *et al.*, *JHEP* **01**, 003 (2000), [hep-ph/9911323].
- [63] J. Scherk and J. H. Schwarz, *Phys. Lett.* **82B**, 60 (1979); J. Scherk and J. H. Schwarz, *Nucl. Phys.* **B153**, 61 (1979).
- [64] R. Barbieri, L. J. Hall and Y. Nomura, *Phys. Rev.* **D66**, 045025 (2002), [hep-ph/0106190]; R. Barbieri, L. J. Hall and Y. Nomura, *Nucl. Phys.* **B624**, 63 (2002), [hep-th/0107004]; I. Garcia Garcia, K. Howe and J. March-Russell, *JHEP* **12**, 005 (2015), [arXiv:1510.07045].
- [65] J. D. Wells, in “11th International Conference on Supersymmetry and the Unification of Fundamental Interactions (SUSY 2003) Tucson, Arizona, June 5-10, 2003,” (2003), [hep-ph/0306127]; J. D. Wells, *Phys. Rev.* **D71**, 015013 (2005), [hep-ph/0411041].
- [66] N. Arkani-Hamed and S. Dimopoulos, *JHEP* **06**, 073 (2005), [hep-th/0405159]; G. F. Giudice and A. Romanino, *Nucl. Phys.* **B699**, 65 (2004), [Erratum: **B706**, 487 (2005)], [hep-ph/0406088].
- [67] G. F. Giudice and A. Strumia, *Nucl. Phys.* **B858**, 63 (2012), [arXiv:1108.6077].
- [68] A. Arvanitaki *et al.*, *JHEP* **02**, 126 (2013), [arXiv:1210.0555]; N. Arkani-Hamed *et al.* (2012), [arXiv:1212.6971].
- [69] E. Bagnaschi *et al.*, *JHEP* **09**, 092 (2014), [arXiv:1407.4081].
- [70] J. Pardo Vega and G. Villadoro, *JHEP* **07**, 159 (2015), [arXiv:1504.05200].
- [71] B. C. Allanach and A. Voigt, *Eur. Phys. J.* **C78**, 573 (2018), [arXiv:1804.09410].
- [72] Y. Kahn, M. McCullough and J. Thaler, *JHEP* **11**, 161 (2013), [arXiv:1308.3490].
- [73] L. J. Hall and Y. Nomura, *JHEP* **01**, 082 (2012), [arXiv:1111.4519]; M. Ibe and T. T. Yanagida, *Phys. Lett.* **B709**, 374 (2012), [arXiv:1112.2462].
- [74] H. E. Haber and L. Stephenson Haskins (2018), *Supersymmetric Theory and Models*, in *Anticipating the Next Discoveries in Particle Physics*, Proceedings of the 2016 Theoretical Advanced Study Institute in Elementary Particle Physics, edited by Rouven Essig and Ian Low (World Scientific, Singapore, 2018) pp. 355–499, [arXiv:1712.05926].
- [75] B. C. Allanach *et al.*, *Comput. Phys. Commun.* **180**, 8 (2009), [arXiv:0801.0045].
- [76] J. M. Frere, D. R. T. Jones and S. Raby, *Nucl. Phys.* **B222**, 11 (1983); J. P. Derendinger and C. A. Savoy, *Nucl. Phys.* **B237**, 307 (1984); J. F. Gunion, H. E. Haber and M. Sher, *Nucl. Phys.* **B306**, 1 (1988); D. Chowdhury *et al.*, *JHEP* **02**, 110 (2014), [Erratum: **03**, 149 (2018)], [arXiv:1310.1932]; W. G. Hollik, *JHEP* **08**, 126 (2016), [arXiv:1606.08356].
- [77] J. A. Casas, A. Lleyda and C. Munoz, *Nucl. Phys.* **B471**, 3 (1996), [hep-ph/9507294].
- [78] C. S. Ün *et al.*, *Phys. Rev.* **D91**, 105033 (2015), [arXiv:1412.1440].
- [79] G. G. Ross, K. Schmidt-Hoberg and F. Staub, *Phys. Lett.* **B759**, 110 (2016), [arXiv:1603.09347].
- [80] G. G. Ross, K. Schmidt-Hoberg and F. Staub, *JHEP* **03**, 021 (2017), [arXiv:1701.03480].
- [81] S. P. Martin, *Phys. Rev.* **D61**, 035004 (2000), [hep-ph/9907550].
- [82] S. Dimopoulos and D. W. Sutter, *Nucl. Phys.* **B452**, 496 (1995), [hep-ph/9504415]; D.W. Sutter, Stanford Ph. D. thesis, arXiv:hep-ph/9704390.
- [83] H.E. Haber, *Nucl. Phys. B (Proc. Suppl.)* **62A-C**, 469 (1998).
- [84] R. M. Barnett, J. F. Gunion and H. E. Haber, *Phys. Lett.* **B315**, 349 (1993), [hep-ph/9306204]; H. Baer, X. Tata and J. Woodside, *Phys. Rev.* **D41**, 906 (1990).
- [85] S. M. Bilenky, N. P. Nedelcheva and E. K. Khristova, *Phys. Lett.* **161B**, 397 (1985); S. M. Bilenky, E. K. Khristova and N. P. Nedelcheva, *Bulg. J. Phys.* **13**, 283 (1986).
- [86] J. Rosiek, *Phys. Rev.* **D41**, 3464 (1990).
- [87] J. Alwall *et al.*, *JHEP* **09**, 028 (2007), [arXiv:0706.2334].
- [88] T. Hahn, *Comput. Phys. Commun.* **140**, 418 (2001), [hep-ph/0012260].
- [89] A. Pukhov *et al.*, INP MSU report 98-41/542 (arXiv:hep-ph/9908288); E. Boos *et al.* [CompHEP Collab.], *Nucl. Instrum. Methods* **A534**, 50 (2004); CompHEP webpage, <https://theory.sinp.msu.ru/dokuwiki/doku.php/comphep/news>.
- [90] D. M. Pierce *et al.*, *Nucl. Phys.* **B491**, 3 (1997), [hep-ph/9606211].
- [91] P. Z. Skands *et al.*, *JHEP* **07**, 036 (2004), [hep-ph/0311123].
- [92] For further details, see *e.g.*, Appendix C of Ref. [22] and Appendix A of Ref. [28].
- [93] J. L. Kneur and G. Moultaka, *Phys. Rev.* **D59**, 015005 (1999), [hep-ph/9807336].
- [94] R.A. Horn and C.R. Johnson, *Matrix Analysis*, 2nd Edition (Cambridge University Press, Cambridge, UK, 2003).
- [95] H. K. Dreiner, H. E. Haber and S. P. Martin, *Phys. Rept.* **494**, 1 (2010), [arXiv:0812.1594].
- [96] L. Autonne, *Annals de l'Université de Lyon, Nouvelle Série I, Fasc.* **38**, 1 (1915); T. Takagi, *Japan J. Math.* **1**, 83 (1925).
- [97] S. Y. Choi *et al.*, *Nucl. Phys.* **B778**, 85 (2007), [hep-ph/0612218].
- [98] S. Y. Choi *et al.*, *Eur. Phys. J.* **C22**, 563 (2001), [Addendum: *Eur. Phys. J.* **C23**, 769 (2002)], [hep-ph/0108117].
- [99] M. M. El Kheishen, A. A. Aboshousha and A. A. Shafik, *Phys. Rev.* **D45**, 4345 (1992).
- [100] T. Hahn (2006), [arXiv:physics/0607103].
- [101] K.-i. Hikasa and M. Kobayashi, *Phys. Rev.* **D36**, 724 (1987); F. Gabbiani and A. Masiero, *Nucl. Phys.* **B322**, 235 (1989); P. Brax and C. A. Savoy, *Nucl. Phys.* **B447**, 227 (1995), [hep-ph/9503306].
- [102] J. R. Ellis and S. Rudaz, *Phys. Lett.* **128B**, 248 (1983); F. Browning, D. Chang and W.-Y. Keung, *Phys. Rev.* **D64**, 015010 (2001), [hep-ph/0012258]; A. Bartl *et al.*, *Phys. Lett.* **B573**, 153 (2003), [hep-ph/0307317]; A. Bartl *et al.*, *Phys. Rev.* **D70**, 035003 (2004), [hep-ph/0311338].
- [103] J.F. Gunion *et al.*, *The Higgs Hunter's Guide* (Westview Press, Boulder, CO, 2000); M. Carena and H. E. Haber, *Prog. Part. Nucl. Phys.* **50**, 63 (2003), [hep-ph/0208209]; A. Djouadi, *Phys. Rept.* **459**, 1 (2008), [hep-ph/0503173].
- [104] E. Bagnaschi *et al.*, *Eur. Phys. J.* **C79**, 617 (2019), [arXiv:1808.07542].
- [105] H. E. Haber and M. Sher, *Phys. Rev.* **D35**, 2206 (1987).
- [106] L. J. Hall, D. Pinner and J. T. Ruderman, *JHEP* **04**, 131 (2012), [arXiv:1112.2703].
- [107] L. J. Hall and M. B. Wise, *Nucl. Phys.* **B187**, 397 (1981).
- [108] H. E. Haber and R. Hempfling, *Phys. Rev. Lett.* **66**, 1815 (1991); Y. Okada, M. Yamaguchi and T. Yanagida, *Prog. Theor. Phys.* **85**, 1 (1991); J. R. Ellis, G. Rüdolf and F. Zwirner, *Phys. Lett.* **B257**, 83 (1991).

- [109] P. Draper and H. Rzehak, Phys. Rept. **619**, 1 (2016), [arXiv:1601.01890].
- [110] A. Pilaftsis and C. E. M. Wagner, Nucl. Phys. **B553**, 3 (1999), [hep-ph/9902371]; D. A. Demir, Phys. Rev. **D60**, 055006 (1999), [hep-ph/9901389]; S. Y. Choi, M. Drees and J. S. Lee, Phys. Lett. **B481**, 57 (2000), [hep-ph/0002287]; M. Carena *et al.*, Nucl. Phys. **B586**, 92 (2000), [hep-ph/0003180]; M. Carena *et al.*, Phys. Lett. **B495**, 155 (2000), [hep-ph/0009212]; M. Carena *et al.*, Nucl. Phys. **B625**, 345 (2002), [hep-ph/0111245]; M. Frank *et al.*, JHEP **02**, 047 (2007), [hep-ph/0611326]; S. Heinemeyer *et al.*, Phys. Lett. **B652**, 300 (2007), [arXiv:0705.0746].
- [111] H. E. Haber and J. D. Mason, Phys. Rev. **D77**, 115011 (2008), [arXiv:0711.2890].
- [112] M. Carena *et al.*, Phys. Rev. **D93**, 035013 (2016), [arXiv:1510.09137].
- [113] S. Khalil, Int. J. Mod. Phys. **A18**, 1697 (2003), [hep-ph/0212050].
- [114] W. Fischler, S. Paban and S. D. Thomas, Phys. Lett. **B289**, 373 (1992), [hep-ph/9205233].
- [115] A. Masiero and L. Silvestrini, in *Perspectives on Supersymmetry*, edited by G.L. Kane (World Scientific, Singapore, 1998) pp. 423–441.
- [116] M. Pospelov and A. Ritz, Annals Phys. **318**, 119 (2005), [hep-ph/0504231].
- [117] J. M. Pendlebury *et al.*, Phys. Rev. **D92**, 092003 (2015), [arXiv:1509.04411]; V. Andreev *et al.* (ACME Collaboration), Nature **562**, 7727, 355 (2018).
- [118] F. Gabbiani *et al.*, Nucl. Phys. **B477**, 321 (1996), [hep-ph/9604387].
- [119] M. J. Ramsey-Musolf and S. Su, Phys. Rept. **456**, 1 (2008), [hep-ph/0612057].
- [120] M. Carena, A. Menon and C. E. M. Wagner, Phys. Rev. **D79**, 075025 (2009), [arXiv:0812.3594].
- [121] M. B. Einhorn and D. R. T. Jones, Nucl. Phys. **B196**, 475 (1982).
- [122] W. J. Marciano and G. Senjanovic, Phys. Rev. **D25**, 3092 (1982).
- [123] R.N. Mohapatra, *Unification and Supersymmetry*, Third Edition (Springer Science, New York, 2003).
- [124] S. P. Martin and M. T. Vaughn, Phys. Rev. **D50**, 2282 (1994), [Erratum: Phys. Rev. **D78**, 039903 (2008)], [hep-ph/9311340]; R. M. Fonseca *et al.*, Nucl. Phys. **B854**, 28 (2012), [arXiv:1107.2670]; F. Staub, Comput. Phys. Commun. **182**, 808 (2011), [arXiv:1002.0840].
- [125] F. Staub, Comput. Phys. Commun. **185**, 1773 (2014), [arXiv:1309.7223]; F. Staub, Adv. High Energy Phys. **2015**, 840780 (2015), [arXiv:1503.04200]; The SARAH homepage is <https://sarah.hepforge.org/>.
- [126] B. C. Allanach, Comput. Phys. Commun. **143**, 305 (2002), [hep-ph/0104145]; The SOFTSUSY homepage is <http://softsusy.hepforge.org/>; A. Djouadi, J.-L. Kneur and G. Moultaka, Comput. Phys. Commun. **176**, 426 (2007), [hep-ph/0211331]; The Suspect homepage is <http://suspect.in2p3.fr/>; F. E. Paige *et al.* (2003), [hep-ph/0312045]; Isajet may be obtained from <http://www.nhn.ou.edu/~isajet/>; W. Porod, Comput. Phys. Commun. **153**, 275 (2003), [hep-ph/0301101]; Spheno may be obtained from <https://spheno.hepforge.org/>; P. Athron *et al.*, Comput. Phys. Commun. **190**, 139 (2015), [arXiv:1406.2319]; The FlexibleSUSY homepage is <https://flexiblesusy.hepforge.org/>.
- [127] L. E. Ibanez and G. G. Ross, Phys. Lett. **110B**, 215 (1982).
- [128] J. Abdallah *et al.* (DELPHI Collaboration), Eur. Phys. J. **C31**, 421 (2003), [hep-ex/0311019].
- [129] H. K. Dreiner *et al.*, Eur. Phys. J. **C62**, 547 (2009), [arXiv:0901.3485].
- [130] G. F. Giudice *et al.*, JHEP **12**, 027 (1998), [hep-ph/9810442]; A. Pomarol and R. Rattazzi, JHEP **05**, 013 (1999), [hep-ph/9903448]; D.-W. Jung and J. Y. Lee, JHEP **03**, 123 (2009), [arXiv:0902.0464].
- [131] J. F. Gunion and H. E. Haber, Phys. Rev. **D37**, 2515 (1988); S. Y. Choi, M. Drees and B. Gaissmaier, Phys. Rev. **D70**, 014010 (2004), [hep-ph/0403054].
- [132] H. Baer, V. Barger and D. Sengupta, Phys. Rev. **D98**, 015039 (2018), [arXiv:1801.09730].
- [133] J. L. Feng *et al.*, Phys. Rev. Lett. **83**, 1731 (1999), [hep-ph/9904250]; J. F. Gunion and S. Mrenna, Phys. Rev. **D62**, 015002 (2000), [hep-ph/9906270].
- [134] T. Gherghetta, G. F. Giudice and J. D. Wells, Nucl. Phys. **B559**, 27 (1999), [hep-ph/9904378].
- [135] M. Endo, M. Yamaguchi and K. Yoshioka, Phys. Rev. **D72**, 015004 (2005), [hep-ph/0504036]; K. Choi, K. S. Jeong and K.-i. Okumura, JHEP **09**, 039 (2005), [hep-ph/0504037]; O. Loaiza-Brito *et al.*, AIP Conf. Proc. **805**, 198 (2005), [hep-th/0509158].
- [136] See *e.g.*, G. D'Ambrosio *et al.*, Nucl. Phys. **B645**, 155 (2002).
- [137] C. Smith, Acta Phys. Polon. Supp. **3**, 53 (2010), [arXiv:0909.4444].
- [138] M. Drees and S.P. Martin, in *Electroweak Symmetry Breaking and New Physics at the TeV Scale*, edited by T. Barklow *et al.* (World Scientific, Singapore, 1996) pp. 146–215.
- [139] G. L. Kane *et al.*, Phys. Rev. **D49**, 6173 (1994), [hep-ph/9312272].
- [140] J. R. Ellis *et al.*, Phys. Lett. **B573**, 162 (2003), [hep-ph/0305212]; J. R. Ellis *et al.*, Phys. Rev. **D70**, 055005 (2004), [hep-ph/0405110].
- [141] H. Baer *et al.*, Phys. Rev. **D71**, 095008 (2005), [hep-ph/0412059].
- [142] V. Berezhinsky *et al.*, Astropart. Phys. **5**, 1 (1996), [hep-ph/9508249]; J. R. Ellis *et al.*, Nucl. Phys. **B652**, 259 (2003), [hep-ph/0210205].
- [143] L. E. Ibanez and D. Lust, Nucl. Phys. **B382**, 305 (1992), [hep-th/9202046]; B. de Carlos, J. A. Casas and C. Munoz, Phys. Lett. **B299**, 234 (1993), [hep-ph/9211266]; V. S. Kaplunovsky and J. Louis, Phys. Lett. **B306**, 269 (1993), [hep-th/9303040]; A. Brignole, L. E. Ibanez and C. Munoz, Nucl. Phys. **B422**, 125 (1994), [Erratum: **B436**, 747 (1995)], [hep-ph/9308271].
- [144] A. Arbey *et al.*, Phys. Rev. **D87**, 115020 (2013), [arXiv:1304.0381].
- [145] G. R. Dvali, G. F. Giudice and A. Pomarol, Nucl. Phys. **B478**, 31 (1996), [hep-ph/9603238].
- [146] P. Draper *et al.*, Phys. Rev. **D85**, 095007 (2012), [arXiv:1112.3068].
- [147] P. Meade, N. Seiberg and D. Shih, Prog. Theor. Phys. Suppl. **177**, 143 (2009), [arXiv:0801.3278]; M. Buican *et al.*, JHEP **03**, 016 (2009), [arXiv:0812.3668].
- [148] A. Rajaraman *et al.*, Phys. Lett. **B678**, 367 (2009), [arXiv:0903.0668]; L. M. Carpenter *et al.*, Phys. Rev. **D79**, 035002 (2009), [arXiv:0805.2944].
- [149] S. Ambrosanio, G. D. Kribs and S. P. Martin, Nucl. Phys. **B516**, 55 (1998), [hep-ph/9710217].
- [150] For a review and guide to the literature, see J.F. Gunion and H.E. Haber, in *Perspectives on Supersymmetry II*, edited by G.L. Kane (World Scientific, Singapore, 2010) pp. 420–445.
- [151] T. S. Roy and M. Schmaltz, Phys. Rev. **D77**, 095008 (2008), [arXiv:0708.3593].
- [152] A. de Gouvea, A. Friedland and H. Murayama, Phys. Rev. **D57**, 5676 (1998), [hep-ph/9711264].

- [153] T. Han, D. Marfatia and R.-J. Zhang, Phys. Rev. **D61**, 013007 (2000), [hep-ph/9906508]; Z. Chacko and E. Ponton, Phys. Rev. **D66**, 095004 (2002), [hep-ph/0112190]; A. Delgado, G. F. Giudice and P. Slavich, Phys. Lett. **B653**, 424 (2007), [arXiv:0706.3873]; T. Liu and C. E. M. Wagner, JHEP **06**, 073 (2008), [arXiv:0803.2895].
- [154] B. Allanach *et al.*, Phys. Rev. **D92**, 015006 (2015), [arXiv:1502.05836].
- [155] A. Djouadi, J.L. Kneur, and G. Moultaka, Comp. Phys. Comm. **176**, 426 (2007); C. F. Berger *et al.*, JHEP **02**, 023 (2009), [arXiv:0812.0980].
- [156] S. P. Martin and J. D. Wells, Phys. Rev. **D64**, 035003 (2001), [hep-ph/0103067].
- [157] J. Berger *et al.*, Phys. Rev. **D93**, 035017 (2016), [arXiv:1510.08840].
- [158] K. J. de Vries *et al.*, Eur. Phys. J. **C75**, 422 (2015), [arXiv:1504.03260].
- [159] M. Cahill-Rowley *et al.*, Phys. Rev. **D90**, 095017 (2014), [arXiv:1407.7021]; M. Cahill-Rowley *et al.*, Phys. Rev. **D91**, 055011 (2015), [arXiv:1405.6716]; A. Barr and J. Liu, Eur. Phys. J. **C77**, 202 (2017), [arXiv:1608.05379].
- [160] G. Bertone *et al.*, JCAP **1604**, 037 (2016), [arXiv:1507.07008].
- [161] N. Arkani-Hamed *et al.* (2007), [hep-ph/0703088]; J. Alwall *et al.*, Phys. Rev. **D79**, 015005 (2009), [arXiv:0809.3264]; J. Alwall, P. Schuster and N. Toro, Phys. Rev. **D79**, 075020 (2009), [arXiv:0810.3921]; D. S. M. Alves, E. Izaguirre and J. G. Wacker, Phys. Lett. **B702**, 64 (2011), [arXiv:1008.0407]; D. S. M. Alves, E. Izaguirre and J. G. Wacker, JHEP **10**, 012 (2011), [arXiv:1102.5338]; D. Alves (LHC New Physics Working Group), J. Phys. **G39**, 105005 (2012), [arXiv:1105.2838].
- [162] F. Ambrogio *et al.*, Eur. Phys. J. **C78**, 215 (2018), [arXiv:1707.09036].
- [163] R. Barbieri and G.F. Giudice, Nucl. Phys. **B305**, 63 (1988).
- [164] J. R. Ellis *et al.*, Mod. Phys. Lett. **A1**, 57 (1986).
- [165] G. W. Anderson and D. J. Castano, Phys. Lett. **B347**, 300 (1995), [hep-ph/9409419]; G. W. Anderson and D. J. Castano, Phys. Rev. **D52**, 1693 (1995), [hep-ph/9412322]; G. W. Anderson and D. J. Castano, Phys. Rev. **D53**, 2403 (1996), [hep-ph/9509212]; P. Athron and D. J. Miller, Phys. Rev. **D76**, 075010 (2007), [arXiv:0705.2241]; M. E. Cabrera, J. A. Casas and R. Ruiz de Austri, JHEP **03**, 075 (2009), [arXiv:0812.0536]; H. Baer *et al.*, Phys. Rev. Lett. **109**, 161802 (2012), [arXiv:1207.3343].
- [166] J. L. Feng, K. T. Matchev and T. Moroi, Phys. Rev. **D61**, 075005 (2000), [hep-ph/9909334].
- [167] D. M. Ghilencea and G. G. Ross, Nucl. Phys. **B868**, 65 (2013), [arXiv:1208.0837].
- [168] H. Baer, V. Barger and D. Mickelson, Phys. Rev. **D88**, 095013 (2013), [arXiv:1309.2984].
- [169] M. van Beekveld, S. Caron and R. Ruiz de Austri, JHEP **01**, 147 (2020), [arXiv:1906.10706].
- [170] G. L. Kane and S. F. King, Phys. Lett. **B451**, 113 (1999), [hep-ph/9810374]; M. Bastero-Gil, G. L. Kane and S. F. King, Phys. Lett. **B474**, 103 (2000), [hep-ph/9910506]; J. A. Casas, J. R. Espinosa and I. Hidalgo, JHEP **01**, 008 (2004), [hep-ph/0310137]; H. Abe, T. Kobayashi and Y. Omura, Phys. Rev. **D76**, 015002 (2007), [hep-ph/0703044]; R. Essig and J.-F. Fortin, JHEP **04**, 073 (2008), [arXiv:0709.0980].
- [171] B. de Carlos and J. A. Casas, Phys. Lett. **B309**, 320 (1993), [hep-ph/9303291]; S. Cassel, D. M. Ghilencea and G. G. Ross, Nucl. Phys. **B825**, 203 (2010), [arXiv:0903.1115]; S. Cassel, D. M. Ghilencea and G. G. Ross, Nucl. Phys. **B835**, 110 (2010), [arXiv:1001.3884].
- [172] O. Buchmueller *et al.*, Eur. Phys. J. **C74**, 6, 2922 (2014), [arXiv:1312.5250].
- [173] P. Bechtle *et al.*, Eur. Phys. J. **C76**, 96 (2016), [arXiv:1508.05951].
- [174] H. Baer *et al.*, Phys. Rev. **D89**, 115019 (2014), [arXiv:1404.2277].
- [175] R. Barbieri and A. Strumia, in “4th Rencontres du Vietnam: Physics at Extreme Energies (Particle Physics and Astrophysics) Hanoi, Vietnam, July 19-25, 2000,” (2000), [hep-ph/0007265].
- [176] L. Giusti, A. Romanino and A. Strumia, Nucl. Phys. **B550**, 3 (1999), [hep-ph/9811386]; H.-C. Cheng and I. Low, JHEP **09**, 051 (2003), [hep-ph/0308199]; H.-C. Cheng and I. Low, JHEP **08**, 061 (2004), [hep-ph/0405243]; R. Harnik *et al.*, Phys. Rev. **D70**, 015002 (2004), [hep-ph/0311349].
- [177] H. Baer *et al.*, Phys. Rev. **D87**, 035017 (2013), [arXiv:1210.3019]; H. Baer *et al.*, Phys. Rev. **D87**, 115028 (2013), [arXiv:1212.2655]; J. L. Feng, Ann. Rev. Nucl. Part. Sci. **63**, 351 (2013), [arXiv:1302.6587].
- [178] J. L. Feng, K. T. Matchev and T. Moroi, Phys. Rev. Lett. **84**, 2322 (2000), [hep-ph/9908309]; J. L. Feng and F. Wilczek, Phys. Lett. **B631**, 170 (2005), [hep-ph/0507032]; D. Horton and G. G. Ross, Nucl. Phys. **B830**, 221 (2010), [arXiv:0908.0857].
- [179] M. Drees, Phys. Rev. **D33**, 1468 (1986); S. Dimopoulos and G. F. Giudice, Phys. Lett. **B357**, 573 (1995), [hep-ph/9507282]; A. Pomarol and D. Tommasini, Nucl. Phys. **B466**, 3 (1996), [hep-ph/9507462].
- [180] M. Dine, A. Kagan and S. Samuel, Phys. Lett. **B243**, 250 (1990); A. G. Cohen, D. B. Kaplan and A. E. Nelson, Phys. Lett. **B388**, 588 (1996), [hep-ph/9607394].
- [181] C. Brust *et al.*, JHEP **03**, 103 (2012), [arXiv:1110.6670].
- [182] S. P. Martin, Phys. Rev. **D75**, 115005 (2007), [hep-ph/0703097]; S. P. Martin, Phys. Rev. **D78**, 055019 (2008), [arXiv:0807.2820].
- [183] J. Fan, M. Reece and J. T. Ruderman, JHEP **11**, 012 (2011), [arXiv:1105.5135]; J. Fan, M. Reece and J. T. Ruderman, JHEP **07**, 196 (2012), [arXiv:1201.4875].
- [184] H. Murayama, Y. Nomura and D. Poland, Phys. Rev. **D77**, 015005 (2008), [arXiv:0709.0775]; G. Perez, T. S. Roy and M. Schmaltz, Phys. Rev. **D79**, 095016 (2009), [arXiv:0811.3206].
- [185] R. Dermisek and J. F. Gunion, Phys. Rev. Lett. **95**, 041801 (2005), [hep-ph/0502105]; Phys. Rev. **D75**, 095019 (2007); R. Dermisek and J. F. Gunion, Phys. Rev. **D76**, 095006 (2007), [arXiv:0705.4387].
- [186] G. G. Ross and K. Schmidt-Hoberg, Nucl. Phys. **B862**, 710 (2012), [arXiv:1108.1284]; G. G. Ross, K. Schmidt-Hoberg and F. Staub, JHEP **08**, 074 (2012), [arXiv:1205.1509]; A. Kaminska, G. G. Ross and K. Schmidt-Hoberg, JHEP **11**, 209 (2013), [arXiv:1308.4168].
- [187] S. P. Martin and J. D. Wells, Phys. Rev. **D86**, 035017 (2012), [arXiv:1206.2956].
- [188] B. Bellazzini *et al.*, Phys. Rev. **D79**, 095003 (2009), [arXiv:0902.0015].
- [189] M. Dine, Ann. Rev. Nucl. Part. Sci. **65**, 43 (2015), [arXiv:1501.01035].
- [190] H. Baer, V. Barger and M. Savoy, Phys. Rev. **D93**, 035016 (2016), [arXiv:1509.02929].
- [191] M.L. Mangano, editor, *Physics at the FCC-hh, a 100 TeV pp collider*, CERN Yellow Report, CERN-2017-003-M (2017).
- [192] D. Stockinger, J. Phys. **G34**, R45 (2007), [hep-ph/0609168]; P. Athron *et al.*, Eur. Phys. J. **C76**, 62 (2016), [arXiv:1510.08071].
- [193] F. Jegerlehner, Acta Phys. Polon. **B49**, 1157 (2018), [arXiv:1804.07409]; M. Davier *et al.*, Eur. Phys. J. **C80**, 3, 241 (2020), [arXiv:1908.00921].

- [194] M. Ibe, T. T. Yanagida and N. Yokozaki, *JHEP* **08**, 067 (2013), [arXiv:1303.6995].
- [195] R. H. Parker *et al.*, *Science* **360**, 191 (2018), [arXiv:1812.04130].
- [196] D. Hanneke, S. Fogwell and G. Gabrielse, *Phys. Rev. Lett.* **100**, 120801 (2008), [arXiv:0801.1134].
- [197] B. Dutta and Y. Mimura, *Phys. Lett.* **B790**, 563 (2019), [arXiv:1811.10209]; M. Endo and W. Yin, *JHEP* **08**, 122 (2019), [arXiv:1906.08768]; M. Badziak and K. Sakurai, *JHEP* **10**, 024 (2019), [arXiv:1908.03607].
- [198] A. Limosani *et al.* (Belle Collaboration), *Phys. Rev. Lett.* **103**, 241801 (2009), [arXiv:0907.1384]; J. P. Lees *et al.* (BaBar Collaboration), *Phys. Rev. Lett.* **109**, 191801 (2012), [arXiv:1207.2690]; J. P. Lees *et al.* (BaBar Collaboration), *Phys. Rev.* **D86**, 112008 (2012), [arXiv:1207.5772].
- [199] M. Misiak *et al.*, *Phys. Rev. Lett.* **114**, 221801 (2015), [arXiv:1503.01789]; M. Czakon *et al.*, *JHEP* **04**, 168 (2015), [arXiv:1503.01791].
- [200] H. Baer and M. Brhlik, *Phys. Rev.* **D55**, 3201 (1997), [hep-ph/9610224]; M. Ciuchini *et al.*, *Phys. Rev.* **D67**, 075016 (2003), [Erratum: **D68**, 079901 (2003)], [hep-ph/0212397]; T. Hurth, *Rev. Mod. Phys.* **75**, 1159 (2003), [hep-ph/0212304]; F. Mahmoudi, *JHEP* **12**, 026 (2007), [arXiv:0710.3791]; K. A. Olive and L. Velasco-Sevilla, *JHEP* **05**, 052 (2008), [arXiv:0801.0428].
- [201] S. R. Choudhury and N. Gaur, *Phys. Lett.* **B451**, 86 (1999), [hep-ph/9810307]; K. S. Babu and C. F. Kolda, *Phys. Rev. Lett.* **84**, 228 (2000), [hep-ph/9909476]; G. Isidori and A. Retico, *JHEP* **11**, 001 (2001), [hep-ph/0110121]; G. Isidori and A. Retico, *JHEP* **09**, 063 (2002), [hep-ph/0208159].
- [202] S. Chatrchyan *et al.* (CMS Collaboration), *Phys. Rev. Lett.* **111**, 101804 (2013), [arXiv:1307.5025]; V. Khachatryan *et al.* (CMS and LHCb Collaborations), *Nature* **522**, 68 (2015), [arXiv:1411.4413]; M. Aaboud *et al.* (ATLAS Collaboration), *JHEP* **04**, 098 (2019), [arXiv:1812.03017]; R. Aaij *et al.* (LHCb Collaboration), *Phys. Rev. Lett.* **118**, 191801 (2017), [arXiv:1703.05747].
- [203] J. Aebischer *et al.*, *Eur. Phys. J. C* **80**, 3, 252 (2020), [arXiv:1903.10434].
- [204] C. Bobeth *et al.*, *Phys. Rev. Lett.* **112**, 101801 (2014), [arXiv:1311.0903].
- [205] M. Bona *et al.* (UTfit Collaboration), *Phys. Lett.* **B687**, 61 (2010), [arXiv:0908.3470].
- [206] J. P. Lees *et al.* (BaBar Collaboration), *Phys. Rev. Lett.* **109**, 101802 (2012), [arXiv:1205.5442]; J. P. Lees *et al.* (BaBar Collaboration), *Phys. Rev.* **D88**, 072012 (2013), [arXiv:1303.0571].
- [207] R. Aaij *et al.* (LHCb Collaboration), *Phys. Rev. Lett.* **115**, 111803 (2015), [Erratum: **115**, 159901 (2015)], [arXiv:1506.08614]; R. Aaij *et al.* (LHCb Collaboration), *Phys. Rev. Lett.* **120**, 171802 (2018), [arXiv:1708.08856]; M. Huschle *et al.* (Belle Collaboration), *Phys. Rev.* **D92**, 072014 (2015), [arXiv:1507.03233]; Y. Sato *et al.* (Belle Collaboration), *Phys. Rev.* **D94**, 072007 (2016), [arXiv:1607.07923]; S. Hirose *et al.* (Belle Collaboration), *Phys. Rev. Lett.* **118**, 211801 (2017), [arXiv:1612.00529]; S. Hirose *et al.* (Belle Collaboration), *Phys. Rev.* **D97**, 012004 (2018), [arXiv:1709.00129].
- [208] G. Caria *et al.* (Belle Collaboration), *Phys. Rev. Lett.* **124**, 16, 161803 (2020), [arXiv:1910.05864].
- [209] S. Klaver (LHCb Collaboration), in "Proceedings of the 17th Conference on Flavor Physics and CP Violation (FPCP 2019) Victoria, BC, Canada, May 6-10, 2019," (2019), [arXiv:1907.01500].
- [210] F. Mahmoudi, S. Neshatpour and J. Orloff, *JHEP* **08**, 092 (2012), [arXiv:1205.1845]; A. Arbey *et al.*, *JHEP* **11**, 132 (2017), [arXiv:1707.00426].
- [211] A. J. Buras, *Acta Phys. Polon.* **B49**, 1043 (2018), [arXiv:1805.11096].
- [212] V. Cirigliano *et al.*, *JHEP* **02**, 032 (2020), [arXiv:1911.01359].
- [213] J. R. Ellis *et al.*, *JHEP* **08**, 083 (2007), [arXiv:0706.0652]; S. Heinemeyer *et al.*, *JHEP* **08**, 087 (2008), [arXiv:0805.2359]; G.-C. Cho *et al.*, *JHEP* **11**, 068 (2011), [arXiv:1104.1769]; E. Bagnaschi *et al.*, *Eur. Phys. J.* **C78**, 256 (2018), [arXiv:1710.11091].
- [214] A. J. Buras *et al.*, *Nucl. Phys.* **B592**, 55 (2001), [hep-ph/0007313].
- [215] I. Esteban *et al.*, *JHEP* **01**, 106 (2019), [arXiv:1811.05487].
- [216] K. Zuber, *Phys. Rept.* **305**, 295 (1998), [hep-ph/9811267]; S. F. King, *J. Phys.* **G42**, 123001 (2015), [arXiv:1510.02091]; S. F. King, *Prog. Part. Nucl. Phys.* **94**, 217 (2017), [arXiv:1701.04413].
- [217] For a review of neutrino masses in supersymmetry, see e.g., B. Mukhopadhyaya, *Proc. Indian National Science Academy* **A70**, 239 (2004); M. Hirsch and J. W. F. Valle, *New J. Phys.* **6**, 76 (2004), [hep-ph/0405015].
- [218] F. Borzumati and Y. Nomura, *Phys. Rev.* **D64**, 053005 (2001), [hep-ph/0007018].
- [219] P. Minkowski, *Phys. Lett.* **67B**, 421 (1977); M. Gell-Mann, P. Ramond, and R. Slansky, in *Supergravity*, edited by D. Freedman and P. van Nieuwenhuizen (North Holland, Amsterdam, 1979) p. 315; T. Yanagida, *Prog. Theor. Phys.* **64**, 1103 (1980); R. N. Mohapatra and G. Senjanovic, *Phys. Rev. Lett.* **44**, 912 (1980); R. N. Mohapatra and G. Senjanovic, *Phys. Rev.* **D23**, 165 (1981).
- [220] J. Hisano *et al.*, *Phys. Lett.* **B357**, 579 (1995), [hep-ph/9501407]; J. Hisano *et al.*, *Phys. Rev.* **D53**, 2442 (1996), [hep-ph/9510309]; J. A. Casas and A. Ibarra, *Nucl. Phys.* **B618**, 171 (2001), [hep-ph/0103065]; J. R. Ellis *et al.*, *Phys. Rev.* **D66**, 115013 (2002), [hep-ph/0206110]; A. Masiero, S. K. Vempati and O. Vives, *New J. Phys.* **6**, 202 (2004), [hep-ph/0407325]; E. Arganda *et al.*, *Phys. Rev.* **D71**, 035011 (2005), [hep-ph/0407302]; F. R. Joaquim and A. Rossi, *Phys. Rev. Lett.* **97**, 181801 (2006), [hep-ph/0604083]; J. R. Ellis and O. Lebedev, *Phys. Lett.* **B653**, 411 (2007), [arXiv:0707.3419].
- [221] Y. Grossman and H. E. Haber, *Phys. Rev. Lett.* **78**, 3438 (1997), [hep-ph/9702421]; A. Dedes, H. E. Haber and J. Rosiek, *JHEP* **11**, 059 (2007), [arXiv:0707.3718].
- [222] M. Hirsch, H. V. Klapdor-Kleingrothaus and S. G. Kovalenko, *Phys. Lett.* **B398**, 311 (1997), [hep-ph/9701253]; L. J. Hall, T. Moroi and H. Murayama, *Phys. Lett.* **B424**, 305 (1998), [hep-ph/9712515]; K. Choi, K. Hwang and W. Y. Song, *Phys. Rev. Lett.* **88**, 141801 (2002), [hep-ph/0108028]; T. Honkavaara, K. Huitu and S. Roy, *Phys. Rev.* **D73**, 055011 (2006), [hep-ph/0512277].
- [223] L. Basso *et al.*, *Comput. Phys. Commun.* **184**, 698 (2013), [arXiv:1206.4563].
- [224] M. Chemtob, *Prog. Part. Nucl. Phys.* **54**, 71 (2005), [hep-ph/0406029]; R. Barbier *et al.*, *Phys. Rept.* **420**, 1 (2005), [hep-ph/0406039].
- [225] H. Dreiner, in *Perspectives on Supersymmetry II*, edited by G.L. Kane (World Scientific, Singapore, 2010) pp. 565–583.
- [226] B. C. Allanach, A. Dedes and H. K. Dreiner, *Phys. Rev.* **D60**, 075014 (1999), [hep-ph/9906209].
- [227] L. E. Ibanez and G. G. Ross, *Nucl. Phys.* **B368**, 3 (1992); L. E. Ibanez, *Nucl. Phys.* **B398**, 301 (1993), [hep-ph/9210211].
- [228] A. Dedes, S. Rimmer and J. Rosiek, *JHEP* **08**, 005 (2006), [hep-ph/0603225]; B. C. Allanach and C. H. Kom, *JHEP* **04**, 081 (2008), [arXiv:0712.0852]; H. K. Dreiner *et al.*, *Phys. Rev.* **D84**, 113005 (2011), [arXiv:1106.4338].
- [229] H. K. Dreiner, C. Luhn and M. Thormeier, *Phys. Rev.* **D73**, 075007 (2006), [hep-ph/0512163].

- [230] K. Tamvakis, Phys. Lett. **B382**, 251 (1996), [hep-ph/9604343]; G. Eyal and Y. Nir, JHEP **06**, 024 (1999), [hep-ph/9904473]; A. Florez *et al.*, Phys. Rev. **D87**, 095010 (2013), [arXiv:1303.0278].
- [231] C. Csaki, Y. Grossman and B. Heidenreich, Phys. Rev. **D85**, 095009 (2012), [arXiv:1111.1239].
- [232] D. Dercks *et al.*, Eur. Phys. J. **C77**, 856 (2017), [arXiv:1706.09418].
- [233] B. C. Allanach and B. Gripaios, JHEP **05**, 062 (2012), [arXiv:1202.6616]; M. Asano, K. Rolbiecki and K. Sakurai, JHEP **01**, 128 (2013), [arXiv:1209.5778]; N. Chamoun *et al.*, JHEP **08**, 142 (2014), [arXiv:1407.2248].
- [234] J. C. Romao, Nucl. Phys. Proc. Suppl. **81**, 231 (2000), [hep-ph/9907466]; Y. Grossman and S. Rakshit, Phys. Rev. **D69**, 093002 (2004), [hep-ph/0311310].
- [235] R. N. Mohapatra, Phys. Rev. **D34**, 3457 (1986); K. S. Babu and R. N. Mohapatra, Phys. Rev. Lett. **75**, 2276 (1995), [hep-ph/9506354]; M. Hirsch, H. V. Klapdor-Kleingrothaus and S. G. Kovalenko, Phys. Rev. Lett. **75**, 17 (1995); M. Hirsch, H. V. Klapdor-Kleingrothaus and S. G. Kovalenko, Phys. Rev. **D53**, 1329 (1996), [hep-ph/9502385].
- [236] Y. Grossman and H. E. Haber, Phys. Rev. **D59**, 093008 (1999), [hep-ph/9810536].
- [237] S. Dimopoulos and L. J. Hall, Phys. Lett. **B207**, 210 (1988); J. Kalinowski *et al.*, Phys. Lett. **B406**, 314 (1997), [hep-ph/9703436]; J. Erler, J. L. Feng and N. Polonsky, Phys. Rev. Lett. **78**, 3063 (1997), [hep-ph/9612397].
- [238] H. K. Dreiner, P. Richardson and M. H. Seymour, Phys. Rev. **D63**, 055008 (2001), [hep-ph/0007228].
- [239] J. E. Kim and H. P. Nilles, Phys. Lett. **138B**, 150 (1984).
- [240] J. E. Kim and H. P. Nilles, Mod. Phys. Lett. **A9**, 3575 (1994), [hep-ph/9406296].
- [241] G. F. Giudice and A. Masiero, Phys. Lett. **B206**, 480 (1988); J. A. Casas and C. Munoz, Phys. Lett. **B306**, 288 (1993), [hep-ph/9302227]; K. J. Bae *et al.*, Phys. Rev. **D99**, 115027 (2019), [arXiv:1902.10748].
- [242] M. Cvetič *et al.*, Phys. Rev. **D56**, 2861 (1997), [Erratum: **D58**, 119905 (1998)], [hep-ph/9703317].
- [243] R. D. Peccei, Lect. Notes Phys. **741**, 3 (2008), [hep-ph/0607268].
- [244] R. D. Peccei and H. R. Quinn, Phys. Rev. Lett. **38**, 1440 (1977); R. D. Peccei and H. R. Quinn, Phys. Rev. **D16**, 1791 (1977).
- [245] H. Murayama, H. Suzuki and T. Yanagida, Phys. Lett. **B291**, 418 (1992); T. Gherghetta and G. L. Kane, Phys. Lett. **B354**, 300 (1995), [hep-ph/9504420]; K. J. Bae, H. Baer and H. Serce, Phys. Rev. **D91**, 1, 015003 (2015), [arXiv:1410.7500]; H. Baer, V. Barger and D. Sengupta, Phys. Lett. **B790**, 58 (2019), [arXiv:1810.03713].
- [246] A. Delgado, G. Nardini and M. Quiros, Phys. Rev. **D86**, 115010 (2012), [arXiv:1207.6596].
- [247] P. Fayet, Phys. Lett. **78B**, 417 (1978).
- [248] K. Benakli, Fortsch. Phys. **59**, 1079 (2011), [arXiv:1106.1649].
- [249] P. J. Fox, A. E. Nelson and N. Weiner, JHEP **08**, 035 (2002), [hep-ph/0206096].
- [250] K. Benakli and M. D. Goodsell, Nucl. Phys. **B816**, 185 (2009), [arXiv:0811.4409]; K. Benakli and M. D. Goodsell, Nucl. Phys. **B840**, 1 (2010), [arXiv:1003.4957].
- [251] U. Sarkar and R. Adhikari, Phys. Rev. **D55**, 3836 (1997), [hep-ph/9608209]; R. Fok *et al.*, Phys. Rev. **D87**, 055018 (2013), [arXiv:1208.2784].
- [252] G. D. Kribs, E. Poppitz and N. Weiner, Phys. Rev. **D78**, 055010 (2008), [arXiv:0712.2039].
- [253] K. Benakli, M. D. Goodsell and F. Staub, JHEP **06**, 073 (2013), [arXiv:1211.0552].
- [254] J. L. Hewett and T. G. Rizzo, Phys. Rept. **183**, 193 (1989).
- [255] S. F. King, S. Moretti and R. Nevzorov, Phys. Lett. **B634**, 278 (2006), [hep-ph/0511256]; S. F. King, S. Moretti and R. Nevzorov, Phys. Rev. **D73**, 035009 (2006), [hep-ph/0510419].

90. Supersymmetry, Part II (Experiment)

Revised September 2019 by O. Buchmuller (Imperial Coll. London) and P. de Jong (NIKHEF).

90.1 Introduction

Supersymmetry (SUSY), a transformation relating fermions to bosons and vice versa [1–9] is one of the most compelling possible extensions of the Standard Model of particle physics (SM).

On theoretical grounds SUSY is motivated as a generalization of space-time symmetries. A low-energy realization of SUSY, *i.e.*, SUSY at the TeV scale, is, however, not a necessary consequence. Instead, low-energy SUSY is motivated by the possible cancellation of quadratic divergences in radiative corrections to the Higgs boson mass [10–15]. Furthermore, it is intriguing that a weakly interacting, (meta)stable supersymmetric particle might make up some or all of the dark matter in the universe [16–18]. In addition, SUSY predicts that gauge couplings, as measured experimentally at the electroweak scale, unify at an energy scale $\mathcal{O}(10^{16})$ GeV (“GUT scale”) near the Planck scale [19–24].

In the minimal supersymmetric extension to the Standard Model, the so called MSSM [11,25,26], a supersymmetry transformation relates every chiral fermion and gauge boson in the SM to a supersymmetric partner with half a unit of spin difference, but otherwise with the same properties (such as mass) and quantum numbers. These are the “sfermions”: squarks (\tilde{q}) and sleptons ($\tilde{\ell}$, $\tilde{\nu}$), and the “gauginos”. The MSSM Higgs sector contains two doublets, for up-type quarks and for down-type quarks and charged leptons respectively. After electroweak symmetry breaking, five Higgs bosons arise, of which two are charged. The supersymmetric partners of the Higgs doublets are known as “higgsinos.” The weak gauginos and higgsinos mix, giving rise to charged mass eigenstates called “charginos” ($\tilde{\chi}^{\pm}$), and neutral mass eigenstates called “neutralinos” ($\tilde{\chi}^0$). The SUSY partners of the gluons are known as “gluinos” (\tilde{g}). The fact that such particles are not yet observed leads to the conclusion that, if supersymmetry is realized, it is a broken symmetry. A description of SUSY in the form of an effective Lagrangian with only “soft” SUSY breaking terms and SUSY masses at the TeV scale maintains the cancellation of quadratic divergences of soft SUSY breaking scalar mass squared parameters.

The phenomenology of SUSY is to a large extent determined by the SUSY breaking mechanism and the SUSY breaking scale. This determines the SUSY particle masses, the mass hierarchy, the field contents of physical particles, and their decay modes. In addition, phenomenology crucially depends on whether the multiplicative quantum number of R-parity [26], $R = (-1)^{3(B-L)+2S}$, where B and L are baryon and lepton numbers and S is the spin, is conserved or violated. If R-parity is conserved, SUSY particles (sparticles), which have odd R-parity, are produced in pairs and the decays of each SUSY particle must involve an odd number of lighter SUSY particles. The lightest SUSY particle (LSP) is then stable and often assumed to be a weakly interacting massive particle (WIMP). If R-parity is violated, new terms λ_{ijk} , λ'_{ijk} and λ''_{ijk} appear in the superpotential, where ijk are generation indices; λ -type couplings appear between lepton superfields only, λ' -type are between quark superfields only, and λ'' -type couplings connect the two. R-parity violation implies lepton and/or baryon number violation. More details of the theoretical framework of SUSY are discussed elsewhere in this volume [27].

Today, low-energy data from flavor physics experiments, high-precision electroweak observables as well as astrophysical data impose strong constraints on the allowed SUSY parameter space. Recent examples of such data include measurements of the rare B-meson decay $B_s \rightarrow \mu^+ \mu^-$ [28,29], measurements of the anomalous magnetic moment of the muon [30], and accurate determinations of the cosmological dark matter relic density constraint [31,32].

These indirect constraints are often more sensitive to higher SUSY mass scales than experiments searching for direct sparticle production at colliders, but the interpretation of these results is often strongly model dependent. In contrast, direct searches for sparticle production at collider experiments are less subject to interpretation ambiguities and therefore they play a crucial role in the search for SUSY.

The discovery of a Higgs boson with a mass around 125 GeV imposes constraints on SUSY models, which are discussed elsewhere [27,33].

In this review we limit ourselves to direct searches, covering data analyses at LEP, HERA, the Tevatron and the LHC, with emphasis on the latter. For more details on LEP and Tevatron constraints, see earlier PDG reviews [34].

90.2 Experimental search program

The electron-positron collider LEP was operational at CERN between 1989 and 2000. In the initial phase, center-of-mass energies around the Z-peak were probed, but after 1995 the LEP experiments collected a significant amount of luminosity at higher center-of-mass energies, some 235 pb⁻¹ per experiment at $\sqrt{s} \geq 204$ GeV, with a maximum \sqrt{s} of 209 GeV.

Searches for new physics at e^+e^- colliders benefit from the clean experimental environment and the fact that momentum balance can be measured not only in the plane transverse to the beam, but also in the direction along the beam (up to the beam pipe holes), defined as the longitudinal direction. Searches at LEP are dominated by the data samples taken at the highest center-of-mass energies.

Constraints on SUSY have been set by the CDF and D0 experiments at the Tevatron, a proton-antiproton collider at a center-of-mass energy of up to 1.96 TeV. CDF and D0 collected integrated luminosities between 10 and 11 fb⁻¹ each up to the end of collider operations in 2011.

The electron-proton collider HERA provided collisions to the H1 and ZEUS experiments between 1992 and 2007, at a center-of-mass energy up to 318 GeV. A total integrated luminosity of approximately 0.5 fb⁻¹ was collected by each experiment. Since at HERA baryons collide with leptons, SUSY searches at HERA typically look for R-parity violating production of single SUSY particles.

The Large Hadron Collider (LHC) at CERN started proton-proton operation at a center-of-mass energy of 7 TeV in 2010. By the end of 2011 the experiments ATLAS and CMS had collected about 5 fb⁻¹ of integrated luminosity each, and the LHCb experiment had collected approximately 1 fb⁻¹. In 2012, the LHC operated at a center-of-mass energy of 8 TeV, and ATLAS and CMS collected approximately 20 fb⁻¹ each, whereas LHCb collected 2 fb⁻¹. In 2015, the LHC started Run 2, with a center-of-mass energy of 13 TeV. At the end of Run 2 in November 2018, ATLAS and CMS had both collected approximately 140 fb⁻¹, and LHCb had collected almost 6 fb⁻¹.

Proton-(anti)proton colliders produce interactions at higher center-of-mass energies than those available at LEP, and cross sections of QCD-mediated processes are larger, which is reflected in the higher sensitivity for SUSY particles carrying color charge: squarks and gluinos. Large background contributions from Standard Model processes, however, pose challenges to the trigger and analysis. Such backgrounds are dominated by multijet production processes, including, particularly at the LHC, those of top quark production, as well as jet production in association with vector bosons. The proton momentum is shared between its parton constituents, and in each collision only a fraction of the total center-of-mass energy is available in the hard parton-parton scattering. Since the parton momenta in the longitudinal direction are not known on an event-by-event basis, use of momentum conservation constraints in an analysis is restricted to the transverse plane, leading to the definition of transverse variables, such as the missing transverse momentum, and the transverse mass. Proton-proton collisions at the LHC differ from proton-antiproton collisions at the Tevatron in the sense that there are no valence anti-quarks in the proton, and that gluon-initiated processes play a more dominant role. The increased center-of-mass energy of the LHC compared to the Tevatron, as well as the increase at the LHC between Run 1 and Run 2, significantly extends the kinematic reach for SUSY searches. This is reflected foremost in the sensitivity for squarks and gluinos, but also for other SUSY particles.

The main production mechanisms of massive colored sparticles at hadron colliders are squark-squark, squark-gluino and gluino-

gluino production; when “squark” is used “antisquark” is also implied. Assuming R-parity conservation, the typical SUSY search signature at hadron colliders contains high- p_T jets, which are produced in the decay chains of heavy squarks and gluinos, and significant missing momentum originating from the two LSPs produced at the end of the decay chain, which escape experimental detection. Standard Model backgrounds with missing transverse momentum include leptonic W/Z -boson decays, heavy-flavor decays to neutrinos, and multijet events that may be affected by instrumental effects such as jet mismeasurement.

Selection variables designed to separate the SUSY signal from the Standard Model backgrounds include H_T , E_T^{miss} , and m_{eff} . The quantities H_T and E_T^{miss} refer to the measured transverse energy and the missing transverse momentum in the event, respectively. They are usually defined as the scalar sum of the transverse jet momenta or calorimeter clusters transverse energies measured in the event (H_T), or the magnitude (E_T^{miss}) of the negative vector sum of transverse momenta of reconstructed objects like jets and leptons in the event (\vec{p}_T^{miss}). The quantity m_{eff} is referred to as the effective mass of the event and is defined as $m_{\text{eff}} = H_T + E_T^{\text{miss}}$. The peak of the m_{eff} distribution for SUSY signal events correlates with the SUSY mass scale, in particular with the mass difference between the primary produced SUSY particle and the LSP [35], whereas the Standard Model backgrounds dominate at low m_{eff} . Additional reduction of multijet backgrounds can be achieved by demanding isolated leptons or photons in the final states; in such events the lepton or photon transverse momentum may be added to H_T or m_{eff} for further signal-background separation.

At the LHC, alternative approaches have been developed to increase the sensitivity to pair production of heavy sparticles with TeV-scale masses focusing on the kinematics of their decays, and to further suppress the background from multijet production. Prominent examples of these new approaches are searches using the α_T [36–40], *razor* [41], *stransverse mass* (m_{T2}) [42], and *contransverse mass* (m_{CT}) [43] variables. Recently, the topological event reconstruction methods have expanded with the *super-razor* [44] and *recursive jigsaw reconstruction* [45] techniques. Furthermore, frequently the searches for massive SUSY particles attempt to identify their decay into top quarks or vector bosons, which are themselves unstable. If these are produced with a significant boost, jets from their decay will typically overlap, and such topologies are searched for with *jet-substructure* [46] techniques.

90.3 Interpretation of results

Since the mechanism by which SUSY is broken is unknown, a general approach to SUSY via the most general soft SUSY breaking Lagrangian adds a significant number of new free parameters. For the minimal supersymmetric standard model, MSSM, *i.e.*, the model with the minimal particle content, these comprise 105 new real degrees of freedom. A phenomenological analysis of SUSY searches leaving all these parameters free is not feasible. For the practical interpretation of SUSY searches at colliders several approaches are taken to reduce the number of free parameters.

One approach is to assume a SUSY breaking mechanism and lower the number of free parameters through the assumption of additional constraints. Before the start of the LHC, interpretations of experimental results were predominately performed in constrained models of gravity mediated [50, 51], gauge-mediated [52–54], and anomaly mediated [55, 56] SUSY breaking. The most popular model was the constrained MSSM (CMSSM) [50, 57, 58], which in the literature is also referred to as minimal supergravity, or MSUGRA.

These constrained SUSY models are theoretically well motivated and provide a rich spectrum of experimental signatures. However, with universality relations imposed on the soft SUSY breaking parameters, they do not cover all possible kinematic signatures and mass relations of SUSY. In such scenarios the squarks are often nearly degenerate in mass, in particular for the first and second generation. The exclusion of parameter space in the CMSSM and in CMSSM-inspired models is mainly driven by first and second generation squark production together with gluino production. As shown in Fig. 90.1 [47–49] these processes possess

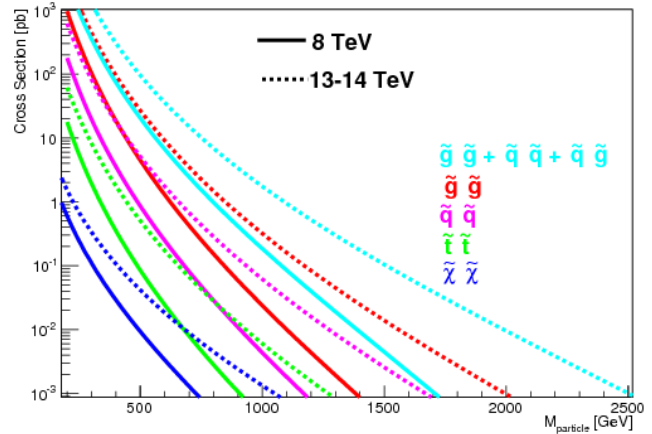


Figure 90.1: Cross sections for pair production of different sparticles as a function of their mass at the LHC for a center-of-mass energy of 8 TeV (solid curves) and 13–14 TeV (dotted curves), taken from Ref. [47]. Typically the production cross section of colored squarks and gluinos, calculated with NLL-FAST [48] at $\sqrt{s} = 8$ and 13 TeV, is several orders of magnitude larger than the one for electroweak gauginos, calculated with Prospino [49] at $\sqrt{s} = 8$ and 14 TeV for higgsino-like neutralinos. Except for the explicitly shown pair production of stops, production cross sections for squarks assumes mass degeneracy of left- and right-handed u , d , s , c and b squarks.

the largest production cross sections in proton-proton collisions, and thus the LHC searches typically provide the tightest mass limits on these colored sparticles. This, however, implies that the allowed parameter space of constrained SUSY models today has been restrained significantly by searches from ATLAS and CMS. Furthermore, confronting the remaining allowed parameter space with other collider and non-collider measurements, which are directly or indirectly sensitive to contributions from SUSY, the overall compatibility of these models with all data is significantly worse than in the pre-LHC era (see section II.8 for further discussion), indicating that very constrained models like the CMSSM are no longer good benchmark scenarios to solely characterize the results of SUSY searches at the LHC.

For these reasons, an effort has been made to complement the traditional constrained models with more flexible approaches.

One approach to study a broader and more comprehensive subset of the MSSM is via the phenomenological-MSSM, or pMSSM [59–61]. It is derived from the MSSM, using experimental data to eliminate parameters that are free in principle but have already been highly constrained by measurements of *e.g.*, flavor mixing and CP-violation. This effective approach reduces the number of free parameters in the MSSM to typically 19 or even less, making it a practical compromise between the full MSSM and highly constrained models such as the CMSSM.

Even less dependent on fundamental assumptions are interpretations in terms of so-called simplified models [62–65]. Such models assume a limited set of SUSY particle production and decay modes and leave open the possibility to vary masses and other parameters freely. Therefore, simplified models enable comprehensive studies of individual SUSY topologies, and are useful for optimization of the experimental searches over a wide parameter space without limitations on fundamental kinematic properties such as masses, production cross sections, and decay modes.

As a consequence, ATLAS and CMS have adopted simplified models as the primary framework to provide interpretations of their searches. In addition to using simplified models that describe prompt decays of SUSY particles, the experiments are now also focusing more on the use of simplified models that allow for decays of long-lived SUSY particles as they can arise in different SUSY scenarios (see Section 90.7 for further discussion). Today, almost every individual search provides interpretations of their results in one or even several simplified models that are characteristic of

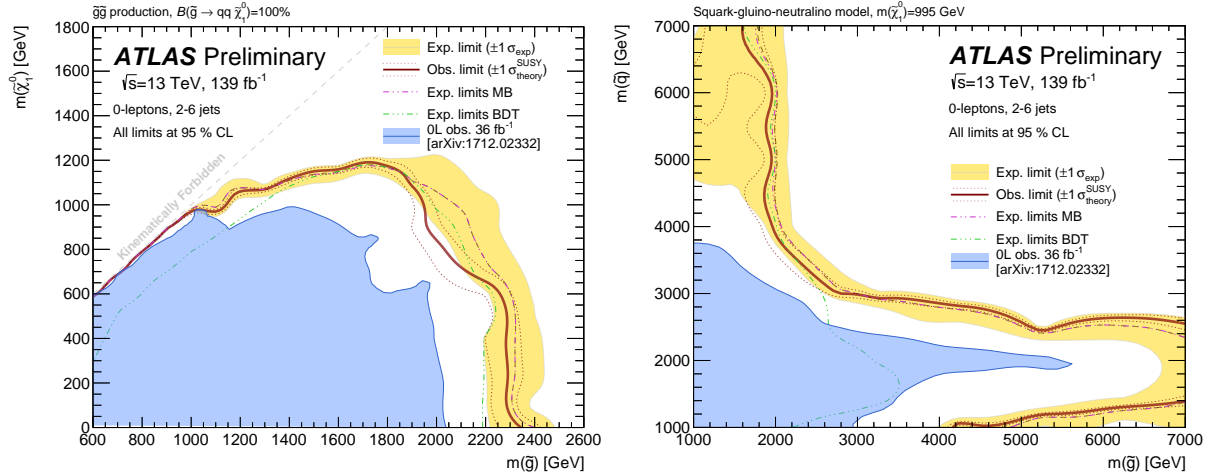


Figure 90.2: Left: lower mass limits, at 95% C.L., on gluino pair production and decay in a simplified model with $\tilde{g} \rightarrow q\bar{q}\tilde{\chi}_1^0$. Right: 95% C.L. mass limits on gluinos and squarks assuming gluino and squark production, and $m_{\tilde{\chi}_1^0} = 995$ GeV. Results of the ATLAS collaboration.

SUSY topologies probed by the analysis.

However, while these models are very convenient for the interpretation of individual SUSY production and decay topologies, care must be taken when applying these limits to more complex SUSY spectra. Therefore, in practice, simplified model limits are often used as an approximation of the constraints that can be placed on sparticle masses in more complex SUSY spectra. Yet, depending on the assumed SUSY spectrum, the sparticle of interest, and the considered simplified model limit, this approximation can lead to a significant mistake, typically an overestimation, in the assumed constraint on the sparticle mass (see for example [66]). Only on a case-by-case basis can it be determined whether the limit of a given simplified model represents a good approximation of the true underlying constraint that can be applied on a sparticle mass in a complex SUSY spectrum. In the following, we will point out explicitly the assumptions that have entered the limits when quoting interpretations from simplified models.

This review covers results up to September 2019 and since none of the searches performed so far have shown significant excess above the SM background prediction, the interpretation of the presented results are exclusion limits on SUSY parameter space. Unless stated differently, all quoted exclusion limits are at 95% confidence level.

90.4 Exclusion limits on gluino and squark masses

Gluinos and squarks are the SUSY partners of gluons and quarks, and thus carry color charge. Limits on squark masses of the order 100 GeV have been set by the LEP experiments [67], in the decay to quark plus neutralino, and for a mass difference between squark and quark plus neutralino of typically at least a few GeV. However, due to the colored production of these particles at hadron colliders (see e.g. Fig. 90.1), hadron collider experiments are able to set much tighter mass limits.

Pair production of these massive colored sparticles at hadron colliders usually involve both the s-channel and t-channel parton-parton interactions. Since there is a negligible amount of bottom and top quark content in the proton, top- and bottom squark production proceeds through s-channel diagrams only. In the past, experimental analyses of squark and/or gluino production typically assumed the first and second generation squarks to be approximately degenerate in mass. However, in order to have even less model dependent interpretations of the searches, the experiments have started to also provide simplified model limits on individual first or second generation squarks.

Assuming R-parity conservation and assuming gluinos to be heavier than squarks, squarks will predominantly decay to a quark and a neutralino or chargino, if kinematically allowed. The de-

cay may involve the lightest neutralino (typically the LSP) or chargino, but, depending on the masses and couplings of the gauginos, may involve heavier neutralinos or charginos. For pair production of first and second generation squarks, the simplest decay modes involve two jets and missing momentum, with potential extra jets stemming from initial state or final state radiation (ISR/FSR) or from decay modes with longer decay chains (cascades). Similarly, gluino pair production leads to four jets and missing momentum, and possibly additional jets from ISR/FSR or cascades. Associated production of a gluino and a (anti-)squark is also possible, in particular if squarks and gluinos have similar masses, typically leading to three or more jets in the final state. In cascades, isolated photons or leptons may appear from the decays of sparticles such as neutralinos or charginos. Final states are thus characterized by significant missing transverse momentum, and at least two, and possibly many more high p_T jets, which can be accompanied by one or more isolated objects like photons or leptons, including τ leptons, in the final state. Table 90.1 shows a schematic overview of characteristic final state signatures of gluino and squark production for different mass hierarchy hypotheses and assuming decays involving the lightest neutralino.

Table 90.1: Typical search signatures at hadron colliders for direct gluino and first- and second-generation squark production assuming different mass hierarchies.

Mass Hierarchy	Main Production	Dominant Decay	Typical Signature
$m_{\tilde{q}} \ll m_{\tilde{g}}$	$\tilde{q}\tilde{q}, \tilde{q}\tilde{q}$	$\tilde{q} \rightarrow q\tilde{\chi}_1^0$	≥ 2 jets + E_T^{miss} + X
$m_{\tilde{q}} \approx m_{\tilde{g}}$	$\tilde{q}\tilde{q}, \tilde{q}\tilde{g}$	$\tilde{q} \rightarrow q\tilde{\chi}_1^0$ $\tilde{g} \rightarrow q\tilde{q}\tilde{\chi}_1^0$	≥ 3 jets + E_T^{miss} + X
$m_{\tilde{q}} \gg m_{\tilde{g}}$	$\tilde{g}\tilde{g}$	$\tilde{g} \rightarrow q\tilde{q}\tilde{\chi}_1^0$	≥ 4 jets + E_T^{miss} + X

90.4.1 Exclusion limits on the gluino mass

Limits set by the Tevatron experiments on the gluino mass assume the framework of the CMSSM, with $\tan\beta = 5$ (CDF) or $\tan\beta = 3$ (D0), where $\tan\beta$ is the ratio of vacuum expectation values of the Higgs fields for up-type and down-type fermions. Furthermore, $A_0 = 0$ and $\mu < 0$ is assumed, and the resulting lower mass limits are about 310 GeV for all squark masses, or 390 GeV for the case $m_{\tilde{q}} = m_{\tilde{g}}$ [68, 69]. These limits have been superseded by those provided by ATLAS and CMS, and the tightest constraints have been set with up to approximately 140 fb^{-1} of data recorded at the LHC at a center-of-mass energy of 13 TeV.

Limits on the gluino mass have been established in the framework of simplified models. Assuming only gluino pair production, in particular three primary decay chains of the gluino have been

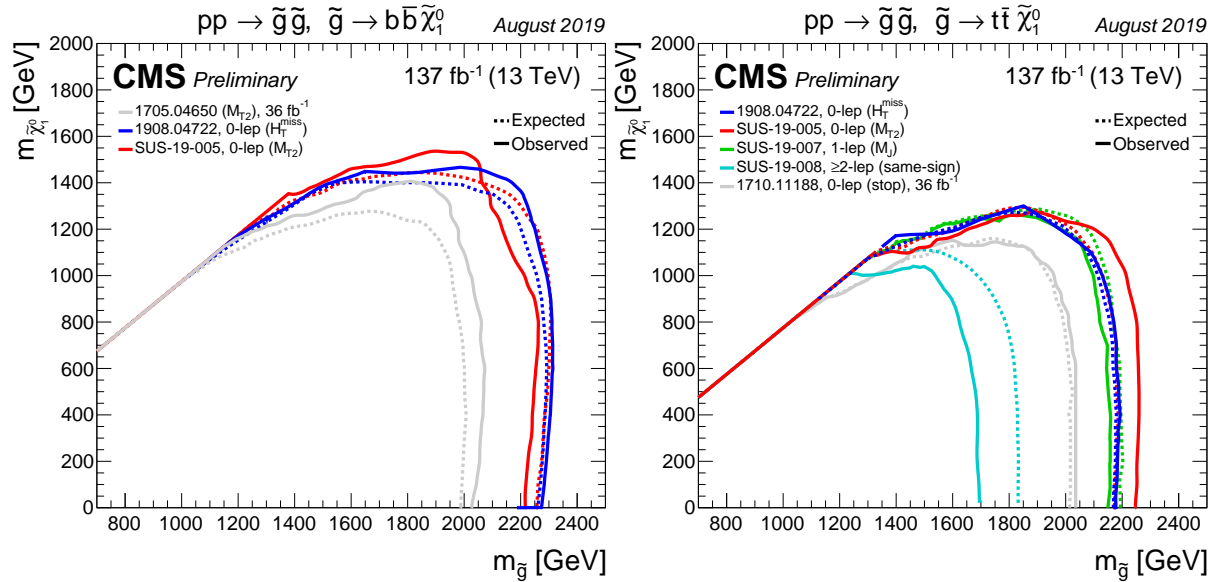


Figure 90.3: Lower mass limits, at 95% C.L., on gluino pair production for various decay chains in the framework of simplified models. Left: $\tilde{g} \rightarrow b\bar{b}\tilde{\chi}_1^0$. Right: $\tilde{g} \rightarrow t\bar{t}\tilde{\chi}_1^0$. Results of the CMS collaboration.

considered by the LHC experiments for interpretations of their search results. The first decay chain $\tilde{g} \rightarrow q\bar{q}\tilde{\chi}_1^0$ assumes gluino mediated production of first and second generation squarks (on-shell or off-shell) which leads to four light flavor quarks in the final state. Therefore, inclusive all-hadronic analyses searching for multijet plus E_T^{miss} final states are utilized to put limits on this simplified model. These limits are derived as a function of the gluino and neutralino (LSP) mass. As shown in Fig. 90.2 (left), using the cross section from next-to-leading order QCD corrections and the resummation of soft gluon emission at next-to-leading-logarithmic accuracy as reference [48], the ATLAS collaboration [70] excludes in this simplified model gluino masses below approximately 2.3 TeV, for a massless neutralino. In scenarios where neutralinos are not very light, the efficiency of the analyses is reduced by the fact that jets are less energetic, and there is less missing transverse momentum in the event. This leads to weaker limits when the mass difference $\Delta m = m_{\tilde{g}} - m_{\tilde{\chi}_1^0}$ is reduced. For example, for neutralino masses above about 1.2 TeV no limit on the gluino mass can be set for this decay chain. Therefore, limits on gluino masses are strongly affected by the assumption of the neutralino mass. Similar results for this simplified model have been obtained by CMS [71].

The second important decay chain of the gluino considered for interpretation in a simplified model is $\tilde{g} \rightarrow b\bar{b}\tilde{\chi}_1^0$. Here the decay is mediated via bottom squarks and thus leads to four jets from b quarks and E_T^{miss} in the final state. Also for this topology inclusive all-hadronic searches provide the highest sensitivity. However, with four b quarks in the final state, the use of secondary vertex reconstruction for the identification of jets originating from b quarks provides a powerful handle on the SM background. Therefore, in addition to a multijet plus E_T^{miss} signature these searches also require several jets to be tagged as b -jets. As shown in Fig. 90.3 (left), for this simplified model CMS [71] excludes gluino masses below ≈ 2.3 TeV for a massless neutralino, while for neutralino masses above ≈ 1.5 TeV no limit on the gluino mass can be set. Comparable limits for this simplified model are provided by searches from ATLAS [72].

Gluino decays are not limited to first and second generation squarks or bottom squarks; if kinematically allowed, decays to top squarks via $\tilde{g} \rightarrow t\bar{t}$ are also possible. This leads to a “four tops” final state $ttt\tilde{\chi}_1^0$ and defines the third important simplified model, $\tilde{g} \rightarrow t\bar{t}\tilde{\chi}_1^0$, characterizing gluino pair production. The topology of this decay is very rich in different experimental signatures: as many as four isolated leptons, four b -jets, several light flavor quark jets, and significant missing momentum from the neu-

trinos in the W decay and from the two neutralinos. As shown in Fig. 90.3 (right), the CMS search based on the m_{T2} variable [73] rules out gluinos with masses below ≈ 2.25 TeV for massless neutralinos in this model. For neutralino masses above ≈ 1.3 TeV, no limit can be placed on the gluino mass. The ATLAS multiple b -jets search [72] obtains similar limits.

The ATLAS collaboration also provides limits in a pMSSM-inspired model with only gluinos and first and second generation squarks, and a bino-like $\tilde{\chi}_1^0$ [70]. As shown in Fig. 90.2 (right), assuming $m_{\tilde{\chi}_1^0} = 995$ GeV, gluinos with masses below ≈ 1.6 TeV are excluded for any squark mass. For $m_{\tilde{q}} \approx m_{\tilde{g}}$, the mass exclusion is about 3.0 TeV. The dependence of these limits on $m_{\tilde{\chi}_1^0}$ is illustrated in Ref. [70]. For massless $\tilde{\chi}_1^0$, gluino masses below 2.2 TeV are excluded for all squark masses.

R-parity violating gluino decays are searched for in a number of final states. Searches in multilepton final states set lower mass limits of 1 to 1.4 TeV, depending on neutralino mass and lepton flavor, on decays mediated by λ and λ' couplings [74–78], assuming prompt decays. Searches for displaced vertices are sensitive to non-prompt decays [79–82]. Multijet final states have been used to search for fully hadronic gluino decays involving λ'' , by CDF [83], ATLAS [79, 84–86] and CMS [87–89]. Lower gluino mass limits range between 600 and 2000 GeV depending on neutralino mass and flavor content of the final state.

90.4.2 Exclusion limits on squark masses

Limits on first and second generation squark masses set by the Tevatron experiments assume the CMSSM, and amount to lower limits of about 380 GeV for all gluino masses, or 390 GeV for the case $m_{\tilde{q}} = m_{\tilde{g}}$ [68, 69].

At the LHC, limits on squark masses have been set using up to approximately 140 fb^{-1} of data at 13 TeV. Interpretations in simplified models typically characterize squark pair production with only one decay chain of $\tilde{q} \rightarrow q\tilde{\chi}_1^0$. Here it is assumed that the left and right-handed \tilde{u} , \tilde{d} , \tilde{s} and \tilde{c} squarks are degenerate in mass. Furthermore, it is assumed that the mass of the gluino is very high and thus contributions of the corresponding t -channel diagrams to squark pair production are negligible. Therefore, the total production cross section for this simplified model is eight times the production cross section of an individual squark (e.g. \tilde{u}_L). Under these assumptions, ATLAS obtains a lower squark mass limit of ≈ 1.9 TeV for light neutralinos [70], as shown in Fig. 90.4 (left). The effects of heavy neutralinos on squark limits are similar to those discussed in the gluino case (see Section 90.4.1), and only for neutralino masses below ≈ 800 GeV can any squark masses

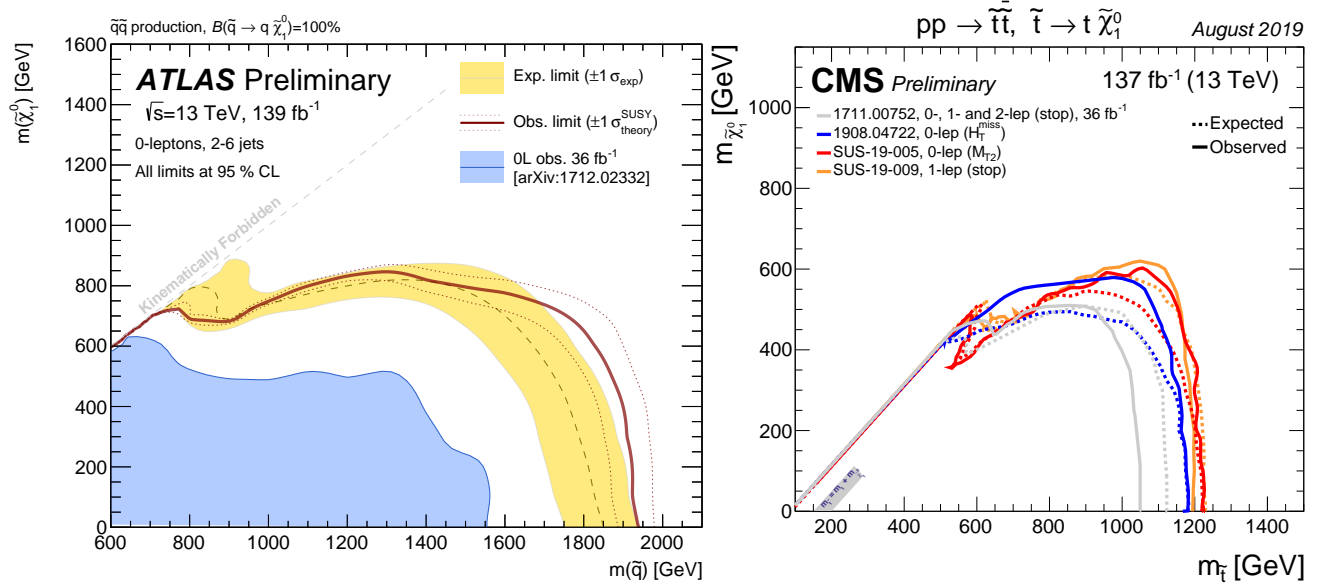


Figure 90.4: Left: 95% C.L. exclusion contours in the squark-neutralino mass plane defined in the framework of simplified models assuming a single decay chain of $\tilde{q} \rightarrow q\tilde{\chi}_1^0$, obtained by ATLAS. Right: the 95% C.L. exclusion contours in the stop-neutralino mass plane defined in the framework of a simplified model assuming a single decay chain of $\tilde{t} \rightarrow t\tilde{\chi}_1^0$ as obtained by CMS.

be excluded.

For the same analysis ATLAS also provides an interpretation of their search result in the aforementioned pMSSM-inspired model with only gluinos and first and second generation squarks, and a bino-like $\tilde{\chi}_1^0$ [70], as shown in Fig. 90.2 (right). In this model, squark production can take place with non-decoupled gluinos, enhancing the squark production cross section through gluino exchange diagrams.

If the assumption of mass degenerate first and second generation squarks is dropped and only the production of a single light squark is assumed, the limits weaken significantly. For example, the CMS limit on degenerate squarks of 1750 GeV for light neutralinos drops to ≈ 1300 GeV for pair production of a single light squark, and for neutralinos heavier than ≈ 600 GeV no squark mass limit can be placed [73]. It should be noted that this limit is not a result of a simple scaling of the above mentioned mass limits assuming eightfold mass degeneracy but it also takes into account that for an eight times lower production cross section the analyses must probe kinematic regions of phase space that are closer to the ones of SM background production. Since signal acceptance and the ratio of expected signal to SM background events of the analyses are typically worse in this region of phase space not only the 1/8 reduction in production cross section but also a worse analysis sensitivity are responsible for the much weaker limit on single squark pair production.

For single light squarks ATLAS also reports results of a dedicated search for pair production of scalar partners of charm quarks [90]. Assuming that the scalar-charm state exclusively decays into a charm quark and a neutralino, scalar-charm masses up to 800 GeV are excluded for neutralino masses below 260 GeV.

Besides placing stringent limits on first and second generation squark masses, the LHC experiments also search for the production of third generation squarks. SUSY at the TeV-scale is often motivated by naturalness arguments, most notably as a solution to cancel quadratic divergences in radiative corrections to the Higgs boson mass. In this context, the most relevant terms for SUSY phenomenology arise from the interplay between the masses of the third generation squarks and the Yukawa coupling of the top quark to the Higgs boson. This motivates a potential constraint on the masses of the top squarks and the left-handed bottom squark. Due to the large top quark mass, significant mixing between \tilde{t}_L and \tilde{t}_R is expected, leading to a lighter mass state \tilde{t}_1 and a heavier mass state \tilde{t}_2 . In the MSSM, the lightest top squark (\tilde{t}_1) can be the lightest squark.

Bottom squarks are expected to decay predominantly to $b\tilde{\chi}_1^0$ giving rise to the characteristic multi b -jet and E_T^{miss} signature. Direct production of bottom squark pairs has been searched for at the Tevatron and at the LHC. Limits from the Tevatron are $m_{\tilde{b}} > 247$ GeV for a massless neutralino [91] [92]. The LHC experiments have surpassed these limits, and the latest results are based on up to 140 fb^{-1} of data collected at $\sqrt{s} = 13$ TeV. CMS has set a lower limit of $m_{\tilde{b}} > \approx 1250$ GeV for massless neutralinos in this model [73]. For $m_{\tilde{\chi}_1^0} \approx 700$ GeV or higher no limit can be placed on direct bottom squark pair production in this simplified model. Limits from ATLAS are comparable [93]. Further bottom squark decay modes have also been searched for by ATLAS [94,95] and CMS [71,76,96].

The top squark decay modes depend on the SUSY mass spectrum, and on the \tilde{t}_L - \tilde{t}_R mixture of the top squark mass eigenstate. If kinematically allowed, the two-body decays $\tilde{t} \rightarrow t\tilde{\chi}_1^0$ (which requires $m_{\tilde{t}} - m_{\tilde{\chi}_1^0} > m_t$) and $\tilde{t} \rightarrow b\tilde{\chi}_1^\pm$ (which requires $m_{\tilde{t}} - m_{\tilde{\chi}_1^\pm} > m_b$) are expected to dominate. If not, the top squark decay may proceed either via the two-body decay $\tilde{t} \rightarrow c\tilde{\chi}_1^0$ or through $\tilde{t} \rightarrow bf\tilde{f}'\tilde{\chi}_1^0$ (where f and \tilde{f}' denote a fermion-antifermion pair with appropriate quantum numbers). For $m_{\tilde{t}} - m_{\tilde{\chi}_1^0} > m_b$ the latter decay chain represents a four-body decay with a W boson, charged Higgs H , slepton $\tilde{\ell}$, or light flavor squark \tilde{q} , exchange. If the exchanged W boson and/or sleptons are kinematically allowed to be on-shell ($(m_{\tilde{t}} - m_{\tilde{\chi}_1^\pm}) > (m_b + m_W)$ and/or $(m_{\tilde{t}} - m_{\tilde{\chi}_1^\pm}) > m_b$), the three-body decays $\tilde{t} \rightarrow Wb\tilde{\chi}_1^0$ and/or $\tilde{t} \rightarrow b\tilde{\ell}\tilde{\chi}_1^0$ will become dominant. For further discussion on top squark decays see for example Ref. [97].

Limits from LEP on the \tilde{t}_1 mass are $m_{\tilde{t}} > 96$ GeV in the charm plus neutralino final state, and > 93 GeV in the lepton, b -quark and sneutrino final state [67].

The Tevatron experiments have performed a number of searches for top squarks, often assuming direct pair production. In the $b\tilde{\nu}$ decay channel, and assuming a 100% branching fraction, limits are set as $m_{\tilde{t}} > 210$ GeV for $m_{\tilde{\nu}} < 110$ GeV and $m_{\tilde{t}} - m_{\tilde{\nu}} > 30$ GeV, or $m_{\tilde{t}} > 235$ GeV for $m_{\tilde{\nu}} < 50$ GeV [98] [99]. In the $\tilde{t} \rightarrow c\tilde{\chi}_1^0$ decay mode, a top squark with a mass below 180 GeV is excluded for a neutralino lighter than 95 GeV [100] [101]. In both analyses, no limits on the top squark can be set for heavy sneutrinos or neutralinos. In the $\tilde{t} \rightarrow b\tilde{\chi}_1^\pm$ decay channel, searches for a relatively light top squark have been performed in the dilepton final state [102] [103]. The CDF experiment sets limits in the $\tilde{t} - \tilde{\chi}_1^0$

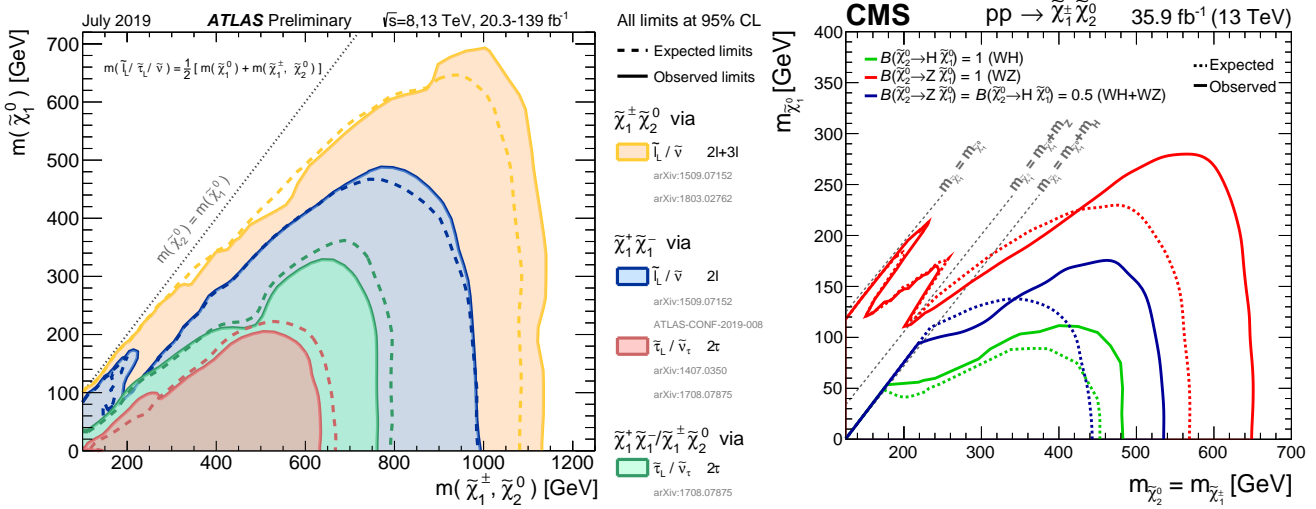


Figure 90.5: LHC exclusion limits on chargino and neutralino masses in a number of simplified models. Left: limits on chargino and neutralino masses for pair production of charginos, pair production of heavier neutralinos, or pair production of chargino and neutralino, under the assumption of light sleptons mediating the decays. Right: limits on chargino and neutralino masses for pair production of chargino and neutralino, under the assumption of decoupled sleptons, and chargino/neutralino decay through W^* , Z^* or H .

mass plane for various branching fractions of the chargino decay to leptons and for two values of $m_{\tilde{\chi}_1^\pm}$. For $m_{\tilde{\chi}_1^\pm} = 105.8$ GeV and $m_{\tilde{\chi}_1^0} = 47.6$ GeV, top squarks between 128 and 135 GeV are excluded for W -like leptonic branching fractions of the chargino.

The LHC experiments have improved these limits substantially. As shown in the right plot of Fig. 90.4, limits on the top squark mass assuming a simplified model with a single decay chain of $\tilde{t} \rightarrow t\tilde{\chi}_1^0$ now surpass 1 TeV. The most important searches for this top squark decay topology are dedicated searches requiring zero or one isolated lepton, modest E_T^{miss} , and four or more jets out of which at least one jet must be reconstructed as a b -jet [71, 73, 104–106]. For example, CMS excludes top squarks with masses below about 1200 GeV in this model for massless neutralinos, while for $m_{\tilde{\chi}_1^0} > 600$ GeV no limits can be provided.

Assuming that the top squark decay exclusively proceeds via the chargino mediated decay chain $\tilde{t} \rightarrow b\tilde{\chi}_1^\pm, \tilde{\chi}_1^\pm \rightarrow W^{\pm(*)}\tilde{\chi}_1^0$ yields stop mass exclusion limits that vary strongly with the assumptions made on the $\tilde{t} - \tilde{\chi}_1^\pm - \tilde{\chi}_1^0$ mass hierarchy. For example, for $m_{\tilde{\chi}_1^\pm} = (m_{\tilde{t}} + m_{\tilde{\chi}_1^0})/2$, a stop mass below ≈ 1150 GeV for a light $\tilde{\chi}_1^0$ is excluded, while no limit can be placed for $m_{\tilde{\chi}_1^0} > 550$ GeV [104]. These limits, however, can weaken significantly when other assumptions about the mass hierarchy or the decay of the charginos are imposed [104, 106–108].

If the decays $\tilde{t} \rightarrow t\tilde{\chi}_1^0$ and $\tilde{t} \rightarrow b\tilde{\chi}_1^\pm, \tilde{\chi}_1^\pm \rightarrow W^{\pm(*)}\tilde{\chi}_1^0$ are kinematically forbidden, the decay chains $\tilde{t} \rightarrow Wb\tilde{\chi}_1^0$ and $\tilde{t} \rightarrow c\tilde{\chi}_1^0$ can become important. The one-lepton ATLAS search provides for the kinematic region $m_{\tilde{t}} - m_{\tilde{\chi}_1^\pm} > m_b + m_W$ lower limits on the top squark mass of ≈ 700 GeV for a neutralino lighter than ≈ 570 GeV [109]. Other analyses with zero, one or two leptons also target this kinematic region [105, 106, 110–114].

For the kinematic region in which even the production of real W bosons is not allowed, ATLAS and CMS improve the Tevatron limit on $\tilde{t} \rightarrow c\tilde{\chi}_1^0$ substantially. Based on a monojet analysis [115] ATLAS excludes top squark masses below $m_{\tilde{\chi}_1^0} \approx 450$ GeV along the kinematic boundary for the $\tilde{t} \rightarrow c\tilde{\chi}_1^0$ decay. A dedicated analysis for $\tilde{t} \rightarrow c\tilde{\chi}_1^0$ excludes stop masses below 500 GeV for $m_{\tilde{\chi}_1^0}$ below 420 GeV [90]. The CMS collaboration uses the hadronic searches [111, 113] to place constraints on this particular stop decay and excludes $m_{\tilde{t}} \approx 550$ GeV for $m_{\tilde{\chi}_1^0}$ below 450 GeV. The exclusion at $m_{\tilde{t}} \approx m_{\tilde{\chi}_1^0}$ is also about 550 GeV.

The other decay chain relevant in this phase region is $\tilde{t} \rightarrow$

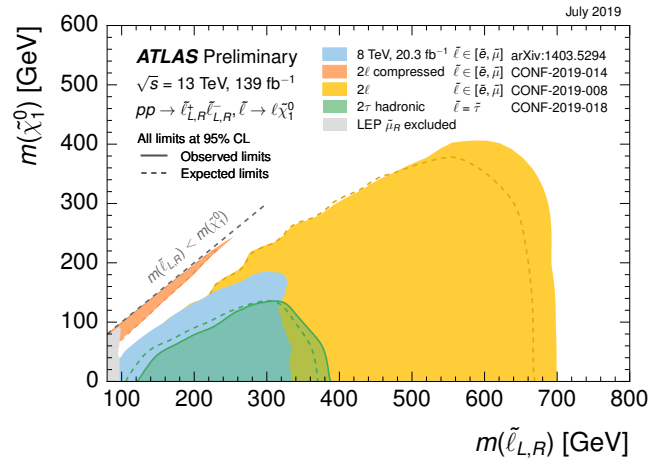


Figure 90.6: LHC exclusion limits on slepton (selectron and smuon) masses, assuming equal masses of selectrons and smuons, degeneracy of $\tilde{\ell}_L$ and $\tilde{\ell}_R$, and a 100% branching fraction for $\tilde{\ell} \rightarrow \ell \tilde{\chi}_1^0$.

$bf\tilde{f}'\tilde{\chi}_1^0$. Here the ATLAS one-lepton [106] and two-lepton [110] searches exclude up to $m_{\tilde{t}} \approx 440$ GeV for $m_{\tilde{\chi}_1^0}$ below 340 GeV, while the monojet analysis [115] excludes at the kinematic boundary top squarks below 400 GeV. As for the $\tilde{t} \rightarrow c\tilde{\chi}_1^0$ decay, CMS uses the zero-lepton searches [111, 113] to also place constraints on $\tilde{t} \rightarrow bf\tilde{f}'\tilde{\chi}_1^0$. Also in this case CMS excludes $m_{\tilde{t}} \approx 550$ GeV for $m_{\tilde{\chi}_1^0}$ below 450 GeV.

In general, the variety of top squark decay chains in the phase space region where $\tilde{t} \rightarrow t\tilde{\chi}_1^0$ is kinematically forbidden represents a challenge for the experimental search program and more data and refined analyses will be required to further improve the sensitivity in this difficult but important region of SUSY parameter space.

R-parity violating production of single squarks via a λ' -type coupling has been studied at HERA. In such models, a lower limit on the squark mass of the order of 275 GeV has been set for electromagnetic-strength-like couplings $\lambda' = 0.3$ [116]. At the LHC, both prompt [75, 78, 117] and non-prompt [80, 118] R-parity violating squark decays have been searched for, but no signal was found. Squark mass limits are very model-dependent.

R-parity violating production of single top squarks has been

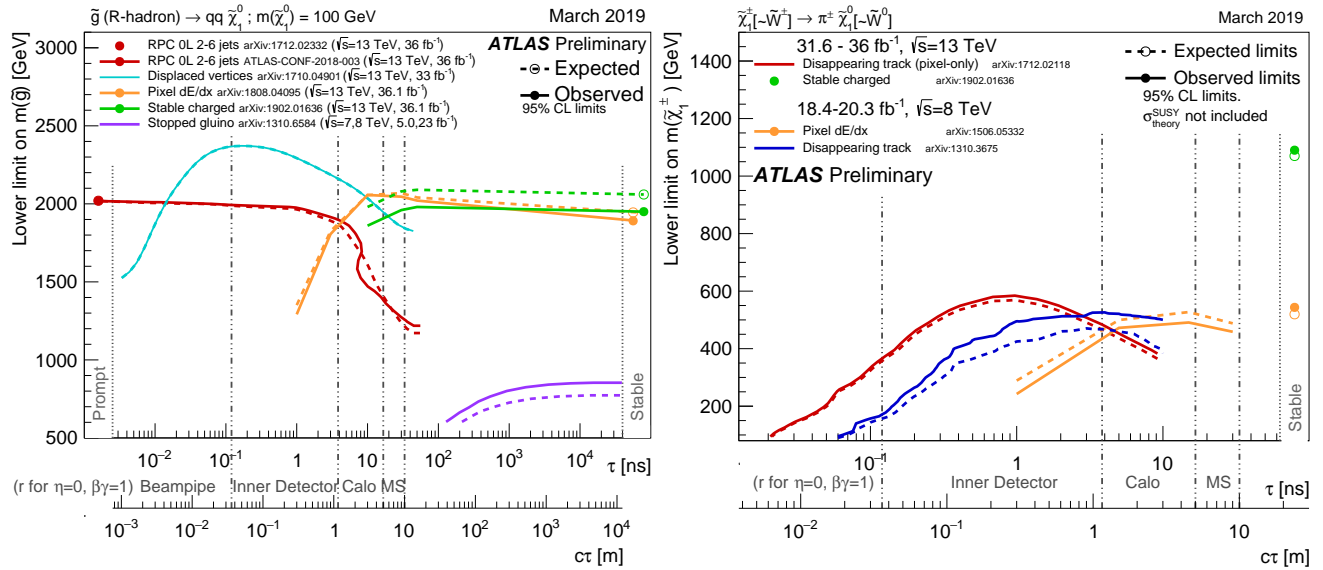


Figure 90.7: Limits at 95% C.L. on the gluino mass in R-hadron models (left), and on the chargino mass in a model where the wino-like chargino is almost degenerate with the LSP (right), as a function of gluino or chargino lifetime, as obtained by ATLAS.

searched for at LEP, HERA, and the Tevatron. For example, an analysis from the ZEUS collaboration [119] makes an interpretation of its search result assuming top squarks to be produced via a λ' coupling and decay either to $b\tilde{\chi}_1^\pm$ or R-parity-violating to a lepton and a jet. Limits are set on λ'_{131} as a function of the top squark mass in an MSSM framework with gaugino mass unification at the GUT scale.

The search for top squark pair production in the context of R-parity violating supersymmetry has now also become a focus point for searches at the LHC. CMS and ATLAS have performed searches for top squarks using a variety of multilepton final states [75, 120]. The λ' -mediated top squark decay $\tilde{t} \rightarrow b\ell$ has been studied by ATLAS for prompt decays [121], and by ATLAS and CMS for non-prompt decays [122–124], setting limits up to 1.4–1.6 TeV in simplified models for this mode. CMS also searched for the λ' -mediated decay $\tilde{t} \rightarrow b\ell q\bar{q}$, setting lower stop mass limits of 890 GeV (e) or 1000 GeV (μ) [125]. The fully hadronic R-parity violating top squark decays $\tilde{t} \rightarrow bs$, $\tilde{t} \rightarrow ds$, and $\tilde{t} \rightarrow bd$, involving λ'' , have been searched for by ATLAS [75, 79, 94, 126], and CMS [127, 128], and lower top squark mass limits up to 610 GeV were set.

It should be noted that limits discussed in this section belong to different top and bottom squark decay channels, different particle mass hierarchies, and different simplified decay scenarios. Therefore, care must be taken when interpreting these limits in the context of more complete SUSY models.

90.4.3 Summary of exclusion limits on squarks and gluinos assuming R-Parity conservation

A summary of the most important squark and gluino mass limits for different interpretation approaches assuming R-parity conservation is shown in Table 90.2.

For gluino masses rather similar limits of about 2.3 TeV are obtained from different model assumptions, indicating that the LHC is indeed probing direct gluino production at the TeV scale and beyond. However, for neutralino masses above approximately 1 to 1.4 TeV, in the best case scenarios, ATLAS and CMS searches do not place any limits on the gluino mass.

Limits on direct squark production, on the other hand, depend strongly on the chosen model. Especially for direct production of top squarks there are still large regions in parameter space where masses below 1 TeV cannot be excluded. This is also true for first and second generation squarks when only one single squark is considered. Furthermore, for neutralino masses above ≈ 500 GeV no limits on any direct squark production scenario are placed by the LHC.

90.5 Exclusion limits on the masses of charginos and neutralinos

Charginos and neutralinos result from mixing of the charged wino and higgsino states, and the neutral bino, wino and higgsino states, respectively. The mixing is determined by a limited number of parameters. For charginos these are the wino mass parameter M_2 , the higgsino mass parameter μ , and $\tan\beta$, and for neutralinos these are the same parameters plus the bino mass parameter M_1 . If any of the parameters M_1 , M_2 or μ happened to be substantially smaller than the others, the chargino/neutralino composition would be dominated by specific states, which are referred to as bino-like ($M_1 \ll M_2, \mu$), wino-like ($M_2 \ll M_1, \mu$), or higgsino-like ($\mu \ll M_1, M_2$). If gaugino mass unification at the GUT scale is assumed, a relation between M_1 and M_2 at the electroweak scale follows: $M_1 = 5/3 \tan^2\theta_W M_2 \approx 0.5M_2$, with θ_W the weak mixing angle. Charginos and neutralinos carry no color charge.

90.5.1 Exclusion limits on chargino masses

If kinematically allowed, two body decay modes such as $\tilde{\chi}^\pm \rightarrow \tilde{f}\tilde{f}'$ (including $\ell\tilde{\nu}$ and $\tilde{\ell}\nu$) are dominant. If not, three body decays $\tilde{\chi}^\pm \rightarrow f\tilde{f}'\tilde{\chi}^0$, mediated through virtual W bosons or sfermions, become dominant. If sfermions are heavy, the W mediation dominates, and $f\tilde{f}'$ are distributed with branching fractions similar to W decay products (barring phase space effects for small mass gaps between $\tilde{\chi}^\pm$ and $\tilde{\chi}^0$). If, on the other hand, sleptons are light enough to play a significant role in the decay, leptonic final states will be enhanced.

At LEP, charginos have been searched for in fully-hadronic, semi-leptonic and fully leptonic decay modes [129] [130]. A general lower limit on the lightest chargino mass of 103.5 GeV is derived, except in corners of phase space with low electron sneutrino mass, where destructive interference in chargino production, or two-body decay modes, play a role. The limit is also affected if the mass difference between $\tilde{\chi}_1^\pm$ and $\tilde{\chi}_1^0$ is small; dedicated searches for such scenarios set a lower limit of 92 GeV.

At the Tevatron, charginos have been searched for via associated production of $\tilde{\chi}_1^\pm \tilde{\chi}_2^0$ [131] [132]. Decay modes involving multilepton final states provide the best discrimination against the large multijet background. Analyses have looked for at least three charged isolated leptons, for two leptons with missing transverse momentum, or for two leptons with the same charge. Depending on the $(\tilde{\chi}_1^\pm - \tilde{\chi}_1^0)$ and/or $(\tilde{\chi}_2^0 - \tilde{\chi}_1^0)$ mass differences, leptons may be soft.

At the LHC, the search strategy is similar to that at the Teva-

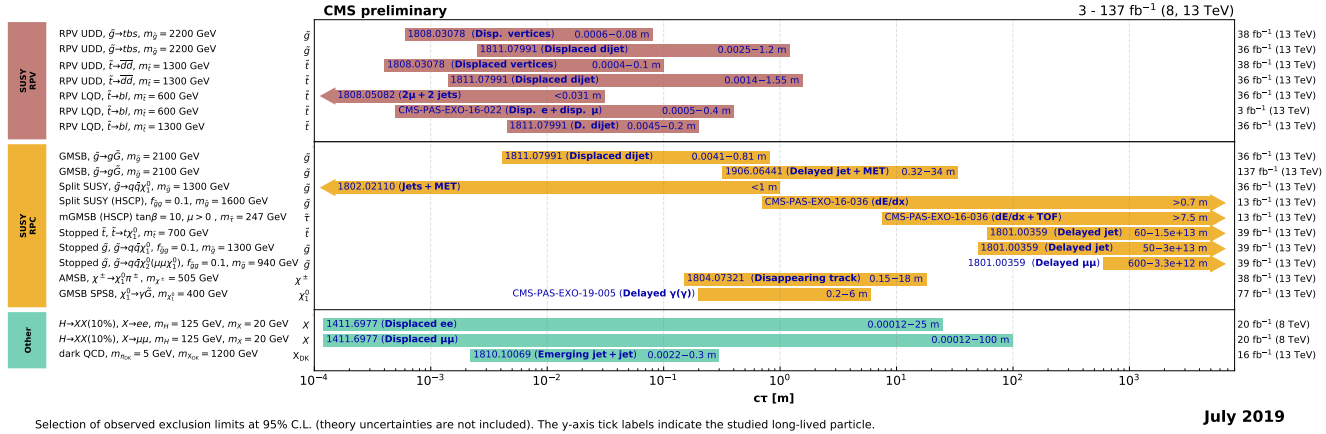


Figure 90.8: Excluded regions, at 95% C.L., in the lifetimes of long-lived particles in several models, as obtained by CMS.

Table 90.2: Summary of squark mass and gluino mass limits using different interpretation approaches assuming R-parity conservation. Masses in this table are provided in GeV. Further details about the assumptions and analyses from which these limits are obtained are discussed in the corresponding sections of the text.

Model	Assumption	$m_{\tilde{q}}$	$m_{\tilde{g}}$
Simplified model $\tilde{g}\tilde{q}, \tilde{g}\tilde{\bar{q}}$	$m_{\tilde{\chi}_1^0} = 0, m_{\tilde{q}} \approx m_{\tilde{g}}$	≈ 3000	≈ 3000
	$m_{\tilde{\chi}_1^0} = 0, \text{ all } m_{\tilde{q}}$	-	≈ 2200
	$m_{\tilde{\chi}_1^0} = 0, \text{ all } m_{\tilde{g}}$	≈ 2600	-
Simplified models $\tilde{g}\tilde{g}$			
$\tilde{g} \rightarrow q\tilde{q}\tilde{\chi}_1^0$	$m_{\tilde{\chi}_1^0} = 0$	-	≈ 2300
	$m_{\tilde{\chi}_1^0} > \approx 1200$	-	no limit
$\tilde{g} \rightarrow b\tilde{b}\tilde{\chi}_1^0$	$m_{\tilde{\chi}_1^0} = 0$	-	≈ 2300
	$m_{\tilde{\chi}_1^0} > \approx 1500$	-	no limit
$\tilde{g} \rightarrow t\tilde{t}\tilde{\chi}_1^0$	$m_{\tilde{\chi}_1^0} = 0$	-	≈ 2250
	$m_{\tilde{\chi}_1^0} > \approx 1300$	-	no limit
Simplified models $\tilde{q}\tilde{q}$			
$\tilde{q} \rightarrow q\tilde{\chi}_1^0$	$m_{\tilde{\chi}_1^0} = 0$	≈ 1900	-
	$m_{\tilde{\chi}_1^0} > \approx 800$	no limit	-
$\tilde{u}_L \rightarrow q\tilde{\chi}_1^0$	$m_{\tilde{\chi}_1^0} = 0$	≈ 1300	-
	$m_{\tilde{\chi}_1^0} > \approx 600$	no limit	-
$\tilde{b} \rightarrow b\tilde{\chi}_1^0$	$m_{\tilde{\chi}_1^0} = 0$	≈ 1250	-
	$m_{\tilde{\chi}_1^0} > \approx 700$	no limit	-
$\tilde{t} \rightarrow t\tilde{\chi}_1^0$	$m_{\tilde{\chi}_1^0} = 0$	≈ 1200	-
	$m_{\tilde{\chi}_1^0} > \approx 600$	no limit	-
$\tilde{t} \rightarrow b\tilde{\chi}_1^\pm$	$m_{\tilde{\chi}_1^0} = 0$	≈ 1150	-
	$m_{\tilde{\chi}_1^0} > \approx 550$	no limit	-
$(m_{\tilde{\chi}_1^\pm} = (m_{\tilde{t}} - m_{\tilde{\chi}_1^0})/2)$	$m_{\tilde{\chi}_1^0} < \approx 570$	≈ 700	-
$(m_W < m_{\tilde{t}} - m_{\tilde{\chi}_1^0} < m_t)$	$\tilde{t} \rightarrow Wb\tilde{\chi}_1^0$	$m_{\tilde{\chi}_1^0} < \approx 450$	≈ 550
	$\tilde{t} \rightarrow c\tilde{\chi}_1^0$	$m_{\tilde{t}} \approx m_{\tilde{\chi}_1^0}$	≈ 550
	$\tilde{t} \rightarrow bff'\tilde{\chi}_1^0$	$m_{\tilde{\chi}_1^0} < \approx 450$	≈ 550
	$(m_{\tilde{t}} - m_{\tilde{\chi}_1^0} < m_W)$	$m_{\tilde{t}} \approx m_{\tilde{\chi}_1^0}$	≈ 550

tron. As shown in Fig. 90.1, the cross section of pair production of electroweak gauginos at the LHC, for masses of several hundreds of GeV, is at least two orders of magnitude smaller than for colored SUSY particles (e.g. top squark pair production). For this reason a large data sample is required to improve the sensitivity

of LEP and Tevatron searches for direct chargino/neutralino production. With the full LHC Run 1 and Run 2 data sets, ATLAS and CMS have surpassed the limits from LEP and Tevatron in regions of SUSY parameter space.

Chargino pair production is searched for in the dilepton plus missing momentum final state. In a simplified model interpretation of the results, assuming mediation of the chargino decay by light sleptons (\tilde{e} and $\tilde{\mu}$), ATLAS [133] and CMS [134] set limits on the chargino mass up to 1 TeV for massless LSPs, but no limits on the chargino mass can be set for $\tilde{\chi}_1^0$ heavier than 480 GeV. Limits are fairly robust against variation of the slepton mass, unless the mass gap between chargino and slepton becomes small. For decays mediated through $\tilde{\tau}$ or $\tilde{\nu}_\tau$, limits of 630 GeV are set by ATLAS [135] for LSPs not heavier than 200 GeV. The CMS experiment provides similar limits [136]. ATLAS also sets limits on charginos decaying via a W boson [133]: chargino masses below 420 GeV are excluded for massless LSPs, but no limits are set for LSPs heavier than 120 GeV.

The trilepton plus missing momentum final state is used to set limits on $\tilde{\chi}_1^\pm \tilde{\chi}_2^0$ production, assuming wino-like $\tilde{\chi}_1^\pm$ and bino-like $\tilde{\chi}_2^0$, and $m_{\tilde{\chi}_1^\pm} = m_{\tilde{\chi}_2^0}$, leaving $m_{\tilde{\chi}_1^\pm}$ and $m_{\tilde{\chi}_1^0}$ free. Again, the branching fraction of leptonic final states is determined by the slepton masses. If the decay is predominantly mediated by a light $\tilde{\ell}_L$, i.e. $\tilde{\ell}_R$ is assumed to be heavy, the three charged-lepton flavors will be produced in equal amounts. It is assumed that $\tilde{\ell}_L$ and sneutrino masses are equal, and diagrams with sneutrinos are included. In this scenario, ATLAS [137] and CMS [138] exclude chargino masses below 1140 GeV for massless LSPs; no limits are set for LSP masses above 700 GeV. If the decay is dominated by a light $\tilde{\ell}_R$, the chargino cannot be a pure wino but needs to have a large higgsino component, preferring the decays to tau leptons. Limits are set in various scenarios. If, like for $\tilde{\ell}_L$, a flavor-democratic scenario is assumed, CMS sets limits of 1060 GeV on the chargino mass for massless LSPs, but under the assumption that both $\tilde{\chi}_1^\pm$ and $\tilde{\chi}_2^0$ decay leads to tau leptons in the final state, the chargino mass limit deteriorates to 620 GeV for massless LSPs [138]. ATLAS assumes a simplified model in which staus are significantly lighter than the other sleptons in order to search for a similar multi-tau final state, and sets a lower limit on the chargino mass of 760 GeV in this model [135]. The CMS experiment provides similar limits [136].

If sleptons are heavy, the chargino is assumed to decay to a W boson plus LSP, and the $\tilde{\chi}_2^0$ into Z plus LSP or H plus LSP. In the WZ channel, ATLAS [137, 139] and CMS [140] limits on the chargino mass reach 650 GeV for massless LSPs, but no limits are set for LSPs heavier than 300 GeV. In the WH channel, for $m_H = 125$ GeV and using various Higgs decay modes, ATLAS [141–143] and CMS [140] set lower limits on the chargino mass up to 740 GeV for massless LSPs, but vanish for LSP masses above 240 GeV.

The results on electroweak gaugino searches interpreted in sim-

plified models are summarized in Fig. 90.5 for the two cases of light or decoupled sleptons. For both cases, ATLAS and CMS have comparable limits.

In both the wino region (a characteristic of anomaly-mediated SUSY breaking models) and the higgsino region of the MSSM, the mass splitting between $\tilde{\chi}_1^\pm$ and $\tilde{\chi}_1^0$ is small. The chargino decay products are very soft and may escape detection. These compressed spectra are hard to detect, and have triggered dedicated search strategies. ATLAS has performed a search for charginos and neutralinos in a compressed mass spectrum using initial state radiation [144]. For wino-like charginos, assuming degenerate $\tilde{\chi}_1^\pm$ and $\tilde{\chi}_2^0$, exclusion contours in the chargino-mass versus $\Delta m(\tilde{\chi}_1^\pm - \tilde{\chi}_1^0)$ plane are derived. As an example, such charginos are excluded below 200 GeV for $\Delta m(\tilde{\chi}_1^\pm - \tilde{\chi}_1^0) = 10$ GeV. CMS has searched for chargino-pair production through vector-boson-fusion [145], also targetting compressed mass spectra. Assuming degenerate $\tilde{\chi}_1^\pm$ and $\tilde{\chi}_2^0$, charginos with a mass below 112 GeV are excluded for $\Delta m(\tilde{\chi}_1^\pm - \tilde{\chi}_1^0) = 1$ GeV. CMS has published further searches for such compressed spectra with soft leptons [146] or a soft tau lepton [147].

90.5.2 Exclusion limits on neutralino masses

In a considerable part of the MSSM parameter space, and in particular when demanding that the LSP carries no electric or color charge, the lightest neutralino $\tilde{\chi}_1^0$ is the LSP. If R-parity is conserved, such a $\tilde{\chi}_1^0$ is stable. Since it is weakly interacting, it will typically escape detectors unseen. Limits on the invisible width of the Z boson apply to neutralinos with a mass below 45.5 GeV, but depend on the Z -neutralino coupling. Such a coupling could be small or even absent; in such a scenario there is no general lower limit on the mass of the lightest neutralino [148]. In models with gaugino mass unification and sfermion mass unification at the GUT scale, a lower limit on the neutralino mass is derived from limits from direct searches, notably for charginos and sleptons, and amounts to 47 GeV [149]. Assuming a constrained model like the CMSSM, this limit increases to 50 GeV at LEP; however the strong constraints now set by the LHC increase such CMSSM-derived $\tilde{\chi}_1^0$ mass limits to well above 200 GeV [150–152].

In gauge-mediated SUSY breaking models (GMSB), the LSP is typically a gravitino, and the phenomenology is determined by the nature of the next-to-lightest supersymmetric particle (NLSP). A NLSP neutralino will decay to a gravitino and a SM particle whose nature is determined by the neutralino composition. Final states with two high p_T photons and missing momentum are searched for, and interpreted in gauge mediation models with bino-like neutralinos [153–158].

Assuming the production of at least two neutralinos per event, neutralinos with large non-bino components can also be searched for by their decay in final states with missing momentum plus any two bosons out of the collection γ, Z, H . A number of searches at the LHC have tried to cover the rich phenomenology of the various Z and H decay modes [74, 96, 138, 140, 142, 156, 159–165].

Heavier neutralinos, in particular $\tilde{\chi}_2^0$, have been searched for in their decays to the lightest neutralino plus a γ , a Z boson or a Higgs boson. Limits on electroweak production of $\tilde{\chi}_2^0$ plus $\tilde{\chi}_1^\pm$ from trilepton analyses have been discussed in the section on charginos; the assumption of equal mass of $\tilde{\chi}_2^0$ and $\tilde{\chi}_1^\pm$ make the limits on chargino masses apply to $\tilde{\chi}_2^0$ as well. Multilepton analyses have also been used to set limits on $\tilde{\chi}_2^0\tilde{\chi}_3^0$ production; assuming equal mass and decay through light sleptons, limits are set up to 680 GeV for massless LSPs [166]. Again, compressed spectra with small mass differences between the heavier neutralinos and the LSP form the most challenging region.

In $\tilde{\chi}_2^0$ decays to $\tilde{\chi}_1^0$ and a lepton pair, the lepton pair invariant mass distribution may show a structure that can be used to measure the $\tilde{\chi}_2^0 - \tilde{\chi}_1^0$ mass difference in case of a signal [35]. This structure, however, can also be used in the search strategy itself, as demonstrated by ATLAS [167, 168] and CMS [96, 169].

In models with R-parity violation, the lightest neutralino can decay even if it is the lightest supersymmetric particle. If the decay involves a non-zero λ coupling, the final state will be a

Table 90.3: Summary of weak gaugino mass limits in simplified models, assuming R-parity conservation. Masses in the table are provided in GeV. Further details about assumptions and analyses from which these limits are obtained are discussed in the text.

Assumption	m_χ
$\tilde{\chi}_1^\pm$, all $\Delta m(\tilde{\chi}_1^\pm, \tilde{\chi}_1^0)$	> 92
$\tilde{\chi}_1^\pm$ $\Delta m > 5$, $m_{\tilde{\nu}} > 300$	> 103.5
$\tilde{\chi}_1^\pm$, $m_{(\tilde{\ell}, \tilde{\nu})} = (m_{\tilde{\chi}_1^\pm} + m_{\tilde{\chi}_1^0})/2$	
$m_{\tilde{\chi}_1^0} \approx 0$	> 1000
$\tilde{\chi}_1^\pm$, $m_{\tilde{\chi}_1^0} > 480$	no LHC limit
$\tilde{\chi}_1^\pm$, $m_{\tilde{\ell}} > m_{\tilde{\chi}_1^\pm}$	
$m_{\tilde{\chi}_1^0} \approx 0$	> 420
$\tilde{\chi}_1^\pm$, $m_{\tilde{\chi}_1^0} > 120$	no LHC limit
$m_{\tilde{\chi}_1^\pm} = m_{\tilde{\chi}_2^0}$, $m_{\tilde{\ell}_L} = (m_{\tilde{\chi}_1^\pm} + m_{\tilde{\chi}_1^0})/2$	
$m_{\tilde{\chi}_1^0} \approx 0$	> 1140
$m_{\tilde{\chi}_1^0} > 700$	no LHC limit
$m_{\tilde{\chi}_1^\pm} = m_{\tilde{\chi}_2^0}$, $m_{\tilde{\ell}_R} = (m_{\tilde{\chi}_1^\pm} + m_{\tilde{\chi}_1^0})/2$	flavor-democratic
$m_{\tilde{\chi}_1^0} \approx 0$	> 1060
$m_{\tilde{\chi}_1^0} > 600$	no LHC limit
$m_{\tilde{\chi}_1^\pm} = m_{\tilde{\chi}_2^0}$, $m_{\tilde{\tau}} = (m_{\tilde{\chi}_1^\pm} + m_{\tilde{\chi}_1^0})/2$	$\tilde{\tau}$ -dominated
$m_{\tilde{\chi}_1^0} \approx 0$	> 620
$m_{\tilde{\chi}_1^0} > 260$	no LHC limit
$m_{\tilde{\chi}_1^\pm} = m_{\tilde{\chi}_2^0}$, $m_{\tilde{\ell}} > m_{\tilde{\chi}_1^\pm}$, $\text{BF}(WZ) = 1$	
$m_{\tilde{\chi}_1^0} \approx 0$	> 650
$m_{\tilde{\chi}_1^0} > 300$	no LHC limit
$m_{\tilde{\chi}_1^\pm} = m_{\tilde{\chi}_2^0}$, $m_{\tilde{\ell}} > m_{\tilde{\chi}_1^\pm}$, $\text{BF}(WH) = 1$	
$m_{\tilde{\chi}_1^0} \approx 0$	> 740
$m_{\tilde{\chi}_1^0} > 240$	no LHC limit

multi-lepton one. Searches for events with four or more isolated charged leptons by ATLAS [74] and CMS [78] are interpreted in such models. With very small coupling values, the neutralino would be long-lived, leading to lepton pairs with a displaced vertex, which have also been searched for [118, 124, 170].

Various searches, including searches for multi-lepton and lepton plus jets events, and searches for events with a displaced hadronic vertex, with or without a matched lepton, are interpreted in a model with R-parity violating neutralino decays involving a non-zero λ' coupling [75, 80, 86, 171]. Neutralino decays involving non-zero λ'' lead to fully hadronic final states, and searches for multi-jet events and jet-pair resonances are used to set limits, typically on the production of colored particles like top squarks or gluinos, which are assumed to be the primary produced sparticles in these interpretations, as discussed earlier [79, 84, 86].

The limits on weak gauginos in simplified models are summarized in Table 90.3. Interpretations of the search results outside simplified models, such as in the phenomenological MSSM [172–176], show that the simplified model limits must be interpreted with care. Electroweak gauginos in models that are compatible with the relic density of dark matter in the universe, for example, have particularly tuned mixing parameters and mass spectra, which are not always captured by the simplified models used.

90.6 Exclusion limits on slepton masses

In models with slepton and gaugino mass unification at the GUT scale, the right-handed slepton, $\tilde{\ell}_R$, is expected to be lighter than the left-handed slepton, $\tilde{\ell}_L$. For tau sleptons there may be considerable mixing between the L and R states, leading to a significant mass difference between the lighter $\tilde{\tau}_1$ and the heavier $\tilde{\tau}_2$.

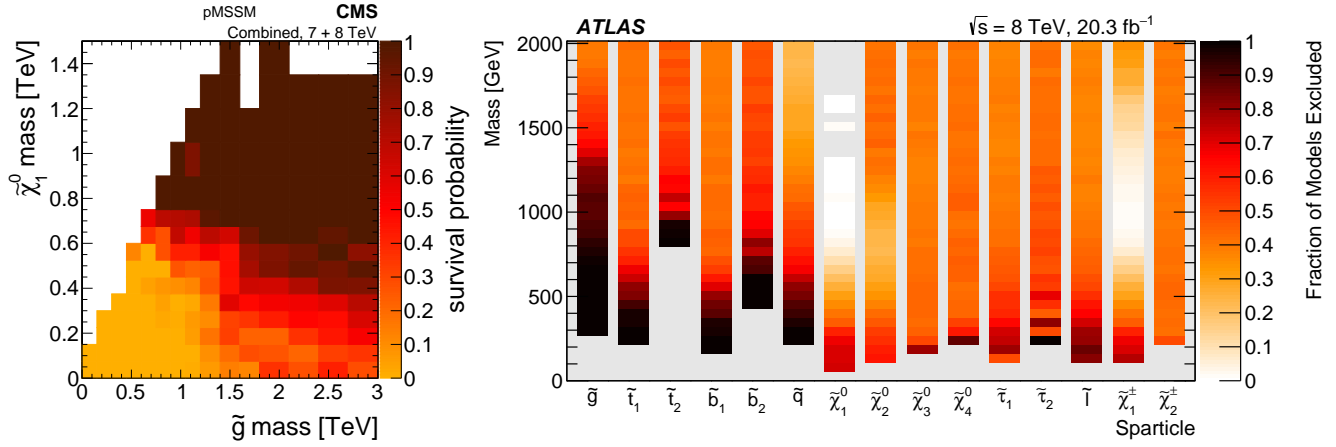


Figure 90.9: The plot on the left shows the survival probability of a pMSSM parameter space model in the gluino-neutralino mass plane after the application of the relevant CMS search results. The plot on the right shows a graphical representation of the ATLAS exclusion power in a pMSSM model. Each vertical bar is a one-dimensional projection of the fraction of models points excluded for each sparticle by ATLAS analyses. The experimental results are obtained from data taken at $\sqrt{s} = 7$ and 8 TeV.

90.6.1 Exclusion limits on the masses of charged sleptons

The most model-independent searches for selectrons, smuons and staus originate from the LEP experiments [177]. Smuon production only takes place via s-channel γ^*/Z exchange. Search results are often quoted for $\tilde{\mu}_R$, since it is typically lighter than $\tilde{\mu}_L$ and has a weaker coupling to the Z boson; limits are therefore conservative. Decays are expected to be dominated by $\tilde{\mu}_R \rightarrow \mu \tilde{\chi}_1^0$, leading to two non-back-to-back muons and missing momentum. Slepton mass limits are calculated in the MSSM under the assumption of gaugino mass unification at the GUT scale, and depend on the mass difference between the smuon and $\tilde{\chi}_1^0$. A $\tilde{\mu}_R$ with a mass below 94 GeV is excluded for $m_{\tilde{\mu}_R} - m_{\tilde{\chi}_1^0} > 10$ GeV. The selectron case is similar to the smuon case, except that an additional production mechanism is provided by t-channel neutralino exchange. The \tilde{e}_R lower mass limit is 100 GeV for $m_{\tilde{\chi}_1^0} < 85$ GeV. Due to the t-channel neutralino exchange, $\tilde{e}_R \tilde{e}_L$ pair production was possible at LEP, and a lower limit of 73 GeV was set on the selectron mass regardless of the neutralino mass by scanning over MSSM parameter space [178]. The potentially large mixing between $\tilde{\tau}_L$ and $\tilde{\tau}_R$ not only makes the $\tilde{\tau}_1$ light, but can also make its coupling to the Z boson small. LEP lower limits on the $\tilde{\tau}$ mass range between 87 and 93 GeV depending on the $\tilde{\chi}_1^0$ mass, for $m_{\tilde{\tau}} - m_{\tilde{\chi}_1^0} > 7$ GeV [177].

At the LHC, pair production of sleptons is not only heavily suppressed with respect to pair production of colored SUSY particles but the cross section is also almost two orders of magnitude smaller than the one of pair production of charginos and neutralinos. With the full data sets of Run 1 and Run 2, however, ATLAS and CMS have surpassed the sensitivity of the LEP analyses under certain assumptions.

Table 90.4: Summary of slepton mass limits from LEP and LHC, assuming R-parity conservation and 100% branching fraction for $\tilde{\ell} \rightarrow \ell \tilde{\chi}_1^0$. Masses in this table are provided in GeV.

Assumption	$m_{\tilde{\ell}}$
$\tilde{\mu}_R, \Delta m(\tilde{\mu}_R, \tilde{\chi}_1^0) > 10$	> 94
$\tilde{e}_R, \Delta m(\tilde{e}_R, \tilde{\chi}_1^0) > 10$	> 94
$\tilde{e}_R, \text{any } \Delta m$	> 73
$\tilde{\tau}_R, \Delta m(\tilde{\tau}_R, \tilde{\chi}_1^0) > 7$	> 87
$\tilde{\nu}_e, \Delta m(\tilde{e}_R, \tilde{\chi}_1^0) > 10$	> 94
$m_{\tilde{e}_{L,R}} = m_{\tilde{\mu}_{L,R}}, m_{\tilde{\chi}_1^0} \approx 0$	> 700
$m_{\tilde{\chi}_1^0} \approx 400$	no LHC limit
$m_{\tilde{\tau}_L} = m_{\tilde{\tau}_R}, m_{\tilde{\chi}_1^0} \approx 0$	> 390
$m_{\tilde{\chi}_1^0} \approx 130$	no LHC limit

ATLAS and CMS have searched for direct production of selectron pairs and smuon pairs at the LHC, with each slepton decaying to its corresponding SM partner lepton and the $\tilde{\chi}_1^0$ LSP. In simplified models, ATLAS [133] and CMS [179] set lower mass limits on sleptons of 700 GeV for degenerate $\tilde{\ell}_L$ and $\tilde{\ell}_R$, for a massless $\tilde{\chi}_1^0$ and assuming equal selectron and smuon masses, as shown in Fig. 90.6. The limits deteriorate with increasing $\tilde{\chi}_1^0$ mass due to decreasing missing momentum and lepton momentum. As a consequence, no limits are set for $\tilde{\chi}_1^0$ masses above 400 GeV. Limits are also derived without the assumption of slepton mass degeneracy [133, 179]. A dedicated search for sleptons with small mass difference between $\tilde{\ell}$ and $\tilde{\chi}_1^0$ is performed by ATLAS [144] demanding the presence of ISR jets.

ATLAS and CMS have also searched for $\tilde{\tau}$ -pair production. In simplified models, ATLAS excludes $\tilde{\tau}$ masses between 120 and 390 GeV assuming light $\tilde{\chi}_1^0$, combining the production of degenerate left- and right-handed $\tilde{\tau}$ s [180]. The CMS analysis [181] covers lower masses and closes the mass gap with LEP. No limits are set for $\tilde{\chi}_1^0$ masses above 130 GeV.

In gauge-mediated SUSY breaking models, sleptons can be (co-)NLSPs, *i.e.*, the next-to-lightest SUSY particles and almost degenerate in mass, decaying to a lepton and a gravitino. This decay can either be prompt, or the slepton can have a non-zero lifetime. Combining several analyses, lower mass limits on $\tilde{\mu}_R$ of 96.3 GeV and on \tilde{e}_R of 66 GeV are set for all slepton lifetimes at LEP [182]. In a considerable part of parameter space in these models, the $\tilde{\tau}$ is the NLSP. The LEP experiments have set lower limits on the mass of such a $\tilde{\tau}$ between 87 and 97 GeV, depending on the $\tilde{\tau}$ lifetime. ATLAS and CMS have searched for final states with τ s, jets and missing transverse momentum, and has interpreted the results in GMSB models setting limits on the model parameters [183, 184]. CMS has interpreted a multilepton analysis in terms of limits on gauge mediation models with slepton NLSP [185]. CDF has put limits on gauge mediation models at high $\tan \beta$ and slepton NLSP using an analysis searching for like-charge light leptons and taus [186].

Limits also exist on sleptons in R-parity violating models, both from LEP and the Tevatron experiments. From LEP, lower limits on $\tilde{\mu}_R$ and \tilde{e}_R masses in such models are 97 GeV, and the limits on the stau mass are very close: 96 GeV [187]. CMS has searched for resonant smuon production in a modified CMSSM scenario [188], putting limits on λ_{211}^2 as a function of $m_0, m_{1/2}$.

90.6.2 Exclusion limits on sneutrino masses

The invisible width of the Z boson puts a lower limit on the sneutrino mass of about 45 GeV. Tighter limits are derived from other searches, notably for gauginos and sleptons, under the assumption of gaugino and sfermion mass universality at the GUT scale, and amount to approximately 94 GeV in the MSSM [189].

It is possible that the lightest sneutrino is the LSP; however, a left-handed sneutrino LSP is ruled out as a cold dark matter candidate [190, 191].

Production of pairs of sneutrinos in R-parity violating models has been searched for at LEP [187]. Assuming fully leptonic decays via λ -type couplings, lower mass limits between 85 and 100 GeV are set. At the Tevatron [192, 193] and at the LHC [188, 194–196], searches have focused on scenarios with resonant production of a sneutrino, decaying to $e\mu$, $\mu\tau$ and $e\tau$ final states. No signal has been seen, and limits have been set on sneutrino masses as a function of the value of relevant RPV couplings. As an example, the LHC experiments exclude a resonant tau sneutrino with a mass below 2.3 TeV for $\lambda_{312} = \lambda_{321} > 0.07$ and $\lambda'_{311} > 0.11$.

The limits on sleptons in simplified models are summarized in Table 90.4.

90.7 Exclusion limits on long-lived particles

Long-lived sparticles arise in many different SUSY models. In particular in co-annihilation scenarios, where the NLSP and LSP are nearly mass-degenerate, this is rather common in order to obtain the correct Dark Matter relic density. Prominent examples are scenarios featuring stau co-annihilation, or models of SUSY breaking, e.g. minimal anomaly-mediated SUSY breaking (AMSB), in which the appropriate Dark Matter density is obtained by co-annihilation of the LSP with an almost degenerate long-lived wino. However, in general, also other sparticles can be long-lived and it is desirable to establish a comprehensive search program for these special long-lived cases, which lead to distinct experimental search signatures, including displaced vertices or disappearing tracks, etc.

Past experiments have performed dedicated searches for long-lived SUSY signatures, but given the absence of any experimental evidence for SUSY so far, more effort and focus has gone into such searches at the LHC recently. As for the interpretation of more standard searches for e.g. R-parity conserving SUSY, simplified models are also a convenient tool to benchmark long-lived scenarios (see e.g. [197, 198]).

If the decay of gluinos is suppressed, for example if squark masses are high, gluinos may live longer than typical hadronization times. It is expected that such gluinos will hadronize to long-living strongly interacting particles known as R-hadrons. In particular, if the suppression of the gluino decay is strong, as in the case that the squark masses are much higher than the TeV scale, these R-hadrons can be (semi-)stable in collider timescales. Searches for such R-hadrons exploit the typical signature of stable charged massive particles in the detector. R-hadrons decaying in the detector are searched for using dE/dx measurements and searches for displaced vertices. As shown in the left plot of Fig. 90.7, the ATLAS experiment excludes semi-stable gluino R-hadrons with masses below 1.9 – 2.3 TeV for all lifetimes in a simplified model where such gluinos always form R-hadrons, and decay into jets and a light neutralino, by combining a number of analyses [79, 199–201]. A combination of CMS searches for long-lived particles, as shown in Fig. 90.8, reaches similar limits [82, 202–204].

Alternatively, since such R-hadrons are strongly interacting, they may be stopped in the calorimeter or in other material, and decay later into energetic jets. These decays are searched for by identifying the jets [205–207] or muons [207] outside the time window associated with bunch-bunch collisions. As shown in Fig. 90.8, the CMS collaboration sets limits on such stopped R-hadrons over 13 orders of magnitude in gluino lifetime, up to masses of 1390 GeV [207].

Top squarks can also be long-lived and hadronize to a R-hadron, for example in the scenario where the top squark is the next-to-lightest SUSY particle (NLSP), with a small mass difference to the LSP. Searches for massive stable charged particles are sensitive to such top squarks. Tevatron limits are approximately $m_{\tilde{t}} > 300$ GeV [208, 209]. ATLAS sets a limit of 1340 GeV on such top squarks [200], the CMS limits are comparable [204].

In addition to colored sparticles, also sparticles like charginos may be long-lived, especially in scenarios with compressed mass spectra. Charginos decaying in the detectors away from the pri-

mary vertex could lead to signatures such as kinked-tracks, or apparently disappearing tracks, since, for example, the pion in $\tilde{\chi}_1^\pm \rightarrow \pi^\pm \tilde{\chi}_1^0$ might be too soft to be reconstructed. At the LHC, searches have been performed for such disappearing tracks, and interpreted within anomaly-mediated SUSY breaking models [210–212]. The right plot of Fig. 90.7 shows constraints for different ATLAS searches on the chargino mass-vs-lifetime plane for an AMSB model ($\tan\beta = 5$, $\mu > 0$) in which a wino-like $\tilde{\chi}^\pm$ decays to a soft pion and an almost mass-degenerated wino-like $\tilde{\chi}_1^0$ [200, 201, 211, 212]. For a similar model, CMS excludes $c\tau$ values between 0.15 and 18 m for a chargino mass of 505 GeV [210], see Fig. 90.8. Charginos with a lifetime longer than the time needed to pass through the detector appear as charged stable massive particles. Limits have been derived by the LEP experiments [213], by D0 at the Tevatron [209], and by the LHC experiments [200, 214], and such charginos with mass below 1090 GeV are excluded.

In gauge mediation models, NLSP neutralino decays need not be prompt, and experiments have searched for late decays with photons in the final state. CDF have searched for delayed $\tilde{\chi}_1^0 \rightarrow \gamma\tilde{G}$ decays using the timing of photon signals in the calorimeter [215]. CMS has used the same technique at the LHC [216]. Results are given as exclusion contours in the neutralino mass versus lifetime plane, and for example in a GMSB model with a neutralino mass of 300 GeV, $c\tau$ values between 10 and 2000 cm are excluded [216]. D0 has looked at the direction of showers in the electromagnetic calorimeter with a similar goal [217], and ATLAS has searched for photon candidates that do not point back to the primary vertex, as well as for delayed photons [218].

Charged slepton decays may be kinematically suppressed, for example in the scenario of a NLSP slepton with a very small mass difference to the LSP. Such a slepton may appear to be a stable charged massive particle. Interpretation of searches at LEP for such signatures within GMSB models with stau NLSP or slepton co-NLSP exclude masses up to 99 GeV [213]. Searches of stable charged particles at the Tevatron [208, 209] and at the LHC [200, 204] are also interpreted in terms of limits on stable charged sleptons. The limits obtained at the LHC exclude stable staus with masses below 430 GeV when produced directly in pairs, and below 660 GeV when staus are produced both directly and indirectly in the decay of other particles in a GMSB model.

90.8 Global interpretations

Apart from the interpretation of direct searches for sparticle production at colliders in terms of limits on masses of individual SUSY particles, model-dependent interpretations of allowed SUSY parameter space are derived from global SUSY fits. Typically these fits combine the results from collider experiments with indirect constraints on SUSY as obtained from low-energy experiments, flavor physics, high-precision electroweak results, and astrophysical data.

In the pre-LHC era these fits were mainly dominated by indirect constraints. Even for very constrained models like the CMSSM, the allowed parameter space, in terms of squark and gluino masses, ranged from several hundreds of GeV to a few TeV. Furthermore, these global fits indicated that squarks and gluino masses in the range of 500 to 1000 GeV were the preferred region of parameter space, although values as high as few TeV were allowed with lower probabilities [219–226].

With ATLAS and CMS now probing mass scales around 1 TeV and beyond, the importance of the direct searches for global analyses of allowed SUSY parameter space has increased. For example, imposing the new experimental limits on constrained supergravity models pushes the most likely values of first generation squark and gluino masses significantly beyond 2 TeV, typically resulting in overall values of fit quality much worse than those in the pre-LHC era [150–152, 174, 227–234]. Also the measured value of m_h pushes the sparticle masses upwards. Although these constrained models are not yet ruled out, the extended experimental limits impose very tight constraints on the allowed parameter space.

For this reason, the emphasis of global SUSY fits has shifted towards less-constrained SUSY models. Especially interpretations in the pMSSM [172–176, 214, 227] but also in simplified models have been useful to generalize SUSY searches, for example to re-

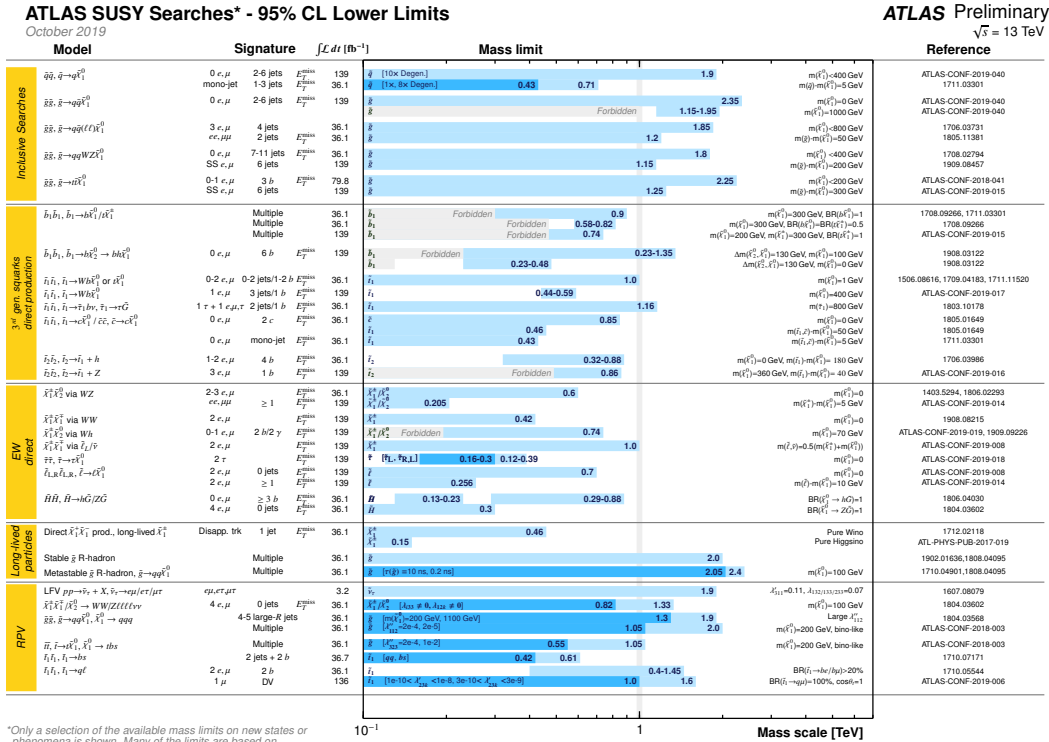


Figure 90.10: Overview of the current landscape of SUSY searches at the LHC. The plot shows exclusion mass limits of ATLAS for different searches and interpretation assumptions. The corresponding results of the CMS experiment are similar.

design experimental analyses in order to increase their sensitivity for compressed spectra, where the mass of the LSP is much closer to squark and gluino masses than predicted, for example, by the CMSSM. As shown in Table 90.2, for neutralino masses above 0.5 – 1 TeV the current set of ATLAS and CMS searches, interpreted in simplified models, cannot exclude the existence of squarks or gluinos with masses only marginally above the neutralino mass. However, as these exclusion limits are defined in the context of simplified models, they are only valid for the assumptions in which these models are defined.

As an alternative approach, both ATLAS [172] and CMS [173] have performed an analysis of the impact of their searches on the parameter space of the pMSSM. Fig. 90.9 shows graphically the LHC exclusion power in the pMSSM based on searches performed at $\sqrt{s} = 7$ and 8 TeV. The plot on the left shows the survival probability in the gluino-neutralino mass plane, which is a measure of the parameter space that remains after inclusion of the relevant CMS search results. As can be seen, gluino masses below about 1.2 TeV are almost fully excluded. This result agrees well with the typical exclusion obtained at 8 TeV in simplified models for gluino production. However, as shown in the right plot of Fig. 90.9, when a similar analysis for other sparticles is performed it becomes apparent that exclusions on the pMSSM parameter can be significantly less stringent than simplified model limits might suggest. This is especially apparent for the electroweak sector, where even at rather low masses several of the pMSSM test points still survive the constraint of ATLAS searches at $\sqrt{s} = 7$ and 8 TeV. This again indicates that care must be taken when interpreting results from the LHC searches and there are still several scenarios where sparticles below the 1 TeV scale are not excluded, even when considering the most recent results at $\sqrt{s} = 13 \text{ TeV}$.

Furthermore, the discovery of a Higgs boson with a mass around 125 GeV has triggered many studies regarding the compatibility of SUSY parameter space with this new particle. Much of it is still work in progress and it will be interesting to see how the interplay between the results from direct SUSY searches and more precise measurements of the properties of the Higgs boson will unfold in the future.

90.9 Summary and Outlook

The absence of any observation of new phenomena at the first run of the LHC at $\sqrt{s} = 7/8 \text{ TeV}$, and after the second run at $\sqrt{s} = 13 \text{ TeV}$, place significant constraints on SUSY parameter space. Today, inclusive searches probe production of gluinos at about 2.3 TeV, first and second generation squarks in the range of about 1 to 1.9 TeV, third generation squarks at scales around 600 GeV to 1.2 TeV, electroweak gauginos at scales around 400 – 1100 GeV, and sleptons around 700 GeV. However, depending on the assumptions made on the underlying SUSY spectrum these limits can also weaken considerably.

With the LHC having reached almost its maximum energy of about $\sqrt{s} = 14 \text{ TeV}$, future sensitivity improvement will have to originate from more data, the improvement of experimental analysis techniques and the focus of special signatures like the one arising in long-lived sparticle decays. Therefore, it is expected that the current landscape of SUSY searches and corresponding exclusion limits at the LHC, as, for example, shown in Fig. 90.10 from the ATLAS experiment [235] (CMS results are similar [236]), will not change as rapidly anymore as it did in the past, when the LHC underwent several successive increases of collision energy.

The interpretation of results at the LHC has moved away from constrained models like the CMSSM towards a large set of simplified models, or the pMSSM. On the one hand this move is because the LHC limits have put constrained models like the CMSSM under severe pressure, while on the other hand simplified models leave more freedom to vary parameters and form a better representation of the underlying sensitivity of analyses. However, these interpretations in simplified models do not come without a price: the decomposition of a potentially complicated reality in a limited set of individual decay chains can be significantly incomplete. Therefore, quoted limits in simplified models are only valid under the explicit assumptions made in these models. The recent addition of more comprehensive interpretations in the pMSSM will complement those derived from simplified models and, thus, will enable an even more refined understanding of the probed SUSY parameter space.

In this context, the limit range of 1.5 – 2.3 TeV on generic

colored SUSY particles only holds for light neutralinos, in the R-parity conserving MSSM. Limits on third generation squarks and electroweak gauginos also only hold for light neutralinos, and under specific assumptions for decay modes and slepton masses.

The next LHC runs at $\sqrt{s} = 13$ or 14 TeV with significantly larger integrated luminosities (notably the High-Luminosity LHC), will provide a large data sample for future SUSY searches. As mentioned above, the improvement in sensitivity will largely have to come from a larger data set, and evolution of trigger and analysis techniques, since there will be no significant energy increase at the LHC anymore. Although the sensitivity for colored sparticles will increase somewhat as well, the expanded data set will be particularly beneficial for electroweak gaugino searches, and for the more difficult final states presented by compressed particle spectra, stealth SUSY, long-lived sparticles, or R-parity violating scenarios.

References

- [1] H. Miyazawa, Prog. Theor. Phys. **36**, 6, 1266 (1966).
- [2] Yu. A. Golfand and E. P. Likhtman, JETP Lett. **13**, 323 (1971), [Pisma Zh. Eksp. Teor. Fiz.13,452(1971)].
- [3] J.-L. Gervais and B. Sakita, Nucl. Phys. **B34**, 632 (1971).
- [4] D. V. Volkov and V. P. Akulov, Phys. Lett. **46B**, 109 (1973).
- [5] J. Wess and B. Zumino, Phys. Lett. **49B**, 52 (1974).
- [6] J. Wess and B. Zumino, Nucl. Phys. **B70**, 39 (1974).
- [7] A. Salam and J. A. Strathdee, Nucl. Phys. **B76**, 477 (1974).
- [8] H. P. Nilles, Phys. Rept. **110**, 1 (1984).
- [9] H. E. Haber and G. L. Kane, Phys. Rept. **117**, 75 (1985).
- [10] E. Witten, Nucl. Phys. **B188**, 513 (1981).
- [11] S. Dimopoulos and H. Georgi, Nucl. Phys. **B193**, 150 (1981).
- [12] M. Dine, W. Fischler and M. Srednicki, Nucl. Phys. **B189**, 575 (1981).
- [13] S. Dimopoulos and S. Raby, Nucl. Phys. **B192**, 353 (1981).
- [14] N. Sakai, Z. Phys. **C11**, 153 (1981).
- [15] R. K. Kaul and P. Majumdar, Nucl. Phys. **B199**, 36 (1982).
- [16] H. Goldberg, Phys. Rev. Lett. **50**, 1419 (1983).
- [17] J. R. Ellis *et al.*, Nucl. Phys. **B238**, 453 (1984).
- [18] G. Jungman, M. Kamionkowski and K. Griest, Phys. Rept. **267**, 195 (1996), [hep-ph/9506380].
- [19] S. Dimopoulos, S. Raby and F. Wilczek, Phys. Rev. **D24**, 1681 (1981).
- [20] W. J. Marciano and G. Senjanovic, Phys. Rev. **D25**, 3092 (1982).
- [21] M. B. Einhorn and D. R. T. Jones, Nucl. Phys. **B196**, 475 (1982).
- [22] L. E. Ibanez and G. G. Ross, Phys. Lett. **105B**, 439 (1981).
- [23] U. Amaldi, W. de Boer and H. Furstenau, Phys. Lett. **B260**, 447 (1991).
- [24] P. Langacker and N. Polonsky, Phys. Rev. **D52**, 3081 (1995), [hep-ph/9503214].
- [25] P. Fayet, Phys. Lett. **64B**, 159 (1976).
- [26] G. R. Farrar and P. Fayet, Phys. Lett. **76B**, 575 (1978).
- [27] B.C. Allanach and H.E. Haber, *Supersymmetry, Part I (Theory)*, in this Review.
- [28] V. Khachatryan *et al.* (CMS, LHCb), Nature **522**, 68 (2015), [arXiv:1411.4413].
- [29] R. Aaij *et al.* (LHCb), Phys. Rev. Lett. **118**, 19, 191801 (2017), [arXiv:1703.05747].
- [30] A. Höcker and W.J. Marciano, *Muon Anomalous Magnetic Moment*, in this Review.
- [31] G. Hinshaw *et al.* (WMAP), Astrophys. J. Suppl. **208**, 19 (2013), [arXiv:1212.5226].
- [32] Planck Collab., Astron. & Astrophys. **594**, A13 (2016).
- [33] M. Carena *et al.*, *Status of Higgs Boson Physics*, in this Review.
- [34] K. Nakamura *et al.* (Particle Data Group), J. Phys. **G37**, 075021 (2010).
- [35] I. Hinchliffe *et al.*, Phys. Rev. **D55**, 5520 (1997), [hep-ph/9610544].
- [36] L. Randall and D. Tucker-Smith, Phys. Rev. Lett. **101**, 221803 (2008), [arXiv:0806.1049].
- [37] V. Khachatryan *et al.* (CMS), Phys. Lett. **B698**, 196 (2011), [arXiv:1101.1628].
- [38] S. Chatrchyan *et al.* (CMS), Phys. Rev. Lett. **107**, 221804 (2011), [arXiv:1109.2352].
- [39] S. Chatrchyan *et al.* (CMS), JHEP **01**, 077 (2013), [arXiv:1210.8115].
- [40] S. Chatrchyan *et al.* (CMS), Eur. Phys. J. **C73**, 9, 2568 (2013), [arXiv:1303.2985].
- [41] S. Chatrchyan *et al.* (CMS), Phys. Rev. **D85**, 012004 (2012), [arXiv:1107.1279].
- [42] C. G. Lester and D. J. Summers, Phys. Lett. **B463**, 99 (1999), [hep-ph/9906349].
- [43] D. R. Tovey, JHEP **04**, 034 (2008), [arXiv:0802.2879].
- [44] M. R. Buckley *et al.*, Phys. Rev. **D89**, 5, 055020 (2014), [arXiv:1310.4827].
- [45] P. Jackson, C. Rogan and M. Santoni, Phys. Rev. **D95**, 3, 035031 (2017), [arXiv:1607.08307].
- [46] J. M. Butterworth *et al.*, Phys. Rev. Lett. **100**, 242001 (2008), [arXiv:0802.2470].
- [47] E. Halkiadakis, G. Redlinger and D. Shih, Ann. Rev. Nucl. Part. Sci. **64**, 319 (2014), [arXiv:1411.1427].
- [48] W. Beenakker *et al.*, Int. J. Mod. Phys. **A26**, 2637 (2011), [arXiv:1105.1110].
- [49] W. Beenakker *et al.*, Nucl. Phys. **B492**, 51 (1997), [hep-ph/9610490].
- [50] A.H. Chamseddine, R. Arnowitt, and P. Nath, Phys. Rev. Lett. **49**, 970 (1982).
- [51] E. Cremmer *et al.*, Nucl. Phys. **B212**, 413 (1983).
- [52] P. Fayet, Phys. Lett. **70B**, 461 (1977).
- [53] M. Dine, A. E. Nelson and Y. Shirman, Phys. Rev. **D51**, 1362 (1995), [hep-ph/9408384].
- [54] P. Meade, N. Seiberg and D. Shih, Prog. Theor. Phys. Suppl. **177**, 143 (2009), [arXiv:0801.3278].
- [55] G. F. Giudice *et al.*, JHEP **12**, 027 (1998), [hep-ph/9810442].
- [56] L. Randall and R. Sundrum, Nucl. Phys. **B557**, 79 (1999), [hep-th/9810155].
- [57] R. L. Arnowitt and P. Nath, Phys. Rev. Lett. **69**, 725 (1992).
- [58] G. L. Kane *et al.*, Phys. Rev. **D49**, 6173 (1994), [hep-ph/9312272].
- [59] A. Djouadi, J.-L. Kneur and G. Moutaka, Comput. Phys. Commun. **176**, 426 (2007), [hep-ph/0211331].
- [60] C. F. Berger *et al.*, JHEP **02**, 023 (2009), [arXiv:0812.0980].
- [61] H. Baer *et al.*, in “Workshop on Physics at Current Accelerators and the Supercollider Argonne, Illinois, June 2-5, 1993,” 0703–720 (1993), [hep-ph/9305342], URL http://lss.fnal.gov/cgi-bin/find_paper.pl?other/ssc/sscl-preprint-441.
- [62] R. M. Barnett, H. E. Haber and G. L. Kane, Nucl. Phys. **B267**, 625 (1986).
- [63] H. Baer, D. Karatas and X. Tata, Phys. Lett. **B183**, 220 (1987).
- [64] J. Alwall, P. Schuster and N. Toro, Phys. Rev. **D79**, 075020 (2009), [arXiv:0810.3921].
- [65] J. Alwall *et al.*, Phys. Rev. **D79**, 015005 (2009), [arXiv:0809.3264].

- [66] O. Buchmueller and J. Marrouche, *Int. J. Mod. Phys. A* **29**, 06, 1450032 (2014), [arXiv:1304.2185].
- [67] LEP2 SUSY Working Group, ALEPH, DELPHI, L3 and OPAL experiments, note LEPSUSYWG/04-02.1, <http://lepsusy.web.cern.ch/lepsusy>.
- [68] T. Aaltonen *et al.* (CDF), *Phys. Rev. Lett.* **102**, 121801 (2009), [arXiv:0811.2512].
- [69] V. M. Abazov *et al.* (D0), *Phys. Lett.* **B660**, 449 (2008), [arXiv:0712.3805].
- [70] ATLAS Collab., ATLAS-CONF-2019-040 (2019).
- [71] A. M. Sirunyan *et al.* (CMS) (2019), [arXiv:1908.04722].
- [72] ATLAS Collab., ATLAS-CONF-2018-041 (2018).
- [73] A. M. Sirunyan *et al.* (CMS) (2019), [arXiv:1909.03460].
- [74] M. Aaboud *et al.* (ATLAS), *Phys. Rev.* **D98**, 3, 032009 (2018), [arXiv:1804.03602].
- [75] M. Aaboud *et al.* (ATLAS), *JHEP* **09**, 084 (2017), [arXiv:1706.03731].
- [76] CMS Collab., CMS-PAS-SUS-19-008 (2019).
- [77] V. Khachatryan *et al.* (CMS), *Phys. Rev.* **D94**, 11, 112009 (2016), [arXiv:1606.08076].
- [78] CMS Collab., CMS-PAS-SUS-13-010 (2013).
- [79] ATLAS Collab., ATLAS-CONF-2018-003 (2018).
- [80] G. Aad *et al.* (ATLAS), *Phys. Rev.* **D92**, 7, 072004 (2015), [arXiv:1504.05162].
- [81] A. M. Sirunyan *et al.* (CMS), *Phys. Rev.* **D98**, 9, 092011 (2018), [arXiv:1808.03078].
- [82] A. M. Sirunyan *et al.* (CMS), *Phys. Rev.* **D99**, 3, 032011 (2019), [arXiv:1811.07991].
- [83] T. Aaltonen *et al.* (CDF), *Phys. Rev. Lett.* **107**, 042001 (2011), [arXiv:1105.2815].
- [84] M. Aaboud *et al.* (ATLAS), *Phys. Lett.* **B785**, 136 (2018), [arXiv:1804.03568].
- [85] ATLAS Collab., ATLAS-CONF-2016-057 (2016).
- [86] M. Aaboud *et al.* (ATLAS), *JHEP* **09**, 088 (2017), [arXiv:1704.08493].
- [87] A. M. Sirunyan *et al.* (CMS), *Phys. Lett.* **B783**, 114 (2018), [arXiv:1712.08920].
- [88] S. Chatrchyan *et al.* (CMS), *Phys. Lett.* **B730**, 193 (2014), [arXiv:1311.1799].
- [89] V. Khachatryan *et al.* (CMS), *Phys. Lett.* **B770**, 257 (2017), [arXiv:1608.01224].
- [90] M. Aaboud *et al.* (ATLAS), *JHEP* **09**, 050 (2018), [arXiv:1805.01649].
- [91] T. Aaltonen *et al.* (CDF), *Phys. Rev. Lett.* **105**, 081802 (2010), [arXiv:1005.3600].
- [92] V. M. Abazov *et al.* (D0), *Phys. Lett.* **B693**, 95 (2010), [arXiv:1005.2222].
- [93] M. Aaboud *et al.* (ATLAS), *JHEP* **11**, 195 (2017), [arXiv:1708.09266].
- [94] G. Aad *et al.* (ATLAS) (2019), [arXiv:1909.08457].
- [95] G. Aad *et al.* (ATLAS) (2019), [arXiv:1908.03122].
- [96] A. M. Sirunyan *et al.* (CMS), *JHEP* **03**, 076 (2018), [arXiv:1709.08908].
- [97] C. Boehm, A. Djouadi and Y. Mambrini, *Phys. Rev.* **D61**, 095006 (2000), [hep-ph/9907428].
- [98] T. Aaltonen *et al.* (CDF), *Phys. Rev.* **D82**, 092001 (2010), [arXiv:1009.0266].
- [99] V. M. Abazov *et al.* (D0), *Phys. Lett.* **B696**, 321 (2011), [arXiv:1009.5950].
- [100] T. Aaltonen *et al.* (CDF), *JHEP* **10**, 158 (2012), [arXiv:1203.4171].
- [101] V. M. Abazov *et al.* (D0), *Phys. Lett.* **B665**, 1 (2008), [arXiv:0803.2263].
- [102] T. Aaltonen *et al.* (CDF), *Phys. Rev. Lett.* **104**, 251801 (2010), [arXiv:0912.1308].
- [103] V. M. Abazov *et al.* (D0), *Phys. Lett.* **B674**, 4 (2009), [arXiv:0901.1063].
- [104] CMS Collab., CMS-PAS-SUS-19-009 (2019).
- [105] M. Aaboud *et al.* (ATLAS), *JHEP* **12**, 085 (2017), [arXiv:1709.04183].
- [106] M. Aaboud *et al.* (ATLAS), *JHEP* **06**, 108 (2018), [arXiv:1711.11520].
- [107] M. Aaboud *et al.* (ATLAS), *Phys. Rev.* **D98**, 3, 032008 (2018), [arXiv:1803.10178].
- [108] CMS Collab., CMS-PAS-SUS-19-003 (2019).
- [109] ATLAS Collab., ATLAS-CONF-2019-017 (2019).
- [110] M. Aaboud *et al.* (ATLAS), *Eur. Phys. J.* **C77**, 12, 898 (2017), [arXiv:1708.03247].
- [111] A. M. Sirunyan *et al.* (CMS), *Eur. Phys. J.* **C77**, 10, 710 (2017), [arXiv:1705.04650].
- [112] A. M. Sirunyan *et al.* (CMS), *Phys. Rev.* **D96**, 3, 032003 (2017), [arXiv:1704.07781].
- [113] A. M. Sirunyan *et al.* (CMS), *JHEP* **10**, 005 (2017), [arXiv:1707.03316].
- [114] A. M. Sirunyan *et al.* (CMS), *JHEP* **10**, 019 (2017), [arXiv:1706.04402].
- [115] M. Aaboud *et al.* (ATLAS), *JHEP* **01**, 126 (2018), [arXiv:1711.03301].
- [116] F. D. Aaron *et al.* (H1), *Eur. Phys. J.* **C71**, 1572 (2011), [arXiv:1011.6359].
- [117] ATLAS Collab., ATLAS-CONF-2015-018 (2015).
- [118] V. Khachatryan *et al.* (CMS), *Phys. Rev.* **D91**, 5, 052012 (2015), [arXiv:1411.6977].
- [119] S. Chekanov *et al.* (ZEUS), *Eur. Phys. J.* **C50**, 269 (2007), [hep-ex/0611018].
- [120] S. Chatrchyan *et al.* (CMS), *Phys. Rev. Lett.* **111**, 22, 221801 (2013), [arXiv:1306.6643].
- [121] M. Aaboud *et al.* (ATLAS), *Phys. Rev.* **D97**, 3, 032003 (2018), [arXiv:1710.05544].
- [122] ATLAS Collab., ATLAS-CONF-2019-006 (2019).
- [123] A. M. Sirunyan *et al.* (CMS), *Phys. Rev.* **D99**, 3, 032014 (2019), [arXiv:1808.05082].
- [124] CMS Collab., CMS-PAS-EXO-16-022 (2016).
- [125] V. Khachatryan *et al.* (CMS), *Phys. Lett.* **B760**, 178 (2016), [arXiv:1602.04334].
- [126] M. Aaboud *et al.* (ATLAS), *Eur. Phys. J.* **C78**, 3, 250 (2018), [arXiv:1710.07171].
- [127] V. Khachatryan *et al.* (CMS), *Phys. Rev.* **D95**, 1, 012009 (2017), [arXiv:1610.05133].
- [128] V. Khachatryan *et al.* (CMS), *Phys. Lett.* **B747**, 98 (2015), [arXiv:1412.7706].
- [129] LEP2 SUSY Working Group, ALEPH, DELPHI, L3 and OPAL experiments, note LEPSUSYWG/01-03.1, <http://lepsusy.web.cern.ch/lepsusy>.
- [130] LEP2 SUSY Working Group, ALEPH, DELPHI, L3 and OPAL experiments, note LEPSUSYWG/02-04.1, <http://lepsusy.web.cern.ch/lepsusy>.
- [131] CDF Collab., CDF Note 10636 (2011).
- [132] V. M. Abazov *et al.* (D0), *Phys. Lett.* **B680**, 34 (2009), [arXiv:0901.0646].
- [133] G. Aad *et al.* (ATLAS) (2019), [arXiv:1908.08215].
- [134] A. M. Sirunyan *et al.* (CMS), *JHEP* **11**, 079 (2018), [arXiv:1807.07799].
- [135] M. Aaboud *et al.* (ATLAS), *Eur. Phys. J.* **C78**, 2, 154 (2018), [arXiv:1708.07875].

- [136] A. M. Sirunyan *et al.* (CMS), JHEP **11**, 151 (2018), [arXiv:1807.02048].
- [137] M. Aaboud *et al.* (ATLAS), Eur. Phys. J. **C78**, 12, 995 (2018), [arXiv:1803.02762].
- [138] A. M. Sirunyan *et al.* (CMS), JHEP **03**, 166 (2018), [arXiv:1709.05406].
- [139] M. Aaboud *et al.* (ATLAS), Phys. Rev. **D98**, 9, 092012 (2018), [arXiv:1806.02293].
- [140] A. M. Sirunyan *et al.* (CMS), JHEP **03**, 160 (2018), [arXiv:1801.03957].
- [141] M. Aaboud *et al.* (ATLAS), Phys. Rev. **D100**, 1, 012006 (2019), [arXiv:1812.09432].
- [142] ATLAS Collab., ATLAS-CONF-2019-019 (2019).
- [143] G. Aad *et al.* (ATLAS) (2019), [arXiv:1909.09226].
- [144] ATLAS Collab., ATLAS-CONF-2019-014 (2019).
- [145] A. M. Sirunyan *et al.* (CMS), JHEP **08**, 150 (2019), [arXiv:1905.13059].
- [146] A. M. Sirunyan *et al.* (CMS), Phys. Lett. **B782**, 440 (2018), [arXiv:1801.01846].
- [147] A. M. Sirunyan *et al.* (CMS) (2019), [arXiv:1910.01185].
- [148] H. K. Dreiner *et al.*, Eur. Phys. J. **C62**, 547 (2009), [arXiv:0901.3485].
- [149] LEP2 SUSY Working Group, ALEPH, DELPHI, L3 and OPAL experiments, note LEPSUSYWG/04-07.1, <http://lepsusy.web.cern.ch/lepsusy>.
- [150] O. Buchmueller *et al.*, Eur. Phys. J. **C74**, 6, 2922 (2014), [arXiv:1312.5250].
- [151] C. Strege *et al.*, JCAP **1304**, 013 (2013), [arXiv:1212.2636].
- [152] A. Fowlie *et al.*, Phys. Rev. **D86**, 075010 (2012), [arXiv:1206.0264].
- [153] LEP2 SUSY Working Group, ALEPH, DELPHI, L3 and OPAL experiments, note LEPSUSYWG/04-09.1, <http://lepsusy.web.cern.ch/lepsusy>.
- [154] T. Aaltonen *et al.* (CDF), Phys. Rev. Lett. **104**, 011801 (2010), [arXiv:0910.3606].
- [155] V. M. Abazov *et al.* (D0), Phys. Rev. Lett. **105**, 221802 (2010), [arXiv:1008.2133].
- [156] M. Aaboud *et al.* (ATLAS), Phys. Rev. **D97**, 9, 092006 (2018), [arXiv:1802.03158].
- [157] A. M. Sirunyan *et al.* (CMS), JHEP **06**, 143 (2019), [arXiv:1903.07070].
- [158] A. M. Sirunyan *et al.* (CMS) (2019), [arXiv:1907.00857].
- [159] M. Aaboud *et al.* (ATLAS), Phys. Rev. **D98**, 9, 092002 (2018), [arXiv:1806.04030].
- [160] M. Aaboud *et al.* (ATLAS), Phys. Rev. **D99**, 1, 012001 (2019), [arXiv:1808.03057].
- [161] A. M. Sirunyan *et al.* (CMS), Eur. Phys. J. **C79**, 5, 444 (2019), [arXiv:1901.06726].
- [162] A. M. Sirunyan *et al.* (CMS), JHEP **01**, 154 (2019), [arXiv:1812.04066].
- [163] A. M. Sirunyan *et al.* (CMS), Phys. Lett. **B780**, 118 (2018), [arXiv:1711.08008].
- [164] A. M. Sirunyan *et al.* (CMS), Phys. Rev. **D97**, 3, 032007 (2018), [arXiv:1709.04896].
- [165] A. M. Sirunyan *et al.* (CMS), Phys. Lett. **B779**, 166 (2018), [arXiv:1709.00384].
- [166] G. Aad *et al.* (ATLAS), Phys. Rev. **D93**, 5, 052002 (2016), [arXiv:1509.07152].
- [167] M. Aaboud *et al.* (ATLAS), Eur. Phys. J. **C78**, 8, 625 (2018), [arXiv:1805.11381].
- [168] M. Aaboud *et al.* (ATLAS), Eur. Phys. J. **C77**, 3, 144 (2017), [arXiv:1611.05791].
- [169] C. P. Herzog and M. Spillane, JHEP **04**, 124 (2016), [arXiv:1506.06757].
- [170] G. Aad *et al.* (ATLAS) (2019), [arXiv:1907.10037].
- [171] V. Khachatryan *et al.* (CMS), Phys. Rev. **D91**, 1, 012007 (2015), [arXiv:1411.6530].
- [172] G. Aad *et al.* (ATLAS), JHEP **10**, 134 (2015), [arXiv:1508.06608].
- [173] V. Khachatryan *et al.* (CMS), JHEP **10**, 129 (2016), [arXiv:1606.03577].
- [174] P. Athron *et al.* (GAMBIT), Eur. Phys. J. **C77**, 12, 879 (2017), [arXiv:1705.07917].
- [175] K. J. de Vries *et al.*, Eur. Phys. J. **C75**, 9, 422 (2015), [arXiv:1504.03260].
- [176] C. Strege *et al.*, JHEP **09**, 081 (2014), [arXiv:1405.0622].
- [177] LEP2 SUSY Working Group, ALEPH, DELPHI, L3 and OPAL experiments, note LEPSUSYWG/04-01.1, <http://lepsusy.web.cern.ch/lepsusy>.
- [178] A. Heister *et al.* (ALEPH), Phys. Lett. **B544**, 73 (2002), [hep-ex/0207056].
- [179] A. M. Sirunyan *et al.* (CMS), Phys. Lett. **B790**, 140 (2019), [arXiv:1806.05264].
- [180] ATLAS Collab., ATLAS-CONF-2019-018 (2019).
- [181] A. M. Sirunyan *et al.* (CMS) (2019), [arXiv:1907.13179].
- [182] LEP2 SUSY Working Group, ALEPH, DELPHI, L3 and OPAL experiments, note LEPSUSYWG/02-09.2, <http://lepsusy.web.cern.ch/lepsusy>.
- [183] M. Aaboud *et al.* (ATLAS), Phys. Rev. **D99**, 1, 012009 (2019), [arXiv:1808.06358].
- [184] S. Chatrchyan *et al.* (CMS), Eur. Phys. J. **C73**, 2493 (2013), [arXiv:1301.3792].
- [185] S. Chatrchyan *et al.* (CMS), Phys. Rev. **D90**, 032006 (2014), [arXiv:1404.5801].
- [186] T. Aaltonen *et al.* (CDF), Phys. Rev. Lett. **110**, 20, 201802 (2013), [arXiv:1302.4491].
- [187] LEP2 SUSY Working Group, ALEPH, DELPHI, L3 and OPAL experiments, note LEPSUSYWG/02-10.1, <http://lepsusy.web.cern.ch/lepsusy>.
- [188] A. M. Sirunyan *et al.* (CMS), Eur. Phys. J. **C79**, 4, 305 (2019), [arXiv:1811.09760].
- [189] DELPHI Collab., Eur. Phys. J. **C31**, 412 (2003).
- [190] T. Falk, K. A. Olive and M. Srednicki, Phys. Lett. **B339**, 248 (1994), [hep-ph/9409270].
- [191] C. Arina and N. Fornengo, JHEP **11**, 029 (2007), [arXiv:0709.4477].
- [192] T. Aaltonen *et al.* (CDF), Phys. Rev. Lett. **105**, 191801 (2010), [arXiv:1004.3042].
- [193] V. M. Abazov *et al.* (D0), Phys. Rev. Lett. **105**, 191802 (2010), [arXiv:1007.4835].
- [194] G. Aad *et al.* (ATLAS), Phys. Rev. Lett. **115**, 3, 031801 (2015), [arXiv:1503.04430].
- [195] M. Aaboud *et al.* (ATLAS), Eur. Phys. J. **C76**, 10, 541 (2016), [arXiv:1607.08079].
- [196] V. Khachatryan *et al.* (CMS), Eur. Phys. J. **C76**, 6, 317 (2016), [arXiv:1604.05239].
- [197] O. Buchmueller *et al.*, JHEP **09**, 076 (2017), [arXiv:1704.06515].
- [198] V. V. Khoze, A. D. Plascencia and K. Sakurai, JHEP **06**, 041 (2017), [arXiv:1702.00750].
- [199] M. Aaboud *et al.* (ATLAS), Phys. Rev. **D97**, 5, 052012 (2018), [arXiv:1710.04901].
- [200] M. Aaboud *et al.* (ATLAS), Phys. Rev. **D99**, 9, 092007 (2019), [arXiv:1902.01636].
- [201] G. Aad *et al.* (ATLAS), Eur. Phys. J. **C75**, 9, 407 (2015), [arXiv:1506.05332].
- [202] A. M. Sirunyan *et al.* (CMS), Phys. Lett. **B797**, 134876 (2019), [arXiv:1906.06441].

- [203] A. M. Sirunyan *et al.* (CMS), JHEP **05**, 025 (2018), [arXiv:1802.02110].
- [204] CMS Collab., CMS-PAS-EXO-16-036 (2016).
- [205] V. M. Abazov *et al.* (D0), Phys. Rev. Lett. **99**, 131801 (2007), [arXiv:0705.0306].
- [206] G. Aad *et al.* (ATLAS), Phys. Rev. **D88**, 11, 112003 (2013), [arXiv:1310.6584].
- [207] A. M. Sirunyan *et al.* (CMS), JHEP **05**, 127 (2018), [arXiv:1801.00359].
- [208] T. Aaltonen *et al.* (CDF), Phys. Rev. Lett. **103**, 021802 (2009), [arXiv:0902.1266].
- [209] V. M. Abazov *et al.* (D0), Phys. Rev. **D87**, 5, 052011 (2013), [arXiv:1211.2466].
- [210] A. M. Sirunyan *et al.* (CMS), JHEP **08**, 016 (2018), [arXiv:1804.07321].
- [211] M. Aaboud *et al.* (ATLAS), JHEP **06**, 022 (2018), [arXiv:1712.02118].
- [212] G. Aad *et al.* (ATLAS), Phys. Rev. **D88**, 11, 112006 (2013), [arXiv:1310.3675].
- [213] LEP2 SUSY Working Group, ALEPH, DELPHI, L3 and OPAL experiments, note LEPSUSYWG/02-05.1, <http://lepsusy.web.cern.ch/lepsusy>.
- [214] V. Khachatryan *et al.* (CMS), Eur. Phys. J. **C75**, 7, 325 (2015), [arXiv:1502.02522].
- [215] T. Aaltonen *et al.* (CDF), Phys. Rev. **D88**, 3, 031103 (2013), [arXiv:1307.0474].
- [216] A. M. Sirunyan *et al.* (CMS) (2019), [arXiv:1909.06166].
- [217] V. M. Abazov *et al.* (D0), Phys. Rev. Lett. **101**, 111802 (2008), [arXiv:0806.2223].
- [218] G. Aad *et al.* (ATLAS), Phys. Rev. **D90**, 11, 112005 (2014), [arXiv:1409.5542].
- [219] O. Buchmueller *et al.*, Eur. Phys. J. **C71**, 1722 (2011), [arXiv:1106.2529].
- [220] E. A. Baltz and P. Gondolo, JHEP **10**, 052 (2004), [hep-ph/0407039].
- [221] B. C. Allanach and C. G. Lester, Phys. Rev. **D73**, 015013 (2006), [hep-ph/0507283].
- [222] R. Ruiz de Austri, R. Trotta and L. Roszkowski, JHEP **05**, 002 (2006), [hep-ph/0602028].
- [223] R. Lafaye *et al.*, Eur. Phys. J. **C54**, 617 (2008), [arXiv:0709.3985].
- [224] M. Shaposhnikov, JHEP **08**, 008 (2008), [arXiv:0804.4542].
- [225] R. Trotta *et al.*, JHEP **12**, 024 (2008), [arXiv:0809.3792].
- [226] P. Bechtle *et al.*, Eur. Phys. J. **C66**, 215 (2010), [arXiv:0907.2589].
- [227] E. Bagnaschi *et al.*, Eur. Phys. J. C **78**, 256, 1 (2018).
- [228] J. Costa *et al.*, Eur. Phys. J. C **78**, 158, 1 (2018).
- [229] E. Bagnaschi *et al.*, Eur. Phys. J. **C77**, 4, 268 (2017), [arXiv:1612.05210].
- [230] E. Bagnaschi *et al.*, Eur. Phys. J. **C77**, 2, 104 (2017), [arXiv:1610.10084].
- [231] L. A. Harland-Lang, V. A. Khoze and M. G. Ryskin, Eur. Phys. J. **C76**, 1, 9 (2016), [arXiv:1508.02718].
- [232] E. A. Bagnaschi *et al.*, Eur. Phys. J. **C75**, 500 (2015), [arXiv:1508.01173].
- [233] O. Buchmueller *et al.*, Eur. Phys. J. **C74**, 12, 3212 (2014), [arXiv:1408.4060].
- [234] M. Citron *et al.*, Phys. Rev. **D87**, 3, 036012 (2013), [arXiv:1212.2886].
- [235] Supersymmetry Physics Results, ATLAS experiment, <http://twiki.cern.ch/twiki/bin/view/AtlasPublic/SupersymmetryPublicResults/>.
- [236] Supersymmetry Physics Results, CMS experiment, <http://cms-results.web.cern.ch/cms-results/public-results/publications/SUS/index.html>.

91. Axions and Other Similar Particles

Revised October 2019 by A. Ringwald (DESY, Hamburg), L.J. Rosenberg (U. Washington) and G. Rybka (U. Washington).

91.1 Introduction

In this section, we list coupling-strength and mass limits for light neutral scalar or pseudoscalar bosons that couple weakly to normal matter and radiation. Such bosons may arise from the spontaneous breaking of a global U(1) symmetry, resulting in a massless Nambu-Goldstone (NG) boson. If there is a small explicit symmetry breaking, either already in the Lagrangian or due to quantum effects such as anomalies, the boson acquires a mass and is called a pseudo-NG boson. Typical examples are axions (A^0) [1–4] and majorons [5], associated, respectively, with a spontaneously broken Peccei-Quinn and lepton-number symmetry.

A common feature of these light bosons ϕ is that their coupling to Standard-Model particles is suppressed by the energy scale that characterizes the symmetry breaking, *i.e.*, the decay constant f . The interaction Lagrangian is

$$\mathcal{L} = f^{-1} J^\mu \partial_\mu \phi, \quad (91.1)$$

where J^μ is the Noether current of the spontaneously broken global symmetry. If f is very large, these new particles interact very weakly. Detecting them would provide a window to physics far beyond what can be probed at accelerators.

Axions are of particular interest because the Peccei-Quinn (PQ) mechanism remains perhaps the most credible scheme to preserve CP-symmetry in QCD. Moreover, the cold dark matter (CDM) of the universe may well consist of axions and they are searched for in dedicated experiments with a realistic chance of discovery.

Originally it was assumed that the PQ scale f_A was related to the electroweak symmetry-breaking scale $v_{EW} = (\sqrt{2}G_F)^{-1/2} = 247$ GeV. However, the associated “standard” and “variant” axions were quickly excluded—we refer to the Listings for detailed limits. Here we focus on “invisible axions” with $f_A \gg v_{EW}$ as the main possibility.

Axions have a characteristic two-photon vertex, inherited from their mixing with π^0 and η . This coupling allows for the main search strategy based on axion-photon conversion in external magnetic fields [6], an effect that also can be of astrophysical interest. While for axions the product “ $A\gamma\gamma$ interaction strength \times mass” is essentially fixed by the corresponding π^0 properties, one may consider a more general class of axion-like particles (ALPs) where the two parameters (coupling and mass) are independent. A number of experiments explore this more general parameter space. ALPs populating the latter are predicted to arise generically, in addition to the axion, in low-energy effective field theories emerging from string theory [7–14]. The latter often contain also very light Abelian vector bosons under which the Standard-Model particles are not charged: so-called hidden-sector photons, dark photons or paraxions. They share a number of phenomenological features with the axion and ALPs, notably the possibility of hidden photon to photon conversion. Their physics cases and the current constraints are compiled in Refs. [15–17].

91.2 Theory

91.2.1 Peccei-Quinn mechanism and axions

The QCD Lagrangian includes a CP-violating term $\mathcal{L}_\Theta = -\bar{\Theta}(\alpha_s/8\pi)G^{\mu\nu a}\tilde{G}_{\mu\nu}^a$, where $-\pi \leq \bar{\Theta} \leq +\pi$ is the effective Θ parameter after diagonalizing quark masses, $G_{\mu\nu}^a$ is the color field strength tensor, and $\tilde{G}^{a,\mu\nu} \equiv \epsilon^{\mu\nu\lambda\rho}G_{\lambda\rho}^a/2$, with $\epsilon^{0123} = 1$, its dual. Limits on the neutron electric dipole moment [18] imply $|\bar{\Theta}| \lesssim 10^{-10}$ even though $\bar{\Theta} = \mathcal{O}(1)$ is otherwise completely satisfactory. The spontaneously broken global Peccei-Quinn symmetry U(1)_{PQ} was introduced to solve this “strong CP problem” [1, 2], the axion being the pseudo-NG boson of U(1)_{PQ} [3, 4]. This symmetry is broken due to the axion’s anomalous triangle coupling to gluons,

$$\mathcal{L} = \left(\frac{\phi_A}{f_A} - \bar{\Theta} \right) \frac{\alpha_s}{8\pi} G^{\mu\nu a} \tilde{G}_{\mu\nu}^a, \quad (91.2)$$

where ϕ_A is the axion field and f_A the axion decay constant. Color anomaly factors have been absorbed in the normalization of f_A which is defined by this Lagrangian. Thus normalized, f_A

is the quantity that enters all low-energy phenomena [19]. Non-perturbative topological fluctuations of the gluon fields in QCD induce a potential for ϕ_A whose minimum is at $\phi_A = \bar{\Theta} f_A$, thereby canceling the $\bar{\Theta}$ term in the QCD Lagrangian and thus restoring CP symmetry.

The resulting axion mass, in units of the PQ scale f_A , is identical to the square root of the topological susceptibility in QCD, $m_A f_A = \sqrt{\chi}$. The latter can be evaluated further [20, 21], exploiting the chiral limit (masses of up and down quarks much smaller than the scale of QCD), yielding $m_A f_A = \sqrt{\chi} \approx f_\pi m_\pi$, where $m_\pi = 135$ MeV and $f_\pi \approx 92$ MeV. In more detail one finds, to next-to-next-to-leading order in chiral perturbation theory [22],

$$m_A = 5.691(51) \left(\frac{10^9 \text{ GeV}}{f_A} \right) \text{meV}. \quad (91.3)$$

A direct calculation of the topological susceptibility via QCD lattice simulations finds almost the same central value, albeit with an about five times larger error bar [23].

Axions with $f_A \gg v_{EW}$ evade all current experimental limits. One generic class of models invokes “hadronic axions” where new heavy quarks carry U(1)_{PQ} charges, leaving ordinary quarks and leptons without tree-level axion couplings. The archetype is the KSVZ model [24], where in addition the heavy new quarks are electrically neutral. Another generic class requires at least two Higgs doublets and ordinary quarks and leptons carry PQ charges, the archetype being the DFSZ model [25]. All of these models contain at least one electroweak singlet scalar that acquires a vacuum expectation value and thereby breaks the PQ symmetry. The KSVZ and DFSZ models are frequently used as benchmark examples, but other models exist where both heavy quarks and Higgs doublets carry PQ charges. In supersymmetric models, the axion is part of a supermultiplet and thus inevitably accompanied by a spin-0 saxion and a spin-1 axino, which both also have couplings suppressed by f_A and are expected to have large masses due to supersymmetry breaking [26].

91.2.2 Model-dependent axion couplings

Although the generic axion interactions scale approximately with f_π/f_A from the corresponding π^0 couplings, there are non-negligible model-dependent factors and uncertainties. The axion’s two-photon interaction plays a key role for many searches,

$$\mathcal{L}_{A\gamma\gamma} = -\frac{g_{A\gamma\gamma}}{4} F_{\mu\nu} \tilde{F}^{\mu\nu} \phi_A = g_{A\gamma\gamma} \mathbf{E} \cdot \mathbf{B} \phi_A, \quad (91.4)$$

where F is the electromagnetic field-strength tensor and $\tilde{F}^{\mu\nu} \equiv \epsilon^{\mu\nu\lambda\rho} F_{\lambda\rho}/2$, with $\epsilon^{0123} = 1$, its dual. The coupling constant is [27]

$$g_{A\gamma\gamma} = \frac{\alpha}{2\pi f_A} \left(\frac{E}{N} - 1.92(4) \right) = \left(0.203(3) \frac{E}{N} - 0.39(1) \right) \frac{m_A}{\text{GeV}^2}, \quad (91.5)$$

where E and N are the electromagnetic and color anomalies of the axial current associated with the axion. In grand unified models, and notably for DFSZ [25], $E/N = 8/3$, whereas for KSVZ [24] $E/N = 0$ if the electric charge of the new heavy quark is taken to vanish. In general, a broad range of E/N values is possible [28, 29], as indicated by the diagonal yellow band in Fig. 91.1. However, this band still does not exhaust all the possibilities. In fact, there exist classes of QCD axion models whose photon couplings populate the entire still allowed region above the yellow band in Fig. 91.1, motivating axion search efforts over a wide range of masses and couplings [30, 31].

The two-photon decay width is

$$\Gamma_{A \rightarrow \gamma\gamma} = \frac{g_{A\gamma\gamma}^2 m_A^3}{64\pi} = 1.1 \times 10^{-24} \text{ s}^{-1} \left(\frac{m_A}{\text{eV}} \right)^5. \quad (91.6)$$

The second expression uses Eq. (91.5) with $E/N = 0$. Axions decay faster than the age of the universe if $m_A \gtrsim 20$ eV. The interaction with fermions f has derivative form and is invariant under a shift $\phi_A \rightarrow \phi_A + \phi_0$ as behaves a NG boson,

$$\mathcal{L}_{Aff} = \frac{C_f}{2f_A} \bar{\Psi}_f \gamma^\mu \gamma_5 \Psi_f \partial_\mu \phi_A. \quad (91.7)$$

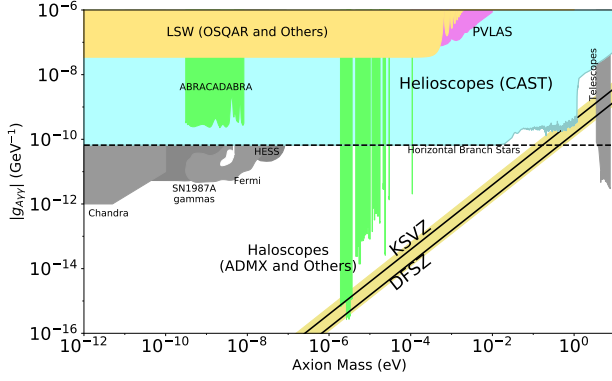


Figure 91.1: Exclusion plot for ALPs as described in the text.

Here, Ψ_f is the fermion field, m_f its mass, and C_f a model-dependent coefficient. The dimensionless combination $g_{Aff} \equiv C_f m_f / f_A$ plays the role of a Yukawa coupling and $\alpha_{Aff} \equiv g_{Aff}^2 / 4\pi$ of a “fine-structure constant.” The often-used pseudoscalar form $\mathcal{L}_{Aff} = -i(C_f m_f / f_A) \bar{\Psi}_f \gamma_5 \Psi_f \phi_A$ need not be equivalent to the appropriate derivative structure, for example when two NG bosons are attached to one fermion line as in axion emission by nucleon bremsstrahlung [32].

In the DFSZ model [25], the tree-level coupling coefficient to electrons is [33]

$$C_e = \frac{\sin^2 \beta}{3}, \quad (91.8)$$

where $\tan \beta$ is the ratio of the vacuum expectation values of the two Higgs doublets giving masses to the up- and down-type quarks, respectively: $\tan \beta = v_u / v_d$.

For nucleons, $C_{p,n}$ have been determined as [27]

$$\begin{aligned} C_p &= -0.47(3) + 0.88(3)C_u - 0.39(2)C_d - 0.038(5)C_s \\ &\quad - 0.012(5)C_c - 0.009(2)C_b - 0.0035(4)C_t, \\ C_n &= -0.02(3) + 0.88(3)C_d - 0.39(2)C_u - 0.038(5)C_s \\ &\quad - 0.012(5)C_c - 0.009(2)C_b - 0.0035(4)C_t, \end{aligned} \quad (91.9)$$

in terms of the corresponding model-dependent quark couplings C_q , $q = u, d, s, c, b, t$.

For hadronic axions with $C_q = 0$, C_n is compatible with zero whereas C_p does not vanish. In the DFSZ model, on the other hand, $C_u = C_c = C_t = \frac{1}{3} \cos^2 \beta$ and $C_d = C_s = C_b = \frac{1}{3} \sin^2 \beta$, and C_p and C_n , as functions of β ,

$$\begin{aligned} C_p &= -0.435 \sin^2 \beta + (-0.182 \pm 0.025), \\ C_n &= 0.414 \sin^2 \beta + (-0.160 \pm 0.025), \end{aligned} \quad (91.10)$$

do not vanish simultaneously.

The axion-pion interaction is given by the Lagrangian [34]

$$\mathcal{L}_{A\pi} = \frac{C_{A\pi}}{f_\pi f_A} (\pi^0 \pi^+ \partial_\mu \pi^- + \pi^0 \pi^- \partial_\mu \pi^+ - 2\pi^+ \pi^- \partial_\mu \pi^0) \partial_\mu \phi_A, \quad (91.11)$$

where $C_{A\pi} = (1-z)/[3(1+z)]$ in hadronic models, with $0.38 < z = m_u / m_d < 0.58$ [35, 36]. The chiral symmetry-breaking Lagrangian provides an additional term $\mathcal{L}'_{A\pi} \propto (m_\pi^2 / f_\pi f_A) (\pi^0 \pi^0 + 2\pi^- \pi^+) \pi^0 \phi_A$. For hadronic axions it vanishes identically, in contrast to the DFSZ model (Roberto Peccei, private communication).

91.3 Laboratory Searches

91.3.1 Light shining through walls

Searching for “invisible axions” is extremely challenging due to its extraordinarily feeble coupling to normal matter and radiation. Currently, the most promising approaches rely on the axion-two-photon interaction, allowing for axion-photon conversion in external electric or magnetic fields [6]. For the Coulomb field of a charged particle, the conversion is best viewed as a scattering process, $\gamma + Ze \leftrightarrow Ze + A$, called Primakoff effect [37].

In the other extreme of a macroscopic field, usually a large-scale B -field, the momentum transfer is small, the interaction is coherent over a large distance, and the conversion is best viewed as an axion-photon oscillation phenomenon in analogy to neutrino flavor oscillations [38].

Photons propagating through a transverse magnetic field, with incident \mathbf{E}_γ and magnetic field \mathbf{B} parallel, may convert into axions. For $m_A^2 L / 2\omega \ll 2\pi$, where L is the length of the B field region and ω the photon energy, the resultant axion beam is coherent with the incident photon beam and the conversion probability is $\Pi \sim (1/4)(g_{A\gamma\gamma} B L)^2$. A practical realization uses a laser beam propagating down the bore of a superconducting dipole magnet (like the bending magnets in high-energy accelerators). If another magnet is in line with the first, but shielded by an optical barrier, then photons may be regenerated from the pure axion beam [39, 40]. The overall probability is $P(\gamma \rightarrow A \rightarrow \gamma) = \Pi^2$.

The first such Light-Shining-through-Walls (LSW) experiment was performed by the BFRT collaboration. It utilized two magnets of length $L = 4.4$ m and $B = 3.7$ T and found $|g_{A\gamma\gamma}| < 6.7 \times 10^{-7} \text{ GeV}^{-1}$ at 95% CL for $m_A < 1$ meV [41]. More recently, several such experiments were performed (see Listings) [42–48]. The current best limit, $|g_{A\gamma\gamma}| < 3.5 \times 10^{-8} \text{ GeV}^{-1}$ at 95% CL for $m_A \lesssim 0.3$ meV (see Fig. 91.1), has been achieved by the OSQAR (Optical Search for QED Vacuum Birefringence, Axions, and Photon Regeneration) experiment, which exploited two 9 T LHC dipole magnets and an 18.5 W continuous wave laser emitting at the wavelength of 532 nm [48]. Some of these experiments have also reported limits for scalar bosons where the photon \mathbf{E}_γ must be chosen perpendicular to the magnetic field \mathbf{B} .

The concept of resonantly enhanced photon regeneration may open unexplored regions of coupling strength [49, 50]. In this scheme, both the production and detection magnets are within Fabry-Perot optical cavities and actively locked in frequency. The $\gamma \rightarrow A \rightarrow \gamma$ rate is enhanced by a factor $\mathcal{F}\mathcal{F}'/\pi^2$ relative to a single-pass experiment, where \mathcal{F} and \mathcal{F}' are the finesses of the two cavities. The resonant enhancement could be of order $10^{(10-12)}$, improving the $g_{A\gamma\gamma}$ sensitivity by $10^{(2.5-3)}$. The experiment ALPS II (Any Light Particle Search II) is based on this concept and aims at an improvement of the current laboratory bound on $g_{A\gamma\gamma}$ by a factor $\sim 10^3$ in the year 2020 [51].

Resonantly enhanced photon regeneration has already been exploited in experiments searching for ‘radiowaves shining through a shielding’ [52–55]. For $m_A \lesssim 10^{-5}$ eV, the upper bound on $g_{A\gamma\gamma}$ established by the CROWS (CERN Resonant Weakly Interacting sub-eV Particle Search) experiment [56] is slightly less stringent than the one set by OSQAR.

91.3.2 Photon polarization

An alternative to regenerating the lost photons is to use the beam itself to detect conversion: the polarization of light propagating through a transverse B field suffers dichroism and birefringence [57]. Dichroism: The E_{\parallel} component, but not E_{\perp} , is depleted by axion production, causing a small rotation of linearly polarized light. For $m_A^2 L / 2\omega \ll 2\pi$, the effect is independent of m_A . For heavier axions, it oscillates and diminishes as m_A increases, and it vanishes for $m_A > \omega$. Birefringence: This effect occurs because there is mixing of virtual axions in the E_{\parallel} state, but not for E_{\perp} . Hence, linearly polarized light will develop elliptical polarization. Higher-order QED also induces vacuum magnetic birefringence (VMB). A search for these effects was performed in the same dipole magnets of the BFRT experiment mentioned before [58]. The dichroic rotation gave a stronger limit than the ellipticity rotation: $|g_{A\gamma\gamma}| < 3.6 \times 10^{-7} \text{ GeV}^{-1}$ at 95% CL, for $m_A < 5 \times 10^{-4}$ eV. The ellipticity limits are better at higher masses, as they fall off smoothly and do not terminate at m_A .

In 2006, the PVLAS collaboration reported a signature of magnetically induced vacuum dichroism that could be interpreted as the effect of a pseudoscalar with $m_A = 1\text{--}1.5$ meV and $|g_{A\gamma\gamma}| = (1.6\text{--}5) \times 10^{-6} \text{ GeV}^{-1}$ [59]. Later, it turned out that these findings are due to instrumental artifacts [60]. This particle interpretation is also excluded by the above photon regeneration searches that were inspired by the original PVLAS result. The fourth generation setup of the PVLAS experiment has published results on searches for VMB (see Fig. 91.1) and dichroism [61].

The bounds from the non-observation of the latter on $g_{A\gamma\gamma}$ are slightly weaker than the ones from OSQAR.

91.3.3 Long-range forces

New bosons would mediate long-range forces, which are severely constrained by “fifth force” experiments [62]. Those looking for new mass-spin couplings provide significant constraints on pseudoscalar bosons [63]. Presently, the most restrictive limits are obtained from combining long-range force measurements with stellar cooling arguments [64]. For the moment, any of these limits are far from realistic values expected for axions. Still, these efforts provide constraints on more general low-mass bosons.

In Ref. [65], a method was proposed that can extend the search for axion-mediated spin-dependent forces by several orders of magnitude. By combining techniques used in nuclear magnetic resonance and short-distance tests of gravity, this method appears to be sensitive to axions in the $\mu\text{eV} - \text{meV}$ mass range, independent of the cosmic axion abundance, if axions have a CP-violating interaction with nuclei as large as the current experimental bound on the electric dipole moment of the neutron allows. Experimental tests to demonstrate the requirements of ARIADNE (Axion Resonant InterAction DetectioN Experiment) are under way [66].

91.4 Axions from Astrophysical Sources

91.4.1 Stellar energy-loss limits

Low-mass weakly-interacting particles (neutrinos, gravitons, axions, baryonic or leptonic gauge bosons, *etc.*) are produced in hot astrophysical plasmas, and can thus transport energy out of stars. The coupling strength of these particles with normal matter and radiation is bounded by the constraint that stellar lifetimes or energy-loss rates are not in conflict with observation [67, 68].

We begin this discussion with our Sun and concentrate on hadronic axions. They are produced predominantly by the Primakoff process $\gamma + Ze \rightarrow Ze + A$. Integrating over a standard solar model yields the axion luminosity [69]

$$L_A = g_{10}^2 \times 1.85 \times 10^{-3} L_\odot, \quad (91.12)$$

where $g_{10} = |g_{A\gamma\gamma}| \times 10^{10} \text{ GeV}$. The maximum of the spectrum is at 3.0 keV, the average at 4.2 keV, and the number flux at Earth is $g_{10}^2 \times 3.75 \times 10^{11} \text{ cm}^{-2} \text{ s}^{-1}$. The solar photon luminosity is fixed, so energy losses due to the Primakoff process require enhanced nuclear energy production and thus enhanced neutrino fluxes. The all-flavor measurements by SNO (Solar Neutrino Observatory), together with a standard solar model, imply $L_A \lesssim 0.10 L_\odot$, corresponding to $g_{10} \lesssim 7$ [70], mildly superseding a similar limit from helioseismology [71]. In Ref. [72], this limit was improved to $g_{10} < 4.1$ (at 3σ), exploiting a new statistical analysis that combined helioseismology (sound speed, surface helium and convective radius) and solar neutrino observations, including theoretical and observational errors, and accounting for tensions between input parameters of solar models, in particular the solar element abundances.

A more restrictive limit derives from globular-cluster (GC) stars that allow for detailed tests of stellar-evolution theory. The stars on the horizontal branch (HB) in the color-magnitude diagram have reached helium burning with a core-averaged energy release of about $80 \text{ erg g}^{-1} \text{ s}^{-1}$, compared to Primakoff axion losses of $g_{10}^2 30 \text{ erg g}^{-1} \text{ s}^{-1}$. The accelerated consumption of helium reduces the HB lifetime by about $80/(80+30 g_{10}^2)$. Number counts of HB stars in a large sample of 39 Galactic GCs compared with the number of red giants (that are not much affected by Primakoff losses) give a weak indication of non-standard losses which may be accounted by Primakoff-like axion emission, if the photon coupling is in the range $|g_{A\gamma\gamma}| = (2.9 \pm 1.8) \times 10^{-11} \text{ GeV}^{-1}$ [73, 74]. Still, the upper bound found in this analysis,

$$|g_{A\gamma\gamma}| < 6.6 \times 10^{-11} \text{ GeV}^{-1} \text{ (95\% CL)}, \quad (91.13)$$

represents the strongest limit on $g_{A\gamma\gamma}$ for a wide mass range, see Fig. 91.1. The conservative constraint, Eq. (91.13), on $g_{A\gamma\gamma}$ may be translated to $f_A > 3.4 \times 10^7 \text{ GeV}$ ($m_A < 0.2 \text{ eV}$), using $E/N = 0$ as in the KSVZ model, or to $f_A > 1.3 \times 10^7 \text{ GeV}$ ($m_A < 0.5 \text{ eV}$), for the DFSZ axion model, with $E/N = 8/3$, see Fig. 91.1.

If axions couple directly to electrons, the dominant emission processes are atomic axio-recombination and axio-deexcitation, axio-bremsstrahlung in electron-ion or electron-electron collisions, and Compton scattering [75]. Stars in the red giant (RG) branch of the color-magnitude diagram of GCs are particularly sensitive to these processes. In fact, they would lead to an extension of the latter to larger brightness. Reference [76] provided high-precision photometry for the Galactic globular cluster M5 (NGC 5904), allowing for a detailed comparison between the observed tip of the RG branch with predictions based on state-of-the-art stellar evolution theory. It was found that, within the uncertainties, the observed and predicted tip of the RG branch brightness agree reasonably well, leading to the bound

$$|g_{Aee}| < 4.3 \times 10^{-13} \text{ (95\% CL)}, \quad (91.14)$$

implying an upper bound on the axion mass in the DFSZ model,

$$m_A \sin^2 \beta < 15 \text{ meV (95\% CL)}, \quad (91.15)$$

see Fig. 91.2 (left panel). Intriguingly, the agreement would improve with a small amount of extra cooling that slightly postpones helium ignition, preferring an electron coupling around $|g_{Aee}| \sim 1.9 \times 10^{-13}$, corresponding to $m_A \sin^2 \beta \sim 7 \text{ meV}$.

Bremsstrahlung is also efficient in white dwarfs (WDs), where the Primakoff and Compton processes are suppressed by the large plasma frequency. A comparison of the predicted and observed luminosity function of WDs can be used to put limits on $|g_{Aee}|$ [78]. A recent analysis, based on detailed WD cooling treatment and new data on the WD luminosity function (WDLF) of the Galactic Disk, found that electron couplings above $|g_{Aee}| \gtrsim 3 \times 10^{-13}$, corresponding to a DFSZ axion mass $m_A \sin^2 \beta \gtrsim 10 \text{ meV}$, are disfavoured [79], see Fig. 91.2 (left panel). Lower couplings cannot be discarded from the current knowledge of the WDLF of the Galactic Disk. On the contrary, features in some WDLFs can be interpreted as suggestions for electron couplings in the range $7.2 \times 10^{-14} \lesssim |g_{Aee}| \lesssim 2.2 \times 10^{-13}$, corresponding to $2.5 \text{ meV} \lesssim m_A \sin^2 \beta \lesssim 7.5 \text{ meV}$ [79, 80]. This hypothesis will be further scrutinized by the Large Synoptic Survey Telescope (LSST) which is expected to increase the sample of WDs in the Galactic halo to hundreds of thousands [81]. This will allow for the determination of independent WDLFs from different Galactic populations, greatly reducing the uncertainties related to star formation histories. For pulsationally unstable WDs (ZZ Ceti stars), the period decrease \dot{P}/P is a measure of the cooling speed. The corresponding observations of the pulsating WDs G117-B15A and R548 imply additional cooling that can be interpreted also in terms of similar axion losses [82, 83].

Recently, it has been pointed out that the hints of excessive cooling of WDs, RGs and HB stars can be explained at one stroke by an ALP coupling to electrons and photons, with couplings $|g_{Aee}| \sim 1.5 \times 10^{-13}$ and $|g_{A\gamma\gamma}| \sim 1.4 \times 10^{-11} \text{ GeV}^{-1}$, respectively [84, 85]. Intriguingly, good fits to the data can be obtained employing the DFSZ axion with a mass in the range $4 \text{ meV} \lesssim m_A \lesssim 250 \text{ meV}$ [84].

Similar constraints derive from the measured duration of the neutrino signal of the supernova SN 1987A. Numerical simulations for a variety of cases, including axions and Kaluza-Klein gravitons, reveal that the energy-loss rate of a nuclear medium at the density $3 \times 10^{14} \text{ g cm}^{-3}$ and temperature 30 MeV should not exceed about $1 \times 10^{19} \text{ erg g}^{-1} \text{ s}^{-1}$ [86]. The energy-loss rate from nucleon bremsstrahlung, $N+N \rightarrow N+N+A$, is $(C_N/2f_A)^2 (T^4/\pi^2 m_N) F$. Here F is a numerical factor that represents an integral over the dynamical spin-density structure function because axions couple to the nucleon spin. For realistic conditions, even after considerable effort, one is limited to a heuristic estimate leading to $F \approx 1$ [68]. The SN 1987A limits are of particular interest for hadronic axions where the bounds on $|g_{Aee}|$ are moot. Using a proton fraction of 0.3, $g_{Ann} = 0$, $F = 1$, and $T = 30 \text{ MeV}$, one finds $f_A \gtrsim 4 \times 10^8 \text{ GeV}$ and $m_A \lesssim 16 \text{ meV}$ [68], see Fig. 91.2 (right panel). A more detailed numerical calculation [87] with state of the art SN models, again assuming $g_{Ann} = 0$, found that a coupling larger than $|g_{App}| \gtrsim 6 \times 10^{-10}$, would shorten significantly the timescale of the neutrino emission. This result is, not surprisingly, rather close to the estimate in Ref. [68]. Improving the

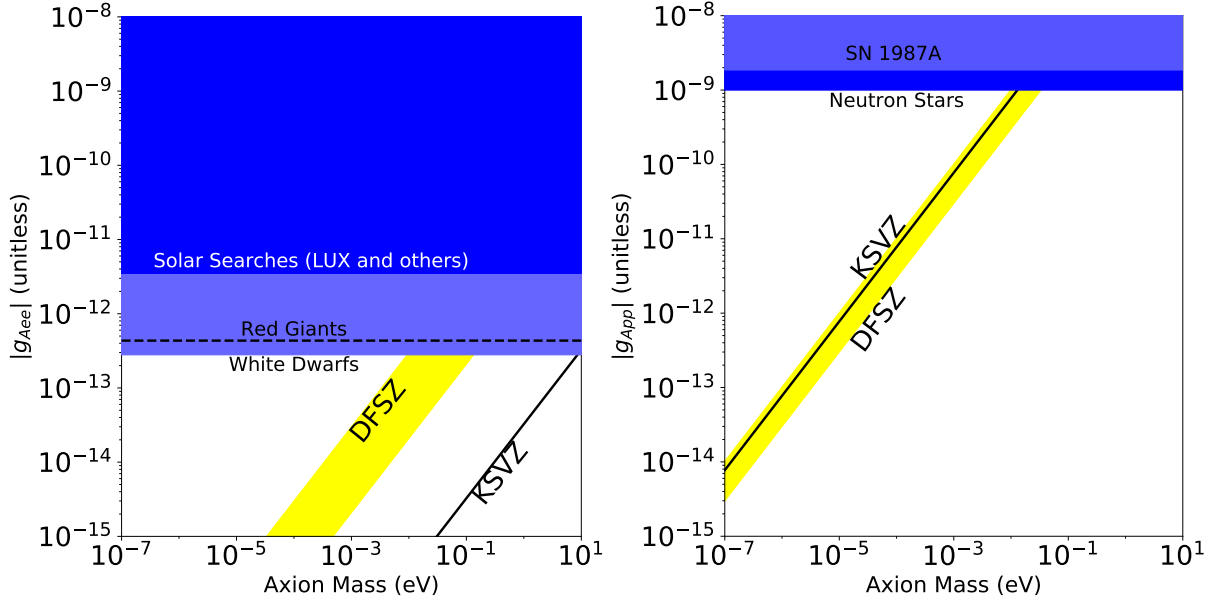


Figure 91.2: Exclusion plots for ALPs as described in the text. For the DFSZ range we have taken into account the constraint $0.28 \lesssim \tan \beta \lesssim 140$ [77] arising from the requirement of perturbative unitarity of the Yukawa couplings of Standard Model fermions.

calculation of axion emission via nucleon-nucleon bremsstrahlung beyond the basic one-pion exchange approximation appears to loosen the bound [88, 89]. The latter analysis finds a reduction of the axion emissivity by an order of magnitude if one takes into account the non-vanishing mass of the exchanged pion, the contribution from two-pion exchange, effective in-medium nucleon masses and multiple nucleon scattering, leading to a looser bound (Maurizio Giannotti and Alessandro Mirizzi, private communication)

$$g_{Ann}^2 + 0.29 g_{App}^2 + 0.27 g_{Ann} g_{App} < 3.25 \times 10^{-18}. \quad (91.16)$$

However, with the present understanding of SNe (current lack of self-consistent 3D SN simulations) and the sparse data from SN 1987A, the constraint on the axion-nucleon couplings from SN 1987A should be considered more as indicative than as a sharp bound [87].

If axions interact sufficiently strongly they are trapped. Only about three orders of magnitude in g_{ANN} or m_A are excluded. For even larger couplings, the axion flux would have been negligible, yet it would have triggered additional events in the detectors, excluding a further range [90]. A possible gap between these two SN 1987A arguments was discussed as the “hadronic axion window” under the assumption that $g_{A\gamma\gamma}$ was anomalously small [91]. This range is now excluded by hot dark matter (HDM) bounds (see below).

There is another hint for excessive stellar energy losses from the neutron star (NS) in the supernova remnant Cassiopeia A (Cas A): its surface temperature measured over 10 years reveals an unusually fast cooling rate. This rapid cooling of the Cas A NS may be explained by NS minimal cooling with neutron superfluidity and proton superconductivity [92, 93]. The rapid cooling may also arise from a phase transition of the neutron condensate into a multicomponent state [94]. Recently, Ref. [95] analyzed Cas A NS cooling in the presence of axion emission and obtained

$$g_{App}^2 + 1.6g_{Ann}^2 < 1 \times 10^{-18}, \quad (91.17)$$

which is comparable to the SN 1987A bound. Refs. [96] put a more conservative bound without an attempt to fit a transient behavior of Cas A,

$$g_{App}^2 < (1 - 6) \times 10^{-17} \text{ (or } f_A > (5 - 10) \times 10^7 \text{ GeV)}, \quad (91.18)$$

from the temperatures of Cas A and other NSs. The Cas A NS cooling may also be interpreted as a hint for extra cooling caused

by the emission of axions from the breaking and re-formation of neutron triplet Cooper pairs [97], requiring a coupling to the neutron of

$$g_{Ann}^2 = (1.4 \pm 0.5) \times 10^{-19}, \quad (91.19)$$

corresponding to an axion mass

$$m_A = (2.3 \pm 0.4) \text{ meV}/C_n. \quad (91.20)$$

On the other hand, Ref. [98] considered another hot young NS in the supernova remnant HESS J1731-347. Its high temperature implies that all the neutrino emission processes except neutron-neutron bremsstrahlung must be strongly suppressed, which can be realized with a negligible neutron triplet gap and a large proton singlet gap. In this setup, the bremsstrahlung from neutrons is the dominant channel for axion emission, from which one obtains a limit

$$g_{Ann}^2 < 7.7 \times 10^{-20}, \quad (91.21)$$

see Fig. 91.3 (left panel).

Finally, let us note that if the interpretation of the various hints for additional cooling of stars reported in this section in terms of emission of axions with $m_A \sim \text{meV}$ were correct, SNe would lose a large fraction of their energy as axions. This would lead to a diffuse SN axion background in the universe with an energy density comparable to the extra-galactic background light [99]. However, there is no apparent way of detecting it or the axion burst from the next nearby SN. On the other hand, neutrino detectors such as IceCube, Super-Kamiokande or a future mega-ton water Cherenkov detector will probe exactly the mass region of interest by measuring the neutrino pulse duration of the next galactic SN [87].

91.4.2 Searches for solar axions and ALPs

Instead of using stellar energy losses to derive axion limits, one can also search directly for these fluxes, notably from the Sun. The main focus has been on ALPs with a two-photon vertex. They are produced by the Primakoff process with a flux given by Eq. (91.12) and an average energy of 4.2 keV, and can be detected at Earth with the reverse process in a macroscopic B -field (“axion helioscope”) [6]. In order to extend the sensitivity in mass towards larger values, one can endow the photon with an effective mass in a gas, $m_\gamma = \omega_{\text{plas}}$, thus matching the axion and photon dispersion relations [100].

An early implementation of these ideas used a conventional dipole magnet, with a conversion volume of variable-pressure gas with a xenon proportional chamber as x-ray detector [101]. The

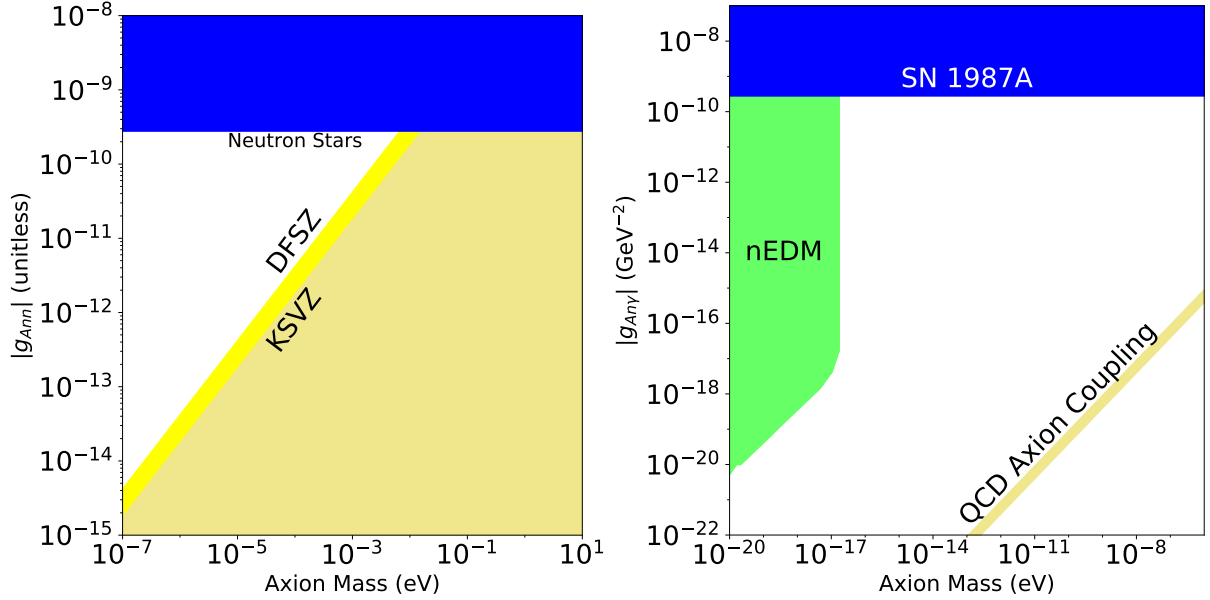


Figure 91.3: Exclusion plots for ALPs as described in the text.

conversion magnet was fixed in orientation and collected data for about 1000 s/day. Axions were excluded for $|g_{A\gamma\gamma}| < 3.6 \times 10^{-9} \text{ GeV}^{-1}$ for $m_A < 0.03 \text{ eV}$, and $|g_{A\gamma\gamma}| < 7.7 \times 10^{-9} \text{ GeV}^{-1}$ for $0.03 < m_A < 0.11 \text{ eV}$ at 95% CL.

Later, the Tokyo axion helioscope used a superconducting magnet on a tracking mount, viewing the Sun continuously. They reported $|g_{A\gamma\gamma}| < 6 \times 10^{-10} \text{ GeV}^{-1}$ for $m_A < 0.3 \text{ eV}$ [102]. This experiment was recommissioned and a similar limit for masses around 1 eV was reported [103].

The most recent helioscope CAST (CERN Axion Solar Telescope) uses a decommissioned LHC dipole magnet on a tracking mount. The hardware includes grazing-incidence x-ray optics with solid-state x-ray detectors, as well as novel x-ray Micromegas position-sensitive gaseous detectors. Exploiting a IAXO (see below) pathfinder system, CAST has established the limit

$$|g_{A\gamma\gamma}| < 6.6 \times 10^{-11} \text{ GeV}^{-1} \quad (95\% \text{ CL}), \quad (91.22)$$

for $m_A < 0.02 \text{ eV}$ [104]. To cover larger masses, the magnet bores are filled with a gas at varying pressure. The runs with ^4He cover masses up to about 0.4 eV [105], providing the ^4He limits shown in Fig. 91.1. To cover yet larger masses, ^3He was used to achieve a larger pressure at cryogenic temperatures. Limits up to 1.17 eV allowed CAST to “cross the axion line” for the KSVZ model [106], see Fig. 91.1.

Going to yet larger masses in a helioscope search is not well motivated because of the cosmic HDM bound of $m_A \lesssim 1 \text{ eV}$ (see below). Sensitivity to significantly smaller values of $g_{A\gamma\gamma}$ can be achieved with a next-generation axion helioscope with a much larger magnetic-field cross section. Realistic design options for this “International Axion Observatory” (IAXO) have been studied in some detail [107] and its physics potential has been reviewed recently [108]. Such a next-generation axion helioscope may also push the sensitivity in the product of couplings to photons and to electrons, $g_{A\gamma\gamma}g_{Aee}$, into a range beyond stellar energy-loss limits and test the hypothesis that WD, RG, and HB cooling is dominated by axion emission [84, 109]. As a first step towards IAXO, an intermediate experimental stage called BabyIAXO is currently under preparation at DESY (for a short introduction, see Ref. [108]).

Other Primakoff searches for solar axions and ALPs have been carried out using crystal detectors, exploiting the coherent conversion of axions into photons when the axion angle of incidence satisfies a Bragg condition with a crystal plane [110]. However, none of these limits is more restrictive than the one derived from the constraint on the solar axion luminosity ($L_A \lesssim 0.10 L_\odot$) discussed earlier.

Another idea is to look at the Sun with an x-ray satellite when the Earth is in between. Solar axions and ALPs would convert in the Earth magnetic field on the far side and could be detected [111]. The sensitivity to $g_{A\gamma\gamma}$ could be comparable to CAST, but only for much smaller m_A . Deep solar x-ray measurements with existing satellites, using the solar magnetosphere as conversion region, have reported preliminary limits on $g_{A\gamma\gamma}$ [112].

Direct detection experiments searching for dark matter (DM) consisting of weakly interacting massive particles, such as EDELWEISS-II, LUX, and XENON100, have also the capability to search for solar axions and ALPs [113, 114]. Recently, the LUX experiment [114] has put a bound on the axion-electron coupling constant by exploiting the axio-electric effect in liquid xenon,

$$|g_{Aee}| < 3.5 \times 10^{-12} \quad (90\% \text{ CL}), \quad (91.23)$$

excluding the DFSZ model with $m_A \sin^2 \beta > 0.12 \text{ eV}$, cf. see Fig. 91.2 (left panel). However, as obvious from the same figure, this technique has not reached the sensitivity of energy-loss considerations in stars (RGs and WDs).

91.4.3 Conversion of astrophysical photon fluxes

Large-scale B fields exist in astrophysics that can induce axion-photon oscillations. In practical cases, B is much smaller than in the laboratory, whereas the conversion region L is much larger. Therefore, while the product BL can be large, realistic sensitivities are usually restricted to very low-mass particles, far away from the “axion band” in a plot like Fig. 91.1.

One example is SN 1987A, which would have emitted a burst of ALPs due to the Primakoff production in its core. They would have partially converted into γ -rays in the galactic B -field. The lack of a gamma-ray signal in the GRS instrument of the SMM satellite in coincidence with the observation of the neutrinos emitted from SN 1987A therefore provides a strong bound on their coupling to photons [115]. This bound has been revisited and the underlying physics has been brought to the current state-of-the-art, as far as modelling of the supernova and the Milky-Way magnetic field are concerned, resulting in the limit [116]

$$|g_{A\gamma\gamma}| < 5.3 \times 10^{-12} \text{ GeV}^{-1}, \text{ for } m_A \lesssim 4.4 \times 10^{-10} \text{ eV}, \quad (91.24)$$

see Fig. 91.1. Magnetically induced oscillations between photons and ALPs can modify the photon fluxes from distant sources in various ways, featuring (i) frequency-dependent dimming, (ii) modified polarization, and (iii) avoiding absorption by propagation in the form of axions.

For example, dimming of SNe Ia could influence the interpretation in terms of cosmic acceleration [117], although it has become

clear that photon-ALP conversion could only be a subdominant effect [118]. Searches for linearly polarised emission from magnetised white dwarfs [119] and changes of the linear polarisation from radio galaxies (see, e.g., Ref. [120]) provide limits close to $g_{A\gamma\gamma} \sim 10^{-11} \text{ GeV}^{-1}$, for masses $m_A \lesssim 10^{-7} \text{ eV}$ and $m_A \lesssim 10^{-15} \text{ eV}$, respectively, albeit with uncertainties related to the underlying assumptions. Even stronger limits, $g_{A\gamma\gamma} \lesssim 2 \times 10^{-13} \text{ GeV}^{-1}$, for $m_A \lesssim 10^{-14} \text{ eV}$, have been obtained by exploiting high-precision measurements of quasar polarisations [121].

Remarkably, it appears that the universe could be too transparent to TeV γ -rays that should be absorbed by pair production on the extra-galactic background light [122–126]. The situation is not conclusive at present [127–129], but the possible role of photon-ALP oscillations in TeV γ -ray astronomy is tantalizing [130]. Fortunately, the region in ALP parameter space, $g_{A\gamma\gamma} \sim 10^{-12} - 10^{-10} \text{ GeV}^{-1}$ for $m_A \lesssim 10^{-7} \text{ eV}$ [131], required to explain the anomalous TeV transparency of the universe, could be conceivably probed by the next generation of laboratory experiments (ALPS II) and helioscopes (IAXO) mentioned above. This parameter region can also be probed by searching for an irregular behavior of the gamma ray spectrum of distant active galactic nuclei (AGN), expected to arise from photon-ALP mixing in a limited energy range. The H.E.S.S. collaboration has set a limit of $|g_{A\gamma\gamma}| \lesssim 2.1 \times 10^{-11} \text{ GeV}^{-1}$, for $1.5 \times 10^{-8} \text{ eV} \lesssim m_A \lesssim 6.0 \times 10^{-8} \text{ eV}$, from the non-observation of an irregular behavior of the spectrum of the AGN PKS 2155-304 [132], see Fig. 91.1. The Fermi-LAT collaboration has put an even more stringent limit on the ALP-photon coupling [133] from observations of the gamma ray spectrum of NGC 1275, the central galaxy of the Perseus cluster, see Fig. 91.1. A similar analysis has been carried out in Ref. [134] using Fermi-LAT data of PKS 2155-304.

Evidence for spectral irregularities has been reported in Galactic sources, such as pulsars and supernova remnants, and has been interpreted as hints for ALPs [135, 136]. However, the inferred ALP parameters are in tension with the CAST helioscope bounds. It should also be noted that the high signal-to-noise spectra of Galactic gamma-ray sources are dominated by uncertainties of the instrumental systematics rather than statistical errors. Furthermore, it has been shown that additional care has to be taken when deriving confidence intervals on ALP parameters based on Wilks' theorem [137], since it has been shown that it does not apply for testing the ALP hypothesis [133].

At smaller masses, $m_A \lesssim 10^{-12} \text{ eV}$, galaxy clusters become highly efficient at interconverting ALPs and photons at x-ray energies. Constraints on spectral irregularities in the spectra of luminous x-ray sources (Hydra A, M87, NGC 1275, NGC 3862, Seyfert galaxy 2E3140; taken by Chandra and XMM-Newton) located in or behind galaxy clusters then lead to stringent upper limits on the ALP-photon coupling [138–143]. In this type of studies, the uncertainty in the cluster magnetic field needs to be taken into account. This typically leads to a range of limits on the ALP-photon coupling that depend on the modelling assumptions. Reference [143] recently performed the most sensitive x-ray searches for ALPs to date by employing Chandra's High-Energy Transmission Gratings that allow for an unsurpassed spectral resolution. New observations of the AGN NGC 1275 then led to the bound

$$|g_{A\gamma\gamma}| < 8 \times 10^{-13} \text{ GeV}^{-1} \quad (99.7\% \text{ CL}) \quad (91.25)$$

for light ALPs, see Fig. 91.1.

91.4.4 Superradiance of black holes

Light bosonic fields such as axions or ALPs can affect the dynamics and gravitational wave emission of rapidly rotating astrophysical black holes through the superradiance mechanism. When their Compton wavelength is of order of the black hole size, they form gravitational bound states around the black hole. Their occupation number grows exponentially by extracting energy and angular momentum from the black hole, forming a coherent axion or ALP bound state emitting gravitational waves. When accretion cannot replenish the spin of the black hole, superradiance dominates the black hole spin evolution; this is true for both su-

permassive and stellar mass black holes. The existence of destabilizing light bosonic fields thus leads to gaps in the mass vs. spin plot of rotating black holes. Stellar black hole spin measurements – exploiting well-studied binaries and two independent techniques – exclude a mass range $6 \times 10^{-13} \text{ eV} < m_A < 2 \times 10^{-11} \text{ eV}$ at 2σ , which for the axion excludes $3 \times 10^{17} \text{ GeV} < f_A < 1 \times 10^{19} \text{ GeV}$ [11, 144, 145]. These bounds apply when gravitational interactions dominate over the axion self-interaction, which is true for the QCD axion in this mass range. Long lasting, monochromatic gravitational wave signals, which can be distinguished from ordinary astrophysical sources by their clustering in a narrow frequency range, are expected to be produced by axions or ALPs annihilating to gravitons. Gravitational waves could also be sourced by axions/ALPs transitioning between gravitationally bound levels. Accordingly, the gravitational wave detector Advanced LIGO should be sensitive to the axion in the $m_A \lesssim 10^{-10} \text{ eV}$ region. LIGO measurements of black hole spins in binary merger events could also provide statistical evidence for the presence of an axion [146, 147]. Similar signatures could arise for supermassive black holes for particle with masses $\lesssim 10^{-15} \text{ eV}$. Gravitational waves from such sources could be detected at lower-frequency observatories such as LISA.

91.5 Cosmic Axions

91.5.1 Cosmic axion populations

In the early universe, axions are produced by processes involving quarks and gluons [148]. After color confinement, the dominant thermalization process is $\pi + \pi \leftrightarrow \pi + A$ [34]. The resulting axion population would contribute an HDM component in analogy to massive neutrinos. Cosmological precision data provide restrictive constraints on a possible HDM fraction that translate into $m_A \lesssim 1 \text{ eV}$ [149], but in detail depend on the used data set and assumed cosmological model. In the future, data from a EUCLID-like survey combined with Planck CMB data can detect HDM axions with a mass $m_A \gtrsim 0.15 \text{ eV}$ at very high significance [150].

For $m_A \gtrsim 20 \text{ eV}$, axions decay fast on a cosmic time scale, removing the axion population while injecting photons. This excess radiation provides additional limits up to very large axion masses [151]. An anomalously small $g_{A\gamma\gamma}$ provides no loophole because suppressing decays leads to thermal axions overdominating the mass density of the universe.

The main cosmological interest in axions derives from their possible role as CDM. In addition to thermal processes, axions are abundantly produced by the vacuum re-alignment (VR) mechanism [152].

The axion DM abundance crucially depends on the cosmological history. Let us first consider the so called *pre-inflationary PQ symmetry breaking scenario*, in which the PQ symmetry is broken before and during inflation and not restored afterwards. After the breakdown of the PQ symmetry, the axion field relaxes somewhere in the bottom of the “wine-bottle-bottom” potential. Near the QCD epoch, topological fluctuations of the gluon fields such as instantons explicitly break the PQ symmetry. This tilting of the “wine-bottle-bottom” drives the axion field toward the CP-conserving minimum, thereby exciting coherent oscillations of the axion field that ultimately represent a condensate of CDM. The fractional cosmic mass density in this homogeneous field mode, created by the VR mechanism, is [23, 153–155],

$$\begin{aligned} \Omega_A^{\text{VR}} h^2 &\approx 0.12 \left(\frac{f_A}{9 \times 10^{11} \text{ GeV}} \right)^{1.165} F \Theta_i^2 \\ &\approx 0.12 \left(\frac{6 \mu\text{eV}}{m_A} \right)^{1.165} F \Theta_i^2, \end{aligned} \quad (91.26)$$

where h is the present-day Hubble expansion parameter in units of $100 \text{ km s}^{-1} \text{ Mpc}^{-1}$, and $-\pi \leq \Theta_i \leq \pi$ is the initial “misalignment angle” relative to the CP-conserving position attained in the causally connected region which evolved into today's observable universe. $F = F(\Theta_i, f_A)$ is a factor accounting for anharmonicities in the axion potential. For $F \Theta_i^2 = \mathcal{O}(1)$, m_A should be above $\sim 6 \mu\text{eV}$ in order that the cosmic axion density does not exceed the observed CDM density, $\Omega_{\text{CDM}} h^2 = 0.12$. However, much smaller

axion masses (much higher PQ scales) are still possible if the initial value Θ_i just happens to be small enough in today's observable universe ("anthropic axion window" [156]). In this cosmological scenario, however, quantum fluctuations of the axion field during inflation are expected to lead to isocurvature density fluctuations which get imprinted to the temperature fluctuations of the CMB [157, 158]. Their non-observation puts severe constraints on the Hubble expansion rate H_I during inflation [159–163], which read, in the simplest cosmological inflationary scenario,

$$H_I \lesssim 5.7 \times 10^8 \text{ GeV} \left(\frac{5 \text{ neV}}{m_a} \right)^{0.4175}, \quad (91.27)$$

if axions represent all of DM.

In the *post-inflationary PQ symmetry breaking scenario*, on the other hand, Θ_i will take on different values in different patches of the present universe. The average contribution is [23, 153–155]

$$\Omega_A^{\text{VR}} h^2 \approx 0.12 \left(\frac{30 \text{ } \mu\text{eV}}{m_A} \right)^{1.165}. \quad (91.28)$$

The decay of cosmic strings and domain walls gives rise to a further population of CDM axions, whose abundance suffers from significant uncertainties [154, 155, 164–172] which arise from the difficulty in understanding the energy loss process of topological defects and the generated axion spectrum in a quantitative way. In fact, in the present state-of-the-art it is still possible that the CDM contribution from the decay of topological defects is subdominant or overwhelmingly large in comparison to the one from the VR mechanism. Correspondingly, the plausible range of axion masses providing all of CDM in scenarios with postinflationary PQ symmetry breaking is still rather large, namely

$$m_A \approx 25 \text{ } \mu\text{eV} - 4.4 \text{ meV}, \quad (91.29)$$

for models with short-lived (requiring unit color anomaly $N = 1$) domain walls, such as the KSVZ model. For models with long-lived ($N > 1$) domain walls, such as an accidental DFSZ model [173], where the PQ symmetry is broken by higher dimensional Planck suppressed operators, the mass is predicted to be significantly higher [168, 173, 174],

$$m_A \approx (0.58 - 130) \text{ meV}. \quad (91.30)$$

However, the upper part of the predicted range is in conflict with stellar energy-loss limits on the axion, cf. Fig. 91.2 (right panel) and Fig. 91.3 (left panel).

In this post-inflationary PQ symmetry breakdown scenario, the spatial axion density variations are large at the QCD transition and they are not erased by free streaming. Gravitationally bound "axion miniclusters" form before and around matter-radiation equality [175–177]. A significant fraction of CDM axions can reside in these bound objects [171, 178]. Remarkably, the minicluster fraction can be bounded by gravitational lensing [179–181].

In the above predictions of the fractional cosmic mass density in axions, the exponent, 1.165, arises from the non-trivial temperature dependence of the topological susceptibility $\chi(T) = m_A^2(T) f_A^2$ at temperatures slightly above the QCD quark-hadron phase transition. Lattice QCD calculations of this exponent [23, 182–186], but also Ref. [187], found it to be remarkably close to the prediction of the dilute instanton gas approximation [188] which was previously exploited. Therefore, the state-of-the-art prediction of the axion mass relevant for DM for a fixed initial misalignment angle Θ_i differs from the previous prediction by just a factor of order one.

The non-thermal production mechanisms attributed to axions are generic to light bosonic weakly interacting particles such as ALPs [189]. The relic abundance is set by the epoch when the axion mass becomes significant, $3H(t) \approx m_A(t)$, and ALP field oscillations begin. For ALPs to contribute to the DM density this epoch must precede that of matter radiation equality. For a temperature independent ALP mass this leads to the bound:

$$m_A \gtrsim 7 \times 10^{-28} \text{ eV} \left(\frac{\Omega_m h^2}{0.15} \right)^{1/2} \left(\frac{1 + z_{\text{eq}}}{3.4 \times 10^3} \right)^{3/2}. \quad (91.31)$$

ALPs lighter than this bound are allowed if their cosmic energy density is small, but they are quite distinct from other forms of DM [190]. Ignoring anharmonicities in the ALP potential, and taking the ALP mass to be temperature independent, the relic density in DM ALPs due to the VR mechanism is given by

$$\Omega_{\text{ALP}}^{\text{VR}} h^2 = 0.12 \left(\frac{m_A}{4.7 \times 10^{-19} \text{ eV}} \right)^{1/2} \left(\frac{f_A}{10^{16} \text{ GeV}} \right)^2 \times \left(\frac{\Omega_m h^2}{0.15} \right)^{3/4} \left(\frac{1 + z_{\text{eq}}}{3.4 \times 10^3} \right)^{-3/4} \Theta_i^2. \quad (91.32)$$

An ALP decay constant near the GUT scale gives the correct relic abundance for *ultralight ALPs* (ULAs), which we now define. Extended discussions of ULAs can be found in Refs. [191, 192].

The standard CDM model treats DM as a distribution of cold, collisionless particles interacting only via gravity. Below the Compton wavelength, $\lambda_c = 2\pi/m_A$, the particle description of ALPs breaks down. For large occupation numbers we can model ALPs below the Compton wavelength as a coherent classical field. Taking as a reference length scale the Earth radius, $R_{\oplus} = 6371 \text{ km}$, we define ULAs to be those axions with $\lambda_c > R_{\oplus}$, leading to the defining bound

$$m_{\text{ULA}} < 2 \times 10^{-13} \text{ eV}. \quad (91.33)$$

ULAs encompass the entire Earth in a single coherent field. The coherence time of the ULA field on Earth can be estimated from the crossing time of the de Broglie wavelength at the virial velocity in the Milky Way, $\tau_{\text{coh}} \sim 1/m_{\text{ULA}} v_{\text{vir}}^2$.

We notice that by the definition, Eq. (91.33), an ultralight QCD axion must have a super-Planckian decay constant, $f_A > 3 \times 10^{19} \text{ GeV}$ and would require fine tuning of θ_i to provide the relic abundance. Natural models for ULAs can be found in string and M-theory compactifications [7–14], in field theory with accidental symmetries [193], or new hidden strongly coupled sectors [194].

In addition to the gravitational potential energy, the ULA field also carries gradient energy. On scales where the gradient energy is non-negligible, ULAs acquire an effective pressure and do not behave as CDM. The gradient energy opposes gravitational collapse, leading to a Jeans scale below which perturbations are stable [195]. The Jeans scale suppresses linear cosmological structure formation relative to CDM [196]. The Jeans scale at matter-radiation equality in the case that ULAs make up all of CDM is:

$$k_{\text{J,eq}} = 8.7 \text{ Mpc}^{-1} \left(\frac{1 + z_{\text{eq}}}{3.4 \times 10^3} \right)^{-1/4} \left(\frac{\Omega_{\text{ALP}}^{\text{VR}}}{0.12} \right)^{1/4} \times \left(\frac{m_{\text{ULA}}}{10^{-22} \text{ eV}} \right)^{1/2}. \quad (91.34)$$

On non-linear scales the gradient energy leads to the existence of a class of pseudo-solitons known as oscillatons, or axion stars [197].

Cosmological and astrophysical observations are consistent with the CDM model, and departures from it are only allowed on the scales of the smallest observed DM structures with $M \sim 10^{6-8} M_{\odot}$. The CMB power spectrum and galaxy auto-correlation power spectrum limit the ULA mass to $m_{\text{ULA}} > 10^{-24} \text{ eV}$ from linear theory of structure formation [190, 198]. Analytic models [199] and N -body simulations [200] for non-linear structures show that halo formation is suppressed in ULA models relative to CDM. This leads to constraints on the ULA mass of $m_{\text{ULA}} > 10^{-22} \text{ eV}$ from observations of high- z galaxies [200, 201], and $m_{\text{ULA}} > 10^{-21} \text{ eV}$ from the Lyman-alpha forest flux power spectrum [202]. Including the effects of anharmonicities on structure formation with ALPs can weaken these bounds if the misalignment angle $\Theta_i \approx \pi$ [203]. Cosmological simulations that treat gradient energy in the ULA field beyond the N -body approximation have just recently become available [204, 205], and show, among other things, evidence for the formation of axion stars in the centres of ULA halos (various consequences of axion stars are considered in Refs. [206]). These central axion stars have been conjectured to play a role in the apparently cored density

profiles of dwarf spheroidal galaxies, and other central galactic regions [204, 207–209]. However, the relationship between the halo mass and the axion star mass [210] leads to problems with this scenario in some galaxies [211–213]. It should be emphasised that many of the conclusions about the role of ULA axion stars in galactic dynamics are based on use of simulation results that do not contain baryons (however, see Ref. [214]), and feedback [215] could be important.

Inside DM halos the axion gradient energy causes coherence on the de Broglie wavelength and fluctuations on the coherence time [204, 216]. These fluctuations can be thought of as short-lived quasiparticles and lead to relaxation processes that can be described statistically [192, 217] (this relaxation processes also leads to the gravitational condensation of axion stars [218]). The typical relaxation time is:

$$t \sim 10^{10} \text{ years} \left(\frac{m_{\text{ULA}}}{10^{-22} \text{ eV}} \right)^3 \left(\frac{v}{100 \text{ km s}^{-1}} \right)^2 \left(\frac{r}{5 \text{ kpc}} \right)^4, \quad (91.35)$$

where v and r are the velocity and radius of the orbit in the host DM halo.

Relaxation processes such as these are not observed in galaxies, though there are some circumstances where they may be desirable [192]. An absence of observed relaxation can be used to set limits on the ULA mass. An absence of observed Milky Way disk thickening excludes $m_{\text{ULA}} > 0.6 \times 10^{-22} \text{ eV}$ [219], while stellar streams give the stronger bound $m_{\text{ULA}} > 1.5 \times 10^{-22} \text{ eV}$ [220]. The survival of the old star cluster in Eridanus II [221] excludes the range of masses $10^{-21} \text{ eV} \lesssim m_{\text{ULA}} \lesssim 10^{-19} \text{ eV}$ [222]. As in the case of ULA axion stars, current constraints from heating do not fully account for the possible role of baryons.

Finally, one should note that the beyond-CDM physics of ULAs (Jeans scale, relaxation, axion star formation) of course also applies to the QCD axion on smaller length scales. This is of particular interest inside axion miniclusters [175, 176, 218, 223].

91.5.2 Telescope searches

The two-photon decay is extremely slow for axions with masses in the CDM regime, but could be detectable for eV masses. The signature would be a quasi-monochromatic emission line from galaxies and galaxy clusters. The expected optical line intensity for DFSZ axions is similar to the continuum night emission. An early search in three rich Abell clusters [224] and a recent search in two rich Abell clusters [225] exclude the “Telescope” range in Fig. 91.1. Of course, axions in this mass range would anyway provide an excessive hot DM contribution.

Very low-mass axions in halos produce a weak quasi-monochromatic radio line. Virial velocities in undisrupted dwarf galaxies are very low, and the axion decay line would therefore be extremely narrow. A search with the Haystack radio telescope on three nearby dwarf galaxies provided a limit $|g_{A\gamma\gamma}| < 1.0 \times 10^{-9} \text{ GeV}^{-1}$ at 96% CL for $298 < m_A < 363 \mu\text{eV}$ [226]. However, this combination of m_A and $g_{A\gamma\gamma}$ does not exclude plausible axion models.

A monochromatic signal is also produced in the conversion of DM axions in the background of slowly varying galactic B -fields [227]. The signal is, however, sensitive to magnetic field power on the scale of the axion mass [228]. Present and future radio telescopes appear to be able to probe ALP DM in the mass range $0.1 - 100 \mu\text{eV}$ for couplings $g_{A\gamma\gamma} \gtrsim 10^{-13} \text{ GeV}^{-1}$ [228] – unfortunately not reaching down to the benchmark QCD axion sensitivity.

Resonant conversion of QCD axion DM in neutron star magnetospheres may give a detectable signal from individual neutron stars for axion masses in the μeV range [229]. Furthermore, stimulated ALP decays in high radiation environments may be detectable, by next-generation radio telescopes such as the Square Kilometer Array, down to $g_{A\gamma\gamma} \gtrsim 10^{-11} \text{ GeV}^{-1}$, for masses between μeV and 0.1 meV [230].

Photon propagation on an ULA DM background can induce birefringence that can be compared with upper limits from the CMB [231] and may also be probed with other sources such as pulsars [232].

91.5.3 Microwave cavity experiments

In a big part of the plausible m_A range for CDM, galactic halo axions may be detected by their resonant conversion into a quasi-monochromatic microwave signal in a high-Q electromagnetic cavity permeated by a strong static B field [6, 233, 234]. The cavity frequency is tunable, and the signal is maximized when the frequency is the total axion energy, rest mass plus kinetic energy, of $\nu = (m_A/2\pi) [1 + \mathcal{O}(10^{-6})]$, the width above the rest mass representing the virial distribution in the galaxy. The frequency spectrum may also contain finer structure from axions more recently fallen into the galactic potential and not yet completely virialized [235, 236].

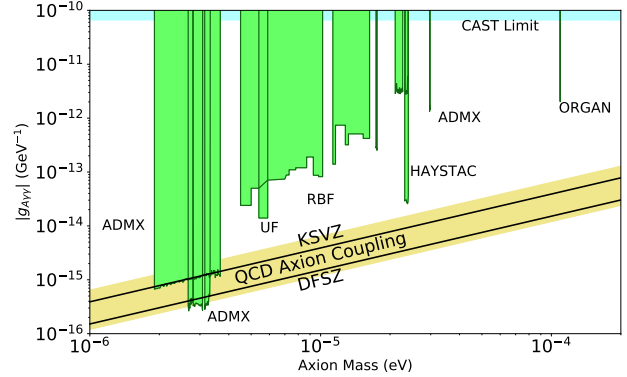


Figure 91.4: Exclusion plot for ALPs as described in the text.

The feasibility of this technique was established in early experiments (RBF and UF) of relatively small sensitive volume, $\mathcal{O}(1)$ liter), with HFET-based amplifiers, setting limits in the range $4.5 < m_A < 16.3 \mu\text{eV}$ [237], but lacking by 2–3 orders of magnitude the sensitivity required to detect realistic axions, see Fig. 91.4. Later, ADMX ($B \sim 8 \text{ T}$, $V \sim 200$ liters) has achieved sensitivity to KSVZ axions, assuming they saturate the local DM density and are well virialized, over the mass range $1.9 - 3.3 \mu\text{eV}$ [238]. Should halo axions have a significant component not yet virialized, ADMX is sensitive to DFSZ axions over the entire mass range [239]. The corresponding 90% CL exclusion regions shown in Fig. 91.4 are normalized to an assumed local CDM density of $7.5 \times 10^{-25} \text{ g cm}^{-3}$ (450 MeV cm^{-3}). More recently, the ADMX experiment commissioned an upgrade [240] that replaces the microwave HFET amplifiers by near quantum-limited low-noise dc SQUID microwave amplifiers [241]. It has reached an unprecedented axion DM sensitivity in the mass range between 2.66 and $3.31 \mu\text{eV}$ [242, 243], down to the DFSZ benchmark axion-photon coupling, see Fig. 91.4. This apparatus is also sensitive to other hypothetical light bosons, such as hidden photons or chameleons, over a limited parameter space [189, 244, 245]. ADMX has also done a testbed experiment to probe higher masses. This experiment lives inside of and operates in tandem with the main ADMX experiment, searches in three widely spaced frequency ranges (4202–4249 MHz, 5086–5799 MHz and 7173–7203 MHz), uses both the TM_{010} and TM_{020} cavity modes, and demonstrates the successful use of a piezoelectric actuator for cavity tuning [246]. Recently, the HAYSTAC experiment reported on first results from a new microwave cavity search for DM axions with masses above $20 \mu\text{eV}$. They exclude axions with two-photon coupling $|g_{A\gamma\gamma}| \gtrsim 2 \times 10^{-14} \text{ GeV}^{-1}$ over the range $23.15 \mu\text{eV} < m_A < 24.0 \mu\text{eV}$ [247, 248], a factor of 2.7 above the KSVZ benchmark, see Fig. 91.4. Exploiting a Josephson parametric amplifier, this experiment has demonstrated total noise approaching the standard quantum limit for the first time in an axion search. A Rydberg atom single-photon detector [249], like any photon counter, can in principle evade the standard quantum limit for coherent photon detection. The ORGAN experiment is designed to probe axions in the mass range $60 \mu\text{eV} < m_A < 210 \mu\text{eV}$. In a pathfinding run, it has set the limit $|g_{A\gamma\gamma}| < 2 \times 10^{-12} \text{ GeV}^{-1}$ at $110 \mu\text{eV}$, in a span of 2.5 neV [250]. There are further microwave cavity axion DM experiments recently in operation (CULTASK [251]), under construction (RADES [252]) or proposed (KLASH [253]).

91.5.4 New concepts for axion DM direct detection

Other new concepts for searching for axion DM are also being investigated. An alternative to the microwave cavity technique is based on a novel detector architecture consisting of an open, Fabry-Perot resonator and a series of current-carrying wire planes [254]. The Orpheus detector has demonstrated this new technique, excluding DM ALPs with masses between 68.2 and 76.5 μeV and axion-photon couplings greater than $4 \times 10^{-7} \text{ GeV}^{-1}$. This technique may be able to probe DM axions in the mass range from 40 to 700 μeV . Another detector concept exploits the fact that a magnetized mirror would radiate photons in the background of axion DM, which could be collected like in a dish antenna [255]. Searches for hidden photon DM exploiting this technique are already underway [256]. The proposed MADMAX experiment will place a stack of dielectric layers in a magnetic field in order to resonantly enhance the photon signal, aiming a sensitivity to probe the mass range $40 \mu\text{eV} \lesssim m_A \lesssim 200 \mu\text{eV}$ [257, 258]. Optical dielectric haloscopes with single photon signal detection have been proposed to search for axions in the 50 meV – 10 eV mass range [259]. Absorption of axions on molecular transitions can be sensitive to the axion pseudoscalar coupling g_{ANN} to nucleons or the pseudoscalar coupling g_{Aee} to electrons in the 0.5 – 20 eV range [260]. Another proposed axion DM search method sensitive in the 100 μeV mass range is to cool a kilogram-sized sample to mK temperatures and count axion induced atomic transitions using laser techniques [261].

The oscillating galactic DM axion field induces oscillating nuclear electric dipole moments (EDMs) [262],

$$d_N(t) = g_{AN\gamma} \sqrt{2\rho_{\text{ADM}}} \cos(m_A t) / m_A, \quad (91.36)$$

where $g_{AN\gamma}$ is the coupling of the axion to the nucleon EDM operator,

$$\mathcal{L}_A \supset -\frac{i}{2} g_{AN\gamma} A \bar{\Psi}_N \sigma_{\mu\nu} \gamma_5 \Psi_N F^{\mu\nu}. \quad (91.37)$$

For the QCD axion, this coupling is predicted as [263]

$$\begin{aligned} g_{AN\gamma} = -g_{Ap\gamma} &= (3.7 \pm 1.5) \times 10^{-3} \left(\frac{1}{f_A} \right) \frac{1}{\text{GeV}} = \\ &= (6.5 \pm 2.6) \times 10^{-13} \left(\frac{m_A}{\text{meV}} \right) \frac{1}{\text{GeV}^2} \end{aligned} \quad (91.38)$$

and plotted as a yellow diagonal band in Fig. 91.3 (right panel). An analysis of the ratio of spin-precession frequencies of stored ultracold neutrons and ^{199}Hg atoms measured by neutron EDM experiments for an axion-induced oscillating neutron EDM revealed no signal consistent with axion DM, excluding a sizeable region of parameter space in the mass region $10^{-24} \text{ eV} \leq m_A \leq 10^{-17} \text{ eV}$ [264], which surpass the limits on anomalous energy loss of SN 1987A [262] by more than seven orders of magnitude, but are still a few orders of magnitude above the QCD axion expectations, see Fig. 91.3 (right panel). The oscillating EDMs cause also the precession of nuclear spins in a nucleon spin polarized sample in the presence of an electric field. The resulting transverse magnetization can be searched for by exploiting magnetic-resonance (MR) techniques, which are most sensitive in the range of low oscillation frequencies corresponding to sub-neV axion masses. The aim of the corresponding Cosmic Axion Spin Precession Experiment (CASPER) [265] is to probe axion DM in the anthropic window, $f_A \gtrsim 10^{15} \text{ GeV}$ ($m_A \lesssim \text{neV}$), motivated from Grand Unification [266–269]. Sub- μeV ALP masses can also be probed by using the storage ring EDM method proposed in Ref. [270] which exploits a combination of B and E-fields to produce a resonance between the $g - 2$ spin precession frequency and the DM ALP field oscillation frequency. This method, however, does not reach the sensitivity to probe the QCD axion prediction for $g_{AN\gamma}$.

In the intermediate mass region, $\text{neV} \lesssim m_A \lesssim 0.1 \mu\text{eV}$, one may exploit a cooled LC circuit and precision magnetometry to search for the oscillating electric current induced by DM axions in a strong magnetic field [271]. A similar approach is followed by the proposed ABRACADABRA [272] and DM-Radio Pathfinder [273] experiments. Recently, ABRACADABRA-10 cm – a small-scale prototype for a future detector that could be sensitive to the QCD

axion – established upper limits on the axion-photon coupling in the mass range $3.1 \times 10^{-10} \text{ eV} - 8.3 \times 10^{-9} \text{ eV}$ [274], which are, however, not competitive yet with other limits in this mass range, see Fig. 91.1.

An eventually non-zero axion electron coupling g_{Aee} will lead to an electron spin precession about the axion DM wind [275]. The QUAX (QUAerere AXions) experiment aims at exploiting MR inside a magnetized material [276]. Because of the higher Larmor frequency of the electron, it is sensitive in the classic window.

91.6 Conclusions

There is a strengthening physics case for very weakly coupled light particles beyond the Standard Model. The elegant solution of the strong CP problem proposed by Peccei and Quinn yields a particularly strong motivation for the axion. In many theoretically appealing ultraviolet completions of the Standard Model axions and ALPs occur automatically. Moreover, they are natural CDM candidates. Perhaps the first hints of their existence have already been seen in the anomalous excessive cooling of stars and the anomalous transparency of the Universe for VHE gamma rays. Interestingly, a significant portion of previously unexplored, but phenomenologically very interesting and theoretically very well motivated axion and ALP parameter space can be tackled in the foreseeable future by a number of terrestrial experiments searching for axion/ALP DM, for solar axions/ALPs, and for light apparently shining through a wall.

References

- [1] R. D. Peccei and H. R. Quinn, Phys. Rev. Lett. **38**, 1440 (1977).
- [2] R. D. Peccei and H. R. Quinn, Phys. Rev. **D16**, 1791 (1977).
- [3] S. Weinberg, Phys. Rev. Lett. **40**, 223 (1978).
- [4] F. Wilczek, Phys. Rev. Lett. **40**, 279 (1978).
- [5] Y. Chikashige, R.N. Mohapatra, and R.D. Peccei, Phys. Lett. **B98**, 265 (1981); G. B. Gelmini and M. Roncadelli, Phys. Lett. **99B**, 411 (1981).
- [6] P. Sikivie, Phys. Rev. Lett. **51**, 1415 (1983) and Erratum *ibid.*, **52**, 695 (1984).
- [7] E. Witten, Phys. Lett. **149B**, 351 (1984).
- [8] J. P. Conlon, JHEP **05**, 078 (2006), [hep-th/0602233].
- [9] P. Svrcek and E. Witten, JHEP **06**, 051 (2006), [hep-th/0605206].
- [10] K.-S. Choi *et al.*, Phys. Lett. **B675**, 381 (2009), [arXiv:0902.3070].
- [11] A. Arvanitaki *et al.*, Phys. Rev. **D81**, 123530 (2010), [arXiv:0905.4720].
- [12] B. S. Acharya, K. Bobkov and P. Kumar, JHEP **11**, 105 (2010), [arXiv:1004.5138].
- [13] M. Cicoli, M. Goodsell and A. Ringwald, JHEP **10**, 146 (2012), [arXiv:1206.0819].
- [14] J. Halverson, C. Long and P. Nath, Phys. Rev. **D96**, 5, 056025 (2017), [arXiv:1703.07779].
- [15] J. Jaeckel and A. Ringwald, Ann. Rev. Nucl. Part. Sci. **60**, 405 (2010), [arXiv:1002.0329].
- [16] A. Ringwald, Phys. Dark Univ. **1**, 116 (2012), [arXiv:1210.5081].
- [17] J. Jaeckel, Frascati Phys. Ser. **56**, 172 (2012), [arXiv:1303.1821].
- [18] C. A. Baker *et al.*, Phys. Rev. Lett. **97**, 131801 (2006), [hep-ex/0602020].
- [19] H. Georgi, D. B. Kaplan and L. Randall, Phys. Lett. **169B**, 73 (1986).
- [20] R. J. Crewther, Phys. Lett. **70B**, 349 (1977).
- [21] P. Di Vecchia and G. Veneziano, Nucl. Phys. **B171**, 253 (1980).
- [22] M. Gorghetto and G. Villadoro, JHEP **03**, 033 (2019), [arXiv:1812.01008].

- [23] S. Borsanyi *et al.*, Nature **539**, 7627, 69 (2016), [arXiv:1606.07494].
- [24] J. E. Kim, Phys. Rev. Lett. **43**, 103 (1979); M. A. Shifman, A. I. Vainshtein and V. I. Zakharov, Nucl. Phys. **B166**, 493 (1980).
- [25] M. Dine, W. Fischler and M. Srednicki, Phys. Lett. **104B**, 199 (1981); A. R. Zhitnitsky, Sov. J. Nucl. Phys. **31**, 260 (1980), [Yad. Fiz.31,497(1980)].
- [26] J. E. Kim and G. Carosi, Rev. Mod. Phys. **82**, 557 (2010), [arXiv:0807.3125].
- [27] G. Grilli di Cortona *et al.*, JHEP **01**, 034 (2016), [arXiv:1511.02867].
- [28] J. E. Kim, Phys. Rev. **D58**, 055006 (1998), [hep-ph/9802220].
- [29] L. Di Luzio, F. Mescia and E. Nardi, Phys. Rev. Lett. **118**, 3, 031801 (2017), [arXiv:1610.07593]; L. Di Luzio, F. Mescia and E. Nardi, Phys. Rev. **D96**, 7, 075003 (2017), [arXiv:1705.05370].
- [30] M. Farina *et al.*, JHEP **01**, 095 (2017), [arXiv:1611.09855].
- [31] P. Agrawal *et al.*, JHEP **02**, 006 (2018), [arXiv:1709.06085].
- [32] G. Raffelt and D. Seckel, Phys. Rev. Lett. **60**, 1793 (1988); M. Carena and R. D. Peccei, Phys. Rev. **D40**, 652 (1989); K. Choi, K. Kang and J. E. Kim, Phys. Rev. Lett. **62**, 849 (1989).
- [33] M. Srednicki, Nucl. Phys. **B260**, 689 (1985).
- [34] S. Chang and K. Choi, Phys. Lett. **B316**, 51 (1993), [hep-ph/9306216].
- [35] H. Leutwyler, Phys. Lett. **B378**, 313 (1996), [hep-ph/9602366].
- [36] C. Patrignani *et al.* (Particle Data Group), Chin. Phys. **C40**, 10, 100001 (2016).
- [37] D. A. Dicus *et al.*, Phys. Rev. **D18**, 1829 (1978).
- [38] G. Raffelt and L. Stodolsky, Phys. Rev. **D37**, 1237 (1988).
- [39] A. A. Anselm, Yad. Fiz. **42**, 1480 (1985).
- [40] K. van Bibber *et al.*, Phys. Rev. Lett. **59**, 759 (1987).
- [41] G. Ruoso *et al.*, Z. Phys. **C56**, 505 (1992); R. Cameron *et al.*, Phys. Rev. **D47**, 3707 (1993).
- [42] M. Fouche *et al.*, Phys. Rev. **D78**, 032013 (2008), [arXiv:0808.2800].
- [43] P. Pagnat *et al.* (OSQAR), Phys. Rev. **D78**, 092003 (2008), [arXiv:0712.3362].
- [44] A. S. Chou *et al.* (GammeV (T-969)), Phys. Rev. Lett. **100**, 080402 (2008), [arXiv:0710.3783].
- [45] A. Afanasev *et al.*, Phys. Rev. Lett. **101**, 120401 (2008), [arXiv:0806.2631].
- [46] K. Ehret *et al.* (ALPS), Phys. Lett. **B689**, 149 (2010), [arXiv:1004.1313].
- [47] P. Pagnat *et al.* (OSQAR), Eur. Phys. J. **C74**, 8, 3027 (2014), [arXiv:1306.0443].
- [48] R. Ballou *et al.* (OSQAR), Phys. Rev. **D92**, 9, 092002 (2015), [arXiv:1506.08082].
- [49] F. Hoogeveen and T. Ziegenhagen, Nucl. Phys. **B358**, 3 (1991).
- [50] P. Sikivie, D. B. Tanner and K. van Bibber, Phys. Rev. Lett. **98**, 172002 (2007), [hep-ph/0701198]; G. Mueller *et al.*, Phys. Rev. **D80**, 072004 (2009), [arXiv:0907.5387].
- [51] R. Baehre *et al.* (ALPS Collab.), JINST **1308**, T09001 (2013).
- [52] F. Hoogeveen, Phys. Lett. **B288**, 195 (1992).
- [53] J. Jaeckel and A. Ringwald, Phys. Lett. **B659**, 509 (2008), [arXiv:0707.2063].
- [54] F. Caspers, J. Jaeckel and A. Ringwald, JINST **4**, P11013 (2009), [arXiv:0908.0759].
- [55] R. Povey, J. Hartnett and M. Tobar, Phys. Rev. **D82**, 052003 (2010), [arXiv:1003.0964].
- [56] M. Betz *et al.*, Phys. Rev. **D88**, 7, 075014 (2013), [arXiv:1310.8098].
- [57] L. Maiani, R. Petronzio and E. Zavattini, Phys. Lett. **B175**, 359 (1986).
- [58] Y. Semertzidis *et al.*, Phys. Rev. Lett. **64**, 2988 (1990).
- [59] E. Zavattini *et al.* (PVLAS), Phys. Rev. Lett. **96**, 110406 (2006), [Erratum: Phys. Rev. Lett.99,129901(2007)], [hep-ex/0507107].
- [60] E. Zavattini *et al.* (PVLAS), Phys. Rev. **D77**, 032006 (2008), [arXiv:0706.3419].
- [61] F. Della Valle *et al.*, Eur. Phys. J. **C76**, 1, 24 (2016), [arXiv:1510.08052].
- [62] E. Fischbach and C. Talmadge, Nature **356**, 207 (1992).
- [63] J. E. Moody and F. Wilczek, Phys. Rev. **D30**, 130 (1984); A. N. Youdin *et al.*, Phys. Rev. Lett. **77**, 2170 (1996); W.-T. Ni *et al.*, Phys. Rev. Lett. **82**, 2439 (1999); D. F. Phillips *et al.*, Phys. Rev. **D63**, 111101 (2001), [arXiv:physics/0008230]; B. R. Heckel *et al.*, Phys. Rev. Lett. **97**, 021603 (2006), [hep-ph/0606218]; S. A. Hoedl *et al.*, Phys. Rev. Lett. **106**, 041801 (2011).
- [64] G. Raffelt, Phys. Rev. **D86**, 015001 (2012), [arXiv:1205.1776].
- [65] A. Arvanitaki and A. A. Geraci, Phys. Rev. Lett. **113**, 16, 161801 (2014), [arXiv:1403.1290].
- [66] A. A. Geraci *et al.* (ARIADNE), Springer Proc. Phys. **211**, 151 (2018), [arXiv:1710.05413].
- [67] M. S. Turner, Phys. Rept. **197**, 67 (1990).
- [68] G. G. Raffelt, Lect. Notes Phys. **741**, 51 (2008), [51(2006)], [hep-ph/0611350].
- [69] S. Andriamonje *et al.* (CAST), JCAP **0704**, 010 (2007), [hep-ex/0702006].
- [70] P. Gondolo and G. G. Raffelt, Phys. Rev. **D79**, 107301 (2009), [arXiv:0807.2926].
- [71] H. Schlattl, A. Weiss and G. Raffelt, Astropart. Phys. **10**, 353 (1999), [hep-ph/9807476].
- [72] N. Vinyoles *et al.*, JCAP **1510**, 10, 015 (2015), [arXiv:1501.01639].
- [73] A. Ayala *et al.*, Phys. Rev. Lett. **113**, 19, 191302 (2014), [arXiv:1406.6053].
- [74] O. Straniero *et al.*, in "Proceedings, 11th Patras Workshop on Axions, WIMPs and WISPs (Axion-WIMP 2015): Zaragoza, Spain, June 22-26, 2015," 77–81 (2015).
- [75] J. Redondo, JCAP **1312**, 008 (2013), [arXiv:1310.0823].
- [76] N. Viaux *et al.*, Phys. Rev. Lett. **111**, 231301 (2013), [arXiv:1311.1669].
- [77] C.-Y. Chen and S. Dawson, Phys. Rev. **D87**, 055016 (2013), [arXiv:1301.0309].
- [78] G. G. Raffelt, Phys. Lett. **166B**, 402 (1986); S. I. Blinnikov and N. V. Dunina-Barkovskaya, Mon. Not. Roy. Astron. Soc. **266**, 289 (1994).
- [79] M. M. Miller Bertolami *et al.*, JCAP **1410**, 10, 069 (2014), [arXiv:1406.7712].
- [80] J. Isern *et al.*, Astrophys. J. **682**, L109 (2008), [arXiv:0806.2807]; J. Isern *et al.*, J. Phys. Conf. Ser. **172**, 012005 (2009), [arXiv:0812.3043].
- [81] A. Drlica-Wagner *et al.* (LSST Dark Matter Group) (2019), [arXiv:1902.01055].
- [82] J. Isern *et al.*, Astron. & Astrophys. **512**, A86 (2010); A. H. Corsico *et al.*, Mon. Not. Roy. Astron. Soc. **424**, 2792 (2012), [arXiv:1205.6180]; A. H. Corsico *et al.*, JCAP **1212**, 010 (2012), [arXiv:1211.3389].
- [83] A. H. Córscico *et al.* (2019), [arXiv:1907.00115].

- [84] M. Giannotti *et al.*, JCAP **1710**, 10, 010 (2017), [arXiv:1708.02111].
- [85] M. Giannotti *et al.*, JCAP **1605**, 05, 057 (2016), [arXiv:1512.08108].
- [86] G.G. Raffelt, *Stars as Laboratories for Fundamental Physics*, (Univ. of Chicago Press, Chicago, 1996).
- [87] T. Fischer *et al.*, Phys. Rev. **D94**, 8, 085012 (2016), [arXiv:1605.08780].
- [88] J. H. Chang, R. Essig and S. D. McDermott, JHEP **09**, 051 (2018), [arXiv:1803.00993].
- [89] P. Carena *et al.* (2019), [arXiv:1906.11844].
- [90] J. Engel, D. Seckel and A. C. Hayes, Phys. Rev. Lett. **65**, 960 (1990).
- [91] T. Moroi and H. Murayama, Phys. Lett. **B440**, 69 (1998), [hep-ph/9804291].
- [92] D. Page *et al.*, Phys. Rev. Lett. **106**, 081101 (2011), [arXiv:1011.6142].
- [93] P. S. Shternin *et al.*, Mon. Not. Roy. Astron. Soc. **412**, L108 (2011), [arXiv:1012.0045].
- [94] L. B. Leinson, Phys. Lett. **B741**, 87 (2015), [arXiv:1411.6833].
- [95] K. Hamaguchi *et al.*, Phys. Rev. **D98**, 10, 103015 (2018), [arXiv:1806.07151].
- [96] J. Keller and A. Sedrakian, Nucl. Phys. **A897**, 62 (2013), [arXiv:1205.6940]; A. Sedrakian, Phys. Rev. **D93**, 6, 065044 (2016), [arXiv:1512.07828].
- [97] L. B. Leinson, JCAP **1408**, 031 (2014), [arXiv:1405.6873].
- [98] M. V. Beznogov *et al.*, Phys. Rev. **C98**, 3, 035802 (2018), [arXiv:1806.07991].
- [99] G. G. Raffelt, J. Redondo and N. Viaux Maira, Phys. Rev. **D84**, 103008 (2011), [arXiv:1110.6397].
- [100] K. van Bibber *et al.*, Phys. Rev. **D39**, 2089 (1989).
- [101] D. M. Lazarus *et al.*, Phys. Rev. Lett. **69**, 2333 (1992).
- [102] S. Moriyama *et al.*, Phys. Lett. **B434**, 147 (1998), [hep-ex/9805026]; Y. Inoue *et al.*, Phys. Lett. **B536**, 18 (2002), [arXiv:astro-ph/0204388].
- [103] Y. Inoue *et al.*, Phys. Lett. **B668**, 93 (2008), [arXiv:0806.2230].
- [104] V. Anastassopoulos *et al.* (CAST), Nature Phys. **13**, 584 (2017), [arXiv:1705.02290].
- [105] E. Arik *et al.* (CAST), JCAP **0902**, 008 (2009), [arXiv:0810.4482].
- [106] S. Aune *et al.* (CAST), Phys. Rev. Lett. **107**, 261302 (2011), [arXiv:1106.3919]; M. Arik *et al.* (CAST), Phys. Rev. Lett. **112**, 9, 091302 (2014), [arXiv:1307.1985]; M. Arik *et al.* (CAST), Phys. Rev. **D92**, 2, 021101 (2015), [arXiv:1503.00610].
- [107] E. Armengaud *et al.*, JINST **9**, T05002 (2014), [arXiv:1401.3233].
- [108] E. Armengaud *et al.* (IAXO), JCAP **1906**, 06, 047 (2019), [arXiv:1904.09155].
- [109] K. Barth *et al.*, JCAP **1305**, 010 (2013), [arXiv:1302.6283].
- [110] F. T. Avignone, III *et al.* (SOLAX), Phys. Rev. Lett. **81**, 5068 (1998), [arXiv:astro-ph/9708008]; S. Cebrian *et al.*, Astropart. Phys. **10**, 397 (1999), [arXiv:astro-ph/9811359]; A. Morales *et al.* (COSME), Astropart. Phys. **16**, 325 (2002), [hep-ex/0101037]; R. Bernabei *et al.*, Phys. Lett. **B515**, 6 (2001); Z. Ahmed *et al.* (CDMS), Phys. Rev. Lett. **103**, 141802 (2009), [arXiv:0902.4693].
- [111] H. Davoudiasl and P. Huber, Phys. Rev. Lett. **97**, 141302 (2006), [hep-ph/0509293].
- [112] H. S. Hudson *et al.*, ASP Conf. Ser. **455**, 25 (2012), [arXiv:1201.4607].
- [113] E. Armengaud *et al.*, JCAP **1311**, 067 (2013), [arXiv:1307.1488]; E. Aprile *et al.* (XENON100), Phys. Rev. **D90**, 6, 062009 (2014), [Erratum: Phys. Rev. D95, no.2, 029904(2017)], [arXiv:1404.1455].
- [114] D. S. Akerib *et al.* (LUX), Phys. Rev. Lett. **118**, 26, 261301 (2017), [arXiv:1704.02297].
- [115] J. W. Brockway, E. D. Carlson and G. G. Raffelt, Phys. Lett. **B383**, 439 (1996), [arXiv:astro-ph/9605197]; J. A. Grifols, E. Masso and R. Toldra, Phys. Rev. Lett. **77**, 2372 (1996), [arXiv:astro-ph/9606028].
- [116] A. Payez *et al.*, JCAP **1502**, 02, 006 (2015), [arXiv:1410.3747].
- [117] C. Csaki, N. Kaloper and J. Terning, Phys. Rev. Lett. **88**, 161302 (2002), [hep-ph/0111311].
- [118] A. Mirizzi, G.G. Raffelt, and P.D. Serpico, Lect. Notes Phys. **741**, 115 (2008).
- [119] R. Gill and J. S. Heyl, Phys. Rev. **D84**, 085001 (2011), [arXiv:1105.2083].
- [120] D. Horns *et al.*, Phys. Rev. **D85**, 085021 (2012), [arXiv:1203.2184].
- [121] A. Payez, J. R. Cudell and D. Hutsemekers, JCAP **1207**, 041 (2012), [arXiv:1204.6187].
- [122] A. Dominguez, M. A. Sanchez-Conde and F. Prada, JCAP **1111**, 020 (2011), [arXiv:1106.1860].
- [123] W. Essey and A. Kusenko, Astrophys. J. **751**, L11 (2012), [arXiv:1111.0815].
- [124] D. Horns and M. Meyer, JCAP **1202**, 033 (2012), [arXiv:1201.4711].
- [125] G. I. Rubtsov and S. V. Troitsky, JETP Lett. **100**, 6, 355 (2014), [Pisma Zh. Eksp. Teor. Fiz.100,no.6,397(2014)], [arXiv:1406.0239].
- [126] K. Kohri and H. Kodama, Phys. Rev. **D96**, 5, 051701 (2017), [arXiv:1704.05189].
- [127] D. A. Sanchez, S. Fegan and B. Giebels, Astron. Astrophys. **554**, A75 (2013), [arXiv:1303.5923].
- [128] J. Biteau and D. A. Williams, Astrophys. J. **812**, 1, 60 (2015), [arXiv:1502.04166].
- [129] A. Domínguez and M. Ajello, Astrophys. J. **813**, 2, L34 (2015), [arXiv:1510.07913].
- [130] A. De Angelis, G. Galanti and M. Roncadelli, Phys. Rev. **D84**, 105030 (2011), [Erratum: Phys. Rev. D87, no.10, 109903(2013)], [arXiv:1106.1132]; M. Simet, D. Hooper and P. D. Serpico, Phys. Rev. **D77**, 063001 (2008), [arXiv:0712.2825]; M. A. Sanchez-Conde *et al.*, Phys. Rev. **D79**, 123511 (2009), [arXiv:0905.3270].
- [131] M. Meyer, D. Horns and M. Raue, Phys. Rev. **D87**, 3, 035027 (2013), [arXiv:1302.1208].
- [132] A. Abramowski *et al.* (H.E.S.S.), Phys. Rev. **D88**, 10, 102003 (2013), [arXiv:1311.3148].
- [133] M. Ajello *et al.* (Fermi-LAT), Phys. Rev. Lett. **116**, 16, 161101 (2016), [arXiv:1603.06978].
- [134] C. Zhang *et al.*, Phys. Rev. **D97**, 6, 063009 (2018), [arXiv:1802.08420].
- [135] Z.-Q. Xia *et al.*, Phys. Rev. **D97**, 6, 063003 (2018), [arXiv:1801.01646].
- [136] J. Majumdar, F. Calore and D. Horns, JCAP **1804**, 04, 048 (2018), [arXiv:1801.08813].
- [137] S. S. Wilks, Annals Math. Statist. **9**, 1, 60 (1938).
- [138] D. Wouters and P. Brun, Astrophys. J. **772**, 44 (2013), [arXiv:1304.0989].
- [139] M. Berg *et al.*, Astrophys. J. **847**, 2, 101 (2017), [arXiv:1605.01043].
- [140] M. C. D. Marsh *et al.*, JCAP **1712**, 12, 036 (2017), [arXiv:1703.07354].

- [141] J. P. Conlon *et al.*, JCAP **1707**, 07, 005 (2017), [arXiv:1704.05256].
- [142] L. Chen and J. P. Conlon, Mon. Not. Roy. Astron. Soc. **479**, 2, 2243 (2018), [arXiv:1712.08313].
- [143] C. S. Reynolds *et al.* (2019), [arXiv:1907.05475].
- [144] A. Arvanitaki and S. Dubovsky, Phys. Rev. **D83**, 044026 (2011), [arXiv:1004.3558].
- [145] A. Arvanitaki, M. Baryakhtar and X. Huang, Phys. Rev. **D91**, 8, 084011 (2015), [arXiv:1411.2263].
- [146] A. Arvanitaki *et al.*, Phys. Rev. **D95**, 4, 043001 (2017), [arXiv:1604.03958].
- [147] K. K. Y. Ng *et al.* (2019), [arXiv:1908.02312].
- [148] M. S. Turner, Phys. Rev. Lett. **59**, 2489 (1987), [Erratum: Phys. Rev. Lett. **60**, 1101(1988)]; E. Masso, F. Rota and G. Zsembinszki, Phys. Rev. **D66**, 023004 (2002), [hep-ph/0203221]; P. Graf and F. D. Steffen, Phys. Rev. **D83**, 075011 (2011), [arXiv:1008.4528].
- [149] S. Hannestad *et al.*, JCAP **1008**, 001 (2010), [arXiv:1004.0695]; M. Archidiacono *et al.*, JCAP **1310**, 020 (2013), [arXiv:1307.0615]; E. Di Valentino *et al.*, Phys. Lett. **B752**, 182 (2016), [arXiv:1507.08665].
- [150] M. Archidiacono *et al.*, JCAP **1505**, 05, 050 (2015), [arXiv:1502.03325].
- [151] E. Masso and R. Toldra, Phys. Rev. **D55**, 7967 (1997), [hep-ph/9702275]; D. Cadamuro and J. Redondo, JCAP **1202**, 032 (2012), [arXiv:1110.2895].
- [152] J. Preskill, M. B. Wise and F. Wilczek, Phys. Lett. **B120**, 127 (1983); L. F. Abbott and P. Sikivie, Phys. Lett. **B120**, 133 (1983); M. Dine and W. Fischler, Phys. Lett. **B120**, 137 (1983).
- [153] K. J. Bae, J.-H. Huh and J. E. Kim, JCAP **0809**, 005 (2008), [arXiv:0806.0497].
- [154] O. Wantz and E. P. S. Shellard, Phys. Rev. **D82**, 123508 (2010), [arXiv:0910.1066].
- [155] G. Ballesteros *et al.*, JCAP **1708**, 08, 001 (2017), [arXiv:1610.01639].
- [156] M. Tegmark *et al.*, Phys. Rev. **D73**, 023505 (2006), [arXiv:astro-ph/0511774].
- [157] A. D. Linde, Phys. Lett. **158B**, 375 (1985).
- [158] D. Seckel and M. S. Turner, Phys. Rev. **D32**, 3178 (1985).
- [159] M. Beltran, J. Garcia-Bellido and J. Lesgourgues, Phys. Rev. **D75**, 103507 (2007), [hep-ph/0606107].
- [160] M. P. Hertzberg, M. Tegmark and F. Wilczek, Phys. Rev. **D78**, 083507 (2008), [arXiv:0807.1726].
- [161] J. Hamann *et al.*, JCAP **0906**, 022 (2009), [arXiv:0904.0647].
- [162] P. A. R. Ade *et al.* (Planck), Astron. Astrophys. **571**, A22 (2014), [arXiv:1303.5082].
- [163] P. A. R. Ade *et al.* (Planck), Astron. Astrophys. **594**, A20 (2016), [arXiv:1502.02114].
- [164] S. Chang, C. Hagmann and P. Sikivie, Phys. Rev. **D59**, 023505 (1999), [hep-ph/9807374].
- [165] C. Hagmann, S. Chang and P. Sikivie, Phys. Rev. **D63**, 125018 (2001), [hep-ph/0012361].
- [166] T. Hiramatsu *et al.*, Phys. Rev. **D83**, 123531 (2011), [arXiv:1012.5502].
- [167] T. Hiramatsu *et al.*, Phys. Rev. **D85**, 105020 (2012), [Erratum: Phys. Rev. **D86**, 089902(2012)], [arXiv:1202.5851].
- [168] M. Kawasaki, K. Saikawa and T. Sekiguchi, Phys. Rev. **D91**, 6, 065014 (2015), [arXiv:1412.0789].
- [169] V. B. Klaer and G. D. Moore, JCAP **1711**, 11, 049 (2017), [arXiv:1708.07521].
- [170] M. Gorghetto, E. Hardy and G. Villadoro, JHEP **07**, 151 (2018), [arXiv:1806.04677].
- [171] M. Buschmann, J. W. Foster and B. R. Safdi (2019), [arXiv:1906.00967].
- [172] M. Hindmarsh *et al.* (2019), [arXiv:1908.03522].
- [173] A. Ringwald and K. Saikawa, Phys. Rev. **D93**, 8, 085031 (2016), [Addendum: Phys. Rev. **D94**, no.4, 049908(2016)], [arXiv:1512.06436].
- [174] T. Hiramatsu *et al.*, JCAP **1301**, 001 (2013), [arXiv:1207.3166].
- [175] C. J. Hogan and M. J. Rees, Phys. Lett. **B205**, 228 (1988).
- [176] E. W. Kolb and I. I. Tkachev, Phys. Rev. Lett. **71**, 3051 (1993), [hep-ph/9303313].
- [177] K. M. Zurek, C. J. Hogan and T. R. Quinn, Phys. Rev. **D75**, 043511 (2007), [arXiv:astro-ph/0607341].
- [178] A. Vaquero, J. Redondo and J. Stadler (2018), [JCAP1904,no.04,012(2019)], [arXiv:1809.09241].
- [179] E. W. Kolb and I. I. Tkachev, Astrophys. J. **460**, L25 (1996), [arXiv:astro-ph/9510043].
- [180] M. Fairbairn, D. J. E. Marsh and J. Quevillon, Phys. Rev. Lett. **119**, 2, 021101 (2017), [arXiv:1701.04787].
- [181] A. Katz *et al.*, JCAP **1812**, 005 (2018), [arXiv:1807.11495].
- [182] E. Berkowitz, M. I. Buchoff and E. Rinaldi, Phys. Rev. **D92**, 3, 034507 (2015), [arXiv:1505.07455].
- [183] S. Borsanyi *et al.*, Phys. Lett. **B752**, 175 (2016), [arXiv:1508.06917].
- [184] R. Kitano and N. Yamada, JHEP **10**, 136 (2015), [arXiv:1506.00370].
- [185] P. Petreczky, H.-P. Schadler and S. Sharma, Phys. Lett. **B762**, 498 (2016), [arXiv:1606.03145].
- [186] Y. Taniguchi *et al.*, Phys. Rev. **D95**, 5, 054502 (2017), [arXiv:1611.02411].
- [187] M. Dine *et al.*, Phys. Rev. **D96**, 9, 095001 (2017), [arXiv:1705.00676].
- [188] R. D. Pisarski and L. G. Yaffe, Phys. Lett. **97B**, 110 (1980).
- [189] P. Arias *et al.*, JCAP **1206**, 013 (2012), [arXiv:1201.5902].
- [190] R. Hlozek *et al.*, Phys. Rev. **D91**, 10, 103512 (2015), [arXiv:1410.2896].
- [191] D. J. E. Marsh, Phys. Rept. **643**, 1 (2016), [arXiv:1510.07633].
- [192] L. Hui *et al.*, Phys. Rev. **D95**, 4, 043541 (2017), [arXiv:1610.08297].
- [193] A. G. Dias *et al.*, JHEP **06**, 037 (2014), [arXiv:1403.5760]; J. E. Kim and D. J. E. Marsh, Phys. Rev. **D93**, 2, 025027 (2016), [arXiv:1510.01701].
- [194] H. Davoudiasl and C. W. Murphy, Phys. Rev. Lett. **118**, 14, 141801 (2017), [arXiv:1701.01136].
- [195] M. Khlopov, B. A. Malomed and I. B. Zeldovich, Mon. Not. Roy. Astron. Soc. **215**, 575 (1985).
- [196] W. Hu, R. Barkana and A. Gruzinov, Phys. Rev. Lett. **85**, 1158 (2000), [arXiv:astro-ph/0003365]; L. Amendola and R. Barbieri, Phys. Lett. **B642**, 192 (2006), [hep-ph/0509257]; D. J. E. Marsh and P. G. Ferreira, Phys. Rev. **D82**, 103528 (2010), [arXiv:1009.3501].
- [197] E. Seidel and W. M. Suen, Phys. Rev. Lett. **66**, 1659 (1991).
- [198] R. Hlozek, D. J. E. Marsh and D. Grin, Mon. Not. Roy. Astron. Soc. **476**, 3, 3063 (2018), [arXiv:1708.05681].
- [199] D. J. E. Marsh and J. Silk, Mon. Not. Roy. Astron. Soc. **437**, 3, 2652 (2014), [arXiv:1307.1705].
- [200] H.-Y. Schive *et al.*, Astrophys. J. **818**, 1, 89 (2016), [arXiv:1508.04621].
- [201] B. Bozek *et al.*, Mon. Not. Roy. Astron. Soc. **450**, 1, 209 (2015), [arXiv:1409.3544]; P. S. Corasaniti *et al.*, Phys. Rev. **D95**, 8, 083512 (2017), [arXiv:1611.05892].

- [202] E. Armengaud *et al.*, *Mon. Not. Roy. Astron. Soc.* **471**, 4, 4606 (2017), [arXiv:1703.09126]; V. Iršič *et al.*, *Phys. Rev. Lett.* **119**, 3, 031302 (2017), [arXiv:1703.04683]; T. Kobayashi *et al.*, *Phys. Rev.* **D96**, 12, 123514 (2017), [arXiv:1708.00015].
- [203] H.-Y. Schive and T. Chiueh, *Mon. Not. Roy. Astron. Soc.* **473**, 1, L36 (2018), [arXiv:1706.03723].
- [204] H.-Y. Schive, T. Chiueh and T. Broadhurst, *Nature Phys.* **10**, 496 (2014), [arXiv:1406.6586].
- [205] B. Schwabe, J. C. Niemeyer and J. F. Engels, *Phys. Rev.* **D94**, 4, 043513 (2016), [arXiv:1606.05151]; J. Veltmaat and J. C. Niemeyer, *Phys. Rev.* **D94**, 12, 123523 (2016), [arXiv:1608.00802]; P. Mocz *et al.*, *Mon. Not. Roy. Astron. Soc.* **471**, 4, 4559 (2017), [arXiv:1705.05845].
- [206] D. G. Levkov, A. G. Panin and I. I. Tkachev, *Phys. Rev. Lett.* **118**, 011301 (2017); T. Helfer *et al.*, *JCAP* **1703**, 03, 055 (2017), [arXiv:1609.04724].
- [207] D. J. E. Marsh and A.-R. Pop, *Mon. Not. Roy. Astron. Soc.* **451**, 3, 2479 (2015), [arXiv:1502.03456]; S.-R. Chen, H.-Y. Schive and T. Chiueh, *Mon. Not. Roy. Astron. Soc.* **468**, 2, 1338 (2017), [arXiv:1606.09030]; A. X. González-Morales *et al.*, *Mon. Not. Roy. Astron. Soc.* **472**, 2, 1346 (2017), [arXiv:1609.05856].
- [208] I. De Martino *et al.* (2018), [arXiv:1807.08153].
- [209] T. Broadhurst *et al.* (2019), [arXiv:1902.10488].
- [210] H.-Y. Schive *et al.*, *Phys. Rev. Lett.* **113**, 26, 261302 (2014), [arXiv:1407.7762].
- [211] V. H. Robles, J. S. Bullock and M. Boylan-Kolchin, *Mon. Not. Roy. Astron. Soc.* **483**, 1, 289 (2019), [arXiv:1807.06018].
- [212] V. Desjacques and A. Nusser (2019), [arXiv:1905.03450].
- [213] M. Safarzadeh and D. N. Spergel (2019), [arXiv:1906.11848].
- [214] J. H. H. Chan *et al.*, *Mon. Not. R. Astron. Soc.* **478**, 2686 (2018), [arXiv:1712.01947].
- [215] A. Pontzen and F. Governato, *Nature* **506**, 171 (2014), [arXiv:1402.1764].
- [216] J. Veltmaat, J. C. Niemeyer and B. Schwabe, *Phys. Rev.* **D98**, 4, 043509 (2018), [arXiv:1804.09647].
- [217] B. Bar-Or, J.-B. Fouvry and S. Tremaine, *Astrophys. J.* **871**, 1, 28 (2019), [arXiv:1809.07673].
- [218] D. G. Levkov, A. G. Panin and I. I. Tkachev, *Phys. Rev. Lett.* **121**, 15, 151301 (2018), [arXiv:1804.05857].
- [219] B. V. Church, P. Mocz and J. P. Ostriker, *Mon. Not. R. Astron. Soc.* **485**, 2861 (2019), [arXiv:1809.04744].
- [220] N. C. Amorisco and A. Loeb (2018), [arXiv:1808.00464].
- [221] T. S. Li *et al.* (DES), *Astrophys. J.* **838**, 1, 8 (2017), [arXiv:1611.05052].
- [222] D. J. E. Marsh and J. C. Niemeyer, *Phys. Rev. Lett.* **123**, 5, 051103 (2019), [arXiv:1810.08543].
- [223] B. Eggemeier and J. C. Niemeyer (2019), [arXiv:1906.01348].
- [224] M. A. Bershadsky, M. T. Ressel and M. S. Turner, *Phys. Rev. Lett.* **66**, 1398 (1991); M. T. Ressel, *Phys. Rev.* **D44**, 3001 (1991).
- [225] D. Grin *et al.*, *Phys. Rev.* **D75**, 105018 (2007), [arXiv:astro-ph/0611502].
- [226] B. D. Blout *et al.*, *Astrophys. J.* **546**, 825 (2001), [arXiv:astro-ph/0006310].
- [227] K. Kelley and P. J. Quinn, *Astrophys. J.* **845**, 1, L4 (2017), [arXiv:1708.01399].
- [228] G. Sigl, *Phys. Rev.* **D96**, 10, 103014 (2017), [arXiv:1708.08908].
- [229] A. Hook *et al.*, *Phys. Rev. Lett.* **121**, 24, 241102 (2018), [arXiv:1804.03145].
- [230] A. Caputo *et al.*, *JCAP* **1903**, 03, 027 (2019), [arXiv:1811.08436].
- [231] M. A. Fedderke, P. W. Graham and S. Rajendran, *Phys. Rev.* **D100**, 1, 015040 (2019), [arXiv:1903.02666].
- [232] T. Liu, G. Smoot and Y. Zhao (2019), [arXiv:1901.10981].
- [233] P. Sikivie, *Phys. Rev.* **D32**, 2988 (1985), [Erratum: *Phys. Rev.* **D36**, 974 (1987)].
- [234] R. Bradley *et al.*, *Rev. Mod. Phys.* **75**, 777 (2003).
- [235] P. Sikivie and J. R. Ipser, *Phys. Lett.* **B291**, 288 (1992).
- [236] P. Sikivie, I. I. Tkachev and Y. Wang, *Phys. Rev. Lett.* **75**, 2911 (1995), [arXiv:astro-ph/9504052].
- [237] S. De Panfilis *et al.*, *Phys. Rev. Lett.* **59**, 839 (1987); W. Wuensch *et al.*, *Phys. Rev.* **D40**, 3153 (1989); C. Hagmann *et al.*, *Phys. Rev.* **D42**, 1297 (1990).
- [238] S. J. Asztalos *et al.* (ADMX), *Phys. Rev.* **D69**, 011101 (2004), [arXiv:astro-ph/0310042].
- [239] L. Duffy *et al.*, *Phys. Rev. Lett.* **95**, 091304 (2005), [arXiv:astro-ph/0505237]; J. Hoskins *et al.*, *Phys. Rev.* **D84**, 121302 (2011), [arXiv:1109.4128].
- [240] S. J. Asztalos *et al.* (ADMX), *Phys. Rev. Lett.* **104**, 041301 (2010), [arXiv:0910.5914].
- [241] S. J. Asztalos *et al.* (ADMX), *Nucl. Instrum. Meth.* **A656**, 39 (2011), [arXiv:1105.4203].
- [242] N. Du *et al.* (ADMX), *Phys. Rev. Lett.* **120**, 15, 151301 (2018), [arXiv:1804.05750].
- [243] T. Braine *et al.* (ADMX) (2019), [arXiv:1910.08638].
- [244] G. Rybka *et al.* (ADMX), *Phys. Rev. Lett.* **105**, 051801 (2010), [arXiv:1004.5160].
- [245] A. Wagner *et al.* (ADMX), *Phys. Rev. Lett.* **105**, 171801 (2010), [arXiv:1007.3766].
- [246] C. Boutan *et al.* (ADMX), *Phys. Rev. Lett.* **121**, 26, 261302 (2018), [arXiv:1901.00920].
- [247] B. M. Brubaker *et al.*, *Phys. Rev. Lett.* **118**, 6, 061302 (2017), [arXiv:1610.02580].
- [248] L. Zhong *et al.* (HAYSTAC), *Phys. Rev.* **D97**, 9, 092001 (2018), [arXiv:1803.03690].
- [249] I. Ogawa, S. Matsuki and K. Yamamoto, *Phys. Rev.* **D53**, R1740 (1996).
- [250] B. T. McAllister *et al.*, *Phys. Dark Univ.* **18**, 67 (2017), [arXiv:1706.00209].
- [251] W. Chung, *PoS CORFU2015*, 047 (2016).
- [252] A. A. Melcon *et al.* (RADES), *JCAP* **1805**, 05, 040 (2018), [arXiv:1803.01243].
- [253] D. Alesini *et al.* (KLASH) (2017), [arXiv:1707.06010].
- [254] G. Rybka *et al.*, *Phys. Rev.* **D91**, 1, 011701 (2015), [arXiv:1403.3121].
- [255] D. Horns *et al.*, *JCAP* **1304**, 016 (2013), [arXiv:1212.2970].
- [256] J. Suzuki *et al.*, *JCAP* **1509**, 09, 042 (2015), [arXiv:1504.00118].
- [257] A. Caldwell *et al.* (MADMAX Working Group), *Phys. Rev. Lett.* **118**, 9, 091801 (2017), [arXiv:1611.05865].
- [258] P. Brun *et al.* (MADMAX), *Eur. Phys. J.* **C79**, 3, 186 (2019), [arXiv:1901.07401].
- [259] M. Baryakhtar, J. Huang and R. Lasenby, *Phys. Rev.* **D98**, 3, 035006 (2018), [arXiv:1803.11455].
- [260] A. Arvanitaki, S. Dimopoulos and K. Van Tilburg, *Phys. Rev.* **X8**, 4, 041001 (2018), [arXiv:1709.05354].
- [261] P. Sikivie, *Phys. Rev. Lett.* **113**, 20, 201301 (2014), [arXiv:1409.2806].
- [262] P. W. Graham and S. Rajendran, *Phys. Rev.* **D88**, 035023 (2013), [arXiv:1306.6088].
- [263] M. Pospelov and A. Ritz, *Nucl. Phys.* **B573**, 177 (2000), [hep-ph/9908508].

- [264] C. Abel *et al.*, Phys. Rev. **X7**, 4, 041034 (2017), [arXiv:1708.06367].
- [265] D. Budker *et al.*, Phys. Rev. **X4**, 2, 021030 (2014), [arXiv:1306.6089].
- [266] M. B. Wise, H. Georgi and S. L. Glashow, Phys. Rev. Lett. **47**, 402 (1981).
- [267] A. Ernst, A. Ringwald and C. Tamarit, JHEP **02**, 103 (2018), [arXiv:1801.04906].
- [268] L. Di Luzio, A. Ringwald and C. Tamarit, Phys. Rev. **D98**, 9, 095011 (2018), [arXiv:1807.09769].
- [269] P. Fileviez Perez, C. Murgui and A. D. Plascencia (2019), [arXiv:1908.01772].
- [270] S. P. Chang *et al.*, Phys. Rev. **D99**, 8, 083002 (2019), [arXiv:1710.05271].
- [271] P. Sikivie, N. Sullivan, and D. B. Tanner, Phys. Rev. Lett. **112**, 131301 (2014).
- [272] Y. Kahn, B. R. Safdi and J. Thaler, Phys. Rev. Lett. **117**, 14, 141801 (2016), [arXiv:1602.01086].
- [273] M. Silva-Feaver *et al.*, IEEE Trans. Appl. Supercond. **27**, 4, 1400204 (2017), [arXiv:1610.09344].
- [274] J. L. Ouellet *et al.* (ABRACADABRA), Phys. Rev. Lett. **122**, 12, 121802 (2019), [arXiv:1810.12257].
- [275] L. Krauss *et al.*, Phys. Rev. Lett. **55**, 1797 (1985).
- [276] R. Barbieri *et al.*, Phys. Dark Univ. **15**, 135 (2017).

92. Searches for Quark and Lepton Compositeness

Revised 2019 by K. Hikasa (Tohoku University), M. Tanabashi (Nagoya University), K. Terashi (ICEPP, University of Tokyo), and N. Varelas (University of Illinois at Chicago)

92.1. Limits on contact interactions

If quarks and leptons are made of constituents, then at the scale of constituent binding energies (compositeness scale) there should appear new interactions among them. At energies much below the compositeness scale (Λ), these interactions are suppressed by inverse powers of Λ . The dominant effect of the compositeness of fermion ψ should come from the lowest dimensional interactions with four fermions (contact terms), whose most general flavor-diagonal color-singlet chirally invariant form reads [1,2]

$$\mathcal{L} = \mathcal{L}_{LL} + \mathcal{L}_{RR} + \mathcal{L}_{LR} + \mathcal{L}_{RL},$$

with

$$\begin{aligned} \mathcal{L}_{LL} &= \frac{g_{\text{contact}}^2}{2\Lambda^2} \sum_{i,j} \eta_{LL}^{ij} (\bar{\psi}_L^i \gamma_\mu \psi_L^i) (\bar{\psi}_L^j \gamma^\mu \psi_L^j), \\ \mathcal{L}_{RR} &= \frac{g_{\text{contact}}^2}{2\Lambda^2} \sum_{i,j} \eta_{RR}^{ij} (\bar{\psi}_R^i \gamma_\mu \psi_R^i) (\bar{\psi}_R^j \gamma^\mu \psi_R^j), \\ \mathcal{L}_{LR} &= \frac{g_{\text{contact}}^2}{2\Lambda^2} \sum_{i,j} \eta_{LR}^{ij} (\bar{\psi}_L^i \gamma_\mu \psi_L^i) (\bar{\psi}_R^j \gamma^\mu \psi_R^j), \\ \mathcal{L}_{RL} &= \frac{g_{\text{contact}}^2}{2\Lambda^2} \sum_{i,j} \eta_{RL}^{ij} (\bar{\psi}_R^i \gamma_\mu \psi_R^i) (\bar{\psi}_L^j \gamma^\mu \psi_L^j), \end{aligned} \quad (92.1)$$

where i, j are the indices of fermion species. Color and other indices are suppressed in Eq. (92.1). Chiral invariance provides a natural explanation why quark and lepton masses are much smaller than their inverse size Λ . Note $\eta_{\alpha\beta}^{ij} = \eta_{\beta\alpha}^{ji}$, therefore, in order to specify the contact interaction among the same fermion species $i = j$, it is enough to use η_{LL} , η_{RR} and η_{LR} . We will suppress the indices of fermion species hereafter. We may determine the scale Λ unambiguously by using the above form of the effective interactions; the conventional method [1] is to fix its scale by setting $g_{\text{contact}}^2/4\pi = g_{\text{contact}}^2(\Lambda)/4\pi = 1$ for the new strong interaction coupling and by setting the largest magnitude of the coefficients $\eta_{\alpha\beta}$ to be unity. In the following, we denote

$$\begin{aligned} \Lambda &= \Lambda_{LL}^\pm \text{ for } (\eta_{LL}, \eta_{RR}, \eta_{LR}) = (\pm 1, 0, 0), \\ \Lambda &= \Lambda_{RR}^\pm \text{ for } (\eta_{LL}, \eta_{RR}, \eta_{LR}) = (0, \pm 1, 0), \\ \Lambda &= \Lambda_{VV}^\pm \text{ for } (\eta_{LL}, \eta_{RR}, \eta_{LR}) = (\pm 1, \pm 1, \pm 1), \\ \Lambda &= \Lambda_{AA}^\pm \text{ for } (\eta_{LL}, \eta_{RR}, \eta_{LR}) = (\pm 1, \pm 1, \mp 1), \\ \Lambda &= \Lambda_{V-A}^\pm \text{ for } (\eta_{LL}, \eta_{RR}, \eta_{LR}) = (0, 0, \pm 1). \end{aligned} \quad (92.2)$$

Such interactions can arise by interchanging constituents (when the fermions have common constituents), and/or by exchanging the binding quanta (whenever binding quanta couple to constituents of both particles).

Fermion scattering amplitude induced from the contact interaction in Eq. (92.1) interferes with the Standard Model (SM) amplitude destructively or constructively [2]. The sign of interference depends on the sign of $\eta_{\alpha\beta}$ ($\alpha, \beta = L, R$). For instance, in the parton level $qq \rightarrow qq$ scattering cross section in the Λ_{LL}^\pm model, the contact interaction amplitude and the SM gluon exchange amplitude interfere destructively for $\eta_{LL} = +1$, while they interfere constructively for $\eta_{LL} = -1$. In models of quark compositeness, the quark scattering cross sections induced from the contact interactions receive sizable QCD radiative corrections. Ref. 3 provides the exact next-to-leading order (NLO) QCD corrections to the contact interaction induced quark scattering cross sections.

Over the last three decades experiments at the CERN SpS [4,5], the Fermilab Tevatron [6,7], and the CERN LHC [8–12] have searched for quark contact interactions, characterized by the four-fermion effective Lagrangian in Eq. (92.1), using jet final states. These searches have been performed primarily by studying the angular distribution of the two highest transverse momentum, p_T , jets (dijets), and the inclusive jet p_T spectrum. The variable $\chi = \exp(|(y_1 - y_2)|)$ is used to measure the dijet angular distribution, where y_1 and y_2 are the rapidities of the two jets with the highest transverse momenta. For collinear massless parton scattering, χ is related to the polar scattering angle θ^* in the partonic center-of-mass frame by $\chi = (1 + |\cos\theta^*|)/(1 - |\cos\theta^*|)$. The choice of χ is motivated by the fact that the angular distribution for Rutherford scattering, which is proportional to $1/(1 - \cos\theta^*)^2$, is independent of χ . In perturbative QCD the χ distributions are relatively uniform and only mildly modified by higher-order QCD or electroweak corrections. Signatures of quark contact interactions exhibit more isotropic angular distribution than QCD and they can be identified as an excess at low values of χ . In the inclusive jet cross section measurement, quark contact interaction effects are searched for as deviations from the predictions of perturbative QCD in the tails of the high- p_T jet spectrum [11].

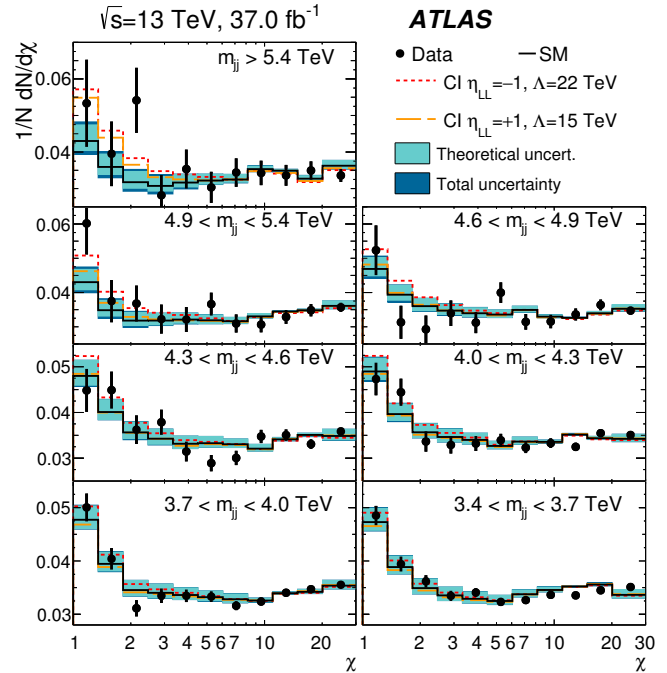


Figure 92.1: Normalized dijet angular distributions in several dijet mass (m_{jj}) ranges. The data distributions are compared to PYTHIA8 predictions with NLO and electroweak corrections applied (solid line) and with the predictions including a contact interaction (CI) term in which only left-handed quarks participate of compositeness scale $\Lambda_{LL}^+ = 15$ TeV (dashed line) and $\Lambda_{LL}^- = 22$ TeV (dotted line). The theoretical uncertainties and the total theoretical and experimental uncertainties in the predictions are displayed as shaded bands around the SM prediction. Figure adopted from Ref. 9.

Recent results from the LHC, using data collected at proton-proton center-of-mass energy of $\sqrt{s} = 13$ TeV, extend previous limits on quark contact interactions. Figure 92.1 shows the normalized dijet angular distributions for several dijet mass ranges measured in ATLAS [9] at $\sqrt{s} = 13$ TeV. The data distributions are compared with SM predictions, estimated using PYTHIA8 [13] with GEANT4-based [14] ATLAS detector simulation and corrected to NLO QCD calculation provided by NLO Jet++ [15] including electroweak corrections [16], and with predictions including a contact interaction term in which only

left-handed quarks participate at compositeness scale $\Lambda_{LL}^+ = 15$ TeV ($\Lambda_{LL}^- = 22$ TeV) with destructive (constructive) interference. Over a wide range of χ and dijet mass the data are well described by the SM predictions. Using the dijet angular distributions measured at high dijet masses and $\sqrt{s} = 13$ TeV, the ATLAS [9] and CMS [12] Collaborations have set 95% confidence level (C.L.) lower limits on the contact interaction scale Λ , ranging from 9.2 to 29.5 TeV for different quark contact interaction models that correspond to various combinations of $(\eta_{LL}, \eta_{RR}, \eta_{LR})$, as summarized in Figure 92.2. The contact interaction scale limits extracted using the dijet angular distributions include the exact NLO QCD corrections to dijet production induced by contact interactions [3]. In proton-proton collisions, the Λ_{LL}^\pm and Λ_{RR}^\pm contact interaction models result in identical tree-level cross sections and NLO QCD corrections and yield the same exclusion limits. For Λ_{VV}^\pm and Λ_{AA}^\pm , the contact interaction predictions are identical at tree level, but exhibit different NLO QCD corrections and yield different exclusion limits.

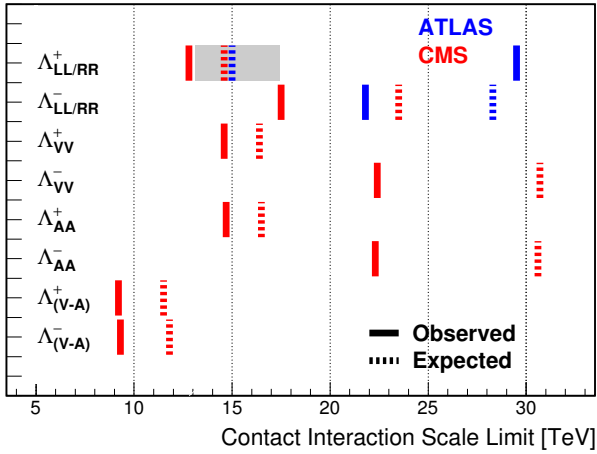


Figure 92.2: Observed (solid lines) and expected (dashed lines) 95% C.L. lower limits on the contact interaction scale Λ for different contact interaction models from ATLAS [9] and CMS [12] using the dijet angular distributions. The contact interaction models used for the dijet angular distributions include the exact NLO QCD corrections to dijet production. The shaded band for the $\Lambda_{LL/RR}^+$ model indicates the range of contact interaction scale that was not excluded in ATLAS [9] due to statistical fluctuation of observed data.

If leptons (l) and quarks (q) are composite with common constituents, the interaction of these constituents will manifest itself in the form of a $llqq$ -type four-fermion contact interaction Lagrangian at energies below the compositeness scale Λ . The $llqq$ terms in the contact interaction Lagrangian can be expressed as

$$\begin{aligned}\mathcal{L}_{LL} &= \frac{g_{\text{contact}}^2}{\Lambda^2} \sum_{i,j} \eta_{LL}^{ij} (\bar{q}_L^i \gamma_\mu q_L^i) (\bar{l}_L^j \gamma^\mu l_L^j), \\ \mathcal{L}_{RR} &= \frac{g_{\text{contact}}^2}{\Lambda^2} \sum_{i,j} \eta_{RR}^{ij} (\bar{q}_R^i \gamma_\mu q_R^i) (\bar{l}_R^j \gamma^\mu l_R^j), \\ \mathcal{L}_{LR} &= \frac{g_{\text{contact}}^2}{\Lambda^2} \sum_{i,j} \eta_{LR}^{ij} (\bar{q}_L^i \gamma_\mu q_L^i) (\bar{l}_R^j \gamma^\mu l_R^j), \\ \mathcal{L}_{RL} &= \frac{g_{\text{contact}}^2}{\Lambda^2} \sum_{i,j} \eta_{RL}^{ij} (\bar{q}_R^i \gamma_\mu q_R^i) (\bar{l}_L^j \gamma^\mu l_L^j).\end{aligned}\quad (92.3)$$

Searches on quark-lepton compositeness have been reported from experiments at LEP [17–20], HERA [21,22], the Tevatron [23,24], and recently from the ATLAS [25,26] and CMS [27–29] experiments at

the LHC. The most stringent searches for $llqq$ contact interactions are performed by the LHC experiments using high-mass oppositely-charged lepton pairs produced through the $q\bar{q} \rightarrow l^+l^-$ Drell-Yan process. The contact interaction amplitude of the $u\bar{u} \rightarrow l^+l^-$ process ($l = e$ or μ) interferes with the corresponding SM amplitude constructively (destructively) for $\eta_{\alpha\beta}^{ul} = -1$ ($\eta_{\alpha\beta}^{ul} = +1$). The ATLAS Collaboration has extracted limits on the $llqq$ contact interaction at $\sqrt{s} = 13$ TeV for the right-right ($\eta_{RR} = \pm 1$, $\eta_{LL} = \eta_{LR} = \eta_{RL} = 0$), left-left ($\eta_{LL} = \pm 1$, $\eta_{RR} = \eta_{LR} = \eta_{RL} = 0$), and left-right ($\eta_{LR} = \eta_{RL} = \pm 1$, $\eta_{RR} = \eta_{LL} = 0$) models. Combining the dielectron and dimuon channels, the 95% C.L. lower limits on the $llqq$ contact interaction scale Λ are 35 TeV (28 TeV) for the right-right model, 40 TeV (25 TeV) for the left-left model, and 36 TeV (28 TeV) for the left-right model, each with constructive (destructive) interference [26]. The CMS Collaboration, using a 36 fb^{-1} dataset at 13 TeV, has set 95% C.L. exclusion limits on the $llqq$ contact interaction scale that range from $\Lambda_{LL} > 20$ TeV for the destructive interference to $\Lambda_{RR} > 32$ TeV for the constructive interference, for the left-left and the right-right models, respectively [29].

Note that the contact interactions arising from the compositeness of quarks and leptons in Eq. (92.1) can also be regarded as a part of more general dimension six operators in the context of low energy standard model effective theory. For a complete list of these dimension six operators, see [30,31].

Interactions of hypothetical dark matter candidate particles with SM particles through mediators can also be described as contact interactions at low energy. See “Searches for WIMPs and Other Particles” in this volume for limits on the interactions involving dark matter candidate particles.

92.2. Limits on excited fermions

Another typical consequence of compositeness is the appearance of excited leptons and quarks (l^* and q^*). Phenomenologically, an excited lepton is defined to be a heavy lepton which shares a leptonic quantum number with one of the existing leptons (an excited quark is defined similarly). For example, an excited electron e^* is characterized by a nonzero transition-magnetic coupling with electrons. Smallness of the lepton mass and the success of QED prediction for $g - 2$ suggest chirality conservation, *i.e.*, an excited lepton should not couple to both left- and right-handed components of the corresponding lepton [32–34].

Excited leptons may be classified by $SU(2) \times U(1)$ quantum numbers. Typical examples are:

1. Sequential type

$$\begin{pmatrix} \nu^* \\ l^* \end{pmatrix}_L, \quad [\nu_R^*], \quad l_R^*.$$

ν_R^* is necessary unless ν^* has a Majorana mass.

2. Mirror type

$$[\nu_L^*], \quad l_L^*, \quad \begin{pmatrix} \nu^* \\ l^* \end{pmatrix}_R.$$

3. Homodoublet type

$$\begin{pmatrix} \nu^* \\ l^* \end{pmatrix}_L, \quad \begin{pmatrix} \nu^* \\ l^* \end{pmatrix}_R.$$

Similar classification can be made for excited quarks.

Excited fermions can be pair produced via their minimal gauge couplings. The couplings of excited leptons with Z are given by

$$\begin{aligned}& \frac{e}{2 \sin \theta_W \cos \theta_W} (-1 + 2 \sin^2 \theta_W) \bar{l}^* \gamma^\mu l^* Z_\mu \\ & + \frac{e}{2 \sin \theta_W \cos \theta_W} \bar{\nu}^* \gamma^\mu \nu^* Z_\mu\end{aligned}$$

in the homodoublet model. The corresponding couplings of excited quarks can be easily obtained. Although form factor effects can be present for the gauge couplings at $q^2 \neq 0$, they are usually neglected.

Excited fermions may also be produced via the contact interactions with ordinary quarks and leptons [35]

$$\mathcal{L} = \frac{g_{\text{contact}}^2}{\Lambda^2} [\eta'_{LL}(\bar{\psi}_L \gamma_\mu \psi_L)(\bar{\psi}_L^* \gamma^\mu \psi_L^*) + (\eta''_{LL}(\bar{\psi}_L \gamma_\mu \psi_L)(\bar{\psi}_L^* \gamma^\mu \psi_L) + \text{h.c.}) + \dots]. \quad (92.4)$$

Again, the coefficient is conventionally taken $g_{\text{contact}}^2 = 4\pi$. It is widely assumed $\eta'_{LL} = \eta''_{LL} = 1$, $\eta'_{LR} = \eta''_{LR} = \eta'_{RL} = \eta''_{RL} = \eta'_{RR} = \eta''_{RR} = 0$ in experimental analyses for simplicity.

In addition, transition-magnetic type couplings with a gauge boson are expected. These couplings can be generally parameterized as follows:

$$\begin{aligned} \mathcal{L} = & \frac{\lambda_\gamma^{(\psi^*)} e}{2m_{\psi^*}} \bar{\psi}^* \sigma^{\mu\nu} (\eta_L \frac{1-\gamma_5}{2} + \eta_R \frac{1+\gamma_5}{2}) \psi F_{\mu\nu} \\ & + \frac{\lambda_Z^{(\psi^*)} e}{2m_{\psi^*}} \bar{\psi}^* \sigma^{\mu\nu} (\eta_L \frac{1-\gamma_5}{2} + \eta_R \frac{1+\gamma_5}{2}) \psi Z_{\mu\nu} \\ & + \frac{\lambda_W^{(l^*)} g}{2m_{l^*}} \bar{l}^* \sigma^{\mu\nu} \frac{1-\gamma_5}{2} \nu W_{\mu\nu} \\ & + \frac{\lambda_W^{(\nu^*)} g}{2m_{\nu^*}} \bar{\nu}^* \sigma^{\mu\nu} (\eta_L \frac{1-\gamma_5}{2} + \eta_R \frac{1+\gamma_5}{2}) l W_{\mu\nu}^\dagger \\ & + \text{h.c.}, \end{aligned} \quad (92.5)$$

where $g = e/\sin\theta_W$, $\psi = \nu$ or l , $F_{\mu\nu} = \partial_\mu A_\nu - \partial_\nu A_\mu$ is the photon field strength, $Z_{\mu\nu} = \partial_\mu Z_\nu - \partial_\nu Z_\mu$, etc.. The normalization of the coupling is chosen such that

$$\max(|\eta_L|, |\eta_R|) = 1.$$

Chirality conservation requires

$$\eta_L \eta_R = 0. \quad (92.6)$$

These couplings in Eq. (92.5) can arise from $SU(2) \times U(1)$ -invariant higher-dimensional interactions. A well-studied model is the interaction of homodoublet type l^* with the Lagrangian (see [36,37])

$$\mathcal{L} = \frac{1}{2\Lambda} \bar{L}^* \sigma^{\mu\nu} (g f \frac{\tau^a}{2} W_{\mu\nu}^a + g' f' Y B_{\mu\nu}) \frac{1-\gamma_5}{2} L + \text{h.c.}, \quad (92.7)$$

where L denotes the lepton doublet (ν, l) , Λ is the compositeness scale, g, g' are $SU(2)$ and $U(1)_Y$ gauge couplings, and $W_{\mu\nu}^a$ and $B_{\mu\nu}$ are the field strengths for $SU(2)$ and $U(1)_Y$ gauge fields. These couplings satisfy the relation

$$\lambda_W = -\sqrt{2} \sin^2 \theta_W (\lambda_Z \cot \theta_W + \lambda_\gamma), \quad (92.8)$$

with $\lambda_{W,Z,\gamma}$ being defined in Eq. (92.5) with $\lambda_{W,Z,\gamma} = \lambda_{W,Z,\gamma}^{(l^*)}$ or $\lambda_{W,Z,\gamma} = \lambda_{W,Z,\gamma}^{(\nu^*)}$. Here $(\eta_L, \eta_R) = (1, 0)$ is assumed. It should be noted that the electromagnetic radiative decay of l^* (ν^*) is forbidden if $f = -f'$ ($f = f'$).

Additional coupling with gluons is possible for excited quarks:

$$\begin{aligned} \mathcal{L} = & \frac{1}{2\Lambda} \bar{Q}^* \sigma^{\mu\nu} \left(g_s f_s \frac{\lambda^a}{2} G_{\mu\nu}^a + g f \frac{\tau^a}{2} W_{\mu\nu}^a + g' f' Y B_{\mu\nu} \right) \\ & \times \frac{1-\gamma_5}{2} Q + \text{h.c.}, \end{aligned} \quad (92.9)$$

where Q denotes a quark doublet, g_s is the QCD gauge coupling, and $G_{\mu\nu}^a$ the gluon field strength.

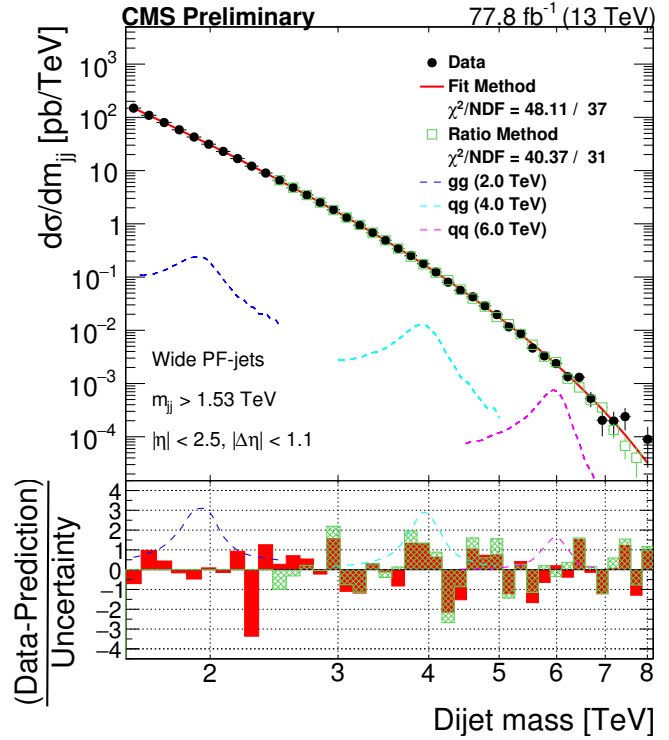


Figure 92.3: Dijet mass distribution measured by CMS using wide jets reconstructed from two highest transverse momentum jets by adding nearby jets within $\Delta R = \sqrt{\Delta\eta^2 + \Delta\phi^2} < 1.1$. The data distribution is compared to a fit representing a smooth background spectrum (solid curve). The excited quark signal with mass of 4.0 TeV (labeled as $q\bar{q}$) is shown together with other benchmark signals. Shown at the bottom panel is the difference between the data and the fitted parametrization divided by the statistical uncertainty of the data. Figure adopted from Ref. 62.

If leptons are made of color triplet and antitriplet constituents, we may expect their color-octet partners. Transitions between the octet leptons (l_8) and the ordinary lepton (l) may take place via the dimension-five interactions

$$\mathcal{L} = \frac{1}{2\Lambda} \sum_l \{ \bar{l}_8^\alpha g_S F_{\mu\nu}^\alpha \sigma^{\mu\nu} (\eta_L l_L + \eta_R l_R) + \text{h.c.} \} \quad (92.10)$$

where the summation is over charged leptons and neutrinos. The leptonic chiral invariance implies $\eta_L \eta_R = 0$ as before.

Searches for the excited quarks and leptons have been performed over the last decades in experiments at the LEP [38–41], HERA [42,43], Tevatron [44,45], and LHC [46–71]. Most stringent constraints, which are described below at 95% confidence level, come from the LHC experiments.

The signature of excited quarks q^* at hadron colliders is characterized by a narrow resonant peak in the reconstructed invariant mass distribution of the q^* decay products. The decays via the transition-magnetic type operator in Eq. (92.9) are considered for excited quarks in LHC searches, and the final states to search for are dijet ($q\bar{q}$) [46, 47, 59–62] or a jet in association with a photon ($q\gamma$) [48, 49, 63, 64] or a weak gauge boson (qW, qZ) [65, 66]. All analyses consider only spin-1/2 excited states of first generation quarks (u^*, d^*) with degenerate masses, expected to be predominantly produced in proton-proton collisions except for the excited b quark searches described below. Only the minimal gauge interactions and the transition-magnetic couplings with the form given in Eq. (92.9) are considered in the production process, and hence the contact interactions in Eq. (92.4) are not considered. The compositeness scale Λ is taken to be the same as the excited quark mass m_{q^*} . The transition-magnetic coupling coefficients f_s, f and f' are assumed to be equal to 1 (denoted by f).

With proton-proton collision data recorded at $\sqrt{s} = 13$ TeV at the LHC, the excited quark masses are excluded in dijet resonance searches up to 6.7 TeV in ATLAS using 140 fb^{-1} [47] and 6.0 TeV in CMS using 77.8 fb^{-1} [62]. Figure 92.3 shows the dijet mass distribution measured in CMS [62] by using the two highest p_T jets reconstructed with the anti- k_T algorithm [72] of a distance parameter of 0.4, and by combining nearby jets within $\Delta R = \sqrt{\Delta\eta^2 + \Delta\phi^2} < 1.1$ around the leading two jets. The measured dijet mass spectrum is compared to a fit with smoothly falling background shape (solid curve) to look for a narrow resonance; an excited quark signal with mass of 4.0 TeV is shown in the figure (denoted by qg) as one of the benchmark signals considered in the analysis.

The photon + jet resonance searches, targeting excited quarks decaying into a quark and a photon ($q^* \rightarrow q + \gamma$), have excluded q^* masses up to 5.3 TeV in ATLAS [49] and 5.5 TeV in CMS [64] using collision data at $\sqrt{s} = 13$ TeV. The W/Z boson + jet final states are examined to look for the $q^* \rightarrow q + W$ and $q + Z$ signal in CMS [66], exploiting jet substructure technique designed to provide sensitivity for highly-boosted hadronically decaying W and Z bosons. The lower mass limit of 5.0 (4.8) TeV is obtained from the $W + \text{jet}$ ($Z + \text{jet}$) search using dataset recorded at $\sqrt{s} = 13$ TeV.

The excited b quarks (b^*) are also considered in the present searches at the LHC. Assuming the similar production processes to the first-generation excited quarks, the b^* has been searched for in final states containing at least one jet identified as originating from a b quark (b -tagging). The searches using two jets including at least one b -tagged jet have been performed at 8 and 13 TeV [50, 51, 60], resulting in b^* lower mass limits of 2.6 TeV in ATLAS using 36.1 fb^{-1} at $\sqrt{s} = 13$ TeV [50] and 1.6 TeV in CMS using 19.7 fb^{-1} at $\sqrt{s} = 8$ TeV [60]. The CMS Collaboration also performed a search for $b^* \rightarrow b + \gamma$ in events with a b -tagged jet in association with a photon using data at $\sqrt{s} = 13$ TeV [64], and excluded b^* masses up to 1.8 TeV. Excited b quarks with charged-current decay into a W -boson and a top quark ($b^* \rightarrow t + W$) were looked for in both ATLAS and CMS using the full 8 TeV data [52, 67]. ATLAS excluded b^* masses below 1.5 TeV for the b^* with left- and right-handed couplings [52] while CMS excluded the masses below 1.39(1.43) TeV for the left(right)-handed couplings [67].

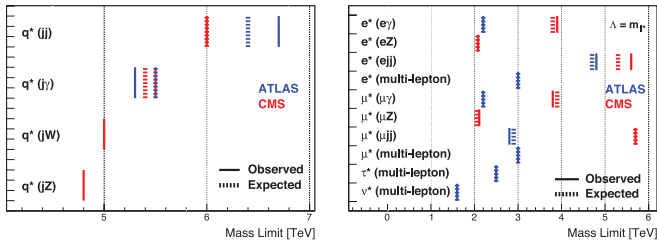


Figure 92.4: 95% C.L. lower mass limits for the excited quarks (left) and excited leptons (right) at ATLAS [47,49,55–57] and CMS [62,64,66] [69–71] experiments. Shown are the most stringent limits for each final state (denoted in parentheses) of the excited fermions from both experiments. Only first generation quarks (u, d) with transition-magnetic type interactions with $f_s = f = f' = 1$ are considered for the excited quarks. The excited lepton limits are given for the production via contact interactions with $\Lambda = m_{l^*}$.

Searches for excited leptons l^* are also performed at the LHC using proton-proton collision data recorded at $\sqrt{s} = 7$ and 8 TeV [54–58, 68, 69] as well as at 13 TeV [70]. Considering single l^* production in contact interactions (Eq. (92.4)) and electromagnetic radiative decay to a SM lepton and a photon ($l^* \rightarrow l + \gamma$ where $l = e, \mu$), the excited electron and muon masses are excluded for $\Lambda = m_{l^*}$ up to 3.9 and 3.8 TeV, respectively, using 35.9 fb^{-1} at $\sqrt{s} = 13$ TeV in CMS [70] and 2.2 TeV using 13 fb^{-1} at $\sqrt{s} = 8$ TeV in ATLAS [55].

With the full 20.3 fb^{-1} data at $\sqrt{s} = 8$ TeV, the inclusive search on multi-lepton signatures with 3 or more charged leptons

in ATLAS [56] further constrains the excited charged leptons and neutrinos. Considering both the transition-magnetic (Eq. (92.7)) and contact interaction (Eq. (92.4)) processes, the lower mass limits for the e^*, μ^*, τ^* and ν_i^* (for every excited neutrino flavor) are obtained to be 3.0, 3.0, 2.5 and 1.6 TeV, respectively, for $\Lambda = m_{e^*}, m_{\mu^*}, m_{\tau^*}$ and $m_{\nu_i^*}$. The rate of pair-produced excited leptons is independent of Λ for the minimal gauge interaction processes, and it allows to improve search sensitivity with multi-lepton signatures at high Λ , especially for excited neutrinos because the predominant $\nu_i^* \rightarrow l + W$ decays result in a higher acceptance for ≥ 3 charged lepton final states.

Both ATLAS and CMS Collaborations performed searches for singly produced excited leptons. The single excited leptons, both produced and decayed in contact interaction processes (Eq. (92.4)), were searched for in CMS using 77.4 fb^{-1} at 13 TeV [71] and in ATLAS using 20.3 fb^{-1} at 8 TeV [57] using the final states with two leptons and two jets ($q\bar{q} \rightarrow ll^* \rightarrow llq\bar{q}$). The CMS search [71] considered both excited electrons and excited muons, using the invariant mass of the combination of the two leptons and two jets as a discriminating variable to separate signal from background. The ATLAS search [57] considered only excited muons. The single excited electrons, produced in contact interactions and decayed either in contact interaction or charged-current processes, were considered in ATLAS using 36.1 fb^{-1} at 13 TeV [58] in the final states with two electrons and two jets ($q\bar{q} \rightarrow ee^* \rightarrow eeq\bar{q}$) or an electron, missing transverse momentum and a hadronically decaying W -boson candidate ($q\bar{q} \rightarrow ee^* \rightarrow e\nu W$). The excited electron (muon) mass was excluded up to 5.6 (5.7) TeV in CMS [71] at $\Lambda = m_{e^*}$ ($\Lambda = m_{\mu^*}$), which is the best limit to date on the excited electrons (muons).

The CMS Collaboration also performed an excited lepton search in the final states containing a Z boson [69], probing the excited leptons produced in contact interactions and decayed in neutral-current processes ($l^* \rightarrow l + Z$) with $f = f' = 1$ or $f = -f' = 1$. The leptonic and hadronic decays of Z bosons have been considered in the search, and the most stringent limits are obtained from the hadronic Z decay to be 2.08 (2.34) TeV and 2.11 (2.37) TeV for the e^* and μ^* , respectively, with $f = f' = 1$ ($f = -f' = 1$) at $\Lambda = m_{l^*}$.

Figure 92.4 summarizes the most stringent 95% C.L. lower mass limits for excited quarks and leptons obtained from the LHC experiments.

References:

1. E.J. Eichten, K.D. Lane, and M.E. Peskin, Phys. Rev. Lett. **50**, 811 (1983).
2. E.J. Eichten *et al.*, Rev. Mod. Phys. **56**, 579 (1984); Erratum *ibid.* **58**, 1065 (1986).
3. J. Gao *et al.*, Phys. Rev. Lett. **106**, 142001 (2011).
4. G. Arnison *et al.* [UA1 Collab.], Phys. Lett. **B177**, 244 (1986).
5. J.A. Appel *et al.* [UA2 Collab.], Phys. Lett. **B160**, 349 (1985).
6. F. Abe *et al.* [CDF Collab.], Phys. Rev. Lett. **62**, 613 (1989); F. Abe *et al.* [CDF Collab.], Phys. Rev. Lett. **69**, 2896 (1992); F. Abe *et al.* [CDF Collab.], Phys. Rev. Lett. **77**, 5336 (1996); F. Abe *et al.* [CDF Collab.], Erratum Phys. Rev. Lett. **78**, 4307 (1997).
7. B. Abbott *et al.* [DØ Collab.], Phys. Rev. Lett. **80**, 666 (1998); B. Abbott *et al.* [DØ Collab.], Phys. Rev. Lett. **82**, 2457 (1999); B. Abbott *et al.* [DØ Collab.], Phys. Rev. **D62**, 031101 (2000); B. Abbott *et al.* [DØ Collab.], Phys. Rev. **D64**, 032003 (2001); B. Abbott *et al.* [DØ Collab.], Phys. Rev. Lett. **103**, 191803 (2009).
8. G. Aad *et al.* [ATLAS Collab.], Phys. Lett. **B694**, 327 (2011); G. Aad *et al.* [ATLAS Collab.], New J. Phys. **13**, 053044 (2011); G. Aad *et al.* [ATLAS Collab.], JHEP **01**, 029 (2013); G. Aad *et al.* [ATLAS Collab.], Phys. Rev. Lett. **114**, 221802 (2015); G. Aad *et al.* [ATLAS Collab.], Phys. Lett. **B754**, 302 (2016).
9. G. Aad *et al.* [ATLAS Collab.], Phys. Rev. **D96**, 052004 (2017).
10. V. Khachatryan *et al.* [CMS Collab.], Phys. Rev. Lett. **105**, 262001 (2010); V. Khachatryan *et al.* [CMS Collab.], Phys. Rev. Lett. **106**, 201804 (2011); S. Chatrchyan *et al.* [CMS Collab.], JHEP **1205**, 055 (2012);

- V. Khachatryan *et al.* [CMS Collab.], Phys. Lett. **B746**, 79 (2015);
A.M. Sirunyan *et al.* [CMS Collab.], JHEP **07**, 013 (2017).
11. S. Chatrchyan *et al.* [CMS Collab.], Phys. Rev. **D87**, 052017 (2013).
 12. A.M. Sirunyan *et al.* [CMS Collab.], Eur. Phys. J. **C78**, 789 (2018).
 13. T. Sjöstrand, S. Mrenna, and P. Skands, Comp. Phys. Comm. **178**, 852 (2008).
 14. S. Agostinelli *et al.* [GEANT4 Collab.], GEANT4: a simulation toolkit, Nucl. Instrum. Methods **A506**, 250 (2003).
 15. Z. Nagy, Phys. Rev. Lett. **88**, 122003 (2002);
Z. Nagy, Phys. Rev. **D68**, 094002, (2003).
 16. S. Dittmaier, A. Huss, and C. Speckner, JHEP **1211**, 095 (2012).
 17. S. Schael *et al.* [ALEPH Collab.], Eur. Phys. J. **C49**, 411 (2007).
 18. J. Abdallah *et al.* [DELPHI Collab.], Eur. Phys. J. **C45**, 589 (2006).
 19. M. Acciarri *et al.* [L3 Collab.], Phys. Lett. **B489**, 81 (2000).
 20. K. Ackerstaff *et al.* [OPAL Collab.], Phys. Lett. **B391**, 221 (1997);
G. Abbiendi *et al.* [OPAL Collab.], Eur. Phys. J. **C33**, 173 (2004).
 21. F.D. Aaron *et al.* [H1 Collab.], Phys. Lett. **B705**, 52 (2011).
 22. S. Chekanov *et al.* [ZEUS Collab.], Phys. Lett. **B591**, 23 (2004).
 23. F. Abe *et al.* [CDF Collab.], Phys. Rev. Lett. **68**, 1463 (1992);
F. Abe *et al.* [CDF Collab.], Phys. Rev. Lett. **79**, 2198 (1997);
T. Affolder *et al.* [CDF Collab.], Phys. Rev. Lett. **87**, 231803 (2001);
A. Abulencia *et al.* [CDF Collab.], Phys. Rev. Lett. **96**, 211801 (2006).
 24. B. Abbott *et al.* [DØ Collab.], Phys. Rev. Lett. **82**, 4769 (1999).
 25. G. Aad *et al.* [ATLAS Collab.], Phys. Rev. **D84**, 011101 (2011);
G. Aad *et al.* [ATLAS Collab.], Phys. Lett. **B712**, 40 (2012);
G. Aad *et al.* [ATLAS Collab.], Phys. Rev. **D87**, 015010 (2013);
G. Aad *et al.* [ATLAS Collab.], Eur. Phys. J. **C74**, 3134 (2014);
M. Aaboud *et al.* [ATLAS Collab.], Phys. Lett. **B761**, 372 (2016).
 26. M. Aaboud *et al.* [ATLAS Collab.], JHEP **10**, 182 (2017).
 27. S. Chatrchyan *et al.* [CMS Collab.], Phys. Rev. **D87**, 032001 (2013).
 28. V. Khachatryan *et al.* [CMS Collab.], JHEP **04**, 025 (2015).
 29. A.M. Sirunyan *et al.* [CMS Collab.], JHEP **04**, 114 (2019).
 30. W. Buchmüller and D. Wyler, Nucl. Phys. **B268**, 621 (1986).
 31. B. Grzadkowski *et al.*, JHEP **1010**, 085 (2010).
 32. F.M. Renard, Phys. Lett. **B116**, 264 (1982).
 33. F. del Aguila, A. Mendez, and R. Pascual, Phys. Lett. **B140**, 431 (1984).
 34. M. Suzuki, Phys. Lett. **B143**, 237 (1984).
 35. U. Baur, M. Spira, and P.M. Zerwas, Phys. Rev. **D42**, 815 (1990).
 36. K. Hagiwara, D. Zeppenfeld, and S. Komamiya, Z. Phys. **C29**, 115 (1985).
 37. N. Cabibbo, L. Maiani, and Y. Srivastava, Phys. Lett. **B139**, 459 (1984).
 38. D. Decamp *et al.* [ALEPH Collab.], Phys. Reports **216**, 253 (1992);
P. Barate *et al.* [ALEPH Collab.], Eur. Phys. J. **C4**, 571 (1998).
 39. P. Abreu *et al.* [DELPHI Collab.], Nucl. Phys. **B367**, 511 (1991);
J. Abdallah *et al.* [DELPHI Collab.], Eur. Phys. J. **C37**, 405 (2004).
 40. O. Adriani *et al.* [L3 Collab.], Phys. Reports **236**, 1 (1993);
P. Achard *et al.* [L3 Collab.], Phys. Lett. **B531**, 28 (2002);
P. Achard *et al.* [L3 Collab.], Phys. Lett. **B568**, 23 (2003).
 41. G. Abbiendi *et al.* [OPAL Collab.], Phys. Lett. **B544**, 57 (2002);
G. Abbiendi *et al.* [OPAL Collab.], Phys. Lett. **B602**, 167 (2004).
 42. C. Adloff *et al.* [H1 Collab.], Phys. Lett. **B525**, 9 (2002);
F.D. Aaron *et al.* [H1 Collab.], Phys. Lett. **B663**, 382 (2008);
F.D. Aaron *et al.* [H1 Collab.], Phys. Lett. **B666**, 131 (2008).
 43. S. Chekanov *et al.* [ZEUS Collab.], Phys. Lett. **B549**, 32 (2002).
 44. D. Acosta *et al.* [CDF Collab.], Phys. Rev. Lett. **94**, 101802 (2005);
A. Abulencia *et al.* [CDF Collab.], Phys. Rev. Lett. **97**, 191802 (2006);
T. Aaltonen *et al.* [CDF Collab.], Phys. Rev. **D79**, 112002 (2009).
 45. V.M. Abazov *et al.* [DØ Collab.], Phys. Rev. **D73**, 111102 (2006);
V.M. Abazov *et al.* [DØ Collab.], Phys. Rev. **D77**, 091102 (2008);
V.M. Abazov *et al.* [DØ Collab.], Phys. Rev. Lett. **103**, 191803 (2009).
 46. G. Aad *et al.* [ATLAS Collab.], Phys. Lett. **B708**, 37 (2012);
G. Aad *et al.* [ATLAS Collab.], JHEP **1301**, 29 (2013);
G. Aad *et al.* [ATLAS Collab.], Phys. Rev. **D91**, 052007 (2015);
G. Aad *et al.* [ATLAS Collab.], Phys. Lett. **B754**, 302 (2016);
M. Aaboud *et al.* [ATLAS Collab.], Phys. Rev. **D96**, 052004 (2017).
 47. ATLAS Collaboration, ATLAS-CONF-2019-007 (2019).
 48. G. Aad *et al.* [ATLAS Collab.], Phys. Rev. Lett. **108**, 211802 (2012);
G. Aad *et al.* [ATLAS Collab.], Phys. Lett. **B728**, 562 (2014);
G. Aad *et al.* [ATLAS Collab.], JHEP **1603**, 41 (2016).
 49. M. Aaboud *et al.* [ATLAS Collab.], Eur. Phys. J. **C78**, 102 (2018).
 50. M. Aaboud *et al.* [ATLAS Collab.], Phys. Rev. **D98**, 032016 (2018).
 51. M. Aaboud *et al.* [ATLAS Collab.], Phys. Lett. **B759**, 229 (2016).
 52. G. Aad *et al.* [ATLAS Collab.], JHEP **1602**, 110 (2016).
 53. G. Aad *et al.* [ATLAS Collab.], Phys. Lett. **B721**, 171 (2013).
 54. G. Aad *et al.* [ATLAS Collab.], Phys. Rev. **D85**, 072003 (2012).
 55. G. Aad *et al.* [ATLAS Collab.], New J. Phys. **15**, 093011 (2013).
 56. G. Aad *et al.* [ATLAS Collab.], JHEP **1508**, 138 (2015).
 57. G. Aad *et al.* [ATLAS Collab.], New J. Phys. **18**, 073021 (2016).
 58. M. Aaboud *et al.* [ATLAS Collab.], Eur. Phys. J. **C79**, 803 (2019).
 59. S. Chatrchyan *et al.* [CMS Collab.], Phys. Lett. **B704**, 123 (2011);
S. Chatrchyan *et al.* [CMS Collab.], JHEP **1301**, 13 (2013);
S. Chatrchyan *et al.* [CMS Collab.], Phys. Rev. **D87**, 114015 (2013).
 60. V. Khachatryan *et al.* [CMS Collab.], Phys. Rev. **D91**, 052009 (2015).
 61. V. Khachatryan *et al.* [CMS Collab.], Phys. Rev. Lett. **116**, 071801 (2016);
V. Khachatryan *et al.* [CMS Collab.], Phys. Rev. Lett. **117**, 031802 (2016);
A.M. Sirunyan *et al.* [CMS Collab.], Phys. Lett. **B769**, 520 (2017);
A.M. Sirunyan *et al.* [CMS Collab.], JHEP **1808**, 130 (2018).
 62. CMS Collaboration, CMS-PAS-EXO-17-026 (2018).
 63. V. Khachatryan *et al.* [CMS Collab.], Phys. Lett. **B738**, 274 (2014).
 64. A.M. Sirunyan *et al.* [CMS Collab.], Phys. Lett. **B781**, 390 (2018).
 65. S. Chatrchyan *et al.* [CMS Collab.], Phys. Lett. **B722**, 28 (2013);
S. Chatrchyan *et al.* [CMS Collab.], Phys. Lett. **B723**, 280 (2013);
V. Khachatryan *et al.* [CMS Collab.], JHEP **1408**, 173 (2014).
 66. A.M. Sirunyan *et al.* [CMS Collab.], Phys. Rev. **D97**, 072006 (2018).
 67. V. Khachatryan *et al.* [CMS Collab.], JHEP **1601**, 166 (2016).
 68. S. Chatrchyan *et al.* [CMS Collab.], Phys. Lett. **B704**, 143 (2011);
S. Chatrchyan *et al.* [CMS Collab.], Phys. Lett. **B720**, 309 (2013).
 69. V. Khachatryan *et al.* [CMS Collab.], JHEP **1603**, 125 (2016).
 70. A.M. Sirunyan *et al.* [CMS Collab.], JHEP **1904**, 015 (2019).
 71. CMS Collaboration, CMS-PAS-EXO-18-013 (2019).
 72. M. Cacciari, G.P. Salam, and G. Soyez, JHEP **0804**, 063 (2008).
 73. T. Sjöstrand *et al.*, Comp. Phys. Comm. **135**, 238 (2001).

93. Dynamical Electroweak Symmetry Breaking: Implications of the H^0

Revised August 2019 by K.M. Black (Wisconsin U.), R.Sekhar Chivukula (UC San Diego) and M. Narain (Brown U.).

93.1 Introduction and Phenomenology

In theories of dynamical electroweak symmetry breaking, the electroweak interactions are broken to electromagnetism by the vacuum expectation value of a composite operator, typically a fermion bilinear. In these theories, the longitudinal components of the massive weak bosons are identified with composite Nambu-Goldstone bosons arising from dynamical symmetry breaking in a strongly-coupled extension of the standard model. Viable theories of dynamical electroweak symmetry breaking must also explain (or at least accommodate) the presence of an additional composite scalar state to be identified with the H^0 scalar boson [1,2] – a state unlike any other observed previously.

Theories of dynamical electroweak symmetry breaking can be classified by the nature of the composite singlet state to be associated with the H^0 and the corresponding dimensional scales f , the analog of the pion decay-constant in QCD, and Λ , the scale of the underlying strong dynamics.¹ Of particular importance is the ratio v/f , where $v^2 = 1/(\sqrt{2}G_F) \approx (246 \text{ GeV})^2$, since this ratio measures the expected size of the deviations of the couplings of a composite Higgs boson from those expected in the standard model. The basic possibilities, and the additional states that they predict, are described below.

93.1.1 Technicolor, $v/f \simeq 1$, $\Lambda \simeq 1 \text{ TeV}$

Technicolor models [7–9] provided the first examples of theories of dynamical electroweak symmetry breaking. These theories incorporate a new asymptotically free gauge theory (“technicolor”) and additional massless fermions (“technifermions” transforming under a vectorial representation of the gauge group). The global chiral symmetry of the fermions is spontaneously broken by the formation of a technifermion condensate, just as the approximate chiral symmetry in QCD is broken down to isospin by the formation of a quark condensate. The $SU(2)_W \times U(1)_Y$ interactions are embedded in the global technifermion chiral symmetries in such a way that the only unbroken gauge symmetry after chiral symmetry breaking is $U(1)_{em}$.² The theories naturally provide the Nambu-Goldstone bosons “eaten” by the W and Z boson. There would also typically be additional heavy states (e.g. vector mesons, analogous to the ρ and ω mesons in QCD) with TeV masses [13,14], and the WW and ZZ scattering amplitudes would be expected to be strong at energies of order 1 TeV.

There are various possibilities for the scalar H^0 in technicolor models. First, the H^0 could be identified as a singlet scalar resonance, analogous to the σ particle expected in pion-scattering in QCD [15,16]. Alternatively, the H^0 could be identified as a dilaton, a (pseudo-)Goldstone boson of scale invariance in theories of “walking technicolor” [17–21].³ Finally, the H^0 could be identified as an additional isosinglet state if the chiral symmetry breaking pattern of the technicolor theory provides for such a state.⁴ In all of these cases, however, one expects large deviations in the couplings of this particle from those of the standard model Higgs boson. Since the couplings observed for the H^0 approximate those of the Higgs boson to the 10% level, models of this kind are very highly constrained.

¹In a strongly interacting theory “Naive Dimensional Analysis” [3,4] implies that, in the absence of fine-tuning, $\Lambda \simeq g^* f$ where $g^* \simeq 4\pi$ is the typical size of a strong coupling in the low-energy theory [5,6]. This estimate is modified in the presence of multiple flavors or colors [7].

²For a review of technicolor models, see [10–12].

³If both the electroweak symmetry and the approximate scale symmetry are broken only by electroweak doublet condensate(s), then the decay-constants for scale and electroweak symmetry breaking may be approximately equal – differing only by terms formally proportional to the amount of explicit scale-symmetry breaking.

⁴In this case, however, the coupling strength of the singlet state to WW and ZZ pairs would be comparable to the couplings to gluon and photon pairs, and these would all arise from loop-level couplings in the underlying technicolor theory [22].

93.1.2 The Higgs doublet as a pseudo-Nambu-Goldstone Boson, $v/f < 1$, $\Lambda > 1 \text{ TeV}$

In technicolor models, the symmetry-breaking properties of the underlying strong dynamics necessarily breaks the electroweak gauge symmetries. An alternative possibility is that the underlying strong dynamics itself does not break the electroweak interactions, and that the entire quartet of bosons in the Higgs doublet (including the state associated with the H^0) are composite (pseudo-) Nambu-Goldstone particles [23,24]. In this case, the underlying dynamics can occur at energies exceeding 1 TeV and additional interactions with the top-quark mass generating sector (and possibly with additional weakly-coupled gauge bosons) cause the vacuum energy to be minimized when the composite Higgs doublet gains a vacuum expectation value [25,26]. In these theories, the couplings of the remaining singlet scalar state would naturally be equal to that of the standard model Higgs boson up to corrections of order $(v/f)^2$ and, therefore, constraints on the size of deviations of the H^0 couplings from that of the standard model Higgs [27] give rise to lower bounds on the scales f and Λ .⁵

The electroweak gauge interactions, as well as the interactions responsible for the top-quark mass, explicitly break the chiral symmetries of the composite Higgs model and lead generically to sizable corrections to the mass-squared of the Higgs-doublet – the so-called “Little Hierarchy Problem” [28]. “Little Higgs” theories [29–32] are examples of composite Higgs models in which the (collective) symmetry-breaking structure is selected so as to suppress these contributions to the Higgs mass-squared.

Composite Higgs models typically require a larger global symmetry of the underlying theory, and hence additional relatively light (compared to Λ) scalar particles, extra electroweak vector bosons (e.g. an additional $SU(2) \times U(1)$ gauge group), and vector-like partners of the top-quark of charge $+2/3$ and possibly also $+5/3$ [33]. In addition to these states, one would expect the underlying dynamics to yield additional scalar and vector resonances with masses of order Λ . If the theory respects a custodial symmetry [34], the couplings of these additional states to the electroweak and Higgs boson will be related – and, for example, one might expect a charged vector resonance to have similar branching ratios to WZ and WH . Different composite Higgs models utilize different mechanisms for arranging for the hierarchy of scales $v < f$ and arranging for a scalar Higgs self-coupling small enough to produce an H^0 of mass of order 125 GeV, for a review see [35]. If the additional states in these models carry color, they can provide additional contributions to Higgs production via gluon fusion [36]. The extent to which Higgs production at the LHC conforms with standard model predictions provides additional constraints (typically lower bounds on the masses of the additional colored states of order 0.7 TeV) on these models.

In addition, if the larger symmetry of the underlying composite Higgs theory does not commute with the standard model gauge group, then the additional states found in those models – especially those related to the top-quark, which tend to have the largest couplings to the electroweak sector – may be *colorless*. For example, in twin Higgs models [37], the top-partners carry no standard model charges. The phenomenology of the additional states in twin Higgs theories is rather different, since lacking color the production of these particles at the LHC will be suppressed – and, their decays may occur only via the electroweak symmetry breaking sector, leading to their being long-lived.

93.1.3 Top-Condensate, Top-Color, Top-Seesaw and related theories, $v/f < 1$, $\Lambda > 1 \text{ TeV}$

A final alternative is to consider a strongly interacting theory with a high (compared to a TeV) underlying dynamical scale that would naturally break the electroweak interactions, but whose

⁵In these models v/f is an adjustable parameter, and in the limit $v/f \rightarrow 1$ they reduce, essentially, to the technicolor models discussed in the previous subsection. Our discussion here is consistent with that given there, since we expect corrections to the SM Higgs couplings to be large for $v/f \simeq 1$. Current measurements constrain the couplings of the H^0 to equal those predicted for the Higgs in the standard model to about the 10% level [27], suggesting that f must have values of order a TeV or higher and, therefore, a dynamical scale Λ of at least several TeV.

strength is adjusted (“fine-tuned”) to produce electroweak symmetry breaking at 1 TeV. This alternative is possible if the electroweak (quantum) phase transition is continuous (second order) in the strength of the strong dynamics [38]. If the fine tuning can be achieved, the underlying strong interactions will produce a light composite Higgs bound state with couplings equal to that of the standard model Higgs boson up to corrections of order $(1 \text{ TeV}/\Lambda)^2$. As in theories in which electroweak symmetry breaking occurs through vacuum alignment, therefore, constraints on the size of deviations of the H^0 couplings from that of the standard model Higgs give rise to lower bounds on the scale Λ . Formally, in the limit $\Lambda \rightarrow \infty$ (a limit which requires arbitrarily fine adjustment of the strength of the high-energy interactions), these theories are equivalent to a theory with a fundamental Higgs boson – and the fine adjustment of the coupling strength is a manifestation of the hierarchy problem of theories with a fundamental scalar particle.

In many of these theories the top-quark itself interacts strongly (at high energies), potentially through an extended color gauge sector [39, 39–43]. In these theories, top-quark condensation (or the condensation of an admixture of the top with additional vector-like quarks) is responsible for electroweak symmetry breaking, and the H^0 is identified with a bound state involving the third generation of quarks. These theories typically include an extra set of massive color-octet vector bosons (top-gluons), and an extra $U(1)$ interaction (giving rise to a top-color Z') which couple preferentially to the third generation and whose masses define the scale Λ of the underlying physics.

93.1.4 Flavor

In addition to the electroweak symmetry breaking dynamics described above, which gives rise to the masses of the W and Z particles, additional interactions must be introduced to produce the masses of the standard model fermions. Two general avenues have been suggested for these new interactions. In “extended technicolor” (ETC) theories [44, 45], the gauge interactions in the underlying strongly interacting theory are extended to incorporate flavor. This extended gauge symmetry is broken down (possibly sequentially, at several different mass scales) to the residual strong interaction responsible for electroweak symmetry breaking. The massive gauge-bosons corresponding to the broken symmetries then mediate interactions between mass operators for the quarks/leptons and the corresponding bilinears of the strongly-interacting fermions, giving rise to the masses of the ordinary fermions after electroweak symmetry breaking.

In the case of “partial compositeness” [46], the additional flavor-dependent interactions arise from mixing between the ordinary quarks and leptons and massive composite fermions in the strongly-interacting underlying theory. Theories incorporating partial compositeness include additional vector-like partners of the ordinary quarks and leptons, typically with masses of order a TeV or less.

In both cases, the effects of flavor interactions on the electroweak properties of the ordinary quarks and leptons are likely to be most pronounced in the third generation of fermions.⁶ The additional particles present in these theories, especially the additional scalars, often couple more strongly to heavier fermions.

Moreover, since the flavor interactions must give rise to quark mixing, we expect that a generic theory of this kind could give rise to large flavor-changing neutral-currents [45]. In ETC theories, these constraints are typically somewhat relaxed if the theory incorporates approximate generational flavor symmetries [47], the theory has a slowly running coupling constant or “walks” [17–21], or if $\Lambda > 1 \text{ TeV}$ [48]. In theories of partial compositeness, the masses of the ordinary fermions depend on the scaling-dimension of the operators corresponding to the composite fermions with which they mix. This leads to a new mechanism for generating the mass-hierarchy of the observed quarks and leptons that, potentially, ameliorates flavor-changing neutral current problems and can provide new contributions to the composite Higgs poten-

tial which allow for $v/f < 1$ [49–53].

Alternatively, one can assume that the underlying flavor dynamics respect flavor symmetries (“minimal” [54, 55] or “next-to-minimal” [56] flavor violation) that suppress flavor-changing neutral currents in the two light generations. Additional considerations apply when extending these arguments to potential explanation of neutrino masses (see, for example, [57, 58]).

Since the underlying high-energy dynamics in these theories are strongly coupled, there are no reliable calculation techniques that can be applied to analyze their properties. Instead, most phenomenological studies depend on the construction of a “low-energy” effective theory describing additional scalar, fermion, or vector boson degrees of freedom, which incorporates the relevant symmetries and, when available, dynamical principles. In some cases, motivated by the AdS/CFT correspondence [59], the strongly-interacting theories described above have been investigated by analyzing a dual compactified five-dimensional gauge theory. In these cases, the AdS/CFT “dictionary” is used to map the features of the underlying strongly coupled high-energy dynamics onto the low-energy weakly coupled dual theory [60].

More recently, progress has been made in investigating strongly-coupled models using lattice gauge theory [61]. These calculations offer the prospect of establishing which strongly coupled theories of electroweak symmetry breaking have a particle with properties consistent with those observed for the H^0 – and for establishing concrete predictions for these theories at the LHC [62].

93.2 Experimental Searches

As discussed above, the extent to which the couplings of the H^0 conform to the expectations for a standard model Higgs boson constrains the viability of each of these models. Measurements of the H^0 couplings, and their interpretation in terms of effective field theory, are summarized in the H^0 review in this volume. In what follows, we will focus on searches for the additional particles that might be expected to accompany the singlet scalar: extra scalars, fermions, and vector bosons. In some cases, detailed model-specific searches have been made for the particles described above (though generally not yet taking account of the demonstrated existence of the H^0 boson).

In most cases, however, generic searches (e.g. for extra W' or Z' particles, extra scalars in the context of multi-Higgs models, or for fourth-generation quarks) are quoted that can be used – when appropriately translated – to derive bounds on a specific model of interest.

The mass scale of the new particles implied by the interpretations of the low mass of H^0 discussed above, and existing studies from the Tevatron and lower-energy colliders, suggests that only the Large Hadron Collider has any real sensitivity. A number of analyses already carried out by ATLAS and CMS use relevant final states and might have been expected to observe a deviation from standard model expectations – in no case so far has any such deviation been reported. The detailed implications of these searches in various model frameworks are described below.

Except where otherwise noted, all limits in this section are quoted at a confidence level of 95%. The searches at $\sqrt{s} = 8 \text{ TeV}$ (Run 1) are based on 20.3 fb^{-1} of data recorded by ATLAS, and an integrated luminosity of 19.7 fb^{-1} analyzed by CMS. The datasets collected at $\sqrt{s} = 13 \text{ TeV}$ during Run 2 of the LHC since 2015 are based on analyses with varied integrated luminosities ranging from $\sim 2\text{--}140 \text{ fb}^{-1}$.

93.2.1 Searches for Z' or W' Bosons

Massive vector bosons or particles with similar decay channels would be expected to arise in Little Higgs theories, in theories of Technicolor, or models involving a dilaton, adjusted to produce a light Higgs boson, consistent with the observed H^0 . These particles would be expected to decay to pairs of vector bosons, or to third generation quarks, or to leptons. The generic searches for W' and Z' vector bosons listed below can, therefore, be used to constrain models incorporating a composite Higgs-like boson.

A general review of searches for Z' and W' bosons is also included in this volume [63, 64]. In the context of the dynamical electroweak symmetry breaking models, we emphasize their decays to third generation fermions by including a detailed overview,

⁶Indeed, from this point of view, the vector-like partners of the top-quark in top-seesaw and little Higgs models can be viewed as incorporating partial compositeness to explain the origin of the top quark’s large mass.

while also briefly summarizing the other searches.

$Z' \rightarrow \ell\ell$:

ATLAS [65] and CMS [66] have both searched for Z' production with $Z' \rightarrow ee$ or $\mu\mu$. No deviation from the standard model prediction was seen in the dielectron and dimuon invariant mass spectra, by either the ATLAS or the CMS analysis, and lower limits on possible Z' boson masses were set. A Z'_{SSM} with couplings equal to the standard model Z' (a “sequential standard model” Z') and a mass below 5.1 TeV was excluded by ATLAS, while CMS set a lower mass limit of 5.15 TeV. The experiments also place limits on the parameters of extra dimension models and in the case of ATLAS on the parameters of a minimal walking technicolor model [17–21], consistent with a 125 GeV Higgs boson [67]. For a general review of searches in these channels see the PDG review of Z prime in this volume [63].

In addition, both experiments have also searched for Z' decaying to a ditau final state [68, 69]. An excess in $\tau^+\tau^-$ could have interesting implications for models in which lepton universality is not a requirement and enhanced couplings to the third generation are allowed. This analysis led to lower limits on the mass of a Z'_{SSM} of 2.4 and 2.1 TeV from ATLAS and CMS respectively.

$Z' \rightarrow q\bar{q}$:

The ability to relatively cleanly select $t\bar{t}$ pairs at the LHC together with the existence of enhanced couplings to the third generation in many models makes it worthwhile to search for new particles decaying in this channel. Both ATLAS [70] and CMS [71] have carried out searches for new particles decaying into $t\bar{t}$.

Both the ATLAS and CMS collaborations searched for $t\bar{t}$ in the all hadronic mode [72] [73] in both the resolved and boosted regions. No evidence of resonance production were seen and limits were produced for various models including the Z' boson in topcolor-assisted technicolor which excludes masses less than 3.1 to 3.6 TeV (ATLAS) depending on the details of the model and 3.3, 5.25, and 6.65 TeV for widths of 1, 10 and 30 percent relative to the mass of the resonance.

ATLAS also presented results on the lepton plus jets final state, where the top quark pair decays as $t\bar{t} \rightarrow WbWb$ with one W boson decaying leptonically and the other hadronically; CMS used final states where both, one or neither W decays leptonically and then combined the results. The $t\bar{t}$ invariant mass spectrum was analyzed for any excess, and no evidence for any resonance was seen. ATLAS excluded a narrow ($\Gamma/m = 1.2\%$) leptophobic topcolor Z' boson with masses between 0.7 and 2.1 TeV and with $\Gamma/m = 3\%$ between 0.7 and 3.2 TeV. CMS set limits on leptophobic Z' bosons for three different assumed widths $\Gamma/m = 1.0\%$, $\Gamma/m = 10.0\%$, and $\Gamma/m = 30.0\%$ of 3.9 TeV to 4.0 TeV and exclude RS KK gluons up to 3.3 TeV.

Both ATLAS [74] and CMS [75] have also searched for resonances decaying into $q\bar{q}$, qg or gg using the dijet invariant mass spectrum. Excited quarks are excluded up to masses of 6.7 TeV and model-independent upper limits on cross sections with a gaussian signal shape were set. CMS excluded string resonances with masses below 7.9 TeV, scalar diquarks below 7.5 TeV, axigluons and colorons below 6.6 TeV, excited quarks below 6.3 TeV, color-octet scalars below 3.7 TeV, W' bosons below 3.6 TeV, Z' bosons with SM-like couplings below 2.9 TeV and between 3.1 TeV and 3.3 TeV, Randall–Sundrum Gravitons below 2.6 TeV.

$W' \rightarrow \ell\nu$:

Both LHC experiments have also searched for massive charged vector bosons. In this section we include a summary of the results, with emphasis on final states with third generation fermions, while the details on other decays are discussed in the mini-review of W' [64]. ATLAS searched for a heavy W' decaying to $e\nu$ or $\mu\nu$ and find no excess over the standard model expectation. A sequential standard model (SSM) W' boson (assuming zero branching ratio to WZ) with mass less than 7 TeV was excluded [76] using 139 fb $^{-1}$ dataset at $\sqrt{s} = 13$ TeV, as well as setting model independent cross-section limits as a function of mass. Based on a smaller dataset, the CMS experiment excluded a SSM W' boson with mass up to 4.1 TeV [77] and presented the upper limits on the production of generic W' bosons decaying into this final state using a model-independent approach.

CMS [78] has carried out a complementary search in the $\tau\nu$ final state. As noted above, such searches place limits on models with enhanced couplings to the third generation. No excess was observed and limits between 2.0 and 2.7 TeV were set on the mass of a W' decaying preferentially to the third generation; a W' with universal fermion couplings was also excluded for masses less than 2.7 TeV.

$W' \rightarrow t\bar{b}$:

Heavy new gauge bosons can couple to left-handed fermions like the SM W boson or to right-handed fermions. W' bosons that couple only to right-handed fermions (W'_R) may not have leptonic decay modes, depending on the mass of the right-handed neutrino. For these W' bosons, the $t\bar{b}$ ($\bar{t}b + \bar{t}b$) decay mode is especially important because in many models the W' boson is expected to have enhanced couplings to the third generation of quarks relative to those in the first and second generations. It is also the hadronic decay mode with the best signal-to-background. ATLAS and CMS have performed searches for W' bosons via the $W' \rightarrow t\bar{b}$ decay channel in the lepton+jets and all-hadronic final state.

The CMS lepton+jets search [79–82], $W' \rightarrow t\bar{b} \rightarrow Wbb \rightarrow \ell\nu b\bar{b}$, proceeded via selecting events with an isolated lepton (electron or muon), and at least two jets, one of which is identified to originate from a b-quark. The mass of the W' boson ($M_{t\bar{b}}$) was reconstructed using the four-momentum vectors of the final state objects ($b\bar{b}\ell\nu$). The distribution of $M_{t\bar{b}}$ is used as the search discriminant. A search [82] using 35.9 fb $^{-1}$ of data, collected at $\sqrt{s} = 13$ TeV, led to an exclusion of W'_R bosons with masses below 3.4 TeV (3.6 TeV) if $M_{W'_R} \gg M_{\nu_R}$ ($M_{W'_R} < M_{\nu_R}$), where M_{ν_R} is the mass of the right-handed neutrino.

The CMS search for $W' \rightarrow t\bar{b}$ decays using the all-hadronic final state focused on W' masses above 1 TeV [81]. In this region, the top quark gets a large Lorentz boost and hence the three hadronic products from its decay merge into a single large-radius jet. Techniques which rely on substructure information of the jets [83] are employed to identify boosted all hadronic W boson and top quark jets and compute the mass of the jet. W' candidate mass was computed from back-to-back boosted top-tagged jet and a low mass b-tagged jet. From this all-hadronic search, W' bosons were excluded for masses up to 2.02 TeV.

ATLAS has searched for W'_R bosons in the $t\bar{b}$ final state both for lepton+jets [84] and all-hadronic [85] decays of the top. No significant deviations from the standard model were seen in either analysis and limits were set on the $W' \rightarrow t\bar{b}$ cross section times branching ratio and W' bosons with purely right-handed couplings to fermions were excluded for masses below 3.15 TeV when the two channels are combined.

In addition, the above studies also provided upper limits on the W' effective couplings to right- and left-handed fermions. In Fig. 93.1 (bottom) the upper limits on W' couplings normalized to the SM W boson couplings derived by ATLAS [86] are shown. The top panel of Fig. 93.1 shows the upper limits for arbitrary combinations of left- and right-handed couplings of the W' boson to fermions set using a model independent approach by CMS [82].

93.2.2 Searches for Resonances decaying to Vector Bosons and/or Higgs Bosons

Both the ATLAS and CMS experiments have used the data collected at $\sqrt{s} = 13$ TeV to search for resonances decaying to pairs of bosons. Overall no significant excesses were seen in the full datasets that were analyzed and the results are interpreted in models with heavy vector triplets (HVT) [87], models with strong gravity and extra spatial dimensions, as well as setting model independent limits as a function of mass. For a full review of models including extra spatial dimensions including the interpretation of many of these results in that context please see the review of extra dimensions in this volume [60].

Utilizing data collected at $\sqrt{s} = 13$ TeV, ATLAS [88] and CMS [89], have both looked for a resonant state decaying into VV (with $V = W$ or Z), VH (with H representing the SM Higgs boson), and HH. Both collaborations have analyzed bosonic decay modes. ATLAS searches in the $q\bar{q}q\bar{q}$, $\nu\nu q\bar{q}$, $\nu\nu q\bar{q}$, $llq\bar{q}$, $l\nu l\nu$, $ll\nu\nu$, $ll\nu\nu$, $llll$, $llll$, $q\bar{q}b\nu\nu b\bar{b}$, $l\nu b\bar{b}$, and $llb\bar{b}$ final states and combined the results

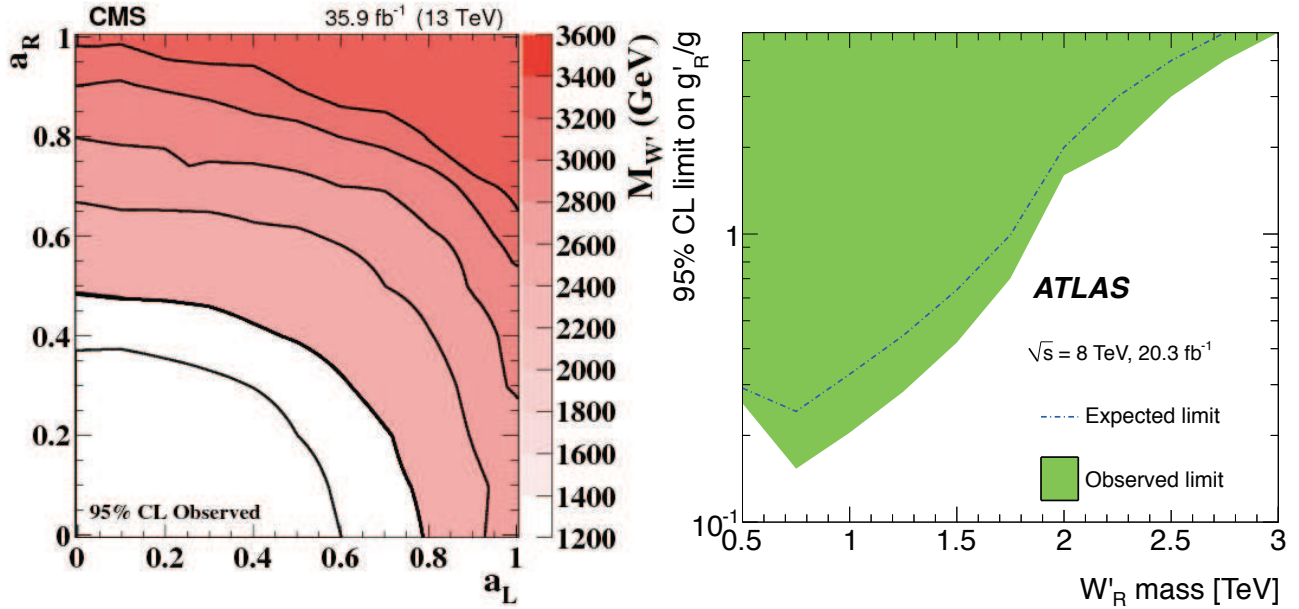


Figure 93.1: Left panel: Observed limits on the W' boson mass as function of the left-handed (a_L) and right-handed (a_R) couplings. Black lines represent contours of equal W' boson mass [82]. Right panel: Observed and expected regions, on the g'/g vs mass of the W' boson plane, that are excluded at 95% CL, for right-handed W' bosons [86].

(separately within each experiment). While CMS analyzes the $qqqq$, $\nu\nu qq$, $lvqq$, $llqq$, $ll\nu\nu$, $\nu\nu bb$, $lvbb$, $llbb$, $bbbb$, $\tau\tau bb$, and $qq\tau\tau$ final states.

The combined limits are expressed both as limits on the cross-section as a function resonance mass as well as constraints on the coupling of the heavy boson triplet to quarks, leptons, and the Higgs boson.

$X \rightarrow WZ$:

ATLAS searches for new heavy resonances decaying into WZ in the channels $WZ \rightarrow qqqq$ [90], $lvqq$ [91], and $lvll$ [92]. In the fully leptonic channel, the invariant mass of the WZ pair is obtained by considering all possible four lepton permutations in each event. The dominant background is Standard Model continuum WZ production, ZZ production where one lepton is not identified or falls outside the detector acceptance, and top quark plus vector boson production. No resonant production is seen in data and lower limits on the mass of a HVT decaying into WZ are set at 2260 (2460) GeV assuming a coupling constant of $g_V = 1$ ($g_V = 3$). In the $WZ \rightarrow lvqq$ mode, ATLAS searches in both the cases that the quarks are observed as individual jets (resolved) and where they merge into one jet in the detector (boosted) which probe the low and high p_T regime of the Z boson. No significant excess is seen in either channel and combined lower mass limits are placed at 2900 (3000) GeV for $g_V = 1$ ($g_V = 3$) in the HVT model. In the all hadronic decay mode, ATLAS searches for two high p_T hadronically decaying vector bosons looking for a resonant structure. No excess is seen and limits are placed excluding 1200-3000 (1200-3300) GeV for $g_V = 1$ ($g_V = 3$) in the HVT model.

The CMS collaboration searches for $VV \rightarrow qqqq$ [93] in the large R dijet search. The W and Z boson are identified through the mass of the large R jet and substructure variables. No excess is seen and limits are set for charged HVT bosons with masses lower than 3200 (3800) GeV for $g_V = 1$ ($g_V = 3$). Cross-section limits as function of mass are reported for the charged spin-1 resonance interpretation and are placed at 44.4 fb at 1.4 TeV to 0.7 pb at 4 TeV. In the $\nu\nu qq$ final state [94], the CMS collaboration searches for a charged spin 1 resonance decaying into a VZ final state with a Z boson decaying into a pair of neutrinos and the other boson decaying into two collimated quarks reconstructed as a large R-jet. The transverse mass of the VZ candidate is reconstructed and utilized to search for evidence of resonant VZ production. No excess is seen and lower mass limits are placed on the charged resonance at 3100 (3400) GeV for $g_V = 1$ ($g_V = 3$).

In the $2l2q$ final state, the CMS collaboration searches for a heavy resonance decaying into ZV [95] looking for events with one large R-jet consistent with the hadronic decay of a vector boson and a Z boson reconstructed in the charged lepton decay channel (e or μ). Limits are set for a HVT W' with a lower mass of 2270 (2330) for $g_V = 1$ ($g_V = 3$).

$X \rightarrow WW$:

The ATLAS collaboration searches for a new heavy resonance decaying into WW in the channels $WW \rightarrow qqqq$ [90], $lvqq$ [91], and $lv\nu\nu$ [96]. In the case where both W 's decay leptonically, ATLAS utilizes the transverse of the two lepton and two neutrino final state and searches for an excess in this distribution between 200 GeV and 5 TeV. No excess is seen and the mass of a HVT is excluded below 1300 GeV. Further vector boson fusion is also considered and cross-section limits as a function of mass are placed ranging from 1.3 pb to 0.006 pb at 200 GeV to 3 TeV, respectively. In the $lvqq$ mode, ATLAS completed a companion analysis to the $WZ \rightarrow$ analysis discussed above and places lower mass limits of 2850 (3150) GeV for $g_V = 1$ ($g_V = 3$) in the HVT model. ATLAS also interprets the all hadronic mode analysis in the hypothesis that $WW \rightarrow qqqq$ and places limits on a HVT boson decaying into WW in the all hadronic mode between 1200 to 2200 (1200 to 2800) GeV for $g_V = 1$ ($g_V = 3$).

The CMS collaboration searches for $VV \rightarrow qqqq$ [93] in the large R dijet search. The W and Z boson are identified through the mass of the large R jet and substructure variables. No excess is seen and limits are set for charged HVT bosons with masses lower than 2700 (2800) GeV for $g_V = 1$ ($g_V = 3$). Cross-section limits as function of mass are reported for the uncharged spin-1 resonance interpretation and are placed at 41.6 fb at 1.4 TeV to 0.6 pb at 4 TeV.

$X \rightarrow VH$:

The ATLAS Collaboration searches for a new heavy resonance decaying into WH and ZH in the qbb (WH and ZH) [97], $lvbb$ (WH), $\nu\nu bb$ (ZH), $llbb$ (ZH) [98]. In the all hadronic mode, ATLAS searches for boosted VH production looking for two large R jets where the larger invariant mass large R jet is interpreted as the Higgs boson decay products while the lesser the hadronically decaying vector boson requiring b tagging on the Higgs boson subjects. The invariant mass is reconstructed and a search is done for resonant production of ZH . None is found and limits from

1100 to 2500 (1300 to 3800 GeV) are placed for $g_V = 1$ ($g_V = 3$). ATLAS also searches for ZH where the W or Z boson decays into $\nu\nu$, $l\nu$, and ll . The analysis searches for both resolved and merged (boosted) b jets from the decay of the Higgs boson as well as defining signal regions based on the number of reconstructed charged leptons (0,1,or 2). In the dilepton channel the invariant mass is explicitly reconstructed of the entire diboson system, the single lepton channel reconstructs the diboson final state constraining the lepton and missing transverse momentum utilizing the known W boson mass, while the 0 charged lepton channel reconstructs the transverse mass of the diboson system. No excess is seen in any channel and limits on the production of a HVT are placed at 2800 GeV (2930) GeV for $g_V = 1$ ($g_V = 3$).

The CMS Collaboration searches for a heavy resonance decaying into VH [99] searching for resonances decaying into a Higgs boson and either a hadronically decaying W or Z boson. The search identifies events with two large- R jets using substructure variables and requires one large- R jets is tagged with a pair of b -hadrons clustered in a single jet. The invariant mass of the VH bosons is reconstructed and evidence for resonance production is sought. No excess is seen and limits are placed. With $g_V = 1$ (3) a narrow W' resonance with $m_{W'} < 2470(3150)$ GeV and $m_{Z'} < 1150(1190)$ GeV. Summary of Searches with Diboson Final States:

Both ATLAS [88] and CMS [89] provide plots summarizing the various searches results and limits combining. The results are shown in the context of HVT models and models of strong gravity with extra spatial dimensions. No excess is seen in any search and limits on the 4.3 (4.5) TeV (ATLAS) and (CMS). Inclusion of decays directly to fermions increase these limits to 5.3 (5.5) TeV and 5.0 (5.2) TeV from the ATLAS and CMS combinations, respectively. Both collaborations also place varying limits on the coupling strength as a function of HVT boson mass as well.

93.2.3 Vector-like third generation quarks

Vector-like quarks (VLQ) have non-chiral couplings to W bosons, i.e. their left- and right-handed components couple in the same way. They therefore have vectorial couplings to W bosons. Vector-like quarks arise in Little Higgs theories, top-coloron-models, and theories of a composite Higgs boson with partial compositeness. In the following, the notation T quark refers to a vector-like quark with charge $2/3$ and the notation B quark refers to a vector-like quark with charge $-1/3$, the same charges as the SM top and b quarks respectively. The exotic vector-like quarks $X_{5/3}$ and $Y_{-4/3}$ have charges $5/3$, and $-4/3$ respectively. Vector-like quarks couple with SM quarks with Yukawa interactions and may exist as $SU(2)$ singlets (T , and B), doublets $[(X_{5/3}, T), (T, B), (B, Y_{-4/3})]$, or triplets $[(X_{5/3}, T, B), (T, B, Y_{-4/3})]$. At the LHC, VLQs can be pair produced via the dominant gluon-gluon fusion. VLQs can also be produced singly by their electroweak effective couplings to a weak boson and a standard model quark. Single production rate is expected to dominate over the rate of pair production at large VLQ masses. T quarks can decay to bW , tZ , or tH^0 . Weak isospin singlets are expected to decay to all three final states with (asymptotic) branching fractions of 50%, 25%, 25%, respectively. Weak isospin doublets are expected to decay exclusively to tZ and to tH^0 [100] with equal branching ratios. Analogously, B quarks can decay to tW , bZ , or bH^0 . The $Y_{-4/3}$ and $X_{5/3}$ quarks decay exclusively to bW and to tW . While these are taken as the benchmark scenarios, other representations are possible and hence the final results are interpreted for many allowed branching fraction combinations.

Given the multiple decay modes of the VLQs, the final state signatures of both pair produced and the singly produced VLQs are fairly rich with leptons, jets, b jets, and missing energy. Depending on the mass of the VLQ, the top quarks and $W/Z/H^0$ bosons may be Lorentz boosted and identified using jet substructure techniques. Thus the searches are performed using lepton+jets signatures, multi-lepton and all-hadronic decays. In addition, T or B quarks with their antiparticles can result in events with same-sign leptons, for example if the decay $T \rightarrow tH \rightarrow bWW^+W^-$ is present, followed by leptonic decays of two same-sign W bosons. In the following subsections, while we describe the searches for each of the decay modes of the VLQs, the same analysis can be

re-interpreted to obtain the sensitivity to a combination with varied branching fractions to the different decay modes.

In the following sections, the results obtained for T (B) quarks assuming 100% branching ratio to Wb (Wt) are also applicable to heavy vector-like $Y_{-4/3}$ ($X_{5/3}$) with charge $4/3$ ($5/3$).

93.2.3.1 Searches for T quarks that decay to W , Z and H^0 bosons

$T/Y \rightarrow bW$:

CMS has searched for pair production of heavy T quarks that decay exclusively to bW [101–103]. The analysis selected events with exactly one charged lepton, assuming that the W boson from the second T quark decays hadronically. Under this hypothesis, a 2-constraint kinematic fit can be performed to reconstruct the mass of the T quark as a narrow mass peak with a mass resolution of around 7%. In Refs. [102] and [103], the two-dimensional distribution of reconstructed mass vs S_T was used to test for the signal, where S_T is the scalar sum of the missing p_T and the transverse momenta of the lepton and the leading four jets. This analysis, when combined with the search in the fully hadronic final state [104] excluded new quarks that decay 100% to bW for masses below 0.89 TeV [103]. At times the hadronically-decaying W boson is produced with a large Lorentz boost, leading to the W decay products merged into a large-radius jet. Algorithms such as jet pruning [105] were used to remove contributions from soft, wide angle radiation, from large-radius jets, leading to better discrimination between QCD jets and those arising from decays of the heavy particles. If the mass of the boosted jet was compatible with the W boson mass, then the W boson candidate jet and its subjects were used in the kinematic reconstruction of the T quark. No excess over standard model backgrounds was observed. Upper limits on the production cross section as a function of the mass of T quarks were measured. By comparing them with the predicted cross section for vector like quark pair production, the strong pair production of T quarks was excluded for masses below 1.30 TeV (1.28 TeV expected) [101].

Another “cut-based” search for pair produced T quarks in the all-hadronic final state targeting the Wb decay mode [106], relies on mass reconstruction of two highest p_T Wb combinations using boosted W boson candidates with $p_T > 200$ GeV and b -tagged jets. H_T is used as the signal discriminator, with selected events divided into nine categories based on the multiplicity of W and b jets in the event. From this search T quarks with pure Wb decays are excluded for masses below 1.04 TeV (1.07 TeV expected).

An analogous search has been carried out by ATLAS [107, 108] for the pair production of heavy T quarks. It used the lepton+jets final state with an isolated electron or muon and at least four jets, including a b jet and required reconstruction of the T quark mass. Given the mass range of the T quark being explored was from a 0.4 TeV to a couple of TeV, the W boson from the T quark may fall in two categories: those with a high boost leading to merged decay products, and others where the two jets from the W boson were resolved. In addition, the selection was optimized to require large angular separation between the high p_T W bosons and the b jets.

The $T \rightarrow Wb$ candidates were constructed from both the leptonically and hadronically decaying W bosons by pairing them with the two highest p_T b -tagged jets in the event. The pairing of b jets with W bosons which minimizes the difference between the masses of leptonically decaying T ($m_{lep}(T)$) and the hadronic T ($m_{had}(T)$) was chosen. Finally, $m_{lep}(T)$ was used as the discriminating variable in a signal region defined by high S'_T (here S'_T is defined as the scalar sum of the missing p_T , the p_T of the lepton and jets) and the opening angle between the lepton and the neutrino ($\Delta R(e, \nu)$). With the 36.1 fb^{-1} data collected during Run 2 at $\sqrt{s} = 13$ TeV, assuming 100% branching ratio to the Wb decay, the observed lower limit on the T mass was 1.35 TeV, and in the $SU(2)$ singlet scenario, the lower mass limit was obtained to be 1.17 TeV [107].

A targeted search for a T quark, produced singly in association with a light flavor quark and a b quark and decaying into bW , was carried out by CMS at $\sqrt{s}=13$ TeV and a dataset corresponding to 2.3 fb^{-1} [109]. The analysis used lepton+jets events, with at least

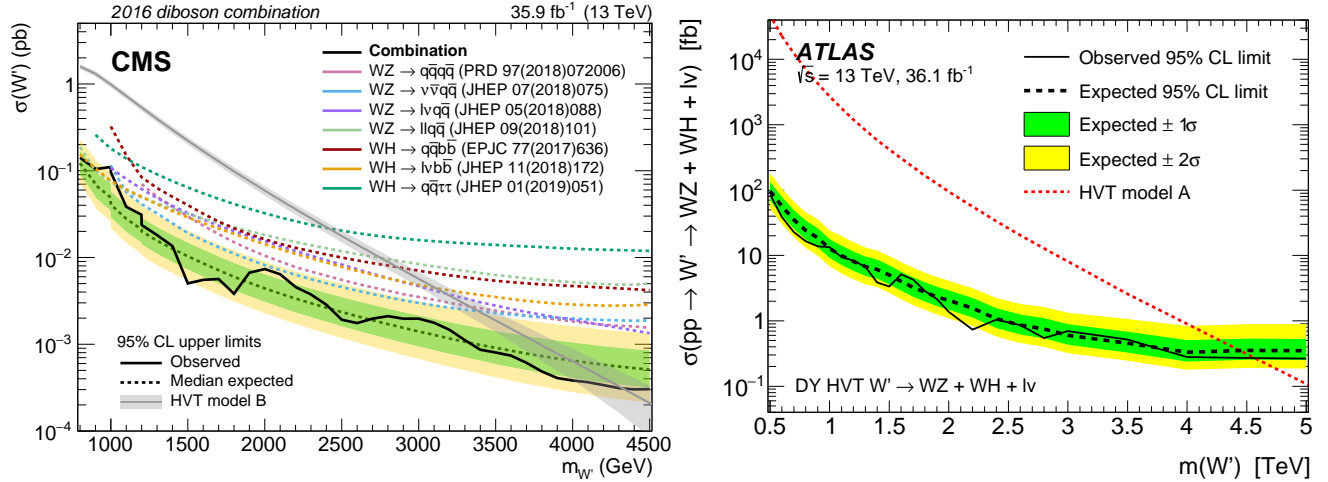


Figure 93.2: Left panel: Observed limits from W' to diboson from CMS [89]. Right panel: Observed limits from W' to diboson decays from ATLAS [88].

one b-tagged jet with large transverse momentum, and a jet in the forward η region. Selected events were required to have $S_T'' > 500$ GeV, where S_T'' is defined as the scalar sum of the transverse momenta of the lepton, the leading central jet, and the missing transverse momentum. The invariant mass of the T candidate was used as the discriminating variable and was reconstructed using the four-vectors of the leptonically decaying W boson and the leading central jet. No excess over the standard model prediction was observed. As the VLQ width is proportional to the square of the coupling, upper limits were set on the production cross section assuming a narrow width VLQ with coupling greater than 0.5. For Y/T quarks with a coupling of 0.5 and a 100% branching fraction for the decay to bW the excluded masses were in the range from 0.85 to 1.40 TeV [109]. A similar search [110, 111] performed by ATLAS singly produced T or $Y_{-4/3}$ quark decaying to Wb using a dataset corresponding to 36.1 fb^{-1} . The search was performed using lepton+jets events with a high p_T b-tagged jet, and at least one forward jet. The reconstructed mass of the $T/Y_{-4/3}$ quark, was used as the discriminating variable and showed no excess above the expectation from SM. Interference effects with the SM background are included in the study. This search led to 95% CL upper limits on the mixing angle $|\sin(\theta_L)|$ (C_L^{Wb}) in the range of 0.18–0.35 (0.25–0.49) for singlet T quark mass between 0.8–1.2 TeV. This search also provided limits as a function of the $Y_{-4/3}$ quark mass, on the coupling of the $Y_{-4/3}$ quark to bW , and the mixing parameter $|\sin\theta_R|$ (C_R^{Wb}) for a $(B, Y_{-4/3})$ doublet model [110]. For VLQ masses between 0.08–1.8 TeV, the limits on $|\sin(\theta_R)|$ (C_R^{Wb}) is in the range 0.17–0.55 (0.24–0.77), where limits on $|\sin\theta_R|$ are around 0.18–0.19 and below the constraints from electroweak precision observables for $Y_{-4/3}$ quark mass between 0.9–1.25 TeV. For $Y_{-4/3}$ quark in the triplets $(T, B, Y_{-4/3})$, limits on $|\sin(\theta_L)|$ (C_L^{Wb}) are between 0.16–0.39 (0.31–0.78) for masses between 0.8 GeV–1.6 TeV [110].

$T \rightarrow tH^0$:

ATLAS has performed a search for $T\bar{T}$ production with $T \rightarrow tH^0$ [108, 112]. Given the dominant decay mode $H^0 \rightarrow b\bar{b}$, these events are characterized by a large number of jets, many of which are b jets. Thus the event selection required one isolated electron or muon and high jet multiplicity (including b-tagged jets). The sample is categorized by the jet multiplicity (5 and ≥ 6 jets in the 1-lepton channel; 6 and ≥ 7 jets in the 0-lepton channel), b tag multiplicity (2, 3 and ≥ 4) and mass-tagged jet multiplicity (0, 1 and ≥ 2). The distribution of m_{eff} , defined as the scalar sum of the lepton and jet p_T and the missing E_T , for each category were used as the discriminant for the final signal and background separation. No excess of events were found. Weak isospin doublet T quarks were excluded below 1.16 TeV.

A search by ATLAS for pair produced VLQs with an all-hadronic final state signature yields an exclusion of pure decays

$T \rightarrow tH^0$ upto a T quark mass of 1.01 TeV [113]. This analysis used a deep neural network technique to identify jets originating from boosted bosons and top-quarks and described further in subsection 93.2.3.2.

The CMS search for $T\bar{T}$ production, with $T \rightarrow tH^0$ decays has been performed in both lepton+jets, multilepton and all-hadronic final states. The lepton+jets analysis [114] emphasizes the presence of large number of b-tagged jets, and combined with other kinematic variables in a Boosted Decision Tree (BDT) for enhancing signal to background discrimination. The multilepton analysis [114] was optimized for the presence of b jets and the large hadronic activity. For $\mathcal{B}(T \rightarrow Wb) = 1$, the combined lepton+jets and multilepton analyses led to a lower limit on T quark masses of 0.71 TeV. A search for $T \rightarrow tH^0$ in all-hadronic decays [115], optimized for a high mass T quark, and based on identifying boosted top quark jets has been carried out by CMS. This search aimed to resolve subjets within the jets arising from boosted top quark decays, including b tagging of the subjets. A likelihood discriminator was defined based on the distributions of H_T , and the invariant mass of the two b jets in the events for signal and background. No excess above background expectations was observed. Assuming 100% branching ratio for $T \rightarrow tH^0$, this analysis led to a lower limit of 0.75 TeV on the mass of the T quark.

Searches for T quarks at $\sqrt{s}=13$ TeV, based on a 2.6 fb^{-1} dataset [116] have been performed by CMS using the lepton+jets final state. This search has been optimized for high mass T quarks by exploiting techniques to identify W or Higgs bosons decaying hadronically with large transverse momenta. The boosted W channel excluded T quarks decaying only to bW with masses below 0.91 TeV, and the boosted tH channel excluded T quarks decaying only to tH for masses below 0.89 TeV.

A CMS search for $T \rightarrow tH^0$ with $H^0 \rightarrow \gamma\gamma$ decays has been performed [117] in pair production of T quarks. To identify the Higgs boson produced in the decay of the heavy T quark, and the subsequent $H^0 \rightarrow \gamma\gamma$ decay, the analysis focused on identification of two photons in events with one or more high p_T lepton+jets or events with no leptons and large hadronic activity. A search for a resonance in the invariant mass distribution of the two photons in events with large hadronic activity defined by the H_T variable showed no excess above the prediction from standard model processes. The analysis resulted in exclusion of T quark masses below 0.54 TeV.

A search for electroweak single production of T quark decaying to tH^0 using boosted topologies in fully hadronic [118] and lepton+jets [119] in the final states has been performed by CMS. The electroweak couplings of the T quarks to the SM third generation quarks are highly model dependent and hence these couplings determine the rates of the single T quark production. In both analyses, T quark candidate invariant mass was reconstructed using the

Implications of the H^0

boosted Higgs boson jets and the top quark. Higgs boson jets were identified using jet substructure techniques and subjet b tagging. For the lepton+jets analysis the top quark was reconstructed from the leptonically decaying W and the b jet, while in the all-hadronic analysis the top quark jet was tagged using substructure analysis. There was no excess of events observed above background. Exclusion limits on the product of the production cross section and the branching fraction ($\sigma(pp \rightarrow Tqt/b) \times \mathcal{B}(T \rightarrow tH^0)$) were derived for the T quark masses in the range 0.70–1.8 TeV. From the lepton+jets analysis, for a mass of 1.0 TeV, values of ($\sigma(pp \rightarrow Tqt/b) \times \mathcal{B}(T \rightarrow tH^0)$) greater than 0.8 and 0.7 pb were excluded assuming left- and right-handed coupling of the T quark to standard model fermions, respectively [119]. For the all-hadronic analysis, upper limits between 0.31 and 0.93 pb were obtained on ($\sigma(pp \rightarrow Tqt/b) \times \mathcal{B}(T \rightarrow tH^0)$) for T quark masses in the range 1.0–1.8 TeV [118].

 $T \rightarrow tZ$:

Both ATLAS and CMS searched for T quarks that decay exclusively into tZ in pp collisions at $\sqrt{s} = 13$ TeV. No excesses were found in either search.

ATLAS performed a search [120] for optimized pair production of vector-like top quarks decaying into tZ where the Z boson subsequently decays into neutrino pairs utilizing 36.1 fb^{-1} of data. The search selected events with one lepton, multiple jets, and significant missing transverse momentum. No significant excesses were found and lower limits on the mass of a vector like top quark were placed, excluding masses below 0.87 TeV (weak-isospin singlet), 1.05 TeV (weak-isospin doublet), and 1.16 TeV (pure tZ mode).

Another search by ATLAS for pair produced T decaying to tZ has been carried out by reconstructing the high transverse momentum Z boson from a pair of opposite-sign same-flavor lepton, using events with two or three charged leptons [121]. The final analysis is based on three final signatures. In the trilepton events, at least one b -tagged jet is required and S_T is used as the discriminating variable. In events with two leptons, at least 2 b jets are requested and those with zero or one high p_T top-tagged jet, use H_T as the discriminator. The second dilepton analysis with two top-tagged high p_T jets focuses on hadronically decaying heavy resonances and the invariant mass of the Z boson and the highest p_T b -tagged jet if found to be a good discriminating variable. No excess was observed over the background expectations. The combined analysis yields a lower limit on T quark mass of 1.03 TeV (1.21 TeV) in the singlet (doublet) model or 100% branching ratio for $T \rightarrow tZ$ a lower limit on the T quark mass of 1.34 TeV is obtained.

ATLAS has subsequently carried out a search [122] for singly produced T quark decaying to tZ where the Z boson decays into neutrino pairs. The search is carried out using 36.1 fb^{-1} of data in events with two different final state signatures: one with jets, and significant missing p_T (0L) and the other with single lepton, jets and missing p_T (1L). Events are divided into signal and dedicated W +jets and $t\bar{t}$ background control regions. The sensitivity to T quark signal is extracted using distributions of missing p_T for 1L and the distributions of transverse mass T quark constructed from missing p_T and the high p_T large-radius top-tagged jet for 0L analysis. The is no excess found over the expected background and lower limits on the production of T singlets is obtained as a function of the left- and right-handed couplings $c_{L,W}$ and $c_{R,W}$ to top quarks and W bosons, where c_W above 0.7 are excluded for T quark mass of 1.4 TeV. The limits on c_W are also recasted into expected and observed 95% CL upper limits for the mixing angle (θ_L) of a singlet T with the top quark.

CMS searched [123] for single production of T quarks decaying into tZ with the Z boson decaying to pairs of charged leptons (electrons and muons) and the top quark decaying hadronically using 35.9 fb^{-1} of data. Limits were placed on T quarks with masses between 0.7 and 1.7 TeV excluding the product of cross section and branching fraction above values of 0.27 to 0.04 pb. Additionally, limits on the product of cross section and branching fractions for a Z' boson decaying into tZ were set between 0.13 and 0.06 pb for Z' boson masses in the range from 1.5 to 2.5 TeV.

Similar searches by ATLAS for singly produced T decaying to

Zt have been performed in final state signatures with two or three charged leptons [121]. The analysis relies on tagging b jets and high p_T large-radius jets originating from top-quarks. Additional selections are devised to reduce the contributions from pair production of T quarks. For events with dilepton analysis, the discriminating variable is the mass of the T quark formed using the invariant mass of the Z boson candidate and the highest p_T top-tagged jet, while for the trilepton analysis, the variable S_T is used to search for an excess of data over the expected SM background. No excess above the SM expectations is observed. The two final states (dilepton and trileptons) are combined to obtain the final results. For the coupling parameter κ_T between 0.1–1.6, the 95% CL upper limits on the production cross section times branching fraction into Zt is between 0.16–0.18 (0.03–0.05) pb at T quark mass of 0.7 (2) TeV.

Combination of $T \rightarrow bW/tZ/tH^0$:

Most of the analyses described above targeted an individual decay mode of the T quark, with 100% branching ratio to either bW , tZ or tH^0 and were optimized accordingly. However, they have varied sensitivity to all three decay modes and the results can be interpreted as a function of branching ratios to each of the three decay modes, with the total adding up to unity ($\mathcal{B}(tH) + \mathcal{B}(tZ) + \mathcal{B}(Wb) = 1$).

Combinations of analyses have been performed by both ATLAS and CMS. The limits set by ATLAS searches in $W(\ell\nu)b = X$, $H(bb)b + X$, $Z(\ell\bar{\nu})$, $Z(\ell\ell)t/b + X$, dileptons with same-sign charge, trileptons, all-hadronic final states have been combined and the results obtained for various sets of branching fractions for T quark decays to bW , tH^0 and tZ are shown in Fig. 93.3 (left). In the combined analysis, ATLAS sets lower T quarks mass limit of 1.31 TeV for all possible values of the branching fractions to the three decay modes [107, 120, 124]. In Fig. 93.3, exclusion is shown in the plane of $\mathcal{B}(T \rightarrow Ht)$ versus $\mathcal{B}(T \rightarrow Wb)$, for different values of the T quark mass. The default branching ratio values for the weak-isospin singlet and doublet cases are also shown in Fig. 93.3 as yellow circle and star symbols respectively. Assuming a weak isospin (T, B) doublet and $|V_{Tb}| \ll |V_{tB}|$, T quark mass below 1.37 TeV is excluded.

CMS analysis for pair production of T , combined three channels with lepton final states: single lepton, two leptons with the same sign of the electric charge (SS), or at least three leptons (trilepton) [125]. For various combinations of branching fractions for T quark decays to bW , tH^0 and tZ , the combined results exclude T quarks with masses below 1.14–1.3 TeV and are shown in Figure 93.3 (right). Single lepton events are classified into 16 signal categories and 6 background control regions based on multiplicity of b -tagged, high p_T H^0 and W -tagged jets. The discriminating variables are H_T for H^0 -tagged and the minimum invariant mass constructed from the lepton and the b jet, $\min[M_{l\bar{b}}]$, for zero H^0 -tagged events. For the same-sign dilepton and trilepton analyses, the non-prompt backgrounds due to misidentified jets and leptons are derived from data control regions. In the trilepton analysis the S_T variable is used as the signal discriminator binned in four categories based on the lepton flavor combinations (eee , $e\mu\mu$, $e\mu\mu$, $\mu\mu\mu$). The single lepton analysis is most sensitive for $tHbW$ and $WbWb$ decay modes, within the the SS dilepton analysis $tHtH$ and $tHtZ$ have the best efficiency and for trileptons the $tZtZ$ and $tHtZ$ decays modes have the highest efficiency. CMS excludes singlet (doublet) T quark masses below 1.2 (1.28) TeV. Masses below 800 GeV were excluded in previous searches. For T quark masses in the range 0.8–1.8 TeV, cross sections smaller than 30.4–9.4 fb (21.2–6.1 fb) are excluded for the singlet (doublet) scenario.

Another inclusive search for pair produced T in all-hadronic final state [106] has been performed by CMS using the boosted event shape tagger (BEST) neural network technique to classify jets in six categories W , Z , H^0 , t , b , and light. This search does not focus on a given VLQ mode, but on various combinations of the boson and quark jets in the final state. Anti- k_T jets with a distance parameter of 0.8 are used. The BEST NN algorithm simultaneously classifies jets according to heavy object type. For each of the six particle hypothesis, it boosts each jet constituent into corresponding frame along jet momentum direction, and cal-

culates event shape and angular variables in the boosted frame, with the expectation that when boosting to the correct rest frame, jet constituents will be isotropic and show the expected N-prong structure of the decaying object in its rest frame. A neural network is trained using the event shape and angular variables in the boosted frame to classify jets according to one of those six possibilities (W, Z, H, t, b , or light). The analysis bins the events into 126 categories depending on the number of W, Z, H, t, b , or light jets in the final state with a maximum of four such objects. For each category H_T^{AK8} , the scalar sum of p_T of all AK8 jets, is used as the signal discriminator. A scan over a combination of various branching fractions is also performed. This search excludes T quark masses in the range 0.74–1.37 TeV for the tH decay mode in the NN analysis.

An inclusive search for VLQs has been carried out by CMS targeted at heavy T quarks decaying to any combination of bW, tZ , or tH^0 is described in [114]. Selected events have at least one isolated charged lepton. Events were categorized according to number and flavour of the leptons, the number of jets, and the presence of hadronic vector boson and top quark decays that are merged into a single jet. The use of jet substructure to identify hadronic decays significantly increases the acceptance for high T quark masses. No excess above standard model backgrounds was observed. Limits on the pair production cross section of the new quarks are set, combining all event categories, for all combinations of branching fractions into the three final states. For T quarks that exclusively decay to $bW/tZ/tH^0$, masses below 0.70/0.78/0.71 TeV are excluded.

93.2.3.2 Searches for B quarks that decay to W, Z and H^0 bosons

ATLAS and CMS have performed searches for pair production of heavy B quarks which subsequently decay to Wt, bZ or bH^0 . The searches have been carried out in final states with single leptons, dileptons (with same charge or opposite charge), multileptons, as well as in fully hadronic final states.

$B \rightarrow bH^0 X$:

Using 36.1 fb^{-1} of data, ATLAS has performed a search for pair produced VLQs with all-hadronic final state signature [113]. While this analysis provides exclusion limits for all third generation VLQs, it provides the strongest results for $B \rightarrow bH^0$ decay mode and excludes pure $B \rightarrow bH^0$ decays for B masses up to 1.01 TeV. The limits are also casted as a two-dimensional plane of branching ratio values of $B \rightarrow bH^0$ vs. $B \rightarrow Wb$. This analysis required the presence of high p_T jets and multiple b tags. It used a multi-class DNN to classify jets arising from W, Z, H^0 bosons and top-quarks. In addition, the matrix element method is used to compute the likelihood for the event to arise from a particular VLQ final state and used to construct the final discriminator. To increase the performance sensitivity, processes with the same number of top quarks, W/Z bosons, and H^0 Higgs bosons are combined into a single hypothesis.

$B \rightarrow WtX$:

A search for $B \rightarrow tW$ in B pair produced events has been performed by the ATLAS experiment [107] using lepton+jets events with one hadronically decaying W and one leptonically decaying W utilizing 36.1 fb^{-1} of data at $\sqrt{s} = 13 \text{ TeV}$. The search was optimized for T production decaying into Wb . Since the analysis was optimized for $T \rightarrow Wb$ rather than Wt decays the analysis does not reconstruct the full B mass. As discussed earlier, the hadronically and leptonically decaying heavy quarks were required to have similar reconstructed masses (within 300 GeV). The interpretation of the $T \rightarrow Wb$ in the context of $B \rightarrow tW$ production led to the exclusion of heavy B like VLQs for masses less than 1.25 TeV and 1.08 TeV, assuming a 100% branching fraction to tW or $SU(2)$ singlet B scenario, respectively.

A similar search by CMS [126], using 19.8 fb^{-1} of $\sqrt{s} = 8 \text{ TeV}$ data, selected events with one lepton and four or more jets, with at least one b -tagged jet, significant missing p_T , and further categorizes them based on the number of jets tagged as arising from the decay of boosted W, Z or H^0 bosons. The S_T distributions of the events in different categories showed no excess of events

above the expected background and yielded a lower limit on the B quark mass of 0.73 TeV for $BR(B \rightarrow Wt) = 1$.

CMS [116] also searched for pair production of both TT and BB with collisions from 2.5 fb^{-1} of $\sqrt{s} = 13 \text{ TeV}$ data. The analysis searches for events with one high p_T lepton, multiple jets, and highly boosted W or Higgs bosons decaying hadronically. The analysis focuses on pair production and selects events with either a boosted W or Higgs candidate and then proceeds to search for anomalous production in excess of standard model production. Seeing no significant excesses CMS then proceeded to set limits in many different interpretations. The strongest was from the the $B \rightarrow Wt$ interpretation leading to excluding heavy vector-like B quark less than 0.73 TeV.

The all-hadronic inclusive analysis [106] performed by CMS using the BEST NN technique to classify $W/Z/H^0/t/b$ light jets also gives exclusion limits on B quark production for various combinations of branching fractions for decays to tW, bZ, bH^0 . By considering categories based on various combinations of the boson and quark jets in the final state it excludes B quarks with masses up to 1230 GeV, for B decays to tW with a 100% branching fraction.

Electroweak production of single heavy $B+b$ productions has been studied by CMS in the decay to tW with lepton+jets final state [127]. Single lepton events with hadronic jets, including a forward jet, missing p_T are selected and divided into 10 different categories based on lepton flavor (e/μ), top-tagged, W -tagged, and $0/1/2$ b -tagged jets. B quark mass m_{reco} is fully reconstructed from lepton, jets, and missing p_T , where the neutrino four-momentum is computed using the missing p_T and the W mass constraint (assuming massless ν). For events within top-tagged category, the high p_T top-tagged hadronic jet and the leptonically decaying W boson is used to compute m_{reco} . The m_{reco} distribution is used as the signal discriminator. In the absence of an excess over the expected SM background, the exclusion limits on the production cross section is for B quark masses between 0.7–2 TeV varies between 0.3 to 0.03 pb. In addition, B quarks with left-handed couplings and a relative width of 10, 20, and 30% are excluded for masses below 1.49, 1.59, and 1.66 TeV respectively.

$B \rightarrow bZX$:

A search by CMS [128] for the pair-production of a heavy B quark and its antiparticle has been performed, where one the heavy B quark decays to bZ . Events with a Z boson decaying to e^+e^- or $\mu^+\mu^-$ and at least one b jet are selected. The signal from $B \rightarrow bZ$ decays are expected to appear as a local enhancement in the bZ mass distribution. No such enhancement was found and B quarks that decay 100% into bZ are excluded below 0.70 TeV. This analysis also set upper limits on the branching fraction for $B \rightarrow bZ$ decays of 30–100% in the B quark mass range 0.45–0.70 TeV. A complementary search has been carried out by ATLAS for new heavy quarks decaying into a Z boson and a b -quark [129]. Selected dilepton events contain a high transverse momentum Z boson that decays leptonically, together with two b jets. If the dilepton events have an extra lepton in addition to those from the Z boson, then only one b -jet is required. No significant excess of events above the standard model expectation was observed, and mass limits were set depending on the assumed branching ratios, as shown in Fig. 93.4. In a weak-isospin singlet scenario, a B quark with mass lower than 0.65 TeV was excluded, while for a particular weak-isospin doublet scenario, a B quark with mass lower than 0.73 TeV was ruled out.

ATLAS has searched for the electroweak production of single B quarks, which is accompanied by a b jet and a light jet [129]. The dilepton selection for double B production was modified for the single B production study by requiring the presence of an additional energetic jet in the forward region. An upper limit of 200 fb was obtained for the process $\sigma(pp \rightarrow B\bar{b}q) \times B(B \rightarrow Zb)$ with a heavy B quark mass at 0.70 TeV. This search indicated that the electroweak mixing parameter X_{Bb} below 0.5 is neither expected or observed to be excluded for any values of B quark mass.

Combination of $B \rightarrow tW/bZ/bH^0$:

The ATLAS experiment has combined the various analyses tar-

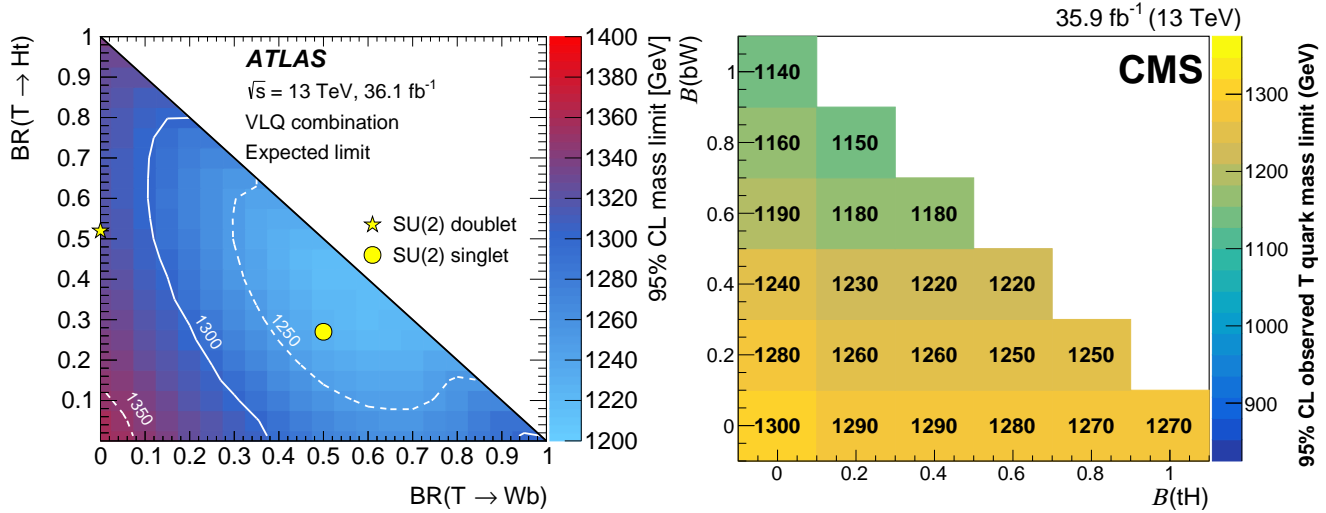


Figure 93.3: Left panel: observed limits on the mass of the T quark in the plane of $\mathcal{B}(T \rightarrow tH^0)$ versus $\mathcal{B}(T \rightarrow bW)$ from a combination [124] of all ATLAS searches for TT production. The markers indicate the default branching ratios for the SU(2) singlet and doublet scenarios. Right panel: the observed lower limits on the T quark mass (in GeV), from CMS searches after combining all lepton channels [125], for various branching fraction scenarios. $\mathcal{B}(T \rightarrow Wb) + \mathcal{B}(T \rightarrow tZ) + \mathcal{B}(T \rightarrow tH^0) = 1$ is assumed.

geted for specific decay modes to obtain the most sensitive limits on the pair production of B quarks [107, 108, 124]. Various searches ($W(\ell\nu)t + X, Z(\ell\ell)t/b + X$, same sign charge dilepton events, trilepton events, and all-hadronic) are combined to obtain lower limits on the mass of the B quark in the plane of $BR(B \rightarrow Wt)$ vs $BR(B \rightarrow bH)$. The searches were optimized for 100% branching fractions and hence are most sensitive at large $BR(B \rightarrow Wt)$, and also at large $BR(B \rightarrow bH^0)$. For all possible values of branching ratios in the three decay modes tW , bZ , or bH^0 , the lower limits on the B quark mass was found to be 1.03 TeV and shown in Fig. 93.4 (left) as a function of both B mass and branching ratio.

CMS combined three channels with lepton final states: single lepton, two leptons with the same sign of the electric charge (SS), or at least three leptons (trilepton) [125]. For various combinations of branching fractions for B quark decays to tW , bH^0 and bZ , the combined results exclude b quarks with masses below 0.91–1.24 TeV and are shown in Figure 93.4 (right) the details are provided earlier in subsection 93.2.3.1. The single lepton analysis is most sensitive for $tHbW$ and $WbWb$ decay modes, within the the SS dilepton analysis $tHtH$ and $tHtZ$ have the best efficiency and for trileptons the $tZtZ$ and $tHtZ$ decays modes have the highest efficiency. CMS excludes singlet (doublet) B quark masses below 1.17 (0.94) TeV. Masses below 800 GeV were excluded in previous searches. For B quark masses in the range 0.8–1.8 TeV, cross sections smaller than 40.6–9.4 fb (101–49.0 fb) are excluded for the singlet (doublet) scenario.

93.2.3.3 Searches for top-partner quark $X_{5/3}$

Searches for a heavy top vector-like quark $X_{5/3}$, with exotic charge $\pm 5/3$, such as that proposed in Refs. [131, 132], have been performed by both ATLAS and CMS [107, 133].

The analyses assumed pair-production or single-production of $X_{5/3}$ with $X_{5/3}$ decaying with 100% branching fraction to tW . Searches for $X_{5/3}$ have been performed using two final state signatures: same-sign leptons and lepton+jets.

The analysis based on searching for same-sign leptons, from the two W bosons from one of the $X_{5/3}$, has smaller backgrounds compared to the lepton+jets signature. Requiring same-sign leptons eliminates most of the standard model background processes, leaving those with smaller cross sections: $t\bar{t}$, W , $t\bar{t}Z$, WWW , and same-sign WW . In addition, backgrounds from instrumental effects due to charge misidentification were considered. Assuming pair production of $X_{5/3}$, the analyses by CMS using H_T as the discriminating variable restrict the $X_{5/3}$ mass to be higher than 1.16 (1.10) TeV for a right (left) handed chirality particle [133–135]. The limits obtained by ATLAS, by classifying the signal region by

number of b jets, H_T , and missing p_T in the event, corresponded to a lower mass limit on $X_{5/3}$ of 1.19 TeV [136, 137].

Searches for $X_{5/3}$ using leptons+jets final state signatures are based on either full or partial reconstruction of the T mass from the lepton, jets (including b jets) and missing p_T . The CMS search [133, 138] also utilized jet substructure techniques to identify boosted $X_{5/3}$ topologies. The discriminating variable used was the mass constructed from the lepton and b -tagged jet, $M_{(\ell,b)}$, which corresponds to the visible mass of leptonically decaying top quark. To optimize the search sensitivity, the events were further separated into categories based on lepton flavor (e, μ), the number of b -tagged jets, the number of W -tagged jets, and the number of t -tagged jets. In the absence of a signal, the CMS analysis excluded $X_{5/3}$ quark masses with right-handed (left-handed) couplings below 1.32 (1.30) TeV [138]. Combining the lepton+jets with the same-sign leptons analyses leads to a slight improvement and excludes $X_{5/3}$ quark masses with right-handed (left-handed) couplings below 1.33 (1.30) TeV.

The ATLAS lepton+jets search for $X_{5/3}$ utilized events with high p_T W bosons and b jets. The search described earlier for T pair production, with $T \rightarrow Wb$ decays, can be reinterpreted as a search for $X \rightarrow tW$. This analysis excluded $X_{5/3}$ with masses below 1.25 TeV [107].

The single $X_{5/3}$ production cross section depends on the coupling constant λ of the tWX vertex. ATLAS has performed an analysis of same-sign dileptons which includes both the single and pair production. This analysis led to a lower limit on the mass of the $X_{5/3}$ of 0.75 TeV for both values of $\lambda = 0.5$ and 1.0 [139].

Single heavy $X_{5/3}+t$ production has been studied by CMS in the decay to tW with lepton+jets final state [127]. The description of the analysis is provided earlier in the discussion of $B \rightarrow WtX$ decays, where the reconstructed mass of $X_{5/3}$, m_{reco} distribution is used as the signal discriminator. In the absence of an excess over the expected SM background, the exclusion limits on the production cross section is for $X_{5/3}$ quark masses between 0.7–2 TeV varies between 0.3 to 0.03 pb, depending on the width of $X_{5/3}$ between 1–10%. In addition, $X_{5/3}$ quarks with left-handed couplings and a relative width of 10, 20, and 30% are excluded for masses below 0.92, 1.3, and 1.45 TeV respectively.

93.2.4 Heavy resonances decaying to VLQ

CMS has performed search for VLQ production in the decay of massive resonances such as Z' and W' bosons.

$Z' \rightarrow tT$: Specifically searches are presented by CMS in Refs. [140] and [141] for massive spin-1 Z' resonances decaying to a top quark and heavy VLQ top quark partner T . The results of this search for a heavy spin-1 resonance are interpreted in the

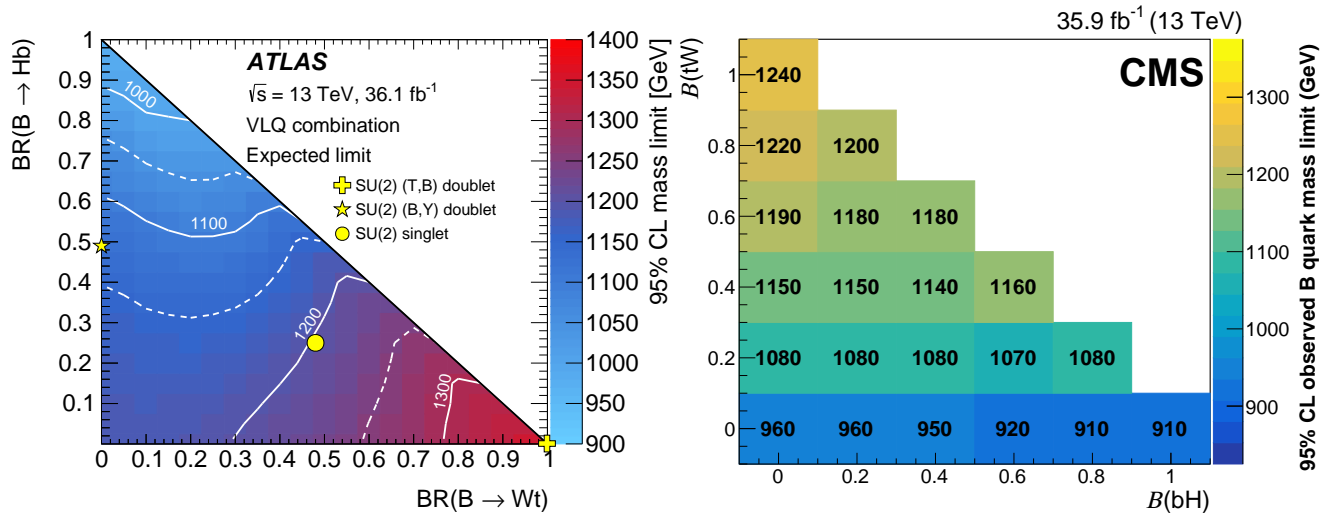


Figure 93.4: Observed limits on the mass of the B quark in the plane of $BR(B \rightarrow bH^0)$ versus $BR(B \rightarrow tW)$ from ATLAS searches [124] on the left panel, and CMS searches [125] on the right panel, for BB production. $B(B \rightarrow \mathcal{H}) + B(B \rightarrow \mathcal{Z}) + B(B \rightarrow \mathcal{W}\mathcal{L}) = 1$ is assumed. The yellow markers indicate the branching ratios for the SU(2) singlet and doublet scenarios.

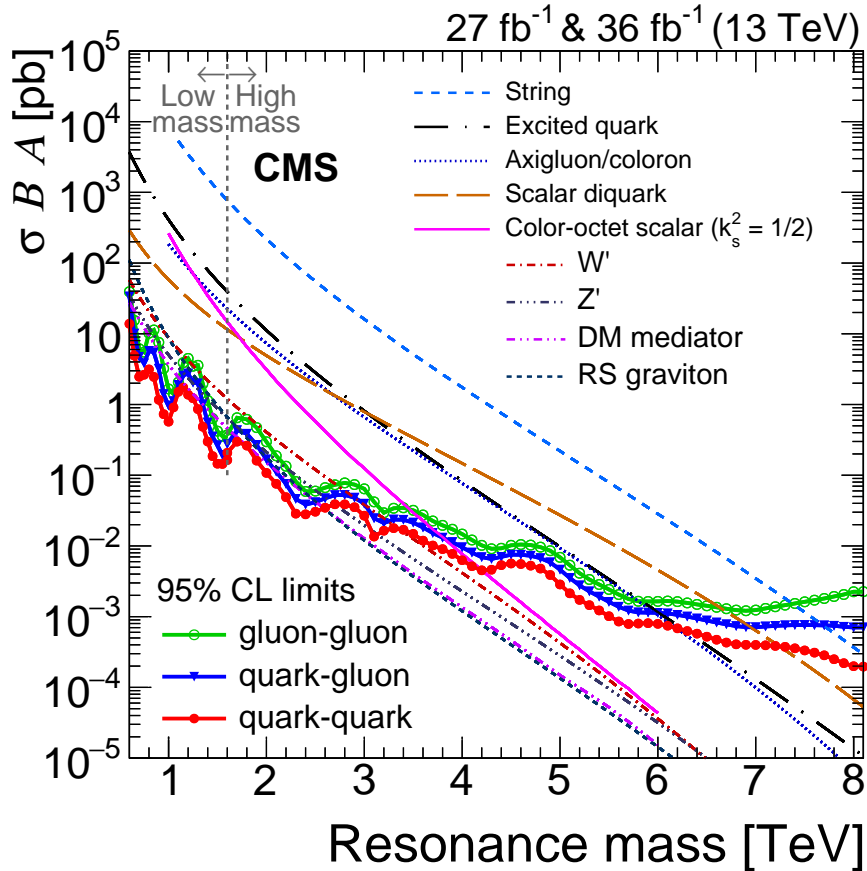


Figure 93.5: Observed 95% C.L. limits on $\sigma \times B \times A$ for string resonances, excited quarks, axigluons, colorons, E6 diquarks, s8 resonances, W' and Z' bosons, and Randall-Sundrum Gravitons g_{KK} from [130].

context of two different models. In the G^* model which predicts ten VLQs ($T, B, \tilde{T}, \tilde{B}, T_{5/3}, T_{2/3}, T', B', B_{-1/3}, B_{-4/3}$) with the mass relationship $M(T_{5/3}) = M(T_{2/3}) = M(T)\cos(\phi_L)$. For the benchmark scenario [142], $\cos(\phi_L)=0.84$ and the branching fractions $T \rightarrow tH^0, tZ, Wb$ are 0.25, 0.25 and 0.5 respectively. The ρ^0 model predicts a multiple of four new VLQs $T, B, X_{2/3}, X_{5/3}$, and in the benchmark scenario [143], the branching fractions $T \rightarrow tH^0, tZ, Wb$ are 0.5, 0.5 and 0 respectively.

Two of the three different decays of the $Z' \rightarrow tT$ with $T \rightarrow$

tH^0, tZ, Wb are characterized by the presence of two top quark decays and a boson (H^0/Z). A search [141] by CMS, optimized for $T \rightarrow tH/Zt$ decays is carried out in the lepton+jets final state using a dataset corresponding to an integrated luminosity of 35.9 fb^{-1} . Jet substructure techniques are used to identify (or tag) the high p_T large-radius jets originating from H^0, Z bosons and merged top quarks. The mass of the Z' boson is used as the signal discriminator and constructed using H^0 or Z -tagged dijet, the hadronic and leptonic top quark four vectors. For the

leptonic top quark reconstruction ($t \rightarrow b\ell\nu_\ell$), the neutrino four vector is obtained from the event missing p_T using the W boson mass constraint. While the high p_T hadronic top quark jets from decays of massive Z' bosons are mostly merged and identified by top tagging techniques, those from T decays maybe resolved. The reconstructed Z' candidate events are classified into six different categories requiring the presence of either H^0 -tagged jet with 2 b-tagged subjets or one b-tagged subjet or a Z -tagged boson, each with either zero or one top-tagged jet. This search does not observe any significant deviation in data over the expectation from standard model backgrounds. Within the context of the G^* model, for a T mass of 1.2 (1.5), this search excludes G^* [142] resonances with masses between 1.5–2.3 (2.0–2.4) TeV.

The search in the all-hadronic final state is based on a 2.6 fb^{-1} dataset [140], and optimized for $T \rightarrow Wb$ decays. Jet substructure techniques are deployed for tagging jets from high p_T W boson and top quarks. Events are categorized into two groups based on the presence of b-tagged subjet in the top-tagged jet. Multijet background estimation is challenging and determined using sidebands defined by inverting the b tagging requirement. Upper limits on cross section for $Z' \rightarrow tT$ are obtained in the range of 0.13–10 pb. With additional data, this search has the potential to exclude scenarios in composite Higgs and extra dimension models.

$W' \rightarrow Tb/Bt$: W' bosons are predicted to decay to VLQ third generation partners T , B quarks within composite Higgs and warped extra dimensional models [144]. In the benchmark scenarios of this framework, W' decays to Tb or Bt are equally distributed and the subsequent VLQ decays $T \rightarrow tH$ and $B \rightarrow bH^0$ each are assumed to have a branching fraction of 0.5. The search for $W' \rightarrow Tb/bH^0 \rightarrow tbH^0$ is performed using a sample of 35.9 fb^{-1} by CMS [145] in the final state with all-hadronic decays of both the Higgs boson ($H^0 \rightarrow b\bar{b}$) and the top quark. Both the H^0 boson and the top quark are expected to be boosted in the decay of a heavy W' , and hence jet substructure techniques, including subjet b-tagging and double b-tagging are deployed to identify the H^0 -tagged and the top-tagged jets. The three particle mass m_{tbH^0} , is used as the signal discriminant to observe the W' resonance. There is no excess observed in data above the expected SM background. This search excludes W' production cross section above 0.01–0.43 pb for masses between 1.5–4.0 TeV.

93.2.5 Colorons and Colored Scalars

These particles are associated with top-condensate and top-seesaw models, which involve an enlarged color gauge group. The new particles decay to dijets, $t\bar{t}$, and $b\bar{b}$.

Direct searches for colorons, color-octet scalars and other heavy objects decaying to $q\bar{q}$, qg , qg , or gg has been performed using LHC data from pp collisions at $\sqrt{s} = 7, 8$ and 13 TeV. Based on the analysis of dijet events from a data sample corresponding to a luminosity of 19.6 fb^{-1} , at $\sqrt{s} = 8$ TeV the CMS experiment excluded pair production of colorons with mass between 1.20–3.60 and 3.90–4.08 TeV [146]. Analyses of inclusive 8- and 10-jet final states with low missing transverse momentum by CMS [147], set limits in several benchmark models. Colorons (axigluons) with masses between 0.6 and 0.75 (up to 1.15) TeV were excluded, and gluinos in R-parity violating supersymmetric scenarios were ruled out from 0.6 up to 1.1 TeV.

A search for pair-produced colorons based on an integrated luminosity of 5.0 fb^{-1} at $\sqrt{s} = 7$ TeV by CMS excluded colorons with masses between 0.25 TeV and 0.74 TeV, assuming colorons decay 100% into $q\bar{q}$ [148]. This analysis was based on events with at least four jets and two dijet combinations with similar dijet mass. Color-octet scalars (s8) with masses between 1.20–2.79 TeV were excluded by CMS [146], and below 2.7 TeV by ATLAS [149].

These studies have now been extended to take advantage of the increased center-of-mass energy during Run 2 of the LHC. Using the 35.9 fb^{-1} of data collected at $\sqrt{s} = 13$ TeV, searches for narrow resonances have been performed by CMS. An analysis of the dijet invariant mass spectrum formed using wide jets [130, 150, 151], separated by $\Delta\eta_{jj} \leq 1.3$, led to limits on new particles decaying to parton pairs ($q\bar{q}$, qg , gg). Specific exclusions on the masses of colorons and color-octet scalars were obtained and are shown in Fig. 93.5. Exclusions have been obtained for axigluons and

colorons below 6.1 TeV, and color-octet scalars below 3.4 TeV.

93.3 Conclusions

As the above analyses have demonstrated, there is already substantial sensitivity to possible new particles predicted to accompany the H^0 in dynamical frameworks of electroweak symmetry breaking. No significant hints of any deviations from the standard model have been observed, and limits typically at the scale of a few hundred GeV to a few TeV are set.

Given the need to better understand the H^0 and to determine in detail how it behaves, such analyses continue to be a major theme of Run 2 the LHC, and we look forward to increased sensitivity as a result of the higher luminosity at the increased center of mass energy of collisions.

References

- [1] G. Aad *et al.* (ATLAS), Phys. Lett. **B716**, 1 (2012), [arXiv:1207.7214].
- [2] S. Chatrchyan *et al.* (CMS), Phys. Lett. **B716**, 30 (2012), [arXiv:1207.7235].
- [3] S. Weinberg, Physica **A96**, 1-2, 327 (1979).
- [4] A. Manohar and H. Georgi, Nucl. Phys. **B234**, 189 (1984).
- [5] H. Georgi, Nucl. Phys. **B266**, 274 (1986).
- [6] R. S. Chivukula, in “Flavor physics for the millennium. Proceedings, Theoretical Advanced Study Institute in elementary particle physics, TASI 2000, Boulder, USA, June 4-30, 2000,” 731–772 (2000), [hep-ph/0011264].
- [7] R. S. Chivukula, M. J. Dugan and M. Golden, Phys. Rev. **D47**, 2930 (1993), [hep-ph/9206222].
- [8] S. Weinberg, Phys. Rev. **D13**, 974 (1976), [Addendum: Phys. Rev. **D19**, 1277(1979)].
- [9] L. Susskind, Phys. Rev. **D20**, 2619 (1979).
- [10] K. Lane (2002), [hep-ph/0202255].
- [11] C. T. Hill and E. H. Simmons, Phys. Rept. **381**, 235 (2003), [Erratum: Phys. Rept. **390**, 553(2004)], [hep-ph/0203079].
- [12] R. Shrock, in “The origin of mass and strong coupling gauge theories. Proceedings, 5th International Workshop, SCGT’06, Nagoya, Japan November 21-24, 2006,” 227–241 (2007), [hep-ph/0703050].
- [13] E. Eichten *et al.*, Rev. Mod. Phys. **56**, 579 (1984), [Addendum: Rev. Mod. Phys. **58**, 1065(1986)].
- [14] E. Eichten *et al.*, Phys. Rev. **D34**, 1547 (1986).
- [15] R. S. Chivukula and V. Koulovassilopoulos, Phys. Lett. **B309**, 371 (1993), [hep-ph/9304293].
- [16] R. Foadi, M. T. Frandsen and F. Sannino, Phys. Rev. **D87**, 9, 095001 (2013), [arXiv:1211.1083].
- [17] B. Holdom, Phys. Lett. **150B**, 301 (1985).
- [18] K. Yamawaki, M. Bando, and K.-i. Matumoto, Phys. Rev. Lett. **56**, 1335 (1986).
- [19] T. W. Appelquist, D. Karabali and L. C. R. Wijewardhana, Phys. Rev. Lett. **57**, 957 (1986).
- [20] T. Appelquist and L. C. R. Wijewardhana, Phys. Rev. **D35**, 774 (1987).
- [21] T. Appelquist and L. C. R. Wijewardhana, Phys. Rev. **D36**, 568 (1987).
- [22] E. Eichten, K. Lane and A. Martin (2012), [arXiv:1210.5462].
- [23] D. B. Kaplan and H. Georgi, Phys. Lett. **136B**, 183 (1984).
- [24] D. B. Kaplan, H. Georgi and S. Dimopoulos, Phys. Lett. **136B**, 187 (1984).
- [25] M. E. Peskin, Nucl. Phys. **B175**, 197 (1980).
- [26] J. Preskill, Nucl. Phys. **B177**, 21 (1981).
- [27] See “Status of Higgs Boson Physics” review in this volume.
- [28] R. Barbieri and A. Strumia, in “4th Rencontres du Vietnam: Physics at Extreme Energies (Particle Physics and Astrophysics) Hanoi, Vietnam, July 19-25, 2000,” (2000), [hep-ph/0007265].

- [29] N. Arkani-Hamed, A. G. Cohen and H. Georgi, Phys. Lett. **B513**, 232 (2001), [hep-ph/0105239].
- [30] N. Arkani-Hamed *et al.*, JHEP **08**, 020 (2002), [hep-ph/0202089].
- [31] N. Arkani-Hamed *et al.*, JHEP **07**, 034 (2002), [hep-ph/0206021].
- [32] M. Schmaltz and D. Tucker-Smith, Ann. Rev. Nucl. Part. Sci. **55**, 229 (2005), [hep-ph/0502182].
- [33] K. Agashe *et al.*, Phys. Lett. **B641**, 62 (2006), [hep-ph/0605341].
- [34] P. Sikivie *et al.*, Nucl. Phys. **B173**, 189 (1980).
- [35] B. Bellazzini, C. Csáki and J. Serra, Eur. Phys. J. **C74**, 5, 2766 (2014), [arXiv:1401.2457].
- [36] R. Essig *et al.*, JHEP **09**, 085 (2017), [arXiv:1707.03399].
- [37] Z. Chacko, H.-S. Goh and R. Harnik, Phys. Rev. Lett. **96**, 231802 (2006), [hep-ph/0506256].
- [38] R. S. Chivukula, A. G. Cohen and K. D. Lane, Nucl. Phys. **B343**, 554 (1990).
- [39] V. A. Miransky, M. Tanabashi and K. Yamawaki, Mod. Phys. Lett. **A4**, 1043 (1989).
- [40] W. A. Bardeen, C. T. Hill and M. Lindner, Phys. Rev. **D41**, 1647 (1990).
- [41] C. T. Hill, Phys. Lett. **B266**, 419 (1991).
- [42] B. A. Dobrescu and C. T. Hill, Phys. Rev. Lett. **81**, 2634 (1998), [hep-ph/9712319].
- [43] R. S. Chivukula *et al.*, Phys. Rev. **D59**, 075003 (1999), [hep-ph/9809470].
- [44] S. Dimopoulos and L. Susskind, Nucl. Phys. **B155**, 237 (1979), [2,930(1979)].
- [45] E. Eichten and K. D. Lane, Phys. Lett. **90B**, 125 (1980).
- [46] D. B. Kaplan, Nucl. Phys. **B365**, 259 (1991).
- [47] T. Appelquist, M. Piai and R. Shrock, Phys. Rev. **D69**, 015002 (2004), [hep-ph/0308061].
- [48] R.S. Chivukula, B.A. Dobrescu, and E.H. Simmons, Phys. Lett. **B401**, 74 (1997).
- [49] Y. Grossman and M. Neubert, Phys. Lett. **B474**, 361 (2000), [hep-ph/9912408].
- [50] S. J. Huber and Q. Shafi, Phys. Lett. **B498**, 256 (2001), [hep-ph/0010195].
- [51] T. Gherghetta and A. Pomarol, Nucl. Phys. **B586**, 141 (2000), [hep-ph/0003129].
- [52] K. Agashe, R. Contino and A. Pomarol, Nucl. Phys. **B719**, 165 (2005), [hep-ph/0412089].
- [53] G. F. Giudice *et al.*, JHEP **06**, 045 (2007), [hep-ph/0703164].
- [54] R. S. Chivukula and H. Georgi, Phys. Lett. **B188**, 99 (1987).
- [55] G. D'Ambrosio *et al.*, Nucl. Phys. **B645**, 155 (2002), [hep-ph/0207036].
- [56] K. Agashe *et al.* (2005), [hep-ph/0509117].
- [57] T. Appelquist and R. Shrock, Phys. Lett. **B548**, 204 (2002), [hep-ph/0204141].
- [58] K. Sakai, Nucl. Phys. **B867**, 429 (2013), [arXiv:1207.4057].
- [59] J. M. Maldacena, Int. J. Theor. Phys. **38**, 1113 (1999), [Adv. Theor. Math. Phys.2,231(1998)], [hep-th/9711200].
- [60] For a review, see C. Csaki, J. Hubisz, and P. Meade, hep-ph/0510275 (2005), and “Extra Dimensions” review in this volume.
- [61] C. Pica, PoS **LATTICE2016**, 015 (2016), [arXiv:1701.07782].
- [62] T. Appelquist *et al.*, Phys. Rev. **D93**, 11, 114514 (2016), [arXiv:1601.04027].
- [63] PDG review of Zprime boson in this volume.
- [64] PDG review of Wprime boson in this volume.
- [65] M. Aaboud *et al.* (ATLAS), Phys. Lett. **B**, 68 (2019), [arXiv:1903.06248].
- [66] CMS Collaboration, Technical Report CMS-PAS-EXO-19-019, CERN, Geneva (2019), URL <http://cds.cern.ch/record/2684757>.
- [67] G. Aad *et al.* (ATLAS), Phys. Rev. **D90**, 5, 052005 (2014), [arXiv:1405.4123].
- [68] M. Aaboud *et al.* (ATLAS), JHEP **01**, 055 (2018), [arXiv:1709.07242].
- [69] CMS Collaboration, JHEP **0217**, 48 (2017).
- [70] ATLAS Collaboration, ATLAS-CONF-2016-014 (2016).
- [71] CMS Collaboration, JHEP **0717**, 001 (2016).
- [72] M. Aaboud *et al.* (ATLAS), Phys. Rev. D. **99**, 092004 (2019), [arXiv:1902.10077].
- [73] A. M. Sirunyan *et al.* (CMS), JHEP **04**, 031 (2019), [arXiv:1810.05905].
- [74] ATLAS Collaboration, ATLAS-CONF-2019-007 (2019).
- [75] CMS Collaboration, CMS-PAS-EXO-19-012 (2019).
- [76] M. Aaboud *et al.* (ATLAS), Accepted by Phys. Rev. [arXiv:1906.05609].
- [77] V. Khachatryan *et al.* (CMS), Phys. Lett. **B770**, 278 (2017), [arXiv:1612.09274].
- [78] V. Khachatryan *et al.* (CMS), Phys. Lett. **B755**, 196 (2016), [arXiv:1508.04308].
- [79] S. Chatrchyan *et al.* (CMS), JHEP **05**, 108 (2014), [arXiv:1402.2176].
- [80] V. Khachatryan *et al.* (CMS), JHEP **02**, 122 (2016), [arXiv:1509.06051].
- [81] A. M. Sirunyan *et al.* (CMS), JHEP **08**, 029 (2017), [arXiv:1706.04260].
- [82] A. M. Sirunyan *et al.* (CMS), Phys. Lett. **B777**, 39 (2018), [arXiv:1708.08539].
- [83] CMS Collaboration, Technical Report CMS-PAS-JME-15-002, CERN, Geneva (2016), URL <http://cds.cern.ch/record/2126325>.
- [84] G. Aad *et al.* (ATLAS), Phys. Lett. **B788**, 347 (2019), [arXiv:1807.10473].
- [85] G. Aad *et al.* (ATLAS), Eur. Phys. J. **C75**, 4, 165 (2015), [arXiv:1408.0886].
- [86] G. Aad *et al.* (ATLAS), Phys. Lett. **B743**, 235 (2015), [arXiv:1410.4103].
- [87] D. Pappadopulo *et al.*, JHEP **09**, 060 (2014), [arXiv:1402.4431].
- [88] M. Aaboud *et al.* (ATLAS), Phys. Rev. **D98**, 5, 052008 (2018), [arXiv:1601.04027].
- [89] A. M. Sirunyan *et al.* (CMS), Phys. Lett. **B798**, 134952 (2019), [arXiv:1906.00057].
- [90] M. Aaboud *et al.* (ATLAS), Phys. Lett. **B**, 91 (2017), [arXiv:1708.04445].
- [91] M. Aaboud *et al.* (ATLAS), JHEP **03**, 042 (2018), [arXiv:1710.07235].
- [92] M. Aaboud *et al.* (ATLAS), Phys. Lett. **B**, 68 (2018), [arXiv:1806.10532].
- [93] A. M. Sirunyan *et al.* (CMS), Phys. Rev. **D97**, 072006, [arXiv:1708.05379].
- [94] A. M. Sirunyan *et al.* (CMS), JHEP **07**, 075, [arXiv:1802.09407].
- [95] A. M. Sirunyan *et al.* (CMS), JHEP **09**, 101, [arXiv:1803.10093].
- [96] M. Aaboud *et al.* (ATLAS), Eur. Phys. J. **C**, 78 (2017), [arXiv:1710.01123].
- [97] M. Aaboud *et al.* (ATLAS), Phys. Lett. **B**, 774 (2017), [arXiv:1707.06858].

- [98] M. Aaboud *et al.* (ATLAS), JHEP **B**, 174 (2018), [arXiv:1712.06518].
- [99] A. M. Sirunyan *et al.* (CMS), Eur. Phys. J. **C**, 636, [arXiv:1707.01303].
- [100] F. del Aguila *et al.*, Nucl. Phys. **B334**, 1 (1990).
- [101] A. M. Sirunyan *et al.* (CMS), Phys. Lett. **B779**, 82 (2018), [arXiv:1710.01539].
- [102] CMS Collaboration, Technical report (2014).
- [103] V. Khachatryan *et al.* (CMS), Phys. Rev. **D93**, 1, 012003 (2016), [arXiv:1509.04177].
- [104] CMS Collaboration, Technical report (2012).
- [105] S. D. Ellis, C. K. Vermilion and J. R. Walsh, Phys. Rev. **D80**, 051501 (2009), [arXiv:0903.5081].
- [106] A. M. Sirunyan *et al.* (CMS) (2019), [arXiv:1906.11903].
- [107] M. Aaboud *et al.* (ATLAS), JHEP **10**, 141 (2017), [arXiv:1707.03347].
- [108] G. Aad *et al.* (ATLAS), JHEP **08**, 105 (2015), [arXiv:1505.04306].
- [109] A. M. Sirunyan *et al.* (CMS), Phys. Lett. **B772**, 634 (2017), [arXiv:1701.08328].
- [110] M. Aaboud *et al.* (ATLAS), JHEP **05**, 164 (2019), [arXiv:1812.07343].
- [111] G. Aad *et al.* (ATLAS), Eur. Phys. J. **C76**, 8, 442 (2016), [arXiv:1602.05606].
- [112] ATLAS collaboration (ATLAS), Technical report (2016).
- [113] M. Aaboud *et al.* (ATLAS), Phys. Rev. **D98**, 9, 092005 (2018), [arXiv:1808.01771].
- [114] S. Chatrchyan *et al.* (CMS), Phys. Lett. **B729**, 149 (2014), [arXiv:1311.7667].
- [115] V. Khachatryan *et al.* (CMS), JHEP **06**, 080 (2015), [arXiv:1503.01952].
- [116] A. M. Sirunyan *et al.* (CMS), JHEP **11**, 085 (2017), [arXiv:1706.03408].
- [117] CMS Collaboration, cds.cern.ch/record/1709129 (2014).
- [118] A. M. Sirunyan *et al.* (CMS), JHEP **04**, 136 (2017), [arXiv:1612.05336].
- [119] V. Khachatryan *et al.* (CMS), Phys. Lett. **B771**, 80 (2017), [arXiv:1612.00999].
- [120] M. Aaboud *et al.* (ATLAS), JHEP **08**, 052 (2017), [arXiv:1705.10751].
- [121] M. Aaboud *et al.* (ATLAS), Phys. Rev. **D98**, 11, 112010 (2018), [arXiv:1806.10555].
- [122] M. Aaboud *et al.* (ATLAS), JHEP **05**, 041 (2019), [arXiv:1812.09743].
- [123] A. M. Sirunyan *et al.* (CMS), Phys. Lett. **B781**, 574 (2018), [arXiv:1708.01062].
- [124] M. Aaboud *et al.* (ATLAS), Phys. Rev. Lett. **121**, 21, 211801 (2018), [arXiv:1808.02343].
- [125] A. M. Sirunyan *et al.* (CMS), JHEP **08**, 177 (2018), [arXiv:1805.04758].
- [126] CMS Collaboration, Technical report (2012).
- [127] A. M. Sirunyan *et al.* (CMS), Eur. Phys. J. **C79**, 90 (2019), [arXiv:1809.08597].
- [128] V. Khachatryan *et al.* (CMS), Phys. Rev. **D93**, 11, 112009 (2016), [arXiv:1507.07129].
- [129] G. Aad *et al.* (ATLAS), JHEP **11**, 104 (2014), [arXiv:1409.5500].
- [130] A. M. Sirunyan *et al.* (CMS), JHEP **08**, 130 (2018), [arXiv:1806.00843].
- [131] R. Contino and G. Servant, JHEP **06**, 026 (2008), [arXiv:0801.1679].
- [132] J. Mrazek and A. Wulzer, Phys. Rev. **D81**, 075006 (2010), [arXiv:0909.3977].
- [133] A. M. Sirunyan *et al.* (CMS), JHEP **08**, 073 (2017), [arXiv:1705.10967].
- [134] CMS Collaboration, Technical report (2017).
- [135] S. Chatrchyan *et al.* (CMS), Phys. Rev. Lett. **112**, 17, 171801 (2014), [arXiv:1312.2391].
- [136] M. Aaboud *et al.* (ATLAS), JHEP **12**, 039 (2018), [arXiv:1807.11883].
- [137] G. Aad *et al.* (ATLAS), Phys. Rev. **D91**, 11, 112011 (2015), [arXiv:1503.05425].
- [138] A. M. Sirunyan *et al.* (CMS), JHEP **03**, 082 (2019), [arXiv:1810.03188].
- [139] G. Aad *et al.* (ATLAS), JHEP **10**, 150 (2015), [arXiv:1504.04605].
- [140] A. M. Sirunyan *et al.* (CMS), JHEP **09**, 053 (2017), [arXiv:1703.06352].
- [141] A. M. Sirunyan *et al.* (CMS), Eur. Phys. J. **C79**, 3, 208 (2019), [arXiv:1812.06489].
- [142] C. Bini, R. Contino and N. Vignaroli, JHEP **01**, 157 (2012), [arXiv:1110.6058].
- [143] D. Greco and D. Liu, JHEP **12**, 126 (2014), [arXiv:1410.2883].
- [144] N. Vignaroli, Phys. Rev. **D89**, 9, 095027 (2014), [arXiv:1404.5558].
- [145] A. M. Sirunyan *et al.* (CMS), JHEP **03**, 127 (2019), [arXiv:1811.07010].
- [146] V. Khachatryan *et al.* (CMS), Phys. Rev. **D91**, 5, 052009 (2015), [arXiv:1501.04198].
- [147] V. Khachatryan *et al.* (CMS), Phys. Lett. **B770**, 257 (2017), [arXiv:1608.01224].
- [148] S. Chatrchyan *et al.* (CMS), Phys. Rev. Lett. **110**, 14, 141802 (2013), [arXiv:1302.0531].
- [149] G. Aad *et al.* (ATLAS), Phys. Rev. **D91**, 5, 052007 (2015), [arXiv:1407.1376].
- [150] A. M. Sirunyan *et al.* (CMS), Phys. Lett. **B769**, 520 (2017), [Erratum: Phys. Lett. **B772**, 882 (2017)], [arXiv:1611.03568].
- [151] CMS Collaboration, Technical report (2015).

94. Grand Unified Theories

Revised August 2019 by A. Hebecker (Heidelberg U.) and J. Hisano (KMI, Nagoya U.).

94.1 The standard model

The Standard Model (SM) may be defined as the renormalizable field theory with gauge group $G_{SM} = SU(3)_C \times SU(2)_L \times U(1)_Y$, with 3 generations of fermions in the representation

$$(\mathbf{3}, \mathbf{2})_{1/3} + (\bar{\mathbf{3}}, \mathbf{1})_{-4/3} + (\bar{\mathbf{3}}, \mathbf{1})_{2/3} + (\mathbf{1}, \mathbf{2})_{-1} + (\mathbf{1}, \mathbf{1})_2, \quad (94.1)$$

and a scalar Higgs doublet H transforming as $(\mathbf{1}, \mathbf{2})_1$. Here and below we use boldface numbers to specify the dimension of representations of non-Abelian groups (in this case fundamental and antifundamental) and lower indices for $U(1)$ charges. The fields of Eq. (94.1) should also be familiar as $[Q, u^c, d^c, L, e^c]$, with $Q = (u, d)$ and $L = (\nu, e)$ being the quark and lepton $SU(2)$ -doublets and u^c, d^c, e^c charge conjugate $SU(2)$ -singlets.¹ Especially after the discovery of the Higgs, this model is remarkably complete and consistent with almost all experimental data.

A notable exception are neutrino masses, which are known to be non-zero but are absent in the SM even after the Higgs acquires its vacuum expectation value (VEV). The minimalist attitude is to allow for the dimension-five operator $(HL)^2$ [1], which induces (Majorana) neutrino masses. In the seesaw mechanism [2–4] this operator is generated by integrating out heavy singlet fermions (right-handed (r.h.) neutrinos). Alternatively, neutrinos can have Dirac masses if light singlet neutrinos are added to the SM spectrum.

Conceptual problems of the SM include the absence of a Dark Matter candidate, of a mechanism for generating the baryon asymmetry of the universe, and of any reason for the observed smallness of the θ parameter of QCD (θ_{QCD}). In addition, the apparently rather complex group-theoretic data of Eq. (94.1) remains unexplained. Together with the abundance of seemingly arbitrary coupling constants, this disfavors the SM as a candidate fundamental theory, even before quantum gravity problems arise at energies near the Planck mass M_P .

To be precise, there are 19 SM parameters which have to be fitted to data: Three gauge couplings² g_3, g_2 and g_1 , 13 parameters associated with the Yukawa couplings (9 charged fermion masses, three mixing angles and one CP phase in the CKM matrix.), the Higgs mass and quartic coupling, and θ_{QCD} . In addition, Majorana neutrinos introduce 3 more masses and 6 mixing angles and phases. As we will see, the paradigm of grand unification addresses mainly the group theoretic data of Eq. (94.1) and the values of the three gauge couplings. In many concrete realizations, it then impacts also the other mentioned issues of the SM, such as the family structure and fermion mass hierarchy.

More specifically, after precision measurements of the Weinberg angle θ_W in the LEP experiments, supersymmetric GUTs (SUSY GUTs) have become the leading candidates in the search for ‘Physics beyond the SM’. Supersymmetry (SUSY) is a symmetry between bosons and fermions which requires the addition of superpartners to the SM spectrum. If SUSY is motivated as a solution to the gauge hierarchy problem (i.e. to the naturalness or fine-tuning problem of the electroweak scale) [5], superpartners have to be present near the weak scale. SUSY GUTs [6] then lead to the prediction of θ_W , in good agreement with subsequent observations [7]. However, the non-discovery of new particles at the LHC puts into question the presence of new physics at the TeV scale in general and in particular of low-scale supersymmetry. Still, SUSY may be present just outside the presently explored energy domain.

The measured Higgs mass (125 GeV) is in principle consistent with this picture, assuming superpartners in the region of roughly 10 TeV. Such heavy superpartners then induce radiative corrections raising the Higgs mass above the Z boson mass m_Z [8, 9]. However, from the vantage point of the hierarchy problem, heavy

superpartners are problematic: They also contribute to SUSY-breaking Higgs mass parameters and thereby to the Higgs potential, tending to raise the Z mass. As a result, the incarnation of SUSY in terms of the minimal supersymmetric SM (MSSM) is becoming questionable. Turning the logic around, one may say that compared to expectations based on the MSSM with superpartner masses below about 1 TeV, the measured Higgs mass value of 125 GeV is somewhat too high [10]. Independently, the LHC has disfavored light colored superpartners (which does not imply that *all* superpartners are heavy). These facts represent new hints for future work on SUSY GUTs or on GUTs without TeV-scale supersymmetry.

94.2 Basic group theory and charge quantization

94.2.1 $SU(4)_C \times SU(2)_L \times SU(2)_R$

Historically, the first attempt at unification was the Pati-Salam model with gauge group $G_{PS} = SU(4)_C \times SU(2)_L \times SU(2)_R$ [11]. It unifies SM fermions in the sense that one generation (plus an extra SM singlet) now comes from the $(\mathbf{4}, \mathbf{2}, \mathbf{1}) + (\bar{\mathbf{4}}, \mathbf{1}, \mathbf{2})$ of G_{PS} . This is easy to verify from the breaking pattern $SU(4)_C \rightarrow SU(3)_C \times U(1)_{B-L}$ together with the identification of SM hypercharge as a linear combination between $B-L$ (baryon minus lepton number) and the T_3 generator of $SU(2)_R$. This model explains charge quantization, that is, why all electric charges are integer multiples of some smallest charge in the SM. Concretely, the $\mathbf{4}$ and $\bar{\mathbf{4}}$ of $SU(4)_C$ identify lepton number as the 4th colour and the tracelessness of the diagonal generator implies that quark charges are expressed in terms of $1/N_c$ fractions of lepton charges. However, G_{PS} is not simple (containing three simple factors), and thus it does not predict gauge coupling unification.

94.2.2 $SU(5)$

Since G_{SM} has rank four (two for $SU(3)_C$ and one for $SU(2)_L$ and $U(1)_Y$, respectively), the rank-four group $SU(5)$ is the minimal choice for unification in a simple group [12]. The three SM gauge coupling constants derive from a universal coupling α_G at the GUT scale M_G . Explicitly embedding G_{SM} in $SU(5)$ is straightforward, with $SU(3)_C$ and $SU(2)_L$ corresponding e.g. to the upper-left 3×3 and lower-right 2×2 blocks, respectively, in traceless 5×5 matrices for $SU(5)$ generators of the fundamental representation. The $U(1)_Y$ corresponds to matrices generated by $\text{diag}(-2/3, -2/3, -2/3, 1, 1)$ and hence commutes with $SU(3)_C \times SU(2)_L \subset SU(5)$. It is then easy to derive how one SM generation precisely comes from the $\mathbf{10} + \bar{\mathbf{5}}$ of $SU(5)$ (where $\mathbf{10}$ is the antisymmetric rank-2 tensor):

$$\mathbf{10} : \begin{pmatrix} 0 & u_b^c & -u_g^c & u_r & d_r \\ -u_b^c & 0 & u_r^c & u_g & d_g \\ u_g^c & -u_r^c & 0 & u_b & d_b \\ -u_r & -u_g & -u_b & 0 & e^c \\ -d_r & -d_g & -d_b & -e^c & 0 \end{pmatrix} \quad \text{and} \quad \bar{\mathbf{5}} : \begin{pmatrix} d_r^c \\ d_b^c \\ d_g^c \\ e \\ -\nu_e \end{pmatrix}. \quad (94.2)$$

In addition to charge quantisation this structure explains why the l.h. quark and lepton states fall in $SU(2)_L$ doublets while the r.h. states are singlets.

Since $SU(5)$ has 24 generators, $SU(5)$ GUTs have 12 new gauge bosons known as X bosons (or X/Y bosons) in addition to the SM. X bosons form an $SU(3)_C$ -triplet and $SU(2)_L$ -doublet. Their interaction connects quarks and leptons such that baryon and lepton numbers are not conserved and nucleon decay is predicted. Furthermore, $U(1)_Y$ hypercharge is automatically quantized since it is embedded in $SU(5)$.

In order to break the electroweak symmetry at the weak scale and give mass to quarks and leptons, Higgs doublets are needed. In the minimal $SU(5)$ model, they can sit in either a $\mathbf{5}_H$ or $\bar{\mathbf{5}}_H$. The three additional states are referred to as color-triplet Higgs scalars. Their couplings also violate baryon and lepton numbers, inducing nucleon decay. In order not to violently disagree with the non-observation of nucleon decay, the triplet mass must be greater than $\sim 10^{11}$ GeV [13]. Moreover, in SUSY GUTs [6], in order to cancel anomalies as well as give mass to both up and down quarks, both Higgs multiplets $\mathbf{5}_H$ and $\bar{\mathbf{5}}_H$ are required. As we shall discuss later, nucleon decay now constrains the Higgs triplets to have

¹ In our convention the electric charge is $Q = T_3 + Y/2$ and all our spinor fields are left-handed (l.h.).

² Equivalently, the $SU(2)_L$ and $U(1)_Y$ couplings are denoted as $g = g_2$ and $g' = \sqrt{3/5} g_1$. One also uses $\alpha_s = \alpha_3 = (g_3^2/4\pi)$, $\alpha_{EM} = (e^2/4\pi)$ with $e = g \sin \theta_W$ and $\sin^2 \theta_W = (g')^2/(g^2 + (g')^2)$.

mass significantly greater than M_G in the minimal SUSY $SU(5)$ GUT since integrating out the Higgs triplets generates dimension-five baryon-number-violating operators [14]. The mass splitting between doublet and triplet in the $\mathbf{5}_H$ (and $\bar{\mathbf{5}}_H$) comes from their interaction with the $SU(5)$ breaking sector.

94.2.3 $SO(10)$

While $SU(5)$ allows for the minimal GUT models, unification is not complete: Two independent representations, $\mathbf{10}$ and $\bar{\mathbf{5}}$, are required for one SM generation. A further representation, an $SU(5)$ singlet, has to be added to serve as r.h. neutrino in the seesaw mechanism. In this case, the r.h. neutrino masses are not necessarily related to the GUT scale. By contrast, a single $\mathbf{16}$ -dimensional spinor representation of $SO(10)$ accommodates a full SM generation together with an extra singlet, potentially providing a r.h. neutrino [15]. This is most easily understood from the breaking pattern $SO(10) \rightarrow SU(5) \times U(1)_X$ and the associated branching rule³ $\mathbf{16} = \mathbf{10}_{-1} + \bar{\mathbf{5}}_3 + \mathbf{1}_{-4}$. Here the indices refer to charges under the $U(1)_X$ subgroup, which is orthogonal to $SU(5)$ and reflects the fact that $SO(10)$ has rank five. From the above, it is easy to see that $U(1)_X$ charges can be given as $2Y - 5(B - L)$. Intriguingly, all representations of $SO(10)$ are anomaly free in four dimensions (4d). Thus, the absence of anomalies in an $SU(5)$ -GUT or a SM generation can be viewed as deriving from this feature.

We now describe in more detail how one family of quarks and leptons appears in the $\mathbf{16}$. To understand this, recall that the Γ -matrices of the 10d Clifford algebra give rise to five independent, anticommuting ‘creation-annihilation’ operators $\Gamma^{a\pm} = (\Gamma^{2a-1} \pm i\Gamma^{2a})/2$ with $a = 1, \dots, 5$. These correspond to five fermionic harmonic oscillators or ‘spin’ 1/2 systems. The 32-dimensional tensor product of those is reducible since the 10d rotation generators $M_{mn} = -i[\Gamma^m, \Gamma^n]/4$ ($m, n = 1, \dots, 10$) always flip an even number of ‘spins’. This gives rise to the $\mathbf{16}$ as displayed in Table 94.1. Next, one also recalls that the natural embedding of $SU(5)$ in $SO(10)$ relies on ‘pairing up’ the 10 real dimensions to produce 5 complex dimensions, $\mathbb{R}^{10} \equiv \mathbb{C}^5$, similarly to the pairing up of Γ^m s used above. This makes it clear how to associate one $|\pm\rangle$ system to each complex dimension of $SU(5)$, which explains the labeling of the ‘spin’ columns in Table 94.1: The first three and last two ‘spins’ correspond to $SU(3)_C$ and $SU(2)_L$, respectively. In fact, an $SU(3)_C$ rotation just raises one color index and lowers another, changing colors $\{r, g, b\}$, or changes relative phases between the three spin states. Similarly, an $SU(2)_L$ rotation raises one weak index and lowers another, thereby flipping the weak isospin from up to down or vice versa, or changes the relative phase between the two spin states. In this representation $U(1)_Y$ hypercharge is simply given by $Y = -2/3(\sum \text{color spins}) + (\sum \text{weak spins})$. $SU(5)$ rotations corresponding to X bosons then raise (or lower) a color index, while at the same time lowering (or raising) a weak index. It is easy to see that such rotations can mix the states $\{Q, u^c, e^c\}$ and $\{d^c, L\}$ among themselves and ν^c is a singlet. Since $SO(10)$ has 45 generators, additional 21 gauge bosons are introduced including the $U(1)_X$ above. The 20 new $SO(10)$ rotations not in $SU(5)$ are then given by either raising any two spins or lowering them. With these rotations, $\mathbf{1}$ and $\bar{\mathbf{5}}$ are connected with $\mathbf{10}$. The last $SO(10)$ rotation changes phases of states with weight $2(\sum \text{color spins}) + 2(\sum \text{weak spins})$, which corresponds to $U(1)_X$.

$SO(10)$ has two inequivalent maximal subgroups and hence breaking patterns, $SO(10) \rightarrow SU(5) \times U(1)_X$ and $SO(10) \rightarrow SU(4)_C \times SU(2)_L \times SU(2)_R$. In the first case, one can carry on breaking to $G_{SM} \subset SU(5)$ precisely as in the minimal $SU(5)$ case above. Alternatively, one can identify $U(1)_Y$ as an appropriate linear combination of $U(1)_X$ and the $U(1)$ factor from $SU(5)$, leading to the so-called flipped $SU(5)$ [17] as an intermediate step in breaking $SO(10)$ to G_{SM} . In the second case, we have an intermediate Pati-Salam model thanks to the branching rule $\mathbf{16} = (\mathbf{4}, \mathbf{2}, \mathbf{1}) + (\bar{\mathbf{4}}, \mathbf{1}, \mathbf{2})$. Finally, $SO(10)$ can break directly to the SM at M_G . Gauge coupling unification remains intact in

Table 94.1: Quantum numbers of $\mathbf{16}$ -dimensional representation of $SO(10)$.

state	Y	Color	Weak	$SU(5)$	$SO(10)$
ν^c	0	---	--	1	16
e^c	2	---	++	10	
u_r	1/3	+--	-+		
d_r	1/3	+--	+-		
u_g	1/3	-+-	-+		
d_g	1/3	-+-	+-		
u_b	1/3	--+	-+		
d_b	1/3	--+	+-		
u_r^c	-4/3	-++	--		
u_g^c	-4/3	+-+	--		
u_b^c	-4/3	++-	--		
d_r^c	2/3	-++	++	5	
d_g^c	2/3	+-+	++		
d_b^c	2/3	++-	++		
ν	-1	+++	-+		
e	-1	+++	+-		

the case of this ‘direct’ breaking and for the breaking pattern $SO(10) \rightarrow SU(5) \rightarrow G_{SM}$ (with $SU(5)$ broken at M_G). In the case of intermediate-scale Pati-Salam or flipped $SU(5)$ models, gauge coupling predictions are modified. The Higgs multiplets in the minimal $SO(10)$ come from the fundamental representation, $\mathbf{10}_H = \mathbf{5}_H + \bar{\mathbf{5}}_H$. Note, only in $SO(10)$ does the representation type distinguish SM matter from Higgs fields.

94.2.4 Beyond $SO(10)$

Finally, larger symmetry groups can be considered. For example, the exceptional group E_6 has maximal subgroup $SO(10) \times U(1)$ [18]. Its fundamental representation branches as $\mathbf{27} = \mathbf{16}_1 + \mathbf{10}_{-2} + \mathbf{1}_4$. Another maximal subgroup is $SU(3)_C \times SU(3)_L \times SU(3)_R \subset E_6$ with branching rule $\mathbf{27} = (\mathbf{3}, \mathbf{3}, \mathbf{1}) + (\bar{\mathbf{3}}, \mathbf{1}, \bar{\mathbf{3}}) + (\mathbf{1}, \bar{\mathbf{3}}, \mathbf{3})$. Independently of any underlying E_6 , the group $[SU(3)]^3$ with additional permutation symmetry Z_3 interchanging the three factors can be considered. This is known as ‘trification’ [19]. The $E_6 \rightarrow [SU(3)]^3$ breaking pattern has been used in phenomenological analyses of the heterotic string [20]. However, in larger symmetry groups, such as E_6 , $SU(6)$, etc., there are now many more states which have not been observed and must be removed from the effective low-energy theory.

Intriguingly, the logic by which G_{SM} is a maximal subgroup of $SU(5)$, which together with $U(1)_X$ is a maximal subgroup of $SO(10)$, continues in a very elegant and systematic way up to the largest exceptional group. The resulting famous breaking chain $E_8 \rightarrow E_7 \rightarrow E_6 \rightarrow SO(10) \rightarrow SU(5) \rightarrow G_{SM}$ together with the special role played by E_8 in group and in string theory is a tantalizing hint at deeper structures. However, since all representations of E_8 and E_7 are real and can not lead to 4d chiral fermions, this is necessarily outside the 4d GUT framework.

94.3 GUT breaking and doublet-triplet splitting

In the standard, 4d field-theoretic approach to GUTs, the unified gauge group is broken spontaneously by an appropriate GUT Higgs sector. Scalar potentials (or superpotentials in SUSY GUTs) exist whose vacua spontaneously break $SU(5)$ or $SO(10)$. While these potentials are ad hoc (just like the Higgs potential in the SM), the most naive expectation is that all their dimensional parameters are $O(M_G)$. In the simplest case of $SU(5)$, the $\mathbf{24}$ (adjoint) GUT Higgs develops a VEV along the G_{SM} -singlet direction as $\langle \Phi \rangle \propto \text{diag}(-2/3, -2/3, -2/3, 1, 1)$. In order for $SO(10)$ to break to $SU(5)$, the $\mathbf{16}$ or $\mathbf{126}$, which have a G_{SM} -singlet with non-zero $U(1)_X$ charge, get a VEV.

The masses of doublet and triplet in the $\mathbf{5}_H$ (and $\bar{\mathbf{5}}_H$) generically split due to their coupling to the GUT Higgs. In addition, both the doublet and the triplet masses also get an equal contribution from an $SU(5)$ -invariant GUT-scale mass term. Without any further structure, an extreme fine-tuning between two large effects is then necessary to keep the doublet mass at the electroweak scale. Supersymmetry plays an important role in for-

³ Useful references on group theory in the present context include [16] and refs. therein.

bidding large radiative correction to the doublet mass due to the non-renormalization theorem [5]. However, even in this case we have to fine tune parameters at tree level. This is the doublet-triplet splitting problem which, in the SUSY context, is clearly related the μ -term problem of the MSSM (the smallness of the coefficient of $\mu H_u H_d$).

Several mechanisms for natural doublet-triplet splitting have been suggested under the assumption of supersymmetry, such as the sliding singlet [21], missing partner [22], missing VEV [23], and pseudo-Nambu-Goldstone boson mechanisms [24]. Particular examples of the missing partner mechanism for $SU(5)$ [25], the missing VEV mechanism for $SO(10)$ [26, 27] and the pseudo-Nambu-Goldstone boson mechanism for $SU(6)$ [28] have been shown to be consistent with gauge coupling unification and nucleon decay. From the GUT-scale perspective, one is satisfied if the triplets are naturally heavy and the doublets are massless ($\mu \simeq 0$). There are also several mechanisms for resolving the subsequent issue of why μ is of order the SUSY breaking scale [29].⁴ For a review of the μ problem and some suggested solutions in SUSY GUTs and string theory, see [30–33] and references therein.

In general, GUT-breaking sectors successfully resolving the doublet-triplet splitting problem, dynamically stabilizing all GUT-scale VEVs and allowing for realistic neutrino masses and Yukawa couplings (including the GUT-symmetry violation in the latter) require a number of ingredients. However, for validity of the effective theory, introduction of higher or many representations is limited, otherwise a Landau pole may appear below the Planck scale. In addition, GUTs are only effective theories below the Planck scale in the 4d field-theoretic approach. Since M_G is close to this scale, the effects of higher-dimension operators are not obviously negligible. In particular, operators including the GUT-breaking Higgs may affect low-energy predictions, such as quark and lepton masses.

Thus, especially in the context of GUT breaking and doublet-triplet splitting, models beyond 4d field theory appear attractive. While this is mainly the subject of the next section, some advantages can already be noted: In models with extra dimensions, in particular string constructions, GUT breaking may occur due to boundary conditions in the compactified dimensions [34–37]. No complicated GUT breaking sector is then required. Moreover, boundary conditions can give mass only to the triplet, leaving the doublet massless. This is similar to the ‘missing partner mechanism’ since the effective mass term does not ‘pair up’ the triplets from $\mathbf{5}_H$ and $\bar{\mathbf{5}}_H$ but rather each of them with further fields which are automatically present in the higher-dimensional theory. This can eliminate dimension-five nucleon decay (cf. Sec. 94.6).

94.4 String-theoretic and higher-dimensional unified models

As noted earlier, the GUT scale is dangerously close to the scale of quantum gravity. It may hence be necessary to discuss unified models of particle physics in the latter, more ambitious context. Among the models of quantum gravity, superstring or M-theory stands out as the best-studied and technically most developed proposal, possessing in particular a high level of internal, mathematical consistency. For our purposes, it is sufficient to know that five 10d and one 11d low-energy effective supergravity theories arise in this setting (cf. [38] and refs. therein).

Grand unification is realized most naturally in the context of the two ‘heterotic’ theories with gauge groups $E_8 \times E_8$ and $SO(32)$, respectively [36, 39] (see [40] for some of the more recent results). Justified in part by the intriguing breaking path $E_8 \rightarrow \dots \rightarrow G_{SM}$ mentioned above, the focus has historically largely been on $E_8 \times E_8$. To describe particle physics, solutions of the 10d theory with geometry $\mathbb{R}^{1,3} \times M_6$ are considered, where M_6 is a Calabi-Yau (CY) 3-fold (with 6 real dimensions) [36]. The background solution involves expectation values of higher-dimensional components of the $E_8 \times E_8$ gauge fields. This includes

both Wilson lines [34] and non-vanishing field-strength and leads, in general, to a reduced gauge symmetry and to chirality in the resulting 4d effective theory. The 4d fermions arise from 10d gauginos.

Given an appropriate embedding⁵ of G_{SM} in $E_8 \times E_8$, gauge coupling unification is automatic at leading order. Corrections arise mainly through (string)-loop effects and are similar to the familiar field-theory thresholds of 4d GUTs⁶ [41]. Thus, one may say that coupling unification is a generic prediction in spite of the complete absence⁷ of a 4d GUT at any energy scale. This absence is both an advantage and a weakness. On the up side, GUT breaking and doublet-triplet splitting [43] are more naturally realized and dimension-five nucleon decay is relatively easy to avoid. On the down side, there is no reason to expect full GUT representations in the matter sector and flavor model building is much less tied to the GUT structure than in 4d.

Let us pause to explain the beautiful idea behind the advertised solution of the doublet-triplet splitting problem: One starts with a simply connected CY X and mods out the action of a discrete group G (say \mathbb{Z}_2). In the absence of fixed points, X/G is smooth and has a non-contractible 1-cycle. Furthermore, let G also act on the gauge bundle, according to an embedding $G \rightarrow E_8$. Now the parallel transport around the 1-cycle is tied to a gauge rotation (one says a non-trivial Wilson-line is present). Moreover, this Wilson line can not be continuously turned off since, e.g. in the case of \mathbb{Z}_2 , its square is the unit element of the group. The induced ‘Wilson-line breaking’, which comes on top of the breaking by non-zero field strengths, may remove certain sub-representations (e.g. the triplet of $SU(5) \rightarrow G_{SM}$) while keeping others exactly massless. A simpler and, due to fixed points, singular version of this will appear below in the context of orbifold GUTs.

One technical problem of heterotic constructions is the dependence on the numerous size and shape parameters of M_6 (the so-called moduli), the stabilization of which is poorly understood (see [44] for recent developments). Another is the sheer mathematical complexity of the analysis, involving in particular the study of (non-Abelian) gauge-bundles on CY spaces [45] (see however [46]).

An interesting aspect of heterotic string constructions is represented by orbifold models [35]. Here the internal space is given by a six-torus, modded out by a discrete symmetry group (e.g. T^6/\mathbb{Z}_n). More recent progress is reported in [47, 48], including in particular the systematic exploration of the phenomenological advantages of so-called ‘non-prime’ (referring to n) orbifolds. The symmetry breaking to G_{SM} as well as the survival of Higgs doublets without triplet partners is ensured by the appropriate embedding of the discrete orbifold group in $E_8 \times E_8$. String theory on such spaces, which are locally flat but include singularities, is much more calculable than in the CY case. The orbifold geometries can be viewed as singular limits of CYs.

An even simpler approach to unified models, which includes many of the advantages of full-fledged string constructions, is provided by Orbifold GUTs [37]. These are (mostly) 5d or 6d SUSY field theories with unified gauge group (e.g. $SU(5)$ or $SO(10)$), broken in the process of compactifying to 4d. To give a particularly simple example, consider $SU(5)$ on $\mathbb{R}^{1,3} \times S^1/(\mathbb{Z}_2 \times \mathbb{Z}'_2)$. Here the compact space is an interval of length $\pi R/2$ and the embedding of \mathbb{Z}'_2 in the hypercharge direction of $SU(5)$ realizes the breaking to G_{SM} . Concretely, 5d X bosons are given Dirichlet BCs at one endpoint of the interval and thus have no Kaluza-Klein (KK) zero mode. Their lightest modes have mass $\sim 1/R$, making the KK-scale the effective GUT scale. As an implication, the boundary theory has no $SU(5)$ invariance. Nevertheless, since the $SU(5)$ -symmetric 5d bulk dominates 4d gauge couplings, unification remains a prediction. Many other features but also problems

⁴ The solution of [29] relies on the absence of the fundamental superpotential term $\mu H_u H_d$ (or $\mu \mathbf{5}_H \bar{\mathbf{5}}_H$). This can be ensured either by a discrete R symmetry or by a $U(1)_R$. The latter clashes with typical superpotentials for the GUT breaking sector. However, higher-dimensional or stringy GUTs, where the triplet Higgs is simply projected out, can be consistent with the $U(1)_R$ symmetry.

⁵ All embeddings of G_{SM} in one E_8 factor which are consistent with a breaking-pattern $E_8 \rightarrow SU(5) \rightarrow G_{SM}$ are suitable (cf. for example the natural breaking chain from E_8 to G_{SM} through maximal subgroups mentioned at the end of Sect. 94.3). Other embeddings can change the ratios between the three resulting G_{SM} couplings at the GUT scale by group-theoretic factors. Crucially, due to the single 10d gauge coupling, no continuous tuning is possible.

⁶ Field-theory thresholds of 4d GUTs are discussed in 94.5.

⁷ See however [42].

of 4d GUTs can be circumvented, especially doublet-triplet splitting is easily realized.

With the advent of the string-theory ‘flux landscape’ [49], which is best understood in 10d type-IIB supergravity, the focus in string model building has shifted to this framework. While type II string theories have no gauge group in 10d, brane-stacks support gauge dynamics. A particularly appealing setting (see e.g. [50]) is provided by type IIB models with D7 branes (defining 8d submanifolds). However, in the $SO(10)$ context the $\mathbf{16}$ is not available and, for $SU(5)$, the top-Yukawa coupling vanishes at leading order [51]. As a crucial insight, this can be overcome on the non-perturbative branch of type IIB, also known as F-theory [52, 53]. This setting allows for more general branes, thus avoiding constraints of the Dp -brane framework. GUT breaking can be realized using hypercharge flux (the VEV of the $U(1)_Y$ field strength), an option not available in heterotic models. The whole framework combines the advantages of the heterotic or higher-dimensional unification approach with the more recent progress in understanding moduli stabilization. It thus represents at this moment the most active and promising branch of theory-driven GUT model building (see e.g. [54] and refs. therein).

As a result of the flux-breaking, a characteristic ‘type IIB’ or ‘F-theoretic’ tree-level correction to gauge unification arises [55]. The fact that this correction can be rather significant numerically is occasionally held against the framework of F-theory GUTs. However, at a parametric level, this correction nevertheless behaves like a 4d threshold, i.e., it provides $\mathcal{O}(1)$ additive contributions to the inverse 4d gauge couplings $\alpha_i^{-1}(M_G)$.

A final important issue in string GUTs is the so-called string-scale/GUT-scale problem [56]. It arises since, in heterotic compactifications, the Planck scale and the high-scale value of the gauge coupling unambiguously fix the string-scale to about 10^{18} GeV. As the compactification radius R is raised above the string length, the GUT scale (identified with $1/R$) goes down and the string coupling goes up. Within the domain of perturbative string theory, a gap of about a factor ~ 20 remains between the lowest GUT scale achievable in this way and the phenomenological goal of 2×10^{16} GeV. The situation can be improved by venturing into the non-perturbative regime [56], by considering ‘anisotropic’ geometries with hierarchically different radii R [56, 57] or by including GUT scale threshold corrections [58, 59].

In F-theory GUTs, the situation is dramatically improved since the gauge theory lives only in four out of the six compact dimensions. This allows for models with a ‘decoupling limit’, where the GUT scale is parametrically below the Planck scale [53]. However, moduli stabilization may not be without problems in such constructions, in part due to a tension between the required large volume and the desirable low SUSY breaking scale.

94.5 Gauge coupling unification

The quantitative unification of the three SM gauge couplings at the energy scale M_G is one of the cornerstones of the GUT paradigm. It is obviously of direct phenomenological relevance. Gauge coupling unification is well understood in the framework of effective field theory (EFT) [60]. In the simplest case, the relevant EFT at energies $\mu \gg M_G$ has a unified gauge symmetry (say $SU(5)$ for definiteness) and a single running gauge coupling $\alpha_G(\mu)$. At energies $\mu \ll M_G$, states with mass $\sim M_G$ (such as X bosons, GUT Higgs, color-triplet Higgs) have to be integrated out. The EFT now has three independent couplings and SM (or SUSY SM) matter content. One-loop renormalization group equations readily allow for an extrapolation to the weak scale,

$$\alpha_i^{-1}(m_Z) = \alpha_G^{-1}(M_G) + \frac{b_i}{2\pi} \log\left(\frac{M_G}{m_Z}\right) + \delta_i, \quad (94.3)$$

($i = 1, 2, 3$). Here we defined δ_i to absorb all sub-leading effects, such as threshold corrections at or near the weak scale (e.g. from superpartners and the additional Higgs bosons in the case of the MSSM) and at the GUT scale, and also higher-order corrections. We will discuss them momentarily.

It is apparent from Eq. (94.3) that the three low-scale couplings can be very different. This is due to the large energy range $m_Z \ll \mu \ll M_G$ and the non-universal β -function coefficients

($b_i^{\text{SM}} = \{41/10, -19/6, -7\}$ or $b_i^{\text{MSSM}} = \{33/5, 1, -3\}$). Incomplete GUT multiplets, such as gauge and Higgs bosons in the SM and also their superpartners and the additional Higgs bosons in the MSSM, contribute to the differences between the β functions. Inverting the argument, one expects that extrapolating the measured couplings to the high scale, we find quantitative unification at $\mu \sim M_G$. While this fails in the SM, it works intriguingly well in the MSSM (cf. Fig. 94.1).

The three equations contained in Eq. (94.3) can be used to determine the three ‘unknowns’ $\alpha_3(m_Z)$, $\alpha_G(M_G)$ and M_G , assuming that all other parameters entering the equations are given. Focusing on the SUSY case and using the $\overline{\text{MS}}$ coupling constants $\alpha_{\text{EM}}^{-1}(m_Z)$ and $\sin^2 \theta_W(m_Z)$ from [62],

$$\alpha_{\text{EM}}^{-1}(m_Z) = 127.955 \pm 0.010, \quad (94.4)$$

$$\sin^2 \theta_W(m_Z) = 0.23122 \pm 0.00003, \quad (94.5)$$

as input, one determines $\alpha_{1,2}^{-1}(m_Z)$, which then gives

$$\alpha_G^{-1}(M_G) \simeq 24.3 \quad \text{and} \quad M_G \simeq 2 \times 10^{16} \text{ GeV}. \quad (94.6)$$

Here we have set $\delta_i = 0$ for simplicity. Crucially, one in addition obtains a prediction for the low-energy observable α_3 ,

$$\alpha_3^{-1}(m_Z) = -\frac{5}{7}\alpha_1^{-1}(m_Z) + \frac{12}{7}\alpha_2^{-1}(m_Z) + \Delta_3, \quad (94.7)$$

where

$$\Delta_3 = \frac{5}{7}\delta_1 - \frac{12}{7}\delta_2 + \delta_3. \quad (94.8)$$

Here we followed the elegant formulation in Ref. [63] of the classical analyses of [7]. Of course, it is a matter of convention which of the three low-energy gauge coupling parameters one ‘predicts’ and indeed, early works on the subject discussed the prediction of $\sin^2 \theta_W$ in terms of α_{EM} and α_3 [64, 65].

Remarkably, the leading order result (i.e. Eq. (94.7) with $\delta_i = 0$) is in excellent agreement with experiments [62]:

$$\alpha_3^{\text{LO}}(m_Z) = 0.117 \quad \text{vs.} \quad \alpha_3^{\text{EXP}}(m_Z) = 0.1181 \pm 0.0011. \quad (94.9)$$

However, this near perfection is to some extent accidental. To see this, we now discuss the various contributions to the δ_i (and hence to Δ_3).

The two-loop running correction from the gauge sector $\Delta_3^{(2)}$ and the low-scale threshold correction $\Delta_3^{(l)}$ from superpartners can be summarized as [63]

$$\Delta_3^{(2)} \simeq -0.82 \quad \text{and} \quad \Delta_3^{(l)} \simeq \frac{19}{28\pi} \log\left(\frac{m_{\text{SUSY}}}{m_Z}\right). \quad (94.10)$$

The relevant scale m_{SUSY} can be estimated as [66]

$$m_{\text{SUSY}} \rightarrow m_H^{3/19} m_{\tilde{H}}^{12/19} m_{\tilde{W}}^{4/19} \times \left(\frac{m_{\tilde{W}}}{m_{\tilde{g}}}\right)^{28/19} \left(\frac{m_{\tilde{t}}}{m_{\tilde{q}}}\right)^{3/19}, \quad (94.11)$$

where m_H stands for the masses of non-SM Higgs states and superpartner masses are given in self-evident notation. Detailed analyses including the above effects are best done using appropriate software packages, such as SOFTSUSY [61] (or alternatively SuSpect [67] or SPheno [68]). See also [61] for references to the underlying theoretical two-loop analyses.

To get a very rough feeling for these effects, let us assume that all superpartners are degenerate at $m_{\text{SUSY}} = 1$ TeV, except for heavier gluinos: $m_{\tilde{W}}/m_{\tilde{g}} \simeq 1/3$. This gives $\Delta_3^{(l)} \simeq -0.35 + 0.22 \ln(m_{\text{SUSY}}/m_Z) \simeq 0.18$. The resulting prediction of $\alpha_3(m_Z) \simeq 0.126$ significantly upsets the perfect one-loop agreement found earlier. Before discussing this issue further, it is useful to introduce yet another important type of correction, the high or GUT scale thresholds.

To discuss high scale thresholds, let us set all other corrections to zero for the moment and write down a version of Eq. (94.3)

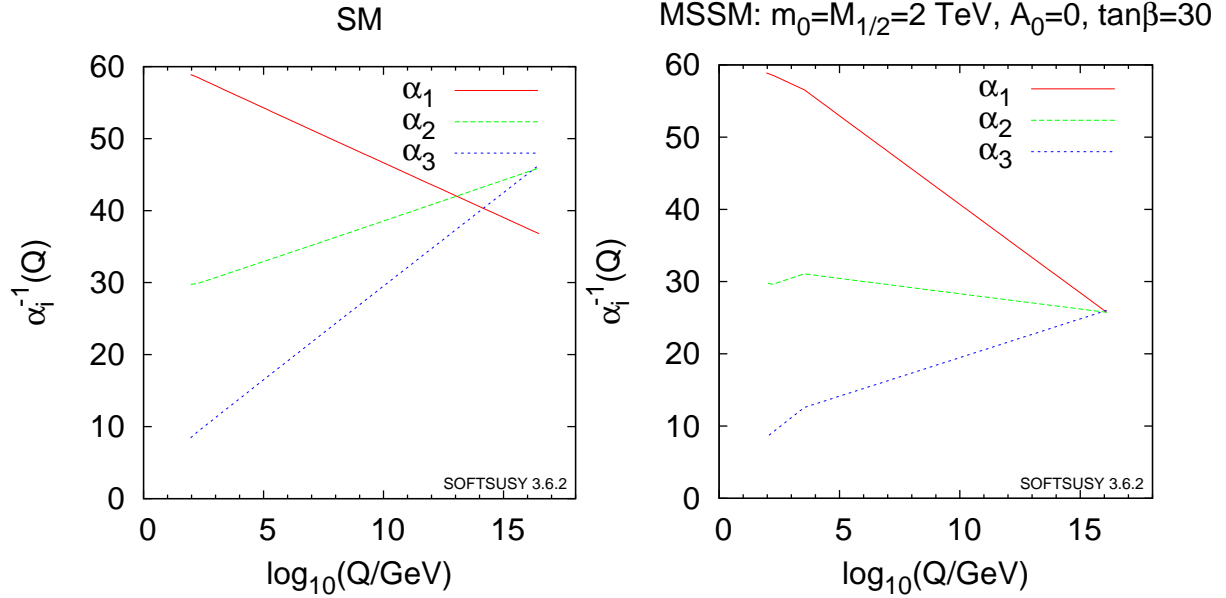


Figure 94.1: Running couplings in SM and MSSM using two-loop RG evolution. The SUSY threshold at 2 TeV is clearly visible on the MSSM side. (We thank Ben Allanach for providing the plots created using SOFTSUSY [61].)

that captures the running near and above the GUT scale more correctly. The threshold correction at one-loop level can be evaluated accurately by the simple step-function approximation for the β functions in the $\overline{\text{DR}}$ scheme⁸ [72],

$$\alpha_i^{-1}(m_Z) = \alpha_G^{-1}(\mu) + \frac{1}{2\pi} \left[b_i \ln \frac{\mu}{m_Z} + b_i^C \ln \frac{\mu}{M_C} + b_i^X \ln \frac{\mu}{M_X} + b_i^\Phi \ln \frac{\mu}{M_\Phi} \right]. \quad (94.12)$$

Here we started the running at some scale $\mu \gg M_G$, including the contribution of the minimal set of states relevant for the transition from the high-scale $SU(5)$ model to the MSSM. These are the color-triplet Higgs multiplets with mass M_C , massive vector multiplets of X -bosons with mass M_X (including GUT Higgs degrees of freedom), and the remaining GUT-Higgs fields and superpartners with mass M_Φ . The coefficients $b_i^{C,X,\Phi}$ can be found in Ref. [73]. Crucially, the b_i in Eq. (94.12) conspire to make the running GUT-universal at high scales, such that the resulting prediction for α_3 does not depend on the value of μ .

To relate this to our previous discussion, we can, for example, define $M_G \equiv M_X$ and then choose $\mu = M_G$ in Eq. (94.12). This gives the high-scale threshold corrections

$$\delta_i^{(h)} = \frac{1}{2\pi} \left[b_i^C \ln \frac{M_G}{M_C} + b_i^\Phi \ln \frac{M_G}{M_\Phi} \right], \quad (94.13)$$

and a corresponding correction $\Delta_3^{(h)}$. To get some intuition for the magnitude, one can furthermore assume $M_\Phi = M_G$, finding (with $b_i^C = \{2/5, 0, 1\}$)

$$\Delta_3^{(h)} = \frac{9}{14\pi} \ln \left(\frac{M_G}{M_C} \right). \quad (94.14)$$

To obtain the desired effect of $-\Delta_3^{(2)} - \Delta_3^{(l)} \simeq +0.64$, the triplet Higgs would have to be by about a factor 20 lighter than the GUT scale. While this is ruled out by nucleon decay in the minimal model [74] as will be discussed Sec. 94.6, it is also clear that threshold corrections of this order of magnitude can, in general, be realized with a certain amount of GUT-scale model building, e.g. in specific $SU(5)$ [25] or $SO(10)$ [26,27] constructions. Corrections

⁸The $\overline{\text{DR}}$ scheme is frequently used in a supersymmetric regularization [69]. The renormalization transformation of the gauge coupling constants from $\overline{\text{MS}}$ to $\overline{\text{DR}}$ scheme is given in Ref. [70]. For an alternative treatment using holomorphic gauge couplings and NSVZ β -functions see e.g. [71].

can also be much larger or of different sign if, as is required in many fully realistic 4d GUT models, many additional (and in particular higher) representations are introduced. Thus, there is considerable model building freedom. Nevertheless, a significant constraint from getting the right GUT threshold corrections while keeping the triplet Higgs heavy remains.

The above analysis implicitly assumes universal soft SUSY breaking masses at the GUT scale, which directly affect the spectrum of SUSY particles at the weak scale. In the simplest case we have a universal gaugino mass $M_{1/2}$, a universal mass for squarks and sleptons m_{16} and a universal Higgs mass m_{10} , as motivated by $SO(10)$. In some cases, threshold corrections to gauge coupling unification can be exchanged for threshold corrections to soft SUSY parameters (see [75] and refs. therein). For example, if gaugino masses were not unified at M_G and, in particular, gluinos were lighter than winos at the weak scale (cf. Eq. (94.11)), then it is possible that, due to weak scale threshold corrections, a much smaller or even slightly negative threshold correction at the GUT scale would be consistent with gauge coupling unification [76].

It is also noteworthy that perfect unification can be realized without significant GUT-scale corrections, simply by slightly raising the (universal) SUSY breaking scale. In this case the dark matter abundance produced by thermal processes in the early universe (if the lightest neutralino is the dark matter particle) is too high. However, even if the gaugino mass in the MSSM is about 1 TeV to explain the dark matter abundance, if the Higgsino and the non-SM Higgs boson masses are about 10-100 TeV, the effective SUSY scale can be raised [77]. This setup is realized in split SUSY [78] or the pure gravity mediation model [79] based on anomaly mediation [80]. Since the squarks and sleptons are much heavier than the gaugino masses in those setups, a gauge hierarchy problem is reintroduced. The facts that no superpartners have so far been seen at the LHC and that the observed Higgs mass favors heavier stop masses than about 1 TeV force one to accept a certain amount of fine-tuning anyway.

For non-SUSY GUTs or GUTs with a very high SUSY breaking scale to fit the data, new light states in incomplete GUT multiplets or multiple GUT breaking scales are required. For example, non-SUSY models $SO(10) \rightarrow SU(4)_C \times SU(2)_L \times SU(2)_R \rightarrow \text{SM}$, with the second breaking scale of order an intermediate scale, determined by light neutrino masses using the see-saw mechanism, can fit the low-energy data for gauge couplings [81] and at the same time survive nucleon decay bounds [82]. Alternatively, one can appeal to string-theoretic corrections discussed in Sec. 94.4 to compensate for a high SUSY breaking scale. This has, for ex-

ample, been concretely analyzed in the context of F-theory GUTs in [83]. Similarly, one may even wonder whether particularly large GUT threshold corrections could be sufficient to ensure non-SUSY precision unification. Notice here that the gauge coupling unification predicts just one parameter. When introducing new states, typically one can fit the data by choice of their masses. This is not the case in SUSY GUTs with low-scale SUSY breaking scale where the masses are constrained by fine tuning.

In 5d or 6d orbifold GUTs, certain “GUT scale” threshold corrections come from the Kaluza-Klein modes between the compactification scale, $M_c \sim 1/R$, and the effective cutoff scale M_* . In string theory, this cutoff scale is the string scale. Gauge coupling unification at two loops then constrains the values of M_c and M_* .⁹ Often, one finds M_c to be lower than the 4d GUT scale. Since the X -bosons, responsible for nucleon decay, get mass at the compactification scale, this has significant consequences for nucleon decay.

Finally, it has been shown that non-supersymmetric GUTs in warped 5d orbifolds can be consistent with gauge coupling unification. This assumes (in 4d language) that the r.h. top quark and the Higgs doublets are composite-like objects with a compositeness scale in the TeV range [85].

94.6 Nucleon decay

Quarks and leptons are indistinguishable in any 4d GUT, and both the baryon (B) and lepton number (L) are not conserved. This leads to baryon-number-violating nucleon decay. In addition to baryon-number violation, lepton-number violation is also required for nucleon decay since, in the SM, leptons are the only free fermions which are lighter than nucleons. The lowest-dimension operators relevant for nucleon decay are $(B+L)$ violating dimension-six four-fermion-terms in the SM, and all baryon-violating operators with dimension less than seven preserve $(B-L)$ [1, 86].

In $SU(5)$ GUTs, the dimension-six operators are induced by X boson exchange. These operators are suppressed by $(1/M_X^2)$ (M_X is the X boson mass), and the nucleon lifetime is given by $\tau_N \propto M_X^4/(\alpha_G^2 m_p^5)$ (m_p is proton mass). The dominant decay mode of the proton (and the baryon-violating decay mode of the neutron), via X boson exchange, is $p \rightarrow e^+ \pi^0$ ($n \rightarrow e^+ \pi^-$). In any simple gauge symmetry, with one universal GUT coupling α_G and scale M_X , the nucleon lifetime from gauge boson exchange is calculable. Hence, the GUT scale may be directly observed via the extremely rare decay of the nucleon. Experimental searches for nucleon decay began with the Kolar Gold Mine, Homestake, Soudan, NUSEX, Frejus, HPW, IMB, and Kamiokande detectors [64]. The present experimental bounds on the modes come from Super-Kamiokande. With 306 kton-years of data they find $\tau_p/\text{Br}(p \rightarrow e^+ \pi^0) > 1.67 \times 10^{34}$ years at 90% CL [87]. In addition, Hyper-Kamiokande [88] is planned to reach to $\tau_p/\text{Br}(p \rightarrow e^+ \pi^0) \sim 10^{35}$ years. The hadronic matrix elements for baryon-number-violating operators are evaluated with lattice QCD simulations [89]. In SUSY $SU(5)$ GUTs, the lower bound on the X boson mass from null results in nucleon decay searches is approaching 10^{16} GeV [90], which is close to the GUT scale suggested by gauge coupling unification. On the other hand, the prediction for nucleon decay in non-SUSY GUTs is hard to quantify. The reason is that gauge couplings do not unify with just the SM particle content. Once extra states or large thresholds are included to ensure precision unification, a certain range of unification scales is allowed.

In SUSY GUTs there are additional sources for baryon and/or lepton-number violation – dimension-four and five operators [14]. These arise since, in the SUSY SM, quarks and leptons have scalar partners (squarks and sleptons). Although our notation does not change, when discussing SUSY models our fields are chiral superfields and both fermionic and bosonic matter is implicitly represented by those. In this language, baryon- and/or lepton-number-violating dimension-four and five operators are given as so-called F terms of products of chiral superfields, which con-

tain two fermionic components and the rest scalars or products of scalars. Within the context of $SU(5)$ the dimension-four and five operators have the form

$$(10 \bar{5} \bar{5}) \supset (u^c d^c d^c) + (Q L d^c) + (e^c L L),$$

$$(10 10 10 \bar{5}) \supset (Q Q Q L) + (u^c u^c d^c e^c) + B\text{- and }L\text{-conserving terms,}$$

respectively.

The dimension-four operators in $(10 \bar{5} \bar{5})$ violate either baryon number or lepton number. The nucleon lifetime is extremely short if both types of dimension-four operators are present in the SUSY SM since squark or slepton exchange induces the dangerous dimension-six SM operators. Even in the case that they violate baryon number or lepton number only but not both, they are constrained by various phenomena [91]. For example, the primordial baryon number in the universe is washed out unless the dimensionless coupling constants are less than 10^{-7} . Both types of operators can be eliminated by requiring R parity, which distinguishes Higgs from ordinary matter multiplets. R parity [92] or its cousin, matter parity [6, 93], act as $F \rightarrow -F$, $H \rightarrow H$ with $F = \{10, \bar{5}\}$, $H = \{\bar{5}_H, 5_H\}$ in $SU(5)$.¹⁰ In $SU(5)$, the Higgs multiplet $\bar{5}_H$ and the matter multiplets $\bar{5}$ have identical gauge quantum numbers. In E_6 , Higgs and matter multiplets could be unified within the fundamental 27 representation. Only in $SO(10)$ are Higgs and matter multiplets distinguished by their gauge quantum numbers. The Z_4 center of $SO(10)$ distinguishes 10_s from 16_s and can be associated with R parity [94].

The baryon-number violating dimension-five operators have a dimensionful coupling. They are generated by integrating out the color-triplet Higgs with GUT-scale mass in SUSY GUTs such that the coefficient is suppressed by $1/M_G$. Note that both triplet Higgsinos (due to their fermionic nature) and Higgs scalars (due to their mass-enhanced trilinear coupling with matter) contribute to the operators. The dimension-five operators include squarks and/or sleptons. To allow for nucleon decay, these must be converted to light quarks or leptons by exchange of a gaugino or Higgsino in the SUSY SM. The nucleon lifetime is proportional to $M_G^2 m_{\text{SUSY}}^2/m_p^5$, where m_{SUSY} is the SUSY breaking scale. Thus, dimension-five operators may predict a shorter nucleon lifetime than dimension-six operators. Unless accidental cancellations are present, the dominant decay modes from dimension-five operators include a K meson, such as $p \rightarrow K^+ \bar{\nu}$ ($n \rightarrow K^0 \bar{\nu}$). This is due to a simple symmetry argument: The operators are given as $(Q_i Q_j Q_k L_l)$ and $(u_i^c u_j^c d_k^c e_l^c)$, where $i, j, k, l (= 1, 2, 3)$ are family indices and color and weak indices are implicit. They must be invariant under $SU(3)_C$ and $SU(2)_L$ so that their color and weak doublet indices must be anti-symmetrized. Since these operators are given by bosonic superfields, they must be totally symmetric under interchange of all indices. Thus the first operator vanishes for $i = j = k$ and the second vanishes for $i = j$. Hence a second or third generation member exists in the dominant modes of nucleon decay unless these modes are accidentally suppressed [93].

The Super-Kamiokande bounds on the proton lifetime severely constrain the dimension-five operators. With 306 kton-years of data they find $\tau_p/\text{Br}(p \rightarrow K^+ \bar{\nu}) > 6.61 \times 10^{33}$ years at 90% CL [87]. In the minimal SUSY $SU(5)$, $\tau_p/\text{Br}(p \rightarrow K^+ \bar{\nu})$ is smaller than about 10^{31} years if the triplet Higgs mass is 10^{16} GeV and $m_{\text{SUSY}} = 1$ TeV [95]. The triplet Higgs mass bound from nucleon decay is then in conflict with gauge coupling unification so that this model is considered to be ruled out [74].

Since nucleon decay induced by the triplet Higgs is a severe problem in SUSY GUTs, various proposals for its suppression have been made. First, some accidental symmetry or accidental structure in non-minimal Higgs sectors in $SU(5)$ or $SO(10)$ theories may suppress the dimension-five operators [22, 26, 27, 96].

⁹ It is interesting to note that a ratio $M_*/M_c \sim 100$, needed for gauge coupling unification to work in orbifold GUTs, is typically the maximum value for this ratio consistent with perturbativity [84].

¹⁰ This forbids the dimension-four operator $(10 \bar{5} \bar{5})$, but allows the Yukawa couplings for quark and lepton masses of the form $(10 \bar{5} \bar{5}_H)$ and $(10 10 \bar{5}_H)$. It also forbids the dimension-three, lepton-number-violating operator $(\bar{5} 5_H) \supset (L H_u)$ as well as the dimension-five, baryon-number-violating operator $(10 10 10 \bar{5}_H) \supset (Q Q Q H_d) + \dots$

Symmetries to suppress the dimension-five operators are typically broken by the VEVs responsible for the color-triplet Higgs masses. Consequently the dimension-five operators are generically generated via the triplet Higgs exchange in SUSY $SU(5)$ GUTs, as mentioned above. In other words, the nucleon decay is suppressed if the Higgs triplets in $\bar{\mathbf{5}}_H$ and $\mathbf{5}_H$ do not have a common mass term but, instead, their mass terms involve partners from other $SU(5)$ multiplets. Second, the SUSY breaking scale may be around $\mathcal{O}(10\text{--}100)$ TeV in order to explain the observed Higgs boson mass at the LHC. In this case, nucleon decay is automatically suppressed [78, 97, 98]. Third, accidental cancellations among diagrams due to a fine-tuned structure of squark and slepton flavor mixing might suppress nucleon decay [99]. Last, we have also implicitly assumed a hierarchical structure for Yukawa matrices in the analysis. It is however possible to fine-tune a hierarchical structure for quarks and leptons which baffles the family structure so that the nucleon decay is suppressed [100]. The upper bound on the proton lifetime from some of these theories is approximately a factor of 10 above the experimental bounds. Future experiments with larger neutrino detectors, such as JUNO [101], Hyper-Kamiokande [88] and DUNE [102], are planned and will have higher sensitivities to nucleon decay.

Are there ways to avoid the stringent predictions for proton decay discussed above? Orbifold GUTs and string theories, see Sec. 94.4, contain grand unified symmetries realized in higher dimensions. In the process of compactification and GUT symmetry breaking, the triplet Higgs states may be removed (projected out of the massless sector of the theory). In such models, the nucleon decay due to dimension-five operators can be severely suppressed or eliminated completely. However, nucleon decay due to dimension-six operators may be enhanced, since the gauge-bosons mediating proton decay obtain mass at the compactification scale, M_c , which is typically less than the 4d GUT scale (cf. Sec. 94.5). Alternatively, the same projections which eliminate the triplet Higgs may rearrange the quark and lepton states such that the massless states of one family come from different higher-dimensional GUT multiplets. This can suppress or completely eliminate even dimension-six proton decay. Thus, enhancement or suppression of dimension-six proton decay is model-dependent. In some complete 5d orbifold GUT models [63, 103] the lifetime for the decay $\tau_p/\text{Br}(p \rightarrow e^+\pi^0)$ can be near the bound of 1×10^{34} years with, however, large model-dependence and/or theoretical uncertainties. In other cases, the modes $p \rightarrow K^+\bar{\nu}$ and $p \rightarrow K^0\mu^+$ may be dominant [63]. Thus, interestingly, the observation of nucleon decay may distinguish string or higher-dimensional GUTs from 4d ones.

In orbifold GUTs or string theory, new discrete symmetries consistent with SUSY GUTs can forbid all dimension-three and four baryon- and lepton-number-violating operators. Even the μ term and dimension-five baryon- and lepton-number-violating operators can be forbidden to all orders in perturbation theory [33]. The μ term and dimension-five baryon- and lepton-number-violating operators may then be generated, albeit sufficiently suppressed, via non-perturbative effects. The simplest example of this is a Z_4^R symmetry which is the unique discrete R symmetry consistent with $SO(10)$ [33]. Even though it forbids the dimension-five proton decay operator to the desired level, it allows the required dimension-five neutrino mass term. In this case, proton decay is dominated by dimension-six operators, leading to decays such as $p \rightarrow e^+\pi^0$.

94.7 Yukawa coupling unification

In the SM, masses and mixings for quarks and leptons come from the Yukawa couplings with the Higgs doublet, but the values of these couplings remain a mystery. GUTs provide at least a partial understanding since each generation is embedded in unified multiplet(s). Specifically, since quarks and leptons are two sides of the same coin, the GUT symmetry relates the Yukawa couplings (and hence the masses) of quarks and leptons.

In $SU(5)$, there are two types of independent renormalizable Yukawa interactions given by $\lambda_{ij}(\mathbf{10}_i \mathbf{10}_j \mathbf{5}_H) + \lambda'_{ij}(\mathbf{10}_i \bar{\mathbf{5}}_j \bar{\mathbf{5}}_H)$. These contain the SM interactions $\lambda_{ij}(Q_i u_j^c H_u) + \lambda'_{ij}(Q_i d_j^c H_d + e_i^c L_j H_d)$. Here $i, j (= 1, 2, 3)$

are, as before, family indices. Hence, at the GUT scale we have tree-level relations between Yukawa coupling constants for charged lepton and down quark masses, such as $\lambda_b = \lambda_\tau$ in which $\lambda_{b/\tau}$ are the bottom quark / τ lepton Yukawa coupling constants [104, 105]. In $SO(10)$, there is only one type of independent renormalizable Yukawa interaction given by $\lambda_{ij}(\mathbf{16}_i \mathbf{16}_j \mathbf{10}_H)$, leading to relations among all Yukawa coupling constants and quark and lepton masses within one generation [106, 107] (such as $\lambda_t = \lambda_b = \lambda_\tau$, with λ_t the top quark Yukawa coupling constant).

In addition to gauge coupling unification, the ratio of bottom quark and τ lepton mass has been a central target in the study of GUTs since it was found that this ratio was almost consistent with observations after including the QCD correction [104]. Today the quark masses and the gauge coupling constants are known precisely such that, as discussed below, the ratio of bottom quark and τ lepton mass has become a target of precision analyses in the GUT context.

94.7.1 The third generation, $b\text{--}\tau$ or $t\text{--}b\text{--}\tau$ unification

Third generation Yukawa couplings are larger than those of the first two generations. Hence, the fermion mass relations predicted from renormalizable GUT interactions which we introduced above are expected to be more reliable. In order to compare them with data, we have to include the radiative correction to these relations from the RG evolution between GUT and fermion mass scale, from integrating out heavy particles at the GUT scale, and from weak scale thresholds.

Since testing Yukawa coupling unification is only possible in models with successful gauge coupling unification, we here focus on SUSY GUTs. In the MSSM, top and bottom quark and τ lepton masses are related to the Yukawa coupling constants at the scale m_Z as

$$\begin{aligned} m_t(m_Z) &= \lambda_t(m_Z) v_u(1 + \delta m_t/m_t), \\ m_{b/\tau}(m_Z) &= \lambda_{b/\tau}(m_Z) v_d(1 + \delta m_{b/\tau}/m_{b/\tau}), \end{aligned}$$

where $\langle H_u^0 \rangle \equiv v_u = \sin \beta v/\sqrt{2}$, $\langle H_d^0 \rangle \equiv v_d = \cos \beta v/\sqrt{2}$, $v_u/v_d \equiv \tan \beta$ and $v \sim 246$ GeV is fixed by the Fermi constant, G_μ . Here, $\delta m_f/m_f$ ($f = t, b, \tau$) represents the threshold correction due to integrating out SUSY partners. For the bottom quark mass, it is found [108] that the dominant corrections come from the gluino-sbottom and from the Higgsino-stop loops,

$$\begin{aligned} \left(\frac{\delta m_b}{m_b}\right)_{g_3} &\sim \frac{g_3^2}{6\pi^2} \frac{m_{\tilde{g}}\mu}{m_{\text{SUSY}}^2} \tan \beta \quad \text{and} \\ \left(\frac{\delta m_b}{m_b}\right)_{\lambda_t} &\sim \frac{\lambda_t^2}{16\pi^2} \frac{A_t \mu}{m_{\text{SUSY}}^2} \tan \beta, \end{aligned} \quad (94.16)$$

where $m_{\tilde{g}}$, μ , and A_t stand for gluino and Higgsino masses and trilinear stop coupling, respectively. Note that Eq. (94.16) only illustrates the structure of the corrections – non-trivial functional dependences on several soft parameters $\sim m_{\text{SUSY}}$ have been suppressed. For the full one-loop correction to the bottom quark mass see, for example, Ref. [109].

Note also that the corrections do not go to zero as SUSY particles become much heavier than m_Z . They may change the bottom quark mass at the $\mathcal{O}(10)\%$ level for $\tan \beta = \mathcal{O}(10)$. The total effect is sensitive to the relative phase between gluino and Higgsino masses since $A_t \sim -m_{\tilde{g}}$ due to the infrared fixed point nature of the RG equation for A_t [110] in settings where SUSY breaking terms come from Planck scale dynamics, such as gravity mediation. The τ lepton mass also receives a similar correction, though only at the few % level. The top quark mass correction, not being proportional to $\tan \beta$, is at most 10% [111].

Including one loop threshold corrections at m_Z and additional RG running, one finds the top, bottom and τ pole masses. In SUSY GUTs, $b\text{--}\tau$ unification has two possible solutions with $\tan \beta \sim 1$ or $\mathcal{O}(10)$. The small $\tan \beta$ solution may be realized in the MSSM if superpartner masses are $\mathcal{O}(10)$ TeV, as suggested by the observed Higgs mass [97]. The large $\tan \beta$ limit such as $\tan \beta \sim 40\text{--}50$ overlaps the $SO(10)$ symmetry relation [111, 112]. When $\tan \beta$ is large, there are significant threshold corrections to

down quark masses as mentioned above, and Yukawa unification is only consistent with low-energy data in a restricted region of SUSY parameter space, with important consequences for SUSY searches [111, 113]. More recent analyses of Yukawa unification after LHC Run-I are found in Ref. [114].

Gauge coupling unification is also successful in the scenario of split supersymmetry [78], in which squarks and sleptons have mass at a scale $\tilde{m} \gg m_Z$, while gauginos and/or Higgsinos have masses of order the weak scale. Unification of b - τ Yukawa couplings requires $\tan\beta$ to be fine-tuned close to 1 [97]. If by contrast, $\tan\beta \gtrsim 1.5$, b - τ Yukawa unification only works for $\tilde{m} \lesssim 10^4$ GeV. This is because the effective theory between the gaugino mass scale and \tilde{m} includes only one Higgs doublet, as in the standard model. As a result, the large top quark Yukawa coupling tends to increase the ratio λ_b/λ_τ due to the vertex correction, which is absent in supersymmetric theories, as one runs down in energy below \tilde{m} . This is opposite to what happens in the MSSM where the large top quark Yukawa coupling lowers the ratio λ_b/λ_τ [105].

94.7.2 Beyond leading order: three-family models

Simple Yukawa unification is not possible for the first two generations. Indeed, the simplest implementation of $SU(5)$ implies $\lambda_s = \lambda_\mu$, $\lambda_d = \lambda_e$ and hence $\lambda_s/\lambda_d = \lambda_\mu/\lambda_e$. This is an RG-invariant relation which extrapolates to $m_s/m_d = m_\mu/m_e$ at the weak scale, in serious disagreement with data ($m_s/m_d \sim 20$ and $m_\mu/m_e \sim 200$). An elegant solution to this problem was given by Georgi and Jarlskog [115] (for a recent analysis in the SUSY context see [116]).

More generally, we have to recall that in all of the previous discussion of Yukawa couplings, we assumed renormalizable interactions as well as the minimal matter and Higgs content. Since the GUT scale is close to the Planck scale, higher-dimension operators involving the GUT-breaking Higgs may modify the predictions, especially for lower generations. An example is provided by the operators $\mathbf{10} \bar{\mathbf{5}} \bar{\mathbf{5}}_H \mathbf{24}_H$ with $\mathbf{24}_H$ the GUT-breaking Higgs of $SU(5)$. We can fit parameters to the observed fermion masses with these operators, though some fine-tuning is introduced in doing so. The SM Higgs doublet may come in part from higher representations of the GUT group. For example, the $\mathbf{45}$ of $SU(5)$ includes an $SU(2)_L$ doublet with appropriate $U(1)_Y$ charge [115]. This $\mathbf{45}$ can, in turn, come from the $\mathbf{120}$ or $\mathbf{126}$ of $SO(10)$ after its breaking to $SU(5)$ [117, 118]. These fields may also have renormalizable couplings with quarks and leptons. The relations among the Yukawa coupling constants in the SM are modified if the SM Higgs doublet is a linear combination of several such doublets from different $SU(5)$ multiplets. Finally, the SM fermions may not be embedded in GUT multiplets in the minimal way. Indeed, if all quarks and leptons are embedded in $\mathbf{16}$ s of $SO(10)$, the renormalizable interactions with $\mathbf{10}_H$ cannot explain the observed CKM mixing angles. This situation improves when extra matter multiplets, such as $\mathbf{10}$, are introduced: After $U(1)_X$, which distinguishes the $\bar{\mathbf{5}}$ s coming from the $\mathbf{16}$ and the $\mathbf{10}$ of $SO(10)$, is broken (e.g. by a VEV of $\mathbf{16}_H$ or $\mathbf{126}_H$), the r.h. down quarks and l.h. leptons in the SM can be linear combinations of components in $\mathbf{16}$ s and $\mathbf{10}$ s. As a result, $\lambda \neq \lambda'$ in $SU(5)$ [119].

To construct realistic three-family models, some or all of the above effects can be used. Even so, to achieve significant predictions for fermion masses and mixing angles grand unification alone is not sufficient. Other ingredients, for example additional global family symmetries are needed (in particular, non-Abelian symmetries can strongly reduce the number of free parameters). These family symmetries constrain the set of effective higher-dimensional fermion mass operators discussed above. In addition, sequential breaking of the family symmetry can be correlated with the hierarchy of fermion masses [120]. One simple, widely known idea in this context is to ensure that each $\mathbf{10}_i$ enters Yukawa interactions together with a suppression factor e^{3-i} (e being a small parameter). This way one automatically generates a stronger hierarchy in up-type quark Yukawas as compared to down-type quark and lepton Yukawas and no hierarchy for neutrinos, which agrees with observations at the $\mathcal{O}(1)$ -level. Three-family models exist which fit all the data, including neutrino masses and mixing [27, 121].

Finally, a particularly ambitious variant of unification is to re-

quire that the fermions of all three generations come from a single representation of a large gauge group. A somewhat weaker assumption is that the flavor group (e.g. $SU(3)$) unifies with the SM gauge group in a simple gauge group at some energy scale $M \geq M_G$. Early work on such ‘flavor-unified GUTs’, see e.g. [119, 122], has been reviewed in [123, 124]. For a selection of more recent papers see [125]. In such settings, Yukawa couplings are generally determined by gauge couplings together with symmetry breaking VEVs. This is reminiscent of heterotic string GUTs, where all couplings come from the 10d gauge coupling. However, while the $E_8 \rightarrow SU(3) \times E_6$ branching rule $\mathbf{248} = (\mathbf{8}, \mathbf{1}) + (\mathbf{1}, \mathbf{78}) + (\mathbf{3}, \mathbf{27}) + (\bar{\mathbf{3}}, \mathbf{27})$ looks very suggestive in this context, the way in which most modern heterotic models arrive at three generations is actually more complicated.

94.8 Neutrino masses

We see from atmospheric and solar neutrino oscillation observations, along with long baseline accelerator and reactor experiments, that neutrinos have finite masses. By adding three ‘sterile’ neutrinos ν_i^c with Yukawa couplings $\lambda_{\nu,ij} (\nu_i^c L_j H_u)$ ($i, j = 1, 2, 3$), one easily obtains three massive Dirac neutrinos with mass $m_\nu = \lambda_\nu v_u$, analogously to quark and charged lepton masses. However, in order to obtain a τ neutrino with mass of order 0.1 eV, one requires the exceedingly small coupling ratio $\lambda_{\nu\tau}/\lambda_\tau \lesssim 10^{-10}$. By contrast, in GUTs the seesaw mechanism *naturally* explains such tiny neutrino masses as follows [2–4]: The sterile neutrinos have no SM gauge quantum numbers so that there is no symmetry other than global lepton number which forbids the Majorana mass term $\frac{1}{2} M_{ij} \nu_i^c \nu_j^c$. Note also that sterile neutrinos can be identified with the r.h. neutrinos necessarily contained in complete families of $SO(10)$ or Pati-Salam models. Since the Majorana mass term violates $U(1)_X$ in $SO(10)$, one might expect $M_{ij} \sim M_G$. The heavy sterile neutrinos can be integrated out, defining an effective low-energy theory with only three light active Majorana neutrinos with the effective dimension-five operator

$$- \mathcal{L}_{eff} = \frac{1}{2} c_{ij} (L_i H_u) (L_j H_u), \tag{94.17}$$

where $c = \lambda_\nu^T M^{-1} \lambda_\nu$. This then leads to a 3×3 Majorana neutrino mass matrix $m = m_\nu^T M^{-1} m_\nu$.

The seesaw mechanism implemented by r.h. neutrinos is sometimes called the type-I seesaw model. There are variant models in which the dimension-five operator for neutrino masses is induced in different ways: In the type-II model, an $SU(2)_L$ triplet Higgs boson Σ is introduced to have couplings ΣL^2 and also ΣH_u^2 [117, 126]. In the type-III model, an $SU(2)_L$ triplet of fermions $\tilde{\Sigma}$ with a Yukawa coupling $\tilde{\Sigma} L H_u$ is introduced [127]. In these models, the dimension-five operator is induced by integrating out the triplet Higgs boson or fermions. Such models can also be implemented in GUTs by introducing Higgs bosons in the $\mathbf{15}$ or fermions in the $\mathbf{24}$ in $SU(5)$ GUTs or the $\mathbf{126}$ in $SO(10)$ GUTs. Notice that the gauge non-singlet fields in the type-II and III models have masses at the intermediate scale. Thus, gauge coupling unification is not automatic if these variant mechanisms are implemented in SUSY GUTs.

Atmospheric neutrino oscillations discovered by Super-Kamiokande [128] require neutrino masses with $\Delta m_\nu^2 \sim 2.5 \times 10^{-3}$ eV² with maximal mixing [62], in the simplest scenario of two neutrino dominance. With hierarchical neutrino masses this implies $m_{\nu\tau} = \sqrt{\Delta m_\nu^2} \sim 0.05$ eV. Next, we can try to relate the neutrino Yukawa coupling to the top quark Yukawa coupling, $\lambda_{\nu\tau} = \lambda_t$ at the GUT scale, as in $SO(10)$ or $SU(4) \times SU(2)_L \times SU(2)_R$ models. This gives $M \sim 10^{14}$ GeV, which is remarkably close to the GUT scale.

Neutrinos pose a special problem for GUTs. The question is why the quark mixing angles in the CKM matrix are small while there are two large lepton mixing angles in the PMNS matrix. Global fits of neutrino masses and mixing angles can, for example, be found in Refs. [129] and [130]. For SUSY GUT models which fit quark and lepton masses, see Ref. [131] for reviews. Finally, for a compilation of the range of SUSY GUT predictions for neutrino mixing, see [132].

94.9 Selected topics

94.9.1 Global symmetries

As we discussed, global symmetries are frequently introduced to control higher-dimension operators in GUT models. This is particularly important in the context of nucleon decay but also plays a role in GUT-based flavor model building and cosmological applications, such as baryogenesis and inflation. However, we should note that appealing to global symmetries to suppress specific interactions may not be as straightforward as it naively seems. Indeed, there are two possibilities: On the one hand, the relevant symmetry might be gauged at a higher scale. Effects of the VEVs responsible for the spontaneous breaking are then in principle dangerous and need to be quantified. On the other hand, the symmetry might be truly only global. This must e.g. be the case for anomalous symmetries, which are then also violated by field-theoretic non-perturbative effects. The latter can in principle be exponentially small. It is, however, widely believed that global symmetries are always broken in quantum gravity (see e.g. [133]). One then needs to understand which power or functional form the Planck scale suppression of the relevant interaction has. For example, dimension-five baryon number violating operators suppressed by just one unit of the Planck or string scale are completely excluded.

In view of the above, it is also useful to recall that in string models 4d global symmetries generally originate in higher-dimensional gauge symmetries [38, 134]. Here ‘global’ implies that the gauge boson has acquired a Stückelberg-mass. This is a necessity in the anomalous case (Green-Schwarz mechanism [135]) but can also happen to non-anomalous symmetries. One expects no symmetry violation beyond the well-understood non-perturbative effects. Discrete symmetries arise as subgroups of continuous gauge symmetries, such as $\mathbb{Z}_N \subset U(1)$. In particular, non-anomalous subgroups of Stückelberg-massive $U(1)$ s represent unbroken discrete gauge symmetries and as such are non-perturbatively exact (see e.g. [136]). Of course, such discrete gauge symmetries may also arise as remnants of continuous gauge symmetries after conventional 4d spontaneous breaking.

94.9.2 Anomaly constraints vs. GUT paradigm

As emphasized at the very beginning, the fact that the SM fermions of one generation fill out the $\mathbf{10} + \bar{\mathbf{5}}$ of $SU(5)$ appears to provide overwhelming evidence for some form of GUT embedding. However, one should be aware that a counterargument can be made which is related to the issue of ‘charge quantization by anomaly cancellation’ (see [137, 138] for some early papers and [139] for a more detailed reference list): Imagine we only knew that the low-energy gauge group were G_{SM} and the matter content included the $(\mathbf{3}, \mathbf{2})_Y$, i.e. a ‘quark doublet’ with $U(1)$ -charge Y . One can then ask which possibilities exist of adding further matter to ensure the cancellation of all triangle anomalies. It turns out that this problem has only three different, minimal¹¹ solutions [138]. One of those is precisely a single SM generation, with the apparent ‘ $SU(5)$ -ness’ emerging accidentally. Thus, if one randomly picks models from the set of consistent gauge theories, preconditioning on G_{SM} and $(\mathbf{3}, \mathbf{2})_Y$, one may easily end up with ‘ $\mathbf{10} + \bar{\mathbf{5}}$ ’ of an $SU(5)$ that is in no way dynamically present. This is precisely what happens in the context of non-GUT string model building [140].

94.9.3 Magnetic monopoles

In the broken phase of a GUT there are typically localized classical solutions carrying magnetic charge under an unbroken $U(1)$ symmetry [141]. These magnetic monopoles with mass of order M_G/α_G can be produced during a possible GUT phase transition in the early universe. The flux of magnetic monopoles is experimentally found to be less than $\sim 10^{-16} \text{ cm}^{-2} \text{ s}^{-1} \text{ sr}^{-1}$ [142]. Many more are however predicted, hence the GUT monopole problem. In fact, one of the original motivations for inflation was to solve the monopole problem by exponential expansion after the GUT phase transition [143] and hence dilution of the

monopole density. Other possible solutions to the monopole problem include: sweeping them away by domain walls [144], $U(1)$ electromagnetic symmetry breaking at high temperature [145] or GUT symmetry non-restoration [146]. Parenthetically, it was also shown that GUT monopoles can catalyze nucleon decay [147]. A significantly stronger bound on the monopole flux can then be obtained by considering X-ray emission from radio pulsars due to monopole capture and the subsequent nucleon decay catalysis [148].

Note that the present upper bound on the inflationary vacuum energy density is very close to the GUT scale, $V_{inf}^{1/4} = (1.88 \times 10^{16} \text{ GeV}) \times (r/0.10)^{1/4}$, with the scalar-to-tensor ratio constrained to $r < 0.07$ [149]. This guarantees that reheating does not lead to temperatures above M_G and hence the monopole problem is solved by inflation (unless M_G is unexpectedly low).

94.9.4 Flavor violation

Yukawa interactions of GUT-scale particles with quarks and leptons may leave imprints on the flavor violation induced by SUSY breaking parameters [150]. To understand this, focus first on the MSSM with universal Planck-scale boundary conditions (as e.g. in gravity mediation). Working in a basis where up-quark and lepton Yukawas are diagonal, one finds that the large top-quark Yukawa coupling reduces the l.h. squark mass squareds in the third generation radiatively. It turns out that only the l.h. down-type squark mass matrix has sizable off-diagonal terms in the flavor basis after CKM-rotation. However, in GUTs the color-triplet Higgs has flavor violating interactions from the Yukawa coupling $\lambda_{ij}(\mathbf{10}_i \mathbf{10}_j \mathbf{5}_H)$, such that flavor-violating r.h. slepton mass terms are radiatively generated in addition [151]. In $SU(5)$ extension of the type-I seesaw model, where r.h. neutrinos are introduced as $SU(5)$ singlets with interactions $\lambda''_{ij}(\mathbf{1}_i \bar{\mathbf{5}}_j \mathbf{5}_H)$, the doublet and color-triplet Higgses acquire another type of Yukawa coupling, respectively. They then radiatively generate flavor-violating l.h. slepton [152] and r.h. down squark masses [153]. These flavor-violating SUSY breaking terms induce new contributions to FCNC processes in quark and lepton sectors, such as $\mu \rightarrow e\gamma$ and $K^0-\bar{K}^0$ and $B^0-\bar{B}^0$ mixing. Note that even if the SUSY breaking terms are generated at M_G , the r.h. neutrino Yukawa coupling may induce sizable flavor violation in l.h. slepton masses due to the running between M_G and the right-handed-neutrino mass scale.

EDMs are also induced when both l.h. and r.h. squarks/sleptons have flavor-violating mass terms with relative phases, as discussed for $SO(10)$ in [154] or for $SU(5)$ with r.h. neutrinos in [155]. Thus, such low-energy observables constrain GUT-scale interactions.

94.9.5 From GUT baryogenesis to leptogenesis and B/L-violating transitions

During inflation, any conserved quantum number is extremely diluted. Thus, one expects the observed baryon asymmetry of the universe to originate at reheating or in the subsequent cosmological evolution. In detail, the situation is slightly more involved: Both baryon number B and lepton number L are global symmetries of the SM. However, $(B+L)$ is anomalous and violated by thermal fluctuations in the early universe, via so-called sphaleron processes. Moreover, it is violated in GUT models, as is most apparent in proton decay. By contrast, $(B-L)$ is anomaly free and preserved by both the SM as well as $SU(5)$ or $SO(10)$ gauge interactions.

Now, the old idea of GUT baryogenesis [156, 157] is to generate a $(B+L)$ and hence a baryon asymmetry by the out-of-equilibrium decay of the color-triplet Higgs. However such an asymmetry, generated at GUT temperatures, is washed out by sphalerons¹². This can be overcome [159] using lepton-number violating interaction of neutrinos to create a $(B-L)$ from the $(B+L)$ asymmetry, before sphaleron processes become sufficiently fast at $T < 10^{12}$ GeV. This $(B-L)$ asymmetry can then survive the subsequent sphaleron dominated phase. Note that this does not work in the minimal SUSY GUT setting, with the triplet Higgs above the

¹¹ Adding extra vector-like sets of fields, e.g. two fermions which only transform under $U(1)$ and have charges Y and $-Y$, is considered to violate minimality.

¹² To be precise, if lepton flavor numbers L_i ($i = 1-3$) are nonzero and $(L_i - L_j) \neq 0$ ($i \neq j$), one may obtain nonzero values for B and L even if $(B-L) = 0$ [158].

GUT scale. The reason is that a correspondingly high reheating temperature would be required which, as explained above, is ruled out by Planck data.

However, the most widely accepted simple way out of the dilemma is to directly generate a net $(B-L)$ asymmetry dynamically in the early universe, also using r.h. neutrinos. Indeed, we have seen that neutrino oscillations suggest a new scale of physics of order 10^{14} GeV. This scale is associated with heavy Majorana neutrinos in the seesaw mechanism. If in the early universe, the decay of the heavy neutrinos is out of equilibrium and violates both lepton number and CP, then a net lepton number may be generated. This lepton number will then be partially converted into baryon number via electroweak processes [160]. This mechanism is called leptogenesis.

If the three heavy Majorana neutrino masses are hierarchical, the net lepton number is produced by decay of the lightest one, and it is proportional to the CP asymmetry in the decay. The CP asymmetry is bounded from above, and the lightest neutrino mass is required to be larger than 10^9 GeV in order to explain the observed baryon asymmetry [161]. This implies that the reheating temperature after inflation should be larger than 10^9 GeV so that the heavy neutrinos are thermally produced¹³. In supersymmetric models, there is a tension between leptogenesis and Big Bang Nucleosynthesis (BBN) if gravitinos decay in the BBN era. The gravitino problem gives a constraint on the reheating temperature $\lesssim 10^{6-10}$ GeV though the precise value depends on the SUSY breaking parameters [163]. Recent reviews of leptogenesis can be found in Ref. [164].

One of the important tests of leptogenesis are searches for neutrinoless double- β ($0\nu\beta\beta$) decays¹⁴. In a $0\nu\beta\beta$ decay, only two electrons but no (anti-)neutrinos are emitted by the decaying nucleus. This is in contrast to ordinary double- β decay. Thus, $0\nu\beta\beta$ decays are lepton-number-violating with $\Delta L = 2$. At the nucleon level, this is described by dimension-nine effective operators for $nn \rightarrow ppee$. These operators may in turn come from SM operators of with dimension less than nine, in combination with SM weak interactions. The lowest one is the dimension-five operator generating the Majorana neutrino mass terms (Eq. (94.17)). Thus, if the lepton-number violating effective interactions come from physics at energies much above the weak scale, the $0\nu\beta\beta$ decay rates are proportional to the Majorana neutrino masses. The latest experimental results are reviewed in [62]. For recent studies of the $0\nu\beta\beta$ decay including SM operators up to mass dimension nine, see [165] and refs. therein.

In addition to L -violation, one can consider $(B-L)$ and B violating phenomena. They are interesting in their own right and may also be relevant to baryogenesis. The relevant operators have higher mass dimension than the familiar dimension-six $(B+L)$ -violating operators (cf. Sec. 94.6). They may be predicted in $SO(10)$ GUTs with an intermediate scale, at which baryogenesis is realized, such as in [166]. First, one may have nucleon decays with $\Delta(B-L) = 2$, such as $n \rightarrow e^-\pi^+$. This is induced by dimension-seven effective operators in the SM, which are suppressed by the SM Higgs VEV or derivatives. Second, there are neutron-antineutron ($n-\bar{n}$) oscillations, which are induced by $\Delta B = 2$ dimension-nine effective operators in the SM. The upper bound on the mean time for $n-\bar{n}$ transitions is directly derived using free neutrons [167]. It is also constrained from the lower limit on the lifetime for neutrons bound in ^{16}O , derived by Super-Kamiokande [168]. Their results are very similar. Super-Kamiokande also searches for dinucleon decays with $\Delta B = 2$, such as $pp \rightarrow \pi^+\pi^+$ and $nn \rightarrow \pi^+\pi^-$ [169].

94.10 Conclusion

Most conservatively, grand unification means that (some of) the SM gauge interactions of $U(1)_Y$, $SU(2)_L$ and $SU(3)_C$ become

¹³ This constraint may be avoided in resonant leptogenesis [162], in which the right-handed neutrinos are required to be almost degenerate in mass.

¹⁴ Another important test of leptogenesis would be the observation of CP violation in neutrino oscillations. Strictly speaking, the CP phase in the PMNS matrix does not contribute to ϵ_1 in the seesaw model. Nevertheless, the observation of CP violation in neutrino oscillations would suggest that the seesaw mechanism is associated with a large CP violation, similarly to the quark sector.

part of a larger, unifying gauge symmetry at a high energy scale. In most models, especially in the simplest and most appealing variants of $SU(5)$ and $SO(10)$ unification, the statement is much stronger: One expects the three gauge couplings to unify (up to small threshold corrections) at a unique scale, M_G , and the proton to be unstable due to exchange of gauge bosons of the larger symmetry group. Supersymmetric grand unified theories provide, by far, the most predictive and economical framework allowing for perturbative unification. Many more details than could be discussed in the present article can be found in some of the classic reviews [123,170] and the two books [171] (see also [172] for two recent overviews).

Thus, the three classical pillars of GUTs are gauge coupling unification at $M_G \sim 2 \times 10^{16}$ GeV, low-energy supersymmetry (with a large SUSY desert), and nucleon decay. The first of these may be viewed as predicting the value of the strong coupling – a prediction which has already been verified (see Fig. 94.1). Numerically, this prediction remains intact even if SUSY partner masses are somewhat above the weak scale. However, at the conceptual level a continuously increasing lower bound on the SUSY scale is nevertheless problematic for the GUT paradigm: Indeed, if the independent, gauge-hierarchy-based motivation for SUSY is completely abandoned, the SUSY scale and hence α_3 become simply free parameters and the first two pillars crumble. Thus, it is important to keep pushing bounds on proton decay which, although again not completely universal in all GUT constructions, is arguably a more generic part of the GUT paradigm than low-energy SUSY.

Whether or not Yukawa couplings unify is more model dependent. However, irrespective of possible (partial) Yukawa unification, there certainly exists a very interesting and potentially fruitful interplay between flavor model building and grand unification. Especially in the neutrino sector this is strongly influenced by the developing experimental situation.

Another phenomenological signature of grand unification is the strength of the direct coupling of the QCD axion to photons, relative to its coupling to gluons. It is quantified by the predicted anomaly ratio $E/N = 8/3$ (see [173,174]). This arises in field-theoretic axion models consistent with GUT symmetry (such as DFSZ [175]) and in string-theoretic GUTs [174,176]. In the latter, the axion does not come from the phase of a complex scalar but is a fundamental shift-symmetric real field, coupling through a higher-dimension operator directly to the product of the GUT field-strength and its dual.

It is probably fair to say that, due to limitations of the 4d approach, including especially remaining ambiguities (free parameters or ad hoc assumptions) in models of flavor and GUT breaking, the string theoretic approach has become more important in GUT model building. In this framework, challenges include learning how to deal with the many vacua of the ‘landscape’ as well as, for each vacuum, developing the tools for reliably calculating detailed, phenomenological observables. Finally, due to limitations of space, the present article has barely touched on the interesting cosmological implications of GUTs. They may become more important in the future, especially in the case that a high inflationary energy scale is established observationally.

References

- [1] S. Weinberg, Phys. Rev. Lett. **43**, 1566 (1979).
- [2] P. Minkowski, Phys. Lett. **67B**, 421 (1977).
- [3] T. Yanagida, in *Proceedings of the Workshop on the Unified Theory and the Baryon Number of the Universe*, eds. O. Sawada and A. Sugamoto, KEK report No. 79-18, Tsukuba, Japan, 1979; S. Glashow, Quarks and leptons, published in *Proceedings of the Cargèse Lectures*, M. Levy (ed.), Plenum Press, New York, (1980); M. Gell-Mann, P. Ramond and R. Slansky, in *Supergravity*, ed. P. van Nieuwenhuizen *et al.*, North-Holland, Amsterdam, (1979), p. 315 [arXiv:1306.4669].
- [4] F. Wilczek, eConf **C790823**, 437 (1979); E. Witten, Phys. Lett. **91B**, 81 (1980); R. N. Mohapatra and G. Senjanovic, Phys. Rev. Lett. **44**, 912 (1980), [231(1979)].

- [5] G. 't Hooft, NATO Sci. Ser. B **59**, 135 (1980); M. J. G. Veltman, Acta Phys. Polon. **B12**, 437 (1981); L. Maiani, Gif-sur-Yvette Summer School on Particle Physics, 11th, Gif-sur-Yvette, France, 1979 (Inst. Nat. Phys. Nucl. Phys. Particules, Paris, 1979); E. Witten, Nucl. Phys. **B188**, 513 (1981).
- [6] S. Dimopoulos, S. Raby and F. Wilczek, Phys. Rev. **D24**, 1681 (1981); S. Dimopoulos and H. Georgi, Nucl. Phys. **B193**, 150 (1981); L. E. Ibanez and G. G. Ross, Phys. Lett. **105B**, 439 (1981); N. Sakai, Z. Phys. **C11**, 153 (1981); M. B. Einhorn and D. R. T. Jones, Nucl. Phys. **B196**, 475 (1982); W. J. Marciano and G. Senjanovic, Phys. Rev. **D25**, 3092 (1982).
- [7] U. Amaldi, W. de Boer and H. Furstenau, Phys. Lett. **B260**, 447 (1991); J. R. Ellis, S. Kelley and D. V. Nanopoulos, Phys. Lett. **B260**, 131 (1991); P. Langacker and M.-x. Luo, Phys. Rev. **D44**, 817 (1991); C. Giunti, C.W. Kim and U.W. Lee, Mod. Phys. Lett. **A6**, 1745 (1991); P. Langacker and N. Polonsky, Phys. Rev. **D47**, 4028 (1993), [hep-ph/9210235]; M. Carena, S. Pokorski and C. E. M. Wagner, Nucl. Phys. **B406**, 59 (1993), [hep-ph/9303202]; See also the review by S. Dimopoulos, S.A. Raby and F. Wilczek, Physics Today, p. 25 October (1991).
- [8] Y. Okada, M. Yamaguchi and T. Yanagida, Prog. Theor. Phys. **85**, 1 (1991); J. R. Ellis, G. Ridolfi and F. Zwirner, Phys. Lett. **B257**, 83 (1991); H. E. Haber and R. Hempfling, Phys. Rev. Lett. **66**, 1815 (1991).
- [9] M. Carena *et al.*, Phys. Lett. **B355**, 209 (1995), [hep-ph/9504316]; G. Degrandi *et al.*, Eur. Phys. J. **C28**, 133 (2003), [hep-ph/0212020]; P. Kant *et al.*, JHEP **08**, 104 (2010), [arXiv:1005.5709].
- [10] J. L. Feng *et al.*, Phys. Rev. Lett. **111**, 131802 (2013), [arXiv:1306.2318]; S. Heinemeyer (2014), [arXiv:1405.3781]; P. Draper and H. Rzehak, Phys. Rept. **619**, 1 (2016), [arXiv:1601.01890].
- [11] J. C. Pati and A. Salam, Phys. Rev. **D8**, 1240 (1973); For more discussion on the standard charge assignments in this formalism, see A. Davidson, Phys. Rev. **D20**, 776 (1979) and R.N. Mohapatra and R.E. Marshak, Phys. Lett. **B91**, 222 (1980); see also J. C. Pati, Int. J. Mod. Phys. A **32**, 1741013 (2017), arXiv:1706.09531 for a recent account.
- [12] H. Georgi and S. L. Glashow, Phys. Rev. Lett. **32**, 438 (1974).
- [13] J. R. Ellis, M. K. Gaillard and D. V. Nanopoulos, Phys. Lett. **80B**, 360 (1979), [Erratum: Phys. Lett. **82B**, 464 (1979)]; E. Golowich, Phys. Rev. **D24**, 2899 (1981).
- [14] S. Weinberg, Phys. Rev. **D26**, 287 (1982); N. Sakai and T. Yanagida, Nucl. Phys. **B197**, 533 (1982).
- [15] H. Georgi, Particles and Fields, *Proceedings of the APS Div. of Particles and Fields*, ed. C. Carlson, p. 575 (1975); H. Fritzsch and P. Minkowski, Annals Phys. **93**, 193 (1975).
- [16] R. Slansky, Phys. Rept. **79**, 1 (1981); H. Georgi, Front. Phys. **54**, 1 (1982); R. Feger and T. W. Kephart, Comput. Phys. Commun. **192**, 166 (2015), [arXiv:1206.6379]; N. Yamatsu, PTEP **2016**, 4, 043B02 (2016), [arXiv:1512.05559].
- [17] S. M. Barr, Phys. Lett. **112B**, 219 (1982); J. P. Derendinger, J. E. Kim and D. V. Nanopoulos, Phys. Lett. **139B**, 170 (1984); I. Antoniadis *et al.*, Phys. Lett. **B194**, 231 (1987); I. Antoniadis *et al.*, Phys. Lett. **B231**, 65 (1989).
- [18] F. Gursev, P. Ramond and P. Sikivie, Phys. Lett. **60B**, 177 (1976).
- [19] A. de Rujula, H. Georgi and S. L. Glashow, *5th Workshop on Grand Unification*, ed. K. Kang, H. Fried and P. Frampton, World Scientific, Singapore (1984), p. 88; See also earlier paper by Y. Achiman and B. Stech, p. 303, "New Phenomena in Lepton-Hadron Physics," ed. D.E.C. Fries and J. Wess, Plenum, NY (1979).
- [20] B. R. Greene *et al.*, Nucl. Phys. **B278**, 667 (1986); B. R. Greene *et al.*, Nucl. Phys. **B292**, 606 (1987); B. R. Greene, C. A. Lutken and G. G. Ross, Nucl. Phys. **B325**, 101 (1989); J. E. Kim, Phys. Lett. **B591**, 119 (2004), [hep-ph/0403196].
- [21] E. Witten, Phys. Lett. **105B**, 267 (1981).
- [22] A. Masiero *et al.*, Phys. Lett. **115B**, 380 (1982); B. Grinstein, Nucl. Phys. **B206**, 387 (1982).
- [23] S. Dimopoulos and F. Wilczek, *Proceedings Erice Summer School*, ed. A. Zichichi (1981); M. Srednicki, Nucl. Phys. **B202**, 327 (1982).
- [24] K. Inoue, A. Kakuto and H. Takano, Prog. Theor. Phys. **75**, 664 (1986).
- [25] Y. Yamada, Z. Phys. **C60**, 83 (1993); J. Hisano *et al.*, Phys. Lett. **B342**, 138 (1995), [hep-ph/9406417]; G. Altarelli, F. Feruglio and I. Masina, JHEP **11**, 040 (2000), [hep-ph/0007254].
- [26] K. S. Babu and S. M. Barr, Phys. Rev. **D48**, 5354 (1993), [hep-ph/9306242]; K. S. Babu and S. M. Barr, Phys. Rev. **D50**, 3529 (1994), [hep-ph/9402291]; K. S. Babu, J. C. Pati and Z. Tavartkiladze, JHEP **06**, 084 (2010), [arXiv:1003.2625].
- [27] K. S. Babu and R. N. Mohapatra, Phys. Rev. Lett. **74**, 2418 (1995), [hep-ph/9410326]; V. Lucas and S. Raby, Phys. Rev. **D54**, 2261 (1996), [hep-ph/9601303]; T. Blazek *et al.*, Phys. Rev. **D56**, 6919 (1997), [hep-ph/9611217]; S. M. Barr and S. Raby, Phys. Rev. Lett. **79**, 4748 (1997), [hep-ph/9705366]; K. S. Babu, J. C. Pati and F. Wilczek, Nucl. Phys. **B566**, 33 (2000), [hep-ph/9812538]; R. Dermisek, A. Mafi and S. Raby, Phys. Rev. **D63**, 035001 (2001), [hep-ph/0007213].
- [28] R. Barbieri, G. R. Dvali and A. Strumia, Nucl. Phys. **B391**, 487 (1993); Z. Berezhiani, C. Csaki and L. Randall, Nucl. Phys. **B444**, 61 (1995), [hep-ph/9501336]; Q. Shafi and Z. Tavartkiladze, Phys. Lett. **B522**, 102 (2001), [hep-ph/0105140].
- [29] G. F. Giudice and A. Masiero, Phys. Lett. **B206**, 480 (1988); J. E. Kim and H. P. Nilles, Mod. Phys. Lett. **A9**, 3575 (1994), [hep-ph/9406296].
- [30] L. Randall and C. Csaki, in "Supersymmetry and unification of fundamental interactions. Proceedings, International Workshop, SUSY 95, Palaiseau, France, May 15-19, 1995," 99-109 (1995), [235(1995)], [hep-ph/9508208].
- [31] E. Witten, in "Supersymmetry and unification of fundamental interactions. Proceedings, 10th International Conference, SUSY'02, Hamburg, Germany, June 17-23, 2002," 472-491 (2001), [hep-ph/0201018], URL http://www-library.desy.de/preparch/desy/proc/proc02-02/Proceedings/susy02/special/hertz_pr.ps; M. Dine, Y. Nir and Y. Shadmi, Phys. Rev. **D66**, 115001 (2002), [hep-ph/0206268].
- [32] A. Hebecker, J. March-Russell and R. Ziegler, JHEP **08**, 064 (2009), [arXiv:0801.4101]; F. Brummer *et al.*, JHEP **08**, 011 (2009), [arXiv:0906.2957]; F. Brummer *et al.*, JHEP **04**, 006 (2010), [arXiv:1003.0084].
- [33] H. M. Lee *et al.*, Phys. Lett. **B694**, 491 (2011), [arXiv:1009.0905]; R. Kappl *et al.*, Nucl. Phys. **B847**, 325 (2011), [arXiv:1012.4574]; H. M. Lee *et al.*, Nucl. Phys. **B850**, 1 (2011), [arXiv:1102.3595].
- [34] Y. Hosotani, Phys. Lett. **126B**, 309 (1983).
- [35] L. J. Dixon *et al.*, Nucl. Phys. **B261**, 678 (1985), [678(1985)]; L. J. Dixon *et al.*, Nucl. Phys. **B274**, 285 (1986); L. E. Ibanez, H. P. Nilles and F. Quevedo, Phys. Lett. **B187**, 25 (1987); L. E. Ibanez *et al.*, Phys. Lett. **B191**, 282 (1987).
- [36] P. Candelas *et al.*, Nucl. Phys. **B258**, 46 (1985).
- [37] Y. Kawamura, Prog. Theor. Phys. **103**, 613 (2000), [hep-ph/9902423]; Y. Kawamura, Prog. Theor. Phys. **105**, 999 (2001), [hep-ph/0012125]; G. Altarelli and F. Feruglio, Phys. Lett. **B511**, 257 (2001), [hep-ph/0102301];

- L. J. Hall and Y. Nomura, *Phys. Rev.* **D64**, 055003 (2001), [hep-ph/0103125]; A. Hebecker and J. March-Russell, *Nucl. Phys.* **B613**, 3 (2001), [hep-ph/0106166]; T. Asaka, W. Buchmuller and L. Covi, *Phys. Lett.* **B523**, 199 (2001), [hep-ph/0108021]; L. J. Hall *et al.*, *Phys. Rev.* **D65**, 035008 (2002), [hep-ph/0108071]; R. Dermisek and A. Mafi, *Phys. Rev.* **D65**, 055002 (2002), [hep-ph/0108139]; H. D. Kim and S. Raby, *JHEP* **01**, 056 (2003), [hep-ph/0212348].
- [38] L.E. Ibanez and A.M. Uranga, “String theory and particle physics: An introduction to string phenomenology,” Cambridge University Press 2012; K.-S. Choi and J. E. Kim, *Lect. Notes Phys.* **696**, 1 (2006); R. Blumenhagen *et al.*, *Phys. Rept.* **445**, 1 (2007), [hep-th/0610327].
- [39] D. J. Gross *et al.*, *Phys. Rev. Lett.* **54**, 502 (1985).
- [40] V. Braun *et al.*, *JHEP* **05**, 043 (2006), [hep-th/0512177]; V. Bouchard and R. Donagi, *Phys. Lett.* **B633**, 783 (2006), [hep-th/0512149]; L. B. Anderson *et al.*, *Phys. Rev.* **D84**, 106005 (2011), [arXiv:1106.4804].
- [41] L. J. Dixon, V. Kaplunovsky and J. Louis, *Nucl. Phys.* **B355**, 649 (1991).
- [42] G. Aldazabal *et al.*, *Nucl. Phys.* **B452**, 3 (1995), [hep-th/9410206]; Z. Kakushadze *et al.*, *Int. J. Mod. Phys.* **A13**, 2551 (1998), [hep-th/9710149].
- [43] E. Witten, *Nucl. Phys.* **B258**, 75 (1985).
- [44] S. Gukov *et al.*, *Phys. Rev.* **D69**, 086008 (2004), [hep-th/0310159]; G. Curio, A. Krause and D. Lust, *Fortsch. Phys.* **54**, 225 (2006), [hep-th/0502168]; L. B. Anderson *et al.*, *Phys. Rev.* **D83**, 106011 (2011), [arXiv:1102.0011].
- [45] R. Friedman, J. Morgan and E. Witten, *Commun. Math. Phys.* **187**, 679 (1997), [hep-th/9701162].
- [46] R. Blumenhagen, G. Honecker and T. Weigand, *JHEP* **08**, 009 (2005), [hep-th/0507041]; L. B. Anderson *et al.*, *JHEP* **01**, 047 (2014), [arXiv:1307.4787].
- [47] T. Kobayashi, S. Raby and R.-J. Zhang, *Phys. Lett.* **B593**, 262 (2004), [hep-ph/0403065].
- [48] S. Forste *et al.*, *Phys. Rev.* **D70**, 106008 (2004), [hep-th/0406208]; T. Kobayashi, S. Raby and R.-J. Zhang, *Nucl. Phys.* **B704**, 3 (2005), [hep-ph/0409098]; W. Buchmuller *et al.*, *Nucl. Phys.* **B712**, 139 (2005), [hep-ph/0412318]; W. Buchmuller *et al.*, *Phys. Rev. Lett.* **96**, 121602 (2006), [hep-ph/0511035]; W. Buchmuller *et al.*, *Nucl. Phys.* **B785**, 149 (2007), [hep-th/0606187]; O. Lebedev *et al.*, *Phys. Lett.* **B645**, 88 (2007), [hep-th/0611095]; J. E. Kim, J.-H. Kim and B. Kyae, *JHEP* **06**, 034 (2007), [hep-ph/0702278]; O. Lebedev *et al.*, *Phys. Rev.* **D77**, 046013 (2008), [arXiv:0708.2691].
- [49] S. B. Giddings, S. Kachru and J. Polchinski, *Phys. Rev.* **D66**, 106006 (2002), [hep-th/0105097]; S. Kachru *et al.*, *Phys. Rev.* **D68**, 046005 (2003), [hep-th/0301240].
- [50] R. Blumenhagen *et al.*, *Nucl. Phys.* **B815**, 1 (2009), [arXiv:0811.2936].
- [51] R. Blumenhagen *et al.*, *Nucl. Phys.* **B616**, 3 (2001), [hep-th/0107138].
- [52] R. Donagi and M. Wijnholt, *Adv. Theor. Math. Phys.* **15**, 5, 1237 (2011), [arXiv:0802.2969].
- [53] C. Beasley, J. J. Heckman and C. Vafa, *JHEP* **01**, 058 (2009), [arXiv:0802.3391]; C. Beasley, J. J. Heckman and C. Vafa, *JHEP* **01**, 059 (2009), [arXiv:0806.0102].
- [54] T. Weigand, *Class. Quant. Grav.* **27**, 214004 (2010), [arXiv:1009.3497]; J. J. Heckman, *Ann. Rev. Nucl. Part. Sci.* **60**, 237 (2010), [arXiv:1001.0577]; M. Cvetič, I. Garcia-Etxebarria and J. Halverson, *JHEP* **01**, 073 (2011), [arXiv:1003.5337]; A. Maharana and E. Palti, *Int. J. Mod. Phys.* **A28**, 1330005 (2013), [arXiv:1212.0555]; S. Krippendorf, S. Schafer-Nameki and J.-M. Wong, *JHEP* **11**, 008 (2015), [arXiv:1507.05961].
- [55] R. Donagi and M. Wijnholt, *Adv. Theor. Math. Phys.* **15**, 6, 1523 (2011), [arXiv:0808.2223]; R. Blumenhagen, *Phys. Rev. Lett.* **102**, 071601 (2009), [arXiv:0812.0248]; K.-S. Choi and J. E. Kim, *Phys. Rev.* **D83**, 065016 (2011), [arXiv:1012.0847]; C. Mayrhofer, E. Palti and T. Weigand, *JHEP* **09**, 082 (2013), [arXiv:1303.3589]; G. K. Leontaris and Q. Shafi, *Phys. Rev.* **D96**, 6, 066023 (2017), [arXiv:1706.08372].
- [56] E. Witten, *Nucl. Phys.* **B471**, 135 (1996), [hep-th/9602070].
- [57] A. Hebecker and M. Trapletti, *Nucl. Phys.* **B713**, 173 (2005), [hep-th/0411131].
- [58] B. Dundee and S. Raby (2008), [arXiv:0808.0992].
- [59] G. G. Ross (2004), [hep-ph/0411057].
- [60] H. Georgi, H. R. Quinn and S. Weinberg, *Phys. Rev. Lett.* **33**, 451 (1974); S. Weinberg, *Phys. Lett.* **91B**, 51 (1980); L. J. Hall, *Nucl. Phys.* **B178**, 75 (1981).
- [61] B. C. Allanach, *Comput. Phys. Commun.* **143**, 305 (2002), [hep-ph/0104145].
- [62] M. Tanabashi *et al.* (Particle Data Group), *Phys. Rev.* **D98**, 3, 030001 (2018).
- [63] M. L. Alciati *et al.*, *JHEP* **03**, 054 (2005), [hep-ph/0501086].
- [64] See talks on proposed and running nucleon decay experiments, and theoretical talks by P. Langacker, p. 131, and W.J. Marciano and A. Sirlin, p. 151, in *The Second Workshop on Grand Unification*, eds. J.P. Leveille *et al.*, Birkhäuser, Boston (1981).
- [65] W.J. Marciano, p. 190, *Eighth Workshop on Grand Unification*, ed. K. Wali, World Scientific Publishing Co., Singapore (1987).
- [66] M.S. Carena *et al.*, in Ref. [7].
- [67] A. Djouadi, J.-L. Kneur and G. Moultaka, *Comput. Phys. Commun.* **176**, 426 (2007), [hep-ph/0211331].
- [68] W. Porod and F. Staub, *Comput. Phys. Commun.* **183**, 2458 (2012), [arXiv:1104.1573].
- [69] W. Siegel, *Phys. Lett.* **94B**, 37 (1980).
- [70] I. Antoniadis, C. Kounnas, and R. Lacaze, *Nucl. Phys.* **B221**, 377 (1983).
- [71] M. A. Shifman, *Int. J. Mod. Phys.* **A11**, 5761 (1996), [hep-ph/9606281]; N. Arkani-Hamed and H. Murayama, *JHEP* **06**, 030 (2000), [hep-th/9707133]; I. Jack, D. R. T. Jones and A. Pickering, *Phys. Lett.* **B435**, 61 (1998), [hep-ph/9805482].
- [72] M.B. Einhorn and D.R.T. Jones in Ref. [6]; I. Antoniadis, C. Kounnas and K. Tamvakis, *Phys. Lett.* **119B**, 377 (1982).
- [73] J. Hisano, H. Murayama and T. Yanagida, *Phys. Rev. Lett.* **69**, 1014 (1992); J. Hisano, H. Murayama and T. Yanagida, *Nucl. Phys.* **B402**, 46 (1993), [hep-ph/9207279].
- [74] H. Murayama and A. Pierce, *Phys. Rev.* **D65**, 055009 (2002), [hep-ph/0108104].
- [75] G. Anderson *et al.*, eConf **C960625**, SUP107 (1996) [hep-ph/9609457].
- [76] L. Roszkowski and M. A. Shifman, *Phys. Rev.* **D53**, 404 (1996), [hep-ph/9503358]; S. Raby, M. Ratz and K. Schmidt-Hoberg, *Phys. Lett.* **B687**, 342 (2010), [arXiv:0911.4249].
- [77] J. Hisano, T. Kuwahara and N. Nagata, *Phys. Lett.* **B723**, 324 (2013), [arXiv:1304.0343].
- [78] N. Arkani-Hamed, A. Delgado and G. F. Giudice, *Nucl. Phys.* **B741**, 108 (2006), [hep-ph/0601041].
- [79] M. Ibe, T. Moroi and T. T. Yanagida, *Phys. Lett.* **B644**, 355 (2007), [hep-ph/0610277].
- [80] G. F. Giudice *et al.*, *JHEP* **12**, 027 (1998), [hep-ph/9810442]; L. Randall and R. Sundrum, *Nucl. Phys.* **B557**, 79 (1999), [hep-th/9810155].
- [81] R. N. Mohapatra and M. K. Parida, *Phys. Rev.* **D47**, 264 (1993), [hep-ph/9204234].

- [82] D.-G. Lee *et al.*, Phys. Rev. **D51**, 229 (1995), [hep-ph/9404238].
- [83] L. E. Ibanez *et al.*, JHEP **07**, 195 (2012), [arXiv:1206.2655].
- [84] K. R. Dienes, E. Dudas and T. Gherghetta, Phys. Rev. Lett. **91**, 061601 (2003), [hep-th/0210294].
- [85] K. Agashe, R. Contino and R. Sundrum, Phys. Rev. Lett. **95**, 171804 (2005), [hep-ph/0502222].
- [86] F. Wilczek and A. Zee, Phys. Rev. Lett. **43**, 1571 (1979).
- [87] K. Abe *et al.* (Super-Kamiokande), Phys. Rev. **D95**, 1, 012004 (2017), [arXiv:1610.03597]; S. Mine (Super Kamiokande), J. Phys. Conf. Ser. **718**, 6, 062044 (2016).
- [88] K. Abe *et al.* (Hyper-Kamiokande) (2018), [arXiv:1805.04163].
- [89] Y. Aoki *et al.*, Phys. Rev. **D96**, 1, 014506 (2017), [arXiv:1705.01338].
- [90] J. Hisano, T. Kuwahara and Y. Omura, Nucl. Phys. **B898**, 1 (2015), [Erratum: Nucl. Phys. B907,476(2016)], [arXiv:1503.08561].
- [91] R. Barbier *et al.*, Phys. Rept. **420**, 1 (2005), [hep-ph/0406039]; F. Domingo *et al.*, JHEP **02**, 066 (2019), [arXiv:1810.08228].
- [92] G. R. Farrar and P. Fayet, Phys. Lett. **76B**, 575 (1978).
- [93] S. Dimopoulos, S. Raby and F. Wilczek, Phys. Lett. **112B**, 133 (1982); J. R. Ellis, D. V. Nanopoulos and S. Rudaz, Nucl. Phys. **B202**, 43 (1982).
- [94] C. S. Aulakh *et al.*, Nucl. Phys. **B597**, 89 (2001), [hep-ph/0004031].
- [95] T. Goto and T. Nihei, Phys. Rev. **D59**, 115009 (1999), [hep-ph/9808255].
- [96] G. D. Coughlan *et al.*, Phys. Lett. **160B**, 249 (1985); J. L. Chkareuli and I. G. Gogoladze, Phys. Rev. **D58**, 055011 (1998), [hep-ph/9803335].
- [97] G. F. Giudice and A. Romanino, Nucl. Phys. **B699**, 65 (2004), [Erratum: Nucl. Phys. B706,487(2005)], [hep-ph/0406088].
- [98] J. Hisano *et al.*, JHEP **07**, 038 (2013), [arXiv:1304.3651].
- [99] B. Bajc, P. Fileviez Perez and G. Senjanovic, Phys. Rev. **D66**, 075005 (2002), [hep-ph/0204311].
- [100] K.-S. Choi, Phys. Lett. **B668**, 392 (2008), [arXiv:0807.2766].
- [101] F. An *et al.* (JUNO), J. Phys. **G43**, 3, 030401 (2016), [arXiv:1507.05613].
- [102] R. Acciarri *et al.* (DUNE) (2015), [arXiv:1512.06148].
- [103] L. J. Hall and Y. Nomura, Phys. Rev. **D66**, 075004 (2002), [hep-ph/0205067]; H. D. Kim, S. Raby and L. Schradin, JHEP **05**, 036 (2005), [hep-ph/0411328].
- [104] M.S. Chanowitz, J.R. Ellis and M.K. Gaillard, Nucl. Phys. **B128**, 506 (1977); A. J. Buras *et al.*, Nucl. Phys. **B135**, 66 (1978).
- [105] K. Inoue *et al.*, Prog. Theor. Phys. **67**, 1889 (1982); L. E. Ibanez and C. Lopez, Nucl. Phys. **B233**, 511 (1984).
- [106] H. Georgi and D. V. Nanopoulos, Nucl. Phys. **B159**, 16 (1979); J. A. Harvey, P. Ramond and D. B. Reiss, Phys. Lett. **92B**, 309 (1980); J. A. Harvey, D. B. Reiss and P. Ramond, Nucl. Phys. **B199**, 223 (1982).
- [107] T. Banks, Nucl. Phys. **B303**, 172 (1988); M. Olechowski and S. Pokorski, Phys. Lett. **B214**, 393 (1988); S. Pokorski, Nucl. Phys. Proc. Suppl. **13**, 606 (1990); B. Ananthanarayan, G. Lazarides and Q. Shafi, Phys. Rev. **D44**, 1613 (1991); Q. Shafi and B. Ananthanarayan, ICTP Summer School lectures (1991); S. Dimopoulos, L. J. Hall and S. Raby, Phys. Rev. Lett. **68**, 1984 (1992); S. Dimopoulos, L. J. Hall and S. Raby, Phys. Rev. **D45**, 4192 (1992); G. W. Anderson *et al.*, Phys. Rev. **D47**, R3702 (1993), [hep-ph/9209250]; B. Ananthanarayan, G. Lazarides and Q. Shafi, Phys. Lett. **B300**, 245 (1993); G. Anderson *et al.*, Phys. Rev. **D49**, 3660 (1994), [hep-ph/9308333]; B. Ananthanarayan, Q. Shafi and X. M. Wang, Phys. Rev. **D50**, 5980 (1994), [hep-ph/9311225].
- [108] L. J. Hall, R. Rattazzi and U. Sarid, Phys. Rev. **D50**, 7048 (1994), [hep-ph/9306309]; M. Carena *et al.*, Nucl. Phys. **B426**, 269 (1994), [hep-ph/9402253].
- [109] A. Anandakrishnan, B. C. Bryant and S. Raby, JHEP **05**, 088 (2015), [arXiv:1411.7035].
- [110] M. Lanzagorta and G. G. Ross, Phys. Lett. **B364**, 163 (1995), [hep-ph/9507366].
- [111] K. Tobe and J. D. Wells, Nucl. Phys. **B663**, 123 (2003), [hep-ph/0301015].
- [112] G. Ross and M. Serna, Phys. Lett. **B664**, 97 (2008), [arXiv:0704.1248].
- [113] T. Blazek, R. Dermisek and S. Raby, Phys. Rev. Lett. **88**, 111804 (2002), [hep-ph/0107097]; T. Blazek, R. Dermisek and S. Raby, Phys. Rev. **D65**, 115004 (2002), [hep-ph/0201081]; D. Auto *et al.*, JHEP **06**, 023 (2003), [hep-ph/0302155]; R. Dermisek *et al.*, JHEP **04**, 037 (2003), [hep-ph/0304101]; R. Dermisek *et al.*, JHEP **09**, 029 (2005), [hep-ph/0507233].
- [114] A. Anandakrishnan, S. Raby and A. Wingerter, Phys. Rev. **D87**, 5, 055005 (2013), [arXiv:1212.0542]; M. Adeel Ajaib *et al.*, JHEP **07**, 139 (2013), [arXiv:1303.6964]; Z. Poh and S. Raby, Phys. Rev. **D92**, 1, 015017 (2015), [arXiv:1505.00264]; M. Badziak, M. Olechowski and S. Pokorski, JHEP **10**, 088 (2013), [arXiv:1307.7999].
- [115] H. Georgi and C. Jarlskog, Phys. Lett. **86B**, 297 (1979).
- [116] S. Antusch and M. Spinrath, Phys. Rev. **D79**, 095004 (2009), [arXiv:0902.4644].
- [117] G. Lazarides, Q. Shafi and C. Wetterich, Nucl. Phys. **B181**, 287 (1981).
- [118] T. E. Clark, T.-K. Kuo and N. Nakagawa, Phys. Lett. **115B**, 26 (1982); K. S. Babu and R. N. Mohapatra, Phys. Rev. Lett. **70**, 2845 (1993), [hep-ph/9209215].
- [119] R. Barbieri and D. V. Nanopoulos, Phys. Lett. **91B**, 369 (1980).
- [120] C. D. Froggatt and H. B. Nielsen, Nucl. Phys. **B147**, 277 (1979).
- [121] R. Barbieri *et al.*, Nucl. Phys. **B493**, 3 (1997), [hep-ph/9610449]; T. Blazek, S. Raby and K. Tobe, Phys. Rev. **D60**, 113001 (1999), [hep-ph/9903340]; T. Blazek, S. Raby and K. Tobe, Phys. Rev. **D62**, 055001 (2000), [hep-ph/9912482]; Q. Shafi and Z. Tavartkiladze, Phys. Lett. **B487**, 145 (2000), [hep-ph/9910314]; C. H. Albright and S. M. Barr, Phys. Rev. Lett. **85**, 244 (2000), [hep-ph/0002155]; Z. Berezhiani and A. Rossi, Nucl. Phys. **B594**, 113 (2001), [hep-ph/0003084]; C. H. Albright and S. M. Barr, Phys. Rev. **D64**, 073010 (2001), [hep-ph/0104294]; M.-C. Chen and K. T. Mahanthappa, Int. J. Mod. Phys. **A18**, 5819 (2003), [hep-ph/0305088]; R. Dermisek and S. Raby, Phys. Lett. **B622**, 327 (2005), [hep-ph/0507045].
- [122] H. Georgi, Nucl. Phys. **B156**, 126 (1979); P. H. Frampton, Phys. Lett. **88B**, 299 (1979); P. Frampton and S. Nandi, Phys. Rev. Lett. **43**, 1460 (1979); J.E. Kim, Phys. Rev. Lett. **45**, 1916 (1980), Phys. Rev. **D23**, 2706 (1981) and Phys. Rev. **D26**, 674 (1982); Y. Fujimoto, Phys. Rev. **D26**, 3183 (1982).
- [123] P. Langacker, Phys. Rept. **72**, 185 (1981).
- [124] H. Georgi, Conf. Proc. C **820726**, 705 (1982).
- [125] S. M. Barr, Phys. Rev. **D78**, 055008 (2008), [arXiv:0805.4808]; Y. Goto, Y. Kawamura and T. Miura, Phys. Rev. **D88**, 5, 055016 (2013), [arXiv:1307.2631]; J. E. Kim, JHEP **06**, 114 (2015), [arXiv:1503.03104]; C.H. Albright, R.P. Feger and T.W. Kephart, arXiv:1601.07523; M. Reig, J. W. F. Valle, C. A. Vaquera-Araujo and F. Wilczek, arXiv:1706.03116.

- [126] M. Magg and C. Wetterich, Phys. Lett. **94B**, 61 (1980); J. Schechter and J. W. F. Valle, Phys. Rev. **D22**, 2227 (1980); R. N. Mohapatra and G. Senjanovic, Phys. Rev. **D23**, 165 (1981); G. B. Gelmini and M. Roncadelli, Phys. Lett. **99B**, 411 (1981).
- [127] R. Foot *et al.*, Z. Phys. **C44**, 441 (1989).
- [128] Y. Fukuda *et al.* (Super-Kamiokande), Phys. Rev. Lett. **81**, 1562 (1998), [hep-ex/9807003].
- [129] G. L. Fogli *et al.*, Phys. Rev. **D84**, 053007 (2011), [arXiv:1106.6028].
- [130] T. Schwetz, M. Tortola and J. W. F. Valle, New J. Phys. **13**, 109401 (2011), [arXiv:1108.1376].
- [131] G. Altarelli, Soryushiron Kenkyu Electron. **116**, A29 (2008), [arXiv:0711.0161]; S. F. King and C. Luhn, Rept. Prog. Phys. **76**, 056201 (2013), [arXiv:1301.1340].
- [132] C. H. Albright and M.-C. Chen, Phys. Rev. **D74**, 113006 (2006), [hep-ph/0608137].
- [133] R. Kallosh *et al.*, Phys. Rev. **D52**, 912 (1995), [hep-th/9502069].
- [134] H. Ruegg and M. Ruiz-Altaba, Int. J. Mod. Phys. **A19**, 3265 (2004), [hep-th/0304245].
- [135] M. B. Green and J. H. Schwarz, Phys. Lett. **149B**, 117 (1984).
- [136] L. E. Ibanez and G. G. Ross, Nucl. Phys. **B368**, 3 (1992); M. Berasaluce-Gonzalez *et al.*, JHEP **12**, 113 (2011), [arXiv:1106.4169].
- [137] N.G. Deshpande, OITS-107; C. Q. Geng and R. E. Marshak, Phys. Rev. **D39**, 693 (1989); A. Font, L. E. Ibanez and F. Quevedo, Phys. Lett. **B228**, 79 (1989); K. S. Babu and R. N. Mohapatra, Phys. Rev. Lett. **63**, 938 (1989).
- [138] R. Foot *et al.*, Phys. Rev. **D39**, 3411 (1989).
- [139] M. Nowakowski and A. Pilaftsis, Phys. Rev. **D48**, 259 (1993), [hep-ph/9304312].
- [140] T. P. T. Dijkstra, L. R. Huiszoon and A. N. Schellekens, Phys. Lett. **B609**, 408 (2005), [hep-th/0403196]; F. Gmeiner *et al.*, JHEP **01**, 004 (2006), [hep-th/0510170]; B. Gato-Rivera and A. N. Schellekens, Nucl. Phys. **B883**, 529 (2014), [arXiv:1401.1782].
- [141] G. 't Hooft, Nucl. Phys. **B79**, 276 (1974) A.M. Polyakov, Pis'ma Zh. Eksp. Teor. Fiz. **20**, 430 (1974) [Sov. Phys. JETP Lett. **20**, 194 (1974)]; For a pedagogical introduction, see S. Coleman, in *Aspects of Symmetry*, Selected Erice Lectures, Cambridge University Press, Cambridge, (1985), and P. Goddard and D. Olive, Rept. on Prog. in Phys. **41**, 1357 (1978).
- [142] M. Ambrosio *et al.* (MACRO), Eur. Phys. J. **C25**, 511 (2002), [hep-ex/0207020]; S. Balestra *et al.* (2011), [arXiv:1105.5587]; L. Patrizii and M. Spurio, Ann. Rev. Nucl. Part. Sci. **65**, 279 (2015), [arXiv:1510.07125].
- [143] For a review, see A.D. Linde, *Particle Physics and Inflationary Cosmology*, Harwood Academic, Switzerland (1990).
- [144] G. R. Dvali, H. Liu and T. Vachaspati, Phys. Rev. Lett. **80**, 2281 (1998), [hep-ph/9710301].
- [145] P. Langacker and S.-Y. Pi, Phys. Rev. Lett. **45**, 1 (1980).
- [146] G. R. Dvali, A. Melfo and G. Senjanovic, Phys. Rev. Lett. **75**, 4559 (1995), [hep-ph/9507230].
- [147] V. Rubakov, Nucl. Phys. **B203**, 311 (1982) and Institute of Nuclear Research Report No. P-0211, Moscow (1981), unpublished; C. G. Callan, Jr., Phys. Rev. **D26**, 2058 (1982); F. Wilczek, Phys. Rev. Lett. **48**, 1146 (1982); S. Dawson and A. N. Schellekens, Phys. Rev. **D27**, 2119 (1983).
- [148] K. Freese, M. S. Turner and D. N. Schramm, Phys. Rev. Lett. **51**, 1625 (1983).
- [149] P. A. R. Ade *et al.* (BICEP2, Keck Array), Phys. Rev. Lett. **116**, 031302 (2016), [arXiv:1510.09217]; N. Aghanim *et al.* (Planck) (2018), [arXiv:1807.06209].
- [150] L. J. Hall, V. A. Kostelecky and S. Raby, Nucl. Phys. **B267**, 415 (1986).
- [151] R. Barbieri and L. J. Hall, Phys. Lett. **B338**, 212 (1994), [hep-ph/9408406]; R. Barbieri, L. J. Hall and A. Strumia, Nucl. Phys. **B445**, 219 (1995), [hep-ph/9501334].
- [152] F. Borzumati and A. Masiero, Phys. Rev. Lett. **57**, 961 (1986); J. Hisano *et al.*, Phys. Lett. **B357**, 579 (1995), [hep-ph/9501407]; J. Hisano *et al.*, Phys. Rev. **D53**, 2442 (1996), [hep-ph/9510309]; J. Hisano and D. Nomura, Phys. Rev. **D59**, 116005 (1999), [hep-ph/9810479].
- [153] T. Moroi, JHEP **03**, 019 (2000), [hep-ph/0002208]; D. Chang, A. Masiero and H. Murayama, Phys. Rev. **D67**, 075013 (2003), [hep-ph/0205111].
- [154] S. Dimopoulos and L. J. Hall, Phys. Lett. **B344**, 185 (1995), [hep-ph/9411273].
- [155] J. Hisano *et al.*, Phys. Lett. **B604**, 216 (2004), [hep-ph/0407169].
- [156] A. Yu. Ignatiev *et al.*, Phys. Lett. **76B**, 436 (1978); M. Yoshimura, Phys. Rev. Lett. **41**, 281 (1978), [Erratum: Phys. Rev. Lett. **42**, 746 (1979)].
- [157] D. Toussaint *et al.*, Phys. Rev. **D19**, 1036 (1979); S. Weinberg, Phys. Rev. Lett. **42**, 850 (1979); M. Yoshimura, Phys. Lett. **88B**, 294 (1979); S. M. Barr, G. Segre and H. A. Weldon, Phys. Rev. **D20**, 2494 (1979); D. V. Nanopoulos and S. Weinberg, Phys. Rev. **D20**, 2484 (1979); A. Yildiz and P. H. Cox, Phys. Rev. **D21**, 906 (1980).
- [158] H. K. Dreiner and G. G. Ross, Nucl. Phys. **B410**, 188 (1993), [hep-ph/9207221].
- [159] M. Fukugita and T. Yanagida, Phys. Rev. Lett. **89**, 131602 (2002), [hep-ph/0203194].
- [160] M. Fukugita and T. Yanagida, Phys. Lett. **B174**, 45 (1986).
- [161] S. Davidson and A. Ibarra, Phys. Lett. **B535**, 25 (2002), [hep-ph/0202239]; K. Hamaguchi, H. Murayama and T. Yanagida, Phys. Rev. **D65**, 043512 (2002), [hep-ph/0109030].
- [162] A. Pilaftsis and T. E. J. Underwood, Phys. Rev. **D72**, 113001 (2005), [hep-ph/0506107].
- [163] M. Kawasaki *et al.*, Phys. Rev. **D78**, 065011 (2008), [arXiv:0804.3745].
- [164] W. Buchmuller, R. D. Peccei and T. Yanagida, Ann. Rev. Nucl. Part. Sci. **55**, 311 (2005), [hep-ph/0502169]; C. S. Fong, E. Nardi and A. Riotto, Adv. High Energy Phys. **2012**, 158303 (2012), [arXiv:1301.3062].
- [165] V. Cirigliano *et al.*, JHEP **12**, 097 (2018), [arXiv:1806.02780].
- [166] K. S. Babu and R. N. Mohapatra, Phys. Rev. **D86**, 035018 (2012), [arXiv:1203.5544]; K. S. Babu and R. N. Mohapatra, Phys. Lett. **B715**, 328 (2012), [arXiv:1206.5701]; K. S. Babu and R. N. Mohapatra, Phys. Rev. Lett. **109**, 091803 (2012), [arXiv:1207.5771].
- [167] M. Baldo-Ceolin *et al.*, Z. Phys. **C63**, 409 (1994).
- [168] K. Abe *et al.* (Super-Kamiokande), Phys. Rev. **D91**, 072006 (2015), [arXiv:1109.4227].
- [169] J. Gustafson *et al.* (Super-Kamiokande), Phys. Rev. **D91**, 7, 072009 (2015), [arXiv:1504.01041].
- [170] K. R. Dienes, Phys. Rept. **287**, 447 (1997), [hep-th/9602045]; P. Nath and P. Fileviez Perez, Phys. Rept. **441**, 191 (2007), [hep-ph/0601023].
- [171] G.G. Ross, "Grand Unified Theories", Benjamin/Cummings, 1984.; S. Raby, Lect. Notes Phys. **939**, 1 (2017).
- [172] P. Nath, Int. J. Mod. Phys. **A33**, 20, 1830017 (2018), [arXiv:1807.05302]; D. Croon *et al.*, Front.in Phys. **7**, 76 (2019), [arXiv:1903.04977].
- [173] A. Ringwald, L.J. Rosenberg and G. Rybka, Review of 'Axions and other Similar Particles' in Ref. [62].

- [174] P. Svrcek and E. Witten, JHEP **06**, 051 (2006), [hep-th/0605206].
- [175] M. Dine, W. Fischler and M. Srednicki, Phys. Lett. **104B**, 199 (1981); A. R. Zhitnitsky, Sov. J. Nucl. Phys. **31**, 260 (1980), [Yad. Fiz.31,497(1980)].
- [176] J. P. Conlon, JHEP **05**, 078 (2006), [hep-th/0602233].

95. Leptoquarks

Updated August 2019 by S. Rolli (US Department of Energy) and M. Tanabashi (Nagoya U.)

Leptoquarks are hypothetical particles carrying both baryon number (B) and lepton number (L). The possible quantum numbers of leptoquark states can be restricted by assuming that their direct interactions with the ordinary standard model (SM) fermions are dimensionless and invariant under the SM gauge group. Table 95.1 shows the list of all possible quantum numbers with this assumption [1]. The columns of $SU(3)_C$, $SU(2)_W$, and $U(1)_Y$ in Table 95.1 indicate the QCD representation, the weak isospin representation, and the weak hypercharge, respectively. The spin of a leptoquark state is taken to be 1 (vector leptoquark) or 0 (scalar leptoquark).

Table 95.1: Possible leptoquarks and their quantum numbers.

Spin	$3B + L$	$SU(3)_c$	$SU(2)_W$	$U(1)_Y$	Allowed coupling
0	-2	$\bar{3}$	1	1/3	$\bar{q}_L^c \ell_L$ or $\bar{u}_R^c e_R$
0	-2	$\bar{3}$	1	4/3	$\bar{d}_R^c e_R$
0	-2	$\bar{3}$	3	1/3	$\bar{q}_L^c \ell_L$
1	-2	$\bar{3}$	2	5/6	$\bar{q}_L^c \gamma^\mu e_R$ or $\bar{d}_R^c \gamma^\mu \ell_L$
1	-2	$\bar{3}$	2	-1/6	$\bar{u}_R^c \gamma^\mu \ell_L$
0	0	3	2	7/6	$\bar{q}_L e_R$ or $\bar{u}_R \ell_L$
0	0	3	2	1/6	$\bar{d}_R \ell_L$
1	0	3	1	2/3	$\bar{q}_L \gamma^\mu \ell_L$ or $\bar{d}_R \gamma^\mu e_R$
1	0	3	1	5/3	$\bar{u}_R \gamma^\mu e_R$
1	0	3	3	2/3	$\bar{q}_L \gamma^\mu \ell_L$

If we do not require leptoquark states to couple directly with SM fermions, different assignments of quantum numbers become possible [2,3].

Leptoquark states are expected to exist in various extensions of the SM. The Pati-Salam model [4] is an example predicting the existence of a leptoquark state. Leptoquark states also exist in grand unification theories based on $SU(5)$ [5], $SO(10)$ [6], which includes Pati-Salam color $SU(4)$, and larger gauge groups. Scalar quarks in supersymmetric models with R-parity violation may also have leptoquark-type Yukawa couplings. The bounds on the leptoquark states can therefore be applied to constrain R-parity-violating supersymmetric models. Scalar leptoquarks are expected to exist at the TeV scale in extended technicolor models [7,8] where leptoquark states appear as the bound states of techni-fermions. Compositeness of quarks and leptons also provides examples of models which may have light leptoquark states [9].

Bounds on leptoquark states are obtained both directly and indirectly. Direct limits are from their production cross sections at colliders, while indirect limits are calculated from bounds on leptoquark-induced four-fermion interactions, which are obtained from low-energy experiments, or from collider experiments below threshold. These four-fermion interactions often cause lepton-flavor non-universalities in heavy quark decays. Anomalies observed recently in the R_K and R_D ratios [10,11] in the semi-leptonic B decays may be explained in models with TeV scale leptoquarks.

If a leptoquark couples to quarks (leptons) belonging to more than a single generation in the mass eigenbasis, it can induce four-fermion interactions causing flavor-changing neutral currents (lepton-family-number violations). The quantum number assignment of Table 1 allows several leptoquark states to couple to both left- and right-handed quarks simultaneously. Such leptoquark states are called non-chiral and may cause four-fermion interactions affecting the $(\pi \rightarrow e\nu)/(\pi \rightarrow \mu\nu)$ ratio [12]. Non-chiral scalar leptoquarks also contribute to the muon anomalous magnetic moment [13,14]. Since indirect limits provide more stringent constraints on these types of leptoquarks, it is often assumed that a leptoquark state couples only to a single generation of quarks and a single generation of leptons in a chiral interaction, for which indirect limits become much weaker.

Additionally, this assumption gives strong constraints on models of leptoquarks.

Refs. [15,16,17] give extensive lists of the bounds on the leptoquark-induced four-fermion interactions. For the isoscalar scalar and vector leptoquarks S_0 and V_0 , for example, which couple with the first- (second-) generation left-handed quark, and the first-generation left-handed lepton, the bounds $\lambda^2 < 0.07 \times (M_{LQ}/1 \text{ TeV})^2$ for S_0 , and $\lambda^2 < 0.4 \times (M_{LQ}/1 \text{ TeV})^2$ for V_0 ($\lambda^2 < 0.7 \times (M_{LQ}/1 \text{ TeV})^2$ for S_0 , and $\lambda^2 < 0.5 \times (M_{LQ}/1 \text{ TeV})^2$ for V_0) with λ being the leptoquark coupling strength, can be derived from the limits listed in Ref. [17]. The e^+e^- experiments are sensitive to the indirect effects coming from t - and u -channel exchanges of leptoquarks in the $e^+e^- \rightarrow q\bar{q}$ process. The HERA experiments give bounds on the leptoquark-induced four-fermion interaction. For detailed bounds obtained in this way, see the Boson Particle Listings for “Indirect Limits for Leptoquarks” and its references.

Collider experiments provide direct limits on the leptoquark states through limits on the pair- and single-production cross sections. The leading-order cross sections of the parton processes

$$\begin{aligned}
 q + \bar{q} &\rightarrow LQ + \bar{LQ} \\
 g + g &\rightarrow LQ + \bar{LQ} \\
 e + q &\rightarrow LQ
 \end{aligned}
 \tag{95.1}$$

may be written as [21]

$$\begin{aligned}
 \hat{\sigma}_{LO} [q\bar{q} \rightarrow LQ + \bar{LQ}] &= \frac{2\alpha_s^2 \pi}{27\hat{s}} \beta^3, \\
 \hat{\sigma}_{LO} [gg \rightarrow LQ + \bar{LQ}] &= \frac{\alpha_s^2 \pi}{96\hat{s}} \\
 &\times \left[\beta(41 - 31\beta^2) + (18\beta^2 - \beta^4 - 17) \log \frac{1+\beta}{1-\beta} \right], \\
 \hat{\sigma}_{LO} [eq \rightarrow LQ] &= \frac{\pi\lambda^2}{4} \delta(\hat{s} - M_{LQ}^2)
 \end{aligned}
 \tag{95.2}$$

for a scalar leptoquark. Here $\sqrt{\hat{s}}$ is the invariant energy of the parton subprocess, and $\beta \equiv \sqrt{1 - 4M_{LQ}^2/\hat{s}}$. The leptoquark Yukawa coupling is given by λ . Leptoquarks are also produced singly at hadron colliders through $g + q \rightarrow LQ + \ell$ [22], which allows extending to higher masses the collider reach in the leptoquark search [23], depending on the leptoquark Yukawa coupling. See also Ref. [24] for a comprehensive review on the leptoquark phenomenology in precision experiments and particle colliders.

Leptoquark states which couple only to left- or right-handed quarks are called chiral leptoquarks. Leptoquark states which couple only to the first (second, third) generation are referred as the first- (second-, third-) generation leptoquarks.

The LHC, Tevatron and LEP experiments have been searching for pair production of the leptoquark states, which arises from the leptoquark gauge interaction. Due to the typical decay of the leptoquark into charged and neutral leptons and quarks, the searches are carried on in signatures including high P_T charged leptons, high E_T jets and large missing transverse energy. Additionally searches for pair produced LQs are often organized by the decay mode of the pair of LQs, via the decay parameter β , which represents the branching fraction into a charge lepton vs a neutrino: $\beta = 1$ for both LQs decaying into a charged lepton, $\beta = 0.5$ for one LQ decaying into a charged lepton and one into a neutrino. The gauge couplings of a scalar leptoquark are determined uniquely according to its quantum numbers in Table 95.1. Since all of the leptoquark states belong to color-triplet representation, the scalar leptoquark pair-production cross section at the Tevatron and LHC can be determined solely as a function of the leptoquark mass without making further assumptions. This is in contrast to the indirect or single-production limits, which give constraints in the leptoquark mass-coupling plane.

Older results from the Tevatron run can be found here: [26], [27], [28] and [29].

Since the previous version of this review, both ATLAS and CMS have updated their results concerning searches for first, second, and third generation LQs and leptoquark states which couple only with the i -th generation quarks and the j -th generation leptons ($i \neq j$) without causing conflicts with severe indirect constraints. The datasets were almost all collected at center of mass energy of 13 TeV and corresponding to the latest integrated luminosity collected before the shutdown of the LHC occurring in 2019 and 2020.

It is worthy to note that organizing LQs by flavor quantum number first before organizing them by gauge quantum number is becoming more common and advantageous because it relates more closely to some of the experimental searches being performed. The traditional nomenclature for 1st, 2nd, and 3rd generation LQ encourages only looking for the diagonal elements in a flavor matrix of possibilities, which has been the traditional experimental search strategy.

Current results extend previous mass limits for scalar leptoquarks to > 1435 GeV (first generation, CMS, $\beta = 1, \sqrt{s} = 13$ TeV) and > 1270 GeV (first generation, CMS, $\beta = 0.5, \sqrt{s} = 13$ TeV) [30]; > 1400 GeV (first generation, ATLAS, $\beta = 1, \sqrt{s} = 13$ TeV) and > 1290 GeV (first generation, ATLAS, $\beta = 0.5, \sqrt{s} = 13$ TeV) [31]; > 1530 GeV (second generation, CMS, $\beta = 1, \sqrt{s} = 13$ TeV) and > 1285 GeV (second generation, CMS, $\beta = 0.5, \sqrt{s} = 13$ TeV) [32]; and > 1560 GeV (second generation, ATLAS, $\beta = 1, \sqrt{s} = 13$ TeV) and > 1230 GeV (second generation, ATLAS, $\beta = 0.5, \sqrt{s} = 13$ TeV) [31]. All limits are presented at 95% C.L.

As for third generation leptoquarks, CMS results are the following: 1) assuming that all leptoquarks decay to a top quark and a τ lepton, the existence of pair produced, third-generation leptoquark up to a mass of 900 GeV ($\beta = 1, 13$ TeV) is excluded at 95% confidence level [33]; 2) assuming that all leptoquarks decay to a bottom quark and a τ lepton, the existence of pair produced, third-generation leptoquark up to a mass of 1020 GeV ($\beta = 1, 13$ TeV) is excluded at 95% confidence level [34]; 3) assuming that all leptoquarks decay to a bottom quark and a τ neutrino, the existence of pair produced, third-generation leptoquark up to a mass of 450 GeV ($\beta = 0, 7$ TeV) is excluded at 95% confidence level [35]. In a recent paper [36], the ATLAS collaboration has limits on pair production of third generation scalar leptoquarks where all possible decays of the leptoquark into a quark (t, b) and a lepton (τ, ν) of the third generation are considered. The limits are presented as a function of the leptoquark mass and the branching ratio into charged leptons for leptoquark of up-type ($LQ_3^{up} \rightarrow \tau\nu/b\tau$) and down-type ($LQ_3^d \rightarrow b\nu/t\tau$); many results are re-interpretation of previously published ATLAS searches. The collaboration finds that masses below 800 GeV are excluded for both LQ_3^u and LQ_3^d independently of the branching ratio, with masses below about 1 TeV being excluded for the limiting cases of branching ratios equal to zero or unity.

It is also possible to consider leptoquark states which couple only with the i -th generation quarks and the j -th generation leptons ($i \neq j$) without causing conflicts with severe indirect constraints. Such couplings have received renewed attention because they may provide an explanation to anomalies in rare $B - meson$ decays and the anomalous magnetic moment of the muon. See Ref. [37], [38] and [39] and references therein for collider search strategies and limits on the pair production cross sections of this class of leptoquark states. In this framework, a novel CMS result [40] presents a non-traditional search for pair production of LQs coupled to a top quark and a muon. As no deviation from the standard model prediction was observed, scalar LQs decaying exclusively into $top - \mu$ are excluded up to masses of 1420 GeV.

The magnetic-dipole-type and the electric-quadrupole-type interactions of a vector leptoquark are not determined even if we fix its gauge quantum numbers as listed in the Table 95.1 [41]. The production of vector leptoquarks depends in general on additional assumptions, where the leptoquark couplings and their pair production cross sections are enhanced relative to the scalar leptoquark contributions. The most stringent limits on vector LQ production are now from CMS [42] where previous searches for squarks and gluinos have been reinterpreted to constrain models of leptoquark production. LQ masses below 1530 GeV are excluded assuming the Yang-Mills case with coupling $\kappa = 1$, or 1115 GeV in the minimal coupling case

where $\kappa = 0$, placing the most stringent constraint to date from pair production of vector LQs.

The leptoquark pair-production cross sections in e^+e^- collisions depend on the leptoquark $SU(2) \times U(1)$ quantum numbers and Yukawa coupling with electron [43].

Searches for first generation leptoquark singly produced were performed by the HERA experiments. Since the leptoquark single-production cross section depends on its Yukawa coupling, the leptoquark mass limits from HERA are usually displayed in the mass-coupling plane. For leptoquark Yukawa coupling $\lambda = 0.1$, early ZEUS Collaboration bounds on the first-generation leptoquarks range from 248 to 290 GeV, depending on the leptoquark species [45]. The ZEUS Collaboration has recently released a new paper [46] where data corresponding to a luminosity of around 1 fb^{-1} have been used in the framework of $eeqq$ contact interactions (CI) to set limits on possible high-energy contributions beyond the Standard Model to electron-quark scattering. The analysis of the ep data has been based on simultaneous fits of parton distribution functions including contributions of Contact Interaction (CI) couplings to ep scattering. Several general CI models and scenarios with heavy leptoquarks were considered. As unambiguous deviations from the SM cannot be established, limits for CI compositeness scales and LQ mass scales were set that are in the TeV range. The H1 Collaboration has a comprehensive summary of searches for first generation leptoquarks using the full data sample collected in ep collisions at HERA (446 pb^{-1}). No evidence of production of leptoquarks was observed in final states with a large transverse momentum electron or large missing transverse momentum. For a coupling strength $\lambda = 0.3$, first generation leptoquarks with masses up to 800 GeV are excluded at 95% C.L. [48].

At the LHC, the CMS collaboration performed searches for single production of first and second generation leptoquarks [49], which is complementary to the HERA searches in the high λ region (for coupling strength $\lambda = 1.0$, first generation leptoquarks are excluded for masses up to 1.73 TeV and second generation leptoquark are excluded up to masses of 530 GeV). CMS also recently searched for third generation LQ decaying into τ and *bottom* in [50]. Assuming unit Yukawa coupling (λ), a third generation scalar leptoquark is excluded for masses below 740 GeV. Limits are also set on λ of the hypothesized leptoquark as a function of its mass. Above $\lambda = 1.4$, the results provide the best upper limit on the mass of a third-generation scalar leptoquark decaying to a τ lepton and a bottom quark.

Searches for LQ will continue with more LHC data, particularly in light of the renewed interest in this type of particle to explain violation of lepton flavor universality and other anomalies, which point to explanations laying outside the Standard Model.

References:

1. W. Buchmüller, R. Rückl, and D. Wyler, Phys. Lett. **B191**, 442 (1987).
2. K.S. Babu, C.F. Kolda, and J. March-Russell, Phys. Lett. **B408**, 261 (1997).
3. J.L. Hewett and T.G. Rizzo, Phys. Rev. **D58**, 055005 (1998).
4. J.C. Pati and A. Salam, Phys. Rev. **D10**, 275 (1974).
5. H. Georgi and S.L. Glashow, Phys. Rev. Lett. **32**, 438 (1974).
6. H. Georgi, AIP Conf. Proc. **23**, 575 (1975);
H. Fritzsch and P. Minkowski, Ann. Phys. **93**, 193 (1975).
7. For a review, see, E. Farhi and L. Susskind, Phys. Reports **74**, 277 (1981).
8. K. Lane and M. Ramana, Phys. Rev. **D44**, 2678 (1991).
9. See, for example, B. Schrepf and F. Schrepf, Phys. Lett. **153B**, 101 (1985).
10. R. Aaij *et al.* [LHCb Collab.], Phys. Rev. Lett. **113**, 151601 (2014);
R. Aaij *et al.* [LHCb Collab.], JHEP **08**, 055 (2017);
R. Aaij *et al.* [LHCb Collab.], Phys. Rev. Lett. **122**, 191801 (2019).
11. Y. Amhis *et al.*, [HFLAV Collab.], Eur. Phys. J. **C77**, 895 (2017), updated results and plots available at hf.lav.web.cern.ch/.
12. O. Shanker, Nucl. Phys. **B204**, 375, (1982).

13. U. Mahanta, Eur. Phys. J. **C21**, 171 (2001) [Phys. Lett. **B515**, 111 (2001)].
14. K. Cheung, Phys. Rev. **D64**, 033001 (2001).
15. S. Davidson, D.C. Bailey, and B.A. Campbell, Z. Phys. **C61**, 613 (1994).
16. M. Leurer, Phys. Rev. **D49**, 333 (1994); Phys. Rev. **D50**, 536 (1994).
17. M. Carpentier and S. Davidson, Eur. Phys. J. **C70**, 1071 (2010).
18. A. Falkowski, M. González-Alonso and K. Mimouni, JHEP **08**, 123 (2017).
19. S. Davidson and A. Saporta, Phys. Rev. **D99**, 015032 (2019).
20. M. Chala, J. Santiago and M. Spannowsky, JHEP **04**, 014 (2019).
21. T. Plehn *et al.*, Z. Phys. **C74**, 611 (1997); M. Kramer *et al.*, Phys. Rev. Lett. **79**, 341 (1997); and references therein.
22. J.L. Hewett and S. Pakvasa, Phys. Rev. **D37**, 3165 (1988); O.J.P. Eboli and A.V. Olinto, Phys. Rev. **D38**, 3461 (1988); A. Dobado, M.J. Herrero, and C. Muñoz, Phys. Lett. **207B**, 97 (1988); V.D. Barger *et al.*, Phys. Lett. **B220**, 464 (1989); M. De Montigny and L. Marleau, Phys. Rev. **D40**, 2869 (1989) [Erratum-*ibid.* **D56**, 3156 (1997)].
23. A. Belyaev *et al.*, JHEP **0509**, 005 (2005).
24. I. Doršner *et al.*, Phys. Reports **641**, 1 (2016).
25. D. Acosta *et al.* [CDF Collab.], Phys. Rev. **D72**, 051107 (2005).
26. V.M. Abazov *et al.* [DØCollab.], Phys. Lett. **B681**, 224 (2009).
27. A. Abulencia *et al.* [CDF Collab.], Phys. Rev. **D73**, 051102 (2006).
28. V.M. Abazov *et al.* [DØCollab.], Phys. Lett. **B671**, 224 (2009).
29. V. Abazov *et al.* [DØCollab.], Phys. Lett. **B693**, 95 (2010).
30. [CMS Collab.], Phys. Rev. **D99**, 052002 (2019).
31. [ATLAS Collab.], Eur. Phys. J. **C79**, 733 (2019).
32. [CMS Collab.], Phys. Rev. **D99**, 032014 (2019).
33. [CMS Collab.], Eur. Phys. J. **C78**, 707 (2018).
34. [CMS Collab.], JHEP **03**, 170 (2019).
35. [CMS Collab.], JHEP **1212**, 055 (2012).
36. [ATLAS Collab.], JHEP **06**, 144 (2019).
37. B. Diaz, M. Schmaltz, and Y. M. Zhong, JHEP **10**, 097 (2017).
38. M. Schmaltz, and Y. M. Zhong, JHEP **01**, 132 (2019).
39. D. Muller, EPJ Web Conf. **179**, 01015 (2018)..
40. [CMS Collab.] Phys. Rev. Lett. **121**, 241802 (2018).
41. J. Blümlein, E. Boos, and A. Kryukov, Z. Phys. **C76**, 137 (1997).
42. [CMS Collab.] Phys. Rev. **D98**, 032005 (2018).
43. J. Blümlein and R. Ruckl, Phys. Lett. **B304**, 337 (1993).
44. G. Abbiendi *et al.* [OPAL Collab.], Eur. Phys. J. **C31**, 281 (2003).
45. S. Chekanov *et al.* [ZEUS Collab.], Phys. Rev. **D68**, 052004 (2003).
46. H. Abramowicz *et al.* [ZEUS Collab.], Phys. Rev. **D99**, 092006 (2019).
47. A. Aktas *et al.* [H1 Collab.], Phys. Lett. **B629**, 9 (2005).
48. F.D. Aaron *et al.* [H1 Collab.], Phys. Lett. **B704**, 388 (2011).
49. V. Khachatryan *et al.* [CMS Collab.], Phys. Rev. **D93**, 032005 (2016).
50. [CMS Collab.] JHEP **07**, 115 (2018).

96. Magnetic Monopoles

Revised August 2019 by D. Milstead (Stockholm U.) and E.J. Weinberg (Columbia U.).

96.1 Theory of magnetic monopoles

The symmetry between electric and magnetic fields in the source-free Maxwell's equations naturally suggests that electric charges might have magnetic counterparts, known as magnetic monopoles. Although the greatest interest has been in the super-massive monopoles that are a firm prediction of all grand unified theories, one cannot exclude the possibility of lighter monopoles.

In either case, the magnetic charge is constrained by a quantization condition first found by Dirac [1]. Consider a monopole with magnetic charge Q_M and a Coulomb magnetic field

$$\mathbf{B} = \frac{Q_M}{4\pi} \frac{\hat{\mathbf{r}}}{r^2}. \quad (96.1)$$

Any vector potential \mathbf{A} whose curl is equal to \mathbf{B} must be singular along some line running from the origin to spatial infinity. This Dirac string singularity could potentially be detected through the extra phase that the wavefunction of a particle with electric charge Q_E would acquire if it moved along a loop encircling the string. For the string to be unobservable, this phase must be a multiple of 2π . Requiring that this be the case for any pair of electric and magnetic charges gives the condition that all charges be integer multiples of minimum charges Q_E^{\min} and Q_M^{\min} obeying

$$Q_E^{\min} Q_M^{\min} = 2\pi. \quad (96.2)$$

(For monopoles which also carry an electric charge, called dyons [2], the quantization conditions on their electric charges can be modified. However, the constraints on magnetic charges, as well as those on all purely electric particles, will be unchanged.)

Another way to understand this result is to note that the conserved orbital angular momentum of a point electric charge moving in the field of a magnetic monopole has an additional component, with

$$\mathbf{L} = m\mathbf{r} \times \mathbf{v} - 4\pi Q_E Q_M \hat{\mathbf{r}} \quad (96.3)$$

Requiring the radial component of \mathbf{L} to be quantized in half-integer units yields Eq. 96.1.

If there are unbroken gauge symmetries in addition to the U(1) of electromagnetism, the above analysis must be modified [3] [4]. For example, a monopole could have both a U(1) magnetic charge and a color magnetic charge. The latter could combine with the color charge of a quark to give an additional contribution to the phase factor associated with a loop around the Dirac string, so that the U(1) charge could be the Dirac charge $Q_M^D \equiv 2\pi/e$, the result that would be obtained by substituting the electron charge into Eq. (96.1). On the other hand, for monopoles without color-magnetic charge, one would simply insert the quark electric charges into Eq. 96.1 and conclude that Q_M must be a multiple of $6\pi/e$.

The prediction of GUT monopoles arises from the work of 't Hooft [5] and Polyakov [6], who showed that certain spontaneously broken gauge theories have nonsingular classical solutions that lead to magnetic monopoles in the quantum theory. The simplest example occurs in a theory where the vacuum expectation value of a triplet Higgs field \mathbf{CE} breaks an SU(2) gauge symmetry down to the U(1) of electromagnetism and gives a mass M_V to two of the gauge bosons. In order to have finite energy, \mathbf{CE} must approach a vacuum value at infinity. However, there is a continuous family of possible vacua, since the scalar field potential determines only the magnitude v of $\langle \mathbf{CE} \rangle$, but not its orientation in the internal SU(2) space. In the monopole solution, the direction of \mathbf{CE} in internal space is correlated with the position in physical space; *i.e.*, $\phi^a \sim v\hat{r}^a$. The stability of the solution follows from the fact that this twisting Higgs field cannot be smoothly deformed to a spatially uniform vacuum configuration. Reducing the energetic cost of the spatial variation of \mathbf{CE} requires a nonzero gauge potential, which turns out to yield the magnetic field corresponding to a charge $Q_M = 4\pi/e$. Numerical solution of the classical field equations shows that the mass of this monopole is

$$M_{\text{mon}} \sim \frac{4\pi M_V}{e^2}. \quad (96.4)$$

The essential ingredient here was the fact that the Higgs fields at spatial infinity could be arranged in a topologically nontrivial configuration. A discussion of the general conditions under which this is possible is beyond the scope of this review, so we restrict ourselves to the two phenomenologically most important cases.

The first is the standard electroweak theory, with SU(2) \times U(1) broken to U(1). There are no topologically nontrivial configurations of the Higgs field, and hence no topologically stable monopole solutions.

The second is when any simple Lie group is broken to a subgroup with a U(1) factor, a case that includes all grand unified theories. The monopole mass is determined by the mass scale of the symmetry breaking that allows nontrivial topology. For example, an SU(5) model with

$$\text{SU}(5) \xrightarrow{M_X} \text{SU}(3) \times \text{SU}(2) \times \text{U}(1) \xrightarrow{M_W} \text{SU}(3) \times \text{U}(1) \quad (96.5)$$

has a monopole [7] with $Q_M = 2\pi/e$ and mass

$$M_{\text{mon}} \sim \frac{4\pi M_X}{g^2}, \quad (96.6)$$

where g is the SU(5) gauge coupling. For a unification scale of 10^{16} GeV, these monopoles would have a mass $M_{\text{mon}} \sim 10^{17} - 10^{18}$ GeV.

In theories with several stages of symmetry breaking, monopoles of different mass scales can arise. In an SO(10) theory with

$$\text{SO}(10) \xrightarrow{M_1} \text{SU}(4) \times \text{SU}(2) \times \text{SU}(2) \xrightarrow{M_2} \text{SU}(3) \times \text{SU}(2) \times \text{U}(1) \quad (96.7)$$

there is monopole with $Q_M = 2\pi/e$ and mass $\sim 4\pi M_1/g^2$ and a much lighter monopole with $Q_M = 4\pi/e$ and mass $\sim 4\pi M_2/g^2$ [8].

The central core of a GUT monopole contains the fields of the superheavy gauge bosons that mediate baryon number violation, so one might expect that baryon number conservation could be violated in baryon-monopole scattering. The surprising feature, pointed out by Callan [9] and Rubakov [10], is that these processes are not suppressed by powers of the gauge boson mass. Instead, the cross-sections for catalysis processes such as $p + \text{monopole} \rightarrow e^+ + \pi^0 + \text{monopole}$ are essentially geometric; *i.e.*, $\sigma_{\Delta B} \beta \sim 10^{-27} \text{ cm}^2$, where $\beta = v/c$. Note, however, that this catalysis is model-dependent and is not even a universal property of all GUT monopoles.

96.2 Production and Annihilation

GUT monopoles are far too massive to be produced in any foreseeable accelerator. However, they could have been produced in the early universe as topological defects arising via the Kibble mechanism [11] in a symmetry-breaking phase transition. Estimates of the initial monopole abundance, and of the degree to which it can be reduced by monopole-antimonopole annihilation, predict a present-day monopole abundance that exceeds by many orders of magnitude the astrophysical and experimental bounds described below [12]. Cosmological inflation and other proposed solutions to this primordial monopole problem generically lead to present-day abundances exponentially smaller than could be plausibly detected, although potentially observable abundances can be obtained in scenarios with carefully tuned parameters.

If monopoles light enough to be produced at colliders exist, one would expect that these could be produced by analogs of the electromagnetic processes that produce pairs of electrically charged particles. Because of the large size of the magnetic charge, this is a strong coupling problem for which perturbation theory cannot be trusted. Indeed, the problem of obtaining reliable quantitative estimates of the production cross-sections remains an open one, on which there is no clear consensus.

96.3 Astrophysical and Cosmological Bounds

If there were no galactic magnetic field, one would expect monopoles in the galaxy to have typical velocities of the order of $10^{-3}c$, comparable to the virial velocity in the galaxy (relevant if the monopoles cluster with the galaxy) and the peculiar velocity of the galaxy with respect to the CMB rest frame (relevant

if the monopoles are not bound to the galaxy). This situation is modified by the existence of a galactic magnetic field $B \sim 3\mu\text{G}$. A monopole with the Dirac charge and mass M would be accelerated by this field to a velocity

$$v_{\text{mag}} \sim \begin{cases} c, & M \lesssim 10^{11} \text{ GeV}, \\ 10^{-3}c \left(\frac{10^{17} \text{ GeV}}{M} \right)^{1/2}, & M \gtrsim 10^{11} \text{ GeV}. \end{cases} \quad (96.8)$$

Accelerating these monopoles drains energy from the magnetic field. Parker [13] obtained an upper bound on the flux of monopoles in the galaxy by requiring that the rate of this energy loss be small compared to the time scale on which the galactic field can be regenerated. With reasonable choices for the astrophysical parameters (see Ref. [14] for details), this Parker bound is

$$F < \begin{cases} 10^{-15} \text{ cm}^{-2} \text{ sr}^{-1} \text{ sec}^{-1}, & M \lesssim 10^{17} \text{ GeV}, \\ 10^{-15} \left(\frac{M}{10^{17} \text{ GeV}} \right) \text{ cm}^{-2} \text{ sr}^{-1} \text{ sec}^{-1}, & M \gtrsim 10^{17} \text{ GeV}. \end{cases} \quad (96.9)$$

Applying similar arguments to an earlier seed field that was the progenitor of the current galactic field leads to a tighter bound [15],

$$F < \left[\frac{M}{10^{17} \text{ GeV}} + (3 \times 10^{-6}) \right] 10^{-16} \text{ cm}^{-2} \text{ sr}^{-1} \text{ sec}^{-1}. \quad (96.10)$$

Considering magnetic fields in galactic clusters gives a bound [16] which, although less secure, is about three orders of magnitude lower than the Parker bound.

A flux bound can also be inferred from the total mass of monopoles in the universe. If the monopole mass density is a fraction Ω_M of the critical density, and the monopoles were uniformly distributed throughout the universe, there would be a monopole flux

$$F_{\text{uniform}} = 1.3 \times 10^{-16} \Omega_M \left(\frac{10^{17} \text{ GeV}}{M} \right) \left(\frac{v}{10^{-3}c} \right) \text{ cm}^{-2} \text{ sr}^{-1} \text{ sec}^{-1}. \quad (96.11)$$

If we assume that $\Omega_M \sim 0.1$, this gives a stronger constraint than the Parker bound for $M \sim 10^{15}$ GeV. However, monopoles with masses $\sim 10^{17}$ GeV are not ejected by the galactic field and can be gravitationally bound to the galaxy. In this case their flux within the galaxy is increased by about five orders of magnitude for a given value of Ω_M , and the mass density bound only becomes stronger than the Parker bound for $M \sim 10^{18}$ GeV.

A much more stringent flux bound applies to GUT monopoles that catalyze baryon number violation. The essential idea is that compact astrophysical objects would capture monopoles at a rate proportional to the galactic flux. These monopoles would then catalyze proton decay, with the energy released in the decay leading to an observable increase in the luminosity of the object. A variety of bounds, based on neutron stars [17–21], white dwarfs [22], and Jovian planets [23] have been obtained. These depend in the obvious manner on the catalysis cross section, but also on the details of the astrophysical scenarios; *e.g.*, on how much the accumulated density is reduced by monopole-antimonopole annihilation, and on whether monopoles accumulated in the progenitor star survive its collapse to a white dwarf or neutron star. The bounds obtained in this manner lie in the range

$$F \left(\frac{\sigma_{\Delta B \beta}}{10^{-27} \text{ cm}^2} \right) \sim (10^{-18} - 10^{-29}) \text{ cm}^{-2} \text{ sr}^{-1} \text{ sec}^{-1}. \quad (96.12)$$

It is important to remember that not all GUT monopoles catalyze baryon number nonconservation. In particular, the intermediate mass monopoles that arise in some GUTs at later stages of symmetry-breaking are examples of theoretically motivated monopoles that are exempt from the bound of the above equation.

96.4 Searches for Magnetic Monopoles

To date there have been no confirmed observations of exotic particles possessing magnetic charge. Precision measurements of the properties of known particles have led to tight limits on the values of magnetic charge they may possess. Using the induction method (see below), the electron’s magnetic charge has been found to be $Q_e^m < 10^{-24} Q_M^D$ [24] (where Q_M^D is the Dirac charge). Furthermore, measurements of the anomalous magnetic moment of the muon have been used to place a model dependent lower limit of 120 GeV on the monopole mass¹ [25]. Nevertheless, guided mainly by Dirac’s argument and the predicted existence of monopoles from spontaneous symmetry breaking mechanisms, searches have been routinely made for monopoles produced at accelerators, in cosmic rays, and bound in matter [26]. Although the resultant limits from such searches are usually made under the assumption of a particle possessing only magnetic charge, most of the searches are also sensitive to dyons.

96.5 Search Techniques

Search strategies are determined by the expected interactions of monopoles as they pass through matter. These would give rise to a number of striking characteristic signatures. Since a complete description of monopole search techniques falls outside of the scope of this minireview, only the most common methods are described below. More comprehensive descriptions of search techniques can be found in Refs. [27] [28].

The induction method exploits the long-ranged electromagnetic interaction of the monopole with the quantum state of a superconducting ring which would lead to a monopole which passes through such a ring inducing a permanent current. The induction technique typically uses Superconducting Quantum Interference Devices (SQUID) technology for detection and is employed for searches for monopoles in cosmic rays and matter. Another approach is to exploit the electromagnetic energy loss of monopoles. Monopoles with Dirac charge would typically lose energy at a rate which is several thousand times larger than that expected from particles possessing the elementary electric charge. Consequently, scintillators, gas chambers and nuclear track detectors (NTDs) have been used in cosmic ray and collider experiments. A further approach, which has been used at colliders, is to search for particles describing a non-helical path in a uniform magnetic field.

96.5.1 Searches for Monopoles Bound in Matter

Monopoles have been sought in a range of bulk materials which it is assumed would have absorbed incident cosmic ray monopoles over a long exposure time of order million years. Materials which have been studied include moon rock, meteorites, manganese modules, and sea water [29, 30]. A stringent upper limit on the monopoles per nucleon ratio of $\sim 10^{-29}$ has been obtained [30].

96.5.2 Searches in Cosmic Rays

Direct searches for monopoles in cosmic rays refer to those experiments in which the passage of the monopole is measured by an active detector. Searches made assuming a catalysis processes in which GUT monopoles could induce nucleon decay are discussed in the next section. To interpret the results of the non-catalysis searches, the cross section for the catalysis process is typically either set to zero [31] or assigned a modest value (1mb) [32].

Although early cosmic ray searches using the induction technique [33] and NTDs [34] observed monopole candidates, none of these apparent observations have been confirmed. Recent experiments have typically employed large scale detectors. The MACRO experiment at the Gran Sasso underground laboratory comprised three different types of detector: liquid scintillator, limited stream tubes, and NTDs, which provided a total acceptance of $\sim 10000\text{m}^2$ for an isotropic flux. As shown in Fig. 96.1, this experiment has so far provided the most extensive β -dependent flux limits for GUT monopoles with Dirac charge [32]. Also shown are limits from an experiment at the OHYA mine in Japan [31], which used a 2000m^2 array of NTDs.

In Fig. 96.1, upper flux limits are also shown as a function of mass for monopole speed $\beta > 0.05$. In addition to MACRO

¹Where no ambiguity is likely to arise, a reference to a monopole implies a particle possessing Dirac charge.

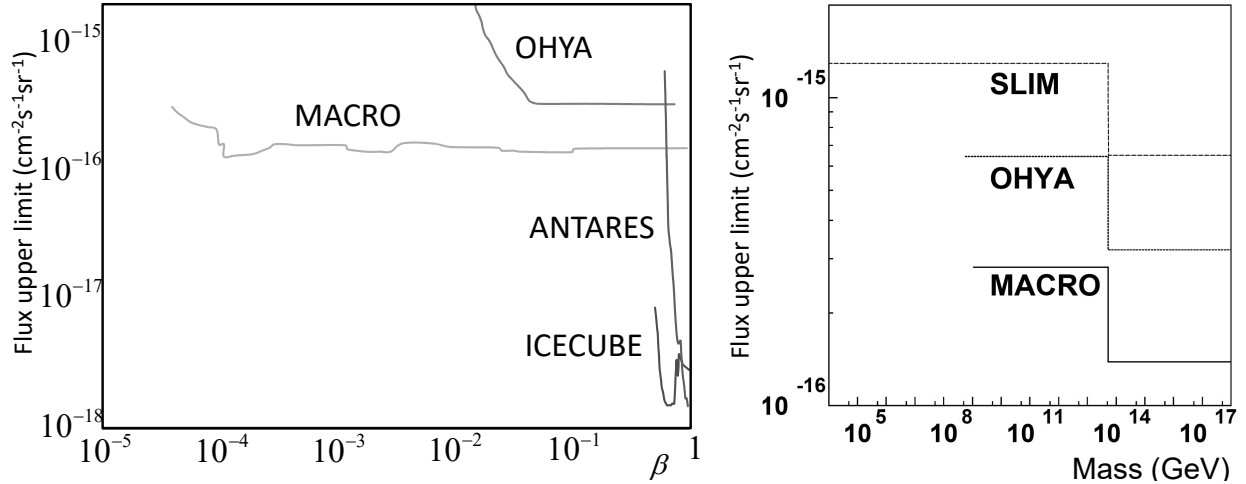


Figure 96.1: Upper flux limits for (left) GUT monopoles as a function of β (right) Monopoles as a function of mass for $\beta > 0.05$.

and OYHA flux limits, results from the SLIM [35] high-altitude experiment are shown. The SLIM experiment provided a good sensitivity to intermediate mass monopoles ($10^5 \lesssim M \lesssim 10^{12}$ GeV). In addition to the results shown in Fig. 96.1, limits as low as $\sim 1.5 \times 10^{-18} \text{ cm}^{-2} \text{ s}^{-1} \text{ sr}^{-1}$ were obtained for monopoles with $\beta > 0.51$ and $\beta > 0.6$ by the IceCube [36] and Antares [37] experiments, respectively. Stringent constraints on the flux of ultra-relativistic monopoles have been obtained at the Pierre Auger Observatory [38] which was sensitive to monopoles with γ values ranging from 10^9 to 10^{12} , leading to flux limits in the range $10^{-15} - 2.5 \times 10^{-21} \text{ cm}^{-2} \text{ s}^{-1} \text{ sr}^{-1}$. The RICE [39] and ANITA-II experiments [40] at the South Pole have also sought ultra-relativistic monopoles with γ values of $10^7 \lesssim \gamma \lesssim 10^{12}$ and $10^9 \lesssim \gamma \lesssim 10^{13}$, respectively, and which produced flux limits as low as $2.5 \times 10^{-21} \text{ cm}^{-2} \text{ s}^{-1} \text{ sr}^{-1}$.

96.5.3 Searches via the Catalysis of Nucleon-Decay

Searches have been performed for evidence of the catalysed decay of a nucleon by a monopole, as predicted by the Callan-Rubakov mechanism. The searches are thus sensitive to the assumed value of the catalysis decay cross section. Searches have been made with the Soudan [41] and Macro [42] experiments, using tracking detectors. Searches at IMB [43], the underwater Lake Baikal experiment [44] and the The IceCube experiment [45] which exploit the Cerenkov effect have also been made. The resulting β -dependent flux limits from these experiments typically vary between $\sim 10^{-18}$ and $\sim 10^{-14} \text{ cm}^{-2} \text{ sr}^{-1} \text{ s}^{-1}$. A recent search for low energy neutrinos (assumed to be produced from induced proton decay in the sun) was made at Super-Kamiokande [46]. A model- and β -dependent of limit of $6.3 \times 10^{-24} (\frac{\beta}{10^{-3}})^2 \text{ cm}^{-2} \text{ sr}^{-1} \text{ s}^{-1}$ was obtained.

96.5.4 Searches at Colliders

Searches have been performed at hadron-hadron, electron-positron and lepton-hadron experiments. Collider searches can be broadly classed as being direct or indirect. In a direct search, evidence of the passage of a monopole through material, such as a charged particle track, is sought. In indirect searches, virtual monopole processes are assumed to influence the production rates of certain final states.

96.5.4.1 Direct Searches at Colliders

Collider experiments typically express their results in terms of upper limits on a production cross section and/or monopole mass. To calculate these limits, ansatzes are used to model the kinematics of monopole-antimonopole pair production processes since perturbative field theory cannot be used to calculate the rate and kinematic properties of produced monopoles. Limits therefore suffer from a degree of model-dependence, implying that a comparison between the results of different experiments can be problematic, in particular when this concerns excluded mass re-

gions. A conservative approach with as little model-dependence as possible is thus to present representative values of the upper cross-section limits as a function of one half the centre-of-mass energy of the collisions, as shown in Fig. 96.2 for recent results from high energy colliders.

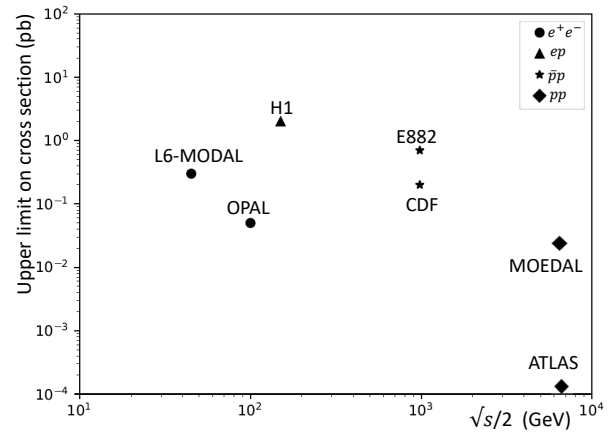


Figure 96.2: Upper limits on the production cross sections of monopoles from various collider-based experiments.

Searches for monopoles produced at the highest available energies in hadron-hadron collisions were made in pp collisions at the LHC by the ATLAS [47, 48] and MoEDAL [49, 50] experiments. The experiments looked for highly ionising particles leaving characteristic energy deposition profiles and stopped monopoles with the induction method, respectively. The charge-dependent mass limits extend up to around 4 TeV. The ATLAS work considers monopoles with $0.5Q_M^D$ and $2Q_M^D$ while MoEDAL quotes limits for monopoles with charges from Q_M^D to $5Q_M^D$. MoEDAL considered monopole-pair production via photon fusion along with, as is commonly used in hadron-hadron collisions, Drell-Yan processes [51]. Tevatron searches have also been carried out by the CDF [52] and E882 [53] experiments. The CDF experiment used a dedicated time-of-flight system whereas the E882 experiment employed the induction technique to search for stopped monopoles in discarded detector material which had been part of the CDF and D0 detectors using periods of luminosity. Earlier searches at the Tevatron, such as [54], used NTDs and were based on comparatively modest amounts of integrated luminosity. Lower energy hadron-hadron experiments have employed a variety of search techniques including plastic track detectors [55] and searches for trapped monopoles [56].

The only LEP-2 search was made by OPAL [57] which quoted

cross section limits for the production of monopoles possessing masses up to around 103 GeV. At LEP-1, searches were made with NTDs deployed around an interaction region. This allowed a range of charges to be sought for masses up to ~ 45 GeV. The L6-MODAL experiment [58] gave limits for monopoles with charges in the range $0.9Q_M^D$ and $3.6Q_M^D$, whilst an earlier search by the MODAL experiment was sensitive to monopoles with charges as low as $0.1Q_M^D$ [59]. The deployment of NTDs around the beam interaction point was also used at earlier e^+e^- colliders such as KEK [60] and PETRA [61]. Searches at e^+e^- facilities have also been made for particles following non-helical trajectories [62] [63].

There has so far been one search for monopole production in lepton-hadron scattering. Using the induction method, monopoles were sought which could have stopped in the aluminium beampipe which had been used by the H1 experiment at HERA [64]. Cross section limits were set for monopoles with charges in the range $Q_M^D - 6Q_M^D$ for masses up to around 140 GeV.

96.5.4.2 Indirect Searches at Colliders

It has been proposed that virtual monopoles can mediate processes which give rise to multi-photon final-states [65] [66]. Photon-based searches were made by the D0 [67] and L3 [68] experiments. The D0 work led to spin-dependent lower mass limits of between 610 and 1580 GeV, while L3 reported a lower mass limit of 510 GeV. However, it should be stressed that uncertainties on the theoretical calculations which were used to derive these limits are difficult to estimate.

References

- [1] P. A. M. Dirac, Proc. Roy. Soc. Lond. **A133**, 821, 60 (1931).
- [2] J. S. Schwinger, Science **165**, 757 (1969).
- [3] F. Englert and P. Windey, Phys. Rev. **D14**, 2728 (1976).
- [4] P. Goddard, J. Nuyts and D. I. Olive, Nucl. Phys. **B125**, 1 (1977).
- [5] G. 't Hooft, Nucl. Phys. **B79**, 276 (1974).
- [6] A. M. Polyakov, JETP Lett. **20**, 194 (1974).
- [7] C. P. Dokos and T. N. Tomaras, Phys. Rev. **D21**, 2940 (1980).
- [8] G. Lazarides and Q. Shafi, Phys. Lett. **94B**, 149 (1980).
- [9] C. G. Callan, Jr., Phys. Rev. **D26**, 2058 (1982).
- [10] V. A. Rubakov, Nucl. Phys. **B203**, 311 (1982).
- [11] T. W. B. Kibble, J. Phys. **A9**, 1387 (1976).
- [12] J. Preskill, Phys. Rev. Lett. **43**, 1365 (1979).
- [13] E. N. Parker, Astrophys. J. **160**, 383 (1970).
- [14] M. S. Turner, E. N. Parker and T. J. Bogdan, Phys. Rev. **D26**, 1296 (1982).
- [15] F. C. Adams *et al.*, Phys. Rev. Lett. **70**, 2511 (1993).
- [16] Y. Rephaeli and M. S. Turner, Phys. Lett. **121B**, 115 (1983).
- [17] E. W. Kolb, S. A. Colgate and J. A. Harvey, Phys. Rev. Lett. **49**, 1373 (1982).
- [18] S. Dimopoulos, J. Preskill and F. Wilczek, Phys. Lett. **119B**, 320 (1982).
- [19] K. Freese, M. S. Turner and D. N. Schramm, Phys. Rev. Lett. **51**, 1625 (1983).
- [20] E. W. Kolb and M. S. Turner, Astrophys. J. **286**, 702 (1984).
- [21] J. A. Harvey, Nucl. Phys. **B236**, 255 (1984).
- [22] K. Freese and E. Krasteva, Phys. Rev. **D59**, 063007 (1999), [arXiv:astro-ph/9804148].
- [23] J. Arafune, M. Fukugita and S. Yanagita, Phys. Rev. **D32**, 2586 (1985).
- [24] L. L. Vant-Hull, Phys. Rev. **173**, 1412 (1968).
- [25] S. Graf, A. Schaefer and W. Greiner, Phys. Lett. **B262**, 463 (1991).
- [26] Review of Particle Physics 2020 (*this paper*), listing on *Searches for Magnetic Monopoles*.
- [27] L. Patrizii and M. Spurio, Ann. Rev. Nucl. Part. Sci. **65**, 279 (2015), [arXiv:1510.07125].
- [28] M. Fairbairn *et al.*, Phys. Rept. **438**, 1 (2007), [hep-ph/0611040].
- [29] J. M. Kovalik and J. L. Kirschvink, Phys. Rev. **A33**, 1183 (1986).
- [30] H. Jeon and M. J. Longo, Phys. Rev. Lett. **75**, 1443 (1995), [Erratum: Phys. Rev. Lett. 76,159(1996)], [hep-ex/9508003].
- [31] S. Orito *et al.*, Phys. Rev. Lett. **66**, 1951 (1991).
- [32] M. Ambrosio *et al.* (MACRO), Eur. Phys. J. **C25**, 511 (2002), [hep-ex/0207020].
- [33] B. Cabrera, Phys. Rev. Lett. **48**, 1378 (1982).
- [34] P. B. Price *et al.*, Phys. Rev. Lett. **35**, 487 (1975).
- [35] S. Balestra *et al.*, Eur. Phys. J. **C55**, 57 (2008), [arXiv:0801.4913].
- [36] M. G. Aartsen *et al.* (IceCube), Eur. Phys. J. **C76**, 3, 133 (2016), [arXiv:1511.01350].
- [37] A. Albert *et al.* (ANTARES), JHEP **07**, 054 (2017), [arXiv:1703.00424].
- [38] A. Aab *et al.* (Pierre Auger), Phys. Rev. **D94**, 8, 082002 (2016), [arXiv:1609.04451].
- [39] D. P. Hogan *et al.*, Phys. Rev. **D78**, 075031 (2008), [arXiv:0806.2129].
- [40] M. Detrixhe *et al.* (ANITA-II), Phys. Rev. **D83**, 023513 (2011), [arXiv:1008.1282].
- [41] J.E. Bartelt *et al.*, Phys. Rev. **D36**, 1990 (1987) [Erratum-ibid. **D40**, 1701 (1989)].
- [42] M. Ambrosio *et al.* (MACRO), Eur. Phys. J. **C26**, 163 (2002), [hep-ex/0207024].
- [43] R. Becker-Szendy *et al.*, Phys. Rev. **D49**, 2169 (1994).
- [44] V. A. Balkanov *et al.* (Baikal), Prog. Part. Nucl. Phys. **40**, 391 (1998), [arXiv:astro-ph/9801044].
- [45] M. G. Aartsen *et al.* (IceCube), Eur. Phys. J. **C74**, 7, 2938 (2014), [Erratum: Eur. Phys. J. C79,no.2,124(2019)], [arXiv:1402.3460].
- [46] K. Ueno *et al.* (Super-Kamiokande), Astropart. Phys. **36**, 131 (2012), [arXiv:1203.0940].
- [47] G. Aad *et al.* (ATLAS), Phys. Rev. **D93**, 5, 052009 (2016), [arXiv:1509.08059].
- [48] G. Aad *et al.* (ATLAS) (2019), [arXiv:1905.10130].
- [49] B. Acharya *et al.* (MoEDAL), Phys. Rev. Lett. **118**, 6, 061801 (2017), [arXiv:1611.06817].
- [50] B. Acharya *et al.* (MoEDAL), Phys. Rev. Lett. **123**, 2, 021802 (2019), [arXiv:1903.08491].
- [51] S. Baines *et al.*, Eur. Phys. J. **C78**, 11, 966 (2018), [Erratum: Eur. Phys. J. C79,no.2,166(2019)], [arXiv:1808.08942].
- [52] A. Abulencia *et al.* (CDF), Phys. Rev. Lett. **96**, 201801 (2006), [hep-ex/0509015].
- [53] G. R. Kalbfleisch *et al.*, Phys. Rev. **D69**, 052002 (2004), [hep-ex/0306045].
- [54] P. B. Price, G.-X. Ren and K. Kinoshita, Phys. Rev. Lett. **59**, 2523 (1987).
- [55] B. Aubert *et al.*, Phys. Lett. **120B**, 465 (1983).
- [56] R. A. Carrigan, F. A. Nezrick and B. P. Strauss, Phys. Rev. **D8**, 3717 (1973).
- [57] G. Abbiendi *et al.* (OPAL), Phys. Lett. **B663**, 37 (2008), [arXiv:0707.0404].
- [58] J. L. Pinfold *et al.*, Phys. Lett. **B316**, 407 (1993).
- [59] K. Kinoshita *et al.*, Phys. Rev. **D46**, R881 (1992).
- [60] K. Kinoshita *et al.*, Phys. Lett. **B228**, 543 (1989).
- [61] P. Musset, M. Price and E. Lohrmann, Phys. Lett. **128B**, 333 (1983).
- [62] T. Gentile *et al.* (CLEO), Phys. Rev. **D35**, 1081 (1987).
- [63] W. Braunschweig *et al.* (TASSO), Z. Phys. **C38**, 543 (1988).

-
- [64] A. Aktas *et al.* (H1), *Eur. Phys. J.* **C41**, 133 (2005), [hep-ex/0501039].
- [65] A. De Rujula, *Nucl. Phys.* **B435**, 257 (1995), [hep-th/9405191].
- [66] I. F. Ginzburg and A. Schiller, *Phys. Rev.* **D60**, 075016 (1999), [hep-ph/9903314].
- [67] B. Abbott *et al.* (D0), *Phys. Rev. Lett.* **81**, 524 (1998), [hep-ex/9803023].
- [68] M. Acciarri *et al.* (L3), *Phys. Lett.* **B345**, 609 (1995).



VOLUME II: TABLE OF CONTENTS

PARTICLE LISTINGS*

Illustrative key and abbreviations	999
Gauge and Higgs bosons	
(γ , gluon, graviton, W , Z , Higgs, Axions)	1013
Leptons	
(e , μ , τ , Heavy-charged lepton searches, Neutrino properties, Number of neutrino types Double- β decay, Neutrino mixing, Heavy-neutral lepton searches)	1101
Quarks	
(u , d , s , c , b , t , b' , t' (4^{th} gen.), Free quarks)	1173
Mesons	
Light unflavored (π , ρ , a , b) (η , ω , f , ϕ , h)	1209
Other light unflavored	1332
Strange (K , K^*)	1337
Charmed (D , D^*)	1391
Charmed, strange (D_s , D_s^* , D_{sJ})	1448
Bottom (B , V_{cb}/V_{ub} , B^* , B_J^*)	1465
Bottom, strange (B_s , B_s^* , B_{sJ}^*)	1640
Bottom, charmed (B_c)	1664
$c\bar{c}$ (η_c , $J/\psi(1S)$, χ_c , h_c , ψ)	1668
$b\bar{b}$ (η_b , Υ , χ_b , h_b)	1782
Baryons	
N	1825
Δ	1878
Λ	1902
Σ	1927
Ξ	1959
Ω	1971
Charmed (Λ_c , Σ_c , Ξ_c , Ω_c)	1974
Doubly charmed (Ξ_{cc})	1996
Bottom (Λ_b , Σ_b , Ξ_b , Ω_b , b -baryon admixture)	1997
Exotic baryons (P_c pentaquarks)	2014
Searches not in Other Sections	
Magnetic monopole searches	2017
Supersymmetric particle searches	2019
Technicolor	2062
Searches for quark and lepton compositeness	2063
Extra dimensions	2067
WIMP and dark matter searches	2073
Other particle searches	2085

*The divider sheets give more detailed indices for each main section of the Particle Listings.

INTRODUCTION TO THE PARTICLE LISTINGS

Illustrative key	999
Abbreviations	1000

Illustrative Key to the Particle Listings

Name of particle. "Old" name used before 1986 renaming scheme also given if different. See the section "Naming Scheme for Hadrons" for details.

$a_0(1200)$

$$I^G(J^{PC}) = 1^-(0^{++})$$

Particle quantum numbers (where known).

OMITTED FROM SUMMARY TABLE
Evidence not compelling, may be a kinematic effect.

Indicates particle omitted from Particle Physics Summary Table, implying particle's existence is not confirmed.

Quantity tabulated below.

$a_0(1200)$ MASS

Top line gives our best value (and error) of quantity tabulated here, based on weighted average of measurements used. Could also be from fit, best limit, estimate, or other evaluation. See next page for details.

VALUE (MeV)	EVTS	DOCUMENT ID	TECN	CHG	COMMENT
1206 ± 7 OUR AVERAGE					
1210 ± 8 ± 9	3000	FENNER 87	MMS	-	3.5 $\pi^- p$
1198 ± 10		PIERCE 83	ASPK	+	2.1 $K^- p$
1216 ± 11 ± 9	1500	MERRILL 81	HBC	0	3.2 $K^- p$
• • • We do not use the following data for averages, fits, limits, etc. • • •					
1192 ± 16		LYNCH 81	HBC	±	2.7 $\pi^- p$
¹ Systematic error was added quadratically by us in our 1986 edition.					

General comments on particle.

"Document id" for this result; full reference given below.

Measurement technique. (See abbreviations on next page.)

Footnote number linking measurement to text of footnote.

$a_0(1200)$ WIDTH

Number of events above background. Measured value used in averages, fits, limits, etc.

VALUE (MeV)	EVTS	DOCUMENT ID	TECN	CHG	COMMENT
41 ± 11 OUR AVERAGE					Error includes scale factor of 1.8. See the ideogram below.
50 ± 8		PIERCE 83	ASPK	+	2.1 $K^- p$
70 +30 -20	200	LYNCH 81	HBC	±	2.7 $\pi^- p$
25 ± 5 ± 7		MERRILL 81	HBC	0	3.2 $K^- p$
• • • We do not use the following data for averages, fits, limits, etc. • • •					
<60		FENNER 87	MMS	±	3.5 $\pi^- p$

Scale factor > 1 indicates possibly inconsistent data.

Reaction producing particle, or general comments.

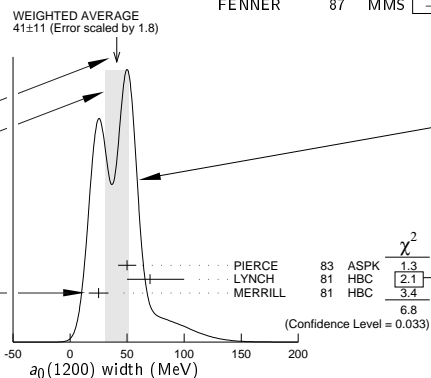
"Change bar" indicates result added or changed since previous edition.

Error in measured value (often statistical only; followed by systematic if separately known; the two are combined in quadrature for averaging and fitting.)

Measured value not used in averages, fits, limits, etc. See the Introductory Text for explanations.

Arrow points to weighted average.

Shaded pattern extends ±1σ (scaled by "scale factor" S) from weighted average.



Charge(s) of particle(s) detected. Ideogram to display possibly inconsistent data. Curve is sum of Gaussians, one for each experiment (area of Gaussian = 1/error; width of Gaussian = ±error). See Introductory Text for discussion.

Value and error for each experiment.

Contribution of experiment to χ^2 (if no entry present, experiment not used in calculating χ^2 or scale factor because of very large error).

$a_0(1200)$ DECAY MODES

Mode	Fraction (Γ_i/Γ)	Scale factor/ Confidence level
Γ_1 3π	(65.2 ± 1.3) %	S=1.7
Γ_2 $K\bar{K}$	(34.8 ± 1.3) %	S=1.7
Γ_3 $\eta\pi^\pm$	< 5 × 10 ⁻⁴	CL=95%

Partial decay mode (labeled by Γ_i).

Our best value for branching fraction as determined from data averaging, fitting, evaluating, limit selection, etc. This list is basically a compact summary of results in the Branching Ratio section below.

$a_0(1200)$ BRANCHING RATIOS

Branching ratio.

Our best value (and error) of quantity tabulated, as determined from constrained fit (using all significant measured branching ratios for this particle).

Weighted average of measurements of this ratio only.

Footnote (referring to LYNCH 81).

$\Gamma(3\pi)/\Gamma_{total}$	VALUE	DOCUMENT ID	TECN	CHG	COMMENT
0.652 ± 0.013 OUR FIT					Error includes scale factor of 1.7.
0.643 ± 0.010 OUR AVERAGE					
0.64 ± 0.01		PIERCE 83	ASPK	+	2.1 $K^- p$
0.74 ± 0.06		MERRILL 81	HBC	0	3.2 $K^- p$
• • • We do not use the following data for averages, fits, limits, etc. • • •					
0.48 ± 0.15		² LYNCH 81	HBC	±	2.7 $\pi^- p$
² Data has questionable background subtraction.					

Confidence level for measured upper limit.

References, ordered inversely by year, then author.

"Document id" used on data entries above.

Journal, report, preprint, etc. (See abbreviations on next page.)

$\Gamma(K\bar{K})/\Gamma_{total}$	VALUE	DOCUMENT ID	TECN	CHG	COMMENT	
0.348 ± 0.013 OUR FIT					Error includes scale factor of 1.7.	
0.35 ± 0.05		PIERCE 83	ASPK	+	2.1 $K^- p$	
$\Gamma(K\bar{K})/\Gamma(3\pi)$	VALUE	DOCUMENT ID	TECN	CHG	COMMENT	
0.535 ± 0.030 OUR FIT					Error includes scale factor of 1.7.	
0.50 ± 0.03		MERRILL 81	HBC	0	3.2 $K^- p$	
$\Gamma(\eta(\text{neutral decay})\pi^\pm)/\Gamma_{total}$	VALUE (units 10 ⁻⁴)	CL%	DOCUMENT ID	TECN	CHG	COMMENT
<3.5		95	PIERCE 83	ASPK	+	2.1 $K^- p$

References, ordered inversely by year, then author.

$a_0(1200)$ REFERENCES

FENNER 87	PRL 55 14	H. Fenner et al.	(SLAC)
PIERCE 83	PL 123B 230	J.H. Pierce	(FNAL) JUP
LYNCH 81	PR D24 610	G.R. Lynch et al.	(CLEO Collab.)
MERRILL 81	PRL 47 143	D.W. Merrill et al.	(SACL, CERN)

Partial list of author(s) in addition to first author.

Quantum number determinations in this reference.

Institution(s) of author(s). (See abbreviations on next page.)

Abbreviations Used in the Particle Listings

Indicator of Procedure Used to Obtain Our Result

OUR AVERAGE	From a weighted average of selected data.
OUR FIT	From a constrained or overdetermined multiparameter fit of selected data.
OUR EVALUATION	Not from a direct measurement, but evaluated from measurements of other quantities.
OUR ESTIMATE	Based on the observed range of the data. Not from a formal statistical procedure.
OUR LIMIT	For special cases where the limit is evaluated by us from measured ratios or other data. Not from a direct measurement.

Measurement Techniques

(i.e., Detectors and Methods of Analysis)

A1	A1 Collaboration at MAMI
A2MM	A2 spectrometer at the Mainz Microtron, MAMI
ABRA	ABRACADABRA QCD axion dark matter search
ACCM	ACCMOR Collaboration
ADMX	Axion Dark Matter Experiment
AEMS	Argonne effective mass spectrometer
ALEP	ALEPH – CERN LEP detector
ALPS	Photon regeneration experiment
AMND	AMANDA South Pole neutrino detector
AMY	AMY detector at KEK-TRISTAN
ANAI	Direct DM detection exp. with NaI at Canfranc Underground Lab, Spain
ANIT	Antarctic Impulsive Transient Antenna balloon mission
ANTR	ANTARES underwater neutrino telescope in the Western Mediterranean Sea
APEX	FNAL APEX Collab.
ARG	ARGUS detector at DORIS
ARGD	Fit to semicircular amplitude path on Argand diagram
ASP	Anomalous single-photon detector
ASPK	Automatic spark chambers
ASTE	ASTERIX detector at LEAR
ASTR	Astronomy
ATLS	ATLAS detector at CERN LHC
AUGE	Pierre Auger Observatory
AURG	Resonant-mass gravitational wave AURIGA detector
B787	BNL experiment 787 detector
B791	BNL experiment 791 detector
B845	BNL experiment 845 detector
B852	BNL E-852
B865	BNL E865 detector
B871	BNL experiment 871 detector
B949	BNL E949 detector at AGS
BABR	BaBar Collab.
BAIK	Lake Baikal neutrino telescope
BAKS	Baksan underground scintillation telescope
BC	Bubble chamber
BDMP	Beam dump
BEAT	CERN BEATRICE Collab.
BEBC	Big European bubble chamber at CERN
BELL	Belle Collab.
BES	BES Beijing Spectrometer at Beijing Electron-Positron Collider
BES2	BES Beijing Spectrometer at Beijing Electron-Positron Collider
BES3	BES Beijing Spectrometer at Beijing Electron-Positron Collider
BIS2	BIS-2 spectrometer at Serpukhov
BKEI	BENKEI spectrometer system at KEK Proton Synchrotron
BOLO	Bolometer, a cryogenic thermal detector
BONA	Bonanza nonmagnetic detector at DORIS
BORX	BOREXINO
BPWA	Barrelet-zero partial-wave analysis
C100	COSINE-100 experiment in South Korea
CALO	Calorimeter
CAST	CAST experiment at CERN
CBAL	Crystal Ball detector at SLAC-SPEAR or DORIS
CBAR	Crystal Barrel detector at CERN-LEAR
CBOX	Crystal Box at LAMPF
CBTP	CBELSA/TAPS Collaboration
CC	Cloud chamber
CCFR	Columbia-Chicago-Fermilab-Rochester detector
CDEX	China Dark Matter Experiment
CDF	Collider detector at Fermilab
CDF2	CDF-II Collab.
CDHS	CDHS neutrino detector at CERN
CDM2	CDMS II, Cryogenic Dark Matter Search at Soudan Underground Lab.

CDMS	CDMS Collaboration
CELL	CELLO detector at DESY
CGNT	CoGeNT dark matter search experiment
CHER	Cherenkov detector
CHM2	CHARM-II neutrino detector (glass) at CERN
CHOZ	Nuclear Power Station near Chooz, France
CHRM	CHARM neutrino detector (marble) at CERN
CHRS	CHORUS Collaboration – CERN SPS
CIB	Cosmic Infrared Background
CIBS	CERN-IHEP boson spectrometer
CLAS	Jefferson CLAS Collab.
CLE2	CLEO II detector at CESR
CLE3	CLEO III detector at CESR
CLEC	CLEO-c detector at CESR
CLEO	Cornell magnetic detector at CESR
CMB	Cosmic Microwave Background
CMD	Cryogenic magnetic detector at VEPP-2M, Novosibirsk
CMD2	Cryogenic magnetic detector 2 at VEPP-2M, Novosibirsk
CMD3	Cryogenic magnetic detector 3 at VEPP-2000, Novosibirsk
CMS	CMS detector at CERN LHC
CNTR	Counters
COMB	Combined analysis of data from independent experiments.
COMP	COMPASS experiment at the CERN SPS
COSM	Cosmology and astrophysics
COSY	COSY-TOF Collaboration
COUP	COUPP (the Chicagoland Observatory for Underground Particle Physics) Collab.
CPLR	CLEAR Collaboration
CRBT	Crystal Ball and TAPS detector at MAMI
CRES	CRESST cryogenic detector
CRYB	Crystal Ball at BNL
CRYM	Crystal Ball detector at Mainz Microtron MAMI
CSB2	Columbia U. - Stony Brook BGO calorimeter inserted in NaI array
CSME	COSME Collaboration
CUOR	CUORICINO experiment at Gran Sasso Laboratory.
CUSB	Columbia U. - Stony Brook segmented NaI detector at CESR
D0	D0 detector at Fermilab Tevatron Collider
DAMA	DAMA, dark matter detector at Gran Sasso National Lab.
DASP	DESY double-arm spectrometer
DAYA	Daya Bay Collaboration
DBC	Deuterium bubble chamber
DCHZ	Double Chooz Collaboration
DEAP	DEAP-3600 DM search with argon at SNOLAB
DISP	Graviton mass measurement based on dispersion measure
DLCO	DELCO detector at SLAC-SPEAR or SLAC-PEP
DLPH	DELPHI detector at LEP
DM1	Magnetic detector no. 1 at Orsay DCI collider
DM2	Magnetic detector no. 2 at Orsay DCI collider
DMIC	DAMIC Dark Matter in CCD experiment at Fermilab
DMTP	Dark Matter Time Projection Chamber (DMTPC) directional detection experiment
DONU	DONUT Collab.
DPWA	Energy-dependent partial-wave analysis
DRFT	Directional dark matter detector at Boulby Underground Science Facility
DS50	DarkSide-50 Liquid Argon TPC at Gran Sasso National Laboratory
E137	SLAC E137 beam-dump experiment
E621	Fermilab E621 detector
E653	Fermilab E653 detector
E665	Fermilab E665 detector
E687	Fermilab E687 detector
E691	Fermilab E691 detector
E705	Fermilab E705 Spectrometer-Calorimeter
E731	Fermilab E731 Spectrometer-Calorimeter
E756	Fermilab E756 detector
E760	Fermilab E760 detector
E761	Fermilab E761 detector
E771	Fermilab E771 detector
E773	Fermilab E773 Spectrometer-Calorimeter
E789	Fermilab E789 detector
E791	Fermilab E791 detector
E799	Fermilab E799 Spectrometer-Calorimeter
E835	Fermilab E835 detector
EDE2	EDELWEISS II dark matter search Collaboration
EDE3	EDELWEISS III dark matter search Collaboration
EDEL	EDELWEISS dark matter search Collaboration
EHS	Four-pi detector at CERN

Abbreviations Used in the Particle Listings

ELEC	Electronic combination	KOLR	Kolar Gold Field underground detector
EMC	European muon collaboration detector at CERN	KOTO	KOTO experiment with K_L^0 beam at J-PARC
EMUL	Emulsions	KTEV	KTeV Collaboration
ESR	Electron spin resonance spectroscopy	L3	L3 detector at LEP
FAST	Fiber Active Scintillator Target detector at PSI	LASR	Laser
FBC	Freon bubble chamber	LASS	Large-angle superconducting solenoid spectrometer at SLAC
FENI	FENICE (at the ADONE collider of Frascati)	LATT	Lattice calculations
FIT	Fit to previously existing data	LEBC	Little European bubble chamber at CERN
FLAT	Large Area Telescope onboard the Fermi Gamma-Ray Space Telescope (Fermi-LAT)	LEGS	BNL LEGS Collab.
FMPS	Fermilab Multiparticle Spectrometer	LENA	Nonmagnetic lead-glass NaI detector at DORIS
FOCS	FNAL E831 FOCUS Collab.	LEP	From combination of all 4 LEP experiments: ALEPH, DELPHI, L3, OPAL
FRAB	ADONE $B\bar{B}$ group detector	LEPS	Low-Energy Pion Spectrometer at the Paul Scherrer Institute
FRAG	ADONE $\gamma\gamma$ group detector	LGW	Lead Glass Wall collaboration at SPEAR/SLAC
FRAM	ADONE MEA group detector	LHC	Combined analysis of LHC experiments
FREJ	FREJUS Collaboration – modular flash chamber detector (calorimeter)	LHCB	LHCb detector at CERN LHC
GA24	Hodoscope Cherenkov γ calorimeter (IHEP GAMS-2000) (CERN GAMS-4000)	L+P	Multichannel L + P model fit
GALX	GALLEX solar neutrino detector in the Gran Sasso Underground Lab.	LSD	Mont Blanc liquid scintillator detector
GAM2	IHEP hodoscope Cherenkov γ calorimeter GAMS-2000	LSND	Liquid Scintillator Neutrino Detector
GAM4	CERN hodoscope Cherenkov γ calorimeter GAMS-4000	LSW	Light Shining through a Wall
GAMS	IHEP hodoscope Cherenkov γ calorimeter GAMS-4 π	LUX	Large Underground Xenon experiment at SURF
GNO	Gallium Neutrino Observatory in the Gran Sasso Underground Lab.	MAC	MAC detector at PEP/SLAC
GOLI	CERN Goliath spectrometer	MAJD	Majorana Demonstrator experiment at SURF
GRAL	GRAAL Collaboration	MBNE	Fermilab MiniBooNE neutrino experiment
H1	H1 detector at DESY/HERA	MBR	Molecular beam resonance technique
HAWC	High Altitude Water Cherenkov Observatory experiment at Sierra Negra, Mexico	MCRO	MACRO detector in Gran Sasso
HBC	Hydrogen bubble chamber	MD1	Magnetic detector at VEPP-4, Novosibirsk
HDBC	Hydrogen and deuterium bubble chambers	MDRP	Millikan drop measurement
HDES	HADES Collaboration at GSI in Darmstadt	MEG	Muon to electron conversion detector at PSI
HDMO	Heidelberg-Moscow Experiment	MGFL	MAGIC and Fermi-LAT Collaborations
HDMS	Heidelberg Dark Matter Search Experiment	MGIC	MAGIC Telescopes gamma-ray observatory
HEBC	Helium bubble chamber	MICA	Underground mica deposits
HEPT	Helium proportional tubes	MICR	MICROSCOPE satellite test of weak equivalence principle
HERA	H1 and ZEUS Collaborations at DESY/HERA	MINS	Fermilab MINOS experiment
HERB	HERA-B detector at DESY/HERA	MIRA	MIRABELLE Liquid-hydrogen bubble chamber
HERM	HERMES detector at DESY/HERA	MLEV	Magnetic levitation
HESS	High Energy Stereoscopic System gamma-ray instrument	MLS	Modified Laurent Series
HFS	Hyperfine structure	MMS	Missing mass spectrometer
HLBC	Heavy-liquid bubble chamber	MOED	MoEDAL magnetic monopoles search experiment at LHC
HOME	Homestake underground scintillation detector	MPS	Multiparticle spectrometer at BNL
HPGE	High-purity Germanium detector	MPS2	Multiparticle spectrometer upgrade at BNL
HPS	Heavy Photon Search experiment at JLAB	MPSF	Multiparticle spectrometer at Fermilab
HPW	Harvard-Pennsylvania-Wisconsin detector	MPWA	Model-dependent partial-wave analysis
HRS	SLAC high-resolution spectrometer	MRK1	SLAC Mark-I detector
HYBR	Hybrid: bubble chamber + electronics	MRK2	SLAC Mark-II detector
HYCP	HyperCP Collab. (FNAL E-871)	MRK3	SLAC Mark-III detector
HYST	HAYSTAC axion search experiment	MRKJ	Mark-J detector at DESY
IACT	Imaging Air Cherenkov Telescope	MRS	Magnetic resonance spectrometer
ICAR	ICARUS experiment at Gran Sasso Laboratory.	MUG2	Muon ($g-2$)
ICCB	IceCube neutrino detector at South Pole	MWPC	Multi-Wire Proportional Chamber
IGEX	IGEX Collab.	NA14	CERN NA14
IMB	Irvine-Michigan-Brookhaven underground Cherenkov detector	NA31	CERN NA31 Spectrometer-Calorimeter
IMB3	Irvine-Michigan-Brookhaven underground Cherenkov detector	NA32	CERN NA32 Spectrometer
INDU	Magnetic induction	NA48	CERN NA48 Collaboration
IPWA	Energy-independent partial-wave analysis	NA49	CERN NA49 Collaboration
ISTR	IHEP ISTR+ spectrometer-calorimeter	NA60	CERN NA60 Collaboration
JADE	JADE detector at DESY	NA62	CERN NA62 Experiment
JPAC	Joint Physics Analysis Center (JPAC) Collaboration	NA64	CERN SPS NA64 Experiment
K246	KEK E246 detector with polarimeter	NAGE	NEWAGE, New generation WIMP-search experiment with advanced gaseous tracking
K2K	KEK to Super-Kamiokande	NAIA	NAIAD (NaI Advanced Detector) dark matter search experiment
K391	KEK E391a detector	ND	NaI detector at VEPP-2M, Novosibirsk
K470	KEK-E470 Stopping K detector	NEOS	NEOS Collaboration
KAM2	KAMIOKANDE-II underground Cherenkov detector	NEWS	NEWS-G direct dark matter search at LSM
KAMI	KAMIOKANDE underground Cherenkov detector	NICE	Serpukhov nonmagnetic precision spectrometer
KAR2	KARMEN2 calorimeter at the ISIS neutron spallation source at Rutherford	NMR	Nuclear magnetic resonance
KARM	KARMEN calorimeter at the ISIS neutron spallation source at Rutherford	NOMD	NOMAD Collaboration, CERN SPS
KEDR	detector operating at VEPP-4M collider (Novosibirsk)	NOVA	NOvA experiment with Fermilab's NuMI neutrino beam
KIMS	Korea Invisible Mass Search experiment at YangYang, Korea	NTEV	NuTeV Collab. at Fermilab
KLND	KamLand Collab. (Japan)	nTRV	neutron Time-Reversal Violation
KLOE	KLOE detector at DAFNE (the Frascati e+e- collider Italy)	NUSX	Mont Blanc NUSEX underground detector
		OBLX	OBELIX detector at LEAR
		OKA	OKA collaboration at U70 accelerator in Protvino, Russia
		OLYA	Detector at VEPP-2M and VEPP-4, Novosibirsk
		OMEG	CERN OMEGA spectrometer
		OPAL	OPAL detector at LEP
		OPER	OPERA experiment with emulsion tracking at Gran Sasso

Abbreviations Used in the Particle Listings

OSPK	Optical spark chamber	WA89	CERN WA89 experiment
PIBE	The PIBETA detector at the Paul Scherrer Institute (PSI), Switzerland.	WARP	Liquid argon detector for CDM searches at Gran Sasso
PICA	PICASSO dark matter search experiment	WASA	WASA detector at CELSIUS, Uppsala and at COSY, Juelich
PICO	PICO bubble chamber experiment in SNOLAB underground laboratory	WDMX	WISP Dark Matter eXperiment (WISPDIMX) for direct hidden photon search
PIE3	π E3 beam-line of Paul Scherrer Institute	WIRE	Wire chamber
PLAS	Plastic detector	X100	XENON100 dark matter search experiment at Gran Sasso National Laboratory
PLUT	DESY PLUTO detector	XE10	XENON10 experiment at Gran Sasso National Laboratory
PMLA	PAMELA space spectrometer on Resurs-DK1 satellite	XE1T	XENON1T dark matter search experiment at Gran Sasso National Laboratory
PNDX	PandaX dual-phase liquid xenon dark matter experiment at Jin-Ping	XEBC	Xenon bubble chamber
PPTA	Parkees Pulsar Timing Array	XMAS	XMASS, liquid xenon scintillation detector at Kamioka Observatory
PRMX	The PRIMEX detector in Hall B at TJNAF	YUKA	Graviton mass measurement based on Yukawa potential
PWA	Partial-wave analysis	ZEP2	ZEPLIN-II dark matter detector
QUAX	QUAX axion search experiment	ZEP3	ZEPLIN-III dark matter detector at Palmer Underground Lab.
RDK2	NIST rare radioactive decay experiment	ZEPL	ZEPLIN-I galactic dark matter detector
REDE	Resonance depolarization	ZEUS	ZEUS detector at DESY/HERA
RENO	RENO Collaboration		
RICE	Radio Ice Cherenkov Experiment		
RVUE	Review of previous data		
SAGE	US - Russian Gallium Experiment		
SCDM	SuperCDMS experiment at Soudan Underground Lab.		
SELX	FNAL SELEX Collab.		
SENS	Sub-Electron-Noise Skipper CCD Experimental Instrument (SENSEI)		
SFM	CERN split-field magnet		
SHF	SLAC Hybrid Facility Photon Collaboration		
SHUK	SHUKET: search for U(1) dark matter with an electromagnetic telescope		
SIGM	Serpukhov CERN-IHEP magnetic spectrometer (SIGMA)		
SILI	Silicon detector		
SIMP	SIMPLE, dark matter detector at Laboratori Nazionali del Sud		
SKAM	Super-Kamiokande Collab.		
SLAX	Solar Axion Experiment in Canfranc Underground Laboratory		
SLD	SLC Large Detector for e^+e^- colliding beams at SLAC		
SMPL	SIMPLE, Superheated Instrument for Massive Particle Experiments		
SND	Novosibirsk Spherical neutral detector at VEPP-2M		
SNDR	SINDRUM spectrometer at PSI		
SNO	SNO Collaboration (Sudbury Neutrino Observatory)		
SNO+	SNO+ Collaboration (Sudbury Neutrino Observatory)		
SOU2	Soudan 2 underground detector		
SODU	Soudan underground detector		
SPEC	Spectrometer		
SPED	From maximum of speed plot or resonant amplitude		
SPHR	Bonn SAPHIR Collab.		
SPNX	SPHINX spectrometer at IHEP accelerator		
SPRK	Spark chamber		
SQID	SQUID device		
STRC	Streamer chamber		
SVD2	SVD-2 experiment at IHEP, Protvino		
T2K	T2K Collaboration		
TASS	DESY TASSO detector		
TEVA	Combined analysis of CDF and DØ experiments		
TEXO	TEXONO Collab., ultra low energy Ge detector at Kuo-Sheng Laboratory		
THEO	Theoretical or heavily model-dependent result		
TNF	TNF-IHEP facility at 70 GeV IHEP accelerator		
TOF	Time-of-flight		
TOPZ	TOPAZ detector at KEK-TRISTAN		
TPC	TPC detector at PEP/SLAC		
TPS	Tagged photon spectrometer at Fermilab		
TRAP	Penning trap		
TWST	TWIST spectrometer at TRIUMF		
UA1	UA1 detector at CERN		
UA2	UA2 detector at CERN		
UA5	UA5 detector at CERN		
UCNA	UCNA collaboration using polarized ultracold neutrons at LANSCE		
UKDM	UK Dark Matter Collab.		
VES	Vertex Spectrometer Facility at 70 GeV IHEP accelerator		
VLBI	Very Long Baseline Interferometer		
VNS	VENUS detector at KEK-TRISTAN		
VRTS	Very Energetic Radiation Imaging Telescope Array System (VERITAS)		
WA75	CERN WA75 experiment		
WA82	CERN WA82 experiment		

Conferences

Conferences are generally referred to by the location at which they were held (e.g., HAMBURG, TORONTO, CORNELL, BRIGHTON, etc.).

Journals

AA	Astronomy and Astrophysics
ADVP	Advances in Physics
AFIS	Anales de Fisica
AJP	American Journal of Physics
AL	Astronomy Letters
ANP	Annals of Physics
ANPL	Annals of Physics (Leipzig)
ANYAS	Annals of the New York Academy of Sciences
AP	Atomic Physics
APAH	Acta Physica Academiae Scientiarum Hungaricae
APJ	Astrophysical Journal
APJS	Astrophysical Journal Suppl.
APP	Acta Physica Polonica
APS	Acta Physica Slovaca
ARNPS	Annual Review of Nuclear and Particle Science
ARNS	Annual Review of Nuclear Science
ASP	Astroparticle Physics
AST	American Statistician
BAPS	Bulletin of the American Physical Society
BASUP	Bulletin of the Academy of Science, USSR (Physics)
CJNP	Chinese Journal of Nuclear Physics
CJP	Canadian Journal of Physics
CNPP	Comments on Nuclear and Particle Physics
CP	Chinese Physics
CPC	Chinese Physics C
CTP	Communications in Theoretical Physics
CZJP	Czechoslovak Journal of Physics
DANS	Doklady Akademii nauk SSSR
DP	Doklady Physics (Magazine)
EPJ	The European Physical Journal
EPL	Europhysics Letters
FECAY	Fizika Elementarnykh Chastits i Atomnogo Yadra
HADJ	Hadronic Journal
IJMP	International Journal of Modern Physics
JAP	Journal of Applied Physics
JCAP	Journal of Cosmology and Astroparticle Physics
JETP	English Translation of Soviet Physics ZETF
JETPL	English Translation of Soviet Physics ZETF Letters
JHEP	Journal of High Energy Physics
JINR	Joint Inst. for Nuclear Research
JINRRC	JINR Rapid Communications
JP	Journal of Physics
JPA	Journal of Physics, A
JPB	Journal of Physics, B
JPCRD	Journal of Physical and Chemical Reference Data
JPCS	Journal of Physics: Conference Series
JPG	Journal of Physics, G
JPSJ	Journal of the Physical Society of Japan
LCN	Lettere Nuovo Cimento
MNRAS	Monthly Notices of the Royal Astronomical Society
MPL	Modern Physics Letters

Abbreviations Used in the Particle Listings

BOSK	“ Rudjer Bošković ” Inst.	Zagreb, Croatia	COLO	Univ. of Colorado	Boulder, CO, USA
BOST	Boston Univ.	Boston, MA, USA	COLU	Columbia Univ.	New York, NY, USA
BRAN	Brandeis Univ.	Waltham, MA, USA	CONC	Concordia University	Montreal, PQ, Canada
BRCO	Univ. of British Columbia	Vancouver, BC, Canada	CORN	Cornell Univ.	Ithaca, NY, USA
BRIS	Univ. of Bristol	Bristol, United Kingdom	COSU	Colorado State Univ.	Fort Collins, CO, USA
BROW	Brown Univ.	Providence, RI, USA	CPPM	Centre National de la Recherche Scientifique, Lu- miny	Marseille , France
BRUN	Brunel Univ.	Uxbridge, Middlesex, United Kingdom	CRAC	Henryk Niewodniczański Inst. of Nuclear Physics	Kraków , Poland
BRUX	Univ. Libre de Bruxelles ; Physique des Particules Elémentaires	Bruxelles, Belgium	CRNL	Chalk River Labs.	Chalk River, ON, Canada
BRUXT	Univ. Libre de Bruxelles ; Physique Théorique	Bruxelles, Belgium	CSOK	Oklahoma Central State Univ.	Edmond, OK, USA
BUCH	Univ. of Bucharest	Bucharest-Magurele, Romania	CST	Univ. of Science and Tech- nology of China	Hefei , Anhui 230026, China
BUDA	Wigner Research Centre for Physics	Budapest , Hungary	CSULB	California State Univ.	Long Beach, CA, USA
BUFF	SUNY at Buffalo	Buffalo, NY, USA	CSUS	California State Univ.	Sacramento, CA, USA
BURE	Inst. des Hautes Etudes Scien- tifiques	Bures-sur-Yvette , France	CUNY	City College of New York	New York, NY, USA
CAEN	Lab. de Physique Corpuscu- laire, ENSICAEN	Caen , France	CURCP	Univ. Pierre et Marie Curie (Paris VI), LCP	Paris, France
CAGL	Univ. degli Studi di Cagliari	Monserato (CA), Italy	CURIN	Univ. Pierre et Marie Curie (Paris VI), LPNHE	Paris, France
CAIR	Cairo University	Orman, Giza, Cairo, Egypt	CURIT	Univ. Pierre et Marie Curie (Paris VI), LPTHE	Paris, France
CAIW	Carnegie Inst. of Washing- ton	Washington, DC, USA	DALH	Dalhousie Univ.	Halifax, NS, Canada
CALB	Univ. della Calabria	Cosenza, Italy	DALI	Dalian Univ. of Tech.	Dalian, China
CALC	Univ. of Calcutta	Calcutta, India	DARE	Daresbury Lab	Cheshire, United Kingdom
CAMB	DAMTP	Cambridge, United Kingdom	DARM	Tech. Hochschule Darmstadt	Darmstadt, Germany
CAMP	Univ. Estadual de Campinas (UNICAMP)	Campinas , SP, Brazil	DELA	Univ. of Delaware ; Dept. of Physics & Astronomy	Newark, DE, USA
CANB	Australian National Univ.	Canberra, ACT, Australia	DELH	Univ. of Delhi	Delhi, India
CANTB	Inst. de Física de Cantabria (CSIC–Univ. Cantabria)	Santander, Spain	DESY	DESY , Deutsches Elektronen-Synchrotron	Hamburg , Germany
CAPE	University of Cape Town	Rondebosch, Cape Town, South Africa	DFAB	Escuela de Ingenieros	Bilbao , Spain
CARA	Univ. Central de Venezuela	Caracas, Venezuela	DOE	Department of Energy	Washington, DC, USA
CARL	Carleton Univ.	Ottawa, ON, Canada	DORT	Technische Univ. Dortmund	Dortmund, Germany
CARLC	Carleton College	Northfield, MN, USA	DUKE	Duke Univ.	Durham, NC, USA
CASE	Case Western Reserve Univ.	Cleveland, OH, USA	DURH	Univ. of Durham	Durham, United Kingdom
CAST	China Center of Advanced Science and Technology	Beijing, China	DUUC	University College Dublin	Dublin, Ireland
CATA	Univ. di Catania	Catania, Italy	EDIN	Univ. of Edinburgh	Edinburgh, United Kingdom
CATH	Catholic Univ. of America	Washington, DC, USA	EFI	Univ. of Chicago, The En- rico Fermi Inst.	Chicago , IL, USA
CAVE	Cavendish Lab.	Cambridge, United Kingdom	ELMT	Elmhurst College	Elmhurst, IL, USA
CBNM	CBNM	Geel , Belgium	ENSP	l’Ecole Normale Supérieure	Paris , France
CBPF	Centro Brasileiro de Pesquisas Físicas – BIB/CDI/CBPF	Rio de Janeiro , RJ, Brazil	EOTV	Eötvös University	Budapest, Hungary
CCAC	Allegheny College	Meadville, PA, USA	EPOL	École Polytechnique	Palaiseau , France
CDEF	Univ. Paris VII, Denis Diderot	Paris, France	ERLA	Univ. Erlangen-Nurnberg	Erlangen, Germany
CEA	Cambridge Electron Accelera- tor (Historical in <i>Review</i>)	Cambridge, MA , USA	ETH	Univ. Zürich	Zürich, Switzerland
CEADE	Center for Apl. Studies for Nuclear Physics	Havana, Cuba	FERR	Univ. di Ferrara	Ferrara, Italy
CEBAF	Jefferson Lab—Thomas Jefferson National Accel- erator Facility	Newport News , VA, USA	FIRZ	Univ. degli Studi di Firenze	Sesto Fiorentino, Italy
CENG	Centre d’Etudes Nucleaires	Grenoble , France	FISK	Fisk Univ.	Nashville, TN, USA
CERN	CERN , European Organiza- tion for Nuclear Research	Genève, Switzerland	FLOR	Univ. of Florida	Gainesville, FL, USA
CFPA	Univ. of California, (Berke- ley)	Berkeley, CA, USA	FNAL	Fermilab	Batavia, IL, USA
CHIC	Univ. of Chicago	Chicago, IL, USA	FOM	FOM , Stichting voor Funda- menteel Onderzoek der Ma- terie	JP Utrecht , The Netherlands
CIAE	State Nuclear Power Re- search Inst.	Beijing , China	FRAN	Frankfurt Inst. for Ad- vanced Studies (FIAS)	Frankfurt am Main, Germany
CINC	Univ. of Cincinnati	Cincinnati, OH, USA	FRAS	Lab. Nazionali di Frascati dell’INFN	Frascati (Roma), Italy
CINV	CINVESTAV-IPN Centro de Investigacion y de Estudios Avanzados del IPN	México , DF, Mexico	FREIB	Albert-Ludwigs Univ.	Freiburg , Germany
CIT	California Inst. of Tech.	Pasadena, CA, USA	FREIE	Freie Univ. Berlin	Berlin, Germany
CLER	Univ. de Clermont-Ferrand	Aubière, France	FRIB	Univ. de Fribourg	Fribourg, Switzerland
CLEV	Cleveland State Univ.	Cleveland, OH, USA	FSU	Florida State Univ.; High Energy Physics	Tallahassee, FL, USA
CMNS	Comenius Univ. (FMFI UK)	Bratislava , Slovakia	FSUSC	Florida State Univ.; SCS (School of Computational Science)	Tallahassee, FL, USA
CMU	Carnegie Mellon Univ.	Pittsburgh, PA, USA	FUKI	Fukui Univ.	Fukui, Japan
CNEA	Comisión Nacional de En- ergía Atómica	Buenos Aires, Argentina	FUKU	Fukushima Univ.	Fukushima, Japan
CNRC	Centre for Research in Partic- le Physics	Ottawa, ON, Canada	GENO	Univ. di Genova	Genova, Italy
COIM	Univ. de Coimbra	Coimbra , Portugal	GEOR	E. Andronikashvili Inst. of Physics	Tbilisi, Republic of Georgia
			GESC	General Electric Co.	Schenectady, NY, USA
			GEVA	Univ. de Genève	Genève, Switzerland
			GIES	Univ. Giessen	Giessen, Germany
			GIFU	Gifu Univ.	Gifu, Japan

Abbreviations Used in the Particle Listings

GLAS	Univ. of Glasgow	Glasgow, United Kingdom	IOFF	A.F. Ioffe Phys. Tech. Inst.	St. Petersburg , Russian Federation
GMAS	George Mason Univ.	Fairfax, VA, USA	IOWA	Univ. of Iowa	Iowa City, IA, USA
GOET	Univ. Göttingen	Göttingen, Germany	IPN	IPN , Inst. de Phys. Nucl.	Orsay , France
GOML	Gomel State Univ.	Gomel, Belarus	IPNP	Univ. Pierre et Marie Curie (Paris VI)	Paris, France
GRAN	Univ. de Granada	Granada, Spain	IRAD	Inst. du Radium (Historical)	Paris , France
GRAZ	Univ. Graz	Graz, Austria	ISNG	Lab. de Physique Subatomique et de Cosmologie (LPSC)	Grenoble , France
GRON	Univ. of Groningen	Groningen, The Netherlands	ISU	Iowa State Univ.	Ames, IA, USA
GSCO	Geological Survey of Canada	Ottawa, ON, Canada	ISUT	Isfahan University of Technology	Isfahan, Iran
GSI	GSI Helmholtzzentrum für Schwerionenforschung GmbH	Darmstadt , Germany	ITEP	ITEP , Inst. of Theor. and Exp. Physics	Moscow , Russian Federation
GUAN	Univ. de Guanajuato	León, Gto., Mexico	ITHA	Ithaca College	Ithaca, NY, USA
GUEL	Univ. of Guelph	Guelph, ON, Canada	IUPU	Indiana Univ., Purdue Univ. Indianapolis	Indianapolis, IN, USA
GWU	George Washington Univ.	Washington, DC, USA	JADA	Jadavpur Univ.	Calcutta, India
HAHN	Hahn-Meitner Inst. Berlin GmbH	Berlin, Germany	JAGL	Jagiellonian Univ.	Kraków, Poland
HAIF	Technion – Israel Inst. of Tech.	Technion, Haifa, Israel	JHU	Johns Hopkins Univ.	Baltimore, MD, USA
HAMB	Univ. Hamburg	Hamburg, Germany	JINR	JINR , Joint Inst. for Nuclear Research	Dubna , Russian Federation
HANN	Univ. Hannover	Hannover, Germany	JULI	Forschungszentrum Jülich	Jülich, Germany
HARC	Houston Advanced Research Ctr.	The Woodlands, TX, USA	JYV	Univ. of Jyväskylä	Jyväskylä, Finland
HARV	Harvard Univ.	Cambridge, MA, USA	KAGO	Univ. of Kagoshima	Kagoshima-shi, Japan
HARV	Harvard Univ. (LPPC)	Cambridge, MA, USA	KAIST	Korea Advanced Inst. of Science and Technology	Yusung ku, Daejeon, Republic of Korea
HAWA	Univ. of Hawai'i	Honolulu, HI, USA	KANP	Indian Inst. of Tech.	Kanpur , UT, India
HEBR	Hebrew Univ.	Jerusalem, Israel	KANS	Univ. of Kansas	Lawrence, KS, USA
HEID	Univ. Heidelberg ; (unspecified division) (Historical in <i>Review</i>)	Heidelberg, Germany	KARL	Univ. Karlsruhe (Historical in <i>Review</i>)	Karlsruhe, Germany
HEIDH	Ruprecht-Karls Univ. Heidelberg	Heidelberg, Germany	KARLE	Karlsruhe Inst. of Technology (KIT); Inst. for Experimental Nuclear Physics	Karlsruhe, Germany
HEIDP	Univ. Heidelberg ; Physics Inst.	Heidelberg, Germany	KARLK	Karlsruhe Inst. of Technology (KIT)	Eggenstein-Leopoldshafen, Germany
HEIDT	Ruprecht-Karls-Universität Heidelberg	Heidelberg, Germany	KARLT	Karlsruhe Inst. of Technology (KIT); Inst. for Theoretical Physics	Karlsruhe, Germany
HELS	Univ. of Helsinki	University of Helsinki, Finland	KAZA	Kazakh Inst. of High Energy Physics	Alma Ata, Kazakhstan
HINR	Inst. of Nuclear Research (ATOMKI)	Debrecen , Hungary	KEK	KEK , High Energy Accelerator Research Organization	Ibaraki-ken, Japan
HIRO	Hiroshima Univ.	Higashi-Hiroshima, Japan	KENT	Univ. of Kent	Canterbury, United Kingdom
HOUS	Univ. of Houston	Houston, TX, USA	KEYN	Open Univ.	Milton Keynes, United Kingdom
HPC	Hewlett-Packard Corp.	Cupertino, CA, USA	KFTI	Kharkov Inst. of Physics and Tech. (NSC KIPT)	Kharkov, Ukraine
HSCA	Harvard-Smithsonian Center for Astrophysics	Cambridge, MA, USA	KIAE	Kurchatov Inst.	Moscow , Russian Federation
HYDER	Indian Inst. of Technology	Hyderabad, India	KIAM	Keldysh Inst. of Applied Math., Acad. Sci., Russia	Moscow , Russian Federation
IAS	Inst. for Advanced Study	Princeton, NJ, USA	KIDR	Vinča Inst. of Nuclear Sciences	Belgrade, Serbia
IASD	Dublin Inst. for Advanced Studies	Dublin, Ireland	KIEV	Institute for Nuclear Research	Kyiv , Ukraine
IBAR	Ibaraki Univ.	Ibaraki, Japan	KINK	Kinki Univ.	Osaka, Japan
IBM	IBM Corp.	Palo Alto, CA, USA	KNTY	Univ. of Kentucky	Lexington, KY, USA
IBMY	IBM	Yorktown Heights, NY, USA	KOBE	Kobe Univ.	Kobe, Japan
IBS	Inst. for Boson Studies	Pasadena, CA, USA	KOMAB	Univ. of Tokyo , Komaba	Tokyo, Japan
ICEPP	The Univ. of Tokyo	Tokyo, Japan	KONAN	Konan Univ.	Kobe, Japan
ICRR	Univ. of Tokyo	Chiba, Japan	KOSI	Inst. of Experimental Physics SAS	Košice , Slovakia
ICTP	Abdus Salam International Centre for Theoretical Physics	Trieste , Italy	KYOT	Kyoto Univ.; Dept. of Physics, Graduate School of Science	Kyoto, Japan
IFIC	IFIC (Instituto de Física Corpuscular)	Paterna (Valencia) , Spain	KYOTU	Kyoto Univ.; Yukawa Inst. for Theor. Physics	Kyoto, Japan
IFRJ	Univ. Federal do Rio de Janeiro	Rio de Janeiro, RJ, Brazil	KYUN	Kyungpook National Univ.	Daegu, Republic of Korea
IIT	Illinois Inst. of Tech.	Chicago, IL, USA	KYUSH	Kyushu Univ.; Elementary Particle Theory Group; Exp. Particle Physics Group; Research Center for Advanced Particle Physics	Fukuoka, Japan
ITI	Indian Inst. of Tech. (of IIT Indore)	Simrol, Indore, India	LALO	LAL , Laboratoire de l'Accélérateur Linéaire	Orsay , France
ILL	Univ. of Illinois at Urbana-Champaign	Urbana, IL, USA	LANC	Lancaster Univ.	Lancaster, United Kingdom
ILLC	Univ. of Illinois at Chicago	Chicago, IL, USA	LANL	Los Alamos National Lab. (LANL)	Los Alamos, NM, USA
ILLG	Inst. Laue-Langevin	Grenoble, France	LAPL	Univ. Nacional de La Plata	La Plata, Argentina
IND	Indiana Univ.	Bloomington, IN, USA			
INEL	E G and G Idaho , Inc.	Idaho Falls, ID, USA			
INFN	Ist. Nazionale di Fisica Nucleare (Generic INFN, unknown location)	Various places, Italy			
INNS	Univ. of Innsbruck	Innsbruck , Austria			
INPK	Henryk Niewodniczański Inst. of Nuclear Physics	Kraków , Poland			
INRM	INR , Inst. for Nucl. Research	Moscow , Russian Federation			
INUS	KEK , High Energy Accelerator Research Organization	Tokyo, Japan			
IOAN	Univ. of Ioannina	Ioannina, Greece			

Abbreviations Used in the Particle Listings

LAPP	LAPP , Lab. d'Annecy-le-Vieux de Phys. des Particules	Annecy-le-Vieux , France	MICH	Univ. of Michigan	Ann Arbor, MI, USA
LASL	U.C. Los Alamos Scientific Lab. (Old name for LANL)	Los Alamos, NM, USA	MILA	Univ. di Milano	Milano, Italy
LATV	Latvian State Univ.	Riga, Latvia	MILAI	INFN , Sez. di Milano	Milano, Italy
LAUS	EPFL Lausanne	Lausanne, Switzerland	MINN	Univ. of Minnesota	Minneapolis, MN, USA
LAVL	Univ. Laval	Quebec, QC, Canada	MIPT	Moscow Institute of Physics and Technology	Moscow, Russian Federation
LBL	Lawrence Berkeley National Lab.	Berkeley, CA, USA	MISS	Univ. of Mississippi	University, MS, USA
LCGT	Univ. di Torino	Turin, Italy	MISSR	Univ. of Missouri	Rolla, MO, USA
LEBD	Lebedev Physical Inst.	Moscow , Russian Federation	MIT	MIT Massachusetts Inst. of Technology	Cambridge, MA, USA
LECE	Univ. di Lecce	Lecce, Italy	MIU	Maharishi International Univ.	Fairfield, IA, USA
LEED	Univ. of Leeds	Leeds, United Kingdom	MIYA	Miyazaki Univ.	Miyazaki-shi, Japan
LEGN	Lab. Naz. di Legnaro	Legnaro , Italy	MONP	Univ. de Montpellier II	Montpellier, France
LEHI	Lehigh Univ.	Bethlehem, PA, USA	MONS	Univ. of Mons	Mons , Belgium
LEHM	Lehman College of CUNY	Bronx, NY, USA	MONT	Univ. de Montréal ; Pavillon René-J.-A.-Lévesque	Montréal, PQ, Canada
LEID	Univ. Leiden	Leiden, The Netherlands	MONTC	Univ. de Montréal ; Centre de recherches mathématiques	Montréal, PQ, Canada
LEMO	Le Moyne Coll.	Syracuse, NY, USA	MOSU	Skobeltsyn Inst. of Nuclear Physics , Lomonosov Moscow State Univ.; Experimental HEP Division; Theoretical HEP Division	Moscow , Russian Federation
LENSU	Saint-Petersburg State Univ.	St. Petersburg , Russian Federation	MPCM	Max Planck Inst. fur Chemie	Mainz , Germany
LEUV	Katholieke Univ. Leuven	Leuven, Belgium	MPEI	Moscow Physical Engineering Inst.	Moscow, Russian Federation
LIEG	Univ. de Liège	Liège, Belgium	MPIG	Max-Planck-Institute für Astrophysik	Garching, Germany
LINZ	Univ. Linz	Linz, Austria	MPIH	Max-Planck-Inst. für Kernphysik	Heidelberg , Germany
LISB	Inst. Nacional de Investigacion Cientifica	Lisboa CODEX, Portugal	MPIM	Max-Planck-Inst. für Physik	München , Germany
LISBT	Centro de Física Teórica de Particulas (CFTP)	Lisboa , Portugal	MSST	Mississippi State University	Mississippi State, MS, USA
LIVP	Univ. of Liverpool	Liverpool, United Kingdom	MSU	Michigan State Univ.	East Lansing, MI, USA
LLL	Lawrence Livermore Lab. (Old name for LLNL)	Livermore, CA, USA	MTHO	Mount Holyoke College	South Hadley, MA, USA
LLNL	Lawrence Livermore National Lab.	Livermore, CA, USA	MULH	Centre Univ. du Haut-Rhin	Mulhouse, France
LNUDA		Dalian, China	MUNI	Ludwig-Maximilians-Univ. München	Garching, Germany
LOCK	Lockheed Palo Alto Res. Lab	Palo Alto, CA, USA	MUNT	Tech. Univ. München	Garching, Germany
LOIC	Imperial College of Science Tech. & Medicine	London, United Kingdom	MURA	Midwestern Univ. Research Assoc. (Historical in <i>Review</i>)	Stroughton, WI, USA
LOKC	Univ. of London , King's College	London, United Kingdom	MURC	Univ. of Murcia	Murcia, Spain
LOQM	Queen Mary, Univ. of London	London, United Kingdom	NAAS	North Americal Aviation Science Center (Historical in <i>Review</i>)	Thousand Oaks, CA, USA
LOUC	University College London	London, United Kingdom	NAGO	Nagoya Univ.	Nagoya, Japan
LOUV	Univ. Catholique de Louvain	Louvain-la-Neuve, Belgium	NANJ	Nanjing Univ.	Nanjing, China
LOWC	Westfield College (Historical, see LOQM (Queen Mary and Westfield joined))	London, United Kingdom	NAPL	Univ. di Napoli "Federico II"	Napoli, Italy
LRL	U.C. Lawrence Radiation Lab. (Old name for LBL)	Berkeley , CA, USA	NASA	NASA	Greenbelt, MD, USA
LSU	Louisiana State Univ.	Baton Rouge, LA, USA	NBS	U.S. National Bureau of Standards (Old name for NIST)	Gaithersburg, MD, USA
LUND	Fysiska Institutionen	Lund , Sweden	NBSB	National Inst. Standards Tech.	Boulder, CO, USA
LUND	Lund Univ.	Lund, Sweden	NCAR	National Center for Atmospheric Research	Boulder, CO, USA
LYON	Institute de Physique Nucléaire de Lyon (IPN)	Villeurbanne, France	NCSU	North Carolina State Univ.	Raleigh , NC, USA
MADE	UAM/CSIC , Inst. de Física Teórica	Madrid , Cantoblanco, Spain	NDAM	Univ. of Notre Dame	Notre Dame, IN, USA
MADR	C.I.E.M.A.T	Madrid , Spain	NEAS	Northeastern Univ.	Boston, MA, USA
MADRA	Univ. of Madras	Madras, India	NEBR	Univ. of Nebraska	Lincoln, NE, USA
MADU	Univ. Autónoma de Madrid	Cantoblanco, Madrid, Spain	NEUC	Univ. de Neuchâtel	Neuchâtel, Switzerland
MANI	Univ. of Manitoba	Winnipeg, MB, Canada	NICEA	Univ. de Nice	Nice, France
MANZ	Johannes-Gutenberg-Univ. ; Inst. für Kernphysik, J.-J.-Becher-Weg 45; Inst. für Physik, Staudingerweg 7	Mainz , Germany	NICEO	Observatoire de Nice	Nice, France
MARB	Univ. Marburg	Marburg, Germany	NIHO	Nihon Univ.	Tokyo, Japan
MARS	Centre de Physique des Particules de Marseille	Marseille, France	NIIG	Niigata Univ.	Niigata, Japan
MASA	Univ. of Massachusetts Amherst	Amherst , MA, USA	NIJM	Radboud Univ. Nijmegen	AJ Nijmegen , The Netherlands
MASB	Univ. of Massachusetts Boston	Boston , MA, USA	NIRS	Nat. Inst. Radiological Sciences	Chiba , Japan
MASD	Univ. of Massachusetts Dartmouth	North Dartmouth , MA, USA	NIST	National Institute of Standards & Technology	Gaithersburg, MD, USA
MCGI	McGill Univ.	Montreal, QC, Canada	NIU	Northern Illinois Univ.	De Kalb, IL, USA
MCHS	Univ. of Manchester	Manchester, United Kingdom	NMSU	New Mexico State Univ. ; Dept. of Physics, MSC 3D; Part. & Nucl. Phys. Group, Box 30001/Dept.	Las Cruces, NM, USA
MCMS	McMaster Univ.	Hamilton, ON, Canada	NORD	Nordita	Stockholm, Sweden
MEHTA	Harish-Chandra Research Inst.	Allahabad, India	NOTT	Univ. of Nottingham	Nottingham, United Kingdom
MEIS	Meisei Univ.	Tokyo, Japan			
MELB	Univ. of Melbourne	Victoria, Australia			
MEUD	Observatoire de Meudon	Meudon, France			

Abbreviations Used in the Particle Listings

NOVM	Inst. of Mathematics	Novosibirsk , Russian Federation	RHEL	Rutherford High Energy Lab (Old name for RAL)	Chilton, Didcot, Oxon., United Kingdom
NOVO	BINP, Budker Inst. of Nuclear Physics	Novosibirsk , Russian Federation	RICE	Rice Univ.	Houston, TX, USA
NPOL	Polytechnic of North London	London, United Kingdom	RIKEN	Riken Nishina Center for Accelerator-Based Science	Saitama, Japan
NRL	Naval Research Lab	Washington, DC, USA	RIKK	Rikkyo Univ.	Tokyo, Japan
NSF	National Science Foundation	Arlington, VA, USA	RIS	Rowland Inst. for Science	Cambridge, MA, USA
NTHU	National Tsing Hua Univ.	Hsinchu, Taiwan	RISC	Rockwell International	Thousand Oaks, CA, USA
NTUA	National Tech. Univ. of Athens	Athens, Greece	RISL	Universities Research Reactor	Risley , Warrington, United Kingdom
NWES	Northwestern Univ.	Evanston, IL, USA	RISO	Riso National Laboratory	Roskilde, Denmark
NYU	New York Univ.	New York, NY, USA	RITS	Royal Inst. of Technology (KTH)	Stockholm , Sweden
OBER	Oberlin College	Oberlin, OH, USA	RL	Rutherford High Energy Lab (Old name for RAL)	Chilton, Didcot, Oxon., United Kingdom
OCH	Ochanomizu Univ.	Tokyo, Japan	RMCS	Royal Military Coll. of Science	Swindon, Wilts., United Kingdom
OHIO	Ohio Univ.	Athens, OH, USA	ROCH	Univ. of Rochester	Rochester, NY, USA
OKAY	Okayama Univ.	Okayama, Japan	ROCK	Rockefeller Univ.	New York, NY, USA
OKLA	Univ. of Oklahoma	Norman, OK, USA	ROMA	Univ. di Roma (Historical)	Roma , Italy
OKSU	Oklahoma State Univ.	Stillwater, OK, USA	ROMA2	Univ. di Roma , "Tor Vergata"	Roma, Italy
OREG	Univ. of Oregon ; Inst. of Theoretical Science; U.O. Center for High Energy Physics	Eugene, OR, USA	ROMA3	INFN, Sez. di Roma Tre	Roma , Italy
ORNL	Oak Ridge National Laboratory	Oak Ridge, TN, USA	ROMAI	INFN, Sez. di Roma	Roma, Italy
ORSAY	Univ. de Paris Sud 11	Orsay CEDEX , France	ROSE	Rose-Hulman Inst. of Technology	Terre Haute, IN, USA
ORST	Oregon State Univ.	Corvallis, OR, USA	RPI	Rensselaer Polytechnic Inst.	Troy, NY, USA
OSAK	Osaka Univ.	Osaka, Japan	RUTG	Rutgers , the State Univ. of New Jersey	Piscataway, NJ, USA
OSKC	Osaka City Univ.	Osaka, Japan	S0GA	Sogang University	Seoul, Republic of Korea
OSLO	Univ. of Oslo	Oslo, Norway	SACL	CEA Saclay , IRFU	Gif-sur-Yvette, France
OSU	Ohio State Univ.	Columbus, OH, USA	SACL5	CEA Saclay – IPhT	Gif-sur-Yvette, France
OTTA	Univ. of Ottawa	Ottawa, ON, Canada	SACL6	CEA Saclay (Essonne)	Gif-sur-Yvette, France
OXF	University of Oxford	Oxford, United Kingdom	SAGA	Saga Univ.	Saga-shi, Japan
OXFTP	Univ. of Oxford	Oxford, United Kingdom	SAHA	Saha Inst. of Nuclear Physics	Bidhan Nagar, Calcutta, India
PADO	Univ. degli Studi di Padova	Padova, Italy	SANG	Kyoto Sangyo Univ.	Kyoto-shi, Japan
PARIN	LPNHE, IN²P³/CNRS	Paris, France	SANI	Ist. Superiore di Sanità	Roma , Italy
PARIS	Univ. de Paris (Historical)	Paris , France	SASK	Univ. of Saskatchewan	Saskatoon, SK, Canada
PARIT	Univ. Paris VII , LPTHE	Paris, France	SASSO	Lab. Naz. Gran Sasso dell'INFN	Assergi (AQ), Italy
PARM	INFN , Gruppo Collegato di Parma	Parma, Italy	SAVO	Univ. de Savoie	Chambery, France
PAST	Institut Pasteur	Paris , France	SBER	California State Univ.	San Bernardino , CA, USA
PATR	Univ. of Patras	Patras, Greece	SCHAF	W.J. Schafer Assoc.	Livermore, DA, USA
PAVI	Univ. di Pavia	Pavia, Italy	SCIT	Science Univ. of Tokyo	Tokyo, Japan
PAVII	INFN, Sez. di Pavia	Pavia , Italy	SCOT	Scottish Univ. Research and Reactor Ctr.	Glasgow, United Kingdom
PENN	Univ. of Pennsylvania	Philadelphia, PA, USA	SCUC	Univ. of South Carolina	Columbia, SC, USA
PGIA	INFN , Sezione di Perugia	Perugia, Italy	SEAT	Seattle Pacific Coll.	Seattle, WA, USA
PISA	Univ. di Pisa	Pisa, Italy	SEIB	Austrian Research Center, Seibersdorf LTD.	Seibersdorf, Austria
PISAI	INFN, Sez. di Pisa	Pisa, Italy	SEOU	Korea Univ. ; Dept. of Physics; HEP Group	Seoul, Republic of Korea
PITT	Univ. of Pittsburgh	Pittsburgh, PA, USA	SEOUL	Seoul National Univ. ; Center for Theoretical Physics; Dept. of Physics & Astronomy, Coll. of Natural Sciences	Seoul, Republic of Korea
PLAT	SUNY at Plattsburgh	Plattsburgh, NY, USA	SERP	IHEP , Inst. for High Energy Physics	Protvino, Russian Federation
PLRM	Univ. di Palermo	Palermo, Italy	SETO	Seton Hall Univ.	South Orange, NJ, USA
PNL	Battelle Memorial Inst.	Richland, WA, USA	SFLA	Univ. of South Florida	Tampa, FL, USA
PNPI	Petersburg Nuclear Physics Inst. of Russian Academy of Sciences	Gatchina, Russian Federation	SFRA	Simon Fraser University	Burnaby, BC, Canada
PPA	Princeton-Penn. Proton Accelerator (Historical in <i>Review</i>)	Princeton, NJ, USA	SFSU	California State Univ.	San Francisco , CA, USA
PRAG	Inst. of Physics, ASCR	Prague , Czech Republic	SHAMS	Ain Shams University	Abbassia, Cairo, Egypt
PRIN	Princeton Univ.	Princeton, NJ, USA	SHDN	Shandong Univ.	Jinan, Shandong, China
PSI	Paul Scherrer Inst.	Villigen PSI , Switzerland	SHEF	Univ. of Sheffield	Sheffield, United Kingdom
PSLL	Physical Science Lab	Las Cruces, NM, USA	SHMP	Univ. of Southampton	Southampton, United Kingdom
PSU	Penn State Univ.	University Park, PA, USA	SHRZ	Shiraz Univ.	Shiraz, Iran
PUCB	Pontificia Univ. Católica do Rio de Janeiro	Rio de Janeiro, RJ, Brazil	SIEG	Univ. of Siegen	Siegen, Germany
PUEB	Univ. Autonoma de Puebla	Puebla , Pue, Mexico	SILES	Univ. of Silesia	Katowice, Poland
PURD	Purdue Univ.	West Lafayette, IN, USA	SIN	Swiss Inst. of Nuclear Research (Old name for VILL)	Villigen , Switzerland
QUKI	Queen's Univ.	Kingston, ON, Canada	SING	National Univ. of Singapore	Kent Ridge, Singapore
RAL	STFC Rutherford Appleton Lab.	Chilton, Didcot, Oxfordshire, United Kingdom	SISSA	Scuola Internazionale Superiore di Studi Avanzati	Trieste , Italy
REGE	Univ. Regensburg	Regensburg, Germany	SLAC	SLAC National Accelerator Laboratory	Menlo Park, CA, USA
REHO	Weizmann Inst. of Science	Rehovot, Israel	SLOV	Inst. of Physics, Slovak Acad. of Sciences	Bratislava 45 , Slovakia
REZ	Nuclear Physics Inst. AVČR	Řež , Czech Republic			
RGSUL	Univ. Federal do Rio Grande do Sul (UFRGS)	Porto Alegre, RS, Brazil			
RHBL	Royal Holloway, Univ. of London	Egham, Surrey, United Kingdom			

Abbreviations Used in the Particle Listings

SMU	Southern Methodist Univ.	Dallas, TX, USA	TUZL	Tuzla Univ.	Tuzla, Argentina
SNSP	Scuola Normale Superiore	Pisa, Italy	UBA	Univ. de Buenos Aires	Buenos Aires, Argentina
SOFI	Inst. for Nuclear Research and Nuclear Energy	Sofia , Bulgaria	UCB	Univ. of California (Berkeley)	Berkeley, CA, USA
SOFU	Univ. of Sofia "St. Kliment Ohridski"	Sofia, Bulgaria	UCD	Univ. of California (Davis)	Davis, CA, USA
SORB	Sorbonne Université	Paris, France	UCI	Univ. of California (Irvine)	Irvine, CA, USA
SPAUL	Univ. de São Paulo	São Paulo, SP, Brazil	UCLA	Univ. of California (Los Angeles)	Los Angeles, CA, USA
SPIFT	Inst. de Física Teórica (IFT)	São Paulo , SP, Brazil	UCND	Union Carbide Corp.	Oak Ridge, TN, USA
SSL	Univ. of California (Berkeley)	Berkeley, CA, USA	UCR	Univ. of California (Riverside)	Riverside, CA, USA
STAN	Stanford Univ.	Stanford, CA, USA	UCSB	Univ. of California (Santa Barbara) ; Physics Dept., High Energy Physics Experiment	Santa Barbara, CA, USA
STEV	Stevens Inst. of Tech.	Hoboken, NJ, USA	UCSBT	Univ. of California (Santa Barbara) ; Kavli Inst. for Theoretical Physics	Santa Barbara, CA, USA
STFN	Jožef Stefan Institute	Ljubljana , Slovenia	UCSC	Univ. of California (Santa Cruz)	Santa Cruz, CA, USA
STLO	St. Louis Univ.	St. Louis, MO, USA	UCSD	Univ. of California (San Diego)	La Jolla, CA, USA
STOH	Stockholm Univ.	Stockholm, Sweden	UGAZ	Univ. of Gaziantep	Gaziantep, Turkey
STON	SUNY at Stony Brook	Stony Brook, NY, USA	UMD	Univ. of Maryland	College Park, MD, USA
STRB	Inst. Pluridisciplinaire Hubert Curien (CNRS)	Strasbourg , France	UNAM	Univ. Nac. Autónoma de México (UNAM)	México, DF, Mexico
STUT	Univ. Stuttgart	Stuttgart, Germany	UNAM	Univ. Nacional Autónoma de México (UNAM)	México, DF, Mexico
STUTM	Max-Planck-Inst.	Stuttgart , Germany	UNC	Univ. of North Carolina	Greensboro, NC, USA
SUGI	Sugiyama Jogakuen Univ.	Aichi, Japan	UNCCH	Univ. of North Carolina at Chapel Hill	Chapel Hill, NC, USA
SUNG	Sungkyunkwan Univ.	Suwon, Republic of Korea	UNCS	Union College	Schenectady, NY, USA
SURR	Univ. of Surrey	Guildford, Surrey, United Kingdom	UNESP	UNESP	Botucatu, Brazil
SUSS	Univ. of Sussex	Brighton, United Kingdom	UNH	Univ. of New Hampshire	Durham, NH, USA
SVR	Savannah River Labs.	Aiken, SC, USA	UNM	Univ. of New Mexico	Albuquerque, NM, USA
SYDN	Univ. of Sydney	Sydney, NSW, Australia	UOEH	Univ. of Occupational and Environmental Health	Kitakyushu , Japan
SYRA	Syracuse Univ.	Syracuse, NY, USA	UPNJ	Uppsala College	East Orange, NJ, USA
TAJK	Acad. Sci., Tadjik SSR	Dushanbe , Tadjikistan	UPPS	Uppsala Univ.	Uppsala , Sweden
TAMU	Texas A&M Univ.	College Station, TX, USA	UPR	Univ. of Puerto Rico	San Juan , PR, USA
TATA	Tata Inst. of Fundamental Research	Bombay, India	URI	Univ. of Rhode Island	Kingston, RI, USA
TBIL	Tbilisi State University	Tbilisi, Republic of Georgia	USC	Univ. of Southern California	Los Angeles, CA, USA
TELA	Tel-Aviv Univ.	Tel Aviv, Israel	USF	Univ. of San Francisco	San Francisco, CA, USA
TELE	Teledyne Brown Engineering	Huntsville, AL, USA	UTAH	Univ. of Utah	Salt Lake City, UT, USA
TEMP	Temple Univ.	Philadelphia, PA, USA	UTRE	Univ. of Utrecht	Utrecht, The Netherlands
TENN	Univ. of Tennessee	Knoxville, TN, USA	UTRO	Norwegian Univ. of Science & Technology	Trondheim, Norway
TEXA	Univ. of Texas at Austin	Austin, TX, USA	UVA	Univ. of Virginia	Charlottesville, VA, USA
TGAK	Tokyo Gakugei Univ.	Tokyo, Japan	UZINR	Acad. Sci., Ukrainian SSR	Uzhgorod , Ukraine
TGU	Tohoku Gakuin Univ.	Miyagi, Japan	VALE	Univ. de Valencia	Burjassot, Valencia , Spain
THES	Aristotle Univ. of Thessaloniki (ATh)	Thessaloniki, Greece	VALP	Valparaiso Univ.	Valparaiso, IN, USA
TINT	Tokyo Inst. of Technology	Tokyo, Japan	VAND	Vanderbilt Univ.	Nashville, TN, USA
TISA	Sagamihara Inst. of Space & Astronautical Sci.	Kanagawa, Japan	VASS	Vassar College	Poughkeepsie, NY, USA
TMSK	Tomsk Polytechnic Univ.	Tomsk , Russian Federation	VICT	Univ. of Victoria	Victoria, BC, Canada
TMTC	Tokyo Metropolitan Coll. Tech.	Tokyo, Japan	VIEN	Inst. für Hochenergiephysik (HEPHY)	Vienna , Austria
TMU	Tokyo Metropolitan Univ.	Tokyo, Japan	VILL	ETH Zürich	Zürich, Switzerland
TNTO	Univ. of Toronto	Toronto, ON, Canada	VPI	Virginia Tech.	Blacksburg, VA, USA
TOHO	Toho Univ.	Chiba, Japan	VRIJ	Vrije Univ.	HV Amsterdam , The Netherlands
TOHOK	Tohoku Univ.	Sendai, Japan	WABRNE	Eidgenössisches Amt für Messwesen	Waber , Switzerland
TOKA	Tokai Univ.	Shimizu, Japan	WARS	Univ. of Warsaw	Warsaw, Poland
TOKAH	Tokai Univ.	Hiratsuka, Japan	WASCR	Waseda Univ. ; Cosmic Ray Division	Tokyo, Japan
TOKMS	Univ. of Tokyo ; Meson Science Laboratory	Tokyo, Japan	WASH	Univ. of Washington ; Elem. Particle Experiment (EPE); Particle Astrophysics (PA)	Seattle, WA, USA
TOKU	Univ. of Tokushima	Tokushima-shi, Japan	WASU	Waseda Univ. ; Dept. of Physics, High Energy Physics Group	Tokyo, Japan
TOKY	Univ. of Tokyo ; High-Energy Physics Theory Group	Tokyo, Japan	WAYN	Wayne State Univ.	Detroit, MI, USA
TOKYC	Univ. of Tokyo ; Dept. of Chemistry	Tokyo, Japan	WESL	Wesleyan Univ.	Middletown, CT, USA
TORI	Univ. degli Studi di Torino	Torino, Italy	WIEN	Univ. Wien	Vienna, Austria
TPTI	Uzbek Academy of Sciences	Tashkent , Republic of Uzbekistan	WILL	Coll. of William and Mary	Williamsburg, VA, USA
TRIN	Trinity College Dublin	Dublin, Ireland	WINR	National Centre for Nuclear Research	Warsaw , Poland
TRIU	TRIUMF	Vancouver, BC, Canada	WISC	Univ. of Wisconsin	Madison, WI, USA
TRST	Univ. di Trieste	Trieste, Italy			
TRSTI	INFN, Sez. di Trieste	Trieste, Italy			
TRSTT	Univ. degli Studi di Trieste	Trieste, Italy			
TSUK	Univ. of Tsukuba	Ibaraki-ken, Japan			
TTAM	Tamagawa Univ.	Tokyo, Japan			
TUAT	Tokyo Univ. of Agriculture Tech.	Tokyo, Japan			
TUBIN	Univ. Tübingen	Tübingen, Germany			
TUFTS	Tufts Univ.	Medford, MA, USA			
TUW	Technische Univ. Wien	Vienna, Austria			

Abbreviations Used in the Particle Listings

WITW	Univ. of the Witwatersrand	Wits, South Africa	YERE	Yerevan Physics Inst.	Yerevan, Armenia
WMIU	Western Michigan Univ.	Kalamazoo, MI, USA	YOKO	Yokohama National Univ.	Yokohama-shi, Japan
WONT	The Univ. of Western Ontario	London, ON, Canada	YORKC	York Univ.	Toronto, Canada
WOOD	Woodstock College (No longer in existence)	Woodstock, MD, USA	ZAGR	Zagreb Univ.	Zagreb, Croatia
WUPP	Bergische Univ. Wuppertal	Wuppertal , Germany	ZARA	Univ. de Zaragoza	Zaragoza, Spain
WURZ	Univ. Würzburg	Würzburg, Germany	ZEEM	Univ. van Amsterdam	TV Amsterdam, The Netherlands
WUSL	Washington Univ.	St. Louis, MO, USA	ZHON	Zhongshan (Sun Yat-Sen) Univ.	Guangzhou, China
WYOM	Univ. of Wyoming	Laramie, WY, USA	ZHZH	Zhengzhou Univ.	Zhengzhou, Henan, China
YALE	Yale Univ.	New Haven, CT, USA	ZURI	Univ. Zürich	Zürich, Switzerland
YARO	Yaroslavl State Univ.	Yaroslavl, Russian Federation			
YCC	Yokohama Coll. of Commerce	Yokohama, Japan			

GAUGE AND HIGGS BOSONS

γ	1013
g (gluon)	1014
graviton	1014
W	1014
Z	1026
H^0	1046
Neutral Higgs Bosons, Searches for	1056
Charged Higgs Bosons (H^\pm and $H^{\pm\pm}$), Searches for	1065
New Heavy Bosons	1068
Axions (A^0) and Other Very Light Bosons	1084

Notes in the Listings

Extraction of triple gauge couplings (TGC's) (rev.)	1017
Anomalous $ZZ\gamma$, $Z\gamma\gamma$, and ZZV couplings	1042
Anomalous W/Z quartic couplings (rev.)	1043

Related Reviews in Volume 1

53. Mass and width of the W boson (rev.)	715
54. Z boson (rev.)	717



GAUGE AND HIGGS BOSONS

γ (photon)

$$I(J^{PC}) = 0,1(1^{- -})$$

γ MASS

Results prior to 2008 are critiqued in GOLDHABER 10. All experimental results published prior to 2005 are summarized in detail by TU 05.

The following conversions are useful: $1 \text{ eV} = 1.783 \times 10^{-33} \text{ g} = 1.957 \times 10^{-6} m_e$; $\chi_C = (1.973 \times 10^{-7} \text{ m})(1 \text{ eV}/m_\gamma)$.

VALUE (eV)	CL%	DOCUMENT ID	COMMENT
<1 × 10⁻¹⁸		1 RYUTOV 07	MHD of solar wind
••• We do not use the following data for averages, fits, limits, etc. •••			
<2.2 × 10 ⁻¹⁴		2 BONETTI 17	Fast Radio Bursts, FRB 121102
<1.8 × 10 ⁻¹⁴		3 BONETTI 16	Fast Radio Bursts, FRB 150418
<1.9 × 10 ⁻¹⁵		4 RETINO 16	Ampere's Law in solar wind
<2.3 × 10 ⁻⁹	95	5 EGOROV 14	Lensed quasar position
		6 ACCIOLY 10	Anomalous magn. mom.
<1 × 10 ⁻²⁶		7 ADELBERGER 07A	Proca galactic field
no limit feasible		7 ADELBERGER 07A	γ as Higgs particle
<1 × 10 ⁻¹⁹		8 TU 06	Torque on rotating magnetized toroid
<1.4 × 10 ⁻⁷		ACCIOLY 04	Dispersion of GHz radio waves by sun
<2 × 10 ⁻¹⁶		9 FULLEKRUG 04	Speed of 5-50 Hz radiation in atmosphere
<7 × 10 ⁻¹⁹		10 LUO 03	Torque on rotating magnetized toroid
<1 × 10 ⁻¹⁷		11 LAKES 98	Torque on toroid balance
<6 × 10 ⁻¹⁷		12 RYUTOV 97	MHD of solar wind
<8 × 10 ⁻¹⁶	90	13 FISCHBACH 94	Earth magnetic field
<5 × 10 ⁻¹³		14 CHERNIKOV 92	Ampere's Law null test
<1.5 × 10 ⁻⁹	90	15 RYAN 85	Coulomb's Law null test
<3 × 10 ⁻²⁷		16 CHIBISOV 76	Galactic magnetic field
<6 × 10 ⁻¹⁶	99.7	17 DAVIS 75	Jupiter's magnetic field
<7.3 × 10 ⁻¹⁶		HOLLWEG 74	Alfvén waves
<6 × 10 ⁻¹⁷		18 FRANKEN 71	Low freq. res. circuit
<2.4 × 10 ⁻¹³		19 KROLL 71A	Dispersion in atmosphere
<1 × 10 ⁻¹⁴		20 WILLIAMS 71	Tests Coulomb's Law
<2.3 × 10 ⁻¹⁵		GOLDHABER 68	Satellite data

- RYUTOV 07 extends the method of RYUTOV 97 to the radius of Pluto's orbit.
- BONETTI 17 uses frequency-dependent time delays of repeating FRB with well-determined redshift, assuming the DM is caused by expected dispersion in IGM. There are several uncertainties, leading to mass limit $2.2 \times 10^{-14} \text{ eV}$.
- BONETTI 16 uses frequency-dependent time delays of FRB, assuming the DM is caused by expected dispersion in IGM. There are several uncertainties, leading to mass limit $1.8 \times 10^{-14} \text{ eV}$, if indeed the FRB is at the initially reported redshift.
- RETINO 16 looks for deviations from Ampere's law in the solar wind, using Cluster four spacecraft data. Authors quote a range of limits from $1.9 \times 10^{-15} \text{ eV}$ to $7.9 \times 10^{-14} \text{ eV}$ depending on the assumptions of the vector potential from the interplanetary magnetic field.
- EGOROV 14 studies chromatic dispersion of lensed quasar positions ("gravitational rainbows") that could be produced by any of several mechanisms, among them via photon mass. Limit not competitive but obtained on cosmological distance scales.
- ACCIOLY 10 limits come from possible alterations of anomalous magnetic moment of electron and gravitational deflection of electromagnetic radiation. Reported limits are not "claimed" by the authors and in any case are not competitive.
- When trying to measure m one must distinguish between measurements performed on large and small scales. If the photon acquires mass by the Higgs mechanism, the large-scale behavior of the photon might be effectively Maxwellian. If, on the other hand, one postulates the Proca regime for all scales, the very existence of the galactic field implies $m < 10^{-26} \text{ eV}$, as correctly calculated by YAMAGUCHI 59 and CHIBISOV 76.
- TU 06 continues the work of LUO 03, with extended LAKES 98 method, reporting the improved limit $\mu^2 A = (0.7 \pm 1.7) \times 10^{-13} \text{ T/m}$ if $A = 0.2 \mu\text{G}$ out to $4 \times 10^{22} \text{ m}$. Reported result $\mu = (0.9 \pm 1.5) \times 10^{-52} \text{ g}$ reduces to the frequentist mass limit $1.2 \times 10^{-19} \text{ eV}$ (FELDMAN 98).
- FULLEKRUG 04 adopted KROLL 71A method with newer and better Schumann resonance data. Result questionable because assumed frequency shift with photon mass is assumed to be linear. It is quadratic according to theorem by GOLDHABER 71B, KROLL 71, and PARK 71.
- LUO 03 extends LAKES 98 technique to set a limit on $\mu^2 A$, where μ^{-1} is the Compton wavelength χ_C of the massive photon and A is the ambient vector potential. The important departure is that the apparatus rotates, removing sensitivity to the direction of A . They take $A = 10^{12} \text{ Tm}$, due to "cluster level fields." But see comment of GOLDHABER 03 and reply by LUO 03B.
- LAKES 98 reports limits on torque on a toroid Cavendish balance, obtaining a limit on $\mu^2 A < 2 \times 10^{-9} \text{ Tm/m}^2$ via the Maxwell-Proca equations, where μ^{-1} is the characteristic length associated with the photon mass and A is the ambient vector potential in the Lorentz gauge. Assuming $A \approx 1 \times 10^{12} \text{ Tm}$ due to cluster fields he obtains $\mu^{-1} > 2 \times 10^{10} \text{ m}$, corresponding to $\mu < 1 \times 10^{-17} \text{ eV}$. A more conservative limit, using $A \approx (1 \mu\text{G})(600 \text{ pc})$ based on the galactic field, is $\mu^{-1} > 1 \times 10^9 \text{ m}$ or $\mu < 2 \times 10^{-16} \text{ eV}$.
- RYUTOV 97 uses a magnetohydrodynamics argument concerning survival of the Sun's field to the radius of the Earth's orbit. "To reconcile observations to theory, one has to

- reduce [the photon mass] by approximately an order of magnitude compared with" per DAVIS 75. "Secure limit, best by this method" (per GOLDHABER 10).
- FISCHBACH 94 analysis is based on terrestrial magnetic fields; approach analogous to DAVIS 75. Similar result based on a much smaller planet probably follows from more precise B field mapping. "Secure limit, best by this method" (per GOLDHABER 10).
 - CHERNIKOV 92, motivated by possibility that photon exhibits mass only below some unknown critical temperature, searches for departure from Ampere's Law at 1.24 K. See also RYAN 85.
 - RYAN 85, motivated by possibility that photon exhibits mass only below some unknown critical temperature, sets mass limit at $< (1.5 \pm 1.4) \times 10^{-42} \text{ g}$ based on Coulomb's Law departure limit at 1.36 K. We report the result as frequentist 90% CL (FELDMAN 98).
 - CHIBISOV 76 depends in critical way on assumptions such as applicability of virial theorem. Some of the arguments given only in unpublished references.
 - DAVIS 75 analysis of Pioneer-10 data on Jupiter's magnetic field. "Secure limit, best by this method" (per GOLDHABER 10).
 - FRANKEN 71 method is of dubious validity (KROLL 71A, JACKSON 99, GOLDHABER 10, and references therein).
 - KROLL 71A used low frequency Schumann resonances in cavity between the conducting earth and resistive ionosphere, overcoming objections to resonant-cavity methods (JACKSON 99, GOLDHABER 10, and references therein). "Secure limit, best by this method" (per GOLDHABER 10).
 - WILLIAMS 71 is landmark test of Coulomb's law. "Secure limit, best by this method" (per GOLDHABER 10).

γ CHARGE

OKUN 06 has argued that schemes in which all photons are charged are inconsistent. He says that if a neutral photon is also admitted to avoid this problem, then other problems emerge, such as those connected with the emission and absorption of charged photons by charged particles. He concludes that in the absence of a self-consistent phenomenological basis, interpretation of experimental data is at best difficult.

VALUE (e)	CHARGE	DOCUMENT ID	TECN	COMMENT
<1 × 10⁻⁴⁶	mixed	1 ALTSCHUL 07B	VLBI	Aharonov-Bohm effect
<1 × 10⁻³⁵	single	2 CAPRINI 05	CMB	Isotropy constraint
••• We do not use the following data for averages, fits, limits, etc. •••				
<1 × 10 ⁻³²	single	1 ALTSCHUL 07B	VLBI	Aharonov-Bohm effect
<3 × 10 ⁻³³	mixed	3 KOBYCHEV 05	VLBI	Smear as function of B-E _γ
<4 × 10 ⁻³¹	single	3 KOBYCHEV 05	VLBI	Deflection as function of B-E _γ
<8.5 × 10 ⁻¹⁷		4 SEMERTZIDIS 03		Laser light deflection in B-field
<3 × 10 ⁻²⁸	single	5 SIVARAM 95	CMB	For $\Omega_M = 0.3, h^2 = 0.5$
<5 × 10 ⁻³⁰		6 RAFFELT 94	TOF	Pulsar $t_1 - t_2$
<2 × 10 ⁻²⁸		7 COCCONI 92		VLBA radio telescope resolution
<2 × 10 ⁻³²		COCCONI 88	TOF	Pulsar $t_1 - t_2$ TOF

- ALTSCHUL 07B looks for Aharonov-Bohm phase shift in addition to geometric phase shift in radio interference fringes (VSOP mission).
- CAPRINI 05 uses isotropy of the cosmic microwave background to place stringent limits on possible charge asymmetry of the Universe. Charge limits are set on the photon, neutrino, and dark matter particles. Valid if charge asymmetries produced by different particles are not anticorrelated.
- KOBYCHEV 05 considers a variety of observable effects of photon charge for extragalactic compact radio sources. Best limits if source observed through a foreground cluster of galaxies.
- SEMERTZIDIS 03 reports the first laboratory limit on the photon charge in the last 30 years. Straightforward improvements in the apparatus could attain a sensitivity of 10^{-20} e .
- SIVARAM 95 requires that CMB photon charge density not overwhelm gravity. Result scales as $\Omega_M h^2$.
- RAFFELT 94 notes that COCCONI 88 neglects the fact that the time delay due to dispersion by free electrons in the interstellar medium has the same photon energy dependence as that due to bending of a charged photon in the magnetic field. His limit is based on the assumption that the entire observed dispersion is due to photon charge. It is a factor of 200 less stringent than the COCCONI 88 limit.
- See COCCONI 92 for less stringent limits in other frequency ranges. Also see RAFFELT 94 note.

γ REFERENCES

BONETTI 17	PL B768 326	L. Bonetti et al.	(ORLEANS, CERN)
BONETTI 16	PL B757 548	L. Bonetti et al.	
RETINO 16	ASP 82 49	A. Retino, A.D.A.M. Spallicci, A. Vaivads (CURCP+)	
EGOROV 14	MNRAS 437 L90	P. Egorov et al.	(MOSU, MIPT, INRM)
ACCIOLY 10	PR D82 065026	A. Accioly, J. Helayel-Neto, E. Scatena (LABEX+)	
GOLDHABER 10	RMP 82 939	A.S. Goldhaber, M.M. Nieto (STON, LANL)	
ADELBERGER 07A	PRL 98 010402	E. Adelberger, G. Dvali, A. Gruzinov (WASH, NYU)	
ALTSCHUL 07B	PRL 98 261801	B. Altschul (IND)	
Also	ASP 29 230	B. Altschul (SUC)	
RYUTOV 07	PPCF 49 B429	D.D. Ryutov	(LLNL)
OKUN 06	APP B37 555	L.B. Okun	(ITEP)
TU 06	PL A352 267	L.-C. Tu et al.	
CAPRINI 05	JCAP 0502 006	C. Caprini, P.G. Ferreira (GEVA, OXFPT)	
KOBYCHEV 05	AL 31 147	V.V. Kobychiev, S.B. Popov (KIEV, PADO)	
TU 05	RPP 68 77	L.-C. Tu, J. Luo, G.T. Gillies	
ACCIOLY 04	PR D69 107501	A. Accioly, R. Paszko	
FULLEKRUG 04	PRL 93 043901	M. Fullekrug	
GOLDHABER 03	PRL 91 149101	A.S. Goldhaber, M.M. Nieto	
LUO 03	PRL 90 081801	J. Luo et al.	
LUO 03B	PRL 91 149102	J. Luo et al.	
SEMERTZIDIS 03	PR D67 017701	Y.K. Semertzidis, G.T. Danby, D.M. Lazarus	
JACKSON 99	Classical Electrodynamics (3rd ed., J. Wiley and Sons (1999))	J.D. Jackson	
FELDMAN 98	PR D57 3873	G.J. Feldman, R.D. Cousins	
LAKES 98	PRL 80 1826	R. Lakes	(WISC)
RYUTOV 97	PPCF 39 A73	D.D. Ryutov	(LLNL)

Gauge & Higgs Boson Particle Listings

$\gamma, g, \text{graviton}, W$

SIVARAM	95	AJP 63 473	C. Sivaram	(BANG)
FISCHBACH	94	PRL 73 514	E. Fischbach <i>et al.</i>	(PURD, JHU+)
RAFFELT	94	PR D50 7729	G. Raffelt	(MPIM)
CHERNIKOV	92	PRL 68 3383	M.A. Chernikov <i>et al.</i>	(ETH)
Also		PRL 69 2999 (erratum)	M.A. Chernikov <i>et al.</i>	(ETH)
COCCONI	92	AJP 60 750	G. Cocconi	(CERN)
COCCONI	88	PL B206 705	G. Cocconi	(CERN)
RYAN	85	PR D32 802	J.J. Ryan, F. Accetta, R.H. Austin	(PRIN)
CHIBISOV	76	SPU 19 524	G.V. Chibisov	(LEBD)
		Translated from UFN 119 551.		
DAVIS	75	PRL 35 1402	L. Davis, A.S. Goldhaber, M.M. Nieto	(CIT, STON+)
HOLLWEG	74	PRL 32 961	J.V. Hollweg	(NCAR)
FRANKEN	71	PRL 26 115	P.A. Franken, G.W. Ampulski	(MICH)
GOLDHABER	71B	RMP 43 277	A.S. Goldhaber, M.M. Nieto	(STON, BOHR, UCSB)
KROLL	71	PRL 26 1395	N.M. Kroll	(SLAC)
KROLL	71A	PRL 27 340	N.M. Kroll	(SLAC)
PARK	71	PRL 26 1393	D. Park, E.R. Williams	(WISC)
WILLIAMS	71	PRL 26 721	E.R. Williams, J.E. Faller, H.A. Hill	(WESL)
GOLDHABER	68	PRL 21 567	A.S. Goldhaber, M.M. Nieto	(STON)
YAMAGUCHI	59	PTPS 11 37	Y. Yamaguchi	

g or gluon

$$I(J^P) = 0(1^-)$$

SU(3) color octet

Mass $m = 0$. Theoretical value. A mass as large as a few MeV may not be precluded, see YNDURAIN 95.

VALUE	DOCUMENT ID	TECN	COMMENT
••• We do not use the following data for averages, fits, limits, etc. •••			
	ABREU	92E DLPH	Spin 1, not 0
	ALEXANDER	91H OPAL	Spin 1, not 0
	BEHREND	82D CELL	Spin 1, not 0
	BERGER	80D PLUT	Spin 1, not 0
	BRANDELIK	80C TASS	Spin 1, not 0

gluon REFERENCES

YNDURAIN	95	PL B345 524	F.J. Yndurain	(MADU)
ABREU	92E	PL B274 490	P. Abreu <i>et al.</i>	(DELPHI Collab.)
ALEXANDER	91H	ZPHY C52 543	G. Alexander <i>et al.</i>	(OPAL Collab.)
BEHREND	82D	PL B110 329	H.J. Behrend <i>et al.</i>	(CELLO Collab.)
BERGER	80D	PL B97 459	C. Berger <i>et al.</i>	(PLUTO Collab.)
BRANDELIK	80C	PL B97 453	R. Brandelik <i>et al.</i>	(TASSO Collab.)

graviton

$$J = 2$$

graviton MASS

Van Dam and Veltman (VANDAM 70), Iwasaki (IWASAKI 70), and Zakharov (ZAKHAROV 70) almost simultaneously showed that "... there is a discrete difference between the theory with zero-mass and a theory with finite mass, no matter how small as compared to all external momenta." The resolution of this "vDVZ discontinuity" has to do with whether the linear approximation is valid. De Rham *et al.* (DE-RHAM 11) have shown that nonlinear effects not captured in their linear treatment can give rise to a screening mechanism, allowing for massive gravity theories. See also GOLDHABER 10 and DE-RHAM 17 and references therein. Experimental limits have been set based on a Yukawa potential or signal dispersion. h_0 is the Hubble constant in units of $100 \text{ km s}^{-1} \text{ Mpc}^{-1}$.

The following conversions are useful: $1 \text{ eV} = 1.783 \times 10^{-33} \text{ g} = 1.957 \times 10^{-6} m_e$; $\chi_C = (1.973 \times 10^{-7} \text{ m}) \times (1 \text{ eV}/m_e)$.

VALUE (eV)	DOCUMENT ID	TECN	COMMENT
$< 6 \times 10^{-32}$	1	CHOUDHURY 04	YUKA Weak gravitational lensing
••• We do not use the following data for averages, fits, limits, etc. •••			
$< 6.8 \times 10^{-23}$		BERNUS 19	YUKA Planetary ephemeris INPOP17b
$< 1.4 \times 10^{-29}$	2	DESAI 18	YUKA Gal cluster Abell 1689
$< 5 \times 10^{-30}$	3	GUPTA 18	YUKA SPT-SZ
$< 3 \times 10^{-30}$	3	GUPTA 18	YUKA Planck all-sky SZ
$< 1.3 \times 10^{-29}$	3	GUPTA 18	YUKA redMaPPer SDSS-DR8
$< 6 \times 10^{-30}$	4	RANA 18	YUKA Weak lensing in massive clusters
$< 8 \times 10^{-30}$	5	RANA 18	YUKA SZ effect in massive clusters
$< 7 \times 10^{-23}$	6	ABBOTT 17	DISP Combined dispersion limit from three BH mergers
$< 1.2 \times 10^{-22}$	6	ABBOTT 16	DISP Combined dispersion limit from two BH mergers
$< 2.9 \times 10^{-21}$	7	ZAKHAROV 16	YUKA S2 star orbit
$< 5 \times 10^{-23}$	8	BRITO 13	Spinning black holes bounds
$< 4 \times 10^{-25}$	9	BASKARAN 08	Graviton phase velocity fluctuations
$< 6 \times 10^{-32}$	10	GRUZINOV 05	YUKA Solar System observations
$< 9.0 \times 10^{-34}$	11	GRSHTEIN 04	From Ω_{tot} value assuming RTG
$> 6 \times 10^{-34}$	12	DVALI 03	Horizon scales
$< 8 \times 10^{-20}$	13,14	FINN 02	DISP Binary pulsar orbital period decrease
	14,15	DAMOUR 91	Binary pulsar PSR 1913+16
$< 7 \times 10^{-23}$		TALMADGE 88	YUKA Solar system planetary astrometric data
$< 2 \times 10^{-29} h_0^{-1}$		GOLDHABER 74	Rich clusters
$< 7 \times 10^{-28}$		HARE 73	Galaxy
$< 8 \times 10^4$		HARE 73	2 γ decay

- CHOUDHURY 04 concludes from a study of weak-lensing data that masses heavier than about the inverse of 100 Mpc seem to be ruled out if the gravitation field has the Yukawa form.
- DESAI 18 limit based on dynamical mass models of galaxy cluster Abell 1689.
- GUPTA 18 obtains graviton mass limits using stacked clusters from 3 disparate surveys.
- RANA 18 limit, 68% CL, obtained using weak lensing mass profiles out to the radius at which the cluster density falls to 200 times the critical density of the Universe. Limit is based on the fractional change between Newtonian and Yukawa accelerations for the 50 most massive galaxy clusters in the Local Cluster Substructure Survey. Limits for other CL's and other density cuts are also given.
- RANA 18 limit, 68% CL, obtained using mass measurements via the SZ effect out to the radius at which the cluster density falls to 500 times the critical density of the Universe for 182 optically confirmed galaxy clusters in an Altacama Cosmology Telescope survey. Limits for other CL's and other density cuts are also given.
- ABBOTT 16 and ABBOTT 17 assumed a dispersion relation for gravitational waves modified relative to GR.
- ZAKHAROV 16 constrains range of Yukawa gravity interaction from S2 star orbit about black hole at Galactic center. The limit is $< 2.9 \times 10^{-21} \text{ eV}$ for $\delta = 100$.
- BRITO 13 explore massive graviton (spin-2) fluctuations around rotating black holes.
- BASKARAN 08 consider fluctuations in pulsar timing due to photon interactions ("surfing") with background gravitational waves.
- GRUZINOV 05 uses the DGP model (DVALI 00) showing that non-perturbative effects restore continuity with Einstein's equations as the graviton mass approaches 0, then bases his limit on Solar System observations.
- GRSHTEIN 04 use non-Einstein field relativistic theory of gravity (RTG), with a massive graviton, to obtain the 95% CL mass limit implied by the value of $\Omega_{tot} = 1.02 \pm 0.02$ current at the time of publication.
- DVALI 03 suggest scale of horizon distance via DGP model (DVALI 00). For a horizon distance of $3 \times 10^{26} \text{ m}$ (about age of Universe/ c ; GOLDHABER 10) this graviton mass limit is implied.
- FINN 02 analyze the orbital decay rates of PSR B1913+16 and PSR B1534+12 with a possible graviton mass as a parameter. The combined frequentist mass limit is at 90% CL.
- As of 2014, limits on dP/dt are now about 0.1% (see T. Damour, "Experimental tests of gravitational theory," in this Review).
- DAMOUR 91 is an analysis of the orbital period change in binary pulsar PSR 1913+16, and confirms the general relativity prediction to 0.8%. "The theoretical importance of the [rate of orbital period decay] measurement has long been recognized as a direct confirmation that the gravitational interaction propagates with velocity c (which is the immediate cause of the appearance of a damping force in the binary pulsar system) and thereby as a test of the existence of gravitational radiation and of its quadrupolar nature." TAYLOR 93 adds that orbital parameter studies now agree with general relativity to 0.5%, and set limits on the level of scalar contribution in the context of a family of tensor [spin 2]-biscalar theories.

graviton REFERENCES

BERNUS	19	PRL 123 161103	L. Bernus <i>et al.</i>	
DESAI	18	PL B778 325	S. Desai	(HYDER)
GUPTA	18	ANP 399 85	S. Gupta, S. Desai	
RANA	18	PL B781 220	A. Rana <i>et al.</i>	(DELHI)
ABBOTT	17	PRL 118 221101	B.P. Abbott <i>et al.</i>	(LIGO and Virgo Collabs.)
DE-RHAM	17	RMP 89 025004	C. de Rham <i>et al.</i>	
ABBOTT	16	PRL 116 061102	B.P. Abbott <i>et al.</i>	(LIGO and Virgo Collabs.)
ZAKHAROV	16	JCAP 1605 045	A.F. Zakharov <i>et al.</i>	
BRITO	13	PR D88 023514	R. Brito, V. Cardoso, P. Pani	(LISB, MISS, HSCA+)
DE-RHAM	11	PRL 106 231101	C. de Rham, G. Gabadadze, A.J. Tolley	
GOLDHABER	10	RMP 82 939	A.S. Goldhaber, M.M. Nieto	(STON, LANL)
BASKARAN	08	PR D78 044018	D. Baskaran <i>et al.</i>	
GRUZINOV	05	NAST 10 311	A. Gruzinov	(NYU)
CHOUDHURY	04	ASP 21 559	S.R. Choudhury <i>et al.</i>	(DELPHI, MELB)
GRSHTEIN	04	PAN 67 1596	S.S. Gershtein <i>et al.</i>	(SERP)
DVALI	03	Translated from YAF 67 1618.	G.R. Dvali, A. Gruzinov, M. Zaldarriaga	(NYU)
FINN	02	PR D65 044022	L.S. Finn, P.J. Sutton	
DVALI	00	PL B485 208	G.R. Dvali, G. Gabadadze, M. Porrati	(NYU)
TAYLOR	93	NAT 355 132	J.N. Taylor <i>et al.</i>	(PRIN, ARCO, BURE+)
DAMOUR	91	APJ 366 501	T. Damour, J.H. Taylor	(BURE, MEUD, PRIN)
TALMADGE	88	PRL 61 1159	C. Talmadge <i>et al.</i>	(JPL)
GOLDHABER	74	PR D9 1119	A.S. Goldhaber, M.M. Nieto	(LANL, STON)
HARE	73	CJP 51 431	M.G. Hare	(SASK)
IWASAKI	70	PR D2 2255	Y. Iwasaki	
VANDAM	70	NP B22 397	H. van Dam, M. Veltman	(UTRE)
ZAKHAROV	70	JETPL 12 312	V.I. Zakharov <i>et al.</i>	

W

$$J = 1$$

See the related review(s):
Mass and Width of the W Boson

W MASS

The W-mass listed here corresponds to the mass parameter in a Breit-Wigner distribution with mass-dependent width. To obtain the world average, common systematic uncertainties between experiments are properly taken into account. The LEP-2 average W mass based on published results is $80.376 \pm 0.033 \text{ GeV}$ [SCHAEL 13a]. The combined Tevatron data yields an average W mass of $80.387 \pm 0.016 \text{ GeV}$ [AALTONEN 13n]. A combination of the LEP average with this Tevatron average and the ATLAS value [AABOUD 18j], assuming a common systematic error of 7 MeV between the latter two [Jens Erler, 52nd Rencontres de Moriond

EW, March 2017], the world average W mass of 80.379 ± 0.012 GeV is obtained. OUR FIT quotes this value for the W mass.

VALUE (GeV)	EVTS	DOCUMENT ID	TECN	COMMENT
80.379 ± 0.012 OUR FIT				
80.370 ± 0.007 ± 0.017	13.7M	¹ AABOUD	18J ATLS	$E_{cm}^{pp} = 7$ TeV
80.375 ± 0.023	2177k	² ABAZOV	14N D0	$E_{cm}^{pp} = 1.96$ TeV
80.387 ± 0.019	1095k	³ AALTONEN	12E CDF	$E_{cm}^{pp} = 1.96$ TeV
80.336 ± 0.055 ± 0.039	10.3k	⁴ ABDALLAH	08A DLPH	$E_{cm}^{ee} = 161-209$ GeV
80.415 ± 0.042 ± 0.031	11830	⁵ ABBIENDI	06 OPAL	$E_{cm}^{ee} = 170-209$ GeV
80.270 ± 0.046 ± 0.031	9909	⁶ ACHARD	06 L3	$E_{cm}^{ee} = 161-209$ GeV
80.440 ± 0.043 ± 0.027	8692	⁷ SCHAEEL	06 ALEP	$E_{cm}^{ee} = 161-209$ GeV
80.483 ± 0.084	49247	⁸ ABAZOV	02D D0	$E_{cm}^{pp} = 1.8$ TeV
80.433 ± 0.079	53841	⁹ AFFOLDER	01E CDF	$E_{cm}^{pp} = 1.8$ TeV
• • • We do not use the following data for averages, fits, limits, etc. • • •				
80.520 ± 0.115		¹⁰ ANDREEV	18A H1	$e^\pm p$
80.367 ± 0.026	1677k	¹¹ ABAZOV	12F D0	$E_{cm}^{pp} = 1.96$ TeV
80.401 ± 0.043	500k	¹² ABAZOV	09AB D0	$E_{cm}^{pp} = 1.96$ TeV
80.413 ± 0.034 ± 0.034	115k	¹³ AALTONEN	07F CDF	$E_{cm}^{pp} = 1.96$ TeV
82.87 ± 1.82 ± $\begin{smallmatrix} +0.30 \\ -0.16 \end{smallmatrix}$	1500	¹⁴ AKTAS	06 H1	$e^\pm p \rightarrow \mathcal{T}_e(\nu_e)X$, $\sqrt{s} \approx 300$ GeV
80.3 ± 2.1 ± 1.2 ± 1.0	645	¹⁵ CHEKANOV	02C ZEUS	$e^- p \rightarrow \nu_e X$, $\sqrt{s} = 318$ GeV
81.4 ± $\begin{smallmatrix} +2.7 \\ -2.6 \end{smallmatrix}$ ± 2.0 ± $\begin{smallmatrix} +3.3 \\ -3.0 \end{smallmatrix}$	1086	¹⁶ BREITWEG	00D ZEUS	$e^+ p \rightarrow \mathcal{T}_e X$, $\sqrt{s} \approx 300$ GeV
80.84 ± 0.22 ± 0.83	2065	¹⁷ ALITTI	92B UA2	See W/Z ratio below
80.79 ± 0.31 ± 0.84		¹⁸ ALITTI	90B UA2	$E_{cm}^{pp} = 546,630$ GeV
80.0 ± 3.3 ± 2.4	22	¹⁹ ABE	89I CDF	$E_{cm}^{pp} = 1.8$ TeV
82.7 ± 1.0 ± 2.7	149	²⁰ ALBAJAR	89 UA1	$E_{cm}^{pp} = 546,630$ GeV
81.8 ± $\begin{smallmatrix} +6.0 \\ -5.3 \end{smallmatrix}$ ± 2.6	46	²¹ ALBAJAR	89 UA1	$E_{cm}^{pp} = 546,630$ GeV
89 ± 3 ± 6	32	²² ALBAJAR	89 UA1	$E_{cm}^{pp} = 546,630$ GeV
81. ± 5.	6	ARNISON	83 UA1	$E_{cm}^{ee} = 546$ GeV
80. ± $\begin{smallmatrix} +10. \\ -6. \end{smallmatrix}$	4	BANNER	83B UA2	Repl. by ALITTI 90B

¹ AABOUD 18J select $4.61M W^+ \rightarrow \mu^+ \nu_\mu$, $3.40M W^+ \rightarrow e^+ \nu_e$, $3.23M W^- \rightarrow \mu^- \bar{\nu}_\mu$ and $2.49M W^- \rightarrow e^- \bar{\nu}_e$ events in $4.6 \text{ fb}^{-1} pp$ data at 7 TeV. The W mass is determined using the transverse mass and transverse lepton momentum distributions, accounting for correlations. The systematic error includes 0.011 GeV experimental and 0.014 GeV modelling uncertainties.

² ABAZOV 14N is a combination of ABAZOV 09AB and ABAZOV 12F, also giving more details on the analysis.

³ AALTONEN 12E select $470k W \rightarrow e \nu$ decays and $625k W \rightarrow \mu \nu$ decays in 2.2 fb^{-1} of Run-II data. The mass is determined using the transverse mass, transverse lepton momentum and transverse missing energy distributions, accounting for correlations. This result supersedes AALTONEN 07F. AALTONEN 14D gives more details on the procedures followed by the authors.

⁴ ABDALLAH 08A use direct reconstruction of the kinematics of $W^+ W^- \rightarrow q \bar{q} \ell \nu$ and $W^+ W^- \rightarrow q \bar{q} q \bar{q}$ events for energies 172 GeV and above. The W mass was also extracted from the dependence of the WW cross section close to the production threshold and combined appropriately to obtain the final result. The systematic error includes ± 0.025 GeV due to final state interactions and ± 0.009 GeV due to LEP energy uncertainty.

⁵ ABBIENDI 06 use direct reconstruction of the kinematics of $W^+ W^- \rightarrow q \bar{q} \ell \nu \ell$ and $W^+ W^- \rightarrow q \bar{q} q \bar{q}$ events. The result quoted here is obtained combining this mass value with the results using $W^+ W^- \rightarrow \ell \nu \ell \ell \nu \ell$ events in the energy range 183–207 GeV (ABBIENDI 03C) and the dependence of the WW production cross-section on m_{WW} at threshold. The systematic error includes ± 0.009 GeV due to the uncertainty on the LEP beam energy.

⁶ ACHARD 06 use direct reconstruction of the kinematics of $W^+ W^- \rightarrow q \bar{q} \ell \nu \ell$ and $W^+ W^- \rightarrow q \bar{q} q \bar{q}$ events in the C.M. energy range 189–209 GeV. The result quoted here is obtained combining this mass value with the results obtained from a direct W mass reconstruction at 172 and 183 GeV and with those from the dependence of the WW production cross-section on m_{WW} at 161 and 172 GeV (ACCIARRI 99).

⁷ SCHAEEL 06 use direct reconstruction of the kinematics of $W^+ W^- \rightarrow q \bar{q} \ell \nu \ell$ and $W^+ W^- \rightarrow q \bar{q} q \bar{q}$ events in the C.M. energy range 183–209 GeV. The result quoted here is obtained combining this mass value with those obtained from the dependence of the W pair production cross-section on m_{WW} at 161 and 172 GeV (BARATE 97 and BARATE 97s respectively). The systematic error includes ± 0.009 GeV due to possible effects of final state interactions in the $q \bar{q} q \bar{q}$ channel and ± 0.009 GeV due to the uncertainty on the LEP beam energy.

⁸ ABAZOV 02D improve the measurement of the W -boson mass including $W \rightarrow e \nu_e$ events in which the electron is close to a boundary of a central electromagnetic calorimeter module. Properly combining the results obtained by fitting $m_T(W)$, $p_T(e)$, and $p_T(\nu)$, this sample provides a mass value of 80.574 ± 0.045 GeV. The value reported here is a combination of this measurement with all previous DØ W -boson mass measurements.

⁹ AFFOLDER 01E fit the transverse mass spectrum of 30115 $W \rightarrow e \nu_e$ events ($M_{WW} = 80.473 \pm 0.065 \pm 0.092$ GeV) and of 14740 $W \rightarrow \mu \nu_\mu$ events ($M_{WW} = 80.465 \pm 0.100 \pm 0.103$ GeV) obtained in the run IB (1994–95). Combining the electron and muon results, accounting for correlated uncertainties, yields $M_{WW} = 80.470 \pm 0.089$ GeV. They combine this value with their measurement of ABE 95P reported in run IA (1992–93) to obtain the quoted value.

¹⁰ ANDREEV 18A obtain this result in a combined electroweak and QCD analysis using all deep-inelastic $e^+ p$ and $e^- p$ neutral current and charged current scattering cross sections published by the H1 Collaboration, including data with longitudinally polarized lepton beams.

¹¹ ABAZOV 12F select $1677k W \rightarrow e \nu$ decays in 4.3 fb^{-1} of Run-II data. The mass is determined using the transverse mass and transverse lepton momentum distributions, accounting for correlations.

¹² ABAZOV 09AB study the transverse mass, transverse electron momentum, and transverse missing energy in a sample of 0.5 million $W \rightarrow e \nu$ decays selected in Run-II data. The quoted result combines all three methods, accounting for correlations.

¹³ AALTONEN 07F obtain high purity $W \rightarrow e \nu_e$ and $W \rightarrow \mu \nu_\mu$ candidate samples totaling 63,964 and 51,128 events respectively. The W mass value quoted above is derived by simultaneously fitting the transverse mass and the lepton, and neutrino p_T distributions.

¹⁴ AKTAS 06 fit the Q^2 dependence ($300 < Q^2 < 30,000 \text{ GeV}^2$) of the charged-current differential cross section with a propagator mass. The first error is experimental and the second corresponds to uncertainties due to input parameters and model assumptions.

¹⁵ CHEKANOV 02c fit the Q^2 dependence ($200 < Q^2 < 60000 \text{ GeV}^2$) of the charged-current differential cross sections with a propagator mass fit. The last error is due to the uncertainty on the probability density functions.

¹⁶ BREITWEG 00D fit the Q^2 dependence ($200 < Q^2 < 22500 \text{ GeV}^2$) of the charged-current differential cross sections with a propagator mass fit. The last error is due to the uncertainty on the probability density functions.

¹⁷ ALITTI 92B result has two contributions to the systematic error (± 0.83); one (± 0.81) cancels in m_W/m_Z and one (± 0.17) is noncancelling. These were added in quadrature. We choose the ALITTI 92B value without using the LEP m_Z value, because we perform our own combined fit.

¹⁸ There are two contributions to the systematic error (± 0.84): one (± 0.81) which cancels in m_W/m_Z and one (± 0.21) which is non-cancelling. These were added in quadrature.

¹⁹ ABE 89I systematic error dominated by the uncertainty in the absolute energy scale.

²⁰ ALBAJAR 89 result is from a total sample of 299 $W \rightarrow e \nu$ events.

²¹ ALBAJAR 89 result is from a total sample of 67 $W \rightarrow \mu \nu$ events.

²² ALBAJAR 89 result is from $W \rightarrow \tau \nu$ events.

W/Z MASS RATIO

VALUE	EVTS	DOCUMENT ID	TECN	COMMENT
0.88147 ± 0.00013		¹ PDG	19	
• • • We do not use the following data for averages, fits, limits, etc. • • •				
0.8821 ± 0.0011 ± 0.0008	28323	² ABBOTT	98N D0	$E_{cm}^{pp} = 1.8$ TeV
0.88114 ± 0.00154 ± 0.00252	5982	³ ABBOTT	98P D0	$E_{cm}^{pp} = 1.8$ TeV
0.8813 ± 0.0036 ± 0.0019	156	⁴ ALITTI	92B UA2	$E_{cm}^{pp} = 630$ GeV

¹ This value was obtained using the world average values of m_Z and m_W as listed in these listings.

² ABBOTT 98N obtain this from a study of 28323 $W \rightarrow e \nu_e$ and 3294 $Z \rightarrow e^+ e^-$ decays. Of this latter sample, 2179 events are used to calibrate the electron energy scale.

³ ABBOTT 98P obtain this from a study of 5982 $W \rightarrow e \nu_e$ events. The systematic error includes an uncertainty of ± 0.00175 due to the electron energy scale.

⁴ Scale error cancels in this ratio.

$m_Z - m_W$

VALUE (GeV)	DOCUMENT ID	TECN	COMMENT
10.809 ± 0.012	¹ PDG	19	
• • • We do not use the following data for averages, fits, limits, etc. • • •			
10.4 ± 1.4 ± 0.8	ALBAJAR	89 UA1	$E_{cm}^{pp} = 546,630$ GeV
11.3 ± 1.3 ± 0.9	ANSARI	87 UA2	$E_{cm}^{pp} = 546,630$ GeV

¹ This value was obtained using the world average values of m_Z and m_W as listed in these listings.

$m_{W^+} - m_{W^-}$

Test of CPT invariance.

VALUE (GeV)	EVTS	DOCUMENT ID	TECN	COMMENT
-0.029 ± 0.028 OUR AVERAGE				
-0.029 ± 0.013 ± 0.025	13.7M	¹ AABOUD	18J ATLS	$E_{cm}^{pp} = 7$ TeV
-0.19 ± 0.58	1722	ABE	90G CDF	$E_{cm}^{pp} = 1.8$ TeV

¹ AABOUD 18J select $4.61M W^+ \rightarrow \mu^+ \nu_\mu$, $3.40M W^+ \rightarrow e^+ \nu_e$, $3.23M W^- \rightarrow \mu^- \bar{\nu}_\mu$ and $2.49M W^- \rightarrow e^- \bar{\nu}_e$ events in $4.6 \text{ fb}^{-1} pp$ data at 7 TeV. The W mass is determined using the transverse mass and transverse lepton momentum distributions, accounting for correlations. The systematic error includes 0.007 GeV experimental and 0.024 GeV modelling uncertainties.

W WIDTH

The W width listed here corresponds to the width parameter in a Breit-Wigner distribution with mass-dependent width. To obtain the world average, common systematic uncertainties between experiments are properly taken into account. The LEP-2 average W width based on published results is 2.195 ± 0.083 GeV [SCHAEEL 13A]. The combined Tevatron data yields an average W width of 2.046 ± 0.049 GeV [FERMLAB-TM-2460-E].

OUR FIT uses these average LEP and Tevatron width values and combines them assuming no correlations.

VALUE (GeV)	EVTS	DOCUMENT ID	TECN	COMMENT
2.085 ± 0.042 OUR FIT				
2.028 ± 0.072	5272	¹ ABAZOV	09AK D0	$E_{cm}^{pp} = 1.96$ GeV
2.032 ± 0.045 ± 0.057	6055	² AALTONEN	08B CDF	$E_{cm}^{pp} = 1.96$ TeV
2.404 ± 0.140 ± 0.101	10.3k	³ ABDALLAH	08A DLPH	$E_{cm}^{ee} = 183-209$ GeV
1.996 ± 0.096 ± 0.102	10729	⁴ ABBIENDI	06 OPAL	$E_{cm}^{ee} = 170-209$ GeV

Gauge & Higgs Boson Particle Listings

W

2.18 ± 0.11 ± 0.09	9795	⁵ ACHARD	06 L3	$E_{cm}^{ee} = 172\text{--}209$ GeV
2.14 ± 0.09 ± 0.06	8717	⁶ SCHAEEL	06 ALEP	$E_{cm}^{ee} = 183\text{--}209$ GeV
2.23 $^{+0.15}_{-0.14}$ ± 0.10	294	⁷ ABAZOV	02E D0	$E_{cm}^{pp} = 1.8$ TeV
2.05 ± 0.10 ± 0.08	662	⁸ AFFOLDER	00M CDF	$E_{cm}^{pp} = 1.8$ TeV
• • • We do not use the following data for averages, fits, limits, etc. • • •				
2.152 ± 0.066	79176	⁹ ABBOTT	00B D0	Extracted value
2.064 ± 0.060 ± 0.059		¹⁰ ABE	95W CDF	Extracted value
2.10 $^{+0.14}_{-0.13}$ ± 0.09	3559	¹¹ ALITTI	92 UA2	Extracted value
2.18 $^{+0.26}_{-0.24}$ ± 0.04		¹² ALBAJAR	91 UA1	Extracted value

- ABAZOV 09AK obtain this result fitting the high-end tail (100–200 GeV) of the transverse mass spectrum in $W \rightarrow e\nu$ decays.
- AALTONEN 08B obtain this result fitting the high-end tail (90–200 GeV) of the transverse mass spectrum in semileptonic $W \rightarrow e\nu_e$ and $W \rightarrow \mu\nu_\mu$ decays.
- ABDALLAH 08A use direct reconstruction of the kinematics of $W^+W^- \rightarrow q\bar{q}\ell\nu$ and $W^+W^- \rightarrow q\bar{q}q\bar{q}$ events. The systematic error includes ±0.065 GeV due to final state interactions.
- ABBIENDI 06 use direct reconstruction of the kinematics of $W^+W^- \rightarrow q\bar{q}\ell\nu_\ell$ and $W^+W^- \rightarrow q\bar{q}q\bar{q}$ events. The systematic error includes ±0.003 GeV due to the uncertainty on the LEP beam energy.
- ACHARD 06 use direct reconstruction of the kinematics of $W^+W^- \rightarrow q\bar{q}\ell\nu_\ell$ and $W^+W^- \rightarrow q\bar{q}q\bar{q}$ events in the C.M. energy range 189–209 GeV. The result quoted here is obtained combining this value of the width with the result obtained from a direct W mass reconstruction at 172 and 183 GeV (ACCIARRI 99).
- SCHAEEL 06 use direct reconstruction of the kinematics of $W^+W^- \rightarrow q\bar{q}\ell\nu_\ell$ and $W^+W^- \rightarrow q\bar{q}q\bar{q}$ events. The systematic error includes ±0.05 GeV due to possible effects of final state interactions in the $q\bar{q}q\bar{q}$ channel and ±0.01 GeV due to the uncertainty on the LEP beam energy.
- ABAZOV 02E obtain this result fitting the high-end tail (90–200 GeV) of the transverse-mass spectrum in semileptonic $W \rightarrow e\nu_e$ decays.
- AFFOLDER 00M fit the high transverse mass (100–200 GeV) $W \rightarrow e\nu_e$ and $W \rightarrow \mu\nu_\mu$ events to obtain $\Gamma(W) = 2.04 \pm 0.11(\text{stat}) \pm 0.09(\text{syst})$ GeV. This is combined with the earlier CDF measurement (ABE 95C) to obtain the quoted result.
- ABBOTT 00B measure $R = 10.43 \pm 0.27$ for the $W \rightarrow e\nu_e$ decay channel. They use the SM theoretical predictions for $\sigma(W)/\sigma(Z)$ and $\Gamma(W \rightarrow e\nu_e)$ and the world average for $B(Z \rightarrow ee)$. The value quoted here is obtained combining this result (2.169 ± 0.070 GeV) with that of ABBOTT 99H.
- ABE 95W measured $R = 10.90 \pm 0.32 \pm 0.29$. They use $m_W = 80.23 \pm 0.18$ GeV, $\sigma(W)/\sigma(Z) = 3.35 \pm 0.03$, $\Gamma(W \rightarrow e\nu) = 225.9 \pm 0.9$ MeV, $\Gamma(Z \rightarrow e^+e^-) = 83.98 \pm 0.18$ MeV, and $\Gamma(Z) = 2.4969 \pm 0.0038$ GeV.
- ALITTI 92 measured $R = 10.4^{+0.7}_{-0.6} \pm 0.3$. The values of $\sigma(Z)$ and $\sigma(W)$ come from $O(\alpha_s^2)$ calculations using $m_W = 80.14 \pm 0.27$ GeV, and $m_Z = 91.175 \pm 0.021$ GeV along with the corresponding value of $\sin^2\theta_W = 0.2274$. They use $\sigma(W)/\sigma(Z) = 3.26 \pm 0.07 \pm 0.05$ and $\Gamma(Z) = 2.487 \pm 0.010$ GeV.
- ALBAJAR 91 measured $R = 9.5^{+1.1}_{-1.0}(\text{stat.} + \text{syst.})$. $\sigma(W)/\sigma(Z)$ is calculated in QCD at the parton level using $m_W = 80.18 \pm 0.28$ GeV and $m_Z = 91.172 \pm 0.031$ GeV along with $\sin^2\theta_W = 0.2322 \pm 0.0014$. They use $\sigma(W)/\sigma(Z) = 3.23 \pm 0.05$ and $\Gamma(Z) = 2.498 \pm 0.020$ GeV. This measurement is obtained combining both the electron and muon channels.

W+ DECAY MODES

W^- modes are charge conjugates of the modes below.

Mode	Fraction (Γ_i/Γ)	Confidence level
Γ_1 $\ell^+\nu$	[a] (10.86 ± 0.09) %	
Γ_2 $e^+\nu$	(10.71 ± 0.16) %	
Γ_3 $\mu^+\nu$	(10.63 ± 0.15) %	
Γ_4 $\tau^+\nu$	(11.38 ± 0.21) %	
Γ_5 hadrons	(67.41 ± 0.27) %	
Γ_6 $\pi^+\gamma$	< 7 × 10 ⁻⁶	95%
Γ_7 $D_s^+\gamma$	< 1.3 × 10 ⁻³	95%
Γ_8 cX	(33.3 ± 2.6) %	
Γ_9 $c\bar{s}$	(31 $^{+13}_{-11}$) %	
Γ_{10} invisible	[b] (1.4 ± 2.9) %	
Γ_{11} $\pi^+\pi^+\pi^-$	< 1.01 × 10 ⁻⁶	95%

[a] ℓ indicates each type of lepton (e , μ , and τ), not sum over them.

[b] This represents the width for the decay of the W boson into a charged particle with momentum below detectability, $p < 200$ MeV.

W PARTIAL WIDTHS

$\Gamma(\text{invisible})$ Γ_{10}
 This represents the width for the decay of the W boson into a charged particle with momentum below detectability, $p < 200$ MeV.

VALUE (MeV)	DOCUMENT ID	TECN	COMMENT
30⁺⁵²₋₄₈ ± 33	¹ BARATE	99I ALEP	$E_{cm}^{ee} = 161+172+183$ GeV
• • • We do not use the following data for averages, fits, limits, etc. • • •			
	² BARATE	99L ALEP	$E_{cm}^{ee} = 161+172+183$ GeV

- BARATE 99I measure this quantity using the dependence of the total cross section σ_W upon a change in the total width. The fit is performed to the WW measured cross sections at 161, 172, and 183 GeV. This partial width is < 139 MeV at 95%CL.
- BARATE 99L use W -pair production to search for effectively invisible W decays, tagging with the decay of the other W boson to Standard Model particles. The partial width for effectively invisible decay is < 27 MeV at 95%CL.

W BRANCHING RATIOS

Overall fits are performed to determine the branching ratios of the W boson. Averages on $W \rightarrow e\nu$, $W \rightarrow \mu\nu$, and $W \rightarrow \tau\nu$, and their correlations are obtained by combining results from the four LEP experiments properly taking into account the common systematic uncertainties and their correlations [SCHAEEL 13A]. A first fit determines the three individual leptonic branching ratios $B(W \rightarrow e\nu)$, $B(W \rightarrow \mu\nu)$, and $B(W \rightarrow \tau\nu)$. This fit has a $\chi^2 = 6.3$ for 9 degrees of freedom. The correlation coefficients between the branching fractions are 0.14 ($e-\mu$), -0.20 ($e-\tau$), -0.12 ($\mu-\tau$). A second fit assumes lepton universality and determines the leptonic branching ratio $B(W \rightarrow \ell\nu)$ and the hadronic branching ratio is derived as $B(W \rightarrow \text{hadrons}) = 1 - 3 B(W \rightarrow \ell\nu)$. This fit has a $\chi^2 = 15.4$ for 11 degrees of freedom.

$\Gamma(\ell^+\nu)/\Gamma_{\text{total}}$ Γ_1/Γ
 ℓ indicates average over e , μ , and τ modes, not sum over modes.

VALUE (units 10 ⁻²)	EVTs	DOCUMENT ID	TECN	COMMENT
10.86 ± 0.09 OUR FIT				
10.86 ± 0.12 ± 0.08	16438	ABBIENDI	07A OPAL	$E_{cm}^{ee} = 161\text{--}209$ GeV
10.85 ± 0.14 ± 0.08	13600	ABDALLAH	04G DLPH	$E_{cm}^{ee} = 161\text{--}209$ GeV
10.83 ± 0.14 ± 0.10	11246	ACHARD	04J L3	$E_{cm}^{ee} = 161\text{--}209$ GeV
10.96 ± 0.12 ± 0.05	16116	SCHAEEL	04A ALEP	$E_{cm}^{ee} = 183\text{--}209$ GeV
• • • We do not use the following data for averages, fits, limits, etc. • • •				
11.02 ± 0.52	11858	¹ ABBOTT	99H D0	$E_{cm}^{pp} = 1.8$ TeV
10.4 ± 0.8	3642	² ABE	92I CDF	$E_{cm}^{pp} = 1.8$ TeV

- ABBOTT 99H measure $R \equiv [\sigma_W B(W \rightarrow \ell\nu_\ell)]/[\sigma_Z B(Z \rightarrow \ell\ell)] = 10.90 \pm 0.52$ combining electron and muon channels. They use $m_W = 80.39 \pm 0.06$ GeV and the SM theoretical predictions for $\sigma(W)/\sigma(Z)$ and $B(Z \rightarrow \ell\ell)$.
- 1216 ± 38 $^{+27}_{-31}$ $W \rightarrow \mu\nu$ events from ABE 92I and 2426 $W \rightarrow e\nu$ events of ABE 91C. ABE 92I give the inverse quantity as 9.6 ± 0.7 and we have inverted.

$\Gamma(e^+\nu)/\Gamma_{\text{total}}$ Γ_2/Γ

VALUE (units 10 ⁻²)	EVTs	DOCUMENT ID	TECN	COMMENT
10.71 ± 0.16 OUR FIT				
10.71 ± 0.25 ± 0.11	2374	ABBIENDI	07A OPAL	$E_{cm}^{ee} = 161\text{--}209$ GeV
10.55 ± 0.31 ± 0.14	1804	ABDALLAH	04G DLPH	$E_{cm}^{ee} = 161\text{--}209$ GeV
10.78 ± 0.29 ± 0.13	1576	ACHARD	04J L3	$E_{cm}^{ee} = 161\text{--}209$ GeV
10.78 ± 0.27 ± 0.10	2142	SCHAEEL	04A ALEP	$E_{cm}^{ee} = 183\text{--}209$ GeV
• • • We do not use the following data for averages, fits, limits, etc. • • •				
10.61 ± 0.28		¹ ABAZOV	04D TEVA	$E_{cm}^{pp} = 1.8$ TeV

- ABAZOV 04D take into account all correlations to properly combine the CDF (ABE 95W) and DØ (ABBOTT 00B) measurements of the ratio R in the electron channel. The ratio R is defined as $[\sigma_W \cdot B(W \rightarrow e\nu_e)] / [\sigma_Z \cdot B(Z \rightarrow ee)]$. The combination gives $R^{\text{TeVatron}} = 10.59 \pm 0.23$. σ_W/σ_Z is calculated at next-to-next-to-leading order (3.360 ± 0.051). The branching fraction $B(Z \rightarrow ee)$ is taken from this Review as (3.363 ± 0.004) %.

$\Gamma(\mu^+\nu)/\Gamma_{\text{total}}$ Γ_3/Γ

VALUE (units 10 ⁻²)	EVTs	DOCUMENT ID	TECN	COMMENT
10.63 ± 0.15 OUR FIT				
10.78 ± 0.24 ± 0.10	2397	ABBIENDI	07A OPAL	$E_{cm}^{ee} = 161\text{--}209$ GeV
10.65 ± 0.26 ± 0.08	1998	ABDALLAH	04G DLPH	$E_{cm}^{ee} = 161\text{--}209$ GeV
10.03 ± 0.29 ± 0.12	1423	ACHARD	04J L3	$E_{cm}^{ee} = 161\text{--}209$ GeV
10.87 ± 0.25 ± 0.08	2216	SCHAEEL	04A ALEP	$E_{cm}^{ee} = 183\text{--}209$ GeV

$\Gamma(\mu^+\nu)/\Gamma(e^+\nu)$ Γ_3/Γ_2

VALUE	EVTs	DOCUMENT ID	TECN	COMMENT
0.996 ± 0.008 OUR AVERAGE				
1.003 ± 0.010		¹ AABOUD	17Q ATLS	$E_{cm}^{pp} = 7$ TeV
0.980 ± 0.018		² AAIJ	16AJ LHCB	$E_{cm}^{pp} = 8$ TeV
0.993 ± 0.019		SCHAEEL	13A LEP	$E_{cm}^{ee} = 130\text{--}209$ GeV
0.89 ± 0.10	13k	³ ABACHI	95D D0	$E_{cm}^{pp} = 1.8$ TeV
1.02 ± 0.08	1216	⁴ ABE	92I CDF	$E_{cm}^{pp} = 1.8$ TeV
1.00 ± 0.14 ± 0.08	67	ALBAJAR	89 UA1	$E_{cm}^{pp} = 546,630$ GeV
• • • We do not use the following data for averages, fits, limits, etc. • • •				
1.24 $^{+0.6}_{-0.4}$	14	ARNISON	84D UA1	Repl. by ALBAJAR 89

- AABOUD 17Q make a precise determination of $W \rightarrow e\nu$ and $W \rightarrow \mu\nu$ production in the following fiducial phase space: lepton pseudo-rapidity range $|\eta| < 2.5$, lepton and neutrino transverse momenta larger than 25 GeV each, and W transverse mass larger than 25 GeV. They determine the ratio of the W branching fractions $B(W \rightarrow e\nu)/B(W \rightarrow \mu\nu) = 0.9967 \pm 0.0004 \pm 0.0101 = 0.997 \pm 0.010$.

See key on page 999

Gauge & Higgs Boson Particle Listings

W

² AAIJ 16AJ make precise measurements of forward $W \rightarrow e\nu$ and $W \rightarrow \mu\nu$ production in proton-proton collisions at 8 TeV and determine the ratio of the W branching fractions $B(W \rightarrow e\nu)/B(W \rightarrow \mu\nu) = 1.020 \pm 0.002 \pm 0.019$.

³ ABACHI 95D obtain this result from the measured $\sigma_W B(W \rightarrow \mu\nu) = 2.09 \pm 0.23 \pm 0.11$ nb and $\sigma_W B(W \rightarrow e\nu) = 2.36 \pm 0.07 \pm 0.13$ nb in which the first error is the combined statistical and systematic uncertainty, the second reflects the uncertainty in the luminosity.

⁴ ABE 92I obtain $\sigma_W B(W \rightarrow \mu\nu) = 2.21 \pm 0.07 \pm 0.21$ and combine with ABE 91C $\sigma_W B(W \rightarrow e\nu)$ to give a ratio of the couplings from which we derive this measurement.

$\Gamma(\tau^+\nu)/\Gamma_{\text{total}}$		Γ_4/Γ			
VALUE (units 10^{-2})	EVTS	DOCUMENT ID	TECN	COMMENT	
11.38 ± 0.21 OUR FIT					
11.14 ± 0.31 ± 0.17	2177	ABBIENDI	07A OPAL	$E_{\text{cm}}^{\text{e}e} = 161\text{--}209$ GeV	
11.46 ± 0.39 ± 0.19	2034	ABDALLAH	04G DLPH	$E_{\text{cm}}^{\text{e}e} = 161\text{--}209$ GeV	
11.89 ± 0.40 ± 0.20	1375	ACHARD	04J L3	$E_{\text{cm}}^{\text{e}e} = 161\text{--}209$ GeV	
11.25 ± 0.32 ± 0.20	2070	SCHAEEL	04A ALEP	$E_{\text{cm}}^{\text{e}e} = 183\text{--}209$ GeV	

$\Gamma(\tau^+\nu)/\Gamma(e^+\nu)$		Γ_4/Γ_2			
VALUE	EVTS	DOCUMENT ID	TECN	COMMENT	
1.043 ± 0.024 OUR AVERAGE					
1.063 ± 0.027		SCHAEEL	13A LEP	$E_{\text{cm}}^{\text{e}e} = 130\text{--}209$ GeV	
0.961 ± 0.061	980	¹ ABBOTT	00D D0	$E_{\text{cm}}^{\text{p}p} = 1.8$ TeV	
0.94 ± 0.14	179	² ABE	92E CDF	$E_{\text{cm}}^{\text{p}p} = 1.8$ TeV	
1.04 ± 0.08 ± 0.08	754	³ ALITTI	92F UA2	$E_{\text{cm}}^{\text{p}p} = 630$ GeV	
1.02 ± 0.20 ± 0.12	32	ALBAJAR	89 UA1	$E_{\text{cm}}^{\text{p}p} = 546, 630$ GeV	
• • • We do not use the following data for averages, fits, limits, etc. • • •					
0.995 ± 0.112 ± 0.083	198	ALITTI	91c UA2	Repl. by ALITTI 92F	
1.02 ± 0.20 ± 0.10	32	ALBAJAR	87 UA1	Repl. by ALBAJAR 89	

¹ ABBOTT 00D measure $\sigma_W \times B(W \rightarrow \tau\nu_\tau) = 2.22 \pm 0.09 \pm 0.10 \pm 0.10$ nb. Using the ABBOTT 00B result $\sigma_W \times B(W \rightarrow e\nu_e) = 2.31 \pm 0.01 \pm 0.05 \pm 0.10$ nb, they quote the ratio of the couplings from which we derive this measurement.

² ABE 92E use two procedures for selecting $W \rightarrow \tau\nu_\tau$ events. The missing E_T trigger leads to 132 ± 14 ± 8 events and the τ trigger to 47 ± 9 ± 4 events. Proper statistical and systematic correlations are taken into account to arrive at $\sigma_B(W \rightarrow \tau\nu) = 2.05 \pm 0.27$ nb. Combined with ABE 91C result on $\sigma_B(W \rightarrow e\nu)$, ABE 92E quote a ratio of the couplings from which we derive this measurement.

³ This measurement is derived by us from the ratio of the couplings of ALITTI 92F.

$\Gamma(\tau^+\nu)/\Gamma(\mu^+\nu)$		Γ_4/Γ_3			
VALUE	DOCUMENT ID	TECN	COMMENT		
1.070 ± 0.026	SCHAEEL	13A LEP	$E_{\text{cm}}^{\text{e}e} = 130\text{--}209$ GeV		

$\Gamma(\text{hadrons})/\Gamma_{\text{total}}$		Γ_5/Γ			
VALUE (units 10^{-2})	EVTS	DOCUMENT ID	TECN	COMMENT	
67.41 ± 0.27 OUR FIT					
67.41 ± 0.37 ± 0.23	16438	ABBIENDI	07A OPAL	$E_{\text{cm}}^{\text{e}e} = 161\text{--}209$ GeV	
67.45 ± 0.41 ± 0.24	13600	ABDALLAH	04G DLPH	$E_{\text{cm}}^{\text{e}e} = 161\text{--}209$ GeV	
67.50 ± 0.42 ± 0.30	11246	ACHARD	04J L3	$E_{\text{cm}}^{\text{e}e} = 161\text{--}209$ GeV	
67.13 ± 0.37 ± 0.15	16116	SCHAEEL	04A ALEP	$E_{\text{cm}}^{\text{e}e} = 183\text{--}209$ GeV	

$\Gamma(\pi^+\gamma)/\Gamma(e^+\nu)$		Γ_6/Γ_2			
VALUE	CL%	DOCUMENT ID	TECN	COMMENT	
< 6.4 × 10⁻⁵	95	AALTONEN	12W CDF	$E_{\text{cm}}^{\text{p}p} = 1.96$ TeV	
< 7 × 10 ⁻⁴	95	ABE	98H CDF	$E_{\text{cm}}^{\text{p}p} = 1.8$ TeV	
< 4.9 × 10 ⁻³	95	¹ ALITTI	92D UA2	$E_{\text{cm}}^{\text{p}p} = 630$ GeV	
< 58 × 10 ⁻³	95	² ALBAJAR	90 UA1	$E_{\text{cm}}^{\text{p}p} = 546, 630$ GeV	

¹ ALITTI 92D limit is 3.8×10^{-3} at 90%CL.

² ALBAJAR 90 obtain < 0.048 at 90%CL.

$\Gamma(D_s^+\gamma)/\Gamma(e^+\nu)$		Γ_7/Γ_2			
VALUE	CL%	DOCUMENT ID	TECN	COMMENT	
< 1.2 × 10⁻²	95	ABE	98P CDF	$E_{\text{cm}}^{\text{p}p} = 1.8$ TeV	

$\Gamma(cX)/\Gamma(\text{hadrons})$		Γ_8/Γ_5			
VALUE	EVTS	DOCUMENT ID	TECN	COMMENT	
0.49 ± 0.04 OUR AVERAGE					
0.481 ± 0.042 ± 0.032	3005	¹ ABBIENDI	00V OPAL	$E_{\text{cm}}^{\text{e}e} = 183 + 189$ GeV	
0.51 ± 0.05 ± 0.03	746	² BARATE	99M ALEP	$E_{\text{cm}}^{\text{e}e} = 172 + 183$ GeV	

¹ ABBIENDI 00V tag $W \rightarrow cX$ decays using measured jet properties, lifetime information, and leptons produced in charm decays. From this result, and using the additional measurements of $\Gamma(W)$ and $B(W \rightarrow \text{hadrons})$, $|V_{cs}|$ is determined to be $0.969 \pm 0.045 \pm 0.036$.

² BARATE 99M tag c jets using a neural network algorithm. From this measurement $|V_{cs}|$ is determined to be $1.00 \pm 0.11 \pm 0.07$.

$\Gamma(\pi^+\pi^+\pi^-)/\Gamma_{\text{total}}$		Γ_{11}/Γ			
VALUE (units 10^{-6})	CL%	DOCUMENT ID	TECN	COMMENT	
< 1.01	95	¹ SIRUNYAN	19BG CMS	$E_{\text{cm}}^{\text{p}p} = 13$ TeV	

¹ SIRUNYAN 19BG search for the rare decay of a W boson into three charged pions. Three pion candidates are required in each event, with transverse momentum larger than 35 GeV, 35 GeV, 18 GeV, respectively, while the transverse momentum of the three-pion system is required to be larger than 40 GeV. Analyzing the three-pion invariant mass, no excess is observed in the W mass region, leading to the 95% C.L. upper limit on the branching fraction.

$R_{cs} = \Gamma(c\bar{s})/\Gamma(\text{hadrons})$		Γ_9/Γ_5			
VALUE	DOCUMENT ID	TECN	COMMENT		
0.46^{+0.18}_{-0.14} ± 0.07	¹ ABREU	98N DLPH	$E_{\text{cm}}^{\text{e}e} = 161 + 172$ GeV		

¹ ABREU 98N tag c and s jets by identifying a charged kaon as the highest momentum particle in a hadronic jet. They also use a lifetime tag to independently identify a c jet, based on the impact parameter distribution of charged particles in a jet. From this measurement $|V_{cs}|$ is determined to be $0.94^{+0.32}_{-0.26} ± 0.13$.

AVERAGE PARTICLE MULTIPLICITIES IN HADRONIC W DECAY

Summed over particle and antiparticle, when appropriate.

$\langle N_{\pi^\pm} \rangle$					
VALUE	DOCUMENT ID	TECN	COMMENT		
15.70 ± 0.35	¹ ABREU,P	00F DLPH	$E_{\text{cm}}^{\text{e}e} = 189$ GeV		

¹ ABREU,P 00F measure $\langle N_{\pi^\pm} \rangle = 31.65 \pm 0.48 \pm 0.76$ and $15.51 \pm 0.38 \pm 0.40$ in the fully hadronic and semileptonic final states respectively. The value quoted is a weighted average without assuming any correlations.

$\langle N_{K^\pm} \rangle$					
VALUE	DOCUMENT ID	TECN	COMMENT		
2.20 ± 0.19	¹ ABREU,P	00F DLPH	$E_{\text{cm}}^{\text{e}e} = 189$ GeV		

¹ ABREU,P 00F measure $\langle N_{K^\pm} \rangle = 4.38 \pm 0.42 \pm 0.12$ and $2.23 \pm 0.32 \pm 0.17$ in the fully hadronic and semileptonic final states respectively. The value quoted is a weighted average without assuming any correlations.

$\langle N_p \rangle$					
VALUE	DOCUMENT ID	TECN	COMMENT		
0.92 ± 0.14	¹ ABREU,P	00F DLPH	$E_{\text{cm}}^{\text{e}e} = 189$ GeV		

¹ ABREU,P 00F measure $\langle N_p \rangle = 1.82 \pm 0.29 \pm 0.16$ and $0.94 \pm 0.23 \pm 0.06$ in the fully hadronic and semileptonic final states respectively. The value quoted is a weighted average without assuming any correlations.

$\langle N_{\text{charged}} \rangle$					
VALUE	DOCUMENT ID	TECN	COMMENT		
19.39 ± 0.08 OUR AVERAGE					
19.38 ± 0.05 ± 0.08	¹ ABBIENDI	06A OPAL	$E_{\text{cm}}^{\text{e}e} = 189\text{--}209$ GeV		
19.44 ± 0.17	² ABREU,P	00F DLPH	$E_{\text{cm}}^{\text{e}e} = 183 + 189$ GeV		
19.3 ± 0.3 ± 0.3	³ ABBIENDI	99N OPAL	$E_{\text{cm}}^{\text{e}e} = 183$ GeV		
19.23 ± 0.74	⁴ ABREU	98C DLPH	$E_{\text{cm}}^{\text{e}e} = 172$ GeV		

¹ ABBIENDI 06A measure $\langle N_{\text{charged}} \rangle = 38.74 \pm 0.12 \pm 0.26$ when both W bosons decay hadronically and $\langle N_{\text{charged}} \rangle = 19.39 \pm 0.11 \pm 0.09$ when one W boson decays semileptonically. The value quoted here is obtained under the assumption that there is no color reconnection between W bosons; the value is a weighted average taking into account correlations in the systematic uncertainties.

² ABREU,P 00F measure $\langle N_{\text{charged}} \rangle = 39.12 \pm 0.33 \pm 0.36$ and $38.11 \pm 0.57 \pm 0.44$ in the fully hadronic final states at 189 and 183 GeV respectively, and $\langle N_{\text{charged}} \rangle = 19.49 \pm 0.31 \pm 0.27$ and $19.78 \pm 0.49 \pm 0.43$ in the semileptonic final states. The value quoted is a weighted average without assuming any correlations.

³ ABBIENDI 99N use the final states $W^+ W^- \rightarrow q\bar{q}l\bar{l}$ to derive this value.

⁴ ABREU 98C combine results from both the fully hadronic as well semileptonic WW final states after demonstrating that the W decay charged multiplicity is independent of the topology within errors.

TRIPLE GAUGE COUPLINGS (TGC'S)

Revised April 2017 by M.W. Grunewald (U. College Dublin) and A. Gurtu (Formerly Tata Inst.).

Fourteen independent couplings, seven each for ZWW and γWW , completely describe the VWW vertices within the most general framework of the electroweak Standard Model (SM) consistent with Lorentz invariance and U(1) gauge invariance. Of each of the seven TGCs, three conserve C and P individually, three violate CP , and one violates C and P individually while conserving CP . Assumption of C and P conservation and electromagnetic gauge invariance reduces the number of independent VWW couplings to five: one common set [1,2]

Gauge & Higgs Boson Particle Listings

W

is $(\kappa_\gamma, \kappa_Z, \lambda_\gamma, \lambda_Z, g_1^Z)$, where $\kappa_\gamma = \kappa_Z = g_1^Z = 1$ and $\lambda_\gamma = \lambda_Z = 0$ in the Standard Model at tree level. The parameters κ_Z and λ_Z are related to the other three due to constraints of gauge invariance as follows: $\kappa_Z = g_1^Z - (\kappa_\gamma - 1) \tan^2 \theta_W$ and $\lambda_Z = \lambda_\gamma$, where θ_W is the weak mixing angle. The W magnetic dipole moment, μ_W , and the W electric quadrupole moment, q_W , are expressed as $\mu_W = e(1 + \kappa_\gamma + \lambda_\gamma)/2M_W$ and $q_W = -e(\kappa_\gamma - \lambda_\gamma)/M_W^2$.

Precision measurements of suitable observables at LEP1 has already led to an exploration of much of the TGC parameter space. At LEP2, the VWW coupling arises in W -pair production via s -channel exchange, or in single W production via the radiation of a virtual photon off the incident e^+ or e^- . At the Tevatron and the LHC, hard-photon bremsstrahlung off a produced W or Z signals the presence of a triple-gauge vertex. In order to extract the value of one TGC, the others are generally kept fixed to their SM values. While most analyses use the above gauge constraints in the extraction of TGCs, one analysis of W -pair events also determines the real and imaginary parts of all 14 couplings using unconstrained single-parameter fits [3]. The results are consistent. Some experiments have determined limits on the couplings under various non-LEP scenarios and assuming different values of the form factor Λ , where the coupling parameters are scaled by $1/(1 + s/\Lambda^2)^2$. For practical reasons it is not possible to quote all such determinations in the listings. For that the individual papers may be consulted. Recently, EFT-inspired sets of couplings [4,5], such as $c_{WWW}/\Lambda^2, c_W/\Lambda^2, c_B/\Lambda^2$ which are linearly related to the couplings discussed above, are also determined by the LHC experiments.

References

1. K. Hagiwara *et al.*, Nucl. Phys. **B282**, 253 (1987).
2. G. Gounaris *et al.*, CERN 96-01 p. 525.
3. S. Schael *et al.* (ALEPH Collab.), Phys. Lett. **B614**, 7 (2005).
4. K. Hagiwara *et al.*, Phys. Rev. **D48**, 2182 (1993).
5. C. Degrande *et al.*, Annals Phys. **335** (2013) 21-32.

g_1^Z

OUR FIT below is taken from [SCHAE1 13A].

VALUE	EVTS	DOCUMENT ID	TECN	COMMENT
$0.984^{+0.018}_{-0.020}$				OUR FIT
$0.975^{+0.033}_{-0.030}$	7872	1 ABDALLAH	10 DLPH	$E_{cm}^{pp} = 189-209$ GeV
$1.001 \pm 0.027 \pm 0.013$	9310	2 SCHAE1	05A ALEP	$E_{cm}^{ee} = 183-209$ GeV
$0.987^{+0.034}_{-0.033}$	9800	3 ABBIENDI	04D OPAL	$E_{cm}^{ee} = 183-209$ GeV
$0.966^{+0.034}_{-0.032} \pm 0.015$	8325	4 ACHARD	04D L3	$E_{cm}^{ee} = 161-209$ GeV
• • •				We do not use the following data for averages, fits, limits, etc. • • •
		5 SIRUNYAN	19CL CMS	$E_{cm}^{pp} = 13$ TeV
		6 SIRUNYAN	18BZ CMS	$E_{cm}^{pp} = 13$ TeV
		7 AABOUD	17s ATLS	$E_{cm}^{pp} = 7+8$ TeV
		8 AABOUD	17u ATLS	$E_{cm}^{pp} = 8$ TeV
		9 KHACHATRY...	17o CMS	$E_{cm}^{pp} = 8$ TeV
		10 SIRUNYAN	17x CMS	$E_{cm}^{pp} = 8$ TeV
		11 AAD	16AR ATLS	$E_{cm}^{pp} = 8$ TeV
		12 AAD	16P ATLS	$E_{cm}^{pp} = 8$ TeV
		13 AAD	14Y ATLS	$E_{cm}^{pp} = 8$ TeV
		14 AAD	13AL ATLS	$E_{cm}^{pp} = 7$ TeV

		15 CHATRCHYAN	13BF CMS	$E_{cm}^{pp} = 7$ TeV
		16 AAD	12CD ATLS	$E_{cm}^{pp} = 7$ TeV
		17 AALTONEN	12AC CDF	$E_{cm}^{pp} = 1.96$ TeV
		18 ABAZOV	12AG D0	$E_{cm}^{pp} = 1.96$ TeV
		34 19 ABAZOV	11 D0	$E_{cm}^{pp} = 1.96$ TeV
		334 20 AALTONEN	10K CDF	$E_{cm}^{pp} = 1.96$ TeV
1.04 ± 0.09		21 ABAZOV	09AD D0	$E_{cm}^{pp} = 1.96$ TeV
		22 ABAZOV	09AJ D0	$E_{cm}^{pp} = 1.96$ TeV
$1.07^{+0.08}_{-0.12}$	1880	23 ABDALLAH	08c DLPH	Superseded by ABDAL-LAH 10
		13 24 ABAZOV	07Z D0	$E_{cm}^{pp} = 1.96$ TeV
		2.3 25 ABAZOV	05s D0	$E_{cm}^{pp} = 1.96$ TeV
$0.98 \pm 0.07 \pm 0.01$	2114	26 ABREU	01i DLPH	$E_{cm}^{ee} = 183+189$ GeV
		331 27 ABBOTT	99i D0	$E_{cm}^{pp} = 1.8$ TeV

- 1 ABDALLAH 10 use data on the final states $e^+e^- \rightarrow jj\ell\nu, jjjj, jjX, \ell X$, at center-of-mass energies between 189-209 GeV at LEP2, where $j = \text{jet}$, $\ell = \text{lepton}$, and X represents missing momentum. The fit is carried out keeping all other parameters fixed at their SM values.
- 2 SCHAE1 05A study single-photon, single- W , and WW -pair production from 183 to 209 GeV. The result quoted here is derived from the WW -pair production sample. Each parameter is determined from a single-parameter fit in which the other parameters assume their Standard Model values.
- 3 ABBIENDI 04D combine results from W^+W^- in all decay channels. Only CP -conserving couplings are considered and each parameter is determined from a single-parameter fit in which the other parameters assume their Standard Model values. The 95% confidence interval is $0.923 < g_1^Z < 1.054$.
- 4 ACHARD 04b study WW -pair production, single- W production and single-photon production with missing energy from 189 to 209 GeV. The result quoted here is obtained from the WW -pair production sample including data from 161 to 183 GeV, ACCIARRI 99q. Each parameter is determined from a single-parameter fit in which the other parameters assume their Standard Model values.
- 5 SIRUNYAN 19CL study WW and WZ production in lepton + jet events, with one W boson decaying leptonically (electron or muon), and another W or Z boson decaying hadronically, reconstructed as a single massive large-radius jet. In the electron channel 2,456 (2,235) events are selected in the $WW(WZ)$ category, while in the muon channel 3,996 (3,572) events are selected in the $WW(WZ)$ category. Analysing the di-boson invariant mass distribution, the following 95% C.L. limit is obtained: $0.9939 < g_1^Z < 1.0074$.
- 6 SIRUNYAN 18BZ study $pp \rightarrow Z$ jet jet events at 13 TeV where $Z \rightarrow e^+e^-/\mu^+\mu^-$. Isolated electrons and muons are selected with p_T of the leading/sub-leading lepton $> 30/20$ GeV and $|\eta| < 2.4$, with the di-lepton invariant mass within 15 GeV of the Z mass. The two highest p_T jets are selected with p_T of the leading/sub-leading jet $> 50/30$ GeV respectively and dijet invariant mass > 200 GeV. Templates in the transverse momentum of the Z are utilized to set limits on the triple gauge couplings in the EFT and the LEP parametrizations. The following 95% C.L. limit is obtained: $0.965 < g_1^Z < 1.042$.
- 7 AABOUD 17s analyze electroweak production of a W boson in association with two jets at high dijet invariant mass, with the W boson decaying to electron or muon plus neutrino. In the signal region of dijet mass larger than 1 TeV and leading-jet transverse momentum larger than 600 GeV, 30 events are observed in the data with 39 ± 4 events expected in the Standard Model, yielding the following limit at 95% CL for the form factor cut-off scale $\Lambda_{FF} \rightarrow \infty$: $0.87 < g_1^Z < 1.12$.
- 8 AABOUD 17u analyze production of WW or WZ boson pairs with one W boson decaying to electron or muon plus neutrino, and the other W or Z boson decaying hadronically. The hadronic decay system is reconstructed as either a resolved two-jet system or as a single large jet. Analysing the transverse momentum distribution of the hadronic system above 100 GeV yields the following limit at 95% CL for the form factor cut-off scale $\Lambda_{FF} \rightarrow \infty$: $0.979 < g_1^Z < 1.024$.
- 9 KHACHATRYAN 17o analyse WZ production where each boson decays into electrons or muons. Events are required to have a tri-lepton invariant mass larger than 100 GeV, with one of the lepton pairs having an invariant mass within 20 GeV of the Z boson mass. The Z transverse momentum spectrum is analyzed to set a 95% C.L. limit of: $0.982 < g_1^Z < 1.035$.
- 10 SIRUNYAN 17x study $pp \rightarrow WW/WZ \rightarrow \ell\nu q\bar{q}$ production at 8 TeV where ℓ is an electron or muon with $p_T > 30$ or 25 GeV respectively. Suitable cuts are put on the p_T of the dijet system and the missing E_T of the event yielding a total of 285 and 204 WW events observed in the electron and muon channels. The following 95% C.L. limit is obtained: $0.9913 < g_1^Z < 1.024$.
- 11 AAD 16AR study WW production in pp collisions and select 6636 WW candidates in decay modes with electrons or muons with an expected background of 1546 ± 157 events. Assuming the LEP formulation and setting the form-factor Λ to infinity, a fit to the transverse momentum distribution of the leading charged lepton, leads to a 95% C.L. range of $0.984 < g_1^Z < 1.027$.
- 12 AAD 16P study WZ production in pp collisions and select 2091 WZ candidates in 4 decay modes with electrons and muons, with an expected background of 1825 ± 7 events. Analysing the WZ transverse momentum distribution, the resulting 95% C.L. limit is: $0.981 < g_1^Z < 1.029$.
- 13 AAD 14Y determine the electroweak Z -dijet cross section in 8 TeV pp collisions. $Z \rightarrow ee$ and $Z \rightarrow \mu\mu$ decays are selected with the di-lepton $p_T > 20$ GeV and mass in the 81-101 GeV range. Minimum two jets are required with $p_T > 55$ and 45 GeV and no additional jets with $p_T > 25$ GeV in the rapidity interval between them. The normalized p_T balance between the Z and the two jets is required to be < 0.15 . This leads to a selection of 900 events with dijet mass > 1 TeV. The number of signal and background events expected is 261 and 592 respectively. A Poisson likelihood method is used on an event by event basis to obtain the 95% CL limit $0.5 < g_1^Z < 1.26$ for a form factor value $\Lambda = \infty$.
- 14 AAD 13AL study WW production in pp collisions and select 1325 WW candidates in decay modes with electrons or muons with an expected background of 369 ± 61 events. Assuming the LEP formulation and setting the form-factor $\Lambda = \text{infinity}$, a fit to the

- transverse momentum distribution of the leading charged lepton, leads to a 95% C.L. range of $0.961 < g_1^Z < 1.052$. Supersedes AAD 12Ac.
- 15 CHATRCHYAN 13BF determine the $W^+ W^-$ production cross section using unlike sign di-lepton (e or μ) events with high p_T . The leptons have $p_T > 20$ GeV/c and are isolated. 1134 candidate events are observed with an expected SM background of 247 ± 34 . The p_T distribution of the leading lepton is fitted to obtain 95% C.L. limits of $0.905 \leq g_1^Z \leq 1.095$.
- 16 AAD 12CD study WZ production in pp collisions and select 317 WZ candidates in three $\ell\nu$ decay modes with an expected background of 68.0 ± 10.0 events. The resulting 95% C.L. range is: $0.943 < g_1^Z < 1.093$. Supersedes AAD 12v.
- 17 AALTONEN 12AC study WZ production in $p\bar{p}$ collisions and select 63 WZ candidates in three $\ell\nu$ decay modes with an expected background of 7.9 ± 1.0 events. Based on the cross section and shape of the Z transverse momentum spectrum, the following 95% C.L. range is reported: $0.92 < g_1^Z < 1.20$ for a form factor of $\Lambda = 2$ TeV.
- 18 ABZOV 12AG combine new results with already published results on $W\gamma, WW$ and WZ production in order to determine the couplings with increased precision, superseding ABZOV 08R, ABZOV 11AC, ABZOV 09AJ, ABZOV 09AD. The 68% C.L. result for a formfactor cutoff of $\Lambda = 2$ TeV is $g_1^Z = 1.022^{+0.032}_{-0.030}$.
- 19 ABZOV 11 study the $p\bar{p} \rightarrow 3\ell\nu$ process arising in WZ production. They observe 34 WZ candidates with an estimated background of 6 events. An analysis of the p_T spectrum of the Z boson leads to a 95% C.L. limit of $0.944 < g_1^Z < 1.154$, for a form factor $\Lambda = 2$ TeV.
- 20 AALTONEN 10K study $p\bar{p} \rightarrow W^+ W^-$ with $W \rightarrow e/\mu\nu$. The p_T of the leading (second) lepton is required to be > 20 (10) GeV. The final number of events selected is 654 of which 320 ± 47 are estimated to be background. The 95% C.L. interval is $0.76 < g_1^Z < 1.34$ for $\Lambda = 1.5$ TeV and $0.78 < g_1^Z < 1.30$ for $\Lambda = 2$ TeV.
- 21 ABZOV 09AD study the $p\bar{p} \rightarrow \ell\nu 2\text{jet}$ process arising in WW and WZ production. They select 12,473 (14,392) events in the electron (muon) channel with an expected di-boson signal of 436 (527) events. The results on the anomalous couplings are derived from an analysis of the p_T spectrum of the 2-jet system and quoted at 68% C.L. and for a form factor of 2 TeV. This measurement is not used for obtaining the mean as it is for a specific form factor. The 95% confidence interval is $0.88 < g_1^Z < 1.20$.
- 22 ABZOV 09AJ study the $p\bar{p} \rightarrow 2\ell 2\nu$ process arising in WW production. They select 100 events with an expected WW signal of 65 events. An analysis of the p_T spectrum of the two charged leptons leads to 95% C.L. limits of $0.86 < g_1^Z < 1.3$, for a form factor $\Lambda = 2$ TeV.
- 23 ABDALLAH 08c determine this triple gauge coupling from the measurement of the spin density matrix elements in $e^+ e^- \rightarrow W^+ W^- \rightarrow (qq)(\ell\nu)$, where $\ell = e$ or μ . Values of all other couplings are fixed to their standard model values.
- 24 ABZOV 07z set limits on anomalous TGCs using the measured cross section and $p_T(Z)$ distribution in WZ production with both the W and the Z decaying leptonically into electrons and muons. Setting the other couplings to their standard model values, the 95% C.L. limit for a form factor scale $\Lambda = 2$ TeV is $0.86 < g_1^Z < 1.35$.
- 25 ABZOV 05s study $p\bar{p} \rightarrow WZ$ production with a subsequent trilepton decay to $\ell\nu\ell'\bar{\ell}'$ (ℓ and $\ell' = e$ or μ). Three events (estimated background 0.71 ± 0.08 events) with WZ decay characteristics are observed from which they derive limits on the anomalous WWZ couplings. The 95% CL limit for a form factor scale $\Lambda = 1.5$ TeV is $0.51 < g_1^Z < 1.66$, fixing λ_Z and κ_Z to their Standard Model values.
- 26 ABREU 01i combine results from $e^+ e^-$ interactions at 189 GeV leading to $W^+ W^-$ and $W\nu_e$ final states with results from ABREU 99L at 183 GeV. The 95% confidence interval is $0.84 < g_1^Z < 1.13$.
- 27 ABBOTT 99i perform a simultaneous fit to the $W\gamma, WW \rightarrow$ dilepton, $WW/WZ \rightarrow e\nu jj, WW/WZ \rightarrow \mu\nu jj$, and $WZ \rightarrow$ trilepton data samples. For $\Lambda = 2.0$ TeV, the 95%CL limits are $0.63 < g_1^Z < 1.57$, fixing λ_Z and κ_Z to their Standard Model values, and assuming Standard Model values for the $WW\gamma$ couplings.

κ_γ OUR FIT below is taken from [SCHAE 13A].

VALUE	EVTS	DOCUMENT ID	TECN	COMMENT
0.982±0.042 OUR FIT				
$1.024^{+0.077}_{-0.081}$	7872	1 ABDALLAH	10 DLPH	$E_{cm}^{pp} = 189-209$ GeV
$0.971 \pm 0.055 \pm 0.030$	10689	2 SCHAE 13A	05A ALEP	$E_{cm}^{pp} = 183-209$ GeV
$0.88^{+0.09}_{-0.08}$	9800	3 ABBIENDI	04D OPAL	$E_{cm}^{pp} = 183-209$ GeV
$1.013^{+0.067}_{-0.064} \pm 0.026$	10575	4 ACHARD	04D L3	$E_{cm}^{pp} = 161-209$ GeV
• • • We do not use the following data for averages, fits, limits, etc. • • •				
		5 AABOUD	17U ATLS	$E_{cm}^{pp} = 8$ TeV
		6 SIRUNYAN	17X CMS	$E_{cm}^{pp} = 8$ TeV
		7 CHATRCHYAN 14AB	CMS	$E_{cm}^{pp} = 7$ TeV
		8 AAD	13AN ATLS	$E_{cm}^{pp} = 7$ TeV
		9 CHATRCHYAN 13BF	CMS	$E_{cm}^{pp} = 7$ TeV
		10 ABZOV	12AG D0	$E_{cm}^{pp} = 1.96$ TeV
		11 ABZOV	11AC D0	$E_{cm}^{pp} = 1.96$ TeV
		12 CHATRCHYAN 11M	CMS	$E_{cm}^{pp} = 7$ TeV
	334	13 AALTONEN	10K CDF	$E_{cm}^{pp} = 1.96$ TeV
	53	14 AARON	09B H1	$E_{cm}^{pp} = 0.3$ TeV
		15 ABZOV	09AD D0	$E_{cm}^{pp} = 1.96$ TeV
		16 ABZOV	09AJ D0	$E_{cm}^{pp} = 1.96$ TeV
$1.07^{+0.26}_{-0.29}$		17 ABZOV	08R D0	$E_{cm}^{pp} = 1.96$ TeV

- 0.68 $^{+0.17}_{-0.15}$ 1880 18 ABDALLAH 08c DLPH Superseded by ABDALLAH 10
- 1617 19 AALTONEN 07L CDF $E_{cm}^{pp} = 1.96$ GeV
- 17 20 ABZOV 06H D0 $E_{cm}^{pp} = 1.96$ TeV
- 141 21 ABZOV 05J D0 $E_{cm}^{pp} = 1.96$ TeV
- 1.25 $^{+0.21}_{-0.20} \pm 0.06$ 2298 22 ABREU 01i DLPH $E_{cm}^{pp} = 183+189$ GeV
- 23 BREITWEG 00 ZEUS $e^+ p \rightarrow e^+ W^+ X$, $\sqrt{s} \approx 300$ GeV
- 0.92 ± 0.34 331 24 ABBOTT 99i D0 $E_{cm}^{pp} = 1.8$ TeV
- 1 ABDALLAH 10 use data on the final states $e^+ e^- \rightarrow jj\ell\nu, jjjj, jjX, \ell X$, at center-of-mass energies between 189-209 GeV at LEP2, where $j = \text{jet}$, $\ell = \text{lepton}$, and X represents missing momentum. The fit is carried out keeping all other parameters fixed at their SM values.
- 2 SCHAE 05A study single-photon, single- W , and WW -pair production from 183 to 209 GeV. Each parameter is determined from a single-parameter fit in which the other parameters assume their Standard Model values.
- 3 ABBIENDI 04d combine results from $W^+ W^-$ in all decay channels. Only CP -conserving couplings are considered and each parameter is determined from a single-parameter fit in which the other parameters assume their Standard Model values. The 95% confidence interval is $0.73 < \kappa_\gamma < 1.07$.
- 4 ACHARD 04d study WW -pair production, single- W production and single-photon production with missing energy from 189 to 209 GeV. The result quoted here is obtained including data from 161 to 183 GeV, ACCIARRI 99q. Each parameter is determined from a single-parameter fit in which the other parameters assume their Standard Model values.
- 5 AABOUD 17U analyze production of WW or WZ boson pairs with one W boson decaying to electron or muon plus neutrino, and the other W or Z boson decaying hadronically. The hadronic decay system is reconstructed as either a resolved two-jet system or as a single large jet. Analysing the transverse momentum distribution of the hadronic system above 100 GeV yields the following limit at 95% CL for the form factor cut-off scale $\Lambda_{FF} \rightarrow \infty$: $0.939 < \kappa_\gamma < 1.064$.
- 6 SIRUNYAN 17x study $pp \rightarrow WW/WZ \rightarrow \ell\nu q\bar{q}$ production at 8 TeV where ℓ is an electron or muon with $p_T > 30$ or 25 GeV respectively. Suitable cuts are put on the p_T of the dijet system and the missing E_T of the event yielding a total of 285 and 204 WV events observed in the electron and muon channels. The following 95% C.L. limit is obtained: $0.956 < \kappa_\gamma < 1.063$.
- 7 CHATRCHYAN 14AB measure $W\gamma$ production cross section for $p_T^\gamma > 15$ GeV and $R(\ell,\gamma) > 0.7$, which is the separation between the γ and the final state charged lepton (e or μ) in the azimuthal angle-pseudorapidity ($\phi - \eta$) plane. After background subtraction the number of $e\nu\gamma$ and $\mu\nu\gamma$ events is determined to be 3200 ± 325 and 4970 ± 543 respectively, compatible with expectations from the SM. This leads to a 95% CL limit of $0.62 < \kappa_\gamma < 1.29$, assuming other parameters have SM values.
- 8 AAD 13AN study $W\gamma$ production in pp collisions. In events with no additional jet, 4449 (6578) W decays to electron (muon) are selected, with an expected background of 1662 ± 262 (2538 ± 362) events. Analysing the photon p_T spectrum above 100 GeV yields a 95% C.L. limit of $0.59 < \kappa_\gamma < 1.46$. Supersedes AAD 12Bx.
- 9 CHATRCHYAN 13BF determine the $W^+ W^-$ production cross section using unlike sign di-lepton (e or μ) events with high p_T . The leptons have $p_T > 20$ GeV/c and are isolated. 1134 candidate events are observed with an expected SM background of 247 ± 34 . The p_T distribution of the leading lepton is fitted to obtain 95% C.L. limits of $0.79 \leq \kappa_\gamma \leq 1.22$.
- 10 ABZOV 12AG combine new results with already published results on $W\gamma, WW$ and WZ production in order to determine the couplings with increased precision, superseding ABZOV 08R, ABZOV 11AC, ABZOV 09AJ, ABZOV 09AD. The 68% C.L. result for a formfactor cutoff of $\Lambda = 2$ TeV is $\kappa_\gamma = 1.048^{+0.106}_{-0.105}$.
- 11 ABZOV 11AC study $W\gamma$ production in $p\bar{p}$ collisions at 1.96 TeV, with the W decay products containing an electron or a muon. They select 196 (363) events in the electron (muon) mode, with a SM expectation of 190 (372) events. A likelihood fit to the photon E_T spectrum above 15 GeV yields at 95% C.L. the result: $0.6 < \kappa_\gamma < 1.4$ for a formfactor $\Lambda = 2$ TeV.
- 12 CHATRCHYAN 11M study $W\gamma$ production in pp collisions at $\sqrt{s} = 7$ TeV using 36 pb^{-1} pp data with the W decaying to electron and muon. The total cross section is measured for photon transverse energy $E_T^\gamma > 10$ GeV and spatial separation from charged leptons in the plane of pseudo rapidity and azimuthal angle $\Delta R(\ell,\gamma) > 0.7$. The number of candidate (background) events is 452 (228 ± 21) for the electron channel and 520 (277 ± 25) for the muon channel. Setting other couplings to their standard model value, they derive a 95% CL limit of $-0.11 < \kappa_\gamma < 2.04$.
- 13 AALTONEN 10K study $p\bar{p} \rightarrow W^+ W^-$ with $W \rightarrow e/\mu\nu$. The p_T of the leading (second) lepton is required to be > 20 (10) GeV. The final number of events selected is 654 of which 320 ± 47 are estimated to be background. The 95% C.L. interval is $0.37 < \kappa_\gamma < 1.72$ for $\Lambda = 1.5$ TeV and $0.43 < \kappa_\gamma < 1.65$ for $\Lambda = 2$ TeV.
- 14 AARON 09B study single- W production in ep collisions at 0.3 TeV C.M. energy. They select 53 $W \rightarrow e/\mu$ events with a standard model expectation of 54.1 ± 7.4 events. Fitting the transverse momentum spectrum of the hadronic recoil system they obtain a 95% C.L. limit of $-3.7 < \kappa_\gamma < -1.5$ or $0.3 < \kappa_\gamma < 1.5$, where the ambiguity is due to the quadratic dependence of the cross section to the coupling parameter.
- 15 ABZOV 09AD study the $p\bar{p} \rightarrow \ell\nu 2\text{jet}$ process arising in WW and WZ production. They select 12,473 (14,392) events in the electron (muon) channel with an expected di-boson signal of 436 (527) events. The results on the anomalous couplings are derived from an analysis of the p_T spectrum of the 2-jet system and quoted at 68% C.L. and for a form factor of 2 TeV. This measurement is not used for obtaining the mean as it is for a specific form factor. The 95% confidence interval is $0.56 < \kappa_\gamma < 1.55$.
- 16 ABZOV 09AJ study the $p\bar{p} \rightarrow 2\ell 2\nu$ process arising in WW production. They select 100 events with an expected WW signal of 65 events. An analysis of the p_T spectrum of the two charged leptons leads to 95% C.L. limits of $0.46 < \kappa_\gamma < 1.83$, for a form factor $\Lambda = 2$ TeV.
- 17 ABZOV 08R use 0.7 fb^{-1} $p\bar{p}$ data at $\sqrt{s} = 1.96$ TeV to select 263 $W\gamma + X$ events, of which 187 constitute signal, with the W decaying into an electron or a muon, which is required to be well separated from a photon with $E_T > 9$ GeV. A likelihood fit to the photon E_T spectrum yields a 95% CL limit $0.49 < \kappa_\gamma < 1.51$ with other couplings fixed to their Standard Model values.

Gauge & Higgs Boson Particle Listings

W

- ¹⁸ ABDALLAH 08c determine this triple gauge coupling from the measurement of the spin density matrix elements in $e^+e^- \rightarrow W^+W^- \rightarrow (qq)(\ell\nu)$, where $\ell = e$ or μ . Values of all other couplings are fixed to their standard model values.
- ¹⁹ AALTONEN 07L set limits on anomalous TGCs using the $p_T(W)$ distribution in WW and WZ production with the W decaying to an electron or muon and the Z to 2 jets. Setting other couplings to their standard model value, the 95% C.L. limits are $0.54 < \kappa_\gamma < 1.39$ for a form factor scale $\Lambda = 1.5$ TeV.
- ²⁰ ABAZOV 06H study $\bar{p}p \rightarrow WW$ production with a subsequent decay $WW \rightarrow e^+\nu_e e^- \bar{\nu}_e$, $WW \rightarrow e^\pm \nu_e \mu^\mp \nu_\mu$ or $WW \rightarrow \mu^\pm \nu_\mu \mu^\mp \bar{\nu}_\mu$. The 95% C.L. limit for a form factor scale $\Lambda = 1$ TeV is $-0.05 < \kappa_\gamma < 2.29$, fixing $\lambda_\gamma = 0$. With the assumption that the $WW\gamma$ and WWZ couplings are equal the 95% C.L. one-dimensional limit ($\Lambda = 2$ TeV) is $0.68 < \kappa < 1.45$.
- ²¹ ABAZOV 05J perform a likelihood fit to the photon E_T spectrum of $W\gamma + X$ events, where the W decays to an electron or muon which is required to be well separated from the photon. For $\Lambda = 2.0$ TeV the 95% CL limits are $0.12 < \kappa_\gamma < 1.96$. In the fit λ_γ is kept fixed to its Standard Model value.
- ²² ABREU 01i combine results from e^+e^- interactions at 189 GeV leading to W^+W^- , $W\nu_e$, and $\nu\bar{\nu}\gamma$ final states with results from ABREU 99L at 183 GeV. The 95% confidence interval is $0.87 < \kappa_\gamma < 1.68$.
- ²³ BREITWEG 00 search for W production in events with large hadronic p_T . For $p_T > 20$ GeV, the upper limit on the cross section gives the 95% CL limit $-3.7 < \kappa_\gamma < 2.5$ (for $\lambda_\gamma = 0$).
- ²⁴ ABBOTT 99i perform a simultaneous fit to the $W\gamma$, $WW \rightarrow$ dilepton, $WW/WZ \rightarrow e\nu jj$, $WW/WZ \rightarrow \mu\nu jj$, and $WZ \rightarrow$ trilepton data samples. For $\Lambda = 2.0$ TeV, the 95% CL limits are $0.75 < \kappa_\gamma < 1.39$.

 λ_γ

OUR FIT below is taken from [SCHAEEL 13A].

VALUE	EVTS	DOCUMENT ID	TECN	COMMENT
-0.022 ± 0.019 OUR FIT				
0.002 ± 0.035	7872	1 ABDALLAH	10 DLPH	$E_{cm}^{ee} = 189-209$ GeV
-0.012 ± 0.027 ± 0.011	10689	2 SCHAEEL	05A ALEP	$E_{cm}^{ee} = 183-209$ GeV
-0.060 + 0.034 -0.033	9800	3 ABBIENDI	04D OPAL	$E_{cm}^{ee} = 183-209$ GeV
-0.021 + 0.035 -0.034 ± 0.017	10575	4 ACHARD	04D L3	$E_{cm}^{ee} = 161-209$ GeV
• • • We do not use the following data for averages, fits, limits, etc. • • •				
		5 CHATRCHYAN14AB	CMS	$E_{cm}^{pp} = 7$ TeV
		6 AAD	13AN ATLS	$E_{cm}^{pp} = 7$ TeV
		7 ABAZOV	12AG D0	$E_{cm}^{pp} = 1.96$ TeV
		8 ABAZOV	11AC D0	$E_{cm}^{pp} = 1.96$ TeV
		9 CHATRCHYAN11M	CMS	$E_{cm}^{pp} = 7$ TeV
	53	10 AARON	09B H1	$E_{cm}^{ep} = 0.3$ TeV
0.00 ± 0.06		11 ABAZOV	09AD D0	$E_{cm}^{pp} = 1.96$ TeV
		12 ABAZOV	09AJ D0	$E_{cm}^{pp} = 1.96$ TeV
		13 ABAZOV	08R D0	$E_{cm}^{pp} = 1.96$ TeV
0.16 + 0.12 -0.13	1880	14 ABDALLAH	08c DLPH	Superseded by ABDAL-LAH 10
	1617	15 AALTONEN	07L CDF	$E_{cm}^{pp} = 1.96$ GeV
	17	16 ABAZOV	06H D0	$E_{cm}^{pp} = 1.96$ TeV
	141	17 ABAZOV	05J D0	$E_{cm}^{pp} = 1.96$ TeV
0.05 ± 0.09 ± 0.01	2298	18 ABREU	01i DLPH	$E_{cm}^{ee} = 183+189$ GeV
		19 BREITWEG	00 ZEUS	$e^+p \rightarrow e^+W^\pm X$, $\sqrt{s} \approx 300$ GeV
0.00 + 0.10 -0.09	331	20 ABBOTT	99i D0	$E_{cm}^{pp} = 1.8$ TeV

- ¹ ABDALLAH 10 use data on the final states $e^+e^- \rightarrow jj\ell\nu$, $jjjj$, jjX , ℓX , at center-of-mass energies between 189–209 GeV at LEP2, where $j =$ jet, $\ell =$ lepton, and X represents missing momentum. The fit is carried out keeping all other parameters fixed at their SM values.
- ² SCHAEEL 05A study single-photon, single- W , and WW -pair production from 183 to 209 GeV. Each parameter is determined from a single-parameter fit in which the other parameters assume their Standard Model values.
- ³ ABBIENDI 04d combine results from W^+W^- in all decay channels. Only CP -conserving couplings are considered and each parameter is determined from a single-parameter fit in which the other parameters assume their Standard Model values. The 95% confidence interval is $-0.13 < \lambda_\gamma < 0.01$.
- ⁴ ACHARD 04b study WW -pair production, single- W production and single-photon production with missing energy from 189 to 209 GeV. The result quoted here is obtained including data from 161 to 183 GeV, ACCIARRI 99q. Each parameter is determined from a single-parameter fit in which the other parameters assume their Standard Model values.
- ⁵ CHATRCHYAN 14AB measure $W\gamma$ production cross section for $p_T^\gamma > 15$ GeV and $R(\ell\gamma) > 0.7$, which is the separation between the γ and the final state charged lepton (e or μ) in the azimuthal angle-pseudorapidity ($\phi - \eta$) plane. After background subtraction the number of $e\nu\gamma$ and $\mu\nu\gamma$ events is determined to be 3200 ± 325 and 4970 ± 543 respectively, compatible with expectations from the SM. This leads to a 95% CL limit of $-0.050 < \lambda_\gamma < 0.037$, assuming all other parameters have SM values.
- ⁶ AAD 13AN study $W\gamma$ production in pp collisions. In events with no additional jet, 4449 (6578) W decays to electron (muon) are selected, with an expected background of 1662 ± 262 (2538 \pm 362) events. Analysing the photon p_T spectrum above 100 GeV yields a 95% C.L. limit of $-0.065 < \lambda_\gamma < 0.061$. Supersedes AAD 12bx.
- ⁷ ABAZOV 12AG combine new results with already published results on $W\gamma$, WW and WZ production in order to determine the couplings with increased precision, superseding ABAZOV 08R, ABAZOV 11AC, ABAZOV 09AJ, ABAZOV 09AD. The 68% C.L. result for a formfactor cutoff of $\Lambda = 2$ TeV is $\lambda_\gamma = 0.007^{+0.021}_{-0.022}$.

- ⁸ ABAZOV 11AC study $W\gamma$ production in $p\bar{p}$ collisions at 1.96 TeV, with the W decay products containing an electron or a muon. They select 196 (363) events in the electron (muon) mode, with a SM expectation of 190 (372) events. A likelihood fit to the photon E_T spectrum above 15 GeV yields at 95% C.L. the result: $-0.08 < \lambda_\gamma < 0.07$ for a formfactor $\Lambda = 2$ TeV.
- ⁹ CHATRCHYAN 11M study $W\gamma$ production in pp collisions at $\sqrt{s} = 7$ TeV using 36 pb⁻¹ pp data with the W decaying to electron and muon. The total cross section is measured for photon transverse energy $E_T^\gamma > 10$ GeV and spatial separation from charged leptons in the plane of pseudo rapidity and azimuthal angle $\Delta R(\ell, \gamma) > 0.7$. The number of candidate (background) events is 452 (228 \pm 21) for the electron channel and 520 (277 \pm 25) for the muon channel. Setting other couplings to their standard model value, they derive a 95% CL limit of $-0.18 < \lambda_\gamma < 0.17$.
- ¹⁰ AARON 09B study single- W production in ep collisions at 0.3 TeV C.M. energy. They select 53 $W \rightarrow e/\mu$ events with a standard model expectation of 54.1 ± 7.4 events. Fitting the transverse momentum spectrum of the hadronic recoil system they obtain a 95% C.L. limit of $-2.5 < \lambda_\gamma < 2.5$.
- ¹¹ ABAZOV 09AD study the $p\bar{p} \rightarrow \ell\nu$ 2jet process arising in WW and WZ production. They select 12,473 (14,392) events in the electron (muon) channel with an expected di-boson signal of 436 (527) events. The results on the anomalous couplings are derived from an analysis of the p_T spectrum of the 2-jet system and quoted at 68% C.L. and for a form factor of 2 TeV. This measurement is not used for obtaining the mean as it is for a specific form factor. The 95% confidence interval is $-0.10 < \lambda_\gamma < 0.11$.
- ¹² ABAZOV 09AJ study the $p\bar{p} \rightarrow 2\ell\nu$ process arising in WW production. They select 100 events with an expected WW signal of 65 events. An analysis of the p_T spectrum of the two charged leptons leads to 95% C.L. limits of $-0.14 < \lambda_\gamma < 0.18$, for a form factor $\Lambda = 2$ TeV.
- ¹³ ABAZOV 08R use 0.7 fb⁻¹ $p\bar{p}$ data at $\sqrt{s} = 1.96$ TeV to select 263 $W\gamma + X$ events, of which 187 constitute signal, with the W decaying into an electron or a muon, which is required to be well separated from a photon with $E_T > 9$ GeV. A likelihood fit to the photon E_T spectrum yields a 95% CL limit $-0.12 < \lambda_\gamma < 0.13$ with other couplings fixed to their Standard Model values.
- ¹⁴ ABDALLAH 08c determine this triple gauge coupling from the measurement of the spin density matrix elements in $e^+e^- \rightarrow W^+W^- \rightarrow (qq)(\ell\nu)$, where $\ell = e$ or μ . Values of all other couplings are fixed to their standard model values.
- ¹⁵ AALTONEN 07L set limits on anomalous TGCs using the $p_T(W)$ distribution in WW and WZ production with the W decaying to an electron or muon and the Z to 2 jets. Setting other couplings to their standard model value, the 95% C.L. limits are $-0.18 < \lambda_\gamma < 0.17$ for a form factor scale $\Lambda = 1.5$ TeV.
- ¹⁶ ABAZOV 06H study $\bar{p}p \rightarrow WW$ production with a subsequent decay $WW \rightarrow e^+\nu_e e^- \bar{\nu}_e$, $WW \rightarrow e^\pm \nu_e \mu^\mp \nu_\mu$ or $WW \rightarrow \mu^\pm \nu_\mu \mu^\mp \bar{\nu}_\mu$. The 95% C.L. limit for a form factor scale $\Lambda = 1$ TeV is $-0.29 < \lambda < 0.30$. With the assumption that the $WW\gamma$ and WWZ couplings are equal the 95% C.L. one-dimensional limit ($\Lambda = 2$ TeV) is $-0.29 < \lambda < 0.30$.
- ¹⁷ ABAZOV 05J perform a likelihood fit to the photon E_T spectrum of $W\gamma + X$ events, where the W decays to an electron or muon which is required to be well separated from the photon. For $\Lambda = 2.0$ TeV the 95% CL limits are $-0.20 < \lambda_\gamma < 0.20$. In the fit κ_γ is kept fixed to its Standard Model value.
- ¹⁸ ABREU 01i combine results from e^+e^- interactions at 189 GeV leading to W^+W^- , $W\nu_e$, and $\nu\bar{\nu}\gamma$ final states with results from ABREU 99L at 183 GeV. The 95% confidence interval is $-0.11 < \lambda_\gamma < 0.23$.
- ¹⁹ BREITWEG 00 search for W production in events with large hadronic p_T . For $p_T > 20$ GeV, the upper limit on the cross section gives the 95% CL limit $-3.2 < \lambda_\gamma < 3.2$ for κ_γ fixed to its Standard Model value.
- ²⁰ ABBOTT 99i perform a simultaneous fit to the $W\gamma$, $WW \rightarrow$ dilepton, $WW/WZ \rightarrow e\nu jj$, $WW/WZ \rightarrow \mu\nu jj$, and $WZ \rightarrow$ trilepton data samples. For $\Lambda = 2.0$ TeV, the 95% CL limits are $-0.18 < \lambda_\gamma < 0.19$.

 κ_Z This coupling is CP -conserving (C and P -separately conserving).

VALUE	EVTS	DOCUMENT ID	TECN	COMMENT
0.924 + 0.059 ± 0.024 -0.056 ± 0.024	7171	1 ACHARD	04D L3	$E_{cm}^{ee} = 189-209$ GeV
• • • We do not use the following data for averages, fits, limits, etc. • • •				
		2 SIRUNYAN	19CL CMS	$E_{cm}^{pp} = 13$ TeV
		3 AABOUD	17s ATLS	$E_{cm}^{pp} = 7+8$ TeV
		4 KHACHATRY...17o	CMS	$E_{cm}^{pp} = 8$ TeV
		5 AAD	16AR ATLS	$E_{cm}^{pp} = 8$ TeV
		6 AAD	16P ATLS	$E_{cm}^{pp} = 8$ TeV
		7 AAD	13AL ATLS	$E_{cm}^{pp} = 7$ TeV
		8 AAD	12CD ATLS	$E_{cm}^{pp} = 7$ TeV
		9 AALTONEN	12AC CDF	$E_{cm}^{pp} = 1.96$ TeV
	34	10 ABAZOV	11 D0	$E_{cm}^{pp} = 1.96$ TeV
	17	11 ABAZOV	06H D0	$E_{cm}^{pp} = 1.96$ TeV
	2.3	12 ABAZOV	05s D0	$E_{cm}^{pp} = 1.96$ TeV

- ¹ ACHARD 04b study WW -pair production, single- W production and single-photon production with missing energy from 189 to 209 GeV. The result quoted here is obtained using the WW -pair production sample. Each parameter is determined from a single-parameter fit in which the other parameters assume their Standard Model values.
- ² SIRUNYAN 19CL study WW and WZ production in lepton + jet events, with one W boson decaying leptonically (electron or muon), and another W or Z boson decaying hadronically, reconstructed as a single massive large-radius jet. In the electron channel 2,456 (2,235) events are selected in the $WW(WZ)$ category, while in the muon channel 3,996 (3572) events are selected in the $WW(WZ)$ category. Analysing the di-boson invariant mass distribution, the following 95% C.L. limit is obtained: $0.9921 < \kappa_Z < 1.0082$.
- ³ AABOUD 17s analyze electroweak production of a W boson in association with two jets at high dijet invariant mass, with the W boson decaying to electron or muon plus neutrino. In the signal region of dijet mass larger than 1 TeV and leading-jet transverse

- momentum larger than 600 GeV, 30 events are observed in the data with 39 ± 4 events expected in the Standard Model, yielding the following limit at 95% CL for the form factor cut-off scale $\Lambda_{FF} \rightarrow \infty$: $0.85 < \kappa_Z < 1.16$.
- 4 KHACHATRYAN 17o analyse WZ production where each boson decays into electrons or muons. Events are required to have a tri-lepton invariant mass larger than 100 GeV, with one of the lepton pairs having an invariant mass within 20 GeV of the Z boson mass. The Z transverse momentum spectrum is analyzed to set a 95% C.L. limit of: $0.79 < \kappa_Z < 1.25$.
 - 5 AAD 16AR study WW production in pp collisions and select 6636 WW candidates in decay modes with electrons or muons with an expected background of 1546 ± 157 events. Assuming the LEP formulation and setting the form-factor Λ to infinity, a fit to the transverse momentum distribution of the leading charged lepton, leads to a 95% C.L. range of $0.975 < \kappa_Z < 1.020$.
 - 6 AAD 16P study WZ production in pp collisions and select 2091 WZ candidates in 4 decay modes with electrons and muons, with an expected background of 1825 ± 7 events. Analyzing the WZ transverse momentum distribution, the resulting 95% C.L. limit is: $0.81 < \kappa_Z < 1.30$.
 - 7 AAD 13AL study WW production in pp collisions and select 1325 WW candidates in decay modes with electrons or muons with an expected background of 369 ± 61 events. Assuming the LEP formulation and setting the form-factor $\Lambda = \infty$, a fit to the transverse momentum distribution of the leading charged lepton, leads to a 95% C.L. range of $0.957 < \kappa_Z < 1.043$. Supersedes AAD 12AC.
 - 8 AAD 12CD study WZ production in pp collisions and select 317 WZ candidates in three $\ell\nu$ decay modes with an expected background of 68.0 ± 10.0 events. The resulting 95% C.L. range is: $0.63 < \kappa_Z < 1.57$. Supersedes AAD 12V.
 - 9 AALTONEN 12AC study WZ production in $p\bar{p}$ collisions and select 63 WZ candidates in three $\ell\nu$ decay modes with an expected background of 7.9 ± 1.0 events. Based on the cross section and shape of the Z transverse momentum spectrum, the following 95% C.L. range is reported: $0.61 < \kappa_Z < 1.90$ for a form factor of $\Lambda = 2$ TeV.
 - 10 ABAZOV 11 study the $p\bar{p} \rightarrow 3\ell\nu$ process arising in WZ production. They observe 34 WZ candidates with an estimated background of 6 events. An analysis of the p_T spectrum of the Z boson leads to a 95% C.L. limit of $0.600 < \kappa_Z < 1.675$, for a form factor $\Lambda = 2$ TeV.
 - 11 ABAZOV 06H study $p\bar{p} \rightarrow WW$ production with a subsequent decay $WW \rightarrow e^+ \nu_e e^- \bar{\nu}_e$, $WW \rightarrow e^\pm \nu_e \mu^\mp \nu_\mu$ or $WW \rightarrow \mu^+ \nu_\mu \mu^- \bar{\nu}_\mu$. The 95% C.L. limit for a form factor scale $\Lambda = 2$ TeV is $0.55 < \kappa_Z < 1.55$, fixing $\lambda_Z = 0$. With the assumption that the $WW\gamma$ and WWZ couplings are equal the 95% C.L. one-dimensional limit ($\Lambda = 2$ TeV) is $0.68 < \kappa < 1.45$.
 - 12 ABAZOV 05s study $p\bar{p} \rightarrow WZ$ production with a subsequent trilepton decay to $\ell\nu\ell'\bar{\ell}'$ (ℓ and $\ell' = e$ or μ). Three events (estimated background 0.71 ± 0.08 events) with WZ decay characteristics are observed from which they derive limits on the anomalous WWZ couplings. The 95% CL limit for a form factor scale $\Lambda = 1$ TeV is $-1.0 < \kappa_Z < 3.4$, fixing λ_Z and g_1^Z to their Standard Model values.

λ_Z This coupling is CP-conserving (C- and P- separately conserving).

VALUE	EVTS	DOCUMENT ID	TECN	COMMENT
-0.088 ± 0.060 -0.057 ± 0.023	7171	1 ACHARD 04D L3	$E_{cm}^{ee} = 189-209$ GeV	
••• We do not use the following data for averages, fits, limits, etc. •••				
		2 SIRUNYAN 19CL CMS	$E_{cm}^{pp} = 13$ TeV	
		3 SIRUNYAN 18bz CMS	$E_{cm}^{pp} = 13$ TeV	
		4 ABOUD 17s ATLS	$E_{cm}^{pp} = 7+8$ TeV	
		5 ABOUD 17u ATLS	$E_{cm}^{pp} = 8$ TeV	
		6 KHACHATRYAN 17o CMS	$E_{cm}^{pp} = 8$ TeV	
		7 SIRUNYAN 17X CMS	$E_{cm}^{pp} = 8$ TeV	
		8 AAD 16AR ATLS	$E_{cm}^{pp} = 8$ TeV	
		9 AAD 16P ATLS	$E_{cm}^{pp} = 8$ TeV	
		10 AAD 14Y ATLS	$E_{cm}^{pp} = 8$ TeV	
		11 AAD 13AL ATLS	$E_{cm}^{pp} = 7$ TeV	
		12 CHATRCHYAN 13BF CMS	$E_{cm}^{pp} = 7$ TeV	
		13 AAD 12CD ATLS	$E_{cm}^{pp} = 7$ TeV	
		14 AALTONEN 12AC CDF	$E_{cm}^{pp} = 1.96$ TeV	
	34	15 ABAZOV 11 D0	$E_{cm}^{pp} = 1.96$ TeV	
	334	16 AALTONEN 10K CDF	$E_{cm}^{pp} = 1.96$ TeV	
	13	17 ABAZOV 07Z D0	$E_{cm}^{pp} = 1.96$ TeV	
	17	18 ABAZOV 06H D0	$E_{cm}^{pp} = 1.96$ TeV	
	2.3	19 ABAZOV 05s D0	$E_{cm}^{pp} = 1.96$ TeV	

- 1 ACHARD 04D study WW -pair production, single- W production and single-photon production with missing energy from 189 to 209 GeV. The result quoted here is obtained using the WW -pair production sample. Each parameter is determined from a single-parameter fit in which the other parameters assume their Standard Model values.
- 2 SIRUNYAN 19CL study WW and WZ production in lepton + jet events, with one W boson decaying leptonically (electron or muon), and another W or Z boson decaying hadronically, reconstructed as a single massive large-radius jet. In the electron channel 2,456 (2,235) events are selected in the $W(W)WZ$ category, while in the muon channel 3,996 (3,572) events are selected in the $W(W)WZ$ category. Analysing the di-boson invariant mass distribution, the following 95% C.L. limit is obtained: $-0.0065 < \lambda_Z < 0.0066$.
- 3 SIRUNYAN 18bz study $pp \rightarrow Z$ jet jet events at 13 TeV where $Z \rightarrow e^+ e^- / \mu^+ \mu^-$. Isolated electrons and muons are selected with p_T of the leading/sub-leading lepton $> 30/20$ GeV and $|\eta| < 2.4$, with the di-lepton invariant mass within 15 GeV of the Z mass. The two highest p_T jets are selected with p_T of the leading/sub-leading jet $> 50/30$ GeV respectively and dijet invariant mass > 200 GeV. Templates in the transverse momentum of the Z are utilized to set limits on the triple gauge couplings in the EFT and the LEP parametrizations. The following 95% C.L. limit is obtained $-0.010 < \lambda_Z < 0.010$.

- 4 ABOUD 17s analyze electroweak production of a W boson in association with two jets at high dijet invariant mass, with the W boson decaying to electron or muon plus neutrino. In the signal region of dijet mass larger than 1 TeV and leading-jet transverse momentum larger than 600 GeV, 30 events are observed in the data with 39 ± 4 events expected in the Standard Model, yielding the following limit at 95% CL for the form factor cut-off scale $\Lambda_{FF} \rightarrow \infty$: $-0.053 < \lambda_Z < 0.042$.
- 5 ABOUD 17u analyze production of WW or WZ boson pairs with one W boson decaying to electron or muon plus neutrino, and the other W or Z boson decaying hadronically. The hadronic decay system is reconstructed as either a resolved two-jet system or as a single large jet. Analysing the transverse momentum distribution of the hadronic system above 100 GeV yields the following limit at 95% CL for the form factor cut-off scale $\Lambda_{FF} \rightarrow \infty$: $-0.013 < \lambda_Z < 0.013$.
- 6 KHACHATRYAN 17o analyse WZ production where each boson decays into electrons or muons. Events are required to have a tri-lepton invariant mass larger than 100 GeV, with one of the lepton pairs having an invariant mass within 20 GeV of the Z boson mass. The Z transverse momentum spectrum is analyzed to set a 95% C.L. limit of: $-0.018 < \lambda_Z < 0.016$.
- 7 SIRUNYAN 17X study $pp \rightarrow WW/WZ \rightarrow \ell\nu q\bar{q}$ production at 8 TeV where ℓ is an electron or muon with $p_T > 30$ or 25 GeV respectively. Suitable cuts are put on the p_T of the dijet system and the missing E_T of the event yielding a total of 285 and 204 WW events observed in the electron and muon channels. The following 95% C.L. limit is obtained: $-0.011 < \lambda_Z < 0.011$.
- 8 AAD 16AR study WW production in pp collisions and select 6636 WW candidates in decay modes with electrons or muons with an expected background of 1546 ± 157 events. Assuming the LEP formulation and setting the form-factor Λ to infinity, a fit to the transverse momentum distribution of the leading charged lepton, leads to a 95% C.L. range of $-0.019 < \lambda_Z < 0.019$.
- 9 AAD 16P study WZ production in pp collisions and select 2091 WZ candidates in 4 decay modes with electrons and muons, with an expected background of 1825 ± 7 events. Analyzing the WZ transverse momentum distribution, the resulting 95% C.L. limit is: $-0.016 < \lambda_Z < 0.016$.
- 10 AAD 14Y determine the electroweak Z -dijet cross section in 8 TeV pp collisions. $Z \rightarrow ee$ and $Z \rightarrow \mu\mu$ decays are selected with the di-lepton $p_T > 20$ GeV and mass in the 81–101 GeV range. Minimum two jets are required with $p_T > 55$ and 45 GeV and no additional jets with $p_T > 25$ GeV in the rapidity interval between them. The normalized p_T balance between the Z and the two jets is required to be < 0.15 . This leads to a selection of 900 events with dijet mass > 1 TeV. The number of signal and background events expected is 261 and 592 respectively. A Poisson likelihood method is used on an event by event basis to obtain the 95% CL limit $-0.15 < \lambda_Z < 0.13$ for a form factor value $\Lambda = \infty$.
- 11 AAD 13AL study WW production in pp collisions and select 1325 WW candidates in decay modes with electrons or muons with an expected background of 369 ± 61 events. Assuming the LEP formulation and setting the form-factor $\Lambda = \infty$, a fit to the transverse momentum distribution of the leading charged lepton, leads to a 95% C.L. range of $-0.062 < \lambda_Z < 0.059$. Supersedes AAD 12AC.
- 12 CHATRCHYAN 13BF determine the W^+W^- production cross section using unlike sign di-lepton (e or μ) events with high p_T . The leptons have $p_T > 20$ GeV/c and are isolated. 1134 candidate events are observed with an expected SM background of 247 \pm 34. The p_T distribution of the leading lepton is fitted to obtain 95% C.L. limits of $-0.048 < \lambda_Z < 0.048$.
- 13 AAD 12CD study WZ production in pp collisions and select 317 WZ candidates in three $\ell\nu$ decay modes with an expected background of 68.0 ± 10.0 events. The resulting 95% C.L. range is: $-0.046 < \lambda_Z < 0.047$. Supersedes AAD 12V.
- 14 AALTONEN 12AC study WZ production in $p\bar{p}$ collisions and select 63 WZ candidates in three $\ell\nu$ decay modes with an expected background of 7.9 ± 1.0 events. Based on the cross section and shape of the Z transverse momentum spectrum, the following 95% C.L. range is reported: $-0.08 < \lambda_Z < 0.10$ for a form factor of $\Lambda = 2$ TeV.
- 15 ABAZOV 11 study the $p\bar{p} \rightarrow 3\ell\nu$ process arising in WZ production. They observe 34 WZ candidates with an estimated background of 6 events. An analysis of the p_T spectrum of the Z boson leads to a 95% C.L. limit of $-0.077 < \lambda_Z < 0.093$, for a form factor $\Lambda = 2$ TeV.
- 16 AALTONEN 10K study $p\bar{p} \rightarrow W^+W^-$ with $W \rightarrow e/\mu\nu$. The p_T of the leading (second) lepton is required to be > 20 (10) GeV. The final number of events selected is 654 of which 320 \pm 47 are estimated to be background. The 95% C.L. interval is $-0.16 < \lambda_Z < 0.16$ for $\Lambda = 1.5$ TeV and $-0.14 < \lambda_Z < 0.15$ for $\Lambda = 2$ TeV.
- 17 ABAZOV 07Z set limits on anomalous TGCs using the measured cross section and $p_T(Z)$ distribution in WZ production with both the W and the Z decaying leptonically into electrons and muons. Setting the other couplings to their standard model values, the 95% C.L. limit for a form factor scale $\Lambda = 2$ TeV is $-0.17 < \lambda_Z < 0.21$.
- 18 ABAZOV 06H study $p\bar{p} \rightarrow WW$ production with a subsequent decay $WW \rightarrow e^+ \nu_e e^- \bar{\nu}_e$, $WW \rightarrow e^\pm \nu_e \mu^\mp \nu_\mu$ or $WW \rightarrow \mu^+ \nu_\mu \mu^- \bar{\nu}_\mu$. The 95% C.L. limit for a form factor scale $\Lambda = 2$ TeV is $-0.39 < \lambda_Z < 0.39$, fixing $\kappa_{\mathcal{P}} = 1$. With the assumption that the $WW\gamma$ and WWZ couplings are equal the 95% C.L. one-dimensional limit ($\Lambda = 2$ TeV) is $-0.29 < \lambda < 0.30$.
- 19 ABAZOV 05s study $p\bar{p} \rightarrow WZ$ production with a subsequent trilepton decay to $\ell\nu\ell'\bar{\ell}'$ (ℓ and $\ell' = e$ or μ). Three events (estimated background 0.71 ± 0.08 events) with WZ decay characteristics are observed from which they derive limits on the anomalous WWZ couplings. The 95% CL limit for a form factor scale $\Lambda = 1.5$ TeV is $-0.48 < \lambda_Z < 0.48$, fixing g_1^Z and κ_Z to their Standard Model values.

κ_Z This coupling is CP-conserving but C- and P-violating.

VALUE	EVTS	DOCUMENT ID	TECN	COMMENT
-0.07 ± 0.09 OUR AVERAGE		Error includes scale factor of 1.1.		
-0.04 ± 0.13 -0.12	9800	1 ABBIENDI 04D OPAL	$E_{cm}^{ee} = 183-209$ GeV	
$0.00 \pm 0.13 \pm 0.05$	7171	2 ACHARD 04D L3	$E_{cm}^{ee} = 189-209$ GeV	
-0.44 ± 0.23 -0.22 ± 0.12	1154	3 ACCIARRI 99Q L3	$E_{cm}^{ee} = 161+172+183$ GeV	
••• We do not use the following data for averages, fits, limits, etc. •••				
-0.31 ± 0.23		4 EBOLI 00 THES	LEP1, SLC+ Tevatron	

Gauge & Higgs Boson Particle Listings

W

¹ ABBIENDI 04d combine results from W^+W^- in all decay channels. Only CP -conserving couplings are considered and each parameter is determined from a single-parameter fit in which the other parameters assume their Standard Model values. The 95% confidence interval is $-0.28 < g_5^Z < +0.21$.

² ACHARD 04d study WW -pair production, single- W production and single-photon production with missing energy from 189 to 209 GeV. The result quoted here is obtained using the WW -pair production sample. Each parameter is determined from a single-parameter fit in which the other parameters assume their Standard Model values.

³ ACCIARRI 99q study W -pair, single- W , and single photon events.

⁴ EBOL 00 extract this indirect value of the coupling studying the non-universal one-loop contributions to the experimental value of the $Z \rightarrow b\bar{b}$ width ($\Lambda=1$ TeV is assumed).

 g_4^Z

This coupling is CP -violating (C -violating and P -conserving).

VALUE	EVTS	DOCUMENT ID	TECN	COMMENT
-0.30 ± 0.17 OUR AVERAGE				
$-0.39^{+0.19}_{-0.20}$	1880	1 ABDALLAH	08c DLPH	$E_{cm}^{ee} = 189-209$ GeV
$-0.02^{+0.32}_{-0.33}$	1065	2 ABBIENDI	01H OPAL	$E_{cm}^{ee} = 189$ GeV

¹ ABDALLAH 08c determine this triple gauge coupling from the measurement of the spin density matrix elements in $e^+e^- \rightarrow W^+W^- \rightarrow (qq)(\ell\nu)$, where $\ell = e$ or μ . Values of all other couplings are fixed to their standard model values.

² ABBIENDI 01H study W -pair events, with one leptonically and one hadronically decaying W . The coupling is extracted using information from the W production angle together with decay angles from the leptonically decaying W .

 $\tilde{\kappa}_Z$

This coupling is CP -violating (C -conserving and P -violating).

VALUE	EVTS	DOCUMENT ID	TECN	COMMENT
$-0.12^{+0.06}_{-0.04}$ OUR AVERAGE				
$-0.09^{+0.08}_{-0.05}$	1880	1 ABDALLAH	08c DLPH	$E_{cm}^{ee} = 189-209$ GeV
$-0.20^{+0.10}_{-0.07}$	1065	2 ABBIENDI	01H OPAL	$E_{cm}^{ee} = 189$ GeV
• • • We do not use the following data for averages, fits, limits, etc. • • •				
		3 AABOUD	17s ATLS	$E_{cm}^{pp} = 7+8$ TeV
		4 BLINOV	11 LEP	$E_{cm}^{ee} = 183-207$ GeV

¹ ABDALLAH 08c determine this triple gauge coupling from the measurement of the spin density matrix elements in $e^+e^- \rightarrow W^+W^- \rightarrow (qq)(\ell\nu)$, where $\ell = e$ or μ . Values of all other couplings are fixed to their standard model values.

² ABBIENDI 01H study W -pair events, with one leptonically and one hadronically decaying W . The coupling is extracted using information from the W production angle together with decay angles from the leptonically decaying W .

³ AABOUD 17s analyze electroweak production of a W boson in association with two jets at high dijet invariant mass, with the W boson decaying to electron or muon plus neutrino. In the signal region of dijet mass larger than 1 TeV and leading-jet transverse momentum larger than 600 GeV, 30 events are observed in the data with 39 ± 4 events expected in the Standard Model, yielding the following limit at 95% CL for the form factor cut-off scale $A_{FF} \rightarrow \infty$: $-0.56 < \tilde{\kappa}_Z < 0.56$.

⁴ BLINOV 11 use the LEP-average $e^+e^- \rightarrow W^+W^-$ cross section data for $\sqrt{s} = 183-207$ GeV to determine an upper limit on the TGC $\tilde{\kappa}_Z$. The average values of the cross sections as well as their correlation matrix, and standard model expectations of the cross sections are taken from the LEPWWG note hep-ex/0612034. At 95% confidence level $|\tilde{\kappa}_Z| < 0.13$.

 $\tilde{\lambda}_Z$

This coupling is CP -violating (C -conserving and P -violating).

VALUE	EVTS	DOCUMENT ID	TECN	COMMENT
-0.09 ± 0.07 OUR AVERAGE				
-0.08 ± 0.07	1880	1 ABDALLAH	08c DLPH	$E_{cm}^{ee} = 189-209$ GeV
$-0.18^{+0.24}_{-0.16}$	1065	2 ABBIENDI	01H OPAL	$E_{cm}^{ee} = 189$ GeV
• • • We do not use the following data for averages, fits, limits, etc. • • •				
		3 AABOUD	17s ATLS	$E_{cm}^{pp} = 7+8$ TeV
		4 BLINOV	11 LEP	$E_{cm}^{ee} = 183-207$ GeV

¹ ABDALLAH 08c determine this triple gauge coupling from the measurement of the spin density matrix elements in $e^+e^- \rightarrow W^+W^- \rightarrow (qq)(\ell\nu)$, where $\ell = e$ or μ . Values of all other couplings are fixed to their standard model values.

² ABBIENDI 01H study W -pair events, with one leptonically and one hadronically decaying W . The coupling is extracted using information from the W production angle together with decay angles from the leptonically decaying W .

³ AABOUD 17s analyze electroweak production of a W boson in association with two jets at high dijet invariant mass, with the W boson decaying to electron or muon plus neutrino. In the signal region of dijet mass larger than 1 TeV and leading-jet transverse momentum larger than 600 GeV, 30 events are observed in the data with 39 ± 4 events expected in the Standard Model, yielding the following limit at 95% CL for the form factor cut-off scale $A_{FF} \rightarrow \infty$: $-0.047 < \tilde{\lambda}_Z < 0.046$.

⁴ BLINOV 11 use the LEP-average $e^+e^- \rightarrow W^+W^-$ cross section data for $\sqrt{s} = 183-207$ GeV to determine an upper limit on the TGC $\tilde{\lambda}_Z$. The average values of the cross sections as well as their correlation matrix, and standard model expectations of the cross sections are taken from the LEPWWG note hep-ex/0612034. At 95% confidence level $|\tilde{\lambda}_Z| < 0.31$.

of these moments and additional references can be found in HAGIWARA 87 and BAUR 88. The parameter Λ appearing in the theoretical limits below is a regularization cutoff which roughly corresponds to the energy scale where the structure of the W boson becomes manifest.

VALUE ($\epsilon/2m_W$)	EVTS	DOCUMENT ID	TECN	COMMENT
$2.22^{+0.20}_{-0.19}$	2298	1 ABREU	01i DLPH	$E_{cm}^{ee} = 183+189$ GeV
• • • We do not use the following data for averages, fits, limits, etc. • • •				
		2 ABE	95G CDF	
		3 ALITTI	92C UA2	
		4 SAMUEL	92 THEO	
		5 SAMUEL	91 THEO	
		6 GRIFOLS	88 THEO	
		7 GROTC	87 THEO	
		8 VANDERBIJ	87 THEO	
		9 GRAU	85 THEO	
		10 SUZUKI	85 THEO	
		11 HERZOG	84 THEO	

¹ ABREU 01i combine results from e^+e^- interactions at 189 GeV leading to W^+W^- , $W\nu_e$, and $\nu\bar{\nu}\gamma$ final states with results from ABREU 99L at 183 GeV to determine Δg_4^Z , $\Delta\kappa_\gamma$, and λ_γ . $\Delta\kappa_\gamma$ and λ_γ are simultaneously floated in the fit to determine μ_W .

² ABE 95G report $-1.3 < \kappa < 3.2$ for $\lambda=0$ and $-0.7 < \lambda < 0.7$ for $\kappa=1$ in $p\bar{p} \rightarrow e\nu_e\gamma X$ and $\mu\nu_\mu\gamma X$ at $\sqrt{s} = 1.8$ TeV.

³ ALITTI 92C measure $\kappa = 1^{+2.5}_{-2.9}$ and $\lambda = 0^{+1.7}_{-1.8}$ in $p\bar{p} \rightarrow e\nu\gamma + X$ at $\sqrt{s} = 630$ GeV. At 95%CL they report $-3.5 < \kappa < 5.9$ and $-3.6 < \lambda < 3.5$.

⁴ SAMUEL 92 use preliminary CDF and UA2 data and find $-2.4 < \kappa < 3.7$ at 96%CL and $-3.1 < \kappa < 4.2$ at 95%CL respectively. They use data for $W\gamma$ production and radiative W decay.

⁵ SAMUEL 91 use preliminary CDF data for $p\bar{p} \rightarrow W\gamma X$ to obtain $-11.3 \leq \Delta\kappa \leq 10.9$. Note that their $\kappa = 1 - \Delta\kappa$.

⁶ GRIFOLS 88 uses deviation from ρ parameter to set limit $\Delta\kappa \lesssim 65 (M_W^2/\Lambda^2)$.

⁷ GROTC 87 finds the limit $-37 < \Delta\kappa < 73.5$ (90% CL) from the experimental limits on $e^+e^- \rightarrow \nu\bar{\nu}\gamma$ assuming three neutrino generations and $-19.5 < \Delta\kappa < 56$ for four generations. Note their $\Delta\kappa$ has the opposite sign as our definition.

⁸ VANDERBIJ 87 uses existing limits to the photon structure to obtain $|\Delta\kappa| < 33 (m_W/\Lambda)$. In addition VANDERBIJ 87 discusses problems with using the ρ parameter of the Standard Model to determine $\Delta\kappa$.

⁹ GRAU 85 uses the muon anomaly to derive a coupled limit on the anomalous magnetic dipole and electric quadrupole (λ) moments $1.05 > \Delta\kappa \ln(\Lambda/m_W) + \lambda/2 > -2.77$. In the Standard Model $\lambda = 0$.

¹⁰ SUZUKI 85 uses partial-wave unitarity at high energies to obtain $|\Delta\kappa| \lesssim 190 (m_W/\Lambda)^2$. From the anomalous magnetic moment of the muon, SUZUKI 85 obtains $|\Delta\kappa| \lesssim 2.2/\ln(\Lambda/m_W)$. Finally SUZUKI 85 uses deviations from the ρ parameter and obtains a very qualitative, order-of-magnitude limit $|\Delta\kappa| \lesssim 150 (m_W/\Lambda)^4$ if $|\Delta\kappa| \ll 1$.

¹¹ HERZOG 84 consider the contribution of W -boson to muon magnetic moment including anomalous coupling of $WW\gamma$. Obtain a limit $-1 < \Delta\kappa < 3$ for $\Lambda \gtrsim 1$ TeV.

 $c_{WW}/\Lambda^2, c_W/\Lambda^2, c_B/\Lambda^2$

These couplings are used in EFT-based approaches to anomalous couplings. They are linearly related to the couplings discussed above.

VALUE	DOCUMENT ID	TECN	COMMENT
• • • We do not use the following data for averages, fits, limits, etc. • • •			
	1 AABOUD	19BA ATLS	$E_{cm}^{pp} = 13$ TeV
	2 SIRUNYAN	19AD CMS	$E_{cm}^{pp} = 13$ TeV
	3 SIRUNYAN	19CL CMS	$E_{cm}^{pp} = 13$ TeV
	4 AABOUD	18Q ATLS	$E_{cm}^{pp} = 13$ TeV
	5 SIRUNYAN	18BZ CMS	$E_{cm}^{pp} = 13$ TeV
	6 AABOUD	17s ATLS	$E_{cm}^{pp} = 7+8$ TeV
	7 AABOUD	17U ATLS	$E_{cm}^{pp} = 8$ TeV
	8 KHACHATRY..17O	CMS	$E_{cm}^{pp} = 8$ TeV
	9 SIRUNYAN	17X CMS	$E_{cm}^{pp} = 8$ TeV
	10 AAD	16AR ATLS	$E_{cm}^{pp} = 8$ TeV
	11 AAD	16P ATLS	$E_{cm}^{pp} = 8$ TeV
	12 KHACHATRY..16BI	CMS	$E_{cm}^{pp} = 8$ TeV

¹ AABOUD 19BA study WW production in decay modes with an electron and a muon. The charged leptons are each required to have a transverse momentum larger than 27 GeV and rapidity less than 2.5. The electron-muon system is required to have a mass larger than 55 GeV and a transverse momentum larger than 30 GeV. The missing transverse energy must be larger than 20 GeV. Events containing a jet with transverse momentum exceeding 35 GeV and rapidity smaller than 4.5 are rejected. A total of 12,659 events are selected in the data, with an expected background of 4240 ± 477 events. Analysing the transverse momentum spectrum of the leading charged lepton, the following 95% C.L. limits are derived in units of TeV^{-2} : $-3.4 < c_{WW}/\Lambda^2 < 3.3$, $-7.4 < c_W/\Lambda^2 < 4.1$, $-21 < c_B/\Lambda^2 < 18$, $-1.6 < c_{\overline{W}W}/\Lambda^2 < 1.6$, $-76 < c_{\overline{W}W}/\Lambda^2 < 76$.

W ANOMALOUS MAGNETIC MOMENT

The full magnetic moment is given by $\mu_W = e(1+\kappa+\lambda)/2m_W$. In the Standard Model, at tree level, $\kappa = 1$ and $\lambda = 0$. Some papers have defined $\Delta\kappa = 1-\kappa$ and assume that $\lambda = 0$. Note that the electric quadrupole moment is given by $-e(\kappa-\lambda)/m_W^2$. A description of the parameterization

- ² SIRUNYAN 19AD study inclusive WZ production, with W and Z decaying to electrons or muons. The leading (subleading) charged lepton candidate from the Z boson decay is required to have a transverse momentum larger than 25 GeV (10 GeV). The charged lepton candidate from the W boson decay is required to have a transverse momentum larger than 25 GeV. The invariant mass of the two leptons from Z decay is required to be within 15 GeV of the Z mass, while the invariant mass of the tri-lepton system is required to exceed 100 GeV. A total of 3,831 tri-lepton events are observed, with a fitted SM WZ signal of 3166 ± 62 events and a fitted background of 666 ± 45 events. The approximated WZ invariant mass distribution is analyzed to set 95% C.L. limits as follows: $-4.1 < c_{WW}/\Lambda^2 < 1.1$, $-2.0 < c_{WWW}/\Lambda^2 < 2.1$, $-100 < c_B/\Lambda^2 < 160$, in units of TeV^{-2} .
- ³ SIRUNYAN 19cl study WW and WZ production in lepton + jet events, with one W boson decaying leptonically (electron or muon), and another W or Z boson decaying hadronically, reconstructed as a single massive large-radius jet. In the electron channel 2,456 (2,235) events are selected in the $WW(WZ)$ category, while in the muon channel 3,996 (3,572) events are selected in the $WW(WZ)$ category. Analysing the di-boson invariant mass distribution, the following 95% C.L. limits are obtained in units of TeV^{-2} : $-1.58 < c_{WWW}/\Lambda^2 < 1.59$, $-2.00 < c_W/\Lambda^2 < 2.65$, $-8.78 < c_B/\Lambda^2 < 8.54$.
- ⁴ AABOUD 18q study $pp \rightarrow ZZ$ events at $\sqrt{s} = 13$ TeV with $Z \rightarrow e^+e^-$ or $Z \rightarrow \mu^+\mu^-$. The number of events observed in the $4e$, $2e2\mu$, and 4μ channels is 249, 465, and 303 respectively. Analysing the p_T spectrum of the leading Z boson, the following the following 95% C.L. limits are derived in units of TeV^{-4} : $-5.9 < c_{\tilde{B}W}/\Lambda^4 < 5.9$, $-3.0 < c_{WW}/\Lambda^4 < 3.0$, $-3.3 < c_{BW}/\Lambda^4 < 3.3$, $-2.7 < c_{BB}/\Lambda^4 < 2.8$.
- ⁵ SIRUNYAN 18bz study $pp \rightarrow Z$ jet events at 13 TeV where $Z \rightarrow e^+e^-/\mu^+\mu^-$. Isolated electrons and muons are selected with p_T of the leading/sub-leading lepton $> 30/20$ GeV and $|\eta| < 2.4$, with the di-lepton invariant mass within 15 GeV of the Z mass. The two highest p_T jets are selected with p_T of the leading/sub-leading jet $> 50/30$ GeV respectively and dijet invariant mass > 200 GeV. Templates in the transverse momentum of the Z are utilized to set limits on the triple gauge couplings in the EFT and the LEP parametrizations. The following 95% C.L. limits are obtained in units of TeV^{-2} : $-2.6 < c_{WWW}/\Lambda^2 < 2.6$ and $-8.4 < c_W/\Lambda^2 < 10.1$.
- ⁶ AABOUD 17s analyze electroweak production of a W boson in association with two jets at high dijet invariant mass, with the W boson decaying to electron or muon plus neutrino. In the signal region of dijet mass larger than 1 TeV and leading-jet transverse momentum larger than 600 GeV, 30 events are observed in the data with 39 ± 4 events expected in the Standard Model, yielding the following limits at 95% CL for the form factor cut-off scale $\Lambda_{FF} \rightarrow \infty$: $-33 < c_{WW}/\Lambda^2 < 30$, $-170 < c_B/\Lambda^2 < 160$, $-13 < c_{WWW}/\Lambda^2 < 9$, $-580 < c_{\tilde{W}W}/\Lambda^2 < 580$, $-11 < c_{\tilde{W}W}/\Lambda^2 < 11$, in units of TeV^{-2} .
- ⁷ AABOUD 17u analyze production of WW or WZ boson pairs with one W boson decaying to electron or muon plus neutrino, and the other W or Z boson decaying hadronically. The hadronic decay system is reconstructed as either a resolved two-jet system or as a single large jet. Analysing the transverse momentum distribution of the hadronic system above 100 GeV yields the following limits at 95% CL for the form factor cut-off scale $\Lambda_{FF} \rightarrow \infty$: $-3.1 < c_{WWW}/\Lambda^2 < 3.1$, $-19 < c_B/\Lambda^2 < 20$, $-5.1 < c_W/\Lambda^2 < 5.8$, in units of TeV^{-2} .
- ⁸ KHACHATRYAN 17o analyse WZ production where each boson decays into electrons or muons. Events are required to have a tri-lepton invariant mass larger than 100 GeV, with one of the lepton pairs having an invariant mass within 20 GeV of the Z boson mass. The Z transverse momentum spectrum is analyzed to set 95% C.L. limits of: $-260 < c_B/\Lambda^2 < 210$, $-4.2 < c_W/\Lambda^2 < 8.0$, $-4.6 < c_{WWW}/\Lambda^2 < 4.2$, in units of TeV^{-2} .
- ⁹ SIRUNYAN 17x study $pp \rightarrow WW/WZ \rightarrow \ell\nu q\bar{q}$ production at 8 TeV where ℓ is an electron or muon with $p_T > 30$ or 25 GeV respectively. Suitable cuts are put on the p_T of the dijet system and the missing E_T of the event yielding a total of 285 and 204 WV events observed in the electron and muon channels. The following 95% C.L. limits in units of TeV^{-2} are obtained: $-2.7 < c_{WWW}/\Lambda^2 < 2.7$, $-14 < c_B/\Lambda^2 < 17$, $-2.0 < c_W/\Lambda^2 < 5.7$.
- ¹⁰ AAD 16AR study WW production in pp collisions and select 6636 WW candidates in decay modes with electrons or muons with an expected background of 1546 ± 157 events. Assuming an EFT formulation, a fit to the transverse momentum distribution of the leading charged lepton, leads to 95% C.L. ranges of: $-4.61 < c_{WWW}/\Lambda^2 < 4.60$, $-5.87 < c_W/\Lambda^2 < 10.54$ and $-20.9 < c_B/\Lambda^2 < 26.3$, in units of TeV^{-2} .
- ¹¹ AAD 16P study WZ production in pp collisions and select 2091 WZ candidates in 4 decay modes with electrons and muons, with an expected background of 1825 ± 7 events. Analysing the WZ transverse momentum distribution, the resulting 95% C.L. limits are: $-3.9 < c_{WWW}/\Lambda^2 < 4.0$, $-4.3 < c_W/\Lambda^2 < 6.8$, and $-320 < c_B/\Lambda^2 < 210$, in units of TeV^{-2} .
- ¹² KHACHATRYAN 16Bi determine the W^+W^- production cross section using unlike sign di-lepton (e or μ) events with high p_T . The leptons have $p_T > 20$ GeV/ c and are isolated. Events are required to have no jets above p_T of 30 GeV/ c . 4847 (2233) events are selected with different (same) flavor leptons, with an expected total background of 1179 ± 123 (643 \pm 73) events. Analysing the di-lepton invariant mass spectrum, the following values are obtained: $c_{WWW}/\Lambda^2 = 0.1 \pm 3.2$, $c_W/\Lambda^2 = -3.6^{+5.0}_{-4.5}$ and $c_B/\Lambda^2 = -3.2^{+15.0}_{-14.5}$, in units of TeV^{-2} . The limits at 95% C.L. are: $-5.7 < c_{WWW}/\Lambda^2 < 5.9$, $-11.4 < c_W/\Lambda^2 < 5.4$ and $-29.2 < c_B/\Lambda^2 < 23.9$, in units of TeV^{-2} .

ANOMALOUS W/Z QUARTIC COUPLINGS

Revised November 2015 by M.W. Grunewald (U. College Dublin) and A. Gurtu (Formerly Tata Inst.).

Quartic couplings, $WWZZ$, $WWZ\gamma$, $WW\gamma\gamma$, and $ZZ\gamma\gamma$, were studied at LEP and Tevatron at energies at which the Standard Model predicts negligible contributions to multiboson production. Thus, to parametrize limits on these couplings, an

effective theory approach is adopted which supplements the Standard Model Lagrangian with higher dimensional operators which include quartic couplings. The LEP collaborations chose the lowers dimensional representation of operators (dimension 6) which presumes the $SU(2) \times U(1)$ gauge symmetry is broken by means other than the conventional Higgs scalar doublet [1–3]. In this representation possible quartic couplings, a_0, a_c, a_n , are expressed in terms of the following dimension-6 operators [1,2];

$$\begin{aligned} L_6^0 &= -\frac{e^2}{16\Lambda^2} a_0 F^{\mu\nu} F_{\mu\nu} \vec{W}^\alpha \cdot \vec{W}_\alpha \\ L_6^c &= -\frac{e^2}{16\Lambda^2} a_c F^{\mu\alpha} F_{\mu\beta} \vec{W}^\beta \cdot \vec{W}_\alpha \\ L_6^n &= -i\frac{e^2}{16\Lambda^2} a_n \epsilon_{ijk} W_{\mu\alpha}^{(i)} W_\nu^{(j)} W^{(k)\alpha} F^{\mu\nu} \\ \tilde{L}_6^0 &= -\frac{e^2}{16\Lambda^2} \tilde{a}_0 F^{\mu\nu} \tilde{F}_{\mu\nu} \vec{W}^\alpha \cdot \vec{W}_\alpha \\ \tilde{L}_6^n &= -i\frac{e^2}{16\Lambda^2} \tilde{a}_n \epsilon_{ijk} W_{\mu\alpha}^{(i)} W_\nu^{(j)} W^{(k)\alpha} \tilde{F}^{\mu\nu} \end{aligned}$$

where F, W are photon and W fields, L_6^0 and L_6^c conserve C, P separately (\tilde{L}_6^0 conserves only C) and generate anomalous $W^+W^-\gamma\gamma$ and $ZZ\gamma\gamma$ couplings, L_6^n violates CP (\tilde{L}_6^n violates both C and P) and generates an anomalous $W^+W^-Z\gamma$ coupling, and Λ is an energy scale for new physics. For the $ZZ\gamma\gamma$ coupling the CP -violating term represented by L_6^n does not contribute. These couplings are assumed to be real and to vanish at tree level in the Standard Model.

Within the same framework as above, a more recent description of the quartic couplings [3] treats the anomalous parts of the $WW\gamma\gamma$ and $ZZ\gamma\gamma$ couplings separately, leading to two sets parametrized as a_0^V/Λ^2 and a_c^V/Λ^2 , where $V = W$ or Z .

With the discovery of a Higgs at the LHC in 2012, it is then useful to go to the next higher dimensional representation (dimension 8 operators) in which the gauge symmetry is broken by the conventional Higgs scalar doublet [3,4]. There are 14 operators which can contribute to the anomalous quartic coupling signal. Some of the operators have analogues in the dimension 6 scheme. The CMS collaboration, [5], have used this parametrization, in which the connections between the two schemes are also summarized:

$$\begin{aligned} \mathcal{L}_{AQGC} &= -\frac{e^2 a_0^W}{8 \Lambda^2} F_{\mu\nu} F^{\mu\nu} W^{+a} W_a^- \\ &\quad -\frac{e^2 a_c^W}{16 \Lambda^2} F_{\mu\nu} F^{\mu\alpha} (W^{+\nu} W_a^- + W^{-\nu} W_a^+) \\ &\quad -e^2 g^2 \frac{\kappa_0^W}{\Lambda^2} F_{\mu\nu} Z^{\mu\nu} W^{+a} W_a^- \\ &\quad -\frac{e^2 g^2 \kappa_c^W}{2 \Lambda^2} F_{\mu\nu} Z^{\mu\alpha} (W^{+\nu} W_a^- + W^{-\nu} W_a^+) \\ &\quad + \frac{f_{T,0}}{\Lambda^4} Tr[\widehat{W}_{\mu\nu} \widehat{W}^{\mu\nu}] \times Tr[\widehat{W}_{\alpha\beta} \widehat{W}^{\alpha\beta}] \end{aligned}$$

The energy scale of possible new physics is Λ , and $g = e/\sin(\theta_W)$, e being the unit electric charge and θ_W the Weinberg angle. The field tensors are described in [3,4].

The two dimension 6 operators a_0^W/Λ^2 and a_c^W/Λ^2 are associated with the $WW\gamma\gamma$ vertex. Among dimension 8 operators, κ_0^W/Λ^2 and κ_c^W/Λ^2 are associated with the $WWZ\gamma$ vertex, whereas the parameter $f_{T,0}/\Lambda^4$ contributes to both vertices. There is a relationship between these two dimension 6 parameters and the dimension 8 parameters $f_{M,i}/\Lambda^4$ as follows [3]:

Gauge & Higgs Boson Particle Listings

W

$$\frac{a_0^W}{\Lambda^2} = -\frac{4M_W^2 f_{M,0}}{g^2 \Lambda^4} - \frac{8M_W^2 f_{M,2}}{g'^2 \Lambda^4}$$

$$\frac{a_c^W}{\Lambda^2} = -\frac{4M_W^2 f_{M,1}}{g^2 \Lambda^4} - \frac{8M_W^2 f_{M,3}}{g'^2 \Lambda^4}$$

where $g' = e/\cos(\theta_W)$ and M_W is the invariant mass of the W boson. This relation provides a translation between limits on dimension 6 operators $a_{0,c}^W$ and $f_{M,j}/\Lambda^4$. It is further required [4] that $f_{M,0} = 2f_{M,2}$ and $f_{M,1} = 2f_{M,3}$ which suppresses contributions to the $WWZ\gamma$ vertex. The complete set of Lagrangian contributions as presented in [4] corresponds to 19 anomalous couplings in total – $f_{S,i}$, $i = 1, 2$, $f_{M,i}$, $i = 0, \dots, 8$ and $f_{T,i}$, $i = 0, \dots, 9$ – each scaled by $1/\Lambda^4$.

The ATLAS collaboration [6], on the other hand, follows a K-matrix driven approach of Ref. 7 in which the anomalous couplings can be expressed in terms of two parameters α_4 and α_5 , which account for all BSM effects.

It is the early stages in the determination of quartic couplings by the LHC experiments. It is hoped that the two collaborations, ATLAS and CMS, will agree to use at least one common set of parameters to express these limits to enable the reader to make a comparison and allow for a possible LHC combination.

References

1. G. Belanger and F. Boudjema, Phys. Lett. **B288**, 201 (1992).
2. J.W. Stirling and A. Werthenbach, Eur. Phys. J. **C14**, 103 (2000);
J.W. Stirling and A. Werthenbach, Phys. Lett. **B466**, 369 (1999);
A. Denner *et al.*, Eur. Phys. J. **C20**, 201 (2001);
G. Montagna *et al.*, Phys. Lett. **B515**, 197 (2001).
3. G. Belanger *et al.*, Eur. Phys. J. **C13**, 283 (2000).
4. O.J.P. Éboli, M.C. Gonzalez-Garcia, and S.M. Lietti, Phys. Rev. **D69**, 095005 (2004);
O.J.P. Éboli, M.C. Gonzalez-Garcia, and J.K. Mizukoshi, Phys. Rev. **D77**, 073005 (2006).
5. S. Chatrchyan *et al.*, Phys. Rev. **D90**, 032008 (2014);
S. Chatrchyan *et al.*, Phys. Rev. Lett. **114**, 051801 (2015).
6. G. Aad *et al.*, Phys. Rev. Lett. **113**, 141803 (2014).
7. A. Albateanu, W. Killian, and J. Reuter, JHEP **0811**, 010 (2008).

a_0/Λ^2 , a_c/Λ^2 , a_n/Λ^2 , κ_0^W/Λ^2 , κ_c^W/Λ^2 , $f_{T,0}/\Lambda^4$, $f_{M,i}/\Lambda^4$, α_4 , α_5 ,
 $F_{S,i}/\Lambda^4$, $F_{M,i}/\Lambda^4$, $F_{T,i}/\Lambda^4$

Anomalous W quartic couplings are measured by the experiments at LEP, the Tevatron, and the LHC. Some of the recent results from the Tevatron and LHC experiments individually surpass the combined LEP-2 results in precision (see below). As discussed in the review on the “Anomalous W/Z quartic couplings (QGCS),” the measurements are typically done using different operator expansions which then do not allow the results to be compared and averaged. At least one common framework should be agreed upon for the use in the future publications by the experiments.

Some publications from LHC experiments derive limits for various assumed values of the form-factor cutoff Λ_{FF} . The values quoted below are for $\Lambda_{FF} \rightarrow \infty$.

VALUE	DOCUMENT ID	TECN	COMMENT
•••	We do not use the following data for averages, fits, limits, etc.	•••	
	1 SIRUNYAN	19BM CMS	$E_{cm}^{pp} = 13$ TeV
	2 SIRUNYAN	19BP CMS	$E_{cm}^{pp} = 13$ TeV
	3 SIRUNYAN	19CQ CMS	$E_{cm}^{pp} = 13$ TeV

4 SIRUNYAN	18CC CMS	$E_{cm}^{pp} = 13$ TeV
5 AABOUD	17AA ATLS	$E_{cm}^{pp} = 8$ TeV
6 AABOUD	17AG ATLS	$E_{cm}^{pp} = 8$ TeV
7 AABOUD	17D ATLS	$E_{cm}^{pp} = 8$ TeV
8 AABOUD	17J ATLS	$E_{cm}^{pp} = 8$ TeV
9 AABOUD	17M ATLS	$E_{cm}^{pp} = 8$ TeV
10 KHACHATRY...	17AA CMS	$E_{cm}^{pp} = 8$ TeV
11 KHACHATRY...	17M CMS	$E_{cm}^{pp} = 8$ TeV
12 SIRUNYAN	17AD CMS	$E_{cm}^{pp} = 13$ TeV
13 SIRUNYAN	17AR CMS	$E_{cm}^{pp} = 8$ TeV
14 AABOUD	16E ATLS	$E_{cm}^{pp} = 8$ TeV
15 AAD	16Q ATLS	$E_{cm}^{pp} = 8$ TeV
16 KHACHATRY...	16AX CMS	$E_{cm}^{pp} = 8$ TeV
17 AAD	15N ATLS	$E_{cm}^{pp} = 8$ TeV
18 KHACHATRY...	15D CMS	$E_{cm}^{pp} = 8$ TeV
19 AAD	14AM ATLS	
20 CHATRCHYAN	14Q CMS	
21 ABZOV	13D D0	
22 CHATRCHYAN	13AA CMS	
23 ABBIENDI	04B OPAL	
24 ABBIENDI	04L OPAL	
25 HEISTER	04A ALEP	
26 ABDALLAH	03I DLPH	
27 ACHARD	02F L3	

¹ SIRUNYAN 19BM search for the final state $W^+W^-W^\pm$ using W decays to electrons or muons. Two event samples are considered, events with three leptons, or events with two oppositely charged leptons accompanied by two jets. In a kinematic region selected to enhance the effect of anomalous couplings, no events are selected in the data, and 95% C.L. upper limits are obtained as follows: $-1.2 < f_{T,0}/\Lambda^4 < 1.2$, $-3.3 < f_{T,1}/\Lambda^4 < 3.3$, $-2.7 < f_{T,2}/\Lambda^4 < 2.6$, in units of TeV^{-4} and without application of a form factor.

² SIRUNYAN 19BP study WZ plus 2 jets production, using W and Z decay channels with electrons or muons. In the data, 75 events are selected, with a fitted SM signal of 15.1 ± 1.6 events and a fitted background of 62.4 ± 2.8 events. The transverse mass distribution of the WZ system is analyzed to set the following limits at 95% C.L., in units of TeV^{-4} : $-9.15 < f_{M,0}/\Lambda^4 < 9.15$, $-9.15 < f_{M,1}/\Lambda^4 < 9.45$, $-26.5 < f_{S,0}/\Lambda^4 < 27.5$, $-41.2 < f_{S,1}/\Lambda^4 < 42.8$, $-0.75 < f_{T,0}/\Lambda^4 < 0.81$, $-0.49 < f_{T,1}/\Lambda^4 < 0.55$, $-1.49 < f_{T,2}/\Lambda^4 < 1.85$.

³ SIRUNYAN 19CQ search for anomalous electroweak production of vector boson pairs in association with two jets. Events are selected by requiring two jets with a large invariant mass and rapidity separation, one or two leptons (electrons or muons), and a W or Z boson decaying hadronically. In the $WV(ZV)$ channel, 347 (47) events are selected in the data, with a total expected background of 352 ± 19 (50.3 ± 5.8) events. Analysing the mass distribution of the WV or ZV system, the following 95% C.L. limits are obtained: $-2.7 < f_{S,0}/\Lambda^4 < 2.7$, $-3.4 < f_{S,1}/\Lambda^4 < 3.4$, $-0.69 < f_{M,0}/\Lambda^4 < 0.70$, $-2.0 < f_{M,1}/\Lambda^4 < 2.1$, $-1.3 < f_{M,6}/\Lambda^4 < 1.3$, $-3.4 < f_{M,7}/\Lambda^4 < 3.4$, $-0.12 < f_{T,0}/\Lambda^4 < 0.11$, $-0.12 < f_{T,1}/\Lambda^4 < 0.13$, $-0.28 < f_{T,2}/\Lambda^4 < 0.28$, in units of TeV^{-4} .

⁴ SIRUNYAN 18CC study pp collisions at $\sqrt{s} = 13$ TeV leading to a pair of same-sign W pairs decaying leptonically (e or μ) associated with a pair of jets. Isolated leptons with $p_T > 25$ (20) GeV for the leading (trailing) lepton, with $|\eta| < 2.5$ (2.4) for e (μ) and jets with $p_T > 30$ GeV, $|\eta| < 5.0$, $|\Delta\eta_{jj}| > 2.5$ and $m_{jj} > 500$ GeV is required. Further cuts are applied to minimize $Z \rightarrow ee$ events, non-prompt leptons and hadronically decaying taus. The number of selected events is 201, with an expected SM signal of 66.9 ± 2.4 and background of 138 ± 13 events. Analysing the dilepton invariant mass spectrum the following 95% C.L. limits are derived: $-7.7 < f_{S,0}/\Lambda^4 < 7.7$, $-21.6 < f_{S,1}/\Lambda^4 < 21.8$, $-6.0 < f_{M,0}/\Lambda^4 < 5.9$, $-8.7 < f_{M,1}/\Lambda^4 < 9.1$, $-11.9 < f_{M,6}/\Lambda^4 < 11.8$, $-13.3 < f_{M,7}/\Lambda^4 < 12.9$, $-0.62 < f_{T,0}/\Lambda^4 < 0.65$, $-0.28 < f_{T,1}/\Lambda^4 < 0.31$, $-0.89 < f_{T,2}/\Lambda^4 < 1.02$.

⁵ AABOUD 17AA analyze $W^\pm W^\pm$ production in association with two jets and W decay modes with electrons or muons. In the kinematic region of VBS the effect of anomalous QGCs is enhanced by requiring the transverse mass of the WW system to be larger than 400 GeV. In the data, 8 events are selected with a total background expected from SM processes of 3.8 ± 0.6 events. Assuming the other QGC coupling to have the SM value of zero, the observed event yield is used to determine 95% CL limits on the QGCs: $-0.14 < \alpha_4 < 0.15$ and $-0.22 < \alpha_5 < 0.22$. Supersedes AAD 14AM.

⁶ AABOUD 17AG determine the $WV\gamma$ and $WZ\gamma$ cross sections in 8 TeV pp interactions by studying the final states $e\nu\mu\nu\gamma$ and $e\nu j j \gamma$ of $\mu\nu j j \gamma$. Upper limits on the production cross sections are derived in a fiducial region optimized for BSM physics. These are used to derive the following 95% C.L. upper limits for quartic couplings assuming the form scale factor, $\Lambda_{FF} = \infty$ (all in units of 10^3TeV^{-4}): $-0.3 < f_{M,0}/\Lambda^4 < 0.3$, $-0.5 < f_{M,1}/\Lambda^4 < 0.5$, $-1.8 < f_{M,2}/\Lambda^4 < 1.8$, $-1.1 < f_{M,4}/\Lambda^4 < 1.1$, $-1.7 < f_{M,5}/\Lambda^4 < 1.7$, $-0.6 < f_{M,6}/\Lambda^4 < 0.6$, $-1.1 < f_{M,7}/\Lambda^4 < 1.1$, $-0.1 < f_{T,0}/\Lambda^4 < 0.1$, $-0.2 < f_{T,1}/\Lambda^4 < 0.2$, $-0.4 < f_{T,4}/\Lambda^4 < 0.4$, $-1.5 < f_{T,5}/\Lambda^4 < 1.6$, $-1.9 < f_{T,6}/\Lambda^4 < 1.9$, $-4.3 < f_{T,7}/\Lambda^4 < 4.3$.

⁷ AABOUD 17D analyze electroweak diboson (WV , $V = W, Z$) production in association with a high-mass dijet system. In the data, 32 events are selected with an expected total background of 32 ± 12 events. Analysing the transverse mass distribution of the WV system, the following limits are set at 95% C.L.: $-0.024 < \alpha_4 < 0.030$ and $-0.028 < \alpha_5 < 0.033$.

- ⁸ AABOUD 17J analyze the $Z\gamma$ production in association with a high-mass dijet system, with the Z boson decaying into a pair of electrons, muons, or neutrinos. In the charged lepton (neutrino) channel, events are selected with a dijet mass larger than 500 (600) GeV and a transverse photon energy larger than 250 (150) GeV, with 2 (4) events selected in the data and 0.30 ± 0.08 (1.6 ± 0.5) expected background events. The observed event yield is used to determine 95% CL limits as follows: $-4.1 \times 10^3 < f_{T,9}/\Lambda^4 < 4.2 \times 10^3$, $-1.9 \times 10^3 < f_{T,8}/\Lambda^4 < 2.1 \times 10^3$, $-1.9 \times 10^1 < f_{T,0}/\Lambda^4 < 1.6 \times 10^1$, $-1.6 \times 10^2 < f_{M,0}/\Lambda^4 < 1.8 \times 10^2$, $-3.5 \times 10^2 < f_{M,1}/\Lambda^4 < 3.4 \times 10^2$, $-8.9 \times 10^2 < f_{M,2}/\Lambda^4 < 8.9 \times 10^2$, $-1.7 \times 10^3 < f_{M,3}/\Lambda^4 < 1.7 \times 10^3$, in units of TeV^{-4} and without application of a form factor.
- ⁹ AABOUD 17M analyze tri-boson $W^\pm W^\pm W^\mp$ production in decay channels with three charged leptons or two like-sign charged leptons with two jets, where the lepton can be an electron or muon. In the data, 24 tri-lepton events and 21 di-lepton plus jets events are selected, compared to a total event yield expected in the SM of 30.8 ± 3.0 and 21.9 ± 2.0 , respectively. Analysing the tri-lepton transverse mass or the transverse momentum sum of the two leptons, two jets and the missing transverse energy, the following limits at 95% CL are derived for the form factor cut-off scale $\Lambda_{FF} \rightarrow \infty$: $-0.13 < f_{S,0}/\Lambda^4 < 0.18$, $-0.21 < f_{S,1}/\Lambda^4 < 0.27$, in units of 10^4 TeV^{-4} , which are converted into the following limits: $-0.49 < \alpha_4 < 0.75$ and $-0.48 < \alpha_5 < 0.62$.
- ¹⁰ KHACHATRYAN 17AA analyse electroweak production of $Z\gamma$ in association with two hadronic jets, with the Z boson decaying to electron or muon pairs. Events with photon transverse momentum larger than 60 GeV and di-jet invariant mass larger than 400 GeV are selected. The $Z\gamma$ invariant mass spectrum is analysed to set 95% C.L. limits as follows: $-71 < f_{M,0}/\Lambda^4 < 75$, $-190 < f_{M,1}/\Lambda^4 < 182$, $-32 < f_{M,2}/\Lambda^4 < 31$, $-58 < f_{M,3}/\Lambda^4 < 59$, $-3.8 < f_{T,0}/\Lambda^4 < 3.4$, $-4.4 < f_{T,1}/\Lambda^4 < 4.4$, $-9.9 < f_{T,2}/\Lambda^4 < 9.0$, $-1.8 < f_{T,8}/\Lambda^4 < 1.8$, $-4.0 < f_{T,9}/\Lambda^4 < 4.0$, in units of TeV^{-4} and without application of a form factor.
- ¹¹ KHACHATRYAN 17M analyse electroweak production of $W\gamma$ in association with two hadronic jets, with the W boson decaying to electrons or muons. Events with photon transverse momentum larger than 200 GeV and di-jet invariant mass larger than 200 GeV are selected. The W transverse momentum spectrum is analysed to set 95% C.L. limits as follows: $-77 < f_{M,0}/\Lambda^4 < 74$, $-125 < f_{M,1}/\Lambda^4 < 129$, $-26 < f_{M,2}/\Lambda^4 < 26$, $-43 < f_{M,3}/\Lambda^4 < 44$, $-40 < f_{M,4}/\Lambda^4 < 40$, $-65 < f_{M,5}/\Lambda^4 < 65$, $-129 < f_{M,6}/\Lambda^4 < 129$, $-164 < f_{M,7}/\Lambda^4 < 162$, $-5.4 < f_{T,0}/\Lambda^4 < 5.6$, $-3.7 < f_{T,1}/\Lambda^4 < 4.0$, $-11 < f_{T,2}/\Lambda^4 < 12$, $-3.8 < f_{T,5}/\Lambda^4 < 3.8$, $-2.8 < f_{T,6}/\Lambda^4 < 3.0$, $-7.3 < f_{T,7}/\Lambda^4 < 7.7$, in units of TeV^{-4} and without application of a form factor.
- ¹² SIRUNYAN 17AD study pp collisions at $\sqrt{s} = 13 \text{ TeV}$ to determine the cross section of $ZZjj$ with the Z decaying to ee or $\mu\mu$. The ZZ mass distribution is used to set upper limits on the anomalous quartic couplings. The 95% upper limits for the relevant quartic couplings in units of TeV^{-4} are: $-0.46 < f_{T,0}/\Lambda^4 < 0.44$, $-0.61 < f_{T,1}/\Lambda^4 < 0.61$, $-1.2 < f_{T,2}/\Lambda^4 < 1.2$, $-0.84 < f_{T,8}/\Lambda^4 < 0.84$, $-1.8 < f_{T,9}/\Lambda^4 < 1.8$.
- ¹³ SIRUNYAN 17AR study pp collisions at $\sqrt{s} = 8 \text{ TeV}$ to determine the cross section of $pp \rightarrow W\gamma\gamma$ and $pp \rightarrow Z\gamma\gamma$ where $W \rightarrow \ell\nu$ and $Z \rightarrow \ell^+\ell^-$, ℓ being an electron or a muon. The number of W events in the e and μ channels is 63 and 108 respectively, and the number of Z events in the e and μ channels is 117 and 141. To increase sensitivity, the transverse momentum of the leading photon is required to be larger than 70 GeV. The 95% C.L. upper limits in units of TeV^{-4} are $-701 < f_{M,2}/\Lambda^4 < 683$, $-1170 < f_{M,3}/\Lambda^4 < 1220$, $-33.5 < f_{T,0}/\Lambda^4 < 34.0$, $-44.3 < f_{T,1}/\Lambda^4 < 44.8$, $-93.8 < f_{T,2}/\Lambda^4 < 93.2$.
- ¹⁴ AABOUD 16E study WW production in two-photon mediated pp collisions at 8 TeV where the W boson decays into an electron or muon, probing the $\gamma\gamma WW$ vertex for anomalous quartic gauge couplings. The lepton p_T is required to be larger than 30 GeV. Limits on anomalous couplings are determined from events with p_T larger than 120 GeV where the aQGC effect is enhanced and the SM background reduced; in the data corresponding to an integrated luminosity of 20.2fb^{-1} , 1 event is selected with an expected SM background of 0.37 ± 0.13 events. The 95% C.L. limits without a form-factor cutoff ($\Lambda_{\text{cutoff}} \rightarrow \infty$) are as follows: $-1.7 < a_0^W/\Lambda^2 < 1.7$ and $-6.4 < a_C^W/\Lambda^2 < 6.3$ in units of 10^{-6} GeV^{-2} . In terms of another set of variables: $-6.6 < f_{M,0}/\Lambda^4 < 6.6$ and $-24 < f_{M,1}/\Lambda^4 < 25$ in units of $10^{-11} \text{ GeV}^{-4}$.
- ¹⁵ AAD 16Q study $Z\gamma\gamma$ production in pp collisions. In events with no additional jets, 29 (22) Z decays to electron (muon) pairs are selected, with an expected background of 3.3 ± 1.1 (6.5 ± 2.0) events, as well as 19 Z decays to neutrino pairs with an expected background of 8.3 ± 4.4 events. Analysing the photon transverse momentum distribution for $m_{\gamma\gamma}$ above 200 GeV (300 GeV) for lepton (neutrino) events, yields the 95% C.L. limits: $-1.6 \times 10^4 < f_{M,2}/\Lambda^4 < 1.6 \times 10^4$, $-2.9 \times 10^4 < f_{M,3}/\Lambda^4 < 2.7 \times 10^4$, $-0.86 \times 10^2 < f_{T,0}/\Lambda^4 < 1.03 \times 10^2$, $-0.69 \times 10^3 < f_{T,5}/\Lambda^4 < 0.68 \times 10^3$, $-0.74 \times 10^4 < f_{T,9}/\Lambda^4 < 0.74 \times 10^4$ in units of TeV^{-4} and without application of a form factor Λ_{FF} .
- ¹⁶ KHACHATRYAN 16AX searches for anomalous $WW\gamma\gamma$ quartic gauge couplings in the two-photon-mediated process $pp \rightarrow ppWW$, assuming the $WW\gamma$ triple gauge boson couplings to be at their Standard Model values. 13 events containing an $e^\pm\mu^\mp$ pair with $p_T(e, \mu) > 30 \text{ GeV}$ are selected in a total luminosity of 19.7 fb^{-1} , with an expected $\gamma\gamma$ to WW signal of 5.3 ± 0.1 events and an expected background of 3.9 ± 0.5 events. When combining with the data collected at 7 TeV (KHACHATRYAN 13AA), and not assuming a form factor, the following 1-parameter limits at 95% C.L. are obtained from the $p_T(e, \mu)$ spectrum: $|a_0^W/\Lambda^2| < 1.1 \times 10^{-6} \text{ GeV}^{-2}$ ($a_C^W = 0$), and $|a_C^W/\Lambda^2| < 4.1 \times 10^{-6} \text{ GeV}^{-2}$ ($a_0^W = 0$). In terms of another set of variables: $|f_{M,0}/\Lambda^4| < 4.2 \times 10^{-12} \text{ GeV}^{-4}$, $|f_{M,1}/\Lambda^4| < 16 \times 10^{-12} \text{ GeV}^{-4}$, $|f_{M,2}/\Lambda^4| < 2.1 \times 10^{-12} \text{ GeV}^{-4}$, $|f_{M,3}/\Lambda^4| < 7.8 \times 10^{-12} \text{ GeV}^{-4}$.
- ¹⁷ AAD 15N study $W\gamma\gamma$ events in 8 TeV pp interactions, where the W decays into an electron or a muon. The events are characterized by an isolated lepton, a missing transverse energy due to the decay neutrino, and two isolated photons, with the p_T of the lepton and the photons being $> 20 \text{ GeV}$. The number of candidate events observed in the
- electron channel for $N(\text{jet}) \geq 0$ and $N(\text{jet}) = 0$ is 47 and 15, the corresponding numbers for the muon channel being 110 and 53. The backgrounds expected are 30.2 ± 7.4 , 8.7 ± 3.0 , 52.1 ± 12.2 , and 24.4 ± 8.3 respectively. The 95% C.L. limits on the values of the parameters $f_{T,0}/\Lambda^4$, $f_{M,2}/\Lambda^4$ and $f_{M,3}/\Lambda^4$ are $-0.9-0.9 \times 10^2$, $-0.8-0.8 \times 10^4$, and $-1.5-1.4 \times 10^4$ respectively, without application of a form factor Λ_{FF} .
- ¹⁸ KHACHATRYAN 15D study vector-boson-scattering tagged by two jets, requiring two same-sign charged leptons arising from $W^\pm W^\pm$ production and decay. The two jets must have a transverse momentum larger than 30 GeV, while the leptons, electrons or muons, must have a transverse momentum $> 20 \text{ GeV}$. The dijet mass is required to be $> 500 \text{ GeV}$, the dilepton mass $> 50 \text{ GeV}$, with additional requirement of differing from the Z mass by $> 15 \text{ GeV}$. In the two categories W^+W^+ and W^-W^- , 10 and 2 data events are observed in a data sample corresponding to an integrated luminosity of 19.4 fb^{-1} , with an expected background of 3.1 ± 0.6 and 2.6 ± 0.5 events. Analysing the distribution of the dilepton invariant mass, the following limits at 95% C.L. are obtained, in units of TeV^{-4} : $-38 < f_{S,0}/\Lambda^4 < 40$, $-118 < f_{S,1}/\Lambda^4 < 120$, $-33 < f_{M,0}/\Lambda^4 < 32$, $-44 < f_{M,1}/\Lambda^4 < 47$, $-65 < f_{M,6}/\Lambda^4 < 63$, $-70 < f_{M,7}/\Lambda^4 < 66$, $-4.2 < f_{T,0}/\Lambda^4 < 4.6$, $-1.9 < f_{T,1}/\Lambda^4 < 2.2$, $-5.2 < f_{T,2}/\Lambda^4 < 6.4$.
- ¹⁹ AAD 14AM analyze electroweak production of WW jet jet same-charge diboson plus two jets production, with the W bosons decaying to electron or muon, to study the quartic $WWWW$ coupling. In a kinematic region enhancing the electroweak production over the strong production, 34 events are observed in the data while 29.8 ± 2.4 events are expected with a background of 15.9 ± 1.9 events. Assuming the other QGC coupling to have the SM value of zero, the observed event yield is used to determine 95% CL limits on the quartic gauge couplings: $-0.14 < \alpha_4 < 0.16$ and $-0.23 < \alpha_5 < 0.24$.
- ²⁰ CHATRCHYAN 14Q study $WV\gamma$ production in 8 TeV pp collisions, in the single lepton final state, with $W \rightarrow \ell\nu$, $Z \rightarrow \text{dijet}$ or $W \rightarrow \ell\nu$, $W \rightarrow \text{dijet}$, the dijet mass resolution precluding differentiation between the W and Z. p_T and pseudo-rapidity cuts are put on the lepton, the photon and the two jets to minimize backgrounds. The dijet mass is required to be between 70–100 GeV and $|\Delta\eta_{jj}| < 1.4$. The selected number of muon (electron) events are 183 (139), with SM expectation being 194.2 ± 11.5 (147.9 ± 10.7) including signal and background. The photon E_T distribution is used to set limits on the anomalous quartic couplings. The following 95% CL limits are deduced (all in units of TeV^{-2} or TeV^{-4}): $-21 < a_0^W/\Lambda^2 < 20$, $-34 < a_C^W/\Lambda^2 < 32$, $-12 < \kappa_0^W/\Lambda^2 < 10$ and $-18 < \kappa_C^W/\Lambda^2 < 17$; and $-25 < f_{T,0}/\Lambda^4 < 24 \text{ TeV}^{-4}$.
- ²¹ ABAZOV 13D searches for anomalous $WW\gamma\gamma$ quartic gauge couplings in the two-photon-mediated process $pp \rightarrow ppWW$, assuming the $WW\gamma$ triple gauge boson couplings to be at their Standard Model values. 946 events containing an e^+e^- pair with missing energy are selected in a total luminosity of 9.7 fb^{-1} , with an expectation of 983 ± 108 events from Standard-Model processes. The following 1-parameter limits at 95% CL are obtained: $|a_0^W/\Lambda^2| < 4.3 \times 10^{-4} \text{ GeV}^{-2}$ ($a_C^W = 0$), $|a_C^W/\Lambda^2| < 1.5 \times 10^{-3} \text{ GeV}^{-2}$ ($a_0^W = 0$).
- ²² CHATRCHYAN 13AA searches for anomalous $WW\gamma\gamma$ quartic gauge couplings in the two-photon-mediated process $pp \rightarrow ppWW$, assuming the $WW\gamma$ triple gauge boson couplings to be at their Standard Model values. 2 events containing an $e^\pm\mu^\mp$ pair with $p_T(e, \mu) > 30 \text{ GeV}$ are selected in a total luminosity of 5.05 fb^{-1} , with an expected $ppWW$ signal of 2.2 ± 0.4 events and an expected background of 0.84 ± 0.15 events. The following 1-parameter limits at 95% CL are obtained from the $p_T(e, \mu)$ spectrum: $|a_0^W/\Lambda^2| < 4.0 \times 10^{-6} \text{ GeV}^{-2}$ ($a_C^W = 0$), $|a_C^W/\Lambda^2| < 1.5 \times 10^{-5} \text{ GeV}^{-2}$ ($a_0^W = 0$).
- ²³ ABBIENDI 04B select 187 $e^+e^- \rightarrow W^+W^-\gamma$ events in the C.M. energy range 180–209 GeV, where $E_\gamma > 2.5 \text{ GeV}$, the photon has a polar angle $|\cos\theta_\gamma| < 0.975$ and is well isolated from the nearest jet and charged lepton, and the effective masses of both fermion-antifermion systems agree with the W mass within $3\Gamma_W$. The measured differential cross section as a function of the photon energy and photon polar angle is used to extract the 95% CL limits: $-0.020 \text{ GeV}^{-2} < a_0/\Lambda^2 < 0.020 \text{ GeV}^{-2}$, $-0.053 \text{ GeV}^{-2} < a_C/\Lambda^2 < 0.037 \text{ GeV}^{-2}$ and $-0.16 \text{ GeV}^{-2} < a_n/\Lambda^2 < 0.15 \text{ GeV}^{-2}$.
- ²⁴ ABBIENDI 04L select 20 $e^+e^- \rightarrow \nu\bar{\nu}\gamma$ acoplanar events in the energy range 180–209 GeV and 176 $e^+e^- \rightarrow q\bar{q}\gamma$ events in the energy range 130–209 GeV. These samples are used to constrain possible anomalous $W^+W^-\gamma\gamma$ and $ZZ\gamma\gamma$ quartic couplings. Further combining with the $W^+W^-\gamma$ sample of ABBIENDI 04B the following one-parameter 95% CL limits are obtained: $-0.007 < a_0^Z/\Lambda^2 < 0.023 \text{ GeV}^{-2}$, $-0.029 < a_C^Z/\Lambda^2 < 0.029 \text{ GeV}^{-2}$, $-0.020 < a_0^W/\Lambda^2 < 0.020 \text{ GeV}^{-2}$, $-0.052 < a_C^W/\Lambda^2 < 0.037 \text{ GeV}^{-2}$.
- ²⁵ In the CM energy range 183 to 209 GeV HEISTER 04A select 30 $e^+e^- \rightarrow \nu\bar{\nu}\gamma$ events with two acoplanar, high energy and high transverse momentum photons. The photon-photon acoplanarity is required to be $> 5^\circ$, $E_\gamma/\sqrt{s} > 0.025$ (the more energetic photon having energy $> 0.2\sqrt{s}$), $p_{T,\gamma}/E_{\text{beam}} > 0.05$ and $|\cos\theta_\gamma| < 0.94$. A likelihood fit to the photon energy and recoil missing mass yields the following one-parameter 95% CL limits: $-0.012 < a_0^Z/\Lambda^2 < 0.019 \text{ GeV}^{-2}$, $-0.041 < a_C^Z/\Lambda^2 < 0.044 \text{ GeV}^{-2}$, $-0.060 < a_0^W/\Lambda^2 < 0.055 \text{ GeV}^{-2}$, $-0.099 < a_C^W/\Lambda^2 < 0.093 \text{ GeV}^{-2}$.
- ²⁶ ABDALLAH 03I select 122 $e^+e^- \rightarrow W^+W^-\gamma$ events in the C.M. energy range 189–209 GeV, where $E_\gamma > 5 \text{ GeV}$, the photon has a polar angle $|\cos\theta_\gamma| < 0.95$ and is well isolated from the nearest charged fermion. A fit to the photon energy spectra yields $a_C/\Lambda^2 = 0.000 \pm 0.019 \text{ GeV}^{-2}$, $a_0/\Lambda^2 = -0.004 \pm 0.018 \text{ GeV}^{-2}$, $\bar{a}_0/\Lambda^2 = -0.007 \pm 0.019 \text{ GeV}^{-2}$, $\bar{a}_n/\Lambda^2 = -0.09 \pm 0.16 \text{ GeV}^{-2}$, and $\bar{a}_n/\Lambda^2 = +0.05 \pm 0.07 \text{ GeV}^{-2}$, keeping the other parameters fixed to their Standard Model values (0). The 95% CL limits are: $-0.063 \text{ GeV}^{-2} < a_C/\Lambda^2 < +0.032 \text{ GeV}^{-2}$, $-0.020 \text{ GeV}^{-2} < a_0/\Lambda^2 < +0.020 \text{ GeV}^{-2}$, $-0.020 \text{ GeV}^{-2} < \bar{a}_0/\Lambda^2 < +0.020 \text{ GeV}^{-2}$, $-0.18 \text{ GeV}^{-2} < \bar{a}_n/\Lambda^2 < +0.14 \text{ GeV}^{-2}$, $-0.16 \text{ GeV}^{-2} < \bar{a}_n/\Lambda^2 < +0.17 \text{ GeV}^{-2}$.
- ²⁷ ACHARD 02F select 86 $e^+e^- \rightarrow W^+W^-\gamma$ events at 192–207 GeV, where $E_\gamma > 5 \text{ GeV}$ and the photon is well isolated. They also select 43 acoplanar $e^+e^- \rightarrow \nu\bar{\nu}\gamma$ events in this energy range, where the photon energies are $> 5 \text{ GeV}$ and $> 1 \text{ GeV}$ and the photon polar angles are between 14° and 166° . All these 43 events are in the recoil mass region corresponding to the Z (75–110 GeV). Using the shape and normalization of the photon spectra in the $W^+W^-\gamma$ events, and combining with the 42 event sample from

Gauge & Higgs Boson Particle Listings

W, Z

189 GeV data (ACCIARRI 00T), they obtain: $a_0/\Lambda^2 = 0.000 \pm 0.010 \text{ GeV}^{-2}$, $a_C/\Lambda^2 = -0.013 \pm 0.023 \text{ GeV}^{-2}$, and $a_N/\Lambda^2 = -0.002 \pm 0.076 \text{ GeV}^{-2}$. Further combining the analyses of $W^+ W^- \gamma$ events with the low recoil mass region of $\nu\bar{\nu}\gamma\gamma$ events (including samples collected at 183 + 189 GeV), they obtain the following one-parameter 95% CL limits: $-0.015 \text{ GeV}^{-2} < a_0/\Lambda^2 < 0.015 \text{ GeV}^{-2}$, $-0.048 \text{ GeV}^{-2} < a_C/\Lambda^2 < 0.026 \text{ GeV}^{-2}$, and $-0.14 \text{ GeV}^{-2} < a_N/\Lambda^2 < 0.13 \text{ GeV}^{-2}$.

W REFERENCES

AABOUD 19BA EPJ C79 884 M. Aaboud et al. (ATLAS Collab.)
 PDG 19 RPP 2019 at pgg.lbl.gov M. Tanabashi et al. (PDG Collab.)
 SIRUNYAN 19AD JHEP 1904 122 A.M. Sirunyan et al. (CMS Collab.)
 SIRUNYAN 19BG PRL 122 151802 A.M. Sirunyan et al. (CMS Collab.)
 SIRUNYAN 19BM PR D100 012004 A.M. Sirunyan et al. (CMS Collab.)
 SIRUNYAN 19BP PL B795 281 A.M. Sirunyan et al. (CMS Collab.)
 SIRUNYAN 19CL JHEP 1912 062 A.M. Sirunyan et al. (CMS Collab.)
 SIRUNYAN 19CQ PL B798 134985 A.M. Sirunyan et al. (CMS Collab.)
 AABOUD 18J EPJ C78 110 M. Aaboud et al. (ATLAS Collab.)
 Also EPJ C78 898 (errata) (errat.) (ATLAS Collab.)
 AABOUD 18Q PR D97 032005 M. Aaboud et al. (ATLAS Collab.)
 ANDREEV 18A EPJ C78 777 V. Andreev et al. (HI Collab.)
 SIRUNYAN 18BZ EPJ C78 589 A.M. Sirunyan et al. (CMS Collab.)
 SIRUNYAN 18CC PRL 120 081801 A.M. Sirunyan et al. (CMS Collab.)
 AABOUD 17AA PR D96 012007 M. Aaboud et al. (ATLAS Collab.)
 AABOUD 17AG EPJ C77 646 M. Aaboud et al. (ATLAS Collab.)
 AABOUD 17D PR D95 032001 M. Aaboud et al. (ATLAS Collab.)
 AABOUD 17J JHEP 1707 107 M. Aaboud et al. (ATLAS Collab.)
 AABOUD 17M EPJ C77 141 M. Aaboud et al. (ATLAS Collab.)
 AABOUD 17Q EPJ C77 367 M. Aaboud et al. (ATLAS Collab.)
 AABOUD 17S EPJ C77 474 M. Aaboud et al. (ATLAS Collab.)
 AABOUD 17U EPJ C77 563 M. Aaboud et al. (ATLAS Collab.)
 KHACHATRYAN... 17AA PL B770 380 V. Khachatryan et al. (CMS Collab.)
 KHACHATRYAN... 17M JHEP 1706 106 V. Khachatryan et al. (CMS Collab.)
 KHACHATRYAN... 17O EPJ C77 236 V. Khachatryan et al. (CMS Collab.)
 SIRUNYAN 17AD PL B774 682 A.M. Sirunyan et al. (CMS Collab.)
 SIRUNYAN 17AR JHEP 1710 072 A.M. Sirunyan et al. (CMS Collab.)
 SIRUNYAN 17X PL B772 21 A.M. Sirunyan et al. (CMS Collab.)
 AABOUD 16E PR D94 032011 M. Aaboud et al. (ATLAS Collab.)
 AAD 16AR JHEP 1609 029 G. Aad et al. (ATLAS Collab.)
 AAD 16P PR D93 092004 G. Aad et al. (ATLAS Collab.)
 AAD 16Q PR D93 112002 G. Aad et al. (ATLAS Collab.)
 AAJ 16AJ JHEP 1610 030 R. Aaij et al. (LHCb Collab.)
 KHACHATRYAN... 16AX JHEP 1608 119 V. Khachatryan et al. (CMS Collab.)
 KHACHATRYAN... 16BI EPJ C76 401 V. Khachatryan et al. (CMS Collab.)
 AAD 15N PRL 115 031802 G. Aad et al. (ATLAS Collab.)
 KHACHATRYAN... 15D PRL 114 051801 V. Khachatryan et al. (CMS Collab.)
 AAD 14AM PRL 113 141803 G. Aad et al. (ATLAS Collab.)
 AAD 14Y JHEP 1404 031 G. Aad et al. (ATLAS Collab.)
 AALTONEN 14D PR D89 072003 T. Aaltonen et al. (CDF Collab.)
 ABZOV 14N PR D89 012005 V.M. Abazov et al. (DO Collab.)
 CHATRCHYAN 14AB PR D89 092005 S. Chatrchyan et al. (CMS Collab.)
 CHATRCHYAN 14Q PR D90 032008 S. Chatrchyan et al. (CMS Collab.)
 AAD 13AL PR D87 112001 G. Aad et al. (ATLAS Collab.)
 Also PR D88 079906 (errata) (errat.) (ATLAS Collab.)
 AAD 13AN PR D87 112003 G. Aad et al. (ATLAS Collab.)
 Also PR D91 119901 (errata) (errat.) (ATLAS Collab.)
 AALTONEN 13N PR D88 052018 T. Aaltonen et al. (CDF and DO Collabs.)
 ABZOV 13D PR D88 012005 V.M. Abazov et al. (DO Collab.)
 CHATRCHYAN 13AA JHEP 1307 116 S. Chatrchyan et al. (CMS Collab.)
 CHATRCHYAN 13BF EPJ C73 2610 S. Chatrchyan et al. (CMS Collab.)
 SCHAE 13A PRL 110 241803 V.M. Abazov et al. (DO Collab.)
 AAD 12AC PL B712 289 G. Aad et al. (ATLAS Collab.)
 AAD 12BX PL B717 49 G. Aad et al. (ATLAS Collab.)
 AAD 12CD EPJ C72 2173 G. Aad et al. (ATLAS Collab.)
 AAD 12V PL B709 341 G. Aad et al. (ATLAS Collab.)
 AALTONEN 12AC PR D86 031104 T. Aaltonen et al. (CDF Collab.)
 AALTONEN 12E PRL 108 151803 T. Aaltonen et al. (CDF Collab.)
 AALTONEN 12W PR D85 032001 T. Aaltonen et al. (CDF Collab.)
 ABZOV 12AG PL B718 451 V.M. Abazov et al. (DO Collab.)
 ABZOV 12AF PR D86 012004 V.M. Abazov et al. (DO Collab.)
 ABZOV 11 PL B695 87 V.M. Abazov et al. (DO Collab.)
 ABZOV 11AC PRL 107 241803 V.M. Abazov et al. (DO Collab.)
 BLINOV 11 PL B699 287 A.E. Blinov, A.S. Rudenko (NOVO Collab.)
 CHATRCHYAN 11M PL B701 535 S. Chatrchyan et al. (CMS Collab.)
 AALTONEN 10K PRL 104 201801 T. Aaltonen et al. (CDF Collab.)
 Also PRL 105 019905 (errata) (errat.) (CDF Collab.)
 ABDALLAH 10 EPJ C66 35 F.J. Abdallah et al. (DELPHI Collab.)
 AARON 09B EPJ C64 251 F.D. Aaron et al. (HI Collab.)
 ABZOV 09AB PRL 103 141801 V.M. Abazov et al. (DO Collab.)
 ABZOV 09AD PR D80 053012 V.M. Abazov et al. (DO Collab.)
 ABZOV 09AJ PRL 103 191801 V.M. Abazov et al. (DO Collab.)
 ABZOV 09AK PRL 103 231802 V.M. Abazov et al. (DO Collab.)
 AALTONEN 08B PRL 100 071801 T. Aaltonen et al. (CDF Collab.)
 ABZOV 08R PRL 100 241805 V.M. Abazov et al. (DO Collab.)
 ABDALLAH 08A EPJ C55 1 J. Abdallah et al. (DELPHI Collab.)
 ABDALLAH 08C EPJ C54 345 J. Abdallah et al. (DELPHI Collab.)
 AALTONEN 07F PRL 99 151801 T. Aaltonen et al. (CDF Collab.)
 Also PR D77 112001 T. Aaltonen et al. (CDF Collab.)
 AALTONEN 07L PR D76 111103 T. Aaltonen et al. (CDF Collab.)
 ABZOV 07Z PR D76 111104 V.M. Abazov et al. (DO Collab.)
 ABBIENDI 07A EPJ C52 767 G. Abbiendi et al. (OPAL Collab.)
 ABZOV 06H PR D74 057101 V.M. Abazov et al. (DO Collab.)
 Also PR D74 059404 (errata) (errat.) (DO Collab.)
 ABBIENDI 06 EPJ C45 307 G. Abbiendi et al. (OPAL Collab.)
 ABBIENDI 06A EPJ C45 291 G. Abbiendi et al. (OPAL Collab.)
 ACHARD 06 EPJ C45 569 P. Achard et al. (L3 Collab.)
 AKTAS 06 PL B632 35 A. Aktas et al. (HI Collab.)
 SCHAE 06 EPJ C47 309 S. Schae et al. (ALEPH Collab.)
 ABZOV 05J PR D71 091108 V.M. Abazov et al. (DO Collab.)
 ABZOV 05S PRL 95 141802 V.M. Abazov et al. (DO Collab.)
 SCHAE 05A PL B614 7 S. Schae et al. (ALEPH Collab.)
 ABZOV 04D PR D70 092008 V.M. Abazov et al. (DO Collab.)
 ABBIENDI 04B PL B580 17 G. Abbiendi et al. (OPAL Collab.)
 ABBIENDI 04D EPJ C33 463 G. Abbiendi et al. (OPAL Collab.)
 ABBIENDI 04L PR D70 032005 G. Abbiendi et al. (OPAL Collab.)
 ABDALLAH 04G EPJ C34 127 J. Abdallah et al. (DELPHI Collab.)
 ACHARD 04D PL B586 151 P. Achard et al. (L3 Collab.)
 ACHARD 04J PL B600 22 P. Achard et al. (L3 Collab.)
 HEISTER 04A PL B602 31 A. Heister et al. (ALEPH Collab.)
 SCHAE 04A EPJ C38 147 S. Schae et al. (ALEPH Collab.)
 ABBIENDI 03C EPJ C26 321 G. Abbiendi et al. (OPAL Collab.)
 ABDALLAH 03I EPJ C31 139 J. Abdallah et al. (DELPHI Collab.)
 ABZOV 02D PR D66 012001 V.M. Abazov et al. (DO Collab.)
 ABZOV 02E PR D66 032008 V.M. Abazov et al. (DO Collab.)
 ACHARD 02H EPJ C33 463 P. Achard et al. (L3 Collab.)
 CHEKANOV 02C PL B539 197 S. Chekanov et al. (ZEUS Collab.)
 ABBIENDI 01H EPJ C19 229 G. Abbiendi et al. (OPAL Collab.)

ABREU 01I PL B502 9 P. Abreu et al. (DELPHI Collab.)
 AFFOLDER 01E PR D64 052001 T. Affolder et al. (CDF Collab.)
 ABBIENDI 00P PL B490 71 G. Abbiendi et al. (OPAL Collab.)
 ABBOTT 00B PR D61 072001 B. Abbott et al. (DO Collab.)
 ABBOTT 00D PRL 84 5710 B. Abbott et al. (DO Collab.)
 ABREU.P 00F EPJ C18 203 P. Abreu et al. (DELPHI Collab.)
 Also EPJ C25 493 (errata) (errat.) (DELPHI Collab.)
 ACCIARRI 00T PL B490 187 M. Acciari et al. (L3 Collab.)
 AFFOLDER 00M PRL 85 3347 T. Affolder et al. (CDF Collab.)
 BREITWEG 00 PL B471 411 J. Breitweg et al. (ZEUS Collab.)
 BREITWEG 00D EPJ C12 411 J. Breitweg et al. (ZEUS Collab.)
 EBOLI 00 MPL A15 1 O. Eboli, M. Gonzalez-Garcia, S. Novaes
 ABBIENDI 99N PL B453 153 G. Abbiendi et al. (OPAL Collab.)
 ABBOTT 99H PR D60 052003 B. Abbott et al. (DO Collab.)
 ABBOTT 99I PR D60 072002 B. Abbott et al. (DO Collab.)
 ABREU 99L PL B459 382 P. Abreu et al. (DELPHI Collab.)
 ACCIARRI 99 PL B454 386 M. Acciari et al. (L3 Collab.)
 ACCIARRI 99Q PL B467 171 M. Acciari et al. (L3 Collab.)
 BARATE 99I PL B453 107 R. Barate et al. (ALEPH Collab.)
 BARATE 99L PL B463 389 R. Barate et al. (ALEPH Collab.)
 BARATE 99M PL B465 349 R. Barate et al. (ALEPH Collab.)
 ABBOTT 98N PR D58 092003 B. Abbott et al. (DO Collab.)
 ABBOTT 98P PR D58 012002 B. Abbott et al. (DO Collab.)
 ABE 98H PR D58 031101 F. Abe et al. (CDF Collab.)
 ABE 98R PR D58 091101 F. Abe et al. (CDF Collab.)
 ABREU 98C PL B416 233 P. Abreu et al. (DELPHI Collab.)
 ABREU 98N PL B439 209 P. Abreu et al. (DELPHI Collab.)
 BARATE 97 PL B401 347 R. Barate et al. (ALEPH Collab.)
 BARATE 97S PL B415 435 R. Barate et al. (ALEPH Collab.)
 ABACHI 95D PRL 75 19456 S. Abachi et al. (DO Collab.)
 ABE 95C PRL 74 341 F. Abe et al. (CDF Collab.)
 ABE 95D PRL 74 1936 F. Abe et al. (CDF Collab.)
 ABE 95P PRL 75 11 F. Abe et al. (CDF Collab.)
 Also PR D52 4784 F. Abe et al. (CDF Collab.)
 ABE 95W PR D52 2624 F. Abe et al. (CDF Collab.)
 Also PRL 73 220 F. Abe et al. (CDF Collab.)
 ABE 92E PRL 68 3398 F. Abe et al. (CDF Collab.)
 ABE 92I PRL 69 28 F. Abe et al. (CDF Collab.)
 ALITTI 92 PL B276 365 J. Alitti et al. (UA2 Collab.)
 ALITTI 92B PL B276 354 J. Alitti et al. (UA2 Collab.)
 ALITTI 92C PL B277 194 J. Alitti et al. (UA2 Collab.)
 ALITTI 92D PL B277 203 J. Alitti et al. (UA2 Collab.)
 ALITTI 92F PL B280 137 J. Alitti et al. (UA2 Collab.)
 SAMUEL 92 PL B280 124 M.A. Samuel et al. (OKSU, CARL)
 ABE 91C PR D44 29 F. Abe et al. (CDF Collab.)
 ALBAJAR 91 PL B253 503 C. Albajar et al. (UA1 Collab.)
 ALITTI 91C ZPHY C52 209 J. Alitti et al. (UA2 Collab.)
 SAMUEL 91 PRL 67 9 M.A. Samuel et al. (OKSU, CARL)
 Also PRL 67 2920 (erratum) (errat.) (CDF Collab.)
 ABE 90G PRL 65 2243 F. Abe et al. (CDF Collab.)
 Also PR D43 2070 F. Abe et al. (CDF Collab.)
 ALBAJAR 90 PL B241 283 C. Albajar et al. (UA1 Collab.)
 ALITTI 90B PL B241 150 J. Alitti et al. (UA2 Collab.)
 ABE 89I PRL 62 1005 F. Abe et al. (CDF Collab.)
 ALBAJAR 89 ZPHY C44 15 C. Albajar et al. (UA1 Collab.)
 BAUR 88 NP B308 127 U. Baur, D. Zeppenfeld (FSU, WISC)
 GRIFOLS 88 IJMP A3 225 J.A. Grifols, S. Peris, J. Sola (BARC, DESY)
 Also PL B197 437 J.A. Grifols, S. Peris, J. Sola (BARC, DESY)
 ALBAJAR 87 PL B185 233 C. Albajar et al. (UA1 Collab.)
 ANSARI 87 PL B186 440 R. Ansari et al. (UA2 Collab.)
 GROTH 87 PR D36 2153 H. Groth, R.W. Robinett (FSU)
 HAGIWARA 87 NP B282 253 K. Hagiwara et al. (KEK, UCLA, PSU)
 VANDERBIJ 87 PR D35 1088 J.J. van der Bij (FNAL)
 GRAU 85 PL 154B 283 A. Grau, J.A. Grifols (BARC)
 SUZUKI 85 PL 153B 289 M. Suzuki (LBL)
 ARNISON 84D PL 134B 469 G.T.J. Arnison et al. (UA1 Collab.)
 HERZOG 84 PL 148B 355 F. Herzog (WISC)
 Also PL 155B 468 (erratum) (errat.) (WISC)
 ARNISON 83 PL 122B 103 G.T.J. Arnison et al. (UA1 Collab.)
 BANNER 83B PL 122B 476 M. Banner et al. (UA2 Collab.)



J = 1

See the related review(s):

Z Boson

Z MASS

OUR FIT is obtained using the fit procedure and correlations as determined by the LEP Electroweak Working Group (see the note "The Z boson" and ref. LEP-SLC 06). The fit is performed using the Z mass and width, the Z hadronic pole cross section, the ratios of hadronic to leptonic partial widths, and the Z pole forward-backward lepton asymmetries. This set is believed to be most free of correlations.

The Z-boson mass listed here corresponds to the mass parameter in a Breit-Wigner distribution with mass dependent width. The value is 34 MeV greater than the real part of the position of the pole (in the energy-squared plane) in the Z-boson propagator. Also the LEP experiments term based on the standard model. Keeping this term as free parameter leads to a somewhat larger error on the fitted Z mass. See ACCIARRI 00q and ABBIENDI 04g for a detailed investigation of both these issues.

VALUE (GeV)	EVTS	DOCUMENT ID	TECN	COMMENT
91.1876 ± 0.0021 OUR FIT				
91.1852 ± 0.0030	4.57M	¹ ABBIENDI 01A	OPAL	$E_{cm}^{ee} = 88-94$ GeV
91.1863 ± 0.0028	4.08M	² ABREU 00F	DLPH	$E_{cm}^{ee} = 88-94$ GeV
91.1898 ± 0.0031	3.96M	³ ACCIARRI 00C	L3	$E_{cm}^{ee} = 88-94$ GeV
91.1885 ± 0.0031	4.57M	⁴ BARATE 00C	ALEP	$E_{cm}^{ee} = 88-94$ GeV

• • • We do not use the following data for averages, fits, limits, etc. • • •

91.084 ± 0.107		5	ANDREEV	18A	H1	$e^\pm \rho$
91.1872 ± 0.0033		6	ABBIENDI	04G	OPAL	$E_{cm}^{ee} = \text{LEP1} + 130\text{--}209 \text{ GeV}$
91.272 ± 0.032 ± 0.033		7	ACHARD	04c	L3	$E_{cm}^{ee} = 183\text{--}209 \text{ GeV}$
91.1875 ± 0.0039	3.97M	8	ACCIARRI	00Q	L3	$E_{cm}^{ee} = \text{LEP1} + 130\text{--}189 \text{ GeV}$
91.151 ± 0.008		9	MIYABAYASHI	95	TOPZ	$E_{cm}^{ee} = 57.8 \text{ GeV}$
91.74 ± 0.28 ± 0.93	156	10	ALITTI	92B	UA2	$E_{cm}^{ee} = 630 \text{ GeV}$
90.9 ± 0.3 ± 0.2	188	11	ABE	89c	CDF	$E_{cm}^{pp} = 1.8 \text{ TeV}$
91.14 ± 0.12	480	12	ABRAMS	89B	MRK2	$E_{cm}^{ee} = 89\text{--}93 \text{ GeV}$
93.1 ± 1.0 ± 3.0	24	13	ALBAJAR	89	UA1	$E_{cm}^{pp} = 546,630 \text{ GeV}$

- ABBIENDI 01A error includes approximately 2.3 MeV due to statistics and 1.8 MeV due to LEP energy uncertainty.
- The error includes 1.6 MeV due to LEP energy uncertainty.
- The error includes 1.8 MeV due to LEP energy uncertainty.
- BARATE 00c error includes approximately 2.4 MeV due to statistics, 0.2 MeV due to experimental systematics, and 1.7 MeV due to LEP energy uncertainty.
- ANDREEV 18A obtain this result in a combined electroweak and QCD analysis using all deep-inelastic e^+p and e^-p neutral current and charged current scattering cross sections published by the H1 Collaboration, including data with longitudinally polarized lepton beams.
- ABBIENDI 04G obtain this result using the S-matrix formalism for a combined fit to their cross section and asymmetry data at the Z peak and their data at 130–209 GeV. The authors have corrected the measurement for the 34 MeV shift with respect to the Breit-Wigner fits.
- ACHARD 04c select $e^+e^- \rightarrow Z\gamma$ events with hard initial-state radiation. Z decays to $q\bar{q}$ and muon pairs are considered. The fit results obtained in the two samples are found consistent to each other and combined considering the uncertainty due to ISR modelling as fully correlated.
- ACCIARRI 00q interpret the s-dependence of the cross sections and lepton forward-backward asymmetries in the framework of the S-matrix formalism. They fit to their cross section and asymmetry data at high energies, using the results of S-matrix fits to Z-peak data (ACCIARRI 00c) as constraints. The 130–189 GeV data constrains the γ/Z interference term. The authors have corrected the measurement for the 34.1 MeV shift with respect to the Breit-Wigner fits. The error contains a contribution of $\pm 2.3 \text{ MeV}$ due to the uncertainty on the γZ interference.
- MIYABAYASHI 95 combine their low energy total hadronic cross-section measurement with the ACTON 93D data and perform a fit using an S-matrix formalism. As expected, this result is below the mass values obtained with the standard Breit-Wigner parametrization.
- Enters fit through W/Z mass ratio given in the W Particle Listings. The ALITTI 92B systematic error (± 0.93) has two contributions: one (± 0.92) cancels in m_W/m_Z and one (± 0.12) is noncancelling. These were added in quadrature.
- First error of ABE 89 is combination of statistical and systematic contributions; second is mass scale uncertainty.
- ABRAMS 89B uncertainty includes 35 MeV due to the absolute energy measurement.
- ALBAJAR 89 result is from a total sample of $33 Z \rightarrow e^+e^-$ events.

Z WIDTH

OUR FIT is obtained using the fit procedure and correlations as determined by the LEP Electroweak Working Group (see the note "The Z boson" and ref. LEP-SLC 06).

VALUE (GeV)	EVTS	DOCUMENT ID	TECN	COMMENT
2.4952 ± 0.0023 OUR FIT				
2.4948 ± 0.0041	4.57M	1 ABBIENDI	01A OPAL	$E_{cm}^{ee} = 88\text{--}94 \text{ GeV}$
2.4876 ± 0.0041	4.08M	2 ABREU	00F DLPH	$E_{cm}^{ee} = 88\text{--}94 \text{ GeV}$
2.5024 ± 0.0042	3.96M	3 ACCIARRI	00c L3	$E_{cm}^{ee} = 88\text{--}94 \text{ GeV}$
2.4951 ± 0.0043	4.57M	4 BARATE	00c ALEP	$E_{cm}^{ee} = 88\text{--}94 \text{ GeV}$
• • • We do not use the following data for averages, fits, limits, etc. • • •				
2.4943 ± 0.0041		5 ABBIENDI	04G OPAL	$E_{cm}^{ee} = \text{LEP1} + 130\text{--}209 \text{ GeV}$
2.5025 ± 0.0041	3.97M	6 ACCIARRI	00Q L3	$E_{cm}^{ee} = \text{LEP1} + 130\text{--}189 \text{ GeV}$
2.50 ± 0.21 ± 0.06		7 ABREU	96R DLPH	$E_{cm}^{ee} = 91.2 \text{ GeV}$
3.8 ± 0.8 ± 1.0	188	8 ABE	89c CDF	$E_{cm}^{pp} = 1.8 \text{ TeV}$
2.42 $\begin{smallmatrix} +0.45 \\ -0.35 \end{smallmatrix}$ ± 1.0	480	9 ABRAMS	89B MRK2	$E_{cm}^{ee} = 89\text{--}93 \text{ GeV}$
2.7 $\begin{smallmatrix} +1.2 \\ -1.0 \end{smallmatrix}$ ± 1.3	24	10 ALBAJAR	89 UA1	$E_{cm}^{pp} = 546,630 \text{ GeV}$
2.7 ± 2.0 ± 1.0	25	11 ANSARI	87 UA2	$E_{cm}^{pp} = 546,630 \text{ GeV}$

- ABBIENDI 01A error includes approximately 3.6 MeV due to statistics, 1 MeV due to event selection systematics, and 1.3 MeV due to LEP energy uncertainty.
- The error includes 1.2 MeV due to LEP energy uncertainty.
- The error includes 1.3 MeV due to LEP energy uncertainty.
- BARATE 00c error includes approximately 3.8 MeV due to statistics, 0.9 MeV due to experimental systematics, and 1.3 MeV due to LEP energy uncertainty.
- ABBIENDI 04G obtain this result using the S-matrix formalism for a combined fit to their cross section and asymmetry data at the Z peak and their data at 130–209 GeV. The authors have corrected the measurement for the 1 MeV shift with respect to the Breit-Wigner fits.
- ACCIARRI 00q interpret the s-dependence of the cross sections and lepton forward-backward asymmetries in the framework of the S-matrix formalism. They fit to their cross section and asymmetry data at high energies, using the results of S-matrix fits to Z-peak data (ACCIARRI 00c) as constraints. The 130–189 GeV data constrains the γ/Z interference term. The authors have corrected the measurement for the 0.9 MeV shift with respect to the Breit-Wigner fits.

- ABREU 96R obtain this value from a study of the interference between initial and final state radiation in the process $e^+e^- \rightarrow Z \rightarrow \mu^+\mu^-$.
- ABRAMS 89B uncertainty includes 50 MeV due to the miniSAM background subtraction error.
- ALBAJAR 89 result is from a total sample of $33 Z \rightarrow e^+e^-$ events.
- Quoted values of ANSARI 87 are from direct fit. Ratio of Z and W production gives either $\Gamma(Z) < (1.09 \pm 0.07) \times \Gamma(W)$, CL = 90% or $\Gamma(Z) = (0.82^{+0.19}_{-0.14} \pm 0.06) \times \Gamma(W)$. Assuming Standard-Model value $\Gamma(W) = 2.65 \text{ GeV}$ then gives $\Gamma(Z) < 2.89 \pm 0.19$ or $= 2.17^{+0.50}_{-0.37} \pm 0.16$.

Z DECAY MODES

Mode	Fraction (Γ_i/Γ)	Scale factor / Confidence level
Γ ₁ e^+e^-	[a] (3.3632 ± 0.0042) %	
Γ ₂ $\mu^+\mu^-$	[a] (3.3662 ± 0.0066) %	
Γ ₃ $\tau^+\tau^-$	[a] (3.3696 ± 0.0083) %	
Γ ₄ $\ell^+\ell^-$	[a,b] (3.3658 ± 0.0023) %	
Γ ₅ $\mu^+\mu^-\mu^+\mu^-$		
Γ ₆ $\ell^+\ell^-\ell^+\ell^-$	[c] (4.63 ± 0.21) × 10 ⁻⁶	
Γ ₇ invisible	[a] (20.000 ± 0.055) %	
Γ ₈ hadrons	[a] (69.911 ± 0.056) %	
Γ ₉ $(u\bar{u} + c\bar{c})/2$	(11.6 ± 0.6) %	
Γ ₁₀ $(d\bar{d} + s\bar{s} + b\bar{b})/3$	(15.6 ± 0.4) %	
Γ ₁₁ $c\bar{c}$	(12.03 ± 0.21) %	
Γ ₁₂ $b\bar{b}$	(15.12 ± 0.05) %	
Γ ₁₃ $b\bar{b}b\bar{b}$	(3.6 ± 1.3) × 10 ⁻⁴	
Γ ₁₄ ggg	< 1.1 %	CL=95%
Γ ₁₅ $\pi^0\gamma$	< 2.01 × 10 ⁻⁵	CL=95%
Γ ₁₆ $\eta\gamma$	< 5.1 × 10 ⁻⁵	CL=95%
Γ ₁₇ $\rho^0\gamma$	< 2.5 × 10 ⁻⁵	CL=95%
Γ ₁₈ $\omega\gamma$	< 6.5 × 10 ⁻⁴	CL=95%
Γ ₁₉ $\eta'(958)\gamma$	< 4.2 × 10 ⁻⁵	CL=95%
Γ ₂₀ $\phi\gamma$	< 9 × 10 ⁻⁷	CL=95%
Γ ₂₁ $\gamma\gamma$	< 1.46 × 10 ⁻⁵	CL=95%
Γ ₂₂ $\pi^0\pi^0$	< 1.52 × 10 ⁻⁵	CL=95%
Γ ₂₃ $\gamma\gamma\gamma$	< 2.2 × 10 ⁻⁶	CL=95%
Γ ₂₄ $\pi^\pm W^\mp$	[d] < 7 × 10 ⁻⁵	CL=95%
Γ ₂₅ $\rho^\pm W^\mp$	[d] < 8.3 × 10 ⁻⁵	CL=95%
Γ ₂₆ $J/\psi(1S)X$	(3.51 $\begin{smallmatrix} +0.23 \\ -0.25 \end{smallmatrix}$) × 10 ⁻³	S=1.1
Γ ₂₇ $J/\psi(1S)\gamma$	< 1.4 × 10 ⁻⁶	CL=95%
Γ ₂₈ $\psi(2S)X$	(1.60 ± 0.29) × 10 ⁻³	
Γ ₂₉ $\psi(2S)\gamma$	< 4.5 × 10 ⁻⁶	CL=95%
Γ ₃₀ $J/\psi(1S)\ell^+\ell^-$		
Γ ₃₁ $J/\psi(1S)J/\psi(1S)$	< 2.2 × 10 ⁻⁶	CL=95%
Γ ₃₂ $\chi_{c1}(1P)X$	(2.9 ± 0.7) × 10 ⁻³	
Γ ₃₃ $\chi_{c2}(1P)X$	< 3.2 × 10 ⁻³	CL=90%
Γ ₃₄ $\Upsilon(1S)X + \Upsilon(2S)X + \Upsilon(3S)X$	(1.0 ± 0.5) × 10 ⁻⁴	
Γ ₃₅ $\Upsilon(1S)X$	< 3.4 × 10 ⁻⁶	CL=95%
Γ ₃₆ $\Upsilon(1S)\gamma$	< 2.8 × 10 ⁻⁶	CL=95%
Γ ₃₇ $\Upsilon(2S)X$	< 6.5 × 10 ⁻⁶	CL=95%
Γ ₃₈ $\Upsilon(2S)\gamma$	< 1.7 × 10 ⁻⁶	CL=95%
Γ ₃₉ $\Upsilon(3S)X$	< 5.4 × 10 ⁻⁶	CL=95%
Γ ₄₀ $\Upsilon(3S)\gamma$	< 4.8 × 10 ⁻⁶	CL=95%
Γ ₄₁ $\Upsilon(1,2,3S)\Upsilon(1,2,3S)$	< 1.5 × 10 ⁻⁶	CL=95%
Γ ₄₂ $(D^0/\bar{D}^0)X$	(20.7 ± 2.0) %	
Γ ₄₃ $D^\pm X$	(12.2 ± 1.7) %	
Γ ₄₄ $D^*(2010)^\pm X$	[d] (11.4 ± 1.3) %	
Γ ₄₅ $D_{s1}(2536)^\pm X$	(3.6 ± 0.8) × 10 ⁻³	
Γ ₄₆ $D_{sJ}(2573)^\pm X$	(5.8 ± 2.2) × 10 ⁻³	
Γ ₄₇ $D^{*'}(2629)^\pm X$	searched for	
Γ ₄₈ BX		
Γ ₄₉ B^*X		
Γ ₅₀ B^+X	[e] (6.08 ± 0.13) %	
Γ ₅₁ B^0X	[e] (1.59 ± 0.13) %	
Γ ₅₂ $B_s^\pm X$	searched for	
Γ ₅₃ $\Lambda_c^+ X$	(1.54 ± 0.33) %	
Γ ₅₄ $\Xi_c^0 X$	seen	
Γ ₅₅ $\Xi_b X$	seen	
Γ ₅₆ b -baryon X	[e] (1.38 ± 0.22) %	
Γ ₅₇ anomalous γ + hadrons	[f] < 3.2 × 10 ⁻³	CL=95%
Γ ₅₈ $e^+e^- \gamma$	[f] < 5.2 × 10 ⁻⁴	CL=95%
Γ ₅₉ $\mu^+\mu^- \gamma$	[f] < 5.6 × 10 ⁻⁴	CL=95%
Γ ₆₀ $\tau^+\tau^- \gamma$	[f] < 7.3 × 10 ⁻⁴	CL=95%
Γ ₆₁ $\ell^+\ell^- \gamma\gamma$	[g] < 6.8 × 10 ⁻⁶	CL=95%

Gauge & Higgs Boson Particle Listings

Z

Γ_{62}	$q\bar{q}\gamma\gamma$		$[g] < 5.5$	$\times 10^{-6}$	CL=95%
Γ_{63}	$\nu\bar{\nu}\gamma\gamma$		$[g] < 3.1$	$\times 10^{-6}$	CL=95%
Γ_{64}	$e^{\pm}\mu^{\mp}$	LF	$[d] < 7.5$	$\times 10^{-7}$	CL=95%
Γ_{65}	$e^{\pm}\tau^{\mp}$	LF	$[d] < 9.8$	$\times 10^{-6}$	CL=95%
Γ_{66}	$\mu^{\pm}\tau^{\mp}$	LF	$[d] < 1.2$	$\times 10^{-5}$	CL=95%
Γ_{67}	ρe	L,B	< 1.8	$\times 10^{-6}$	CL=95%
Γ_{68}	$\rho\mu$	L,B	< 1.8	$\times 10^{-6}$	CL=95%

[a] This parameter is not directly used in the overall fit but is derived using the fit results; see the note "The Z boson" and ref. LEP-SLC 06 (Physics Reports (Physics Letters C) **427** 257 (2006)).

[b] ℓ indicates each type of lepton (e , μ , and τ), not sum over them.

[c] Here ℓ indicates e or μ .

[d] The value is for the sum of the charge states or particle/antiparticle states indicated.

[e] This value is updated using the product of (i) the $Z \rightarrow b\bar{b}$ fraction from this listing and (ii) the b -hadron fraction in an unbiased sample of weakly decaying b -hadrons produced in Z-decays provided by the Heavy Flavor Averaging Group (HFLAV, http://www.slac.stanford.edu/xorg/hflav/osc/PDG_2009/#FRACZ).

[f] See the Particle Listings below for the γ energy range used in this measurement.

[g] For $m_{\gamma\gamma} = (60 \pm 5)$ GeV.

Z PARTIAL WIDTHS

$\Gamma(e^+e^-)$ Γ_1
For the LEP experiments, this parameter is not directly used in the overall fit but is derived using the fit results; see the note "The Z boson" and ref. LEP-SLC 06.

VALUE (MeV)	EVTS	DOCUMENT ID	TECN	COMMENT
83.91 ± 0.12 OUR FIT				
83.66 ± 0.20	137.0K	ABBIENDI	01A OPAL	$E_{cm}^{ee} = 88-94$ GeV
83.54 ± 0.27	117.8k	ABREU	00F DLPH	$E_{cm}^{ee} = 88-94$ GeV
84.16 ± 0.22	124.4k	ACCIARRI	00c L3	$E_{cm}^{ee} = 88-94$ GeV
83.88 ± 0.19		BARATE	00c ALEP	$E_{cm}^{ee} = 88-94$ GeV
82.89 ± 1.20 ± 0.89		¹ ABE	95J SLD	$E_{cm}^{ee} = 91.31$ GeV

¹ ABE 95J obtain this measurement from Bhabha events in a restricted fiducial region to improve systematics. They use the values 91.187 and 2.489 GeV for the Z mass and total decay width to extract this partial width.

$\Gamma(\mu^+\mu^-)$ Γ_2
This parameter is not directly used in the overall fit but is derived using the fit results; see the note "The Z boson" and ref. LEP-SLC 06.

VALUE (MeV)	EVTS	DOCUMENT ID	TECN	COMMENT
83.99 ± 0.18 OUR FIT				
84.03 ± 0.30	182.8K	ABBIENDI	01A OPAL	$E_{cm}^{ee} = 88-94$ GeV
84.48 ± 0.40	157.6k	ABREU	00F DLPH	$E_{cm}^{ee} = 88-94$ GeV
83.95 ± 0.44	113.4k	ACCIARRI	00c L3	$E_{cm}^{ee} = 88-94$ GeV
84.02 ± 0.28		BARATE	00c ALEP	$E_{cm}^{ee} = 88-94$ GeV

$\Gamma(\tau^+\tau^-)$ Γ_3
This parameter is not directly used in the overall fit but is derived using the fit results; see the note "The Z boson" and ref. LEP-SLC 06.

VALUE (MeV)	EVTS	DOCUMENT ID	TECN	COMMENT
84.08 ± 0.22 OUR FIT				
83.94 ± 0.41	151.5K	ABBIENDI	01A OPAL	$E_{cm}^{ee} = 88-94$ GeV
83.71 ± 0.58	104.0k	ABREU	00F DLPH	$E_{cm}^{ee} = 88-94$ GeV
84.23 ± 0.58	103.0k	ACCIARRI	00c L3	$E_{cm}^{ee} = 88-94$ GeV
84.38 ± 0.31		BARATE	00c ALEP	$E_{cm}^{ee} = 88-94$ GeV

$\Gamma(\ell^+\ell^-)$ Γ_4
 ℓ indicates each type of lepton (e , μ , and τ), not sum over them.

In our fit $\Gamma(\ell^+\ell^-)$ is defined as the partial Z width for the decay into a pair of massless charged leptons. This parameter is not directly used in the 5-parameter fit assuming lepton universality but is derived using the fit results. See the note "The Z boson" and ref. LEP-SLC 06.

VALUE (MeV)	EVTS	DOCUMENT ID	TECN	COMMENT
83.984 ± 0.086 OUR FIT				
83.82 ± 0.15	471.3K	ABBIENDI	01A OPAL	$E_{cm}^{ee} = 88-94$ GeV
83.85 ± 0.17	379.4k	ABREU	00F DLPH	$E_{cm}^{ee} = 88-94$ GeV
84.14 ± 0.17	340.8k	ACCIARRI	00c L3	$E_{cm}^{ee} = 88-94$ GeV
84.02 ± 0.15	500k	BARATE	00c ALEP	$E_{cm}^{ee} = 88-94$ GeV

$\Gamma(\text{invisible})$ Γ_7
We use only direct measurements of the invisible partial width using the single photon channel to obtain the average value quoted below. OUR FIT value is obtained as a difference between the total and the observed partial widths assuming lepton universality.

VALUE (MeV)	EVTS	DOCUMENT ID	TECN	COMMENT
499.0 ± 1.5 OUR FIT				
503 ± 16 OUR AVERAGE	Error	includes scale factor of 1.2.		
498 ± 12 ± 12	1791	ACCIARRI	98G L3	$E_{cm}^{ee} = 88-94$ GeV
539 ± 26 ± 17	410	AKERS	95c OPAL	$E_{cm}^{ee} = 88-94$ GeV
450 ± 34 ± 34	258	BUSKULIC	93L ALEP	$E_{cm}^{ee} = 88-94$ GeV
540 ± 80 ± 40	52	ADEVA	92 L3	$E_{cm}^{ee} = 88-94$ GeV
• • • We do not use the following data for averages, fits, limits, etc. • • •				
498.1 ± 2.6		¹ ABBIENDI	01A OPAL	$E_{cm}^{ee} = 88-94$ GeV
498.1 ± 3.2		¹ ABREU	00F DLPH	$E_{cm}^{ee} = 88-94$ GeV
499.1 ± 2.9		¹ ACCIARRI	00c L3	$E_{cm}^{ee} = 88-94$ GeV
499.1 ± 2.5		¹ BARATE	00c ALEP	$E_{cm}^{ee} = 88-94$ GeV

¹ This is an indirect determination of $\Gamma(\text{invisible})$ from a fit to the visible Z decay modes.

$\Gamma(\text{hadrons})$ Γ_8
This parameter is not directly used in the 5-parameter fit assuming lepton universality, but is derived using the fit results. See the note "The Z boson" and ref. LEP-SLC 06.

VALUE (MeV)	EVTS	DOCUMENT ID	TECN	COMMENT
1744.4 ± 2.0 OUR FIT				
1745.4 ± 3.5	4.10M	ABBIENDI	01A OPAL	$E_{cm}^{ee} = 88-94$ GeV
1738.1 ± 4.0	3.70M	ABREU	00F DLPH	$E_{cm}^{ee} = 88-94$ GeV
1751.1 ± 3.8	3.54M	ACCIARRI	00c L3	$E_{cm}^{ee} = 88-94$ GeV
1744.0 ± 3.4	4.07M	BARATE	00c ALEP	$E_{cm}^{ee} = 88-94$ GeV

Z BRANCHING RATIOS

OUR FIT is obtained using the fit procedure and correlations as determined by the LEP Electroweak Working Group (see the note "The Z boson" and ref. LEP-SLC 06).

VALUE	DOCUMENT ID	TECN	COMMENT	Γ_2/Γ_1
1.0001 ± 0.0024 OUR AVERAGE				
0.9974 ± 0.0050	¹ AABOUD	17Q ATLS	$E_{cm}^{pp} = 7$ TeV	
1.0009 ± 0.0028	² LEP-SLC	06	$E_{cm}^{ee} = 88-94$ GeV	

¹ AABOUD 17Q make a precise determination of $Z \rightarrow ee$ and $Z \rightarrow \mu\mu$ production in the lepton pseudo-rapidity range $|\eta| < 2.5$ and determine the ratio of the Z branching fractions $B(Z \rightarrow ee)/B(Z \rightarrow \mu\mu) = 1.0026 \pm 0.0013 \pm 0.0048 = 1.0026 \pm 0.0050$.

² This parameter is not directly used in the overall fit but is derived using the fit results; see the note "The Z boson" and ref. LEP-SLC 06.

VALUE	DOCUMENT ID	TECN	COMMENT	Γ_3/Γ_1
1.0020 ± 0.0032 OUR AVERAGE				
1.02 ± 0.06	¹ AAIJ	18AR LHCB	$E_{cm}^{pp} = 8$ TeV	
1.0019 ± 0.0032	² LEP-SLC	06	$E_{cm}^{ee} = 88-94$ GeV	

¹ AAIJ 18AR obtain the result from the ratio of the measured $pp \rightarrow Z + X$ cross sections in the corresponding Z decay channels.

² This parameter is not directly used in the overall fit but is derived using the fit results; see the note "The Z boson" and ref. LEP-SLC 06.

VALUE	DOCUMENT ID	TECN	COMMENT	Γ_3/Γ_2
1.0010 ± 0.0026 OUR AVERAGE				
1.01 ± 0.05	¹ AAIJ	18AR LHCB	$E_{cm}^{pp} = 8$ TeV	
1.0010 ± 0.0026	² LEP-SLC	06	$E_{cm}^{ee} = 88-94$ GeV	

¹ AAIJ 18AR obtain the result from the ratio of the measured $pp \rightarrow Z + X$ cross sections in the corresponding Z decay channels.

² This parameter is not directly used in the overall fit but is derived using the fit results; see the note "The Z boson" and ref. LEP-SLC 06.

VALUE (units 10^{-6})	EVTS	DOCUMENT ID	TECN	COMMENT	$\Gamma_6/\Gamma_{\text{total}}$
4.63 ± 0.21 OUR AVERAGE					
4.70 ± 0.32 ± 0.25		¹ AABOUD	19N ATLS	$E_{cm}^{pp} = 13$ TeV	
4.83 ^{+0.23+0.35} _{-0.22-0.32}	509	² SIRUNYAN	18BT CMS	$E_{cm}^{pp} = 13$ TeV	
4.9 ^{+0.8+0.4} _{-0.7-0.2}	39	³ KHACHATRY...	16cc CMS	$E_{cm}^{pp} = 13$ TeV	
4.31 ± 0.34 ± 0.17	172	AAD	14N ATLS	$E_{cm}^{pp} = 7, 8$ TeV	
4.6 ^{+1.0} _{-0.9} ± 0.2	28	⁴ CHATRCHYAN12BN	CMS	$E_{cm}^{pp} = 7$ TeV	

Here ℓ indicates either e or μ . The branching fractions in this note are given within the phase-space defined by the requirements that (i) the 4-lepton invariant mass is between 80 GeV and 100 GeV, and (ii) any opposite-sign same-flavor lepton pair has a di-lepton invariant mass larger than 4 GeV.

- ¹ AABOUD 19N reports $(4.70 \pm 0.32 \pm 0.21 \pm 0.14) \times 10^{-6}$, where the uncertainties are statistical, systematic, and luminosity. We have combined the latter two in quadrature.
- ² SIRUNYAN 18BT report the $Z \rightarrow 4\ell$ branching fraction = $(4.83^{+0.23+0.32}_{-0.22-0.29} \pm 0.08 \pm 0.12) \times 10^{-6}$, where the uncertainties are statistical, systematic, due to theory, and luminosity. The last three have been added in quadrature to obtain the total systematic error.
- ³ KHACHATRYAN 16CC reports $(4.9^{+0.8+0.3+0.2+0.1}_{-0.7-0.2-0.1-0.1}) \times 10^{-6}$ value, where the uncertainties are statistical, systematic, theory, and due to luminosity. We have combined uncertainties in quadrature.
- ⁴ CHATRCHYAN 12BN reports $(4.2^{+0.9}_{-0.3} \pm 0.2) \times 10^{-6}$ value. Their result (both central value and uncertainties) is scaled up by 10% to account for the different phase-space definition used here (see RAINBOLT 19).

$\Gamma(\text{hadrons})/\Gamma(e^+e^-)$ Γ_8/Γ_1

VALUE	EVTs	DOCUMENT ID	TECN	COMMENT
20.804 ± 0.050 OUR FIT				
20.902 ± 0.084	137.0K	¹ ABBIENDI 01A	OPAL	$E_{cm}^{ee} = 88-94$ GeV
20.88 ± 0.12	117.8k	ABREU 00F	DLPH	$E_{cm}^{ee} = 88-94$ GeV
20.816 ± 0.089	124.4k	ACCIARRI 00C	L3	$E_{cm}^{ee} = 88-94$ GeV
20.677 ± 0.075		² BARATE 00C	ALEP	$E_{cm}^{ee} = 88-94$ GeV
27.0 $^{+11.7}_{-8.8}$	12	³ ABRAMS 89D	MRK2	$E_{cm}^{ee} = 89-93$ GeV

- • • We do not use the following data for averages, fits, limits, etc. • • •
- ¹ ABBIENDI 01A error includes approximately 0.067 due to statistics, 0.040 due to event selection systematics, 0.027 due to the theoretical uncertainty in t -channel prediction, and 0.014 due to LEP energy uncertainty.
- ² BARATE 00C error includes approximately 0.062 due to statistics, 0.033 due to experimental systematics, and 0.026 due to the theoretical uncertainty in t -channel prediction.
- ³ ABRAMS 89D have included both statistical and systematic uncertainties in their quoted errors.

$\Gamma(\text{hadrons})/\Gamma(\mu^+\mu^-)$ Γ_8/Γ_2

OUR FIT is obtained using the fit procedure and correlations as determined by the LEP Electroweak Working Group (see the note "The Z boson" and ref. LEP-SLC 06).

VALUE	EVTs	DOCUMENT ID	TECN	COMMENT
20.785 ± 0.033 OUR FIT				
20.811 ± 0.058	182.8K	¹ ABBIENDI 01A	OPAL	$E_{cm}^{ee} = 88-94$ GeV
20.65 ± 0.08	157.6k	ABREU 00F	DLPH	$E_{cm}^{ee} = 88-94$ GeV
20.861 ± 0.097	113.4k	ACCIARRI 00C	L3	$E_{cm}^{ee} = 88-94$ GeV
20.799 ± 0.056		² BARATE 00C	ALEP	$E_{cm}^{ee} = 88-94$ GeV
18.9 $^{+7.1}_{-5.3}$	13	³ ABRAMS 89D	MRK2	$E_{cm}^{ee} = 89-93$ GeV

- • • We do not use the following data for averages, fits, limits, etc. • • •
- ¹ ABBIENDI 01A error includes approximately 0.050 due to statistics and 0.027 due to event selection systematics.
- ² BARATE 00C error includes approximately 0.053 due to statistics and 0.021 due to experimental systematics.
- ³ ABRAMS 89D have included both statistical and systematic uncertainties in their quoted errors.

$\Gamma(\text{hadrons})/\Gamma(\tau^+\tau^-)$ Γ_8/Γ_3

OUR FIT is obtained using the fit procedure and correlations as determined by the LEP Electroweak Working Group (see the note "The Z boson" and ref. LEP-SLC 06).

VALUE	EVTs	DOCUMENT ID	TECN	COMMENT
20.764 ± 0.045 OUR FIT				
20.832 ± 0.091	151.5K	¹ ABBIENDI 01A	OPAL	$E_{cm}^{ee} = 88-94$ GeV
20.84 ± 0.13	104.0k	ABREU 00F	DLPH	$E_{cm}^{ee} = 88-94$ GeV
20.792 ± 0.133	103.0k	ACCIARRI 00C	L3	$E_{cm}^{ee} = 88-94$ GeV
20.707 ± 0.062		² BARATE 00C	ALEP	$E_{cm}^{ee} = 88-94$ GeV
15.2 $^{+4.8}_{-3.9}$	21	³ ABRAMS 89D	MRK2	$E_{cm}^{ee} = 89-93$ GeV

- • • We do not use the following data for averages, fits, limits, etc. • • •
- ¹ ABBIENDI 01A error includes approximately 0.055 due to statistics and 0.071 due to event selection systematics.
- ² BARATE 00C error includes approximately 0.054 due to statistics and 0.033 due to experimental systematics.
- ³ ABRAMS 89D have included both statistical and systematic uncertainties in their quoted errors.

$\Gamma(\text{hadrons})/\Gamma(\ell^+\ell^-)$ Γ_8/Γ_4

ℓ indicates each type of lepton (e , μ , and τ), not sum over them.

Our fit result is obtained requiring lepton universality.

VALUE	EVTs	DOCUMENT ID	TECN	COMMENT
20.767 ± 0.025 OUR FIT				
20.823 ± 0.044	471.3K	¹ ABBIENDI 01A	OPAL	$E_{cm}^{ee} = 88-94$ GeV
20.730 ± 0.060	379.4k	ABREU 00F	DLPH	$E_{cm}^{ee} = 88-94$ GeV
20.810 ± 0.060	340.8k	ACCIARRI 00C	L3	$E_{cm}^{ee} = 88-94$ GeV
20.725 ± 0.039	500k	² BARATE 00C	ALEP	$E_{cm}^{ee} = 88-94$ GeV
18.9 $^{+3.6}_{-3.2}$	46	ABRAMS 89B	MRK2	$E_{cm}^{ee} = 89-93$ GeV

- • • We do not use the following data for averages, fits, limits, etc. • • •
- ¹ ABBIENDI 01A error includes approximately 0.034 due to statistics and 0.027 due to event selection systematics.
- ² BARATE 00C error includes approximately 0.033 due to statistics, 0.020 due to experimental systematics, and 0.005 due to the theoretical uncertainty in t -channel prediction.

$\Gamma((u\bar{u} + c\bar{c})/2)/\Gamma(\text{hadrons})$ Γ_9/Γ_8

This quantity is the branching ratio of $Z \rightarrow$ "up-type" quarks to $Z \rightarrow$ hadrons. Except ACKERSTAFF 97T the values of $Z \rightarrow$ "up-type" and $Z \rightarrow$ "down-type" branchings are extracted from measurements of $\Gamma(\text{hadrons})$, and $\Gamma(Z \rightarrow \gamma + \text{jets})$ where γ is a high-energy (>5 or 7 GeV) isolated photon. As the experiments use different procedures and slightly different values of M_Z , $\Gamma(\text{hadrons})$ and α_s in their extraction procedures, our average has to be taken with caution.

VALUE	DOCUMENT ID	TECN	COMMENT
0.166 ± 0.009 OUR AVERAGE			
0.172 $^{+0.011}_{-0.010}$	¹ ABBIENDI 04E	OPAL	$E_{cm}^{ee} = 91.2$ GeV
0.160 ± 0.019 ± 0.019	² ACKERSTAFF 97T	OPAL	$E_{cm}^{ee} = 88-94$ GeV
0.137 $^{+0.038}_{-0.054}$	³ ABREU 95X	DLPH	$E_{cm}^{ee} = 88-94$ GeV
0.137 ± 0.033	⁴ ADRIANI 93	L3	$E_{cm}^{ee} = 91.2$ GeV

- ¹ ABBIENDI 04E select photons with energy > 7 GeV and use $\Gamma(\text{hadrons}) = 1744.4 \pm 2.0$ MeV and $\alpha_s = 0.1172 \pm 0.002$ to obtain $\Gamma_u = 300^{+19}_{-18}$ MeV.
- ² ACKERSTAFF 97T measure $\Gamma_{u\bar{u}}/(\Gamma_{d\bar{d}} + \Gamma_{u\bar{u}} + \Gamma_{s\bar{s}}) = 0.258 \pm 0.031 \pm 0.032$. To obtain this branching ratio authors use $R_c + R_b = 0.380 \pm 0.010$. This measurement is fully negatively correlated with the measurement of $\Gamma_{d\bar{d},s\bar{s}}/(\Gamma_{d\bar{d}} + \Gamma_{u\bar{u}} + \Gamma_{s\bar{s}})$ given in the next data block.
- ³ ABREU 95X use $M_Z = 91.187 \pm 0.009$ GeV, $\Gamma(\text{hadrons}) = 1725 \pm 12$ MeV and $\alpha_s = 0.123 \pm 0.005$. To obtain this branching ratio we divide their value of $C_{2/3} = 0.91^{+0.25}_{-0.36}$ by their value of $(3C_{1/3} + 2C_{2/3}) = 6.66 \pm 0.05$.
- ⁴ ADRIANI 93 use $M_Z = 91.181 \pm 0.022$ GeV, $\Gamma(\text{hadrons}) = 1742 \pm 19$ MeV and $\alpha_s = 0.125 \pm 0.009$. To obtain this branching ratio we divide their value of $C_{2/3} = 0.92 \pm 0.22$ by their value of $(3C_{1/3} + 2C_{2/3}) = 6.720 \pm 0.076$.

$\Gamma((d\bar{d} + s\bar{s} + b\bar{b})/3)/\Gamma(\text{hadrons})$ Γ_{10}/Γ_8

This quantity is the branching ratio of $Z \rightarrow$ "down-type" quarks to $Z \rightarrow$ hadrons. Except ACKERSTAFF 97T the values of $Z \rightarrow$ "up-type" and $Z \rightarrow$ "down-type" branchings are extracted from measurements of $\Gamma(\text{hadrons})$, and $\Gamma(Z \rightarrow \gamma + \text{jets})$ where γ is a high-energy (>5 or 7 GeV) isolated photon. As the experiments use different procedures and slightly different values of M_Z , $\Gamma(\text{hadrons})$ and α_s in their extraction procedures, our average has to be taken with caution.

VALUE	DOCUMENT ID	TECN	COMMENT
0.223 ± 0.006 OUR AVERAGE			
0.218 ± 0.007	¹ ABBIENDI 04E	OPAL	$E_{cm}^{ee} = 91.2$ GeV
0.230 ± 0.010 ± 0.010	² ACKERSTAFF 97T	OPAL	$E_{cm}^{ee} = 88-94$ GeV
0.243 $^{+0.036}_{-0.026}$	³ ABREU 95X	DLPH	$E_{cm}^{ee} = 88-94$ GeV
0.243 ± 0.022	⁴ ADRIANI 93	L3	$E_{cm}^{ee} = 91.2$ GeV

- ¹ ABBIENDI 04E select photons with energy > 7 GeV and use $\Gamma(\text{hadrons}) = 1744.4 \pm 2.0$ MeV and $\alpha_s = 0.1172 \pm 0.002$ to obtain $\Gamma_d = 381 \pm 12$ MeV.
- ² ACKERSTAFF 97T measure $\Gamma_{d\bar{d},s\bar{s}}/(\Gamma_{d\bar{d}} + \Gamma_{u\bar{u}} + \Gamma_{s\bar{s}}) = 0.371 \pm 0.016 \pm 0.016$. To obtain this branching ratio authors use $R_c + R_b = 0.380 \pm 0.010$. This measurement is fully negatively correlated with the measurement of $\Gamma_{u\bar{u}}/(\Gamma_{d\bar{d}} + \Gamma_{u\bar{u}} + \Gamma_{s\bar{s}})$ presented in the previous data block.
- ³ ABREU 95X use $M_Z = 91.187 \pm 0.009$ GeV, $\Gamma(\text{hadrons}) = 1725 \pm 12$ MeV and $\alpha_s = 0.123 \pm 0.005$. To obtain this branching ratio we divide their value of $C_{1/3} = 1.62^{+0.24}_{-0.17}$ by their value of $(3C_{1/3} + 2C_{2/3}) = 6.66 \pm 0.05$.
- ⁴ ADRIANI 93 use $M_Z = 91.181 \pm 0.022$ GeV, $\Gamma(\text{hadrons}) = 1742 \pm 19$ MeV and $\alpha_s = 0.125 \pm 0.009$. To obtain this branching ratio we divide their value of $C_{1/3} = 1.63 \pm 0.15$ by their value of $(3C_{1/3} + 2C_{2/3}) = 6.720 \pm 0.076$.

$R_c = \Gamma(c\bar{c})/\Gamma(\text{hadrons})$ Γ_{11}/Γ_8

OUR FIT is obtained by a simultaneous fit to several c - and b -quark measurements as explained in the note "The Z boson" and ref. LEP-SLC 06.

The Standard Model predicts $R_c = 0.1723$ for $m_t = 174.3$ GeV and $M_H = 150$ GeV.

VALUE	DOCUMENT ID	TECN	COMMENT
0.1721 ± 0.0030 OUR FIT			
0.1744 ± 0.0031 ± 0.0021	¹ ABE 05F	SLD	$E_{cm}^{ee} = 91.28$ GeV
0.1665 ± 0.0051 ± 0.0081	² ABREU 00	DLPH	$E_{cm}^{ee} = 88-94$ GeV
0.1698 ± 0.0069	³ BARATE 00B	ALEP	$E_{cm}^{ee} = 88-94$ GeV
0.180 ± 0.011 ± 0.013	⁴ ACKERSTAFF 98E	OPAL	$E_{cm}^{ee} = 88-94$ GeV
0.167 ± 0.011 ± 0.012	⁵ ALEXANDER 96R	OPAL	$E_{cm}^{ee} = 88-94$ GeV
0.1623 ± 0.0085 ± 0.0209	⁶ ABREU 95D	DLPH	$E_{cm}^{ee} = 88-94$ GeV

- • • We do not use the following data for averages, fits, limits, etc. • • •
- ¹ ABE 05F use hadronic Z decays collected during 1996-98 to obtain an enriched sample of $c\bar{c}$ events using a double tag method. The single c -tag is obtained with a neural network trained to perform flavor discrimination using as input several signatures (corrected secondary vertex mass, vertex decay length, multiplicity and total momentum of the hemisphere). A multitag approach is used, defining 4 regions of the output value of the neural network and R_c is extracted from a simultaneous fit to the count rates of the 4 different tags. The quoted systematic error includes an uncertainty of ± 0.0006 due to the uncertainty on R_b .
- ² ABREU 00 obtain this result properly combining the measurement from the D^{*+} production rate ($R_c = 0.1610 \pm 0.0104 \pm 0.0077 \pm 0.0043$ (BR)) with that from the overall charm counting ($R_c = 0.1692 \pm 0.0047 \pm 0.0063 \pm 0.0074$ (BR)) in $c\bar{c}$ events. The systematic error includes an uncertainty of ± 0.0054 due to the uncertainty on the charmed hadron branching fractions.
- ³ BARATE 00B use exclusive decay modes to independently determine the quantities $R_c \times f(c \rightarrow X)$, $X = D^0, D^+, D_s^+, \text{ and } \Lambda_c$. Estimating $R_c \times f(c \rightarrow \Xi_c / \Omega_c) = 0.0034$, they simply sum over all the charm decays to obtain $R_c = 0.1738 \pm 0.0047 \pm 0.0088 \pm$

Gauge & Higgs Boson Particle Listings

Z

0.0075(BR). This is combined with all previous ALEPH measurements (BARATE 98T and BUSKULIC 94G, $R_C = 0.1681 \pm 0.0054 \pm 0.0062$) to obtain the quoted value.

⁴ACKERSTAFF 98E use an inclusive/exclusive double tag. In one jet $D^{*\pm}$ mesons are exclusively reconstructed in several decay channels and in the opposite jet a slow pion (opposite charge inclusive $D^{*\pm}$) tag is used. The b content of this sample is measured by the simultaneous detection of a lepton in one jet and an inclusively reconstructed $D^{*\pm}$ meson in the opposite jet. The systematic error includes an uncertainty of ± 0.006 due to the external branching ratios.

⁵ALEXANDER 96R obtain this value via direct charm counting, summing the partial contributions from D^0 , D^+ , D_S^+ , and Λ_C^+ , and assuming that strange-charmed baryons account for the 15% of the Λ_C^+ production. An uncertainty of ± 0.005 due to the uncertainties in the charm hadron branching ratios is included in the overall systematics.

⁶ABREU 95D perform a maximum likelihood fit to the combined p and p_T distributions of single and dilepton samples. The second error includes an uncertainty of ± 0.0124 due to models and branching ratios.

$R_b = \Gamma(b\bar{b})/\Gamma(\text{hadrons})$ Γ_{12}/Γ_8

OUR FIT is obtained by a simultaneous fit to several c - and b -quark measurements as explained in the note "The Z boson" and ref. LEP-SLC 06.

The Standard Model predicts $R_b = 0.21581$ for $m_t = 174.3$ GeV and $M_H = 150$ GeV.

VALUE	DOCUMENT ID	TECN	COMMENT
0.21629 ± 0.00066 OUR FIT			
0.21594 ± 0.00094 ± 0.00075	¹ ABE	05F SLD	$E_{cm}^{ee} = 91.28$ GeV
0.2174 ± 0.0015 ± 0.0028	² ACCIARRI	00 L3	$E_{cm}^{ee} = 89-93$ GeV
0.2178 ± 0.0011 ± 0.0013	³ ABBIENDI	99B OPAL	$E_{cm}^{ee} = 88-94$ GeV
0.21634 ± 0.00067 ± 0.00060	⁴ ABREU	99B DLPH	$E_{cm}^{ee} = 88-94$ GeV
0.2159 ± 0.0009 ± 0.0011	⁵ BARATE	97F ALEP	$E_{cm}^{ee} = 88-94$ GeV
• • • We do not use the following data for averages, fits, limits, etc. • • •			
0.2145 ± 0.0089 ± 0.0067	⁶ ABREU	95D DLPH	$E_{cm}^{ee} = 88-94$ GeV
0.219 ± 0.006 ± 0.005	⁷ BUSKULIC	94G ALEP	$E_{cm}^{ee} = 88-94$ GeV
0.251 ± 0.049 ± 0.030	⁸ JACOBSEN	91 MRK2	$E_{cm}^{ee} = 91$ GeV

¹ABE 05F use hadronic Z decays collected during 1996-98 to obtain an enriched sample of $b\bar{b}$ events using a double tag method. The single b-tag is obtained with a neural network trained to perform flavor discrimination using as input several signatures (corrected secondary vertex mass, vertex decay length, multiplicity and total momentum of the hemisphere; the key tag is obtained requiring the secondary vertex corrected mass to be above the D -meson mass). ABE 05F obtain $R_b = 0.21604 \pm 0.00098 \pm 0.00074$ where the systematic error includes an uncertainty of ± 0.00012 due to the uncertainty on R_C . The value reported here is obtained properly combining with ABE 98D. The quoted systematic error includes an uncertainty of ± 0.00012 due to the uncertainty on R_C .

²ACCIARRI 00 obtain this result using a double-tagging technique, with a high p_T lepton tag and an impact parameter tag in opposite hemispheres.

³ABBIENDI 99B tag $Z \rightarrow b\bar{b}$ decays using leptons and/or separated decay vertices. The b-tagging efficiency is measured directly from the data using a double-tagging technique.

⁴ABREU 99B obtain this result combining in a multivariate analysis several tagging methods (impact parameter and secondary vertex reconstruction, complemented by event shape variables). For R_C different from its Standard Model value of 0.172, R_b varies as $-0.024 \times (R_C - 0.172)$.

⁵BARATE 97F combine the lifetime-mass hemisphere tag (BARATE 97E) with event shape information and lepton tag to identify $Z \rightarrow b\bar{b}$ candidates. They further use c - and u d -selection tags to identify the background. For R_C different from its Standard Model value of 0.172, R_b varies as $-0.019 \times (R_C - 0.172)$.

⁶ABREU 95D perform a maximum likelihood fit to the combined p and p_T distributions of single and dilepton samples. The second error includes an uncertainty of ± 0.0023 due to models and branching ratios.

⁷BUSKULIC 94G perform a simultaneous fit to the p and p_T spectra of both single and dilepton events.

⁸JACOBSEN 91 tagged $b\bar{b}$ events by requiring coincidence of ≥ 3 tracks with significant impact parameters using vertex detector. Systematic error includes lifetime and decay uncertainties (± 0.014).

$\Gamma(b\bar{b}b\bar{b})/\Gamma(\text{hadrons})$ Γ_{13}/Γ_8

VALUE (units 10^{-4})	DOCUMENT ID	TECN	COMMENT
5.2 ± 1.9 OUR AVERAGE			
3.6 ± 1.7 ± 2.7	¹ ABBIENDI	01G OPAL	$E_{cm}^{ee} = 88-94$ GeV
6.0 ± 1.9 ± 1.4	² ABREU	99u DLPH	$E_{cm}^{ee} = 88-94$ GeV

¹ABBIENDI 01G use a sample of four-jet events from hadronic Z decays. To enhance the $b\bar{b}b\bar{b}$ signal, at least three of the four jets are required to have a significantly detached secondary vertex.

²ABREU 99u force hadronic Z decays into 3jets to use all the available phase space and require a b tag for every jet. This decay mode includes primary and secondary 4b production, e.g. from gluon splitting to $b\bar{b}$.

$\Gamma(ggg)/\Gamma(\text{hadrons})$ Γ_{14}/Γ_8

VALUE	CL%	DOCUMENT ID	TECN	COMMENT
<1.6 × 10⁻²	95	¹ ABREU	96S DLPH	$E_{cm}^{ee} = 88-94$ GeV

¹This branching ratio is slightly dependent on the jet-finder algorithm. The value we quote is obtained using the JADE algorithm, while using the DURHAM algorithm ABREU 96S obtain an upper limit of 1.5×10^{-2} .

$\Gamma(\pi^0\gamma)/\Gamma_{\text{total}}$ Γ_{15}/Γ

VALUE	CL%	DOCUMENT ID	TECN	COMMENT
<2.01 × 10⁻⁵	95	AALTONEN	14E CDF	$E_{cm}^{pp} = 1.96$ TeV
<5.2 × 10 ⁻⁵	95	¹ ACCIARRI	95G L3	$E_{cm}^{ee} = 88-94$ GeV
<5.5 × 10 ⁻⁵	95	ABREU	94B DLPH	$E_{cm}^{ee} = 88-94$ GeV
<2.1 × 10 ⁻⁴	95	DECAMP	92 ALEP	$E_{cm}^{ee} = 88-94$ GeV
<1.4 × 10 ⁻⁴	95	AKRAWY	91F OPAL	$E_{cm}^{ee} = 88-94$ GeV

¹This limit is for both decay modes $Z \rightarrow \pi^0\gamma/\gamma\gamma$ which are indistinguishable in ACCIARRI 95G.

$\Gamma(\eta\gamma)/\Gamma_{\text{total}}$ Γ_{16}/Γ

VALUE	CL%	DOCUMENT ID	TECN	COMMENT
<7.6 × 10 ⁻⁵	95	ACCIARRI	95G L3	$E_{cm}^{ee} = 88-94$ GeV
<8.0 × 10 ⁻⁵	95	ABREU	94B DLPH	$E_{cm}^{ee} = 88-94$ GeV
<5.1 × 10⁻⁵	95	DECAMP	92 ALEP	$E_{cm}^{ee} = 88-94$ GeV
<2.0 × 10 ⁻⁴	95	AKRAWY	91F OPAL	$E_{cm}^{ee} = 88-94$ GeV

$\Gamma(\rho^0\gamma)/\Gamma_{\text{total}}$ Γ_{17}/Γ

VALUE	CL%	EVTS	DOCUMENT ID	TECN	COMMENT
<2.5 × 10⁻⁵	95	12.5k	¹ AABOUD	18AU ATLS	$E_{cm}^{pp} = 13$ TeV

¹AABOUD 18AU search for the $Z \rightarrow \rho\gamma$ decay mode where the ρ is identified through its decay $\rho \rightarrow \pi^+\pi^-$. In the data corresponding to 32.3 fb^{-1} , 12,583 events are selected for $635 < m(\pi^+\pi^-) < 915$ MeV.

$\Gamma(\omega\gamma)/\Gamma_{\text{total}}$ Γ_{18}/Γ

VALUE	CL%	DOCUMENT ID	TECN	COMMENT
<6.5 × 10⁻⁴	95	ABREU	94B DLPH	$E_{cm}^{ee} = 88-94$ GeV

$\Gamma(\eta'(958)\gamma)/\Gamma_{\text{total}}$ Γ_{19}/Γ

VALUE	CL%	DOCUMENT ID	TECN	COMMENT
<4.2 × 10⁻⁵	95	DECAMP	92 ALEP	$E_{cm}^{ee} = 88-94$ GeV

$\Gamma(\phi\gamma)/\Gamma_{\text{total}}$ Γ_{20}/Γ

VALUE	CL%	EVTS	DOCUMENT ID	TECN	COMMENT
<9 × 10⁻⁷	95	3.3k	¹ AABOUD	18AU ATLS	$E_{cm}^{pp} = 13$ TeV

• • • We do not use the following data for averages, fits, limits, etc. • • •

<8.3 × 10⁻⁶ 95 1.0k ²AABOUD 16k ATLS $E_{cm}^{pp} = 13$ TeV

¹AABOUD 18AU search for the $Z \rightarrow \phi\gamma$ decay mode where the ϕ is identified through its decay $\phi \rightarrow K^+K^-$. In the data corresponding to 32.3 fb^{-1} , 3,364 events are selected for $1012 < m(K^+K^-) < 1028$ MeV.

²AABOUD 16k search for the $Z \rightarrow \phi\gamma$ decay mode where the ϕ is identified through its decay into K^+K^- . In the data corresponding to a total luminosity of 2.7 fb^{-1} , 1065 events are selected and their $K^+K^-\gamma$ invariant mass spectrum is analyzed.

$\Gamma(\gamma\gamma)/\Gamma_{\text{total}}$ Γ_{21}/Γ

This decay would violate the Landau-Yang theorem.

VALUE	CL%	DOCUMENT ID	TECN	COMMENT
<1.46 × 10⁻⁵	95	AALTONEN	14E CDF	$E_{cm}^{pp} = 1.96$ TeV
<5.2 × 10 ⁻⁵	95	¹ ACCIARRI	95G L3	$E_{cm}^{ee} = 88-94$ GeV
<5.5 × 10 ⁻⁵	95	ABREU	94B DLPH	$E_{cm}^{ee} = 88-94$ GeV
<1.4 × 10 ⁻⁴	95	AKRAWY	91F OPAL	$E_{cm}^{ee} = 88-94$ GeV

¹This limit is for both decay modes $Z \rightarrow \pi^0\gamma/\gamma\gamma$ which are indistinguishable in ACCIARRI 95G.

$\Gamma(\pi^0\pi^0)/\Gamma_{\text{total}}$ Γ_{22}/Γ

VALUE	CL%	DOCUMENT ID	TECN	COMMENT
<1.52 × 10⁻⁵	95	AALTONEN	14E CDF	$E_{cm}^{pp} = 1.96$ TeV

$\Gamma(\gamma\gamma\gamma)/\Gamma_{\text{total}}$ Γ_{23}/Γ

VALUE	CL%	DOCUMENT ID	TECN	COMMENT
<2.2 × 10⁻⁶	95	AAD	16L ATLS	$E_{cm}^{pp} = 8$ TeV

• • • We do not use the following data for averages, fits, limits, etc. • • •

<1.0 × 10⁻⁵ 95 ¹ ACCIARRI 95c L3 $E_{cm}^{ee} = 88-94$ GeV

<1.7 × 10⁻⁵ 95 ¹ ABREU 94B DLPH $E_{cm}^{ee} = 88-94$ GeV

<6.6 × 10⁻⁵ 95 AKRAWY 91F OPAL $E_{cm}^{ee} = 88-94$ GeV

¹Limit derived in the context of composite Z model.

$\Gamma(\pi^\pm W^\mp)/\Gamma_{\text{total}}$ Γ_{24}/Γ

The value is for the sum of the charge states indicated.

VALUE	CL%	DOCUMENT ID	TECN	COMMENT
<7 × 10⁻⁵	95	DECAMP	92 ALEP	$E_{cm}^{ee} = 88-94$ GeV

$\Gamma(\rho^\pm W^\mp)/\Gamma_{\text{total}}$ Γ_{25}/Γ

The value is for the sum of the charge states indicated.

VALUE	CL%	DOCUMENT ID	TECN	COMMENT
<8.3 × 10⁻⁵	95	DECAMP	92 ALEP	$E_{cm}^{ee} = 88-94$ GeV

$\Gamma(J/\psi(1S)X)/\Gamma_{\text{total}}$ Γ_{26}/Γ

VALUE (units 10^{-3})	EVTS	DOCUMENT ID	TECN	COMMENT
$3.51^{+0.23}_{-0.25}$ OUR AVERAGE				Error includes scale factor of 1.1.
$3.21 \pm 0.21^{+0.19}_{-0.28}$	553	¹ ACCIARRI	99F L3	$E_{\text{cm}}^{pp} = 88\text{--}94$ GeV
$3.9 \pm 0.2 \pm 0.3$	511	² ALEXANDER	96B OPAL	$E_{\text{cm}}^{pp} = 88\text{--}94$ GeV
$3.73 \pm 0.39 \pm 0.36$	153	³ ABREU	94P DLPH	$E_{\text{cm}}^{pp} = 88\text{--}94$ GeV

¹ ACCIARRI 99F combine $\mu^+\mu^-$ and $e^+e^- J/\psi(1S)$ decay channels. The branching ratio for prompt $J/\psi(1S)$ production is measured to be $(2.1 \pm 0.6 \pm 0.4^{+0.4}_{-0.2}(\text{theor.})) \times 10^{-4}$.

² ALEXANDER 96B identify $J/\psi(1S)$ from the decays into lepton pairs. $(4.8 \pm 2.4)\%$ of this branching ratio is due to prompt $J/\psi(1S)$ production (ALEXANDER 96N).

³ Combining $\mu^+\mu^-$ and e^+e^- channels and taking into account the common systematic errors. $(7.7^{+6.3}_{-5.4})\%$ of this branching ratio is due to prompt $J/\psi(1S)$ production.

 $\Gamma(J/\psi(1S)\gamma)/\Gamma_{\text{total}}$ Γ_{27}/Γ

VALUE	CL%	DOCUMENT ID	TECN	COMMENT
$<1.4 \times 10^{-6}$	95	¹ SIRUNYAN	19AJ CMS	$E_{\text{cm}}^{pp} = 13$ TeV
$<2.3 \times 10^{-6}$	95	² AABOUD	18BL ATLS	$E_{\text{cm}}^{pp} = 13$ TeV
$<2.6 \times 10^{-6}$	95	³ AAD	15I ATLS	$E_{\text{cm}}^{pp} = 8$ TeV

¹ SIRUNYAN 19AJ study $Z \rightarrow J/\psi\gamma$ with $J/\psi \rightarrow \mu^+\mu^-$. Candidate events are selected by requiring a pair of oppositely charged muons and a well isolated photon. The leading (subleading) muon is required to have a transverse momentum larger than 20 GeV (4 GeV), while the photon must have a transverse energy larger than 33 GeV. Requiring the invariant mass of the $\mu\mu$ ($\mu\mu\gamma$) system in the range 3.0 to 3.2 (81 to 101) GeV, selects 183 data events which is consistent with the expected background. The 95% C.L. limit on the Z branching fraction is obtained assuming the J/ψ to be unpolarized.

² AABOUD 18BL study $Z \rightarrow J/\psi\gamma$ in 13 TeV pp interactions. Two triggers were used: isolated photon of $p_T > 35(25)$ GeV and a muon with $p_T > 18(24)$ GeV. The J/ψ is detected via its dimuon decay and it is required that the azimuthal angle between the photon and the J/ψ in the plane transverse to the beam direction is $> \pi/2$. The number of observed/expected background events is 92/89 ± 6 in the dimuon mass range 2.9–3.3 GeV leading to the quoted 95% C.L. limit.

³ AAD 15I use events with the highest p_T muon in the pair required to have $p_T > 20$ GeV, the dimuon mass required to be within 0.2 GeV of the $J/\psi(1S)$ mass and its transverse momentum required to be > 36 GeV. The photon is also required to have its $p_T > 36$ GeV.

 $\Gamma(\psi(2S)X)/\Gamma_{\text{total}}$ Γ_{28}/Γ

VALUE (units 10^{-3})	EVTS	DOCUMENT ID	TECN	COMMENT
1.60 ± 0.29 OUR AVERAGE				
$1.6 \pm 0.5 \pm 0.3$	39	¹ ACCIARRI	97J L3	$E_{\text{cm}}^{pp} = 88\text{--}94$ GeV
$1.6 \pm 0.3 \pm 0.2$	46.9	² ALEXANDER	96B OPAL	$E_{\text{cm}}^{pp} = 88\text{--}94$ GeV
$1.60 \pm 0.73 \pm 0.33$	5.4	³ ABREU	94P DLPH	$E_{\text{cm}}^{pp} = 88\text{--}94$ GeV

¹ ACCIARRI 97J measure this branching ratio via the decay channel $\psi(2S) \rightarrow \ell^+\ell^-$ ($\ell = \mu, e$).

² ALEXANDER 96B measure this branching ratio via the decay channel $\psi(2S) \rightarrow J/\psi\pi^+\pi^-$, with $J/\psi \rightarrow \ell^+\ell^-$.

³ ABREU 94P measure this branching ratio via decay channel $\psi(2S) \rightarrow J/\psi\pi^+\pi^-$, with $J/\psi \rightarrow \mu^+\mu^-$.

 $\Gamma(\psi(2S)\gamma)/\Gamma_{\text{total}}$ Γ_{29}/Γ

VALUE	CL%	DOCUMENT ID	TECN	COMMENT
$<4.5 \times 10^{-6}$	95	¹ AABOUD	18BL ATLS	$E_{\text{cm}}^{pp} = 13$ TeV

¹ AABOUD 18BL study $Z \rightarrow \psi(2S)\gamma$ in 13 TeV pp interactions. Two triggers were used: isolated photon of $p_T > 35(25)$ GeV and a muon with $p_T > 18(24)$ GeV. The $\psi(2S)$ is detected via its dimuon decay and it is required that the azimuthal angle between the photon and the $\psi(2S)$ in the plane transverse to the beam direction is $> \pi/2$. The number of observed/expected background events is 43/42 ± 5 in the dimuon mass range 3.5–3.9 GeV leading to the quoted 95% C.L. limit.

 $\Gamma(J/\psi(1S)\ell^+\ell^-)/\Gamma(\mu^+\mu^-\mu^+\mu^-)$ Γ_{30}/Γ_5

VALUE	DOCUMENT ID	TECN	COMMENT
$0.67 \pm 0.18 \pm 0.05$	¹ SIRUNYAN	18DZ CMS	pp at 13 TeV

¹ SIRUNYAN 18DZ observe the decay $Z \rightarrow \Psi\ell^+\ell^-$ in pp collisions at $\sqrt{s} = 13$ TeV, where Ψ includes J/ψ as well as $\psi(2S) \rightarrow J/\psi X$, and $\ell^+\ell^-$ represents an electron or muon pair while the J/ψ is detected via its $\mu^+\mu^-$ decay channel. To reduce systematic errors they determine the ratio of the branching fraction of this decay to that of $Z \rightarrow \mu^+\mu^- \mu^+\mu^-$ within phase-space cuts imposed on lepton transverse momentum and pseudo rapidity, dilepton invariant mass, and J/ψ transverse momentum. The number of selected $\Psi\mu^+\mu^-$ (Ψe^+e^-) candidate events is 29 (18). Analyzing the $\mu^+\mu^-$ and $\mu^+\mu^- \ell^+\ell^-$ invariant mass distributions, a yield of 13.0 ± 3.9 (11.2 ± 3.4) events for the $\Psi\mu^+\mu^-$ (Ψe^+e^-) mode is obtained. The ratio of the branching fractions is determined as $0.67 \pm 0.18 \pm 0.05$ within the selected phase-space cuts. Assuming extrapolation to full phase space cancels in the ratio, and using their measured value of $B(Z \rightarrow \mu^+\mu^- \mu^+\mu^-) = (1.20 \pm 0.08) \times 10^{-6}$, they estimate $B(Z \rightarrow J/\psi\ell^+\ell^-) = 8 \times 10^{-7}$.

 $\Gamma(J/\psi(1S)J/\psi(1S))/\Gamma_{\text{total}}$ Γ_{31}/Γ

VALUE	CL%	EVTS	DOCUMENT ID	TECN	COMMENT
$<2.2 \times 10^{-6}$	95	189	¹ SIRUNYAN	19BR CMS	$E_{\text{cm}}^{pp} = 13$ TeV

¹ SIRUNYAN 19BR search for Z decays to a pair of J/ψ mesons in the channel $J/\psi \rightarrow \mu^+\mu^-$. The invariant masses of the higher/lower- p_T J/ψ candidates have to be within 0.1/0.15 GeV of the nominal J/ψ mass. A total of 189 events are selected in the 40–140 GeV 4-muon invariant mass range. An un-binned extended maximum likelihood fit leads to the 95% C.L. upper limit, obtained assuming the J/ψ mesons to be unpolarised.

 $\Gamma(\chi_{c1}(1P)X)/\Gamma_{\text{total}}$ Γ_{32}/Γ

VALUE (units 10^{-3})	EVTS	DOCUMENT ID	TECN	COMMENT
2.9 ± 0.7 OUR AVERAGE				
$2.7 \pm 0.6 \pm 0.5$	33	¹ ACCIARRI	97J L3	$E_{\text{cm}}^{pp} = 88\text{--}94$ GeV
$5.0 \pm 2.1^{+1.5}_{-0.9}$	6.4	² ABREU	94P DLPH	$E_{\text{cm}}^{pp} = 88\text{--}94$ GeV

¹ ACCIARRI 97J measure this branching ratio via the decay channel $\chi_{c1} \rightarrow J/\psi + \gamma$, with $J/\psi \rightarrow \ell^+\ell^-$ ($\ell = \mu, e$). The $M(\ell^+\ell^-\gamma) - M(\ell^+\ell^-)$ mass difference spectrum is fitted with two gaussian shapes for χ_{c1} and χ_{c2} .

² This branching ratio is measured via the decay channel $\chi_{c1} \rightarrow J/\psi + \gamma$, with $J/\psi \rightarrow \mu^+\mu^-$.

 $\Gamma(\chi_{c2}(1P)X)/\Gamma_{\text{total}}$ Γ_{33}/Γ

VALUE	CL%	DOCUMENT ID	TECN	COMMENT
$<3.2 \times 10^{-3}$	90	¹ ACCIARRI	97J L3	$E_{\text{cm}}^{pp} = 88\text{--}94$ GeV

¹ ACCIARRI 97J derive this limit via the decay channel $\chi_{c2} \rightarrow J/\psi + \gamma$, with $J/\psi \rightarrow \ell^+\ell^-$ ($\ell = \mu, e$). The $M(\ell^+\ell^-\gamma) - M(\ell^+\ell^-)$ mass difference spectrum is fitted with two gaussian shapes for χ_{c1} and χ_{c2} .

 $\Gamma(\Upsilon(1S)X + \Upsilon(2S)X + \Upsilon(3S)X)/\Gamma_{\text{total}}$ $\Gamma_{34}/\Gamma = (\Gamma_{35} + \Gamma_{37} + \Gamma_{39})/\Gamma$

VALUE (units 10^{-4})	EVTS	DOCUMENT ID	TECN	COMMENT
$1.0 \pm 0.4 \pm 0.22$	6.4	¹ ALEXANDER	96F OPAL	$E_{\text{cm}}^{pp} = 88\text{--}94$ GeV

¹ ALEXANDER 96F identify the Υ (which refers to any of the three lowest bound states) through its decay into e^+e^- and $\mu^+\mu^-$. The systematic error includes an uncertainty of ± 0.2 due to the production mechanism.

 $\Gamma(\Upsilon(1S)X)/\Gamma_{\text{total}}$ Γ_{35}/Γ

VALUE	CL%	DOCUMENT ID	TECN	COMMENT
$<3.4 \times 10^{-6}$	95	¹ AAD	15I ATLS	$E_{\text{cm}}^{pp} = 8$ TeV
$<4.4 \times 10^{-5}$	95	² ACCIARRI	99F L3	$E_{\text{cm}}^{pp} = 88\text{--}94$ GeV

¹ AAD 15I use events with the highest p_T muon in the pair required to have $p_T > 20$ GeV, the dimuon mass required to be in the range 8–12 GeV and its transverse momentum required to be > 36 GeV. The photon is also required to have its $p_T > 36$ GeV.

² ACCIARRI 99F search for $\Upsilon(1S)$ through its decay into $\ell^+\ell^-$ ($\ell = e$ or μ).

 $\Gamma(\Upsilon(1S)\gamma)/\Gamma_{\text{total}}$ Γ_{36}/Γ

VALUE	CL%	DOCUMENT ID	TECN	COMMENT
$<2.8 \times 10^{-6}$	95	¹ AABOUD	18BL ATLS	$E_{\text{cm}}^{pp} = 13$ TeV

¹ AABOUD 18BL study $Z \rightarrow \Upsilon(1S)\gamma$ in 13 TeV pp interactions. Two triggers were used: isolated photon of $p_T > 35(25)$ GeV and a muon with $p_T > 18(24)$ GeV. The $\Upsilon(1S)$ is detected via its dimuon decay and it is required that the azimuthal angle between the photon and the $\Upsilon(1S)$ in the plane transverse to the beam direction is $> \pi/2$. The number of observed/expected background events is 115/126 ± 8 in the dimuon mass range 9.0–10.0 GeV leading to the quoted 95% C.L. limit.

 $\Gamma(\Upsilon(2S)X)/\Gamma_{\text{total}}$ Γ_{37}/Γ

VALUE	CL%	DOCUMENT ID	TECN	COMMENT
$<6.5 \times 10^{-6}$	95	¹ AAD	15I ATLS	$E_{\text{cm}}^{pp} = 8$ TeV
$<13.9 \times 10^{-5}$	95	² ACCIARRI	97R L3	$E_{\text{cm}}^{pp} = 88\text{--}94$ GeV

¹ AAD 15I use events with the highest p_T muon in the pair required to have $p_T > 20$ GeV, the dimuon mass required to be in the range 8–12 GeV and its transverse momentum required to be > 36 GeV. The photon is also required to have its $p_T > 36$ GeV.

² ACCIARRI 97R search for $\Upsilon(2S)$ through its decay into $\ell^+\ell^-$ ($\ell = e$ or μ).

 $\Gamma(\Upsilon(2S)\gamma)/\Gamma_{\text{total}}$ Γ_{38}/Γ

VALUE	CL%	DOCUMENT ID	TECN	COMMENT
$<1.7 \times 10^{-6}$	95	¹ AABOUD	18BL ATLS	$E_{\text{cm}}^{pp} = 13$ TeV

¹ AABOUD 18BL study $Z \rightarrow \Upsilon(2S)\gamma$ in 13 TeV pp interactions. Two triggers were used: isolated photon of $p_T > 35(25)$ GeV and a muon with $p_T > 18(24)$ GeV. The $\Upsilon(2S)$ is detected via its dimuon decay and it is required that the azimuthal angle between the photon and the $\Upsilon(2S)$ in the plane transverse to the beam direction is $> \pi/2$. The number of observed/expected background events is 106/121 ± 8 in the dimuon mass range 9.5–10.5 GeV leading to the quoted 95% C.L. limit.

 $\Gamma(\Upsilon(3S)X)/\Gamma_{\text{total}}$ Γ_{39}/Γ

VALUE	CL%	DOCUMENT ID	TECN	COMMENT
$<5.4 \times 10^{-6}$	95	¹ AAD	15I ATLS	$E_{\text{cm}}^{pp} = 8$ TeV
$<9.4 \times 10^{-5}$	95	² ACCIARRI	97R L3	$E_{\text{cm}}^{pp} = 88\text{--}94$ GeV

¹ AAD 15I use events with the highest p_T muon in the pair required to have $p_T > 20$ GeV, the dimuon mass required to be in the range 8–12 GeV and its transverse momentum required to be > 36 GeV. The photon is also required to have its $p_T > 36$ GeV.

² ACCIARRI 97R search for $\Upsilon(3S)$ through its decay into $\ell^+\ell^-$ ($\ell = e$ or μ).

Gauge & Higgs Boson Particle Listings

Z

$\Gamma(\Upsilon(3S)\gamma)/\Gamma_{\text{total}}$ Γ_{40}/Γ

VALUE	CL%	DOCUMENT ID	TECN	COMMENT
$<4.8 \times 10^{-6}$	95	1 AABOUD	18BL ATLS	$E_{\text{cm}}^{pp} = 13 \text{ TeV}$

1 AABOUD 18BL study $Z \rightarrow \Upsilon(3S)\gamma$ in 13 TeV pp interactions. Two triggers were used: isolated photon of $p_T > 35(25) \text{ GeV}$ and a muon with $p_T > 18(24) \text{ GeV}$. The $\Upsilon(3S)$ is detected via its dimuon decay and it is required that the azimuthal angle between the photon and the $\Upsilon(3S)$ in the plane transverse to the beam direction is $> \pi/2$. The number of observed/expected background events is $112/113 \pm 8$ in the dimuon mass range $10.0\text{--}11.0 \text{ GeV}$ leading to the quoted 95% C.L. limit.

$\Gamma(\Upsilon(1,2,3S)\Upsilon(1,2,3S))/\Gamma_{\text{total}}$ Γ_{41}/Γ

VALUE	CL%	EVTS	DOCUMENT ID	TECN	COMMENT
$<1.5 \times 10^{-6}$	95	106	1 SIRUNYAN	19BR CMS	$E_{\text{cm}}^{pp} = 13 \text{ TeV}$

1 SIRUNYAN 19BR search for Z decays to a pair of Υ mesons in the channel $\Upsilon \rightarrow \mu^+\mu^-$. The invariant mass of the Υ candidates has to be in the range of 8.5 to 11 GeV. A total of 106 events are selected in the 20–140 GeV 4-muon invariant mass range. An un-binned extended maximum likelihood fit leads to the 95% C.L. upper limit, obtained assuming the Υ mesons to be unpolarised.

$\Gamma((D^0/\bar{D}^0)X)/\Gamma(\text{hadrons})$ Γ_{42}/Γ_8

VALUE	EVTS	DOCUMENT ID	TECN	COMMENT
$0.296 \pm 0.019 \pm 0.021$	369	1 ABREU	93I DLPH	$E_{\text{cm}}^{ee} = 88\text{--}94 \text{ GeV}$

1 The (D^0/\bar{D}^0) states in ABREU 93I are detected by the $K\pi$ decay mode. This is a corrected result (see the erratum of ABREU 93I).

$\Gamma(D^{\pm}X)/\Gamma(\text{hadrons})$ Γ_{43}/Γ_8

VALUE	EVTS	DOCUMENT ID	TECN	COMMENT
$0.174 \pm 0.016 \pm 0.018$	539	1 ABREU	93I DLPH	$E_{\text{cm}}^{ee} = 88\text{--}94 \text{ GeV}$

1 The D^{\pm} states in ABREU 93I are detected by the $K\pi\pi$ decay mode. This is a corrected result (see the erratum of ABREU 93I).

$\Gamma(D^*(2010)^{\pm}X)/\Gamma(\text{hadrons})$ Γ_{44}/Γ_8

VALUE	EVTS	DOCUMENT ID	TECN	COMMENT
0.163 ± 0.019 OUR AVERAGE	Error includes scale factor of 1.3.			
$0.155 \pm 0.010 \pm 0.013$	358	1 ABREU	93I DLPH	$E_{\text{cm}}^{ee} = 88\text{--}94 \text{ GeV}$
0.21 ± 0.04	362	2 DECAMP	91J ALEP	$E_{\text{cm}}^{ee} = 88\text{--}94 \text{ GeV}$

1 $D^*(2010)^{\pm}$ in ABREU 93I are reconstructed from $D^0\pi^{\pm}$, with $D^0 \rightarrow K^-\pi^+$. The new CLEO II measurement of $B(D^{*\pm} \rightarrow D^0\pi^{\pm}) = (68.1 \pm 1.6)\%$ is used. This is a corrected result (see the erratum of ABREU 93I).

2 DECAMP 91J report $B(D^*(2010)^+ \rightarrow D^0\pi^+) B(D^0 \rightarrow K^-\pi^+) \Gamma(D^*(2010)^{\pm}X)/\Gamma(\text{hadrons}) = (5.11 \pm 0.34) \times 10^{-3}$. They obtained the above number assuming $B(D^0 \rightarrow K^-\pi^+) = (3.62 \pm 0.34 \pm 0.44)\%$ and $B(D^*(2010)^+ \rightarrow D^0\pi^+) = (55 \pm 4)\%$. We have rescaled their original result of 0.26 ± 0.05 taking into account the new CLEO II branching ratio $B(D^*(2010)^+ \rightarrow D^0\pi^+) = (68.1 \pm 1.6)\%$.

$\Gamma(D_{s1}(2536)^{\pm}X)/\Gamma(\text{hadrons})$ Γ_{45}/Γ_8

VALUE (%)	EVTS	DOCUMENT ID	TECN	COMMENT
$0.52 \pm 0.09 \pm 0.06$	92	1 HEISTER	02B ALEP	$E_{\text{cm}}^{ee} = 88\text{--}94 \text{ GeV}$

1 HEISTER 02B reconstruct this meson in the decay modes $D_{s1}(2536)^{\pm} \rightarrow D^{\pm}K^0$ and $D_{s1}(2536)^{\pm} \rightarrow D^*0K^{\pm}$. The quoted branching ratio assumes that the decay width of the $D_{s1}(2536)$ is saturated by the two measured decay modes.

$\Gamma(D_{sJ}(2573)^{\pm}X)/\Gamma(\text{hadrons})$ Γ_{46}/Γ_8

VALUE (%)	EVTS	DOCUMENT ID	TECN	COMMENT
$0.83 \pm 0.29 \pm 0.07$ 0.13	64	1 HEISTER	02B ALEP	$E_{\text{cm}}^{ee} = 88\text{--}94 \text{ GeV}$

1 HEISTER 02B reconstruct this meson in the decay mode $D_{s2}^*(2573)^{\pm} \rightarrow D^0K^{\pm}$. The quoted branching ratio assumes that the detected decay mode represents 45% of the full decay width.

$\Gamma(D^{*'}(2629)^{\pm}X)/\Gamma(\text{hadrons})$ Γ_{47}/Γ_8

VALUE	DOCUMENT ID	TECN	COMMENT
searched for	1 ABBIENDI 01N OPAL	$E_{\text{cm}}^{ee} = 88\text{--}94 \text{ GeV}$	

1 ABBIENDI 01N searched for the decay mode $D^{*'}(2629)^{\pm} \rightarrow D^{*\pm}\pi^+\pi^-$ with $D^{*+} \rightarrow D^0\pi^+$, and $D^0 \rightarrow K^-\pi^+$. They quote a 95% CL limit for $Z \rightarrow D^{*'}(2629)^{\pm} \times B(D^{*'}(2629)^+ \rightarrow D^{*+}\pi^+\pi^-) < 3.1 \times 10^{-3}$.

$\Gamma(B^*X)/[\Gamma(BX) + \Gamma(B^*X)]$ $\Gamma_{49}/(\Gamma_{48} + \Gamma_{49})$

VALUE	EVTS	DOCUMENT ID	TECN	COMMENT
0.75 ± 0.04 OUR AVERAGE				
$0.760 \pm 0.036 \pm 0.083$		1 ACKERSTAFF 97M OPAL	$E_{\text{cm}}^{ee} = 88\text{--}94 \text{ GeV}$	
$0.771 \pm 0.026 \pm 0.070$		2 BUSKULIC 96D ALEP	$E_{\text{cm}}^{ee} = 88\text{--}94 \text{ GeV}$	
$0.72 \pm 0.03 \pm 0.06$		3 ABREU 95R DLPH	$E_{\text{cm}}^{ee} = 88\text{--}94 \text{ GeV}$	
$0.76 \pm 0.08 \pm 0.06$	1378	4 ACCIARRI 95B L3	$E_{\text{cm}}^{ee} = 88\text{--}94 \text{ GeV}$	

As the experiments assume different values of the b -baryon contribution, our average should be taken with caution.

1 ACKERSTAFF 97M use an inclusive B reconstruction method and assume a $(13.2 \pm 4.1)\%$ b -baryon contribution. The value refers to a b -flavored meson mixture of B_u, B_d , and B_s .

2 BUSKULIC 96D use an inclusive reconstruction of B hadrons and assume a $(12.2 \pm 4.3)\%$ b -baryon contribution. The value refers to a b -flavored mixture of B_u, B_d , and B_s .

3 ABREU 95R use an inclusive B -reconstruction method and assume a $(10 \pm 4)\%$ b -baryon contribution. The value refers to a b -flavored meson mixture of B_u, B_d , and B_s .

4 ACCIARRI 95B assume a 9.4% b -baryon contribution. The value refers to a b -flavored mixture of B_u, B_d , and B_s .

$\Gamma(B^+X)/\Gamma(\text{hadrons})$ Γ_{50}/Γ_8

"OUR EVALUATION" is obtained using our current values for $f(\bar{b} \rightarrow B^+)$ and $R_b = \Gamma(b\bar{b})/\Gamma(\text{hadrons})$. We calculate $\Gamma(B^+X)/\Gamma(\text{hadrons}) = R_b \times f(\bar{b} \rightarrow B^+)$. The decay fraction $f(\bar{b} \rightarrow B^+)$ was provided by the Heavy Flavor Averaging Group (HFLAV, <https://hflav.web.cern.ch/>).

VALUE	DOCUMENT ID	TECN	COMMENT
0.0869 ± 0.0019 OUR EVALUATION			
0.0887 ± 0.0030	1 ABDALLAH 03k DLPH	$E_{\text{cm}}^{ee} = 88\text{--}94 \text{ GeV}$	

1 ABDALLAH 03k measure the production fraction of B^+ mesons in hadronic Z decays $f(B^+) = (40.99 \pm 0.82 \pm 1.11)\%$. The value quoted here is obtained multiplying this production fraction by our value of $R_b = \Gamma(\bar{b}b)/\Gamma(\text{hadrons})$.

$\Gamma(B_s^0X)/\Gamma(\text{hadrons})$ Γ_{51}/Γ_8

"OUR EVALUATION" is obtained using our current values for $f(\bar{b} \rightarrow B_s^0)$ and $R_b = \Gamma(b\bar{b})/\Gamma(\text{hadrons})$. We calculate $\Gamma(B_s^0X)/\Gamma(\text{hadrons}) = R_b \times f(\bar{b} \rightarrow B_s^0)$. The decay fraction $f(\bar{b} \rightarrow B_s^0)$ was provided by the Heavy Flavor Averaging Group (HFLAV, <https://hflav.web.cern.ch/>).

VALUE	DOCUMENT ID	TECN	COMMENT
0.0227 ± 0.0019 OUR EVALUATION			

seen	DOCUMENT ID	TECN	COMMENT
1 ABREU 92M DLPH	$E_{\text{cm}}^{ee} = 88\text{--}94 \text{ GeV}$		
2 ACTON 92N OPAL	$E_{\text{cm}}^{ee} = 88\text{--}94 \text{ GeV}$		
3 BUSKULIC 92E ALEP	$E_{\text{cm}}^{ee} = 88\text{--}94 \text{ GeV}$		

1 ABREU 92M reported value is $\Gamma(B_s^0X) \times B(B_s^0 \rightarrow D_s\mu\nu\mu X) \times B(D_s \rightarrow \phi\pi)/\Gamma(\text{hadrons}) = (18 \pm 8) \times 10^{-5}$.

2 ACTON 92N find evidence for B_s^0 production using $D_s\text{--}\ell$ correlations, with $D_s^+ \rightarrow \phi\pi^+$ and $K^*(892)K^+$. Assuming R_b from the Standard Model and averaging over the e and μ channels, authors measure the product branching fraction to be $f(\bar{b} \rightarrow B_s^0) \times B(B_s^0 \rightarrow D_s^-\ell^+\nu_\ell X) \times B(D_s^- \rightarrow \phi\pi^-) = (3.9 \pm 1.1 \pm 0.8) \times 10^{-4}$.

3 BUSKULIC 92E find evidence for B_s^0 production using $D_s\text{--}\ell$ correlations, with $D_s^+ \rightarrow \phi\pi^+$ and $K^*(892)K^+$. Using $B(D_s^+ \rightarrow \phi\pi^+) = (2.7 \pm 0.7)\%$ and summing up the e and μ channels, the weighted average product branching fraction is measured to be $B(\bar{b} \rightarrow B_s^0) \times B(B_s^0 \rightarrow D_s^-\ell^+\nu_\ell X) = 0.040 \pm 0.011 \pm 0.012$.

$\Gamma(B_c^+X)/\Gamma(\text{hadrons})$ Γ_{52}/Γ_8

VALUE	DOCUMENT ID	TECN	COMMENT
searched for	1 ACKERSTAFF 98O OPAL	$E_{\text{cm}}^{ee} = 88\text{--}94 \text{ GeV}$	
searched for	2 ABREU 97E DLPH	$E_{\text{cm}}^{ee} = 88\text{--}94 \text{ GeV}$	
searched for	3 BARATE 97H ALEP	$E_{\text{cm}}^{ee} = 88\text{--}94 \text{ GeV}$	

1 ACKERSTAFF 98O searched for the decay modes $B_c \rightarrow J/\psi\pi^+, J/\psi a_1^+$, and $J/\psi\ell^+\nu_\ell$, with $J/\psi \rightarrow \ell^+\ell^-, \ell = e, \mu$. The number of candidates (background) for the three decay modes is $2(0.63 \pm 0.2), 0(1.10 \pm 0.22)$, and $1(0.82 \pm 0.19)$ respectively. Interpreting the $2B_c \rightarrow J/\psi\pi^+$ candidates as signal, they report $\Gamma(B_c^+X) \times B(B_c \rightarrow J/\psi\pi^+)/\Gamma(\text{hadrons}) = (3.8 \pm 5.0 \pm 0.5) \times 10^{-5}$. Interpreted as background, the 90% CL bounds are $\Gamma(B_c^+X) \times B(B_c \rightarrow J/\psi\pi^+)/\Gamma(\text{hadrons}) < 1.06 \times 10^{-4}$, $\Gamma(B_c^+X) \times B(B_c \rightarrow J/\psi a_1^+)/\Gamma(\text{hadrons}) < 5.29 \times 10^{-4}$, $\Gamma(B_c^+X) \times B(B_c \rightarrow J/\psi\ell^+\nu_\ell)/\Gamma(\text{hadrons}) < 6.96 \times 10^{-5}$.

2 ABREU 97E searched for the decay modes $B_c \rightarrow J/\psi\pi^+, J/\psi\ell^+\nu_\ell$, and $J/\psi(3\pi^+)$, with $J/\psi \rightarrow \ell^+\ell^-, \ell = e, \mu$. The number of candidates (background) for the three decay modes is $1(1.7), 0(0.3)$, and $1(2.3)$ respectively. They report the following 90% CL limits: $\Gamma(B_c^+X) \times B(B_c \rightarrow J/\psi\pi^+)/\Gamma(\text{hadrons}) < (1.05\text{--}0.84) \times 10^{-4}$, $\Gamma(B_c^+X) \times B(B_c \rightarrow J/\psi\ell^+\nu_\ell)/\Gamma(\text{hadrons}) < (5.8\text{--}5.0) \times 10^{-5}$, $\Gamma(B_c^+X) \times B(B_c \rightarrow J/\psi(3\pi^+))/\Gamma(\text{hadrons}) < 1.75 \times 10^{-4}$, where the ranges are due to the predicted B_c lifetime (0.4–1.4) ps.

3 BARATE 97H searched for the decay modes $B_c \rightarrow J/\psi\pi^+$ and $J/\psi\ell^+\nu_\ell$ with $J/\psi \rightarrow \ell^+\ell^-, \ell = e, \mu$. The number of candidates (background) for the two decay modes is $0(0.44)$ and $2(0.81)$ respectively. They report the following 90% CL limits: $\Gamma(B_c^+X) \times B(B_c \rightarrow J/\psi\pi^+)/\Gamma(\text{hadrons}) < 3.6 \times 10^{-5}$ and $\Gamma(B_c^+X) \times B(B_c \rightarrow J/\psi\ell^+\nu_\ell)/\Gamma(\text{hadrons}) < 5.2 \times 10^{-5}$.

$\Gamma(A_c^+X)/\Gamma(\text{hadrons})$ Γ_{53}/Γ_8

VALUE	DOCUMENT ID	TECN	COMMENT
0.022 ± 0.005 OUR AVERAGE			
$0.024 \pm 0.003 \pm 0.006$	1 ALEXANDER 96R OPAL	$E_{\text{cm}}^{ee} = 88\text{--}94 \text{ GeV}$	
$0.021 \pm 0.005 \pm 0.005$	2 BUSKULIC 96Y ALEP	$E_{\text{cm}}^{ee} = 88\text{--}94 \text{ GeV}$	

¹ ALEXANDER 96R measure $R_b \times f(b \rightarrow \Lambda_c^+ X) \times B(\Lambda_c^+ \rightarrow p K^- \pi^+) = (0.122 \pm 0.023 \pm 0.010)\%$ in hadronic Z decays; the value quoted here is obtained using our best value $B(\Lambda_c^+ \rightarrow p K^- \pi^+) = (5.0 \pm 1.3)\%$. The first error is the total experiment's error and the second error is the systematic error due to the branching fraction uncertainty.

² BUSKULIC 96V obtain the production fraction of Λ_c^+ baryons in hadronic Z decays $f(b \rightarrow \Lambda_c^+ X) = 0.110 \pm 0.014 \pm 0.006$ using $B(\Lambda_c^+ \rightarrow p K^- \pi^+) = (4.4 \pm 0.6)\%$; we have rescaled using our best value $B(\Lambda_c^+ \rightarrow p K^- \pi^+) = (5.0 \pm 1.3)\%$ obtaining $f(b \rightarrow \Lambda_c^+ X) = 0.097 \pm 0.013 \pm 0.025$ where the first error is their total experiment's error and the second error is the systematic error due to the branching fraction uncertainty. The value quoted here is obtained multiplying this production fraction by our value of $R_b = \Gamma(b\bar{b})/\Gamma(\text{hadrons})$.

$\Gamma(\Xi_c^0 X)/\Gamma(\text{hadrons})$ Γ_{54}/Γ_8

••• We do not use the following data for averages, fits, limits, etc. •••

VALUE	DOCUMENT ID	TECN	COMMENT
seen	¹ ABDALLAH 05c	DLPH	$E_{cm}^{ee} = 88-94$ GeV

¹ ABDALLAH 05c searched for the charmed strange baryon Ξ_c^0 in the decay channel $\Xi_c^0 \rightarrow \Xi^- \pi^+$ ($\Xi^- \rightarrow \Lambda \pi^-$). The production rate is measured to be $f_{\Xi_c^0}^b \times B(\Xi_c^0 \rightarrow \Xi^- \pi^+) = (4.7 \pm 1.4 \pm 1.1) \times 10^{-4}$ per hadronic Z decay.

$\Gamma(\Xi_b X)/\Gamma(\text{hadrons})$ Γ_{55}/Γ_8

Here Ξ_b is used as a notation for the strange b-baryon states Ξ_b^- and Ξ_b^0 .

VALUE	DOCUMENT ID	TECN	COMMENT
••• We do not use the following data for averages, fits, limits, etc. •••			
seen	¹ ABDALLAH 05c	DLPH	$E_{cm}^{ee} = 88-94$ GeV
seen	² BUSKULIC 96t	ALEP	$E_{cm}^{ee} = 88-94$ GeV
seen	³ ABREU 95v	DLPH	$E_{cm}^{ee} = 88-94$ GeV

¹ ABDALLAH 05c searched for the beauty strange baryon Ξ_b in the inclusive semileptonic decay channel $\Xi_b \rightarrow \Xi^- \ell^+ \nu_\ell X$. Evidence for the Ξ_b production is seen from the observation of Ξ^\mp production accompanied by a lepton of the same sign. From the excess of "right-sign" pairs $\Xi^\mp \ell^\mp$ compared to "wrong-sign" pairs $\Xi^\mp \ell^\pm$ the production rate is measured to be $B(b \rightarrow \Xi_b) \times B(\Xi_b \rightarrow \Xi^- \ell^+ X) = (3.0 \pm 1.0 \pm 0.3) \times 10^{-4}$ per lepton species, averaged over electrons and muons.

² BUSKULIC 96t investigate Ξ -lepton correlations and find a significant excess of "right-sign" pairs $\Xi^\mp \ell^\mp$ compared to "wrong-sign" pairs $\Xi^\mp \ell^\pm$. This excess is interpreted as evidence for Ξ_b semileptonic decay. The measured product branching ratio is $B(b \rightarrow \Xi_b) \times B(\Xi_b \rightarrow X_c X \ell^+ \nu_\ell) \times B(X_c \rightarrow \Xi^- X') = (5.4 \pm 1.1 \pm 0.8) \times 10^{-4}$ per lepton species, averaged over electrons and muons, with X_c a charmed baryon.

³ ABREU 95v observe an excess of "right-sign" pairs $\Xi^\mp \ell^\mp$ compared to "wrong-sign" pairs $\Xi^\mp \ell^\pm$ in jets; this excess is interpreted as evidence for the beauty strange baryon Ξ_b production, with $\Xi_b \rightarrow \Xi^- \ell^+ \nu_\ell X$. They find that the probability for this signal to come from non b-baryon decays is less than 5×10^{-4} and that Λ_b decays can account for less than 10% of these events. The Ξ_b production rate is then measured to be $B(b \rightarrow \Xi_b) \times B(\Xi_b \rightarrow \Xi^- \ell^+ X) = (5.9 \pm 2.1 \pm 1.0) \times 10^{-4}$ per lepton species, averaged over electrons and muons.

$\Gamma(b\text{-baryon } X)/\Gamma(\text{hadrons})$ Γ_{56}/Γ_8

"OUR EVALUATION" is obtained using our current values for $f(b \rightarrow b\text{-baryon})$ and $R_b = \Gamma(b\bar{b})/\Gamma(\text{hadrons})$. We calculate $\Gamma(b\text{-baryon } X)/\Gamma(\text{hadrons}) = R_b \times f(b \rightarrow b\text{-baryon})$. The decay fraction ($f(b \rightarrow b\text{-baryon})$) was provided by the Heavy Flavor Averaging Group (<https://inflav.web.cern.ch/>).

VALUE	DOCUMENT ID	TECN	COMMENT
0.0197 ± 0.0032 OUR EVALUATION			
0.0221 ± 0.0015 ± 0.0058	¹ BARATE 98v	ALEP	$E_{cm}^{ee} = 88-94$ GeV

¹ BARATE 98v use the overall number of identified protons in b-hadron decays to measure $f(b \rightarrow b\text{-baryon}) = 0.102 \pm 0.007 \pm 0.027$. They assume $BR(b\text{-baryon} \rightarrow p X) = (58 \pm 6)\%$ and $BR(B_s^0 \rightarrow p X) = (8.0 \pm 4.0)\%$. The value quoted here is obtained multiplying this production fraction by our value of $R_b = \Gamma(b\bar{b})/\Gamma(\text{hadrons})$.

$\Gamma(\text{anomalous } \gamma + \text{hadrons})/\Gamma_{\text{total}}$ Γ_{57}/Γ

Limits on additional sources of prompt photons beyond expectations for final-state bremsstrahlung.

VALUE	CL%	DOCUMENT ID	TECN	COMMENT
<3.2 × 10⁻³	95	¹ AKRAWY 90j	OPAL	$E_{cm}^{ee} = 88-94$ GeV

¹ AKRAWY 90j report $\Gamma(\gamma X) < 8.2$ MeV at 95%CL. They assume a three-body $\gamma q\bar{q}$ distribution and use $E(\gamma) > 10$ GeV.

$\Gamma(e^+ e^- \gamma)/\Gamma_{\text{total}}$ Γ_{58}/Γ

VALUE	CL%	DOCUMENT ID	TECN	COMMENT
<5.2 × 10⁻⁴	95	¹ ACTON 91b	OPAL	$E_{cm}^{ee} = 91.2$ GeV

¹ ACTON 91b looked for isolated photons with $E > 2\%$ of beam energy (> 0.9 GeV).

$\Gamma(\mu^+ \mu^- \gamma)/\Gamma_{\text{total}}$ Γ_{59}/Γ

VALUE	CL%	DOCUMENT ID	TECN	COMMENT
<5.6 × 10⁻⁴	95	¹ ACTON 91b	OPAL	$E_{cm}^{ee} = 91.2$ GeV

¹ ACTON 91b looked for isolated photons with $E > 2\%$ of beam energy (> 0.9 GeV).

$\Gamma(\tau^+ \tau^- \gamma)/\Gamma_{\text{total}}$ Γ_{60}/Γ

VALUE	CL%	DOCUMENT ID	TECN	COMMENT
<7.3 × 10⁻⁴	95	¹ ACTON 91b	OPAL	$E_{cm}^{ee} = 91.2$ GeV

¹ ACTON 91b looked for isolated photons with $E > 2\%$ of beam energy (> 0.9 GeV).

$\Gamma(\ell^+ \ell^- \gamma\gamma)/\Gamma_{\text{total}}$ Γ_{61}/Γ

The value is the sum over $\ell = e, \mu, \tau$.

VALUE	CL%	DOCUMENT ID	TECN	COMMENT
<6.8 × 10⁻⁶	95	¹ ACTON 93E	OPAL	$E_{cm}^{ee} = 88-94$ GeV

¹ For $m_{\gamma\gamma} = 60 \pm 5$ GeV.

$\Gamma(q\bar{q}\gamma\gamma)/\Gamma_{\text{total}}$ Γ_{62}/Γ

VALUE	CL%	DOCUMENT ID	TECN	COMMENT
<5.5 × 10⁻⁶	95	¹ ACTON 93E	OPAL	$E_{cm}^{ee} = 88-94$ GeV

¹ For $m_{\gamma\gamma} = 60 \pm 5$ GeV.

$\Gamma(\nu\bar{\nu}\gamma\gamma)/\Gamma_{\text{total}}$ Γ_{63}/Γ

VALUE	CL%	DOCUMENT ID	TECN	COMMENT
<3.1 × 10⁻⁶	95	¹ ACTON 93E	OPAL	$E_{cm}^{ee} = 88-94$ GeV

¹ For $m_{\gamma\gamma} = 60 \pm 5$ GeV.

$\Gamma(e^\pm \mu^\mp)/\Gamma_{\text{total}}$ Γ_{64}/Γ

Test of lepton family number conservation. The value is for the sum of the charge states indicated.

VALUE	CL%	DOCUMENT ID	TECN	COMMENT
<7.5 × 10⁻⁷	95	AAD 14AU	ATLS	$E_{cm}^{pp} = 8$ TeV
<2.5 × 10 ⁻⁶	95	ABREU 97c	DLPH	$E_{cm}^{ee} = 88-94$ GeV
<1.7 × 10 ⁻⁶	95	AKERS 95w	OPAL	$E_{cm}^{ee} = 88-94$ GeV
<0.6 × 10 ⁻⁵	95	ADRIANI 93i	L3	$E_{cm}^{ee} = 88-94$ GeV
<2.6 × 10 ⁻⁵	95	DECAMP 92	ALEP	$E_{cm}^{ee} = 88-94$ GeV

$\Gamma(e^\pm \mu^\mp)/\Gamma(e^+ e^-)$ Γ_{64}/Γ_1

Test of lepton family number conservation. The value is for the sum of the charge states indicated.

VALUE	CL%	DOCUMENT ID	TECN	COMMENT
<0.07	90	ALBAJAR 89	UA1	$E_{cm}^{pp} = 546,630$ GeV

$\Gamma(e^\pm \tau^\mp)/\Gamma_{\text{total}}$ Γ_{65}/Γ

Test of lepton family number conservation. The value is for the sum of the charge states indicated.

VALUE	CL%	DOCUMENT ID	TECN	COMMENT
<5.8 × 10 ⁻⁵	95	AABOUD 18CN	ATLS	$E_{cm}^{pp} = 13$ TeV
<2.2 × 10 ⁻⁵	95	ABREU 97c	DLPH	$E_{cm}^{ee} = 88-94$ GeV
<9.8 × 10⁻⁶	95	AKERS 95w	OPAL	$E_{cm}^{ee} = 88-94$ GeV
<1.3 × 10 ⁻⁵	95	ADRIANI 93i	L3	$E_{cm}^{ee} = 88-94$ GeV
<1.2 × 10 ⁻⁴	95	DECAMP 92	ALEP	$E_{cm}^{ee} = 88-94$ GeV

$\Gamma(\mu^\pm \tau^\mp)/\Gamma_{\text{total}}$ Γ_{66}/Γ

Test of lepton family number conservation. The value is for the sum of the charge states indicated.

VALUE	CL%	DOCUMENT ID	TECN	COMMENT
<1.3 × 10 ⁻⁵	95	AABOUD 18CN	ATLS	$E_{cm}^{pp} = 8, 13$ TeV
<1.2 × 10⁻⁵	95	ABREU 97c	DLPH	$E_{cm}^{ee} = 88-94$ GeV
<1.7 × 10 ⁻⁵	95	AKERS 95w	OPAL	$E_{cm}^{ee} = 88-94$ GeV
<1.9 × 10 ⁻⁵	95	ADRIANI 93i	L3	$E_{cm}^{ee} = 88-94$ GeV
<1.0 × 10 ⁻⁴	95	DECAMP 92	ALEP	$E_{cm}^{ee} = 88-94$ GeV

$\Gamma(p\bar{e})/\Gamma_{\text{total}}$ Γ_{67}/Γ

Test of baryon number and lepton number conservations. Charge conjugate states are implied.

VALUE	CL%	DOCUMENT ID	TECN	COMMENT
<1.8 × 10⁻⁶	95	¹ ABBIENDI 99i	OPAL	$E_{cm}^{ee} = 88-94$ GeV

¹ ABBIENDI 99i give the 95%CL limit on the partial width $\Gamma(Z^0 \rightarrow p\bar{e}) < 4.6$ KeV and we have transformed it into a branching ratio.

$\Gamma(p\bar{\mu})/\Gamma_{\text{total}}$ Γ_{68}/Γ

Test of baryon number and lepton number conservations. Charge conjugate states are implied.

VALUE	CL%	DOCUMENT ID	TECN	COMMENT
<1.8 × 10⁻⁶	95	¹ ABBIENDI 99i	OPAL	$E_{cm}^{ee} = 88-94$ GeV

¹ ABBIENDI 99i give the 95%CL limit on the partial width $\Gamma(Z^0 \rightarrow p\bar{\mu}) < 4.4$ KeV and we have transformed it into a branching ratio.

AVERAGE PARTICLE MULTIPLICITIES IN HADRONIC Z DECAY

Summed over particle and antiparticle, when appropriate.

$\langle N_\gamma \rangle$	VALUE	DOCUMENT ID	TECN	COMMENT
	20.97 ± 0.02 ± 1.15	ACKERSTAFF 98A	OPAL	$E_{cm}^{ee} = 91.2$ GeV

$\langle N_{\pi^\pm} \rangle$	VALUE	DOCUMENT ID	TECN	COMMENT
	17.03 ± 0.16 OUR AVERAGE			
	17.007 ± 0.209	ABE 04c	SLD	$E_{cm}^{ee} = 91.2$ GeV
	17.26 ± 0.10 ± 0.88	ABREU 98L	DLPH	$E_{cm}^{ee} = 91.2$ GeV
	17.04 ± 0.31	BARATE 98v	ALEP	$E_{cm}^{ee} = 91.2$ GeV
	17.05 ± 0.43	AKERS 94P	OPAL	$E_{cm}^{ee} = 91.2$ GeV

Gauge & Higgs Boson Particle Listings

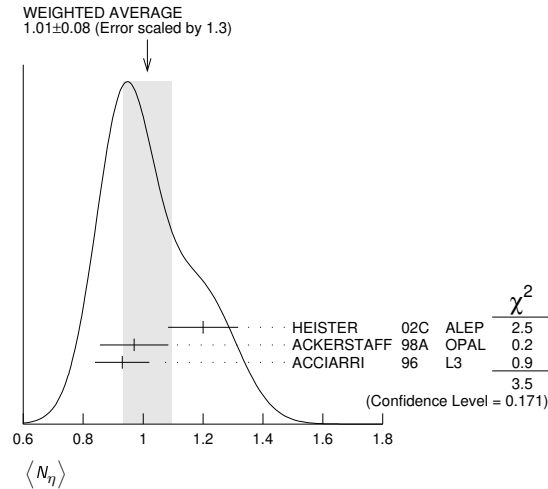
Z

$\langle N_{\pi^0} \rangle$

VALUE	DOCUMENT ID	TECN	COMMENT
9.76 ± 0.26 OUR AVERAGE			
9.55 ± 0.06 ± 0.75	ACKERSTAFF 98A	OPAL	$E_{cm}^{ee} = 91.2$ GeV
9.63 ± 0.13 ± 0.63	BARATE 97J	ALEP	$E_{cm}^{ee} = 91.2$ GeV
9.90 ± 0.02 ± 0.33	ACCIARRI 96	L3	$E_{cm}^{ee} = 91.2$ GeV
9.2 ± 0.2 ± 1.0	ADAM 96	DLPH	$E_{cm}^{ee} = 91.2$ GeV

$\langle N_{\eta} \rangle$

VALUE	DOCUMENT ID	TECN	COMMENT
1.01 ± 0.08 OUR AVERAGE			Error includes scale factor of 1.3. See the ideogram below.
1.20 ± 0.04 ± 0.11	HEISTER 02c	ALEP	$E_{cm}^{ee} = 91.2$ GeV
0.97 ± 0.03 ± 0.11	ACKERSTAFF 98A	OPAL	$E_{cm}^{ee} = 91.2$ GeV
0.93 ± 0.01 ± 0.09	ACCIARRI 96	L3	$E_{cm}^{ee} = 91.2$ GeV



$\langle N_{\rho^\pm} \rangle$

VALUE	DOCUMENT ID	TECN	COMMENT
2.57 ± 0.15 OUR AVERAGE			
2.59 ± 0.03 ± 0.16	¹ BEDDALL 09	ALEPH archive,	$E_{cm}^{ee} = 91.2$ GeV
2.40 ± 0.06 ± 0.43	ACKERSTAFF 98A	OPAL	$E_{cm}^{ee} = 91.2$ GeV

¹ BEDDALL 09 analyse 3.2 million hadronic Z decays as archived by ALEPH collaboration and report a value of $2.59 \pm 0.03 \pm 0.15 \pm 0.04$. The first error is statistical, the second systematic, and the third arises from extrapolation to full phase space. We combine the systematic errors in quadrature.

$\langle N_{\rho^0} \rangle$

VALUE	DOCUMENT ID	TECN	COMMENT
1.24 ± 0.10 OUR AVERAGE			Error includes scale factor of 1.1.
1.19 ± 0.10	ABREU 99J	DLPH	$E_{cm}^{ee} = 91.2$ GeV
1.45 ± 0.06 ± 0.20	BUSKULIC 96H	ALEP	$E_{cm}^{ee} = 91.2$ GeV

$\langle N_{\omega} \rangle$

VALUE	DOCUMENT ID	TECN	COMMENT
1.02 ± 0.06 OUR AVERAGE			
1.00 ± 0.03 ± 0.06	HEISTER 02c	ALEP	$E_{cm}^{ee} = 91.2$ GeV
1.04 ± 0.04 ± 0.14	ACKERSTAFF 98A	OPAL	$E_{cm}^{ee} = 91.2$ GeV
1.17 ± 0.09 ± 0.15	ACCIARRI 97D	L3	$E_{cm}^{ee} = 91.2$ GeV

$\langle N_{\eta'} \rangle$

VALUE	DOCUMENT ID	TECN	COMMENT
0.17 ± 0.05 OUR AVERAGE			Error includes scale factor of 2.4.
0.14 ± 0.01 ± 0.02	ACKERSTAFF 98A	OPAL	$E_{cm}^{ee} = 91.2$ GeV
0.25 ± 0.04	¹ ACCIARRI 97D	L3	$E_{cm}^{ee} = 91.2$ GeV

• • • We do not use the following data for averages, fits, limits, etc. • • •
 0.068 ± 0.018 ± 0.016 ²BUSKULIC 92D ALEP $E_{cm}^{ee} = 91.2$ GeV
¹ACCIARRI 97D obtain this value averaging over the two decay channels $\eta' \rightarrow \pi^+ \pi^- \eta$ and $\eta' \rightarrow \rho^0 \gamma$.
²BUSKULIC 92D obtain this value for $x > 0.1$.

$\langle N_{f_0(980)} \rangle$

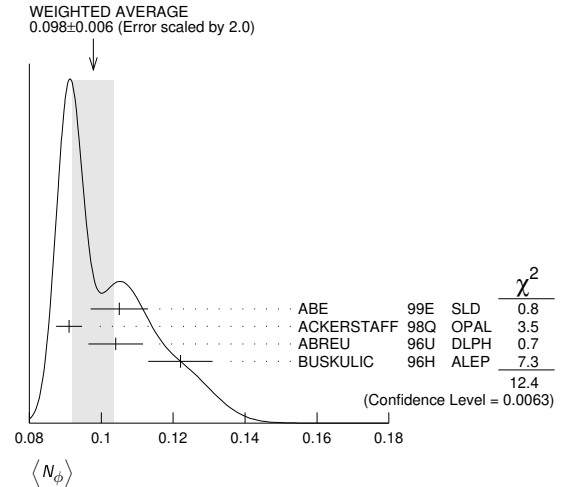
VALUE	DOCUMENT ID	TECN	COMMENT
0.147 ± 0.011 OUR AVERAGE			
0.164 ± 0.021	ABREU 99J	DLPH	$E_{cm}^{ee} = 91.2$ GeV
0.141 ± 0.007 ± 0.011	ACKERSTAFF 98Q	OPAL	$E_{cm}^{ee} = 91.2$ GeV

$\langle N_{\rho_0(980)^\pm} \rangle$

VALUE	DOCUMENT ID	TECN	COMMENT
0.27 ± 0.04 ± 0.10	ACKERSTAFF 98A	OPAL	$E_{cm}^{ee} = 91.2$ GeV

$\langle N_{\phi} \rangle$

VALUE	DOCUMENT ID	TECN	COMMENT
0.098 ± 0.006 OUR AVERAGE			Error includes scale factor of 2.0. See the ideogram below.
0.105 ± 0.008	ABE 99E	SLD	$E_{cm}^{ee} = 91.2$ GeV
0.091 ± 0.002 ± 0.003	ACKERSTAFF 98Q	OPAL	$E_{cm}^{ee} = 91.2$ GeV
0.104 ± 0.003 ± 0.007	ABREU 96U	DLPH	$E_{cm}^{ee} = 91.2$ GeV
0.122 ± 0.004 ± 0.008	BUSKULIC 96H	ALEP	$E_{cm}^{ee} = 91.2$ GeV



$\langle N_{f_1(1270)} \rangle$

VALUE	DOCUMENT ID	TECN	COMMENT
0.169 ± 0.025 OUR AVERAGE			Error includes scale factor of 1.4.
0.214 ± 0.038	ABREU 99J	DLPH	$E_{cm}^{ee} = 91.2$ GeV
0.155 ± 0.011 ± 0.018	ACKERSTAFF 98Q	OPAL	$E_{cm}^{ee} = 91.2$ GeV

$\langle N_{f_1(1285)} \rangle$

VALUE	DOCUMENT ID	TECN	COMMENT
0.165 ± 0.051	¹ ABDALLAH 03H	DLPH	$E_{cm}^{ee} = 91.2$ GeV

¹ ABDALLAH 03H assume a $K\bar{K}\pi$ branching ratio of $(9.0 \pm 0.4)\%$.

$\langle N_{f_1(1420)} \rangle$

VALUE	DOCUMENT ID	TECN	COMMENT
0.056 ± 0.012	¹ ABDALLAH 03H	DLPH	$E_{cm}^{ee} = 91.2$ GeV

¹ ABDALLAH 03H assume a $K\bar{K}\pi$ branching ratio of 100%.

$\langle N_{f_2'(1525)} \rangle$

VALUE	DOCUMENT ID	TECN	COMMENT
0.012 ± 0.006	ABREU 99J	DLPH	$E_{cm}^{ee} = 91.2$ GeV

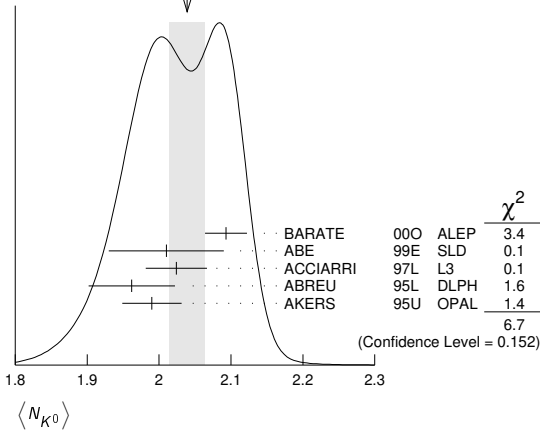
$\langle N_{K^{\pm}} \rangle$

VALUE	DOCUMENT ID	TECN	COMMENT
2.24 ± 0.04 OUR AVERAGE			
2.203 ± 0.071	ABE 04c	SLD	$E_{cm}^{ee} = 91.2$ GeV
2.21 ± 0.05 ± 0.05	ABREU 98L	DLPH	$E_{cm}^{ee} = 91.2$ GeV
2.26 ± 0.12	BARATE 98v	ALEP	$E_{cm}^{ee} = 91.2$ GeV
2.42 ± 0.13	AKERS 94P	OPAL	$E_{cm}^{ee} = 91.2$ GeV

$\langle N_{K^0} \rangle$

VALUE	DOCUMENT ID	TECN	COMMENT
2.039 ± 0.025 OUR AVERAGE			Error includes scale factor of 1.3. See the ideogram below.
2.093 ± 0.004 ± 0.029	BARATE 00o	ALEP	$E_{cm}^{ee} = 91.2$ GeV
2.01 ± 0.08	ABE 99E	SLD	$E_{cm}^{ee} = 91.2$ GeV
2.024 ± 0.006 ± 0.042	ACCIARRI 97L	L3	$E_{cm}^{ee} = 91.2$ GeV
1.962 ± 0.022 ± 0.056	ABREU 95L	DLPH	$E_{cm}^{ee} = 91.2$ GeV
1.99 ± 0.01 ± 0.04	AKERS 95U	OPAL	$E_{cm}^{ee} = 91.2$ GeV

WEIGHTED AVERAGE
2.039±0.025 (Error scaled by 1.3)



$\langle N_{K^*(892)^\pm} \rangle$

VALUE	DOCUMENT ID	TECN	COMMENT
0.72 ± 0.05 OUR AVERAGE			
0.712 ± 0.031 ± 0.059	ABREU 95L DLPH	$E_{cm}^{ee} = 91.2$ GeV	
0.72 ± 0.02 ± 0.08	ACTON 93 OPAL	$E_{cm}^{ee} = 91.2$ GeV	

$\langle N_{K^*(892)^0} \rangle$

VALUE	DOCUMENT ID	TECN	COMMENT
0.739 ± 0.022 OUR AVERAGE			
0.707 ± 0.041	ABE 99E SLD	$E_{cm}^{ee} = 91.2$ GeV	
0.74 ± 0.02 ± 0.02	ACKERSTAFF 97S OPAL	$E_{cm}^{ee} = 91.2$ GeV	
0.77 ± 0.02 ± 0.07	ABREU 96U DLPH	$E_{cm}^{ee} = 91.2$ GeV	
0.83 ± 0.01 ± 0.09	BUSKULIC 96H ALEP	$E_{cm}^{ee} = 91.2$ GeV	
0.97 ± 0.18 ± 0.31	ABREU 93 DLPH	$E_{cm}^{ee} = 91.2$ GeV	

$\langle N_{K_2^*(1430)} \rangle$

VALUE	DOCUMENT ID	TECN	COMMENT
0.073 ± 0.023	ABREU 99J DLPH	$E_{cm}^{ee} = 91.2$ GeV	
0.19 ± 0.04 ± 0.06	¹ AKERS 95X OPAL	$E_{cm}^{ee} = 91.2$ GeV	

• • • We do not use the following data for averages, fits, limits, etc. • • •

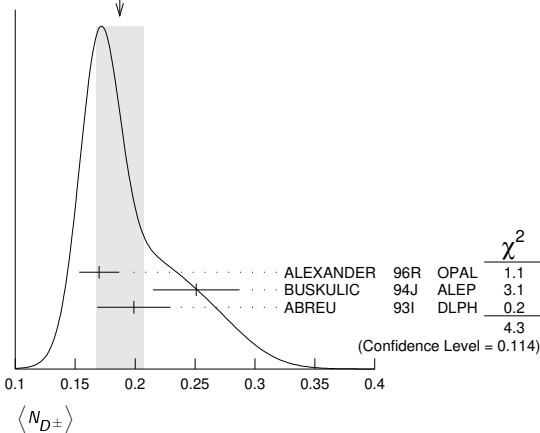
¹ AKERS 95X obtain this value for $x < 0.3$.

$\langle N_{D^\pm} \rangle$

VALUE	DOCUMENT ID	TECN	COMMENT
0.187 ± 0.020 OUR AVERAGE			Error includes scale factor of 1.5. See the ideogram below.
0.170 ± 0.009 ± 0.014	ALEXANDER 96R OPAL	$E_{cm}^{ee} = 91.2$ GeV	
0.251 ± 0.026 ± 0.025	BUSKULIC 94J ALEP	$E_{cm}^{ee} = 91.2$ GeV	
0.199 ± 0.019 ± 0.024	¹ ABREU 93I DLPH	$E_{cm}^{ee} = 91.2$ GeV	

¹ See ABREU 95 (erratum).

WEIGHTED AVERAGE
0.187±0.020 (Error scaled by 1.5)



$\langle N_{D^0} \rangle$

VALUE	DOCUMENT ID	TECN	COMMENT
0.462 ± 0.026 OUR AVERAGE			
0.465 ± 0.017 ± 0.027	ALEXANDER 96R OPAL	$E_{cm}^{ee} = 91.2$ GeV	
0.518 ± 0.052 ± 0.035	BUSKULIC 94J ALEP	$E_{cm}^{ee} = 91.2$ GeV	
0.403 ± 0.038 ± 0.044	¹ ABREU 93I DLPH	$E_{cm}^{ee} = 91.2$ GeV	

¹ See ABREU 95 (erratum).

$\langle N_{D_s^\pm} \rangle$

VALUE	DOCUMENT ID	TECN	COMMENT
0.183 ± 0.010 ± 0.018	ALEXANDER 96R OPAL	$E_{cm}^{ee} = 91.2$ GeV	

$\langle N_{D^*(2010)^\pm} \rangle$

VALUE	DOCUMENT ID	TECN	COMMENT
0.183 ± 0.008 OUR AVERAGE			
0.1854 ± 0.0041 ± 0.0091	¹ ACKERSTAFF 98E OPAL	$E_{cm}^{ee} = 91.2$ GeV	
0.187 ± 0.015 ± 0.013	BUSKULIC 94J ALEP	$E_{cm}^{ee} = 91.2$ GeV	
0.171 ± 0.012 ± 0.016	² ABREU 93I DLPH	$E_{cm}^{ee} = 91.2$ GeV	

¹ ACKERSTAFF 98E systematic error includes an uncertainty of ± 0.0069 due to the branching ratios $B(D^{*+} \rightarrow D^0 \pi^+) = 0.683 \pm 0.014$ and $B(D^0 \rightarrow K^- \pi^+) = 0.0383 \pm 0.0012$.

² See ABREU 95 (erratum).

$\langle N_{D_{s1}(2536)^+} \rangle$

VALUE (units 10 ⁻³)	DOCUMENT ID	TECN	COMMENT
2.9^{+0.7}_{-0.6} ± 0.2	¹ ACKERSTAFF 97W OPAL	$E_{cm}^{ee} = 91.2$ GeV	

• • • We do not use the following data for averages, fits, limits, etc. • • •

¹ ACKERSTAFF 97W obtain this value for $x > 0.6$ and with the assumption that its decay width is saturated by the $D^* K$ final states.

$\langle N_{B^*} \rangle$

VALUE	DOCUMENT ID	TECN	COMMENT
0.28 ± 0.01 ± 0.03	¹ ABREU 95R DLPH	$E_{cm}^{ee} = 91.2$ GeV	

¹ ABREU 95R quote this value for a flavor-averaged excited state.

$\langle N_{J/\psi(1S)} \rangle$

VALUE	DOCUMENT ID	TECN	COMMENT
0.0056 ± 0.0003 ± 0.0004	¹ ALEXANDER 96B OPAL	$E_{cm}^{ee} = 91.2$ GeV	

¹ ALEXANDER 96B identify $J/\psi(1S)$ from the decays into lepton pairs.

$\langle N_{\psi(2S)} \rangle$

VALUE	DOCUMENT ID	TECN	COMMENT
0.0023 ± 0.0004 ± 0.0003	ALEXANDER 96B OPAL	$E_{cm}^{ee} = 91.2$ GeV	

$\langle N_p \rangle$

VALUE	DOCUMENT ID	TECN	COMMENT
1.046 ± 0.026 OUR AVERAGE			
1.054 ± 0.035	ABE 04C SLD	$E_{cm}^{ee} = 91.2$ GeV	
1.08 ± 0.04 ± 0.03	ABREU 98L DLPH	$E_{cm}^{ee} = 91.2$ GeV	
1.00 ± 0.07	BARATE 98V ALEP	$E_{cm}^{ee} = 91.2$ GeV	
0.92 ± 0.11	AKERS 94P OPAL	$E_{cm}^{ee} = 91.2$ GeV	

$\langle N_{\Delta(1232)^{++}} \rangle$

VALUE	DOCUMENT ID	TECN	COMMENT
0.087 ± 0.033 OUR AVERAGE			Error includes scale factor of 2.4.
0.079 ± 0.009 ± 0.011	ABREU 95W DLPH	$E_{cm}^{ee} = 91.2$ GeV	
0.22 ± 0.04 ± 0.04	ALEXANDER 95D OPAL	$E_{cm}^{ee} = 91.2$ GeV	

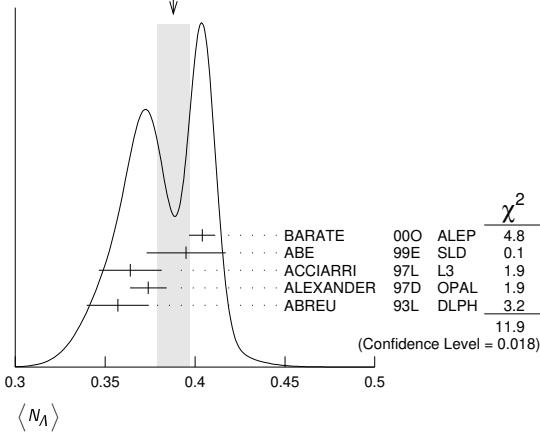
$\langle N_\Lambda \rangle$

VALUE	DOCUMENT ID	TECN	COMMENT
0.388 ± 0.009 OUR AVERAGE			Error includes scale factor of 1.7. See the ideogram below.
0.404 ± 0.002 ± 0.007	BARATE 00O ALEP	$E_{cm}^{ee} = 91.2$ GeV	
0.395 ± 0.022	ABE 99E SLD	$E_{cm}^{ee} = 91.2$ GeV	
0.364 ± 0.004 ± 0.017	ACCIARRI 97L L3	$E_{cm}^{ee} = 91.2$ GeV	
0.374 ± 0.002 ± 0.010	ALEXANDER 97D OPAL	$E_{cm}^{ee} = 91.2$ GeV	
0.357 ± 0.003 ± 0.017	ABREU 93L DLPH	$E_{cm}^{ee} = 91.2$ GeV	

Gauge & Higgs Boson Particle Listings

Z

WEIGHTED AVERAGE
0.388±0.009 (Error scaled by 1.7)



$\langle N_{\Lambda(1520)} \rangle$

VALUE	DOCUMENT ID	TECN	COMMENT
0.0224 ± 0.0027 OUR AVERAGE			
0.029 ± 0.005 ± 0.005	ABREU 00P	DLPH	$E_{cm}^{ee} = 91.2$ GeV
0.0213 ± 0.0021 ± 0.0019	ALEXANDER 97D	OPAL	$E_{cm}^{ee} = 91.2$ GeV

$\langle N_{\Sigma^+} \rangle$

VALUE	DOCUMENT ID	TECN	COMMENT
0.107 ± 0.010 OUR AVERAGE			
0.114 ± 0.011 ± 0.009	ACCIARRI 00J	L3	$E_{cm}^{ee} = 91.2$ GeV
0.099 ± 0.008 ± 0.013	ALEXANDER 97E	OPAL	$E_{cm}^{ee} = 91.2$ GeV

$\langle N_{\Sigma^-} \rangle$

VALUE	DOCUMENT ID	TECN	COMMENT
0.082 ± 0.007 OUR AVERAGE			
0.081 ± 0.002 ± 0.010	ABREU 00P	DLPH	$E_{cm}^{ee} = 91.2$ GeV
0.083 ± 0.006 ± 0.009	ALEXANDER 97E	OPAL	$E_{cm}^{ee} = 91.2$ GeV

$\langle N_{\Sigma^+ + \Sigma^-} \rangle$

VALUE	DOCUMENT ID	TECN	COMMENT
0.181 ± 0.018 OUR AVERAGE			
0.182 ± 0.010 ± 0.016	¹ ALEXANDER 97E	OPAL	$E_{cm}^{ee} = 91.2$ GeV
0.170 ± 0.014 ± 0.061	ABREU 95O	DLPH	$E_{cm}^{ee} = 91.2$ GeV

¹ We have combined the values of $\langle N_{\Sigma^+} \rangle$ and $\langle N_{\Sigma^-} \rangle$ from ALEXANDER 97E adding the statistical and systematic errors of the two final states separately in quadrature. If isospin symmetry is assumed this value becomes $0.174 \pm 0.010 \pm 0.015$.

$\langle N_{\Sigma^0} \rangle$

VALUE	DOCUMENT ID	TECN	COMMENT
0.076 ± 0.010 OUR AVERAGE			
0.095 ± 0.015 ± 0.013	ACCIARRI 00J	L3	$E_{cm}^{ee} = 91.2$ GeV
0.071 ± 0.012 ± 0.013	ALEXANDER 97E	OPAL	$E_{cm}^{ee} = 91.2$ GeV
0.070 ± 0.010 ± 0.010	ADAM 96B	DLPH	$E_{cm}^{ee} = 91.2$ GeV

$\langle N_{(\Sigma^+ + \Sigma^- + \Sigma^0)/3} \rangle$

VALUE	DOCUMENT ID	TECN	COMMENT
0.084 ± 0.005 ± 0.008	ALEXANDER 97E	OPAL	$E_{cm}^{ee} = 91.2$ GeV

$\langle N_{\Sigma(1385)^+} \rangle$

VALUE	DOCUMENT ID	TECN	COMMENT
0.0239 ± 0.0009 ± 0.0012	ALEXANDER 97D	OPAL	$E_{cm}^{ee} = 91.2$ GeV

$\langle N_{\Sigma(1385)^-} \rangle$

VALUE	DOCUMENT ID	TECN	COMMENT
0.0240 ± 0.0010 ± 0.0014	ALEXANDER 97D	OPAL	$E_{cm}^{ee} = 91.2$ GeV

$\langle N_{\Sigma(1385)^+ + \Sigma(1385)^-} \rangle$

VALUE	DOCUMENT ID	TECN	COMMENT
0.046 ± 0.004 OUR AVERAGE			
0.0479 ± 0.0013 ± 0.0026	ALEXANDER 97D	OPAL	$E_{cm}^{ee} = 91.2$ GeV
0.0382 ± 0.0028 ± 0.0045	ABREU 95O	DLPH	$E_{cm}^{ee} = 91.2$ GeV

Error includes scale factor of 1.6.

$\langle N_{\Xi^-} \rangle$

VALUE	DOCUMENT ID	TECN	COMMENT
0.0258 ± 0.0009 OUR AVERAGE			
0.0247 ± 0.0009 ± 0.0025	ABDALLAH 06E	DLPH	$E_{cm}^{ee} = 91.2$ GeV
0.0259 ± 0.0004 ± 0.0009	ALEXANDER 97D	OPAL	$E_{cm}^{ee} = 91.2$ GeV

$\langle N_{\Xi(1530)^0} \rangle$

VALUE	DOCUMENT ID	TECN	COMMENT
0.0059 ± 0.0011 OUR AVERAGE			Error includes scale factor of 2.3.
0.0045 ± 0.0005 ± 0.0006	ABDALLAH 05C	DLPH	$E_{cm}^{ee} = 91.2$ GeV
0.0068 ± 0.0005 ± 0.0004	ALEXANDER 97D	OPAL	$E_{cm}^{ee} = 91.2$ GeV

$\langle N_{\Omega^-} \rangle$

VALUE	DOCUMENT ID	TECN	COMMENT
0.00164 ± 0.00028 OUR AVERAGE			
0.0018 ± 0.0003 ± 0.0002	ALEXANDER 97D	OPAL	$E_{cm}^{ee} = 91.2$ GeV
0.0014 ± 0.0002 ± 0.0004	ADAM 96B	DLPH	$E_{cm}^{ee} = 91.2$ GeV

$\langle N_{\Lambda_c^+} \rangle$

VALUE	DOCUMENT ID	TECN	COMMENT
0.078 ± 0.012 ± 0.012	ALEXANDER 96R	OPAL	$E_{cm}^{ee} = 91.2$ GeV

$\langle N_D \rangle$

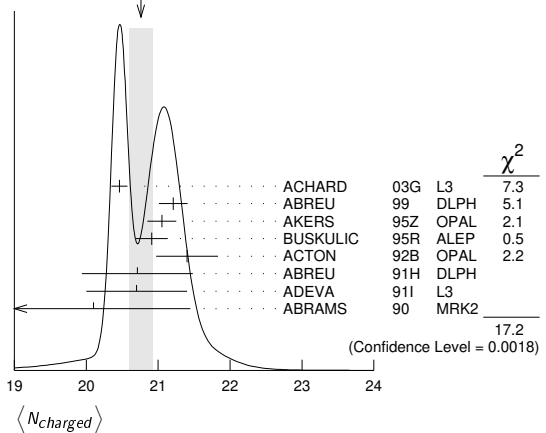
VALUE (units 10^{-6})	DOCUMENT ID	TECN	COMMENT
5.9 ± 1.8 ± 0.5	¹ SCHAEAL 06A	ALEP	$E_{cm}^{ee} = 91.2$ GeV

¹ SCHAEAL 06A obtain this anti-deuteron production rate per hadronic Z decay in the anti-deuteron momentum range from 0.62 to 1.03 GeV/c.

$\langle N_{\text{charged}} \rangle$

VALUE	DOCUMENT ID	TECN	COMMENT
20.76 ± 0.16 OUR AVERAGE			Error includes scale factor of 2.1. See the ideogram below.
20.46 ± 0.01 ± 0.11	ACHARD 03G	L3	$E_{cm}^{ee} = 91.2$ GeV
21.21 ± 0.01 ± 0.20	ABREU 99	DLPH	$E_{cm}^{ee} = 91.2$ GeV
21.05 ± 0.20	AKERS 95Z	OPAL	$E_{cm}^{ee} = 91.2$ GeV
20.91 ± 0.03 ± 0.22	BUSKULIC 95R	ALEP	$E_{cm}^{ee} = 91.2$ GeV
21.40 ± 0.43	ACTON 92B	OPAL	$E_{cm}^{ee} = 91.2$ GeV
20.71 ± 0.04 ± 0.77	ABREU 91H	DLPH	$E_{cm}^{ee} = 91.2$ GeV
20.7 ± 0.7	ADEVA 91I	L3	$E_{cm}^{ee} = 91.2$ GeV
20.1 ± 1.0 ± 0.9	ABRAMS 90	MRK2	$E_{cm}^{ee} = 91.1$ GeV

WEIGHTED AVERAGE
20.76±0.16 (Error scaled by 2.1)



Z HADRONIC POLE CROSS SECTION

OUR FIT is obtained using the fit procedure and correlations as determined by the LEP Electroweak Working Group (see the note "The Z boson" and ref. LEP-SLC 06). This quantity is defined as

$$\sigma_h^0 = \frac{12\pi}{M_Z^2} \frac{\Gamma(e^+e^-)\Gamma(\text{hadrons})}{\Gamma_Z^2}$$

It is one of the parameters used in the Z lineshape fit.

VALUE (nb)	EVTS	DOCUMENT ID	TECN	COMMENT
41.541 ± 0.037 OUR FIT				
41.501 ± 0.055	4.10M	¹ ABBIENDI 01A	OPAL	$E_{cm}^{ee} = 88-94$ GeV
41.578 ± 0.069	3.70M	ABREU 00F	DLPH	$E_{cm}^{ee} = 88-94$ GeV
41.535 ± 0.055	3.54M	ACCIARRI 00C	L3	$E_{cm}^{ee} = 88-94$ GeV
41.559 ± 0.058	4.07M	² BARATE 00C	ALEP	$E_{cm}^{ee} = 88-94$ GeV
42 ± 4	450	ABRAMS 89B	MRK2	$E_{cm}^{ee} = 89.2-93.0$ GeV

¹ ABBIENDI 01A error includes approximately 0.031 due to statistics, 0.033 due to event selection systematics, 0.029 due to uncertainty in luminosity measurement, and 0.011 due to LEP energy uncertainty.

² BARATE 00C error includes approximately 0.030 due to statistics, 0.026 due to experimental systematics, and 0.025 due to uncertainty in luminosity measurement.

Z VECTOR COUPLINGS

These quantities are the effective vector couplings of the Z to charged leptons and quarks. Their magnitude is derived from a measurement of the Z lineshape and the forward-backward lepton asymmetries as a function of energy around the Z mass. The relative sign among the vector to axial-vector couplings is obtained from a measurement of the Z asymmetry parameters, A_e , A_μ , and A_τ . By convention the sign of g_A^e is fixed to be negative (and opposite to that of g^{V_e} obtained using ν_e scattering measurements). For the light quarks, the sign of the couplings is assigned consistently with this assumption. The LEP/SLD-based fit values quoted below correspond to global nine- or five-parameter fits to lineshape, lepton forward-backward asymmetry, and A_e , A_μ , and A_τ measurements. See the note "The Z boson" and ref. LEP-SLC 06 for details. Where $p\bar{p}$ and $e\bar{p}$ data is quoted, OUR FIT value corresponds to a weighted average of this with the LEP/SLD fit result.

VALUE	EVTS	DOCUMENT ID	TECN	COMMENT
-0.03817 ± 0.00047 OUR FIT				
$-0.058 \pm 0.016 \pm 0.007$	5026	1 ACOSTA	05M CDF	$E_{cm}^{p\bar{p}} = 1.96$ TeV
-0.0346 ± 0.0023	137.0K	2 ABBIENDI	01o OPAL	$E_{cm}^{ee} = 88-94$ GeV
-0.0412 ± 0.0027	124.4k	3 ACCIARRI	00c L3	$E_{cm}^{ee} = 88-94$ GeV
-0.0400 ± 0.0037		BARATE	00c ALEP	$E_{cm}^{ee} = 88-94$ GeV
-0.0414 ± 0.0020		4 ABE	95J SLD	$E_{cm}^{ee} = 91.31$ GeV

- ACOSTA 05M determine the forward-backward asymmetry of e^+e^- pairs produced via $q\bar{q} \rightarrow Z/\gamma^* \rightarrow e^+e^-$ in 15 M(e^+e^-) effective mass bins ranging from 40 GeV to 600 GeV. These results are used to obtain the vector and axial-vector couplings of the Z to e^+e^- , assuming the quark couplings are as predicted by the standard model. Higher order radiative corrections have not been taken into account.
- ABBIENDI 01o use their measurement of the τ polarization in addition to the lineshape and forward-backward lepton asymmetries.
- ACCIARRI 00c use their measurement of the τ polarization in addition to forward-backward lepton asymmetries.
- ABE 95J obtain this result combining polarized Bhabha results with the A_{LR} measurement of ABE 94c. The Bhabha results alone give $-0.0507 \pm 0.0096 \pm 0.0020$.

VALUE	EVTS	DOCUMENT ID	TECN	COMMENT
-0.0367 ± 0.0023 OUR FIT				
$-0.0388 \pm 0.0060 \pm 0.0064$	182.8K	1 ABBIENDI	01o OPAL	$E_{cm}^{ee} = 88-94$ GeV
-0.0386 ± 0.0073	113.4k	2 ACCIARRI	00c L3	$E_{cm}^{ee} = 88-94$ GeV
-0.0362 ± 0.0061		BARATE	00c ALEP	$E_{cm}^{ee} = 88-94$ GeV
-0.0413 ± 0.0060	66143	3 ABBIENDI	01k OPAL	$E_{cm}^{ee} = 89-93$ GeV

- We do not use the following data for averages, fits, limits, etc.
- ABBIENDI 01o use their measurement of the τ polarization in addition to the lineshape and forward-backward lepton asymmetries.
 - ACCIARRI 00c use their measurement of the τ polarization in addition to forward-backward lepton asymmetries.
 - ABBIENDI 01k obtain this from an angular analysis of the muon pair asymmetry which takes into account effects of initial state radiation on an event by event basis and of initial-final state interference.

VALUE	EVTS	DOCUMENT ID	TECN	COMMENT
-0.0366 ± 0.0010 OUR FIT				
-0.0365 ± 0.0023	151.5K	1 ABBIENDI	01o OPAL	$E_{cm}^{ee} = 88-94$ GeV
-0.0384 ± 0.0026	103.0k	2 ACCIARRI	00c L3	$E_{cm}^{ee} = 88-94$ GeV
-0.0361 ± 0.0068		BARATE	00c ALEP	$E_{cm}^{ee} = 88-94$ GeV

- ABBIENDI 01o use their measurement of the τ polarization in addition to the lineshape and forward-backward lepton asymmetries.
- ACCIARRI 00c use their measurement of the τ polarization in addition to forward-backward lepton asymmetries.

VALUE	EVTS	DOCUMENT ID	TECN	COMMENT
-0.03783 ± 0.00041 OUR FIT				
-0.0358 ± 0.0014	471.3K	1 ABBIENDI	01o OPAL	$E_{cm}^{ee} = 88-94$ GeV
-0.0397 ± 0.0020	379.4k	2 ABREU	00f DLPH	$E_{cm}^{ee} = 88-94$ GeV
-0.0397 ± 0.0017	340.8k	3 ACCIARRI	00c L3	$E_{cm}^{ee} = 88-94$ GeV
-0.0383 ± 0.0018	500k	BARATE	00c ALEP	$E_{cm}^{ee} = 88-94$ GeV

- ABBIENDI 01o use their measurement of the τ polarization in addition to the lineshape and forward-backward lepton asymmetries.
- Using forward-backward lepton asymmetries.
- ACCIARRI 00c use their measurement of the τ polarization in addition to forward-backward lepton asymmetries.

VALUE	EVTS	DOCUMENT ID	TECN	COMMENT
0.266 ± 0.034 OUR AVERAGE				
0.270 ± 0.037		1 ANDREEV	18A H1	$e^\pm p$
0.201 ± 0.112	156k	2 ABAZOV	11D D0	$E_{cm}^{p\bar{p}} = 1.97$ TeV
$0.24 \pm 0.28 \pm 0.11$		3 LEP-SLC	06	$E_{cm}^{ee} = 88-94$ GeV
$0.399 \pm 0.152 \pm 0.188$	5026	4 ACOSTA	05M CDF	$E_{cm}^{p\bar{p}} = 1.96$ TeV

• • • We do not use the following data for averages, fits, limits, etc. • • •

$0.14 \pm 0.09 \pm 0.09$		5 ABRAMOWICZ16A	ZEUS	
$0.144 \pm 0.066 \pm 0.058$		6 ABT	16	
0.27 ± 0.13	1500	7 AKTAS	06 H1	$e^\pm p \rightarrow \mathcal{P}_e(\nu_e)X$, $\sqrt{s} \approx 300$ GeV

- ANDREEV 18A obtain this result in a combined electroweak and QCD analysis using all deep-inelastic e^+p and e^-p neutral current and charged current scattering cross sections published by the H1 Collaboration, including data with longitudinally polarized lepton beams.
- ABAZOV 11D study $p\bar{p} \rightarrow Z/\gamma^* e^+e^-$ events using 5 fb⁻¹ data at $\sqrt{s} = 1.96$ TeV. The candidate events are selected by requiring two isolated electromagnetic showers with $E_T > 25$ GeV, at least one electron in the central region and the di-electron mass in the range 50–1000 GeV. From the forward-backward asymmetry, determined as a function of the di-electron mass, they derive the axial and vector couplings of the u - and d -quarks and the value of $\sin^2\theta_{eff}^l = 0.2309 \pm 0.0008(\text{stat}) \pm 0.0006(\text{syst})$.
- LEP-SLC 06 is a combination of the results from LEP and SLC experiments using light quark tagging. s - and d -quark couplings are assumed to be identical.
- ACOSTA 05M determine the forward-backward asymmetry of e^+e^- pairs produced via $q\bar{q} \rightarrow Z/\gamma^* \rightarrow e^+e^-$ in 15 M(e^+e^-) effective mass bins ranging from 40 GeV to 600 GeV. These results are used to obtain the vector and axial-vector couplings of the Z to the light quarks, assuming the electron couplings are as predicted by the Standard Model. Higher order radiative corrections have not been taken into account.
- ABRAMOWICZ 16A determine the Z⁰ couplings to u - and d -quarks using the ZEUS polarised data for Run II together with the unpolarised data from both ZEUS and H1 Collaborations for Run I and unpolarised H1 data from Run II.
- ABT 16 determine the Z⁰ couplings to u - and d -quarks using the same techniques and data as ABRAMOWICZ 16A but additionally use the published H1 polarised data.
- AKTAS 06 fit the neutral current ($1.5 \leq Q^2 \leq 30,000$ GeV²) and charged current ($1.5 \leq Q^2 \leq 15,000$ GeV²) differential cross sections. In the determination of the u -quark couplings the electron and d -quark couplings are fixed to their standard model values.

VALUE	EVTS	DOCUMENT ID	TECN	COMMENT
$-0.38 \pm 0.04 \pm 0.05$ OUR AVERAGE				
-0.488 ± 0.092		1 ANDREEV	18A H1	$e^\pm p$
-0.351 ± 0.251	156k	2 ABAZOV	11D D0	$E_{cm}^{p\bar{p}} = 1.97$ TeV
$-0.33 \pm 0.05 \pm 0.07$		3 LEP-SLC	06	$E_{cm}^{ee} = 88-94$ GeV
$-0.226 \pm 0.635 \pm 0.290$	5026	4 ACOSTA	05M CDF	$E_{cm}^{p\bar{p}} = 1.96$ TeV

• • • We do not use the following data for averages, fits, limits, etc. • • •

$-0.41 \pm 0.25 \pm 0.20$		5 ABRAMOWICZ16A	ZEUS	
$-0.503 \pm 0.171 \pm 0.103$		6 ABT	16	
-0.33 ± 0.33	1500	7 AKTAS	06 H1	$e^\pm p \rightarrow \mathcal{P}_e(\nu_e)X$, $\sqrt{s} \approx 300$ GeV

- ANDREEV 18A obtain this result in a combined electroweak and QCD analysis using all deep-inelastic e^+p and e^-p neutral current and charged current scattering cross sections published by the H1 Collaboration, including data with longitudinally polarized lepton beams.
- ABAZOV 11D study $p\bar{p} \rightarrow Z/\gamma^* e^+e^-$ events using 5 fb⁻¹ data at $\sqrt{s} = 1.96$ TeV. The candidate events are selected by requiring two isolated electromagnetic showers with $E_T > 25$ GeV, at least one electron in the central region and the di-electron mass in the range 50–1000 GeV. From the forward-backward asymmetry, determined as a function of the di-electron mass, they derive the axial and vector couplings of the u - and d -quarks and the value of $\sin^2\theta_{eff}^l = 0.2309 \pm 0.0008(\text{stat}) \pm 0.0006(\text{syst})$.
- LEP-SLC 06 is a combination of the results from LEP and SLC experiments using light quark tagging. s - and d -quark couplings are assumed to be identical.
- ACOSTA 05M determine the forward-backward asymmetry of e^+e^- pairs produced via $q\bar{q} \rightarrow Z/\gamma^* \rightarrow e^+e^-$ in 15 M(e^+e^-) effective mass bins ranging from 40 GeV to 600 GeV. These results are used to obtain the vector and axial-vector couplings of the Z to the light quarks, assuming the electron couplings are as predicted by the Standard Model. Higher order radiative corrections have not been taken into account.
- ABRAMOWICZ 16A determine the Z⁰ couplings to u - and d -quarks using the ZEUS polarised data for Run II together with the unpolarised data from both ZEUS and H1 Collaborations for Run I and unpolarised H1 data from Run II.
- ABT 16 determine the Z⁰ couplings to u - and d -quarks using the same techniques and data as ABRAMOWICZ 16A but additionally use the published H1 polarised data.
- AKTAS 06 fit the neutral current ($1.5 \leq Q^2 \leq 30,000$ GeV²) and charged current ($1.5 \leq Q^2 \leq 15,000$ GeV²) differential cross sections. In the determination of the d -quark couplings the electron and u -quark couplings are fixed to their standard model values.

Z AXIAL-VECTOR COUPLINGS

These quantities are the effective axial-vector couplings of the Z to charged leptons and quarks. Their magnitude is derived from a measurement of the Z lineshape and the forward-backward lepton asymmetries as a function of energy around the Z mass. The relative sign among the vector to axial-vector couplings is obtained from a measurement of the Z asymmetry parameters, A_e , A_μ , and A_τ . By convention the sign of g_A^e is fixed to be negative (and opposite to that of g^{V_e} obtained using ν_e scattering measurements). For the light quarks, the sign of the couplings is assigned consistently with this assumption. The LEP/SLD-based fit values quoted below correspond to global nine- or five-parameter fits to lineshape, lepton forward-backward asymmetry, and A_e , A_μ , and A_τ measurements. See

Gauge & Higgs Boson Particle Listings

Z

the note "The Z boson" and ref. LEP-SLC 06 for details. Where $p\bar{p}$ and ep data is quoted, OUR FIT value corresponds to a weighted average of this with the LEP/SLD fit result.

 g_A^e

VALUE	EVTS	DOCUMENT ID	TECN	COMMENT
-0.50111 ± 0.00035 OUR FIT				
-0.528 ± 0.123 ± 0.059	5026	1 ACOSTA	05M CDF	$E_{cm}^{p\bar{p}} = 1.96$ TeV
-0.50062 ± 0.00062	137.0K	2 ABBIENDI	01o OPAL	$E_{cm}^{ee} = 88-94$ GeV
-0.5015 ± 0.0007	124.4k	3 ACCIARRI	00c L3	$E_{cm}^{ee} = 88-94$ GeV
-0.50166 ± 0.00057		BARATE	00c ALEP	$E_{cm}^{ee} = 88-94$ GeV
-0.4977 ± 0.0045		4 ABE	95J SLD	$E_{cm}^{ee} = 91.31$ GeV

¹ ACOSTA 05M determine the forward-backward asymmetry of e^+e^- pairs produced via $q\bar{q} \rightarrow Z/\gamma^* \rightarrow e^+e^-$ in 15 M(e^+e^-) effective mass bins ranging from 40 GeV to 600 GeV. These results are used to obtain the vector and axial-vector couplings of the Z to e^+e^- , assuming the quark couplings are as predicted by the standard model. Higher order radiative corrections have not been taken into account.

² ABBIENDI 01o use their measurement of the τ polarization in addition to the lineshape and forward-backward lepton asymmetries.

³ ACCIARRI 00c use their measurement of the τ polarization in addition to forward-backward lepton asymmetries.

⁴ ABE 95J obtain this result combining polarized Bhabha results with the A_{FB} measurement of ABE 94c. The Bhabha results alone give $-0.4968 \pm 0.0039 \pm 0.0027$.

 g_A^{μ}

VALUE	EVTS	DOCUMENT ID	TECN	COMMENT
-0.50120 ± 0.00054 OUR FIT				
-0.50117 ± 0.00099	182.8K	1 ABBIENDI	01o OPAL	$E_{cm}^{ee} = 88-94$ GeV
-0.5009 ± 0.0014	113.4k	2 ACCIARRI	00c L3	$E_{cm}^{ee} = 88-94$ GeV
-0.50046 ± 0.00093		BARATE	00c ALEP	$E_{cm}^{ee} = 88-94$ GeV
• • • We do not use the following data for averages, fits, limits, etc. • • •				
-0.520 ± 0.015	66143	3 ABBIENDI	01k OPAL	$E_{cm}^{ee} = 89-93$ GeV

¹ ABBIENDI 01o use their measurement of the τ polarization in addition to the lineshape and forward-backward lepton asymmetries.

² ACCIARRI 00c use their measurement of the τ polarization in addition to forward-backward lepton asymmetries.

³ ABBIENDI 01k obtain this from an angular analysis of the muon pair asymmetry which takes into account effects of initial state radiation on an event by event basis and of initial-final state interference.

 g_A^{τ}

VALUE	EVTS	DOCUMENT ID	TECN	COMMENT
-0.50204 ± 0.00064 OUR FIT				
-0.50165 ± 0.00124	151.5K	1 ABBIENDI	01o OPAL	$E_{cm}^{ee} = 88-94$ GeV
-0.5023 ± 0.0017	103.0K	2 ACCIARRI	00c L3	$E_{cm}^{ee} = 88-94$ GeV
-0.50216 ± 0.00100		BARATE	00c ALEP	$E_{cm}^{ee} = 88-94$ GeV

¹ ABBIENDI 01o use their measurement of the τ polarization in addition to the lineshape and forward-backward lepton asymmetries.

² ACCIARRI 00c use their measurement of the τ polarization in addition to forward-backward lepton asymmetries.

 g_A^l

VALUE	EVTS	DOCUMENT ID	TECN	COMMENT
-0.50123 ± 0.00026 OUR FIT				
-0.50089 ± 0.00045	471.3K	1 ABBIENDI	01o OPAL	$E_{cm}^{ee} = 88-94$ GeV
-0.5007 ± 0.0005	379.4k	ABREU	00f DLPH	$E_{cm}^{ee} = 88-94$ GeV
-0.50153 ± 0.00053	340.8k	2 ACCIARRI	00c L3	$E_{cm}^{ee} = 88-94$ GeV
-0.50150 ± 0.00046	500k	BARATE	00c ALEP	$E_{cm}^{ee} = 88-94$ GeV

¹ ABBIENDI 01o use their measurement of the τ polarization in addition to the lineshape and forward-backward lepton asymmetries.

² ACCIARRI 00c use their measurement of the τ polarization in addition to forward-backward lepton asymmetries.

 g_A^u

VALUE	EVTS	DOCUMENT ID	TECN	COMMENT
0.519 ± 0.028 OUR AVERAGE				
0.548 ± 0.036		1 ANDREEV	18A H1	$e^\pm p$
0.501 ± 0.110	156k	2 ABAZOV	11D D0	$E_{cm}^{p\bar{p}} = 1.97$ TeV
0.47 ± 0.05 -0.33		3 LEP-SLC	06	$E_{cm}^{ee} = 88-94$ GeV
0.441 ± 0.207 -0.173 ± 0.067	5026	4 ACOSTA	05M CDF	$E_{cm}^{p\bar{p}} = 1.96$ TeV
• • • We do not use the following data for averages, fits, limits, etc. • • •				
0.50 ± 0.12 -0.05		5 ABRAMOWICZ16A	ZEUS	
0.532 ± 0.107 -0.063		6 ABT	16	
0.57 ± 0.08	1500	7 AKTAS	06 H1	$e^\pm p \rightarrow \bar{\nu}_e(\nu_e)X$, $\sqrt{s} \approx 300$ GeV

¹ ANDREEV 18A obtain this result in a combined electroweak and QCD analysis using all deep-inelastic e^+p and e^-p neutral current and charged current scattering cross sections published by the H1 Collaboration, including data with longitudinally polarized lepton beams.

² ABAZOV 11D study $p\bar{p} \rightarrow Z/\gamma^* e^+e^-$ events using 5 fb⁻¹ data at $\sqrt{s} = 1.96$ TeV. The candidate events are selected by requiring two isolated electromagnetic showers with $E_T > 25$ GeV, at least one electron in the central region and the di-electron mass in the range 50–1000 GeV. From the forward-backward asymmetry, determined as a function of the di-electron mass, they derive the axial and vector couplings of the u - and d -quarks and the value of $\sin^2\theta_{eff}^l = 0.2309 \pm 0.0008(\text{stat}) \pm 0.0006(\text{syst})$.

³ LEP-SLC 06 is a combination of the results from LEP and SLC experiments using light quark tagging. s - and d -quark couplings are assumed to be identical.

⁴ ACOSTA 05M determine the forward-backward asymmetry of e^+e^- pairs produced via $q\bar{q} \rightarrow Z/\gamma^* \rightarrow e^+e^-$ in 15 M(e^+e^-) effective mass bins ranging from 40 GeV to 600 GeV. These results are used to obtain the vector and axial-vector couplings of the Z to the light quarks, assuming the electron couplings are as predicted by the Standard Model. Higher order radiative corrections have not been taken into account.

⁵ ABRAMOWICZ16A determine the Z^0 couplings to u - and d -quarks using the ZEUS polarised data from Run II together with the unpolarised data from both ZEUS and H1 Collaborations for Run I and unpolarised H1 data from Run II.

⁶ ABT 16 determine the Z^0 couplings to u - and d -quarks using the same techniques and data as ABRAMOWICZ16A but additionally use the published H1 polarised data.

⁷ AKTAS 06 fit the neutral current ($1.5 \leq Q^2 \leq 30,000$ GeV²) and charged current ($1.5 \leq Q^2 \leq 15,000$ GeV²) differential cross sections. In the determination of the d -quark couplings the electron and u -quark couplings are fixed to their standard model values.

¹ ANDREEV 18A obtain this result in a combined electroweak and QCD analysis using all deep-inelastic e^+p and e^-p neutral current and charged current scattering cross sections published by the H1 Collaboration, including data with longitudinally polarized lepton beams.

² ABAZOV 11D study $p\bar{p} \rightarrow Z/\gamma^* e^+e^-$ events using 5 fb⁻¹ data at $\sqrt{s} = 1.96$ TeV. The candidate events are selected by requiring two isolated electromagnetic showers with $E_T > 25$ GeV, at least one electron in the central region and the di-electron mass in the range 50–1000 GeV. From the forward-backward asymmetry, determined as a function of the di-electron mass, they derive the axial and vector couplings of the u - and d -quarks and the value of $\sin^2\theta_{eff}^l = 0.2309 \pm 0.0008(\text{stat}) \pm 0.0006(\text{syst})$.

³ LEP-SLC 06 is a combination of the results from LEP and SLC experiments using light quark tagging. s - and d -quark couplings are assumed to be identical.

⁴ ACOSTA 05M determine the forward-backward asymmetry of e^+e^- pairs produced via $q\bar{q} \rightarrow Z/\gamma^* \rightarrow e^+e^-$ in 15 M(e^+e^-) effective mass bins ranging from 40 GeV to 600 GeV. These results are used to obtain the vector and axial-vector couplings of the Z to the light quarks, assuming the electron couplings are as predicted by the Standard Model. Higher order radiative corrections have not been taken into account.

⁵ ABRAMOWICZ16A determine the Z^0 couplings to u - and d -quarks using the ZEUS polarised data from Run II together with the unpolarised data from both ZEUS and H1 Collaborations for Run I and unpolarised H1 data from Run II.

⁶ ABT 16 determine the Z^0 couplings to u - and d -quarks using the same techniques and data as ABRAMOWICZ16A but additionally use the published H1 polarised data.

⁷ AKTAS 06 fit the neutral current ($1.5 \leq Q^2 \leq 30,000$ GeV²) and charged current ($1.5 \leq Q^2 \leq 15,000$ GeV²) differential cross sections. In the determination of the u -quark couplings the electron and d -quark couplings are fixed to their standard model values.

 g_A^d

VALUE	EVTS	DOCUMENT ID	TECN	COMMENT
-0.527 ± 0.040 OUR AVERAGE				
-0.619 ± 0.108		1 ANDREEV	18A H1	$e^\pm p$
-0.497 ± 0.165	156k	2 ABAZOV	11D D0	$E_{cm}^{p\bar{p}} = 1.97$ TeV
-0.52 ± 0.05 -0.03		3 LEP-SLC	06	$E_{cm}^{ee} = 88-94$ GeV
-0.016 ± 0.346 -0.536 ± 0.091	5026	4 ACOSTA	05M CDF	$E_{cm}^{p\bar{p}} = 1.96$ TeV
• • • We do not use the following data for averages, fits, limits, etc. • • •				
-0.56 ± 0.41 -0.15		5 ABRAMOWICZ16A	ZEUS	
-0.409 ± 0.373 -0.213		6 ABT	16	
-0.80 ± 0.24	1500	7 AKTAS	06 H1	$e^\pm p \rightarrow \bar{\nu}_e(\nu_e)X$, $\sqrt{s} \approx 300$ GeV

¹ ANDREEV 18A obtain this result in a combined electroweak and QCD analysis using all deep-inelastic e^+p and e^-p neutral current and charged current scattering cross sections published by the H1 Collaboration, including data with longitudinally polarized lepton beams.

² ABAZOV 11D study $p\bar{p} \rightarrow Z/\gamma^* e^+e^-$ events using 5 fb⁻¹ data at $\sqrt{s} = 1.96$ TeV. The candidate events are selected by requiring two isolated electromagnetic showers with $E_T > 25$ GeV, at least one electron in the central region and the di-electron mass in the range 50–1000 GeV. From the forward-backward asymmetry, determined as a function of the di-electron mass, they derive the axial and vector couplings of the u - and d -quarks and the value of $\sin^2\theta_{eff}^l = 0.2309 \pm 0.0008(\text{stat}) \pm 0.0006(\text{syst})$.

³ LEP-SLC 06 is a combination of the results from LEP and SLC experiments using light quark tagging. s - and d -quark couplings are assumed to be identical.

⁴ ACOSTA 05M determine the forward-backward asymmetry of e^+e^- pairs produced via $q\bar{q} \rightarrow Z/\gamma^* \rightarrow e^+e^-$ in 15 M(e^+e^-) effective mass bins ranging from 40 GeV to 600 GeV. These results are used to obtain the vector and axial-vector couplings of the Z to the light quarks, assuming the electron couplings are as predicted by the Standard Model. Higher order radiative corrections have not been taken into account.

⁵ ABRAMOWICZ16A determine the Z^0 couplings to u - and d -quarks using the ZEUS polarised data from Run II together with the unpolarised data from both ZEUS and H1 Collaborations for Run I and unpolarised H1 data from Run II.

⁶ ABT 16 determine the Z^0 couplings to u - and d -quarks using the same techniques and data as ABRAMOWICZ16A but additionally use the published H1 polarised data.

⁷ AKTAS 06 fit the neutral current ($1.5 \leq Q^2 \leq 30,000$ GeV²) and charged current ($1.5 \leq Q^2 \leq 15,000$ GeV²) differential cross sections. In the determination of the d -quark couplings the electron and u -quark couplings are fixed to their standard model values.

Z COUPLINGS TO NEUTRAL LEPTONS

Averaging over neutrino species, the invisible Z decay width determines the effective neutrino coupling $g^{\nu e}$. For $g^{\nu e}$ and $g^{\nu \mu}$, $\nu_e e$ and $\nu_\mu e$ scattering results are combined with g_A^e and g_V^e measurements at the Z mass to obtain $g^{\nu e}$ and $g^{\nu \mu}$ following NOVIKOV 93c.

 $g^{\nu e}$

VALUE	DOCUMENT ID	COMMENT
0.50076 ± 0.00076	1 LEP-SLC 06	$E_{cm}^{ee} = 88-94$ GeV

¹ From invisible Z-decay width.

 $g^{\nu \mu}$

VALUE	DOCUMENT ID	TECN	COMMENT
0.528 ± 0.085	1 VILAIN 94	CHM2	From $\nu_\mu e$ and $\nu_e e$ scattering

¹ VILAIN 94 derive this value from their value of $g^{\nu \mu}$ and their ratio $g^{\nu e}/g^{\nu \mu} = 1.05 \pm 0.15$.

$g^{\nu\mu}$

VALUE	DOCUMENT ID	TECN	COMMENT
0.502 ± 0.017	1 VILAIN	94	CHM2 From $\nu_\mu e$ scattering

1 VILAIN 94 derive this value from their measurement of the couplings $g_A^{\nu\mu} = -0.503 \pm 0.017$ and $g_V^{\nu\mu} = -0.035 \pm 0.017$ obtained from $\nu_\mu e$ scattering. We have re-evaluated this value using the current PDG values for g_A^e and g_V^e .

Z ASYMMETRY PARAMETERS

For each fermion-antifermion pair coupling to the Z these quantities are defined as

$$A_f = \frac{2g_V^f g_A^f}{(g_V^f)^2 + (g_A^f)^2}$$

where g_V^f and g_A^f are the effective vector and axial-vector couplings. For their relation to the various lepton asymmetries see the note "The Z boson" and ref. LEP-SLC 06.

A_e Using polarized beams, this quantity can also be measured as $(\sigma_L - \sigma_R) / (\sigma_L + \sigma_R)$, where σ_L and σ_R are the e^+e^- production cross sections for Z bosons produced with left-handed and right-handed electrons respectively.

VALUE	EVTS	DOCUMENT ID	TECN	COMMENT
0.1515 ± 0.0019 OUR AVERAGE				
0.1454 ± 0.0108 ± 0.0036	144810	1 ABBIENDI	010 OPAL	$E_{cm}^{ee} = 88-94$ GeV
0.1516 ± 0.0021	559000	2 ABE	01B SLD	$E_{cm}^{ee} = 91.24$ GeV
0.1504 ± 0.0068 ± 0.0008		3 HEISTER	01 ALEP	$E_{cm}^{ee} = 88-94$ GeV
0.1382 ± 0.0116 ± 0.0005	105000	4 ABREU	00E DLPH	$E_{cm}^{ee} = 88-94$ GeV
0.1678 ± 0.0127 ± 0.0030	137092	5 ACCIARRI	98H L3	$E_{cm}^{ee} = 88-94$ GeV
0.162 ± 0.041 ± 0.014	89838	6 ABE	97 SLD	$E_{cm}^{ee} = 91.27$ GeV
0.202 ± 0.038 ± 0.008		7 ABE	95J SLD	$E_{cm}^{ee} = 91.31$ GeV

- 1 ABBIENDI 010 fit for A_e and A_τ from measurements of the τ polarization at varying τ production angles. The correlation between A_e and A_τ is less than 0.03.
- 2 ABE 01B use the left-right production and left-right forward-backward decay asymmetries in leptonic Z decays to obtain a value of 0.1544 ± 0.0060. This is combined with left-right production asymmetry measurement using hadronic Z decays (ABE 00B) to obtain the quoted value.
- 3 HEISTER 01 obtain this result fitting the τ polarization as a function of the polar production angle of the τ .
- 4 ABREU 00E obtain this result fitting the τ polarization as a function of the polar τ production angle. This measurement is a combination of different analyses (exclusive τ decay modes, inclusive hadronic 1-prong reconstruction, and a neural network analysis).
- 5 Derived from the measurement of forward-backward τ polarization asymmetry.
- 6 ABE 97 obtain this result from a measurement of the observed left-right charge asymmetry, $A_{LR}^{Obs} = 0.225 \pm 0.056 \pm 0.019$, in hadronic Z decays. If they combine this value of A_{LR}^{Obs} with their earlier measurement of A_{LR}^{Obs} they determine A_e to be 0.1574 ± 0.0197 ± 0.0067 independent of the beam polarization.
- 7 ABE 95J obtain this result from polarized Bhabha scattering.

A_μ This quantity is directly extracted from a measurement of the left-right forward-backward asymmetry in $\mu^+\mu^-$ production at SLC using a polarized electron beam. This double asymmetry eliminates the dependence on the Z-e-e coupling parameter A_e .

VALUE	EVTS	DOCUMENT ID	TECN	COMMENT
0.142 ± 0.015	16844	1 ABE	01B SLD	$E_{cm}^{ee} = 91.24$ GeV
• • • We do not use the following data for averages, fits, limits, etc. • • •				
0.153 ± 0.012	1.7M	2 AAD	15BT ATLS	$E_{cm}^{pp} = 7$ TeV

- 1 ABE 01B obtain this direct measurement using the left-right production and left-right forward-backward polar angle asymmetries in $\mu^+\mu^-$ decays of the Z boson obtained with a polarized electron beam.
- 2 AAD 15BT study $pp \rightarrow Z \rightarrow \ell^+\ell^-$ events where ℓ is an electron or a muon in the dilepton mass region 70–1000 GeV. The background in the Z peak region is estimated to be < 1% for the muon channel. The muon asymmetry parameter is derived from the measured forward-backward asymmetry assuming the value of the quark asymmetry parameter from the SM. For this reason it is not used in the average.

A_τ The LEP Collaborations derive this quantity from the measurement of the τ polarization in $Z \rightarrow \tau^+\tau^-$. The SLD Collaboration directly extracts this quantity from its measured left-right forward-backward asymmetry in $Z \rightarrow \tau^+\tau^-$ produced using a polarized e^- beam. This double asymmetry eliminates the dependence on the Z-e-e coupling parameter A_e .

VALUE	EVTS	DOCUMENT ID	TECN	COMMENT
0.143 ± 0.004 OUR AVERAGE				
0.1456 ± 0.0076 ± 0.0057	144810	1 ABBIENDI	010 OPAL	$E_{cm}^{ee} = 88-94$ GeV
0.136 ± 0.015	16083	2 ABE	01B SLD	$E_{cm}^{ee} = 91.24$ GeV
0.1451 ± 0.0052 ± 0.0029		3 HEISTER	01 ALEP	$E_{cm}^{ee} = 88-94$ GeV
0.1359 ± 0.0079 ± 0.0055	105000	4 ABREU	00E DLPH	$E_{cm}^{ee} = 88-94$ GeV
0.1476 ± 0.0088 ± 0.0062	137092	ACCIARRI	98H L3	$E_{cm}^{ee} = 88-94$ GeV

- 1 ABBIENDI 010 fit for A_e and A_τ from measurements of the τ polarization at varying τ production angles. The correlation between A_e and A_τ is less than 0.03.
- 2 ABE 01B obtain this direct measurement using the left-right production and left-right forward-backward polar angle asymmetries in $\tau^+\tau^-$ decays of the Z boson obtained with a polarized electron beam.
- 3 HEISTER 01 obtain this result fitting the τ polarization as a function of the polar production angle of the τ .
- 4 ABREU 00E obtain this result fitting the τ polarization as a function of the polar τ production angle. This measurement is a combination of different analyses (exclusive τ decay modes, inclusive hadronic 1-prong reconstruction, and a neural network analysis).

A_S The SLD Collaboration directly extracts this quantity by a simultaneous fit to four measured s-quark polar angle distributions corresponding to two states of e^- polarization (positive and negative) and to the K^+K^- and $K^\pm K_S^0$ strange particle tagging modes in the hadronic final states.

VALUE	EVTS	DOCUMENT ID	TECN	COMMENT
0.895 ± 0.066 ± 0.062	2870	1 ABE	00D SLD	$E_{cm}^{ee} = 91.2$ GeV

- 1 ABE 00D tag $Z \rightarrow s\bar{s}$ events by an absence of B or D hadrons and the presence in each hemisphere of a high momentum K^\pm or K_S^0 .

A_C This quantity is directly extracted from a measurement of the left-right forward-backward asymmetry in $c\bar{c}$ production at SLC using polarized electron beam. This double asymmetry eliminates the dependence on the Z-e-e coupling parameter A_e . OUR FIT is obtained by a simultaneous fit to several c- and b-quark measurements as explained in the note "The Z boson" and ref. LEP-SLC 06.

VALUE	EVTS	DOCUMENT ID	TECN	COMMENT
0.670 ± 0.027 OUR FIT				
0.6712 ± 0.0224 ± 0.0157		1 ABE	05 SLD	$E_{cm}^{ee} = 91.24$ GeV
• • • We do not use the following data for averages, fits, limits, etc. • • •				
0.583 ± 0.055 ± 0.055		2 ABE	02G SLD	$E_{cm}^{ee} = 91.24$ GeV
0.688 ± 0.041		3 ABE	01c SLD	$E_{cm}^{ee} = 91.25$ GeV

- 1 ABE 05 use hadronic Z decays collected during 1996–98 to obtain an enriched sample of $c\bar{c}$ events tagging on the invariant mass of reconstructed secondary decay vertices. The charge of the underlying c-quark is obtained with an algorithm that takes into account the net charge of the vertex as well as the charge of tracks emanating from the vertex and identified as kaons. This yields (9970 events) $A_C = 0.6747 \pm 0.0290 \pm 0.0233$. Taking into account all correlations with earlier results reported in ABE 02G and ABE 01c, they obtain the quoted overall SLD result.
- 2 ABE 02G tag b and c quarks through their semileptonic decays into electrons and muons. A maximum likelihood fit is performed to extract simultaneously A_b and A_c .
- 3 ABE 01c tag $Z \rightarrow c\bar{c}$ events using two techniques: exclusive reconstruction of D^{*+}, D^+ and D^0 mesons and the soft pion tag for $D^{*+} \rightarrow D^0\pi^+$. The large background from D mesons produced in $b\bar{b}$ events is separated efficiently from the signal using precision vertex information. When combining the A_C values from these two samples, care is taken to avoid double counting of events common to the two samples, and common systematic errors are properly taken into account.

A_b This quantity is directly extracted from a measurement of the left-right forward-backward asymmetry in $b\bar{b}$ production at SLC using polarized electron beam. This double asymmetry eliminates the dependence on the Z-e-e coupling parameter A_e . OUR FIT is obtained by a simultaneous fit to several c- and b-quark measurements as explained in the note "The Z boson" and ref. LEP-SLC 06.

VALUE	EVTS	DOCUMENT ID	TECN	COMMENT
0.923 ± 0.020 OUR FIT				
0.9170 ± 0.0147 ± 0.0145		1 ABE	05 SLD	$E_{cm}^{ee} = 91.24$ GeV
• • • We do not use the following data for averages, fits, limits, etc. • • •				
0.907 ± 0.020 ± 0.024	48028	2 ABE	03F SLD	$E_{cm}^{ee} = 91.24$ GeV
0.919 ± 0.030 ± 0.024		3 ABE	02G SLD	$E_{cm}^{ee} = 91.24$ GeV
0.855 ± 0.088 ± 0.102	7473	4 ABE	99L SLD	$E_{cm}^{ee} = 91.27$ GeV

- 1 ABE 05 use hadronic Z decays collected during 1996–98 to obtain an enriched sample of $b\bar{b}$ events tagging on the invariant mass of reconstructed secondary decay vertices. The charge of the underlying b-quark is obtained with an algorithm that takes into account the net charge of the vertex as well as the charge of tracks emanating from the vertex and identified as kaons. This yields (25917 events) $A_b = 0.9173 \pm 0.0184 \pm 0.0173$. Taking into account all correlations with earlier results reported in ABE 03F, ABE 02G and ABE 99L, they obtain the quoted overall SLD result.
- 2 ABE 03F obtain an enriched sample of $b\bar{b}$ events tagging on the invariant mass of a 3-dimensional topologically reconstructed secondary decay. The charge of the underlying b quark is obtained using a self-calibrating track-charge method. For the 1996–1998 data sample they measure $A_b = 0.906 \pm 0.022 \pm 0.023$. The value quoted here is obtained combining the above with the result of ABE 981 (1993–1995 data sample).
- 3 ABE 02G tag b and c quarks through their semileptonic decays into electrons and muons. A maximum likelihood fit is performed to extract simultaneously A_b and A_c .
- 4 ABE 99L obtain an enriched sample of $b\bar{b}$ events tagging with an inclusive vertex mass cut. For distinguishing b and \bar{b} quarks they use the charge of identified K^\pm .

TRANSVERSE SPIN CORRELATIONS IN $Z \rightarrow \tau^+\tau^-$

The correlations between the transverse spin components of $\tau^+\tau^-$ produced in Z decays may be expressed in terms of the vector and axial-vector couplings:

$$C_{TT} = \frac{|g_A^\tau|^2 - |g_V^\tau|^2}{|g_A^\tau|^2 + |g_V^\tau|^2}$$

Gauge & Higgs Boson Particle Listings

Z

$$C_{TN} = -2 \frac{|g_A^\tau| |g_V^\tau|}{|g_A^\tau|^2 + |g_V^\tau|^2} \sin(\Phi_{g_V^\tau} - \Phi_{g_A^\tau})$$

C_{TT} refers to the transverse-transverse (within the collision plane) spin correlation and C_{TN} refers to the transverse-normal (to the collision plane) spin correlation.

The longitudinal τ polarization P_τ ($= -A_\tau$) is given by:

$$P_\tau = -2 \frac{|g_A^\tau| |g_V^\tau|}{|g_A^\tau|^2 + |g_V^\tau|^2} \cos(\Phi_{g_V^\tau} - \Phi_{g_A^\tau})$$

Here Φ is the phase and the phase difference $\Phi_{g_V^\tau} - \Phi_{g_A^\tau}$ can be obtained using both the measurements of C_{TN} and P_τ .

C_{TT}				
VALUE	EVTS	DOCUMENT ID	TECN	COMMENT
1.01 ± 0.12 OUR AVERAGE				
0.87 ± 0.20 ^{+0.10} _{-0.12}	9.1k	ABREU	97G DLPH	$E_{cm}^{ee} = 91.2$ GeV
1.06 ± 0.13 ± 0.05	120k	BARATE	97D ALEP	$E_{cm}^{ee} = 91.2$ GeV

C_{TN}				
VALUE	EVTS	DOCUMENT ID	TECN	COMMENT
0.08 ± 0.13 ± 0.04				
	120k	1 BARATE	97D ALEP	$E_{cm}^{ee} = 91.2$ GeV

¹ BARATE 97D combine their value of C_{TN} with the world average $P_\tau = -0.140 \pm 0.007$ to obtain $\tan(\Phi_{g_V^\tau} - \Phi_{g_A^\tau}) = -0.57 \pm 0.97$.

FORWARD-BACKWARD $e^+e^- \rightarrow f\bar{f}$ CHARGE ASYMMETRIES

These asymmetries are experimentally determined by tagging the respective lepton or quark flavor in e^+e^- interactions. Details of heavy flavor (c - or b -quark) tagging at LEP are described in the note on "The Z boson" and ref. LEP-SLC 06. The Standard Model predictions for LEP data have been (re)computed using the ZFITTER package (version 6.36) with input parameters $M_Z = 91.187$ GeV, $M_{top} = 174.3$ GeV, $M_{Higgs} = 150$ GeV, $\alpha_s = 0.119$, $\alpha^{(5)}(M_Z) = 1/128.877$ and the Fermi constant $G_F = 1.16637 \times 10^{-5} \text{ GeV}^{-2}$ (see the note on "The Z boson" for references). For non-LEP data the Standard Model predictions are as given by the authors of the respective publications.

$A_{FB}^{(0,e)}$ CHARGE ASYMMETRY IN $e^+e^- \rightarrow e^+e^-$

OUR FIT is obtained using the fit procedure and correlations as determined by the LEP Electroweak Working Group (see the note "The Z boson" and ref. LEP-SLC 06). For the Z peak, we report the pole asymmetry defined by $(3/4)A_e^2$ as determined by the nine-parameter fit to cross-section and lepton forward-backward asymmetry data.

ASYMMETRY (%)	STD. MODEL	\sqrt{s} (GeV)	DOCUMENT ID	TECN
1.45 ± 0.25 OUR FIT				
0.89 ± 0.44	1.57	91.2	¹ ABBIENDI 01A	OPAL
1.71 ± 0.49	1.57	91.2	ABREU 00F	DLPH
1.06 ± 0.58	1.57	91.2	ACCIARRI 00c	L3
1.88 ± 0.34	1.57	91.2	² BARATE 00c	ALEP

¹ ABBIENDI 01A error includes approximately 0.38 due to statistics, 0.16 due to event selection systematics, and 0.18 due to the theoretical uncertainty in t -channel prediction.
² BARATE 00c error includes approximately 0.31 due to statistics, 0.06 due to experimental systematics, and 0.13 due to the theoretical uncertainty in t -channel prediction.

$A_{FB}^{(0,\mu)}$ CHARGE ASYMMETRY IN $e^+e^- \rightarrow \mu^+\mu^-$

OUR FIT is obtained using the fit procedure and correlations as determined by the LEP Electroweak Working Group (see the note "The Z boson" and ref. LEP-SLC 06). For the Z peak, we report the pole asymmetry defined by $(3/4)A_e A_\mu$ as determined by the nine-parameter fit to cross-section and lepton forward-backward asymmetry data.

ASYMMETRY (%)	STD. MODEL	\sqrt{s} (GeV)	DOCUMENT ID	TECN
1.69 ± 0.13 OUR FIT				
1.59 ± 0.23	1.57	91.2	¹ ABBIENDI 01A	OPAL
1.65 ± 0.25	1.57	91.2	ABREU 00F	DLPH
1.88 ± 0.33	1.57	91.2	ACCIARRI 00c	L3
1.71 ± 0.24	1.57	91.2	² BARATE 00c	ALEP

• • • We do not use the following data for averages, fits, limits, etc. • • •

9 ± 30	-1.3	20	³ ABREU 95M	DLPH
7 ± 26	-8.3	40	³ ABREU 95M	DLPH
-11 ± 33	-24.1	57	³ ABREU 95M	DLPH
-62 ± 17	-44.6	69	³ ABREU 95M	DLPH
-56 ± 10	-63.5	79	³ ABREU 95M	DLPH
-13 ± 5	-34.4	87.5	³ ABREU 95M	DLPH
-29.0 ± 5.0 ± 4.8 ± 0.5	-32.1	56.9	⁴ ABE 90I	VNS
-9.9 ± 1.5 ± 0.5	-9.2	35	HEGNER 90	JADE
0.05 ± 0.22	0.026	91.14	⁵ ABRAMS 89D	MRK2
-43.4 ± 17.0	-24.9	52.0	⁶ BACALA 89	AMY
-11.0 ± 16.5	-29.4	55.0	⁶ BACALA 89	AMY

-30.0 ± 12.4	-31.2	56.0	⁶ BACALA 89	AMY
-46.2 ± 14.9	-33.0	57.0	⁶ BACALA 89	AMY
-29 ± 13	-25.9	53.3	ADACHI 88c	TOPZ
+ 5.3 ± 5.0 ± 0.5	-1.2	14.0	ADEVA 88	MRKJ
-10.4 ± 1.3 ± 0.5	-8.6	34.8	ADEVA 88	MRKJ
-12.3 ± 5.3 ± 0.5	-10.7	38.3	ADEVA 88	MRKJ
-15.6 ± 3.0 ± 0.5	-14.9	43.8	ADEVA 88	MRKJ
-1.0 ± 6.0	-1.2	13.9	BRAUNSCH... 88D	TASS
-9.1 ± 2.3 ± 0.5	-8.6	34.5	BRAUNSCH... 88D	TASS
-10.6 ± 2.2 ± 2.3 ± 0.5	-8.9	35.0	BRAUNSCH... 88D	TASS
-17.6 ± 4.4 ± 4.3 ± 0.5	-15.2	43.6	BRAUNSCH... 88D	TASS
-4.8 ± 6.5 ± 1.0	-11.5	39	BEHREND 87c	CELL
-18.8 ± 4.5 ± 1.0	-15.5	44	BEHREND 87c	CELL
+ 2.7 ± 4.9	-1.2	13.9	BARTEL 86c	JADE
-11.1 ± 1.8 ± 1.0	-8.6	34.4	BARTEL 86c	JADE
-17.3 ± 4.8 ± 1.0	-13.7	41.5	BARTEL 86c	JADE
-22.8 ± 5.1 ± 1.0	-16.6	44.8	BARTEL 86c	JADE
-6.3 ± 0.8 ± 0.2	-6.3	29	ASH 85	MAC
-4.9 ± 1.5 ± 0.5	-5.9	29	DERRICK 85	HRS
-7.1 ± 1.7	-5.7	29	LEVI 83	MRK2
-16.1 ± 3.2	-9.2	34.2	BRANDELIK 82c	TASS

¹ ABBIENDI 01A error is almost entirely on account of statistics.
² BARATE 00c error is almost entirely on account of statistics.
³ ABREU 95M perform this measurement using radiative muon-pair events associated with high-energy isolated photons.
⁴ ABE 90I measurements in the range $50 \leq \sqrt{s} \leq 60.8$ GeV.
⁵ ABRAMS 89D asymmetry includes both $9 \mu^+ \mu^-$ and $15 \tau^+ \tau^-$ events.
⁶ BACALA 89 systematic error is about 5%.

$A_{FB}^{(0,\tau)}$ CHARGE ASYMMETRY IN $e^+e^- \rightarrow \tau^+\tau^-$

OUR FIT is obtained using the fit procedure and correlations as determined by the LEP Electroweak Working Group (see the note "The Z boson" and ref. LEP-SLC 06). For the Z peak, we report the pole asymmetry defined by $(3/4)A_e A_\tau$ as determined by the nine-parameter fit to cross-section and lepton forward-backward asymmetry data.

ASYMMETRY (%)	STD. MODEL	\sqrt{s} (GeV)	DOCUMENT ID	TECN
1.88 ± 0.17 OUR FIT				
1.45 ± 0.30	1.57	91.2	¹ ABBIENDI 01A	OPAL
2.41 ± 0.37	1.57	91.2	ABREU 00F	DLPH
2.60 ± 0.47	1.57	91.2	ACCIARRI 00c	L3
1.70 ± 0.28	1.57	91.2	² BARATE 00c	ALEP

• • • We do not use the following data for averages, fits, limits, etc. • • •

-32.8 ± 6.4 ± 6.2 ± 1.5	-32.1	56.9	³ ABE 90I	VNS
-8.1 ± 2.0 ± 0.6	-9.2	35	HEGNER 90	JADE
-18.4 ± 19.2	-24.9	52.0	⁴ BACALA 89	AMY
-17.7 ± 26.1	-29.4	55.0	⁴ BACALA 89	AMY
-45.9 ± 16.6	-31.2	56.0	⁴ BACALA 89	AMY
-49.5 ± 18.0	-33.0	57.0	⁴ BACALA 89	AMY
-20 ± 14	-25.9	53.3	ADACHI 88c	TOPZ
-10.6 ± 3.1 ± 1.5	-8.5	34.7	ADEVA 88	MRKJ
-8.5 ± 6.6 ± 1.5	-15.4	43.8	ADEVA 88	MRKJ
-6.0 ± 2.5 ± 1.0	8.8	34.6	BARTEL 85F	JADE
-11.8 ± 4.6 ± 1.0	14.8	43.0	BARTEL 85F	JADE
-5.5 ± 1.2 ± 0.5	-0.063	29.0	FERNANDEZ 85	MAC
-4.2 ± 2.0	0.057	29	LEVI 83	MRK2
-10.3 ± 5.2	-9.2	34.2	BEHREND 82	CELL
-0.4 ± 6.6	-9.1	34.2	BRANDELIK 82c	TASS

¹ ABBIENDI 01A error includes approximately 0.26 due to statistics and 0.14 due to event selection systematics.
² BARATE 00c error includes approximately 0.26 due to statistics and 0.11 due to experimental systematics.
³ ABE 90I measurements in the range $50 \leq \sqrt{s} \leq 60.8$ GeV.
⁴ BACALA 89 systematic error is about 5%.

$A_{FB}^{(0,\ell)}$ CHARGE ASYMMETRY IN $e^+e^- \rightarrow \ell^+\ell^-$

For the Z peak, we report the pole asymmetry defined by $(3/4)A_e^2$ as determined by the five-parameter fit to cross-section and lepton forward-backward asymmetry data assuming lepton universality. For details see the note "The Z boson" and ref. LEP-SLC 06.

ASYMMETRY (%)	STD. MODEL	\sqrt{s} (GeV)	DOCUMENT ID	TECN
1.71 ± 0.10 OUR FIT				
1.45 ± 0.17	1.57	91.2	¹ ABBIENDI 01A	OPAL
1.87 ± 0.19	1.57	91.2	ABREU 00F	DLPH
1.92 ± 0.24	1.57	91.2	ACCIARRI 00c	L3
1.73 ± 0.16	1.57	91.2	² BARATE 00c	ALEP

¹ ABBIENDI 01A error includes approximately 0.15 due to statistics, 0.06 due to event selection systematics, and 0.03 due to the theoretical uncertainty in t -channel prediction.
² BARATE 00c error includes approximately 0.15 due to statistics, 0.04 due to experimental systematics, and 0.02 due to the theoretical uncertainty in t -channel prediction.

$A_{FB}^{(0,u)}$ CHARGE ASYMMETRY IN $e^+ e^- \rightarrow u\bar{u}$

ASYMMETRY (%)	STD. MODEL	\sqrt{s} (GeV)	DOCUMENT ID	TECN
4.0 ± 6.7 ± 2.8	7.2	91.2	¹ ACKERSTAFF 97T	OPAL

¹ ACKERSTAFF 97T measure the forward-backward asymmetry of various fast hadrons made of light quarks. Then using SU(2) isospin symmetry and flavor independence for down and strange quarks authors solve for the different quark types.

$A_{FB}^{(0,s)}$ CHARGE ASYMMETRY IN $e^+ e^- \rightarrow s\bar{s}$

The s-quark asymmetry is derived from measurements of the forward-backward asymmetry of fast hadrons containing an s quark.

ASYMMETRY (%)	STD. MODEL	\sqrt{s} (GeV)	DOCUMENT ID	TECN
9.8 ± 1.1 OUR AVERAGE				
10.08 ± 1.13 ± 0.40	10.1	91.2	¹ ABREU 00B	DLPH
6.8 ± 3.5 ± 1.1	10.1	91.2	² ACKERSTAFF 97T	OPAL

¹ ABREU 00B tag the presence of an s quark requiring a high-momentum-identified charged kaon. The s-quark pole asymmetry is extracted from the charged-kaon asymmetry taking the expected d- and u-quark asymmetries from the Standard Model and using the measured values for the c- and b-quark asymmetries.
² ACKERSTAFF 97T measure the forward-backward asymmetry of various fast hadrons made of light quarks. Then using SU(2) isospin symmetry and flavor independence for down and strange quarks authors solve for the different quark types. The value reported here corresponds then to the forward-backward asymmetry for "down-type" quarks.

$A_{FB}^{(0,c)}$ CHARGE ASYMMETRY IN $e^+ e^- \rightarrow c\bar{c}$

OUR FIT, which is obtained by a simultaneous fit to several c- and b-quark measurements as explained in the note "The Z boson" and ref. LEP-SLC 06, refers to the Z pole asymmetry. The experimental values, on the other hand, correspond to the measurements carried out at the respective energies.

ASYMMETRY (%)	STD. MODEL	\sqrt{s} (GeV)	DOCUMENT ID	TECN
7.07 ± 0.35 OUR FIT				
6.31 ± 0.93 ± 0.65	6.35	91.26	¹ ABDALLAH 04F	DLPH
5.68 ± 0.54 ± 0.39	6.3	91.25	² ABBIENDI 03P	OPAL
6.45 ± 0.57 ± 0.37	6.10	91.21	³ HEISTER 02H	ALEP
6.59 ± 0.94 ± 0.35	6.2	91.235	⁴ ABREU 99Y	DLPH
6.3 ± 0.9 ± 0.3	6.1	91.22	⁵ BARATE 98O	ALEP
6.3 ± 1.2 ± 0.6	6.1	91.22	⁶ ALEXANDER 97C	OPAL
8.3 ± 3.8 ± 2.7	6.2	91.24	⁷ ADRIANI 92D	L3
• • • We do not use the following data for averages, fits, limits, etc. • • •				
3.1 ± 3.5 ± 0.5	-3.5	89.43	¹ ABDALLAH 04F	DLPH
11.0 ± 2.8 ± 0.7	12.3	92.99	¹ ABDALLAH 04F	DLPH
-6.8 ± 2.5 ± 0.9	-3.0	89.51	² ABBIENDI 03P	OPAL
14.6 ± 2.0 ± 0.8	12.2	92.95	² ABBIENDI 03P	OPAL
-12.4 ± 15.9 ± 2.0	-9.6	88.38	³ HEISTER 02H	ALEP
-2.3 ± 2.6 ± 0.2	-3.8	89.38	³ HEISTER 02H	ALEP
-0.3 ± 8.3 ± 0.6	0.9	90.21	³ HEISTER 02H	ALEP
10.6 ± 7.7 ± 0.7	9.6	92.05	³ HEISTER 02H	ALEP
11.9 ± 2.1 ± 0.6	12.2	92.94	³ HEISTER 02H	ALEP
12.1 ± 11.0 ± 1.0	14.2	93.90	³ HEISTER 02H	ALEP
-4.96 ± 3.68 ± 0.53	-3.5	89.434	⁴ ABREU 99Y	DLPH
11.80 ± 3.18 ± 0.62	12.3	92.990	⁴ ABREU 99Y	DLPH
-1.0 ± 4.3 ± 1.0	-3.9	89.37	⁵ BARATE 98O	ALEP
11.0 ± 3.3 ± 0.8	12.3	92.96	⁵ BARATE 98O	ALEP
3.9 ± 5.1 ± 0.9	-3.4	89.45	⁶ ALEXANDER 97C	OPAL
15.8 ± 4.1 ± 1.1	12.4	93.00	⁶ ALEXANDER 97C	OPAL
-12.9 ± 7.8 ± 5.5	-13.6	35	BEHREND 90D	CELL
7.7 ± 13.4 ± 5.0	-22.1	43	BEHREND 90D	CELL
-12.8 ± 4.4 ± 4.1	-13.6	35	ELSEN 90	JADE
-10.9 ± 12.9 ± 4.6	-23.2	44	ELSEN 90	JADE
-14.9 ± 6.7	-13.3	35	OULD-SAADA 89	JADE

¹ ABDALLAH 04F tag b- and c-quarks using semileptonic decays combined with charge flow information from the hemisphere opposite to the lepton. Enriched samples of c \bar{c} and b \bar{b} events are obtained using lifetime information.
² ABBIENDI 03P tag heavy flavors using events with one or two identified leptons. This allows the simultaneous fitting of the b and c quark forward-backward asymmetries as well as the average B⁰-B⁰ mixing.
³ HEISTER 02H measure simultaneously b and c quark forward-backward asymmetries using their semileptonic decays to tag the quark charge. The flavor separation is obtained with a discriminating multivariate analysis.
⁴ ABREU 99Y tag Z → b \bar{b} and Z → c \bar{c} events by an exclusive reconstruction of several D meson decay modes (D^{*+}, D⁰, and D⁺ with their charge-conjugate states).
⁵ BARATE 98O tag Z → c \bar{c} events requiring the presence of high-momentum reconstructed D^{*+}, D⁺, or D⁰ mesons.
⁶ ALEXANDER 97C identify the b and c events using a D/D* tag.
⁷ ADRIANI 92D use both electron and muon semileptonic decays.

$A_{FB}^{(0,b)}$ CHARGE ASYMMETRY IN $e^+ e^- \rightarrow b\bar{b}$

OUR FIT, which is obtained by a simultaneous fit to several c- and b-quark measurements as explained in the note "The Z boson" and ref. LEP-SLC 06, refers to the Z pole asymmetry. The experimental values,

on the other hand, correspond to the measurements carried out at the respective energies.

ASYMMETRY (%)	STD. MODEL	\sqrt{s} (GeV)	DOCUMENT ID	TECN
9.92 ± 0.16 OUR FIT				
9.58 ± 0.32 ± 0.14	9.68	91.231	¹ ABDALLAH 05	DLPH
10.04 ± 0.56 ± 0.25	9.69	91.26	² ABDALLAH 04F	DLPH
9.72 ± 0.42 ± 0.15	9.67	91.25	³ ABBIENDI 03P	OPAL
9.77 ± 0.36 ± 0.18	9.69	91.26	⁴ ABBIENDI 02I	OPAL
9.52 ± 0.41 ± 0.17	9.59	91.21	⁵ HEISTER 02H	ALEP
10.00 ± 0.27 ± 0.11	9.63	91.232	⁶ HEISTER 01D	ALEP
7.62 ± 1.94 ± 0.85	9.64	91.235	⁷ ABREU 99Y	DLPH
9.60 ± 0.66 ± 0.33	9.69	91.26	⁸ ACCIARRI 99D	L3
9.31 ± 1.01 ± 0.55	9.65	91.24	⁹ ACCIARRI 98U	L3
9.4 ± 2.7 ± 2.2	9.61	91.22	¹⁰ ALEXANDER 97C	OPAL

• • • We do not use the following data for averages, fits, limits, etc. • • •

6.37 ± 1.43 ± 0.17	5.8	89.449	¹ ABDALLAH 05	DLPH
10.41 ± 1.15 ± 0.24	12.1	92.990	¹ ABDALLAH 05	DLPH
6.7 ± 2.2 ± 0.2	5.7	89.43	² ABDALLAH 04F	DLPH
11.2 ± 1.8 ± 0.2	12.1	92.99	² ABDALLAH 04F	DLPH
4.7 ± 1.8 ± 0.1	5.9	89.51	³ ABBIENDI 03P	OPAL
10.3 ± 1.5 ± 0.2	12.0	92.95	³ ABBIENDI 03P	OPAL
5.82 ± 1.53 ± 0.12	5.9	89.50	⁴ ABBIENDI 02I	OPAL
12.21 ± 1.23 ± 0.25	12.0	92.91	⁴ ABBIENDI 02I	OPAL
-13.1 ± 13.5 ± 1.0	3.2	88.38	⁵ HEISTER 02H	ALEP
5.5 ± 1.9 ± 0.1	5.6	89.38	⁵ HEISTER 02H	ALEP
-0.4 ± 6.7 ± 0.8	7.5	90.21	⁵ HEISTER 02H	ALEP
11.1 ± 6.4 ± 0.5	11.0	92.05	⁵ HEISTER 02H	ALEP
10.4 ± 1.5 ± 0.3	12.0	92.94	⁵ HEISTER 02H	ALEP
13.8 ± 9.3 ± 1.1	12.9	93.90	⁵ HEISTER 02H	ALEP
4.36 ± 1.19 ± 0.11	5.8	89.472	⁶ HEISTER 01D	ALEP
11.72 ± 0.97 ± 0.11	12.0	92.950	⁶ HEISTER 01D	ALEP
5.67 ± 7.56 ± 1.17	5.7	89.434	⁷ ABREU 99Y	DLPH
8.82 ± 6.33 ± 1.22	12.1	92.990	⁷ ABREU 99Y	DLPH
6.11 ± 2.93 ± 0.43	5.9	89.50	⁸ ACCIARRI 99D	L3
13.71 ± 2.40 ± 0.44	12.2	93.10	⁸ ACCIARRI 99D	L3
4.95 ± 5.23 ± 0.40	5.8	89.45	⁹ ACCIARRI 98U	L3
11.37 ± 3.99 ± 0.65	12.1	92.99	⁹ ACCIARRI 98U	L3
-8.6 ± 10.8 ± 2.9	5.8	89.45	¹⁰ ALEXANDER 97C	OPAL
-2.1 ± 9.0 ± 2.6	12.1	93.00	¹⁰ ALEXANDER 97C	OPAL
-71 ± 34 ± 7	-58	58.3	SHIMONAKA 91	TOPZ
-22.2 ± 7.7 ± 3.5	-26.0	35	BEHREND 90D	CELL
-49.1 ± 16.0 ± 5.0	-39.7	43	BEHREND 90D	CELL
-28 ± 11	-23	35	BRAUNSCH... 90	TASS
-16.6 ± 7.7 ± 4.8	-24.3	35	ELSEN 90	JADE
-33.6 ± 22.2 ± 5.2	-39.9	44	ELSEN 90	JADE
3.4 ± 7.0 ± 3.5	-16.0	29.0	BAND 89	MAC
-72 ± 28 ± 13	-56	55.2	SAGAWA 89	AMY

¹ ABDALLAH 05 obtain an enriched samples of b \bar{b} events using lifetime information. The quark (or antiquark) charge is determined with a neural network using the secondary vertex charge, the jet charge and particle identification.
² ABDALLAH 04F tag b- and c-quarks using semileptonic decays combined with charge flow information from the hemisphere opposite to the lepton. Enriched samples of c \bar{c} and b \bar{b} events are obtained using lifetime information.
³ ABBIENDI 03P tag heavy flavors using events with one or two identified leptons. This allows the simultaneous fitting of the b and c quark forward-backward asymmetries as well as the average B⁰-B⁰ mixing.
⁴ ABBIENDI 02I tag Z⁰ → b \bar{b} decays using a combination of secondary vertex and lepton tags. The sign of the b-quark charge is determined using an inclusive tag based on jet, vertex, and kaon charges.
⁵ HEISTER 02H measure simultaneously b and c quark forward-backward asymmetries using their semileptonic decays to tag the quark charge. The flavor separation is obtained with a discriminating multivariate analysis.
⁶ HEISTER 01D tag Z → b \bar{b} events using the impact parameters of charged tracks complemented with information from displaced vertices, event shape variables, and lepton identification. The b-quark direction and charge is determined using the hemisphere charge method along with information from fast kaon tagging and charge estimators of primary and secondary vertices. The change in the quoted value due to variation of A_{FB}^c and R_b is given as +0.103 (A_{FB}^c - 0.0651) - 0.440 (R_b - 0.21585).
⁷ ABREU 99Y tag Z → b \bar{b} and Z → c \bar{c} events by an exclusive reconstruction of several D meson decay modes (D^{*+}, D⁰, and D⁺ with their charge-conjugate states).
⁸ ACCIARRI 99D tag Z → b \bar{b} events using high p and p \bar{p} leptons. The analysis determines simultaneously a mixing parameter $\chi_b = 0.1192 \pm 0.0068 \pm 0.0051$ which is used to correct the observed asymmetry.
⁹ ACCIARRI 98U tag Z → b \bar{b} events using lifetime and measure the jet charge using the hemisphere charge.
¹⁰ ALEXANDER 97C identify the b and c events using a D/D* tag.

CHARGE ASYMMETRY IN $e^+ e^- \rightarrow q\bar{q}$

Summed over five lighter flavors.

Experimental and Standard Model values are somewhat event-selection dependent. Standard Model expectations contain some assumptions on B⁰-B⁰ mixing and on other electroweak parameters.

ASYMMETRY (%)	STD. MODEL	\sqrt{s} (GeV)	DOCUMENT ID	TECN
• • • We do not use the following data for averages, fits, limits, etc. • • •				
- 0.76 ± 0.12 ± 0.15		91.2	¹ ABREU 92l	DLPH
4.0 ± 0.4 ± 0.63	4.0	91.3	² ACTON 92L	OPAL
9.1 ± 1.4 ± 1.6	9.0	57.9	ADACHI 91	TOPZ
- 0.84 ± 0.15 ± 0.04		91	DECAMP 91B	ALEP
8.3 ± 2.9 ± 1.9	8.7	56.6	STUART 90	AMY
11.4 ± 2.2 ± 2.1	8.7	57.6	ABE 89L	VNS
6.0 ± 1.3	5.0	34.8	GREENSHAW 89	JADE
8.2 ± 2.9	8.5	43.6	GREENSHAW 89	JADE

¹ ABREU 92l has 0.14 systematic error due to uncertainty of quark fragmentation.

² ACTON 92L use the weight function method on 259k selected $Z \rightarrow$ hadrons events.

The systematic error includes a contribution of 0.2 due to $B^0\bar{B}^0$ mixing effect, 0.4 due to Monte Carlo (MC) fragmentation uncertainties and 0.3 due to MC statistics. ACTON 92L derive a value of $\sin^2\theta_{\text{eff}}^W$ to be $0.2321 \pm 0.0017 \pm 0.0028$.

CHARGE ASYMMETRY IN $p\bar{p} \rightarrow Z \rightarrow e^+e^-$

ASYMMETRY (%)	STD. MODEL	\sqrt{s} (GeV)	DOCUMENT ID	TECN
• • • We do not use the following data for averages, fits, limits, etc. • • •				
5.2 ± 5.9 ± 0.4		91	ABE 91E	CDF

ANOMALOUS $ZZ\gamma$, $Z\gamma\gamma$, AND ZZV COUPLINGS

Revised September 2013 by M.W. Gr unewald (U. College Dublin and U. Ghent) and A. Gurtu (Formerly Tata Inst.).

In on-shell $Z\gamma$ production, deviations from the Standard Model for the $Z\gamma\gamma^*$ and $Z\gamma Z^*$ couplings may be described in terms of eight parameters, h_i^V ($i = 1, 4; V = \gamma, Z$) [1]. The parameters h_i^γ describe the $Z\gamma\gamma^*$ couplings and the parameters h_i^Z the $Z\gamma Z^*$ couplings. In this formalism h_1^V and h_2^V lead to CP -violating and h_3^V and h_4^V to CP -conserving effects. All these anomalous contributions to the cross section increase rapidly with center-of-mass energy. In order to ensure unitarity, these parameters are usually described by a form-factor representation, $h_i^V(s) = h_{i0}^V/(1 + s/\Lambda^2)^n$, where Λ is the energy scale for the manifestation of a new phenomenon and n is a sufficiently large power. By convention one uses $n = 3$ for $h_{1,3}^V$ and $n = 4$ for $h_{2,4}^V$. Usually limits on h_i^V 's are put assuming some value of Λ , sometimes ∞ .

In on-shell ZZ production, deviations from the Standard Model for the $ZZ\gamma^*$ and ZZZ^* couplings may be described by means of four anomalous couplings f_i^V ($i = 4, 5; V = \gamma, Z$) [2]. As above, the parameters f_i^γ describe the $ZZ\gamma^*$ couplings and the parameters f_i^Z the ZZZ^* couplings. The anomalous couplings f_5^V lead to violation of C and P symmetries while f_4^V introduces CP violation. Also here, formfactors depending on a scale Λ are used.

All these couplings h_i^V and f_i^V are zero at tree level in the Standard Model; they are measured in e^+e^- , $p\bar{p}$ and pp collisions at LEP, Tevatron and LHC.

References

- U. Baur and E.L. Berger, Phys. Rev. **D47**, 4889 (1993).
- K. Hagiwara *et al.*, Nucl. Phys. **B282**, 253 (1987).

h_i^V

Combining the LEP-2 results taking into account the correlations, the following 95% CL limits are derived [SCHAEL 13A]:

$$\begin{aligned} -0.12 < h_1^\gamma < +0.11, & \quad -0.07 < h_2^\gamma < +0.07, \\ -0.19 < h_3^\gamma < +0.06, & \quad -0.04 < h_4^\gamma < +0.13, \\ -0.05 < h_1^Z < +0.05, & \quad -0.04 < h_2^Z < +0.02, \\ -0.05 < h_3^Z < +0.00, & \quad +0.01 < h_4^Z < +0.05. \end{aligned}$$

Some of the recent results from the Tevatron and LHC experiments individually surpass the combined LEP-2 results in precision (see below).

VALUE	DOCUMENT ID	TECN	COMMENT
• • • We do not use the following data for averages, fits, limits, etc. • • •			
¹ AAD 16Q	ATLS	$E_{\text{cm}}^{pp} = 8$ TeV	
² KHACHATRYAN 16AE	CMS	$E_{\text{cm}}^{pp} = 8$ TeV	
³ KHACHATRYAN 15AC	CMS	$E_{\text{cm}}^{pp} = 8$ TeV	
⁴ CHATRCHYAN 14AB	CMS	$E_{\text{cm}}^{pp} = 7$ TeV	
⁵ AAD 13AN	ATLS	$E_{\text{cm}}^{pp} = 7$ TeV	
⁶ CHATRCHYAN 13BI	CMS	$E_{\text{cm}}^{pp} = 7$ TeV	
⁷ ABAZOV 12S	D0	$E_{\text{cm}}^{pp} = 1.96$ TeV	
⁸ AALTONEN 11S	CDF	$E_{\text{cm}}^{pp} = 1.96$ TeV	
⁹ CHATRCHYAN 11M	CMS	$E_{\text{cm}}^{pp} = 7$ TeV	
¹⁰ ABAZOV 09L	D0	$E_{\text{cm}}^{pp} = 1.96$ TeV	
¹¹ ABAZOV 07M	D0	$E_{\text{cm}}^{pp} = 1.96$ TeV	
¹² ABDALLAH 07C	DLPH	$E_{\text{cm}}^{ee} = 183\text{--}208$ GeV	
¹³ ACHARD 04H	L3	$E_{\text{cm}}^{ee} = 183\text{--}208$ GeV	
¹⁴ ABBIENDI, G	OPAL	$E_{\text{cm}}^{ee} = 189$ GeV	
¹⁵ ABBOTT 98M	D0	$E_{\text{cm}}^{pp} = 1.8$ TeV	
¹⁶ ABREU 98K	DLPH	$E_{\text{cm}}^{ee} = 161, 172$ GeV	

¹ AAD 16Q study $Z\gamma$ production in pp collisions. In events with no additional jets, 10268 (12738) Z decays to electron (muon) pairs are selected, with an expected background of 1291 ± 340 (1537 ± 408) events, as well as 1039 Z decays to neutrino pairs with an expected background of 450 ± 96 events. Analyzing the photon transverse momentum distribution above 250 GeV (400 GeV) for lepton (neutrino) events, yields the 95% C.L. limits: $-7.8 \times 10^{-4} < h_3^Z < 8.6 \times 10^{-4}$, $-3.0 \times 10^{-6} < h_4^Z < 2.9 \times 10^{-6}$, $-9.5 \times 10^{-4} < h_3^\gamma < 9.9 \times 10^{-4}$, $-3.2 \times 10^{-6} < h_4^\gamma < 3.2 \times 10^{-6}$.

² KHACHATRYAN 16AE determine the $Z\gamma \rightarrow \nu\bar{\nu}\gamma$ cross section by selecting events with a photon of $E_T > 145$ GeV and $\cancel{E}_T > 140$ GeV. 630 candidate events are observed with an expected SM background of 269 ± 26 . The E_T spectrum of the photon is used to set 95% C.L. limits as follows: $-1.5 \times 10^{-3} < h_3^Z < 1.6 \times 10^{-3}$, $-3.9 \times 10^{-6} < h_4^Z < 4.5 \times 10^{-6}$, $-1.1 \times 10^{-3} < h_3^\gamma < 0.9 \times 10^{-3}$, $-3.8 \times 10^{-6} < h_4^\gamma < 4.3 \times 10^{-6}$.

³ KHACHATRYAN 15AC study $Z\gamma$ events in 8 TeV pp interactions, where the Z decays into 2 same-flavor, opposite sign leptons (e or μ) and a photon with $p_T > 15$ GeV. The p_T of a lepton is required to be > 20 GeV/ c , their effective mass > 50 GeV, and the photon should have a separation $\Delta R > 0.7$ with each lepton. The observed p_T distribution of the photons is used to extract the 95% C.L. limits: $-3.8 \times 10^{-3} < h_3^Z < 3.7 \times 10^{-3}$, $-3.1 \times 10^{-5} < h_4^Z < 3.0 \times 10^{-5}$, $-4.6 \times 10^{-3} < h_3^\gamma < 4.6 \times 10^{-3}$, $-3.6 \times 10^{-5} < h_4^\gamma < 3.5 \times 10^{-5}$.

⁴ CHATRCHYAN 14AB measure $Z\gamma$ production cross section for $p_T^\gamma > 15$ GeV and $R(\ell\gamma) > 0.7$, which is the separation between the γ and the final state charged lepton (e or μ) in the azimuthal angle-pseudorapidity ($\phi - \eta$) plane. The di-lepton mass is required to be > 50 GeV. After background subtraction the number of $e\gamma$ and $\mu\mu\gamma$ events is determined to be 3160 ± 120 and 5030 ± 233 respectively, compatible with expectations from the SM. This leads to a 95% CL limits of $-1 \times 10^{-2} < h_3^\gamma < 1 \times 10^{-2}$, $-9 \times 10^{-5} < h_4^\gamma < 9 \times 10^{-5}$, $-9 \times 10^{-3} < h_3^Z < 9 \times 10^{-3}$, $-8 \times 10^{-5} < h_4^Z < 8 \times 10^{-5}$, assuming h_1^V and h_2^V have SM values, $V = \gamma$ or Z .

⁵ AAD 13AN study $Z\gamma$ production in pp collisions. In events with no additional jet, 1417 (2031) Z decays to electron (muon) pairs are selected, with an expected background of 156 ± 54 (244 ± 64) events, as well as 662 Z decays to neutrino pairs with an expected background of 302 ± 42 events. Analysing the photon p_T spectrum above 100 GeV yields the 95% C.L. limits: $-0.013 < h_3^Z < 0.014$, $-8.7 \times 10^{-5} < h_4^Z < 8.7 \times 10^{-5}$, $-0.015 < h_3^\gamma < 0.016$, $-9.4 \times 10^{-5} < h_4^\gamma < 9.2 \times 10^{-5}$. Supersedes AAD 12BX.

⁶ CHATRCHYAN 13BI determine the $Z\gamma \rightarrow \nu\bar{\nu}\gamma$ cross section by selecting events with a photon of $E_T > 145$ GeV and a $\cancel{E}_T > 130$ GeV. 73 candidate events are observed with an expected SM background of 30.2 ± 6.5 . The E_T spectrum of the photon is used to set 95% C.L. limits as follows: $|h_3^Z| < 2.7 \times 10^{-3}$, $|h_4^Z| < 1.3 \times 10^{-5}$, $|h_3^\gamma| < 2.9 \times 10^{-3}$, $|h_4^\gamma| < 1.5 \times 10^{-5}$.

⁷ ABAZOV 12S study $Z\gamma$ production in $p\bar{p}$ collisions at $\sqrt{s} = 1.96$ TeV using 6.2 fb^{-1} of data where the Z decays to electron (muon) pairs and the photon has at least 10 GeV of transverse momentum. In data, 304 (308) di-electron (di-muon) events are observed with an expected background of 255 ± 16 (285 ± 24) events. Based on the photon p_T spectrum, and including also earlier data and the $Z \rightarrow \nu\bar{\nu}$ decay mode (from ABAZOV 09L), the following 95% C.L. limits are reported: $|h_{03}^Z| < 0.026$, $|h_{04}^Z| < 0.0013$, $|h_{03}^\gamma| < 0.027$, $|h_{04}^\gamma| < 0.0014$ for a form factor scale of $\Lambda = 1.5$ TeV.

⁸ AALTONEN 11S study $Z\gamma$ events in $p\bar{p}$ interactions at $\sqrt{s} = 1.96$ TeV with integrated luminosity 5.1 fb^{-1} for $Z \rightarrow e^+e^-/\mu^+\mu^-$ and 4.9 fb^{-1} for $Z \rightarrow \nu\bar{\nu}$. For the charged lepton case, the two leptons must be of the same flavor with the transverse momentum/energy of one > 20 GeV and the other > 10 GeV. The isolated photon must have $E_T > 50$ GeV. They observe 91 events with 87.2 ± 7.8 events expected from standard model processes. For the $\nu\bar{\nu}$ case they require solitary photons with $E_T > 25$ GeV and missing $E_T > 25$ GeV and observe 85 events with standard model expectation of 85.9 ± 5.6 events. Taking the form factor $\Lambda = 1.5$ TeV they derive 95% C.L. limits as $|h_{3,4}^Z| < 0.022$ and $|h_{3,4}^\gamma| < 0.0009$.

⁹ CHATRCHYAN 11M study $Z\gamma$ production in pp collisions at $\sqrt{s} = 7$ TeV using 36 pb^{-1} pp data, where the Z decays to e^+e^- or $\mu^+\mu^-$. The total cross sections are measured for photon transverse energy $E_T^\gamma > 10$ GeV and spatial separation from charged leptons in the plane of pseudo rapidity and azimuthal angle $\Delta R(\ell, \gamma) > 0.7$ with

- the dilepton invariant mass requirement of $M_{\ell\ell} > 50$ GeV. The number of $e^+e^- \gamma$ and $\mu^+\mu^- \gamma$ candidates is 81 and 90 with estimated backgrounds of 20.5 ± 2.5 and 27.3 ± 3.2 events respectively. The 95% CL limits for $ZZ\gamma$ couplings are $-0.05 < h_3^Z < 0.06$ and $-0.0005 < h_4^Z < 0.0005$, and for $Z\gamma\gamma$ couplings are $-0.07 < h_3^\gamma < 0.07$ and $-0.0005 < h_4^\gamma < 0.0006$.
- ¹⁰ ABAZOV 09L study $Z\gamma, Z \rightarrow \nu\bar{\nu}$ production in $p\bar{p}$ collisions at 1.96 TeV C.M. energy. They select 51 events with a photon of transverse energy E_T larger than 90 GeV, with an expected background of 17 events. Based on the photon E_T spectrum and including also Z decays to charged leptons (from ABAZOV 07M), the following 95% CL limits are reported: $|h_{30}^\gamma| < 0.033, |h_{40}^\gamma| < 0.0017, |h_{30}^Z| < 0.033, |h_{40}^Z| < 0.0017$.
- ¹¹ ABAZOV 07M use 968 $p\bar{p} \rightarrow e^+e^-/\mu^+\mu^- \gamma X$ candidates, at 1.96 TeV center of mass energy, to tag $p\bar{p} \rightarrow Z\gamma$ events by requiring $E_T(\gamma) > 7$ GeV, lepton-gamma separation $\Delta R_{\ell\gamma} > 0.7$, and di-lepton invariant mass > 30 GeV. The cross section is in agreement with the SM prediction. Using these $Z\gamma$ events they obtain 95% C.L. limits on each h_i^V , keeping all others fixed at their SM values. They report: $-0.083 < h_{30}^Z < 0.082, -0.0053 < h_{40}^Z < 0.0054, -0.085 < h_{30}^\gamma < 0.084, -0.0053 < h_{40}^\gamma < 0.0054$, for the form factor scale $\Lambda = 1.2$ TeV.
- ¹² Using data collected at $\sqrt{s} = 183\text{--}208$, ABDALLAH 07c select 1,877 $e^+e^- \rightarrow Z\gamma$ events with $Z \rightarrow q\bar{q}$ or $\nu\bar{\nu}$, 171 $e^+e^- \rightarrow ZZ$ events with $Z \rightarrow q\bar{q}$ or lepton pair (except an explicit τ pair), and 74 $e^+e^- \rightarrow Z\gamma^*$ events with a $q\bar{q}\mu^+\mu^-$ or $q\bar{q}e^+e^-$ signature, to derive 95% CL limits on h_i^V . Each limit is derived with other parameters set to zero. They report: $-0.23 < h_1^Z < 0.23, -0.30 < h_2^Z < 0.16, -0.14 < h_1^\gamma < 0.14, -0.049 < h_2^\gamma < 0.044$.
- ¹³ ACHARD 04H select 3515 $e^+e^- \rightarrow Z\gamma$ events with $Z \rightarrow q\bar{q}$ or $\nu\bar{\nu}$ at $\sqrt{s} = 189\text{--}209$ GeV to derive 95% CL limits on h_i^V . For deriving each limit the other parameters are fixed at zero. They report: $-0.153 < h_1^Z < 0.141, -0.087 < h_2^Z < 0.079, -0.220 < h_3^Z < 0.112, -0.068 < h_4^Z < 0.148, -0.057 < h_1^\gamma < 0.057, -0.050 < h_2^\gamma < 0.023, -0.059 < h_3^\gamma < 0.004, -0.004 < h_4^\gamma < 0.024$.
- ¹⁴ ABBIENDI, G 00c study $e^+e^- \rightarrow Z\gamma$ events (with $Z \rightarrow q\bar{q}$ and $Z \rightarrow \nu\bar{\nu}$) at 189 GeV to obtain the central values (and 95% CL limits) of these couplings: $h_1^Z = 0.000 \pm 0.100$ ($-0.190, 0.190$), $h_2^Z = 0.000 \pm 0.068$ ($-0.128, 0.128$), $h_3^Z = -0.074 \pm_{-0.103}^{+0.102}$ ($-0.269, 0.119$), $h_4^Z = 0.046 \pm 0.068$ ($-0.084, 0.175$), $h_1^\gamma = 0.000 \pm 0.061$ ($-0.115, 0.115$), $h_2^\gamma = 0.000 \pm 0.041$ ($-0.077, 0.077$), $h_3^\gamma = -0.080 \pm_{-0.041}^{+0.039}$ ($-0.164, -0.006$), $h_4^\gamma = 0.064 \pm_{-0.030}^{+0.033}$ ($+0.007, +0.134$). The results are derived assuming that only one coupling at a time is different from zero.
- ¹⁵ ABBOTT 98M study $p\bar{p} \rightarrow Z\gamma + X$, with $Z \rightarrow e^+e^-, \mu^+\mu^-, \nu\bar{\nu}$ at 1.8 TeV, to obtain 95% CL limits at $\Lambda = 750$ GeV: $|h_{30}^Z| < 0.36, |h_{40}^Z| < 0.05$ (keeping $h_i^Z = 0$), and $|h_{30}^\gamma| < 0.37, |h_{40}^\gamma| < 0.05$ (keeping $h_i^\gamma = 0$). Limits on the CP-violating couplings are $|h_{10}^Z| < 0.36, |h_{20}^Z| < 0.05$ (keeping $h_i^Z = 0$), and $|h_{10}^\gamma| < 0.37, |h_{20}^\gamma| < 0.05$ (keeping $h_i^\gamma = 0$).
- ¹⁶ ABREU 98k determine a 95% CL upper limit on $\sigma(e^+e^- \rightarrow \gamma + \text{invisible particles}) < 2.5$ pb using 161 and 172 GeV data. This is used to set 95% CL limits on $|h_{30}^\gamma| < 0.8$ and $|h_{30}^Z| < 1.3$, derived at a scale $\Lambda = 1$ TeV and with $n = 3$ in the form factor representation.
- f_i^V**
Combining the LEP-2 results taking into account the correlations, the following 95% CL limits are derived [SCHAEL 13A]:
- $$\begin{aligned} -0.28 < f_4^Z < +0.32, & \quad -0.34 < f_5^Z < +0.35, \\ -0.17 < f_4^\gamma < +0.19, & \quad -0.35 < f_5^\gamma < +0.32. \end{aligned}$$
- Some of the recent results from the Tevatron and LHC experiments individually surpass the combined LEP-2 results in precision (see below).
- | VALUE | DOCUMENT ID | TECN | COMMENT |
|-------|---|-----------|-------------------------------------|
| • • • | We do not use the following data for averages, fits, limits, etc. | • • • | |
| 1 | AABOUD | 19AY ATLS | $E_{cm}^{pp} = 13$ TeV |
| 2 | AABOUD | 18Q ATLS | $E_{cm}^{pp} = 13$ TeV |
| 3 | SIRUNYAN | 18BT CMS | $E_{cm}^{pp} = 13$ TeV |
| 4 | KHACHATRYAN...15B | CMS | $E_{cm}^{pp} = 8$ TeV |
| 5 | KHACHATRYAN...15Bc | CMS | $E_{cm}^{pp} = 7, 8$ TeV |
| 6 | AAD | 13z ATLS | $E_{cm}^{pp} = 7$ TeV |
| 7 | CHATRCHYAN13B | CMS | $E_{cm}^{pp} = 7$ TeV |
| 8 | SCHAEL | 09 ALEP | $E_{cm}^{ee} = 192\text{--}209$ GeV |
| 9 | ABAZOV | 08k D0 | $E_{cm}^{pp} = 1.96$ TeV |
| 10 | ABDALLAH | 07c DLPH | $E_{cm}^{ee} = 183\text{--}208$ GeV |
| 11 | ABBIENDI | 04c OPAL | |
| 12 | ACHARD | 03D L3 | |
- ¹ AABOUD 19AY study ZZ production in the $\ell\ell\nu\nu$ decay channel. Events with a pair of isolated high-transverse momentum charged leptons (electron pairs or muon pairs), and with large missing energy, are selected. In the data, 371 (416) di-electron (di-muon) events are found, with a total expected background of 128 ± 8 (143 ± 8) events. Analysing the transverse momentum distribution of the charged dilepton system above 150 GeV, the following 95% C.L. limits are derived in units of 10^{-3} : $-1.2 < f_4^Z < 1.2, -1.0 < f_4^\gamma < 1.0, -1.2 < f_5^Z < 1.2, -1.0 < f_5^\gamma < 1.0$.
- ² AABOUD 18Q study $pp \rightarrow ZZ$ events at $\sqrt{s} = 13$ TeV with $Z \rightarrow e^+e^-$ or $Z \rightarrow \mu^+\mu^-$. The number of events observed in the $4e, 2e2\mu$, and 4μ channels is 249, 465, and 303 respectively. Analysing the p_T spectrum of the leading Z boson, the following the following 95% C.L. limits are derived in units of 10^{-4} : $-1.8 < f_4^Z < 1.8, -1.5 < f_4^\gamma < 1.5, -1.8 < f_5^Z < 1.8, -1.5 < f_5^\gamma < 1.5$.
- ³ SIRUNYAN 18BT study $ppZZ$ events at $\sqrt{s} = 13$ TeV with $Z \rightarrow e^+e^-$ or $Z \rightarrow \mu^+\mu^-$. The number of events observed in the $4e, 2e2\mu$, and 4μ channels is 220, 543 and 335 respectively. Analysing the 4-lepton invariant mass spectrum, the following 95% C.L. limits are derived in units of 10^{-3} : $-1.2 < f_4^Z < 1.3, -1.2 < f_4^\gamma < 1.0, -1.2 < f_5^Z < 1.3, -1.0 < f_5^\gamma < 1.3$.
- ⁴ KHACHATRYAN 15B study ZZ production in 8 TeV pp collisions. In the decay modes $ZZ \rightarrow 4e, 4\mu, 2e2\mu, 54, 75, 148$ events are observed, with an expected background of $2.2 \pm 0.9, 1.2 \pm 0.6$, and 2.4 ± 1.0 events, respectively. Analysing the 4-lepton invariant mass spectrum in the range from 110 GeV to 1200 GeV, the following 95% C.L. limits are obtained: $|f_4^Z| < 0.004, |f_5^Z| < 0.004, |f_4^\gamma| < 0.005, |f_5^\gamma| < 0.005$.
- ⁵ KHACHATRYAN 15Bc use the cross section measurement of the final state $pp \rightarrow ZZ \rightarrow 2\ell 2\ell'$ (ℓ being an electron or a muon) at 7 and 8 TeV to put limits on these triple gauge couplings. Effective mass of the charged lepton pair is required to be in the range 83.5–98.5 GeV and the dilepton $p_T > 45$ GeV. The reduced missing E_T is required to be > 65 GeV, which takes into account the fake missing E_T due to detector effects. The numbers of e^+e^- and $\mu^+\mu^-$ events selected are 35 and 40 at 7 TeV and 176 and 271 at 8 TeV respectively. The production cross sections so obtained are in agreement with SM predictions. The following 95% C.L. limits are set: $-0.0028 < f_4^Z < 0.0032, -0.0037 < f_4^\gamma < 0.0033, -0.0029 < f_5^Z < 0.0031, -0.0033 < f_5^\gamma < 0.0037$. Combining with previous results (KHACHATRYAN 15B and CHATRCHYAN 13B) which include 7 TeV and 8 TeV data on the final states $pp \rightarrow ZZ \rightarrow 2\ell 2\ell'$ where ℓ and ℓ' are an electron or a muon, the best limits are $-0.0022 < f_4^Z < 0.0026, -0.0029 < f_4^\gamma < 0.0026, -0.0023 < f_5^Z < 0.0023, -0.0026 < f_5^\gamma < 0.0027$.
- ⁶ AAD 13z study ZZ production in pp collisions at $\sqrt{s} = 7$ TeV. In the $ZZ \rightarrow \ell^+\ell^-\ell'^+\ell'^-$ final state they observe a total of 66 events with an expected background of 0.9 ± 1.3 . In the $ZZ \rightarrow \ell^+\ell^-\nu\nu$ final state they observe a total of 87 events with an expected background of 46.9 ± 5.2 . The limits on anomalous TGCs are determined using the observed and expected numbers of these ZZ events binned in p_T^Z . The 95% C.L. are as follows: for form factor scale $\Lambda = \infty, -0.015 < f_4^Z < 0.015, -0.013 < f_4^\gamma < 0.013, -0.016 < f_5^Z < 0.015, -0.013 < f_5^\gamma < 0.013$; for form factor scale $\Lambda = 3$ TeV, $-0.022 < f_4^Z < 0.023, -0.019 < f_4^\gamma < 0.019, -0.023 < f_5^Z < 0.023, -0.020 < f_5^\gamma < 0.019$.
- ⁷ CHATRCHYAN 13B study ZZ production in pp collisions and select 54 ZZ candidates in the Z decay channel with electrons or muons with an expected background of 1.4 ± 0.5 events. The resulting 95% C.L. ranges are: $-0.013 < f_4^Z < 0.015, -0.011 < f_4^\gamma < 0.012, -0.014 < f_5^Z < 0.014, -0.012 < f_5^\gamma < 0.012$.
- ⁸ Using data collected in the center of mass energy range 192–209 GeV, SCHAEL 09 select 318 $e^+e^- \rightarrow ZZ$ events with 319.4 expected from the standard model. Using this data they derive the following 95% CL limits: $-0.321 < f_4^Z < 0.318, -0.534 < f_4^\gamma < 0.534, -0.724 < f_5^Z < 0.733, -1.194 < f_5^\gamma < 1.190$.
- ⁹ ABAZOV 08k search for ZZ and $Z\gamma^*$ events with $1\text{fb}^{-1} p\bar{p}$ data at $\sqrt{s} = 1.96$ TeV in $(e\ell)(e\ell), (\mu\mu)(\mu\mu), (e\ell)(\mu\mu)$ final states requiring the lepton pair masses to be > 30 GeV. They observe 1 event, which is consistent with an expected signal of 1.71 ± 0.15 events and a background of 0.13 ± 0.03 events. From this they derive the following limits, for a form factor (Λ) value of 1.2 TeV: $-0.28 < f_{40}^Z < 0.28, -0.31 < f_{50}^Z < 0.29, -0.26 < f_{40}^\gamma < 0.26, -0.30 < f_{50}^\gamma < 0.28$.
- ¹⁰ Using data collected at $\sqrt{s} = 183\text{--}208$ GeV, ABDALLAH 07c select 171 $e^+e^- \rightarrow ZZ$ events with $Z \rightarrow q\bar{q}$ or lepton pair (except an explicit τ pair), and 74 $e^+e^- \rightarrow Z\gamma^*$ events with a $q\bar{q}\mu^+\mu^-$ or $q\bar{q}e^+e^-$ signature, to derive 95% CL limits on f_i^V . Each limit is derived with other parameters set to zero. They report: $-0.40 < f_4^Z < 0.42, -0.38 < f_5^Z < 0.62, -0.23 < f_4^\gamma < 0.25, -0.52 < f_5^\gamma < 0.48$.
- ¹¹ ABBIENDI 04c study ZZ production in e^+e^- collisions in the C.M. energy range 190–209 GeV. They select 340 events with an expected background of 180 events. Including the ABBIENDI 00N data at 183 and 189 GeV (118 events with an expected background of 65 events) they report the following 95% CL limits: $-0.45 < f_4^Z < 0.58, -0.94 < f_5^Z < 0.25, -0.32 < f_4^\gamma < 0.33, \text{ and } -0.71 < f_5^\gamma < 0.59$.
- ¹² ACHARD 03D study Z-boson pair production in e^+e^- collisions in the C.M. energy range 200–209 GeV. They select 549 events with an expected background of 432 events. Including the ACCIARRI 99G and ACCIARRI 99o data (183 and 189 GeV respectively, 286 events with an expected background of 241 events) and the 192–202 GeV ACCIARRI 01i results (656 events, expected background of 512 events), they report the following 95% CL limits: $-0.48 \leq f_4^Z \leq 0.46, -0.36 \leq f_5^Z \leq 1.03, -0.28 \leq f_4^\gamma \leq 0.28, \text{ and } -0.40 \leq f_5^\gamma \leq 0.47$.

ANOMALOUS W/Z QUARTIC COUPLINGS

Revised November 2015 by M.W. Grunewald (U. College Dublin) and A. Gurtu (Formerly Tata Inst.).

Quartic couplings, $WWZZ, WWZ\gamma, WW\gamma\gamma$, and $ZZ\gamma\gamma$, were studied at LEP and Tevatron at energies at which the Standard Model predicts negligible contributions to multiboson production. Thus, to parametrize limits on these couplings, an

effective theory approach is adopted which supplements the Standard Model Lagrangian with higher dimensional operators which include quartic couplings. The LEP collaborations chose the lower dimensional representation of operators (dimension 6) which presumes the $SU(2) \times U(1)$ gauge symmetry is broken by means other than the conventional Higgs scalar doublet [1–3]. In this representation possible quartic couplings, a_0, a_c, a_n , are expressed in terms of the following dimension-6 operators [1,2];

$$\begin{aligned} L_6^0 &= -\frac{e^2}{16\Lambda^2} a_0 F^{\mu\nu} F_{\mu\nu} \vec{W}^\alpha \cdot \vec{W}_\alpha \\ L_6^c &= -\frac{e^2}{16\Lambda^2} a_c F^{\mu\alpha} F_{\mu\beta} \vec{W}^\beta \cdot \vec{W}_\alpha \\ L_6^n &= -i\frac{e^2}{16\Lambda^2} a_n \epsilon_{ijk} W_{\mu\alpha}^{(i)} W_\nu^{(j)} W^{(k)\alpha} F^{\mu\nu} \\ \tilde{L}_6^0 &= -\frac{e^2}{16\Lambda^2} \tilde{a}_0 F^{\mu\nu} \tilde{F}_{\mu\nu} \vec{W}^\alpha \cdot \vec{W}_\alpha \\ \tilde{L}_6^n &= -i\frac{e^2}{16\Lambda^2} \tilde{a}_n \epsilon_{ijk} W_{\mu\alpha}^{(i)} W_\nu^{(j)} W^{(k)\alpha} \tilde{F}^{\mu\nu} \end{aligned}$$

where F, W are photon and W fields, L_6^0 and L_6^c conserve C, P separately (\tilde{L}_6^0 conserves only C) and generate anomalous $W^+W^-\gamma\gamma$ and $ZZ\gamma\gamma$ couplings, L_6^n violates CP (\tilde{L}_6^n violates both C and P) and generates an anomalous $W^+W^-Z\gamma$ coupling, and Λ is an energy scale for new physics. For the $ZZ\gamma\gamma$ coupling the CP -violating term represented by L_6^n does not contribute. These couplings are assumed to be real and to vanish at tree level in the Standard Model.

Within the same framework as above, a more recent description of the quartic couplings [3] treats the anomalous parts of the $WW\gamma\gamma$ and $ZZ\gamma\gamma$ couplings separately, leading to two sets parametrized as a_0^V/Λ^2 and a_c^V/Λ^2 , where $V = W$ or Z .

With the discovery of a Higgs at the LHC in 2012, it is then useful to go to the next higher dimensional representation (dimension 8 operators) in which the gauge symmetry is broken by the conventional Higgs scalar doublet [3,4]. There are 14 operators which can contribute to the anomalous quartic coupling signal. Some of the operators have analogues in the dimension 6 scheme. The CMS collaboration, [5], have used this parametrization, in which the connections between the two schemes are also summarized:

$$\begin{aligned} \mathcal{L}_{AQGC} &= -\frac{e^2 a_0^W}{8 \Lambda^2} F_{\mu\nu} F^{\mu\nu} W^{+\alpha} W_a^- \\ &\quad -\frac{e^2 a_c^W}{16 \Lambda^2} F_{\mu\nu} F^{\mu\alpha} (W^{+\nu} W_a^- + W^{-\nu} W_a^+) \\ &\quad -e^2 g^2 \frac{\kappa_0^W}{\Lambda^2} F_{\mu\nu} Z^{\mu\nu} W^{+\alpha} W_a^- \\ &\quad -\frac{e^2 g^2 \kappa_c^W}{2 \Lambda^2} F_{\mu\nu} Z^{\mu\alpha} (W^{+\nu} W_a^- + W^{-\nu} W_a^+) \\ &\quad + \frac{f_{T,0}}{\Lambda^4} Tr[\widehat{W}_{\mu\nu} \widehat{W}^{\mu\nu}] \times Tr[\widehat{W}_{\alpha\beta} \widehat{W}^{\alpha\beta}] \end{aligned}$$

The energy scale of possible new physics is Λ , and $g = e/\sin(\theta_W)$, e being the unit electric charge and θ_W the Weinberg angle. The field tensors are described in [3,4].

The two dimension 6 operators a_0^W/Λ^2 and a_c^W/Λ^2 are associated with the $WW\gamma\gamma$ vertex. Among dimension 8 operators, κ_0^W/Λ^2 and κ_c^W/Λ^2 are associated with the $WWZ\gamma$ vertex, whereas the parameter $f_{T,0}/\Lambda^4$ contributes to both vertices. There is a relationship between these two dimension 6 parameters and the dimension 8 parameters $f_{M,i}/\Lambda^4$ as follows [3]:

$$\frac{a_0^W}{\Lambda^2} = -\frac{4M_W^2}{g^2} \frac{f_{M,0}}{\Lambda^4} - \frac{8M_W^2}{g'^2} \frac{f_{M,2}}{\Lambda^4}$$

$$\frac{a_c^W}{\Lambda^2} = -\frac{4M_W^2}{g^2} \frac{f_{M,1}}{\Lambda^4} - \frac{8M_W^2}{g'^2} \frac{f_{M,3}}{\Lambda^4}$$

where $g' = e/\cos(\theta_W)$ and M_W is the invariant mass of the W boson. This relation provides a translation between limits on dimension 6 operators $a_{0,c}^W$ and $f_{M,j}/\Lambda^4$. It is further required [4] that $f_{M,0} = 2f_{M,2}$ and $f_{M,1} = 2f_{M,3}$ which suppresses contributions to the $WWZ\gamma$ vertex. The complete set of Lagrangian contributions as presented in [4] corresponds to 19 anomalous couplings in total – $f_{S,i}$, $i = 1, 2$, $f_{M,i}$, $i = 0, \dots, 8$ and $f_{T,i}$, $i = 0, \dots, 9$ – each scaled by $1/\Lambda^4$.

The ATLAS collaboration [6], on the other hand, follows a K-matrix driven approach of Ref. 7 in which the anomalous couplings can be expressed in terms of two parameters α_4 and α_5 , which account for all BSM effects.

It is the early stages in the determination of quartic couplings by the LHC experiments. It is hoped that the two collaborations, ATLAS and CMS, will agree to use at least one common set of parameters to express these limits to enable the reader to make a comparison and allow for a possible LHC combination.

References

1. G. Belanger and F. Boudjema, Phys. Lett. **B288**, 201 (1992).
2. J.W. Stirling and A. Werthenbach, Eur. Phys. J. **C14**, 103 (2000);
J.W. Stirling and A. Werthenbach, Phys. Lett. **B466**, 369 (1999);
A. Denner *et al.*, Eur. Phys. J. **C20**, 201 (2001);
G. Montagna *et al.*, Phys. Lett. **B515**, 197 (2001).
3. G. Belanger *et al.*, Eur. Phys. J. **C13**, 283 (2000).
4. O.J.P. Éboli, M.C. Gonzalez-Garcia, and S.M. Lietti, Phys. Rev. **D69**, 095005 (2004);
O.J.P. Éboli, M.C. Gonzalez-Garcia, and J.K. Mizukoshi, Phys. Rev. **D77**, 073005 (2006).
5. S. Chatrchyan *et al.*, Phys. Rev. **D90**, 032008 (2014);
S. Chatrchyan *et al.*, Phys. Rev. Lett. **114**, 051801 (2015).
6. G. Aad *et al.*, Phys. Rev. Lett. **113**, 141803 (2014).
7. A. Albateanu, W. Killian, and J. Reuter, JHEP **0811**, 010 (2008).

$a_0/\Lambda^2, a_c/\Lambda^2$

Combining published and unpublished preliminary LEP results the following 95% CL intervals for the QGCs associated with the $ZZ\gamma\gamma$ vertex are derived (CERN-PH-EP/2005-051 or hep-ex/0511027):

$$\begin{aligned} -0.008 < a_0^Z/\Lambda^2 < +0.021 \\ -0.029 < a_c^Z/\Lambda^2 < +0.039 \end{aligned}$$

Anomalous Z quartic couplings have also been measured by the Tevatron and LHC experiments. As discussed in the review on "Anomalous W/Z quartic couplings," the coupling parameters in the Anomalous QGC Lagrangian may relate to processes involving only the W or only to the Z or to both. Thus, results on all other AQGCs are reported together in the W listings.

VALUE	DOCUMENT ID	TECN
•••	We do not use the following data for averages, fits, limits, etc. •••	
1	ABBIENDI	04L OPAL
2	HEISTER	04A ALEP
3	ACHARD	02G L3

- 1** ABBIENDI 04L select $20 e^+ e^- \rightarrow \nu \bar{\nu} \gamma \gamma$ acoplanar events in the energy range 180–209 GeV and $176 e^+ e^- \rightarrow q \bar{q} \gamma \gamma$ events in the energy range 130–209 GeV. These samples are used to constrain possible anomalous $W^+ W^- \gamma \gamma$ and $Z Z \gamma \gamma$ quartic couplings. Further combining with the $W^+ W^- \gamma$ sample of ABBIENDI 04B the following one-parameter 95% CL limits are obtained: $-0.007 < a_0^Z/\Lambda^2 < 0.023 \text{ GeV}^{-2}$, $-0.029 < a_C^Z/\Lambda^2 < 0.029 \text{ GeV}^{-2}$, $-0.020 < a_0^W/\Lambda^2 < 0.020 \text{ GeV}^{-2}$, $-0.052 < a_C^W/\Lambda^2 < 0.037 \text{ GeV}^{-2}$.
- 2** In the CM energy range 183 to 209 GeV HEISTER 04A select $30 e^+ e^- \rightarrow \nu \bar{\nu} \gamma \gamma$ events with two acoplanar, high energy and high transverse momentum photons. The photon-photon acoplanarity is required to be $> 5^\circ$, $E_\gamma/\sqrt{s} > 0.025$ (the more energetic photon having energy $> 0.2 \sqrt{s}$), $p_{T\gamma}/E_{\text{beam}} > 0.05$ and $|\cos \theta_\gamma| < 0.94$. A likelihood fit to the photon energy and recoil missing mass yields the following one-parameter 95% CL limits: $-0.012 < a_0^Z/\Lambda^2 < 0.019 \text{ GeV}^{-2}$, $-0.041 < a_C^Z/\Lambda^2 < 0.044 \text{ GeV}^{-2}$, $-0.060 < a_0^W/\Lambda^2 < 0.055 \text{ GeV}^{-2}$, $-0.099 < a_C^W/\Lambda^2 < 0.093 \text{ GeV}^{-2}$.
- 3** ACHARD 02c study $e^+ e^- \rightarrow Z \gamma \gamma \rightarrow q \bar{q} \gamma \gamma$ events using data at center-of-mass energies from 200 to 209 GeV. The photons are required to be isolated, each with energy $> 5 \text{ GeV}$ and $|\cos \theta| < 0.97$, and the di-jet invariant mass to be compatible with that of the Z boson (74–111 GeV). Cuts on Z velocity ($\beta < 0.73$) and on the energy of the most energetic photon reduce the backgrounds due to non-resonant production of the $q \bar{q} \gamma \gamma$ state and due to ISR respectively, yielding a total of 40 candidate events of which 8.6 are expected to be due to background. The energy spectra of the least energetic photon are fitted for all ten center-of-mass energy values from 130 GeV to 209 GeV (as obtained adding to the present analysis 130–202 GeV data of ACCIARRI 01E, for a total of 137 events with an expected background of 34.1 events) to obtain the fitted values $a_0/\Lambda^2 = 0.00 \pm 0.02 \text{ GeV}^{-2}$ and $a_C/\Lambda^2 = 0.03 \pm 0.01 \text{ GeV}^{-2}$, where the other parameter is kept fixed to its Standard Model value (0). A simultaneous fit to both parameters yields the 95% CL limits $-0.02 \text{ GeV}^{-2} < a_0/\Lambda^2 < 0.03 \text{ GeV}^{-2}$ and $-0.07 \text{ GeV}^{-2} < a_C/\Lambda^2 < 0.05 \text{ GeV}^{-2}$.

Z REFERENCES

AABOUD 19AY JHEP 1910 127
 AABOUD 19N JHEP 1904 048
 RAINBOLT 19 PR D99 013004
 SIRUNYAN 19AJ EPJ C79 94
 SIRUNYAN 19BR PL B797 134811
 AABOUD 18AL JHEP 1807 127
 AABOUD 18BL PL B786 134
 AABOUD 18CM PR D98 092010
 AABOUD 18Q PR D97 032005
 AAU 18AR JHEP 1809 159
 ANDREEV 18A EPJ C78 777
 SIRUNYAN 18BT EPJ C78 165
 SIRUNYAN 18DZ PRL 121 141801
 AABOUD 17Q EPJ C77 367
 AABOUD 16K PRL 117 111802
 AAD 16L EPJ C76 210
 AAD 16Q PR D93 112002
 ABRAMOWICZ 16A PR D93 02002
 ABT 16 PR D94 052007
 KHACHATRYAN 16AF PL B760 448
 KHACHATRYAN 16CC PL B763 280
 AAD 15B JHEP 1509 049
 AAD 15I PRL 114 121801
 KHACHATRYAN 15AC JHEP 1504 164
 KHACHATRYAN 15BC PL B740 250
 KHACHATRYAN 15BC EPJ C75 511
 AAD 14AU PR D90 072010
 AAD 14N PRL 112 231806
 AALTONEN 14E PRL 112 111803
 CHATRCHYAN 14AB PR D89 092005
 AAD 13AN PR D87 112003
 Also PR D91 119901 (erratum)
 AAD 13Z JHEP 1303 128
 CHATRCHYAN 13B JHEP 1301 063
 CHATRCHYAN 13BI JHEP 1310 164
 SCHAE 13A PRPL 532 119
 AAD 12XB PL B717 49
 ABAZOV 12S PR D85 052001
 CHATRCHYAN 12BM JHEP 1212 034
 AALTONEN 11S PRL 107 051802
 AABOUD 11D PR D84 012007
 CHATRCHYAN 11M PL B701 535
 ABAZOV 09L PRL 102 201802
 BEDDALL 09 PL B670 300
 SCHAE 09 JHEP 0904 124
 ABAZOV 08K PRL 100 131801
 ABAZOV 07M PL B653 378
 ABDALLAH 07C EPJ C51 525
 ABDALLAH 06E PL B639 179
 AKTAS 06 PL B632 35
 LEP-SLC 06 PRL 427 257
 SCHAE 06A PL B639 192
 ABDALLAH 05 EPJ C40 1
 ABDALLAH 05C EPJ C44 299
 ABE 05 PRL 94 091801
 ABE 05F PR D71 112004
 ACOSTA 05M PR D71 052002
 ABBIENDI 04B PL B580 17
 ABBIENDI 04C EPJ C32 303
 ABBIENDI 04E PL B586 167
 ABBIENDI 04G EPJ C33 173
 ABBIENDI 04L PR D70 032005
 ABDALLAH 04F EPJ C34 109
 ABE 04C PR D69 072003
 ACHARD 04C PL B585 42
 ACHARD 04H PL B597 119
 HEISTER 04A PL B602 31
 ABBIENDI 03P PL B577 18
 ABDALLAH 03H PL B569 129
 ABDALLAH 03K PL B576 29
 ABE 03F PRL 90 141804
 ACHARD 03D PL B572 133
 ACHARD 03G PL B577 109
 ABBIENDI 02I PL B548 29
 ABE 02G PRL 88 151801
 ACHARD 02G PL B540 43
 HEISTER 02B PL B526 34
 HEISTER 02C PL B528 19

HEISTER 02H EPJ C24 177
 ABBIENDI 01A EPJ C19 587
 ABBIENDI 01G EPJ C18 447
 ABBIENDI 01K PL B516 1
 ABBIENDI 01N EPJ C20 445
 ABBIENDI 01O EPJ C21 1
 ABE 01B PRL 86 1162
 ABE 01C PR D63 032005
 ACCIARRI 01E PL B505 47
 ACCIARRI 01I PL B497 23
 HEISTER 01I EPJ C20 401
 HEISTER 01D EPJ C22 201
 ABBIENDI 00N PL B476 256
 ABBIENDI,G 00C EPJ C17 553
 ABE 00B PRL 84 5945
 ABE 00D PRL 85 5059
 ABREU 00E EPJ C12 225
 ABREU 00B EPJ C14 613
 ABREU 00E EPJ C14 585
 ABREU 00F EPJ C16 371
 ABREU 00P PL B475 429
 ACCIARRI 00E EPJ C13 47
 ACCIARRI 00C EPJ C16 1
 ACCIARRI 00Q PL B479 79
 ACCIARRI 00J PL B489 93
 BARATE 00E EPJ C16 597
 BARATE 00C EPJ C14 1
 BARATE 00O EPJ C16 613
 ABBIENDI 99B EPJ C8 217
 ABBIENDI 99I PL B447 157
 ABE 99E PR D59 052001
 ABE 99L PRL 83 1902
 ABREU 99E EPJ C6 19
 ABREU 99B EPJ C10 415
 ABREU 99J PL B449 364
 ABREU 99U PL B462 425
 ABREU 99Y EPJ C10 219
 ACCIARRI 99D PL B448 152
 ACCIARRI 99F PL B453 94
 ACCIARRI 99G PL B450 281
 ACCIARRI 99O PL B465 363
 ABBOTT 98M PR D52 0817
 ABE 98D PRL 80 660
 ABE 98I PRL 81 942
 ABREU 98K PL B423 194
 ABREU 98L EPJ C5 585
 ACCIARRI 98G PL B431 199
 ACCIARRI 98H PL B429 387
 ACCIARRI 98U PL B439 225
 ACKERSTAFF 98A EPJ C5 411
 ACKERSTAFF 98E EPJ C1 439
 ACKERSTAFF 98O PL B420 157
 ACKERSTAFF 98Q EPJ C4 19
 BARATE 98M PL B434 415
 BARATE 98T EPJ C4 557
 BARATE 98V EPJ C5 205
 ABE 97 PRL 78 17
 ABREU 97C ZPHY C73 243
 ABREU 97E PL B398 207
 ABREU 97G PL B404 194
 ACCIARRI 97D PL B393 465
 ACCIARRI 97J PL B407 351
 ACCIARRI 97L PL B407 389
 ACCIARRI 97R PL B413 167
 ACKERSTAFF 97M ZPHY C74 413
 ACKERSTAFF 97S PL B412 210
 ACKERSTAFF 97T ZPHY C76 387
 ACKERSTAFF 97W ZPHY C76 425
 ALEXANDER 97C ZPHY C73 379
 ALEXANDER 97D ZPHY C73 569
 ALEXANDER 97E ZPHY C73 587
 BARATE 97E PL B405 191
 BARATE 97F PL B401 150
 BARATE 97G PL B401 163
 BARATE 97H PL B404 213
 BARATE 97J ZPHY C74 451
 ABREU 96R ZPHY C72 31
 ABREU 96S PL B389 405
 ABREU 96U ZPHY C73 61
 ACCIARRI 96 PL B371 126
 ADAM 96 ZPHY C69 561
 ADAM 96B ZPHY C70 371
 ALEXANDER 96B ZPHY C70 197
 ALEXANDER 96F PL B370 185
 ALEXANDER 96N PL B384 343
 ALEXANDER 96R ZPHY C72 1
 BUSKULIC 96D ZPHY C69 393
 BUSKULIC 96H ZPHY C69 379
 BUSKULIC 96T PL B384 449
 BUSKULIC 96Y PL B388 648
 ABE 95J PRL 74 2880
 ABREU 95 ZPHY C65 709 (erratum)
 ABREU 95D ZPHY C66 323
 ABREU 95M ZPHY C65 587
 ABREU 95P ZPHY C65 603
 ABREU 95R ZPHY C67 543
 ABREU 95S ZPHY C68 353
 ABREU 95V ZPHY C68 541
 ABREU 95W PL B361 207
 ABREU 95X ZPHY C69 1
 ACCIARRI 95B PL B345 589
 ACCIARRI 95C PL B345 609
 ACCIARRI 95G PL B353 136
 AKERS 95C ZPHY C65 47
 AKERS 95U ZPHY C67 389
 AKERS 95V ZPHY C67 555
 AKERS 95Z ZPHY C68 203
 AKERS 95Z ZPHY C68 203
 ALEXANDER 95D PL B358 162
 BUSKULIC 95R ZPHY C69 15
 MIYABAYASHI 95 PL B347 171
 ABE 94C PRL 73 25
 ABREU 94B PL B327 386
 ABREU 94P PL B341 109
 AKERS 94 ZPHY C63 181
 BUSKULIC 94G ZPHY C62 179
 BUSKULIC 94J ZPHY C62 1
 VILAIN 94 PL B320 203
 ABREU 93Z PL B229 236
 ABREU 93I ZPHY C59 533
 Also ZPHY C65 709 (erratum)
 ABREU 93L PL B318 249

Downloaded from https://academic.oup.com/ptep/article/2020/08/30/15891211 by guest on 20 August 2020

Gauge & Higgs Boson Particle Listings

 Z, H^0

ACTON	93	PL B305 407	P.D. Acton <i>et al.</i>	(OPAL Collab.)
ACTON	93D	ZPHY C58 219	P.D. Acton <i>et al.</i>	(OPAL Collab.)
ACTON	93E	PL B311 391	P.D. Acton <i>et al.</i>	(OPAL Collab.)
ADRIANI	93	PL B301 136	O. Adriani <i>et al.</i>	(L3 Collab.)
ADRIANI	93I	PL B316 427	O. Adriani <i>et al.</i>	(L3 Collab.)
BUSKULIC	93L	PL B313 520	D. Buskulic <i>et al.</i>	(ALEPH Collab.)
NOVIKOV	93C	PL B298 453	V.A. Novikov, L.B. Okun, M.I. Vysotsky	(DELPHI Collab.)
ABREU	92I	PL B277 371	P. Abreu <i>et al.</i>	(DELPHI Collab.)
ABREU	92M	PL B289 199	P. Abreu <i>et al.</i>	(DELPHI Collab.)
ACTON	92B	ZPHY C53 539	D.P. Acton <i>et al.</i>	(OPAL Collab.)
ACTON	92L	PL B294 436	P.D. Acton <i>et al.</i>	(OPAL Collab.)
ACTON	92N	PL B295 357	P.D. Acton <i>et al.</i>	(OPAL Collab.)
ADEVA	92	PL B275 209	B. Adeva <i>et al.</i>	(L3 Collab.)
ADRIANI	92D	PL B292 454	O. Adriani <i>et al.</i>	(L3 Collab.)
ALITTI	92B	PL B276 354	J. Alitti <i>et al.</i>	(UA2 Collab.)
BUSKULIC	92D	PL B292 210	D. Buskulic <i>et al.</i>	(ALEPH Collab.)
BUSKULIC	92E	PL B294 145	D. Buskulic <i>et al.</i>	(ALEPH Collab.)
DECAMP	92	PRL 216 253	D. Decamp <i>et al.</i>	(CDF Collab.)
ABE	91E	PRL 67 1502	F. Abe <i>et al.</i>	(CDF Collab.)
ABREU	91H	ZPHY C50 185	F. Abreu <i>et al.</i>	(DELPHI Collab.)
ACTON	91B	PL B273 338	D.P. Acton <i>et al.</i>	(OPAL Collab.)
ADACHI	91	PL B255 613	I. Adachi <i>et al.</i>	(TOPAZ Collab.)
ADEVA	91I	PL B259 199	B. Adeva <i>et al.</i>	(L3 Collab.)
AKRAWY	91F	PL B257 531	M.Z. Akrawy <i>et al.</i>	(OPAL Collab.)
DECAMP	91B	PL B259 377	D. Decamp <i>et al.</i>	(ALEPH Collab.)
DECAMP	91J	PL B266 218	D. Decamp <i>et al.</i>	(ALEPH Collab.)
JACOBSEN	91	PRL 67 3347	R.G. Jacobsen <i>et al.</i>	(Mark II Collab.)
SHIMONAKA	91	PL B268 457	A. Shimonaka <i>et al.</i>	(TOPAZ Collab.)
ABE	90I	ZPHY C48 13	K. Abe <i>et al.</i>	(VENUS Collab.)
ABRAMS	90	PRL 64 1334	G.S. Abrams <i>et al.</i>	(Mark II Collab.)
AKRAWY	90J	PL B246 205	M.Z. Akrawy <i>et al.</i>	(OPAL Collab.)
BEHREND	90D	ZPHY C47 333	H.J. Behrend <i>et al.</i>	(CELLO Collab.)
BRAUNSCHEWIG	90	ZPHY C48 433	W. Braunschweig <i>et al.</i>	(TASSO Collab.)
ELSEN	90	ZPHY C46 349	E. Elsen <i>et al.</i>	(JADE Collab.)
HEGNER	90	ZPHY C46 547	S. Hegner <i>et al.</i>	(JADE Collab.)
STUART	90	PRL 64 983	D. Stuart <i>et al.</i>	(AMY Collab.)
ABE	89	PRL 62 613	F. Abe <i>et al.</i>	(CDF Collab.)
ABE	89C	PRL 63 720	F. Abe <i>et al.</i>	(CDF Collab.)
ABE	89L	PL B232 425	K. Abe <i>et al.</i>	(VENUS Collab.)
ABRAMS	89B	PRL 63 2173	G.S. Abrams <i>et al.</i>	(Mark II Collab.)
ABRAMS	89D	PRL 63 2780	G.S. Abrams <i>et al.</i>	(Mark II Collab.)
ALBAJAR	89	ZPHY C44 15	C. Albajar <i>et al.</i>	(UA1 Collab.)
BACALA	89	PL B218 112	A. Bacala <i>et al.</i>	(AMY Collab.)
BAND	89	PL B218 369	H.R. Band <i>et al.</i>	(MAC Collab.)
GREENSHAW	89	ZPHY C42 1	T. Greenshaw <i>et al.</i>	(JADE Collab.)
OULD-SAAD	89	ZPHY C44 567	F. Ould-Saada <i>et al.</i>	(JADE Collab.)
SAGAWA	89	PRL 63 2341	H. Sagawa <i>et al.</i>	(AMY Collab.)
ADACHI	88C	PL B208 319	I. Adachi <i>et al.</i>	(TOPAZ Collab.)
ADEVA	88	PL D38 2665	B. Adeva <i>et al.</i>	(Mark-J Collab.)
BRAUNSCHEWIG	88D	ZPHY C40 163	W. Braunschweig <i>et al.</i>	(TASSO Collab.)
ANSARI	87	PL B186 440	R. Ansari <i>et al.</i>	(UA2 Collab.)
BEHREND	87C	PL B191 209	H.J. Behrend <i>et al.</i>	(CELLO Collab.)
BARTEL	86C	ZPHY C30 371	W. Bartel <i>et al.</i>	(JADE Collab.)
Also		ZPHY C26 507	W. Bartel <i>et al.</i>	(JADE Collab.)
Also		PL 108B 140	W. Bartel <i>et al.</i>	(JADE Collab.)
ASH	85	PRL 55 1831	W.W. Ash <i>et al.</i>	(MAC Collab.)
BARTEL	85F	PL 161B 188	W. Bartel <i>et al.</i>	(JADE Collab.)
DERRICK	85	PR D31 2352	M. Derrick <i>et al.</i>	(HRS Collab.)
FERNANDEZ	85	PRL 54 1624	E. Fernandez <i>et al.</i>	(MAC Collab.)
LEVI	83	PRL 51 1941	M.E. Levi <i>et al.</i>	(Mark II Collab.)
BEHREND	82	PL 114B 282	H.J. Behrend <i>et al.</i>	(CELLO Collab.)
BRANDELIK	82C	PL 110B 173	R. Brandelik <i>et al.</i>	(TASSO Collab.)

 H^0 $J = 0$

In the following H^0 refers to the signal that has been discovered in the Higgs searches. Whereas the observed signal is labeled as a spin 0 particle and is called a Higgs Boson, the detailed properties of H^0 and its role in the context of electroweak symmetry breaking need to be further clarified. These issues are addressed by the measurements listed below.

Concerning mass limits and cross section limits that have been obtained in the searches for neutral and charged Higgs bosons, see the sections "Searches for Neutral Higgs Bosons" and "Searches for Charged Higgs Bosons (H^\pm and $H^{\pm\pm}$)", respectively.

 H^0 MASS

VALUE (GeV)	DOCUMENT ID	TECN	COMMENT
125.10 ± 0.14 OUR AVERAGE			
124.86 ± 0.27	1 AABOUD	18BM ATLS	$pp, 13 \text{ TeV}, 36.1 \text{ fb}^{-1}, \gamma\gamma, ZZ^* \rightarrow 4\ell$
125.26 ± 0.20 ± 0.08	2 SIRUNYAN	17AV CMS	$pp, 13 \text{ TeV}, ZZ^* \rightarrow 4\ell$
125.09 ± 0.21 ± 0.11	1,3 AAD	15B LHC	$pp, 7, 8 \text{ TeV}$
••• We do not use the following data for averages, fits, limits, etc. •••			
124.79 ± 0.37	4 AABOUD	18BM ATLS	$pp, 13 \text{ TeV}, 36.1 \text{ fb}^{-1}, ZZ^* \rightarrow 4\ell$
124.93 ± 0.40	5 AABOUD	18BM ATLS	$pp, 13 \text{ TeV}, 36.1 \text{ fb}^{-1}, \gamma\gamma$
124.97 ± 0.24	1,6 AABOUD	18BM ATLS	$pp, 7, 8, 13 \text{ TeV}, \gamma\gamma, ZZ^* \rightarrow 4\ell$
125.07 ± 0.25 ± 0.14	3 AAD	15B LHC	$pp, 7, 8 \text{ TeV}, \gamma\gamma$
125.15 ± 0.37 ± 0.15	3 AAD	15B LHC	$pp, 7, 8 \text{ TeV}, ZZ^* \rightarrow 4\ell$
126.02 ± 0.43 ± 0.27	AAD	15B ATLS	$pp, 7, 8 \text{ TeV}, \gamma\gamma$
124.51 ± 0.52 ± 0.04	AAD	15B ATLS	$pp, 7, 8 \text{ TeV}, ZZ^* \rightarrow 4\ell$
125.59 ± 0.42 ± 0.17	AAD	15B CMS	$pp, 7, 8 \text{ TeV}, ZZ^* \rightarrow 4\ell$
125.02 ± 0.26 ± 0.14 0.27 ± 0.15	7 KHACHATRYAN	15AM CMS	$pp, 7, 8 \text{ TeV}$
125.36 ± 0.37 ± 0.18	1,8 AAD	14W ATLS	$pp, 7, 8 \text{ TeV}$
125.98 ± 0.42 ± 0.28	8 AAD	14W ATLS	$pp, 7, 8 \text{ TeV}, \gamma\gamma$

124.51 ± 0.52 ± 0.06	8 AAD	14W ATLS	$pp, 7, 8 \text{ TeV}, ZZ^* \rightarrow 4\ell$
125.6 ± 0.4 ± 0.2	9 CHATRCHYAN	14AA CMS	$pp, 7, 8 \text{ TeV}, ZZ^* \rightarrow 4\ell$
122 ± 7	10 CHATRCHYAN	14K CMS	$pp, 7, 8 \text{ TeV}, \tau\tau$
124.70 ± 0.31 ± 0.15	11 KHACHATRYAN	14P CMS	$pp, 7, 8 \text{ TeV}, \gamma\gamma$
125.5 ± 0.2 +0.5 -0.6	1,12 AAD	13AK ATLS	$pp, 7, 8 \text{ TeV}$
126.8 ± 0.2 ± 0.7	12 AAD	13AK ATLS	$pp, 7, 8 \text{ TeV}, \gamma\gamma$
124.3 +0.6 +0.5 -0.5 -0.3	12 AAD	13AK ATLS	$pp, 7, 8 \text{ TeV}, ZZ^* \rightarrow 4\ell$
125.8 ± 0.4 ± 0.4	1,13 CHATRCHYAN	13J CMS	$pp, 7, 8 \text{ TeV}$
126.2 ± 0.6 ± 0.2	13 CHATRCHYAN	13J CMS	$pp, 7, 8 \text{ TeV}, ZZ^* \rightarrow 4\ell$
126.0 ± 0.4 ± 0.4	1,14 AAD	12AI ATLS	$pp, 7, 8 \text{ TeV}$
125.3 ± 0.4 ± 0.5	1,15 CHATRCHYAN	12N CMS	$pp, 7, 8 \text{ TeV}$

1 Combined value from $\gamma\gamma$ and $ZZ^* \rightarrow 4\ell$ final states.

2 SIRUNYAN 17AV use 35.9 fb^{-1} of pp collisions at $E_{\text{cm}} = 13 \text{ TeV}$ with $H^0 \rightarrow ZZ^* \rightarrow 4\ell$ where $\ell = e, \mu$.

3 ATLAS and CMS data are fitted simultaneously.

4 AABOUD 18BM use 36.1 fb^{-1} of pp collisions at $E_{\text{cm}} = 13 \text{ TeV}$ with $H^0 \rightarrow ZZ^* \rightarrow 4\ell$ where $\ell = e, \mu$.

5 AABOUD 18BM use 36.1 fb^{-1} of pp collisions at $E_{\text{cm}} = 13 \text{ TeV}$ with $H^0 \rightarrow \gamma\gamma$.

6 AABOUD 18BM combine 13 TeV results with 7 and 8 TeV results. Other combined results are summarized in their Fig. 4.

7 KHACHATRYAN 15AM use up to 5.1 fb^{-1} of pp collisions at $E_{\text{cm}} = 7 \text{ TeV}$ and up to 19.7 fb^{-1} at $E_{\text{cm}} = 8 \text{ TeV}$.

8 AAD 14W use 4.5 fb^{-1} of pp collisions at $E_{\text{cm}} = 7 \text{ TeV}$ and 20.3 fb^{-1} at 8 TeV.

9 CHATRCHYAN 14AA use 5.1 fb^{-1} of pp collisions at $E_{\text{cm}} = 7 \text{ TeV}$ and 19.7 fb^{-1} at $E_{\text{cm}} = 8 \text{ TeV}$.

10 CHATRCHYAN 14K use 4.9 fb^{-1} of pp collisions at $E_{\text{cm}} = 7 \text{ TeV}$ and 19.7 fb^{-1} at $E_{\text{cm}} = 8 \text{ TeV}$.

11 KHACHATRYAN 14P use 5.1 fb^{-1} of pp collisions at $E_{\text{cm}} = 7 \text{ TeV}$ and 19.7 fb^{-1} at $E_{\text{cm}} = 8 \text{ TeV}$.

12 AAD 13AK use 4.7 fb^{-1} of pp collisions at $E_{\text{cm}} = 7 \text{ TeV}$ and 20.7 fb^{-1} at $E_{\text{cm}} = 8 \text{ TeV}$. Superseded by AAD 14W.

13 CHATRCHYAN 13J use 5.1 fb^{-1} of pp collisions at $E_{\text{cm}} = 7 \text{ TeV}$ and 12.2 fb^{-1} at $E_{\text{cm}} = 8 \text{ TeV}$.

14 AAD 12AI obtain results based on 4.6–4.8 fb^{-1} of pp collisions at $E_{\text{cm}} = 7 \text{ TeV}$ and 5.8–5.9 fb^{-1} at $E_{\text{cm}} = 8 \text{ TeV}$. An excess of events over background with a local significance of 5.9 σ is observed at $m_{H^0} = 126 \text{ GeV}$. See also AAD 12DA.

15 CHATRCHYAN 12N obtain results based on 4.9–5.1 fb^{-1} of pp collisions at $E_{\text{cm}} = 7 \text{ TeV}$ and 5.1–5.3 fb^{-1} at $E_{\text{cm}} = 8 \text{ TeV}$. An excess of events over background with a local significance of 5.0 σ is observed at about $m_{H^0} = 125 \text{ GeV}$. See also CHATRCHYAN 12BY and CHATRCHYAN 13J.

 H^0 SPIN AND CP PROPERTIES

The observation of the signal in the $\gamma\gamma$ final state rules out the possibility that the discovered particle has spin 1, as a consequence of the Landau-Yang theorem. This argument relies on the assumptions that the decaying particle is an on-shell resonance and that the decay products are indeed two photons rather than two pairs of boosted photons, which each could in principle be misidentified as a single photon.

Concerning distinguishing the spin 0 hypothesis from a spin 2 hypothesis, some care has to be taken in modelling the latter in order to ensure that the discriminating power is actually based on the spin properties rather than on unphysical behavior that may affect the model of the spin 2 state.

Under the assumption that the observed signal consists of a single state rather than an overlap of more than one resonance, it is sufficient to discriminate between distinct hypotheses in the spin analyses. On the other hand, the determination of the CP properties is in general much more difficult since in principle the observed state could consist of any admixture of CP-even and CP-odd components. As a first step, the compatibility of the data with distinct hypotheses of pure CP-even and pure CP-odd states with different spin assignments has been investigated. In order to treat the case of a possible mixing of different CP states, certain cross section ratios are considered. Those cross section ratios need to be distinguished from the amount of mixing between a CP-even and a CP-odd state, as the cross section ratios depend in addition also on the coupling strengths of the CP-even and CP-odd components to the involved particles. A small relative coupling implies a small sensitivity of the corresponding cross section ratio to effects of CP mixing.

VALUE	DOCUMENT ID	TECN	COMMENT
••• We do not use the following data for averages, fits, limits, etc. •••			
1	SIRUNYAN	19BL CMS	$pp, 7, 8, 13 \text{ TeV}, ZZ^* / ZZ \rightarrow 4\ell$
2	SIRUNYAN	19BZ CMS	$pp \rightarrow H^0 + 2\text{jets (VBF, ggF, V H)}, H^0 \rightarrow \tau\tau, 13 \text{ TeV}$
3	AABOUD	18AJ ATLS	$H^0 \rightarrow ZZ^* \rightarrow 4\ell (\ell = e, \mu), 13 \text{ TeV}$
4	SIRUNYAN	17AM CMS	$pp \rightarrow H^0 + \geq 2\ell, H^0 \rightarrow 4\ell (\ell = e, \mu)$
5	AAD	16 ATLS	$H^0 \rightarrow \gamma\gamma$
6	AAD	16BL ATLS	$pp \rightarrow H^0 jjX (\text{VBF}), H^0 \rightarrow \tau\tau, 8 \text{ TeV}$
7	KHACHATRYAN	16AB CMS	$pp \rightarrow WH^0, ZH^0, H^0 \rightarrow b\bar{b}, 8 \text{ TeV}$
8	AAD	15AX ATLS	$H^0 \rightarrow WW^*$
9	AAD	15CI ATLS	$H^0 \rightarrow ZZ^*, WW^*, \gamma\gamma$
10	AALTONEN	15 TEVA	$p\bar{p} \rightarrow WH^0, ZH^0, H^0 \rightarrow b\bar{b}$
11	AALTONEN	15B CDF	$p\bar{p} \rightarrow WH^0, ZH^0, H^0 \rightarrow b\bar{b}$
12	KHACHATRYAN	15Y CMS	$H^0 \rightarrow 4\ell, WW^*, \gamma\gamma$
13	ABAZOV	14F D0	$p\bar{p} \rightarrow WH^0, ZH^0, H^0 \rightarrow b\bar{b}$
14	CHATRCHYAN	14AA CMS	$H^0 \rightarrow ZZ^*$
15	CHATRCHYAN	14G CMS	$H^0 \rightarrow WW^*$
16	KHACHATRYAN	14P CMS	$H^0 \rightarrow \gamma\gamma$
17	AAD	13AJ ATLS	$H^0 \rightarrow \gamma\gamma, ZZ^* \rightarrow 4\ell, WW^* \rightarrow \ell\nu\ell\nu$
18	CHATRCHYAN	13J CMS	$H^0 \rightarrow ZZ^* \rightarrow 4\ell$

- ¹ SIRUNYAN 19BL measure the anomalous HVV couplings from on-shell and off-shell production in the 4ℓ final state. Data of 80.2 fb^{-1} at 13 TeV, 19.7 fb^{-1} at 8 TeV, and 5.1 fb^{-1} at 7 TeV are used. See their Tables VI and VII for anomalous HVV couplings of CP -violating and CP -conserving parameters with on- and off-shells.
- ² SIRUNYAN 19BZ constrain anomalous HVV couplings of the Higgs boson with data of 35.9 fb^{-1} at $E_{\text{cm}} = 13 \text{ TeV}$ using Higgs boson candidates with two jets produced in VBF, ggF, and VH that decay to $\tau\tau$. See their Table 2 and Fig. 10, which show 68% CL and 95% CL intervals. Combining those with the $H^0 \rightarrow 4\ell$ (SIRUNYAN 19BL, on-shell scenario), results shown in their Tables 3, 4, and Fig. 11 are obtained. A CP -violating parameter is set to be $f_{a3}\cos(\phi_{a3}) = (0.00 \pm 0.27) \times 10^{-3}$ and CP -conserving parameters are $f_{a2}\cos(\phi_{a2}) = (0.06 \pm 1.04) \times 10^{-3}$, $f_{\Lambda 1}\cos(\phi_{\Lambda 1}) = (0.00 \pm 0.53) \times 10^{-3}$, and $f_{\Lambda 1}^{\prime}\cos(\phi_{\Lambda 1}^{\prime}) = (0.0 \pm 1.1) \times 10^{-3}$.
- ³ AABOUD 18AJ study the tensor structure of the Higgs boson couplings using an effective Lagrangian using 36.1 fb^{-1} of pp collision data at $E_{\text{cm}} = 13 \text{ TeV}$. Constraints are set on the non-Standard-Model CP -even and CP -odd couplings to Z bosons and on the CP -odd coupling to gluons. See their Figs. 9 and 10, and Tables 10 and 11.
- ⁴ SIRUNYAN 17AM constrain anomalous couplings of the Higgs boson with 5.1 fb^{-1} of pp collisions at $E_{\text{cm}} = 7 \text{ TeV}$, 19.7 fb^{-1} at $E_{\text{cm}} = 8 \text{ TeV}$, and 38.6 fb^{-1} at $E_{\text{cm}} = 13 \text{ TeV}$. See their Table 3 and Fig. 3, which show 68% CL and 95% CL intervals. A CP violation parameter f_{a3} is set to be $f_{a3}\cos(\phi_{a3}) = [-0.38, 0.46]$ at 95% CL ($\phi_{a3} = 0$ or π).
- ⁵ AAD 16 study $H^0 \rightarrow \gamma\gamma$ with an effective Lagrangian including CP even and odd terms in 20.3 fb^{-1} of pp collisions at $E_{\text{cm}} = 8 \text{ TeV}$. The data is consistent with the expectations for the Higgs boson of the Standard Model. Limits on anomalous couplings are also given.
- ⁶ AAD 16BL study VBF $H^0 \rightarrow \tau\tau$ with an effective Lagrangian including a CP odd term in 20.3 fb^{-1} of pp collisions at $E_{\text{cm}} = 8 \text{ TeV}$. The measurement is consistent with the expectation of the Standard Model. The CP -mixing parameter \bar{d} (a dimensionless coupling $\bar{d} = -(m_W^2/\Lambda^2)f_{\bar{d}}/W$) is constrained to the interval of $(-0.11, 0.05)$ at 68% CL under the assumption of $\bar{d} = \bar{d}_B$.
- ⁷ KHACHATRYAN 16AB search for anomalous pseudoscalar couplings of the Higgs boson to W and Z with 18.9 fb^{-1} of pp collisions at $E_{\text{cm}} = 8 \text{ TeV}$. See their Table 5 and Figs 5 and 6 for limits on possible anomalous pseudoscalar coupling parameters.
- ⁸ AAD 15AX compare the $J^{CP} = 0^+$ Standard Model assignment with other J^{CP} hypotheses in 20.3 fb^{-1} of pp collisions at $E_{\text{cm}} = 8 \text{ TeV}$, using the process $H^0 \rightarrow WW^* \rightarrow e\nu\mu\nu$. 2^+ hypotheses are excluded at 84.5–99.4%CL, 0^- at 96.5%CL, 0^+ (field strength coupling) at 70.8%CL. See their Fig. 19 for limits on possible CP mixture parameters.
- ⁹ AAD 15CI compare the $J^{CP} = 0^+$ Standard Model assignment with other J^{CP} hypotheses in 4.5 fb^{-1} of pp collisions at $E_{\text{cm}} = 7 \text{ TeV}$ and 20.3 fb^{-1} at $E_{\text{cm}} = 8 \text{ TeV}$, using the processes $H^0 \rightarrow ZZ^* \rightarrow 4\ell$, $H^0 \rightarrow \gamma\gamma$ and combine with AAD 15AX data. 0^+ (field strength coupling), 0^- and several 2^+ hypotheses are excluded at more than 99.9% CL. See their Tables 7–9 for limits on possible CP mixture parameters.
- ¹⁰ AALTONEN 15 combine AALTONEN 15B and ABAZOV 14F data. An upper limit of 0.36 of the Standard Model production rate at 95% CL is obtained both for a 0^- and a 2^+ state. Assuming the SM event rate, the $J^{CP} = 0^-$ (2^+) hypothesis is excluded at the 5.0σ (4.9σ) level.
- ¹¹ AALTONEN 15B compare the $J^{CP} = 0^+$ Standard Model assignment with other J^{CP} hypotheses in 9.45 fb^{-1} of $p\bar{p}$ collisions at $E_{\text{cm}} = 1.96 \text{ TeV}$, using the processes $ZH^0 \rightarrow \ell\ell b\bar{b}$, $WH^0 \rightarrow \ell\nu b\bar{b}$, and $ZH^0 \rightarrow \nu\nu b\bar{b}$. Bounds on the production rates of 0^- and 2^+ (graviton-like) states are set, see their tables II and III.
- ¹² KHACHATRYAN 15Y compare the $J^{CP} = 0^+$ Standard Model assignment with other J^{CP} hypotheses in up to 5.1 fb^{-1} of pp collisions at $E_{\text{cm}} = 7 \text{ TeV}$ and up to 19.7 fb^{-1} at $E_{\text{cm}} = 8 \text{ TeV}$, using the processes $H^0 \rightarrow 4\ell$, $H^0 \rightarrow WW^*$, and $H^0 \rightarrow \gamma\gamma$. 0^- is excluded at 99.98% CL, and several 2^+ hypotheses are excluded at more than 99% CL. Spin 1 models are excluded at more than 99.999% CL in ZZ^* and WW^* modes. Limits on anomalous couplings and several cross section fractions, treating the case of CP -mixed states, are also given.
- ¹³ ABAZOV 14F compare the $J^{CP} = 0^+$ Standard Model assignment with $J^{CP} = 0^-$ and 2^+ (graviton-like coupling) hypotheses in up to 9.7 fb^{-1} of $p\bar{p}$ collisions at $E_{\text{cm}} = 1.96 \text{ TeV}$. They use kinematic correlations between the decay products of the vector boson and the Higgs boson in the final states $ZH \rightarrow \ell\ell b\bar{b}$, $WH \rightarrow \ell\nu b\bar{b}$, and $ZH \rightarrow \nu\nu b\bar{b}$. The 0^- (2^+) hypothesis is excluded at 97.6% CL (99.0% CL). In order to treat the case of a possible mixture of a 0^+ state with another J^{CP} state, the cross section fractions $f_X = \sigma_X/(\sigma_{0^+} + \sigma_X)$ are considered, where $X = 0^-, 2^+$. Values for f_{0^-} (f_{2^+}) above 0.80 (0.67) are excluded at 95% CL under the assumption that the total cross section is that of the SM Higgs boson.
- ¹⁴ CHATRCHYAN 14AA compare the $J^{CP} = 0^+$ Standard Model assignment with various J^{CP} hypotheses in 5.1 fb^{-1} of pp collisions at $E_{\text{cm}} = 7 \text{ TeV}$ and 19.7 fb^{-1} at $E_{\text{cm}} = 8 \text{ TeV}$. $J^{CP} = 0^-$ and 1^{\pm} hypotheses are excluded at 99% CL, and several $J = 2$ hypotheses are excluded at 95% CL. In order to treat the case of a possible mixture of a 0^+ state with another J^{CP} state, the cross section fraction $f_{a3} = |a_3|^2 \sigma_3 / (|a_1|^2 \sigma_1 + |a_2|^2 \sigma_2 + |a_3|^2 \sigma_3)$ is considered, where the case $a_3 = 1$, $a_1 = a_2 = 0$ corresponds to a pure CP -odd state. Assuming $a_2 = 0$, a value for f_{a3} above 0.51 is excluded at 95% CL.
- ¹⁵ CHATRCHYAN 14G compare the $J^{CP} = 0^+$ Standard Model assignment with $J^{CP} = 0^-$ and 2^+ (graviton-like coupling) hypotheses in 4.9 fb^{-1} of pp collisions at $E_{\text{cm}} = 7 \text{ TeV}$ and 19.4 fb^{-1} at $E_{\text{cm}} = 8 \text{ TeV}$. Varying the fraction of the production of the 2^+ state via $g\bar{g}$ and $q\bar{q}$, 2^+ hypotheses are disfavored at CL between 83.7 and 99.8%. The 0^- hypothesis is disfavored against 0^+ at the 65.3% CL.
- ¹⁶ KHACHATRYAN 14P compare the $J^{CP} = 0^+$ Standard Model assignment with a 2^+ (graviton-like coupling) hypothesis in 5.1 fb^{-1} of pp collisions at $E_{\text{cm}} = 7 \text{ TeV}$ and 19.7 fb^{-1} at $E_{\text{cm}} = 8 \text{ TeV}$. Varying the fraction of the production of the 2^+ state via $g\bar{g}$ and $q\bar{q}$, 2^+ hypotheses are disfavored at CL between 71 and 94%.
- ¹⁷ AAD 13AJ compare the spin 0, CP -even hypothesis with specific alternative hypotheses of spin 0, CP -odd, spin 1, CP -even and CP -odd, and spin 2, CP -even models using the

Higgs boson decays $H \rightarrow \gamma\gamma$, $H \rightarrow ZZ^* \rightarrow 4\ell$ and $H \rightarrow WW^* \rightarrow \ell\nu\ell\nu$ and combinations thereof. The data are compatible with the spin 0, CP -even hypothesis, while all other tested hypotheses are excluded at confidence levels above 97.8%.

- ¹⁸ CHATRCHYAN 13J study angular distributions of the lepton pairs in the ZZ^* channel where both Z bosons decay to e or μ pairs. Under the assumption that the observed particle has spin 0, the data are found to be consistent with the pure CP -even hypothesis, while the pure CP -odd hypothesis is disfavored.

H^0 DECAY WIDTH

The total decay width for a light Higgs boson with a mass in the observed range is not expected to be directly observable at the LHC. For the case of the Standard Model the prediction for the total width is about 4 MeV, which is three orders of magnitude smaller than the experimental mass resolution. There is no indication from the results observed so far that the natural width is broadened by new physics effects to such an extent that it could be directly observable. Furthermore, as all LHC Higgs channels rely on the identification of Higgs decay products, the total Higgs width cannot be measured indirectly without additional assumptions. The different dependence of on-peak and off-peak contributions on the total width in Higgs decays to ZZ^* and interference effects between signal and background in Higgs decays to $\gamma\gamma$ can provide additional information in this context. Constraints on the total width from the combination of on-peak and off-peak contributions in Higgs decays to ZZ^* rely on the assumption of equal on- and off-shell effective couplings. Without an experimental determination of the total width or further theoretical assumptions, only ratios of couplings can be determined at the LHC rather than absolute values of couplings.

VALUE (GeV)	CL%	DOCUMENT ID	TECN	COMMENT
0.0032 \pm 0.0028 \pm 0.0022		1 SIRUNYAN	19BL CMS	pp , 7, 8, 13 TeV, $ZZ^*/ZZ \rightarrow 4\ell$
<0.0144	95	2 AABOUD	18BP ATLS	pp , 13 TeV, $ZZ \rightarrow 4\ell, 2\ell 2\nu$
<1.10	95	3 SIRUNYAN	17AV CMS	pp , 13 TeV, $ZZ^* \rightarrow 4\ell$
<0.013	95	4 KHACHATRYAN	16BA CMS	pp , 7, 8 TeV, ZZ^*, WW^*
<1.7	95	5 KHACHATRYAN	15AM CMS	pp , 7, 8 TeV
> 3.5 $\times 10^{-12}$	95	6 KHACHATRYAN	15BA CMS	pp , 7, 8 TeV, flight distance
<5.0	95	7 AAD	14W ATLS	pp , 7, 8 TeV, $\gamma\gamma$
<2.6	95	7 AAD	14W ATLS	pp , 7, 8 TeV, $ZZ^* \rightarrow 4\ell$
• • • We do not use the following data for averages, fits, limits, etc. • • •				
<0.026	95	8 KHACHATRYAN	16BA CMS	pp , 7, 8 TeV, WW^*
<0.0227	95	9 AAD	15BE ATLS	pp , 8 TeV, ZZ^*, WW^*
<0.046	95	10 KHACHATRYAN	15BA CMS	pp , 7, 8 TeV, $ZZ^* \rightarrow 4\ell$
<3.4	95	11 CHATRCHYAN	14AA CMS	pp , 7, 8 TeV, $ZZ^* \rightarrow 4\ell$
<0.022	95	12 KHACHATRYAN	14D CMS	pp , 7, 8 TeV, ZZ^*
<2.4	95	13 KHACHATRYAN	14P CMS	pp , 7, 8 TeV, $\gamma\gamma$

- ¹ SIRUNYAN 19BL measure the width and anomalous HVV couplings from on-shell and off-shell production in the 4ℓ final state. Data of 80.2 fb^{-1} at 13 TeV, 19.7 fb^{-1} at 8 TeV, and 5.1 fb^{-1} at 7 TeV are used. The total width for the SM-like couplings is measured to be also $[0.08, 9.16]$ MeV with 95% CL, assuming SM-like couplings for on- and off-shells (see their Table VIII). Constraints on the total width for anomalous HVV interaction cases are found in their Table IX. See their Table X for the Higgs boson signal strength in the off-shell region.
- ² AABOUD 18BP use 36.1 fb^{-1} at $E_{\text{cm}} = 13 \text{ TeV}$. An observed upper limit on the off-shell Higgs signal strength of 3.8 is obtained at 95% CL using off-shell Higgs boson production in the $ZZ \rightarrow 4\ell$ and $ZZ \rightarrow 2\ell 2\nu$ decay channels ($\ell = e, \mu$). Combining with the on-shell signal strength measurements, the quoted upper limit on the Higgs boson total width is obtained, assuming the ratios of the relevant Higgs-boson couplings to the SM predictions are constant with energy from on-shell production to the high-mass range.
- ³ SIRUNYAN 17AV obtain an upper limit on the width from the $m_{4\ell}$ distribution in $ZZ^* \rightarrow 4\ell$ ($\ell = e, \mu$) decays. Data of 35.9 fb^{-1} pp collisions at $E_{\text{cm}} = 13 \text{ TeV}$ is used. The expected limit is 1.60 GeV.
- ⁴ KHACHATRYAN 16BA combine the WW^* result with ZZ^* results of KHACHATRYAN 15BA and KHACHATRYAN 14D.
- ⁵ KHACHATRYAN 15AM combine $\gamma\gamma$ and $ZZ^* \rightarrow 4\ell$ results. The expected limit is 2.3 GeV.
- ⁶ KHACHATRYAN 15BA derive a lower limit on the total width from an upper limit on the decay flight distance $\tau < 1.9 \times 10^{-13} \text{ s}$. 5.1 fb^{-1} of pp collisions at $E_{\text{cm}} = 7 \text{ TeV}$ and 19.7 fb^{-1} at $E_{\text{cm}} = 8 \text{ TeV}$ are used.
- ⁷ AAD 14W use 4.5 fb^{-1} of pp collisions at $E_{\text{cm}} = 7 \text{ TeV}$ and 20.3 fb^{-1} at 8 TeV. The expected limit is 6.2 GeV.
- ⁸ KHACHATRYAN 16BA derive constraints on the total width from comparing WW^* production via on-shell and off-shell H^0 using 4.9 fb^{-1} of pp collisions at $E_{\text{cm}} = 7 \text{ TeV}$ and 19.4 fb^{-1} at 8 TeV.
- ⁹ AAD 15BE derive constraints on the total width from comparing ZZ^* and WW^* production via on-shell and off-shell H^0 using 20.3 fb^{-1} of pp collisions at $E_{\text{cm}} = 8 \text{ TeV}$. The K factor for the background processes is assumed to be equal to that for the signal.
- ¹⁰ KHACHATRYAN 15BA derive constraints on the total width from comparing ZZ^* production via on-shell and off-shell H^0 with an unconstrained anomalous coupling. 4ℓ final states in 5.1 fb^{-1} of pp collisions at $E_{\text{cm}} = 7 \text{ TeV}$ and 19.7 fb^{-1} at $E_{\text{cm}} = 8 \text{ TeV}$ are used.
- ¹¹ CHATRCHYAN 14AA use 5.1 fb^{-1} of pp collisions at $E_{\text{cm}} = 7 \text{ TeV}$ and 19.7 fb^{-1} at $E_{\text{cm}} = 8 \text{ TeV}$. The expected limit is 2.8 GeV.
- ¹² KHACHATRYAN 14D derive constraints on the total width from comparing ZZ^* production via on-shell and off-shell H^0 . 4ℓ and $\ell\nu\nu\ell$ final states in 5.1 fb^{-1} of pp collisions at $E_{\text{cm}} = 7 \text{ TeV}$ and 19.7 fb^{-1} at $E_{\text{cm}} = 8 \text{ TeV}$ are used.
- ¹³ KHACHATRYAN 14P use 5.1 fb^{-1} of pp collisions at $E_{\text{cm}} = 7 \text{ TeV}$ and 19.7 fb^{-1} at $E_{\text{cm}} = 8 \text{ TeV}$. The expected limit is 3.1 GeV.

Gauge & Higgs Boson Particle Listings

 H^0 H^0 DECAY MODES

Mode	Fraction (Γ_i/Γ)	Confidence level
Γ_1 $W W^*$		
Γ_2 $Z Z^*$		
Γ_3 $\gamma\gamma$		
Γ_4 $b\bar{b}$		
Γ_5 $e^+ e^-$	$<3.6 \times 10^{-4}$	95%
Γ_6 $\mu^+ \mu^-$		
Γ_7 $\tau^+ \tau^-$		
Γ_8 $Z\gamma$		
Γ_9 $\gamma^* \gamma$		
Γ_{10} $J/\psi\gamma$	$<3.5 \times 10^{-4}$	95%
Γ_{11} $J/\psi J/\psi$	$<1.8 \times 10^{-3}$	95%
Γ_{12} $\psi(2S)\gamma$	$<2.0 \times 10^{-3}$	95%
Γ_{13} $\Upsilon(1S)\gamma$	$<4.9 \times 10^{-4}$	95%
Γ_{14} $\Upsilon(2S)\gamma$	$<5.9 \times 10^{-4}$	95%
Γ_{15} $\Upsilon(3S)\gamma$	$<5.7 \times 10^{-4}$	95%
Γ_{16} $\Upsilon(nS)\Upsilon(mS)$	$<1.4 \times 10^{-3}$	95%
Γ_{17} $\rho(770)\gamma$	$<8.8 \times 10^{-4}$	95%
Γ_{18} $\phi(1020)\gamma$	$<4.8 \times 10^{-4}$	95%
Γ_{19} $e\mu$	LF $<6.1 \times 10^{-5}$	95%
Γ_{20} $e\tau$	LF $<4.7 \times 10^{-3}$	95%
Γ_{21} $\mu\tau$	LF $<2.5 \times 10^{-3}$	95%
Γ_{22} invisible		
Γ_{23} γ invisible	$<4.6\%$	95%

 H^0 BRANCHING RATIOS $\Gamma(e^+ e^-)/\Gamma_{\text{total}}$ Γ_5/Γ

VALUE	CL%	DOCUMENT ID	TECN	COMMENT
$<3.6 \times 10^{-4}$	95	¹ AAD	20F ATLS	pp , 13 TeV
••• We do not use the following data for averages, fits, limits, etc. •••				
$<1.9 \times 10^{-3}$	95	² KHACHATRYAN...15H	CMS	pp , 7, 8 TeV
¹ AAD 20F use 139 fb ⁻¹ of pp collisions at $E_{\text{cm}} = 13$ TeV. The best-fit value of the $H^0 \rightarrow ee$ branching fraction is $(0.0 \pm 1.7 \pm 0.6) \times 10^{-4}$ for $m_{H^0} = 125$ GeV.				
² KHACHATRYAN 15H use 5.0 fb ⁻¹ of pp collisions at $E_{\text{cm}} = 7$ TeV and 19.7 fb ⁻¹ at 8 TeV.				

 $\Gamma(J/\psi\gamma)/\Gamma_{\text{total}}$ Γ_{10}/Γ

VALUE	CL%	DOCUMENT ID	TECN	COMMENT
$<7.6 \times 10^{-4}$	95	¹ SIRUNYAN	19AJ CMS	13 TeV, 35.9 fb ⁻¹
$<3.5 \times 10^{-4}$	95	² AABOUD	18BL ATLS	13 TeV, 36.1 fb ⁻¹
••• We do not use the following data for averages, fits, limits, etc. •••				
$<1.5 \times 10^{-3}$	95	³ KHACHATRYAN...16B	CMS	8 TeV
$<1.5 \times 10^{-3}$	95	⁴ AAD	15I ATLS	8 TeV
¹ SIRUNYAN 19AJ search for $H^0 \rightarrow J/\psi\gamma, J/\psi \rightarrow \mu^+\mu^-$ with 35.9 fb ⁻¹ of pp collision data at $E_{\text{cm}} = 13$ TeV. The upper limit corresponds to 260 times the SM prediction and by combining the KHACHATRYAN 16B, it is 220 times the SM prediction.				
² AABOUD 18BL search for $H^0 \rightarrow J/\psi\gamma, J/\psi \rightarrow \mu^+\mu^-$ with 36.1 fb ⁻¹ of pp collision data at $E_{\text{cm}} = 13$ TeV.				
³ KHACHATRYAN 16B use 19.7 fb ⁻¹ of pp collision data at 8 TeV.				
⁴ AAD 15I use 19.7 fb ⁻¹ of pp collision data at 8 TeV.				

 $\Gamma(J/\psi J/\psi)/\Gamma_{\text{total}}$ Γ_{11}/Γ

VALUE	CL%	DOCUMENT ID	TECN	COMMENT
$<1.8 \times 10^{-3}$	95	¹ SIRUNYAN	19BR CMS	pp at 13 TeV
¹ SIRUNYAN 19BR search for $H^0 \rightarrow J/\psi J/\psi, J/\psi \rightarrow \mu^+\mu^-$ with 37.5 fb ⁻¹ of pp collision data at $E_{\text{cm}} = 13$ TeV. J/ψ s from the Higgs decay are assumed to be unpolarized. For fully longitudinal (transverse) polarized J/ψ s, limits change by -22% ($+10\%$).				

 $\Gamma(\psi(2S)\gamma)/\Gamma_{\text{total}}$ Γ_{12}/Γ

VALUE	CL%	DOCUMENT ID	TECN	COMMENT
$<2.0 \times 10^{-3}$	95	¹ AABOUD	18BL ATLS	13 TeV, 36.1 fb ⁻¹
¹ AABOUD 18BL search for $H^0 \rightarrow \psi(2S)\gamma, \psi(2S) \rightarrow \mu^+\mu^-$ with 36.1 fb ⁻¹ of pp collision data at $E_{\text{cm}} = 13$ TeV.				

 $\Gamma(\Upsilon(1S)\gamma)/\Gamma_{\text{total}}$ Γ_{13}/Γ

VALUE	CL%	DOCUMENT ID	TECN	COMMENT
$<4.9 \times 10^{-4}$	95	¹ AABOUD	18BL ATLS	13 TeV, 36.1 fb ⁻¹
••• We do not use the following data for averages, fits, limits, etc. •••				
$<1.3 \times 10^{-3}$	95	² AAD	15I ATLS	8 TeV
¹ AABOUD 18BL search for $H^0 \rightarrow \Upsilon(1S)\gamma, \Upsilon(1S) \rightarrow \mu^+\mu^-$ with 36.1 fb ⁻¹ of pp collision data at $E_{\text{cm}} = 13$ TeV.				
² AAD 15I use 19.7 fb ⁻¹ of pp collision data at 8 TeV.				

 $\Gamma(\Upsilon(2S)\gamma)/\Gamma_{\text{total}}$ Γ_{14}/Γ

VALUE	CL%	DOCUMENT ID	TECN	COMMENT
$<5.9 \times 10^{-4}$	95	¹ AABOUD	18BL ATLS	13 TeV, 36.1 fb ⁻¹
••• We do not use the following data for averages, fits, limits, etc. •••				
$<1.9 \times 10^{-3}$	95	² AAD	15I ATLS	8 TeV
¹ AABOUD 18BL search for $H^0 \rightarrow \Upsilon(2S)\gamma, \Upsilon(2S) \rightarrow \mu^+\mu^-$ with 36.1 fb ⁻¹ of pp collision data at $E_{\text{cm}} = 13$ TeV.				
² AAD 15I use 19.7 fb ⁻¹ of pp collision data at 8 TeV.				

 $\Gamma(\Upsilon(3S)\gamma)/\Gamma_{\text{total}}$ Γ_{15}/Γ

VALUE	CL%	DOCUMENT ID	TECN	COMMENT
$<5.7 \times 10^{-4}$	95	¹ AABOUD	18BL ATLS	13 TeV, 36.1 fb ⁻¹
••• We do not use the following data for averages, fits, limits, etc. •••				
$<1.3 \times 10^{-3}$	95	² AAD	15I ATLS	8 TeV
¹ AABOUD 18BL search for $H^0 \rightarrow \Upsilon(3S)\gamma, \Upsilon(3S) \rightarrow \mu^+\mu^-$ with 36.1 fb ⁻¹ of pp collision data at $E_{\text{cm}} = 13$ TeV.				
² AAD 15I use 19.7 fb ⁻¹ of pp collision data at 8 TeV.				

 $\Gamma(\Upsilon(nS)\Upsilon(mS))/\Gamma_{\text{total}}$ Γ_{16}/Γ

VALUE	CL%	DOCUMENT ID	TECN	COMMENT
$<1.4 \times 10^{-3}$	95	¹ SIRUNYAN	19BR CMS	pp at 13 TeV
¹ SIRUNYAN 19BR search for $H^0 \rightarrow \Upsilon(nS)\Upsilon(mS)$ with $\Upsilon(nS), \Upsilon(mS) \rightarrow \mu^+\mu^-$ ($n, m = 1, 2, 3$) for 37.5 fb ⁻¹ of pp collision data at $E_{\text{cm}} = 13$ TeV. Υ s from the Higgs decay are assumed to be unpolarized. For fully longitudinal (transverse) polarized Υ s, limits change by -22% ($+10\%$). The three Υ states selected in a mass range of 8.5–11 GeV are not distinguished.				

 $\Gamma(\rho(770)\gamma)/\Gamma_{\text{total}}$ Γ_{17}/Γ

VALUE	CL%	DOCUMENT ID	TECN	COMMENT
$<8.8 \times 10^{-4}$	95	¹ AABOUD	18AU ATLS	pp , 13 TeV
¹ AABOUD 18AU use 35.6 fb ⁻¹ of pp collision data at 13 TeV.				

 $\Gamma(\phi(1020)\gamma)/\Gamma_{\text{total}}$ Γ_{18}/Γ

VALUE	CL%	DOCUMENT ID	TECN	COMMENT
$<4.8 \times 10^{-4}$	95	¹ AABOUD	18AU ATLS	pp , 13 TeV
••• We do not use the following data for averages, fits, limits, etc. •••				
$<1.4 \times 10^{-3}$	95	² AABOUD	16K ATLS	pp , 13 TeV
¹ AABOUD 18AU use 35.6 fb ⁻¹ of pp collision data at 13 TeV.				
² AABOUD 16K use 2.7 fb ⁻¹ of pp collision data at 13 TeV.				

 $\Gamma(e\mu)/\Gamma_{\text{total}}$ Γ_{19}/Γ

VALUE	CL%	DOCUMENT ID	TECN	COMMENT
$<6.1 \times 10^{-5}$	95	¹ AAD	20F ATLS	pp , 13 TeV
••• We do not use the following data for averages, fits, limits, etc. •••				
$<3.5 \times 10^{-4}$	95	² KHACHATRYAN...16CD	CMS	pp , 8 TeV
¹ AAD 20F use 139 fb ⁻¹ of pp collisions at $E_{\text{cm}} = 13$ TeV. The best-fit value of the $H^0 \rightarrow e\mu$ branching fraction is $(0.4 \pm 2.9 \pm 0.3) \times 10^{-5}$ for $m_{H^0} = 125$ GeV.				
² KHACHATRYAN 16CD search for $H^0 \rightarrow e\mu$ in 19.7 fb ⁻¹ of pp collisions at $E_{\text{cm}} = 8$ TeV. The limit constrains the $Y_{e\mu}$ Yukawa coupling to $\sqrt{ Y_{e\mu} ^2 + Y_{\mu e} ^2} < 5.4 \times 10^{-4}$ at 95% CL (see their Fig. 6).				

 $\Gamma(e\tau)/\Gamma_{\text{total}}$ Γ_{20}/Γ

VALUE	CL%	DOCUMENT ID	TECN	COMMENT
$<4.7 \times 10^{-3}$	95	¹ AAD	20A ATLS	pp , 13 TeV
••• We do not use the following data for averages, fits, limits, etc. •••				
$<6.1 \times 10^{-3}$	95	² SIRUNYAN	18BH CMS	pp , 13 TeV
$<1.04 \times 10^{-2}$	95	³ AAD	17 ATLS	pp , 8 TeV
$<6.9 \times 10^{-3}$	95	⁴ KHACHATRYAN...16CD	CMS	pp , 8 TeV
¹ AAD 20A search for $H^0 \rightarrow e\tau$ in 36.1 fb ⁻¹ of pp collisions at $E_{\text{cm}} = 13$ TeV. The limit constrains the $Y_{e\tau}$ Yukawa coupling to $\sqrt{ Y_{e\tau} ^2 + Y_{\tau e} ^2} < 2.0 \times 10^{-3}$ at 95% CL (see their Fig. 5).				
² SIRUNYAN 18BH search for $H^0 \rightarrow e\tau$ in 35.9 fb ⁻¹ of pp collisions at $E_{\text{cm}} = 13$ TeV. The limit constrains the $Y_{e\tau}$ Yukawa coupling to $\sqrt{ Y_{e\tau} ^2 + Y_{\tau e} ^2} < 2.26 \times 10^{-3}$ at 95% CL (see their Fig. 10).				
³ AAD 17 search for $H^0 \rightarrow e\tau$ in 20.3 fb ⁻¹ of pp collisions at $E_{\text{cm}} = 8$ TeV.				
⁴ KHACHATRYAN 16CD search for $H^0 \rightarrow e\tau$ in 19.7 fb ⁻¹ of pp collisions at $E_{\text{cm}} = 8$ TeV. The limit constrains the $Y_{e\tau}$ Yukawa coupling to $\sqrt{ Y_{e\tau} ^2 + Y_{\tau e} ^2} < 2.4 \times 10^{-3}$ at 95% CL (see their Fig. 6).				

 $\Gamma(\mu\tau)/\Gamma_{\text{total}}$ Γ_{21}/Γ

VALUE	CL%	DOCUMENT ID	TECN	COMMENT
$<2.5 \times 10^{-3}$	95	¹ SIRUNYAN	18BH CMS	pp , 13 TeV
••• We do not use the following data for averages, fits, limits, etc. •••				
$<2.8 \times 10^{-3}$	95	² AAD	20A ATLS	pp , 13 TeV
<0.26	95	³ AAIJ	18AMLHCB	pp , 8 TeV
$<1.43 \times 10^{-2}$	95	⁴ AAD	17 ATLS	pp , 8 TeV
$<1.51 \times 10^{-2}$	95	⁵ KHACHATRYAN...15Q	CMS	pp , 8 TeV

See key on page 999

Gauge & Higgs Boson Particle Listings

H^0

- 1 SIRUNYAN 18BH search for $H^0 \rightarrow \mu\tau$ in 35.9 fb⁻¹ of pp collisions at $E_{cm} = 13$ TeV. The limit constrains the $Y_{\mu\tau}$ Yukawa coupling to $\sqrt{|Y_{\mu\tau}|^2 + |Y_{\tau\mu}|^2} < 1.43 \times 10^{-3}$ at 95% CL (see their Fig. 10).
- 2 AAD 20A search for $H^0 \rightarrow \mu\tau$ in 36.1 fb⁻¹ of pp collisions at $E_{cm} = 13$ TeV. The limit constrains the $Y_{\mu\tau}$ Yukawa coupling to $\sqrt{|Y_{\mu\tau}|^2 + |Y_{\tau\mu}|^2} < 1.5 \times 10^{-3}$ at 95% CL (see their Fig. 5).
- 3 AAIJ 18AM search for $H^0 \rightarrow \mu\tau$ in 2.0 fb⁻¹ of pp collisions at $E_{cm} = 8$ TeV. The limit constrains the $Y_{\mu\tau}$ Yukawa coupling to $\sqrt{|Y_{\mu\tau}|^2 + |Y_{\tau\mu}|^2} < 1.7 \times 10^{-2}$ at 95% CL assuming SM production cross sections.
- 4 AAD 17 search for $H^0 \rightarrow \mu\tau$ in 20.3 fb⁻¹ of pp collisions at $E_{cm} = 8$ TeV.
- 5 KHACHATRYAN 15Q search for $H^0 \rightarrow \mu\tau$ with τ decaying electronically or hadronically in 19.7 fb⁻¹ of pp collisions at $E_{cm} = 8$ TeV. The fit gives $B(H^0 \rightarrow \mu\tau) = (0.84_{-0.39}^{+0.37})\%$ with a significance of 2.4 σ .

$\Gamma(\text{invisible})/\Gamma_{\text{total}}$		Γ_{22}/Γ			
VALUE	CL%	DOCUMENT ID	TECN	COMMENT	
<0.26	95	1 AABOUD	19AL ATLS	$pp, 7, 8, 13$ TeV, $H \rightarrow \text{inv}$	
<0.19	95	2 SIRUNYAN	19Bo CMS	$pp, 7, 8, 13$ TeV	
• • • We do not use the following data for averages, fits, limits, etc. • • •					
<0.37	95	3 AABOUD	19AI ATLS	$pp \rightarrow qqH^0X, H^0 \rightarrow \text{inv}, 13$ TeV	
<0.38	95	4 AABOUD	19AL ATLS	$pp, 13$ TeV, $H \rightarrow \text{inv}$	
<0.22	95	5 SIRUNYAN	19AT CMS	$pp, 13$ TeV, $H \rightarrow \text{inv}$	
<0.33	95	6 SIRUNYAN	19Bo CMS	$pp \rightarrow qqH^0X, H^0 \rightarrow \text{inv}, 13$ TeV	
<0.26	95	7 SIRUNYAN	19Bo CMS	$pp, 13$ TeV	
<0.67	95	8 AABOUD	18 ATLS	$pp \rightarrow H^0ZX, H^0 \rightarrow \text{inv}, 13$ TeV	
<0.83	95	9 AABOUD	18CA ATLS	$pp \rightarrow H^0W/Z, W/Z \rightarrow jj, 13$ TeV	
<0.40	95	10 SIRUNYAN	18BV CMS	$pp \rightarrow Z(\ell\ell)H^0, H^0 \rightarrow \text{inv}, 13$ TeV	
<0.53	95	11 SIRUNYAN	18s CMS	$pp, 13$ TeV, jet or $V(\rightarrow q\bar{q}), H^0 \rightarrow \text{inv}$	
<0.46	95	12 AABOUD	17BD ATLS	$pp \rightarrow gH^0X, qqH^0X, H^0 \rightarrow \text{inv}, 13$ TeV	
<0.24	95	13 KHACHATRY..17F	CMS	$pp, 7, 8, 13$ TeV	
<0.28	95	14 AAD	16AF ATLS	$pp \rightarrow qqH^0X, 8$ TeV	
<0.34	95	15 AAD	16AN LHC	$pp, 7, 8$ TeV	
<0.78	95	16 AAD	15BD ATLS	$pp \rightarrow H^0W/ZX, 8$ TeV	
<0.25	95	17 AAD	15CX ATLS	$pp, 7, 8$ TeV, $H \rightarrow \text{inv}$	
<0.75	95	18 AAD	14O ATLS	$pp \rightarrow H^0ZX, 7, 8$ TeV	
<0.58	95	19 CHATRCHYAN14B	CMS	$pp \rightarrow H^0ZX, qqH^0X$	
<0.81	95	20 CHATRCHYAN14B	CMS	$pp \rightarrow H^0ZX, 7, 8$ TeV	
<0.65	95	21 CHATRCHYAN14B	CMS	$pp \rightarrow qqH^0X, 8$ TeV	

- 1 AABOUD 19AL combine results of 7, 8 (AAD 15CX), and 13 TeV for H^0 decaying to invisible final states.
- 2 SIRUNYAN 19Bo combine 13 TeV 35.9 fb⁻¹ results with 7, 8, 13 TeV (KHACHATRYAN 17F) for H^0 decaying to invisible final states. The quoted limit on the branching ratio is given for $m_{H^0} = 125.09$ GeV and assumes the Standard Model production rates. The branching ratio is obtained to be 0.05 ± 0.03 (stat) ± 0.07 (syst).
- 3 AABOUD 19AI search for $pp \rightarrow qqH^0X$ (VBF) with H^0 decaying to invisible final states using 36.1 fb⁻¹ of data. The quoted limit on the branching ratio is given for $m_{H^0} = 125$ GeV and assumes the Standard Model rates for VBF and gluon-fusion production.
- 4 AABOUD 19AL combine results of H^0 decaying to invisible final states with VBF(AABOUD 19AI), ZH , and WH productions (AABOUD 18, AABOUD 18CA), which use 36.1 fb⁻¹ of data at 13 TeV. The quoted limit is given for $m_{H^0} = 125$ GeV and assumes the Standard Model rates for gluon fusion, VBF, ZH , and WH productions.
- 5 SIRUNYAN 19AT perform a combined fit with visible decay using 35.9 fb⁻¹ of data at 13 TeV.
- 6 SIRUNYAN 19Bo search for $pp \rightarrow qqH^0X$ (VBF) with H^0 decaying to invisible final states using 35.9 fb⁻¹ of data. The quoted limit on the branching ratio is given for $m_{H^0} = 125.09$ GeV and assumes the Standard Model production rates.
- 7 SIRUNYAN 19Bo combine the VBF channel with results of other 13 TeV analyses: SIRUNYAN 18BV and SIRUNYAN 18s. The quoted limit on the branching ratio is given for $m_{H^0} = 125.09$ GeV and assumes the Standard Model production rates.
- 8 AABOUD 18 search for $pp \rightarrow H^0ZX, Z \rightarrow ee, \mu\mu$ with H^0 decaying to invisible final states in 36.1 fb⁻¹ at $E_{cm} = 13$ TeV. The quoted limit on the branching ratio is given for $m_{H^0} = 125$ GeV and assumes the Standard Model rate for H^0Z production.
- 9 AABOUD 18CA search for H^0 decaying to invisible final states using WH, ZH and ZH productions, where W and Z hadronically decay. The data of 36.1 fb⁻¹ at $E_{cm} = 13$ TeV is used. The quoted limit assumes SM production cross sections with combining the contributions from WH, ZH, ggF and VBF production modes.
- 10 SIRUNYAN 18BV search for H^0 decaying to invisible final states associated with a $Z, Z \rightarrow \ell\ell$ using 35.9 fb⁻¹ at 13 TeV. The limit is obtained for $m_{H^0} = 125$ GeV and assuming the SM ZH^0 production cross section.
- 11 SIRUNYAN 18s search for H^0 decaying to invisible final states associated with an energetic jet or a $V, V \rightarrow q\bar{q}$ using 35.9 fb⁻¹ at 13 TeV.
- 12 AABOUD 17BD search for H^0 decaying to invisible final states with ≥ 1 jet and VBF events using 3.2 fb⁻¹ of pp collisions at $E_{cm} = 13$ TeV. A cross-section ratio R^{miss} is used in the measurement. The quoted limit is given for $m_{H^0} = 125$ GeV.
- 13 KHACHATRYAN 17F search for H^0 decaying to invisible final states with gluon fusion, VBF, ZH , and WH productions using 2.3 fb⁻¹ of pp collisions at $E_{cm} = 13$ TeV, 19.7 fb⁻¹ at 8 TeV, and 5.1 fb⁻¹ at 7 TeV. The quoted limit is given for $m_{H^0} =$

- 125 GeV and assumes the Standard Model rates for gluon fusion, VBF, ZH , and WH productions.
- 14 AAD 16AF search for $pp \rightarrow qqH^0X$ (VBF) with H^0 decaying to invisible final states in 20.3 fb⁻¹ at $E_{cm} = 8$ TeV. The quoted limit on the branching ratio is given for $m_{H^0} = 125$ GeV and assumes the Standard Model rates for VBF and gluon-fusion production.
- 15 AAD 16AN perform fits to the ATLAS and CMS data at $E_{cm} = 7$ and 8 TeV. The branching fraction of decays into BSM particles that are invisible or into undetected decay modes is measured for $m_{H^0} = 125.09$ GeV.
- 16 AAD 15BD search for $pp \rightarrow H^0WX$ and $pp \rightarrow H^0ZX$ with W or Z decaying hadronically and H^0 decaying to invisible final states using data at $E_{cm} = 8$ TeV. The quoted limit is given for $m_{H^0} = 125$ GeV, assumes the Standard Model rates for the production processes and is based on a combination of the contributions from H^0W, H^0Z and the gluon-fusion process.
- 17 AAD 15CX search for H^0 decaying to invisible final states with VBF, ZH , and WH productions using 20.3 fb⁻¹ at 8 TeV, and 4.7 fb⁻¹ at 7 TeV. The quoted limit is given for $m_{H^0} = 125.36$ GeV and assumes the Standard Model rates for gluon fusion, VBF, ZH , and WH productions. The upper limit is improved to 0.23 by adding the measured visible decay rates.
- 18 AAD 14O search for $pp \rightarrow H^0ZX, Z \rightarrow \ell\ell$, with H^0 decaying to invisible final states in 4.5 fb⁻¹ at $E_{cm} = 7$ TeV and 20.3 fb⁻¹ at $E_{cm} = 8$ TeV. The quoted limit on the branching ratio is given for $m_{H^0} = 125.5$ GeV and assumes the Standard Model rate for H^0Z production.
- 19 CHATRCHYAN 14B search for $pp \rightarrow H^0ZX, Z \rightarrow \ell\ell$ and $Z \rightarrow b\bar{b}$, and also $pp \rightarrow qqH^0X$ with H^0 decaying to invisible final states using data at $E_{cm} = 7$ and 8 TeV. The quoted limit on the branching ratio is obtained from a combination of the limits from H^0Z and qqH^0X . It is given for $m_{H^0} = 125$ GeV and assumes the Standard Model rates for the two production processes.
- 20 CHATRCHYAN 14B search for $pp \rightarrow H^0ZX$ with H^0 decaying to invisible final states and $Z \rightarrow \ell\ell$ in 4.9 fb⁻¹ at $E_{cm} = 7$ TeV and 19.7 fb⁻¹ at $E_{cm} = 8$ TeV, and also with $Z \rightarrow b\bar{b}$ in 18.9 fb⁻¹ at $E_{cm} = 8$ TeV. The quoted limit on the branching ratio is given for $m_{H^0} = 125$ GeV and assumes the Standard Model rate for H^0Z production.
- 21 CHATRCHYAN 14B search for $pp \rightarrow qqH^0X$ (vector boson fusion) with H^0 decaying to invisible final states in 19.5 fb⁻¹ at $E_{cm} = 8$ TeV. The quoted limit on the branching ratio is given for $m_{H^0} = 125$ GeV and assumes the Standard Model rate for qqH^0X production.

$\Gamma(\gamma\text{invisible})/\Gamma_{\text{total}}$		Γ_{23}/Γ			
VALUE	CL%	DOCUMENT ID	TECN	COMMENT	
<0.046	95	1 SIRUNYAN	19CG CMS	$pp \rightarrow H^0Z, H^0 \rightarrow \gamma\text{invisible}, Z \rightarrow \ell\ell, 13$ TeV	
1 SIRUNYAN 19CG search for $pp \rightarrow H^0Z, Z \rightarrow ee, \mu\mu$ with H^0 decaying to invisible final states plus a γ in 137 fb ⁻¹ at $E_{cm} = 13$ TeV. The quoted limit on the branching ratio is given for $m_{H^0} = 125$ GeV assuming the Standard Model rate for H^0Z production and is obtained in the context of a theoretical model, where the undetected (invisible) is massless.					

H^0 SIGNAL STRENGTHS IN DIFFERENT CHANNELS

The H^0 signal strength in a particular final state xx is given by the cross section times branching ratio in this channel normalized to the Standard Model (SM) value, $\sigma \cdot B(H^0 \rightarrow xx) / (\sigma \cdot B(H^0 \rightarrow xx))_{\text{SM}}$, for the specified mass value of H^0 . For the SM predictions, see DITTMAYER 11, DITTMAYER 12, and HEINEMEYER 13A. Results for fiducial and differential cross sections are also listed below.

Combined Final States		DOCUMENT ID	TECN	COMMENT
1.13 ± 0.06 OUR AVERAGE				
1.11 +0.09 -0.08		1 AAD	20 ATLS	$pp, 13$ TeV
1.17 ± 0.10		2 SIRUNYAN	19AT CMS	$pp, 13$ TeV
1.09 ± 0.07 ± 0.04 ± 0.03 +0.07 -0.06		3,4 AAD	16AN LHC	$pp, 7, 8$ TeV
1.44 +0.59 -0.56		5 AALTONEN	13M TEVA	$p\bar{p} \rightarrow H^0X, 1.96$ TeV
• • • We do not use the following data for averages, fits, limits, etc. • • •				
1.20 ± 0.10 ± 0.06 ± 0.04 +0.08 -0.07		4 AAD	16AN ATLS	$pp, 7, 8$ TeV
0.97 ± 0.09 ± 0.05 +0.04 +0.07 -0.03 -0.06		4 AAD	16AN CMS	$pp, 7, 8$ TeV
1.18 ± 0.10 ± 0.07 +0.08 -0.07		7 AAD	16K ATLS	$pp, 7, 8$ TeV
0.75 +0.28 +0.13 +0.08 -0.26 -0.11 -0.05		7 AAD	16K ATLS	$pp, 7$ TeV
1.28 ± 0.11 ± 0.08 +0.10 -0.07 -0.08		7 AAD	16K ATLS	$pp, 8$ TeV
1.00 ± 0.09 ± 0.07 +0.08 -0.07		8 AAD	15P ATLS	$pp, 8$ TeV, cross section
1.33 +0.14 -0.10 ± 0.15		9 KHACHATRY...15AM	CMS	$pp, 7, 8$ TeV
1.54 +0.77 -0.73		10 AAD	13AK ATLS	$pp, 7$ and 8 TeV
1.40 +0.92 -0.88		11 AALTONEN	13L CDF	$p\bar{p} \rightarrow H^0X, 1.96$ TeV
1.4 ± 0.3		12 ABAZOV	13L D0	$p\bar{p} \rightarrow H^0X, 1.96$ TeV
1.2 ± 0.4		13 AAD	12AI ATLS	$pp \rightarrow H^0X, 7, 8$ TeV
1.5 ± 0.4		13 AAD	12AI ATLS	$pp \rightarrow H^0X, 7$ TeV
0.87 ± 0.23		13 AAD	12AI ATLS	$pp \rightarrow H^0X, 8$ TeV
		14 CHATRCHYAN12N	CMS	$pp \rightarrow H^0X, 7, 8$ TeV

Gauge & Higgs Boson Particle Listings

 H^0

- ¹ AAD 20 combine results of up to 79.8 fb^{-1} of data at $E_{\text{cm}} = 13 \text{ TeV}$, assuming $m_{H^0} = 125.09 \text{ GeV}$: $\gamma\gamma$, ZZ^* , WW^* , $\tau\tau$, $b\bar{b}$, $\mu\mu$, invisible, and off-shell analyses (see their Table I). The signal strengths for individual production processes are 1.04 ± 0.09 for gluon fusion, $1.21^{+0.24}_{-0.22}$ for vector boson fusion, $1.30^{+0.40}_{-0.38}$ for WH^0 production, $1.05^{+0.31}_{-0.29}$ for ZH^0 production, and $1.21^{+0.26}_{-0.24}$ for $t\bar{t}H^0 + tH^0$ production (see their Fig. 2 and Table IV). Several results with the simplified template cross section and κ -frameworks are presented: see their Figs. 9–11, Figs 20, 21 and Table VIII for stage-1 simplified template cross sections, their Figs. 12–17 and Tables X–XII for the κ -framework.
- ² SIRUNYAN 19AT combine results of 35.9 fb^{-1} of data at $E_{\text{cm}} = 13 \text{ TeV}$, assuming $m_{H^0} = 125.09 \text{ GeV}$. The signal strengths for individual production processes are $1.22^{+0.14}_{-0.12}$ for gluon fusion, $0.73^{+0.30}_{-0.27}$ for vector boson fusion, $2.18^{+0.58}_{-0.55}$ for WH^0 production, $0.87^{+0.44}_{-0.42}$ for ZH^0 production, and $1.18^{+0.30}_{-0.27}$ for $t\bar{t}H^0$ production. Several results with the simplified template cross section and κ -frameworks are presented: see their Fig. 8 and Table 5 for stage-0 simplified template cross sections, their Figs. 9–18 and Tables 7–11 for the κ -framework.
- ³ AAD 16AN perform fits to the ATLAS and CMS data at $E_{\text{cm}} = 7$ and 8 TeV . The signal strengths for individual production processes are $1.03^{+0.16}_{-0.14}$ for gluon fusion, $1.18^{+0.25}_{-0.23}$ for vector boson fusion, $0.89^{+0.40}_{-0.38}$ for WH^0 production, $0.79^{+0.38}_{-0.36}$ for ZH^0 production, and $2.3^{+0.7}_{-0.6}$ for $t\bar{t}H^0$ production.
- ⁴ AAD 16AN: The uncertainties represent statistics, experimental systematics, theory systematics on the background, and theory systematics on the signal. The quoted signal strengths are given for $m_{H^0} = 125.09 \text{ GeV}$. In the fit, relative branching ratios and relative production cross sections are fixed to those in the Standard Model.
- ⁵ AALTONEN 13M combine all Tevatron data from the CDF and D0 Collaborations with up to 10.0 fb^{-1} and 9.7 fb^{-1} , respectively, of $p\bar{p}$ collisions at $E_{\text{cm}} = 1.96 \text{ TeV}$. The quoted signal strength is given for $m_{H^0} = 125 \text{ GeV}$.
- ⁶ SIRUNYAN 19BA measure differential cross sections for the Higgs boson transverse momentum, the number of jets, the rapidity of the Higgs boson and the transverse momentum of the leading jet using 35.9 fb^{-1} of data at $E_{\text{cm}} = 13 \text{ TeV}$ with $H^0 \rightarrow \gamma\gamma$, $H^0 \rightarrow ZZ^*$, and $H^0 \rightarrow b\bar{b}$. The total cross section for Higgs boson production is measured to be $61.1 \pm 6.0 \pm 3.7 \text{ pb}$ using $H^0 \rightarrow \gamma\gamma$ and $H^0 \rightarrow ZZ^*$ channels. Several coupling measurements in the κ -framework are performed.
- ⁷ AAD 16K use up to 4.7 fb^{-1} of pp collisions at $E_{\text{cm}} = 7 \text{ TeV}$ and up to 20.3 fb^{-1} at $E_{\text{cm}} = 8 \text{ TeV}$. The third uncertainty in the measurement is theory systematics. The signal strengths for individual production modes are $1.23 \pm 0.14^{+0.09}_{-0.08}$ for gluon fusion, $1.23^{+0.28}_{-0.27} + 0.13^{+0.11}_{-0.09}$ for vector boson fusion, $0.80^{+0.31}_{-0.30} \pm 0.17^{+0.10}_{-0.05}$ for W/ZH^0 production, and $1.81^{+0.52}_{-0.50} + 0.58^{+0.31}_{-0.55} - 0.12^{+0.12}_{-0.05}$ for $t\bar{t}H^0$ production. The quoted signal strengths are given for $m_{H^0} = 125.36 \text{ GeV}$.
- ⁸ AAD 15P measure total and differential cross sections of the process $pp \rightarrow H^0 X$ at $E_{\text{cm}} = 8 \text{ TeV}$ with 20.3 fb^{-1} . $\gamma\gamma$ and 4ℓ final states are used. $\sigma(pp \rightarrow H^0 X) = 33.0 \pm 5.3 \pm 1.6 \text{ pb}$ is given. See their Figs. 2 and 3 for data on differential cross sections.
- ⁹ KHACHATRYAN 15AM use up to 5.1 fb^{-1} of pp collisions at $E_{\text{cm}} = 7 \text{ TeV}$ and up to 19.7 fb^{-1} at $E_{\text{cm}} = 8 \text{ TeV}$. The third uncertainty in the measurement is theory systematics. Fits to each production mode give the value of $0.85^{+0.19}_{-0.16}$ for gluon fusion, $1.16^{+0.37}_{-0.34}$ for vector boson fusion, $0.92^{+0.38}_{-0.36}$ for WH^0 , ZH^0 production, and $2.90^{+1.08}_{-0.94}$ for $t\bar{t}H^0$ production.
- ¹⁰ AAD 13AK use 4.7 fb^{-1} of pp collisions at $E_{\text{cm}} = 7 \text{ TeV}$ and 20.7 fb^{-1} at $E_{\text{cm}} = 8 \text{ TeV}$. The combined signal strength is based on the $\gamma\gamma$, $ZZ^* \rightarrow 4\ell$, and $WW^* \rightarrow \ell\nu\ell\nu$ channels. The quoted signal strength is given for $m_{H^0} = 125.5 \text{ GeV}$. Reported statistical error value modified following private communication with the experiment.
- ¹¹ AALTONEN 13L combine all CDF results with $9.45\text{--}10.0 \text{ fb}^{-1}$ of $p\bar{p}$ collisions at $E_{\text{cm}} = 1.96 \text{ TeV}$. The quoted signal strength is given for $m_{H^0} = 125 \text{ GeV}$.
- ¹² ABAZOV 13L combine all D0 results with up to 9.7 fb^{-1} of $p\bar{p}$ collisions at $E_{\text{cm}} = 1.96 \text{ TeV}$. The quoted signal strength is given for $m_{H^0} = 125 \text{ GeV}$.
- ¹³ AAD 12AI obtain results based on $4.6\text{--}4.8 \text{ fb}^{-1}$ of pp collisions at $E_{\text{cm}} = 7 \text{ TeV}$ and $5.8\text{--}5.9 \text{ fb}^{-1}$ at $E_{\text{cm}} = 8 \text{ TeV}$. An excess of events over background with a local significance of 5.9σ is observed at $m_{H^0} = 126 \text{ GeV}$. The quoted signal strengths are given for $m_{H^0} = 126 \text{ GeV}$. See also AAD 12DA.
- ¹⁴ CHATRCHYAN 12N obtain results based on $4.9\text{--}5.1 \text{ fb}^{-1}$ of pp collisions at $E_{\text{cm}} = 7 \text{ TeV}$ and $5.1\text{--}5.3 \text{ fb}^{-1}$ at $E_{\text{cm}} = 8 \text{ TeV}$. An excess of events over background with a local significance of 5.0σ is observed at about $m_{H^0} = 125 \text{ GeV}$. The combined signal strength is based on the $\gamma\gamma$, ZZ^* , WW^* , $\tau^+\tau^-$, and $b\bar{b}$ channels. The quoted signal strength is given for $m_{H^0} = 125.5 \text{ GeV}$. See also CHATRCHYAN 13Y.

WW* Final State

VALUE	DOCUMENT ID	TECN	COMMENT
1.19±0.12 OUR AVERAGE			
$1.28^{+0.17}_{-0.16}$	1	SIRUNYAN 19AT CMS	pp , 13 TeV
$1.09^{+0.18}_{-0.16}$	2,3	AAD 16AN LHC	pp , 7, 8 TeV
$0.94^{+0.85}_{-0.83}$	4	AALTONEN 13M TEVA	$p\bar{p} \rightarrow H^0 X$, 1.96 TeV
••• We do not use the following data for averages, fits, limits, etc. •••			
	5	AABOUD 19F ATLS	pp , 13 TeV, cross sections
$2.5^{+0.9}_{-0.8}$	6	AAD 19A ATLS	$pp \rightarrow H^0 W/H^0 Z$, $H^0 \rightarrow WW^*$, 13 TeV

$1.28^{+0.18}_{-0.17}$	7	SIRUNYAN 19AX CMS	pp , 13 TeV
$1.22^{+0.23}_{-0.21}$	3	AAD 16AN ATLS	pp , 7, 8 TeV
$0.90^{+0.23}_{-0.21}$	3	AAD 16AN CMS	pp , 7, 8 TeV
	8	AAD 16AO ATLS	pp , 8 TeV, cross sections
$1.18 \pm 0.16^{+0.17}_{-0.14}$	9	AAD 16K ATLS	pp , 7, 8 TeV
$1.09^{+0.16}_{-0.15} + 0.17^{+0.17}_{-0.14}$	10	AAD 15AA ATLS	pp , 7, 8 TeV
$3.0^{+1.3}_{-1.1} + 1.0^{+1.0}_{-0.7}$	11	AAD 15AQ ATLS	$pp \rightarrow H^0 W/ZX$, 7, 8 TeV
$1.16^{+0.16}_{-0.15} + 0.18^{+0.18}_{-0.15}$	12	AAD 15AQ ATLS	pp , 7, 8 TeV
$0.72 \pm 0.12 \pm 0.10^{+0.12}_{-0.10}$	13	CHATRCHYAN 14G CMS	pp , 7, 8 TeV
$0.99^{+0.31}_{-0.28}$	14	AAD 13AK ATLS	pp , 7 and 8 TeV
$0.00^{+0.17}_{-0.00}$	15	AALTONEN 13L CDF	$p\bar{p} \rightarrow H^0 X$, 1.96 TeV
$1.90^{+1.63}_{-1.52}$	16	ABAZOV 13L D0	$p\bar{p} \rightarrow H^0 X$, 1.96 TeV
1.3 ± 0.5	17	AAD 12AI ATLS	$pp \rightarrow H^0 X$, 7, 8 TeV
0.5 ± 0.6	17	AAD 12AI ATLS	$pp \rightarrow H^0 X$, 7 TeV
1.9 ± 0.7	17	AAD 12AI ATLS	$pp \rightarrow H^0 X$, 8 TeV
$0.60^{+0.42}_{-0.37}$	18	CHATRCHYAN 12N CMS	$pp \rightarrow H^0 X$, 7, 8 TeV

- ¹ SIRUNYAN 19AT perform a combine fit to 35.9 fb^{-1} of data at $E_{\text{cm}} = 13 \text{ TeV}$.
- ² AAD 16AN perform fits to the ATLAS and CMS data at $E_{\text{cm}} = 7$ and 8 TeV . The signal strengths for individual production processes are 0.84 ± 0.17 for gluon fusion, 1.2 ± 0.4 for vector boson fusion, $1.6^{+1.2}_{-1.0}$ for WH^0 production, $5.9^{+2.8}_{-2.2}$ for ZH^0 production, and $5.0^{+1.8}_{-1.7}$ for $t\bar{t}H^0$ production.
- ³ AAD 16AN: In the fit, relative production cross sections are fixed to those in the Standard Model. The quoted signal strength is given for $m_{H^0} = 125.09 \text{ GeV}$.
- ⁴ AALTONEN 13M combine all Tevatron data from the CDF and D0 Collaborations with up to 10.0 fb^{-1} and 9.7 fb^{-1} , respectively, of $p\bar{p}$ collisions at $E_{\text{cm}} = 1.96 \text{ TeV}$. The quoted signal strength is given for $m_{H^0} = 125 \text{ GeV}$.
- ⁵ AABOUD 19F measure cross-sections times the $H^0 \rightarrow WW^*$ branching fraction in the $H^0 \rightarrow WW^* \rightarrow e\nu\mu\nu$ channel using 36.1 fb^{-1} of pp collisions at $E_{\text{cm}} = 13 \text{ TeV}$: $\sigma_{ggF} \times B(H^0 \rightarrow WW^*) = 11.4^{+1.2}_{-1.1} + 1.8^{+1.8}_{-1.7} \text{ pb}$ and $\sigma_{VBF} \times B(H^0 \rightarrow WW^*) = 0.50^{+0.24}_{-0.22} \pm 0.17 \text{ pb}$.
- ⁶ AAD 19A use 36.1 fb^{-1} data at 13 TeV . The cross section times branching fraction values are measured to be $0.67^{+0.31}_{-0.27} + 0.18^{+0.18}_{-0.14} \text{ pb}$ for WH^0 , $H^0 \rightarrow WW^*$ and $0.54^{+0.31}_{-0.24} + 0.15^{+0.15}_{-0.07} \text{ pb}$ for ZH^0 , $H^0 \rightarrow WW^*$.
- ⁷ SIRUNYAN 19AX measure the signal strengths, cross sections and so on using gluon fusion, VBF and VH^0 production processes with 35.9 fb^{-1} of data. The quoted signal strength is given for $m_{H^0} = 125.09 \text{ GeV}$. Signal strengths for each production process is found in their Fig. 9. Measured cross sections and ratios to the SM predictions in the stage-0 simplified template cross section framework are shown in their Fig. 10. $\kappa_F = 1.52^{+0.48}_{-0.41}$ and $\kappa_V = 1.10 \pm 0.08$ are obtained (see their Fig. 11 (right)).
- ⁸ AAD 16AO measure fiducial total and differential cross sections of gluon fusion process at $E_{\text{cm}} = 8 \text{ TeV}$ with 20.3 fb^{-1} using $H^0 \rightarrow WW^* \rightarrow e\nu\mu\nu$. The measured fiducial total cross section is $36.0 \pm 9.7 \text{ fb}$ in their fiducial region (Table 7). See their Fig. 6 for fiducial differential cross sections. The results are given for $m_{H^0} = 125 \text{ GeV}$.
- ⁹ AAD 16K use up to 4.7 fb^{-1} of pp collisions at $E_{\text{cm}} = 7 \text{ TeV}$ and up to 20.3 fb^{-1} at $E_{\text{cm}} = 8 \text{ TeV}$. The quoted signal strength is given for $m_{H^0} = 125.36 \text{ GeV}$.
- ¹⁰ AAD 15AA use 4.5 fb^{-1} of pp collisions at $E_{\text{cm}} = 7 \text{ TeV}$ and 20.3 fb^{-1} at $E_{\text{cm}} = 8 \text{ TeV}$. The quoted signal strength for the gluon fusion and vector boson fusion mode is $1.02 \pm 0.19^{+0.22}_{-0.18}$ and $1.27^{+0.44}_{-0.40} + 0.30^{+0.30}_{-0.21}$, respectively. The quoted signal strengths are given for $m_{H^0} = 125.36 \text{ GeV}$.
- ¹¹ AAD 15AQ use 4.5 fb^{-1} of pp collisions at $E_{\text{cm}} = 7 \text{ TeV}$ and 20.3 fb^{-1} at $E_{\text{cm}} = 8 \text{ TeV}$. The quoted signal strength is given for $m_{H^0} = 125.36 \text{ GeV}$.
- ¹² AAD 15AQ combine their result on W/ZH^0 production with the results of AAD 15AA (gluon fusion and vector boson fusion, slightly updated). The quoted signal strength is given for $m_{H^0} = 125.36 \text{ GeV}$.
- ¹³ CHATRCHYAN 14G use 4.9 fb^{-1} of pp collisions at $E_{\text{cm}} = 7 \text{ TeV}$ and 19.4 fb^{-1} at $E_{\text{cm}} = 8 \text{ TeV}$. The last uncertainty in the measurement is theory systematics. The quoted signal strength is given for $m_{H^0} = 125.6 \text{ GeV}$.
- ¹⁴ AAD 13AK use 4.7 fb^{-1} of pp collisions at $E_{\text{cm}} = 7 \text{ TeV}$ and 20.7 fb^{-1} at $E_{\text{cm}} = 8 \text{ TeV}$. The quoted signal strength is given for $m_{H^0} = 125.5 \text{ GeV}$. Superseded by AAD 15AA.
- ¹⁵ AALTONEN 13L combine all CDF results with $9.45\text{--}10.0 \text{ fb}^{-1}$ of $p\bar{p}$ collisions at $E_{\text{cm}} = 1.96 \text{ TeV}$. The quoted signal strength is given for $m_{H^0} = 125 \text{ GeV}$.
- ¹⁶ ABAZOV 13L combine all D0 results with up to 9.7 fb^{-1} of $p\bar{p}$ collisions at $E_{\text{cm}} = 1.96 \text{ TeV}$. The quoted signal strength is given for $m_{H^0} = 125 \text{ GeV}$.
- ¹⁷ AAD 12AI obtain results based on 4.7 fb^{-1} of pp collisions at $E_{\text{cm}} = 7 \text{ TeV}$ and 5.8 fb^{-1} at $E_{\text{cm}} = 8 \text{ TeV}$. The quoted signal strengths are given for $m_{H^0} = 126 \text{ GeV}$. See also AAD 12DA.
- ¹⁸ CHATRCHYAN 12N obtain results based on 4.9 fb^{-1} of pp collisions at $E_{\text{cm}} = 7 \text{ TeV}$ and 5.1 fb^{-1} at $E_{\text{cm}} = 8 \text{ TeV}$. The quoted signal strength is given for $m_{H^0} = 125.5 \text{ GeV}$. See also CHATRCHYAN 13Y.

Z Z* Final State

VALUE	CL%	DOCUMENT ID	TECN	COMMENT
$1.20^{+0.12}_{-0.11}$				OUR AVERAGE
$1.06^{+0.19}_{-0.17}$		1 SIRUNYAN	19AT CMS	pp , 13 TeV
$1.28^{+0.21}_{-0.19}$		2 AABOUD	18AJ ATLS	pp , 13 TeV
$1.29^{+0.26}_{-0.23}$		3,4 AAD	16AN LHC	pp , 7, 8 TeV
• • • We do not use the following data for averages, fits, limits, etc. • • •				
<6.5	95	5 AABOUD	19N ATLS	pp , 13 TeV, off-shell
<3.8	95	6 AABOUD	18BP ATLS	pp , 13 TeV, off-shell
$1.05^{+0.15+0.11}_{-0.14-0.09}$		7 SIRUNYAN	17AV CMS	pp , 13 TeV
$1.52^{+0.40}_{-0.34}$		4 AAD	16AN ATLS	pp , 7, 8 TeV
$1.04^{+0.32}_{-0.26}$		4 AAD	16AN CMS	pp , 7, 8 TeV
$1.46^{+0.35+0.19}_{-0.31-0.13}$		8 AAD	16K ATLS	pp , 7, 8 TeV
		9 KHACHATRYAN	16AR CMS	pp , 7, 8 TeV cross sections
$1.44^{+0.34+0.21}_{-0.31-0.11}$		10 AAD	15F ATLS	$pp \rightarrow H^0 X$, 7, 8 TeV
		11 AAD	14AR ATLS	pp , 8 TeV, differential cross section
$0.93^{+0.26+0.13}_{-0.23-0.09}$		12 CHATRCHYAN	14AA CMS	pp , 7, 8 TeV
$1.43^{+0.40}_{-0.35}$		13 AAD	13AK ATLS	pp , 7 and 8 TeV
$0.80^{+0.35}_{-0.28}$		14 CHATRCHYAN	13J CMS	$pp \rightarrow H^0 X$, 7, 8 TeV
1.2 ± 0.6		15 AAD	12AI ATLS	$pp \rightarrow H^0 X$, 7, 8 TeV
1.4 ± 1.1		15 AAD	12AI ATLS	$pp \rightarrow H^0 X$, 7 TeV
1.1 ± 0.8		15 AAD	12AI ATLS	$pp \rightarrow H^0 X$, 8 TeV
$0.73^{+0.45}_{-0.33}$		16 CHATRCHYAN	12N CMS	$pp \rightarrow H^0 X$, 7, 8 TeV

- 1 SIRUNYAN 19AT perform a combine fit to 35.9 fb^{-1} of data at $E_{\text{cm}} = 13 \text{ TeV}$.
- 2 AABOUD 18AJ perform analyses using $H^0 \rightarrow ZZ^* \rightarrow 4\ell$ ($\ell = e, \mu$) with data of 36.1 fb^{-1} at $E_{\text{cm}} = 13 \text{ TeV}$. Results are given for $m_{H^0} = 125.09 \text{ GeV}$. The inclusive cross section times branching ratio for $H^0 \rightarrow ZZ^*$ decay ($|\eta(H^0)| < 2.5$) is measured to be $1.73^{+0.26}_{-0.24} \text{ pb}$ (with $1.34^{+0.09}_{-0.09} \text{ pb}$ expected in the SM).
- 3 AAD 16AN perform fits to the ATLAS and CMS data at $E_{\text{cm}} = 7$ and 8 TeV . The signal strengths for individual production processes are $1.13^{+0.34}_{-0.31}$ for gluon fusion and $0.1^{+1.1}_{-0.6}$ for vector boson fusion.
- 4 AAD 16AN: In the fit, relative production cross sections are fixed to those in the Standard Model. The quoted signal strength is given for $m_{H^0} = 125.09 \text{ GeV}$.
- 5 AABOUD 19N measure the spectrum of the four-lepton invariant mass $m_{4\ell}$ ($\ell = e$ or μ) using 36.1 fb^{-1} of data at $E_{\text{cm}} = 13 \text{ TeV}$. The quoted signal strength upper limit is obtained from $180 \text{ GeV} < m_{4\ell} < 1200 \text{ GeV}$.
- 6 AABOUD 18BP measure an off-shell Higgs boson production using $ZZ \rightarrow 4\ell$ and $ZZ \rightarrow 2\ell 2\nu$ ($\ell = e, \mu$) decay channels with 36.1 fb^{-1} of data at $E_{\text{cm}} = 13 \text{ TeV}$. The quoted signal strength upper limit is obtained from a combination of these two channels, where $220 \text{ GeV} < m_{4\ell} < 2000 \text{ GeV}$ for $ZZ \rightarrow 4\ell$ and $250 \text{ GeV} < m_{\ell\ell}^{ZZ} < 2000 \text{ GeV}$ for $ZZ \rightarrow 2\ell 2\nu$ ($m_{\ell\ell}^{ZZ}$ is defined in their Section 5). See their Table 2 for each measurement.
- 7 SIRUNYAN 17AV use 35.9 fb^{-1} of pp collisions at $E_{\text{cm}} = 13 \text{ TeV}$. The quoted signal strength, obtained from the analysis of $H^0 \rightarrow ZZ^* \rightarrow 4\ell$ ($\ell = e, \mu$) decays, is given for $m_{H^0} = 125.09 \text{ GeV}$. The signal strengths for different production modes are given in their Table 3. The fiducial and differential cross sections are shown in their Fig. 10.
- 8 AAD 16K use up to 4.7 fb^{-1} of pp collisions at $E_{\text{cm}} = 7 \text{ TeV}$ and up to 20.3 fb^{-1} at $E_{\text{cm}} = 8 \text{ TeV}$. The quoted signal strength is given for $m_{H^0} = 125.36 \text{ GeV}$.
- 9 KHACHATRYAN 16AR use data of 5.1 fb^{-1} at $E_{\text{cm}} = 7 \text{ TeV}$ and 19.7 fb^{-1} at 8 TeV . The fiducial cross sections for the production of 4 leptons via $H^0 \rightarrow 4\ell$ decays are measured to be $0.56^{+0.67+0.21}_{-0.44-0.06} \text{ fb}$ at 7 TeV and $1.11^{+0.41+0.14}_{-0.35-0.10} \text{ fb}$ at 8 TeV in their fiducial region (Table 2). The differential cross sections at $E_{\text{cm}} = 8 \text{ TeV}$ are also shown in Figs. 4 and 5. The results are given for $m_{H^0} = 125 \text{ GeV}$.
- 10 AAD 15F use 4.5 fb^{-1} of pp collisions at $E_{\text{cm}} = 7 \text{ TeV}$ and 20.3 fb^{-1} at $E_{\text{cm}} = 8 \text{ TeV}$. The quoted signal strength is given for $m_{H^0} = 125.36 \text{ GeV}$. The signal strength for the gluon fusion production mode is $1.66^{+0.45+0.25}_{-0.41-0.15}$, while the signal strength for the vector boson fusion production mode is $0.26^{+1.60+0.36}_{-0.91-0.23}$.
- 11 AAD 14AR measure the cross section for $pp \rightarrow H^0 X$, $H^0 \rightarrow ZZ^*$ using 20.3 fb^{-1} at $E_{\text{cm}} = 8 \text{ TeV}$. They give $\sigma \cdot B = 2.11^{+0.53}_{-0.47} \pm 0.08 \text{ fb}$ in their fiducial region, where $1.30 \pm 0.13 \text{ fb}$ is expected in the Standard Model for $m_{H^0} = 125.4 \text{ GeV}$. Various differential cross sections are also given, which are in agreement with the Standard Model expectations.
- 12 CHATRCHYAN 14AA use 5.1 fb^{-1} of pp collisions at $E_{\text{cm}} = 7 \text{ TeV}$ and 19.7 fb^{-1} at $E_{\text{cm}} = 8 \text{ TeV}$. The quoted signal strength is given for $m_{H^0} = 125.6 \text{ GeV}$. The signal strength for the gluon fusion and $t\bar{t}H$ production mode is $0.80^{+0.46}_{-0.36}$, while the signal strength for the vector boson fusion and WH^0 , ZH^0 production mode is $1.7^{+2.2}_{-2.1}$.
- 13 AAD 13AK use 4.7 fb^{-1} of pp collisions at $E_{\text{cm}} = 7 \text{ TeV}$ and 20.7 fb^{-1} at $E_{\text{cm}} = 8 \text{ TeV}$. The quoted signal strength is given for $m_{H^0} = 125.5 \text{ GeV}$.
- 14 CHATRCHYAN 13J obtain results based on $ZZ \rightarrow 4\ell$ final states in 5.1 fb^{-1} of pp collisions at $E_{\text{cm}} = 7 \text{ TeV}$ and 12.2 fb^{-1} at $E_{\text{cm}} = 8 \text{ TeV}$. The quoted signal strength is given for $m_{H^0} = 125.8 \text{ GeV}$. Superseded by CHATRCHYAN 14AA.

15 AAD 12AI obtain results based on $4.7\text{--}4.8 \text{ fb}^{-1}$ of pp collisions at $E_{\text{cm}} = 7 \text{ TeV}$ and 5.8 fb^{-1} at $E_{\text{cm}} = 8 \text{ TeV}$. The quoted signal strengths are given for $m_{H^0} = 126 \text{ GeV}$.

See also AAD 12DA.
 16 CHATRCHYAN 12N obtain results based on $4.9\text{--}5.1 \text{ fb}^{-1}$ of pp collisions at $E_{\text{cm}} = 7 \text{ TeV}$ and $5.1\text{--}5.3 \text{ fb}^{-1}$ at $E_{\text{cm}} = 8 \text{ TeV}$. An excess of events over background with a local significance of 5.0σ is observed at about $m_{H^0} = 125 \text{ GeV}$. The quoted signal strengths are given for $m_{H^0} = 125.5 \text{ GeV}$. See also CHATRCHYAN 12BY and CHATRCHYAN 13Y.

 $\gamma\gamma$ Final State

VALUE	DOCUMENT ID	TECN	COMMENT
$1.11^{+0.10}_{-0.09}$			OUR AVERAGE
$1.20^{+0.18}_{-0.14}$	1 SIRUNYAN	19AT CMS	pp , 13 TeV
$0.99^{+0.15}_{-0.14}$	2 AABOUD	18BO ATLS	pp , 13 TeV, 36.1 fb^{-1}
$1.14^{+0.19}_{-0.18}$	3,4 AAD	16AN LHC	pp , 7, 8 TeV
$5.97^{+3.39}_{-3.12}$	5 AALTONEN	13M TEVA	$p\bar{p} \rightarrow H^0 X$, 1.96 TeV
• • • We do not use the following data for averages, fits, limits, etc. • • •			
$1.18^{+0.17}_{-0.14}$	6 SIRUNYAN	19L CMS	pp , 13 TeV, diff. x-section
	7 SIRUNYAN	18DS CMS	pp , $H^0 \rightarrow \gamma\gamma$, 13 TeV, floated m_{H^0}
$1.14^{+0.27}_{-0.25}$	4 AAD	16AN ATLS	pp , 7, 8 TeV
$1.11^{+0.25}_{-0.23}$	4 AAD	16AN CMS	pp , 7, 8 TeV
	8 KHACHATRYAN	16G CMS	pp , 8 TeV, diff. x-section
$1.17 \pm 0.23^{+0.10+0.12}_{-0.08-0.08}$	9 AAD	14BC ATLS	$pp \rightarrow H^0 X$, 7, 8 TeV
	10 AAD	14BJ ATLS	pp , 8 TeV, diff. x-section
$1.14 \pm 0.21^{+0.09+0.13}_{-0.05-0.09}$	11 KHACHATRYAN	14P CMS	pp , 7, 8 TeV
$1.55^{+0.33}_{-0.28}$	12 AAD	13AK ATLS	pp , 7 and 8 TeV
$7.81^{+4.61}_{-4.42}$	13 AALTONEN	13L CDF	$p\bar{p} \rightarrow H^0 X$, 1.96 TeV
$4.20^{+4.60}_{-4.20}$	14 ABAZOV	13L D0	$p\bar{p} \rightarrow H^0 X$, 1.96 TeV
1.8 ± 0.5	15 AAD	12AI ATLS	$pp \rightarrow H^0 X$, 7, 8 TeV
2.2 ± 0.7	15 AAD	12AI ATLS	$pp \rightarrow H^0 X$, 7 TeV
1.5 ± 0.6	15 AAD	12AI ATLS	$pp \rightarrow H^0 X$, 8 TeV
$1.54^{+0.46}_{-0.42}$	16 CHATRCHYAN	12N CMS	$pp \rightarrow H^0 X$, 7, 8 TeV

- 1 SIRUNYAN 19AT perform a combine fit to 35.9 fb^{-1} of data at $E_{\text{cm}} = 13 \text{ TeV}$.
- 2 AABOUD 18BO use 36.1 fb^{-1} of pp collisions at $E_{\text{cm}} = 13 \text{ TeV}$. The signal strengths for the individual production modes are: $0.81^{+0.19}_{-0.18}$ for gluon fusion, $2.0^{+0.6}_{-0.5}$ for vector boson fusion, $0.7^{+0.9}_{-0.8}$ for VH^0 production ($V = W, Z$), and 0.5 ± 0.6 for $t\bar{t}H^0$ and tH^0 production. Other measurements of cross sections and couplings are summarized in their Section 10. The quoted values are given for $m_{H^0} = 125.09 \text{ GeV}$.
- 3 AAD 16AN perform fits to the ATLAS and CMS data at $E_{\text{cm}} = 7$ and 8 TeV . The signal strengths for individual production processes are $1.10^{+0.23}_{-0.22}$ for gluon fusion, 1.3 ± 0.5 for vector boson fusion, $0.5^{+1.3}_{-1.2}$ for WH^0 production, $0.5^{+3.0}_{-2.5}$ for ZH^0 production, and $2.2^{+1.6}_{-1.3}$ for $t\bar{t}H^0$ production.
- 4 AAD 16AN: In the fit, relative production cross sections are fixed to those in the Standard Model. The quoted signal strength is given for $m_{H^0} = 125.09 \text{ GeV}$.
- 5 AALTONEN 13M combine all Tevatron data from the CDF and D0 Collaborations with up to 10.0 fb^{-1} and 9.7 fb^{-1} , respectively, of $p\bar{p}$ collisions at $E_{\text{cm}} = 1.96 \text{ TeV}$. The quoted signal strength is given for $m_{H^0} = 125 \text{ GeV}$.
- 6 SIRUNYAN 19L measure fiducial and differential cross sections of the process $pp \rightarrow H^0 \rightarrow \gamma\gamma$ at $E_{\text{cm}} = 13 \text{ TeV}$ with 35.9 fb^{-1} . See their Figs. 4–11.
- 7 SIRUNYAN 18DS use 35.9 fb^{-1} of $pp \rightarrow H^0$ collisions with $H^0 \rightarrow \gamma\gamma$ at $E_{\text{cm}} = 13 \text{ TeV}$. The Higgs mass is floated in the measurement of a signal strength. The result is $1.18^{+0.12}_{-0.11}(\text{stat.})^{+0.09}_{-0.07}(\text{syst.})^{+0.07}_{-0.06}(\text{theory})$, which is largely insensitive to the Higgs mass around 125 GeV .
- 8 KHACHATRYAN 16G measure fiducial and differential cross sections of the process $pp \rightarrow H^0 X$, $H^0 \rightarrow \gamma\gamma$ at $E_{\text{cm}} = 8 \text{ TeV}$ with 19.7 fb^{-1} . See their Figs. 4–6 and Table 1 for data.
- 9 AAD 14BC use 4.5 fb^{-1} of pp collisions at $E_{\text{cm}} = 7 \text{ TeV}$ and 20.3 fb^{-1} at $E_{\text{cm}} = 8 \text{ TeV}$. The last uncertainty in the measurement is theory systematics. The quoted signal strength is given for $m_{H^0} = 125.4 \text{ GeV}$. The signal strengths for the individual production modes are: 1.32 ± 0.38 for gluon fusion, 0.8 ± 0.7 for vector boson fusion, 1.0 ± 1.6 for WH^0 production, $0.1^{+3.7}_{-0.1}$ for ZH^0 production, and $1.6^{+2.7}_{-1.8}$ for $t\bar{t}H^0$ production.
- 10 AAD 14BJ measure fiducial and differential cross sections of the process $pp \rightarrow H^0 X$, $H^0 \rightarrow \gamma\gamma$ at $E_{\text{cm}} = 8 \text{ TeV}$ with 20.3 fb^{-1} . See their Table 3 and Figs. 3–12 for data.
- 11 KHACHATRYAN 14P use 5.1 fb^{-1} of pp collisions at $E_{\text{cm}} = 7 \text{ TeV}$ and 19.7 fb^{-1} at $E_{\text{cm}} = 8 \text{ TeV}$. The last uncertainty in the measurement is theory systematics. The quoted signal strength is given for $m_{H^0} = 124.7 \text{ GeV}$. The signal strength for the gluon fusion and $t\bar{t}H$ production mode is $1.13^{+0.37}_{-0.31}$, while the signal strength for the vector boson fusion and WH^0 , ZH^0 production mode is $1.16^{+0.63}_{-0.58}$.
- 12 AAD 13AK use 4.7 fb^{-1} of pp collisions at $E_{\text{cm}} = 7 \text{ TeV}$ and 20.7 fb^{-1} at $E_{\text{cm}} = 8 \text{ TeV}$. The quoted signal strength is given for $m_{H^0} = 125.5 \text{ GeV}$.
- 13 AALTONEN 13L combine all CDF results with $9.45\text{--}10.0 \text{ fb}^{-1}$ of $p\bar{p}$ collisions at $E_{\text{cm}} = 1.96 \text{ TeV}$. The quoted signal strength is given for $m_{H^0} = 125 \text{ GeV}$.

Gauge & Higgs Boson Particle Listings

 H^0

- ¹⁴ ABAZOV 13L combine all D0 results with up to 9.7 fb^{-1} of $p\bar{p}$ collisions at $E_{\text{cm}} = 1.96 \text{ TeV}$. The quoted signal strength is given for $m_{H^0} = 125 \text{ GeV}$.
- ¹⁵ AAD 12A1 obtain results based on 4.8 fb^{-1} of pp collisions at $E_{\text{cm}} = 7 \text{ TeV}$ and 5.9 fb^{-1} at $E_{\text{cm}} = 8 \text{ TeV}$. The quoted signal strengths are given for $m_{H^0} = 126 \text{ GeV}$. See also AAD 12DA.
- ¹⁶ CHATRCHYAN 12N obtain results based on 5.1 fb^{-1} of pp collisions at $E_{\text{cm}} = 7 \text{ TeV}$ and 5.3 fb^{-1} at $E_{\text{cm}} = 8 \text{ TeV}$. The quoted signal strength is given for $m_{H^0} = 125.5 \text{ GeV}$. See also CHATRCHYAN 13Y.

 $c\bar{c}$ Final State

VALUE	CL%	DOCUMENT ID	TECN	COMMENT
<110	95	¹ AABOUD	18M ATLS	pp , 13 TeV

- ¹ AABOUD 18M use 36.1 fb^{-1} at of pp collisions at $E_{\text{cm}} = 13 \text{ TeV}$. The upper limit on $\sigma(pp \rightarrow ZH^0) \cdot B(H^0 \rightarrow c\bar{c})$ is 2.7 pb at 95% CL. The quoted values are given for $m_{H^0} = 125 \text{ GeV}$.

 $b\bar{b}$ Final State

VALUE	DOCUMENT ID	TECN	COMMENT
1.04 ± 0.13 OUR AVERAGE			

1.12 ± 0.29	¹ SIRUNYAN	19AT CMS	pp , 13 TeV
$1.16^{+0.27}_{-0.25}$	² AABOUD	18BN ATLS	$pp \rightarrow H^0 W/H^0 Z, H^0 \rightarrow b\bar{b}$, 13 TeV, 79.8 fb^{-1}
1.06 ± 0.26	³ SIRUNYAN	18DB CMS	$pp \rightarrow H^0 W/H^0 Z, H^0 \rightarrow b\bar{b}$, 13 TeV, 77.2 fb^{-1}
$0.70^{+0.29}_{-0.27}$	^{4,5} AAD	16AN LHC	pp , 7, 8 TeV
$1.59^{+0.69}_{-0.72}$	⁶ AALTONEN	13M TEVA	$p\bar{p} \rightarrow H^0 X$, 1.96 TeV
$0.98^{+0.22}_{-0.21}$	⁸ AABOUD	18BN ATLS	$pp \rightarrow H^0 W/H^0 Z, H^0 \rightarrow b\bar{b}$, 7, 8, 13 TeV
1.01 ± 0.20	⁹ AABOUD	18BN ATLS	$pp \rightarrow H^0 X, \text{ggF}, \text{VBF}, V H^0, t\bar{t}H^0$, 7, 8, 13 TeV
$2.5^{+1.4}_{-1.3}$	^{10,11} AABOUD	18BQ ATLS	$pp \rightarrow H^0 X, \text{VBF}, \text{ggF}, V H^0, t\bar{t}H^0$, 13 TeV
$3.0^{+1.7}_{-1.6}$	^{10,12} AABOUD	18BQ ATLS	$pp \rightarrow H^0 X, \text{VBF}$, 13 TeV
$1.19^{+0.40}_{-0.38}$	¹⁴ SIRUNYAN	18AE CMS	$pp \rightarrow H^0 W/H^0 Z, H^0 \rightarrow b\bar{b}$, 13 TeV
$1.06^{+0.31}_{-0.29}$	¹⁵ SIRUNYAN	18AE CMS	$pp \rightarrow H^0 W/H^0 Z, H^0 \rightarrow b\bar{b}$, 7, 8, 13 TeV
1.01 ± 0.22	¹⁶ SIRUNYAN	18DB CMS	$pp \rightarrow H^0 W/H^0 Z, H^0 \rightarrow b\bar{b}$, 7, 8, 13 TeV
1.04 ± 0.20	¹⁷ SIRUNYAN	18DB CMS	$pp \rightarrow H^0 X, \text{ggF}, \text{VBF}, V H^0, t\bar{t}H^0$, 7, 8, 13 TeV
$2.3^{+1.8}_{-1.6}$	¹⁸ SIRUNYAN	18E CMS	$pp \rightarrow H^0 X$, boosted, 13 TeV
$1.20^{+0.24+0.34}_{-0.23-0.28}$	¹⁹ AABOUD	17BA ATLS	$pp \rightarrow H^0 W/ZX, H^0 \rightarrow b\bar{b}$, 13 TeV, 36.1 fb^{-1}
$0.90 \pm 0.18^{+0.21}_{-0.19}$	²⁰ AABOUD	17BA ATLS	$pp \rightarrow H^0 W/ZX, H^0 \rightarrow b\bar{b}$, 7, 8, 13 TeV
$-0.8 \pm 1.3^{+1.8}_{-1.9}$	²¹ AABOUD	16X ATLS	$pp \rightarrow H^0 X, \text{VBF}$, 8 TeV
0.62 ± 0.37	⁵ AAD	16AN ATLS	pp , 7, 8 TeV
$0.81^{+0.45}_{-0.43}$	⁵ AAD	16AN CMS	pp , 7, 8 TeV
$0.63^{+0.31+0.24}_{-0.30-0.23}$	²² AAD	16K ATLS	pp , 7, 8 TeV
$0.52 \pm 0.32 \pm 0.24$	²³ AAD	15G ATLS	$pp \rightarrow H^0 W/ZX$, 7, 8 TeV
$2.8^{+1.6}_{-1.4}$	²⁴ KHACHATRYAN..15Z	CMS	$pp \rightarrow H^0 X, \text{VBF}$, 8 TeV
$1.03^{+0.44}_{-0.42}$	²⁵ KHACHATRYAN..15Z	CMS	pp , 8 TeV, combined
1.0 ± 0.5	²⁶ CHATRCHYAN14A1	CMS	$pp \rightarrow H^0 W/ZX$, 7, 8 TeV
$1.72^{+0.92}_{-0.87}$	²⁷ AALTONEN	13L CDF	$p\bar{p} \rightarrow H^0 X$, 1.96 TeV
$1.23^{+1.24}_{-1.17}$	²⁸ ABAZOV	13L D0	$p\bar{p} \rightarrow H^0 X$, 1.96 TeV
0.5 ± 2.2	²⁹ AAD	12A1 ATLS	$pp \rightarrow H^0 W/ZX$, 7 TeV
	³⁰ AALTONEN	12T TEVA	$p\bar{p} \rightarrow H^0 W/ZX$, 1.96 TeV
$0.48^{+0.81}_{-0.70}$	³¹ CHATRCHYAN12N	CMS	$pp \rightarrow H^0 W/ZX$, 7, 8 TeV

- ¹ SIRUNYAN 19AT perform a combine fit to 35.9 fb^{-1} of data at $E_{\text{cm}} = 13 \text{ TeV}$.
- ² AABOUD 18BN search for $VH^0, H^0 \rightarrow b\bar{b}$ ($V = W, Z$) using 79.8 fb^{-1} of pp collision data at $E_{\text{cm}} = 13 \text{ TeV}$. The quoted signal strength corresponds to a significance of 4.9 standard deviations and is given for $m_{H^0} = 125 \text{ GeV}$.
- ³ SIRUNYAN 18DB search for $VH^0, H^0 \rightarrow b\bar{b}$ ($V = W, Z$) using 77.2 fb^{-1} of pp collision data at $E_{\text{cm}} = 13 \text{ TeV}$. The quoted signal strength corresponds to a significance of 4.4 standard deviations and is given for $m_{H^0} = 125.09 \text{ GeV}$.
- ⁴ AAD 16AN perform fits to the ATLAS and CMS data at $E_{\text{cm}} = 7$ and 8 TeV . The signal strengths for individual production processes are 1.0 ± 0.5 for WH^0 production, 0.4 ± 0.4 for ZH^0 production, and 1.1 ± 1.0 for $t\bar{t}H^0$ production.
- ⁵ AAD 16AN: In the fit, relative production cross sections are fixed to those in the Standard Model. The quoted signal strength is given for $m_{H^0} = 125.09 \text{ GeV}$.

- ⁶ AALTONEN 13M combine all Tevatron data from the CDF and D0 Collaborations with up to 10.0 fb^{-1} and 9.7 fb^{-1} , respectively, of $p\bar{p}$ collisions at $E_{\text{cm}} = 1.96 \text{ TeV}$. The quoted signal strength is given for $m_{H^0} = 125 \text{ GeV}$.
- ⁷ AABOUD 19U measure cross sections of $pp \rightarrow VH^0, H^0 \rightarrow b\bar{b}$ production as a function of the gauge boson transverse momentum using data of 79.8 fb^{-1} . The kinematic fiducial volumes used is based on the simplified template cross section framework (reduced stage-1). See their Table 3 and Fig. 3.
- ⁸ AABOUD 18BN combine results of 79.8 fb^{-1} at $E_{\text{cm}} = 13 \text{ TeV}$ with results of VH^0 at $E_{\text{cm}} = 7$ and 8 TeV .
- ⁹ AABOUD 18BN combine results of VH^0 at $E_{\text{cm}} = 7, 8$ and 13 TeV with results of VBF (+gluon fusion) and $t\bar{t}H^0$ at $E_{\text{cm}} = 7, 8$, and 13 TeV to perform a search for the $H^0 \rightarrow b\bar{b}$ decay. The quoted signal strength assumes a SM production strength and corresponds to a significance of 5.4 standard deviations.
- ¹⁰ AABOUD 18BQ search for $H^0 \rightarrow b\bar{b}$ produced through vector-boson fusion (VBF) and VBF+ γ with 30.6 fb^{-1} pp collision data at $E_{\text{cm}} = 13 \text{ TeV}$. The quoted signal strength is given for $m_{H^0} = 125 \text{ GeV}$.
- ¹¹ The signal strength is measured including all production modes (VBF, ggF, $VH^0, t\bar{t}H^0$).
- ¹² The signal strength is measured for VBF-only and others (ggF, $VH^0, t\bar{t}H^0$) are constrained to Standard Model expectations with uncertainties described in their Section VIII B.
- ¹³ AALTONEN 18C use 5.4 fb^{-1} of $p\bar{p}$ collisions at $E_{\text{cm}} = 1.96 \text{ TeV}$. The upper limit at 95% CL on $p\bar{p} \rightarrow H^0 \rightarrow b\bar{b}$ is 33 times the SM prediction, which corresponds to a cross section of 40.6 pb .
- ¹⁴ SIRUNYAN 18AE use 35.9 fb^{-1} of pp collision data at $E_{\text{cm}} = 13 \text{ TeV}$. The quoted signal strength corresponds to 3.3 standard deviations and is given for $m_{H^0} = 125.09 \text{ GeV}$.
- ¹⁵ SIRUNYAN 18AE combine the result of 35.9 fb^{-1} at $E_{\text{cm}} = 13 \text{ TeV}$ with results obtained from data of up to 5.1 fb^{-1} at $E_{\text{cm}} = 7 \text{ TeV}$ and up to 18.9 fb^{-1} at $E_{\text{cm}} = 8 \text{ TeV}$ (CHATRCHYAN 14A1 and KHACHATRYAN 15Z). The quoted signal strength corresponds to 3.8 standard deviations and is given for $m_{H^0} = 125.09 \text{ GeV}$.
- ¹⁶ SIRUNYAN 18DB combine the result of 77.2 fb^{-1} at $E_{\text{cm}} = 13 \text{ TeV}$ with the results obtained from data of up to 5.1 fb^{-1} at $E_{\text{cm}} = 7 \text{ TeV}$ and up to 18.9 fb^{-1} at $E_{\text{cm}} = 8 \text{ TeV}$. The quoted signal strength corresponds to a significance of 4.8 standard deviations and is given for $m_{H^0} = 125.09 \text{ GeV}$.
- ¹⁷ SIRUNYAN 18DB combine results of 77.2 fb^{-1} at $E_{\text{cm}} = 13 \text{ TeV}$ with results of gluon fusion (ggF), VBF and $t\bar{t}H^0$ at $E_{\text{cm}} = 7 \text{ TeV}$, 8 TeV and 13 TeV to perform a search for the $H^0 \rightarrow b\bar{b}$ decay. The quoted signal strength assumes a SM production strength and corresponds to a significance of 5.6 standard deviations and is given for $m_{H^0} = 125.09 \text{ GeV}$.
- ¹⁸ SIRUNYAN 18E use 35.9 fb^{-1} at $E_{\text{cm}} = 13 \text{ TeV}$. The quoted signal strength is given for $m_{H^0} = 125 \text{ GeV}$. They measure $\sigma \cdot B$ for gluon fusion production of $H^0 \rightarrow b\bar{b}$ with $p_T > 450 \text{ GeV}$, $|\eta| < 2.5$ to be $74 \pm 48^{+17}_{-10} \text{ fb}$.
- ¹⁹ AABOUD 17BA use 36.1 fb^{-1} at $E_{\text{cm}} = 13 \text{ TeV}$. The quoted signal strength is given for $m_{H^0} = 125 \text{ GeV}$. They give $\sigma(WH) \cdot B(H^0 \rightarrow b\bar{b}) = 1.08^{+0.54}_{-0.47} \text{ pb}$ and $\sigma(ZH) \cdot B(H^0 \rightarrow b\bar{b}) = 0.57^{+0.26}_{-0.23} \text{ pb}$.
- ²⁰ AABOUD 17BA combine 7, 8 and 13 TeV analyses. The quoted signal strength is given for $m_{H^0} = 125 \text{ GeV}$.
- ²¹ AABOUD 16X search for vector-boson fusion production of H^0 decaying to $b\bar{b}$ in 20.2 fb^{-1} of pp collisions at $E_{\text{cm}} = 8 \text{ TeV}$. The quoted signal strength is given for $m_{H^0} = 125 \text{ GeV}$.
- ²² AAD 16K use up to 4.7 fb^{-1} of pp collisions at $E_{\text{cm}} = 7 \text{ TeV}$ and up to 20.3 fb^{-1} at $E_{\text{cm}} = 8 \text{ TeV}$. The quoted signal strength is given for $m_{H^0} = 125.36 \text{ GeV}$.
- ²³ AAD 15G use 4.7 fb^{-1} of pp collisions at $E_{\text{cm}} = 7 \text{ TeV}$ and 20.3 fb^{-1} at $E_{\text{cm}} = 8 \text{ TeV}$. The quoted signal strength is given for $m_{H^0} = 125.36 \text{ GeV}$.
- ²⁴ KHACHATRYAN 15Z search for vector-boson fusion production of H^0 decaying to $b\bar{b}$ in up to 19.8 fb^{-1} of pp collisions at $E_{\text{cm}} = 8 \text{ TeV}$. The quoted signal strength is given for $m_{H^0} = 125 \text{ GeV}$.
- ²⁵ KHACHATRYAN 15Z combined vector boson fusion, WH^0, ZH^0 production, and $t\bar{t}H^0$ production results. The quoted signal strength is given for $m_{H^0} = 125 \text{ GeV}$.
- ²⁶ CHATRCHYAN 14A1 use up to 5.1 fb^{-1} of pp collisions at $E_{\text{cm}} = 7 \text{ TeV}$ and up to 18.9 fb^{-1} at $E_{\text{cm}} = 8 \text{ TeV}$. The quoted signal strength is given for $m_{H^0} = 125 \text{ GeV}$. See also CHATRCHYAN 14A1.
- ²⁷ AALTONEN 13L combine all CDF results with $9.45\text{--}10.0 \text{ fb}^{-1}$ of $p\bar{p}$ collisions at $E_{\text{cm}} = 1.96 \text{ TeV}$. The quoted signal strength is given for $m_{H^0} = 125 \text{ GeV}$.
- ²⁸ ABAZOV 13L combine all D0 results with up to 9.7 fb^{-1} of $p\bar{p}$ collisions at $E_{\text{cm}} = 1.96 \text{ TeV}$. The quoted signal strength is given for $m_{H^0} = 125 \text{ GeV}$.
- ²⁹ AAD 12A1 obtain results based on $4.6\text{--}4.8 \text{ fb}^{-1}$ of pp collisions at $E_{\text{cm}} = 7 \text{ TeV}$. The quoted signal strengths are given in their Fig. 10 for $m_{H^0} = 126 \text{ GeV}$. See also Fig. 13 of AAD 12DA.
- ³⁰ AALTONEN 12T combine AALTONEN 12Q, AALTONEN 12R, AALTONEN 12S, ABAZOV 12P, ABAZOV 12P, and ABAZOV 12K. An excess of events over background is observed which is most significant in the region $m_{H^0} = 120\text{--}135 \text{ GeV}$, with a local significance of up to 3.3σ . The local significance at $m_{H^0} = 125 \text{ GeV}$ is 2.8σ , which corresponds to $(\sigma(H^0 W) + \sigma(H^0 Z)) \cdot B(H^0 \rightarrow b\bar{b}) = (0.23^{+0.09}_{-0.08}) \text{ pb}$, compared to the Standard Model expectation at $m_{H^0} = 125 \text{ GeV}$ of $0.12 \pm 0.01 \text{ pb}$. Superseded by AALTONEN 13M.
- ³¹ CHATRCHYAN 12N obtain results based on 5.0 fb^{-1} of pp collisions at $E_{\text{cm}} = 7 \text{ TeV}$ and 5.1 fb^{-1} at $E_{\text{cm}} = 8 \text{ TeV}$. The quoted signal strength is given for $m_{H^0} = 125.5 \text{ GeV}$. See also CHATRCHYAN 13Y.

$\mu^+ \mu^-$ Final State

VALUE	CL%	DOCUMENT ID	TECN	COMMENT
0.6 ± 0.8		OUR AVERAGE		
1.0 ± 1.0 ± 0.1		1 SIRUNYAN	19E CMS	pp , 7, 8, 13 TeV
-0.1 ± 1.4		2 AABOUD	17Y ATLS	pp , 7, 8, 13 TeV
• • • We do not use the following data for averages, fits, limits, etc. • • •				
0.68 ^{+1.25} _{-1.24}		3 SIRUNYAN	19AT CMS	pp , 13 TeV
0.7 ± 1.0 ^{+0.2} _{-0.1}		1 SIRUNYAN	19E CMS	pp , 13 TeV, 35.9 fb ⁻¹
-0.1 ± 1.5		2 AABOUD	17Y ATLS	pp , 13 TeV
0.1 ± 2.5		4 AAD	16AN LHC	pp , 7, 8 TeV
-0.6 ± 3.6		4 AAD	16AN ATLS	pp , 7, 8 TeV
0.9 ± 3.6 _{-3.5}		4 AAD	16AN CMS	pp , 7, 8 TeV
< 7.4	95	5 KHACHATRYAN...15H	CMS	$pp \rightarrow H^0 X$, 7, 8 TeV
< 7.0	95	6 AAD	14AS ATLS	$pp \rightarrow H^0 X$, 7, 8 TeV
1 SIRUNYAN 19E search for $H^0 \rightarrow \mu^+ \mu^-$ using 35.9 fb ⁻¹ of pp collisions at $E_{cm} = 13$ TeV and combine with results of 7 TeV (5.0 fb ⁻¹) and 8 TeV (19.7 fb ⁻¹). The upper limit at 95% CL on the signal strength is 2.9, which corresponds to the SM Higgs boson branching fraction to a muon pair of 6.4×10^{-4} .				
2 AABOUD 17Y use 36.1 fb ⁻¹ of pp collisions at $E_{cm} = 13$ TeV, 20.3 fb ⁻¹ at 8 TeV and 4.5 fb ⁻¹ at 7 TeV. The quoted signal strength is given for $m_{H^0} = 125$ GeV.				
3 SIRUNYAN 19AT perform a combine fit to 35.9 fb ⁻¹ of data at $E_{cm} = 13$ TeV.				
4 AAD 16AN: In the fit, relative production cross sections are fixed to those in the Standard Model. The quoted signal strength is given for $m_{H^0} = 125.09$ GeV.				
5 KHACHATRYAN 15H use 5.0 fb ⁻¹ of pp collisions at $E_{cm} = 7$ TeV and 19.7 fb ⁻¹ at 8 TeV. The quoted signal strength is given for $m_{H^0} = 125$ GeV.				
6 AAD 14AS search for $H^0 \rightarrow \mu^+ \mu^-$ in 4.5 fb ⁻¹ of pp collisions at $E_{cm} = 7$ TeV and 20.3 fb ⁻¹ at $E_{cm} = 8$ TeV. The quoted signal strength is given for $m_{H^0} = 125.5$ GeV.				

 $\tau^+ \tau^-$ Final State

VALUE	CL%	DOCUMENT ID	TECN	COMMENT
1.15 ± 0.16		OUR AVERAGE		
1.09 ^{+0.18} _{-0.17} + 0.26 ^{+0.16} _{-0.22} - 0.11		1 AABOUD	19AQ ATLS	pp , 13 TeV, $H \rightarrow \tau\tau$
1.24 ^{+0.29} _{-0.27}		2 SIRUNYAN	19AF CMS	pp , 13 TeV
1.11 ^{+0.24} _{-0.22}		3,4 AAD	16AN LHC	pp , 7, 8 TeV
1.68 ^{+2.28} _{-1.68}		5 AALTONEN	13M TEVA	$p\bar{p} \rightarrow H^0 X$, 1.96 TeV
• • • We do not use the following data for averages, fits, limits, etc. • • •				
2.5 ^{+1.4} _{-1.3}		6 SIRUNYAN	19AF CMS	$pp \rightarrow H^0 W/H^0 Z$, $H^0 \rightarrow \tau\tau$, 13 TeV
1.02 ^{+0.26} _{-0.24}		7 SIRUNYAN	19AT CMS	pp , 13 TeV
1.09 ^{+0.27} _{-0.26}		8 SIRUNYAN	18Y CMS	pp , 13 TeV
0.98 ± 0.18		9 SIRUNYAN	18Y CMS	pp , 7, 8, 13 TeV
2.3 ± 1.6		10 AAD	16AC ATLS	$pp \rightarrow H^0 W/ZX$, 8 TeV
1.41 ^{+0.40} _{-0.36}		4 AAD	16AN ATLS	pp , 7, 8 TeV
0.88 ^{+0.30} _{-0.28}		4 AAD	16AN CMS	pp , 7, 8 TeV
1.44 ^{+0.30} _{-0.29} - 0.23		11 AAD	16K ATLS	pp , 7, 8 TeV
1.43 ^{+0.27} _{-0.26} ± 0.09		12 AAD	15AH ATLS	$pp \rightarrow H^0 X$, 7, 8 TeV
0.78 ± 0.27		13 CHATRCHYAN 14K	CMS	$pp \rightarrow H^0 X$, 7, 8 TeV
0.00 ^{+8.44} _{-0.00}		14 AALTONEN	13L D0	$p\bar{p} \rightarrow H^0 X$, 1.96 TeV
3.96 ^{+4.11} _{-3.38}		15 ABAZOV	13L D0	$p\bar{p} \rightarrow H^0 X$, 1.96 TeV
0.4 ^{+1.6} _{-2.0}		16 AAD	12AI ATLS	$pp \rightarrow H^0 X$, 7 TeV
0.00 ^{+0.76} _{-0.74}		17 CHATRCHYAN 12N	CMS	$pp \rightarrow H^0 X$, 7, 8 TeV
1 AABOUD 19AQ use 36.1 fb ⁻¹ of data. The first, second and third quoted errors are statistical, experimental systematic and theory systematic uncertainties, respectively. The quoted signal strength is given for $m_{H^0} = 125$ GeV and corresponds to 4.4 standard deviations. Combining with 7 TeV and 8 TeV results (AAD 15AH), the observed significance is 6.4 standard deviations. The cross sections in the $H^0 \rightarrow \tau\tau$ decay channel ($m_{H^0} = 125$ GeV) are measured to $3.77^{+0.60}_{-0.59}$ (stat) ± 0.87 (syst) pb for the inclusive, $0.28 \pm 0.09^{+0.11}_{-0.09}$ pb for VBF, and $3.1 \pm 1.0^{+1.6}_{-1.3}$ pb for gluon-fusion production. See their Table XI for the cross sections in the framework of simplified template cross sections.				
2 SIRUNYAN 19AF use 35.9 fb ⁻¹ of data. $H^0 W/Z$ channels are added with a few updates on gluon fusion and vector boson fusion with respect to SIRUNYAN 18Y. The quoted signal strength is given for $m_{H^0} = 125$ GeV and corresponds to 5.5 standard deviations. The signal strengths for the individual production modes are: $1.12^{+0.53}_{-0.50}$ for gluon fusion, $1.13^{+0.45}_{-0.42}$ for vector boson fusion, $3.39^{+1.68}_{-1.54}$ for WH^0 and $1.23^{+1.62}_{-1.35}$ for ZH^0 . See their Fig. 7 for other couplings (κ_V, κ_f).				
3 AAD 16AN perform fits to the ATLAS and CMS data at $E_{cm} = 7$ and 8 TeV. The signal strengths for individual production processes are 1.0 ± 0.6 for gluon fusion, 1.3 ± 0.4 for vector boson fusion, -1.4 ± 1.4 for WH^0 production, $2.2^{+2.2}_{-1.8}$ for ZH^0 production, and $-1.9^{+3.7}_{-3.3}$ for $t\bar{t}H^0$ production.				

- 4 AAD 16AN: In the fit, relative production cross sections are fixed to those in the Standard Model. The quoted signal strength is given for $m_{H^0} = 125.09$ GeV.
- 5 AALTONEN 13M combine all Tevatron data from the CDF and D0 Collaborations with up to 10.0 fb⁻¹ and 9.7 fb⁻¹, respectively, of $p\bar{p}$ collisions at $E_{cm} = 1.96$ TeV. The quoted signal strength is given for $m_{H^0} = 125$ GeV.
- 6 SIRUNYAN 19AF use 35.9 fb⁻¹ of data. The quoted signal strength is given for $m_{H^0} = 125$ GeV and corresponds to 2.3 standard deviations.
- 7 SIRUNYAN 19AT perform a combine fit to 35.9 fb⁻¹ of data at $E_{cm} = 13$ TeV. This combination is based on SIRUNYAN 18Y.
- 8 SIRUNYAN 18Y use 35.9 fb⁻¹ of pp collisions at $E_{cm} = 13$ TeV. The quoted signal strength is given for $m_{H^0} = 125.09$ GeV and corresponds to 4.9 standard deviations.
- 9 SIRUNYAN 18Y combine the result of 35.9 fb⁻¹ at $E_{cm} = 13$ TeV with the results obtained from data of 4.9 fb⁻¹ at $E_{cm} = 7$ TeV and 19.7 fb⁻¹ at $E_{cm} = 8$ TeV (KHACHATRYAN 15AM). The quoted signal strength is given for $m_{H^0} = 125.09$ GeV and corresponds to 5.9 standard deviations.
- 10 AAD 16AC measure the signal strength with $pp \rightarrow H^0 W/ZX$ processes using 20.3 fb⁻¹ of $E_{cm} = 8$ TeV. The quoted signal strength is given for $m_{H^0} = 125$ GeV.
- 11 AAD 16K use up to 4.7 fb⁻¹ of pp collisions at $E_{cm} = 7$ TeV and up to 20.3 fb⁻¹ at $E_{cm} = 8$ TeV. The quoted signal strength is given for $m_{H^0} = 125.36$ GeV.
- 12 AAD 15AH use 4.5 fb⁻¹ of pp collisions at $E_{cm} = 7$ TeV and 20.3 fb⁻¹ at $E_{cm} = 8$ TeV. The third uncertainty in the measurement is theory systematics. The signal strength for the gluon fusion mode is $2.0 \pm 0.8^{+1.2}_{-0.8} \pm 0.3$ and that for vector boson fusion and W/ZH^0 production modes is $1.24^{+0.49+0.31}_{-0.45-0.29} \pm 0.08$. The quoted signal strength is given for $m_{H^0} = 125.36$ GeV.
- 13 CHATRCHYAN 14K use 4.9 fb⁻¹ of pp collisions at $E_{cm} = 7$ TeV and 19.7 fb⁻¹ at $E_{cm} = 8$ TeV. The quoted signal strength is given for $m_{H^0} = 125$ GeV. See also CHATRCHYAN 14AJ.
- 14 AALTONEN 13L combine all CDF results with 9.45–10.0 fb⁻¹ of $p\bar{p}$ collisions at $E_{cm} = 1.96$ TeV. The quoted signal strength is given for $m_{H^0} = 125$ GeV.
- 15 ABAZOV 13L combine all D0 results with up to 9.7 fb⁻¹ of $p\bar{p}$ collisions at $E_{cm} = 1.96$ TeV. The quoted signal strength is given for $m_{H^0} = 125$ GeV.
- 16 AAD 12AI obtain results based on 4.7 fb⁻¹ of pp collisions at $E_{cm} = 7$ TeV. The quoted signal strengths are given in their Fig. 10 for $m_{H^0} = 126$ GeV. See also Fig. 13 of AAD 12DA.
- 17 CHATRCHYAN 12N obtain results based on 4.9 fb⁻¹ of pp collisions at $E_{cm} = 7$ TeV and 5.1 fb⁻¹ at $E_{cm} = 8$ TeV. The quoted signal strength is given for $m_{H^0} = 125.5$ GeV. See also CHATRCHYAN 13Y.

 $Z\gamma$ Final State

VALUE	CL%	DOCUMENT ID	TECN	COMMENT
< 6.6	95	1 AABOUD	17AW ATLS	$pp \rightarrow H^0 X$, 13 TeV
• • • We do not use the following data for averages, fits, limits, etc. • • •				
< 7.4	95	2 SIRUNYAN	18DQ CMS	$pp \rightarrow H^0 X$, 13 TeV, $H^0 \rightarrow Z\gamma$
< 11	95	3 AAD	14I ATLS	$pp \rightarrow H^0 X$, 7, 8 TeV
< 9.5	95	4 CHATRCHYAN 13BK	CMS	$pp \rightarrow H^0 X$, 7, 8 TeV
1 AABOUD 17AW search for $H^0 \rightarrow Z\gamma, Z \rightarrow ee, \mu\mu$ in 36.1 fb ⁻¹ of pp collisions at $E_{cm} = 13$ TeV. The quoted signal strength is given for $m_{H^0} = 125.09$ GeV. The upper limit on the branching ratio of $H^0 \rightarrow Z\gamma$ is 1.0% at 95% CL assuming the SM Higgs boson production.				
2 SIRUNYAN 18DQ search for $H^0 \rightarrow Z\gamma, Z \rightarrow ee, \mu\mu$ in 35.9 fb ⁻¹ of pp collisions at $E_{cm} = 13$ TeV. The quoted signal strength (see their Figs. 6 and 7) is given for $m_{H^0} = 125$ GeV.				
3 AAD 14I search for $H^0 \rightarrow Z\gamma \rightarrow \ell\ell\gamma$ in 4.5 fb ⁻¹ of pp collisions at $E_{cm} = 7$ TeV and 20.3 fb ⁻¹ at $E_{cm} = 8$ TeV. The quoted signal strength is given for $m_{H^0} = 125.5$ GeV.				
4 CHATRCHYAN 13BK search for $H^0 \rightarrow Z\gamma \rightarrow \ell\ell\gamma$ in 5.0 fb ⁻¹ of pp collisions at $E_{cm} = 7$ TeV and 19.6 fb ⁻¹ at $E_{cm} = 8$ TeV. A limit on cross section times branching ratio which corresponds to (4–25) times the expected Standard Model cross section is given in the range $m_{H^0} = 120$ –160 GeV at 95% CL. The quoted limit is given for $m_{H^0} = 125$ GeV, where 10 is expected for no signal.				

 $\gamma^* \gamma$ Final State

VALUE	CL%	DOCUMENT ID	TECN	COMMENT
• • • We do not use the following data for averages, fits, limits, etc. • • •				
< 4.0	95	1 SIRUNYAN	18DQ CMS	$pp \rightarrow H^0 X$, 13 TeV, $H^0 \rightarrow \gamma^* \gamma$
< 6.7	95	2 KHACHATRYAN...16B	CMS	pp , 8 TeV, $e e \gamma, \mu \mu \gamma$
1 SIRUNYAN 18DQ search for $H^0 \rightarrow \gamma^* \gamma, \gamma^* \rightarrow \mu\mu$ in 35.9 fb ⁻¹ of pp collisions at $E_{cm} = 13$ TeV. The mass of γ^* is smaller than 50 GeV except in J/ψ and Υ mass regions. The quoted signal strength (see their Figs. 6 and 7) is given for $m_{H^0} = 125$ GeV.				
2 KHACHATRYAN 16B search for $H^0 \rightarrow \gamma^* \gamma \rightarrow e^+ e^- \gamma$ and $\mu^+ \mu^- \gamma$ (with $m(e^+ e^-) < 3.5$ GeV and $m(\mu^+ \mu^-) < 20$ GeV) in 19.7 fb ⁻¹ of pp collisions at $E_{cm} = 8$ TeV. See their Fig. 6 for limits on individual channels.				

Higgs Yukawa couplings

top Yukawa coupling

VALUE	CL%	DOCUMENT ID	TECN	COMMENT
< 1.7	95	1 SIRUNYAN	20c CMS	pp , 13 TeV
• • • We do not use the following data for averages, fits, limits, etc. • • •				
< 1.67	95	2 SIRUNYAN	19BY CMS	pp , 13 TeV
< 2.1	95	3 SIRUNYAN	18BU CMS	pp , 13 TeV

Gauge & Higgs Boson Particle Listings

 H^0

- 1 SIRUNYAN 20c search for the production of four top quarks with same-sign and multilepton final states with 137 fb^{-1} pp collision data at $E_{\text{cm}} = 13 \text{ TeV}$. The results constrain the ratio of the top quark Yukawa coupling y_t to its Standard Model by comparing to the central value of a theoretical prediction (see their Refs. [1-2]), yielding $|y_t/y_t^{\text{SM}}| < 1.7$ at 95% CL. See their Fig. 5.
- 2 SIRUNYAN 19By measure the top quark Yukawa coupling from $t\bar{t}$ kinematic distributions, the invariant mass of the top quark pair and the rapidity difference between t and \bar{t} , in the ℓ -jets final state with 35.8 fb^{-1} pp collision data at $E_{\text{cm}} = 13 \text{ TeV}$. The results constrain the ratio of the top quark Yukawa coupling to its Standard Model to be $1.07^{+0.34}_{-0.43}$ with an upper limit of 1.67 at 95% CL (see their Table III).
- 3 SIRUNYAN 18Bu search for the production of four top quarks with same-sign and multilepton final states with 35.9 fb^{-1} pp collision data at $E_{\text{cm}} = 13 \text{ TeV}$. The results constrain the ratio of the top quark Yukawa coupling y_t to its Standard Model by comparing to the central value of a theoretical prediction (see their Ref. [16]), yielding $|y_t/y_t^{\text{SM}}| < 2.1$ at 95% CL.

OTHER H^0 PRODUCTION PROPERTIES $t\bar{t}H^0$ Production

Signal strength relative to the Standard Model cross section.

VALUE	CL%	DOCUMENT ID	TECN	COMMENT
1.28 ± 0.20 OUR AVERAGE				
1.2 ± 0.3		1 AABOUD	18Ac ATLS	$pp, 13 \text{ TeV}, H^0 \rightarrow b\bar{b}, \tau\tau, \gamma\gamma, WW^*, ZZ^*$
$1.26^{+0.31}_{-0.26}$		2 SIRUNYAN	18L CMS	$pp, 7, 8, 13 \text{ TeV}, H^0 \rightarrow b\bar{b}, \tau\tau, \gamma\gamma, WW^*, ZZ^*$
$1.9^{+0.8}_{-0.7}$		3 AAD	16AN ATLS	$pp, 7, 8 \text{ TeV}$
• • • We do not use the following data for averages, fits, limits, etc. • • •				
$0.72 \pm 0.24 \pm 0.38$		4 SIRUNYAN	19R CMS	$pp, 13 \text{ TeV}, H^0 \rightarrow b\bar{b}$
$1.6^{+0.5}_{-0.4}$		5 AABOUD	18Ac ATLS	$pp, 13 \text{ TeV}, H^0 \rightarrow \tau\tau, WW^*, ZZ^*$
		6 AABOUD	18Bk ATLS	$pp, 13 \text{ TeV}, H^0 \rightarrow b\bar{b}, \tau\tau, \gamma\gamma, WW^*, ZZ^*$
$0.84^{+0.64}_{-0.61}$		7 AABOUD	18T ATLS	$pp, 13 \text{ TeV}, H^0 \rightarrow b\bar{b}$
0.9 ± 1.5		8 SIRUNYAN	18Bd CMS	$pp, 13 \text{ TeV}, H^0 \rightarrow b\bar{b}$
$1.23^{+0.45}_{-0.43}$		9 SIRUNYAN	18Bq CMS	$pp, 13 \text{ TeV}, H^0 \rightarrow \tau\tau, WW^*, ZZ^*$
1.7 ± 0.8		10 AAD	16AL ATLS	$pp, 7, 8 \text{ TeV}, H^0 \rightarrow b\bar{b}, \tau\tau, \gamma\gamma, WW^*, \text{ and } ZZ^*$
$2.3^{+0.7}_{-0.6}$		3.11 AAD	16AN LHC	$pp, 7, 8 \text{ TeV}$
$2.9^{+1.0}_{-0.9}$		3 AAD	16AN CMS	$pp, 7, 8 \text{ TeV}$
$1.81^{+0.52+0.58+0.31}_{-0.50-0.55-0.12}$		12 AAD	16K ATLS	$pp, 7, 8 \text{ TeV}$
$1.4^{+2.1+0.6}_{-1.4-0.3}$		13 AAD	15 ATLS	$pp, 7, 8 \text{ TeV}$
1.5 ± 1.1		14 AAD	15Bc ATLS	$pp, 8 \text{ TeV}$
$2.1^{+1.4}_{-1.2}$		15 AAD	15T ATLS	$pp, 8 \text{ TeV}$
$1.2^{+1.6}_{-1.5}$		16 KHACHATRY...15AN	CMS	$pp, 8 \text{ TeV}$
$2.8^{+1.0}_{-0.9}$		17 KHACHATRY...14H	CMS	$pp, 7, 8 \text{ TeV}$
$9.49^{+6.60}_{-6.28}$		18 AALTONEN	13L CDF	$p\bar{p}, 1.96 \text{ TeV}$
<5.8	95	19 CHATRCHYAN 13x	CMS	$pp, 7, 8 \text{ TeV}, H^0 \rightarrow b\bar{b}$

- 1 AABOUD 18Ac combine results of $t\bar{t}H^0, H^0 \rightarrow \tau\tau, WW^*(\rightarrow \ell\nu\nu, \ell\nu q\bar{q}), ZZ^*(\rightarrow \ell\nu\nu, \ell\nu q\bar{q})$ with results of $t\bar{t}H^0, H^0 \rightarrow b\bar{b}$ (AABOUD 18T), $\gamma\gamma$ (AABOUD 18Bo), $ZZ^*(\rightarrow 4\ell)$ (AABOUD 18Aj) in 36.1 fb^{-1} of pp collisions at $E_{\text{cm}} = 13 \text{ TeV}$. The quoted signal strength is given for $m_{H^0} = 125 \text{ GeV}$. See their Table 14.
- 2 SIRUNYAN 18L use up to 5.1, 19.7 and 35.9 fb^{-1} of pp collisions at $E_{\text{cm}} = 7, 8,$ and 13 TeV , respectively. The quoted signal strength corresponds to a significance of 5.2 standard deviations and is given for $m_{H^0} = 125.09 \text{ GeV}$. H^0 decay channels of $WW^*, ZZ^*, \gamma\gamma, \tau\tau,$ and $b\bar{b}$ are used. See their Table 1 and Fig. 2 for results on individual channels.
- 3 AAD 16AN: In the fit, relative branching ratios are fixed to those in the Standard Model. The quoted signal strength is given for $m_{H^0} = 125.09 \text{ GeV}$.
- 4 SIRUNYAN 19R search for $t\bar{t}H^0$ production with H^0 decaying to $b\bar{b}$ in 35.9 fb^{-1} of data at $E_{\text{cm}} = 13 \text{ TeV}$. The quoted signal strength is given for $m_{H^0} = 125 \text{ GeV}$.
- 5 AABOUD 18Ac search for $t\bar{t}H^0$ production with H^0 decaying to $\tau\tau, WW^*(\rightarrow \ell\nu\nu, \ell\nu q\bar{q}), ZZ^*(\rightarrow \ell\nu\nu, \ell\nu q\bar{q})$ in 36.1 fb^{-1} of pp collisions at $E_{\text{cm}} = 13 \text{ TeV}$. The quoted signal strength is given for $m_{H^0} = 125 \text{ GeV}$. See their Table 13 and Fig. 13.
- 6 AABOUD 18Bk use 79.8 fb^{-1} data for $t\bar{t}H^0$ production with $H^0 \rightarrow \gamma\gamma$ and $ZZ^* \rightarrow 4\ell$ ($\ell = e, \mu$) and 36.1 fb^{-1} for other decay channels at $E_{\text{cm}} = 13 \text{ TeV}$. A significance of 5.8 standard deviations is observed for $m_{H^0} = 125.09 \text{ GeV}$ and its signal strength without the uncertainty of the $t\bar{t}H^0$ cross section is $1.32^{+0.28}_{-0.26}$. Combining with results of 7 and 8 TeV (AAD 16K), the significance is 6.3 standard deviations. Assuming Standard Model branching fractions, the total $t\bar{t}H^0$ production cross section at 13 TeV is measured to be $670 \pm 90^{+110}_{-100} \text{ fb}$.

- 7 AABOUD 18T search for $t\bar{t}H^0$ production with H^0 decaying to $b\bar{b}$ in 36.1 fb^{-1} of pp collisions at $E_{\text{cm}} = 13 \text{ TeV}$. The quoted signal strength is given for $m_{H^0} = 125 \text{ GeV}$.
- 8 SIRUNYAN 18Bd search for $t\bar{t}H^0, H^0 \rightarrow b\bar{b}$ in the all-jet final state with 35.9 fb^{-1} pp collision data at $E_{\text{cm}} = 13 \text{ TeV}$. The quoted signal strength is given for $m_{H^0} = 125 \text{ GeV}$.
- 9 SIRUNYAN 18Bq search for $t\bar{t}H^0$ in final states with electrons, muons and hadronically decaying τ leptons ($H^0 \rightarrow WW^*, ZZ^*, \tau\tau$) with 35.9 fb^{-1} of pp collision data at $E_{\text{cm}} = 13 \text{ TeV}$. The quoted signal strength corresponds to a significance of 3.2 standard deviations and is given for $m_{H^0} = 125 \text{ GeV}$.
- 10 AAD 16AL search for $t\bar{t}H^0$ production with H^0 decaying to $\gamma\gamma$ in 4.5 fb^{-1} of pp collisions at $E_{\text{cm}} = 7 \text{ TeV}$ and $b\bar{b}, \tau\tau, \gamma\gamma, WW^*,$ and ZZ^* in 20.3 fb^{-1} at $E_{\text{cm}} = 8 \text{ TeV}$. The quoted signal strength is given for $m_{H^0} = 125 \text{ GeV}$. This paper combines the results of previous papers, and the new result of this paper only is: $\mu = 1.6 \pm 2.6$.
- 11 AAD 16AN perform fits to the ATLAS and CMS data at $E_{\text{cm}} = 7$ and 8 TeV .
- 12 AAD 16K use up to 4.7 fb^{-1} of pp collisions at $E_{\text{cm}} = 7 \text{ TeV}$ and up to 20.3 fb^{-1} at $E_{\text{cm}} = 8 \text{ TeV}$. The third uncertainty in the measurement is theory systematics. The quoted signal strength is given for $m_{H^0} = 125.36 \text{ GeV}$.
- 13 AAD 15 search for $t\bar{t}H^0$ production with H^0 decaying to $\gamma\gamma$ in 4.5 fb^{-1} of pp collisions at $E_{\text{cm}} = 7 \text{ TeV}$ and 20.3 fb^{-1} at $E_{\text{cm}} = 8 \text{ TeV}$. The quoted result on the signal strength is equivalent to an upper limit of 6.7 at 95% CL and is given for $m_{H^0} = 125.4 \text{ GeV}$.
- 14 AAD 15Bc search for $t\bar{t}H^0$ production with H^0 decaying to $b\bar{b}$ in 20.3 fb^{-1} of pp collisions at $E_{\text{cm}} = 8 \text{ TeV}$. The corresponding upper limit is 3.4 at 95% CL. The quoted signal strength is given for $m_{H^0} = 125 \text{ GeV}$.
- 15 AAD 15T search for $t\bar{t}H^0$ production with H^0 resulting in multilepton final states (mainly from $WW^*, \tau\tau, ZZ^*$) in 20.3 fb^{-1} of pp collisions at $E_{\text{cm}} = 8 \text{ TeV}$. The quoted result on the signal strength is given for $m_{H^0} = 125 \text{ GeV}$ and corresponds to an upper limit of 4.7 at 95% CL. The data sample is independent from AAD 15 and AAD 15Bc.
- 16 KHACHATRYAN 15AN search for $t\bar{t}H^0$ production with H^0 decaying to $b\bar{b}$ in 19.5 fb^{-1} of pp collisions at $E_{\text{cm}} = 8 \text{ TeV}$. The quoted result on the signal strength is equivalent to an upper limit of 4.2 at 95% CL and is given for $m_{H^0} = 125 \text{ GeV}$.
- 17 KHACHATRYAN 14H search for $t\bar{t}H^0$ production with H^0 decaying to $b\bar{b}, \tau\tau, \gamma\gamma, WW^*,$ and ZZ^* , in 5.1 fb^{-1} of pp collisions at $E_{\text{cm}} = 7 \text{ TeV}$ and 19.7 fb^{-1} at $E_{\text{cm}} = 8 \text{ TeV}$. The quoted signal strength is given for $m_{H^0} = 125.6 \text{ GeV}$.
- 18 AALTONEN 13L combine all CDF results with $9.45\text{--}10.0 \text{ fb}^{-1}$ of $p\bar{p}$ collisions at $E_{\text{cm}} = 1.96 \text{ TeV}$. The quoted signal strength is given for $m_{H^0} = 125 \text{ GeV}$.
- 19 CHATRCHYAN 13x search for $t\bar{t}H^0$ production followed by $H^0 \rightarrow b\bar{b}$, one top decaying to $\ell\nu$ and the other to either $\ell\nu$ or $q\bar{q}$ in 5.0 fb^{-1} and 5.1 fb^{-1} of pp collisions at $E_{\text{cm}} = 7$ and 8 TeV . A limit on cross section times branching ratio which corresponds to $(4.0\text{--}8.6)$ times the expected Standard Model cross section is given for $m_{H^0} = 110\text{--}140 \text{ GeV}$ at 95% CL. The quoted limit is given for $m_{H^0} = 125 \text{ GeV}$, where 5.2 is expected for no signal.

 H^0H^0 ProductionThe 95% CL limits are for the cross section (CS) and Higgs self coupling (κ_λ) scaling factors both relative to the SM predictions.

CS	κ_λ	CL%	DOCUMENT ID	TECN	COMMENT
• • • We do not use the following data for averages, fits, limits, etc. • • •					
< 6.9	-5.0 to 12.0	95	1 AAD	20c ATLS	13 TeV, $b\bar{b}\gamma\gamma, b\bar{b}\tau\tau, b\bar{b}b\bar{b}, b\bar{b}WW^*, WW^*\gamma\gamma, WW^*WW^*$
< 40		95	2 AAD	20E ATLS	13 TeV, $H^0H^0 \rightarrow b\bar{b}\ell\nu\ell\nu$
< 12.9		95	3 AABOUD	19A ATLS	13 TeV, $b\bar{b}b\bar{b}$
< 300		95	4 AABOUD	19O ATLS	13 TeV, $b\bar{b}WW^*$
< 160		95	5 AABOUD	19T ATLS	13 TeV, WW^*WW^*
< 24	-11 to 17	95	6 SIRUNYAN	19 CMS	13 TeV, $\gamma\gamma b\bar{b}$
< 75		95	7 SIRUNYAN	19AB CMS	13 TeV, $b\bar{b}b\bar{b}$
< 22.2	-11.8 to 18.8	95	8 SIRUNYAN	19BE CMS	13 TeV, $b\bar{b}\gamma\gamma, b\bar{b}\tau\tau, b\bar{b}b\bar{b}, b\bar{b}WW^*, b\bar{b}ZZ^*$
< 179		95	9 SIRUNYAN	19H CMS	13 TeV, $b\bar{b}b\bar{b}$
< 230		95	10 AABOUD	18Bu ATLS	13 TeV, $\gamma\gamma WW^*$
< 12.7		95	11 AABOUD	18Cq ATLS	13 TeV, $b\bar{b}\tau\tau$
< 22	-8.2 to 13.2	95	12 AABOUD	18Cw ATLS	13 TeV, $\gamma\gamma b\bar{b}$
< 30		95	13 SIRUNYAN	18A CMS	13 TeV, $b\bar{b}\tau\tau$
< 79		95	14 SIRUNYAN	18F CMS	13 TeV, $b\bar{b}\ell\nu\ell\nu$
< 43		95	15 SIRUNYAN	17CN CMS	8 TeV, $b\bar{b}\tau\tau, \gamma\gamma b\bar{b}, b\bar{b}b\bar{b}$
< 108		95	16 AABOUD	16i ATLS	13 TeV, $b\bar{b}b\bar{b}$
< 74		95	17 KHACHATRY...16Bq	CMS	8 TeV, $\gamma\gamma b\bar{b}$
< 70		95	18 AAD	15CE ATLS	8 TeV, $b\bar{b}b\bar{b}, b\bar{b}\tau\tau, \gamma\gamma b\bar{b}, \gamma\gamma WW^*$

- 1 AAD 20c combine results of up to 36.1 fb^{-1} data at $E_{\text{cm}} = 13 \text{ TeV}$ for $pp \rightarrow H^0H^0 \rightarrow b\bar{b}\gamma\gamma, b\bar{b}\tau\tau, b\bar{b}b\bar{b}, b\bar{b}WW^*, WW^*\gamma\gamma, WW^*WW^*$ (AABOUD 18Cw, AABOUD 18Cq, AABOUD 19A, AABOUD 19O, AABOUD 18Bu, and AABOUD 19T).
- 2 AAD 20e search non-resonant for H^0H^0 production using $H^0H^0 \rightarrow b\bar{b}\ell\nu\ell\nu$, where one of the Higgs bosons decays to $b\bar{b}$ and the other decays to either $WW^*, ZZ^*,$ or $\tau\tau$, with data of 139 fb^{-1} at $E_{\text{cm}} = 13 \text{ TeV}$. The upper limit on the $pp \rightarrow H^0H^0$ production cross section at 95% CL is measured to be 1.2 pb, which corresponds to about 40 times the SM prediction.
- 3 AABOUD 19A search for H^0H^0 production using $H^0H^0 \rightarrow b\bar{b}b\bar{b}$ with data of 36.1 fb^{-1} at $E_{\text{cm}} = 13 \text{ TeV}$. The upper limit on the $pp \rightarrow H^0H^0 \rightarrow b\bar{b}b\bar{b}$ production cross section at 95% is measured to be 147 fb, which corresponds to about 12.9 times the SM prediction.

- 4 AABOUD 19o search for $H^0 H^0$ production using $H^0 H^0 \rightarrow b\bar{b} W W^*$ with data of 36.1 fb^{-1} at $E_{\text{cm}} = 13 \text{ TeV}$. The upper limit on the $pp \rightarrow H^0 H^0$ production cross section at 95% CL is calculated to be 10 pb from the observed upper limit on the $pp \rightarrow H^0 H^0 \rightarrow b\bar{b} W W^*$ production cross section of 2.5 pb assuming the SM branching fractions. The former corresponds to about 300 times the SM prediction.
- 5 AABOUD 19T search for $H^0 H^0$ production using $H^0 H^0 \rightarrow W W^* W W^*$ with data of 36.1 fb^{-1} at $E_{\text{cm}} = 13 \text{ TeV}$. The upper limit on the $pp \rightarrow H^0 H^0$ production cross section at 95% is measured to be 5.3 pb, which corresponds to about 160 times the SM prediction.
- 6 SIRUNYAN 19 search for $H^0 H^0$ production using $H^0 H^0 \rightarrow \gamma\gamma b\bar{b}$ with data of 35.9 fb^{-1} at $E_{\text{cm}} = 13 \text{ TeV}$. The upper limit on the $pp \rightarrow H^0 H^0 \rightarrow \gamma\gamma b\bar{b}$ production cross section at 95% CL is measured to be 2.0 fb, which corresponds to about 24 times the SM prediction. The effective Higgs boson self-coupling $\kappa_\lambda (\lambda = \lambda_{HHH} / \lambda_{HHH}^{\text{SM}})$ is constrained to be $-11 < \kappa_\lambda < 17$ at 95% CL assuming all other Higgs boson couplings are at their SM value.
- 7 SIRUNYAN 19AB search for $H^0 H^0$ production using $H^0 H^0 \rightarrow b\bar{b} b\bar{b}$, where 4 heavy flavor jets from two Higgs bosons are resolved, with data of 35.9 fb^{-1} at $E_{\text{cm}} = 13 \text{ TeV}$. The upper limit on the $pp \rightarrow H^0 H^0 \rightarrow b\bar{b} b\bar{b}$ production cross section at 95% is measured to be 847 fb, which corresponds to about 75 times the SM prediction.
- 8 SIRUNYAN 19BE combine results of 13 TeV 35.9 fb^{-1} data: SIRUNYAN 19, SIRUNYAN 18A, SIRUNYAN 19AB, SIRUNYAN 19H, and SIRUNYAN 18F.
- 9 SIRUNYAN 19H search for $H^0 H^0$ production using $H^0 H^0 \rightarrow b\bar{b} b\bar{b}$, where one of $b\bar{b}$ pairs is highly boosted and the other one is resolved, with data of 35.9 fb^{-1} at $E_{\text{cm}} = 13 \text{ TeV}$. The upper limit on the $pp \rightarrow H^0 H^0 \rightarrow b\bar{b} b\bar{b}$ production cross section at 95% is measured to be 1980 fb, which corresponds to about 179 times the SM prediction.
- 10 AABOUD 18BU search for $H^0 H^0$ production using $\gamma\gamma W W^*$ with the final state of $\gamma\gamma \ell\nu j j$ using data of 36.1 fb^{-1} at $E_{\text{cm}} = 13 \text{ TeV}$. The upper limit on the $pp \rightarrow H^0 H^0$ production cross section at 95% CL is measured to be 7.7 pb, which corresponds to about 230 times the SM prediction. The upper limit on the $pp \rightarrow H^0 H^0 \rightarrow \gamma\gamma W W^*$ at 95% CL is measured to be 7.5 fb (see their Table 6).
- 11 AABOUD 18CQ search for $H^0 H^0$ production using $H^0 H^0 \rightarrow b\bar{b} \tau\tau$ with data of 36.1 fb^{-1} at $E_{\text{cm}} = 13 \text{ TeV}$. The upper limit on the $pp \rightarrow H^0 H^0 \rightarrow b\bar{b} \tau\tau$ production cross section at 95% is measured to be 30.9 fb, which corresponds to about 12.7 times the SM prediction.
- 12 AABOUD 18CW search for $H^0 H^0$ production using $H^0 H^0 \rightarrow \gamma\gamma b\bar{b}$ with data of 36.1 fb^{-1} at $E_{\text{cm}} = 13 \text{ TeV}$. The upper limit on the $pp \rightarrow H^0 H^0$ production cross section at 95% is measured to be 0.73 pb, which corresponds to about 22 times the SM prediction. The effective Higgs boson self-coupling κ_λ is constrained to be $-8.2 < \kappa_\lambda < 13.2$ at 95% CL assuming all other Higgs boson couplings are at their SM value.
- 13 SIRUNYAN 18A search for $H^0 H^0$ production using $H^0 H^0 \rightarrow b\bar{b} \tau\tau$ with data of 35.9 fb^{-1} at $E_{\text{cm}} = 13 \text{ TeV}$. The upper limit on the $pp \rightarrow H^0 H^0 \rightarrow b\bar{b} \tau\tau$ production cross section is measured to be 75.4 fb, which corresponds to about 30 times the SM prediction. Limits on Higgs-boson trilinear coupling λ_{HHH} and top Yukawa coupling y_t are also given (see their Fig. 6).
- 14 SIRUNYAN 18F search non-resonant for $H^0 H^0$ production using $H^0 H^0 \rightarrow b\bar{b} \ell\nu\ell\nu$, where $\ell\nu\ell\nu$ is either $W W \rightarrow \ell\nu\nu$ or $Z Z \rightarrow \ell\nu\nu$ (ℓ is e, μ or a leptonically decaying τ), with data of 35.9 fb^{-1} at $E_{\text{cm}} = 13 \text{ TeV}$. The upper limit on the $pp \rightarrow H^0 H^0 \rightarrow b\bar{b} \ell\nu\ell\nu$ production cross section at 95% CL is measured to be 72 fb, which corresponds to about 79 times the SM prediction.
- 15 SIRUNYAN 17CN search for $H^0 H^0$ production using $H^0 H^0 \rightarrow b\bar{b} \tau\tau$ with data of 18.3 fb^{-1} at $E_{\text{cm}} = 8 \text{ TeV}$. Results are then combined with the published results of the $H^0 H^0 \rightarrow \gamma\gamma b\bar{b}$ and $H^0 H^0 \rightarrow b\bar{b} b\bar{b}$, which use data of up to 19.7 fb^{-1} at $E_{\text{cm}} = 8 \text{ TeV}$. The upper limit on the $pp \rightarrow H^0 H^0$ production cross section is measured to be 0.59 pb from $b\bar{b} \tau\tau$, which corresponds to about 59 times the SM prediction (gluon fusion). The combined upper limit is 0.43 pb, which is about 43 times the SM prediction. The quoted values are given for $m_{H^0} = 125 \text{ GeV}$.
- 16 AABOUD 16I search for $H^0 H^0$ production using $H^0 H^0 \rightarrow b\bar{b} b\bar{b}$ with data of 3.2 fb^{-1} at $E_{\text{cm}} = 13 \text{ TeV}$. The upper limit on the $pp \rightarrow H^0 H^0 \rightarrow b\bar{b} b\bar{b}$ production cross section is measured to be 1.22 pb. This result corresponds to about 108 times the SM prediction (gluon fusion), which is $11.3^{+0.9}_{-1.0} \text{ fb}$ (NNLO+NNLL) including top quark mass effects. The quoted values are given for $m_{H^0} = 125 \text{ GeV}$.
- 17 KHACHATRYAN 16BQ search for $H^0 H^0$ production using $H^0 H^0 \rightarrow \gamma\gamma b\bar{b}$ with data of 19.7 fb^{-1} at $E_{\text{cm}} = 8 \text{ TeV}$. The upper limit on the $pp \rightarrow H^0 H^0 \rightarrow \gamma\gamma b\bar{b}$ production is measured to be 1.85 fb, which corresponds to about 74 times the SM prediction and is translated into 0.71 pb for $gg \rightarrow H^0 H^0$ production cross section. Limits on Higgs-boson trilinear coupling λ are also given.
- 18 AAD 15CE search for $H^0 H^0$ production using $H^0 H^0 \rightarrow b\bar{b} \tau\tau$ and $H^0 H^0 \rightarrow \gamma\gamma W W$ with data of 20.3 fb^{-1} at $E_{\text{cm}} = 8 \text{ TeV}$. These results are then combined with the published results of the $H^0 H^0 \rightarrow \gamma\gamma b\bar{b}$ and $H^0 H^0 \rightarrow b\bar{b} b\bar{b}$, which use data of up to 20.3 fb^{-1} at $E_{\text{cm}} = 8 \text{ TeV}$. The upper limits on the $pp \rightarrow H^0 H^0$ production cross section are measured to be 1.6 pb, 11.4 pb, 2.2 pb and 0.62 pb from $b\bar{b} \tau\tau, \gamma\gamma W W, \gamma\gamma b\bar{b}$ and $b\bar{b} b\bar{b}$, respectively. The combined upper limit is 0.69 pb, which corresponds to about 70 times the SM prediction. The quoted results are given for $m_{H^0} = 125.4 \text{ GeV}$. See their Table 4.

$t H^0$ associated production cross section

VALUE	DOCUMENT ID	TECN	COMMENT
••• We do not use the following data for averages, fits, limits, etc. •••			
	1 SIRUNYAN 19BK CMS	$pp, 13 \text{ TeV}$	
	2 KHACHATRYAN...16AU CMS	$pp, 8 \text{ TeV}$	
1 SIRUNYAN 19BK search for the $t H^0$ associated production using multipion signatures ($H^0 \rightarrow W W^*, H^0 \rightarrow \tau\tau, H^0 \rightarrow Z Z^*$) and signatures with a single lepton and a $b\bar{b}$ pair ($H^0 \rightarrow b\bar{b}$) using 35.9 fb^{-1} at $E_{\text{cm}} = 13 \text{ TeV}$. Results are combined with $H^0 \rightarrow \gamma\gamma$ (SIRUNYAN 18DS). The observed 95% CL upper limit on the $t H^0$ production cross section times $H^0 \rightarrow W W^* + \tau\tau + Z Z^* + b\bar{b} + \gamma\gamma$ branching fraction is 1.94 pb (assuming SM $t\bar{t} H^0$ production cross section). See their Table X and Fig. 14. The values outside the ranges of $[-0.9, -0.5]$ and $[1.0, 2.1]$ times the standard model top quark Yukawa coupling are excluded at 95% CL.			

- 2 KHACHATRYAN 16AU search for the $t H^0$ associated production in 19.7 fb^{-1} at $E_{\text{cm}} = 8 \text{ TeV}$. The 95% CL upper limits on the $t H^0$ associated production cross section is measured to be 600–1000 fb depending on the assumed $\gamma\gamma$ branching ratios of the Higgs boson. The $\gamma\gamma$ branching ratio is varied to be by a factor of 0.5–3.0 of the Standard Model Higgs boson ($m_{H^0} = 125 \text{ GeV}$). The results of the signal strengths for a negative Higgs-boson trilinear coupling are given. The results are given for $m_{H^0} = 125 \text{ GeV}$.

H^0 Production Cross Section in pp Collisions at $\sqrt{s} = 13 \text{ TeV}$

Assumes $m_{H^0} = 125 \text{ GeV}$

VALUE (pb)	DOCUMENT ID	TECN	COMMENT
59 ± 5 OUR AVERAGE			
61.1 ± 6.0 ± 3.7	1 SIRUNYAN 19BA CMS	$pp, 13 \text{ TeV}, \gamma\gamma, Z Z^* \rightarrow 4\ell (\ell = e, \mu)$	
57.0 ± 6.0 + 4.0 / 5.9 - 3.3	2 AABOUD 18CG ATLAS	$pp, 13 \text{ TeV}, \gamma\gamma, Z Z^* \rightarrow 4\ell (\ell = e, \mu)$	
••• We do not use the following data for averages, fits, limits, etc. •••			
47.9 ± 9.1 / 8.6	2 AABOUD 18CG ATLAS	$pp, 13 \text{ TeV}, \gamma\gamma$	
68 ± 11 / -10	2 AABOUD 18CG ATLAS	$pp, 13 \text{ TeV}, Z Z^* \rightarrow 4\ell (\ell = e, \mu)$	
69 ± 10 / -9 ± 5	3 AABOUD 17CO ATLAS	$pp, 13 \text{ TeV}, Z Z^* \rightarrow 4\ell$	
1 SIRUNYAN 19BA use 35.9 fb^{-1} of pp collisions at $E_{\text{cm}} = 13 \text{ TeV}$.			
2 AABOUD 18CG use 36.1 fb^{-1} of pp collisions at $E_{\text{cm}} = 13 \text{ TeV}$.			
3 AABOUD 17CO use 36.1 fb^{-1} of pp collisions at $E_{\text{cm}} = 13 \text{ TeV}$ with $H^0 \rightarrow Z Z^* \rightarrow 4\ell$ where $\ell = e, \mu$ for $m_{H^0} = 125 \text{ GeV}$. Differential cross sections for the Higgs boson transverse momentum, Higgs boson rapidity, and other related quantities are measured as shown in their Figs. 8 and 9.			

H^0 REFERENCES

AAD	20	PR D101 012002	G. Aad et al.	(ATLAS Collab.)
AAD	20A	PL B800 135069	G. Aad et al.	(ATLAS Collab.)
AAD	20C	PL B800 135103	G. Aad et al.	(ATLAS Collab.)
AAD	20E	PL B801 135145	G. Aad et al.	(ATLAS Collab.)
AAD	20F	PL B801 135148	G. Aad et al.	(ATLAS Collab.)
SIRUNYAN	20C	EPJ C80 75	A.M. Sirunyan et al.	(CMS Collab.)
AABOUD	19A	JHEP 1901 030	M. Aaboud et al.	(ATLAS Collab.)
AABOUD	19AI	PL B793 499	M. Aaboud et al.	(ATLAS Collab.)
AABOUD	19AL	PRL 122 231801	M. Aaboud et al.	(ATLAS Collab.)
AABOUD	19AQ	PR D99 072001	M. Aaboud et al.	(ATLAS Collab.)
AABOUD	19F	PL B789 508	M. Aaboud et al.	(ATLAS Collab.)
AABOUD	19N	JHEP 1904 048	M. Aaboud et al.	(ATLAS Collab.)
AABOUD	19O	JHEP 1904 092	M. Aaboud et al.	(ATLAS Collab.)
AABOUD	19T	JHEP 1905 124	M. Aaboud et al.	(ATLAS Collab.)
AABOUD	19U	JHEP 1905 141	M. Aaboud et al.	(ATLAS Collab.)
AAD	19A	PL B798 134949	G. Aad et al.	(ATLAS Collab.)
SIRUNYAN	19	PL B788 7	A.M. Sirunyan et al.	(CMS Collab.)
SIRUNYAN	19AB	JHEP 1904 112	A.M. Sirunyan et al.	(CMS Collab.)
SIRUNYAN	19AF	JHEP 1906 093	A.M. Sirunyan et al.	(CMS Collab.)
SIRUNYAN	19AJ	EPJ C79 94	A.M. Sirunyan et al.	(CMS Collab.)
SIRUNYAN	19AJ	EPJ C79 421	A.M. Sirunyan et al.	(CMS Collab.)
SIRUNYAN	19AX	PL B791 96	A.M. Sirunyan et al.	(CMS Collab.)
SIRUNYAN	19BA	PL B792 369	A.M. Sirunyan et al.	(CMS Collab.)
SIRUNYAN	19BE	PRL 122 121803	A.M. Sirunyan et al.	(CMS Collab.)
SIRUNYAN	19BK	PR D99 092005	A.M. Sirunyan et al.	(CMS Collab.)
SIRUNYAN	19BL	PR D99 112003	A.M. Sirunyan et al.	(CMS Collab.)
SIRUNYAN	19BO	PL B793 520	A.M. Sirunyan et al.	(CMS Collab.)
SIRUNYAN	19BR	PL B797 134811	A.M. Sirunyan et al.	(CMS Collab.)
SIRUNYAN	19BY	PR D100 072007	A.M. Sirunyan et al.	(CMS Collab.)
SIRUNYAN	19BZ	PR D100 112002	A.M. Sirunyan et al.	(CMS Collab.)
SIRUNYAN	19CG	JHEP 1910 139	A.M. Sirunyan et al.	(CMS Collab.)
SIRUNYAN	19E	PRL 122 021801	A.M. Sirunyan et al.	(CMS Collab.)
SIRUNYAN	19H	JHEP 1901 040	A.M. Sirunyan et al.	(CMS Collab.)
SIRUNYAN	19I	JHEP 1901 183	A.M. Sirunyan et al.	(CMS Collab.)
SIRUNYAN	19R	JHEP 1903 026	A.M. Sirunyan et al.	(CMS Collab.)
AABOUD	18	PL B776 318	M. Aaboud et al.	(ATLAS Collab.)
AABOUD	18AC	PR D97 072003	M. Aaboud et al.	(ATLAS Collab.)
AABOUD	18AJ	JHEP 1803 095	M. Aaboud et al.	(ATLAS Collab.)
AABOUD	18AU	JHEP 1807 127	M. Aaboud et al.	(ATLAS Collab.)
AABOUD	18BK	PL B784 173	M. Aaboud et al.	(ATLAS Collab.)
AABOUD	18BL	PL B786 134	M. Aaboud et al.	(ATLAS Collab.)
AABOUD	18BM	PL B784 345	M. Aaboud et al.	(ATLAS Collab.)
AABOUD	18BN	PL B786 59	M. Aaboud et al.	(ATLAS Collab.)
AABOUD	18BO	PR D98 052005	M. Aaboud et al.	(ATLAS Collab.)
AABOUD	18BP	PL B786 223	M. Aaboud et al.	(ATLAS Collab.)
AABOUD	18BQ	PR D98 052003	M. Aaboud et al.	(ATLAS Collab.)
AABOUD	18BU	EPJ C78 1007	M. Aaboud et al.	(ATLAS Collab.)
AABOUD	18CA	JHEP 1810 180	M. Aaboud et al.	(ATLAS Collab.)
AABOUD	18CG	PL B786 114	M. Aaboud et al.	(ATLAS Collab.)
AABOUD	18CQ	PRL 121 191801	M. Aaboud et al.	(ATLAS Collab.)
AABOUD	18CW	JHEP 1811 040	M. Aaboud et al.	(ATLAS Collab.)
AABOUD	18M	PRL 120 211802	M. Aaboud et al.	(ATLAS Collab.)
AABOUD	18T	PR D97 072016	M. Aaboud et al.	(ATLAS Collab.)
AATJ	18AM	EPJ C78 1008	R. Aaij et al.	(LHCb Collab.)
AALTONEN	18E	PR D98 072002	T. Aaltonen et al.	(CDF Collab.)
SIRUNYAN	18A	PL B778 101	A.M. Sirunyan et al.	(CMS Collab.)
SIRUNYAN	18AE	PL B780 501	A.M. Sirunyan et al.	(CMS Collab.)
SIRUNYAN	18BD	JHEP 1806 101	A.M. Sirunyan et al.	(CMS Collab.)
SIRUNYAN	18BH	JHEP 1806 001	A.M. Sirunyan et al.	(CMS Collab.)
SIRUNYAN	18BQ	JHEP 1808 066	A.M. Sirunyan et al.	(CMS Collab.)
SIRUNYAN	18BU	EPJ C78 140	A.M. Sirunyan et al.	(CMS Collab.)
SIRUNYAN	18BV	EPJ C78 291	A.M. Sirunyan et al.	(CMS Collab.)
SIRUNYAN	18DB	PRL 121 121801	A.M. Sirunyan et al.	(CMS Collab.)
SIRUNYAN	18DQ	JHEP 1811 152	A.M. Sirunyan et al.	(CMS Collab.)
SIRUNYAN	18DS	JHEP 1811 185	A.M. Sirunyan et al.	(CMS Collab.)
SIRUNYAN	18E	PRL 120 071802	A.M. Sirunyan et al.	(CMS Collab.)
SIRUNYAN	18F	JHEP 1801 054	A.M. Sirunyan et al.	(CMS Collab.)
SIRUNYAN	18L	PRL 120 231801	A.M. Sirunyan et al.	(CMS Collab.)
SIRUNYAN	18S	PR D97 092005	A.M. Sirunyan et al.	(CMS Collab.)
SIRUNYAN	18Y	PL B779 283	A.M. Sirunyan et al.	(CMS Collab.)
AABOUD	17AW	JHEP 1710 112	M. Aaboud et al.	(ATLAS Collab.)
AABOUD	17BA	JHEP 1712 024	M. Aaboud et al.	(ATLAS Collab.)
AABOUD	17BD	EPJ C77 765	M. Aaboud et al.	(ATLAS Collab.)
AABOUD	17CO	JHEP 1710 132	M. Aaboud et al.	(ATLAS Collab.)
AABOUD	17Y	PRL 119 051802	M. Aaboud et al.	(ATLAS Collab.)
AAD	17	EPJ C77 70	G. Aad et al.	(ATLAS Collab.)
KHACHATRYAN...	17F	JHEP 1702 135	V. Khachatryan et al.	(CMS Collab.)
SIRUNYAN	17AM	PL B775 1	A.M. Sirunyan et al.	(CMS Collab.)
SIRUNYAN	17AV	JHEP 1711 047	A.M. Sirunyan et al.	(CMS Collab.)

Gauge & Higgs Boson Particle Listings

 H^0 , Neutral Higgs Bosons, Searches for

SIRUNYAN	17CN	PR D96 072004	A.M. Sirunyan et al.	(CMS Collab.)
AABOUD	16I	PR D94 052002	M. Aaboud et al.	(ATLAS Collab.)
AABOUD	16K	PRL 117 111802	M. Aaboud et al.	(ATLAS Collab.)
AABOUD	16X	JHEP 1611 112	M. Aaboud et al.	(ATLAS Collab.)
AAD	16	PL B753 69	G. Aad et al.	(ATLAS Collab.)
AAD	16AC	PR D93 092005	G. Aad et al.	(ATLAS Collab.)
AAD	16AF	JHEP 1601 172	G. Aad et al.	(ATLAS Collab.)
AAD	16AL	JHEP 1605 160	G. Aad et al.	(ATLAS Collab.)
AAD	16AN	JHEP 1608 045	G. Aad et al.	(ATLAS and CMS Collabs.)
AAD	16AO	JHEP 1608 104	G. Aad et al.	(ATLAS Collab.)
AAD	16BL	EPJ C76 658	G. Aad et al.	(ATLAS Collab.)
AAD	16K	EPJ C76 6	G. Aad et al.	(ATLAS Collab.)
KHACHATRYAN	16AB	PL B759 672	V. Khachatryan et al.	(CMS Collab.)
KHACHATRYAN	16AR	JHEP 1604 005	V. Khachatryan et al.	(CMS Collab.)
KHACHATRYAN	16AU	JHEP 1606 177	V. Khachatryan et al.	(CMS Collab.)
KHACHATRYAN	16B	PL B753 341	V. Khachatryan et al.	(CMS Collab.)
KHACHATRYAN	16BA	JHEP 1609 051	V. Khachatryan et al.	(CMS Collab.)
KHACHATRYAN	16BQ	PR D94 052012	V. Khachatryan et al.	(CMS Collab.)
KHACHATRYAN	16CD	PL B763 472	V. Khachatryan et al.	(CMS Collab.)
KHACHATRYAN	16G	EPJ C76 13	V. Khachatryan et al.	(CMS Collab.)
AAD	15	PL B740 222	G. Aad et al.	(ATLAS Collab.)
AAD	15AA	PR D92 012006	G. Aad et al.	(ATLAS Collab.)
AAD	15AH	JHEP 1504 117	G. Aad et al.	(ATLAS Collab.)
AAD	15AQ	JHEP 1508 137	G. Aad et al.	(ATLAS Collab.)
AAD	15AX	EPJ C75 231	G. Aad et al.	(ATLAS Collab.)
AAD	15B	PRL 114 191803	G. Aad et al.	(ATLAS and CMS Collabs.)
AAD	15BC	EPJ C75 349	G. Aad et al.	(ATLAS Collab.)
AAD	15BD	EPJ C75 337	G. Aad et al.	(ATLAS Collab.)
AAD	15BE	EPJ C75 335	G. Aad et al.	(ATLAS Collab.)
AAD	15CE	PR D92 092004	G. Aad et al.	(ATLAS Collab.)
AAD	15CI	EPJ C76 476	G. Aad et al.	(ATLAS Collab.)
Also		EPJ C76 152 (err.)	G. Aad et al.	(ATLAS Collab.)
AAD	15CX	JHEP 1511 206	G. Aad et al.	(ATLAS Collab.)
AAD	15F	PR D91 012006	G. Aad et al.	(ATLAS Collab.)
AAD	15G	JHEP 1501 069	G. Aad et al.	(ATLAS Collab.)
AAD	15I	PRL 114 121801	G. Aad et al.	(ATLAS Collab.)
AAD	15P	PRL 115 091801	G. Aad et al.	(ATLAS Collab.)
AAD	15T	PL B749 519	G. Aad et al.	(ATLAS Collab.)
AALTONEN	15	PRL 114 151802	T. Aaltonen et al.	(CDF and DO Collabs.)
AALTONEN	15B	PRL 114 141802	T. Aaltonen et al.	(CDF Collab.)
KHACHATRYAN	15AM	EPJ C75 212	V. Khachatryan et al.	(CMS Collab.)
KHACHATRYAN	15AN	EPJ C75 251	V. Khachatryan et al.	(CMS Collab.)
KHACHATRYAN	15BA	PR D92 072010	V. Khachatryan et al.	(CMS Collab.)
KHACHATRYAN	15H	PL B744 184	V. Khachatryan et al.	(CMS Collab.)
KHACHATRYAN	15Q	PL B749 337	V. Khachatryan et al.	(CMS Collab.)
KHACHATRYAN	15R	PR D92 012004	V. Khachatryan et al.	(CMS Collab.)
KHACHATRYAN	15Z	PR D92 032008	V. Khachatryan et al.	(CMS Collab.)
AAD	14AR	PL B738 234	G. Aad et al.	(ATLAS Collab.)
AAD	14AS	PL B738 68	G. Aad et al.	(ATLAS Collab.)
AAD	14BC	PR D90 112015	G. Aad et al.	(ATLAS Collab.)
AAD	14BJ	JHEP 1409 112	G. Aad et al.	(ATLAS Collab.)
AAD	14J	PL B732 8	G. Aad et al.	(ATLAS Collab.)
AAD	14O	PRL 112 201802	G. Aad et al.	(ATLAS Collab.)
AAD	14W	PR D90 052004	G. Aad et al.	(ATLAS Collab.)
ABAZOV	14F	PRL 113 161802	V.M. Abazov et al.	(DO Collab.)
CHATRCHYAN	14AA	PR D89 092007	S. Chatrchyan et al.	(CMS Collab.)
CHATRCHYAN	14AI	PR D89 012003	S. Chatrchyan et al.	(CMS Collab.)
CHATRCHYAN	14AJ	NATP 10 557	S. Chatrchyan et al.	(CMS Collab.)
CHATRCHYAN	14B	EPJ C74 2980	S. Chatrchyan et al.	(CMS Collab.)
CHATRCHYAN	14G	JHEP 1401 096	S. Chatrchyan et al.	(CMS Collab.)
CHATRCHYAN	14K	JHEP 1405 104	S. Chatrchyan et al.	(CMS Collab.)
KHACHATRYAN	14D	PL B736 64	V. Khachatryan et al.	(CMS Collab.)
KHACHATRYAN	14H	JHEP 1409 087	V. Khachatryan et al.	(CMS Collab.)
KHACHATRYAN	14P	EPJ C74 3076	V. Khachatryan et al.	(CMS Collab.)
AAD	13AJ	PL B726 120	G. Aad et al.	(ATLAS Collab.)
AAD	13AK	PL B726 88	G. Aad et al.	(ATLAS Collab.)
Also		PL B734 406 (err.)	G. Aad et al.	(ATLAS Collab.)
AALTONEN	13L	PR D88 052013	T. Aaltonen et al.	(CDF Collab.)
AALTONEN	13M	PR D88 052014	T. Aaltonen et al.	(CDF and DO Collabs.)
ABAZOV	13L	PR D88 052011	V.M. Abazov et al.	(DO Collab.)
CHATRCHYAN	13BK	PL B726 587	S. Chatrchyan et al.	(CMS Collab.)
CHATRCHYAN	13J	PRL 110 081803	S. Chatrchyan et al.	(CMS Collab.)
CHATRCHYAN	13X	JHEP 1305 145	S. Chatrchyan et al.	(CMS Collab.)
CHATRCHYAN	13Y	JHEP 1306 081	S. Chatrchyan et al.	(CMS Collab.)
HEINEMEYER	13A	arXiv:1307.1347	S. Heinemeyer et al.	(LHC Higgs CS Working Group)
AAD	12AI	PL B716 1	G. Aad et al.	(ATLAS Collab.)
AAD	12DA	SCI 338 1576	G. Aad et al.	(ATLAS Collab.)
AALTONEN	12Q	PRL 109 111803	T. Aaltonen et al.	(CDF Collab.)
AALTONEN	12R	PRL 109 111804	T. Aaltonen et al.	(CDF Collab.)
AALTONEN	12S	PRL 109 111805	T. Aaltonen et al.	(CDF Collab.)
AALTONEN	12T	PRL 109 071804	T. Aaltonen et al.	(CDF and DO Collabs.)
ABAZOV	12K	PL B716 285	V.M. Abazov et al.	(DO Collab.)
ABAZOV	12O	PRL 109 121803	V.M. Abazov et al.	(DO Collab.)
ABAZOV	12P	PRL 109 121804	V.M. Abazov et al.	(DO Collab.)
CHATRCHYAN	12BY	SCI 338 1569	S. Chatrchyan et al.	(CMS Collab.)
CHATRCHYAN	12N	PL B716 30	S. Chatrchyan et al.	(CMS Collab.)
DIETMAIER	12	arXiv:1201.3084	S. Dittmaier et al.	(LHC Higgs CS Working Group)
DIETMAIER	11	arXiv:1101.0593	S. Dittmaier et al.	(LHC Higgs CS Working Group)

Neutral Higgs Bosons, Searches for

CONTENTS:

- Mass Limits for Neutral Higgs Bosons in Supersymmetric Models
 - Mass Limits for heavy neutral Higgs bosons (H_2^0, A^0) in the MSSM
 - Mass Limits for H_1^0 (Higgs Boson) in Supersymmetric Models
- Mass Limits for Neutral Higgs Bosons in Extended Higgs Models
 - Mass Limits in General two-Higgs-doublet Models
 - Mass Limits for H^0 with Vanishing Yukawa Couplings
 - Mass Limits for H^0 Decaying to Invisible Final States
 - Mass Limits for Light A^0
 - Other Mass Limits
- Searches for a Higgs Boson with Standard Model Couplings
 - Direct Mass Limits for H^0
 - Indirect Mass Limits for H^0 from Electroweak Analysis

MASS LIMITS FOR NEUTRAL HIGGS BOSONS IN SUPERSYMMETRIC MODELS

The minimal supersymmetric model has two complex doublets of Higgs bosons. The resulting physical states are two scalars [H_1^0 and H_2^0], where we define $m_{H_1^0} < m_{H_2^0}$, a pseudoscalar (A^0), and a charged Higgs pair

(H^\pm). H_1^0 and H_2^0 are also called h and H in the literature. There are two free parameters in the Higgs sector which can be chosen to be m_{A^0} and $\tan\beta = v_2/v_1$, the ratio of vacuum expectation values of the two Higgs doublets. Tree-level Higgs masses are constrained by the model to be $m_{H_1^0} \leq m_Z$, $m_{H_2^0} \geq m_Z$, $m_{A^0} \geq m_{H^0}$, and $m_{H^\pm} \geq m_W$.

However, as described in the review on “Status of Higgs Boson Physics” in this Volume these relations are violated by radiative corrections.

The observed signal at about 125 GeV, see section “ H^0 ”, can be interpreted as one of the neutral Higgs bosons of supersymmetric models. Unless otherwise noted, we identify the lighter scalar H_1^0 with the Higgs discovered at 125 GeV at the LHC (AAD 12AI, CHATRCHYAN 12N).

Unless otherwise noted, the experiments in e^+e^- collisions search for the processes $e^+e^- \rightarrow H_1^0 Z^0$ in the channels used for the Standard Model Higgs searches and $e^+e^- \rightarrow H_2^0 A^0$ in the final states $b\bar{b}b\bar{b}$ and $b\bar{b}\tau^+\tau^-$. Unless otherwise stated, the following results assume no invisible H_1^0 or A^0 decays. Unless otherwise noted, the results are given in the m_h^{max} scenario, CARENA 13.

In $p\bar{p}$ and pp collisions the experiments search for a variety of processes, as explicitly specified for each entry. Limits on the A^0 mass arise from these direct searches, as well as from the relations valid in the minimal supersymmetric model between m_{A^0} and $m_{H_1^0}$. As discussed in the review on “Status of Higgs Boson Physics” in this Volume, these relations depend, via potentially large radiative corrections, on the mass of the t quark and on the supersymmetric parameters, in particular those of the stop sector. These indirect limits are weaker for larger t and \bar{t} masses. To include the radiative corrections to the Higgs masses, unless otherwise stated, the listed papers use theoretical predictions incorporating two-loop corrections, and the results are given for the m_h^{mod+} benchmark scenario, see CARENA 13.

Mass Limits for heavy neutral Higgs bosons (H_2^0, A^0) in the MSSM

The limits rely on $pp \rightarrow H_2^0/A^0 \rightarrow \tau^+\tau^-$ and assume that H_2^0 and A^0 are (sufficiently) mass degenerate. The limits depend on $\tan\beta$.

VALUE (GeV)	CL%	DOCUMENT ID	TECN	COMMENT
> 377	95	1 AABOUD	18G ATLS	$\tan\beta = 10$ GeV
> 863	95	1 AABOUD	18G ATLS	$\tan\beta = 20$ GeV
>1157	95	1 AABOUD	18G ATLS	$\tan\beta = 30$ GeV
>1328	95	1 AABOUD	18G ATLS	$\tan\beta = 40$ GeV
>1483	95	1 AABOUD	18G ATLS	$\tan\beta = 50$ GeV
>1613	95	1 AABOUD	18G ATLS	$\tan\beta = 60$ GeV
> 389	95	2 SIRUNYAN	18CX CMS	$\tan\beta = 10$ GeV
> 832	95	2 SIRUNYAN	18CX CMS	$\tan\beta = 20$ GeV
>1148	95	2 SIRUNYAN	18CX CMS	$\tan\beta = 30$ GeV
>1341	95	2 SIRUNYAN	18CX CMS	$\tan\beta = 40$ GeV
>1496	95	2 SIRUNYAN	18CX CMS	$\tan\beta = 50$ GeV
>1613	95	2 SIRUNYAN	18CX CMS	$\tan\beta = 60$ GeV

• • • We do not use the following data for averages, fits, limits, etc. • • •

3 AAD	20 ATLS	H^0 properties
4 AAD	20C ATLS	$H_2^0 \rightarrow H^0 H^0$
5 SIRUNYAN	19CR CMS	$H_2^0/A^0 \rightarrow \mu^+\mu^-$
6 SIRUNYAN	18A CMS	$H_2^0 \rightarrow H^0 H^0$
7 SIRUNYAN	18BP CMS	$pp \rightarrow H_2^0/A^0 + b + X,$ $H_2^0/A^0 \rightarrow b\bar{b}$
8 AABOUD	16AA ATLS	$A^0 \rightarrow \tau^+\tau^-$
9 KHACHATRYAN	16A CMS	$H_{1,2}^0/A^0 \rightarrow \mu^+\mu^-$
10 KHACHATRYAN	16P CMS	$H_2^0 \rightarrow H^0 H^0, A^0 \rightarrow Z H^0$
11 KHACHATRYAN	15AY CMS	$pp \rightarrow H_{1,2}^0/A^0 + b + X,$ $H_{1,2}^0/A^0 \rightarrow b\bar{b}$
12 AAD	14AW ATLS	$pp \rightarrow H_{1,2}^0/A^0 + X,$ $H_{1,2}^0/A^0 \rightarrow \tau\tau$
13 KHACHATRYAN	14M CMS	$pp \rightarrow H_{1,2}^0/A^0 + X,$ $H_{1,2}^0/A^0 \rightarrow \tau\tau$
14 AAD	13O ATLS	$pp \rightarrow H_{1,2}^0/A^0 + X,$ $H_{1,2}^0/A^0 \rightarrow \tau^+\tau^-$
15 AAIJ	13T LHCB	$pp \rightarrow H_{1,2}^0/A^0 + X,$ $H_{1,2}^0/A^0 \rightarrow \tau^+\tau^-$
16 CHATRCHYAN	13AG CMS	$pp \rightarrow H_{1,2}^0/A^0 + b + X,$ $H_{1,2}^0/A^0 \rightarrow b\bar{b}$
17 AALTONEN	12AQ TEVA	$p\bar{p} \rightarrow H_{1,2}^0/A^0 + b + X,$ $H_{1,2}^0/A^0 \rightarrow b\bar{b}$

	18	AALTONEN	12X	CDF	$p\bar{p} \rightarrow H_{1,2}^0/A^0 + b + X,$ $H_{1,2}^0/A^0 \rightarrow b\bar{b}$		
	19	ABAZOV	12G	D0	$p\bar{p} \rightarrow H_{1,2}^0/A^0 + X,$ $H_{1,2}^0/A^0 \rightarrow \tau^+\tau^-$		
	20	CHATRCHYAN	12K	CMS	$p\bar{p} \rightarrow H_{1,2}^0/A^0 + X,$ $H_{1,2}^0/A^0 \rightarrow \tau^+\tau^-$		
	21	ABAZOV	11K	D0	$p\bar{p} \rightarrow H_{1,2}^0/A^0 + b + X,$ $H_{1,2}^0/A^0 \rightarrow b\bar{b}$		
	22	ABAZOV	11W	D0	$p\bar{p} \rightarrow H_{1,2}^0/A^0 + b + X,$ $H_{1,2}^0/A^0 \rightarrow \tau^+\tau^-$		
	23	AALTONEN	09AR	CDF	$p\bar{p} \rightarrow H_{1,2}^0/A^0 + X,$ $H_{1,2}^0/A^0 \rightarrow \tau^+\tau^-$		
>	90.4	24	ABDALLAH	08B	DLPH	$E_{cm} \leq 209$ GeV	
>	93.4	95	25	SCHAEEL	06B	LEP	$E_{cm} \leq 209$ GeV
		26	ACOSTA	05Q	CDF	$p\bar{p} \rightarrow H_{1,2}^0/A^0 + X$	
>	85.0	95	27,28	ABBIENDI	04M	OPAL	$E_{cm} \leq 209$ GeV
		29	ABBIENDI	03G	OPAL	$H_1^0 \rightarrow A^0 A^0$	
>	86.5	95	27,30	ACHARD	02H	L3	$E_{cm} \leq 209$ GeV, $\tan\beta > 0.4$
		31	AKERROYD	02	RVUE		
>	90.1	95	27,32	HEISTER	02	ALEP	$E_{cm} \leq 209$ GeV, $\tan\beta > 0.5$
		1	ABOUD	18G	search for production of $H_{2,3}^0/A^0 \rightarrow \tau^+\tau^-$ by gluon fusion and b -associated production in 36.1 fb^{-1} of pp collisions at $E_{cm} = 13$ TeV. See their Fig. 10 for excluded regions in the $m_{A^0} - \tan\beta$ plane in several MSSM scenarios.		
		2	SIRUNYAN	18CX	search for production of $H_{1,2}^0/A^0 \rightarrow \tau^+\tau^-$ by gluon fusion and b -associated production in 35.9 fb^{-1} of pp collisions at $E_{cm} = 13$ TeV. See their Fig. 9 for excluded regions in the $m_{A^0} - \tan\beta$ plane in several MSSM scenarios.		
		3	AAD	20	combine measurements of H^0 production and decay using data taken in years 2015–2017 (up to 79.8 fb^{-1}) of pp collisions at $E_{cm} = 13$ TeV. See their Fig. 19 for excluded region in the hMSSM parameter space.		
		4	AAD	20C	combine searches for a scalar resonance decaying to $H^0 H^0$ in 36.1 fb^{-1} of pp collisions at $E_{cm} = 13$ TeV from ABOUD 19A, ABOUD 19O, ABOUD 18CQ, ABOUD 19T, ABOUD 18CW, and ABOUD 18BU. See their Fig. 7(b) for the excluded region in the hMSSM parameter space.		
		5	SIRUNYAN	19CR	search for production of $H_{2,3}^0/A^0$ in gluon fusion and in association with a $b\bar{b}$ pair, decaying to $\mu^+\mu^-$ in 35.9 fb^{-1} of pp collisions at $E_{cm} = 13$ TeV. See their Fig. 5 for the excluded region in the MSSM parameter space in the $m_h^{\text{mod+}}$ and hMSSM scenarios.		
		6	SIRUNYAN	18A	search for production of a scalar resonance decaying to $H^0 H^0 \rightarrow b\bar{b}\tau^+\tau^-$ in 35.9 fb^{-1} of pp collisions at $E_{cm} = 13$ TeV. See their Fig. 5 (lower) for excluded regions in the $m_{A^0} - \tan\beta$ plane in the hMSSM scenario.		
		7	SIRUNYAN	18BP	search for production of $H_{2,3}^0/A^0 \rightarrow b\bar{b}$ by b -associated production in 35.7 fb^{-1} of pp collisions at $E_{cm} = 13$ TeV. See their Fig. 6 for the limits on cross section times branching ratio for $m_{H_{2,3}^0}, m_{A^0} = 0.3\text{--}1.3$ TeV, and Fig. 7 for excluded regions in the $m_{A^0} - \tan\beta$ plane in several MSSM scenarios.		
		8	ABOUD	16AA	search for production of a Higgs boson in gluon fusion and in association with a $b\bar{b}$ pair followed by the decay $A^0 \rightarrow \tau^+\tau^-$ in 3.2 fb^{-1} of pp collisions at $E_{cm} = 13$ TeV. See their Fig. 5(a, b) for limits on cross section times branching ratio for $m_{A^0} = 200\text{--}1200$ GeV, and Fig. 5(c, d) for the excluded region in the MSSM parameter space in the $m_h^{\text{mod+}}$ and hMSSM scenarios.		
		9	KHACHATRYAN	16A	search for production of a Higgs boson in gluon fusion and in association with a $b\bar{b}$ pair followed by the decay $H_{1,2}^0/A^0 \rightarrow \mu^+\mu^-$ in 5.1 fb^{-1} of pp collisions at $E_{cm} = 7$ TeV and 19.3 fb^{-1} at $E_{cm} = 8$ TeV. See their Fig. 7 for the excluded region in the MSSM parameter space in the $m_h^{\text{mod+}}$ benchmark scenario and Fig. 9 for limits on cross section times branching ratio.		
		10	KHACHATRYAN	16P	search for gluon fusion production of an $H_{2,3}^0$ decaying to $H^0 H^0 \rightarrow b\bar{b}\tau^+\tau^-$ and an A^0 decaying to $ZH^0 \rightarrow \ell^+\ell^-\tau^+\tau^-$ in 19.7 fb^{-1} of pp collisions at $E_{cm} = 8$ TeV. See their Fig. 12 for excluded region in the $\tan\beta - \cos(\beta - \alpha)$ plane for $m_{H_{2,3}^0} = m_{A^0} = 300$ GeV.		
		11	KHACHATRYAN	15AY	search for production of a Higgs boson in association with a b quark in the decay $H_{1,2}^0/A^0 \rightarrow b\bar{b}$ in 19.7 fb^{-1} of pp collisions at $E_{cm} = 8$ TeV and combine with CHATRCHYAN 13AG 7 TeV data. See their Fig. 6 for the limits on cross section times branching ratio for $m_{A^0} = 100\text{--}900$ GeV and Figs. 7–9 for the excluded region in the MSSM parameter space in various benchmark scenarios.		
		12	AAD	14AW	search for production of a Higgs boson followed by the decay $H_{1,2}^0/A^0 \rightarrow \tau^+\tau^-$ in $19.5\text{--}20.3 \text{ fb}^{-1}$ of pp collisions at $E_{cm} = 8$ TeV. See their Fig. 11 for the limits on cross section times branching ratio and their Figs. 9 and 10 for the excluded region in the MSSM parameter space. For $m_{A^0} = 140$ GeV, the region $\tan\beta > 5.4$ is excluded at 95% CL in the m_h^{max} scenario.		
		13	KHACHATRYAN	14M	search for production of a Higgs boson in gluon fusion and in association with a b quark followed by the decay $H_{1,2}^0/A^0 \rightarrow \tau^+\tau^-$ in 4.9 fb^{-1} of pp collisions at $E_{cm} = 7$ TeV and 19.7 fb^{-1} at $E_{cm} = 8$ TeV. See their Figs. 7 and 8 for one- and two-dimensional limits on cross section times branching ratio and their Figs. 5 and 6 for the excluded region in the MSSM parameter space. For $m_{A^0} = 140$ GeV, the region $\tan\beta > 3.8$ is excluded at 95% CL in the m_h^{max} scenario.		
		14	AAD	13O	search for production of a Higgs boson in the decay $H_{1,2}^0/A^0 \rightarrow \tau^+\tau^-$ and $\mu^+\mu^-$ with $4.7\text{--}4.8 \text{ fb}^{-1}$ of pp collisions at $E_{cm} = 7$ TeV. See their Fig. 6 for the excluded region in the MSSM parameter space and their Fig. 7 for the limits on cross		

section times branching ratio. For $m_{A^0} = 110\text{--}170$ GeV, $\tan\beta \gtrsim 10$ is excluded, and for $\tan\beta = 50$, m_{A^0} below 470 GeV is excluded at 95% CL in the m_h^{max} scenario.

- 15 AAIJ 13T search for production of a Higgs boson in the forward region in the decay $H_{1,2}^0/A^0 \rightarrow \tau^+\tau^-$ in 1.0 fb^{-1} of pp collisions at $E_{cm} = 7$ TeV. See their Fig. 2 for the limits on cross section times branching ratio and the excluded region in the MSSM parameter space.
- 16 CHATRCHYAN 13AG search for production of a Higgs boson in association with a b quark in the decay $H_{1,2}^0/A^0 \rightarrow b\bar{b}$ in $2.7\text{--}4.8 \text{ fb}^{-1}$ of pp collisions at $E_{cm} = 7$ TeV. See their Fig. 6 for the excluded region in the MSSM parameter space and Fig. 5 for the limits on cross section times branching ratio. For $m_{A^0} = 90\text{--}350$ GeV, upper bounds on $\tan\beta$ of 18–42 at 95% CL are obtained in the m_h^{max} scenario with $\mu = +200$ GeV.
- 17 AALTONEN 12AQ combine AALTONEN 12X and ABAZOV 11K. See their Table I and Fig. 1 for the limit on cross section times branching ratio and Fig. 2 for the excluded region in the MSSM parameter space.
- 18 AALTONEN 12X search for associated production of a Higgs boson and a b quark in the decay $H_{1,2}^0/A^0 \rightarrow b\bar{b}$, with 2.6 fb^{-1} of $p\bar{p}$ collisions at $E_{cm} = 1.96$ TeV. See their Table III and Fig. 15 for the limit on cross section times branching ratio and Figs. 17, 18 for the excluded region in the MSSM parameter space.
- 19 ABAZOV 12G search for production of a Higgs boson in the decay $H_{1,2}^0/A^0 \rightarrow \tau^+\tau^-$ with 7.3 fb^{-1} of $p\bar{p}$ collisions at $E_{cm} = 1.96$ TeV and combine with ABAZOV 11W and ABAZOV 11K. See their Figs. 4, 5, and 6 for the excluded region in the MSSM parameter space. For $m_{A^0} = 90\text{--}180$ GeV, $\tan\beta \gtrsim 30$ is excluded at 95% CL in the m_h^{max} scenario.
- 20 CHATRCHYAN 12K search for production of a Higgs boson in the decay $H_{1,2}^0/A^0 \rightarrow \tau^+\tau^-$ with 4.6 fb^{-1} of pp collisions at $E_{cm} = 7$ TeV. See their Fig. 3 and Table 4 for the excluded region in the MSSM parameter space. For $m_{A^0} = 160$ GeV, the region $\tan\beta > 7.1$ is excluded at 95% CL in the m_h^{max} scenario. Superseded by KHACHATRYAN 14M.
- 21 ABAZOV 11K search for associated production of a Higgs boson and a b quark, followed by the decay $H_{1,2}^0/A^0 \rightarrow b\bar{b}$, in 5.2 fb^{-1} of $p\bar{p}$ collisions at $E_{cm} = 1.96$ TeV. See their Fig. 5/Table 2 for the limit on cross section times branching ratio and Fig. 6 for the excluded region in the MSSM parameter space for $\mu = -200$ GeV.
- 22 ABAZOV 11W search for associated production of a Higgs boson and a b quark, followed by the decay $H_{1,2}^0/A^0 \rightarrow \tau\tau$, in 7.3 fb^{-1} of $p\bar{p}$ collisions at $E_{cm} = 1.96$ TeV. See their Fig. 2 for the limit on cross section times branching ratio and for the excluded region in the MSSM parameter space.
- 23 AALTONEN 09AR search for Higgs bosons decaying to $\tau^+\tau^-$ in two doublet models in 1.8 fb^{-1} of $p\bar{p}$ collisions at $E_{cm} = 1.96$ TeV. See their Fig. 2 for the limit on $\sigma \cdot B(H_{1,2}^0/A^0 \rightarrow \tau^+\tau^-)$ for different Higgs masses, and see their Fig. 3 for the excluded region in the MSSM parameter space.
- 24 ABDALLAH 08B give limits in eight CP -conserving benchmark scenarios and some CP -violating scenarios. See paper for excluded regions for each scenario. Supersedes ABDALLAH 04.
- 25 SCHAEEL 06B make a combined analysis of the LEP data. The quoted limit is for the m_h^{max} scenario with $m_t = 174.3$ GeV. In the CP -violating CPX scenario no lower bound on $m_{H_{1,2}^0}$ can be set at 95% CL. See paper for excluded regions in various scenarios. See Figs. 2–6 and Tabs. 14–21 for limits on $\sigma(ZH^0) \cdot B(H^0 \rightarrow b\bar{b}, \tau^+\tau^-)$ and $\sigma(H_1^0 H_2^0) \cdot B(H_1^0 H_2^0 \rightarrow b\bar{b}, \tau^+\tau^-)$.
- 26 ACOSTA 05Q search for $H_{1,2}^0/A^0$ production in $p\bar{p}$ collisions at $E_{cm} = 1.8$ TeV with $H_{1,2}^0/A^0 \rightarrow \tau^+\tau^-$. At $m_{A^0} = 100$ GeV, the obtained cross section upper limit is above theoretical expectation.
- 27 Search for $e^+e^- \rightarrow H_{1,2}^0/A^0$ in the final states $b\bar{b}b\bar{b}$ and $b\bar{b}\tau^+\tau^-$, and $e^+e^- \rightarrow H_{1,2}^0 Z$. Universal scalar mass of 1 TeV, $SU(2)$ gaugino mass of 200 GeV, and $\mu = -200$ GeV are assumed, and two-loop radiative corrections incorporated. The limits hold for $m_t = 175$ GeV, and for the m_h^{max} scenario.
- 28 ABBIENDI 04M exclude $0.7 < \tan\beta < 1.9$, assuming $m_t = 174.3$ GeV. Limits for other MSSM benchmark scenarios, as well as for CP violating cases, are also given.
- 29 ABBIENDI 03G search for $e^+e^- \rightarrow H_1^0 Z$ followed by $H_1^0 \rightarrow A^0 A^0, A^0 \rightarrow c\bar{c}, gg$, or $\tau^+\tau^-$. In the no-mixing scenario, the region $m_{H_1^0} = 45\text{--}85$ GeV and $m_{A^0} = 2\text{--}9.5$ GeV is excluded at 95% CL.
- 30 ACHARD 02H also search for the final state $H_1^0 Z \rightarrow 2A^0 q\bar{q}, A^0 \rightarrow q\bar{q}$. In addition, the MSSM parameter set in the “large- μ ” and “no-mixing” scenarios are examined.
- 31 AKEROYD 02 examine the possibility of a light A^0 with $\tan\beta < 1$. Electroweak measurements are found to be inconsistent with such a scenario.
- 32 HEISTER 02 excludes the range $0.7 < \tan\beta < 2.3$. A wider range is excluded with different stop mixing assumptions. Updates BARATE 01C.

Mass Limits for H_1^0 (Higgs Boson) in Supersymmetric Models

VALUE (GeV)	CL%	DOCUMENT ID	TECN	COMMENT
>89.7		1	ABDALLAH	08B DLPH $E_{cm} \leq 209$ GeV
>92.8	95	2	SCHAEEL	06B LEP $E_{cm} \leq 209$ GeV
>84.5	95	3,4	ABBIENDI	04M OPAL $E_{cm} \leq 209$ GeV
>86.0	95	3,5	ACHARD	02H L3 $E_{cm} \leq 209$ GeV, $\tan\beta > 0.4$
>89.8	95	3,6	HEISTER	02 ALEP $E_{cm} \leq 209$ GeV, $\tan\beta > 0.5$

- We do not use the following data for averages, fits, limits, etc. •••
- 7 AALTONEN 12AQ TEVA $p\bar{p} \rightarrow H_{1,2}^0/A^0 + b + X,$
 $H_{1,2}^0/A^0 \rightarrow b\bar{b}$

1 ABDALLAH 08B give limits in eight CP -conserving benchmark scenarios and some CP -violating scenarios. See paper for excluded regions for each scenario. Supersedes ABDALLAH 04.

2 SCHAEEL 06B make a combined analysis of the LEP data. The quoted limit is for the m_h^{max} scenario with $m_t = 174.3$ GeV. In the CP -violating CPX scenario no lower bound

Gauge & Higgs Boson Particle Listings

Neutral Higgs Bosons, Searches for

on $m_{H_1^0}$ can be set at 95% CL. See paper for excluded regions in various scenarios. See

Figs. 2–6 and Tabs. 14–21 for limits on $\sigma(ZH^0) \cdot \text{B}(H^0 \rightarrow b\bar{b}, \tau^+\tau^-)$ and $\sigma(H_1^0 H_2^0) \cdot \text{B}(H_1^0, H_2^0 \rightarrow b\bar{b}, \tau^+\tau^-)$.

³ Search for $e^+e^- \rightarrow H_1^0 A^0$ in the final states $b\bar{b}b\bar{b}$ and $b\bar{b}\tau^+\tau^-$, and $e^+e^- \rightarrow H_1^0 Z$. Universal scalar mass of 1 TeV, SU(2) gaugino mass of 200 GeV, and $\mu = -200$ GeV are assumed, and two-loop radiative corrections incorporated. The limits hold for $m_t = 175$ GeV, and for the m_h^{max} scenario.

⁴ ABBIENDI 04M exclude $0.7 < \tan\beta < 1.9$, assuming $m_t = 174.3$ GeV. Limits for other MSSM benchmark scenarios, as well as for CP violating cases, are also given.

⁵ ACHARD 02H also search for the final state $H_1^0 Z \rightarrow 2A^0 q\bar{q}$, $A^0 \rightarrow q\bar{q}$. In addition, the MSSM parameter set in the “large- μ ” and “no-mixing” scenarios are examined.

⁶ HEISTER 02 excludes the range $0.7 < \tan\beta < 2.3$. A wider range is excluded with different stop mixing assumptions. Updates BARATE 01c.

⁷ AALTONEN 12A0 combine AALTONEN 12x and ABAZOV 11k. See their Table I and Fig. 1 for the limit on cross section times branching ratio and Fig. 2 for the excluded region in the MSSM parameter space.

MASS LIMITS FOR NEUTRAL HIGGS BOSONS IN EXTENDED HIGGS MODELS

This Section covers models which do not fit into either the Standard Model or its simplest minimal Supersymmetric extension (MSSM), leading to anomalous production rates, or nonstandard final states and branching ratios. In particular, this Section covers limits which may apply to generic two-Higgs-doublet models (2HDM), or to special regions of the MSSM parameter space where decays to invisible particles or to photon pairs are dominant (see the review on “Status of Higgs Boson Physics”). Concerning the mass limits for H^0 and A^0 listed below, see the footnotes or the comment lines for details on the nature of the models to which the limits apply.

The observed signal at about 125 GeV, see section “ H^0 ”, can be interpreted as one of the neutral Higgs bosons of an extended Higgs sector.

Mass Limits in General two-Higgs-doublet Models

VALUE (GeV)	CL%	DOCUMENT ID	TECN	COMMENT
• • •				We do not use the following data for averages, fits, limits, etc. • • •
		1 AAD 20 ATLS	H^0	properties
		2 SIRUNYAN 19AE CMS	$A^0 \rightarrow \tau^+\tau^-$	
		3 SIRUNYAN 19AV CMS	$A^0 \rightarrow ZH^0$	
		4 AABOUD 18AH ATLS	$A^0 \rightarrow ZH_2^0$	
		5 AABOUD 18AI ATLS	$A^0 \rightarrow ZH_1^0$	
		6 AABOUD 18BF ATLS	$H_2^0 \rightarrow ZZ$	
		7 AABOUD 18CE ATLS	$pp \rightarrow H_2^0/A^0 t\bar{t}$, $H_2^0/A^0 \rightarrow t\bar{t}$	
		8 HALLER 18 RVUE	global fits	
		9 SIRUNYAN 18BP CMS	$pp \rightarrow H_2^0/A^0 + b + X$, $H_2^0/A^0 \rightarrow b\bar{b}$	
		10 SIRUNYAN 18ED CMS	$A^0 \rightarrow ZH^0$	
		11 AABOUD 17AN ATLS	$H_2^0, A^0 \rightarrow t\bar{t}$	
		12 SIRUNYAN 17AX CMS	$A^0 b\bar{b}, A^0 \rightarrow \mu^+\mu^-$	
		13 AAD 16AX ATLS	$H_2^0 \rightarrow ZZ$	
		14 KHACHATRYAN 16P CMS	$H_2^0 \rightarrow H^0 H^0, A^0 \rightarrow ZH^0$	
		15 KHACHATRYAN 16W CMS	$A^0 b\bar{b}, A^0 \rightarrow \tau^+\tau^-$	
		16 KHACHATRYAN 16Z CMS	$H_2^0 \rightarrow ZA^0$ or $A^0 \rightarrow ZH_2^0$	
		17 AAD 15BK ATLS	$H_2^0 \rightarrow H^0 H^0$	
		18 AAD 15S ATLS	$A^0 \rightarrow ZH^0$	
		19 KHACHATRYAN 15BB CMS	$H_2^0, A^0 \rightarrow \gamma\gamma$	
		20 KHACHATRYAN 15N CMS	$A^0 \rightarrow ZH^0$	
		21 AAD 14M ATLS	$H_2^0 \rightarrow H^\pm W^\mp \rightarrow H^0 W^\pm W^\mp, H^0 \rightarrow b\bar{b}$	
		22 KHACHATRYAN 14Q CMS	$H_2^0 \rightarrow H^0 H^0, A^0 \rightarrow ZH^0$	
		23 AALTONEN 09AR CDF	$p\bar{p} \rightarrow H_{1,2}^0/A^0 + X$, $H_{1,2}^0/A^0 \rightarrow \tau^+\tau^-$	
none 1–55	95	24 ABBIENDI 05A OPAL	H_1^0 , Type II model	
>110.6	95	25 ABDALLAH 05D DLPH	$H^0 \rightarrow 2$ jets	
		26 ABDALLAH 04O DLPH	$Z \rightarrow t\bar{t}H$	
		27 ABDALLAH 04O DLPH	$e^+e^- \rightarrow H^0 Z, H^0 A^0$	
		28 ABBIENDI 02D OPAL	$e^+e^- \rightarrow b\bar{b}H$	
none 1–44	95	29 ABBIENDI 01E OPAL	H_1^0 , Type-II model	
> 68.0	95	30 ABBIENDI 99E OPAL	$\tan\beta > 1$	
		31 ABREU 95H DLPH	$Z \rightarrow H^0 Z^*, H^0 A^0$	
		32 PICH 92 RVUE	Very light Higgs	

¹ AAD 20 combine measurements on H^0 production and decay using data taken in years 2015–2017 (up to 79.8 fb^{-1}) of pp collisions at $E_{\text{cm}} = 13$ TeV. See their Fig. 18 for excluded regions in various 2HDMs.

² SIRUNYAN 19AE search for a pseudoscalar resonance produced in association with a $b\bar{b}$ pair, decaying to $\tau^+\tau^-$ in 35.9 fb^{-1} of pp collisions at $E_{\text{cm}} = 13$ TeV. See their Fig. 4 for cross section limits for $m_{A^0} = 25\text{--}70$ GeV and comparison with some representative 2HDMs.

³ SIRUNYAN 19AV search for a scalar resonance produced by gluon fusion or b associated production, decaying to $ZH^0 \rightarrow \ell^+\ell^- b\bar{b}$ ($\ell = e, \mu$) or $\nu\bar{\nu}b\bar{b}$ in 35.9 fb^{-1} of pp collisions at $E_{\text{cm}} = 13$ TeV. See their Figs. 6 and 7 for excluded regions in the parameter space of various 2HDMs.

⁴ AABOUD 18AH search for production of an A^0 in gluon-gluon fusion and in association with a $b\bar{b}$, decaying to $ZH_2^0 \rightarrow \ell^+\ell^- b\bar{b}$ in 36.1 fb^{-1} of pp collisions at $E_{\text{cm}} = 13$ TeV. See their Fig. 6 for excluded regions in the parameter space of various 2HDMs.

⁵ AABOUD 18AI search for production of an A^0 in gluon-gluon fusion and in association with a $b\bar{b}$, decaying to ZH^0 in the final states $\nu\bar{\nu}b\bar{b}$ and $\ell^+\ell^- b\bar{b}$ in 36.1 fb^{-1} of pp collisions at $E_{\text{cm}} = 13$ TeV. See their Figs. 7 and 8 for excluded regions in the parameter space in various 2HDMs.

⁶ AABOUD 18BF search for production of a heavy H_2^0 state decaying to ZZ in the final states $\ell^+\ell^- \ell^+\ell^-$ and $\ell^+\ell^- \nu\bar{\nu}$ in 36.1 fb^{-1} of pp collisions at $E_{\text{cm}} = 13$ TeV. See their Figs. 8 and 9 for excluded parameter regions in 2HDM Type I and II.

⁷ AABOUD 18CE search for the process $pp \rightarrow H_2^0/A^0 t\bar{t}$ followed by the decay $H_2^0/A^0 \rightarrow t\bar{t}$ in 36.1 fb^{-1} of pp collisions at $E_{\text{cm}} = 13$ TeV. See their Fig. 12 for limits on cross section times branching ratio, and for lower limits on $\tan\beta$ for $m_{H_2^0}, m_{A^0} = 0.4\text{--}1.0$ TeV in the 2HDM type II.

⁸ HALLER 18 perform global fits in the framework of two-Higgs-doublet models (type I, II, lepton specific, flipped). See their Fig. 8 for excluded parameter regions from fits to LHC H^0 measurements, Fig. 9 bottom and charm decays, Fig. 10 muon anomalous magnetic moment, Fig. 11 electroweak precision data, and Fig. 12 by combination of all data.

⁹ SIRUNYAN 18BP search for production of $H_2^0/A^0 \rightarrow b\bar{b}$ by b -associated production in 35.7 fb^{-1} of pp collisions at $E_{\text{cm}} = 13$ TeV. See their Fig. 6 for the limits on cross section times branching ratio for $m_{H_2^0}, m_{A^0} = 0.3\text{--}1.3$ TeV, and Figs. 8 and 9 for excluded regions in the parameter space of type-I and flipped 2HDMs.

¹⁰ SIRUNYAN 18ED search for production of an A^0 in gluon-gluon fusion and in association with a $b\bar{b}$, decaying to ZH^0 in the final states $\nu\bar{\nu}b\bar{b}$ or $\ell^+\ell^- b\bar{b}$ in 35.9 fb^{-1} of pp collisions at $E_{\text{cm}} = 13$ TeV. See their Fig. 9 for excluded regions in the parameter space in Type I and II 2HDMs.

¹¹ AABOUD 17AN search for production of a heavy H_2^0 and/or A^0 decaying to $t\bar{t}$ in 20.3 fb^{-1} of pp collisions at $E_{\text{cm}} = 8$ TeV. See their Fig. 3 and Table III for excluded parameter regions in Type II two-Higgs-Doublet-Models.

¹² SIRUNYAN 17AX search for $A^0 b\bar{b}$ production followed by the decay $A^0 \rightarrow \mu^+\mu^-$ in 19.7 fb^{-1} of pp collisions at $E_{\text{cm}} = 8$ TeV. Limits are set in the range $m_{A^0} = 25\text{--}60$ GeV. See their Fig. 5 for upper limits on $\sigma(A^0 b\bar{b}) \cdot \text{B}(A^0 \rightarrow \mu^+\mu^-)$.

¹³ AAD 16AX search for production of a heavy H^0 state decaying to ZZ in the final states $\ell^+\ell^- \ell^+\ell^-$, $\ell^+\ell^- \nu\bar{\nu}$, $\ell^+\ell^- q\bar{q}$, and $\nu\bar{\nu}q\bar{q}$ in 20.3 fb^{-1} of pp collisions at $E_{\text{cm}} = 8$ TeV. See their Figs. 13 and 14 for excluded parameter regions in Type I and II models.

¹⁴ KHACHATRYAN 16P search for gluon fusion production of an H_2^0 decaying to $H^0 H^0 \rightarrow b\bar{b}\tau^+\tau^-$ and an A^0 decaying to $ZH^0 \rightarrow \ell^+\ell^- \tau^+\tau^-$ in 19.7 fb^{-1} of pp collisions at $E_{\text{cm}} = 8$ TeV. See their Fig. 11 for limits on $\tan\beta$ for $m_{A^0} = 230\text{--}350$ GeV.

¹⁵ KHACHATRYAN 16W search for $A^0 b\bar{b}$ production followed by the decay $A^0 \rightarrow \tau^+\tau^-$ in 19.7 fb^{-1} of pp collisions at $E_{\text{cm}} = 8$ TeV. See their Fig. 3 for upper limits on $\sigma(A^0 b\bar{b}) \cdot \text{B}(A^0 \rightarrow \tau^+\tau^-)$.

¹⁶ KHACHATRYAN 16Z search for $H_2^0 \rightarrow ZA^0$ followed by $A^0 \rightarrow b\bar{b}$ or $\tau^+\tau^-$, and $A^0 \rightarrow ZH_2^0$ followed by $H_2^0 \rightarrow b\bar{b}$ or $\tau^+\tau^-$, in 19.8 fb^{-1} of pp collisions at $E_{\text{cm}} = 8$ TeV. See their Fig. 4 for cross section limits and Fig. 5 for excluded region in the parameter space.

¹⁷ AAD 15BK search for production of a heavy H_2^0 decaying to $H^0 H^0$ in the final state $b\bar{b}b\bar{b}$ in 19.5 fb^{-1} of pp collisions at $E_{\text{cm}} = 8$ TeV. See their Figs. 15–18 for excluded regions in the parameter space.

¹⁸ AAD 15S search for production of A^0 decaying to $ZH^0 \rightarrow \ell^+\ell^- b\bar{b}$, $\nu\bar{\nu}b\bar{b}$ and $\ell^+\ell^- \tau^+\tau^-$ in 20.3 fb^{-1} of pp collisions at $E_{\text{cm}} = 8$ TeV. See their Figs. 4 and 5 for excluded regions in the parameter space.

¹⁹ KHACHATRYAN 15BB search for $H_2^0, A^0 \rightarrow \gamma\gamma$ in 19.7 fb^{-1} of pp collisions at $E_{\text{cm}} = 8$ TeV. See their Fig. 10 for excluded regions in the two-Higgs-doublet model parameter space.

²⁰ KHACHATRYAN 15N search for production of A^0 decaying to $ZH^0 \rightarrow \ell^+\ell^- b\bar{b}$ in 19.7 fb^{-1} of pp collisions at $E_{\text{cm}} = 8$ TeV. See their Fig. 5 for excluded regions in the $\tan\beta - \cos(\beta - \alpha)$ plane for $m_{A^0} = 300$ GeV.

²¹ AAD 14M search for the decay cascade $H_2^0 \rightarrow H^\pm W^\mp \rightarrow H^0 W^\pm W^\mp, H^0$ decaying to $b\bar{b}$ in 20.3 fb^{-1} of pp collisions at $E_{\text{cm}} = 8$ TeV. See their Table IV for limits in a two-Higgs-doublet model for $m_{H_2^0} = 325\text{--}1025$ GeV and $m_{H^\pm} = 225\text{--}825$ GeV.

²² KHACHATRYAN 14Q search for $H_2^0 \rightarrow H^0 H^0$ and $A^0 \rightarrow ZH^0$ in 19.5 fb^{-1} of pp collisions at $E_{\text{cm}} = 8$ TeV. See their Figs. 4 and 5 for limits on cross section times branching ratio for $m_{H_2^0, A^0} = 260\text{--}360$ GeV and their Figs. 7–9 for limits in two-Higgs-doublet models.

²³ AALTONEN 09AR search for Higgs bosons decaying to $\tau^+\tau^-$ in two doublet models in 1.8 fb^{-1} of $p\bar{p}$ collisions at $E_{\text{cm}} = 1.96$ TeV. See their Fig. 2 for the limit on $\sigma \cdot \text{B}(H_{1,2}^0/A^0 \rightarrow \tau^+\tau^-)$ for different Higgs masses, and see their Fig. 3 for the excluded region in the MSSM parameter space.

²⁴ ABBIENDI 05A search for $e^+e^- \rightarrow H_1^0 A^0$ in general Type-II two-doublet models, with decays $H_1^0, A^0 \rightarrow q\bar{q}, gg, \tau^+\tau^-$, and $H_1^0 \rightarrow A^0 A^0$.

²⁵ ABDALLAH 05D search for $e^+e^- \rightarrow H^0 Z$ and $H^0 A^0$ with H^0, A^0 decaying to two jets of any flavor including gg . The limit is for SM $H^0 Z$ production cross section with $\text{B}(H^0 \rightarrow jj) = 1$.

²⁶ ABDALLAH 04O search for $Z \rightarrow b\bar{b}H^0, b\bar{b}A^0, \tau^+\tau^- H^0$ and $\tau^+\tau^- A^0$ in the final states $4b, b\bar{b}\tau^+\tau^-$, and 4τ . See paper for limits on Yukawa couplings.

²⁷ ABDALLAH 04O search for $e^+e^- \rightarrow H^0 Z$ and $H^0 A^0$, with H^0, A^0 decaying to $b\bar{b}, \tau^+\tau^-$, or $H^0 \rightarrow A^0 A^0$ at $E_{\text{cm}} = 189\text{--}208$ GeV. See paper for limits on couplings.

²⁸ ABBIENDI 02D search for $Z \rightarrow b\bar{b}H^0$ and $b\bar{b}A^0$ with $H_1^0/A^0 \rightarrow \tau^+\tau^-$, in the range $4 < m_H < 12$ GeV. See their Fig. 8 for limits on the Yukawa coupling.

See key on page 999

Gauge & Higgs Boson Particle Listings

Neutral Higgs Bosons, Searches for

- 29 ABBIENDI 01E search for neutral Higgs bosons in general Type-II two-doublet models, at $E_{cm} \leq 189$ GeV. In addition to usual final states, the decays $H_1^0, A^0 \rightarrow q\bar{q}, gg$ are searched for. See their Figs. 15,16 for excluded regions.
- 30 ABBIENDI 99E search for $e^+e^- \rightarrow H^0 A^0$ and $H^0 Z$ at $E_{cm} = 183$ GeV. The limit is with $m_H = m_A$ in general two Higgs-doublet models. See their Fig. 18 for the exclusion limit in the $m_H - m_A$ plane. Updates the results of ACKERSTAFF 98s.
- 31 See Fig. 4 of ABREU 95H for the excluded region in the $m_{H^0} - m_{A^0}$ plane for general two-doublet models. For $\tan\beta > 1$, the region $m_{H^0} + m_{A^0} \lesssim 87$ GeV, $m_{H^0} < 47$ GeV is excluded at 95% CL.
- 32 PICH 92 analyse H^0 with $m_{H^0} < 2m_\mu$ in general two-doublet models. Excluded regions in the space of mass-mixing angles from LEP, beam dump, and π^\pm, η rare decays are shown in Figs. 3,4. The considered mass region is not totally excluded.

Mass Limits for H^0 with Vanishing Yukawa Couplings

These limits assume that H^0 couples to gauge bosons with the same strength as the Standard Model Higgs boson, but has no coupling to quarks and leptons (this is often referred to as "fermiophobic").

VALUE (GeV)	CL%	DOCUMENT ID	TECN	COMMENT
• • •		We do not use the following data for averages, fits, limits, etc. • • •		
none 100-113	95	1 AALTONEN	13K CDF	$H^0 \rightarrow WW^*$
none 100-116	95	2 AALTONEN	13L CDF	$H^0 \rightarrow \gamma\gamma, WW^*, ZZ^*$
none 100-113	95	3 AALTONEN	13M TEVA	$H^0 \rightarrow \gamma\gamma, WW^*, ZZ^*$
none 100-113	95	4 ABAZOV	13G D0	$H^0 \rightarrow WW^*$
none 100-114	95	5 ABAZOV	13H D0	$H^0 \rightarrow \gamma\gamma$
none 100-114	95	6 ABAZOV	13I D0	$H^0 \rightarrow WW^*$
none 100-114	95	7 ABAZOV	13J D0	$H^0 \rightarrow WW^*, ZZ^*$
none 100-114	95	8 ABAZOV	13L D0	$H^0 \rightarrow \gamma\gamma, WW^*, ZZ^*$
none 110-147	95	9 CHATRCHYAN	13AL CMS	$H^0 \rightarrow \gamma\gamma$
none 110-118, 119.5-121	95	10 AAD	12N ATLS	$H^0 \rightarrow \gamma\gamma$
none 100-114	95	11 AALTONEN	12AN CDF	$H^0 \rightarrow \gamma\gamma$
none 110-194	95	12 CHATRCHYAN	12AO CMS	$H^0 \rightarrow \gamma\gamma, WW^*, ZZ^*$
none 70-106	95	13 AALTONEN	09AB CDF	$H^0 \rightarrow \gamma\gamma$
none 70-100	95	14 ABAZOV	08U D0	$H^0 \rightarrow \gamma\gamma$
>105.8	95	15 SCHAEEL	07 ALEP	$e^+e^- \rightarrow H^0 Z, H^0 \rightarrow WW^*$
>104.1	95	16,17 ABDALLAH	04L DLPH	$e^+e^- \rightarrow H^0 Z, H^0 \rightarrow \gamma\gamma$
>107	95	18 ACHARD	03C L3	$H^0 \rightarrow WW^*, ZZ^*, \gamma\gamma$
>105.5	95	16,19 ABBIENDI	02F OPAL	$H^0 \rightarrow \gamma\gamma$
>105.4	95	20 ACHARD	02C L3	$H^0 \rightarrow \gamma\gamma$
none 60-82	95	21 AFFOLDER	01H CDF	$p\bar{p} \rightarrow H^0 W/Z, H^0 \rightarrow \gamma\gamma$
> 94.9	95	22 ACCIARRI	00s L3	$e^+e^- \rightarrow H^0 Z, H^0 \rightarrow \gamma\gamma$
>100.7	95	23 BARATE	00L ALEP	$e^+e^- \rightarrow H^0 Z, H^0 \rightarrow \gamma\gamma$
> 96.2	95	24 ABBIENDI	99O OPAL	$e^+e^- \rightarrow H^0 Z, H^0 \rightarrow \gamma\gamma$
> 78.5	95	25 ABBOTT	99B D0	$p\bar{p} \rightarrow H^0 W/Z, H^0 \rightarrow \gamma\gamma$
		26 ABREU	99P DLPH	$e^+e^- \rightarrow H^0 \gamma$ and/or $H^0 \rightarrow \gamma\gamma$

- 1 AALTONEN 13K search for $H^0 \rightarrow WW^*$ in 9.7 fb^{-1} of $p\bar{p}$ collisions at $E_{cm} = 1.96$ TeV. A limit on cross section times branching ratio which corresponds to (1.3-6.6) times the expected cross section is given in the range $m_{H^0} = 110-200$ GeV at 95% CL.
- 2 AALTONEN 13L combine all CDF searches with $9.45-10.0 \text{ fb}^{-1}$ of $p\bar{p}$ collisions at $E_{cm} = 1.96$ TeV.
- 3 AALTONEN 13M combine all Tevatron data from the CDF and D0 Collaborations of $p\bar{p}$ collisions at $E_{cm} = 1.96$ TeV.
- 4 ABAZOV 13G search for $H^0 \rightarrow WW^*$ in 9.7 fb^{-1} of $p\bar{p}$ collisions at $E_{cm} = 1.96$ TeV. A limit on cross section times branching ratio which corresponds to (2-9) times the expected cross section is given for $m_{H^0} = 100-200$ GeV at 95% CL.
- 5 ABAZOV 13H search for $H^0 \rightarrow \gamma\gamma$ in 9.6 fb^{-1} of $p\bar{p}$ collisions at $E_{cm} = 1.96$ TeV.
- 6 ABAZOV 13I search for H^0 production in the final state with one lepton and two or more jets plus missing E_T in 9.7 fb^{-1} of $p\bar{p}$ collisions at $E_{cm} = 1.96$ TeV. The search is sensitive to WH^0, ZH^0 and vector-boson fusion Higgs production with $H^0 \rightarrow WW^*$. A limit on cross section times branching ratio which corresponds to (8-30) times the expected cross section is given in the range $m_{H^0} = 100-200$ GeV at 95% CL.
- 7 ABAZOV 13J search for H^0 production in the final states $e e \mu, e \mu \mu, \mu \tau \tau$, and $e^\pm \mu^\pm$ in $8.6-9.7 \text{ fb}^{-1}$ of $p\bar{p}$ collisions at $E_{cm} = 1.96$ TeV. The search is sensitive to WH^0, ZH^0 production with $H^0 \rightarrow WW^*, ZZ^*$, decaying to leptonic final states. A limit on cross section times branching ratio which corresponds to (2.4-13.0) times the expected cross section is given in the range $m_{H^0} = 100-200$ GeV at 95% CL.
- 8 ABAZOV 13L combine all D0 results with up to 9.7 fb^{-1} of $p\bar{p}$ collisions at $E_{cm} = 1.96$ TeV.
- 9 CHATRCHYAN 13AL search for $H^0 \rightarrow \gamma\gamma$ in 5.1 fb^{-1} and 5.3 fb^{-1} of pp collisions at $E_{cm} = 7$ and 8 TeV.
- 10 AAD 12N search for $H^0 \rightarrow \gamma\gamma$ with 4.9 fb^{-1} of pp collisions at $E_{cm} = 7$ TeV in the mass range $m_{H^0} = 110-150$ GeV.
- 11 AALTONEN 12AN search for $H^0 \rightarrow \gamma\gamma$ with 10 fb^{-1} of $p\bar{p}$ collisions at $E_{cm} = 1.96$ TeV in the mass range $m_{H^0} = 100-150$ GeV.
- 12 CHATRCHYAN 12AO use data from CHATRCHYAN 12G, CHATRCHYAN 12E, CHATRCHYAN 12H, CHATRCHYAN 12I, CHATRCHYAN 12D, and CHATRCHYAN 12C.
- 13 AALTONEN 09AB search for $H^0 \rightarrow \gamma\gamma$ in 3.0 fb^{-1} of $p\bar{p}$ collisions at $E_{cm} = 1.96$ TeV in the mass range $m_{H^0} = 70-150$ GeV. Associated $H^0 W, H^0 Z$ production and WW, ZZ fusion are considered.
- 14 ABAZOV 08U search for $H^0 \rightarrow \gamma\gamma$ in $p\bar{p}$ collisions at $E_{cm} = 1.96$ TeV in the mass range $m_{H^0} = 70-150$ GeV. Associated $H^0 W, H^0 Z$ production and WW, ZZ fusion are considered. See their Tab. 1 for the limit on $\sigma \cdot B(H^0 \rightarrow \gamma\gamma)$, and see their Fig. 3 for the excluded region in the $m_{H^0} - B(H^0 \rightarrow \gamma\gamma)$ plane.

- 15 SCHAEEL 07 search for Higgs bosons in association with a fermion pair and decaying to WW^* . The limit is from this search and HEISTER 02L for a H^0 with SM production cross section.
- 16 Search for associated production of a $\gamma\gamma$ resonance with a Z boson, followed by $Z \rightarrow q\bar{q}, \ell^+ \ell^-$, or $\nu\bar{\nu}$, at $E_{cm} \leq 209$ GeV. The limit is for a H^0 with SM production cross section.
- 17 Updates ABREU 01F.
- 18 ACHARD 03C search for $e^+e^- \rightarrow ZH^0$ followed by $H^0 \rightarrow WW^*$ or ZZ^* at $E_{cm} = 200-209$ GeV and combine with the ACHARD 02c result. The limit is for a H^0 with SM production cross section. For $B(H^0 \rightarrow WW^*) + B(H^0 \rightarrow ZZ^*) = 1$, $m_{H^0} > 108.1$ GeV is obtained. See Fig. 6 for the limits under different BR assumptions.
- 19 For $B(H^0 \rightarrow \gamma\gamma) = 1$, $m_{H^0} > 117$ GeV is obtained.
- 20 ACHARD 02c search for associated production of a $\gamma\gamma$ resonance with a Z boson, followed by $Z \rightarrow q\bar{q}, \ell^+ \ell^-$, or $\nu\bar{\nu}$, at $E_{cm} \leq 209$ GeV. The limit is for a H^0 with SM production cross section. For $B(H^0 \rightarrow \gamma\gamma) = 1$, $m_{H^0} > 114$ GeV is obtained.
- 21 AFFOLDER 01H search for associated production of a $\gamma\gamma$ resonance and a W or Z (tagged by two jets, an isolated lepton, or missing E_T). The limit assumes Standard Model values for the production cross section and for the couplings of the H^0 to W and Z bosons. See their Fig. 11 for limits with $B(H^0 \rightarrow \gamma\gamma) < 1$.
- 22 ACCIARRI 00s search for associated production of a $\gamma\gamma$ resonance with a $q\bar{q}, \nu\bar{\nu}$, or $\ell^+ \ell^-$ pair in e^+e^- collisions at $E_{cm} = 189$ GeV. The limit is for a H^0 with SM production cross section. For $B(H^0 \rightarrow \gamma\gamma) = 1$, $m_{H^0} > 98$ GeV is obtained. See their Fig. 5 for limits on $B(H \rightarrow \gamma\gamma) \cdot \sigma(e^+e^- \rightarrow H f \bar{f}) / \sigma(e^+e^- \rightarrow H f \bar{f})$ (SM).
- 23 BARATE 00L search for associated production of a $\gamma\gamma$ resonance with a $q\bar{q}, \nu\bar{\nu}$, or $\ell^+ \ell^-$ pair in e^+e^- collisions at $E_{cm} = 88-202$ GeV. The limit is for a H^0 with SM production cross section. For $B(H^0 \rightarrow \gamma\gamma) = 1$, $m_{H^0} > 109$ GeV is obtained. See their Fig. 3 for limits on $B(H \rightarrow \gamma\gamma) \cdot \sigma(e^+e^- \rightarrow H f \bar{f}) / \sigma(e^+e^- \rightarrow H f \bar{f})$ (SM).
- 24 ABBIENDI 99O search for associated production of a $\gamma\gamma$ resonance with a $q\bar{q}, \nu\bar{\nu}$, or $\ell^+ \ell^-$ pair in e^+e^- collisions at 189 GeV. The limit is for a H^0 with SM production cross section. See their Fig. 4 for limits on $\sigma(e^+e^- \rightarrow H^0 Z^0) \times B(H^0 \rightarrow \gamma\gamma) \times B(X^0 \rightarrow f \bar{f})$ for various masses. Updates the results of ACKERSTAFF 98Y.
- 25 ABBOTT 99B search for associated production of a $\gamma\gamma$ resonance and a dijet pair. The limit assumes Standard Model values for the production cross section and for the couplings of the H^0 to W and Z bosons. Limits in the range of $\sigma(H^0 + Z/W) \cdot B(H^0 \rightarrow \gamma\gamma) = 0.80-0.34$ pb are obtained in the mass range $m_{H^0} = 65-150$ GeV.
- 26 ABREU 99P search for $e^+e^- \rightarrow H^0 \gamma$ with $H^0 \rightarrow b\bar{b}$ or $\gamma\gamma$, and $e^+e^- \rightarrow H^0 q\bar{q}$ with $H^0 \rightarrow \gamma\gamma$. See their Fig. 4 for limits on $\sigma \times B$. Explicit limits within an effective interaction framework are also given.

Mass Limits for H^0 Decaying to Invisible Final States

These limits are for a neutral scalar H^0 which predominantly decays to invisible final states. Standard Model values are assumed for the couplings of H^0 to ordinary particles unless otherwise stated.

VALUE (GeV)	CL%	DOCUMENT ID	TECN	COMMENT
• • •		We do not use the following data for averages, fits, limits, etc. • • •		
>108.2	95	1 AABOUD	19AI ATLS	$W W/Z$ fusion
>112.3	95	2 AAD	15BD ATLS	$p\bar{p} \rightarrow H^0 W X, H^0 Z X$
>112.1	95	3 AAD	15BH ATLS	jet + missing E_T
>114.1	95	4 AAD	14BA ATLS	secondary vertex
>106.4	95	5 AAD	14O ATLS	$p\bar{p} \rightarrow H^0 Z X$
> 89.2	95	6 CHATRCHYAN	14B CMS	$p\bar{p} \rightarrow H^0 Z X, q\bar{q} H^0 X$
		7 AAD	13AG ATLS	secondary vertex
		8 AAD	13AT ATLS	electron jets
		9 CHATRCHYAN	13BI CMS	
		10 AAD	12AQ ATLS	secondary vertex
		11 AALTONEN	12AB CDF	secondary vertex
		12 AALTONEN	12U CDF	secondary vertex
		13 ABBIENDI	10 OPAL	
		14 ABBIENDI	07 OPAL	large width
		15 ACHARD	05 L3	
		16 ABDALLAH	04B DLPH	
		17 HEISTER	02 ALEP	$E_{cm} \leq 209$ GeV
		18 BARATE	01C ALEP	$E_{cm} \leq 202$ GeV
		19 ACCIARRI	00M L3	

- 1 AABOUD 19AI search for $H_{1,2}^0$ production by vector boson fusion and decay to invisible final states in 36.1 fb^{-1} of pp collisions at $E_{cm} = 13$ TeV. See their Fig. 6(b) for limits on cross section times branching ratios for $m_{H_{1,2}^0} = 0.1-3$ TeV.
- 2 AAD 15BD search for $p\bar{p} \rightarrow H^0 W X$ and $p\bar{p} \rightarrow H^0 Z X$ with W or Z decaying hadronically and H^0 decaying to invisible final states in 20.3 fb^{-1} at $E_{cm} = 8$ TeV. See their Fig. 6 for a limit on the cross section times branching ratio for $m_{H^0} = 115-300$ GeV.
- 3 AAD 15BH search for events with a jet and missing E_T in 20.3 fb^{-1} of pp collisions at $E_{cm} = 8$ TeV. Limits on $\sigma(H^0) B(H^0 \rightarrow \text{invisible}) < (44-10)$ pb (95%CL) is given for $m_{H^0} = 115-300$ GeV.
- 4 AAD 14BA search for H^0 production in the decay mode $H^0 \rightarrow X^0 X^0$, where X^0 is a long-lived particle which decays to collimated pairs of $e^+e^-, \mu^+\mu^-,$ or $\pi^+\pi^-$ plus invisible particles, in 20.3 fb^{-1} of pp collisions at $E_{cm} = 8$ TeV. See their Figs. 15 and 16 for limits on cross section times branching ratio.
- 5 AAD 14O search for $p\bar{p} \rightarrow H^0 Z X, Z \rightarrow \ell\ell$, with H^0 decaying to invisible final states in 4.5 fb^{-1} at $E_{cm} = 7$ TeV and 20.3 fb^{-1} at $E_{cm} = 8$ TeV. See their Fig. 3 for a limit on the cross section times branching ratio for $m_{H^0} = 110-400$ GeV.
- 6 CHATRCHYAN 14B search for $p\bar{p} \rightarrow H^0 Z X, Z \rightarrow \ell\ell$ and $Z \rightarrow b\bar{b}$, and also $p\bar{p} \rightarrow q\bar{q} H^0 X$ with H^0 decaying to invisible final states using data at $E_{cm} = 7$ and 8 TeV. See their Figs. 10, 11 for limits on the cross section times branching ratio for $m_{H^0} = 100-400$ GeV.

Gauge & Higgs Boson Particle Listings

Neutral Higgs Bosons, Searches for

- ⁷ AAD 13AG search for H^0 production in the decay mode $H^0 \rightarrow X^0 X^0$, where X^0 is a long-lived particle which decays to $\mu^+ \mu^- X^0$, in 1.9 fb^{-1} of pp collisions at $E_{\text{cm}} = 7 \text{ TeV}$. See their Fig. 7 for limits on cross section times branching ratio.
- ⁸ AAD 13AT search for H^0 production in the decay $H^0 \rightarrow X^0 X^0$, where X^0 eventually decays to clusters of collimated $e^+ e^-$ pairs, in 2.04 fb^{-1} of pp collisions at $E_{\text{cm}} = 7 \text{ TeV}$. See their Fig. 3 for limits on cross section times branching ratio.
- ⁹ CHATRCHYAN 13BJ search for H^0 production in the decay chain $H^0 \rightarrow X^0 X^0, X^0 \rightarrow \mu^+ \mu^- X^0$ in 5.3 fb^{-1} of pp collisions at $E_{\text{cm}} = 7 \text{ TeV}$. See their Fig. 2 for limits on cross section times branching ratio.
- ¹⁰ AAD 12AQ search for H^0 production in the decay mode $H^0 \rightarrow X^0 X^0$, where X^0 is a long-lived particle which decays mainly to $b\bar{b}$ in the muon detector, in 1.94 fb^{-1} of pp collisions at $E_{\text{cm}} = 7 \text{ TeV}$. See their Fig. 3 for limits on cross section times branching ratio for $m_{H^0} = 120, 140 \text{ GeV}$, $m_{X^0} = 20, 40 \text{ GeV}$ in the $c\tau$ range of 0.5–35 m.
- ¹¹ AALTONEN 12AB search for H^0 production in the decay $H^0 \rightarrow X^0 X^0$, where X^0 eventually decays to clusters of collimated $\ell^+ \ell^-$ pairs, in 5.1 fb^{-1} of $p\bar{p}$ collisions at $E_{\text{cm}} = 1.96 \text{ TeV}$. Cross section limits are provided for a benchmark MSSM model incorporating the parameters given in Table VI.
- ¹² AALTONEN 12U search for H^0 production in the decay mode $H^0 \rightarrow X^0 X^0$, where X^0 is a long-lived particle with $c\tau \approx 1 \text{ cm}$ which decays mainly to $b\bar{b}$, in 3.2 fb^{-1} of $p\bar{p}$ collisions at $E_{\text{cm}} = 1.96 \text{ TeV}$. See their Figs. 9 and 10 for limits on cross section times branching ratio for $m_{H^0} = (130\text{--}170) \text{ GeV}$, $m_{X^0} = 20, 40 \text{ GeV}$.
- ¹³ ABBIENDI 10 search for $e^+ e^- \rightarrow H^0 Z$ with H^0 decaying invisibly. The limit assumes SM production cross section and $B(H^0 \rightarrow \text{invisible}) = 1$.
- ¹⁴ ABBIENDI 07 search for $e^+ e^- \rightarrow H^0 Z$ with $Z \rightarrow q\bar{q}$ and H^0 decaying to invisible final states. The H^0 width is varied between 1 GeV and 3 TeV. A limit $\sigma \cdot B(H^0 \rightarrow \text{invisible}) < (0.07\text{--}0.57) \text{ pb}$ (95%CL) is obtained at $E_{\text{cm}} = 206 \text{ GeV}$ for $m_{H^0} = 60\text{--}114 \text{ GeV}$.
- ¹⁵ Search for $e^+ e^- \rightarrow H^0 Z$ with H^0 decaying invisibly. The limit assumes SM production cross section and $B(H^0 \rightarrow \text{invisible}) = 1$.
- ¹⁶ ACCIARRI 00M search for $e^+ e^- \rightarrow ZH^0$ with H^0 decaying invisibly at $E_{\text{cm}} = 183\text{--}189 \text{ GeV}$. The limit assumes SM production cross section and $B(H^0 \rightarrow \text{invisible}) = 1$. See their Fig. 6 for limits for smaller branching ratios.

Mass Limits for Light A^0

These limits are for a pseudoscalar A^0 in the mass range below $\mathcal{O}(10) \text{ GeV}$.

VALUE (GeV)	DOCUMENT ID	TECN	COMMENT
• • •	We do not use the following data for averages, fits, limits, etc. • • •		
1	AABOUD 18AP ATLAS	$H^0 \rightarrow A^0 A^0$	
2	KHACHATRYAN 17AZ CMS	$H^0 \rightarrow A^0 A^0$	
3	ABLIKIM 16E BES3	$J/\psi \rightarrow A^0 \gamma$	
4	KHACHATRYAN 16F CMS	$H^0 \rightarrow A^0 A^0$	
5	LEES 15H BABR	$\Upsilon(1S) \rightarrow A^0 \gamma$	
6	LEES 13C BABR	$\Upsilon(1S) \rightarrow A^0 \gamma$	
7	LEES 13L BABR	$\Upsilon(1S) \rightarrow A^0 \gamma$	
8	LEES 13R BABR	$\Upsilon(1S) \rightarrow A^0 \gamma$	
9	ABLIKIM 12E BES3	$J/\psi \rightarrow A^0 \gamma$	
10	CHATRCHYAN 12V CMS	$A^0 \rightarrow \mu^+ \mu^-$	
11	AALTONEN 11P CDF	$t \rightarrow bH^+, H^+ \rightarrow W^+ A^0$	
12,13	ABOUZAID 11A KTEV	$K_L \rightarrow \pi^0 \pi^0 A^0, A^0 \rightarrow \mu^+ \mu^-$	
14	DEL-AMO-SANCHEZ 11J BABR	$\Upsilon(1S) \rightarrow A^0 \gamma$	
15	LEES 11H BABR	$\Upsilon(2S, 3S) \rightarrow A^0 \gamma$	
16	ANDREAS 10 RVUE		
13,17	HYUN 10 BELL	$B^0 \rightarrow K^{*0} A^0, A^0 \rightarrow \mu^+ \mu^-$	
13,18	HYUN 10 BELL	$B^0 \rightarrow \rho^0 A^0, A^0 \rightarrow \mu^+ \mu^-$	
19	AUBERT 09P BABR	$\Upsilon(3S) \rightarrow A^0 \gamma$	
20	AUBERT 09Z BABR	$\Upsilon(2S) \rightarrow A^0 \gamma$	
21	AUBERT 09Z BABR	$\Upsilon(3S) \rightarrow A^0 \gamma$	
13,22	TUNG 09 K391	$K_L \rightarrow \pi^0 \pi^0 A^0, A^0 \rightarrow \gamma \gamma$	
23	LOVE 08 CLEO	$\Upsilon(1S) \rightarrow A^0 \gamma$	
24	BESSION 07 CLEO	$\Upsilon(1S) \rightarrow \eta_b \gamma$	
25	PARK 05 HYCP	$\Sigma^+ \rightarrow p A^0, A^0 \rightarrow \mu^+ \mu^-$	
26	BALEST 95 CLE2	$\Upsilon(1S) \rightarrow A^0 \gamma$	
27	ANTREASIAN 90C CBAL	$\Upsilon(1S) \rightarrow A^0 \gamma$	

- ¹ AABOUD 18AP search for the decay $H^0 \rightarrow A^0 A^0 \rightarrow \mu^+ \mu^- \mu^+ \mu^-$ in 36.1 fb^{-1} of pp collisions at $E_{\text{cm}} = 13 \text{ TeV}$. See their Fig. 10(b) for limits on $B(H^0 \rightarrow A^0 A^0)$ in the range $m_{A^0} = 1\text{--}2.5, 4.5\text{--}8 \text{ GeV}$, assuming a type-II two-doublet plus singlet model with $\tan(\beta) = 5$.
- ² KHACHATRYAN 17AZ search for the decay $H^0 \rightarrow A^0 A^0 \rightarrow \tau^+ \tau^- \tau^+ \tau^-$, $\mu^+ \mu^- b\bar{b}$, and $\mu^+ \mu^- \tau^+ \tau^-$ in 19.7 fb^{-1} of pp collisions at $E_{\text{cm}} = 8 \text{ TeV}$. See their Figs. 4, 5, and 6 for cross section limits in the range $m_{A^0} = 5\text{--}62.5 \text{ GeV}$. See also their Figs. 7, 8, and 9 for interpretation of the data in terms of models with two Higgs doublets and a singlet.
- ³ ABLIKIM 16E search for the process $J/\psi \rightarrow A^0 \gamma$ with A^0 decaying to $\mu^+ \mu^-$ and give limits on $B(J/\psi \rightarrow A^0 \gamma) \cdot B(A^0 \rightarrow \mu^+ \mu^-)$ in the range $2.8 \times 10^{-8}\text{--}5.0 \times 10^{-6}$ (90% CL) for $0.212 \leq m_{A^0} \leq 3.0 \text{ GeV}$. See their Fig. 5.
- ⁴ KHACHATRYAN 16F search for the decay $H^0 \rightarrow A^0 A^0 \rightarrow \tau^+ \tau^- \tau^+ \tau^-$ in 19.7 fb^{-1} of pp collisions at $E_{\text{cm}} = 8 \text{ TeV}$. See their Fig. 8 for cross section limits for $m_{A^0} = 4\text{--}8 \text{ GeV}$.
- ⁵ LEES 15H search for the process $\Upsilon(2S) \rightarrow \Upsilon(1S) \pi^+ \pi^- \rightarrow A^0 \gamma \pi^+ \pi^-$ with A^0 decaying to $c\bar{c}$ and give limits on $B(\Upsilon(1S) \rightarrow A^0 \gamma) \cdot B(A^0 \rightarrow c\bar{c})$ in the range $7.4 \times 10^{-5}\text{--}2.4 \times 10^{-3}$ (90% CL) for $4.00 \leq m_{A^0} \leq 8.95$ and $9.10 \leq m_{A^0} \leq 9.25 \text{ GeV}$. See their Fig. 6.
- ⁶ LEES 13C search for the process $\Upsilon(2S, 3S) \rightarrow \Upsilon(1S) \pi^+ \pi^- \rightarrow A^0 \gamma \pi^+ \pi^-$ with A^0 decaying to $\mu^+ \mu^-$ and give limits on $B(\Upsilon(1S) \rightarrow A^0 \gamma) \cdot B(A^0 \rightarrow \mu^+ \mu^-)$ in the range $(0.3\text{--}9.7) \times 10^{-6}$ (90% CL) for $0.212 \leq m_{A^0} \leq 9.20 \text{ GeV}$. See their Fig. 5(e) for limits on the $b\text{--}A^0$ Yukawa coupling derived by combining this result with AUBERT 09Z.

- ⁷ LEES 13L search for the process $\Upsilon(2S) \rightarrow \Upsilon(1S) \pi^+ \pi^- \rightarrow A^0 \gamma \pi^+ \pi^-$ with A^0 decaying to $g\bar{g}$ or $s\bar{s}$ and give limits on $B(\Upsilon(1S) \rightarrow A^0 \gamma) \cdot B(A^0 \rightarrow g\bar{g})$ between 1×10^{-6} and 2×10^{-2} (90% CL) for $0.5 \leq m_{A^0} \leq 9.0 \text{ GeV}$, and $B(\Upsilon(1S) \rightarrow A^0 \gamma) \cdot B(A^0 \rightarrow s\bar{s})$ between 4×10^{-6} and 1×10^{-3} (90%CL) for $1.5 \leq m_{A^0} \leq 9.0 \text{ GeV}$. See their Fig. 4.
- ⁸ LEES 13R search for the process $\Upsilon(2S) \rightarrow \Upsilon(1S) \pi^+ \pi^- \rightarrow A^0 \gamma \pi^+ \pi^-$ with A^0 decaying to $\tau^+ \tau^-$ and give limits on $B(\Upsilon(1S) \rightarrow A^0 \gamma) \cdot B(A^0 \rightarrow \tau^+ \tau^-)$ in the range $0.9\text{--}13 \times 10^{-5}$ (90% CL) for $3.6 \leq m_{A^0} \leq 9.2 \text{ GeV}$ for limits on the $b\text{--}A^0$ Yukawa coupling derived by combining this result with AUBERT 09P.
- ⁹ ABLIKIM 12 searches for the process $\psi(3686) \rightarrow \pi \pi J/\psi, J/\psi \rightarrow A^0 \gamma$ with A^0 decaying to $\mu^+ \mu^-$. It gives mass dependent limits on $B(J/\psi \rightarrow A^0 \gamma) \cdot B(A^0 \rightarrow \mu^+ \mu^-)$ in the range $4 \times 10^{-7}\text{--}2.1 \times 10^{-5}$ (90% C.L.) for $0.212 \leq m_{A^0} \leq 3.0 \text{ GeV}$. See their Fig. 2.
- ¹⁰ CHATRCHYAN 12V search for A^0 production in the decay $A^0 \rightarrow \mu^+ \mu^-$ with 1.3 fb^{-1} of pp collisions at $E_{\text{cm}} = 7 \text{ TeV}$. A limit on $\sigma(A^0) \cdot B(A^0 \rightarrow \mu^+ \mu^-)$ in the range $(1.5\text{--}7.5) \text{ pb}$ is given for $m_{A^0} = (5.5\text{--}8.7)$ and $(11.5\text{--}14) \text{ GeV}$ at 95% CL.
- ¹¹ AALTONEN 11P search in 2.7 fb^{-1} of $p\bar{p}$ collisions at $E_{\text{cm}} = 1.96 \text{ TeV}$ for the decay chain $t \rightarrow bH^+, H^+ \rightarrow W^+ A^0, A^0 \rightarrow \tau^+ \tau^-$ with m_{A^0} between 4 and 9 GeV. See their Fig. 4 for limits on $B(t \rightarrow bH^+)$ for $90 < m_{H^+} < 160 \text{ GeV}$.
- ¹² ABOUZAID 11A search for the decay chain $K_L \rightarrow \pi^0 \pi^0 A^0, A^0 \rightarrow \mu^+ \mu^-$ and give a limit $B(K_L \rightarrow \pi^0 \pi^0 A^0) \cdot B(A^0 \rightarrow \mu^+ \mu^-) < 1.0 \times 10^{-10}$ at 90% CL for $m_{A^0} = 214.3 \text{ MeV}$.
- ¹³ The search was motivated by PARK 05.
- ¹⁴ DEL-AMO-SANCHEZ 11J search for the process $\Upsilon(2S) \rightarrow \Upsilon(1S) \pi^+ \pi^- \rightarrow A^0 \gamma \pi^+ \pi^-$ with A^0 decaying to invisible final states. They give limits on $B(\Upsilon(1S) \rightarrow A^0 \gamma) \cdot B(A^0 \rightarrow \text{invisible})$ in the range $(1.9\text{--}4.5) \times 10^{-6}$ (90% CL) for $0 \leq m_{A^0} \leq 8.0 \text{ GeV}$, and $(2.7\text{--}37) \times 10^{-6}$ for $8.0 \leq m_{A^0} \leq 9.2 \text{ GeV}$.
- ¹⁵ LEES 11H search for the process $\Upsilon(2S, 3S) \rightarrow A^0 \gamma$ with A^0 decaying hadronically and give limits on $B(\Upsilon(2S, 3S) \rightarrow A^0 \gamma) \cdot B(A^0 \rightarrow \text{hadrons})$ in the range $1 \times 10^{-6}\text{--}8 \times 10^{-5}$ (90% CL) for $0.3 < m_{A^0} < 7 \text{ GeV}$. The decay rates for $\Upsilon(2S)$ and $\Upsilon(3S)$ are assumed to be equal up to the phase space factor. See their Fig. 5.
- ¹⁶ ANDREAS 10 analyze constraints from rare decays and other processes on a light A^0 with $m_{A^0} < 2m_\mu$ and give limits on its coupling to fermions at the level of 10^{-4} times the Standard Model value.
- ¹⁷ HYUN 10 search for the decay chain $B^0 \rightarrow K^{*0} A^0, A^0 \rightarrow \mu^+ \mu^-$ and give a limit on $B(B^0 \rightarrow K^{*0} A^0) \cdot B(A^0 \rightarrow \mu^+ \mu^-)$ in the range $(2.26\text{--}5.53) \times 10^{-8}$ at 90%CL for $m_{A^0} = 212\text{--}300 \text{ MeV}$. The limit for $m_{A^0} = 214.3 \text{ MeV}$ is 2.26×10^{-8} .
- ¹⁸ HYUN 10 search for the decay chain $B^0 \rightarrow \rho^0 A^0, A^0 \rightarrow \mu^+ \mu^-$ and give a limit on $B(B^0 \rightarrow \rho^0 A^0) \cdot B(A^0 \rightarrow \mu^+ \mu^-)$ in the range $(1.73\text{--}4.51) \times 10^{-8}$ at 90%CL for $m_{A^0} = 212\text{--}300 \text{ MeV}$. The limit for $m_{A^0} = 214.3 \text{ MeV}$ is 1.73×10^{-8} .
- ¹⁹ AUBERT 09P search for the process $\Upsilon(3S) \rightarrow A^0 \gamma$ with $A^0 \rightarrow \tau^+ \tau^-$ for $4.03 < m_{A^0} < 9.52$ and $9.61 < m_{A^0} < 10.10 \text{ GeV}$, and give limits on $B(\Upsilon(3S) \rightarrow A^0 \gamma) \cdot B(A^0 \rightarrow \tau^+ \tau^-)$ in the range $(1.5\text{--}16) \times 10^{-5}$ (90% CL).
- ²⁰ AUBERT 09Z search for the process $\Upsilon(2S) \rightarrow A^0 \gamma$ with $A^0 \rightarrow \mu^+ \mu^-$ for $0.212 < m_{A^0} < 9.3 \text{ GeV}$ and give limits on $B(\Upsilon(2S) \rightarrow A^0 \gamma) \cdot B(A^0 \rightarrow \mu^+ \mu^-)$ in the range $(0.3\text{--}8) \times 10^{-6}$ (90% CL).
- ²¹ AUBERT 09Z search for the process $\Upsilon(3S) \rightarrow A^0 \gamma$ with $A^0 \rightarrow \mu^+ \mu^-$ for $0.212 < m_{A^0} < 9.3 \text{ GeV}$ and give limits on $B(\Upsilon(3S) \rightarrow A^0 \gamma) \cdot B(A^0 \rightarrow \mu^+ \mu^-)$ in the range $(0.3\text{--}5) \times 10^{-6}$ (90% CL).
- ²² TUNG 09 search for the decay chain $K_L \rightarrow \pi^0 \pi^0 A^0, A^0 \rightarrow \gamma \gamma$ and give a limit on $B(K_L \rightarrow \pi^0 \pi^0 A^0) \cdot B(A^0 \rightarrow \gamma \gamma)$ in the range $(2.4\text{--}10.7) \times 10^{-7}$ at 90%CL for $m_{A^0} = 194.3\text{--}219.3 \text{ MeV}$. The limit for $m_{A^0} = 214.3 \text{ MeV}$ is 2.4×10^{-7} .
- ²³ LOVE 08 search for the process $\Upsilon(1S) \rightarrow A^0 \gamma$ with $A^0 \rightarrow \mu^+ \mu^-$ (for $m_{A^0} < 2m_\tau$) and $A^0 \rightarrow \tau^+ \tau^-$. Limits on $B(\Upsilon(1S) \rightarrow A^0 \gamma) \cdot B(A^0 \rightarrow \ell^+ \ell^-)$ in the range $10^{-6}\text{--}10^{-4}$ (90% CL) are given.
- ²⁴ BESSION 07 give a limit $B(\Upsilon(1S) \rightarrow \eta_b \gamma) \cdot B(\eta_b \rightarrow \tau^+ \tau^-) < 0.27\%$ (95% CL), which constrains a possible A^0 exchange contribution to the η_b decay.
- ²⁵ PARK 05 found three candidate events for $\Sigma^+ \rightarrow p \mu^+ \mu^-$ in the HyperCP experiment. Due to a narrow spread in dimuon mass, they hypothesize the events as a possible signal of a new boson. It can be interpreted as a neutral particle with $m_{A^0} = 214.3 \pm 0.5 \text{ MeV}$ and the branching fraction $B(\Sigma^+ \rightarrow p A^0) \cdot B(A^0 \rightarrow \mu^+ \mu^-) = (3.1^{+2.4}_{-1.9} \pm 1.5) \times 10^{-8}$.
- ²⁶ BALEST 95 give limits $B(\Upsilon(1S) \rightarrow A^0 \gamma) \cdot 1.5 \times 10^{-5}$ at 90% CL for $m_{A^0} < 5 \text{ GeV}$. The limit becomes $< 10^{-4}$ for $m_{A^0} < 7.7 \text{ GeV}$.
- ²⁷ ANTREASIAN 90C give limits $B(\Upsilon(1S) \rightarrow A^0 \gamma) \cdot 5.6 \times 10^{-5}$ at 90% CL for $m_{A^0} < 7.2 \text{ GeV}$. A^0 is assumed not to decay in the detector.

Other Mass Limits

We use a symbol H_1^0 if mass $< 125 \text{ GeV}$ or H_2^0 if mass $> 125 \text{ GeV}$. The notation H^0 is reserved for the 125 GeV particle.

VALUE (GeV)	CL%	DOCUMENT ID	TECN	COMMENT
• • •	We do not use the following data for averages, fits, limits, etc. • • •			
1	AAD	20C ATLAS	$H_2^0 \rightarrow H^0 H^0$	
2	SIRUNYAN	20 CMS	$H^0 \rightarrow A^0 A^0$	
3	AABOUD	19A ATLAS	$H_2^0 \rightarrow H^0 H^0$	
4	AABOUD	19AG ATLAS	$H^0 \rightarrow A^0 A^0$	
5	AABOUD	19O ATLAS	$H_2^0 \rightarrow H^0 H^0$	
6	AABOUD	19T ATLAS	$H_2^0 \rightarrow H^0 H^0$	
7	AABOUD	19V ATLAS	two doublet + pseudoscalar model	
8	AABOUD	19Y ATLAS	$H_2^0 \rightarrow \mu^+ \mu^-$	

Gauge & Higgs Boson Particle Listings

Neutral Higgs Bosons, Searches for

9	AALTONEN	19	CDF	$H_{1,2}^0 \rightarrow b\bar{b}$
10	SIRUNYAN	19	CMS	$H_2^0 \rightarrow H^0 H^0$
11	SIRUNYAN	19AE	CMS	$A_2^0 \rightarrow \tau^+ \tau^-$
12	SIRUNYAN	19AN	CMS	$A_2^0 \rightarrow H^0 A_1^0$
13	SIRUNYAN	19AV	CMS	$A_2^0 \rightarrow Z H^0$
14	SIRUNYAN	19B	CMS	$H_{1,2}^0/A^0 \rightarrow b\bar{b}$
15	SIRUNYAN	19BB	CMS	$H_1^0 \rightarrow \gamma\gamma$
16	SIRUNYAN	19BD	CMS	$H^0 \rightarrow A^0 A^0$
17	SIRUNYAN	19BE	CMS	$H_2^0 \rightarrow H^0 H^0$
18	SIRUNYAN	19BQ	CMS	$H_{1,2}^0 \rightarrow A^0 A^0$
19	SIRUNYAN	19CR	CMS	$H_2^0/A^0 \rightarrow \mu^+ \mu^-$
20	SIRUNYAN	19H	CMS	$H_2^0 \rightarrow H^0 H^0$
21	AABOUD	18AA	ATLS	$H_2^0 \rightarrow Z\gamma$
22	AABOUD	18AG	ATLS	$H^0 \rightarrow A^0 A^0$
23	AABOUD	18AH	ATLS	$A^0 \rightarrow Z H_2^0$
24	AABOUD	18AI	ATLS	$A^0 \rightarrow Z H^0$
25	AABOUD	18BF	ATLS	$H_2^0 \rightarrow ZZ$
26	AABOUD	18BU	ATLS	$H_2^0 \rightarrow H^0 H^0$
27	AABOUD	18BX	ATLS	$H^0 \rightarrow A^0 A^0$
28	AABOUD	18CQ	ATLS	$H_2^0 \rightarrow H^0 H^0$
29	AABOUD	18F	ATLS	$H_2^0 \rightarrow W^+ W^-, ZZ$
30	AAIJ	18AMLHCB		$H_{1,2}^0 \rightarrow \mu\tau$
31	AAIJ	18AQ	LHCB	$A^0 \rightarrow \mu^+ \mu^-$
32	AAIJ	18AQ	LHCB	$H^0 \rightarrow A^0 A^0, A^0 \rightarrow \mu^+ \mu^-$
33	SIRUNYAN	18AF	CMS	$H_2^0 \rightarrow H^0 H^0$
34	SIRUNYAN	18BA	CMS	$H_2^0 \rightarrow ZZ$
35	SIRUNYAN	18CW	CMS	$H_2^0 \rightarrow H^0 H^0$
36	SIRUNYAN	18DK	CMS	$H_2^0 \rightarrow Z\gamma$
37	SIRUNYAN	18DT	CMS	$H^0 \rightarrow A^0 A^0$
38	SIRUNYAN	18DU	CMS	$H_2^0 \rightarrow \gamma\gamma$
39	SIRUNYAN	18ED	CMS	$A^0 \rightarrow Z H^0$
40	SIRUNYAN	18EE	CMS	$H^0 \rightarrow A^0 A^0$
41	SIRUNYAN	18F	CMS	$pp, 13 \text{ TeV}, H_2^0 \rightarrow H^0 H^0$
42	AABOUD	17	ATLS	$H_2^0 \rightarrow Z\gamma$
43	AABOUD	17AW	ATLS	$H_2^0 \rightarrow Z\gamma$
44	KHACHATRY...	17AZ	CMS	$H^0 \rightarrow A^0 A^0$
45	KHACHATRY...	17D	CMS	$pp, 8, 13 \text{ TeV}, H_2^0 \rightarrow Z\gamma$
46	KHACHATRY...	17R	CMS	$H_2^0 \rightarrow \gamma\gamma$
47	SIRUNYAN	17CN	CMS	$pp, 8 \text{ TeV}, H_2^0 \rightarrow H^0 H^0$
48	SIRUNYAN	17Y	CMS	$pp, 8, 13 \text{ TeV}, H_2^0 \rightarrow Z\gamma$
49	AABOUD	16AB	ATLS	$H^0 \rightarrow A^0 A^0$
50	AABOUD	16AE	ATLS	$H_2^0 \rightarrow W^+ W^-, ZZ$
51	AABOUD	16H	ATLS	$H_2^0 \rightarrow \gamma\gamma$
52	AABOUD	16I	ATLS	$H_2^0 \rightarrow H^0 H^0$
53	AAD	16AX	ATLS	$H^0 \rightarrow ZZ$
54	AAD	16C	ATLS	$H^0 \rightarrow W^+ W^-$
55	AAD	16L	ATLS	$H^0 \rightarrow A^0 A^0$
56	AAD	16L	ATLS	$H_2^0 \rightarrow A^0 A^0$
57	AALTONEN	16C	CDF	$H_1^0 H^\pm \rightarrow H_1^0 H_1^0 W^*$, $H_1^0 \rightarrow \gamma\gamma$
58	KHACHATRY...	16BG	CMS	$H_2^0 \rightarrow H^0 H^0$
59	KHACHATRY...	16BQ	CMS	$pp, 8 \text{ TeV}, H_2^0 \rightarrow H^0 H^0$
60	KHACHATRY...	16F	CMS	$H^0 \rightarrow H_1^0 H_1^0$
61	KHACHATRY...	16M	CMS	$H_2^0 \rightarrow \gamma\gamma$
62	KHACHATRY...	16P	CMS	$H_2^0 \rightarrow H^0 H^0$
63	KHACHATRY...	16P	CMS	$A^0 \rightarrow Z H^0$
64	AAD	15BK	ATLS	$H_2^0 \rightarrow H^0 H^0$
65	AAD	15BZ	ATLS	$H^0 \rightarrow A^0 A^0$
66	AAD	15BZ	ATLS	$H_2^0 \rightarrow A^0 A^0$
67	AAD	15CE	ATLS	$H_2^0 \rightarrow H^0 H^0$
68	AAD	15H	ATLS	$H_2^0 \rightarrow H^0 H^0$
69	AAD	15S	ATLS	$A^0 \rightarrow Z H^0$
70	KHACHATRY...	15AW	CMS	$H_2^0 \rightarrow W^+ W^-, ZZ$
71	KHACHATRY...	15BB	CMS	$H^0 \rightarrow \gamma\gamma$
72	KHACHATRY...	15N	CMS	$A^0 \rightarrow Z H^0$
73	KHACHATRY...	15O	CMS	$A^0 \rightarrow Z H^0$
74	KHACHATRY...	15R	CMS	$H_2^0 \rightarrow H^0 H^0$
75	AAD	14AP	ATLS	$H^0 \rightarrow \gamma\gamma$
76	AAD	14M	ATLS	$H_2^0 \rightarrow H^\pm W^\mp \rightarrow H^0 W^\pm W^\mp, H^0 \rightarrow b\bar{b}$
77	CHATRCHYAN	14G	CMS	$H^0 \rightarrow WW^*$
78	KHACHATRY...	14P	CMS	$H^0 \rightarrow \gamma\gamma$
79	AALTONEN	13P	CDF	$H^0 \rightarrow H^\pm W^\mp \rightarrow H^0 W^\pm W^\mp$
80	CHATRCHYAN	13BJ	CMS	$H^0 \rightarrow A^0 A^0$

81	AALTONEN	11P	CDF	$t \rightarrow bH^+, H^+ \rightarrow W^+ A^0$
82	ABBIENDI	10	OPAL	$H^0 \rightarrow \tilde{\chi}_1^0 \tilde{\chi}_2^0$
83	SCHAELE	10	ALEP	$H^0 \rightarrow A^0 A^0$
84	ABAZOV	09V	D0	$H^0 \rightarrow A^0 A^0$
85	ABBIENDI	05A	OPAL	A^0 , Type II model
86	ABBIENDI	04K	OPAL	$H^0 \rightarrow 2 \text{ jets}$
87	ABDALLAH	04	DLPH	$H^0 VV$ couplings
88	ACHARD	04B	L3	$H^0 \rightarrow 2 \text{ jets}$
89	ACHARD	04F	L3	Anomalous coupling
90	ABBIENDI	03F	OPAL	$e^+ e^- \rightarrow H^0 Z, H^0 \rightarrow \text{any}$
91	ABBIENDI	03G	OPAL	$H^0 \rightarrow A^0 A^0$
92,93	HEISTER	02L	ALEP	$H^0 \rightarrow \gamma\gamma$
94	HEISTER	02M	ALEP	$H^0 \rightarrow 2 \text{ jets or } \tau^+ \tau^-$
95	ABBIENDI	01E	OPAL	A^0 , Type-II model
96	ACCIARRI	00R	L3	$e^+ e^- \rightarrow H^0 \gamma$ and/or $H^0 \rightarrow \gamma\gamma$
97	ACCIARRI	00R	L3	$e^+ e^- \rightarrow e^+ e^- H^0$
98	GONZALEZ...	98B	RVUE	Anomalous coupling
99	KRAWCZYK	97	RVUE	$(g-2)_\mu$
100	ALEXANDER	96H	OPAL	$Z \rightarrow H^0 \gamma$

- AAD 20c combine searches for a scalar resonance decaying to $H^0 H^0$ in 36.1 fb^{-1} of pp collisions at $E_{\text{cm}} = 13 \text{ TeV}$ from AABOUD 19A, AABOUD 19O, AABOUD 18CQ, AABOUD 19T, AABOUD 18CW, and AABOUD 18BU. See their Fig. 5(a) for limits on cross section times branching ratio for $m_{H_2^0} = 0.26\text{--}3 \text{ TeV}$.
- SIRUNYAN 20 search for the decay $H^0 \rightarrow A^0 A^0 \rightarrow \tau^+ \tau^- \tau^+ \tau^-$ or $\tau^+ \tau^- \mu^+ \mu^-$ in 35.9 fb^{-1} of pp collisions at $E_{\text{cm}} = 13 \text{ TeV}$. See their Fig. 10 for limits on the product of production cross section (normalized to the SM) and branching ratios in the range $m_{A^0} = 4\text{--}15 \text{ GeV}$.
- AABOUD 19A search for a narrow scalar resonance decaying to $H^0 H^0 \rightarrow b\bar{b}b\bar{b}$ in $27.5\text{--}36.1 \text{ fb}^{-1}$ of pp collisions at $E_{\text{cm}} = 13 \text{ TeV}$. See their Fig. 9(a) for limits on cross section times branching ratios for $m_{H_2^0} = 0.26\text{--}3 \text{ TeV}$.
- AABOUD 19AG search for the decay $H^0 \rightarrow A^0 A^0 \rightarrow \mu^+ \mu^- b\bar{b}$ in 36.7 fb^{-1} of pp collisions at $E_{\text{cm}} = 13 \text{ TeV}$. See their Fig. 6 (a) for limits on the product of production cross section (normalized to the SM) and branching ratios in the range $m_{A^0} = 20\text{--}60 \text{ GeV}$.
- AABOUD 19O search for a scalar resonance decaying to $H^0 H^0 \rightarrow b\bar{b}WW^*$ in 36.1 fb^{-1} of pp collisions at $E_{\text{cm}} = 13 \text{ TeV}$. See their Fig. 12 (left) for limits on cross section times branching ratio for $m_{H_2^0} = 0.5\text{--}3 \text{ TeV}$.
- AABOUD 19T search for a scalar resonance decaying to $H^0 H^0 \rightarrow WW^* WW^*$ in 36.1 fb^{-1} of pp collisions at $E_{\text{cm}} = 13 \text{ TeV}$. See their Fig. 3 for limits on cross section times branching ratio for $m_{H_2^0} = 260\text{--}500 \text{ GeV}$, assuming SM decay rates for the H^0 .
- AABOUD 19V combine published ATLAS data to constrain two-Higgs-doublet plus singlet pseudoscalar model with A_1^0 decaying to invisible final states. See their Fig. 19 for excluded parameter regions.
- AABOUD 19Y search for a narrow scalar resonance produced by gluon fusion or b associated production, decaying to $\mu^+ \mu^-$ in 36.1 fb^{-1} of pp collisions at $E_{\text{cm}} = 13 \text{ TeV}$. See their Figs. 4 and 5(a) for cross section limits for $m_{H_2^0} = 0.2\text{--}1.0 \text{ TeV}$.
- AALTONEN 19 search for b associated production of a scalar particle decaying to $b\bar{b}$ in 5.4 fb^{-1} of $p\bar{p}$ collisions at $E_{\text{cm}} = 1.96 \text{ TeV}$. See their Fig. 3 for limits on cross section times branching ratio for $m_{H_{1,2}^0} = 100\text{--}300 \text{ GeV}$.
- SIRUNYAN 19 search for a narrow scalar resonance decaying to $H^0 H^0 \rightarrow \gamma\gamma b\bar{b}$ in 35.9 fb^{-1} of pp collisions at $E_{\text{cm}} = 13 \text{ TeV}$. See their Fig. 9 (left) for limits on cross section times branching ratios for $m_{H_2^0} = 260\text{--}900 \text{ GeV}$.
- SIRUNYAN 19AE search for a scalar resonance produced in association with a $b\bar{b}$ pair, decaying to $\tau^+ \tau^-$ in 35.9 fb^{-1} of pp collisions at $E_{\text{cm}} = 13 \text{ TeV}$. See their Fig. 4 for cross section limits for $m_{A^0} = 25\text{--}70 \text{ GeV}$.
- SIRUNYAN 19AN search for production of A_2^0 decaying to $H^0 A_1^0$ followed by $H^0 \rightarrow b\bar{b}, A_1^0 \rightarrow \text{invisible}$ in 35.9 fb^{-1} of pp collisions at $E_{\text{cm}} = 13 \text{ TeV}$, in the mass range $m_{A_2^0} = 0.2\text{--}1.6 \text{ TeV}$, $m_{A_1^0} = 0.15\text{--}0.5 \text{ TeV}$. See their Fig. 6 for limits in terms of two-Higgs-doublet plus singlet pseudoscalar model.
- SIRUNYAN 19AV search for a scalar resonance produced by gluon fusion or b -associated production, decaying to $Z H^0 \rightarrow \ell^+ \ell^- b\bar{b}$ ($\ell = e, \mu$) or $\nu\bar{\nu}b\bar{b}$ in 35.9 fb^{-1} of pp collisions at $E_{\text{cm}} = 13 \text{ TeV}$. See their Fig. 5 for cross section limits for $m_{A^0} = 0.22\text{--}1.0 \text{ TeV}$.
- SIRUNYAN 19B search for gluon fusion production of narrow scalar resonance with large transverse momentum, decaying to $b\bar{b}$, in 35.9 fb^{-1} of pp collisions at $E_{\text{cm}} = 13 \text{ TeV}$. See their Figs. 7 and 8 for limits on cross section times branching ratio for the resonance mass of $50\text{--}350 \text{ GeV}$.
- SIRUNYAN 19BB search for the decay $H_1^0 \rightarrow \gamma\gamma$ in 19.7 fb^{-1} of pp collisions at $E_{\text{cm}} = 8 \text{ TeV}$ and 35.9 fb^{-1} at $E_{\text{cm}} = 13 \text{ TeV}$. See their Figs. 4–6 for limits on cross section times branching ratio for $m_{H_1^0} = 80\text{--}110 \text{ GeV}$ (some results in Fig. 5 for $m_{H_1^0} = 70\text{--}110 \text{ GeV}$).
- SIRUNYAN 19BD search for the decay $H^0 \rightarrow A^0 A^0 \rightarrow \mu^+ \mu^- b\bar{b}$ in 35.9 fb^{-1} of pp collisions at $E_{\text{cm}} = 13 \text{ TeV}$. See their Fig. 5 for limits on the product of cross section times branching ratios in the range $m_{A^0} = 20\text{--}62.5 \text{ GeV}$. See also their Figs. 6 and 7 for interpretation of the data in terms of models with two Higgs doublets and a singlet.
- SIRUNYAN 19BE combine searches for $H_2^0 \rightarrow H^0 H^0$ in 35.9 fb^{-1} of pp collisions at $E_{\text{cm}} = 13 \text{ TeV}$ in various H^0 decay modes, from SIRUNYAN 18A, SIRUNYAN 18AF, SIRUNYAN 18CW, SIRUNYAN 19, and SIRUNYAN 19H. See their Fig. 3 for limits on cross section times branching ratios for $m_{H_2^0} = 0.25\text{--}3 \text{ TeV}$.

Gauge & Higgs Boson Particle Listings

Neutral Higgs Bosons, Searches for

- 18 SIRUNYAN 19BQ search for production of $H_{1,2}^0$ decaying to $A^0 A^0 \rightarrow \mu^+ \mu^- \mu^+ \mu^-$ in 35.9 fb⁻¹ of pp collisions at $E_{\text{cm}} = 13$ TeV. See their Fig. 2 for limits on cross section times branching ratio for $m_{H_{1,2}^0} = 90\text{--}150$ GeV, $m_{A^0} = 0.25\text{--}3.55$ GeV.
- 19 SIRUNYAN 19CR search for production of $H_{2,3}^0/A^0$ in gluon fusion and in association with a $b\bar{b}$ pair, decaying to $\mu^+ \mu^-$ in 35.9 fb⁻¹ of pp collisions at $E_{\text{cm}} = 13$ TeV. See their Fig. 6 for limits on cross section times branching ratio.
- 20 SIRUNYAN 19H search for a narrow scalar resonance decaying to $H^0 H^0 \rightarrow b\bar{b}b\bar{b}$ in 35.9 fb⁻¹ of pp collisions at $E_{\text{cm}} = 13$ TeV, where one $b\bar{b}$ pair is resolved and the other not. Limits on cross section times branching ratios for $m_{H_2^0} = 0.75\text{--}1.6$ TeV are obtained and combined with data from SIRUNYAN 18AF. See their Fig. 5 (right).
- 21 AABOUD 18AA search for production of a scalar resonance decaying to $Z\gamma$, with Z decaying hadronically, in 36.1 fb⁻¹ of pp collisions at $E_{\text{cm}} = 13$ TeV. See their Fig. 8(a) for limits on cross section times branching ratio for $m_{H_2^0} = 1.0\text{--}6.8$ TeV.
- 22 AABOUD 18AG search for the decay $H^0 \rightarrow A^0 A^0 \rightarrow \gamma\gamma gg$ in 36.7 fb⁻¹ of pp collisions at $E_{\text{cm}} = 13$ TeV. See their Fig. 2 and Table 6 for cross section limits in the range $m_{A^0} = 20\text{--}60$ GeV.
- 23 AABOUD 18AH search for production of an A^0 in gluon-gluon fusion and in association with a $b\bar{b}$, decaying to $ZH_2^0 \rightarrow \ell^+ \ell^- b\bar{b}$ in 36.1 fb⁻¹ of pp collisions at $E_{\text{cm}} = 13$ TeV. See their Fig. 5 for cross section limits for $m_{A^0} = 230\text{--}800$ GeV and $m_{H_2^0} = 130\text{--}700$ GeV.
- 24 AABOUD 18AI search for production of an A^0 in gluon-gluon fusion and in association with a $b\bar{b}$, decaying to ZH^0 in the final states $\nu\bar{\nu}b\bar{b}$ and $\ell^+ \ell^- b\bar{b}$ in 36.1 fb⁻¹ of pp collisions at $E_{\text{cm}} = 13$ TeV. See their Fig. 6 for cross section limits for $m_{A^0} = 0.2\text{--}2$ TeV. See also AABOUD 18CC.
- 25 AABOUD 18BF search for production of a heavy H_2^0 state decaying to ZZ in the final states $\ell^+ \ell^- \ell^+ \ell^-$ and $\ell^+ \ell^- \nu\bar{\nu}$ in 36.1 fb⁻¹ of pp collisions at $E_{\text{cm}} = 13$ TeV. See their Fig. 6 for upper limits on cross section times branching ratio for $m_{H_2^0} = 0.2\text{--}1.2$ TeV assuming ggF or VBF with the NWA. See their Fig. 7 for upper limits on cross section times branching ratio for $m_{H_2^0} = 0.4\text{--}1.0$ TeV assuming ggF, and with several assumptions on its width.
- 26 AABOUD 18BU search for a narrow scalar resonance decaying to $H^0 H^0 \rightarrow \gamma\gamma WW^*$ in 36.1 fb⁻¹ of pp collisions at $E_{\text{cm}} = 13$ TeV. See their Fig. 4 for limits on cross section times branching ratios for $m_{H_2^0} = 260\text{--}500$ GeV.
- 27 AABOUD 18BX search for associated production of WH^0 or ZH^0 followed by the decay $H^0 \rightarrow A^0 A^0 \rightarrow b\bar{b}b\bar{b}$ in 36.1 fb⁻¹ of pp collisions at $E_{\text{cm}} = 13$ TeV. See their Fig. 9 for limits on cross section times branching ratios for $m_{A^0} = 20\text{--}60$ GeV. See also their Fig. 10 for the dependence of the limit on A^0 lifetime.
- 28 AABOUD 18CQ search for a narrow scalar resonance decaying to $H^0 H^0 \rightarrow b\bar{b}\tau^+ \tau^-$ in 36.1 fb⁻¹ of pp collisions at $E_{\text{cm}} = 13$ TeV. See their Fig. 2 (above) for limits on cross section times branching ratios for $m_{H_2^0} = 260\text{--}1000$ GeV.
- 29 AABOUD 18F search for production of a narrow scalar resonance decaying to $W^+ W^-$ and ZZ , followed by hadronic decays of W and Z , in 36.7 fb⁻¹ of pp collisions at $E_{\text{cm}} = 13$ TeV. See their Fig. 5(c) for limits on cross section times branching ratio for $m_{H_2^0} = 1.2\text{--}3.0$ TeV.
- 30 AAIJ 18AM search for gluon-fusion production of $H_{1,2}^0$ decaying to $\mu\tau$ in 2 fb⁻¹ of pp collisions at $E_{\text{cm}} = 8$ TeV. See their Fig. 2 for limits on cross section times branching ratio for $m_{H_{1,2}^0} = 45\text{--}195$ GeV.
- 31 AAIJ 18AQ search for gluon-fusion production of a scalar particle A^0 decaying to $\mu^+ \mu^-$ in 1.99 fb⁻¹ of pp collisions at $E_{\text{cm}} = 8$ TeV and 0.98 fb⁻¹ at $E_{\text{cm}} = 7$ TeV. See their Fig. 4 for limits on cross section times branching ratio for $m_{A^0} = 5.5\text{--}15$ GeV (using the $E_{\text{cm}} = 8$ TeV data set).
- 32 AAIJ 18AQ search for the decay $H^0 \rightarrow A^0 A^0$, with one of the A^0 decaying to $\mu^+ \mu^-$, in 1.99 fb⁻¹ of pp collisions at $E_{\text{cm}} = 8$ TeV and 0.98 fb⁻¹ at $E_{\text{cm}} = 7$ TeV. See their Fig. 5 (right) for limits on the product of branching ratios for $m_{A^0} = 5.5\text{--}15$ GeV (using the $E_{\text{cm}} = 8$ TeV data set).
- 33 SIRUNYAN 18AF search for a narrow scalar resonance decaying to $H^0 H^0 \rightarrow b\bar{b}b\bar{b}$ in 35.9 fb⁻¹ of pp collisions at $E_{\text{cm}} = 13$ TeV, where both $b\bar{b}$ pairs are not resolved. See their Fig. 9 for limits on cross section times branching ratios for $m_{H_2^0} = 0.75\text{--}3$ TeV.
- 34 SIRUNYAN 18BA search for production of a heavy H_2^0 state decaying to ZZ in the final states $\ell^+ \ell^- \ell^+ \ell^-$, $\ell^+ \ell^- q\bar{q}$, and $\ell^+ \ell^- \nu\bar{\nu}$ in 35.9 fb⁻¹ of pp collisions at $E_{\text{cm}} = 13$ TeV. See their Figs. 10 and 11 for upper limits on cross section times branching ratio for $m_{H_2^0} = 0.13\text{--}3$ TeV with several assumptions on its width and on the fraction of Vector-Boson-Fusion of the total production cross section.
- 35 SIRUNYAN 18CW search for a narrow scalar resonance decaying to $H^0 H^0 \rightarrow b\bar{b}b\bar{b}$ in 35.9 fb⁻¹ of pp collisions at $E_{\text{cm}} = 13$ TeV, where both $b\bar{b}$ pairs are resolved. See their Fig. 9 for limits on cross section times branching ratios for $m_{H_2^0} = 260\text{--}1200$ GeV.
- 36 SIRUNYAN 18DK search for production of a scalar resonance decaying to $Z\gamma$, with Z decaying to $\ell^+ \ell^-$ or hadronically, in 35.9 fb⁻¹ of pp collisions at $E_{\text{cm}} = 13$ TeV. See their Fig. 7 for limits on cross section times branching ratio for $m_{H_2^0} = 0.35\text{--}4$ TeV for different assumptions on the width of the resonance.
- 37 SIRUNYAN 18DT search for the decay $H^0 \rightarrow A^0 A^0 \rightarrow \tau^+ \tau^- b\bar{b}$ in 35.9 fb⁻¹ of pp collisions at $E_{\text{cm}} = 13$ TeV. See their Fig. 7 for limits on the product of branching ratios in the range $m_{A^0} = 15\text{--}60$ GeV. See also their Fig. 8 for interpretation of the data in terms of models with two Higgs doublets and a singlet.
- 38 SIRUNYAN 18DU search for production of a narrow scalar resonance decaying to $\gamma\gamma$ in 35.9 fb⁻¹ (taken in 2016) of pp collisions at $E_{\text{cm}} = 13$ TeV. See their Fig. 3 (right) for limits on cross section times branching ratio for $m_{H_2^0} = 0.5\text{--}5$ TeV for several values of its width-to-mass ratio.
- 39 SIRUNYAN 18ED search for production of an A^0 in gluon-gluon fusion and in association with a $b\bar{b}$, decaying to ZH^0 in the final states $\nu\bar{\nu}b\bar{b}$ or $\ell^+ \ell^- b\bar{b}$ in 35.9 fb⁻¹ of pp collisions at $E_{\text{cm}} = 13$ TeV. See their Fig. 8 for cross section limits for $m_{A^0} = 0.8\text{--}2$ TeV.
- 40 SIRUNYAN 18EE search for the decay $H^0 \rightarrow A^0 A^0 \rightarrow \mu^+ \mu^- \tau^+ \tau^-$ in 35.9 fb⁻¹ of pp collisions at $E_{\text{cm}} = 13$ TeV. See their Fig. 4 for limits on the product of branching ratios in the range $m_{A^0} = 15\text{--}62.5$ GeV, normalized to the SM production cross section. See also their Fig. 5 for interpretation of the data in terms of models with two Higgs doublets and a singlet.
- 41 SIRUNYAN 18F search for a narrow scalar resonance decaying to $H^0 H^0 \rightarrow WWb\bar{b}$ or $ZZb\bar{b}$ in the final state $\ell\ell\nu\nu b\bar{b}$ in 35.9 fb⁻¹ of pp collisions at $E_{\text{cm}} = 13$ TeV. See their Fig. 7 for limits on cross section times branching ratios for $m_{H_2^0} = 250\text{--}900$ GeV.
- 42 AABOUD 17 search for production of a scalar resonance decaying to $Z\gamma$ in 3.2 fb⁻¹ of pp collisions at $E_{\text{cm}} = 13$ TeV. See their Fig. 4 for the limits on cross section times branching ratio for $m_{H_2^0} = 0.25\text{--}3.0$ TeV.
- 43 AABOUD 17AW search for production of a scalar resonance decaying to $Z\gamma$ in 36.1 fb⁻¹ of pp collisions at $E_{\text{cm}} = 13$ TeV. See their Fig. 7 for limits on cross section times branching ratio for $m_{H_2^0} = 0.25\text{--}2.4$ TeV.
- 44 KHACHATRYAN 17AZ search for the decay $H^0 \rightarrow A^0 A^0 \rightarrow \tau^+ \tau^- \tau^+ \tau^-$, $\mu^+ \mu^- b\bar{b}$, and $\mu^+ \mu^- \tau^+ \tau^-$ in 19.7 fb⁻¹ of pp collisions at $E_{\text{cm}} = 8$ TeV. See their Figs. 4, 5, and 6 for cross section limits in the range $m_{A^0} = 5\text{--}62.5$ GeV. See also their Figs. 7, 8, and 9 for interpretation of the data in terms of models with two Higgs doublets and a singlet.
- 45 KHACHATRYAN 17D search for production of a scalar resonance decaying to $Z\gamma$ in 19.7 fb⁻¹ of pp collisions at $E_{\text{cm}} = 8$ TeV and 2.7 fb⁻¹ at $E_{\text{cm}} = 13$ TeV. See their Figs. 3 and 4 for the limits on cross section times branching ratio for $m_{H_2^0} = 0.2\text{--}2.0$ TeV.
- 46 KHACHATRYAN 17R search for production of a narrow scalar resonance decaying to $\gamma\gamma$ in 12.9 fb⁻¹ (taken in 2016) of pp collisions at $E_{\text{cm}} = 13$ TeV. See their Fig. 2 for limits on cross section times branching ratio for $m_{H_2^0} = 0.5\text{--}4.5$ TeV for several values of its width-to-mass ratio. Limits from combination with KHACHATRYAN 16M are shown in their Figs. 4 and 6.
- 47 SIRUNYAN 17CN search for a narrow scalar resonance decaying to $H^0 H^0 \rightarrow b\bar{b}\tau^+ \tau^-$ in 18.3 fb⁻¹ of pp collisions at $E_{\text{cm}} = 8$ TeV. See their Fig. 5 (above) and Table II for limits on the cross section times branching ratios for $m_{H_2^0} = 0.3\text{--}1$ TeV, and Fig. 6 (above) and Table III for the corresponding limits by combining with data from KHACHATRYAN 16BQ and KHACHATRYAN 15R.
- 48 SIRUNYAN 17Y search for production of a scalar resonance decaying to $Z\gamma$ in 19.7 fb⁻¹ of pp collisions at $E_{\text{cm}} = 8$ TeV and 2.7 fb⁻¹ at $E_{\text{cm}} = 13$ TeV. See their Figs. 3, 4 and Table 3 for limits on cross section times branching ratio for $m_{H_2^0} = 0.7\text{--}3.0$ TeV, and Fig. 5 for the corresponding limits for $m_{H_2^0} = 0.2\text{--}3.0$ TeV from combination with KHACHATRYAN 17D data.
- 49 AABOUD 16AB search for associated production of WH^0 with the decay $H^0 \rightarrow A^0 A^0 \rightarrow b\bar{b}b\bar{b}$ in 3.2 fb⁻¹ of pp collisions at $E_{\text{cm}} = 13$ TeV. See their Fig. 8 for limits on cross section times branching ratios for $m_{A^0} = 20\text{--}60$ GeV.
- 50 AABOUD 16AE search for production of a narrow scalar resonance decaying to $W^+ W^-$ and ZZ in 3.2 fb⁻¹ of pp collisions at $E_{\text{cm}} = 13$ TeV. See their Fig. 4 for limits on cross section times branching ratio for $m_{H_2^0} = 0.5\text{--}3$ TeV.
- 51 AABOUD 16H search for production of a scalar resonance decaying to $\gamma\gamma$ in 3.2 fb⁻¹ of pp collisions at $E_{\text{cm}} = 13$ TeV. See their Fig. 12 for limits on cross section times branching ratio for $m_{H_2^0} = 0.2\text{--}2$ TeV with different assumptions on the width.
- 52 AABOUD 16I search for a narrow scalar resonance decaying to $H^0 H^0 \rightarrow b\bar{b}b\bar{b}$ in 3.2 fb⁻¹ of pp collisions at $E_{\text{cm}} = 13$ TeV. See their Fig. 10(c) for limits on cross section times branching ratios for $m_{H_2^0} = 0.5\text{--}3$ TeV.
- 53 AAD 16AX search for production of a heavy H^0 state decaying to ZZ in the final states $\ell^+ \ell^- \ell^+ \ell^-$, $\ell^+ \ell^- \nu\bar{\nu}$, $\ell^+ \ell^- q\bar{q}$, and $\nu\bar{\nu}q\bar{q}$ in 20.3 fb⁻¹ of pp collisions at $E_{\text{cm}} = 8$ TeV. See their Fig. 12 for upper limits on $\sigma(H^0) B(H^0 \rightarrow ZZ)$ for m_{H^0} ranging from 140 GeV to 1000 GeV.
- 54 AAD 16C search for production of a heavy H^0 state decaying to $W^+ W^-$ in the final states $\ell\nu\ell\nu$ and $\ell\nu q\bar{q}$ in 20.3 fb⁻¹ of pp collisions at $E_{\text{cm}} = 8$ TeV. See their Figs. 12, 13, and 16 for upper limits on $\sigma(H^0) B(H^0 \rightarrow W^+ W^-)$ for m_{H^0} ranging from 300 GeV to 1000 or 1500 GeV with various assumptions on the total width of H^0 .
- 55 AAD 16L search for the decay $H^0 \rightarrow A^0 A^0 \rightarrow \gamma\gamma\gamma\gamma$ in 20.3 fb⁻¹ of pp collisions at $E_{\text{cm}} = 8$ TeV. See their Fig. 4 (upper right) for limits on cross section times branching ratios (normalized to the SM H^0 cross section) for $m_{A^0} = 10\text{--}60$ GeV.
- 56 AAD 16L search for the decay $H_2^0 \rightarrow A^0 A^0 \rightarrow \gamma\gamma\gamma\gamma$ in 20.3 fb⁻¹ of pp collisions at $E_{\text{cm}} = 8$ TeV. See their Fig. 4 (lower right) for limits on cross section times branching ratios for $m_{H_2^0} = 600$ GeV and $m_{A^0} = 10\text{--}245$ GeV, and Table 5 for limits for $m_{H_2^0} = 300$ and 900 GeV.
- 57 AALTONEN 16C search for electroweak associated production of $H_1^0 H_{\pm}^{\pm}$ followed by the decays $H_{\pm}^{\pm} \rightarrow H_1^0 W^*$, $H_1^0 \rightarrow \gamma\gamma$ for $m_{H_1^0} = 10\text{--}105$ GeV and $m_{H_{\pm}^{\pm}} = 30\text{--}300$ GeV. See their Fig. 3 for excluded parameter region in a two-doublet model in which H_1^0 has no direct decay to fermions.
- 58 KHACHATRYAN 16BG search for a narrow scalar resonance decaying to $H^0 H^0 \rightarrow b\bar{b}b\bar{b}$ in 19.7 fb⁻¹ of pp collisions at $E_{\text{cm}} = 8$ TeV. See their Fig. 6 for limits on the cross section times branching ratios for $m_{H_2^0} = 1.15\text{--}3$ TeV.
- 59 KHACHATRYAN 16BQ search for a resonance decaying to $H^0 H^0 \rightarrow \gamma\gamma b\bar{b}$ in 19.7 fb⁻¹ of pp collisions at $E_{\text{cm}} = 8$ TeV. See their Fig. 9 for limits on the cross section times branching ratios for $m_{H_2^0} = 0.26\text{--}1.1$ TeV.
- 60 KHACHATRYAN 16F search for the decay $H^0 \rightarrow H_1^0 H_1^0 \rightarrow \tau^+ \tau^- \tau^+ \tau^-$ in 19.7 fb⁻¹ of pp collisions at $E_{\text{cm}} = 8$ TeV. See their Fig. 8 for cross section limits for $m_{H_1^0} = 4\text{--}8$ GeV.

See key on page 999

Gauge & Higgs Boson Particle Listings

Neutral Higgs Bosons, Searches for

- 61 KHACHATRYAN 16M search for production of a narrow resonance decaying to $\gamma\gamma$ in 19.7 fb^{-1} of pp collisions at $E_{\text{cm}} = 8 \text{ TeV}$ and 3.3 fb^{-1} at $E_{\text{cm}} = 13 \text{ TeV}$. See their Fig. 3 (top) for limits on cross section times branching ratio for $m_{H_2^0} = 0.5\text{--}4 \text{ TeV}$.
- 62 KHACHATRYAN 16P search for gluon fusion production of an H_2^0 decaying to $H^0 H^0 \rightarrow b\bar{b}\tau^+\tau^-$ in 19.7 fb^{-1} of pp collisions at $E_{\text{cm}} = 8 \text{ TeV}$. See their Fig. 8 (lower right) for cross section limits for $m_{H_2^0} = 260\text{--}350 \text{ GeV}$.
- 63 KHACHATRYAN 16P search for gluon fusion production of an A^0 decaying to $ZH^0 \rightarrow \ell^+\ell^-\tau^+\tau^-$ in 19.7 fb^{-1} of pp collisions at $E_{\text{cm}} = 8 \text{ TeV}$. See their Fig. 10 for cross section limits for $m_{H_2^0} = 220\text{--}350 \text{ GeV}$.
- 64 AAD 15BK search for production of a heavy H_2^0 decaying to $H^0 H^0$ in the final state $b\bar{b}b\bar{b}$ in 19.5 fb^{-1} of pp collisions at $E_{\text{cm}} = 8 \text{ TeV}$. See their Fig. 14(c) for $\sigma(H_2^0) B(H_2^0 \rightarrow H^0 H^0)$ for $m_{H_2^0} = 500\text{--}1500 \text{ GeV}$ with $\Gamma_{H_2^0} = 1 \text{ GeV}$.
- 65 AAD 15BZ search for the decay $H^0 \rightarrow A^0 A^0 \rightarrow \mu^+\mu^-\tau^+\tau^-$ ($m_{H^0} = 125 \text{ GeV}$) in 20.3 fb^{-1} of pp collisions at $E_{\text{cm}} = 8 \text{ TeV}$. See their Fig. 6 for limits on cross section times branching ratio for $m_{A^0} = 3.7\text{--}50 \text{ GeV}$.
- 66 AAD 15BZ search for a state H_2^0 via the decay $H_2^0 \rightarrow A^0 A^0 \rightarrow \mu^+\mu^-\tau^+\tau^-$ in 20.3 fb^{-1} of pp collisions at $E_{\text{cm}} = 8 \text{ TeV}$. See their Fig. 6 for limits on cross section times branching ratio for $m_{H_2^0} = 100\text{--}500 \text{ GeV}$ and $m_{A^0} = 5 \text{ GeV}$.
- 67 AAD 15CE search for production of a heavy H_2^0 decaying to $H^0 H^0$ in the final states $b\bar{b}\tau^+\tau^-$ and $\gamma\gamma WW^*$ in 20.3 fb^{-1} of pp collisions at $E_{\text{cm}} = 8 \text{ TeV}$ and combine with data from AAD 15H and AAD 15BK. A limit $\sigma(H_2^0) B(H_2^0 \rightarrow H^0 H^0) < 2.1\text{--}0.011 \text{ pb}$ (95% CL) is given for $m_{H_2^0} = 260\text{--}1000 \text{ GeV}$. See their Fig. 6.
- 68 AAD 15H search for production of a heavy H_2^0 decaying to $H^0 H^0$ in the final state $\gamma\gamma b\bar{b}$ in 20.3 fb^{-1} of pp collisions at $E_{\text{cm}} = 8 \text{ TeV}$. A limit of $\sigma(H_2^0) B(H_2^0 \rightarrow H^0 H^0) < 3.5\text{--}0.7 \text{ pb}$ is given for $m_{H_2^0} = 260\text{--}500 \text{ GeV}$ at 95% CL. See their Fig. 3.
- 69 AAD 15S search for production of A^0 decaying to $ZH^0 \rightarrow \ell^+\ell^-b\bar{b}, \nu\bar{\nu}b\bar{b}$ and $\ell^+\ell^-\tau^+\tau^-$ in 20.3 fb^{-1} of pp collisions at $E_{\text{cm}} = 8 \text{ TeV}$. See their Fig. 3 for cross section limits for $m_{A^0} = 200\text{--}1000 \text{ GeV}$.
- 70 KHACHATRYAN 15AW search for production of a heavy state H_2^0 of an electroweak singlet extension of the Standard Model via the decays of H_2^0 to W^+W^- and ZZ in up to 5.1 fb^{-1} of pp collisions at $E_{\text{cm}} = 7 \text{ TeV}$ and up to 19.7 fb^{-1} at $E_{\text{cm}} = 8 \text{ TeV}$ in the range $m_{H_2^0} = 145\text{--}1000 \text{ GeV}$. See their Figs. 8 and 9 for limits in the parameter space of the model.
- 71 KHACHATRYAN 15BB search for production of a resonance H^0 decaying to $\gamma\gamma$ in 19.7 fb^{-1} of pp collisions at $E_{\text{cm}} = 8 \text{ TeV}$. See their Fig. 7 for limits on cross section times branching ratio for $m_{H^0} = 150\text{--}850 \text{ GeV}$.
- 72 KHACHATRYAN 15N search for production of A^0 decaying to $ZH^0 \rightarrow \ell^+\ell^-b\bar{b}$ in 19.7 fb^{-1} of pp collisions at $E_{\text{cm}} = 8 \text{ TeV}$. See their Fig. 3 for limits on cross section times branching ratios for $m_{A^0} = 225\text{--}600 \text{ GeV}$.
- 73 KHACHATRYAN 15O search for production of a high-mass narrow resonance A^0 decaying to $ZH^0 \rightarrow q\bar{q}\tau^+\tau^-$ in 19.7 fb^{-1} of pp collisions at $E_{\text{cm}} = 8 \text{ TeV}$. See their Fig. 6 for limits on cross section times branching ratios for $m_{A^0} = 800\text{--}2500 \text{ GeV}$.
- 74 KHACHATRYAN 15R search for a narrow scalar resonance decaying to $H^0 H^0 \rightarrow b\bar{b}b\bar{b}$ in 17.9 fb^{-1} of pp collisions at $E_{\text{cm}} = 8 \text{ TeV}$. See their Fig. 5 (top) for limits on cross section times branching ratios for $m_{H_2^0} = 0.27\text{--}1.1 \text{ TeV}$.
- 75 AAD 14AP search for a second H^0 state decaying to $\gamma\gamma$ in addition to the state at about 125 GeV in 20.3 fb^{-1} of pp collisions at $E_{\text{cm}} = 8 \text{ TeV}$. See their Fig. 4 for limits on cross section times branching ratio for $m_{H^0} = 65\text{--}600 \text{ GeV}$.
- 76 AAD 14M search for the decay cascade $H_2^0 \rightarrow H^\pm W^\mp \rightarrow H^0 W^\pm W^\mp, H^0$ decaying to $b\bar{b}$ in 20.3 fb^{-1} of pp collisions at $E_{\text{cm}} = 8 \text{ TeV}$. See their Table III for limits on cross section times branching ratio for $m_{H_2^0} = 325\text{--}1025 \text{ GeV}$ and $m_{H^\pm} = 225\text{--}925 \text{ GeV}$.
- 77 CHATRYAN 14G search for a second H^0 state decaying to $WW^{(*)}$ in addition to the observed signal at about 125 GeV using 4.9 fb^{-1} of pp collisions at $E_{\text{cm}} = 7 \text{ TeV}$ and 19.4 fb^{-1} at $E_{\text{cm}} = 8 \text{ TeV}$. See their Fig. 21 (right) for cross section limits in the mass range $110\text{--}600 \text{ GeV}$.
- 78 KHACHATRYAN 14P search for a second H^0 state decaying to $\gamma\gamma$ in addition to the observed signal at about 125 GeV using 5.1 fb^{-1} of pp collisions at $E_{\text{cm}} = 7 \text{ TeV}$ and 19.7 fb^{-1} at $E_{\text{cm}} = 8 \text{ TeV}$. See their Figs. 27 and 28 for cross section limits in the mass range $110\text{--}150 \text{ GeV}$.
- 79 AALTONEN 13P search for production of a heavy Higgs boson H^0 that decays into a charged Higgs boson H^\pm and a lighter Higgs boson H^0 via the decay chain $H^0 \rightarrow H^\pm W^\mp, H^\pm \rightarrow W^\pm H^0, H^0 \rightarrow b\bar{b}$ in the final state $\ell\nu$ plus 4 jets in 8.7 fb^{-1} of $p\bar{p}$ collisions at $E_{\text{cm}} = 1.96 \text{ TeV}$. See their Fig. 4 for limits on cross section times branching ratio in the $m_{H^\pm}\text{--}m_{H^0}$ plane for $m_{H^0} = 126 \text{ GeV}$.
- 80 CHATRYAN 13BJ search for H^0 production in the decay chain $H^0 \rightarrow A^0 A^0, A^0 \rightarrow \mu^+\mu^-$ in 5.3 fb^{-1} of pp collisions at $E_{\text{cm}} = 7 \text{ TeV}$. See their Fig. 2 for limits on cross section times branching ratio.
- 81 AALTONEN 11P search in 2.7 fb^{-1} of $p\bar{p}$ collisions at $E_{\text{cm}} = 1.96 \text{ TeV}$ for the decay chain $t \rightarrow bH^+, H^+ \rightarrow W^+ A^0, A^0 \rightarrow \tau^+\tau^-$ with m_{A^0} between 4 and 9 GeV. See their Fig. 4 for limits on $B(t \rightarrow bH^+)$ for $90 < m_{H^+} < 160 \text{ GeV}$.
- 82 ABBIENDI 10 search for $e^+e^- \rightarrow ZH^0$ with the decay chain $H^0 \rightarrow \tilde{\chi}_1^0 \tilde{\chi}_2^0, \tilde{\chi}_2^0 \rightarrow \tilde{\chi}_1^0 + (\gamma \text{ or } Z^*)$, when $\tilde{\chi}_1^0$ and $\tilde{\chi}_2^0$ are nearly degenerate. For a mass difference of 2 (4) GeV, a lower limit on m_{H^0} of 108.4 (107.0) GeV (95% CL) is obtained for SM ZH^0 cross section and $B(H^0 \rightarrow \tilde{\chi}_1^0 \tilde{\chi}_2^0) = 1$.
- 83 SCHAEEL 10 search for the process $e^+e^- \rightarrow H^0 Z$ followed by the decay chain $H^0 \rightarrow A^0 A^0 \rightarrow \tau^+\tau^-\tau^+\tau^-$ with $Z \rightarrow \ell^+\ell^-, \nu\bar{\nu}$ at $E_{\text{cm}} = 183\text{--}209 \text{ GeV}$. For a $H^0 Z Z$ coupling equal to the SM value, $B(H^0 \rightarrow A^0 A^0) = B(A^0 \rightarrow \tau^+\tau^-) = 1$, and $m_{A^0} = 4\text{--}10 \text{ GeV}$, m_{H^0} up to 107 GeV is excluded at 95% CL.
- 84 ABAZOV 09v search for H^0 production followed by the decay chain $H^0 \rightarrow A^0 A^0 \rightarrow \mu^+\mu^-\mu^+\mu^-$ or $\mu^+\mu^-\tau^+\tau^-$ in 4.2 fb^{-1} of $p\bar{p}$ collisions at $E_{\text{cm}} = 1.96 \text{ TeV}$. See their Fig. 3 for limits on $\sigma(H^0) \cdot B(H^0 \rightarrow A^0 A^0)$ for $m_{A^0} = 3.6\text{--}19 \text{ GeV}$.
- 85 ABBIENDI 05A search for $e^+e^- \rightarrow H_1^0 A^0$ in general Type-II two-doublet models, with decays $H_1^0, A^0 \rightarrow q\bar{q}, gg, \tau^+\tau^-$, and $H_1^0 \rightarrow A^0 A^0$.
- 86 ABBIENDI 04k search for $e^+e^- \rightarrow H^0 Z$ with H^0 decaying to two jets of any flavor including gg . The limit is for SM production cross section with $B(H^0 \rightarrow jj) = 1$.
- 87 ABDALLAH 04 consider the full combined LEP and LEP2 datasets to set limits on the Higgs coupling to W or Z bosons, assuming SM decays of the Higgs. Results in Fig. 26.
- 88 ACHARD 04B search for $e^+e^- \rightarrow H^0 Z$ with H^0 decaying to $b\bar{b}, c\bar{c}$, or gg . The limit is for SM production cross section with $B(H^0 \rightarrow jj) = 1$.
- 89 ACHARD 04F search for H^0 with anomalous coupling to gauge boson pairs in the processes $e^+e^- \rightarrow H^0 \gamma, e^+e^- H^0, H^0 Z$ with decays $H^0 \rightarrow f\bar{f}, \gamma\gamma, Z\gamma$, and $W^* W^*$ at $E_{\text{cm}} = 189\text{--}209 \text{ GeV}$. See paper for limits.
- 90 ABBIENDI 03f search for $H^0 \rightarrow$ anything in $e^+e^- \rightarrow H^0 Z$, using the recoil mass spectrum of $Z \rightarrow e^+e^-$ or $\mu^+\mu^-$. In addition, it searched for $Z \rightarrow \nu\bar{\nu}$ and $H^0 \rightarrow e^+e^-$ or photons. Scenarios with large width or continuum H^0 mass distribution are considered. See their Figs. 11–14 for the results.
- 91 ABBIENDI 03G search for $e^+e^- \rightarrow H_1^0 Z$ followed by $H_1^0 \rightarrow A^0 A^0, A^0 \rightarrow c\bar{c}, gg$, or $\tau^+\tau^-$ in the region $m_{H_1^0} = 45\text{--}86 \text{ GeV}$ and $m_{A^0} = 2\text{--}11 \text{ GeV}$. See their Fig. 7 for the limits.
- 92 Search for associated production of a $\gamma\gamma$ resonance with a Z boson, followed by $Z \rightarrow q\bar{q}, \ell^+\ell^-, \nu\bar{\nu}$, at $E_{\text{cm}} \leq 209 \text{ GeV}$. The limit is for a H^0 with SM production cross section and $B(H^0 \rightarrow f\bar{f})=0$ for all fermions f .
- 93 For $B(H^0 \rightarrow \gamma\gamma)=1, m_{H^0} > 113.1 \text{ GeV}$ is obtained.
- 94 HEISTER 02M search for $e^+e^- \rightarrow H^0 Z$, assuming that H^0 decays to $q\bar{q}, gg$, or $\tau^+\tau^-$ only. The limit assumes SM production cross section.
- 95 ABBIENDI 01E search for neutral Higgs bosons in general Type-II two-doublet models, at $E_{\text{cm}} \leq 189 \text{ GeV}$. In addition to usual final states, the decays $H_1^0, A^0 \rightarrow q\bar{q}, gg$ are searched for. See their Figs. 15,16 for excluded regions.
- 96 ACCIARRI 00R search for $e^+e^- \rightarrow H^0 \gamma$ with $H^0 \rightarrow b\bar{b}, Z\gamma$, or $\gamma\gamma$. See their Fig. 3 for limits on $\sigma\text{--}B$. Explicit limits within an effective interaction framework are also given, for which the Standard Model Higgs search results are used in addition.
- 97 ACCIARRI 00R search for the two-photon type processes $e^+e^- \rightarrow e^+e^- H^0$ with $H^0 \rightarrow b\bar{b}$ or $\gamma\gamma$. See their Fig. 4 for limits on $\Gamma(H^0 \rightarrow \gamma\gamma) \cdot B(H^0 \rightarrow \gamma\gamma \text{ or } b\bar{b})$ for $m_{H^0} = 70\text{--}170 \text{ GeV}$.
- 98 GONZALEZ-GARCIA 98B use $D\bar{0}$ limit for $\gamma\gamma$ events with missing E_T in $p\bar{p}$ collisions (ABBOTT 98) to constrain possible ZH or WH production followed by unconventional $H \rightarrow \gamma\gamma$ decay which is induced by higher-dimensional operators. See their Figs. 1 and 2 for limits on the anomalous couplings.
- 99 KRAWCZYK 97 analyse the muon anomalous magnetic moment in a two-doublet Higgs model (with type II Yukawa couplings) assuming no $H_1^0 Z Z$ coupling and obtain $m_{H_1^0} \gtrsim 5 \text{ GeV}$ or $m_{A^0} \gtrsim 5 \text{ GeV}$ for $\tan\beta > 50$. Other Higgs bosons are assumed to be much heavier.
- 100 ALEXANDER 96H give $B(Z \rightarrow H^0 \gamma) \times B(H^0 \rightarrow q\bar{q}) < 1\text{--}4 \times 10^{-5}$ (95%CL) and $B(Z \rightarrow H^0 \gamma) \times B(H^0 \rightarrow b\bar{b}) < 0.7\text{--}2 \times 10^{-5}$ (95%CL) in the range $20 < m_{H^0} < 80 \text{ GeV}$.

SEARCHES FOR A HIGGS BOSON WITH STANDARD MODEL COUPLINGS

These listings are based on experimental searches for a scalar boson whose couplings to W, Z and fermions are precisely those of the Higgs boson predicted by the three-generation Standard Model with the minimal Higgs sector.

For a review and a bibliography, see the review on "Status of Higgs Boson Physics."

Indirect Mass Limits for H^0 from Electroweak Analysis

The mass limits shown below apply to a Higgs boson H^0 with Standard Model couplings whose mass is a priori unknown.

For limits obtained before the direct measurement of the top quark mass, see the 1996 (Physical Review D54 1 (1996)) Edition of this Review. Other studies based on data available prior to 1996 can be found in the 1998 Edition (The European Physical Journal C 3 1 (1998)) of this Review.

VALUE (GeV)	DOCUMENT ID	TECN
90^{+21}_{-18}	1 HALLER	18 RVUE
91^{+30}_{-23}	2 BAAK	12 RVUE
94^{+25}_{-22}	3 BAAK	12A RVUE
91^{+31}_{-24}	4 ERLER	10A RVUE
129^{+74}_{-49}	5 LEP-SLC	06 RVUE

••• We do not use the following data for averages, fits, limits, etc. •••

See key on page 999

Gauge & Higgs Boson Particle Listings

Neutral Higgs Bosons, Searches for, Charged Higgs Bosons (H^\pm and $H^{\pm\pm}$), Searches for

PDG	98	EPJ C3 1	C. Caso et al.	(PDG Collab.)
KRAWCZYK	97	PR D55 6968	M. Krawczyk, J. Zochowski	(WARS)
ALEXANDER	96H	ZPHY C71 1	G. Alexander et al.	(OPAL Collab.)
PDG	96	PR D54 1	R. M. Barnett et al.	(PDG Collab.)
ABREU	95H	ZPHY C67 69	P. Abreu et al.	(DELPHI Collab.)
BALEST	95	PR D51 2053	R. Balest et al.	(CLEO Collab.)
PICH	92	NP B388 31	A. Pich, J. Prades, P. Yepes	(CERN, CPPM)
ANTREASANYAN	90C	PL B251 204	D. Antreasyan et al.	(Crystal Ball Collab.)

Charged Higgs Bosons (H^\pm and $H^{\pm\pm}$), Searches for

CONTENTS:

- H^\pm (charged Higgs) mass limits for $m_{H^\pm} < m(\text{top})$
- H^\pm (charged Higgs) mass limits for $m_{H^\pm} > m(\text{top})$
- $H^{\pm\pm}$ (doubly-charged Higgs boson) mass limits
 - Limits for $H^{\pm\pm}$ with $T_3 = \pm 1$
 - Limits for $H^{\pm\pm}$ with $T_3 = 0$

H^\pm (charged Higgs) mass limits for $m_{H^\pm} < m(\text{top})$

Unless otherwise stated, LEP limits assume $B(H^+ \rightarrow \tau^+ \nu) + B(H^+ \rightarrow c\bar{s}) = 1$, and hold for all values of $B(H^+ \rightarrow \tau^+ \nu_\tau)$, and assume H^+ weak isospin of $T_3 = +1/2$. In the following, $\tan\beta$ is the ratio of the two vacuum expectation values in two-doublet models (2HDM).

The limits are also applicable to point-like technipions. For a discussion of techniparticles, see the Review of Dynamical Electroweak Symmetry Breaking in this Review.

Limits obtained at the LHC are given in the $m_h^{\text{mod-}}$ benchmark scenario, see CARENA 13, and hold for all $\tan\beta$ values.

For limits obtained in hadronic collisions before the observation of the top quark, and based on the top mass values inconsistent with the current measurements, see the 1996 (Physical Review D54 1 (1996)) Edition of this Review.

Searches in e^+e^- collisions at and above the Z pole have conclusively ruled out the existence of a charged Higgs in the region $m_{H^\pm} \lesssim 45$ GeV, and are meanwhile superseded by the searches in higher energy e^+e^- collisions at LEP. Results that are by now obsolete are therefore not included in this compilation, and can be found in a previous Edition (The European Physical Journal C15 1 (2000)) of this Review.

In the following, and unless otherwise stated, results from the LEP experiments (ALEPH, DELPHI, L3, and OPAL) are assumed to derive from the study of the $e^+e^- \rightarrow H^+H^-$ process. Limits from $b \rightarrow s\gamma$ decays are usually stronger in generic 2HDM models than in Supersymmetric models.

VALUE (GeV)	CL%	DOCUMENT ID	TECN	COMMENT
none 80–140	95	1 AAD	15AF ATLS	$t \rightarrow bH^+$
none 90–155	95	2 KHACHATRYAN..15AX	CMS	$t \rightarrow bH^+, H^+ \rightarrow \tau^+ \nu$
> 80	95	3 LEP	13 LEP	$e^+e^- \rightarrow H^+H^-, E_{\text{cm}} \leq 209\text{GeV}$
> 76.3	95	4 ABBIENDI	12 OPAL	$e^+e^- \rightarrow H^+H^-, E_{\text{cm}} \leq 209\text{GeV}$
> 74.4	95	ABDALLAH	04i DLPH	$E_{\text{cm}} \leq 209\text{ GeV}$
> 76.5	95	ACHARD	03E L3	$E_{\text{cm}} \leq 209\text{ GeV}$
> 79.3	95	HEISTER	02P ALEP	$E_{\text{cm}} \leq 209\text{ GeV}$
• • • We do not use the following data for averages, fits, limits, etc. • • •				
		5 SIRUNYAN	19AH CMS	$H^+ \rightarrow \tau^+ \nu$
		6 SIRUNYAN	19BP CMS	$H^+ \rightarrow W^+ Z$
		7 SIRUNYAN	19CC CMS	$t \rightarrow bH^+, H^+ \rightarrow W^+ A^0, A^0 \rightarrow \mu^+ \mu^-$
		8 SIRUNYAN	19CQ CMS	$H^+ \rightarrow W^+ Z$
		9 AABOUD	18BWATLS	$\bar{t}bH^+$ or $t \rightarrow bH^+, H^+ \rightarrow \tau^+ \nu$
		10 AABOUD	18CD ATLS	$\bar{t}bH^+, H^+ \rightarrow t\bar{b}$
		11 AABOUD	18CH ATLS	$H^\pm \rightarrow W^\pm Z$
		12 HALLER	18 RVUE	$b \rightarrow s\gamma$
		13 SIRUNYAN	18DO CMS	$t \rightarrow bH^+, H^+ \rightarrow c\bar{b}$
		14 MISIAK	17 RVUE	$b \rightarrow s(d)\gamma$
		15 SIRUNYAN	17AE CMS	$H^\pm \rightarrow W^\pm Z$
		16 AABOUD	16A ATLS	$t(b)H^+, H^+ \rightarrow \tau^+ \nu$
		17 AAD	16AJ ATLS	$t(b)H^+, H^+ \rightarrow t\bar{b}$
		18 AAD	16AJ ATLS	$qq \rightarrow H^+, H^+ \rightarrow t\bar{b}$
		19 AAD	15AF ATLS	tH^\pm
		20 AAD	15M ATLS	$H^\pm \rightarrow W^\pm Z$
		21 KHACHATRYAN..15AX	CMS	$tH^+, H^+ \rightarrow t\bar{b}$
		22 KHACHATRYAN..15AX	CMS	$tH^\pm, H^\pm \rightarrow \tau^\pm \nu$
		23 KHACHATRYAN..15BF	CMS	$t \rightarrow bH^+, H^+ \rightarrow c\bar{s}$
		24 AAD	14M ATLS	$H_2^0 \rightarrow H^\pm W^\mp \rightarrow H^0 W^\pm W^\mp, H^0 \rightarrow b\bar{b}$
		25 AALTONEN	14A CDF	$t \rightarrow b\tau\nu$
		26 AAD	13AC ATLS	$t \rightarrow bH^+$

		27 AAD	13V ATLS	$t \rightarrow bH^+, \text{lepton non-universality}$
		28 AAD	12BH ATLS	$t \rightarrow bH^+$
		29 CHATRCHYAN	12AA CMS	$t \rightarrow bH^+$
		30 AALTONEN	11P CDF	$t \rightarrow bH^+, H^+ \rightarrow W^+ A^0$
		31 DESCHAMPS	10 RVUE	Type II, flavor physics data
		32 AALTONEN	09AJ OPAL	$t \rightarrow bH^+$
		33 ABAZOV	09AC D0	$t \rightarrow bH^+$
		34 ABAZOV	09AG D0	$t \rightarrow bH^+$
		35 ABAZOV	09AI D0	$t \rightarrow bH^+$
		36 ABAZOV	09P D0	$H^+ \rightarrow t\bar{b}$
		37 ABULENCIA	06E CDF	$t \rightarrow bH^+$
> 92.0	95	ABBIENDI	04 OPAL	$B(\tau\nu) = 1$
> 76.7	95	ABDALLAH	04i DLPH	Type I
		39 ABBIENDI	03 OPAL	$\tau \rightarrow \mu\bar{\nu}\nu, e\bar{\nu}\nu$
		40 ABAZOV	02B D0	$t \rightarrow bH^+, H \rightarrow \tau\nu$
		41 BORZUMATI	02 RVUE	
		42 ABBIENDI	01Q OPAL	$B \rightarrow \tau\nu_\tau X$
		43 BARATE	01E ALEP	$B \rightarrow \tau\nu_\tau$
		44 GAMBINO	01 RVUE	$b \rightarrow s\gamma$
> 315	99	45 AFFOLDER	00i CDF	$t \rightarrow bH^+, H \rightarrow \tau\nu$
> 59.5	95	ABBIENDI	99E OPAL	$E_{\text{cm}} \leq 183\text{ GeV}$
		46 ABBOTT	99E D0	$t \rightarrow bH^+$
		47 ACKERSTAFF	99D OPAL	$\tau \rightarrow e\nu\nu, \mu\nu\nu$
		48 ACCIARRI	97F L3	$B \rightarrow \tau\nu_\tau$
		49 AMMAR	97B CLEO	$\tau \rightarrow \mu\nu\nu$
		50 COARASA	97 RVUE	$B \rightarrow \tau\nu_\tau X$
		51 GUCHAIT	97 RVUE	$t \rightarrow bH^+, H \rightarrow \tau\nu$
		52 MANGANO	97 RVUE	$B_{u(c)} \rightarrow \tau\nu_\tau$
		53 STAHL	97 RVUE	$\tau \rightarrow \mu\nu\nu$
> 244	95	54 ALAM	95 CLE2	$b \rightarrow s\gamma$
		55 BUSKULIC	95 ALEP	$b \rightarrow \tau\nu_\tau X$

- 1 AAD 15AF search for $t\bar{t}$ production followed by $t \rightarrow bH^+, H^+ \rightarrow \tau^+ \nu$ in 19.5 fb^{-1} of pp collisions at $E_{\text{cm}} = 8\text{ TeV}$. Upper limits on $B(t \rightarrow bH^+) B(H^+ \rightarrow \tau\nu)$ between 2.3×10^{-3} and 1.3×10^{-2} (95% CL) are given for $m_{H^\pm} = 80\text{--}160\text{ GeV}$. See their Fig. 8 for the excluded regions in different benchmark scenarios of the MSSM. The region $m_{H^\pm} < 140\text{ GeV}$ is excluded for $\tan\beta > 1$ in the considered scenarios.
- 2 KHACHATRYAN 15AX search for $t\bar{t}$ production followed by $t \rightarrow bH^+, H^+ \rightarrow \tau^+ \nu$ in 19.7 fb^{-1} of pp collisions at $E_{\text{cm}} = 8\text{ TeV}$. Upper limits on $B(t \rightarrow bH^+) B(H^+ \rightarrow \tau\nu)$ between 1.2×10^{-2} and 1.5×10^{-3} (95% CL) are given for $m_{H^\pm} = 80\text{--}160\text{ GeV}$. See their Fig. 11 for the excluded regions in different benchmark scenarios of the MSSM. The region $m_{H^\pm} < 155\text{ GeV}$ is excluded for $\tan\beta > 1$ in the considered scenarios.
- 3 LEP 13 give a limit that refers to the Type II scenario. The limit for $B(H^+ \rightarrow \tau\nu) = 1$ is 94 GeV (95% CL), and for $B(H^+ \rightarrow c\bar{s}) = 1$ the region below 80.5 as well as the region $83\text{--}88\text{ GeV}$ is excluded (95% CL). LEP 13 also search for the decay mode $H^+ \rightarrow A^0 W^+$ with $A^0 \rightarrow b\bar{b}$, which is not negligible in Type I models. The limit in Type I models is 72.5 GeV (95% CL) if $m_{A^0} > 12\text{ GeV}$.
- 4 ABBIENDI 12 also search for the decay mode $H^+ \rightarrow A^0 W^+$ with $A^0 \rightarrow b\bar{b}$.
- 5 SIRUNYAN 19AH search for H^+ in the decay of a pair-produced t quark, or in associated tbH^+ or nonresonant $b\bar{b}H^+ W^-$ production, followed by $H^+ \rightarrow \tau^+ \nu$, in 35.9 fb^{-1} of pp collisions at $E_{\text{cm}} = 13\text{ TeV}$. Upper limits on cross section times branching ratio between 6 pb and 5 fb (95% CL) are given for $m_{H^\pm} = 80\text{--}3000\text{ GeV}$ (including the non-resonant production near the top quark mass), see their Fig. 6 (left). See their Fig. 6 (right) for the excluded regions in the $m_h^{\text{mod-}}$ scenario of the MSSM.
- 6 SIRUNYAN 19BP search for vector boson fusion production of H^+ decaying to $H^+ \rightarrow W^+ Z \rightarrow \ell^+ \nu \ell^+ \ell^-$ in 35.9 fb^{-1} of pp collisions at $E_{\text{cm}} = 13\text{ TeV}$. See their Fig. 7 for limits on cross section times branching ratio for $m_{H^\pm} = 0.3\text{--}2.0\text{ TeV}$, and also for limits on the triplet vacuum expectation value fraction in the Georgi-Machacek model.
- 7 SIRUNYAN 19CC search for $t \rightarrow bH^+$ from pair produced top quarks, with the decay chain $H^+ \rightarrow W^+ A^0, A^0 \rightarrow \mu^+ \mu^-$ in 35.9 fb^{-1} of pp collisions at $E_{\text{cm}} = 13\text{ TeV}$. See their Fig. 2 for limits on the product of branching ratios for $m_{A^0} = 15\text{--}75\text{ GeV}$.
- 8 SIRUNYAN 19CQ search for vector boson fusion production of H^+ decaying to $H^+ \rightarrow W^+ Z \rightarrow \ell^+ \nu q \bar{q}$ or $q \bar{q} \ell^+ \ell^-$ in 35.9 fb^{-1} of pp collisions at $E_{\text{cm}} = 13\text{ TeV}$. See their Fig. 5 for limits on cross section times branching ratio for $m_{H^\pm} = 0.6\text{--}2.0\text{ TeV}$, and also for limits on the triplet vacuum expectation value fraction in the Georgi-Machacek model.
- 9 AABOUD 18BW search for $\bar{t}bH^+$ associated production or the decay $t \rightarrow bH^+$, followed by $H^+ \rightarrow \tau^+ \nu$, in 36.1 fb^{-1} of pp collisions at $E_{\text{cm}} = 13\text{ TeV}$. See their Fig. 8(a) for upper limits on cross section times branching ratio for $m_{H^\pm} = 90\text{--}2000\text{ GeV}$, and Fig. 8(b) for limits on $B(t \rightarrow bH^+) B(H^+ \rightarrow \tau^+ \nu)$ for $m_{H^\pm} = 90\text{--}160\text{ GeV}$. See also their Fig. 9 for the excluded region in the hMSSM parameter space.
- 10 AABOUD 18CD search for $\bar{t}bH^+$ associated production followed by $H^+ \rightarrow t\bar{b}$ in 36.1 fb^{-1} of pp collisions at $E_{\text{cm}} = 13\text{ TeV}$. See their Fig. 8 for upper limits on cross section times branching ratio for $m_{H^\pm} = 0.2\text{--}2\text{ TeV}$. See also their Fig. 9 for the excluded region in the parameter space of the $m_h^{\text{mod-}}$ and hMSSM scenarios of the MSSM. The theory predictions overlaid to the experimental limits to determine the excluded m_{H^\pm} range are shown without their respective uncertainty band.
- 11 AABOUD 18CH search for vector boson fusion production of H^\pm decaying to $H^\pm \rightarrow W^\pm Z \rightarrow \ell^\pm \nu \ell^\pm \ell^-$ in 36.1 fb^{-1} of pp collisions at $E_{\text{cm}} = 13\text{ TeV}$. See their Fig. 7 for limits on cross section times branching ratio for $m_{H^\pm} = 0.2\text{--}0.9\text{ TeV}$, and also for limits on the triplet vacuum expectation value fraction in the Georgi-Machacek model.
- 12 HALLER 18 give 95% CL lower limits on m_{H^\pm} of 590 GeV in type II two Higgs doublet model from combined data (including an unpublished BELLE result) for $(b \rightarrow s\gamma)$.

Gauge & Higgs Boson Particle Listings

Charged Higgs Bosons (H^\pm and $H^{\pm\pm}$), Searches for

- 13 SIRUNYAN 18DO search for $t\bar{t}$ production followed by $t \rightarrow bH^+$, $H^+ \rightarrow c\bar{b}$ in 19.7 fb^{-1} of pp collisions at $E_{\text{cm}} = 8 \text{ TeV}$. See their Fig. 3 for upper limits on $\text{B}(t \rightarrow bH^+)$ for $m_{H^+} = 90\text{--}150 \text{ GeV}$ assuming that $\text{B}(H^+ \rightarrow c\bar{b}) = 1$ and $\text{B}(t \rightarrow bH^+) + \text{B}(t \rightarrow bW^+) = 1$.
- 14 MISIAK 17 give 95% CL lower limits on m_{H^\pm} between 570 and 800 GeV in type II two Higgs doublet model from combined data (including an unpublished BELLE result) for $\text{B}(b \rightarrow s(d)\gamma)$.
- 15 SIRUNYAN 17AE search for vector boson fusion production of H^\pm decaying to $H^\pm \rightarrow W^\pm Z \rightarrow \ell^\pm \nu \ell^+ \ell^-$ in 15.2 fb^{-1} of pp collisions at $E_{\text{cm}} = 13 \text{ TeV}$. See their Fig. 3 for limits on cross section times branching ratio for $m_{H^\pm} = 0.2\text{--}2.0 \text{ TeV}$, and also for limits on the triplet vacuum expectation value fraction in the Georgi-Machacek model.
- 16 AABOUD 16A search for $t(b) H^\pm$ associated production followed by $H^\pm \rightarrow \tau^\pm \nu$ in 3.2 fb^{-1} of pp collisions at $E_{\text{cm}} = 13 \text{ TeV}$. Upper limits on $\sigma(t(b) H^\pm) \text{B}(H^\pm \rightarrow \tau \nu)$ between 1.9 pb and 15 fb (95% CL) are given for $m_{H^\pm} = 200\text{--}2000 \text{ GeV}$, see their Fig. 6. See their Fig. 7 for the excluded regions in the hMSSM scenario.
- 17 AAD 16AJ search for $t(b) H^\pm$ associated production followed by $H^\pm \rightarrow tb$ in 20.3 fb^{-1} of pp collisions at $E_{\text{cm}} = 8 \text{ TeV}$. See their Fig. 6 for upper limits on $\sigma(t(b) H^\pm) \text{B}(H^\pm \rightarrow tb)$ for $m_{H^\pm} = 200\text{--}600 \text{ GeV}$.
- 18 AAD 16AJ search for H^\pm production from quark-antiquark annihilation, followed by $H^\pm \rightarrow tb$, in 20.3 fb^{-1} of pp collisions at $E_{\text{cm}} = 8 \text{ TeV}$. See their Fig. 10 for upper limits on $\sigma(H^\pm) \text{B}(H^\pm \rightarrow tb)$ for $m_{H^\pm} = 400\text{--}3000 \text{ GeV}$.
- 19 AAD 15AF search for tH^\pm associated production followed by $H^\pm \rightarrow \tau^\pm \nu$ in 19.5 fb^{-1} of pp collisions at $E_{\text{cm}} = 8 \text{ TeV}$. Upper limits on $\sigma(tH^\pm) \text{B}(H^\pm \rightarrow \tau \nu)$ between 760 and 4.5 fb (95% CL) are given for $m_{H^\pm} = 180\text{--}1000 \text{ GeV}$. See their Fig. 8 for the excluded regions in different benchmark scenarios of the MSSM.
- 20 AAD 15M search for vector boson fusion production of H^\pm decaying to $H^\pm \rightarrow W^\pm Z \rightarrow q\bar{q}\ell^+\ell^-$ in 20.3 fb^{-1} of pp collisions at $E_{\text{cm}} = 8 \text{ TeV}$. See their Fig. 2 for limits on cross section times branching ratio for $m_{H^\pm} = 200\text{--}1000 \text{ GeV}$, and Fig. 3 for limits on the triplet vacuum expectation value fraction in the Georgi-Machacek model.
- 21 KHACHATRYAN 15AX search for tH^\pm associated production followed by $H^\pm \rightarrow tb$ in 19.7 fb^{-1} of pp collisions at $E_{\text{cm}} = 8 \text{ TeV}$. Upper limits on $\sigma(tH^\pm) \text{B}(H^\pm \rightarrow t\bar{b})$ between 2.0 and 0.13 pb (95% CL) are given for $m_{H^\pm} = 180\text{--}600 \text{ GeV}$. See their Fig. 11 for the excluded regions in different benchmark scenarios of the MSSM.
- 22 KHACHATRYAN 15AX search for tH^\pm associated production followed by $H^\pm \rightarrow \tau^\pm \nu$ in 19.7 fb^{-1} of pp collisions at $E_{\text{cm}} = 8 \text{ TeV}$. Upper limits on $\sigma(tH^\pm) \text{B}(H^\pm \rightarrow \tau \nu)$ between 380 and 25 fb (95% CL) are given for $m_{H^\pm} = 180\text{--}600 \text{ GeV}$. See their Fig. 11 for the excluded regions in different benchmark scenarios of the MSSM.
- 23 KHACHATRYAN 15BF search for $t\bar{t}$ production followed by $t \rightarrow bH^+$, $H^+ \rightarrow c\bar{s}$ in 19.7 fb^{-1} of pp collisions at $E_{\text{cm}} = 8 \text{ TeV}$. Upper limits on $\text{B}(t \rightarrow bH^+) \text{B}(H^+ \rightarrow c\bar{s})$ between 1.2×10^{-2} and 6.5×10^{-2} (95% CL) are given for $m_{H^+} = 90\text{--}160 \text{ GeV}$.
- 24 AAD 14M search for the decay cascade $H_2^0 \rightarrow H^\pm W^\mp \rightarrow H^0 W^\pm W^\mp$, H^0 decaying to $b\bar{b}$ in 20.3 fb^{-1} of pp collisions at $E_{\text{cm}} = 8 \text{ TeV}$. See their Table III for limits on cross section times branching ratio for $m_{H_2^0} = 325\text{--}1025 \text{ GeV}$ and $m_{H^\pm} = 225\text{--}925 \text{ GeV}$.
- 25 AALTONEN 14A measure $\text{B}(t \rightarrow b\tau\nu) = 0.096 \pm 0.028$ using 9 fb^{-1} of $p\bar{p}$ collisions at $E_{\text{cm}} = 1.96 \text{ TeV}$. For $m_{H^\pm} = 80\text{--}140 \text{ GeV}$, this measured value is translated to a limit $\text{B}(t \rightarrow bH^+) < 0.059$ at 95% CL assuming $\text{B}(H^+ \rightarrow \tau^+\nu) = 1$.
- 26 AAD 13AC search for $t\bar{t}$ production followed by $t \rightarrow bH^+$, $H^+ \rightarrow c\bar{s}$ (flavor unidentified) in 4.7 fb^{-1} of pp collisions at $E_{\text{cm}} = 7 \text{ TeV}$. Upper limits on $\text{B}(t \rightarrow bH^+) \text{B}(H^+ \rightarrow c\bar{s})$ between 0.05 and 0.01 (95% CL) are given for $m_{H^+} = 90\text{--}150 \text{ GeV}$ and $\text{B}(H^+ \rightarrow c\bar{s}) = 1$.
- 27 AAD 13V search for $t\bar{t}$ production followed by $t \rightarrow bH^+$, $H^+ \rightarrow \tau^+\nu$ through violation of lepton universality with 4.6 fb^{-1} of pp collisions at $E_{\text{cm}} = 7 \text{ TeV}$. Upper limits on $\text{B}(t \rightarrow bH^+) \text{B}(H^+ \rightarrow \tau^+\nu) = 1$. By combining with AAD 12BH, the limits improve to 0.008 to 0.034 for $m_{H^+} = 90\text{--}160 \text{ GeV}$. See their Fig. 7 for the excluded region in the $m_{H^+}^{\text{max}}$ scenario of the MSSM.
- 28 AAD 12BH search for $t\bar{t}$ production followed by $t \rightarrow bH^+$, $H^+ \rightarrow \tau^+\nu$ with 4.6 fb^{-1} of pp collisions at $E_{\text{cm}} = 7 \text{ TeV}$. Upper limits on $\text{B}(t \rightarrow bH^+) \text{B}(H^+ \rightarrow \tau^+\nu) = 1$ (95% CL) are given for $m_{H^+} = 90\text{--}160 \text{ GeV}$ and $\text{B}(H^+ \rightarrow \tau^+\nu) = 1$. See their Fig. 8 for the excluded region in the $m_{H^+}^{\text{max}}$ scenario of the MSSM.
- 29 CHATRCHYAN 12AA search for $t\bar{t}$ production followed by $t \rightarrow bH^+$, $H^+ \rightarrow \tau^+\nu$ with 2 fb^{-1} of pp collisions at $E_{\text{cm}} = 7 \text{ TeV}$. Upper limits on $\text{B}(t \rightarrow bH^+) \text{B}(H^+ \rightarrow \tau^+\nu) = 1$ (95% CL) are given for $m_{H^+} = 80\text{--}160 \text{ GeV}$ and $\text{B}(H^+ \rightarrow \tau^+\nu) = 1$.
- 30 AALTONEN 11P search in 2.7 fb^{-1} of $p\bar{p}$ collisions at $E_{\text{cm}} = 1.96 \text{ TeV}$ for the decay chain $t \rightarrow bH^+$, $H^+ \rightarrow W^+ A^0$, $A^0 \rightarrow \tau^+ \tau^-$ with m_{A^0} between 4 and 9 GeV. See their Fig. 4 for limits on $\text{B}(t \rightarrow bH^+) \text{B}(H^+ \rightarrow \tau^+ \tau^-)$ for $90 < m_{H^+} < 160 \text{ GeV}$.
- 31 DESCHAMPS 10 make Type II two Higgs doublet model fits to weak leptonic and semileptonic decays, $b \rightarrow s\gamma$, B_s mixings, and $Z \rightarrow b\bar{b}$. The limit holds irrespective of $\tan\beta$.
- 32 AALTONEN 09AJ search for $t \rightarrow bH^+$, $H^+ \rightarrow c\bar{s}$ in $t\bar{t}$ events in 2.2 fb^{-1} of $p\bar{p}$ collisions at $E_{\text{cm}} = 1.96 \text{ TeV}$. Upper limits on $\text{B}(t \rightarrow bH^+) \text{B}(H^+ \rightarrow c\bar{s})$ between 0.08 and 0.32 (95% CL) are given for $m_{H^+} = 60\text{--}150 \text{ GeV}$ and $\text{B}(H^+ \rightarrow c\bar{s}) = 1$.
- 33 ABZOV 09AC search for $t \rightarrow bH^+$, $H^+ \rightarrow \tau^+\nu$ in $t\bar{t}$ events in 0.9 fb^{-1} of $p\bar{p}$ collisions at $E_{\text{cm}} = 1.96 \text{ TeV}$. Upper limits on $\text{B}(t \rightarrow bH^+) \text{B}(H^+ \rightarrow \tau^+\nu) = 1$ (95% CL) are given for $m_{H^+} = 80\text{--}155 \text{ GeV}$ and $\text{B}(H^+ \rightarrow \tau^+\nu) = 1$. See their Fig. 4 for an excluded region in a MSSM scenario.
- 34 ABZOV 09AG measure $t\bar{t}$ cross sections in final states with ℓ + jets ($\ell = e, \mu$), $\ell\ell$, and $\tau\ell$ in 1 fb^{-1} of $p\bar{p}$ collisions at $E_{\text{cm}} = 1.96 \text{ TeV}$, which constrains possible $t \rightarrow bH^+$ branching fractions. Upper limits (95% CL) on $\text{B}(t \rightarrow bH^+) \text{B}(H^+ \rightarrow \tau^+\nu) = 1$ ($\text{B}(H^+ \rightarrow c\bar{s}) = 1$) for $m_{H^+} = 80\text{--}155 \text{ GeV}$.
- 35 ABZOV 09AI search for $t \rightarrow bH^+$ in $t\bar{t}$ events in 1 fb^{-1} of $p\bar{p}$ collisions at $E_{\text{cm}} = 1.96 \text{ TeV}$. Final states with ℓ + jets ($\ell = e, \mu$), $\ell\ell$, and $\tau\ell$ are examined. Upper limits on

- $\text{B}(t \rightarrow bH^+) \text{B}(H^+ \rightarrow \tau^+\nu) = 1$ ($\text{B}(H^+ \rightarrow c\bar{s}) = 1$) for $m_{H^+} = 80\text{--}155 \text{ GeV}$. For $\text{B}(H^+ \rightarrow \tau^+\nu) = 1$ also a simultaneous extraction of $\text{B}(t \rightarrow bH^+)$ and the $t\bar{t}$ cross section is performed, yielding a limit on $\text{B}(t \rightarrow bH^+) \text{B}(H^+ \rightarrow \tau^+\nu) = 1$ between 0.12 and 0.26 for $m_{H^+} = 80\text{--}155 \text{ GeV}$. See their Figs. 5–8 for excluded regions in several MSSM scenarios.
- 36 ABZOV 09P search for H^\pm production by $q\bar{q}'$ annihilation followed by $H^\pm \rightarrow t\bar{b}$ decay in 0.9 fb^{-1} of $p\bar{p}$ collisions at $E_{\text{cm}} = 1.96 \text{ TeV}$. Cross section limits in several two-doublet models are given for $m_{H^\pm} = 180\text{--}300 \text{ GeV}$. A region with $20 \lesssim \tan\beta \lesssim 70$ is excluded (95% CL) for $180 \text{ GeV} \lesssim m_{H^\pm} \lesssim 184 \text{ GeV}$ in type-I models.
- 37 ABULENCIA 06E search for associated $H^0 W$ production in $p\bar{p}$ collisions at $E_{\text{cm}} = 1.96 \text{ TeV}$. A fit is made for $t\bar{t}$ production processes in dilepton, lepton + jets, and lepton + τ final states, with the decays $t \rightarrow W^+ b$ and $t \rightarrow H^+ b$ followed by $H^+ \rightarrow \tau^+ \nu$, $c\bar{s}$, $t^* \bar{b}$, or $W^+ H^0$. Within the MSSM the search is sensitive to the region $\tan\beta < 1$ or > 30 in the mass range $m_{H^\pm} = 80\text{--}160 \text{ GeV}$. See Fig. 2 for the excluded region in a certain MSSM scenario.
- 38 ABDALLAH 04I search for $e^+ e^- \rightarrow H^\pm H^\mp$ with H^\pm decaying to $\tau\nu$, $c\bar{s}$, or $W^* A^0$ in Type-I two-Higgs-doublet models.
- 39 ABBIENDI 03 give a limit $m_{H^\pm} > 1.28 \tan\beta \text{ GeV}$ (95%CL) in Type II two-doublet models.
- 40 ABZOV 02B search for a charged Higgs boson in top decays with $H^\pm \rightarrow \tau^\pm \nu$ at $E_{\text{cm}} = 1.8 \text{ TeV}$. For $m_{H^\pm} = 75 \text{ GeV}$, the region $\tan\beta > 32.0$ is excluded at 95% CL. The excluded mass region extends to over 140 GeV for $\tan\beta$ values above 100.
- 41 BORZUMATI 02 point out that the decay modes such as $b\bar{b} W$, $A^0 W$, and supersymmetric ones can have substantial branching fractions in the mass range explored at LEP II and Tevatron.
- 42 ABBIENDI 01Q give a limit $\tan\beta/m_{H^\pm} < 0.53 \text{ GeV}^{-1}$ (95%CL) in Type II two-doublet models.
- 43 BARATE 01E give a limit $\tan\beta/m_{H^\pm} < 0.40 \text{ GeV}^{-1}$ (90% CL) in Type II two-doublet models. An independent measurement of $B \rightarrow \tau\nu X$ gives $\tan\beta/m_{H^\pm} < 0.49 \text{ GeV}^{-1}$ (90% CL).
- 44 GAMBINO 01 use the world average data in the summer of 2001 $\text{B}(b \rightarrow s\gamma) = (3.23 \pm 0.42) \times 10^{-4}$. The limit applies for Type-II two-doublet models.
- 45 AFFOLDER 00I search for a charged Higgs boson in top decays with $H^\pm \rightarrow \tau^\pm \nu$ in $p\bar{p}$ collisions at $E_{\text{cm}} = 1.8 \text{ TeV}$. The excluded mass region extends to over 120 GeV for $\tan\beta$ values above 100 and $\text{B}(\tau\nu) = 1$. If $\text{B}(t \rightarrow bH^+) \gtrsim 0.6$, m_{H^+} up to 160 GeV is excluded. Updates ABE 97L.
- 46 ABBOTT 99E search for a charged Higgs boson in top decays in $p\bar{p}$ collisions at $E_{\text{cm}} = 1.8 \text{ TeV}$, by comparing the observed $t\bar{t}$ cross section (extracted from the data assuming the dominant decay $t \rightarrow bW^+$) with theoretical expectation. The search is sensitive to regions of the domains $\tan\beta \lesssim 1$, $50 < m_{H^\pm} (\text{GeV}) \lesssim 120$ and $\tan\beta \gtrsim 40$, $50 < m_{H^\pm} (\text{GeV}) \lesssim 160$. See Fig. 3 for the details of the excluded region.
- 47 ACKERSTAFF 99D measure the Michel parameters ρ , ξ , η , and $\xi\delta$ in leptonic τ decays from $Z \rightarrow \tau\tau$. Assuming $e\text{--}\mu$ universality, the limit $m_{H^\pm} > 0.97 \tan\beta \text{ GeV}$ (95%CL) is obtained for two-doublet models in which only one doublet couples to leptons.
- 48 ACCIARRI 97F give a limit $m_{H^\pm} > 2.6 \tan\beta \text{ GeV}$ (90% CL) from their limit on the exclusive $B \rightarrow \tau\nu X$ branching ratio.
- 49 AMMAR 97B measure the Michel parameter ρ from $\tau \rightarrow e\nu\nu$ decays and assumes e/μ universality to extract the Michel η parameter from $\tau \rightarrow \mu\nu\nu$ decays. The measurement is translated to a lower limit on m_{H^\pm} in a two-doublet model $m_{H^\pm} > 0.97 \tan\beta \text{ GeV}$ (90% CL).
- 50 COARASA 97 reanalyzed the constraint on the $(m_{H^\pm}, \tan\beta)$ plane derived from the inclusive $B \rightarrow \tau\nu X$ branching ratio in GROSSMAN 95B and BUSKULIC 95. They show that the constraint is quite sensitive to supersymmetric one-loop effects.
- 51 GUCHAIT 97 studies the constraints on m_{H^\pm} set by Tevatron data on $\ell\tau$ final states in $t\bar{t} \rightarrow (Wb)(Hb)$, $W \rightarrow \ell\nu$, $H \rightarrow \tau\nu$. See Fig. 2 for the excluded region.
- 52 MANGANO 97 reconsiders the limit in ACCIARRI 97F including the effect of the potentially large $B_c \rightarrow \tau\nu$ background to $B_u \rightarrow \tau\nu$ decays. Stronger limits are obtained.
- 53 STAHL 97 fit τ lifetime, leptonic branching ratios, and the Michel parameters and derive limit $m_{H^\pm} > 1.5 \tan\beta \text{ GeV}$ (90% CL) for a two-doublet model. See also STAHL 94.
- 54 ALAM 95 measure the inclusive $b \rightarrow s\gamma$ branching ratio at $\mathcal{T}(4S)$ and give $\text{B}(b \rightarrow s\gamma) < 4.2 \times 10^{-4}$ (95% CL), which translates to the limit $m_{H^\pm} > [244 + 63/(\tan\beta)^{1.3}] \text{ GeV}$ in the Type II two-doublet model. Light supersymmetric particles can invalidate this bound.
- 55 BUSKULIC 95 give a limit $m_{H^\pm} > 1.9 \tan\beta \text{ GeV}$ (90% CL) for Type-II models from $b \rightarrow \tau\nu X$ branching ratio, as proposed in GROSSMAN 94.

H^\pm (charged Higgs) mass limits for $m_{H^\pm} > m(\text{top})$

Limits obtained at the LHC are given in the $m_h^{\text{mod-}}$ benchmark scenario, see CARENA 13, and depend on the $\tan\beta$ values.

VALUE (GeV)	CL%	DOCUMENT ID	TECN	COMMENT
> 181	95	1 AABOUD	18BWATLS	$\tan\beta = 10$
> 249	95	1 AABOUD	18BWATLS	$\tan\beta = 20$
> 390	95	1 AABOUD	18BWATLS	$\tan\beta = 30$
> 894	95	1 AABOUD	18BWATLS	$\tan\beta = 40$
> 1017	95	1 AABOUD	18BWATLS	$\tan\beta = 50$
> 1103	95	1 AABOUD	18BWATLS	$\tan\beta = 60$

1 AABOUD 18Bw search for $\bar{t}bH^+$ associated production in 36.1 fb^{-1} of pp collisions at $E_{\text{cm}} = 13 \text{ TeV}$. See also their Fig. 9 for the excluded region in the hMSSM parameter space.

See key on page 999

Gauge & Higgs Boson Particle Listings
Charged Higgs Bosons (H^\pm and $H^{\pm\pm}$), Searches for $H^{\pm\pm}$ (doubly-charged Higgs boson) mass limits

This section covers searches for a doubly-charged Higgs boson with couplings to lepton pairs. Its weak isospin T_3 is thus restricted to two possibilities depending on lepton chiralities: $T_3(H^{\pm\pm}) = \pm 1$, with the coupling $g_{\ell\ell}$ to $\ell_L^-\ell_L^-$ and $\ell_R^+\ell_R^+$ ("left-handed") and $T_3(H^{\pm\pm}) = 0$, with the coupling to $\ell_R^-\ell_R^-$ and $\ell_L^+\ell_L^+$ ("right-handed"). These Higgs bosons appear in some left-right symmetric models based on the gauge group $SU(2)_L \times SU(2)_R \times U(1)$, the type-II seesaw model, and the Zee-Babu model. The two cases are listed separately in the following. Unless noted, one of the lepton flavor combinations is assumed to be dominant in the decay.

Limits for $H^{\pm\pm}$ with $T_3 = \pm 1$

VALUE (GeV)	CL%	DOCUMENT ID	TECN	COMMENT
>220	95	1 AABOUD	19K ATLS	$W^\pm W^\pm$
>768	95	2 AABOUD	18Bc ATLS	$e\bar{e}$
>846	95	2 AABOUD	18Bc ATLS	$\mu\bar{\mu}$
>468	95	3 AAD	15AG ATLS	$e\mu$
>400	95	4 AAD	15AP ATLS	$e\tau$
>400	95	4 AAD	15AP ATLS	$\mu\tau$
>169	95	5 CHATRCHYAN12AU	CMS	$\tau\tau$
>300	95	5 CHATRCHYAN12AU	CMS	$\mu\tau$
>293	95	5 CHATRCHYAN12AU	CMS	$e\tau$
>395	95	5 CHATRCHYAN12AU	CMS	$\mu\mu$
>391	95	5 CHATRCHYAN12AU	CMS	$e\mu$
>382	95	5 CHATRCHYAN12AU	CMS	$e\bar{e}$
> 98.1	95	6 ABDALLAH	03 DLPH	$\tau\tau$
> 99.0	95	7 ABBIENDI	02c OPAL	$\tau\tau$
••• We do not use the following data for averages, fits, limits, etc. •••				
		8 SIRUNYAN	19CQ CMS	$W^\pm W^\pm$
		9 SIRUNYAN	18CC CMS	$W^\pm W^\pm$
>551	95	3 AAD	15AG ATLS	$e\bar{e}$
>516	95	3 AAD	15AG ATLS	$\mu\bar{\mu}$
		10 KANEMURA	15 RVUE	$W^{(*)}\pm W^{(*)}\pm$
		11 KHACHATRYAN15D	CMS	$W^\pm W^\pm$
		12 KANEMURA	14 RVUE	$W^{(*)}\pm W^{(*)}\pm$
>330	95	13 AAD	13Y ATLS	$\mu\mu$
>237	95	13 AAD	13Y ATLS	$\mu\tau$
>355	95	14 AAD	12AY ATLS	$\mu\mu$
>398	95	15 AAD	12CQ ATLS	$\mu\mu$
>375	95	15 AAD	12CQ ATLS	$e\mu$
>409	95	15 AAD	12CQ ATLS	$e\bar{e}$
>128	95	16 ABAZOV	12A D0	$\tau\tau$
>144	95	16 ABAZOV	12A D0	$\mu\tau$
>245	95	17 AALTONEN	11AF CDF	$\mu\mu$
>210	95	17 AALTONEN	11AF CDF	$e\mu$
>225	95	17 AALTONEN	11AF CDF	$e\bar{e}$
>114	95	18 AALTONEN	08AA CDF	$e\tau$
>112	95	18 AALTONEN	08AA CDF	$\mu\tau$
>168	95	19 ABAZOV	08V D0	$\mu\mu$
		20 AKTAS	06A H1	single $H^{\pm\pm}$
>133	95	21 ACOSTA	05L CDF	stable
>118.4	95	22 ABAZOV	04E D0	$\mu\mu$
		23 ABBIENDI	03Q OPAL	$E_{cm} \leq 209$ GeV, single $H^{\pm\pm}$
		24 GORDEEV	97 SPEC	muonium conversion
		25 ASAKA	95 THEO	
> 45.6	95	26 ACTON	92M OPAL	
> 30.4	95	27 ACTON	92M OPAL	
none 6.5–36.6	95	28 SWARTZ	90 MRK2	

1 AABOUD 19K search for pair production of $H^{++}H^{--}$ followed by the decay $H^{\pm\pm} \rightarrow W^\pm W^\pm$ in 36.1 fb^{-1} of pp collisions at $E_{cm} = 13$ TeV. The search is interpreted in a doublet-triplet extension of the scalar sector with a vev of 0.1 GeV, leading to $B(H^{\pm\pm} \rightarrow W^\pm W^\pm) = 1$. See their Fig. 5 for limits on the cross section for $m_{H^{++}}$ between 200 and 700 GeV.

2 See their Figs. 11(b) and 13 for limits with smaller branching ratios.

3 AAD 15AG search for $H^{++}H^{--}$ production in 20.3 fb^{-1} of pp collisions at $E_{cm} = 8$ TeV. The limit assumes 100% branching ratio to the specified final state. See their Fig. 5 for limits for arbitrary branching ratios.

4 AAD 15AP search for $H^{++}H^{--}$ production in 20.3 fb^{-1} of pp collisions at $E_{cm} = 8$ TeV. The limit assumes 100% branching ratio to the specified final state.

5 CHATRCHYAN 12AU search for $H^{++}H^{--}$ production with 4.9 fb^{-1} of pp collisions at $E_{cm} = 7$ TeV. The limit assumes 100% branching ratio to the specified final state. See their Table 6 for limits including associated $H^{++}H^-$ production or assuming different scenarios.

6 ABDALLAH 03 search for $H^{++}H^{--}$ pair production either followed by $H^{++} \rightarrow \tau^+\tau^+$, or decaying outside the detector.

7 ABBIENDI 02c searches for pair production of $H^{++}H^{--}$, with $H^{\pm\pm} \rightarrow \ell^\pm\ell^\pm$ ($\ell, \ell' = e, \mu, \tau$). The limit holds for $\ell = \ell' = \tau$, and becomes stronger for other combinations of leptonic final states. To ensure the decay within the detector, the limit only applies for $g(H\ell\ell) \gtrsim 10^{-7}$.

8 SIRUNYAN 19CQ search for $H^{\pm\pm}$ production by vector boson fusion followed by the decay $H^{\pm\pm} \rightarrow W^\pm W^\pm \rightarrow qq\ell\nu$ in 35.9 fb^{-1} of pp collisions at $E_{cm} = 13$ TeV. See their Fig. 5 for limits on cross section times branching ratio for $m_{H^{\pm\pm}}$ between 0.6 and 2 TeV.

9 SIRUNYAN 18CC search for $H^{\pm\pm}$ production by vector boson fusion followed by the decay $H^{\pm\pm} \rightarrow W^\pm W^\pm$ in 35.9 fb^{-1} of pp collisions at $E_{cm} = 13$ TeV. See their Fig. 3 for limits on cross section times branching ratio for $m_{H^{\pm\pm}}$ between 200 and 1000 GeV.

10 KANEMURA 15 examine the case where H^{++} decays preferentially to $W^{(*)}W^{(*)}$ and estimate that a lower mass limit of ~ 84 GeV can be derived from the same-sign dilepton data of AAD 15AG if H^{++} decays with 100% branching ratio to $W^{(*)}W^{(*)}$.

11 KHACHATRYAN 15D search for $H^{\pm\pm}$ production by vector boson fusion followed by the decay $H^{\pm\pm} \rightarrow W^\pm W^\pm$ in 19.4 fb^{-1} of pp collisions at $E_{cm} = 8$ TeV. See their Fig. 4 for limits on cross section times branching ratio for $m_{H^{++}}$ between 160 and 800 GeV.

12 KANEMURA 14 examine the case where H^{++} decays preferentially to $W^{(*)}W^{(*)}$ and estimate that a lower mass limit of ~ 60 GeV can be derived from the same-sign dilepton data of AAD 12CQ.

13 AAD 13Y search for $H^{++}H^{--}$ production in a generic search of events with three charged leptons in 4.6 fb^{-1} of pp collisions at $E_{cm} = 7$ TeV. The limit assumes 100% branching ratio to the specified final state.

14 AAD 12AY search for $H^{++}H^{--}$ production with 1.6 fb^{-1} of pp collisions at $E_{cm} = 7$ TeV. The limit assumes 100% branching ratio to the specified final state.

15 AAD 12CQ search for $H^{++}H^{--}$ production with 4.7 fb^{-1} of pp collisions at $E_{cm} = 7$ TeV. The limit assumes 100% branching ratio to the specified final state. See their Table 1 for limits assuming smaller branching ratios.

16 ABAZOV 12A search for $H^{++}H^{--}$ production in 7.0 fb^{-1} of $p\bar{p}$ collisions at $E_{cm} = 1.96$ TeV.

17 AALTONEN 11AF search for $H^{++}H^{--}$ production in 6.1 fb^{-1} of $p\bar{p}$ collisions at $E_{cm} = 1.96$ TeV.

18 AALTONEN 08AA search for $H^{++}H^{--}$ production in $p\bar{p}$ collisions at $E_{cm} = 1.96$ TeV. The limit assumes 100% branching ratio to the specified final state.

19 ABAZOV 08V search for $H^{++}H^{--}$ production in $p\bar{p}$ collisions at $E_{cm} = 1.96$ TeV. The limit is for $B(H \rightarrow \mu\mu) = 1$. The limit is updated in ABAZOV 12A.

20 AKTAS 06A search for single $H^{\pm\pm}$ production in ep collisions at HERA. Assuming that H^{++} only couples to $e^+\mu^+$ with $g_{e\mu} = 0.3$ (electromagnetic strength), a limit $m_{H^{++}} > 141$ GeV (95% CL) is derived. For the case where H^{++} couples to $e\tau$ only the limit is 112 GeV.

21 ACOSTA 05L search for $H^{++}H^{--}$ pair production in $p\bar{p}$ collisions. The limit is valid for $g_{\ell\ell} \leq 10^{-8}$ so that the Higgs decays outside the detector.

22 ABAZOV 04E search for $H^{++}H^{--}$ pair production in $H^{\pm\pm} \rightarrow \mu^\pm\mu^\pm$. The limit is valid for $g_{\mu\mu} \gtrsim 10^{-7}$.

23 ABBIENDI 03Q searches for single $H^{\pm\pm}$ via direct production in $e^+e^- \rightarrow e\bar{\tau}e\bar{H}^{\pm\pm}$, and via t -channel exchange in $e^+e^- \rightarrow e^+e^-$. In the direct case, and assuming $B(H^{\pm\pm} \rightarrow \ell^\pm\ell^\pm) = 1$, a 95% CL limit on $h_{ee} < 0.071$ is set for $m_{H^{\pm\pm}} \leq 160$ GeV (see Fig. 6). In the second case, indirect limits on h_{ee} are set for $m_{H^{\pm\pm}} < 2$ TeV (see Fig. 8).

24 GORDEEV 97 search for muonium-antimuonium conversion and find $G_{M\bar{M}}/G_F < 0.14$ (90% CL), where $G_{M\bar{M}}$ is the lepton-flavor violating effective four-fermion coupling. This limit may be converted to $m_{H^{++}} > 210$ GeV if the Yukawa couplings of H^{++} to ee and $\mu\mu$ are as large as the weak gauge coupling. For similar limits on muonium-antimuonium conversion, see the muon Particle Listings.

25 ASAKA 95 point out that H^{++} decays dominantly to four fermions in a large region of parameter space where the limit of ACTON 92M from the search of dilepton modes does not apply.

26 ACTON 92M limit assumes $H^{\pm\pm} \rightarrow \ell^\pm\ell^\pm$ or $H^{\pm\pm}$ does not decay in the detector. Thus the region $g_{\ell\ell} \approx 10^{-7}$ is not excluded.

27 ACTON 92M from $\Delta\Gamma_Z < 40$ MeV.

28 SWARTZ 90 assume $H^{\pm\pm} \rightarrow \ell^\pm\ell^\pm$ (any flavor). The limits are valid for the Higgs-lepton coupling $g(H\ell\ell) \gtrsim 7.4 \times 10^{-7} [m_{H^{\pm\pm}}/\text{GeV}]^{1/2}$. The limits improve somewhat for ee and $\mu\mu$ decay modes.

Limits for $H^{\pm\pm}$ with $T_3 = 0$

VALUE (GeV)	CL%	DOCUMENT ID	TECN	COMMENT
> 58	95	1 AABOUD	18Bc ATLS	$e\bar{e}$
>723	95	1 AABOUD	18Bc ATLS	$\mu\bar{\mu}$
>402	95	2 AAD	15AG ATLS	$e\mu$
>290	95	3 AAD	15AP ATLS	$e\tau$
>290	95	3 AAD	15AP ATLS	$\mu\tau$
> 97.3	95	4 ABDALLAH	03 DLPH	$\tau\tau$
> 97.3	95	5 ACHARD	03F L3	$\tau\tau$
> 98.5	95	6 ABBIENDI	02c OPAL	$\tau\tau$
••• We do not use the following data for averages, fits, limits, etc. •••				
>374	95	2 AAD	15AG ATLS	$e\bar{e}$
>438	95	2 AAD	15AG ATLS	$\mu\bar{\mu}$
>251	95	7 AAD	12AY ATLS	$\mu\mu$
>306	95	8 AAD	12CQ ATLS	$\mu\mu$
>310	95	8 AAD	12CQ ATLS	$e\mu$
>322	95	8 AAD	12CQ ATLS	$e\bar{e}$
>113	95	9 ABAZOV	12A D0	$\mu\tau$
>205	95	10 AALTONEN	11AF CDF	$\mu\mu$
>190	95	10 AALTONEN	11AF CDF	$e\mu$
>205	95	10 AALTONEN	11AF CDF	$e\bar{e}$
>145	95	11 ABAZOV	08V D0	$\mu\mu$
		12 AKTAS	06A H1	single $H^{\pm\pm}$
>109	95	13 ACOSTA	05L CDF	stable
> 98.2	95	14 ABAZOV	04E D0	$\mu\mu$
		15 ABBIENDI	03Q OPAL	$E_{cm} \leq 209$ GeV, single $H^{\pm\pm}$
		16 GORDEEV	97 SPEC	muonium conversion
> 45.6	95	17 ACTON	92M OPAL	
> 25.5	95	18 ACTON	92M OPAL	
none 7.3–34.3	95	19 SWARTZ	90 MRK2	

Gauge & Higgs Boson Particle Listings

Charged Higgs Bosons (H^\pm and $H^{\pm\pm}$), Searches for, New Heavy Bosons

- 1 See their Figs. 12(b) and 14 for limits with smaller branching ratios.
- 2 AAD 15AG search for $H^{++}H^{--}$ production in 20.3 fb^{-1} of pp collisions at $E_{\text{cm}} = 8 \text{ TeV}$. The limit assumes 100% branching ratio to the specified final state. See their Fig. 5 for limits for arbitrary branching ratios.
- 3 AAD 15AP search for $H^{++}H^{--}$ production in 20.3 fb^{-1} of pp collisions at $E_{\text{cm}} = 8 \text{ TeV}$. The limit assumes 100% branching ratio to the specified final state.
- 4 ABDALLAH 03 search for $H^{++}H^{--}$ pair production either followed by $H^{++} \rightarrow \tau^+ \tau^+$, or decaying outside the detector.
- 5 ACHARD 03F search for $e^+e^- \rightarrow H^{\pm\pm}$ with $H^{\pm\pm} \rightarrow \ell^\pm \ell^\pm$. The limit holds for $\ell = \ell' = \tau$, and slightly different limits apply for other flavor combinations. The limit is valid for $g_{\ell\ell} \gtrsim 10^{-7}$.
- 6 ABBIENDI 02c searches for pair production of $H^{++}H^{--}$, with $H^{\pm\pm} \rightarrow \ell^\pm \ell^\pm (\ell, \ell' = e, \mu, \tau)$, the limit holds for $\ell = \ell' = \tau$, and becomes stronger for other combinations of leptonic final states. To ensure the decay within the detector, the limit only applies for $g(H\ell\ell) \gtrsim 10^{-7}$.
- 7 AAD 12AY search for $H^{++}H^{--}$ production with 1.6 fb^{-1} of pp collisions at $E_{\text{cm}} = 7 \text{ TeV}$. The limit assumes 100% branching ratio to the specified final state.
- 8 AAD 12CQ search for $H^{++}H^{--}$ production with 4.7 fb^{-1} of pp collisions at $E_{\text{cm}} = 7 \text{ TeV}$. The limit assumes 100% branching ratio to the specified final state. See their Table 1 for limits assuming smaller branching ratios.
- 9 ABZOV 12A search for $H^{++}H^{--}$ production in 7.0 fb^{-1} of $p\bar{p}$ collisions at $E_{\text{cm}} = 1.96 \text{ TeV}$.
- 10 AALTONEN 11AF search for $H^{++}H^{--}$ production in 6.1 fb^{-1} of $p\bar{p}$ collisions at $E_{\text{cm}} = 1.96 \text{ TeV}$.
- 11 ABZOV 08V search for $H^{++}H^{--}$ production in $p\bar{p}$ collisions at $E_{\text{cm}} = 1.96 \text{ TeV}$. The limit is for $B(H \rightarrow \mu\mu) = 1$. The limit is updated in ABZOV 12A.
- 12 AKTAS 06A search for single $H^{\pm\pm}$ production in ep collisions at HERA. Assuming that H^{++} only couples to $e^+ \mu^+$ with $g_{e\mu} = 0.3$ (electromagnetic strength), a limit $m_{H^{++}} > 141 \text{ GeV}$ (95% CL) is derived. For the case where H^{++} couples to $e\tau$ only the limit is 112 GeV .
- 13 ACOSTA 05L search for $H^{++}H^{--}$ pair production in $p\bar{p}$ collisions. The limit is valid for $g_{\ell\ell} < 10^{-8}$ so that the Higgs decays outside the detector.
- 14 ABZOV 04E search for $H^{++}H^{--}$ pair production in $H^{\pm\pm} \rightarrow \mu^\pm \mu^\pm$. The limit is valid for $g_{\mu\mu} \gtrsim 10^{-7}$.
- 15 ABBIENDI 03Q searches for single $H^{\pm\pm}$ via direct production in $e^+e^- \rightarrow e^\mp e^\mp H^{\pm\pm}$, and via t -channel exchange in $e^+e^- \rightarrow e^+e^-$. In the direct case, and assuming $B(H^{\pm\pm} \rightarrow \ell^\pm \ell^\pm) = 1$, a 95% CL limit on $h_{ee} < 0.071$ is set for $m_{H^{\pm\pm}} < 160 \text{ GeV}$ (see Fig. 6). In the second case, indirect limits on h_{ee} are set for $m_{H^{\pm\pm}} < 2 \text{ TeV}$ (see Fig. 8).
- 16 GORDEEV 97 search for muonium-antimuonium conversion and find $G_{MM}/G_F < 0.14$ (90% CL), where G_{MM} is the lepton-flavor violating effective four-fermion coupling. This limit may be converted to $m_{H^{++}} > 210 \text{ GeV}$ if the Yukawa couplings of H^{++} to ee and $\mu\mu$ are as large as the weak gauge coupling. For similar limits on muonium-antimuonium conversion, see the muon Particle Listings.
- 17 ACTON 92M limit assumes $H^{\pm\pm} \rightarrow \ell^\pm \ell^\pm$ or $H^{\pm\pm}$ does not decay in the detector. Thus the region $g_{\ell\ell} \approx 10^{-7}$ is not excluded.
- 18 ACTON 92M from $\Delta\Gamma_Z < 40 \text{ MeV}$.
- 19 SWARTZ 90 assume $H^{\pm\pm} \rightarrow \ell^\pm \ell^\pm$ (any flavor). The limits are valid for the Higgs-lepton coupling $g(H\ell\ell) \gtrsim 7.4 \times 10^{-7} / [m_H/\text{GeV}]^{1/2}$. The limits improve somewhat for ee and $\mu\mu$ decay modes.

H^\pm and $H^{\pm\pm}$ REFERENCES

ABOUD	19K	EPJ C79 58	M. Aaboud et al.	(ATLAS Collab.)
SIRUNYAN	19AH	JHEP 1907 142	A.M. Sirunyan et al.	(CMS Collab.)
SIRUNYAN	19BP	PL B795 281	A.M. Sirunyan et al.	(CMS Collab.)
SIRUNYAN	19CC	PRL 123 131802	A.M. Sirunyan et al.	(CMS Collab.)
SIRUNYAN	19CQ	PL B798 134985	A.M. Sirunyan et al.	(CMS Collab.)
ABOUD	18BC	EPJ C78 199	M. Aaboud et al.	(ATLAS Collab.)
ABOUD	18BW	JHEP 1809 139	M. Aaboud et al.	(ATLAS Collab.)
ABOUD	18CD	JHEP 1811 085	M. Aaboud et al.	(ATLAS Collab.)
ABOUD	18CH	PL B787 68	M. Aaboud et al.	(ATLAS Collab.)
HALLER	18	EPJ C78 675	J. Haller et al.	(Glitter Group)
SIRUNYAN	18CC	PRL 120 081801	A.M. Sirunyan et al.	(CMS Collab.)
SIRUNYAN	18DO	JHEP 1811 115	A.M. Sirunyan et al.	(CMS Collab.)
MISIJK	17	EPJ C77 201	M. Misiak, M. Steinhäuser	(ATLAS Collab.)
SIRUNYAN	17AE	PRL 119 141802	A.M. Sirunyan et al.	(CMS Collab.)
ABOUD	16A	PL B759 555	M. Aaboud et al.	(ATLAS Collab.)
AAD	16AJ	JHEP 1603 127	G. Aad et al.	(ATLAS Collab.)
AAD	15AF	JHEP 1503 088	G. Aad et al.	(ATLAS Collab.)
AAD	15AG	JHEP 1503 041	G. Aad et al.	(ATLAS Collab.)
AAD	15AP	JHEP 1508 138	G. Aad et al.	(ATLAS Collab.)
AAD	15M	PRL 114 231801	G. Aad et al.	(ATLAS Collab.)
KANEMURA	15	PTEP 2015 051B02	S. Kanemura et al.	(CMS Collab.)
KHACHATRYAN	15AX	JHEP 1511 018	V. Khachatryan et al.	(CMS Collab.)
KHACHATRYAN	15BF	JHEP 1512 178	V. Khachatryan et al.	(CMS Collab.)
KHACHATRYAN	15D	PRL 114 051801	V. Khachatryan et al.	(ATLAS Collab.)
AALTONEN	14A	PR D89 032002	G. Aad et al.	(ATLAS Collab.)
AALTONEN	14A	PR D89 091101	T. Aaltonen et al.	(CDF Collab.)
KANEMURA	14	PR D90 115018	S. Kanemura et al.	(CDF Collab.)
AAD	13AC	EPJ C73 2465	G. Aad et al.	(ATLAS Collab.)
AAD	13V	JHEP 1303 076	G. Aad et al.	(ATLAS Collab.)
AAD	13Y	PR D87 052002	G. Aad et al.	(ATLAS Collab.)
CARENA	13	EPJ C73 2552	M. Carena et al.	(ATLAS Collab.)
LEP	13	EPJ C73 2463	LEP Collab.	(ALEPH, DELPHI, L3, OPAL, LEP)
AAD	12AY	PR D85 032004	G. Aad et al.	(ATLAS Collab.)
AAD	12BH	JHEP 1206 039	G. Aad et al.	(ATLAS Collab.)
AAD	12CQ	EPJ C72 2244	G. Aad et al.	(ATLAS Collab.)
AAD	12CY	JHEP 1212 007	G. Aad et al.	(ATLAS Collab.)
ABZOV	12A	PRL 108 021801	V.M. Abazov et al.	(DO Collab.)
ABBIENDI	12	EPJ C72 2076	G. Abbiendi et al.	(OPAL Collab.)
CHATRCHYAN	12AA	JHEP 1207 143	S. Chatrchyan et al.	(CMS Collab.)
CHATRCHYAN	12AU	EPJ C72 2189	S. Chatrchyan et al.	(CMS Collab.)
AALTONEN	11AF	PRL 107 181801	T. Aaltonen et al.	(CDF Collab.)
AALTONEN	11P	PRL 107 031801	T. Aaltonen et al.	(CDF Collab.)
DESCHAMPS	10	PR D82 073012	O. Deschamps et al.	(CLER, ORSAY, LAPP)
AALTONEN	09AJ	PRL 103 101803	T. Aaltonen et al.	(CDF Collab.)
ABZOV	09AC	PR D80 051107	V.M. Abazov et al.	(DO Collab.)
ABZOV	09AG	PR D80 071102	V.M. Abazov et al.	(DO Collab.)

ABZOV	09AI	PL B682 278	V.M. Abazov et al.	(DO Collab.)
ABZOV	09P	PRL 102 191802	V.M. Abazov et al.	(DO Collab.)
AALTONEN	08AA	PRL 101 121801	T. Aaltonen et al.	(CDF Collab.)
ABZOV	08V	PRL 101 071803	V.M. Abazov et al.	(DO Collab.)
ABULENCIA	06E	PRL 96 042003	A. Abulencia et al.	(CDF Collab.)
AKTAS	06A	PL B638 432	A. Aktas et al.	(H1 Collab.)
ACOSTA	05L	PRL 95 071801	D. Acosta et al.	(CDF Collab.)
ABZOV	04E	PRL 93 141801	V.M. Abazov et al.	(DO Collab.)
ABBIENDI	04	EPJ C32 453	G. Abbiendi et al.	(OPAL Collab.)
ABDALLAH	04I	EPJ C34 399	J. Abdallah et al.	(DELPHI Collab.)
ABBIENDI	03Q	PL B551 35	G. Abbiendi et al.	(OPAL Collab.)
ABBIENDI	03P	PL B577 93	G. Abbiendi et al.	(OPAL Collab.)
ABDALLAH	03E	PL B552 127	J. Abdallah et al.	(DELPHI Collab.)
ACHARD	03E	PL B575 208	P. Achard et al.	(L3 Collab.)
ACHARD	03F	PL B576 18	P. Achard et al.	(L3 Collab.)
ABZOV	02B	PRL 88 151803	V.M. Abazov et al.	(DO Collab.)
ABBIENDI	02C	PL B526 221	G. Abbiendi et al.	(OPAL Collab.)
BORZUMATI	02	PL B549 170	F.M. Borzumati, A. Djouadi	(OPAL Collab.)
HEISTER	02P	PL B543 1	A. Heister et al.	(ALEPH Collab.)
ABBIENDI	01Q	PL B520 1	G. Abbiendi et al.	(OPAL Collab.)
BARATE	01E	EPJ C19 213	R. Barate et al.	(ALEPH Collab.)
GAMBINO	01	NP B611 338	P. Gambino, M. Misiak	(ALEPH Collab.)
AFFOLDER	00I	PR D62 012004	T. Affolder et al.	(CDF Collab.)
PDG	00	EPJ C15 1	D.E. Groom et al.	(PDG Collab.)
ABBIENDI	99E	EPJ C7 407	G. Abbiendi et al.	(OPAL Collab.)
ABBOTT	99E	PRL 82 4975	B. Abbott et al.	(DO Collab.)
ACKERSTAFF	99D	EPJ C8 3	K. Ackerstaff et al.	(OPAL Collab.)
ABE	97L	PRL 79 357	F. Abe et al.	(CDF Collab.)
ACCIARRI	97L	PL B396 327	M. Acciarri et al.	(L3 Collab.)
AMMAR	97B	PRL 78 4686	R. Ammar et al.	(CLEO Collab.)
COARASA	97B	PL B406 337	J.A. Coarasa, R.A. Jimenez, J. Sola	(CLEO Collab.)
GORDEEV	97	PAN 60 1164	V.A. Gordeev et al.	(PNPI)
		Translated from YAF 60 1291		
GUCHAIT	97	PR D55 7263	M. Guchait, D.P. Roy	(TATA)
MANGANO	97	PL B410 299	M. Mangano, S. Slabospitsky	(TATA)
STAHL	97	ZPHY C74 73	A. Stahl, H. Voss	(BONN)
PDG	96	PR D54 1	R. M. Barnett et al.	(PDG Collab.)
ALAM	95	PRL 74 2885	M.S. Alam et al.	(CLEO Collab.)
ASAKA	95	PL B345 36	T. Asaka, K.I. Hikasa	(TOHOK)
BUSKULIC	95	PL B343 444	D. Buskulic et al.	(ALEPH Collab.)
GROSSMAN	95B	PL B357 520	Y. Grossman, H. Haber, Y. Nir	(ALEPH Collab.)
GROSSMAN	94	PL B332 373	Y. Grossman, Z. Ligeti	(ALEPH Collab.)
STAHL	94	PL B324 121	A. Stahl	(BONN)
ACTON	92M	PL B295 347	P.D. Acton et al.	(OPAL Collab.)
SWARTZ	90	PRL 64 2877	M.L. Swartz et al.	(Mark II Collab.)

New Heavy Bosons (W' , Z' , leptoquarks, etc.), Searches for

We list here various limits on charged and neutral heavy vector bosons (other than W 's and Z 's), heavy scalar bosons (other than Higgs bosons), vector or scalar leptoquarks, and axiglons. The latest unpublished results are described in " W' Searches" and " Z' Searches" reviews. For recent searches on scalar bosons which could be identified as Higgs bosons, see the listings in the Higgs boson section.

CONTENTS:

Mass Limits for W' (Heavy Charged Vector Boson Other Than W) in Hadron Collider Experiments
W_R (Right-Handed W Boson) Mass Limits
Limit on W_L - W_R Mixing Angle ζ
Mass Limits for Z' (Heavy Neutral Vector Boson Other Than Z)
– Limits for Z'_{SM}
– Limits for Z'_{LR}
– Limits for Z'_X
– Limits for Z'_{η}
– Limits for other Z'
– Searches for Z' with Lepton-Flavor-Violating decays
Indirect Constraints on Kaluza-Klein Gauge Bosons
Mass Limits for Leptoquarks from Pair Production
Mass Limits for Leptoquarks from Single Production
Indirect Limits for Leptoquarks
Mass Limits for Diquarks
Mass Limits for g_A (axigluon) and Other Color-Octet Gauge Bosons
Mass Limits for Color-Octet Scalar Bosons
X^0 (Heavy Boson) Searches in Z Decays
Mass Limits for a Heavy Neutral Boson Coupling to e^+e^-
Search for X^0 Resonance in e^+e^- Collisions
Search for X^0 Resonance in ep Collisions
Search for X^0 Resonance in Two-Photon Process
Search for X^0 Resonance in $e^+e^- \rightarrow X^0 \gamma$
Search for X^0 Resonance in $Z \rightarrow f\bar{f}X^0$
Search for X^0 Resonance in $W X^0$ final state
Search for X^0 Resonance in Quarkonium Decays

See the related review(s):

W' -Boson Searches

MASS LIMITS FOR W' (HEAVY CHARGED VECTOR BOSON OTHER THAN W) IN HADRON COLLIDER EXPERIMENTS

Couplings of W' to quarks and leptons are taken to be identical with those of W . The following limits are obtained from $p\bar{p}$ or $pp \rightarrow W'X$ with W' decaying to the mode indicated in the comments. New decay channels (e.g., $W' \rightarrow WZ$) are assumed to

See key on page 999

Gauge & Higgs Boson Particle Listings

New Heavy Bosons

be suppressed. The most recent preliminary results can be found in the “ W' -boson searches” review above.

VALUE (GeV)	CL%	DOCUMENT ID	TECN	COMMENT
>5200 (CL = 95%) OUR LIMIT				
none 500–3250	95	1 AABOUD 19B ATLS	$W' \rightarrow N\ell \rightarrow \ell\ell j$	
>6000	95	2 AABOUD 19E ATLS	$W' \rightarrow t\bar{b}$	
none 1300–3600	95	3 AAD 19C ATLS	$W' \rightarrow e\nu, \mu\nu$	
none 400–4000	95	4 AAD 19D ATLS	$W' \rightarrow WZ$	
>4300	95	5 SIRUNYAN 19AY CMS	$W' \rightarrow \tau\nu$	
>2600	95	6 SIRUNYAN 19CP CMS	$W' \rightarrow WZ, WH, \ell\nu$	
none 1000–3000	95	7 SIRUNYAN 19I CMS	$W' \rightarrow WH$	
none 500–2820	95	8 AABOUD 18AF ATLS	$W' \rightarrow t\bar{b}$	
none 300–3000	95	9 AABOUD 18AI ATLS	$W' \rightarrow WH$	
none 800–3200	95	10 AABOUD 18AK ATLS	$W' \rightarrow WZ$	
>5100	95	11 AABOUD 18AL ATLS	$W' \rightarrow WZ$	
none 250–2460	95	12 AABOUD 18BG ATLS	$W' \rightarrow e\nu, \mu\nu$	
none 1200–3300	95	13 AABOUD 18CH ATLS	$W' \rightarrow WZ$	
none 500–3700	95	14 AABOUD 18F ATLS	$W' \rightarrow WZ$	
none 1000–3600	95	15 AABOUD 18K ATLS	$W' \rightarrow \tau\nu$	
none 1000–3050	95	16 SIRUNYAN 18 CMS	$W' \rightarrow t\bar{b}$	
none 1000–5200	95	17 SIRUNYAN 18AX CMS	$W' \rightarrow WZ$	
none 1000–3400	95	18 SIRUNYAN 18AZ CMS	$W' \rightarrow e\nu, \mu\nu$	
none 600–3300	95	19 SIRUNYAN 18BK CMS	$W' \rightarrow WZ$	
none 900–4400	95	20 SIRUNYAN 18BO CMS	$W' \rightarrow q\bar{q}$	
none 800–2330	95	21 SIRUNYAN 18CV CMS	$W' \rightarrow N\ell \rightarrow \ell\ell j$	
>2800	95	22 SIRUNYAN 18DJ CMS	$W' \rightarrow WZ$	
none 1200–3200, 3300–3600	95	23 SIRUNYAN 18ED CMS	$W' \rightarrow WH$	
>3600	95	24 SIRUNYAN 18P CMS	$W' \rightarrow WZ$	
none 1100–2500	95	25 AABOUD 17AK ATLS	$W' \rightarrow q\bar{q}$	
>2220	95	26 AABOUD 17AO ATLS	$W' \rightarrow WH$	
>2300	95	27 AABOUD 17B ATLS	$W' \rightarrow WH$	
none 600–2700	95	28 KHACHATRY...17J CMS	$W' \rightarrow N\tau \rightarrow \tau\tau j$	
>4100	95	29 KHACHATRY...17W CMS	$W' \rightarrow q\bar{q}$	
>2200	95	30 KHACHATRY...17Z CMS	$W' \rightarrow e\nu, \mu\nu$	
>2300	95	31 SIRUNYAN 17A CMS	$W' \rightarrow WZ$	
>2900	95	32 SIRUNYAN 17AK CMS	$W' \rightarrow WZ, WH$	
>2600	95	33 SIRUNYAN 17H CMS	$W' \rightarrow \tau N$	
>2450	95	34 SIRUNYAN 17I CMS	$W' \rightarrow t\bar{b}$	
none 2780–3150	95	35 SIRUNYAN 17R CMS	$W' \rightarrow WH$	
>2600	95	36 AABOUD 16AE ATLS	$W' \rightarrow WZ$	
>4070	95	37 AABOUD 16V ATLS	$W' \rightarrow e\nu, \mu\nu$	
>1810	95	38 AAD 16R ATLS	$W' \rightarrow WZ$	
>2600	95	39 AAD 16S ATLS	$W' \rightarrow q\bar{q}$	
>2150	95	40 KHACHATRY...16AO CMS	$W' \rightarrow t\bar{b}$	
none 1000–1600	95	41 KHACHATRY...16AP CMS	$W' \rightarrow WH$	
none 800–1500	95	42 KHACHATRY...16BD CMS	$W' \rightarrow WH \rightarrow b\bar{b}\ell\nu$	
none 1500–2600	95	43 KHACHATRY...16K CMS	$W' \rightarrow q\bar{q}$	
none 500–1600	95	44 KHACHATRY...16L CMS	$W' \rightarrow q\bar{q}$	
none 300–2700	95	45 KHACHATRY...16O CMS	$W' \rightarrow \tau\nu$	
none 400–1590	95	46 AAD 15AU ATLS	$W' \rightarrow WZ$	
none 1500–1760	95	47 AAD 15AV ATLS	$W' \rightarrow t\bar{b}$	
none 300–1490	95	48 AAD 15AZ ATLS	$W' \rightarrow WZ$	
none 1300–1500	95	49 AAD 15CP ATLS	$W' \rightarrow WZ$	
none 500–1920	95	50 AAD 15R ATLS	$W' \rightarrow t\bar{b}$	
none 800–2450	95	51 AAD 15V ATLS	$W' \rightarrow q\bar{q}$	
>1470	95	52 KHACHATRY...15C CMS	$W' \rightarrow WZ$	
>3710	95	53 KHACHATRY...15T CMS	$W' \rightarrow e\nu, \mu\nu$	
none 1000–3010	95	54 KHACHATRY...14O CMS	$W' \rightarrow N\ell \rightarrow \ell\ell j$	
• • • We do not use the following data for averages, fits, limits, etc. • • •				
		55 AABOUD 19BB ATLS	$W' \rightarrow N\ell \rightarrow j\ell\ell$	
		56 SIRUNYAN 19V CMS	$W' \rightarrow B\tau, T\bar{b}$	
		57 AABOUD 18AA ATLS	$W' \rightarrow W\gamma$	
		58 AABOUD 18AD ATLS	$W' \rightarrow HX$	
>4500	95	59 AABOUD 18CJ ATLS	$W' \rightarrow WZ, WH, \ell\nu$	
		60 KHACHATRY...17U CMS	$W' \rightarrow WH$	
		61 AAD 15BB ATLS	$W' \rightarrow WH$	
none 300–880	95	62 AALTONEN 15c CDF	$W' \rightarrow t\bar{b}$	
none 1200–1900 and 2000–2200	95	63 KHACHATRY...15V CMS	$W' \rightarrow q\bar{q}$	
>3240	95	AAD 14AI ATLS	$W' \rightarrow e\nu, \mu\nu$	
		64 AAD 14AT ATLS	$W' \rightarrow W\gamma$	
none 200–1520	95	65 AAD 14S ATLS	$W' \rightarrow WZ$	
none 1000–1700	95	66 KHACHATRY...14 CMS	$W' \rightarrow WZ$	
		67 KHACHATRY...14A CMS	$W' \rightarrow WZ$	
none 500–950	95	68 AAD 13AO ATLS	$W' \rightarrow WZ$	
none 1100–1680	95	AAD 13D ATLS	$W' \rightarrow q\bar{q}$	
none 1000–1920	95	CHATRCHYAN13A CMS	$W' \rightarrow q\bar{q}$	
		69 CHATRCHYAN13AJ CMS	$W' \rightarrow WZ$	
		70 CHATRCHYAN13AQ CMS	$W' \rightarrow e\nu, \mu\nu$	
>2900	95	71 CHATRCHYAN13E CMS	$W' \rightarrow t\bar{b}$	
none 800–1510	95	72 CHATRCHYAN13U CMS	$W' \rightarrow WZ$	
none 700–940	95	73 AAD 12AV ATLS	$W' \rightarrow t\bar{b}$	

none 200–760	95	74 AAD 12BB ATLS	$W' \rightarrow WZ$
		75 AAD 12CK ATLS	$W' \rightarrow \tau q$
>2550	95	76 AAD 12CR ATLS	$W' \rightarrow e\nu, \mu\nu$
		77 AAD 12M ATLS	$W' \rightarrow N\ell \rightarrow \ell\ell j$
		78 AALTONEN 12N CDF	$W' \rightarrow \tau q$
none 200–1143	95	74 CHATRCHYAN12AF CMS	$W' \rightarrow WZ$
		79 CHATRCHYAN12AR CMS	$W' \rightarrow \tau q$
		80 CHATRCHYAN12BG CMS	$W' \rightarrow N\ell \rightarrow \ell\ell j$
>1120	95	AALTONEN 11c CDF	$W' \rightarrow e\nu$
none 180–690	95	81 ABAZOV 11H D0	$W' \rightarrow WZ$
none 600–863	95	82 ABAZOV 11L D0	$W' \rightarrow t\bar{b}$
none 285–516	95	83 AALTONEN 10N CDF	$W' \rightarrow WZ$
none 280–840	95	84 AALTONEN 09AC CDF	$W' \rightarrow q\bar{q}$
>1000	95	ABAZOV 08c D0	$W' \rightarrow e\nu$
none 300–800	95	ABAZOV 04c D0	$W' \rightarrow q\bar{q}$
none 225–536	95	85 ACOSTA 03B CDF	$W' \rightarrow t\bar{b}$
none 200–480	95	86 AFFOLDER 02c CDF	$W' \rightarrow WZ$
> 786	95	87 AFFOLDER 01i CDF	$W' \rightarrow e\nu, \mu\nu$
none 300–420	95	88 ABE 97G CDF	$W' \rightarrow q\bar{q}$
> 720	95	89 ABACHI 96c D0	$W' \rightarrow e\nu$
> 610	95	90 ABACHI 95e D0	$W' \rightarrow e\nu, \tau\nu$
none 260–600	95	91 RIZZO 93 RVUE	$W' \rightarrow q\bar{q}$

- AABOUD 19B search for right-handed W'_R in pp collisions at $\sqrt{s} = 13$ TeV. W'_R is assumed to decay into ℓ and hypothetical heavy neutrino N , with N decaying to ℓj . See their Figs. 7 and 8 for excluded regions in $M_{W'_R} - M_N$ plane.
- AABOUD 19E search for right-handed W' in pp collisions at $\sqrt{s} = 13$ TeV. See their Fig. 8 for limit on $\sigma \cdot B$.
- AAD 19c search for W' with SM-like couplings in pp collisions at $\sqrt{s} = 13$ TeV. Bosonic decays and $W - W'$ interference are neglected. The limits on e and μ separately are 6.0 and 5.1 TeV respectively. See their Fig. 2 for limits on $\sigma \cdot B$.
- AAD 19d search for resonances decaying to WZ in pp collisions at $\sqrt{s} = 13$ TeV. The quoted limit is for heavy-vector-triplet W' with $g_V = 3$. The limit becomes $M_{W'} > 3400$ GeV for $g_V = 1$. If we assume $M_{W'} = M_{Z'}$, the limit increases $M_{W'} > 3800$ GeV and $M_{W'} > 3500$ GeV for $g_V = 3$ and $g_V = 1$, respectively. See their Fig. 9 for limits on $\sigma \cdot B$.
- SIRUNYAN 19AY limits shown for W' with SM-like coupling using pp collisions at $\sqrt{s} = 13$ TeV. $W - W'$ interference and bosonic decays of W' are not included. See their Fig. 5 for limits on $\sigma \cdot B$. Limits in the context of a nonuniversal gauge interaction are shown in Fig. 7. Model independent limits on $\sigma B A \epsilon$ can be seen in Fig. 8.
- SIRUNYAN 19CP present a statistical combinations of searches for W' decaying to pairs of bosons or leptons in pp collisions at $\sqrt{s} = 13$ TeV. The quoted limit is for heavy-vector-triplet W' with $g_V = 3$. If we assume $M_{W'} = M_{Z'}$, the limit becomes $M_{W'} > 4500$ GeV for $g_V = 3$ and $M_{W'} > 5000$ GeV for $g_V = 1$. See their Figs. 2 and 3 for limits on $\sigma \cdot B$.
- SIRUNYAN 19I search for resonances decaying to HW in pp collisions at $\sqrt{s} = 13$ TeV. The quoted limit is for heavy-vector-triplet W' with $g_V = 3$. The limit becomes $M_{W'} > 2800$ GeV if we assume $M_{W'} = M_{Z'}$.
- AABOUD 18AF give the limit above for right-handed W' using pp collisions at $\sqrt{s} = 13$ TeV. These limits also exclude W bosons with left-handed couplings with masses below 2.9 TeV, at the 95% confidence level. $W' \rightarrow \ell\nu_R$ is assumed to be forbidden. See their Fig. 5 for limits on $\sigma \cdot B$ for both cases of left- and right-handed W' .
- AABOUD 18AI search for resonances decaying to HW in pp collisions at $\sqrt{s} = 13$ TeV. The quoted limit is for heavy-vector-triplet W' with $g_V = 3$. The limit becomes $M_{W'} > 2670$ GeV for $g_V = 1$. If we assume $M_{W'} = M_{Z'}$, the limit increases $M_{W'} > 2930$ GeV and $M_{W'} > 2800$ GeV for $g_V = 3$ and $g_V = 1$, respectively. See their Fig. 5 for limits on $\sigma \cdot B$.
- AABOUD 18AK search for resonances decaying to WZ in pp collisions at $\sqrt{s} = 13$ TeV. The limit quoted above is for heavy-vector-triplet W' with $g_V = 3$. The limit becomes $M_{W'} > 2800$ GeV for $g_V = 1$.
- AABOUD 18AL search for resonances decaying to WZ in pp collisions at $\sqrt{s} = 13$ TeV. The limit quoted above is for heavy-vector-triplet W' with $g_V = 3$. The limit becomes $M_{W'} > 2900$ GeV for $g_V = 1$.
- AABOUD 18BG limit is for W' with SM-like couplings using pp collisions at $\sqrt{s} = 13$ TeV. Bosonic decays of W' and $W - W'$ interference are neglected. See Fig. 2 for limits on $\sigma \cdot B$.
- AABOUD 18CH search for resonances decaying to WZ in pp collisions at $\sqrt{s} = 13$ TeV. The limit quoted above is for heavy-vector-triplet W' with $g_V = 3$. The limit becomes $M_{W'} > 2260$ GeV for $g_V = 1$.
- AABOUD 18F search for resonances decaying to WZ in pp collisions at $\sqrt{s} = 13$ TeV. The quoted limit is for heavy-vector-triplet W' with $g_V = 3$. The limit becomes $M_{W'} > 3000$ GeV for $g_V = 1$. If we assume $M_{Z'} = M_{W'}$, the limit increases $M_{W'} > 3500$ GeV and $M_{W'} > 3100$ GeV for $g_V = 3$ and $g_V = 1$, respectively. See their Fig. 5 for limits on $\sigma \cdot B$.
- AABOUD 18K limit is for W' with SM-like coupling using pp collisions at $\sqrt{s} = 13$ TeV. $W - W'$ interference and bosonic decays of W' are not included. See their Fig. 4 for limit on $\sigma \cdot B$.
- SIRUNYAN 18 limit is for right-handed W' using pp collisions at $\sqrt{s} = 13$ TeV. $W' \rightarrow \ell\nu_R$ decay is assumed to be forbidden. The limit becomes $M_{W'} > 3.4$ TeV if $M_{\nu_R} \ll M_{W'}$. See their Fig. 5 for exclusion limits on W' models having both left- and right-handed couplings.
- SIRUNYAN 18AX search for resonances decaying to WZ in pp collisions at $\sqrt{s} = 13$ TeV. The quoted limit is for heavy-vector-triplet W' with $g_V = 3$. See their Fig. 6 for limits on $\sigma \cdot B$.
- SIRUNYAN 18AZ limit is derived for W' with SM-like coupling using pp collisions at $\sqrt{s} = 13$ TeV. No interference with SM W process is considered. The bosonic decays are assumed to be negligible. See their Fig. 6 for limits on $\sigma \cdot B$.

Gauge & Higgs Boson Particle Listings

New Heavy Bosons

- 19 SIRUNYAN 18BK search for resonances decaying to WZ in pp collisions at $\sqrt{s} = 13$ TeV. The limit quoted above is for heavy-vector-triplet W' with $g_V = 3$. The limit becomes $M_{W'} > 3100$ GeV for $g_V = 1$.
- 20 SIRUNYAN 18BO limit is for W' with SM-like coupling using pp collisions at $\sqrt{s} = 13$ TeV.
- 21 SIRUNYAN 18CV search for right-handed W_R in pp collisions at $\sqrt{s} = 13$ TeV. W_R is assumed to decay into ℓ and hypothetical heavy neutrino N , with N decaying to ℓj . The quoted limit is for $M_N = M_{W_R}/2$. See their Fig. 6 for excluded regions in the $M_{W_R} - M_N$ plane.
- 22 SIRUNYAN 18DJ search for resonances decaying to WZ in pp collisions at $\sqrt{s} = 13$ TeV. The limit quoted above is for heavy-vector-triplet W' with $g_V = 3$. The limit becomes $M_{W'} > 2270$ GeV for $g_V = 1$.
- 23 SIRUNYAN 18ED search for resonances decaying to HW in pp collisions at $\sqrt{s} = 13$ TeV. The limit above is for heavy-vector-triplet W' with $g_V = 3$. If we assume $M_{W'} = M_{Z'}$, the limit increases $M_{W'} > 2900$ GeV and $M_{W'} > 2800$ GeV for $g_V = 3$ and $g_V = 1$, respectively.
- 24 SIRUNYAN 18P give this limit for a heavy-vector-triplet W' with $g_V = 3$. If they assume $M_{Z'} = M_{W'}$, the limit increases to $M_{W'} > 3800$ GeV.
- 25 AABOUD 17AK search for a new resonance decaying to dijets in pp collisions at $\sqrt{s} = 13$ TeV. The limit above is for a W' boson having axial-vector SM couplings and decaying to quarks with 75% branching fraction.
- 26 AABOUD 17AO search for resonances decaying to HW in pp collisions at $\sqrt{s} = 13$ TeV. The limit quoted above is for a W' in the heavy-vector-triplet model with $g_V = 3$. See their Fig.4 for limits on $\sigma \cdot B$.
- 27 AABOUD 17B search for resonances decaying to HW ($H \rightarrow b\bar{b}, c\bar{c}; W \rightarrow \ell\nu$) in pp collisions at $\sqrt{s} = 13$ TeV. The quoted limit is for heavy-vector-triplet W' with $g_V = 3$. The limit becomes $M_{W'} > 1750$ GeV for $g_V = 1$. If we assume $M_{W'} = M_{Z'}$, the limit increases $M_{W'} > 2310$ GeV and $M_{W'} > 1730$ GeV for $g_V = 3$ and $g_V = 1$, respectively. See their Fig.3 for limits on $\sigma \cdot B$.
- 28 KHACHATRYAN 17J search for right-handed W_R in pp collisions at $\sqrt{s} = 13$ TeV. W_R is assumed to decay into τ and hypothetical heavy neutrino N_τ , with N_τ decaying into τj . The quoted limit is for $M_{N_\tau} = M_{W_R}/2$. The limit becomes $M_{W_R} > 2350$ GeV (1630 GeV) for $M_{W_R}/M_{N_\tau} = 0.8$ (0.2). See their Fig. 4 for excluded regions in the $M_{W_R} - M_{N_\tau}$ plane.
- 29 KHACHATRYAN 17W search for resonances decaying to dijets in pp collisions at $\sqrt{s} = 13$ TeV.
- 30 KHACHATRYAN 17Z limit is for W' with SM-like coupling using pp collisions at $\sqrt{s} = 13$ TeV. The bosonic decays of W' and the interference with SM W process are neglected.
- 31 SIRUNYAN 17A search for resonances decaying to WZ with $WZ \rightarrow \ell\nu q\bar{q}, q\bar{q}q\bar{q}$ in pp collisions at $\sqrt{s} = 13$ TeV. The quoted limit is for heavy-vector-triplet W' with $g_V = 3$. The limit becomes $M_{W'} > 2000$ GeV for $g_V = 1$. If we assume $M_{Z'} = M_{W'}$, the limit increases $M_{W'} > 2400$ GeV and $M_{W'} > 2300$ GeV for $g_V = 3$ and $g_V = 1$, respectively. See their Fig.6 for limits on $\sigma \cdot B$.
- 32 SIRUNYAN 17AK search for resonances decaying to WZ or HW in pp collisions at $\sqrt{s} = 8$ and 13 TeV. The quoted limit is for heavy-vector-triplet W' with $g_V = 3$. The limit becomes $M_{W'} > 2300$ GeV for $g_V = 1$. If we assume $M_{W'} = M_{Z'}$, the limit increases $M_{W'} > 2400$ GeV for both $g_V = 3$ and $g_V = 1$. See their Fig.1 and 2 for limits on $\sigma \cdot B$.
- 33 SIRUNYAN 17H search for right-handed W' in pp collisions at $\sqrt{s} = 13$ TeV. W' is assumed to decay into τ and a heavy neutrino N , with N decaying to $\tau q\bar{q}$. The limit above assumes $M_N = M_{W'}/2$.
- 34 SIRUNYAN 17I limit is for a right-handed W' using pp collisions at $\sqrt{s} = 13$ TeV. The limit becomes $M_{W'} > 2400$ GeV for $M_{\nu R} \ll M_{W'}$.
- 35 SIRUNYAN 17R search for resonances decaying to HW in pp collisions at $\sqrt{s} = 13$ TeV. The quoted limit is for heavy-vector-triplet W' with $g_V = 3$. Mass regions $M_{W'} < 2370$ GeV and $2870 < M_{W'} < 2970$ GeV are excluded for $g_V = 1$. If we assume $M_{Z'} = M_{W'}$, the excluded mass regions are $1000 < M_{W'} < 2500$ GeV and $2760 < M_{W'} < 3300$ GeV for $g_V = 3$; $1000 < M_{W'} < 2430$ GeV and $2810 < M_{W'} < 3130$ GeV for $g_V = 1$. See their Fig.5 for limits on $\sigma \cdot B$.
- 36 AABOUD 16AE search for resonances decaying to VV ($V = W$ or Z) in pp collisions at $\sqrt{s} = 13$ TeV. Results from $\nu\nu q\bar{q}, \nu\ell q\bar{q}, \ell\ell q\bar{q}$ and qqq final states are combined. The quoted limit is for a heavy-vector-triplet W' with $g_V = 3$ and $M_{W'} = M_{Z'}$.
- 37 AABOUD 16V limit is for W' with SM-like coupling using pp collisions at $\sqrt{s} = 13$ TeV. The bosonic decays of W' and the interference with SM W process are neglected.
- 38 AAD 16R search for $W' \rightarrow WZ$ in pp collisions at $\sqrt{s} = 8$ TeV. $\ell\nu\ell'\ell', \ell\ell q\bar{q}, \ell\nu q\bar{q}$, and all hadronic channels are combined. The quoted limit assumes $g_{W'WZ}/g_{WWZ} = (M_{W'}/M_{W'})^2$.
- 39 AAD 16S search for a new resonance decaying to dijets in pp collisions at $\sqrt{s} = 13$ TeV. The limit quoted above is for a W' having SM-like couplings to quarks.
- 40 KHACHATRYAN 16AO limit is for a SM-like right-handed W' using pp collisions at $\sqrt{s} = 8$ TeV. The quoted limit combines $t \rightarrow qq\bar{b}$ and $t \rightarrow \ell\nu b$ events.
- 41 KHACHATRYAN 16AP search for a resonance decaying to HW in pp collisions at $\sqrt{s} = 8$ TeV. Both H and W are assumed to decay to fat jets. The quoted limit is for heavy-vector-triplet W' with $g_V = 3$.
- 42 KHACHATRYAN 16BD search for resonance decaying to HW in pp collisions at $\sqrt{s} = 8$ TeV. The quoted limit is for heavy-vector-triplet (HVT) W' with $g_V = 3$. The HVT model $m_{W'} = m_{Z'} > 1.8$ TeV is also obtained by combining $W'/Z' \rightarrow WH/ZH \rightarrow \ell\nu b\bar{b}, qq\tau\tau, qq\bar{b}b$, and $qqqqqq$ channels.
- 43 KHACHATRYAN 16K search for resonances decaying to dijets in pp collisions at $\sqrt{s} = 13$ TeV.
- 44 KHACHATRYAN 16L search for resonances decaying to dijets in pp collisions at $\sqrt{s} = 8$ TeV with the data scouting technique, increasing the sensitivity to the low mass resonances.
- 45 KHACHATRYAN 16O limit is for W' having universal couplings. Interferences with the SM amplitudes are assumed to be absent.
- 46 AAD 15AU search for W' decaying into the WZ final state with $W \rightarrow q\bar{q}'$, $Z \rightarrow \ell^+\ell^-$ using pp collisions at $\sqrt{s} = 8$ TeV. The quoted limit assumes $g_{W'WZ}/g_{WWZ} = (M_{W'}/M_{W'})^2$.
- 47 AAD 15AV limit is for a SM like right-handed W' using pp collisions at $\sqrt{s} = 8$ TeV. $W' \rightarrow \ell\nu$ decay is assumed to be forbidden.
- 48 AAD 15AZ search for W' decaying into the WZ final state with $W \rightarrow \ell\nu$, $Z \rightarrow q\bar{q}$ using pp collisions at $\sqrt{s} = 8$ TeV. The quoted limit assumes $g_{W'WZ}/g_{WWZ} = (M_{W'}/M_{W'})^2$.
- 49 AAD 15CP search for W' decaying into the WZ final state with $W \rightarrow q\bar{q}$, $Z \rightarrow q\bar{q}$ using pp collisions at $\sqrt{s} = 8$ TeV. The quoted limit assumes $g_{W'WZ}/g_{WWZ} = (M_{W'}/M_{W'})^2$.
- 50 AAD 15R limit is for a SM like right-handed W' using pp collisions at $\sqrt{s} = 8$ TeV. $W' \rightarrow \ell\nu$ decay is assumed to be forbidden.
- 51 AAD 15V search for new resonance decaying to dijets in pp collisions at $\sqrt{s} = 8$ TeV.
- 52 KHACHATRYAN 15C search for W' decaying via WZ to fully leptonic final states using pp collisions at $\sqrt{s}=8$ TeV. The quoted limit assumes $g_{W'WZ}/g_{WWZ} = M_{W'}/M_{Z'}$.
- 53 KHACHATRYAN 15T limit is for W' with SM-like coupling which interferes the SM W boson constructively using pp collisions at $\sqrt{s} = 8$ TeV. For W' without interference, the limit becomes > 3280 GeV.
- 54 KHACHATRYAN 14O search for right-handed W_R in pp collisions at $\sqrt{s} = 8$ TeV. W_R is assumed to decay into ℓ and hypothetical heavy neutrino N , with N decaying into ℓj . The quoted limit is for $M_{\nu eR} = M_{\nu \mu R} = M_{W_R}/2$. See their Fig. 3 and Fig. 5 for excluded regions in the $M_{W_R} - M_\nu$ plane.
- 55 AABOUD 19BB search for right handed W_R in pp collisions at $\sqrt{s} = 13$ TeV. W_R is assumed to decay into ℓ and a boosted hypothetical heavy neutrino N , with N decaying to ℓ and a large radius jet $j = q\bar{q}$. See their Fig. 7 for excluded regions in $M_{W_R} - M_N$ plane.
- 56 SIRUNYAN 19V search for a new resonance decaying to a top quark and a heavy vector-like bottom partner B decaying to Hb (or a bottom quark and a heavy vector-like top partner T decaying to Ht) in pp collisions at $\sqrt{s} = 13$ TeV. See their Fig. 8 for limits on $\sigma \cdot B$.
- 57 AABOUD 18AA search for a narrow charged vector boson decaying to $W\gamma$. See their Fig. 9 for the exclusion limit in $M_{W'} - \sigma B$ plane.
- 58 AABOUD 18AD search for resonances decaying to HX ($H \rightarrow b\bar{b}$, $X \rightarrow q\bar{q}'$) in pp collisions at $\sqrt{s} = 13$ TeV. See their Figs. 3-5 for limits on $\sigma \cdot B$.
- 59 AABOUD 18CJ search for heavy-vector-triplet W' in pp collisions at $\sqrt{s} = 13$ TeV. The limit quoted above is for model with $g_V = 3$ assuming $M_{W'} = M_{Z'}$. The limit becomes $M_{W'} > 5500$ GeV for model with $g_V = 1$.
- 60 KHACHATRYAN 17U search for resonances decaying to HW ($H \rightarrow b\bar{b}$; $W \rightarrow \ell\nu$) in pp collisions at $\sqrt{s} = 13$ TeV. The limit on the heavy-vector-triplet model is $M_{Z'} = M_{W'} > 2$ TeV for $g_V = 3$, in which constraints from the $Z' \rightarrow HZ$ ($H \rightarrow b\bar{b}$; $Z \rightarrow \ell^+\ell^-, \nu\bar{\nu}$) are combined. See their Fig.3 and Fig.4 for limits on $\sigma \cdot B$.
- 61 AAD 15BB search for W' decaying into WH with $W \rightarrow \ell\nu$, $H \rightarrow b\bar{b}$. See their Fig. 4 for the exclusion limits in the heavy vector triplet benchmark model parameter space.
- 62 AALTONEN 15C limit is for a SM-like right-handed W' assuming $W' \rightarrow \ell\nu$ decays are forbidden, using $p\bar{p}$ collisions at $\sqrt{s}=1.96$ TeV. See their Fig. 3 for limit on $g_{W'}/g_W$.
- 63 KHACHATRYAN 15V search new resonance decaying to dijets in pp collisions at $\sqrt{s} = 8$ TeV.
- 64 AAD 14AT search for a narrow charged vector boson decaying to $W\gamma$. See their Fig. 3a for the exclusion limit in $m_{W'} - \sigma B$ plane.
- 65 AAD 14S search for W' decaying into the WZ final state with $W \rightarrow \ell\nu$, $Z \rightarrow \ell\ell$ using pp collisions at $\sqrt{s}=8$ TeV. The quoted limit assumes $g_{W'WZ}/g_{WWZ} = (M_{W'}/M_{W'})^2$.
- 66 KHACHATRYAN 14 search for W' decaying into WZ final state with $W \rightarrow q\bar{q}$, $Z \rightarrow q\bar{q}$ using pp collisions at $\sqrt{s}=8$ TeV. The quoted limit assumes $g_{W'WZ}/g_{WWZ} = (M_{W'}/M_{W'})^2$.
- 67 KHACHATRYAN 14A search for W' decaying into the WZ final state with $W \rightarrow \ell\nu$, $Z \rightarrow q\bar{q}$, or $W \rightarrow q\bar{q}$, $Z \rightarrow \ell\ell$. pp collisions data at $\sqrt{s}=8$ TeV are used for the search. See their Fig. 13 for the exclusion limit on the number of events in the mass-width plane.
- 68 AAD 13AO search for W' decaying into the WZ final state with $W \rightarrow \ell\nu$, $Z \rightarrow 2j$ using pp collisions at $\sqrt{s}=7$ TeV. The quoted limit assumes $g_{W'WZ}/g_{WWZ} = (M_{W'}/M_{W'})^2$.
- 69 CHATRYAN 13AJ search for resonances decaying to WZ pair, using the hadronic decay modes of W and Z , in pp collisions at $\sqrt{s}=7$ TeV. See their Fig. 7 for the limit on the cross section.
- 70 CHATRYAN 13AQ limit is for W' with SM-like coupling which interferes with the SM W boson using pp collisions at $\sqrt{s}=7$ TeV.
- 71 CHATRYAN 13E limit is for W' with SM-like coupling which interferes with the SM W boson using pp collisions at $\sqrt{s}=7$ TeV. For W' with right-handed coupling, the bound becomes >1850 GeV (>1910 GeV) if W' decays to both leptons and quarks (only to quarks). If both left- and right-handed couplings are present, the limit becomes >1640 GeV.
- 72 CHATRYAN 13U search for W' decaying to the WZ final state, with W decaying into jets, in pp collisions at $\sqrt{s}=7$ TeV. The quoted limit assumes $g_{W'WZ}/g_{WWZ} = (M_{W'}/M_{W'})^2$.
- 73 The AAD 12AV quoted limit is for a SM-like right-handed W' using pp collisions at $\sqrt{s}=7$ TeV. $W' \rightarrow \ell\nu$ decay is assumed to be forbidden.
- 74 AAD 12BB use pp collisions data at $\sqrt{s}=7$ TeV. The quoted limit assumes $g_{W'WZ}/g_{WWZ} = (M_{W'}/M_{W'})^2$.
- 75 AAD 12CK search for $pp \rightarrow tW'$, $W' \rightarrow Tq$ events in pp collisions. See their Fig. 5 for the limit on $\sigma \cdot B$.
- 76 AAD 12CR use pp collisions at $\sqrt{s}=7$ TeV.

See key on page 999

Gauge & Higgs Boson Particle Listings

New Heavy Bosons

- 77 AAD 12M search for right-handed W_R in pp collisions at $\sqrt{s} = 7$ TeV. W_R is assumed to decay into ℓ and hypothetical heavy neutrino N , with N decaying into ℓjj . See their Fig. 4 for the limit in the $m_N - m_{W_R}$ plane.
- 78 AALTONEN 12N search for $p\bar{p} \rightarrow tW', W' \rightarrow \bar{t}d$ events in $p\bar{p}$ collisions. See their Fig. 3 for the limit on $\sigma \cdot B$.
- 79 CHATRCHYAN 12AR search for $pp \rightarrow tW', W' \rightarrow \bar{t}d$ events in pp collisions. See their Fig. 2 for the limit on $\sigma \cdot B$.
- 80 CHATRCHYAN 12BG search for right-handed W_R in pp collisions $\sqrt{s} = 7$ TeV. W_R is assumed to decay into ℓ and hypothetical heavy neutrino N , with N decaying into ℓjj . See their Fig. 3 for the limit in the $m_N - m_{W_R}$ plane.
- 81 ABAZOV 11H use data from $p\bar{p}$ collisions at $\sqrt{s}=1.96$ TeV. The quoted limit is obtained assuming $W'WZ$ coupling strength is the same as the ordinary WZ coupling strength in the Standard Model.
- 82 ABAZOV 11L limit is for W' with SM-like coupling which interferes with the SM W boson, using $p\bar{p}$ collisions at $\sqrt{s}=1.96$ TeV. For W' with right-handed coupling, the bound becomes >885 GeV (>890 GeV) if W' decays to both leptons and quarks (only to quarks). If both left- and right-handed couplings present, the limit becomes >916 GeV.
- 83 AALTONEN 10N use $p\bar{p}$ collision data at $\sqrt{s}=1.96$ TeV. The quoted limit assumes $g_{W'WZ}/g_{WZ} = (M_{W'}/M_W)^2$. See their Fig. 4 for limits in mass-coupling plane.
- 84 AALTONEN 09AC search for new particle decaying to dijets using $p\bar{p}$ collisions at $\sqrt{s}=1.96$ TeV.
- 85 The ACOSTA 03B quoted limit is for $M_{W'} \gg M_{\nu_R}$, using $p\bar{p}$ collisions at $\sqrt{s}=1.8$ TeV. For $M_{W'} < M_{\nu_R}$, $M_{W'}$ between 225 and 566 GeV is excluded.
- 86 The quoted limit is obtained assuming $W'WZ$ coupling strength is the same as the ordinary WZ coupling strength in the Standard Model, using $p\bar{p}$ collisions at $\sqrt{s}=1.8$ TeV. See their Fig. 2 for the limits on the production cross sections as a function of the W' width.
- 87 AFFOLDER 01i combine a new bound on $W' \rightarrow e\nu$ of 754 GeV, using $p\bar{p}$ collisions at $\sqrt{s}=1.8$ TeV, with the bound of ABE 00 on $W' \rightarrow \mu\nu$ to obtain quoted bound.
- 88 ABE 97G search for new particle decaying to dijets using $p\bar{p}$ collisions at $\sqrt{s}=1.8$ TeV.
- 89 For bounds on W_R with nonzero right-handed mass, see Fig. 5 from ABACHI 96c.
- 90 ABACHI 95E assume that the decay $W' \rightarrow WZ$ is suppressed and that the neutrino from W' decay is stable and has a mass significantly less $m_{W'}$.
- 91 RIZZO 93 analyses CDF limit on possible two-jet resonances. The limit is sensitive to the inclusion of the assumed K factor.

W_R (Right-Handed W Boson) MASS LIMITS

Assuming a light right-handed neutrino, except for BEALL 82, LANGACKER 89b, and COLANGELO 91. $g_R = g_L$ assumed. [Limits in the section MASS LIMITS for W' below are also valid for W_R if $m_{\nu_R} \ll m_{W_R}$.] Some limits assume manifest left-right symmetry, i.e., the equality of left- and right Cabibbo-Kobayashi-Maskawa matrices. For a comprehensive review, see LANGACKER 89b. Limits on the $W_L - W_R$ mixing angle ζ are found in the next section. Values in brackets are from cosmological and astrophysical considerations and assume a light right-handed neutrino.

VALUE (GeV)	CL%	DOCUMENT ID	TECN	COMMENT
> 5.92	90	1 BUENO	11 TWST	μ decay
> 715	90	2 CZAKON	99 RVUE	Electroweak
• • • We do not use the following data for averages, fits, limits, etc. • • •				
> 235	90	3 PRIEELS	14 PIE3	μ decay
> 245	90	4 WAUTERS	10 CNTR	^{60}Co β decay
>2500		5 ZHANG	08 THEO	$m_{K_L^0} - m_{K_S^0}$
> 180	90	6 MELCONIAN	07 CNTR	^{37}K β^+ decay
> 290.7	90	7 SCHUMANN	07 CNTR	Polarized neutron decay
[> 3300]	95	8 CYBURT	05 COSM	Nucleosynthesis; light ν_R
> 310	90	9 THOMAS	01 CNTR	β^+ decay
> 137	95	10 ACKERSTAFF	99D OPAL	τ decay
>1400	68	11 BARENBOIM	98 RVUE	Electroweak, $Z-Z'$ mixing
> 549	68	12 BARENBOIM	97 RVUE	μ decay
> 220	95	13 STAHL	97 RVUE	τ decay
> 220	90	14 ALLET	96 CNTR	β^+ decay
> 281	90	15 KUZNETSOV	95 CNTR	Polarized neutron decay
> 282	90	16 KUZNETSOV	94b CNTR	Polarized neutron decay
> 439	90	17 BHATTACH...	93 RVUE	$Z-Z'$ mixing
> 250	90	18 SEVERIJNS	93 CNTR	β^+ decay
		19 IMAZATO	92 CNTR	K^+ decay
> 475	90	20 POLAK	92b RVUE	μ decay
> 240	90	21 AQUINO	91 RVUE	Neutron decay
> 496	90	21 AQUINO	91 RVUE	Neutron and muon decay
> 700		22 COLANGELO	91 THEO	$m_{K_L^0} - m_{K_S^0}$
> 477	90	23 POLAK	91 RVUE	μ decay
[none 540-23000]		24 BARBIERI	89b ASTR	SN 1987A; light ν_R
> 300	90	25 LANGACKER	89b RVUE	General
> 160	90	26 BALKE	88 CNTR	$\mu \rightarrow e\nu\bar{\nu}$
> 406	90	27 JODIDIO	86 ELEC	Any ζ
> 482	90	27 JODIDIO	86 ELEC	$\zeta = 0$
> 800		MOHAPATRA	86 RVUE	$\text{SU}(2)_L \times \text{SU}(2)_R \times \text{U}(1)$
> 400	95	28 STOKER	85 ELEC	Any ζ
> 475	95	28 STOKER	85 ELEC	$\zeta < 0.041$
		29 BERGSMA	83 CHRM	$\nu_\mu e \rightarrow \mu\nu e$
> 380	90	30 CARR	83 ELEC	μ^+ decay
>1600		31 BEALL	82 THEO	$m_{K_L^0} - m_{K_S^0}$

1 The quoted limit is for manifest left-right symmetric model.

2 CZAKON 99 perform a simultaneous fit to charged and neutral sectors.

- 3 PRIEELS 14 limit is from $\mu^+ \rightarrow e^+ \nu\bar{\nu}$ decay parameter ξ'' , which is determined by the positron polarization measurement.
- 4 WAUTERS 10 limit is from a measurement of the asymmetry parameter of polarized ^{60}Co β decays. The listed limit assumes no mixing.
- 5 ZHANG 08 limit uses a lattice QCD calculation of the relevant hadronic matrix elements, while BEALL 82 limit used the vacuum saturation approximation.
- 6 MELCONIAN 07 measure the neutrino angular asymmetry in β^+ -decays of polarized ^{37}K , stored in a magneto-optical trap. Result is consistent with SM prediction and does not constrain the $W_L - W_R$ mixing angle appreciably.
- 7 SCHUMANN 07 limit is from measurements of the asymmetry $\langle \bar{\beta}_\nu \cdot \sigma_n \rangle$ in the β decay of polarized neutrons. Zero mixing is assumed.
- 8 CYBURT 05 limit follows by requiring that three light ν_R 's decouple when $T_{dec} > 140$ MeV. For different T_{dec} , the bound becomes $M_{W_R} > 3.3 \text{ TeV } (T_{dec} / 140 \text{ MeV})^{3/4}$.
- 9 THOMAS 01 limit is from measurement of β^+ polarization in decay of polarized ^{12}N . The listed limit assumes no mixing.
- 10 ACKERSTAFF 99D limit is from τ decay parameters. Limit increase to 145 GeV for zero mixing.
- 11 BARENBOIM 98 assumes minimal left-right model with Higgs of $\text{SU}(2)_R$ in $\text{SU}(2)_L$ doublet. For Higgs in $\text{SU}(2)_L$ triplet, $m_{W_R} > 1100$ GeV. Bound calculated from effect of corresponding Z_{LR} on electroweak data through $Z-Z_{LR}$ mixing.
- 12 The quoted limit is from μ decay parameters. BARENBOIM 97 also evaluate limit from $K_L - K_S$ mass difference.
- 13 STAHL 97 limit is from fit to τ -decay parameters.
- 14 ALLET 96 measured polarization-asymmetry correlation in ^{12}N β^+ decay. The listed limit assumes zero $L-R$ mixing.
- 15 KUZNETSOV 95 limit is from measurements of the asymmetry $\langle \bar{\beta}_\nu \cdot \sigma_n \rangle$ in the β decay of polarized neutrons. Zero mixing assumed. See also KUZNETSOV 94b.
- 16 KUZNETSOV 94b limit is from measurements of the asymmetry $\langle \bar{\beta}_\nu \cdot \sigma_n \rangle$ in the β decay of polarized neutrons. Zero mixing assumed.
- 17 BHATTACHARYYA 93 uses $Z-Z'$ mixing limit from LEP '90 data, assuming a specific Higgs sector of $\text{SU}(2)_L \times \text{SU}(2)_R \times \text{U}(1)$ gauge model. The limit is for $m_t = 200$ GeV and slightly improves for smaller m_t .
- 18 SEVERIJNS 93 measured polarization-asymmetry correlation in ^{107}In β^+ decay. The listed limit assumes zero $L-R$ mixing. Value quoted here is from SEVERIJNS 94 erratum.
- 19 IMAZATO 92 measure positron asymmetry in $K^+ \rightarrow \mu^+ \nu_\mu$ decay and obtain $\xi_{P,\mu} > 0.990$ (90% CL). If W_R couples to $u\bar{s}$ with full weak strength ($V_{us}^R = 1$), the result corresponds to $m_{W_R} > 653$ GeV. See their Fig. 4 for m_{W_R} limits for general $|V_{us}^R|^2 = 1 - |V_{ud}^R|^2$.
- 20 POLAK 92b limit is from fit to muon decay parameters and is essentially determined by JODIDIO 86 data assuming $\zeta=0$. Supersedes POLAK 91.
- 21 AQUINO 91 limits obtained from neutron lifetime and asymmetries together with unitarity of the CKM matrix. Manifest left-right symmetry assumed. Stronger of the two limits also includes muon decay results.
- 22 COLANGELO 91 limit uses hadronic matrix elements evaluated by QCD sum rule and is less restrictive than BEALL 82 limit which uses vacuum saturation approximation. Manifest left-right symmetry assumed.
- 23 POLAK 91 limit is from fit to muon decay parameters and is essentially determined by JODIDIO 86 data assuming $\zeta=0$. Superseded by POLAK 92b.
- 24 BARBIERI 89b limit holds for $m_{\nu_R} \leq 10$ MeV.
- 25 LANGACKER 89b limit is for any ν_R mass (either Dirac or Majorana) and for a general class of right-handed quark mixing matrices.
- 26 BALKE 88 limit is for $m_{\nu_{eR}} = 0$ and $m_{\nu_{\mu R}} \leq 50$ MeV. Limits come from precise measurements of the muon decay asymmetry as a function of the positron energy.
- 27 JODIDIO 86 is the same TRIUMF experiment as STOKER 85 (and CARR 83); however, it uses a different technique. The results given here are combined results of the two techniques. The technique here involves precise measurement of the end-point e^+ spectrum in the decay of the highly polarized μ^+ .
- 28 STOKER 85 is same TRIUMF experiment as CARR 83. Here they measure the decay e^+ spectrum asymmetry above 46 MeV/c using a muon-spin-rotation technique. Assumed a light right-handed neutrino. Quoted limits are from combining with CARR 83.
- 29 BERGSMA 83 set limit $m_{W_2}/m_{W_1} > 1.9$ at CL = 90%.
- 30 CARR 83 is TRIUMF experiment with a highly polarized μ^+ beam. Looked for deviation from $V-A$ at the high momentum end of the decay e^+ energy spectrum. Limit from previous world-average muon polarization parameter is $m_{W_R} > 240$ GeV. Assumes a light right-handed neutrino.
- 31 BEALL 82 limit is obtained assuming that W_R contribution to $K_L^0 - K_S^0$ mass difference is smaller than the standard one, neglecting the top quark contributions. Manifest left-right symmetry assumed.

Limit on $W_L - W_R$ Mixing Angle ζ

Lighter mass eigenstate $W_1 = W_L \cos \zeta - W_R \sin \zeta$. Light ν_R assumed unless noted. Values in brackets are from cosmological and astrophysical considerations.

VALUE	CL%	DOCUMENT ID	TECN	COMMENT
• • • We do not use the following data for averages, fits, limits, etc. • • •				
-0.020 to 0.017	90	BUENO	11 TWST	$\mu \rightarrow e\nu\bar{\nu}$
< 0.022	90	MACDONALD	08 TWST	$\mu \rightarrow e\nu\bar{\nu}$
< 0.12	95	1 ACKERSTAFF	99D OPAL	τ decay
< 0.013	90	2 CZAKON	99 RVUE	Electroweak
< 0.0333		3 BARENBOIM	97 RVUE	μ decay
< 0.04	90	4 MISHRA	92 CCFR	νN scattering
-0.0006 to 0.0028	90	5 AQUINO	91 RVUE	
[none 0.00001-0.02]		6 BARBIERI	89b ASTR	SN 1987A
< 0.040	90	7 JODIDIO	86 ELEC	μ decay
-0.056 to 0.040	90	7 JODIDIO	86 ELEC	μ decay

Gauge & Higgs Boson Particle Listings

New Heavy Bosons

- ¹ ACKERSTAFF 99D limit is from τ decay parameters.
² CZAKON 99 perform a simultaneous fit to charged and neutral sectors.
³ The quoted limit is from μ decay parameters. BARENBOIM 97 also evaluate limit from $K_L - K_S$ mass difference.
⁴ MISHRA 92 limit is from the absence of extra large- x , large- y $\bar{\nu}_\mu N \rightarrow \bar{\nu}_\mu X$ events at Tevatron, assuming left-handed ν and right-handed $\bar{\nu}$ in the neutrino beam. The result gives $\zeta^2(1-2m_{W_1}^2/m_{W_2}^2) < 0.0015$. The limit is independent of ν_{R^c} mass.
⁵ AQUINO 91 limits obtained from neutron lifetime and asymmetries together with unitarity of the CKM matrix. Manifest left-right asymmetry is assumed.
⁶ BARBIERI 89B limit holds for $m_{\nu_R} \leq 10$ MeV.
⁷ First JODIDIO 86 result assumes $m_{W_R} = \infty$, second is for unconstrained m_{W_R} .

- ⁹ KHACHATRYAN 17W search for resonances decaying to dijets in pp collisions at $\sqrt{s} = 13$ TeV.
¹⁰ AABOUD 16U search for resonances decaying to $\ell^+ \ell^-$ in pp collisions at $\sqrt{s} = 13$ TeV.
¹¹ KHACHATRYAN 15AE search for resonances decaying to $e^+ e^-, \mu^+ \mu^-$ in pp collisions at $\sqrt{s} = 8$ TeV.
¹² KHACHATRYAN 15V search for resonances decaying to dijets in pp collisions at $\sqrt{s} = 8$ TeV.
¹³ AAD 14V search for resonances decaying to $e^+ e^-, \mu^+ \mu^-$ in pp collisions at $\sqrt{s} = 8$ TeV.
¹⁴ BOBOVNIKOV 18 use the ATLAS limits on $\sigma(pp \rightarrow Z')B(Z' \rightarrow W^+ W^-)$ to constrain the $Z-Z'$ mixing parameter ξ . See their Fig. 11 for limits in $M_{Z'} - \xi$ plane.
¹⁵ AABOUD 16AA search for resonances decaying to $\tau^+ \tau^-$ in pp collisions at $\sqrt{s} = 13$ TeV.
¹⁶ AAD 15AM search for resonances decaying to $\tau^+ \tau^-$ in pp collisions at $\sqrt{s} = 8$ TeV.
¹⁷ AAD 13S search for resonances decaying to $\tau^+ \tau^-$ in pp collisions at $\sqrt{s} = 7$ TeV.
¹⁸ CHATRCHYAN 13A use pp collisions at $\sqrt{s} = 7$ TeV.
¹⁹ CHATRCHYAN 13AF search for resonances decaying to $e^+ e^-, \mu^+ \mu^-$ in pp collisions at $\sqrt{s} = 7$ TeV and 8 TeV.
²⁰ AAD 12CC search for resonances decaying to $e^+ e^-, \mu^+ \mu^-$ in pp collisions at $\sqrt{s} = 7$ TeV.
²¹ CHATRCHYAN 12O search for resonances decaying to $\tau^+ \tau^-$ in pp collisions at $\sqrt{s} = 7$ TeV.
²² AALTONEN 11I search for resonances decaying to $\mu^+ \mu^-$ in $p\bar{p}$ collisions at $\sqrt{s} = 1.96$ TeV.
²³ ABZOV 11A, AALTONEN 09T, AALTONEN 07H, and ABULENCIA 06L search for resonances decaying to $e^+ e^-$ in $p\bar{p}$ collisions at $\sqrt{s} = 1.96$ TeV.
²⁴ The quoted limit assumes $g_{WWZ'}/g_{WWZ} = (M_W/M_{Z'})^2$. See their Fig. 4 for limits in mass-coupling plane.
²⁵ AALTONEN 09AC search for new particle decaying to dijets.
²⁶ ERLER 09 give 95% CL limit on the $Z-Z'$ mixing $-0.0026 < \theta < 0.0006$.
²⁷ ABDALLAH 06c use data $\sqrt{s} = 130-207$ GeV.
²⁸ ACOSTA 05R search for resonances decaying to tau lepton pairs in $p\bar{p}$ collisions at $\sqrt{s} = 1.96$ TeV.
²⁹ ABBIENDI 04c give 95% CL limit on $Z-Z'$ mixing $-0.00422 < \theta < 0.00091$. $\sqrt{s} = 91$ to 207 GeV.
³⁰ ABZOV 01B search for resonances in $p\bar{p} \rightarrow e^+ e^-$ at $\sqrt{s} = 1.8$ TeV. They find $\sigma \cdot B(Z' \rightarrow ee) < 0.06$ pb for $M_{Z'} > 500$ GeV.
³¹ CHEUNG 01B limit is derived from bounds on contact interactions in a global electroweak analysis.
³² ABREU 00s uses LEP data at $\sqrt{s} = 90$ to 189 GeV.
³³ BARATE 00i search for deviations in cross section and asymmetries in $e^+ e^- \rightarrow$ fermions at $\sqrt{s} = 90$ to 183 GeV. Assume $\theta = 0$. Bounds in the mass-mixing plane are shown in their Figure 18.
³⁴ ERLER 99 give 90%CL limit on the $Z-Z'$ mixing $-0.0041 < \theta < 0.0003$. $\rho_0 = 1$ is assumed.
³⁵ ABE 97s find $\sigma(Z') \times B(e^+ e^-, \mu^+ \mu^-) < 40$ fb for $M_{Z'} > 600$ GeV at $\sqrt{s} = 1.8$ TeV.
³⁶ VILAIN 94B assume $m_t = 150$ GeV.
³⁷ ALITTI 93 search for resonances in the two-jet invariant mass. The limit assumes $B(Z' \rightarrow q\bar{q}) = 0.7$. See their Fig. 5 for limits in the $m_{Z'} - B(q\bar{q})$ plane.
³⁸ RIZZO 93 analyses CDF limit on possible two-jet resonances.
³⁹ ABE 90f use data for $R, R_{\ell\ell}$, and $A_{\ell\ell}$. They fix $m_W = 80.49 \pm 0.43 \pm 0.24$ GeV and $m_Z = 91.13 \pm 0.03$ GeV.

See the related review(s):

Z'-Boson Searches

MASS LIMITS for Z' (Heavy Neutral Vector Boson Other Than Z)

Limits for Z'_{SM}

Z'_{SM} is assumed to have couplings with quarks and leptons which are identical to those of Z, and decays only to known fermions. The most recent preliminary results can be found in the "Z'-boson searches" review above.

VALUE (GeV)	CL%	DOCUMENT ID	TECN	COMMENT
none 250-5100	95	1 AAD	19L ATLS	$pp; Z'_{SM} \rightarrow e^+ e^-, \mu^+ \mu^-$
none 600-2000	95	2 AABOUD	18AB ATLS	$pp; Z'_{SM} \rightarrow b\bar{b}$
>2420	95	3 AABOUD	18G ATLS	$pp; Z'_{SM} \rightarrow \tau^+ \tau^-$
none 200-4500	95	4 SIRUNYAN	18BB CMS	$pp; Z'_{SM} \rightarrow e^+ e^-, \mu^+ \mu^-$
none 600-2700	95	5 SIRUNYAN	18BO CMS	$pp; Z'_{SM} \rightarrow q\bar{q}$
>4500	95	6 AABOUD	17AT ATLS	$pp; Z'_{SM} \rightarrow e^+ e^-, \mu^+ \mu^-$
>2100	95	7 KHACHATRYAN	17H CMS	$pp; Z'_{SM} \rightarrow \tau^+ \tau^-$
>3370	95	8 KHACHATRYAN	17T CMS	$pp; Z'_{SM} \rightarrow e^+ e^-, \mu^+ \mu^-$
none 600-2100, 2300-2600	95	9 KHACHATRYAN	17W CMS	$pp; Z'_{SM} \rightarrow q\bar{q}$
>3360	95	10 AABOUD	16U ATLS	$pp; Z'_{SM} \rightarrow e^+ e^-, \mu^+ \mu^-$
>2900	95	11 KHACHATRYAN	15AE CMS	$pp; Z'_{SM} \rightarrow e^+ e^-, \mu^+ \mu^-$
none 1200-1700	95	12 KHACHATRYAN	15V CMS	$pp; Z'_{SM} \rightarrow q\bar{q}$
>2900	95	13 AAD	14V ATLS	$pp; Z'_{SM} \rightarrow e^+ e^-, \mu^+ \mu^-$
• • • We do not use the following data for averages, fits, limits, etc. • • •				
>1900	95	14 BOBOVNIKOV	18 RVUE	$pp, Z'_{SM} \rightarrow W^+ W^-$
>2020	95	15 AABOUD	16AA ATLS	$pp; Z'_{SM} \rightarrow \tau^+ \tau^-$
>1400	95	16 AAD	15AM ATLS	$pp; Z'_{SM} \rightarrow \tau^+ \tau^-$
>1470	95	17 AAD	13S ATLS	$pp; Z'_{SM} \rightarrow \tau^+ \tau^-$
>1470	95	18 CHATRCHYAN	13A CMS	$pp; Z'_{SM} \rightarrow q\bar{q}$
>2590	95	19 CHATRCHYAN	13AF CMS	$pp; Z'_{SM} \rightarrow e^+ e^-, \mu^+ \mu^-$
>2220	95	20 AAD	12CC ATLS	$pp; Z'_{SM} \rightarrow e^+ e^-, \mu^+ \mu^-$
>1400	95	21 CHATRCHYAN	12O CMS	$pp; Z'_{SM} \rightarrow \tau^+ \tau^-$
>1071	95	22 AALTONEN	11I CDF	$p\bar{p}; Z'_{SM} \rightarrow \mu^+ \mu^-$
>1023	95	23 ABZOV	11A D0	$p\bar{p}; Z'_{SM} \rightarrow e^+ e^-$
none 247-544	95	24 AALTONEN	10N CDF	$Z' \rightarrow WW$
none 320-740	95	25 AALTONEN	09AC CDF	$Z' \rightarrow q\bar{q}$
> 963	95	26 AALTONEN	09T CDF	$p\bar{p}; Z'_{SM} \rightarrow e^+ e^-$
>1403	95	27 ERLER	09 RVUE	Electroweak
>1305	95	28 ABDALLAH	06C DLPH	$e^+ e^-$
> 399	95	29 ACOSTA	05R CDF	$p\bar{p}; Z'_{SM} \rightarrow \tau^+ \tau^-$
none 400-640	95	30 ABZOV	04C D0	$p\bar{p}; Z'_{SM} \rightarrow q\bar{q}$
>1018	95	31 ABBIENDI	04G OPAL	$e^+ e^-$
> 670	95	32 ABZOV	01B D0	$p\bar{p}; Z'_{SM} \rightarrow e^+ e^-$
>1500	95	33 CHEUNG	01B RVUE	Electroweak
> 710	95	34 ABREU	00s DLPH	$e^+ e^-$
> 898	95	35 BARATE	00i ALEP	$e^+ e^-$
> 809	95	36 ERLER	99 RVUE	Electroweak
> 690	95	37 ABE	97s CDF	$p\bar{p}; Z'_{SM} \rightarrow e^+ e^-, \mu^+ \mu^-$
> 398	95	38 VILAIN	94B CHM2	$\nu_\mu e \rightarrow \nu_\mu e$ and $\bar{\nu}_\mu e \rightarrow \bar{\nu}_\mu e$
> 237	90	39 ALITTI	93 UA2	$p\bar{p}; Z'_{SM} \rightarrow q\bar{q}$
none 260-600	95	40 RIZZO	93 RVUE	$p\bar{p}; Z'_{SM} \rightarrow q\bar{q}$
> 426	90	41 ABE	90F VNS	$e^+ e^-$

- ¹ AAD 19L search for resonances decaying to $\ell^+ \ell^-$ in pp collisions at $\sqrt{s} = 13$ TeV.
² AABOUD 18AB search for resonances decaying to $b\bar{b}$ in pp collisions at $\sqrt{s} = 13$ TeV.
³ AABOUD 18G search for resonances decaying to $\tau^+ \tau^-$ in pp collisions at $\sqrt{s} = 13$ TeV.
⁴ SIRUNYAN 18BB search for resonances decaying to $\ell^+ \ell^-$ in pp collisions at $\sqrt{s} = 13$ TeV. See their Fig. 5 for limits on the Z' coupling strengths with light quarks.
⁵ SIRUNYAN 18BO search for resonances decaying to dijets in pp collisions at $\sqrt{s} = 13$ TeV.
⁶ AABOUD 17AT search for resonances decaying to $\ell^+ \ell^-$ in pp collisions at $\sqrt{s} = 13$ TeV.
⁷ KHACHATRYAN 17H search for resonances decaying to $\tau^+ \tau^-$ in pp collisions at $\sqrt{s} = 13$ TeV.
⁸ KHACHATRYAN 17T search for resonances decaying to $e^+ e^-, \mu^+ \mu^-$ in pp collisions at $\sqrt{s} = 8, 13$ TeV.

Limits for Z'_{LR}

Z'_{LR} is the extra neutral boson in left-right symmetric models. $g_L = g_R$ is assumed unless noted. Values in parentheses assume stronger constraint on the Higgs sector, usually motivated by specific left-right symmetric models (see the Note on the W'). Values in brackets are from cosmological and astrophysical considerations and assume a light right-handed neutrino. Direct search bounds assume decays to Standard Model fermions only, unless noted.

VALUE (GeV)	CL%	DOCUMENT ID	TECN	COMMENT
>1162	95	1 DEL-AGUILA	10 RVUE	Electroweak
> 630	95	2 ABE	97s CDF	$p\bar{p}; Z'_{LR} \rightarrow e^+ e^-, \mu^+ \mu^-$
• • • We do not use the following data for averages, fits, limits, etc. • • •				
> 998	95	3 BOBOVNIKOV	18 RVUE	$pp, Z'_{LR} \rightarrow W^+ W^-$
> 600	95	4 ERLER	09 RVUE	Electroweak
> 455	95	5 SCHAEEL	07A ALEP	$e^+ e^-$
> 518	95	6 ABDALLAH	06C DLPH	$e^+ e^-$
> 860	95	7 ABBIENDI	04G OPAL	$e^+ e^-$
> 380	95	8 CHEUNG	01B RVUE	Electroweak
> 436	95	9 ABREU	00s DLPH	$e^+ e^-$
> 550	95	10 BARATE	00i ALEP	Repl. by SCHAEEL 07A
> 1205	90	11 CHAY	00 RVUE	Electroweak
> 564	95	12 ERLER	00 RVUE	Cs
> 1673	95	13 ERLER	99 RVUE	Electroweak
> 1700	68	14 BARENBOIM	98 RVUE	Electroweak
> 244	95	15 CONRAD	98 RVUE	$\nu_\mu N$ scattering
> 253	95	16 VILAIN	94B CHM2	$\nu_\mu e \rightarrow \nu_\mu e$ and $\bar{\nu}_\mu e \rightarrow \bar{\nu}_\mu e$
none 200-600	95	17 RIZZO	93 RVUE	$p\bar{p}; Z'_{LR} \rightarrow q\bar{q}$
[> 2000]		18 WALKER	91 COSM	Nucleosynthesis; light ν_R
none 200-500		19 GRIFOLS	90 ASTR	SN 1987A; light ν_R
none 350-2400		20 BARBIERI	89B ASTR	SN 1987A; light ν_R

- 1 DEL-AGUILA 10 give 95% CL limit on the Z-Z' mixing $-0.0012 < \theta < 0.0004$.
- 2 ABE 97s find $\sigma(Z') \times B(e^+ e^-, \mu^+ \mu^-) < 40 \text{ fb}$ for $m_{Z'} > 600 \text{ GeV}$ at $\sqrt{s} = 1.8 \text{ TeV}$.
- 3 BOBOVNIKOV 18 use the ATLAS limits on $\sigma(pp \rightarrow Z') \cdot B(Z' \rightarrow W^+ W^-)$ to constrain the Z-Z' mixing parameter ξ . See their Fig. 10 for limits in $M_{Z'} - \xi$ plane.
- 4 ERLER 09 give 95% CL limit on the Z-Z' mixing $-0.0013 < \theta < 0.0006$.
- 5 ABDALLAH 06c give 95% CL limit $|\theta| < 0.0028$. See their Fig. 14 for limit contours in the mass-mixing plane.
- 6 ABBIENDI 04g give 95% CL limit on Z-Z' mixing $-0.00098 < \theta < 0.00190$. See their Fig. 20 for the limit contour in the mass-mixing plane. $\sqrt{s} = 91$ to 207 GeV.
- 7 CHEUNG 01b limit is derived from bounds on contact interactions in a global electroweak analysis.
- 8 ABREU 00s give 95% CL limit on Z-Z' mixing $|\theta| < 0.0018$. See their Fig. 6 for the limit contour in the mass-mixing plane. $\sqrt{s} = 90$ to 189 GeV.
- 9 BARATE 00i search for deviations in cross section and asymmetries in $e^+ e^- \rightarrow$ fermions at $\sqrt{s} = 90$ to 183 GeV. Assume $\theta = 0$. Bounds in the mass-mixing plane are shown in their Figure 18.
- 10 CHAY 00 also find $-0.0003 < \theta < 0.0019$. For g_R free, $m_{Z'} > 430 \text{ GeV}$.
- 11 ERLER 00 discuss the possibility that a discrepancy between the observed and predicted values of $Q_{W'}(Cs)$ is due to the exchange of Z'. The data are better described in a certain class of the Z' models including Z_{LR} and Z_χ .
- 12 CASALBUONI 99 discuss the discrepancy between the observed and predicted values of $Q_{W'}(Cs)$. It is shown that the data are better described in a class of models including the Z_{LR} model.
- 13 CZAKON 99 perform a simultaneous fit to charged and neutral sectors. Assumes manifest left-right symmetric model. Finds $|\theta| < 0.0042$.
- 14 ERLER 99 give 90% CL limit on the Z-Z' mixing $-0.0009 < \theta < 0.0017$.
- 15 ERLER 99 assumes 2 Higgs doublets, transforming as 10 of SO(10), embedded in E_6 .
- 16 BARENBOIM 98 also gives 68% CL limits on the Z-Z' mixing $-0.0005 < \theta < 0.0033$. Assumes Higgs sector of minimal left-right model.
- 17 CONRAD 98 limit is from measurements at CCFR, assuming no Z-Z' mixing.
- 18 VILAIN 94b assume $m_t = 150 \text{ GeV}$ and $\theta = 0$. See Fig. 2 for limit contours in the mass-mixing plane.
- 19 RIZZO 93 analyses CDF limit on possible two-jet resonances.
- 20 GRIFOLS 90 limit holds for $m_{\nu_R} \lesssim 1 \text{ MeV}$. A specific Higgs sector is assumed. See also GRIFOLS 90d, RIZZO 91.
- 21 BARBIERI 89b limit holds for $m_{\nu_R} \lesssim 10 \text{ MeV}$. Bounds depend on assumed supernova core temperature.

Limits for Z_χ

Z_χ is the extra neutral boson in $\text{SO}(10) \rightarrow \text{SU}(5) \times \text{U}(1)_\chi$. $g_\chi = e/\cos\theta_W$ is assumed unless otherwise stated. We list limits with the assumption $\rho = 1$ but with no further constraints on the Higgs sector. Values in parentheses assume stronger constraint on the Higgs sector motivated by superstring models. Values in brackets are from cosmological and astrophysical considerations and assume a light right-handed neutrino.

VALUE (GeV)	CL%	DOCUMENT ID	TECN	COMMENT
none 250-4800	95	1 AAD	19L ATLS	$pp; Z'_\chi \rightarrow e^+ e^-, \mu^+ \mu^-$
>4100	95	2 AABOUD	17AT ATLS	$pp; Z'_\chi \rightarrow e^+ e^-, \mu^+ \mu^-$
••• We do not use the following data for averages, fits, limits, etc. •••				
>3050	95	3 BOBOVNIKOV 18	RVUE	$pp, Z'_\chi \rightarrow W^+ W^-$
>2620	95	4 AABOUD	16u ATLS	$pp; Z'_\chi \rightarrow e^+ e^-, \mu^+ \mu^-$
>1970	95	5 AAD	14v ATLS	$pp, Z'_\chi \rightarrow e^+ e^-, \mu^+ \mu^-$
>1970	95	6 AAD	12cc ATLS	$pp, Z'_\chi \rightarrow e^+ e^-, \mu^+ \mu^-$
> 930	95	7 AALTONEN	11i CDF	$p\bar{p}; Z'_\chi \rightarrow \mu^+ \mu^-$
> 903	95	8 ABAZOV	11A D0	$p\bar{p}; Z'_\chi \rightarrow e^+ e^-$
>1022	95	9 DEL-AGUILA	10 RVUE	Electroweak
> 862	95	8 AALTONEN	09T CDF	$p\bar{p}; Z'_\chi \rightarrow e^+ e^-$
> 892	95	10 AALTONEN	09v CDF	Repl. by AALTONEN 11i
>1141	95	11 ERLER	09 RVUE	Electroweak
> 822	95	8 AALTONEN	07H CDF	Repl. by AALTONEN 09T
> 680	95	SCHAEEL	07A ALEP	$e^+ e^-$
> 545	95	12 ABDALLAH	06c DLPH	$e^+ e^-$
> 740	95	8 ABULENCIA	06L CDF	Repl. by AALTONEN 07H
> 690	95	13 ABULENCIA	05A CDF	$p\bar{p}; Z'_\chi \rightarrow e^+ e^-, \mu^+ \mu^-$
> 781	95	14 ABBIENDI	04g OPAL	$e^+ e^-$
>2100	95	15 BARGER	03b COSM	Nucleosynthesis; light ν_R
> 680	95	16 CHEUNG	01b RVUE	Electroweak
> 440	95	17 ABREU	00s DLPH	$e^+ e^-$
> 533	95	18 BARATE	00i ALEP	Repl. by SCHAEEL 07A
> 554	95	19 CHO	00 RVUE	Electroweak
		20 ERLER	00 RVUE	Cs
		21 ROSNER	00 RVUE	Cs
> 545	95	22 ERLER	99 RVUE	Electroweak
(> 1368)	95	23 ERLER	99 RVUE	Electroweak
> 215	95	24 CONRAD	98 RVUE	$\nu_\mu N$ scattering
> 595	95	25 ABE	97s CDF	$p\bar{p}; Z'_\chi \rightarrow e^+ e^-, \mu^+ \mu^-$
> 190	95	26 ARIMA	97 VNS	Bhabha scattering
> 262	95	27 VILAIN	94b CHM2	$\nu_\mu e \rightarrow \nu_\mu e; \bar{\nu}_\mu e \rightarrow \bar{\nu}_\mu e$
[>1470]		28 FARAGGI	91 COSM	Nucleosynthesis; light ν_R
> 231	90	29 ABE	90F VNS	$e^+ e^-$
[> 1140]		30 GONZALEZ...	90d COSM	Nucleosynthesis; light ν_R
[> 2100]		31 GRIFOLS	90 ASTR	SN 1987A; light ν_R

- 1 AAD 19L search for resonances decaying to $\ell^+ \ell^-$ in pp collisions at $\sqrt{s} = 13 \text{ TeV}$.
- 2 AABOUD 17AT search for resonances decaying to $\ell^+ \ell^-$ in pp collisions at $\sqrt{s} = 13 \text{ TeV}$.
- 3 BOBOVNIKOV 18 use the ATLAS limits on $\sigma(pp \rightarrow Z') \cdot B(Z' \rightarrow W^+ W^-)$ to constrain the Z-Z' mixing parameter ξ . See their Fig. 9 for limits in $M_{Z'} - \xi$ plane.
- 4 AABOUD 16u search for resonances decaying to $\ell^+ \ell^-$ in pp collisions at $\sqrt{s} = 13 \text{ TeV}$.
- 5 AAD 14v search for resonances decaying to $e^+ e^-, \mu^+ \mu^-$ in pp collisions at $\sqrt{s} = 8 \text{ TeV}$.
- 6 AAD 12cc search for resonances decaying to $e^+ e^-, \mu^+ \mu^-$ in pp collisions at $\sqrt{s} = 7 \text{ TeV}$.
- 7 AALTONEN 11i search for resonances decaying to $\mu^+ \mu^-$ in $p\bar{p}$ collisions at $\sqrt{s} = 1.96 \text{ TeV}$.
- 8 ABIZOVI 11A, AALTONEN 09T, AALTONEN 07H, and ABULENCIA 06L search for resonances decaying to $e^+ e^-$ in $p\bar{p}$ collisions at $\sqrt{s} = 1.96 \text{ TeV}$.
- 9 DEL-AGUILA 10 give 95% CL limit on the Z-Z' mixing $-0.0011 < \theta < 0.0007$.
- 10 AALTONEN 09v search for resonances decaying to $\mu^+ \mu^-$ in $p\bar{p}$ collisions at $\sqrt{s} = 1.96 \text{ TeV}$.
- 11 ERLER 09 give 95% CL limit on the Z-Z' mixing $-0.0016 < \theta < 0.0006$.
- 12 ABDALLAH 06c give 95% CL limit $|\theta| < 0.0031$. See their Fig. 14 for limit contours in the mass-mixing plane.
- 13 ABULENCIA 05A search for resonances decaying to electron or muon pairs in $p\bar{p}$ collisions at $\sqrt{s} = 1.96 \text{ TeV}$.
- 14 ABBIENDI 04g give 95% CL limit on Z-Z' mixing $-0.00099 < \theta < 0.00194$. See their Fig. 20 for the limit contour in the mass-mixing plane. $\sqrt{s} = 91$ to 207 GeV.
- 15 BARGER 03b limit is from the nucleosynthesis bound on the effective number of light neutrino $\delta N_\nu < 1$. The quark-hadron transition temperature $T_C = 150 \text{ MeV}$ is assumed. The limit with $T_C = 400 \text{ MeV}$ is $>4300 \text{ GeV}$.
- 16 CHEUNG 01b limit is derived from bounds on contact interactions in a global electroweak analysis.
- 17 ABREU 00s give 95% CL limit on Z-Z' mixing $|\theta| < 0.0017$. See their Fig. 6 for the limit contour in the mass-mixing plane. $\sqrt{s} = 90$ to 189 GeV.
- 18 BARATE 00i search for deviations in cross section and asymmetries in $e^+ e^- \rightarrow$ fermions at $\sqrt{s} = 90$ to 183 GeV. Assume $\theta = 0$. Bounds in the mass-mixing plane are shown in their Figure 18.
- 19 CHO 00 use various electroweak data to constrain Z' models assuming $m_H = 100 \text{ GeV}$. See Fig. 3 for limits in the mass-mixing plane.
- 20 ERLER 00 discuss the possibility that a discrepancy between the observed and predicted values of $Q_{W'}(Cs)$ is due to the exchange of Z'. The data are better described in a certain class of the Z' models including Z_{LR} and Z_χ .
- 21 ROSNER 00 discusses the possibility that a discrepancy between the observed and predicted values of $Q_{W'}(Cs)$ is due to the exchange of Z'. The data are better described in a certain class of the Z' models including Z_χ .
- 22 ERLER 99 give 90% CL limit on the Z-Z' mixing $-0.0020 < \theta < 0.0015$.
- 23 ERLER 99 assumes 2 Higgs doublets, transforming as 10 of SO(10), embedded in E_6 .
- 24 CONRAD 98 limit is from measurements at CCFR, assuming no Z-Z' mixing.
- 25 ABE 97s find $\sigma(Z') \times B(e^+ e^-, \mu^+ \mu^-) < 40 \text{ fb}$ for $m_{Z'} > 600 \text{ GeV}$ at $\sqrt{s} = 1.8 \text{ TeV}$.
- 26 Z-Z' mixing is assumed to be zero. $\sqrt{s} = 57.77 \text{ GeV}$.
- 27 VILAIN 94b assume $m_t = 150 \text{ GeV}$ and $\theta = 0$. See Fig. 2 for limit contours in the mass-mixing plane.
- 28 FARAGGI 91 limit assumes the nucleosynthesis bound on the effective number of neutrinos $\Delta N_\nu < 0.5$ and is valid for $m_{\nu_R} < 1 \text{ MeV}$.
- 29 ABE 90F use data for $R, R_{\ell\ell}$, and $A_{\ell\ell}$. ABE 90F fix $m_W = 80.49 \pm 0.43 \pm 0.24 \text{ GeV}$ and $m_Z = 91.13 \pm 0.03 \text{ GeV}$.
- 30 Assumes the nucleosynthesis bound on the effective number of light neutrinos ($\delta N_\nu < 1$) and that ν_R is light ($\lesssim 1 \text{ MeV}$).
- 31 GRIFOLS 90 limit holds for $m_{\nu_R} \lesssim 1 \text{ MeV}$. See also GRIFOLS 90d, RIZZO 91.

Limits for Z_ψ

Z_ψ is the extra neutral boson in $E_6 \rightarrow \text{SO}(10) \times \text{U}(1)_\psi$. $g_\psi = e/\cos\theta_W$ is assumed unless otherwise stated. We list limits with the assumption $\rho = 1$ but with no further constraints on the Higgs sector. Values in brackets are from cosmological and astrophysical considerations and assume a light right-handed neutrino.

VALUE (GeV)	CL%	DOCUMENT ID	TECN	COMMENT
>3900 (CL = 95%) OUR LIMIT				
none 250-4500	95	1 AAD	19L ATLS	$pp; Z'_\psi \rightarrow e^+ e^-, \mu^+ \mu^-$
none 200-3900	95	2 SIRUNYAN	18BB CMS	$pp; Z'_\psi \rightarrow e^+ e^-, \mu^+ \mu^-$
>3800	95	3 AABOUD	17AT ATLS	$pp; Z'_\psi \rightarrow e^+ e^-, \mu^+ \mu^-$
>2820	95	4 KHACHATRY...17T	CMS	$pp; Z'_\psi \rightarrow e^+ e^-, \mu^+ \mu^-$
>1100	95	5 CHATRCHYAN12o	CMS	$pp, Z'_\psi \rightarrow \tau^+ \tau^-$
••• We do not use the following data for averages, fits, limits, etc. •••				
>2740	95	6 BOBOVNIKOV 18	RVUE	$pp, Z'_\psi \rightarrow W^+ W^-$
>2570	95	7 AABOUD	16u ATLS	$pp; Z'_\psi \rightarrow e^+ e^-, \mu^+ \mu^-$
>2510	95	8 KHACHATRY...15AE	CMS	$pp; Z'_\psi \rightarrow e^+ e^-, \mu^+ \mu^-$
>2510	95	9 AAD	14v ATLS	$pp, Z'_\psi \rightarrow e^+ e^-, \mu^+ \mu^-$
>2260	95	10 CHATRCHYAN13AF	CMS	$pp, Z'_\psi \rightarrow e^+ e^-, \mu^+ \mu^-$
>1790	95	11 AAD	12cc ATLS	$pp, Z'_\psi \rightarrow e^+ e^-, \mu^+ \mu^-$
>2000	95	12 CHATRCHYAN12M	CMS	Repl. by CHATRCHYAN 13AF
> 917	95	13 AALTONEN	11i CDF	$p\bar{p}; Z'_\psi \rightarrow \mu^+ \mu^-$
> 891	95	14 ABAZOV	11A D0	$p\bar{p}; Z'_\psi \rightarrow e^+ e^-$
> 476	95	15 DEL-AGUILA	10 RVUE	Electroweak
> 851	95	14 AALTONEN	09T CDF	$p\bar{p}; Z'_\psi \rightarrow e^+ e^-$
> 878	95	16 AALTONEN	09v CDF	Repl. by AALTONEN 11i
> 147	95	17 ERLER	09 RVUE	Electroweak

Gauge & Higgs Boson Particle Listings

New Heavy Bosons

> 822	95	14	AALTONEN	07H	CDF	Repl. by AALTONEN 09T
> 410	95		SCHAEEL	07A	ALEP	e^+e^-
> 475	95		ABDALLAH	06C	DLPH	e^+e^-
> 725		14	ABULENCIA	06L	CDF	Repl. by AALTONEN 07H
> 675	95	19	ABULENCIA	05A	CDF	Repl. by AALTONEN 11i and AALTONEN 09T
> 366	95	20	ABBIENDI	04G	OPAL	e^+e^-
> 600		21	BARGER	03B	COSM	Nucleosynthesis; light ν_R
> 350	95	22	ABREU	00S	DLPH	e^+e^-
> 294	95	23	BARATE	00i	ALEP	Repl. by SCHAEEL 07A
> 137	95	24	CHO	00	RVUE	Electroweak
> 146	95	25	ERLER	99	RVUE	Electroweak
> 54	95	26	CONRAD	98	RVUE	$\nu_\mu N$ scattering
> 590	95	27	ABE	97S	CDF	$p\bar{p}; Z'_\psi \rightarrow e^+e^-, \mu^+\mu^-$
> 135	95	28	VILAIN	94B	CHM2	$\nu_\mu e \rightarrow \nu_\mu e; \bar{\nu}_\mu e \rightarrow \bar{\nu}_\mu e$
> 105	90	29	ABE	90F	VNS	e^+e^-
[> 160]		30	GONZALEZ...	90D	COSM	Nucleosynthesis; light ν_R
[> 2000]		31	GRIFOLS	90D	ASTR	SN 1987A; light ν_R

- AAD 19L search for resonances decaying to $\ell^+\ell^-$ in pp collisions at $\sqrt{s} = 13$ TeV.
- SIRUNYAN 18BB search for resonances decaying to $\ell^+\ell^-$ in pp collisions at $\sqrt{s} = 13$ TeV.
- AABOUD 17AT search for resonances decaying to $\ell^+\ell^-$ in pp collisions at $\sqrt{s} = 13$ TeV.
- KHACHATRYAN 17T search for resonances decaying to $e^+e^-, \mu^+\mu^-$ in pp collisions at $\sqrt{s} = 8, 13$ TeV.
- CHATRCHYAN 12C search for resonances decaying to $\tau^+\tau^-$ in pp collisions at $\sqrt{s} = 7$ TeV.
- BOBOVNIKOV 18 use the ATLAS limits on $\sigma(pp \rightarrow Z')B(Z' \rightarrow W^+W^-)$ to constrain the Z - Z' mixing parameter ξ . See their Fig. 10 for limits in $M_{Z'}-\xi$ plane.
- AABOUD 16U search for resonances decaying to $\ell^+\ell^-$ in pp collisions at $\sqrt{s} = 13$ TeV.
- KHACHATRYAN 15AE search for resonances decaying to $e^+e^-, \mu^+\mu^-$ in pp collisions at $\sqrt{s} = 8$ TeV.
- AAD 14V search for resonances decaying to $e^+e^-, \mu^+\mu^-$ in pp collisions at $\sqrt{s} = 8$ TeV.
- CHATRCHYAN 13AF search for resonances decaying to $e^+e^-, \mu^+\mu^-$ in pp collisions at $\sqrt{s} = 7$ TeV and 8 TeV.
- AAD 12CC search for resonances decaying to $e^+e^-, \mu^+\mu^-$ in pp collisions at $\sqrt{s} = 7$ TeV.
- CHATRCHYAN 12M search for resonances decaying to e^+e^- or $\mu^+\mu^-$ in pp collisions at $\sqrt{s} = 7$ TeV.
- AALTONEN 11i search for resonances decaying to $\mu^+\mu^-$ in $p\bar{p}$ collisions at $\sqrt{s} = 1.96$ TeV.
- ABAZOV 11A, AALTONEN 09T, AALTONEN 07H, and ABULENCIA 06L search for resonances decaying to e^+e^- in $p\bar{p}$ collisions at $\sqrt{s} = 1.96$ TeV.
- DEL-AGUILA 10 give 95% CL limit on the Z - Z' mixing $-0.0019 < \theta < 0.0007$.
- AALTONEN 09V search for resonances decaying to $\mu^+\mu^-$ in $p\bar{p}$ collisions at $\sqrt{s} = 1.96$ TeV.
- ERLER 09 give 95% CL limit on the Z - Z' mixing $-0.0018 < \theta < 0.0009$.
- ABDALLAH 06C give 95% CL limit $|\theta| < 0.0027$. See their Fig. 14 for limit contours in the mass-mixing plane.
- ABULENCIA 05A search for resonances decaying to electron or muon pairs in $p\bar{p}$ collisions at $\sqrt{s} = 1.96$ TeV.
- ABBIENDI 04G give 95% CL limit on Z - Z' mixing $-0.00129 < \theta < 0.00258$. See their Fig. 20 for the limit contour in the mass-mixing plane. $\sqrt{s} = 91$ to 207 GeV.
- BARGER 03B limit is from the nucleosynthesis bound on the effective number of light neutrino $\delta N_\nu < 1$. The quark-hadron transition temperature $T_C = 150$ MeV is assumed. The limit with $T_C = 400$ MeV is > 1100 GeV.
- ABREU 00S give 95% CL limit on Z - Z' mixing $|\theta| < 0.0018$. See their Fig. 6 for the limit contour in the mass-mixing plane. $\sqrt{s} = 90$ to 189 GeV.
- BARATE 00i search for deviations in cross section and asymmetries in $e^+e^- \rightarrow$ fermions at $\sqrt{s} = 90$ to 183 GeV. Assume $\theta = 0$. Bounds in the mass-mixing plane are shown in their Figure 18.
- CHO 00 use various electroweak data to constrain Z' models assuming $m_H = 100$ GeV. See Fig. 3 for limits in the mass-mixing plane.
- ERLER 99 give 90% CL limit on the Z - Z' mixing $-0.0013 < \theta < 0.0024$.
- CONRAD 98 limit is from measurements at CCFR, assuming no Z - Z' mixing.
- ABE 97S find $\sigma(Z') \times B(e^+e^-, \mu^+\mu^-) < 40$ fb for $m_{Z'} > 600$ GeV at $\sqrt{s} = 1.8$ TeV.
- VILAIN 94B assume $m_t = 150$ GeV and $\theta = 0$. See Fig. 2 for limit contours in the mass-mixing plane.
- ABE 90F use data for $R, R_{\ell\ell}$, and $A_{\ell\ell}$. ABE 90F fix $m_W = 80.49 \pm 0.43 \pm 0.24$ GeV and $m_Z = 91.13 \pm 0.03$ GeV.
- Assumes the nucleosynthesis bound on the effective number of light neutrinos ($\delta N_\nu < 1$) and that ν_R is light ($\lesssim 1$ MeV).
- GRIFOLS 90D limit holds for $m_{\nu_R} \lesssim 1$ MeV. See also RIZZO 91.

Limits for Z_η

Z_η is the extra neutral boson in E_6 models, corresponding to $Q_\eta = \sqrt{3/8} Q_X - \sqrt{5/8} Q_\psi$. $g_\eta = e/\cos\theta_W$ is assumed unless otherwise stated. We list limits with the assumption $\rho = 1$ but with no further constraints on the Higgs sector. Values in parentheses assume stronger constraint on the Higgs sector motivated by superstring models. Values in brackets are from cosmological and astrophysical considerations and assume a light right-handed neutrino.

VALUE (GeV)	CL%	DOCUMENT ID	TECN	COMMENT
>3900	95	1 AABOUD	17AT ATLS	$p\bar{p}; Z'_\eta \rightarrow e^+e^-, \mu^+\mu^-$

• • • We do not use the following data for averages, fits, limits, etc. • • •

>2810	95	2	BOBOVNIKOV	18	RVUE	$p\bar{p}; Z'_\eta \rightarrow W^+W^-$
>1870	95	3	AABOUD	16U	ATLS	$p\bar{p}; Z'_\eta \rightarrow e^+e^-, \mu^+\mu^-$
> 938	95	4	AAD	12CC	ATLS	$p\bar{p}; Z'_\eta \rightarrow e^+e^-, \mu^+\mu^-$
> 923	95	5	AALTONEN	11i	CDF	$p\bar{p}; Z'_\eta \rightarrow \mu^+\mu^-$
> 488	95	6	ABAZOV	11A	D0	$p\bar{p}; Z'_\eta \rightarrow e^+e^-$
> 877	95	7	DEL-AGUILA	10	RVUE	Electroweak
> 904	95	8	AALTONEN	09T	CDF	$p\bar{p}; Z'_\eta \rightarrow e^+e^-$
> 427	95	9	ERLER	09	RVUE	Electroweak
> 891	95	10	AALTONEN	07H	CDF	Repl. by AALTONEN 09T
> 350	95		SCHAEEL	07A	ALEP	e^+e^-
> 360	95	11	ABULENCIA	06L	CDF	Repl. by AALTONEN 07H
> 745	95	12	ABULENCIA	05A	CDF	Repl. by AALTONEN 11i and AALTONEN 09T
> 720	95	13	ABBIENDI	04G	OPAL	e^+e^-
> 515	95	14	BARGER	03B	COSM	Nucleosynthesis; light ν_R
>1600		15	ABREU	00S	DLPH	e^+e^-
> 310	95	16	BARATE	00i	ALEP	Repl. by SCHAEEL 07A
> 329	95	17	CHO	00	RVUE	Electroweak
> 619	95	18	ERLER	99	RVUE	Electroweak
> 365	95	19	CONRAD	98	RVUE	$\nu_\mu N$ scattering
> 87	95	20	ABE	97S	CDF	$p\bar{p}; Z'_\eta \rightarrow e^+e^-, \mu^+\mu^-$
> 620	95	21	VILAIN	94B	CHM2	$\nu_\mu e \rightarrow \nu_\mu e; \bar{\nu}_\mu e \rightarrow \bar{\nu}_\mu e$
> 100	95	22	ABE	90F	VNS	e^+e^-
> 125	90	23	GONZALEZ...	90D	COSM	Nucleosynthesis; light ν_R
[> 820]		24	GRIFOLS	90	ASTR	SN 1987A; light ν_R
[> 3300]		25	LOPEZ	90	COSM	Nucleosynthesis; light ν_R
[> 1040]		26				

- AABOUD 17AT search for resonances decaying to $\ell^+\ell^-$ in pp collisions at $\sqrt{s} = 13$ TeV.
- BOBOVNIKOV 18 use the ATLAS limits on $\sigma(pp \rightarrow Z')B(Z' \rightarrow W^+W^-)$ to constrain the Z - Z' mixing parameter ξ . See their Fig. 9 for limits in $M_{Z'}-\xi$ plane.
- AABOUD 16U search for resonances decaying to $\ell^+\ell^-$ in pp collisions at $\sqrt{s} = 13$ TeV.
- AAD 12CC search for resonances decaying to $e^+e^-, \mu^+\mu^-$ in pp collisions at $\sqrt{s} = 7$ TeV.
- AALTONEN 11i search for resonances decaying to $\mu^+\mu^-$ in $p\bar{p}$ collisions at $\sqrt{s} = 1.96$ TeV.
- ABAZOV 11A, AALTONEN 09T, AALTONEN 07H, and ABULENCIA 06L search for resonances decaying to e^+e^- in $p\bar{p}$ collisions at $\sqrt{s} = 1.96$ TeV.
- DEL-AGUILA 10 give 95% CL limit on the Z - Z' mixing $-0.0023 < \theta < 0.0027$.
- AALTONEN 09V search for resonances decaying to $\mu^+\mu^-$ in $p\bar{p}$ collisions at $\sqrt{s} = 1.96$ TeV.
- ERLER 09 give 95% CL limit on the Z - Z' mixing $-0.0047 < \theta < 0.0021$.
- ABDALLAH 06C give 95% CL limit $|\theta| < 0.0092$. See their Fig. 14 for limit contours in the mass-mixing plane.
- ABULENCIA 05A search for resonances decaying to electron or muon pairs in $p\bar{p}$ collisions at $\sqrt{s} = 1.96$ TeV.
- ABBIENDI 04G give 95% CL limit on Z - Z' mixing $-0.00447 < \theta < 0.00331$. See their Fig. 20 for the limit contour in the mass-mixing plane. $\sqrt{s} = 91$ to 207 GeV.
- BARGER 03B limit is from the nucleosynthesis bound on the effective number of light neutrino $\delta N_\nu < 1$. The quark-hadron transition temperature $T_C = 150$ MeV is assumed. The limit with $T_C = 400$ MeV is > 3300 GeV.
- ABREU 00S give 95% CL limit on Z - Z' mixing $|\theta| < 0.0024$. See their Fig. 6 for the limit contour in the mass-mixing plane. $\sqrt{s} = 90$ to 189 GeV.
- BARATE 00i search for deviations in cross section and asymmetries in $e^+e^- \rightarrow$ fermions at $\sqrt{s} = 90$ to 183 GeV. Assume $\theta = 0$. Bounds in the mass-mixing plane are shown in their Figure 18.
- CHO 00 use various electroweak data to constrain Z' models assuming $m_H = 100$ GeV. See Fig. 3 for limits in the mass-mixing plane.
- ERLER 99 give 90% CL limit on the Z - Z' mixing $-0.0062 < \theta < 0.0011$.
- CONRAD 98 limit is from measurements at CCFR, assuming no Z - Z' mixing.
- ABE 97S find $\sigma(Z') \times B(e^+e^-, \mu^+\mu^-) < 40$ fb for $m_{Z'} > 600$ GeV at $\sqrt{s} = 1.8$ TeV.
- VILAIN 94B assume $m_t = 150$ GeV and $\theta = 0$. See Fig. 2 for limit contours in the mass-mixing plane.
- ABE 90F use data for $R, R_{\ell\ell}$, and $A_{\ell\ell}$. ABE 90F fix $m_W = 80.49 \pm 0.43 \pm 0.24$ GeV and $m_Z = 91.13 \pm 0.03$ GeV.
- These authors claim that the nucleosynthesis bound on the effective number of light neutrinos ($\delta N_\nu < 1$) constrains Z' masses if ν_R is light ($\lesssim 1$ MeV).
- GRIFOLS 90 limit holds for $m_{\nu_R} \lesssim 1$ MeV. See also GRIFOLS 90D, RIZZO 91.

Limits for other Z'

VALUE (GeV)	CL%	DOCUMENT ID	TECN	COMMENT
none 580-3100	95	1 AABOUD	19AS ATLS	$Z' \rightarrow t\bar{t}$
none 1300-3100	95	2 AAD	19D ATLS	$Z' \rightarrow WW$
>3800	95	3 SIRUNYAN	19AA CMS	$Z' \rightarrow t\bar{t}$
>3700	95	4 SIRUNYAN	19CP CMS	$Z' \rightarrow WW, HZ, \ell^+\ell^-$
>1800	95	5 SIRUNYAN	19I CMS	$Z' \rightarrow HZ$
none 600-2100	95	6 AABOUD	18AB ATLS	$Z' \rightarrow b\bar{b}$
none 500-2830	95	7 AABOUD	18AI ATLS	$Z' \rightarrow HZ$
none 300-3000	95	8 AABOUD	18AK ATLS	$Z' \rightarrow WW$
>1300	95	9 AABOUD	18B ATLS	$Z' \rightarrow WW$
none 400-3000	95	10 AABOUD	18BI ATLS	$Z' \rightarrow t\bar{t}$
none 1200-2800	95	11 AABOUD	18F ATLS	$Z' \rightarrow WW$
>2300	95	12 SIRUNYAN	18ED CMS	$Z' \rightarrow HZ$

See key on page 999

Gauge & Higgs Boson Particle Listings
New Heavy Bosons

none 1200–2700	95	13	SIRUNYAN	18P	CMS	$Z' \rightarrow WW$
>2900	95	14	AABOUD	17AK	ATLS	$Z' \rightarrow q\bar{q}$
none 1100–2600	95	15	AABOUD	17AO	ATLS	$Z' \rightarrow HZ$
>2300	95	16	SIRUNYAN	17AK	CMS	$Z' \rightarrow WW, HZ$
>2500	95	17	SIRUNYAN	17Q	CMS	$Z' \rightarrow t\bar{t}$
>1190	95	18	SIRUNYAN	17R	CMS	$Z' \rightarrow HZ$
none 1210–2260	95	18	SIRUNYAN	17R	CMS	$Z' \rightarrow HZ$
••• We do not use the following data for averages, fits, limits, etc. •••						
		19	AABOUD	19AJ	ATLS	$Z' \rightarrow q\bar{q}$
		20	AABOUD	19D	ATLS	$Z' \rightarrow q\bar{q}$
		21	AABOUD	19V	ATLS	DM simplified Z'
		22	AAD	19L	ATLS	$Z' \rightarrow e^+e^-, \mu^+\mu^-$
		23	LONG	19	RVUE	Electroweak
		24	PANDEY	19	RVUE	neutrino NSI
		25	SIRUNYAN	19AL	CMS	$Z' \rightarrow tT, T \rightarrow Ht, Zt, Wb$
		26	SIRUNYAN	19AN	CMS	DM simplified Z'
		27	SIRUNYAN	19CB	CMS	$Z' \rightarrow q\bar{q}$
		28	SIRUNYAN	19CD	CMS	$Z' \rightarrow q\bar{q}$
		29	SIRUNYAN	19D	CMS	$Z' \rightarrow H\gamma$
		30	AABOUD	18AA	ATLS	$Z' \rightarrow H\gamma$
>4500	95	31	AABOUD	18CJ	ATLS	$Z' \rightarrow WW, HZ, \ell^+\ell^-$
		32	AABOUD	18N	ATLS	$Z' \rightarrow q\bar{q}$
		33	AAIJ	18AQ	LHCB	$Z' \rightarrow \mu^+\mu^-$
		34	SIRUNYAN	18DR	CMS	$Z' \rightarrow \mu^+\mu^-$
		35	SIRUNYAN	18G	CMS	$Z' \rightarrow q\bar{q}$
		36	SIRUNYAN	18I	CMS	$Z' \rightarrow b\bar{b}$
>1580	95	37	AABOUD	17B	ATLS	$Z' \rightarrow HZ$
		38	KHACHATRY...	17AX	CMS	$Z' \rightarrow \ell\ell\ell$
		39	KHACHATRY...	17U	CMS	$Z' \rightarrow HZ$
>1700	95	40	SIRUNYAN	17A	CMS	$Z' \rightarrow WW$
		41	SIRUNYAN	17AP	CMS	$Z' \rightarrow HA$
		42	SIRUNYAN	17T	CMS	$Z' \rightarrow q\bar{q}$
		43	SIRUNYAN	17V	CMS	$Z' \rightarrow Tt$
none 1100–1500	95	44	AABOUD	16	ATLS	$Z' \rightarrow b\bar{b}$
		45	AAD	16L	ATLS	$Z' \rightarrow a\gamma, a \rightarrow \gamma\gamma$
none 1500–2600	95	46	AAD	16S	ATLS	$Z' \rightarrow q\bar{q}$
none 1000–1100, none 1300–1500	95	47	KHACHATRY...	16AP	CMS	$Z' \rightarrow HZ$
>2400	95	48	KHACHATRY...	16E	CMS	$Z' \rightarrow t\bar{t}$
		49	AAD	15AO	ATLS	$Z' \rightarrow t\bar{t}$
		50	AAD	15AT	ATLS	monotop
		51	AAD	15CD	ATLS	$H \rightarrow ZZ', Z'Z'; Z' \rightarrow \ell^+\ell^-$
		52	KHACHATRY...	15F	CMS	monotop
		53	KHACHATRY...	15O	CMS	$Z' \rightarrow HZ$
		54	AAD	14AT	ATLS	$Z' \rightarrow Z\gamma$
		55	KHACHATRY...	14A	CMS	$Z' \rightarrow VV$
		56	MARTINEZ	14	RVUE	Electroweak
none 500–1740	95	57	AAD	13AQ	ATLS	$Z' \rightarrow t\bar{t}$
>1320 or 1000–1280	95	58	AAD	13G	ATLS	$Z' \rightarrow t\bar{t}$
> 915	95	58	AALTONEN	13A	CDF	$Z' \rightarrow t\bar{t}$
>1300	95	59	CHATRCHYAN	13AP	CMS	$Z' \rightarrow t\bar{t}$
>2100	95	58	CHATRCHYAN	13BM	CMS	$Z' \rightarrow t\bar{t}$
		60	AAD	12BV	ATLS	$Z' \rightarrow t\bar{t}$
		61	AAD	12K	ATLS	$Z' \rightarrow t\bar{t}$
		62	AALTONEN	12AR	CDF	Chromophilic
		63	AALTONEN	12N	CDF	$Z' \rightarrow \tau\nu$
> 835	95	64	ABAZOV	12R	D0	$Z' \rightarrow t\bar{t}$
		65	CHATRCHYAN	12AI	CMS	$Z' \rightarrow t\bar{t}$
		66	CHATRCHYAN	12AQ	CMS	$Z' \rightarrow t\bar{t}$
>1490	95	58	CHATRCHYAN	12BL	CMS	$Z' \rightarrow t\bar{t}$
		67	AALTONEN	11AD	CDF	$Z' \rightarrow t\bar{t}$
		68	AALTONEN	11AE	CDF	$Z' \rightarrow t\bar{t}$
		69	CHATRCHYAN	11O	CMS	$pp \rightarrow tt$
		70	AALTONEN	08D	CDF	$Z' \rightarrow t\bar{t}$
		70	AALTONEN	08Y	CDF	$Z' \rightarrow t\bar{t}$
		70	ABAZOV	08AA	D0	$Z' \rightarrow t\bar{t}$
		71	ABAZOV	04A	D0	Repl. by ABAZOV 08AA
		72	BARGER	03B	COSM	Nucleosynthesis; light ν_R
		73	CHO	00	RVUE	E_6 -motivated
		74	CHO	98	RVUE	E_6 -motivated
		75	ABE	97G	CDF	$Z' \rightarrow q\bar{q}$

¹ AABOUD 19As search for a resonance decaying to $t\bar{t}$ in pp collisions at $\sqrt{s} = 13$ TeV. The quoted limit is for a top-color Z' with $\Gamma_{Z'}/M_{Z'} = 0.01$. Limits are also set on Z' masses in simplified Dark Matter models.

² AAD 19D search for resonances decaying to WW in pp collisions at $\sqrt{s} = 13$ TeV. The quoted limit is for heavy-vector-triplet Z' with $g_V = 3$. The limit becomes $M_{Z'} > 2900$ GeV for $g_V = 1$. If we assume $M_{Z'} = M_{W'}$, the limit increases $M_{Z'} > 3800$ GeV and $M_{Z'} > 3500$ GeV for $g_V = 3$ and $g_V = 1$, respectively. See their Fig. 9 for limits on $\sigma \cdot B$.

³ SIRUNYAN 19AA search for a resonance decaying to $t\bar{t}$ in pp collisions at $\sqrt{s} = 13$ TeV. The quoted limit is for a leptophobic top-color Z' with $\Gamma_{Z'}/M_{Z'} = 0.01$.

⁴ SIRUNYAN 19CP present a statistical combinations of searches for Z' decaying to pairs of bosons or leptons in pp collisions at $\sqrt{s} = 13$ TeV. The quoted limit is for heavy-vector-triplet Z' with $g_V = 3$. If we assume $M_{Z'} = M_{W'}$, the limit becomes $M_{Z'} > 4500$ GeV for $g_V = 3$ and $M_{Z'} > 5000$ GeV for $g_V = 1$. See their Figs. 2 and 3 for limits on $\sigma \cdot B$.

⁵ SIRUNYAN 19I search for resonances decaying to ZW in pp collisions at $\sqrt{s} = 13$ TeV. The quoted limit is for heavy-vector-triplet Z' with $g_V = 3$. The limit becomes $M_{Z'} > 2800$ GeV if we assume $M_{Z'} = M_{W'}$.

⁶ AABOUD 18AB search for resonances decaying to $b\bar{b}$ in pp collisions at $\sqrt{s} = 13$ TeV. The limit quoted above is for a leptophobic Z' with SM-like couplings to quarks. See their Fig. 6 for limits on $\sigma \cdot B$.

⁷ AABOUD 18AI search for resonances decaying to HZ in pp collisions at $\sqrt{s} = 13$ TeV. The quoted limit is for heavy-vector-triplet Z' with $g_V = 3$. The limit becomes $M_{Z'} > 2650$ GeV for $g_V = 1$. If we assume $M_{W'} = M_{Z'}$, the limit increases $M_{Z'} > 2930$ GeV and $M_{Z'} > 2800$ GeV for $g_V = 3$ and $g_V = 1$, respectively. See their Fig. 5 for limits on $\sigma \cdot B$.

⁸ AABOUD 18AK search for resonances decaying to WW in pp collisions at $\sqrt{s} = 13$ TeV. The limit quoted above is for heavy-vector-triplet Z' with $g_V = 3$. The limit becomes $M_{Z'} > 2750$ GeV for $g_V = 1$.

⁹ AABOUD 18B search for resonances decaying to WW in pp collisions at $\sqrt{s} = 13$ TeV. The quoted limit is for heavy-vector-triplet Z' with $g_V = 1$. See their Fig.11 for limits on $\sigma \cdot B$.

¹⁰ AABOUD 18BI search for a resonance decaying to $t\bar{t}$ in pp collisions at $\sqrt{s} = 13$ TeV. The quoted limit is for a top-color assisted TC Z' with $\Gamma_{Z'}/M_{Z'} = 0.01$. The limits for wider resonances are available. See their Fig. 14 for limits on $\sigma \cdot B$.

¹¹ AABOUD 18F search for resonances decaying to WW in pp collisions at $\sqrt{s} = 13$ TeV. The quoted limit is for heavy-vector-triplet Z' with $g_V = 3$. The limit becomes $M_{Z'} > 2200$ GeV for $g_V = 1$. If we assume $M_{Z'} = M_{W'}$, the limit increases $M_{Z'} > 3500$ GeV and $M_{Z'} > 3100$ GeV for $g_V = 3$ and $g_V = 1$, respectively. See their Fig.5 for limits on $\sigma \cdot B$.

¹² SIRUNYAN 18ED search for resonances decaying to HZ in pp collisions at $\sqrt{s} = 13$ TeV. The limit above is for heavy-vector-triplet Z' with $g_V = 3$. If we assume $M_{Z'} = M_{W'}$, the limit increases $M_{Z'} > 2900$ GeV and $M_{Z'} > 2800$ GeV for $g_V = 3$ and $g_V = 1$, respectively.

¹³ SIRUNYAN 18P give this limit for a heavy-vector-triplet Z' with $g_V = 3$. If they assume $M_{Z'} = M_{W'}$, the limit increases to $M_{Z'} > 3800$ GeV.

¹⁴ AABOUD 17AK search for a new resonance decaying to dijets in pp collisions at $\sqrt{s} = 13$ TeV. The limit quoted above is for a leptophobic Z' boson having axial-vector coupling strength with quarks $g_q = 0.2$. The limit is 2100 GeV if $g_q = 0.1$.

¹⁵ AABOUD 17AO search for resonances decaying to HZ in pp collisions at $\sqrt{s} = 13$ TeV. The limit quoted above is for a Z' in the heavy-vector-triplet model with $g_V = 3$. See their Fig.4 for limits on $\sigma \cdot B$.

¹⁶ SIRUNYAN 17AK search for resonances decaying to WW or HZ in pp collisions at $\sqrt{s} = 8$ and 13 TeV. The quoted limit is for heavy-vector-triplet Z' with $g_V = 3$. The limit becomes $M_{Z'} > 2200$ GeV for $g_V = 1$. If we assume $M_{Z'} = M_{W'}$, the limit increases $M_{Z'} > 2400$ GeV for both $g_V = 3$ and $g_V = 1$. See their Fig.1 and 2 for limits on $\sigma \cdot B$.

¹⁷ SIRUNYAN 17Q search for a resonance decaying to $t\bar{t}$ in pp collisions at $\sqrt{s} = 13$ TeV. The limit quoted above is for a resonance with relative width $\Gamma_{Z'}/M_{Z'} = 0.01$. Limits for wider resonances are available. See their Fig.6 for limits on $\sigma \cdot B$.

¹⁸ SIRUNYAN 17R search for resonances decaying to HZ in pp collisions at $\sqrt{s} = 13$ TeV. The quoted limit is for heavy-vector-triplet Z' with $g_V = 3$. Mass regions $M_{Z'} < 1150$ GeV and 1250 GeV $< M_{Z'} < 1670$ GeV are excluded for $g_V = 1$. If we assume $M_{Z'} = M_{W'}$, the excluded mass regions are $1000 < M_{Z'} < 2500$ GeV and $2760 < M_{Z'} < 3300$ GeV for $g_V = 3$; $1000 < M_{Z'} < 2430$ GeV and $2810 < M_{Z'} < 3130$ GeV for $g_V = 1$. See their Fig.5 for limits on $\sigma \cdot B$.

¹⁹ AABOUD 19AJ search in pp collisions at $\sqrt{s} = 13$ TeV for a new resonance decaying to $q\bar{q}$ and produced in association with a high p_T photon. For a leptophobic axial-vector Z' in the mass region 250 GeV $< M_{Z'} < 950$ GeV, the Z' coupling with quarks g_q is constrained below 0.18. See their Fig.2 for limits in $M_{Z'} - g_q$ plane.

²⁰ AABOUD 19D search in pp collisions at $\sqrt{s} = 13$ TeV for a new resonance decaying to $q\bar{q}$ and produced in association with a high- p_T photon or jet. For a leptophobic axial-vector Z' in the mass region 100 GeV $< M_{Z'} < 220$ GeV, the Z' coupling with quarks g_q is constrained below 0.23. See their Fig. 6 for limits in $M_{Z'} - g_q$ plane.

²¹ AABOUD 19V search for Dark Matter simplified Z' decaying invisibly or decaying to fermion pair in pp collisions at $\sqrt{s} = 13$ TeV.

²² AAD 19L search for resonances decaying to $\ell^+\ell^-$ in pp collisions at $\sqrt{s} = 13$ TeV. See their Fig. 4 for limits in the heavy vector triplet model couplings.

²³ LONG 19 uses the weak charge data of Cesium and proton to constrain mass of Z' in the 3–3.1 models.

²⁴ PANDEY 19 obtain limits on Z' induced neutrino non-standard interaction (NSI) parameter ϵ from LHC and IceCube data. See their Fig.2 for limits in $M_{Z'} - \epsilon$ plane, where $\epsilon = g_q g_V v^2 / (2 M_{Z'}^2)$.

²⁵ SIRUNYAN 19AL search for a new resonance decaying to a top quark and a heavy vector-like top partner in pp collisions at $\sqrt{s} = 13$ TeV. See their Fig. 8 for limits on Z' production cross section.

²⁶ SIRUNYAN 19AN search for a Dark Matter (DM) simplified model Z' decaying to H DM in pp collisions at $\sqrt{s} = 13$ TeV. See their Fig. 7 for limits on the signal strength modifiers.

²⁷ SIRUNYAN 19CB search in pp collisions at $\sqrt{s} = 13$ TeV for a new resonance decaying to $q\bar{q}$. For a leptophobic Z' in the mass region 50–300 GeV, the Z' coupling with quarks g'_q is constrained below 0.2. See their Figs. 4 and 5 for limits on g'_q in the mass range $50 < M_{Z'} < 450$ GeV.

²⁸ SIRUNYAN 19CD search in pp collisions at $\sqrt{s} = 13$ TeV for a leptophobic Z' produced in association of high p_T ISR photon and decaying to $q\bar{q}$. See their Fig. 2 for limits on the Z' coupling strength g'_q to $q\bar{q}$ in the mass range between 10 and 125 GeV.

Gauge & Higgs Boson Particle Listings

New Heavy Bosons

- 29 SIRUNYAN 19D search for a narrow neutral vector resonance decaying to $H\gamma$. See their Fig. 3 for exclusion limit in $M_{Z'}$ - $\sigma \cdot B$ plane. Upper limits on the production of $H\gamma$ resonances are set as a function of the resonance mass in the range of 720–3250 GeV.
- 30 AABOUD 18AA search for a narrow neutral vector boson decaying to $H\gamma$. See their Fig. 10 for the exclusion limit in $M_{Z'}$ - $\sigma \cdot B$ plane.
- 31 AABOUD 18CJ search for heavy-vector-triplet Z' in pp collisions at $\sqrt{s} = 13$ TeV. The limit quoted above is for model with $g_V = 3$ assuming $M_{Z'} = M_{W'}$. The limit becomes $M_{Z'} > 5500$ GeV for model with $g_V = 1$.
- 32 AABOUD 18N search for a narrow resonance decaying to $q\bar{q}$ in pp collisions at $\sqrt{s} = 13$ TeV using trigger level analysis to improve the low mass region sensitivity. See their Fig. 5 for limits in the mass-coupling plane in the Z' mass range 450–1800 GeV.
- 33 ALIJ 18AQ search for spin-0 and spin-1 resonances decaying to $\mu^+\mu^-$ in pp collisions at $\sqrt{s} = 7$ and 8 TeV in the mass region near 10 GeV. See their Figs. 4 and 5 for limits on $\sigma \cdot B$.
- 34 SIRUNYAN 18DR searches for $\mu^+\mu^-$ resonances produced in association with b -jets in the pp collision data with $\sqrt{s} = 8$ TeV and 13 TeV. An excess of events near $m_{\mu\mu} = 28$ GeV is observed in the 8 TeV data. See their Fig. 3 for the measured fiducial signal cross sections at $\sqrt{s} = 8$ TeV and the 95% CL upper limits at $\sqrt{s} = 13$ TeV.
- 35 SIRUNYAN 18E search for a new resonance decaying to dijets in pp collisions at $\sqrt{s} = 13$ TeV in the mass range 50–300 GeV. See their Fig.7 for limits in the mass-coupling plane.
- 36 SIRUNYAN 18I search for a narrow resonance decaying to $b\bar{b}$ in pp collisions at $\sqrt{s} = 8$ TeV using dedicated b -tagged dijet triggers to improve the sensitivity in the low mass region. See their Fig. 3 for limits on $\sigma \cdot B$ in the Z' mass range 325–1200 GeV.
- 37 AABOUD 17B search for resonances decaying to HZ ($H \rightarrow b\bar{b}, c\bar{c}, Z \rightarrow \ell^+\ell^-, \nu\bar{\nu}$) in pp collisions at $\sqrt{s} = 13$ TeV. The quoted limit is for heavy-vector-triplet Z' with $g_V = 3$. The limit becomes $M_{Z'} > 1490$ GeV for $g_V = 1$. If we assume $M_{Z'} = M_{W'}$, the limit increases $M_{Z'} > 2310$ GeV and $M_{Z'} > 1730$ GeV for $g_V = 3$ and $g_V = 1$, respectively. See their Fig.3 for limits on $\sigma \cdot B$.
- 38 KHACHATRYAN 17AX search for lepto-phobic resonances decaying to four leptons in pp collisions at $\sqrt{s} = 8$ TeV.
- 39 KHACHATRYAN 17U search for resonances decaying to HZ ($H \rightarrow b\bar{b}, c\bar{c}, Z \rightarrow \ell^+\ell^-, \nu\bar{\nu}$) in pp collisions at $\sqrt{s} = 13$ TeV. The limit on the heavy-vector-triplet model is $M_{Z'} = M_{W'} > 2$ TeV for $g_V = 3$, in which constraints from the $W' \rightarrow HW$ ($H \rightarrow b\bar{b}, W \rightarrow \ell\nu$) are combined. See their Fig.3 and Fig.4 for limits on $\sigma \cdot B$.
- 40 SIRUNYAN 17A search for resonances decaying to WW with $WW \rightarrow \ell\nu q\bar{q}, q\bar{q}q\bar{q}$ in pp collisions at $\sqrt{s} = 13$ TeV. The quoted limit is for heavy-vector-triplet Z' with $g_V = 3$. The limit becomes $M_{Z'} > 1600$ GeV for $g_V = 1$. If we assume $M_{Z'} = M_{W'}$, the limit increases $M_{Z'} > 2400$ GeV and $M_{Z'} > 2300$ GeV for $g_V = 3$ and $g_V = 1$, respectively. See their Fig.6 for limits on $\sigma \cdot B$.
- 41 SIRUNYAN 17AP search for resonances decaying into a SM-like Higgs scalar H and a light pseudo scalar A . A is assumed to decay invisibly. See their Fig.9 for limits on $\sigma \cdot B$.
- 42 SIRUNYAN 17T search for a new resonance decaying to dijets in pp collisions at $\sqrt{s} = 13$ TeV in the mass range 100–300 GeV. See their Fig.3 for limits in the mass-coupling plane.
- 43 SIRUNYAN 17V search for a new resonance decaying to a top quark and a heavy vector-like top partner T in pp collisions at $\sqrt{s} = 13$ TeV. See their table 5 for limits on the Z' production cross section for various values of $M_{Z'}$ and M_T in the range of $M_{Z'} = 1500$ –2500 GeV and $M_T = 700$ –1500 GeV.
- 44 AABOUD 16 search for a narrow resonance decaying into $b\bar{b}$ in pp collisions at $\sqrt{s} = 13$ TeV. The limit quoted above is for a leptophobic Z' with SM-like couplings to quarks. See their Fig.6 for limits on $\sigma \cdot B$.
- 45 AAD 16L search for $Z' \rightarrow a\gamma, a \rightarrow \gamma\gamma$ in pp collisions at $\sqrt{s} = 8$ TeV. See their Table 6 for limits on $\sigma \cdot B$.
- 46 AAD 16S search for a new resonance decaying to dijets in pp collisions at $\sqrt{s} = 13$ TeV. The limit quoted above is for a leptophobic Z' having coupling strength with quark $g_q = 0.3$ and is taken from their Figure 3.
- 47 KHACHATRYAN 16AP search for a resonance decaying to HZ in pp collisions at $\sqrt{s} = 8$ TeV. Both H and Z' are assumed to decay to fat jets. The quoted limit is for heavy-vector-triplet Z' with $g_V = 3$.
- 48 KHACHATRYAN 16E search for a leptophobic top-color Z' decaying to $t\bar{t}$ using pp collisions at $\sqrt{s} = 8$ TeV. The quoted limit assumes that $\Gamma_{Z'}/M_{Z'} = 0.012$. Also $m_{Z'} < 2.9$ TeV is excluded for wider topcolor Z' with $\Gamma_{Z'}/M_{Z'} = 0.1$.
- 49 AAD 15A search for narrow resonance decaying to $t\bar{t}$ using pp collisions at $\sqrt{s} = 8$ TeV. See Fig. 11 for limit on $\sigma \cdot B$.
- 50 AAD 15AT search for monoton production plus large missing E_T events in pp collisions at $\sqrt{s} = 8$ TeV and give constraints on a Z' model having $Z' u\bar{t}$ coupling. Z' is assumed to decay invisibly. See their Fig. 6 for limits on $\sigma \cdot B$.
- 51 AAD 15CD search for decays of Higgs bosons to 4ℓ states via Z' bosons, $H \rightarrow Z'Z' \rightarrow 4\ell$ or $H \rightarrow Z'Z' \rightarrow 4\ell$. See Fig. 5 for the limit on the signal strength of the $H \rightarrow Z'Z' \rightarrow 4\ell$ process and Fig. 16 for the limit on $H \rightarrow Z'Z' \rightarrow 4\ell$.
- 52 KHACHATRYAN 15F search for monoton production plus large missing E_T events in pp collisions at $\sqrt{s} = 8$ TeV and give constraints on a Z' model having $Z' u\bar{t}$ coupling. Z' is assumed to decay invisibly. See Fig. 3 for limits on $\sigma \cdot B$.
- 53 KHACHATRYAN 15O search for narrow Z' resonance decaying to ZH in pp collisions at $\sqrt{s} = 8$ TeV. See their Fig. 6 for limit on $\sigma \cdot B$.
- 54 AAD 14AT search for a narrow neutral vector boson decaying to $Z\gamma$. See their Fig. 3b for the exclusion limit in $M_{Z'} - \sigma \cdot B$ plane.
- 55 KHACHATRYAN 14A search for new resonance in the WW ($\ell\nu q\bar{q}$) and the ZZ ($\ell\ell q\bar{q}$) channels using pp collisions at $\sqrt{s}=8$ TeV. See their Fig.13 for the exclusion limit on the number of events in the mass-width plane.
- 56 MARTINEZ 14 use various electroweak data to constrain the Z' boson in the 3-3-1 models.
- 57 AAD 13AQ search for a leptophobic top-color Z' decaying to $t\bar{t}$. The quoted limit assumes that $\Gamma_{Z'}/M_{Z'} = 0.012$.
- 58 CHATRCHYAN 13BM search for top-color Z' decaying to $t\bar{t}$ using pp collisions at $\sqrt{s}=8$ TeV. The quoted limit is for $\Gamma_{Z'}/M_{Z'} = 0.012$.
- 59 CHATRCHYAN 13AP search for top-color leptophobic Z' decaying to $t\bar{t}$ using pp collisions at $\sqrt{s}=7$ TeV. The quoted limit is for $\Gamma_{Z'}/M_{Z'} = 0.012$.

- 60 AAD 12BV search for narrow resonance decaying to $t\bar{t}$ using pp collisions at $\sqrt{s}=7$ TeV. See their Fig. 7 for limit on $\sigma \cdot B$.
- 61 AAD 12K search for narrow resonance decaying to $t\bar{t}$ using pp collisions at $\sqrt{s}=7$ TeV. See their Fig. 5 for limit on $\sigma \cdot B$.
- 62 AALTONEN 12AR search for chromophilic Z' in $p\bar{p}$ collisions at $\sqrt{s} = 1.96$ TeV. See their Fig. 5 for limit on $\sigma \cdot B$.
- 63 AALTONEN 12N search for $p\bar{p} \rightarrow tZ', Z' \rightarrow T\bar{u}$ events in $p\bar{p}$ collisions. See their Fig. 3 for the limit on $\sigma \cdot B$.
- 64 ABASOV 12R search for top-color Z' boson decaying exclusively to $t\bar{t}$. The quoted limit is for $\Gamma_{Z'}/M_{Z'} = 0.012$.
- 65 CHATRCHYAN 12AI search for $pp \rightarrow tt$ events and give constraints on a Z' model having $Z'\bar{t}t$ coupling. See their Fig. 4 for the limit in mass-coupling plane.
- 66 Search for resonance decaying to $t\bar{t}$. See their Fig. 6 for limit on $\sigma \cdot B$.
- 67 Search for narrow resonance decaying to $t\bar{t}$. See their Fig. 4 for limit on $\sigma \cdot B$.
- 68 Search for narrow resonance decaying to $t\bar{t}$. See their Fig. 3 for limit on $\sigma \cdot B$.
- 69 CHATRCHYAN 11O search for same-sign top production in pp collisions induced by a hypothetical FCNC Z' at $\sqrt{s} = 7$ TeV. See their Fig. 3 for limit in mass-coupling plane.
- 70 Search for narrow resonance decaying to $t\bar{t}$. See their Fig. 3 for limit on $\sigma \cdot B$.
- 71 Search for narrow resonance decaying to $t\bar{t}$. See their Fig. 2 for limit on $\sigma \cdot B$.
- 72 BARGER 03b use the nucleosynthesis bound on the effective number of light neutrino δN_{ν} . See their Figs.4–5 for limits in general E_6 motivated models.
- 73 CHO 00 use various electroweak data to constrain Z' models assuming $m_H=100$ GeV. See Fig. 2 for limits in general E_6 -motivated models.
- 74 CHO 98 study constraints on four-Fermi contact interactions obtained from low-energy electroweak experiments, assuming no Z - Z' mixing.
- 75 Search for Z' decaying to dijets at $\sqrt{s}=1.8$ TeV. For Z' with electromagnetic strength coupling, no bound is obtained.

Searches for Z' with Lepton-Flavor-Violating decays

The following limits are obtained from $p\bar{p}$ or $pp \rightarrow Z'X$ with Z' decaying to the mode indicated in the comments.

VALUE	DOCUMENT ID	TECN	COMMENT
• • •	We do not use the following data for averages, fits, limits, etc. • • •		
1	AABOUD 18CMATLS	18CMATLS	$Z' \rightarrow e\mu, e\tau, \mu\tau$
2	SIRUNYAN 18AT CMS	18AT CMS	$Z' \rightarrow e\mu$
3	AABOUD 16P ATLS	16P ATLS	$Z' \rightarrow e\mu, e\tau, \mu\tau$
4	KHACHATRYAN 16BE CMS	16BE CMS	$Z' \rightarrow e\mu$
5	AAD 15O ATLS	15O ATLS	$Z' \rightarrow e\mu, e\tau, \mu\tau$
6	AAD 11H ATLS	11H ATLS	$Z' \rightarrow e\mu$
7	AAD 11Z ATLS	11Z ATLS	$Z' \rightarrow e\mu$
8	ABULENCIA 06M CDF	06M CDF	$Z' \rightarrow e\mu$

- 1 AABOUD 18CM search for a new particle with lepton-flavor violating decay in pp collisions at $\sqrt{s} = 13$ TeV. See their Figs. 4, 5, and 6 for limits on $\sigma \cdot B$.
- 2 SIRUNYAN 18AT search for a narrow resonance Z' decaying into $e\mu$ in pp collisions at $\sqrt{s} = 13$ TeV. See their Fig.5 for limit on $\sigma \cdot B$ in the range of $600 \text{ GeV} < M_{Z'} < 5000$ GeV.
- 3 AABOUD 16P search for new particle with lepton flavor violating decay in pp collisions at $\sqrt{s} = 13$ TeV. See their Figs. 2, 3, and 4 for limits on $\sigma \cdot B$.
- 4 KHACHATRYAN 16BE search for new particle Z' with lepton flavor violating decay in pp collisions at $\sqrt{s} = 8$ TeV in the range of $200 \text{ GeV} < M_{Z'} < 2000$ GeV. See their Fig.4 for limits on $\sigma \cdot B$ and their Table 5 for bounds on various masses.
- 5 AAD 15O search for new particle Z' with lepton flavor violating decay in pp collisions at $\sqrt{s} = 8$ TeV in the range of $500 \text{ GeV} < M_{Z'} < 3000$ GeV. See their Fig. 2 for limits on $\sigma \cdot B$.
- 6 AAD 11H search for new particle Z' with lepton flavor violating decay in pp collisions at $\sqrt{s} = 7$ TeV in the range of $700 \text{ GeV} < M_{Z'} < 1000$ GeV. See their Fig. 3 for limits on $\sigma \cdot B$.
- 7 AAD 11Z search for new particle Z' with lepton flavor violating decay in pp collisions at $\sqrt{s} = 7$ TeV in the range $700 \text{ GeV} < M_{Z'} < 2000$ GeV. See their Fig. 3 for limits on $\sigma \cdot B$.
- 8 ABULENCIA 06M search for new particle Z' with lepton flavor violating decay in $p\bar{p}$ collisions at $\sqrt{s} = 1.96$ TeV in the range of $100 \text{ GeV} < M_{Z'} < 800$ GeV. See their Fig. 4 for limits in the mass-coupling plane.

Indirect Constraints on Kaluza-Klein Gauge Bosons

Bounds on a Kaluza-Klein excitation of the Z boson or photon in $d=1$ extra dimension. These bounds can also be interpreted as a lower bound on $1/R$, the size of the extra dimension. Unless otherwise stated, bounds assume all fermions live on a single brane and all gauge fields occupy the $4+d$ -dimensional bulk. See also the section on "Extra Dimensions" in the "Searches" Listings in this Review.

VALUE (TeV)	CL%	DOCUMENT ID	TECN	COMMENT
• • •	We do not use the following data for averages, fits, limits, etc. • • •			
> 4.7		1 MUECK 02	RVUE	Electroweak
> 3.3	95	2 CORNET 00	RVUE	$e\nu qq'$
>5000		3 DELGADO 00	RVUE	e_K
> 2.6	95	4 DELGADO 00	RVUE	Electroweak
> 3.3	95	5 RIZZO 00	RVUE	Electroweak
> 2.9	95	6 MARCIANO 99	RVUE	Electroweak
> 2.5	95	7 MASIP 99	RVUE	Electroweak
> 1.6	90	8 NATH 99	RVUE	Electroweak
> 3.4	95	9 STRUMIA 99	RVUE	Electroweak

- 1 MUECK 02 limit is 2σ and is from global electroweak fit ignoring correlations among observables. Higgs is assumed to be confined on the brane and its mass is fixed. For scenarios of bulk Higgs, of brane-SU(2)_L, bulk-U(1)_Y, and of bulk-SU(2)_L, brane-U(1)_Y, the corresponding limits are > 4.6 TeV, > 4.3 TeV and > 3.0 TeV, respectively.
- 2 Bound is derived from limits on $e\nu qq'$ contact interaction, using data from HERA and the Tevatron.

See key on page 999

Gauge & Higgs Boson Particle Listings

New Heavy Bosons

- ³ Bound holds only if first two generations of quarks lives on separate branes. If quark mixing is not complex, then bound lowers to 400 TeV from Δm_K .
- ⁴ See Figs. 1 and 2 of DELGADO 00 for several model variations. Special boundary conditions can be found which permit KK states down to 950 GeV and that agree with the measurement of $Q_{WW}(Cs)$. Quoted bound assumes all Higgs bosons confined to brane; placing one Higgs doublet in the bulk lowers bound to 2.3 TeV.
- ⁵ Bound is derived from global electroweak analysis assuming the Higgs field is trapped on the matter brane. If the Higgs propagates in the bulk, the bound increases to 3.8 TeV.
- ⁶ Bound is derived from global electroweak analysis but considering only presence of the KK W bosons.
- ⁷ Global electroweak analysis used to obtain bound independent of position of Higgs on brane or in bulk.
- ⁸ Bounds from effect of KK states on G_F , α , $M_{W\prime}$, and M_Z . Hard cutoff at string scale determined using gauge coupling unification. Limits for $d=2,3,4$ rise to 3.5, 5.7, and 7.8 TeV.
- ⁹ Bound obtained for Higgs confined to the matter brane with $m_H=500$ GeV. For Higgs in the bulk, the bound increases to 3.5 TeV.

See the related review(s): Leptoquarks

MASS LIMITS for Leptoquarks from Pair Production

These limits rely only on the color or electroweak charge of the leptoquark.

VALUE (GeV)	CL%	DOCUMENT ID	TECN	COMMENT
>1185	95	1 SIRUNYAN 20A	CMS	Scalar LQ. $B(\nu b) = 1$
>1140	95	2 SIRUNYAN 20A	CMS	Scalar LQ. $B(\nu t) = 1$
>1140	95	3 SIRUNYAN 20A	CMS	Scalar LQ. $B(\mu q) = 1$ with $q = u, d, s, c$
>1925	95	4 SIRUNYAN 20A	CMS	Vector LQ. $\kappa = 1$. $B(\nu b) = 1$
>1825	95	5 SIRUNYAN 20A	CMS	Vector LQ. $\kappa = 1$. $B(\nu t) = 1$
>1980	95	6 SIRUNYAN 20A	CMS	Vector LQ. $\kappa = 1$. $B(\nu q) = 1$ with $q = u, d, s, c$
>1400	95	7 AABOUD 19AX	ATLS	Scalar LQ. $B(e q) = 1$
>1560	95	8 AABOUD 19AX	ATLS	Scalar LQ. $B(\mu q) = 1$
>1000	95	9 AABOUD 19X	ATLS	Scalar LQ. $B(\tau \nu) = 1$
>1030	95	10 AABOUD 19X	ATLS	Scalar LQ. $B(b \tau) = 1$
> 970	95	11 AABOUD 19X	ATLS	Scalar LQ. $B(b \nu) = 1$
> 920	95	12 AABOUD 19X	ATLS	Scalar LQ. $B(\tau \tau) = 1$
>1530	95	13 SIRUNYAN 19BI	CMS	Scalar LQ. $B(\mu q)+B(\nu q) = 1$
>1435	95	14 SIRUNYAN 19BJ	CMS	Scalar LQ. $B(e q)+B(\nu q) = 1$
>1020	95	15 SIRUNYAN 19Y	CMS	Scalar LQ. $B(\tau b) = 1$
none 300-900	95	16 SIRUNYAN 18CZ	CMS	Scalar LQ. $B(\tau t) = 1$
>1420	95	17 SIRUNYAN 18EC	CMS	Scalar LQ. $B(\mu t) = 1$
>1190	95	18 SIRUNYAN 18EC	CMS	Vector LQ. $\mu, t, \tau, \nu b$
>1100	95	19 SIRUNYAN 18U	CMS	Scalar LQ. $B(\nu b) = 1$
> 980	95	20 SIRUNYAN 18U	CMS	Scalar LQ. $B(\nu q) = 1$ with $q = u, d, s, c$
>1020	95	21 SIRUNYAN 18U	CMS	Scalar LQ. $B(\nu t) = 1$
>1810	95	22 SIRUNYAN 18U	CMS	Vector LQ. $\kappa=1$. $LQ \rightarrow b\nu$
>1790	95	23 SIRUNYAN 18U	CMS	Vector LQ. $\kappa=1$. $LQ \rightarrow q\nu$ with $q = u, d, s, c$
>1780	95	24 SIRUNYAN 18U	CMS	Vector LQ. $\kappa=1$. $LQ \rightarrow t\nu$
> 740	95	25 KHACHATRY...17J	CMS	Scalar LQ. $B(\tau b) = 1$
> 850	95	26 SIRUNYAN 17H	CMS	Scalar LQ. $B(\tau b) = 1$
>1050	95	27 AAD 16G	ATLS	Scalar LQ. $B(e q) = 1$
>1000	95	28 AAD 16G	ATLS	Scalar LQ. $B(\mu q) = 1$
> 625	95	29 AAD 16G	ATLS	Scalar LQ. $B(\nu b) = 1$
none 200-640	95	30 AAD 16G	ATLS	Scalar LQ. $B(\nu t) = 1$
>1010	95	31 KHACHATRY...16AF	CMS	Scalar LQ. $B(e q) = 1$
>1080	95	32 KHACHATRY...16AF	CMS	Scalar LQ. $B(\mu q) = 1$
> 685	95	33 KHACHATRY...15AJ	CMS	Scalar LQ. $B(\tau t) = 1$
> 740	95	34 KHACHATRY...14T	CMS	Scalar LQ. $B(\tau b) = 1$
••• We do not use the following data for averages, fits, limits, etc. •••				
> 534	95	35 SIRUNYAN 19bc	CMS	Scalar LQ ($\rightarrow \mu q$) LQ ($\rightarrow X + DM$)
> 525	95	36 AAD 13AE	ATLS	Third generation
> 660	95	37 CHATRCHYAN 13M	CMS	Third generation
> 685	95	38 AAD 12H	ATLS	First generation
> 830	95	39 AAD 12o	ATLS	Second generation
> 840	95	40 CHATRCHYAN 12AG	CMS	First generation
> 450	95	41 CHATRCHYAN 12AG	CMS	Second generation
> 376	95	42 CHATRCHYAN 12Bo	CMS	Third generation
> 422	95	43 AAD 11D	ATLS	Superseded by AAD 12H
> 326	95	44 AAD 11D	ATLS	Superseded by AAD 12o
> 339	95	45 ABAZOV 11V	D0	First generation
> 384	95	46 CHATRCHYAN 11N	CMS	Superseded by CHATRCHYAN 12AG
> 394	95	47 KHACHATRY...11D	CMS	Superseded by CHATRCHYAN 12AG
> 247	95	48 KHACHATRY...11E	CMS	Superseded by CHATRCHYAN 12AG
> 316	95	49 ABAZOV 10L	D0	Third generation
> 299	95	50 ABAZOV 09 D0	D0	Second generation
> 153	95	51 ABAZOV 09AF	D0	Superseded by ABAZOV 11V
> 205	95	52 AALTONEN 08P	CDF	Third generation
> 210	95	53 AALTONEN 08Z	CDF	Third generation
> 229	95	54 ABAZOV 08AD	D0	All generations
> 251	95	55 ABAZOV 08AN	D0	Third generation
> 136	95	56 ABAZOV 07J	D0	Superseded by ABAZOV 10L
> 226	95	57 ABAZOV 06A	D0	Superseded by ABAZOV 09
> 226	95	58 ABAZOV 06L	D0	Superseded by ABAZOV 08AD
> 226	95	59 ABULENCIA 06T	CDF	Second generation

> 256	95	59 ABAZOV 05H	D0	First generation
> 117	95	54 ACOSTA 05I	CDF	First generation
> 236	95	60 ACOSTA 05P	CDF	First generation
> 99	95	61 ABBIENDI 03R	OPAL	First generation
> 100	95	61 ABBIENDI 03R	OPAL	Second generation
> 98	95	61 ABBIENDI 03R	OPAL	Third generation
> 98	95	62 ABAZOV 02	D0	All generations
> 225	95	63 ABAZOV 01D	D0	First generation
> 85.8	95	64 ABBIENDI 00M	OPAL	Superseded by ABBIENDI 03R
> 85.5	95	64 ABBIENDI 00M	OPAL	Superseded by ABBIENDI 03R
> 82.7	95	64 ABBIENDI 00M	OPAL	Superseded by ABBIENDI 03R
> 200	95	65 ABBOTT 00C	D0	Second generation
> 123	95	66 AFFOLDER 00K	CDF	Second generation
> 148	95	67 AFFOLDER 00K	CDF	Third generation
> 160	95	68 ABBOTT 99J	D0	Second generation
> 225	95	69 ABBOTT 98E	D0	First generation
> 94	95	70 ABBOTT 98J	D0	Third generation
> 202	95	71 ABE 98S	CDF	Second generation
> 242	95	72 GROSS-PILCH.98		First generation
> 99	95	73 ABE 97F	CDF	Third generation
> 213	95	74 ABE 97X	CDF	First generation
> 45.5	95	75,76 ABREU 93J	DLPH	First + second generation
> 44.4	95	77 ADRIANI 93M	L3	First generation
> 44.5	95	77 ADRIANI 93M	L3	Second generation
> 45	95	77 DECAMP 92	ALEP	Third generation
none 8.9-22.6	95	78 KIM 90	AMY	First generation
none 10.2-23.2	95	78 KIM 90	AMY	Second generation
none 5-20.8	95	79 BARTEL 87B	JADE	
none 7-20.5	95	80 BEHREND 86B	CELL	

- 1 SIRUNYAN 20A search for scalar and vector leptoquarks decaying to $t\nu, b\nu$, and $q\nu$ ($q = u, d, s, c$). The limit quoted above assumes scalar leptoquark with $B(\nu b) = 1$.
- 2 SIRUNYAN 20A search for scalar and vector leptoquarks decaying to $t\nu, b\nu$, and $q\nu$ ($q = u, d, s, c$). The limit quoted above assumes scalar leptoquark with $B(\nu t) = 1$.
- 3 SIRUNYAN 20A search for scalar and vector leptoquarks decaying to $t\nu, b\nu$, and $q\nu$ ($q = u, d, s, c$). The limit quoted above assumes scalar leptoquark with $B(\nu q) = 1$.
- 4 SIRUNYAN 20A search for scalar and vector leptoquarks decaying to $t\nu, b\nu$, and $q\nu$ ($q = u, d, s, c$). The limit quoted above assumes vector leptoquark with $B(\nu b) = 1$ and $\kappa = 1$. If we assume $\kappa = 0$, the limit becomes $M_{LQ} > 1560$ GeV.
- 5 SIRUNYAN 20A search for scalar and vector leptoquarks decaying to $t\nu, b\nu$, and $q\nu$ ($q = u, d, s, c$). The limit quoted above assumes vector leptoquark with $B(\nu t) = 1$ and $\kappa = 1$. If we assume $\kappa = 0$, the limit becomes $M_{LQ} > 1475$ GeV.
- 6 SIRUNYAN 20A search for scalar and vector leptoquarks decaying to $t\nu, b\nu$, and $q\nu$ ($q = u, d, s, c$). The limit quoted above assumes vector leptoquark with $B(\nu q) = 1$ and $\kappa = 1$. If we assume $\kappa = 0$, the limit becomes $M_{LQ} > 1560$ GeV.
- 7 AABOUD 19AX search for leptoquarks using $e\bar{e}jj$ events in pp collisions at $\sqrt{s} = 13$ TeV. The limit above assumes $B(eq) = 1$.
- 8 AABOUD 19AX search for leptoquarks using $\mu\mu jj$ events in pp collisions at $\sqrt{s} = 13$ TeV. The limit above assumes $B(\mu q) = 1$.
- 9 AABOUD 19X search for scalar leptoquarks decaying to $t\nu$ in pp collisions at $\sqrt{s} = 13$ TeV.
- 10 AABOUD 19X search for scalar leptoquarks decaying to $b\tau$ in pp collisions at $\sqrt{s} = 13$ TeV.
- 11 AABOUD 19X search for scalar leptoquarks decaying to $b\nu$ in pp collisions at $\sqrt{s} = 13$ TeV.
- 12 AABOUD 19X search for scalar leptoquarks decaying to $\tau\tau$ in pp collisions at $\sqrt{s} = 13$ TeV.
- 13 SIRUNYAN 19BI search for a pair of scalar leptoquarks decaying to $\mu\mu jj$ and to $\mu\nu jj$ final states in pp collisions at $\sqrt{s} = 13$ TeV. Limits are shown as a function of β where β is the branching fraction to a muon and a quark. For $\beta = 1.0$ (0.5) LQ masses up to 1530 (1285) GeV are excluded. See Fig. 9 for exclusion limits in the plane of β and LQ mass.
- 14 SIRUNYAN 19BJ search for a pair of scalar leptoquarks decaying to $e\bar{e}jj$ and $e\nu jj$ final states in pp collisions at $\sqrt{s} = 13$ TeV. Limits are shown as a function of the branching fraction β to an electron and a quark. For $\beta = 1.0$ (0.5) LQ masses up to 1435 (1270) GeV are excluded. See Fig. 9 for exclusion limits in the plane of β and LQ mass.
- 15 SIRUNYAN 19Y search for a pair of third generation scalar leptoquarks, each decaying to τ and a jet. Assuming $B(\tau b) = 1$, leptoquark masses below 1.02 TeV are excluded.
- 16 SIRUNYAN 18CZ search for scalar leptoquarks decaying to τt in pp collisions at $\sqrt{s} = 13$ TeV. The limit above assumes $B(\tau t) = 1$.
- 17 SIRUNYAN 18EC set limits for scalar and vector leptoquarks decaying to $\mu t, \tau t$, and νb . The limit quoted above assumes scalar leptoquark with $B(\mu t) = 1$.
- 18 SIRUNYAN 18EC set limits for scalar and vector leptoquarks decaying to $\mu t, \tau t$, and νb . The limit quoted above assumes vector leptoquark with all possible combinations of branching fractions to μ, τ, t , and νb .
- 19 SIRUNYAN 18U set limits for scalar and vector leptoquarks decaying to $t\nu, b\nu$, and $q\nu$. The limit quoted above assumes scalar leptoquark with $B(b\nu) = 1$. Vector leptoquarks with $\kappa = 1$ are excluded below masses of 1810 GeV.
- 20 SIRUNYAN 18U set limits for scalar and vector leptoquarks decaying to $t\nu, b\nu$, and $q\nu$. The limit quoted above assumes scalar leptoquark with $B(q\nu) = 1$. Vector leptoquarks with $\kappa = 1$ are excluded below masses of 1790 GeV.
- 21 SIRUNYAN 18U set limits for scalar and vector leptoquarks decaying to $t\nu, b\nu$, and $q\nu$. The limit quoted above assumes scalar leptoquark with $B(\nu t) = 1$. Vector leptoquarks with $\kappa = 1$ are excluded below masses of 1780 GeV.
- 22 SIRUNYAN 18U set limits for scalar and vector leptoquarks decaying to $t\nu, b\nu$, and $q\nu$. $\kappa = 1$ and $LQ \rightarrow b\nu$ are assumed.
- 23 SIRUNYAN 18U set limits for scalar and vector leptoquarks decaying to $t\nu, b\nu$, and $q\nu$. $\kappa = 1$ and $LQ \rightarrow q\nu$ with $q = u, d, s, c$ are assumed.
- 24 SIRUNYAN 18U set limits for scalar and vector leptoquarks decaying to $t\nu, b\nu$, and $q\nu$. $\kappa = 1$ and $LQ \rightarrow t\nu$ are assumed.
- 25 KHACHATRYAN 17J search for scalar leptoquarks decaying to τb using pp collisions at $\sqrt{s} = 13$ TeV. The limit above assumes $B(\tau b) = 1$.
- 26 SIRUNYAN 17H search for scalar leptoquarks using $\tau\tau bb$ events in pp collisions at $\sqrt{s} = 8$ TeV. The limit above assumes $B(\tau b) = 1$.

Gauge & Higgs Boson Particle Listings

New Heavy Bosons

- 27 AAD 16G search for scalar leptoquarks using $eejj$ events in collisions at $\sqrt{s} = 8$ TeV. The limit above assumes $B(eq) = 1$.
- 28 AAD 16G search for scalar leptoquarks using $\mu\mu jj$ events in collisions at $\sqrt{s} = 8$ TeV. The limit above assumes $B(\mu q) = 1$.
- 29 AAD 16G search for scalar leptoquarks decaying to $b\nu$. The limit above assumes $B(b\nu) = 1$.
- 30 AAD 16G search for scalar leptoquarks decaying to $t\nu$. The limit above assumes $B(t\nu) = 1$.
- 31 KHACHATRYAN 16AF search for scalar leptoquarks using $eejj$ and $e\nu jj$ events in pp collisions at $\sqrt{s} = 8$ TeV. The limit above assumes $B(eq) = 1$. For $B(eq) = 0.5$, the limit becomes 850 GeV.
- 32 KHACHATRYAN 16AF search for scalar leptoquarks using $\mu\mu jj$ and $\mu\nu jj$ events in pp collisions at $\sqrt{s} = 8$ TeV. The limit above assumes $B(\mu q) = 1$. For $B(\mu q) = 0.5$, the limit becomes 760 GeV.
- 33 KHACHATRYAN 15AJ search for scalar leptoquarks using $\tau\tau tt$ events in pp collisions at $\sqrt{s} = 8$ TeV. The limit above assumes $B(\tau t) = 1$.
- 34 KHACHATRYAN 14T search for scalar leptoquarks decaying to τb using pp collisions at $\sqrt{s} = 8$ TeV. The limit above assumes $B(\tau b) = 1$. See their Fig. 5 for the exclusion limit as function of $B(\tau b)$.
- 35 SIRUNYAN 19bc search for scalar leptoquark (LQ) pair production in pp collisions at $\sqrt{s} = 13$ TeV. One LQ is assumed to decay to μq , while the other decays to dark matter pair and SM particles. See their Fig. 4 for limits in $M_{LQ} - M_{DM}$ plane.
- 36 AAD 13AE search for scalar leptoquarks using $\tau\tau bb$ events in pp collisions at $E_{cm} = 7$ TeV. The limit above assumes $B(\tau b) = 1$.
- 37 CHATRCHYAN 13M search for scalar and vector leptoquarks decaying to τb in pp collisions at $E_{cm} = 7$ TeV. The limit above is for scalar leptoquarks with $B(\tau b) = 1$.
- 38 AAD 12H search for scalar leptoquarks using $eejj$ and $e\nu jj$ events in pp collisions at $E_{cm} = 7$ TeV. The limit above assumes $B(eq) = 1$. For $B(eq) = 0.5$, the limit becomes 607 GeV.
- 39 AAD 12o search for scalar leptoquarks using $\mu\mu jj$ and $\mu\nu jj$ events in pp collisions at $E_{cm} = 7$ TeV. The limit above assumes $B(\mu q) = 1$. For $B(\mu q) = 0.5$, the limit becomes 594 GeV.
- 40 CHATRCHYAN 12AG search for scalar leptoquarks using $eejj$ and $e\nu jj$ events in pp collisions at $E_{cm} = 7$ TeV. The limit above assumes $B(eq) = 1$. For $B(eq) = 0.5$, the limit becomes 640 GeV.
- 41 CHATRCHYAN 12AG search for scalar leptoquarks using $\mu\mu jj$ and $\mu\nu jj$ events in pp collisions at $E_{cm} = 7$ TeV. The limit above assumes $B(\mu q) = 1$. For $B(\mu q) = 0.5$, the limit becomes 650 GeV.
- 42 CHATRCHYAN 12Bo search for scalar leptoquarks decaying to νb in pp collisions at $\sqrt{s} = 7$ TeV. The limit above assumes $B(\nu b) = 1$.
- 43 AAD 11b search for scalar leptoquarks using $eejj$ and $e\nu jj$ events in pp collisions at $E_{cm} = 7$ TeV. The limit above assumes $B(eq) = 1$. For $B(eq) = 0.5$, the limit becomes 319 GeV.
- 44 AAD 11b search for scalar leptoquarks using $\mu\mu jj$ and $\mu\nu jj$ events in pp collisions at $E_{cm} = 7$ TeV. The limit above assumes $B(\mu q) = 1$. For $B(\mu q) = 0.5$, the limit becomes 362 GeV.
- 45 ABYZOV 11v search for scalar leptoquarks using $e\nu jj$ events in $p\bar{p}$ collisions at $E_{cm} = 1.96$ TeV. The limit above assumes $B(eq) = 0.5$.
- 46 CHATRCHYAN 11N search for scalar leptoquarks using $e\nu jj$ events in pp collisions at $E_{cm} = 7$ TeV. The limit above assumes $B(eq) = 0.5$.
- 47 KHACHATRYAN 11D search for scalar leptoquarks using $eejj$ events in pp collisions at $E_{cm} = 7$ TeV. The limit above assumes $B(eq) = 1$.
- 48 KHACHATRYAN 11E search for scalar leptoquarks using $\mu\mu jj$ events in pp collisions at $E_{cm} = 7$ TeV. The limit above assumes $B(\mu q) = 1$.
- 49 ABYZOV 10L search for pair productions of scalar leptoquark state decaying to νb in $p\bar{p}$ collisions at $E_{cm} = 1.96$ TeV. The limit above assumes $B(\nu b) = 1$.
- 50 ABYZOV 09 search for scalar leptoquarks using $\mu\mu jj$ and $\mu\nu jj$ events in $p\bar{p}$ collisions at $E_{cm} = 1.96$ TeV. The limit above assumes $B(\mu q) = 1$. For $B(\mu q) = 0.5$, the limit becomes 270 GeV.
- 51 ABYZOV 09AF search for scalar leptoquarks using $eejj$ and $e\nu jj$ events in $p\bar{p}$ collisions at $E_{cm} = 1.96$ TeV. The limit above assumes $B(eq) = 1$. For $B(eq) = 0.5$ the bound becomes 284 GeV.
- 52 AALTONEN 08P search for vector leptoquarks using $\tau^+\tau^-b\bar{b}$ events in $p\bar{p}$ collisions at $E_{cm} = 1.96$ TeV. Assuming Yang-Mills (minimal) couplings, the mass limit is >317 GeV (251 GeV) at 95% CL for $B(\tau b) = 1$.
- 53 Search for pair production of scalar leptoquark state decaying to τb in $p\bar{p}$ collisions at $E_{cm} = 1.96$ TeV. The limit above assumes $B(\tau b) = 1$.
- 54 Search for scalar leptoquarks using $\nu\nu jj$ events in $p\bar{p}$ collisions at $E_{cm} = 1.96$ TeV. The limit above assumes $B(\nu q) = 1$.
- 55 ABYZOV 07J search for pair productions of scalar leptoquark state decaying to νb in $p\bar{p}$ collisions at $E_{cm} = 1.96$ TeV. The limit above assumes $B(\nu b) = 1$.
- 56 ABYZOV 06A search for scalar leptoquarks using $\mu\mu jj$ events in $p\bar{p}$ collisions at $E_{cm} = 1.8$ TeV and 1.96 TeV. The limit above assumes $B(\mu q) = 1$. For $B(\mu q) = 0.5$, the limit becomes 204 GeV.
- 57 ABYZOV 06L search for scalar leptoquarks using $\nu\nu jj$ events in $p\bar{p}$ collisions at $E_{cm} = 1.8$ TeV and at 1.96 TeV. The limit above assumes $B(\nu q) = 1$.
- 58 ABULENCA 06T search for scalar leptoquarks using $\mu\mu jj$, $\mu\nu jj$, and $\nu\nu jj$ events in $p\bar{p}$ collisions at $E_{cm} = 1.96$ TeV. The quoted limit assumes $B(\mu q) = 1$. For $B(\mu q) = 0.5$ or 0.1, the bound becomes 208 GeV or 143 GeV, respectively. See their Fig. 4 for the exclusion limit as a function of $B(\mu q)$.
- 59 ABYZOV 05H search for scalar leptoquarks using $eejj$ and $e\nu jj$ events in $p\bar{p}$ collisions at $E_{cm} = 1.8$ TeV and 1.96 TeV. The limit above assumes $B(eq) = 1$. For $B(eq) = 0.5$ the bound becomes 234 GeV.
- 60 ACOSTA 05P search for scalar leptoquarks using $eejj$, $e\nu jj$ events in $p\bar{p}$ collisions at $E_{cm} = 1.96$ TeV. The limit above assumes $B(eq) = 1$. For $B(eq) = 0.5$ and 0.1, the bound becomes 205 GeV and 145 GeV, respectively.
- 61 ABBIENDI 03R search for scalar/vector leptoquarks in e^+e^- collisions at $\sqrt{s} = 189-209$ GeV. The quoted limits are for charge $-4/3$ isospin 0 scalar-leptoquark with $B(\ell q) = 1$. See their table 12 for other cases.
- 62 ABYZOV 02 search for scalar leptoquarks using $\nu\nu jj$ events in $p\bar{p}$ collisions at $E_{cm} = 1.8$ TeV. The bound holds for all leptoquark generations. Vector leptoquarks are likewise constrained to lie above 200 GeV.
- 63 ABYZOV 01b search for scalar leptoquarks using $e\nu jj$, $eejj$, and $\nu\nu jj$ events in $p\bar{p}$ collisions at $E_{cm} = 1.8$ TeV. The limit above assumes $B(eq) = 1$. For $B(eq) = 0.5$ and 0, the bound becomes 204 and 79 GeV, respectively. Bounds for vector leptoquarks are also given. Supersedes ABBOTT 98E.
- 64 ABBIENDI 00M search for scalar/vector leptoquarks in e^+e^- collisions at $\sqrt{s} = 183$ GeV. The quoted limits are for charge $-4/3$ isospin 0 scalar-leptoquarks with $B(\ell q) = 1$. See their Table 8 and Figs. 6-9 for other cases.
- 65 ABBOTT 00c search for scalar leptoquarks using $\mu\mu jj$, $\mu\nu jj$, and $\nu\nu jj$ events in $p\bar{p}$ collisions at $E_{cm} = 1.8$ TeV. The limit above assumes $B(\mu q) = 1$. For $B(\mu q) = 0.5$ and 0, the bound becomes 180 and 79 GeV respectively. Bounds for vector leptoquarks are also given.
- 66 AFFOLDER 00k search for scalar leptoquark using $\nu\nu cc$ events in $p\bar{p}$ collisions at $E_{cm} = 1.8$ TeV. The quoted limit assumes $B(\nu c) = 1$. Bounds for vector leptoquarks are also given.
- 67 AFFOLDER 00k search for scalar leptoquark using $\nu\nu bb$ events in $p\bar{p}$ collisions at $E_{cm} = 1.8$ TeV. The quoted limit assumes $B(\nu b) = 1$. Bounds for vector leptoquarks are also given.
- 68 ABBOTT 99j search for leptoquarks using $\mu\nu jj$ events in $p\bar{p}$ collisions at $E_{cm} = 1.8$ TeV. The quoted limit is for a scalar leptoquark with $B(\nu b) = 1$.
- 69 ABBOTT 98E search for scalar leptoquarks using $e\nu jj$, $eejj$, and $\nu\nu jj$ events in $p\bar{p}$ collisions at $E_{cm} = 1.8$ TeV. The limit above assumes $B(eq) = 1$. For $B(eq) = 0.5$ and 0, the bound becomes 204 and 79 GeV, respectively.
- 70 ABBOTT 98j search for charge $-1/3$ third generation scalar and vector leptoquarks in $p\bar{p}$ collisions at $E_{cm} = 1.8$ TeV. The quoted limit is for scalar leptoquark with $B(\nu b) = 1$.
- 71 ABE 98s search for scalar leptoquarks using $\mu\mu jj$ events in $p\bar{p}$ collisions at $E_{cm} = 1.8$ TeV. The limit is for $B(\mu q) = 1$. For $B(\mu q) = B(\nu q) = 0.5$, the limit is > 160 GeV.
- 72 GROSS-PILCHER 98 is the combined limit of the CDF and DØ Collaborations as determined by a joint CDF/DØ working group and reported in this FNAL Technical Memo. Original data published in ABE 97x and ABBOTT 98E.
- 73 ABE 97f search for third generation scalar and vector leptoquarks in $p\bar{p}$ collisions at $E_{cm} = 1.8$ TeV. The quoted limit is for scalar leptoquark with $B(\tau b) = 1$.
- 74 ABE 97x search for scalar leptoquarks using $eejj$ events in $p\bar{p}$ collisions at $E_{cm} = 1.8$ TeV. The limit is for $B(eq) = 1$.
- 75 Limit is for charge $-1/3$ isospin-0 leptoquark with $B(\ell q) = 2/3$.
- 76 First and second generation leptoquarks are assumed to be degenerate. The limit is slightly lower for each generation.
- 77 Limits are for charge $-1/3$, isospin-0 scalar leptoquarks decaying to $\ell^- q$ or νq with any branching ratio. See paper for limits for other charge-isospin assignments of leptoquarks.
- 78 KIM 90 assume pair production of charge 2/3 scalar-leptoquark via photon exchange. The decay of the first (second) generation leptoquark is assumed to be any mixture of $d e^+$ and $u \bar{\nu}$ ($s \mu^+$ and $c \bar{\nu}$). See paper for limits for specific branching ratios.
- 79 BARTEL 87B limit is valid when a pair of charge 2/3 spinless leptoquarks X is produced with point coupling, and when they decay under the constraint $B(X \rightarrow c \bar{\nu}_\mu) + B(X \rightarrow s \mu^+) = 1$.
- 80 BEHREND 86B assumed that a charge 2/3 spinless leptoquark, χ , decays either into $s \mu^+$ or $c \bar{\nu}$: $B(\chi \rightarrow s \mu^+) + B(\chi \rightarrow c \bar{\nu}) = 1$.

MASS LIMITS for Leptoquarks from Single Production

These limits depend on the q - ℓ -leptoquark coupling g_{LQ} . It is often assumed that $g_{LQ}^2/4\pi = 1/137$. Limits shown are for a scalar, weak isoscalar, charge $-1/3$ leptoquark.

VALUE (GeV)	CL%	DOCUMENT ID	TECN	COMMENT
none 150-740	95	1 SIRUNYAN 18BJ CMS		Third generation
>1755	95	2 KHACHATRY..16AG CMS		First generation
> 660	95	3 KHACHATRY..16AG CMS		Second generation
> 304	95	4 ABRAMOWICZ12A ZEUS		First generation
> 73	95	5 ABREU 93J DLPH		Second generation
> 300	95	6 DEY 16 ICCB	$\nu q \rightarrow LQ \rightarrow \nu q$	
		7 AARON 11A H1		Lepton-flavor violation
		8 AARON 11B H1		First generation
		9 ABYZOV 07E D0		Second generation
> 295	95	10 AKTAS 05B H1		First generation
		11 CHEKANOV 05A ZEUS		Lepton-flavor violation
> 298	95	12 CHEKANOV 03B ZEUS		First generation
> 197	95	13 ABBIENDI 02B OPAL		First generation
		14 CHEKANOV 02 ZEUS		Repl. by CHEKANOV 05A
> 290	95	15 ADLOFF 01C H1		First generation
> 204	95	16 BREITWEG 01 ZEUS		First generation
		17 BREITWEG 00E ZEUS		First generation
> 161	95	18 ABREU 99G DLPH		First generation
> 200	95	19 ADLOFF 99 H1		First generation
		20 DERRICK 97 ZEUS		Lepton-flavor violation
> 168	95	21 DERRICK 93 ZEUS		First generation

- 1 SIRUNYAN 18BJ search for single production of charge 2/3 scalar leptoquarks decaying to τb in pp collisions at $\sqrt{s} = 13$ TeV. The limit above assumes $B(\tau b) = 1$ and the leptoquark coupling strength $\lambda = 1$.
- 2 KHACHATRYAN 16AG search for single production of charge $\pm 1/3$ scalar leptoquarks using $eejj$ events in pp collisions at $\sqrt{s} = 8$ TeV. The limit above assumes $B(eq) = 1$ and the leptoquark coupling strength $\lambda = 1$.
- 3 KHACHATRYAN 16AG search for single production of charge $\pm 1/3$ scalar leptoquarks using $\mu\mu jj$ events in pp collisions at $\sqrt{s} = 8$ TeV. The limit above assumes $B(\mu q) = 1$ and the leptoquark coupling strength $\lambda = 1$.
- 4 ABRAMOWICZ 12A limit is for a scalar, weak isoscalar, charge $-1/3$ leptoquark coupled with e_R . See their Figs. 12-17 and Table 4 for states with different quantum numbers.
- 5 Limit from single production in Z decay. The limit is for a leptoquark coupling of electromagnetic strength and assumes $B(\ell q) = 2/3$. The limit is 77 GeV if first and second leptoquarks are degenerate.
- 6 DEY 16 use the 2010-2012 IceCube PeV energy data set to constrain the leptoquark production cross section through the $\nu q \rightarrow LQ \rightarrow \nu q$ process. See their Figure 4 for the exclusion limit in the mass-coupling plane.
- 7 AARON 11A search for various leptoquarks with lepton-flavor violating couplings. See their Figs. 2-3 and Tables 1-4 for detailed limits.

See key on page 999

Gauge & Higgs Boson Particle Listings

New Heavy Bosons

- ⁸ The quoted limit is for a scalar, weak isoscalar, charge $-1/3$ leptoquark coupled with e_R . See their Figs. 3–5 for limits on states with different quantum numbers.
- ⁹ ABAZOV 07E search for leptoquark single production through qg fusion process in $p\bar{p}$ collisions. See their Fig. 4 for exclusion plot in mass-coupling plane.
- ¹⁰ AKTAS 05B limit is for a scalar, weak isoscalar, charge $-1/3$ leptoquark coupled with e_R . See their Fig. 3 for limits on states with different quantum numbers.
- ¹¹ CHEKANOV 05 search for various leptoquarks with lepton-flavor violating couplings. See their Figs.6–10 and Tables 1–8 for detailed limits.
- ¹² CHEKANOV 03B limit is for a scalar, weak isoscalar, charge $-1/3$ leptoquark coupled with e_R . See their Figs. 11–12 and Table 5 for limits on states with different quantum numbers.
- ¹³ For limits on states with different quantum numbers and the limits in the mass-coupling plane, see their Fig. 4 and Fig. 5.
- ¹⁴ CHEKANOV 02 search for various leptoquarks with lepton-flavor violating couplings. See their Figs. 6–7 and Tables 5–6 for detailed limits.
- ¹⁵ For limits on states with different quantum numbers and the limits in the mass-coupling plane, see their Fig. 3.
- ¹⁶ See their Fig. 14 for limits in the mass-coupling plane.
- ¹⁷ BREITWEG 00E search for $F=0$ leptoquarks in e^+p collisions. For limits in mass-coupling plane, see their Fig. 11.
- ¹⁸ ABREU 99G limit obtained from process $e\gamma \rightarrow LQ+q$. For limits on vector and scalar states with different quantum numbers and the limits in the coupling-mass plane, see their Fig. 4 and Table 2.
- ¹⁹ For limits on states with different quantum numbers and the limits in the mass-coupling plane, see their Fig. 13 and Fig. 14. ADLOFF 99 also search for leptoquarks with lepton-flavor violating couplings. ADLOFF 99 supersedes AID 96B.
- ²⁰ DERRICK 97 search for various leptoquarks with lepton-flavor violating couplings. See their Figs. 5–8 and Table 1 for detailed limits.
- ²¹ DERRICK 93 search for single leptoquark production in ep collisions with the decay $e q$ and νq . The limit is for leptoquark coupling of electromagnetic strength and assumes $B(eq) = B(\nu q) = 1/2$. The limit for $B(eq) = 1$ is 176 GeV. For limits on states with different quantum numbers, see their Table 3.

- ³ ZHANG 18A give bounds on leptoquark induced four-fermion interactions from $D \rightarrow K\ell\nu$. The authors inform us that the shape parameter of the vector form factor in both the abstract and the conclusions of ZHANG 18A should be $r_{+1} = 2.16 \pm 0.07$ rather than ± 0.007 . The numbers listed in their Table 7 are correct.
- ⁴ BARRANCO 16 give bounds on leptoquark induced four-fermion interactions from $D \rightarrow K\ell\nu$ and $D_S \rightarrow \ell\nu$.
- ⁵ KUMAR 16 gives bound on SU(2) singlet scalar leptoquark with charge $-1/3$ from $K^0 - \bar{K}^0$ mixing, $K \rightarrow \pi\nu\bar{\nu}$, $K_L^0 \rightarrow \mu^+\mu^-$, and $K_L^0 \rightarrow \mu^\pm e^\mp$ decays.
- ⁶ BESSAA 15 obtain limit on leptoquark induced four-fermion interactions from the ATLAS and CMS limit on the $\bar{q}q\bar{e}e$ contact interactions.
- ⁷ SAHO 15A obtain limit on leptoquark induced four-fermion interactions from $B_{s,d} \rightarrow \mu^+\mu^-$ for $\lambda \simeq O(1)$.
- ⁸ SAKAKI 13 explain the $B \rightarrow D^{(*)}\tau\bar{\nu}$ anomaly using Wilson coefficients of leptoquark-induced four-fermion operators.
- ⁹ KOSNIK 12 obtains limits on leptoquark induced four-fermion interactions from $b \rightarrow s\ell^+\ell^-$ decays.
- ¹⁰ AARON 11c limit is for weak isotriplet spin-0 leptoquark at strong coupling $\lambda = \sqrt{4\pi}$. For the limits of leptoquarks with different quantum numbers, see their Table 3. Limits are derived from bounds of eq contact interactions.
- ¹¹ DORSNER 11 give bounds on scalar, weak singlet, charge $4/3$ leptoquark from K, B, τ decays, meson mixings, $LFV, g-2$ and $Z \rightarrow b\bar{b}$.
- ¹² AKTAS 07A search for lepton-flavor violation in ep collision. See their Tables 4–7 for limits on lepton-flavor violating four-fermion interactions induced by various leptoquarks.
- ¹³ SCHAEEL 07A limit is for the weak-isoscalar spin-0 left-handed leptoquark with the coupling of electromagnetic strength. For the limits of leptoquarks with different quantum numbers, see their Table 35.
- ¹⁴ SMIRNOV 07 obtains mass limits for the vector and scalar chiral leptoquark states from $K \rightarrow e\mu, B \rightarrow e\tau$ decays.
- ¹⁵ CHEKANOV 05 search for various leptoquarks with lepton-flavor violating couplings. See their Figs.6–10 and Tables 1–8 for detailed limits.
- ¹⁶ ADLOFF 03 limit is for the weak isotriplet spin-0 leptoquark at strong coupling $\lambda = \sqrt{4\pi}$. For the limits of leptoquarks with different quantum numbers, see their Table 3. Limits are derived from bounds on $e^\pm q$ contact interactions.
- ¹⁷ The bound is derived from $B(B^0 \rightarrow e^\pm\mu^\mp) < 1.7 \times 10^{-7}$.
- ¹⁸ CHEKANOV 02 search for lepton-flavor violation in ep collisions. See their Tables 1–4 for limits on lepton-flavor violating and four-fermion interactions induced by various leptoquarks.
- ¹⁹ CHEUNG 01B quoted limit is for a scalar, weak isoscalar, charge $-1/3$ leptoquark with a coupling of electromagnetic strength. The limit is derived from bounds on contact interactions in a global electroweak analysis. For the limits of leptoquarks with different quantum numbers, see Table 5.
- ²⁰ ACCIARRI 00P limit is for the weak isoscalar spin-0 leptoquark with the coupling of electromagnetic strength. For the limits of leptoquarks with different quantum numbers, see their Table 4.
- ²¹ ADLOFF 00 limit is for the weak isotriplet spin-0 leptoquark at strong coupling, $\lambda = \sqrt{4\pi}$. For the limits of leptoquarks with different quantum numbers, see their Table 2. ADLOFF 00 limits are from the Q^2 spectrum measurement of $e^+p \rightarrow e^+X$.
- ²² BARATE 00i search for deviations in cross section and jet-charge asymmetry in $e^+e^- \rightarrow q\bar{q}$ due to t -channel exchange of a leptoquark at $\sqrt{s}=130$ to 183 GeV. Limits for other scalar and vector leptoquarks are also given in their Table 22.
- ²³ BARGER 00 explain the deviation of atomic parity violation in cesium atoms from prediction is explained by scalar leptoquark exchange.
- ²⁴ GABRIELLI 00 calculate various process with lepton flavor violation in leptoquark models.
- ²⁵ ZARNECKI 00 limit is derived from data of HERA, LEP, and Tevatron and from various low-energy data including atomic parity violation. Leptoquark coupling with electromagnetic strength is assumed.
- ²⁶ ABBIENDI 99 limits are from $e^+e^- \rightarrow q\bar{q}$ cross section at 130–136, 161–172, 183 GeV. See their Fig. 8 and Fig. 9 for limits in mass-coupling plane.
- ²⁷ ABE 98v quoted limit is from $B(B_S \rightarrow e^\pm\mu^\mp) < 8.2 \times 10^{-6}$. ABE 98v also obtain a similar limit on $M_{LQ} > 20.4$ TeV from $B(B_{d,s} \rightarrow e^\pm\mu^\mp) < 4.5 \times 10^{-6}$. Both bounds assume the non-canonical association of the b quark with electrons or muons under SU(4).
- ²⁸ ACCIARRI 98j limit is from $e^+e^- \rightarrow q\bar{q}$ cross section at $\sqrt{s}=130$ –172 GeV which can be affected by the t - and u -channel exchanges of leptoquarks. See their Fig. 4 and Fig. 5 for limits in the mass-coupling plane.
- ²⁹ ACKERSTAFF 98v limits are from $e^+e^- \rightarrow q\bar{q}$ and $e^+e^- \rightarrow b\bar{b}$ cross sections at $\sqrt{s}=130$ –172 GeV, which can be affected by the t - and u -channel exchanges of leptoquarks. See their Fig. 21 and Fig. 22 for limits of leptoquarks in mass-coupling plane.
- ³⁰ DEANDREA 97 limit is for \bar{R}_2 leptoquark obtained from atomic parity violation (APV). The coupling of leptoquark is assumed to be electromagnetic strength. See Table 2 for limits of the four-fermion interactions induced by various scalar leptoquark exchange. DEANDREA 97 combines APV limit and limits from Tevatron and HERA. See Fig. 1–4 for combined limits of leptoquark in mass-coupling plane.
- ³¹ DERRICK 97 search for lepton-flavor violation in ep collision. See their Tables 2–5 for limits on lepton-flavor violating four-fermion interactions induced by various leptoquarks.
- ³² GROSSMAN 97 estimate the upper bounds on the branching fraction $B \rightarrow \tau^+\tau^- (X)$ from the absence of the B decay with large missing energy. These bounds can be used to constrain leptoquark induced four-fermion interactions.
- ³³ JADACH 97 limit is from $e^+e^- \rightarrow q\bar{q}$ cross section at $\sqrt{s}=172.3$ GeV which can be affected by the t - and u -channel exchanges of leptoquarks. See their Fig. 1 for limits on vector leptoquarks in mass-coupling plane.
- ³⁴ KUZNETSOV 95b use π, K, B, τ decays and μe conversion and give a list of bounds on the leptoquark mass and the fermion mixing matrix in the Pati-Salam model. The quoted limit is from $K_L \rightarrow \mu e$ decay assuming zero mixing.
- ³⁵ MIZUKOSHI 95 calculate the one-loop radiative correction to the Z-physics parameters in various scalar leptoquark models. See their Fig. 4 for the exclusion plot of third generation leptoquark models in mass-coupling plane.
- ³⁶ BHATTACHARYYA 94 limit is from one-loop radiative correction to the leptonic decay width of the Z. $m_H=250$ GeV, $\alpha_S(m_Z)=0.12$, $m_t=180$ GeV, and the electroweak strength of leptoquark coupling are assumed. For leptoquark coupled to $\bar{t}_L t_R, \bar{\tau}_L \tau_R$, and $\bar{\nu}_\tau$, see Fig. 2 in BHATTACHARYYA 94b erratum and Fig. 3.
- ³⁷ DAVIDSON 94 gives an extensive list of the bounds on leptoquark-induced four-fermion interactions from π, K, D, B, μ, τ decays and meson mixings, etc. See Table 15 of DAVIDSON 94 for detail.

Indirect Limits for Leptoquarks

VALUE (TeV)	CL%	DOCUMENT ID	TECN	COMMENT
• • • We do not use the following data for averages, fits, limits, etc. • • •				
> 3.1	95	1 ABRAMOWICZ19	ZEUS	First generation
		2 MANDAL 19	RVUE	τ, μ, e, K
		3 ZHANG 18A	RVUE	D decays
		4 BARRANCO 16	RVUE	D decays
		5 KUMAR 16	RVUE	neutral K mixing, rare K decays
		6 BESSAA 15	RVUE	$q\bar{q} \rightarrow e^+e^-$
> 14	95	7 SAHO 15A	RVUE	$B_{s,d} \rightarrow \mu^+\mu^-$
		8 SAKAKI 13	RVUE	$B \rightarrow D^{(*)}\tau\bar{\nu}, B \rightarrow X_S\nu\bar{\nu}$
		9 KOSNIK 12	RVUE	$b \rightarrow s\ell^+\ell^-$
> 2.5	95	10 AARON 11c	H1	First generation
		11 DORSNER 11	RVUE	scalar, weak singlet, charge $4/3$
		12 AKTAS 07A	H1	Lepton-flavor violation
> 0.49	95	13 SCHAEEL 07A	ALEP	$e^+e^- \rightarrow q\bar{q}$
		14 SMIRNOV 07	RVUE	$K \rightarrow e\mu, B \rightarrow e\tau$
		15 CHEKANOV 05A	ZEUS	Lepton-flavor violation
> 1.7	96	16 ADLOFF 03	H1	First generation
> 46	90	17 CHANG 03	BELL	Pati-Salam type
		18 CHEKANOV 02	ZEUS	Repl. by CHEKANOV 05A
> 1.7	95	19 CHEUNG 01B	RVUE	First generation
> 0.39	95	20 ACCIARRI 00P	L3	$e^+e^- \rightarrow q\bar{q}$
> 1.5	95	21 ADLOFF 00	H1	First generation
> 0.2	95	22 BARATE 00i	ALEP	Repl. by SCHAEEL 07A
		23 BARGER 00	RVUE	Cs
		24 GABRIELLI 00	RVUE	Lepton flavor violation
> 0.74	95	25 ZARNECKI 00	RVUE	S_1 leptoquark
		26 ABBIENDI 99	OPAL	
> 19.3	95	27 ABE 98v	CDF	$B_S \rightarrow e^\pm\mu^\mp$, Pati-Salam type
		28 ACCIARRI 98j	L3	$e^+e^- \rightarrow q\bar{q}$
		29 ACKERSTAFF 98v	OPAL	$e^+e^- \rightarrow q\bar{q}, e^+e^- \rightarrow b\bar{b}$
> 0.76	95	30 DEANDREA 97	RVUE	\bar{R}_2 leptoquark
		31 DERRICK 97	ZEUS	Lepton-flavor violation
		32 GROSSMAN 97	RVUE	$B \rightarrow \tau^+\tau^- (X)$
		33 JADACH 97	RVUE	$e^+e^- \rightarrow q\bar{q}$
> 1200		34 KUZNETSOV 95b	RVUE	Pati-Salam type
		35 MIZUKOSHI 95	RVUE	Third generation scalar leptoquark
> 0.3	95	36 BHATTACH... 94	RVUE	Spin-0 leptoquark coupled to $\bar{\nu}_R t_L$
		37 DAVIDSON 94	RVUE	
		38 KUZNETSOV 94	RVUE	Pati-Salam type
> 0.43	95	39 LEURER 94	RVUE	First generation spin-1 leptoquark
> 0.44	95	39 LEURER 94b	RVUE	First generation spin-0 leptoquark
		40 MAHANTA 94	RVUE	P and T violation
> 1		41 SHANKER 82	RVUE	Nonchiral spin-0 leptoquark
> 125		41 SHANKER 82	RVUE	Nonchiral spin-1 leptoquark

- ¹ ABRAMOWICZ 19 obtain a limit on $\lambda/M_{LQ} > 1.16$ TeV $^{-1}$ for weak isotriplet spin-0 leptoquark S_1^+ . We obtain the limit quoted above by converting the limit on λ/M_{LQ} for S_1^+ assuming $\lambda = \sqrt{4\pi}$. See their Table 5 for the limits of leptoquarks with different quantum numbers. These limits are derived from bounds of eq contact interactions.
- ² MANDAL 19 give bounds on leptoquarks from τ -decays, leptonic dipole moments, lepton-flavor-violating processes, and K decays.

Gauge & Higgs Boson Particle Listings

New Heavy Bosons

- ³⁸ KUZNETSOV 94 gives mixing independent bound of the Pati-Salam leptoquark from the cosmological limit on $\pi^0 \rightarrow \nu\bar{\nu}$.
- ³⁹ LEURER 94, LEURER 94B limits are obtained from atomic parity violation and apply to any chiral leptoquark which couples to the first generation with electromagnetic strength. For a nonchiral leptoquark, universality in $\pi_{\ell 2}$ decay provides a much more stringent bound.
- ⁴⁰ MAHANTA 94 gives bounds of P - and T -violating scalar-leptoquark couplings from atomic and molecular experiments.
- ⁴¹ From $(\pi \rightarrow e\nu)/(\pi \rightarrow \mu\nu)$ ratio. SHANKER 82 assumes the leptoquark induced four-fermion coupling $4g^2/M^2 (\bar{\nu}_e \ell u_R) (\bar{\ell} \ell e_R)$ with $g=0.004$ for spin-0 leptoquark and $g^2/M^2 (\bar{\nu}_e \ell u_L) (\bar{\ell} \ell e_R)$ with $g \approx 0.6$ for spin-1 leptoquark.

MASS LIMITS for Diquarks

VALUE (GeV)	CL%	DOCUMENT ID	TECN	COMMENT
>6000 (CL = 95%) OUR LIMIT				
none 600–7200	95	1 SIRUNYAN 18B0 CMS	E_6	diquark
none 600–6900	95	2 KHACHATRYAN...17W CMS	E_6	diquark
none 1500–6000	95	3 KHACHATRYAN...16K CMS	E_6	diquark
none 500–1600	95	4 KHACHATRYAN...16L CMS	E_6	diquark
none 1200–4700	95	5 KHACHATRYAN...15V CMS	E_6	diquark
• • • We do not use the following data for averages, fits, limits, etc. • • •				
>3750	95	6 CHATRCHYAN 13A CMS	E_6	diquark
none 1000–4280	95	7 CHATRCHYAN 13AS CMS	Superseded by KHACHATRYAN 15V	
>3520	95	8 CHATRCHYAN 11Y CMS	Superseded by CHATRCHYAN 13A	
none 970–1080, 1450–1600	95	9 KHACHATRYAN...10 CMS	Superseded by CHATRCHYAN 13A	
none 290–630	95	10 AALTONEN 09AC CDF	E_6	diquark
none 290–420	95	11 ABE 97G CDF	E_6	diquark
none 15–31.7	95	12 ABREU 94O DLPH	SUSY E_6	diquark

- ¹ SIRUNYAN 18B0 search for resonances decaying to dijets in pp collisions at $\sqrt{s} = 13$ TeV.
- ² KHACHATRYAN 17W search for resonances decaying to dijets in pp collisions at $\sqrt{s} = 13$ TeV.
- ³ KHACHATRYAN 16K search for resonances decaying to dijets in pp collisions at $\sqrt{s} = 13$ TeV.
- ⁴ KHACHATRYAN 16L search for resonances decaying to dijets in pp collisions at $\sqrt{s} = 8$ TeV with the data scouting technique, increasing the sensitivity to the low mass resonances.
- ⁵ KHACHATRYAN 15V search for resonances decaying to dijets in pp collisions at $\sqrt{s} = 8$ TeV.
- ⁶ CHATRCHYAN 13A search for new resonance decaying to dijets in pp collisions at $\sqrt{s} = 7$ TeV.
- ⁷ CHATRCHYAN 13AS search for new resonance decaying to dijets in pp collisions at $\sqrt{s} = 8$ TeV.
- ⁸ CHATRCHYAN 11Y search for new resonance decaying to dijets in pp collisions at $\sqrt{s} = 7$ TeV.
- ⁹ KHACHATRYAN 10 search for new resonance decaying to dijets in pp collisions at $\sqrt{s} = 7$ TeV.
- ¹⁰ AALTONEN 09AC search for new narrow resonance decaying to dijets.
- ¹¹ ABE 97G search for new particle decaying to dijets.
- ¹² ABREU 94O limit is from $e^+e^- \rightarrow \tau\bar{\tau}c$ s. Range extends up to 43 GeV if diquarks are degenerate in mass.

MASS LIMITS for g_A (axigluon) and Other Color-Octet Gauge Bosons

Axigluons are massive color-octet gauge bosons in chiral color models and have axial-vector coupling to quarks with the same coupling strength as gluons.

VALUE (GeV)	CL%	DOCUMENT ID	TECN	COMMENT
>6100 (CL = 95%) OUR LIMIT				
none 600–6100	95	1 SIRUNYAN 18B0 CMS	$pp \rightarrow g_A X, g_A \rightarrow 2j$	
none 600–5500	95	2 KHACHATRYAN...17W CMS	$pp \rightarrow g_A X, g_A \rightarrow 2j$	
none 1500–5100	95	3 KHACHATRYAN...16K CMS	$pp \rightarrow g_A X, g_A \rightarrow 2j$	
none 500–1600	95	4 KHACHATRYAN...16L CMS	$pp \rightarrow g_A X, g_A \rightarrow 2j$	
none 1300–3600	95	5 KHACHATRYAN...15V CMS	$pp \rightarrow g_A X, g_A \rightarrow 2j$	
• • • We do not use the following data for averages, fits, limits, etc. • • •				
>2800	95	6 KHACHATRYAN...17Y CMS	$pp \rightarrow g_A g_A \rightarrow 8j$	
		7 AAD 16W ATLS	$pp \rightarrow g_A X, g_A \rightarrow b\bar{b}b\bar{b}$	
		8 KHACHATRYAN...16E CMS	$pp \rightarrow g_{KK} X, g_{KK} \rightarrow t\bar{t}$	
		9 KHACHATRYAN...15AV CMS	$pp \rightarrow \theta^0 \theta^0 \rightarrow b\bar{b}Zg$	
		10 AALTONEN 13R CDF	$pp \rightarrow g_A X, g_A \rightarrow \sigma\sigma, \sigma \rightarrow 2j$	
>3360	95	11 CHATRCHYAN 13A CMS	$pp \rightarrow g_A X, g_A \rightarrow 2j$	
none 1000–3270	95	12 CHATRCHYAN 13AS CMS	Superseded by KHACHATRYAN 15V	
none 250–740	95	13 CHATRCHYAN 13AU CMS	$pp \rightarrow 2g_A X, g_A \rightarrow 2j$	
> 775	95	14 ABAZOV 12R D0	$p\bar{p} \rightarrow g_A X, g_A \rightarrow t\bar{t}$	
>2470	95	15 CHATRCHYAN 11Y CMS	Superseded by CHATRCHYAN 13A	
none 1470–1520	95	16 AALTONEN 10L CDF	$p\bar{p} \rightarrow g_A X, g_A \rightarrow t\bar{t}$	
		17 KHACHATRYAN...10 CMS	Superseded by CHATRCHYAN 13A	
none 260–1250	95	18 AALTONEN 09AC CDF	$p\bar{p} \rightarrow g_A X, g_A \rightarrow 2j$	
> 910	95	19 CHOUDHURY 07 RVUE	$p\bar{p} \rightarrow t\bar{t}X$	
> 365	95	20 DONCHESKI 98 RVUE	$\Gamma(Z \rightarrow \text{hadron})$	

none 200–980	95	21 ABE 97G CDF	$p\bar{p} \rightarrow g_A X, g_A \rightarrow 2j$
none 200–870	95	22 ABE 95N CDF	$p\bar{p} \rightarrow g_A X, g_A \rightarrow q\bar{q}$
none 240–640	95	23 ABE 93G CDF	$p\bar{p} \rightarrow g_A X, g_A \rightarrow 2j$
> 50	95	24 CUYPERS 91 RVUE	$\sigma(e^+e^- \rightarrow \text{hadrons})$
none 120–210	95	25 ABE 90H CDF	$p\bar{p} \rightarrow g_A X, g_A \rightarrow 2j$
> 29		26 ROBINETT 89 THEO	Partial-wave unitarity
none 150–310	95	27 ALBAJAR 88B UA1	$p\bar{p} \rightarrow g_A X, g_A \rightarrow 2j$
> 20		BERGSTROM 88 RVUE	$p\bar{p} \rightarrow TX$ via $g_A g$
> 9		28 CUYPERS 88 RVUE	T decay
> 25		29 DONCHESKI 88B RVUE	T decay

- ¹ SIRUNYAN 18B0 search for resonances decaying to dijets in pp collisions at $\sqrt{s} = 13$ TeV.
- ² KHACHATRYAN 17W search for resonances decaying to dijets in pp collisions at $\sqrt{s} = 13$ TeV.
- ³ KHACHATRYAN 16K search for resonances decaying to dijets in pp collisions at $\sqrt{s} = 13$ TeV.
- ⁴ KHACHATRYAN 16L search for resonances decaying to dijets in pp collisions at $\sqrt{s} = 8$ TeV with the data scouting technique, increasing the sensitivity to the low mass resonances.
- ⁵ KHACHATRYAN 15V search for resonances decaying to dijets in pp collisions at $\sqrt{s} = 8$ TeV.
- ⁶ KHACHATRYAN 17Y search for pair production of color-octet gauge boson g_A each decaying to $4j$ in pp collisions at $\sqrt{s} = 8$ TeV.
- ⁷ AAD 16W search for a new resonance decaying to a pair of b and B_H in pp collisions at $\sqrt{s} = 8$ TeV. The vector-like quark B_H is assumed to decay to bH . See their Fig. 3 and Fig. 4 for limits on $\sigma \cdot B$.
- ⁸ KHACHATRYAN 16E search for KK gluon decaying to $t\bar{t}$ in pp collisions at $\sqrt{s} = 8$ TeV.
- ⁹ KHACHATRYAN 15AV search for pair productions of neutral color-octet weak-triplet scalar particles (θ^0), decaying to $b\bar{b}$, Zg or γg , in pp collisions at $\sqrt{s} = 8$ TeV. The θ^0 particle is often predicted in coloron (G' , color-octet gauge boson) models and appear in the pp collisions through $G' \rightarrow \theta^0 \theta^0$ decays. Assuming $B(\theta^0 \rightarrow b\bar{b}) = 0.5$, they give limits $m_{\theta^0} > 623$ GeV (426 GeV) for $m_{G'} = 2.3 m_{\theta^0}$ ($m_{G'} = 5 m_{\theta^0}$).
- ¹⁰ AALTONEN 13R search for new resonance decaying to $\sigma\sigma$, with hypothetical strongly interacting σ particle subsequently decaying to 2 jets, in $p\bar{p}$ collisions at $\sqrt{s} = 1.96$ TeV, using data corresponding to an integrated luminosity of 6.6 fb⁻¹. For 50 GeV $< m_\sigma < m_{g_A}/2$, axigluons in mass range 150–400 GeV are excluded.
- ¹¹ CHATRCHYAN 13A search for new resonance decaying to dijets in pp collisions at $\sqrt{s} = 7$ TeV.
- ¹² CHATRCHYAN 13AS search for new resonance decaying to dijets in pp collisions at $\sqrt{s} = 8$ TeV.
- ¹³ CHATRCHYAN 13AU search for the pair produced color-octet vector bosons decaying to $q\bar{q}$ pairs in pp collisions. The quoted limit is for $B(g_A \rightarrow q\bar{q}) = 1$.
- ¹⁴ ABAZOV 12R search for massive color octet vector particle decaying to $t\bar{t}$. The quoted limit assumes g_A couplings with light quarks are suppressed by 0.2.
- ¹⁵ CHATRCHYAN 11Y search for new resonance decaying to dijets in pp collisions at $\sqrt{s} = 7$ TeV.
- ¹⁶ AALTONEN 10L search for massive color octet non-chiral vector particle decaying into $t\bar{t}$ pair with mass in the range 400 GeV $< M < 800$ GeV. See their Fig. 6 for limit in the mass-coupling plane.
- ¹⁷ KHACHATRYAN 10 search for new resonance decaying to dijets in pp collisions at $\sqrt{s} = 7$ TeV.
- ¹⁸ AALTONEN 09AC search for new narrow resonance decaying to dijets.
- ¹⁹ CHOUDHURY 07 limit is from the $t\bar{t}$ production cross section measured at CDF.
- ²⁰ DONCHESKI 98 compare α_s derived from low-energy data and that from $\Gamma(Z \rightarrow \text{hadrons})/\Gamma(Z \rightarrow \text{leptons})$.
- ²¹ ABE 97G search for new particle decaying to dijets.
- ²² ABE 95N assume axigluons decaying to quarks in the Standard Model only.
- ²³ ABE 93G assume $\Gamma(g_A) = N\alpha_s m_{g_A}/6$ with $N = 10$.
- ²⁴ CUYPERS 91 compare α_s measured in T decay and that from R at PEP/PETRA energies.
- ²⁵ ABE 90H assumes $\Gamma(g_A) = N\alpha_s m_{g_A}/6$ with $N = 5$ ($\Gamma(g_A) = 0.09 m_{g_A}$). For $N = 10$, the excluded region is reduced to 120–150 GeV.
- ²⁶ ROBINETT 89 result demands partial-wave unitarity of $J = 0$ $t\bar{t} \rightarrow t\bar{t}$ scattering amplitude and derives a limit $m_{g_A} > 0.5 m_t$. Assumes $m_t > 56$ GeV.
- ²⁷ ALBAJAR 88B result is from the nonobservation of a peak in two-jet invariant mass distribution. $\Gamma(g_A) < 0.4 m_{g_A}$ assumed. See also BAGGER 88.
- ²⁸ CUYPERS 88 requires $\Gamma(T \rightarrow g g_A) < \Gamma(T \rightarrow g g g)$. A similar result is obtained by DONCHESKI 88.
- ²⁹ DONCHESKI 88B requires $\Gamma(T \rightarrow g q\bar{q})/\Gamma(T \rightarrow g g g) < 0.25$, where the former decay proceeds via axigluon exchange. A more conservative estimate of < 0.5 leads to $m_{g_A} > 21$ GeV.

MASS LIMITS for Color-Octet Scalar Bosons

VALUE (GeV)	CL%	DOCUMENT ID	TECN	COMMENT
• • • We do not use the following data for averages, fits, limits, etc. • • •				
none 600–3400	95	1 SIRUNYAN 18B0 CMS	$pp \rightarrow S_8 X, S_8 \rightarrow g g$	
		2 KHACHATRYAN...15AV CMS	$pp \rightarrow \theta^0 \theta^0 \rightarrow b\bar{b}Zg$	
none 150–287	95	3 AAD 13K ATLS	$pp \rightarrow S_8 S_8 X, S_8 \rightarrow 2j$	
		1 SIRUNYAN 18B0	search for color octet scalar boson produced through gluon fusion process in pp collisions at $\sqrt{s} = 13$ TeV. The limit above assumes S_{8gg} coupling $k_s^2 = 1/2$.	
		2 KHACHATRYAN 15AV	search for pair productions of neutral color-octet weak-triplet scalar particles (θ^0), decaying to $b\bar{b}$, Zg or γg , in pp collisions at $\sqrt{s} = 8$ TeV. The θ^0 particle is often predicted in coloron (G' , color-octet gauge boson) models and appear in the pp collisions through $G' \rightarrow \theta^0 \theta^0$ decays. Assuming $B(\theta^0 \rightarrow b\bar{b}) = 0.5$, they give limits $m_{\theta^0} > 623$ GeV (426 GeV) for $m_{G'} = 2.3 m_{\theta^0}$ ($m_{G'} = 5 m_{\theta^0}$).	

See key on page 999

Gauge & Higgs Boson Particle Listings

New Heavy Bosons

³AAD 13k search for pair production of color-octet scalar particles in pp collisions at $\sqrt{s} = 7$ TeV. Cross section limits are interpreted as mass limits on scalar partners of a Dirac gluino.

X^0 (Heavy Boson) Searches in Z Decays

Searches for radiative transition of Z to a lighter spin-0 state X^0 decaying to hadrons, a lepton pair, a photon pair, or invisible particles as shown in the comments. The limits are for the product of branching ratios.

VALUE	CL%	DOCUMENT ID	TECN	COMMENT
• • • We do not use the following data for averages, fits, limits, etc. • • •				
		1 RAINBOLT 19	RVUE	$X^0 \rightarrow \ell^+ \ell^-$
		2 SIRUNYAN 19AZ	CMS	$X^0 \rightarrow \mu^+ \mu^-$
		3 BARATE 98U	ALEP	$X^0 \rightarrow \ell \bar{\ell}, q \bar{q}, gg, \gamma\gamma, \nu\bar{\nu}$
		4 ACCIARRI 97Q	L3	$X^0 \rightarrow$ invisible particle(s)
		5 ACTON 93E	OPAL	$X^0 \rightarrow \gamma\gamma$
		6 ABREU 92D	DLPH	$X^0 \rightarrow$ hadrons
		7 ADRIANI 92F	L3	$X^0 \rightarrow$ hadrons
		8 ACTON 91	OPAL	$X^0 \rightarrow$ anything
		9 ACTON 91B	OPAL	$X^0 \rightarrow e^+ e^-$
$<1.1 \times 10^{-4}$	95	9 ACTON 91B	OPAL	$X^0 \rightarrow \mu^+ \mu^-$
$<9 \times 10^{-5}$	95	9 ACTON 91B	OPAL	$X^0 \rightarrow \tau^+ \tau^-$
$<1.1 \times 10^{-4}$	95	9 ACTON 91B	OPAL	$X^0 \rightarrow \tau^+ \tau^-$
$<2.8 \times 10^{-4}$	95	10 ADEVA 91D	L3	$X^0 \rightarrow e^+ e^-$
$<2.3 \times 10^{-4}$	95	10 ADEVA 91D	L3	$X^0 \rightarrow \mu^+ \mu^-$
$<4.7 \times 10^{-4}$	95	11 ADEVA 91D	L3	$X^0 \rightarrow$ hadrons
$<8 \times 10^{-4}$	95	12 AKRAWY 90J	OPAL	$X^0 \rightarrow$ hadrons

- RAINBOLT 19 limits are from $B(Z \rightarrow \ell^+ \ell^- \ell^+ \ell^-)$. See their Figs. 5 and 6 for limits in mass-coupling plane.
- SIRUNYAN 19AZ search for $pp \rightarrow Z \rightarrow X^0 \mu^+ \mu^- \rightarrow \mu^+ \mu^- \mu^+ \mu^-$ events in pp collisions at $\sqrt{s} = 13$ TeV. See their Fig. 5 for limits on $\sigma(pp \rightarrow X^0 \mu^+ \mu^-) \cdot B(X^0 \rightarrow \mu^+ \mu^-)$.
- BARATE 98U obtain limits on $B(Z \rightarrow \gamma X^0) \cdot B(X^0 \rightarrow \ell \bar{\ell}, q \bar{q}, gg, \gamma\gamma, \nu\bar{\nu})$. See their Fig. 17.
- See Fig. 4 of ACCIARRI 97Q for the upper limit on $B(Z \rightarrow \gamma X^0; E_\gamma > E_{\min})$ as a function of E_{\min} .
- ACTON 93E give $\sigma(e^+ e^- \rightarrow X^0 \gamma) \cdot B(X^0 \rightarrow \gamma\gamma) < 0.4$ pb (95%CL) for $m_{X^0} = 60 \pm 2.5$ GeV. If the process occurs via s-channel γ exchange, the limit translates to $\Gamma(X^0) \cdot B(X^0 \rightarrow \gamma\gamma)^2 < 20$ MeV for $m_{X^0} = 60 \pm 1$ GeV.
- ABREU 92D give $\sigma_Z \cdot B(Z \rightarrow \gamma X^0) \cdot B(X^0 \rightarrow \text{hadrons}) < (3-10)$ pb for $m_{X^0} = 10-78$ GeV. A very similar limit is obtained for spin-1 X^0 .
- ADRIANI 92F search for isolated γ in hadronic Z decays. The limit $\sigma_Z \cdot B(Z \rightarrow \gamma X^0) \cdot B(X^0 \rightarrow \text{hadrons}) < (2-10)$ pb (95%CL) is given for $m_{X^0} = 25-85$ GeV.
- ACTON 91 searches for $Z \rightarrow Z^* X^0, Z^* \rightarrow e^+ e^-, \mu^+ \mu^-,$ or $\nu\bar{\nu}$. Excludes any new scalar X^0 with $m_{X^0} < 9.5$ GeV/c if it has the same coupling to ZZ^* as the MSM Higgs boson.
- ACTON 91B limits are for $m_{X^0} = 60-85$ GeV.
- ADEVA 91D limits are for $m_{X^0} = 30-89$ GeV.
- ADEVA 91D limits are for $m_{X^0} = 30-86$ GeV.
- AKRAWY 90J give $\Gamma(Z \rightarrow \gamma X^0) \cdot B(X^0 \rightarrow \text{hadrons}) < 1.9$ MeV (95%CL) for $m_{X^0} = 32-80$ GeV. We divide by $\Gamma(Z) = 2.5$ GeV to get product of branching ratios. For nonresonant transitions, the limit is $B(Z \rightarrow \gamma q \bar{q}) < 8.2$ MeV assuming three-body phase space distribution.

MASS LIMITS for a Heavy Neutral Boson Coupling to $e^+ e^-$

VALUE (GeV)	CL%	DOCUMENT ID	TECN	COMMENT
• • • We do not use the following data for averages, fits, limits, etc. • • •				
none 55-61		1 ODAKA 89	VNS	$\Gamma(X^0 \rightarrow e^+ e^-) \cdot B(X^0 \rightarrow \text{had.}) \gtrsim 0.2$ MeV
>45	95	2 DERRICK 86	HRS	$\Gamma(X^0 \rightarrow e^+ e^-) = 6$ MeV
>46.6	95	3 ADEVA 85	MRKJ	$\Gamma(X^0 \rightarrow e^+ e^-) = 10$ keV
>48	95	3 ADEVA 85	MRKJ	$\Gamma(X^0 \rightarrow e^+ e^-) = 4$ MeV
		4 BERGER 85B	PLUT	
none 39.8-45.5		5 ADEVA 84	MRKJ	$\Gamma(X^0 \rightarrow e^+ e^-) = 10$ keV
>47.8	95	5 ADEVA 84	MRKJ	$\Gamma(X^0 \rightarrow e^+ e^-) = 4$ MeV
none 39.8-45.2		5 BEHREND 84c	CELL	
>47	95	5 BEHREND 84c	CELL	$\Gamma(X^0 \rightarrow e^+ e^-) = 4$ MeV

- ODAKA 89 looked for a narrow or wide scalar resonance in $e^+ e^- \rightarrow$ hadrons at $E_{cm} = 55.0-60.8$ GeV.
- DERRICK 86 found no deviation from the Standard Model Bhabha scattering at $E_{cm} = 29$ GeV and set limits on the possible scalar boson $e^+ e^-$ coupling. See their figure 4 for excluded region in the $\Gamma(X^0 \rightarrow e^+ e^-) \cdot m_{X^0}$ plane. Electronic chiral invariance requires a parity doublet of X^0 , in which case the limit applies for $\Gamma(X^0 \rightarrow e^+ e^-) = 3$ MeV.
- ADEVA 85 first limit is from $2\gamma, \mu^+ \mu^-,$ hadrons assuming X^0 is a scalar. Second limit is from $e^+ e^-$ channel. $E_{cm} = 40-47$ GeV. Supersedes ADEVA 84.
- BERGER 85B looked for effect of spin-0 boson exchange in $e^+ e^- \rightarrow e^+ e^-$ and $\mu^+ \mu^-$ at $E_{cm} = 34.7$ GeV. See Fig. 5 for excluded region in the $m_{X^0} - \Gamma(X^0)$ plane.
- ADEVA 84 and BEHREND 84c have $E_{cm} = 39.8-45.5$ GeV. MARK-J searched X^0 in $e^+ e^- \rightarrow$ hadrons, $2\gamma, \mu^+ \mu^-, e^+ e^-$ and CELLO in the same channels plus τ pair. No narrow or broad X^0 is found in the energy range. They also searched for the effect of X^0 with $m_X > E_{cm}$. The second limits are from Bhabha data and for spin-0 singlet.

The same limits apply for $\Gamma(X^0 \rightarrow e^+ e^-) = 2$ MeV if X^0 is a spin-0 doublet. The second limit of BEHREND 84c was read off from their figure 2. The original papers also list limits in other channels.

Search for X^0 Resonance in $e^+ e^-$ Collisions

The limit is for $\Gamma(X^0 \rightarrow e^+ e^-) \cdot B(X^0 \rightarrow f)$, where f is the specified final state. Spin 0 is assumed for X^0 .

VALUE (keV)	CL%	DOCUMENT ID	TECN	COMMENT
• • • We do not use the following data for averages, fits, limits, etc. • • •				
$<10^3$	95	1 ABE 93c	VNS	$\Gamma(ee)$
$<(0.4-10)$	95	2 ABE 93c	VNS	$f = \gamma\gamma$
$<(0.3-5)$	95	3,4 ABE 93d	TOPZ	$f = \gamma\gamma$
$<(2-12)$	95	3,4 ABE 93d	TOPZ	$f = \text{hadrons}$
$<(4-200)$	95	4,5 ABE 93d	TOPZ	$f = ee$
$<(0.1-6)$	95	4,5 ABE 93d	TOPZ	$f = \mu\mu$
$<(0.5-8)$	90	6 STERNER 93	AMY	$f = \gamma\gamma$

- Limit is for $\Gamma(X^0 \rightarrow e^+ e^-) m_{X^0} = 56-63.5$ GeV for $\Gamma(X^0) = 0.5$ GeV.
- Limit is for $m_{X^0} = 56-61.5$ GeV and is valid for $\Gamma(X^0) \ll 100$ MeV. See their Fig. 5 for limits for $\Gamma = 1, 2$ GeV.
- Limit is for $m_{X^0} = 57.2-60$ GeV.
- Limit is valid for $\Gamma(X^0) \ll 100$ MeV. See paper for limits for $\Gamma = 1$ GeV and those for $J = 2$ resonances.
- Limit is for $m_{X^0} = 56.6-60$ GeV.
- STERNER 93 limit is for $m_{X^0} = 57-59.6$ GeV and is valid for $\Gamma(X^0) < 100$ MeV. See their Fig. 2 for limits for $\Gamma = 1, 3$ GeV.

Search for X^0 Resonance in ep Collisions

VALUE	DOCUMENT ID	TECN	COMMENT
-------	-------------	------	---------

- • • We do not use the following data for averages, fits, limits, etc. • • •
- 1 CHEKANOV 02B ZEUS $X \rightarrow jj$
- 1 CHEKANOV 02B search for photoproduction of X decaying into dijets in ep collisions. See their Fig. 5 for the limit on the photoproduction cross section.

Search for X^0 Resonance in $e^+ e^- \rightarrow X^0 \gamma$

VALUE (GeV)	DOCUMENT ID	TECN	COMMENT
-------------	-------------	------	---------

- • • We do not use the following data for averages, fits, limits, etc. • • •
- 1 ABBIENDI 03D OPAL $X^0 \rightarrow \gamma\gamma$
- 2 ABREU 00Z DLPH X^0 decaying invisibly
- 3 ADAM 96c DLPH X^0 decaying invisibly
- 1 ABBIENDI 03D measure the $e^+ e^- \rightarrow \gamma\gamma\gamma$ cross section at $\sqrt{s}=181-209$ GeV. The upper bound on the production cross section, $\sigma(e^+ e^- \rightarrow X^0 \gamma)$ times the branching ratio for $X^0 \rightarrow \gamma\gamma$, is less than 0.03 pb at 95%CL for X^0 masses between 20 and 180 GeV. See their Fig. 9b for the limits in the mass-cross section plane.
- 2 ABREU 00Z is from the single photon cross section at $\sqrt{s}=183, 189$ GeV. The production cross section upper limit is less than 0.3 pb for X^0 mass between 40 and 160 GeV. See their Fig. 4 for the limit in mass-cross section plane.
- 3 ADAM 96c is from the single photon production cross at $\sqrt{s}=130, 136$ GeV. The upper bound is less than 3 pb for X^0 masses between 60 and 130 GeV. See their Fig. 5 for the exact bound on the cross section $\sigma(e^+ e^- \rightarrow \gamma X^0)$.

Search for X^0 Resonance in $Z \rightarrow f \bar{f} X^0$

The limit is for $B(Z \rightarrow f \bar{f} X^0) \cdot B(X^0 \rightarrow F)$ where f is a fermion and F is the specified final state. Spin 0 is assumed for X^0 .

VALUE	CL%	DOCUMENT ID	TECN	COMMENT
• • • We do not use the following data for averages, fits, limits, etc. • • •				
$<3.7 \times 10^{-6}$	95	1 ABREU 96T	DLPH	$f=e, \mu, \tau; F=\gamma\gamma$
		2 ABREU 96T	DLPH	$f=\nu; F=\gamma\gamma$
		3 ABREU 96T	DLPH	$f=q; F=\gamma\gamma$
$<6.8 \times 10^{-6}$	95	2 ACTON 93E	OPAL	$f=e, \mu, \tau; F=\gamma\gamma$
$<5.5 \times 10^{-6}$	95	2 ACTON 93E	OPAL	$f=q; F=\gamma\gamma$
$<3.1 \times 10^{-6}$	95	2 ACTON 93E	OPAL	$f=\nu; F=\gamma\gamma$
$<6.5 \times 10^{-6}$	95	2 ACTON 93E	OPAL	$f=e, \mu; F=\ell \bar{\ell}, q \bar{q}, \nu\bar{\nu}$
$<7.1 \times 10^{-6}$	95	2 BUSKULIC 93F	ALEP	$f=e, \mu; F=\ell \bar{\ell}, q \bar{q}, \nu\bar{\nu}$
		4 ADRIANI 92F	L3	$f=q; F=\gamma\gamma$

- ABREU 96T obtain limit as a function of m_{X^0} . See their Fig. 6.
- Limit is for m_{X^0} around 60 GeV.
- ABREU 96T obtain limit as a function of m_{X^0} . See their Fig. 15.
- ADRIANI 92F give $\sigma_Z \cdot B(Z \rightarrow q \bar{q} X^0) \cdot B(X^0 \rightarrow \gamma\gamma) < (0.75-1.5)$ pb (95%CL) for $m_{X^0} = 10-70$ GeV. The limit is 1 pb at 60 GeV.

Search for X^0 Resonance in $W X^0$ final state

VALUE (MeV)	DOCUMENT ID	TECN	COMMENT
-------------	-------------	------	---------

- • • We do not use the following data for averages, fits, limits, etc. • • •
- 1 AALTONEN 13AA CDF $X^0 \rightarrow jj$
- 2 CHATRCHYAN 12BR CMS $X^0 \rightarrow jj$
- 3 ABAZOV 11i D0 $X^0 \rightarrow jj$
- 4 ABE 97W CDF $X^0 \rightarrow b \bar{b}$

Gauge & Higgs Boson Particle Listings

New Heavy Bosons

- 1 AALTONEN 13AA search for X^0 production associated with W (or Z) in $p\bar{p}$ collisions at $E_{cm} = 1.96$ TeV. The upper limit on the cross section $\sigma(p\bar{p} \rightarrow WX^0)$ is 2.2 pb for $M_{X^0} = 145$ GeV.
- 2 CHATRCHYAN 12BR search for X^0 production associated with W in pp collisions at $E_{cm} = 7$ TeV. The upper limit on the cross section is 5.0 pb at 95% CL for $m_{X^0} = 150$ GeV.
- 3 ABAZOV 111 search for X^0 production associated with W in $p\bar{p}$ collisions at $E_{cm} = 1.96$ TeV. The 95% CL upper limit on the cross section ranges from 2.57 to 1.28 pb for X^0 mass between 110 and 170 GeV.
- 4 ABE 97W search for X^0 production associated with W in $p\bar{p}$ collisions at $E_{cm} = 1.8$ TeV. The 95% CL upper limit on the production cross section times the branching ratio for $X^0 \rightarrow b\bar{b}$ ranges from 14 to 19 pb for X^0 mass between 70 and 120 GeV. See their Fig. 3 for upper limits of the production cross section as a function of m_{X^0} .

Search for X^0 Resonance in Quarkonium Decays

Limits are for branching ratios to modes shown. Spin 1 is assumed for X^0 .

VALUE	CL%	DOCUMENT ID	TECN	COMMENT
$< 3 \times 10^{-5} - 6 \times 10^{-3}$	90	¹ BALEST	95 CLE2	$\Gamma(1S) \rightarrow \chi^0 X^0 \gamma$, $m_{X^0} < 3.9$ GeV.

- • • We do not use the following data for averages, fits, limits, etc. • • •
- ¹BALEST 95 three-body limit is for phase-space photon energy distribution and angular distribution same as for $\Upsilon \rightarrow g g \gamma$.

Search for X^0 Resonance in $H(125)$ Decays

Spin 1 is assumed for X^0 . See neutral Higgs search listing for pseudoscalar X^0 .

VALUE	DOCUMENT ID	TECN	COMMENT
$\bullet \bullet \bullet$	We do not use the following data for averages, fits, limits, etc. • • •		

- • • We do not use the following data for averages, fits, limits, etc. • • •
- | | | |
|---------------------|-----------|------------------------------|
| ¹ AABOUD | 18AP ATLS | $H(125) \rightarrow Z X^0$ |
| ² AABOUD | 18AP ATLS | $H(125) \rightarrow X^0 X^0$ |
- ¹AABOUD 18AP use pp collision data at $\sqrt{s} = 13$ TeV. $X^0 \rightarrow \ell^+ \ell^-$ decay is assumed. See their Fig. 9 for limits on $\sigma_{H(125)} \cdot B(Z X^0)$.
- ²AABOUD 18AP use pp collision data at $\sqrt{s} = 13$ TeV. $X^0 \rightarrow \ell^+ \ell^-$ decay is assumed. See their Fig. 10 for limits on $\sigma_{H(125)} \cdot B(X^0 X^0)$.

REFERENCES FOR Searches for New Heavy Bosons (W' , Z' , leptiquarks, etc.)

SIRUNYAN	20A EPJ C80 3	A.M. Sirunyan et al.	(CMS Collab.)
AABOUD	19AJ PL B795 56	M. Aaboud et al.	(ATLAS Collab.)
AABOUD	19AS PR D99 092004	M. Aaboud et al.	(ATLAS Collab.)
AABOUD	19AX EPJ C79 733	M. Aaboud et al.	(ATLAS Collab.)
AABOUD	19B JHEP 1901 016	M. Aaboud et al.	(ATLAS Collab.)
AABOUD	19BB PL B798 134942	M. Aaboud et al.	(ATLAS Collab.)
AABOUD	19D PL B788 316	M. Aaboud et al.	(ATLAS Collab.)
AABOUD	19E PL B788 347	M. Aaboud et al.	(ATLAS Collab.)
AABOUD	19V JHEP 1905 142	M. Aaboud et al.	(ATLAS Collab.)
AABOUD	19X JHEP 1906 144	M. Aaboud et al.	(ATLAS Collab.)
AAD	19C PR D100 052013	G. Aad et al.	(ATLAS Collab.)
AAD	19D JHEP 1909 091	G. Aad et al.	(ATLAS Collab.)
AAD	19L PL B796 68	G. Aad et al.	(ATLAS Collab.)
ABRAMOWICZ	19 PR D99 092006	H. Abramowicz et al.	(ZEUS Collab.)
LONG	19 NP B943 114629	H.N. Long et al.	(VALE, SIEG)
MANDAL	19 JHEP 1912 089	R. Mandal, A. Pich	(VALE, SIEG)
PANDEY	19 JHEP 1911 046	S. Pandey, S. Karmakar, S. Rakshit	(IITB)
RAIBOLT	19 PR D99 013004	J.L. Raibolt, M. Schmidt	(NWES)
SIRUNYAN	19AA JHEP 1904 031	A.M. Sirunyan et al.	(CMS Collab.)
SIRUNYAN	19AL EPJ C79 208	A.M. Sirunyan et al.	(CMS Collab.)
SIRUNYAN	19AN EPJ C79 280	A.M. Sirunyan et al.	(CMS Collab.)
SIRUNYAN	19AY PL B792 107	A.M. Sirunyan et al.	(CMS Collab.)
SIRUNYAN	19AZ PL B792 345	A.M. Sirunyan et al.	(CMS Collab.)
SIRUNYAN	19BC PL B795 76	A.M. Sirunyan et al.	(CMS Collab.)
SIRUNYAN	19BI PR D99 032014	A.M. Sirunyan et al.	(CMS Collab.)
SIRUNYAN	19BJ PR D99 052002	A.M. Sirunyan et al.	(CMS Collab.)
SIRUNYAN	19CB PR D100 112007	A.M. Sirunyan et al.	(CMS Collab.)
SIRUNYAN	19CD PRL 123 231803	A.M. Sirunyan et al.	(CMS Collab.)
SIRUNYAN	19CP PL B798 134952	A.M. Sirunyan et al.	(CMS Collab.)
SIRUNYAN	19D PRL 122 081804	A.M. Sirunyan et al.	(CMS Collab.)
SIRUNYAN	19I JHEP 1901 051	A.M. Sirunyan et al.	(CMS Collab.)
SIRUNYAN	19V JHEP 1903 127	A.M. Sirunyan et al.	(CMS Collab.)
SIRUNYAN	19Y JHEP 1903 170	A.M. Sirunyan et al.	(CMS Collab.)
AABOUD	18AA PR D98 032015	M. Aaboud et al.	(ATLAS Collab.)
AABOUD	18AB PR D98 032016	M. Aaboud et al.	(ATLAS Collab.)
AABOUD	18AD PL B779 24	M. Aaboud et al.	(ATLAS Collab.)
AABOUD	18AF PL B781 327	M. Aaboud et al.	(ATLAS Collab.)
AABOUD	18AI JHEP 1803 174	M. Aaboud et al.	(ATLAS Collab.)
AABOUD	18AJ JHEP 1811 051 (errat.)	M. Aaboud et al.	(ATLAS Collab.)
AABOUD	18AK JHEP 1803 042	M. Aaboud et al.	(ATLAS Collab.)
AABOUD	18AL JHEP 1803 009	M. Aaboud et al.	(ATLAS Collab.)
AABOUD	18AP JHEP 1806 166	M. Aaboud et al.	(ATLAS Collab.)
AABOUD	18B EPJ C78 24	M. Aaboud et al.	(ATLAS Collab.)
AABOUD	18BG EPJ C78 401	M. Aaboud et al.	(ATLAS Collab.)
AABOUD	18BI EPJ C78 565	M. Aaboud et al.	(ATLAS Collab.)
AABOUD	18CH PL B787 68	M. Aaboud et al.	(ATLAS Collab.)
AABOUD	18CJ PR D98 052008	M. Aaboud et al.	(ATLAS Collab.)
AABOUD	18CM PR D98 092008	M. Aaboud et al.	(ATLAS Collab.)
AABOUD	18F PL B777 91	M. Aaboud et al.	(ATLAS Collab.)
AABOUD	18G JHEP 1801 055	M. Aaboud et al.	(ATLAS Collab.)
AABOUD	18K PRL 120 161802	M. Aaboud et al.	(ATLAS Collab.)
AABOUD	18N PRL 121 081801	M. Aaboud et al.	(ATLAS Collab.)
AALJ	18AQ JHEP 1809 147	R. Aaij et al.	(LHCb Collab.)
BOBOVNIKOV	18 PR D98 095029	I.D. Bobovnikov, P. Osland, A.A. Pankov	(BERG+)
SIRUNYAN	18 PL B777 39	A.M. Sirunyan et al.	(CMS Collab.)
SIRUNYAN	18AT JHEP 1804 073	A.M. Sirunyan et al.	(CMS Collab.)
SIRUNYAN	18AX JHEP 1805 088	A.M. Sirunyan et al.	(CMS Collab.)
SIRUNYAN	18AZ JHEP 1806 128	A.M. Sirunyan et al.	(CMS Collab.)
SIRUNYAN	18BB JHEP 1806 120	A.M. Sirunyan et al.	(CMS Collab.)
SIRUNYAN	18BJ JHEP 1807 115	A.M. Sirunyan et al.	(CMS Collab.)
SIRUNYAN	18BK JHEP 1807 075	A.M. Sirunyan et al.	(CMS Collab.)
SIRUNYAN	18BD JHEP 1808 130	A.M. Sirunyan et al.	(CMS Collab.)
SIRUNYAN	18CV JHEP 1805 148	A.M. Sirunyan et al.	(CMS Collab.)
SIRUNYAN	18CZ EPJ C78 707	A.M. Sirunyan et al.	(CMS Collab.)
SIRUNYAN	18DJ JHEP 1809 101	A.M. Sirunyan et al.	(CMS Collab.)
SIRUNYAN	18DR JHEP 1811 161	A.M. Sirunyan et al.	(CMS Collab.)
SIRUNYAN	18EC PRL 121 241802	A.M. Sirunyan et al.	(CMS Collab.)
SIRUNYAN	18ED JHEP 1811 172	A.M. Sirunyan et al.	(CMS Collab.)
SIRUNYAN	18E JHEP 1801 097	A.M. Sirunyan et al.	(CMS Collab.)
SIRUNYAN	18I PRL 120 201801	A.M. Sirunyan et al.	(CMS Collab.)
SIRUNYAN	18J PR D97 072006	A.M. Sirunyan et al.	(CMS Collab.)
SIRUNYAN	18K PR D98 032005	A.M. Sirunyan et al.	(CMS Collab.)
ZHANG	18A EPJ C78 695	J. Zhang, C.-X. Yue, C.-H. Li	(LHUJDA)
AABOUD	17AK PR D96 052004	M. Aaboud et al.	(ATLAS Collab.)
AABOUD	17AO PL B774 494	M. Aaboud et al.	(ATLAS Collab.)
AABOUD	17AT JHEP 1710 182	M. Aaboud et al.	(ATLAS Collab.)
AABOUD	17B PL B765 32	M. Aaboud et al.	(ATLAS Collab.)
KHACHATRYAN	17AX PL B773 563	V. Khachatryan et al.	(CMS Collab.)
KHACHATRYAN	17X JHEP 1702 048	V. Khachatryan et al.	(CMS Collab.)
KHACHATRYAN	17Y JHEP 1703 077	V. Khachatryan et al.	(CMS Collab.)
KHACHATRYAN	17Z PL B768 57	V. Khachatryan et al.	(CMS Collab.)
KHACHATRYAN	17W PL B768 137	V. Khachatryan et al.	(CMS Collab.)
KHACHATRYAN	17U PL B769 520	V. Khachatryan et al.	(CMS Collab.)
KHACHATRYAN	17Y PL B770 257	V. Khachatryan et al.	(CMS Collab.)
KHACHATRYAN	17Z PL B770 278	V. Khachatryan et al.	(CMS Collab.)
SIRUNYAN	17A JHEP 1703 162	A.M. Sirunyan et al.	(CMS Collab.)
SIRUNYAN	17AK PL B774 533	A.M. Sirunyan et al.	(CMS Collab.)
SIRUNYAN	17AP JHEP 1710 180	A.M. Sirunyan et al.	(CMS Collab.)
SIRUNYAN	17H JHEP 1707 121	A.M. Sirunyan et al.	(CMS Collab.)
SIRUNYAN	17I JHEP 1708 029	A.M. Sirunyan et al.	(CMS Collab.)
SIRUNYAN	17J JHEP 1707 001	A.M. Sirunyan et al.	(CMS Collab.)
SIRUNYAN	17K EPJ C77 636	A.M. Sirunyan et al.	(CMS Collab.)
SIRUNYAN	17T PRL 119 111802	A.M. Sirunyan et al.	(CMS Collab.)
SIRUNYAN	17V JHEP 1709 053	A.M. Sirunyan et al.	(CMS Collab.)
AABOUD	16E PL B759 229	M. Aaboud et al.	(ATLAS Collab.)
AABOUD	16AA EPJ C76 565	M. Aaboud et al.	(ATLAS Collab.)
AABOUD	16AE JHEP 1609 173	M. Aaboud et al.	(ATLAS Collab.)
AABOUD	16P EPJ C76 541	M. Aaboud et al.	(ATLAS Collab.)
AABOUD	16U PL B761 372	M. Aaboud et al.	(ATLAS Collab.)
AABOUD	16V PL B762 334	M. Aaboud et al.	(ATLAS Collab.)
AAD	16G EPJ C76 5	G. Aad et al.	(ATLAS Collab.)
AAD	16L EPJ C76 210	G. Aad et al.	(ATLAS Collab.)
AAD	16R PL B755 285	G. Aad et al.	(ATLAS Collab.)
AAD	16S PL B754 302	G. Aad et al.	(ATLAS Collab.)
AAD	16W PL B758 249	G. Aad et al.	(ATLAS Collab.)
BARRANCO	16 JP G43 115004	J. Barranco et al.	(CMS Collab.)
DEY	16E JHEP 1604 187	H.K. Dey, S. Mohanty	(ATLAS Collab.)
KHACHATRYAN	16AF PR D95 032004	V. Khachatryan et al.	(CMS Collab.)
KHACHATRYAN	16AG PR D93 032005	V. Khachatryan et al.	(CMS Collab.)
Also	PR D95 039906 (errat.)	V. Khachatryan et al.	(CMS Collab.)
KHACHATRYAN	16AO JHEP 1602 122	V. Khachatryan et al.	(CMS Collab.)
KHACHATRYAN	16AP JHEP 1602 145	V. Khachatryan et al.	(CMS Collab.)
KHACHATRYAN	16BD EPJ C76 237	V. Khachatryan et al.	(CMS Collab.)
KHACHATRYAN	16BE EPJ C76 317	V. Khachatryan et al.	(CMS Collab.)
KHACHATRYAN	16E PR D93 012001	V. Khachatryan et al.	(CMS Collab.)
KHACHATRYAN	16K PRL 116 071801	V. Khachatryan et al.	(CMS Collab.)
KHACHATRYAN	16L PRL 117 031802	V. Khachatryan et al.	(CMS Collab.)
KHACHATRYAN	16O PL B755 196	V. Khachatryan et al.	(CMS Collab.)
KUMAR	16 PR D96 014022	G. Kumar	(CMS Collab.)
AAD	15AM JHEP 1507 157	G. Aad et al.	(ATLAS Collab.)
AAD	15AO JHEP 1508 148	G. Aad et al.	(ATLAS Collab.)
AAD	15AT EPJ C75 79	G. Aad et al.	(ATLAS Collab.)
AAD	15AU EPJ C75 69	G. Aad et al.	(ATLAS Collab.)
AAD	15AV EPJ C75 165	G. Aad et al.	(ATLAS Collab.)
AAD	15AZ EPJ C75 209	G. Aad et al.	(ATLAS Collab.)
Also	EPJ C75 370 (errat.)	G. Aad et al.	(ATLAS Collab.)
AAD	15BB EPJ C75 263	G. Aad et al.	(ATLAS Collab.)
AAD	15CD PR D92 092001	G. Aad et al.	(ATLAS Collab.)
AAD	15CF EPJ C75 152	G. Aad et al.	(ATLAS Collab.)
AAD	15O PRL 115 031801	G. Aad et al.	(ATLAS Collab.)
AAD	15R PL B743 235	G. Aad et al.	(ATLAS Collab.)
AAD	15S PR D91 052007	G. Aad et al.	(ATLAS Collab.)
AALTONEN	15C PRL 115 061801	T. Aaltonen et al.	(CDF Collab.)
BESSAA	15 EPJ C75 97	A. Bessaa, S. Davidson	(CDF Collab.)
KHACHATRYAN	15AE JHEP 1504 025	V. Khachatryan et al.	(CMS Collab.)
KHACHATRYAN	15AJ JHEP 1507 042	V. Khachatryan et al.	(CMS Collab.)
KHACHATRYAN	15AV JHEP 1509 201	V. Khachatryan et al.	(CMS Collab.)
KHACHATRYAN	15C PL B740 83	V. Khachatryan et al.	(CMS Collab.)
KHACHATRYAN	15F PRL 114 101801	V. Khachatryan et al.	(CMS Collab.)
KHACHATRYAN	15G PL B748 265	V. Khachatryan et al.	(CMS Collab.)
KHACHATRYAN	15H PR D91 092005	V. Khachatryan et al.	(CMS Collab.)
KHACHATRYAN	15I PR D91 052009	V. Khachatryan et al.	(CMS Collab.)
SAHOO	15A PR D91 094019	S. Sahoo, R. Mohanta	(CDF Collab.)
AAD	14AI JHEP 1409 037	G. Aad et al.	(ATLAS Collab.)
AAD	14AT PL B738 428	G. Aad et al.	(ATLAS Collab.)
AAD	14S PL B737 223	G. Aad et al.	(ATLAS Collab.)
AAD	14V PR D90 052005	G. Aad et al.	(ATLAS Collab.)
KHACHATRYAN	14A JHEP 1408 173	V. Khachatryan et al.	(CMS Collab.)
KHACHATRYAN	14A JHEP 1408 174	V. Khachatryan et al.	(CMS Collab.)
KHACHATRYAN	14O EPJ C74 3149	V. Khachatryan et al.	(CMS Collab.)
KHACHATRYAN	14T PL B739 229	V. Khachatryan et al.	(CMS Collab.)
MARTINEZ	14 PR D90 015028	R. Martinez, F. Ochoa	(CMS Collab.)
PRIEELS	14 PR D90 112003	R. Priees et al.	(LOUV, ETH, PSI+)
AAD	13AE JHEP 1306 033	G. Aad et al.	(ATLAS Collab.)
AAD	13AO PR D87 112006	G. Aad et al.	(ATLAS Collab.)
AAD	13AQ PR D88 012004	G. Aad et al.	(ATLAS Collab.)
AAD	13D JHEP 1301 029	G. Aad et al.	(ATLAS Collab.)
AAD	13G JHEP 1301 116	G. Aad et al.	(ATLAS Collab.)
AAD	13K EPJ C73 2263	G. Aad et al.	(ATLAS Collab.)
AAD	13S PL B719 242	G. Aad et al.	(ATLAS Collab.)
AALTONEN	13A PRL 110 121802	T. Aaltonen et al.	(CDF Collab.)
AALTONEN	13AA PR D88 092004	T. Aaltonen et al.	(CDF Collab.)
AALTONEN	13R PRL 111 031802	T. Aaltonen et al.	(CDF Collab.)
CHATRCHYAN	13A JHEP 1301 013	S. Chatrchyan et al.	(CMS Collab.)
CHATRCHYAN	13AF PL B720 63	S. Chatrchyan et al.	(CMS Collab.)
CHATRCHYAN	13AJ PL B723 280	S. Chatrchyan et al.	(CMS Collab.)
CHATRCHYAN	13AP PR D87 072002	S. Chatrchyan et al.	(CMS Collab.)
CHATRCHYAN	13AQ PR D87 072005	S. Chatrchyan et al.	(CMS Collab.)
CHATRCHYAN	13AS PR D87 114015	S. Chatrchyan et al.	(CMS Collab.)
CHATRCHYAN	13AU PRL 110 141802	S. Chatrchyan et al.	(CMS Collab.)
CHATRCHYAN	13BM PRL 111 211804	S. Chatrchyan et al.	(CMS Collab.)
Also	PRL 112 119903 (errat.)	S. Chatrchyan et al.	(CMS Collab.)
CHATRCHYAN	13E PL B718 1229	S. Chatrchyan et al.	(CMS Collab.)
CHATRCHYAN	13M PRL 110 081801	S. Chatrchyan et al.	(CMS Collab.)
CHATRCHYAN	13U JHEP 1302 036	S. Chatrchyan et al.	(CMS Collab.)
SAKAKI	13 PR D88 094012	Y. Sakaki et al.	(CMS Collab.)
AAD	12AV PRL 109 081801	G. Aad et al.	(ATLAS Collab.)
AAD	12BB PR D85 112012	G. Aad et al.	(ATLAS Collab.)
AAD	12BV JHEP 1209 041	G. Aad et al.	(ATLAS Collab.)
AAD	12CC JHEP 1211 138	G. Aad et al.	(ATLAS Collab.)
AAD	12CK		

Gauge & Higgs Boson Particle Listings

New Heavy Bosons, Axions (A^0) and Other Very Light Bosons

BARTEL	87B	ZPHY C36 15	W. Bartel <i>et al.</i>	(JADE Collab.)
BEHREND	86B	PL B178 452	H.J. Behrend <i>et al.</i>	(CELLO Collab.)
DERRICK	86	PL 166B 463	M. Derrick <i>et al.</i>	(HRS Collab.)
Also		PR D34 3286	M. Derrick <i>et al.</i>	(HRS Collab.)
JODIDIO	86	PR D34 1967	A. Jodidio <i>et al.</i>	(LBL, NWES, TRIU)
Also		PR D37 237 (erratum)	A. Jodidio <i>et al.</i>	(LBL, NWES, TRIU)
MOHAPATRA	86	PR D34 909	R.N. Mohapatra	(UMD)
ADEVA	85	PL 152B 439	B. Adeva <i>et al.</i>	(Mark-J Collab.)
BERGER	85B	ZPHY C27 341	C. Berger <i>et al.</i>	(PLUTO Collab.)
STOKER	85	PRL 54 1887	D.P. Stoker <i>et al.</i>	(LBL, NWES, TRIU)
ADEVA	84	PRL 53 134	B. Adeva <i>et al.</i>	(Mark-J Collab.)
BEHREND	84C	PL 140B 130	H.J. Behrend <i>et al.</i>	(CELLO Collab.)
BERGSMAN	83	PL 122B 465	F. Bergsma <i>et al.</i>	(CHARM Collab.)
CARR	83	PRL 51 627	J. Carr <i>et al.</i>	(LBL, NWES, TRIU)
BEALL	82	PRL 48 848	G. Beall, M. Bander, A. Soni	(UCI, UCLA)
SHANKER	82	NP B204 375	O. Shanker	(TRIUM)

Axions (A^0) and Other Very Light Bosons, Searches for

See the related review(s):

[Axions and Other Similar Particles](#)

A^0 (Axion) MASS LIMITS from Astrophysics and Cosmology

These bounds depend on model-dependent assumptions (i.e. — on a combination of axion parameters).

VALUE (MeV)	DOCUMENT ID	TECN	COMMENT
••• We do not use the following data for averages, fits, limits, etc. •••			
>0.2	BARROSO 82	ASTR	Standard Axion
>0.25	1 RAFFELT 82	ASTR	Standard Axion
>0.2	2 DICUS 78C	ASTR	Standard Axion
	MIKHAELIAN 78	ASTR	Stellar emission
>0.3	2 SATO 78	ASTR	Standard Axion
>0.2	VYSOTSKII 78	ASTR	Standard Axion

1 Lower bound from 5.5 MeV γ -ray line from the sun.

2 Lower bound from requiring the red giants' stellar evolution not be disrupted by axion emission.

A^0 (Axion) and Other Light Boson (X^0) Searches in Hadron Decays

Limits are for branching ratios.

VALUE	CL%	DOCUMENT ID	TECN	COMMENT
••• We do not use the following data for averages, fits, limits, etc. •••				
<2 $\times 10^{-10}$	95	1 AAIJ 17A	LHCB	$B^+ \rightarrow K^+ X^0 (X^0 \rightarrow \mu^+ \mu^-)$
<3.7 $\times 10^{-8}$	90	2 AHN 17	KOTO	$K_L^0 \rightarrow \pi^0 X^0, m_{X^0} = 135$ MeV
<6 $\times 10^{-11}$	90	3 BATLEY 17	NA48	$K^\pm \rightarrow \pi^\pm X^0 (X^0 \rightarrow \mu^+ \mu^-)$
		4 WON 16	BELL	$\eta \rightarrow \gamma X^0 (X^0 \rightarrow \pi^+ \pi^-)$
<1 $\times 10^{-9}$	95	5 AAIJ 15AZ	LHCB	$B^0 \rightarrow K^{*0} X^0 (X^0 \rightarrow \mu^+ \mu^-)$
<1.5 $\times 10^{-6}$	90	6 ADLARSON 13	WASA	$\pi^0 \rightarrow \gamma X^0 (X^0 \rightarrow e^+ e^-), m_{X^0} = 100$ MeV
<2 $\times 10^{-8}$	90	7 BABUSCI 13B	KLOE	$\phi \rightarrow \eta X^0 (X^0 \rightarrow e^+ e^-)$
		8 ARCHILLI 12A	KLOE	$\phi \rightarrow \eta X^0 (X^0 \rightarrow e^+ e^-)$
<2 $\times 10^{-15}$	90	9 GNINENKO 12A	BDMP	$\pi^0 \rightarrow \gamma X^0 (X^0 \rightarrow e^+ e^-)$
<3 $\times 10^{-14}$	90	10 GNINENKO 12B	BDMP	$\eta(\eta') \rightarrow \gamma X^0 (X^0 \rightarrow e^+ e^-)$
<7 $\times 10^{-10}$	90	11 ADLER 04	B787	$K^+ \rightarrow \pi^+ X^0$
<7.3 $\times 10^{-11}$	90	12 ANISIMOVSK. 04	B949	$K^+ \rightarrow \pi^+ X^0$
<4.5 $\times 10^{-11}$	90	13 ADLER 02C	B787	$K^+ \rightarrow \pi^+ X^0$
<4 $\times 10^{-5}$	90	14 ADLER 01	B787	$K^+ \rightarrow \pi^+ \pi^0 A^0$
<4.9 $\times 10^{-5}$	90	AMMAR 01B	CLEO	$B^\pm \rightarrow \pi^\pm (K^\pm) X^0$
<5.3 $\times 10^{-5}$	90	AMMAR 01B	CLEO	$B^0 \rightarrow K_S^0 X^0$
<3.3 $\times 10^{-5}$	90	15 ALTEGOER 98	NOMD	$\pi^0 \rightarrow \gamma X^0, m_{X^0} < 120$ MeV
<5.0 $\times 10^{-8}$	90	16 KITCHING 97	B787	$K^+ \rightarrow \pi^+ X^0 (X^0 \rightarrow \gamma\gamma)$
<5.2 $\times 10^{-10}$	90	17 ADLER 96	B787	$K^+ \rightarrow \pi^+ X^0$
<2.8 $\times 10^{-4}$	90	18 AMSLER 96B	CBAR	$\pi^0 \rightarrow \gamma X^0, m_{X^0} < 65$ MeV
<3 $\times 10^{-4}$	90	18 AMSLER 96B	CBAR	$\eta \rightarrow \gamma X^0, m_{X^0} = 50-200$ MeV
<4 $\times 10^{-5}$	90	18 AMSLER 96B	CBAR	$\eta' \rightarrow \gamma X^0, m_{X^0} = 50-925$ MeV
<6 $\times 10^{-5}$	90	18 AMSLER 94B	CBAR	$\pi^0 \rightarrow \gamma X^0, m_{X^0} = 65-125$ MeV
<6 $\times 10^{-5}$	90	18 AMSLER 94B	CBAR	$\eta \rightarrow \gamma X^0, m_{X^0} = 200-525$ MeV
<7 $\times 10^{-3}$	90	19 MEIJERDREES 94	CNTR	$\pi^0 \rightarrow \gamma X^0, m_{X^0} = 25$ MeV
<2 $\times 10^{-3}$	90	19 MEIJERDREES 94	CNTR	$\pi^0 \rightarrow \gamma X^0, m_{X^0} = 100$ MeV
<2 $\times 10^{-7}$	90	20 ATIYA 93B	B787	Sup. by ADLER 04
<3 $\times 10^{-13}$	90	21 NG 93	COSM	$\pi^0 \rightarrow \gamma X^0$
<1.1 $\times 10^{-8}$	90	22 ALLIEGRO 92	SPEC	$K^+ \rightarrow \pi^+ X^0 (X^0 \rightarrow e^+ e^-)$
<5 $\times 10^{-4}$	90	23 ATIYA 92	B787	$\pi^0 \rightarrow \gamma X^0$
<1 $\times 10^{-12}$	95	24 BARABASH 92	BDMP	$\pi^\pm \rightarrow e^\pm \nu X^0 (X^0 \rightarrow e^+ e^-, \gamma\gamma), m_{X^0} = 8$ MeV
<1 $\times 10^{-12}$	95	25 BARABASH 92	BDMP	$K^\pm \rightarrow \pi^\pm X^0 (X^0 \rightarrow e^+ e^-, \gamma\gamma), m_{X^0} = 10$ MeV
<1 $\times 10^{-11}$	95	26 BARABASH 92	BDMP	$K_L^0 \rightarrow \pi^0 X^0 (X^0 \rightarrow e^+ e^-, \gamma\gamma), m_{X^0} = 10$ MeV
<1 $\times 10^{-14}$	95	27 BARABASH 92	BDMP	$\eta' \rightarrow \eta X^0 (X^0 \rightarrow e^+ e^-, \gamma\gamma), m_{X^0} = 10$ MeV

<4 $\times 10^{-6}$	90	28 MEIJERDREES 92	SPEC	$\pi^0 \rightarrow \gamma X^0 (X^0 \rightarrow e^+ e^-), m_{X^0} = 100$ MeV
<1 $\times 10^{-7}$	90	29 ATIYA 90B	B787	Sup. by KITCHING 97
<1.3 $\times 10^{-8}$	90	30 KORENCHENKO 87	SPEC	$\pi^+ \rightarrow e^+ \nu A^0 (A^0 \rightarrow e^+ e^-)$
<1 $\times 10^{-9}$	90	31 EICHLER 86	SPEC	Stopped $\pi^+ \rightarrow e^+ \nu A^0$
<2 $\times 10^{-5}$	90	32 YAMAZAKI 84	SPEC	For $160 < m < 260$ MeV
<(1.5-4) $\times 10^{-6}$	90	32 YAMAZAKI 84	SPEC	K decay, $m_{X^0} \ll 100$ MeV
		33 ASANO 82	CNTR	Stopped $K^+ \rightarrow \pi^+ X^0$
		34 ASANO 81B	CNTR	Stopped $K^+ \rightarrow \pi^+ X^0$
		35 ZHITNITSKII 79		Heavy axion

1 The limit is for $\tau_{X^0} = 10$ ps. See their Fig. 4 for limits in the range of $m_{X^0} = 250-4700$ MeV and $\tau_{X^0} = 0.1-1000$ ps.

2 The limit as a function of m_{X^0} from 0 to 250 MeV is provided in their Fig. 5.

3 The limit is for $m_{X^0} = 216$ MeV and $\tau_{X^0} \leq 10$ ps. See their Fig. 4(c) for limits in the range of $m_{X^0} = 211-354$ MeV and longer lifetimes.

4 WON 16 look for a vector boson coupled to baryon number. Derived limits on $\alpha' < 10^{-3}-10^{-2}$ for $m_{X^0} = 290-520$ MeV at 95% CL. See their Fig. 4 for mass-dependent limits.

5 The limit is for $\tau_{X^0} = 10$ ps and $m_{X^0} = 214-4350$ MeV. See their Fig. 4 for mass- and lifetime-dependent limits.

6 Limits between 2.0×10^{-5} and 1.5×10^{-6} are obtained for $m_{X^0} = 20-100$ MeV (see their Fig. 8). Angular momentum conservation requires that X^0 has spin ≥ 1 .

7 The limit is for $B(\phi \rightarrow \eta X^0) \cdot B(X^0 \rightarrow e^+ e^-)$ and applies to $m_{X^0} = 410$ MeV. It is derived by analyzing $\eta \rightarrow \pi^0 \pi^0 \pi^0$ and $\pi^- \pi^+ \pi^0$. Limits between 1×10^{-6} and 2×10^{-8} are obtained for $m_{X^0} \leq 450$ MeV (see their Fig. 6).

8 ARCHILLI 12 analyzed $\eta \rightarrow \pi^+ \pi^- \pi^0$ decays. Derived limits on $\alpha'/\alpha < 2 \times 10^{-5}$ for $m_{X^0} = 50-420$ MeV at 90% CL. See their Fig. 8 for mass-dependent limits.

9 This limit is for $B(\pi^0 \rightarrow \gamma X^0) \cdot B(X^0 \rightarrow e^+ e^-)$ and applies for $m_{X^0} = 90$ MeV and $\tau_{X^0} \approx 1 \times 10^{-8}$ sec. Limits between 10^{-8} and 2×10^{-15} are obtained for $m_{X^0} = 3-120$ MeV and $\tau_{X^0} = 1 \times 10^{-11}-1$ sec. See their Fig. 3 for limits at different masses and lifetimes.

10 This limit is for $B(\eta \rightarrow \gamma X^0) \cdot B(X^0 \rightarrow e^+ e^-)$ and applies for $m_{X^0} = 100$ MeV and $\tau_{X^0} \approx 6 \times 10^{-9}$ sec. Limits between 10^{-5} and 3×10^{-14} are obtained for $m_{X^0} \lesssim 550$ MeV and $\tau_{X^0} = 10^{-10}-10$ sec. See their Fig. 5 for limits at different mass and lifetime and for η' decays.

11 This limit applies for a mass near 180 MeV. For other masses in the range $m_{X^0} = 150-250$ MeV the limit is less restrictive, but still improves ADLER 02c and ATIYA 93b.

12 ANISIMOVSKY 04 bound is for $m_{X^0} = 0$.

13 ADLER 02c bound is for $m_{X^0} < 60$ MeV. See Fig. 2 for limits at higher masses.

14 The quoted limit is for $m_{X^0} = 0-80$ MeV. See their Fig. 5 for the limit at higher mass. The branching fraction limit assumes pure phase space decay distributions.

15 ALTEGOER 98 looked for X^0 from π^0 decay which penetrate the shielding and convert to π^0 in the external Coulomb field of a nucleus.

16 KITCHING 97 limit is for $B(K^+ \rightarrow \pi^+ X^0) \cdot B(X^0 \rightarrow \gamma\gamma)$ and applies for $m_{X^0} \approx 50$ MeV, $\tau_{X^0} < 10^{-10}$ s. Limits are provided for $0 < m_{X^0} < 100$ MeV, $\tau_{X^0} < 10^{-8}$ s.

17 ADLER 96 looked for a peak in missing-mass distribution. This work is an update of ATIYA 93. The limit is for massless stable X^0 particles and extends to $m_{X^0} = 80$ MeV at the same level. See paper for dependence on finite lifetime.

18 AMSLER 94b and AMSLER 96b looked for a peak in missing-mass distribution.

19 The MEIJERDREES 94 limit is based on inclusive photon spectrum and is independent of X^0 decay modes. It applies to $\tau(X^0) > 10^{-23}$ sec.

20 ATIYA 93b looked for a peak in missing mass distribution. The bound applies for stable X^0 of $m_{X^0} = 150-250$ MeV, and the limit becomes stronger (10^{-8}) for $m_{X^0} = 180-240$ MeV.

21 NG 93 studied the production of X^0 via $\gamma\gamma \rightarrow \pi^0 \rightarrow \gamma X^0$ in the early universe at $T \approx 1$ MeV. The bound on extra neutrinos from nucleosynthesis $\Delta N_\nu < 0.3$ (WALKER 91) is employed. It applies to $m_{X^0} \ll 1$ MeV in order to be relativistic down to nucleosynthesis temperature. See paper for heavier X^0 .

22 ALLIEGRO 92 limit applies for $m_{X^0} = 150-340$ MeV and is the branching ratio times the decay probability. Limit is $< 1.5 \times 10^{-8}$ at 99% CL.

23 ATIYA 92 looked for a peak in missing mass distribution. The limit applies to $m_{X^0} = 0-130$ MeV in the narrow resonance limit. See paper for the dependence on lifetime. Covariance requires X^0 to be a vector particle.

24 BARABASH 92 is a beam dump experiment that searched for a light Higgs. Limits between 1×10^{-12} and 1×10^{-7} are obtained for $3 < m_{X^0} < 40$ MeV.

25 Limits between 1×10^{-12} and 1 are obtained for $4 < m_{X^0} < 69$ MeV.

26 Limits between 1×10^{-11} and 5×10^{-3} are obtained for $4 < m_{X^0} < 63$ MeV.

27 Limits between 1×10^{-14} and 1 are obtained for $3 < m_{X^0} < 82$ MeV.

28 MEIJERDREES 92 limit applies for $\tau_{X^0} = 10^{-23}-10^{-11}$ sec. Limits between 2×10^{-4} and 4×10^{-6} are obtained for $m_{X^0} = 25-120$ MeV. Angular momentum conservation requires that X^0 has spin ≥ 1 .

29 ATIYA 90b limit is for $B(K^+ \rightarrow \pi^+ X^0) \cdot B(X^0 \rightarrow \gamma\gamma)$ and applies for $m_{X^0} = 50$ MeV, $\tau_{X^0} < 10^{-10}$ s. Limits are also provided for $0 < m_{X^0} < 100$ MeV, $\tau_{X^0} < 10^{-8}$ s.

30 KORENCHENKO 87 limit assumes $m_{A^0} = 1.7$ MeV, $\tau_{A^0} \lesssim 10^{-12}$ s, and $B(A^0 \rightarrow e^+ e^-) = 1$.

31 EICHLER 86 looked for $\pi^+ \rightarrow e^+ \nu A^0$ followed by $A^0 \rightarrow e^+ e^-$. Limits on the branching fraction depend on the mass and lifetime of A^0 . The quoted limits are valid when $\tau(A^0) \gtrsim 3 \times 10^{-10}$ s if the decays are kinematically allowed.

See key on page 999

Gauge & Higgs Boson Particle Listings

Axions (A^0) and Other Very Light Bosons

- ³² YAMAZAKI 84 looked for a discrete line in $K^+ \rightarrow \pi^+ X$. Sensitive to wide mass range (5–300 MeV), independent of whether X decays promptly or not.
- ³³ ASANO 82 at KEK set limits for $B(K^+ \rightarrow \pi^+ X^0)$ for $m_{X^0} < 100$ MeV as $BR < 4. \times 10^{-8}$ for $\tau(X^0 \rightarrow n\gamma\text{'s}) > 1. \times 10^{-9}$ s, $BR < 1.4 \times 10^{-6}$ for $\tau < 1. \times 10^{-9}$ s.
- ³⁴ ASANO 81B is KEK experiment. Set $B(K^+ \rightarrow \pi^+ X^0) < 3.8 \times 10^{-8}$ at CL = 90%.
- ³⁵ ZHITNITSKII 79 argue that a heavy axion predicted by YANG 78 ($3 < m < 40$ MeV) contradicts experimental muon anomalous magnetic moments.

A^0 (Axion) Searches in Quarkonium Decays

Decay or transition of quarkonium. Limits are for branching ratio.

VALUE	CL%	DOCUMENT ID	TECN	COMMENT
• • • We do not use the following data for averages, fits, limits, etc. • • •				
$< 2.8 \times 10^{-8}$	90	1 ABLIKIM 16E	BES3	$J/\psi \rightarrow A^0 \gamma (A^0 \rightarrow \mu^+ \mu^-)$
$< 4 \times 10^{-7}$	90	2 ABLIKIM 12	BES3	$J/\psi \rightarrow A^0 \gamma (A^0 \rightarrow \mu^+ \mu^-)$
$< 4.0 \times 10^{-5}$	90	3 ANTREASYAN 90c	CBAL	$\Upsilon(1S) \rightarrow A^0 \gamma$
$< 5 \times 10^{-5}$	90	4 DRUZHININ 87	ND	$\phi \rightarrow A^0 \gamma (A^0 \rightarrow e^+ e^-)$
$< 2 \times 10^{-3}$	90	5 DRUZHININ 87	ND	$\phi \rightarrow A^0 \gamma (A^0 \rightarrow \gamma \gamma)$
$< 7 \times 10^{-6}$	90	6 DRUZHININ 87	ND	$\phi \rightarrow A^0 \gamma (A^0 \rightarrow \text{missing})$
$< 1.4 \times 10^{-5}$	90	7 EDWARDS 82	CBAL	$J/\psi \rightarrow A^0 \gamma$
1 ABLIKIM 16E limits between $2.8\text{--}495.3 \times 10^{-8}$ were obtained for $0.212 \text{ GeV} < m_{A^0} < 3.0$ GeV. See their Fig. 5 for mass-dependent limits.				
2 ABLIKIM 12 derived limits between $4 \times 10^{-7}\text{--}2.1 \times 10^{-5}$ for $0.212 \text{ GeV} < m_{A^0} < 3.0$ GeV. See their Fig. 2(c) for mass-dependent limits.				
3 ANTREASYAN 90c assume that A^0 does not decay in the detector.				
4 The first DRUZHININ 87 limit is valid when $\tau_{A^0}/m_{A^0} < 3 \times 10^{-13}$ s/MeV and $m_{A^0} < 20$ MeV.				
5 The second DRUZHININ 87 limit is valid when $\tau_{A^0}/m_{A^0} < 5 \times 10^{-13}$ s/MeV and $m_{A^0} < 20$ MeV.				
6 The third DRUZHININ 87 limit is valid when $\tau_{A^0}/m_{A^0} > 7 \times 10^{-12}$ s/MeV and $m_{A^0} < 200$ MeV.				
7 EDWARDS 82 looked for $J/\psi \rightarrow \gamma A^0$ decays by looking for events with a single γ [of energy $\sim 1/2$ the $J/\psi(1S)$ mass], plus nothing else in the detector. The limit is inconsistent with the axion interpretation of the FAISSNER 81B result.				

A^0 (Axion) Searches in Positronium Decays

Decay or transition of positronium. Limits are for branching ratio.

VALUE	CL%	DOCUMENT ID	TECN	COMMENT
• • • We do not use the following data for averages, fits, limits, etc. • • •				
$< 4.4 \times 10^{-5}$	90	1 BADERT... 02	CNTR	$\alpha\text{-Ps} \rightarrow \gamma X_1 X_2, m_{X_1} + m_{X_2} \leq 900 \text{ keV}$
$< 2 \times 10^{-4}$	90	MAENO 95	CNTR	$\alpha\text{-Ps} \rightarrow A^0 \gamma, m_{A^0} = 850\text{--}1013 \text{ keV}$
$< 3.0 \times 10^{-4}$	90	2 ASAI 94	CNTR	$\alpha\text{-Ps} \rightarrow A^0 \gamma, m_{A^0} = 30\text{--}500 \text{ keV}$
$< 2.8 \times 10^{-5}$	90	3 AKOPYAN 91	CNTR	$\alpha\text{-Ps} \rightarrow A^0 \gamma (A^0 \rightarrow \gamma \gamma), m_{A^0} < 30 \text{ keV}$
$< 1.1 \times 10^{-6}$	90	4 ASAI 91	CNTR	$\alpha\text{-Ps} \rightarrow A^0 \gamma, m_{A^0} < 800 \text{ keV}$
$< 3.8 \times 10^{-4}$	90	GNINENKO 90	CNTR	$\alpha\text{-Ps} \rightarrow A^0 \gamma, m_{A^0} < 30 \text{ keV}$
$< (1\text{--}5) \times 10^{-4}$	95	5 TSUCHIAKI 90	CNTR	$\alpha\text{-Ps} \rightarrow A^0 \gamma, m_{A^0} = 300\text{--}900 \text{ keV}$
$< 6.4 \times 10^{-5}$	90	6 ORITO 89	CNTR	$\alpha\text{-Ps} \rightarrow A^0 \gamma, m_{A^0} < 30 \text{ keV}$
		7 AMALDI 85	CNTR	Ortho-positronium
		8 CARBONI 83	CNTR	Ortho-positronium
1 BADERTSCHER 02 looked for a three-body decay of ortho-positronium into a photon and two penetrating (neutral or milli-charged) particles.				
2 The ASAI 94 limit is based on inclusive photon spectrum and is independent of A^0 decay modes.				
3 The AKOPYAN 91 limit applies for a short-lived A^0 with $\tau_{A^0} < 10^{-13} m_{A^0} [\text{keV}]$ s.				
4 ASAI 91 limit translates to $g_{A^0 e^+ e^-}^2 / 4\pi < 1.1 \times 10^{-11}$ (90% CL) for $m_{A^0} < 800 \text{ keV}$.				
5 The TSUCHIAKI 90 limit is based on inclusive photon spectrum and is independent of A^0 decay modes.				
6 ORITO 89 limit translates to $g_{A^0 e^+ e^-}^2 / 4\pi < 6.2 \times 10^{-10}$. Somewhat more sensitive limits are obtained for larger m_{A^0} : $B < 7.6 \times 10^{-6}$ at 100 keV.				
7 AMALDI 85 set limits $B(A^0 \gamma) / B(\gamma \gamma \gamma) < (1\text{--}5) \times 10^{-6}$ for $m_{A^0} = 900\text{--}100 \text{ keV}$ which are about 1/10 of the CARBONI 83 limits.				
8 CARBONI 83 looked for ortho-positronium $\rightarrow A^0 \gamma$. Set limit for A^0 electron coupling squared, $(g_{e e A^0})^2 / (4\pi) < 6. \times 10^{-10}\text{--}7. \times 10^{-9}$ for m_{A^0} from 150–900 keV (CL = 99.7%). This is about 1/10 of the bound from $g\text{--}2$ experiments.				

A^0 (Axion) Search in Photoproduction

VALUE	DOCUMENT ID	COMMENT
• • • We do not use the following data for averages, fits, limits, etc. • • •		
	1 BASSOMPIERRE... 95	$m_{A^0} = 1.8 \pm 0.2 \text{ MeV}$
1 BASSOMPIERRE 95 is an extension of BASSOMPIERRE 93. They looked for a peak in the invariant mass of $e^+ e^-$ pairs in the region $m_{e^+ e^-} = 1.8 \pm 0.2 \text{ MeV}$. They obtained bounds on the production rate A^0 for $\tau(A^0) = 10^{-18}\text{--}10^{-9}$ sec. They also found an excess of events in the range $m_{e^+ e^-} = 2.1\text{--}3.5 \text{ MeV}$.		

A^0 (Axion) Production in Hadron Collisions

Limits are for $\sigma(A^0) / \sigma(\pi^0)$.

VALUE	CL%	EVENTS	DOCUMENT ID	TECN	COMMENT
• • • We do not use the following data for averages, fits, limits, etc. • • •					
			1 SIRUNYAN 19Bq	CMS	$X^0 \rightarrow \mu^+ \mu^-$
			2 JAIN 07	CNTR	$A^0 \rightarrow e^+ e^-$
			3 AHMAD 97	SPEC	e^+ production
			4 LEINBERGER 97	SPEC	$A^0 \rightarrow e^+ e^-$
			5 GANZ 96	SPEC	$A^0 \rightarrow e^+ e^-$
			6 KAMEL 96	EMUL	^{32}S emulsion, $A^0 \rightarrow e^+ e^-$
			7 BLUEMLEIN 92	BDMP	$A^0 N_Z \rightarrow \ell^+ \ell^- N_Z$
			8 MEIJERDREES 92	SPEC	$\pi^- p \rightarrow n A^0, A^0 \rightarrow e^+ e^-$
			9 BLUEMLEIN 91	BDMP	$A^0 \rightarrow e^+ e^-, 2\gamma$
			10 FAISSNER 89	OSPCK	Beam dump, $A^0 \rightarrow e^+ e^-$
			11 DEBOER 88	RVUE	$A^0 \rightarrow e^+ e^-$
			12 EL-NADI 88	EMUL	$A^0 \rightarrow e^+ e^-$
			13 FAISSNER 88	OSPCK	Beam dump, $A^0 \rightarrow 2\gamma$
			14 BADIER 86	BDMP	$A^0 \rightarrow e^+ e^-$
			15 BERGSMA 85	CHRM	CERN beam dump
			15 BERGSMA 85	CHRM	CERN beam dump
			16 FAISSNER 83	OSPCK	Beam dump, $A^0 \rightarrow 2\gamma$
			17 FAISSNER 83B	RVUE	LAMPF beam dump
			18 FRANK 83B	RVUE	LAMPF beam dump
			19 HOFFMAN 83	CNTR	$\pi p \rightarrow n A^0 (A^0 \rightarrow e^+ e^-)$
			20 FETSCHER 82	RVUE	See FAISSNER 81B
			21 FAISSNER 81	OSPCK	CERN PS ν wideband
			22 FAISSNER 81B	OSPCK	Beam dump, $A^0 \rightarrow 2\gamma$
			23 KIM 81	OSPCK	26 GeV $pN \rightarrow A^0 X$
			24 FAISSNER 80	OSPCK	Beam dump, $A^0 \rightarrow e^+ e^-$
$< 2. \times 10^{-11}$	90	0	25 JACQUES 80	HLBC	28 GeV protons
$< 1. \times 10^{-13}$	90	0	25 JACQUES 80	HLBC	Beam dump
			26 SOUKAS 80	CALO	28 GeV p beam dump
			27 BECHIS 79	CNTR	
			28 COTEUS 79	OSPCK	Beam dump
			29 DISHAW 79	CALO	400 GeV pp
			ALIBRAN 78	HYBR	Beam dump
			ASRATYAN 78B	CALO	Beam dump
			30 BELLOTTI 78	HLBC	Beam dump
			30 BELLOTTI 78	HLBC	$m_{A^0} = 1.5 \text{ MeV}$
			30 BELLOTTI 78	HLBC	$m_{A^0} = 1 \text{ MeV}$
			31 BOSETTI 78B	HYBR	Beam dump
			32 DONNELLY 78		
			HANSL 78D	WIRE	Beam dump
			33 MICELMAC... 78		
			34 VYSOTSKII 78		

- 1 SIRUNYAN 19Bq look for the pair production of a new light boson decaying into a pair of muons, and set limits on the product of the production cross section times branching fraction to dimuons squared times acceptance over a range of $m_{X^0} = 0.25\text{--}8.5 \text{ GeV}$. See the right panel of their Fig. 1 for mass-dependent limits.
- 2 JAIN 07 claims evidence for $A^0 \rightarrow e^+ e^-$ produced in 207Pb collision on nuclear emulsion (Ag/Br) for $m(A^0) = 7 \pm 1$ or $19 \pm 1 \text{ MeV}$ and $\tau(A^0) \leq 10^{-13} \text{ s}$.
- 3 AHMAD 97 reports a result of APEX Collaboration which studied positron production in $^{238}\text{U} \rightarrow ^{232}\text{Ta}$ and $^{238}\text{U} \rightarrow ^{181}\text{Ta}$ collisions, without requiring a coincident electron. No narrow lines were found for $250 < E_{e^+} < 750 \text{ keV}$.
- 4 LEINBERGER 97 (ORANGE Collaboration) at GSI looked for a narrow sum-energy $e^+ e^-$ line at $\sim 635 \text{ keV}$ in $^{238}\text{U} \rightarrow ^{181}\text{Ta}$ collision. Limits on the production probability for a narrow sum-energy $e^+ e^-$ line are set. See their Table 2.
- 5 GANZ 96 (EPOS II Collaboration) has placed upper bounds on the production cross section of $e^+ e^-$ pairs from $^{238}\text{U} \rightarrow ^{181}\text{Ta}$ and $^{238}\text{U} \rightarrow ^{232}\text{Th}$ collisions at GSI. See Table 2 for limits both for back-to-back and isotropic configurations of $e^+ e^-$ pairs. These limits rule out the existence of peaks in the $e^+ e^-$ sum-energy distribution, reported by an earlier version of this experiment.
- 6 KAMEL 96 looked for $e^+ e^-$ pairs from the collision of ^{32}S (200 GeV/nucleon) and emulsion. No evidence of mass peaks is found in the region of sensitivity $m_{e e} > 2 \text{ MeV}$.
- 7 BLUEMLEIN 92 is a proton beam dump experiment at Serpukhov with a secondary target to induce Bethe-Heitler production of $e^+ e^-$ or $\mu^+ \mu^-$ from the produce A^0 . See Fig. 5 for the excluded region in m_{A^0} - x plane. For the standard axion, $0.3 < x < 25$ is excluded at 95% CL. If combined with BLUEMLEIN 91, $0.008 < x < 32$ is excluded.
- 8 MEIJERDREES 92 give $\Gamma(\pi^- p \rightarrow n A^0) \cdot B(A^0 \rightarrow e^+ e^-) / \Gamma(\pi^- p \rightarrow \text{all}) < 10^{-5}$ (90% CL) for $m_{A^0} = 100 \text{ MeV}$, $\tau_{A^0} = 10^{-11}\text{--}10^{-23} \text{ sec}$. Limits ranging from 2.5×10^{-3} to 10^{-7} are given for $m_{A^0} = 25\text{--}136 \text{ MeV}$.
- 9 BLUEMLEIN 91 is a proton beam dump experiment at Serpukhov. No candidate event for $A^0 \rightarrow e^+ e^-, 2\gamma$ are found. Fig. 6 gives the excluded region in m_{A^0} - x plane ($x = \tan\beta = v_2/v_1$). Standard axion is excluded for $0.2 < m_{A^0} < 3.2 \text{ MeV}$ for most $x > 1$, $0.2\text{--}11 \text{ MeV}$ for most $x < 1$.
- 10 FAISSNER 89 searched for $A^0 \rightarrow e^+ e^-$ in a proton beam dump experiment at SIN. No excess of events was observed over the background. A standard axion with mass $2m_e\text{--}20 \text{ MeV}$ is excluded. Lower limit on f_{A^0} of $\sim 10^4 \text{ GeV}$ is given for $m_{A^0} = 2m_e\text{--}20 \text{ MeV}$.
- 11 DEBOER 88 reanalyze EL-NADI 88 data and claim evidence for three distinct states with mass $\sim 1.1, \sim 2.1, \text{ and } \sim 9 \text{ MeV}$, lifetimes $10^{-16}\text{--}10^{-15} \text{ s}$ decaying to $e^+ e^-$

Gauge & Higgs Boson Particle Listings

Axions (A^0) and Other Very Light Bosons

- and note the similarity of the data with those of a cosmic-ray experiment by Bristol group (B. M. Anand, Proc. of the Royal Society of London, Section A **A22** 183 (1953)). For a criticism see PERKINS 89, who suggests that the events are compatible with π^0 Dalitz decay. DEBOER 89B is a reply which contests the criticism.
- 12 EL-NADI 88 claim the existence of a neutral particle decaying into e^+e^- with mass 1.60 ± 0.59 MeV, lifetime $(0.15 \pm 0.01) \times 10^{-14}$ s, which is produced in heavy ion interactions with emulsion nuclei at ~ 4 GeV/c/nucleon.
 - 13 FAISSNER 88 is a proton beam dump experiment at SIN. They found no candidate event for $A^0 \rightarrow \gamma\gamma$. A standard axion decaying to 2γ is excluded except for a region $x \approx 1$. Lower limit on f_{A^0} of 10^2 – 10^3 GeV is given for $m_{A^0} = 0.1$ –1 MeV.
 - 14 BADIER 86 did not find long-lived A^0 in 300 GeV π^- Beam Dump Experiment that decays into e^+e^- in the mass range $m_{A^0} = (20$ – $200)$ MeV, which excludes the A^0 decay constant $f(A^0)$ in the interval (60–600) GeV. See their figure 6 for excluded region on $f(A^0)$ – m_{A^0} plane.
 - 15 BERGSMÄ 85 look for $A^0 \rightarrow 2\gamma, e^+e^-, \mu^+\mu^-$. First limit above is for $m_{A^0} = 1$ MeV; second is for 200 MeV. See their figure 4 for excluded region on f_{A^0} – m_{A^0} plane, where f_{A^0} is A^0 decay constant. For Peccei-Quinn PECCER 77 $A^0, m_{A^0} < 180$ keV and $\tau > 0.037$ s. (CL = 90%). For the axion of FAISSNER 81B at 250 keV, BERGSMÄ 85 expect 15 events but observe zero.
 - 16 FAISSNER 83 observed 19 $1\text{-}\gamma$ and 12 $2\text{-}\gamma$ events where a background of 4.8 and 2.3 respectively is expected. A small-angle peak is observed even if iron wall is set in front of the decay region.
 - 17 FAISSNER 83B extrapolate SIN γ signal to LAMPF ν experimental condition. Resulting 370 γ 's are not at variance with LAMPF upper limit of 450 γ 's. Derived from LAMPF limit that $[d\sigma(A^0)/d\omega \text{ at } 90^\circ] m_{A^0} / \tau_{A^0} < 14 \times 10^{-35} \text{ cm}^2 \text{ sr}^{-1} \text{ MeV ms}^{-1}$. See comment on FRANK 83B.
 - 18 FRANK 83B stress the importance of LAMPF data bins with negative net signal. By statistical analysis say that LAMPF and SIN-A0 are at variance when extrapolation by phase-space model is done. They find LAMPF upper limit is 248 not 450 γ 's. See comment on FAISSNER 83B.
 - 19 HOFFMAN 83 set CL = 90% limit $d\sigma/dt B(e^+e^-) < 3.5 \times 10^{-32} \text{ cm}^2/\text{GeV}^2$ for $140 < m_{A^0} < 160$ MeV. Limit assumes $\tau(A^0) < 10^{-9}$ s.
 - 20 FETSCHER 82 reanalyzes SIN beam-dump data of FAISSNER 81. Claims no evidence for axion since $2\text{-}\gamma$ peak rate remarkably decreases if iron wall is set in front of the decay region.
 - 21 FAISSNER 81 see excess μe events. Suggest axion interactions.
 - 22 FAISSNER 81B is SIN 590 MeV proton beam dump. Observed 14.5 ± 5.0 events of 2γ decay of long-lived neutral penetrating particle with $m_{2\gamma} \lesssim 1$ MeV. Axion interpretation with η - A^0 mixing gives $m_{A^0} = 250 \pm 25$ keV, $\tau_{(2\gamma)} = (7.3 \pm 3.7) \times 10^{-3}$ s from above rate. See critical remarks below in comments of FETSCHER 82, FAISSNER 83, FAISSNER 83B, FRANK 83B, and BERGSMÄ 85. Also see in the next subsection ALEKSEEV 82B, CAVIGNAC 83, and ANANEV 85.
 - 23 KIM 81 analyzed 8 candidates for $A^0 \rightarrow 2\gamma$ obtained by Aachen-Padova experiment at CERN with 26 GeV protons on Be. Estimated axion mass is about 300 keV and lifetime is $(0.86$ – $5.6) \times 10^{-3}$ s depending on models. Faisner (private communication), says axion production underestimated and mass overestimated. Correct value around 200 keV.
 - 24 FAISSNER 80 is SIN beam dump experiment with 590 MeV protons looking for $A^0 \rightarrow e^+e^-$ decay. Assuming $A^0/\pi^0 = 5.5 \times 10^{-7}$, obtained decay rate limit $20/(A^0 \text{ mass}) \text{ MeV/s}$ (CL = 90%), which is about 10^{-7} below theory and interpreted as upper limit to $m_{A^0} < 2m_{e^-}$.
 - 25 JACQUES 80 is a BNL beam dump experiment. First limit above comes from nonobservation of excess neutral-current-type events $[\sigma(\text{production})\sigma(\text{interaction}) < 7. \times 10^{-68} \text{ cm}^4, \text{ CL} = 90\%]$. Second limit is from nonobservation of axion decays into 2γ 's or e^+e^- , and for axion mass a few MeV.
 - 26 SOUKAS 80 at BNL observed no excess of neutral-current-type events in beam dump.
 - 27 BECHIS 79 looked for the axion production in low energy electron Bremsstrahlung and the subsequent decay into either 2γ or e^+e^- . No signal found. CL = 90% limits for model parameter(s) are given.
 - 28 COTEUS 79 is a beam dump experiment at BNL.
 - 29 DISHAW 79 is a calorimetric experiment and looks for low energy tail of energy distributions due to energy lost to weakly interacting particles.
 - 30 BELLOTTI 78 first value comes from search for $A^0 \rightarrow e^+e^-$. Second value comes from search for $A^0 \rightarrow 2\gamma$, assuming mass $< 2m_{e^-}$. For any mass satisfying this, limit is above value $\times (\text{mass}^{-4})$. Third value uses data of PL 60B 401 and quotes $\sigma(\text{production})\sigma(\text{interaction}) < 10^{-67} \text{ cm}^4$.
 - 31 BOSETTI 78B quotes $\sigma(\text{production})\sigma(\text{interaction}) < 2. \times 10^{-67} \text{ cm}^4$.
 - 32 DONNELLY 78 examines data from reactor neutrino experiments of REINES 76 and GURR 74 as well as SLAC beam dump experiment. Evidence is negative.
 - 33 MICELMACHER 78 finds no evidence of axion existence in reactor experiments of REINES 76 and GURR 74. (See reference under DONNELLY 78 below).
 - 34 VYSOTSKII 78 derived lower limit for the axion mass 25 keV from luminosity of the sun and 200 keV from red supergiants.

A^0 (Axion) Searches in Reactor Experiments

VALUE	DOCUMENT ID	TECN	COMMENT
• • • We do not use the following data for averages, fits, limits, etc. • • •			
1	CHANG 07		Primakoff or Compton
2	ALTMANN 95	CNTR	Reactor; $A^0 \rightarrow e^+e^-$
3	KETOV 86	SPEC	Reactor; $A^0 \rightarrow \gamma\gamma$
4	KOCH 86	SPEC	Reactor; $A^0 \rightarrow \gamma\gamma$
5	DATAR 82	CNTR	Light water reactor
6	VUILLEUMIER 81	CNTR	Reactor; $A^0 \rightarrow 2\gamma$

- 1 CHANG 07 looked for monochromatic photons from Primakoff or Compton conversion of axions from the Kuo-Sheng reactor due to axion coupling to photon or electron, respectively. The search places model-independent limits on the products $G_{A\gamma\gamma}G_{ANN}$ and $G_{Aee}G_{ANN}$ for $m(A^0)$ less than the MeV range.
- 2 ALTMANN 95 looked for A^0 decaying into e^+e^- from the Bugey 5 nuclear reactor. They obtain an upper limit on the A^0 production rate of $\omega(A^0)/\omega(\gamma) \times B(A^0 \rightarrow e^+e^-) < 10^{-16}$ for $m_{A^0} = 1.5$ MeV at 90% CL. The limit is weaker for heavier A^0 . In the case of a standard axion, this limit excludes a mass in the range $2m_e < m_{A^0} < 4.8$ MeV at 90% CL. See Fig. 5 of their paper for exclusion limits of axion-like resonances Z^0 in the (m_{X^0}, f_{X^0}) plane.
- 3 KETOV 86 searched for A^0 at the Rovno nuclear power plant. They found an upper limit on the A^0 production probability of $0.8 [100 \text{ keV}/m_{A^0}]^6 \times 10^{-6}$ per fission. In the standard axion model, this corresponds to $m_{A^0} > 150$ keV. Not valid for $m_{A^0} \gtrsim 1$ MeV.
- 4 KOCH 86 searched for $A^0 \rightarrow \gamma\gamma$ at nuclear power reactor Biblis A. They found an upper limit on the A^0 production rate of $\omega(A^0)/\omega(\gamma(M1)) < 1.5 \times 10^{-10}$ (CL=95%). Standard axion with $m_{A^0} = 250$ keV gives 10^{-5} for the ratio. Not valid for $m_{A^0} > 1022$ keV.
- 5 DATAR 82 looked for $A^0 \rightarrow 2\gamma$ in neutron capture ($np \rightarrow dA^0$) at Tarapur 500 MW reactor. Sensitive to sum of $l = 0$ and $l = 1$ amplitudes. With ZEHNDER 81 [$(l = 0) - (l = 1)$] result, assert nonexistence of standard A^0 .
- 6 VUILLEUMIER 81 is at Grenoble reactor. Set limit $m_{A^0} < 280$ keV.

A^0 (Axion) and Other Light Boson (X^0) Searches in Nuclear Transitions

VALUE	CL%	DOCUMENT ID	TECN	COMMENT
• • • We do not use the following data for averages, fits, limits, etc. • • •				
$< 8.5 \times 10^{-6}$	90	1 DERBIN 02	CNTR	^{125m}Te decay
		2 DEBOER 97C	RVUE	M1 transitions
$< 5.5 \times 10^{-10}$	95	3 TSUNODA 95	CNTR	^{252}Cf fission, $A^0 \rightarrow e^+e^-$
$< 1.2 \times 10^{-6}$	95	4 MINOWA 93	CNTR	$^{139}\text{La}^* \rightarrow ^{139}\text{La}A^0$
$< 2 \times 10^{-4}$	90	5 HICKS 92	CNTR	^{35}S decay, $A^0 \rightarrow \gamma\gamma$
$< 1.5 \times 10^{-9}$	95	6 ASANUMA 90	CNTR	^{241}Am decay
$< (0.4\text{--}10) \times 10^{-3}$	95	7 DEBOER 90	CNTR	$^8\text{Be}^* \rightarrow ^8\text{Be}A^0, A^0 \rightarrow e^+e^-, ^{16}\text{O}^* \rightarrow ^{16}\text{O}X^0,$
$< (0.2\text{--}1) \times 10^{-3}$	90	8 BINI 89	CNTR	$X^0 \rightarrow e^+e^-, \text{Cu}^* \rightarrow \text{Cu}A^0 (A^0 \rightarrow 2\gamma, A^0 \rightarrow \gamma e, A^0 Z \rightarrow \gamma Z)$
$< 1.5 \times 10^{-4}$	90	10 DATAR 88	CNTR	$^{12}\text{C}^* \rightarrow ^{12}\text{C}A^0,$
$< 5 \times 10^{-3}$	90	11 DEBOER 88c	CNTR	$^{16}\text{O}^* \rightarrow ^{16}\text{O}X^0, X^0 \rightarrow e^+e^-,$
$< 3.4 \times 10^{-5}$	95	12 DOEHNER 88	SPEC	$^2\text{H}^*, A^0 \rightarrow e^+e^-$
$< 4 \times 10^{-4}$	95	13 SAVAGE 88	CNTR	Nuclear decay (isovector)
$< 3 \times 10^{-3}$	95	13 SAVAGE 88	CNTR	Nuclear decay (isoscalar)
$< 10.6 \times 10^{-2}$	90	14 HALLIN 86	SPEC	^6Li isovector decay
< 10.8	90	14 HALLIN 86	SPEC	^{10}B isoscalar decays
< 2.2	90	14 HALLIN 86	SPEC	^{14}N isoscalar decays
$< 4 \times 10^{-4}$	90	15 SAVAGE 86B	CNTR	$^{14}\text{N}^*$
		16 ANANEV 85	CNTR	$\text{Li}^*, \text{deut}^* A^0 \rightarrow 2\gamma$
		17 CAVIGNAC 83	CNTR	$^{97}\text{Nb}^*, \text{deut}^* \text{ transition } A^0 \rightarrow 2\gamma$
		18 ALEKSEEV 82B	CNTR	$\text{Li}^*, \text{deut}^* \text{ transition } A^0 \rightarrow 2\gamma$
		19 LEHMANN 82	CNTR	$\text{Cu}^* \rightarrow \text{Cu}A^0 (A^0 \rightarrow 2\gamma)$
		20 ZEHNDER 82	CNTR	$\text{Li}^*, \text{Nb}^* \text{ decay, } n\text{-capt.}$
		21 ZEHNDER 81	CNTR	$\text{Ba}^* \rightarrow \text{Ba}A^0 (A^0 \rightarrow 2\gamma)$
		22 CALAPRICE 79		Carbon

- 1 DERBIN 02 looked for the axion emission in an M1 transition in ^{125m}Te decay. They looked for a possible presence of a shifted energy spectrum in gamma rays due to the undetected axion.
- 2 DEBOER 97C reanalyzed the existent data on Nuclear M1 transitions and find that a 9 MeV boson decaying into e^+e^- would explain the excess of events with large opening angles. See also DEBOER 01 for follow-up experiments.
- 3 TSUNODA 95 looked for axion emission when ^{252}Cf undergoes a spontaneous fission, with the axion decaying into e^+e^- . The bound is for $m_{A^0} = 40$ MeV. It improves to 2.5×10^{-5} for $m_{A^0} = 200$ MeV.
- 4 MINOWA 93 studied chain process, $^{139}\text{Ce} \rightarrow ^{139}\text{La}^*$ by electron capture and M1 transition of $^{139}\text{La}^*$ to the ground state. It does not assume decay modes of A^0 . The bound applies for $m_{A^0} < 166$ keV.
- 5 HICKS 92 bound is applicable for $\tau_{X^0} < 4 \times 10^{-11}$ sec.
- 6 THE ASANUMA 90 limit is for the branching fraction of X^0 emission per ^{241}Am α decay and valid for $\tau_{X^0} < 3 \times 10^{-11}$ s.
- 7 THE DEBOER 90 limit is for the branching ratio $^8\text{Be}^* (18.15 \text{ MeV}, 1^+) \rightarrow ^8\text{Be}A^0, A^0 \rightarrow e^+e^-$ for the mass range $m_{A^0} = 4$ –15 MeV.
- 8 THE BINI 89 limit is for the branching fraction of $^{16}\text{O}^* (6.05 \text{ MeV}, 0^+) \rightarrow ^{16}\text{O}X^0, X^0 \rightarrow e^+e^-$ for $m_{X^0} = 1.5$ –3.1 MeV. $\tau_{X^0} \lesssim 10^{-11}$ s is assumed. The spin-parity of X is restricted to 0^+ or 1^- .
- 9 AVIGNONE 88 looked for the 1115 keV transition $\text{C}^* \rightarrow \text{Cu}A^0$, either from $A^0 \rightarrow 2\gamma$ in-flight decay or from the secondary A^0 interactions by Compton and by Primakoff processes. Limits for axion parameters are obtained for $m_{A^0} < 1.1$ MeV.

Gauge & Higgs Boson Particle Listings

Axions (A^0) and Other Very Light Bosons

- ¹⁰DATAR 88 rule out light pseudoscalar particle emission through its decay $A^0 \rightarrow e^+e^-$ in the mass range 1.02–2.5 MeV and lifetime range 10^{-13} – 10^{-8} s. The above limit is for $\tau = 5 \times 10^{-13}$ s and $m = 1.7$ MeV; see the paper for the τ - m dependence of the limit.
- ¹¹The limit is for the branching fraction of $^{16}\text{O}^*(6.05 \text{ MeV}, 0^+) \rightarrow ^{16}\text{O}X^0, X^0 \rightarrow e^+e^-$ against internal pair conversion for $m_{X^0} = 1.7$ MeV and $\tau_{X^0} < 10^{-11}$ s. Similar limits are obtained for $m_{X^0} = 1.3$ – 3.2 MeV. The spin parity of X^0 must be either 0^+ or 1^- . The limit at 1.7 MeV is translated into a limit for the X^0 -nucleon coupling constant: $g_{X^0 NN}^2/4\pi < 2.3 \times 10^{-9}$.
- ¹²The DOEHNER 88 limit is for $m_{A^0} = 1.7$ MeV, $\tau(A^0) < 10^{-10}$ s. Limits less than 10^{-4} are obtained for $m_{A^0} = 1.2$ – 2.2 MeV.
- ¹³SAVAGE 88 looked for A^0 that decays into e^+e^- in the decay of the 9.17 MeV $J^P = 2^+$ state in ^{14}N , 17.64 MeV state $J^P = 1^+$ in ^8Be , and the 18.15 MeV state $J^P = 1^+$ in ^8Be . This experiment constrains the isovector coupling of A^0 to hadrons, if $m_{A^0} = (1.1 \rightarrow 2.2)$ MeV and the isoscalar coupling of A^0 to hadrons, if $m_{A^0} = (1.1 \rightarrow 2.6)$ MeV. Both limits are valid only if $\tau(A^0) \lesssim 1 \times 10^{-11}$ s.
- ¹⁴Limits are for $\Gamma(A^0(1.8 \text{ MeV}))/\Gamma(\pi\text{M}1)$; i.e., for 1.8 MeV axion emission normalized to the rate for internal emission of e^+e^- pairs. Valid for $\tau_{A^0} < 2 \times 10^{-11}$ s. ^6Li isovector decay data strongly disfavor PECCCI 86 model I, whereas the ^{10}B and ^{14}N isoscalar decay data strongly reject PECCCI 86 model II and III.
- ¹⁵SAVAGE 86b looked for A^0 that decays into e^+e^- in the decay of the 9.17 MeV $J^P = 2^+$ state in ^{14}N . Limit on the branching fraction is valid if $\tau_{A^0} \lesssim 1 \times 10^{-11}$ s for $m_{A^0} = (1.1$ – $1.7)$ MeV. This experiment constrains the iso-vector coupling of A^0 to hadrons.
- ¹⁶ANANEV 85 with IBR-2 pulsed reactor exclude standard A^0 at CL = 95% masses below 470 keV (Li^* decay) and below $2m_e$ for deuterium* decay.
- ¹⁷CAVAIGNAC 83 at Bugey reactor exclude axion at any $m_{97\text{Nb}^*}$ decay and axion with m_{A^0} between 275 and 288 keV (deuteron* decay).
- ¹⁸ALEKSEEV 82 with IBR-2 pulsed reactor exclude standard A^0 at CL = 95% mass-ranges $m_{A^0} < 400$ keV (Li^* decay) and 330 keV $< m_{A^0} < 2.2$ MeV. (deuteron* decay).
- ¹⁹LEHMANN 82 obtained $A^0 \rightarrow 2\gamma$ rate $< 6.2 \times 10^{-5}/\text{s}$ (CL = 95%) excluding m_{A^0} between 100 and 1000 keV.
- ²⁰ZEHNDER 82 used Gogsen 2.8GW light-water reactor to check A^0 production. No 2γ peak in Li^* , Nb^* decay (both single p transition) nor in n capture (combined with previous Ba^* negative result) rules out standard A^0 . Set limit $m_{A^0} < 60$ keV for any A^0 .
- ²¹ZEHNDER 81 looked for $\text{Ba}^* \rightarrow A^0\text{Ba}$ transition with $A^0 \rightarrow 2\gamma$. Obtained 2γ coincidence rate $< 2.2 \times 10^{-5}/\text{s}$ (CL = 95%) excluding $m_{A^0} > 160$ keV (or 200 keV depending on Higgs mixing). However, see BARROSO 81.
- ²²CALAPRICE 79 saw no axion emission from excited states of carbon. Sensitive to axion mass between 1 and 15 MeV.

A^0 (Axion) Limits from Its Electron Coupling

Limits are for $\tau(A^0 \rightarrow e^+e^-)$.

VALUE (s)	CL%	DOCUMENT ID	TECN	COMMENT
• • • We do not use the following data for averages, fits, limits, etc. • • •				
none 4×10^{-16} – 4.5×10^{-12}	90	1 BROSS	91	BDMP $eN \rightarrow eA^0N$ ($A^0 \rightarrow ee$)
		2 GUO	90	BDMP $eN \rightarrow eA^0N$ ($A^0 \rightarrow ee$)
		3 BJORKEN	88	CALO $A \rightarrow e^+e^-$ or 2γ
		4 BLINOV	88	MD1 $ee \rightarrow eeA^0$ ($A^0 \rightarrow ee$)
none 1×10^{-14} – 1×10^{-10}	90	5 RIORDAN	87	BDMP $eN \rightarrow eA^0N$ ($A^0 \rightarrow ee$)
none 1×10^{-14} – 1×10^{-11}	90	6 BROWN	86	BDMP $eN \rightarrow eA^0N$ ($A^0 \rightarrow ee$)
none 6×10^{-14} – 9×10^{-11}	95	7 DAVIER	86	BDMP $eN \rightarrow eA^0N$ ($A^0 \rightarrow ee$)
none 3×10^{-13} – 1×10^{-7}	90	8 KONAKA	86	BDMP $eN \rightarrow eA^0N$ ($A^0 \rightarrow ee$)

- ¹The listed BROSS 91 limit is for $m_{A^0} = 1.14$ MeV. $B(A^0 \rightarrow e^+e^-) = 1$ assumed. Excluded domain in the τ_{A^0} - m_{A^0} plane extends up to $m_{A^0} \approx 7$ MeV (see Fig. 5). Combining with electron g -2 constraint, axions coupling only to e^+e^- ruled out for $m_{A^0} < 4.8$ MeV (90% CL).
- ²GUO 90 use the same apparatus as BROWN 86 and improve the previous limit in the shorter lifetime region. Combined with g -2 constraint, axions coupling only to e^+e^- are ruled out for $m_{A^0} < 2.7$ MeV (90% CL).
- ³BJORKEN 88 reports limits on axion parameters (f_A, m_A, τ_A) for $m_{A^0} < 200$ MeV from electron beam-dump experiment with production via Primakoff photoproduction, bremsstrahlung from electrons, and resonant annihilation of positrons on atomic electrons.
- ⁴BLINOV 88 assume zero spin, $m = 1.8$ MeV and lifetime $< 5 \times 10^{-12}$ s and find $\Gamma(A^0 \rightarrow \gamma\gamma)B(A^0 \rightarrow e^+e^-) < 2$ eV (CL=90%).
- ⁵Assumes $A^0\gamma\gamma$ coupling is small and hence Primakoff production is small. Their figure 2 shows limits on axions for $m_{A^0} < 15$ MeV.
- ⁶Uses electrons in hadronic showers from an incident 800 GeV proton beam. Limits for $m_{A^0} < 15$ MeV are shown in their figure 3.
- ⁷ $m_{A^0} = 1.8$ MeV assumed. The excluded domain in the τ_{A^0} - m_{A^0} plane extends up to $m_{A^0} \approx 14$ MeV, see their figure 4.
- ⁸The limits are obtained from their figure 3. Also given is the limit on the $A^0\gamma\gamma$ - $A^0e^+e^-$ coupling plane by assuming Primakoff production.

Search for A^0 (Axion) Resonance in Bhabha Scattering

The limit is for $\Gamma(A^0)[B(A^0 \rightarrow e^+e^-)]^2$.

VALUE (10^{-3} eV)	CL%	DOCUMENT ID	TECN	COMMENT
• • • We do not use the following data for averages, fits, limits, etc. • • •				
< 1.3	97	1 HALLIN	92	CNTR $m_{A^0} = 1.75$ – 1.88 MeV
none 0.0016–0.47	90	2 HENDERSON	92c	CNTR $m_{A^0} = 1.5$ – 1.86 MeV
< 2.0	90	3 WU	92	CNTR $m_{A^0} = 1.56$ – 1.86 MeV
< 0.013	95	TSERTOS	91	CNTR $m_{A^0} = 1.832$ MeV
none 0.19–3.3	95	4 WIDMANN	91	CNTR $m_{A^0} = 1.78$ – 1.92 MeV
< 5	97	BAUER	90	CNTR $m_{A^0} = 1.832$ MeV
none 0.09–1.5	95	5 JUDGE	90	CNTR $m_{A^0} = 1.832$ MeV, $m_{A^0}^{\text{elastic}}$
< 1.9	97	6 TSERTOS	89	CNTR $m_{A^0} = 1.82$ MeV
$<(10-40)$	97	6 TSERTOS	89	CNTR $m_{A^0} = 1.51$ – 1.65 MeV
$<(1-2.5)$	97	6 TSERTOS	89	CNTR $m_{A^0} = 1.80$ – 1.86 MeV
< 31	95	LORENZ	88	CNTR $m_{A^0} = 1.646$ MeV
< 94	95	LORENZ	88	CNTR $m_{A^0} = 1.726$ MeV
< 23	95	LORENZ	88	CNTR $m_{A^0} = 1.782$ MeV
< 19	95	LORENZ	88	CNTR $m_{A^0} = 1.837$ MeV
< 3.8	97	7 TSERTOS	88	CNTR $m_{A^0} = 1.832$ MeV
		8 VANKLINKEN	88	CNTR
		9 MAIER	87	CNTR
< 2500	90	MILLS	87	CNTR $m_{A^0} = 1.8$ MeV
		10 VONWIMMER	87	CNTR

- ¹HALLIN 92 quote limits on lifetime, 8×10^{-14} – 5×10^{-13} sec depending on mass, assuming $B(A^0 \rightarrow e^+e^-) = 100\%$. They say that TSERTOS 91 overestimated their sensitivity by a factor of 3.
- ²HENDERSON 92c exclude axion with lifetime $\tau_{A^0} = 1.4 \times 10^{-12}$ – 4.0×10^{-10} s, assuming $B(A^0 \rightarrow e^+e^-) = 100\%$. HENDERSON 92c also exclude a vector boson with $\tau = 1.4 \times 10^{-12}$ – 6.0×10^{-10} s.
- ³WU 92 quote limits on lifetime $> 3.3 \times 10^{-13}$ s assuming $B(A^0 \rightarrow e^+e^-) = 100\%$. They say that TSERTOS 89 overestimate the limit by a factor of $\pi/2$. WU 92 also quote a bound for vector boson, $\tau > 8.2 \times 10^{-13}$ s.
- ⁴WIDMANN 91 bound applies exclusively to the case $B(A^0 \rightarrow e^+e^-) = 1$, since the detection efficiency varies substantially as $\Gamma(A^0)_{\text{total}}$ changes. See their Fig. 6.
- ⁵JUDGE 90 excludes an elastic pseudoscalar e^+e^- resonance for 4.5×10^{-13} s $< \tau(A^0) < 7.5 \times 10^{-12}$ s (95% CL) at $m_{A^0} = 1.832$ MeV. Comparable limits can be set for $m_{A^0} = 1.776$ – 1.856 MeV.
- ⁶See also TSERTOS 88b in references.
- ⁷The upper limit listed in TSERTOS 88 is too large by a factor of 4. See TSERTOS 88b, footnote 3.
- ⁸VANKLINKEN 88 looked for relatively long-lived resonance ($\tau = 10^{-10}$ – 10^{-12} s). The sensitivity is not sufficient to exclude such a narrow resonance.
- ⁹MAIER 87 obtained limits $R\Gamma \lesssim 60$ eV (100 eV) at $m_{A^0} \approx 1.64$ MeV (1.83 MeV) for energy resolution $\Delta E_{\text{cm}} \approx 3$ keV, where R is the resonance cross section normalized to that of Bhabha scattering, and $\Gamma = \Gamma_{e^+e^-}^2/\Gamma_{\text{total}}$. For a discussion implying that $\Delta E_{\text{cm}} \approx 10$ keV, see TSERTOS 89.
- ¹⁰VONWIMMERSPERG 87 measured Bhabha scattering for $E_{\text{cm}} = 1.37$ – 1.86 MeV and found a possible peak at 1.73 with $\int \sigma dE_{\text{cm}} = 14.5 \pm 6.8$ keV·b. For a comment and a reply, see VANKLINKEN 88b and VONWIMMERSPERG 88. Also see CONNELL 88.

Search for A^0 (Axion) Resonance in $e^+e^- \rightarrow \gamma\gamma$

The limit is for $\Gamma(A^0 \rightarrow e^+e^-)\Gamma(A^0 \rightarrow \gamma\gamma)/\Gamma_{\text{total}}$.

VALUE (10^{-3} eV)	CL%	DOCUMENT ID	TECN	COMMENT
• • • We do not use the following data for averages, fits, limits, etc. • • •				
< 0.18	95	VO	94	CNTR $m_{A^0} = 1.1$ MeV
< 1.5	95	VO	94	CNTR $m_{A^0} = 1.4$ MeV
< 12	95	VO	94	CNTR $m_{A^0} = 1.7$ MeV
< 6.6	95	1 TRZASKA	91	CNTR $m_{A^0} = 1.8$ MeV
< 4.4	95	WIDMANN	91	CNTR $m_{A^0} = 1.78$ – 1.92 MeV
		2 FOX	89	CNTR
< 0.11	95	3 MINOWA	89	CNTR $m_{A^0} = 1.062$ MeV
< 33	97	CONNELL	88	CNTR $m_{A^0} = 1.580$ MeV
< 42	97	CONNELL	88	CNTR $m_{A^0} = 1.642$ MeV
< 73	97	CONNELL	88	CNTR $m_{A^0} = 1.782$ MeV
< 79	97	CONNELL	88	CNTR $m_{A^0} = 1.832$ MeV

- ¹TRZASKA 91 also give limits in the range $(6.6$ – $30) \times 10^{-3}$ eV (95% CL) for $m_{A^0} = 1.6$ – 2.0 MeV.
- ²FOX 89 measured positron annihilation with an electron in the source material into two photons and found no signal at 1.062 MeV ($< 9 \times 10^{-5}$ of two-photon annihilation at rest).
- ³Similar limits are obtained for $m_{A^0} = 1.045$ – 1.085 MeV.

Search for X^0 (Light Boson) Resonance in $e^+e^- \rightarrow \gamma\gamma\gamma$

The limit is for $\Gamma(X^0 \rightarrow e^+e^-)\Gamma(X^0 \rightarrow \gamma\gamma\gamma)/\Gamma_{\text{total}}$. C invariance forbids spin-0 X^0 coupling to both e^+e^- and $\gamma\gamma\gamma$.

VALUE (10^{-3} eV)	CL%	DOCUMENT ID	TECN	COMMENT
• • • We do not use the following data for averages, fits, limits, etc. • • •				

Gauge & Higgs Boson Particle Listings

Axions (A^0) and Other Very Light Bosons

< 0.2	95	1 VO	94 CNTR	$m_{X^0}=1.1-1.9$ MeV
< 1.0	95	2 VO	94 CNTR	$m_{X^0}=1.1$ MeV
< 2.5	95	2 VO	94 CNTR	$m_{X^0}=1.4$ MeV
<120	95	2 VO	94 CNTR	$m_{X^0}=1.7$ MeV
< 3.8	95	3 SKALSEY	92 CNTR	$m_{X^0}=1.5$ MeV

¹ VO 94 looked for $X^0 \rightarrow \gamma\gamma$ decaying at rest. The precise limits depend on m_{X^0} . See Fig. 2(b) in paper.

² VO 94 looked for $X^0 \rightarrow \gamma\gamma$ decaying in flight.

³ SKALSEY 92 also give limits 4.3 for $m_{X^0} = 1.54$ and 7.5 for 1.64 MeV. The spin of X^0 is assumed to be one.

Light Boson (X^0) Search in Nonresonant e^+e^- Annihilation at Rest

Limits are for the ratio of $n\gamma + X^0$ production relative to $\gamma\gamma$.

VALUE (units 10^{-6})	CL%	DOCUMENT ID	TECN	COMMENT
< 4.2	90	1 MITSUI	96 CNTR	γX^0
< 4	68	2 SKALSEY	95 CNTR	γX^0
<40	68	3 SKALSEY	95 RVUE	γX^0
< 0.18	90	4 ADACHI	94 CNTR	$\gamma\gamma X^0, X^0 \rightarrow \gamma\gamma$
< 0.26	90	5 ADACHI	94 CNTR	$\gamma\gamma X^0, X^0 \rightarrow \gamma\gamma$
< 0.33	90	6 ADACHI	94 CNTR	$\gamma X^0, X^0 \rightarrow \gamma\gamma$

¹ MITSUI 96 looked for a monochromatic γ . The bound applies for a vector X^0 with $C=-1$ and $m_{X^0} < 200$ keV. They derive an upper bound on eX^0 coupling and hence on the branching ratio $B(\rho\text{-Ps} \rightarrow \gamma X^0) < 6.2 \times 10^{-6}$. The bounds weaken for heavier X^0 .

² SKALSEY 95 looked for a monochromatic γ without an accompanying γ in e^+e^- annihilation. The bound applies for scalar and vector X^0 with $C = -1$ and $m_{X^0} = 100-1000$ keV.

³ SKALSEY 95 reinterpreted the bound on γA^0 decay of ρ -Ps by ASA1 91 where 3% of delayed annihilations are not from 3S_1 states. The bound applies for scalar and vector X^0 with $C = -1$ and $m_{X^0} = 0-800$ keV.

⁴ ADACHI 94 looked for a peak in the $\gamma\gamma$ invariant mass distribution in $\gamma\gamma\gamma\gamma$ production from e^+e^- annihilation. The bound applies for $m_{X^0} = 70-800$ keV.

⁵ ADACHI 94 looked for a peak in the missing-mass distribution in $\gamma\gamma$ channel, using $\gamma\gamma\gamma\gamma$ production from e^+e^- annihilation. The bound applies for $m_{X^0} < 800$ keV.

⁶ ADACHI 94 looked for a peak in the missing mass distribution in $\gamma\gamma\gamma$ channel, using $\gamma\gamma\gamma\gamma$ production from e^+e^- annihilation. The bound applies for $m_{X^0} = 200-900$ keV.

Searches for Goldstone Bosons (X^0)

(Including Horizontal Bosons and Majorons.) Limits are for branching ratios.

VALUE	CL%	DOCUMENT ID	TECN	COMMENT
<9 $\times 10^{-6}$	90	1 BAYES	15 TWST	$\mu^+ \rightarrow e^+ X^0$, Familon
		2 LATTANZI	13 COSM	Majoron dark matter decay
		3 LESSA	07 RVUE	Meson, ℓ decays to Majoron
		4 DIAZ	98 THEO	$H^0 \rightarrow X^0 X^0, A^0 \rightarrow X^0 X^0 X^0$, Majoron
		5 BOBRAKOV	91	Electron quasi-magnetic interaction
<3.3 $\times 10^{-2}$	95	6 ALBRECHT	90E ARG	$\tau \rightarrow \mu X^0$, Familon
<1.8 $\times 10^{-2}$	95	6 ALBRECHT	90E ARG	$\tau \rightarrow e X^0$, Familon
<6.4 $\times 10^{-9}$	90	7 ATIYA	90 B787	$K^+ \rightarrow \pi^+ X^0$, Familon
<1.4 $\times 10^{-5}$	90	8 BALKE	88 CNTR	$\mu^+ \rightarrow e^+ X^0$, Familon
<1.1 $\times 10^{-9}$	90	9 BOLTON	88 CBOX	$\mu^+ \rightarrow e^+ \gamma X^0$, Familon
		10 CHANDA	88 ASTR	Sun, Majoron
		11 CHOI	88 ASTR	Majoron, SN 1987A
<5 $\times 10^{-6}$	90	12 PICCIOTTO	88 CNTR	$\pi \rightarrow e \nu X^0$, Majoron
<1.3 $\times 10^{-9}$	90	13 GOLDMAN	87 CNTR	$\mu \rightarrow e \gamma X^0$, Familon
<3 $\times 10^{-4}$	90	14 BRYMAN	86E RVUE	$\mu \rightarrow e X^0$, Familon
<1 $\times 10^{-10}$	90	15 EICHLER	86 SPEC	$\mu^+ \rightarrow e^+ X^0$, Familon
<2.6 $\times 10^{-6}$	90	16 JODIDIO	86 SPEC	$\mu^+ \rightarrow e^+ X^0$, Familon
		17 BALTRUSAITIS	85 MRK3	$\tau \rightarrow \ell X^0$, Familon
		18 DICUS	83 COSM	$\nu(\text{hvy}) \rightarrow \nu(\text{light}) X^0$

¹ BAYES 15 limits are the average over $m_{X^0} = 13-80$ MeV for the isotropic decay distribution of positrons. See their Fig. 4 and Table II for the mass-dependent limits as well as the dependence on the decay anisotropy. In particular, they find a limit $< 58 \times 10^{-6}$ at 90% CL for massless familons and for the same asymmetry as normal muon decay, a case not covered by JODIDIO 86.

² LATTANZI 13 use WMAP 9 year data as well as X-ray and γ -ray observations to derive limits on decaying majoron dark matter. A limit on the decay width $\Gamma(X^0 \rightarrow \nu\bar{\nu}) < 6.4 \times 10^{-19} \text{ s}^{-1}$ at 95% CL is found if majorons make up all of the dark matter.

³ LESSA 07 consider decays of the form Meson $\rightarrow \ell\nu$ Majoron and $\ell \rightarrow \ell'\nu\bar{\nu}$ Majoron and use existing data to derive limits on the neutrino-Majoron Yukawa couplings $g_{\alpha\beta}$ ($\alpha, \beta = e, \mu, \tau$). Their best limits are $|g_{e\alpha}|^2 < 5.5 \times 10^{-6}$, $|g_{\mu\alpha}|^2 < 4.5 \times 10^{-5}$, $|g_{\tau\alpha}|^2 < 5.5 \times 10^{-2}$ at CL = 90%.

⁴ DIAZ 98 studied models of spontaneously broken lepton number with both singlet and triplet Higgses. They obtain limits on the parameter space from invisible decay $Z \rightarrow H^0 A^0 \rightarrow X^0 X^0 X^0 X^0$ and $e^+e^- \rightarrow Z H^0$ with $H^0 \rightarrow X^0 X^0$.

⁵ BOBRAKOV 91 searched for anomalous magnetic interactions between polarized electrons expected from the exchange of a massless pseudoscalar boson (arion). A limit

$x_e^2 < 2 \times 10^{-4}$ (95%CL) is found for the effective anomalous magneton parametrized as $x_e(G_F/8\pi\sqrt{2})^{1/2}$.

⁶ ALBRECHT 90E limits are for $B(\tau \rightarrow \ell X^0)/B(\tau \rightarrow \ell\nu\bar{\nu})$. Valid for $m_{X^0} < 100$ MeV. The limits rise to 7.1% (for μ), 5.0% (for e) for $m_{X^0} = 500$ MeV.

⁷ ATIYA 90 limit is for $m_{X^0} = 0$. The limit $B < 1 \times 10^{-8}$ holds for $m_{X^0} < 95$ MeV.

For the reduction of the limit due to finite lifetime of X^0 , see their Fig. 3.

⁸ BALKE 88 limits are for $B(\mu^+ \rightarrow e^+ X^0)$. Valid for $m_{X^0} < 80$ MeV and $\tau_{X^0} > 10^{-8}$ sec.

⁹ BOLTON 88 limit corresponds to $F > 3.1 \times 10^9$ GeV, which does not depend on the chirality property of the coupling.

¹⁰ CHANDA 88 find $v_T < 10$ MeV for the weak-triplet Higgs vacuum expectation value in Gelmini-Roncadelli model, and $v_S > 5.8 \times 10^6$ GeV in the singlet Majoron model.

¹¹ CHOI 88 used the observed neutrino flux from the supernova SN 1987A to exclude the neutrino Majoron Yukawa coupling h in the range $2 \times 10^{-5} < h < 3 \times 10^{-4}$ for the interaction $L_{\text{int}} = \frac{1}{2} i h \bar{\nu}_\nu \gamma_5 \psi_\nu \phi_X$. For several families of neutrinos, the limit applies for $(\sum h_i^2)^{1/4}$.

¹² PICCIOTTO 88 limit applies when $m_{X^0} < 55$ MeV and $\tau_{X^0} > 2$ ns, and it decreases to 4×10^{-7} at $m_{X^0} = 125$ MeV, beyond which no limit is obtained.

¹³ GOLDMAN 87 limit corresponds to $F > 2.9 \times 10^9$ GeV for the family symmetry breaking scale from the Lagrangian $L_{\text{int}} = (1/F) \bar{\psi}_\mu \gamma^\mu (a + b\gamma_5) \psi_e \theta_\mu \phi_{X^0}$ with $a^2 + b^2 = 1$.

This is not as sensitive as the limit $F > 9.9 \times 10^9$ GeV derived from the search for $\mu^+ \rightarrow e^+ X^0$ by JODIDIO 86, but does not depend on the chirality property of the coupling.

¹⁴ Limits are for $\Gamma(\mu \rightarrow e X^0)/\Gamma(\mu \rightarrow e\nu\bar{\nu})$. Valid when $m_{X^0} = 0-93.4, 98.1-103.5$ MeV.

¹⁵ EICHLER 86 looked for $\mu^+ \rightarrow e^+ X^0$ followed by $X^0 \rightarrow e^+ e^-$. Limits on the branching fraction depend on the mass and lifetime of X^0 . The quoted limits are valid when $\tau_{X^0} \lesssim 3 \times 10^{-10}$ s if the decays are kinematically allowed.

¹⁶ JODIDIO 86 corresponds to $F > 9.9 \times 10^9$ GeV for the family symmetry breaking scale with the parity-conserving effective Lagrangian $L_{\text{int}} = (1/F) \bar{\psi}_\mu \gamma^\mu \psi_e \theta_\mu \phi_{X^0}$.

¹⁷ BALTRUSAITIS 85 search for light Goldstone boson (X^0) of broken U(1). CL = 95% limits are $B(\tau \rightarrow \mu^+ X^0)/B(\tau \rightarrow \mu^+ \nu\bar{\nu}) < 0.125$ and $B(\tau \rightarrow e^+ X^0)/B(\tau \rightarrow e^+ \nu\bar{\nu}) < 0.04$. Inferred limit for the symmetry breaking scale is $m > 3000$ TeV.

¹⁸ The primordial heavy neutrino must decay into ν and familon, f_A , early so that the red-shifted decay products are below critical density, see their table. In addition, $K \rightarrow \pi f_A$ and $\mu \rightarrow e f_A$ are unseen. Combining these excludes $m_{\text{heavy}\nu}$ between 5×10^{-5} and 5×10^{-4} MeV (μ decay) and $m_{\text{heavy}\nu}$ between 5×10^{-5} and 0.1 MeV (K -decay).

Majoron Searches in Neutrinoless Double β Decay

Limits are for the half-life of neutrinoless $\beta\beta$ decay with a Majoron emission.

No experiment currently claims any such evidence. Only the best or comparable limits for each isotope are reported.

$t_{1/2}(10^{21} \text{ yr})$	CL%	ISOTOPE	TRANSITION	METHOD	DOCUMENT ID
>7200	90	128Te	CNTR		1 BERNATOW... 92
> 4.4	90	100Mo	0 ν 1 χ	NEMO-3	2 ARNOLD 19
> 37	90	82Se	0 ν 1 χ	NEMO-3	3 ARNOLD 18
> 420	90	76Ge	0 ν 1 χ	GERDA	4 AGOSTINI 15A
> 400	90	100Mo	0 ν 1 χ	NEMO-3	5 ARNOLD 15
>1200	90	136Xe	0 ν 1 χ	EXO-200	6 ALBERT 14A
>2600	90	136Xe	0 ν 1 χ	KamLAND-Zen	7 GANDO 12
> 16	90	130Te	0 ν 1 χ	NEMO-3	8 ARNOLD 11
> 1.9	90	96Zr	2 ν 1 χ	NEMO-3	9 ARGYRADES 10
> 1.52	90	150Nd	0 ν 1 χ	NEMO-3	10 ARGYRADES 09
> 27	90	100Mo	0 ν 1 χ	NEMO-3	11 ARNOLD 06
> 15	90	82Se	0 ν 1 χ	NEMO-3	12 ARNOLD 06
> 14	90	100Mo	0 ν 1 χ	NEMO-3	13 ARNOLD 04
> 12	90	82Se	0 ν 1 χ	NEMO-3	14 ARNOLD 04
> 2.2	90	130Te	0 ν 1 χ	Cryo. det.	15 ARNABOLDI 03
> 0.9	90	130Te	0 ν 2 χ	Cryo. det.	16 ARNABOLDI 03
> 8	90	116Cd	0 ν 1 χ	CdWO ₄ scint.	17 DANEVICH 03
> 0.8	90	116Cd	0 ν 2 χ	CdWO ₄ scint.	18 DANEVICH 03
> 500	90	136Xe	0 ν 1 χ	Liquid Xe Scint.	19 BERNABEI 02D
> 5.8	90	100Mo	0 ν 1 χ	ELEGANT V	20 FUSHIMI 02
> 0.32	90	100Mo	0 ν 1 χ	Liq. Ar ioniz.	21 ASHITKOV 01
> 0.0035	90	160Gd	0 ν 1 χ	¹⁶⁰ Gd ₂ SiO ₅ :Ce	22 DANEVICH 01
> 0.013	90	160Gd	0 ν 2 χ	¹⁶⁰ Gd ₂ SiO ₅ :Ce	23 DANEVICH 01
> 2.3	90	82Se	0 ν 1 χ	NEMO 2	24 ARNOLD 00
> 0.31	90	96Zr	0 ν 1 χ	NEMO 2	25 ARNOLD 00
> 0.63	90	82Se	0 ν 2 χ	NEMO 2	26 ARNOLD 00
> 0.063	90	96Zr	0 ν 2 χ	NEMO 2	26 ARNOLD 00
> 0.16	90	100Mo	0 ν 2 χ	NEMO 2	26 ARNOLD 00
> 2.4	90	82Se	0 ν 1 χ	NEMO 2	27 ARNOLD 98
> 7.2	90	136Xe	0 ν 2 χ	TPC	28 LUESCHER 98
> 7.91	90	76Ge	SPEC		29 GUENTHER 96
> 17	90	76Ge	CNTR		BECK 93

¹ BERNATOWICZ 92 studied double- β decays of ¹²⁸Te and ¹³⁰Te, and found the ratio $\tau(130\text{Te})/\tau(128\text{Te}) = (3.52 \pm 0.11) \times 10^{-4}$ in agreement with relatively stable theoretical predictions. The bound is based on the requirement that Majoron-emitting decay cannot be larger than the observed double-beta rate of ¹²⁸Te of $(7.7 \pm 0.4) \times 10^{24}$ year. We calculated 90% CL limit as $(7.7-1.28 \times 0.4=7.2) \times 10^{24}$.

See key on page 999

Gauge & Higgs Boson Particle Listings

Axions (A^0) and Other Very Light Bosons

² ARNOLD 19 uses the NEMO-3 tracking calorimeter to determine limits for the Majoron emitting double beta decay, with spectral index $n = 3$. The limit corresponds to the range of the g_{ee} coupling of 0.013–0.035; depending on the nuclear matrix elements used.

³ ARNOLD 18 use the NEMO-3 tracking detector. The limit corresponds to $\langle g_{ee} \rangle < 3.2\text{--}8.0 \times 10^{-5}$; the range corresponds to different nuclear matrix element calculations.

⁴ AGOSTINI 15A analyze a 20.3 kg yr of data set of the GERDA calorimeter to determine $g_{\nu\chi} < 3.4\text{--}8.7 \times 10^{-5}$ on the Majoron-neutrino coupling constant. The range reflects the spread of the nuclear matrix elements.

⁵ ARNOLD 15 use the NEMO-3 tracking calorimeter with 3.43 kg yr exposure to determine the limit on Majoron emission. The limit corresponds to $g_{\nu\chi} < 1.6\text{--}3.0 \times 10^{-4}$. The spread reflects different nuclear matrix elements. Supersedes ARNOLD 06.

⁶ ALBERT 14A utilize 100 kg yr of exposure of the EXO-200 tracking calorimeter to place a limit on the $g_{\nu\chi} < 0.8\text{--}1.7 \times 10^{-5}$ on the Majoron-neutrino coupling constant. The range reflects the spread of the nuclear matrix elements.

⁷ GANDO 12 use the KamLAND-Zen detector to obtain the limit on the $0\nu\chi$ decay with Majoron emission. It implies that the coupling constant $g_{\nu\chi} < 0.8\text{--}1.6 \times 10^{-5}$ depending on the nuclear matrix elements used.

⁸ ARNOLD 11 use the NEMO-3 detector to obtain the reported limit on Majoron emission. It implies that the coupling constant $g_{\nu\chi} < 0.6\text{--}1.6 \times 10^{-4}$ depending on the nuclear matrix element used. Supersedes ARNOLD 03.

⁹ ARGYRIADES 10 use the NEMO-3 tracking detector and ^{96}Zr to derive the reported limit. No limit for the Majoron electron coupling is given.

¹⁰ ARGYRIADES 09 use ^{150}Nd data taken with the NEMO-3 tracking detector. The reported limit corresponds to $\langle g_{\nu\chi} \rangle < 1.7\text{--}3.0 \times 10^{-4}$ using a range of nuclear matrix elements that include the effect of nuclear deformation.

¹¹ ARNOLD 06 use ^{100}Mo data taken with the NEMO-3 tracking detector. The reported limit corresponds to $\langle g_{\nu\chi} \rangle < (0.4\text{--}1.8) \times 10^{-4}$ using a range of matrix element calculations. Superseded by ARNOLD 15.

¹² NEMO-3 tracking calorimeter is used in ARNOLD 06. Reported half-life limit for ^{82}Se corresponds to $\langle g_{\nu\chi} \rangle < (0.66\text{--}1.9) \times 10^{-4}$ using a range of matrix element calculations. Supersedes ARNOLD 04.

¹³ ARNOLD 04 use the NEMO-3 tracking detector. The limit corresponds to $\langle g_{\nu\chi} \rangle < (0.5\text{--}0.9)10^{-4}$ using the matrix elements of SIMKOVIĆ 99, STOICA 01 and CIVITARESE 03. Superseded by ARNOLD 06.

¹⁴ ARNOLD 04 use the NEMO-3 tracking detector. The limit corresponds to $\langle g_{\nu\chi} \rangle < (0.7\text{--}1.6)10^{-4}$ using the matrix elements of SIMKOVIĆ 99, STOICA 01 and CIVITARESE 03.

¹⁵ Supersedes ALESSANDRELLO 00. Array of TeO_2 crystals in high resolution cryogenic calorimeter. Some enriched in ^{130}Te . Derive $\langle g_{\nu\chi} \rangle < 17\text{--}33 \times 10^{-5}$ depending on matrix element.

¹⁶ Supersedes ALESSANDRELLO 00. Cryogenic calorimeter search.

¹⁷ Limit for the $0\nu\chi$ decay with Majoron emission of ^{116}Cd using enriched CdWO_4 scintillators. $\langle g_{\nu\chi} \rangle < 4.6\text{--}8.1 \times 10^{-5}$ depending on the matrix element. Supersedes DANEVICH 00.

¹⁸ Limit for the $0\nu 2\chi$ decay of ^{116}Cd . Supersedes DANEVICH 00.

¹⁹ BERNABEI 02b obtain limit for $0\nu\chi$ decay with Majoron emission of ^{136}Xe using liquid Xe scintillation detector. They derive $\langle g_{\nu\chi} \rangle < 2.0\text{--}3.0 \times 10^{-5}$ with several nuclear matrix elements.

²⁰ Replaces TANAKA 93. FUSHIMI 02 derive half-life limit for the $0\nu\chi$ decay by means of tracking calorimeter ELEGANT V. Considering various matrix element calculations, a range of limits for the Majoron-neutrino coupling is given: $\langle g_{\nu\chi} \rangle < (6.3\text{--}360) \times 10^{-5}$.

²¹ ASHITKOV 01 result for $0\nu\chi$ of ^{100}Mo is less stringent than ARNOLD 00.

²² DANEVICH 01 obtain limit for the $0\nu\chi$ decay with Majoron emission of ^{160}Gd using $\text{Gd}_2\text{SiO}_5\text{:Ce}$ crystal scintillators.

²³ DANEVICH 01 obtain limit for the $0\nu 2\chi$ decay with 2 Majoron emission of ^{160}Gd .

²⁴ ARNOLD 00 reports limit for the $0\nu\chi$ decay with Majoron emission derived from tracking calorimeter NEMO 2. Using ^{82}Se source: $\langle g_{\nu\chi} \rangle < 1.6 \times 10^{-4}$. Matrix element from GUENTHER 96.

²⁵ Using ^{96}Zr source: $\langle g_{\nu\chi} \rangle < 2.6 \times 10^{-4}$. Matrix element from ARNOLD 99.

²⁶ ARNOLD 00 reports limit for the $0\nu 2\chi$ decay with two Majoron emission derived from tracking calorimeter NEMO 2.

²⁷ ARNOLD 98 determine the limit for $0\nu\chi$ decay with Majoron emission of ^{82}Se using the NEMO-2 tracking detector. They derive $\langle g_{\nu\chi} \rangle < 2.3\text{--}4.3 \times 10^{-4}$ with several nuclear matrix elements.

²⁸ LUESCHER 98 report a limit for the 0ν decay with Majoron emission of ^{136}Xe using Xe TPC. This result is more stringent than BARABASH 89. Using the matrix elements of ENGEL 88, they obtain a limit on $\langle g_{\nu\chi} \rangle$ of 2.0×10^{-4} .

²⁹ See Table 1 in GUENTHER 96 for limits on the Majoron coupling in different models.

< 1.2	95	12	HANNESTAD	07	COSM	K, hot dark matter
< 0.42	95	13	MELCHIORRI	07A	COSM	K, hot dark matter
< 1.05	95	14	HANNESTAD	05A	COSM	K, hot dark matter
3 to 20		15	MOROI	98	COSM	K, hot dark matter
< 0.007		16	BORISOV	97	ASTR	D, neutron star
< 4		17	KACHELRIESS	97	ASTR	D, neutron star cooling
< (0.5–6) × 10 ⁻³		18	KEIL	97	ASTR	SN 1987A
< 0.018		19	RAFFELT	95	ASTR	D, red giant
< 0.010		20	ALTHERR	94	ASTR	D, red giants, white dwarfs
< 0.01		21	CHANG	93	ASTR	K, SN 1987A
< 0.03			WANG	92	ASTR	D, white dwarf
none 3–8			WANG	92C	ASTR	D, C-O burning
< 10		22	BERSHADY	91	ASTR	D, K, intergalactic light
< 1 × 10 ⁻³		23	KIM	91C	COSM	D, K, mass density of the universe, super-symmetry
none 10 ⁻³ –3		24	RAFFELT	91B	ASTR	D, K, SN 1987A
< 0.02		25	RESSELL	91	ASTR	K, intergalactic light
< 1 × 10 ⁻³			BURROWS	90	ASTR	D, K, SN 1987A
< (1.4–10) × 10 ⁻³		26	ENGEL	90	ASTR	D, K, SN 1987A
< 3.6 × 10 ⁻⁴		27	RAFFELT	90D	ASTR	D, red giant
< 12		28	BURROWS	89	ASTR	D, K, SN 1987A
< 1 × 10 ⁻³		29	ERICSON	89	ASTR	D, K, SN 1987A
		30	MAYLE	89	ASTR	D, K, SN 1987A
			CHANDA	88	ASTR	D, Sun
			RAFFELT	88	ASTR	D, K, SN 1987A
		31	RAFFELT	88B	ASTR	red giant
< 0.07			FRIEMAN	87	ASTR	D, red giant
< 0.7		32	RAFFELT	87	ASTR	K, red giant
< 2–5			TURNER	87	COSM	K, thermal production
< 0.01		33	DEARBORN	86	ASTR	D, red giant
< 0.06			RAFFELT	86	ASTR	D, red giant
< 0.7		34	RAFFELT	86	ASTR	K, red giant
< 0.03			RAFFELT	86B	ASTR	D, white dwarf
< 1		35	KAPLAN	85	ASTR	K, red giant
< 0.003–0.02			IWAMOTO	84	ASTR	D, K, neutron star
> 1 × 10 ⁻⁵			ABBOTT	83	COSM	D, K, mass density of the universe
> 1 × 10 ⁻⁵			DINE	83	COSM	D, K, mass density of the universe
> 0.04			ELLIS	83B	ASTR	D, red giant
> 1 × 10 ⁻⁵			PRESKILL	83	COSM	D, K, mass density of the universe
< 0.1			BARROSO	82	ASTR	D, red giant
< 1		36	FUKUGITA	82	ASTR	D, stellar cooling
< 0.07			FUKUGITA	82B	ASTR	D, red giant

¹ PALOMBA 19 used the LIGO O2 dataset to derive limits on nearly monochromatic gravitational waves emitted by boson clouds formed around a stellar-mass black hole. They exclude boson masses in a range of 1.1×10^{-13} and 4×10^{-13} eV for high initial black hole spin, and 1.2×10^{-13} and 1.8×10^{-13} eV for moderate spin. See their Figs. 2 and 3 for limits based on various values of black hole initial spin, boson cloud age, and distance.

² CHANG 18 update axion bremsstrahlung emission rates in nucleon-nucleon collisions, shifting the excluded mass range to higher values. They rule out the hadronic axion with mass up to a few hundred eV, closing the hadronic axion window. See their Fig. 11 for results based on several different choices of the temperature and density profile of the proto-neutron star.

³ ARCHIDIACONO 13A is analogous to HANNESTAD 05A. The limit is based on the CMB temperature power spectrum of the Planck data, the CMB polarization from the WMAP 9-yr data, the matter power spectrum from SDSS-DR7, and the local Hubble parameter measurement by the Carnegie Hubble program.

⁴ CADAMURO 11 use the deuterium abundance to show that the m_{A0} range 0.7 eV – 300 keV is excluded for axions, complementing HANNESTAD 10.

⁵ DERBIN 11A look for solar axions produced by Compton and bremsstrahlung processes, in the resonant excitation of ^{169}Tm , constraining the axion-electron × axion nucleon couplings.

⁶ ANDRIAMONJE 10 search for solar axions produced from ^7Li (478 keV) and $\text{D}(\rho, \gamma)^3\text{He}$ (5.5 MeV) nuclear transitions. They show limits on the axion-photon coupling for two reference values of the axion-nucleon coupling for $m_A < 100$ eV.

⁷ This is an update of HANNESTAD 08 including 7 years of WMAP data.

⁸ ANDRIAMONJE 09 look for solar axions produced from the thermally excited 14.4 keV level of ^{57}Fe . They show limits on the axion-nucleon × axion-photon coupling assuming $m_A < 0.03$ eV.

⁹ DERBIN 09A look for Primakoff-produced solar axions in the resonant excitation of ^{169}Tm , constraining the axion-photon × axion-nucleon couplings.

¹⁰ KEKEZ 09 look at axio-electric effect of solar axions in HPGe detectors. The one-loop axion-electron coupling for hadronic axions is used.

¹¹ This is an update of HANNESTAD 07 including 5 years of WMAP data.

¹² This is an update of HANNESTAD 05a with new cosmological data, notably WMAP (3 years) and baryon acoustic oscillations (BAO). Lyman- α data are left out, in contrast to HANNESTAD 05a and MELCHIORRI 07A, because it is argued that systematic errors are large. It uses Bayesian statistics and marginalizes over a possible neutrino hot dark matter component.

¹³ MELCHIORRI 07A is analogous to HANNESTAD 05A, with updated cosmological data, notably WMAP (3 years). Uses Bayesian statistics and marginalizes over a possible neutrino hot dark matter component. Leaving out Lyman- α data, a conservative limit is 1.4 eV.

¹⁴ HANNESTAD 05A puts an upper limit on the mass of hadronic axion because in this mass range it would have been thermalized and contribute to the hot dark matter component of the universe. The limit is based on the CMB anisotropy from WMAP, SDSS large

Invisible A^0 (Axion) MASS LIMITS from Astrophysics and Cosmology

$v_1 = v_2$ is usually assumed ($v_j =$ vacuum expectation values). For a review of these limits, see RAFFELT 91 and TURNER 90. In the comment lines below, D and K refer to DFSZ and KSVZ axion types, discussed in the above minireview.

VALUE (eV)	CL%	DOCUMENT ID	TECN	COMMENT
•••		We do not use the following data for averages, fits, limits, etc. •••		
none $1\text{--}4 \times 10^{-13}$	95	1	PALOMBA 19	ASTR BH superradiance
< 0.06		2	CHANG 18	ASTR K, SN 1987A
< 0.67	95	3	ARCHIDIACO...13A	COSM K, hot dark matter
none $0.7\text{--}3 \times 10^5$		4	CADAMURO 11	COSM D abundance
<105	90	5	DERBIN 11A	CNTR D, solar axion
		6	ANDRIAMON...10	CAST K, solar axions
< 0.72	95	7	HANNESTAD 10	COSM K, hot dark matter
		8	ANDRIAMON...09	CAST K, solar axions
<191	90	9	DERBIN 09A	CNTR K, solar axions
<334	95	10	KEKEZ 09	HPGE K, solar axions
< 1.02	95	11	HANNESTAD 08	COSM K, hot dark matter

Gauge & Higgs Boson Particle Listings

Axions (A^0) and Other Very Light Bosons

- scale structure, Lyman α , and the prior Hubble parameter from HST Key Project. A χ^2 statistic is used. Neutrinos are assumed not to contribute to hot dark matter.
- 15 MORIO 98 points out that a KSVZ axion of this mass range (see CHANG 93) can be a viable hot dark matter of Universe, as long as the model-dependent $g_{A\gamma}$ is accidentally small enough as originally emphasized by KAPLAN 85; see Fig. 1.
- 16 BORISOV 97 bound is on the axion-electron coupling $g_{ae} < 1 \times 10^{-13}$ from the photo-production of axions off of magnetic fields in the outer layers of neutron stars.
- 17 KACHELRIESS 97 bound is on the axion-electron coupling $g_{ae} < 1 \times 10^{-10}$ from the production of axions in strongly magnetized neutron stars. The authors also quote a stronger limit, $g_{ae} < 9 \times 10^{-13}$ which is strongly dependent on the strength of the magnetic field in white dwarfs.
- 18 KEIL 97 uses new measurements of the axial-vector coupling strength of nucleons, as well as a reanalysis of many-body effects and pion-emission processes in the core of the neutron star, to update limits on the invisible-axion mass.
- 19 RAFFELT 95 reexamined the constraints on axion emission from red giants due to the axion-electron coupling. They improve on DEARBORN 86 by taking into proper account degeneracy effects in the bremsstrahlung rate. The limit comes from requiring the red giant core mass at helium ignition not to exceed its standard value by more than 5% (0.025 solar masses).
- 20 ALTHERR 94 bound is on the axion-electron coupling $g_{ae} < 1.5 \times 10^{-13}$, from energy loss via axion emission.
- 21 CHANG 93 updates ENGEL 90 bound with the Kaplan-Manohar ambiguity in $z=m_{\psi}/m_{\phi}$ (see the Note on the Quark Masses in the Quark Particle Listings). It leaves the window $f_A = 3 \times 10^5 - 3 \times 10^6$ GeV open. The constraint from Big-Bang Nucleosynthesis is satisfied in this window as well.
- 22 BERSHADY 91 searched for a line at wave length from 3100–8300 Å expected from 2 γ decays of relic thermal axions in intergalactic light of three rich clusters of galaxies.
- 23 KIM 91c argues that the bound from the mass density of the universe will change drastically for the supersymmetric models due to the entropy production of saxion (scalar component in the axionic chiral multiplet) decay. Note that it is an *upperbound* rather than a lowerbound.
- 24 RAFFELT 91b argue that previous SN1987A bounds must be relaxed due to corrections to nucleon bremsstrahlung processes.
- 25 RESSELL 91 uses absence of any intracuster line emission to set limit.
- 26 ENGEL 90 rule out $10^{-10} \lesssim g_{AN} \lesssim 10^{-3}$, which for a hadronic axion with EMC motivated axion-nucleon couplings corresponds to $2.5 \times 10^{-3} \text{ eV} \lesssim m_{A^0} \lesssim 2.5 \times 10^4 \text{ eV}$. The constraint is loose in the middle of the range, i.e. for $g_{AN} \sim 10^{-6}$.
- 27 RAFFELT 90d is a re-analysis of DEARBORN 86.
- 28 The region $m_{A^0} \gtrsim 2 \text{ eV}$ is also allowed.
- 29 ERICSON 89 considered various nuclear corrections to axion emission in a supernova core, and found a reduction of the previous limit (MAYLE 88) by a large factor.
- 30 MAYLE 89 limit based on naive quark model couplings of axion to nucleons. Limit based on couplings motivated by EMC measurements is 2–4 times weaker. The limit from axion-electron coupling is weak: see HATSUDA 88b.
- 31 RAFFELT 88b derives a limit for the energy generation rate by exotic processes in helium-burning stars $\epsilon < 100 \text{ erg g}^{-1} \text{ s}^{-1}$, which gives a firmer basis for the axion limits based on red giant cooling.
- 32 RAFFELT 87 also gives a limit $g_{A\gamma} < 1 \times 10^{-10} \text{ GeV}^{-1}$.
- 33 DEARBORN 86 also gives a limit $g_{A\gamma} < 1.4 \times 10^{-11} \text{ GeV}^{-1}$.
- 34 RAFFELT 86 gives a limit $g_{A\gamma} < 1.1 \times 10^{-10} \text{ GeV}^{-1}$ from red giants and $< 2.4 \times 10^{-9} \text{ GeV}^{-1}$ from the sun.
- 35 KAPLAN 85 says $m_{A^0} < 23 \text{ eV}$ is allowed for a special choice of model parameters.
- 36 FUKUGITA 82 gives a limit $g_{A\gamma} < 2.3 \times 10^{-10} \text{ GeV}^{-1}$.

Search for Relic Invisible Axions

Limits are for $[G_{A\gamma\gamma}/m_{A^0}]^2 \rho_A$ where $G_{A\gamma\gamma}$ denotes the axion two-photon coupling, $L_{\text{int}} = -\frac{G_{A\gamma\gamma}}{4} \phi_A F_{\mu\nu} \tilde{F}^{\mu\nu} = G_{A\gamma\gamma} \phi_A \mathbf{E} \cdot \mathbf{B}$, and ρ_A is the axion energy density near the earth.

VALUE	CL%	DOCUMENT ID	TECN	COMMENT
$< 2.6 \times 10^{-39}$	95	1 ALESINI 19	QUAX	$m_{A^0} = 37.5 \mu\text{eV}$
$< 6 \times 10^{-5}$		2 FUJITA 19	ASTR	$m_{A^0} < 10^{-21} \text{ eV}$
$< 2 \times 10^{-27}$	95	3 OUELLET 19a	ABRA	$m_{A^0} = 0.31\text{--}8.3 \text{ neV}$
$< 7.3 \times 10^{-40}$	90	4 BOUTAN 18	ADMX	$m_{A^0} = 17.38\text{--}17.57 \mu\text{eV}$
$< 1.8 \times 10^{-39}$	90	4 BOUTAN 18	ADMX	$m_{A^0} = 21.03\text{--}23.98 \mu\text{eV}$
$< 3.4 \times 10^{-39}$	90	4 BOUTAN 18	ADMX	$m_{A^0} = 29.67\text{--}29.79 \mu\text{eV}$
$< 1.4 \times 10^{-44}$	90	5 DU 18	ADMX	$m_{A^0} = 2.66\text{--}2.81 \mu\text{eV}$
$< 2.87 \times 10^{-42}$	90	6 ZHONG 18	HYST	$m_{A^0} = 23.15\text{--}24 \mu\text{eV}$
		7 BRANCA 17	AURG	$m_{S^0} = 3.5\text{--}3.9 \text{ peV}$
$< 3 \times 10^{-42}$	90	8 BRUBAKER 17	HYST	$m_{A^0} = 23.55\text{--}24.0 \mu\text{eV}$
$< 1.0 \times 10^{-29}$	95	9 CHOI 17		$m_{A^0} = 24.7\text{--}29.1 \mu\text{eV}$
$< 8.6 \times 10^{-42}$	90	10 HOSKINS 16	ADMX	$m_{A^0} = 3.36\text{--}3.52$ or $3.55\text{--}3.69 \mu\text{eV}$
		11 BECK 13		$m_{A^0} = 0.11 \text{ meV}$
$< 3.5 \times 10^{-43}$		12 HOSKINS 11	ADMX	$m_{A^0} = 3.3\text{--}3.69 \times 10^{-6} \text{ eV}$
$< 2.9 \times 10^{-43}$	90	13 ASZTALOS 10	ADMX	$m_{A^0} = 3.34\text{--}3.53 \times 10^{-6} \text{ eV}$
$< 1.9 \times 10^{-43}$	97.7	14 DUFFY 06	ADMX	$m_{A^0} = 1.98\text{--}2.17 \times 10^{-6} \text{ eV}$
$< 5.5 \times 10^{-43}$	90	15 ASZTALOS 04	ADMX	$m_{A^0} = 1.9\text{--}3.3 \times 10^{-6} \text{ eV}$
		16 KIM 98	THEO	
$< 2 \times 10^{-41}$		17 HAGMANN 90	CNTR	$m_{A^0} = (5.4\text{--}5.9) \times 10^{-6} \text{ eV}$
$< 6.3 \times 10^{-42}$	95	18 WUENSCH 89	CNTR	$m_{A^0} = (4.5\text{--}10.2) \times 10^{-6} \text{ eV}$
$< 5.4 \times 10^{-41}$	95	18 WUENSCH 89	CNTR	$m_{A^0} = (11.3\text{--}16.3) \times 10^{-6} \text{ eV}$

- 1 ALESINI 19 used a superconducting resonant cavity made of NbTi to increase the quality factor. The limit applies to a mass range of 0.2 neV around $m_{A^0} = 37.5 \mu\text{eV}$.
- 2 FUJITA 19 look for photon birefringence under the oscillating axion background using the polarimetric imaging observation of a protoplanetary disk, AB Aur. See their Fig. 2 for a more conservative limit taking account of possible systematic effects.
- 3 OUELLET 19a look for the axion-induced oscillating magnetic field generated by a toroidal magnetic field. The quoted limit applies at $m_{A^0} = 8 \text{ neV}$. See their Fig. 3 for the mass-dependent limits.
- 4 BOUTAN 18 use a small high frequency cavity installed above the main ADMX cavity to look for heavier axion dark matter. See their Fig. 4 for mass-dependent limits.
- 5 DU 18 is analogous to DUFFY 06. They upgraded a dilution refrigerator to reduce the system noise. The quoted limit is around $m_{A^0} = 2.69 \mu\text{eV}$ for the boosted Maxwellian axion line shape. See Fig. 4 for their mass-dependent limits.
- 6 ZHONG 18 is analogous to BRUBAKER 17. The quoted limit applies at $m_{A^0} = 23.76 \mu\text{eV}$. See Fig. 4 for their mass-dependent limits.
- 7 BRANCA 17 look for modulations of the fine-structure constant and the electron mass due to moduli dark matter by using the cryogenic resonant-mass AURIGA detector. The limit on the assumed dilatonic coupling implies $G_{S\gamma\gamma} < 1.5 \times 10^{-24} \text{ GeV}^{-1}$ for the scalar to two-photon coupling. See Fig. 5 for the mass-dependent limits.
- 8 BRUBAKER 17 used a microwave cavity detector at the Yale Wright Laboratory to search for dark matter axions. See Fig. 3 for the mass-dependent limits.
- 9 CHOI 17 used a microwave cavity detector with toroidal geometry. See Fig. 4 for their mass-dependent limits.
- 10 HOSKINS 16 is analogous to DUFFY 06. See Fig. 12 for mass-dependent limits in terms of the local dark matter density.
- 11 BECK 13 argues that dark-matter axions passing through Earth may generate a small observable signal in resonant S/N/S Josephson junctions. A measurement by HOFFMANN 04 [Physical Review B70 1805 03 (2004)] is interpreted in terms of subdominant dark matter axions with $m_{A^0} = 0.11 \text{ meV}$.
- 12 HOSKINS 11 is analogous to DUFFY 06. See Fig. 4 for the mass-dependent limit in terms of the local density.
- 13 ASZTALOS 10 used the upgraded detector of ASZTALOS 04 to search for halo axions. See their Fig. 5 for the m_{A^0} dependence of the limit.
- 14 DUFFY 06 used the upgraded detector of ASZTALOS 04, while assuming a smaller velocity dispersion than the isothermal model as in Eq. (8) of their paper. See Fig. 10 of their paper on the axion mass dependence of the limit.
- 15 ASZTALOS 04 looked for a conversion of halo axions to microwave photons in magnetic field. At 90% CL, the KSVZ axion cannot have a local halo density more than 0.45 GeV/cm^3 in the quoted mass range. See Fig. 7 of their paper on the axion mass dependence of the limit.
- 16 KIM 98 calculated the axion-to-photon couplings for various axion models and compared them to the HAGMANN 90 bounds. This analysis demonstrates a strong model dependence of $G_{A\gamma\gamma}$ and hence the bound from relic axion search.
- 17 HAGMANN 90 experiment is based on the proposal of SIKIVIE 83.
- 18 WUENSCH 89 looks for condensed axions near the earth that could be converted to photons in the presence of an intense electromagnetic field via the Primakoff effect, following the proposal of SIKIVIE 83. The theoretical prediction with $[G_{A\gamma\gamma}/m_{A^0}]^2 = 2 \times 10^{-14} \text{ MeV}^{-4}$ (the three generation DFSZ model) and $\rho_A = 300 \text{ MeV/cm}^3$ that makes up galactic halos gives $(G_{A\gamma\gamma}/m_{A^0})^2 \rho_A = 4 \times 10^{-44}$. Note that our definition of $G_{A\gamma\gamma}$ is $(1/4\pi)$ smaller than that of WUENSCH 89.

Invisible A^0 (Axion) Limits from Photon Coupling

Limits are for the modulus of the axion-two-photon coupling $G_{A\gamma\gamma}$ defined by $L = -G_{A\gamma\gamma} \phi_A \mathbf{E} \cdot \mathbf{B}$. For scalars S^0 the limit is on the coupling constant in $L = G_{S\gamma\gamma} \phi_S (\mathbf{E}^2 - \mathbf{B}^2)$. The relation between $G_{A\gamma\gamma}$ and m_{A^0} is not used unless stated otherwise, i.e., many of these bounds apply to low-mass axion-like particles (ALPs), not to QCD axions.

VALUE (GeV^{-1})	CL%	DOCUMENT ID	TECN	COMMENT
$< 1 \times 10^{-3}$	95	1 ALONI 19	PRMX	$m_{A^0} = 0.16 \text{ GeV}$
$< 1.4 \times 10^{-14}$	95	2 CAPUTO 19	ASTR	$m_{A^0} = 5 \times 10^{-24} \text{ eV}$
$< 9.6 \times 10^{-14}$	95	3 FEDDERKE 19	CMB	$m_{A^0} = 10^{-22} \text{ eV}$
$< 7 \times 10^{-13}$	95	4 IVANOV 19	ASTR	$m_{A^0} = 5 \times 10^{-23} \text{ eV}$
$< 4 \times 10^{-11}$	95	5 LIANG 19	ASTR	$m_{A^0} = 1.2 \times 10^{-7} \text{ eV}$
		6 FORTIN 18	ASTR	Axion-like particles
		7 YAMAJI 18	LSW	$m_{A^0} = 46\text{--}1020 \text{ eV}$
$< 5.0 \times 10^{-3}$	90	8 ZHANG 18	ASTR	$m_{A^0} = 0.6\text{--}4 \text{ neV}$
$< 1 \times 10^{-11}$	99.9	9 ADE 17	CMB	Axion-like particles
$< 6.6 \times 10^{-11}$	95	10 ANASTASSO...17	CAST	$m_{A^0} < 0.02 \text{ eV}$
		11 DOLAN 17	RVUE	Axion-like particles
		12 INADA 17	LSW	$m_{A^0} < 0.1 \text{ eV}$
$< 2.51 \times 10^{-4}$	95	13 KOHRI 17	ASTR	$m_{A^0} = 0.7\text{--}50 \text{ neV}$
$> 1.5 \times 10^{-11}$	95	14 MARSH 17	ASTR	$m_{A^0} \leq 10^{-13} \text{ eV}$
$< 2.6 \times 10^{-12}$	95	15 TIWARI 17	COSM	$m_{A^0} \leq 10^{-15} \text{ eV}$
$< 6 \times 10^{-13}$		16 AJELLO 16	ASTR	$m_{A^0} = 0.5\text{--}5 \text{ neV}$
$< 5 \times 10^{-12}$	95	17 DELLA-VALLE 16	LASR	$m_{A^0} = 1.3 \text{ meV}$
$< 1.2 \times 10^{-7}$	95	18 DELLA-VALLE 16	LASR	$m_{A^0} < 0.5 \text{ meV}$
$< 7.2 \times 10^{-8}$	95	19 JAECKEL 16	ALPS	$m_{A^0} = 0.1\text{--}100 \text{ GeV}$
$< 8 \times 10^{-4}$		20 LEEFER 16		$m_{S^0} < 10^{-18} \text{ eV}$
$< 6 \times 10^{-21}$		21 ANASTASSO...15	CAST	Chameleons
		22 ARIK 15	CAST	$m_{A^0} = 0.39\text{--}0.42 \text{ eV}$
$< 1.47 \times 10^{-10}$	95	23 BALLOU 15	LSW	$m_{A^0} < 2 \times 10^{-4} \text{ eV}$
$< 3.5 \times 10^{-8}$	95	24 BRAX 15	ASTR	$m_{S^0} < 4 \times 10^{-12} \text{ eV}$

See key on page 999

Gauge & Higgs Boson Particle Listings
Axions (A^0) and Other Very Light Bosons

$<5.42 \times 10^{-4}$	95	25	HASEBE	15	LASR	$m_{A^0} = 0.15$ eV
		26	MILLEA	15	COSM	Axion-like particles
		27	VANTILBURG	15		Dilaton-like dark matter
$<4.1 \times 10^{-10}$	99.7	28	VINYOLES	15	ASTR	$m_{A^0} = 0.6\text{--}185$ eV
$<3.3 \times 10^{-10}$	95	29	ARIK	14	CAST	$m_{A^0} = 0.64\text{--}1.17$ eV
$<6.6 \times 10^{-11}$	95	30	AYALA	14	ASTR	Globular clusters
$<1.4 \times 10^{-7}$	95	31	DELLA-VALLE	14	LASR	$m_{A^0} = 1$ meV
		32	EJLLI	14	COSM	$m_{A^0} = 2.66\text{--}48.8$ μ eV
$<8 \times 10^{-8}$	95	33	PUGNAT	14	LSW	$m_{A^0} < 0.3$ meV
$<1 \times 10^{-11}$		34	REESMAN	14	ASTR	$m_{A^0} < 1 \times 10^{-10}$ eV
$<2.1 \times 10^{-11}$	95	35	ABRAMOWSKI13A	13A	IACT	$m_{A^0} = 15\text{--}60$ neV
$<2.15 \times 10^{-9}$	95	36	ARMENGAUD	13	EDEL	$m_{A^0} < 7 \times 10^6$ eV
$<4.5 \times 10^{-8}$	95	37	BETZ	13	LSW	$m_{A^0} = 7.2 \times 10^{-6}$ eV
$<8 \times 10^{-11}$		38	FRIEDLAND	13	ASTR	Red giants
$>2 \times 10^{-11}$		39	MEYER	13	ASTR	$m_{A^0} < 1 \times 10^{-7}$ eV
$<8.3 \times 10^{-12}$	95	40	WOUTERS	13	ASTR	$m_{A^0} < 7 \times 10^{-12}$ eV
		41	CADAMURO	12	COSM	Axion-like particles
$<2.5 \times 10^{-13}$	95	42	PAYEZ	12	ASTR	$m_{A^0} < 4.2 \times 10^{-14}$ eV
$<2.3 \times 10^{-10}$		43	ARIK	11	CAST	$m_{A^0} = 0.39\text{--}0.64$ eV
$<6.5 \times 10^{-8}$	95	44	EHRET	10	ALPS	$m_{A^0} < 0.7$ meV
$<2.4 \times 10^{-9}$	95	45	AHMED	09A	CDMS	$m_{A^0} < 100$ eV
$<1.2\text{--}2.8 \times 10^{-10}$	95	46	ARIK	09	CAST	$m_{A^0} = 0.02\text{--}0.39$ eV
		47	CHOU	09		Chameleons
$<7 \times 10^{-10}$		48	GONDOLO	09	ASTR	$m_{A^0} < \text{few keV}$
$<1.3 \times 10^{-6}$	95	49	AFANA SEV	08		$m_{S^0} < 1$ meV
$<3.5 \times 10^{-7}$	99.7	50	CHOU	08		$m_{A^0} < 0.5$ meV
$<1.1 \times 10^{-6}$	99.7	51	FOUCHE	08		$m_{A^0} < 1$ meV
$<5.6\text{--}13.4 \times 10^{-10}$	95	52	INOUE	08		$m_{A^0} = 0.84\text{--}1.00$ eV
$<5 \times 10^{-7}$		53	ZAVATTINI	08		$m_{A^0} < 1$ meV
$<8.8 \times 10^{-11}$	95	54	ANDRIAMON..07	07	CAST	$m_{A^0} < 0.02$ eV
$<1.25 \times 10^{-6}$	95	55	ROBILLIARD	07		$m_{A^0} < 1$ meV
$2\text{--}5 \times 10^{-6}$		56	ZAVATTINI	06		$m_{A^0} = 1\text{--}1.5$ meV
$<1.1 \times 10^{-9}$	95	57	INOUE	02		$m_{A^0} = 0.05\text{--}0.27$ eV
$<2.78 \times 10^{-9}$	95	58	MORALES	02B		$m_{A^0} < 1$ keV
$<1.7 \times 10^{-9}$	95	59	BERNABEI	01B		$m_{A^0} < 100$ eV
$<1.5 \times 10^{-4}$	90	60	ASTIER	00B	NOMD	$m_{A^0} < 40$ eV
		61	MASSO	00	THEO	induced γ coupling
$<2.7 \times 10^{-9}$	95	62	AVIGNONE	98	SLAX	$m_{A^0} < 1$ keV
$<6.0 \times 10^{-10}$	95	63	MORIYAMA	98		$m_{A^0} < 0.03$ eV
$<3.6 \times 10^{-7}$	95	64	CAMERON	93		$m_{A^0} < 10^{-3}$ eV, optical rotation
$<6.7 \times 10^{-7}$	95	65	CAMERON	93		$m_{A^0} < 10^{-3}$ eV, photon regeneration
$<3.6 \times 10^{-9}$	99.7	66	LAZARUS	92		$m_{A^0} < 0.03$ eV
$<7.7 \times 10^{-9}$	99.7	66	LAZARUS	92		$m_{A^0} = 0.03\text{--}0.11$ eV
$<7.7 \times 10^{-7}$	99	67	RUOSO	92		$m_{A^0} < 10^{-3}$ eV
$<2.5 \times 10^{-6}$		68	SEMERTZIDIS	90		$m_{A^0} < 7 \times 10^{-4}$ eV

- 1 ALONI 19 used the data collected by the PRIMEX experiment to derive a limit based on a data-driven method. See their Fig. 2 for mass-dependent limits.
- 2 CAPUTO 19 look for an oscillating variation of the polarization angle of the pulsar J0437-4715, where they assume the local axion energy density $\rho_A = 0.3$ GeV/cm³. See their Fig. 2 for mass-dependent limits for 5×10^{-24} eV $\leq m_{A^0} \leq 2 \times 10^{-19}$ eV.
- 3 FEDDERKE 19 look for a uniform reduction of the CMB polarization at large scales, which is induced by the oscillating axion background during CMB decoupling. The quoted limit is based on the assumption that axions make up all of the dark matter. See their Fig. 3 for mass-dependent limits for $m_{A^0} = 10^{-22}\text{--}10^{-19}$ eV.
- 4 IVANOV 19 look for the axion-induced periodic changes in the polarization angle of parsec-scale jets in active galactic nuclei observed by the MOJAVE program, where they use the axion energy density $\rho_A = 20$ GeV/cm³. See their Fig. 6 for mass-dependent limits for 5×10^{-23} eV $\leq m_{A^0} \leq 1.2 \times 10^{-21}$ eV.
- 5 LIANG 19 look for spectral irregularities in the spectrum of 10 bright H.E.S.S. sources in the Galactic plane, assuming photon-ALP mixing in the Galactic magnetic fields. See their Fig. 2 for mass-dependent limits with different Galactic magnetic field models.
- 6 FORTIN 18 studied the conversion of axion-like particles produced in the core of a magnetar to hard X-rays in the magnetosphere. See their Fig. 5 for mass-dependent limits with different values of the magnetar core temperature.
- 7 YAMAJI 18 search for axions with an x-ray LSW at Spring-8, using the Laue-case conversion in a silicon crystal. They also obtain $G_{A\gamma\gamma} < 4.2 \times 10^{-9}$ GeV⁻¹ for $m_{A^0} < 10$ eV. See their Fig. 5 for mass-dependent limits.
- 8 ZHANG 18 look for spectral irregularities in the spectrum of PKS 2155-304 measured by Fermi-LAT, assuming photon-ALP mixing in the intercluster and Galactic magnetic fields. See their Figs. 2 and 3 for mass-dependent limits with different values of the intercluster magnetic field parameters.
- 9 ADE 17 look for cosmic birefringence from axion-like particles using CMB polarization data taken by the BICEP2 and Keck Array experiments. They set a limit $G_{A\gamma\gamma} H_I < 7.2 \times 10^{-2}$ at 95%CL for $m_{A^0} < 10^{-28}$ eV, where H_I is the Hubble parameter during inflation.
- 10 ANASTASSOPOULOS 17 looked for solar axions by the CAST axion helioscope in the vacuum phase, and supersedes ANDRIAMONJE 07.

- 11 DOLAN 17 update existing limits on $G_{A\gamma\gamma}$ for axion-like particles. See their Fig. 2 for mass-dependent limits.
- 12 INADA 17 search for axions with an x-ray LSW at Spring-8. See their Fig. 4 for mass-dependent limits.
- 13 KOHRI 17 attributed to axion-photon oscillations the excess of cosmic infrared background observed by the CIBER experiment. See their Fig. 5 for the region preferred by their scenario.
- 14 MARSH 17 is similar to WOUTERS 13, using Chandra observations of M87. See their Fig. 6 for mass-dependent limits.
- 15 TIWARI 17 use observed limits of the cosmic distance-duality relation to constrain the photon-ALP mixing based on 3D simulations of the magnetic field configuration. The quoted value is for the averaged magnetic field of 1nG with a coherent length of 1 Mpc. See their Fig. 5 for mass-dependent limits.
- 16 AJELLO 16 look for irregularities in the energy spectrum of the NGC1275 measured by Fermi LAT, assuming photon-ALP mixing in the intra-cluster and Galactic magnetic fields. See their Fig. 2 for mass-dependent limits.
- 17 DELLA-VALLE 16 look for the birefringence induced by axion-like particles. See their Fig. 14 for mass-dependent limits.
- 18 DELLA-VALLE 16 look for the dichroism induced by axion-like particles. See their Fig. 14 for mass-dependent limits.
- 19 JAECKEL 16 use the LEP data of $Z \rightarrow 2\gamma$ and $Z \rightarrow 3\gamma$ to constrain the ALP production via $e^+e^- \rightarrow Z \rightarrow A^0\gamma$ ($A^0 \rightarrow \gamma\gamma$), assuming the ALP coupling with two hypercharge bosons. See their Fig. 4 for mass-dependent limits.
- 20 LEEFER 16 derived limits by using radio-frequency spectroscopy of dysprosium and atomic clock measurements. See their Fig. 1 for mass-dependent limits as well as limits on Yukawa-type couplings of the scalar to the electron and nucleons.
- 21 ANASTASSOPOULOS 15 search for solar chameleons with CAST and derived limits on the chameleon coupling to photons and matter. See their Fig. 12 for the exclusion region.
- 22 ARIK 15 is analogous to ARIK 09, and search for solar axions for m_{A^0} around 0.2 and 0.4 eV. See their Figs. 1 and 3 for the mass-dependent limits.
- 23 Based on OSQAR photon regeneration experiment. See their Fig. 6 for mass-dependent limits on scalar and pseudoscalar bosons.
- 24 BRAX 15 derived limits on conformal and disformal couplings of a scalar to photons by searching for a chaotic absorption pattern in the X-ray and UV bands of the Hydra A galaxy cluster and a BL lac object, respectively. See their Fig. 8.
- 25 HASEBE 15 look for an axion via a four-wave mixing process at quasi-parallel colliding laser beams. They also derived limits on a scalar coupling to photons $G_{S\gamma\gamma} < 2.62 \times 10^{-4}$ GeV⁻¹ at $m_{S^0} = 0.15$ eV. See their Figs. 11 and 12 for mass-dependent limits.
- 26 MILLEA 15 is similar to CADAMURO 12, including the Planck data and the latest inferences of primordial deuterium abundance. See their Fig. 3 for mass-dependent limits.
- 27 VANTILBURG 15 look for harmonic variations in the dysprosium transition frequency data, induced by coherent oscillations of the fine-structure constant due to dilaton-like dark matter, and set the limits, $G_{S\gamma\gamma} < 6 \times 10^{-27}$ GeV⁻¹ at $m_{S^0} = 6 \times 10^{-23}$ eV. See their Fig. 4 for mass-dependent limits between $1 \times 10^{-24} < m_{S^0} < 1 \times 10^{-15}$ eV.
- 28 VINYOLES 15 performed a global fit analysis based on helioseismology and solar neutrino observations. See their Fig. 9.
- 29 ARIK 14 is similar to ARIK 11. See their Fig. 2 for mass-dependent limits.
- 30 AYALA 14 derived the limit from the helium-burning lifetime of horizontal-branch stars based on number counts in globular clusters.
- 31 DELLA-VALLE 14 use the new PVLAS apparatus to set a limit on vacuum magnetic birefringence induced by axion-like particles. See their Fig. 6 for the mass-dependent limits.
- 32 EJLLI 14 set limits on a product of primordial magnetic field and the axion mass using CMB distortion induced by resonant axion production from CMB photons. See their Fig. 1 for limits applying specifically to the DFSZ and KSVZ axion models.
- 33 PUGNAT 14 is analogous to EHRET 10. See their Fig. 5 for mass-dependent limits on scalar and pseudoscalar bosons.
- 34 REESMAN 14 derive limits by requiring effects of axion-photon interconversion on gamma-ray spectra from distant blazars to be no larger than errors in the best-fit optical depth based on a certain extragalactic background light model. See their Fig. 5 for mass-dependent limits.
- 35 ABRAMOWSKI 13A look for irregularities in the energy spectrum of the BL Lac object PKS 2155-304 measured by H.E.S.S. The limits depend on assumed magnetic field around the source. See their Fig. 7 for mass-dependent limits.
- 36 ARMENGAUD 13 is analogous to AVIGNONE 98. See Fig. 6 for the limit.
- 37 BETZ 13 performed a microwave-based light shining through the wall experiment. See their Fig. 13 for mass-dependent limits.
- 38 FRIEDLAND 13 derived the limit by considering blue-loop suppression of the evolution of red giants with 7-12 solar masses.
- 39 MEYER 13 attributed to axion-photon oscillations the observed excess of very high-energy γ -rays with respect to predictions based on extragalactic background light models. See their Fig. 4 for mass-dependent lower limits for various magnetic field configurations.
- 40 WOUTERS 13 look for irregularities in the X-ray spectrum of the Hydra cluster observed by Chandra. See their Fig. 4 for mass-dependent limits.
- 41 CADAMURO 12 derived cosmological limits on $G_{A\gamma\gamma}$ for axion-like particles. See their Fig. 1 for mass-dependent limits.
- 42 PAYEZ 12 derive limits from polarization measurements of quasar light (see their Fig. 3). The limits depend on assumed magnetic field strength in galaxy clusters. The limits depend on assumed magnetic field and electron density in the local galaxy supercluster.
- 43 ARIK 11 search for solar axions using ³He buffer gas in CAST, continuing from the ⁴He version of ARIK 09. See Fig. 2 for the exact mass-dependent limits.
- 44 ALPS is a photon regeneration experiment. See their Fig. 4 for mass-dependent limits on scalar and pseudoscalar bosons.
- 45 AHMED 09A is analogous to AVIGNONE 98.
- 46 ARIK 09 is the ⁴He filling version of the CAST axion helioscope in analogy to INOUE 02 and INOUE 08. See their Fig. 7 for mass-dependent limits.
- 47 CHOU 09 use the GammeV apparatus in the afterglow mode to search for chameleons, (pseudo)scalar bosons with a mass depending on the environment. For pseudoscalars they exclude at 3 σ the range 2.6×10^{-7} GeV⁻¹ $< G_{A\gamma\gamma} < 4.2 \times 10^{-6}$ GeV⁻¹ for vacuum m_{A^0} roughly below 6 meV for density scaling index exceeding 0.8.

Gauge & Higgs Boson Particle Listings

Axions (A^0) and Other Very Light Bosons

- ⁴⁸ GONDOLO 09 use the all-flavor measured solar neutrino flux to constrain solar interior temperature and thus energy losses.
- ⁴⁹ LIPSS photon regeneration experiment, assuming scalar particle S^0 . See Fig. 4 for mass-dependent limits.
- ⁵⁰ CHOU 08 perform a variable-baseline photon regeneration experiment. See their Fig. 3 for mass-dependent limits. Excludes the PVLAS result of ZAVATTINI 06.
- ⁵¹ FOCHE 08 is an update of ROBILLIARD 07. See their Fig. 12 for mass-dependent limits.
- ⁵² INOUE 08 is an extension of INOUE 02 to larger axion masses, using the Tokyo axion helioscope. See their Fig. 4 for mass-dependent limits.
- ⁵³ ZAVATTINI 08 is an upgrade of ZAVATTINI 06, see their Fig. 8 for mass-dependent limits. They now exclude the parameter range where ZAVATTINI 06 had seen a positive signature.
- ⁵⁴ ANDRIAMONJE 07 looked for Primakoff conversion of solar axions in 9T superconducting magnet into X-rays. Supersedes ZIOUTAS 05.
- ⁵⁵ ROBILLIARD 07 perform a photon regeneration experiment with a pulsed laser and pulsed magnetic field. See their Fig. 4 for mass-dependent limits. Excludes the PVLAS result of ZAVATTINI 06 with a CL exceeding 99.9%.
- ⁵⁶ ZAVATTINI 06 propagate a laser beam in a magnetic field and observe dichroism and birefringence effects that could be attributed to an axion-like particle. This result is now excluded by ROBILLIARD 07, ZAVATTINI 08, and CHOU 08.
- ⁵⁷ INOUE 02 looked for Primakoff conversion of solar axions in 4T superconducting magnet into X-ray.
- ⁵⁸ MORALES 02b looked for the coherent conversion of solar axions to photons via the Primakoff effect in Germanium detector.
- ⁵⁹ BERNABE 01b looked for Primakoff coherent conversion of solar axions into photons via Bragg scattering in NaI crystal in DAMA dark matter detector.
- ⁶⁰ ASTIER 00b looked for production of axions from the interaction of high-energy photons with the horn magnetic field and their subsequent re-conversion to photons via the interaction with the NOMAD dipole magnetic field.
- ⁶¹ MASSO 00 studied limits on axion-proton coupling using the induced axion-photon coupling through the proton loop and CAMERON 93 bound on the axion-photon coupling using optical rotation. They obtained the bound $g_{p\gamma}^2/4\pi < 1.7 \times 10^{-9}$ for the coupling $g_{p\gamma}^2 P^0 A$.
- ⁶² AVIGNONE 98 result is based on the coherent conversion of solar axions to photons via the Primakoff effect in a single crystal germanium detector.
- ⁶³ Based on the conversion of solar axions to X-rays in a strong laboratory magnetic field.
- ⁶⁴ Experiment based on proposal by MAIANI 86.
- ⁶⁵ Experiment based on proposal by VANBIBBER 87.
- ⁶⁶ LAZARUS 92 experiment is based on proposal found in VANBIBBER 89.
- ⁶⁷ RUOSO 92 experiment is based on the proposal by VANBIBBER 87.
- ⁶⁸ SEMERTZIDIS 90 experiment is based on the proposal of MAIANI 86. The limit is obtained by taking the noise amplitude as the upper limit. Limits extend to $m_{A^0} = 4 \times 10^{-3}$ where $G_{A\gamma\gamma} < 1 \times 10^{-4} \text{ GeV}^{-1}$.

Limit on Invisible A^0 (Axion) Electron Coupling

The limit is for $g_{Aee} \phi_A \bar{\psi}(\gamma_5)\psi$, or equivalently, the dipole-dipole potential

$$-\frac{g_{Aee}^2}{16\pi m_{A^0}^2} ((\sigma_1 \cdot \sigma_2) - 3(\sigma_1 \cdot \mathbf{n})(\sigma_2 \cdot \mathbf{n}))/r^3 \text{ where } \mathbf{n} = \mathbf{r}/r \text{ and the sign of the potential was corrected based on DAIDO 17.}$$

VALUE	CL%	DOCUMENT ID	TECN	COMMENT
$<1.7 \times 10^{-11}$	90	1 ADHIKARI 19B	C100	Solar axions
$<2.3 \times 10^{-14}$	90	2 APRILE 19D	XE1T	$m_{A^0} = 0.186\text{--}1 \text{ keV}$
		3 DESSERT 19	ASTR	Magnetic white dwarf
$<2.6 \times 10^{-10}$	95	4 TERRANO 19		Torsion pendulum
$<1.5 \times 10^{-13}$	90	5 ABE 18F	XMAS	$m_{A^0} = 40\text{--}120 \text{ keV}$
$<1.1 \times 10^{-11}$	90	6 ARMENGAUD 18	EDE3	Solar axions
$<4 \times 10^{-13}$	90	7 ARMENGAUD 18	EDE3	$m_{A^0} = 0.8\text{--}500 \text{ keV}$
$<4.9 \times 10^{-10}$	95	8 CRESCINI 18	QUAX	$m_{A^0} = 58 \mu\text{eV}$
		9 FICEK 18	THEO	$m_{A^0} < 10 \text{ keV}$
$<4.5 \times 10^{-13}$	90	10 ABGRALL 17	HPGE	$m_{A^0} = 11.8 \text{ keV}$
$<3.5 \times 10^{-12}$	90	11 AKERIB 17B	LUX	Solar axions
$<4.2 \times 10^{-13}$	90	12 AKERIB 17B	LUX	$m_{A^0} = 1\text{--}16 \text{ keV}$
$<2.3 \times 10^{-13}$	90	13 APRILE 17B	X100	$m_{A^0} = 6 \text{ keV}$
$<4 \times 10^{-4}$	90	14 FICEK 17	THEO	$m_{A^0} < 1 \text{ keV}$
$<4.35 \times 10^{-12}$	90	15 FU 17A	PNDX	Solar axions
$<4.3 \times 10^{-14}$	90	16 FU 17A	PNDX	$m_{A^0} = 2 \text{ keV}$
$<5 \times 10^{-13}$	90	17 LIU 17A	CDEX	$m_{A^0} = 13 \text{ keV}$
$<2.5 \times 10^{-11}$	90	18 LIU 17A	CDEX	Solar axions
<0.15	95	19 LUO 17		$m_{A^0} = 300 \text{ eV}$
$<3.3 \times 10^{-13}$	68	20 BATTICH 16	ASTR	White dwarf cooling
$<7 \times 10^{-13}$		21 CORSICO 16	ASTR	White dwarf cooling
$<1.39 \times 10^{-11}$	90	22 YOON 16	KIMS	Solar axions
$<7.4 \times 10^{-9}$	95	23 TERRANO 15		$m_{A^0} < 30 \mu\text{eV}$
$<8 \times 10^{-13}$	90	24 ABE 14F	XMAS	$m_{A^0} = 60 \text{ keV}$
$<7.7 \times 10^{-12}$	90	25 APRILE 14B	X100	Solar axions
		26 APRILE 14B	X100	$m_{A^0} = 5\text{--}7 \text{ keV}$
$< 0.96\text{--}8.2 \times 10^{-8}$	90	27 DERBIN 14	CNTR	$m_{A^0} = 0.1\text{--}1 \text{ MeV}$
$<2.8 \times 10^{-13}$	99	28 MILLER-BER... 14	ASTR	White dwarf cooling
$<5.4 \times 10^{-11}$	90	29 ABE 13D	XMAS	Solar axions
$<1.07 \times 10^{-12}$	90	30 ARMENGAUD 13	EDEL	$m_{A^0} = 12.5 \text{ keV}$
$<2.59 \times 10^{-11}$	90	31 ARMENGAUD 13	EDEL	Solar axions

$< 1.4\text{--}9.7 \times 10^{-7}$	90	32 BARTH 13	CAST	Solar axions
$<1.5 \times 10^{-8}$	68	33 DERBIN 13	CNTR	$m_{A^0} = 0.1\text{--}1 \text{ MeV}$
$<4.3 \times 10^{-13}$	95	34 HECKEL 13		$m_{A^0} \leq 0.1 \mu\text{eV}$
$<7 \times 10^{-13}$	95	35 VIAUX 13A	ASTR	Low-mass red giants
$<2.2 \times 10^{-10}$	90	36 CORSICO 12	ASTR	White dwarf cooling
$<0.02\text{--}1 \times 10^{-10}$	90	37 DERBIN 12	CNTR	Solar axions
$<1.4 \times 10^{-12}$	90	38 AALSETH 11	CNTR	$m_{A^0} = 0.3\text{--}8 \text{ keV}$
$<4 \times 10^{-9}$	66	39 AHMED 09A	CDMS	$m_{A^0} = 2.5 \text{ keV}$
$<2.7 \times 10^{-8}$		40 DAVOUDIASL 09	ASTR	Earth cooling
		41 NI 94		Induced magnetism
		41 CHUI 93		Induced magnetism
$<3.6 \times 10^{-7}$	66	42 PAN 92		Torsion pendulum
$<2.9 \times 10^{-8}$	95	41 BOBRAKOV 91		Induced magnetism
$<1.9 \times 10^{-6}$	66	43 WINELAND 91	NMR	
$<7 \times 10^{-7}$	66	42 RITTER 90		Torsion pendulum
$<6.6 \times 10^{-8}$	95	41 VOROBYOV 88		Induced magnetism

¹ ADHIKARI 19B is analogous to LIU 17A.

² APRILE 19D is analogous to APRILE 17B, but they use only ionization signals. The quoted limit applies to $m_{A^0} = 0.7 \text{ keV}$. See their Fig. 5(e) for mass-dependent limits.

³ DESSERT 19 used the Suzaku observations of a magnetic white dwarf (RE J0317-853) to look for X-ray signatures converted from axions in the surrounding magnetic fields. They obtained the limit, $g_{Aee} \cdot G_{A\gamma\gamma} < 1.6 \times 10^{-24} \text{ GeV}^{-1}$ at 95%CL for $m_{A^0} \sim 10^{-5} \text{ eV}$. See their Fig. 2 for mass-dependent limits.

⁴ TERRANO 19 look for the axion-induced oscillating magnetic field acting on the electron spin, using data taken with a rotating torsion pendulum containing polarized electrons. The quoted limit applies to $m_{A^0} = 10^{-23}\text{--}10^{-18} \text{ eV}$ and assumes a local axion dark matter density, $\rho_A = 0.45 \text{ GeV}/\text{cm}^3$. See their Fig. 5 for mass-dependent limits.

⁵ ABE 18F is an update of ABE 14F. The quoted limit applies to $m_{A^0} = 60 \text{ keV}$. See their Fig. 5 for mass-dependent limits.

⁶ ARMENGAUD 18 is analogous to LIU 17A.

⁷ ARMENGAUD 18 is analogous to AHMED 09A. See the left panel of Fig. 5 for mass-dependent limits.

⁸ CRESCINI 18 look for collective excitations of the electron spins caused by dark matter axions. The quoted limit assumes the local dark matter density, $\rho_A = 0.45 \text{ GeV}/\text{cm}^3$.

⁹ FICEK 18 use the measurements of the hyperfine structure of antiprotonic helium to constrain a dipole-dipole potential between electron and antiproton. See their Fig. 3 for limits on various spin- and velocity-dependent potentials.

¹⁰ ABGRALL 17 is analogous to AHMED 09A using the MAJORANA DEMONSTRATOR. See their Fig. 2 for limits between $6 \text{ keV} < m_{A^0} < 97 \text{ keV}$.

¹¹ AKERIB 17B is analogous to LIU 17A.

¹² AKERIB 17B is analogous to AHMED 09A. See their Fig. 7 for mass-dependent limits.

¹³ APRILE 17B is analogous to AHMED 09A. They found a bug in their code and needed to correct the limits in Fig. 7 of APRILE 14B. See their Fig. 1 for the corrected limits between $1 \text{ keV} < m_{A^0} < 40 \text{ keV}$.

¹⁴ FICEK 17 look for spin-dependent interactions between electrons by comparing precision spectroscopic measurements in ^4He with theoretical calculations. See their Fig. 1 for limits up to $m_{A^0} = 10 \text{ keV}$.

¹⁵ FU 17A is analogous to LIU 17A. See their Fig. 3 for mass-dependent limits.

¹⁶ FU 17A is analogous to AHMED 09A. See their Fig. 4 for mass-dependent limits.

¹⁷ LIU 17A is analogous to AHMED 09A. See their Fig. 9 for limits between $0.25 \text{ keV} < m_{A^0} < 20 \text{ keV}$.

¹⁸ LIU 17A look for solar axions produced from Compton, bremsstrahlung, atomic-recombination and deexcitation channels, and set a limit for $m_{A^0} < 1 \text{ keV}$.

¹⁹ LUO 17 use a recent measurement of the dipole-dipole interaction between two iron atoms at the nanometer scale and set a limit for $m_{A^0} < 1 \text{ keV}$. See their Fig. 3 for mass-dependent limits.

²⁰ BATTICH 16 is analogous to CORSICO 16 and used the pulsating DB white dwarf PG 1351+489.

²¹ CORSICO 16 studied the cooling rate of the pulsating DA white dwarf L19-2 based on an asteroseismic model.

²² YOON 16 look for solar axions with the axio-electric effect in CsI(Tl) crystals and set a limit for $m_{A^0} < 1 \text{ keV}$.

²³ TERRANO 15 used a torsion pendulum and rotating attractor with 20-pole electron-spin distributions. See their Fig. 4 for a mass-dependent limit up to $m_{A^0} = 500 \mu\text{eV}$.

²⁴ ABE 14F set limits on the axioelectric effect in the XMAS detector assuming the pseudoscalar constitutes all the local dark matter. See their Fig. 3 for limits between $m_{A^0} = 40\text{--}120 \text{ keV}$.

²⁵ APRILE 14B look for solar axions using the XENON100 detector.

²⁶ APRILE 14B is analogous to AHMED 09A. Their Fig. 7 was later found to be incorrect due to a bug in their code. See Fig. 1 in APRILE 17B for the corrected limits.

²⁷ DERBIN 14 is an update of DERBIN 13 with a BGO scintillating bolometer. See their Fig. 3 for mass-dependent limits.

²⁸ MILLER-BERTOLAMI 14 studied the impact of axion emission on white dwarf cooling in a self-consistent way.

²⁹ ABE 13D is analogous to DERBIN 12, using the XMAS detector.

³⁰ ARMENGAUD 13 is similar to AALSETH 11. See their Fig. 10 for limits between $3 \text{ keV} < m_{A^0} < 100 \text{ keV}$.

³¹ ARMENGAUD 13 is similar to DERBIN 12, and take account of axio-recombination and axio-deexcitation effects. See their Fig. 12 for mass-dependent limits.

³² BARTH 13 search for solar axions produced by axion-electron coupling, and obtained the limit, $g_{Aee} \cdot G_{A\gamma\gamma} < 8.1 \times 10^{-23} \text{ GeV}^{-1}$ at 95%CL.

³³ DERBIN 13 looked for 5.5 MeV solar axions produced in $p\bar{d} \rightarrow ^3\text{He} A^0$ in a BGO detector through the axioelectric effect. See their Fig. 4 for mass-dependent limits.

³⁴ HECKEL 13 studied the influence of 2 or 4 stationary sources each containing 6.0×10^{24} polarized electrons, on a rotating torsion pendulum containing 9.8×10^{24} polarized electrons. See their Fig. 4 for mass-dependent limits.

35 VIAUX 13A constrain axion emission using the observed brightness of the tip of the red-giant branch in the globular cluster M5.
 36 CORSICO 12 attributed the excessive cooling rate of the pulsating white dwarf R548 to emission of axions with $g_{Aee} \simeq 4.8 \times 10^{-13}$.
 37 DERBIN 12 look for solar axions with the axio-electric effect in a Si(Li) detector. The solar production is based on Compton and bremsstrahlung processes.
 38 AALSETH 11 is analogous to AHMED 09A. See their Fig. 4 for mass-dependent limits.
 39 AHMED 09A assume keV-mass pseudoscalars are the local dark matter and constrain the axio-electric effect in the CDMS detector. See their Fig. 5 for mass-dependent limits.
 40 DAVOUDIASL 09 use geophysical constraints on Earth cooling by axion emission.
 41 These experiments measured induced magnetization of a bulk material by the spin-dependent potential generated from other bulk material with aligned electron spins, where the magnetic field is shielded with superconductor. The sign of the limit set by CHUI 93 is opposite to that of the axion-mediated dipole-dipole potential.
 42 These experiments used a torsion pendulum to measure the potential between two bulk matter objects where the spins are polarized but without a net magnetic field in either of them. The limits reflect the corrected sign of the dipole-dipole potential.
 43 WINELAND 91 looked for an effect of bulk matter with aligned electron spins on atomic hyperfine splitting using nuclear magnetic resonance.

Invisible A^0 (Axion) Limits from Nucleon Coupling

Limits are for the axion mass in eV.

VALUE (eV)	CL%	DOCUMENT ID	TECN	COMMENT
••• We do not use the following data for averages, fits, limits, etc. •••				
< 0.03		1 LEINSON 19	ASTR	Neutron star cooling
< 9.6×10^{-3}	95	2 LLOYD 19	ASTR	γ -rays from NS
		3 SMORRA 19	19	\bar{p} g-factor
		4 WU 19	NMR	Axion dark matter
< 65	95	5 AKHMATOV 18	CNTR	Solar axion
< 6.6	90	6 ARMENGAUD 18	EDE3	Solar axion
< 0.085	90	7 BEZNOGOV 18	ASTR	Neutron star cooling
< 12.7	95	8 GAVRILYUK 18	CNTR	Solar axion
< 0.01		9 HAMAGUCHI 18	ASTR	Neutron star cooling
		10 ABEL 17		Neutron EDM
< 93	90	11 ABGRALL 17	HPGE	Solar axion
< 4	90	12 FU 17A	PNDX	Solar axion
		13 KLIMCHITSK...17A		Casimir effect
<177	90	14 LIU 17A	CDEX	Solar axion
< 0.079	95	15 BERENJI 16	ASTR	γ -rays from NS
<100	95	16 GAVRILYUK 15	CNTR	Solar axion
		17 KLIMCHITSK...15		Casimir-less
		18 BEZERRA 14		Casimir effect
		19 BEZERRA 14A		Casimir effect
		20 BEZERRA 14B		Casimir effect
		21 BEZERRA 14C		Casimir effect
		22 BLUM 14	COSM	^4He abundance
		23 LEINSON 14	ASTR	Neutron star cooling
<250	95	24 ALESSANDRIA 13	CNTR	Solar axion
<155	90	25 ARMENGAUD 13	EDEL	Solar axion
< 8.6×10^3	90	26 BELLI 12	CNTR	Solar axion
< 1.4×10^4	90	27 BELLINI 12B	BORX	Solar axion
<145	95	28 DERBIN 11	CNTR	Solar axion
		29 BELLINI 08	CNTR	Solar axion
		30 ADELBERGER 07		Test of Newton's law

1 LEINSON 19 is analogous to BEZNOGOV 18, but estimating the axion luminosity based on the Tolman's analytic solution to the Einstein equations of spherical fluids in hydrostatic equilibrium. The dimensionless axion-neutron coupling is constrained as $g_{ANN} < 1.0 \times 10^{-10}$.
 2 LLOYD 19 is analogous to BERENJI 16. They highlight that the limit obtained with this technique strongly depends on the assumed NS core temperature.
 3 SMORRA 19 look for spin-precession effects from ultra-light axion dark matter in the \bar{p} spin-flip resonance data. Assuming $\rho_A = 0.4 \text{ GeV/cm}^3$, they constrain the dimensionless axion-antiproton coupling as $g_{A\bar{p}p} < 2-9$ at 95% CL for $m_{A^0} = 2 \times 10^{-23}-4 \times 10^{-17} \text{ eV}$. See the right panel of their Fig. 3.
 4 WU 19 look for axion-induced time-oscillating features of the NMR spectrum of acetonitrile- d_3 . Assuming $C_p = C_n$ and $\rho_A = 0.4 \text{ GeV/cm}^3$, they constrain the dimensionless axion-nucleon coupling as $g_{ANN} < 6 \times 10^{-5}$ for $m_{A^0} = 10^{-21}-1.3 \times 10^{-17} \text{ eV}$. Note that the limits for $m_{A^0} < 10^{-21} \text{ eV}$ in their Fig. 3(a) should be weaker than those for heavier masses. See ADELBERGER 19 and WU 19c on this issue.
 5 AKHMATOV 18 is an update of GAVRILYUK 15.
 6 ARMENGAUD 18 is analogous to ALESSANDRIA 13. The quoted limit assumes the DFSZ axion model. See their Fig. 4 for the limit on product of axion couplings to electrons and nucleons.
 7 BEZNOGOV 18 constrain the axion-neutron coupling by assuming that thermal evolution of the hot neutron star HESS J1731-347 is dominated by the lowest possible neutrino emission. The quoted limit assumes the KSVZ axion with the effective Peccei-Quinn charge of the neutron $C_n = -0.02$. The dimensionless axion-neutron coupling is constrained as $g_{ANN} < 2.8 \times 10^{-10}$.
 8 GAVRILYUK 18 look for the resonant excitation of ^{83}Kr (9.4 keV) by solar axions produced via the Primakoff effect. The mass bound assumes $m_H/m_d = 0.56$ and $S = 0.5$.
 9 HAMAGUCHI 18 studied the axion emission from the neutron star in Cassiopeia A based on the minimal cooling scenario which explains the observed rapid cooling rate. The quoted limit corresponds to $f_A > 5 \times 10^8 \text{ GeV}$ obtained for the KSVZ axion with $C_p = -0.47$ and $C_n = -0.02$.

10 ABEL 17 look for a time-oscillating neutron EDM and an axion-wind spin-precession effect respectively induced by axion dark matter couplings to gluons and nucleons. See their Fig. 4 for limits in the range of $m_{A^0} = 10^{-24}-10^{-17} \text{ eV}$.
 11 ABGRALL 17 limit assumes the hadronic axion model used in ALESSANDRIA 13. See their Fig. 4 for the limit on product of axion couplings to electrons and nucleons.
 12 FU 17A look for the 14.4 keV ^{57}Fe solar axions. The limit assumes the DFSZ axion model. See their Fig. 3 for mass-dependent limits on the axion-electron coupling. Notice that in this figure the DFSZ and KSVZ lines should be interchanged.
 13 KLIMCHITSKAYA 17A use the differential measurement of the Casimir force between a Ni-coated sphere and Au and Ni sectors of the structured disc to constrain the axion coupling to nucleons for $2.61 \text{ meV} < m_{A^0} < 0.9 \text{ eV}$. See their Figs. 1 and 2 for mass dependent limits.
 14 LIU 17 is analogous to ALESSANDRIA 13. The limit assumes the hadronic axion model. See their Fig. 6(b) for the limit on product of axion couplings to electrons and nucleons.
 15 BERENJI 16 used the Fermi LAT observations of neutron stars to look for photons from axion decay. They assume the effective Peccei-Quinn charge of the neutron $C_n = 0.1$ and a neutron-star core temperature of 20 MeV.
 16 GAVRILYUK 15 look for solar axions emitted by the M1 transition of ^{83}Kr (9.4 keV). The mass bound assumes $m_H/m_d = 0.56$ and $S = 0.5$.
 17 KLIMCHITSKAYA 15 use the measurement of differential forces between a test mass and rotating source masses of Au and Si to constrain the force due to two-axion exchange for $1.7 \times 10^{-3} < m_{A^0} < 0.9 \text{ eV}$. See their Figs. 1 and 2 for mass dependent limits.
 18 BEZERRA 14 use the measurement of the thermal Casimir-Polder force between a Bose-Einstein condensate of ^{87}Rb atoms and a SiO_2 plate to constrain the force mediated by exchange of two pseudoscalars for $0.1 \text{ meV} < m_{A^0} < 0.3 \text{ eV}$. See their Fig. 2 for the mass-dependent limit on pseudoscalar coupling to nucleons.
 19 BEZERRA 14A is analogous to BEZERRA 14. They use the measurement of the Casimir pressure between two Au-coated plates to constrain pseudoscalar coupling to nucleons for $1 \times 10^{-3} \text{ eV} < m_{A^0} < 15 \text{ eV}$. See their Figs. 1 and 2 for the mass-dependent limit.
 20 BEZERRA 14B is analogous to BEZERRA 14. BEZERRA 14B use the measurement of the normal and lateral Casimir forces between sinusoidally corrugated surfaces of a sphere and a plate to constrain pseudoscalar coupling to nucleons for $1 \text{ eV} < m_{A^0} < 20 \text{ eV}$. See their Figs. 1-3 for mass-dependent limits.
 21 BEZERRA 14C is analogous to BEZERRA 14. They use the measurement of the gradient of the Casimir force between Au- and Ni-coated surfaces of a sphere and a plate to constrain pseudoscalar coupling to nucleons for $3 \times 10^{-5} \text{ eV} < m_{A^0} < 1 \text{ eV}$. See their Figs. 1, 3, and 4 for the mass-dependent limits.
 22 BLUM 14 studied effects of an oscillating strong CP phase induced by axion dark matter on the primordial ^4He abundance. See their Fig. 1 for mass-dependent limits.
 23 LEINSON 14 attributes the excessive cooling rate of the neutron star in Cassiopeia A to axion emission from the superfluid core, and found $C_n^2 m_{A^0}^2 \simeq 5.7 \times 10^{-6} \text{ eV}^2$, where C_n is the effective Peccei-Quinn charge of the neutron.
 24 ALESSANDRIA 13 used the CUORE experiment to look for 14.4 keV solar axions produced from the M1 transition of thermally excited ^{57}Fe nuclei in the solar core, using the axio-electric effect. The limit assumes the hadronic axion model. See their Fig. 4 for the limit on product of axion couplings to electrons and nucleons.
 25 ARMENGAUD 13 is analogous to ALESSANDRIA 13. The limit assumes the hadronic axion model. See their Fig. 8 for the limit on product of axion couplings to electrons and nucleons.
 26 BELLI 12 looked for solar axions emitted by the M1 transition of $^7\text{Li}^*$ (478 keV) after the electron capture of ^7Be , using the resonant excitation ^7Li in the LiF crystal. The mass bound assumes $m_H/m_d = 0.55$, $m_H/m_S = 0.029$, and the flavor-singlet axial vector matrix element $S = 0.4$.
 27 BELLINI 12B looked for 5.5 MeV solar axions produced in the $p d \rightarrow ^3\text{He} A^0$. The limit assumes the hadronic axion model. See their Figs. 6 and 7 for mass-dependent limits on product of axion couplings to photons, electrons, and nucleons.
 28 DERBIN 11 looked for solar axions emitted by the M1 transition of thermally excited ^{57}Fe nuclei in the Sun, using their possible resonant capture on ^{57}Fe in the laboratory. The mass bound assumes $m_H/m_d = 0.56$ and the flavor-singlet axial vector matrix element $S = 3F - D \simeq 0.5$.
 29 BELLINI 08 consider solar axions emitted in the M1 transition of $^7\text{Li}^*$ (478 keV) and look for a peak at 478 keV in the energy spectra of the Counting Test Facility (CTF), a Borexino prototype. For $m_{A^0} < 450 \text{ keV}$ they find mass-dependent limits on products of axion couplings to photons, electrons, and nucleons.
 30 ADELBERGER 07 use precision tests of Newton's law to constrain a force contribution from the exchange of two pseudoscalars. See their Fig. 5 for limits on the pseudoscalar coupling to nucleons, relevant for m_{A^0} below about 1 meV.

Axion Limits from T-violating Medium-Range Forces

The limit is for the coupling $g = g_p g_s$ in a T-violating potential between nucleons or nucleon and electron of the form $V = \frac{g_p^2}{8\pi m_p} (\boldsymbol{\sigma} \cdot \boldsymbol{r}) \left(\frac{1}{r^2} + \frac{1}{\lambda r} \right) e^{-r/\lambda}$, where g_p and g_s are dimensionless scalar and pseudoscalar coupling constants and $\lambda = \hbar/(m_A c)$ is the range of the force.

VALUE	DOCUMENT ID	TECN	COMMENT
••• We do not use the following data for averages, fits, limits, etc. •••			
	1 DZUBA 18	THEO	atomic EDM
	2 STADNIK 18	THEO	atomic and molecular EDMs
	3 CRESCINI 17	SQID	paramagnetic GSO crystal
	4 AFACH 15		ultracold neutrons
	5 STADNIK 15	THEO	nucleon spin contributions for nuclei
	6 TERRANO 15		torsion pendulum
	7 BULATOWICZ 13	NMR	polarized ^{129}Xe and ^{131}Xe
	8 CHU 13		polarized ^3He
	9 TULLNEY 13	SQID	polarized ^3He and ^{129}Xe
	10 RAFFELT 12		stellar energy loss
	11 HOEDL 11		torsion pendulum
	12 PETUKHOV 10		polarized ^3He

See key on page 999

Gauge & Higgs Boson Particle Listings
Axions (A^0) and Other Very Light Bosons

- <1 $\times 10^{-3}$ 90 64 ABRAHAMY... 11 $m_{\gamma'}$ = 175–250 MeV
- <9 $\times 10^{-8}$ 95 65 BLUEMLEIN 11 BDMP $m_{\gamma'}$ = 70 MeV
- <1 $\times 10^{-7}$ 66 BJORKEN 09 BDMP $m_{\gamma'}$ = 2–400 MeV
- <5 $\times 10^{-9}$ 67 BJORKEN 09 ASTR $m_{\gamma'}$ = 2–50 MeV
- 1 AAIJ 20c look for hidden photons produced from the pp collision in the decay channel $\gamma' \rightarrow \mu^+ \mu^-$. For prompt decaying hidden photons, limits at the level of 10^{-4} – 10^{-3} are obtained for $m_{\gamma'} = 0.214$ –30 GeV. See their Fig. 2 for mass-dependent limits.
- 2 AAIJ 20c look for hidden photons produced from the pp collision in the decay channel $\gamma' \rightarrow \mu^+ \mu^-$. For hidden photons with lifetimes of order ps, limits at the level of 10^{-5} are obtained for $m_{\gamma'} = 218$ –315 MeV. See their Fig. 4 for mass-dependent limits.
- 3 AABOUD 19g look for $h \rightarrow \gamma' \gamma'$ ($\gamma' \rightarrow \mu^+ \mu^-$) and exclude a kinetic mixing around 10^{-9} – 10^{-8} for $B(h \rightarrow \gamma' \gamma') = 0.01$ and 0.1. See their Fig. 9 for mass-dependent limits.
- 4 ABLIKIM 19A look for $J/\psi \rightarrow \gamma' \eta$ ($\gamma' \rightarrow e^+ e^-$). Limits between 6×10^{-3} and 5×10^{-2} are obtained (see their Fig. 8).
- 5 ABLIKIM 19H look for $J/\psi \rightarrow \gamma' \eta'$ ($\gamma' \rightarrow e^+ e^-$). Limits between 3.4×10^{-3} and 2.6×10^{-2} are obtained. See their Fig. 5 for mass-dependent limits.
- 6 AGUILAR-AREVALO 19A look for the absorption signal of hidden photon dark matter by using a CCD. The quoted limit applies to $m_{\gamma'} = 17$ eV. The local density $\rho_{\gamma'} = 0.3$ GeV/cm³ is assumed. See their Fig. 4 for mass-dependent limits.
- 7 APRILE 19D is analogous to ABE 14F. The quoted limit applies to $m_{\gamma'} = 0.7$ keV. See their Fig. 5(f) for mass-dependent limits.
- 8 BANERJEE 19 is an update of BANERJEE 18A. The quoted limit is at $m_{\gamma'} = 1$ MeV. See their Fig. 3 for mass-dependent limits.
- 9 BHONAH 19 examine heating of Galactic Center gas clouds by hidden photon dark matter. The quoted limit applies to $m_{\gamma'} \simeq 10^{-12}$ eV. See their Fig. 2 for mass-dependent limits.
- 10 BRUN 19 is analogous to SUZUKI 15. The limit is derived under an assumption that hidden photons constitute the local dark matter density $\rho_{\gamma'} = 0.3$ GeV/cm³.
- 11 CORTINA-GIL 19 look for an invisible hidden photon in the reaction $K^+ \rightarrow \pi^+ \pi^0$ ($\pi^0 \rightarrow \gamma \gamma'$). The quoted limit applies to $m_{\gamma'} = 62.5$ –65 MeV. See their Figs. 6 and 7 for mass-dependent limits.
- 12 DANILOV 19 examined the hidden photon production in nuclear reactors, correctly taking account of the effective photon mass in the reactor and detector. The limit gets weaker for $m_{\gamma'}$ less than the effective photon mass in proportion to $1/m_{\gamma'}^2$. See their Fig. 1 for mass-dependent limits.
- 13 HOCHBERG 19 look for the absorption signal of hidden photon dark matter by using superconducting-nanowire single-photon detectors. The quoted limit applies to $m_{\gamma'} \simeq 1$ eV. The local density $\rho_{\gamma'} = 0.3$ GeV/cm³ is assumed. See their Fig. 4 for mass-dependent limits.
- 14 KOPYLOV 19 look for hidden-photon dark matter using a counter with an aluminum cathode and derive limits assuming it constitute all the local dark matter. The quoted limit applies to $m_{\gamma'} = 12$ eV. See their Fig. 7 for mass-dependent limits.
- 15 KOVETZ 19 examine heating of the early Universe plasma by hidden photon dark matter, and derive the limits by requiring that the cosmic mean 21 cm brightness temperature relative to the CMB temperature satisfy $T_{21} > -100$ mK. The quoted limit applies to $m_{\gamma'} \simeq 2 \times 10^{-14}$ eV. See their Fig. 3 for mass-dependent limits.
- 16 NGUYEN 19 look for hidden photon dark matter with a resonant cavity, and set limits $\sim 10^{-12}$ for $m_{\gamma'} = 0.2$ –2.07 μ eV. The quoted limit applies to $m_{\gamma'} = 1.3$ μ eV. The local density $\rho_{\gamma'} = 0.3$ GeV/cm³ is assumed. See their Fig. 19 for mass-dependent limits.
- 17 ABE 18f is an update of ABE 14f. The quoted limit applies to $m_{\gamma'} \simeq 40$ keV. See their Fig. 5 for mass-dependent limits.
- 18 ADRIAN 18 look for a hidden photon resonance in the reaction $e^- Z \rightarrow e^- Z \gamma'$ ($\gamma' \rightarrow e^+ e^-$). The quoted limit applies to $m_{\gamma'} = 40$ MeV. See their Fig. 4 for mass-dependent limits.
- 19 ANASTASI 18b look for a hidden photon resonance in the reaction $e^+ e^- \rightarrow \gamma' \gamma$ ($\gamma' \rightarrow \mu^+ \mu^-$). The quoted limit is obtained by combining the result of ANASTASI 16 and it applies to $m_{\gamma'} \simeq 519$ –987 MeV. See their Fig. 9 for mass-dependent limits.
- 20 ARMENGAUD 18 is analogous to ABE 14f. The quoted limits applies to $m_{\gamma'} = 1.6$ keV. See the right panel of Fig. 5 for mass-dependent limits.
- 21 BANERJEE 18 look for hidden photons produced in the reaction $e^- Z \rightarrow e^- Z \gamma'$ ($\gamma' \rightarrow e^+ e^-$), and exclude $9.2 \times 10^{-5} \lesssim \chi \lesssim 1 \times 10^{-2}$ for $m_{\gamma'} = 1$ –23 MeV. They also set a limit on the electron coupling to a 16.7 MeV gauge boson suggested by the ATOMKI (KRASZNAHORKAY 16) experiment. See their Fig. 3 for mass-dependent limits.
- 22 BANERJEE 18A look for invisible decays of hidden photons produced in the reaction $e^- Z \rightarrow e^- Z \gamma'$. The quoted limit is at $m_{\gamma'} = 1$ MeV. See their Fig. 15 for mass-dependent limits.
- 23 KNIRCK 18 is analogous to SUZUKI 15. See their Fig. 5 for mass-dependent limits.
- 24 ABRALL 17 is analogous to ABE 14f using the MAJORANA DEMONSTRATOR. See their Fig. 3 for limits between 6 keV < $m_{\gamma'} < 97$ keV.
- 25 ABLIKIM 17AA look for $e^+ e^- \rightarrow \gamma \gamma'$ ($\gamma' \rightarrow e^+ e^-$ or $\mu^+ \mu^-$). Limits between 10^{-3} and 10^{-4} are obtained (see their Fig. 3).
- 26 ANGLÖHER 17 is analogous to ABE 14f. The quoted limit is at $m_{\gamma'} = 0.7$ keV. See their Fig. 8 for mass-dependent limits.
- 27 BANERJEE 17 look for invisible decays of hidden photons produced in the reaction $e^- Z \rightarrow e^- Z \gamma'$. The quoted limit applies to $m_{\gamma'} = 2$ MeV. See their Fig. 3 for mass-dependent limits.
- 28 CHANG 17 examine the hidden photon emission from SN1987A, including the effects of finite temperature and density on χ and obtain limits χ ($m_{\gamma'}/\text{MeV}$) $\lesssim 3 \times 10^{-9}$ for $m_{\gamma'} < 15$ MeV and $\chi \lesssim 10^{-9}$ for $m_{\gamma'} = 15$ –120 MeV.
- 29 DUBININA 17 look for $\mu^+ \rightarrow e^+ \bar{\nu}_\mu \nu_e \gamma'$ ($\gamma' \rightarrow e^+ e^-$) in a nuclear photoemulsion. The quoted limit applies to $m_{\gamma'} = 1.1$ MeV. Limits between 4.5×10^{-3} and 10^{-2} are obtained (see their Fig. 3).
- 30 LEES 17E look for invisible decays of hidden photons produced in the reaction $e^+ e^- \rightarrow \gamma \gamma'$. See their Fig. 5 for limits in the mass range $m_{\gamma'} \leq 8$ GeV.
- 31 AAD 16AG look for hidden photons promptly decaying into collimated electrons and/or muons, assuming that they are produced in the cascade decays of squarks or the Higgs boson. See their Fig. 10 and Fig.13 for their limits on the cross section times branching fractions.
- 32 ANASTASI 16 look for the decay $\gamma' \rightarrow \pi^+ \pi^-$ in the reaction $e^+ e^- \rightarrow \gamma \gamma'$. Limits between 4.3×10^{-3} and 4.4×10^{-4} are obtained for $527 < m_{\gamma'} < 987$ MeV (see their Fig. 9).
- 33 KHACHATRYAN 16 look for $\gamma' \rightarrow \mu^+ \mu^-$ in a dark SUSY scenario where the SM-like Higgs boson decays into a pair of the visible lightest neutralinos with mass 10 GeV, both of which decay into γ' and a hidden neutralino with mass 1 GeV. See the right panel in their Fig. 2.
- 34 AAD 15CD look for $H \rightarrow Z \gamma' \rightarrow 4\ell$ with the ATLAS detector at LHC and find $\chi < 4$ – 17×10^{-2} for $m_{\gamma'} = 15$ –55 GeV. See their Fig. 6.
- 35 ADARE 15 look for a hidden photon in $\pi^0, \eta^0 \rightarrow \gamma e^+ e^-$ at the PHENIX experiment. See their Fig. 4 for mass-dependent limits.
- 36 AN 15A derived limits from the absence of ionization signals in the XENON10 and XENON100 experiments, assuming hidden photons constitute all the local dark matter. Their best limit is $\chi < 1.3 \times 10^{-15}$ at $m_{\gamma'} = 18$ eV. See their Fig. 1 for mass-dependent limits.
- 37 ANASTASI 15 look for a production of a hidden photon and a hidden Higgs boson with the KLOE detector at DAΦNE, where the hidden photon decays into a pair of muons and the hidden Higgs boson lighter than $m_{\gamma'}$ escape detection. See their Figs. 6 and 7 for mass-dependent limits on a product of the hidden fine structure constant and the kinetic mixing.
- 38 ANASTASI 15A look for the decay $\gamma' \rightarrow e^+ e^-$ in the reaction $e^+ e^- \rightarrow e^+ e^- \gamma$. Limits between 1.7×10^{-3} and 1×10^{-2} are obtained for $m_{\gamma'} = 5$ –320 MeV (see their Fig. 7).
- 39 BATLEY 15A look for $\pi^0 \rightarrow \gamma \gamma'$ ($\gamma' \rightarrow e^+ e^-$) at the NA48/2 experiment. Limits between 4.2×10^{-4} and 8.8×10^{-3} are obtained for $m_{\gamma'} = 9$ –120 MeV (see their Fig. 4).
- 40 JAEGLER 15 look for the decay $\gamma' \rightarrow e^+ e^-, \mu^+ \mu^-,$ or $\pi^+ \pi^-$ in the dark Higgsstrahlung channel, $e^+ e^- \rightarrow \gamma' H'$ ($H' \rightarrow \gamma' \gamma'$) at the BELLE experiment. They set limits on a product of the branching fraction and the Born cross section as well as a product of the hidden fine structure constant and the kinetic mixing. See their Figs. 3 and 4.
- 41 KAZANAS 15 set limits by studying the decay of hidden photons $\gamma' \rightarrow e^+ e^-$ inside and near the progenitor star of SN1987A. See their Fig. 6 for mass-dependent limits.
- 42 SUZUKI 15 looked for hidden-photon dark matter with a dish antenna and derived limits assuming they constitute all the local dark matter. Their limits are $\chi < 6 \times 10^{-12}$ for $m_{\gamma'} = 1.9$ –4.3 eV. See their Fig. 7 for mass-dependent limits.
- 43 VINOLES 15 performed a global fit analysis based on helioseismology and solar neutrino observations, and set the limits $\chi m_{\gamma'} < 1.8 \times 10^{-12}$ eV for $m_{\gamma'} = 3 \times 10^{-5}$ –8 eV. See their Fig. 11.
- 44 ABE 14f look for the photoelectric-like interaction in the XMASS detector assuming the hidden photon constitutes all the local dark matter. Limits between 2×10^{-13} and 1×10^{-12} are obtained, where the relation $\chi^2 = \alpha'/\alpha$ is used to translate the original bound on the ratio of the hidden and EM fine-structure constants. See their Fig. 3 for mass-dependent limits.
- 45 AGA KISHIEV 14 look for hidden photons $\gamma' \rightarrow e^+ e^-$ at the HADES experiment, and set limits on χ for $m_{\gamma'} = 0.02$ –0.6 GeV. See their Fig. 5 for mass-dependent limits.
- 46 BABUSCI 14 look for the decay $\gamma' \rightarrow \mu^+ \mu^-$ in the reaction $e^+ e^- \rightarrow \mu^+ \mu^- \gamma$. Limits between 4×10^{-3} and 9.0×10^{-4} are obtained for 520 MeV < $m_{\gamma'} < 980$ MeV (see their Fig. 7).
- 47 BATELL 14 derived limits from the electron beam dump experiment at SLAC (E-137) by searching for events with recoil electrons by sub-GeV dark matter produced from the decay of the hidden photon. Limits at the level of 10^{-4} – 10^{-1} are obtained for $m_{\gamma'} = 10^{-3}$ –1 GeV, depending on the dark matter mass and the hidden gauge coupling (see their Fig. 2).
- 48 BLUEMLEIN 14 analyzed the beam dump data taken at the U-70 accelerator to look for γ' -bremsstrahlung and the subsequent decay into muon pairs and hadrons. See their Fig. 4 for mass-dependent excluded region.
- 49 FRADETTE 14 studied effects of decay of relic hidden photons on BBN and CMB to set constraints on very small values of the kinetic mixing. See their Figs. 4 and 7 for mass-dependent excluded regions.
- 50 LEES 14I look for hidden photons in the reaction $e^+ e^- \rightarrow \gamma \gamma'$ ($\gamma' \rightarrow e^+ e^-, \mu^+ \mu^-$). Limits at the level of 10^{-4} – 10^{-3} are obtained for 0.02 GeV < $m_{\gamma'} < 10.2$ GeV. See their Fig. 4 for mass-dependent limits.
- 51 MERKEL 14 look for $\gamma' \rightarrow e^+ e^-$ at the A1 experiment at the Mainz Microtron (MAMI). See their Fig. 3 for mass-dependent limits.
- 52 AN 13B examined the stellar production of hidden photons, correcting an important error of the production rate of the longitudinal mode which now dominates. See their Fig. 2 for mass-dependent limits based on solar energy loss.
- 53 AN 13c use the solar flux of hidden photons to set a limit on the atomic ionization rate in the XENON10 experiment. They find $\chi m_{\gamma'} < 3 \times 10^{-12}$ eV for $m_{\gamma'} < 1$ eV. See their Fig. 2 for mass-dependent limits.
- 54 DIAMOND 13 analyzed the beam dump data taken at the SLAC millicharge experiment to constrain a hidden photon invisibly decaying into lighter long-lived particles, which undergo elastic scattering off nuclei in the detector. Limits between 8×10^{-4} – 2×10^{-2}

See key on page 999

Gauge & Higgs Boson Particle Listings
Axions (A⁰) and Other Very Light Bosons

Table listing particle experiments and collaborations. Columns include author names, publication details (journal, volume, page, year), and collaboration names. Entries range from GANDO 12 PR C86 021601 to AMSLER 94B PL B333 271.

Downloaded from https://academic.oup.com/ptep/article/2018/08/30/15891211 by guest on 20 August 2020

Gauge & Higgs Boson Particle Listings

Axions (A^0) and Other Very Light Bosons

MAIER	87	ZPHY A326 527	K. Maier <i>et al.</i>	(STUT, GSI)	DATAR	82	PL 114B 63	V.M. Datar <i>et al.</i>	(BHAB)
MILLS	87	PR D36 707	A.P. Mills, J. Levy	(BELL)	EDWARDS	82	PRL 48 903	C. Edwards <i>et al.</i>	(Crystal Ball Collab.)
RAFFELT	87	PR D36 2211	G.G. Raffelt, D.S.P. Dearborn	(LLL, UCB)	FETSCHER	82	JP G8 L147	W. Fetscher	(ETH)
RIORDAN	87	PRL 59 755	E.M. Riordan <i>et al.</i>	(ROCH, CIT+)	FUKUGITA	82	PRL 48 1522	M. Fukugita, S. Watamura, M. Yoshimura	(KEK)
TURNER	87	PRL 59 2489	M.S. Turner	(FNAL, EFI)	FUKUGITA	82B	PR D26 1840	M. Fukugita, S. Watamura, M. Yoshimura	(KEK)
VANBIBBER	87	PRL 59 759	K. van Bibber <i>et al.</i>	(LLL, CIT, MIT+)	LEHMANN	82	PL 115B 270	P. Lehmann <i>et al.</i>	(SACL)
VONWIMMER	87	PRL 59 266	U. von Wimmersperg <i>et al.</i>	(WITW)	RAFFELT	82	PL 119B 323	G. Raffelt, L. Stodolsky	(MPIM)
BADIER	86	ZPHY C31 21	J. Badier <i>et al.</i>	(NA3 Collab.)	ZEHNDER	82	PL 110B 419	A. Zehnder, K. G��bath��ler, J.L. Vuilleumier	(ETH+)
BROWN	86	PRL 57 2101	C.N. Brown <i>et al.</i>	(FNAL, WASH, KYOT+)	ASANO	81B	PL 107B 159	Y. Asano <i>et al.</i>	(KEK, TOKY, INUS, OSAK)
BRYMAN	86B	PRL 57 2787	D.A. Bryman, E.T.H. Clifford	(TRIUM)	BARROSO	81	PL 106B 91	A. Barroso, N.C. Mukhopadhyay	(SIN)
DAVIER	86	PL B180 295	M. Davier, J. Jeanjean, H. Nguyen Ngoc	(LALO)	FAISSNER	81	ZPHY C10 95	H. Faissner <i>et al.</i>	(AACH3)
DEARBORN	86	PRL 56 26	D.S.P. Dearborn, D.N. Schramm, G. Steigman	(LLL+)	FAISSNER	81B	PL 103B 234	H. Faissner <i>et al.</i>	(AACH3)
EICHLER	86	PL B175 101	R.A. Eichler <i>et al.</i>	(SINDRUM Collab.)	KIM	81	PL 105B 55	B.R. Kim, C. Stamm	(AACH3)
HALLIN	86	PRL 57 2105	A.L. Hallin <i>et al.</i>	(PRIN)	VUILLEUMIER	81	PL 101B 341	J.L. Vuilleumier <i>et al.</i>	(CIT, MUNI)
JODIDIO	86	PR D34 1967	A. Jodidio <i>et al.</i>	(LBL, NWES, TRIU)	ZEHNDER	81	PL 104B 494	A. Zehnder	(ETH)
Also		PR D37 237 (erratum)	A. Jodidio <i>et al.</i>	(LBL, NWES, TRIU)	FAISSNER	80	PL 96B 201	H. Faissner <i>et al.</i>	(AACH3)
KETOV	86	JETPL 44 146	S.N. Ketov <i>et al.</i>	(KIAE)	JACQUES	80	PR D21 1206	P.F. Jacques <i>et al.</i>	(RUTG, STEV, COLU)
		Translated from ZETFP 44 114			SOUKAS	80	PRL 44 564	A. Soukas <i>et al.</i>	(BNL, HARV, ORNL, PENN)
KOCH	86	NC 96A 182	H.R. Koch, O.W.B. Schult	(JULI)	BECHIS	79	PRL 42 1511	D.J. Bechis <i>et al.</i>	(UMD, COLU, AFRR)
KONAKA	86	PRL 57 659	A. Konaka <i>et al.</i>	(KYOT, KEK)	CALAPRICE	79	PR D20 2708	F.P. Calaprice <i>et al.</i>	(PRIN)
MAIANI	86	PL B175 359	L. Maiani, R. Petronzio, E. Zavattini	(CERN)	COTEUS	79	PRL 42 1438	P. Coteus <i>et al.</i>	(COLU, ILL, BNL)
PECCCI	86	PL B172 435	R.D. Peccci, T.T. Wu, T. Yanagida	(DESY)	DISHAW	79	PL 85B 142	J.P. Dishaw <i>et al.</i>	(SLAC, CIT)
RAFFELT	86	PR D33 897	G.G. Raffelt	(MPIM)	ZHITNITSKII	79	SJNP 29 517	A.R. Zhitnitsky, Y.I. Skovpen	(NOVO)
RAFFELT	86B	PL 166B 402	G.G. Raffelt	(MPIM)			Translated from YAF 29 1001		
SAVAGE	86B	PRL 57 178	M.J. Savage <i>et al.</i>	(CIT)	ALIBRAN	78	PL 74B 134	P. Alibrant <i>et al.</i>	(Gargamelle Collab.)
AMALDI	85	PL 153B 444	U. Amaldi <i>et al.</i>	(CERN)	ASRATYAN	78B	PL 79B 497	A.E. Asratyan <i>et al.</i>	(ITEP, SERP)
ANANEV	85	SJNP 41 585	V.D. Ananev <i>et al.</i>	(JINR)	BELLOTTI	78	PL 76B 223	E. Bellotti, E. Fiorini, L. Zanotti	(MILA)
		Translated from YAF 41 912			BOSETTI	78B	PL 74B 143	P.C. Bosetti <i>et al.</i>	(BEBC Collab.)
BALTRUSAITIS	85	PRL 55 1842	R.M. Baltrusaitis <i>et al.</i>	(Mark III Collab.)	DICUS	78C	PR D18 1829	D.A. Dicus <i>et al.</i>	(TEXA, VPI, STAN)
BERGSM��	85	PL 157B 458	F. Bergsma <i>et al.</i>	(CHARM Collab.)	DONNELLY	78	PR D18 1607	T.W. Donnelly <i>et al.</i>	(STAN)
KAPLAN	85	NP B260 215	D.B. Kaplan	(HARV)	Also		PRL 37 315	F. Reines, H.S. Gurr, H.W. Sobel	(UCI)
IWAMOTO	84	PRL 53 1198	N. Iwamoto	(UCSB, WUSL)	Also		PRL 33 179	H.S. Gurr, F. Reines, H.W. Sobel	(UCI)
YAMAZAKI	84	PL 52 1089	T. Yamazaki <i>et al.</i>	(INUS, KEK)	HANSL	78D	PL 74B 139	T. Hanst <i>et al.</i>	(CDHS Collab.)
ABBOTT	83	PL 120B 133	L.F. Abbott, P. Sikivie	(BRAN, FLOR)	MICELMAC	78	LNC 21 441	G.V. Mitselmakher, B. Pontecorvo	(JINR)
CARBONI	83	PL 123B 349	G. Carboni, W. Dahme	(CERN, MUNI)	MIKAELIAN	78	PR D18 3605	K.O. Mikaelian	(FNAL, NWES)
CAVAIGNAC	83	PL 121B 193	J.F. Cavaignac <i>et al.</i>	(ISNG, LAPP)	SATO	78	PTP 60 1942	K. Sato	(KYOT)
DICUS	83	PR D28 1778	D.A. Dicus, V.L. Teplitz	(TEXA, UMD)	VYSOTSKII	78	JETPL 27 502	M.L. Vysotsky <i>et al.</i>	(ASCI)
DINE	83	PL 120B 137	M. Dine, W. Fischler	(IAS, PENN)			Translated from ZETFP 27 533		
ELLIS	83B	NP B223 252	J. Ellis, K.A. Olive	(CERN)	YANG	78	PRL 41 523	T.C. Yang	(MASA)
FAISSNER	83	PR D28 1198	H. Faissner <i>et al.</i>	(AACH)	PECCEI	77	PR D16 1791	R.D. Peccci, H.R. Quinn	(STAN, SLAC)
FAISSNER	83B	PR D28 1787	H. Faissner <i>et al.</i>	(AACH3)	Also		PRL 38 1440	R.D. Peccci, H.R. Quinn	(STAN, SLAC)
FRANK	83B	PR D28 1790	J.S. Frank <i>et al.</i>	(LANL, YALE, LBL+)	REINES	76	PRL 37 315	F. Reines, H.S. Gurr, H.W. Sobel	(UCI)
HOFFMAN	83	PR D28 660	C.M. Hoffman <i>et al.</i>	(LANL, ARZS)	GURR	74	PRL 33 179	H.S. Gurr, F. Reines, H.W. Sobel	(UCI)
PRESKILL	83	PL 120B 127	J. Preskill, M.B. Wise, F. Wilczek	(HARV, UCSBT)	ANAND	53	PRSL A22 183	B.M. Anand	
SIKIVIE	83	PRL 51 1415	P. Sikivie	(FLOR)					
Also		PRL 52 695 (erratum)	P. Sikivie	(FLOR)					
ALEKSEEV	82	JETP 55 591	E.A. Alekseeva <i>et al.</i>	(KIAE)					
		Translated from ZETFP 82 1007			SREDNICKI	85	NP B260 689	M. Srednicki	(UCSB)
ALEKSEEV	82B	JETPL 36 116	G.D. Alekseev <i>et al.</i>	(MOSU, JINR)	BARDEEN	78	PL 74B 229	W.A. Bardeen, S.-H.H. Tye	(FNAL)
		Translated from ZETFP 36 94							
ASANO	82	PL 113B 195	Y. Asano <i>et al.</i>	(KEK, TOKY, INUS, OSAK)					
BARROS O	82	PL 116B 247	A. Barroso, G.C. Branco	(LIBS)					

OTHER RELATED PAPERS

SREDNICKI	85	NP B260 689	M. Srednicki	(UCSB)
BARDEEN	78	PL 74B 229	W.A. Bardeen, S.-H.H. Tye	(FNAL)

LEPTONS

e	1101
μ	1102
τ	1106
Heavy Charged Lepton Searches	1134
Neutrino Properties	1135
Number of Neutrino Types	1143
Double- β Decay	1145
Neutrino Mixing	1149
Heavy Neutral Leptons, Searches for	1168

Notes in the Listings

Neutrino properties	1135
Sum of neutrino masses (rev.)	1138
Number of light neutrino types from collider experiments	1143
Neutrinoless double- β decay (rev.)	1145
Three-neutrino mixing parameters (rev.)	1155

Related Reviews in Volume 1

55. Muon anomalous magnetic moment (rev.)	722
56. Muon decay parameters (rev.)	725
57. τ branching fractions (rev.)	728
58. τ -lepton decay parameters	731



LEPTONS

e

$$J = \frac{1}{2}$$

e MASS (atomic mass units u)

The primary determination of an electron's mass comes from measuring the ratio of the mass to that of a nucleus, so that the result is obtained in u (atomic mass units). The conversion factor to MeV is more uncertain than the mass of the electron in u; indeed, the recent improvements in the mass determination are not evident when the result is given in MeV. In this datablock we give the result in u, and in the following datablock in MeV.

VALUE (10 ⁻⁶ u)	DOCUMENT ID	TECN	COMMENT
548.5799070 ± 0.00000016	MOHR	16	RVUE 2014 CODATA value
••• We do not use the following data for averages, fits, limits, etc. •••			
548.57990946 ± 0.00000022	MOHR	12	RVUE 2010 CODATA value
548.57990943 ± 0.00000023	MOHR	08	RVUE 2006 CODATA value
548.57990945 ± 0.00000024	MOHR	05	RVUE 2002 CODATA value
548.5799092 ± 0.00000004	¹ BEIER	02	CNTR Penning trap
548.5799110 ± 0.00000012	MOHR	99	RVUE 1998 CODATA value
548.5799111 ± 0.00000012	² FARNHAM	95	CNTR Penning trap
548.579903 ± 0.0000013	COHEN	87	RVUE 1986 CODATA value

¹ BEIER 02 compares Larmor frequency of the electron bound in a ¹²C⁵⁺ ion with the cyclotron frequency of a single trapped ¹²C⁵⁺ ion.
² FARNHAM 95 compares cyclotron frequency of trapped electrons with that of a single trapped ¹²C⁶⁺ ion.

e MASS

2010 CODATA (MOHR 12) gives the conversion factor from u (atomic mass units, see the above datablock) to MeV as 931.494 061 (21). Earlier values use the then-current conversion factor. The conversion error dominates the uncertainty of the masses given below.

VALUE (MeV)	DOCUMENT ID	TECN	COMMENT
0.5109989461 ± 0.0000000031	MOHR	16	RVUE 2014 CODATA value
••• We do not use the following data for averages, fits, limits, etc. •••			
0.510998928 ± 0.000000011	MOHR	12	RVUE 2010 CODATA value
0.510998910 ± 0.000000013	MOHR	08	RVUE 2006 CODATA value
0.510998918 ± 0.000000044	MOHR	05	RVUE 2002 CODATA value
0.510998901 ± 0.000000020	^{1,2} BEIER	02	CNTR Penning trap
0.510998902 ± 0.000000021	MOHR	99	RVUE 1998 CODATA value
0.510998903 ± 0.000000020	^{1,3} FARNHAM	95	CNTR Penning trap
0.510998895 ± 0.000000024	¹ COHEN	87	RVUE 1986 CODATA value
0.5110034 ± 0.0000014	COHEN	73	RVUE 1973 CODATA value

¹ Converted to MeV using the 1998 CODATA value of the conversion constant, 931.494013 ± 0.000037 MeV/u.
² BEIER 02 compares Larmor frequency of the electron bound in a ¹²C⁵⁺ ion with the cyclotron frequency of a single trapped ¹²C⁵⁺ ion.
³ FARNHAM 95 compares cyclotron frequency of trapped electrons with that of a single trapped ¹²C⁶⁺ ion.

$$(m_{e^+} - m_{e^-}) / m_{average}$$

A test of CPT invariance.

VALUE	CL%	DOCUMENT ID	TECN	COMMENT
< 8 × 10⁻⁹	90	¹ FEE	93	CNTR Positronium spectroscopy
••• We do not use the following data for averages, fits, limits, etc. •••				
< 4 × 10 ⁻²³	90	² DOLGOV	14	From photon mass limit
< 4 × 10 ⁻⁸	90	CHU	84	CNTR Positronium spectroscopy

¹ FEE 93 value is obtained under the assumption that the positronium Rydberg constant is exactly half the hydrogen one.
² DOLGOV 14 result is obtained under the assumption that any mass difference between electron and positron would lead to a non-zero photon mass. The PDG 12 limit of 1 × 10⁻¹⁸ eV on the photon mass is in turn used to derive the value quoted here.

$$|q_{e^+} + q_{e^-}|/e$$

A test of CPT invariance. See also similar tests involving the proton.

VALUE	DOCUMENT ID	TECN	COMMENT
< 4 × 10⁻⁸	¹ HUGHES	92	RVUE
••• We do not use the following data for averages, fits, limits, etc. •••			
< 2 × 10 ⁻¹⁸	² SCHAEFER	95	THEO Vacuum polarization
< 1 × 10 ⁻¹⁸	³ MUELLER	92	THEO Vacuum polarization

¹ HUGHES 92 uses recent measurements of Rydberg-energy and cyclotron-frequency ratios.
² SCHAEFER 95 removes model dependency of MUELLER 92.
³ MUELLER 92 argues that an inequality of the charge magnitudes would, through higher-order vacuum polarization, contribute to the net charge of atoms.

e MAGNETIC MOMENT ANOMALY

$$\mu_e / \mu_B - 1 = (g-2)/2$$

VALUE (units 10 ⁻⁶)	DOCUMENT ID	TECN	CHG	COMMENT
1159.65218091 ± 0.00000026	MOHR	16	RVUE	2014 CODATA value
••• We do not use the following data for averages, fits, limits, etc. •••				
1159.65218076 ± 0.00000027	MOHR	12	RVUE	2010 CODATA value
1159.65218073 ± 0.00000028	HANNEKE	08	MRS	Single electron
1159.65218111 ± 0.00000074	¹ MOHR	08	RVUE	2006 CODATA value
1159.65218085 ± 0.00000076	² ODOM	06	MRS	Single electron
1159.6521859 ± 0.00000038	MOHR	05	RVUE	2002 CODATA value
1159.6521869 ± 0.00000041	MOHR	99	RVUE	1998 CODATA value
1159.652193 ± 0.000010	COHEN	87	RVUE	1986 CODATA value
1159.6521884 ± 0.00000043	VANDYCK	87	MRS	Single electron
1159.6521879 ± 0.00000043	VANDYCK	87	MRS	Single positron

¹ MOHR 08 average is dominated by ODOM 06.

² Superseded by HANNEKE 08 per private communication with Gerald Gabrielse.

$$(g_{e^+} - g_{e^-}) / g_{average}$$

A test of CPT invariance.

VALUE (units 10 ⁻¹²)	CL%	DOCUMENT ID	TECN	COMMENT
- 0.5 ± 2.1		¹ VANDYCK	87	MRS Penning trap
••• We do not use the following data for averages, fits, limits, etc. •••				
< 12 ± 64	95	² VASSERMAN	87	CNTR Assumes m _{e+} = m _{e-}
		SCHWINBERG	81	MRS Penning trap

¹ VANDYCK 87 measured (g₋/g₊) - 1 and we converted it.

² VASSERMAN 87 measured (g₊ - g₋)/(g - 2). We multiplied by (g - 2)/g = 1.2 × 10⁻³.

e ELECTRIC DIPOLE MOMENT (d)

A nonzero value is forbidden by both T invariance and P invariance.

VALUE (10 ⁻²⁸ ecm)	CL%	DOCUMENT ID	TECN	COMMENT
< 0.11	90	¹ ANDREEV	18	CNTR ThO molecules
••• We do not use the following data for averages, fits, limits, etc. •••				
< 1.3	90	² CAIRNCROSS	17	ESR 180Hf19F molecules
- 5570 ± 7980 ± 120		KIM	15	CNTR Gd ₃ Ga ₅ O ₁₂ molecules
< 0.87	90	³ BARON	14	CNTR ThO molecules
< 6050	90	⁴ ECKEL	12	CNTR Eu _{0.5} Ba _{0.5} TiO ₃ molecules
< 10.5	90	⁵ HUDSON	11	NMR YbF molecules
6.9 ± 7.4		REGAN	02	MRS 205-Tl beams
18 ± 12 ± 10		⁶ COMMINS	94	MRS 205-Tl beams
- 27 ± 83		⁶ ABDULLAH	90	MRS 205-Tl beams
- 1400 ± 2400		CHO	89	NMR TlF molecules
- 150 ± 550 ± 150		MURTHY	89	Cs, no B field
- 5000 ± 11000		LA MOREAUX	87	NMR 199Hg
19000 ± 34000	90	SANDARS	75	MRS Thallium
7000 ± 22000	90	PLAYER	70	MRS Xenon
< 30000	90	WEISSKOPF	68	MRS Cesium

¹ ANDREEV 18 gives a measurement corresponding to this limit as (4.3 ± 3.1 ± 2.6) × 10⁻³⁰ ecm.

² CAIRNCROSS 17 gives a measurement corresponding to this limit as (0.09 ± 0.77 ± 0.17) × 10⁻²⁸ ecm.

³ BARON 14 gives a measurement corresponding to this limit as (-0.21 ± 0.37 ± 0.25) × 10⁻²⁸ ecm.

⁴ ECKEL 12 gives a measurement corresponding to this limit as (-1.07 ± 3.06 ± 1.74) × 10⁻²⁵ ecm.

⁵ HUDSON 11 gives a measurement corresponding to this limit as (-2.4 ± 5.7 ± 1.5) × 10⁻²⁸ ecm.

⁶ ABDULLAH 90, COMMINS 94, and REGAN 02 use the relativistic enhancement of a valence electron's electric dipole moment in a high-Z atom.

e⁻ MEAN LIFE / BRANCHING FRACTION

A test of charge conservation. See the "Note on Testing Charge Conservation and the Pauli Exclusion Principle" following this section in our 1992 edition (Physical Review **D45** S1 (1992), p. VI.10).

Most of these experiments are one of three kinds: Attempts to observe (a) the 255.5 keV gamma ray produced in e⁻ → ν_eγ, (b) the (K) shell x-ray produced when an electron decays without additional energy deposit, e.g., e⁻ → ν_eν̄_eν_e ("disappearance" experiments), and (c) nuclear de-excitation gamma rays after the electron disappears from an atomic shell and the nucleus is left in an excited state. The last can include both weak boson and photon mediating processes. We use the best e⁻ → ν_eγ limit for the Summary Tables.

Note that we use the mean life rather than the half life, which is often reported.

e → ν_eγ and astrophysical limits

VALUE (yr)	CL%	DOCUMENT ID	TECN	COMMENT
> 6.6 × 10²⁸	90	AGOSTINI	15b	BORX e ⁻ → ν _e γ

Lepton Particle Listings

e, μ

• • • We do not use the following data for averages, fits, limits, etc. • • •

>1.2 × 10 ²⁴	90	ABGRALL	17	HPGE	electron decay to invisible
>1.22 × 10 ²⁶	68	¹ KLAPDOR-K...	07	CNTR	e ⁻ → νγ
>4.6 × 10 ²⁶	90	BACK	02	BORX	e ⁻ → νγ
>3.4 × 10 ²⁶	68	BELLI	00b	DAMA	e ⁻ → νγ, liquid Xe
>3.7 × 10 ²⁵	68	AHARONOV	95b	CNTR	e ⁻ → νγ
>2.35 × 10 ²⁵	68	BALYSH	93	CNTR	e ⁻ → νγ, ⁷⁶ Ge detector
>1.5 × 10 ²⁵	68	AVIGNONE	86	CNTR	e ⁻ → νγ
>1 × 10 ³⁹		² ORITO	85	ASTR	Astrophysical argument
>3 × 10 ²³	68	BELLOTTI	83b	CNTR	e ⁻ → νγ

¹The authors of A. Derbin et al, arXiv:0704.2047v1 argue that this limit is overestimated by at least a factor of 5.

²ORITO 85 assumes that electromagnetic forces extend out to large enough distances and that the age of our galaxy is 10¹⁰ years.

Disappearance and nuclear-de-excitation experiments

VALUE (yr)	CL%	DOCUMENT ID	TECN	COMMENT
>6.4 × 10 ²⁴	68	¹ BELLI	99b	DAMA De-excitation of ¹²⁹ Xe

• • • We do not use the following data for averages, fits, limits, etc. • • •

>4.2 × 10 ²⁴	68	BELLI	99	DAMA Iodine L-shell disappearance
>2.4 × 10 ²³	90	² BELLI	99d	DAMA De-excitation of ¹²⁷ I (in Na)
>4.3 × 10 ²³	68	AHARONOV	95b	CNTR Ge K-shell disappearance
>2.7 × 10 ²³	68	REUSSER	91	CNTR Ge K-shell disappearance
>2 × 10 ²²	68	BELLOTTI	83b	CNTR Ge K-shell disappearance

¹BELLI 99b limit on charge nonconserving e⁻ capture involving excitation of the 236.1 keV nuclear state of ¹²⁹Xe; the 90% CL limit is 3.7 × 10²⁴ yr. Less stringent limits for other states are also given.

²BELLI 99d limit on charge nonconserving e⁻ capture involving excitation of the 57.6 keV nuclear state of ¹²⁷I. Less stringent limits for the other states and for the state of ²³Na are also given.

LIMITS ON LEPTON-FLAVOR VIOLATION IN PRODUCTION

Forbidden by lepton family number conservation.

This section was added for the 2008 edition of this Review and is not complete. For a list of further measurements see references in the papers listed below.

σ(e⁺e⁻ → e[±]τ[∓]) / σ(e⁺e⁻ → μ[±]μ⁻)

VALUE	CL%	DOCUMENT ID	TECN	COMMENT
<8.9 × 10 ⁻⁶	95	AUBERT	07p	BABR e ⁺ e ⁻ at E _{cm} = 10.58 GeV

• • • We do not use the following data for averages, fits, limits, etc. • • •

<1.8 × 10 ⁻³	95	GOMEZ-CAD...	91	MRK2 e ⁺ e ⁻ at E _{cm} = 29 GeV
-------------------------	----	--------------	----	--

σ(e⁺e⁻ → μ[±]τ[∓]) / σ(e⁺e⁻ → μ[±]μ⁻)

VALUE	CL%	DOCUMENT ID	TECN	COMMENT
<4.0 × 10 ⁻⁶	95	AUBERT	07p	BABR e ⁺ e ⁻ at E _{cm} = 10.58 GeV

• • • We do not use the following data for averages, fits, limits, etc. • • •

<6.1 × 10 ⁻³	95	GOMEZ-CAD...	91	MRK2 e ⁺ e ⁻ at E _{cm} = 29 GeV
-------------------------	----	--------------	----	--

e REFERENCES

ANDREEV 18 NAT 562 355	V. Andreev et al.	(ACME Collab.)
ABGRALL 17 PRL 118 161801	N. Abgrall et al.	(MAJORANA Collab.)
CAIRN CROSS 17 PRL 119 153001	W.B. Cairncross et al.	(NIST, COLO)
MOHR 16 RMP 88 035009	P.J. Mohr, D.B. Newell, B.N. Taylor	(NIST)
AGOSTINI 15B PRL 115 231802	M. Agostini et al.	(Borexino Collab.)
KIM 15 PR D91 102004	Y.J. Kim et al.	(IND, YALE, LANL)
BARON 14 SCIENCE 343 269	J. Baron et al.	(ACME Collab.)
DOLGOV 14 PL B732 244	A.D. Dolgov, V.A. Novikov	
BEIER 12 PRL 109 193003	S. Eckel, A.O. Sushkov, S.K. Lamoreaux	(YALE)
MOHR 12 RMP 84 1527	P.J. Mohr, B.N. Taylor, D.B. Newell	(NIST)
PDG 12 PR D86 010001	J. Berlinger et al.	(PDG Collab.)
HUDSON 11 NAT 473 493	J.J. Hudson et al.	(LOIC)
HANNEKE 08 PRL 100 120801	D. Hanneke, S. Fogwell, G. Gabrielse	(HARV)
MOHR 08 RMP 80 633	P.J. Mohr, B.N. Taylor, D.B. Newell	(NIST)
AUBERT 07P PR D75 031103	B. Aubert et al.	(BABAR Collab.)
KLAPDOR-K... 07 PL B644 109	H.V. Klapdor-Kleingrothaus, I.V. Krivosheina, I.V. Titkova	
ODOM 06 PRL 97 030801	B. Odom et al.	(HARV)
MOHR 05 RMP 77 1	P.J. Mohr, B.N. Taylor	(NIST)
BACK 02 PL B525 29	H.O. Back et al.	(Borexino/SASSO Collab.)
BEIER 02 PRL 88 011603	T. Beier et al.	
REGAN 02 PRL 88 071805	B.C. Regan et al.	
BELLI 00b PR D61 117301	P. Belli et al.	(DAMA Collab.)
BELLI 99 PL B460 236	P. Belli et al.	(DAMA Collab.)
BELLI 99b PL B465 315	P. Belli et al.	(DAMA Collab.)
BELLI 99d PR C60 065501	P. Belli et al.	(DAMA Collab.)
MOHR 99 JPCRD 28 1713	P.J. Mohr, B.N. Taylor	(NIST)
Also RMP 72 351	P.J. Mohr, B.N. Taylor	(NIST)
AHARONOV 95b PR D52 3785	Y. Aharonov et al.	(SCUC, PNL, ZARA+)
Also PL B353 168	Y. Aharonov et al.	(SCUC, PNL, ZARA+)
FARNHAM 95 PRL 75 3598	D.L. Farnham, R.S. van Dyck, P.B. Schwinberg	(WASH)
SCHAEFER 95 PR A51 838	A. Schaefer, J. Reinhardt	(FRAN)
COMMINS 94 PR A50 2960	E.D. Commings et al.	
BALYSH 93 PL B298 278	A. Balysh et al.	(KIAE, MPIH, SASSO)
FEF 93 PR A48 192	M.S. Fef et al.	
HUGHES 92 PRL 69 578	R.J. Hughes, B.J. Deutch	(LANL, AARH)
MUELLER 92 PRL 69 3432	B. Mueller, M.H. Thoma	(DUKE)
PDG 92 PR D45 51	K. Hikasa et al.	(KEK, LBL, BOST+)
GOMEZ-CAD... 91 PRL 66 1007	J.J. Gomez-Cadenas et al.	(SLAC MARK-2 Collab.)
REUSSER 91 PL B255 143	D. Reusser et al.	(NEUC, CIT, PSI)
ABDULLAH 90 PRL 65 2347	K. Abdullah et al.	(LBL, UCB)
CHO 89 PRL 63 2559	D. Cho, K. Sangster, E.A. Hinds	(YALE)
MURTHY 89 PRL 63 965	S.A. Murthy et al.	(AMHT)
COHEN 87 RMP 59 1121	E.R. Cohen, B.N. Taylor	(RISC, NBS)

LAMOREAUX 87 PRL 59 2275	S.K. Lamoreaux et al.	(WASH)
VANDYCK 87 PRL 59 26	R.S. van Dyck, P.B. Schwinberg, H.G. Dehmelt	(WASH)
VASSERMAN 87 PL B198 302	I.B. Vasserma et al.	(NOVO)
Also PL B187 172	I.B. Vasserma et al.	(NOVO)
AVIGNONE 86 PR D34 97	F.T. Avignone et al.	(PNL, SCUC)
ORITO 85 PR 54 2457	S. Orto, M. Yoshimura	(TOKY, KEK)
CHU 84 PRL 52 1689	S. Chu, A.P. Mills, J.L. Hall	(BELL, NBS, COLO)
BELLOTTI 83b PL 124B 435	E. Bellotti et al.	(MILA)
SCHWINBERG 81 PRL 47 1579	P.B. Schwinberg, R.S. van Dyck, H.G. Dehmelt	(WASH)
SANDARS 75 PR A11 473	P.G.H. Sandars, D.M. Sternheimer	(OXF, BNL)
COHEN 73 JPCRD 2 664	E.R. Cohen, B.N. Taylor	(RISC, NBS)
PLAYER 70 JP B3 1620	M.A. Player, P.G.H. Sandars	(OXF)
WEISSKOPF 68 PRL 21 1645	M.C. Weisskopf et al.	(BRAN)



$$J = \frac{1}{2}$$

μ MASS (atomic mass units u)

The muon's mass is obtained from the muon-electron mass ratio as determined from the measurement of Zeeman transition frequencies in muonium (μ⁺e⁻ atom). Since the electron's mass is most accurately known in u, the muon's mass is also most accurately known in u. The conversion factor to MeV has approximately the same relative uncertainty as the mass of the muon in u. In this datablock we give the result in u, and in the following datablock in MeV.

VALUE (u)	DOCUMENT ID	TECN	COMMENT
0.113428925 ± 0.000000025	MOHR	16	RVUE 2014 CODATA value
• • • We do not use the following data for averages, fits, limits, etc. • • •			
0.1134289267 ± 0.000000029	MOHR	12	RVUE 2010 CODATA value
0.1134289256 ± 0.000000029	MOHR	08	RVUE 2006 CODATA value
0.1134289264 ± 0.000000030	MOHR	05	RVUE 2002 CODATA value
0.1134289168 ± 0.000000034	¹ MOHR	99	RVUE 1998 CODATA value
0.113428913 ± 0.000000017	² COHEN	87	RVUE 1986 CODATA value

¹MOHR 99 make use of other 1998 CODATA entries below.
²COHEN 87 make use of other 1986 CODATA entries below.

μ MASS

2010 CODATA (MOHR 12) gives the conversion factor from u (atomic mass units, see the above datablock) to MeV as 931.494 061 (21). Earlier values use the then-current conversion factor. The conversion error contributes significantly to the uncertainty of the masses given below.

VALUE (MeV)	DOCUMENT ID	TECN	CHG	COMMENT
105.6583745 ± 0.0000024	MOHR	16	RVUE	2014 CODATA value
• • • We do not use the following data for averages, fits, limits, etc. • • •				
105.6583715 ± 0.0000035	MOHR	12	RVUE	2010 CODATA value
105.6583668 ± 0.0000038	MOHR	08	RVUE	2006 CODATA value
105.6583692 ± 0.0000094	MOHR	05	RVUE	2002 CODATA value
105.6583568 ± 0.0000052	MOHR	99	RVUE	1998 CODATA value
105.658353 ± 0.000016	¹ COHEN	87	RVUE	1986 CODATA value
105.658386 ± 0.000044	² MARIAM	82	CNTR +	
105.65836 ± 0.00026	³ CROWE	72	CNTR	
105.65865 ± 0.00044	⁴ CRANE	71	CNTR	

¹Converted to MeV using the 1998 CODATA value of the conversion constant, 931.494013 ± 0.000037 MeV/u.

²MARIAM 82 give m_μ/m_e = 206.768259(62).

³CROWE 72 give m_μ/m_e = 206.7682(5).

⁴CRANE 71 give m_μ/m_e = 206.76878(85).

μ MEAN LIFE τ

Measurements with an error > 0.001 × 10⁻⁶ s have been omitted.

VALUE (10 ⁻⁶ s)	DOCUMENT ID	TECN	CHG	COMMENT
2.1969811 ± 0.0000022 OUR AVERAGE				
2.1969803 ± 0.0000021 ± 0.0000007 ¹	TISHCHENKO	13	CNTR +	Surface μ ⁺ at PSI
2.197083 ± 0.000032 ± 0.000015	BARCZYK	08	CNTR +	Muons from π ⁺ decay at rest
2.197013 ± 0.000021 ± 0.000011	CHITWOOD	07	CNTR +	Surface μ ⁺ at PSI
2.197078 ± 0.000073	BARDIN	84	CNTR +	
2.197025 ± 0.000155	BARDIN	84	CNTR -	
2.19695 ± 0.000006	GIOVANNETTI	84	CNTR +	
2.19711 ± 0.000008	BALANDIN	74	CNTR +	
2.1973 ± 0.0003	DUCLOS	73	CNTR +	
• • • We do not use the following data for averages, fits, limits, etc. • • •				
2.1969803 ± 0.0000022	WEBBER	11	CNTR +	Surface μ ⁺ at PSI

¹TISHCHENKO 13 uses 1.6 × 10¹² μ⁺ events and supersedes WEBBER 11.

τ_{μ⁺}/τ_{μ⁻} MEAN LIFE RATIO

A test of CPT invariance.

VALUE	DOCUMENT ID	TECN	COMMENT
1.000024 ± 0.000078	BARDIN	84	CNTR

• • • We do not use the following data for averages, fits, limits, etc. • • •

1.0008 ± 0.0010	BAILEY	79	CNTR	Storage ring
1.000 ± 0.001	MEYER	63	CNTR	Mean life μ^+ / μ^-

$$(\tau_{\mu^+} - \tau_{\mu^-}) / \tau_{\text{average}}$$

A test of *CPT* invariance. Calculated from the mean-life ratio, above.

VALUE	DOCUMENT ID
$(2 \pm 8) \times 10^{-5}$	OUR EVALUATION

μ/p MAGNETIC MOMENT RATIO

This ratio is used to obtain a precise value of the muon mass and to reduce experimental muon Larmor frequency measurements to the muon magnetic moment anomaly. Measurements with an error > 0.00001 have been omitted. By convention, the minus sign on this ratio is omitted. CODATA values were fitted using their selection of data, plus other data from multiparameter fits.

VALUE	DOCUMENT ID	TECN	CHG	COMMENT
3.183345142 ± 0.000000071	MOHR	16	RVUE	2014 CODATA value
• • • We do not use the following data for averages, fits, limits, etc. • • •				
3.183345107 ± 0.000000084	MOHR	12	RVUE	2010 CODATA value
3.183345137 ± 0.000000085	MOHR	08	RVUE	2006 CODATA value
3.183345118 ± 0.000000089	MOHR	05	RVUE	2002 CODATA value
3.18334513 ± 0.000000039	LIU	99	CNTR +	HFS in muonium
3.18334539 ± 0.000000010	MOHR	99	RVUE	1998 CODATA value
3.18334547 ± 0.000000047	COHEN	87	RVUE	1986 CODATA value
3.1833441 ± 0.00000017	KLEMPPT	82	CNTR +	Precession strob
3.1833461 ± 0.00000011	MARIAM	82	CNTR +	HFS splitting
3.1833448 ± 0.00000029	CAMANI	78	CNTR +	See KLEMPPT 82
3.1833403 ± 0.00000044	CASPERSON	77	CNTR +	HFS splitting
3.1833402 ± 0.00000072	COHEN	73	RVUE	1973 CODATA value
3.1833467 ± 0.00000082	CROWE	72	CNTR +	Precession phase

See the related review(s):
 Muon Anomalous Magnetic Moment

μ MAGNETIC MOMENT ANOMALY

The parity-violating decay of muons in a storage ring is observed. The difference frequency ω_3 between the muon spin precession and the orbital angular frequency ($e/m_\mu c$)(B) is measured, as is the free proton NMR frequency ω_p , thus determining the ratio $R = \omega_3 / \omega_p$. Given the magnetic moment ratio $\lambda = \mu_\mu / \mu_p$ (from hyperfine structure in muonium), $(g-2)/2 = R / (\lambda - R)$.

$$\mu_\mu / (e\hbar/2m_\mu) - 1 = (g_\mu - 2)/2$$

VALUE (units 10^{-10})	DOCUMENT ID	TECN	CHG	COMMENT
11659208.9 ± 5.4 ± 3.3	¹ BENNETT	06	MUG2	Average μ^+ and μ^-
• • • We do not use the following data for averages, fits, limits, etc. • • •				
11659208 ± 6	BENNETT	04	MUG2	Average μ^+ and μ^-
11659214 ± 8 ± 3	BENNETT	04	MUG2 -	Storage ring
11659203 ± 6 ± 5	BENNETT	04	MUG2 +	Storage ring
11659204 ± 7 ± 5	BENNETT	02	MUG2 +	Storage ring
11659202 ± 14 ± 6	BROWN	01	MUG2 +	Storage ring
11659191 ± 59	BROWN	00	MUG2 +	
11659100 ± 110	² BAILEY	79	CNTR +	Storage ring
11659360 ± 120	² BAILEY	79	CNTR -	Storage ring
11659230 ± 85	² BAILEY	79	CNTR ±	Storage ring
11620000 ± 5000	CHARPAK	62	CNTR +	

¹ BENNETT 06 reports $(g_\mu - 2)/2 = (11659208.0 \pm 5.4 \pm 3.3) \times 10^{-10}$. We rescaled this value using μ/p magnetic moment ratio of 3.183345137(85) from MOHR 08.

² BAILEY 79 values recalculated by HUGHES 99 using the COHEN 87 μ/p magnetic moment. The improved MOHR 99 value does not change the result.

$$(g_{\mu^+} - g_{\mu^-}) / g_{\text{average}}$$

A test of *CPT* invariance.

VALUE (units 10^{-8})	DOCUMENT ID	TECN
-0.11 ± 0.12	BENNETT	04 MUG2
• • • We do not use the following data for averages, fits, limits, etc. • • •		
-2.6 ± 1.6	BAILEY	79 CNTR

μ ELECTRIC DIPOLE MOMENT (d)

A nonzero value is forbidden by both *T* invariance and *P* invariance.

VALUE (10^{-19} e cm)	CL%	DOCUMENT ID	TECN	CHG	COMMENT
< 1.8	95	¹ BENNETT	09	MUG2 ±	Storage ring

• • • We do not use the following data for averages, fits, limits, etc. • • •

-0.1 ± 1.0	² BENNETT	09	MUG2 +	Storage ring
-0.1 ± 0.7	³ BENNETT	09	MUG2 -	Storage ring
-3.7 ± 3.4	⁴ BAILEY	78	CNTR ±	Storage ring
8.6 ± 4.5	BAILEY	78	CNTR +	Storage ring
0.8 ± 4.3	BAILEY	78	CNTR -	Storage ring

¹ This is the combination of the two BENNETT 09 measurements quoted here separately for μ^+ and μ^- . The result is also presented as a measurement of $(0.0 \pm 0.9) \times 10^{-19}$ e cm.

² Also reported as the limit of $|d(\mu^+)| < 2.1 \times 10^{-19}$ e cm at 95% CL.

³ Also reported as the limit of $|d(\mu^-)| < 1.5 \times 10^{-19}$ e cm at 95% CL.

⁴ This is the combination of the two BAILEY 78 results quoted here separately for μ^+ and μ^- . BAILEY 78 uses the convention $d = 1/2 \cdot (d_{\mu^+} - d_{\mu^-})$ and reports 3.7 ± 3.4 . We convert their result to use the same convention as BENNETT 09.

MUON-ELECTRON CHARGE RATIO ANOMALY $q_{\mu^+}/q_{e^-} - 1$

VALUE	DOCUMENT ID	TECN	CHG	COMMENT
(1.1 ± 2.1) × 10⁻⁹	¹ MEYER	00	CNTR +	1s-2s muonium interval
• • • We do not use the following data for averages, fits, limits, etc. • • •				
	¹ MEYER	00		measure the 1s-2s muonium interval, and then interpret the result in terms of muon-electron charge ratio q_{μ^+}/q_{e^-} .

μ^- DECAY MODES

μ^+ modes are charge conjugates of the modes below.

Mode	Fraction (Γ_i/Γ)	Confidence level
Γ_1 $e^- \bar{\nu}_e \nu_\mu$	$\approx 100\%$	
Γ_2 $e^- \bar{\nu}_e \nu_\mu \gamma$	[a] $(6.0 \pm 0.5) \times 10^{-8}$	
Γ_3 $e^- \bar{\nu}_e \nu_\mu e^+ e^-$	[b] $(3.4 \pm 0.4) \times 10^{-5}$	

Lepton Family number (LF) violating modes

Mode	LF	Confidence level
Γ_4 $e^- \nu_e \bar{\nu}_\mu$	[c] < 1.2	90%
Γ_5 $e^- \gamma$	< 4.2	$\times 10^{-13}$ 90%
Γ_6 $e^- e^+ e^-$	< 1.0	$\times 10^{-12}$ 90%
Γ_7 $e^- 2\gamma$	< 7.2	$\times 10^{-11}$ 90%

[a] This only includes events with energy of $e > 45$ MeV and energy of $\gamma > 40$ MeV. Since the $e^- \bar{\nu}_e \nu_\mu$ and $e^- \bar{\nu}_e \nu_\mu \gamma$ modes cannot be clearly separated, we regard the latter mode as a subset of the former.

[b] See the Particle Listings below for the energy limits used in this measurement.

[c] A test of additive vs. multiplicative lepton family number conservation.

μ^- BRANCHING RATIOS

$\Gamma(e^- \bar{\nu}_e \nu_\mu \gamma) / \Gamma_{\text{total}}$	Γ_2/Γ			
$6.03 \pm 0.14 \pm 0.53 \times 10^{-8}$				
VALUE (units 10^{-8})	EVTS	DOCUMENT ID	TECN	COMMENT
$(3.3 \pm 1.3) \times 10^{-3}$	13k	¹ BALDINI	16A	SPEC γ KE > 40 MeV
$(1.4 \pm 0.4) \times 10^{-2}$	862	BOGART	67	CNTR γ KE > 14.5 MeV
		CRITTENDEN	61	CNTR γ KE > 20 MeV
		CRITTENDEN	61	CNTR γ KE > 10 MeV
	27	ASHKIN	59	CNTR

¹ BALDINI 16 measurement refers to $\mu^+ \rightarrow e^+ \nu \bar{\nu} \gamma$ decay and requires energy of $e^+ > 45$ MeV and energy $\gamma > 40$ MeV.

$\Gamma(e^- \bar{\nu}_e \nu_\mu e^+ e^-) / \Gamma_{\text{total}}$	Γ_3/Γ				
$3.4 \pm 0.2 \pm 0.3$					
VALUE (units 10^{-5})	EVTS	DOCUMENT ID	TECN	CHG	COMMENT
2.2 ± 1.5	7	² CRITTENDEN	61	HLBC +	$E(e^+ e^-) > 10$ MeV
2	1	³ GUREVICH	60	EMUL +	
1.5 ± 1.0	3	LEE	59	HBC +	

¹ BERTL 85 has transverse momentum cut $p_T > 17$ MeV/c. Systematic error was increased by us.

² CRITTENDEN 61 count only those decays where total energy of either (e^+ , e^-) combination is >10 MeV.

³ GUREVICH 60 interpret their event as either virtual or real photon conversion. e^+ and e^- energies not measured.

⁴ In the three LEE 59 events, the sum of energies $E(e^+) + E(e^-) + E(\gamma)$ was 51 MeV, 55 MeV, and 33 MeV.

$\Gamma(e^- \nu_e \bar{\nu}_\mu) / \Gamma_{\text{total}}$	Γ_4/Γ				
< 0.012					
VALUE	CL%	DOCUMENT ID	TECN	CHG	COMMENT
< 0.012	90	¹ FREEDMAN	93	CNTR +	ν oscillation search

Forbidden by the additive conservation law for lepton family number. A multiplicative law predicts this branching ratio to be 1/2. For a review see NEMETHY 81.

Lepton Particle Listings

μ

• • • We do not use the following data for averages, fits, limits, etc. • • •

VALUE	CL%	DOCUMENT ID	TECN	CHG	COMMENT
< 0.018	90	KRAKAUER 91B	CALO	+	
< 0.05	90	² BERGSMA 83	CALO		$\bar{\nu}_\mu e \rightarrow \mu^- \bar{\nu}_e$
< 0.09	90	JONKER 80	CALO		See BERGSMA 83
-0.001 ± 0.061		WILLIS 80	CNTR	+	
0.13 ± 0.15		BLIETSCHAU 78	HLBC	±	Avg. of 4 values
< 0.25	90	EICHTEN 73	HLBC	+	

¹ FREEDMAN 93 limit on $\bar{\nu}_e$ observation is here interpreted as a limit on lepton family number violation.
² BERGSMA 83 gives a limit on the inverse muon decay cross-section ratio $\sigma(\bar{\nu}_\mu e^- \rightarrow \mu^- \bar{\nu}_e) / \sigma(\nu_\mu e^- \rightarrow \mu^- \nu_e)$, which is essentially equivalent to $\Gamma(e^- \nu_e \bar{\nu}_\mu) / \Gamma_{\text{total}}$ for small values like that quoted.

$\Gamma(e^- \gamma) / \Gamma_{\text{total}}$ Γ_5 / Γ

Forbidden by lepton family number conservation.

VALUE (units 10^{-11})	CL%	DOCUMENT ID	TECN	CHG	COMMENT
< 0.042	90	BALDINI 16	SPEC	+	MEG at PSI

• • • We do not use the following data for averages, fits, limits, etc. • • •

< 0.057	90	ADAM 13B	SPEC	+	MEG at PSI
< 0.24	90	ADAM 11	SPEC	+	MEG at PSI
< 2.8	90	ADAM 10	SPEC	+	MEG at PSI
< 1.2	90	AHMED 02	SPEC	+	MEGA
< 1.2	90	BROOKS 99	SPEC	+	LAMPF
< 4.9	90	BOLTON 88	CBOX	+	LAMPF
<100	90	AZUELOS 83	CNTR	+	TRIUMF
< 17	90	KINNISON 82	SPEC	+	LAMPF
<100	90	SCHAAF 80	ELEC	+	SIN

$\Gamma(e^- e^+ e^-) / \Gamma_{\text{total}}$ Γ_6 / Γ

Forbidden by lepton family number conservation.

VALUE (units 10^{-12})	CL%	DOCUMENT ID	TECN	CHG	COMMENT
< 1.0	90	¹ BELLGARDT 88	SPEC	+	SINDRUM

• • • We do not use the following data for averages, fits, limits, etc. • • •

< 36	90	BARANOV 91	SPEC	+	ARES
< 35	90	BOLTON 88	CBOX	+	LAMPF
< 2.4	90	¹ BERTL 85	SPEC	+	SINDRUM
<160	90	¹ BERTL 84	SPEC	+	SINDRUM
<130	90	¹ BOLTON 84	CNTR		LAMPF

¹ These experiments assume a constant matrix element.

$\Gamma(e^- 2\gamma) / \Gamma_{\text{total}}$ Γ_7 / Γ

Forbidden by lepton family number conservation.

VALUE (units 10^{-11})	CL%	DOCUMENT ID	TECN	CHG	COMMENT
< 7.2	90	BOLTON 88	CBOX	+	LAMPF

• • • We do not use the following data for averages, fits, limits, etc. • • •

< 840	90	¹ AZUELOS 83	CNTR	+	TRIUMF
<5000	90	² BOWMAN 78	CNTR		DEPOMMIER 77 data

¹ AZUELOS 83 uses the phase space distribution of BOWMAN 78.
² BOWMAN 78 assumes an interaction Lagrangian local on the scale of the inverse μ mass.

LIMIT ON $\mu^- \rightarrow e^-$ CONVERSION

Forbidden by lepton family number conservation.

$\sigma(\mu^- 32S \rightarrow e^- 32S) / \sigma(\mu^- 32S \rightarrow \nu_\mu 32P^*)$

VALUE	CL%	DOCUMENT ID	TECN	COMMENT
< 7×10^{-11}	90	BADERT...	80	STRC SIN

• • • We do not use the following data for averages, fits, limits, etc. • • •

< 4×10^{-10}	90	BADERT...	77	STRC SIN
-----------------------	----	-----------	----	----------

$\sigma(\mu^- Cu \rightarrow e^- Cu) / \sigma(\mu^- Cu \rightarrow \text{capture})$

VALUE	CL%	DOCUMENT ID	TECN	COMMENT
< 1.6×10^{-8}	90	BRYMAN 72	SPEC	

$\sigma(\mu^- Ti \rightarrow e^- Ti) / \sigma(\mu^- Ti \rightarrow \text{capture})$

VALUE	CL%	DOCUMENT ID	TECN	COMMENT
< 4.3×10^{-12}	90	¹ DOHMEN 93	SPEC	SINDRUM II

• • • We do not use the following data for averages, fits, limits, etc. • • •

< 4.6×10^{-12}	90	AHMAD 88	TPC	TRIUMF
< 1.6×10^{-11}	90	BRYMAN 85	TPC	TRIUMF

¹ DOHMEN 93 assumes $\mu^- \rightarrow e^-$ conversion leaves the nucleus in its ground state, a process enhanced by coherence and expected to dominate.

$\sigma(\mu^- Pb \rightarrow e^- Pb) / \sigma(\mu^- Pb \rightarrow \text{capture})$

VALUE	CL%	DOCUMENT ID	TECN	COMMENT
< 4.6×10^{-11}	90	HONECKER 96	SPEC	SINDRUM II

• • • We do not use the following data for averages, fits, limits, etc. • • •

< 4.9×10^{-10}	90	AHMAD 88	TPC	TRIUMF
-------------------------	----	----------	-----	--------

$\sigma(\mu^- Au \rightarrow e^- Au) / \sigma(\mu^- Au \rightarrow \text{capture})$

VALUE	CL%	DOCUMENT ID	TECN	CHG	COMMENT
< 7×10^{-13}	90	BERTL 06	SPEC	-	SINDRUM II

LIMIT ON $\mu^- \rightarrow e^+$ CONVERSION

Forbidden by total lepton number conservation.

$\sigma(\mu^- 32S \rightarrow e^+ 32Si^*) / \sigma(\mu^- 32S \rightarrow \nu_\mu 32P^*)$

VALUE	CL%	DOCUMENT ID	TECN	COMMENT
< 9×10^{-10}	90	BADERT...	80	STRC SIN

• • • We do not use the following data for averages, fits, limits, etc. • • •

< 1.5×10^{-9}	90	BADERT...	78	STRC SIN
------------------------	----	-----------	----	----------

$\sigma(\mu^- 127I \rightarrow e^+ 127Sb^*) / \sigma(\mu^- 127I \rightarrow \text{anything})$

VALUE	CL%	DOCUMENT ID	TECN	COMMENT
< 3×10^{-10}	90	¹ ABELA 80	CNTR	Radiochemical tech.

¹ ABELA 80 is upper limit for $\mu^- e^+$ conversion leading to particle-stable states of ¹²⁷Sb. Limit for total conversion rate is higher by a factor less than 4 (G. Backenstoss, private communication).

$\sigma(\mu^- Cu \rightarrow e^+ Co) / \sigma(\mu^- Cu \rightarrow \nu_\mu Ni)$

VALUE	CL%	DOCUMENT ID	TECN	COMMENT
< 2.6×10^{-8}	90	BRYMAN 72	SPEC	
< 2.2×10^{-7}	90	CONFORTO 62	OSPK	

• • • We do not use the following data for averages, fits, limits, etc. • • •

$\sigma(\mu^- Ti \rightarrow e^+ Ca) / \sigma(\mu^- Ti \rightarrow \text{capture})$

VALUE	CL%	EVTS	DOCUMENT ID	TECN	CHG	COMMENT
< 3.6×10^{-11}	90	1	^{1,2} KAULARD 98	SPEC	-	SINDRUM II

• • • We do not use the following data for averages, fits, limits, etc. • • •

< 1.7×10^{-12}	90	1	^{2,3} KAULARD 98	SPEC	-	SINDRUM II
< 4.3×10^{-12}	90		³ DOHMEN 93	SPEC		SINDRUM II
< 8.9×10^{-11}	90		¹ DOHMEN 93	SPEC		SINDRUM II
< 1.7×10^{-10}	90		⁴ AHMAD 88	TPC		TRIUMF

¹ This limit assumes a giant resonance excitation of the daughter Ca nucleus (mean energy and width both 20 MeV).
² KAULARD 98 obtained these same limits using the unified classical analysis of FELDMAN 98.
³ This limit assumes the daughter Ca nucleus is left in the ground state. However, the probability of this is unknown.
⁴ Assuming a giant-resonance-excitation model.

LIMIT ON MUONIUM \rightarrow ANTIMUONIUM CONVERSION

Forbidden by lepton family number conservation.

$$R_g = G_C / G_F$$

The effective Lagrangian for the $\mu^+ e^- \rightarrow \mu^- e^+$ conversion is assumed to be

$$\mathcal{L} = 2^{-1/2} G_C [\bar{\nu}_\mu \gamma_\lambda (1 - \gamma_5) \psi_e] [\bar{\psi}_\mu \gamma_\lambda (1 - \gamma_5) \psi_e] + \text{h.c.}$$

The experimental result is then an upper limit on G_C / G_F , where G_F is the Fermi coupling constant.

VALUE	CL%	EVTS	DOCUMENT ID	TECN	CHG	COMMENT
< 0.0030	90	1	¹ WILLMANN 99	SPEC	+	μ^+ at 26 GeV/c

• • • We do not use the following data for averages, fits, limits, etc. • • •

< 0.14	90	1	² GORDEEV 97	SPEC	+	JINR phasotron
< 0.018	90	0	³ ABELA 96	SPEC	+	μ^+ at 24 MeV
< 6.9	90		NI 93	CBOX		LAMPF
< 0.16	90		MATTHIAS 91	SPEC		LAMPF
< 0.29	90		HUBER 90B	CNTR		TRIUMF
< 20	95		BEER 86	CNTR		TRIUMF
< 42	95		MARSHALL 82	CNTR		

¹ WILLMANN 99 quote both probability $P_{M\bar{M}} < 8.3 \times 10^{-11}$ at 90%CL in a 0.1 T field and $R_g = G_C / G_F$.
² GORDEEV 97 quote limits on both $f = G_{MM} / G_F$ and the probability $W_{MM} < 4.7 \times 10^{-7}$ (90% CL).
³ ABELA 96 quote both probability $P_{M\bar{M}} < 8 \times 10^{-9}$ at 90% CL and $R_g = G_C / G_F$.

See the related review(s):

[Muon Decay Parameters](#)

μ DECAY PARAMETERS

ρ PARAMETER
 (V-A) theory predicts $\rho = 0.75$.

VALUE	CL%	EVTS	DOCUMENT ID	TECN	CHG	COMMENT	
0.74979 ± 0.00026 OUR AVERAGE							
0.74977 ± 0.00012 ± 0.00023			¹ BAYES	11	TWST	+	Surface μ^+
0.7518 ± 0.0026			DERENZO	69	RVUE		

• • • We do not use the following data for averages, fits, limits, etc. • • •

0.75014 ± 0.00017 ± 0.00045	2	MACDONALD	08	TWST	+	Surface μ^+	
0.75080 ± 0.00032 ± 0.00100	6G	3	MUSSER	05	TWST	+	Surface μ^+
0.72 ± 0.06 ± 0.08		4	AMORUSO	04	ICAR		Liquid Ar TPC
0.762 ± 0.008	170k	4	FRYBERGER	68	ASPK	+	25–53 MeV e^+
0.760 ± 0.009	280k	4	SHERWOOD	67	ASPK	+	25–53 MeV e^+
0.7503 ± 0.0026	800k	4	PEOPLES	66	ASPK	+	20–53 MeV e^+

- The quoted systematic error includes a contribution of 0.00013 (added in quadrature) from uncertainties on radiative corrections and on the Michel parameter η .
- The quoted systematic error includes a contribution of 0.00011 (added in quadrature) from the dependence on the Michel parameter η .
- The quoted systematic error includes a contribution of 0.00023 (added in quadrature) from the dependence on the Michel parameter η .
- η constrained = 0. These values incorporated into a two parameter fit to ρ and η by DERENZO 69.

η PARAMETER

(V–A) theory predicts $\eta = 0$.

VALUE	EVTS	DOCUMENT ID	TECN	CHG	COMMENT		
0.057 ± 0.034 OUR AVERAGE							
0.071 ± 0.037 ± 0.005	30M	DANNEBERG	05	CNTR	+	7–53 MeV e^+	
0.011 ± 0.081 ± 0.026	5.3M	1	BURKARD	85B	CNTR	+	9–53 MeV e^+
–0.12 ± 0.21	6346	DERENZO	69	HBC	+	1.6–6.8 MeV e^+	
–0.0021 ± 0.0070 ± 0.0010	30M	2	DANNEBERG	05	CNTR	+	7–53 MeV e^+
–0.012 ± 0.015 ± 0.003	5.3M	2	BURKARD	85B	CNTR	+	9–53 MeV e^+
–0.007 ± 0.013	5.3M	3	BURKARD	85B	FIT		9–53 MeV e^+
–0.7 ± 0.5	170k	4	FRYBERGER	68	ASPK	+	25–53 MeV e^+
–0.7 ± 0.6	280k	4	SHERWOOD	67	ASPK	+	25–53 MeV e^+
0.05 ± 0.5	800k	4	PEOPLES	66	ASPK	+	20–53 MeV e^+
–2.0 ± 0.9	9213	5	PLANO	60	HBC	+	Whole spectrum

- • • We do not use the following data for averages, fits, limits, etc. • • •
- Previously we used the global fit result from BURKARD 85B in OUR AVERAGE, we now only include their actual measurement.
 - $\alpha = \alpha' = 0$ assumed.
 - Global fit to all measured parameters. The fit correlation coefficients are given in BURKARD 85B.
 - ρ constrained = 0.75.
 - Two parameter fit to ρ and η ; PLANO 60 discounts value for η .

δ PARAMETER

(V–A) theory predicts $\delta = 0.75$.

VALUE	EVTS	DOCUMENT ID	TECN	CHG	COMMENT		
0.75047 ± 0.00034 OUR AVERAGE							
0.75049 ± 0.00021 ± 0.00027		1	BAYES	11	TWST	+	Surface μ^+
0.7486 ± 0.0026 ± 0.0028		2	BALKE	88	SPEC	+	Surface μ^+
0.75067 ± 0.00030 ± 0.00067		MACDONALD	08	TWST	+	Surface μ^+	
0.74964 ± 0.00066 ± 0.00112	6G	GAPONENKO	05	TWST	+	Surface μ^+	
		3	VOSSLER	69			
0.752 ± 0.009	490k	FRYBERGER	68	ASPK	+	25–53 MeV e^+	
0.782 ± 0.031		KRUGER	61				
0.78 ± 0.05	8354	PLANO	60	HBC	+	Whole spectrum	

- • • We do not use the following data for averages, fits, limits, etc. • • •
- The quoted systematic error includes a contribution of 0.00006 (added in quadrature) from uncertainties on radiative corrections and on the Michel parameter η .
 - BALKE 88 uses $\rho = 0.752 \pm 0.003$.
 - VOSSLER 69 has measured the asymmetry below 10 MeV. See comments about radiative corrections in VOSSLER 69.

$(\xi \text{ PARAMETER}) \times (\mu \text{ LONGITUDINAL POLARIZATION})$

(V–A) theory predicts $\xi = 1$, longitudinal polarization = 1.

VALUE	EVTS	DOCUMENT ID	TECN	CHG	COMMENT		
1.0009 ± 0.0016 OUR AVERAGE							
1.00084 ± 0.00029 ± 0.00165		BUENO	11	TWST	Surface μ^+ beam		
1.0027 ± 0.0079 ± 0.0030		BELTRAMI	87	CNTR	SIN, π decay in flight		
1.0003 ± 0.0006 ± 0.0038		JAMIESON	06	TWST	+	surface μ^+ beam	
1.0013 ± 0.0030 ± 0.0053		1	IMAZATO	92	SPEC	+	$K^+ \rightarrow \mu^+ \nu_\mu$
0.975 ± 0.015		AKHMANOV	68	EMUL			140 kG
0.975 ± 0.030		GUREVICH	64	EMUL			See AKHMANOV 68
0.903 ± 0.027		2	ALI-ZADE	61	EMUL	+	27 kG
0.93 ± 0.06		PLANO	60	HBC	+		8.8 kG
0.97 ± 0.05		BARDON	59	CNTR			Bromoform target

- • • We do not use the following data for averages, fits, limits, etc. • • •
- The corresponding 90% confidence limit from IMAZATO 92 is $|\xi P_\mu| > 0.990$. This measurement is of K^+ decay, not π^+ decay, so we do not include it in an average, nor do we yet set up a separate data block for K results.
 - Depolarization by medium not known sufficiently well.

$\xi \times (\mu \text{ LONGITUDINAL POLARIZATION}) \times \delta / \rho$

VALUE	CL%	DOCUMENT ID	TECN	CHG	COMMENT		
1.00179 ± 0.00156 OUR AVERAGE							
1.00179 ± 0.00156		1	BAYES	11	TWST	+	Surface μ^+ beam
>0.99682	90	2	JODIDIO	86	SPEC	+	TRIUMF
>0.9966	90	3	STOKER	85	SPEC	+	μ -spin rotation
>0.9959	90	CARR	83	SPEC	+		11 kG

- BAYES 11 obtains the limit > 0.99909 (90% CL) with the constraint that $\xi \times (\mu \text{ LONGITUDINAL POLARIZATION}) \times \delta / \rho \leq 1.0$.
- JODIDIO 86 includes data from CARR 83 and STOKER 85. The value here is from the erratum.
- STOKER 85 find $(\xi P_\mu \delta / \rho) > 0.9955$ and > 0.9966 , where the first limit is from new μ spin-rotation data and the second is from combination with CARR 83 data. In V–A theory, $(\delta / \rho) = 1.0$.

$\xi' = \text{LONGITUDINAL POLARIZATION OF } e^+$

(V–A) theory predicts the longitudinal polarization = ± 1 for e^\pm , respectively. We have flipped the sign for e^- so our programs can average.

VALUE	EVTS	DOCUMENT ID	TECN	CHG	COMMENT	
1.00 ± 0.04 OUR AVERAGE						
0.998 ± 0.045	1M	BURKARD	85	CNTR	+	Bhabha + annihl
0.89 ± 0.28	29k	SCHWARTZ	67	OSPK	–	Moller scattering
0.94 ± 0.38		BLOOM	64	CNTR	+	Brems. transmiss.
1.04 ± 0.18		DUCLOS	64	CNTR	+	Bhabha scattering
1.05 ± 0.30		BUHLER	63	CNTR	+	Annihilation

ξ'' PARAMETER

VALUE	EVTS	DOCUMENT ID	TECN	CHG	COMMENT		
0.98 ± 0.04 OUR AVERAGE							
0.981 ± 0.045 ± 0.003	3.87M	PRIEELS	14	CNTR	+	Bhabha + annihl	
0.65 ± 0.36	326k	1	BURKARD	85	CNTR	+	Bhabha + annihl

- • • We do not use the following data for averages, fits, limits, etc. • • •
- BURKARD 85 measure $(\xi'' - \xi \xi') / \xi$ and set $\xi = 1$.

TRANSVERSE e^+ POLARIZATION IN PLANE OF μ SPIN, e^+ MOMENTUM

VALUE (units 10^{-3})	EVTS	DOCUMENT ID	TECN	CHG	COMMENT	
–2 ± 8 OUR AVERAGE						
6.3 ± 7.7 ± 3.4	30M	DANNEBERG	05	CNTR	+	7–53 MeV e^+
16 ± 21 ± 10	5.3M	BURKARD	85B	CNTR	+	Annihil 9–53 MeV

TRANSVERSE e^+ POLARIZATION NORMAL TO PLANE OF μ SPIN, e^+ MOMENTUM

Zero if T invariance holds.

VALUE (units 10^{-3})	EVTS	DOCUMENT ID	TECN	CHG	COMMENT	
–2 ± 8 OUR AVERAGE						
–3.7 ± 7.7 ± 3.4	30M	DANNEBERG	05	CNTR	+	7–53 MeV e^+
7 ± 22 ± 7	5.3M	BURKARD	85B	CNTR	+	Annihil 9–53 MeV

α/A

VALUE (units 10^{-3})	EVTS	DOCUMENT ID	TECN	CHG	COMMENT	
0.4 ± 4.3						
15 ± 50 ± 14	5.3M	BURKARD	85B	CNTR	+	9–53 MeV e^+

- • • We do not use the following data for averages, fits, limits, etc. • • •
- Global fit to all measured parameters. Correlation coefficients are given in BURKARD 85B.

α'/A

Zero if T invariance holds.

VALUE (units 10^{-3})	EVTS	DOCUMENT ID	TECN	CHG	COMMENT		
–10 ± 20 OUR AVERAGE							
–3.4 ± 21.3 ± 4.9	30M	DANNEBERG	05	CNTR	+	7–53 MeV e^+	
–47 ± 50 ± 14	5.3M	1	BURKARD	85B	CNTR	+	9–53 MeV e^+
–0.2 ± 4.3		2	BURKARD	85B	FIT		

- • • We do not use the following data for averages, fits, limits, etc. • • •
- Previously we used the global fit result from BURKARD 85B in OUR AVERAGE, we now only include their actual measurement. BURKARD 85B measure e^+ polarizations P_{T1} and P_{T2} versus e^+ energy.
 - Global fit to all measured parameters. The fit correlation coefficients are given in BURKARD 85B.

β/A

VALUE (units 10^{-3})	EVTS	DOCUMENT ID	TECN	CHG	COMMENT	
3.9 ± 6.2						
2 ± 17 ± 6	5.3M	BURKARD	85B	CNTR	+	9–53 MeV e^+

- • • We do not use the following data for averages, fits, limits, etc. • • •
- Global fit to all measured parameters. The fit correlation coefficients are given in BURKARD 85B.

β'/A

Zero if T invariance holds.

VALUE (units 10^{-3})	EVTS	DOCUMENT ID	TECN	CHG	COMMENT		
2 ± 7 OUR AVERAGE							
–0.5 ± 7.8 ± 1.8	30M	DANNEBERG	05	CNTR	+	7–53 MeV e^+	
17 ± 17 ± 6	5.3M	1	BURKARD	85B	CNTR	+	9–53 MeV e^+
–1.3 ± 3.5 ± 0.6	30M	2	DANNEBERG	05	CNTR	+	7–53 MeV e^+
1.5 ± 6.3		3	BURKARD	85B	FIT		

- • • We do not use the following data for averages, fits, limits, etc. • • •
- Previously we used the global fit result from BURKARD 85B in OUR AVERAGE, we now only include their actual measurement. BURKARD 85B measure e^+ polarizations P_{T1} and P_{T2} versus e^+ energy.
 - $\alpha = \alpha' = 0$ assumed.
 - Global fit to all measured parameters. The fit correlation coefficients are given in BURKARD 85B.

Lepton Particle Listings

μ, τ

a/A

This comes from an alternative parameterization to that used in the Summary Table (see the "Note on Muon Decay Parameters" above).

VALUE (units 10^{-3})	CL%	DOCUMENT ID	TECN
<15.9	90	¹ BURKARD 85B	FIT

¹ Global fit to all measured parameters. Correlation coefficients are given in BURKARD 85b.

a'/A

This comes from an alternative parameterization to that used in the Summary Table (see the "Note on Muon Decay Parameters" above).

VALUE (units 10^{-3})	CL%	DOCUMENT ID	TECN
5.3 ± 4.1		¹ BURKARD 85B	FIT

¹ Global fit to all measured parameters. Correlation coefficients are given in BURKARD 85b.

(b'+b)/A

This comes from an alternative parameterization to that used in the Summary Table (see the "Note on Muon Decay Parameters" above).

VALUE (units 10^{-3})	CL%	DOCUMENT ID	TECN
<1.04	90	¹ BURKARD 85B	FIT

¹ Global fit to all measured parameters. Correlation coefficients are given in BURKARD 85b.

c/A

This comes from an alternative parameterization to that used in the Summary Table (see the "Note on Muon Decay Parameters" above).

VALUE (units 10^{-3})	CL%	DOCUMENT ID	TECN
<6.4	90	¹ BURKARD 85B	FIT

¹ Global fit to all measured parameters. Correlation coefficients are given in BURKARD 85b.

c'/A

This comes from an alternative parameterization to that used in the Summary Table (see the "Note on Muon Decay Parameters" above).

VALUE (units 10^{-3})	CL%	DOCUMENT ID	TECN
3.5 ± 2.0		¹ BURKARD 85B	FIT

¹ Global fit to all measured parameters. Correlation coefficients are given in BURKARD 85b.

$\overline{\eta}$ PARAMETER

($V-A$) theory predicts $\overline{\eta} = 0$. $\overline{\eta}$ affects spectrum of radiative muon decay.

VALUE	DOCUMENT ID	TECN	CHG	COMMENT
0.02 ± 0.08 OUR AVERAGE				
-0.014 ± 0.090	EICHENBER... 84	ELEC	+	ρ free
+0.09 ± 0.14	BOGART 67	CNTR	+	
-0.035 ± 0.098	EICHENBER... 84	ELEC	+	$\rho=0.75$ assumed

μ REFERENCES

BALDINI 16 EPJ C76 434	A.M. Baldini et al.	(MEG Collab.)
BALDINI 16A EPJ C76 108	A.M. Baldini et al.	(MEG Collab.)
MOHR 16 RMP 88 035009	P.J. Mohr, D.B. Newell, B.N. Taylor	(NIST)
PRIEELS 14 PR D90 112003	R. Priests et al.	(LOUV, ETH, PSI+)
ADAM 13B PRL 110 201801	J. Adam et al.	(MEG Collab.)
TISHCHENKO 13 PR D87 052003	V. Tishchenko et al.	(MuLan Collab.)
MOHR 12 RMP 84 1527	P.J. Mohr, B.N. Taylor, D.B. Newell	(NIST)
ADAM 11 PRL 107 171801	J. Adam et al.	(MEG Collab.)
BAYES 11 PRL 106 041804	R. Bayes et al.	(TWIST Collab.)
Also PR D85 092013	A. Hillairet et al.	(TWIST Collab.)
BUENO 11 PR D84 032005	J.F. Bueno et al.	(TWIST Collab.)
Also PR D85 039908 (err.)	J.F. Bueno et al.	(TWIST Collab.)
WEBBER 11 PRL 106 041803	D.M. Webber et al.	(MuLan Collab.)
Also PRL 106 079901 (err.)	D.M. Webber et al.	(MuLan Collab.)
ADAM 10 NP B834 1	J. Adam et al.	(MEG Collab.)
BENNETT 09 PR D80 052008	G.W. Bennett et al.	(MUG-2 Collab.)
BARCZYK 08 PL B663 172	A. Barczyk et al.	(FAST Collab.)
MACDONALD 08 PR D78 032010	R.P. MacDonald et al.	(MEGA Collab.)
MOHR 08 RMP 80 633	P.J. Mohr, B.N. Taylor, D.B. Newell	(NIST)
CHITWOOD 07 PRL 99 032001	D.B. Chitwood et al.	(MULAN Collab.)
BENNETT 06 PR D73 072003	G.W. Bennett et al.	(MUG-2 Collab.)
BERTL 06 EPJ C47 337	W. Bertl et al.	(SINDRUM II Collab.)
JAMIESON 06 PR D74 072007	B. Jamieson et al.	(TWIST Collab.)
DANNEBERG 05 PRL 94 021802	N. Danneberg et al.	(ETH, JAGL, PSI+)
GAPONENKO 05 PR D71 071101	A. Gaponenko et al.	(TWIST Collab.)
MOHR 05 RMP 77 1	P.J. Mohr, B.N. Taylor	(NIST)
MUSSER 05 PRL 94 101805	J.R. Musser et al.	(TWIST Collab.)
AMORUSO 04 EPJ C33 233	S. Amoroso et al.	(ICARUS Collab.)
BENNETT 04 PRL 92 161802	G.W. Bennett et al.	(Muon(g-2) Collab.)
AHMED 02 PR D65 112002	M. Ahmed et al.	(MEGA Collab.)
BENNETT 02 PRL 89 101804	G.W. Bennett et al.	(Muon(g-2) Collab.)
BROWN 01 PRL 86 2227	H.N. Brown et al.	(Muon(g-2) Collab.)
BROWN 00 PR D62 091101	H.N. Brown et al.	(BNL/G-2 Collab.)
MEYER 00 PRL 84 1136	V. Meyer et al.	
BROOKS 99 PRL 83 1521	M.L. Brooks et al.	(MEGA/LAMPF Collab.)
HUGHES 99 RMP 71 5133	V.W. Hughes, T. Kinoshita	
LIU 99 PRL 82 711	W. Liu et al.	(LAMPF Collab.)
MOHR 99 JPCRD 28 1713	P.J. Mohr, B.N. Taylor	(NIST)
Also RMP 72 351	P.J. Mohr, B.N. Taylor	(NIST)
WILLMANN 99 PRL 82 49	L. Willmann et al.	
FELDMAN 98 PR D57 3873	G.J. Feldman, R.D. Cousins	

KAULARD 98 PL B422 334	J. Kaulard et al.	(SINDRUM-II Collab.)
GORDEEV 97 PAN 60 1164	V.A. Gordeev et al.	(PNPI)
Translated from YAF 60 1291.		
ABELA 96 PRL 77 1950	R. Abela et al.	(PSI, ZURI, HEIDH, TBIL+)
HONECKER 96 PRL 76 200	W. Honecker et al.	(SINDRUM II Collab.)
DOHMEN 93 PL B317 631	C. Dohmen et al.	(PSI SINDRUM-II Collab.)
FREDMAN 93 PR D47 911	S.J. Freedman et al.	(LAMPF E645 Collab.)
NI 93 PR D48 1976	B. Ni et al.	(LAMPF Crystal-Box Collab.)
IMAZATO 92 PRL 69 877	J. Imazato et al.	(KEK, INUS, TOKY+)
BARANOV 91 SJNP 53 802	V.A. Baranov et al.	(JINR)
Translated from YAF 53 1302.		
KRAKAUER 91B PL B263 534	D.A. Krakauer et al.	(UMD, UCI, LANL)
MATTHIAS 91 PRL 66 2716	B.E. Matthias et al.	(YALE, HEIDP, WILL+)
Also PRL 67 532 (erratum)	B.E. Matthias et al.	(YALE, HEIDP, WILL+)
HUBER 90B PR D38 2102	T.M. Huber et al.	(WYOM, VICT, ARIZ+)
AHMAD 90 PRL 59 970	S. Ahmad et al.	(TRIUM, VICT, VPI, BRCO+)
Also PRL 59 2102	S. Ahmad et al.	(TRIUM, VPI, VICT, BRCO+)
BALKE 88 PR D37 587	B. Balke et al.	(LBL, UCB, COLO, NWES+)
BELLEGARDT 88 NP B299 1	U. Bellgardt et al.	(SINDRUM Collab.)
BOLTON 88 PR D38 2077	R.D. Bolton et al.	(LANL, STAN, CHIC+)
Also PRL 56 2461	R.D. Bolton et al.	(LANL, STAN, CHIC+)
Also PRL 57 3241	D. Gronskic et al.	(CHIC, LANL, STAN+)
BELTRAMI 87 PL B194 326	I. Beltrami et al.	(ETH, SIN, MANZ)
COHEN 87 RMP 59 1121	E.R. Cohen, B.N. Taylor	(RIS, CN)
BEER 86 PRL 57 571	G.A. Beer et al.	(VICT, TRIUM, WYOM)
JODIDIO 86 PR D34 1967	A. Jodidio et al.	(LBL, NWES, TRIUM)
Also PR D37 237 (erratum)	A. Jodidio et al.	(LBL, NWES, TRIUM)
BERTL 85 NP B260 1	W. Bertl et al.	(SINDRUM Collab.)
BRYMAN 85 PRL 55 465	D.A. Bryman et al.	(TRIUM, CNCR, BRCO+)
BURKARD 85 PL 150B 242	H. Burkhardt et al.	(ETH, SIN, MANZ)
BURKARD 85B PL 160B 343	H. Burkhardt et al.	(ETH, SIN, MANZ)
Also PR D24 2004	F. Corriveau et al.	(ETH, SIN, MANZ)
Also PL 129B 260	F. Corriveau et al.	(ETH, SIN, MANZ)
STOKER 85 PRL 54 1887	D.P. Stoker et al.	(LBL, NWES, TRIUM)
BARDIN 84 PL 137B 135	G. Bardin et al.	(SACL, CERN, BGNA, FIRZ)
BERTL 84 PL 140B 299	W. Bertl et al.	(SINDRUM Collab.)
BOLTON 84 PRL 53 1415	R.D. Bolton et al.	(LANL, CHIC, STAN+)
EICHENBER... 84 NP A412 523	W. Eichenberger, R. Engfer, A. van der Schaff	
GIOVANETTI 84 PR D29 343	K.L. Giovanetti et al.	(WILL)
AZUELOS 83 PRL 51 164	G. Azuelos et al.	(MONT, TRIUM, BRCO)
Also PRL 39 1113	P. Depommier et al.	(MONT, BRCO, TRIUM+)
BERGSM 83 PL 122B 465	F. Bergsma et al.	(CHARM Collab.)
CARR 83 PRL 51 627	J. Carr et al.	(LBL, NWES, TRIUM)
KINNISON 82 PR D25 2846	W.W. Kinnison et al.	(EFI, STAN, LANL)
Also PRL 42 556	J.D. Bowman et al.	(LASL, EFI, STAN)
KLEMP 82 PR D25 652	E. Klemp et al.	(MANZ, ETH)
MARIAM 82 PRL 49 993	F.G. Mariani et al.	(YALE, HEIDH, BERN)
MARSHALL 82 PR D25 1174	G.M. Marshall et al.	(BRCO)
NEMETHY 81 CNR 29 147	P. Nemethy, V.W. Hughes	(LBL, YALE)
ABELA 80 PL 95B 318	R. Abela et al.	(BASL, KARLK, KARLE)
BADERT... 80 LNC 28 401	A. Badertscher et al.	(BERN)
Also NP A377 406	A. Badertscher et al.	(BERN)
JONKER 80 PL 93B 203	M. Jonker et al.	(CHARM Collab.)
SCHAAF 80 NP A340 249	A. van der Schaaf et al.	(ZURI, ETH+)
Also PL 72B 183	H.P. Povel et al.	(ZURI, ETH, SIN)
WILLIS 80 PRL 44 522	S.E. Willis et al.	(YALE, LBL, LASL+)
Also PRL 45 1370	S.E. Willis et al.	(YALE, LBL, LASL+)
BAILEY 79 NP B150 1	J.M. Bailey	(CERN, DARE, MANZ)
BADERT... 78 PL 79B 371	A. Badertscher et al.	(BERN)
BAILEY 78 JP 64 345	J.M. Bailey	(DARE, BERN, SHEF, MANZ, RUCS+)
Also NP B150 1	J.M. Bailey	(CERN, DARE, MANZ)
BLIETSCHAU 78 NP B133 205	J. Blietschau et al.	(Gargamelle Collab.)
BOWMAN 78 PRL 41 442	J.D. Bowman et al.	(LASL, IAS, CMU+)
CAMANI 78 PL 77B 326	M. Camani et al.	(ETH, MANZ)
BADERT... 77 PRL 39 1385	A. Badertscher et al.	(BERN, BRNO)
CASPERSON 77 PRL 38 956	D.E. Caspersen et al.	(BERN, HEIDH, LASL+)
DEPOMMIER 77 PRL 39 1113	P. Depommier et al.	(MONT, BRCO, TRIUM+)
BALANDIN 74 JETP 40 811	M.P. Balandin et al.	(JINR)
Translated from ZETF 67 1631.		
COHEN 73 JPCRD 2 664	E.R. Cohen, B.N. Taylor	(RIS, NBS)
DUCLOS 73 PL 47B 491	J. Duclos, A. Magnon, J. Picant	(SACL)
EICHTEN 73 PL 46B 281	T. Eichten et al.	(Gargamelle Collab.)
BRYMAN 72 PRL 28 1469	D.A. Bryman et al.	(VPI)
CROWE 72 PR D5 2145	K.M. Crowe et al.	(LBL, WASH)
CRANE 71 PRL 27 474	T. Crane et al.	(YALE)
DERENZO 69 PR 181 1854	S.E. Denzno	(EFI)
VOSSLER 69 NC 63A 423	C. Vossler	(EFI)
AKHMANOV 68 SJNP 6 230	V.V. Akhmanov et al.	(KIAE)
Translated from YAF 6 316.		
FRYBERGER 68 PR 166 1379	D. Fryberger	(EFI)
BOGART 67 PR 156 1405	E. Bogart et al.	(COLU)
SCHWARTZ 67 PR 162 1306	D.M. Schwartz	(EFI)
SHERWOOD 67 PR 156 1475	B.A. Sherwood	(EFI)
PEOPLES 66 Nevis 147 unpub.	J. Peoples	(COLU)
BLOOM 64 PL 8 87	S. Bloom et al.	(CERN)
DUCLOS 64 PL 9 62	J. Duclos et al.	(CERN)
GUREVICH 64 PL 11 185	I.I. Gurevich et al.	(KIAE)
BUHLER 63 PL 7 368	A. Buhler-Broglin et al.	(CERN)
MEYER 63 PR 132 2693	S.L. Meyer et al.	(COLU)
CHARPAK 62 PL 1 16	G. Charpak et al.	(CERN)
CONFORTO 62 NC 26 261	G. Conforto et al.	(INFN, ROMA, CERN)
ALI-ZADE 61 JETP 13 313	S.A. Ali-Zade, I.I. Gurevich, B.A. Nikolsky	
Translated from ZETF 40 452.		
CRITTENDEN 61 PR 121 1823	R.R. Crittenden, W.D. Walker, J. Ballam	(WIS+)
KRUGER 61 UCRL 9322 unpub.	H. Kruger	(LRL)
GUREVICH 60 JETP 10 225	I.I. Gurevich, B.A. Nikolsky, L.V. Surkova	(ITEP)
Translated from ZETF 37 338.		
PLANO 60 PR 119 1400	R.J. Plano	(COLU)
ASHKIN 59 NC 14 1266	J. Ashkin et al.	(CERN)
BARDON 59 PRL 2 56	M. Bardon, D. Berley, L.M. Lederman	(COLU)
LEE 59 PRL 3 55	J. Lee, N.P. Samios	(COLU)

τ

$$J = \frac{1}{2}$$

τ discovery paper was PERL 75. $e^+e^- \rightarrow \tau^+\tau^-$ cross-section threshold behavior and magnitude are consistent with pointlike spin-1/2 Dirac particle. BRANDELIK 78 ruled out pointlike spin-0 or spin-1 particle. FELDMAN 78 ruled out $J = 3/2$. KIRKBY 79 also ruled out $J = \text{integer}$, $J = 3/2$.

τ MASS

VALUE (MeV)	EVTS	DOCUMENT ID	TECN	COMMENT
1776.86 ± 0.12 OUR AVERAGE				
1776.91 ± 0.12 ^{+0.10} _{-0.13}	1171	¹ ABLKIK	14d BES3	23.3 pb ⁻¹ , $E_{cm}^{ee} = 3.54\text{-}3.60$ GeV

1776.68 ± 0.12 ± 0.41	682k	² AUBERT	09AK BABR	423 fb ⁻¹ , E _{cm} ^{ee} =10.6 GeV
1776.81 ^{+0.25} _{-0.23} ± 0.15	81	ANASHIN	07 KEDR	6.7 pb ⁻¹ , E _{cm} ^{ee} =3.54-3.78 GeV
1776.61 ± 0.13 ± 0.35		² BELOUS	07 BELL	414 fb ⁻¹ , E _{cm} ^{ee} =10.6 GeV
1775.1 ± 1.6 ± 1.0	13.3k	³ ABBIENDI	00A OPAL	1990-1995 LEP runs
1778.2 ± 0.8 ± 1.2		ANASTASSOV	97 CLEO	E _{cm} ^{ee} = 10.6 GeV
1776.96 ^{+0.18} _{-0.21} ± 0.25 ± 0.17	65	⁴ BAI	96 BES	E _{cm} ^{ee} = 3.54-3.57 GeV
1776.3 ± 2.4 ± 1.4	11k	⁵ ALBRECHT	92M ARG	E _{cm} ^{ee} = 9.4-10.6 GeV
1783 ⁺³ ₋₄	692	⁶ BACINO	78B DLCO	E _{cm} ^{ee} = 3.1-7.4 GeV

• • • We do not use the following data for averages, fits, limits, etc. • • •
 1777.8 ± 0.7 ± 1.7 35k ⁷BALEST 93 CLEO Repl. by ANASTASSOV 97
 1776.9^{+0.4}_{-0.5} ± 0.2 14 ⁸BAI 92 BES Repl. by BAI 96

- 1 ABLIKIM 14D fit $\sigma(e^+e^- \rightarrow \tau^+\tau^-)$ at different energies near threshold.
- 2 AUBERT 09AK and BELOUS 07 fit τ pseudomass spectrum in $\tau \rightarrow \pi\pi^+\pi^-\nu_\tau$ decays. Result assumes $m_{\nu_\tau} = 0$.
- 3 ABBIENDI 00A fit τ pseudomass spectrum in $\tau \rightarrow \pi^\pm \leq 2\pi^0\nu_\tau$ and $\tau \rightarrow \pi^\pm\pi^+\pi^- \leq 1\pi^0\nu_\tau$ decays. Result assumes $m_{\nu_\tau} = 0$.
- 4 BAI 96 fit $\sigma(e^+e^- \rightarrow \tau^+\tau^-)$ at different energies near threshold.
- 5 ALBRECHT 92M fit τ pseudomass spectrum in $\tau^- \rightarrow 2\pi^-\pi^+\nu_\tau$ decays. Result assumes $m_{\nu_\tau} = 0$.
- 6 BACINO 78B value comes from $e^\pm X^\mp$ threshold. Published mass 1782 MeV increased by 1 MeV using the high precision $\psi(2S)$ mass measurement of ZHOLENTZ 80 to eliminate the absolute SPEAR energy calibration uncertainty.
- 7 BALEST 93 fit spectra of minimum kinematically allowed τ mass in events of the type $e^+e^- \rightarrow \tau^+\tau^- \rightarrow (\pi^+n\pi^0\nu_\tau)(\pi^-m\pi^0\nu_\tau)$ $n \leq 2, m \leq 2, 1 \leq n+m \leq 3$. If $m_{\nu_\tau} \neq 0$, result increases by $(m_{\nu_\tau}^2/1100)$ MeV.
- 8 BAI 92 fit $\sigma(e^+e^- \rightarrow \tau^+\tau^-)$ near threshold using $e\mu$ events.

$(m_{\tau^+} - m_{\tau^-})/m_{\text{average}}$

A test of CPT invariance.

VALUE	CL%	DOCUMENT ID	TECN	COMMENT
<2.8 × 10⁻⁴	90	BELOUS	07 BELL	414 fb ⁻¹ , E _{cm} ^{ee} =10.6 GeV
• • • We do not use the following data for averages, fits, limits, etc. • • •				
<5.5 × 10 ⁻⁴	90	¹ AUBERT	09AK BABR	423 fb ⁻¹ , E _{cm} ^{ee} =10.6 GeV
<3.0 × 10 ⁻³	90	ABBIENDI	00A OPAL	1990-1995 LEP runs
¹ AUBERT 09AK quote both the listed upper limit and $(m_{\tau^+} - m_{\tau^-})/m_{\text{average}} = (-3.4 \pm 1.3 \pm 0.3) \times 10^{-4}$.				

τ MEAN LIFE

VALUE (10 ⁻¹⁵ s)	EVTS	DOCUMENT ID	TECN	COMMENT
290.3 ± 0.5 OUR AVERAGE				
290.17 ± 0.53 ± 0.33	1.1M	BELOUS	14 BELL	711 fb ⁻¹ , E _{cm} ^{ee} =10.6 GeV
290.9 ± 1.4 ± 1.0		ABDALLAH	04T DLPH	1991-1995 LEP runs
293.2 ± 2.0 ± 1.5		ACCIARRI	00B L3	1991-1995 LEP runs
290.1 ± 1.5 ± 1.1		BARATE	97R ALEP	1989-1994 LEP runs
289.2 ± 1.7 ± 1.2		ALEXANDER	96E OPAL	1990-1994 LEP runs
289.0 ± 2.8 ± 4.0	57.4k	BALEST	96 CLEO	E _{cm} ^{ee} = 10.6 GeV
• • • We do not use the following data for averages, fits, limits, etc. • • •				
291.2 ± 2.0 ± 1.2		BARATE	97I ALEP	Repl. by BARATE 97R
291.4 ± 3.0		ABREU	96B DLPH	Repl. by ABDALLAH 04T
290.1 ± 4.0	34k	ACCIARRI	96K L3	Repl. by ACCIARRI 00B
297 ± 9 ± 5	1671	ABE	95Y SLD	1992-1993 SLC runs
304 ± 14 ± 7	4100	BATTLE	92 CLEO	E _{cm} ^{ee} = 10.6 GeV
301 ± 29	3780	KLEINWORT	89 JADE	E _{cm} ^{ee} = 35-46 GeV
288 ± 16 ± 17	807	AMIDEI	88 MRK2	E _{cm} ^{ee} = 29 GeV
306 ± 20 ± 14	695	BRAUNSCH...	88C TASS	E _{cm} ^{ee} = 36 GeV
299 ± 15 ± 10	1311	ABACHI	87C HRS	E _{cm} ^{ee} = 29 GeV
295 ± 14 ± 11	5696	ALBRECHT	87P ARG	E _{cm} ^{ee} = 9.3-10.6 GeV
309 ± 17 ± 7	3788	BAND	87B MAC	E _{cm} ^{ee} = 29 GeV
325 ± 14 ± 18	8470	BEBEK	87C CLEO	E _{cm} ^{ee} = 10.5 GeV
460 ± 190	102	FELDMAN	82 MRK2	E _{cm} ^{ee} = 29 GeV

$(\tau_+ - \tau_-) / \tau_{\text{average}}$

Test of CPT invariance.

VALUE	CL%	DOCUMENT ID	TECN	COMMENT
<7.0 × 10⁻³	90	¹ BELOUS	14 BELL	711 fb ⁻¹ , E _{cm} ^{ee} = 10.6 GeV
¹ BELOUS 14 quote limit on the absolute value of the relative lifetime difference.				

τ MAGNETIC MOMENT ANOMALY

The q^2 dependence is expected to be small providing no thresholds are nearby.

$\mu_\tau / (e\hbar/2m_\tau) - 1 = (g_\tau - 2)/2$

For a theoretical calculation $[(g_\tau - 2)/2 = 117721(5) \times 10^{-8}]$, see EIDELMAN 07.

VALUE	CL%	DOCUMENT ID	TECN	COMMENT
> -0.052 and < 0.013 (CL = 95%) OUR LIMIT				
> -0.052 and < 0.013	95	¹ ABDALLAH	04k DLPH	$e^+e^- \rightarrow e^+e^-\tau^+\tau^-$ at LEP2
• • • We do not use the following data for averages, fits, limits, etc. • • •				
<0.107	95	² ACHARD	04G L3	$e^+e^- \rightarrow e^+e^-\tau^+\tau^-$ at LEP2
> -0.007 and < 0.005	95	³ GONZALEZ-S.	00 RVUE	$e^+e^- \rightarrow \tau^+\tau^-$ and $W \rightarrow \tau\nu_\tau$
> -0.052 and < 0.058	95	⁴ ACCIARRI	98E L3	1991-1995 LEP runs
> -0.068 and < 0.065	95	⁵ ACKERSTAFF	98N OPAL	1990-1995 LEP runs
> -0.004 and < 0.006	95	⁶ ESCRIBANO	97 RVUE	$Z \rightarrow \tau^+\tau^-$ at LEP
<0.01	95	⁷ ESCRIBANO	93 RVUE	$Z \rightarrow \tau^+\tau^-$ at LEP
<0.12	90	GRIFOLS	91 RVUE	$Z \rightarrow \tau\tau\gamma$ at LEP
<0.023	95	⁸ SILVERMAN	83 RVUE	$e^+e^- \rightarrow \tau^+\tau^-$ at PETRA

- 1 ABDALLAH 04k limit is derived from $e^+e^- \rightarrow e^+e^-\tau^+\tau^-$ total cross-section measurements at \sqrt{s} between 183 and 208 GeV. In addition to the limits, the authors also quote a value of -0.018 ± 0.017 .
- 2 ACHARD 04G limit is derived from $e^+e^- \rightarrow e^+e^-\tau^+\tau^-$ total cross-section measurements at \sqrt{s} between 189 and 206 GeV, and is on the absolute value of the magnetic moment anomaly.
- 3 GONZALEZ-SPRINBERG 00 use data on tau lepton production at LEP1, SLC, and LEP2, and data from colliders and LEP2 to determine limits. Assume imaginary component is zero.
- 4 ACCIARRI 98E use $Z \rightarrow \tau^+\tau^-\gamma$ events. In addition to the limits, the authors also quote a value of $0.004 \pm 0.027 \pm 0.023$.
- 5 ACKERSTAFF 98N use $Z \rightarrow \tau^+\tau^-\gamma$ events. The limit applies to an average of the form factor for off-shell τ 's having p^2 ranging from m_τ^2 to $(M_Z - m_\tau)^2$.
- 6 ESCRIBANO 97 use preliminary experimental results.
- 7 ESCRIBANO 93 limit derived from $\Gamma(Z \rightarrow \tau^+\tau^-)$, and is on the absolute value of the magnetic moment anomaly.
- 8 SILVERMAN 83 limit is derived from $e^+e^- \rightarrow \tau^+\tau^-$ total cross-section measurements for q^2 up to (37 GeV)².

τ ELECTRIC DIPOLE MOMENT (d_τ)

A nonzero value is forbidden by both T invariance and P invariance.

The q^2 dependence is expected to be small providing no thresholds are nearby.

Re(d_τ)

VALUE (10 ⁻¹⁶ e cm)	CL%	DOCUMENT ID	TECN	COMMENT
- 0.22 to 0.45	95	¹ INAMI	03 BELL	E _{cm} ^{ee} = 10.6 GeV
• • • We do not use the following data for averages, fits, limits, etc. • • •				
< 2.3	90	² GROZIN	09A RVUE	From e EDM limit
< 3.7	95	³ ABDALLAH	04k DLPH	$e^+e^- \rightarrow e^+e^-\tau^+\tau^-$ at LEP2
< 11.4	95	⁴ ACHARD	04G L3	$e^+e^- \rightarrow e^+e^-\tau^+\tau^-$ at LEP2
< 4.6	95	⁵ ALBRECHT	00 ARG	E _{cm} ^{ee} = 10.4 GeV
> -3.1 and < 3.1	95	ACCIARRI	98E L3	1991-1995 LEP runs
> -3.8 and < 3.6	95	⁶ ACKERSTAFF	98N OPAL	1990-1995 LEP runs
< 0.11	95	^{7,8} ESCRIBANO	97 RVUE	$Z \rightarrow \tau^+\tau^-$ at LEP
< 0.5	95	⁹ ESCRIBANO	93 RVUE	$Z \rightarrow \tau^+\tau^-$ at LEP
< 7	90	GRIFOLS	91 RVUE	$Z \rightarrow \tau\tau\gamma$ at LEP
< 1.6	90	DELAGUILA	90 RVUE	$e^+e^- \rightarrow \tau^+\tau^-$ E _{cm} ^{ee} = 35 GeV

- 1 INAMI 03 use $e^+e^- \rightarrow \tau^+\tau^-$ events.
- 2 GROZIN 09A calculate the contribution to the electron electric dipole moment from the τ electric dipole moment appearing in loops, which is $\Delta d_e = 6.9 \times 10^{-12} d_\tau$. Dividing the REGAN 02 upper limit $|d_e| \leq 1.6 \times 10^{-27}$ e cm at CL=90% by 6.9×10^{-12} gives this limit.
- 3 ABDALLAH 04k limit is derived from $e^+e^- \rightarrow e^+e^-\tau^+\tau^-$ total cross-section measurements at \sqrt{s} between 183 and 208 GeV and is on the absolute value of d_τ .
- 4 ACHARD 04G limit is derived from $e^+e^- \rightarrow e^+e^-\tau^+\tau^-$ total cross-section measurements at \sqrt{s} between 189 and 206 GeV, and is on the absolute value of d_τ .
- 5 ALBRECHT 00 use $e^+e^- \rightarrow \tau^+\tau^-$ events. Limit is on the absolute value of Re(d_τ).
- 6 ACKERSTAFF 98N use $Z \rightarrow \tau^+\tau^-\gamma$ events. The limit applies to an average of the form factor for off-shell τ 's having p^2 ranging from m_τ^2 to $(M_Z - m_\tau)^2$.
- 7 ESCRIBANO 97 derive the relationship $|d_\tau| = \cot \theta_W |d_W^W|$ using effective Lagrangian methods, and use a conference result $|d_W^W| < 5.8 \times 10^{-18}$ e cm at 95% CL (L. Silvestris, ICHEP96) to obtain this result.
- 8 ESCRIBANO 97 use preliminary experimental results.
- 9 ESCRIBANO 93 limit derived from $\Gamma(Z \rightarrow \tau^+\tau^-)$, and is on the absolute value of the electric dipole moment.

Lepton Particle Listings

τ

$\text{Im}(d_\tau)$

VALUE ($10^{-16} e\text{cm}$)	CL%	DOCUMENT ID	TECN	COMMENT
-0.25 to 0.008	95	¹ INAMI	03	BELL $E_{\text{cm}}^e = 10.6 \text{ GeV}$

- • • We do not use the following data for averages, fits, limits, etc. • • •
- < 1.8 95 ² ALBRECHT 00 ARG $E_{\text{cm}}^e = 10.4 \text{ GeV}$
- ¹ INAMI 03 use $e^+e^- \rightarrow \tau^+\tau^-$ events.
- ² ALBRECHT 00 use $e^+e^- \rightarrow \tau^+\tau^-$ events. Limit is on the absolute value of $\text{Im}(d_\tau)$.

τ WEAK DIPOLE MOMENT (d_τ^W)

A nonzero value is forbidden by CP invariance.
The q^2 dependence is expected to be small providing no thresholds are nearby.

$\text{Re}(d_\tau^W)$

VALUE ($10^{-17} e\text{cm}$)	CL%	DOCUMENT ID	TECN	COMMENT
<0.50	95	¹ HEISTER	03F	ALEP 1990-1995 LEP runs

- • • We do not use the following data for averages, fits, limits, etc. • • •
- <3.0 90 ¹ ACCIARRI 98c L3 1991-1995 LEP runs
- <0.56 95 ACKERSTAFF 97L OPAL 1991-1995 LEP runs
- <0.78 95 ² AKERS 95F OPAL Repl. by ACKERSTAFF 97L
- <1.5 95 ² BUSKULIC 95c ALEP Repl. by HEISTER 03F
- <7.0 95 ² ACTON 92F OPAL $Z \rightarrow \tau^+\tau^-$ at LEP
- <3.7 95 ² BUSKULIC 92J ALEP Repl. by BUSKULIC 95c
- ¹ Limit is on the absolute value of the real part of the weak dipole moment.
- ² Limit is on the absolute value of the real part of the weak dipole moment, and applies for $q^2 = m_Z^2$.

$\text{Im}(d_\tau^W)$

VALUE ($10^{-17} e\text{cm}$)	CL%	DOCUMENT ID	TECN	COMMENT
<1.1	95	¹ HEISTER	03F	ALEP 1990-1995 LEP runs

- • • We do not use the following data for averages, fits, limits, etc. • • •
- <1.5 95 ACKERSTAFF 97L OPAL 1991-1995 LEP runs
- <4.5 95 ² AKERS 95F OPAL Repl. by ACKERSTAFF 97L
- ¹ HEISTER 03F limit is on the absolute value of the imaginary part of the weak dipole moment.
- ² Limit is on the absolute value of the imaginary part of the weak dipole moment, and applies for $q^2 = m_Z^2$.

τ WEAK ANOMALOUS MAGNETIC DIPOLE MOMENT (α_τ^W)

Electroweak radiative corrections are expected to contribute at the 10^{-6} level. See BERNABEU 95.
The q^2 dependence is expected to be small providing no thresholds are nearby.

$\text{Re}(\alpha_\tau^W)$

VALUE	CL%	DOCUMENT ID	TECN	COMMENT
<1.1 $\times 10^{-3}$	95	¹ HEISTER	03F	ALEP 1990-1995 LEP runs

- • • We do not use the following data for averages, fits, limits, etc. • • •
- > -0.0024 and < 0.0025 95 ² GONZALEZ-S...00 RVUE $e^+e^- \rightarrow \tau^+\tau^-$ and $W \rightarrow \tau\nu_\tau$
- <4.5 $\times 10^{-3}$ 90 ¹ ACCIARRI 98c L3 1991-1995 LEP runs
- ¹ Limit is on the absolute value of the real part of the weak anomalous magnetic dipole moment.
- ² GONZALEZ-SPRINGER 00 use data on tau lepton production at LEP1, SLC, and LEP2, and data from colliders and LEP2 to determine limits. Assume imaginary component is zero.

$\text{Im}(\alpha_\tau^W)$

VALUE	CL%	DOCUMENT ID	TECN	COMMENT
<2.7 $\times 10^{-3}$	95	¹ HEISTER	03F	ALEP 1990-1995 LEP runs

- • • We do not use the following data for averages, fits, limits, etc. • • •
- <9.9 $\times 10^{-3}$ 90 ¹ ACCIARRI 98c L3 1991-1995 LEP runs
- ¹ Limit is on the absolute value of the imaginary part of the weak anomalous magnetic dipole moment.

τ^\pm DECAY MODES

τ^\pm modes are charge conjugates of the modes below. " h^\pm " stands for π^\pm or K^\pm . " e^\pm " stands for e or μ . "Neutrals" stands for γ 's and/or π^0 's.

Mode	Fraction (Γ_i/Γ)	Scale factor/ Confidence level
------	--------------------------------	-----------------------------------

Modes with one charged particle

Γ_1 particle $^- \geq 0$ neutrals $\geq 0K^0\nu_\tau$ ("1-prong")	(85.24 \pm 0.06) %	
Γ_2 particle $^- \geq 0$ neutrals $\geq 0K_L^0\nu_\tau$	(84.58 \pm 0.06) %	
Γ_3 $\mu^- \bar{\nu}_\mu \nu_\tau$	[a] (17.39 \pm 0.04) %	
Γ_4 $\mu^- \bar{\nu}_\mu \nu_\tau \gamma$	[b] (3.67 \pm 0.08) $\times 10^{-3}$	
Γ_5 $e^- \bar{\nu}_e \nu_\tau$	[a] (17.82 \pm 0.04) %	
Γ_6 $e^- \bar{\nu}_e \nu_\tau \gamma$	[b] (1.83 \pm 0.05) %	
Γ_7 $h^- \geq 0K_L^0 \nu_\tau$	(12.03 \pm 0.05) %	
Γ_8 $h^- \nu_\tau$	(11.51 \pm 0.05) %	
Γ_9 $\pi^- \nu_\tau$	[a] (10.82 \pm 0.05) %	
Γ_{10} $K^- \nu_\tau$	[a] (6.96 \pm 0.10) $\times 10^{-3}$	
Γ_{11} $h^- \geq 1$ neutrals ν_τ	(37.01 \pm 0.09) %	
Γ_{12} $h^- \geq 1\pi^0 \nu_\tau$ (ex. K^0)	(36.51 \pm 0.09) %	
Γ_{13} $h^- \pi^0 \nu_\tau$	(25.93 \pm 0.09) %	
Γ_{14} $\pi^- \pi^0 \nu_\tau$	[a] (25.49 \pm 0.09) %	
Γ_{15} $\pi^- \pi^0$ non- $\rho(770)\nu_\tau$	(3.0 \pm 3.2) $\times 10^{-3}$	
Γ_{16} $K^- \pi^0 \nu_\tau$	[a] (4.33 \pm 0.15) $\times 10^{-3}$	
Γ_{17} $h^- \geq 2\pi^0 \nu_\tau$	(10.81 \pm 0.09) %	
Γ_{18} $h^- 2\pi^0 \nu_\tau$	(9.48 \pm 0.10) %	
Γ_{19} $h^- 2\pi^0 \nu_\tau$ (ex. K^0)	(9.32 \pm 0.10) %	
Γ_{20} $\pi^- 2\pi^0 \nu_\tau$ (ex. K^0)	[a] (9.26 \pm 0.10) %	
Γ_{21} $\pi^- 2\pi^0 \nu_\tau$ (ex. K^0), scajar	< 9 $\times 10^{-3}$ CL=95%	
Γ_{22} $\pi^- 2\pi^0 \nu_\tau$ (ex. K^0), vector	< 7 $\times 10^{-3}$ CL=95%	
Γ_{23} $K^- 2\pi^0 \nu_\tau$ (ex. K^0)	[a] (6.5 \pm 2.2) $\times 10^{-4}$	
Γ_{24} $h^- \geq 3\pi^0 \nu_\tau$	(1.34 \pm 0.07) %	
Γ_{25} $h^- \geq 3\pi^0 \nu_\tau$ (ex. K^0)	(1.25 \pm 0.07) %	
Γ_{26} $h^- 3\pi^0 \nu_\tau$	(1.18 \pm 0.07) %	
Γ_{27} $\pi^- 3\pi^0 \nu_\tau$ (ex. K^0)	[a] (1.04 \pm 0.07) %	
Γ_{28} $K^- 3\pi^0 \nu_\tau$ (ex. K^0, η)	[a] (4.8 \pm 2.1) $\times 10^{-4}$	
Γ_{29} $h^- 4\pi^0 \nu_\tau$ (ex. K^0)	(1.6 \pm 0.4) $\times 10^{-3}$	
Γ_{30} $h^- 4\pi^0 \nu_\tau$ (ex. K^0, η)	[a] (1.1 \pm 0.4) $\times 10^{-3}$	
Γ_{31} $a_1(1260)\nu_\tau \rightarrow \pi^- \gamma \nu_\tau$	(3.8 \pm 1.5) $\times 10^{-4}$	
Γ_{32} $K^- \geq 0\pi^0 \geq 0K^0 \geq 0\gamma \nu_\tau$	(1.552 \pm 0.029) %	
Γ_{33} $K^- \geq 1(\pi^0 \text{ or } K^0 \text{ or } \gamma) \nu_\tau$	(8.59 \pm 0.28) $\times 10^{-3}$	

Modes with K^0 's

Γ_{34} K_S^0 (particles) $^- \nu_\tau$	(9.43 \pm 0.28) $\times 10^{-3}$	
Γ_{35} $h^- K^0 \nu_\tau$	(9.87 \pm 0.14) $\times 10^{-3}$	
Γ_{36} $\pi^- K^0 \nu_\tau$	[a] (8.38 \pm 0.14) $\times 10^{-3}$	
Γ_{37} $\pi^- K^0$ (non- $K^*(892)^-\nu_\tau$)	(5.4 \pm 2.1) $\times 10^{-4}$	
Γ_{38} $K^- K^0 \nu_\tau$	[a] (1.486 \pm 0.034) $\times 10^{-3}$	
Γ_{39} $K^- K^0 \geq 0\pi^0 \nu_\tau$	(2.99 \pm 0.07) $\times 10^{-3}$	
Γ_{40} $h^- K^0 \pi^0 \nu_\tau$	(5.32 \pm 0.13) $\times 10^{-3}$	
Γ_{41} $\pi^- K^0 \pi^0 \nu_\tau$	[a] (3.82 \pm 0.13) $\times 10^{-3}$	
Γ_{42} $\bar{K}^0 \rho^- \nu_\tau$	(2.2 \pm 0.5) $\times 10^{-3}$	
Γ_{43} $K^- K^0 \pi^0 \nu_\tau$	[a] (1.50 \pm 0.07) $\times 10^{-3}$	
Γ_{44} $\pi^- K^0 \geq 1\pi^0 \nu_\tau$	(4.08 \pm 0.25) $\times 10^{-3}$	
Γ_{45} $\pi^- K^0 \pi^0 \pi^0 \nu_\tau$ (ex. K^0)	[a] (2.6 \pm 2.3) $\times 10^{-4}$	
Γ_{46} $K^- K^0 \pi^0 \pi^0 \nu_\tau$	< 1.6 $\times 10^{-4}$ CL=95%	
Γ_{47} $\pi^- K^0 \bar{K}^0 \nu_\tau$	(1.55 \pm 0.24) $\times 10^{-3}$	
Γ_{48} $\pi^- K_S^0 K_S^0 \nu_\tau$	[a] (2.35 \pm 0.06) $\times 10^{-4}$	
Γ_{49} $\pi^- K_S^0 K_L^0 \nu_\tau$	[a] (1.08 \pm 0.24) $\times 10^{-3}$	
Γ_{50} $\pi^- K_L^0 K_L^0 \nu_\tau$	(2.35 \pm 0.06) $\times 10^{-4}$	
Γ_{51} $\pi^- K^0 \bar{K}^0 \pi^0 \nu_\tau$	(3.6 \pm 1.2) $\times 10^{-4}$	
Γ_{52} $\pi^- K_S^0 K_S^0 \pi^0 \nu_\tau$	[a] (1.82 \pm 0.21) $\times 10^{-5}$	
Γ_{53} $K^* K^0 \pi^0 \nu_\tau \rightarrow \pi^- K_S^0 K_S^0 \pi^0 \nu_\tau$	(1.08 \pm 0.21) $\times 10^{-5}$	
Γ_{54} $f_1(1285)\pi^- \nu_\tau \rightarrow \pi^- K_S^0 K_S^0 \pi^0 \nu_\tau$	(6.8 \pm 1.5) $\times 10^{-6}$	
Γ_{55} $f_1(1420)\pi^- \nu_\tau \rightarrow \pi^- K_S^0 K_S^0 \pi^0 \nu_\tau$	(2.4 \pm 0.8) $\times 10^{-6}$	
Γ_{56} $\pi^- K_S^0 K_L^0 \pi^0 \nu_\tau$	[a] (3.2 \pm 1.2) $\times 10^{-4}$	
Γ_{57} $\pi^- K_L^0 K_L^0 \pi^0 \nu_\tau$	(1.82 \pm 0.21) $\times 10^{-5}$	
Γ_{58} $K^- K_S^0 K_S^0 \nu_\tau$	< 6.3 $\times 10^{-7}$ CL=90%	
Γ_{59} $K^- K_S^0 K_S^0 \pi^0 \nu_\tau$	< 4.0 $\times 10^{-7}$ CL=90%	
Γ_{60} $K^0 h^+ h^- h^- \geq 0$ neutrals ν_τ	< 1.7 $\times 10^{-3}$ CL=95%	
Γ_{61} $K^0 h^+ h^- h^- \nu_\tau$	[a] (2.5 \pm 2.0) $\times 10^{-4}$	

Modes with three charged particles

Γ ₆₂	$h^- h^- h^+ \geq 0$ neutrals $\geq 0 K_L^0 \nu_\tau$	(15.20 ± 0.06) %	
Γ ₆₃	$h^- h^- h^+ \geq 0$ neutrals ν_τ (ex. $K_S^0 \rightarrow \pi^+ \pi^-$) ("3-prong")	(14.55 ± 0.06) %	
Γ ₆₄	$h^- h^- h^+ \nu_\tau$	(9.80 ± 0.05) %	
Γ ₆₅	$h^- h^- h^+ \nu_\tau$ (ex. K^0)	(9.46 ± 0.05) %	
Γ ₆₆	$h^- h^- h^+ \nu_\tau$ (ex. K^0, ω)	(9.43 ± 0.05) %	
Γ ₆₇	$\pi^- \pi^+ \pi^- \nu_\tau$	(9.31 ± 0.05) %	
Γ ₆₈	$\pi^- \pi^+ \pi^- \nu_\tau$ (ex. K^0)	(9.02 ± 0.05) %	
Γ ₆₉	$\pi^- \pi^+ \pi^- \nu_\tau$ (ex. K^0), non-axial vector	< 2.4 %	CL=95%
Γ ₇₀	$\pi^- \pi^+ \pi^- \nu_\tau$ (ex. K^0, ω)	[a] (8.99 ± 0.05) %	
Γ ₇₁	$h^- h^- h^+ \geq 1$ neutrals ν_τ	(5.29 ± 0.05) %	
Γ ₇₂	$h^- h^- h^+ \geq 1 \pi^0 \nu_\tau$ (ex. K^0)	(5.09 ± 0.05) %	
Γ ₇₃	$h^- h^- h^+ \pi^0 \nu_\tau$	(4.76 ± 0.05) %	
Γ ₇₄	$h^- h^- h^+ \pi^0 \nu_\tau$ (ex. K^0)	(4.57 ± 0.05) %	
Γ ₇₅	$h^- h^- h^+ \pi^0 \nu_\tau$ (ex. K^0, ω)	(2.79 ± 0.07) %	
Γ ₇₆	$\pi^- \pi^+ \pi^- \pi^0 \nu_\tau$	(4.62 ± 0.05) %	
Γ ₇₇	$\pi^- \pi^+ \pi^- \pi^0 \nu_\tau$ (ex. K^0)	(4.49 ± 0.05) %	
Γ ₇₈	$\pi^- \pi^+ \pi^- \pi^0 \nu_\tau$ (ex. K^0, ω)	[a] (2.74 ± 0.07) %	
Γ ₇₉	$h^- \rho^0 \nu_\tau$		
Γ ₈₀	$h^- \rho^+ h^- \nu_\tau$		
Γ ₈₁	$h^- \rho^- h^+ \nu_\tau$		
Γ ₈₂	$h^- h^- h^+ \geq 2 \pi^0 \nu_\tau$ (ex. K^0)	(5.17 ± 0.31) × 10 ⁻³	
Γ ₈₃	$h^- h^- h^+ 2 \pi^0 \nu_\tau$	(5.05 ± 0.31) × 10 ⁻³	
Γ ₈₄	$h^- h^- h^+ 2 \pi^0 \nu_\tau$ (ex. K^0)	(4.95 ± 0.31) × 10 ⁻³	
Γ ₈₅	$h^- h^- h^+ 2 \pi^0 \nu_\tau$ (ex. K^0, ω, η)	[a] (10 ± 4) × 10 ⁻⁴	
Γ ₈₆	$h^- h^- h^+ 3 \pi^0 \nu_\tau$	(2.13 ± 0.30) × 10 ⁻⁴	
Γ ₈₇	$2 \pi^- \pi^+ 3 \pi^0 \nu_\tau$ (ex. K^0)	(1.95 ± 0.30) × 10 ⁻⁴	
Γ ₈₈	$2 \pi^- \pi^+ 3 \pi^0 \nu_\tau$ (ex. $K^0, \eta, f_1(1285)$)	(1.7 ± 0.4) × 10 ⁻⁴	
Γ ₈₉	$2 \pi^- \pi^+ 3 \pi^0 \nu_\tau$ (ex. $K^0, \eta, \omega, f_1(1285)$)	[a] (1.4 ± 2.7) × 10 ⁻⁵	
Γ ₉₀	$K^- h^+ h^- \geq 0$ neutrals ν_τ	(6.29 ± 0.14) × 10 ⁻³	
Γ ₉₁	$K^- h^+ \pi^- \nu_\tau$ (ex. K^0)	(4.37 ± 0.07) × 10 ⁻³	
Γ ₉₂	$K^- h^+ \pi^- \pi^0 \nu_\tau$ (ex. K^0)	(8.6 ± 1.2) × 10 ⁻⁴	
Γ ₉₃	$K^- \pi^+ \pi^- \geq 0$ neutrals ν_τ	(4.77 ± 0.14) × 10 ⁻³	
Γ ₉₄	$K^- \pi^+ \pi^- \geq 0 \pi^0 \nu_\tau$ (ex. K^0)	(3.73 ± 0.13) × 10 ⁻³	
Γ ₉₅	$K^- \pi^+ \pi^- \nu_\tau$	(3.45 ± 0.07) × 10 ⁻³	
Γ ₉₆	$K^- \pi^+ \pi^- \nu_\tau$ (ex. K^0)	(2.93 ± 0.07) × 10 ⁻³	
Γ ₉₇	$K^- \pi^+ \pi^- \nu_\tau$ (ex. K^0, ω)	[a] (2.93 ± 0.07) × 10 ⁻³	
Γ ₉₈	$K^- \rho^0 \nu_\tau \rightarrow K^- \pi^+ \pi^- \nu_\tau$	(1.4 ± 0.5) × 10 ⁻³	
Γ ₉₉	$K^- \pi^+ \pi^- \pi^0 \nu_\tau$	(1.31 ± 0.12) × 10 ⁻³	
Γ ₁₀₀	$K^- \pi^+ \pi^- \pi^0 \nu_\tau$ (ex. K^0)	(7.9 ± 1.2) × 10 ⁻⁴	
Γ ₁₀₁	$K^- \pi^+ \pi^- \pi^0 \nu_\tau$ (ex. K^0, η)	(7.6 ± 1.2) × 10 ⁻⁴	
Γ ₁₀₂	$K^- \pi^+ \pi^- \pi^0 \nu_\tau$ (ex. K^0, ω)	(3.7 ± 0.9) × 10 ⁻⁴	
Γ ₁₀₃	$K^- \pi^+ \pi^- \pi^0 \nu_\tau$ (ex. K^0, ω, η)	[a] (3.9 ± 1.4) × 10 ⁻⁴	
Γ ₁₀₄	$K^- \pi^+ K^- \geq 0$ neut. ν_τ	< 9 × 10 ⁻⁴	CL=95%
Γ ₁₀₅	$K^- K^+ \pi^- \geq 0$ neut. ν_τ	(1.496 ± 0.033) × 10 ⁻³	
Γ ₁₀₆	$K^- K^+ \pi^- \nu_\tau$	[a] (1.435 ± 0.027) × 10 ⁻³	
Γ ₁₀₇	$K^- K^+ \pi^- \pi^0 \nu_\tau$	[a] (6.1 ± 1.8) × 10 ⁻⁵	
Γ ₁₀₈	$K^- K^+ K^- \nu_\tau$	(2.2 ± 0.8) × 10 ⁻⁵	S=5.4
Γ ₁₀₉	$K^- K^+ K^- \nu_\tau$ (ex. ϕ)	< 2.5 × 10 ⁻⁶	CL=90%
Γ ₁₁₀	$K^- K^+ K^- \pi^0 \nu_\tau$	< 4.8 × 10 ⁻⁶	CL=90%
Γ ₁₁₁	$\pi^- K^+ \pi^- \geq 0$ neut. ν_τ	< 2.5 × 10 ⁻³	CL=95%
Γ ₁₁₂	$e^- e^- e^+ \bar{\nu}_e \nu_\tau$	(2.8 ± 1.5) × 10 ⁻⁵	
Γ ₁₁₃	$\mu^- e^- e^+ \bar{\nu}_\mu \nu_\tau$	< 3.2 × 10 ⁻⁵	CL=90%
Γ ₁₁₄	$\pi^- e^- e^+ \nu_\tau$		
Γ ₁₁₅	$\pi^- \mu^- \mu^+ \nu_\tau$	< 1.14 × 10 ⁻⁵	CL=90%

Modes with five charged particles

Γ ₁₁₆	$3h^- 2h^+ \geq 0$ neutrals ν_τ (ex. $K_S^0 \rightarrow \pi^- \pi^+$) ("5-prong")	(9.9 ± 0.4) × 10 ⁻⁴	
Γ ₁₁₇	$3h^- 2h^+ \nu_\tau$ (ex. K^0)	(8.29 ± 0.31) × 10 ⁻⁴	
Γ ₁₁₈	$3\pi^- 2\pi^+ \nu_\tau$ (ex. K^0, ω)	(8.27 ± 0.31) × 10 ⁻⁴	
Γ ₁₁₉	$3\pi^- 2\pi^+ \nu_\tau$ (ex. $K^0, \omega, f_1(1285)$)	[a] (7.75 ± 0.30) × 10 ⁻⁴	
Γ ₁₂₀	$K^- 2\pi^- 2\pi^+ \nu_\tau$ (ex. K^0)	[a] (6 ± 12) × 10 ⁻⁷	
Γ ₁₂₁	$K^+ 3\pi^- \pi^+ \nu_\tau$	< 5.0 × 10 ⁻⁶	CL=90%
Γ ₁₂₂	$K^+ K^- 2\pi^- \pi^+ \nu_\tau$	< 4.5 × 10 ⁻⁷	CL=90%

Γ ₁₂₃	$3h^- 2h^+ \pi^0 \nu_\tau$ (ex. K^0)	(1.65 ± 0.11) × 10 ⁻⁴	
Γ ₁₂₄	$3\pi^- 2\pi^+ \pi^0 \nu_\tau$ (ex. K^0)	(1.63 ± 0.11) × 10 ⁻⁴	
Γ ₁₂₅	$3\pi^- 2\pi^+ \pi^0 \nu_\tau$ (ex. $K^0, \eta, f_1(1285)$)	(1.11 ± 0.10) × 10 ⁻⁴	
Γ ₁₂₆	$3\pi^- 2\pi^+ \pi^0 \nu_\tau$ (ex. $K^0, \eta, \omega, f_1(1285)$)	[a] (3.8 ± 0.9) × 10 ⁻⁵	
Γ ₁₂₇	$K^- 2\pi^- 2\pi^+ \pi^0 \nu_\tau$ (ex. K^0)	[a] (1.1 ± 0.6) × 10 ⁻⁶	
Γ ₁₂₈	$K^+ 3\pi^- \pi^+ \pi^0 \nu_\tau$	< 8 × 10 ⁻⁷	CL=90%
Γ ₁₂₉	$3h^- 2h^+ 2\pi^0 \nu_\tau$	< 3.4 × 10 ⁻⁶	CL=90%

Miscellaneous other allowed modes

Γ ₁₃₀	$(5\pi^-) \nu_\tau$	(7.8 ± 0.5) × 10 ⁻³	
Γ ₁₃₁	$4h^- 3h^+ \geq 0$ neutrals ν_τ ("7-prong")	< 3.0 × 10 ⁻⁷	CL=90%
Γ ₁₃₂	$4h^- 3h^+ \nu_\tau$	< 4.3 × 10 ⁻⁷	CL=90%
Γ ₁₃₃	$4h^- 3h^+ \pi^0 \nu_\tau$	< 2.5 × 10 ⁻⁷	CL=90%
Γ ₁₃₄	$X^- (S=-1) \nu_\tau$	(2.92 ± 0.04) %	
Γ ₁₃₅	$K^*(892)^- \geq 0$ neutrals $\geq 0 K_L^0 \nu_\tau$	(1.42 ± 0.18) %	S=1.4
Γ ₁₃₆	$K^*(892)^- \nu_\tau$	(1.20 ± 0.07) %	S=1.8
Γ ₁₃₇	$K^*(892)^- \nu_\tau \rightarrow \pi^- \bar{K}^0 \nu_\tau$	(7.82 ± 0.26) × 10 ⁻³	
Γ ₁₃₈	$K^*(892)^0 K^- \geq 0$ neutrals ν_τ	(3.2 ± 1.4) × 10 ⁻³	
Γ ₁₃₉	$K^*(892)^0 K^- \nu_\tau$	(2.1 ± 0.4) × 10 ⁻³	
Γ ₁₄₀	$\bar{K}^*(892)^0 \pi^- \geq 0$ neutrals ν_τ	(3.8 ± 1.7) × 10 ⁻³	
Γ ₁₄₁	$\bar{K}^*(892)^0 \pi^- \nu_\tau$	(2.2 ± 0.5) × 10 ⁻³	
Γ ₁₄₂	$(\bar{K}^*(892) \pi^-) \nu_\tau \rightarrow \pi^- \bar{K}^0 \pi^0 \nu_\tau$	(1.0 ± 0.4) × 10 ⁻³	
Γ ₁₄₃	$K_1^*(1270)^- \nu_\tau$	(4.7 ± 1.1) × 10 ⁻³	
Γ ₁₄₄	$K_1^*(1400)^- \nu_\tau$	(1.7 ± 2.6) × 10 ⁻³	S=1.7
Γ ₁₄₅	$K^*(1410)^- \nu_\tau$	(1.5 ± 1.4) × 10 ⁻³	
Γ ₁₄₆	$K_0^*(1430)^- \nu_\tau$	< 5 × 10 ⁻⁴	CL=95%
Γ ₁₄₇	$K_2^*(1430)^- \nu_\tau$	< 3 × 10 ⁻³	CL=95%
Γ ₁₄₈	$a_0(980)^- \geq 0$ neutrals ν_τ		
Γ ₁₄₉	$\eta \pi^- \nu_\tau$	< 9.9 × 10 ⁻⁵	CL=95%
Γ ₁₅₀	$\eta \pi^- \pi^0 \nu_\tau$	[a] (1.39 ± 0.07) × 10 ⁻³	
Γ ₁₅₁	$\eta \pi^- \pi^0 \pi^0 \nu_\tau$	[a] (2.0 ± 0.4) × 10 ⁻⁴	
Γ ₁₅₂	$\eta K^- \nu_\tau$	[a] (1.55 ± 0.08) × 10 ⁻⁴	
Γ ₁₅₃	$\eta K^*(892)^- \nu_\tau$	(1.38 ± 0.15) × 10 ⁻⁴	
Γ ₁₅₄	$\eta K^- \pi^0 \nu_\tau$	[a] (4.8 ± 1.2) × 10 ⁻⁵	
Γ ₁₅₅	$\eta K^- \pi^0$ (non- $K^*(892)$) ν_τ	< 3.5 × 10 ⁻⁵	CL=90%
Γ ₁₅₆	$\eta \bar{K}^0 \pi^- \nu_\tau$	[a] (9.4 ± 1.5) × 10 ⁻⁵	
Γ ₁₅₇	$\eta \bar{K}^0 \pi^- \pi^0 \nu_\tau$	< 5.0 × 10 ⁻⁵	CL=90%
Γ ₁₅₈	$\eta K^- K^0 \nu_\tau$	< 9.0 × 10 ⁻⁶	CL=90%
Γ ₁₅₉	$\eta \pi^+ \pi^- \pi^- \geq 0$ neutrals ν_τ	< 3 × 10 ⁻³	CL=90%
Γ ₁₆₀	$\eta \pi^- \pi^+ \pi^- \nu_\tau$ (ex. K^0)	[a] (2.20 ± 0.13) × 10 ⁻⁴	
Γ ₁₆₁	$\eta \pi^- \pi^+ \pi^- \nu_\tau$ (ex. $K^0, f_1(1285)$)	(9.9 ± 1.6) × 10 ⁻⁵	
Γ ₁₆₂	$\eta a_1(1260)^- \nu_\tau \rightarrow \eta \pi^- \rho^0 \nu_\tau$	< 3.9 × 10 ⁻⁴	CL=90%
Γ ₁₆₃	$\eta \eta \pi^- \nu_\tau$	< 7.4 × 10 ⁻⁶	CL=90%
Γ ₁₆₄	$\eta \eta \pi^- \pi^0 \nu_\tau$	< 2.0 × 10 ⁻⁴	CL=95%
Γ ₁₆₅	$\eta \eta K^- \nu_\tau$	< 3.0 × 10 ⁻⁶	CL=90%
Γ ₁₆₆	$\eta'(958) \pi^- \nu_\tau$	< 4.0 × 10 ⁻⁶	CL=90%
Γ ₁₆₇	$\eta'(958) \pi^- \pi^0 \nu_\tau$	< 1.2 × 10 ⁻⁵	CL=90%
Γ ₁₆₈	$\eta'(958) K^- \nu_\tau$	< 2.4 × 10 ⁻⁶	CL=90%
Γ ₁₆₉	$\phi \pi^- \nu_\tau$	(3.4 ± 0.6) × 10 ⁻⁵	
Γ ₁₇₀	$\phi K^- \nu_\tau$	[a] (4.4 ± 1.6) × 10 ⁻⁵	
Γ ₁₇₁	$f_1(1285) \pi^- \nu_\tau$	(3.9 ± 0.5) × 10 ⁻⁴	S=1.9
Γ ₁₇₂	$f_1(1285) \pi^- \nu_\tau \rightarrow \eta \pi^- \pi^+ \pi^- \nu_\tau$	(1.18 ± 0.07) × 10 ⁻⁴	S=1.3
Γ ₁₇₃	$f_1(1285) \pi^- \nu_\tau \rightarrow 3\pi^- 2\pi^+ \nu_\tau$	[a] (5.2 ± 0.4) × 10 ⁻⁵	
Γ ₁₇₄	$\pi(1300)^- \nu_\tau \rightarrow (\rho \pi)^- \nu_\tau \rightarrow (3\pi)^- \nu_\tau$	< 1.0 × 10 ⁻⁴	CL=90%
Γ ₁₇₅	$\pi(1300)^- \nu_\tau \rightarrow ((\pi \pi)_{S\text{-wave}} \pi)^- \nu_\tau \rightarrow (3\pi)^- \nu_\tau$	< 1.9 × 10 ⁻⁴	CL=90%
Γ ₁₇₆	$h^- \omega \geq 0$ neutrals ν_τ	(2.40 ± 0.08) %	
Γ ₁₇₇	$h^- \omega \nu_\tau$	(1.99 ± 0.06) %	
Γ ₁₇₈	$\pi^- \omega \nu_\tau$	[a] (1.95 ± 0.06) %	
Γ ₁₇₉	$K^- \omega \nu_\tau$	[a] (4.1 ± 0.9) × 10 ⁻⁴	
Γ ₁₈₀	$h^- \omega \pi^0 \nu_\tau$	[a] (4.1 ± 0.4) × 10 ⁻³	
Γ ₁₈₁	$h^- \omega 2\pi^0 \nu_\tau$	(1.4 ± 0.5) × 10 ⁻⁴	
Γ ₁₈₂	$\pi^- \omega 2\pi^0 \nu_\tau$	[a] (7.2 ± 1.6) × 10 ⁻⁵	
Γ ₁₈₃	$h^- 2\omega \nu_\tau$	< 5.4 × 10 ⁻⁷	CL=90%
Γ ₁₈₄	$2h^- h^+ \omega \nu_\tau$	(1.20 ± 0.22) × 10 ⁻⁴	
Γ ₁₈₅	$2\pi^- \pi^+ \omega \nu_\tau$ (ex. K^0)	[a] (8.4 ± 0.6) × 10 ⁻⁵	

Lepton Particle Listings

T

ments of $B(\tau \rightarrow 3\text{-prong})$ and $B(\tau \rightarrow 5\text{-prong})$ are -0.98 and -0.08 respectively.
 2 The correlation coefficients between this measurement and the ACHARD 01D measurements of $B(\tau \rightarrow "3\text{-prong}")$ and $B(\tau \rightarrow "5\text{-prong}")$ are -0.978 and -0.082 respectively.

$\Gamma(\text{particle}^- \geq 0 \text{ neutrals} \geq 0K_L^0 \nu_\tau)/\Gamma_{\text{total}} \quad \Gamma_2/\Gamma$
 $\Gamma_2/\Gamma = (\Gamma_3 + \Gamma_5 + \Gamma_9 + \Gamma_{10} + \Gamma_{14} + \Gamma_{16} + \Gamma_{20} + \Gamma_{23} + \Gamma_{27} + \Gamma_{28} + \Gamma_{30} + 0.6534\Gamma_{36} + 0.6534\Gamma_{38} + 0.6534\Gamma_{41} + 0.6534\Gamma_{43} + 0.6534\Gamma_{45} + 0.0942\Gamma_{48} + 0.3069\Gamma_{49} + \Gamma_{50} + 0.0942\Gamma_{52} + 0.3069\Gamma_{56} + \Gamma_{57} + 0.7212\Gamma_{150} + 0.7212\Gamma_{152} + 0.7212\Gamma_{154} + 0.4712\Gamma_{156} + 0.1049\Gamma_{170} + 0.0840\Gamma_{178} + 0.0840\Gamma_{179} + 0.0840\Gamma_{180})/\Gamma$

VALUE (%)	EVTS	DOCUMENT ID	TECN	COMMENT
84.58 ± 0.06 OUR FIT				
85.1 ± 0.4 OUR AVERAGE				
• • • We use the following data for averages but not for fits. • • •				
85.6 ± 0.6 ± 0.3	3300	1 ADEVA	91F L3	$E_{\text{cm}}^{\text{ee}} = 88.3\text{--}94.3$ GeV
84.9 ± 0.4 ± 0.3		BEHREND	89B CELL	$E_{\text{cm}}^{\text{ee}} = 14\text{--}47$ GeV
84.7 ± 0.8 ± 0.6		2 AIHARA	87B TPC	$E_{\text{cm}}^{\text{ee}} = 29$ GeV
• • • We do not use the following data for averages, fits, limits, etc. • • •				
86.4 ± 0.3 ± 0.3		ABACHI	89B HRS	$E_{\text{cm}}^{\text{ee}} = 29$ GeV
87.1 ± 1.0 ± 0.7		3 BURCHAT	87 MRK2	$E_{\text{cm}}^{\text{ee}} = 29$ GeV
87.2 ± 0.5 ± 0.8		SCHMIDKE	86 MRK2	$E_{\text{cm}}^{\text{ee}} = 29$ GeV
84.7 ± 1.1 ± 1.6	169	4 ALTHOFF	85 TASS	$E_{\text{cm}}^{\text{ee}} = 34.5$ GeV
86.1 ± 0.5 ± 0.9		BARTEL	85F JADE	$E_{\text{cm}}^{\text{ee}} = 34.6$ GeV
87.8 ± 1.3 ± 3.9		5 BERGER	85 PLUT	$E_{\text{cm}}^{\text{ee}} = 34.6$ GeV
86.7 ± 0.3 ± 0.6		FERNANDEZ	85 MAC	$E_{\text{cm}}^{\text{ee}} = 29$ GeV

1 Not independent of ADEVA 91F $\Gamma(h^- h^- h^+ \geq 0 \text{ neutrals} \geq 0K_L^0 \nu_\tau)/\Gamma_{\text{total}}$ value.
 2 Not independent of AIHARA 87B $\Gamma(\mu^- \bar{\nu}_\mu \nu_\tau)/\Gamma_{\text{total}}$, $\Gamma(e^- \bar{\nu}_e \nu_\tau)/\Gamma_{\text{total}}$, and $\Gamma(h^- \geq 0 \text{ neutrals} \geq 0K_L^0 \nu_\tau)/\Gamma_{\text{total}}$ values.
 3 Not independent of SCHMIDKE 86 value (also not independent of BURCHAT 87 value for $\Gamma(h^- h^- h^+ \geq 0 \text{ neutrals} \geq 0K_L^0 \nu_\tau)/\Gamma_{\text{total}}$.
 4 Not independent of ALTHOFF 85 $\Gamma(\mu^- \bar{\nu}_\mu \nu_\tau)/\Gamma_{\text{total}}$, $\Gamma(e^- \bar{\nu}_e \nu_\tau)/\Gamma_{\text{total}}$, $\Gamma(h^- \geq 0 \text{ neutrals} \geq 0K_L^0 \nu_\tau)/\Gamma_{\text{total}}$, and $\Gamma(h^- h^- h^+ \geq 0 \text{ neutrals} \geq 0K_L^0 \nu_\tau)/\Gamma_{\text{total}}$ values.
 5 Not independent of (1-prong + $0\pi^0$) and (1-prong + $\geq 1\pi^0$) values.

$\Gamma(\mu^- \bar{\nu}_\mu \nu_\tau)/\Gamma_{\text{total}} \quad \Gamma_3/\Gamma$
 To minimize the effect of experiments with large systematic errors, we exclude experiments which together would contribute 5% of the weight in the average.

VALUE (%)	EVTS	DOCUMENT ID	TECN	COMMENT
17.39 ± 0.04 OUR FIT				
17.33 ± 0.05 OUR AVERAGE				
17.319 ± 0.070 ± 0.032	54k	1 SCHAEEL	05c ALEP	1991-1995 LEP runs
17.34 ± 0.09 ± 0.06	31.4k	ABBIENDI	03 OPAL	1990-1995 LEP runs
17.342 ± 0.110 ± 0.067	21.5k	2 ACCIARRI	01F L3	1991-1995 LEP runs
17.325 ± 0.095 ± 0.077	27.7k	ABREU	99X DLPH	1991-1995 LEP runs
• • • We use the following data for averages but not for fits. • • •				
17.37 ± 0.08 ± 0.18		3 ANASTASSOV	97 CLEO	$E_{\text{cm}}^{\text{ee}} = 10.6$ GeV
• • • We do not use the following data for averages, fits, limits, etc. • • •				
17.31 ± 0.11 ± 0.05	20.7k	BUSKULIC	96c ALEP	Repl. by SCHAEEL 05c
17.02 ± 0.19 ± 0.24	6586	ABREU	95T DLPH	Repl. by ABREU 99X
17.36 ± 0.27	7941	AKERS	95I OPAL	Repl. by ABBIENDI 03
17.6 ± 0.4 ± 0.4	2148	ADRIANI	93M L3	Repl. by ACCIARRI 01F
17.4 ± 0.3 ± 0.5		4 ALBRECHT	93G ARG	$E_{\text{cm}}^{\text{ee}} = 9.4\text{--}10.6$ GeV
17.35 ± 0.41 ± 0.37		DECAMP	92c ALEP	1989-1990 LEP runs
17.7 ± 0.8 ± 0.4	568	BEHREND	90 CELL	$E_{\text{cm}}^{\text{ee}} = 35$ GeV
17.4 ± 1.0	2197	ADEVA	88 MRKJ	$E_{\text{cm}}^{\text{ee}} = 14\text{--}16$ GeV
17.7 ± 1.2 ± 0.7		AIHARA	87B TPC	$E_{\text{cm}}^{\text{ee}} = 29$ GeV
18.3 ± 0.9 ± 0.8		BURCHAT	87 MRK2	$E_{\text{cm}}^{\text{ee}} = 29$ GeV
18.6 ± 0.8 ± 0.7	558	5 BARTEL	86D JADE	$E_{\text{cm}}^{\text{ee}} = 34.6$ GeV
12.9 ± 1.7 ± 0.7		ALTHOFF	85B TASS	$E_{\text{cm}}^{\text{ee}} = 34.5$ GeV
18.0 ± 0.9 ± 0.5	473	5 ASH	85B MAC	$E_{\text{cm}}^{\text{ee}} = 29$ GeV
18.0 ± 1.0 ± 0.6		6 BALTRUSAITIS...	85 MRK3	$E_{\text{cm}}^{\text{ee}} = 3.77$ GeV
19.4 ± 1.6 ± 1.7	153	BERGER	85 PLUT	$E_{\text{cm}}^{\text{ee}} = 34.6$ GeV
17.6 ± 2.6 ± 2.1	47	BEHREND	83c CELL	$E_{\text{cm}}^{\text{ee}} = 34$ GeV
17.8 ± 2.0 ± 1.8		BERGER	81B PLUT	$E_{\text{cm}}^{\text{ee}} = 9\text{--}32$ GeV

1 See footnote to SCHAEEL 05c $\Gamma(\tau^- \rightarrow e^- \bar{\nu}_e \nu_\tau)/\Gamma_{\text{total}}$ measurement for correlations with other measurements.
 2 The correlation coefficient between this measurement and the ACCIARRI 01F measurement of $B(\tau^- \rightarrow e^- \bar{\nu}_e \nu_\tau)$ is 0.08.
 3 The correlation coefficients between this measurement and the ANASTASSOV 97 measurements of $B(e^- \bar{\nu}_e \nu_\tau)$, $B(\mu^- \bar{\nu}_\mu \nu_\tau)$, $B(h^- \nu_\tau)$, and $B(h^- \nu_\tau)/B(e^- \bar{\nu}_e \nu_\tau)$ are 0.50, 0.58, 0.50, and 0.08 respectively.
 4 Not independent of ALBRECHT 92D $\Gamma(\mu^- \bar{\nu}_\mu \nu_\tau)/\Gamma_{\text{total}}$ and ALBRECHT 93G $\Gamma(\mu^- \bar{\nu}_\mu \nu_\tau) \times \Gamma(e^- \bar{\nu}_e \nu_\tau)/\Gamma_{\text{total}}$ values.
 5 Modified using $B(e^- \bar{\nu}_e \nu_\tau)/B("1 \text{ prong}"), = 0.855$.
 6 Error correlated with BALTRUSAITIS 85 $e^- \bar{\nu}_e \nu_\tau$.

$\Gamma(\mu^- \bar{\nu}_\mu \nu_\tau \gamma)/\Gamma_{\text{total}} \quad \Gamma_4/\Gamma$
 VALUE (%) EVTS DOCUMENT ID TECN COMMENT

0.367 ± 0.008 OUR AVERAGE				
0.363 ± 0.002 ± 0.015	22K	1 SHIMIZU	18A BELL	711 fb ⁻¹ $E_{\text{cm}}^{\text{ee}} = 10.6$ GeV
0.369 ± 0.003 ± 0.010	16k	2 LEES	15G BABR	431 fb ⁻¹ $E_{\text{cm}}^{\text{ee}} = 10.6$ GeV
0.361 ± 0.016 ± 0.035		3 BERGFELD	00 CLEO	$E_{\text{cm}}^{\text{ee}} = 10.6$ GeV
• • • We do not use the following data for averages, fits, limits, etc. • • •				
0.30 ± 0.04 ± 0.05	116	4 ALEXANDER	96S OPAL	1991-1994 LEP runs
0.23 ± 0.10	10	5 WU	90 MRK2	$E_{\text{cm}}^{\text{ee}} = 29$ GeV

1 SHIMIZU 18A impose requirements on detected γ 's corresponding to a τ -rest-frame energy cutoff $E_\gamma^* > 10$ MeV.
 2 LEES 15G impose requirements on detected γ 's corresponding to a τ -rest-frame energy cutoff $E_\gamma^* > 10$ MeV.
 3 BERGFELD 00 impose requirements on detected γ 's corresponding to a τ -rest-frame energy cutoff $E_\gamma^* > 10$ MeV. For $E_\gamma^* > 20$ MeV, they quote $(3.04 \pm 0.14 \pm 0.30) \times 10^{-3}$.
 4 ALEXANDER 96S impose requirements on detected γ 's corresponding to a τ -rest-frame energy cutoff $E_\gamma > 20$ MeV.
 5 WU 90 reports $\Gamma(\mu^- \bar{\nu}_\mu \nu_\tau \gamma)/\Gamma(\mu^- \bar{\nu}_\mu \nu_\tau) = 0.013 \pm 0.006$, which is converted to $\Gamma(\mu^- \bar{\nu}_\mu \nu_\tau \gamma)/\Gamma_{\text{total}}$ using $\Gamma(\mu^- \bar{\nu}_\mu \nu_\tau \gamma)/\Gamma_{\text{total}} = 17.35\%$. Requirements on detected γ 's correspond to a τ rest frame energy cutoff $E_\gamma > 37$ MeV.

$\Gamma(e^- \bar{\nu}_e \nu_\tau)/\Gamma_{\text{total}} \quad \Gamma_5/\Gamma$
 To minimize the effect of experiments with large systematic errors, we exclude experiments which together would contribute 5% of the weight in the average.

VALUE (%)	EVTS	DOCUMENT ID	TECN	COMMENT
17.82 ± 0.04 OUR FIT				
17.82 ± 0.05 OUR AVERAGE				
17.837 ± 0.072 ± 0.036	5.6k	1 SCHAEEL	05c ALEP	1991-1995 LEP runs
17.806 ± 0.104 ± 0.076	24.7k	2 ACCIARRI	01F L3	1991-1995 LEP runs
17.81 ± 0.09 ± 0.06	33.1k	ABBIENDI	99H OPAL	1991-1995 LEP runs
17.877 ± 0.109 ± 0.110	23.3k	ABREU	99X DLPH	1991-1995 LEP runs
17.76 ± 0.06 ± 0.17		3 ANASTASSOV	97 CLEO	$E_{\text{cm}}^{\text{ee}} = 10.6$ GeV
• • • We do not use the following data for averages, fits, limits, etc. • • •				
17.78 ± 0.10 ± 0.09	25.3k	ALEXANDER	96D OPAL	Repl. by ABBI- ENDI 99H
17.79 ± 0.12 ± 0.06	20.6k	BUSKULIC	96c ALEP	Repl. by SCHAEEL 05c
17.51 ± 0.23 ± 0.31	5059	ABREU	95T DLPH	Repl. by ABREU 99X
17.9 ± 0.4 ± 0.4	2892	ADRIANI	93M L3	Repl. by ACCIARRI 01F
17.5 ± 0.3 ± 0.5		4 ALBRECHT	93G ARG	$E_{\text{cm}}^{\text{ee}} = 9.4\text{--}10.6$ GeV
17.97 ± 0.14 ± 0.23	3970	AKERIB	92 CLEO	Repl. by ANA S- TASSOV 97
19.1 ± 0.4 ± 0.6	2960	5 AMMAR	92 CLEO	$E_{\text{cm}}^{\text{ee}} = 10.5\text{--}10.9$ GeV
18.09 ± 0.45 ± 0.45		DECAMP	92c ALEP	Repl. by SCHAEEL 05c
17.0 ± 0.5 ± 0.6	1.7k	ABACHI	90 HRS	$E_{\text{cm}}^{\text{ee}} = 29$ GeV
18.4 ± 0.8 ± 0.4	644	BEHREND	90 CELL	$E_{\text{cm}}^{\text{ee}} = 35$ GeV
16.3 ± 0.3 ± 3.2		JANSEN	89 CBAL	$E_{\text{cm}}^{\text{ee}} = 9.4\text{--}10.6$ GeV
18.4 ± 1.2 ± 1.0		AIHARA	87B TPC	$E_{\text{cm}}^{\text{ee}} = 29$ GeV
19.1 ± 0.8 ± 1.1		BURCHAT	87 MRK2	$E_{\text{cm}}^{\text{ee}} = 29$ GeV
16.8 ± 0.7 ± 0.9	515	5 BARTEL	86D JADE	$E_{\text{cm}}^{\text{ee}} = 34.6$ GeV
20.4 ± 3.0 ± 1.4		ALTHOFF	85 TASS	$E_{\text{cm}}^{\text{ee}} = 34.5$ GeV
17.8 ± 0.9 ± 0.6	390	5 ASH	85B MAC	$E_{\text{cm}}^{\text{ee}} = 29$ GeV
18.2 ± 0.7 ± 0.5		6 BALTRUSAITIS...	85 MRK3	$E_{\text{cm}}^{\text{ee}} = 3.77$ GeV
13.0 ± 1.9 ± 2.9		BERGER	85 PLUT	$E_{\text{cm}}^{\text{ee}} = 34.6$ GeV
18.3 ± 2.4 ± 1.9	60	BEHREND	83c CELL	$E_{\text{cm}}^{\text{ee}} = 34$ GeV
16.0 ± 1.3	459	7 BACINO	78B DLCO	$E_{\text{cm}}^{\text{ee}} = 3.1\text{--}7.4$ GeV

1 Correlation matrix for SCHAEEL 05c branching fractions, in percent:
 (1) $\Gamma(\tau^- \rightarrow e^- \bar{\nu}_e \nu_\tau)/\Gamma_{\text{total}}$
 (2) $\Gamma(\tau^- \rightarrow \mu^- \bar{\nu}_\mu \nu_\tau)/\Gamma_{\text{total}}$
 (3) $\Gamma(\tau^- \rightarrow \pi^- \nu_\tau)/\Gamma_{\text{total}}$
 (4) $\Gamma(\tau^- \rightarrow \pi^- \pi^0 \nu_\tau)/\Gamma_{\text{total}}$
 (5) $\Gamma(\tau^- \rightarrow \pi^- 2\pi^0 \nu_\tau (\text{ex. } K^0))/\Gamma_{\text{total}}$
 (6) $\Gamma(\tau^- \rightarrow \pi^- 3\pi^0 \nu_\tau (\text{ex. } K^0))/\Gamma_{\text{total}}$
 (7) $\Gamma(\tau^- \rightarrow h^- 4\pi^0 \nu_\tau (\text{ex. } K^0, \eta))/\Gamma_{\text{total}}$
 (8) $\Gamma(\tau^- \rightarrow \pi^- \pi^+ \pi^- \nu_\tau (\text{ex. } K^0, \omega))/\Gamma_{\text{total}}$
 (9) $\Gamma(\tau^- \rightarrow \pi^- \pi^+ \pi^- \pi^0 \nu_\tau (\text{ex. } K^0))/\Gamma_{\text{total}}$
 (10) $\Gamma(\tau^- \rightarrow h^- h^- h^+ 2\pi^0 \nu_\tau (\text{ex. } K^0))/\Gamma_{\text{total}}$
 (11) $\Gamma(\tau^- \rightarrow h^- h^- h^+ 3\pi^0 \nu_\tau)/\Gamma_{\text{total}}$
 (12) $\Gamma(\tau^- \rightarrow 3h^- 2h^+ \nu_\tau (\text{ex. } K^0))/\Gamma_{\text{total}}$
 (13) $\Gamma(\tau^- \rightarrow 3h^- 2h^+ \pi^0 \nu_\tau (\text{ex. } K^0))/\Gamma_{\text{total}}$

(1)	(2)	(3)	(4)	(5)	(6)	(7)	(8)	(9)	(10)	(11)	(12)
(2)	-20										
(3)	-9	-6									
(4)	-16	-12	2								
(5)	-5	-5	-17	-37							
(6)	0	-4	-15	2	-27						
(7)	-2	-4	-24	-15	20	-47					
(8)	-14	-9	15	-5	-17	-14	-8				

(9)	-13	-12	-25	-30	4	-2	16	-15				
(10)	0	-2	-23	-14	4	10	13	-6	-17			
(11)	1	0	-5	1	4	6	0	-9	-2	-11		
(12)	0	1	9	4	-8	-4	-6	9	-5	-4	-2	
(13)	1	-4	-3	-5	3	2	-4	-3	-1	4	1	-24

- ² The correlation coefficient between this measurement and the ACCIARRI 01F measurement of $B(\tau^- \rightarrow \mu^- \bar{\nu}_\mu \nu_\tau)$ is 0.08.
- ³ The correlation coefficients between this measurement and the ANASTASSOV 97 measurements of $B(\mu \bar{\nu}_\mu \nu_\tau)$, $B(\mu \bar{\nu}_\mu \nu_\tau)/B(e \bar{\nu}_e \nu_\tau)$, $B(h^- \nu_\tau)$, and $B(h^- \nu_\tau)/B(e \bar{\nu}_e \nu_\tau)$ are 0.50, -0.42, 0.48, and -0.39 respectively.
- ⁴ Not independent of ALBRECHT 92D $\Gamma(\mu^- \bar{\nu}_\mu \nu_\tau)/\Gamma(e^- \bar{\nu}_e \nu_\tau)$ and ALBRECHT 93G $\Gamma(\mu^- \bar{\nu}_\mu \nu_\tau) \times \Gamma(e^- \bar{\nu}_e \nu_\tau)/\Gamma_{\text{total}}^2$ values.
- ⁵ Modified using $B(e^- \bar{\nu}_e \nu_\tau)/B(\text{"1 prong"})$ and $B(h^- \nu_\tau)$, = 0.855.
- ⁶ Error correlated with BALTRUSAITIS 85 $\Gamma(\mu^- \bar{\nu}_\mu \nu_\tau)/\Gamma_{\text{total}}$.
- ⁷ BACINO 78B value comes from fit to events with e^\pm and one other nonelectron charged prong.

$\Gamma(\mu^- \bar{\nu}_\mu \nu_\tau)/\Gamma(e^- \bar{\nu}_e \nu_\tau)$ Γ_3/Γ_5

Standard Model prediction including mass effects is 0.9726.

VALUE (units 10^{-2})	EVTS	DOCUMENT ID	TECN	COMMENT
97.62 ± 0.28 OUR FIT				
97.9 ± 0.4 OUR AVERAGE				
97.96 ± 0.16 ± 0.36	731k	¹ AUBERT	10F	BABR 467 fb ⁻¹ $E_{\text{cm}}^{\text{ee}} = 10.6$ GeV
97.77 ± 0.63 ± 0.87		² ANASTASSOV 97	CLEO	$E_{\text{cm}}^{\text{ee}} = 10.6$ GeV
99.7 ± 3.5 ± 4.0		ALBRECHT 92D	ARG	$E_{\text{cm}}^{\text{ee}} = 9.4\text{--}10.6$ GeV

- ¹ Correlation matrix for AUBERT 10F branching fractions:
 - $\Gamma(\tau^- \rightarrow \mu^- \bar{\nu}_\mu \nu_\tau) / \Gamma(\tau^- \rightarrow e^- \bar{\nu}_e \nu_\tau)$
 - $\Gamma(\tau^- \rightarrow \pi^- \nu_\tau) / \Gamma(\tau^- \rightarrow e^- \bar{\nu}_e \nu_\tau)$
 - $\Gamma(\tau^- \rightarrow K^- \nu_\tau) / \Gamma(\tau^- \rightarrow e^- \bar{\nu}_e \nu_\tau)$

(1)	(2)
(2)	0.25
(3)	0.12 0.33

- ² The correlation coefficients between this measurement and the ANASTASSOV 97 measurements of $B(\mu \bar{\nu}_\mu \nu_\tau)$, $B(e \bar{\nu}_e \nu_\tau)$, $B(h^- \nu_\tau)$, and $B(h^- \nu_\tau)/B(e \bar{\nu}_e \nu_\tau)$ are 0.58, -0.42, 0.07, and 0.45 respectively.

$\Gamma(e^- \bar{\nu}_e \nu_\tau)/\Gamma_{\text{total}}$ Γ_6/Γ

VALUE (%)	EVTS	DOCUMENT ID	TECN	COMMENT
1.83 ± 0.05 OUR AVERAGE				
1.79 ± 0.02 ± 0.10	12K	¹ SHIMIZU	18A	BELL 711 fb ⁻¹ $E_{\text{cm}}^{\text{ee}} = 10.6$ GeV
1.847 ± 0.015 ± 0.052	18k	² LEES	15G	BABR 431 fb ⁻¹ $E_{\text{cm}}^{\text{ee}} = 10.6$ GeV
1.75 ± 0.06 ± 0.17		³ BERGFELD	00	CLEO $E_{\text{cm}}^{\text{ee}} = 10.6$ GeV

- ¹ SHIMIZU 18A impose requirements on detected γ 's corresponding to a τ -rest-frame energy cutoff $E_\gamma^* > 10$ MeV.
- ² LEES 15G impose requirements on detected γ 's corresponding to a τ -rest-frame energy cutoff $E_\gamma^* > 10$ MeV.
- ³ BERGFELD 00 impose requirements on detected γ 's corresponding to a τ -rest-frame energy cutoff $E_\gamma^* > 10$ MeV.

$\Gamma(h^- \geq 0K_L^0 \nu_\tau)/\Gamma_{\text{total}}$ Γ_7/Γ

$\Gamma_7/\Gamma = (\Gamma_9 + \Gamma_{10} + \frac{1}{2}\Gamma_{36} + \frac{1}{2}\Gamma_{38} + \Gamma_{50})/\Gamma$

VALUE (%)	EVTS	DOCUMENT ID	TECN	COMMENT
12.03 ± 0.05 OUR FIT				
12.2 ± 0.4 OUR AVERAGE				
12.47 ± 0.26 ± 0.43	2967	¹ ACCIARRI	95	L3 1992 LEP run
12.4 ± 0.7 ± 0.7	283	² ABREU	92N	DLPH 1990 LEP run
12.1 ± 0.7 ± 0.5	309	ALEXANDER	91D	OPAL 1990 LEP run
• • • We use the following data for averages but not for fits. • • •				
11.3 ± 0.5 ± 0.8	798	³ FORD	87	MAC $E_{\text{cm}}^{\text{ee}} = 29$ GeV
• • • We do not use the following data for averages, fits, limits, etc. • • •				
12.44 ± 0.11 ± 0.11	15k	⁴ BUSKULIC	96	ALEP Repl. by SCHAEEL 05c
11.7 ± 0.6 ± 0.8		⁵ ALBRECHT	92D	ARG $E_{\text{cm}}^{\text{ee}} = 9.4\text{--}10.6$ GeV
12.98 ± 0.44 ± 0.33		⁶ DECAMP	92c	ALEP Repl. by SCHAEEL 05c
12.3 ± 0.9 ± 0.5	1338	BEHREND	90	CELL $E_{\text{cm}}^{\text{ee}} = 35$ GeV
11.1 ± 1.1 ± 1.4		⁷ BURCHAT	87D	MRK2 $E_{\text{cm}}^{\text{ee}} = 29$ GeV
12.3 ± 0.6 ± 1.1	328	⁸ BARTEL	86D	JADE $E_{\text{cm}}^{\text{ee}} = 34.6$ GeV
13.0 ± 2.0 ± 4.0		BERGER	85	PLUT $E_{\text{cm}}^{\text{ee}} = 34.6$ GeV
11.2 ± 1.7 ± 1.2	34	⁹ BEHREND	83c	CELL $E_{\text{cm}}^{\text{ee}} = 34$ GeV

- ¹ ACCIARRI 95 with 0.65% added to remove their correction for $\pi^- K_L^0$ backgrounds.
- ² ABREU 92N with 0.5% added to remove their correction for $K^*(892)^-$ backgrounds.
- ³ FORD 87 result for $B(\pi^- \nu_\tau)$ with 0.67% added to remove their K^- correction and adjusted for 1992 B("1 prong").
- ⁴ BUSKULIC 96 quote $11.78 \pm 0.11 \pm 0.13$ We add 0.66 to undo their correction for unseen K_L^0 and modify the systematic error accordingly.
- ⁵ Not independent of ALBRECHT 92D $\Gamma(\mu^- \bar{\nu}_\mu \nu_\tau)/\Gamma(e^- \bar{\nu}_e \nu_\tau)$, $\Gamma(\mu^- \bar{\nu}_\mu \nu_\tau) \times \Gamma(e^- \bar{\nu}_e \nu_\tau)$, and $\Gamma(h^- \geq 0K_L^0 \nu_\tau)/\Gamma(e^- \bar{\nu}_e \nu_\tau)$ values.
- ⁶ DECAMP 92c quote $B(h^- \geq 0K_L^0 \nu_\tau) \geq 0(K_S^0 \rightarrow \pi^+ \pi^-) \nu_\tau = 13.32 \pm 0.44 \pm 0.33$. We subtract 0.35 to correct for their inclusion of the K_S^0 decays.

- ⁷ BURCHAT 87 with 1.1% added to remove their correction for K^- and $K^*(892)^-$ backgrounds.
- ⁸ BARTEL 86D result for $B(\pi^- \nu_\tau)$ with 0.59% added to remove their K^- correction and adjusted for 1992 B("1 prong").
- ⁹ BEHREND 83c quote $B(\pi^- \nu_\tau) = 9.9 \pm 1.7 \pm 1.3$ after subtracting 1.3 ± 0.5 to correct for $B(K^- \nu_\tau)$.

$\Gamma(h^- \nu_\tau)/\Gamma_{\text{total}}$ $\Gamma_8/\Gamma = (\Gamma_9 + \Gamma_{10})/\Gamma$

VALUE (%)	EVTS	DOCUMENT ID	TECN	COMMENT
11.61 ± 0.05 OUR FIT				
11.63 ± 0.12 OUR AVERAGE				Error includes scale factor of 1.4. See the ideogram below.
11.571 ± 0.120 ± 0.114	19k	¹ ABDALLAH	06A	DLPH 1992-1995 LEP runs
11.98 ± 0.13 ± 0.16		ACKERSTAFF 98M	OPAL	1991-1995 LEP runs
11.52 ± 0.05 ± 0.12		² ANASTASSOV 97	CLEO	$E_{\text{cm}}^{\text{ee}} = 10.6$ GeV

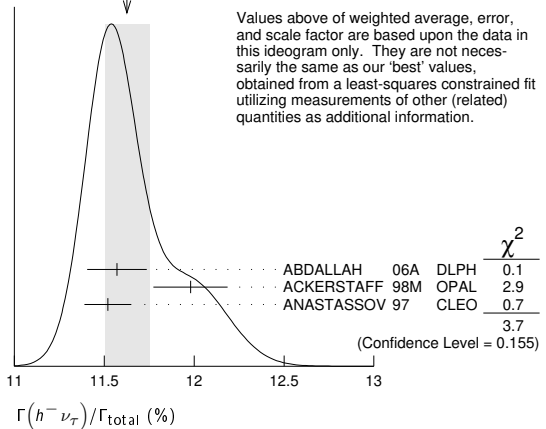
- ¹ Correlation matrix for ABDALLAH 06A branching fractions, in percent:

(1)	$\Gamma(\tau^- \rightarrow h^- \nu_\tau)/\Gamma_{\text{total}}$
(2)	$\Gamma(\tau^- \rightarrow h^- \pi^0 \nu_\tau)/\Gamma_{\text{total}}$
(3)	$\Gamma(\tau^- \rightarrow h^- \geq 1\pi^0 \nu_\tau (\text{ex. } K^0))/\Gamma_{\text{total}}$
(4)	$\Gamma(\tau^- \rightarrow h^- 2\pi^0 \nu_\tau (\text{ex. } K^0))/\Gamma_{\text{total}}$
(5)	$\Gamma(\tau^- \rightarrow h^- \geq 3\pi^0 \nu_\tau (\text{ex. } K^0))/\Gamma_{\text{total}}$
(6)	$\Gamma(\tau^- \rightarrow h^- h^- h^+ \nu_\tau (\text{ex. } K^0))/\Gamma_{\text{total}}$
(7)	$\Gamma(\tau^- \rightarrow h^- h^- h^+ \pi^0 \nu_\tau (\text{ex. } K^0))/\Gamma_{\text{total}}$
(8)	$\Gamma(\tau^- \rightarrow h^- h^- h^+ \geq 1\pi^0 \nu_\tau (\text{ex. } K^0))/\Gamma_{\text{total}}$
(9)	$\Gamma(\tau^- \rightarrow h^- h^- h^+ \geq 2\pi^0 \nu_\tau (\text{ex. } K^0))/\Gamma_{\text{total}}$
(10)	$\Gamma(\tau^- \rightarrow 3h^- 2h^+ \nu_\tau (\text{ex. } K^0))/\Gamma_{\text{total}}$
(11)	$\Gamma(\tau^- \rightarrow 3h^- 2h^+ \pi^0 \nu_\tau (\text{ex. } K^0))/\Gamma_{\text{total}}$

(1)	(2)	(3)	(4)	(5)	(6)	(7)	(8)	(9)	(10)	
(2)	-34									
(3)	-47	56								
(4)	6	-66	15							
(5)	-6	38	11	-86						
(6)	-7	-8	15	0	-2					
(7)	-2	-1	-5	-3	3	-53				
(8)	-4	-4	-13	-4	-2	-56	75			
(9)	-1	-1	-4	3	-6	26	-78	-16		
(10)	-1	-1	1	0	0	-2	-3	-1	3	
(11)	0	0	0	0	0	1	0	-5	5	-57

- ² The correlation coefficients between this measurement and the ANASTASSOV 97 measurements of $B(\mu \bar{\nu}_\mu \nu_\tau)$, $B(e \bar{\nu}_e \nu_\tau)$, $B(\mu \bar{\nu}_\mu \nu_\tau)/B(e \bar{\nu}_e \nu_\tau)$, and $B(h^- \nu_\tau)/B(e \bar{\nu}_e \nu_\tau)$ are 0.50, 0.48, 0.07, and 0.63 respectively.

WEIGHTED AVERAGE
11.63±0.12 (Error scaled by 1.4)



$\Gamma(h^- \nu_\tau)/\Gamma(e^- \bar{\nu}_e \nu_\tau)$ $\Gamma_8/\Gamma_5 = (\Gamma_9 + \Gamma_{10})/\Gamma_5$

VALUE (units 10^{-2})	EVTS	DOCUMENT ID	TECN	COMMENT
64.62 ± 0.33 OUR FIT				
64.0 ± 0.7 OUR AVERAGE				Error includes scale factor of 1.6.
63.33 ± 0.14 ± 0.61	394k	¹ AUBERT	10F	BABR 467 fb ⁻¹ $E_{\text{cm}}^{\text{ee}} = 10.6$ GeV
64.84 ± 0.41 ± 0.60		² ANASTASSOV 97	CLEO	$E_{\text{cm}}^{\text{ee}} = 10.6$ GeV

- ¹ Not independent of AUBERT 10F $\Gamma(\tau^- \rightarrow \pi^- \nu_\tau)/\Gamma(\tau^- \rightarrow e^- \bar{\nu}_e \nu_\tau)$ and $\Gamma(\tau^- \rightarrow K^- \nu_\tau)/\Gamma(\tau^- \rightarrow e^- \bar{\nu}_e \nu_\tau)$.
- ² The correlation coefficients between this measurement and the ANASTASSOV 97 measurements of $B(\mu \bar{\nu}_\mu \nu_\tau)$, $B(e \bar{\nu}_e \nu_\tau)$, $B(\mu \bar{\nu}_\mu \nu_\tau)/B(e \bar{\nu}_e \nu_\tau)$, and $B(h^- \nu_\tau)$ are 0.08, -0.39, 0.45, and 0.63 respectively.

Lepton Particle Listings

 τ $\Gamma(\pi^- \nu_\tau)/\Gamma_{\text{total}}$ Γ_9/Γ

VALUE (%)	EVTS	DOCUMENT ID	TECN	COMMENT
10.82 ± 0.05 OUR FIT				
10.828 ± 0.070 ± 0.078	38k	1 SCHAEL	05c ALEP	1991-1995 LEP runs
11.06 ± 0.11 ± 0.14		2 BUSKULIC	96 ALEP	Repl. by SCHAEL 05c
11.7 ± 0.4 ± 1.8	1138	BLOCKER	82D MRK2	$E_{\text{cm}}^{\text{ee}} = 3.5\text{--}6.7$ GeV

1 See footnote to SCHAEL 05c $\Gamma(\tau^- \rightarrow e^- \bar{\nu}_e \nu_\tau)/\Gamma_{\text{total}}$ measurement for correlations with other measurements.

2 Not independent of BUSKULIC 96 B($h^- \nu_\tau$) and B($K^- \nu_\tau$) values.

 $\Gamma(\pi^- \nu_\tau)/\Gamma(e^- \bar{\nu}_e \nu_\tau)$ Γ_9/Γ_5

VALUE (units 10^{-2})	EVTS	DOCUMENT ID	TECN	COMMENT
60.71 ± 0.32 OUR FIT				
59.45 ± 0.14 ± 0.61	369k	1 AUBERT	10F BABR	467 fb^{-1} $E_{\text{cm}}^{\text{ee}} = 10.6$ GeV

1 See footnote to AUBERT 10F $\Gamma(\tau^- \rightarrow \mu^- \bar{\nu}_\mu \nu_\tau)/\Gamma(\tau^- \rightarrow e^- \bar{\nu}_e \nu_\tau)$ for correlations with other measurements.

 $\Gamma(K^- \nu_\tau)/\Gamma_{\text{total}}$ Γ_{10}/Γ

VALUE (%)	EVTS	DOCUMENT ID	TECN	COMMENT
0.696 ± 0.010 OUR FIT				
0.685 ± 0.023 OUR AVERAGE				
0.658 ± 0.027 ± 0.029		1 ABBIENDI	01J OPAL	1990-1995 LEP runs
0.696 ± 0.025 ± 0.014	2032	BARATE	99K ALEP	1991-1995 LEP runs
0.85 ± 0.18	27	ABREU	94K DLPH	LEP 1992 Z data
0.66 ± 0.07 ± 0.09	99	BATTLE	94 CLEO	$E_{\text{cm}}^{\text{ee}} \approx 10.6$ GeV
0.72 ± 0.04 ± 0.04	728	BUSKULIC	96 ALEP	Repl. by BARATE 99K
0.59 ± 0.18	16	MILLS	84 DLCO	$E_{\text{cm}}^{\text{ee}} = 29$ GeV
1.3 ± 0.5	15	BLOCKER	82B MRK2	$E_{\text{cm}}^{\text{ee}} = 3.9\text{--}6.7$ GeV

1 The correlation coefficient between this measurement and the ABBIENDI 01J B($\tau^- \rightarrow K^- \nu_\tau$) is 0.60.

 $\Gamma(K^- \nu_\tau)/\Gamma(e^- \bar{\nu}_e \nu_\tau)$ Γ_{10}/Γ_5

VALUE (units 10^{-2})	EVTS	DOCUMENT ID	TECN	COMMENT
3.91 ± 0.05 OUR FIT				
3.882 ± 0.032 ± 0.057	25k	1 AUBERT	10F BABR	467 fb^{-1} $E_{\text{cm}}^{\text{ee}} = 10.6$ GeV

1 See footnote to AUBERT 10F $\Gamma(\tau^- \rightarrow \mu^- \bar{\nu}_\mu \nu_\tau)/\Gamma(\tau^- \rightarrow e^- \bar{\nu}_e \nu_\tau)$ for correlations with other measurements.

 $\Gamma(K^- \nu_\tau)/\Gamma(\pi^- \nu_\tau)$ Γ_{10}/Γ_9

VALUE (units 10^{-2})	DOCUMENT ID	TECN	COMMENT
6.44 ± 0.09 OUR FIT			
6.531 ± 0.056 ± 0.093	1 AUBERT	10F BABR	467 fb^{-1} $E_{\text{cm}}^{\text{ee}} = 10.6$ GeV

1 Not independent of AUBERT 10F $\Gamma(\tau^- \rightarrow \pi^- \nu_\tau)/\Gamma(\tau^- \rightarrow e^- \bar{\nu}_e \nu_\tau)$ and $\Gamma(\tau^- \rightarrow K^- \nu_\tau)/\Gamma(\tau^- \rightarrow e^- \bar{\nu}_e \nu_\tau)$.

 $\Gamma(h^- \geq 1 \text{ neutrals } \nu_\tau)/\Gamma_{\text{total}}$ Γ_{11}/Γ

$$\Gamma_{11}/\Gamma = (\Gamma_{14} + \Gamma_{16} + \Gamma_{20} + \Gamma_{23} + \Gamma_{27} + \Gamma_{28} + \Gamma_{30} + 0.15344\Gamma_{36} + 0.15344\Gamma_{38} + 0.15344\Gamma_{41} + 0.15344\Gamma_{43} + 0.0942\Gamma_{48} + 0.0942\Gamma_{52} + 0.7212\Gamma_{150} + 0.7212\Gamma_{152} + 0.7212\Gamma_{154} + 0.1107\Gamma_{156} + 0.0840\Gamma_{178} + 0.0840\Gamma_{179} + 0.0840\Gamma_{180})/\Gamma$$

VALUE (%)	DOCUMENT ID	TECN	COMMENT
37.01 ± 0.09 OUR FIT			
36.14 ± 0.33 ± 0.58	1 AKERS	94E OPAL	1991-1992 LEP runs
38.4 ± 1.2 ± 1.0	2 BURCHAT	87 MRK2	$E_{\text{cm}}^{\text{ee}} = 29$ GeV
42.7 ± 2.0 ± 2.9	BERGER	85 PLUT	$E_{\text{cm}}^{\text{ee}} = 34.6$ GeV

1 Not independent of ACKERSTAFF 98M B($h^- \pi^0 \nu_\tau$) and B($h^- \geq 2\pi^0 \nu_\tau$) values.

2 BURCHAT 87 quote for B($\pi^\pm \rightarrow 1 \text{ neutral } \nu_\tau$) = $0.378 \pm 0.012 \pm 0.010$. We add 0.006 to account for contribution from ($K^* \nu_\tau$) which they fixed at BR = 0.013.

 $\Gamma(h^- \geq 1\pi^0 \nu_\tau \text{ (ex. } K^0))/\Gamma_{\text{total}}$ Γ_{12}/Γ

$$\Gamma_{12}/\Gamma = (\Gamma_{14} + \Gamma_{16} + \Gamma_{20} + \Gamma_{23} + \Gamma_{27} + \Gamma_{28} + \Gamma_{30} + 0.3268\Gamma_{150} + 0.3268\Gamma_{152} + 0.3268\Gamma_{154})/\Gamma$$

VALUE (%)	EVTS	DOCUMENT ID	TECN	COMMENT
36.51 ± 0.09 OUR FIT				
36.64 ± 0.155 ± 0.127	45k	1 ABDALLAH	06A DLPH	1992-1995 LEP runs

1 See footnote to ABDALLAH 06A $\Gamma(\tau^- \rightarrow h^- \nu_\tau)/\Gamma_{\text{total}}$ measurement for correlations with other measurements.

 $\Gamma(h^- \pi^0 \nu_\tau)/\Gamma_{\text{total}}$ $\Gamma_{13}/\Gamma = (\Gamma_{14} + \Gamma_{16})/\Gamma$

VALUE (%)	EVTS	DOCUMENT ID	TECN	COMMENT
25.93 ± 0.09 OUR FIT				
25.73 ± 0.16 OUR AVERAGE				
25.67 ± 0.01 ± 0.39	5.4M	FUJIKAWA	08 BELL	72 fb^{-1} $E_{\text{cm}}^{\text{ee}} = 10.6$ GeV
25.740 ± 0.201 ± 0.138	35k	1 ABDALLAH	06A DLPH	1992-1995 LEP runs
25.89 ± 0.17 ± 0.29		ACKERSTAFF	98M OPAL	1991-1995 LEP runs
25.05 ± 0.35 ± 0.50	6613	ACCIARRI	95 L3	1992 LEP run
25.87 ± 0.12 ± 0.42	51k	2 ARTUSO	94 CLEO	$E_{\text{cm}}^{\text{ee}} = 10.6$ GeV

• • • We do not use the following data for averages, fits, limits, etc. • • •

25.76 ± 0.15 ± 0.13	31k	BUSKULIC	96 ALEP	Repl. by SCHAEL 05c
25.98 ± 0.36 ± 0.52		3 AKERS	94E OPAL	Repl. by ACKER-STAFF 98M
22.9 ± 0.8 ± 1.3	283	4 ABREU	92N DLPH	$E_{\text{cm}}^{\text{ee}} = 88.2\text{--}94.2$ GeV
23.1 ± 0.4 ± 0.9	1249	5 ALBRECHT	92Q ARG	$E_{\text{cm}}^{\text{ee}} = 10$ GeV
25.02 ± 0.64 ± 0.88	1849	DECAMP	92C ALEP	1989-1990 LEP runs
22.0 ± 0.8 ± 1.9	779	ANTREASNYAN	91 CBAL	$E_{\text{cm}}^{\text{ee}} = 9.4\text{--}10.6$ GeV
22.6 ± 1.5 ± 0.7	1101	BEHREND	90 CELL	$E_{\text{cm}}^{\text{ee}} = 35$ GeV
23.1 ± 1.9 ± 1.6		BEHREND	84 CELL	$E_{\text{cm}}^{\text{ee}} = 14,22$ GeV

1 See footnote to ABDALLAH 06A $\Gamma(\tau^- \rightarrow h^- \nu_\tau)/\Gamma_{\text{total}}$ measurement for correlations with other measurements.

2 ARTUSO 94 reports the combined result from three independent methods, one of which (23% of the $\tau^- \rightarrow h^- \pi^0 \nu_\tau$) is normalized to the inclusive one-prong branching fraction, taken as 0.854 ± 0.004 . Renormalization to the present value causes negligible change.

3 AKERS 94E quote ($26.25 \pm 0.36 \pm 0.52$) $\times 10^{-2}$; we subtract 0.27% from their number to correct for $\tau^- \rightarrow h^- K_L^0 \nu_\tau$.

4 ABREU 92N with 0.5% added to remove their correction for $K^*(892)^-$ backgrounds.

5 ALBRECHT 92Q with 0.5% added to remove their correction for $\tau^- \rightarrow K^*(892)^- \nu_\tau$ background.

 $\Gamma(\pi^- \pi^0 \nu_\tau)/\Gamma_{\text{total}}$ Γ_{14}/Γ

VALUE (%)	EVTS	DOCUMENT ID	TECN	COMMENT
25.49 ± 0.09 OUR FIT				
25.46 ± 0.12 OUR AVERAGE				
25.471 ± 0.097 ± 0.085	81k	1 SCHAEL	05c ALEP	1991-1995 LEP runs
25.36 ± 0.44		2 ARTUSO	94 CLEO	$E_{\text{cm}}^{\text{ee}} = 10.6$ GeV
25.30 ± 0.15 ± 0.13		3 BUSKULIC	96 ALEP	Repl. by SCHAEL 05c
21.5 ± 0.4 ± 1.9	4400	4,5 ALBRECHT	88L ARG	$E_{\text{cm}}^{\text{ee}} = 10$ GeV
23.0 ± 1.3 ± 1.7	582	ADLER	87B MRK3	$E_{\text{cm}}^{\text{ee}} = 3.77$ GeV
25.8 ± 1.7 ± 2.5		6 BURCHAT	87 MRK2	$E_{\text{cm}}^{\text{ee}} = 29$ GeV
22.3 ± 0.6 ± 1.4	629	5 YELTON	86 MRK2	$E_{\text{cm}}^{\text{ee}} = 29$ GeV

1 See footnote to SCHAEL 05c $\Gamma(\tau^- \rightarrow e^- \bar{\nu}_e \nu_\tau)/\Gamma_{\text{total}}$ measurement for correlations with other measurements.

2 Not independent of ARTUSO 94 B($h^- \pi^0 \nu_\tau$) and BATTLE 94 B($K^- \pi^0 \nu_\tau$) values.

3 Not independent of BUSKULIC 96 B($h^- \pi^0 \nu_\tau$) and B($K^- \pi^0 \nu_\tau$) values.

4 The authors divide by $(\Gamma_3 + \Gamma_5 + \Gamma_9 + \Gamma_{10})/\Gamma = 0.467$ to obtain this result.

5 Experiment had no hadron identification. Kaon corrections were made, but insufficient information is given to permit their removal.

6 BURCHAT 87 value is not independent of YELTON 86 value. Nonresonant decays included.

 $\Gamma(\pi^- \pi^0 \text{ non-}\rho(770) \nu_\tau)/\Gamma_{\text{total}}$ Γ_{15}/Γ

VALUE (%)	DOCUMENT ID	TECN	COMMENT
0.3 ± 0.1 ± 0.3	1 BEHREND	84 CELL	$E_{\text{cm}}^{\text{ee}} = 14,22$ GeV

1 BEHREND 84 assume a flat nonresonant mass distribution down to the $\rho(770)$ mass, using events with mass above 1300 to set the level.

 $\Gamma(K^- \pi^0 \nu_\tau)/\Gamma_{\text{total}}$ Γ_{16}/Γ

VALUE (%)	EVTS	DOCUMENT ID	TECN	COMMENT
0.433 ± 0.015 OUR FIT				
0.426 ± 0.016 OUR AVERAGE				
0.416 ± 0.003 ± 0.018	78k	AUBERT	07AP BABR	230 fb^{-1} $E_{\text{cm}}^{\text{ee}} = 10.6$ GeV
0.471 ± 0.059 ± 0.023	360	ABBIENDI	04J OPAL	1991-1995 LEP runs
0.444 ± 0.026 ± 0.024	923	BARATE	99K ALEP	1991-1995 LEP runs
0.51 ± 0.10 ± 0.07	37	BATTLE	94 CLEO	$E_{\text{cm}}^{\text{ee}} \approx 10.6$ GeV
0.52 ± 0.04 ± 0.05	395	BUSKULIC	96 ALEP	Repl. by BARATE 99K

 $\Gamma(h^- \geq 2\pi^0 \nu_\tau)/\Gamma_{\text{total}}$ Γ_{17}/Γ

$$\Gamma_{17}/\Gamma = (\Gamma_{20} + \Gamma_{23} + \Gamma_{27} + \Gamma_{28} + \Gamma_{30} + 0.15344\Gamma_{36} + 0.15344\Gamma_{38} + 0.15344\Gamma_{41} + 0.15344\Gamma_{43} + 0.09419\Gamma_{48} + 0.0942\Gamma_{52} + 0.3268\Gamma_{150} + 0.3268\Gamma_{152} + 0.3268\Gamma_{154})/\Gamma$$

VALUE (%)	EVTS	DOCUMENT ID	TECN	COMMENT
10.81 ± 0.09 OUR FIT				
9.91 ± 0.31 ± 0.27		ACKERSTAFF	98M OPAL	1991-1995 LEP runs
9.89 ± 0.34 ± 0.55		1 AKERS	94E OPAL	Repl. by ACKER-STAFF 98M
14.0 ± 1.2 ± 0.6	938	2 BEHREND	90 CELL	$E_{\text{cm}}^{\text{ee}} = 35$ GeV
12.0 ± 1.4 ± 2.5		3 BURCHAT	87 MRK2	$E_{\text{cm}}^{\text{ee}} = 29$ GeV
13.9 ± 2.0 ± 1.9		4 AIHARA	86E TPC	$E_{\text{cm}}^{\text{ee}} = 29$ GeV

1 AKERS 94E not independent of AKERS 94E B($h^- \geq 1\pi^0 \nu_\tau$) and B($h^- \pi^0 \nu_\tau$) measurements.

2 No independent of BEHREND 90 $\Gamma(h^- 2\pi^0 \nu_\tau \text{ (exp. } K^0))$ and $\Gamma(h^- \geq 3\pi^0 \nu_\tau)$.

3 Error correlated with BURCHAT 87 $\Gamma(\rho^- \nu_e)/\Gamma(\text{total})$ value.

4 AIHARA 86E (TPC) quote B($2\pi^0 \pi^- \nu_\tau$) + 1.6B($3\pi^0 \pi^- \nu_\tau$) + 1.1B($\pi^0 \eta \pi^- \nu_\tau$).

$$\Gamma(h^- 2\pi^0 \nu_\tau) / \Gamma_{\text{total}} \quad \Gamma_{18} / \Gamma$$

$$\Gamma_{18} / \Gamma = (\Gamma_{20} + \Gamma_{23} + 0.15344\Gamma_{36} + 0.15344\Gamma_{38}) / \Gamma$$

VALUE (%)	EVTS	DOCUMENT ID	TECN	COMMENT
9.48 ± 0.10 OUR FIT				
• • • We do not use the following data for averages, fits, limits, etc. • • •				
9.48 ± 0.13 ± 0.10	12k	¹ BUSKULIC	96 ALEP	Repl. by SCHAELE 05c
¹ BUSKULIC 96 quote 9.29 ± 0.13 ± 0.10. We add 0.19 to undo their correction for $\tau^- \rightarrow h^- K^0 \nu_\tau$.				

$$\Gamma(h^- 2\pi^0 \nu_\tau \text{ (ex. } K^0)) / \Gamma_{\text{total}} \quad \Gamma_{19} / \Gamma$$

$$\Gamma_{19} / \Gamma = (\Gamma_{20} + \Gamma_{23}) / \Gamma$$

VALUE (%)	EVTS	DOCUMENT ID	TECN	COMMENT
9.32 ± 0.10 OUR FIT				
9.17 ± 0.27 OUR AVERAGE				
9.498 ± 0.320 ± 0.275	9.5k	¹ ABDALLAH	06A DLPH	1992–1995 LEP runs
8.88 ± 0.37 ± 0.42	1060	ACCIARRI	95 L3	1992 LEP run
• • • We use the following data for averages but not for fits. • • •				
8.96 ± 0.16 ± 0.44		² PROCARIO	93 CLEO	$E_{\text{cm}}^{\text{ee}} \approx 10.6$ GeV
• • • We do not use the following data for averages, fits, limits, etc. • • •				
10.38 ± 0.66 ± 0.82	809	³ DECAMP	92c ALEP	Repl. by SCHAELE 05c
5.7 ± 0.5 ± 1.7	133	⁴ ANTREASIAN	91 CBAL	$E_{\text{cm}}^{\text{ee}} = 9.4\text{--}10.6$ GeV
10.0 ± 1.5 ± 1.1	333	⁵ BEHREND	90 CELL	$E_{\text{cm}}^{\text{ee}} = 35$ GeV
8.7 ± 0.4 ± 1.1	815	⁶ BAND	87 MAC	$E_{\text{cm}}^{\text{ee}} = 29$ GeV
6.2 ± 0.6 ± 1.2		⁷ GAN	87 MRK2	$E_{\text{cm}}^{\text{ee}} = 29$ GeV
6.0 ± 3.0 ± 1.8		BEHREND	84 CELL	$E_{\text{cm}}^{\text{ee}} = 14.22$ GeV

¹ See footnote to ABDALLAH 06A $\Gamma(\tau^- \rightarrow h^- \nu_\tau) / \Gamma_{\text{total}}$ measurement for correlations with other measurements.
² PROCARIO 93 entry is obtained from $B(h^- 2\pi^0 \nu_\tau) / B(h^- \pi^0 \nu_\tau)$ using ARTUSO 94 result for $B(h^- \pi^0 \nu_\tau)$.
³ We subtract 0.0015 to account for $\tau^- \rightarrow K^*(892)^- \nu_\tau$ contribution.
⁴ ANTREASIAN 91 subtract 0.001 to account for the $\tau^- \rightarrow K^*(892)^- \nu_\tau$ contribution.
⁵ BEHREND 90 subtract 0.002 to account for the $\tau^- \rightarrow K^*(892)^- \nu_\tau$ contribution.
⁶ BAND 87 assume $B(\pi^- 3\pi^0 \nu_\tau) = 0.01$ and $B(\pi^- \pi^0 \eta \nu_\tau) = 0.005$.
⁷ GAN 87 analysis use photon multiplicity distribution.

$$\Gamma(h^- 2\pi^0 \nu_\tau \text{ (ex. } K^0)) / \Gamma(h^- \pi^0 \nu_\tau) \quad \Gamma_{19} / \Gamma_{13}$$

$$\Gamma_{19} / \Gamma_{13} = (\Gamma_{20} + \Gamma_{23}) / (\Gamma_{14} + \Gamma_{16})$$

VALUE (units 10^{-2})	DOCUMENT ID	TECN	COMMENT
36.0 ± 0.4 OUR FIT			
34.2 ± 0.6 ± 1.6	¹ PROCARIO	93 CLEO	$E_{\text{cm}}^{\text{ee}} \approx 10.6$ GeV

¹ PROCARIO 93 quote 0.345 ± 0.006 ± 0.016 after correction for 2 kaon backgrounds assuming $B(K^* \nu_\tau) = 1.42 \pm 0.18\%$ and $B(h^- K^0 \pi^0 \nu_\tau) = 0.48 \pm 0.48\%$. We multiply by 0.990 ± 0.010 to remove these corrections to $B(h^- \pi^0 \nu_\tau)$.

$$\Gamma(\pi^- 2\pi^0 \nu_\tau \text{ (ex. } K^0)) / \Gamma_{\text{total}} \quad \Gamma_{20} / \Gamma$$

VALUE (%)	EVTS	DOCUMENT ID	TECN	COMMENT
9.26 ± 0.10 OUR FIT				
9.239 ± 0.086 ± 0.090	31k	¹ SCHAELE	05c ALEP	1991–1995 LEP runs
• • • We do not use the following data for averages, fits, limits, etc. • • •				
9.21 ± 0.13 ± 0.11		² BUSKULIC	96 ALEP	Repl. by SCHAELE 05c

¹ See footnote to SCHAELE 05c $\Gamma(\tau^- \rightarrow e^- \bar{\nu}_e \nu_\tau) / \Gamma_{\text{total}}$ measurement for correlations with other measurements.
² Not independent of BUSKULIC 96 $B(h^- 2\pi^0 \nu_\tau \text{ (ex. } K^0))$ and $B(K^- 2\pi^0 \nu_\tau \text{ (ex. } K^0))$ values.

$$\Gamma(\pi^- 2\pi^0 \nu_\tau \text{ (ex. } K^0), \text{ scalar}) / \Gamma(\pi^- 2\pi^0 \nu_\tau \text{ (ex. } K^0)) \quad \Gamma_{21} / \Gamma_{20}$$

VALUE	CL%	DOCUMENT ID	TECN	COMMENT
< 0.094	95	¹ BROWDER	00 CLEO	$4.7 \text{ fb}^{-1} E_{\text{cm}}^{\text{ee}} = 10.6$ GeV

¹ Model-independent limit from structure function analysis on contribution to $B(\tau^- \rightarrow \pi^- 2\pi^0 \nu_\tau \text{ (ex. } K^0))$ from scalars.

$$\Gamma(\pi^- 2\pi^0 \nu_\tau \text{ (ex. } K^0), \text{ vector}) / \Gamma(\pi^- 2\pi^0 \nu_\tau \text{ (ex. } K^0)) \quad \Gamma_{22} / \Gamma_{20}$$

VALUE	CL%	DOCUMENT ID	TECN	COMMENT
< 0.073	95	¹ BROWDER	00 CLEO	$4.7 \text{ fb}^{-1} E_{\text{cm}}^{\text{ee}} = 10.6$ GeV

¹ Model-independent limit from structure function analysis on contribution to $B(\tau^- \rightarrow \pi^- 2\pi^0 \nu_\tau \text{ (ex. } K^0))$ from vectors.

$$\Gamma(K^- 2\pi^0 \nu_\tau \text{ (ex. } K^0)) / \Gamma_{\text{total}} \quad \Gamma_{23} / \Gamma$$

VALUE (units 10^{-4})	EVTS	DOCUMENT ID	TECN	COMMENT
6.5 ± 2.2 OUR FIT				
5.8 ± 2.4 OUR AVERAGE				
5.6 ± 2.0 ± 1.5	131	BARATE	99K ALEP	1991–1995 LEP runs
9 ± 10 ± 3	3	¹ BATTLE	94 CLEO	$E_{\text{cm}}^{\text{ee}} \approx 10.6$ GeV
• • • We do not use the following data for averages, fits, limits, etc. • • •				
8 ± 2 ± 2	59	BUSKULIC	96 ALEP	Repl. by BARATE 99K

¹ BATTLE 94 quote $(14 \pm 10 \pm 3) \times 10^{-4}$ or $< 30 \times 10^{-4}$ at 90% CL. We subtract $(5 \pm 2) \times 10^{-4}$ to account for $\tau^- \rightarrow K^- (K^0 \rightarrow \pi^0 \pi^0) \nu_\tau$ background.

$$\Gamma(h^- \geq 3\pi^0 \nu_\tau) / \Gamma_{\text{total}} \quad \Gamma_{24} / \Gamma$$

$$\Gamma_{24} / \Gamma = (\Gamma_{27} + \Gamma_{28} + \Gamma_{30} + 0.15344\Gamma_{41} + 0.15344\Gamma_{43} + 0.0942\Gamma_{48} + 0.0942\Gamma_{52} + 0.3268\Gamma_{150} + 0.3268\Gamma_{152} + 0.3268\Gamma_{154} + 0.0501\Gamma_{156}) / \Gamma$$

VALUE (%)	EVTS	DOCUMENT ID	TECN	COMMENT
1.34 ± 0.07 OUR FIT				
• • • We do not use the following data for averages, fits, limits, etc. • • •				
1.53 ± 0.40 ± 0.46	186	DECAMP	92c ALEP	Repl. by SCHAELE 05c
3.2 ± 1.0 ± 1.0		BEHREND	90 CELL	$E_{\text{cm}}^{\text{ee}} = 35$ GeV

$$\Gamma(h^- \geq 3\pi^0 \nu_\tau \text{ (ex. } K^0)) / \Gamma_{\text{total}} \quad \Gamma_{25} / \Gamma$$

$$\Gamma_{25} / \Gamma = (\Gamma_{27} + \Gamma_{28} + \Gamma_{30} + 0.3268\Gamma_{150} + 0.3268\Gamma_{152} + 0.3268\Gamma_{154}) / \Gamma$$

VALUE (%)	EVTS	DOCUMENT ID	TECN	COMMENT
1.25 ± 0.07 OUR FIT				
1.403 ± 0.214 ± 0.224	1.1k	¹ ABDALLAH	06A DLPH	1992–1995 LEP runs
¹ See footnote to ABDALLAH 06A $\Gamma(\tau^- \rightarrow h^- \nu_\tau) / \Gamma_{\text{total}}$ measurement for correlations with other measurements.				

$$\Gamma(h^- 3\pi^0 \nu_\tau) / \Gamma_{\text{total}} \quad \Gamma_{26} / \Gamma$$

$$\Gamma_{26} / \Gamma = (\Gamma_{27} + \Gamma_{28} + 0.15344\Gamma_{41} + 0.15344\Gamma_{43} + 0.3268\Gamma_{152}) / \Gamma$$

VALUE (%)	EVTS	DOCUMENT ID	TECN	COMMENT
1.18 ± 0.07 OUR FIT				
1.21 ± 0.17 OUR AVERAGE				Error includes scale factor of 1.2.
1.70 ± 0.24 ± 0.38	293	ACCIARRI	95 L3	1992 LEP run
• • • We use the following data for averages but not for fits. • • •				
1.15 ± 0.08 ± 0.13		¹ PROCARIO	93 CLEO	$E_{\text{cm}}^{\text{ee}} \approx 10.6$ GeV
• • • We do not use the following data for averages, fits, limits, etc. • • •				
1.24 ± 0.09 ± 0.11	2.3k	² BUSKULIC	96 ALEP	Repl. by SCHAELE 05c
0.0 ± 1.4 ± 1.1		³ GAN	87 MRK2	$E_{\text{cm}}^{\text{ee}} = 29$ GeV

¹ PROCARIO 93 entry is obtained from $B(h^- 3\pi^0 \nu_\tau) / B(h^- \pi^0 \nu_\tau)$ using ARTUSO 94 result for $B(h^- \pi^0 \nu_\tau)$.
² BUSKULIC 96 quote $B(h^- 3\pi^0 \nu_\tau \text{ (ex. } K^0)) = 1.17 \pm 0.09 \pm 0.11$. We add 0.07 to remove their correction for K^0 backgrounds.
³ Highly correlated with GAN 87 $\Gamma(\eta \pi^- \pi^0 \nu_\tau) / \Gamma_{\text{total}}$ value. Authors quote $B(\pi^\pm 3\pi^0 \nu_\tau) + 0.67B(\pi^\pm \eta \pi^0 \nu_\tau) = 0.047 \pm 0.010 \pm 0.011$.

$$\Gamma(h^- 3\pi^0 \nu_\tau) / \Gamma(h^- \pi^0 \nu_\tau) \quad \Gamma_{26} / \Gamma_{13}$$

$$\Gamma_{26} / \Gamma_{13} = (\Gamma_{27} + \Gamma_{28} + 0.15344\Gamma_{41} + 0.15344\Gamma_{43} + 0.3268\Gamma_{152}) / (\Gamma_{14} + \Gamma_{16})$$

VALUE (units 10^{-2})	DOCUMENT ID	TECN	COMMENT
4.54 ± 0.28 OUR FIT			
4.4 ± 0.3 ± 0.5	¹ PROCARIO	93 CLEO	$E_{\text{cm}}^{\text{ee}} \approx 10.6$ GeV

¹ PROCARIO 93 quote 0.041 ± 0.003 ± 0.005 after correction for 2 kaon backgrounds assuming $B(K^* \nu_\tau) = 1.42 \pm 0.18\%$ and $B(h^- K^0 \pi^0 \nu_\tau) = 0.48 \pm 0.48\%$. We add 0.003 ± 0.003 and multiply the sum by 0.990 ± 0.010 to remove these corrections.

$$\Gamma(\pi^- 3\pi^0 \nu_\tau \text{ (ex. } K^0)) / \Gamma_{\text{total}} \quad \Gamma_{27} / \Gamma$$

VALUE (%)	EVTS	DOCUMENT ID	TECN	COMMENT
1.04 ± 0.07 OUR FIT				
0.977 ± 0.069 ± 0.058	6.1k	¹ SCHAELE	05c ALEP	1991–1995 LEP runs

¹ See footnote to SCHAELE 05c $\Gamma(\tau^- \rightarrow e^- \bar{\nu}_e \nu_\tau) / \Gamma_{\text{total}}$ measurement for correlations with other measurements.

$$\Gamma(K^- 3\pi^0 \nu_\tau \text{ (ex. } K^0, \eta)) / \Gamma_{\text{total}} \quad \Gamma_{28} / \Gamma$$

VALUE (units 10^{-4})	EVTS	DOCUMENT ID	TECN	COMMENT
4.8 ± 2.1 OUR FIT				
3.7 ± 2.1 ± 1.1	22	BARATE	99K ALEP	1991–1995 LEP runs
• • • We do not use the following data for averages, fits, limits, etc. • • •				
5 ± 13		¹ BUSKULIC	94E ALEP	Repl. by BARATE 99K

¹ BUSKULIC 94E quote $B(K^- \geq 0\pi^0 \geq 0K^0 \nu_\tau) - [B(K^- \nu_\tau) + B(K^- \pi^0 \nu_\tau) + B(K^- K^0 \nu_\tau) + B(K^- \pi^0 \pi^0 \nu_\tau) + B(K^- \pi^0 K^0 \nu_\tau)] = (5 \pm 13) \times 10^{-4}$ accounting for common systematic errors in BUSKULIC 94E and BUSKULIC 94F measurements of these modes. We assume $B(K^- \geq 2K^0 \nu_\tau)$ and $B(K^- \geq 4\pi^0 \nu_\tau)$ are negligible.

$$\Gamma(h^- 4\pi^0 \nu_\tau \text{ (ex. } K^0)) / \Gamma_{\text{total}} \quad \Gamma_{29} / \Gamma$$

$$\Gamma_{29} / \Gamma = (\Gamma_{30} + 0.3268\Gamma_{150} + 0.3268\Gamma_{154}) / \Gamma$$

VALUE (%)	EVTS	DOCUMENT ID	TECN	COMMENT
0.16 ± 0.04 OUR FIT				
0.16 ± 0.05 ± 0.05		¹ PROCARIO	93 CLEO	$E_{\text{cm}}^{\text{ee}} \approx 10.6$ GeV
• • • We do not use the following data for averages, fits, limits, etc. • • •				
0.16 ± 0.04 ± 0.09	232	² BUSKULIC	96 ALEP	Repl. by SCHAELE 05c

¹ PROCARIO 93 quotes $B(h^- 4\pi^0 \nu_\tau) / B(h^- \pi^0 \nu_\tau) = 0.006 \pm 0.002 \pm 0.002$. We multiply by the ARTUSO 94 result for $B(h^- \pi^0 \nu_\tau)$ to obtain $B(h^- 4\pi^0 \nu_\tau)$. PROCARIO 93 assume $B(h^- \geq 5\pi^0 \nu_\tau)$ is small and do not correct for it.
² BUSKULIC 96 quote result for $\tau^- \rightarrow h^- \geq 4\pi^0 \nu_\tau$. We assume $B(h^- \geq 5\pi^0 \nu_\tau)$ is negligible.

$$\Gamma(h^- 4\pi^0 \nu_\tau \text{ (ex. } K^0, \eta)) / \Gamma_{\text{total}} \quad \Gamma_{30} / \Gamma$$

VALUE (%)	EVTS	DOCUMENT ID	TECN	COMMENT
0.11 ± 0.04 OUR FIT				
0.112 ± 0.037 ± 0.035	957	¹ SCHAELE	05c ALEP	1991–1995 LEP runs

¹ See footnote to SCHAELE 05c $\Gamma(\tau^- \rightarrow e^- \bar{\nu}_e \nu_\tau) / \Gamma_{\text{total}}$ measurement for correlations with other measurements.

Lepton Particle Listings

τ

$\Gamma(a_1(1260)\nu_\tau \rightarrow \pi^- \gamma \nu_\tau)/\Gamma_{\text{total}}$ $\Gamma_{31}/\Gamma = (0.0021\Gamma_{20} + 0.0021\Gamma_{70})/\Gamma$

The uncertainty on $\Gamma(\tau^- \rightarrow a_1(1260)\nu_\tau \rightarrow \pi^- \gamma \nu_\tau)/\Gamma_{\text{total}}$ is the sum in quadrature of the uncertainty on the fit result for $\Gamma(\tau^- \rightarrow a_1(1260)\nu_\tau \rightarrow \pi^- \gamma \nu_\tau)/\Gamma_{\text{total}}$ and of the uncertainty on $\Gamma(a_1(1260) \rightarrow \pi\gamma)/\Gamma_{\text{total}} = ((2.1 \pm 0.8) \times 10^{-3})$ as reported in SCHAEF 05c, which is the coefficient of the relationship that defines $\Gamma(\tau^- \rightarrow a_1(1260)\nu_\tau \rightarrow \pi^- \gamma \nu_\tau)/\Gamma_{\text{total}}$ in terms of $\Gamma(\tau^- \rightarrow \pi^- 2\pi^0 \nu_\tau (\text{ex. } K^0))/\Gamma_{\text{total}}$ and $\Gamma(\tau^- \rightarrow \pi^- \pi^+ \pi^- \nu_\tau (\text{ex. } K^0, \omega))/\Gamma_{\text{total}}$.

VALUE (units 10^{-4})	EVTS	DOCUMENT ID	TECN	COMMENT
3.8 ± 1.5 OUR FIT				

$\Gamma(K^- \geq 0\pi^0 \geq 0K^0 \geq 0\gamma \nu_\tau)/\Gamma_{\text{total}}$ Γ_{32}/Γ

$\Gamma_{32}/\Gamma = (\Gamma_{10} + \Gamma_{16} + \Gamma_{23} + \Gamma_{28} + \Gamma_{38} + \Gamma_{43} + 0.7212\Gamma_{152} + 0.1049\Gamma_{170})/\Gamma$

VALUE (%)	EVTS	DOCUMENT ID	TECN	COMMENT
1.552 ± 0.029 OUR FIT				
1.53 ± 0.04 OUR AVERAGE				

1.528 ± 0.039 ± 0.040	1	ABBIENDI	01J	OPAL 1990-1995 LEP runs
1.54 ± 0.24		ABREU	94K	DLPH LEP 1992 Z data
1.70 ± 0.12 ± 0.19	202	2	BATTLE	94 CLEO $E_{\text{cm}}^{\text{ee}} \approx 10.6$ GeV

- • • We use the following data for averages but not for fits. • • •
 - • • We do not use the following data for averages, fits, limits, etc. • • •
- | | | | | |
|-----------------------|------|---|----------|--|
| 1.520 ± 0.040 ± 0.041 | 4006 | 3 | BARATE | 99K ALEP 1991-1995 LEP runs |
| 1.70 ± 0.05 ± 0.06 | 1610 | 4 | BUSKULIC | 96 ALEP Repl. by BARATE 99K |
| 1.6 ± 0.4 ± 0.2 | 35 | | AIHARA | 87B TPC $E_{\text{cm}}^{\text{ee}} = 29$ GeV |
| 1.71 ± 0.29 | 53 | | MILLS | 84 DLCO $E_{\text{cm}}^{\text{ee}} = 29$ GeV |

- The correlation coefficient between this measurement and the ABBIENDI 01J $B(\tau^- \rightarrow K^- \nu_\tau)$ is 0.60.
- BATTLE 94 quote $1.60 \pm 0.12 \pm 0.19$. We add 0.10 ± 0.02 to correct for their rejection of $K_S^0 \rightarrow \pi^+ \pi^-$ decays.
- Not independent of BARATE 99K $B(K^- \nu_\tau)$, $B(K^- \pi^0 \nu_\tau)$, $B(K^- 2\pi^0 \nu_\tau (\text{ex. } K^0))$, $B(K^- 3\pi^0 \nu_\tau (\text{ex. } K^0))$, $B(K^- K^0 \nu_\tau)$, and $B(K^- K^0 \pi^0 \nu_\tau)$ values.
- Not independent of BUSKULIC 96 $B(K^- \nu_\tau)$, $B(K^- \pi^0 \nu_\tau)$, $B(K^- 2\pi^0 \nu_\tau)$, $B(K^- K^0 \nu_\tau)$, and $B(K^- K^0 \pi^0 \nu_\tau)$ values.

$\Gamma(K^- \geq 1(\pi^0 \text{ or } K^0 \text{ or } \gamma) \nu_\tau)/\Gamma_{\text{total}}$ Γ_{33}/Γ

$\Gamma_{33}/\Gamma = (\Gamma_{16} + \Gamma_{23} + \Gamma_{28} + \Gamma_{38} + \Gamma_{43} + 0.7212\Gamma_{152} + 0.7212\Gamma_{154} + 0.1049\Gamma_{170})/\Gamma$

VALUE (%)	EVTS	DOCUMENT ID	TECN	COMMENT
0.859 ± 0.028 OUR FIT				
0.86 ± 0.05 OUR AVERAGE				

0.869 ± 0.031 ± 0.034	1	ABBIENDI	01J	OPAL 1990-1995 LEP runs
0.69 ± 0.25		2	ABREU	94K DLPH LEP 1992 Z data
1.2 ± 0.5 ± 0.2	9		AIHARA	87B TPC $E_{\text{cm}}^{\text{ee}} = 29$ GeV

- • • We use the following data for averages but not for fits. • • •
- • • We do not use the following data for averages, fits, limits, etc. • • •

$\Gamma(K_S^0 (\text{particles})^- \nu_\tau)/\Gamma_{\text{total}}$ Γ_{34}/Γ

$\Gamma_{34}/\Gamma = (\frac{1}{2}\Gamma_{36} + \frac{1}{2}\Gamma_{38} + \frac{1}{2}\Gamma_{41} + \frac{1}{2}\Gamma_{43} + \frac{1}{2}\Gamma_{45} + \Gamma_{48} + \Gamma_{49} + \Gamma_{52} + \Gamma_{56} + 0.3606\Gamma_{156} + 0.340\Gamma_{170})/\Gamma$

VALUE (%)	EVTS	DOCUMENT ID	TECN	COMMENT
0.943 ± 0.028 OUR FIT				
0.918 ± 0.015 OUR AVERAGE				

0.970 ± 0.058 ± 0.062	929		BARATE	98E ALEP 1991-1995 LEP runs
0.97 ± 0.09 ± 0.06	141		AKERS	94G OPAL $E_{\text{cm}}^{\text{ee}} = 88-94$ GeV
0.915 ± 0.001 ± 0.015	398k	1	RYU	14 BELL $669 \text{ fb}^{-1} E_{\text{cm}}^{\text{ee}} = 10.6$ GeV

- • • We use the following data for averages but not for fits. • • •
- • • We do not use the following data for averages, fits, limits, etc. • • •

$\Gamma(h^- \bar{K}^0 \nu_\tau)/\Gamma_{\text{total}}$ $\Gamma_{35}/\Gamma = (\Gamma_{36} + \Gamma_{38})/\Gamma$

VALUE (%)	EVTS	DOCUMENT ID	TECN	COMMENT
0.987 ± 0.014 OUR FIT				
0.90 ± 0.07 OUR AVERAGE				

0.855 ± 0.036 ± 0.073	1242		COAN	96 CLEO $E_{\text{cm}}^{\text{ee}} \approx 10.6$ GeV
1.01 ± 0.11 ± 0.07	555	1	BARATE	98E ALEP 1991-1995 LEP runs

- • • We use the following data for averages but not for fits. • • •
- • • We do not use the following data for averages, fits, limits, etc. • • •

$\Gamma(\pi^- \bar{K}^0 \nu_\tau)/\Gamma_{\text{total}}$ Γ_{36}/Γ

VALUE (units 10^{-3})	EVTS	DOCUMENT ID	TECN	COMMENT
8.38 ± 0.14 OUR FIT				
8.39 ± 0.22 OUR AVERAGE				

8.32 ± 0.02 ± 0.16	158k	1	RYU	14 BELL $669 \text{ fb}^{-1} E_{\text{cm}}^{\text{ee}} = 10.6$ GeV
9.33 ± 0.68 ± 0.49	377		ABBIENDI	00C OPAL 1991-1995 LEP runs
9.28 ± 0.45 ± 0.34	937	2	BARATE	99K ALEP 1991-1995 LEP runs
9.5 ± 1.5 ± 0.6		3	ACCIARRI	95F L3 1991-1993 LEP runs

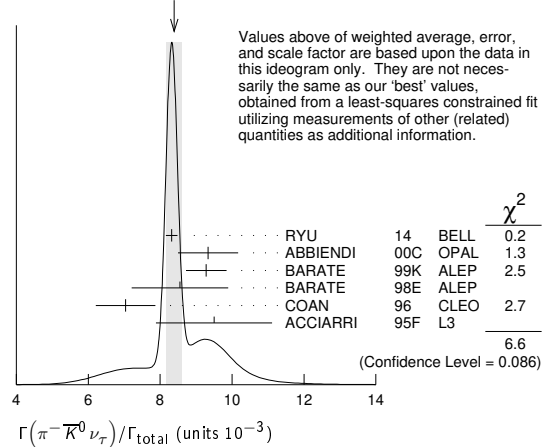
- • • We use the following data for averages but not for fits. • • •
- • • We do not use the following data for averages, fits, limits, etc. • • •

8.55 ± 1.17 ± 0.66	509	4	BARATE	98E ALEP 1991-1995 LEP runs
7.04 ± 0.41 ± 0.72		5	COAN	96 CLEO $E_{\text{cm}}^{\text{ee}} \approx 10.6$ GeV

8.08 ± 0.04 ± 0.26	53k		EPIFANOV	07 BELL Repl. by RYU 14
7.9 ± 1.0 ± 0.9	98	6	BUSKULIC	96 ALEP Repl. by BARATE 99K

- RYU 14 reconstruct K^0 's using $K_S^0 \rightarrow \pi^+ \pi^-$ decays.
- BARATE 99K measure K^0 's by detecting K_L^0 's in their hadron calorimeter.
- ACCIARRI 95F do not identify π^-/K^- and assume $B(K^- K^0 \nu_\tau) = (0.29 \pm 0.12)\%$.
- BARATE 98E reconstruct K^0 's using $K_S^0 \rightarrow \pi^+ \pi^-$ decays. Not independent of BARATE 98E $B(K^0 \text{ particles}^- \nu_\tau)$ value.
- Not independent of COAN 96 $B(h^- K^0 \nu_\tau)$ and $B(K^- K^0 \nu_\tau)$ measurements.
- BUSKULIC 96 measure K^0 's by detecting K_L^0 's in their hadron calorimeter.

WEIGHTED AVERAGE
8.39±0.22 (Error scaled by 1.5)



$\Gamma(\pi^- \bar{K}^0 (\text{non-}K^*(892)^- \nu_\tau)/\Gamma_{\text{total}}$ Γ_{37}/Γ

VALUE (units 10^{-4})	CL%	DOCUMENT ID	TECN	COMMENT
5.4 ± 2.1		1	EPIFANOV	07 BELL $351 \text{ fb}^{-1} E_{\text{cm}}^{\text{ee}} = 10.6$ GeV

- • • We do not use the following data for averages, fits, limits, etc. • • •
- • • We do not use the following data for averages, fits, limits, etc. • • •

$\Gamma(K^- K^0 \nu_\tau)/\Gamma_{\text{total}}$ Γ_{38}/Γ

VALUE (units 10^{-4})	EVTS	DOCUMENT ID	TECN	COMMENT
14.86 ± 0.34 OUR FIT				
14.83 ± 0.35 OUR AVERAGE				

14.78 ± 0.22 ± 0.40	29k	1	LEES	18B BABR $468 \text{ fb}^{-1} E_{\text{cm}}^{\text{ee}} = 10.6$ GeV
14.80 ± 0.14 ± 0.54	33k	2	RYU	14 BELL $669 \text{ fb}^{-1} E_{\text{cm}}^{\text{ee}} = 10.6$ GeV
16.2 ± 2.1 ± 1.1	150	3	BARATE	99K ALEP 1991-1995 LEP runs
15.8 ± 4.2 ± 1.7	46	4	BARATE	98E ALEP 1991-1995 LEP runs
15.1 ± 2.1 ± 2.2	111		COAN	96 CLEO $E_{\text{cm}}^{\text{ee}} \approx 10.6$ GeV

- • • We do not use the following data for averages, fits, limits, etc. • • •
- • • We do not use the following data for averages, fits, limits, etc. • • •

$\Gamma(K^- K^0 \geq 0\pi^0 \nu_\tau)/\Gamma_{\text{total}}$ $\Gamma_{39}/\Gamma = (\Gamma_{38} + \Gamma_{43})/\Gamma$

VALUE (%)	EVTS	DOCUMENT ID	TECN	COMMENT
0.299 ± 0.007 OUR FIT				
0.330 ± 0.055 ± 0.039	124		ABBIENDI	00C OPAL 1991-1995 LEP runs

$\Gamma(h^- \bar{K}^0 \pi^0 \nu_\tau)/\Gamma_{\text{total}}$ $\Gamma_{40}/\Gamma = (\Gamma_{41} + \Gamma_{43})/\Gamma$

VALUE (%)	EVTS	DOCUMENT ID	TECN	COMMENT
0.532 ± 0.013 OUR FIT				
0.50 ± 0.06 OUR AVERAGE				

0.562 ± 0.050 ± 0.048	264		COAN	96 CLEO $E_{\text{cm}}^{\text{ee}} \approx 10.6$ GeV
0.446 ± 0.052 ± 0.046	157	1	BARATE	98E ALEP 1991-1995 LEP runs

- • • We use the following data for averages but not for fits. • • •
- • • We do not use the following data for averages, fits, limits, etc. • • •

1 Not independent of BARATE 98E $B(\tau^- \rightarrow \pi^- \bar{K}^0 \pi^0 \nu_\tau)$ and $B(\tau^- \rightarrow K^- K^0 \pi^0 \nu_\tau)$ values.

$\Gamma(\pi^- \bar{K}^0 \pi^0 \nu_\tau)/\Gamma_{total}$ Γ_{41}/Γ

Table with columns: VALUE (%), EVTS, DOCUMENT ID, TECN, COMMENT. Includes OUR FIT 0.382±0.013 and OUR AVERAGE 0.383±0.014. Lists experiments like RYU, BARATE, ACCIARRI, COAN, BUSKULIC.

$\Gamma(\bar{K}^0 \rho^- \nu_\tau)/\Gamma_{total}$ Γ_{42}/Γ

Table with columns: VALUE (%), DOCUMENT ID, TECN, COMMENT. Includes OUR FIT 0.22±0.05 and OUR AVERAGE 0.250±0.057±0.044. Lists experiments BARATE.

$\Gamma(K^- K^0 \pi^0 \nu_\tau)/\Gamma_{total}$ Γ_{43}/Γ

Table with columns: VALUE (units 10^-4), EVTS, DOCUMENT ID, TECN, COMMENT. Includes OUR FIT 15.0±0.7 and OUR AVERAGE 14.9±0.7. Lists experiments RYU, BARATE, COAN, BUSKULIC.

$\Gamma(\pi^- \bar{K}^0 \ge 1\pi^0 \nu_\tau)/\Gamma_{total}$ $\Gamma_{44}/\Gamma = (\Gamma_{41} + \Gamma_{45})/\Gamma$

Table with columns: VALUE (%), EVTS, DOCUMENT ID, TECN, COMMENT. Includes OUR FIT 0.408±0.025 and OUR AVERAGE 0.324±0.074±0.066. Lists experiment ABBIENDI.

$\Gamma(\pi^- \bar{K}^0 \pi^0 \pi^0 \nu_\tau (ex. K^0))/\Gamma_{total}$ Γ_{45}/Γ

Table with columns: VALUE (units 10^-3), CL%, EVTS, DOCUMENT ID, TECN, COMMENT. Includes OUR FIT 0.26±0.23 and OUR FIT 0.26±0.24. Lists experiments BARATE.

$\Gamma(K^- K^0 \pi^0 \pi^0 \nu_\tau)/\Gamma_{total}$ Γ_{46}/Γ

Table with columns: VALUE, CL%, DOCUMENT ID, TECN, COMMENT. Includes OUR FIT 0.16 x 10^-3. Lists experiment BARATE.

$\Gamma(\pi^- K^0 \bar{K}^0 \nu_\tau)/\Gamma_{total}$ $\Gamma_{47}/\Gamma = (\Gamma_{48} + \Gamma_{49} + \Gamma_{50})/\Gamma$

Table with columns: VALUE (%), EVTS, DOCUMENT ID, TECN, COMMENT. Includes OUR FIT 0.155±0.024 and OUR AVERAGE 0.153±0.030±0.016. Lists experiment BARATE.

• • • We do not use the following data for averages, fits, limits, etc. • • •
0.31 ± 0.12 ± 0.04 ² ACCIARRI 95F L3 1991-1993 LEP runs

¹ BARATE 98E obtain this value by adding twice their $B(\pi^- K_S^0 K_L^0 \nu_\tau)$ value to their $B(\pi^- K_S^0 K_L^0 \nu_\tau)$ value.
² ACCIARRI 95F assume $B(\pi^- K_S^0 K_S^0 \nu) = B(\pi^- K_S^0 K_L^0 \nu) = 1/2 B(\pi^- K_S^0 K_L^0 \nu)$.

$\Gamma(\pi^- K_S^0 K_S^0 \nu_\tau)/\Gamma_{total}$ Γ_{48}/Γ

Table with columns: VALUE (units 10^-4), EVTS, DOCUMENT ID, TECN, COMMENT. Includes OUR FIT 2.35±0.06 and OUR AVERAGE 2.32±0.06. Lists experiments RYU, LEES, BARATE, COAN.

¹ The correlation coefficient between this measurement and the LEES 12Y $\Gamma(\tau^- \rightarrow \pi^- K_S^0 K_S^0 \pi^0 \nu_\tau)/\Gamma_{total}$ one is 0.0828.

$\Gamma(\pi^- K_S^0 K_L^0 \nu_\tau)/\Gamma_{total}$ Γ_{49}/Γ

Table with columns: VALUE (units 10^-4), EVTS, DOCUMENT ID, TECN, COMMENT. Includes OUR FIT 10.8±2.4 and OUR FIT 10.1±2.3±1.3. Lists experiment BARATE.

$\Gamma(\pi^- K_L^0 K_L^0 \nu_\tau)/\Gamma_{total}$ $\Gamma_{50}/\Gamma = \Gamma_{48}/\Gamma$

Table with columns: VALUE (units 10^-4), DOCUMENT ID. Includes OUR FIT 2.35±0.06.

$\Gamma(\pi^- K^0 \bar{K}^0 \pi^0 \nu_\tau)/\Gamma_{total}$ $\Gamma_{51}/\Gamma = (\Gamma_{52} + \Gamma_{56} + \Gamma_{57})/\Gamma$

Table with columns: VALUE (units 10^-4), DOCUMENT ID, TECN, COMMENT. Includes OUR FIT 3.6±1.2. Lists experiment BARATE.

$\Gamma(\pi^- K_S^0 K_S^0 \pi^0 \nu_\tau)/\Gamma_{total}$ Γ_{52}/Γ

Table with columns: VALUE (units 10^-5), CL% EVTS, DOCUMENT ID, TECN, COMMENT. Includes OUR FIT 1.82±0.21 and OUR AVERAGE 1.80±0.21. Lists experiments RYU, LEES.

$\Gamma(K^+ K^0 \pi^0 \nu_\tau \rightarrow \pi^- K_S^0 K_S^0 \pi^0 \nu_\tau)/\Gamma_{total}$ Γ_{53}/Γ

Table with columns: VALUE (units 10^-6), DOCUMENT ID, TECN, COMMENT. Includes OUR FIT 10.8±1.4±1.5. Lists experiment RYU.

$\Gamma(f_1(1285) \pi^- \nu_\tau \rightarrow \pi^- K_S^0 K_S^0 \pi^0 \nu_\tau)/\Gamma_{total}$ Γ_{54}/Γ

Table with columns: VALUE (units 10^-6), DOCUMENT ID, TECN, COMMENT. Includes OUR FIT 6.8±1.3±0.7. Lists experiment RYU.

$\Gamma(f_1(1420) \pi^- \nu_\tau \rightarrow \pi^- K_S^0 K_S^0 \pi^0 \nu_\tau)/\Gamma_{total}$ Γ_{55}/Γ

Table with columns: VALUE (units 10^-6), DOCUMENT ID, TECN, COMMENT. Includes OUR FIT 2.4±0.5±0.6. Lists experiment RYU.

$\Gamma(\pi^- K_S^0 K_L^0 \pi^0 \nu_\tau)/\Gamma_{total}$ Γ_{56}/Γ

Table with columns: VALUE (units 10^-4), EVTS, DOCUMENT ID, TECN, COMMENT. Includes OUR FIT 3.2±1.2 and OUR FIT 3.1±1.1±0.5. Lists experiment BARATE.

$\Gamma(\pi^- K_L^0 K_L^0 \pi^0 \nu_\tau)/\Gamma_{total}$ $\Gamma_{57}/\Gamma = \Gamma_{52}/\Gamma$

Table with columns: VALUE (units 10^-5), DOCUMENT ID. Includes OUR FIT 1.82±0.21.

$\Gamma(K^- K_S^0 K_S^0 \nu_\tau)/\Gamma_{total}$ Γ_{58}/Γ

Table with columns: VALUE, CL%, DOCUMENT ID, TECN, COMMENT. Includes OUR FIT <6.3 x 10^-7. Lists experiment LEES.

$\Gamma(K^- K_S^0 K_S^0 \pi^0 \nu_\tau)/\Gamma_{total}$ Γ_{59}/Γ

Table with columns: VALUE, CL%, DOCUMENT ID, TECN, COMMENT. Includes OUR FIT <4.0 x 10^-7. Lists experiment LEES.

Lepton Particle Listings

T

$\Gamma(K^0 h^+ h^- h^- \geq 0 \text{ neutrals } \nu_\tau)/\Gamma_{\text{total}}$ Γ_{60}/Γ

VALUE (%)	CL%	DOCUMENT ID	TECN	COMMENT
<0.17	95	TSCHIRHART 88	HRS	$E_{\text{cm}}^{\text{ee}} = 29 \text{ GeV}$

• • • We do not use the following data for averages, fits, limits, etc. • • •

<0.27	90	BELTRAMI 85	HRS	$E_{\text{cm}}^{\text{ee}} = 29 \text{ GeV}$
-------	----	-------------	-----	--

$\Gamma(K^0 h^+ h^- h^- \nu_\tau)/\Gamma_{\text{total}}$ Γ_{61}/Γ

VALUE (units 10^{-4})	EVTS	DOCUMENT ID	TECN	COMMENT
2.5 ± 2.0 OUR FIT				
2.3 ± 1.9 ± 0.7	6	¹ BARATE 98E	98E	ALEP 1991–1995 LEP runs

¹ BARATE 98E reconstruct K^0 's using $K_S^0 \rightarrow \pi^+ \pi^-$ decays.

$\Gamma(h^- h^- h^+ \geq 0 \text{ neutrals } \geq 0 K^0 \nu_\tau)/\Gamma_{\text{total}}$ Γ_{62}/Γ

$$\Gamma_{62}/\Gamma = (0.34598\Gamma_{36} + 0.34598\Gamma_{38} + 0.34598\Gamma_{41} + 0.34598\Gamma_{43} + 0.4247\Gamma_{48} + 0.6920\Gamma_{49} + 0.4247\Gamma_{52} + 0.6920\Gamma_{56} + 0.6534\Gamma_{61} + \Gamma_{70} + \Gamma_{78} + \Gamma_{85} + \Gamma_{86} + \Gamma_{97} + \Gamma_{103} + \Gamma_{106} + \Gamma_{107} + 0.2789\Gamma_{150} + 0.2789\Gamma_{152} + 0.2789\Gamma_{154} + 0.2628\Gamma_{156} + 0.7259\Gamma_{170} + 0.9078\Gamma_{178} + 0.9078\Gamma_{179} + 0.9078\Gamma_{180})/\Gamma$$

VALUE (%)	EVTS	DOCUMENT ID	TECN	COMMENT
15.20 ± 0.06 OUR FIT				
14.8 ± 0.4 OUR AVERAGE				

14.4 ± 0.6 ± 0.3		ADEVA 91F	L3	$E_{\text{cm}}^{\text{ee}} = 88.3\text{--}94.3 \text{ GeV}$
15.0 ± 0.4 ± 0.3		BEHREND 89B	CELL	$E_{\text{cm}}^{\text{ee}} = 14\text{--}47 \text{ GeV}$
15.1 ± 0.8 ± 0.6		AIHARA 87B	TPC	$E_{\text{cm}}^{\text{ee}} = 29 \text{ GeV}$

• • • We do not use the following data for averages, fits, limits, etc. • • •

13.5 ± 0.3 ± 0.3		ABACHI 89B	HRS	$E_{\text{cm}}^{\text{ee}} = 29 \text{ GeV}$
12.8 ± 1.0 ± 0.7		¹ BURCHAT 87	MRK2	$E_{\text{cm}}^{\text{ee}} = 29 \text{ GeV}$
12.1 ± 0.5 ± 1.2		RUCKSTUHL 86	DLCO	$E_{\text{cm}}^{\text{ee}} = 29 \text{ GeV}$
12.8 ± 0.5 ± 0.8	1420	SCHMIDKE 86	MRK2	$E_{\text{cm}}^{\text{ee}} = 29 \text{ GeV}$
15.3 ± 1.1 $\begin{smallmatrix} +1.3 \\ -1.6 \end{smallmatrix}$	367	ALTHOFF 85	TASS	$E_{\text{cm}}^{\text{ee}} = 34.5 \text{ GeV}$
13.6 ± 0.5 ± 0.8		BARTEL 85F	JADE	$E_{\text{cm}}^{\text{ee}} = 34.6 \text{ GeV}$
12.2 ± 1.3 ± 3.9		² BERGER 85	PLUT	$E_{\text{cm}}^{\text{ee}} = 34.6 \text{ GeV}$
13.3 ± 0.3 ± 0.6		FERNANDEZ 85	MAC	$E_{\text{cm}}^{\text{ee}} = 29 \text{ GeV}$
24 ± 6	35	BRANDELIK 80	TASS	$E_{\text{cm}}^{\text{ee}} = 30 \text{ GeV}$
32 ± 5	692	³ BACINO 78B	DLCO	$E_{\text{cm}}^{\text{ee}} = 3.1\text{--}7.4 \text{ GeV}$
35 ± 11		³ BRANDELIK 78	DASP	Assumes V–A decay
18 ± 6.5	33	³ JAROS 78	LGW	$E_{\text{cm}}^{\text{ee}} > 6 \text{ GeV}$

- ¹ BURCHAT 87 value is not independent of SCHMIDKE 86 value.
- ² Not independent of BERGER 85 $\Gamma(\mu^- \bar{\nu}_\mu \nu_\tau)/\Gamma_{\text{total}}$, $\Gamma(e^- \bar{\nu}_e \nu_\tau)/\Gamma_{\text{total}}$, $\Gamma(h^- \geq 1 \text{ neutrals } \nu_\tau)/\Gamma_{\text{total}}$, and $\Gamma(h^- \geq 0 K_L^0 \nu_\tau)/\Gamma_{\text{total}}$, and therefore not used in the fit.
- ³ Low energy experiments are not in average or fit because the systematic errors in background subtraction are judged to be large.

$\Gamma(h^- h^- h^+ \geq 0 \text{ neutrals } \nu_\tau \text{ (ex. } K_S^0 \rightarrow \pi^+ \pi^-) \text{ ("3-prong")})/\Gamma_{\text{total}}$ Γ_{63}/Γ

$$\Gamma_{63}/\Gamma = (\Gamma_{70} + \Gamma_{78} + \Gamma_{85} + \Gamma_{86} + \Gamma_{97} + \Gamma_{103} + \Gamma_{106} + \Gamma_{107} + 0.2789\Gamma_{150} + 0.2789\Gamma_{152} + 0.2789\Gamma_{154} + 0.492\Gamma_{170} + 0.9078\Gamma_{178} + 0.9078\Gamma_{179} + 0.9078\Gamma_{180})/\Gamma$$

VALUE (%)	EVTS	DOCUMENT ID	TECN	COMMENT
14.55 ± 0.06 OUR FIT				
14.61 ± 0.06 OUR AVERAGE				

14.556 ± 0.105 ± 0.076		¹ ACHARD 01D	L3	1992–1995 LEP runs
14.96 ± 0.09 ± 0.22	10.4k	AKERS 95Y	OPAL	1991–1994 LEP runs

• • • We use the following data for averages but not for fits. • • •

14.652 ± 0.067 ± 0.086		SCHAEEL 05c	ALEP	1991–1995 LEP runs
14.569 ± 0.093 ± 0.048	23k	² ABREU 01m	DLPH	1992–1995 LEP runs
14.22 ± 0.10 ± 0.37		³ BALEST 95c	CLEO	$E_{\text{cm}}^{\text{ee}} \approx 10.6 \text{ GeV}$

• • • We do not use the following data for averages, fits, limits, etc. • • •

15.26 ± 0.26 ± 0.22		ACTON 92H	OPAL	Repl. by AKERS 95Y
13.3 ± 0.3 ± 0.8		⁴ ALBRECHT 92D	ARG	$E_{\text{cm}}^{\text{ee}} = 9.4\text{--}10.6 \text{ GeV}$
14.35 $\begin{smallmatrix} +0.40 \\ -0.45 \end{smallmatrix}$ ± 0.24		DECAMP 92c	ALEP	1989–1990 LEP runs

- ¹ The correlation coefficients between this measurement and the ACHARD 01D measurements of $B(\tau \rightarrow \text{"1-prong"})$ and $B(\tau \rightarrow \text{"5-prong"})$ are -0.978 and -0.19 respectively.
- ² The correlation coefficients between this measurement and the ABREU 01M measurements of $B(\tau \rightarrow \text{1-prong})$ and $B(\tau \rightarrow \text{5-prong})$ are -0.98 and -0.08 respectively.
- ³ Not independent of BALEST 95c $B(h^- h^- h^+ \nu_\tau)$ and $B(h^- h^- h^+ \pi^0 \nu_\tau)$ values, and BORTOLETTO 93 $B(h^- h^- h^+ 2\pi^0 \nu_\tau)/B(h^- h^- h^+ \geq 0 \text{ neutrals } \nu_\tau)$ value.
- ⁴ This ALBRECHT 92D value is not independent of their $\Gamma(\mu^- \bar{\nu}_\mu \nu_\tau)/\Gamma_{\text{total}}$, $\Gamma(e^- \bar{\nu}_e \nu_\tau)/\Gamma_{\text{total}}$ value.

$\Gamma(h^- h^- h^+ \nu_\tau)/\Gamma_{\text{total}}$ Γ_{64}/Γ

$$\Gamma_{64}/\Gamma = (0.34598\Gamma_{36} + 0.34598\Gamma_{38} + \Gamma_{70} + \Gamma_{97} + \Gamma_{106} + 0.492\Gamma_{170} + 0.0153\Gamma_{178} + 0.0153\Gamma_{179})/\Gamma$$

VALUE (%)	EVTS	DOCUMENT ID	TECN	COMMENT
9.80 ± 0.05 OUR FIT				

• • • We use the following data for averages but not for fits. • • •

7.6 ± 0.1 ± 0.5	7.5k	¹ ALBRECHT 96E	ARG	$E_{\text{cm}}^{\text{ee}} = 9.4\text{--}10.6 \text{ GeV}$
------------------------	------	---------------------------	-----	--

• • • We do not use the following data for averages, fits, limits, etc. • • •

9.92 ± 0.10 ± 0.09	11.2k	² BUSKULIC 96	ALEP	Repl. by SCHAEEL 05c
9.49 ± 0.36 ± 0.63		DECAMP 92c	ALEP	Repl. by SCHAEEL 05c
8.7 ± 0.7 ± 0.3	694	³ BEHREND 90	CELL	$E_{\text{cm}}^{\text{ee}} = 35 \text{ GeV}$
7.0 ± 0.3 ± 0.7	1566	⁴ BAND 87	MAC	$E_{\text{cm}}^{\text{ee}} = 29 \text{ GeV}$
6.7 ± 0.8 ± 0.9		⁵ BURCHAT 87	MRK2	$E_{\text{cm}}^{\text{ee}} = 29 \text{ GeV}$
6.4 ± 0.4 ± 0.9		⁶ RUCKSTUHL 86	DLCO	$E_{\text{cm}}^{\text{ee}} = 29 \text{ GeV}$
7.8 ± 0.5 ± 0.8	890	SCHMIDKE 86	MRK2	$E_{\text{cm}}^{\text{ee}} = 29 \text{ GeV}$
8.4 ± 0.4 ± 0.7	1255	⁶ FERNANDEZ 85	MAC	$E_{\text{cm}}^{\text{ee}} = 29 \text{ GeV}$
9.7 ± 2.0 ± 1.3		BEHREND 84	CELL	$E_{\text{cm}}^{\text{ee}} = 14,22 \text{ GeV}$

- ¹ ALBRECHT 96E not independent of ALBRECHT 93c $\Gamma(h^- h^- h^+ \nu_\tau \text{ (ex. } K^0)) \times \Gamma(\text{particle}^- \geq 0 \text{ neutrals } \geq 0 K_L^0 \nu_\tau)/\Gamma_{\text{total}}$ value.
- ² BUSKULIC 96 quote $B(h^- h^- h^+ \nu_\tau \text{ (ex. } K^0)) = 9.50 \pm 0.10 \pm 0.11$. We add 0.42 to remove their K^0 correction and reduce the systematic error accordingly.
- ³ BEHREND 90 subtract 0.3% to account for the $\tau^- \rightarrow K^*(892)^- \nu_\tau$ contribution to measured events.
- ⁴ BAND 87 subtract for charged kaon modes; not independent of FERNANDEZ 85 value.
- ⁵ BURCHAT 87 value is not independent of SCHMIDKE 86 value.
- ⁶ Value obtained by multiplying paper's $R = B(h^- h^- h^+ \nu_\tau)/B(3\text{-prong})$ by $B(3\text{-prong}) = 0.143$ and subtracting 0.3% for $K^*(892)$ background.

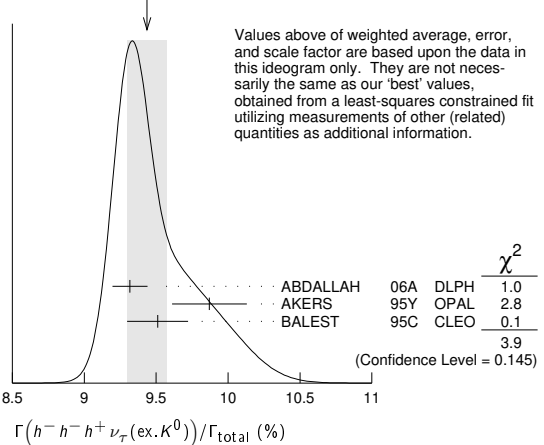
$\Gamma(h^- h^- h^+ \nu_\tau \text{ (ex. } K^0))/\Gamma_{\text{total}}$ Γ_{65}/Γ

$$\Gamma_{65}/\Gamma = (\Gamma_{70} + \Gamma_{97} + \Gamma_{106} + 0.492\Gamma_{170} + 0.0153\Gamma_{178} + 0.0153\Gamma_{179})/\Gamma$$

VALUE (%)	EVTS	DOCUMENT ID	TECN	COMMENT
9.46 ± 0.05 OUR FIT				
9.44 ± 0.14 OUR AVERAGE				Error includes scale factor of 1.4. See the ideogram below.

- 9.317 ± 0.090 ± 0.082 12.2k ¹ ABDALLAH 06A DLPH 1992–1995 LEP runs
 - 9.51 ± 0.07 ± 0.20 37.7k BALEST 95c CLEO $E_{\text{cm}}^{\text{ee}} \approx 10.6 \text{ GeV}$
 - • • We use the following data for averages but not for fits. • • •
 - 9.87 ± 0.10 ± 0.24 ² AKERS 95Y OPAL 1991–1994 LEP runs
 - • • We do not use the following data for averages, fits, limits, etc. • • •
 - 9.50 ± 0.10 ± 0.11 11.2k ³ BUSKULIC 96 ALEP Repl. by SCHAEEL 05c
- ¹ See footnote to ABDALLAH 06A $\Gamma(\tau^- \rightarrow h^- \nu_\tau)/\Gamma_{\text{total}}$ measurement for correlations with other measurements.
 - ² Not independent of AKERS 95Y $B(h^- h^- h^+ \geq 0 \text{ neutrals } \nu_\tau \text{ (ex. } K_S^0 \rightarrow \pi^+ \pi^-))$ and $B(h^- h^- h^+ \nu_\tau \text{ (ex. } K^0))/B(h^- h^- h^+ \geq 0 \text{ neutrals } \nu_\tau \text{ (ex. } K_S^0 \rightarrow \pi^+ \pi^-))$ values.
 - ³ Not independent of BUSKULIC 96 $B(h^- h^- h^+ \nu_\tau)$ value.

WEIGHTED AVERAGE
9.44 ± 0.14 (Error scaled by 1.4)



$\Gamma(h^- h^- h^+ \nu_\tau \text{ (ex. } K^0))/\Gamma_{\text{total}}$ Γ_{65}/Γ_{63} ("3-prong")

$$\Gamma_{65}/\Gamma_{63} = (\Gamma_{70} + \Gamma_{97} + \Gamma_{106} + 0.492\Gamma_{170} + 0.0153\Gamma_{178} + 0.0153\Gamma_{179}) / (0.4247\Gamma_{52} + \Gamma_{70} + \Gamma_{78} + \Gamma_{85} + \Gamma_{89} + \Gamma_{97} + \Gamma_{103} + \Gamma_{106} + \Gamma_{107} + 0.2789\Gamma_{150} + 0.2292\Gamma_{151} + 0.2789\Gamma_{152} + 0.2789\Gamma_{154} + 0.1131\Gamma_{156} + 0.3268\Gamma_{160} + 0.492\Gamma_{170} + 0.9078\Gamma_{178} + 0.9078\Gamma_{179} + 0.9078\Gamma_{180} + 0.893\Gamma_{182})$$

VALUE (units 10^{-2})	DOCUMENT ID	TECN	COMMENT
64.98 ± 0.31 OUR FIT			
66.0 ± 0.4 ± 1.4	AKERS 95Y	OPAL	1991–1994 LEP runs

$\Gamma(h^- h^- h^+ \nu_\tau \text{ (ex. } K^0, \mu))/\Gamma_{\text{total}}$ Γ_{66}/Γ

$$\Gamma_{66}/\Gamma = (\Gamma_{70} + \Gamma_{97} + \Gamma_{106} + 0.492\Gamma_{170})/\Gamma$$

VALUE (%)	DOCUMENT ID	TECN	COMMENT
9.43 ± 0.05 OUR FIT			

$\Gamma(\pi^- \pi^+ \pi^- \nu_\tau)/\Gamma_{\text{total}}$ $\Gamma_{67}/\Gamma = (0.34598\Gamma_{36} + \Gamma_{70} + 0.0153\Gamma_{178})/\Gamma$

VALUE (%)	DOCUMENT ID	TECN	COMMENT
9.31 ± 0.05 OUR FIT			

$\Gamma(\pi^- \pi^+ \pi^- \nu_\tau \text{ (ex. } K^0)) / \Gamma_{\text{total}}$ $\Gamma_{68} / \Gamma = (\Gamma_{70} + 0.0153\Gamma_{178}) / \Gamma$

Table with columns: VALUE (%), EVTS, DOCUMENT ID, TECN, COMMENT. Includes entries for LEE, AUBERT, BRIERE.

1 Quoted statistical error is 0.003%. Correlation matrix for LEE 10 branching fractions:

- (1) $\Gamma(\tau^- \rightarrow \pi^- \pi^+ \pi^- \nu_\tau \text{ (ex. } K^0)) / \Gamma_{\text{total}}$
(2) $\Gamma(\tau^- \rightarrow K^- \pi^+ \pi^- \nu_\tau \text{ (ex. } K^0)) / \Gamma_{\text{total}}$
(3) $\Gamma(\tau^- \rightarrow K^- K^+ \pi^- \nu_\tau) / \Gamma_{\text{total}}$
(4) $\Gamma(\tau^- \rightarrow K^- K^+ K^- \nu_\tau) / \Gamma_{\text{total}}$

Correlation matrix table with columns (1), (2), (3) and values.

2 Correlation matrix for AUBERT 08 branching fractions:

- (1) $\Gamma(\tau^- \rightarrow \pi^- \pi^+ \pi^- \nu_\tau \text{ (ex. } K^0)) / \Gamma_{\text{total}}$
(2) $\Gamma(\tau^- \rightarrow K^- \pi^+ \pi^- \nu_\tau \text{ (ex. } K^0)) / \Gamma_{\text{total}}$
(3) $\Gamma(\tau^- \rightarrow K^- K^+ \pi^- \nu_\tau) / \Gamma_{\text{total}}$
(4) $\Gamma(\tau^- \rightarrow K^- K^+ K^- \nu_\tau) / \Gamma_{\text{total}}$

Correlation matrix table with columns (1), (2), (3) and values.

3 47% correlated with BRIERE 03 $\tau^- \rightarrow K^- \pi^+ \pi^- \nu_\tau$ and 71% correlated with $\tau^- \rightarrow K^- K^+ \pi^- \nu_\tau$ because of a common 5% normalization error.

$\Gamma(\pi^- \pi^+ \pi^- \nu_\tau \text{ (ex. } K^0, \text{ non-axial vector)}) / \Gamma(\pi^- \pi^+ \pi^- \nu_\tau \text{ (ex. } K^0))$ $\Gamma_{69} / \Gamma_{68}$

Table with columns: VALUE, CL%, DOCUMENT ID, TECN, COMMENT.

1 Model-independent limit from structure function analysis on contribution to $B(\tau^- \rightarrow \pi^- \pi^+ \pi^- \nu_\tau \text{ (ex. } K^0))$ from non-axial vectors.

$\Gamma(\pi^- \pi^+ \pi^- \nu_\tau \text{ (ex. } K^0, \omega)) / \Gamma_{\text{total}}$ Γ_{70} / Γ

Table with columns: VALUE (%), EVTS, DOCUMENT ID, TECN, COMMENT.

1 See footnote to SCHAEEL 05c $\Gamma(\tau^- \rightarrow e^- \bar{\nu}_e \nu_\tau) / \Gamma_{\text{total}}$ measurement for correlations with other measurements.

$\Gamma(h^- h^- h^+ \geq 1 \text{ neutrals } \nu_\tau) / \Gamma_{\text{total}}$ Γ_{71} / Γ

Table with columns: VALUE (%), EVTS, DOCUMENT ID, TECN, COMMENT.

$\Gamma(\pi^- \pi^+ \pi^- \pi^0 \nu_\tau \text{ (ex. } K^0, \omega)) / \Gamma_{\text{total}}$ Γ_{72} / Γ

Table with columns: VALUE (%), EVTS, DOCUMENT ID, TECN, COMMENT.

- • • We do not use the following data for averages, fits, limits, etc. • • •
- 5.6 ± 0.7 ± 0.3 352 1 BEHREND 90 CELL $E_{\text{cm}}^{\text{ex}} = 35 \text{ GeV}$
- 4.2 ± 0.5 ± 0.9 203 2 ALBRECHT 87L ARG $E_{\text{cm}}^{\text{ex}} = 10 \text{ GeV}$
- 6.1 ± 0.8 ± 0.9 3 BURCHAT 87 MRK2 $E_{\text{cm}}^{\text{ex}} = 29 \text{ GeV}$
- 7.6 ± 0.4 ± 0.9 4,5 RUCKSTUHL 86 DLCO $E_{\text{cm}}^{\text{ex}} = 29 \text{ GeV}$
- 4.7 ± 0.5 ± 0.8 530 6 SCHMIDKE 86 MRK2 $E_{\text{cm}}^{\text{ex}} = 29 \text{ GeV}$
- 5.6 ± 0.4 ± 0.7 5 FERNANDEZ 85 MAC $E_{\text{cm}}^{\text{ex}} = 29 \text{ GeV}$
- 6.2 ± 2.3 ± 1.7 BEHREND 84 CELL $E_{\text{cm}}^{\text{ex}} = 14,22 \text{ GeV}$

1 BEHREND 90 value is not independent of BEHREND 90 $B(3h\nu_\tau \geq 1 \text{ neutrals}) + B(5\text{-prong})$.
2 ALBRECHT 87L measure the product of branching ratios $B(3\pi^\pm \pi^0 \nu_\tau) B((e\bar{\nu}_e \mu\bar{\nu}_\mu \text{ or } \pi^0 \text{ or } K^0 \text{ or } \rho) \nu_\tau) = 0.029$ and use the PDG 86 values for the second branching ratio which sum to 0.69 ± 0.03 to get the quoted value.
3 BURCHAT 87 value is not independent of SCHMIDKE 86 value.
4 Contributions from kaons and from $>1\pi^0$ are subtracted. Not independent of (3-prong + $0\pi^0$) and (3-prong + $\geq 0\pi^0$) values.
5 Value obtained using paper's $R = B(h^- h^- h^+ \nu_\tau) / B(3\text{-prong})$ and current $B(3\text{-prong}) = 0.143$.
6 Not independent of SCHMIDKE 86 $h^- h^- h^+ \nu_\tau$ and $h^- h^- h^+ (\geq 0\pi^0) \nu_\tau$ values.

$\Gamma(h^- h^- h^+ \geq 1\pi^0 \nu_\tau \text{ (ex. } K^0)) / \Gamma_{\text{total}}$ Γ_{72} / Γ

Table with columns: VALUE (%), EVTS, DOCUMENT ID, TECN, COMMENT.

- • • We use the following data for averages but not for fits. • • •
- 5.106 ± 0.083 ± 0.103 10.1k 1 ABDALLAH 06A DLPH 1992–1995 LEP runs
- 5.09 ± 0.10 ± 0.23 2 AKERS 95Y OPAL 1991–1994 LEP runs
- • • We do not use the following data for averages, fits, limits, etc. • • •
- 4.95 ± 0.29 ± 0.65 570 DECAMP 92c ALEP Repl. by SCHAEEL 05c

1 See footnote to ABDALLAH 06A $\Gamma(\tau^- \rightarrow h^- \nu_\tau) / \Gamma_{\text{total}}$ measurement for correlations with other measurements.
2 Not independent of AKERS 95Y $B(h^- h^- h^+ \geq 0 \text{ neutrals } \nu_\tau \text{ (ex. } K_S^0 \rightarrow \pi^+ \pi^-))$ and $B(h^- h^- h^+ \geq 0 \text{ neutrals } \nu_\tau \text{ (ex. } K_S^0)) / B(h^- h^- h^+ \geq 0 \text{ neutrals } \nu_\tau \text{ (ex. } K_S^0 \rightarrow \pi^+ \pi^-))$ values.

$\Gamma(h^- h^- h^+ \pi^0 \nu_\tau) / \Gamma_{\text{total}}$ Γ_{73} / Γ

Table with columns: VALUE (%), EVTS, DOCUMENT ID, TECN, COMMENT.

- • • We do not use the following data for averages, fits, limits, etc. • • •
- 4.45 ± 0.09 ± 0.07 6.1k 1 BUSKULIC 96 ALEP Repl. by SCHAEEL 05c
- 1 BUSKULIC 96 quote $B(h^- h^- h^+ \pi^0 \nu_\tau \text{ (ex. } K^0)) = 4.30 \pm 0.09 \pm 0.09$. We add 0.15 to remove their K^0 correction and reduce the systematic error accordingly.

$\Gamma(h^- h^- h^+ \pi^0 \nu_\tau \text{ (ex. } K^0)) / \Gamma_{\text{total}}$ Γ_{74} / Γ

Table with columns: VALUE (%), EVTS, DOCUMENT ID, TECN, COMMENT.

- • • We do not use the following data for averages, fits, limits, etc. • • •
- 4.57 ± 0.05 OUR FIT
- 4.545 ± 0.106 ± 0.103 8.9k 1 ABDALLAH 06A DLPH 1992–1995 LEP runs
- 4.23 ± 0.06 ± 0.22 7.2k BALEST 95c CLEO $E_{\text{cm}}^{\text{ex}} \approx 10.6 \text{ GeV}$
- 1 See footnote to ABDALLAH 06A $\Gamma(\tau^- \rightarrow h^- \nu_\tau) / \Gamma_{\text{total}}$ measurement for correlations with other measurements.

$\Gamma(h^- h^- h^+ \pi^0 \nu_\tau \text{ (ex. } K^0, \omega)) / \Gamma_{\text{total}}$ $\Gamma_{75} / \Gamma = (\Gamma_{78} + \Gamma_{103} + \Gamma_{107} + 0.2292\Gamma_{152}) / \Gamma$

Table with columns: VALUE (%), EVTS, DOCUMENT ID, TECN, COMMENT.

$\Gamma(\pi^- \pi^+ \pi^- \pi^0 \nu_\tau) / \Gamma_{\text{total}}$ Γ_{76} / Γ

Table with columns: VALUE (%), EVTS, DOCUMENT ID, TECN, COMMENT.

$\Gamma(\pi^- \pi^+ \pi^- \pi^0 \nu_\tau \text{ (ex. } K^0)) / \Gamma_{\text{total}}$ Γ_{77} / Γ

Table with columns: VALUE (%), EVTS, DOCUMENT ID, TECN, COMMENT.

$\Gamma(\pi^- \pi^+ \pi^- \pi^0 \nu_\tau \text{ (ex. } K^0, \omega)) / \Gamma_{\text{total}}$ Γ_{78} / Γ

Table with columns: VALUE (%), EVTS, DOCUMENT ID, TECN, COMMENT.

1 SCHAEEL 05c quote (4.590 ± 0.057 ± 0.064)%. We add 0.008% to remove their correction for $\tau^- \rightarrow \pi^- \pi^0 \omega \nu_\tau \rightarrow \pi^- \pi^0 \pi^+ \pi^- \nu_\tau$ decays. See footnote to SCHAEEL 05c $\Gamma(\tau^- \rightarrow e^- \bar{\nu}_e \nu_\tau) / \Gamma_{\text{total}}$ measurement for correlations with other measurements.
2 EDWARDS 00A quote (4.19 ± 0.10) × 10⁻² with a 5% systematic error.

$\Gamma(h^- \rho \pi^0 \nu_\tau) / \Gamma(h^- h^- h^+ \pi^0 \nu_\tau)$ $\Gamma_{79} / \Gamma_{73}$

Table with columns: VALUE (%), EVTS, DOCUMENT ID, TECN, COMMENT.

- • • We do not use the following data for averages, fits, limits, etc. • • •
- 0.30 ± 0.04 ± 0.02 393 ALBRECHT 91D ARG $E_{\text{cm}}^{\text{ex}} = 9.4\text{--}10.6 \text{ GeV}$

$\Gamma(h^- \rho^+ h^- \nu_\tau) / \Gamma(h^- h^- h^+ \pi^0 \nu_\tau)$ $\Gamma_{80} / \Gamma_{73}$

Table with columns: VALUE (%), EVTS, DOCUMENT ID, TECN, COMMENT.

- • • We do not use the following data for averages, fits, limits, etc. • • •
- 0.10 ± 0.03 ± 0.04 142 ALBRECHT 91D ARG $E_{\text{cm}}^{\text{ex}} = 9.4\text{--}10.6 \text{ GeV}$

$\Gamma(h^- \rho^- h^+ \nu_\tau) / \Gamma(h^- h^- h^+ \pi^0 \nu_\tau)$ $\Gamma_{81} / \Gamma_{73}$

Table with columns: VALUE (%), EVTS, DOCUMENT ID, TECN, COMMENT.

- • • We do not use the following data for averages, fits, limits, etc. • • •
- 0.26 ± 0.05 ± 0.01 370 ALBRECHT 91D ARG $E_{\text{cm}}^{\text{ex}} = 9.4\text{--}10.6 \text{ GeV}$

$\Gamma(h^- h^- h^+ \geq 2\pi^0 \nu_\tau \text{ (ex. } K^0)) / \Gamma_{\text{total}}$ Γ_{82} / Γ

Table with columns: VALUE (%), EVTS, DOCUMENT ID, TECN, COMMENT.

- • • We do not use the following data for averages, fits, limits, etc. • • •
- 5.17 ± 0.031 OUR FIT
- 5.61 ± 0.068 ± 0.095 1.3k 1 ABDALLAH 06A DLPH 1992–1995 LEP runs
- 1 See footnote to ABDALLAH 06A $\Gamma(\tau^- \rightarrow h^- \nu_\tau) / \Gamma_{\text{total}}$ measurement for correlations with other measurements.

$\Gamma(h^- h^- h^+ 2\pi^0 \nu_\tau) / \Gamma_{\text{total}}$ Γ_{83} / Γ

Table with columns: VALUE (%), EVTS, DOCUMENT ID, TECN, COMMENT.

- • • We do not use the following data for averages, fits, limits, etc. • • •
- 5.05 ± 0.031 OUR FIT

Lepton Particle Listings

τ

$$\Gamma(h^- h^- h^+ 2\pi^0 \nu_\tau (\text{ex. } K^0)) / \Gamma_{\text{total}} \quad \Gamma_{84} / \Gamma$$

$$\Gamma_{84} / \Gamma = (\Gamma_{85} + 0.2292\Gamma_{150} + 0.2292\Gamma_{154} + 0.893\Gamma_{180}) / \Gamma$$

VALUE (%)	EVTS	DOCUMENT ID	TECN	COMMENT
-----------	------	-------------	------	---------

0.495 ± 0.031 OUR FIT
0.435 ± 0.030 ± 0.035 2.6k 1 SCHAEL 05c ALEP 1991-1995 LEP runs

• • • We do not use the following data for averages, fits, limits, etc. • • •
 0.50 ± 0.07 ± 0.07 1.8k BUSKULIC 96 ALEP Repl. by SCHAEL 05c

¹ SCHAEL 05c quote (0.392 ± 0.030 ± 0.035)%. We add 0.043% to remove their correction for $\tau^- \rightarrow \pi^- \eta \pi^0 \nu_\tau \rightarrow \pi^- \pi^+ \pi^- 2\pi^0 \nu_\tau$ and $\tau^- \rightarrow K^*(892)^- \eta \nu_\tau \rightarrow K^- \pi^+ \pi^- 2\pi^0 \nu_\tau$ decays. See footnote to SCHAEL 05c $\Gamma(\tau^- \rightarrow e^- \bar{\nu}_e \nu_\tau) / \Gamma_{\text{total}}$ measurement for correlations with other measurements.

$$\Gamma(h^- h^- h^+ 2\pi^0 \nu_\tau (\text{ex. } K^0)) / \Gamma(h^- h^- h^+ \geq 0 \text{ neutrals } \nu_\tau) \geq 0 K^0 \nu_\tau \quad \Gamma_{84} / \Gamma_{62}$$

$$\Gamma_{84} / \Gamma_{62} = (\Gamma_{85} + 0.2292\Gamma_{150} + 0.2292\Gamma_{154} + 0.893\Gamma_{180}) / (0.34598\Gamma_{36} + 0.34598\Gamma_{38} + 0.34598\Gamma_{41} + 0.34598\Gamma_{43} + 0.4247\Gamma_{48} + 0.6920\Gamma_{49} + 0.8494\Gamma_{52} + 0.6920\Gamma_{56} + 0.6534\Gamma_{61} + \Gamma_{70} + \Gamma_{78} + \Gamma_{85} + \Gamma_{89} + \Gamma_{97} + \Gamma_{103} + \Gamma_{106} + \Gamma_{107} + 0.2789\Gamma_{150} + 0.2292\Gamma_{151} + 0.2789\Gamma_{152} + 0.2789\Gamma_{154} + 0.3759\Gamma_{156} + 0.3268\Gamma_{160} + 0.7259\Gamma_{170} + 0.9078\Gamma_{178} + 0.9078\Gamma_{179} + 0.9078\Gamma_{180} + 0.893\Gamma_{182})$$

VALUE (units 10 ⁻²)	EVTS	DOCUMENT ID	TECN	COMMENT
---------------------------------	------	-------------	------	---------

3.26 ± 0.20 OUR FIT
3.4 ± 0.2 ± 0.3 668 BORTOLETTO93 CLEO $E_{\text{cm}}^{\text{ee}} \approx 10.6$ GeV

$$\Gamma(h^- h^- h^+ 2\pi^0 \nu_\tau (\text{ex. } K^0, \omega, \eta)) / \Gamma_{\text{total}} \quad \Gamma_{85} / \Gamma$$

VALUE (units 10 ⁻⁴)	DOCUMENT ID	TECN	COMMENT
---------------------------------	-------------	------	---------

10 ± 4 OUR FIT

$$\Gamma(h^- h^- h^+ 3\pi^0 \nu_\tau) / \Gamma_{\text{total}} \quad \Gamma_{86} / \Gamma = (0.4247\Gamma_{52} + \Gamma_{87} + 0.1131\Gamma_{156}) / \Gamma$$

VALUE (units 10 ⁻⁴)	CL%	EVTS	DOCUMENT ID	TECN	COMMENT
---------------------------------	-----	------	-------------	------	---------

2.13 ± 0.30 OUR FIT

2.2 ± 0.3 ± 0.4 139 ANASTASSOV 01 CLEO $E_{\text{cm}}^{\text{ee}} = 10.6$ GeV

• • • We do not use the following data for averages, fits, limits, etc. • • •

< 4.9 95 SCHAEL 05c ALEP 1991-1995 LEP runs

2.85 ± 0.56 ± 0.51 57 ANDERSON 97 CLEO Repl. by ANAS-

11 ± 4 ± 5 440 ¹BUSKULIC 96 ALEP Repl. by SCHAEL 05c

¹ BUSKULIC 96 state their measurement is for $B(h^- h^- h^+ \geq 3\pi^0 \nu_\tau)$. We assume that $B(h^- h^- h^+ \geq 4\pi^0 \nu_\tau)$ is very small.

$$\Gamma(2\pi^- \pi^+ 3\pi^0 \nu_\tau (\text{ex. } K^0)) / \Gamma_{\text{total}} \quad \Gamma_{87} / \Gamma$$

$$\Gamma_{87} / \Gamma = (\Gamma_{89} + 0.2292\Gamma_{151} + 0.3268\Gamma_{160} + 0.893\Gamma_{182}) / \Gamma$$

VALUE (units 10 ⁻⁴)	DOCUMENT ID	TECN	COMMENT
---------------------------------	-------------	------	---------

1.95 ± 0.30 OUR FIT

• • • We use the following data for averages but not for fits. • • •

2.07 ± 0.18 ± 0.37 ¹LEES 12x BABR 468 fb⁻¹ $E_{\text{cm}}^{\text{ee}} = 10.6$ GeV

¹ Not independent of LEES 12x $\Gamma(\tau^- \rightarrow \eta \pi^- \pi^+ \pi^- \nu_\tau (\text{ex. } K^0)) / \Gamma$, $\Gamma(\tau^- \rightarrow \eta \pi^- \pi^0 \pi^0 \nu_\tau) / \Gamma$, $\Gamma(\tau^- \rightarrow \pi^- \omega 2\pi^0 \nu_\tau) / \Gamma$, and $\Gamma(\tau^- \rightarrow f_1(1285) \pi^- \nu_\tau \rightarrow \eta \pi^- \pi^+ \pi^- \nu_\tau) / \Gamma$ values.

$$\Gamma(2\pi^- \pi^+ 3\pi^0 \nu_\tau (\text{ex. } K^0, \eta, f_1(1285))) / \Gamma_{\text{total}} \quad \Gamma_{88} / \Gamma$$

VALUE (units 10 ⁻⁴)	DOCUMENT ID	TECN	COMMENT
---------------------------------	-------------	------	---------

1.69 ± 0.08 ± 0.43 LEES 12x BABR 468 fb⁻¹ $E_{\text{cm}}^{\text{ee}} = 10.6$ GeV

$$\Gamma(2\pi^- \pi^+ 3\pi^0 \nu_\tau (\text{ex. } K^0, \eta, \omega, f_1(1285))) / \Gamma_{\text{total}} \quad \Gamma_{89} / \Gamma$$

VALUE (units 10 ⁻⁵)	DOCUMENT ID	TECN	COMMENT
---------------------------------	-------------	------	---------

1.4 ± 2.7 OUR FIT

1.0 ± 0.8 ± 3.0 ¹LEES 12x BABR 468 fb⁻¹ $E_{\text{cm}}^{\text{ee}} = 10.6$ GeV

¹ LEES 12x measurement corresponds to the lower limit of $< 5.8 \times 10^{-5}$ at 90% CL.

$$\Gamma(K^- h^+ h^- \geq 0 \text{ neutrals } \nu_\tau) / \Gamma_{\text{total}} \quad \Gamma_{90} / \Gamma$$

$$\Gamma_{90} / \Gamma = (0.34598\Gamma_{38} + 0.34598\Gamma_{43} + \Gamma_{97} + \Gamma_{103} + \Gamma_{106} + \Gamma_{107} + 0.2789\Gamma_{152} + 0.492\Gamma_{170} + 0.9078\Gamma_{179}) / \Gamma$$

VALUE (%)	CL%	DOCUMENT ID	TECN	COMMENT
-----------	-----	-------------	------	---------

0.629 ± 0.014 OUR FIT

< 0.6 90 AIHARA 84c TPC $E_{\text{cm}}^{\text{ee}} = 29$ GeV

$$\Gamma(K^- h^+ \pi^- \nu_\tau (\text{ex. } K^0)) / \Gamma_{\text{total}} \quad \Gamma_{91} / \Gamma = (\Gamma_{97} + \Gamma_{106} + 0.0153\Gamma_{179}) / \Gamma$$

VALUE (%)	DOCUMENT ID	TECN	COMMENT
-----------	-------------	------	---------

0.437 ± 0.007 OUR FIT

$$\Gamma(K^- h^+ \pi^- \nu_\tau (\text{ex. } K^0)) / \Gamma(\pi^- \pi^+ \pi^- \nu_\tau (\text{ex. } K^0)) \quad \Gamma_{91} / \Gamma_{68}$$

$$\Gamma_{91} / \Gamma_{68} = (\Gamma_{97} + \Gamma_{106} + 0.0153\Gamma_{179}) / (\Gamma_{70} + 0.0153\Gamma_{178})$$

VALUE (%)	EVTS	DOCUMENT ID	TECN	COMMENT
-----------	------	-------------	------	---------

4.85 ± 0.08 OUR FIT

5.44 ± 0.21 ± 0.53 7.9k RICHICHI 99 CLEO $E_{\text{cm}}^{\text{ee}} = 10.6$ GeV

$$\Gamma(K^- h^+ \pi^- \pi^0 \nu_\tau (\text{ex. } K^0)) / \Gamma_{\text{total}} \quad \Gamma_{92} / \Gamma$$

$$\Gamma_{92} / \Gamma = (\Gamma_{103} + \Gamma_{107} + 0.2292\Gamma_{152} + 0.893\Gamma_{179}) / \Gamma$$

VALUE (units 10 ⁻⁴)	DOCUMENT ID	TECN	COMMENT
---------------------------------	-------------	------	---------

8.6 ± 1.2 OUR FIT

$$\Gamma(K^- h^+ \pi^- \pi^0 \nu_\tau (\text{ex. } K^0)) / \Gamma(\pi^- \pi^+ \pi^- \pi^0 \nu_\tau (\text{ex. } K^0)) \quad \Gamma_{92} / \Gamma_{77}$$

$$\Gamma_{92} / \Gamma_{77} = (\Gamma_{103} + \Gamma_{107} + 0.2292\Gamma_{152} + 0.893\Gamma_{179}) / (\Gamma_{78} + 0.893\Gamma_{178} + 0.0153\Gamma_{180})$$

VALUE (%)	EVTS	DOCUMENT ID	TECN	COMMENT
-----------	------	-------------	------	---------

1.91 ± 0.26 OUR FIT
2.61 ± 0.45 ± 0.42 719 RICHICHI 99 CLEO $E_{\text{cm}}^{\text{ee}} = 10.6$ GeV

$$\Gamma(K^- \pi^+ \pi^- \geq 0 \text{ neutrals } \nu_\tau) / \Gamma_{\text{total}} \quad \Gamma_{93} / \Gamma$$

$$\Gamma_{93} / \Gamma = (0.34598\Gamma_{38} + 0.34598\Gamma_{43} + \Gamma_{97} + \Gamma_{103} + 0.2789\Gamma_{152} + 0.9078\Gamma_{179}) / \Gamma$$

VALUE (%)	EVTS	DOCUMENT ID	TECN	COMMENT
-----------	------	-------------	------	---------

0.477 ± 0.014 OUR FIT

0.58 +0.15 -0.13 ± 0.12 20 ¹BAUER 94 TPC $E_{\text{cm}}^{\text{ee}} = 29$ GeV

• • • We do not use the following data for averages, fits, limits, etc. • • •

0.22 +0.16 ± 0.05 9 ²MILLS 85 DLCO $E_{\text{cm}}^{\text{ee}} = 29$ GeV

¹ We multiply 0.58% by 0.20, the relative systematic error quoted by BAUER 94, to obtain the systematic error.

² Error correlated with MILLS 85 ($K K \pi \nu$) value. We multiply 0.22% by 0.23, the relative systematic error quoted by MILLS 85, to obtain the systematic error.

$$\Gamma(K^- \pi^+ \pi^- \geq 0\pi^0 \nu_\tau (\text{ex. } K^0)) / \Gamma_{\text{total}} \quad \Gamma_{94} / \Gamma$$

$$\Gamma_{94} / \Gamma = (\Gamma_{97} + \Gamma_{103} + 0.2292\Gamma_{152} + 0.9078\Gamma_{179}) / \Gamma$$

VALUE (%)	DOCUMENT ID	TECN	COMMENT
-----------	-------------	------	---------

0.373 ± 0.013 OUR FIT

0.30 ± 0.05 OUR AVERAGE

• • • We use the following data for averages but not for fits. • • •

0.343 ± 0.073 ± 0.031 ¹ABBIENDI 00D OPAL 1990-1995 LEP runs

0.275 ± 0.064 ¹BARATE 98 ALEP 1991-1995 LEP runs

¹ Not independent of BARATE 98 $\Gamma(\tau^- \rightarrow K^- \pi^+ \pi^- \nu_\tau) / \Gamma_{\text{total}}$ and $\Gamma(\tau^- \rightarrow K^- \pi^+ \pi^- \pi^0 \nu_\tau) / \Gamma_{\text{total}}$ values.

$$\Gamma(K^- \pi^+ \pi^- \nu_\tau) / \Gamma_{\text{total}} \quad \Gamma_{95} / \Gamma = (0.34598\Gamma_{38} + \Gamma_{97} + 0.0153\Gamma_{179}) / \Gamma$$

VALUE (%)	DOCUMENT ID	TECN	COMMENT
-----------	-------------	------	---------

0.345 ± 0.007 OUR FIT

$$\Gamma(K^- \pi^+ \pi^- \nu_\tau (\text{ex. } K^0)) / \Gamma_{\text{total}} \quad \Gamma_{96} / \Gamma = (\Gamma_{97} + 0.0153\Gamma_{179}) / \Gamma$$

VALUE (%)	EVTS	DOCUMENT ID	TECN	COMMENT
-----------	------	-------------	------	---------

0.293 ± 0.007 OUR FIT

0.290 ± 0.018 OUR AVERAGE Error includes scale factor of 2.4. See the ideogram below.

0.330 ± 0.001 ± 0.016 ¹LEE 10 BELL 666 fb⁻¹ $E_{\text{cm}}^{\text{ee}} = 10.6$ GeV

0.273 ± 0.002 ± 0.009 70k ²AUBERT 08 BABR 342 fb⁻¹ $E_{\text{cm}}^{\text{ee}} = 10.6$ GeV

0.415 ± 0.053 ± 0.040 269 ABBIENDI 04J OPAL 1991-1995 LEP runs

0.384 ± 0.014 ± 0.038 3.5k ³BRIERE 03 CLE3 $E_{\text{cm}}^{\text{ee}} = 10.6$ GeV

0.214 ± 0.037 ± 0.029 BARATE 98 ALEP 1991-1995 LEP runs

• • • We use the following data for averages but not for fits. • • •

0.346 ± 0.023 ± 0.056 158 ⁴RICHICHI 99 CLEO $E_{\text{cm}}^{\text{ee}} = 10.6$ GeV

• • • We do not use the following data for averages, fits, limits, etc. • • •

0.360 ± 0.082 ± 0.048 ABBIENDI 00D OPAL 1990-1995 LEP runs

¹ See footnote to LEE 10 $\Gamma(\tau^- \rightarrow \pi^- \pi^+ \pi^- \nu_\tau (\text{ex. } K^0)) / \Gamma_{\text{total}}$ measurement for correlations with other measurements. Not independent of LEE 10 $\Gamma(\tau^- \rightarrow K^- \pi^+ \pi^- \nu_\tau (\text{ex. } K^0)) / \Gamma_{\text{total}}$ value.

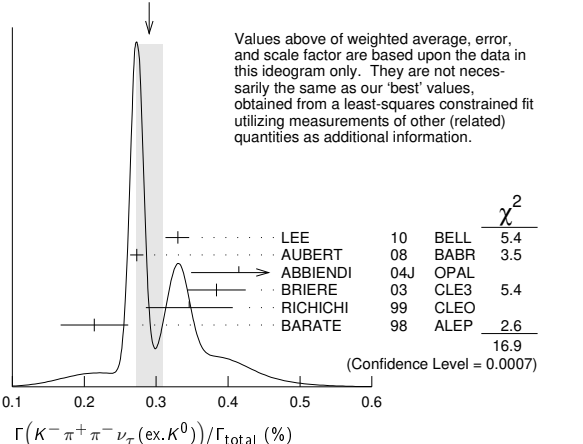
² See footnote to AUBERT 08 $\Gamma(\tau^- \rightarrow \pi^- \pi^+ \pi^- \nu_\tau (\text{ex. } K^0)) / \Gamma_{\text{total}}$ measurement for correlations with other measurements.

³ 47% correlated with BRIERE 03 $\tau^- \rightarrow \pi^- \pi^+ \pi^- \nu_\tau$ and 34% correlated with $\tau^- \rightarrow K^- K^+ \pi^- \nu_\tau$ because of a common 5% normalization error.

⁴ Not independent of RICHICHI 99

$\Gamma(\tau^- \rightarrow K^- h^+ \pi^- \nu_\tau (\text{ex. } K^0)) / \Gamma(\tau^- \rightarrow \pi^- \pi^+ \pi^- \nu_\tau (\text{ex. } K^0))$, $\Gamma(\tau^- \rightarrow K^- K^+ \pi^- \nu_\tau) / \Gamma(\tau^- \rightarrow \pi^- \pi^+ \pi^- \nu_\tau (\text{ex. } K^0))$ and BALEST 95c $\Gamma(\tau^- \rightarrow h^- h^- h^+ \nu_\tau (\text{ex. } K^0)) / \Gamma_{\text{total}}$ values.

WEIGHTED AVERAGE
 0.290 ± 0.018 (Error scaled by 2.4)



$$\Gamma(K^- \pi^+ \pi^- \nu_\tau(\text{ex.}K^0))/\Gamma(\pi^- \pi^+ \pi^- \nu_\tau(\text{ex.}K^0)) \quad \Gamma_{96}/\Gamma_{68}$$

$$\Gamma_{96}/\Gamma_{68} = (\Gamma_{97} + 0.0153\Gamma_{179})/(\Gamma_{70} + 0.0153\Gamma_{178})$$

VALUE (units 10 ⁻²)	EVTS	DOCUMENT ID	TECN	COMMENT
3.25 ± 0.07 OUR FIT				

• • • We use the following data for averages but not for fits. • • •

3.92 ± 0.02 ± 0.15 794k 1 LEE 10 BELL 666 fb⁻¹ E_{cm}^{ee} = 10.6 GeV

1 Not independent of LEE 10 $\Gamma(\tau^- \rightarrow K^- \pi^+ \pi^- \nu_\tau(\text{ex.}K^0))/\Gamma_{\text{total}}$ and $\Gamma(\tau^- \rightarrow \pi^- \pi^+ \pi^- \nu_\tau(\text{ex.}K^0))/\Gamma_{\text{total}}$ values.

$$\Gamma(K^- \pi^+ \pi^- \nu_\tau(\text{ex.}K^0, \omega))/\Gamma_{\text{total}} \quad \Gamma_{97}/\Gamma$$

VALUE (units 10 ⁻³)	DOCUMENT ID
2.93 ± 0.07 OUR FIT	

$$\Gamma(K^- \rho^0 \nu_\tau \rightarrow K^- \pi^+ \pi^- \nu_\tau)/\Gamma(K^- \pi^+ \pi^- \nu_\tau(\text{ex.}K^0)) \quad \Gamma_{98}/\Gamma_{96}$$

VALUE	DOCUMENT ID	TECN	COMMENT
0.48 ± 0.14 ± 0.10	1 ASNER 00B CLEO	E _{cm} ^{ee} = 10.6 GeV	

• • • We do not use the following data for averages, fits, limits, etc. • • •

0.39 ± 0.14 2 BARATE 99R ALEP 1991-1995 LEP runs

1 ASNER 00B assume $\tau^- \rightarrow K^- \pi^+ \pi^- \nu_\tau(\text{ex.}K^0)$ decays proceed only through $K\rho$ and $K^* \pi$ intermediate states. They assume the resonance structure of $\tau^- \rightarrow K^- \pi^+ \pi^- \nu_\tau(\text{ex.}K^0)$ decays is dominated by $K_1(1270)^-$ and $K_1(1400)^-$ resonances, and assume $B(K_1(1270) \rightarrow K^*(892)\pi) = (16 \pm 5)\%$, $B(K_1(1270) \rightarrow K\rho) = (42 \pm 6)\%$, and $B(K_1(1400) \rightarrow K\rho) = 0$.

2 BARATE 99R assume $\tau^- \rightarrow K^- \pi^+ \pi^- \nu_\tau(\text{ex.}K^0)$ decays proceed only through $K\rho$ and $K^* \pi$ intermediate states. The quoted error is statistical only.

$$\Gamma(K^- \pi^+ \pi^- \pi^0 \nu_\tau)/\Gamma_{\text{total}} \quad \Gamma_{99}/\Gamma$$

$$\Gamma_{99}/\Gamma = (0.3459\Gamma_{43} + \Gamma_{103} + 0.2292\Gamma_{152} + 0.893\Gamma_{179})/\Gamma$$

VALUE (units 10 ⁻⁴)	DOCUMENT ID
13.1 ± 1.2 OUR FIT	

$$\Gamma(K^- \pi^+ \pi^- \pi^0 \nu_\tau(\text{ex.}K^0))/\Gamma_{\text{total}} \quad \Gamma_{100}/\Gamma$$

$$\Gamma_{100}/\Gamma = (\Gamma_{103} + 0.2292\Gamma_{152} + 0.893\Gamma_{179})/\Gamma$$

VALUE (units 10 ⁻⁴)	CL%	DOCUMENT ID	TECN	COMMENT
7.9 ± 1.2 OUR FIT				
7.3 ± 1.2 OUR AVERAGE				

7.4 ± 0.8 ± 1.1 1 ARMS 05 CLE3 7.6 fb⁻¹, E_{cm}^{ee} = 10.6 GeV

6.1 ± 3.9 ± 1.8 BARATE 98 ALEP 1991-1995 LEP runs

• • • We use the following data for averages but not for fits. • • •

7.5 ± 2.6 ± 1.8 2 RICHICHI 99 CLEO E_{cm}^{ee} = 10.6 GeV

• • • We do not use the following data for averages, fits, limits, etc. • • •

<17 95 ABBIENDI 00D OPAL 1990-1995 LEP runs

1 Not independent of ARMS 05 $\Gamma(\tau^- \rightarrow K^- \pi^+ \pi^- \pi^0 \nu_\tau(\text{ex.}K^0, \omega))/\Gamma_{\text{total}}$ and $\Gamma(\tau^- \rightarrow K^- \omega \nu_\tau)/\Gamma_{\text{total}}$ values.

2 Not independent of RICHICHI 99 $\Gamma(\tau^- \rightarrow K^- h^+ \pi^- \nu_\tau(\text{ex.}K^0))/\Gamma(\tau^- \rightarrow \pi^- \pi^+ \pi^- \nu_\tau(\text{ex.}K^0))$, $\Gamma(\tau^- \rightarrow K^- K^+ \pi^- \nu_\tau)/\Gamma(\tau^- \rightarrow \pi^- \pi^+ \pi^- \nu_\tau(\text{ex.}K^0))$ and BALEST 95c $\Gamma(\tau^- \rightarrow h^- h^- h^+ \nu_\tau(\text{ex.}K^0))/\Gamma_{\text{total}}$ values.

$$\Gamma(K^- \pi^+ \pi^- \pi^0 \nu_\tau(\text{ex.}K^0, \eta))/\Gamma_{\text{total}} \quad \Gamma_{101}/\Gamma = (\Gamma_{103} + 0.893\Gamma_{179})/\Gamma$$

VALUE (units 10 ⁻⁴)	DOCUMENT ID
7.6 ± 1.2 OUR FIT	

$$\Gamma(K^- \pi^+ \pi^- \pi^0 \nu_\tau(\text{ex.}K^0, \omega))/\Gamma_{\text{total}} \quad \Gamma_{102}/\Gamma$$

VALUE (units 10 ⁻⁴)	EVTS	DOCUMENT ID	TECN	COMMENT
3.7 ± 0.5 ± 0.8	833	ARMS 05 CLE3		7.6 fb ⁻¹ , E _{cm} ^{ee} = 10.6 GeV

$$\Gamma(K^- \pi^+ \pi^- \pi^0 \nu_\tau(\text{ex.}K^0, \omega, \eta))/\Gamma_{\text{total}} \quad \Gamma_{103}/\Gamma$$

VALUE (units 10 ⁻⁴)	DOCUMENT ID
3.9 ± 1.4 OUR FIT	

$$\Gamma(K^- \pi^+ K^- \geq 0 \text{ neut. } \nu_\tau)/\Gamma_{\text{total}} \quad \Gamma_{104}/\Gamma$$

VALUE (%)	CL%	DOCUMENT ID	TECN	COMMENT
<0.09	95	BAUER 94 TPC		E _{cm} ^{ee} = 29 GeV

$$\Gamma(K^- K^+ \pi^- \geq 0 \text{ neut. } \nu_\tau)/\Gamma_{\text{total}} \quad \Gamma_{105}/\Gamma = (\Gamma_{106} + \Gamma_{107})/\Gamma$$

VALUE (%)	EVTS	DOCUMENT ID	TECN	COMMENT
0.1496 ± 0.0033 OUR FIT				
0.203 ± 0.031 OUR AVERAGE				

0.159 ± 0.053 ± 0.020 ABBIENDI 00D OPAL 1990-1995 LEP runs

0.15 ± 0.09 ± 0.03 4 1 BAUER 94 TPC E_{cm}^{ee} = 29 GeV

• • • We use the following data for averages but not for fits. • • •

0.238 ± 0.042 2 BARATE 98 ALEP 1991-1995 LEP runs

1 We multiply 0.15% by 0.20, the relative systematic error quoted by BAUER 94, to obtain the systematic error.

2 Not independent of BARATE 98 $\Gamma(\tau^- \rightarrow K^- K^+ \pi^- \nu_\tau)/\Gamma_{\text{total}}$ and $\Gamma(\tau^- \rightarrow K^- K^+ \pi^- \pi^0 \nu_\tau)/\Gamma_{\text{total}}$ values.

$$\Gamma(K^- K^+ \pi^- \nu_\tau)/\Gamma_{\text{total}} \quad \Gamma_{106}/\Gamma$$

VALUE (units 10 ⁻³)	EVTS	DOCUMENT ID	TECN	COMMENT
1.43 ± 0.07 OUR FIT				
1.43 ± 0.07 OUR AVERAGE				

Error includes scale factor of 2.4. See the ideogram below.

1.55 ± 0.01 ± 0.06 108k 1 LEE 10 BELL 666 fb⁻¹ E_{cm}^{ee} = 10.6 GeV

1.346 ± 0.010 ± 0.036 18k 2 AUBERT 08 BABR 342 fb⁻¹ E_{cm}^{ee} = 10.6 GeV

1.55 ± 0.06 ± 0.09 932 3 BRIERE 03 CLE3 E_{cm}^{ee} = 10.6 GeV

1.63 ± 0.21 ± 0.17 BARATE 98 ALEP 1991-1995 LEP runs

• • • We use the following data for averages but not for fits. • • •

0.87 ± 0.56 ± 0.40 ABBIENDI 00D OPAL 1990-1995 LEP runs

1.45 ± 0.13 ± 0.28 2.3k 4 RICHICHI 99 CLEO E_{cm}^{ee} = 10.6 GeV

• • • We do not use the following data for averages, fits, limits, etc. • • •

2.2 ± 1.7 ± 1.1 9 5 MILLS 85 DLCO E_{cm}^{ee} = 29 GeV

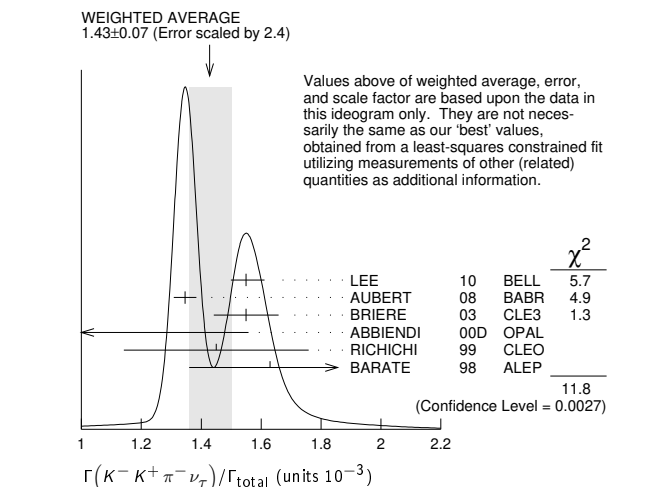
1 See footnote to LEE 10 $\Gamma(\tau^- \rightarrow \pi^- \pi^+ \pi^- \nu_\tau(\text{ex.}K^0))/\Gamma_{\text{total}}$ measurement for correlations with other measurements. Not independent of LEE 10 $\Gamma(\tau^- \rightarrow K^- K^+ \pi^- \nu_\tau)/\Gamma(\tau^- \rightarrow \pi^- \pi^+ \pi^- \nu_\tau(\text{ex.}K^0))$ value.

2 See footnote to AUBERT 08 $\Gamma(\tau^- \rightarrow \pi^- \pi^+ \pi^- \nu_\tau(\text{ex.}K^0))/\Gamma_{\text{total}}$ measurement for correlations with other measurements.

3 71% correlated with BRIERE 03 $\tau^- \rightarrow \pi^- \pi^+ \pi^- \nu_\tau$ and 34% correlated with $\tau \rightarrow K^- \pi^+ \pi^- \nu_\tau$ because of a common 5% normalization error.

4 Not independent of RICHICHI 99 $\Gamma(\tau^- \rightarrow K^- K^+ \pi^- \nu_\tau)/\Gamma(\tau^- \rightarrow \pi^- \pi^+ \pi^- \nu_\tau(\text{ex.}K^0))$ and BALEST 95c $\Gamma(\tau^- \rightarrow h^- h^- h^+ \nu_\tau(\text{ex.}K^0))/\Gamma_{\text{total}}$ values.

5 Error correlated with MILLS 85 ($K \pi \pi^0 \nu$) value. We multiply 0.22% by 0.23, the relative systematic error quoted by MILLS 85, to obtain the systematic error.



$$\Gamma(K^- K^+ \pi^- \nu_\tau)/\Gamma(\pi^- \pi^+ \pi^- \nu_\tau(\text{ex.}K^0)) \quad \Gamma_{106}/\Gamma_{68}$$

$$\Gamma_{106}/\Gamma_{68} = \Gamma_{106}/(\Gamma_{70} + 0.0153\Gamma_{178})$$

VALUE (%)	EVTS	DOCUMENT ID	TECN	COMMENT
1.592 ± 0.030 OUR FIT				
1.83 ± 0.05 OUR AVERAGE				

1.60 ± 0.15 ± 0.30 2.3k RICHICHI 99 CLEO E_{cm}^{ee} = 10.6 GeV

• • • We use the following data for averages but not for fits. • • •

1.84 ± 0.01 ± 0.05 108k 1 LEE 10 BELL 666 fb⁻¹ E_{cm}^{ee} = 10.6 GeV

1 Not independent of LEE 10 $\Gamma(\tau^- \rightarrow K^- K^+ \pi^- \nu_\tau)/\Gamma_{\text{total}}$ and $\Gamma(\tau^- \rightarrow \pi^- \pi^+ \pi^- \nu_\tau(\text{ex.}K^0))/\Gamma_{\text{total}}$ values.

$$\Gamma(K^- K^+ \pi^- \pi^0 \nu_\tau)/\Gamma_{\text{total}} \quad \Gamma_{107}/\Gamma$$

VALUE (units 10 ⁻⁴)	CL%	EVTS	DOCUMENT ID	TECN	COMMENT
0.61 ± 0.18 OUR FIT					
0.60 ± 0.18 OUR AVERAGE					

0.55 ± 0.14 ± 0.12 48 ARMS 05 CLE3 7.6 fb⁻¹, E_{cm}^{ee} = 10.6 GeV

7.5 ± 2.9 ± 1.5 BARATE 98 ALEP 1991-1995 LEP runs

• • • We use the following data for averages but not for fits. • • •

3.3 ± 1.8 ± 0.7 158 1 RICHICHI 99 CLEO E_{cm}^{ee} = 10.6 GeV

• • • We do not use the following data for averages, fits, limits, etc. • • •

<27 95 ABBIENDI 00D OPAL 1990-1995 LEP runs

1 Not independent of RICHICHI 99 $\Gamma(\tau^- \rightarrow K^- K^+ \pi^- \nu_\tau)/\Gamma(\tau^- \rightarrow \pi^- \pi^+ \pi^- \nu_\tau(\text{ex.}K^0))$ and BALEST 95c $\Gamma(\tau^- \rightarrow h^- h^- h^+ \nu_\tau(\text{ex.}K^0))/\Gamma_{\text{total}}$ values.

$$\Gamma(K^- K^+ \pi^- \pi^0 \nu_\tau)/\Gamma(\pi^- \pi^+ \pi^- \pi^0 \nu_\tau(\text{ex.}K^0)) \quad \Gamma_{107}/\Gamma_{77}$$

$$\Gamma_{107}/\Gamma_{77} = \Gamma_{107}/(\Gamma_{78} + 0.893\Gamma_{178} + 0.0153\Gamma_{180})$$

VALUE (%)	EVTS	DOCUMENT ID	TECN	COMMENT
0.14 ± 0.04 OUR FIT				
0.79 ± 0.44 ± 0.16	158	1 RICHICHI 99 CLEO		E _{cm} ^{ee} = 10.6 GeV

1 RICHICHI 99 also quote a 95%CL upper limit of 0.0157 for this measurement.

Lepton Particle Listings

 τ $\Gamma(K^- K^+ K^- \nu_\tau)/\Gamma_{\text{total}}$ $\Gamma_{108}/\Gamma = 0.492\Gamma_{170}/\Gamma$

VALUE (units 10^{-5})	CL%	EVTS	DOCUMENT ID	TECN	COMMENT
2.2 ± 0.8 OUR FIT					Error includes scale factor of 5.4.
2.1 ± 0.8 OUR AVERAGE					Error includes scale factor of 5.4.
3.29 ± 0.17 ± 0.19 -0.20		3.2k	¹ LEE	10 BELL	666 fb ⁻¹ $E_{\text{cm}}^{ee} = 10.6$ GeV
1.58 ± 0.13 ± 0.12		275	² AUBERT	08 BABR	342 fb ⁻¹ $E_{\text{cm}}^{ee} = 10.6$ GeV

• • • We do not use the following data for averages, fits, limits, etc. • • •

< 3.7	90		BRIERE	03 CLE3	$E_{\text{cm}}^{ee} = 10.6$ GeV
< 19	90		BARATE	98 ALEP	1991-1995 LEP runs

¹ See footnote to LEE 10 $\Gamma(\tau^- \rightarrow \pi^- \pi^+ \pi^- \nu_\tau \text{ (ex. } K^0)) / \Gamma_{\text{total}}$ measurement for correlations with other measurements. Not independent of LEE 10 $\Gamma(\tau^- \rightarrow K^- K^+ K^- \nu_\tau) / \Gamma(\tau^- \rightarrow \pi^- \pi^+ \pi^- \nu_\tau \text{ (ex. } K^0))$ value.

² See footnote to AUBERT 08 $\Gamma(\tau^- \rightarrow \pi^- \pi^+ \pi^- \nu_\tau \text{ (ex. } K^0)) / \Gamma_{\text{total}}$ measurement for correlations with other measurements.

 $\Gamma(K^- K^+ K^- \nu_\tau) / \Gamma(\pi^- \pi^+ \pi^- \nu_\tau \text{ (ex. } K^0))$ Γ_{108}/Γ_{68}

VALUE (units 10^{-4})	EVTS	DOCUMENT ID	TECN	COMMENT
3.90 ± 0.02 ± 0.22 -0.23	3.2k	¹ LEE	10 BELL	666 fb ⁻¹ $E_{\text{cm}}^{ee} = 10.6$ GeV

• • • We do not use the following data for averages, fits, limits, etc. • • •

¹ Not independent of LEE 10 $\Gamma(\tau^- \rightarrow K^- K^+ K^- \nu_\tau) / \Gamma_{\text{total}}$ and $\Gamma(\tau^- \rightarrow \pi^- \pi^+ \pi^- \nu_\tau \text{ (ex. } K^0)) / \Gamma_{\text{total}}$ values.

 $\Gamma(K^- K^+ K^- \nu_\tau \text{ (ex. } \phi)) / \Gamma_{\text{total}}$ Γ_{109}/Γ

VALUE	CL%	DOCUMENT ID	TECN	COMMENT
< 2.5 × 10⁻⁶	90	AUBERT	08 BABR	342 fb ⁻¹ $E_{\text{cm}}^{ee} = 10.6$ GeV

• • • We do not use the following data for averages, fits, limits, etc. • • •

¹ See footnote to LEE 10 $\Gamma(\tau^- \rightarrow K^- K^+ K^- \nu_\tau) / \Gamma_{\text{total}}$ and $\Gamma(\tau^- \rightarrow \pi^- \pi^+ \pi^- \nu_\tau \text{ (ex. } K^0)) / \Gamma_{\text{total}}$ values.

 $\Gamma(K^- K^+ K^- \pi^0 \nu_\tau) / \Gamma_{\text{total}}$ Γ_{110}/Γ

VALUE	CL%	DOCUMENT ID	TECN	COMMENT
< 4.8 × 10⁻⁶	90	ARMS	05 CLE3	7.6 fb ⁻¹ , $E_{\text{cm}}^{ee} = 10.6$ GeV

• • • We do not use the following data for averages, fits, limits, etc. • • •

¹ See footnote to LEE 10 $\Gamma(\tau^- \rightarrow K^- K^+ K^- \nu_\tau) / \Gamma_{\text{total}}$ and $\Gamma(\tau^- \rightarrow \pi^- \pi^+ \pi^- \nu_\tau \text{ (ex. } K^0)) / \Gamma_{\text{total}}$ values.

 $\Gamma(K^- K^+ K^- \pi^0 \nu_\tau) / \Gamma_{\text{total}}$ Γ_{111}/Γ

VALUE (%)	CL%	DOCUMENT ID	TECN	COMMENT
< 0.25	95	BAUER	94 TPC	$E_{\text{cm}}^{ee} = 29$ GeV

• • • We do not use the following data for averages, fits, limits, etc. • • •

¹ See footnote to LEE 10 $\Gamma(\tau^- \rightarrow K^- K^+ K^- \nu_\tau) / \Gamma_{\text{total}}$ and $\Gamma(\tau^- \rightarrow \pi^- \pi^+ \pi^- \nu_\tau \text{ (ex. } K^0)) / \Gamma_{\text{total}}$ values.

 $\Gamma(e^- e^- e^+ \nu_e \nu_\tau) / \Gamma_{\text{total}}$ Γ_{112}/Γ

VALUE (units 10^{-5})	EVTS	DOCUMENT ID	TECN	COMMENT
2.8 ± 1.4 ± 0.4	5	ALAM	96 CLEO	$E_{\text{cm}}^{ee} = 10.6$ GeV

• • • We do not use the following data for averages, fits, limits, etc. • • •

¹ See footnote to LEE 10 $\Gamma(\tau^- \rightarrow K^- K^+ K^- \nu_\tau) / \Gamma_{\text{total}}$ and $\Gamma(\tau^- \rightarrow \pi^- \pi^+ \pi^- \nu_\tau \text{ (ex. } K^0)) / \Gamma_{\text{total}}$ values.

 $\Gamma(\mu^- e^- e^+ \nu_\mu \nu_\tau) / \Gamma_{\text{total}}$ Γ_{113}/Γ

VALUE (units 10^{-5})	CL%	DOCUMENT ID	TECN	COMMENT
< 3.2	90	ALAM	96 CLEO	$E_{\text{cm}}^{ee} = 10.6$ GeV

• • • We do not use the following data for averages, fits, limits, etc. • • •

¹ See footnote to LEE 10 $\Gamma(\tau^- \rightarrow K^- K^+ K^- \nu_\tau) / \Gamma_{\text{total}}$ and $\Gamma(\tau^- \rightarrow \pi^- \pi^+ \pi^- \nu_\tau \text{ (ex. } K^0)) / \Gamma_{\text{total}}$ values.

 $\Gamma(\pi^- e^- e^+ \nu_\tau) / \Gamma_{\text{total}}$ Γ_{114}/Γ

VALUE (units 10^{-5})	EVTS	DOCUMENT ID	TECN	COMMENT
1.46 ± 0.13 ± 0.21	400	¹ JIN	19 BELL	axial-vector, 562 fb ⁻¹ , $E_{\text{cm}}^{ee} = 10.6$ GeV
3.01 ± 0.27 ± 0.43	400	¹ JIN	19 BELL	vector, 562 fb ⁻¹ , $E_{\text{cm}}^{ee} = 10.6$ GeV

• • • We do not use the following data for averages, fits, limits, etc. • • •

¹ JIN 19 measures $B(\tau^- \rightarrow \pi^- e^- e^+ \nu_\tau (m_{\pi^- e^- e^+} > 1.05 \text{ GeV}/c^2)) = (5.90 \pm 0.53 \pm 0.86) \times 10^{-6}$, which is only sensitive to the structure-dependent contribution, and assumes that the decay proceeds with either a pure axial-vector current or a pure vector current to obtain the two respective branching fraction measurements for this mode, which are 100% correlated.

 $\Gamma(\pi^- \mu^- \mu^+ \nu_\tau) / \Gamma_{\text{total}}$ Γ_{115}/Γ

VALUE	CL%	DOCUMENT ID	TECN	COMMENT
< 1.14 × 10⁻⁵	90	JIN	19 BELL	562 fb ⁻¹ , $E_{\text{cm}}^{ee} = 10.6$ GeV

• • • We do not use the following data for averages, fits, limits, etc. • • •

¹ See footnote to LEE 10 $\Gamma(\tau^- \rightarrow K^- K^+ K^- \nu_\tau) / \Gamma_{\text{total}}$ and $\Gamma(\tau^- \rightarrow \pi^- \pi^+ \pi^- \nu_\tau \text{ (ex. } K^0)) / \Gamma_{\text{total}}$ values.

 $\Gamma(3h^- 2h^+ \geq 0 \text{ neutrals } \nu_\tau \text{ (ex. } K_S^0 \rightarrow \pi^- \pi^+ \text{ ("5-prong"))} / \Gamma_{\text{total}}$ Γ_{116}/Γ

VALUE (%)	EVTS	DOCUMENT ID	TECN	COMMENT
0.099 ± 0.004 OUR FIT				
0.107 ± 0.007 OUR AVERAGE				Error includes scale factor of 1.1.
0.170 ± 0.022 ± 0.026		¹ ACHARD	01D L3	1992-1995 LEP runs
0.097 ± 0.005 ± 0.011	419	GIBAUT	94B CLEO	$E_{\text{cm}}^{ee} = 10.6$ GeV
0.102 ± 0.029	13	BYLSMA	87 HRS	$E_{\text{cm}}^{ee} = 29$ GeV

• • • We do not use the following data for averages, fits, limits, etc. • • •

¹ See footnote to LEE 10 $\Gamma(\tau^- \rightarrow K^- K^+ K^- \nu_\tau) / \Gamma_{\text{total}}$ and $\Gamma(\tau^- \rightarrow \pi^- \pi^+ \pi^- \nu_\tau \text{ (ex. } K^0)) / \Gamma_{\text{total}}$ values.

² See footnote to AUBERT 08 $\Gamma(\tau^- \rightarrow \pi^- \pi^+ \pi^- \nu_\tau \text{ (ex. } K^0)) / \Gamma_{\text{total}}$ measurement for correlations with other measurements.

³ See footnote to ACKERSTAFF 99E $\Gamma(\tau^- \rightarrow \pi^- \pi^+ \pi^- \nu_\tau \text{ (ex. } K^0)) / \Gamma_{\text{total}}$ measurement for correlations with other measurements.

• • • We do not use the following data for averages, fits, limits, etc. • • •

¹ See footnote to LEE 10 $\Gamma(\tau^- \rightarrow K^- K^+ K^- \nu_\tau) / \Gamma_{\text{total}}$ and $\Gamma(\tau^- \rightarrow \pi^- \pi^+ \pi^- \nu_\tau \text{ (ex. } K^0)) / \Gamma_{\text{total}}$ values.

² See footnote to AUBERT 08 $\Gamma(\tau^- \rightarrow \pi^- \pi^+ \pi^- \nu_\tau \text{ (ex. } K^0)) / \Gamma_{\text{total}}$ measurement for correlations with other measurements.

³ See footnote to ACKERSTAFF 99E $\Gamma(\tau^- \rightarrow \pi^- \pi^+ \pi^- \nu_\tau \text{ (ex. } K^0)) / \Gamma_{\text{total}}$ measurement for correlations with other measurements.

• • • We do not use the following data for averages, fits, limits, etc. • • •

¹ See footnote to LEE 10 $\Gamma(\tau^- \rightarrow K^- K^+ K^- \nu_\tau) / \Gamma_{\text{total}}$ and $\Gamma(\tau^- \rightarrow \pi^- \pi^+ \pi^- \nu_\tau \text{ (ex. } K^0)) / \Gamma_{\text{total}}$ values.

² See footnote to AUBERT 08 $\Gamma(\tau^- \rightarrow \pi^- \pi^+ \pi^- \nu_\tau \text{ (ex. } K^0)) / \Gamma_{\text{total}}$ measurement for correlations with other measurements.

³ See footnote to ACKERSTAFF 99E $\Gamma(\tau^- \rightarrow \pi^- \pi^+ \pi^- \nu_\tau \text{ (ex. } K^0)) / \Gamma_{\text{total}}$ measurement for correlations with other measurements.

0.16 ± 0.08 ± 0.04	4	BURCHAT	85 MRK2	$E_{\text{cm}}^{ee} = 29$ GeV
1.0 ± 0.4	10	BEHREND	82 CELL	Repl. by BEHREND 89B

¹ The correlation coefficients between this measurement and the ACHARD 01D measurements of $B(\tau^- \rightarrow \text{"1-prong"})$ and $B(\tau^- \rightarrow \text{"3-prong"})$ are -0.082 and -0.19 respectively.

² The correlation coefficients between this measurement and the ABREU 01M measurements of $B(\tau^- \rightarrow \text{1-prong})$ and $B(\tau^- \rightarrow \text{3-prong})$ are -0.08 and -0.08 respectively.

³ Not independent of ACKERSTAFF 99E $B(\tau^- \rightarrow 3h^- 2h^+ \nu_\tau \text{ (ex. } K^0))$ and $B(\tau^- \rightarrow 3h^- 2h^+ \pi^0 \nu_\tau \text{ (ex. } K^0))$ measurements.

 $\Gamma(3h^- 2h^+ \nu_\tau \text{ (ex. } K^0)) / \Gamma_{\text{total}}$ $\Gamma_{117}/\Gamma = (\Gamma_{118} + \Gamma_{120} + 0.0153\Gamma_{185}) / \Gamma$

VALUE (units 10^{-4})	EVTS	DOCUMENT ID	TECN	COMMENT
8.29 ± 0.31 OUR FIT				
8.32 ± 0.35 OUR AVERAGE				
9.7 ± 1.5 ± 0.5	96	¹ ABDALLAH	06A DLPH	1992-1995 LEP runs
7.2 ± 0.9 ± 1.2	165	² SCHAEEL	05c ALEP	1991-1995 LEP runs
9.1 ± 1.4 ± 0.6	97	ACKERSTAFF	99E OPAL	1991-1995 LEP runs
7.7 ± 0.5 ± 0.9	295	GIBAUT	94B CLEO	$E_{\text{cm}}^{ee} = 10.6$ GeV
6.4 ± 2.3 ± 1.0	12	ALBRECHT	88B ARG	$E_{\text{cm}}^{ee} = 10$ GeV
5.1 ± 2.0	7	BYLSMA	87 HRS	$E_{\text{cm}}^{ee} = 29$ GeV

• • • We use the following data for averages but not for fits. • • •

¹ See footnote to ABDALLAH 06A $\Gamma(\tau^- \rightarrow h^- \nu_\tau) / \Gamma_{\text{total}}$ measurement for correlations with other measurements.

² See footnote to SCHAEEL 05c $\Gamma(\tau^- \rightarrow e^- \bar{\nu}_e \nu_\tau) / \Gamma_{\text{total}}$ measurement for correlations with other measurements.

³ The error quoted is statistical only.

• • • We do not use the following data for averages, fits, limits, etc. • • •

¹ See footnote to LEE 10 $\Gamma(\tau^- \rightarrow K^- K^+ K^- \nu_\tau) / \Gamma_{\text{total}}$ and $\Gamma(\tau^- \rightarrow \pi^- \pi^+ \pi^- \nu_\tau \text{ (ex. } K^0)) / \Gamma_{\text{total}}$ values.

² See footnote to AUBERT 08 $\Gamma(\tau^- \rightarrow \pi^- \pi^+ \pi^- \nu_\tau \text{ (ex. } K^0)) / \Gamma_{\text{total}}$ measurement for correlations with other measurements.

³ See footnote to ACKERSTAFF 99E $\Gamma(\tau^- \rightarrow \pi^- \pi^+ \pi^- \nu_\tau \text{ (ex. } K^0)) / \Gamma_{\text{total}}$ measurement for correlations with other measurements.

• • • We do not use the following data for averages, fits, limits, etc. • • •

¹ See footnote to LEE 10 $\Gamma(\tau^- \rightarrow K^- K^+ K^- \nu_\tau) / \Gamma_{\text{total}}$ and $\Gamma(\tau^- \rightarrow \pi^- \pi^+ \pi^- \nu_\tau \text{ (ex. } K^0)) / \Gamma_{\text{total}}$ values.

² See footnote to AUBERT 08 $\Gamma(\tau^- \rightarrow \pi^- \pi^+ \pi^- \nu_\tau \text{ (ex. } K^0)) / \Gamma_{\text{total}}$ measurement for correlations with other measurements.

³ The error quoted is statistical only.

• • • We do not use the following data for averages but not for fits. • • •

¹ See footnote to LEE 10 $\Gamma(\tau^- \rightarrow K^- K^+ K^- \nu_\tau) / \Gamma_{\text{total}}$ and $\Gamma(\tau^- \rightarrow \pi^- \pi^+ \pi^- \nu_\tau \text{ (ex. } K^0)) / \Gamma_{\text{total}}$ values.

² See footnote to AUBERT 08 $\Gamma(\tau^- \rightarrow \pi^- \pi^+ \pi^- \nu_\tau \text{ (ex. } K^0)) / \Gamma_{\text{total}}$ measurement for correlations with other measurements.

³ See footnote to ACKERSTAFF 99E $\Gamma(\tau^- \rightarrow \pi^- \pi^+ \pi^- \nu_\tau \text{ (ex. } K^0)) / \Gamma_{\text{total}}$ measurement for correlations with other measurements.

• • • We do not use the following data for averages, fits, limits, etc. • • •

¹ See footnote to LEE 10 $\Gamma(\tau^- \rightarrow K^- K^+ K^- \nu_\tau) / \Gamma_{\text{total}}$ and $\Gamma(\tau^- \rightarrow \pi^- \pi^+ \pi^- \nu_\tau \text{ (ex. } K^0)) / \Gamma_{\text{total}}$ values.

² See footnote to AUBERT 08 $\Gamma(\tau^- \rightarrow \pi^- \pi^+ \pi^- \nu_\tau \text{ (ex. } K^0)) / \Gamma_{\text{total}}$ measurement for correlations with other measurements.

³ See footnote to ACKERSTAFF 99E $\Gamma(\tau^- \rightarrow \pi^- \pi^+ \pi^- \nu_\tau \text{ (ex. } K^0)) / \Gamma_{\text{total}}$ measurement for correlations with other measurements.

• • • We do not use the following data for averages, fits, limits, etc. • • •

¹ See footnote to LEE 10 $\Gamma(\tau^- \rightarrow K^- K^+ K^- \nu_\tau) / \Gamma_{\text{total}}$ and $\Gamma(\tau^- \rightarrow \pi^- \pi^+ \pi^- \nu_\tau \text{ (ex. } K^0)) / \Gamma_{\text{total}}$ values.

² See footnote to AUBERT 08 $\Gamma(\tau^- \rightarrow \pi^- \pi^+ \pi^- \nu_\tau \text{ (ex. } K^0)) / \Gamma_{\text{total}}$ measurement for correlations with other measurements.

³ See footnote to ACKERSTAFF 99E $\Gamma(\tau^- \rightarrow \pi^- \pi^+ \pi^- \nu_\tau \text{ (ex. } K^0)) / \Gamma_{\text{total}}$ measurement for correlations with other measurements.

• • • We do not use the following data for averages, fits, limits, etc. • • •

¹ See footnote to LEE 10 $\Gamma(\tau^- \rightarrow K^- K^+ K^- \nu_\tau) / \Gamma_{\text{total}}$ and $\Gamma(\tau^- \rightarrow \pi^- \pi^+ \pi^- \nu_\tau \text{ (ex. } K^0)) / \Gamma_{\text{total}}$ values.

² See footnote to AUBERT 08 $\Gamma(\tau^- \rightarrow \pi^- \pi^+ \pi^- \nu_\tau \text{ (ex. } K^0)) / \Gamma_{\text{total}}$ measurement for correlations with other measurements.

³ See footnote to ACKERSTAFF 99E $\Gamma(\tau^- \rightarrow \pi^- \pi^+ \pi^- \nu_\tau \text{ (ex. } K^0)) / \Gamma_{\text{total}}$ measurement for correlations with other measurements.

• • • We do not use the following data for averages, fits, limits, etc. • • •

¹ See footnote to LEE 10 $\Gamma(\tau^- \rightarrow K^- K^+ K^- \nu_\tau) / \Gamma_{\text{total}}$ and $\Gamma(\tau^- \rightarrow \pi^- \pi^+ \pi^- \nu_\tau \text{ (ex. } K^0)) / \Gamma_{\text{total}}$ values.

² See footnote to AUBERT 08 $\Gamma(\tau^- \rightarrow \pi^- \pi^+ \pi^- \nu_\tau \text{ (ex. } K^0)) / \Gamma_{\text{total}}$ measurement for correlations with other measurements.

³ See footnote to ACKERSTAFF 99E $\Gamma(\tau^- \rightarrow \pi^- \pi^+ \pi^- \nu_\tau \text{ (ex. } K^0)) / \Gamma_{\text{total}}$ measurement for correlations with other measurements.

• • • We do not use the following data for averages, fits, limits, etc. • • •

¹ See footnote to LEE 10 $\Gamma(\tau^- \rightarrow K^- K^+ K^- \nu_\tau) / \Gamma_{\text{total}}$ and $\Gamma(\tau^- \rightarrow \pi^- \pi^+ \pi^- \nu_\tau \text{ (ex. } K^0)) / \Gamma_{\text{total}}$ values.

² See footnote to AUBERT 08 $\Gamma(\tau^- \rightarrow \pi^- \pi^+ \pi^- \nu_\tau \text{ (ex. } K^0)) / \Gamma_{\text{total}}$ measurement for correlations with other measurements.

³ See footnote to ACKERSTAFF 99E $\Gamma(\tau^- \rightarrow \pi^- \pi^+ \pi^- \nu_\tau \text{ (ex. } K^0)) / \Gamma_{\text{total}}$ measurement for correlations with other measurements.

• • • We do not use the following data for averages, fits, limits, etc. • • •

¹ See footnote to LEE 10 $\Gamma(\tau^- \rightarrow K^- K^+ K^- \nu_\tau) / \Gamma_{\text{total}}$ and $\Gamma(\tau^- \rightarrow \pi^- \pi^+ \pi^- \nu_\tau \text{ (ex. } K^0)) / \Gamma_{\text{total}}$ values.

$\Gamma(3\pi^- 2\pi^+ \pi^0 \nu_\tau (\text{ex. } K^0))/\Gamma_{\text{total}}$ Γ_{124}/Γ
 $\Gamma_{124}/\Gamma = (\Gamma_{126} + 0.2292\Gamma_{160} + 0.893\Gamma_{185})/\Gamma$

VALUE (units 10^{-4})	DOCUMENT ID	TECN	COMMENT
1.63 ± 0.11 OUR FIT			
• • • We use the following data for averages but not for fits. • • •			
1.65 ± 0.05 ± 0.09	¹ LEES	12X	BABR 468 fb ⁻¹ $E_{\text{cm}}^{\text{ee}} = 10.6$ GeV
¹ Not independent of LEES 12X measurements of $\Gamma(\tau^- \rightarrow 2\pi^- \pi^+ \omega \nu_\tau (\text{ex. } K^0))/\Gamma$, $\Gamma(\tau^- \rightarrow \eta \pi^- \pi^+ \pi^- \nu_\tau (\text{ex. } K^0))/\Gamma$, and $\Gamma(\tau^- \rightarrow 3\pi^- 2\pi^+ \pi^0 \nu_\tau (\text{ex. } K^0, \eta, \omega, f_1(1285)))/\Gamma$.			

$\Gamma(3\pi^- 2\pi^+ \pi^0 \nu_\tau (\text{ex. } K^0, \eta, f_1(1285)))/\Gamma_{\text{total}}$ Γ_{125}/Γ

VALUE (units 10^{-4})	DOCUMENT ID	TECN	COMMENT
1.11 ± 0.04 ± 0.09	¹ LEES	12X	BABR 468 fb ⁻¹ $E_{\text{cm}}^{\text{ee}} = 10.6$ GeV
¹ Not independent of LEES 12X $\Gamma(\tau^- \rightarrow 2\pi^- \pi^+ \omega \nu_\tau (\text{ex. } K^0))/\Gamma$ and $\Gamma(\tau^- \rightarrow 3\pi^- 2\pi^+ \pi^0 \nu_\tau (\text{ex. } K^0, \eta, \omega, f_1(1285)))/\Gamma$ values.			

$\Gamma(3\pi^- 2\pi^+ \pi^0 \nu_\tau (\text{ex. } K^0, \eta, \omega, f_1(1285)))/\Gamma_{\text{total}}$ Γ_{126}/Γ

VALUE (units 10^{-4})	EVTS	DOCUMENT ID	TECN	COMMENT
0.38 ± 0.09 OUR FIT				
0.36 ± 0.03 ± 0.09	7.3k	LEES	12X	BABR 468 fb ⁻¹ $E_{\text{cm}}^{\text{ee}} = 10.6$ GeV

$\Gamma(K^- 2\pi^- 2\pi^+ \pi^0 \nu_\tau (\text{ex. } K^0))/\Gamma_{\text{total}}$ Γ_{127}/Γ

VALUE (units 10^{-6})	DOCUMENT ID	TECN	COMMENT
1.1 ± 0.6 OUR FIT			
1.1 ± 0.4 ± 0.4	¹ LEES	12X	BABR 468 fb ⁻¹ $E_{\text{cm}}^{\text{ee}} = 10.6$ GeV
¹ LEES 12X measurement corresponds to the lower limit of $< 1.9 \times 10^{-6}$ at 90% CL.			

$\Gamma(K^+ 3\pi^- \pi^+ \pi^0 \nu_\tau)/\Gamma_{\text{total}}$ Γ_{128}/Γ

VALUE	CL%	DOCUMENT ID	TECN	COMMENT
$< 8 \times 10^{-7}$	90	LEES	12X	BABR 468 fb ⁻¹ $E_{\text{cm}}^{\text{ee}} = 10.6$ GeV

$\Gamma(3h^- 2h^+ 2\pi^0 \nu_\tau)/\Gamma_{\text{total}}$ Γ_{129}/Γ

VALUE	CL%	DOCUMENT ID	TECN	COMMENT
$< 3.4 \times 10^{-6}$	90	AUBERT,B	06	BABR 232 fb ⁻¹ $E_{\text{cm}}^{\text{ee}} = 10.6$ GeV
• • • We do not use the following data for averages, fits, limits, etc. • • •				
$< 1.1 \times 10^{-4}$	90	GIBAUT	94B	CLEO $E_{\text{cm}}^{\text{ee}} = 10.6$ GeV

$\Gamma((5\pi^-) - \nu_\tau)/\Gamma_{\text{total}}$ Γ_{130}/Γ
 $\Gamma_{130}/\Gamma = (\Gamma_{30} + \frac{1}{2}\Gamma_{45} + \Gamma_{48} + \frac{1}{2}\Gamma_{61} + \Gamma_{85} + \Gamma_{117} + 0.5559\Gamma_{150} + 0.893\Gamma_{180})/\Gamma$

VALUE (%)	DOCUMENT ID	TECN	COMMENT
0.78 ± 0.05 OUR FIT			
• • • We use the following data for averages but not for fits. • • •			
0.61 ± 0.06 ± 0.08	¹ GIBAUT	94B	CLEO $E_{\text{cm}}^{\text{ee}} = 10.6$ GeV
¹ Not independent of GIBAUT 94B B(3h ⁻ 2h ⁺ ν_τ), PROCARIO 93 B(h ⁻ 4 π^0 ν_τ), and BORTOLETTO 93 B(2h ⁻ h ⁺ 2 π^0 ν_τ)/B("3prong") measurements. Result is corrected for η contributions.			

$\Gamma(4h^- 3h^+ \geq 0 \text{ neutrals } \nu_\tau (\text{"7-prong"}))/\Gamma_{\text{total}}$ Γ_{131}/Γ

VALUE	CL%	DOCUMENT ID	TECN	COMMENT
$< 3.0 \times 10^{-7}$	90	AUBERT,B	05F	BABR 232 fb ⁻¹ , $E_{\text{cm}}^{\text{ee}} = 10.6$ GeV
• • • We do not use the following data for averages, fits, limits, etc. • • •				
$< 1.8 \times 10^{-5}$	95	ACKERSTAFF	97J	OPAL 1990-1995 LEP runs
$< 2.4 \times 10^{-6}$	90	EDWARDS	97B	CLEO $E_{\text{cm}}^{\text{ee}} = 10.6$ GeV
$< 2.9 \times 10^{-4}$	90	BYLSMA	87	HRS $E_{\text{cm}}^{\text{ee}} = 29$ GeV

$\Gamma(4h^- 3h^+ \nu_\tau)/\Gamma_{\text{total}}$ Γ_{132}/Γ

VALUE	CL%	DOCUMENT ID	TECN	COMMENT
$< 4.3 \times 10^{-7}$	90	AUBERT,B	05F	BABR 232 fb ⁻¹ , $E_{\text{cm}}^{\text{ee}} = 10.6$ GeV

$\Gamma(4h^- 3h^+ \pi^0 \nu_\tau)/\Gamma_{\text{total}}$ Γ_{133}/Γ

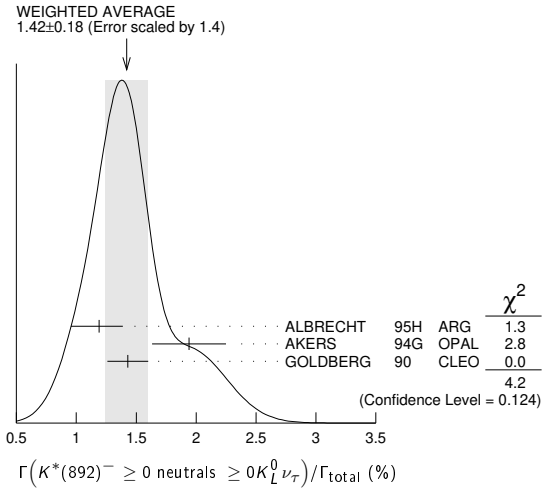
VALUE	CL%	DOCUMENT ID	TECN	COMMENT
$< 2.5 \times 10^{-7}$	90	AUBERT,B	05F	BABR 232 fb ⁻¹ , $E_{\text{cm}}^{\text{ee}} = 10.6$ GeV

$\Gamma(X^-(S=-1)\nu_\tau)/\Gamma_{\text{total}}$ Γ_{134}/Γ
 $\Gamma_{134}/\Gamma = (\Gamma_{10} + \Gamma_{16} + \Gamma_{23} + \Gamma_{28} + \Gamma_{36} + \Gamma_{41} + \Gamma_{45} + \Gamma_{61} + \Gamma_{97} + \Gamma_{103} + \Gamma_{120} + \Gamma_{127} + \Gamma_{152} + \Gamma_{154} + \Gamma_{156} + 0.8312\Gamma_{170} + \Gamma_{179})/\Gamma$

VALUE (%)	DOCUMENT ID	TECN	COMMENT
2.92 ± 0.04 OUR FIT			
• • • We use the following data for averages but not for fits. • • •			
2.87 ± 0.12	¹ BARATE	99R	ALEP 1991-1995 LEP runs
¹ BARATE 99R perform a combined analysis of all ALEPH LEP 1 data on τ branching fraction measurements for decay modes having total strangeness equal to -1.			

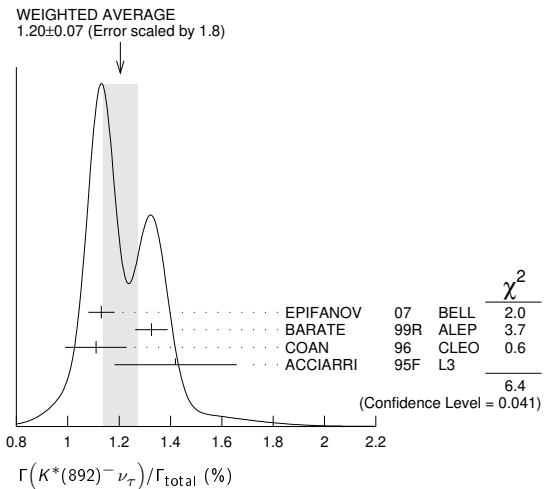
$\Gamma(K^*(892)^- \geq 0 \text{ neutrals } \geq 0 K_L^0 \nu_\tau)/\Gamma_{\text{total}}$ Γ_{135}/Γ

VALUE (%)	EVTS	DOCUMENT ID	TECN	COMMENT
1.42 ± 0.18 OUR AVERAGE				Error includes scale factor of 1.4. See the ideogram below.
1.19 ± 0.15 ^{+0.13} _{-0.18}	104	ALBRECHT	95H	ARG $E_{\text{cm}}^{\text{ee}} = 9.4-10.6$ GeV
1.94 ± 0.27 ± 0.15	74	¹ AKERS	94G	OPAL $E_{\text{cm}}^{\text{ee}} = 88-94$ GeV
1.43 ± 0.11 ± 0.13	475	² GOLDBERG	90	CLEO $E_{\text{cm}}^{\text{ee}} = 9.4-10.9$ GeV
¹ AKERS 94G reject events in which a K_S^0 accompanies the $K^*(892)^-$. We do not correct for them.				
² GOLDBERG 90 estimates that 10% of observed $K^*(892)$ are accompanied by a π^0 .				



$\Gamma(K^*(892)^- \nu_\tau)/\Gamma_{\text{total}}$ Γ_{136}/Γ

VALUE (%)	EVTS	DOCUMENT ID	TECN	COMMENT
1.20 ± 0.07 OUR AVERAGE				Error includes scale factor of 1.8. See the ideogram below.
1.131 ± 0.006 ± 0.051	49k	¹ EPIFANOV	07	BELL 351 fb ⁻¹ $E_{\text{cm}}^{\text{ee}} = 10.6$ GeV
1.326 ± 0.063		BARATE	99R	ALEP 1991-1995 LEP runs
1.11 ± 0.12		² COAN	96	CLEO $E_{\text{cm}}^{\text{ee}} \approx 10.6$ GeV
1.42 ± 0.22 ± 0.09		³ ACCIARRI	95F	L3 1991-1993 LEP runs
• • • We do not use the following data for averages, fits, limits, etc. • • •				
1.39 ± 0.09 ± 0.10		⁴ BUSKULIC	96	ALEP Repl. by BARATE 99R
1.45 ± 0.13 ± 0.11	273	⁵ BUSKULIC	94F	ALEP Repl. by BUSKULIC 96
1.23 ± 0.21 ^{+0.11} _{-0.21}	54	⁶ ALBRECHT	88L	ARG $E_{\text{cm}}^{\text{ee}} = 10$ GeV
1.9 ± 0.3 ± 0.4	44	⁷ TSCHIRHART	88	HRS $E_{\text{cm}}^{\text{ee}} = 29$ GeV
1.5 ± 0.4 ± 0.4	15	⁸ AIHARA	87C	TPC $E_{\text{cm}}^{\text{ee}} = 29$ GeV
1.3 ± 0.3 ± 0.3	31	YELTON	86	MRK2 $E_{\text{cm}}^{\text{ee}} = 29$ GeV
1.7 ± 0.7	11	DORFAN	81	MRK2 $E_{\text{cm}}^{\text{ee}} = 4.2-6.7$ GeV



¹ EPIFANOV 07 quote $B(\tau^- \rightarrow K^*(892)^- \nu_\tau) B(K^*(892)^- \rightarrow K_S^0 \pi^-) = (3.77 \pm 0.02(\text{stat}) \pm 0.12(\text{syst}) \pm 0.12(\text{mod})) \times 10^{-3}$. We add the systematic and model uncertainties in quadrature and divide by $B(K^*(892)^- \rightarrow K_S^0 \pi^-) = 0.3333$.

² Not independent of COAN 96 B($\pi^- \bar{K}^0 \nu_\tau$) and BATTLE 94 B($K^- \pi^0 \nu_\tau$) measurements. K π final states are consistent with and assumed to originate from $K^*(892)^-$ production.

³ This result is obtained from their B($\pi^- \bar{K}^0 \nu_\tau$) assuming all those decays originate in $K^*(892)^-$ decays.

Lepton Particle Listings

 τ

⁴ Not independent of BUSKULIC 96 B($\pi^- \bar{K}^0 \nu_\tau$) and B($K^- \pi^0 \nu_\tau$) measurements.

⁵ BUSKULIC 94F obtain this result from BUSKULIC 94F B($\bar{K}^0 \pi^- \nu_\tau$) and BUSKULIC 94E B($K^- \pi^0 \nu_\tau$) assuming all of those decays originate in $K^*(892)^-$ decays.

⁶ The authors divide by $\Gamma_2/\Gamma = 0.865$ to obtain this result.

⁷ Not independent of TSCHIRHART 88 $\Gamma(\tau^- \rightarrow h^- \bar{K}^0) \geq 0$ neutrals $\geq 0 K_L^0 \nu_\tau / \Gamma$.

⁸ Decay π^- identified in this experiment, is assumed in the others.

$\Gamma(K^*(892)^- \nu_\tau) / \Gamma(\pi^- \pi^0 \nu_\tau)$		$\Gamma_{136} / \Gamma_{14}$	
VALUE	DOCUMENT ID	TECN	COMMENT
0.075 ± 0.027	¹ ABREU	94K	DLPH LEP 1992 Z data

¹ ABREU 94K quote B($\tau^- \rightarrow K^*(892)^- \nu_\tau$)B($K^*(892)^- \rightarrow K^- \pi^0$)/B($\tau^- \rightarrow \rho^- \nu_\tau$) = 0.025 ± 0.009. We divide by B($K^*(892)^- \rightarrow K^- \pi^0$) = 0.333 to obtain this result.

$\Gamma(K^*(892)^- \nu_\tau \rightarrow \pi^- \bar{K}^0 \nu_\tau) / \Gamma(\pi^- \bar{K}^0 \nu_\tau)$		$\Gamma_{137} / \Gamma_{36}$	
VALUE	EVTS	DOCUMENT ID	TECN
0.933 ± 0.027	49k	EPIFANOV	07 BELL

$\Gamma(K^*(892)^0 K^- \geq 0 \text{ neutrals } \nu_\tau) / \Gamma_{\text{total}}$		Γ_{138} / Γ	
VALUE (%)	EVTS	DOCUMENT ID	TECN
0.32 ± 0.08 ± 0.12	119	GOLDBERG	90 CLEO

$\Gamma(K^*(892)^0 K^- \nu_\tau) / \Gamma_{\text{total}}$		Γ_{139} / Γ	
VALUE (%)	EVTS	DOCUMENT ID	TECN
0.21 ± 0.04 OUR AVERAGE			
0.213 ± 0.048		¹ BARATE	98 ALEP
0.20 ± 0.05 ± 0.04	47	ALBRECHT	95H ARG

¹ BARATE 98 measure the $K^- (\rho^0 \rightarrow \pi^+ \pi^-)$ fraction in $\tau^- \rightarrow K^- \pi^+ \pi^- \nu_\tau$ decays to be (35 ± 11)% and derive this result from their measurement of $\Gamma(\tau^- \rightarrow K^- \pi^+ \pi^- \nu_\tau) / \Gamma_{\text{total}}$ assuming the intermediate states are all $K^- \rho$ and $K^- K^*(892)^0$.

$\Gamma(\bar{K}^*(892)^0 \pi^- \geq 0 \text{ neutrals } \nu_\tau) / \Gamma_{\text{total}}$		Γ_{140} / Γ	
VALUE (%)	EVTS	DOCUMENT ID	TECN
0.38 ± 0.11 ± 0.13	105	GOLDBERG	90 CLEO

$\Gamma(\bar{K}^*(892)^0 \pi^- \nu_\tau) / \Gamma_{\text{total}}$		Γ_{141} / Γ	
VALUE (%)	EVTS	DOCUMENT ID	TECN
0.22 ± 0.05 OUR AVERAGE			
0.209 ± 0.058		¹ BARATE	98 ALEP
0.25 ± 0.10 ± 0.05	27	ALBRECHT	95H ARG

¹ BARATE 98 measure the $K^- K^*(892)^0$ fraction in $\tau^- \rightarrow K^- K^+ \pi^- \nu_\tau$ decays to be (87 ± 13)% and derive this result from their measurement of $\Gamma(\tau^- \rightarrow K^- K^+ \pi^- \nu_\tau) / \Gamma_{\text{total}}$.

$\Gamma((\bar{K}^*(892)^0 \pi^-) \nu_\tau \rightarrow \pi^- \bar{K}^0 \pi^0 \nu_\tau) / \Gamma_{\text{total}}$		Γ_{142} / Γ	
VALUE (%)	EVTS	DOCUMENT ID	TECN
0.10 ± 0.04 OUR AVERAGE			
0.097 ± 0.044 ± 0.036		¹ BARATE	99k ALEP
0.106 ± 0.037 ± 0.032		² BARATE	98E ALEP

¹ BARATE 99k measure K^0 's by detecting K_S^0 's in their hadron calorimeter. They determine the $\bar{K}^0 \rho^-$ fraction in $\tau^- \rightarrow \pi^- \bar{K}^0 \pi^0 \nu_\tau$ decays to be (0.72 ± 0.12 ± 0.10) and multiply their B($\pi^- \bar{K}^0 \pi^0 \nu_\tau$) measurement by one minus this fraction to obtain the quoted result.

² BARATE 98E reconstruct K^0 's using $K_S^0 \rightarrow \pi^+ \pi^-$ decays. They determine the $\bar{K}^0 \rho^-$ fraction in $\tau^- \rightarrow \pi^- \bar{K}^0 \pi^0 \nu_\tau$ decays to be (0.64 ± 0.09 ± 0.10) and multiply their B($\pi^- \bar{K}^0 \pi^0 \nu_\tau$) measurement by one minus this fraction to obtain the quoted result.

$\Gamma(K_1(1270)^- \nu_\tau) / \Gamma_{\text{total}}$		Γ_{143} / Γ	
VALUE (%)	EVTS	DOCUMENT ID	TECN
0.47 ± 0.11 OUR AVERAGE			
0.48 ± 0.11		BARATE	99R ALEP
0.41 \pm $\frac{0.41}{0.35}$ ± 0.10	5	¹ BAUER	94 TPC

¹ We multiply 0.41% by 0.25, the relative systematic error quoted by BAUER 94, to obtain the systematic error.

$\Gamma(K_1(1400)^- \nu_\tau) / \Gamma_{\text{total}}$		Γ_{144} / Γ	
VALUE (%)	EVTS	DOCUMENT ID	TECN
0.17 ± 0.26 OUR AVERAGE			
0.05 ± 0.17		BARATE	99R ALEP
0.76 \pm $\frac{0.40}{0.33}$ ± 0.20	11	¹ BAUER	94 TPC

¹ We multiply 0.76% by 0.25, the relative systematic error quoted by BAUER 94, to obtain the systematic error.

$\frac{\Gamma(K_1(1270)^- \nu_\tau) + \Gamma(K_1(1400)^- \nu_\tau)}{\Gamma_{\text{total}}}$		$(\Gamma_{143} + \Gamma_{144}) / \Gamma$	
VALUE (%)	EVTS	DOCUMENT ID	TECN
1.17 \pm $\frac{0.41}{0.37}$ ± 0.29	16	¹ BAUER	94 TPC

¹ We multiply 1.17% by 0.25, the relative systematic error quoted by BAUER 94, to obtain the systematic error. Not independent of BAUER 94 B($K_1(1270)^- \nu_\tau$) and BAUER 94 B($K_1(1400)^- \nu_\tau$) measurements.

$\Gamma(K_1(1270)^- \nu_\tau) / [\Gamma(K_1(1270)^- \nu_\tau) + \Gamma(K_1(1400)^- \nu_\tau)]$		$\Gamma_{143} / (\Gamma_{143} + \Gamma_{144})$	
VALUE	DOCUMENT ID	TECN	COMMENT
0.69 ± 0.15 OUR AVERAGE			
0.71 ± 0.16 ± 0.11		¹ ABBIENDI	00D OPAL
0.66 ± 0.19 ± 0.13		² ASNER	00B CLEO

¹ ABBIENDI 00D assume the resonance structure of $\tau^- \rightarrow K^- \pi^+ \pi^- \nu_\tau$ decays is dominated by the $K_1(1270)^-$ and $K_1(1400)^-$ resonances.

² ASNER 00B assume the resonance structure of $\tau^- \rightarrow K^- \pi^+ \pi^- \nu_\tau$ (ex. K^0) decays is dominated by $K_1(1270)^-$ and $K_1(1400)^-$ resonances.

$\Gamma(K^*(1410)^- \nu_\tau) / \Gamma_{\text{total}}$		Γ_{145} / Γ	
VALUE (units 10^{-3})	DOCUMENT ID	TECN	COMMENT
1.5 \pm $\frac{1.4}{1.0}$	BARATE	99R	ALEP

$\Gamma(K_0^*(1430)^- \nu_\tau) / \Gamma_{\text{total}}$		Γ_{146} / Γ	
VALUE (units 10^{-3})	CL%	DOCUMENT ID	TECN
< 0.5	95	BARATE	99R ALEP

$\Gamma(K_2^*(1430)^- \nu_\tau) / \Gamma_{\text{total}}$		Γ_{147} / Γ	
VALUE (%)	CL%	EVTS	DOCUMENT ID
< 0.3	95		TSCHIRHART 88

• • • We do not use the following data for averages, fits, limits, etc. • • •

< 0.33	95	¹ ACCIARRI	95F L3
< 0.9	95	DORFAN	81 MRK2

¹ ACCIARRI 95F quote B($\tau^- \rightarrow K^*(1430)^- \rightarrow \pi^- \bar{K}^0 \nu_\tau$) < 0.11%. We divide by B($K^*(1430)^- \rightarrow \pi^- \bar{K}^0$) = 0.33 to obtain the limit shown.

$\Gamma(a_0(980)^- \geq 0 \text{ neutrals } \nu_\tau) / \Gamma_{\text{total}} \times B(a_0(980) \rightarrow K^0 K^-)$		$\Gamma_{148} / \Gamma \times B$	
VALUE (units 10^{-4})	CL%	DOCUMENT ID	TECN
< 2.8	90	GOLDBERG	90 CLEO

$\Gamma(\eta \pi^- \nu_\tau) / \Gamma_{\text{total}}$		Γ_{149} / Γ	
VALUE (units 10^{-4})	CL%	EVTS	DOCUMENT ID
< 0.99	95		¹ DEL-AMO-SA...11E

¹ DEL-AMO-SA...11E BABR 470 fb⁻¹ $E_{\text{cm}}^{\text{ee}} = 10.6$ GeV

$\Gamma(\eta \pi^- \pi^0 \nu_\tau) / \Gamma_{\text{total}}$		Γ_{150} / Γ	
VALUE (units 10^{-3})	CL%	EVTS	DOCUMENT ID
1.39 ± 0.07 OUR FIT			
1.38 ± 0.09 OUR AVERAGE			
1.35 ± 0.03 ± 0.07	6.0k	INAMI	09 BELL
1.8 ± 0.4 ± 0.2		BUSKULIC	97c ALEP
1.7 ± 0.2 ± 0.2	125	ARTUSO	92c CLEO

¹ DEL-AMO-SANCHEZ 11E also quote B($\tau^- \rightarrow \eta \pi^- \nu_\tau$) = (3.4 ± 3.4 ± 2.1) × 10⁻⁵.

$\Gamma(\eta \pi^- \pi^0 \nu_\tau) / \Gamma_{\text{total}}$		Γ_{150} / Γ	
VALUE (units 10^{-3})	CL%	EVTS	DOCUMENT ID
1.39 ± 0.07 OUR FIT			
1.38 ± 0.09 OUR AVERAGE			
1.35 ± 0.03 ± 0.07	6.0k	INAMI	09 BELL
1.8 ± 0.4 ± 0.2		BUSKULIC	97c ALEP
1.7 ± 0.2 ± 0.2	125	ARTUSO	92c CLEO

• • • We do not use the following data for averages, fits, limits, etc. • • •

< 11.0	95	ALBRECHT	88M ARG
< 21.0	95	BARINGER	87 CLEO

42.0 \pm $\frac{7.0}{12.0}$ ± 16.0		¹ GAN	87 MRK2
--------------------------------------	--	------------------	---------

¹ Highly correlated with GAN 87 $\Gamma(\pi^- 3\pi^0 \nu_\tau) / \Gamma(\text{total})$ value.

$\Gamma(\eta \pi^- \pi^0 \nu_\tau) / \Gamma_{\text{total}}$		Γ_{151} / Γ	
VALUE (units 10^{-4})	CL%	EVTS	DOCUMENT ID
2.0 ± 0.4 OUR FIT			
1.81 ± 0.31 OUR AVERAGE			
2.01 ± 0.34 ± 0.22	381	LEES	12X BABR

• • • We use the following data for averages but not for fits. • • •

1.5 ± 0.5	30	¹ ANASTASSOV	01 CLEO
1.4 ± 0.6 ± 0.3	15	² BERGFELD	97 CLEO
< 4.3	95	ARTUSO	92 CLEO
< 120	95	ALBRECHT	88M ARG

¹ Weighted average of BERGFELD 97 and ANASTASSOV 01 value of (1.5 ± 0.6 ± 0.3) × 10⁻⁴ obtained using η 's reconstructed from $\eta \rightarrow \pi^+ \pi^- \pi^0$ decays.

² BERGFELD 97 reconstruct η 's using $\eta \rightarrow \gamma \gamma$ decays.

$\Gamma(\eta K^- \nu_\tau)/\Gamma_{\text{total}}$ Γ_{152}/Γ

VALUE (units 10^{-4})	CL%	EVTS	DOCUMENT ID	TECN	COMMENT
1.55 ± 0.08 OUR FIT					
1.54 ± 0.08 OUR AVERAGE					
1.42 ± 0.11 ± 0.07	690		DEL-AMO-SA..11E	BABR	470 fb ⁻¹ $E_{\text{cm}}^{\text{ee}} = 10.6$ GeV
1.58 ± 0.05 ± 0.09	1.6k		INAMI	09 BELL	490 fb ⁻¹ $E_{\text{cm}}^{\text{ee}} = 10.6$ GeV
2.9 ^{+1.3} _{-1.2} ± 0.7			BUSKULIC	97c ALEP	1991-1994 LEP runs
2.6 ± 0.5 ± 0.5	85		BARTELT	96 CLEO	$E_{\text{cm}}^{\text{ee}} \approx 10.6$ GeV
• • • We do not use the following data for averages, fits, limits, etc. • • •					
< 4.7	95		ARTUSO	92 CLEO	$E_{\text{cm}}^{\text{ee}} \approx 10.6$ GeV

 $\Gamma(\eta K^*(892)^- \nu_\tau)/\Gamma_{\text{total}}$ Γ_{153}/Γ

VALUE (units 10^{-4})	EVTS	DOCUMENT ID	TECN	COMMENT
1.38 ± 0.15 OUR AVERAGE				
1.34 ± 0.12 ± 0.09	245	1 INAMI	09 BELL	490 fb ⁻¹ $E_{\text{cm}}^{\text{ee}} = 10.6$ GeV
2.90 ± 0.80 ± 0.42	25	BISHAI	99 CLEO	$E_{\text{cm}}^{\text{ee}} = 10.6$ GeV

¹ Not independent of INAMI 09 $B(\tau^- \rightarrow \eta K^- \pi^0 \nu_\tau)$ and $B(\tau^- \rightarrow \eta \bar{K}^0 \pi^- \nu_\tau)$ values.

 $\Gamma(\eta K^- \pi^0 \nu_\tau)/\Gamma_{\text{total}}$ Γ_{154}/Γ

VALUE (units 10^{-4})	EVTS	DOCUMENT ID	TECN	COMMENT
0.48 ± 0.12 OUR FIT				
0.48 ± 0.12 OUR AVERAGE				
0.46 ± 0.11 ± 0.04	270	INAMI	09 BELL	490 fb ⁻¹ $E_{\text{cm}}^{\text{ee}} = 10.6$ GeV
1.77 ± 0.56 ± 0.71	36	BISHAI	99 CLEO	$E_{\text{cm}}^{\text{ee}} = 10.6$ GeV

 $\Gamma(\eta K^- \pi^0 (\text{non-}K^*(892)) \nu_\tau)/\Gamma_{\text{total}}$ Γ_{155}/Γ

VALUE	CL%	DOCUMENT ID	TECN	COMMENT
< 3.5 × 10 ⁻⁵	90	INAMI	09 BELL	490 fb ⁻¹ $E_{\text{cm}}^{\text{ee}} = 10.6$ GeV

 $\Gamma(\eta \bar{K}^0 \pi^- \nu_\tau)/\Gamma_{\text{total}}$ Γ_{156}/Γ

VALUE (units 10^{-4})	EVTS	DOCUMENT ID	TECN	COMMENT
0.94 ± 0.15 OUR FIT				
0.93 ± 0.15 OUR AVERAGE				
0.88 ± 0.14 ± 0.06	161	1 INAMI	09 BELL	490 fb ⁻¹ $E_{\text{cm}}^{\text{ee}} = 10.6$ GeV
2.20 ± 0.70 ± 0.22	15	2 BISHAI	99 CLEO	$E_{\text{cm}}^{\text{ee}} = 10.6$ GeV

¹ We multiply the INAMI 09 measurement $B(\tau^- \rightarrow \eta K_S^0 \pi^- \nu_\tau) = (0.44 \pm 0.07 \pm 0.03) \times 10^{-4}$ by 2 to obtain the listed value.

² We multiply the BISHAI 99 measurement $B(\tau^- \rightarrow \eta K_S^0 \pi^- \nu_\tau) = (1.10 \pm 0.35 \pm 0.11) \times 10^{-4}$ by 2 to obtain the listed value.

 $\Gamma(\eta \bar{K}^0 \pi^- \pi^0 \nu_\tau)/\Gamma_{\text{total}}$ Γ_{157}/Γ

VALUE	CL%	DOCUMENT ID	TECN	COMMENT
< 5.0 × 10 ⁻⁵	90	1 INAMI	09 BELL	490 fb ⁻¹ $E_{\text{cm}}^{\text{ee}} = 10.6$ GeV

¹ We multiply the INAMI 09 measurement $B(\tau^- \rightarrow \eta K_S^0 \pi^- \pi^0 \nu_\tau) < 2.5 \times 10^{-5}$ by 2 to obtain the listed value.

 $\Gamma(\eta K^- K^0 \nu_\tau)/\Gamma_{\text{total}}$ Γ_{158}/Γ

VALUE	CL%	DOCUMENT ID	TECN	COMMENT
< 9.0 × 10 ⁻⁶	90	1 INAMI	09 BELL	490 fb ⁻¹ $E_{\text{cm}}^{\text{ee}} = 10.6$ GeV

¹ We multiply the INAMI 09 measurement $B(\tau^- \rightarrow \eta K^- K_S^0 \nu_\tau) < 4.5 \times 10^{-6}$ by 2 to obtain the listed value.

 $\Gamma(\eta \pi^+ \pi^- \pi^- \geq 0 \text{ neutrals } \nu_\tau)/\Gamma_{\text{total}}$ Γ_{159}/Γ

VALUE (%)	CL%	DOCUMENT ID	TECN	COMMENT
< 0.3	90	ABACHI	87b HRS	$E_{\text{cm}}^{\text{ee}} = 29$ GeV

 $\Gamma(\eta \pi^- \pi^+ \pi^- \nu_\tau (\text{ex. } K^0))/\Gamma_{\text{total}}$ Γ_{160}/Γ

VALUE (units 10^{-4})	EVTS	DOCUMENT ID	TECN	COMMENT
2.20 ± 0.13 OUR FIT				
2.23 ± 0.12 OUR AVERAGE				
2.10 ± 0.09 ± 0.13	2.9k	1 LEES	12x BABR	$\eta \rightarrow \gamma \gamma$
2.37 ± 0.12 ± 0.18	1.4k	1 LEES	12x BABR	$\eta \rightarrow \pi^+ \pi^- \pi^0$
2.54 ± 0.27 ± 0.25	315	1 LEES	12x BABR	$\eta \rightarrow 3\pi^0$
• • • We use the following data for averages but not for fits. • • •				
2.3 ± 0.5	170	2 ANASTASSOV	01 CLEO	$E_{\text{cm}}^{\text{ee}} = 10.6$ GeV
• • • We do not use the following data for averages, fits, limits, etc. • • •				
1.60 ± 0.05 ± 0.11	1.8 k	AUBERT	08AE BABR	Repl. by LEES 12x
3.4 ^{+0.6} _{-0.5} ± 0.6	89	3 BERGFELD	97 CLEO	Repl. by ANASTASSOV 01

¹ LEES 12x uses 468 fb⁻¹ of data taken at $E_{\text{cm}}^{\text{ee}} = 10.6$ GeV. It gives the average of the three measurements listed here as $(2.25 \pm 0.07 \pm 0.12) \times 10^{-4}$.

² Weighted average of BERGFELD 97 and ANASTASSOV 01 measurements using η 's reconstructed from $\eta \rightarrow \pi^+ \pi^- \pi^0$ and $\eta \rightarrow 3\pi^0$ decays.

³ BERGFELD 97 reconstruct η 's using $\eta \rightarrow \gamma \gamma$ and $\eta \rightarrow 3\pi^0$ decays.

 $\Gamma(\eta \pi^- \pi^+ \pi^- \nu_\tau (\text{ex. } K^0, f_1(1285)))/\Gamma_{\text{total}}$ Γ_{161}/Γ

VALUE (units 10^{-4})	DOCUMENT ID	TECN	COMMENT
0.99 ± 0.09 ± 0.13	1 LEES	12x BABR	468 fb ⁻¹ $E_{\text{cm}}^{\text{ee}} = 10.6$ GeV

¹ LEES 12x obtain this result by subtracting their $B(\tau^- \rightarrow f_1(1285) \pi^- \nu_\tau \rightarrow \eta \pi^- \pi^+ \pi^- \nu_\tau)$ measurement from their $B(\tau^- \rightarrow \eta \pi^- \pi^+ \pi^- \nu_\tau (\text{ex. } K^0))$ measurement.

 $\Gamma(\eta a_1(1260)^- \nu_\tau \rightarrow \eta \pi^- \rho^0 \nu_\tau)/\Gamma_{\text{total}}$ Γ_{162}/Γ

VALUE	CL%	DOCUMENT ID	TECN	COMMENT
< 3.9 × 10 ⁻⁴	90	BERGFELD	97 CLEO	$E_{\text{cm}}^{\text{ee}} = 10.6$ GeV

 $\Gamma(\eta \eta \pi^- \nu_\tau)/\Gamma_{\text{total}}$ Γ_{163}/Γ

VALUE	CL%	DOCUMENT ID	TECN	COMMENT
< 7.4 × 10 ⁻⁶	90	INAMI	09 BELL	490 fb ⁻¹ $E_{\text{cm}}^{\text{ee}} = 10.6$ GeV
< 1.1 × 10 ⁻⁴	95	ARTUSO	92 CLEO	$E_{\text{cm}}^{\text{ee}} \approx 10.6$ GeV
< 8.3 × 10 ⁻³	95	ALBRECHT	88M ARG	$E_{\text{cm}}^{\text{ee}} \approx 10$ GeV

 $\Gamma(\eta \eta \pi^- \pi^0 \nu_\tau)/\Gamma_{\text{total}}$ Γ_{164}/Γ

VALUE (units 10^{-4})	CL%	DOCUMENT ID	TECN	COMMENT
< 2.0	95	ARTUSO	92 CLEO	$E_{\text{cm}}^{\text{ee}} \approx 10.6$ GeV
< 90	95	ALBRECHT	88M ARG	$E_{\text{cm}}^{\text{ee}} \approx 10$ GeV

 $\Gamma(\eta \eta K^- \nu_\tau)/\Gamma_{\text{total}}$ Γ_{165}/Γ

VALUE	CL%	DOCUMENT ID	TECN	COMMENT
< 3.0 × 10 ⁻⁶	90	INAMI	09 BELL	490 fb ⁻¹ $E_{\text{cm}}^{\text{ee}} = 10.6$ GeV

 $\Gamma(\eta'(958) \pi^- \nu_\tau)/\Gamma_{\text{total}}$ Γ_{166}/Γ

VALUE	CL%	DOCUMENT ID	TECN	COMMENT
< 4.0 × 10 ⁻⁶	90	LEES	12x BABR	468 fb ⁻¹ $E_{\text{cm}}^{\text{ee}} = 10.6$ GeV
< 7.2 × 10 ⁻⁶	90	AUBERT	08AE BABR	384 fb ⁻¹ , $E_{\text{cm}}^{\text{ee}} = 10.6$ GeV
< 7.4 × 10 ⁻⁵	90	BERGFELD	97 CLEO	$E_{\text{cm}}^{\text{ee}} = 10.6$ GeV

 $\Gamma(\eta'(958) \pi^- \pi^0 \nu_\tau)/\Gamma_{\text{total}}$ Γ_{167}/Γ

VALUE	CL%	DOCUMENT ID	TECN	COMMENT
< 1.2 × 10 ⁻⁵	90	LEES	12x BABR	468 fb ⁻¹ $E_{\text{cm}}^{\text{ee}} = 10.6$ GeV
< 8.0 × 10 ⁻⁵	90	BERGFELD	97 CLEO	$E_{\text{cm}}^{\text{ee}} = 10.6$ GeV

 $\Gamma(\eta'(958) K^- \nu_\tau)/\Gamma_{\text{total}}$ Γ_{168}/Γ

VALUE	CL%	DOCUMENT ID	TECN	COMMENT
< 2.4 × 10 ⁻⁶	90	LEES	12x BABR	468 fb ⁻¹ $E_{\text{cm}}^{\text{ee}} = 10.6$ GeV

 $\Gamma(\phi \pi^- \nu_\tau)/\Gamma_{\text{total}}$ Γ_{169}/Γ

VALUE (units 10^{-5})	CL%	EVTS	DOCUMENT ID	TECN	COMMENT
3.42 ± 0.55 ± 0.25	344		AUBERT	08 BABR	342 fb ⁻¹ $E_{\text{cm}}^{\text{ee}} = 10.6$ GeV
• • • We do not use the following data for averages, fits, limits, etc. • • •					
< 20	90		1 AVERY	97 CLEO	$E_{\text{cm}}^{\text{ee}} = 10.6$ GeV
< 35	90		ALBRECHT	95H ARG	$E_{\text{cm}}^{\text{ee}} = 9.4-10.6$ GeV

¹ AVERY 97 limit varies from $(1.2-2.0) \times 10^{-4}$ depending on decay model assumptions.

 $\Gamma(\phi K^- \nu_\tau)/\Gamma_{\text{total}}$ Γ_{170}/Γ

VALUE (units 10^{-5})	CL%	EVTS	DOCUMENT ID	TECN	COMMENT
4.4 ± 1.6 OUR FIT					
3.70 ± 0.33 OUR AVERAGE Error includes scale factor of 1.3.					

• • • We use the following data for averages but not for fits. • • •					
3.39 ± 0.20 ± 0.28	274		AUBERT	08 BABR	342 fb ⁻¹ $E_{\text{cm}}^{\text{ee}} = 10.6$ GeV
4.05 ± 0.25 ± 0.26	551		INAMI	06 BELL	401 fb ⁻¹ $E_{\text{cm}}^{\text{ee}} = 10.6$ GeV
• • • We do not use the following data for averages, fits, limits, etc. • • •					
< 6.7	90		1 AVERY	97 CLEO	$E_{\text{cm}}^{\text{ee}} = 10.6$ GeV

¹ AVERY 97 limit varies from $(5.4-6.7) \times 10^{-5}$ depending on decay model assumptions.

 $\Gamma(f_1(1285) \pi^- \nu_\tau)/\Gamma_{\text{total}}$ Γ_{171}/Γ

VALUE (units 10^{-4})	EVTS	DOCUMENT ID	TECN	COMMENT
3.9 ± 0.5 OUR AVERAGE Error includes scale factor of 1.9.				
4.73 ± 0.28 ± 0.45	3.7k	1 LEES	12x BABR	468 fb ⁻¹ $E_{\text{cm}}^{\text{ee}} = 10.6$ GeV
3.60 ± 0.18 ± 0.23	2.5k	2 LEES	12x BABR	468 fb ⁻¹ $E_{\text{cm}}^{\text{ee}} = 10.6$ GeV
• • • We do not use the following data for averages, fits, limits, etc. • • •				
3.19 ± 0.18 ± 1.00	1.3 k	3 AUBERT	08AE BABR	Repl. by LEES 12x
3.9 ± 0.7 ± 0.5	1.4 k	4 AUBERT,B	05W BABR	Repl. by LEES 12x
5.8 ^{+1.4} _{-1.3} ± 1.8	54	5 BERGFELD	97 CLEO	$E_{\text{cm}}^{\text{ee}} = 10.6$ GeV

¹ LEES 12x obtain this value by dividing their $B(\tau^- \rightarrow f_1(1285) \pi^- \nu_\tau \rightarrow 3\pi^- 2\pi^+ \nu_\tau)$ measurement by the PDG 12 value of $B(f_1(1285) \rightarrow 2\pi^+ 2\pi^-) = 0.111^{+0.007}_{-0.006}$.

Lepton Particle Listings

 τ

² LEES 12X obtain this value by dividing their $B(\tau^- \rightarrow f_1(1285)\pi^- \nu_\tau \rightarrow \eta\pi^- \pi^+ \pi^- \nu_\tau)$ measurement by 2/3 of the PDG 12 value of $B(f_1(1285) \rightarrow \eta\pi\pi) = 0.524^{+0.019}_{-0.021}$.

³ AUBERT 08AE obtain this value by dividing their $B(\tau^- \rightarrow f_1(1285)\pi^- \nu_\tau \rightarrow \eta\pi^- \pi^+ \pi^- \nu_\tau)$ measurement by the PDG 06 value of $B(f_1(1285) \rightarrow \eta\pi^- \pi^+) = 0.35 \pm 0.11$. The quote $(3.19 \pm 0.18 \pm 0.16 \pm 0.99) \times 10^{-4}$ where the final error is due to the uncertainty on $B(f_1(1285) \rightarrow \eta\pi^- \pi^+)$. We combine the two systematic errors in quadrature.

⁴ AUBERT,B 05W use the $f_1(1285) \rightarrow 2\pi^+ 2\pi^-$ decay mode and the PDG 04 value of $B(f_1(1285) \rightarrow 2\pi^+ 2\pi^-) = 0.110^{+0.007}_{-0.006}$.

⁵ BERGFELD 97 use the $f_1(1285) \rightarrow \eta\pi^+ \pi^-$ decay mode.

$\Gamma(f_1(1285)\pi^- \nu_\tau \rightarrow \eta\pi^- \pi^+ \pi^- \nu_\tau)/\Gamma_{\text{total}}$ Γ_{172}/Γ

VALUE (units 10^{-4})	EVTS	DOCUMENT ID	TECN	COMMENT
1.18 ± 0.07 OUR AVERAGE				Error includes scale factor of 1.3.
1.26 ± 0.06 ± 0.06	2.5k	LEES	12X BABR	468 fb ⁻¹ $E_{\text{cm}}^{\text{ex}} = 10.6$ GeV
1.11 ± 0.06 ± 0.05	1.3 k	AUBERT	08AE BABR	384 fb ⁻¹ , $E_{\text{cm}}^{\text{ex}} = 10.6$ GeV

$\Gamma(f_1(1285)\pi^- \nu_\tau \rightarrow \eta\pi^- \pi^+ \pi^- \nu_\tau)/\Gamma(\eta\pi^- \pi^+ \pi^- \nu_\tau \text{ (ex. } K^0))$ $\Gamma_{172}/\Gamma_{160}$

VALUE (%)	DOCUMENT ID	TECN	COMMENT
0.69 ± 0.01 ± 0.05	¹ AUBERT	08AE BABR	384 fb ⁻¹ , $E_{\text{cm}}^{\text{ex}} = 10.6$ GeV

• • • We do not use the following data for averages, fits, limits, etc. • • •

0.55 ± 0.14 BERGFELD 97 CLEO $E_{\text{cm}}^{\text{ex}} = 10.6$ GeV

¹ Not independent of AUBERT 08AE $B(\tau^- \rightarrow f_1(1285)\pi^- \nu_\tau \rightarrow \eta\pi^- \pi^+ \pi^- \nu_\tau)$ and $B(\tau^- \rightarrow \eta\pi^- \pi^+ \pi^- \nu_\tau \text{ (ex. } K^0))$ values.

$\Gamma(f_1(1285)\pi^- \nu_\tau \rightarrow 3\pi^- 2\pi^+ \nu_\tau)/\Gamma_{\text{total}}$ Γ_{173}/Γ

VALUE (units 10^{-4})	EVTS	DOCUMENT ID	TECN	COMMENT
0.52 ± 0.04 OUR FIT				
0.520 ± 0.031 ± 0.037	3.7k	LEES	12X BABR	468 fb ⁻¹ $E_{\text{cm}}^{\text{ex}} = 10.6$ GeV

$\Gamma(\pi(1300)^- \nu_\tau \rightarrow (\rho\pi)^- \nu_\tau \rightarrow (3\pi)^- \nu_\tau)/\Gamma_{\text{total}}$ Γ_{174}/Γ

VALUE	CL%	DOCUMENT ID	TECN	COMMENT
< 1.0 × 10⁻⁴	90	ASNER	00 CLEO	$E_{\text{cm}}^{\text{ex}} = 10.6$ GeV

$\Gamma(\pi(1300)^- \nu_\tau \rightarrow ((\pi\pi)_{\text{S-wave}} \pi)^- \nu_\tau \rightarrow (3\pi)^- \nu_\tau)/\Gamma_{\text{total}}$ Γ_{175}/Γ

VALUE	CL%	DOCUMENT ID	TECN	COMMENT
< 1.9 × 10⁻⁴	90	ASNER	00 CLEO	$E_{\text{cm}}^{\text{ex}} = 10.6$ GeV

$\Gamma(h^- \omega \geq 0 \text{ neutrals } \nu_\tau)/\Gamma_{\text{total}}$ Γ_{176}/Γ

VALUE (%)	EVTS	DOCUMENT ID	TECN	COMMENT
2.40 ± 0.08 OUR FIT				
$\Gamma_{176}/\Gamma = (\Gamma_{178} + \Gamma_{179} + \Gamma_{180})/\Gamma$				

• • • We use the following data for averages but not for fits. • • •

1.65 ± 0.3 ± 0.2 1513 ALBRECHT 88M ARG $E_{\text{cm}}^{\text{ex}} \approx 10$ GeV

$\Gamma(h^- \omega \nu_\tau)/\Gamma_{\text{total}}$ $\Gamma_{177}/\Gamma = (\Gamma_{178} + \Gamma_{179})/\Gamma$

VALUE (%)	EVTS	DOCUMENT ID	TECN	COMMENT
1.99 ± 0.06 OUR FIT				
1.92 ± 0.07 OUR AVERAGE				

1.91 ± 0.07 ± 0.06 5803 BUSKULIC 97C ALEP 1991–1994 LEP runs

1.60 ± 0.27 ± 0.41 139 BARINGER 87 CLEO $E_{\text{cm}}^{\text{ex}} = 10.5$ GeV

• • • We use the following data for averages but not for fits. • • •

1.95 ± 0.07 ± 0.11 2223 ¹ BALEST 95C CLEO $E_{\text{cm}}^{\text{ex}} \approx 10.6$ GeV

¹ Not independent of BALEST 95C $B(\tau^- \rightarrow h^- \omega \nu_\tau)/B(\tau^- \rightarrow h^- h^- h^+ \pi^0 \nu_\tau)$ value.

$[\Gamma(\pi^- \omega \nu_\tau) + \Gamma(K^- \omega \nu_\tau)]/\Gamma(h^- h^- h^+ \pi^0 \nu_\tau \text{ (ex. } K^0))$ $(\Gamma_{178} + \Gamma_{179})/\Gamma_{74}$

VALUE (units 10^{-2})	EVTS	DOCUMENT ID	TECN	COMMENT
43.5 ± 1.4 OUR FIT				
45.3 ± 1.9 OUR AVERAGE				

43.1 ± 3.3 2350 ¹ BUSKULIC 96 ALEP LEP 1991–1993 data

46.4 ± 1.6 ± 1.7 2223 ² BALEST 95C CLEO $E_{\text{cm}}^{\text{ex}} \approx 10.6$ GeV

• • • We do not use the following data for averages, fits, limits, etc. • • •

37 ± 5 ± 2 458 ³ ALBRECHT 91D ARG $E_{\text{cm}}^{\text{ex}} = 9.4$ –10.6 GeV

¹ BUSKULIC 96 quote the fraction of $\tau \rightarrow h^- h^- h^+ \pi^0 \nu_\tau \text{ (ex. } K^0)$ decays which originate in a $h^- \omega$ final state = 0.383 ± 0.029 . We divide this by the $\omega(782) \rightarrow \pi^+ \pi^- \pi^0$ branching fraction (0.888).

² BALEST 95C quote the fraction of $\tau^- \rightarrow h^- h^- h^+ \pi^0 \nu_\tau \text{ (ex. } K^0)$ decays which originate in a $h^- \omega$ final state equals $0.412 \pm 0.014 \pm 0.015$. We divide this by the $\omega(782) \rightarrow \pi^+ \pi^- \pi^0$ branching fraction (0.888).

³ ALBRECHT 91D quote the fraction of $\tau^- \rightarrow h^- h^- h^+ \pi^0 \nu_\tau$ decays which originate in a $\pi^- \omega$ final state equals $0.33 \pm 0.04 \pm 0.02$. We divide this by the $\omega(782) \rightarrow \pi^+ \pi^- \pi^0$ branching fraction (0.888).

$\Gamma(\pi^- \omega \nu_\tau)/\Gamma_{\text{total}}$ Γ_{178}/Γ

VALUE (%)	DOCUMENT ID	TECN	COMMENT
1.95 ± 0.06 OUR FIT			

$\Gamma(K^- \omega \nu_\tau)/\Gamma_{\text{total}}$ Γ_{179}/Γ

VALUE (units 10^{-4})	EVTS	DOCUMENT ID	TECN	COMMENT
4.1 ± 0.9 OUR FIT				
4.1 ± 0.6 ± 0.7	500	ARMS	05 CLE3	7.6 fb ⁻¹ , $E_{\text{cm}}^{\text{ex}} = 10.6$ GeV

$\Gamma(h^- \omega \pi^0 \nu_\tau)/\Gamma_{\text{total}}$ Γ_{180}/Γ

VALUE (%)	EVTS	DOCUMENT ID	TECN	COMMENT
0.41 ± 0.04 OUR FIT				
0.43 ± 0.06 ± 0.05	7283	BUSKULIC	97C ALEP	1991–1994 LEP runs

$\Gamma(h^- \omega \pi^0 \nu_\tau)/\Gamma(h^- h^- h^+ \geq 0 \text{ neutrals } \geq 0 K^0 \nu_\tau)$ Γ_{180}/Γ_{62}

VALUE (%)	EVTS	DOCUMENT ID	TECN	COMMENT
(2.69 ± 0.28) × 10⁻² OUR FIT				
$\Gamma_{180}/\Gamma_{62} = \Gamma_{180}/(0.34598\Gamma_{36} + 0.34598\Gamma_{38} + 0.34598\Gamma_{41} + 0.34598\Gamma_{43} + 0.4247\Gamma_{48} + 0.6920\Gamma_{49} + 0.8494\Gamma_{52} + 0.6920\Gamma_{56} + 0.6534\Gamma_{61} + \Gamma_{70} + \Gamma_{78} + \Gamma_{85} + \Gamma_{89} + \Gamma_{97} + \Gamma_{103} + \Gamma_{106} + \Gamma_{107} + 0.2789\Gamma_{150} + 0.2292\Gamma_{151} + 0.2789\Gamma_{152} + 0.2789\Gamma_{154} + 0.3759\Gamma_{156} + 0.3268\Gamma_{160} + 0.7259\Gamma_{170} + 0.9078\Gamma_{178} + 0.9078\Gamma_{179} + 0.9078\Gamma_{180} + 0.893\Gamma_{182})$				

• • • We use the following data for averages but not for fits. • • •

0.028 ± 0.003 ± 0.003 430 ¹ BORTOLETTO 93 CLEO $E_{\text{cm}}^{\text{ex}} \approx 10.6$ GeV

¹ Not independent of BORTOLETTO 93 $\Gamma(\tau^- \rightarrow h^- \omega \pi^0 \nu_\tau)/\Gamma(\tau^- \rightarrow h^- h^- h^+ 2\pi^0 \nu_\tau \text{ (ex. } K^0))$ value.

$\Gamma(h^- \omega \pi^0 \nu_\tau)/\Gamma(h^- h^- h^+ 2\pi^0 \nu_\tau \text{ (ex. } K^0))$ Γ_{180}/Γ_{84}

VALUE (units 10^{-2})	DOCUMENT ID	TECN	COMMENT
82 ± 8 OUR FIT			
81 ± 6 ± 6	BORTOLETTO93	CLEO	$E_{\text{cm}}^{\text{ex}} \approx 10.6$ GeV

$\Gamma(h^- \omega 2\pi^0 \nu_\tau)/\Gamma_{\text{total}}$ Γ_{181}/Γ

VALUE (units 10^{-4})	EVTS	DOCUMENT ID	TECN	COMMENT
1.4 ± 0.4 ± 0.3	53	ANASTASSOV 01	CLEO	$E_{\text{cm}}^{\text{ex}} = 10.6$ GeV

• • • We do not use the following data for averages, fits, limits, etc. • • •

1.89 ± 0.74 ± 0.40 19 ANDERSON 97 CLEO Repl. by ANASTASSOV 01

$\Gamma(\pi^- \omega 2\pi^0 \nu_\tau)/\Gamma_{\text{total}}$ Γ_{182}/Γ

VALUE (units 10^{-4})	EVTS	DOCUMENT ID	TECN	COMMENT
0.72 ± 0.16 OUR FIT				
0.73 ± 0.12 ± 0.12	1.1k	LEES	12X BABR	468 fb ⁻¹ $E_{\text{cm}}^{\text{ex}} = 10.6$ GeV

$\Gamma(h^- 2\omega \nu_\tau)/\Gamma_{\text{total}}$ Γ_{183}/Γ

VALUE	CL%	DOCUMENT ID	TECN	COMMENT
< 5.4 × 10⁻⁷	90	AUBERT,B	06 BABR	232 fb ⁻¹ $E_{\text{cm}}^{\text{ex}} = 10.6$ GeV

$\Gamma(2h^- h^+ \omega \nu_\tau)/\Gamma_{\text{total}}$ Γ_{184}/Γ

VALUE (units 10^{-4})	EVTS	DOCUMENT ID	TECN	COMMENT
1.2 ± 0.2 ± 0.1	110	ANASTASSOV 01	CLEO	$E_{\text{cm}}^{\text{ex}} = 10.6$ GeV

$\Gamma(2\pi^- \pi^+ \omega \nu_\tau \text{ (ex. } K^0))/\Gamma_{\text{total}}$ Γ_{185}/Γ

VALUE (units 10^{-4})	EVTS	DOCUMENT ID	TECN	COMMENT
0.84 ± 0.06 OUR FIT				
0.84 ± 0.04 ± 0.06	2.4k	LEES	12X BABR	468 fb ⁻¹ $E_{\text{cm}}^{\text{ex}} = 10.6$ GeV

$\Gamma(e^- \gamma)/\Gamma_{\text{total}}$ Γ_{186}/Γ

VALUE	CL%	DOCUMENT ID	TECN	COMMENT
< 3.3 × 10⁻⁸	90	AUBERT	10B BABR	516 fb ⁻¹ , $E_{\text{cm}}^{\text{ex}} = 10.6$ GeV

• • • We do not use the following data for averages, fits, limits, etc. • • •

< 1.2 × 10⁻⁷ 90 HAYASAKA 08 BELL 535 fb⁻¹, $E_{\text{cm}}^{\text{ex}} = 10.6$ GeV

< 1.1 × 10⁻⁷ 90 AUBERT 06c BABR 232 fb⁻¹, $E_{\text{cm}}^{\text{ex}} = 10.6$ GeV

< 3.9 × 10⁻⁷ 90 HAYASAKA 05 BELL 86.7 fb⁻¹, $E_{\text{cm}}^{\text{ex}} = 10.6$ GeV

< 2.7 × 10⁻⁶ 90 EDWARDS 97 CLEO

< 1.1 × 10⁻⁴ 90 ABREU 95U DLPH 1990–1993 LEP runs

< 1.2 × 10⁻⁴ 90 ALBRECHT 92k ARG $E_{\text{cm}}^{\text{ex}} = 10$ GeV

< 2.0 × 10⁻⁴ 90 KEH 88 CBAL $E_{\text{cm}}^{\text{ex}} = 10$ GeV

< 6.4 × 10⁻⁴ 90 HAYES 82 MRK2 $E_{\text{cm}}^{\text{ex}} = 3.8$ –6.8 GeV

$\Gamma(\mu^- \gamma)/\Gamma_{\text{total}}$ Γ_{187}/Γ

VALUE	CL%	DOCUMENT ID	TECN	COMMENT
< 4.4 × 10⁻⁸	90	AUBERT	10B BABR	516 fb ⁻¹ , $E_{\text{cm}}^{\text{ex}} = 10.6$ GeV

• • • We do not use the following data for averages, fits, limits, etc. • • •

< 4.5 × 10⁻⁸ 90 HAYASAKA 08 BELL 535 fb⁻¹, $E_{\text{cm}}^{\text{ex}} = 10.6$ GeV

< 6.8 × 10⁻⁸ 90 AUBERT,B 05A BABR 232 fb⁻¹, $E_{\text{cm}}^{\text{ex}} = 10.6$ GeV

< 3.1 × 10⁻⁷ 90 ABE 04B BELL 86.3 fb⁻¹, $E_{\text{cm}}^{\text{ex}} = 10.6$ GeV

< 1.1 × 10⁻⁶ 90 AHMED 00 CLEO $E_{\text{cm}}^{\text{ex}} = 10.6$ GeV

< 3.0 × 10⁻⁶ 90 EDWARDS 97 CLEO

< 6.2 × 10⁻⁵ 90 ABREU 95U DLPH 1990–1993 LEP runs

< 0.42 × 10⁻⁵ 90 BEAN 93 CLEO $E_{\text{cm}}^{\text{ex}} = 10.6$ GeV

< 3.4 × 10⁻⁵ 90 ALBRECHT 92k ARG $E_{\text{cm}}^{\text{ex}} = 10$ GeV

< 5.5 × 10⁻⁵ 90 HAYES 82 MRK2 $E_{\text{cm}}^{\text{ex}} = 3.8$ –6.8 GeV

Lepton Particle Listings

T

$\Gamma(e^- \eta'(958))/\Gamma_{total}$ Γ_{202}/Γ

VALUE	CL%	DOCUMENT ID	TECN	COMMENT
$< 1.6 \times 10^{-7}$	90	MIYAZAKI	07	BELL 401 fb ⁻¹ , $E_{cm}^{ee} = 10.6$ GeV
• • • We do not use the following data for averages, fits, limits, etc. • • •				
$< 2.4 \times 10^{-7}$	90	AUBERT	07I	BABR 339 fb ⁻¹ , $E_{cm}^{ee} = 10.6$ GeV
$< 10. \times 10^{-7}$	90	ENARI	05	BELL 154 fb ⁻¹ , $E_{cm}^{ee} = 10.6$ GeV

$\Gamma(\mu^- \eta'(958))/\Gamma_{total}$ Γ_{203}/Γ

VALUE	CL%	DOCUMENT ID	TECN	COMMENT
$< 1.3 \times 10^{-7}$	90	MIYAZAKI	07	BELL 401 fb ⁻¹ , $E_{cm}^{ee} = 10.6$ GeV
• • • We do not use the following data for averages, fits, limits, etc. • • •				
$< 1.4 \times 10^{-7}$	90	AUBERT	07I	BABR 339 fb ⁻¹ , $E_{cm}^{ee} = 10.6$ GeV
$< 4.7 \times 10^{-7}$	90	ENARI	05	BELL 154 fb ⁻¹ , $E_{cm}^{ee} = 10.6$ GeV

$\Gamma(e^- f_0(980) \rightarrow e^- \pi^+ \pi^-)/\Gamma_{total}$ Γ_{204}/Γ

VALUE	CL%	DOCUMENT ID	TECN	COMMENT
$< 3.2 \times 10^{-8}$	90	MIYAZAKI	09	BELL 671 fb ⁻¹ $E_{cm}^{ee} = 10.6$ GeV

$\Gamma(\mu^- f_0(980) \rightarrow \mu^- \pi^+ \pi^-)/\Gamma_{total}$ Γ_{205}/Γ

VALUE	CL%	DOCUMENT ID	TECN	COMMENT
$< 3.4 \times 10^{-8}$	90	MIYAZAKI	09	BELL 671 fb ⁻¹ $E_{cm}^{ee} = 10.6$ GeV

$\Gamma(e^- \phi)/\Gamma_{total}$ Γ_{206}/Γ

Test of lepton family number conservation.

VALUE	CL%	DOCUMENT ID	TECN	COMMENT
$< 3.1 \times 10^{-8}$	90	MIYAZAKI	11	BELL 854 fb ⁻¹ $E_{cm}^{ee} = 10.6$ GeV
$< 3.1 \times 10^{-8}$	90	AUBERT	09W	BABR 451 fb ⁻¹ $E_{cm}^{ee} = 10.6$ GeV
• • • We do not use the following data for averages, fits, limits, etc. • • •				
$< 7.3 \times 10^{-8}$	90	NISHIO	08	BELL 543 fb ⁻¹ $E_{cm}^{ee} = 10.6$ GeV
$< 7.3 \times 10^{-7}$	90	YUSA	06	BELL 158 fb ⁻¹ $E_{cm}^{ee} = 10.6$ GeV
$< 6.9 \times 10^{-6}$	90	BLISS	98	CLEO $E_{cm}^{ee} = 10.6$ GeV

$\Gamma(\mu^- \phi)/\Gamma_{total}$ Γ_{207}/Γ

Test of lepton family number conservation.

VALUE	CL%	DOCUMENT ID	TECN	COMMENT
$< 8.4 \times 10^{-8}$	90	MIYAZAKI	11	BELL 854 fb ⁻¹ $E_{cm}^{ee} = 10.6$ GeV
• • • We do not use the following data for averages, fits, limits, etc. • • •				
$< 1.9 \times 10^{-7}$	90	AUBERT	09W	BABR 451 fb ⁻¹ $E_{cm}^{ee} = 10.6$ GeV
$< 1.3 \times 10^{-7}$	90	NISHIO	08	BELL 543 fb ⁻¹ $E_{cm}^{ee} = 10.6$ GeV
$< 7.7 \times 10^{-7}$	90	YUSA	06	BELL 158 fb ⁻¹ $E_{cm}^{ee} = 10.6$ GeV
$< 7.0 \times 10^{-6}$	90	BLISS	98	CLEO $E_{cm}^{ee} = 10.6$ GeV

$\Gamma(e^- e^+ e^-)/\Gamma_{total}$ Γ_{208}/Γ

Test of lepton family number conservation.

VALUE	CL%	DOCUMENT ID	TECN	COMMENT
$< 2.7 \times 10^{-8}$	90	HAYASAKA	10	BELL 782 fb ⁻¹ $E_{cm}^{ee} = 10.6$ GeV
• • • We do not use the following data for averages, fits, limits, etc. • • •				
$< 2.9 \times 10^{-8}$	90	LEES	10A	BABR 468 fb ⁻¹ $E_{cm}^{ee} = 10.6$ GeV
$< 3.6 \times 10^{-8}$	90	MIYAZAKI	08	BELL 535 fb ⁻¹ $E_{cm}^{ee} = 10.6$ GeV
$< 4.3 \times 10^{-8}$	90	AUBERT	07BK	BABR 376 fb ⁻¹ $E_{cm}^{ee} = 10.6$ GeV
$< 2.0 \times 10^{-7}$	90	AUBERT	04J	BABR 91.5 fb ⁻¹ $E_{cm}^{ee} = 10.6$ GeV
$< 3.5 \times 10^{-7}$	90	YUSA	04	BELL 87.1 fb ⁻¹ $E_{cm}^{ee} = 10.6$ GeV
$< 2.9 \times 10^{-6}$	90	BLISS	98	CLEO $E_{cm}^{ee} = 10.6$ GeV
$< 0.33 \times 10^{-5}$	90	¹ BARTELT	94	CLEO Repl. by BLISS 98
$< 1.3 \times 10^{-5}$	90	ALBRECHT	92K	ARG $E_{cm}^{ee} = 10$ GeV
$< 2.7 \times 10^{-5}$	90	BOWCOCK	90	CLEO $E_{cm}^{ee} = 10.4-10.9$
$< 40 \times 10^{-5}$	90	HAYES	82	MRK2 $E_{cm}^{ee} = 3.8-6.8$ GeV

¹ BARTELT 94 assume phase space decays.

$\Gamma(e^- \mu^+ \mu^-)/\Gamma_{total}$ Γ_{209}/Γ

Test of lepton family number conservation.

VALUE	CL%	DOCUMENT ID	TECN	COMMENT
$< 2.7 \times 10^{-8}$	90	HAYASAKA	10	BELL 782 fb ⁻¹ $E_{cm}^{ee} = 10.6$ GeV
• • • We do not use the following data for averages, fits, limits, etc. • • •				
$< 3.2 \times 10^{-8}$	90	LEES	10A	BABR 468 fb ⁻¹ $E_{cm}^{ee} = 10.6$ GeV
$< 4.1 \times 10^{-8}$	90	MIYAZAKI	08	BELL 535 fb ⁻¹ $E_{cm}^{ee} = 10.6$ GeV
$< 3.7 \times 10^{-8}$	90	AUBERT	07BK	BABR 376 fb ⁻¹ $E_{cm}^{ee} = 10.6$ GeV
$< 3.3 \times 10^{-7}$	90	AUBERT	04J	BABR 91.5 fb ⁻¹ $E_{cm}^{ee} = 10.6$ GeV
$< 2.0 \times 10^{-7}$	90	YUSA	04	BELL 87.1 fb ⁻¹ $E_{cm}^{ee} = 10.6$ GeV
$< 1.8 \times 10^{-6}$	90	BLISS	98	CLEO $E_{cm}^{ee} = 10.6$ GeV
$< 0.36 \times 10^{-5}$	90	¹ BARTELT	94	CLEO Repl. by BLISS 98
$< 1.9 \times 10^{-5}$	90	ALBRECHT	92K	ARG $E_{cm}^{ee} = 10$ GeV
$< 2.7 \times 10^{-5}$	90	BOWCOCK	90	CLEO $E_{cm}^{ee} = 10.4-10.9$
$< 33 \times 10^{-5}$	90	HAYES	82	MRK2 $E_{cm}^{ee} = 3.8-6.8$ GeV

¹ BARTELT 94 assume phase space decays.

$\Gamma(e^+ \mu^- \mu^-)/\Gamma_{total}$ Γ_{210}/Γ

Test of lepton family number conservation.

VALUE	CL%	DOCUMENT ID	TECN	COMMENT
$< 1.7 \times 10^{-8}$	90	HAYASAKA	10	BELL 782 fb ⁻¹ $E_{cm}^{ee} = 10.6$ GeV
• • • We do not use the following data for averages, fits, limits, etc. • • •				
$< 2.6 \times 10^{-8}$	90	LEES	10A	BABR 468 fb ⁻¹ $E_{cm}^{ee} = 10.6$ GeV
$< 2.3 \times 10^{-8}$	90	MIYAZAKI	08	BELL 535 fb ⁻¹ $E_{cm}^{ee} = 10.6$ GeV
$< 5.6 \times 10^{-8}$	90	AUBERT	07BK	BABR 376 fb ⁻¹ $E_{cm}^{ee} = 10.6$ GeV
$< 1.3 \times 10^{-7}$	90	AUBERT	04J	BABR 91.5 fb ⁻¹ $E_{cm}^{ee} = 10.6$ GeV
$< 2.0 \times 10^{-7}$	90	YUSA	04	BELL 87.1 fb ⁻¹ $E_{cm}^{ee} = 10.6$ GeV
$< 1.5 \times 10^{-6}$	90	BLISS	98	CLEO $E_{cm}^{ee} = 10.6$ GeV
$< 0.35 \times 10^{-5}$	90	¹ BARTELT	94	CLEO Repl. by BLISS 98
$< 1.8 \times 10^{-5}$	90	ALBRECHT	92K	ARG $E_{cm}^{ee} = 10$ GeV
$< 1.6 \times 10^{-5}$	90	BOWCOCK	90	CLEO $E_{cm}^{ee} = 10.4-10.9$

¹ BARTELT 94 assume phase space decays.

$\Gamma(\mu^- e^+ e^-)/\Gamma_{total}$ Γ_{211}/Γ

Test of lepton family number conservation.

VALUE	CL%	DOCUMENT ID	TECN	COMMENT
$< 1.8 \times 10^{-8}$	90	HAYASAKA	10	BELL 782 fb ⁻¹ $E_{cm}^{ee} = 10.6$ GeV
• • • We do not use the following data for averages, fits, limits, etc. • • •				
$< 2.2 \times 10^{-8}$	90	LEES	10A	BABR 468 fb ⁻¹ $E_{cm}^{ee} = 10.6$ GeV
$< 2.7 \times 10^{-8}$	90	MIYAZAKI	08	BELL 535 fb ⁻¹ $E_{cm}^{ee} = 10.6$ GeV
$< 8.0 \times 10^{-8}$	90	AUBERT	07BK	BABR 376 fb ⁻¹ $E_{cm}^{ee} = 10.6$ GeV
$< 2.7 \times 10^{-7}$	90	AUBERT	04J	BABR 91.5 fb ⁻¹ $E_{cm}^{ee} = 10.6$ GeV
$< 1.9 \times 10^{-7}$	90	YUSA	04	BELL 87.1 fb ⁻¹ $E_{cm}^{ee} = 10.6$ GeV
$< 1.7 \times 10^{-6}$	90	BLISS	98	CLEO $E_{cm}^{ee} = 10.6$ GeV
$< 0.34 \times 10^{-5}$	90	¹ BARTELT	94	CLEO Repl. by BLISS 98
$< 1.4 \times 10^{-5}$	90	ALBRECHT	92K	ARG $E_{cm}^{ee} = 10$ GeV
$< 2.7 \times 10^{-5}$	90	BOWCOCK	90	CLEO $E_{cm}^{ee} = 10.4-10.9$
$< 44 \times 10^{-5}$	90	HAYES	82	MRK2 $E_{cm}^{ee} = 3.8-6.8$ GeV

¹ BARTELT 94 assume phase space decays.

$\Gamma(\mu^+ e^- e^-)/\Gamma_{total}$ Γ_{212}/Γ

Test of lepton family number conservation.

VALUE	CL%	DOCUMENT ID	TECN	COMMENT
$< 1.5 \times 10^{-8}$	90	HAYASAKA	10	BELL 782 fb ⁻¹ $E_{cm}^{ee} = 10.6$ GeV
• • • We do not use the following data for averages, fits, limits, etc. • • •				
$< 1.8 \times 10^{-8}$	90	LEES	10A	BABR 468 fb ⁻¹ $E_{cm}^{ee} = 10.6$ GeV
$< 2.0 \times 10^{-8}$	90	MIYAZAKI	08	BELL 535 fb ⁻¹ $E_{cm}^{ee} = 10.6$ GeV
$< 5.8 \times 10^{-8}$	90	AUBERT	07BK	BABR 376 fb ⁻¹ $E_{cm}^{ee} = 10.6$ GeV
$< 1.1 \times 10^{-7}$	90	AUBERT	04J	BABR 91.5 fb ⁻¹ $E_{cm}^{ee} = 10.6$ GeV
$< 2.0 \times 10^{-7}$	90	YUSA	04	BELL 87.1 fb ⁻¹ $E_{cm}^{ee} = 10.6$ GeV
$< 1.5 \times 10^{-6}$	90	BLISS	98	CLEO $E_{cm}^{ee} = 10.6$ GeV
$< 0.34 \times 10^{-5}$	90	¹ BARTELT	94	CLEO Repl. by BLISS 98
$< 1.4 \times 10^{-5}$	90	ALBRECHT	92K	ARG $E_{cm}^{ee} = 10$ GeV
$< 1.6 \times 10^{-5}$	90	BOWCOCK	90	CLEO $E_{cm}^{ee} = 10.4-10.9$

¹ BARTELT 94 assume phase space decays.

$\Gamma(\mu^- \mu^+ \mu^-)/\Gamma_{total}$ Γ_{213}/Γ

Test of lepton family number conservation.

VALUE	CL%	DOCUMENT ID	TECN	COMMENT
$< 2.1 \times 10^{-8}$	90	HAYASAKA	10	BELL 782 fb ⁻¹ $E_{cm}^{ee} = 10.6$ GeV
• • • We do not use the following data for averages, fits, limits, etc. • • •				
$< 3.8 \times 10^{-7}$	90	AAD	16BA	ATLS 20.3 fb ⁻¹ $\sqrt{s} = 8$ TeV
$< 4.6 \times 10^{-8}$	90	AAIJ	15Al	LHCb 3.0 fb ⁻¹ $\sqrt{s} = 7, 8$ TeV
$< 8.0 \times 10^{-8}$	90	¹ AAIJ	13AH	LHCb 1.0 fb ⁻¹ $\sqrt{s} = 7$ TeV
$< 3.3 \times 10^{-8}$	90	LEES	10A	BABR 468 fb ⁻¹ $E_{cm}^{ee} = 10.6$ GeV
$< 3.2 \times 10^{-8}$	90	MIYAZAKI	08	BELL 535 fb ⁻¹ $E_{cm}^{ee} = 10.6$ GeV
$< 5.3 \times 10^{-8}$	90	AUBERT	07BK	BABR 376 fb ⁻¹ $E_{cm}^{ee} = 10.6$ GeV
$< 1.9 \times 10^{-7}$	90	AUBERT	04J	BABR 91.5 fb ⁻¹ $E_{cm}^{ee} = 10.6$ GeV
$< 2.0 \times 10^{-7}$	90	YUSA	04	BELL 87.1 fb ⁻¹ $E_{cm}^{ee} = 10.6$ GeV
$< 1.9 \times 10^{-6}$	90	BLISS	98	CLEO $E_{cm}^{ee} = 10.6$ GeV
$< 0.43 \times 10^{-5}$	90	² BARTELT	94	CLEO Repl. by BLISS 98
$< 1.9 \times 10^{-5}$	90	ALBRECHT	92K	ARG $E_{cm}^{ee} = 10$ GeV
$< 1.7 \times 10^{-5}$	90	BOWCOCK	90	CLEO $E_{cm}^{ee} = 10.4-10.9$
$< 49 \times 10^{-5}$	90	HAYES	82	MRK2 $E_{cm}^{ee} = 3.8-6.8$ GeV

¹ Repl. by AAJJ 15Al.
² BARTELT 94 assume phase space decays.

$\Gamma(e^- \pi^+ \pi^-)/\Gamma_{total}$ Γ_{214}/Γ

Test of lepton family number conservation.

VALUE	CL%	DOCUMENT ID	TECN	COMMENT
$< 2.3 \times 10^{-8}$	90	MIYAZAKI	13	BELL 854 fb ⁻¹ $E_{cm}^{ee} = 10.6$ GeV

• • • We do not use the following data for averages, fits, limits, etc. • • •

Table with 5 columns: VALUE, CL%, DOCUMENT ID, TECN, COMMENT. Rows include MIYAZAKI, YUSA, AUBERT,BE, BLISS, BARTELT, ALBRECHT, BOWCOCK with various decay rates and references.

¹ BARTELT 94 assume phase space decays.

$\Gamma(e^+ \pi^- \pi^-)/\Gamma_{total}$ Test of lepton number conservation. Γ_{215}/Γ

Table with 5 columns: VALUE, CL%, DOCUMENT ID, TECN, COMMENT. Rows include MIYAZAKI, YUSA, AUBERT,BE, BLISS, BARTELT, ALBRECHT, BOWCOCK.

¹ BARTELT 94 assume phase space decays.

$\Gamma(\mu^- \pi^+ \pi^-)/\Gamma_{total}$ Test of lepton family number conservation. Γ_{216}/Γ

Table with 5 columns: VALUE, CL%, DOCUMENT ID, TECN, COMMENT. Rows include MIYAZAKI, YUSA, AUBERT,BE, BLISS, BARTELT, ALBRECHT, BOWCOCK.

¹ BARTELT 94 assume phase space decays.

$\Gamma(\mu^+ \pi^- \pi^-)/\Gamma_{total}$ Test of lepton number conservation. Γ_{217}/Γ

Table with 5 columns: VALUE, CL%, DOCUMENT ID, TECN, COMMENT. Rows include MIYAZAKI, YUSA, AUBERT,BE, BLISS, BARTELT, ALBRECHT, BOWCOCK.

¹ BARTELT 94 assume phase space decays.

$\Gamma(e^- \pi^+ K^-)/\Gamma_{total}$ Test of lepton family number conservation. Γ_{218}/Γ

Table with 5 columns: VALUE, CL%, DOCUMENT ID, TECN, COMMENT. Rows include MIYAZAKI, YUSA, AUBERT,BE, BLISS, BARTELT, ALBRECHT, BOWCOCK.

¹ BARTELT 94 assume phase space decays.

$\Gamma(e^- \pi^- K^+)/\Gamma_{total}$ Test of lepton family number conservation. Γ_{219}/Γ

Table with 5 columns: VALUE, CL%, DOCUMENT ID, TECN, COMMENT. Rows include MIYAZAKI, YUSA, AUBERT,BE, BLISS, BARTELT, BOWCOCK.

¹ BARTELT 94 assume phase space decays.

$\Gamma(e^+ \pi^- K^-)/\Gamma_{total}$ Test of lepton number conservation. Γ_{220}/Γ

Table with 5 columns: VALUE, CL%, DOCUMENT ID, TECN, COMMENT. Rows include MIYAZAKI, YUSA, AUBERT,BE, BLISS, BARTELT, ALBRECHT, BOWCOCK.

¹ BARTELT 94 assume phase space decays.

$\Gamma(e^- K_S^0 K_S^0)/\Gamma_{total}$ Test of lepton family number conservation. Γ_{221}/Γ

Table with 5 columns: VALUE, CL%, DOCUMENT ID, TECN, COMMENT. Rows include MIYAZAKI, YUSA, CHEN.

$\Gamma(e^- K^+ K^-)/\Gamma_{total}$ Test of lepton family number conservation. Γ_{222}/Γ

Table with 5 columns: VALUE, CL%, DOCUMENT ID, TECN, COMMENT. Rows include MIYAZAKI, YUSA, AUBERT,BE, BLISS.

$\Gamma(e^+ K^- K^-)/\Gamma_{total}$ Test of lepton number conservation. Γ_{223}/Γ

Table with 5 columns: VALUE, CL%, DOCUMENT ID, TECN, COMMENT. Rows include MIYAZAKI, YUSA, AUBERT,BE, BLISS.

$\Gamma(\mu^- \pi^+ K^-)/\Gamma_{total}$ Test of lepton family number conservation. Γ_{224}/Γ

Table with 5 columns: VALUE, CL%, DOCUMENT ID, TECN, COMMENT. Rows include MIYAZAKI, YUSA, AUBERT,BE, BLISS, BARTELT, ALBRECHT, BOWCOCK.

¹ BARTELT 94 assume phase space decays.

$\Gamma(\mu^- \pi^- K^+)/\Gamma_{total}$ Test of lepton family number conservation. Γ_{225}/Γ

Table with 5 columns: VALUE, CL%, DOCUMENT ID, TECN, COMMENT. Rows include MIYAZAKI, YUSA, AUBERT,BE, BLISS, BARTELT, BOWCOCK.

¹ BARTELT 94 assume phase space decays.

$\Gamma(\mu^+ \pi^- K^-)/\Gamma_{total}$ Test of lepton number conservation. Γ_{226}/Γ

Table with 5 columns: VALUE, CL%, DOCUMENT ID, TECN, COMMENT. Rows include MIYAZAKI, YUSA, AUBERT,BE, BLISS, BARTELT, ALBRECHT, BOWCOCK.

¹ BARTELT 94 assume phase space decays.

Lepton Particle Listings

T

$\Gamma(\mu^- K_S^0 K_S^0)/\Gamma_{total}$ Γ_{227}/Γ

VALUE	CL%	DOCUMENT ID	TECN	COMMENT
$<8.0 \times 10^{-8}$	90	MIYAZAKI	10A BELL	$671 \text{ fb}^{-1} E_{cm}^{ee} = 10.6 \text{ GeV}$
••• We do not use the following data for averages, fits, limits, etc. •••				
$<3.4 \times 10^{-6}$	90	CHEN	02c CLEO	$E_{cm}^{ee} = 10.6 \text{ GeV}$

$\Gamma(\mu^- K^+ K^-)/\Gamma_{total}$ Γ_{228}/Γ

Test of lepton family number conservation.

VALUE	CL%	DOCUMENT ID	TECN	COMMENT
$<4.4 \times 10^{-8}$	90	MIYAZAKI	13 BELL	$854 \text{ fb}^{-1} E_{cm}^{ee} = 10.6 \text{ GeV}$
••• We do not use the following data for averages, fits, limits, etc. •••				
$<6.8 \times 10^{-8}$	90	MIYAZAKI	10 BELL	Repl. by MIYAZAKI 13
$<8.0 \times 10^{-7}$	90	YUSA	06 BELL	$158 \text{ fb}^{-1} E_{cm}^{ee} = 10.6 \text{ GeV}$
$<2.5 \times 10^{-7}$	90	AUBERT,BE	05D BABR	$221 \text{ fb}^{-1}, E_{cm}^{ee} = 10.6 \text{ GeV}$
$<15 \times 10^{-6}$	90	BLISS	98 CLEO	$E_{cm}^{ee} = 10.6 \text{ GeV}$

$\Gamma(\mu^+ K^- K^-)/\Gamma_{total}$ Γ_{229}/Γ

Test of lepton number conservation.

VALUE	CL%	DOCUMENT ID	TECN	COMMENT
$<4.7 \times 10^{-8}$	90	MIYAZAKI	13 BELL	$854 \text{ fb}^{-1} E_{cm}^{ee} = 10.6 \text{ GeV}$
••• We do not use the following data for averages, fits, limits, etc. •••				
$<9.6 \times 10^{-8}$	90	MIYAZAKI	10 BELL	Repl. by MIYAZAKI 13
$<4.4 \times 10^{-7}$	90	YUSA	06 BELL	$158 \text{ fb}^{-1} E_{cm}^{ee} = 10.6 \text{ GeV}$
$<4.8 \times 10^{-7}$	90	AUBERT,BE	05D BABR	$221 \text{ fb}^{-1}, E_{cm}^{ee} = 10.6 \text{ GeV}$
$<6.0 \times 10^{-6}$	90	BLISS	98 CLEO	$E_{cm}^{ee} = 10.6 \text{ GeV}$

$\Gamma(e^- \pi^0 \pi^0)/\Gamma_{total}$ Γ_{230}/Γ

Test of lepton family number conservation.

VALUE	CL%	DOCUMENT ID	TECN	COMMENT
$<6.5 \times 10^{-6}$	90	BONVICINI	97 CLEO	$E_{cm}^{ee} = 10.6 \text{ GeV}$

$\Gamma(\mu^- \pi^0 \pi^0)/\Gamma_{total}$ Γ_{231}/Γ

Test of lepton family number conservation.

VALUE	CL%	DOCUMENT ID	TECN	COMMENT
$<14 \times 10^{-6}$	90	BONVICINI	97 CLEO	$E_{cm}^{ee} = 10.6 \text{ GeV}$

$\Gamma(e^- \eta \eta)/\Gamma_{total}$ Γ_{232}/Γ

Test of lepton family number conservation.

VALUE	CL%	DOCUMENT ID	TECN	COMMENT
$<35 \times 10^{-6}$	90	BONVICINI	97 CLEO	$E_{cm}^{ee} = 10.6 \text{ GeV}$

$\Gamma(\mu^- \eta \eta)/\Gamma_{total}$ Γ_{233}/Γ

Test of lepton family number conservation.

VALUE	CL%	DOCUMENT ID	TECN	COMMENT
$<60 \times 10^{-6}$	90	BONVICINI	97 CLEO	$E_{cm}^{ee} = 10.6 \text{ GeV}$

$\Gamma(e^- \pi^0 \eta)/\Gamma_{total}$ Γ_{234}/Γ

Test of lepton family number conservation.

VALUE	CL%	DOCUMENT ID	TECN	COMMENT
$<24 \times 10^{-6}$	90	BONVICINI	97 CLEO	$E_{cm}^{ee} = 10.6 \text{ GeV}$

$\Gamma(\mu^- \pi^0 \eta)/\Gamma_{total}$ Γ_{235}/Γ

Test of lepton family number conservation.

VALUE	CL%	DOCUMENT ID	TECN	COMMENT
$<22 \times 10^{-6}$	90	BONVICINI	97 CLEO	$E_{cm}^{ee} = 10.6 \text{ GeV}$

$\Gamma(\rho \mu^- \mu^-)/\Gamma_{total}$ Γ_{236}/Γ

VALUE	CL%	DOCUMENT ID	TECN	COMMENT
$<4.4 \times 10^{-7}$	90	AAIJ	13AH LHCB	$1.0 \text{ fb}^{-1}, \sqrt{s} = 7 \text{ TeV}$

$\Gamma(\bar{\rho} \mu^+ \mu^-)/\Gamma_{total}$ Γ_{237}/Γ

VALUE	CL%	DOCUMENT ID	TECN	COMMENT
$<3.3 \times 10^{-7}$	90	AAIJ	13AH LHCB	$1.0 \text{ fb}^{-1}, \sqrt{s} = 7 \text{ TeV}$

$\Gamma(\bar{\rho} \gamma)/\Gamma_{total}$ Γ_{238}/Γ

Test of lepton number and baryon number conservation.

VALUE	CL%	DOCUMENT ID	TECN	COMMENT
$<3.5 \times 10^{-6}$	90	GODANG	99 CLEO	$E_{cm}^{ee} = 10.6 \text{ GeV}$
••• We do not use the following data for averages, fits, limits, etc. •••				
$<29 \times 10^{-5}$	90	ALBRECHT	92k ARG	$E_{cm}^{ee} = 10 \text{ GeV}$

$\Gamma(\bar{\rho} \pi^0)/\Gamma_{total}$ Γ_{239}/Γ

Test of lepton number and baryon number conservation.

VALUE	CL%	DOCUMENT ID	TECN	COMMENT
$<15 \times 10^{-6}$	90	GODANG	99 CLEO	$E_{cm}^{ee} = 10.6 \text{ GeV}$
••• We do not use the following data for averages, fits, limits, etc. •••				
$<66 \times 10^{-5}$	90	ALBRECHT	92k ARG	$E_{cm}^{ee} = 10 \text{ GeV}$

$\Gamma(\bar{\rho} 2\pi^0)/\Gamma_{total}$ Γ_{240}/Γ

Test of lepton number and baryon number conservation.

VALUE	CL%	DOCUMENT ID	TECN	COMMENT
$<33 \times 10^{-6}$	90	GODANG	99 CLEO	$E_{cm}^{ee} = 10.6 \text{ GeV}$

$\Gamma(\bar{\rho} \eta)/\Gamma_{total}$ Γ_{241}/Γ

Test of lepton number and baryon number conservation.

VALUE	CL%	DOCUMENT ID	TECN	COMMENT
$<8.9 \times 10^{-6}$	90	GODANG	99 CLEO	$E_{cm}^{ee} = 10.6 \text{ GeV}$
••• We do not use the following data for averages, fits, limits, etc. •••				
$<130 \times 10^{-5}$	90	ALBRECHT	92k ARG	$E_{cm}^{ee} = 10 \text{ GeV}$

$\Gamma(\bar{\rho} \pi^0 \eta)/\Gamma_{total}$ Γ_{242}/Γ

Test of lepton number and baryon number conservation.

VALUE	CL%	DOCUMENT ID	TECN	COMMENT
$<27 \times 10^{-6}$	90	GODANG	99 CLEO	$E_{cm}^{ee} = 10.6 \text{ GeV}$

$\Gamma(\Lambda \pi^-)/\Gamma_{total}$ Γ_{243}/Γ

Test of lepton number and baryon number conservation.

VALUE	CL%	DOCUMENT ID	TECN	COMMENT
$<0.72 \times 10^{-7}$	90	MIYAZAKI	06 BELL	$154 \text{ fb}^{-1}, E_{cm}^{ee} = 10.6 \text{ GeV}$

$\Gamma(\bar{\Lambda} \pi^-)/\Gamma_{total}$ Γ_{244}/Γ

Test of lepton number and baryon number conservation.

VALUE	CL%	DOCUMENT ID	TECN	COMMENT
$<1.4 \times 10^{-7}$	90	MIYAZAKI	06 BELL	$154 \text{ fb}^{-1}, E_{cm}^{ee} = 10.6 \text{ GeV}$

$\Gamma(e^- \text{light boson})/\Gamma(e^- \bar{\nu}_e \nu_\tau)$ Γ_{245}/Γ_5

Test of lepton family number conservation.

VALUE	CL%	DOCUMENT ID	TECN	COMMENT
<0.015	95	¹ ALBRECHT	95G ARG	$E_{cm}^{ee} = 9.4\text{--}10.6 \text{ GeV}$
••• We do not use the following data for averages, fits, limits, etc. •••				
<0.018	95	² ALBRECHT	90E ARG	$E_{cm}^{ee} = 9.4\text{--}10.6 \text{ GeV}$
<0.040	95	³ BALTRUSAITIS...85	MRK3	$E_{cm}^{ee} = 3.77 \text{ GeV}$

¹ ALBRECHT 95G limit holds for bosons with mass $< 0.4 \text{ GeV}$. The limit rises to 0.036 for a mass of 1.0 GeV, then falls to 0.006 at the upper mass limit of 1.6 GeV.
² ALBRECHT 90E limit applies for spinless boson with mass $< 100 \text{ MeV}$, and rises to 0.050 for mass = 500 MeV.
³ BALTRUSAITIS 85 limit applies for spinless boson with mass $< 100 \text{ MeV}$.

$\Gamma(\mu^- \text{light boson})/\Gamma(e^- \bar{\nu}_e \nu_\tau)$ Γ_{246}/Γ_5

Test of lepton family number conservation.

VALUE	CL%	DOCUMENT ID	TECN	COMMENT
<0.026	95	¹ ALBRECHT	95G ARG	$E_{cm}^{ee} = 9.4\text{--}10.6 \text{ GeV}$
••• We do not use the following data for averages, fits, limits, etc. •••				
<0.033	95	² ALBRECHT	90E ARG	$E_{cm}^{ee} = 9.4\text{--}10.6 \text{ GeV}$
<0.125	95	³ BALTRUSAITIS...85	MRK3	$E_{cm}^{ee} = 3.77 \text{ GeV}$

¹ ALBRECHT 95G limit holds for bosons with mass $< 1.3 \text{ GeV}$. The limit rises to 0.034 for a mass of 1.4 GeV, then falls to 0.003 at the upper mass limit of 1.6 GeV.
² ALBRECHT 90E limit applies for spinless boson with mass $< 100 \text{ MeV}$, and rises to 0.071 for mass = 500 MeV.
³ BALTRUSAITIS 85 limit applies for spinless boson with mass $< 100 \text{ MeV}$.

τ -DECAY PARAMETERS

See the related review(s):

[τ-Lepton Decay Parameters](#)

$\rho(e \text{ or } \mu)$ PARAMETER

(V-A) theory predicts $\rho = 0.75$.

VALUE	EVTS	DOCUMENT ID	TECN	COMMENT
0.745 ± 0.008 OUR FIT				
0.749 ± 0.008 OUR AVERAGE				
$0.742 \pm 0.014 \pm 0.006$	81k	HEISTER	01E ALEP	1991–1995 LEP runs
$0.775 \pm 0.023 \pm 0.020$	36k	ABREU	00L DLPH	1992–1995 runs
$0.781 \pm 0.028 \pm 0.018$	46k	ACKERSTAFF	99D OPAL	1990–1995 LEP runs
0.762 ± 0.035	54k	ACCIARRI	98R L3	1991–1995 LEP runs
0.731 ± 0.031		¹ ALBRECHT	98 ARG	$E_{cm}^{ee} = 9.5\text{--}10.6 \text{ GeV}$
$0.72 \pm 0.09 \pm 0.03$		² ABE	97O SLD	1993–1995 SLC runs
$0.747 \pm 0.010 \pm 0.006$	55k	ALEXANDER	97F CLEO	$E_{cm}^{ee} = 10.6 \text{ GeV}$
$0.79 \pm 0.10 \pm 0.10$	3732	FORD	87B MAC	$E_{cm}^{ee} = 29 \text{ GeV}$
$0.71 \pm 0.09 \pm 0.03$	1426	BEHRENDTS	85 CLEO	$e^+ e^-$ near $\Upsilon(4S)$
••• We do not use the following data for averages, fits, limits, etc. •••				
$0.735 \pm 0.013 \pm 0.008$	31k	AMMAR	97B CLEO	Repl. by ALEXANDER 97F
$0.794 \pm 0.039 \pm 0.031$	18k	ACCIARRI	96H L3	Repl. by ACCIARRI 98R
$0.732 \pm 0.034 \pm 0.020$	8.2k	³ ALBRECHT	95 ARG	$E_{cm}^{ee} = 9.5\text{--}10.6 \text{ GeV}$
0.738 ± 0.038		⁴ ALBRECHT	95C ARG	Repl. by ALBRECHT 98
$0.751 \pm 0.039 \pm 0.022$		BUSKULIC	95D ALEP	Repl. by HEISTER 01E
$0.742 \pm 0.035 \pm 0.020$	8000	ALBRECHT	90E ARG	$E_{cm}^{ee} = 9.4\text{--}10.6 \text{ GeV}$

¹ Combined fit to ARGUS tau decay parameter measurements in ALBRECHT 98, ALBRECHT 95c, ALBRECHT 93g, and ALBRECHT 94e. ALBRECHT 98 use tau pair events of the type $\tau^- \tau^+ \rightarrow (\ell^- \bar{\nu}_\ell \nu_\tau)(\pi^+ \pi^0 \bar{\nu}_\tau)$, and their charged conjugates.
² ABE 97o assume $\eta = 0$ in their fit. Letting η vary in the fit gives a ρ value of $0.69 \pm 0.13 \pm 0.05$.
³ Value is from a simultaneous fit for the ρ and η decay parameters to the lepton energy spectrum. Not independent of ALBRECHT 90E $\rho(e \text{ or } \mu)$ value which assumes $\eta = 0$. Result is strongly correlated with ALBRECHT 95c.
⁴ Combined fit to ARGUS tau decay parameter measurements in ALBRECHT 95c, ALBRECHT 93g, and ALBRECHT 94e.

ρ(e) PARAMETER

(V-A) theory predicts ρ = 0.75. Table with columns: VALUE, EVTS, DOCUMENT ID, TECN, COMMENT. Includes sub-sections: 0.747±0.010 OUR FIT, 0.744±0.010 OUR AVERAGE, and a list of experimental data points.

••• We do not use the following data for averages, fits, limits, etc. •••
1 ALBRECHT 98 use tau pair events of the type τ-τ+ → (ℓ-νℓντ)(π+π0ντ), and their charged conjugates.
2 ALBRECHT 95 use tau pair events of the type τ-τ+ → (ℓ-νℓντ)(h+h-h+π0ντ) and their charged conjugates.
3 ALBRECHT 93G use tau pair events of the type τ-τ+ → (μ-νμντ)(e+νeντ) and their charged conjugates.

ρ(μ) PARAMETER

(V-A) theory predicts ρ = 0.75. Table with columns: VALUE, EVTS, DOCUMENT ID, TECN, COMMENT. Includes sub-sections: 0.763±0.020 OUR FIT, 0.770±0.022 OUR AVERAGE, and a list of experimental data points.

••• We do not use the following data for averages, fits, limits, etc. •••

ξ(e or μ) PARAMETER

(V-A) theory predicts ξ = 1. Table with columns: VALUE, EVTS, DOCUMENT ID, TECN, COMMENT. Includes sub-sections: 0.985±0.030 OUR FIT, 0.981±0.031 OUR AVERAGE, and a list of experimental data points.

1 Combined fit to ARGUS tau decay parameter measurements in ALBRECHT 98, ALBRECHT 95C, ALBRECHT 93G, and ALBRECHT 94E. ALBRECHT 98 use tau pair events of the type τ-τ+ → (ℓ-νℓντ)(π+π0ντ), and their charged conjugates.
2 ABE 97o assume η = 0 in their fit. Letting η vary in the fit gives a ξ value of 1.02 ± 0.36 ± 0.05.
3 Combined fit to ARGUS tau decay parameter measurements in ALBRECHT 95C, ALBRECHT 93G, and ALBRECHT 94E. ALBRECHT 95C uses events of the type τ-τ+ → (ℓ-νℓντ)(h+h-h+π0ντ) and their charged conjugates.
4 ALBRECHT 93G measurement determines |ξ| for the case ξ(e) = ξ(μ), but the authors point out that other LEP experiments determine the sign to be positive.

ξ(e) PARAMETER

(V-A) theory predicts ξ = 1. Table with columns: VALUE, EVTS, DOCUMENT ID, TECN, COMMENT. Includes sub-sections: 0.994±0.040 OUR FIT, 1.00 ±0.04 OUR AVERAGE, and a list of experimental data points.

••• We do not use the following data for averages, fits, limits, etc. •••
1 ALBRECHT 98 use tau pair events of the type τ-τ+ → (ℓ-νℓντ)(π+π0ντ), and their charged conjugates.
2 ALBRECHT 95 use tau pair events of the type τ-τ+ → (ℓ-νℓντ)(h+h-h+π0ντ) and their charged conjugates.
3 ALBRECHT 93G use tau pair events of the type τ-τ+ → (μ-νμντ)(e+νeντ) and their charged conjugates.

ξ(μ) PARAMETER

(V-A) theory predicts ξ = 1. Table with columns: VALUE, EVTS, DOCUMENT ID, TECN, COMMENT. Includes sub-sections: 1.030±0.059 OUR FIT, 1.06 ±0.06 OUR AVERAGE, and a list of experimental data points.

••• We do not use the following data for averages, fits, limits, etc. •••

η(e or μ) PARAMETER

(V-A) theory predicts η = 0. Table with columns: VALUE, EVTS, DOCUMENT ID, TECN, COMMENT. Includes sub-sections: 0.013±0.020 OUR FIT, 0.015±0.021 OUR AVERAGE, and a list of experimental data points.

••• We do not use the following data for averages, fits, limits, etc. •••

η(μ) PARAMETER

(V-A) theory predicts η = 0. Table with columns: VALUE, EVTS, DOCUMENT ID, TECN, COMMENT. Includes sub-sections: 0.094±0.073 OUR FIT, 0.17 ±0.15 OUR AVERAGE, and a list of experimental data points.

(δξ)(e or μ) PARAMETER

(V-A) theory predicts (δξ) = 0.75. Table with columns: VALUE, EVTS, DOCUMENT ID, TECN, COMMENT. Includes sub-sections: 0.746±0.021 OUR FIT, 0.744±0.022 OUR AVERAGE, and a list of experimental data points.

Downloaded from https://academic.oup.com/ptep/article/2020/8/083C01/5891211 by guest on 20 August 2020

Lepton Particle Listings

τ

¹ Combined fit to ARGUS tau decay parameter measurements in ALBRECHT 98, ALBRECHT 95c, ALBRECHT 93g, and ALBRECHT 94e. ALBRECHT 98 use tau pair events of the type $\tau^- \tau^+ \rightarrow (\ell^- \bar{\nu}_\ell \nu_\tau)(\pi^+ \pi^0 \bar{\nu}_\tau)$, and their charged conjugates.

² ABE 97o assume $\eta = 0$ in their fit. Letting η vary in the fit gives a $(\delta\xi)$ value of $0.87 \pm 0.27 \pm 0.04$.

³ Combined fit to ARGUS tau decay parameter measurements in ALBRECHT 95c, ALBRECHT 93g, and ALBRECHT 94e. ALBRECHT 95c uses events of the type $\tau^- \tau^+ \rightarrow (\ell^- \bar{\nu}_\ell \nu_\tau) (h^+ h^- h^+ \bar{\nu}_\tau)$ and their charged conjugates.

$(\delta\xi)(e)$ PARAMETER

$(V-A)$ theory predicts $(\delta\xi) = 0.75$.

VALUE	EVTS	DOCUMENT ID	TECN	COMMENT
0.734 ± 0.028 OUR FIT				
0.731 ± 0.029 OUR AVERAGE				
0.778 ± 0.066 ± 0.024	44k	HEISTER 01E	ALEP	1991–1995 LEP runs
0.85 ± 0.12 ± 0.04	17k	ABREU 00L	DLPH	1992–1995 runs
0.72 ± 0.31 ± 0.14	25k	ACKERSTAFF 99D	OPAL	1990–1995 LEP runs
0.56 ± 0.14 ± 0.06		¹ ALBRECHT 98	ARG	$E_{cm}^{ee} = 9.5\text{--}10.6$ GeV
0.85 ± 0.43 ± 0.08		ABE 97o	SLD	1993–1995 SLC runs
0.720 ± 0.032 ± 0.010	34k	ALEXANDER 97F	CLEO	$E_{cm}^{ee} = 10.6$ GeV

• • • We do not use the following data for averages, fits, limits, etc. • • •

1.11 ± 0.17 ± 0.07 BUSKULIC 95D ALEP Repl. by HEISTER 01E

¹ ALBRECHT 98 use tau pair events of the type $\tau^- \tau^+ \rightarrow (\ell^- \bar{\nu}_\ell \nu_\tau)(\pi^+ \pi^0 \bar{\nu}_\tau)$, and their charged conjugates.

$(\delta\xi)(\mu)$ PARAMETER

$(V-A)$ theory predicts $(\delta\xi) = 0.75$.

VALUE	EVTS	DOCUMENT ID	TECN	COMMENT
0.778 ± 0.037 OUR FIT				
0.79 ± 0.04 OUR AVERAGE				
0.786 ± 0.066 ± 0.028	46k	HEISTER 01E	ALEP	1991–1995 LEP runs
0.86 ± 0.13 ± 0.04	22k	ABREU 00L	DLPH	1992–1995 runs
0.63 ± 0.23 ± 0.05	27k	ACKERSTAFF 99D	OPAL	1990–1995 LEP runs
0.73 ± 0.18 ± 0.10		¹ ALBRECHT 98	ARG	$E_{cm}^{ee} = 9.5\text{--}10.6$ GeV
0.82 ± 0.32 ± 0.07		ABE 97o	SLD	1993–1995 SLC runs
0.786 ± 0.041 ± 0.032	22k	ALEXANDER 97F	CLEO	$E_{cm}^{ee} = 10.6$ GeV

• • • We do not use the following data for averages, fits, limits, etc. • • •

0.71 ± 0.14 ± 0.06 BUSKULIC 95D ALEP Repl. by HEISTER 01E

¹ ALBRECHT 98 use tau pair events of the type $\tau^- \tau^+ \rightarrow (\ell^- \bar{\nu}_\ell \nu_\tau)(\pi^+ \pi^0 \bar{\nu}_\tau)$, and their charged conjugates.

$\xi(\pi)$ PARAMETER

$(V-A)$ theory predicts $\xi(\pi) = 1$.

VALUE	EVTS	DOCUMENT ID	TECN	COMMENT
0.993 ± 0.022 OUR FIT				
0.994 ± 0.023 OUR AVERAGE				
0.994 ± 0.020 ± 0.014	27k	HEISTER 01E	ALEP	1991–1995 LEP runs
0.81 ± 0.17 ± 0.02		ABE 97o	SLD	1993–1995 SLC runs
1.03 ± 0.06 ± 0.04	2.0k	COAN 97	CLEO	$E_{cm}^{ee} = 10.6$ GeV

• • • We do not use the following data for averages, fits, limits, etc. • • •

0.987 ± 0.057 ± 0.027 BUSKULIC 95D ALEP Repl. by HEISTER 01E

0.95 ± 0.11 ± 0.05 ¹ BUSKULIC 94D ALEP 1990+1991 LEP run

¹ Superseded by BUSKULIC 95D.

$\xi(\rho)$ PARAMETER

$(V-A)$ theory predicts $\xi(\rho) = 1$.

VALUE	EVTS	DOCUMENT ID	TECN	COMMENT
0.994 ± 0.008 OUR FIT				
0.994 ± 0.009 OUR AVERAGE				
0.987 ± 0.012 ± 0.011	59k	HEISTER 01E	ALEP	1991–1995 LEP runs
0.99 ± 0.12 ± 0.04		ABE 97o	SLD	1993–1995 SLC runs
0.995 ± 0.010 ± 0.003	66k	ALEXANDER 97F	CLEO	$E_{cm}^{ee} = 10.6$ GeV
1.022 ± 0.028 ± 0.030	1.7k	¹ ALBRECHT 94E	ARG	$E_{cm}^{ee} = 9.4\text{--}10.6$ GeV

• • • We do not use the following data for averages, fits, limits, etc. • • •

1.045 ± 0.058 ± 0.032 BUSKULIC 95D ALEP Repl. by HEISTER 01E

1.03 ± 0.11 ± 0.05 ² BUSKULIC 94D ALEP 1990+1991 LEP run

¹ ALBRECHT 94e measure the square of this quantity and use the sign determined by ALBRECHT 90i to obtain the quoted result.

² Superseded by BUSKULIC 95D.

$\xi(a_1)$ PARAMETER

$(V-A)$ theory predicts $\xi(a_1) = 1$.

VALUE	EVTS	DOCUMENT ID	TECN	COMMENT
1.001 ± 0.027 OUR FIT				
1.002 ± 0.028 OUR AVERAGE				
1.000 ± 0.016 ± 0.024	35k	¹ HEISTER 01E	ALEP	1991–1995 LEP runs
1.02 ± 0.13 ± 0.03	17.2k	ASNER 00	CLEO	$E_{cm}^{ee} = 10.6$ GeV
1.29 ± 0.26 ± 0.11	7.4k	² ACKERSTAFF 97R	OPAL	1992–1994 LEP runs
0.85 +0.15 -0.17 ± 0.05		ALBRECHT 95c	ARG	$E_{cm}^{ee} = 9.5\text{--}10.6$ GeV
1.25 ± 0.23 +0.15 -0.08 ± 0.08	7.5k	ALBRECHT 93c	ARG	$E_{cm}^{ee} = 9.4\text{--}10.6$ GeV

• • • We do not use the following data for averages, fits, limits, etc. • • •

1.08 +0.46 +0.14 -0.41 -0.25 ± 2.6k ³ AKERS 95P OPAL Repl. by ACKERSTAFF 97R

0.937 ± 0.116 ± 0.064 BUSKULIC 95D ALEP Repl. by HEISTER 01E

¹ HEISTER 01E quote $1.000 \pm 0.016 \pm 0.013 \pm 0.020$ where the errors are statistical, systematic, and an uncertainty due to the final state model. We combine the systematic error and model uncertainty.

² ACKERSTAFF 97R obtain this result with a model independent fit to the hadronic structure functions. Fitting with the model of Kuhn and Santamaria (ZPHY C48, 445 (1990)) gives $0.87 \pm 0.16 \pm 0.04$, and with the model of Isgur *et al.* (PR D39,1357 (1989)) they obtain $1.20 \pm 0.21 \pm 0.14$.

³ AKERS 95P obtain this result with a model independent fit to the hadronic structure functions. Fitting with the model of Kuhn and Santamaria (ZPHY C48, 445 (1990)) gives $0.87 \pm 0.27 +0.05 -0.06 \pm 0.13 -0.14$, and with the model of Isgur *et al.* (PR D39,1357 (1989)) they obtain $1.10 \pm 0.31 +0.13 -0.14$.

$\xi(\text{all hadronic modes})$ PARAMETER

$(V-A)$ theory predicts $\xi = 1$.

VALUE	EVTS	DOCUMENT ID	TECN	COMMENT
0.995 ± 0.007 OUR FIT				
0.997 ± 0.007 OUR AVERAGE				
0.992 ± 0.007 ± 0.008	102k	¹ HEISTER 01E	ALEP	1991–1995 LEP runs
0.997 ± 0.027 ± 0.011	39k	² ABREU 00L	DLPH	1992–1995 runs
1.02 ± 0.13 ± 0.03	17.2k	³ ASNER 00	CLEO	$E_{cm}^{ee} = 10.6$ GeV
1.032 ± 0.031	37k	⁴ ACCIARRI 98R	L3	1991–1995 LEP runs
0.93 ± 0.10 ± 0.04		ABE 97o	SLD	1993–1995 SLC runs
1.29 ± 0.26 ± 0.11	7.4k	⁵ ACKERSTAFF 97R	OPAL	1992–1994 LEP runs
0.995 ± 0.010 ± 0.003	66k	⁶ ALEXANDER 97F	CLEO	$E_{cm}^{ee} = 10.6$ GeV
1.03 ± 0.06 ± 0.04	2.0k	⁷ COAN 97	CLEO	$E_{cm}^{ee} = 10.6$ GeV
1.017 ± 0.039		⁸ ALBRECHT 95c	ARG	$E_{cm}^{ee} = 9.5\text{--}10.6$ GeV
1.25 ± 0.23 +0.15 -0.08 ± 7.5k		⁹ ALBRECHT 93c	ARG	$E_{cm}^{ee} = 9.4\text{--}10.6$ GeV

• • • We do not use the following data for averages, fits, limits, etc. • • •

0.970 ± 0.053 ± 0.011 14k ¹⁰ ACCIARRI 96H L3 Repl. by ACCIARRI 98R

1.08 +0.46 +0.14 -0.41 -0.25 ± 2.6k ¹¹ AKERS 95P OPAL Repl. by ACKERSTAFF 97R

1.006 ± 0.032 ± 0.019 ¹² BUSKULIC 95D ALEP Repl. by HEISTER 01E

1.022 ± 0.028 ± 0.030 1.7k ¹³ ALBRECHT 94E ARG $E_{cm}^{ee} = 9.4\text{--}10.6$ GeV

0.99 ± 0.07 ± 0.04 ¹⁴ BUSKULIC 94D ALEP 1990+1991 LEP run

1.14 ± 0.34 +0.34 -0.17 ± 3.9k ⁹ ALBRECHT 90i ARG Repl. by ALBRECHT 93c

¹ HEISTER 01E quote $0.992 \pm 0.007 \pm 0.006 \pm 0.005$ where the errors are statistical, systematic, and an uncertainty due to the final state model. We combine the systematic error and model uncertainty. They use $\tau \rightarrow \pi \nu_\tau$, $\tau \rightarrow K \nu_\tau$, $\tau \rightarrow \rho \nu_\tau$, and $\tau \rightarrow a_1 \nu_\tau$ decays.

² ABREU 00L use $\tau^- \rightarrow h^- \geq 0\pi^0 \nu_\tau$ decays.

³ ASNER 00 use $\tau^- \rightarrow \pi^- 2\pi^0 \nu_\tau$ decays.

⁴ ACCIARRI 98R use $\tau \rightarrow \pi \nu_\tau$, $\tau \rightarrow K \nu_\tau$, and $\tau \rightarrow \rho \nu_\tau$ decays.

⁵ ACKERSTAFF 97R use $\tau \rightarrow a_1 \nu_\tau$ decays.

⁶ ALEXANDER 97F use $\tau \rightarrow \rho \nu_\tau$ decays.

⁷ COAN 97 use $h^+ h^-$ energy correlations.

⁸ Combined fit to ARGUS tau decay parameter measurements in ALBRECHT 95c, ALBRECHT 93g, and ALBRECHT 94e.

⁹ Uses $\tau \rightarrow a_1 \nu_\tau$ decays. Replaced by ALBRECHT 95c.

¹⁰ ACCIARRI 96H use $\tau \rightarrow \pi \nu_\tau$, $\tau \rightarrow K \nu_\tau$, and $\tau \rightarrow \rho \nu_\tau$ decays.

¹¹ AKERS 95P use $\tau \rightarrow a_1 \nu_\tau$ decays.

¹² BUSKULIC 95D use $\tau \rightarrow \pi \nu_\tau$, $\tau \rightarrow \rho \nu_\tau$, and $\tau \rightarrow a_1 \nu_\tau$ decays.

¹³ ALBRECHT 94e measure the square of this quantity and use the sign determined by ALBRECHT 90i to obtain the quoted result. Uses $\tau \rightarrow a_1 \nu_\tau$ decays. Replaced by ALBRECHT 95c.

¹⁴ BUSKULIC 94D use $\tau \rightarrow \pi \nu_\tau$ and $\tau \rightarrow \rho \nu_\tau$ decays. Superseded by BUSKULIC 95D.

$\bar{\eta}(\mu)$ PARAMETER

$(V-A)$ theory predicts $\bar{\eta}(\mu) = 0$.

VALUE	EVTS	DOCUMENT ID	TECN	COMMENT
-1.3 ± 1.5 ± 0.8				
	71k	¹ SHIMIZU 18A	BELL	$\tau^- \rightarrow \nu_\tau e^- \bar{\nu}_\mu \gamma$

¹ The measurement procedure fits a distribution affected by $\bar{\eta}(\mu)$, $\xi_\kappa(\mu)$ and $\eta''(\mu)$, floating $\bar{\eta}(\mu)$ and $\xi_\kappa(\mu)$ and fixing $\eta''(\mu) = 0$. The contribution of $\eta''(\mu)$ is suppressed by m_μ/m_τ .

$\xi_\kappa(e)$ PARAMETER

$(V-A)$ theory predicts $\xi_\kappa(e) = 0$.

VALUE	EVTS	DOCUMENT ID	TECN	COMMENT
-0.4 ± 0.8 ± 0.9				
	78k	¹ SHIMIZU 18A	BELL	$\tau^- \rightarrow \nu_\tau e^- \bar{\nu}_e \gamma$

¹ The measurement procedure fits a distribution affected by $\bar{\eta}(e)$, $\xi_\kappa(e)$ and $\eta''(e)$, floating $\bar{\eta}(e)$ and $\xi_\kappa(e)$ and fixing $\eta''(e) = 0$. The contribution of $\eta''(e)$ is suppressed by m_e/m_τ .

$\xi_\kappa(\mu)$ PARAMETER

$(V-A)$ theory predicts $\xi_\kappa(\mu) = 0$.

VALUE	EVTS	DOCUMENT ID	TECN	COMMENT
0.8 ± 0.5 ± 0.3				
	71k	¹ SHIMIZU 18A	BELL	$\tau^- \rightarrow \nu_\tau e^- \bar{\nu}_\mu \gamma$

¹ The measurement procedure fits a distribution affected by $\bar{\eta}(\mu)$, $\xi_\kappa(\mu)$ and $\eta''(\mu)$, floating $\bar{\eta}(\mu)$ and $\xi_\kappa(\mu)$ and fixing $\eta''(\mu) = 0$. The contribution of $\eta''(\mu)$ is suppressed by m_μ/m_τ .

See key on page 999

REFERENCES

JIN 19 PR D100 071101 Y. Jin *et al.* (BELLE Collab.)

LEES 18B PR D98 032010 J.P. Lees *et al.* (BABAR Collab.)

SHIMIZU 18A PTEP 2018 023C01 N. Shimizu *et al.* (BELLE Collab.)

AAD 16BA EPJ C76 232 G.Aad *et al.* (ATLAS Collab.)

AJAI 15AI JHEP 1502 121 R. Ajai *et al.* (LHCb Collab.)

LEES 15G PR D91 051103 J.P. Lees *et al.* (BABAR Collab.)

ABLKIM 14D PR D90 012001 M. Ablikim *et al.* (BESII Collab.)

BELOUS 14 PRL 112 031801 K. Belous *et al.* (BELLE Collab.)

RYU 14 PR D89 072009 S. Ryu *et al.* (BELLE Collab.)

AYU 13AH PL B724 36 R. Ayu *et al.* (LHCb Collab.)

MIYAZAKI 13 PL B719 346 Y. Miyazaki *et al.* (BELLE Collab.)

LEES 12M PR D85 031102 J.P. Lees *et al.* (BABAR Collab.)

Also PR D85 099904 (erratum) J.P. Lees *et al.* (BABAR Collab.)

LEES 12X PR D86 092010 J.P. Lees *et al.* (BABAR Collab.)

LEES 12Y PR D86 092013 J.P. Lees *et al.* (BABAR Collab.)

PDG 12 PR D86 010001 J. Beiringer *et al.* (PDG Collab.)

DEL-AMO-SA... 11E PR D83 032002 P. del Amo Sanchez *et al.* (BABAR Collab.)

MIYAZAKI 11 PL B699 251 Y. Miyazaki *et al.* (BELLE Collab.)

AUBERT 10B PRL 104 021802 B. Aubert *et al.* (BABAR Collab.)

AUBERT 10F PRL 105 051602 B. Aubert *et al.* (BABAR Collab.)

HAYASAKA 10 PL B687 139 K. Hayasaka *et al.* (BELLE Collab.)

LEE 10 PR D81 113007 M.J. Lee *et al.* (BELLE Collab.)

LEES 10A PR D81 111101 J.P. Lees *et al.* (BABAR Collab.)

MIYAZAKI 10 PL B682 355 Y. Miyazaki *et al.* (BELLE Collab.)

MIYAZAKI 10A PL B692 4 Y. Miyazaki *et al.* (BELLE Collab.)

AUBERT 09AK PR D80 092005 B. Aubert *et al.* (BABAR Collab.)

AUBERT 09D PR D79 012004 B. Aubert *et al.* (BABAR Collab.)

AUBERT 09W PRL 103 021801 B. Aubert *et al.* (BABAR Collab.)

GROZIN 09A PAN 72 1203 A.G. Grozin, I.B. Khriplovich, A.S. Rudenko (NOVO Collab.)

INAMI 09 PL B672 309 K. Inami *et al.* (BELLE Collab.)

MIYAZAKI 09 PL B672 317 Y. Miyazaki *et al.* (BELLE Collab.)

AUBERT 08 PR 100 011801 B. Aubert *et al.* (BABAR Collab.)

AUBERT 08AE PR D77 112002 B. Aubert *et al.* (BABAR Collab.)

AUBERT 08K PRL 100 071802 B. Aubert *et al.* (BABAR Collab.)

FUJIKAWA 08 PR D78 072006 M. Fujikawa *et al.* (BELLE Collab.)

HAYASAKA 08 PL B666 16 K. Hayasaka *et al.* (BELLE Collab.)

MIYAZAKI 08 PL B660 154 Y. Miyazaki *et al.* (BELLE Collab.)

NISHIO 08 PL B664 35 Y. Nishio *et al.* (BELLE Collab.)

ANASHIN 07 JETPL 85 347 V.V. Anashin *et al.* (KEDR Collab.)

Also translated from ZETFP 85 429

07AP PR D76 051104 B. Aubert *et al.* (BABAR Collab.)

AUBERT 07BK PRL 99 251803 B. Aubert *et al.* (BABAR Collab.)

AUBERT 07I PRL 98 061803 B. Aubert *et al.* (BABAR Collab.)

BELOUS 07 PRL 99 011801 K. Belous *et al.* (BELLE Collab.)

EIDELMAN 07 MPL A22 159 S. Eidelman, M. Passera (NOVO, PADO Collab.)

EPIFANOV 07 PL B654 65 D. Epifanov *et al.* (BELLE Collab.)

MIYAZAKI 07 PL B648 341 Y. Miyazaki *et al.* (BELLE Collab.)

ABDALLAH 06A EPJ C46 1 J. Abdallah *et al.* (DELPHI Collab.)

AUBERT 06C PRL 96 041801 B. Aubert *et al.* (BABAR Collab.)

AUBERT B PR D73 112003 B. Aubert *et al.* (BABAR Collab.)

INAMI 06 PL B643 309 K. Inami *et al.* (BELLE Collab.)

MIYAZAKI 06 PL B632 51 Y. Miyazaki *et al.* (BELLE Collab.)

MIYAZAKI 06A PL B639 159 Y. Miyazaki *et al.* (BELLE Collab.)

PDG 06 JP G33 1 W.-M. Yao *et al.* (PDG Collab.)

YUSA 06 PL B640 138 Y. Yusa *et al.* (BELLE Collab.)

ARMS 05 PRL 94 241802 K. Arms *et al.* (CLEO Collab.)

AUBERT B 05A PRL 95 041802 B. Aubert *et al.* (BABAR Collab.)

AUBERT B 05F PR D72 012003 B. Aubert *et al.* (BABAR Collab.)

AUBERT B 05W PR D72 072001 B. Aubert *et al.* (BABAR Collab.)

AUBERT BE 05D PRL 95 191801 B. Aubert *et al.* (BABAR Collab.)

ENARI 05 PL B622 218 Y. Enari *et al.* (BE Collab.)

HAYASAKA 05 PL B613 20 K. Hayasaka *et al.* (BELLE Collab.)

SCHAEL 05C PRPL 421 191 S. Schael *et al.* (ALEPH Collab.)

ABBIENDI 04J EPJ C35 437 G. Abbiendi *et al.* (OPAL Collab.)

ABDALLAH 04K EPJ C35 159 J. Abdallah *et al.* (DELPHI Collab.)

ABDALLAH 04T EPJ C36 283 J. Abdallah *et al.* (DELPHI Collab.)

ABE 04B PRL 92 171802 K. Abe *et al.* (BELLE Collab.)

ACHARD 04G PL B585 53 P. Achard *et al.* (L3 Collab.)

AUBERT 04J PRL 92 121801 B. Aubert *et al.* (BABAR Collab.)

ENARI 04 PR 93 081803 Y. Enari *et al.* (BELLE Collab.)

PDG 04 PL B592 1 S. Eidelman *et al.* (PDG Collab.)

YUSA 04 PL B589 103 Y. Yusa *et al.* (BELLE Collab.)

ABBIENDI 03 PL B551 35 G. Abbiendi *et al.* (OPAL Collab.)

BRIERE 03 PRL 90 181802 R. A. Briere *et al.* (CLEO Collab.)

HEISTER 03F EPJ C30 291 A. Heister *et al.* (ALEPH Collab.)

INAMI 03 PL B551 16 K. Inami *et al.* (BELLE Collab.)

CHEN 02C PR D66 071101 S. Chen *et al.* (CLEO Collab.)

REGAN 02 PRL 88 071805 B.C. Regan *et al.* (OPAL Collab.)

ABBIENDI 01J EPJ C19 653 G. Abbiendi *et al.* (OPAL Collab.)

ABREU 01M EPJ C20 617 P. Abreu *et al.* (DELPHI Collab.)

ACCIARRI 01F PL B507 47 M. Acciari *et al.* (L3 Collab.)

ACHARD 01D PL B519 189 P. Achard *et al.* (L3 Collab.)

ANASTASSOV 01I PRL 86 4467 A. Anastassov *et al.* (CLEO Collab.)

HEISTER 01E EPJ C22 217 A. Heister *et al.* (ALEPH Collab.)

ABBIENDI 00A PL B492 23 G. Abbiendi *et al.* (OPAL Collab.)

ABBIENDI 00C EPJ C13 213 G. Abbiendi *et al.* (OPAL Collab.)

ABBIENDI 00D EPJ C13 197 G. Abbiendi *et al.* (OPAL Collab.)

ABREU 00L EPJ C16 229 P. Abreu *et al.* (DELPHI Collab.)

ACCIARRI 00B PL B479 67 M. Acciari *et al.* (L3 Collab.)

AHMED 00 PR D61 071101 S. Ahmed *et al.* (CLEO Collab.)

ALBRECHT 00 PL B485 37 H. Albrecht *et al.* (ARGUS Collab.)

ASNER 00 PR D61 012002 D.M. Asner *et al.* (CLEO Collab.)

ASNER 00B PR D62 072006 D.M. Asner *et al.* (CLEO Collab.)

BERGFELD 00 PR 84 830 T. Bergfeld *et al.* (CLEO Collab.)

BROWDER 00 PR D61 052004 T.E. Browder *et al.* (CLEO Collab.)

EDWARDS 00A PR D61 072003 K.W. Edwards *et al.* (CLEO Collab.)

GONZALEZ-S... 00 NP B582 3 G.A. Gonzalez-Sprinberg *et al.* (OPAL Collab.)

ABBIENDI 99H PL B447 134 G. Abbiendi *et al.* (OPAL Collab.)

ABREU 99X EPJ C10 201 P. Abreu *et al.* (DELPHI Collab.)

ACKERSTAFF 99D EPJ C8 3 K. Ackerstaff *et al.* (OPAL Collab.)

ACKERSTAFF 99E EPJ C8 183 K. Ackerstaff *et al.* (OPAL Collab.)

BARATE 99K EPJ C10 1 R. Barate *et al.* (ALEPH Collab.)

BARATE 99R EPJ C11 599 R. Barate *et al.* (ALEPH Collab.)

BISHAI 99 PR 82 281 M. Bishai *et al.* (CLEO Collab.)

GODANG 99 PR D59 091303 S. Godang *et al.* (CLEO Collab.)

RICHICHI 99 PR D60 112002 R.J. Richichi *et al.* (CLEO Collab.)

ACCIARRI 98C PL B426 207 M. Acciari *et al.* (L3 Collab.)

ACCIARRI 98E PL B434 169 M. Acciari *et al.* (L3 Collab.)

ACCIARRI 98R PL B438 405 M. Acciari *et al.* (L3 Collab.)

ACKERSTAFF 98M EPJ C4 193 K. Ackerstaff *et al.* (OPAL Collab.)

ACKERSTAFF 98N PL B431 188 K. Ackerstaff *et al.* (OPAL Collab.)

ALBRECHT 98 PL B431 179 H. Albrecht *et al.* (ARGUS Collab.)

BARATE 98 EPJ C1 65 R. Barate *et al.* (ALEPH Collab.)

BARATE 98E EPJ C4 29 R. Barate *et al.* (ALEPH Collab.)

BLISS 98 PR D57 5903 D.W. Bliss *et al.* (CLEO Collab.)

ABE 97O PRL 78 4691 K. Abe *et al.* (SLD Collab.)

ACKERSTAFF 97J PL B404 213 K. Ackerstaff *et al.* (OPAL Collab.)

ACKERSTAFF 97L ZPHY C74 403 K. Ackerstaff *et al.* (OPAL Collab.)

ACKERSTAFF 97R ZPHY C75 593 K. Ackerstaff *et al.* (OPAL Collab.)

ALEXANDER 97F PR D56 5320 J.P. Alexander *et al.* (CLEO Collab.)

AMMAR 97B PRL 78 4686 R. Ammar *et al.* (CLEO Collab.)

ANASTASSOV 97 PR D55 2559 A. Anastassov *et al.* (CLEO Collab.)

Also PR D58 119903 (erratum) A. Anastassov *et al.* (CLEO Collab.)

ANDERSON 97 PRL 79 3814 S. Anderson *et al.* (CLEO Collab.)

AVERY 97 PR D55 1119 P. Avery *et al.* (CLEO Collab.)

BARATE 97I ZPHY C74 387 R. Barate *et al.* (ALEPH Collab.)

BARATE 97R PL B414 362 R. Barate *et al.* (ALEPH Collab.)

BERGFELD 97 PRL 79 2406 T. Bergfeld *et al.* (CLEO Collab.)

BONVICINI 97 PRL 79 1221 G. Bonvicini *et al.* (CLEO Collab.)

BUSKULIC 97C ZPHY C74 263 D. Buskulic *et al.* (ALEPH Collab.)

COAN 97 PR D55 7291 T.E. Coan *et al.* (CLEO Collab.)

EDWARDS 97 PR D55 3919 K.W. Edwards *et al.* (CLEO Collab.)

EDWARDS 97B PR D56 5297 K.W. Edwards *et al.* (CLEO Collab.)

ESCRIBANO 97 PR B395 369 R. Escríbano, E. Masso (BARC, PART Collab.)

ABREU 96H PL B365 448 P. Abreu *et al.* (DELPHI Collab.)

ACCIARRI 96L PL B377 313 M. Acciari *et al.* (L3 Collab.)

ACCIARRI 96K PL B389 187 M. Acciari *et al.* (L3 Collab.)

ALAM 96 PRL 76 2637 M.S. Alam *et al.* (CLEO Collab.)

ALBRECHT 96E PRPL 276 223 H. Albrecht *et al.* (ARGUS Collab.)

ALEXANDER 96D PL B374 341 G. Alexander *et al.* (OPAL Collab.)

ALEXANDER 96F PL B388 437 G. Alexander *et al.* (OPAL Collab.)

BAI 96 PR D53 20 J.Z. Bai *et al.* (BES Collab.)

BALEST 96 PL B388 402 R. Balest *et al.* (CLEO Collab.)

BARTELT 96 PRL 76 4119 J.E. Bartelt *et al.* (CLEO Collab.)

BUSKULIC 96 ZPHY C70 579 D. Buskulic *et al.* (ALEPH Collab.)

BUSKULIC 96C ZPHY C70 561 D. Buskulic *et al.* (ALEPH Collab.)

COAN 96 PR D53 6037 T.E. Coan *et al.* (CLEO Collab.)

ABE 95Y PR D52 4828 K. Abe *et al.* (SLD Collab.)

ABREU 95T PL B357 715 P. Abreu *et al.* (DELPHI Collab.)

ABREU 95U PL B355 411 P. Abreu *et al.* (DELPHI Collab.)

ACCIARRI 95 PL B345 93 M. Acciari *et al.* (L3 Collab.)

ACCIARRI 95F PL B352 487 M. Acciari *et al.* (L3 Collab.)

AKERS 95F ZPHY C66 31 R. Akers *et al.* (OPAL Collab.)

AKERS 95I ZPHY C66 543 R. Akers *et al.* (OPAL Collab.)

AKERS 95P ZPHY C67 45 R. Akers *et al.* (OPAL Collab.)

AKERS 95Y ZPHY C68 555 R. Akers *et al.* (OPAL Collab.)

ALBRECHT 95 PL B341 441 H. Albrecht *et al.* (ARGUS Collab.)

ALBRECHT 95C PL B349 576 H. Albrecht *et al.* (ARGUS Collab.)

ALBRECHT 95G ZPHY C68 25 H. Albrecht *et al.* (ARGUS Collab.)

ALBRECHT 95H ZPHY C68 215 H. Albrecht *et al.* (ARGUS Collab.)

BALEST 95C PRL 76 3809 R. Balest *et al.* (CLEO Collab.)

BERNABEU 95 NP B436 474 J. Bernabeu *et al.* (TPC/2gamma Collab.)

BUSKULIC 95D PL B346 371 D. Buskulic *et al.* (ALEPH Collab.)

BUSKULIC 95C PL B346 379 D. Buskulic *et al.* (ALEPH Collab.)

Also PL B363 265 (erratum) D. Buskulic *et al.* (ALEPH Collab.)

ABREU 94K PL B334 435 P. Abreu *et al.* (DELPHI Collab.)

AKERS 94G PL B328 207 R. Akers *et al.* (OPAL Collab.)

AKERS 94F PL B339 278 R. Akers *et al.* (OPAL Collab.)

ALBRECHT 94 PL B337 383 H. Albrecht *et al.* (ARGUS Collab.)

ARTUSO 94 PRL 72 3762 M. Artuso *et al.* (CLEO Collab.)

BARTELT 94 PRL 73 1830 J.E. Bartelt *et al.* (CLEO Collab.)

BATTLE 94 PR D50 179 D. Battle *et al.* (CLEO Collab.)

BAUER 94 PR D50 133 A.D. Bauer *et al.* (TPC/2gamma Collab.)

BUSKULIC 94D PL B321 168 D. Buskulic *et al.* (ALEPH Collab.)

BUSKULIC 94E PL B322 209 D. Buskulic *et al.* (ALEPH Collab.)

BUSKULIC 94F PL B332 219 D. Buskulic *et al.* (ALEPH Collab.)

GIBAUT 94B PRL 73 934 D. Gibaut *et al.* (CLEO Collab.)

ADRIANI 93M PRPL 236 1 O. Adriani *et al.* (L3 Collab.)

ALBRECHT 93C ZPHY C58 61 H. Albrecht *et al.* (ARGUS Collab.)

ALBRECHT 93G PL B316 608 H. Albrecht *et al.* (ARGUS Collab.)

BALEST 93 PR D47 3671 R. Balest *et al.* (CLEO Collab.)

BEAN 93 PRL 70 138 A. Bean *et al.* (CLEO Collab.)

DEBORTOLLETTO 93 PR 70 1791 D. DeBortolotto *et al.* (CLEO Collab.)

ESCRIBANO 93 PL B301 419 R. Escríbano, E. Masso (BARC Collab.)

PROCARIO 93 PRL 70 1207 M. Procario *et al.* (CLEO Collab.)

ABREU 92N ZPHY C55 555 P. Abreu *et al.* (DELPHI Collab.)

ACTON 92F PL B281 405 D.P. Acton *et al.* (OPAL Collab.)

ACTON 92H PL B288 373 P.D. Acton *et al.* (OPAL Collab.)

AKERIB 92 PRL 69 3610 D.S. Akerib *et al.* (CLEO Collab.)

Also PRL 71 3395 (erratum) D.S. Akerib *et al.* (CLEO Collab.)

ALBRECHT 92K ZPHY C53 367 H. Albrecht *et al.* (ARGUS Collab.)

ALBRECHT 92D ZPHY C55 179 H. Albrecht *et al.* (ARGUS Collab.)

ALBRECHT 92M PL B292 222 H. Albrecht *et al.* (ARGUS Collab.)

ALBRECHT 92Q ZPHY C56 339 H. Albrecht *et al.* (ARGUS Collab.)

AMMAR 92 PR D45 3976 R. Ammar *et al.* (CLEO Collab.)

ARTUSO 92 PRL 69 3278 M. Artuso *et al.* (CLEO Collab.)

BAI 92 PRL 69 3021 J.Z. Bai *et al.* (BES Collab.)

BATTLE 92 PL B291 488 M. Battle *et al.* (CLEO Collab.)

BUSKULIC 92J PL B297 459 D. Buskulic *et al.* (ALEPH Collab.)

DECAMP 92C ZPHY C54 211 D. Decamp *et al.* (ALEPH Collab.)

ADEVA 91F PL B265 451 B. Adeva *et al.* (L3 Collab.)

ALBRECHT 91D PL B260 259 H. Albrecht *et al.* (ARGUS Collab.)

ALEXANDER 91D PL B266 201 G. Alexander *et al.* (OPAL Collab.)

ANTREASYAN 91 PL B259 212 D. Antreasyan *et al.* (Crystal Ball Collab.)

GRIFOLS 91 PL B255 611 J.A. Grifols, A. Mendez (BARC Collab.)

ABACHI 90 PR D41 1414 S. Abachi *et al.* (HRS Collab.)

ALBRECHT 90E PL B246 278 H. Albrecht *et al.* (ARGUS Collab.)

ALBRECHT 90I PL B250 164 H. Albrecht *et al.* (ARGUS Collab.)

BEHREND 90 ZPHY C46 537 H.J. Behrend *et al.* (CELLO Collab.)

BOWCOCK 90 PR D41 805 T.J.V. Bowcock *et al.* (CLEO Collab.)

DELAGUILLA 90 PL B252 116 F. del Aguila, M. Sher (BARC, WILL Collab.)

GOLDBERG 90 PL B251 223 M. Goldberg *et al.* (CLEO Collab.)

WU 90 PR D41 2339 D.Y. Wu *et al.* (Mark II Collab.)

ABACHI 89B PR D40 902 S. Abachi *et al.* (HRS Collab.)

BEHREND 89B PL B222 163 H.J. Behrend *et al.* (CELLO Collab.)

JANSEN 89 PR D29 273 H. Jansen *et al.* (HRS Collab.)

KLEINWORT 89 ZPHY C42 7 C. Kleinwort *et al.* (Crystal Ball Collab.)

ADEVA 88 PR D38 2665 B. Adeva *et al.* (Mark-J Collab.)

ALBRECHT 88B PL B202 149 H. Albrecht *et al.* (ARGUS Collab.)

ALBRECHT 88L ZPHY C41 1 H. Albrecht *et al.* (ARGUS Collab.)

ALBRECHT 88M ZPHY C41 405 H. Albrecht *et al.* (ARGUS Collab.)

AMIDEI 88 PR D37 1750 D. Amidei *et al.* (Mark II Collab.)

BEHREND 88 PL B200 226 H.J. Behrend *et al.* (CELLO Collab.)

BRÄUNSCHW... 88C ZPHY C39 331 W. Braunschweig *et al.* (TASSO Collab.)

KEH 88 PR B212 123 S. Keh *et al.* (Crystal Ball Collab.)

TSCHIRHART 88 PR B205 407 R. Tschirhart *et al.* (HRS Collab.)

ABACHI 87B PL B197 291 S. Abachi *et al.* (HRS Collab.)

ABACHI 87C PRL 59 2519 S. Abachi *et al.* (HRS Collab.)

ADLER 87B PRL 59 1527 J. Adler *et al.* (Mark III Collab.)

AIHARA 87B PR D35 1553 H. Aihara *et al.* (TPC Collab.)

AIHARA 87C PRL 59 751 H. Aihara *et al.* (TPC Collab.)

ALBRECHT 87L PL B185 223 H. Albrecht *et al.* (ARGUS Collab.)

ALBRECHT 87P PL B199 580 H. Albrecht *et al.* (ARGUS Collab.)

BAND 87 PL B198 297 H.R. Band *et al.* (MAC Collab.)

BAND 87B PRL 59 415 H.R. Band *et al.* (MAC Collab.)

BÄRINGER 87 PR 59 1993 P. Bäringer *et al.* (CLEO Collab.)

BEBEK 87C PR D36 530 C. Bebek *et al.* (CLEO Collab.)

BURCHAT 87 PR D35 273 P.R. Burchat *et al.* (Mark II Collab.)

BYLSMA 87 PR D35 2269 B.C. Bylsma *et al.* (HRS Collab.)

COFFMAN 87 PR D36 2185 D.M. Coffman *et al.* (Mark III Collab.)

DERRICK 87 PL B189 260 M. Derrick *et al.* (HRS Collab.)

Downloaded from https://academic.oup.com/ptep/article/2020/8/083C01/5891211 by guest on 20 August 2020

Lepton Particle Listings

 τ , Heavy Charged Lepton Searches

FORD	87	PR D35 408	W.T. Ford <i>et al.</i>	(MAC Collab.)
FORD	87B	PR D36 1971	W.T. Ford <i>et al.</i>	(MAC Collab.)
GAN	87	PRL 59 411	K.K. Gan <i>et al.</i>	(Mark II Collab.)
GAN	87B	PL B197 561	K.K. Gan <i>et al.</i>	(Mark II Collab.)
AIHARA	86E	PRL 57 1836	H. Aihara <i>et al.</i>	(JADE Collab.)
BARTEL	86D	PL B182 216	W. Bartel <i>et al.</i>	(CERN, CIT+)
PDC	86	PL 170B 1	M. Aguilar-Benítez <i>et al.</i>	(DELCO Collab.)
RUCKSTUHL	86	PRL 56 2132	W. Ruckstuhl <i>et al.</i>	(Mark II Collab.)
SCHMIDKE	86	PRL 57 527	W.B. Schmidke <i>et al.</i>	(Mark II Collab.)
YELTON	86	PRL 56 812	J.M. Yelton <i>et al.</i>	(TASSO Collab.)
ALTHOFF	85	ZPHY C26 521	M. Althoff <i>et al.</i>	(MAC Collab.)
ASH	85B	PRL 55 2118	W.W. Ash <i>et al.</i>	(Mark III Collab.)
BALTUSAITIS...	85	PRL 55 1842	R.M. Baltusaitis <i>et al.</i>	(JADE Collab.)
BARTEL	85F	PL 161B 188	W. Bartel <i>et al.</i>	(CLEO Collab.)
BEHREND	85	PR D32 2468	S. Behrend <i>et al.</i>	(HRS Collab.)
BELTRAMI	85	PRL 54 1775	I. Beltrami <i>et al.</i>	(PLUTO Collab.)
BERGER	85	ZPHY C28 1	C. Berger <i>et al.</i>	(MAC Collab.)
BURCHAT	85	PRL 54 2489	P.R. Burchat <i>et al.</i>	(DELCO Collab.)
FERNANDEZ	85	PL 54 1624	E. Fernandez <i>et al.</i>	(DELCO Collab.)
MILLS	85	PL 54 624	G.B. Mills <i>et al.</i>	(TPC Collab.)
AIHARA	84C	PR D30 2436	H. Aihara <i>et al.</i>	(CELLO Collab.)
BEHREND	84	ZPHY C23 103	H.J. Behrend <i>et al.</i>	(DELCO Collab.)
MILLS	84	PRL 52 1944	G.B. Mills <i>et al.</i>	(CELLO Collab.)
BEHREND	83C	PL 127B 270	H.J. Behrend <i>et al.</i>	(UCI)
SILVERMAN	83	PR D27 1196	D.J. Silverman, G.L. Shaw	(CELLO Collab.)
BEHREND	82	PL 114B 282	H.J. Behrend <i>et al.</i>	(Mark II Collab.)
BLOCKER	82B	PRL 48 1586	C.A. Blocker <i>et al.</i>	(Mark II Collab.)
BLOCKER	82D	PL 109B 119	C.A. Blocker <i>et al.</i>	(Mark II Collab.)
FELDMAN	82	PRL 48 66	G.J. Feldman <i>et al.</i>	(Mark II Collab.)
HAYES	82	PR D25 2869	K.G. Hayes <i>et al.</i>	(PLUTO Collab.)
BERGER	81B	PL 99B 489	C. Berger <i>et al.</i>	(Mark II Collab.)
DORFAN	81	PRL 46 215	J.M. Dorfan <i>et al.</i>	(TASSO Collab.)
BRANDELIK	80	PL 92B 199	R. Brandelik <i>et al.</i>	(NOVO)
ZHOLENTZ	80	PL 96B 214	A.A. Zholents <i>et al.</i>	(NOVO)
Also		SJNP 34 814	A.A. Zholents <i>et al.</i>	(NOVO)
Translated from YAF	34	1471	W.J. Bacino <i>et al.</i>	(DELCO Collab.)
BACINO	79B	PRL 42 749	W.J. Bacino <i>et al.</i>	(SLAC)J
KIRKBY	79	SLAC-PUB-2419	J. Kirkby	(DELCO Collab.)
Batavia Lepton	Photon Conference.			
BACINO	78B	PRL 41 13	W.J. Bacino <i>et al.</i>	(DELCO Collab.)
Also		Tokyo Conf. 249	J. Kirz	(STON)
Also		PL 96B 214	A.A. Zholents <i>et al.</i>	(NOVO)
BRANDELIK	78	PL 73B 109	R. Brandelik <i>et al.</i>	(DASP Collab.)
FELDMAN	78	Tokyo Conf. 777	G.J. Feldman	(SLAC)J
JAROS	78	PRL 40 1120	J. Jaros <i>et al.</i>	(LGV Collab.)
PERL	75	PRL 35 1489	M.L. Perl <i>et al.</i>	(LBL, SLAC)

OTHER RELATED PAPERS

DAVIER	06	RMP 78 1043	M. Davier, A. Hocker, Z. Zhang	(LALO, PARIN+)
RAHAL-CAL...	98	IJMP A13 695	G. Rahal-Callot	(ETH)
GENTILE	96	PRPL 274 287	S. Gentile, M. Pohl	(ROMAI, ETH)
WEINSTEIN	93	ARNPS 43 457	A.J. Weinstein, R. Stroynowski	(CIT, SMU)
PERL	92	RPP 55 653	M.L. Perl	(SLAC)
PICH	90	MPL A5 1995	A. Pich	(VALE)
BARISH	88	PRPL 157 1	B.C. Barish, R. Stroynowski	(CIT)
GAN	88	IJMP A3 531	K.K. Gan, M.L. Perl	(SLAC)
HAYES	88	PR D38 3351	K.G. Hayes, M.L. Perl	(SLAC)
PERL	80	ARNPS 30 299	M.L. Perl	(SLAC)

Heavy Charged Lepton Searches

Charged Heavy Lepton MASS LIMITS

Sequential Charged Heavy Lepton (L^\pm) MASS LIMITS

These experiments assumed that a fourth generation L^\pm decayed to a fourth generation ν_L (or L^0) where ν_L was stable, or that L^\pm decays to a light ν_L via mixing.

See the "Quark and Lepton Compositeness, Searches for" Listings for limits on radiatively decaying excited leptons, *i.e.* $\ell^* \rightarrow \ell\gamma$. See the "WIMPs and other Particle Searches" section for heavy charged particle search limits in which the charged particle could be a lepton.

VALUE (GeV)	CL%	DOCUMENT ID	TECN	COMMENT
>100.8	95	ACHARD 01B L3	L3	Decay to νW
>101.9	95	ACHARD 01B L3	L3	$m_L - m_{L^0} > 15$ GeV
••• We do not use the following data for averages, fits, limits, etc. •••				
> 81.5	95	ACKERSTAFF 98C OPAL	OPAL	Assumed $m_{L^\pm} - m_{L^0} > 8.4$ GeV
> 80.2	95	ACKERSTAFF 98C OPAL	OPAL	$m_{L^0} > m_{L^\pm}$ and $L^\pm \rightarrow \nu W$
< 48 or > 61	95	¹ ACCIARRI 96G L3	L3	
> 63.9	95	ALEXANDER 96P OPAL	OPAL	Decay to massless ν 's
> 63.5	95	BUSKULIC 96S ALEP	ALEP	$m_L - m_{L^0} > 7$ GeV
> 65	95	BUSKULIC 96S ALEP	ALEP	Decay to massless ν 's
none 10-225		² AHMED 94 CNTR	CNTR	HI Collab. at HERA
none 12.6-29.6	95	KIM 91B AMY	AMY	Massless ν assumed
> 44.3	95	AKRAWY 90G OPAL	OPAL	
none 0.5-1.0	95	³ RILES 90 MRK2	MRK2	For $(m_{L^0} - m_{L^+}) > 0.25-0.4$ GeV
> 8		⁴ STOKER 89 MRK2	MRK2	For $(m_{L^+} - m_{L^0}) = 0.4$ GeV
> 12		⁴ STOKER 89 MRK2	MRK2	For $m_{L^0} = 0.9$ GeV
none 18.4-27.6	95	⁵ ABE 88 VNS	VNS	
> 25.5	95	⁶ ADACHI 88B TOPZ	TOPZ	
none 1.5-22.0	95	BEHREND 88C CELL	CELL	
> 41	90	⁷ ALBAJAR 87B UA1	UA1	
> 22.5	95	⁸ ADEVA 85 MRKJ	MRKJ	
> 18.0	95	⁹ BARTEL 83 JADE	JADE	
none 4-14.5	95	¹⁰ BERGER 81B PLUT	PLUT	
> 15.5	95	¹¹ BRANDELIK 81 TASS	TASS	
> 13.		¹² AZIMOV 80		
> 16.	95	¹³ BARBER 80B CNTR	CNTR	
> 0.490		¹⁴ ROTHER 69 RVUE	RVUE	

- ACCIARRI 96G assumes LEP result that the associated neutral heavy lepton mass > 40 GeV.
- THE AHMED 94 limits are from a search for neutral and charged sequential heavy leptons at HERA via the decay channels $L^+ \rightarrow e\gamma$, $L^- \rightarrow \nu W^-$, $L^- \rightarrow eZ$; and $L^0 \rightarrow \nu\gamma$, $L^0 \rightarrow e^- W^+$, $L^- \rightarrow \nu Z$, where the W decays to $\ell\nu_\ell$, or to jets, and Z decays to $\ell^+ \ell^-$ or jets.
- RILES 90 limits were the result of a special analysis of the data in the case where the mass difference $m_{L^-} - m_{L^0}$ was allowed to be quite small, where L^0 denotes the neutrino into which the sequential charged lepton decays. With a slightly reduced m_{L^\pm} range, the mass difference extends to about 4 GeV.
- STOKER 89 (Mark II at PEP) gives bounds on charged heavy lepton (L^\pm) mass for the generalized case in which the corresponding neutral heavy lepton (L^0) in the SU(2) doublet is not of negligible mass.
- ABE 88 search for L^+ and $L^- \rightarrow$ hadrons looking for acoplanar jets. The bound is valid for $m_\nu < 10$ GeV.
- ADACHI 88B search for hadronic decays giving acoplanar events with large missing energy. $E_{cm}^{ee} = 52$ GeV.
- Assumes associated neutrino is approximately massless.
- ADEVA 85 analyze one-isolated-muon data and sensitive to $\tau < 10$ nanosec. Assume $B(\text{lepton}) = 0.30$. $E_{cm} = 40-47$ GeV.
- BARTEL 83 limit is from PETRA e^+e^- experiment with average $E_{cm} = 34.2$ GeV.
- BERGER 81B is DESY DORIS and PETRA experiment. Looking for $e^+e^- \rightarrow L^+L^-$.
- BRANDELIK 81 is DESY-PETRA experiment. Looking for $e^+e^- \rightarrow L^+L^-$.
- AZIMOV 80 estimated probabilities for $M+N$ type events in $e^+e^- \rightarrow L^+L^-$ deducing semi-hadronic decay multiplicities of L from e^+e^- annihilation data at $E_{cm} = (2/3)m_L$. Obtained above limit comparing these with e^+e^- data (BRANDELIK 80).
- BARBER 80B looked for $e^+e^- \rightarrow L^+L^-$, $L \rightarrow \nu_L^+ X$ with MARK-J at DESY-PETRA.
- ROTHER 69 examines previous data on μ pair production and π and K decays.

Stable Charged Heavy Lepton (L^\pm) MASS LIMITS

VALUE (GeV)	CL%	DOCUMENT ID	TECN
>102.6	95	ACHARD 01B L3	L3

- We do not use the following data for averages, fits, limits, etc. •••

> 28.2	95	¹⁵ ADACHI 90C TOPZ	TOPZ
none 18.5-42.8	95	AKRAWY 90O OPAL	OPAL
> 26.5	95	DECAMP 90F ALEP	ALEP
none $m_\mu - 36.3$	95	SODERSTROM90 MRK2	MRK2

- ADACHI 90C put lower limits on the mass of stable charged particles with electric charge Q satisfying $2/3 < Q/e < 4/3$ and with spin 0 or 1/2. We list here the special case for a stable charged heavy lepton.

Charged Long-Lived Heavy Lepton MASS LIMITS

VALUE (GeV)	CL%	DOCUMENT ID	TECN	CHG	COMMENT
>574	95	CHATRCHYAN13AB CMS	CMS		Leptons singlet model
>102.0	95	ABBIENDI 03L OPAL	OPAL		pair produced in e^+e^-
> 0.1		¹⁶ ANSORGE 73B HBC	HBC	-	Long-lived
none 0.55-4.5		¹⁷ BUSHNIN 73 CNTR	CNTR	-	Long-lived
none 0.2-0.92		¹⁸ BARNA 68 CNTR	CNTR	-	Long-lived
none 0.97-1.03		¹⁸ BARNA 68 CNTR	CNTR	-	Long-lived

- We do not use the following data for averages, fits, limits, etc. •••

>574	95	CHATRCHYAN13AB CMS	CMS		Leptons singlet model
>102.0	95	ABBIENDI 03L OPAL	OPAL		pair produced in e^+e^-
> 0.1		¹⁶ ANSORGE 73B HBC	HBC	-	Long-lived
none 0.55-4.5		¹⁷ BUSHNIN 73 CNTR	CNTR	-	Long-lived
none 0.2-0.92		¹⁸ BARNA 68 CNTR	CNTR	-	Long-lived
none 0.97-1.03		¹⁸ BARNA 68 CNTR	CNTR	-	Long-lived

- ANSORGE 73B looks for electron pair production and electron-like Bremsstrahlung.
- BUSHNIN 73 is SERPUKHOV 70 GeV p experiment. Masses assume mean life above 7×10^{-10} and 3×10^{-8} respectively. Calculated from cross section (see "Charged Quasi-Stable Lepton Production Differential Cross Section" below) and 30-GeV muon pair production data.
- BARNA 68 is SLAC photoproduction experiment.

Doubly-Charged Heavy Lepton MASS LIMITS

VALUE (GeV)	CL%	DOCUMENT ID	TECN	CHG
none 1-9 GeV	90	¹⁹ CLARK 81 SPEC	SPEC	++

- We do not use the following data for averages, fits, limits, etc. •••

none 1-9 GeV	90	¹⁹ CLARK 81 SPEC	SPEC	++
¹⁹ CLARK 81 is FNAL experiment with 209 GeV muons. Bounds apply to μ_P which couples with full weak strength to muon. See also section on "Doubly-Charged Lepton Production Cross Section."				

Doubly-Charged Lepton Production Cross Section (μN Scattering)

VALUE (cm ²)	EVTS	DOCUMENT ID	TECN	CHG
$< 6. \times 10^{-38}$	0	²⁰ CLARK 81 SPEC	SPEC	++

- We do not use the following data for averages, fits, limits, etc. •••

²⁰ CLARK 81 is FNAL experiment with 209 GeV muon. Looked for μ^+ nucleon $\rightarrow \bar{P}^0 X$, $\bar{P}^0 \rightarrow \mu^+ \bar{\nu}_\mu$, and $\mu^+ n \rightarrow \mu_P^+ X$, $\mu_P^+ \rightarrow 2\mu^+ \nu_\mu$. Above limits are for $\sigma \times BR$ taken from their mass-dependence plot figure 2.				
--	--	--	--	--

REFERENCES FOR Heavy Charged Lepton Searches

CHATRCHYAN 13AB	JHEP 1307 122	S. Chatrchyan <i>et al.</i>	(CMS Collab.)
ABBIENDI 03L	PL B572 8	G. Abbiendi <i>et al.</i>	(OPAL Collab.)
ACHARD 01B	PL B517 75	P. Achard <i>et al.</i>	(L3 Collab.)
ACKERSTAFF 98C	EJP C1 45	K. Ackerstaff <i>et al.</i>	(OPAL Collab.)
ACCIARRI 96G	PL B377 304	M. Acciarri <i>et al.</i>	(L3 Collab.)
ALEXANDER 96P	PL B385 433	G. Alexander <i>et al.</i>	(OPAL Collab.)
BUSKULIC 96S	PL B384 439	D. Buskulic <i>et al.</i>	(ALEPH Collab.)
AHMED 94	PL B340 205	T. Ahmed <i>et al.</i>	(HI Collab.)

Lepton Particle Listings

Heavy Charged Lepton Searches, Neutrino Properties

KIM	91B	UMP A6 2583	G.N. Kim <i>et al.</i>	(AMY Collab.)
ADACHI	90C	PL B244 352	I. Adachi <i>et al.</i>	(TOPAZ Collab.)
AKRAWY	90G	PL B240 250	M.Z. Akrawy <i>et al.</i>	(OPAL Collab.)
AKRAWY	90O	PL B252 290	M.Z. Akrawy <i>et al.</i>	(OPAL Collab.)
DECAMP	90F	PL B236 511	D. Decamp <i>et al.</i>	(ALEPH Collab.)
RILES	90	PR D42 1	K. Riles <i>et al.</i>	(Mark II Collab.)
SODERSTROM	90	PRL 64 2980	E. Soderstrom <i>et al.</i>	(Mark II Collab.)
STOKER	89	PR D39 1811	D.P. Stoker <i>et al.</i>	(Mark II Collab.)
ABE	88	PRL 61 915	K. Abe <i>et al.</i>	(VENUS Collab.)
ADACHI	85B	PR D37 1339	I. Adachi <i>et al.</i>	(TOPAZ Collab.)
BEHREND	85C	ZPHY C41 7	H.J. Behrend <i>et al.</i>	(CELLO Collab.)
ALBAJAR	87B	PL B185 241	C. Albajar <i>et al.</i>	(UA1 Collab.)
ADEVA	85	PL 152B 439	B. Adeva <i>et al.</i>	(Mark-J Collab.)
Also		PRPL 109 131	B. Adeva <i>et al.</i>	(Mark-J Collab.)
BARTEL	83	PL 123B 353	W. Bartel <i>et al.</i>	(JADE Collab.)
BERGER	81B	PL 99B 489	C. Berger <i>et al.</i>	(PLUTO Collab.)
BRANDELIK	81	PL 99B 163	R. Brandelik <i>et al.</i>	(TASSO Collab.)
CLARK	81	PRL 46 299	A.R. Clark <i>et al.</i>	(UCB, LBL, FNAL+)
Also		PR D25 2762	W.H. Smith <i>et al.</i>	(LBL, FNAL, PRIN)
AZIMOV	80	JETPL 32 664	Y.I. Azimov, V.A. Khoze	(PNPI)
Translated from		ZETFP 32 677		
BARBER	80B	PRL 45 1904	D.P. Barber <i>et al.</i>	(Mark-J Collab.)
BRANDELIK	80	PL 92B 199	R. Brandelik <i>et al.</i>	(TASSO Collab.)
ANSORGE	73B	PR D7 26	R.E. Ansorge <i>et al.</i>	(CAVE)
BUSHNIN	73	NP B58 476	Y.B. Bushnin <i>et al.</i>	(SERP)
Also		PL 42B 136	S.V. Golovkin <i>et al.</i>	(SERP)
ROTHE	69	NP B10 241	K.W. Rothe, A.M. Wolsky	(PENN)
BARNA	68	PR 173 1391	A. Barna <i>et al.</i>	(SLAC, STAN)

OTHER RELATED PAPERS

PERL	81	SLAC-PUB-2752	M.L. Perl	(SLAC)
Physics in		Collision	Conference.	

Neutrino Properties

NEUTRINO PROPERTIES

Revised August 2019 by P. Vogel (Caltech) and A. Piepke (University of Alabama).

The Neutrino Properties Listings concern measurements of various properties of neutrinos. Nearly all of the measurements, so far only limits, actually concern superpositions of the mass eigenstates ν_i , which are in turn related to the weak eigenstates ν_ℓ , via the neutrino mixing matrix

$$|\nu_\ell\rangle = \sum_i U_{\ell i} |\nu_i\rangle.$$

In the analogous case of quark mixing via the CKM matrix, the smallness of the off-diagonal terms (small mixing angles) permits a “dominant eigenstate” approximation. However, the results of neutrino oscillation searches show that the mixing matrix contains two large mixing angles and a third angle that is not exceedingly small. We cannot therefore associate any particular state $|\nu_i\rangle$ with any particular lepton label e, μ or τ . Nevertheless, note that in the standard labeling the $|\nu_1\rangle$ has the largest $|\nu_e\rangle$ component ($\sim 2/3$), $|\nu_2\rangle$ contains $\sim 1/3$ of the $|\nu_e\rangle$ component and $|\nu_3\rangle$ contains only a small $\sim 2.5\%$ $|\nu_e\rangle$ component.

Neutrinos are produced in weak decays with a definite lepton flavor, and are typically detected by the charged current weak interaction again associated with a specific lepton flavor. Hence, the listings for the neutrino mass that follow are separated into the three associated charged lepton categories. Other properties (mean lifetime, magnetic moment, charge and charge radius) are no longer separated this way. If needed, the associated lepton flavor is reported in the footnotes.

Measured quantities (mass-squared, magnetic moments, mean lifetimes, *etc.*) all depend upon the mixing parameters $|U_{\ell i}|^2$, but to some extent also on experimental conditions (e.g., on energy resolution). Many of these observables, in particular

mass-squared, cannot distinguish between Dirac and Majorana neutrinos and are unaffected by CP phases.

Direct neutrino mass measurements are usually based on the analysis of the kinematics of charged particles (leptons, pions) emitted together with neutrinos (flavor states) in various weak decays. The most sensitive neutrino mass measurement to date, involving electron type antineutrinos, is based on fitting the shape of the beta spectrum. The quantity $m_{\nu_e}^{2(eff)} = \sum_i |U_{ei}|^2 m_{\nu_i}^2$ is determined or constrained, where the sum is over all mass eigenvalues m_{ν_i} that are too close together to be resolved experimentally. (The quantity $m_{\nu_e}^{eff} \equiv \sqrt{m_{\nu_e}^{2(eff)}}$ is often denoted $\langle m_\beta \rangle$ in the literature.) If the energy resolution is better than $\Delta m_{ij}^2 \equiv m_{\nu_i}^2 - m_{\nu_j}^2$, the corresponding heavier m_{ν_i} and mixing parameter could be determined by fitting the resulting spectral anomaly (step or kink).

The dependence of m_{ν_e} on the mass of the lightest neutrino is shown in Fig. 14.11 of the *Neutrino Masses, Mixing, and Oscillations* review. In the case of inverted ordering there is a minimum possible value of $m_{\nu_e}^{eff}$, approximately $\sqrt{(\Delta m_{32}^2)} \sim 50$ meV. If $m_{\nu_e}^{eff}$ is found to be larger than this value, it is impossible, based on this information only, to decide which ordering is realized in nature. On the other hand, if the $m_{\nu_e}^{eff}$ is less than ~ 50 meV, only the normal mass ordering is possible.

A limit on $m_{\nu_e}^{2(eff)}$ implies an upper limit on the minimum value m_{min}^2 of $m_{\nu_i}^2$, independent of the mixing parameters U_{ei} : $m_{min}^2 \leq m_{\nu_e}^{2(eff)}$. However, if and when the value of $m_{\nu_e}^{2(eff)}$ is determined then its combination with the results derived from neutrino oscillations that give us the values of the neutrino mass-squared differences $\Delta m_{ij}^2 \equiv m_i^2 - m_j^2$, including eventually also their signs, and the mixing parameters $|U_{ei}|^2$, the individual neutrino mass squares $m_{\nu_j}^2 = m_{\nu_e}^{2(eff)} - \sum_i |U_{ei}|^2 \Delta m_{ij}^2$ can be determined.

So far solar, reactor, atmospheric and accelerator neutrino oscillation experiments can be consistently described using three active neutrino flavors, i.e. two mass splittings and three mixing angles. However, several experiments with radioactive sources, reactors, and accelerators imply the possible existence of one or more non-interacting, i.e. sterile, neutrino species that might be observable since they couple, albeit weakly, to the flavor neutrinos $|\nu_l\rangle$. In that case, the neutrino mixing matrix would be $n \times n$ unitary matrix with $n > 3$.

Combined three neutrino analyses determine the squared mass differences and all three mixing angles to within reasonable accuracy. For given $|\Delta m_{ij}^2|$ a limit on $m_{\nu_e}^{2(eff)}$ from beta decay defines an upper limit on the maximum value m_{max} of m_{ν_i} : $m_{max}^2 \leq m_{\nu_e}^{2(eff)} + \sum_{i < j} |\Delta m_{ij}^2|$. The analysis of the low energy beta decay of tritium, combined with the oscillation results, thus limits *all* active neutrino masses. Traditionally, experimental neutrino mass limits obtained from pion decay $\pi^+ \rightarrow \mu^+ + \nu_\mu$ or the shape of the spectrum of decay products of the τ lepton did not distinguish between flavor and mass eigenstates. These results are reported as limits of the μ and τ based neutrino

Lepton Particle Listings

Neutrino Properties

mass. After the determination of the $|\Delta m_{ij}^2|$'s and the mixing angles θ_{ij} , the corresponding neutrino mass limits are no longer competitive with those derived from low energy beta decays.

The spread of arrival times of the neutrinos from SN1987A, coupled with the measured neutrino energies, provided a time-of-flight limit on a quantity similar to $\langle m_{\beta} \rangle \equiv \sqrt{m_{\nu_e}^{2(eff)}}$. This statement, clothed in various degrees of sophistication, has been the basis for a very large number of papers. The resulting limits, however, are no longer comparable with the limits from tritium beta decay.

Constraint, or eventually a value, of the sum of the neutrino masses m_{tot} can be determined from the analysis of the cosmic microwave background anisotropy, combined with the galaxy redshift surveys and other data. These limits are reported in a separate table (Sum of Neutrino Masses, m_{tot}). Obviously, m_{tot} represents an upper limit for all m_i values. Note that many reported m_{tot} limits are considerably more stringent than the listed $m_{\nu_e}^{eff}$ limits. Discussion concerning the model dependence of the m_{tot} limit is continuing.

\overline{m} MASS (electron based)

Those limits given below are for the square root of $m_{\nu_e}^{2(eff)} \equiv \sum_i |U_{ei}|^2 m_{\nu_i}^2$. Limits that come from the kinematics of ${}^3\text{H}\beta\text{-}\overline{m}$ decay are the square roots of the limits for $m_{\nu_e}^{2(eff)}$. Obtained from the measurements reported in the Listings for " \overline{m} Mass Squared," below.

VALUE (eV)	CL%	DOCUMENT ID	TECN	COMMENT
< 1.1	90	1 AKER	19 SPEC	${}^3\text{H}\beta$ decay
• • • We do not use the following data for averages, fits, limits, etc. • • •				
< 2.05	95	2 ASEEV	11 SPEC	${}^3\text{H}\beta$ decay
< 5.8	95	3 PAGLIAROLI	10 ASTR	SN1987A
< 2.3	95	4 KRAUS	05 SPEC	${}^3\text{H}\beta$ decay
< 21.7	90	5 ARNABOLDI	03A BOLO	${}^{187}\text{Re}\beta$ decay
< 5.7	95	6 LOREDO	02 ASTR	SN1987A
< 2.5	95	7 LOBASHEV	99 SPEC	${}^3\text{H}\beta$ decay
< 2.8	95	8 WEINHEIMER	99 SPEC	${}^3\text{H}\beta$ decay
< 4.35	95	9 BELESEV	95 SPEC	${}^3\text{H}\beta$ decay
< 12.4	95	10 CHING	95 SPEC	${}^3\text{H}\beta$ decay
< 9.2	95	11 HIDDEMANN	95 SPEC	${}^3\text{H}\beta$ decay
15 \pm 32 -15		HIDDEMANN	95 SPEC	${}^3\text{H}\beta$ decay
< 19.6	95	KERNAN	95 ASTR	SN 1987A
< 7.0	95	12 STOEFL	95 SPEC	${}^3\text{H}\beta$ decay
< 7.2	95	13 WEINHEIMER	93 SPEC	${}^3\text{H}\beta$ decay
< 11.7	95	14 HOLZSCHUH	92B SPEC	${}^3\text{H}\beta$ decay
< 13.1	95	15 KAWAKAMI	91 SPEC	${}^3\text{H}\beta$ decay
< 9.3	95	16 ROBERTSON	91 SPEC	${}^3\text{H}\beta$ decay
< 14	95	AVIGNONE	90 ASTR	SN 1987A
< 16		SPERGEL	88 ASTR	SN 1987A
17 to 40		17 BORIS	87 SPEC	${}^3\text{H}\beta$ decay

¹ AKER 19 report a neutrino mass limit, derived from the first month of data collected by the KATRIN tritium endpoint experiment. The analysis of the electron kinematics shows no evidence for neutrino mass.

² ASEEV 11 report the analysis of the entire beta endpoint data, taken with the Troitsk integrating electrostatic spectrometer between 1997 and 2002 (some of the earlier runs were rejected), using a windowless gaseous tritium source. The fitted value of m_{ν} , based on the method of Feldman and Cousins, is obtained from the upper limit of the fit for m_{ν}^2 . Previous analysis problems were resolved by careful monitoring of the tritium gas column density. Supersedes LOBASHEV 99 and BELESEV 95.

³ PAGLIAROLI 10 is critical of the likelihood method used by LOREDO 02.

⁴ KRAUS 05 is a continuation of the work reported in WEINHEIMER 99. This result represents the final analysis of data taken from 1997 to 2001. Various sources of systematic uncertainties have been identified and quantified. The background has been reduced compared to the initial running period. A spectral anomaly at the endpoint, reported in LOBASHEV 99, was not observed.

⁵ ARNABOLDI 03A *et al.* report kinematical neutrino mass limit using β -decay of ${}^{187}\text{Re}$. Bolometric AgReO_4 micro-calorimeters are used. Mass bound is substantially weaker than those derived from tritium β -decays but has different systematic uncertainties.

⁶ LOREDO 02 updates LOREDO 89.

⁷ LOBASHEV 99 report a new measurement which continues the work reported in BELESEV 95. This limit depends on phenomenological fit parameters used to derive their best fit to m_{ν}^2 , making an unambiguous interpretation difficult. See the footnote under " \overline{m} Mass Squared."

⁸ WEINHEIMER 99 presents two analyses which exclude the spectral anomaly and result in an acceptable m_{ν}^2 . We report the most conservative limit, but the other is nearly the same. See the footnote under " \overline{m} Mass Squared."

⁹ BELESEV 95 (Moscow) use an integral electrostatic spectrometer with adiabatic magnetic collimation and a gaseous tritium source. A fit to a normal Kurie plot above 18300–18350 eV (to avoid a low-energy anomaly) plus a monochromatic line 7–15 eV below the endpoint yields $m_{\nu}^2 = -4.1 \pm 10.9 \text{ eV}^2$, leading to this Bayesian limit.

¹⁰ CHING 95 quotes results previously given by SUN 93; no experimental details are given. A possible explanation for consistently negative values of m_{ν}^2 is given.

¹¹ HIDDEMANN 95 (Munich) experiment uses atomic tritium embedded in a metal-dioxide lattice. Bayesian limit calculated from the weighted mean $m_{\nu}^2 = 221 \pm 4244 \text{ eV}^2$ from the two runs listed below.

¹² STOEFL 95 (LLNL) result is the Bayesian limit obtained from the m_{ν}^2 errors given below but with m_{ν}^2 set equal to 0. The anomalous endpoint accumulation leads to a value of m_{ν}^2 which is negative by more than 5 standard deviations.

¹³ WEINHEIMER 93 (Mainz) is a measurement of the endpoint of the tritium β spectrum using an electrostatic spectrometer with a magnetic guiding field. The source is molecular tritium frozen onto an aluminum substrate.

¹⁴ HOLZSCHUH 92B (Zurich) result is obtained from the measurement $m_{\nu}^2 = -24 \pm 48 \pm 61$ (1σ errors), in eV^2 , using the PDG prescription for conversion to a limit in m_{ν} .

¹⁵ KAWAKAMI 91 (Tokyo) experiment uses tritium-labeled arachidic acid. This result is the Bayesian limit obtained from the m_{ν}^2 limit with the errors combined in quadrature. This was also done in ROBERTSON 91, although the authors report a different procedure.

¹⁶ ROBERTSON 91 (LANL) experiment uses gaseous molecular tritium. The result is in strong disagreement with the earlier claims by the ITEP group [LUBIMOV 80, BORIS 87 (+ BORIS 88 erratum)] that m_{ν} lies between 17 and 40 eV. However, the probability of a positive m^2 is only 3% if statistical and systematic error are combined in quadrature.

¹⁷ See also comment in BORIS 87B and erratum in BORIS 88.

\overline{m}^2 MASS SQUARED (electron based)

Given troubling systematics which result in improbably negative estimates of $m_{\nu_e}^{2(eff)} \equiv \sum_i |U_{ei}|^2 m_{\nu_i}^2$, in many experiments, we use only KRAUS 05, LOBASHEV 99, and AKER 19 for our average.

VALUE (eV ²)	DOCUMENT ID	TECN	COMMENT
– 0.9 \pm 0.8 + 1.0	OUR AVERAGE		
– 1.0 \pm 0.9 + 1.1	1 AKER	19 SPEC	${}^3\text{H}\beta$ decay
– 0.67 \pm 2.53	2 ASEEV	11 SPEC	${}^3\text{H}\beta$ decay
– 0.6 \pm 2.2 \pm 2.1	3 KRAUS	05 SPEC	${}^3\text{H}\beta$ decay
• • • We do not use the following data for averages, fits, limits, etc. • • •			
– 1.9 \pm 3.4 \pm 2.2	4 LOBASHEV	99 SPEC	${}^3\text{H}\beta$ decay
– 3.7 \pm 5.3 \pm 2.1	5 WEINHEIMER	99 SPEC	${}^3\text{H}\beta$ decay
– 22 \pm 4.8	6 BELESEV	95 SPEC	${}^3\text{H}\beta$ decay
129 \pm 6010	7 HIDDEMANN	95 SPEC	${}^3\text{H}\beta$ decay
313 \pm 5994	7 HIDDEMANN	95 SPEC	${}^3\text{H}\beta$ decay
– 130 \pm 20 \pm 15	8 STOEFL	95 SPEC	${}^3\text{H}\beta$ decay
– 31 \pm 75 \pm 48	9 SUN	93 SPEC	${}^3\text{H}\beta$ decay
– 39 \pm 34 \pm 15	10 WEINHEIMER	93 SPEC	${}^3\text{H}\beta$ decay
– 24 \pm 48 \pm 61	11 HOLZSCHUH	92B SPEC	${}^3\text{H}\beta$ decay
– 65 \pm 85 \pm 65	12 KAWAKAMI	91 SPEC	${}^3\text{H}\beta$ decay
– 147 \pm 68 \pm 41	13 ROBERTSON	91 SPEC	${}^3\text{H}\beta$ decay

¹ AKER 19 use the first month of data collected by the KATRIN experiment to determine m_{ν}^2 . The result is consistent with a neutrino mass of zero and is used to place a limit on m_{ν} .

² ASEEV 11 report the analysis of the entire beta endpoint data, taken with the Troitsk integrating electrostatic spectrometer between 1997 and 2002, using a windowless gaseous tritium source. The analysis does not use the two additional fit parameters (see LOBASHEV 99) for a step-like structure near the endpoint. Using only the runs where the tritium gas column density was carefully monitored the need for such parameters was eliminated. Supersedes LOBASHEV 99 and BELESEV 95.

³ KRAUS 05 is a continuation of the work reported in WEINHEIMER 99. This result represents the final analysis of data taken from 1997 to 2001. Problems with significantly negative squared neutrino masses, observed in some earlier experiments, have been resolved in this work.

⁴ LOBASHEV 99 report a new measurement which continues the work reported in BELESEV 95. The data were corrected for electron trapping effects in the source, eliminating the dependence of the fitted neutrino mass on the fit interval. The analysis assuming a pure beta spectrum yields significantly negative fitted $m_{\nu}^2 \approx -(20-10) \text{ eV}^2$. This problem is attributed to a discrete spectral anomaly of about 6×10^{-11} intensity with a time-dependent energy of 5–15 eV below the endpoint. The data analysis accounts for this anomaly by introducing two extra phenomenological fit parameters resulting in a best fit of $m_{\nu}^2 = -1.9 \pm 3.4 \pm 2.2 \text{ eV}^2$ which is used to derive a neutrino mass limit. However, the introduction of phenomenological fit parameters which are correlated with the derived m_{ν}^2 limit makes unambiguous interpretation of this result difficult.

See key on page 999

Lepton Particle Listings Neutrino Properties

- ⁵ WEINHEIMER 99 is a continuation of the work reported in WEINHEIMER 93. Using a lower temperature of the frozen tritium source eliminated the dewetting of the T_2 film, which introduced a dependence of the fitted neutrino mass on the fit interval in the earlier work. An indication for a spectral anomaly reported in LOBASHEV 99 has been seen, but its time dependence does not agree with LOBASHEV 99. Two analyses, which exclude the spectral anomaly either by choice of the analysis interval or by using a particular data set which does not exhibit the anomaly, result in acceptable m_ν^2 fits and are used to derive the neutrino mass limit published by the authors. We list the most conservative of the two.
- ⁶ BELESEV 95 (Moscow) use an integral electrostatic spectrometer with adiabatic magnetic collimation and a gaseous tritium sources. This value comes from a fit to a normal Kurie plot above 18300–18350 eV (to avoid a low-energy anomaly), including the effects of an apparent peak 7–15 eV below the endpoint.
- ⁷ HIDDEMANN 95 (Munich) experiment uses atomic tritium embedded in a metal-dioxide lattice. They quote measurements from two data sets.
- ⁸ STOEFL 95 (LLNL) uses a gaseous source of molecular tritium. An anomalous pileup of events at the endpoint leads to the negative value for m_ν^2 . The authors acknowledge that “the negative value for the best fit of m_ν^2 has no physical meaning” and discuss possible explanations for this effect.
- ⁹ SUN 93 uses a tritiated hydrocarbon source. See also CHING 95.
- ¹⁰ WEINHEIMER 93 (Mainz) is a measurement of the endpoint of the tritium β spectrum using an electrostatic spectrometer with a magnetic guiding field. The source is molecular tritium frozen onto an aluminum substrate.
- ¹¹ HOLZSCHUH 92B (Zurich) source is a monolayer of tritiated hydrocarbon.
- ¹² KAWAKAMI 91 (Tokyo) experiment uses tritium-labeled arachidic acid.
- ¹³ ROBERTSON 91 (LANL) experiment uses gaseous molecular tritium. The result is in strong disagreement with the earlier claims by the ITEP group [LUBIMOV 80, BORIS 87 (+ BORIS 88 erratum)] that m_ν lies between 17 and 40 eV. However, the probability of a positive m_ν^2 is only 3% if statistical and systematic error are combined in quadrature.

ν MASS (electron based)

These are measurement of m_ν (in contrast to $m_{\overline{\nu}}$ given above). The masses can be different for a Dirac neutrino in the absence of CPT invariance. The possible distinction between ν and $\overline{\nu}$ properties is usually ignored elsewhere in these Listings.

VALUE (eV)	CL%	DOCUMENT ID	TECN	COMMENT
<460	68	YASUMI 94	CNTR	^{163}Ho decay
<225	95	SPRINGER 87	CNTR	^{163}Ho decay

ν MASS (muon based)

Limits given below are for the square root of $m_\nu^{2(\text{eff})} \equiv \sum_i |U_{\nu i}|^2 m_{\nu_i}^2$.

In some of the COSM papers listed below, the authors did not distinguish between weak and mass eigenstates.

OUR EVALUATION is based on OUR AVERAGE for the π^\pm mass and the ASSAMAGAN 96 value for the muon momentum for the π^+ decay at rest. The limit is calculated using the unified classical analysis of FELDMAN 98 for a Gaussian distribution near a physical boundary. WARNING: since $m_\nu^{2(\text{eff})}$ is calculated from the differences of large numbers, it and the corresponding limits are extraordinarily sensitive to small changes in the pion mass, the decay muon momentum, and their errors. For example, the limits obtained using JECKELMANN 94, LENZ 98, and the weighted averages are 0.15, 0.29, and 0.19 MeV, respectively.

VALUE (MeV)	CL%	DOCUMENT ID	TECN	COMMENT
<0.19 (CL = 90%) OUR EVALUATION				
<0.17	90	1 ASSAMAGAN 96	SPEC	$m_\nu^2 = -0.016 \pm 0.023$

- • • We do not use the following data for averages, fits, limits, etc. • • •
- <0.15 2 DOLGOV 95 COSM Nucleosynthesis
- <0.48 3 ENQVIST 93 COSM Nucleosynthesis
- <0.3 4 FULLER 91 COSM Nucleosynthesis
- <0.42 4 LAM 91 COSM Nucleosynthesis
- <0.50 90 5 ANDERHUB 82 SPEC $m_\nu^2 = -0.14 \pm 0.20$
- <0.65 90 CLARK 74 ASPK $K_{\mu 3}$ decay

- ¹ ASSAMAGAN 96 measurement of p_μ from $\pi^+ \rightarrow \mu^+ \nu$ at rest combined with JECKELMANN 94 Solution B pion mass yields $m_\nu^2 = -0.016 \pm 0.023$ with corresponding Bayesian limit listed above. If Solution A is used, $m_\nu^2 = -0.143 \pm 0.024$ MeV². Replaces ASSAMAGAN 94.
- ² DOLGOV 95 removes earlier assumptions (DOLGOV 93) about thermal equilibrium below T_{QCD} for wrong-helicity Dirac neutrinos (ENQVIST 93, FULLER 91) to set more stringent limits.
- ³ ENQVIST 93 bases limit on the fact that thermalized wrong-helicity Dirac neutrinos would speed up expansion of early universe, thus reducing the primordial abundance. FULLER 91 exploits the same mechanism but in the older calculation obtains a larger production rate for these states, and hence a lower limit. Neutrino lifetime assumed to exceed nucleosynthesis time, ~ 1 s.
- ⁴ Assumes neutrino lifetime > 1 s. For Dirac neutrinos only. See also ENQVIST 93.

⁵ ANDERHUB 82 kinematics is insensitive to the pion mass.

ν MASS (tau based)

The limits given below are the square roots of limits for $m_{\nu_\tau}^{2(\text{eff})} \equiv \sum_i |U_{\tau i}|^2 m_{\nu_i}^2$.

In some of the ASTR and COSM papers listed below, the authors did not distinguish between weak and mass eigenstates.

VALUE (MeV)	CL%	EVTS	DOCUMENT ID	TECN	COMMENT
< 18.2	95		1 BARATE 98F	ALEP	1991–1995 LEP runs
• • • We do not use the following data for averages, fits, limits, etc. • • •					
< 28	95		2 ATHANAS 00	CLEO	$E_{\text{cm}}^{\text{eff}} = 10.6$ GeV
< 27.6	95		3 ACKERSTAFF 98T	OPAL	1990–1995 LEP runs
< 30	95	473	4 AMMAR 98	CLEO	$E_{\text{cm}}^{\text{eff}} = 10.6$ GeV
< 60	95		5 ANASTASSOV 97	CLEO	$E_{\text{cm}}^{\text{eff}} = 10.6$ GeV
< 0.37 or >22			6 FIELDS 97	COSM	Nucleosynthesis
< 68	95		7 SWAIN 97	THEO	m_τ, τ_τ, τ partial widths
< 29.9	95		8 ALEXANDER 96M	OPAL	1990–1994 LEP runs
<149			9 BOTTINO 96	THEO	π, μ, τ leptonic decays
<1 or >25			10 HANNESTAD 96C	COSM	Nucleosynthesis
< 71	95		11 SOBIE 96	THEO	$m_\tau, \tau_\tau, B(\tau^- \rightarrow e^- \overline{\nu}_e \nu_\tau)$
< 24	95	25	12 BUSKULIC 95H	ALEP	1991–1993 LEP runs
< 0.19			13 DOLGOV 95	COSM	Nucleosynthesis
< 3			14 SIGL 95	ASTR	SN 1987A
< 0.4 or > 30			15 DODELSON 94	COSM	Nucleosynthesis
< 0.1 or > 50			16 KAWASAKI 94	COSM	Nucleosynthesis
155–225			17 PERES 94	THEO	π, K, μ, τ weak decays
< 32.6	95	113	18 CINABRO 93	CLEO	$E_{\text{cm}}^{\text{eff}} \approx 10.6$ GeV
< 0.3 or > 35			19 DOLGOV 93	COSM	Nucleosynthesis
< 0.74			20 ENQVIST 93	COSM	Nucleosynthesis
< 31	95	19	21 ALBRECHT 92M	ARG	$E_{\text{cm}}^{\text{eff}} = 9.4\text{--}10.6$ GeV
< 0.3			22 FULLER 91	COSM	Nucleosynthesis
< 0.5 or > 25			23 KOLB 91	COSM	Nucleosynthesis
< 0.42			22 LAM 91	COSM	Nucleosynthesis

- ¹ BARATE 98F result based on kinematics of 2939 $\tau^- \rightarrow 2\pi^- \pi^+ \nu_\tau$ and 52 $\tau^- \rightarrow 3\pi^- 2\pi^+ (\pi^0) \nu_\tau$ decays. If possible 2.5% excited a_1 decay is included in 3-prong sample analysis, limit increases to 19.2 MeV.
- ² ATHANAS 00 bound comes from analysis of $\tau^- \rightarrow \pi^- \pi^+ \pi^- \pi^0 \nu_\tau$ decays.
- ³ ACKERSTAFF 98T use $\tau^- \rightarrow 5\pi^\pm \nu_\tau$ decays to obtain a limit of 43.2 MeV (95%CL). They combine this with ALEXANDER 96M value using $\tau^- \rightarrow 3h^\pm \nu_\tau$ decays to obtain quoted limit.
- ⁴ AMMAR 98 limit comes from analysis of $\tau^- \rightarrow 3\pi^- 2\pi^+ \nu_\tau$ and $\tau^- \rightarrow 2\pi^- \pi^+ 2\pi^0 \nu_\tau$ decay modes.
- ⁵ ANASTASSOV 97 derive limit by comparing their m_τ measurement (which depends on m_{ν_τ}) to BAI 96 m_τ threshold measurement.
- ⁶ FIELDS 97 limit for a Dirac neutrino. For a Majorana neutrino the mass region < 0.93 or > 31 MeV is excluded. These bounds assume $N_\nu < 4$ from nucleosynthesis; a wider excluded region occurs with a smaller N_ν upper limit.
- ⁷ SWAIN 97 derive their limit from the Standard Model relationships between the tau mass, lifetime, branching fractions for $\tau^- \rightarrow e^- \overline{\nu}_e \nu_\tau, \tau^- \rightarrow \mu^- \overline{\nu}_\mu \nu_\tau, \tau^- \rightarrow \pi^- \nu_\tau$, and $\tau^- \rightarrow K^- \nu_\tau$, and the muon mass and lifetime by assuming lepton universality and using world average values. Limit is reduced to 48 MeV when the CLEO τ mass measurement (BALEST 93) is included; see CLEO’s more recent m_{ν_τ} limit (ANASTASSOV 97). Consideration of mixing with a fourth generation heavy neutrino yields $\sin^2 \theta_L < 0.016$ (95%CL).
- ⁸ ALEXANDER 96M bound comes from analyses of $\tau^- \rightarrow 3\pi^- 2\pi^+ \nu_\tau$ and $\tau^- \rightarrow h^- h^- h^+ \nu_\tau$ decays.
- ⁹ BOTTINO 96 assumes three generations of neutrinos with mixing, finds consistency with massless neutrinos with no mixing based on 1995 data for masses, lifetimes, and leptonic partial widths.
- ¹⁰ HANNESTAD 96C limit is on the mass of a Majorana neutrino. This bound assumes $N_\nu < 4$ from nucleosynthesis. A wider excluded region occurs with a smaller N_ν upper limit. This paper is the corrected version of HANNESTAD 96; see the erratum: HANNESTAD 96B.
- ¹¹ SOBIE 96 derive their limit from the Standard Model relationship between the tau mass, lifetime, and leptonic branching fraction, and the muon mass and lifetime, by assuming lepton universality and using world average values.
- ¹² BUSKULIC 95H bound comes from a two-dimensional fit of the visible energy and invariant mass distribution of $\tau^- \rightarrow 5\pi (\pi^0) \nu_\tau$ decays. Replaced by BARATE 98F.
- ¹³ DOLGOV 95 removes earlier assumptions (DOLGOV 93) about thermal equilibrium below T_{QCD} for wrong-helicity Dirac neutrinos (ENQVIST 93, FULLER 91) to set more stringent limits. DOLGOV 96 argues that a possible window near 20 MeV is excluded.
- ¹⁴ SIGL 95 exclude massive Dirac or Majorana neutrinos with lifetimes between 10^{-3} and 10^8 seconds if the decay products are predominantly γ or $e^+ e^-$.
- ¹⁵ DODELSON 94 calculate constraints on ν_τ mass and lifetime from nucleosynthesis for 4 generic decay modes. Limits depend strongly on decay mode. Quoted limit is valid for

Lepton Particle Listings

Neutrino Properties

all decay modes of Majorana neutrinos with lifetime greater than about 300s. For Dirac neutrinos limits change to < 0.3 or > 33 .

¹⁶ KAWASAKI 94 excluded region is for Majorana neutrino with lifetime > 1000 s. Other limits are given as a function of ν_τ lifetime for decays of the type $\nu_\tau \rightarrow \nu_\mu \phi$ where ϕ is a Nambu-Goldstone boson.

¹⁷ PERES 94 used PDG 92 values for parameters to obtain a value consistent with mixing. Reexamination by BOTTINO 96 which included radiative corrections and 1995 PDG parameters resulted in two allowed regions, $m_3 < 70$ MeV and 140 MeV $m_3 < 149$ MeV.

¹⁸ CINABRO 93 bound comes from analysis of $\tau^- \rightarrow 3\pi^- 2\pi^+ \nu_\tau$ and $\tau^- \rightarrow 2\pi^- \pi^+ 2\pi^0 \nu_\tau$ decay modes.

¹⁹ DOLGOV 93 assumes neutrino lifetime > 100 s. For Majorana neutrinos, the low mass limit is 0.5 MeV. KAWANO 92 points out that these bounds can be overcome for a Dirac neutrino if it possesses a magnetic moment. See also DOLGOV 96.

²⁰ ENQVIST 93 bases limit on the fact that thermalized wrong-helicity Dirac neutrinos would speed up expansion of early universe, thus reducing the primordial abundance. FULLER 91 exploits the same mechanism but in the older calculation obtains a larger production rate for these states, and hence a lower limit. Neutrino lifetime assumed to exceed nucleosynthesis time, ~ 1 s.

²¹ ALBRECHT 92M reports measurement of a slightly lower τ mass, which has the effect of reducing the ν_τ mass reported in ALBRECHT 88B. Bound is from analysis of $\tau^- \rightarrow 3\pi^- 2\pi^+ \nu_\tau$ mode.

²² Assumes neutrino lifetime > 1 s. For Dirac neutrinos. See also ENQVIST 93.

²³ KOLB 91 exclusion region is for Dirac neutrino with lifetime > 1 s; other limits are given.

Revised September 2019 by K.A. Olive (University of Minnesota).

Neutrinos decouple from thermal equilibrium in the early universe at temperatures $\mathcal{O}(1)$ MeV. The limits on low mass ($m_\nu \lesssim 1$ MeV) neutrinos apply to m_{tot} given by

$$m_{\text{tot}} = \sum_{\nu} m_{\nu} .$$

Stable neutrinos in this mass range decouple from the thermal bath while still relativistic and make a contribution to the total energy density of the Universe which is given by

$$\rho_{\nu} = m_{\text{tot}} n_{\nu} \simeq m_{\text{tot}} (3/11) (3.045/3)^{3/4} n_{\gamma} ,$$

where the factor $3/11$ is the ratio of (light) neutrinos to photons and the factor $(3.045/3)^{3/4}$ corrects for the fact that the effective number of neutrinos in the standard model is 3.045 when taking into account e^+e^- annihilation during neutrino decoupling. Writing $\Omega_{\nu} = \rho_{\nu}/\rho_c$, where ρ_c is the critical energy density of the Universe, and using $n_{\gamma} = 410.7 \text{ cm}^{-3}$, we have

$$\Omega_{\nu} h^2 \simeq m_{\text{tot}} / (93 \text{ eV}) .$$

While an upper limit to the matter density of $\Omega_m h^2 < 0.12$ would constrain $m_{\text{tot}} < 11$ eV, much stronger constraints are obtained from a combination of observations of the CMB, the amplitude of density fluctuations on smaller scales from the clustering of galaxies and the Lyman- α forest, baryon acoustic oscillations, and new Hubble parameter data. These combine to give an upper limit of around 0.15 eV, and may, in the near future, be able to provide a lower bound on the sum of the neutrino masses. The current lower bound of $m_{\text{tot}} > 0.06$ eV implies a lower limit of $\Omega_{\nu} h^2 > 6 \times 10^{-4}$. See our review on "Neutrinos in Cosmology" for more details.

SUM OF THE NEUTRINO MASSES, m_{tot}

This is a sum of the neutrino masses, m_{tot} , as defined in the above note, of effectively stable neutrinos, i.e. those with mean lifetimes on cosmological scales. When necessary, we have generalized the results reported so they apply to m_{tot} . For other limits, see SZALAY 76, VYSOTSKY 77, BERNSTEIN 81, FREESE 84, SCHRAMM 84, and COWSIK 85. For more information see a note on "Neutrinos in Cosmology" in this Review.

VALUE (eV)	CL%	DOCUMENT ID	TECN	COMMENT
< 0.26	95	¹ LOUREIRO 19	COSM	
< 0.18	95	² UPADHYE 19	COSM	BOSS and CMB
< 0.152	95	³ CHOUDHURY 18	COSM	
0.064 \pm 0.061 -0.005	95	⁴ SIMPSON 17	COSM	
< 0.151	95	⁵ VAGNOZZI 17	COSM	
< 0.14	95	⁶ YECHE 17	COSM	BOSS and XQ-100
< 0.0926	90	⁷ DIVALENTINO 16	COSM	
< 0.18	95	⁸ HUANG 16	COSM	Normal mass hierarchy
< 0.14	95	⁹ ROSSI 15	COSM	
< 0.23	95	¹⁰ ADE 14	COSM	Planck
0.320 \pm 0.081		¹¹ BATTYE 14	COSM	
0.35 \pm 0.10		¹² BEUTLER 14	COSM	BOSS
0.22 \pm 0.09 -0.10		¹³ COSTANZI 14	COSM	
< 0.22	95	¹⁴ GIUSARMA 14	COSM	
0.32 \pm 0.11		¹⁵ HOU 14	COSM	
< 0.26	95	¹⁶ LEISTEDT 14	COSM	
< 0.18	95	¹⁷ RIEMER-SOR...14	COSM	
< 0.24	68	¹⁸ MORESCO 12	COSM	
< 0.29	95	¹⁹ XIA 12	COSM	
< 0.81	95	²⁰ SAITO 11	COSM	SDSS
< 0.44	95	²¹ HANNESTAD 10	COSM	
< 0.6	95	²² SEKIGUCHI 10	COSM	
< 0.28	95	²³ THOMAS 10	COSM	
< 1.1		²⁴ ICHIKI 09	COSM	
< 1.3	95	²⁵ KOMATSU 09	COSM	WMAP
< 1.2		²⁶ TERENO 09	COSM	
< 0.33		²⁷ VIKHLININ 09	COSM	
< 0.28		²⁸ BERNARDIS 08	COSM	
< 0.17-2.3		²⁹ FOGLI 07	COSM	
< 0.42	95	³⁰ KRISTIANSEN 07	COSM	
< 0.63-2.2		³¹ ZUNCKEL 07	COSM	
< 0.24	95	³² CIRELLI 06	COSM	
< 0.62	95	³³ HANNESTAD 06	COSM	
< 1.2		³⁴ SANCHEZ 06	COSM	
< 0.17	95	³² SELJAK 06	COSM	
< 2.0	95	³⁵ ICHIKAWA 05	COSM	
< 0.75		³⁶ BARGER 04	COSM	
< 1.0		³⁷ CROTTY 04	COSM	
< 0.7		³⁸ SPERGEL 03	COSM	WMAP
< 0.9		³⁹ LEWIS 02	COSM	
< 4.2		⁴⁰ WANG 02	COSM	CMB
< 2.7		⁴¹ FUKUGITA 00	COSM	
< 5.5		⁴² CROFT 99	ASTR	Ly α power spec
<180		SZALAY 74	COSM	
<132		COWSIK 72	COSM	
<280		MARX 72	COSM	
<400		GERSHTEIN 66	COSM	

¹ LOUREIRO 19 combines data from large scale structure, cosmic microwave background, type Ia supernovae and big bang nucleosynthesis using physically motivated neutrino mass models.

² UPADHYE 19 uses the shape of the BOSS redshift-space galaxy power spectrum in combination with the CMB, and supernovae data. Limit weakens to < 0.54 eV if the dark energy equation of state is allowed to vary.

³ CHOUDHURY 18 combines 2015 Planck CMB temperature data, information from the optical depth to reionization from Planck 2016 intermediate results together with baryon acoustic oscillation data from BOSS, MGS, and 6dFGS as well as supernovae Type Ia data from the Pantheon Sample. The limit is strengthened to 0.118 eV when high- l CMB polarization data is also included.

⁴ SIMPSON 17 uses a combination of laboratory and cosmological measurements to determine the light neutrino masses and argue that there is strong evidence for the normal mass ordering.

⁵ Combines temperature anisotropies of the CMB from Planck with data on baryon acoustic oscillations and the optical depth to reionization. Limit is strengthened to 0.118 when high multipole polarization data is included. Updates GIUSARMA 16.

⁶ Constrains the total mass of neutrinos using the Lyman-alpha forest power spectrum with BOSS (mid-resolution), XQ-100 (high-resolution) and CMB. Without the CMB data, the limit relaxes to 0.8 eV. Supersedes PALANQUE-DELABROUILLE 15A.

⁷ Constrains the total mass of neutrinos from Planck CMB data combined with baryon acoustic oscillation and Planck cluster data.

⁸ Constrains the total mass of neutrinos from BAO data from SDSS-III/BOSS combined with CMB data from Planck. Limit quoted for normal mass hierarchy. The limit for the inverted mass hierarchy is 0.20 eV and for the degenerate mass hierarchy it is 0.15 eV.

⁹ ROSSI 15 sets limits on the sum of neutrino masses using BOSS Lyman alpha forest data combined with Planck CMB data and baryon acoustic oscillations.

- 10 Constrains the total mass of neutrinos from Planck CMB data along with WMAP polarization, high L, and BAO data.
- 11 Finite neutrino mass fit to resolve discrepancy between CMB and lensing measurements.
- 12 Fit to the total mass of neutrinos from BOSS data along with WMAP CMB data and data from other BAO constraints and weak lensing.
- 13 Fit to the total mass of neutrinos from Planck CMB data along with BAO.
- 14 Constrains the total mass of neutrinos from Planck CMB data combined with baryon acoustic oscillation data from BOSS and HST data on the Hubble parameter.
- 15 Fit based on the SPT-SZ survey combined with CMB, BAO, and H_0 data.
- 16 Constrains the total mass of neutrinos (marginalizing over the effective number of neutrino species) from CMB, CMB lensing, BAO, and galaxy clustering data.
- 17 Constrains the total mass of neutrinos from Planck CMB data combined with baryon acoustic oscillation data from BOSS, 6dFGS, SDSS, WiggleZ data on the galaxy power spectrum, and HST data on the Hubble parameter. The limit is increased to 0.25 eV if a lower bound to the sum of neutrino masses of 0.04 eV is assumed.
- 18 Constrains the total mass of neutrinos from observational Hubble parameter data with seven-year WMAP data and the most recent estimate of H_0 .
- 19 Constrains the total mass of neutrinos from the CFHTLS combined with seven-year WMAP data and a prior on the Hubble parameter. Limit is relaxed to 0.41 eV when small scales affected by non-linearities are removed.
- 20 Constrains the total mass of neutrinos from the Sloan Digital Sky Survey and the five-year WMAP data.
- 21 Constrains the total mass of neutrinos from the 7-year WMAP data including SDSS and HST data. Limit relaxes to 1.19 eV when CMB data is used alone. Supersedes HANNESTAD 06.
- 22 Constrains the total mass of neutrinos from a combination of CMB data, a recent measurement of H_0 (SHOES), and baryon acoustic oscillation data from SDSS.
- 23 Constrains the total mass of neutrinos from SDSS MegaZ LRG DR7 galaxy clustering data combined with CMB, HST, supernovae and baryon acoustic oscillation data. Limit relaxes to 0.47 eV when the equation of state parameter, $w \neq 1$.
- 24 Constrains the total mass of neutrinos from weak lensing measurements when combined with CMB. Limit improves to 0.54 eV when supernovae and baryon acoustic oscillation observations are included. Assumes Λ CDM model.
- 25 Constrains the total mass of neutrinos from five-year WMAP data. Limit improves to 0.67 eV when supernovae and baryon acoustic oscillation observations are included. Limits quoted assume the Λ CDM model. Supersedes SPERGEL 07.
- 26 Constrains the total mass of neutrinos from weak lensing measurements when combined with CMB. Limit improves to $0.03 < \Sigma m_\nu < 0.54$ eV when supernovae and baryon acoustic oscillation observations are included. The slight preference for massive neutrinos at the two-sigma level disappears when systematic errors are taken into account. Assumes Λ CDM model.
- 27 Constrains the total mass of neutrinos from recent Chandra X-ray observations of galaxy clusters when combined with CMB, supernovae, and baryon acoustic oscillation measurements. Assumes flat universe and constant dark-energy equation of state, w .
- 28 Constrains the total mass of neutrinos from recent CMB and SOSS LRG power spectrum data along with bias mass relations from SDSS, DEEP2, and Lyman-Break Galaxies. It assumes Λ CDM model. Limit degrades to 0.59 eV in a more general w CDM model.
- 29 Constrains the total mass of neutrinos from neutrino oscillation experiments and cosmological data. The most conservative limit uses only WMAP three-year data, while the most stringent limit includes CMB, large-scale structure, supernova, and Lyman-alpha data.
- 30 Constrains the total mass of neutrinos from recent CMB, large scale structure, $SN1a$, and baryon acoustic oscillation data. The limit relaxes to 1.75 when WMAP data alone is used with no prior. Paper shows results with several combinations of data sets. Supersedes KRISTIANSEN 06.
- 31 Constrains the total mass of neutrinos from the CMB and the large scale structure data. The most conservative limit is obtained when generic initial conditions are allowed.
- 32 Constrains the total mass of neutrinos from recent CMB, large scale structure, Lyman-alpha forest, and $SN1a$ data.
- 33 Constrains the total mass of neutrinos from recent CMB and large scale structure data. See also GOOBAR 06. Superseded by HANNESTAD 10.
- 34 Constrains the total mass of neutrinos from the CMB and the final 2dF Galaxy Redshift Survey.
- 35 Constrains the total mass of neutrinos from the CMB experiments alone, assuming Λ CDM Universe. FUKUGITA 06 show that this result is unchanged by the 3-year WMAP data.
- 36 Constrains the total mass of neutrinos from the power spectrum of fluctuations derived from the Sloan Digital Sky Survey and the 2dF galaxy redshift survey, WMAP and 27 other CMB experiments and measurements by the HST Key project.
- 37 Constrains the total mass of neutrinos from the power spectrum of fluctuations derived from the Sloan Digital Sky Survey, the 2dF galaxy redshift survey, WMAP and ACBAR. The limit is strengthened to 0.6 eV when measurements by the HST Key project and supernovae data are included.
- 38 Constrains the fractional contribution of neutrinos to the total matter density in the Universe from WMAP data combined with other CMB measurements, the 2dFGRS data, and Lyman α data. The limit does not noticeably change if the Lyman α data are not used.
- 39 LEVVIS 02 constrains the total mass of neutrinos from the power spectrum of fluctuations derived from the CMB, HST Key project, 2dF galaxy redshift survey, supernovae type Ia, and BBN.
- 40 WANG 02 constrains the total mass of neutrinos from the power spectrum of fluctuations derived from the CMB and other cosmological data sets such as galaxy clustering and the Lyman α forest.
- 41 FUKUGITA 00 is a limit on neutrino masses from structure formation. The constraint is based on the clustering scale σ_8 and the COBE normalization and leads to a conservative limit of 0.9 eV assuming 3 nearly degenerate neutrinos. The quoted limit is on the sum of the light neutrino masses.

42 CROFT 99 result based on the power spectrum of the Ly α forest. If $\Omega_{\text{matter}} < 0.5$, the limit is improved to $m_\nu < 2.4 (\Omega_{\text{matter}}/0.17-1)$ eV.

Limits on MASSES of Light Stable Right-Handed ν (with necessarily suppressed interaction strengths)

VALUE (eV)	DOCUMENT ID	TECN	COMMENT
<100-200	1 OLIVE	82 COSM	Dirac ν
<200-2000	1 OLIVE	82 COSM	Majorana ν

• • • We do not use the following data for averages, fits, limits, etc. • • •
 1 Depending on interaction strength G_R where $G_R < G_F$.

Limits on MASSES of Heavy Stable Right-Handed ν (with necessarily suppressed interaction strengths)

VALUE (GeV)	DOCUMENT ID	TECN	COMMENT
> 10	1 OLIVE	82 COSM	$G_R/G_F < 0.1$
>100	1 OLIVE	82 COSM	$G_R/G_F < 0.01$

• • • We do not use the following data for averages, fits, limits, etc. • • •
 1 These results apply to heavy Majorana neutrinos and are summarized by the equation: $m_\nu > 1.2 \text{ GeV } (G_F/G_R)$. The bound saturates, and if G_R is too small no mass range is allowed.

ν CHARGE

e = electron charge is the unit of values listed below.

VALUE (e)	CL%	DOCUMENT ID	TECN	COMMENT
<4 $\times 10^{-35}$	95	1 CAPRINI	05 COSM	charge neutral universe

- • • We do not use the following data for averages, fits, limits, etc. • • •
- 1 CAPRINI 05 limit derived from the lack of a charge asymmetry in the universe. Limit assumes that charge asymmetries between particles are not anti-correlated.
- 2 DELLA-VALLE 16 obtain a limit on the charge of neutrinos valid for masses of less than 10 MeV. For heavier neutrinos the limit increases as a power of mass, reaching 10^{-6} e for $m = 100$ MeV.
- 3 CHEN 14A use the Multi-Configuration RPPA method to analyze reactor $\bar{\nu}_e$ scattering on Ge atoms with 300 eV recoil energy threshold to obtain this limit.
- 4 STUDENIKIN 14 uses the limit on μ_ν from BEDA 13 and the 2.8 keV threshold of the electron recoil energy to obtain this limit.
- 5 GNINENKO 07 use limit on $\bar{\nu}_e$ magnetic moment from LI 03b to derive this result. The limit is considerably weaker than the limits on the charge of ν_e and $\bar{\nu}_e$ from various astrophysics considerations.
- 6 This RAFFELT 99 limit applies to all neutrino flavors which are light enough (<5 keV) to be emitted from globular-cluster red giants.
- 7 This RAFFELT 99 limit is derived from the helioseismological limit on a new energy-loss channel of the Sun, and applies to all neutrino flavors which are light enough (<1 keV) to be emitted from the sun.
- 8 BABU 94 use COOPER-SARKAR 92 limit on ν magnetic moment to derive quoted result. It applies to ν_τ .
- 9 DAVIDSON 91 use data from early SLAC electron beam dump experiment to derive charge limit as a function of neutrino mass. It applies to ν_τ .
- 10 Exact BARBIELLINI 87 limit depends on assumptions about the intergalactic or galactic magnetic fields and about the direct distance and time through the field. It applies to ν_e .
- 11 The limit applies to all flavors.

ν (MEAN LIFE) / MASS

Measures $[\sum |U_{ej}|^2 \Gamma_j m_j]^{-1}$, where the sum is over mass eigenstates which cannot be resolved experimentally. Some of the limits constrain the radiative decay and are based on the limit of the corresponding photon flux. Other apply to the decay of a heavier neutrino into the lighter one and a Majoron or other invisible particle. Many of these limits apply to any ν within the indicated mass range.

Limits on the radiative decay are either directly based on the limits of the corresponding photon flux, or are derived from the limits on the neutrino magnetic moments. In the later case the transition rate for $\nu_i \rightarrow \nu_j + \gamma$

is constrained by $\Gamma_{ij} = \frac{1}{\tau_{ij}} = \frac{(m_i^2 - m_j^2)^3}{m_i^3} \mu_{ij}^2$ where μ_{ij} is the neutrino transition moment in the mass eigenstates basis. Typically, the limits on lifetime based on the magnetic moments are many orders of magnitude more restrictive than limits based on the nonobservation of photons.

Lepton Particle Listings

Neutrino Properties

VALUE (s/eV)	CL%	DOCUMENT ID	TECN	COMMENT
> 15.4	90	1 KRAKAUER	91 CNTR	$\nu_\mu, \bar{\nu}_\mu$ at LAMPF
> 7 × 10 ⁹		2 RAFFELT	85 ASTR	
> 300	90	3 REINES	74 CNTR	$\bar{\nu}_e$
• • • We do not use the following data for averages, fits, limits, etc. • • •				
> 8.08 × 10 ⁻⁵	90	4 AHARMIM	19 SNO	ν_2 invisible nonradiative decay
> 1.92 × 10 ⁻³	90	5 AHARMIM	19 FIT	ν_2 invisible nonradiative decay
6–26 × 10 ⁹	95	6 ESCUDERO	19 COSM	Invisible decay $m_\nu \geq 0.05$ eV
> 10 ⁵ – 10 ¹⁰	95	7 CECCHINI	11 ASTR	$\nu_2 \rightarrow \nu_1$ radiative decay
	90	8 MIRIZZI	07 CMB	radiative decay
	90	9 MIRIZZI	07 CIB	radiative decay
	90	10 WONG	07 CNTR	Reactor $\bar{\nu}_e$
> 0.11	90	11 XIN	05 CNTR	Reactor ν_e
	90	12 XIN	05 CNTR	Reactor ν_e
> 0.004	90	13 AHARMIM	04 SNO	quasidegen. ν masses
> 4.4 × 10 ⁻⁵	90	13 AHARMIM	04 SNO	hierarchical ν masses
> 100	95	14 CECCHINI	04 ASTR	Radiative decay for ν mass > 0.01 eV
> 0.067	90	15 EGUCHI	04 KLND	quasidegen. ν masses
> 1.1 × 10 ⁻³	95	15 EGUCHI	04 KLND	hierarchical ν masses
> 8.7 × 10 ⁻⁵	99	16 BANDYOPA...	03 FIT	nonradiative decay
> 4200	90	17 DERBIN	02B CNTR	Solar pp and Be ν
> 2.8 × 10 ⁻⁵	99	18 JOSHIPURA	02B FIT	nonradiative decay
		19 DOLGOV	99 COSM	
		20 BILLER	98 ASTR	$m_\nu = 0.05$ –1 eV
> 2.8 × 10 ¹⁵		21,22 BLUDMAN	92 ASTR	$m_\nu < 50$ eV
none 10 ⁻¹² – 5 × 10 ⁴		23 DODELSON	92 ASTR	$m_\nu = 1$ –300 keV
< 10 ⁻¹² or > 5 × 10 ⁴		23 DODELSON	92 ASTR	$m_\nu = 1$ –300 keV
		24 GRANEK	91 COSM	Decaying L^0
> 6.4	90	25 KRAKAUER	91 CNTR	ν_e at LAMPF
> 1.1 × 10 ¹⁵		26 WALKER	90 ASTR	$m_\nu = 0.03$ – ~2 MeV
> 6.3 × 10 ¹⁵		22,27 CHUPP	89 ASTR	$m_\nu < 20$ eV
> 1.7 × 10 ¹⁵		22 KOLB	89 ASTR	$m_\nu < 20$ eV
		28 RAFFELT	89 RVUE	$\bar{\nu}$ (Dirac, Majorana)
		29 RAFFELT	89B ASTR	
		30 VONFEILIT...	88 ASTR	
> 8.3 × 10 ¹⁴		31 OBERAUER	87	$\bar{\nu}_R$ (Dirac)
> 22	68	31 OBERAUER	87	$\bar{\nu}$ (Majorana)
> 38	68	31 OBERAUER	87	$\bar{\nu}_L$ (Dirac)
> 59	68	31 OBERAUER	87	
> 30	68	KETOV	86 CNTR	$\bar{\nu}$ (Dirac)
> 20	68	KETOV	86 CNTR	$\bar{\nu}$ (Majorana)
		32 BINETRUY	84 COSM	$m_\nu \sim 1$ MeV
> 0.11	90	33 FRANK	81 CNTR	$\nu\bar{\nu}$ LAMPF
> 2 × 10 ²¹		34 STECKER	80 ASTR	$m_\nu = 10$ –100 eV
> 1.0 × 10 ⁻²	90	33 BLIETSCHAU	78 HLBC	ν_μ , CERN GGM
> 1.7 × 10 ⁻²	90	33 BLIETSCHAU	78 HLBC	$\bar{\nu}_\mu$, CERN GGM
< 3 × 10 ⁻¹¹		35 FALK	78 ASTR	$m_\nu < 10$ MeV
> 2.2 × 10 ⁻³	90	33 BARNES	77 DBC	ν , ANL 12-ft
		36 COWSIK	77 ASTR	
> 3. × 10 ⁻³	90	33 BELLOTTI	76 HLBC	ν , CERN GGM
> 1.3 × 10 ⁻²	90	33 BELLOTTI	76 HLBC	$\bar{\nu}$, CERN GGM

¹ KRAKAUER 91 quotes the limit $\tau/m_{\nu_1} > (0.75a^2 + 21.65a + 26.3) \text{ s/eV}$, where a is a parameter describing the asymmetry in the neutrino decay defined as $dN_{\nu_1}/d\cos\theta = (1/2)(1 + a\cos\theta)$. The parameter $a = 0$ for a Majorana neutrino, but can vary from -1 to 1 for a Dirac neutrino. The bound given by the authors is the most conservative (which applies for $a = -1$).

² RAFFELT 85 limit on the radiative decay is from solar x- and γ -ray fluxes. Limit depends on ν flux from pp , now established from GALLEX and SAGE to be > 0.5 of expectation.

³ REINES 74 looked for ν of nonzero mass decaying radiatively to a neutral of lesser mass + γ . Used liquid scintillator detector near fission reactor. Finds lab lifetime 6×10^7 s or more. Above value of (mean life)/mass assumes average effective neutrino energy of 0.2 MeV. To obtain the limit 6×10^7 s REINES 74 assumed that the full $\bar{\nu}_e$ reactor flux could be responsible for yielding decays with photon energies in the interval 0.1 MeV – 0.5 MeV. This represents some overestimate so their lower limit is an over-estimate of the lab lifetime (VOGEL 84). If so, OBERAUER 87 may be comparable or better.

⁴ AHARMIM 19 quotes the limit τ/m_{ν_2} for invisible nonradiative decay of ν_2 . They obtained this result by analyzing the entire SNO dataset, allowing for the decay of ν_2 which would cause an energy-dependent distortion of the survival probability of electron-type solar neutrinos.

⁵ AHARMIM 19 quotes the limit τ/m_{ν_2} for invisible nonradiative decay of ν_2 . They obtained this result by combining the τ/m_{ν_2} measurements from SNO and other solar neutrino experiments (Super-Kamiokande, KamLAND, and Borexino ^{8B} results; Borexino and KamLAND ^{7Be} results; the combined gallium interaction rate from GNO, GALLEX, and SAGE; and the chlorine interaction rate from Homestake). The quoted limit at 99% CL is $> 1.04 \times 10^{-3}$.

⁶ ESCUDERO 19 sets limits on invisible neutrino decays using Planck 2018 data of $\tau > 1.3$ – 0.3×10^9 s at 95% C.L. Values in the range $\tau = 2$ – 16×10^9 s are preferred at 95% C.L. when Planck polarization data is included. Limits scale as $(m_\nu/0.05 \text{ eV})^3$.

⁷ CECCHINI 11 search for radiative decays of solar neutrinos into visible photons during the 2006 total solar eclipse. The range of (mean life)/mass values corresponds to a range of ν_1 masses between 10^{-4} and 0.1 eV.

⁸ MIRIZZI 07 determine a limit on the neutrino radiative decay from analysis of the maximum allowed distortion of the CMB spectrum as measured by the COBE/FIRAS. For the decay $\nu_2 \rightarrow \nu_1$ the lifetime limit is $\lesssim 4 \times 10^{20}$ s for $m_{min} \lesssim 0.14$ eV. For transition with the $|\Delta m_{31}|$ mass difference the lifetime limit is $\sim 2 \times 10^{19}$ s for $m_{min} \lesssim 0.14$ eV and $\sim 5 \times 10^{20}$ s for $m_{min} \gtrsim 0.14$ eV.

⁹ MIRIZZI 07 determine a limit on the neutrino radiative decay from analysis of the cosmic infrared background (CIB) using the Spitzer Observatory data. For transition with the $|\Delta m_{31}|$ mass difference they obtain the lifetime limit $\sim 10^{20}$ s for $m_{min} \lesssim 0.14$ eV.

¹⁰ WONG 07 use their limit on the neutrino magnetic moment together with the assumed experimental value of $\Delta m_{13}^2 \sim 2 \times 10^{-3} \text{ eV}^2$ to obtain $\tau_{13}/m_1^3 > 3.2 \times 10^{27} \text{ s/eV}^3$ for the radiative decay in the case of the inverted mass hierarchy. Similarly to RAFFELT 89 this limit can be violated if electric and magnetic moments are equal to each other. Analogous, but numerically somewhat different limits are obtained for τ_{23} and τ_{21} .

¹¹ XIN 05 search for the γ from radiative decay of ν_e produced by the electron capture on ⁵¹Cr. No events were seen and the limit on τ/m_ν was derived. This is a weaker limit on the decay of ν_e than KRAKAUER 91.

¹² XIN 05 use their limit on the neutrino magnetic moment of ν_e together with the assumed experimental value of $\Delta m_{1,3}^2 \sim 2 \times 10^{-3} \text{ eV}^2$ to obtain $\tau_{13}/m_1^3 > 1 \times 10^{23} \text{ s/eV}^3$ for the radiative decay in the case of the inverted mass hierarchy. Similarly to RAFFELT 89 this limit can be violated if electric and magnetic moments are equal to each other. Analogous, but numerically somewhat different limits are obtained for τ_{23} and τ_{21} . Again, this limit is specific for ν_e .

¹³ AHARMIM 04 obtained these results from the solar $\bar{\nu}_e$ flux limit set by the SNO measurement assuming ν_2 decay through nonradiative process $\nu_2 \rightarrow \bar{\nu}_1 X$, where X is a Majoron or other invisible particle. Limits are given for the cases of quasidegenerate and hierarchical neutrino masses.

¹⁴ CECCHINI 04 obtained this bound through the observations performed on the occasion of the 21 June 2001 total solar eclipse, looking for visible photons from radiative decays of solar neutrinos. Limit is a τ/m_{ν_2} in $\nu_2 \rightarrow \nu_1 \gamma$. Limit ranges from ~ 100 to 10^7 s/eV for $0.01 < m_{\nu_1} < 0.1 \text{ eV}$.

¹⁵ EGUCHI 04 obtained these results from the solar $\bar{\nu}_e$ flux limit set by the KamLAND measurement assuming ν_2 decay through nonradiative process $\nu_2 \rightarrow \bar{\nu}_1 X$, where X is a Majoron or other invisible particle. Limits are given for the cases of quasidegenerate and hierarchical neutrino masses.

¹⁶ The ratio of the lifetime over the mass derived by BANDYOPADHYAY 03 is for ν_2 . They obtained this result using the following solar-neutrino data: total rates measured in Cl and Ga experiments, the Super-Kamiokande's zenith-angle spectra, and SNO's day and night spectra. They assumed that ν_1 is the lowest mass, stable or nearly stable neutrino state and ν_2 decays through nonradiative Majoron emission process, $\nu_2 \rightarrow \bar{\nu}_1 + J$, or through nonradiative process with all the final state particles being sterile. The best fit is obtained in the region of the LMA solution.

¹⁷ DERBIN 02B (also BACK 03b) obtained this bound for the radiative decay from the results of background measurements with Counting Test Facility (the prototype of the Borexino detector). The laboratory gamma spectrum is given as $dN_\gamma/d\cos\theta = (1/2)(1 + \alpha\cos\theta)$ with $\alpha=0$ for a Majorana neutrino, and α varying to -1 to 1 for a Dirac neutrino. The listed bound is for the case of $\alpha=0$. The most conservative bound $1.5 \times 10^{13} \text{ s eV}^{-1}$ is obtained for the case of $\alpha=-1$.

¹⁸ The ratio of the lifetime over the mass derived by JOSHIPURA 02B is for ν_2 . They obtained this result from the total rates measured in all solar neutrino experiments. They assumed that ν_1 is the lowest mass, stable or nearly stable neutrino state and ν_2 decays through nonradiative process like Majoron emission decay, $\nu_2 \rightarrow \nu'_1 + J$ where ν'_1 state is sterile. The exact limit depends on the specific solution of the solar neutrino problem. The quoted limit is for the LMA solution.

¹⁹ DOLGOV 99 places limits in the (Majorana) τ -associated ν mass-lifetime plane based on nucleosynthesis. Results would be considerably modified if neutrino oscillations exist.

²⁰ BILLER 98 use the observed TeV γ -ray spectra to set limits on the mean life of any radiatively decaying neutrino between 0.05 and 1 eV. Curve shows $\tau_\nu/B_\gamma > 0.15 \times 10^{21} \text{ s}$ at 0.05 eV, $> 1.2 \times 10^{21} \text{ s}$ at 0.17 eV, $> 3 \times 10^{21} \text{ s}$ at 1 eV, where B_γ is the branching ratio to photons.

²¹ BLUDMAN 92 sets additional limits by this method for higher mass ranges. Cosmological limits are also obtained.

²² Limit on the radiative decay based on nonobservation of γ 's in coincidence with ν 's from SN 1987A.

²³ DODELSON 92 range is for wrong-helicity keV mass Dirac ν 's from the core of neutron star in SN 1987A decaying to ν 's that would have interacted in KAM2 or LMB detectors.

²⁴ GRANEK 91 considers heavy neutrino decays to $\gamma\nu_L$ and $3\nu_L$, where $m_{\nu_1} < 100 \text{ keV}$. Lifetime is calculated as a function of heavy neutrino mass, branching ratio into $\gamma\nu_L$, and m_{ν_1} .

²⁵ KRAKAUER 91 quotes the limit for ν_e , $\tau/m_\nu > (0.3a^2 + 9.8a + 15.9) \text{ s/eV}$, where a is a parameter describing the asymmetry in the radiative neutrino decay defined as $dN_\nu/d\cos\theta = (1/2)(1 + a\cos\theta)$ $a=0$ for a Majorana neutrino, but can vary from -1 to 1 for a Dirac neutrino. The bound given by the authors is the most conservative (which applies for $a = -1$).

²⁶ WALKER 90 uses SN 1987A γ flux limits after 289 days.

²⁷ CHUPP 89 should be multiplied by a branching ratio (about 1) and a detection efficiency (about 1/4), and pertains to radiative decay of any neutrino to a lighter or sterile neutrino.

²⁸ RAFFELT 89 uses KYULDJIEV 84 to obtain $\tau m^3 > 3 \times 10^{18} \text{ s eV}^3$ (based on $\bar{\nu}_e e^-$ cross sections). The bound for the radiative decay is not valid if electric and magnetic transition moments are equal for Dirac neutrinos.

See key on page 999

Lepton Particle Listings
Neutrino Properties

- 29 RAFFELT 89B analyze stellar evolution and exclude the region 3 x 10^12 < tau m^3 < 3 x 10^21 s eV^3.
30 Model-dependent theoretical analysis of SN1987A neutrinos. Quoted limit is for [sum_j |U_lj|^2 Gamma_j m_j]^-1, where l=mu, tau. Limit is 3.3 x 10^14 s/eV for l=e.
31 OBERAUER 87 looks for photons and e+e- pairs from radiative decays of reactor neutrinos.
32 BINETRUY 84 finds tau < 10^8 s for neutrinos in a radiation-dominated universe.
33 These experiments look for nu_k -> nu_j gamma or nu_k -> nu_j gamma.
34 STECKER 80 limit based on UV background; result given is tau > 4 x 10^22 s at m_nu = 20 eV.
35 FALK 78 finds lifetime constraints based on supernova energetics.
36 COWSIK 77 considers variety of scenarios. For neutrinos produced in the big bang, present limits on optical photon flux require tau > 10^23 s for m_nu ~ 1 eV. See also COWSIK 79 and GOLDMAN 79.

MAGNETIC MOMENT

The coupling of neutrinos to an electromagnetic field is characterized by a 3x3 matrix lambda of the magnetic (mu) and electric (d) dipole moments (lambda = mu - id). For Majorana neutrinos the matrix lambda is antisymmetric and only transition moments are allowed, while for Dirac neutrinos lambda is a general 3x3 matrix. In the standard electroweak theory extended to include neutrino masses (see FUJIKAWA 80) mu_nu = 3e G_F m_nu / (8 pi^2 sqrt(2)) = 3.2 x 10^-19 (m_nu/eV) mu_B, i.e. it is unobservably small given the known small neutrino masses. In more general models there is no longer a proportionality between neutrino mass and its magnetic moment, even though only massive neutrinos have nonvanishing magnetic moments without fine tuning.

Laboratory bounds on lambda are obtained via elastic nu-e scattering, where the scattered neutrino is not observed. The combinations of matrix elements of lambda that are constrained by various experiments depend on the initial neutrino flavor and on its propagation between source and detector (e.g., solar nu_e and reactor nu_e do not constrain the same combinations). The listings below therefore identify the initial neutrino flavor.

Other limits, e.g. from various stellar cooling processes, apply to all neutrino flavors. Analogous flavor independent, but weaker, limits are obtained from the analysis of e+e- -> nu gamma collider experiments.

Table with columns: VALUE (10^-10 mu_B), CL%, DOCUMENT ID, TECN, COMMENT. Lists various experimental constraints on the magnetic moment of neutrinos from sources like AGOSTINI, BEDA, AUERBACH, etc.

Table with columns: VALUE, DOCUMENT ID, TECN, COMMENT. Lists constraints on neutrino properties from sources like KRAKAUER, RAFFELT, FUKUGITA, GROUCH, etc.

- 1 AGOSTINI 17A obtained this limit using the shape of the recoil electron energy spectrum from the Borexino Phase-II 1291.5 live days of solar neutrino data and the constraints on the sum of the solar neutrino fluxes from the radiochemical gallium experiments SAGE, Gallex, and GNO. Without radiochemical constraints, the 90% C.L. limit of < 4.0 x 10^-11 mu_B is obtained.
2 BEDA 13 report nu_e e- scattering results, using the Kalinin Nuclear Power Plant and a shielded Ge detector. The recoil electron spectrum is analyzed between 2.5 and 55 keV. Supersedes BEDA 07. Supersedes BEDA 10. This is the most stringent limit on the magnetic moment of reactor nu_e.
3 AUERBACH 01 limit is based on the LSND nu_e and nu_mu electron scattering measurements. The limit is slightly more stringent than KRAKAUER 90.
4 SCHWIENHORST 01 quote an experimental sensitivity of 4.9 x 10^-7.
5 ARCEO-DIAZ 15 constrains the neutrino magnetic moment from observation of the tip of the red giant branch in the globular cluster omega-Centauri.
6 CORSICO 14 constrains the neutrino magnetic moment from observations of white dwarf pulsations.
7 MILLER-BERTOLAMI 14B constrains the neutrino magnetic moment from observations of the white dwarf luminosity function of the Galactic disk.
8 VIAUX 13A constrains the neutrino magnetic moment from observations of the globular cluster M5.
9 BEDA 10 report nu_e e- scattering results, using the Kalinin Nuclear Power Plant and a shielded Ge detector. The recoil electron spectrum is analyzed between 2.9 and 45 keV. Supersedes BEDA 07. Supersedes by BEDA 13.
10 DENIZ 10 observe reactor nu_e scattering with recoil kinetic energies 3-8 MeV using CsI(Tl) detectors. The observed rate and spectral shape are consistent with the Standard Model prediction, leading to the reported constraint on nu_e magnetic moment.
11 KUZNETSOV 09 obtain a limit on the flavor averaged magnetic moment of Dirac neutrinos from the time averaged neutrino signal of SN1987A. Improves and supersedes the analysis of BARBIERI 88 and AYALA 99.
12 ARPESELLA 08A obtained this limit using the shape of the recoil electron energy spectrum from the Borexino 192 live days of solar neutrino data.
13 BEDA 07 performed search for electromagnetic nu_e-e scattering at Kalininskaya nuclear reactor. A Ge detector with active and passive shield was used and the electron recoil spectrum between 3.0 and 61.3 keV analyzed. Superseded by BEDA 10.
14 WONG 07 performed search for non-standard nu_e-e scattering at the Kuo-Sheng nuclear reactor. Ge detector equipped with active anti-Compton shield is used. Most stringent laboratory limit on magnetic moment of reactor nu_e. Supersedes LI 03B.
15 DARAKTCHIEVA 05 present the final analysis of the search for non-standard nu_e-e scattering component at Bugey nuclear reactor. Full kinematical event reconstruction of both the kinetic energy above 700 keV and scattering angle of the recoil electron, by use of TPC. Most stringent laboratory limit on magnetic moment. Supersedes DARAKTCHIEVA 03.
16 XIN 05 evaluated the nu_e flux at the Kuo-Sheng nuclear reactor and searched for non-standard nu_e-e scattering. Ge detector equipped with active anti-Compton shield was used. This laboratory limit on magnetic moment is considerably less stringent than the limits for reactor nu_e, but is specific to nu_e.
17 GRIFOLS 04 obtained this bound using the SNO data of the solar 8B neutrino flux measured with deuteron breakup. This bound applies to mu_eff = (mu_21^2 + mu_22^2 + mu_23^2)^1/2.
18 LIU 04 obtained this limit using the shape of the recoil electron energy spectrum from the Super-Kamiokande-I 1496 days of solar neutrino data. Neutrinos are assumed to have only diagonal magnetic moments, mu_j1 = mu_j2. This limit corresponds to the oscillation parameters in the vacuum oscillation region.
19 LIU 04 obtained this limit using the shape of the recoil electron energy spectrum from the Super-Kamiokande-I 1496 live-day solar neutrino data, by limiting the oscillation parameter region in the LMA region allowed by solar neutrino experiments plus KamLAND. mu_j1 = mu_j2 is assumed. In the LMA region, the same limit would be obtained even if neutrinos have off-diagonal magnetic moments.
20 BACK 03B obtained this bound from the results of background measurements with Counting Test Facility (the prototype of the Borexino detector). Standard Solar Model flux was assumed. This mu_nu can be different from the reactor mu_nu in certain oscillation scenarios (see BEACOM 99).
21 DARAKTCHIEVA 03 searched for non-standard nu_e-e scattering component at Bugey nuclear reactor. Full kinematical event reconstruction by use of TPC. Superseded by DARAKTCHIEVA 05.
22 LI 03B used Ge detector in active shield near nuclear reactor to test for nonstandard nu_e-e scattering.
23 GRIMUS 02 obtain stringent bounds on all Majorana neutrino transition moments from a simultaneous fit of LMA-MSW oscillation parameters and transition moments to global

Lepton Particle Listings

Neutrino Properties

- solar neutrino data + reactor data. Using only solar neutrino data, a 90% CL bound of $6.3 \times 10^{-10} \mu_B$ is obtained.
- 24 TANIMOTO 00 combined $e^+ e^- \rightarrow \nu \bar{\nu} \gamma$ data from VENUS, TOPAZ, and AMY.
 - 25 AYALA 99 improves the limit of BARBIERI 88.
 - 26 BEACOM 99 obtain the limit using the shape, but not the absolute magnitude which is affected by oscillations, of the solar neutrino spectrum obtained by Superkamiokande (825 days). This μ_ν can be different from the reactor μ_ν in certain oscillation scenarios.
 - 27 RAFFELT 99 is an update of RAFFELT 90. This limit applies to all neutrino flavors which are light enough (< 5 keV) to be emitted from globular-cluster red giants. This limit pertains equally to electric dipole moments and magnetic transition moments, and it applies to both Dirac and Majorana neutrinos.
 - 28 RAFFELT 99 is essentially an update of BERNSTEIN 63, but is derived from the helioseismological limit on a new energy-loss channel of the Sun. This limit applies to all neutrino flavors which are light enough (< 1 keV) to be emitted from the Sun. This limit pertains equally to electric dipole and magnetic transition moments, and it applies to both Dirac and Majorana neutrinos.
 - 29 ACCIARRI 97q result applies to both direct and transition magnetic moments and for $q^2=0$.
 - 30 ELMFORS 97 calculate the rate of depolarization in a plasma for neutrinos with a magnetic moment and use the constraints from a big-bang nucleosynthesis on additional degrees of freedom.
 - 31 Applies to absolute value of magnetic moment.
 - 32 DERBIN 93 determine the cross section for 0.6–2.0 MeV electron energy as $(1.28 \pm 0.63) \times \sigma_{\text{weak}}$. However, the (reactor on - reactor off)/(reactor off) is only $\sim 1/100$.
 - 33 COOPER-SARKAR 92 assume $f_D/f_\pi = 2$ and D_S, \bar{D}_S production cross section = $2.6 \mu\text{b}$ to calculate ν flux.
 - 34 VIDYAKIN 92 limit is from a $e\bar{\nu}$ elastic scattering experiment. No experimental details are given except for the cross section from which this limit is derived. Signal/noise was 1/10. The limit uses $\sin^2\theta_W = 0.23$ as input.
 - 35 DORENBOSCH 91 corrects an incorrect statement in DORENBOSCH 89 that the ν magnetic moment is $< 1 \times 10^{-9}$ at the 95%CL. DORENBOSCH 89 measures both $\nu_\mu e$ and $\bar{\nu} e$ elastic scattering and assume $\mu(\nu) = \mu(\bar{\nu})$.
 - 36 KRAKAUER 90 experiment fully reported in ALLEN 93.
 - 37 RAFFELT 90 limit applies for a diagonal magnetic moment of a Dirac neutrino, or for a transition magnetic moment of a Majorana neutrino. In the latter case, the same analysis gives $< 1.4 \times 10^{-12}$. Limit at 95%CL obtained from δM_C .
 - 38 Significant dependence on details of stellar models.
 - 39 FUKUGITA 88 find magnetic dipole moments of any two neutrino species are bounded by $\mu < 10^{-16} [10^{-9} G/B_0]$ where B_0 is the present-day intergalactic field strength.
 - 40 GROTCHE 88 combined data from MAC, ASP, CELLO, and Mark J.
 - 41 For $m_\nu = 8\text{--}200$ eV. NUSSINOV 87 examines transition magnetic moments for $\nu_\mu \rightarrow \nu_e$ and obtain $< 3 \times 10^{-15}$ for $m_\nu > 16$ eV and $< 6 \times 10^{-14}$ for $m_\nu > 4$ eV.
 - 42 We obtain above limit from SUTHERLAND 76 using their limit $f < 1/3$.
 - 43 KIM 74 is a theoretical analysis of $\bar{\nu}_\mu$ reaction data.

NEUTRINO CHARGE RADIUS SQUARED

We report limits on the so-called neutrino charge radius squared. While the straight-forward definition of a neutrino charge radius has been proven to be gauge-dependent and, hence, unphysical (LEE 77c), there have been recent attempts to define a physically observable neutrino charge radius (BERNABEU 00, BERNABEU 02). The issue is still controversial (FUJIKAWA 03, BERNABEU 03). A more general interpretation of the experimental results is that they are limits on certain nonstandard contributions to neutrino scattering.

VALUE (10^{-32} cm^2)	CL%	DOCUMENT ID	TECN	COMMENT
-2.1 to 3.3	90	1 DENIZ 10	TEXO	Reactor $\bar{\nu}_e e$
••• We do not use the following data for averages, fits, limits, etc. •••				
-4 to 5.5	90	2 CADEDU 18		ν_μ coherent scat. on CsI
-0.53 to 0.68	90	3 HIRSCH 03		$\nu_\mu e$ scat.
-8.2 to 9.9	90	4 HIRSCH 03		anomalous $e^+ e^- \rightarrow \nu \bar{\nu} \gamma$
-2.97 to 4.14	90	5 AUERBACH 01	LSND	$\nu_e e \rightarrow \nu_e e$
-0.6 to 0.6	90	VILAIN 95B	CHM2	$\nu_\mu e$ elastic scat.
0.9 \pm 2.7		ALLEN 93	CNTR	LAMPF $\nu e \rightarrow \nu e$
< 2.3	95	MOURAO 92	ASTR	HOME/KAM2 ν rates
< 7.3	90	6 VIDYAKIN 92	CNTR	Reactor $\bar{\nu} e \rightarrow \bar{\nu} e$
1.1 \pm 2.3		ALLEN 91	CNTR	Repl. by ALLEN 93
-1.1 \pm 1.0		7 AHRENS 90	CNTR	$\nu_\mu e$ elastic scat.
-0.3 \pm 1.5		7 DORENBOS... 89	CHRM	$\nu_\mu e$ elastic scat.
		8 GRIFOLS 89B	ASTR	SN 1987A

- 1 DENIZ 10 observe reactor $\bar{\nu}_e e$ scattering with recoil kinetic energies 3–8 MeV using CsI(Tl) detectors. The observed rate and spectral shape are consistent with the Standard Model prediction, leading to the reported constraint on $\bar{\nu}_e$ charge radius.
- 2 CADEDU 18 use the data of the COHERENT experiment, AKIMOV 18. The limit is $\langle r_\nu^2 \rangle$ for ν_μ obtained from the time-dependent data. Weaker limits were obtained for charge radii of ν_e and for transition charge radii. The published value was divided by 2 to conform to the convention of this table.

- 3 Based on analysis of CCFR 98 results. Limit is on $\langle r_\nu^2 \rangle + \langle r_A^2 \rangle$. The CHARM II and E734 at BNL results are reanalyzed, and weaker bounds on the charge radius squared than previously published are obtained. The NuTeV result is discussed; when tentatively interpreted as ν_μ charge radius it implies $\langle r_\nu^2 \rangle + \langle r_A^2 \rangle = (4.20 \pm 1.64) \times 10^{-33} \text{ cm}^2$.
- 4 Results of LEP-2 are interpreted as limits on the axial-vector charge radius squared of a Majorana ν_τ . Slightly weaker limits for both vector and axial-vector charge radius squared are obtained for the Dirac case, and somewhat weaker limits are obtained from the analysis of lower energy data (LEP-1.5 and TRISTAN).
- 5 AUERBACH 01 measure $\nu_e e$ elastic scattering with LSND detector. The cross section agrees with the Standard Model expectation, including the charge and neutral current interference. The 90% CL applies to the range shown.
- 6 VIDYAKIN 92 limit is from a $e\bar{\nu}$ elastic scattering experiment. No experimental details are given except for the cross section from which this limit is derived. Signal/noise was 1/10. The limit uses $\sin^2\theta_W = 0.23$ as input.
- 7 Result is obtained from reanalysis given in ALLEN 91, followed by our reduction to obtain 1σ errors.
- 8 GRIFOLS 89b sets a limit of $\langle r^2 \rangle < 0.2 \times 10^{-32} \text{ cm}^2$ for right-handed neutrinos.

REFERENCES FOR Neutrino Properties

AHARMIM 19	PR D99 032013	B. Aharmim et al.	(SNO Collab.)
AKER 19	PRL 123 221802	M. Aker et al.	(KATRIN)
ESCUDERO 19	PR D100 103531	M. Escudero, M. Fairbairn	(LOKX)
LOUREIRO 19	PRL 123 081301	A. Loureiro et al.	
UPADHYE 19	JCAP 1905 041	A. Upadhye	(WISC)
AKIMOV 18	arXiv:1804.09459	D. Akimov et al.	(COHERENT Collab.)
CADEDU 18	PR D98 113010	M. Cadeddu et al.	
CHOUDHURY 18	JCAP 1809 017	S.R. Choudhury, S. Choubey	
AGOSTINI 17A	PR D96 091103	M. Agostini et al.	(Borexino Collab.)
SIMPSON 17	JCAP 1706 029	F. Simpson et al.	(BARC)
VAGNOZZI 17	PR D96 123503	S. Vagnozzi et al.	
YECHÉ 17	JCAP 1706 047	C. Yeché et al.	
DELLA-VALLE 16	EPJ C76 24	F. Della Valle et al.	(PVLAS Collab.)
DIVALENTINO 16	PR D93 083527	E. Di Valentino et al.	
GIUSARMA 16	PR D94 083522	E. Giusarma et al.	
HUANG 16	EPJ C76 489	Q.-G. Huang, K. Wang, S. Wang	
ARCEO-DIAZ 15	ASP 70 1	S. Arceo-Diaz et al.	
PALANQUE... 15A	JCAP 1511 011	N. Palanque-Desabrouille et al.	
ROSSI 15	PR D92 063505	G. Rossi et al.	
ADE 14	AA 571 A16	P.A.R. Ade et al.	(Planck Collab.)
BATTYE 14	PRL 112 051303	R.A. Battye, A. Moss	(MCHS, NOTT)
BEUTLER 14	MNRAS 444 3501	F. Beutler et al.	(BOSS Collab.)
CHEN 14A	PR D90 011301	J.-W. Chen et al.	(TEXONO Collab.)
CORSICO 14	JCAP 1408 054	A.H. Corsico	
COSTANZI 14	JCAP 1410 081	M. Costanzi et al.	(TRST, TRST1)
GIUSARMA 14	PR D90 043507	E. Giusarma et al.	
HOU 14	APJ 782 74	Z. Hou et al.	
LEISTEDT 14	PRL 113 041301	B. Leistedt, H.V. Peiris, L. Verde	
MILLER-BER... 14B	AA 562 A123	M.M. Miller-Berlioni	(MPIG, LAPL)
RIEMER-SOR... 14	PR D89 103505	S. Riemer-Sørensen, D. Parkinson, T.M. Davis	(BOSS Collab.)
STUDENIKIN 14	EPL 107 21001	A.I. Studenikin	(GEMMA Collab.)
BEDA 13	PNPL 10 139	A.G. Beda et al.	
VIAUX 13A	PRL 111 231301	N. Viaux et al.	
MORESCO 12	JCAP 1207 053	M. Moresco et al.	
XIA 12	JCAP 1206 010	J.-Q. Xia et al.	
ASEEV 11	PR D84 112003	V.N. Aseev et al.	
CECCHINI 11	ASP 34 486	S. Cecchini et al.	
SAITO 11	PR D83 043529	S. Saito, M. Takada, A. Taruya	
BEDA 10	PNPL 7 406	A.G. Beda et al.	(GEMMA Collab.)
DENIZ 10	PR D81 072001	M. Deniz et al.	(TEXONO Collab.)
NANNESTAD 10	JCAP 1008 001	S. Hannestad et al.	
PAGLIAROLI 10	ASP 33 287	G. Pagliaroli, F. Rossi-Torres, E. Vissani	(INFN+)
SEKIGUCHI 10	JCAP 1003 015	T. Sekiguchi et al.	
THOMAS 10	PRL 105 031301	S.A. Thomas, F.B. Abdalla, O. Lahav	(LOUC)
ICHIKI 09	PR D79 023520	K. Ichiki, M. Takada, T. Takahashi	
KOMATSU 09	APJS 180 330	E. Komatsu et al.	
KUZNETSOV 09	IJMP A24 5977	A.V. Kuznetsov, N.V. Mikheyev, A.A. Okrugin	(YARO)
TERENO 09	AA 500 657	I. Tereno et al.	
VIKHLININ 09	APJ 692 1060	A. Vikhlinin et al.	
ARPESELLA 08A	PRL 101 091302	C. Arpessella et al.	(Borexino Collab.)
BERNARDIS 08	PR D78 083535	F. De Bernardis et al.	
BEDA 07	PAN 70 1873	A.G. Beda et al.	
	Translated from YAF 70 1925		
FOGLI 07	PR D75 053001	G.L. Fogli et al.	
GNINENKO 07	PR D75 075014	S.N. Gninenko, N.V. Krasnikov, A. Rubbia	
KRISTIANSEN 07	PR D75 083510	J. Kristiansen, O. Elgaroy, H. Dahle	
MIRIZZI 07	PR D76 053007	A. Mirizzi, D. Montanari, P.D. Serpico	
SPERGEL 07	APJS 170 377	D.N. Spergel et al.	
WONG 07	PR D75 012001	H.T. Wong et al.	(TEXONO Collab.)
ZUNCKEL 07	JCAP 0708 004	C. Zunckel, P. Ferreira	
CIRELLI 06	JCAP 0612 013	M. Cirelli et al.	
FUKUGITA 06	PR D74 027302	M. Fukugita et al.	
GOOBAR 06	JCAP 0606 019	A. Goobar et al.	
HANNESTAD 06	JCAP 0611 016	S. Hannestad, G. Raffelt	
KRISTIANSEN 06	PR D74 123005	J. Kristiansen, O. Elgaroy, H. Eriksen	
SANCHEZ 06	MNRAS 366 189	A.G. Sanchez et al.	
SELJAK 06	JCAP 0610 014	U. Seljak, A. Slosar, P. McDonald	
CAPRINI 05	JCAP 0502 006	C. Caprini, P.G. Ferreira	(GEVA, OXFTP)
DARAKTCH... 05	PL B615 153	Z. Daraktchieva et al.	(MUNU Collab.)
ICHIKAWA 05	PR D71 043001	K. Ichikawa, M. Fukugita, M. Kawasaki	(ICRR)
KRAUS 05	EPJ C40 447	Ch. Kraus et al.	
XIN 05	PR D72 012006	B. Xin et al.	(TEXONO Collab.)
AHARMIM 04	PR D70 093014	B. Aharmim et al.	(SNO Collab.)
BARGER 04	PL B595 55	V. Barger, D. Marfatia, A. Tregre	
CECCHINI 04	ASP 21 183	S. Cecchini et al.	(BGNA+)
CROTTY 04	PR D69 123007	P. Crotty, J. Lessingourges, S. Pastor	
EGUCHI 04	PRL 92 071301	K. Eguchi et al.	(KamLAND Collab.)
GRIFOLS 04	PL B587 184	J.A. Grifols, E. Masso, S. Mohanty	(BARC, AHMED)
LIU 04	PRL 93 021802	D.W. Liu et al.	(Super-Kamiokande Collab.)
ARNABOLDI 03A	PRL 91 161802	C. Arnaboldi et al.	
BACK 03B	PL B563 35	H.O. Back et al.	(Borexino Collab.)
BANDYOPA... 03	PL B555 33	A. Bandyopadhyay, S. Choubey, S. Goswami	(SAHA+)
BERNABEU 03	hep-ph/0303202	J. Bernabeu, J. Papavassiliou, J. Vidal	
DARAKTCH... 03	PL B564 190	Z. Daraktchieva et al.	(MUNU Collab.)
FUJIKAWA 03	hep-ph/0303188	K. Fujikawa, R. Shrock	
HIRSCH 03	PR D67 033005	M. Hirsch, E. Nardi, D. Restrepo	
LI 03B	PRL 90 131802	H.B. Li et al.	(TEXONO Collab.)
SPERGEL 03	APJS 148 175	D.N. Spergel et al.	
BERNABEU 02	PRL 89 101802	J. Bernabeu, J. Papavassiliou, J. Vidal	
Also	PRL 89 229902 (errata)	J. Bernabeu, J. Papavassiliou, J. Vidal	
DERBIN 02B	JETPL 76 409	A.V. Derbin, O.Ju. Smirnov	

Translated from ZETFP 76 483.

See key on page 999

Lepton Particle Listings

Neutrino Properties, Number of Neutrino Types

GRIMUS	02	NP B648 376	W. Grimus et al.	
JOSHIPURA	02B	PR D66 113008	A.S. Josphira, E. Masso, S. Mohanty	
LEWIS	02	PR D66 103511	A. Lewis, S. Bridle	
LOREDO	02	PR D65 063002	T.J. Loredo, D.Q. Lamb	
WANG	02	PR D65 123001	X. Wang, M. Tegmark, M. Zaldarriaga	
AUERBACH	01	PR D63 112001	L.B. Auerbach et al.	(LSDN Collab.)
SCHWIENHO...	01	PL B513 23	R. Schwenhorst et al.	(DOMUT Collab.)
ATHANAS	00	PR D61 052002	M. Athanas et al.	(CLEO Collab.)
BERNABEU	00	PR D62 113012	J. Bernabeu et al.	
FUKUGITA	00	PRL 84 1082	M. Fukugita, G.C. Liu, N. Sugiyama	
TANIMOTO	00	PL B478 1	N. Tanimoto et al.	
AYALA	99	PR D59 111901	A. Ayala, J.C. D'Olivo, M. Torres	
BEACOM	99	PRL 83 5222	J.F. Beacom, P. Vogel	
CROFT	99	PRL 83 1092	R.A.C. Croft, W. Hu, R. Dave	
DOLGOV	99	NP B548 385	A.D. Dolgov et al.	
LOBASHEV	99	PL B460 227	V.M. Lobashev et al.	
RAFFELT	99	PRPL 320 319	G.G. Raffelt	
WEINHIMER	99	PL B460 219	Ch. Weinheimer et al.	
ACKERSTAFF	98T	EPJ C5 229	K. Ackerstaff et al.	(OPAL Collab.)
AMMAR	98	PL B431 209	R. Ammar et al.	(CLEO Collab.)
BARATE	98F	EPJ C2 395	R. Barate et al.	(ALEPH Collab.)
BILLER	98	PRL 80 2992	S.D. Biller et al.	(WHIPPLE Collab.)
FELDMAN	98	PR D57 3873	G.J. Feldman, R.D. Cousins	
LENZ	98	PL B416 50	S. Lenz et al.	
ABREU	97J	ZPHY C74 577	P. Abreu et al.	(DELPHI Collab.)
ACCIARRI	97Q	PL B412 201	M. Acciari et al.	(L3 Collab.)
ANASTASSOV	97	PR D55 2559	A. Anastassov et al.	(CLEO Collab.)
	Also	PR D58 119903 (erratum)	A. Anastassov et al.	(CLEO Collab.)
ELMFORS	97	NP B503 3	P. Elmfors et al.	
ESCRIBANO	97	PL B395 369	R. Escríbano, E. Masso	(BARC, PARIT)
FIELDS	97	ASP 6 169	B.D. Fields, K. Kainulainen, K.A. Olive	(NDAM+)
SWAIN	97	PR D55 1	J. Swain, L. Taylor	(NEAS)
ALEXANDER	96M	ZPHY C72 231	G. Alexander et al.	(OPAL Collab.)
ASSAMAGAN	96	PR D53 6065	K.A. Assamagan et al.	(PSI, ZURI, VILL+)
BAI	96	PR D53 20	J.Z. Bai et al.	(BES Collab.)
BOTTINO	96	PR D53 6361	A. Bottino et al.	
DOLGOV	96	PL B383 193	A.D. Dolgov, S. Pastor, J.W.F. Valle	(IFIC, VALE)
HANNESSTAD	96	PRL 76 2848	S. Hannestad, J. Madsen	(AARH)
HANNESSTAD	96B	PRL 77 5148 (erratum)	S. Hannestad, J. Madsen	(AARH)
HANNESSTAD	96C	PR D54 7894	S. Hannestad, J. Madsen	(AARH)
SOBIE	96	ZPHY C70 383	R.J. Sobie, R.K. Keeler, I. Lawson	(VICT)
BELESVE	95	PL B349 263	A.I. Belesve et al.	(INRM, KIAE)
BUSKULIC	95H	PL B349 585	D. Buskulic et al.	(ALEPH Collab.)
CHING	95	UMP A10 2841	C.R. Ching et al.	(CST, BEUT, CIAE)
DOLGOV	95	PR D51 4129	A.D. Dolgov, K. Kainulainen, I.Z. Rothstein	(MICH+)
HIDDEMANN	95	JP G21 639	K.H. Hidde mann, H. Daniel, O. Schwentker	(MUNT)
KERNAN	95	NP B437 243	P.J. Kernan, L.M. Krauss	(CASE)
SIGL	95	PR D51 1499	G. Sigl, M.S. Turner	(FNAL, EFI)
STOEFL	95	PRL 75 3237	W. Stoefl, D.J. Decman	(LNL)
VILAIN	95B	PL B345 115	P. Vilain et al.	(CHARM II Collab.)
ASSAMAGAN	94	PL B335 231	K.A. Assamagan et al.	(PSI, ZURI, VILL+)
BABU	94	PL B321 140	K.S. Babu, T.M. Gould, I.Z. Rothstein	(BART+)
DODELSON	94	PL D49 5068	S. Dodelson, G. Gyuk, M.S. Turner	(FNAL, CHIC+)
GOULD	94	PL B333 545	T.M. Gould, I.Z. Rothstein	(JHU, MICH)
JECKELMANN	94	PL B335 326	B. Jeckelmann, P.F.A. Goudmits, H.J. Leisi	(WABRN+)
KAWASAKI	94	NP B419 105	M. Kawasaki et al.	(OSU)
PERES	94	PR D50 513	O.L.G. Peres, V. Pleitez, R. Zukanovich Funchal	
YASUMI	94	PL B334 229	S. Yasumi et al.	(KEK, TSUK, KYOT+)
ALLEN	93	PR D47 11	R.C. Allen et al.	(UCI, LANL, ANL+)
BALEST	93	PR D47 3671	R. Balest et al.	(CLEO Collab.)
CINABRO	93	PRL 70 3700	D. Cinabro et al.	(CLEO Collab.)
DERBIN	93	JETPL 57 768	A.V. Derbin et al.	(PNPI)
		Translated from ZETFP 57 755.		
DOLGOV	93	PRL 71 476	A.D. Dolgov, I.Z. Rothstein	(MICH)
ENQVIST	93	PL B301 376	K. Enqvist, H. Uibo	(NORD)
SUN	93	CMP 15 261	H.C. Sun et al.	(CIAE, CST)
WEINHIMER	93	PL B300 210	C. Weinheimer et al.	(MANZ)
ALBRECHT	92M	PL B292 221	H. Albrecht et al.	(ARGUS Collab.)
BLUDMAN	92	PR D45 4720	S.A. Bludman	(CFPA)
COOPER...	92	PL B280 153	A.M. Cooper-Sarkar et al.	(BEBC WA66 Collab.)
DODELSON	92	PRL 68 2572	S. Dodelson, J.A. Frieman, M.S. Turner	(FNAL+)
HOLZSCHUH	92B	PL B287 381	E. Holzschuh, M. Fritschl, W. Kundig	(ZURI)
KAWANO	92	PL B275 487	L.H. Kawano et al.	(CIT, UCSD, LLL+)
MOURAO	92	PL B285 364	A.M. Mourao, J. Pulido, J.P. Ralston	(LISB, LISBT+)
PDG	92	PR D45 51	K. Hikasa et al.	(KEK, LBL, BOST+)
VIDYAKIN	92	JETPL 55 206	G.S. Vidyakin et al.	(KIAE)
		Translated from ZETFP 55 212.		
ALLEN	91	PR D43 1	R.C. Allen et al.	(UCI, LANL, UMD)
DAVIDSON	91	PR D43 2314	S. Davidson, B.A. Campbell, D. Bailey	(ALBE+)
DESHPANDE	91	PR D43 943	N.M. Deshpande, K.V.L. Sarna	(OREG, TATA)
DORENBOSCH...	91	ZPHY C51 142 (erratum)	J. Dorenbosch et al.	(CHARM Collab.)
FULLER	91	PR D43 3136	G.M. Fuller, R.A. Malaney	(UCSD)
GRANEK	91	JUMP A6 2387	H. GraneK, B.H.J. McKellar	(MELB)
KAWAKAMI	91	PL B256 105	H. Kawakami et al.	(INUS, TOHOK, TINT+)
KOLB	91	PRL 67 533	E.W. Kolb et al.	(FNAL, CHIC)
KRAKAUER	91	PR D44 6	D.A. Krakaue r et al.	(LAMPF E225 Collab.)
LAM	91	PR D44 3345	W.P. Lam, K.W. Ng	(AST)
ROBERTS ON	91	PRL 67 957	R.G.H. Robertso n et al.	(LASL, LLL)
AHRENS	90	PR D41 3297	L.A. Ahrens et al.	(BNL, BROW, HIRO+)
AVIGNONE	90	PR D41 682	F.T. Avignone, J.I. Collar	(SCUC)
KRAKAUER	90	PL B252 177	D.A. Krakaue r et al.	(LAMPF E225 Collab.)
RAFFELT	90	PRL 64 2856	G.G. Raffelt	(MPIM)
WALKER	90	PR D41 689	T.P. Walker	(HARV)
CHUPP	89	PRL 62 505	E.L. Chupp, W.T. Vestrand, C. Reppin	(UNH, MPIM)
DORENBOSCH...	89	ZPHY C41 567	J. Dorenbosch et al.	(CHARM Collab.)
GRIFOLS	89B	PR D40 3819	J.A. Grifols, E. Masso	(BARC)
KOLB	89	PRL 62 509	E.W. Kolb, M.S. Turner	(CHIC, FNAL)
LOREDO	89	ANYAS 571 601	T.J. Loredo, D.Q. Lamb	(CHIC)
RAFFELT	89	PR D39 2066	G.G. Raffelt	(PRIN, UCB)
RAFFELT	89B	APJ 336 61	H. Raffelt, D. Dearborn, J. Silk	(UCB, LLL)
ALBRECHT	88B	PL B202 149	H. Albrecht et al.	(ARGUS Collab.)
BARBERI	88	PRL 61 27	R. Barberi, R.N. Mohapatra	(PSI, UMD)
BORIS	88	PRL 61 245 (erratum)	S.D. Boris et al.	(ITEP, ASCI)
FUKUGITA	88	PRL 60 879	M. Fukugita et al.	(KYOTU, MPIM, UCB)
GROTC H	88	ZPHY C39 553	H. Grotch, R.W. Robinett	(PSU)
RAFFELT	88B	PR D37 549	G.G. Raffelt, D.S.P. Dearborn	(UCB, LLL)
SPERGEL	88	PL B200 366	D.N. Spergel, J.N. Bahcall	(IAS)
VONFEILITZ...	88	PL B200 580	F. von Feilitzsch, L. Oberauer	(MUNT)
BARBIELLINI	87	NAT 329 21	G. Barbiellini, G. Cocconi	(CERN)
BORIS	87	PRL 58 2019	S.D. Boris et al.	(ITEP, ASCI)
	Also	PRL 61 245 (erratum)	S.D. Boris et al.	(ITEP, ASCI)
BORIS	87B	JETPL 45 333	S.D. Boris et al.	(ITEP)
		Translated from ZETFP 45 267.		
FUKUGITA	87	PR D36 3817	M. Fukugita, S. Yazaki	(KYOTU, TOKY)
MUSKINOV	87	PR D36 2278	M. Muskinov, Y. Rephelli	(TELA)
OBERAUER	87	PL B198 1133	F. Oberauer, F. von Feilitzsch, R.L. Mossbauer	(LLNL)
SPRINGER	87	PR A35 679	P.T. Springer et al.	(LNL)
KETOV	86	JETPL 44 146	S.N. Ketov et al.	(KIAE)
		Translated from ZETFP 44 114.		
COWSIK	85	PL 151B 62	R. Cowisik	(TATA)
RAFFELT	85	PR D31 3002	G.G. Raffelt	(MPIM)
BINETRUY	84	PL 134B 174	P. Binetruy, G. Girardi, P. Salati	(LAPP)
FREESE	84	NP B233 167	K. Freese, D.N. Schramm	(CHIC, FNAL)
KYULDJIEV	84	NP B243 387	A.V. Kyuldjiev	(SOFI)
SCHRAMM	84	PL 141B 337	D.N. Schramm, G. Steigman	(FNAL, BART)
VOGEL	84	PR D30 1505	P. Vogel	
ANDERHUB	82	PL 114B 76	H.B. Anderhub et al.	(ETH, SIN)
OLIVE	82	PR D25 213	K.A. Olive, M.S. Turner	(CHIC, UCSB)
BERNSTEIN	81	PL 101B 39	J. Bernstein, G. Feinberg	(STEV, COLU)
FRANK	81	PR D24 2001	J.S. Frank et al.	(LASL, YALE, MIT+)
MORGAN	81	PL 102B 247	J.A. Morgan	(SUSS)
FUJIKAWA	80	PRL 45 963	K. Fujikawa, R. Shrock	(STON)
LUBIMOV	80	PL 94B 266	V.A. Lyubimov et al.	(ITEP)
STECKER	80	PRL 45 1460	F.W. Stecker	(NASA)
COWSIK	79	PR D19 2219	R. Cowisik	(TATA)
GOLDMAN	79	PR D19 2215	T. Goldman, G.J. Stephenson	(LASL)
BEG	78	PR D17 1395	M.A.B. Beg, W.J. Marciano, M. Ruderman	(ROCK+)
BLIETSCHAU	78	NP B133 205	J. Blietschau et al.	(Gargamelle Collab.)
FALK	78	PL 79B 511	S.W. Falk, D.N. Schramm	(CHIC)
BARNES	77	PRL 38 1049	V.E. Barnes et al.	(PURD, ANL)
COWSIK	77	PRL 39 784	R. Cowisik	(MPIM, TATA)
LEE	77C	PR D16 1444	B.W. Lee, R.E. Shrock	(STON)
VYSOTSKY	77	JETPL 26 188	M.I. Vyso tsky, A.D. Dolgov, Y.B. Zeldovich	(ITEP)
		Translated from ZETFP 26 200.		
BELLOTTI	76	LNC 17 553	E. Bellotti et al.	(MILA)
SUTHERLAND	76	PR D13 2700	P. Sutherland et al.	(PENN, COLU, NYU)
SZALAY	76	AA 49 437	A.S. Szalay, G. Marx	(EOTV)
CLARK	74	PR D9 533	A.R. Clark et al.	(LBL)
KIM	74	PR D9 3050	J.E. Kim, V.S. Mathur, S. Okubo	(ROCH)
REINES	74	PRL 32 180	F. Reines, H.W. Sobel, H.S. Gurr	(UCI)
SZALAY	74	APAH 35 8	A.S. Szalay, G. Marx	(EOTV)
COWSIK	72	PRL 29 511	R. Cowisik, J. McClelland	(UCB)
MARX	72	Nu Conf. Budapest	G. Marx, A.S. Szalay	(EOTV)
GRSHTSTEIN	66	JETPL 4 120	S.S. Gershtein, Y.B. Zeldovich	(KIAM)
		Translated from ZETFP 4 189.		
BERNSTEIN	63	PR 132 1227	J. Bernstein, M. Ruderman, G. Feinberg	(NYU+)
COWAN	57	PR 107 528	C.L. Cowan, F. Reines	(LANL)

Number of Neutrino Types

The neutrinos referred to in this section are those of the Standard SU(2)×U(1) Electroweak Model possibly extended to allow nonzero neutrino masses. Light neutrinos are those with $m < m_Z/2$. The limits are on the number of neutrino mass eigenstates, including ν_1 , ν_2 , and ν_3 .

THE NUMBER OF LIGHT NEUTRINO TYPES FROM COLLIDER EXPERIMENTS

Revised June 2020 by C.-J. Lin (LBNL). Written by D. Karlen (University of Victoria and TRIUMF).

The most precise measurements of the number of light neutrino types, N_ν , come from studies of Z production in e^+e^- collisions. The invisible partial width, Γ_{inv} , is determined by subtracting the measured visible partial widths, corresponding to Z decays into quarks and charged leptons, from the total Z width. The invisible width is assumed to be due to N_ν light neutrino species each contributing the neutrino partial width Γ_ν as given by the Standard Model. In order to reduce the model dependence, the Standard Model value for the ratio of the neutrino to charged leptonic partial widths, $(\Gamma_\nu/\Gamma_\ell)_{SM} = 1.991 \pm 0.001$, is used instead of $(\Gamma_\nu)_{SM}$ to determine the number of light neutrino types:

$$N_\nu = \frac{\Gamma_{inv}}{\Gamma_\ell} \left(\frac{\Gamma_\ell}{\Gamma_\nu} \right)_{SM} \quad (1)$$

The combined result from the four LEP experiments is $N_\nu = 2.984 \pm 0.008$ [1]. Recent analyses applied corrections to the LEP result [1] by including the effect of correlated luminosity systematics and also using an improved Bhabha cross section calculation [2,3] to obtain $N_\nu = 2.9963 \pm 0.0074$.

In the past, when only small samples of Z decays had been recorded by the LEP experiments and by the Mark II at SLC, the uncertainty in N_ν was reduced by using Standard Model fits to the measured hadronic cross sections at several center-of-mass energies near the Z resonance. Since this method is

Downloaded from https://academic.oup.com/ptep/article/2020/8/083C01/5891211 by guest on 20 August 2020

Lepton Particle Listings

Number of Neutrino Types

much more dependent on the Standard Model, the approach described above is favored.

Before SLC and LEP, limits on the number of neutrino generations were placed by experiments at lower-energy e^+e^- colliders by measuring the cross section of the process $e^+e^- \rightarrow \nu\bar{\nu}\gamma$. The ASP, CELLO, MAC, MARK J, and VENUS experiments observed a total of 3.9 events above background [4], leading to a 95% CL limit of $N_\nu < 4.8$. This process has a much larger cross section at center-of-mass energies near the Z mass and has been measured at LEP by the ALEPH, DELPHI, L3, and OPAL experiments [5]. These experiments have observed several thousand such events, and the combined result is $N_\nu = 3.00 \pm 0.08$. The same process has also been measured by the LEP experiments at much higher center-of-mass energies, between 130 and 208 GeV, in searches for new physics [6]. Combined with the lower energy data, the result is $N_\nu = 2.92 \pm 0.05$.

Experiments at $p\bar{p}$ colliders also placed limits on N_ν by determining the total Z width from the observed ratio of $W^\pm \rightarrow \ell^\pm\nu$ to $Z \rightarrow \ell^+\ell^-$ events [7]. This involved a calculation that assumed Standard Model values for the total W width and the ratio of W and Z leptonic partial widths, and used an estimate of the ratio of Z to W production cross sections. Now that the Z width is very precisely known from the LEP experiments, the approach is now one of those used to determine the W width.

References

1. ALEPH, DELPHI, L3, OPAL, and SLD Collaborations, and LEP Electroweak Working Group, and SLD Electroweak Group, and SLD Heavy Flavour Group, Phys. Reports **427**, 257 (2006).
2. P. Janot and S. Jadach, Phys. Lett. **B803**, 135319 (2020).
3. G. Voutsinas *et al.*, Phys. Lett. **B800**, 135068 (2020).
4. VENUS: K. Abe *et al.*, Phys. Lett. **B232**, 431 (1989); ASP: C. Hearty *et al.*, Phys. Rev. **D39**, 3207 (1989); CELLO: H.J. Behrend *et al.*, Phys. Lett. **B215**, 186 (1988); MAC: W.T. Ford *et al.*, Phys. Rev. **D33**, 3472 (1986); MARK J: H. Wu, Ph.D. Thesis, Univ. Hamburg (1986).
5. L3: M. Acciarri *et al.*, Phys. Lett. **B431**, 199 (1998); DELPHI: P. Abreu *et al.*, Z. Phys. **C74**, 577 (1997); OPAL: R. Akers *et al.*, Z. Phys. **C65**, 47 (1995); ALEPH: D. Buskulic *et al.*, Phys. Lett. **B313**, 520 (1993).
6. DELPHI: J. Abdallah *et al.*, Eur. Phys. J. **C38**, 395 (2005); L3: P. Achard *et al.*, Phys. Lett. **B587**, 16 (2004); ALEPH: A. Heister *et al.*, Eur. Phys. J. **C28**, 1 (2003); OPAL: G. Abbiendi *et al.*, Eur. Phys. J. **C18**, 253 (2000).
7. UA1: C. Albajar *et al.*, Phys. Lett. **B198**, 271 (1987); UA2: R. Ansari *et al.*, Phys. Lett. **B186**, 440 (1987).

Number from e^+e^- Colliders

Number of Light ν Types

VALUE	DOCUMENT ID	TECN
2.9963 ± 0.0074	¹ JANOT 20	
2.9918 ± 0.0081	² VOUTSINAS 20	
2.9840 ± 0.0082	³ LEP-SLC 06	RVUE
3.00 ± 0.05	⁴ LEP 92	RVUE

• • • We do not use the following data for averages, fits, limits, etc. • • •

¹ JANOT 20 applies a correction to LEP-SLC 06 using an updated Bhabha cross section calculation. This result also includes a correction to account for correlated luminosity bias as presented in VOUTSINAS 20.

² VOUTSINAS 20 applies a correction to LEP-SLC 06 to account for correlated luminosity bias.

³ Combined fit from ALEPH, DELPHI, L3 and OPAL Experiments.

⁴ Simultaneous fits to all measured cross section data from all four LEP experiments.

Number of Light ν Types from Direct Measurement of Invisible Z Width

In the following, the invisible Z width is obtained from studies of single-photon events from the reaction $e^+e^- \rightarrow \nu\bar{\nu}\gamma$. All are obtained from LEP runs in the E_{cm}^{ee} range 88–209 GeV.

VALUE	DOCUMENT ID	TECN	COMMENT
2.92 ± 0.05 OUR AVERAGE	Error includes scale factor of 1.2.		
2.84 ± 0.10 ± 0.14	ABDALLAH 05B	DLPH	$\sqrt{s} = 180\text{--}209$ GeV
2.98 ± 0.05 ± 0.04	ACHARD 04E	L3	1990–2000 LEP runs
2.86 ± 0.09	HEISTER 03C	ALEP	$\sqrt{s} = 189\text{--}209$ GeV
2.69 ± 0.13 ± 0.11	ABBIENDI,G 00D	OPAL	1998 LEP run
2.89 ± 0.32 ± 0.19	ABREU 97J	DLPH	1993–1994 LEP runs
3.23 ± 0.16 ± 0.10	AKERS 95C	OPAL	1990–1992 LEP runs
2.68 ± 0.20 ± 0.20	BUSKULIC 93L	ALEP	1990–1991 LEP runs
• • • We do not use the following data for averages, fits, limits, etc. • • •			
2.84 ± 0.15 ± 0.14	ABREU 00Z	DLPH	1997–1998 LEP runs
3.01 ± 0.08	ACCIARRI 99R	L3	1991–1998 LEP runs
3.1 ± 0.6 ± 0.1	ADAM 96C	DLPH	$\sqrt{s} = 130, 136$ GeV

Limits from Astrophysics and Cosmology

Effective Number of Light ν Types

"Light" means here with a mass $<$ about 1 MeV. The quoted values correspond to N_{eff} , where $N_{\text{eff}} = 3.045$ in the Standard Model with $N_\nu = 3$. See also reviews on "Big-Bang Nucleosynthesis" and "Neutrinos in Cosmology."

VALUE	CL%	DOCUMENT ID	TECN	COMMENT
• • • We do not use the following data for averages, fits, limits, etc. • • •				
2.3–3.2	95	¹ VERDE 17	COSM	
2.88 ± 0.20	95	² ROSSI 15	COSM	
3.3 ± 0.5	95	³ ADE 14	COSM	Planck
3.78 ^{+0.31} _{-0.30}		⁴ COSTANZI 14	COSM	
3.29 ± 0.31		⁵ HOU 14	COSM	
< 3.80	95	⁶ LEISTEDT 14	COSM	
< 4.10	95	⁷ MORESCO 12	COSM	
< 5.79	95	⁸ XIA 12	COSM	
< 4.08	95	MANGANO 11	COSM	BBN
0.9–8.2		⁹ ICHIKAWA 07	COSM	
3–7	95	¹⁰ CIRELLI 06	COSM	
2.7–4.6	95	¹¹ HANNESTAD 06	COSM	
3.6–7.4	95	¹² SELJAK 06	COSM	
< 4.4		¹⁰ CYBURT 05	COSM	
< 3.3		¹³ BARGER 03C	COSM	
1.4–6.8		¹⁴ CROTTY 03	COSM	
1.9–6.6		¹⁴ PIERPAOLI 03	COSM	
2–4		LISI 99	COSM	BBN
< 4.3		OLIVE 99	COSM	BBN
< 4.9		COPI 97		Cosmology
< 3.6		HATA 97B		High D/H quasar abs.
< 4.0		OLIVE 97		BBN; high ^4He and ^7Li
< 4.7		CARDALL 96B	COSM	High D/H quasar abs.
< 3.9		FIELDS 96	COSM	BBN; high ^4He and ^7Li
< 4.5		KERNAN 96	COSM	High D/H quasar abs.
< 3.6		OLIVE 95		BBN; ≥ 3 massless ν
< 3.3		WALKER 91		Cosmology
< 3.4		OLIVE 90		Cosmology
< 4		YANG 84		Cosmology
< 4		YANG 79		Cosmology
< 7		STEIGMAN 77		Cosmology
< 16		PEEBLES 71		Cosmology
		¹⁵ SHVARTSMAN69		Cosmology
		HOYLE 64		Cosmology

¹ Uses Planck Data combined with an independent standard measure of distance to the sound horizon to set a limit on the total number of neutrinos. Only CMB and early-time information are used.

² ROSSI 15 sets limits on the number of neutrino types using BOSS Lyman alpha forest data combined with Planck CMB data and baryon acoustic oscillations.

³ Fit to the number of neutrino degrees of freedom from Planck CMB data along with WMAP polarization, high L, and BAO data.

⁴ Fit to the number of neutrinos degrees of freedom from Planck CMB data along with BAO, shear and cluster data.

⁵ Fit based on the SPT-SZ survey combined with CMB, BAO, and H_0 data.

⁶ Constrains the number of neutrino degrees of freedom (marginalizing over the total mass) from CMB, CMB lensing, BAO, and galaxy clustering data.

⁷ Limit on the number of light neutrino types from observational Hubble parameter data with seven-year WMAP data, SPT, and the most recent estimate of H_0 . Best fit is 3.45 ± 0.65 .

See key on page 999

Lepton Particle Listings

Number of Neutrino Types, Double- β Decay

- ⁸ Limit on the number of light neutrino types from the CFHTLS combined with seven-year WMAP data and a prior on the Hubble parameter. Best fit is $4.17^{+1.62}_{-1.26}$. Limit is relaxed to $3.98^{+2.02}_{-1.20}$ when small scales affected by non-linearities are removed.
- ⁹ Constrains the number of neutrino types from recent CMB and large scale structure data. No priors on other cosmological parameters are used.
- ¹⁰ Constrains the number of neutrino types from recent CMB, large scale structure, Lyman-alpha forest, and SN1a data. The slight preference for $N_\nu > 3$ comes mostly from the Lyman-alpha forest data.
- ¹¹ Constrains the number of neutrino types from recent CMB and large scale structure data. See also HAMANN 07.
- ¹² Limit on the number of neutrino types based on ⁴He and D/H abundance assuming a baryon density fixed to the WMAP data. Limit relaxes to 4.6 if D/H is not used or to 5.8 if only D/H and the CMB are used. See also CYBURT 01 and CYBURT 03.
- ¹³ Limit on the number of neutrino types based on combination of WMAP data and big-bang nucleosynthesis. The limit from WMAP data alone is 8.3. See also KNELLER 01. $N_\nu \geq 3$ is assumed to compute the limit.
- ¹⁴ 95% confidence level range on the number of neutrino flavors from WMAP data combined with other CMB measurements, the 2dFGRS data, and HST data.
- ¹⁵ SHVARTSMAN 69 limit inferred from his equations.

Number Coupling with Less Than Full Weak Strength

VALUE	DOCUMENT ID	TECN
<20	1 OLIVE	81c COSM
<20	1 STEIGMAN	79 COSM

¹ Limit varies with strength of coupling. See also WALKER 91.

REFERENCES FOR Limits on Number of Neutrino Types

JANOT	20	PL B803 135319	P. Janot, S. Jadach	(CERN, CRAC)
VOUTSINAS	20	PL B800 135068	G. Voutsinas <i>et al.</i>	(CERN, BOHR)
VERDE	17	JCAP 1704 023	L. Verde <i>et al.</i>	
ROSSI	15	PR D92 063505	G. Rossi <i>et al.</i>	
ADE	14	AA 571 A16	P.A.R. Ade <i>et al.</i>	(Planck Collab.)
COSTANZI	14	JCAP 1410 081	M. Costanzi <i>et al.</i>	(TRST, TRST1)
HOU	14	APJ 782 74	Z. Hou <i>et al.</i>	
LEISTEDT	14	PRL 113 041301	B. Leistedt, H.V. Peiris, L. Verde	
MORESCO	12	JCAP 1207 053	M. Moresco <i>et al.</i>	
XIA	12	JCAP 1206 010	J.-Q. Xia <i>et al.</i>	
MANGANO	11	PL B701 296	P. Mangano, P. Serpico	
HAMANN	07	JCAP 0708 021	J. Hamann <i>et al.</i>	
ICHIKAWA	07	JCAP 0705 007	K. Ichikawa, M. Kawasaki, F. Takahashi	
CIRELLI	06	JCAP 0612 013	M. Cirelli <i>et al.</i>	
HANNESSTAD	06	JCAP 0611 016	S. Hannestad, G. Raffelt	
LEP-SLC	06	PRPL 427 257	ALEPH, DELPHI, L3, OPAL, SLD and working groups	
SELJAK	06	JCAP 0610 014	U. Seljak, A. Slosar, P. McDonald	
ABDALLAH	05B	EPJ C38 395	J. Abdallah <i>et al.</i>	(DELPHI Collab.)
CYBURT	05	ASP 23 313	R.H. Cyburt <i>et al.</i>	
ACHARD	04E	PL B587 16	P. Achard <i>et al.</i>	(L3 Collab.)
BARGER	03C	PL B566 8	V. Barger <i>et al.</i>	
CROTTY	03	PR D67 123005	P. Crotty, J. Lesgourgues, S. Pastor	
CYBURT	03	PL B567 227	R.H. Cyburt, B.D. Fields, K.A. Olive	
HEISTER	03C	EPJ C28 1	A. Heister <i>et al.</i>	(ALEPH Collab.)
PIERPAOLI	03	MNRAS 342 L63	E. Pierpaoli	
CYBURT	01	ASP 17 87	R.H. Cyburt, B.D. Fields, K.A. Olive	
KNELLER	01	PR D64 123506	J.P. Kneller <i>et al.</i>	
ABBIENDI.G	00D	EPJ C18 253	G. Abbiendi <i>et al.</i>	(OPAL Collab.)
ABREU	00Z	EPJ C17 53	P. Abreu <i>et al.</i>	(DELPHI Collab.)
ACCIARRI	99R	PL B470 268	M. Acciarri <i>et al.</i>	(L3 Collab.)
LISI	99	PR D59 123520	E. Lisi, S. Sarkar, F.L. Villante	
OLIVE	99	ASP 11 403	K.A. Olive, D. Thomas	
ABREU	97J	ZPHY C74 577	P. Abreu <i>et al.</i>	(DELPHI Collab.)
COPPI	97	PR D55 3389	C.J. Coppi, D.W. Schramm, M.S. Turner	(CHIC)
HATA	97B	PR D55 540	N. Hata <i>et al.</i>	(OSU, PENN)
OLIVE	97	ASP 7 27	K.A. Olive, D. Thomas	(MINN, FLOR)
ADAM	96C	PL B380 471	W. Adam <i>et al.</i>	(DELPHI Collab.)
CARDALL	96B	APJ 472 435	C.Y. Cardall, G.M. Fuller	(UCSD)
FIELDS	96	New Ast 1 77	B.D. Fields <i>et al.</i>	(NDAM, CERN, MINN+)
KERNAN	96	PR D54 3681	P.S. Kernan, S. Sarkar	(CASE, OXFTP)
AKERS	95C	ZPHY C65 47	R. Akers <i>et al.</i>	(OPAL Collab.)
OLIVE	95	PL B354 357	K.A. Olive, G. Steigman	(MINN, OSU)
BUSKULIC	93L	PL B313 520	D. Buskulic <i>et al.</i>	(ALEPH Collab.)
LEP	92	PL B276 247	LEP Collabs.	(LEP, ALEPH, DELPHI, L3, OPAL)
WALKER	91	APJ 376 51	T.P. Walker <i>et al.</i>	(HSCA, OSU, CHIC+)
OLIVE	90	PL B236 454	K.A. Olive <i>et al.</i>	(MINN, CHIC, OSU+)
YANG	84	APJ 281 493	J. Yang <i>et al.</i>	(CHIC, BART)
OLIVE	81C	NP B180 497	K.A. Olive, D.N. Schramm, G. Steigman	(EFI+)
STEIGMAN	79	PRL 43 239	G. Steigman, K.A. Olive, D.N. Schramm	(BART+)
YANG	79	APJ 227 697	J. Yang <i>et al.</i>	(CHIC, YALE, UVA)
STEIGMAN	77	PL 66B 202	G. Steigman, D.N. Schramm, J.E. Gunn	(YALE, CHIC+)
PEEBLES	71	Physical Cosmology	P.Z. Peebles	(PRIN)
SHVARTSMAN	69	Princeton Univ. Press (1971) JETPL 9 184	V.F. Shvartsman	(MOSU)
HOYLE	64	Translated from ZETFP 9 NAT 203 1108	F. Hoyle, R.J. Tayler	(CAMB)

Double- β Decay

OMITTED FROM SUMMARY TABLE

NEUTRINOLESS DOUBLE- β DECAY

Revised August 2019 by A. Piepke (University of Alabama) and P. Vogel (Caltech).

Observation of neutrinoless double-beta ($0\nu\beta\beta$) decay would signal violation of total lepton number conservation. The process can be mediated by an exchange of a light Majorana neutrino, or by an exchange of other particles. However, the existence of $0\nu\beta\beta$ -decay requires a nonvanishing Majorana neutrino mass, no matter what the actual mechanism is. As long as only a limit on the lifetime is available, limits on the effective Majorana neutrino mass, on the lepton-number violating right-handed current or other possible mechanisms mediating $0\nu\beta\beta$ decay can be obtained, independently of the actual mechanism, by assuming that one of these “new physics” possibilities dominates. These limits are listed in the Double- β Decay Listings of the experimental measurements.

In the following we assume that the exchange of light Majorana neutrinos ($m_{\nu_i} \leq 10$ MeV) contributes dominantly to the decay rate. Besides a dependence on the phase space ($G^{0\nu}$) and the nuclear matrix element ($M^{0\nu}$), the observable $0\nu\beta\beta$ -decay rate is proportional then to the square of the effective Majorana mass m_{ee} , $(T_{1/2}^{0\nu})^{-1} = G^{0\nu} \cdot |M^{0\nu}|^2 \cdot m_{ee}^2$, with $m_{ee}^2 = |\sum_i U_{ei}^2 m_{\nu_i}|^2$. The sum contains, in general, complex CP-phases in U_{ei}^2 , i.e., cancellations may occur. For three neutrino flavors there are two physical phases for Majorana neutrinos (η_1, η_2) and one for Dirac neutrinos (δ_{CP}). The relevant Majorana phases affect only processes to which lepton-number changing amplitudes contribute. Given the general 3×3 mixing matrix for Majorana neutrinos, one can construct other analogous lepton number violating quantities, $m_{\ell\ell'} = \sum_i U_{ei} U_{\ell'i} m_{\nu_i}$ (ℓ or $\ell' \neq e$). However, these are currently much less constrained than m_{ee} .

Nuclear structure calculations are needed to deduce m_{ee} from the decay rate. While $G^{0\nu}$ can be calculated accurately, the computation of $M^{0\nu}$ is subject to uncertainty. Comparing different nuclear model evaluations indicates a factor ~ 2 -3 spread in the calculated nuclear matrix elements. Nuclear structure calculation consistently overestimate Gamow-Teller (axial current) matrix elements. This inability of the nuclear models to reproduce Gamow-Teller decay rates is often parametrized in form of a modified coupling constant g_A . Many nuclear theorists interpret this shortcoming as evidence that important physics is missing in the modeling of weak nuclear transitions. It is not clear how these observed uncertainties impact $0\nu\beta\beta$ -matrix elements. Nevertheless, this constitutes an additional element of uncertainty. Recent work, [1] shows how the discrepancy between experimental and theoretical axial current matrix elements might be resolved. However, application of this approach to the $0\nu\beta\beta$ decay remains to be accomplished. The particle physics quantities to be determined are thus nuclear model-dependent, so the half-life measurements are listed first. Where possible, we reference the nuclear matrix elements used in the subsequent analysis. Since rates for the conventional $2\nu\beta\beta$ decay serve to constrain the nuclear theory models, results for this process are also given.

Lepton Particle Listings

Double- β Decay

Oscillation experiments utilizing atmospheric, accelerator, solar, and reactor produced neutrinos and anti-neutrinos show that at least some neutrinos are massive. However, so far the inverted mass ordering (i.e., whether $\Delta m_{31}^2 < 0$) is disfavored only by 2-3 σ compared to the normal mass ordering (when $\Delta m_{31}^2 > 0$), while the absolute neutrino mass values or the properties of neutrinos under CPT-conjugation (Dirac or Majorana) remain undetermined. All confirmed oscillation experiments can be consistently described using three interacting neutrino species with two mass splittings and three mixing angles. (For values of the mixing angles and mass square differences see the corresponding tables.)

Based on the 3-neutrino analysis:

$m_{ee}^2 = |\cos^2 \theta_{13} \cos^2 \theta_{12} m_1 + e^{2i(\eta_2 - \eta_1)} \cos^2 \theta_{13} \sin^2 \theta_{12} m_2 + e^{-2i(\eta_1 + \delta_{CP})} \sin^2 \theta_{13} m_3|^2$, valid for both mass orderings. Given the present knowledge of the neutrino oscillation parameters one can derive a relation between the effective Majorana mass and the mass of the lightest neutrino, as illustrated in Figure 14.11 in the Neutrino Masses, Mixing and Oscillations review. The three mass orderings allowed by the oscillation data: normal ($m_1 < m_2 \ll m_3$), inverted ($m_3 \ll m_1 < m_2$), and degenerate ($m_1 \approx m_2 \approx m_3$), result in different projections. The width of the colored bands reflects the uncertainty introduced by the unknown Majorana and Dirac phases as well as the experimental errors of the oscillation parameters. The latter causes only minor broadening of the bands. Because of the overlap of the different mass scenarios, a measurement of m_{ee} would not reveal which mass ordering is applicable, provided the value of m_{ee} is in the overlapping range.

Analogous plots depict the relation of m_{ee} with the summed neutrino mass $m_{tot} = m_1 + m_2 + m_3$, constrained by observational cosmology, and m_{ee} as a function of the average mass $m_{\nu_e}^{eff} = [\sum |U_{ei}|^2 m_{\nu_i}^2]^{1/2}$ determined through the analysis of the electron energy distribution in low energy beta decays. (See Fig. 1 of [2].) The oscillation data thus allow to test whether observed values of m_{ee} and m_{tot} or $m_{\nu_e}^{eff}$ are consistent within the 3 neutrino framework. The rather large intrinsic width of the $\beta\beta$ -decay constraints essentially does not allow to positively identify the mass ordering, and thus the sign of Δm_{31}^2 , even in combination with these other observables. Naturally, if a value of $0 < m_{ee} \leq 0.01$ eV is ever established, then the normal mass ordering becomes the only possible scenario.

It should be noted that systematic uncertainties of the nuclear matrix elements and possible quenching of the axial current matrix elements are sometimes not folded into the mass limits reported by $\beta\beta$ -decay experiments. Taking this additional uncertainty into account would further widen the projections. The plots are based on a 3-neutrino analysis. If it turns out that additional, i.e. sterile light neutrinos exist, the allowed regions would be modified substantially.

If neutrinoless double-beta decay is observed, it will be possible to fix a range of absolute values of the masses m_{ν_i} . Unlike the direct neutrino mass measurements, however, a limit

on m_{ee} does not allow one to constrain the individual mass values m_{ν_i} even when the mass differences Δm_{ij}^2 are known.

Neutrino oscillation data imply the existence of a lower limit ~ 0.014 eV for the Majorana neutrino mass for the inverted mass ordering pattern, while m_{ee} could, by fine tuning, vanish in the case of the normal mass ordering. Several new double-beta searches have been proposed to probe the interesting m_{ee} mass range, with the prospect of full coverage of the inverted mass ordering region within the next decade.

The $0\nu\beta\beta$ decay mechanism discussed so far is not the only way in which the decay can occur. Numerous other possible scenarios have been proposed, however, all of them requiring new physics. It will be a challenging task to decide which mechanism was responsible once $0\nu\beta\beta$ decay is observed. LHC experiments may reveal corresponding signatures for new physics of lepton number violation. If lepton-number violating right-handed weak current interactions exist, its strength can be characterized by the phenomenological coupling constants η and λ (η describes the coupling between the right-handed lepton current and left-handed quark current while λ describes the coupling when both currents are right-handed). The $0\nu\beta\beta$ decay rate then depends on $\langle \eta \rangle = \eta \sum_i U_{ei} V_{ei}$ and $\langle \lambda \rangle = \lambda \sum_i U_{ei} V_{ei}$ that vanish for massless or unmixed neutrinos (V_{ij} is a matrix analogous to U_{ij} but describing the mixing with the hypothetical right-handed neutrinos). The observation of the single electron spectra could, in principle, allow to distinguish this mechanism of $0\nu\beta\beta$ from the light Majorana neutrino exchange driven mode. The limits on $\langle \eta \rangle$ and $\langle \lambda \rangle$ are listed in a separate table. The reader is cautioned that a number of earlier experiments did not distinguish between η and λ . In addition, see the section on Majoron searches for additional limits set by these experiments.

References

1. P. Gysbers *et al.*, Nature Phys. **15**, 5 (2019); [arXiv:1903.00047].
2. M.J. Dolinski, A.W.P. Poon and W. Rodejohann, Ann. Rev. Nucl. Part. Sci. **49**, 219 (2019); [arXiv:1902.04097].

Half-life 0ν double- β decay

In most cases the transitions $(Z,A) \rightarrow (Z+2,A) + 2e^-$ to the 0^+ ground state of the final nucleus are listed. We also list transitions that decrease the nuclear charge ($2e^+$, e^+ CC and double EC) and transitions to an excited state of the final nucleus (0_2^+ , 2^+ , and 2_1^+). In the following Listings only the best or comparable limits for the half-lives of each transition are reported and only those with about $T_{1/2} > 10^{23}$ years that are relevant for particle physics.

$T_{1/2}(10^{23} \text{ yr})$	CL% ISOTOPE	TRANSITION METHOD	DOCUMENT ID
• • • We do not use the following data for averages, fits, limits, etc. • • •			
> 900	90 ⁷⁶ Ge	GERDA	1 AGOSTINI 19
> 14	90 ¹³⁰ Te	$g.s \rightarrow 0_1^+$ CUORE-0	2 ALDUINO 19
> 0.95	90 ¹⁰⁰ Mo	AMoRE	3 ALENKOV 19
> 270	90 ⁷⁶ Ge	MAJORANA	4 ALVIS 19
> 350	90 ¹³⁶ Xe	EXO-200	5 ANTON 19
> 35	90 ⁸² Se	CUPID-0	6 AZZOLINI 19

> 2.4	90	¹³⁶ Xe	PANDAX-II	7	Ni	19
> 190	90	⁷⁶ Ge	MAJORANA	8	AALSETH	18
> 800	90	⁷⁶ Ge	GERDA	9	AGOSTINI	18
> 180	90	¹³⁶ Xe	EXO-200	10	ALBERT	18
> 150	90	¹³⁰ Te	CUORE	11	ALDUINO	18
> 2.5	90	⁸² Se	NEMO-3	12	ARNOLD	18
> 24	90	⁸² Se	CUPID-0	13	AZZOLINI	18
> 0.81	90	⁸² Se	g.s. → 0 ₁ ⁺	14	AZZOLINI	18A
> 2.2	90	¹¹⁶ Cd	AURORA	15	BARABASH	18
> 530	90	⁷⁶ Ge	GERDA	16	AGOSTINI	17
> 1.1	90	¹³⁴ Xe	EXO-200	17	ALBERT	17C
> 1	90	¹¹⁶ Cd	NEMO-3	18	ARNOLD	17
> 40	90	¹³⁰ Te	CUORE(CINO)	19	ALDUINO	16
> 260	90	¹³⁶ Xe	g.s. → 2 ₁ ⁺	20	ASAKURA	16
> 260	90	¹³⁶ Xe	g.s. → 2 ₂ ⁺	21	ASAKURA	16
> 240	90	¹³⁶ Xe	g.s. → 0 ₁ ⁺	22	ASAKURA	16
>1070	90	¹³⁶ Xe	KamLAND-Zen	23	GANDO	16
> 11	90	¹⁰⁰ Mo	NEMO-3	24	ARNOLD	15
> 110	90	¹³⁶ Xe	EXO-200	25	ALBERT	14B
> 9.4	90	¹³⁰ Te	0 ⁺ → 0 ₁ ⁺	26	ANDREOTTI	12
> 3.6	90	⁸² Se	NEMO-3	27	BARABASH	11A
> 30	90	¹³⁰ Te	CUORICINO	28	ARNABOLDI	08
> 0.58	90	⁴⁸ Ca	CaF ₂ scint.	29	UMEHARA	08
> 0.89	90	¹⁰⁰ Mo	0 ⁺ → 0 ₁ ⁺	30	ARNOLD	07
> 1.6	90	¹⁰⁰ Mo	0 ⁺ → 2 ⁺	31	ARNOLD	07
> 1	90	⁸² Se	NEMO-3	32	ARNOLD	05A
> 1.1	90	¹²⁸ Te	Cryog. det.	33	ARNABOLDI	03
> 1.7	90	¹¹⁶ Cd	¹¹⁶ CdWO ₄ scint.	34	DANEVICH	03
> 157	90	⁷⁶ Ge	Enriched HPGe	35	AALSETH	02B
> 190	90	⁷⁶ Ge	Enriched HPGe	36	KLAPDOR-K...	01

- AGOSTINI 19 use 82.4 kg-yr of data, collected by the GERDA experiment, to search for the 0ν ββ decay of ⁷⁶Ge. High resolution Ge-calorimeters, made from isotopically enriched Ge, are used. A median sensitivity of 1.1 × 10²⁶ yr is reported. Supersedes AGOSTINI 18.
- ALDUINO 19 use the combined data of the CUORICINO and CUORE-0 experiments to place a lower limit on the half life of the 0ν ββ decay of ¹³⁰Te to the first excited 0⁺ state of ¹³⁰Xe. Supersedes ANDREOTTI 12.
- ALENKOV 19 report the 0ν ββ decay half-life limit based on the 52.1 kg-d exposure of ¹⁰⁰Mo, of a cryogenic dual heat and light detector in the Yangyang underground laboratory. The median sensitivity is 1.1 × 10²³ years.
- ALVIS 19 use the MAJORANA Demonstrator with enriched in ⁷⁶Ge detectors to set this limit on 0ν ββ half-life of ⁷⁶Ge. The exposure is 26.0 kg yr. The sensitivity is 4.8 × 10²⁵ yr.
- ANTON 19 uses the complete dataset of the EXO-200 detector to search for the 0ν ββ decay. The exposure is 234.1 kg yr. The median sensitivity is 5.0 × 10²⁵ yr. Supersedes ALBERT 18 and ALBERT 14B.
- AZZOLINI 19 use the CPID-0 scintillating cryogenic bolometer to set this limit on 0ν ββ half-life of ⁸²Se. The exposure is 5.29 kg yr. The sensitivity is 5 × 10²⁴ yr.
- Ni 19 use the PandaX-II dual phase TPC at CJPL to search for the 0ν ββ decay of ¹³⁶Xe. The half-life limit 2.4 × 10²³ yr is obtained from 22.2 kg yr exposure with a sensitivity of 1.9 × 10²³ yr.
- AALSETH 18 uses the MAJORANA Demonstrator to search for the 0ν ββ decay. The exposure is 9.95 kg-year. The median sensitivity is 2.1 × 10²⁵ yr.
- AGOSTINI 18 uses the GERDA detector to search for the 0ν ββ decay. The exposure is 46.7 kg-year. The median sensitivity is 5.8 × 10²⁵ yr. Supersedes AGOSTINI 17.
- ALBERT 18 uses the EXO-200 detector to search for the 0ν ββ decay. The exposure is 177.6 kg-year. The median sensitivity is 3.7 × 10²⁵ years.
- ALDUINO 18 uses the CUORE detector to search for the 0ν ββ decay of ¹³⁰Te. The exposure is 86.3 kg-year of natural TeO₂ corresponding to 24.0 kg-year for ¹³⁰Te. The median sensitivity is 0.7 × 10²⁵ yr. The limit is obtained combining the new data from CUORE with those of CUORE0 (9.8 kg-year of ¹³⁰Te) and Cuoricino (19.8 kg-year of ¹³⁰Te).
- ARNOLD 18 use the NEMO-3 tracking detector to place a limit on the 0ν ββ decay of ⁸²Se. This is a slightly weaker limit than in BARABASH 11A, using the same detector. Supersedes ARNOLD 05A.
- AZZOLINI 18 uses CUPID-0 detector, a novel scintillating cryogenic calorimeter, operated in the LNGS. This results replaces BARABASH 11A (NEMO-3) as the most stringent limit on the 0ν ββ-decay of ⁸²Se.
- AZZOLINI 18A data collected by CUPID-0 based on scintillating bolometers is used to derive a new most stringent limit on the 0ν ββ-decay of ⁸²Se to the 0₁⁺ state of ⁸²Kr.
- BARABASH 18 use 1.162 kg of ¹¹⁶CdWO₄ scintillating crystals to obtain this limit. Supersedes DANEVICH 03 with analogous source and is more sensitive than ARNOLD 17.
- AGOSTINI 17 result corresponds to data collected with GERDA phase 1 and first release of phase 2 for a total of 343 mol-yr exposure. Supersedes AGOSTINI 13A. The median sensitivity is 4.0 10²⁵ yr.
- ALBERT 17C uses the EXO-200 detector that contains 19.098 ± 0.014% admixture of ¹³⁴Xe to search for the 0ν and 2ν ββ decay modes. The exposure is 29.6 kg-year. The median sensitivity is 1.9 × 10²¹ years.
- ARNOLD 17 use the NEMO-3 tracking calorimeter, containing 410 g of enriched ¹¹⁶Cd exposed for 5.26 yr, to determine the half-life limit. Supersedes BARABASH 11A.

- ALDUINO 16 report result obtained with 9.8 kg y of data collected with the CUORE-0 bolometer, combined with data from the CUORICINO. Supersedes ALFONSO 15.
- ASAKURA 16 use the KamLAND-Zen liquid scintillator calorimeter (¹³⁶Xe 89.5 kg yr) to place a limit on the 0ν ββ-decay into the first excited state of the daughter nuclide.
- ASAKURA 16 use the KamLAND-Zen liquid scintillator calorimeter (¹³⁶Xe 89.5 kg yr) to place a limit on the 0ν ββ-decay into the second excited state of the daughter nuclide.
- ASAKURA 16 use the KamLAND-Zen liquid scintillator calorimeter (¹³⁶Xe 89.5 kg yr) to place a limit on the 0ν ββ-decay into the third excited state of the daughter nuclide.
- GANDO 16 use the the KamLAND detector to search for the 0ν decay of ¹³⁶Xe. With a significant background reduction, the combination of results of the first (270.7 days) and the second phase (263.8 days) of the experiment leads to about six fold improvement over the previous limit. Supersedes GANDO 13A. The sensitivity is 5.6 10²⁵ yr.
- ARNOLD 15 use the NEMO-3 tracking calorimeter with 34.3 kg yr exposure to determine the limit of 0ν ββ-half life of ¹⁰⁰Mo. Supersedes ARNOLD 2005A and BARABASH 11A.
- ALBERT 14B use 100 kg yr of exposure of the EXO-200 tracking calorimeter to place a lower limit on the 0ν ββ-half life of ¹³⁶Xe. Supersedes AUGER 12.
- ANDREOTTI 12 use high resolution TeO₂ bolometric calorimeter to search for the 0ν ββ decay of ¹³⁰Te leading to the excited 0₁⁺ state at 1793.5 keV.
- BARABASH 11A use the NEMO-3 detector to measure 2ν ββ rates and place limits on 0ν ββ half lives for various nuclides. Supersedes ARNOLD 05A, ARNOLD 04, ARNOLD 98, and ELLIOTT 92.
- Supersedes ARNABOLDI 04. Bolometric TeO₂ detector array CUORICINO is used for high resolution search for 0ν ββ decay. The half-life limit is derived from 3.09 kg yr ¹³⁰Te exposure.
- UMEHARA 08 use CaF₂ scintillation calorimeter to search for double beta decay of ⁴⁸Ca. Limit is significantly more stringent than quoted sensitivity: 18 × 10²¹ years.
- Limit on 0ν-decay to the first excited 0₁⁺-state of daughter nucleus using NEMO-3 tracking calorimeter. Supersedes DASSIE 95.
- Limit on 0ν-decay to the first excited 2⁺-state of daughter nucleus using NEMO-3 tracking calorimeter.
- NEMO-3 tracking calorimeter is used in ARNOLD 05A to place limit on 0ν ββ half-life of ⁸²Se. Detector contains 0.93 kg of enriched ⁸²Se. Supersedes ARNOLD 04.
- Supersedes ALESSANDRELLO 00. Array of TeO₂ crystals in high resolution cryogenic calorimeter. Some enriched in ¹²⁸Te. Ground state to ground state decay.
- Limit on 0ν ββ decay of ¹¹⁶Cd using enriched CdWO₄ scintillators. Supersedes DANEVICH 00.
- AALSETH 02b limit is based on 117 mol-yr of data using enriched Ge detectors. Background reduction by means of pulse shape analysis is applied to part of the data set. Reported limit is slightly less restrictive than that in KLAPDOR-KLEINGROTHAUS 01 However, it excludes part of the allowed half-life range reported in KLAPDOR-KLEINGROTHAUS 01B for the same nuclide. The analysis has been criticized in KLAPDOR-KLEINGROTHAUS 04B. The criticism was addressed and disputed in AALSETH 04.
- KLAPDOR-KLEINGROTHAUS 01 is a continuation of the work published in BAUDIS 99. Isotopically enriched Ge detectors are used in calorimetric measurement. The most stringent bound is derived from the data set in which pulse-shape analysis has been used to reduce background. Exposure time is 35.5 kg y. Supersedes BAUDIS 99 as most stringent result.

Half-life measurements of the two-neutrino double-β decay

The measured half-life values for the transitions (Z,A) → (Z+2,A) + 2e⁻ + 2ν̄_e to the 0⁺ ground state of the final nucleus are listed. We also list the transitions to an excited state of the final nucleus (0_i⁺, etc.). We report only the measurements with the smallest (or comparable) uncertainty for each transition.

t _{1/2} (10 ²¹ yr)	ISOTOPE	TRANSITION	METHOD	DOCUMENT ID
• • •	We do not use the following data for averages, fits, limits, etc. • • •			
18 ± 5 ± 1	¹²⁴ Xe	2νDEC	XENON1T	1 APRILE 19E
0.00680 ± 0.00001 ± 0.00038	¹⁰⁰ Mo		NEMO-3	2 ARNOLD 19
0.0939 ± 0.0017 ± 0.0058	⁸² Se		NEMO-3	3 ARNOLD 18
0.0263 ± 0.0011 ± 0.0012	¹¹⁶ Cd		AURORA	4 BARABASH 18
> 0.87	¹³⁴ Xe		EXO-200	5 ALBERT 17C
0.82 ± 0.02 ± 0.06	¹³⁰ Te		CUORE-0	6 ALDUINO 17
0.00690 ± 0.00015 ± 0.00037	¹⁰⁰ Mo		CUPID	7 ARMENGAUD 17
0.0274 ± 0.0004 ± 0.0018	¹¹⁶ Cd		NEMO-3	8 ARNOLD 17
0.064 ± 0.007 ± 0.012 ± 0.009	⁴⁸ Ca		NEMO-3	9 ARNOLD 16
0.00934 ± 0.00022 ± 0.00062	¹⁵⁰ Nd		NEMO-3	10 ARNOLD 16A
1.926 ± 0.094	⁷⁶ Ge		GERDA	11 AGOSTINI 15A
0.00693 ± 0.00004	¹⁰⁰ Mo		NEMO-3	12 ARNOLD 15
2.165 ± 0.016 ± 0.059	¹³⁶ Xe		EXO-200	13 ALBERT 14
9.2 ± 5.5 ± 1.3	⁷⁸ Kr		BAKSAN	14 GAVRILYAK 13
2.38 ± 0.02 ± 0.14	¹³⁶ Xe		KamLAND-Zen	15 GANDO 12A
0.7 ± 0.09 ± 0.11	¹³⁰ Te		NEMO-3	16 ARNOLD 11
0.0235 ± 0.0014 ± 0.0016	⁹⁶ Zr		NEMO-3	17 ARGYRADES 10
0.69 ± 0.10 ± 0.08	¹⁰⁰ Mo	0 ⁺ → 0 ₁ ⁺	Ge coinc.	18 BELLI 10
0.57 ± 0.13 ± 0.09	¹⁰⁰ Mo	0 ⁺ → 0 ₁ ⁺	NEMO-3	19 ARNOLD 07

Lepton Particle Listings

Double- β Decay

VALUE (eV)	ISOTOPE	METHOD	DOCUMENT ID
0.096 \pm 0.003 \pm 0.010	^{82}Se	NEMO-3	²⁰ ARNOLD 05A
0.029 \pm 0.004 \pm 0.003	^{116}Cd	$^{116}\text{CdWO}_4$ scint.	²¹ DANEVICH 03
< 0.311–0.638	^{82}Se	CUPID-0	⁵ AZZOLINI 19
< 1.3–3.5	^{136}Xe	PANDAX-II	⁶ NI 19
< 0.24–0.52	^{76}Ge	MAJORANA Dem	⁷ AALSETH 18
< 0.12–0.26	^{76}Ge	GERDA	⁸ AGOSTINI 18
< 0.15–0.40	^{136}Xe	EXO-200	⁹ ALBERT 18
< 0.11–0.52	^{130}Te	CUORE	¹⁰ ALDUINO 18
< 1.2–3.0	^{82}Se	NEMO-3	¹¹ ARNOLD 18
< 0.376–0.770	^{82}Se	CUPID-0	¹² AZZOLINI 18
< 1.0–1.7	^{116}Cd	AURORA	¹³ BARABASH 18
< 0.15–0.33	^{76}Ge	GERDA	¹⁴ AGOSTINI 17
< 1.4–2.5	^{116}Cd	NEMO-3	¹⁵ ARNOLD 17
< 0.27–0.76	^{130}Te	CUORE(CINO)	¹⁶ ALDUINO 16
< 1.6–5.3	^{150}Nd	NEMO-3	¹⁷ ARNOLD 16A
< 0.061–0.165	^{136}Xe	KamLAND-Zen	¹⁸ GANDO 16
< 0.33–0.62	^{100}Mo	NEMO-3	¹⁹ ARNOLD 15
< 0.19–0.45	^{136}Xe	EXO-200	²⁰ ALBERT 14B
< 0.89–2.43	^{82}Se	NEMO-3	²¹ BARABASH 11A
< 7.2–19.5	^{96}Zr	NEMO-3	²² ARGYRIADES 10
< 3.5–2.2	^{48}Ca	CaF_2 scint.	²³ UMEHARA 08
< 0.2–1.1	^{130}Te	Cryog. det.	²⁴ ARNABOLDI 05
< 0.37–1.9	^{130}Te	Cryog. det.	²⁵ ARNABOLDI 04
< 1.5–1.7	^{116}Cd	$^{116}\text{CdWO}_4$ scint.	²⁶ DANEVICH 03
< 0.350	^{76}Ge	Enriched HPGC	²⁷ KLAPDOR-K...01
< 8.3	^{48}Ca	CaF_2 scint.	YOU 91
			¹ AGOSTINI 19 use 82.4 kg-yr of data collected by the isotopically enriched ^{76}Ge detectors of the GERDA experiment to derive an upper limit for $\langle m_{\beta\beta} \rangle$. The range reflects the variability of the theoretically calculated nuclear matrix elements. Supersedes AGOSTINI 18.
			² ALENKOV 19 report the range of the effective masses $\langle m_{\beta\beta} \rangle$ corresponding to the $0\nu\beta\beta$ decay half-life limit. It is based on the 52.1 kg-d exposure of ^{100}Mo , in the Yangyang underground laboratory. The median sensitivity is 1.1×10^{23} years. The range of $\langle m_{\beta\beta} \rangle$ reflects the uncertainty of nuclear matrix elements.
			³ ALVIS 19 use the MAJORANA Demonstrator with enriched in ^{76}Ge detectors to set this limit. The exposure is 26.0 kg yr. The sensitivity is 4.8×10^{25} yr.
			⁴ ANTON 19 uses the complete dataset of the EXO-200 experiment to obtain these limits. The spread reflect the uncertainty in the nuclear matrix elements. Supersedes ALBERT 18 and ALBERT 14B.
			⁵ AZZOLINI 19 use the CPID-0 scintillating cryogenic bolometer to set this limit. The exposure is 5.29 kg yr. The sensitivity is 5×10^{24} yr.
			⁶ NI 19 use the PandaX-II dual phase TPC at CJPL to search for the $0\nu\beta\beta$ decay of ^{136}Xe with 22.2 kg yr exposure. The range in the $m_{\beta\beta}$ limit of 1.3–3.5 eV reflects the range of the calculated nuclear matrix elements. The sensitivity is 1.9×10^{23} yr.
			⁷ AALSETH 18 uses the MAJORANA Demonstrator detector to establish this limit.
			⁸ AGOSTINI 18 uses the GERDA detector to establish this limit.
			⁹ ALBERT 18 uses the EXO-200 experiment to obtain this limit.
			¹⁰ ALDUINO 18 use the combined data of CUORE, CUORE0, and Cuoricino to obtain this limit.
			¹¹ ARNOLD 18 use the NEMO-3 tracking detector to constrain the $0\nu\beta\beta$ decay of ^{82}Se . The limit on $\langle m_{\beta\beta} \rangle$ is obtained assuming light neutrino exchange; the range reflects different calculations of the nuclear matrix elements. This is a somewhat weaker limit than in BARABASH 11A using the same detector.
			¹² AZZOLINI 18 uses data collected by the CUPID-0 scintillating cryogenic calorimeter, operated in the LNGS, to derive a range of limits on $\langle m_{\beta\beta} \rangle$. The reported range reflects the spread of the nuclear matrix element calculations considered in this work. Use $g_A = 1.269$.
			¹³ BARABASH 18 use 1.162 kg of $^{116}\text{CdWO}_4$ scintillating crystals to obtain these limits. The spread reflects the estimated uncertainty in the nuclear matrix element. Supersedes DANEVICH 03.
			¹⁴ AGOSTINI 17 is based on 343 mol yr of data from GERDA phase 1 and phase 2 first part and the corresponding limit on $T_{1/2}$ using the different nuclear matrix elements mentioned by the authors. Supersedes AGOSTINI 13A.
			¹⁵ ARNOLD 17 utilize NEMO-3 data, taken with enriched ^{116}Cd to limit the effective Majorana neutrino mass. The reported range results from the use of different nuclear matrix elements. Supersedes BARABASH 11A.
			¹⁶ ALDUINO 16 place a limit on the effective Majorana neutrino mass using the combined data of the CUORE-0 and CUORICINO experiments. The range reflects the authors' evaluation of the variability of the nuclear matrix elements. Supersedes ALFONSO 15.
			¹⁷ ARNOLD 16A limit is derived from data taken with the NEMO-3 detector and ^{150}Nd . A range of nuclear matrix elements that include the effect of nuclear deformation have been used. Supersedes ARGYRIADES 09.
			¹⁸ GANDO 16 result is based on the 2016 KamLAND-Zen half-life limit. The stated range reflects different nuclear matrix elements, an unquenched $g_A = 1.27$ is used. Supersedes GANDO 13A.
			¹⁹ ARNOLD 15 use the NEMO-3 tracking calorimeter with 34.3 kg yr exposure to determine the neutrino mass limit based on the $0\nu\beta\beta$ -half life of ^{100}Mo . The spread range reflects different nuclear matrix elements. Supersedes ARNOLD 14 and BARABASH 11A.
			²⁰ ALBERT 14B is based on 100 kg yr of exposure of the EXO-200 tracking calorimeter. The mass range reflects the nuclear matrix element calculations. Supersedes AUGER 12.
			²¹ BARABASH 11A limit is based on NEMO-3 data for ^{82}Se . The reported range reflects different nuclear matrix elements. Supersedes ARNOLD 05A and ARNOLD 04.
			²² ARGYRIADES 10 use ^{96}Zr and the NEMO-3 tracking detector to obtain the reported mass limit. The range reflects the fluctuation of the nuclear matrix elements considered.

$\langle m_{ee} \rangle$, The Effective Weighted Sum of Majorana Neutrino Masses Contributing to Neutrinoless Double- β Decay

$\langle m_{ee} \rangle = |\sum U_{ei}^2 m_{\nu_i}|$, $i = 1, 2, 3$. It is assumed that ν_i are Majorana particles and that the transition is dominated by the known (light) neutrinos. Note that U_{ei}^2 and not $|U_{ei}|^2$ occur in the sum, and that consequently cancellations are possible. The experiments obtain the limits on $\langle m_{\nu} \rangle$ from the measured ones on $T_{1/2}$ using a range of nuclear matrix elements (NME), which is reflected in the spread of $\langle m_{\nu} \rangle$. Different experiments may choose different NME. All assume $g_A = 1.27$. In the following Listings, only the best or comparable limits for each isotope are reported. When not mentioned explicitly the transition is between ground states, but transitions between excited states are also reported.

VALUE (eV)	ISOTOPE	METHOD	DOCUMENT ID
< 0.07–0.16	^{76}Ge	GERDA	¹ AGOSTINI 19
< 1.2–2.1	^{100}Mo	AMoRE	² ALENKOV 19
< 0.200–0.433	^{76}Ge	MAJORANA	³ ALVIS 19
< 0.093–0.286	^{136}Xe	EXO-200	⁴ ANTON 19

• • • We do not use the following data for averages, fits, limits, etc. • • •

See key on page 999

Lepton Particle Listings
Double-β Decay, Neutrino Mixing

- 23 Limit was obtained using CaF2 scintillation calorimeter to search for double beta decay of 48Ca. Reported range of limits reflects spread of QRPA and SM matrix element calculations used. Supersedes OGAWA 04.
24 Supersedes ARNABOLDI 04. Reported range of limits due to use of different nuclear matrix element calculations.
25 Supersedes ARNABOLDI 03. Reported range of limits due to use of different nuclear matrix element calculations.
26 Limit for $\langle m_{\nu} \rangle$ is based on the nuclear matrix elements of STAUDT 90 and ARNOLD 96. Supersedes DANEVICH 00.
27 KLAPDOR-KLEINGROTHAUS 01 uses the calculation by STAUDT 90. Using several other models in the literature could worsen the limit up to 1.2eV. This is the most stringent experimental bound on m_{ν}. It supersedes BAUDIS 99B.

Limits on Lepton-Number Violating (V+A) Current Admixture

For reasons given in the discussion at the beginning of this section, we list only results from 1989 and later. $\langle \lambda \rangle = \lambda \sum U_{ej} V_{ej}$ and $\langle \eta \rangle = \eta \sum U_{ej} V_{ej}$, where the sum is over the number of neutrino generations. This sum vanishes for massless or unmixed neutrinos. In the following Listings, only best or comparable limits or lifetimes for each isotope are reported.

Table with columns: $\langle \lambda \rangle (10^{-6})$, CL%, $\langle \eta \rangle (10^{-8})$, CL%, ISOTOPE, METHOD, DOCUMENT ID. Contains various isotopes like 82Se, 116Cd, 100Mo, 76Ge, 130Te, 116CdWO4 scint., 100Mo, 76Ge, 136Xe, 128Te.

- 1 ARNOLD 18 use the NEMO03 tracking detector, with 0.93 kg of 82Se mass and 5.25 y exposure to obtain the limits for the hypothetical right-handed currents. Supersedes ARNOLD 05A.
2 BARABASH 18 use 1.162 kg of 116CdWO4 scintillating crystals to obtain this limits for the hypothetical right-handed currents in the 0νββ decay of 116Cd.
3 ARNOLD 14 is based on 34.7 kg yr of exposure of the NEMO-3 tracking calorimeter. The reported range limit on $\langle \lambda \rangle$ and $\langle \eta \rangle$ reflects the nuclear matrix element uncertainty in 100Mo.
4 ARNOLD 07 use NEMO-3 half life limit for 0ν-decay of 100Mo to the first excited 2+ state of daughter nucleus to limit the right-right handed admixture of weak currents $\langle \lambda \rangle$. This limit is not competitive when compared to the decay to the ground state.
5 Re-analysis of data originally published in KLAPDOR-KLEINGROTHAUS 04A. Modified pulse shape analysis leads the authors to claim 6σ statistical evidence for observation of 0ν-decay. Authors use matrix element of MUTO 89 to determine $\langle \lambda \rangle$ and $\langle \eta \rangle$. Uncertainty of nuclear matrix element is not reflected in stated errors.
6 ARNOLD 05A derive limit for $\langle \lambda \rangle$ based on 100 Mo data collected with NEMO-3 detector. No limit for $\langle \eta \rangle$ is given. Supersedes ARNOLD 04.
7 ARNOLD 05A derive limit for $\langle \lambda \rangle$ based on 82Se data collected with NEMO-3 detector. No limit for $\langle \eta \rangle$ is given. Supersedes ARNOLD 04.
8 ARNOLD 04 use the matrix elements of SUHONEN 94 to obtain a limit for $\langle \lambda \rangle$, no limit for $\langle \eta \rangle$ is given. This limit is more stringent than the limit in EJIRI 01 for the same nucleus.
9 ARNOLD 04 use the matrix elements of TOMODA 91 and SUHONEN 91 to obtain a limit for $\langle \lambda \rangle$, no limit for $\langle \eta \rangle$ is given.
10 Supersedes ALESSANDRELLO 00. Cryogenic calorimeter search. Reported a range reflecting uncertainty in nuclear matrix element calculations.
11 Limits for $\langle \lambda \rangle$ and $\langle \eta \rangle$ are based on nuclear matrix elements of STAUDT 90. Supersedes DANEVICH 00.
12 The range of the reported $\langle \lambda \rangle$ and $\langle \eta \rangle$ values reflects the spread of the nuclear matrix elements. On axis value assuming $\langle m_{\nu} \rangle = 0$ and $\langle \lambda \rangle = \langle \eta \rangle = 0$, respectively.
13 GUENTHER 97 limits use the matrix elements of STAUDT 90. Supersedes BALYSH 95 and BALYSH 92.
14 VUILLEUMIER 93 uses the matrix elements of MUTO 89. Based on a half-life limit 2.6 × 1023 y at 90%CL.
15 BERNATOWICZ 92 takes the measured geochemical decay width as a limit on the 0ν width, and uses the SUHONEN 91 coefficients to obtain the least restrictive limit on η. Further details of the experiment are given in BERNATOWICZ 93.

Table with columns: Author, Year, Reference, Collaboration. Lists various authors and their associated publications and collaborations like NEMO-3, CUORE, MAJORANA, GERDA, EXO-200, CUORICINO, DAMA-INR, CUORICINO, KamLAND-Zen, etc.

Neutrino Mixing

With the possible exceptions of "short-baseline anomalies," such as LSND, all neutrino data can be described within the framework of a 3×3 mixing matrix between the mass eigenstates ν1, ν2, and ν3, leading to the flavor eigenstates νe, νμ, and ντ, as described in the review "Neutrino masses, mixing and oscillations."

The Listings are divided in the following sections:

(A) Neutrino fluxes and event ratios: shows measurements which correspond to various oscillation tests for Accelerator, Reactor, Atmospheric, and Solar neutrino experiments. Typically, ratios involve a measurement in a realm sensitive to oscillations compared to one for which no oscillation effect is expected.

Double-β Decay REFERENCES

Table with columns: Author, Year, Reference, Collaboration. Lists authors like AGOSTINI, ALDUINO, ALENKOV, ALVIS, ANTON, APRILE and their associated references and collaborations.

Downloaded from https://academic.oup.com/ptep/article/2020/8/083C01/5891211 by guest on 20 August 2020

Lepton Particle Listings

Neutrino Mixing

(B) Neutrino mixing parameters: shows measurements of $\sin^2(\theta_{12})$, $\sin^2(\theta_{23})$, $\sin^2(\theta_{13})$, Δm_{21}^2 , Δm_{32}^2 , and δ_{CP} as extracted from the measured data in the quoted publications in the frame of the three-neutrino mixing scheme. The quoted averages are not the result of a global fit, as in the review "Neutrino masses, mixing, and oscillations," and, as a consequence, might slightly differ from them. In some cases, measurements depend on the mass order (normal when $\Delta m_{32}^2 > 0$ or inverted when $\Delta m_{32}^2 < 0$) or octant of θ_{23} (lower when $\theta_{23} < 45^\circ$ or upper when $\theta_{23} > 45^\circ$).

(C) Other neutrino mixing results:

The LSND anomaly [AGUILAR 01], reported a signal which is consistent with $\bar{\nu}_\mu \rightarrow \bar{\nu}_e$ oscillations. In a three neutrino framework, this would be a measurement of θ_{12} and Δm_{21}^2 . This does not appear to be consistent with the interpretation of other neutrino data. It has been interpreted as evidence for a 4th "sterile" neutrino. The following listings include results which might be relevant towards understanding this observation. They include searches for $\nu_\mu \rightarrow \nu_e$, $\bar{\nu}_\mu \rightarrow \bar{\nu}_e$, sterile neutrino oscillations, and others.

(A) Neutrino fluxes and event ratios

Events (observed/expected) from accelerator ν_μ experiments.

Some neutrino oscillation experiments compare the flux in two or more detectors. This is usually quoted as the ratio of the event rate in the far detector to the expected rate based on an extrapolation from the near detector in the absence of oscillations.

VALUE	DOCUMENT ID	TECN	COMMENT
• • •	We do not use the following data for averages, fits, limits, etc. • • •		
1.01 ± 0.10	¹ ABE	14B T2K	ν_e rate in T2K near detect.
0.71 ± 0.08	² AHN	06A K2K	K2K to Super-K
0.64 ± 0.05	³ MICHAEL	06 MINS	All charged current events
0.71 $^{+0.08}_{-0.09}$	⁴ ALIU	05 K2K	KEK to Super-K
0.70 $^{+0.10}_{-0.11}$	⁵ AHN	03 K2K	KEK to Super-K

¹ The rate of ν_e from μ decay was measured to be 0.68 ± 0.30 compared to the predicted flux. From K decay 1.10 ± 0.14 compared to the predicted flux.

² Based on the observation of 112 events when $158.1^{+9.2}_{-8.6}$ were expected without oscillations. Including not only the number of events but also the shape of the energy distribution, the evidence for oscillation is at the level of about 4.3σ . Supersedes ALIU 05.

³ This ratio is based on the observation of 215 events compared to an expectation of 336 ± 14 without oscillations. See also ADAMSON 08.

⁴ This ratio is based on the observation of 107 events at the far detector 250 km away from KEK, and an expectation of 151^{+12}_{-10} .

⁵ This ratio is based on the observation of 56 events with an expectation of $80.1^{+6.2}_{-5.4}$.

Events (observed/expected) from reactor $\bar{\nu}_e$ experiments.

The quoted values are the ratios of the measured reactor $\bar{\nu}_e$ event rate at the quoted distances, and the rate expected without oscillations. The expected rate is based on the experimental data for the most significant reactor fuels (^{235}U , ^{239}Pu , ^{241}Pu) and on calculations for ^{238}U .

A recent re-evaluation of the spectral conversion of electron to $\bar{\nu}_e$ in MUELLER 11 results in an upward shift of the reactor $\bar{\nu}_e$ spectrum by 3% and, thus, might require revisions to the ratios listed in this table.

VALUE	DOCUMENT ID	TECN	COMMENT
• • •	We do not use the following data for averages, fits, limits, etc. • • •		
0.952 ± 0.027	¹ ADEY	19 DAYA	DayaBay, Ling Ao/Ao II reactors
1.08 ± 0.21 ± 0.16	² AN	16 DAYA	DayaBay, Ling Ao/Ao II reactors
0.658 ± 0.044 ± 0.047	³ DENIZ	10 TEXO	Kuo-Sheng reactor, 28 m
0.611 ± 0.085 ± 0.041	⁴ ARAKI	05 KLND	Japanese react. ~ 180 km
1.01 ± 0.024 ± 0.053	⁵ EGUCHI	03 KLND	Japanese react. ~ 180 km
1.01 ± 0.028 ± 0.027	⁶ BOEHM	01	Palo Verde react. 0.75–0.89 km
0.987 ± 0.006 ± 0.037	⁷ APOLLONIO	99 CHOZ	Chooz reactors 1 km
0.988 ± 0.004 ± 0.05	⁸ GREENWOOD	96	Savannah River, 18.2 m
	ACHKAR	95 CNTR	Bugey reactor, 15 m

0.994 ± 0.010 ± 0.05	ACHKAR	95 CNTR	Bugey reactor, 40 m
0.915 ± 0.132 ± 0.05	ACHKAR	95 CNTR	Bugey reactor, 95 m
0.987 ± 0.014 ± 0.027	⁹ DECLAIS	94 CNTR	Bugey reactor, 15 m
0.985 ± 0.018 ± 0.034	KUVSHINN...	91 CNTR	Rovno reactor
1.05 ± 0.02 ± 0.05	VUILLEUMIER	82	Gösgen reactor
0.955 ± 0.035 ± 0.110	¹⁰ KWON	81	$\bar{\nu}_e p \rightarrow e^+ n$
0.89 ± 0.15	¹⁰ BOEHM	80	$\bar{\nu}_e p \rightarrow e^+ n$

¹ ADEY 19 present a re-analysis of 1230 days of Daya Bay near detector data with reduced systematic uncertainties on the neutron detection efficiency. Note that ADEY 19 report the measured to predicted antineutrino ratio using the reactor model of MUELLER 11 (Huber-Mueller model). The ratio using the older ILL-Vogel model is $1.001 \pm 0.015 \pm 0.027$.

² AN 16 use 217 days of data (338k events) to determine the neutrino flux ratio relative to the prediction of Mueller-Huber and ILL-Vogel models (see AN 16 for details). The reported flux ratios were corrected for θ_{13} oscillation effect. The flux measurement is consistent with results from previous short-baseline reactor experiments. The measured inverse beta decay yield is $(1.55 \pm 0.04) \times 10^{-18} \text{ cm}^2/(\text{GW day})$ or $\sigma_f = (5.92 \pm 0.14) \times 10^{-43} \text{ cm}^2/\text{fission}$. About 4σ excess of events was observed in the 4–6 MeV prompt energy region.

³ DENIZ 10 observe reactor $\bar{\nu}_e e$ scattering with recoil kinetic energies 3–8 MeV using CsI(Tl) detectors. The observed rate is consistent with the Standard Model prediction, leading to a constraint on $\sin^2\theta_W = 0.251 \pm 0.031(\text{stat}) \pm 0.024(\text{sys})$.

⁴ Updated result of KamLAND, including the data used in EGUCHI 03. Note that the survival probabilities for different periods are not directly comparable because the effective baseline varies with power output of the reactor sources involved, and there were large variations in the reactor power production in Japan in 2003.

⁵ EGUCHI 03 observe reactor neutrino disappearance at ~ 180 km baseline to various Japanese nuclear power reactors.

⁶ BOEHM 01 search for neutrino oscillations at 0.75 and 0.89 km distance from the Palo Verde reactors.

⁷ APOLLONIO 99, APOLLONIO 98 search for neutrino oscillations at 1.1 km fixed distance from Chooz reactors. They use $\bar{\nu}_e p \rightarrow e^+ n$ in Gd-loaded scintillator target. APOLLONIO 99 supersedes APOLLONIO 98. See also APOLLONIO 03 for detailed description.

⁸ GREENWOOD 96 search for neutrino oscillations at 18 m and 24 m from the reactor at Savannah River.

⁹ DECLAIS 94 result based on integral measurement of neutrons only. Result is ratio of measured cross section to that expected in standard V-A theory. Replaced by ACHKAR 95.

¹⁰ KWON 81 represents an analysis of a larger set of data from the same experiment as BOEHM 80.

Atmospheric neutrinos

Neutrinos and antineutrinos produced in the atmosphere induce μ -like and e -like events in underground detectors. The ratio of the numbers of the two kinds of events is defined as μ/e . It has the advantage that systematic effects, such as flux uncertainty, tend to cancel, for both experimental and theoretical values of the ratio. The "ratio of the ratios" of experimental to theoretical μ/e , $R(\mu/e)$, or that of experimental to theoretical μ/total , $R(\mu/\text{total})$ with $\text{total} = \mu + e$, is reported below. If the actual value is not unity, the value obtained in a given experiment may depend on the experimental conditions. In addition, the measured "up-down asymmetry" for μ ($N_{\text{up}}(\mu)/N_{\text{down}}(\mu)$) or e ($N_{\text{up}}(e)/N_{\text{down}}(e)$) is reported. The expected "up-down asymmetry" is nearly unity if there is no neutrino oscillation.

$R(\mu/e) = (\text{Measured Ratio } \mu/e) / (\text{Expected Ratio } \mu/e)$

VALUE	DOCUMENT ID	TECN	COMMENT
• • •	We do not use the following data for averages, fits, limits, etc. • • •		
0.658 ± 0.016 ± 0.035	¹ ASHIE	05 SKAM	sub-GeV
0.702 $^{+0.032}_{-0.030}$ ± 0.101	² ASHIE	05 SKAM	multi-GeV
0.69 ± 0.10 ± 0.06	³ SANCHEZ	03 SOU2	Calorimeter raw data
1.00 ± 0.15 ± 0.08	⁴ FUKUDA	96B KAMI	Water Cherenkov
0.60 $^{+0.06}_{-0.05}$ ± 0.05	⁵ DAUM	95 FREJ	Calorimeter
0.60 $^{+0.06}_{-0.05}$ ± 0.05	⁶ FUKUDA	94 KAMI	sub-GeV
0.57 $^{+0.08}_{-0.07}$ ± 0.07	⁷ FUKUDA	94 KAMI	multi-GeV
	⁸ BECKER-SZ...	92B IMB	Water Cherenkov

¹ ASHIE 05 results are based on an exposure of 92 kton yr during the complete Super-Kamiokande I running period. The analyzed data sample consists of fully-contained single-ring e -like events with $0.1 \text{ GeV}/c < p_e$ and μ -like events $0.2 \text{ GeV}/c < p_\mu$, both having a visible energy $< 1.33 \text{ GeV}$. These criteria match the definition used by FUKUDA 94.

² ASHIE 05 results are based on an exposure of 92 kton yr during the complete Super-Kamiokande I running period. The analyzed data sample consists of fully-contained single-ring events with visible energy $> 1.33 \text{ GeV}$ and partially-contained events. All partially-contained events are classified as μ -like.

³ SANCHEZ 03 result is based on an exposure of 5.9 kton yr, and updates ALLISON 99 result. The analyzed data sample consists of fully-contained e -flavor and μ -flavor events having lepton momentum $> 0.3 \text{ GeV}/c$.

⁴ FUKUDA 96B studied neutron background in the atmospheric neutrino sample observed in the Kamiokande detector. No evidence for the background contamination was found.

⁵ DAUM 95 results are based on an exposure of 2.0 kton yr which includes the data used by BERGER 90B. This ratio is for the contained and semicontained events. DAUM 95

See key on page 999

Lepton Particle Listings

Neutrino Mixing

also report $R(\mu/e) = 0.99 \pm 0.13 \pm 0.08$ for the total neutrino induced data sample which includes upward going stopping muons and horizontal muons in addition to the contained and semicontained events.

⁶FUKUDA 94 result is based on an exposure of 7.7 kton yr and updates the HIRATA 92 result. The analyzed data sample consists of fully-contained e -like events with $0.1 < p_e < 1.33$ GeV/c and fully-contained μ -like events with $0.2 < p_\mu < 1.5$ GeV/c.

⁷FUKUDA 94 analyzed the data sample consisting of fully contained events with visible energy > 1.33 GeV and partially contained μ -like events.

⁸BECKER-SZENDY 92B reports the fraction of nonshowering events (mostly muons from atmospheric neutrinos) as $0.36 \pm 0.02 \pm 0.02$, as compared with expected fraction $0.51 \pm 0.01 \pm 0.05$. After cutting the energy range to the Kamiokande limits, BEIER 92 finds $R(\mu/e)$ very close to the Kamiokande value.

$R(\nu_\mu) = (\text{Measured Flux of } \nu_\mu) / (\text{Expected Flux of } \nu_\mu)$

VALUE	DOCUMENT ID	TECN	COMMENT
• • • We do not use the following data for averages, fits, limits, etc. • • •			
0.84 ± 0.12	¹ ADAMSON 06	MINS	MINOS atmospheric
$0.72 \pm 0.026 \pm 0.13$	² AMBROSIO 01	MCRO	upward through-going
$0.57 \pm 0.05 \pm 0.15$	³ AMBROSIO 00	MCRO	upgoing partially contained
$0.71 \pm 0.05 \pm 0.19$	⁴ AMBROSIO 00	MCRO	downgoing partially contained + upgoing stopping
$0.74 \pm 0.036 \pm 0.046$	⁵ AMBROSIO 98	MCRO	Streamer tubes
	⁶ CASPER 91	IMB	Water Cherenkov
	⁷ AGLIETTA 89	NUSX	
	⁸ BOLIEV 81	Baksan	
0.95 ± 0.22			Case Western /UCI
0.62 ± 0.17	CROUCH 78		

¹ADAMSON 06 uses a measurement of 107 total neutrinos compared to an expected rate of 127 ± 13 without oscillations.

²AMBROSIO 01 result is based on the upward through-going muon tracks with $E_\mu > 1$ GeV. The data came from three different detector configurations, but the statistics is largely dominated by the full detector run, from May 1994 to December 2000. The total live time, normalized to the full detector configuration, is 6.17 years. The first error is the statistical error, the second is the systematic error, dominated by the theoretical error in the predicted flux.

³AMBROSIO 00 result is based on the upgoing partially contained event sample. It came from 4.1 live years of data taking with the full detector, from April 1994 to February 1999. The average energy of atmospheric muon neutrinos corresponding to this sample is 4 GeV. The first error is statistical, the second is the systematic error, dominated by the 25% theoretical error in the rate (20% in the flux and 15% in the cross section, added in quadrature). Within statistics, the observed deficit is uniform over the zenith angle.

⁴AMBROSIO 00 result is based on the combined samples of downgoing partially contained events and upgoing stopping events. These two subsamples could not be distinguished due to the lack of timing information. The result came from 4.1 live years of data taking with the full detector, from April 1994 to February 1999. The average energy of atmospheric muon neutrinos corresponding to this sample is 4 GeV. The first error is statistical, the second is the systematic error, dominated by the 25% theoretical error in the rate (20% in the flux and 15% in the cross section, added in quadrature). Within statistics, the observed deficit is uniform over the zenith angle.

⁵AMBROSIO 98 result is for all nadir angles and updates AHLEN 95 result. The lower cutoff on the muon energy is 1 GeV. In addition to the statistical and systematic errors, there is a Monte Carlo flux error (theoretical error) of ±0.13. With a neutrino oscillation hypothesis, the fit either to the flux or zenith distribution independently yields $\sin^2 2\theta = 1.0$ and $\Delta(m^2) \sim$ a few times 10^{-3} eV². However, the fit to the observed zenith distribution gives a maximum probability for χ^2 of only 5% for the best oscillation hypothesis.

⁶CASPER 91 correlates showering/nonshowering signature of single-ring events with parent atmospheric-neutrino flavor. They find nonshowering ($\approx \nu_\mu$ induced) fraction is $0.41 \pm 0.03 \pm 0.02$, as compared with expected 0.51 ± 0.05 (syst).

⁷AGLIETTA 89 finds no evidence for any anomaly in the neutrino flux. They define $\rho = (\text{measured number of } \nu_e) / (\text{measured number of } \nu_\mu)$. They report $\rho(\text{measured}) = \rho(\text{expected}) = 0.96 \pm 0.32$.

⁸From this data BOLIEV 81 obtain the limit $\Delta(m^2) \leq 6 \times 10^{-3}$ eV² for maximal mixing, $\nu_\mu \leftrightarrow \nu_\mu$ type oscillation.

$R(\mu/\text{total}) = (\text{Measured Ratio } \mu/\text{total}) / (\text{Expected Ratio } \mu/\text{total})$

VALUE	DOCUMENT ID	TECN	COMMENT
• • • We do not use the following data for averages, fits, limits, etc. • • •			
$1.1 \pm 0.07 \pm 0.11$	¹ CLARK 97	IMB	multi-GeV

¹CLARK 97 obtained this result by an analysis of fully contained and partially contained events in the IMB water-Cherenkov detector with visible energy > 0.95 GeV.

$N_{\text{up}}(\mu) / N_{\text{down}}(\mu)$

VALUE	DOCUMENT ID	TECN	COMMENT
• • • We do not use the following data for averages, fits, limits, etc. • • •			
0.71 ± 0.06	¹ ADAMSON 12B	MINS	contained-vertex muons
$0.551 \pm 0.035 \pm 0.004$	² ASHIE 05	SKAM	multi-GeV

¹ADAMSON 12B reports the atmospheric neutrino results obtained with MINOS far detector in 2,553 live days (an exposure of 37.9 kton-yr). This result is obtained with a sample of high resolution contained-vertex muons. The quoted error is statistical only.

²ASHIE 05 results are based on an exposure of 92 kton yr during the complete Super-Kamiokande I running period. The analyzed data sample consists of fully-contained single-ring μ -like events with visible energy > 1.33 GeV and partially-contained events.

All partially-contained events are classified as μ -like. Upward-going events are those with $-1 < \cos(\text{zenith angle}) < -0.2$ and downward-going events are those with $0.2 < \cos(\text{zenith angle}) < 1$. The μ -like up-down ratio for the multi-GeV data deviates from 1 (the expectation for no atmospheric ν_μ oscillations) by more than 12 standard deviations.

$N_{\text{up}}(e) / N_{\text{down}}(e)$

VALUE	DOCUMENT ID	TECN	COMMENT
• • • We do not use the following data for averages, fits, limits, etc. • • •			
$0.961 \pm 0.086 \pm 0.016$	¹ ASHIE 05	SKAM	multi-GeV

¹ASHIE 05 results are based on an exposure of 92 kton yr during the complete Super-Kamiokande I running period. The analyzed data sample consists of fully-contained single-ring e -like events with visible energy > 1.33 GeV. Upward-going events are those with $-1 < \cos(\text{zenith angle}) < -0.2$ and downward-going events are those with $0.2 < \cos(\text{zenith angle}) < 1$. The e -like up-down ratio for the multi-GeV data is consistent with 1 (the expectation for no atmospheric ν_e oscillations).

$R(\text{up/down}; \mu) = (\text{Measured up/down}; \mu) / (\text{Expected up/down}; \mu)$

VALUE	DOCUMENT ID	TECN	COMMENT
• • • We do not use the following data for averages, fits, limits, etc. • • •			
$0.62 \pm 0.05 \pm 0.02$	¹ ADAMSON 12B	MINS	contained-vertex muons
$0.63 \pm 0.19 \pm 0.02$	² ADAMSON 06	MINS	atmospheric ν with far detector

¹ADAMSON 12B reports the atmospheric neutrino results obtained with MINOS far detector in 2,553 live days (an exposure of 37.9 kton-yr). This result is obtained with a sample of high resolution contained-vertex muons. The expected ratio is calculated with no neutrino oscillation.

²ADAMSON 06 result is obtained with the MINOS far detector with an exposure of 4.54 kton yr. The expected ratio is calculated with no neutrino oscillation.

$N(\mu^+) / N(\mu^-)$

VALUE	DOCUMENT ID	TECN	COMMENT
• • • We do not use the following data for averages, fits, limits, etc. • • •			
$0.46 \pm 0.05 \pm 0.04$	^{1,2} ADAMSON 12B	MINS	contained-vertex muons
$0.63 \pm 0.09 \pm 0.08$	^{1,3} ADAMSON 12B	MINS	ν -induced rock-muons

¹ADAMSON 12B reports the atmospheric neutrino results obtained with MINOS far detector in 2,553 live days (an exposure of 37.9 kton-yr). The muon charge ratio $N(\mu^+) / N(\mu^-)$ represents the $\overline{\nu}_\mu / \nu_\mu$ ratio.

²This result is obtained with a charge-separated sample of high resolution contained-vertex muons. The quoted error is statistical only.

³This result is obtained with a charge-separated sample of high resolution neutrino-induced rock-muons. The quoted error is statistical only.

$R(\mu^+ / \mu^-) = (\text{Measured } N(\mu^+) / N(\mu^-)) / (\text{Expected } N(\mu^+) / N(\mu^-))$

VALUE	DOCUMENT ID	TECN	COMMENT
• • • We do not use the following data for averages, fits, limits, etc. • • •			
$0.93 \pm 0.09 \pm 0.09$	^{1,2} ADAMSON 12B	MINS	contained-vertex muons
$1.29 \pm 0.19 \pm 0.16$	^{1,3} ADAMSON 12B	MINS	ν -induced rock-muons
$1.03 \pm 0.08 \pm 0.08$	^{1,4} ADAMSON 12B	MINS	contained
$1.39 \pm 0.35 \pm 0.08$	⁵ ADAMSON 07	MINS	Upward and horizontal μ with far detector
$0.96 \pm 0.38 \pm 0.15$	⁶ ADAMSON 06	MINS	atmospheric ν with far detector

¹ADAMSON 12B reports the atmospheric neutrino results obtained with MINOS far detector in 2,553 live days (an exposure of 37.9 kton-yr). The muon charge ratio $N(\mu^+) / N(\mu^-)$ represents the $\overline{\nu}_\mu / \nu_\mu$ ratio. As far as the same oscillation parameters are used for ν_s and $\overline{\nu}_s$, the expected $\overline{\nu}_\mu / \nu_\mu$ ratio is almost entirely independent of any input oscillations.

²This result is obtained with a charge-separated sample of high resolution contained-vertex muons.

³This result is obtained with a charge-separated sample of high resolution neutrino-induced rock-muons.

⁴The charge-separated samples of high resolution contained-vertex muons and neutrino-induced rock-muons are combined to obtain this result which is consistent with unity.

⁵ADAMSON 07 result is obtained with the MINOS far detector in 854.24 live days, based on neutrino-induced upward-going and horizontal muons. This result is consistent with CP T conservation.

⁶ADAMSON 06 result is obtained with the MINOS far detector with an exposure of 4.54 kton yr, based on contained events. The expected ratio is calculated by assuming the same oscillation parameters for neutrinos and antineutrinos.

Solar neutrinos

Solar neutrinos are produced by thermonuclear fusion reactions in the Sun. Radiochemical experiments measure particular combinations of fluxes from various neutrino-producing reactions, whereas water-Cherenkov experiments mainly measure a flux of neutrinos from decay of ⁸B. Solar neutrino fluxes are composed of all active neutrino species, ν_e , ν_μ , and ν_τ . In addition, some other mechanisms may cause antineutrino components in solar neutrino fluxes. Each measurement method is sensitive to

Lepton Particle Listings

Neutrino Mixing

a particular component or a combination of components of solar neutrino fluxes.

ν_e Capture Rates from Radiochemical Experiments

1 SNU (Solar Neutrino Unit) = 10^{-36} captures per atom per second.

VALUE (SNU)	DOCUMENT ID	TECN	COMMENT
73.4 $^{+6.1}_{-6.0}$ $^{+3.7}_{-4.1}$	¹ KAETHER	10	GALX reanalysis
67.6 ± 4.0 ± 3.2	² KAETHER	10	GNO+GALX reanalysis combined
65.4 $^{+3.1}_{-3.0}$ $^{+2.6}_{-2.8}$	³ ABDURASHI...	09 SAGE	⁷¹ Ga \rightarrow ⁷¹ Ge
62.9 $^{+5.5}_{-5.3}$ ± 2.5	⁴ ALTMANN	05 GNO	⁷¹ Ga \rightarrow ⁷¹ Ge
69.3 ± 4.1 ± 3.6	⁵ ALTMANN	05 GNO	GNO + GALX combined
77.5 ± 6.2 $^{+4.3}_{-4.7}$	⁶ HAMPEL	99 GALX	⁷¹ Ga \rightarrow ⁷¹ Ge
2.56 ± 0.16 ± 0.16	⁷ CLEVELAND	98 HOME	³⁷ Cl \rightarrow ³⁷ Ar

- • • We do not use the following data for averages, fits, limits, etc. • • •
- ¹ KAETHER 10 reports the reanalysis results of a complete GALLEX data (GALLEX I+II+III+IV, reported in HAMPEL 99) based on the event selection with a new pulse shape analysis, which provides a better background reduction than the rise time analysis adopted in HAMPEL 99.
- ² Combined result of GALLEX I+II+III+IV reanalysis and GNO I+II+III (ALTMANN 05).
- ³ ABDURASHITOV 09 reports a combined analysis of 168 extractions of the SAGE solar neutrino experiment during the period January 1990 through December 2007, and updates the ABDURASHITOV 02 result. The data are consistent with the assumption that the solar neutrino production rate is constant in time. Note that a $\sim 15\%$ systematic uncertainty in the overall normalization may be added to the ABDURASHITOV 09 result, because calibration experiments for gallium solar neutrino measurements using intense ⁵¹Cr (twice by GALLEX and once by SAGE) and ³⁷Ar (by SAGE) result in an average ratio of 0.87 ± 0.05 of the observed to calculated rates.
- ⁴ ALTMANN 05 reports the complete result from the GNO solar neutrino experiment (GNO I+II+III), which is the successor project of GALLEX. Experimental technique of GNO is essentially the same as that of GALLEX. The run data cover the period 20 May 1998 through 9 April 2003.
- ⁵ Combined result of GALLEX I+II+III+IV (HAMPEL 99) and GNO I+II+III.
- ⁶ HAMPEL 99 report the combined result for GALLEX I+II+III+IV (65 runs in total), which update the HAMPEL 96 result. The GALLEX IV result (12 runs) is $118.4 \pm 17.8 \pm 6.6$ SNU. (HAMPEL 99 discuss the consistency of partial results with the mean.) The GALLEX experimental program has been completed with these runs. The total run data cover the period 14 May 1991 through 23 January 1997. A total of 300 ⁷¹Ge events were observed. Note that a $\sim 15\%$ systematic uncertainty in the overall normalization may be added to the HAMPEL 99 result, because calibration experiments for gallium solar neutrino measurements using intense ⁵¹Cr (twice by GALLEX and once by SAGE) and ³⁷Ar (by SAGE) result in an average ratio of 0.87 ± 0.05 of the observed to calculated rates.
- ⁷ CLEVELAND 98 is a detailed report of the ³⁷Cl experiment at the Homestake Mine. The average solar neutrino-induced ³⁷Ar production rate from 108 runs between 1970 and 1994 updates the DAVIS 89 result.

ϕ_{ES} (⁸B)

⁸B solar-neutrino flux measured via νe elastic scattering. This process is sensitive to all active neutrino flavors, but with reduced sensitivity to ν_μ, ν_τ due to the cross-section difference, $\sigma(\nu_{\mu,\tau} e) \sim 0.16\sigma(\nu_e e)$. If the ⁸B solar-neutrino flux involves nonelectron flavor active neutrinos, their contribution to the flux is ~ 0.16 times of ν_e .

VALUE ($10^6 \text{ cm}^{-2} \text{ s}^{-1}$)	DOCUMENT ID	TECN	COMMENT
2.53 $^{+0.31}_{-0.28}$ $^{+0.13}_{-0.10}$	¹ ANDERSON	19 SNO+	Water phase; average flux
2.57 $^{+0.17}_{-0.18}$ $^{+0.07}_{-0.07}$	² AGOSTINI	18B BORX	average flux
2.345 ± 0.014 ± 0.036	³ ABE	16C SKAM	SK-I+II+III+IV average flux
2.308 ± 0.020 $^{+0.039}_{-0.040}$	⁴ ABE	16C SKAM	SK-IV average flux
2.250 $^{+0.030}_{-0.029}$ ± 0.038	⁴ ABE	16C SKAM	SK-IV day flux
2.364 ± 0.029 ± 0.040	⁴ ABE	16C SKAM	SK-IV night flux
2.404 ± 0.039 ± 0.053	⁵ ABE	16C SKAM	SK-III average flux
2.41 ± 0.05 $^{+0.16}_{-0.15}$	⁶ ABE	11 SKAM	SK-II average flux
2.38 ± 0.02 ± 0.08	⁷ ABE	11 SKAM	SK-I average flux
2.77 ± 0.26 ± 0.32	⁸ ABE	11B KLND	average flux
2.4 ± 0.4 ± 0.1	⁹ BELLINI	10A BORX	average flux
1.77 $^{+0.24}_{-0.21}$ $^{+0.09}_{-0.10}$	¹⁰ AHARMIM	08 SNO	Phase III
2.38 ± 0.05 $^{+0.16}_{-0.15}$	¹¹ CRAVENS	08 SKAM	average flux
2.35 ± 0.02 ± 0.08	¹² HOSAKA	06 SKAM	average flux
2.35 ± 0.22 ± 0.15	¹³ AHARMIM	05A SNO	Salty D ₂ O; ⁸ B shape not constrained
2.34 ± 0.23 $^{+0.15}_{-0.14}$	¹³ AHARMIM	05A SNO	Salty D ₂ O; ⁸ B shape constrained
2.39 $^{+0.24}_{-0.23}$ ± 0.12	¹⁴ AHMAD	02 SNO	average flux

• • • We do not use the following data for averages, fits, limits, etc. • • •

2.39 ± 0.34 $^{+0.16}_{-0.14}$	¹⁵ AHMAD	01 SNO	average flux
2.80 ± 0.19 ± 0.33	¹⁶ FUKUDA	96 KAMI	average flux
2.70 ± 0.27	¹⁶ FUKUDA	96 KAMI	day flux
2.87 $^{+0.27}_{-0.26}$	¹⁶ FUKUDA	96 KAMI	night flux

- ¹ ANDERSON 19 reports this result from the $\nu_e e$ elastic scattering rate using a 69.2 kton-day (or 114.7 days) of exposure from May through December, 2017 during the SNO+ detector's water commissioning phase. The events over the reconstructed electron kinetic energy range of 5–15 MeV were analyzed.
- ² AGOSTINI 18B obtained this result from the $\nu_e e$ elastic scattering rate over the period between January 2008 and December 2016.
- ³ ABE 16C reports the combined results of the four phases of the Super-Kamiokande average flux measurements. Here the revised Super-Kamiokande-III result is used.
- ⁴ ABE 16C reports the Super-Kamiokande-IV results for 1664 live days from September 2008 to February 2014. The analysis threshold is total electron energy of 4.0 MeV.
- ⁵ ABE 16C revised the Super-Kamiokande-III average flux value reported in ABE 11. Super-Kamiokande-III results are for 548 live days from August 4, 2006 to August 18, 2008. The analysis threshold is 5.0 MeV, but the event sample in the 5.0–6.5 MeV total electron energy range has a total live time of 298 days.
- ⁶ ABE 11 recalculated the Super-Kamiokande-II results using ⁸B spectrum of WINTER 06A.
- ⁷ ABE 11 recalculated the Super-Kamiokande-I results using ⁸B spectrum of WINTER 06A.
- ⁸ ABE 11B use a 123 kton-day exposure of the KamLAND liquid scintillation detector to measure the ⁸B solar neutrino flux. They utilize $\nu - e$ elastic scattering above a reconstructed-energy threshold of 5.5 MeV, corresponding to 5 MeV electron recoil energy. 299 electron recoil candidate events are reported, of which 157 ± 23.6 are assigned to background.
- ⁹ BELLINI 10A reports the Borexino result with 3 MeV energy threshold for scattered electrons. The data correspond to 345.3 live days with a target mass of 100 t, between July 15, 2007 and August 23, 2009.
- ¹⁰ AHARMIM 08 reports the results from SNO Phase III measurement using an array of ³He proportional counters to measure the rate of NC interactions in heavy water, over the period between November 27, 2004 and November 28, 2006, corresponding to 385.17 live days. A simultaneous fit was made for the number of NC events detected by the proportional counters and the numbers of NC, CC, and ES events detected by the PMTs, where the spectral distributions of the ES and CC events were not constrained to the ⁸B shape.
- ¹¹ CRAVENS 08 reports the Super-Kamiokande-II results for 791 live days from December 2002 to October 2005. The photocathode coverage of the detector is 19% (reduced from 40% of that of Super-Kamiokande-I due to an accident in 2001). The analysis threshold for the average flux is 7 MeV.
- ¹² HOSAKA 06 reports the final results for 1496 live days with Super-Kamiokande-I between May 31, 1996 and July 15, 2001, and replace FUKUDA 02 results. The analysis threshold is 5 MeV except for the first 280 live days (6.5 MeV).
- ¹³ AHARMIM 05A measurements were made with dissolved NaCl (0.195% by weight) in heavy water over the period between July 26, 2001 and August 28, 2003, corresponding to 391.4 live days, and update AHMED 04A. The CC, ES, and NC events were statistically separated. In one method, the ⁸B energy spectrum was not constrained. In the other method, the constraint of an undistorted ⁸B energy spectrum was added for comparison with AHMAD 02 results.
- ¹⁴ AHMAD 02 reports the ⁸B solar-neutrino flux measured via νe elastic scattering above the kinetic energy threshold of 5 MeV. The data correspond to 306.4 live days with SNO between November 2, 1999 and May 28, 2001, and updates AHMAD 01 results.
- ¹⁵ AHMAD 01 reports the ⁸B solar-neutrino flux measured via νe elastic scattering above the kinetic energy threshold of 6.75 MeV. The data correspond to 241 live days with SNO between November 2, 1999 and January 15, 2001.
- ¹⁶ FUKUDA 96 results are for a total of 2079 live days with Kamiokande II and III from January 1987 through February 1995, covering the entire solar cycle 22, with threshold $E_e > 9.3$ MeV (first 449 days), > 7.5 MeV (middle 794 days), and > 7.0 MeV (last 836 days). These results update the HIRATA 90 result for the average ⁸B solar-neutrino flux and HIRATA 91 result for the day-night variation in the ⁸B solar-neutrino flux. The total data sample was also analyzed for short-term variations: within experimental errors, no strong correlation of the solar-neutrino flux with the sunspot numbers was found.

ϕ_{CC} (⁸B)

⁸B solar-neutrino flux measured with charged-current reaction which is sensitive exclusively to ν_e .

VALUE ($10^6 \text{ cm}^{-2} \text{ s}^{-1}$)	DOCUMENT ID	TECN	COMMENT
1.67 $^{+0.05}_{-0.04}$ $^{+0.07}_{-0.08}$	¹ AHARMIM	08 SNO	Phase III
1.68 ± 0.06 $^{+0.08}_{-0.09}$	² AHARMIM	05A SNO	Salty D ₂ O; ⁸ B shape not const.
1.72 ± 0.05 ± 0.11	² AHARMIM	05A SNO	Salty D ₂ O; ⁸ B shape constrained
1.76 $^{+0.06}_{-0.05}$ ± 0.09	³ AHMAD	02 SNO	average flux
1.75 ± 0.07 $^{+0.12}_{-0.11}$ ± 0.05	⁴ AHMAD	01 SNO	average flux

- • • We do not use the following data for averages, fits, limits, etc. • • •
- ¹ AHARMIM 08 reports the results from SNO Phase III measurement using an array of ³He proportional counters to measure the rate of NC interactions in heavy water, over the period between November 27, 2004 and November 28, 2006, corresponding to 385.17 live days. A simultaneous fit was made for the number of NC events detected by the proportional counters and the numbers of NC, CC, and ES events detected by the PMTs, where the spectral distributions of the ES and CC events were not constrained to the ⁸B shape.

See key on page 999

Lepton Particle Listings

Neutrino Mixing

²AHARMIM 05A measurements were made with dissolved NaCl (0.195% by weight) in heavy water over the period between July 26, 2001 and August 28, 2003, corresponding to 391.4 live days, and update AHMED 04A. The CC, ES, and NC events were statistically separated. In one method, the ⁸B energy spectrum was not constrained. In the other method, the constraint of an undistorted ⁸B energy spectrum was added for comparison with AHMAD 02 results.

³AHMAD 02 reports the SNO result of the ⁸B solar-neutrino flux measured with charged-current reaction on deuterium, $\nu_e d \rightarrow pp e^-$, above the kinetic energy threshold of 5 MeV. The data correspond to 306.4 live days with SNO between November 2, 1999 and May 28, 2001, and updates AHMAD 01 results. The complete description of the SNO Phase I data set is given in AHARMIM 07.

⁴AHMAD 01 reports the first SNO result of the ⁸B solar-neutrino flux measured with the charged-current reaction on deuterium, $\nu_e d \rightarrow pp e^-$, above the kinetic energy threshold of 6.75 MeV. The data correspond to 241 live days with SNO between November 2, 1999 and January 15, 2001.

ϕ_{NC} (⁸B)

⁸B solar neutrino flux measured with neutral-current reaction, which is equally sensitive to ν_e , ν_μ , and ν_τ .

VALUE ($10^6 \text{ cm}^{-2} \text{ s}^{-1}$)	DOCUMENT ID	TECN	COMMENT
• • • We do not use the following data for averages, fits, limits, etc. • • •			
5.25 ± 0.16 ^{+0.11} / _{-0.13}	¹ AHARMIM	13	SNO All three phases combined
5.140 ± 0.160 ^{+0.132} / _{-0.158}	² AHARMIM	10	SNO Phase I+II, low threshold
5.54 ± 0.33 ^{+0.36} / _{-0.31}	³ AHARMIM	08	SNO Phase III, prop. counter + PMT
4.94 ± 0.21 ^{+0.38} / _{-0.34}	⁴ AHARMIM	05A	SNO Salty D ₂ O; ⁸ B shape not const.
4.81 ± 0.19 ^{+0.28} / _{-0.27}	⁴ AHARMIM	05A	SNO Salty D ₂ O; ⁸ B shape constrained
5.09 ± 0.44 ^{+0.46} / _{-0.43}	⁵ AHMAD	02	SNO average flux; ⁸ B shape const.
6.42 ± 1.57 ^{+0.55} / _{-0.58}	⁵ AHMAD	02	SNO average flux; ⁸ B shape not const.

¹AHARMIM 13 obtained this result from a combined analysis of the data from all three phases, SNO-I, II, and III. The measurement of the ⁸B flux mostly comes from the NC signal, however, CC contribution is included in the fit.

²AHARMIM 10 reports this result from a joint analysis of SNO Phase I+II data with the "effective electron kinetic energy" threshold of 3.5 MeV. This result is obtained with a "binned-histogram unconstrained fit" where binned probability distribution functions of the neutrino signal observables were used without any model constraints on the shape of the neutrino spectrum.

³AHARMIM 08 reports the results from SNO Phase III measurement using an array of ³He proportional counters to measure the rate of NC interactions in heavy water, over the period between November 27, 2004 and November 28, 2006, corresponding to 385.17 live days. A simultaneous fit was made for the number of NC events detected by the proportional counters and the numbers of NC, CC, and ES events detected by the PMTs, where the spectral distributions of the ES and CC events were not constrained to the ⁸B shape.

⁴AHARMIM 05A measurements were made with dissolved NaCl (0.195% by weight) in heavy water over the period between July 26, 2001 and August 28, 2003, corresponding to 391.4 live days, and update AHMED 04A. The CC, ES, and NC events were statistically separated. In one method, the ⁸B energy spectrum was not constrained. In the other method, the constraint of an undistorted ⁸B energy spectrum was added for comparison with AHMAD 02 results.

⁵AHMAD 02 reports the first SNO result of the ⁸B solar-neutrino flux measured with the neutral-current reaction on deuterium, $\nu_e d \rightarrow np \nu_e$, above the neutral-current reaction threshold of 2.2 MeV. The data correspond to 306.4 live days with SNO between November 2, 1999 and May 28, 2001. The complete description of the SNO Phase I data set is given in AHARMIM 07.

$\phi_{\nu_\mu + \nu_\tau}$ (⁸B)

Nonelectron-flavor active neutrino component (ν_μ and ν_τ) in the ⁸B solar-neutrino flux.

VALUE ($10^6 \text{ cm}^{-2} \text{ s}^{-1}$)	DOCUMENT ID	TECN	COMMENT
• • • We do not use the following data for averages, fits, limits, etc. • • •			
3.26 ± 0.25 ^{+0.40} / _{-0.35}	¹ AHARMIM	05A	SNO From ϕ_{NC} , ϕ_{CC} , and ϕ_{ES} ; ⁸ B shape not const.
3.09 ± 0.22 ^{+0.30} / _{-0.27}	¹ AHARMIM	05A	SNO From ϕ_{NC} , ϕ_{CC} , and ϕ_{ES} ; ⁸ B shape constrained
3.41 ± 0.45 ^{+0.48} / _{-0.45}	² AHMAD	02	SNO From ϕ_{NC} , ϕ_{CC} , and ϕ_{ES}
3.69 ± 1.13	³ AHMAD	01	Derived from SNO+SuperKam, water Cherenkov

¹AHARMIM 05A measurements were made with dissolved NaCl (0.195% by weight) in heavy water over the period between July 26, 2001 and August 28, 2003, corresponding to 391.4 live days, and update AHMED 04A. The CC, ES, and NC events were statistically separated. In one method, the ⁸B energy spectrum was not constrained. In the other method, the constraint of an undistorted ⁸B energy spectrum was added for comparison with AHMAD 02 results.

²AHMAD 02 deduced the nonelectron-flavor active neutrino component (ν_μ and ν_τ) in the ⁸B solar-neutrino flux, by combining the charged-current result, the ν_e elastic-scattering result and the neutral-current result. The complete description of the SNO Phase I data set is given in AHARMIM 07.

³AHMAD 01 deduced the nonelectron-flavor active neutrino component (ν_μ and ν_τ) in the ⁸B solar-neutrino flux, by combining the SNO charged-current result (AHMAD 01) and the Super-Kamiokande ν_e elastic-scattering result (FUKUDA 01).

Total Flux of Active pp Solar Neutrinos

Total flux of active neutrinos (ν_e, ν_μ, ν_τ).

VALUE ($10^{10} \text{ cm}^{-2} \text{ s}^{-1}$)	DOCUMENT ID	TECN	COMMENT
• • • We do not use the following data for averages, fits, limits, etc. • • •			
6.1 ± 0.5 ^{+0.3} / _{-0.5}	¹ AGOSTINI	18B	BORX Use $\nu_e e$ scattering rate

¹AGOSTINI 18B obtained this result from the measured $\nu_e e$ elastic scattering rate over the period between December 2011 and May 2016, assuming the MSW-LMA oscillation parameters derived by ESTEBAN 17. Assuming a high-metallicity standard solar model, the electron neutrino survival probability for the pp solar neutrino is calculated to be 0.57 ± 0.09 .

Total Flux of Active ⁷Be Solar Neutrinos

Total flux of active neutrinos (ν_e, ν_μ, ν_τ).

VALUE ($10^9 \text{ cm}^{-2} \text{ s}^{-1}$)	DOCUMENT ID	TECN	COMMENT
• • • We do not use the following data for averages, fits, limits, etc. • • •			
4.99 ± 0.11 ^{+0.06} / _{-0.08}	¹ AGOSTINI	18B	BORX Use $\nu_e e$ scattering rate

¹AGOSTINI 18B obtained this result from the measured $\nu_e e$ elastic scattering rate over the period between December 2011 and May 2016, assuming the MSW-LMA oscillation parameters derived by ESTEBAN 17. Assuming a high-metallicity standard solar model, the electron neutrino survival probability for the ⁷Be solar neutrino is calculated to be 0.53 ± 0.05 .

Total Flux of Active pep Solar Neutrinos

Total flux of active neutrinos (ν_e, ν_μ, ν_τ).

VALUE ($10^8 \text{ cm}^{-2} \text{ s}^{-1}$)	DOCUMENT ID	TECN	COMMENT
• • • We do not use the following data for averages, fits, limits, etc. • • •			
1.27 ± 0.19 ^{+0.08} / _{-0.12}	¹ AGOSTINI	18B	BORX Use $\nu_e e$ scattering rate

¹AGOSTINI 18B obtained this result from the measured $\nu_e e$ elastic scattering rate over the period between December 2011 and May 2016, assuming the MSW-LMA oscillation parameters derived by ESTEBAN 17 and a high-metallicity standard solar model. The electron neutrino survival probability for the pep solar neutrino is calculated to be 0.43 ± 0.11 .

Total Flux of Active ⁸B Solar Neutrinos

Total flux of active neutrinos (ν_e, ν_μ , and ν_τ).

VALUE ($10^6 \text{ cm}^{-2} \text{ s}^{-1}$)	DOCUMENT ID	TECN	COMMENT
• • • We do not use the following data for averages, fits, limits, etc. • • •			
5.95 ^{+0.75} / _{-0.71} ^{+0.28} / _{-0.30}	¹ ANDERSON	19	SNO+ Water phase; $\nu_e e$ scattering rate
5.68 ^{+0.39} / _{-0.41} ^{+0.03} / _{-0.03}	² AGOSTINI	18B	BORX From $\nu_e e$ scattering rate
5.25 ± 0.16 ^{+0.11} / _{-0.13}	³ AHARMIM	13	SNO All three phases combined
5.046 ± 0.159 ^{+0.107} / _{-0.152} ^{+0.107} / _{-0.123}	⁴ AHARMIM	10	SNO From ϕ_{NC} in Phase I+II, low threshold
5.54 ± 0.33 ^{+0.36} / _{-0.31} ^{+0.36} / _{-0.34}	⁵ AHARMIM	08	SNO ϕ_{NC} in Phase III
4.94 ± 0.21 ^{+0.38} / _{-0.34}	⁶ AHARMIM	05A	SNO From ϕ_{NC} ; ⁸ B shape not const.
4.81 ± 0.19 ^{+0.28} / _{-0.27}	⁶ AHARMIM	05A	SNO From ϕ_{NC} ; ⁸ B shape constrained
5.09 ± 0.44 ^{+0.46} / _{-0.43}	⁷ AHMAD	02	SNO Direct measurement from ϕ_{NC}
5.44 ± 0.99	⁸ AHMAD	01	Derived from SNO+SuperKam, water Cherenkov

¹ANDERSON 19 reports this result from the measured $\nu_e e$ elastic scattering rate using a 69.2 kton-day (or 114.7 days) of exposure from May through December, 2017 during the SNO+ detector's water commissioning phase, assuming the neutrino mixing parameters given in PDG 16 and a standard solar model given in BAHCALL 05.

²AGOSTINI 18B obtained this result from the measured $\nu_e e$ elastic scattering rate over the period between January 2008 and December 2016, assuming the MSW-LMA oscillation parameters derived by ESTEBAN 17. Assuming a high-metallicity standard solar model, the electron neutrino survival probability for the ⁸B solar neutrino is calculated to be 0.37 ± 0.08 .

³AHARMIM 13 obtained this result from a combined analysis of the data from all three phases, SNO-I, II, and III. The measurement of the ⁸B flux mostly comes from the NC signal, however, CC contribution is included in the fit.

⁴AHARMIM 10 reports this result from a joint analysis of SNO Phase I+II data with the "effective electron kinetic energy" threshold of 3.5 MeV. This result is obtained with the assumption of unitarity, which relates the NC, CC, and ES rates. The data were fit with the free parameters directly describing the total ⁸B neutrino flux and the energy-dependent ν_e survival probability.

⁵AHARMIM 08 reports the results from SNO Phase III measurement using an array of ³He proportional counters to measure the rate of NC interactions in heavy water, over the period between November 27, 2004 and November 28, 2006, corresponding to 385.17

Lepton Particle Listings

Neutrino Mixing

live days. A simultaneous fit was made for the number of NC events detected by the proportional counters and the numbers of NC, CC, and ES events detected by the PMTs, where the spectral distributions of the ES and CC events were not constrained to the ^8B shape.

⁶AHARMIM 05A measurements were made with dissolved NaCl (0.195% by weight) in heavy water over the period between July 26, 2001 and August 28, 2003, corresponding to 391.4 live days, and update AHMED 04A. The CC, ES, and NC events were statistically separated. In one method, the ^8B energy spectrum was not constrained. In the other method, the constraint of an undistorted ^8B energy spectrum was added for comparison with AHMAD 02 results.

⁷AHMAD 02 determined the total flux of active ^8B solar neutrinos by directly measuring the neutral-current reaction, $\nu_e d \rightarrow np\nu_e$, which is equally sensitive to ν_e , ν_μ , and ν_τ . The complete description of the SNO Phase I data set is given in AHARMIM 07.

⁸AHMAD 01 deduced the total flux of active ^8B solar neutrinos by combining the SNO charged-current result (AHMAD 01) and the Super-Kamiokande νe elastic-scattering result (FUKUDA 01).

Total Flux of Active CNO Solar Neutrinos

Total flux of active neutrinos (ν_e, ν_μ, ν_τ).

VALUE ($10^8 \text{ cm}^{-2} \text{ s}^{-1}$)	CL%	DOCUMENT ID	TECN	COMMENT
---	-----	-------------	------	---------

• • • We do not use the following data for averages, fits, limits, etc. • • •

<7.9	95	¹ AGOSTINI	18B BORSX	Use $\nu_e e$ scattering rate
------	----	-----------------------	-----------	-------------------------------

¹AGOSTINI 18B obtained this result from an upper limit of the $\nu_e e$ elastic scattering rate for the CNO neutrinos over the period between December 2011 and May 2016, assuming the MSW-LMA oscillation parameters derived by ESTEBAN 17.

Total Flux of Active hep Solar Neutrinos

Total flux of active neutrinos (ν_e, ν_μ, ν_τ).

VALUE ($10^5 \text{ cm}^{-2} \text{ s}^{-1}$)	CL%	DOCUMENT ID	TECN	COMMENT
---	-----	-------------	------	---------

• • • We do not use the following data for averages, fits, limits, etc. • • •

<2.2	90	¹ AGOSTINI	18B BORSX	Use $\nu_e e$ scattering rate
------	----	-----------------------	-----------	-------------------------------

¹AGOSTINI 18B obtained this result from an upper limit of the $\nu_e e$ elastic scattering rate for the hep neutrino using the dataset corresponding to an exposure of 0.8 kt-yr and assuming the MSW-LMA oscillation parameters derived by ESTEBAN 17.

Day-Night Asymmetry (^8B)

$A = (\phi_{\text{night}} - \phi_{\text{day}}) / \phi_{\text{average}}$

VALUE	DOCUMENT ID	TECN	COMMENT
-------	-------------	------	---------

$0.033 \pm 0.010 \pm 0.005$	¹ ABE	16c SKAM	SK combined; Based on ϕ_{ES}
---	------------------	----------	-----------------------------------

• • • We do not use the following data for averages, fits, limits, etc. • • •

$0.036 \pm 0.016 \pm 0.006$	² ABE	16c SKAM	SK-IV; Based on ϕ_{ES}
-----------------------------	------------------	----------	-----------------------------

$0.032 \pm 0.011 \pm 0.005$	³ RENSHAW	14 SKAM	Based on ϕ_{ES}
-----------------------------	----------------------	---------	----------------------

$0.063 \pm 0.042 \pm 0.037$	⁴ CRAVENS	08 SKAM	Based on ϕ_{ES}
-----------------------------	----------------------	---------	----------------------

$0.021 \pm 0.020 \pm 0.012$ -0.013	⁵ HOSAKA	06 SKAM	Based on ϕ_{ES}
---	---------------------	---------	----------------------

$0.017 \pm 0.016 \pm 0.012$ -0.013	⁶ HOSAKA	06 SKAM	Fitted in the LMA region
---	---------------------	---------	--------------------------

$-0.056 \pm 0.074 \pm 0.053$	⁷ AHARMIM	05A SNO	From salty SNO ϕ_{CC}
------------------------------	----------------------	---------	----------------------------

$-0.037 \pm 0.063 \pm 0.032$	⁷ AHARMIM	05A SNO	From salty SNO ϕ_{CC} ; const. of no ϕ_{NC} asymmetry
------------------------------	----------------------	---------	---

$0.14 \pm 0.063 \pm 0.015$ -0.014	⁸ AHMAD	02B SNO	Derived from SNO ϕ_{CC}
--	--------------------	---------	------------------------------

$0.07 \pm 0.049 \pm 0.013$ -0.012	⁹ AHMAD	02B SNO	Const. of no ϕ_{NC} asymmetry
--	--------------------	---------	------------------------------------

¹ABE 16c reports the combined day-night flux asymmetry results of the four phases of the Super-Kamiokande measurements. Amplitude fit method is used. See footnote to RENSHAW 14.

²ABE 16c reports the Super-Kamiokande-IV results for 1664 live days from September 2008 to February 2014. The analysis threshold for day-night flux asymmetry is recoil electron energy of 4.49 MeV (total electron energy of 5.0 MeV). Amplitude fit method is used. See footnote to RENSHAW 14.

³RENSHAW 14 obtains this result by using the "amplitude fit" introduced in SMY 04. The data from the Super-Kamiokande(SK)-I, -II, -III, and 1306 live days of the SK-IV measurements are used. The analysis threshold is recoil-electron kinetic energy of 4.5 MeV for SK-III, and SK-IV except for 250 live days in SK-III (6.0 MeV). The analysis threshold for SK-I and SK-II is the same as in the previous reports. (Note that in the previous SK solar-neutrino results, the analysis threshold is quoted as recoil-electron total energy.) This day-night asymmetry result is consistent with neutrino oscillations for $4 \times 10^{-5} \text{ eV}^2 < \Delta m_{21}^2 < 7 \times 10^{-5} \text{ eV}^2$ and large mixing values of θ_{12} at the 68% CL.

⁴CRAVENS 08 reports the Super-Kamiokande-II results for 791 live days from December 2002 to October 2005. The photocathode coverage of the detector is 19% (reduced from 40% of that of Super-Kamiokande-I due to an accident in 2001). The analysis threshold for the day and night fluxes is 7.5 MeV except for the first 159 live days (8.0 MeV).

⁵HOSAKA 06 reports the final results for 1496 live days with Super-Kamiokande-I between May 31, 1996 and July 15, 2001, and replace FUKUDA 02 results. The analysis threshold is 5 MeV except for the first 280 live days (6.5 MeV).

⁶This result with reduced statistical uncertainty is obtained by assuming two-neutrino oscillations within the LMA (large mixing angle) region and by fitting the time variation of the solar neutrino flux measured via $\nu_e e$ elastic scattering to the variations expected from neutrino oscillations. For details, see SMY 04. There is an additional small systematic error of ± 0.0004 coming from uncertainty of oscillation parameters.

⁷AHARMIM 05A measurements were made with dissolved NaCl (0.195% by weight) in heavy water over the period between July 26, 2001 and August 28, 2003, with 176.5 days of the live time recorded during the day and 214.9 days during the night. This result is obtained with the spectral distribution of the CC events not constrained to the ^8B shape.

⁸AHMAD 02b results are based on the charged-current interactions recorded between November 2, 1999 and May 28, 2001, with the day and night live times of 128.5 and 177.9 days, respectively. The complete description of the SNO Phase I data set is given in AHARMIM 07.

⁹AHMAD 02b results are derived from the charged-current interactions, neutral-current interactions, and νe elastic scattering, with the total flux of active neutrinos constrained to have no asymmetry. The data were recorded between November 2, 1999 and May 28, 2001, with the day and night live times of 128.5 and 177.9 days, respectively. The complete description of the SNO Phase I data set is given in AHARMIM 07.

 $\phi_{ES} (^7\text{Be})$

^7Be solar-neutrino flux measured via $\nu_e e$ elastic scattering. This process is sensitive to all active neutrino flavors, but with reduced sensitivity to ν_μ, ν_τ due to the cross-section difference, $\sigma(\nu_{\mu,\tau} e) \sim 0.2 \sigma(\nu_e e)$. If the ^7Be solar-neutrino flux involves nonelectron flavor active neutrinos, their contribution to the flux is ~ 0.2 times that of ν_e .

VALUE ($10^9 \text{ cm}^{-2} \text{ s}^{-1}$)	DOCUMENT ID	TECN	COMMENT
---	-------------	------	---------

• • • We do not use the following data for averages, fits, limits, etc. • • •

3.26 ± 0.52	¹ GANDO	15 KLND	average flux
-----------------	--------------------	---------	--------------

3.10 ± 0.15	² BELLINI	11A BORSX	average flux
-----------------	----------------------	-----------	--------------

¹GANDO 15 uses 165.4 kton-day exposure of the KamLAND liquid scintillator detector to measure the 862 keV ^7Be solar neutrino flux via $\nu - e$ elastic scattering.

²BELLINI 11A reports the ^7Be solar neutrino flux measured via $\nu - e$ elastic scattering. The data correspond to 740.7 live days between May 16, 2007 and May 8, 2010, and also correspond to 153.6 ton-year fiducial exposure. BELLINI 11A measured the 862 keV ^7Be solar neutrino flux, which is an 89.6% branch of the ^7Be solar neutrino flux, to be $(2.78 \pm 0.13) \times 10^9 \text{ cm}^{-2} \text{ s}^{-1}$. Supersedes ARPESELLA 08A.

 $\phi_{ES} (pep)$

pep solar-neutrino flux measured via $\nu_e e$ elastic scattering. This process is sensitive to all active neutrino flavors, but with reduced sensitivity to ν_μ, ν_τ due to the cross section difference, $\sigma(\nu_{\mu,\tau} e) \sim 0.2 \sigma(\nu_e e)$. If the pep solar-neutrino flux involves non-electron flavor active neutrinos, their contribution to the flux is ~ 0.2 times that of ν_e .

VALUE ($10^8 \text{ cm}^{-2} \text{ s}^{-1}$)	DOCUMENT ID	TECN	COMMENT
---	-------------	------	---------

• • • We do not use the following data for averages, fits, limits, etc. • • •

1.0 ± 0.2	¹ BELLINI	12A BORSX	average flux
---------------	----------------------	-----------	--------------

¹BELLINI 12A reports 1.44 MeV pep solar-neutrino flux measured via $\nu_e e$ elastic scattering. The data were collected between January 13, 2008 and May 9, 2010, corresponding to 20,4009 ton-day fiducial exposure. The listed flux value is calculated from the observed rate of pep solar neutrino interactions in Borexino ($3.1 \pm 0.6 \pm 0.3$ counts/(day-100 ton)) and the corresponding rate expected for no neutrino flavor oscillations (4.47 ± 0.05 counts/(day-100 ton)), using the SSM prediction for the pep solar neutrino flux of $(1.441 \pm 0.012) \times 10^8 \text{ cm}^{-2} \text{ s}^{-1}$.

 $\phi_{ES} (\text{CNO})$

CNO solar-neutrino flux measured via $\nu_e e$ elastic scattering. This process is sensitive to all active neutrino flavors, but with reduced sensitivity to ν_μ, ν_τ due to the cross section difference, $\sigma(\nu_{\mu,\tau} e) \sim 0.2 \sigma(\nu_e e)$. If the CNO solar-neutrino flux involves non-electron flavor active neutrinos, their contribution to the flux is ~ 0.2 times that of ν_e .

VALUE ($10^8 \text{ cm}^{-2} \text{ s}^{-1}$)	CL%	DOCUMENT ID	TECN	COMMENT
---	-----	-------------	------	---------

• • • We do not use the following data for averages, fits, limits, etc. • • •

<7.7	90	¹ BELLINI	12A BORSX	MSW-LMA solution assumed
------	----	----------------------	-----------	--------------------------

¹BELLINI 12A reports an upper limit of the CNO solar neutrino flux measured via $\nu_e e$ elastic scattering. The data were collected between January 13, 2008 and May 9, 2010, corresponding to 20,409 ton-day fiducial exposure.

 $\phi_{ES} (pp)$

pp solar-neutrino flux measured via $\nu_e e$ elastic scattering. This process is sensitive to all active neutrino flavors, but with reduced sensitivity to ν_μ, ν_τ due to the cross section difference, $\sigma(\nu_{\mu,\tau} e) \sim 0.3 \sigma(\nu_e e)$. If the pp solar-neutrino flux involves nonelectron flavor active neutrinos, their contribution to the flux is ~ 0.3 times of ν_e .

VALUE ($10^{10} \text{ cm}^{-2} \text{ s}^{-1}$)	DOCUMENT ID	TECN	COMMENT
--	-------------	------	---------

• • • We do not use the following data for averages, fits, limits, etc. • • •

4.4 ± 0.5	¹ BELLINI	14A BORSX	average flux
---------------	----------------------	-----------	--------------

¹BELLINI 14A reports pp solar-neutrino flux measured via $\nu_e e$ elastic scattering. The data were collected between January 2012 and May 2013, corresponding to 408 days of data. The pp neutrino interaction rate in Borexino is measured to be $144 \pm 13 \pm 10$ counts/(day-100 ton) by fitting the measured energy spectrum of events in the 165–590 keV recoil electron kinetic energy window with the expected signal + background spectrum. The listed flux value $\phi_{ES}(pp)$ is calculated from the observed rate and the number of $(3.307 \pm 0.003) \times 10^{31}$ electrons for 100 tons of the Borexino scintillator, and the $\nu_e e$ integrated cross section over the pp neutrino spectrum, $\sigma(\nu_e e) = 11.38 \times 10^{-46} \text{ cm}^2$.

$\phi_{CC}(pp)$

pp solar-neutrino flux measured with charged-current reaction which is sensitive exclusively to ν_e .

VALUE ($10^{10} \text{ cm}^{-2} \text{ s}^{-1}$)	DOCUMENT ID	TECN	COMMENT
--	-------------	------	---------

• • • We do not use the following data for averages, fits, limits, etc. • • •

3.38 ± 0.47	¹ ABDURASHI...	09	FIT	Fit existing solar- ν data
-------------	---------------------------	----	-----	--------------------------------

¹ ABDURASHITOV 09 reports the pp solar-neutrino flux derived from the Ga solar neutrino capture rate by subtracting contributions from ^8B , ^7Be , $ppep$ and CNO solar neutrino fluxes determined by other solar neutrino experiments as well as neutrino oscillation parameters determined from available world neutrino oscillation data.

 $\phi_{ES}(\text{hep})$

hep solar-neutrino flux measured via νe elastic scattering. This process is sensitive to all active neutrino flavors, but with reduced sensitivity to ν_μ, ν_τ due to the cross-section difference, $\sigma(\nu_{\mu,\tau} e) \sim 0.16\sigma(\nu_e e)$. If the hep solar-neutrino flux involves nonelectron flavor active neutrinos, their contribution to the flux is ~ 0.16 times of ν_e .

VALUE ($10^3 \text{ cm}^{-2} \text{ s}^{-1}$)	CL%	DOCUMENT ID	TECN	COMMENT
---	-----	-------------	------	---------

• • • We do not use the following data for averages, fits, limits, etc. • • •

<73	90	¹ HOSAKA	06	SKAM
-----	----	---------------------	----	------

¹ HOSAKA 06 result is obtained from the recoil electron energy window of 18–21 MeV, and updates FUKUDA 01 result.

 $\phi_{\bar{\nu}_e}(\text{8B})$

Searches are made for electron antineutrino flux from the Sun. Flux limits listed here are derived relative to the BS05(OP) Standard Solar Model ^8B solar neutrino flux ($5.69 \times 10^6 \text{ cm}^{-2} \text{ s}^{-1}$), with an assumption that solar $\bar{\nu}_e$ s follow an unoscillated ^8B neutrino spectrum.

VALUE (%)	CL%	DOCUMENT ID	TECN	COMMENT
-----------	-----	-------------	------	---------

• • • We do not use the following data for averages, fits, limits, etc. • • •

<0.013	90	BELLINI	11	BORX $E_{\bar{\nu}_e} > 1.8 \text{ MeV}$
<1.9	90	¹ BALATA	06	CNTR $1.8 < E_{\bar{\nu}_e} < 20.0 \text{ MeV}$
<0.72	90	AHARMIM	04	SNO $4.0 < E_{\bar{\nu}_e} < 14.8 \text{ MeV}$
<0.022	90	EGUCHI	04	KLND $8.3 < E_{\bar{\nu}_e} < 14.8 \text{ MeV}$
<0.7	90	GANDO	03	SKAM $8.0 < E_{\bar{\nu}_e} < 20.0 \text{ MeV}$
<1.7	90	AGLIETTA	96	LSD $7 < E_{\bar{\nu}_e} < 17 \text{ MeV}$

¹ BALATA 06 obtained this result from the search for $\bar{\nu}_e$ interactions with Counting Test Facility (the prototype of the Borexino detector).

(B) Three-neutrino mixing parameters**THREE-NEUTRINO MIXING PARAMETERS**

Updated July 2019 by M. Goodman (ANL).

Introduction and Notation: With the exception of possible short-baseline anomalies (such as LSND), current accelerator, reactor, solar and atmospheric neutrino data can be described within the framework of a 3×3 mixing matrix between the flavor states ν_e, ν_μ and ν_τ and mass eigenstates ν_1, ν_2 and ν_3 . (See equation 14.34 of the review “Neutrino Mass, Mixing and Oscillations” by M.C. Gonzalez-Garcia and M. Yokoyama.) Whether or not this is the ultimately correct framework, it is currently widely used to parametrize neutrino mixing data and to plan new experiments.

The mass differences are called $\Delta m_{21}^2 \equiv m_2^2 - m_1^2$ and $\Delta m_{32}^2 \equiv m_3^2 - m_2^2$. Until recently, we assumed

$$\Delta m_{32}^2 \sim \Delta m_{31}^2. \quad (1)$$

But the experimental error is comparable to the difference $\Delta m_{31}^2 - \Delta m_{32}^2 = \Delta m_{21}^2$, so we quote them separately when appropriate. The measurements made by ν_μ disappearance at accelerators and by ν_e disappearance at reactors are slightly different mixtures of Δm_{32}^2 and Δm_{31}^2 . The angles are labeled θ_{12}, θ_{23} and θ_{13} . The CP violating phase is called δ_{CP} .

The familiar two neutrino form for oscillations is

$$P(\nu_a \rightarrow \nu_b; a \neq b) = \sin^2(2\theta) \sin^2(\Delta m^2 L/4E). \quad (2)$$

Despite the fact that the mixing angles have been measured to be much larger than in the quark sector, the two neutrino form is often a very good approximation and is used in many situations.

The angles appear in the equations below in many forms. They often appear as $\sin^2(2\theta)$. The listings currently now use $\sin^2(\theta)$ because this distinguishes the octant, i.e. whether θ_{23} is larger or smaller than 45° .

Accelerator neutrino experiments: Ignoring Δm_{21}^2 , CP violation, and matter effects, the equations for the probability of appearance in an accelerator oscillation experiment are:

$$P(\nu_\mu \rightarrow \nu_\tau) = \sin^2(2\theta_{23}) \cos^4(\theta_{13}) \sin^2(\Delta m_{32}^2 L/4E) \quad (3)$$

$$P(\nu_\mu \rightarrow \nu_e) = \sin^2(2\theta_{13}) \sin^2(\theta_{23}) \sin^2(\Delta m_{32}^2 L/4E) \quad (4)$$

$$P(\nu_e \rightarrow \nu_\mu) = \sin^2(2\theta_{13}) \sin^2(\theta_{23}) \sin^2(\Delta m_{32}^2 L/4E) \quad (5)$$

$$P(\nu_e \rightarrow \nu_\tau) = \sin^2(2\theta_{13}) \cos^2(\theta_{23}) \sin^2(\Delta m_{32}^2 L/4E). \quad (6)$$

Current and future long-baseline accelerator experiments are studying non-zero θ_{13} through $P(\nu_\mu \rightarrow \nu_e)$. Including the CP terms and low mass scale, the equation for neutrino oscillation in vacuum is:

$$\begin{aligned} P(\nu_\mu \rightarrow \nu_e) &= P1 + P2 + P3 + P4 \\ P1 &= \sin^2(\theta_{23}) \sin^2(2\theta_{13}) \sin^2(\Delta m_{32}^2 L/4E) \\ P2 &= \cos^2(\theta_{23}) \sin^2(2\theta_{13}) \sin^2(\Delta m_{21}^2 L/4E) \\ P3 &= -/+ J \sin(\delta_{CP}) \sin(\Delta m_{32}^2 L/4E) \\ P4 &= J \cos(\delta_{CP}) \cos(\Delta m_{32}^2 L/4E) \end{aligned} \quad (7)$$

where

$$\begin{aligned} J &= \cos(\theta_{13}) \sin(2\theta_{12}) \sin(2\theta_{13}) \sin(2\theta_{23}) \times \\ &\sin(\Delta m_{32}^2 L/4E) \sin(\Delta m_{21}^2 L/4E) \end{aligned} \quad (8)$$

and the sign in P3 is negative for neutrinos and positive for anti-neutrinos respectively. For most new long-baseline accelerator experiments, P2 can safely be neglected. Also, depending on the distance and the mass order, matter effects need to be included.

Reactor neutrino experiments: Nuclear reactors are prolific sources of $\bar{\nu}_e$ with an energy near 4 MeV. The oscillation probability can be expressed

$$\begin{aligned} P(\bar{\nu}_e \rightarrow \bar{\nu}_e) &= 1 - \cos^4(\theta_{13}) \sin^2(2\theta_{12}) \sin^2(\Delta m_{21}^2 L/4E) \\ &- \cos^2(\theta_{12}) \sin^2(2\theta_{13}) \sin^2(\Delta m_{31}^2 L/4E) \\ &- \sin^2(\theta_{12}) \sin^2(2\theta_{13}) \sin^2(\Delta m_{32}^2 L/4E) \end{aligned} \quad (9)$$

not using the approximation in Eq. (1). For short distances ($L < 5 \text{ km}$) we can ignore the second term on the right and can reimpose approximation Eq. (1). This takes the familiar two neutrino form with θ_{13} and Δm_{32}^2 :

$$P(\bar{\nu}_e \rightarrow \bar{\nu}_e) = 1 - \sin^2(2\theta_{13}) \sin^2(\Delta m_{32}^2 L/4E). \quad (10)$$

Lepton Particle Listings

Neutrino Mixing

Solar and Atmospheric neutrino experiments: Solar neutrino experiments are sensitive to ν_e disappearance and have allowed the measurement of θ_{12} and Δm_{21}^2 . They are also sensitive to θ_{13} . We identify $\Delta m_{\odot}^2 = \Delta m_{21}^2$ and $\theta_{\odot} = \theta_{12}$.

Atmospheric neutrino experiments are primarily sensitive to ν_{μ} disappearance through $\nu_{\mu} \rightarrow \nu_{\tau}$ oscillations, and have allowed the measurement of θ_{23} and Δm_{32}^2 . We identify $\Delta m_A^2 = \Delta m_{32}^2$ and $\theta_A = \theta_{23}$. Despite the large ν_e component of the atmospheric neutrino flux, it is difficult to measure Δm_{21}^2 effects. This is because of a cancellation between $\nu_{\mu} \rightarrow \nu_e$ and $\nu_e \rightarrow \nu_{\mu}$ together with the fact that the ratio of ν_{μ} and ν_e atmospheric fluxes, which arise from sequential π and μ decay, is near 2.

Oscillation Parameter Listings: In Section (B) we encode the three mixing angles θ_{12} , θ_{23} , θ_{13} , δ_{CP} , and two mass squared differences Δm_{21}^2 and Δm_{32}^2 . Our knowledge of θ_{12} and Δm_{21}^2 comes from the KamLAND reactor neutrino experiment together with solar neutrino experiments. Our knowledge of θ_{23} and Δm_{32}^2 comes from atmospheric, reactor and long-baseline accelerator neutrino experiments. For the earlier experiments, we identified the large mass splitting as Δm_{32}^2 . Now that $\sigma(\Delta m_{32}^2) \approx \Delta m_{21}^2$, some experiments report separate values for the two mass orders. Results on θ_{13} come from reactor antineutrino disappearance experiments. There are also results from long-baseline accelerator experiments looking for ν_e appearance. The interpretation of both kinds of results depends on Δm_{32}^2 , and the accelerator results also depend on the mass order, θ_{23} and the CP violating phase δ_{CP} .

Accelerator and atmospheric experiments have some sensitivity to the CP violation phase δ_{CP} through Eq. (7). Note that P3 depends on the sign of Δm_{32}^2 so the sensitivity depends on the mass order. For non-maximal θ_{23} mixing, it also depends on the octant of θ_{23} , i.e. whether $\theta_{23} > \pi/4$ or $\theta_{23} < \pi/4$.

 $\sin^2(\theta_{12})$

If an experiment reports $\sin^2(2\theta_{12})$ we convert the value to $\sin^2(\theta_{12})$.

VALUE	DOCUMENT ID	TECN	COMMENT
$0.307^{+0.013}_{-0.012}$	1 ABE	16c FIT	KamLAND+global solar; 3ν
• • •	We do not use the following data for averages, fits, limits, etc. • • •		
$0.320^{+0.020}_{-0.016}$	DE-SALAS	18 FIT	Global Fit
0.310 ± 0.014	2 ABE	16c FIT	SKAM+SNO; 3ν
$0.334^{+0.027}_{-0.023}$	3 ABE	16c FIT	SK-I+II+III+IV; 3ν
$0.327^{+0.026}_{-0.031}$	4 ABE	16c FIT	SK-IV; 3ν
0.323 ± 0.016	5 FORERO	14 FIT	3ν
$0.304^{+0.013}_{-0.012}$	6 GONZALEZ...	14 FIT	Either mass ordering; global fit
$0.299^{+0.014}_{-0.014}$	7,8 AHARMIM	13 FIT	global solar; 2ν
$0.307^{+0.016}_{-0.013}$	8,9 AHARMIM	13 FIT	global solar; 3ν
$0.304^{+0.022}_{-0.018}$	8,10 AHARMIM	13 FIT	KamLAND + global solar; 3ν
$0.304^{+0.014}_{-0.013}$	11 GANDO	13 FIT	KamLAND + global solar + SBL + accelerator; 3ν
$0.304^{+0.014}_{-0.013}$	12 GANDO	13 FIT	KamLAND + global solar; 3ν
$0.325^{+0.039}_{-0.039}$	13 GANDO	13 FIT	KamLAND; 3ν
$0.30^{+0.02}_{-0.01}$	14 ABE	11 FIT	KamLAND + global solar; 2ν
$0.30^{+0.02}_{-0.01}$	15 ABE	11 FIT	global solar; 2ν

$0.31^{+0.03}_{-0.02}$	16 ABE	11 FIT	KamLAND + global solar; 3ν
$0.31^{+0.03}_{-0.03}$	17 ABE	11 FIT	global solar; 3ν
$0.314^{+0.015}_{-0.012}$	18 BELLINI	11A FIT	KamLAND + global solar; 2ν
$0.319^{+0.017}_{-0.015}$	19 BELLINI	11A FIT	global solar; 2ν
$0.311^{+0.016}_{-0.016}$	20 GANDO	11 FIT	KamLAND + solar; 3ν
$0.304^{+0.046}_{-0.042}$	21 GANDO	11 FIT	KamLAND; 3ν
$0.314^{+0.018}_{-0.014}$	22,23 AHARMIM	10 FIT	KamLAND + global solar; 2ν
$0.314^{+0.017}_{-0.020}$	22,24 AHARMIM	10 FIT	global solar; 2ν
$0.319^{+0.019}_{-0.016}$	22,25 AHARMIM	10 FIT	KamLAND + global solar; 3ν
$0.319^{+0.023}_{-0.024}$	22,26 AHARMIM	10 FIT	global solar; 3ν
$0.36^{+0.05}_{-0.04}$	27 ABE	08A FIT	KamLAND
0.32 ± 0.03	28 ABE	08A FIT	KamLAND + global fit
0.32 ± 0.02	29 AHARMIM	08 FIT	KamLAND + global solar
$0.31^{+0.04}_{-0.04}$	30 HOSAKA	06 FIT	KamLAND + global solar
$0.31^{+0.04}_{-0.03}$	31 HOSAKA	06 FIT	SKAM+SNO+KamLAND
$0.31^{+0.03}_{-0.04}$	32 HOSAKA	06 FIT	SKAM+SNO
$0.31^{+0.02}_{-0.03}$	33 AHARMIM	05A FIT	KamLAND + global solar
0.25-0.39	34 AHARMIM	05A FIT	global solar
0.29 \pm 0.03	35 ARAKI	05 FIT	KamLAND + global solar
$0.29^{+0.03}_{-0.02}$	36 AHMED	04A FIT	KamLAND + global solar
0.23-0.37	37 AHMED	04A FIT	global solar
$0.31^{+0.04}_{-0.04}$	38 SMY	04 FIT	KamLAND + global solar
$0.29^{+0.04}_{-0.04}$	39 SMY	04 FIT	global solar
$0.32^{+0.06}_{-0.05}$	40 SMY	04 FIT	SKAM + SNO
0.19-0.33	41 AHMAD	02B FIT	global solar
0.19-0.39	42 FUKUDA	02 FIT	global solar

¹ ABE 16c obtained this result by a three-neutrino oscillation analysis, with a constraint of $\sin^2(\theta_{13}) = 0.0219 \pm 0.0014$ coming from reactor neutrino experiments, using all solar data and KamLAND data. *CPT* invariance is assumed.

² ABE 16c obtained this result by a three-neutrino oscillation analysis, with a constraint of $\sin^2(\theta_{13}) = 0.0219 \pm 0.0014$ coming from reactor neutrino experiments, using Super-Kamiokande (I+II+III+IV) and SNO data.

³ ABE 16c obtained this result by a three-neutrino oscillation analysis, with a constraint of $\sin^2(\theta_{13}) = 0.0219 \pm 0.0014$ coming from reactor neutrino experiments, by combining the four phases of the Super-Kamiokande solar data.

⁴ ABE 16c obtained this result by a three-neutrino oscillation analysis, with a constraint of $\sin^2(\theta_{13}) = 0.0219 \pm 0.0014$ coming from reactor neutrino experiments, using the Super-Kamiokande-IV data.

⁵ FORERO 14 performs a global fit to neutrino oscillations using solar, reactor, long-baseline accelerator, and atmospheric neutrino data.

⁶ GONZALEZ-GARCIA 14 result comes from a frequentist global fit. The corresponding Bayesian global fit to the same data results are reported in BERGSTROM 15 as $0.304^{+0.013}_{-0.012}$ for normal and $0.305^{+0.012}_{-0.013}$ for inverted mass ordering.

⁷ AHARMIM 13 obtained this result by a two-neutrino oscillation analysis using global solar neutrino data.

⁸ AHARMIM 13 global solar neutrino data include SNO's all-phases-combined analysis results on the total active ^8B neutrino flux and energy-dependent ν_e survival probability parameters, measurements of Cl (CLEVELAND 98), Ga (ABDURASHITOV 09 which contains combined analysis with GNO (ALTMANN 05 and Ph.D. thesis of F. Kaether)), and ^7Be (BELLINI 11A) rates, and ^8B solar-neutrino recoil electron measurements of SK-I (HOSAKA 06) zenith, SK-II (CRAVEN 08) and SK-III (ABE 11) day/night spectra, and Borexino (BELLINI 10A) spectra.

⁹ AHARMIM 13 obtained this result by a three-neutrino oscillation analysis with the value of Δm_{32}^2 fixed to $2.45 \times 10^{-3} \text{ eV}^2$, using global solar neutrino data.

¹⁰ AHARMIM 13 obtained this result by a three-neutrino oscillation analysis with the value of Δm_{32}^2 fixed to $2.45 \times 10^{-3} \text{ eV}^2$, using global solar neutrino and KamLAND (GANDO 11) data. *CPT* invariance is assumed.

¹¹ GANDO 13 obtained this result by a three-neutrino oscillation analysis using KamLAND, global solar neutrino, short-baseline (SBL) reactor, and accelerator data, assuming *CPT* invariance. Supersedes GANDO 11.

¹² GANDO 13 obtained this result by a three-neutrino oscillation analysis using KamLAND and global solar neutrino data, assuming *CPT* invariance. Supersedes GANDO 11.

¹³ GANDO 13 obtained this result by a three-neutrino oscillation analysis using KamLAND data. Supersedes GANDO 11.

¹⁴ ABE 11 obtained this result by a two-neutrino oscillation analysis using solar neutrino data including Super-Kamiokande, SNO, Borexino (ARPESELLA 08a), Homestake, GALLEX/GNO, SAGE, and KamLAND data. *CPT* invariance is assumed.

¹⁵ ABE 11 obtained this result by a two-neutrino oscillation analysis using solar neutrino data including Super-Kamiokande, SNO, Borexino (ARPESELLA 08a), Homestake, GALLEX/GNO, and SAGE data.

- ¹⁶ ABE 11 obtained this result by a three-neutrino oscillation analysis with the value of Δm_{32}^2 fixed to $2.4 \times 10^{-3} \text{ eV}^2$, using solar neutrino data including Super-Kamiokande, SNO, Borexino (ARPESELLA 08A), Homestake, GALLEX/GNO, SAGE, and KamLAND data. The normal neutrino mass ordering and CPT invariance are assumed.
- ¹⁷ ABE 11 obtained this result by a three-neutrino oscillation analysis with the value of Δm_{32}^2 fixed to $2.4 \times 10^{-3} \text{ eV}^2$, using solar neutrino data including Super-Kamiokande, SNO, Borexino (ARPESELLA 08A), Homestake, and GALLEX/GNO data. The normal neutrino mass ordering is assumed.
- ¹⁸ BELLINI 11A obtained this result by a two-neutrino oscillation analysis using KamLAND, Homestake, SAGE, Gallex, GNO, Kamiokande, Super-Kamiokande, SNO, and Borexino (BELLINI 11A) data and the SSM flux prediction in SERENELLI 11 (Astrophysical Journal **743** 24 (2011)) with the exception that the ^8B flux was left free. CPT invariance is assumed.
- ¹⁹ BELLINI 11A obtained this result by a two-neutrino oscillation analysis using Homestake, SAGE, Gallex, GNO, Kamiokande, Super-Kamiokande, SNO, and Borexino (BELLINI 11A) data and the SSM flux prediction in SERENELLI 11 (Astrophysical Journal **743** 24 (2011)) with the exception that the ^8B flux was left free.
- ²⁰ GAND0 11 obtained this result with three-neutrino fit using the KamLAND + solar data. Superseded by GAND0 13.
- ²¹ GAND0 11 obtained this result with three-neutrino fit using the KamLAND data only. Superseded by GAND0 13.
- ²² AHARMIM 10 global solar neutrino data include SNO's low-energy-threshold analysis survival probability day/night curves, SNO Phase III integral rates (AHARMIM 08), Cl (CLEVELAND 98), SAGE (ABDURASHITOV 09), Gallex/GNO (HAMPEL 99, ALTMANN 05), Borexino (ARPESELLA 08A), SK-I zenith (HOSAKA 06), and SK-II day/night spectra (CRAVENS 08).
- ²³ AHARMIM 10 obtained this result by a two-neutrino oscillation analysis using global solar neutrino data and KamLAND data (ABE 08A). CPT invariance is assumed.
- ²⁴ AHARMIM 10 obtained this result by a two-neutrino oscillation analysis using global solar neutrino data.
- ²⁵ AHARMIM 10 obtained this result by a three-neutrino oscillation analysis with the value of Δm_{31}^2 fixed to $2.3 \times 10^{-3} \text{ eV}^2$, using global solar neutrino data and KamLAND data (ABE 08A). CPT invariance is assumed.
- ²⁶ AHARMIM 10 obtained this result by a three-neutrino oscillation analysis with the value of Δm_{31}^2 fixed to $2.3 \times 10^{-3} \text{ eV}^2$, using global solar neutrino data.
- ²⁷ ABE 08A obtained this result by a rate + shape + time combined geoneutrino and reactor two-neutrino fit for Δm_{21}^2 and $\tan^2 \theta_{12}$, using KamLAND data only. Superseded by GAND0 11.
- ²⁸ ABE 08A obtained this result by means of a two-neutrino fit using KamLAND, Homestake, SAGE, GALLEX, GNO, SK (zenith angle and E-spectrum), the SNO χ^2 -map, and solar flux data. CPT invariance is assumed. Superseded by GAND0 11.
- ²⁹ The result given by AHARMIM 08 is $\theta = (34.4^{+1.3}_{-1.2})^\circ$. This result is obtained by a two-neutrino oscillation analysis using solar neutrino data including those of Borexino (ARPESELLA 08A) and Super-Kamiokande-I (HOSAKA 06), and KamLAND data (ABE 08A). CPT invariance is assumed.
- ³⁰ HOSAKA 06 obtained this result by a two-neutrino oscillation analysis using SK ν_e data, CC data from other solar neutrino experiments, and KamLAND data (ARAKI 05). CPT invariance is assumed.
- ³¹ HOSAKA 06 obtained this result by a two-neutrino oscillation analysis using the data from Super-Kamiokande, SNO (AHMAD 02 and AHMAD 02b), and KamLAND (ARAKI 05) experiments. CPT invariance is assumed.
- ³² HOSAKA 06 obtained this result by a two-neutrino oscillation analysis using the Super-Kamiokande and SNO (AHMAD 02 and AHMAD 02b) solar neutrino data.
- ³³ The result given by AHARMIM 05A is $\theta = (33.9 \pm 1.6)^\circ$. This result is obtained by a two-neutrino oscillation analysis using SNO pure deuterium and salt phase data, SK ν_e data, Cl and Ga CC data, and KamLAND data (ARAKI 05). CPT invariance is assumed. AHARMIM 05A also quotes $\theta = (33.9^{+2.4}_{-2.2})^\circ$ as the error enveloping the 68% CL two-dimensional region. This translates into $\sin^2 2\theta = 0.86^{+0.05}_{-0.06}$.
- ³⁴ AHARMIM 05A obtained this result by a two-neutrino oscillation analysis using the data from all solar neutrino experiments. The listed range of the parameter envelops the 95% CL two-dimensional region shown in figure 35a of AHARMIM 05A. AHARMIM 05A also quotes $\tan^2 \theta = 0.45^{+0.09}_{-0.08}$ as the error enveloping the 68% CL two-dimensional region. This translates into $\sin^2 2\theta = 0.86^{+0.05}_{-0.07}$.
- ³⁵ ARAKI 05 obtained this result by a two-neutrino oscillation analysis using KamLAND and solar neutrino data. CPT invariance is assumed. The 1σ error shown here is translated from the number provided by the KamLAND collaboration, $\tan^2 \theta = 0.40^{+0.07}_{-0.05}$. The corresponding number quoted in ARAKI 05 is $\tan^2 \theta = 0.40^{+0.10}_{-0.07}$ ($\sin^2 2\theta = 0.82 \pm 0.07$), which envelops the 68% CL two-dimensional region.
- ³⁶ The result given by AHMED 04A is $\theta = (32.5^{+1.7}_{-1.6})^\circ$. This result is obtained by a two-neutrino oscillation analysis using solar neutrino and KamLAND data (EGUCHI 03). CPT invariance is assumed. AHMED 04A also quotes $\theta = (32.5^{+2.4}_{-2.3})^\circ$ as the error enveloping the 68% CL two-dimensional region. This translates into $\sin^2 2\theta = 0.82 \pm 0.06$.
- ³⁷ AHMED 04A obtained this result by a two-neutrino oscillation analysis using the data from all solar neutrino experiments. The listed range of the parameter envelops the 95% CL two-dimensional region shown in Fig. 5(a) of AHMED 04A. The best-fit point is $\Delta(m^2) = 6.5 \times 10^{-5} \text{ eV}^2$, $\tan^2 \theta = 0.40$ ($\sin^2 2\theta = 0.82$).
- ³⁸ The result given by SMY 04 is $\tan^2 \theta = 0.44 \pm 0.08$. This result is obtained by a two-neutrino oscillation analysis using solar neutrino and KamLAND data (IANNI 03). CPT invariance is assumed.
- ³⁹ SMY 04 obtained this result by a two-neutrino oscillation analysis using the data from all solar neutrino experiments. The 1σ errors are read from Fig. 6(a) of SMY 04.

- ⁴⁰ SMY 04 obtained this result by a two-neutrino oscillation analysis using the Super-Kamiokande and SNO (AHMAD 02 and AHMAD 02b) solar neutrino data. The 1σ errors are read from Fig. 6(a) of SMY 04.
- ⁴¹ AHMAD 02b obtained this result by a two-neutrino oscillation analysis using the data from all solar neutrino experiments. The listed range of the parameter envelops the 95% CL two-dimensional region shown in Fig. 4(b) of AHMAD 02b. The best fit point is $\Delta(m^2) = 5.0 \times 10^{-5} \text{ eV}^2$ and $\tan \theta = 0.34$ ($\sin^2 2\theta = 0.76$).
- ⁴² FUKUDA 02 obtained this result by a two-neutrino oscillation analysis using the data from all solar neutrino experiments. The listed range of the parameter envelops the 95% CL two-dimensional region shown in Fig. 4 of FUKUDA 02. The best fit point is $\Delta(m^2) = 6.9 \times 10^{-5} \text{ eV}^2$ and $\tan^2 \theta = 0.38$ ($\sin^2 2\theta = 0.80$).

 Δm_{21}^2

VALUE (10^{-5} eV^2)	DOCUMENT ID	TECN	COMMENT
7.53 ± 0.18	¹ GAND0	13 FIT	KamLAND + global solar + SBL + accelerator: 3ν
• • • We do not use the following data for averages, fits, limits, etc. • • •			
$7.55^{+0.20}_{-0.16}$	DE-SALAS	18 FIT	Global Fit
$7.49^{+0.19}_{-0.18}$	² ABE	16c FIT	KamLAND+global solar; 3ν
$4.8^{+1.3}_{-0.6}$	³ ABE	16c FIT	SKAM+SNO; 3ν
$4.8^{+1.5}_{-0.8}$	⁴ ABE	16c FIT	SK-I+II+III+IV; 3ν
$3.2^{+2.8}_{-0.2}$	⁵ ABE	16c FIT	SK-IV; 3ν
$7.6^{+0.19}_{-0.18}$	⁶ FORERO	14 FIT	3ν
$7.50^{+0.19}_{-0.17}$	⁷ GONZALEZ...	14 FIT	Either mass ordering; global fit
$5.13^{+1.29}_{-0.96}$	^{8,9} AHARMIM	13 FIT	global solar: 2ν
$5.13^{+1.49}_{-0.98}$	^{9,10} AHARMIM	13 FIT	global solar: 3ν
$7.46^{+0.20}_{-0.19}$	^{9,11} AHARMIM	13 FIT	KamLAND + global solar: 3ν
$7.53^{+0.19}_{-0.18}$	¹² GAND0	13 FIT	KamLAND + global solar: 3ν
$7.54^{+0.19}_{-0.18}$	¹³ GAND0	13 FIT	KamLAND: 3ν
7.6 ± 0.2	¹⁴ ABE	11 FIT	KamLAND + global solar: 2ν
$6.2^{+1.1}_{-1.9}$	¹⁵ ABE	11 FIT	global solar: 2ν
7.7 ± 0.3	¹⁶ ABE	11 FIT	KamLAND + global solar: 3ν
$6.0^{+2.2}_{-2.5}$	¹⁷ ABE	11 FIT	global solar: 3ν
$7.50^{+0.16}_{-0.24}$	¹⁸ BELLINI	11A FIT	KamLAND + global solar: 2ν
$5.2^{+1.5}_{-0.9}$	¹⁹ BELLINI	11A FIT	global solar: 2ν
$7.50^{+0.19}_{-0.20}$	²⁰ GAND0	11 FIT	KamLAND + solar: 3ν
7.49 ± 0.20	²¹ GAND0	11 FIT	KamLAND: 3ν
$7.59^{+0.20}_{-0.21}$	^{22,23} AHARMIM	10 FIT	KamLAND + global solar: 2ν
$5.89^{+2.13}_{-2.16}$	^{22,24} AHARMIM	10 FIT	global solar: 2ν
7.59 ± 0.21	^{22,25} AHARMIM	10 FIT	KamLAND + global solar: 3ν
$6.31^{+2.49}_{-2.58}$	^{22,26} AHARMIM	10 FIT	global solar: 3ν
$7.58^{+0.14}_{-0.13} \pm 0.15$	²⁷ ABE	08A FIT	KamLAND
7.59 ± 0.21	²⁸ ABE	08A FIT	KamLAND + global solar
$7.59^{+0.19}_{-0.21}$	²⁹ AHARMIM	08 FIT	KamLAND + global solar
8.0 ± 0.3	³⁰ HOSAKA	06 FIT	KamLAND + global solar
8.0 ± 0.3	³¹ HOSAKA	06 FIT	SKAM+SNO+KamLAND
$6.3^{+3.7}_{-1.5}$	³² HOSAKA	06 FIT	SKAM+SNO
5–12	³³ HOSAKA	06 FIT	SKAM day/night in the LMA region
$8.0^{+0.4}_{-0.3}$	³⁴ AHARMIM	05A FIT	KamLAND + global solar LMA
3.3–14.4	³⁵ AHARMIM	05A FIT	global solar
$7.9^{+0.4}_{-0.3}$	³⁶ ARAKI	05 FIT	KamLAND + global solar
$7.1^{+1.0}_{-0.3}$	³⁷ AHMED	04A FIT	KamLAND + global solar
3.2–13.7	³⁸ AHMED	04A FIT	global solar
$7.1^{+0.6}_{-0.5}$	³⁹ SMY	04 FIT	KamLAND + global solar
$6.0^{+1.7}_{-1.6}$	⁴⁰ SMY	04 FIT	global solar
$6.0^{+2.5}_{-1.6}$	⁴¹ SMY	04 FIT	SKAM + SNO
2.8–12.0	⁴² AHMAD	02b FIT	global solar
3.2–19.1	⁴³ FUKUDA	02 FIT	global solar

¹ GAND0 13 obtained this result by a three-neutrino oscillation analysis using KamLAND, global solar neutrino, short-baseline (SBL) reactor, and accelerator data, assuming CPT invariance. Supersedes GAND0 11.

² ABE 16c obtained this result by a three-neutrino oscillation analysis, with a constraint of $\sin^2(\theta_{13}) = 0.0219 \pm 0.0014$ coming from reactor neutrino experiments, using all solar data and KamLAND data. CPT invariance is assumed.

Lepton Particle Listings

Neutrino Mixing

- ³ ABE 16c obtained this result by a three-neutrino oscillation analysis, with a constraint of $\sin^2(\theta_{13}) = 0.0219 \pm 0.0014$ coming from reactor neutrino experiments, using Super-Kamiokande (I+II+III+IV) and SNO data.
- ⁴ ABE 16c obtained this result by a three-neutrino oscillation analysis, with a constraint of $\sin^2(\theta_{13}) = 0.0219 \pm 0.0014$ coming from reactor neutrino experiments, by combining the four phases of the Super-Kamiokande solar data.
- ⁵ ABE 16c obtained this result by a three-neutrino oscillation analysis, with a constraint of $\sin^2(\theta_{13}) = 0.0219 \pm 0.0014$ coming from reactor neutrino experiments, using the Super-Kamiokande-IV data.
- ⁶ FORERO 14 performs a global fit to Δm_{21}^2 using solar, reactor, long-baseline accelerator, and atmospheric neutrino data.
- ⁷ GONZALEZ-GARCIA 14 result comes from a frequentist global fit. The corresponding Bayesian global fit to the same data results are reported in BERGSTROM 15 as $(7.50^{+0.19}_{-0.17}) \times 10^{-5} \text{ eV}^2$ for normal and $(7.50^{+0.18}_{-0.17}) \times 10^{-5} \text{ eV}^2$ for inverted mass ordering.
- ⁸ AHARMIM 13 obtained this result by a two-neutrino oscillation analysis using global solar neutrino data.
- ⁹ AHARMIM 13 global solar neutrino data include SNO's all-phases-combined analysis results on the total active ^8B neutrino flux and energy-dependent ν_e survival probability parameters, measurements of Cl (CLEVELAND 98), Ga (ABDURASHITOV 09 which contains combined analysis with GNO (ALTMANN 05 and Ph.D. thesis of F. Kaether)), and ^7Be (BELLINI 11A) rates, and ^8B solar-neutrino recoil electron measurements of SK-I (HOSAKA 06) zenith, SK-II (CRAVENS 08), and SK-III (ABE 11) day/night spectra, and Borexino (BELLINI 10A) spectra.
- ¹⁰ AHARMIM 13 obtained this result by a three-neutrino oscillation analysis with the value of Δm_{31}^2 fixed to $2.45 \times 10^{-3} \text{ eV}^2$, using global solar neutrino data.
- ¹¹ AHARMIM 13 obtained this result by a three-neutrino oscillation analysis with the value of Δm_{31}^2 fixed to $2.45 \times 10^{-3} \text{ eV}^2$, using global solar neutrino and KamLAND data (GANDO 11). *CPT* invariance is assumed.
- ¹² GANDO 13 obtained this result by a three-neutrino oscillation analysis using KamLAND and global solar neutrino data, assuming *CPT* invariance. Supersedes GANDO 11.
- ¹³ GANDO 13 obtained this result by a three-neutrino oscillation analysis using KamLAND data. Supersedes GANDO 11.
- ¹⁴ ABE 11 obtained this result by a two-neutrino oscillation analysis using solar neutrino data including Super-Kamiokande, SNO, Borexino (ARPESELLA 08a), Homestake, GALLEX/GNO, SAGE, and KamLAND data. *CPT* invariance is assumed.
- ¹⁵ ABE 11 obtained this result by a two-neutrino oscillation analysis using solar neutrino data including Super-Kamiokande, SNO, Borexino (ARPESELLA 08a), Homestake, GALLEX/GNO, and SAGE data.
- ¹⁶ ABE 11 obtained this result by a three-neutrino oscillation analysis with the value of Δm_{32}^2 fixed to $2.4 \times 10^{-3} \text{ eV}^2$, using solar neutrino data including Super-Kamiokande, SNO, Borexino (ARPESELLA 08a), Homestake, GALLEX/GNO, SAGE, and KamLAND data. The normal neutrino mass ordering and *CPT* invariance are assumed.
- ¹⁷ ABE 11 obtained this result by a three-neutrino oscillation analysis with the value of Δm_{32}^2 fixed to $2.4 \times 10^{-3} \text{ eV}^2$, using solar neutrino data including Super-Kamiokande, SNO, Borexino (ARPESELLA 08a), Homestake, and GALLEX/GNO data. The normal neutrino mass ordering is assumed.
- ¹⁸ BELLINI 11A obtained this result by a two-neutrino oscillation analysis using KamLAND, Homestake, SAGE, Gallex, GNO, Kamiokande, Super-Kamiokande, SNO, and Borexino (BELLINI 11A) data and the SSM flux prediction in SERENELLI 11 (Astrophysical Journal **743** 24 (2011)) with the exception that the ^8B flux was left free. *CPT* invariance is assumed.
- ¹⁹ BELLINI 11A obtained this result by a two-neutrino oscillation analysis using Homestake, SAGE, Gallex, GNO, Kamiokande, Super-Kamiokande, SNO, and Borexino (BELLINI 11A) data and the SSM flux prediction in SERENELLI 11 (Astrophysical Journal **743** 24 (2011)) with the exception that the ^8B flux was left free.
- ²⁰ GANDO 11 obtain this result with three-neutrino fit using the KamLAND + solar data. Superseded by GANDO 13.
- ²¹ GANDO 11 obtain this result with three-neutrino fit using the KamLAND data only. Supersedes ABE 08a.
- ²² AHARMIM 10 global solar neutrino data include SNO's low-energy-threshold analysis survival probability day/night curves, SNO Phase III integral rates (AHARMIM 08), Cl (CLEVELAND 98), SAGE (ABDURASHITOV 09), Gallex/GNO (HAMPEL 99, ALTMANN 05), Borexino (ARPESELLA 08a), SK-I zenith (HOSAKA 06), and SK-II day/night spectra (CRAVENS 08).
- ²³ AHARMIM 10 obtained this result by a two-neutrino oscillation analysis using global solar neutrino data and KamLAND data (ABE 08a). *CPT* invariance is assumed.
- ²⁴ AHARMIM 10 obtained this result by a two-neutrino oscillation analysis using global solar neutrino data.
- ²⁵ AHARMIM 10 obtained this result by a three-neutrino oscillation analysis with the value of Δm_{31}^2 fixed to $2.3 \times 10^{-3} \text{ eV}^2$, using global solar neutrino data and KamLAND data (ABE 08a). *CPT* invariance is assumed.
- ²⁶ AHARMIM 10 obtained this result by a three-neutrino oscillation analysis with the value of Δm_{31}^2 fixed to $2.3 \times 10^{-3} \text{ eV}^2$, using global solar neutrino data.
- ²⁷ ABE 08a obtained this result by a rate + shape + time combined geoneutrino and reactor two-neutrino fit for Δm_{21}^2 and $\tan^2\theta_{12}$, using KamLAND data only. Superseded by GANDO 11.
- ²⁸ ABE 08a obtained this result by means of a two-neutrino fit using KamLAND, Homestake, SAGE, GALLEX, GNO, SK (zenith angle and E-spectrum), the SNO χ^2 -map, and solar flux data. *CPT* invariance is assumed. Superseded by GANDO 11.
- ²⁹ AHARMIM 08 obtained this result by a two-neutrino oscillation analysis using all solar neutrino data including those of Borexino (ARPESELLA 08a) and Super-Kamiokande-I (HOSAKA 06), and KamLAND data (ABE 08a). *CPT* invariance is assumed.
- ³⁰ HOSAKA 06 obtained this result by a two-neutrino oscillation analysis using solar neutrino and KamLAND data (ARAKI 05). *CPT* invariance is assumed.
- ³¹ HOSAKA 06 obtained this result by a two-neutrino oscillation analysis using the data from Super-Kamiokande, SNO (AHMAD 02 and AHMAD 02b), and KamLAND (ARAKI 05) experiments. *CPT* invariance is assumed.
- ³² HOSAKA 06 obtained this result by a two-neutrino oscillation analysis using the Super-Kamiokande and SNO (AHMAD 02 and AHMAD 02b) solar neutrino data.
- ³³ HOSAKA 06 obtained this result from the consistency between the observed and expected day-night flux asymmetry amplitude. The listed 68% CL range is derived from the 1σ boundary of the amplitude fit to the data. Oscillation parameters are constrained to be in the LMA region. The mixing angle is fixed at $\tan^2\theta = 0.44$ because the fit depends only very weakly on it.
- ³⁴ AHARMIM 05a obtained this result by a two-neutrino oscillation analysis using solar neutrino and KamLAND data (ARAKI 05). *CPT* invariance is assumed. AHARMIM 05a also quotes $\Delta(m^2) = (8.0^{+0.6}_{-0.4}) \times 10^{-5} \text{ eV}^2$ as the error enveloping the 68% CL two-dimensional region.
- ³⁵ AHARMIM 05a obtained this result by a two-neutrino oscillation analysis using the data from all solar neutrino experiments. The listed range of the parameter envelops the 95% CL two-dimensional region shown in figure 35a of AHARMIM 05a. AHARMIM 05a also quotes $\Delta(m^2) = (6.5^{+4.4}_{-2.3}) \times 10^{-5} \text{ eV}^2$ as the error enveloping the 68% CL two-dimensional region.
- ³⁶ ARAKI 05 obtained this result by a two-neutrino oscillation analysis using KamLAND and solar neutrino data. *CPT* invariance is assumed. The 1σ error shown here is provided by the KamLAND collaboration. The error quoted in ARAKI 05, $\Delta(m^2) = (7.9^{+0.6}_{-0.5}) \times 10^{-5}$, envelops the 68% CL two-dimensional region.
- ³⁷ AHMED 04a obtained this result by a two-neutrino oscillation analysis using solar neutrino and KamLAND data (EGUCHI 03). *CPT* invariance is assumed. AHMED 04a also quotes $\Delta(m^2) = (7.1^{+1.2}_{-0.6}) \times 10^{-5} \text{ eV}^2$ as the error enveloping the 68% CL two-dimensional region.
- ³⁸ AHMED 04a obtained this result by a two-neutrino oscillation analysis using the data from all solar neutrino experiments. The listed range of the parameter envelops the 95% CL two-dimensional region shown in Fig. 5(a) of AHMED 04a. The best-fit point is $\Delta(m^2) = 6.5 \times 10^{-5} \text{ eV}^2$, $\tan^2\theta = 0.40$ ($\sin^2 2\theta = 0.82$).
- ³⁹ SMY 04 obtained this result by a two-neutrino oscillation analysis using solar neutrino and KamLAND data (IANNI 03). *CPT* invariance is assumed.
- ⁴⁰ SMY 04 obtained this result by a two-neutrino oscillation analysis using the data from all solar neutrino experiments. The 1σ errors are read from Fig. 6(a) of SMY 04.
- ⁴¹ SMY 04 obtained this result by a two-neutrino oscillation analysis using the Super-Kamiokande and SNO (AHMAD 02 and AHMAD 02b) solar neutrino data. The 1σ errors are read from Fig. 6(a) of SMY 04.
- ⁴² AHMAD 02b obtained this result by a two-neutrino oscillation analysis using the data from all solar neutrino experiments. The listed range of the parameter envelops the 95% CL two-dimensional region shown in Fig. 4(b) of AHMAD 02b. The best fit point is $\Delta(m^2) = 5.0 \times 10^{-5} \text{ eV}^2$ and $\tan\theta = 0.34$ ($\sin^2 2\theta = 0.76$).
- ⁴³ FUKUDA 02 obtained this result by a two-neutrino oscillation analysis using the data from all solar neutrino experiments. The listed range of the parameter envelops the 95% CL two-dimensional region shown in Fig. 4 of FUKUDA 02. The best fit point is $\Delta(m^2) = 6.9 \times 10^{-5} \text{ eV}^2$ and $\tan^2\theta = 0.38$ ($\sin^2 2\theta = 0.80$).

 $\sin^2(\theta_{23})$

The reported limits below correspond to the projection onto the $\sin^2(\theta_{23})$ axis of the 90% CL contours in the $\sin^2(\theta_{23}) - \Delta m_{32}^2$ plane presented by the authors. Unless otherwise specified, the limits are 90% CL and the reported uncertainties are 68% CL.

If an experiment reports $\sin^2(2\theta_{23})$ we convert the value to $\sin^2(\theta_{23})$.

VALUE	DOCUMENT ID	TECN	COMMENT
0.547 ± 0.021 OUR FIT	Assuming inverted mass ordering		
0.545 ± 0.021 OUR FIT	Assuming normal mass ordering		
0.56 ^{+0.04} _{-0.03}	1 ACERO	19 NOVA	Normal mass order; octant II for θ_{23}
0.56 ^{+0.04} _{-0.03}	1,2 ACERO	19 NOVA	Inverted mass order; octant II for θ_{23}
0.51 ^{+0.07} _{-0.09}	3 AARTSEN	18a ICCB	Normal mass ordering
0.588 ^{+0.031} _{-0.064}	4 ABE	18b SKAM	Normal mass ordering, θ_{13} constrained
0.575 ^{+0.036} _{-0.073}	4 ABE	18b SKAM	Inverted mass ordering, θ_{13} constrained
0.526 ^{+0.032} _{-0.036}	5 ABE	18g T2K	Normal mass ordering, θ_{13} constrained
0.530 ^{+0.030} _{-0.034}	5 ABE	18g T2K	Inverted mass ordering, θ_{13} constrained
0.41 ^{+0.23} _{-0.06}	6 ADAMSON	14 MINS	Normal mass ordering
0.41 ^{+0.26} _{-0.07}	6 ADAMSON	14 MINS	Inverted mass ordering
• • • We do not use the following data for averages, fits, limits, etc. • • •			
0.455	7 AARTSEN	20 ICCB	For both mass orderings
0.58 ^{+0.04} _{-0.13}	8 AARTSEN	19c ICCB	
0.48 ^{+0.04} _{-0.03}	1,2 ACERO	19 NOVA	Normal mass order; octant I for θ_{23}
0.47 ^{+0.04} _{-0.03}	1,2 ACERO	19 NOVA	Inverted mass order; octant I for θ_{23}

See key on page 999

Lepton Particle Listings

Neutrino Mixing

0.49 \pm 0.30 -0.28	AGAFONOVA	19	OPER		0.24 to 0.76 ⁵³ HATAKEYAMA 98 KAMI Kamiokande
0.50 \pm 0.20 -0.19	⁹ ALBERT	19	ANTR	Atmospheric ν , deep sea telescope	0.20 to 0.80 ⁵⁴ FUKUDA 94 KAMI Kamiokande
0.587 \pm 0.036 -0.069	¹⁰ ABE	18B	SKAM	3ν osc: normal mass ordering, θ_{13} free	¹ ACERO 19 is based on a sample size of 12.33×10^{20} protons on target. The fit combines both antineutrino and neutrino data to extract the oscillation parameters. The results favor the normal mass ordering by 1.9 σ and θ_{23} values in octant II by 1.6 σ . Supersedes ACERO 18.
0.551 \pm 0.044 -0.075	¹⁰ ABE	18B	SKAM	3ν osc: inverted mass ordering, θ_{13} free	² Errors are from normal mass ordering and θ_{13} octant II fits.
0.56 \pm 0.04	¹¹ ACERO	18	NOVA	Normal mass order; octant II for θ_{23}	³ AARTSEN 18A uses three years (April 2012 – May 2015) of neutrino data from full sky with reconstructed energies between 5.6 and 56 GeV, measured with the low-energy subdetector DeepCore of the IceCube neutrino telescope. AARTSEN 18A also reports the best fit result for the inverted mass ordering as $\Delta m_{32}^2 = -2.32 \times 10^{-3} \text{ eV}^2$ and $\sin^2(\theta_{23}) = 0.51$. Uncertainties for the inverted mass ordering fits were not provided. Supersedes AARTSEN 15A.
0.47 \pm 0.04	¹¹ ACERO	18	NOVA	Normal mass order; octant I for θ_{23}	⁴ ABE 18B uses 328 kton-years of Super-Kamiokande I-IV atmospheric neutrino data to obtain this result. The fit is performed over the three parameters, Δm_{21}^2 , $\sin^2(\theta_{23})$, and δ , while the solar parameters and $\sin^2(\theta_{13})$ are fixed to $\Delta m_{21}^2 = (7.53 \pm 0.18) \times 10^{-5} \text{ eV}^2$, $\sin^2(\theta_{12}) = 0.304 \pm 0.014$, and $\sin^2(\theta_{13}) = 0.0219 \pm 0.0012$.
0.547 \pm 0.020 -0.030	DE-SALAS	18	FIT	Normal mass ordering, global fit	⁵ ABE 18g data prefers normal mass ordering is with a posterior probability of 87%. Supersedes ABE 17F.
0.551 \pm 0.018 -0.030	DE-SALAS	18	FIT	Inverted mass order, global fit	⁶ ADAMSON 14 uses a complete set of accelerator and atmospheric data. The analysis combines the ν_μ disappearance and ν_e appearance data using three-neutrino oscillation fit. The fit results are obtained for normal and inverted mass ordering assumptions. The best fit is for first θ_{23} octant and inverted mass ordering.
0.532 \pm 0.061 -0.087	¹² ABE	17A	T2K	Normal mass ordering	⁷ AARTSEN 20 uses the data taken between May 2012 and April 2014 with the low-energy subdetector DeepCore of the IceCube neutrino telescope. The reconstructed energy range is between 4 (5) and 90 (80) GeV for the main (confirmatory) analysis. Though the observed best-fit is in the lower octant for both mass orderings, a substantial range of $\sin^2(\theta_{23}) > 0.5$ is still compatible with the observed data for both mass orderings.
0.534 \pm 0.061 -0.087	¹² ABE	17A	T2K	Inverted mass ordering	⁸ AARTSEN 19c uses three years (April 2012 – May 2015) of neutrino data from full sky with reconstructed energies between 5.6 and 56 GeV, measured with the low-energy sub-detector DeepCore of the IceCube neutrino telescope. AARTSEN 19c adopts looser event selection criteria to prioritize the efficiency of selecting neutrino events, different from tighter event selection criteria which closely follow the criteria used by AARTSEN 18A to measure the ν_μ disappearance.
0.51 \pm 0.08 -0.07	ABE	17C	T2K	Normal mass ordering with neutrinos	⁹ ALBERT 19 measured the oscillation parameters of atmospheric neutrinos with the ANTARES deep sea neutrino telescope using the data taken from 2007 to 2016 (2830 days of total live time). Supersedes ADRIAN-MARTINEZ 12.
0.42 \pm 0.25 -0.07	ABE	17C	T2K	Normal mass ordering with antineutrinos	¹⁰ ABE 18b uses 328 kton-years of Super-Kamiokande I-IV atmospheric neutrino data to obtain this result. The fit is performed over the four parameters, Δm_{21}^2 , $\sin^2\theta_{23}$, $\sin^2\theta_{13}$, and δ , while the solar parameters are fixed to $\Delta m_{21}^2 = (7.53 \pm 0.18) \times 10^{-5} \text{ eV}^2$ and $\sin^2\theta_{12} = 0.304 \pm 0.014$.
0.52 \pm 0.075 -0.09	ABE	17C	T2K	normal mass ordering with neutrinos and antineutrinos	¹¹ ACERO 18 performs a joint fit to the data for ν_μ disappearance and ν_e appearance. The overall best fit favors normal mass ordering and θ_{23} in octant II. No 1σ confidence intervals are presented for the inverted mass ordering scenarios. Superseded by ACERO 19.
0.55 \pm 0.05 -0.09	¹² ABE	17F	T2K	Normal mass ordering	¹² Errors are from the projections of the 68% contour on 2D plot of Δm^2 versus $\sin^2(\theta_{23})$. ABE 17f supersedes ABE 17A. Superseded by ABE 18g.
0.55 \pm 0.05 -0.08	¹² ABE	17F	T2K	Inverted mass ordering	¹³ Superseded by ACERO 18.
0.404 \pm 0.022 -0.030	¹³ ADAMSON	17A	NOVA	Normal mass ordering; octant I for θ_{23}	¹⁴ ABE 16d reports oscillation results using $\bar{\nu}_\mu$ disappearance in an off-axis beam.
0.624 \pm 0.022 -0.022	¹³ ADAMSON	17A	NOVA	Normal mass ordering; octant II for θ_{23}	¹⁵ ADAMSON 16A obtains $\sin^2(\theta_{23})$ in the 68% C.L. range [0.38, 0.65] ([0.37, 0.64]), with two statistically degenerate best-fit values of 0.44 and 0.59 (0.44 and 0.59) for normal (inverted) mass ordering. Superseded by ADAMSON 17A.
0.398 \pm 0.030 -0.022	¹³ ADAMSON	17A	NOVA	Inverted mass ordering; octant I for θ_{23}	¹⁶ AARTSEN 15A obtains this result by a three-neutrino oscillation analysis using 10–100 GeV muon neutrino sample from a total of 953 days of measurement with the low-energy subdetector DeepCore of the IceCube neutrino telescope. Superseded by AARTSEN 18A.
0.618 \pm 0.022 -0.030	¹³ ADAMSON	17A	NOVA	Inverted mass ordering; octant II for θ_{23}	¹⁷ ABE 14 results are based on ν_μ disappearance using three-neutrino oscillation fit. The confidence intervals are derived from one dimensional profiled likelihoods. Superseded by ABE 17A.
0.45 \pm 0.19 -0.07	¹⁴ ABE	16D	T2K	3ν osc; normal mass ordering; $\bar{\nu}$ beam	¹⁸ FORERO 14 performs a global fit to neutrino oscillations using solar, reactor, long-baseline accelerator, and atmospheric neutrino data.
0.38 to 0.65	¹⁵ ADAMSON	16A	NOVA	normal mass ordering	¹⁹ GONZALEZ-GARCIA 14 result comes from a frequentist global fit. The corresponding Bayesian global fit to the same data results are reported in BERGSTROM 15 as 68% CL intervals of 0.433–0.496 or 0.530–0.594 for normal and 0.514–0.612 for inverted mass ordering.
0.37 to 0.64	¹⁵ ADAMSON	16A	NOVA	Inverted mass ordering	²⁰ AARTSEN 13B obtained this result by a two-neutrino oscillation analysis using 20–100 GeV muon neutrino sample from a total of 318.9 days of live-time measurement with the low-energy subdetector DeepCore of the IceCube neutrino telescope.
0.53 \pm 0.09 -0.12	¹⁶ AARTSEN	15A	ICCB	Normal mass ordering	²¹ The best fit value is $\sin^2(\theta_{23}) = 0.514 \pm 0.082$. Superseded by ABE 14.
0.51 \pm 0.09 -0.11	¹⁶ AARTSEN	15A	ICCB	Inverted mass ordering	²² ADAMSON 13b obtained this result from ν_μ and $\bar{\nu}_\mu$ disappearance using ν_μ (10.71 $\times 10^{20}$ POT) and $\bar{\nu}_\mu$ (3.36 $\times 10^{20}$ POT) beams, and atmospheric (37.88kton-years) data from MINOS. The fit assumed two-flavor neutrino hypothesis and identical ν_μ and $\bar{\nu}_\mu$ oscillation parameters. Superseded by ADAMSON 14.
0.514 \pm 0.055 -0.056	¹⁷ ABE	14	T2K	3ν osc.; normal mass ordering	²³ ABE 12a obtained this result by a two-neutrino oscillation analysis. The best-fit point is $\sin^2(2\theta_{23}) = 0.98$.
0.511 \pm 0.055	¹⁷ ABE	14	T2K	3ν osc.; inverted mass ordering	²⁴ ADAMSON 12 is a two-neutrino oscillation analysis using antineutrinos. The best fit value is $\sin^2(2\theta_{23}) = 0.95 \pm 0.10 \pm 0.01$.
0.567 \pm 0.032 -0.128	¹⁸ FORERO	14	FIT	Normal mass ordering	²⁵ ADAMSON 12B obtained this result by a two-neutrino oscillation analysis of the L/E distribution using 37.9 kton-yr atmospheric neutrino data with the MINOS far detector.
0.573 \pm 0.025 -0.043	¹⁸ FORERO	14	FIT	Inverted mass ordering	²⁶ The best fit point is $\Delta m^2 = 0.0019 \text{ eV}^2$ and $\sin^2 2\theta = 0.99$. The 90% single-parameter confidence interval at the best fit point is $\sin^2 2\theta > 0.86$.
0.452 \pm 0.052 -0.028	¹⁹ GONZALEZ...	14	FIT	Normal mass ordering; global fit	²⁷ The data are separated into pure samples of ν_s and $\bar{\nu}_s$, and separate oscillation parameters for ν_s and $\bar{\nu}_s$ are fit to the data. The best fit point is $(\Delta m^2, \sin^2 2\theta) = (0.0022 \text{ eV}^2, 0.99)$ and $(\Delta \bar{m}^2, \sin^2 2\bar{\theta}) = (0.0016 \text{ eV}^2, 1.00)$. The quoted result is taken from the
0.579 \pm 0.025 -0.037	¹⁹ GONZALEZ...	14	FIT	Inverted mass ordering; global fit	
0.24 to 0.76	²⁰ AARTSEN	13B	ICCB	DeepCore, 2ν oscillation	
0.514 \pm 0.082	²¹ ABE	13G	T2K	3ν osc.; normal mass ordering	
0.388 \pm 0.051 -0.053	²² ADAMSON	13B	MINS	Beam + Atmospheric; identical ν & $\bar{\nu}$	
0.3 to 0.7	²³ ABE	12A	T2K	Off-axis beam	
0.28 to 0.72	²⁴ ADAMSON	12	MINS	$\bar{\nu}$ beam	
0.25 to 0.75	^{25,26} ADAMSON	12B	MINS	MINOS atmospheric	
0.27 to 0.73	^{25,27} ADAMSON	12B	MINS	MINOS pure atmospheric $\bar{\nu}$	
0.21 to 0.79	^{25,27} ADAMSON	12B	MINS	MINOS pure atmospheric ν	
0.15 to 0.85	²⁸ ADRIAN-MAR.	12	ANTR	Atmospheric ν with deep sea telescope	
0.39 to 0.61	²⁹ ABE	11C	SKAM	Super-Kamiokande	
0.34 to 0.66	ADAMSON	11	MINS	2ν osc.; maximal mixing	
0.31 \pm 0.10 -0.07	³⁰ ADAMSON	11B	MINS	$\bar{\nu}$ beam	
0.41 to 0.59	³¹ WENDELL	10	SKAM	3ν osc. with solar terms; $\theta_{13}=0$	
0.39 to 0.61	³² WENDELL	10	SKAM	3ν osc.; normal mass ordering	
0.37 to 0.63	³³ WENDELL	10	SKAM	3ν osc.; inverted mass ordering	
0.31 to 0.69	ADAMSON	08A	MINS	MINOS	
0.05 to 0.95	³⁴ ADAMSON	06	MINS	Atmospheric ν with far detector	
0.18 to 0.82	³⁵ AHN	06A	K2K	KEK to Super-K	
0.23 to 0.77	³⁶ MICHAEL	06	MINS	MINOS	
0.18 to 0.82	³⁷ ALIU	05	K2K	KEK to Super-K	
0.18 to 0.82	³⁸ ALLISON	05	SOU2		
0.36 to 0.64	³⁹ ASHIE	05	SKAM	Super-Kamiokande	
0.28 to 0.72	⁴⁰ AMBROSIO	04	MCRO	MACRO	
0.34 to 0.66	⁴¹ ASHIE	04	SKAM	L/E distribution	
0.08 to 0.92	⁴² AHN	03	K2K	KEK to Super-K	
0.13 to 0.87	⁴³ AMBROSIO	03	MCRO	MACRO	
0.26 to 0.74	⁴⁴ AMBROSIO	03	MCRO	MACRO	
0.15 to 0.85	⁴⁵ SANCHEZ	03	SOU2	Soudan-2 Atmospheric	
0.28 to 0.72	⁴⁶ AMBROSIO	01	MCRO	Upward μ	
0.29 to 0.71	⁴⁷ AMBROSIO	01	MCRO	Upward μ	
0.13 to 0.87	⁴⁸ FUKUDA	99C	SKAM	Upward μ	
0.23 to 0.77	⁴⁹ FUKUDA	99D	SKAM	Upward μ	
0.08 to 0.92	⁵⁰ FUKUDA	99D	SKAM	Stop μ / through	
0.29 to 0.71	⁵¹ FUKUDA	98C	SKAM	Super-Kamiokande	
0.08 to 0.92	⁵² HATAKEYAMA	98	KAMI	Kamiokande	

Lepton Particle Listings

Neutrino Mixing

- 90% C.L. contour in the $(\Delta m^2, \sin^2 2\theta)$ plane obtained by minimizing the four parameter log-likelihood function with respect to the other oscillation parameters.
- ²⁸ADRIAN-MARTINEZ 12 measured the oscillation parameters of atmospheric neutrinos with the ANTARES deep sea neutrino telescope using the data taken from 2007 to 2010 (863 days of total live time). Superseded by ALBERT 19.
- ²⁹ABE 11c obtained this result by a two-neutrino oscillation analysis using the Super-Kamiokande-I+II+III atmospheric neutrino data. ABE 11c also reported results under a two-neutrino disappearance model with separate mixing parameters between ν and $\bar{\nu}$, and obtained $\sin^2 2\theta > 0.93$ for ν and $\sin^2 2\theta > 0.83$ for $\bar{\nu}$ at 90% C.L.
- ³⁰ADAMSON 11b obtained this result by a two-neutrino oscillation analysis of antineutrinos in an antineutrino enhanced beam with 1.71×10^{20} protons on target. This result is consistent with the neutrino measurements of ADAMSON 11 at 2% C.L.
- ³¹WENDELL 10 obtained this result ($\sin^2 \theta_{23} = 0.407\text{--}0.583$) by a three-neutrino oscillation analysis using the Super-Kamiokande-I+II+III atmospheric neutrino data, assuming $\theta_{13} = 0$ but including the solar oscillation parameters Δm_{21}^2 and $\sin^2 \theta_{12}$ in the fit.
- ³²WENDELL 10 obtained this result ($\sin^2 \theta_{23} = 0.43\text{--}0.61$) by a three-neutrino oscillation analysis with one mass scale dominance ($\Delta m_{21}^2 = 0$) using the Super-Kamiokande-I+II+III atmospheric neutrino data, and updates the HOSAKA 06a result.
- ³³WENDELL 10 obtained this result ($\sin^2 \theta_{23} = 0.44\text{--}0.63$) by a three-neutrino oscillation analysis with one mass scale dominance ($\Delta m_{21}^2 = 0$) using the Super-Kamiokande-I+II+III atmospheric neutrino data, and updates the HOSAKA 06a result.
- ³⁴ADAMSON 06 obtained this result by a two-neutrino oscillation analysis of the L/E distribution using 4.54 kton yr atmospheric neutrino data with the MINOS far detector.
- ³⁵Supersedes ALIU 05.
- ³⁶MICHAEL 06 best fit is for maximal mixing. See also ADAMSON 08.
- ³⁷The best fit is for maximal mixing.
- ³⁸ALLISON 05 result is based upon atmospheric neutrino interactions including upward-stopping muons, with an exposure of 5.9 kton yr. From a two-flavor oscillation analysis the best-fit point is $\Delta m^2 = 0.0017 \text{ eV}^2$ and $\sin^2(2\theta) = 0.97$.
- ³⁹ASHIE 05 obtained this result by a two-neutrino oscillation analysis using 92 kton yr atmospheric neutrino data from the complete Super-Kamiokande I running period.
- ⁴⁰AMBROSIO 04 obtained this result, without using the absolute normalization of the neutrino flux, by combining the angular distribution of upward through-going muon tracks with $E_\mu > 1 \text{ GeV}$, N_{low} and N_{high} , and the numbers of InDown + UpStop and InUp events. Here, N_{low} and N_{high} are the number of events with reconstructed neutrino energies $< 30 \text{ GeV}$ and $> 130 \text{ GeV}$, respectively. InDown and InUp represent events with downward and upward-going tracks starting inside the detector due to neutrino interactions, while UpStop represents entering upward-going tracks which stop in the detector. The best fit is for maximal mixing.
- ⁴¹ASHIE 04 obtained this result from the $L(\text{flight length})/E(\text{estimated neutrino energy})$ distribution of ν_μ disappearance probability, using the Super-Kamiokande-I 1489 live-day atmospheric neutrino data.
- ⁴²There are several islands of allowed region from this K2K analysis, extending to high values of Δm^2 . We only include the one that overlaps atmospheric neutrino analyses. The best fit is for maximal mixing.
- ⁴³AMBROSIO 03 obtained this result on the basis of the ratio $R = N_{low}/N_{high}$, where N_{low} and N_{high} are the number of upward through-going muon events with reconstructed neutrino energy $< 30 \text{ GeV}$ and $> 130 \text{ GeV}$, respectively. The data came from the full detector run started in 1994. The method of FELDMAN 98 is used to obtain the limits.
- ⁴⁴AMBROSIO 03 obtained this result by using the ratio R and the angular distribution of the upward through-going muons. R is given in the previous note and the angular distribution is reported in AMBROSIO 01. The method of FELDMAN 98 is used to obtain the limits. The best fit is to maximal mixing.
- ⁴⁵SANCHEZ 03 is based on an exposure of 5.9 kton yr. The result is obtained using a likelihood analysis of the neutrino L/E distribution for a selection μ flavor sample while the e -flavor sample provides flux normalization. The method of FELDMAN 98 is used to obtain the allowed region. The best fit is $\sin^2(2\theta) = 0.97$.
- ⁴⁶AMBROSIO 01 result is based on the angular distribution of upward through-going muon tracks with $E_\mu > 1 \text{ GeV}$. The data came from three different detector configurations, but the statistics is largely dominated by the full detector run, from May 1994 to December 2000. The total live time, normalized to the full detector configuration is 6.17 years. The best fit is obtained outside the physical region. The method of FELDMAN 98 is used to obtain the limits. The best fit is for maximal mixing.
- ⁴⁷AMBROSIO 01 result is based on the angular distribution and normalization of upward through-going muon tracks with $E_\mu > 1 \text{ GeV}$. See the previous footnote.
- ⁴⁸FUKUDA 99c obtained this result from a total of 537 live days of upward through-going muon data in Super-Kamiokande between April 1996 to January 1998. With a threshold of $E_\mu > 1.6 \text{ GeV}$, the observed flux is $(1.74 \pm 0.07 \pm 0.02) \times 10^{-13} \text{ cm}^{-2}\text{s}^{-1}\text{sr}^{-1}$. The best fit is $\sin^2(2\theta) = 0.95$.
- ⁴⁹FUKUDA 99b obtained this result from a simultaneous fitting to zenith angle distributions of upward-stopping and through-going muons. The flux of upward-stopping muons of minimum energy of 1.6 GeV measured between April 1996 and January 1998 is $(0.39 \pm 0.04 \pm 0.02) \times 10^{-13} \text{ cm}^{-2}\text{s}^{-1}\text{sr}^{-1}$. This is compared to the expected flux of $(0.73 \pm 0.16 (\text{theoretical error})) \times 10^{-13} \text{ cm}^{-2}\text{s}^{-1}\text{sr}^{-1}$. The best fit is to maximal mixing.
- ⁵⁰FUKUDA 99d obtained this result from the zenith dependence of the upward-stopping/through-going flux ratio. The best fit is to maximal mixing.
- ⁵¹FUKUDA 98c obtained this result by an analysis of 33.0 kton yr atmospheric neutrino data. The best fit is for maximal mixing.
- ⁵²HATAKEYAMA 98 obtained this result from a total of 2456 live days of upward-going muon data in Kamiokande between December 1985 and May 1995. With a threshold of $E_\mu > 1.6 \text{ GeV}$, the observed flux of upward through-going muons is $(1.94 \pm 0.10^{+0.07}_{-0.06}) \times$

$10^{-13} \text{ cm}^{-2}\text{s}^{-1}\text{sr}^{-1}$. This is compared to the expected flux of $(2.46 \pm 0.54 (\text{theoretical error})) \times 10^{-13} \text{ cm}^{-2}\text{s}^{-1}\text{sr}^{-1}$. The best fit is for maximal mixing.

- ⁵³HATAKEYAMA 98 obtained this result from a combined analysis of Kamiokande contained events (FUKUDA 94) and upward going muon events. The best fit is $\sin^2(2\theta) = 0.95$.

- ⁵⁴FUKUDA 94 obtained the result by a combined analysis of sub- and multi-GeV atmospheric neutrino events in Kamiokande. The best fit is for maximal mixing.

 Δm_{32}^2

The sign of Δm_{32}^2 is not known at this time. If given, values are shown separately for the normal and inverted mass ordering. Unless otherwise specified, the ranges below correspond to the projection onto the Δm_{32}^2 axis of the 90% CL contours in the $\sin^2(2\theta_{23}) - \Delta m_{32}^2$ plane presented by the authors. If uncertainties are reported with the value, they correspond to one standard deviation uncertainty.

VALUE (10^{-3} eV^2)	DOCUMENT ID	TECN	COMMENT
$-2.546^{+0.034}_{-0.040}$ OUR FIT			Assuming inverted ordering
2.453 ± 0.034 OUR FIT			Assuming normal ordering
$2.48^{+0.11}_{-0.06}$	1 ACERO	19 NOVA	Normal mass ordering, octant II for θ_{23}
$-2.54^{+0.06}_{-0.11}$	1 ACERO	19 NOVA	Inverted mass ordering, octant II for θ_{23}
$2.31^{+0.11}_{-0.13}$	2 AARTSEN	18A ICCB	Normal mass ordering
$2.50^{+0.13}_{-0.20}$	3 ABE	18B SKAM	Normal mass ordering, θ_{13} constrained
$-2.58^{+0.08}_{-0.37}$	3 ABE	18B SKAM	Inverted mass ordering, θ_{13} constrained
$2.463^{+0.071}_{-0.070}$	4 ABE	18G T2K	Normal mass ordering, θ_{13} constrained
-2.507 ± 0.070	4.5 ABE	18G T2K	Inverted mass ordering, θ_{13} constrained
$2.471^{+0.068}_{-0.070}$	6 ADEY	18A DAYA	Normal mass ordering
$-2.575^{+0.068}_{-0.070}$	6 ADEY	18A DAYA	Inverted mass ordering
2.63 ± 0.14	7 BAK	18 RENO	Normal mass ordering
-2.73 ± 0.14	7 BAK	18 RENO	Inverted mass ordering
2.37 ± 0.09	8 ADAMSON	14 MINS	Accel., atmospheric, normal mass ordering
$-2.41^{+0.09}_{-0.12}$	8 ADAMSON	14 MINS	Accel., atmospheric, inverted mass ordering
• • • We do not use the following data for averages, fits, limits, etc. • • •			
$2.55^{+0.12}_{-0.11}$	9 AARTSEN	19C ICCB	
< 4.1 at 90% CL	AGAFONOVA	19 OPER	
$2.0^{+0.4}_{-0.3}$	10 ALBERT	19 ANTR	Atmospheric ν , deep sea telescope
$2.50^{+0.13}_{-0.31}$	11 ABE	18B SKAM	3ν osc: normal mass ordering, θ_{13} free
$-2.28^{+0.33}_{-0.13}$	11 ABE	18B SKAM	3ν osc: inverted mass ordering, θ_{13} free
$2.44^{+0.08}_{-0.07}$	12 ACERO	18 NOVA	Normal mass order, octant II for θ_{23}
$2.45^{+0.07}_{-0.08}$	12,13 ACERO	18 NOVA	Normal mass order; octant I for θ_{23}
$2.7^{+0.7}_{-0.6}$	14 AGAFONOVA	18 OPER	OPERA ν_τ appearance
2.42 ± 0.03	DE-SALAS	18 FIT	Normal mass ordering, global fit
$-2.50^{+0.03}_{-0.04}$	DE-SALAS	18 FIT	Inverted mass order, global fit
$2.57^{+0.21}_{-0.23}$	15 SEO	18 RENO	Normal mass ordering
$-2.67^{+0.23}_{-0.21}$	15 SEO	18 RENO	Inverted mass ordering
$2.53^{+0.15}_{-0.13}$	ABE	17C T2K	Normal mass ordering with neutrinos
$2.55^{+0.33}_{-0.27}$	ABE	17C T2K	Normal mass ordering with antineutrinos
$2.55^{+0.08}_{-0.08}$	ABE	17C T2K	Normal mass ordering with neutrinos and antineutrinos
$-2.63^{+0.08}_{-0.08}$	ABE	17C T2K	Inverted mass ordering with neutrinos and antineutrinos
2.54 ± 0.08	16 ABE	17F T2K	Normal mass ordering; $\nu+\bar{\nu}$
-2.51 ± 0.08	16 ABE	17F T2K	Inverted mass ordering; $\nu+\bar{\nu}$
2.67 ± 0.11	17 ADAMSON	17A NOVA	3ν osc; normal mass ordering
-2.72 ± 0.11	17 ADAMSON	17A NOVA	3ν osc; inverted mass ordering
$2.45 \pm 0.06 \pm 0.06$	18 AN	17A DAYA	Normal mass ordering
$-2.56 \pm 0.06 \pm 0.06$	18 AN	17A DAYA	Inverted mass ordering

See key on page 999

Lepton Particle Listings
Neutrino Mixing

2.51 ^{+0.29} _{-0.25}	19	ABE	16D	T2K	3ν osc.; normal mass ordering; $\bar{\nu}$ beam
2.52 ^{+0.20} _{-0.18}	20	ADAMSON	16A	NOVA	3ν osc.; normal mass ordering
-2.56 ± 0.19	20	ADAMSON	16A	NOVA	3ν osc.; inverted mass ordering
2.56 ^{+0.21} _{-0.23}	21	CHOI	16	RENO	3ν osc.; normal mass ordering
2.56 ^{+0.21} _{-0.13}	21	CHOI	16	RENO	3ν osc.; normal mass ordering
-2.69 ^{+0.23} _{-0.21}	21	CHOI	16	RENO	3ν osc.; inverted mass ordering
2.72 ^{+0.19} _{-0.20}	22	AARTSEN	15A	ICCB	Normal mass ordering
-2.73 ^{+0.21} _{-0.18}	22	AARTSEN	15A	ICCB	Inverted mass ordering
2.0-5.0	23	AGAFONOVA	15A	OPER	90% CL, 5 events
2.37 ± 0.11	24	AN	15	DAYA	3ν osc.; normal mass ordering
-2.47 ± 0.11	24	AN	15	DAYA	3ν osc.; inverted mass ordering
2.51 ± 0.10	25	ABE	14	T2K	3ν osc.; normal mass ordering
-2.56 ± 0.10	25	ABE	14	T2K	3ν osc.; inverted mass ordering
2.54 ^{+0.19} _{-0.20}	26	AN	14	DAYA	3ν osc.; normal mass ordering
-2.64 ^{+0.20} _{-0.19}	26	AN	14	DAYA	3ν osc.; inverted mass ordering
2.48 ^{+0.05} _{-0.07}	27	FORERO	14	FIT	3ν; normal mass ordering
-2.38 ^{+0.06} _{-0.05}	27	FORERO	14	FIT	3ν; inverted mass ordering
2.457 ± 0.047	28,29	GONZALEZ...	14	FIT	Normal mass ordering; global fit
-2.449 ^{+0.047} _{-0.048}	28	GONZALEZ...	14	FIT	Inverted mass ordering; global fit
2.3 ^{+0.6} _{-0.5}	30	AARTSEN	13B	ICCB	DeepCore, 2ν oscillation
2.44 ^{+0.17} _{-0.15}	31	ABE	13G	T2K	3ν osc.; normal mass ordering
2.41 ^{+0.09} _{-0.10}	32	ADAMSON	13B	MINS	2ν osc.; beam + atmospheric; identical ν & $\bar{\nu}$ off-axis beam
2.2-3.1	33	ABE	12A	T2K	$\bar{\nu}$ beam
2.62 ^{+0.31} _{-0.28} ± 0.09	34	ADAMSON	12	MINS	$\bar{\nu}$ beam
1.35-2.55	35,36	ADAMSON	12B	MINS	MINOS atmospheric
1.4-5.6	35,37	ADAMSON	12B	MINS	MINOS pure atmospheric ν
0.9-2.5	35,37	ADAMSON	12B	MINS	MINOS pure atmospheric $\bar{\nu}$
1.8-5.0	38	ADRIAN-MAR.	12	ANTR	Atmospheric ν with deep sea telescope
1.3-4.0	39	ABE	11C	SKAM	atmospheric $\bar{\nu}$
2.32 ^{+0.12} _{-0.08}		ADAMSON	11	MINS	2ν oscillation; maximal mixing
3.36 ^{+0.46} _{-0.40}	40	ADAMSON	11B	MINS	$\bar{\nu}$ beam
< 3.37	41	ADAMSON	11C	MINS	MINOS
1.9-2.6	42	WENDELL	10	SKAM	3ν osc.; normal mass ordering
-1.7- -2.7	42	WENDELL	10	SKAM	3ν osc.; inverted mass ordering
2.43 ± 0.13		ADAMSON	08A	MINS	MINOS
0.07-5.0	43	ADAMSON	06	MINS	atmospheric ν with far detector
1.9-4.0	44,45	AHN	06A	K2K	KEK to Super-K
2.2-3.8	46	MICHAEL	06	MINS	MINOS
1.9-3.6	47	ALIU	05	K2K	KEK to Super-K
0.3-1.2	44	ALLISON	05	SOU2	
1.5-3.4	48	ASHIE	05	SKAM	atmospheric neutrino
0.6-8.0	49	AMBROSIO	04	MCRO	MACRO
1.9 to 3.0	50	ASHIE	04	SKAM	L/E distribution
1.5-3.9	51	AHN	03	K2K	KEK to Super-K
0.25-9.0	52	AMBROSIO	03	MCRO	MACRO
0.6-7.0	53	AMBROSIO	03	MCRO	MACRO
0.15-15	54	SANCHEZ	03	SOU2	Soudan-2 Atmospheric
0.6-15	55	AMBROSIO	01	MCRO	upward μ
1.0-6.0	56	AMBROSIO	01	MCRO	upward μ
1.0-5.0	57	FUKUDA	99C	SKAM	upward μ
1.5-15.0	58	FUKUDA	99D	SKAM	upward μ
0.7-18	59	FUKUDA	99D	SKAM	stop μ / through
0.5-6.0	60	FUKUDA	98C	SKAM	Super-Kamiokande
0.55-5.0	61	HATAKEYAMA	98	KAMI	Kamiokande
4-23	62	HATAKEYAMA	98	KAMI	Kamiokande
5-25	63	FUKUDA	94	KAMI	Kamiokande

¹ ACERO 19 is based on a sample size of 12.33×10^{20} protons on target. The fit combines both antineutrino and neutrino data to extract the oscillation parameters. The results favor the normal mass ordering by 1.9σ and θ_{23} values in octant II by 1.6σ . Supersedes ACERO 18A.

² AARTSEN 18A uses three years (April 2012 – May 2015) of neutrino data from full sky with reconstructed energies between 5.6 and 56 GeV, measured with the low-energy subdetector DeepCore of the IceCube neutrino telescope. AARTSEN 18A also reports the best fit values for the inverted mass ordering as $\Delta m_{32}^2 = -2.32 \times 10^{-3} \text{ eV}^2$ and $\sin^2(\theta_{23}) = 0.51$. Uncertainties for the inverted mass ordering fits were not provided. Supersedes AARTSEN 15A.

³ ABE 18B uses 328 kton-years of Super-Kamiokande I-IV atmospheric neutrino data to obtain this result. The fit is performed over the three parameters, Δm_{32}^2 , $\sin^2(\theta_{23})$, and δ , while the solar parameters and $\sin^2(\theta_{13})$ are fixed to $\Delta m_{21}^2 = (7.53 \pm 0.18) \times 10^{-5} \text{ eV}^2$, $\sin^2(\theta_{13}) = 0.304 \pm 0.014$, and $\sin^2(\theta_{13}) = 0.0219 \pm 0.0012$.

⁴ ABE 18C data prefers normal ordering with a posterior probability of 87%. Supersedes ABE 17F.

⁵ ABE 18C reports $\Delta m_{13}^2 = (2.432 \pm 0.070) \times 10^{-3} \text{ eV}^2$ for inverted mass ordering. We convert to Δm_{32}^2 using PDG 18 value of $\Delta m_{21}^2 = (7.53 \pm 0.18) \times 10^{-5} \text{ eV}^2$.

⁶ ADEY 18A reports results from analysis of 1958 days of data taking with the Daya-Bay experiment, with 3.9×10^6 $\bar{\nu}_e$ candidates. The fit to the data gives $\Delta m_{ee}^2 = (2.522^{+0.068}_{-0.070}) \times 10^{-3} \text{ eV}^2$. Solar oscillation parameters are fixed in the analysis using the global averages, $\sin^2(\theta_{12}) = 0.307^{+0.013}_{-0.012}$, $\Delta m_{21}^2 = (7.53 \pm 0.18) \times 10^{-5} \text{ eV}^2$, from PDG 18. Supersedes AN 17A.

⁷ BAK 18 reports results of the RENO experiment using about 2200 live-days of data taken with detectors placed at 410.6 and 1445.7 m from reactors of the Hanbit Nuclear Power Plant. We convert the results to Δm_{32}^2 using the PDG 18 values of $\sin^2\theta_{12} = 0.307^{+0.013}_{-0.012}$ and $\Delta m_{21}^2 = (7.53 \pm 0.18) \times 10^{-5} \text{ eV}^2$. Supersedes SEO 18.

⁸ ADAMSON 14 uses a complete set of accelerator and atmospheric data. The analysis combines the analysis combines the ν_μ disappearance and ν_e appearance data using three-neutrino oscillation fit. The fit results are obtained for normal and inverted mass ordering assumptions.

⁹ AARTSEN 19C uses three years (April 2012 – May 2015) of neutrino data from full sky with reconstructed energies between 5.6 and 56 GeV, measured with the low-energy sub-detector DeepCore of the IceCube neutrino telescope. AARTSEN 19C adopts looser event selection criteria to prioritize the efficiency of selecting neutrino events, different from tighter event selection criteria which closely follow the criteria used by AARTSEN 18A to measure the ν_μ disappearance.

¹⁰ ALBERT 19 measured the oscillation parameters of atmospheric neutrinos with the ANTARES deep sea neutrino telescope using the data taken from 2007 to 2016 (2830 days of total live time). Supersedes ADRIAN-MARTINEZ 12.

¹¹ ABE 18B uses 328 kton-years of Super-Kamiokande I-IV atmospheric neutrino data to obtain this result. The fit is performed over the four parameters, Δm_{32}^2 , $\sin^2\theta_{23}$, $\sin^2\theta_{13}$, and δ , while the solar parameters are fixed to $\Delta m_{21}^2 = (7.53 \pm 0.18) \times 10^{-5} \text{ eV}^2$ and $\sin^2\theta_{12} = 0.304 \pm 0.014$.

¹² ACERO 18 performs a joint fit to the data for ν_μ disappearance and ν_e appearance. The overall best fit favors normal mass ordering and θ_{23} in octant II. No 1σ confidence intervals are presented for the inverted mass ordering scenarios. Superseded by ACERO 19.

¹³ The error for octant I is taken from the result for octant II.

¹⁴ AGAFONOVA 18 assumes maximal θ_{23} mixing.

¹⁵ SEO 18 reports result of the RENO experiment from a rate and shape analysis of 500 days of data. A simultaneous fit to θ_{13} and Δm_{ee}^2 yields $\Delta m_{ee}^2 = (2.62^{+0.21+0.12}_{-0.23-0.13}) \times 10^{-3} \text{ eV}^2$. We convert the results to Δm_{32}^2 using the PDG 18 values of $\sin^2\theta_{12}$ and Δm_{21}^2 . SEO 18 is a detailed description of the results published in CHOI 16, which it supersedes. Superseded by BAK 18.

¹⁶ ABE 17F confidence intervals are obtained using a frequentist analysis including θ_{13} constraint from reactor experiments. Bayesian intervals based on Markov Chain Monte Carlo method are also provided by the authors. Superseded by ABE 18G.

¹⁷ Superseded by ACERO 18.

¹⁸ AN 17A report results from combined rate and spectral shape analysis of 1230 days of data taken with the Daya Bay reactor experiment. The data set contains more than 2.5×10^6 inverse beta-decay events with neutron capture on Gd. The fit to the data gives $\Delta_{ee}^2 = (2.50 \pm 0.06 \pm 0.06) \times 10^{-3} \text{ eV}$. Superseded by ADEY 18A.

¹⁹ ABE 16D reports oscillation results using $\bar{\nu}_\mu$ disappearance in an off-axis beam.

²⁰ Superseded by ADAMSON 17A.

²¹ CHOI 16 reports result of the RENO experiment from a rate and shape analysis of 500 days of data. A simultaneous fit to θ_{13} and Δm_{ee}^2 yields $\Delta m_{ee}^2 = (2.62^{+0.21+0.12}_{-0.23-0.13}) \times 10^{-3} \text{ eV}$. We convert the results to Δm_{32}^2 using PDG 18 values of $\sin^2(\theta_{12})$ and Δm_{21}^2 .

²² AARTSEN 15A obtains this result by a three-neutrino oscillation analysis using 10–100 GeV muon neutrino sample from a total of 953 days of measurements with the low-energy subdetector DeepCore of the IceCube neutrino telescope. Superseded by AARTSEN 18A.

²³ AGAFONOVA 15A result is based on 5 $\nu_\mu \rightarrow \nu_\tau$ appearance candidates with an expected background of 0.25 ± 0.05 events. The best fit is for $\Delta m_{32}^2 = 3.3 \times 10^{-3} \text{ eV}^2$.

²⁴ AN 15 uses all eight identical detectors, with four placed near the reactor cores and the remaining four at the far hall to determine prompt energy spectra. The results correspond to the exposure of $6.9 \times 10^5 \text{ GW}_{th}\text{-ton-days}$. They derive $\Delta m_{ee}^2 = (2.42 \pm 0.11) \times 10^{-3} \text{ eV}^2$. Assuming the normal (inverted) ordering, the fitted $\Delta m_{32}^2 = (2.37 \pm 0.11) \times 10^{-3} ((2.47 \pm 0.11) \times 10^{-3}) \text{ eV}^2$. Superseded by AN 17A.

²⁵ ABE 14 results are based on ν_μ disappearance using three-neutrino oscillation fit. The confidence intervals are derived from one dimensional profiled likelihoods. In ABE 14 the inverted mass ordering result is reported as $\Delta m_{13}^2 = (2.48 \pm 0.10) \times 10^{-3} \text{ eV}^2$ which we converted to Δm_{32}^2 by adding PDG 14 value of $\Delta m_{21}^2 = (7.53 \pm 0.18) \times 10^{-5} \text{ eV}^2$. Superseded by ABE 17C.

²⁶ AN 14 uses six identical detectors, with three placed near the reactor cores (flux-weighted baselines of 512 and 561 m) and the remaining three at the far hall (at the flux averaged distance of 1579 m from all six reactor cores) to determine prompt energy spectra and derive $\Delta m_{ee}^2 = (2.59^{+0.19}_{-0.20}) \times 10^{-3} \text{ eV}^2$. Assuming the normal (inverted) ordering, the fitted $\Delta m_{32}^2 = (2.54^{+0.19}_{-0.20}) \times 10^{-3} ((2.64^{+0.19}_{-0.20}) \times 10^{-3}) \text{ eV}^2$. Superseded by AN 15.

²⁷ FORERO 14 performs a global fit to Δm_{31}^2 using solar, reactor, long-baseline accelerator, and atmospheric neutrino data.

²⁸ GONZALEZ-GARCIA 14 result comes from a frequentist global fit. The corresponding Bayesian global fit to the same data results are reported in BERGSTROM 15 as $(2.460 \pm 0.046) \times 10^{-3} \text{ eV}^2$ for normal and $(2.445^{+0.047}_{-0.045}) \times 10^{-3} \text{ eV}^2$ for inverted mass ordering.

²⁹ The value for normal mass ordering is actually a measurement of Δm_{31}^2 which differs from Δm_{32}^2 by a much smaller value of Δm_{21}^2 .

³⁰ AARTSEN 13B obtained this result by a two-neutrino oscillation analysis using 20–100 GeV muon neutrino sample from a total of 318.9 days of live-time measurement with the low-energy subdetector DeepCore of the IceCube neutrino telescope.

Lepton Particle Listings

Neutrino Mixing

- ³¹ Based on the observation of 58 ν_μ events with 205 ± 17 (syst) expected in the absence of neutrino oscillations. Superseded by ABE 14.
- ³² ADAMSON 13B obtained this result from ν_μ and $\bar{\nu}_\mu$ disappearance using ν_μ (10.71×10^{20} POT) and $\bar{\nu}_\mu$ (3.36×10^{20} POT) beams, and atmospheric (37.88 kton-years) data from MINOS. The fit assumed two-flavor neutrino hypothesis and identical ν_μ and $\bar{\nu}_\mu$ oscillation parameters.
- ³³ ABE 12A obtained this result by a two-neutrino oscillation analysis. The best-fit point is $\Delta m_{32}^2 = 2.65 \times 10^{-3} \text{ eV}^2$.
- ³⁴ ADAMSON 12 is a two-neutrino oscillation analysis using antineutrinos.
- ³⁵ ADAMSON 12B obtained this result by a two-neutrino oscillation analysis of the L/E distribution using 37.9 kton-yr atmospheric neutrino data with the MINOS far detector.
- ³⁶ The 90% single-parameter confidence interval at the best fit point is $\Delta m^2 = 0.0019 \pm 0.0004 \text{ eV}^2$.
- ³⁷ The data are separated into pure samples of ν_s and $\bar{\nu}_s$, and separate oscillation parameters for ν_s and $\bar{\nu}_s$ are fit to the data. The best fit point is $(\Delta m^2, \sin^2 2\theta) = (0.0022 \text{ eV}^2, 0.99)$ and $(\Delta \bar{m}^2, \sin^2 2\bar{\theta}) = (0.0016 \text{ eV}^2, 1.00)$. The quoted result is taken from the 90% C.L. contour in the $(\Delta m^2, \sin^2 2\theta)$ plane obtained by minimizing the four parameter log-likelihood function with respect to the other oscillation parameters.
- ³⁸ ADRIAN-MARTINEZ 12 measured the oscillation parameters of atmospheric neutrinos with the ANTARES deep sea neutrino telescope using the data taken from 2007 to 2010 (863 days of total live time). Superseded by ALBERT 19
- ³⁹ ABE 11c obtained this result by a two-neutrino oscillation analysis with separate mixing parameters between neutrinos and antineutrinos, using the Super-Kamiokande-I+II+III atmospheric neutrino data. The corresponding 90% CL neutrino oscillation parameter range obtained from this analysis is $\Delta m^2 = 1.7\text{--}3.0 \times 10^{-3} \text{ eV}^2$.
- ⁴⁰ ADAMSON 11B obtained this result by a two-neutrino oscillation analysis of antineutrinos in an antineutrino enhanced beam with 1.71×10^{20} protons on target. This result is consistent with the neutrino measurements of ADAMSON 11 at 2% C.L.
- ⁴¹ ADAMSON 11c obtains this result based on a study of antineutrinos in a neutrino beam and assumes maximal mixing in the two-flavor approximation.
- ⁴² WENDELL 10 obtained this result by a three-neutrino oscillation analysis with one mass scale dominance ($\Delta m_{21}^2 = 0$) using the Super-Kamiokande-I+II+III atmospheric neutrino data, and updates the HOSAKA 06A result.
- ⁴³ ADAMSON 06 obtained this result by a two-neutrino oscillation analysis of the L/E distribution using 4.54 kton yr atmospheric neutrino data with the MINOS far detector.
- ⁴⁴ The best fit in the physical region is for $\Delta m^2 = 2.8 \times 10^{-3} \text{ eV}^2$.
- ⁴⁵ Supersedes ALIU 05.
- ⁴⁶ MICHAEL 06 best fit is $2.74 \times 10^{-3} \text{ eV}^2$. See also ADAMSON 08.
- ⁴⁷ ALLISON 05 result is based on an atmospheric neutrino observation with an exposure of 5.9 kton yr. From a two-flavor oscillation analysis the best-fit point is $\Delta m^2 = 0.0017 \text{ eV}^2$ and $\sin^2 2\theta = 0.97$.
- ⁴⁸ ASHIE 05 obtained this result by a two-neutrino oscillation analysis using 92 kton yr atmospheric neutrino data from the complete Super-Kamiokande I running period. The best fit is for $\Delta m^2 = 2.1 \times 10^{-3} \text{ eV}^2$.
- ⁴⁹ AMBROSIO 04 obtained this result, without using the absolute normalization of the neutrino flux, by combining the angular distribution of upward through-going muon tracks with $E_\mu > 1 \text{ GeV}$, N_{low} and N_{high} , and the numbers of InDown + UpStop and InUp events. Here, N_{low} and N_{high} are the number of events with reconstructed neutrino energies $< 30 \text{ GeV}$ and $> 130 \text{ GeV}$, respectively. InDown and InUp represent events with downward and upward-going tracks starting inside the detector due to neutrino interactions, while UpStop represents entering upward-going tracks which stop in the detector. The best fit is for $\Delta m^2 = 2.3 \times 10^{-3} \text{ eV}^2$.
- ⁵⁰ ASHIE 04 obtained this result from the L(flight length)/E(estimated neutrino energy) distribution of ν_μ disappearance probability, using the Super-Kamiokande-I 1489 live-day atmospheric neutrino data. The best fit is for $\Delta m^2 = 2.4 \times 10^{-3} \text{ eV}^2$.
- ⁵¹ There are several islands of allowed region from this K2K analysis, extending to high values of Δm^2 . We only include the one that overlaps atmospheric neutrino analyses. The best fit is for $\Delta m^2 = 2.8 \times 10^{-3} \text{ eV}^2$.
- ⁵² AMBROSIO 03 obtained this result on the basis of the ratio $R = N_{low}/N_{high}$, where N_{low} and N_{high} are the number of upward through-going muon events with reconstructed neutrino energy $< 30 \text{ GeV}$ and $> 130 \text{ GeV}$, respectively. The data came from the full detector run started in 1994. The method of FELDMAN 98 is used to obtain the limits. The best fit is for $\Delta m^2 = 2.5 \times 10^{-3} \text{ eV}^2$.
- ⁵³ AMBROSIO 03 obtained this result by using the ratio R and the angular distribution of the upward through-going muons. R is given in the previous note and the angular distribution is reported in AMBROSIO 01. The method of FELDMAN 98 is used to obtain the limits. The best fit is for $\Delta m^2 = 2.5 \times 10^{-3} \text{ eV}^2$.
- ⁵⁴ SANCHEZ 03 is based on an exposure of 5.9 kton yr. The result is obtained using a likelihood analysis of the neutrino L/E distribution for a selection μ flavor sample while the e -flavor sample provides flux normalization. The method of FELDMAN 98 is used to obtain the allowed region. The best fit is for $\Delta m^2 = 5.2 \times 10^{-3} \text{ eV}^2$.
- ⁵⁵ AMBROSIO 01 result is based on the angular distribution of upward through-going muon tracks with $E_\mu > 1 \text{ GeV}$. The data came from three different detector configurations, but the statistics is largely dominated by the full detector run, from May 1994 to December 2000. The total live time, normalized to the full detector configuration is 6.17 years. The best fit is obtained outside the physical region. The method of FELDMAN 98 is used to obtain the limits.
- ⁵⁶ AMBROSIO 01 result is based on the angular distribution and normalization of upward through-going muon tracks with $E_\mu > 1 \text{ GeV}$. See the previous footnote.
- ⁵⁷ FUKUDA 99c obtained this result from a total of 537 live days of upward through-going muon data in Super-Kamiokande between April 1996 to January 1998. With a threshold of $E_\mu > 1.6 \text{ GeV}$, the observed flux is $(1.74 \pm 0.07 \pm 0.02) \times 10^{-13} \text{ cm}^{-2}\text{s}^{-1}\text{sr}^{-1}$. The best fit is for $\Delta m^2 = 5.9 \times 10^{-3} \text{ eV}^2$.

- ⁵⁸ FUKUDA 99b obtained this result from a simultaneous fitting to zenith angle distributions of upward-stopping and through-going muons. The flux of upward-stopping muons of minimum energy of 1.6 GeV measured between April 1996 and January 1998 is $(0.39 \pm 0.04 \pm 0.02) \times 10^{-13} \text{ cm}^{-2}\text{s}^{-1}\text{sr}^{-1}$. This is compared to the expected flux of $(0.73 \pm 0.16 \text{ (theoretical error)}) \times 10^{-13} \text{ cm}^{-2}\text{s}^{-1}\text{sr}^{-1}$. The best fit is for $\Delta m^2 = 3.9 \times 10^{-3} \text{ eV}^2$.
- ⁵⁹ FUKUDA 99d obtained this result from the zenith dependence of the upward-stopping/through-going flux ratio. The best fit is for $\Delta m^2 = 3.1 \times 10^{-3} \text{ eV}^2$.
- ⁶⁰ FUKUDA 98c obtained this result by an analysis of 33.0 kton yr atmospheric neutrino data. The best fit is for $\Delta m^2 = 2.2 \times 10^{-3} \text{ eV}^2$.
- ⁶¹ HATAKEYAMA 98 obtained this result from a total of 2456 live days of upward-going muon data in Kamiokande between December 1985 and May 1995. With a threshold of $E_\mu > 1.6 \text{ GeV}$, the observed flux of upward through-going muons is $(1.94 \pm 0.10^{+0.07}_{-0.06}) \times 10^{-13} \text{ cm}^{-2}\text{s}^{-1}\text{sr}^{-1}$. This is compared to the expected flux of $(2.46 \pm 0.54 \text{ (theoretical error)}) \times 10^{-13} \text{ cm}^{-2}\text{s}^{-1}\text{sr}^{-1}$. The best fit is for $\Delta m^2 = 2.2 \times 10^{-3} \text{ eV}^2$.
- ⁶² HATAKEYAMA 98 obtained this result from a combined analysis of Kamiokande contained events (FUKUDA 94) and upward going muon events. The best fit is for $\Delta m^2 = 13 \times 10^{-3} \text{ eV}^2$.
- ⁶³ FUKUDA 94 obtained the result by a combined analysis of sub- and multi-GeV atmospheric neutrino events in Kamiokande. The best fit is for $\Delta m^2 = 16 \times 10^{-3} \text{ eV}^2$.

$\sin^2(\theta_{13})$

At present time direct measurements of $\sin^2(\theta_{13})$ are derived from the reactor $\bar{\nu}_e$ disappearance at distances corresponding to the Δm_{32}^2 value, i.e. $L \sim 1\text{km}$. Alternatively, limits can also be obtained from the analysis of the solar neutrino data and accelerator-based $\nu_\mu \rightarrow \nu_e$ experiments.

If an experiment reports $\sin^2(2\theta_{13})$ we convert the value to $\sin^2(\theta_{13})$.

VALUE (units 10^{-2})	CL%	DOCUMENT ID	TECN	COMMENT
2.18 ± 0.07	OUR AVERAGE			
2.188 ± 0.076		¹ ADEY	18A DAYA	DayaBay, LingAo/Ao II reactors
2.29 ± 0.18		² BAK	18 RENO	Yonggwang reactors
2.25 ± 0.87		³ ABE	16B DCHZ	Chooz reactors
1.81 ± 0.29		⁴ AN	16A DAYA	DayaBay, Ling Ao/Ao II reactors
• • • We do not use the following data for averages, fits, limits, etc. • • •				
< 3.9	68	AGAFONOVA	19 OPER	
1.8 ± 2.9		⁵ ABE	18B SKAM	3ν osc: normal mass ordering, θ_{13} free
0.8 ± 1.7		⁵ ABE	18B SKAM	3ν osc: inverted mass ordering, θ_{13} free
<12	90	⁶ AGAFONOVA	18A OPER	OPERA: ν_e appearance
2.160 ⁺ _{-0.069}		DE-SALAS	18 FIT	Normal mass ordering, global fit
2.220 ⁺ _{-0.076}		DE-SALAS	18 FIT	Inverted mass ordering, global fit
2.09 ± 0.23 ± 0.16		⁷ SEO	18 RENO	Yonggwang reactors
2.7 ± 0.7		⁸ ABE	17F T2K	Normal mass ordering, T2K only
2.149 ± 0.071 ± 0.050		⁹ AN	17A DAYA	DayaBay, LingAo/Ao II reactors
2.09 ± 0.23 ± 0.16		¹⁰ CHOI	16 RENO	Yonggwang reactors
2.15 ± 0.13		¹¹ AN	15 DAYA	DayaBay, Ling Ao/Ao II reactors
2.6 ± 1.2		¹² ABE	14A DCHZ	Chooz reactors
3.0 ± 1.3		¹³ ABE	14C T2K	Inverted mass ordering
3.6 ± 1.0		¹³ ABE	14C T2K	Normal mass ordering
2.3 ± 0.9		¹⁴ ABE	14H DCHZ	Chooz reactors
2.3 ± 0.2		¹⁵ AN	14 DAYA	DayaBay, Ling Ao/Ao II reactors
2.12 ± 0.47		¹⁶ AN	14B DAYA	DayaBay, Ling Ao/Ao II reactors
2.34 ± 0.20		¹⁷ FORERO	14 FIT	Normal mass ordering
2.40 ± 0.19		¹⁷ FORERO	14 FIT	Inverted mass ordering
2.18 ± 0.10		¹⁸ GONZALEZ...	14 FIT	Normal mass ordering; global fit
2.19 ± 0.11		¹⁸ GONZALEZ...	14 FIT	Inverted mass ordering; global fit
2.5 ± 0.9 ± 0.9		¹⁹ ABE	13C DCHZ	Chooz reactors
2.3 ± 1.3		²⁰ ABE	13E T2K	Normal mass ordering
2.8 ± 1.6		²⁰ ABE	13E T2K	Inverted mass ordering
1.6 ± 1.3		²¹ ADAMSON	13A MINS	Normal mass ordering
3.0 ± 1.8		²¹ ADAMSON	13A MINS	Inverted mass ordering
<13	90	AGAFONOVA	13 OPER	OPERA: 3ν
< 3.6	95	22 AHARMIM	13 FIT	global solar: 3ν

2.3 ± 0.3 ± 0.1	23	AN	13	DAYA	DayaBay, Ling Ao/Ao II reactors	13 ABE 14C result is for ν_e appearance and assumes $\Delta m_{32}^2 = 2.4 \times 10^{-3} \text{ eV}^2$, $\sin^2(\theta_{23}) = 0.5$, and $\delta = 0$.	
2.2 ± 1.1 ± 0.8	24	ABE	12	DCHZ	Chooz reactors	14 ABE 14H uses 467.9 live days of one detector, 1050 m away from two reactor cores of the Chooz nuclear power station, to determine the mixing parameter $\sin^2(2\theta_{13})$. The Bugey4 data (DECLAIS 94) is used to constrain the neutrino flux. The data set includes 7.24 reactor-off days. A rate and shape analysis is performed. Superseded by ABE 16B.	
2.8 ± 0.8 ± 0.7	25	ABE	12B	DCHZ	Chooz reactors	15 AN 14 uses six identical detectors, with three placed near the reactor cores (flux-weighted baselines of 512 and 561 m) and the remaining three at the far hall (at the flux averaged distance of 1579 m from all six reactor cores) to determine the mixing angle θ_{13} using the $\overline{\nu}_e$ observed interaction rates with neutron capture on Gd and energy spectra. Supersedes AN 13 and superseded by AN 15.	
2.9 ± 0.3 ± 0.5	26	AHN	12	RENO	Yonggwang reactors	16 AN 14B uses six identical anti-neutrino detectors with flux-weighted baselines of ~ 500 m and ~ 1.6 km to six power reactors. This rate analysis uses a 217-day data set and neutron capture on protons (not Gd) only. $\Delta m_{31}^2 = 2.32 \times 10^{-3} \text{ eV}^2$ is assumed. Superseded by AN 16A.	
2.4 ± 0.4 ± 0.1	27	AN	12	DAYA	DayaBay, Ling Ao/Ao II reactors	17 FORERO 14 performs a global fit to neutrino oscillations using solar, reactor, long-baseline accelerator, and atmospheric neutrino data.	
2.5 + 1.8 - 1.6	28	ABE	11	FIT	KamLAND + global solar	18 GONZALEZ-GARCIA 14 result comes from a frequentist global fit. The corresponding Bayesian global fit to the same data results are reported in BERGSTROM 15 as $(2.18^{+0.10}_{-0.11}) \times 10^{-2} \text{ eV}^2$ for normal and $(2.19^{+0.12}_{-0.10}) \times 10^{-2} \text{ eV}^2$ for inverted mass ordering.	
< 6.1	95	29	ABE	11	FIT	Global solar	19 ABE 13C uses delayed neutron capture on hydrogen instead of on Gd used previously. The physical volume is thus three times larger. The fit is based on the rate and shape analysis as in ABE 12B. The Bugey4 data (DECLAIS 94) is used to constrain the neutrino flux. Superseded by ABE 16B.
1.3 to 5.6	68	30	ABE	11A	T2K	Normal mass ordering	20 ABE 13E assumes maximal θ_{23} mixing and CP phase $\delta = 0$.
1.5 to 5.6	68	31	ABE	11A	T2K	Inverted mass ordering	21 ADAMSON 13A results obtained from ν_e appearance, assuming $\delta = 0$, and $\sin^2(2\theta_{23}) = 0.957$.
0.3 to 2.3	68	32	ADAMSON	11D	MINS	Normal mass ordering	22 AHARMIM 13 obtained this result by a three-neutrino oscillation analysis with the value of Δm_{32}^2 fixed to $2.45 \times 10^{-3} \text{ eV}^2$, using global solar neutrino data. AHARMIM 13 global solar neutrino data include SNO's all-phases-combined analysis results on the total active ^8B neutrino flux and energy-dependent ν_e survival probability parameters, measurements of Cl (CLEVELAND 98), Ga (ABDURASHITOV 09 which contains combined analysis with GNO (ALTMANN 05 and Ph.D. thesis of F. Kaether)), and ^7Be (BELLINI 11A) rates, and ^8B solar-neutrino recoil electron measurements of SK-I (HOSAKA 06) zenith, SK-II (CRAVENS 08) and SK-III (ABE 11) day/night spectra, and Borexino (BELLINI 10A) spectra. AHARMIM 13 also reported a result combining global solar and KamLAND data, which is $\sin^2(2\theta_{13}) = (9.1^{+2.9}_{-3.1}) \times 10^{-2}$.
0.8 to 3.9	68	33	ADAMSON	11D	MINS	Inverted mass ordering	23 AN 13 uses six identical detectors, with three placed near the reactor cores (flux-weighted baselines of 498 and 555 m) and the remaining three at the far hall (at the flux averaged distance of 1628 m from all six reactor cores) to determine the $\overline{\nu}_e$ interaction rate ratios. Superseded by AN 14.
8 ± 3		34	FOGLI	11	FIT	Global neutrino data	24 ABE 12 determines the $\overline{\nu}_e$ interaction rate in a single detector, located 1050 m from the cores of two reactors. A rate and shape analysis is performed. The rate normalization is fixed by the results of the Bugey4 reactor experiment, thus avoiding any dependence on possible very short baseline oscillations. The value of $\Delta m_{31}^2 = 2.4 \times 10^{-3} \text{ eV}^2$ is used in the analysis. Superseded by ABE 12B.
7.8 ± 6.2		35	GANDO	11	FIT	KamLAND + solar: 3ν	25 ABE 12B determines the neutrino mixing angle θ_{13} using a single detector, located 1050 m from the cores of two reactors. This result is based on a spectral shape and rate analysis. The Bugey4 data (DECLAIS 94) is used to constrain the neutrino flux. Superseded by ABE 14A.
12.4 ± 13.3		36	GANDO	11	FIT	KamLAND: 3ν	26 AHN 12 uses two identical detectors, placed at flux weighted distances of 408.56 m and 1433.99 m from six reactor cores, to determine the mixing angle θ_{13} . This rate-only analysis excludes the no-oscillation hypothesis at 4.9 standard deviations. The value of $\Delta m_{31}^2 = (2.32^{+0.12}_{-0.08}) \times 10^{-3} \text{ eV}^2$ was assumed in the analysis. Superseded by CHOI 16.
3 + 9 - 7	90	37	ADAMSON	10A	MINS	Normal mass ordering	27 AN 12 uses six identical detectors with three placed near the reactor cores (flux-weighted baselines of 470 m and 576 m) and the remaining three at the far hall (at the flux averaged distance of 1648 m from all six reactor cores) to determine the mixing angle θ_{13} using the $\overline{\nu}_e$ observed interaction rate ratios. This rate-only analysis excludes the no-oscillation hypothesis at 5.2 standard deviations. The value of $\Delta m_{31}^2 = (2.32^{+0.12}_{-0.08}) \times 10^{-3} \text{ eV}^2$ was assumed in the analysis. Superseded by AN 13.
6 + 14 - 6	90	38	ADAMSON	10A	MINS	Inverted mass ordering	28 ABE 11 obtained this result by a three-neutrino oscillation analysis with the value of Δm_{32}^2 fixed to $2.4 \times 10^{-3} \text{ eV}^2$, using solar neutrino data including Super-Kamiokande, SNO, Borexino (ARPESELLA 08A), Homestake, GALLEX/GNO, SAGE, and KamLAND data. This result implies an upper bound of $\sin^2\theta_{13} < 0.059$ (95% CL) or $\sin^2 2\theta_{13} < 0.22$ (95% CL). The normal neutrino mass ordering and CPT invariance are assumed.
8 + 8 - 7	90	39,40	AHARMIM	10	FIT	KamLAND + global solar: 3ν	29 ABE 11 obtained this result by a three-neutrino oscillation analysis with the value of Δm_{32}^2 fixed to $2.4 \times 10^{-3} \text{ eV}^2$, using solar neutrino data including Super-Kamiokande, SNO, Borexino (ARPESELLA 08A), Homestake, and GALLEX/GNO data. The normal neutrino mass ordering is assumed.
< 30	95	39,41	AHARMIM	10	FIT	global solar: 3ν	30 The quoted limit is for $\Delta m_{32}^2 = 2.4 \times 10^{-3} \text{ eV}^2$, $\theta_{23} = \pi/2$, $\delta = 0$, and the normal mass ordering. For other values of δ , the 68% region spans from 0.03 to 0.25, and the 90% region from 0.02 to 0.32.
< 15	90	42	WENDELL	10	SKAM	3ν osc.; normal m ordering	31 The quoted limit is for $\Delta m_{32}^2 = 2.4 \times 10^{-3} \text{ eV}^2$, $\theta_{23} = \pi/2$, $\delta = 0$, and the inverted mass ordering. For other values of δ , the 68% region spans from 0.04 to 0.30, and the 90% region from 0.02 to 0.39.
< 33	90	42	WENDELL	10	SKAM	3ν osc.; inverted m ordering	32 The quoted limit is for $\Delta m_{32}^2 = 2.32 \times 10^{-3} \text{ eV}^2$, $\theta_{23} = \pi/2$, $\delta = 0$, and the normal mass ordering. For other values of δ , the 68% region spans from 0.02 to 0.12, and the 90% region from 0 to 0.16.
11 + 11 - 8		43	ADAMSON	09	MINS	Normal mass ordering	33 The quoted limit is for $\Delta m_{32}^2 = 2.32 \times 10^{-3} \text{ eV}^2$, $\theta_{23} = \pi/2$, $\delta = 0$, and the inverted mass ordering. For other values of δ , the 68% region spans from 0.02 to 0.16, and the 90% region from 0 to 0.21.
18 + 15 - 11		44	ADAMSON	09	MINS	Inverted mass ordering	34 FOGLI 11 obtained this result from an analysis using the atmospheric, accelerator long baseline, CHOOZ, solar, and KamLAND data. Recently, MUELLER 11 suggested an
6 ± 4		45	FOGLI	08	FIT	Global neutrino data	
8 ± 7		46	FOGLI	08	FIT	Solar + KamLAND data	
5 ± 5		47	FOGLI	08	FIT	Atmospheric + LBL + CHOOZ	
< 36	90	48	YAMAMOTO	06	K2K	Accelerator experiment	
< 48	90	49	AHN	04	K2K	Accelerator experiment	
< 36	90	50	BOEHM	01		Palo Verde react.	
< 45	90	51	BOEHM	00		Palo Verde react.	
< 15	90	52	APOLLONIO	99	CHOZ	Reactor Experiment	

1 ADEY 18A reports results from analysis of 1958 days of data taking with the Daya-Bay experiment, with 3.9×10^6 $\overline{\nu}_e$ candidates. The fit to the data gives $\Delta m_{ee}^2 = (2.522^{+0.068}_{-0.070}) \times 10^{-3} \text{ eV}^2$. Solar oscillation parameters are fixed in the analysis using the global averages, $\sin^2(\theta_{12}) = 0.307^{+0.013}_{-0.012}$, $\Delta m_{21}^2 = (7.53 \pm 0.18) \times 10^{-5} \text{ eV}^2$, from PDG 18. Supersedes AN 17A.

2 BAK 18 reports results of the RENO experiment using about 2200 live-days of data taken with detectors placed at 410.6 and 1445.7 m from reactors of the Hanbit Nuclear Power Plant. Supersedes SEO 18.

3 ABE 16B uses 455.57 live days of data from a detector 1050 m away from two reactor cores of the Chooz nuclear power station, to determine the mixing parameter $\sin^2(2\theta_{13})$. This analysis uses 7.15 reactor-off days for constraining backgrounds. A rate and shape analysis is performed on combined neutron captures on H and Gd. Supersedes ABE 14H and ABE 13C.

4 AN 16A uses data from the eight antineutrino detectors (404 days) and six antineutrino detectors (217 days) runs to determine the mixing parameter $\sin^2(2\theta_{13})$ using the neutron capture on H only. Supersedes AN 14B.

5 ABE 18B uses 328 kton-years of Super-Kamiokande I-IV atmospheric neutrino data to obtain this result. The fit is performed over the four parameters, Δm_{32}^2 , $\sin^2\theta_{23}$, $\sin^2\theta_{13}$, and δ , while the solar parameters are fixed to $\Delta m_{21}^2 = (7.53 \pm 0.18) \times 10^{-5} \text{ eV}^2$ and $\sin^2\theta_{12} = 0.304 \pm 0.014$.

6 AGAFONOVA 18A reports $\sin^2(2\theta_{13}) < 0.43$ at 90% C.L. The result on the sterile neutrino search in the context of 3+1 model is also reported. A 90% C.L. upper limit on $\sin^2(2\theta_{\mu e}) = 0.021$ for $\Delta m_{41}^2 \geq 0.1 \text{ eV}^2$ is set.

7 SEO 18 reports results of the RENO experiment using about 500 days of data, performing a rate and shape analysis. Compared to AHN 12, a significant reduction of the systematic uncertainties is reported. A 3% excess of events near 5 MeV of the prompt energy is observed. SEO 18 is a detailed description of the results published in CHOI 16, which it supersedes. Superseded by BAK 18.

8 Using T2K data only. For inverted mass ordering, all values of θ_{13} are ruled out at 68% CL.

9 AN 17A reports results from combined rate and spectral shape analysis of 1230 days of data taken with the Daya Bay reactor experiment. The data set contains more than 2.5×10^6 inverse beta-decay events with neutron capture on Gd. A simultaneous fit to θ_{13} and Δm_{ee}^2 is performed. Superseded by ADEY 18A.

10 CHOI 16 reports results of the RENO experiment using about 500 days of data, performing a rate and shape analysis. Compared to AHN 12, a significant reduction of the systematic uncertainties is reported. A 3% excess of events near 5 MeV of the prompt energy is observed. Supersedes AHN 12.

11 AN 15 uses all eight identical detectors, with four placed near the reactor cores and the remaining four at the far hall to determine the mixing angle θ_{13} using the $\overline{\nu}_e$ observed interaction rates with neutron capture on Gd and energy spectra. The result corresponds to the exposure of $6.9 \times 10^5 \text{ GW}_{th}$ -ton-days. Superseded by AN 17A.

12 ABE 14A uses 467.9 live days of one detector, 1050 m away from two reactor cores of the Chooz nuclear power station, to determine the mixing parameter $\sin^2(2\theta_{13})$. The Bugey4 data (DECLAIS 94) is used to constrain the neutrino flux. The data set includes 7.24 reactor-off days. A "rate-modulation" analysis is performed. Supersedes ABE 12B.

Lepton Particle Listings

Neutrino Mixing

average increase of about 3.5% in normalization of the reactor $\bar{\nu}_e$ fluxes, and using these fluxes, the fitted result becomes 0.10 ± 0.03 .

³⁵ GANDO 11 report $\sin^2\theta_{13} = 0.020 \pm 0.016$. This result was obtained with three-neutrino fit using the KamLAND + solar data.

³⁶ GANDO 11 report $\sin^2\theta_{13} = 0.032 \pm 0.037$. This result was obtained with three-neutrino fit using the KamLAND data only.

³⁷ This result corresponds to the limit of <0.12 at 90% CL for $\Delta m_{32}^2 = 2.43 \times 10^{-3} \text{ eV}^2$, $\theta_{23} = \pi/2$, and $\delta = 0$. For other values of δ , the 90% CL region spans from 0 to 0.16.

³⁸ This result corresponds to the limit of <0.20 at 90% CL for $\Delta m_{32}^2 = 2.43 \times 10^{-3} \text{ eV}^2$, $\theta_{23} = \pi/2$, and $\delta = 0$. For other values of δ , the 90% CL region spans from 0 to 0.21.

³⁹ AHARMIM 10 global solar neutrino data include SNO's low-energy-threshold analysis survival probability day/night curves, SNO Phase III integral rates (AHARMIM 08), CL (CLEVELAND 98), SAGE (ABDURASHITOV 09), Gallex/GNO (HAMPEL 99, ALTMANN 05), Borexino (ARPESELLA 08a), SK-I zenith (HOSAKA 06), and SK-II day/night spectra (CRAVENS 08).

⁴⁰ AHARMIM 10 obtained this result by a three-neutrino oscillation analysis with the value of Δm_{31}^2 fixed to $2.3 \times 10^{-3} \text{ eV}^2$, using global solar neutrino data and KamLAND data (ABE 08a). *CPT* invariance is assumed. This result implies an upper bound of $\sin^2\theta_{13} < 0.057$ (95% CL) or $\sin^2\theta_{13} < 0.22$ (95% CL).

⁴¹ AHARMIM 10 obtained this result by a three-neutrino oscillation analysis with the value of Δm_{31}^2 fixed to $2.3 \times 10^{-3} \text{ eV}^2$, using global solar neutrino data.

⁴² WENDELL 10 obtained this result by a three-neutrino oscillation analysis with one mass scale dominance ($\Delta m_{21}^2 = 0$) using the Super-Kamiokande-I+II+III atmospheric neutrino data, and updates the HOSAKA 06a result.

⁴³ The quoted limit is for $\Delta m_{32}^2 = 2.43 \times 10^{-3} \text{ eV}^2$, $\theta_{23} = \pi/2$, and $\delta = 0$. For other values of δ , the 68% CL region spans from 0.02 to 0.26.

⁴⁴ The quoted limit is for $\Delta m_{32}^2 = 2.43 \times 10^{-3} \text{ eV}^2$, $\theta_{23} = \pi/2$, and $\delta = 0$. For other values of δ , the 68% CL region spans from 0.04 to 0.34.

⁴⁵ FOGLI 08 obtained this result from a global analysis of all neutrino oscillation data, that is, solar + KamLAND + atmospheric + accelerator long baseline + CHOOZ.

⁴⁶ FOGLI 08 obtained this result from an analysis using the solar and KamLAND neutrino oscillation data.

⁴⁷ FOGLI 08 obtained this result from an analysis using the atmospheric, accelerator long baseline, and CHOOZ neutrino oscillation data.

⁴⁸ YAMAMOTO 06 searched for $\nu_\mu \rightarrow \nu_e$ appearance. Assumes $2 \sin^2(2\theta_{\mu e}) = \sin^2(2\theta_{13})$. The quoted limit is for $\Delta m_{32}^2 = 1.9 \times 10^{-3} \text{ eV}^2$. That value of Δm_{32}^2 is the one- σ low value for AHN 06a. For the AHN 06a best fit value of $2.8 \times 10^{-3} \text{ eV}^2$, the $\sin^2(2\theta_{13})$ limit is < 0.26 . Supersedes AHN 04.

⁴⁹ AHN 04 searched for $\nu_\mu \rightarrow \nu_e$ appearance. Assuming $2 \sin^2(2\theta_{\mu e}) = \sin^2(2\theta_{13})$, a limit on $\sin^2(2\theta_{\mu e})$ is converted to a limit on $\sin^2(2\theta_{13})$. The quoted limit is for $\Delta m_{32}^2 = 1.9 \times 10^{-3} \text{ eV}^2$. That value of Δm_{32}^2 is the one- σ low value for ALIU 05. For the ALIU 05 best fit value of $2.8 \times 10^{-3} \text{ eV}^2$, the $\sin^2(2\theta_{13})$ limit is < 0.30 .

⁵⁰ The quoted limit is for $\Delta m_{32}^2 = 1.9 \times 10^{-3} \text{ eV}^2$. That value of Δm_{32}^2 is the 1- σ low value for ALIU 05. For the ALIU 05 best fit value of $2.8 \times 10^{-3} \text{ eV}^2$, the $\sin^2 2\theta_{13}$ limit is < 0.19 . In this range, the θ_{13} limit is larger for lower values of Δm_{32}^2 , and smaller for higher values of Δm_{32}^2 .

⁵¹ The quoted limit is for $\Delta m_{32}^2 = 1.9 \times 10^{-3} \text{ eV}^2$. That value of Δm_{32}^2 is the 1- σ low value for ALIU 05. For the ALIU 05 best fit value of $2.8 \times 10^{-3} \text{ eV}^2$, the $\sin^2 2\theta_{13}$ limit is < 0.23 .

⁵² The quoted limit is for $\Delta m_{32}^2 = 2.43 \times 10^{-3} \text{ eV}^2$. That value of Δm_{32}^2 is the central value for ADAMSON 08. For the ADAMSON 08 1- σ low value of $2.30 \times 10^{-3} \text{ eV}^2$, the $\sin^2 2\theta_{13}$ limit is < 0.16 . See also APOLLONIO 03 for a detailed description of the experiment.

CP violating phase

δ , CP violating phase

Measurements of δ come from atmospheric and accelerator experiments looking at ν_e appearance. We encode values between 0 and 2π , though it is equivalent to use $-\pi$ to π .

VALUE (π rad)	CL%	DOCUMENT ID	TECN	COMMENT
1.36\pm0.17 OUR AVERAGE				
0.0 \pm 1.3 -0.4		¹ ACERO	19 NOVA	Normal mass ordering, octant II for θ_{23}
1.33 \pm 0.45 -0.51		² ABE	18B SKAM	Normal mass ordering, θ_{13} constrained
1.40 \pm 0.20		³ ABE	18G T2K	Normal mass ordering, θ_{13} constrained
• • • We do not use the following data for averages, fits, limits, etc. • • •				
1.33 \pm 0.46 -0.53		⁴ ABE	18B SKAM	3ν osc: normal mass ordering, θ_{13} free
1.22 \pm 0.76 -0.67		⁴ ABE	18B SKAM	3ν osc: inverted mass ordering, θ_{13} free
1.33 \pm 0.48 -0.53		² ABE	18B SKAM	3ν osc: inverted mass ordering, θ_{13} constrained

1.54 \pm 0.14 -0.12	95	³ ABE	18G T2K	Inverted mass ordering, θ_{13} constrained
1.21 \pm 0.91 -0.30		⁵ ACERO	18 NOVA	Normal mass ordering, octant II for θ_{23}
1.46 \pm 0.56 -0.42		⁵ ACERO	18 NOVA	Normal mass order; octant I for θ_{23}
1.32 \pm 0.21 -0.15		DE-SALAS	18 FIT	Normal mass ordering, global fit
1.56 \pm 0.13 -0.15		DE-SALAS	18 FIT	Inverted mass ordering, global fit
1.45 \pm 0.27 -0.26		⁶ ABE	17F T2K	Normal mass ordering
1.54 \pm 0.22 -0.23		⁶ ABE	17F T2K	Inverted mass ordering
1.50 \pm 0.53 -0.57		⁷ ADAMSON	17B NOVA	Inverted mass ordering; θ_{23} in octant II
0.74 \pm 0.57 -0.93		⁷ ADAMSON	17B NOVA	Normal mass ordering; θ_{23} in octant II
1.48 \pm 0.69 -0.58		⁷ ADAMSON	17B NOVA	Normal mass ordering; θ_{23} in octant I
0.0 to 0.1, 0.5 to 2.0	90	^{7,8} ADAMSON	16 NOVA	Inverted mass ordering
0.0 to 2.0 0 to 0.15, 0.83 to 2	90	⁸ ADAMSON	16 NOVA	Normal mass ordering
1.09 to 1.92 0.05 to 1.2	90	ABE	15D T2K	Normal mass ordering
1.34 \pm 0.64 -0.38		⁹ ADAMSON	14 MINS	Inverted mass ordering
1.48 \pm 0.34 -0.32		FORERO	14 FIT	Normal mass ordering
1.48 \pm 0.34 -0.32		FORERO	14 FIT	Inverted mass ordering
1.70 \pm 0.22 -0.39		¹⁰ GONZALEZ...	14 FIT	Normal mass ordering; global fit
1.41 \pm 0.35 -0.34		¹⁰ GONZALEZ...	14 FIT	Inverted mass ordering; global fit
0 to 1.5 or 1.9 to 2	90	¹¹ ADAMSON	13A MINS	Normal mass ordering

¹ ACERO 19 is based on a sample size of 1.33×10^{20} protons on target with combined antineutrino and neutrino data. Supersedes ACERO 18.

² ABE 18B uses 328 kton-years of Super-Kamiokande I-IV atmospheric neutrino data to obtain this result. The fit is performed over the three parameters, Δm_{32}^2 , $\sin^2\theta_{23}$, and δ , while the solar parameters and $\sin^2\theta_{13}$ are fixed to $\Delta m_{21}^2 = (7.53 \pm 0.18) \times 10^{-5} \text{ eV}^2$, $\sin^2\theta_{12} = 0.304 \pm 0.014$, and $\sin^2\theta_{13} = 0.0219 \pm 0.0012$.

³ ABE 18G confidence intervals are marginalized over both mass orderings. Normal order preferred with a posterior probability of 87%. The 1-sigma result for normal mass ordering used in the average was provided by the experiment via private communications. Supersedes ABE 17F.

⁴ ABE 18B uses 328 kton-years of Super-Kamiokande I-IV atmospheric neutrino data to obtain this result. The fit is performed over the four parameters, Δm_{32}^2 , $\sin^2\theta_{23}$, $\sin^2\theta_{13}$, and δ , while the solar parameters are fixed to $\Delta m_{21}^2 = (7.53 \pm 0.18) \times 10^{-5} \text{ eV}^2$ and $\sin^2\theta_{12} = 0.304 \pm 0.014$.

⁵ ACERO 18 performs a joint fit to the data for ν_μ disappearance and ν_e appearance. The overall best fit favors normal mass ordering and θ_{23} in octant II. No 1- σ confidence intervals are presented for the inverted mass ordering scenarios. Superseded by ACERO 19.

⁶ ABE 17F confidence intervals are obtained using a frequentist analysis including θ_{13} constraint from reactor experiments. Bayesian intervals based on Markov Chain Monte Carlo method are also provided by the authors. Superseded by ABE 18G.

⁷ Errors are projections of 68% C.L. curve of δ_{CP} vs. $\sin^2\theta_{23}$.

⁸ ADAMSON 16 result is based on a data sample with 2.74×10^{20} protons on target. The likelihood-based analysis observed 6 ν_e events with an expected background of 0.99 ± 0.11 events.

⁹ ADAMSON 14 result is based on three-flavor formalism and $\theta_{23} > \pi/4$. Likelihood as a function of δ is also shown for the other three combinations of hierarchy and θ_{23} octants; all values of δ are allowed at 90% C.L.

¹⁰ GONZALEZ-GARCIA 14 result comes from a frequentist global fit. The corresponding Bayesian global fit to the same data results are reported in BERGSTROM 15 as 68% CL intervals of 1.24–1.94 for normal and 1.15–1.77 for inverted mass ordering.

¹¹ ADAMSON 13A result is based on ν_e appearance in MINOS and the calculated $\sin^2(2\theta_{23}) = 0.957$, $\theta_{23} > \pi/4$, and normal mass hierarchy. Likelihood as a function of δ is also shown for the other three combinations of hierarchy and θ_{23} octants; all values of δ are allowed at 90% C.L.

(C) Other neutrino mixing results

The LSND collaboration reported in AGUILAR 01 a signal which is consistent with $\bar{\nu}_\mu \rightarrow \bar{\nu}_e$ oscillations. In a three neutrino framework, this would be a measurement of θ_{12} and Δm_{21}^2 . This does not appear to be consistent with most of the other neutrino data. The following listings include results from $\nu_\mu \rightarrow \nu_e$, $\bar{\nu}_\mu \rightarrow \bar{\nu}_e$ appearance and ν_μ , $\bar{\nu}_\mu$, ν_e , and $\bar{\nu}_e$ disappearance experiments, and searches for *CPT* violation.

See key on page 999

Lepton Particle Listings Neutrino Mixing

$\Delta(m^2)$ for $\sin^2(2\theta) = 1$ ($\nu_\mu \rightarrow \nu_e$)

VALUE (eV ²)	CL%	DOCUMENT ID	TECN	COMMENT
0.03 to 0.05	90	1 AGUILAR-AR...18c	MBNE	MiniBooNE $\nu_\mu \bar{\nu}_e$ combined
0.015 to 0.050	90	2 AGUILAR-AR...13A	MBNE	MiniBooNE
<0.34	90	3 MAHN 12	MBNE	MiniBooNE/SciBooNE
<0.034	90	AGUILAR-AR...07	MBNE	MiniBooNE
<0.0008	90	AHN 04	K2K	Water Cherenkov
<0.4	90	ASTIER 03	NOMD	CERN SPS
<2.4	90	AVVAKUMOV 02	NTEV	NUTEV FNAL
0.03 to 0.3	95	4 AGUILAR 01	LSND	$\nu_\mu \rightarrow \nu_e$ osc.prob.
<2.3	90	5 ATHANASSO...98	LSND	$\nu_\mu \rightarrow \nu_e$
<0.9	90	6 LOVERRE 96	CHARM/CDHS	
<0.9	90	VILAIN 94c	CHM2	CERN SPS
<0.09	90	ANGELINI 86	HLBC	BEBC CERN PS

- 1 AGUILAR-AREVALO 18c result is based on $\nu_\mu \rightarrow \nu_e$ appearance of 460.5 ± 99.0 events; The best fit value is $\Delta m^2 = 0.041$ eV².
- 2 AGUILAR-AREVALO 13A result is based on $\nu_\mu \rightarrow \nu_e$ appearance of 162.0 ± 47.8 events; marginally compatible with twoneutrino oscillations. The best fit value is $\Delta m^2 = 3.14$ eV².
- 3 MAHN 12 is a combined spectral fit of MiniBooNE and SciBooNE neutrino data with the range of Δm^2 up to 25 eV². The best limit is 0.04 at 7 eV².
- 4 AGUILAR 01 is the final analysis of the LSND full data set. Search is made for the $\nu_\mu \rightarrow \nu_e$ oscillations using ν_μ from π^+ decay in flight by observing beam-on electron events from $\nu_e C \rightarrow e^- X$. Present analysis results in 8.1 ± 12.2 ± 1.7 excess events in the 60 < E_e < 200 MeV energy range, corresponding to oscillation probability of 0.10 ± 0.16 ± 0.04%. This is consistent, though less significant, with the previous result of ATHANASSOPOULOS 98, which it supersedes. The present analysis uses selection criteria developed for the decay at rest region, and is less effective in removing the background above 60 MeV than ATHANASSOPOULOS 98.
- 5 ATHANASSOPOULOS 98 is a search for the $\nu_\mu \rightarrow \nu_e$ oscillations using ν_μ from π^+ decay in flight. The 40 observed beam-on electron events are consistent with $\nu_e C \rightarrow e^- X$; the expected background is 21.9 ± 2.1. Authors interpret this excess as evidence for an oscillation signal corresponding to oscillations with probability (0.26 ± 0.10 ± 0.05)%. Although the significance is only 2.3 σ , this measurement is an important and consistent cross check of ATHANASSOPOULOS 96 who reported evidence for $\bar{\nu}_\mu \rightarrow \bar{\nu}_e$ oscillations from μ^+ decay at rest. See also ATHANASSOPOULOS 98b.
- 6 LOVERRE 96 uses the charged-current to neutral-current ratio from the combined CHARM (ALLABY 86) and CDHS (ABRAMOWICZ 86) data from 1986.

$\sin^2(2\theta)$ for "Large" $\Delta(m^2)$ ($\nu_\mu \rightarrow \nu_e$)

VALUE (units 10 ⁻³)	CL%	DOCUMENT ID	TECN	COMMENT
< 5	90	1 AGUILAR-AR...18c	MBNE	MiniBooNE; $\nu_\mu \bar{\nu}_e$
< 7.2	90	AGAFONOVA 13	OPER	$\Delta(m^2) > 0.1$ eV ²
0.8 to 3	90	2 AGUILAR-AR...13A	MBNE	MiniBooNE
< 11	90	3 ANTONELLO 13	ICAR	$\nu_\mu \rightarrow \nu_e$
< 6.8	90	4 ANTONELLO 13A	ICAR	$\nu_\mu \rightarrow \nu_e$
<100	90	5 MAHN 12	MBNE	MiniBooNE/SciBooNE
< 1.8	90	6 AGUILAR-AR...07	MBNE	MiniBooNE
<110	90	7 AHN 04	K2K	Water Cherenkov
< 1.4	90	ASTIER 03	NOMD	CERN SPS
< 1.6	90	AVVAKUMOV 02	NTEV	NUTEV FNAL
0.5 to 30	95	8 AGUILAR 01	LSND	$\nu_\mu \rightarrow \nu_e$ osc.prob.
< 3.0	90	9 ATHANASSO...98	LSND	$\nu_\mu \rightarrow \nu_e$
< 9.4	90	10 LOVERRE 96	CHARM/CDHS	
< 5.6	90	VILAIN 94c	CHM2	CERN SPS
< 5.6	90	11 VILAIN 94c	CHM2	CERN SPS

- 1 AGUILAR-AREVALO 18c result is based on $\nu_\mu \rightarrow \nu_e$ appearance of 460.5 ± 99.0 events; The best fit value is $\sin^2(2\theta) = 0.92$. The quoted limit for the two-neutrino mixing angle θ is valid above $\Delta m^2 = 0.59$ eV².
- 2 AGUILAR-AREVALO 13A result is based on $\nu_\mu \rightarrow \nu_e$ appearance of 162.0 ± 47.8 events; marginally compatible with two neutrino oscillations. The best fit value is $\sin^2(2\theta) = 0.002$.
- 3 ANTONELLO 13 use the ICARUS T600 detector at LNGS and ~ 20 GeV beam of ν_μ from CERN 730 km away to search for an excess of ν_e events. Two events are found with 3.7 ± 0.6 expected from conventional sources. This result excludes some parts of the parameter space expected by LSND. Superseded by ANTONELLO 13A.
- 4 Based on four events with a background of 6.4 ± 0.9 from conventional sources with an average energy of 20 GeV and 730 km from the source of ν_μ .
- 5 MAHN 12 is a combined fit of MiniBooNE and SciBooNE neutrino data.
- 6 The limit is $\sin^2 2\theta < 0.9 \times 10^{-3}$ at $\Delta m^2 = 2$ eV². That value of Δm^2 corresponds to the smallest mixing angle consistent with the reported signal from LSND in AGUILAR 01.
- 7 The limit becomes $\sin^2 2\theta < 0.15$ at $\Delta m^2 = 2.8 \times 10^{-3}$ eV², the best-fit value of the ν_μ disappearance analysis in K2K.
- 8 AGUILAR 01 is the final analysis of the LSND full data set of the search for the $\nu_\mu \rightarrow \nu_e$ oscillations. See footnote in preceding table for further details.
- 9 ATHANASSOPOULOS 98 report (0.26 ± 0.10 ± 0.05)% for the oscillation probability; the value of $\sin^2 2\theta$ for large Δm^2 is deduced from this probability. See footnote in

preceding table for further details, and see the paper for a plot showing allowed regions. If effect is due to oscillation, it is most likely to be intermediate $\sin^2 2\theta$ and Δm^2 . See also ATHANASSOPOULOS 98b.

- 10 LOVERRE 96 uses the charged-current to neutral-current ratio from the combined CHARM (ALLABY 86) and CDHS (ABRAMOWICZ 86) data from 1986.
- 11 VILAIN 94c limit derived by combining the ν_μ and $\bar{\nu}_\mu$ data assuming CP conservation.

$\Delta(m^2)$ for $\sin^2(2\theta) = 1$ ($\bar{\nu}_\mu \rightarrow \bar{\nu}_e$)

VALUE (eV ²)	CL%	DOCUMENT ID	TECN	COMMENT
0.023 to 0.060	90	1 AGUILAR-AR...13A	MBNE	MiniBooNE
<0.16	90	2 CHENG 12	MBNE	MiniBooNE/SciBooNE
0.03-0.09	90	3 AGUILAR-AR...10	MBNE	E _ν > 475 MeV
0.03-0.07	90	4 AGUILAR-AR...10	MBNE	E _ν > 200 MeV
<0.06	90	AGUILAR-AR...09b	MBNE	MiniBooNE
<0.055	90	5 ARMBRUSTER02	KAR2	Liquid Sci. calor.
<2.6	90	AVVAKUMOV 02	NTEV	NUTEV FNAL
0.03-0.05	90	6 AGUILAR 01	LSND	LAMPF
0.05-0.08	90	7 ATHANASSO...96	LSND	LAMPF
0.048-0.090	80	8 ATHANASSO...95		
<0.07	90	HILL 95		
<0.9	90	VILAIN 94c	CHM2	CERN SPS
<0.14	90	10 FREEDMAN 93	CNTR	LAMPF

- 1 Based on $\bar{\nu}_\mu \rightarrow \bar{\nu}_e$ appearance of 78.4 ± 28.5 events. The best fit values are $\Delta m^2 = 0.043$ eV² and $\sin^2 2\theta = 0.88$.
- 2 CHENG 12 is a combined fit of MiniBooNE and SciBooNE antineutrino data.
- 3 This value is for a two neutrino oscillation analysis for excess antineutrino events with E_ν > 475 MeV. The best fit is at 0.07. The allowed region is consistent with LSND reported by AGUILAR 01. Supersedes AGUILAR-AREVALO 09b.
- 4 This value is for a two neutrino oscillation analysis for excess antineutrino events with E_ν > 200 MeV with subtraction of the expected 12 events low energy excess seen in the neutrino component of the beam. The best fit value is 0.007 for $\Delta(m^2) = 4.4$ eV².
- 5 ARMBRUSTER 02 is the final analysis of the KARMEN 2 data for 17.7 m distance from the ISIS stopped pion and muon neutrino source. It is a search for $\bar{\nu}_e$, detected by the inverse β -decay reaction on protons and ¹²C. 15 candidate events are observed, and 15.8 ± 0.5 background events are expected, hence no oscillation signal is detected. The results exclude large regions of the parameter area favored by the LSND experiment.
- 6 AGUILAR 01 is the final analysis of the LSND full data set. It is a search for $\bar{\nu}_e$ 30 m from LAMPF beam stop. Neutrinos originate mainly for π^+ decay at rest. $\bar{\nu}_e$ are detected through $\bar{\nu}_e p \rightarrow e^+ n$ (20 < E_{e+} < 60 MeV) in delayed coincidence with $np \rightarrow d \gamma$. Authors observe 87.9 ± 22.4 ± 6.0 total excess events. The observation is attributed to $\bar{\nu}_\mu \rightarrow \bar{\nu}_e$ oscillations with the oscillation probability of 0.264 ± 0.067 ± 0.045%, consistent with the previously published result. Taking into account all constraints, the most favored allowed region of oscillation parameters is a band of $\Delta(m^2)$ from 0.2-2.0 eV². Supersedes ATHANASSOPOULOS 95, ATHANASSOPOULOS 96, and ATHANASSOPOULOS 98.
- 7 ATHANASSOPOULOS 96 is a search for $\bar{\nu}_e$ 30 m from LAMPF beam stop. Neutrinos originate mainly from π^+ decay at rest. $\bar{\nu}_e$ could come from either $\bar{\nu}_\mu \rightarrow \bar{\nu}_e$ or $\nu_e \rightarrow \bar{\nu}_e$; our entry assumes the first interpretation. They are detected through $\bar{\nu}_e p \rightarrow e^+ n$ (20 MeV < E_{e+} < 60 MeV) in delayed coincidence with $np \rightarrow d \gamma$. Authors observe 51 ± 20 ± 8 total excess events over an estimated background 12.5 ± 2.9. ATHANASSOPOULOS 96b is a shorter version of this paper.
- 8 ATHANASSOPOULOS 95 error corresponds to the 1.6 σ band in the plot. The expected background is 2.7 ± 0.4 events. Corresponds to an oscillation probability of (0.34 ± 0.20 ± 0.18 ± 0.07)%. For a different interpretation, see HILL 95. Replaced by ATHANASSOPOULOS 96.
- 9 HILL 95 is a report by one member of the LSND Collaboration, reporting a different conclusion from the analysis of the data of this experiment (see ATHANASSOPOULOS 95). Contrary to the rest of the LSND Collaboration, Hill finds no evidence for the neutrino oscillation $\bar{\nu}_\mu \rightarrow \bar{\nu}_e$ and obtains only upper limits.
- 10 FREEDMAN 93 is a search at LAMPF for $\bar{\nu}_e$ generated from any of the three neutrino types $\nu_\mu, \bar{\nu}_\mu$, and ν_e which come from the beam stop. The $\bar{\nu}_e$'s would be detected by the reaction $\bar{\nu}_e p \rightarrow e^+ n$. FREEDMAN 93 replaces DURKIN 88.

$\sin^2(2\theta)$ for "Large" $\Delta(m^2)$ ($\bar{\nu}_\mu \rightarrow \bar{\nu}_e$)

VALUE (units 10 ⁻³)	CL%	DOCUMENT ID	TECN	COMMENT
<640	90	1 ANTONELLO 13A	ICAR	$\bar{\nu}_e$ appearance
<150	90	2 CHENG 12	MBNE	MiniBooNE/SciBooNE
0.4-9.0	90	3 AGUILAR-AR...10	MBNE	E _ν > 475 MeV
0.4-9.0	99	4 AGUILAR-AR...10	MBNE	E _ν > 200 MeV
< 3.3	90	5 AGUILAR-AR...09b	MBNE	MiniBooNE
< 1.7	90	6 ARMBRUSTER02	KAR2	Liquid Sci. calor.
< 1.1	90	AVVAKUMOV 02	NTEV	NUTEV FNAL
5.3 ± 1.3 ± 9.0		7 AGUILAR 01	LSND	LAMPF
6.2 ± 2.4 ± 1.0		8 ATHANASSO...96	LSND	LAMPF
3-12	80	9 ATHANASSO...95		
< 6	90	10 HILL 95		

- 1 ANTONELLO 13A
- 2 CHENG 12
- 3 AGUILAR-AR...10
- 4 AGUILAR-AR...10
- 5 AGUILAR-AR...09b
- 6 ARMBRUSTER02
- 7 AGUILAR 01
- 8 ATHANASSO...96
- 9 ATHANASSO...95
- 10 HILL 95

Lepton Particle Listings

Neutrino Mixing

- ¹ ANTONELLO 13a obtained the limit by assuming $\bar{\nu}_\mu \rightarrow \bar{\nu}_e$ oscillation from the $\sim 2\%$ of $\bar{\nu}_\mu$ events contamination in the CNGS beam.
- ² CHENG 12 is a combined fit of MiniBooNE and SciBooNE antineutrino data.
- ³ This value is for a two neutrino oscillation analysis for excess antineutrino events with $E_\nu > 475$ MeV. At 90% CL there is no solution at high $\Delta(m^2)$. The best fit is at maximal mixing. The allowed region is consistent with LSND reported by AGUILAR 01. Supersedes AGUILAR-AREVALO 09b.
- ⁴ This value is for a two neutrino oscillation analysis for excess antineutrino events with $E_\nu > 200$ MeV with subtraction of the expected 12 events low energy excess seen in the neutrino component of the beam. At 90% CL there is no solution at high $\Delta(m^2)$. The best fit value is 0.007 for $\Delta(m^2) = 4.4 \text{ eV}^2$.
- ⁵ This result is inconclusive with respect to small amplitude mixing suggested by LSND.
- ⁶ ARMBRUSTER 02 is the final analysis of the KARMEN2 data. See footnote in the preceding table for further details, and the paper for the exclusion plot.
- ⁷ AGUILAR 01 is the final analysis of the LSND full data set. The deduced oscillation probability is $0.264 \pm 0.067 \pm 0.045\%$; the value of $\sin^2 2\theta$ for large $\Delta(m^2)$ is twice this probability (although these values are excluded by other constraints). See footnote in preceding table for further details, and the paper for a plot showing allowed regions. Supersedes ATHANASSOPOULOS 95, ATHANASSOPOULOS 96, and ATHANASSOPOULOS 98.
- ⁸ ATHANASSOPOULOS 96 reports $(0.31 \pm 0.12 \pm 0.05)\%$ for the oscillation probability; the value of $\sin^2 2\theta$ for large $\Delta(m^2)$ should be twice this probability. See footnote in preceding table for further details, and see the paper for a plot showing allowed regions.
- ⁹ ATHANASSOPOULOS 95 error corresponds to the 1.6σ band in the plot. The expected background is 2.7 ± 0.4 events. Corresponds to an oscillation probability of $(0.34^{+0.20}_{-0.18} \pm 0.07)\%$. For a different interpretation, see HILL 95. Replaced by ATHANASSOPOULOS 96.
- ¹⁰ HILL 95 is a report by one member of the LSND Collaboration, reporting a different conclusion than the analysis of the data of this experiment (see ATHANASSOPOULOS 95). Contrary to the rest of the LSND Collaboration, Hill finds no evidence for the neutrino oscillation $\bar{\nu}_\mu \rightarrow \bar{\nu}_e$ and obtains only upper limits.

$\Delta(m^2)$ for $\sin^2(2\theta) = 1$ ($\nu_\mu(\bar{\nu}_\mu) \rightarrow \nu_e(\bar{\nu}_e)$)

VALUE (eV ²)	CL%	DOCUMENT ID	TECN	COMMENT
<0.075	90	BORODOV... 92	CNTR	BNL E776
• • • We do not use the following data for averages, fits, limits, etc. • • •				
<1.6	90	¹ ROMOSAN 97	CCFR	FNAL
¹ ROMOSAN 97 uses wideband beam with a 0.5 km decay region.				

$\sin^2(2\theta)$ for "Large" $\Delta(m^2)$ ($\nu_\mu(\bar{\nu}_\mu) \rightarrow \nu_e(\bar{\nu}_e)$)

VALUE (units 10^{-3})	CL%	DOCUMENT ID	TECN	COMMENT
<1.8	90	¹ ROMOSAN 97	CCFR	FNAL
• • • We do not use the following data for averages, fits, limits, etc. • • •				
<3.8	90	² MCFARLAND 95	CCFR	FNAL
<3	90	BORODOV... 92	CNTR	BNL E776
¹ ROMOSAN 97 uses wideband beam with a 0.5 km decay region.				
² MCFARLAND 95 state that "This result is the most stringent to date for $250 < \Delta(m^2) < 450 \text{ eV}^2$ and also excludes at 90%CL much of the high $\Delta(m^2)$ region favored by the recent LSND observation." See ATHANASSOPOULOS 95 and ATHANASSOPOULOS 96.				

$\Delta(m^2)$ for $\sin^2(2\theta) = 1$ ($\bar{\nu}_e \nrightarrow \bar{\nu}_e$)

VALUE (eV ²)	CL%	DOCUMENT ID	TECN	COMMENT
<0.01	90	¹ ACHKAR 95	CNTR	Bugey reactor
¹ ACHKAR 95 bound is for $L=15, 40,$ and 95 m .				

$\sin^2(2\theta)$ for "Large" $\Delta(m^2)$ ($\bar{\nu}_e \nrightarrow \bar{\nu}_e$)

VALUE	CL%	DOCUMENT ID	TECN	COMMENT
<0.02	90	¹ ACHKAR 95	CNTR	For $\Delta(m^2) = 0.6 \text{ eV}^2$
¹ ACHKAR 95 bound is from data for $L=15, 40,$ and 95 m distance from the Bugey reactor.				

———— Sterile neutrino limits ————

$\Delta(m^2)$ for $\sin^2(2\theta) = 1$ ($\nu_\mu \rightarrow \nu_s$)

ν_s means ν_τ or any sterile (noninteracting) ν .

VALUE (10^{-5} eV^2)	CL%	DOCUMENT ID	TECN	COMMENT
<3000 (or <550)	90	¹ OYAMA 89	KAMI	Water Cherenkov
<4.2 (or >54)	90	BIONTA 88	IMB	Flux has $\nu_\mu, \bar{\nu}_\mu, \nu_e,$ and $\bar{\nu}_e$
• • • We do not use the following data for averages, fits, limits, etc. • • •				

¹ OYAMA 89 gives a range of limits, depending on assumptions in their analysis. They argue that the region $\Delta(m^2) = (100-1000) \times 10^{-5} \text{ eV}^2$ is not ruled out by any data for large mixing.

Search for ν_μ or $\nu_e \rightarrow \nu_s$

VALUE	CL%	DOCUMENT ID	TECN	COMMENT
• • • We do not use the following data for averages, fits, limits, etc. • • •				
<0.1	99	¹ SEREBROV 19		Neutrino-4
<0.01	90	² ALEKSEEV 18		DANSS
<0.06	90	³ ALMAZAN 18		STEREO
<0.1	95	⁴ ASHENFELT... 18		PROSPECT
<0.1	95	⁵ SEREBROV 18A		Neutrino-4
<0.4	90	⁶ AARTSEN 17B	ICCB	IceCube-DeepCore
<8 $\times 10^{-3}$	95	⁷ ABDURASHLI... 17		T β decay
<1 $\times 10^{-2}$	90	⁸ KO 17		NEOS
<2 $\times 10^{-2}$	90	⁹ AARTSEN 16	ICCB	IceCube
<4.5 $\times 10^{-4}$	95	¹⁰ ADAMSON 16B		MINOS, DayaBay
<8.6 $\times 10^{-2}$	95	¹¹ ADAMSON 16C		MINS
<1.1 $\times 10^{-2}$	95	¹² AN 16B		DAYA
		¹³ AMBROSIO 01	MCRO	matter effects
		¹⁴ FUKUDA 00	SKAM	neutral currents + matter effects

- ¹ SEREBROV 19 searches for $\bar{\nu}_e \rightarrow \bar{\nu}_s$ oscillations with baseline 6–12 m with SM-3 research reactor that uses highly enriched ²³⁵U fuel. The spectrum is well described by the $1/L^2$ dependence. However, the shape differs from the theoretical expectations, with the best fit corresponding to $\Delta m_{41}^2 = 7.34 \pm 0.1 \text{ eV}^2$ and $\sin^2(2\theta_{14}) = 0.39 \pm 0.12$ at 3σ significance.
- ² ALEKSEEV 18 searches for $\bar{\nu}_e \rightarrow \bar{\nu}_s$ oscillations using the DANSS detector at 10.7, 11.2, and 12.7 m from the 3.1 GW_{th} power reactor. The DANSS detector is highly segmented and moveable; the positions are changed usually 3 times a week. The analysis is based on the ratio of the events at top and bottom position; the middle position is used for checks of consistency. The best fit point is at $\Delta m_{41}^2 = 1.4 \text{ eV}^2$ and $\sin^2(2\theta_{14}) = 0.05$ with $\Delta\chi^2 = 13.1$ (statistical errors only) compared to the fit with 3 active neutrinos only. The quoted limit of 0.01 for $\sin^2(2\theta_{14})$ corresponds to $\Delta m_{41}^2 \sim 1.0 \text{ eV}^2$.
- ³ ALMAZAN 18 searches for the $\bar{\nu}_e \rightarrow \bar{\nu}_s$ oscillations with baseline from 9.4 to 11.1 m from the ILL research reactor with highly enriched ²³⁵U fuel. The STEREO detector consists of six separated cells with Gd loaded scintillator, with 15 m water equivalent overburden. The detected rate is $396.3 \pm 4.7 \bar{\nu}_e/\text{day}$ with signal to background ratio of about 0.9. The reported results corresponds to 66 days of reactor-on. The analysis uses the relative rates normalized to the cell number 1. No indication of the oscillation to the sterile neutrinos is found, the stated limit on $\sin^2(2\theta_{14})$ correspond to $\Delta m_{41}^2 \sim 3.5 \text{ eV}^2$ where the exclusion is maximal.
- ⁴ ASHENFELT 18 searches for the $\bar{\nu}_e \rightarrow \bar{\nu}_s$ oscillations at baseline from 6.7 to 9.2 m from the 85 MW research reactor with pure ²³⁵U core. The segmented 4 ton ⁶Li-doped liquid scintillator is operated with about 1 m water equivalent overburden and recorded 25461 ± 283 IB events. No indication of oscillations into sterile neutrinos was observed. The stated limit for $\sin^2(2\theta_{14})$ is for $\Delta m_{41}^2 \sim 2 \text{ eV}^2$ where the sensitivity is maximal.
- ⁵ SEREBROV 18A searches for the $\bar{\nu}_e \rightarrow \bar{\nu}_s$ oscillation with baseline 6–12 m from the core of the SM-3 research reactor that uses highly enriched ²³⁵U. They find that oscillations with $\Delta m_{41}^2 \sim 0.7-0.8 \text{ eV}^2$ and $\sin^2(2\theta_{14}) \sim 0.10-0.15$ give better fit to the L and E dependence than the no oscillation scenario. The significance of this is about 2 σ .
- ⁶ AARTSEN 17B uses three years of upward-going atmospheric neutrino data in the energy range of 10–60 GeV to constrain their disappearance into light sterile neutrinos. The reported limit $\sin^2\theta_{24} < 0.11$ at 90% C.L. is for $\Delta m_{41}^2 = 1.0 \text{ eV}^2$. We convert the result to $\sin^2 2\theta_{24}$ for the listing. AARTSEN 17B also reports $\cos^2\theta_{24} \cdot \sin^2\theta_{34} < 0.15$ at 90% C.L. for $\Delta m_{41}^2 = 1.0 \text{ eV}^2$.
- ⁷ ABDURASHITOV 17 use the Troitsk ν -mass experiment to search for sterile neutrinos with mass 0.1 - 2 keV. We convert the reported limit from $U_{e4}^2 < 0.002$ to $\sin^2 2\theta_{14} < 0.008$ assume $U_{e4} \sim \sin\theta_{14}$. The stated limit corresponds to the smallest U_{e4}^2 . The exclusion curve begins at U_{e4}^2 of 0.02 for $m_4 = 0.1 \text{ keV}$.
- ⁸ KO 17 reports on short baseline reactor oscillation search ($\bar{\nu}_e \rightarrow \bar{\nu}_s$), motivated by the so-called "reactor antineutrino anomaly". The experiment is conducted at 23.7 m from the core of unit 5 of the Hanbit Nuclear Power Complex in Korea. The reported limited on $\sin^2(2\theta_{41})$ for sterile neutrinos was determined using the reactor antineutrino spectrum determined by the Daya Bay experiment for Δm_{14}^2 around 0.55 eV^2 where the sensitivity is maximal. A fraction of the parameter space derived from the "reactor antineutrino anomaly" is excluded by this work. Compared to reactor models an event excess is observed at about 5 MeV, in agreement with other experiments.
- ⁹ AARTSEN 16 use one year of upward-going atmospheric muon neutrino data in the energy range of 320 GeV to 20 TeV to constrain their disappearance into light sterile neutrinos. Sterile neutrinos are expected to produce distinctive zenith distribution for these energies for $0.01 \leq \Delta m^2 \leq 10 \text{ eV}^2$. The stated limit is for $\sin^2 2\theta_{24}$ at Δm^2 around 0.3 eV^2 .
- ¹⁰ ADAMSON 16b combine the results of AN 16B, ADAMSON 16C, and Bugey-3 reactor experiments to constrain ν_μ to ν_e mixing through oscillations into light sterile neutrinos. The stated limit for $\sin^2 2\theta_{\mu e}$ is at $|\Delta m_{41}^2| = 1.2 \text{ eV}^2$.
- ¹¹ ADAMSON 16c use the NuMI beam and exposure of 10.56×10^{20} protons on target to search for the oscillation of ν_μ dominated beam into light sterile neutrinos with detector at 1.04 and 735 km. The reported limit $\sin^2(\theta_{24}) < 0.022$ at 95% C.L. is for $|\Delta m_{41}^2| = 0.5 \text{ eV}^2$. We convert the result to $\sin^2(2\theta_{24})$ for the listing.
- ¹² AN 16B utilize 621 days of data to place limits on the $\bar{\nu}_e$ disappearance into a light sterile neutrino. The stated limit corresponds to the smallest $\sin^2(2\theta_{14})$ at $|\Delta m_{41}^2| \sim 3 \times 10^{-2} \text{ eV}^2$ (obtained from Figure 3 in AN 16B). The exclusion curve begins at $|\Delta m_{41}^2| \sim 1.5 \times 10^{-4} \text{ eV}^2$ and extends to $\sim 0.25 \text{ eV}^2$. The analysis assumes $\sin^2(2\theta_{12})$

See key on page 999

Lepton Particle Listings
Neutrino Mixing

= 0.846 ± 0.021, Δm₂₁² = (7.53 ± 0.18) × 10⁻⁵ eV², and |Δm₃₂²| = (2.44 ± 0.06) × 10⁻³ eV².

¹³AMBROSIO 01 tested the pure 2-flavor ν_μ → ν_s hypothesis using matter effects which change the shape of the zenith-angle distribution of upward through-going muons. With maximum mixing and Δm² around 0.0024 eV², the ν_μ → ν_s oscillation is disfavored with 99% confidence level with respect to the ν_μ → ν_τ hypothesis.

¹⁴FUKUDA 00 tested the pure 2-flavor ν_μ → ν_s hypothesis using three complementary atmospheric-neutrino data samples. With this hypothesis, zenith-angle distributions are expected to show characteristic behavior due to neutral currents and matter effects. In the Δm² and sin²2θ region preferred by the Super-Kamiokande data, the ν_μ → ν_s hypothesis is rejected at the 99% confidence level, while the ν_μ → ν_τ hypothesis consistently fits all of the data sample.

CPT tests

Table with columns: (Δm₂₁² - Δm₂₁²), VALUE (10⁻⁴ eV²), CL%, DOCUMENT ID, TECN, COMMENT. Row 1: $\langle \Delta m_{21}^2 - \Delta \bar{m}_{21}^2 \rangle$, -0.11 ± 0.24, 99.7, 1 DEGOUVEA 05, FIT, solar vs. reactor.

¹DEGOUVEA 05 obtained this bound at the 3σ CL from the KamLAND (ARAKI 05) and solar neutrino data.

Table with columns: (Δm₃₂² - Δm₃₂²), VALUE (10⁻³ eV²), CL%, DOCUMENT ID, TECN, COMMENT. Row 1: $\langle \Delta m_{32}^2 - \Delta \bar{m}_{32}^2 \rangle$, -0.12 ± 0.26, 90, 2 ADAMSON 12B, MINS, MINOS atmospheric.

• • • We do not use the following data for averages, fits, limits, etc. • • •

Table with columns: VALUE (10⁻³ eV²), CL%, DOCUMENT ID, TECN, COMMENT. Row 1: 0.6 ± 2.4, 90, 2 ADAMSON 12B, MINS, MINOS atmospheric.

¹ADAMSON 13B quotes this difference as a negative of our convention.

²The quoted result is the single-parameter 90% C.L. interval determined from the 90% C.L. contour in the (Δm², Δm²) plane, which is obtained by minimizing the four parameter log-likelihood function with respect to the other oscillation parameters.

REFERENCES FOR Neutrino Mixing

AARTSEN 20 EPJ C80 9 M.G. Aartsen et al. (IceCube Collab.)
AARTSEN 19C PR D99 032007 M.G. Aartsen et al. (IceCube Collab.)
ACERO 19 PRL 123 151803 M.A. Acero et al. (NOvA Collab.)
ADEY 19 PR D100 052004 D. Adey et al. (Daya Bay Collab.)
AGAFONOVA 19 PR D100 051301 N. Agafonova et al. (OPERA Collab.)
ALBERT 19 JHEP 1906 113 A. Albert et al. (ANTARES Collab.)
ANDERSON 19 PR D99 012012 M. Anderson et al. (SNO+ Collab.)
SEREBROV 19 JETPL 109 213 A.P. Serbrov et al. (Neutrino-4 Collab.)
AARTSEN 18A PRL 120 071801 M.G. Aartsen et al. (IceCube Collab.)
ABE 18B PR D97 072001 K. Abe et al. (Super-Kamiokande Collab.)
ABE 18G PRL 121 171802 K. Abe et al. (T2K Collab.)
ACERO 18 PR D98 032012 M.A. Acero et al. (NOvA Collab.)
ADEY 18A PRL 121 241805 D. Adey et al. (Daya Bay Collab.)
AGAFONOVA 18A JHEP 1806 151 N. Agafonova et al. (OPERA Collab.)
AGOSTINI 18B NAT 562 505 M. Agostini et al. (Borexino Collab.)
AGUILAR-AR... 18C PRL 121 221801 A.A. Aguilar-Arevalo et al. (MiniBooNE Collab.)
ALEKSEEV 18 PR B787 56 I. Alekseev et al. (DANSS Collab.)
ALMAZAN 18 PRL 121 161801 H. Almazan et al. (STEREO Collab.)
ASHENFELT... 18 PRL 121 251802 J. Ashenfelter et al. (PROSPECT Collab.)
BAK 18 PRL 121 201801 G. Bak et al. (RENO Collab.)
DE-SALAS 18 PR B782 633 P.F. de Salas et al. (PDG Collab.)
PDG 18 PR D98 030001 M. Tanabashi et al. (PDG Collab.)
SEO 18 PR D98 012002 S.H. Seo et al. (RENO Collab.)
SEREBROV 18A PPN 49 701 A.P. Serbrov et al. (Neutrino-4 Collab.)
AARTSEN 17B PR D95 112002 M.G. Aartsen et al. (IceCube Collab.)
ABDURASHI... 17B JETPL 105 753 J.N. Abdurashitov et al. (Troitsk non-mass Collab.)
ABE 17A PRL 118 151801 K. Abe et al. (T2K Collab.)
ABE 17C PR D96 011102 K. Abe et al. (T2K Collab.)
ABE 17F PR D96 092006 K. Abe et al. (T2K Collab.)
Also PR D98 019902 (errat.) K. Abe et al. (T2K Collab.)
ADAMSON 17A PRL 118 151802 P. Adamson et al. (NOvA Collab.)
ADAMSON 17B PRL 118 231801 P. Adamson et al. (NOvA Collab.)
AN 17A PR D95 072006 F.P. An et al. (Daya Bay Collab.)
ESTEBAN 17 JHEP 1701 087 I. Esteban et al. (NEOS Collab.)
KO 17 PRL 118 121802 Y.J. Ko et al. (IceCube Collab.)
AARTSEN 16 PR 117 071801 M.G. Aartsen et al. (IceCube Collab.)
ABE 16B JHEP 1601 163 Y. Abe et al. (Double Chooz Collab.)
ABE 16C PR D94 052010 K. Abe et al. (Super-Kamiokande Collab.)
ABE 16D PRL 116 181801 K. Abe et al. (T2K Collab.)
ADAMSON 16 PR D93 051104 P. Adamson et al. (NOvA Collab.)
ADAMSON 16A PR D93 051104 P. Adamson et al. (NOvA Collab.)
ADAMSON 16B PRL 117 151801 P. Adamson et al. (Daya Bay and MINOS Collab.)
ADAMSON 16C PRL 117 151803 P. Adamson et al. (MINOS Collab.)
AN 16 PR 116 061801 F.P. An et al. (Daya Bay Collab.)
AN 16A PR D93 072011 F.P. An et al. (Daya Bay Collab.)
AN 16B PRL 117 151802 F.P. An et al. (Daya Bay Collab.)
CHOI 16 PR 116 211801 J.H. Choi et al. (RENO Collab.)
PDG 16 CP C40 100001 C. Patrignani et al. (PDG Collab.)
AARTSEN 15A PR D91 072004 M.G. Aartsen et al. (IceCube Collab.)
ABE 15D PR D91 072010 K. Abe et al. (T2K Collab.)
AGAFONOVA 15A PRL 115 121802 N. Agafonova et al. (OPERA Collab.)
AN 15 PRL 115 111802 F.P. An et al. (Daya Bay Collab.)
BERGSTROM 15 JHEP 1509 200 J. Bergstrom et al. (BARC, STON, MADU+ Collab.)
GANDO 15 PR C92 055808 A. Gando et al. (KamLAND Collab.)
ABE 14 PRL 112 181801 K. Abe et al. (T2K Collab.)
Also PR D91 072010 K. Abe et al. (T2K Collab.)
ABE 14A PL B735 51 Y. Abe et al. (Double Chooz Collab.)
ABE 14B PR D89 092003 K. Abe et al. (T2K Collab.)
ABE 14C PRL 112 061802 K. Abe et al. (T2K Collab.)
ABE 14H JHEP 1410 086 Y. Abe et al. (Double Chooz Collab.)
Also JHEP 1502 074 (errat.) Y. Abe et al. (Double Chooz Collab.)
ADAMSON 14 PRL 112 191801 P. Adamson et al. (MINOS Collab.)
AN 14 PRL 112 061801 F.P. An et al. (Daya Bay Collab.)
AN 14B PR D90 071101 F.P. An et al. (Daya Bay Collab.)
BELLINI 14A NAT 512 383 G. Bellini et al. (Borexino Collab.)
FORERO 14 PR D90 093006 D.V. Forero, M. Tortola, J.W.F. Valle

GONZALEZ... 14 JHEP 1411 052 M.C. Gonzalez-Garcia, M. Maltoni, T. Schwetz
PDG 14 CP C38 070001 K. Olive et al. (PDG Collab.)
RENSHAW 14 PRL 112 091805 A. Renshaw et al. (Super-Kamiokande Collab.)
AARTSEN 13B PRL 111 081801 M.G. Aartsen et al. (IceCube Collab.)
ABE 13C PL B723 66 Y. Abe et al. (Double Chooz Collab.)
ABE 13E PR D88 032002 K. Abe et al. (T2K Collab.)
ABE 13G PRL 111 211803 K. Abe et al. (T2K Collab.)
ADAMSON 13A PRL 110 171801 P. Adamson et al. (MINOS Collab.)
ADAMSON 13B PRL 110 251801 P. Adamson et al. (MINOS Collab.)
AGAFONOVA 13 JHEP 1307 004 N. Agafonova et al. (OPERA Collab.)
AGUILAR-AR... 13A PRL 110 161801 A.A. Aguilar-Arevalo et al. (MiniBooNE Collab.)
AHARMIM 13 PR C88 02501 B. Aharmim et al. (SNO Collab.)
AN 13 CP C37 011001 F.P. An et al. (Daya Bay Collab.)
ANTONELLO 13 EPJ C73 2345 M. Antonello et al. (ICARUS Collab.)
ANTONELLO 13A EPJ C73 2599 M. Antonello et al. (ICARUS Collab.)
GANDO 13 PR D88 033001 A. Gando et al. (KamLAND Collab.)
ABE 12 PRL 108 131801 Y. Abe et al. (Double Chooz Collab.)
ABE 12A PR D85 031103 K. Abe et al. (T2K Collab.)
ABE 12B PR D86 052008 Y. Abe et al. (Double Chooz Collab.)
ADAMSON 12 PRL 108 191801 P. Adamson et al. (MINOS Collab.)
ADAMSON 12B PR D86 052007 P. Adamson et al. (MINOS Collab.)
ADRIAN-MAR... 12 PL B714 224 S. Adrian-Martinez et al. (ANTARES Collab.)
AHN 12 PRL 108 191802 J.K. Ahn et al. (RENO Collab.)
AN 12 PRL 108 171803 F.P. An et al. (Daya Bay Collab.)
BELLINI 12A PRL 108 051302 G. Bellini et al. (Borexino Collab.)
CHENG 12 PR D86 052009 G. Cheng et al. (MiniBooNE/SciBooNE Collab.)
MAHN 12 PR D85 032007 K.B.M. Mahn et al. (MiniBooNE/SciBooNE Collab.)
ABE 11 PR D83 052010 K. Abe et al. (Super-Kamiokande Collab.)
ABE 11A PRL 107 041801 K. Abe et al. (T2K Collab.)
ABE 11B PR C84 035004 S. Abe et al. (KamLAND Collab.)
ABE 11C PRL 107 241801 K. Abe et al. (Super-Kamiokande Collab.)
ADAMSON 11 PRL 106 181801 P. Adamson et al. (MINOS Collab.)
ADAMSON 11B PRL 107 021801 P. Adamson et al. (MINOS Collab.)
ADAMSON 11C PR D84 071103 P. Adamson et al. (MINOS Collab.)
ADAMSON 11D PRL 107 181802 P. Adamson et al. (MINOS Collab.)
BELLINI 11 PL B696 191 G. Bellini et al. (Borexino Collab.)
BELLINI 11A PRL 107 141302 G. Bellini et al. (Borexino Collab.)
FOGLI 11 PR D84 053007 G.L. Fogli et al. (Borexino Collab.)
GANDO 11 PR D83 052002 A. Gando et al. (KamLAND Collab.)
MUELLER 11 PR C83 054615 Th.A. Mueller et al.
SERENELLI 11 APJ 743 24 A.M. Serenelli, W.C. Haxton, C. Pena-Garay
ADAMSON 10A PR D82 051102 P. Adamson et al. (MINOS Collab.)
AGUILAR-AR... 10 PR 105 181801 A.A. Aguilar-Arevalo et al. (MiniBooNE Collab.)
AHARMIM 10 PR C81 055504 B. Aharmim et al. (SNO Collab.)
BELLINI 10A PR D82 033006 G. Bellini et al. (Borexino Collab.)
DENIZ 10 PR D81 072001 M. Deniz et al. (TEXONO Collab.)
KAETHER 10 PL B685 47 F. Kaether et al. (Super-Kamiokande Collab.)
WENDELL 10 PR D81 092004 R. Wendell et al. (SAGE Collab.)
ABDURASHI... 09 PR C80 015807 J.N. Abdurashitov et al. (SAGE Collab.)
ADAMSON 09 PRL 103 261802 P. Adamson et al. (MINOS Collab.)
AGUILAR-AR... 09B PRL 103 111801 A.A. Aguilar-Arevalo et al. (MiniBooNE Collab.)
ABE 08A PRL 100 221803 S. Abe et al. (KamLAND Collab.)
Also PRL 101 119904 E. Abe et al. (KamLAND Collab.)
ADAMSON 08 PR D77 072002 P. Adamson et al. (MINOS Collab.)
ADAMSON 08A PRL 101 131802 P. Adamson et al. (MINOS Collab.)
AHARMIM 08 PRL 101 111301 B. Aharmim et al. (SNO Collab.)
Also PR C87 015502 B. Aharmim et al. (SNO Collab.)
ARPESELLA 08A PRL 101 091302 C. Arpesella et al. (Borexino Collab.)
CRAVENS 08 PR D78 032002 J.P. Cravens et al. (Super-Kamiokande Collab.)
FOGLI 08 PRL 101 141801 G.L. Fogli
ADAMSON 07 PR D75 092003 P. Adamson et al. (MINOS Collab.)
AGUILAR-AR... 07 PRL 98 231801 A.A. Aguilar-Arevalo et al. (MiniBooNE Collab.)
AHARMIM 07 PR C75 045502 B. Aharmim et al. (SNO Collab.)
ADAMSON 06 PR D73 072002 P. Adamson et al. (MINOS Collab.)
AHN 06A PR D74 072003 M.H. Ahn et al. (K2K Collab.)
BALATA 06 EPJ C47 21 M. Balata et al. (Borexino Collab.)
HOSAKA 06 PR D73 112001 J. Hosaka et al. (Super-Kamiokande Collab.)
HOSAKA 06A PR D74 032002 J. Hosaka et al. (Super-Kamiokande Collab.)
MICHAEL 06 PRL 97 191801 D. Michael et al. (MINOS Collab.)
WINTER 06A PR C73 025503 W.T. Winter et al.
YAMAMOTO 06 PRL 96 181801 S. Yamamoto et al. (K2K Collab.)
AHARMIM 05A PR C72 055502 B. Aharmim et al. (SNO Collab.)
ALIU 05 PR 94 081802 E. Aliu et al. (K2K Collab.)
ALLISON 05 PR D72 052005 W.W.M. Allison et al. (Soudan 2 Collab.)
ALTMANN 05 PR B616 174 M. Altmann et al. (GLO Collab.)
ARAKI 05 PR 94 081801 T. Araki et al. (KamLAND Collab.)
ASHIE 05 PR D71 112005 Y. Ashie et al. (Super-Kamiokande Collab.)
BAHCALL 05 APJ 621 L85 J.N. Bahcall, A.M. Serenelli, S. Basu (IAS+)
DEGOUVEA 05 PR D71 093002 A. de Gouvea, C. Pena-Garay
AHARMIM 04 PR D70 093014 B. Aharmim et al. (SNO Collab.)
AHMED 04A PRL 92 181301 S.N. Ahmed et al. (SNO Collab.)
AHN 04 PRL 93 051801 M.H. Ahn et al. (K2K Collab.)
AMBROSIO 04 EPJ C36 323 M. Ambrosio et al. (MACRO Collab.)
ASHIE 04 PRL 93 101801 Y. Ashie et al. (Super-Kamiokande Collab.)
EGUCHI 04 PRL 92 071301 K. Eguchi et al. (KamLAND Collab.)
SMY 04 PR D69 011104 M.B. Smy et al. (Super-Kamiokande Collab.)
AHN 03 PRL 90 041801 M.H. Ahn et al. (K2K Collab.)
AMBROSIO 03 PL B566 35 M. Ambrosio et al. (MACRO Collab.)
APOLLONIO 03 EPJ C27 331 M. Apollonio et al. (CHOOZ Collab.)
ASTIER 03 PRL 87 019019 P. Astier et al. (NOMAD Collab.)
EGUCHI 03 PRL 90 021802 K. Eguchi et al. (KamLAND Collab.)
GANDO 03 PRL 90 171302 Y. Gando et al. (Super-Kamiokande Collab.)
IANNI 03 JP G29 2107 A. Ianni (INFN Gran Sasso)
SANCHEZ 03 PR D68 113004 M. Sanchez et al. (Soudan 2 Collab.)
ABDURASHI... 02 JETP 95 181 J.N. Abdurashitov et al. (SAGE Collab.)
Translated from ZETF 122 211.
AHMAD 02 PRL 89 011301 Q.R. Ahmad et al. (SNO Collab.)
AHMAD 02B PRL 89 011302 Q.R. Ahmad et al. (SNO Collab.)
ARMBRUSTER 02 PR D65 112001 B. Armbruster et al. (KARMEN 2 Collab.)
AVAKUMOV 02 PRL 89 011804 S. Avakumov et al. (NuTeV Collab.)
FUKUDA 02 PL B539 179 S. Fukuda et al. (Super-Kamiokande Collab.)
AGUILAR 01 PR D64 112007 A. Aguilar et al. (LSND Collab.)
AHMAD 01 PRL 87 071301 Q.R. Ahmad et al. (SNO Collab.)
AMBROSIO 01 PR B517 59 M. Ambrosio et al. (MACRO Collab.)
BOEHM 01 PR D64 112001 F. Boehm et al. (MACRO Collab.)
FUKUDA 01 PRL 86 5651 S. Fukuda et al. (Super-Kamiokande Collab.)
AMBROSIO 00 PRL 84 3764 M. Ambrosio et al. (MACRO Collab.)
BOEHM 00 PRL 84 3764 F. Boehm et al. (MACRO Collab.)
FUKUDA 00 PRL 85 3999 S. Fukuda et al. (Super-Kamiokande Collab.)
ALLISON 99 PL B449 137 W.W.M. Allison et al. (Soudan 2 Collab.)
APOLLONIO 99 PL B466 415 M. Apollonio et al. (CHOOZ Collab.)
Also PL B472 434 (errat.) M. Apollonio et al. (CHOOZ Collab.)
FUKUDA 99C PRL 82 2644 Y. Fukuda et al. (Super-Kamiokande Collab.)
FUKUDA 99D PL B467 185 Y. Fukuda et al. (Super-Kamiokande Collab.)
HAMPPEL 99 PL B447 127 W. Hampel et al. (GALLEX Collab.)
AMBROSIO 98 PL B434 451 M. Ambrosio et al. (MACRO Collab.)
APOLLONIO 98 PL B420 397 M. Apollonio et al. (CHOOZ Collab.)
ATHANASSO... 98 PRL 81 1774 C. Athanassopoulos et al. (LSND Collab.)
ATHANASSO... 98B PR C58 2489 C. Athanassopoulos et al. (LSND Collab.)
CLEVELAND 98 APJ 496 505 B.T. Cleveland et al. (Homestake Collab.)
FELDMAN 98 PR D67 3873 G.J. Feldman, R.D. Cousins

Downloaded from https://academic.oup.com/ptep/article/2020/8/083C01/5891211 by guest on 20 August 2020

Lepton Particle Listings

Neutrino Mixing, Heavy Neutral Leptons, Searches for

FUKUDA	98C	PRL 81 1562	Y. Fukuda <i>et al.</i>	(Super-Kamiokande Collab.)
HATAKEYAMA	98B	PRL 81 2016	S. Hatakeyama <i>et al.</i>	(Kamiokande Collab.)
CLARK	97	PRL 79 345	R. Clark <i>et al.</i>	(IMB Collab.)
ROMOSAN	97	PRL 78 2912	A. Romosan <i>et al.</i>	(CCFR Collab.)
AGLIETTA	96	JETPL 63 791	M. Aglietta <i>et al.</i>	(LSD Collab.)
Translated from ZETFP 63 753.				
ATHANASSO...	96	PR C54 2685	C. Athanassopoulos <i>et al.</i>	(LSND Collab.)
ATHANASSO...	96B	PRL 77 3082	C. Athanassopoulos <i>et al.</i>	(LSND Collab.)
FUKUDA	96	PRL 77 1683	Y. Fukuda <i>et al.</i>	(Kamiokande Collab.)
FUKUDA	96B	PL B388 397	Y. Fukuda <i>et al.</i>	(Kamiokande Collab.)
GREENWOOD	96	PR D53 6054	Z.D. Greenwood <i>et al.</i>	(UCI, SVR, S CUC)
HAMPEL	96	PL B388 384	W. Hampel <i>et al.</i>	(GALLEX Collab.)
LOVERRE	96	PL B370 156	P.F. Loverre	
ACHKAR	95	NP B434 503	B. Achkar <i>et al.</i>	(SING, SACL, CPPM, CDEF+)
AHLEN	95	PL B357 481	S.P. Ahlen <i>et al.</i>	(MACRO Collab.)
ATHANASSO...	95	PRL 75 2650	C. Athanassopoulos <i>et al.</i>	(LSND Collab.)
DAUM	95	ZPHY C66 417	K. Daum <i>et al.</i>	(FREJUS Collab.)
HILL	95	PRL 75 2654	J.E. Hill	(PENN)
MCFARLAND	95	PRL 75 3993	K.S. McFarland <i>et al.</i>	(CCFR Collab.)
DECLAIS	94	PL B338 383	Y. Declais <i>et al.</i>	(Kamiokande Collab.)
FUKUDA	94	PL B335 237	Y. Fukuda <i>et al.</i>	(CHARM II Collab.)
VILAIN	94C	ZPHY C64 539	P. Vilain <i>et al.</i>	(CHARM II Collab.)
FREEDMAN	93	PR D47 811	S.J. Freedman <i>et al.</i>	(LAMPF E645 Collab.)
BECKER-SZ...	92B	PR D46 3720	R.A. Becker-Szendy <i>et al.</i>	(IMB Collab.)
BEIER	92	PL B283 446	E.W. Beier <i>et al.</i>	(KAM2 Collab.)
	Also	PTRSL A346 63	E.W. Beier, E.D. Frank	(PENN)
BORODOV...	92	PRL 68 274	L. Borodovsky <i>et al.</i>	(COLU, JHU, ILL)
HIRATA	92	PL B280 146	K.S. Hirata <i>et al.</i>	(Kamiokande II Collab.)
CASPER	91	PRL 66 2561	D. Casper <i>et al.</i>	(IMB Collab.)
HIRATA	91	PRL 66 9	K.S. Hirata <i>et al.</i>	(Kamiokande II Collab.)
KUVSHINN...	91	JETPL 54 253	A.A. Kuvshinnikov <i>et al.</i>	(KIAE)
BERGER	90B	PL B245 305	C. Berger <i>et al.</i>	(FREJUS Collab.)
HIRATA	90	PRL 65 1297	K.S. Hirata <i>et al.</i>	(Kamiokande II Collab.)
AGLIETTA	89	EPL 8 611	M. Aglietta <i>et al.</i>	(FREJUS Collab.)
DAVIS	89	ARNPS 39 467	R. Davis, A.K. Mann, L. Wolfenstein	(BNL, PENN+)
OYAMA	89	PR D39 1481	Y. Oyama <i>et al.</i>	(Kamiokande II Collab.)
BIONTA	88	PR D38 768	R.M. Bionta <i>et al.</i>	(IMB Collab.)
DURKIN	88	PRL 61 1811	L.S. Durkin <i>et al.</i>	(OSU, ANL, CIT+)
ABRAMOWICZ	86	PRL 57 298	H. Abramowicz <i>et al.</i>	(CDHS Collab.)
ALLABY	86	PL B177 446	J.V. Allaby <i>et al.</i>	(CHARM Collab.)
ANGELINI	86	PL B179 307	C. Angelini <i>et al.</i>	(PISA, ATHU, PADO+)
VUILLEUMIER	82	PL 114B 298	J.L. Vuilleumier <i>et al.</i>	(CIT, SIN, MUNI)
BOLIEV	81	SJNP 34 787	M.M. Boliev <i>et al.</i>	(INRM)
Translated from YAF 34 1418.				
KWON	81	PR D24 1097	H. Kwon <i>et al.</i>	(CIT, ISNG, MUNI)
BOEHM	80	PL 97B 310	F. Boehm <i>et al.</i>	(ILLG, CIT, ISNG, MUNI)
CROUCH	78	PR D18 2239	M.F. Crouch <i>et al.</i>	(CASE, UCI, WITW)

$<2 \times 10^{-9}$	10,11	BERNARDI	88	CNTR	Near $m_K - m_e$ kin. thres.
$<1 \times 10^{-7}$	90	DORENBOS...	86	CHRM	Near $m_D - m_e$ kin. thres.
$<1 \times 10^{-7}$	90	COOPER...	85	BEBC	Near $m_D - m_e$ kin. thres.

••• We do not use the following data for averages, fits, limits, etc. •••

14	PARK	16	BELL	$m_{\nu_x} \sim 0.2-1.4$ GeV
----	------	----	------	------------------------------

- Limit from prompt lepton number violating trilepton search.
- $K^+ \rightarrow e^+ \nu_x$, with ν_x decay through U_{eX} . ABE 19B also considers bounds on $|U_{eX} U_{\ell'X}|$ for combinations of lepton flavors in the ν_x decay final state.
- Searches for a Majorana Heavy Neutral Lepton producing a $\pi^- e^+$ resonance in the same sign dilepton decay $D \rightarrow K \pi^- e^+ e^+$.
- Search for $\pi^+ \rightarrow e^+ \nu_x$.
- Search for $K^+ \rightarrow e^+ \nu_x$.
- Search for prompt ν_x decay signatures.
- Search for displaced ν_x decay signatures.
- Searches for K or $\pi \rightarrow e^+ \nu_x, \nu_x \rightarrow e^+ e^- \nu_e$ using a beam dump experiment at the 70 GeV Serpukhov proton synchrotron. BARANOV 93 also considers limits for $|U_{eX} U_{\mu X}|$ from K or $\pi \rightarrow \mu^+ \nu_x, \nu_x \rightarrow e^+ e^- \nu_e$.
- $\pi^+ \rightarrow e^+ \nu_x$, with ν_x decay through U_{eX} .
- BERNARDI 88 also considers bounds on $|U_{eX} U_{\mu X}|$.
- $K^+ \rightarrow e^+ \nu_x$, with ν_x decay through U_{eX} .
- $D^+ \rightarrow e^+ \nu_x$, with $\nu_x \rightarrow e^- \ell^+ \nu_{\ell}$.
- $D^+ \rightarrow e^+ \nu_x$, with $\nu_x \rightarrow e^- \ell^+ \nu_{\ell}$ or $\nu_x \rightarrow e^- \pi^+$.
- PARK 16 quotes an approximate limit $B(B^+ \rightarrow e^+ \nu_x) < 3 \times 10^{-6}$ in the mass range $m_{\nu_x} \sim 0.2-1.4$ GeV.

Limits on $|U_{\mu X}|^2$

Quoted limits are either the best limit near the kinematic threshold of the experiment, or a characteristic value in the mass range of the experimental sensitivity

VALUE	CL%	DOCUMENT ID	TECN	COMMENT
$<2 \times 10^{-5}$	95	1 AAD	19F ATLS	$m_{\nu_x} \sim 10-50$ GeV
$<2 \times 10^{-6}$	95	2 AAD	19F ATLS	$m_{\nu_x} \sim 10$ GeV
$<1 \times 10^{-9}$	90	3 ABE	19B T2K	Near $m_K - m_{\mu}$ kin. thres.
$<5 \times 10^{-6}$	90	4,5 AGUILAR-AR...	19B PIEN	$m_{\nu_x} \sim 16-30$ MeV
$<1 \times 10^{-5}$	90	5 AGUILAR-AR...	19B PIEN	Near $m_{\pi} - m_{\mu}$ kin. thres.
$<3 \times 10^{-7}$	90	6 CORTINA-GIL	18 NA62	$m_{\nu_x} \sim 250-350$ MeV
$<3 \times 10^{-6}$	90	6 LAZZERONI	17A NA62	Near $m_K - m_{\mu}$ kin. thres.
$<1 \times 10^{-8}$	90	6 ARTAMONOV	15A B949	$m_{\nu_x} \sim 200-300$ MeV
$<2.0 \times 10^{-8}$	95	7 DAUM	00 KARM	$m_{\nu_x} = 33.905$ MeV
$<8 \times 10^{-8}$	90	8 VAITAITIS	99 CCFR	Near $m_K - m_{\mu}$ kin. thres.
$<6 \times 10^{-8}$	90	9 VAITAITIS	99 CCFR	Near $m_{D_s} - m_{\mu}$ kin. thres.
$<3 \times 10^{-5}$	95	10 ABREU	97I DLPH	$m_{\nu_x} \sim 6-50$ GeV
$<2 \times 10^{-5}$	95	11 ABREU	97I DLPH	Near $m_{\nu_x} \sim 3.5$ GeV
$<3 \times 10^{-5}$	90	12 VILAIN	95C CHM2	Near $m_K - m_{\mu}$ kin. thres.
$<3 \times 10^{-8}$	13,14	BERNARDI	88 CNTR	Near $m_{\mu} + m_{\pi}$ kin. thres.
$<2 \times 10^{-9}$	14,15	BERNARDI	88 CNTR	Near $m_K - m_{\mu}$ kin. thres.
$<1 \times 10^{-7}$	90	16 DORENBOS...	86 CHRM	Near $m_D - m_{\mu}$ kin. thres.
$<1 \times 10^{-7}$	90	17 COOPER...	85 BEBC	Near $m_D - m_{\mu}$ kin. thres.

••• We do not use the following data for averages, fits, limits, etc. •••

18	PARK	16	BELL	$m_{\nu_x} \sim 0.2-1.4$ GeV
----	------	----	------	------------------------------

- Limit from prompt lepton number violating trilepton search.
- Limit from displaced lepton violating or conserving trilepton searches.
- $K^+ \rightarrow \mu^+ \nu_x$, with ν_x decay through $U_{\mu X}$. ABE 19B also considers bounds on $|U_{eX} U_{\ell'X}|$ for combinations of lepton flavors in the ν_x decay final state.
- Limit requires muon kinetic energy > 1.2 MeV.
- Search for $\pi^+ \rightarrow \mu^+ \nu_x$.
- Search for $K^+ \rightarrow \mu^+ \nu_x$.
- DAUM 00 quotes a branching ratio bound $B(\pi^+ \rightarrow \mu^+ \nu_x) < 6.0 \times 10^{-10}$ at 95% CL.
- $K^+ \rightarrow \mu^+ \nu_x$, with $\nu_x \rightarrow \mu X$.
- $D_s \rightarrow \mu^+ \nu_x$, with $\nu_x \rightarrow \mu X$.
- Search for prompt ν_x decay signatures.
- Search for displaced ν_x decay signatures.
- Search for Heavy Neutral Leptons produced by neutral current muon neutrino interactions, with $\nu_x \rightarrow \mu^+ \mu^- \nu_{\mu}$.
- $K^+ \rightarrow \mu^+ \nu_x$, with ν_x decay through $U_{\mu X}$ and $m_{\nu_x} < m_{\mu} + m_{\pi}$.
- BERNARDI 88 also considers bounds on $|U_{eX} U_{\mu X}|$.
- $K^+ \rightarrow \mu^+ \nu_x$, with $\nu_x \rightarrow \mu^- \pi^+$.
- $D^+ \rightarrow \mu^+ \nu_x$, with $\nu_x \rightarrow \mu^- \ell^+ \nu_{\ell}$.

Heavy Neutral Leptons, Searches for

OMITTED FROM SUMMARY TABLE

We define searches for Heavy Neutral Leptons (HNLs) as searches for Dirac or Majorana fermions with sterile neutrino quantum numbers, that are heavy enough to not disrupt the simplest Big Bang Nucleosynthesis bounds and/or unstable on cosmological timescales: Typically HNLs have mass \sim MeV or higher.

Searches for these particles generically set bounds on the mixing between the HNL and the active neutrinos, as parametrized by the extended 3×4 PMNS matrix elements $U_{\ell X}$ (see the "Neutrino mass, mixing and oscillations" review) where $\ell = e, \mu$ or τ , and we denote the HNL as ν_x . While many measurements may be interpreted to place bounds on various combinations of these matrix elements, we quote below limits only for those cases in which one matrix element is assumed to be much larger than the other two, i.e. $|U_{\ell X}| \gg |U_{\ell' X}|$ for $\ell' \neq \ell$.

Experimental searches make use of various different strategies, including e.g. resonance searches in missing mass decay distributions or specific final states, searches for lepton number violating decays, and trilepton signatures. The resulting bounds on $U_{\ell X}$ are typically dependent on the HNL mass. The quoted limits below are either the best limit near an experimental kinematic threshold, or a characteristic value in the mass range of the experimental sensitivity.

Limits on heavy neutral lepton mixing parameters

Limits on $|U_{eX}|^2$

Quoted limits are either the best limit near the kinematic threshold of the experiment, or a characteristic value in the mass range of the experimental sensitivity

VALUE	CL%	DOCUMENT ID	TECN	COMMENT
$<2 \times 10^{-5}$	95	1 AAD	19F ATLS	$m_{\nu_x} \sim 15-40$ GeV
$<1 \times 10^{-9}$	90	2 ABE	19B T2K	Near $m_K - m_e$ kin. thres.
$<1 \times 10^{-4}$	90	3 ABLIKIM	19AL BES3	$m_{\nu_x} \sim 0.3-0.7$ GeV
$<1 \times 10^{-8}$	90	4 AGUILAR-AR...	18A PIEN	$m_{\nu_x} \sim 60-120$ MeV i_{br}
$<3 \times 10^{-7}$	90	5 CORTINA-GIL	18 NA62	$m_{\nu_x} \sim 200-400$ MeV
$<3 \times 10^{-5}$	95	6 ABREU	97I DLPH	$m_{\nu_x} \sim 6-50$ GeV
$<2 \times 10^{-5}$	95	7 ABREU	97I DLPH	Near $m_{\nu_x} \sim 3.5$ GeV
$<1 \times 10^{-5}$	90	8 BARANOV	93	Near $m_{\pi} - m_e$ kin. thres.
$<2 \times 10^{-7}$	90	8 BARANOV	93	Near $m_K - m_e$ kin. thres.
$<1 \times 10^{-7}$	9,10	BERNARDI	88 CNTR	Near $m_{\pi} - m_e$ kin. thres.

See key on page 999

Lepton Particle Listings

Heavy Neutral Leptons, Searches for

¹⁷ $D^+ \rightarrow \mu^+ \nu_X$, with $\nu_X \rightarrow \mu^- \ell^+ \nu_\ell$ or $\nu_X \rightarrow \mu^- \pi^+$.
¹⁸ PARK 16 quotes an approximate limit $B(B^+ \rightarrow \mu^+ \nu_X) < 3 \times 10^{-6}$ in the mass range $m_{\nu_X} \sim 0.2-1.4$ GeV.

Limits on $|U_{\tau X}|^2$

Quoted limits are either the best limit near the kinematic threshold of the experiment, or a characteristic value in the mass range of the experimental sensitivity

VALUE	CL%	DOCUMENT ID	TECN	COMMENT
$< 2 \times 10^{-4}$	90	1 ORLOFF	02	CHRM Near $m_D - m_\tau$ kin. thres.
$< 1 \times 10^{-4}$	90	2 ORLOFF	02	CHRM $m_{\nu_X} \sim 200-250$ MeV
$< 3 \times 10^{-5}$	95	3 ABREU	97I	DLPH $m_{\nu_X} \sim 6-50$ GeV
$< 2 \times 10^{-5}$	95	4 ABREU	97I	DLPH Near $m_{\nu_X} \sim 3.5$ GeV

- ¹ $D_S \rightarrow \tau^+ \nu_X$, with ν_X decay via $U_{\tau X}$.
- ² $D_S \rightarrow \nu_\tau \tau^+$, $\tau^+ \rightarrow \nu_X X$, with ν_X decay via $U_{\tau X}$.
- ³ Search for prompt ν_X decay signatures.
- ⁴ Search for displaced ν_X decay signatures. Kinematical suppression of $\nu_X \rightarrow \tau X$ at lower masses leads to rapid loosening of the $|U_{\tau X}|$ bound compared to that for $|U_{eX}|$ and $|U_{\mu X}|$.

REFERENCES FOR Heavy Neutral Leptons, Searches for

AAD	19F	JHEP 1910 265	G. Aad <i>et al.</i>	(ATLAS Collab.)
ABE	19B	PR D100 052006	K. Abe <i>et al.</i>	(T2K Collab.)
ABLIKIM	19AL	PR D99 112002	M. Ablikim <i>et al.</i>	(BESIII Collab.)
AGUILAR-AR...	19B	PL B798 134980	A. Aguilar-Arevalo <i>et al.</i>	(PIENU Collab.)
AGUILAR-AR...	18A	PR D97 072012	A. Aguilar-Arevalo <i>et al.</i>	(PIENU Collab.)
CORTINA-GIL	18	PL B778 137	E. Cortina Gil <i>et al.</i>	(NA62 Collab.)
LAZZERONI	17A	PL B772 712	C. Lazzeroni <i>et al.</i>	(NA62 Collab.)
PARK	16	PR D94 012003	C.-S. Park <i>et al.</i>	(BELLE Collab.)
ARTAMONOV	15A	PR D91 052001	A.V. Artamonov <i>et al.</i>	(E949 Collab.)
ORLOFF	02	PL B550 9	J. Orloff <i>et al.</i>	(CHARM Collab.)
DAUM	00	PRL 85 1815	Im. Daum <i>et al.</i>	(KARMEN Collab.)
VAITAITIS	99	PRL 83 4943	A. Vaitaitis <i>et al.</i>	(CCFR Collab.)
ABREU	97I	ZPHY C74 67	P. Abreu <i>et al.</i>	(DELPHI Collab.)
Also		ZPHY C75 580 (errat.)	P. Abreu <i>et al.</i>	(DELPHI Collab.)
VILAIN	95C	PL B351 387	P. Vilain <i>et al.</i>	(CHARM II Collab.)
Also		PL B343 453	P. Vilain <i>et al.</i>	(CHARM II Collab.)
BARANOV	93	PL B302 336	S.A. Baranov <i>et al.</i>	(JINR, SERP, BUDA)
BERNARDI	88	PL B203 332	G. Bernardi <i>et al.</i>	(PARIN, CERN, INFN+)
DORENBOS...	86	PL 166B 473	J. Dorenbosch <i>et al.</i>	(CHARM Collab.)
COOPER...	85	PL 160B 207	A.M. Cooper-Sarkar <i>et al.</i>	(CERN, LOIC+)

QUARKS

<i>u</i>	1173
<i>d</i>	1173
<i>s</i>	1173
<i>c</i>	1177
<i>b</i>	1179
<i>t</i>	1180
<i>b'</i> (Fourth Generation) Quark	1197
<i>t'</i> (Fourth Generation) Quark	1199
Free Quark Searches	1201

Related Reviews in Volume 1

59. Quark masses (rev.)	733
60. Top quark (rev.)	741



See key on page 999

Quark Particle Listings

Quarks, *u*, *d*, *s*, Light Quarks (*u*, *d*, *s*)

QUARKS

See the related review(s):

Quark Masses

u $I(J^P) = \frac{1}{2}(\frac{1}{2}^+)$

Mass $m = 2.16^{+0.49}_{-0.26}$ MeV Charge = $\frac{2}{3} e$ $I_z = +\frac{1}{2}$

$m_u/m_d = 0.47^{+0.06}_{-0.07}$

d $I(J^P) = \frac{1}{2}(\frac{1}{2}^+)$

Mass $m = 4.67^{+0.48}_{-0.17}$ MeV Charge = $-\frac{1}{3} e$ $I_z = -\frac{1}{2}$

$m_s/m_d = 17-22$

$\bar{m} = (m_u + m_d)/2 = 3.45^{+0.55}_{-0.15}$ MeV

s $I(J^P) = 0(\frac{1}{2}^+)$

Mass $m = 93^{+11}_{-5}$ MeV Charge = $-\frac{1}{3} e$ Strangeness = -1

$(m_s - (m_u + m_d)/2)/(m_d - m_u) = 27.3^{+0.7}_{-1.3}$

Light Quarks (*u*, *d*, *s*)

OMITTED FROM SUMMARY TABLE

u-QUARK MASS

The *u*-, *d*-, and *s*-quark masses are estimates of so-called “current-quark masses,” in a mass-independent subtraction scheme such as \overline{MS} . The ratios m_u/m_d and m_s/m_d are extracted from pion and kaon masses using chiral symmetry. The estimates of *d* and *u* masses are not without controversy and remain under active investigation. Within the literature there are even suggestions that the *u* quark could be essentially massless. The *s*-quark mass is estimated from SU(3) splittings in hadron masses.

We have normalized the \overline{MS} masses at a renormalization scale of $\mu = 2$ GeV. Results quoted in the literature at $\mu = 1$ GeV have been rescaled by dividing by 1.35. The values of “Our Evaluation” were determined in part via Figures 1 and 2.

\overline{MS} MASS (MeV)	DOCUMENT ID	TECN
2.16 \pm 0.49 -0.26 OUR EVALUATION	See the ideogram below.	
2.6 \pm 0.4	1 DOMINGUEZ 19	THEO
2.130 \pm 0.041	2 BAZAVOV 18	LATT
2.27 \pm 0.06 \pm 0.06	3 FODOR 16	LATT
2.36 \pm 0.24	4 CARRASCO 14	LATT
2.57 \pm 0.26 \pm 0.07	5 AOKI 12	LATT
2.24 \pm 0.10 \pm 0.34	6 BLUM 10	LATT
2.01 \pm 0.14	7 MCNEILE 10	LATT
• • • We do not use the following data for averages, fits, limits, etc. • • •		
2.15 \pm 0.03 \pm 0.10	8 DURR 11	LATT
1.9 \pm 0.2	9 BAZAVOV 10	LATT
2.01 \pm 0.14	7 DAVIES 10	LATT
2.9 \pm 0.2	10 DOMINGUEZ 09	THEO
2.9 \pm 0.8	11 DEANDREA 08	THEO
3.02 \pm 0.33	12 BLUM 07	LATT
2.7 \pm 0.4	13 JAMIN 06	THEO
1.9 \pm 0.2	14 MASON 06	LATT
2.8 \pm 0.2	15 NARISON 06	THEO
1.7 \pm 0.3	16 AUBIN 04A	LATT

¹ DOMINGUEZ 19 determine the quark mass from a QCD finite energy sum rule for the divergence of the axial current.

² BAZAVOV 18 determine the quark masses using a lattice computation with staggered fermions and four active quark flavors.

³ FODOR 16 is a lattice simulation with $N_f = 2 + 1$ dynamical flavors and includes partially quenched QED effects.

⁴ CARRASCO 14 is a lattice QCD computation of light quark masses using $2 + 1 + 1$ dynamical quarks, with $m_u = m_d \neq m_s \neq m_c$. The *u* and *d* quark masses are obtained separately by using the *K* meson mass splittings and lattice results for the electromagnetic contributions.

⁵ AOKI 12 is a lattice computation using $1 + 1 + 1$ dynamical quark flavors.

⁶ BLUM 10 determines light quark masses using a QCD plus QED lattice computation of the electromagnetic mass splittings of the low-lying hadrons. The lattice simulations use $2+1$ dynamical quark flavors.

⁷ DAVIES 10 and MCNEILE 10 determine $\bar{m}_c(\mu)/\bar{m}_s(\mu) = 11.85 \pm 0.16$ using a lattice computation with $N_f = 2 + 1$ dynamical fermions of the pseudoscalar meson masses.

Mass m_u is obtained from this using the value of m_c from ALLISON 08 or MCNEILE 10 and the BAZAVOV 10 values for the light quark mass ratios, m_s/\bar{m} and m_u/m_d .

⁸ DURR 11 determine quark mass from a lattice computation of the meson spectrum using $N_f = 2 + 1$ dynamical flavors. The lattice simulations were done at the physical quark mass, so that extrapolation in the quark mass was not needed. The individual m_u , m_d values are obtained using the lattice determination of the average mass m_{ud} and of the ratio m_s/m_{ud} and the value of $Q = (m_s^2 - m_{ud}^2) / (m_d^2 - m_u^2)$ as determined from $\eta \rightarrow 3\pi$ decays.

⁹ BAZAVOV 10 is a lattice computation using $2+1$ dynamical quark flavors.

¹⁰ DOMINGUEZ 09 use QCD finite energy sum rules for the two-point function of the divergence of the axial vector current computed to order α_s^4 .

¹¹ DEANDREA 08 determine $m_u - m_d$ from $\eta \rightarrow 3\pi^0$, and combine with the PDG 06 lattice average value of $m_u + m_d = 7.6 \pm 1.6$ to determine m_u and m_d .

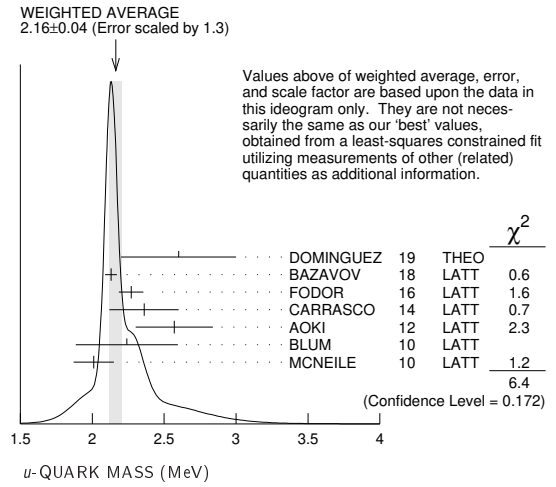
¹² BLUM 07 determine quark masses from the pseudoscalar meson masses using a QED plus QCD lattice computation with two dynamical quark flavors.

¹³ JAMIN 06 determine $m_u(2 \text{ GeV})$ by combining the value of m_s obtained from the spectral function for the scalar *K* π form factor with other determinations of the quark mass ratios.

¹⁴ MASON 06 extract light quark masses from a lattice simulation using staggered fermions with an improved action, and three dynamical light quark flavors with degenerate *u* and *d* quarks. Perturbative corrections were included at NNLO order. The quark masses m_u and m_d were determined from their $(m_u + m_d)/2$ measurement and AUBIN 04A m_u/m_d value.

¹⁵ NARISON 06 uses sum rules for $e^+ e^- \rightarrow$ hadrons to order α_s^3 to determine m_s combined with other determinations of the quark mass ratios.

¹⁶ AUBIN 04A employ a partially quenched lattice calculation of the pseudoscalar meson masses.



d-QUARK MASS

See the comment for the *u* quark above.

We have normalized the \overline{MS} masses at a renormalization scale of $\mu = 2$ GeV. Results quoted in the literature at $\mu = 1$ GeV have been rescaled by dividing by 1.35. The values of “Our Evaluation” were determined in part via Figures 1 and 2.

\overline{MS} MASS (MeV)	DOCUMENT ID	TECN
4.67 \pm 0.48 -0.17 OUR EVALUATION	See the ideogram below.	
5.3 \pm 0.4	1 DOMINGUEZ 19	THEO
4.675 \pm 0.056	2 BAZAVOV 18	LATT
4.67 \pm 0.06 \pm 0.06	3 FODOR 16	LATT
5.03 \pm 0.26	4 CARRASCO 14	LATT
3.68 \pm 0.29 \pm 0.10	5 AOKI 12	LATT
4.65 \pm 0.15 \pm 0.32	6 BLUM 10	LATT
4.77 \pm 0.15	7 MCNEILE 10	LATT
• • • We do not use the following data for averages, fits, limits, etc. • • •		
4.79 \pm 0.07 \pm 0.12	8 DURR 11	LATT
4.6 \pm 0.3	9 BAZAVOV 10	LATT
4.79 \pm 0.16	7 DAVIES 10	LATT
5.3 \pm 0.4	10 DOMINGUEZ 09	THEO
4.7 \pm 0.8	11 DEANDREA 08	THEO
5.49 \pm 0.39	12 BLUM 07	LATT
4.8 \pm 0.5	13 JAMIN 06	THEO
4.4 \pm 0.3	14 MASON 06	LATT
5.1 \pm 0.4	15 NARISON 06	THEO
3.9 \pm 0.5	16 AUBIN 04A	LATT

Quark Particle Listings

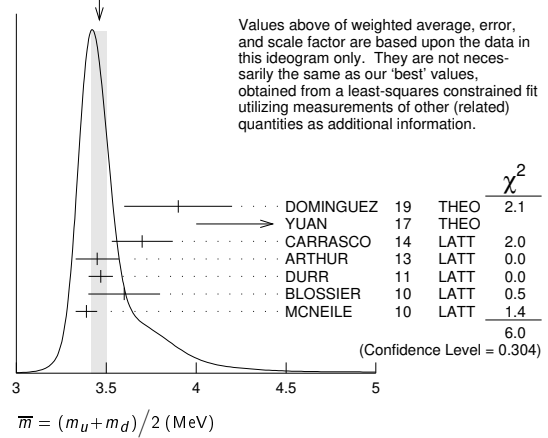
Light Quarks (*u, d, s*)

- ¹ DOMINGUEZ 19 determine the quark mass from a QCD finite energy sum rule for the divergence of the axial current.
- ² BAZAVOV 18 determine the quark masses using a lattice computation with staggered fermions and four active quark flavors.
- ³ FODOR 16 is a lattice simulation with $N_f = 2 + 1$ dynamical flavors and includes partially quenched QED effects.
- ⁴ CARRASCO 14 is a lattice QCD computation of light quark masses using $2 + 1 + 1$ dynamical quarks, with $m_u = m_d \neq m_s \neq m_c$. The *u* and *d* quark masses are obtained separately by using the *K* meson mass splittings and lattice results for the electromagnetic contributions.
- ⁵ AOKI 12 is a lattice computation using $1 + 1 + 1$ dynamical quark flavors.
- ⁶ BLUM 10 determines light quark masses using a QCD plus QED lattice computation of the electromagnetic mass splittings of the low-lying hadrons. The lattice simulations use $2+1$ dynamical quark flavors.
- ⁷ DAVIES 10 and MCNEILE 10 determine $\overline{m}_c(\mu)/\overline{m}_s(\mu) = 11.85 \pm 0.16$ using a lattice computation with $N_f = 2 + 1$ dynamical fermions of the pseudoscalar meson masses. Mass m_d is obtained from this using the value of m_c from ALLISON 08 or MCNEILE 10 and the BAZAVOV 10 values for the light quark mass ratios, m_s/\overline{m} and m_u/m_d .
- ⁸ DURR 11 determine quark mass from a lattice computation of the meson spectrum using $N_f = 2 + 1$ dynamical flavors. The lattice simulations were done at the physical quark mass, so that extrapolation in the quark mass was not needed. The individual m_u, m_d values are obtained using the lattice determination of the average mass m_{ud} and of the ratio m_s/m_{ud} and the value of $Q = (m_s^2 - m_{ud}^2) / (m_d^2 - m_u^2)$ as determined from $\eta \rightarrow 3\pi$ decays.
- ⁹ BAZAVOV 10 is a lattice computation using $2+1$ dynamical quark flavors.
- ¹⁰ DOMINGUEZ 09 use QCD finite energy sum rules for the two-point function of the divergence of the axial vector current computed to order α_s^4 .
- ¹¹ DEANDREA 08 determine $m_u - m_d$ from $\eta \rightarrow 3\pi^0$, and combine with the PDG 06 lattice average value of $m_u + m_d = 7.6 \pm 1.6$ to determine m_u and m_d .
- ¹² BLUM 07 determine quark masses from the pseudoscalar meson masses using a QED plus QCD lattice computation with two dynamical quark flavors.
- ¹³ JAMIN 06 determine $m_d(2 \text{ GeV})$ by combining the value of m_s obtained from the spectral function for the scalar $K\pi$ form factor with other determinations of the quark mass ratios.
- ¹⁴ MASON 06 extract light quark masses from a lattice simulation using staggered fermions with an improved action, and three dynamical light quark flavors with degenerate *u* and *d* quarks. Perturbative corrections were included at NNLO order. The quark masses m_u and m_d were determined from their $(m_u + m_d)/2$ measurement and AUBIN 04A m_u/m_d value.
- ¹⁵ NARISON 06 uses sum rules for $e^+ e^- \rightarrow \text{hadrons}$ to order α_s^3 to determine m_s combined with other determinations of the quark mass ratios.
- ¹⁶ AUBIN 04A perform three flavor dynamical lattice calculation of pseudoscalar meson masses, with continuum estimate of electromagnetic effects in the kaon masses, and one-loop perturbative renormalization constant.

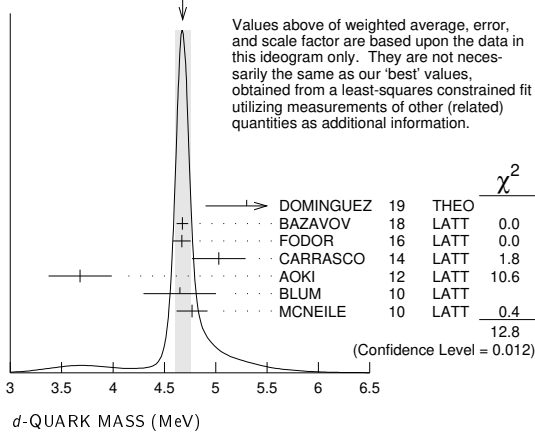
• • • We do not use the following data for averages, fits, limits, etc. • • •

3.59 ± 0.21	⁸ AOKI	11A	LATT
3.40 ± 0.07	⁷ DAVIES	10	LATT
4.1 ± 0.2	⁹ DOMINGUEZ	09	THEO
3.72 ± 0.41	¹⁰ ALLTON	08	LATT
3.85 ± 0.12 ± 0.4	¹¹ BLOSSIER	08	LATT
≥ 4.85 ± 0.20	¹² DOMINGUEZ..08B	THEO	
3.55 ^{+0.65} _{-0.28}	¹³ ISHIKAWA	08	LATT
4.026 ± 0.048	¹⁴ NAKAMURA	08	LATT
4.25 ± 0.35	¹⁵ BLUM	07	LATT
4.08 ± 0.25 ± 0.42	¹⁶ GOCKELER	06	LATT
4.7 ± 0.2 ± 0.3	¹⁷ GOCKELER	06A	LATT
3.2 ± 0.3	¹⁸ MASON	06	LATT
3.95 ± 0.3	¹⁹ NARISON	06	THEO
2.8 ± 0.3	²⁰ AUBIN	04	LATT
4.29 ± 0.14 ± 0.65	²¹ AOKI	03	LATT
3.223 ± 0.3	²² AOKI	03B	LATT
4.4 ± 0.1 ± 0.4	²³ BECIREVIC	03	LATT
4.1 ± 0.3 ± 1.0	²⁴ CHIU	03	LATT

WEIGHTED AVERAGE
3.46±0.04 (Error scaled by 1.1)



WEIGHTED AVERAGE
4.68±0.08 (Error scaled by 1.8)



$$\overline{m} = (m_u + m_d)/2$$

See the comments for the *u* quark above.

We have normalized the \overline{m}_S masses at a renormalization scale of $\mu = 2$ GeV. Results quoted in the literature at $\mu = 1$ GeV have been rescaled by dividing by 1.35. The values of "Our Evaluation" were determined in part via Figures 1 and 2.

\overline{m}_S MASS (MeV)	DOCUMENT ID	TECN
3.45 ^{+0.55} _{-0.15} OUR EVALUATION	See the ideogram below.	
3.9 ± 0.3	¹ DOMINGUEZ 19	THEO
4.7 ^{+0.8} _{-0.7}	² YUAN 17	THEO
3.70 ± 0.17	³ CARRASCO 14	LATT
3.45 ± 0.12	⁴ ARTHUR 13	LATT
3.469 ± 0.047 ± 0.048	⁵ DURR 11	LATT
3.6 ± 0.2	⁶ BLOSSIER 10	LATT
3.39 ± 0.06	⁷ MCNEILE 10	LATT

- ¹ DOMINGUEZ 19 determine the quark mass from a QCD finite energy sum rule for the divergence of the axial current.
- ² YUAN 17 determine \overline{m} using QCD sum rules in the isospin $I=0$ scalar channel. At the end of the "Numerical Results" section of YUAN 17 the authors discuss the significance of their larger value of the light quark mass compared to previous determinations.
- ³ CARRASCO 14 is a lattice QCD computation of light quark masses using $2 + 1 + 1$ dynamical quarks, with $m_u = m_d \neq m_s \neq m_c$. The *u* and *d* quark masses are obtained separately by using the *K* meson mass splittings and lattice results for the electromagnetic contributions.
- ⁴ ARTHUR 13 is a lattice computation using $2+1$ dynamical domain wall fermions. Masses at $\mu = 3$ GeV have been converted to $\mu = 2$ GeV using conversion factors given in their paper.
- ⁵ DURR 11 determine quark mass from a lattice computation of the meson spectrum using $N_f = 2 + 1$ dynamical flavors. The lattice simulations were done at the physical quark mass, so that extrapolation in the quark mass was not needed.
- ⁶ BLOSSIER 10 determines quark masses from a computation of the hadron spectrum using $N_f=2$ dynamical twisted-mass Wilson fermions.
- ⁷ DAVIES 10 and MCNEILE 10 determine $\overline{m}_c(\mu)/\overline{m}_s(\mu) = 11.85 \pm 0.16$ using a lattice computation with $N_f = 2 + 1$ dynamical fermions of the pseudoscalar meson masses. Mass \overline{m} is obtained from this using the value of m_c from ALLISON 08 or MCNEILE 10 and the BAZAVOV 10 values for the light quark mass ratio, m_s/\overline{m} .
- ⁸ AOKI 11A determine quark masses from a lattice computation of the hadron spectrum using $N_f = 2 + 1$ dynamical flavors of domain wall fermions.
- ⁹ DOMINGUEZ 09 use QCD finite energy sum rules for the two-point function of the divergence of the axial vector current computed to order α_s^4 .
- ¹⁰ ALLTON 08 use a lattice computation of the π, K , and Ω masses with $2+1$ dynamical flavors of domain wall quarks, and non-perturbative renormalization.
- ¹¹ BLOSSIER 08 use a lattice computation of pseudoscalar meson masses and decay constants with 2 dynamical flavors and non-perturbative renormalization.
- ¹² DOMINGUEZ-CLARIMON 08B obtain an inequality from sum rules for the scalar two-point correlator.
- ¹³ ISHIKAWA 08 use a lattice computation of the light meson spectrum with $2+1$ dynamical flavors of $C(a)$ improved Wilson quarks, and one-loop perturbative renormalization.
- ¹⁴ NAKAMURA 08 do a lattice computation using quenched domain wall fermions and non-perturbative renormalization.
- ¹⁵ BLUM 07 determine quark masses from the pseudoscalar meson masses using a QED plus QCD lattice computation with two dynamical quark flavors.
- ¹⁶ GOCKELER 06 use an unquenched lattice computation of the axial Ward Identity with $N_f = 2$ dynamical light quark flavors, and non-perturbative renormalization, to obtain $\overline{m}(2 \text{ GeV}) = 4.08 \pm 0.25 \pm 0.19 \pm 0.23$ MeV, where the first error is statistical, the second and third are systematic due to the fit range and force scale uncertainties, respectively. We have combined the systematic errors linearly.
- ¹⁷ GOCKELER 06A use an unquenched lattice computation of the pseudoscalar meson masses with $N_f = 2$ dynamical light quark flavors, and non-perturbative renormalization.

See key on page 999

Quark Particle Listings

Light Quarks (*u, d, s*)

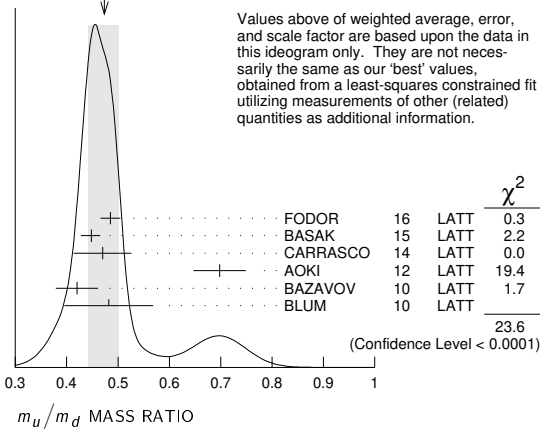
- ¹⁸ MASON 06 extract light quark masses from a lattice simulation using staggered fermions with an improved action, and three dynamical light quark flavors with degenerate *u* and *d* quarks. Perturbative corrections were included at NNLO order.
- ¹⁹ NARISON 06 uses sum rules for $e^+e^- \rightarrow$ hadrons to order α_s^3 to determine m_s combined with other determinations of the quark mass ratios.
- ²⁰ AUBIN 04 perform three flavor dynamical lattice calculation of pseudoscalar meson masses, with one-loop perturbative renormalization constant.
- ²¹ AOKI 03 uses quenched lattice simulation of the meson and baryon masses with degenerate light quarks. The extrapolations are done using quenched chiral perturbation theory.
- ²² The errors given in AOKI 03b were $+0.046$ -0.069 . We changed them to ± 0.3 for calculating the overall best values. AOKI 03b uses lattice simulation of the meson and baryon masses with two dynamical light quarks. Simulations are performed using the $O(a)$ improved Wilson action.
- ²³ BECIREVIC 03 perform quenched lattice computation using the vector and axial Ward identities. Uses $O(a)$ improved Wilson action and nonperturbative renormalization.
- ²⁴ CHIU 03 determines quark masses from the pion and kaon masses using a lattice simulation with a chiral fermion action in quenched approximation.

m_u/m_d MASS RATIO

VALUE	DOCUMENT ID	TECN	COMMENT
0.47 \pm 0.06	OUR EVALUATION		See the ideogram below.
0.485 \pm 0.011 \pm 0.016	1 FODOR	16 LATT	
0.4482 \pm 0.0173 -0.0206	2 BASAK	15 LATT	
0.470 \pm 0.056	3 CARRASCO	14 LATT	
0.698 \pm 0.051	4 AOKI	12 LATT	
0.42 \pm 0.01 \pm 0.04	5 BAZAVOV	10 LATT	
0.4818 \pm 0.0096 \pm 0.0860	6 BLUM	10 LATT	
••• We do not use the following data for averages, fits, limits, etc. •••			
0.550 \pm 0.031	7 BLUM	07 LATT	
0.43 \pm 0.08	8 AUBIN	04A LATT	
0.410 \pm 0.036	9 NELSON	03 LATT	
0.553 \pm 0.043	10 LEUTWYLER	96 THEO	Compilation

- ¹ FODOR 16 is a lattice simulation with $N_f = 2 + 1$ dynamical flavors and includes partially quenched QED effects.
- ² BASAK 15 is a lattice computation using 2+1 dynamical quark flavors.
- ³ CARRASCO 14 is a lattice QCD computation of light quark masses using 2 + 1 + 1 dynamical quarks, with $m_u = m_d \neq m_s \neq m_c$. The *u* and *d* quark masses are obtained separately by using the *K* meson mass splittings and lattice results for the electromagnetic contributions.
- ⁴ AOKI 12 is a lattice computation using 1 + 1 + 1 dynamical quark flavors.
- ⁵ BAZAVOV 10 is a lattice computation using 2+1 dynamical quark flavors.
- ⁶ BLUM 10 is a lattice computation using 2+1 dynamical quark flavors.
- ⁷ BLUM 07 determine quark masses from the pseudoscalar meson masses using a QED plus QCD lattice computation with two dynamical quark flavors.
- ⁸ AUBIN 04a perform three flavor dynamical lattice calculation of pseudoscalar meson masses, with continuum estimate of electromagnetic effects in the kaon masses.
- ⁹ NELSON 03 computes coefficients in the order p^4 chiral Lagrangian using a lattice calculation with three dynamical flavors. The ratio m_u/m_d is obtained by combining this with the chiral perturbation theory computation of the meson masses to order p^4 .
- ¹⁰ LEUTWYLER 96 uses a combined fit to $\eta \rightarrow 3\pi$ and $\psi' \rightarrow J/\psi(\pi, \eta)$ decay rates, and the electromagnetic mass differences of the π and *K*.

WEIGHTED AVERAGE
0.474 \pm 0.029 (Error scaled by 2.4)



s-QUARK MASS

See the comment for the *u* quark above.

We have normalized the \overline{MS} masses at a renormalization scale of $\mu = 2$ GeV. Results quoted in the literature at $\mu = 1$ GeV have been rescaled by dividing by 1.35.

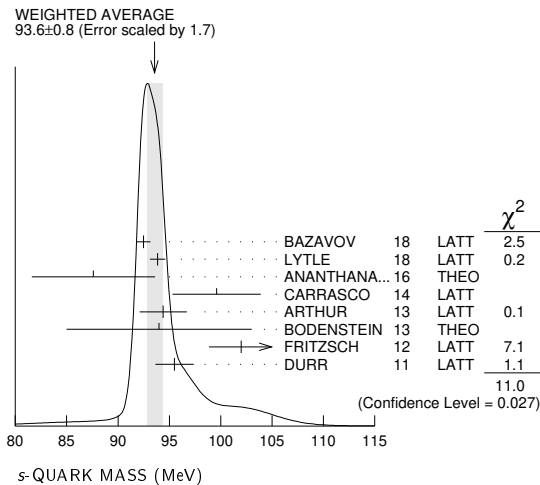
\overline{MS} MASS (MeV)	DOCUMENT ID	TECN
93 \pm 11	OUR EVALUATION	See the ideogram below.
92.47 \pm 0.69	1 BAZAVOV	18 LATT
93.85 \pm 0.75	2 LYTLE	18 LATT
87.6 \pm 6.0	3 ANANTHANA	16 THEO
99.6 \pm 4.3	4 CARRASCO	14 LATT
94.4 \pm 2.3	5 ARTHUR	13 LATT
94 \pm 9	6 BODENSTEIN	13 THEO
102 \pm 3 \pm 1	7 FRITZSCH	12 LATT
95.5 \pm 1.1 \pm 1.5	8 DURR	11 LATT
••• We do not use the following data for averages, fits, limits, etc. •••		
93.6 \pm 0.8	9 CHAKRABORTY	15 LATT
96.2 \pm 2.7	10 AOKI	11A LATT
95 \pm 6	11 BLOSSIER	10 LATT
97.6 \pm 2.9 \pm 5.5	12 BLUM	10 LATT
92.4 \pm 1.5	13 DAVIES	10 LATT
92.2 \pm 1.3	14 MCNEILE	10 LATT
107.3 \pm 11.7	14 ALLTON	08 LATT
105 \pm 3 \pm 9	15 BLOSSIER	08 LATT
102 \pm 8	16 DOMINGUEZ	08A THEO
90.1 \pm 17.2 -6.1	17 ISHIKAWA	08 LATT
105.6 \pm 1.2	18 NAKAMURA	08 LATT
119.5 \pm 9.3	19 BLUM	07 LATT
105 \pm 6 \pm 7	20 CHETYRKIN	06 THEO
111 \pm 6 \pm 10	21 GOCKELER	06 LATT
119 \pm 5 \pm 8	22 GOCKELER	06A LATT
92 \pm 9	23 JAMIN	06 THEO
87 \pm 6	24 MASON	06 LATT
104 \pm 15	25 NARISON	06 THEO
$\geq 71 \pm 4, \leq 151 \pm 14$	26 NARISON	06 THEO
96 \pm 5 \pm 16 -18	27 BAIKOV	05 THEO
81 \pm 22	28 GAMIZ	05 THEO
125 \pm 28	29 GORBUNOV	05 THEO
93 \pm 32	30 NARISON	05 THEO
76 \pm 8	31 AUBIN	04 LATT
116 \pm 6 \pm 0.65	32 AOKI	03 LATT
84.5 \pm 12 -1.7	33 AOKI	03B LATT
106 \pm 2 \pm 8	34 BECIREVIC	03 LATT
92 \pm 9 \pm 16	35 CHIU	03 LATT
117 \pm 17	36 GAMIZ	03 THEO
103 \pm 17	37 GAMIZ	03 THEO

- ¹ BAZAVOV 18 determine the quark masses using a lattice computation with staggered fermions and four active quark flavors.
- ² LYTLE 18 combined with CHAKRABORTY 2015 determine $\overline{m}_s(3 \text{ GeV}) = 84.78 \pm 0.65$ MeV from a lattice simulation with $n_f = 2+1+1$ flavors. They also determine the quoted value $\overline{m}_s(2 \text{ GeV})$ for $n_f = 4$ dynamical flavors.
- ³ ANANTHANARAYAN 16 determine $\overline{m}_s(2 \text{ GeV}) = 106.70 \pm 9.36$ MeV and 74.47 ± 7.77 MeV from fits to ALEPH and OPAL τ decay data, respectively. We have used the weighted average of the two.
- ⁴ CARRASCO 14 is a lattice QCD computation of light quark masses using 2 + 1 + 1 dynamical quarks, with $m_u = m_d \neq m_s \neq m_c$. The *u* and *d* quark masses are obtained separately by using the *K* meson mass splittings and lattice results for the electromagnetic contributions.
- ⁵ ARTHUR 13 is a lattice computation using 2+1 dynamical domain wall fermions. Masses at $\mu = 3$ GeV have been converted to $\mu = 2$ GeV using conversion factors given in their paper.
- ⁶ BODENSTEIN 13 determines m_s from QCD finite energy sum rules, and the perturbative computation of the pseudoscalar correlator to five-loop order.
- ⁷ FRITZSCH 12 determine m_s using a lattice computation with $N_f = 2$ dynamical flavors.
- ⁸ DURR 11 determine quark mass from a lattice computation of the meson spectrum using $N_f = 2 + 1$ dynamical flavors. The lattice simulations were done at the physical quark mass, so that extrapolation in the quark mass was not needed.
- ⁹ CHAKRABORTY 15 is a lattice QCD computation that determines m_c and m_c/m_s using pseudoscalar mesons masses tuned on gluon field configurations with 2+1+1 dynamical flavors of HISQ quarks with *u/d* masses down to the physical value.
- ¹⁰ AOKI 11A determine quark masses from a lattice computation of the hadron spectrum using $N_f = 2 + 1$ dynamical flavors of domain wall fermions.
- ¹¹ BLOSSIER 10 determines quark masses from a computation of the hadron spectrum using $N_f=2$ dynamical twisted-mass Wilson fermions.
- ¹² BLUM 10 determines light quark masses using a QCD plus QED lattice computation of the electromagnetic mass splittings of the low-lying hadrons. The lattice simulations use 2+1 dynamical quark flavors.
- ¹³ DAVIES 10 and MCNEILE 10 determine $\overline{m}_c(\mu)/\overline{m}_s(\mu) = 11.85 \pm 0.16$ using a lattice computation with $N_f = 2 + 1$ dynamical fermions of the pseudoscalar meson masses. Mass m_s is obtained from this using the value of m_c from ALLISON 08 or MCNEILE 10.
- ¹⁴ ALLTON 08 use a lattice computation of the π , *K*, and Ω masses with 2+1 dynamical flavors of domain wall quarks, and non-perturbative renormalization.
- ¹⁵ BLOSSIER 08 use a lattice computation of pseudoscalar meson masses and decay constants with 2 dynamical flavors and non-perturbative renormalization.
- ¹⁶ DOMINGUEZ 08A make determination from QCD finite energy sum rules for the pseudoscalar two-point function computed to order a^4 .
- ¹⁷ ISHIKAWA 08 use a lattice computation of the light meson spectrum with 2+1 dynamical flavors of $O(a)$ improved Wilson quarks, and one-loop perturbative renormalization.
- ¹⁸ NAKAMURA 08 do a lattice computation using quenched domain wall fermions and non-perturbative renormalization.

Quark Particle Listings

Light Quarks (*u, d, s*)

- ¹⁹BLUM 07 determine quark masses from the pseudoscalar meson masses using a QED plus QCD lattice computation with two dynamical quark flavors.
- ²⁰CHETYRKIN 06 use QCD sum rules in the pseudoscalar channel to order α_s^4 .
- ²¹GOCKELER 06 use an unquenched lattice computation of the axial Ward Identity with $N_f = 2$ dynamical light quark flavors, and non-perturbative renormalization, to obtain $\overline{m}_s(2 \text{ GeV}) = 111 \pm 6 \pm 4 \pm 6 \text{ MeV}$, where the first error is statistical, the second and third are systematic due to the fit range and force scale uncertainties, respectively. We have combined the systematic errors linearly.
- ²²GOCKELER 06A use an unquenched lattice computation of the pseudoscalar meson masses with $N_f = 2$ dynamical light quark flavors, and non-perturbative renormalization.
- ²³JAMIN 06 determine $\overline{m}_s(2 \text{ GeV})$ from the spectral function for the scalar $K\pi$ form factor.
- ²⁴MASON 06 extract light quark masses from a lattice simulation using staggered fermions with an improved action, and three dynamical light quark flavors with degenerate u and d quarks. Perturbative corrections were included at NNLO order.
- ²⁵NARISON 06 uses sum rules for $e^+e^- \rightarrow$ hadrons to order α_s^3 .
- ²⁶NARISON 06 obtains the quoted range from positivity of the spectral functions.
- ²⁷BAIKOV 05 determines $\overline{m}_s(M_\tau) = 100^{+5}_{-3} +^{17}_{-19}$ from sum rules using the strange spectral function in τ decay. The computations were done to order α_s^3 , with an estimate of the α_s^4 terms. We have converted the result to $\mu = 2 \text{ GeV}$.
- ²⁸GAMIZ 05 determines $\overline{m}_s(2 \text{ GeV})$ from sum rules using the strange spectral function in τ decay. The computations were done to order α_s^2 , with an estimate of the α_s^3 terms.
- ²⁹GORBUNOV 05 use hadronic tau decays to N3LO, including power corrections.
- ³⁰NARISON 05 determines $\overline{m}_s(2 \text{ GeV})$ from sum rules using the strange spectral function in τ decay. The computations were done to order α_s^3 .
- ³¹AUBIN 04 perform three flavor dynamical lattice calculation of pseudoscalar meson masses, with one-loop perturbative renormalization constant.
- ³²AOKI 03 uses quenched lattice simulation of the meson and baryon masses with degenerate light quarks. The extrapolations are done using quenched chiral perturbation theory. Determines $m_s = 113.8 \pm 2.3^{+5.8}_{-2.9}$ using K mass as input and $m_s = 142.3 \pm 5.8^{+22}_{-0}$ using ϕ mass as input. We have performed a weighted average of these values.
- ³³AOKI 03b uses lattice simulation of the meson and baryon masses with two dynamical light quarks. Simulations are performed using the $\mathcal{O}(a)$ improved Wilson action.
- ³⁴BEČIREVIĆ 03 perform quenched lattice computation using the vector and axial Ward identities. Uses $\mathcal{O}(a)$ improved Wilson action and nonperturbative renormalization. They also quote $\overline{m}/m_s = 24.3 \pm 0.2 \pm 0.6$.
- ³⁵CHIU 03 determines quark masses from the pion and kaon masses using a lattice simulation with a chiral fermion action in quenched approximation.
- ³⁶GAMIZ 03 determines m_s from SU(3) breaking in the τ hadronic width. The value of V_{us} is chosen to satisfy CKM unitarity.
- ³⁷GAMIZ 03 determines m_s from SU(3) breaking in the τ hadronic width. The value of V_{us} is taken from the PDG.



OTHER LIGHT QUARK MASS RATIOS

m_s/m_d MASS RATIO

VALUE	DOCUMENT ID	TECN	COMMENT
17-22 OUR EVALUATION			
20.0	1 GAO	97 THEO	
18.9 ± 0.8	2 LEUTWYLER	96 THEO	Compilation
21	3 DONOGHUE	92 THEO	
18	4 GERARD	90 THEO	
18 to 23	5 LEUTWYLER	90b THEO	

- ¹GAO 97 uses electromagnetic mass splittings of light mesons.
- ²LEUTWYLER 96 uses a combined fit to $\eta \rightarrow 3\pi$ and $\psi' \rightarrow J/\psi(\pi, \eta)$ decay rates, and the electromagnetic mass differences of the π and K .
- ³DONOGHUE 92 result is from a combined analysis of meson masses, $\eta \rightarrow 3\pi$ using second-order chiral perturbation theory including nonanalytic terms, and $(\psi(2S) \rightarrow J/\psi(1S)\pi)/(\psi(2S) \rightarrow J/\psi(1S)\eta)$.
- ⁴GERARD 90 uses large N and η - η' mixing.
- ⁵LEUTWYLER 90b determines quark mass ratios using second-order chiral perturbation theory for the meson and baryon masses, including nonanalytic corrections. Also uses Weinberg sum rules to determine L_7 .

m_s/\overline{m} MASS RATIO

$$\overline{m} \equiv (m_u + m_d)/2$$

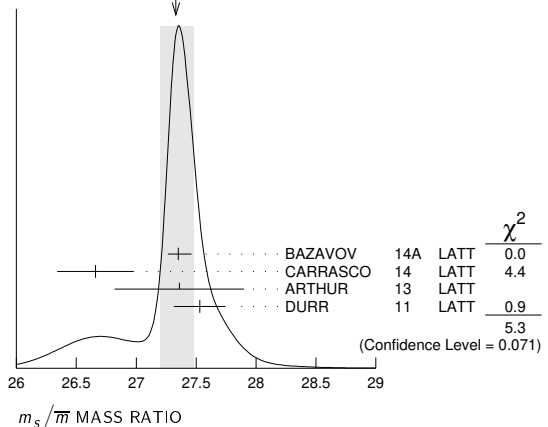
VALUE	DOCUMENT ID	TECN
-------	-------------	------

27.3 ± 0.7 OUR EVALUATION See the ideogram below.

27.35 ± 0.05 ^{+0.10} _{-0.07}	1 BAZAVOV	14A LATT
26.66 ± 0.32	2 CARRASCO	14 LATT
27.36 ± 0.54	3 ARTHUR	13 LATT
27.53 ± 0.20 ± 0.08	4 DURR	11 LATT
26.8 ± 1.4	5 AOKI	11A LATT
27.3 ± 0.9	6 BLOSSIER	10 LATT
28.8 ± 1.65	7 ALLTON	08 LATT
27.3 ± 0.3 ± 1.2	8 BLOSSIER	08 LATT
23.5 ± 1.5	9 OLLER	07A THEO
27.4 ± 0.4	10 AUBIN	04 LATT

- ¹BAZAVOV 14A is a lattice computation using 4 dynamical flavors of HISQ fermions.
- ²CARRASCO 14 is a lattice QCD computation of light quark masses using 2 + 1 + 1 dynamical quarks, with $m_u = m_d \neq m_s \neq m_c$. The u and d quark masses are obtained separately by using the K meson mass splittings and lattice results for the electromagnetic contributions.
- ³ARTHUR 13 is a lattice computation using 2+1 dynamical domain wall fermions.
- ⁴DURR 11 determine quark mass from a lattice computation of the meson spectrum using $N_f = 2 + 1$ dynamical flavors. The lattice simulations were done at the physical quark mass, so that extrapolation in the quark mass was not needed.
- ⁵AOKI 11A determine quark masses from a lattice computation of the hadron spectrum using $N_f = 2 + 1$ dynamical flavors of domain wall fermions.
- ⁶BLOSSIER 10 determines quark masses from a computation of the hadron spectrum using $N_f=2$ dynamical twisted-mass Wilson fermions.
- ⁷ALLTON 08 use a lattice computation of the π , K , and Ω masses with 2+1 dynamical flavors of domain wall quarks, and non-perturbative renormalization.
- ⁸BLOSSIER 08 use a lattice computation of pseudoscalar meson masses and decay constants with 2 dynamical flavors and non-perturbative renormalization.
- ⁹OLLER 07A use unitarized chiral perturbation theory to order p^4 .
- ¹⁰Three flavor dynamical lattice calculation of pseudoscalar meson masses.

WEIGHTED AVERAGE
27.33 ± 0.15 - 0.12 (Error scaled by 1.6)



Q MASS RATIO

$$Q \equiv \sqrt{(m^2_s - \overline{m}^2)/(m^2_d - m^2_u)}; \quad \overline{m} \equiv (m_u + m_d)/2$$

VALUE	DOCUMENT ID	TECN
-------	-------------	------

••• We do not use the following data for averages, fits, limits, etc. •••

22.1 ± 0.7	1 COLANGELO	18 THEO
22.0 ± 0.7	2 COLANGELO	17 THEO
21.6 ± 1.1	3 GUO	17 THEO
23.4 ± 0.4 ± 0.5	4 FODOR	16 LATT
21.4 ± 0.4	5 GUO	15F THEO
22.8 ± 0.4	6 MARTEMYA..	05 THEO
22.7 ± 0.8	7 ANISOVICH	96 THEO

- ¹COLANGELO 18 obtain Q from a dispersive analysis of $\eta \rightarrow 3\pi$ decay.
- ²COLANGELO 17 obtain Q from a dispersive analysis of KLOE collaboration data on $\eta \rightarrow \pi^+\pi^-\pi^0$ decays and chiral perturbation theory input.
- ³GUO 17 determine Q from a dispersive model fit to KLOE and WASA-at-COSY data on $\eta \rightarrow \pi^+\pi^-\pi^0$ decay and matching to chiral perturbation theory.
- ⁴FODOR 16 is a lattice simulation with $N_f = 2 + 1$ dynamical flavors and includes partially quenched QED effects.
- ⁵GUO 15F determine Q from a Khuri-Treiman analysis of $\eta \rightarrow 3\pi$ decays.
- ⁶MARTEMYANOV 05 determine Q from $\eta \rightarrow 3\pi$ decay.
- ⁷ANISOVICH 96 find Q from $\eta \rightarrow \pi^+\pi^-\pi^0$ decay using dispersion relations and chiral perturbation theory.

LIGHT QUARKS (*u, d, s*) REFERENCES

DOMINGUEZ 19	JHEP 1902 057	C.A. Dominguez, A. Mes, K. Schilcher (CAPE, MAINZ)
BAZAVOV 18	PR D98 054517	A. Bazavov et al. (Fermilab Lattice, MILC, TUMQCD)
COLANGELO 18	EJ 078 947	G. Colangelo et al.
LYTLE 18	PR D98 014513	A.T. Lytle et al. (HPQCD Collab.)
COLANGELO 17	PRL 118 022001	G. Colangelo et al. (BERN, IND, JLAB)
GUO 17	PL B771 497	P. Guo et al.
YUAN 17	PR D96 014034	J.-M. Yuan et al.
ANANTHANA... 16	PR D94 116014	Z. Ananthanarayan, D. Das (BANG, AHMED)
FODOR 16	PRL 117 082001	F. Fodor et al. (BMW Collab.)
BASAK 15	JPCS 640 012052	S. Basak et al. (MILC Collab.)
CHAKRABOR... 15	PR D91 054508	B. Chakraborty et al. (HPQCD Collab.)
GUO 15F	PR D92 054016	P. Guo et al.
BAZAVOV 14A	PR D90 074509	A. Bazavov et al. (Fermi-LAT and MILC Collabs.)
CARRASCO 14	NP B887 19	N. Carrasco et al. (European Twisted Mass Collab.)
ARTHUR 13	PR D87 094514	R. Arthur et al. (RBC and UKQCD Collabs.)
BODENSTEIN 13	JHEP 1307 138	S. Bodenstein, C.A. Dominguez, K. Schilcher (MANZ+)
AOKI 12	PR D86 034507	S. Aoki et al. (PACS-CS Collab.)
FRITZSCH 12	NP B865 397	P. Fritzsche et al. (ALPHA Collab.)
AOKI 11A	PR D83 074508	Y. Aoki et al. (RBC-UKQCD Collab.)
DURR 11	PL B701 265	S. Durr et al. (BMW Collab.)
BAZAVOV 10	RMP 82 1349	A. Bazavov et al. (MILC Collab.)
BLOSSIER 10	PR D82 114513	B. Blossier et al. (ETM Collab.)
BLUM 10	PR D82 094508	T. Blum et al.
DAVIES 10	PRL 104 132003	C.H. Davies et al. (HPQCD Collab.)
MCNEILE 10	PR D82 034512	C. McNeile et al. (HPQCD Collab.)
DOMINGUEZ 09	PR D79 014009	C.A. Dominguez et al.
ALLISON 08	PR D78 054513	L. Allison et al. (HPQCD Collab.)
ALLTON 08	PR D78 114509	C. Allton et al. (RBC and UKQCD Collabs.)
BLOSSIER 08	JHEP 0804 020	B. Blossier et al. (ETM Collab.)
DEANDREA 08	PR D78 034032	A. Deandrea, A. Nehme, P. Talavera
DOMINGUEZ 08A	JHEP 0805 020	C.A. Dominguez et al.
DOMINGUEZ... 08B	PL B660 49	A. Dominguez-Clarimon, E. de Rafael, J. Tarón
ISHIKAWA 08	PR D78 011502	T. Ishikawa et al. (CP-PACS and JLQCD Collabs.)
NAKAMURA 08	PR D78 034502	Y. Nakamura et al. (CP-PACS Collab.)
BLUM 07	PR D76 114508	T. Blum et al.
OLLER 07A	EJ A34 371	J.A. Oller, L. Roca
CHETYRKIN 06	EJ 646 721	K.G. Chetyrkin, A. Khodjamirian
GOCKELER 06	PR D73 054508	M. Gockeler et al. (QCDSF and UKQCD Collabs.)
GOCKELER 06A	PL B639 307	M. Gockeler et al. (QCDSF and UKQCD Collabs.)
JAMIN 06	PR D74 074009	M. Jamin, J.A. Oller, A. Pich
MASON 06	PR D73 114501	Q. Mason et al. (HPQCD Collab.)
NARISON 06	PR D74 034013	S. Narison
PDG 06	JG 333 1	W.-M. Yao et al. (PDG Collab.)
BAIKOV 05	PRL 95 012003	P.A. Baikov, K.G. Chetyrkin, J.H. Kuhn
GAMIZ 05	PRL 94 011803	E. Gamiz et al.
GORBUNOV 05	PR D71 013002	D.S. Gorbunov, A.A. Pivovarov
MARTEMYAN... 05	PR D71 017501	V.V. Martemyanov, V.S. Sopot
NARISON 05	PL B626 101	S. Narison
AUBIN 04	PR D70 031504	C. Aubin et al. (HPQCD, MILC, UKQCD Collabs.)
AUBIN 04A	PR D70 114501	C. Aubin et al. (MILC Collab.)
AOKI 03	PR D67 034503	S. Aoki et al. (CP-PACS Collab.)
AOKI 03B	PR D68 054502	S. Aoki et al. (CP-PACS Collab.)
BECIREVIC 03	PL B558 69	D. Becirevic, V. Lubicz, C. Tarantino
CHIU 03	NP B673 217	T.-W. Chiu, T.-H. Hsieh
GAMIZ 03	JHEP 0301 060	E. Gamiz et al.
NELSON 03	PRL 90 021601	D. Nelson, G.T. Fleming, G.W. Kilcup
GAO 97	PR D56 4115	A.N. Gao, B.A. Li, M.-L. Yan
ANISOVICH 96	PL B375 335	A.V. Anisovich, H. Leutwyler
LEUTWYLER 96	PL B378 313	H. Leutwyler
DONOGHUE 92	PRL 69 3444	J.F. Donoghue, B.R. Holstein, D. Wyler (MASA+)
GERARD 90	MPL A5 391	J.M. Gerard (MPIM)
LEUTWYLER 90B	NP B337 108	H. Leutwyler (BERN)

21	ABRAMOWICZ13c	COMB	1.26 ± 0.05 ± 0.04
22	DEHNADI 13	THEO	1.282 ± 0.011 ± 0.022
23	NARISON 13	THEO	1.286 ± 0.066
24	ALEKHIN 12	THEO	1.36 ± 0.04 ± 0.10
25	NARISON 12A	THEO	1.261 ± 0.016
26	ALEKHIN 11	THEO	1.01 ± 0.09 ± 0.03
27	BLOSSIER 10	LATT	1.28 ± 0.04
28	BODENSTEIN 10	THEO	1.299 ± 0.026
29	MCNEILE 10	LATT	1.273 ± 0.006
30	NARISON 10	THEO	1.261 ± 0.018
31	CHETYRKIN 09	THEO	1.279 ± 0.013
32	ALLISON 08	LATT	1.268 ± 0.009
33	KUHN 07	THEO	1.286 ± 0.013
34	BOUGHEZAL 06	THEO	1.295 ± 0.015
35	BUCHMUEL... 06	THEO	1.24 ± 0.09
36	HOANG 06	THEO	1.224 ± 0.017 ± 0.054
37	AUBERT 04x	THEO	1.33 ± 0.10
38	HOANG 04	THEO	1.29 ± 0.07
39	DEDIVITIIS 03	LATT	1.319 ± 0.028
40	EIDEMULLER 03	THEO	1.19 ± 0.11
41	ERLER 03	THEO	1.289 ± 0.043
42	ZYABLYUK 03	THEO	1.26 ± 0.02

- 1 NARISON 20 determines the quark mass using QCD Laplace sum rules from the B_c mass, combined with previous determinations of the QCD condensates and c and b masses.
- 2 ABRAMOWICZ 18 determine $\overline{m}_c(\overline{m}_c) = 1.290 \pm 0.046 \pm 0.062 \pm 0.003$ from the production of c quarks in $e p$ collisions at HERA using combined H1 and ZEUS data. The experimental/fitting errors, and those from modeling and parameterization have been combined in quadrature.
- 3 BAZAVOV 18 determine the quark masses using a lattice computation with staggered fermions and four active quark flavors.
- 4 LYTLE 18 combined with CHAKRABORTY 15 determine $\overline{m}_c(3 \text{ GeV}) = 0.9874(48) \text{ GeV}$ from a lattice simulation with $n_f = 2+1+1$ flavors. They also determine the quoted value $\overline{m}_c(\overline{m}_c)$ for $n_f = 4$ dynamical flavors.
- 5 PESET 18 determine $\overline{m}_c(\overline{m}_c)$ and $\overline{m}_b(\overline{m}_b)$ using an N3LO calculation of the η_c, η_b and B_c masses.
- 6 CHETYRKIN 17 determine $\overline{m}_c(\mu = 3 \text{ GeV}) = 0.993 \pm 0.008 \text{ GeV}$ and $\overline{m}_c(\overline{m}_c)$ from a four-loop sum-rule computation of the cross-section for $e^+e^- \rightarrow$ hadrons in the charm threshold region.
- 7 ERLER 17 determine $\overline{m}_c(\overline{m}_c) = 1.272 \pm 0.008 \text{ GeV}$ from a three-loop QCD sum-rule computation of the vector current correlator. This result is for fixed $\alpha_s(M_Z) = 0.1182$. Including an α_s uncertainty of ± 0.0016 , the charm mass error increases from 8 to 9 MeV.
- 8 KIYO 16 determine $\overline{m}_c(\overline{m}_c)$ from the $J/\psi(1S)$ mass at order α_s^3 (N3LO).
- 9 DEHNADI 15 determine $\overline{m}_c(\overline{m}_c)$ using sum rules for $e^+e^- \rightarrow$ hadrons at order α_s^3 (N3LO), and fitting to both experimental data and lattice results.
- 10 CARRASCO 14 is a lattice QCD computation of light quark masses using $2 + 1 + 1$ dynamical quarks, with $m_u = m_d \neq m_s \neq m_c$. The u and d quark masses are obtained separately by using the K meson mass splittings and lattice results for the electromagnetic contributions.
- 11 ALEKHIN 13 determines m_c from charm production in deep inelastic scattering at HERA using approximate NNLO QCD.
- 12 SAMOYLOV 13 determines m_c from a study of charm dimuon production in neutrino-iron scattering using the NLO QCD result for the charm quark production cross section.
- 13 BODENSTEIN 11 determine $\overline{m}_c(3 \text{ GeV}) = 0.987 \pm 0.009 \text{ GeV}$ and $\overline{m}_c(\overline{m}_c) = 1.278 \pm 0.009 \text{ GeV}$ using QCD sum rules for the charm quark vector current correlator.
- 14 LASCHKA 11 determine the c mass from the charmonium spectrum. The theoretical computation uses the heavy $Q\overline{Q}$ potential to order $1/m_Q$ obtained by matching the short-distance perturbative result onto lattice QCD result at larger scales.
- 15 AUBERT 10A determine the b - and c -quark masses from a fit to the inclusive decay spectra in semileptonic B decays in the kinetic scheme (and convert it to the \overline{MS} scheme).
- 16 SIGNER 09 determines the c -quark mass using non-relativistic sum rules to analyze the $e^+e^- \rightarrow c\overline{c}$ cross-section near threshold. Also determine the PS mass $m_{PS}(\mu_P = 0.7 \text{ GeV}) = 1.50 \pm 0.04 \text{ GeV}$.
- 17 NARISON 18A determines simultaneously $\overline{m}_c(\overline{m}_c)$ and the 4-dimension gluon condensate using QCD exponential sum rules and their ratios evaluated at the optimal scale $\mu = 2.85 \text{ GeV}$ at N2LO-N3LO of perturbative QCD and including condensates up to dimension 6-8 in the (axial-)vector and (pseudo-)scalar charmonium channels.
- 18 NARISON 18B determines $\overline{m}_c(\overline{m}_c)$ using QCD vector moment sum rules and their ratios at N2LO-N3LO of perturbative QCD and including condensates up to dimension 8.
- 19 BERTONE 16 determine $\overline{m}_c(\overline{m}_c)$ from HERA deep inelastic scattering data using the FONLL scheme. Also determine $\overline{m}_c(\overline{m}_c) = 1.318 \pm 0.054 \pm 0.490 \pm 0.022$ using the fixed flavor number scheme.
- 20 CHAKRABORTY 15 is a lattice QCD computation using $2+1+1$ dynamical flavors. Moments of pseudoscalar current-current correlators are matched to α_s^3 -accurate QCD perturbation theory with the η_c meson mass tuned to experiment.
- 21 ABRAMOWICZ 13c determines m_c from charm production in deep inelastic $e p$ scattering, using the QCD prediction at NLO order. The uncertainties from model and parameterization assumptions, and the value of α_s , of ± 0.03 , ± 0.02 , and ± 0.02 respectively, have been combined in quadrature.
- 22 DEHNADI 13 determines m_c using QCD sum rules for the charmonium spectrum and charm continuum to order α_s^3 (N3LO). The statistical and systematic experimental errors of ± 0.006 and ± 0.009 have been combined in quadrature. The theoretical uncertainties ± 0.019 from truncation of the perturbation series, ± 0.010 from α_s , and ± 0.002 from the gluon condensate have been combined in quadrature.
- 23 NARISON 13 determines m_c using QCD spectral sum rules to order α_s^2 (NNLO) and including condensates up to dimension 6.
- 24 ALEKHIN 12 determines m_c from heavy quark production in deep inelastic scattering at HERA using approximate NNLO QCD.
- 25 NARISON 12A determines m_c using sum rules for the vector current correlator to order α_s^3 , including the effect of gluon condensates up to dimension eight.



$$J(J^P) = 0(\frac{1}{2}^+)$$

Charge = $\frac{2}{3} e$ Charm = +1

c-QUARK MASS

The c -quark mass corresponds to the "running" mass $m_c(\mu = m_c)$ in the \overline{MS} scheme. We have converted masses in other schemes to the \overline{MS} scheme using two-loop QCD perturbation theory with $\alpha_s(\mu = m_c) = 0.38 \pm 0.03$. The value $1.27 \pm 0.02 \text{ GeV}$ for the \overline{MS} mass corresponds to $1.67 \pm 0.07 \text{ GeV}$ for the pole mass (see the "Note on Quark Masses").

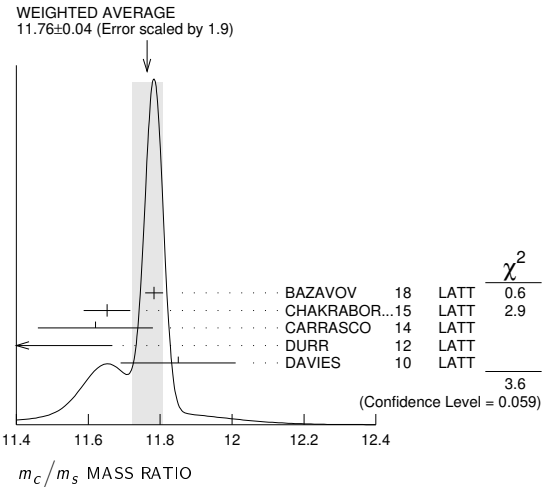
\overline{MS} MASS (GeV)	DOCUMENT ID	TECN
1.27 ± 0.02	OUR EVALUATION	See the ideogram below.
1.266 ± 0.006	1 NARISON 20	THEO
1.290 +0.077 -0.053	2 ABRAMOWICZ18	HERA
1.273 ± 0.010	3 BAZAVOV 18	LATT
1.2737 ± 0.0077	4 LYTLE 18	LATT
1.223 ± 0.033	5 PESET 18	THEO
1.279 ± 0.008	6 CHETYRKIN 17	THEO
1.272 ± 0.008	7 ERLER 17	THEO
1.246 ± 0.023	8 KIYO 16	THEO
1.288 ± 0.020	9 DEHNADI 15	THEO
1.348 ± 0.046	10 CARRASCO 14	LATT
1.24 ± 0.03 +0.03 -0.07	11 ALEKHIN 13	THEO
1.159 ± 0.075	12 SAMOYLOV 13	NOMD
1.278 ± 0.009	13 BODENSTEIN 11	THEO
1.28 +0.07 -0.06	14 LASCHKA 11	THEO
1.196 ± 0.059 ± 0.050	15 AUBERT 10A	BABR
1.25 ± 0.04	16 SIGNER 09	THEO
• • • We do not use the following data for averages, fits, limits, etc. • • •		
1.263 ± 0.014	17 NARISON 18A	THEO
1.264 ± 0.006	18 NARISON 18B	THEO
1.335 ± 0.043 +0.040 -0.011	19 BERTONE 16	THEO
1.2715 ± 0.0095	20 CHAKRABOR...15	LATT

Quark Particle Listings

C

- 26 ALEKHIN 11 determines m_c from heavy quark production in deep inelastic scattering using fixed target and HERA data, and approximate NNLO QCD.
- 27 BLOSSIER 10 determines quark masses from a computation of the hadron spectrum using $N_f=2$ dynamical twisted-mass Wilson fermions.
- 28 BODENSTEIN 10 determines $\overline{m}_c(3 \text{ GeV}) = 1.008 \pm 0.026 \text{ GeV}$ using finite energy sum rules for the vector current correlator. The authors have converted this to $\overline{m}_c(\overline{m}_c)$ using $\alpha_s(M_Z) = 0.1189 \pm 0.0020$.
- 29 MCNEILE 10 determines m_c by comparing the order α_s^3 perturbative results for the pseudo-scalar current to lattice simulations with $N_f = 2+1$ sea-quarks by the HPQCD collaboration.
- 30 NARISON 10 determines m_c from ratios of moments of vector current correlators computed to order α_s^3 and including the dimension-six gluon condensate.
- 31 CHETYRKIN 09 determine m_c and m_b from the $e^+e^- \rightarrow Q\overline{Q}$ cross-section and sum rules, using an order α_s^3 computation of the heavy quark vacuum polarization. They also determine $m_c(3 \text{ GeV}) = 0.986 \pm 0.013 \text{ GeV}$.
- 32 ALLISON 08 determine m_c by comparing four-loop perturbative results for the pseudo-scalar current correlator to lattice simulations by the HPQCD collaboration. The result has been updated in MCNEILE 10.
- 33 KUHN 07 determine $\overline{m}_c(\mu = 3 \text{ GeV}) = 0.986 \pm 0.013 \text{ GeV}$ and $\overline{m}_c(\overline{m}_c)$ from a four-loop sum-rule computation of the cross-section for $e^+e^- \rightarrow$ hadrons in the charm threshold region.
- 34 BOUGHEZAL 06 result comes from the first moment of the hadronic production cross-section to order α_s^3 .
- 35 BUCHMUELLER 06 determine m_b and m_c by a global fit to inclusive B decay spectra.
- 36 HOANG 06 determines $\overline{m}_c(\overline{m}_c)$ from a global fit to inclusive B decay data. The B decay distributions were computed to order $\alpha_s^2\beta_0$, and the conversion between different m_c mass schemes to order α_s^3 .
- 37 AUBERT 04x obtain m_c from a fit to the hadron mass and lepton energy distributions in semileptonic B decay. The paper quotes values in the kinetic scheme. The MS value has been provided by the BABAR collaboration.
- 38 HOANG 04 determines $\overline{m}_c(\overline{m}_c)$ from moments at order α_s^2 of the charm production cross-section in e^+e^- annihilation.
- 39 DEDIVITIIS 03 use a quenched lattice computation of heavy-heavy and heavy-light meson masses.
- 40 EIDEMULLER 03 determines m_b and m_c using QCD sum rules.
- 41 ERLER 03 determines m_b and m_c using QCD sum rules. Includes recent BES data.
- 42 ZYABLYUK 03 determines m_c by using QCD sum rules in the pseudoscalar channel and comparing with the η_c mass.

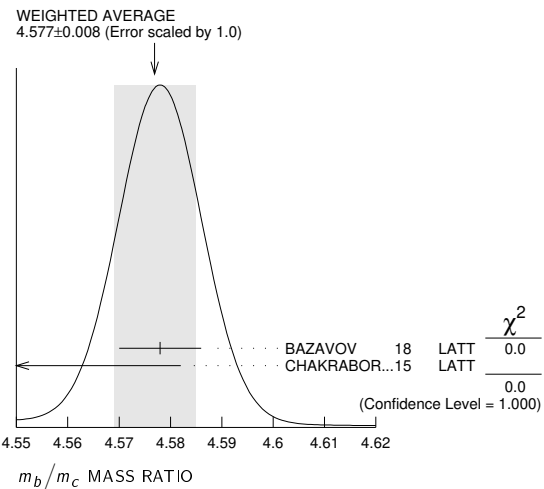
- 5 DAVIES 10 determine m_c/m_s from meson masses calculated on gluon fields including $u, d,$ and s sea quarks with lattice spacing down to 0.045 fm. The Highly Improved Staggered quark formalism is used for the valence quarks.
- 6 BAZAVOV 14A is a lattice computation using 4 dynamical flavors of HISQ fermions.
- 7 BLOSSIER 10 determine m_c/m_s from a computation of the hadron spectrum using $N_f = 2$ dynamical twisted-mass Wilson fermions.



m_b/m_c MASS RATIO

VALUE	DOCUMENT ID	TECN
4.577 ± 0.008 OUR AVERAGE	See the ideogram below.	
4.578 ± 0.008	1 BAZAVOV 18	LATT
4.528 ± 0.054	2 CHAKRABORTY 15	LATT

- 1 BAZAVOV 18 determine the quark masses using a lattice computation with staggered fermions and four active quark flavors for the u, d, s, c quarks and five active flavors for the b quark.
- 2 CHAKRABORTY 15 is a lattice computation using 4 dynamical quark flavors.



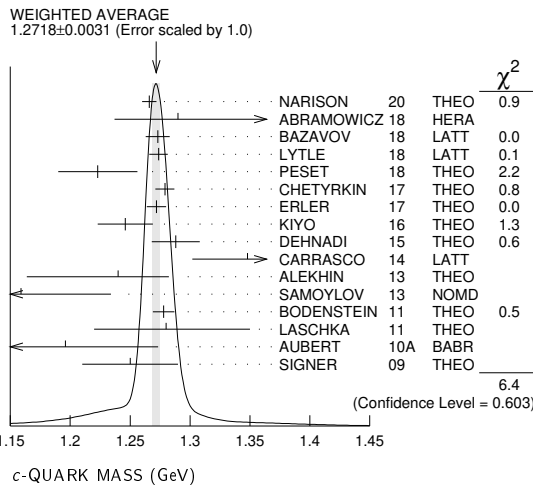
$m_b - m_c$ QUARK MASS DIFFERENCE

VALUE (GeV)	DOCUMENT ID	TECN
3.45 ± 0.05 OUR EVALUATION		
3.472 ± 0.032	1 AUBERT 10A	BABR
3.42 ± 0.06	2 ABDALLAH 06B	DLPH
3.44 ± 0.03	3 AUBERT 04x	BABR
3.41 ± 0.01	3 BAUER 04	THEO

- • • We do not use the following data for averages, fits, limits, etc. • • •
- 1 AUBERT 10A determine the b - and c -quark masses from a fit to the inclusive decay spectra in semileptonic B decays in the kinetic scheme.
- 2 ABDALLAH 06B determine $m_b - m_c$ from moments of the hadron invariant mass and lepton energy spectra in semileptonic inclusive B decays.
- 3 Determine $m_b - m_c$ from a global fit to inclusive B decay spectra.

c-QUARK REFERENCES

NARISON 20	PL B802 135221	S. Narison	(MONP)
ABRAMOWICZ 18	EPJ C78 473	H. Abramowicz et al.	(H1 and ZEUS Collabs.)
BAZAVOV 18	PR D98 054517	A. Bazavov et al.	(Fermilab Lattice, MILC, TUMQCD)
LYTLE 18	PR D98 014513	A.T. Lytle et al.	(HPQCD Collab.)
NARISON 18A	IJMP A33 1850045	S. Narison	(MONP)
NARISON 18B	PL B784 261	S. Narison	(MONP)



m_c/m_s MASS RATIO

VALUE	DOCUMENT ID	TECN
11.72 ± 0.25 OUR EVALUATION	See the ideogram below.	
11.783 ± 0.025	1 BAZAVOV 18	LATT
11.652 ± 0.065	2 CHAKRABORTY 15	LATT
11.62 ± 0.16	3 CARRASCO 14	LATT
11.27 ± 0.30 ± 0.26	4 DURR 12	LATT
11.85 ± 0.16	5 DAVIES 10	LATT
11.747 ± 0.019 ± 0.059 - 0.043	6 BAZAVOV 14A	LATT
12.0 ± 0.3	7 BLOSSIER 10	LATT

- • • We do not use the following data for averages, fits, limits, etc. • • •
- 1 BAZAVOV 18 determine the quark masses using a lattice computation with staggered fermions and four active quark flavors.
- 2 CHAKRABORTY 15 is a lattice QCD computation on gluon field configurations with 2+1+1 dynamical flavors of HISQ quarks with u/d masses down to the physical value. m_c and m_s are tuned from pseudoscalar meson masses.
- 3 CARRASCO 14 is a lattice QCD computation of light quark masses using 2 + 1 + 1 dynamical quarks, with $m_u = m_d \neq m_s \neq m_c$. The u and d quark masses are obtained separately by using the K meson mass splittings and lattice results for the electromagnetic contributions.
- 4 DURR 12 determine m_c/m_s using a lattice computation with $N_f = 2$ dynamical fermions. The result is combined with other determinations of m_c to obtain $m_s(2 \text{ GeV}) = 97.0 \pm 2.6 \pm 2.5 \text{ MeV}$.

PESET	18	JHEP 1809 167	C. Peset, A. Pineda, J. Segovia (BARC, MUNT)
CHETYRKIN	17	PR D96 116007	K.G. Chetyrkin <i>et al.</i>
ERLER	17	EPJ C77 99	J. Erler, P. Masjuan, H. Spiesberger
BERTONE	16	JHEP 1608 050	V. Bertone <i>et al.</i> (xFitter Developers)
KIYO	16	PL B752 122	Y. Kiyo, G. Mishima, Y. Sumino
CHAKRABOR...	15	PR D91 054508	B. Chakraborty <i>et al.</i> (HPQCD Collab.)
DEHNADI	15	JHEP 1508 155	B. Dehnadi, A.H. Hoang, V. Mateu
BAZAVOV	14A	PR D90 074509	A. Bazavov <i>et al.</i> (Fermi-LAT and MILC Collabs.)
CARRASCO	14	NP B887 19	N. Carrasco <i>et al.</i> (European Twisted Mass Collab.)
ABRAMOWICZ	13C	EPJ C73 2311	H. Abramowicz <i>et al.</i> (H1 and Zeuss Collabs.)
ALEKHIN	13	PL B720 172	S. Alekhin <i>et al.</i> (SERP, DESYZ, WUPP+)
DEHNADI	13	JHEP 1309 103	B. Dehnadi <i>et al.</i> (SHRZ, VIEN, MPIM+)
NARISON	13	PL B718 1321	S. Narison (MONP)
SAMOYLOV	13	NP B876 339	O. Samoylov <i>et al.</i> (NOMAD Collab.)
ALEKHIN	12	PL B718 550	S. Alekhin <i>et al.</i> (SERP, WUPP, DESYZ+)
DURR	12	PRL 108 122003	S. Durr, G. Koutsou (WUPP, JULI, CYPR)
NARISON	12A	PL B706 412	S. Narison (MONP)
ALEKHIN	11	PL B699 345	S. Alekhin, S. Moch (DESY, SERP)
BODENSTEIN	11	PR D83 074014	S. Bodenstein <i>et al.</i>
LASCHKA	11	PR D83 094002	A. Laschka, M. Kaiser, W. Weise
AUBERT	10A	PR D81 032003	B. Aubert <i>et al.</i> (BABAR Collab.)
BLOSSIER	10	PR D82 114513	B. Blossier <i>et al.</i> (ETM Collab.)
BODENSTEIN	10	PR D82 114013	S. Bodenstein <i>et al.</i>
DAVIES	10	PRL 104 132003	C.T.H. Davies <i>et al.</i> (HPQCD Collab.)
MCNEILE	10	PR D82 034512	C. McNeile <i>et al.</i> (HPQCD Collab.)
NARISON	10	PL B693 559	S. Narison (MONP)
Also		PL B705 544 (errata.)	S. Narison (MONP)
CHETYRKIN	09	PR D80 074010	K.G. Chetyrkin <i>et al.</i> (KARL, BNL)
SIGNER	09	PL B672 333	A. Signer (DURH)
ALLISON	08	PR D78 054513	I. Allison <i>et al.</i> (HPQCD Collab.)
KUHN	07	NP B779 192	J.H. Kuhn, M. Steinhauser, C. Sturm
ABDALLAH	06B	EPJ C45 35	J. Abdallah <i>et al.</i> (DELPHI Collab.)
BOUGHEZAL	06	PR D74 074006	R. Boughezal, M. Czakon, T. Schutzmeier
BUCHMUEL...	06	PR D73 073008	O.L. Buchmüller, H.U. Flacher (RHBL)
HOANG	06	PL B633 526	A.H. Hoang, A.V. Manohar
AUBERT	04X	PRL 93 011803	B. Aubert <i>et al.</i> (BABAR Collab.)
BAUER	04	PR D70 094017	C. Bauer <i>et al.</i>
HOANG	04	PL B594 127	A.H. Hoang, M. Jamin
DEDIVITIIS	03	NP B675 309	G.M. de Divitiis <i>et al.</i>
EIDEMULLER	03	PR D67 113002	M. Eidemüller
ERLER	03	PL B558 125	J. Erler, M. Luo
ZYABLYUK	03	JHEP 0301 081	K.N. Zybalyuk (ITEP)

b

$$I(J^P) = 0(\frac{1}{2}^+)$$

$$\text{Charge} = -\frac{1}{3} e \quad \text{Bottom} = -1$$

b-QUARK MASS

b -quark mass corresponds to the “running mass” $\overline{m}_b(\mu = \overline{m}_b)$ in the $\overline{\text{MS}}$ scheme. We have converted masses in other schemes to the $\overline{\text{MS}}$ mass using two-loop QCD perturbation theory with $\alpha_s(\mu = \overline{m}_b) = 0.223 \pm 0.008$. The value $4.18^{+0.04}_{-0.03}$ GeV for the $\overline{\text{MS}}$ mass corresponds to 4.78 ± 0.06 GeV for the pole mass, using the two-loop conversion formula. A discussion of masses in different schemes can be found in the “Note on Quark Masses.”

$\overline{\text{MS}}$ MASS (GeV)	DOCUMENT ID	TECN.
$4.18^{+0.03}_{-0.02}$	OUR EVALUATION	of $\overline{\text{MS}}$ Mass. See the ideogram below.
4.197 ± 0.008	1 NARISON 20	THEO
$4.049^{+0.138}_{-0.118}$	2 ABRAMOWICZ18	HERA
4.195 ± 0.014	3 BAZAVOV 18	LATT
4.186 ± 0.037	4 PESET 18	THEO
4.197 ± 0.022	5 KIYO 16	THEO
4.183 ± 0.037	6 ALBERTI 15	THEO
$4.203^{+0.016}_{-0.034}$	7 BENEKE 15	THEO
4.196 ± 0.023	8 COLQUHOUN 15	LATT
4.176 ± 0.023	9 DEHNADI 15	THEO
4.21 ± 0.11	10 BERNARDONI 14	LATT
$4.169 \pm 0.002 \pm 0.008$	11 PENIN 14	THEO
4.166 ± 0.043	12 LEE 13o	LATT
4.247 ± 0.034	13 LUCHA 13	THEO
4.171 ± 0.009	14 BODENSTEIN 12	THEO
4.29 ± 0.14	15 DIMOPOUL... 12	LATT
$4.18^{+0.05}_{-0.04}$	16 LASCHKA 11	THEO
$4.186 \pm 0.044 \pm 0.015$	17 AUBERT 10A	BABR
4.163 ± 0.016	18 CHETYRKIN 09	THEO
4.243 ± 0.049	19 SCHWANDA 08	BELL
• • •	We do not use the following data for averages, fits, limits, etc. • • •	
4.184 ± 0.011	20 NARISON 18A	THEO
4.188 ± 0.008	21 NARISON 18B	THEO
4.07 ± 0.17	22 ABRAMOWICZ14A	ZEUS
4.201 ± 0.043	23 AYALA 14A	THEO
4.236 ± 0.069	24 NARISON 13	THEO
4.213 ± 0.059	25 NARISON 13A	THEO
$4.235 \pm 0.003 \pm 0.055$	26 HOANG 12	THEO
4.212 ± 0.032	27 NARISON 12	THEO
4.177 ± 0.011	28 NARISON 12	THEO
4.171 ± 0.014	29 NARISON 12A	THEO
4.164 ± 0.023	30 MCNEILE 10	LATT
4.173 ± 0.010	31 NARISON 10	THEO
5.26 ± 1.2	32 ABDALLAH 08D	DLPH
$4.42 \pm 0.06 \pm 0.08$	33 GUAZZINI 08	LATT
$4.347 \pm 0.048 \pm 0.08$	34 DELLA-MOR... 07	LATT
4.164 ± 0.025	35 KUHN 07	THEO
4.19 ± 0.40	36 ABDALLAH 06D	DLPH

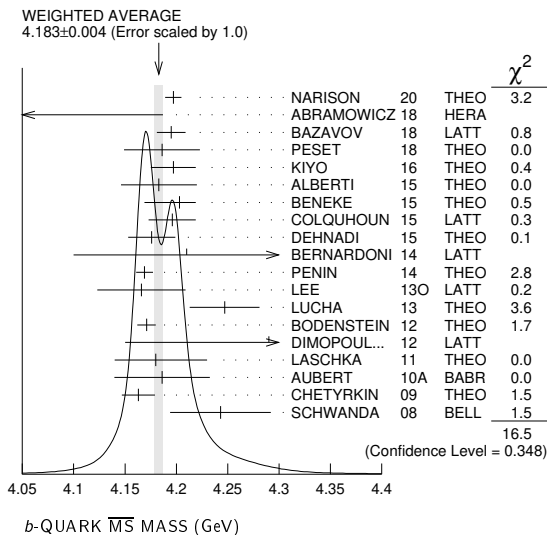
4.205 ± 0.058	37 BOUGHEZAL 06	THEO
4.20 ± 0.04	38 BUCHMUEL... 06	THEO
4.19 ± 0.06	39 PINEDA 06	THEO
4.4 ± 0.3	40 GRAY 05	LATT
4.22 ± 0.06	41 AUBERT 04X	THEO
4.17 ± 0.03	42 BAUER 04	THEO
4.22 ± 0.11	43 HOANG 04	THEO
4.25 ± 0.11	44 MCNEILE 04	LATT
4.22 ± 0.09	45 BAUER 03	THEO
4.19 ± 0.05	46 BORDES 03	THEO
4.20 ± 0.09	47 CORCELLA 03	THEO
4.33 ± 0.10	48 DEDIVITIIS 03	LATT
4.24 ± 0.10	49 EIDEMULLER 03	THEO
4.207 ± 0.03	50 ERLER 03	THEO
$4.33 \pm 0.06 \pm 0.10$	51 MAHMOOD 03	CLEO
4.190 ± 0.032	52 BRAMBILLA 02	THEO
4.346 ± 0.070	53 PENIN 02	THEO

- NARISON 20 determines the quark mass using QCD Laplace sum rules from the B_c mass, combined with previous determinations of the QCD condensates and c and b masses.
- ABRAMOWICZ 18 determine $\overline{m}_b(\overline{m}_b) = 4.049^{+0.104+0.090+0.001}_{-0.109-0.032-0.031}$ from the production of b quarks in $e p$ collisions at HERA using combined H1 and ZEUS data. The experimental/fitting errors, and those from modeling and parameterization have been combined in quadrature.
- BAZAVOV 18 determine the b mass using a lattice computation with staggered fermions and five active quark flavors.
- PESET 18 determine $\overline{m}_c(\overline{m}_c)$ and $\overline{m}_b(\overline{m}_b)$ using an N3LO calculation of the η_c , η_b and B_c masses.
- KIYO 16 determine $\overline{m}_b(\overline{m}_b)$ from the $\Upsilon(1S)$ mass at order α_s^3 (N3LO).
- ALBERTI 15 determine $\overline{m}_b(\overline{m}_b)$ from fits to inclusive $B \rightarrow X_c e \overline{\nu}$ decay. They also find $m_b^{\text{kin}}(1 \text{ GeV}) = 4.553 \pm 0.020$ GeV.
- BENEKE 15 determine $\overline{m}_b(\overline{m}_b)$ using sum rules for $e^+ e^- \rightarrow$ hadrons at order N3LO including finite m_c effects. They find $m_b^{\text{P}}(2 \text{ GeV}) = 4.532^{+0.013}_{-0.039}$ GeV, and $\overline{m}_b(\overline{m}_b) = 4.193^{+0.022}_{-0.035}$ GeV. The value quoted is obtained using the four-loop conversion given in BENEKE 16.
- COLQUHOUN 15 determine $\overline{m}_b(\overline{m}_b)$ from moments of the vector current correlator computed with a lattice simulation using the NRQCD action.
- DEHNADI 15 determine $\overline{m}_b(\overline{m}_b)$ using sum rules for $e^+ e^- \rightarrow$ hadrons at order α_s^3 (N3LO), and fitting to both experimental data and lattice results.
- BERNARDONI 14 determine m_b from $N_f = 2$ lattice calculations using heavy quark effective theory non-perturbatively renormalized and matched to QCD at $1/m$ order.
- PENIN 14 determine $\overline{m}_b(\overline{m}_b) = 4.169 \pm 0.008 \pm 0.002 \pm 0.002$ using an estimate of the order α_s^3 b -quark vacuum polarization function in the threshold region, including finite m_c effects. The errors of ± 0.008 from theoretical uncertainties, and ± 0.002 from α_s have been combined in quadrature.
- LEE 13o determines m_b using lattice calculations of the Υ and B_s binding energies in NRQCD, including three light dynamical quark flavors. The quark mass shift in NRQCD is determined to order α_s^2 , with partial α_s^3 contributions.
- LUCHA 13 determines m_b from QCD sum rules for heavy-light currents using the lattice value for f_B of 191.5 ± 7.3 GeV.
- BODENSTEIN 12 determine m_b using sum rules for the vector current correlator and the $e^+ e^- \rightarrow Q \overline{Q}$ total cross-section.
- DIMOPOULOS 12 determine quark masses from a lattice computation using $N_f = 2$ dynamical flavors of twisted mass fermions.
- LASCHKA 11 determine the b mass from the charmonium spectrum. The theoretical computation uses the heavy $Q \overline{Q}$ potential to order $1/m_Q$ obtained by matching the short-distance perturbative result onto lattice QCD result at larger scales.
- AUBERT 10A determine the b - and c -quark masses from a fit to the inclusive decay spectra in semileptonic B decays in the kinetic scheme (and convert it to the $\overline{\text{MS}}$ scheme).
- CHETYRKIN 09 determine m_c and m_b from the $e^+ e^- \rightarrow Q \overline{Q}$ cross-section and sum rules, using an order α_s^3 (N3LO) computation of the heavy quark vacuum polarization.
- SCHWANDA 08 measure moments of the inclusive photon spectrum in $B \rightarrow X_s \gamma$ decay to determine $m_b^1 S$. We have converted this to $\overline{\text{MS}}$ scheme.
- NARISON 18A determines $\overline{m}_b(\overline{m}_b)$ as a function of α_s using QCD exponential sum rules and their ratios evaluated at the optimal scale $\mu = 9.5$ GeV at N2LO-N3LO of perturbative QCD and including condensates up to dimension 6–8 in the (axial-)vector and (pseudo-)scalar bottomonium channels.
- NARISON 18B determines $\overline{m}_b(\overline{m}_b)$ using QCD vector moment sum rules and their ratios at N2LO-N3LO of perturbative QCD and including condensates up to dimension 8.
- ABRAMOWICZ 14A determine $\overline{m}_b(\overline{m}_b) = 4.07 \pm 0.14^{+0.01+0.05+0.08}_{-0.07-0.00-0.05}$ from the production of b quarks in $e p$ collisions at HERA. The errors due to fitting, modeling, PDF parameterization, and theoretical QCD uncertainties due to the values of α_s , m_c , and the renormalization scale μ have been combined in quadrature.
- AYALA 14A determine $\overline{m}_b(\overline{m}_b)$ from the $\Upsilon(1S)$ mass computed to N3LO order in perturbation theory using a renormalon subtracted scheme.
- NARISON 13 determines m_b using QCD spectral sum rules to order α_s^2 (NNLO) and including condensates up to dimension 6.
- NARISON 13A determines m_b using HQET sum rules to order α_s^2 (NNLO) and the B meson mass and decay constant.
- HOANG 12 determine m_b using non-relativistic sum rules for the Υ system at order α_s^2 (NNLO) with renormalization group improvement.
- NARISON 12 determines m_b using exponential sum rules for the vector current correlator to order α_s^3 , including the effect of gluon condensates up to dimension eight.
- Determines m_b to order α_s^3 (N3LO), including the effect of gluon condensates up to dimension eight combining the methods of NARISON 12 and NARISON 12A.
- NARISON 12A determines m_b using sum rules for the vector current correlator to order α_s^3 , including the effect of gluon condensates up to dimension eight.

Quark Particle Listings

b, t

- 30 MCNEILE 10 determines m_b by comparing order α_s^3 (N3LO) perturbative results for the pseudo-scalar current to lattice simulations with $N_f = 2+1$ sea-quarks by the HPQCD collaboration.
- 31 NARISON 10 determines m_b from ratios of moments of vector current correlators computed to order α_s^2 and including the dimension-six gluon condensate. These values are taken from the erratum to that reference.
- 32 ABDALLAH 08d determine $\overline{m}_b(M_Z) = 3.76 \pm 1.0$ GeV from a leading order study of four-jet rates at LEP.
- 33 GUAZZINI 08 determine $\overline{m}_b(\overline{m}_b)$ from a quenched lattice simulation of heavy meson masses. The ± 0.08 is an estimate of the quenching error.
- 34 DELLA-MORTE 07 determine $\overline{m}_b(\overline{m}_b)$ from a computation of the spin-averaged B meson mass using quenched lattice HQET at order $1/m$. The ± 0.08 is an estimate of the quenching error.
- 35 KUHN 07 determine $\overline{m}_b(\mu = 10 \text{ GeV}) = 3.609 \pm 0.025$ GeV and $\overline{m}_b(\overline{m}_b)$ from a four-loop sum-rule computation of the cross-section for $e^+e^- \rightarrow$ hadrons in the bottom threshold region.
- 36 ABDALLAH 06d determine $m_b(M_Z) = 2.85 \pm 0.32$ GeV from Z -decay three-jet events containing a b -quark.
- 37 BOUGHEZAL 06 $\overline{M_S}$ scheme result comes from the first moment of the hadronic production cross-section to order α_s^3 .
- 38 BUCHMUELLER 06 determine m_b and m_c by a global fit to inclusive B decay spectra.
- 39 PINEDA 06 $\overline{M_S}$ scheme result comes from a partial NNLL evaluation (complete at order α_s^2 (NNLO)) of sum rules of the bottom production cross-section in e^+e^- annihilation.
- 40 GRAY 05 determines $\overline{m}_b(\overline{m}_b)$ from a lattice computation of the Υ spectrum. The simulations have $2+1$ dynamical light flavors. The b quark is implemented using NRQCD.
- 41 AUBERT 04x obtain m_b from a fit to the hadron mass and lepton energy distributions in semileptonic B decay. The paper quotes values in the kinetic scheme. The $\overline{M_S}$ value has been provided by the BABAR collaboration.
- 42 BAUER 04 determine m_b , m_c and $m_b - m_c$ by a global fit to inclusive B decay spectra.
- 43 HOANG 04 determines $\overline{m}_b(\overline{m}_b)$ from moments at order α_s^2 of the bottom production cross-section in e^+e^- annihilation.
- 44 MCNEILE 04 use lattice QCD with dynamical light quarks and a static heavy quark to compute the masses of heavy-light mesons.
- 45 BAUER 03 determine the b quark mass by a global fit to B decay observables. The experimental data includes lepton energy and hadron invariant mass moments in semileptonic $B \rightarrow X_c \ell \nu_\ell$ decay, and the inclusive photon spectrum in $B \rightarrow X_s \gamma$ decay. The theoretical expressions used are of order $1/m^3$, and $\alpha_s^2 \beta_0$.
- 46 BORDES 03 determines m_b using QCD finite energy sum rules to order α_s^2 .
- 47 CORCELLA 03 determines \overline{m}_b using sum rules computed to order α_s^2 . Includes charm quark mass effects.
- 48 DEDIVITIIS 03 use a quenched lattice computation of heavy-heavy and heavy-light meson masses.
- 49 EIDEMULLER 03 determines \overline{m}_b and \overline{m}_c using QCD sum rules.
- 50 ERLER 03 determines \overline{m}_b and \overline{m}_c using QCD sum rules. Includes recent BES data.
- 51 MAHMOOD 03 determines m_b^{1S} by a fit to the lepton energy moments in $B \rightarrow X_c \ell \nu_\ell$ decay. The theoretical expressions used are of order $1/m^3$ and $\alpha_s^2 \beta_0$. We have converted their result to the $\overline{M_S}$ scheme.
- 52 BRAMBILLA 02 determine $\overline{m}_b(\overline{m}_b)$ from a computation of the $\Upsilon(1S)$ mass to order α_s^4 , including finite m_c corrections.
- 53 PENIN 02 determines \overline{m}_b from the spectrum of the Υ system.



m_b/m_s MASS RATIO

VALUE	DOCUMENT ID	TECN
53.94 ± 0.12	1 BAZAVOV	18 LATT

1 BAZAVOV 18 determine the quark masses using a lattice computation with staggered fermions and four active quark flavors for the u, d, s, c quarks and five active flavors for the b quark.

b-QUARK REFERENCES

NARISON 20	PL B802 135221	S. Narison (MONP)
ABRAMOWICZ 18	EPJ C78 473	H. Abramowicz et al. (HI and ZEUS Collabs.)
BAZAVOV 18	PR D98 054517	A. Bazavov et al. (Fermilab Lattice, MILC, TUMQCD)
NARISON 18A	IJMP A33 1850045	S. Narison (MONP)
NARISON 18B	PL B784 261	S. Narison (MONP)
PESET 18	JHEP 1809 167	C. Peset, A. Pineda, J. Segovia (BARC, MUNT)
BENEKE 16	PoS RADCOR2015 035	M. Beneke et al.
KIYO 16	PL B752 122	Y. Kiyo, G. Mishima, Y. Sumino
ALBERTI 15	PRL 114 061802	A. Alberti et al.
BENEKE 15	NP B591 42	M. Beneke et al.
COLQUHOUN 15	PR D91 074514	B. Colquhoun et al. (HPQCD Collab.)
DEHNADI 15	JHEP 1508 155	B. Dehnadi, A.H. Hoang, V. Mateu
ABRAMOWICZ 14A	JHEP 1409 127	H. Abramowicz et al. (ZEUS Collab.)
AYALA 14A	JHEP 1409 045	C. Ayala, G. Cvetič, A. Pineda
BERNARDONI 14	PL B730 171	F. Bernardoni et al. (ALPHA Collab.)
PENIN 14	JHEP 1404 120	A.A. Penin, N. Zerb
LEE 13O	PR D87 074018	A.J. Lee et al. (HPQCD Collab.)
LUCHA 13	PR D88 056011	W. Lucha, D. Melikhov, S. Simuta (WIEN, MOSU+)
NARISON 13	PL B718 1321	S. Narison (MONP)
NARISON 13A	PL B721 269	S. Narison (MONP)
BODENSTEIN 12	PR D85 034003	S. Bodenstein et al. (CAPE, VALE, MANZ+)
DIMOPOL... 12	JHEP 1201 046	P. Dimopoulos et al. (ETM Collab.)
HOANG 12	JHEP 1210 188	A.H. Hoang, P. Ruiz-Femenia, M. Stahlhofen (WIEN+)
NARISON 12	PL B707 259	S. Narison (MONP)
NARISON 12A	PL B706 412	S. Narison (MONP)
LASCHKA 11	PR D83 094002	A. Laschka, N. Kaiser, W. Weise
AUBERT 10A	PR D81 032003	B. Aubert et al. (BABAR Collab.)
MCNEILE 10	PR D82 034512	C. McNeile et al. (HPQCD Collab.)
NARISON 10	PL B693 559	S. Narison (MONP)
Also	PL B705 544 (errata.)	S. Narison (MONP)
CHETYRKIN 09	PR D80 074010	K.G. Chetyrkin et al. (KARL, BNL)
ABDALLAH 08D	EPJ C55 525	J. Abdallah et al. (DELPHI Collab.)
GUAZZINI 08	JHEP 0801 076	D. Guazzini, R. Sommer, N. Tantalo
SCHWANDA 08	PR D78 032016	C. Schwanda et al. (BELLE Collab.)
DELLA-MOR... 07	JHEP 0701 007	M. Della Morte et al.
KUHN 07	NP B778 192	J.H. Kuhn, M. Steinhauser, C. Sturm
ABDALLAH 06D	EPJ C46 569	J. Abdallah et al. (DELPHI Collab.)
BOUGHEZAL 06	PR D74 074006	R. Boughezal, M. Czakon, T. Schutzmeier
BUCHMUELL... 06	PR D73 073008	O.L. Buchmuller, H.U. Flacher (RHBL)
PINEDA 06	PR D73 111501	A. Pineda, A. Signer
GRAY 05	PR D72 094507	A. Gray et al. (HPQCD and UKQCD Collab.)
AUBERT 04X	PRL 93 013803	B. Aubert et al. (BABAR Collab.)
BAUER 04	PR D70 094017	C. Bauer et al.
HOANG 04	PL B594 127	A.H. Hoang, M. Jamin
MCNEILE 04	PL B600 77	C. McNeile, C. Michael, G. Thompson (UKQCD Collab.)
BAUER 03	PR D67 054012	C.W. Bauer et al.
BORDES 03	PL B562 81	J. Bordes, J. Penarrocha, K. Schilcher
CORCELLA 03	PL B554 133	G. Corcella, A.H. Hoang
DEDIVITIIS 03	NP B675 309	G.M. de Divitiis et al.
EIDEMULLER 03	PR D67 113002	M. Eidemuller
ERLER 03	PL B558 125	J. Erler, M. Luo
MAHMOOD 03	PR D67 072001	A.H. Mahmood et al. (CLEO Collab.)
BRAMBILLA 02	PR D65 034001	N. Brambilla, Y. Sumino, A. Vairo
PENIN 02	PL B538 335	A. Penin, M. Steinhauser



$$I(J^P) = 0(\frac{1}{2}^+)$$

$$\text{Charge} = \frac{2}{3} e \quad \text{Top} = +1$$

See the related review(s):
[Top Quark](#)

t-QUARK MASS

We first list the direct measurements of the top quark mass which employ the event kinematics and then list the measurements which extract a top quark mass from the measured $t\bar{t}$ cross-section using theory calculations. A discussion of the definition of the top quark mass in these measurements can be found in the review "The Top Quark."

For earlier search limits see PDG 96, Physical Review **D54** 1 (1996). We no longer include a compilation of indirect top mass determinations from Standard Model Electroweak fits in the Listings (our last compilation can be found in the Listings of the 2007 partial update). For a discussion of current results see the reviews "The Top Quark" and "Electroweak Model and Constraints on New Physics."

t-Quark Mass (Direct Measurements)

The following measurements extract a t -quark mass from the kinematics of $t\bar{t}$ events. They are sensitive to the top quark mass used in the MC generator that is usually interpreted as the pole mass, but the theoretical uncertainty in this interpretation is hard to quantify. See the review "The Top Quark" and references therein for more information.

OUR AVERAGE of 172.76 ± 0.30 GeV is an average of top mass measurements from LHC and Tevatron Runs. The latest Tevatron average, $174.30 \pm 0.35 \pm 0.54$ GeV, was provided by the Tevatron Electroweak Working Group (TEVEWWG).

VALUE (GeV)	DOCUMENT ID	TECN	COMMENT
172.76 ± 0.30 OUR AVERAGE	Error includes scale factor of 1.2.		
172.69 ± 0.25 ± 0.41	1 AABOUD	19AC ATLAS	7, 8 TeV ATLAS combination
172.26 ± 0.07 ± 0.61	2 SIRUNYAN	19AP CMS	lepton+jets, all-jets channels
172.33 ± 0.14 ± 0.66	3 SIRUNYAN	19AR CMS	dilepton channel ($e, \mu, 2e, 2\mu$)
172.95 ± 0.77 ± 0.97	4 SIRUNYAN	17L CMS	t -channel single top production
172.44 ± 0.13 ± 0.47	5 KHACHATRY...16AK	CMS	7, 8 TeV CMS combination
174.30 ± 0.35 ± 0.54	6 TEVEWWG	16 TEVA	Tevatron combination

• • • We do not use the following data for averages, fits, limits, etc. • • •

172.08 ± 0.39 ± 0.82	7	AABOUD	19AC	ATLS	$\ell + \geq 4j$ ($2b$)
172.34 ± 0.20 ± 0.70	8	SIRUNYAN	19AP	CMS	≥ 6 jets ($\geq 2b$)
172.25 ± 0.08 ± 0.62	9	SIRUNYAN	18DE	CMS	$\ell + \geq 4j$ ($2b$)
173.72 ± 0.55 ± 1.01	10	AABOUD	17AH	ATLS	≥ 5 jets ($2b$)
174.95 ± 0.40 ± 0.64	11	ABAZOV	17B	D0	ℓ + jets and dilepton channels
170.8 ± 9.0	12	SIRUNYAN	17N	CMS	jet mass in highly-boosted $t\bar{t}$ events
172.22 ± 0.18 ± 0.89	13	SIRUNYAN	17O	CMS	Dilepton channel
172.99 ± 0.41 ± 0.74	14	AABOUD	16T	ATLS	dilepton channel
172.84 ± 0.34 ± 0.61	15	AABOUD	16T	ATLS	combination of ATLAS
173.32 ± 1.36 ± 0.85	16	ABAZOV	16D	D0	$\ell\ell + \cancel{E}_T + \geq 2j$ ($\geq 2b$)
173.93 ± 1.61 ± 0.88	17	ABAZOV	16D	D0	$\ell\ell + \cancel{E}_T + \geq 2j$ ($\geq 2b$)
172.35 ± 0.16 ± 0.48	18,19	KHACHATRYAN	16AK	CMS	$\ell + \geq 4j$ ($2b$)
172.32 ± 0.25 ± 0.59	18,19	KHACHATRYAN	16AK	CMS	≥ 6 jets ($2b$)
172.82 ± 0.19 ± 1.22	18,20	KHACHATRYAN	16AK	CMS	$(ee/\mu\mu) + \cancel{E}_T + \geq 2b, e\mu + \geq 2b$
173.68 ± 0.20 ± 1.58	21	KHACHATRYAN	16AL	CMS	semi- + di-leptonic channels
173.5 ± 3.0 ± 0.9	22	KHACHATRYAN	16CB	CMS	$t \rightarrow (W \rightarrow \ell\nu)(b \rightarrow J/\psi X \rightarrow \mu^+ \mu^- X)$
175.1 ± 1.4 ± 1.2	23	AAD	15AW	ATLS	small \cancel{E}_T , ≥ 6 jets ($2b$ -tag)
172.99 ± 0.48 ± 0.78	24	AAD	15BF	ATLS	ℓ + jets and dilepton
171.5 ± 1.9 ± 2.5	25	AALTONEN	15D	CDF	$\ell\ell + \cancel{E}_T + \geq 2j$
175.07 ± 1.19 ± 1.55	26	AALTONEN	14N	CDF	small \cancel{E}_T , 6-8 jets ($\geq 1b$ -tag)
174.98 ± 0.58 ± 0.49	27	ABAZOV	14C	D0	$\ell + \cancel{E}_T + 4$ jets ($\geq 1b$ -tag)
173.49 ± 0.69 ± 1.21	28	CHATRCHYAN	14C	D0	≥ 6 jets ($\geq 2b$ -tag)
173.93 ± 1.64 ± 0.87	29	AALTONEN	13H	CDF	$\cancel{E}_T + \geq 4$ jets ($\geq 1b$)
173.9 ± 0.9 ± 1.7	30	CHATRCHYAN	13S	CMS	$\ell\ell + \cancel{E}_T + \geq 2b$ -tag ($MT_2(T)$)
174.5 ± 0.6 ± 2.3	31	AAD	12I	ATLS	$\ell + \cancel{E}_T + \geq 4$ jets ($\geq 1b$), MT
172.85 ± 0.71 ± 0.85	32	AALTONEN	12AI	CDF	$\ell + \cancel{E}_T + \geq 4j$ (0,1,2 b) template
172.7 ± 9.3 ± 3.7	33	AALTONEN	12AL	CDF	$\tau_h + \cancel{E}_T + 4j$ ($\geq 1b$)
173.18 ± 0.56 ± 0.75	34	AALTONEN	12AP	TEVA	CDF, D0 combination
172.5 ± 1.4 ± 1.5	35	AALTONEN	12G	CDF	6-8 jets with $\geq 1b$
173.7 ± 2.8 ± 1.5	36	ABAZOV	12AB	D0	$\ell\ell + \cancel{E}_T + \geq 2j$ (ν WT)
173.9 ± 1.9 ± 1.6	37	ABAZOV	12AB	D0	$\ell\ell + \cancel{E}_T + \geq 2j$ (ν WT+MWT)
172.5 ± 0.4 ± 1.5	38	CHATRCHYAN	12BA	CMS	$\ell\ell + \cancel{E}_T + \geq 2j$ ($\geq 1b$), AMWT
173.49 ± 0.43 ± 0.98	39	CHATRCHYAN	12BP	CMS	$\ell + \cancel{E}_T + \geq 4j$ ($\geq 2b$)
172.4 ± 1.4 ± 1.3	40	AALTONEN	11AC	CDF	$\ell + \cancel{E}_T + 4$ jets ($\geq 1b$ -tag)
172.3 ± 2.4 ± 1.0	41	AALTONEN	11AK	CDF	Repl. by AALTONEN 13H
172.1 ± 1.1 ± 0.9	42	AALTONEN	11E	CDF	ℓ + jets and dilepton
176.9 ± 8.0 ± 2.7	43	AALTONEN	11T	CDF	$\ell + \cancel{E}_T + 4$ jets ($\geq 1b$ -tag), $p_T(\ell)$ shape
174.94 ± 0.83 ± 1.24	44	ABAZOV	11P	D0	$\ell + \cancel{E}_T + 4$ jets ($\geq 1b$ -tag)
174.0 ± 1.8 ± 2.4	45	ABAZOV	11R	D0	dilepton + $\cancel{E}_T + \geq 2$ jets
175.5 ± 4.6 ± 4.6	46	CHATRCHYAN	11F	CMS	dilepton + \cancel{E}_T + jets
173.0 ± 0.9 ± 0.9	47	AALTONEN	10AE	CDF	$\ell + \cancel{E}_T + 4$ jets ($\geq 1b$ -tag), ME method
169.3 ± 2.7 ± 3.2	48	AALTONEN	10C	CDF	dilepton + b -tag (MT2+NWA)
170.7 ± 6.3 ± 2.6	49	AALTONEN	10D	CDF	$\ell + \cancel{E}_T + 4$ jets (b -tag)
174.8 ± 2.4 ± 1.2	50	AALTONEN	10E	CDF	≥ 6 jets, vtx b -tag
180.5 ± 12.0 ± 3.6	51	AALTONEN	09AK	CDF	$\ell + \cancel{E}_T +$ jets (soft μ b -tag)
172.7 ± 1.8 ± 1.2	52	AALTONEN	09J	CDF	$\ell + \cancel{E}_T + 4$ jets (b -tag)
171.1 ± 3.7 ± 2.1	53	AALTONEN	09K	CDF	6 jets, vtx b -tag
171.9 ± 1.7 ± 1.1	54	AALTONEN	09L	CDF	ℓ + jets, $\ell\ell$ + jets
171.2 ± 2.7 ± 2.9	55	AALTONEN	09O	CDF	dilepton
165.5 ± 3.4 ± 3.1	56	AALTONEN	09X	CDF	$\ell\ell + \cancel{E}_T$ ($\nu\phi$ weighting)
174.7 ± 4.4 ± 2.0	57	ABAZOV	09AH	D0	dilepton + b -tag (ν WT+MWT)
170.7 ± 4.2 ± 3.9	58,59	AALTONEN	08C	CDF	dilepton, $\sigma_{t\bar{t}}$ constrained
171.5 ± 1.8 ± 1.1	60	ABAZOV	08AH	D0	$\ell + \cancel{E}_T + 4$ jets
177.1 ± 4.9 ± 4.7	61,62	AALTONEN	07C	CDF	6 jets with $\geq 1b$ vtx
172.3 ± 10.8 ± 9.6	63	AALTONEN	07B	CDF	≥ 4 jets (b -tag)
174.0 ± 2.2 ± 4.8	64	AALTONEN	07D	CDF	≥ 6 jets, vtx b -tag
170.8 ± 2.2 ± 1.4	65,66	AALTONEN	07I	CDF	lepton + jets (b -tag)
173.7 ± 4.4 ± 2.1	62,67	ABAZOV	07F	D0	lepton + jets
176.2 ± 9.2 ± 3.9	68	ABAZOV	07W	D0	dilepton (MWT)
179.5 ± 7.4 ± 5.6	68	ABAZOV	07W	D0	dilepton (ν WT)
164.5 ± 3.9 ± 3.9	66,69	ABULENCIA	07D	CDF	dilepton
180.7 ± 15.5 ± 13.4	70	ABULENCIA	07J	CDF	lepton + jets
170.3 ± 4.1 ± 4.5	66,71	ABAZOV	06U	D0	lepton + jets (b -tag)
173.2 ± 2.6 ± 2.4	72,73	ABULENCIA	06D	CDF	lepton + jets
173.5 ± 3.7 ± 3.6	59,72	ABULENCIA	06D	CDF	lepton + jets
165.2 ± 6.1 ± 3.4	66,74	ABULENCIA	06G	CDF	dilepton
170.1 ± 6.0 ± 4.1	59,75	ABULENCIA	06V	CDF	dilepton
178.5 ± 13.7 ± 7.7	76,77	ABAZOV	05	D0	6 or more jets
180.1 ± 3.6 ± 3.9	78,79	ABAZOV	04G	D0	lepton + jets
176.1 ± 5.1 ± 5.3	80	AFFOLDER	01	CDF	lepton + jets
176.1 ± 6.6	81	AFFOLDER	01	CDF	dilepton, lepton+jets, all-jets
172.1 ± 5.2 ± 4.9	82	ABBOTT	99G	D0	di-lepton, lepton+jets
176.0 ± 6.5	83,84	ABE	99B	CDF	dilepton, lepton+jets, all-jets
167.4 ± 10.3 ± 4.8	84,85	ABE	99B	CDF	dilepton

168.4 ± 12.3 ± 3.6	79	ABBOTT	98D	D0	dilepton
173.3 ± 5.6 ± 5.5	79,86	ABBOTT	98F	D0	lepton + jets
175.9 ± 4.8 ± 5.3	85,87	ABE	98E	CDF	lepton + jets
161 ± 17 ± 10	85	ABE	98F	CDF	dilepton
172.1 ± 5.2 ± 4.9	88	BHAT	98B	RVUE	dilepton and lepton+jets
173.8 ± 5.0	89	BHAT	98B	RVUE	dilepton, lepton+jets, all-jets
173.3 ± 5.6 ± 6.2	79	ABACHI	97E	D0	lepton + jets
186 ± 10 ± 5.7	85,90	ABE	97R	CDF	6 or more jets
199 ± 19 ± 21		ABACHI	95	D0	lepton + jets
176 ± 8 ± 10		ABE	95F	CDF	lepton + b -jet
174 ± 10 ± 13		ABE	94E	CDF	lepton + b -jet

- AABOUD 19AC is an ATLAS combination of 7 and 8 TeV top-quark mass determination in the dilepton, lepton + jets, and all jets channels.
- SIRUNYAN 19AP based on 35.9 fb⁻¹ of pp data at $\sqrt{s} = 13$ TeV. A combined measurement using the lepton+jets and all-jets channels through a single likelihood function. See SIRUNYAN 18DE and SIRUNYAN 19AP below.
- SIRUNYAN 19AR based on 35.9 fb⁻¹ of pp data at $\sqrt{s} = 13$ TeV. Obtained from a simultaneous fit of the cross section and the top quark mass in the POWHEG simulation. The cross section is used also to extract the MS mass and the strong coupling constant for different PDF sets.
- SIRUNYAN 17L based on 19.7 fb⁻¹ of pp data at $\sqrt{s} = 8$ TeV. m_t is reconstructed from a fit to the invariant mass distribution of $\mu\nu b$, where p_T^{miss} and W mass constraint are used to reconstruct ν momentum. The number of events for various contributions, except for the t -channel single top one, are fixed to the values extracted from simulation.
- KHACHATRYAN 16AK based on 19.7 fb⁻¹ of pp data at $\sqrt{s} = 8$ TeV. Combination of the three top mass measurements in KHACHATRYAN 16AK and with the CMS results at $\sqrt{s} = 7$ TeV.
- TEVEVWG 16 is the latest Tevatron average (July 2016) provided by the Tevatron Electroweak Working Group. It takes correlated uncertainties into account and has a χ^2 of 10.8 for 11 degrees of freedom.
- AABOUD 19AC based on 20.2 fb⁻¹ of pp collisions at $\sqrt{s} = 8$ TeV. Uses optimized event selection to suppress less-well-reconstructed events and template fits to determine m_t together with a global jet energy scale factor and a relative b -to-light-jet energy scale factor.
- SIRUNYAN 19AP based on 35.9 fb⁻¹ of pp data at $\sqrt{s} = 13$ TeV. A kinematical fit is applied to each event assuming the signal event topology. m_t is determined simultaneously with a jet energy scale factor (JSF). The second error represents stat.+JSF. Modeling uncertainties are larger than in the measurements at $\sqrt{s} = 7$ and 8 TeV because of the use of new alternative color reconnection models.
- SIRUNYAN 18DE based on 35.9 fb⁻¹ of pp data at $\sqrt{s} = 13$ TeV. m_t is determined simultaneously with an overall jet energy scale factor constrained by the mass of the hadronically decayed W . Compared to the Run 1 analysis a more advanced treatment of modeling uncertainties are employed, in particular concerning color-reconnection models.
- AABOUD 17AH based on 20.2 fb⁻¹ of pp data at $\sqrt{s} = 8$ TeV. Uses template fits to the ratio of the masses of three-jets (from t candidate) and dijets (from W candidate), to suppress jet energy scale uncertainty. Large QCD background is modelled using a data-driven method.
- ABAZOV 17B is a combination of measurements of the top quark mass by D0 in the lepton+jets and dilepton channels, using all data collected in Run I (1992-1996) at $\sqrt{s} = 1.8$ TeV and Run II (2001-2011) at $\sqrt{s} = 1.96$ TeV of the Tevatron, corresponding to integrated luminosities of 0.1 fb⁻¹ and 9.7 fb⁻¹, respectively.
- SIRUNYAN 17N based on 19.7 fb⁻¹ of pp data at $\sqrt{s} = 8$ TeV. The fully hadronic decay of a highly-boosted t is reconstructed in the ℓ +jets channel and unfolded at the particle level. The sensitivity of the peak position of the m_{jet} distribution is used to test quality of the modelling by the simulation.
- SIRUNYAN 17O based on 19.7 fb⁻¹ of pp data at $\sqrt{s} = 8$ TeV. Analysis is based on the kinematical observables $M(b\ell)$, MT_2 and $M(b\ell\nu)$. A fit is performed to determine m_t and an overall jet energy scale factor simultaneously.
- AABOUD 16T based on 20.2 fb⁻¹ of pp data at $\sqrt{s} = 8$ TeV. The analysis is refined using the p_T and invariant mass distributions of ℓ + b -jet system. A combination with measurements from $\sqrt{s} = 7$ TeV data in the dilepton and lepton+jets channels gives $172.84 \pm 0.34 \pm 0.61$ GeV.
- AABOUD 16I is an ATLAS combination of 8 TeV top-quark mass in the dilepton channel with previous measurements from $\sqrt{s} = 7$ TeV data in the dilepton and lepton + jets channels.
- ABAZOV 16 based on 9.7 fb⁻¹ of data in $p\bar{p}$ collisions at $\sqrt{s} = 1.96$ TeV. Employs improved fit to minimize statistical errors and improved jet energy calibration, using lepton + jets mode, which reduces error of jet energy scale. Based on previous determination in ABAZOV 12AB with increased integrated luminosity and improved fit and calibrations.
- ABAZOV 16D based on 9.7 fb⁻¹ of data in $p\bar{p}$ collisions at $\sqrt{s} = 1.96$ TeV, using the matrix element technique. Based on previous determination in ABAZOV 11R with increased integrated luminosity. There is a strong correlation with the determination in ABAZOV 16. (See ABAZOV 17B.)
- KHACHATRYAN 16AK based on 19.7 fb⁻¹ of pp data at $\sqrt{s} = 8$ TeV. Combination of the three top mass measurements in KHACHATRYAN 16AK and with the CMS results at $\sqrt{s} = 7$ TeV gives $172.44 \pm 0.13 \pm 0.47$ GeV.
- The top mass and jet energy scale factor are determined by a fit.
- Uses the analytical matrix weighting technique method.
- KHACHATRYAN 16AL based on 19.7 fb⁻¹ in pp collisions at $\sqrt{s} = 8$ TeV. Determined from the invariant mass distribution of leptons and reconstructed secondary vertices from b decays using only charged particles. The uncertainty is dominated by modeling of b fragmentation and top p_T distribution.
- KHACHATRYAN 16CB based on 666 candidate reconstructed events corresponding to 19.7 fb⁻¹ of pp data at $\sqrt{s} = 8$ TeV. The measurement exploits correlation of m_t with $M(J/\psi X)$ in the same top quark decay, using a high-purity event sample. A study on modeling of b -quark fragmentation is given in Sec.3.3.
- AAD 15AW based on 4.6 fb⁻¹ of pp data at $\sqrt{s} = 7$ TeV. Uses template fits to the ratio of the masses of three-jets (from t candidate) and dijets (from W candidate). Large background from multijet production is modeled with data-driven methods.
- AAD 15BF based on 4.6 fb⁻¹ in pp collisions at $\sqrt{s} = 7$ TeV. Using a three-dimensional template likelihood technique the lepton plus jets ($\geq 1b$ -tagged) channel gives $172.33 \pm 0.75 \pm 1.02$ GeV, while exploiting a one dimensional template method using $m_{\ell b}$ the dilepton channel (1 or 2b-tags) gives $173.79 \pm 0.54 \pm 1.30$ GeV. The results are combined.

Quark Particle Listings

 t

- 25 AALTONEN 15D based on 9.1 fb^{-1} of $p\bar{p}$ data at $\sqrt{s} = 1.96 \text{ TeV}$. Uses a template technique to fit a distribution of a variable defined by a linear combination of variables sensitive and insensitive to jet energy scale to optimize reduction of systematic errors. b -tagged and non- b -tagged events are separately analyzed and combined.
- 26 Based on 9.3 fb^{-1} of $p\bar{p}$ data at $\sqrt{s} = 1.96 \text{ TeV}$. Multivariate algorithm is used to discriminate signal from backgrounds, and templates are used to measure m_t .
- 27 Based on 9.7 fb^{-1} of $p\bar{p}$ data at $\sqrt{s} = 1.96 \text{ TeV}$. A matrix element method is used to calculate the probability of an event to be signal or background, and the overall jet energy scale is constrained *in situ* by m_W . See ABAZOV 15G for further details.
- 28 Based on 3.54 fb^{-1} of pp data at $\sqrt{s} = 7 \text{ TeV}$. The mass is reconstructed for each event employing a kinematic fit of the jets to a $t\bar{t}$ hypothesis. The combination with the previous CMS measurements in the dilepton and the lepton+jets channels gives $173.54 \pm 0.33 \pm 0.96 \text{ GeV}$.
- 29 Based on 8.7 fb^{-1} in $p\bar{p}$ collisions at $\sqrt{s} = 1.96 \text{ TeV}$. Events with an identified charged lepton or small E_T are rejected from the event sample, so that the measurement is statistically independent from those in the $\ell + \text{jets}$ and all hadronic channels while being sensitive to those events with a τ lepton in the final state.
- 30 Based on 5.0 fb^{-1} of pp data at $\sqrt{s} = 7 \text{ TeV}$. CHATRCHYAN 13s studied events with di-lepton + $E_T + \geq 2$ b -jets, and looked for kinematical endpoints of MT2, MT2 $_T$, and subsystem variables.
- 31 AAD 12i based on 1.04 fb^{-1} of pp data at $\sqrt{s} = 7 \text{ TeV}$. Uses 2d-template analysis (MT) with m_t and jet energy scale factor (JSF) from m_W mass fit.
- 32 Based on 8.7 fb^{-1} of data in $p\bar{p}$ collisions at 1.96 TeV . The JES is calibrated by using the dijet mass from the W boson decay.
- 33 Use the ME method based on 2.2 fb^{-1} of data in $p\bar{p}$ collisions at 1.96 TeV .
- 34 Combination based on up to 5.8 fb^{-1} of data in $p\bar{p}$ collisions at 1.96 TeV .
- 35 Based on 5.8 fb^{-1} of data in $p\bar{p}$ collisions at 1.96 TeV the quoted value is $m_t = 172.5 \pm 1.4(\text{stat}) \pm 1.0(\text{JES}) \pm 1.1(\text{syst}) \text{ GeV}$. The measurement is performed with a likelihood fit technique which simultaneously determines m_t and JES (Jet Energy Scale).
- 36 Based on 4.3 fb^{-1} of data in p - p bar collisions at 1.96 TeV . The measurement reduces the JES uncertainty by using the single lepton channel study of ABAZOV 11P.
- 37 Combination with the result in 1 fb^{-1} of preceding data reported in ABAZOV 09AH as well as the MWT result of ABAZOV 11R with a statistical correlation of 60%.
- 38 Based on 5.0 fb^{-1} of pp data at $\sqrt{s} = 7 \text{ TeV}$. Uses an analytical matrix weighting technique (AMWT) and full kinematic analysis (KIN).
- 39 Based on 5.0 fb^{-1} of pp data at $\sqrt{s} = 7 \text{ TeV}$. The first error is statistical and JES combined, and the second is systematic. Ideogram method is used to obtain 2D likelihood for the kinematical fit with two parameters m_{top} and JES.
- 40 Based on 3.2 fb^{-1} in $p\bar{p}$ collisions at $\sqrt{s} = 1.96 \text{ TeV}$. The first error is from statistics and JES combined, and the latter is from the other systematic uncertainties. The result is obtained using an unbinned maximum likelihood method where the top quark mass and the JES are measured simultaneously, with $\Delta_{JES} = 0.3 \pm 0.3(\text{stat})$.
- 41 Based on 5.7 fb^{-1} in $p\bar{p}$ collisions at $\sqrt{s} = 1.96 \text{ TeV}$. Events with an identified charged lepton or small E_T are rejected from the event sample, so that the measurement is statistically independent from those in the $\ell + \text{jets}$ and all hadronic channels while being sensitive to those events with a τ lepton in the final state. Supersedes AALTONEN 07B.
- 42 AALTONEN 11E based on 5.6 fb^{-1} in $p\bar{p}$ collisions at $\sqrt{s} = 1.96 \text{ TeV}$. Employs a multi-dimensional template likelihood technique where the lepton plus jets (one or two b -tags) channel gives $172.2 \pm 1.2 \pm 0.9 \text{ GeV}$ while the dilepton channel yields $170.3 \pm 2.0 \pm 3.1 \text{ GeV}$. The results are combined. OUR EVALUATION includes the measurement in the dilepton channel only.
- 43 Uses a likelihood fit of the lepton p_T distribution based on 2.7 fb^{-1} in $p\bar{p}$ collisions at $\sqrt{s} = 1.96 \text{ TeV}$.
- 44 Based on 3.6 fb^{-1} in $p\bar{p}$ collisions at $\sqrt{s} = 1.96 \text{ TeV}$. ABAZOV 11P reports $174.94 \pm 0.83 \pm 0.78 \pm 0.96 \text{ GeV}$, where the first uncertainty is from statistics, the second from JES, and the last from other systematic uncertainties. We combine the JES and systematic uncertainties. A matrix-element method is used where the JES uncertainty is constrained by the W mass. ABAZOV 11P describes a measurement based on 2.6 fb^{-1} that is combined with ABAZOV 08AH, which employs an independent 1 fb^{-1} of data.
- 45 Based on a matrix-element method which employs 5.4 fb^{-1} in $p\bar{p}$ collisions at $\sqrt{s} = 1.96 \text{ TeV}$. Superseded by ABAZOV 12AB.
- 46 Based on 36 pb^{-1} of pp collisions at $\sqrt{s} = 7 \text{ TeV}$. A Kinematic Method using b -tagging and an analytical Matrix Weighting Technique give consistent results and are combined. Superseded by CHATRCHYAN 12BA.
- 47 Based on 5.6 fb^{-1} in $p\bar{p}$ collisions at $\sqrt{s} = 1.96 \text{ TeV}$. The likelihood calculated using a matrix element method gives $m_t = 173.0 \pm 0.7(\text{stat}) \pm 0.6(\text{JES}) \pm 0.9(\text{syst}) \text{ GeV}$, for a total uncertainty of 1.2 GeV .
- 48 Based on 3.4 fb^{-1} of $p\bar{p}$ collisions at $\sqrt{s} = 1.96 \text{ TeV}$. The result is obtained by combining the MT2 variable method and the NWA (Neutrino Weighting Algorithm). The MT2 method alone gives $m_t = 168.0^{+4.8}_{-4.0}(\text{stat}) \pm 2.9(\text{syst}) \text{ GeV}$ with smaller systematic error due to small JES uncertainty.
- 49 Based on 1.9 fb^{-1} in $p\bar{p}$ collisions at $\sqrt{s} = 1.96 \text{ TeV}$. The result is from the measurement using the transverse decay length of b -hadrons and that using the transverse momentum of the W decay muons, which are both insensitive to the JES (jet energy scale) uncertainty. OUR EVALUATION uses only the measurement exploiting the decay length significance which yields $166.9^{+9.5}_{-8.5}(\text{stat}) \pm 2.9(\text{syst}) \text{ GeV}$. The measurement that uses the lepton transverse momentum is excluded from the average because of a statistical correlation with other samples.
- 50 Based on 2.9 fb^{-1} of $p\bar{p}$ collisions at $\sqrt{s} = 1.96 \text{ TeV}$. The first error is from statistics and JES uncertainty, and the latter is from the other systematics. Neural-network-based kinematical selection of 6 highest E_T jets with a $vt\bar{t}$ b -tag is used to distinguish signal from background. Superseded by AALTONEN 12G.
- 51 Based on 2 fb^{-1} of data at $\sqrt{s} = 1.96 \text{ TeV}$. The top mass is obtained from the measurement of the invariant mass of the lepton (e or μ) from W decays and the soft μ in b -jet. The result is insensitive to jet energy scaling.
- 52 Based on 1.9 fb^{-1} of data at $\sqrt{s} = 1.96 \text{ TeV}$. The first error is from statistics and jet energy scale uncertainty, and the latter is from the other systematics. Matrix element method with effective propagators.
- 53 Based on 943 pb^{-1} of data at $\sqrt{s} = 1.96 \text{ TeV}$. The first error is from statistical and jet-energy-scale uncertainties, and the latter is from other systematics. AALTONEN 09k selected 6 jet events with one or more vertex b -tags and used the tree-level matrix element to construct template models of signal and background.
- 54 Based on 1.9 fb^{-1} of data at $\sqrt{s} = 1.96 \text{ TeV}$. The first error is from statistical and jet-energy-scale (JES) uncertainties, and the second is from other systematics. Events with lepton + jets and those with dilepton + jets were simultaneously fit to constrain m_t and JES. Lepton + jets data only give $m_t = 171.8 \pm 2.2 \text{ GeV}$, and dilepton data only give $m_t = 171.2^{+5.3}_{-5.1} \text{ GeV}$.
- 55 Based on 2 fb^{-1} of data at $\sqrt{s} = 1.96 \text{ TeV}$. Matrix Element method. Optimal selection criteria for candidate events with two high p_T leptons, high E_T , and two or more jets with and without b -tag are obtained by neural network with neuroevolution technique to minimize the statistical error of m_t .
- 56 Based on 2.9 fb^{-1} of data at $\sqrt{s} = 1.96 \text{ TeV}$. Mass m_t is estimated from the likelihood for the eight-fold kinematical solutions in the plane of the azimuthal angles of the two neutrino momenta.
- 57 Based on 1 fb^{-1} of data at $\sqrt{s} = 1.96 \text{ TeV}$. Events with two identified leptons, and those with one lepton plus one isolated track and a b -tag were used to constrain m_t . The result is a combination of the ν WT (ν Weighting Technique) result of $176.2 \pm 4.8 \pm 2.1 \text{ GeV}$ and the MWT (Matrix-element Weighting Technique) result of $173.2 \pm 4.9 \pm 2.0 \text{ GeV}$.
- 58 Reports measurement of $170.7^{+4.2}_{-3.9} \pm 2.6 \pm 2.4 \text{ GeV}$ based on 1.2 fb^{-1} of data at $\sqrt{s} = 1.96 \text{ TeV}$. The last error is due to the theoretical uncertainty on $\sigma_{t\bar{t}}$. Without the cross-section constraint a top mass of $169.7^{+5.2}_{-4.9} \pm 3.1 \text{ GeV}$ is obtained.
- 59 Template method.
- 60 Result is based on 1 fb^{-1} of data at $\sqrt{s} = 1.96 \text{ TeV}$. The first error is from statistics and jet energy scale uncertainty, and the latter is from the other systematics.
- 61 Based on 310 pb^{-1} of data at $\sqrt{s} = 1.96 \text{ TeV}$.
- 62 Ideogram method.
- 63 Based on 311 pb^{-1} of data at $\sqrt{s} = 1.96 \text{ TeV}$. Events with 4 or more jets with $E_T > 15 \text{ GeV}$, significant missing E_T , and secondary vertex b -tag are used in the fit. About 44% of the signal acceptance is from $\tau\nu + 4$ jets. Events with identified e or μ are vetoed to provide a statistically independent measurement.
- 64 Based on 1.02 fb^{-1} of data at $\sqrt{s} = 1.96 \text{ TeV}$. Superseded by AALTONEN 12G.
- 65 Based on 955 pb^{-1} of data at $\sqrt{s} = 1.96 \text{ TeV}$. m_t and JES (Jet Energy Scale) are fitted simultaneously, and the first error contains the JES contribution of 1.5 GeV .
- 66 Matrix element method.
- 67 Based on 425 pb^{-1} of data at $\sqrt{s} = 1.96 \text{ TeV}$. The first error is a combination of statistics and JES (Jet Energy Scale) uncertainty, which has been measured simultaneously to give $\text{JES} = 0.989 \pm 0.029(\text{stat})$.
- 68 Based on 370 pb^{-1} of data at $\sqrt{s} = 1.96 \text{ TeV}$. Combined result of MWT (Matrix-element Weighting Technique) and ν WT (ν Weighting Technique) analyses is $178.1 \pm 6.7 \pm 4.8 \text{ GeV}$.
- 69 Based on 1.0 fb^{-1} of data at $\sqrt{s} = 1.96 \text{ TeV}$. ABULENCIA 07D improves the matrix element description by including the effects of initial-state radiation.
- 70 Based on 695 pb^{-1} of data at $\sqrt{s} = 1.96 \text{ TeV}$. The transverse decay length of the b hadron is used to determine m_t , and the result is free from the JES (jet energy scale) uncertainty.
- 71 Based on $\sim 400 \text{ pb}^{-1}$ of data at $\sqrt{s} = 1.96 \text{ TeV}$. The first error includes statistical and systematic jet energy scale uncertainties, the second error is from the other systematics. The result is obtained with the b -tagging information. The result without b -tagging is $169.2^{+5.0+1.5}_{-7.4-1.4} \text{ GeV}$. Superseded by ABAZOV 08AH.
- 72 Based on 318 pb^{-1} of data at $\sqrt{s} = 1.96 \text{ TeV}$.
- 73 Dynamical likelihood method.
- 74 Based on 340 pb^{-1} of data at $\sqrt{s} = 1.96 \text{ TeV}$.
- 75 Based on 360 pb^{-1} of data at $\sqrt{s} = 1.96 \text{ TeV}$.
- 76 Based on $110.2 \pm 5.8 \text{ pb}^{-1}$ at $\sqrt{s} = 1.8 \text{ TeV}$.
- 77 Based on the all hadronic decays of $t\bar{t}$ pairs. Single b -quark tagging via the decay chain $b \rightarrow c \rightarrow \mu$ was used to select signal enriched multijet events. The result was obtained by the maximum likelihood method after bias correction.
- 78 Obtained by re-analysis of the lepton + jets candidate events that led to ABBOTT 98F. It is based upon the maximum likelihood method which makes use of the leading order matrix elements.
- 79 Based on $125 \pm 7 \text{ pb}^{-1}$ of data at $\sqrt{s} = 1.8 \text{ TeV}$.
- 80 Based on $\sim 106 \text{ pb}^{-1}$ of data at $\sqrt{s} = 1.8 \text{ TeV}$.
- 81 Obtained by combining the measurements in the lepton + jets [AFFOLDER 01], all-jets [ABE 97R, ABE 99B], and dilepton [ABE 99B] decay topologies.
- 82 Obtained by combining the D0 result $m_t(\text{GeV}) = 168.4 \pm 12.3 \pm 3.6$ from 6 di-lepton events (see also ABBOTT 98B) and $m_t(\text{GeV}) = 173.3 \pm 5.6 \pm 5.5$ from lepton+jets events (ABBOTT 98F).
- 83 Obtained by combining the CDF results of $m_t(\text{GeV}) = 167.4 \pm 10.3 \pm 4.8$ from 8 dilepton events, $m_t(\text{GeV}) = 175.9 \pm 4.8 \pm 5.3$ from lepton+jets events (ABE 98E), and $m_t(\text{GeV}) = 186.0 \pm 10.0 \pm 5.7$ from all-jet events (ABE 97R). The systematic errors in the latter two measurements are changed in this paper.
- 84 See AFFOLDER 01 for details of systematic error re-evaluation.
- 85 Based on $109 \pm 7 \text{ pb}^{-1}$ of data at $\sqrt{s} = 1.8 \text{ TeV}$.
- 86 See ABAZOV 04G.
- 87 The updated systematic error is listed. See AFFOLDER 01, appendix C.
- 88 Obtained by combining the D0 results of $m_t(\text{GeV}) = 168.4 \pm 12.3 \pm 3.6$ from 6 dilepton events and $m_t(\text{GeV}) = 173.3 \pm 5.6 \pm 5.5$ from 77 lepton+jets events.
- 89 Obtained by combining the D0 results from dilepton and lepton+jets events, and the CDF results (ABE 99B) from dilepton, lepton+jets events, and all-jet events.
- 90 Based on the first observation of all hadronic decays of $t\bar{t}$ pairs. Single b -quark tagging with jet-shape variable constraints was used to select signal enriched multi-jet events. The updated systematic error is listed. See AFFOLDER 01, appendix C.

 t -Quark Mass from Cross-Section Measurements

The top quark $M\bar{S}$ or pole mass can be extracted from a measurement of $\sigma(t\bar{t})$ by using theory calculations. We quote below the $M\bar{S}$ mass. See the review "The Top Quark" and references therein for more information.

VALUE (GeV)	DOCUMENT ID	TECN	COMMENT
$162.5^{+2.1}_{-1.5}$ OUR AVERAGE			
$162.9 \pm 0.5 \pm 1.0^{+2.1}_{-1.2}$	1 AAD	19G ATLS	$\ell + \cancel{E}_T + \geq 5 j$ ($2b$ -j)
$160.0^{+4.8}_{-4.3}$	2 ABAZOV	11s D0	$\sigma(t\bar{t})$ + theory
	3 ABAZOV	09AG D0	cross sects, theory + exp
	4 ABAZOV	09R D0	cross sects, theory + exp

• • • We do not use the following data for averages, fits, limits, etc. • • •

1 AAD 19g based on 20.2 fb⁻¹ of data in pp collisions at sqrt(s) = 8 TeV. Normalized tT + 1-jet differential cross section as a function of tTj invariant mass is measured in the l + jets mode. The unfolded parton-level distribution is compared with the NLO QCD prediction. The three errors are from statistics, systematics, and theory.

2 Based on 5.3 fb⁻¹ in pP collisions at sqrt(s) = 1.96 TeV. ABAZOV 11s uses the measured tT production cross section of 8.13 +/- 1.02/-0.90 pb [ABAZOV 11E] in the lepton plus jets channel to obtain the top quark MS mass by using an approximate NNLO computation (MOCH 08, LANGENFELD 09). The corresponding top quark pole mass is 167.5 +/- 5.4 GeV. A different theory calculation (AHRENS 10, AHRENS 10A) is also used and yields mT = 154.5 +/- 5.0/-4.3 GeV.

3 Based on 1 fb⁻¹ of data at sqrt(s) = 1.96 TeV. Uses the l + jets, ll, and lT + jets channels. ABAZOV 09Ag extract the pole mass of the top quark using two different calculations that yield 169.1 +/- 5.9/-5.2 GeV (MOCH 08, LANGENFELD 09) and 168.2 +/- 5.4 GeV (KIDONAKIS 08).

4 Based on 1 fb⁻¹ of data at sqrt(s) = 1.96 TeV. Uses the ll and lT + jets channels. ABAZOV 09R extract the pole mass of the top quark using two different calculations that yield 173.3 +/- 9.8/-8.6 GeV (MOCH 08, LANGENFELD 09) and 171.5 +/- 9.9/-8.8 GeV (CACIARI 08).

t-Quark Pole Mass from Cross-Section Measurements

Table with 4 columns: VALUE (GeV), DOCUMENT ID, TECN, COMMENT. Includes 'OUR AVERAGE' and various experimental results from ATLAS, CMS, D0, etc.

1 AAD 19g based on 20.2 fb⁻¹ of data in pp collisions at sqrt(s) = 8 TeV. Normalized tT + 1-jet differential cross section as a function of tTj invariant mass is measured in the l + jets mode. The unfolded parton-level distribution is compared with the NLO QCD prediction. The three errors are from statistics, systematics, and theory.

2 AABOUD 17bc based on 20.2 fb⁻¹ of pp data at sqrt(s) = 8 TeV. The pole mass is extracted from a fit of NLO predictions to eight single lepton and dilepton differential distributions, while simultaneously constraining uncertainties due to PDFs and QCD scales. The three reported uncertainties come from statistics, experimental systematics, and theoretical sources.

3 SIRUNYAN 17w based on 2.2 fb⁻¹ of pp data at sqrt(s) = 13 TeV. Events are categorized according to the jet multiplicity and the number of b-tagged jets. The pole mass is obtained from the inclusive cross section measurement and the NNLO prediction.

4 ABAZOV 16f based on 9.7 fb⁻¹ of data in pP collisions at sqrt(s) = 1.96 TeV. The result is obtained from the inclusive cross section measurement and the NNLO+NNLL prediction.

5 KHACHATRYAN 16Aw based on 5.0 fb⁻¹ of pp collisions at 7 TeV and 19.7 fb⁻¹ at 8 TeV. The 7 TeV data include those used in CHATRCHYAN 14. The result is obtained from the inclusive cross sections.

6 AAD 15Bw based on 4.6 fb⁻¹ of pp data at sqrt(s) = 7 TeV. Uses normalized differential cross section for tT + 1 jet as a function of the inverse of the invariant mass of the tT + 1 jet system. The measured cross section is corrected to the parton level. Then a fit to the data using NLO + parton shower prediction is performed.

7 AAD 14Ay used sigma(tT) for e mu events. The result is a combination of the measurements mt = 171.4 +/- 2.6 GeV based on 4.6 fb⁻¹ of data at 7 TeV and mt = 174.1 +/- 2.6 GeV based on 20.3 fb⁻¹ of data at 8 TeV.

8 CHATRCHYAN 14 used sigma(tT) from pP collisions at sqrt(s) = 7 TeV measured in CHATRCHYAN 12Ax to obtain mt(pole) = 0.1184 +/- 0.0007. The errors have been corrected in KHACHATRYAN 14k.

mt - mT

Test of CPT conservation. OUR AVERAGE assumes that the systematic uncertainties are uncorrelated.

Table with 4 columns: VALUE (GeV), DOCUMENT ID, TECN, COMMENT. Includes 'OUR AVERAGE' and various experimental results.

1 CHATRCHYAN 17 based on 19.6 fb⁻¹ of pp data at sqrt(s) = 8 TeV and an average top mass of 172.84 +/- 0.10 (stat) GeV is obtained.

2 Based on 4.7 fb⁻¹ of pp data at sqrt(s) = 7 TeV and an average top mass of 172.5 GeV/c^2.

3 Based on 8.7 fb⁻¹ of pP collisions at sqrt(s) = 1.96 TeV and an average top mass of 172.5 GeV/c^2.

4 Based on 4.96 fb⁻¹ of pp data at sqrt(s) = 7 TeV. Based on the fitted mt for l+ and l- events using the Ideogram method.

5 Based on a matrix-element method which employs 3.6 fb⁻¹ in pP collisions at sqrt(s) = 1.96 TeV.

6 Based on a template likelihood technique which employs 5.6 fb⁻¹ in pP collisions at sqrt(s) = 1.96 TeV.

7 Based on 1 fb⁻¹ of data in pP collisions at sqrt(s) = 1.96 TeV.

t-quark DECAY WIDTH

Table with 5 columns: VALUE (GeV), CL%, DOCUMENT ID, TECN, COMMENT. Lists various decay width measurements for the t quark.

1 Based on 20.2 fb⁻¹ of pp data at sqrt(s) = 8 TeV. Gamma_t is measured using a template fit to the reconstructed invariant mass of the b-jet of the semileptonically decaying top quark and the corresponding lepton, and the angular distance between jb and jj in hadronic top decay. Signal templates are generated by reweighting events at parton-level to Breit-Wigner distribution with different Gamma_t hypotheses for mt = 172.5 GeV. The result is consistent with the NNLO SM prediction of 1.322 GeV.

2 Based on 19.7 fb⁻¹ of pp data at sqrt(s) = 8 TeV. The result is obtained by combining the measurement of R = Gamma(t -> Wb)/Gamma(t -> Wq (q=b,s,d)) and a previous CMS measurement of the t-channel single top production cross section of CHATRCHYAN 12Bq, by using the theoretical calculation of Gamma(t -> Wb) for mt = 172.5 GeV.

3 Based on 5.4 fb⁻¹ of data in pP collisions at 1.96 TeV. Gamma(t -> bW) = 1.87 +/- 0.44 GeV is obtained from the observed t-channel single top quark production cross section, whereas B(t -> bW) = 0.90 +/- 0.04 is used assuming Sigma_q B(t -> qW) = 1. The result is valid for mt = 172.5 GeV. See the paper for the values for mt = 170 or 175 GeV.

4 Based on 8.7 fb⁻¹ of data. The two sided 68% CL interval is 1.10 GeV < Gamma_t < 4.05 GeV for mt = 172.5 GeV.

5 Based on 2.3 fb⁻¹ in pP collisions at sqrt(s) = 1.96 TeV. ABAZOV 11B extracted Gamma_t from the partial width Gamma(t -> Wb) = 1.92 +/- 0.58/-0.51 GeV measured using the t-channel single top production cross section, and the branching fraction brt -> Wb = 0.962 +/- 0.068 (stat) +/- 0.064 (syst). The Gamma(t -> Wb) measurement gives the 95% CL lowerbound of Gamma(t -> Wb) and hence that of Gamma_t.

6 Results are based on 4.3 fb⁻¹ of data in pP collisions at sqrt(s) = 1.96 TeV. The top quark mass and the hadronically decaying W boson mass are reconstructed for each candidate events and compared with templates of different top quark width. The two sided 68% CL interval is 0.3 GeV < Gamma_t < 4.4 GeV for mt = 172.5 GeV.

7 Based on 955 pb⁻¹ of pP collision data at sqrt(s) = 1.96 TeV. AALTONEN 09m selected tT candidate events for the l + ET + jets channel with one or two b-tags, and examine the decay width dependence of the reconstructed mt distribution. The result is for mt = 175 GeV, whereas the upper limit is lower for smaller mt.

t DECAY MODES

Table with 3 columns: Mode, Fraction (Gamma_i/Gamma), Confidence level. Lists various decay modes for the t quark.

Delta T = 1 weak neutral current (TI) modes

Table with 4 columns: Gamma_i, Mode, TI, Confidence level. Lists TI modes for the t quark.

[a] This limit is for Gamma(t -> gamma q)/Gamma(t -> Wb).

[b] This limit is for Gamma(t -> Z q)/Gamma(t -> Wb).

t BRANCHING RATIOS

Gamma(Wb)/Gamma(Wq (q=b,s,d)) OUR AVERAGE assumes that the systematic uncertainties are uncorrelated.

Table with 4 columns: VALUE, DOCUMENT ID, TECN, COMMENT. Lists branching ratios for the t quark.

1 AALTONEN 14g CDF ll + ET + >= 2j (0,1,2 b-tag)

2 KHACHATRYAN 14E CMS ll + ET + 2,3,4j (0-2b-tag)

3 AALTONEN 13g CDF ll + ET + >= 3jets (>= 1b-tag)

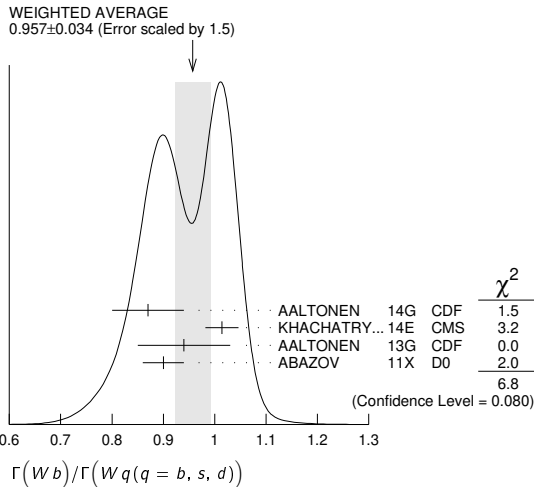
Quark Particle Listings

t

• • • We do not use the following data for averages, fits, limits, etc. • • •

0.97 $\begin{smallmatrix} +0.09 \\ -0.08 \end{smallmatrix}$	5	ABAZOV	08M D0	$\ell + n$ jets with 0,1,2 <i>b</i> -tag
1.03 $\begin{smallmatrix} +0.19 \\ -0.17 \end{smallmatrix}$	6	ABAZOV	06k D0	
1.12 $\begin{smallmatrix} +0.21 & +0.17 \\ -0.19 & -0.13 \end{smallmatrix}$	7	ACOSTA	05A CDF	Repl. by AALTONEN 13G
0.94 $\begin{smallmatrix} +0.26 & +0.17 \\ -0.21 & -0.12 \end{smallmatrix}$	8	AFFOLDER	01c CDF	

- Based on 8.7 fb⁻¹ of data. This measurement gives $|V_{tb}| = 0.93 \pm 0.04$ and $|V_{tb}| > 0.85$ (95% CL) in the SM.
- Based on 19.7 fb⁻¹ of *pp* data at $\sqrt{s} = 8$ TeV. The result is obtained by counting the number of *b* jets per *t* \bar{t} signal events in the dilepton channel. The *t* \bar{t} production cross section is measured to be $\sigma(t\bar{t}) = 238 \pm 1 \pm 15$ pb, in good agreement with the SM prediction and the latest CMS measurement of CHATRCHYAN 14F. The measurement gives $R > 0.995$ (95% CL), or $|V_{tb}| > 0.975$ (95% CL) in the SM, requiring $R \leq 1$.
- Based on 8.7 fb⁻¹ of *p* \bar{p} collisions at $\sqrt{s} = 1.96$ TeV. Measure the fraction of *t* $\rightarrow Wb$ decays simultaneously with the *t* \bar{t} cross section. The correlation coefficient between those two measurements is -0.434 . Assume unitarity of the 3x3 CKM matrix and set $|V_{tb}| > 0.89$ at 95% CL.
- Based on 5.4 fb⁻¹ of data. The error is statistical and systematic combined. The result is a combination of 0.95 ± 0.07 from $\ell +$ jets channel and 0.86 ± 0.05 from $\ell\ell$ channel. $|V_{tb}| = 0.95 \pm 0.02$ follows from the result by assuming unitarity of the 3x3 CKM matrix.
- Result is based on 0.9 fb⁻¹ of data. The 95% CL lower bound $R > 0.79$ gives $|V_{tb}| > 0.89$ (95% CL).
- ABAZOV 06k result is from the analysis of $t\bar{t} \rightarrow \ell\nu_\ell + \geq 3$ jets with 230 pb⁻¹ of data at $\sqrt{s} = 1.96$ TeV. It gives $R > 0.61$ and $|V_{tb}| > 0.78$ at 95% CL. Superseded by ABAZOV 08M.
- ACOSTA 05A result is from the analysis of lepton + jets and di-lepton + jets final states of *t* \bar{t} candidate events with ~ 162 pb⁻¹ of data at $\sqrt{s} = 1.96$ TeV. The first error is statistical and the second systematic. It gives $R > 0.61$, or $|V_{tb}| > 0.78$ at 95% CL.
- AFFOLDER 01c measures the top-quark decay width ratio $R = \Gamma(Wb)/\Gamma(Wq)$, where *q* is a *d*, *s*, or *b* quark, by using the number of events with multiple *b*tags. The first error is statistical and the second systematic. A numerical integration of the likelihood function gives $R > 0.61$ (0.56) at 90% (95%) CL. By assuming three generation unitarity, $|V_{tb}| = 0.97^{+0.16}_{-0.12}$ or $|V_{tb}| > 0.78$ (0.75) at 90% (95%) CL is obtained. The result is based on 109 pb⁻¹ of data at $\sqrt{s} = 1.8$ TeV.



$\Gamma(e\nu_e b)/\Gamma_{total}$	Γ_3/Γ		
VALUE	DOCUMENT ID	TECN	COMMENT
0.111 ± 0.003	1 AAD	15cc ATLS	$\ell +$ jets, $\ell\ell +$ jets, $\ell\tau_h +$ jets

- AAD 15cc based on 4.6 fb⁻¹ of *pp* data at $\sqrt{s} = 7$ TeV. The original value is given by $13.3 \pm 0.4 \pm 0.5\%$, which includes electrons from the decay of τ leptons. It is assumed that the top branching ratios to leptons and jets add up to one and that only SM processes contribute to the background. The event selection criteria are optimized for the $\ell\tau_h +$ jets channel. We have converted the original value to eliminate contributions of electrons from τ 's, by using the AAD 15cc measurements of the branching ratios to μ and τ channels, as well as the PDG values of τ branching ratios into *e* and μ channels.

$\Gamma(\mu\nu_\mu b)/\Gamma_{total}$	Γ_4/Γ		
VALUE	DOCUMENT ID	TECN	COMMENT
0.114 ± 0.002	1 AAD	15cc ATLS	$\ell +$ jets, $\ell\ell +$ jets, $\ell\tau_h +$ jets

- AAD 15cc based on 4.6 fb⁻¹ of *pp* data at $\sqrt{s} = 7$ TeV. The original value is given by $13.4 \pm 0.3 \pm 0.5\%$, which includes muons from the decay of τ leptons. It is assumed that the top branching ratios to leptons and jets add up to one and that only SM processes contribute to the background. The event selection criteria are optimized for the $\ell\tau_h +$ jets channel. We have converted the original value to eliminate contributions of muons from τ 's, by using the AAD 15cc measurements of the branching ratios to μ and τ channels, as well as the PDG values of τ branching ratios into *e* and τ channels.

$\Gamma(\tau\nu_\tau b)/\Gamma_{total}$	Γ_5/Γ		
VALUE	DOCUMENT ID	TECN	COMMENT
0.111 ± 0.009 OUR AVERAGE			
0.112 ± 0.009	1 AAD	15cc ATLS	$\ell +$ jets, $\ell\ell +$ jets, $\ell\tau_h +$ jets
0.096 ± 0.028	2 AALTONEN	14A CDF	$\ell + \tau_h + \geq 2$ jets ($\geq 1b$ -tag)

• • • We do not use the following data for averages, fits, limits, etc. • • •

³ ABULENCIA	06R CDF	$\ell\tau +$ jets
⁴ ABE	97V CDF	$\ell\tau +$ jets

- AAD 15cc based on 4.6 fb⁻¹ of *pp* data at $\sqrt{s} = 7$ TeV. The original value is given by $7.0 \pm 0.3 \pm 0.5\%$, which includes only the hadronic decay of τ leptons. It is assumed that the top branching ratios to leptons and jets add up to one and that only SM processes contribute to the background. The event selection criteria are optimized for the $\ell\tau_h +$ jets channel. We have converted the original value to include leptonic decays of τ 's, by using the AAD 15cc measurements of the branching ratios to *e* and μ channels, as well as the PDG values of τ branching ratios into *e* and μ channels.
- Based on 9 fb⁻¹ of data. The measurement is in the channel $t\bar{t} \rightarrow (b\ell\nu)(b\tau\nu)$, where τ decays into hadrons (τ_h), and ℓ (*e* or μ) include ℓ from τ decays (τ_ℓ). The result is consistent with lepton universality.
- ABULENCIA 06R looked for $t\bar{t} \rightarrow (\ell\nu_\ell)(\tau\nu_\tau) b\bar{b}$ events in 194 pb⁻¹ of *p* \bar{p} collisions at $\sqrt{s} = 1.96$ TeV. 2 events are found where 1.00 ± 0.17 signal and 1.29 ± 0.25 background events are expected, giving a 95% CL upper bound for the partial width ratio $\Gamma(t \rightarrow \tau\nu q) / \Gamma_{SM}(t \rightarrow \tau\nu q) < 5.2$.
- ABE 97V searched for $t\bar{t} \rightarrow (\ell\nu_\ell)(\tau\nu_\tau) b\bar{b}$ events in 109 pb⁻¹ of *p* \bar{p} collisions at $\sqrt{s} = 1.8$ TeV. They observed 4 candidate events where one expects ~ 1 signal and ~ 2 background events. Three of the four observed events have jets identified as *b* candidates.

$\Gamma(q\bar{q}b)/\Gamma_{total}$	Γ_6/Γ		
VALUE	DOCUMENT ID	TECN	COMMENT
0.665 ± 0.004 ± 0.013	1 AAD	15cc ATLS	$\ell +$ jets, $\ell\ell +$ jets, $\ell\tau_h +$ jets

- AAD 15cc based on 4.6 fb⁻¹ of *pp* data at $\sqrt{s} = 7$ TeV. Branching ratio of top quark into *b* and jets. It is assumed that the top branching ratios to leptons and jets add up to one and that only SM processes contribute to the background. The event selection criteria are optimized for the $\ell\tau_h +$ jets channel.

$\Gamma(\gamma q(q=u,c))/\Gamma_{total}$	Γ_7/Γ			
VALUE	CL%	DOCUMENT ID	TECN	COMMENT

<2.8 × 10⁻⁵	95	1 AAD	20B ATLS	$B(t \rightarrow \gamma u)$, left-handed $t u \gamma$ coupling
<6.1 × 10⁻⁵	95	1 AAD	20B ATLS	$B(t \rightarrow \gamma u)$, right-handed $t u \gamma$ coupling
<2.2 × 10⁻⁴	95	1 AAD	20B ATLS	$B(t \rightarrow \gamma c)$, left-handed $t c \gamma$ coupling
<1.8 × 10⁻⁴	95	1 AAD	20B ATLS	$B(t \rightarrow \gamma c)$, right-handed $t c \gamma$ coupling
<1.3 × 10 ⁻⁴	95	2 KHACHATRYAN 16AS	CMS	$B(t \rightarrow \gamma u)$
<1.7 × 10 ⁻³	95	2 KHACHATRYAN 16AS	CMS	$B(t \rightarrow \gamma c)$
<5.9 × 10 ⁻³	95	3 CHEKANOV 03	ZEUS	$B(t \rightarrow \gamma u)$

• • • We do not use the following data for averages, fits, limits, etc. • • •

- <0.0064
- <0.0465
- <0.0132
- <0.041
- <0.032
- AAD 20B based on 81 fb⁻¹ of data in *pp* collisions at $\sqrt{s} = 13$ TeV. FCNC through single top production in association with a photon is searched for in the mode $\ell\gamma + E_T + 1j$ (*b*-tag). Anomalous FCNC left-handed and right-handed couplings are searched for, which result in different kinematical properties of top decay such as the lepton distribution. Limits are set on the $tq\gamma$ couplings in an effective field theory.
- KHACHATRYAN 16AS based on 19.8 fb⁻¹ of data in *pp* collisions at $\sqrt{s} = 8$ TeV. FCNC through single top production in association with a photon is searched for in the mode $\mu + \gamma + E_T + \geq 1j$ (0,1*b*). Bounds on the anomalous FCNC couplings are given by $\kappa_{t u \gamma} < 0.025$ and $\kappa_{t c \gamma} < 0.091$.
- CHEKANOV 03 looked for single top production via FCNC in the reaction $e^\pm p \rightarrow e^\pm (t \text{ or } \bar{t}) X$ in 130.1 pb⁻¹ of data at $\sqrt{s} = 300\text{--}318$ GeV. No evidence for top production and its decay into *bW* was found. The result is obtained for $m_t = 175$ GeV when $B(\gamma c) = B(Z q) = 0$, where *q* is a *u* or *c* quark. Bounds on the effective *t*-*u*- γ and *t*-*u*-*Z* couplings are found in their Fig. 4. The conversion to the constraint listed is from private communication, E. Gallo, January 2004.
- AARON 09A looked for single top production via FCNC in $e^\pm p$ collisions at HERA with 474 pb⁻¹. The upper bound of the cross section gives the bound on the FCNC coupling $\kappa_{t u \gamma} / \Lambda < 1.03$ TeV⁻¹, which corresponds to the result for $m_t = 175$ GeV.
- ABDALLAH 04c looked for single top production via FCNC in the reaction $e^+ e^- \rightarrow \bar{t} c$ or $\bar{t} u$ in 541 pb⁻¹ of data at $\sqrt{s} = 189\text{--}208$ GeV. No deviation from the SM is found, which leads to the bound on $B(t \rightarrow \gamma q)$, where *q* is a *u* or a *c* quark, for $m_t = 175$ GeV when $B(\gamma c) = B(Z q) = 0$ is assumed. The conversion to the listed bound is from private communication, O. Yushchenko, April 2005. The bounds on the effective *t*- γ and *t*-*q*-*Z* couplings are given in their Fig. 7 and Table 4, for $m_t = 170\text{--}180$ GeV, where most conservative bounds are found by choosing the chiral couplings to maximize the negative interference between the virtual γ and *Z* exchange amplitudes.
- AKTAS 04 looked for single top production via FCNC in e^\pm collisions at HERA with 118.3 pb⁻¹, and found 5 events in the *e* or μ channels. By assuming that they are due to statistical fluctuation, the upper bound on the $t u \gamma$ coupling $\kappa_{t u \gamma} < 0.27$ (95% CL) is obtained. The conversion to the partial width limit, when $B(\gamma c) = B(Z u) = B(Z c) = 0$, is from private communication, E. Perez, May 2005.
- ACHARD 02j looked for single top production via FCNC in the reaction $e^+ e^- \rightarrow \bar{t} c$ or $\bar{t} u$ in 634 pb⁻¹ of data at $\sqrt{s} = 189\text{--}209$ GeV. No deviation from the SM is found, which leads to a bound on the top-quark decay branching fraction $B(\gamma q)$, where *q* is a *u* or *c* quark. The bound assumes $B(Z q) = 0$ and is for $m_t = 175$ GeV; bounds for $m_t = 170$ GeV and 180 GeV and $B(Z q) \neq 0$ are given in Fig. 5 and Table 7.
- ABE 98G looked for *t* \bar{t} events where one *t* decays into $q\gamma$ while the other decays into *bW*. The quoted bound is for $\Gamma(\gamma q)/\Gamma(Wb)$.

$\Gamma(H^+ b, H^+ \rightarrow \tau \nu_\tau)/\Gamma_{\text{total}}$		Γ_8/Γ	
VALUE (%)	CL%	DOCUMENT ID	TECN
<0.25	95	1 AABOUD	18BWATLS

¹AABOUD 18BW based on 36.1 fb^{-1} of pp data at $\sqrt{s} = 13 \text{ TeV}$. In the mass range of $m_{H^+} = 90\text{--}160 \text{ GeV}$, assuming the SM cross section for the $t\bar{t}$ production, the upper limit for the branching fraction $B(t \rightarrow bH^+) \times B(H^+ \rightarrow \tau \nu_\tau)$ ranges between 0.25% and 0.031%.

$\Gamma(Z q(q=u,c))/\Gamma_{\text{total}}$		Γ_9/Γ	
VALUE (units 10^{-3})	CL%	DOCUMENT ID	TECN

< 0.17	95	1 AABOUD	18AT ATLS	$t \rightarrow Zu$
< 0.24	95	1 AABOUD	18AT ATLS	$t \rightarrow Zc$
< 0.22	95	2 SIRUNYAN	17E CMS	$t \rightarrow Zu$
< 0.49	95	2 SIRUNYAN	17E CMS	$t \rightarrow Zc$
< 0.7	95	3 AAD	16D ATLS	$t \rightarrow Zq (q = u, c)$
< 0.5	95	4 CHATRCHYAN14s	CMS	$t \rightarrow Zq (q = u, c)$
••• We do not use the following data for averages, fits, limits, etc. •••				
< 0.6	95	5 CHATRCHYAN14s	CMS	$t \rightarrow Zq (q = u, c)$
< 2.1	95	6 CHATRCHYAN13F	CMS	$t \rightarrow Zq (q = u, c)$
< 7.3	95	7 AAD	12BT ATLS	$t\bar{t} \rightarrow \ell^+ \ell^- \ell'^{\pm} + E_T + \text{jets}$
< 32	95	8 ABZOV	11M D0	$t \rightarrow Zq (q = u, c)$
< 83	95	9 AALTONEN	09AL CDF	$t \rightarrow Zq (q = c)$
< 37	95	10 AALTONEN	08AD CDF	$t \rightarrow Zq (q = u, c)$
< 1.59×10^2	95	11 ABDALLAH	04C DLPH	$e^+e^- \rightarrow \bar{t}c \text{ or } \bar{t}u$
< 1.37×10^2	95	12 ACHARD	02J L3	$e^+e^- \rightarrow \bar{t}c \text{ or } \bar{t}u$
< 1.4×10^2	95	13 HEISTER	02Q ALEP	$e^+e^- \rightarrow \bar{t}c \text{ or } \bar{t}u$
< 1.37×10^2	95	14 ABBIENDI	01T OPAL	$e^+e^- \rightarrow \bar{t}c \text{ or } \bar{t}u$
< 1.7×10^2	95	15 BARATE	00s ALEP	$e^+e^- \rightarrow \bar{t}c \text{ or } \bar{t}u$
< 3.3×10^2	95	16 ABE	98G CDF	$t\bar{t} \rightarrow (Wb)(Zc \text{ or } Zu)$

- ¹Based on 36.1 fb^{-1} of pp data at $\sqrt{s} = 13 \text{ TeV}$. The final states $t\bar{t} \rightarrow \ell^+ \ell^- \ell'^{\pm} \nu$ + jets ($\ell, \ell' = e, \mu$) are investigated and no significant excess over the SM background contributions is observed.
- ²SIRUNYAN 17E based on 19.7 fb^{-1} of pp data at $\sqrt{s} = 8 \text{ TeV}$. The final states $t\bar{t} \rightarrow \ell^+ \ell^- \ell'^{\pm} \nu$ + jets ($\ell, \ell' = e, \mu$) are investigated and the cross section $\sigma(pp \rightarrow tZq \rightarrow \ell \nu b \ell^+ \ell^- q) = 10_{-7}^{+8} \text{ fb}$ is measured, giving no sign of FCNC decays of the top quark.
- ³AAD 16D based on 20.3 fb^{-1} of pp data at $\sqrt{s} = 8 \text{ TeV}$. The FCNC decay is searched for in $t\bar{t}$ events in the final state $(bW)(qZ)$ when both W and Z decay leptonically, giving 3 charged leptons.
- ⁴CHATRCHYAN 14s combined search limit from this and CHATRCHYAN 13F data.
- ⁵Based on 19.7 fb^{-1} of pp data at $\sqrt{s} = 8 \text{ TeV}$. The flavor changing decay is searched for in $t\bar{t}$ events in the final state $(bW)(qZ)$ when both W and Z decay leptonically, giving 3 charged leptons.
- ⁶Based on 5.0 fb^{-1} of pp data at $\sqrt{s} = 7 \text{ TeV}$. Search for FCNC decays of the top quark in $t\bar{t} \rightarrow \ell^+ \ell^- \ell'^{\pm} \nu$ + jets ($\ell, \ell' = e, \mu$) final states found no excess of signal events.
- ⁷Based on 2.1 fb^{-1} of pp data at $\sqrt{s} = 7 \text{ TeV}$.
- ⁸Based on 4.1 fb^{-1} of data. ABZOV 11M searched for FCNC decays of the top quark in $t\bar{t} \rightarrow \ell^+ \ell^- \ell'^{\pm} \nu$ + jets ($\ell, \ell' = e, \mu$) final states, and absence of the signal gives the bound.
- ⁹Based on $p\bar{p}$ data of 1.52 fb^{-1} . AALTONEN 09AL compared $t\bar{t} \rightarrow WbWb \rightarrow \ell \nu b j j b$ and $t\bar{t} \rightarrow ZcWb \rightarrow \ell \ell c j j b$ decay chains, and absence of the latter signal gives the bound. The result is for 100% longitudinally polarized Z boson and the theoretical $t\bar{t}$ production cross section. The results for different Z polarizations and those without the cross section assumption are given in their Table XII.
- ¹⁰Result is based on 1.9 fb^{-1} of data at $\sqrt{s} = 1.96 \text{ TeV}$. $t\bar{t} \rightarrow WbZq \text{ or } ZqZq$ processes have been looked for in $Z + \geq 4$ jet events with and without b -tag. No signal leads to the bound $B(t \rightarrow Zq) < 0.037 (0.041)$ for $m_t = 175 (170) \text{ GeV}$.
- ¹¹ABDALLAH 04c looked for single top production via FCNC in the reaction $e^+e^- \rightarrow \bar{t}c \text{ or } \bar{t}u$ in 541 pb^{-1} of data at $\sqrt{s} = 189\text{--}208 \text{ GeV}$. No deviation from the SM is found, which leads to the bound on $B(t \rightarrow Zq)$, where q is a u or a c quark, for $m_t = 175 \text{ GeV}$ when $B(t \rightarrow \gamma q) = 0$ is assumed. The conversion to the listed bound is from private communication, O. Yushchenko, April 2005. The bounds on the effective t - q - γ and t - q - Z couplings are given in their Fig. 7 and Table 4, for $m_t = 170\text{--}180 \text{ GeV}$, where most conservative bounds are found by choosing the chiral couplings to maximize the negative interference between the virtual γ and Z exchange amplitudes.
- ¹²ACHARD 02j looked for single top production via FCNC in the reaction $e^+e^- \rightarrow \bar{t}c \text{ or } \bar{t}u$ in 634 pb^{-1} of data at $\sqrt{s} = 189\text{--}209 \text{ GeV}$. No deviation from the SM is found, which leads to a bound on the top-quark decay branching fraction $B(Zq)$, where q is a u or c quark. The bound assumes $B(\gamma q) = 0$ and is for $m_t = 175 \text{ GeV}$; bounds for $m_t = 170 \text{ GeV}$ and 180 GeV and $B(\gamma q) \neq 0$ are given in Fig. 5 and Table 7. Table 6 gives constraints on t - c - e four-fermi contact interactions.
- ¹³HEISTER 02q looked for single top production via FCNC in the reaction $e^+e^- \rightarrow \bar{t}c \text{ or } \bar{t}u$ in 214 pb^{-1} of data at $\sqrt{s} = 204\text{--}209 \text{ GeV}$. No deviation from the SM is found, which leads to a bound on the branching fraction $B(Zq)$, where q is a u or c quark. The bound assumes $B(\gamma q) = 0$ and is for $m_t = 174 \text{ GeV}$. Bounds on the effective t - $(c \text{ or } u)$ - γ and t - $(c \text{ or } u)$ - Z couplings are given in their Fig. 2.
- ¹⁴ABBIENDI 01T looked for single top production via FCNC in the reaction $e^+e^- \rightarrow \bar{t}c \text{ or } \bar{t}u$ in 600 pb^{-1} of data at $\sqrt{s} = 189\text{--}209 \text{ GeV}$. No deviation from the SM is found, which leads to bounds on the branching fractions $B(Zq)$ and $B(\gamma q)$, where q is a u or c quark. The result is obtained for $m_t = 174 \text{ GeV}$. The upper bound becomes 9.7% (20.6%) for $m_t = 169 (179) \text{ GeV}$. Bounds on the effective t - $(c \text{ or } u)$ - γ and t - $(c \text{ or } u)$ - Z couplings are given in their Fig. 4.
- ¹⁵BARATE 00s looked for single top production via FCNC in the reaction $e^+e^- \rightarrow \bar{t}c \text{ or } \bar{t}u$ in 411 pb^{-1} of data at c.m. energies between 189 and 202 GeV. No deviation from the SM is found, which leads to a bound on the branching fraction. The bound assumes $B(\gamma q) = 0$. Bounds on the effective t - $(c \text{ or } u)$ - γ and t - $(c \text{ or } u)$ - Z couplings are given in their Fig. 4.
- ¹⁶ABE 98g looked for $t\bar{t}$ events where one t decays into three jets and the other decays into qZ with $Z \rightarrow \ell\ell$. The quoted bound is for $\Gamma(Zq)/\Gamma(Wb)$.

$\Gamma(Hu)/\Gamma_{\text{total}}$		Γ_{10}/Γ	
VALUE (units 10^{-3})	CL%	DOCUMENT ID	TECN

<1.2	95	1 AABOUD	19s ATLS	combination of $t \rightarrow Hu$ ($H \rightarrow WW, ZZ, \tau\tau, \gamma\gamma, b\bar{b}$)
••• We do not use the following data for averages, fits, limits, etc. •••				
<5.2	95	2 AABOUD	19s ATLS	$t \rightarrow Hu (H \rightarrow bb)$
<1.7	95	3 AABOUD	19s ATLS	$t \rightarrow Hu (H \rightarrow \tau\tau)$
<1.9	95	4 AABOUD	18x ATLS	$t \rightarrow Hu (H \rightarrow WW, ZZ, \tau\tau)$
<4.7	95	5 SIRUNYAN	18Bc CMS	$t \rightarrow Hu (H \rightarrow bb)$
<2.4	95	6 AABOUD	17AV ATLS	$t \rightarrow Hu (H \rightarrow \gamma\gamma)$
<5.5	95	7 KHACHATRYAN..17l	CMS	$t \rightarrow Hu (H \rightarrow WW, ZZ, \tau\tau, \gamma\gamma, b\bar{b})$
<6.1	95	8 AAD	15c0 ATLS	$t \rightarrow Hu (H \rightarrow bb)$
<7.9	95	9 AAD	14AA ATLS	$t \rightarrow Hq (q=u,c; H \rightarrow \gamma\gamma)$

- ¹AABOUD 19s based on 36.1 fb^{-1} at $\sqrt{s} = 13 \text{ TeV}$ of pp data. The searches using $H \rightarrow bb$ and $H \rightarrow \tau_h \tau_h$ are combined with searches in diphoton and multilepton final states. The upper limit on the Yukawa coupling $|Y_{tH}| < 0.066$ (95% CL) is obtained.
- ²AABOUD 19s based on 36.1 fb^{-1} at $\sqrt{s} = 13 \text{ TeV}$ of pp data. Uses events with one isolated lepton and multiple jets (several of them b -tagged with high purity). A multivariate analysis is performed to distinguish the signal from backgrounds.
- ³AABOUD 19s based on 36.1 fb^{-1} at $\sqrt{s} = 13 \text{ TeV}$ of pp data. Uses events with one or two hadronically decaying τ and multiple jets. A multivariate analysis is performed to distinguish the signal from backgrounds.
- ⁴AABOUD 18x based on 36.1 fb^{-1} at $\sqrt{s} = 13 \text{ TeV}$ of pp data. $\ell\ell$ (same sign) + $\geq 4j$ mode and $\ell\ell\ell + \geq 2j$ mode are targeted and specialized boosted decision trees are used to distinguish signals from backgrounds.
- ⁵SIRUNYAN 18Bc based on 35.9 fb^{-1} at $\sqrt{s} = 13 \text{ TeV}$ of pp data. Two channels $pp \rightarrow tH$ and $pp \rightarrow t\bar{t}$ in final states with one isolated lepton and ≥ 3 jets with ≥ 2 b jets are considered assuming a single tHc FCNC coupling. Reconstructed kinematical variables are fed into a multivariate analysis and no significant deviation is observed from the predicted background.
- ⁶AABOUD 17AV based on 36.1 fb^{-1} at $\sqrt{s} = 13 \text{ TeV}$ of pp data. Search for $t\bar{t}$ events, where the other top quark decays hadronically or semi-leptonically.
- ⁷KHACHATRYAN 17l based on 19.7 fb^{-1} of pp data at $\sqrt{s} = 8 \text{ TeV}$, using the topologies $t\bar{t} \rightarrow Hq + Wb$, where $q = u, c$.
- ⁸AAD 15c0 based on 20.3 fb^{-1} at $\sqrt{s} = 8 \text{ TeV}$ of pp data. Searches for $t\bar{t}$ events, where the other top quark decays semi-leptonically. Exploits high multiplicity of b -jets and uses a likelihood discriminant. Combining with other ATLAS searches for different Higgs decay modes, $B(t \rightarrow Hc) < 0.46\%$ and $B(t \rightarrow Hu) < 0.45\%$ are obtained.
- ⁹AAD 14AA based on 4.7 fb^{-1} at $\sqrt{s} = 7 \text{ TeV}$ and 20.3 fb^{-1} at $\sqrt{s} = 8 \text{ TeV}$ of pp data. The upper-bound is for the sum of $\text{Br}(t \rightarrow Hc)$ and $\text{Br}(t \rightarrow Hu)$. Search for $t\bar{t}$ events, where the other top quark decays hadronically or semi-leptonically. The upper bound constrains the H - t - c Yukawa couplings $\sqrt{|Y_{tH}^c}|^2 + |Y_{tH}^u}|^2 < 0.17$ (95% CL).

$\Gamma(Hc)/\Gamma_{\text{total}}$		Γ_{11}/Γ	
VALUE (units 10^{-3})	CL%	DOCUMENT ID	TECN

< 1.1	95	1 AABOUD	19s ATLS	combination of $t \rightarrow Hc$ ($H \rightarrow WW, ZZ, \tau\tau, \gamma\gamma, b\bar{b}$)
••• We do not use the following data for averages, fits, limits, etc. •••				
< 4.2	95	2 AABOUD	19s ATLS	$t \rightarrow Hc (H \rightarrow bb)$
< 1.9	95	3 AABOUD	19s ATLS	$t \rightarrow Hc (H \rightarrow \tau\tau)$
< 1.6	95	4 AABOUD	18x ATLS	$t \rightarrow Hc (H \rightarrow WW, ZZ, \tau\tau)$
< 4.7	95	5 SIRUNYAN	18Bc CMS	$t \rightarrow Hc (H \rightarrow bb)$
< 2.2	95	6 AABOUD	17AV ATLS	$t \rightarrow Hc (H \rightarrow \gamma\gamma)$
< 4	95	7 KHACHATRYAN..17l	CMS	$t \rightarrow Hc (H \rightarrow WW, ZZ, \tau\tau, \gamma\gamma, b\bar{b})$
< 5.6	95	8 AAD	15c0 ATLS	$t \rightarrow Hc (H \rightarrow bb)$
< 7.9	95	9 AAD	14AA ATLS	$t \rightarrow Hq (q=u,c; H \rightarrow \gamma\gamma)$
< 13	95	10 CHATRCHYAN14R	CMS	$t \rightarrow Hc (H \rightarrow \geq 2 \ell)$
< 5.6	95	11 KHACHATRYAN..14q	CMS	$t \rightarrow Hc (H \rightarrow \gamma\gamma \text{ or } \text{leptons})$

- ¹AABOUD 19s based on 36.1 fb^{-1} at $\sqrt{s} = 13 \text{ TeV}$ of pp data. The searches using $H \rightarrow bb$ and $H \rightarrow \tau_h \tau_h$ are combined with searches in diphoton and multilepton final states. The upper limit on the Yukawa coupling $|Y_{tH}| < 0.064$ (95% CL) is obtained.
- ²AABOUD 19s based on 36.1 fb^{-1} at $\sqrt{s} = 13 \text{ TeV}$ of pp data. Uses events with one isolated lepton and multiple jets (several of them b -tagged with high purity). A multivariate analysis is performed to distinguish the signal from backgrounds.
- ³AABOUD 19s based on 36.1 fb^{-1} at $\sqrt{s} = 13 \text{ TeV}$ of pp data. Uses events with one or two hadronically decaying τ and multiple jets. A multivariate analysis is performed to distinguish the signal from backgrounds.
- ⁴AABOUD 18x based on 36.1 fb^{-1} at $\sqrt{s} = 13 \text{ TeV}$ of pp data. $\ell\ell$ (same sign) + $\geq 4j$ mode and $\ell\ell\ell + \geq 2j$ mode are targeted and specialized boosted decision trees are used to distinguish signals from backgrounds.
- ⁵SIRUNYAN 18Bc based on 35.9 fb^{-1} at $\sqrt{s} = 13 \text{ TeV}$ of pp data. Two channels $pp \rightarrow tH$ and $pp \rightarrow t\bar{t}$ in final states with one isolated lepton and ≥ 3 jets with ≥ 2 b jets are considered assuming a single tHc FCNC coupling. Reconstructed kinematical variables are fed into a multivariate analysis and no significant deviation is observed from the predicted background.
- ⁶AABOUD 17AV based on 36.1 fb^{-1} at $\sqrt{s} = 13 \text{ TeV}$ of pp data. Search for $t\bar{t}$ events, where the other top quark decays hadronically or semi-leptonically. The upper bound on the H - t - c Yukawa couplings is 0.090 (95% CL).
- ⁷KHACHATRYAN 17l based on 19.7 fb^{-1} of pp data at $\sqrt{s} = 8 \text{ TeV}$, using the topologies $t\bar{t} \rightarrow Hq + Wb$, where $q = u, c$.
- ⁸AAD 15c0 based on 20.3 fb^{-1} at $\sqrt{s} = 8 \text{ TeV}$ of pp data. Searches for $t\bar{t}$ events, where the other top quark decays semi-leptonically. Exploits high multiplicity of b -jets

Quark Particle Listings

t

and uses a likelihood discriminant. Combining with other ATLAS searches for different Higgs decay modes, $B(t \rightarrow Hc) < 0.46\%$ and $B(t \rightarrow Hu) < 0.45\%$ are obtained.

- ⁹AAD 14AA based on 4.7 fb^{-1} at $\sqrt{s} = 7 \text{ TeV}$ and 20.3 fb^{-1} at $\sqrt{s} = 8 \text{ TeV}$ of pp data. The upper-bound is for the sum of $B(t \rightarrow Hc)$ and $B(t \rightarrow Hu)$. Search for $t\bar{t}$ events, where the other top quark decays hadronically or semi-leptonically. The upper bound constrains the H - t - c Yukawa couplings $\sqrt{|Y_{t_{c_L}}^H|^2 + |Y_{t_{c_R}}^H|^2} < 0.17$ (95% CL).
- ¹⁰Based on 19.5 fb^{-1} of pp data at $\sqrt{s} = 8 \text{ TeV}$. Search for final states with 3 or more isolated high E_T charged leptons ($\ell = e, \mu$) bounds the $t \rightarrow Hc$ decay in $t\bar{t}$ events when H decays contain a pair of leptons. The upper bound constrains the H - t - c Yukawa couplings $\sqrt{|Y_{t_{c_L}}^H|^2 + |Y_{t_{c_R}}^H|^2} < 0.21$ (95% CL).
- ¹¹KHACHATRYAN 14Q based on 19.5 fb^{-1} at $\sqrt{s} = 8 \text{ TeV}$ of pp data. Search for final states with ≥ 3 isolated charged leptons or with a photon pair accompanied by ≥ 1 lepton(s).

$\Gamma(\ell^+ \bar{q} q' (q=d,s,b; q'=u,c))/\Gamma_{\text{total}}$				Γ_{12}/Γ
VALUE	CL%	DOCUMENT ID	TECN	COMMENT
$< 1.6 \times 10^{-3}$	95	¹ CHATRCHYAN14O	CMS	$\mu + \text{dijets}$
$< 1.7 \times 10^{-3}$	95	¹ CHATRCHYAN14O	CMS	$e + \text{dijets}$

- • • We do not use the following data for averages, fits, limits, etc. • • •
- ¹Based on 19.5 fb^{-1} of pp data at $\sqrt{s} = 8 \text{ TeV}$. Baryon number violating decays of the top quark are searched for in $t\bar{t}$ production events where one of the pair decays into hadronic three jets.

t-quark EW Couplings

W helicity fractions in top decays. F_0 is the fraction of longitudinal and F_{\pm} the fraction of right-handed W bosons. F_{V+A} is the fraction of $V+A$ current in top decays. The effective Lagrangian (cited by ABAZOV 08AI) has terms f_L^L and f_L^R for $V-A$ and $V+A$ couplings, f_2^L and f_2^R for tensor couplings with b_R and b_L respectively.

F_0				
VALUE	DOCUMENT ID	TECN	COMMENT	
0.687 ± 0.018 OUR AVERAGE				
0.70 ± 0.05	¹ AABOUD 17BB	ATLS	$F_0 = 1 - f_1$	
$0.681 \pm 0.012 \pm 0.023$	² KHACHATRYAN 16BU	CMS	$F_0 = B(t \rightarrow W_0 b)$	
$0.726 \pm 0.066 \pm 0.067$	³ AALTONEN 13D	CDF	$F_0 = B(t \rightarrow W_0 b)$	
$0.682 \pm 0.030 \pm 0.033$	⁴ CHATRCHYAN 13BH	CMS	$F_0 = B(t \rightarrow W_0 b)$	
0.67 ± 0.07	⁵ AAD 12BG	ATLS	$F_0 = B(t \rightarrow W_0 b)$	
$0.722 \pm 0.062 \pm 0.052$	⁶ AALTONEN 12Z	TEVA	$F_0 = B(t \rightarrow W_0 b)$	
$0.669 \pm 0.078 \pm 0.065$	⁷ ABAZOV 11C	D0	$F_0 = B(t \rightarrow W_0 b)$	
$0.91 \pm 0.37 \pm 0.13$	⁸ AFFOLDER 00B	CDF	$F_0 = B(t \rightarrow W_0 b)$	
• • • We do not use the following data for averages, fits, limits, etc. • • •				
$0.70 \pm 0.07 \pm 0.04$	⁹ AALTONEN 10Q	CDF	Repl. by AALTONEN 12Z	
$0.62 \pm 0.10 \pm 0.05$	¹⁰ AALTONEN 09Q	CDF	Repl. by AALTONEN 10Q	
$0.425 \pm 0.166 \pm 0.102$	¹¹ ABAZOV 08B	D0	Repl. by ABAZOV 11c	
$0.85^{+0.15}_{-0.22} \pm 0.06$	¹² ABULENCIA 07I	CDF	$F_0 = B(t \rightarrow W_0 b)$	
$0.74^{+0.22}_{-0.34}$	¹³ ABULENCIA 06U	CDF	$F_0 = B(t \rightarrow W_0 b)$	
0.56 ± 0.31	¹⁴ ABAZOV 05G	D0	$F_0 = B(t \rightarrow W_0 b)$	

- ¹AABOUD 17BB based on 20.2 fb^{-1} of pp data at $\sqrt{s} = 8 \text{ TeV}$. Triple-differential decay rate of top quark in the t -channel single-top production is used to simultaneously determine five generalized Wtb couplings as well as the top polarization. No assumption is made for the other couplings. See this paper for constraints on other couplings not included here. The paper reported f_1 , and we converted it to F_0 .
- ²KHACHATRYAN 16BU based on 19.8 fb^{-1} of pp data at $\sqrt{s} = 8 \text{ TeV}$ using $t\bar{t}$ events with $\ell + E_T + \geq 4$ jets ($\geq 2 b$). The errors of F_0 and F_{\pm} are correlated with a correlation coefficient $\rho(F_0, F_{\pm}) = -0.87$. The result is consistent with the NNLO SM prediction of 0.687 ± 0.005 for $m_t = 172.8 \pm 1.3 \text{ GeV}$.
- ³Based on 8.7 fb^{-1} of data in $p\bar{p}$ collisions at $\sqrt{s} = 1.96 \text{ TeV}$ using $t\bar{t}$ events with $\ell + E_T + \geq 4$ jets ($\geq 1 b$), and under the constraint $F_0 + F_{\pm} + F_{\mp} = 1$. The statistical errors of F_0 and F_{\pm} are correlated with correlation coefficient $\rho(F_0, F_{\pm}) = -0.69$.
- ⁴Based on 5.0 fb^{-1} of pp data at $\sqrt{s} = 7 \text{ TeV}$. CHATRCHYAN 13BH studied tt events with large E_T and $\ell + \geq 4$ jets using a constrained kinematic fit.
- ⁵Based on 1.04 fb^{-1} of pp data at $\sqrt{s} = 7 \text{ TeV}$. AAD 12BG studied tt events with large E_T and either $\ell + \geq 4j$ or $\ell\ell + \geq 2j$. The uncertainties are not independent, $\rho(F_0, F_{\pm}) = -0.96$.
- ⁶Based on 2.7 and 5.1 fb^{-1} of CDF data in $\ell +$ jets and dilepton channels, and 5.4 fb^{-1} of D0 data in $\ell +$ jets and dilepton channels. $F_0 = 0.682 \pm 0.035 \pm 0.046$ if $F_{\pm} = 0.0017(1)$, while $F_{\pm} = -0.015 \pm 0.018 \pm 0.030$ if $F_0 = 0.688(4)$, where the assumed fixed values are the SM prediction for $m_t = 173.3 \pm 1.1 \text{ GeV}$ and $m_W = 80.399 \pm 0.023 \text{ GeV}$.
- ⁷Results are based on 5.4 fb^{-1} of data in $p\bar{p}$ collisions at 1.96 TeV , including those of ABAZOV 08B. Under the SM constraint of $f_0 = 0.698$ (for $m_t = 173.3 \text{ GeV}$, $m_W = 80.399 \text{ GeV}$), $f_{\pm} = 0.010 \pm 0.022 \pm 0.030$ is obtained.
- ⁸AFFOLDER 00B studied the angular distribution of leptonic decays of W bosons in $t \rightarrow Wb$ events. The ratio F_0 is the fraction of the helicity zero (longitudinal) W bosons in the decaying top quark rest frame. $B(t \rightarrow W_{\pm} b)$ is the fraction of positive helicity (right-handed) positive charge W bosons in the top quark decays. It is obtained by assuming the Standard Model value of F_0 .
- ⁹Results are based on 2.7 fb^{-1} of data in $p\bar{p}$ collisions at $\sqrt{s} = 1.96 \text{ TeV}$. F_0 result is obtained by assuming $F_{\pm} = 0$, while F_{\pm} result is obtained for $F_0 = 0.70$, the SM value. Model independent fits for the two fractions give $F_0 = 0.88 \pm 0.11 \pm 0.06$ and $F_{\pm} = -0.15 \pm 0.07 \pm 0.06$ with correlation coefficient of -0.59 . The results are for $m_t = 175 \text{ GeV}$.
- ¹⁰Results are based on 1.9 fb^{-1} of data in $p\bar{p}$ collisions at $\sqrt{s} = 1.96 \text{ TeV}$. F_0 result is obtained assuming $F_{\pm} = 0$, while F_{\pm} result is obtained for $F_0 = 0.70$, the SM values.

Model independent fits for the two fractions give $F_0 = 0.66 \pm 0.16 \pm 0.05$ and $F_{\pm} = -0.03 \pm 0.06 \pm 0.03$.

- ¹¹Based on 1 fb^{-1} at $\sqrt{s} = 1.96 \text{ TeV}$.
- ¹²Based on 318 pb^{-1} of data at $\sqrt{s} = 1.96 \text{ TeV}$.
- ¹³Based on 200 pb^{-1} of data at $\sqrt{s} = 1.96 \text{ TeV}$. $t \rightarrow Wb \rightarrow \ell\nu b$ ($\ell = e$ or μ). The errors are stat + syst.
- ¹⁴ABAZOV 05G studied the angular distribution of leptonic decays of W bosons in $t\bar{t}$ candidate events with lepton + jets final states, and obtained the fraction of longitudinally polarized W under the constraint of no right-handed current, $F_{\pm} = 0$. Based on 125 pb^{-1} of data at $\sqrt{s} = 1.8 \text{ TeV}$.

 F_{-}

VALUE	CL%	DOCUMENT ID	TECN	COMMENT
0.320 ± 0.013 OUR AVERAGE				
$> 0.264 \pm 0.044$	95	¹ AABOUD 17BB	ATLS	$F_{-} = f_1(1 - f_1^{\pm})$
$0.323 \pm 0.008 \pm 0.014$		² KHACHATRYAN 16BU	CMS	$F_{-} = B(t \rightarrow W_{-} b)$
$0.310 \pm 0.022 \pm 0.022$		³ CHATRCHYAN 13BH	CMS	$F_{-} = B(t \rightarrow W_{-} b)$
0.32 ± 0.04		⁴ AAD 12BG	ATLS	$F_{-} = B(t \rightarrow W_{-} b)$

- ¹AABOUD 17BB based on 20.2 fb^{-1} of pp data at $\sqrt{s} = 8 \text{ TeV}$. Triple-differential decay rate of top quark in the t -channel single-top production is used to simultaneously determine five generalized Wtb couplings as well as the top polarization. No assumption is made for the other couplings. The authors reported $f_1 = 0.30 \pm 0.05$ and $f_1^{\pm} < 0.120$ which we converted to $F_{-} = f_1(1 - f_1^{\pm})$. See this paper for constraints on other couplings not included here.
- ²KHACHATRYAN 16BU based on 19.8 fb^{-1} of pp data at $\sqrt{s} = 8 \text{ TeV}$ using $t\bar{t}$ events with $\ell + E_T + \geq 4$ jets ($\geq 2 b$). The errors of F_0 and F_{-} are correlated with a correlation coefficient $\rho(F_0, F_{-}) = -0.87$. The result is consistent with the NNLO SM prediction of 0.311 ± 0.005 for $m_t = 172.8 \pm 1.3 \text{ GeV}$.
- ³Based on 5.0 fb^{-1} of pp data at $\sqrt{s} = 7 \text{ TeV}$. CHATRCHYAN 13BH studied tt events with large E_T and $\ell + \geq 4$ jets using a constrained kinematic fit.
- ⁴Based on 1.04 fb^{-1} of pp data at $\sqrt{s} = 7 \text{ TeV}$. AAD 12BG studied tt events with large E_T and either $\ell + \geq 4j$ or $\ell\ell + \geq 2j$. The uncertainties are not independent, $\rho(F_0, F_{-}) = -0.96$.

 F_{+}

VALUE	CL%	DOCUMENT ID	TECN	COMMENT
0.002 ± 0.011 OUR AVERAGE				
$< 0.036 \pm 0.006$	95	¹ AABOUD 17BB	ATLS	$F_{+} = f_1 f_1^{\pm}$
$-0.004 \pm 0.005 \pm 0.014$		² KHACHATRYAN 16BU	CMS	$F_{+} = B(t \rightarrow W_{+} b)$
$-0.045 \pm 0.044 \pm 0.058$		³ AALTONEN 13D	CDF	$F_{+} = B(t \rightarrow W_{+} b)$
$0.008 \pm 0.012 \pm 0.014$		⁴ CHATRCHYAN 13BH	CMS	$F_{+} = B(t \rightarrow W_{+} b)$
0.01 ± 0.05		⁵ AAD 12BG	ATLS	$F_{+} = B(t \rightarrow W_{+} b)$
$0.023 \pm 0.041 \pm 0.034$		⁶ ABAZOV 11C	D0	$F_{+} = B(t \rightarrow W_{+} b)$
0.11 ± 0.15		⁷ AFFOLDER 00B	CDF	$F_{+} = B(t \rightarrow W_{+} b)$
• • • We do not use the following data for averages, fits, limits, etc. • • •				
$-0.033 \pm 0.034 \pm 0.031$		⁸ AALTONEN 12Z	TEVA	$F_{+} = B(t \rightarrow W_{+} b)$
$-0.01 \pm 0.02 \pm 0.05$		⁹ AALTONEN 10Q	CDF	Repl. by AALTONEN 12Z
$-0.04 \pm 0.04 \pm 0.03$		¹⁰ AALTONEN 09Q	CDF	Repl. by AALTONEN 10Q
$0.119 \pm 0.090 \pm 0.053$		¹¹ ABAZOV 08B	D0	Repl. by ABAZOV 11c
$0.056 \pm 0.080 \pm 0.057$		¹² ABAZOV 07D	D0	$F_{+} = B(t \rightarrow W_{+} b)$
$0.05^{+0.11}_{-0.05} \pm 0.03$		¹³ ABULENCIA 07I	CDF	$F_{+} = B(t \rightarrow W_{+} b)$
< 0.26	95	¹³ ABULENCIA 07I	CDF	$F_{+} = B(t \rightarrow W_{+} b)$
< 0.27	95	¹⁴ ABULENCIA 06U	CDF	$F_{+} = B(t \rightarrow W_{+} b)$
$0.00 \pm 0.13 \pm 0.07$		¹⁵ ABAZOV 05L	D0	$F_{+} = B(t \rightarrow W_{+} b)$
< 0.25	95	¹⁵ ABAZOV 05L	D0	$F_{+} = B(t \rightarrow W_{+} b)$
< 0.24	95	¹⁶ ACOSTA 05D	CDF	$F_{+} = B(t \rightarrow W_{+} b)$

- ¹AABOUD 17BB based on 20.2 fb^{-1} of pp data at $\sqrt{s} = 8 \text{ TeV}$. Triple-differential decay rate of top quark in the t -channel single-top production is used to simultaneously determine five generalized Wtb couplings as well as the top polarization. No assumption is made for the other couplings. The authors reported $f_1 = 0.30 \pm 0.05$ and $f_1^{\pm} < 0.120$ which we converted to $F_{+} = f_1 f_1^{\pm}$. See this paper for constraints on other couplings not included here.
- ²KHACHATRYAN 16BU based on 19.8 fb^{-1} of pp data at $\sqrt{s} = 8 \text{ TeV}$ using $t\bar{t}$ events with $\ell + E_T + \geq 4$ jets ($\geq 2 b$). The result is consistent with the NNLO SM prediction of 0.0017 ± 0.0001 for $m_t = 172.8 \pm 1.3 \text{ GeV}$.
- ³Based on 8.7 fb^{-1} of data in $p\bar{p}$ collisions at $\sqrt{s} = 1.96 \text{ TeV}$ using $t\bar{t}$ events with $\ell + E_T + \geq 4$ jets ($\geq 1 b$), and under the constraint $F_0 + F_{\pm} + F_{\mp} = 1$. The statistical errors of F_0 and F_{\pm} are correlated with correlation coefficient $\rho(F_0, F_{\pm}) = -0.69$.
- ⁴Based on 5.0 fb^{-1} of pp data at $\sqrt{s} = 7 \text{ TeV}$. CHATRCHYAN 13BH studied tt events with large E_T and $\ell + \geq 4$ jets using a constrained kinematic fit.
- ⁵Based on 1.04 fb^{-1} of pp data at $\sqrt{s} = 7 \text{ TeV}$. AAD 12BG studied tt events with large E_T and either $\ell + \geq 4j$ or $\ell\ell + \geq 2j$.
- ⁶Results are based on 5.4 fb^{-1} of data in $p\bar{p}$ collisions at 1.96 TeV , including those of ABAZOV 08B. Under the SM constraint of $f_0 = 0.698$ (for $m_t = 173.3 \text{ GeV}$, $m_W = 80.399 \text{ GeV}$), $f_{\pm} = 0.010 \pm 0.022 \pm 0.030$ is obtained.
- ⁷AFFOLDER 00B studied the angular distribution of leptonic decays of W bosons in $t \rightarrow Wb$ events. The ratio F_0 is the fraction of the helicity zero (longitudinal) W bosons in the decaying top quark rest frame. $B(t \rightarrow W_{\pm} b)$ is the fraction of positive helicity (right-handed) positive charge W bosons in the top quark decays. It is obtained by assuming the Standard Model value of F_0 .
- ⁸Based on 2.7 and 5.1 fb^{-1} of CDF data in $\ell +$ jets and dilepton channels, and 5.4 fb^{-1} of D0 data in $\ell +$ jets and dilepton channels. $F_0 = 0.682 \pm 0.035 \pm 0.046$ if $F_{\pm} = 0.0017(1)$, while $F_{\pm} = -0.015 \pm 0.018 \pm 0.030$ if $F_0 = 0.688(4)$, where the assumed

fixed values are the SM prediction for $m_t = 173.3 \pm 1.1$ GeV and $m_W = 80.399 \pm 0.023$ GeV.

- 9 Results are based on 2.7 fb^{-1} of data in $p\bar{p}$ collisions at $\sqrt{s} = 1.96$ TeV. F_0 result is obtained by assuming $F_{\pm} = 0$, while F_{\pm} result is obtained for $F_0 = 0.70$, the SM value. Model independent fits for the two fractions give $F_0 = 0.88 \pm 0.11 \pm 0.06$ and $F_{\pm} = -0.15 \pm 0.07 \pm 0.06$ with correlation coefficient of -0.59 . The results are for $m_t = 175$ GeV.
- 10 Results are based on 1.9 fb^{-1} of data in $p\bar{p}$ collisions at $\sqrt{s} = 1.96$ TeV. F_0 result is obtained assuming $F_{\pm} = 0$, while F_{\pm} result is obtained for $F_0 = 0.70$, the SM values. Model independent fits for the two fractions give $F_0 = 0.66 \pm 0.16 \pm 0.05$ and $F_{\pm} = -0.03 \pm 0.06 \pm 0.03$.
- 11 Based on 1 fb^{-1} at $\sqrt{s} = 1.96$ TeV.
- 12 Based on 370 pb^{-1} of data at $\sqrt{s} = 1.96$ TeV, using the $\ell + \text{jets}$ and dilepton decay channels. The result assumes $F_0 = 0.70$, and it gives $F_{\pm} < 0.23$ at 95% CL.
- 13 Based on 318 pb^{-1} of data at $\sqrt{s} = 1.96$ TeV.
- 14 Based on 200 pb^{-1} of data at $\sqrt{s} = 1.96$ TeV. $t \rightarrow Wb \rightarrow \ell\nu b$ ($\ell = e$ or μ). The errors are stat + syst.
- 15 ABAZOV 05L studied the angular distribution of leptonic decays of W bosons in $t\bar{t}$ events, where one of the W 's from t or \bar{t} decays into e or μ and the other decays hadronically. The fraction of the $+$ helicity W boson is obtained by assuming $F_0 = 0.7$, which is the generic prediction for any linear combination of V and A currents. Based on $230 \pm 15 \text{ pb}^{-1}$ of data at $\sqrt{s} = 1.96$ TeV.
- 16 ACOSTA 05D measures the $m_{\ell^+ b}^2$ distribution in $t\bar{t}$ production events where one or both W 's decay leptonically to $\ell = e$ or μ , and finds a bound on the V+A coupling of the tbW vertex. By assuming the SM value of the longitudinal W fraction $F_0 = B(t \rightarrow W_0 b) = 0.70$, the bound on F_{\pm} is obtained. If the results are combined with those of AFFOLDER 00B, the bounds become $F_{V+A} < 0.61$ (95% CL) and $F_{\pm} < 0.18$ (95% CL), respectively. Based on $109 \pm 7 \text{ pb}^{-1}$ of data at $\sqrt{s} = 1.8$ TeV (run I).

F_{V+A}

VALUE	CL%	DOCUMENT ID	TECN	COMMENT
< 0.29	95	1 ABULENCIA	07G CDF	$F_{V+A} = B(t \rightarrow Wb_R)$
• • • We do not use the following data for averages, fits, limits, etc. • • •				
$-0.06 \pm 0.22 \pm 0.12$		1 ABULENCIA	07G CDF	$F_{V+A} = B(t \rightarrow Wb_R)$
< 0.80	95	2 ACOSTA	05D CDF	$F_{V+A} = B(t \rightarrow Wb_R)$

- 1 Based on 700 pb^{-1} of data at $\sqrt{s} = 1.96$ TeV.
- 2 ACOSTA 05D measures the $m_{\ell^+ b}^2$ distribution in $t\bar{t}$ production events where one or both W 's decay leptonically to $\ell = e$ or μ , and finds a bound on the V+A coupling of the tbW vertex. By assuming the SM value of the longitudinal W fraction $F_0 = B(t \rightarrow W_0 b) = 0.70$, the bound on F_{\pm} is obtained. If the results are combined with those of AFFOLDER 00B, the bounds become $F_{V+A} < 0.61$ (95% CL) and $F_{\pm} < 0.18$ (95% CL), respectively. Based on $109 \pm 7 \text{ pb}^{-1}$ of data at $\sqrt{s} = 1.8$ TeV (run I).

f_1^R

VALUE	CL%	DOCUMENT ID	TECN	COMMENT
• • • We do not use the following data for averages, fits, limits, etc. • • •				
$ f_1^R/f_2^R < 0.37$	95	1 AABOUD	17BB ATLS	t-channel single top
$ f_1^R < 0.16$	95	2 KHACHATRYAN...17G	CMS	t-channel single-t prod.
$-0.20 < \text{Re}(V_{tb} f_1^R) < 0.23$	95	3 AAD	12BG ATLS	Constr. on Wtb vtx
$(V_{tb} f_1^R)^2 < 0.93$	95	4 ABAZOV	12E D0	Single-top
$ f_1^R ^2 < 0.30$	95	5 ABAZOV	12I D0	single-t + W helicity
$ f_1^R ^2 < 1.01$	95	6 ABAZOV	09J D0	$ f_1^L = 1, f_2^L = f_2^R = 0$
$ f_1^R ^2 < 2.5$	95	7 ABAZOV	08AI D0	$ f_1^L ^2 = 1.8^{+1.0}_{-1.3}$

- 1 AABOUD 17BB based on 20.2 fb^{-1} of pp data at $\sqrt{s} = 8$ TeV. Triple-differential decay rate of top quark is used to simultaneously determine five generalized Wtb couplings as well as the top polarization. No assumption is made for the other couplings. See this paper for constraints on other couplings not included here.
- 2 KHACHATRYAN 17G based on 5.0 and 19.7 fb^{-1} of pp data at $\sqrt{s} = 7$ and 8 TeV, respectively. A Bayesian neural network technique is used to discriminate between signal and backgrounds. This is a 95% CL exclusion limit obtained by a three-dimensional fit with simultaneous variation of (f_1^L, f_1^R, f_2^R) .
- 3 Based on 1.04 fb^{-1} of pp data at $\sqrt{s} = 7$ TeV. AAD 12BG studied $t\bar{t}$ events with large E_T and either $\ell + \geq 4j$ or $\ell\ell + \geq 2j$.
- 4 Based on 5.4 fb^{-1} of data. For each value of the form factor quoted the other two are assumed to have their SM value. Their Fig. 4 shows two-dimensional posterior probability density distributions for the anomalous couplings.
- 5 Based on 5.4 fb^{-1} of data in $p\bar{p}$ collisions at 1.96 TeV. Results are obtained by combining the limits from the W helicity measurements and those from the single top quark production.
- 6 Based on 1 fb^{-1} of data at $p\bar{p}$ collisions $\sqrt{s} = 1.96$ TeV. Combined result of the W helicity measurement in $t\bar{t}$ events (ABAZOV 08B) and the search for anomalous tbW couplings in the single top production (ABAZOV 08AI). Constraints when f_1^L and one of the anomalous couplings are simultaneously allowed to vary are given in their Fig. 1 and Table 1.
- 7 Result is based on 0.9 fb^{-1} of data at $\sqrt{s} = 1.96$ TeV. Single top quark production events are used to measure the Lorentz structure of the tbW coupling. The upper bounds on the non-standard couplings are obtained when only one non-standard coupling is allowed to be present together with the SM one, $f_1^L = V_{tb}^*$.

f_2^L

VALUE	CL%	DOCUMENT ID	TECN	COMMENT
• • • We do not use the following data for averages, fits, limits, etc. • • •				
$ f_2^L/f_1^L < 0.29$	95	1 AABOUD	17BB ATLS	t-channel single top
$ f_2^L < 0.057$	95	2 KHACHATRYAN...17G	CMS	t-channel single-t prod.
$-0.14 < \text{Re}(f_2^L) < 0.11$	95	3 AAD	12BG ATLS	Constr. on Wtb vtx

$(V_{tb} f_2^L)^2 < 0.13$	95	4 ABAZOV	12E D0	Single-top
$ f_2^L ^2 < 0.05$	95	5 ABAZOV	12I D0	single-t + W helicity
$ f_2^L ^2 < 0.28$	95	6 ABAZOV	09J D0	$ f_1^L = 1, f_1^R = f_2^R = 0$
$ f_2^L ^2 < 0.5$	95	7 ABAZOV	08AI D0	$ f_1^L ^2 = 1.4^{+0.6}_{-0.5}$

- 1 AABOUD 17BB based on 20.2 fb^{-1} of pp data at $\sqrt{s} = 8$ TeV. Triple-differential decay rate of top quark is used to simultaneously determine five generalized Wtb couplings as well as the top polarization. No assumption is made for the other couplings. See this paper for constraints on other couplings not included here.
- 2 KHACHATRYAN 17G based on 5.0 and 19.7 fb^{-1} of pp data at $\sqrt{s} = 7$ and 8 TeV, respectively. A Bayesian neural network technique is used to discriminate between signal and backgrounds. This is a 95% CL exclusion limit obtained by a three-dimensional fit with simultaneous variation of (f_1^L, f_2^L, f_2^R) .
- 3 Based on 1.04 fb^{-1} of pp data at $\sqrt{s} = 7$ TeV. AAD 12BG studied $t\bar{t}$ events with large E_T and either $\ell + \geq 4j$ or $\ell\ell + \geq 2j$.
- 4 Based on 5.4 fb^{-1} of data. For each value of the form factor quoted the other two are assumed to have their SM value. Their Fig. 4 shows two-dimensional posterior probability density distributions for the anomalous couplings.
- 5 Based on 5.4 fb^{-1} of data in $p\bar{p}$ collisions at 1.96 TeV. Results are obtained by combining the limits from the W helicity measurements and those from the single top quark production.
- 6 Based on 1 fb^{-1} of data at $p\bar{p}$ collisions $\sqrt{s} = 1.96$ TeV. Combined result of the W helicity measurement in $t\bar{t}$ events (ABAZOV 08B) and the search for anomalous tbW couplings in the single top production (ABAZOV 08AI). Constraints when f_1^L and one of the anomalous couplings are simultaneously allowed to vary are given in their Fig. 1 and Table 1.
- 7 Result is based on 0.9 fb^{-1} of data at $\sqrt{s} = 1.96$ TeV. Single top quark production events are used to measure the Lorentz structure of the tbW coupling. The upper bounds on the non-standard couplings are obtained when only one non-standard coupling is allowed to be present together with the SM one, $f_1^L = V_{tb}^*$.

f_2^R

VALUE	CL%	DOCUMENT ID	TECN	COMMENT
• • • We do not use the following data for averages, fits, limits, etc. • • •				
$-0.12 < \text{Re}(f_2^R/f_1^R) < 0.17$	95	1 AABOUD	17BB ATLS	t-channel single top
$-0.07 < \text{Im}(f_2^R/f_1^R) < 0.06$	95	1 AABOUD	17BB ATLS	t-channel single top
$-0.18 < \text{Im}(f_2^R) < 0.06$	95	2 AABOUD	17I ATLS	t-channel single top
$-0.049 < f_2^R < 0.048$	95	3 KHACHATRYAN...17G	CMS	t-channel single top
$-0.36 < \text{Re}(f_2^R/f_1^R) < 0.10$	95	4 AAD	16AK ATLS	Single-top
$-0.17 < \text{Im}(f_2^R/f_1^R) < 0.23$	95	4 AAD	16AK ATLS	Single-top
$-0.08 < \text{Re}(f_2^R) < 0.04$	95	5 AAD	12BG ATLS	Constr. on Wtb vtx
$(V_{tb} f_2^R)^2 < 0.06$	95	6 ABAZOV	12E D0	Single-top
$ f_2^R ^2 < 0.12$	95	7 ABAZOV	12I D0	single-t + W helicity
$ f_2^R ^2 < 0.23$	95	8 ABAZOV	09J D0	$ f_1^L = 1, f_1^R = f_2^L = 0$
$ f_2^R ^2 < 0.3$	95	9 ABAZOV	08AI D0	$ f_1^L ^2 = 1.4^{+0.9}_{-0.8}$

- 1 AABOUD 17BB based on 20.2 fb^{-1} of pp data at $\sqrt{s} = 8$ TeV. Triple-differential decay rate of top quark is used to simultaneously determine five generalized Wtb couplings as well as the top polarization. No assumption is made for the other couplings. See this paper for constraints on other couplings not included here.
- 2 AABOUD 17I based on 20.2 fb^{-1} of pp data at $\sqrt{s} = 8$ TeV. A cut-based analysis is used to discriminate between signal and backgrounds. All anomalous couplings other than $\text{Im}(f_2^R)$ are assumed to be zero. See this paper for a number of other asymmetries and measurements that are not included here.
- 3 KHACHATRYAN 17G based on 5.0 and 19.7 fb^{-1} of pp data at $\sqrt{s} = 7$ and 8 TeV, respectively. A Bayesian neural network technique is used to discriminate between signal and backgrounds. This is a 95% CL exclusion limit obtained by a three-dimensional fit with simultaneous variation of (f_1^L, f_2^L, f_2^R) .
- 4 AAD 16AK based on 4.6 fb^{-1} of pp data at $\sqrt{s} = 7$ TeV. The results are obtained from an analysis of angular distributions of the decay products of single top quarks, assuming $f_1^R = f_2^L = 0$. The fraction of decays containing transversely polarized W is measured to be $F_{\pm} + F_{\mp} = 0.37 \pm 0.07$.
- 5 Based on 1.04 fb^{-1} of pp data at $\sqrt{s} = 7$ TeV. AAD 12BG studied $t\bar{t}$ events with large E_T and either $\ell + \geq 4j$ or $\ell\ell + \geq 2j$.
- 6 Based on 5.4 fb^{-1} of data. For each value of the form factor quoted the other two are assumed to have their SM value. Their Fig. 4 shows two-dimensional posterior probability density distributions for the anomalous couplings.
- 7 Based on 5.4 fb^{-1} of data in $p\bar{p}$ collisions at 1.96 TeV. Results are obtained by combining the limits from the W helicity measurements and those from the single top quark production.
- 8 Based on 1 fb^{-1} of data at $p\bar{p}$ collisions $\sqrt{s} = 1.96$ TeV. Combined result of the W helicity measurement in $t\bar{t}$ events (ABAZOV 08B) and the search for anomalous tbW couplings in the single top production (ABAZOV 08AI). Constraints when f_1^L and one of the anomalous couplings are simultaneously allowed to vary are given in their Fig. 1 and Table 1.
- 9 Result is based on 0.9 fb^{-1} of data at $\sqrt{s} = 1.96$ TeV. Single top quark production events are used to measure the Lorentz structure of the tbW coupling. The upper bounds on the non-standard couplings are obtained when only one non-standard coupling is allowed to be present together with the SM one, $f_1^L = V_{tb}^*$.

$|f_{LV} V_{tb}|$

Assumed that the top-quark-related CKM matrix elements obey the relation $|V_{td}|, |V_{ts}| \ll |V_{tb}|$ and a form factor f_{LV} is determined for each production mode and centre-of-mass energy.

VALUE	DOCUMENT ID	TECN	COMMENT
$1.02 \pm 0.04 \pm 0.02$	1 AABOUD	19R LHC	ATLAS + CMS at $\sqrt{s} = 7, 8$ TeV

- 1 The combination of single-top production cross-section measurements in the t-channel, tW , and s-channel production modes from ATLAS and CMS at $\sqrt{s} = 7$ and 8 TeV.

Quark Particle Listings

t

Chromo-magnetic dipole moment $\mu_t = g_s \hat{\mu}_t / m_t$

VALUE	CL%	DOCUMENT ID	TECN	COMMENT
-------	-----	-------------	------	---------

- • • We do not use the following data for averages, fits, limits, etc. • • •
 - $-0.014 < \hat{\mu}_t < 0.004$ 95 1 SIRUNYAN 19bx CMS $\ell\ell + \geq 2j$ ($\geq 1b$)
 - $-0.053 < \text{Re}(\hat{\mu}_t) < 0.026$ 95 2 KHACHATRYAN...16AI CMS $\ell\ell + \geq 2j$ ($\geq 1b$)
- 1 SIRUNYAN 19bx based on 35.9 fb⁻¹ of pp data at $\sqrt{s} = 13$ TeV. A set of parton-level normalized differential cross sections is measured to extract coefficients of the spin-dependent $t\bar{t}$ production density matrix. The coefficients are compared with the NLO MC simulations and with the NLO QCD calculation including EW corrections.
- 2 KHACHATRYAN 16AI based on 19.5 fb⁻¹ of pp data at $\sqrt{s} = 8$ TeV, using lepton angular distributions as a function of the $t\bar{t}$ -system kinematical variables.

Chromo-electric dipole moment $d_t = g_s \hat{d}_t / m_t$

VALUE	CL%	DOCUMENT ID	TECN	COMMENT
-------	-----	-------------	------	---------

- • • We do not use the following data for averages, fits, limits, etc. • • •
 - $-0.020 < \hat{d}_t < 0.012$ 95 1 SIRUNYAN 19bx CMS $\ell\ell + \geq 2j$ ($\geq 1b$)
 - $-0.068 < \text{Im}(\hat{d}_t) < 0.067$ 95 2 KHACHATRYAN...16AI CMS $\ell\ell + \geq 2j$ ($\geq 1b$)
- 1 SIRUNYAN 19bx based on 35.9 fb⁻¹ of pp data at $\sqrt{s} = 13$ TeV. A set of parton-level normalized differential cross sections is measured to extract coefficients of the spin-dependent $t\bar{t}$ production density matrix and constrain the anomalous chromomagnetic and chromoelectric dipole moments of the top quark. The coefficients are compared with the NLO MC simulations and with the NLO QCD calculation including EW corrections.
- 2 KHACHATRYAN 16AI based on 19.5 fb⁻¹ of pp data at $\sqrt{s} = 8$ TeV, using lepton angular distributions as a function of the $t\bar{t}$ -system kinematical variables.

Spin Correlation in $t\bar{t}$ Production in $p\bar{p}$ Collisions

C is the correlation strength parameter, f is the ratio of events with correlated t and \bar{t} spins (SM prediction: f = 1), and κ is the spin correlation coefficient. See "The Top Quark" review for more information.

VALUE	DOCUMENT ID	TECN	COMMENT
-------	-------------	------	---------

- • • We do not use the following data for averages, fits, limits, etc. • • •
 - 0.89 ± 0.22 1 ABAZOV 16A D0 f ($\ell\ell + \geq 2$ jets, $\ell + \geq 4$ jets)
 - 0.85 ± 0.29 2 ABAZOV 12B D0 f ($\ell\ell + \geq 2$ jets, $\ell + \geq 4$ jets)
 - $1.15^{+0.42}_{-0.43}$ 3 ABAZOV 12B D0 f ($\ell + \cancel{E}_T + \geq 4$ jets)
 - $0.60^{+0.50}_{-0.16}$ 4 AALTONEN 11AR CDF κ ($\ell + \cancel{E}_T + \geq 4$ jets)
 - $0.74^{+0.40}_{-0.41}$ 5 ABAZOV 11AE D0 f ($\ell\ell + \cancel{E}_T + \geq 2$ jets)
 - 0.10 ± 0.45 6 ABAZOV 11AF D0 C ($\ell\ell + \cancel{E}_T + \geq 2$ jets)
- 1 ABAZOV 16A based on 9.7 fb⁻¹ of data. A matrix element method is used. It corresponds to evidence of spin correlation at 4.2 σ and is in agreement with the NLO SM prediction $0.80^{+0.01}_{-0.02}$.
- 2 This is a combination of the lepton + jets analysis presented in ABAZOV 12B and the dilepton measurement of ABAZOV 11AE. It provides a 3.1 σ evidence for the $t\bar{t}$ spin correlation.
- 3 Based on 5.3 fb⁻¹ of data. The error is statistical and systematic combined. A matrix element method is used.
- 4 Based on 4.3 fb⁻¹ of data. The measurement is based on the angular study of the top quark decay products in the helicity basis. The theory prediction is $\kappa \approx 0.40$.
- 5 Based on 5.4 fb⁻¹ of data using a matrix element method. The error is statistical and systematic combined. The no-correlation hypothesis is excluded at the 97.7% CL.
- 6 Based on 5.4 fb⁻¹ of data. The error is statistical and systematic combined. The NLO QCD prediction is C = 0.78 ± 0.03 . The neutrino weighting method is used for reconstruction of kinematics.

Spin Correlation in $t\bar{t}$ Production in pp Collisions

Spin correlation, f_{SM} , measures the strength of the correlation between the spins of the pair produced $t\bar{t}$. $f_{SM} = 1$ for the SM, while $f_{SM} = 0$ for no spin correlation.

VALUE	DOCUMENT ID	TECN	COMMENT
-------	-------------	------	---------

- • • We do not use the following data for averages, fits, limits, etc. • • •
- $0.90 \pm 0.07 \pm 0.09 \pm 0.01$ 1 SIRUNYAN 19BX CMS C_{kk} in $\ell\ell + \geq 2j$ ($\geq 1b$)
- $1.13 \pm 0.32 \pm 0.32^{+0.10}_{-0.13}$ 1 SIRUNYAN 19BX CMS C_{rr} in $\ell\ell + \geq 2j$ ($\geq 1b$)
- $1.01 \pm 0.04 \pm 0.05 \pm 0.01$ 1 SIRUNYAN 19BX CMS C_{nn} in $\ell\ell + \geq 2j$ ($\geq 1b$)
- $0.94 \pm 0.17 \pm 0.26 \pm 0.01$ 1 SIRUNYAN 19BX CMS $C_{rk} + C_{kr}$ in $\ell\ell + \geq 2j$ ($\geq 1b$)
- $0.98 \pm 0.03 \pm 0.04 \pm 0.01$ 1 SIRUNYAN 19BX CMS $(C_{kk} + C_{rr} + C_{nn})/3$ in $\ell\ell + \geq 2j$ ($\geq 1b$)
- $0.74 \pm 0.07 \pm 0.19^{+0.06}_{-0.08}$ 1 SIRUNYAN 19BX CMS $A_{\cos\phi}^{lab}$ in $\ell\ell + \geq 2j$ ($\geq 1b$)
- $1.05 \pm 0.03 \pm 0.08^{+0.09}_{-0.12}$ 1 SIRUNYAN 19BX CMS $A_{|\Delta\phi(\ell\ell)|}$ in $\ell\ell + \geq 2j$ ($\geq 1b$)
- $1.12^{+0.12}_{-0.15}$ 2 KHACHATRYAN...16AI CMS $\ell\ell + \geq 2j$ ($\geq 1b$)
- $0.72 \pm 0.08^{+0.15}_{-0.13}$ 3 KHACHATRYAN...16X CMS $\mu + 4, 5j$
- $1.20 \pm 0.05 \pm 0.13$ 4 AAD 15J ATLS $\Delta\phi(\ell\ell)$ in $\ell\ell + \geq 2j$ ($\geq 1b$)
- $1.19 \pm 0.09 \pm 0.18$ 5 AAD 14BB ATLS $\Delta\phi(\ell\ell)$ in $\ell\ell + \geq 2j$ events
- $1.12 \pm 0.11 \pm 0.22$ 5 AAD 14BB ATLS $\Delta\phi(\ell j)$ in $\ell + \geq 4j$ events
- $0.87 \pm 0.11 \pm 0.14$ 5,6 AAD 14BB ATLS S-ratio in $\ell\ell + \geq 2j$ events
- $0.75 \pm 0.19 \pm 0.23$ 5,7 AAD 14BB ATLS $\cos\theta(\ell^+) \cos\theta(\ell^-)$ in $\ell\ell + \geq 2j$ events
- $0.83 \pm 0.14 \pm 0.18$ 5,8 AAD 14BB ATLS $\cos\theta(\ell^+) \cos\theta(\ell^-)$ in $\ell\ell + \geq 2j$ events

- 1 SIRUNYAN 19bx based on 35.9 fb⁻¹ of pp data at $\sqrt{s} = 13$ TeV. A set of parton-level normalized differential cross sections sensitive to coefficients of the spin-dependent $t\bar{t}$ production density matrix is measured. The distributions and coefficients are compared with the NLO MC simulations and with the NLO QCD calculation including EW corrections. Three errors are from statistics, experimental systematics, and theory.

- 2 KHACHATRYAN 16AI based on 19.5 fb⁻¹ of pp data at $\sqrt{s} = 8$ TeV, using lepton angular distributions as a function of the $t\bar{t}$ -system kinematical variables.
- 3 KHACHATRYAN 16x based on 19.7 fb⁻¹ of pp data at $\sqrt{s} = 8$ TeV. Uses a template fit method. Spin correlation strength in the helicity basis is given by $A_{\text{hel}} = 0.23 \pm 0.03^{+0.05}_{-0.04}$.
- 4 AAD 15J based on 20.3 fb⁻¹ of pp data at $\sqrt{s} = 8$ TeV. Uses a fit including a linear superposition of $\Delta\phi$ distribution from the SM NLO simulation with coefficient f_{SM} and from $t\bar{t}$ simulation without spin correlation with coefficient $(1 - f_{SM})$.
- 5 Based on 4.6 fb⁻¹ of pp data at $\sqrt{s} = 7$ TeV. The results are for $m_t = 172.5$ GeV.
- 6 The S-ratio is defined as the SM spin correlation in the like-helicity gluon-gluon collisions normalized to the no spin correlation case; see eq. (6) for the LO expression.
- 7 The polar angle correlation along the helicity axis.
- 8 The polar angle correlation along the direction which maximizes the correlation.

t-quark FCNC Couplings κ^{tug}/Λ and κ^{ctg}/Λ

VALUE (TeV ⁻¹)	CL%	DOCUMENT ID	TECN	COMMENT
----------------------------	-----	-------------	------	---------

- • • We do not use the following data for averages, fits, limits, etc. • • •
 - < 0.0041 95 1 KHACHATRYAN...17G CMS $|\kappa^{tug}|/\Lambda$
 - < 0.018 95 1 KHACHATRYAN...17G CMS $|\kappa^{ctg}|/\Lambda$
 - < 0.0058 95 2 AAD 16As ATLS κ^{tug}/Λ
 - < 0.013 95 2 AAD 16As ATLS κ^{ctg}/Λ
 - < 0.0069 95 3 AAD 12BP ATLS t^{tug}/Λ ($t^{ctg} = 0$)
 - < 0.016 95 3 AAD 12BP ATLS t^{ctg}/Λ ($t^{tug} = 0$)
 - < 0.013 95 4 ABAZOV 10K D0 κ^{tug}/Λ
 - < 0.057 95 4 ABAZOV 10K D0 κ^{ctg}/Λ
 - < 0.018 95 5 AALTONEN 09N CDF κ^{tug}/Λ ($\kappa^{ctg} = 0$)
 - < 0.069 95 5 AALTONEN 09N CDF κ^{ctg}/Λ ($\kappa^{tug} = 0$)
 - < 0.037 95 6 ABAZOV 07V D0 κ^{tug}/Λ
 - < 0.15 95 6 ABAZOV 07V D0 κ^{ctg}/Λ
- 1 KHACHATRYAN 17G based on 5.0 and 19.7 fb⁻¹ of pp data at $\sqrt{s} = 7$ and 8 TeV, respectively. t-channel single top production is used. The result corresponds to $B(t \rightarrow ug) < 2.0 \times 10^{-5}$ or $B(t \rightarrow cg) < 4.1 \times 10^{-4}$.
- 2 AAD 16As based on 20.3 fb⁻¹ of pp data at $\sqrt{s} = 8$ TeV. The results are obtained from the 95% CL upper limit on the single top-quark production $\sigma(qg \rightarrow t) \cdot B(t \rightarrow bW) < 3.4$ pb, $B(t \rightarrow ug) < 4.0 \times 10^{-5}$ and $B(t \rightarrow cg) < 20 \times 10^{-5}$.
- 3 Based on 2.05 fb⁻¹ of pp data at $\sqrt{s} = 7$ TeV. The results are obtained from the 95% CL upper limit on the single top-quark production $\sigma(qg \rightarrow t) \cdot B(t \rightarrow bW) < 3.9$ pb, for $q=u$ or $q=c$, $B(t \rightarrow ug) < 5.7 \times 10^{-5}$ and $B(t \rightarrow cg) < 2.7 \times 10^{-4}$.
- 4 Based on 2.3 fb⁻¹ of data in $p\bar{p}$ collisions at $\sqrt{s} = 1.96$ TeV. Upper limit of single top quark production cross section 0.20 pb and 0.27 pb via FCNC t-u-g and t-c-g couplings, respectively, lead to the bounds without assuming the absence of the other coupling. $B(t \rightarrow u + g) < 2.0 \times 10^{-4}$ and $B(t \rightarrow c + g) < 3.9 \times 10^{-3}$ follow.
- 5 Based on 2.2 fb⁻¹ of data in $p\bar{p}$ collisions at $\sqrt{s} = 1.96$ TeV. Upper limit of single top quark production cross section $\sigma(u(c) + g \rightarrow t) < 1.8$ pb (95% CL) via FCNC t-u-g and t-c-g couplings lead to the bounds. $B(t \rightarrow u + g) < 3.9 \times 10^{-4}$ and $B(t \rightarrow c + g) < 5.7 \times 10^{-3}$ follow.
- 6 Result is based on 230 pb⁻¹ of data at $\sqrt{s} = 1.96$ TeV. Absence of single top quark production events via FCNC t-u-g and t-c-g couplings lead to the upper bounds on the dimensioned couplings, κ^{tug}/Λ and κ^{ctg}/Λ , respectively.

t-Quark Yukawa Coupling from $t\bar{t}$ Kinematic Distributions in pp Collisions

The ratio of t-quark Yukawa coupling to its standard model predicted value.

VALUE	DOCUMENT ID	TECN	COMMENT
-------	-------------	------	---------

- • • We do not use the following data for averages, fits, limits, etc. • • •
 - $1.07^{+0.34}_{-0.43}$ 1 SIRUNYAN 19BY CMS $\ell + \text{jets}$, $t\bar{t}$ threshold
- 1 SIRUNYAN 19BY based on 35.8 fb⁻¹ of data at $\sqrt{s} = 13$ TeV. Experimental sensitivity is enhanced in the low $M_{t\bar{t}}$ region. The distributions of $M_{t\bar{t}}$, $|y_t - y_{\bar{t}}|$, and the number of reconstructed jets are compared with predictions by different Yukawa couplings which include NNLO QCD and NLO EW corrections.

 $\sigma(H t\bar{t}) / \sigma(H t\bar{t})_{SM}$

VALUE	CL%	DOCUMENT ID	TECN	COMMENT
-------	-----	-------------	------	---------

- • • We do not use the following data for averages, fits, limits, etc. • • •
- $0.72 \pm 0.24 \pm 0.38$ 1 SIRUNYAN 19R CMS $H t\bar{t} (H \rightarrow b\bar{b}, t\bar{t} \rightarrow \ell + \text{jets or dilepton})$
- $0.9 \pm 0.7 \pm 1.3$ 2 SIRUNYAN 18BD CMS $H t\bar{t} (H \rightarrow b\bar{b}, t\bar{t} \rightarrow \text{all jets})$
- $1.26^{+0.31}_{-0.26}$ 3 SIRUNYAN 18L CMS combination of CMS
- < 6.7 95 4 AAD 15 ATLS $H t\bar{t}; H \rightarrow \gamma\gamma$
- 2.8 ± 1.0 5 KHACHATRYAN...14H CMS $H \rightarrow b\bar{b}, \tau\tau, \tau\tau, \gamma\gamma, WW/ZZ(\text{leptons})$

- 1 SIRUNYAN 19R based on 35.9 fb⁻¹ of pp data at 13 TeV. Multivariate techniques are employed to separate the signal from the dominant $t\bar{t} + \text{jets}$ background. The result is for $m_H = 125$ GeV. The measured ratio corresponds to a signal significance of 1.6 σ above the background-only hypothesis.
- 2 SIRUNYAN 18BD based on 35.9 fb⁻¹ of pp data at 13 TeV. A combined fit of signal and background templates to data is performed in six event categories separated by jet and b-jet multiplicities. An upper limit of 3.8 is obtained for the cross section ratio.
- 3 SIRUNYAN 18L based on up to 5.1, 19.7, and 35.9 fb⁻¹ of pp data at 7, 8, and 13 TeV, respectively. An excess of events is observed, with a significance of 5.2 standard deviations, over the expectation from the background-only hypothesis. The result is for the Higgs boson mass of 125.09 GeV.
- 4 Based on 4.5 fb⁻¹ of data at 7 TeV and 20.3 fb⁻¹ at 8 TeV. The result is for $m_H = 125.4$ GeV. The measurement constrains the top quark Yukawa coupling strength parameter $\kappa_t = Y_t/Y_t^{SM}$ to be $-1.3 < \kappa_t < 8.0$ (95% CL).

See key on page 999

⁵ Based on 5.1 fb^{-1} of pp data at 7 TeV and 19.7 fb^{-1} at 8 TeV. The results are obtained by assuming the SM decay branching fractions for the Higgs boson of mass 125.6 GeV. The signal strength for individual Higgs decay channels are given in Fig. 13, and the preferred region in the (κ_V, κ_f) space is given in Fig. 14.

Single t -Quark Production Cross Section in $p\bar{p}$ Collisions at $\sqrt{s} = 1.8 \text{ TeV}$

Direct probe of the $t b W$ coupling and possible new physics at $\sqrt{s} = 1.8 \text{ TeV}$.

VALUE (pb)	CL%	DOCUMENT ID	TECN	COMMENT
<24	95	¹ ACOSTA	04H	CDF $p\bar{p} \rightarrow tb + X, tqb + X$
<18	95	² ACOSTA	02	CDF $p\bar{p} \rightarrow tb + X$
<13	95	³ ACOSTA	02	CDF $p\bar{p} \rightarrow tqb + X$

¹ ACOSTA 04H bounds single top-quark production from the s -channel W -exchange process, $q'\bar{q}' \rightarrow t\bar{b}$, and the t -channel W -exchange process, $q'g \rightarrow qt\bar{b}$. Based on $\sim 106 \text{ pb}^{-1}$ of data.

² ACOSTA 02 bounds the cross section for single top-quark production via the s -channel W -exchange process, $q'\bar{q}' \rightarrow t\bar{b}$. Based on $\sim 106 \text{ pb}^{-1}$ of data.

³ ACOSTA 02 bounds the cross section for single top-quark production via the t -channel W -exchange process, $q'g \rightarrow qt\bar{b}$. Based on $\sim 106 \text{ pb}^{-1}$ of data.

Single t -Quark Production Cross Section in $p\bar{p}$ Collisions at $\sqrt{s} = 1.96 \text{ TeV}$

Direct probes of the $t b W$ coupling and possible new physics at $\sqrt{s} = 1.96 \text{ TeV}$.

OUR AVERAGE assumes that the systematic uncertainties are uncorrelated.

VALUE (pb)	CL%	DOCUMENT ID	TECN	COMMENT
$3.53^{+1.25}_{-1.16}$		¹ AALTONEN	16	CDF $s- + t$ -channels ($0\ell + \cancel{E}_T + 2, 3j$ ($\geq 1b$ -tag))
$2.25^{+0.29}_{-0.31}$		² AALTONEN	15H	TEVA t -channel
$3.30^{+0.52}_{-0.40}$		^{2,3} AALTONEN	15H	TEVA $s- + t$ -channels
$1.12^{+0.61}_{-0.57}$		⁴ AALTONEN	14K	CDF s -channel ($0\ell + \cancel{E}_T + 2, 3j$ ($\geq 1b$ -tag))
$1.41^{+0.44}_{-0.42}$		⁵ AALTONEN	14L	CDF s -channel ($\ell + \cancel{E}_T + 2j$ ($\geq 1b$ -tag))
$1.29^{+0.26}_{-0.24}$		⁶ AALTONEN	14M	TEVA s -channel (CDF + D0)
$3.04^{+0.57}_{-0.53}$		⁷ AALTONEN	14o	CDF $s + t + Wt$ ($\ell + \cancel{E}_T + 2$ or 3 jets ($\geq 1b$ -tag))
$1.10^{+0.33}_{-0.31}$		⁸ ABAZOV	13o	D0 s -channel
$3.07^{+0.54}_{-0.49}$		⁸ ABAZOV	13o	D0 t -channel
$4.11^{+0.60}_{-0.55}$		⁸ ABAZOV	13o	D0 $s- + t$ -channels
$0.98^{+0.63}_{-0.59}$		⁹ ABAZOV	11AA	D0 s -channel
$2.90^{+0.59}_{-0.54}$		⁹ ABAZOV	11AA	D0 t -channel
$3.43^{+0.73}_{-0.74}$		¹⁰ ABAZOV	11AD	D0 $s- + t$ -channels
$1.8^{+0.7}_{-0.5}$		¹¹ AALTONEN	10AB	CDF s -channel
0.8 ± 0.4		¹¹ AALTONEN	10AB	CDF t -channel
$4.9^{+2.5}_{-2.2}$		¹² AALTONEN	10U	CDF $\cancel{E}_T + \text{jets decay}$
$3.14^{+0.94}_{-0.80}$		¹³ ABAZOV	10	D0 t -channel
$1.05^{+0.81}_{-0.80}$		¹³ ABAZOV	10	D0 s -channel
< 7.3	95	¹⁴ ABAZOV	10J	D0 $\tau + \text{jets decay}$
$2.3^{+0.6}_{-0.5}$		¹⁵ AALTONEN	09AT	CDF $s- + t$ -channel
$3.94^{+0.88}_{-0.88}$		¹⁶ ABAZOV	09Z	D0 $s- + t$ -channel
$2.2^{+0.7}_{-0.6}$		¹⁷ AALTONEN	08AH	CDF $s- + t$ -channel
$4.7^{+1.3}_{-1.3}$		¹⁸ ABAZOV	08I	D0 $s- + t$ -channel
$4.9^{+1.4}_{-1.4}$		¹⁹ ABAZOV	07H	D0 $s- + t$ -channel
< 6.4	95	²⁰ ABAZOV	05P	D0 $p\bar{p} \rightarrow tb + X$
< 5.0	95	²⁰ ABAZOV	05P	D0 $p\bar{p} \rightarrow tqb + X$
<10.1	95	²¹ ACOSTA	05N	CDF $p\bar{p} \rightarrow tqb + X$
<13.6	95	²¹ ACOSTA	05N	CDF $p\bar{p} \rightarrow tb + X$
<17.8	95	²¹ ACOSTA	05N	CDF $p\bar{p} \rightarrow tb + X, tqb + X$

¹ AALTONEN 16 based on 9.5 fb^{-1} of data. This includes, as a part, the result of AALTONEN 14K. Combination of this result with that of AALTONEN 14o gives a $s + t$ cross section of $3.02^{+0.49}_{-0.48} \text{ pb}$ and $|V_{tb}| > 0.84$ (95% CL).

² AALTONEN 15H based on 9.7 fb^{-1} of data per experiment. The result is for $m_t = 172.5 \text{ GeV}$, and is a combination of the CDF measurements (AALTONEN 16) and the D0 measurements (ABAZOV 13o) on the t -channel single t -quark production cross section. The result is consistent with the NLO+NNLL SM prediction and gives $|V_{tb}| = 1.02^{+0.06}_{-0.05}$ and $|V_{tb}| > 0.92$ (95% CL).

³ AALTONEN 15H is a combined measurement of s -channel single top cross section by CDF + D0. AALTONEN 14M is not included.

⁴ Based on 9.45 fb^{-1} of data, using neural networks to separate signal from backgrounds. The result is for $m_t = 172.5 \text{ GeV}$. Combination of this result with the CDF measurement in the 1 lepton channel AALTONEN 14K gives $1.36^{+0.37}_{-0.32} \text{ pb}$, consistent with the SM prediction, and is 4.2 sigma away from the background only hypothesis.

⁵ Based on 9.4 fb^{-1} of data, using neural networks to separate signal from backgrounds. The result is for $m_t = 172.5 \text{ GeV}$. The result is 3.8 sigma away from the background only hypothesis.

⁶ Based on 9.7 fb^{-1} of data per experiment. The result is for $m_t = 172.5 \text{ GeV}$, and is a combination of the CDF measurements AALTONEN 14L, AALTONEN 14K and the D0 measurement ABAZOV 13o on the s -channel single t -quark production cross section. The result is consistent with the SM prediction of $1.05 \pm 0.06 \text{ pb}$ and the significance of the observation is of 6.3 standard deviations.

⁷ Based on 7.5 fb^{-1} of data. Neural network is used to discriminate signals (s -, t - and Wt -channel single top production) from backgrounds. The result is consistent with the SM prediction, and gives $|V_{tb}| = 0.95 \pm 0.09$ (stat + syst) ± 0.05 (theory) and $|V_{tb}| > 0.78$ (95% CL). The result is for $m_t = 172.5 \text{ GeV}$.

⁸ Based on 9.7 fb^{-1} of data. Events with $\ell + \cancel{E}_T + 2$ or 3 jets (1 or 2 b -tag) are analysed, assuming $m_t = 172.5 \text{ GeV}$. The combined $s- + t$ -channel cross section gives $|V_{tb} f_1^L| = 1.12^{+0.09}_{-0.08}$, or $|V_{tb}| > 0.92$ at 95% CL for $f_1^L = 1$ and a flat prior within $0 \leq |V_{tb}|^2 \leq 1$.

⁹ Based on 5.4 fb^{-1} of data. The error is statistical + systematic combined. The results are for $m_t = 172.5 \text{ GeV}$. Results for other m_t values are given in Table 2 of ABAZOV 11AA.

¹⁰ Based on 5.4 fb^{-1} of data and for $m_t = 172.5 \text{ GeV}$. The error is statistical + systematic combined. Results for other m_t values are given in Table III of ABAZOV 11AD. The result is obtained by assuming the SM ratio between tb (s -channel) and tqb (t -channel) productions, and gives $|V_{tb} f_1^L| = 1.02^{+0.10}_{-0.11}$, or $|V_{tb}| > 0.79$ at 95% CL for a flat prior within $0 < |V_{tb}|^2 < 1$.

¹¹ Based on 3.2 fb^{-1} of data. For combined $s- + t$ -channel result see AALTONEN 09AT.

¹² Result is based on 2.1 fb^{-1} of data. Events with large missing E_T and jets with at least one b -jet without identified electron or muon are selected. Result is obtained when observed 2.1σ excess over the background originates from the signal for $m_t = 175 \text{ GeV}$, giving $|V_{tb}| = 1.24^{+0.34}_{-0.29} \pm 0.07$ (theory).

¹³ Result is based on 2.3 fb^{-1} of data. Events with isolated $\ell + \cancel{E}_T + 2, 3, 4$ jets with one or two b -tags are selected. The analysis assumes $m_t = 170 \text{ GeV}$.

¹⁴ Result is based on 4.8 fb^{-1} of data. Events with an isolated reconstructed tau lepton, missing $E_T + 2, 3$ jets with one or two b -tags are selected. When combined with ABAZOV 09Z result for $e + \mu$ channels, the s - and t -channels combined cross section is $3.84^{+0.89}_{-0.83} \text{ pb}$.

¹⁵ Based on 3.2 fb^{-1} of data. Events with isolated $\ell + \cancel{E}_T + \text{jets}$ with at least one b -tag are analyzed and s - and t -channel single top events are selected by using the likelihood function, matrix element, neural-network, boosted decision tree, likelihood function optimized for s -channel process, and neural-network based analysis of events with \cancel{E}_T that has sensitivity for $W \rightarrow \tau\nu$ decays. The result is for $m_t = 175 \text{ GeV}$, and the mean value decreases by 0.02 pb/GeV for smaller m_t . The signal has 5.0 sigma significance. The result gives $|V_{tb}| = 0.91 \pm 0.11$ (stat+syst) ± 0.07 (theory), or $|V_{tb}| > 0.71$ at 95% CL.

¹⁶ Based on 2.3 fb^{-1} of data. Events with isolated $\ell + \cancel{E}_T + \geq 2$ jets with 1 or 2 b -tags are analyzed and s - and t -channel single top events are selected by using boosted decision tree, Bayesian neural networks and the matrix element method. The signal has 5.0 sigma significance. The result gives $|V_{tb}| = 1.07 \pm 0.12$, or $|V_{tb}| > 0.78$ at 95% CL. The analysis assumes $m_t = 170 \text{ GeV}$.

¹⁷ Result is based on 2.2 fb^{-1} of data. Events with isolated $\ell + \cancel{E}_T + 2, 3$ jets with at least one b -tag are selected, and s - and t -channel single top events are selected by using likelihood, matrix element, and neural network discriminants. The result can be interpreted as $|V_{tb}| = 0.88^{+0.13}_{-0.12}$ (stat + syst) ± 0.07 (theory), and $|V_{tb}| > 0.66$ (95% CL) under the $|V_{tb}| < 1$ constraint.

¹⁸ Result is based on 0.9 fb^{-1} of data. Events with isolated $\ell + \cancel{E}_T + 2, 3, 4$ jets with one or two b -vertex-tag are selected, and contributions from $W + \text{jets}$, $t\bar{t}$, s - and t -channel single top events are identified by using boosted decision trees, Bayesian neural networks, and matrix element analysis. The result can be interpreted as the measurement of the CKM matrix element $|V_{tb}| = 1.31^{+0.25}_{-0.21}$, or $|V_{tb}| > 0.68$ (95% CL) under the $|V_{tb}| < 1$ constraint.

¹⁹ Result is based on 0.9 fb^{-1} of data. This result constrains V_{tb} to $0.68 < |V_{tb}| \leq 1$ at 95% CL.

²⁰ ABAZOV 05P bounds single top-quark production from either the s -channel W -exchange process, $q'\bar{q}' \rightarrow t\bar{b}$, or the t -channel W -exchange process, $q'g \rightarrow qt\bar{b}$, based on $\sim 230 \text{ pb}^{-1}$ of data.

²¹ ACOSTA 05N bounds single top-quark production from the t -channel W -exchange process ($q'g \rightarrow qt\bar{b}$), the s -channel W -exchange process ($q'\bar{q}' \rightarrow t\bar{b}$), and from the combined cross section of t - and s -channel. Based on $\sim 162 \text{ pb}^{-1}$ of data.

t -channel Single t Production Cross Section in pp Collisions at $\sqrt{s} = 7 \text{ TeV}$

Direct probe of the $t b W$ coupling and possible new physics at $\sqrt{s} = 7 \text{ TeV}$.

VALUE (pb)	DOCUMENT ID	TECN	COMMENT
67.5 ± 5.7	¹ AABOUD	19R	LHC combination of ATLAS+CMS
$68 \pm 2 \pm 8$	² AAD	14BI	ATLS $\ell + \cancel{E}_T + 2j$ or $3j$
$83 \pm 4^{+20}_{-19}$	³ AAD	12CH	ATLS t -channel $\ell + \cancel{E}_T + (2, 3)j$ (1b)
67.2 ± 6.1	⁴ CHATRCHYAN12BQ	CMS	t -channel $\ell + \cancel{E}_T + \geq 2j$ (1b)
$83.6 \pm 29.8 \pm 3.3$	⁵ CHATRCHYAN11R	CMS	t -channel

¹ AABOUD 19R based on 1.17 to 5.1 fb^{-1} of data from ATLAS and CMS at 7 TeV.

² Based on 4.59 fb^{-1} of data, using neural networks for signal and background separation. $\sigma(tq) = 46 \pm 1 \pm 6 \text{ pb}$ and $\sigma(\bar{t}q) = 23 \pm 1 \pm 3 \text{ pb}$ are separately measured, as well as their ratio $R = \sigma(tq)/\sigma(\bar{t}q) = 2.04 \pm 0.13 \pm 0.12$. The results are for $m_t = 172.5 \text{ GeV}$, and those for other m_t values are given by eq.(4) and Table IV. The measurements give $|V_{tb}| = 1.02 \pm 0.07$ or $|V_{tb}| > 0.88$ (95% CL).

³ Based on 1.04 fb^{-1} of data. The result gives $|V_{tb}| = 1.13^{+0.14}_{-0.13}$ from the ratio $\sigma(\text{exp})/\sigma(\text{th})$, where $\sigma(\text{th})$ is the SM prediction for $|V_{tb}| = 1$. The 95% CL lower bound of $|V_{tb}| > 0.75$ is found if $|V_{tb}| < 1$ is assumed. $\sigma(t) = 59^{+18}_{-16} \text{ pb}$ and $\sigma(\bar{t}) = 33^{+13}_{-12} \text{ pb}$ are found for the separate single t and \bar{t} production cross sections, respectively. The results assume $m_t = 172.5 \text{ GeV}$ for the acceptance.

Quark Particle Listings

t

⁴ Based on 1.17 fb^{-1} of data for $\ell = \mu$, 1.56 fb^{-1} of data for $\ell = e$ at 7 TeV collected during 2011. The result gives $|V_{tb}| = 1.020 \pm 0.046(\text{meas}) \pm 0.017(\text{th})$. The 95% CL lower bound of $|V_{tb}| > 0.92$ is found if $|V_{tb}| < 1$ is assumed. The results assume $m_t = 172.5 \text{ GeV}$ for the acceptance.

⁵ Based on 36 pb^{-1} of data. The first error is statistical + systematic combined, the second is luminosity. The result gives $|V_{tb}| = 1.114 \pm 0.22(\text{exp}) \pm 0.02(\text{th})$ from the ratio $\sigma(\text{exp})/\sigma(\text{th})$, where $\sigma(\text{th})$ is the SM prediction for $|V_{tb}| = 1$. The 95% CL lower bound of $|V_{tb}| > 0.62$ (0.68) is found from the 2D (BDT) analysis under the constraint $0 < |V_{tb}|^2 < 1$.

t-channel Single t Production Cross Section in pp Collisions at $\sqrt{s} = 8 \text{ TeV}$

VALUE (pb)	DOCUMENT ID	TECN	COMMENT
•••	We do not use the following data for averages, fits, limits, etc. •••		
87.7 ± 5.8	¹ AABOUD	19R LHC	combination of ATLAS+CMS
$89.6^{+7.1}_{-6.3}$	² AABOUD	17T ATLS	$\ell + \cancel{E}_T + 2j$ (1b j)
$83.6 \pm 2.3 \pm 7.4$	³ KHACHATRYAN...14F	CMS	$\ell + \cancel{E}_T + \geq 2j$ (1, 2 b, 1 forward j)

¹ AABOUD 19R based on 12.2 to 20.3 fb^{-1} of data from ATLAS and CMS at 8 TeV.

² AABOUD 17T based on 20.2 fb^{-1} of data. A maximum-likelihood fit to neural-network discriminant distributions is used to separate signal and background events. Individual cross sections are measured as $\sigma(tq) = 56.7^{+4.3}_{-3.8} \text{ pb}$ and $\sigma(\bar{T}q) = 32.9^{+3.0}_{-2.7} \text{ pb}$, while their ratio is given by $\sigma(tq)/\sigma(\bar{T}q) = 1.72 \pm 0.09$. A lower limit $|V_{tb}| > 0.92$ (95% CL) is obtained. Measured total and differential cross sections are described well by the SM.

³ Based on 19.7 fb^{-1} of data. The t and \bar{T} production cross sections are measured separately as $\sigma_{t\text{-ch.}}(t) = 53.8 \pm 1.5 \pm 4.4 \text{ pb}$ and $\sigma_{t\text{-ch.}}(\bar{T}) = 27.6 \pm 1.3 \pm 3.7 \text{ pb}$, respectively, as well as their ratio $R_{t\text{-ch.}} = \sigma_{t\text{-ch.}}(t)/\sigma_{t\text{-ch.}}(\bar{T}) = 1.95 \pm 0.10 \pm 0.19$, in agreement with the SM predictions. Combination with a previous CMS result at $\sqrt{s} = 7 \text{ TeV}$ [CHATRCHYAN 12Bq] gives $|V_{tb}| = 0.998 \pm 0.038 \pm 0.016$. Also obtained is the ratio $R_{8/7} = \sigma_{t\text{-ch.}}(8\text{TeV})/\sigma_{t\text{-ch.}}(7\text{TeV}) = 1.24 \pm 0.08 \pm 0.12$.

s-channel Single t Production Cross Section in pp Collisions at $\sqrt{s} = 8 \text{ TeV}$

VALUE (pb)	DOCUMENT ID	TECN	COMMENT
•••	We do not use the following data for averages, fits, limits, etc. •••		
4.9 ± 1.4	¹ AABOUD	19R LHC	ATLAS + CMS
$4.8 \pm 0.8^{+1.6}_{-1.3}$	² AAD	16U ATLS	$\ell + \cancel{E}_T + 2b$
13.4 ± 7.3	³ KHACHATRYAN...16AZ	CMS	$\ell + \cancel{E}_T + 2b$
5.0 ± 4.3	⁴ AAD	15A ATLS	$\ell + \cancel{E}_T + 2b$

¹ AABOUD 19R based on 12.2 to 20.3 fb^{-1} of data from ATLAS and CMS at 8 TeV.

² AAD 16U based on 20.3 fb^{-1} of data, using a maximum-likelihood fit of a matrix element method discriminant. The same data set as in AAD 15A is used. The result corresponds to an observed significance of 3.2σ .

³ KHACHATRYAN 16AZ based on 19.7 fb^{-1} of data, using a multivariate analysis to separate signal and backgrounds. The same method is applied to 5.1 fb^{-1} of data at $\sqrt{s} = 7 \text{ TeV}$, giving $7.1 \pm 8.1 \text{ pb}$. Combining both measurements, the observed significance is 2.5σ . A best fit value of 2.0 ± 0.9 is obtained for the combined ratio of the measured values and SM expectations.

⁴ AAD 15A based on 20.3 fb^{-1} of data, using a multivariate analysis to separate signal and backgrounds. The 95% CL upper bound of the cross section is 14.6 pb . The results are consistent with the SM prediction of $5.61 \pm 0.22 \text{ pb}$ at approximate NNLO.

t-channel Single t Production Cross Section in pp Collisions at $\sqrt{s} = 13 \text{ TeV}$

VALUE (pb)	DOCUMENT ID	TECN	COMMENT
•••	We do not use the following data for averages, fits, limits, etc. •••		
$130 \pm 1 \pm 19$	¹ SIRUNYAN	20D CMS	$\sigma(tq), \ell + \cancel{E}_T + \geq 2j$
$77 \pm 1 \pm 12$	¹ SIRUNYAN	20D CMS	$\sigma(\bar{T}q), \ell + \cancel{E}_T + \geq 2j$
$156 \pm 5 \pm 27 \pm 3$	² AABOUD	17H ATLS	$\sigma(tq), \ell + \cancel{E}_T + 2j$ (1b, 1 forward j)
$91 \pm 4 \pm 18 \pm 2$	² AABOUD	17H ATLS	$\sigma(\bar{T}q), \ell + \cancel{E}_T + 2j$ (1b, 1 forward j)
$154 \pm 8 \pm 9 \pm 19 \pm 4$	³ SIRUNYAN	17AA CMS	$\sigma(tq), \mu + \geq 2j$ (1b)
$85 \pm 10 \pm 4 \pm 11 \pm 2$	³ SIRUNYAN	17AA CMS	$\sigma(\bar{T}q), \mu + \geq 2j$ (1b)

¹ SIRUNYAN 20D based on 35.9 fb^{-1} of data. Different categories of jet and b jet multiplicity and multivariate discriminators are used to separate signal and background events. The cross section ratio is measured to be $\sigma(tq)/\sigma(\bar{T}q) = 1.68 \pm 0.02 \pm 0.05$. CKM matrix element is obtained as $|f_{LV} V_{tb}| = 0.98 \pm 0.07(\text{exp}) \pm 0.02(\text{theo})$ where f_{LV} is an anomalous form factor. All results are in agreement with the SM.

² AABOUD 17H based on 3.2 fb^{-1} of data. A maximum-likelihood fit to neural-network discriminant distributions is used to separate signal and background events. The third error is for luminosity. The cross section ratio is measured to be $\sigma(tq)/\sigma(\bar{T}q) = 1.72 \pm 0.09 \pm 0.18$. A lower limit $|V_{tb}| > 0.84$ (95% CL) is obtained. All results are in agreement with the SM.

³ SIRUNYAN 17AA based on 2.2 fb^{-1} of data. A multivariate discriminator is used to separate signal and background events. The four errors are from statistics, experimental systematics, theory, and luminosity. The cross section ratio is measured to be $\sigma(tq)/\sigma(\bar{T}q) = 1.81 \pm 0.18 \pm 0.15$. CKM matrix element is obtained as $|V_{tb}| = 1.05 \pm 0.07(\text{exp}) \pm 0.02(\text{theo})$. All results are in agreement with the SM.

t \bar{T} Production Cross Section in pp Collisions at $\sqrt{s} = 13 \text{ TeV}$

VALUE (fb)	DOCUMENT ID	TECN	COMMENT
•••	We do not use the following data for averages, fits, limits, etc. •••		
$670 \pm 90^{+110}_{-100}$	¹ AABOUD	18BK ATLS	$H \rightarrow b\bar{b}, WW^* \tau\tau, \gamma\gamma, ZZ^*$

¹ AABOUD 18BK based on 79.8 fb^{-1} of data. The observed significance is 5.8σ relative to the background-only hypothesis. The measurement is consistent with the NLO SM prediction of $507^{+35}_{-50} \text{ fb}$. See Table 3 and Fig. 5 for measurements of individual modes. Combined with the measurements at 7 and 8 TeV, the observed significance is 6.3σ .

Wt Production Cross Section in pp Collisions at $\sqrt{s} = 7 \text{ TeV}$

VALUE (pb)	DOCUMENT ID	TECN	COMMENT
•••	We do not use the following data for averages, fits, limits, etc. •••		
16.3 ± 4.1	¹ AABOUD	19R LHC	ATLAS + CMS combined
16^{+5}_{-4}	² CHATRCHYAN13C	CMS	$t + W$ channel, $2\ell + \cancel{E}_T + 1b$
16.3 ± 4.1	¹ AABOUD 19R	based on 1.17 to 5.1 fb^{-1} of data from ATLAS and CMS at 7 TeV.	
16^{+5}_{-4}	² CHATRCHYAN13C	based on 4.9 fb^{-1} of data. The result gives $V_{tb} = 1.01^{+0.16}_{-0.13}(\text{exp})^{+0.03}_{-0.04}(\text{th})$. $V_{tb} > 0.79$ (95% CL) if $V_{tb} < 1$ is assumed. The results assume $m_t = 172.5 \text{ GeV}$ for the acceptance.	

Wt Production Cross Section in pp Collisions at $\sqrt{s} = 8 \text{ TeV}$

VALUE (pb)	DOCUMENT ID	TECN	COMMENT
•••	We do not use the following data for averages, fits, limits, etc. •••		
23.1 ± 3.6	¹ AABOUD	19R LHC	ATLAS + CMS combined
$23.0 \pm 1.3 \pm 3.2 \pm 1.1$	² AAD	16B ATLS	$2\ell + \cancel{E}_T + 1b$
23.4 ± 5.4	³ CHATRCHYAN14AC	CMS	$t + W$ channel, $2\ell + \cancel{E}_T + 1b$
23.1 ± 3.6	¹ AABOUD 19R	based on 12.2 to 20.3 fb^{-1} of data from ATLAS and CMS at 8 TeV.	
$23.0 \pm 1.3 \pm 3.2 \pm 1.1$	² AAD 16B	based on 20.3 fb^{-1} of data. The result gives $ V_{tb} = 1.01 \pm 0.10$ and $ V_{tb} > 0.80$ (95% CL) without assuming unitarity of the CKM matrix. The results assume $m_t = 172.5 \text{ GeV}$ for the acceptance.	
23.4 ± 5.4	³ CHATRCHYAN14AC	based on 12.2 fb^{-1} of data. Events with two oppositely charged leptons, large \cancel{E}_T and a b -tagged jet are selected, and a multivariate analysis is used to separate the signal from the backgrounds. The result is consistent with the SM prediction of $22.2 \pm 0.6(\text{scale}) \pm 1.4(\text{PDF}) \text{ pb}$ at approximate NNLO.	

Wt Production Cross Section in pp Collisions at $\sqrt{s} = 13 \text{ TeV}$

VALUE (pb)	DOCUMENT ID	TECN	COMMENT
•••	We do not use the following data for averages, fits, limits, etc. •••		
$94 \pm 10^{+28}_{-22} \pm 2$	¹ AABOUD	18H ATLS	$\ell^+ \ell^- + \geq 1j$
$63.1 \pm 1.8 \pm 6.4 \pm 2.1$	² SIRUNYAN	18DL CMS	$e^\pm \mu^\mp + \geq 1j(b\text{-tag})$
$94 \pm 10^{+28}_{-22} \pm 2$	¹ AABOUD 18H	based on 3.2 fb^{-1} of data. The last error is from luminosity. A multivariate analysis is used to separate the signal from the backgrounds. The result is consistent with the NLO+NNLL SM prediction of $71.7 \pm 1.8(\text{scale}) \pm 3.4(\text{PDF}) \text{ pb}$.	
$63.1 \pm 1.8 \pm 6.4 \pm 2.1$	² SIRUNYAN 18DL	based on 35.9 fb^{-1} of data. The last error is from luminosity. A multivariate analysis is used to separate the signal from the backgrounds. The result is consistent with the NLO+NNLL SM prediction of $71.7 \pm 1.8(\text{scale}) \pm 3.4(\text{PDF}) \text{ pb}$.	

Zt Production Cross Section in pp Collisions at $\sqrt{s} = 13 \text{ TeV}$

VALUE (fb)	DOCUMENT ID	TECN	COMMENT
•••	We do not use the following data for averages, fits, limits, etc. •••		
$111 \pm 13^{+11}_{-9}$	¹ SIRUNYAN	19BF CMS	$3\ell + \geq 2j$ ($\geq 1b_j$)
$600 \pm 170 \pm 140$	² AABOUD	18AE ATLS	$3\ell + 1j + 1b_j$
$123 \pm 33 \pm 29$	³ SIRUNYAN	18Z CMS	$3\ell + 1j + 1b_j$
$111 \pm 13^{+11}_{-9}$	¹ SIRUNYAN 19BF	based on 77.4 fb^{-1} of data. Two BDT's are used in the analysis: one to discriminate prompt leptons from non-prompt ones; and one to discriminate tZq signal from backgrounds. The result is for the cross section $\sigma(pp \rightarrow tZq \rightarrow t\ell^+ \ell^- q)$ for dilepton invariant masses above 30 GeV and is consistent with the NLO SM prediction of $94.2 \pm 3.1 \text{ fb}$.	
$600 \pm 170 \pm 140$	² AABOUD 18AE	based on 36.1 fb^{-1} of data. A multivariate analysis is used to separate the signal from the backgrounds. The result is consistent with the NLO SM prediction of 800 fb with a scale uncertainty of $+6.1\%$.	
$123 \pm 33 \pm 29$	³ SIRUNYAN 18Z	based on 35.9 fb^{-1} of data. A multivariate analysis is used to separate the signal from the backgrounds. The result is for the cross section $\sigma(pp \rightarrow tZq \rightarrow Wb\ell^+ \ell^- q)$ and is consistent with the NLO SM prediction of $94.2^{+1.9}_{-1.8}(\text{scale}) \pm 2.5(\text{PDF}) \text{ fb}$. Superseded by SIRUNYAN 19BF.	

Single t-Quark Production Cross Section in ep Collisions

VALUE (pb)	CL%	DOCUMENT ID	TECN	COMMENT
•••	We do not use the following data for averages, fits, limits, etc. •••			
< 0.25	95	¹ AARON	09A H1	$e^\pm p \rightarrow e^\pm tX$
< 0.55	95	² AKTAS	04 H1	$e^\pm p \rightarrow e^\pm tX$
< 0.225	95	³ CHEKANOV	03 ZEUS	$e^\pm p \rightarrow e^\pm tX$
< 0.25	95	¹ AARON 09A	looked for single top production via FCNC in $e^\pm p$ collisions at HERA with 474 pb^{-1} of data at $\sqrt{s} = 301\text{--}319 \text{ GeV}$. The result supersedes that of AKTAS 04.	
< 0.55	95	² AKTAS 04	looked for single top production via FCNC in e^\pm collisions at HERA with 118.3 pb^{-1} , and found 5 events in the e or μ channels while 1.31 ± 0.22 events are expected from the Standard Model background. No excess was found for the hadronic channel. The observed cross section of $\sigma(ep \rightarrow etX) = 0.29^{+0.15}_{-0.14} \text{ pb}$ at $\sqrt{s} = 319 \text{ GeV}$ gives the quoted upper bound if the observed events are due to statistical fluctuation.	
< 0.225	95	³ CHEKANOV 03	looked in 130.1 pb^{-1} of data at $\sqrt{s} = 301$ and 318 GeV . The limit is for $\sqrt{s} = 318 \text{ GeV}$ and assumes $m_t = 175 \text{ GeV}$.	

t \bar{T} Production Cross Section in p \bar{p} Collisions at $\sqrt{s} = 1.8 \text{ TeV}$

Only the final combined $t\bar{T}$ production cross sections obtained from Tevatron Run I by the CDF and D0 experiments are quoted below.

VALUE (pb)	DOCUMENT ID	TECN	COMMENT
•••	We do not use the following data for averages, fits, limits, etc. •••		
$5.69 \pm 1.21 \pm 1.04$	¹ ABAZOV	03A D0	Combined Run I data
$6.5^{+1.7}_{-1.4}$	² AFFOLDER	01A CDF	Combined Run I data
$5.69 \pm 1.21 \pm 1.04$	¹ ABAZOV	combined result from 110 pb^{-1} of Tevatron Run I data. Assume $m_t = 172.1 \text{ GeV}$.	
$6.5^{+1.7}_{-1.4}$	² AFFOLDER	combined result from 105 pb^{-1} of Tevatron Run I data. Assume $m_t = 175 \text{ GeV}$.	

t \bar{t} Production Cross Section in p \bar{p} Collisions at $\sqrt{s} = 1.96$ TeV

Unless otherwise noted the first quoted error is from statistics, the second from systematic uncertainties, and the third from luminosity. If only two errors are quoted the luminosity is included in the systematic uncertainties.

VALUE (pb)	DOCUMENT ID	TECN.	COMMENT
7.26 \pm 0.13 $^{+0.57}_{-0.50}$	1 ABAZOV	16F D0	$\ell\ell, \ell+$ jets channels
8.1 \pm 2.1	2 AALTONEN	14A CDF	$\ell + \tau_h + \geq 2$ jets ($\geq 1b$ -tag)
7.60 \pm 0.20 \pm 0.29 \pm 0.21	3 AALTONEN	14H TEVA	$\ell\ell, \ell+$ jets, all-jets channels
8.0 \pm 0.7 \pm 0.6 \pm 0.5	4 ABAZOV	14K D0	$\ell + \cancel{E}_T + \geq 4$ jets ($\geq 1b$ -tag)
7.09 \pm 0.84	5 AALTONEN	13AB CDF	$\ell\ell + \cancel{E}_T + \geq 2$ jets
7.5 \pm 1.0	6 AALTONEN	13G CDF	$\ell + \cancel{E}_T + \geq 3$ jets ($\geq 1b$ -tag)
8.8 \pm 3.3 \pm 2.2	7 AALTONEN	12AL CDF	$\tau_h + \cancel{E}_T + 4j$ ($\geq 1b$)
8.5 \pm 0.6 \pm 0.7	8 AALTONEN	11D CDF	$\ell + \cancel{E}_T + \geq 3$ jets ($\geq 1b$ -tag)
7.64 \pm 0.57 \pm 0.45	9 AALTONEN	11W CDF	$\ell + \cancel{E}_T + \text{jets}$ ($\geq 1b$ -tag)
7.99 \pm 0.55 \pm 0.76 \pm 0.46	10 AALTONEN	11Y CDF	$\cancel{E}_T + \geq 4$ jets (0,1,2 b -tag)
7.78 \pm 0.77 $_{-0.64}$	11 ABAZOV	11E D0	$\ell + \cancel{E}_T + \geq 2$ jets
7.56 \pm 0.63 $_{-0.56}$	12 ABAZOV	11Z D0	Combination
6.27 \pm 0.73 \pm 0.63 \pm 0.39	13 AALTONEN	10AA CDF	Repl. by AALTONEN 13AB
7.2 \pm 0.5 \pm 1.0 \pm 0.4	14 AALTONEN	10E CDF	≥ 6 jets, vtx b -tag
7.8 \pm 2.4 \pm 1.6 \pm 0.5	15 AALTONEN	10V CDF	$\ell + \geq 3$ jets, soft- e b -tag
7.70 \pm 0.52	16 AALTONEN	10W CDF	$\ell + \cancel{E}_T + \geq 3$ jets + b -tag, norm. to $\sigma(Z \rightarrow \ell\ell)_{TH}$
6.9 \pm 2.0	17 ABAZOV	10I D0	≥ 6 jets with 2 b -tags
6.9 \pm 1.2 $^{+0.8}_{-0.7}$ \pm 0.4	18 ABAZOV	10Q D0	τ_h + jets
9.6 \pm 1.2 $^{+0.6}_{-0.5}$ \pm 0.6	19 AALTONEN	09AD CDF	$\ell\ell + \cancel{E}_T$ / vtx b -tag
9.1 \pm 1.1 $^{+1.0}_{-0.9}$ \pm 0.6	20 AALTONEN	09H CDF	$\ell + \geq 3$ jets + \cancel{E}_T / soft μ b -tag
8.18 \pm 0.98 $_{-0.87}$	21 ABAZOV	09AG D0	$\ell + \text{jets}, \ell\ell$ and $\ell\tau + \text{jets}$
7.5 \pm 1.0 $^{+0.7}_{-0.6}$ $^{+0.6}_{-0.5}$	22 ABAZOV	09R D0	$\ell\ell$ and $\ell\tau + \text{jets}$
8.18 \pm 0.90 $_{-0.84}$ \pm 0.50	23 ABAZOV	08M D0	$\ell + n$ jets with 0,1,2 b -tag
7.62 \pm 0.85	24 ABAZOV	08N D0	$\ell + n$ jets + b -tag or kinematics
8.5 \pm 2.7 $_{-2.2}$	25 ABULENCIA	08 CDF	$\ell^+ \ell^-$ ($\ell = e, \mu$)
8.3 \pm 1.0 $^{+2.0}_{-1.5}$ \pm 0.5	26 AALTONEN	07D CDF	≥ 6 jets, vtx b -tag
7.4 \pm 1.4 \pm 1.0	27 ABAZOV	07O D0	$\ell\ell + \text{jets}, \text{vtx } b$ -tag
4.5 $^{+2.0}_{-1.9}$ $^{+1.4}_{-1.1}$ \pm 0.3	28 ABAZOV	07P D0	≥ 6 jets, vtx b -tag
6.4 $^{+1.3}_{-1.2}$ \pm 0.7 \pm 0.4	29 ABAZOV	07R D0	$\ell + \geq 4$ jets
6.6 \pm 0.9 \pm 0.4	30 ABAZOV	06X D0	$\ell + \text{jets}, \text{vtx } b$ -tag
8.7 \pm 0.9 $^{+1.1}_{-0.9}$	31 ABULENCIA	06Z CDF	$\ell + \text{jets}, \text{vtx } b$ -tag
5.8 \pm 1.2 $^{+0.9}_{-0.7}$	32 ABULENCIA,A	06C CDF	missing E_T + jets, vtx b -tag
7.5 \pm 2.1 $^{+3.3}_{-2.2}$ $^{+0.5}_{-0.4}$	33 ABULENCIA,A	06E CDF	6–8 jets, b -tag
8.9 \pm 1.0 $^{+1.1}_{-1.0}$	34 ABULENCIA,A	06F CDF	$\ell + \geq 3$ jets, b -tag
8.6 $^{+1.6}_{-1.5}$ \pm 0.6	35 ABAZOV	05Q D0	$\ell + n$ jets
8.6 $^{+3.2}_{-2.7}$ \pm 1.1 \pm 0.6	36 ABAZOV	05R D0	di-lepton + n jets
6.7 $^{+1.4}_{-1.3}$ $^{+1.6}_{-1.1}$ \pm 0.4	37 ABAZOV	05X D0	$\ell + \text{jets}$ / kinematics
5.3 \pm 3.3 $^{+1.3}_{-1.0}$	38 ACOSTA	05S CDF	$\ell + \text{jets}$ / soft μ b -tag
6.6 \pm 1.1 \pm 1.5	39 ACOSTA	05T CDF	$\ell + \text{jets}$ / kinematics
6.0 $^{+1.5}_{-1.6}$ $^{+1.2}_{-1.3}$	40 ACOSTA	05U CDF	$\ell + \text{jets}/\text{kinematics} + \text{vtx } b$ -tag
5.6 $^{+1.2}_{-1.1}$ $^{+0.9}_{-0.6}$	41 ACOSTA	05V CDF	$\ell + n$ jets
7.0 $^{+2.4}_{-2.1}$ $^{+1.6}_{-1.1}$ \pm 0.4	42 ACOSTA	04I CDF	di-lepton + jets + missing ET

1 ABAZOV 16F based on 9.7 fb $^{-1}$ of data. The result is for $m_t = 172.5$ GeV, and the m_t dependence is shown in Table V and Fig. 9. The result agrees with the NNLO+NNLL SM prediction of 7.35 $^{+0.23}_{-0.27}$ pb.

2 Based on 9 fb $^{-1}$ of data. The measurement is in the channel $t\bar{t} \rightarrow (b\bar{b})\ell(\nu\tau)$, where τ decays into hadrons (τ_h), and ℓ (e or μ) include ℓ from τ decays (τ_ℓ). The result is for $m_t = 173$ GeV.

3 Based on 8.8 fb $^{-1}$ of data. Combination of CDF and D0 measurements given, respectively, by $\sigma(t\bar{t}; \text{CDF}) = 7.63 \pm 0.31 \pm 0.36 \pm 0.16$ pb, $\sigma(t\bar{t}; \text{D0}) = 7.56 \pm 0.20 \pm 0.32 \pm 0.46$ pb. All the results are for $m_t = 172.5$ GeV. The m_t dependence of the mean value is parametrized in eq. (1) and shown in Fig. 2.

4 Based on 9.7 fb $^{-1}$ of data. Differential cross sections with respect to $m_{t\bar{t}}$, $|y(\text{top})|$, $E_T(\text{top})$ are shown in Figs. 9, 10, 11, respectively, and are compared to the predictions of MC models.

5 Based on 8.8 fb $^{-1}$ of p \bar{p} collisions at $\sqrt{s} = 1.96$ TeV.

6 Based on 8.7 fb $^{-1}$ of p \bar{p} collisions at $\sqrt{s} = 1.96$ TeV. Measure the $t\bar{t}$ cross section simultaneously with the fraction of $t \rightarrow Wb$ decays. The correlation coefficient between those two measurements is -0.434 . Assume unitarity of the 3 \times 3 CKM matrix and set $|V_{tb}| > 0.89$ at 95% CL.

7 Based on 2.2 fb $^{-1}$ of data in p \bar{p} collisions at 1.96 TeV. The result assumes the acceptance for $m_t = 172.5$ GeV.

8 Based on 1.12 fb $^{-1}$ and assumes $m_t = 175$ GeV, where the cross section changes by ± 0.1 pb for every ∓ 1 GeV shift in m_t . AALTONEN 11D fits simultaneously the $t\bar{t}$

production cross section and the b -tagging efficiency and find improvements in both measurements.

9 Based on 2.7 fb $^{-1}$. The first error is from statistics and systematics, the second is from luminosity. The result is for $m_t = 175$ GeV. AALTONEN 11W fits simultaneously a jet flavor discriminator between b -, c -, and light-quarks, and find significant reduction in the systematic error.

10 Based on 2.2 fb $^{-1}$. The result is for $m_t = 172.5$ GeV. AALTONEN 11Y selects multi-jet events with large \cancel{E}_T , and vetoes identified electrons and muons.

11 Based on 5.3 fb $^{-1}$. The error is statistical + systematic + luminosity combined. The result is for $m_t = 172.5$ GeV. The results for other m_t values are given in Table XII and eq.(10) of ABAZOV 11E.

12 Combination of dilepton measurement presented in ABAZOV 11Z (based on 5.4 fb $^{-1}$), which yields 7.36 $^{+0.90}_{-0.79}$ (stat+syst) pb, and the lepton + jets measurement of ABAZOV 11E. The result is for $m_t = 172.5$ GeV. The results for other m_t values is given by eq.(5) of ABAZOV 11A.

13 Based on 2.8 fb $^{-1}$. The result is for $m_t = 175$ GeV.

14 Based on 2.9 fb $^{-1}$. Result is obtained from the fraction of signal events in the top quark mass measurement in the all hadronic decay channel.

15 Based on 1.7 fb $^{-1}$. The result is for $m_t = 175$ GeV. AALTONEN 10V uses soft electrons from b -hadron decays to suppress W +jets background events.

16 Based on 4.6 fb $^{-1}$. The result is for $m_t = 172.5$ GeV. The ratio $\sigma(t\bar{t} \rightarrow \ell + \text{jets}) / \sigma(Z/\gamma^* \rightarrow \ell\ell)$ is measured and then multiplied by the theoretical $Z/\gamma^* \rightarrow \ell\ell$ cross section of $\sigma(Z/\gamma^* \rightarrow \ell\ell) = 251.3 \pm 5.0$ pb, which is free from the luminosity error.

17 Based on 1 fb $^{-1}$. The result is for $m_t = 175$ GeV. 7.9 \pm 2.3 pb is found for $m_t = 170$ GeV. ABAZOV 10I uses a likelihood discriminant to separate signal from background, where the background model was created from lower jet-multiplicity data.

18 Based on 1 fb $^{-1}$. The result is for $m_t = 170$ GeV. For $m_t = 175$ GeV, the result is 6.3 $^{+1.2}_{-1.1}$ (stat) \pm 0.7(syst) \pm 0.4(lumi) pb. Cross section of $t\bar{t}$ production has been measured in the $t\bar{t} \rightarrow \tau_h + \text{jets}$ topology, where τ_h denotes hadronically decaying τ leptons. The result for the cross section times the branching ratio is $\sigma(t\bar{t} \rightarrow \tau_h + \text{jets}) = 0.60^{+0.23+0.15}_{-0.22-0.14} \pm 0.04$ pb for $m_t = 170$ GeV.

19 Based on 1.1 fb $^{-1}$. The result is for $B(W \rightarrow \ell\nu) = 10.8\%$ and $m_t = 175$ GeV; the mean value is 9.8 for $m_t = 172.5$ GeV and 10.1 for $m_t = 170$ GeV. AALTONEN 09AD used high p_T e or μ with an isolated track to select $t\bar{t}$ decays into dileptons including $\ell = \tau$. The result is based on the candidate event samples with and without vertex b -tag.

20 Based on 2 fb $^{-1}$. The result is for $m_t = 175$ GeV; the mean value is 3% higher for $m_t = 170$ GeV and 4% lower for $m_t = 180$ GeV.

21 Result is based on 1 fb $^{-1}$ of data. The result is for $m_t = 170$ GeV, and the mean value decreases with increasing m_t ; see their Fig. 2. The result is obtained after combining $\ell + \text{jets}, \ell\ell$, and $\ell\tau$ final states, and the ratios of the extracted cross sections are $R^{\ell\ell/\ell j} = 0.86^{+0.19}_{-0.17}$ and $R^{\ell\tau/\ell\ell - \ell j} = 0.97^{+0.32}_{-0.29}$, consistent with the SM expectation of $R = 1$. This leads to the upper bound of $B(t \rightarrow bH^+)$ as a function of m_{H^+} . Results are shown in their Fig. 1 for $B(H^+ \rightarrow \tau\nu) = 1$ and $B(H^+ \rightarrow c\bar{s}) = 1$ cases. Comparison of the m_t dependence of the extracted cross section and a partial NNLO prediction gives $m_t = 169.1^{+5.9}_{-5.2}$ GeV.

22 Result is based on 1 fb $^{-1}$ of data. The result is for $m_t = 170$ GeV, and the mean value changes by $-0.07 [m_t(\text{GeV}) - 170]$ pb near the reference m_t value. Comparison of the m_t dependence of the extracted cross section and a partial NNLO QCD prediction gives $m_t = 171.5^{+9.9}_{-8.8}$ GeV. The $\ell\tau$ channel alone gives 7.6 $^{+4.9+3.5+1.4}_{-4.3-3.4-0.9}$ pb and the $\ell\ell$ channel gives 7.5 $^{+1.2+0.7+0.7}_{-1.1-0.6-0.5}$ pb.

23 Result is based on 0.9 fb $^{-1}$ of data. The first error is from stat + syst, while the latter error is from luminosity. The result is for $m_t = 175$ GeV, and the mean value changes by $-0.09 \text{ pb} \cdot [m_t(\text{GeV}) - 175]$.

24 Result is based on 0.9 fb $^{-1}$ of data. The cross section is obtained from the $\ell + \geq 3$ jet event rates with 1 or 2 b -tag, and also from the kinematical likelihood analysis of the $\ell + 3, 4$ jet events. The result is for $m_t = 172.6$ GeV, and its m_t dependence shown in Fig. 3 leads to the constraint $m_t = 170 \pm 7$ GeV when compared to the SM prediction.

25 Result is based on 360 pb $^{-1}$ of data. Events with high p_T oppositely charged dileptons $\ell^+ \ell^-$ ($\ell = e, \mu$) are used to obtain cross sections for $t\bar{t}, W^+W^-$, and $Z \rightarrow \tau^+\tau^-$ production processes simultaneously. The other cross sections are given in Table IV.

26 Based on 1.02 fb $^{-1}$ of data. Result is for $m_t = 175$ GeV. Secondary vertex b -tag and neural network selections are used to achieve a signal-to-background ratio of about 1/2.

27 Based on 425 pb $^{-1}$ of data. Result is for $m_t = 175$ GeV. For $m_t = 170.9$ GeV, 7.8 \pm 1.8(stat + syst) pb is obtained.

28 Based on 405 \pm 25 pb $^{-1}$ of data. Result is for $m_t = 175$ GeV. The last error is for luminosity. Secondary vertex b -tag and neural network are used to separate the signal events from the background.

29 Based on 425 pb $^{-1}$ of data. Assumes $m_t = 175$ GeV.

30 Based on ~ 425 pb $^{-1}$. Assuming $m_t = 175$ GeV. The first error is combined statistical and systematic, the second one is luminosity.

31 Based on ~ 318 pb $^{-1}$. Assuming $m_t = 178$ GeV. The cross section changes by ± 0.08 pb for each \mp GeV change in the assumed m_t . Result is for at least one b -tag. For at least two b -tagged jets, $t\bar{t}$ signal of significance greater than 5 σ is found, and the cross section is 10.1 $^{+1.6+2.0}_{-1.4-1.3}$ pb for $m_t = 178$ GeV.

32 Based on ~ 311 pb $^{-1}$. Assuming $m_t = 178$ GeV. For $m_t = 175$ GeV, the result is 6.0 \pm 1.2 $^{+0.9}_{-0.7}$. This is the first CDF measurement without lepton identification, and hence it has sensitivity to the $W \rightarrow \tau\nu$ mode.

33 ABULENCIA,A 06E measures the $t\bar{t}$ production cross section in the all hadronic decay mode by selecting events with 6 to 8 jets and at least one b -jet. $S/B = 1/5$ has been achieved. Based on 311 pb $^{-1}$. Assuming $m_t = 178$ GeV.

34 Based on ~ 318 pb $^{-1}$. Assuming $m_t = 178$ GeV. Result is for at least one b -tag. For at least two b -tagged jets, the cross section is 11.1 $^{+2.3+2.5}_{-1.9-1.9}$ pb.

35 ABAZOV 05Q measures the top-quark pair production cross section with ~ 230 pb $^{-1}$ of data, based on the analysis of W plus n -jet events where W decays into e or μ plus neutrino, and at least one of the jets is b -jet like. The first error is statistical and systematic, and the second accounts for the luminosity uncertainty. The result assumes

Quark Particle Listings

t

- $m_t = 175$ GeV; the mean value changes by $(175 - m_t(\text{GeV})) \times 0.06$ pb in the mass range 160 to 190 GeV.
- ³⁶ ABZOV 05R measures the top-quark pair production cross section with 224–243 pb⁻¹ of data, based on the analysis of events with two charged leptons in the final state. The result assumes $m_t = 175$ GeV; the mean value changes by $(175 - m_t(\text{GeV})) \times 0.08$ pb in the mass range 160 to 190 GeV.
- ³⁷ Based on 230 pb⁻¹. Assuming $m_t = 175$ GeV.
- ³⁸ Based on 194 pb⁻¹. Assuming $m_t = 175$ GeV.
- ³⁹ Based on 194 ± 11 pb⁻¹. Assuming $m_t = 175$ GeV.
- ⁴⁰ Based on 162 ± 10 pb⁻¹. Assuming $m_t = 175$ GeV.
- ⁴¹ ACOSTA 05V measures the top-quark pair production cross section with ~ 162 pb⁻¹ data, based on the analysis of *W* plus *n*-jet events where *W* decays into *e* or μ plus neutrino, and at least one of the jets is *b*-jet like. Assumes $m_t = 175$ GeV.
- ⁴² ACOSTA 04I measures the top-quark pair production cross section with 197 ± 12 pb⁻¹ data, based on the analysis of events with two charged leptons in the final state. Assumes $m_t = 175$ GeV.

Ratio of the Production Cross Sections of $t\bar{t}\gamma$ to $t\bar{t}$ at $\sqrt{s} = 1.96$ TeV

VALUE	DOCUMENT ID	TECN	COMMENT
0.024 ± 0.009	¹ AALTONEN	11z CDF	$E_{T(\gamma)} > 10$ GeV, $ \eta(\gamma) < 1.0$

• • • We do not use the following data for averages, fits, limits, etc. • • •

¹ Based on 6.0 fb⁻¹ of data. The error is statistical and systematic combined. Events with lepton + $\cancel{E}_T + \geq 3$ jets ($\geq 1b$) with and without central, high E_T photon are measured. The result is consistent with the SM prediction of 0.024 ± 0.005. The absolute production cross section is measured to be 0.18 ± 0.08 fb. The statistical significance is 3.0 standard deviations.

t *t* Production Cross Section in *pp* Collisions at $\sqrt{s} = 7$ TeV

VALUE (pb)	CL%	DOCUMENT ID	TECN	COMMENT
< 1.7	95	¹ AAD	12BE ATLS	$\ell^+ \ell^+ + \cancel{E}_T + \geq 2j + HT$

• • • We do not use the following data for averages, fits, limits, etc. • • •

¹ Based on 1.04 fb⁻¹ of *pp* data at $\sqrt{s} = 7$ TeV. The upper bounds are the same for LL, LR and RR chiral components of the two top quarks.

$t\bar{t}$ Production Cross Section in *pp* Collisions at $\sqrt{s} = 5.02$ TeV

Unless otherwise noted the first quoted error is from statistics, the second from systematic uncertainties, and the third from luminosity. If only two errors are quoted the luminosity is included in the systematic uncertainties.

VALUE (pb)	DOCUMENT ID	TECN	COMMENT
69.5 ± 6.1 ± 5.6 ± 1.6	¹ SIRUNYAN	18AQ CMS	$\ell + \text{jets}, \ell\ell + \text{jets}$

• • • We do not use the following data for averages, fits, limits, etc. • • •

¹ SIRUNYAN 18AQ based on 27.4 pb⁻¹ of data from *pp* collisions at $\sqrt{s} = 5.02$ TeV. The result is in agreement with the NNLO SM prediction $68.9_{-2.3}^{+1.9}(\text{scale}) \pm 2.3(\text{PDF}) \pm 1.4(\alpha_s)$ pb.

$t\bar{t}$ Production Cross Section in *pp* Collisions at $\sqrt{s} = 7$ TeV

Unless otherwise noted the first quoted error is from statistics, the second from systematic uncertainties, and the third from luminosity. If only two errors are quoted the luminosity is included in the systematic uncertainties.

VALUE (pb)	DOCUMENT ID	TECN	COMMENT
161.7 ± 6.0 ± 12.0 ± 3.6	¹ KHACHATRYAN...17B	CMS	$\ell + \cancel{E}_T + \geq 4j (\geq 1b)$
173.6 ± 2.1 ± 4.5 ± 3.8	² KHACHATRYAN...16AW	CMS	$e + \mu + \cancel{E}_T + \geq 0j$
181.2 ± 2.8 ± 10.8 ± 10.6	³ AAD	15B0 ATLS	$e + \mu + \cancel{E}_T + \geq 0j$
178 ± 3 ± 16 ± 3	⁴ AAD	15CC ATLS	$\ell + \text{jets}, \ell\ell + \text{jets}, \ell\tau_h + \text{jets}$
	⁵ AAIJ	15R LHCB	$\mu + \geq 1j(b\text{-tag})$ forward region
182.9 ± 3.1 ± 6.4	⁶ AAD	14AY ATLS	$e + \mu + 1$ or $2b$ jets
194 ± 18 ± 46	⁷ AAD	13X ATLS	$\tau_h + \cancel{E}_T + \geq 5j (\geq 2b)$
139 ± 10 ± 26	⁸ CHATRCHYAN13AY	CMS	≥ 6 jets with $2 b\text{-tags}$
158.1 ± 2.1 ± 10.8	⁹ CHATRCHYAN13BB	CMS	$\ell + \cancel{E}_T + \text{jets} (\geq 1 b\text{-tag})$
152 ± 12 ± 32	¹⁰ CHATRCHYAN13BE	CMS	$\tau_h + \cancel{E}_T + \geq 4 \text{ jets} (\geq 1 b)$
177 ± 20 ± 14 ± 7	¹¹ AAD	12B ATLS	Repl. by AAD 12BF
176 ± 5 ± 14 ± 11 ± 8	¹² AAD	12BF ATLS	$\ell\ell + \cancel{E}_T + \geq 2j$
187 ± 11 ± 18 ± 17 ± 6	¹³ AAD	12B0 ATLS	$\ell + \cancel{E}_T + \geq 3j$ with <i>b</i> -tag
186 ± 13 ± 20 ± 7	¹⁴ AAD	12CG ATLS	$\ell + \tau_h + \cancel{E}_T + \geq 2j (\geq 1b)$
143 ± 14 ± 22 ± 3	¹⁵ CHATRCHYAN12AC	CMS	$\ell + \tau_h + \cancel{E}_T + \geq 2j (\geq 1b)$
161.9 ± 2.5 ± 5.1 ± 5.0 ± 3.6	¹⁶ CHATRCHYAN12AX	CMS	$\ell\ell + \cancel{E}_T + \geq 2b$
145 ± 31 ± 42 ± 27	¹⁷ AAD	11A ATLS	$\ell + \cancel{E}_T + \geq 4j, \ell\ell + \cancel{E}_T + \geq 2j$
173 ± 39 ± 32 ± 7	¹⁸ CHATRCHYAN11AA	CMS	$\ell + \cancel{E}_T + \geq 3 \text{ jets}$
168 ± 18 ± 14 ± 7	¹⁹ CHATRCHYAN11F	CMS	$\ell\ell + \cancel{E}_T + \text{jets}$
154 ± 17 ± 6	²⁰ CHATRCHYAN11Z	CMS	Combination
194 ± 72 ± 24 ± 21	²¹ KHACHATRYAN...11A	CMS	$\ell\ell + \cancel{E}_T + \geq 2 \text{ jets}$

- ¹ KHACHATRYAN 17B based on 5.0 fb⁻¹ of data, using a binned likelihood fit of templates to the data. Also the ratio $\sigma(t\bar{t}; 8 \text{ TeV})/\sigma(t\bar{t}; 7 \text{ TeV}) = 1.43 \pm 0.04 \pm 0.07 \pm 0.05$ is reported. The results are in agreement with NNLO SM predictions.
- ² KHACHATRYAN 16AW based on 5.0 fb⁻¹ of data, using a binned likelihood fit to differential distributions of *b*-tagged and non-*b*-tagged jets. The result is in good agreement with NNLO SM predictions.
- ³ Based on 4.6 fb⁻¹ of data. Uses a template fit to distributions of \cancel{E}_T and jet multiplicities to measure simultaneously $t\bar{t}$, *WW*, and $Z/\gamma^* \rightarrow \tau\tau$ cross sections, assuming $m_t = 172.5$ GeV.

- ⁴ AAD 15CC based on 4.6 fb⁻¹ of data. The event selection criteria are optimized for the $\ell\tau_h + \text{jets}$ channel. Using only this channel $183 \pm 9 \pm 23 \pm 3$ pb is derived for the cross section.
- ⁵ AAIJ 15R, based on 1.0 fb⁻¹ of data, reports $0.239 \pm 0.053 \pm 0.033 \pm 0.024$ pb cross section for the forward fiducial region $p_T(\mu) > 25$ GeV, $2.0 < \eta(\mu) < 4.5$, $50 \text{ GeV} < p_T(b) < 100$ GeV, $2.2 < \eta(b) < 4.2$, $\Delta R(\mu, b) > 0.5$, and $p_T(\mu+b) > 20$ GeV. The three errors are from statistics, systematics, and theory. The result agrees with the SM NLO prediction.
- ⁶ AAD 14AY reports $182.9 \pm 3.1 \pm 4.2 \pm 3.6 \pm 3.3$ pb value based on 4.6 fb⁻¹ of data. The four errors are from statistics, systematic, luminosity, and the 0.66% beam energy uncertainty. We have combined the systematic uncertainties in quadrature. The result is for $m_t = 172.5$ GeV; for other m_t , $\sigma(m_t) = \sigma(172.5 \text{ GeV}) \times [1 - 0.0028 \times (m_t - 172.5 \text{ GeV})]$. The result is consistent with the SM prediction at NNLO.
- ⁷ Based on 1.67 fb⁻¹ of data. The result uses the acceptance for $m_t = 172.5$ GeV.
- ⁸ Based on 3.54 fb⁻¹ of data.
- ⁹ Based on 2.3 fb⁻¹ of data.
- ¹⁰ Based on 3.9 fb⁻¹ of data.
- ¹¹ Based on 35 pb⁻¹ of data for an assumed top quark mass of $m_t = 172.5$ GeV.
- ¹² Based on 0.70 fb⁻¹ of data. The 3 errors are from statistics, systematics, and luminosity. The result uses the acceptance for $m_t = 172.5$ GeV.
- ¹³ Based on 35 pb⁻¹ of data. The 3 errors are from statistics, systematics, and luminosity. The result uses the acceptance for $m_t = 172.5$ GeV and $173 \pm 17_{-16}^{+18} \pm 6$ pb is found without the *b*-tag.
- ¹⁴ Based on 2.05 fb⁻¹ of data. The hadronic τ candidates are selected using a BDT technique. The 3 errors are from statistics, systematics, and luminosity. The result uses the acceptance for $m_t = 172.5$ GeV.
- ¹⁵ Based on 2.0 fb⁻¹ and 2.2 fb⁻¹ of data for $\ell = e$ and $\ell = \mu$, respectively. The 3 errors are from statistics, systematics, and luminosity. The result uses the acceptance for $m_t = 172.5$ GeV.
- ¹⁶ Based on 2.3 fb⁻¹ of data. The 3 errors are from statistics, systematics, and luminosity. The result uses the profile likelihood-ratio (PLB) method and an assumed m_t of 172.5 GeV.
- ¹⁷ Based on 2.9 pb⁻¹ of data. The result for single lepton channels is $142 \pm 34_{-31}^{+50}$ pb, while for the dilepton channels is $151 \pm 78_{-62}^{+37} \pm 24$ pb.
- ¹⁸ Result is based on 36 pb⁻¹ of data. The first uncertainty corresponds to the statistical and systematic uncertainties, and the second corresponds to the luminosity.
- ¹⁹ Based on 33 pb⁻¹ of data. The ratio of $t\bar{t}$ and Z/γ^* cross sections is measured as $\sigma(pp \rightarrow t\bar{t})/\sigma(pp \rightarrow Z/\gamma^* \rightarrow e^+e^-/\mu^+\mu^-) = 0.175 \pm 0.018(\text{stat}) \pm 0.015(\text{syst})$ for $60 < m_{\ell\ell} < 120$ GeV, for which they use an NNLO prediction for the denominator cross section of 972 ± 42 pb.
- ²⁰ Result is based on 36 pb⁻¹ of data. The first error is from statistical and systematic uncertainties, and the second from luminosity. This is a combination of a measurement in the dilepton channel (CHATRCHYAN 11F) and the measurement in the $\ell + \text{jets}$ channel (CHATRCHYAN 11Z) which yields $150 \pm 9 \pm 17 \pm 6$ pb.
- ²¹ Result is based on 3.1 ± 0.3 pb⁻¹ of data.

$t\bar{t}$ Production Cross Section in *pp* Collisions at $\sqrt{s} = 8$ TeV

Unless otherwise noted the first quoted error is from statistics, the second from systematic uncertainties, and the third from luminosity. If only two errors are quoted the luminosity is included in the systematic uncertainties.

VALUE (pb)	DOCUMENT ID	TECN	COMMENT
248.3 ± 0.7 ± 13.4 ± 4.7	¹ AABOUD	18BH ATLS	$\ell + \cancel{E}_T + \geq 4j (\geq 1b)$
239 ± 4 ± 28 ± 5	² AABOUD	17Z ATLS	$\tau_h + \cancel{E}_T + \geq 2j (\geq 2b)$
228.5 ± 3.8 ± 13.7 ± 6.0	³ KHACHATRYAN...17B	CMS	$\ell + \cancel{E}_T + \geq 4j (\geq 1b)$
242.9 ± 1.7 ± 8.6	⁴ AAD	16BK ATLS	$e + \mu + 1$ or $2b$ jets
244.9 ± 1.4 ± 6.3 ± 6.4	⁵ KHACHATRYAN...16AW	CMS	$e + \mu + \cancel{E}_T + \geq 0j$
275.6 ± 6.1 ± 37.8 ± 7.2	⁶ KHACHATRYAN...16BC	CMS	$\geq 6j (\geq 2b)$
260 ± 1 ± 24 ± 25	⁷ AAD	15BP ATLS	$\ell + \cancel{E}_T + \geq 3j (\geq 1b)$
242.4 ± 1.7 ± 10.2	⁸ AAIJ	15R LHCB	$\mu + \geq 1j(b\text{-tag})$ forward region
239 ± 2 ± 11 ± 6	⁹ AAD	14AY ATLS	$e + \mu + 1$ or $2b$ jets
257 ± 3 ± 24 ± 7	¹⁰ CHATRCHYAN14F	CMS	$\ell\ell + \cancel{E}_T + \geq 2j (\geq 1 b\text{-tag})$
	¹¹ KHACHATRYAN...14S	CMS	$\ell + \tau_h + \cancel{E}_T + \geq 2j (\geq 1b)$

- ¹ AABOUD 18BH based on 20.2 fb⁻¹ of data. The result is for $m_t = 172.5$ GeV. To reduce effects of uncertainties in the jet energy scale and *b*-tagging efficiency, they are included as nuisance parameters in the fit of discriminant distributions, after separating selected events into three regions. Furthermore the $W + \text{jets}$ background distribution is modelled using $Z + \text{jets}$ event data.
- ² AABOUD 17Z based on 20.2 fb⁻¹ of data, using the mode $t\bar{t} \rightarrow \tau\nu q^* \bar{q} b \bar{b}$ with τ decaying hadronically. Single prong and 3 prong decays of τ are separately analyzed. The result is consistent with the SM. The third quoted uncertainty is due to luminosity.
- ³ KHACHATRYAN 17B based on 19.6 fb⁻¹ of data, using a binned likelihood fit of templates to the data. Also the ratio $\sigma(t\bar{t}; 8 \text{ TeV})/\sigma(t\bar{t}; 7 \text{ TeV}) = 1.43 \pm 0.04 \pm 0.07 \pm 0.05$ is reported. The results are in agreement with NNLO SM predictions.
- ⁴ AAD 16BK is an update of the value from AAD 14AY using the improved luminosity calibration. The value $242.9 \pm 1.7 \pm 5.5 \pm 5.1 \pm 4.2$ pb is reported, where we have combined the systematic uncertainties in quadrature. Also the ratio $\sigma(t\bar{t}; 8 \text{ TeV})/\sigma(t\bar{t}; 7 \text{ TeV}) = 1.328 \pm 0.024 \pm 0.015 \pm 0.038 \pm 0.001$ has been updated. The former result is consistent with the SM predictions at NNLO, while the latter result is 2.1 σ below the expectation.
- ⁵ KHACHATRYAN 16AW based on 19.7 fb⁻¹ of data, using a binned likelihood fit to differential distributions of *b*-tagged and non-*b*-tagged jets. The result is in good agreement with NNLO SM predictions.
- ⁶ KHACHATRYAN 16BC based on 18.4 fb⁻¹ of data. The last uncertainty is due to luminosity. Cuts on kinematical fit probability and $\Delta R(b, b)$ are imposed. The major QCD background is determined from the data. The result is for $m_t = 172.5$ GeV and in agreement with the SM prediction. The top quark p_T spectra, also measured, are significantly softer than theoretical predictions.
- ⁷ AAD 15BP based on 20.3 fb⁻¹ of data. The result is for $m_t = 172.5$ GeV and in agreement with the SM prediction 253_{-15}^{+13} pb at NNLO+NNLL. Superseded by AABOUD 18BH.

⁸ AAIJ 15R, based on 2.0 fb⁻¹ of data, reports 0.289 ± 0.043 ± 0.040 ± 0.029 pb cross section for the forward fiducial region $p_T(\mu) > 25$ GeV, $2.0 < \eta(\mu) < 4.5$, 50 GeV < $p_T(b) < 100$ GeV, $2.2 < \eta(b) < 4.2$, $\Delta R(\mu, b) > 0.5$, and $p_T(\mu+b) > 20$ GeV. The three errors are from statistics, systematics, and theory. The result agrees with the SM NLO prediction.

⁹ AAD 14AY reports 242.4 ± 1.7 ± 5.5 ± 7.5 ± 4.2 pb value based on 20.3 fb⁻¹ of data. The four errors are from statistics, systematic, luminosity, and the 0.66% beam energy uncertainty. We have combined the systematic uncertainties in quadrature. The result is for $m_t = 172.5$ GeV; for other m_t , $\sigma(m_t) = \sigma(172.5 \text{ GeV}) \times [1 - 0.0028 \times (m_t - 172.5 \text{ GeV})]$. Also measured is the ratio $\sigma(t\bar{t}; 8 \text{ TeV})/\sigma(t\bar{t}; 7 \text{ TeV}) = 1.326 \pm 0.024 \pm 0.015 \pm 0.049 \pm 0.001$. The results are consistent with the SM predictions at NNLO.

¹⁰ Based on 5.3 fb⁻¹ of data. The result is for $m_t = 172.5$ GeV, and a parametrization is given in eq.(6.1) for the mean value at other m_t values. The result is in agreement with the SM prediction 252.9^{+6.4}_{-8.6} pb at NNLO.

¹¹ Based on 19.6 fb⁻¹ of data. The measurement is in the channel $t\bar{t} \rightarrow (b\ell\nu)(b\tau\nu)$, where τ decays into hadrons (τ_h). The result is for $m_t = 172.5$ GeV. For $m_t = 173.3$ GeV, the cross section is lower by 3.1 pb.

$t\bar{t}$ Production Cross Section in pp Collisions at $\sqrt{s} = 13$ TeV

VALUE (pb)	DOCUMENT ID	TECN	COMMENT
•••	We do not use the following data for averages, fits, limits, etc. •••		
803 ± 2 ± 25 ± 20	¹ SIRUNYAN 19AR CMS	19AR	dilepton channel ($e\mu, 2e, 2\mu$)
	² SIRUNYAN 19P CMS	19P	dilepton channel
815 ± 9 ± 38 ± 19	³ KHACHATRYAN...17N CMS	17N	$e\mu + \geq 2j$ ($\geq 1b$)
888 ± 2 ⁺²⁶ ₋₂₈ ± 20	⁴ SIRUNYAN 17W CMS	17W	$\ell + \geq 1j$
818 ± 8 ± 35	⁵ AABOUD 16R ATLS	16R	$e + \mu + 1$ or $2b$ jets
746 ± 5 ± 8 ± 53 ± 36	⁶ KHACHATRYAN...16j CMS	16j	$e + \mu + \geq 2j$

¹ SIRUNYAN 19AR based on 35.9 fb⁻¹ of data. Obtained from the visible cross section measured using a template fit to multidifferential distributions categorized according to the b -tagged jet multiplicity. The result is for $m_t = 172.5$ GeV and in agreement with the SM prediction at NNLO+NNLL.

² SIRUNYAN 19P reports differential $t\bar{t}$ cross sections measured using dilepton events at 13 TeV with 35.9 fb⁻¹ and compared to NLO predictions.

³ KHACHATRYAN 17N based on 2.2 fb⁻¹ of data. The last quoted uncertainty is due to the beam luminosity. This measurement supersedes that of KHACHATRYAN 16j.

⁴ SIRUNYAN 17W based on 2.2 fb⁻¹ of pp data at $\sqrt{s} = 13$ TeV. Events are categorized according to the jet multiplicity and the number of b -tagged jets. A likelihood fit is performed to the event distributions to compare to the NNLO+NNLL prediction.

⁵ AABOUD 16R reported value 818 ± 8 ± 27 ± 19 ± 12 pb based on 3.2 fb⁻¹ of data. The four errors are from statistics, systematic, luminosity, and beam energy. We have combined the systematic uncertainties in quadrature. The result is in agreement with the SM prediction 832⁺⁴⁰₋₄₆ pb at NNLO+NNLL for $m_t = 172.5$ GeV.

⁶ KHACHATRYAN 16j based on 4.3 pb⁻¹ of data. The last uncertainty is due to luminosity. The result is for $m_t = 172.5$ GeV and in agreement with the SM prediction 832⁺⁴⁰₋₄₆ pb at NNLO+NNLL.

$t\bar{t} t\bar{t}$ Production Cross Section in pp Collisions at $\sqrt{s} = 8$ TeV

VALUE (fb)	CL%	DOCUMENT ID	TECN	COMMENT
•••	We do not use the following data for averages, fits, limits, etc. •••			
<23	95	¹ AAD 15AR ATLS	15AR	$\ell + \ell^+ \ell^- \geq 5j$ ($\geq 2b$)
<70	95	² AAD 15BY ATLS	15BY	$\geq 2\ell + \ell^+ \ell^- + \geq 2j$ ($\geq 1b$)
<32	95	³ KHACHATRYAN...14R CMS	14R	$\ell + \ell^+ \ell^- + \geq 6j$ ($\geq 2b$)

¹ AAD 15AR based on 20.3 fb⁻¹ of data. A fit to H_T distributions in multi-channels classified by the number of jets and of b -tagged jets is performed.

² AAD 15BY based on 20.3 fb⁻¹ of data. A same-sign lepton pair is required. An excess over the SM prediction reaches 2.5 σ for hypotheses involving heavy resonances decaying into $t\bar{t}t\bar{t}$.

³ Based on 19.6 fb⁻¹ of data, using a multivariate analysis to separate signal from backgrounds. About $\sigma(t\bar{t}t\bar{t}) = 1$ fb is expected in the SM.

$t\bar{t} t\bar{t}$ Production Cross Section in pp Collisions at $\sqrt{s} = 13$ TeV

VALUE (fb)	CL%	DOCUMENT ID	TECN	COMMENT
•••	We do not use the following data for averages, fits, limits, etc. •••			
<47	95	¹ AABOUD 19AP ATLS	19AP	$\ell + \ell^+ \ell^-$ channels
<49	95	² AABOUD 19AP ATLS	19AP	combination of ATLAS
13 ⁺¹¹ ₋₉		³ SIRUNYAN 19CN CMS	19CN	combination of CMS
<48	95	⁴ SIRUNYAN 19CN CMS	19CN	$\ell + \text{jets}, \ell^+ \ell^- + \text{jets}$ channels
<69	95	⁵ AABOUD 18CE ATLS	18CE	$\geq 2\ell$ (same sign) + $\ell^+ \ell^- + \geq 1b$
16.9 ^{+13.8} _{-11.4}		⁶ SIRUNYAN 18BU CMS	18BU	$t\bar{t}t\bar{t} \rightarrow$ (same sign 2ℓ or $\geq 3\ell$) + $\geq 4j$ ($\geq 2b$)
<94	95	⁷ SIRUNYAN 17AB CMS	17AB	$\ell + \text{jets}, \ell^+ \ell^- + \text{jets}$ channels
<42	95	⁸ SIRUNYAN 17S CMS	17S	(same sign 2ℓ) + $\ell^+ \ell^- + \geq 2j$

¹ AABOUD 19AP based on 36.1 fb⁻¹ of data. The upper limit corresponds to 5.1 times the NLO SM cross section.

² AABOUD 19AP limit from data combined with AABOUD 18CE. The upper limit corresponds to 5.3 times the NLO SM cross section. Also a limit on the four-top-quark contact interaction of $|C_{4t}|/\Lambda^2 < 1.9 \text{ TeV}^{-2}$ (95% CL) is obtained in an EFT model.

³ SIRUNYAN 19CN based on 35.8 fb⁻¹ of data, combined with SIRUNYAN 18BU. The results are also interpreted in the effective field theory framework.

⁴ SIRUNYAN 19CN based on 35.8 fb⁻¹ of data. A multivariate analysis using global event and jet properties is performed to discriminate from $t\bar{t}$ background.

⁵ AABOUD 18CE based on 36.1 fb⁻¹ of proton-proton data taken at $\sqrt{s} = 13$ TeV. Events including a same-sign lepton pair are used. The result is consistent with the NLO SM cross section of 9.2 fb.

⁶ SIRUNYAN 18BU based on 35.9 fb⁻¹ of proton-proton data taken at $\sqrt{s} = 13$ TeV. Yields from signal regions and control regions defined based on N_{jets}, N_b and N_l are combined in a maximum-likelihood fit. The result is in agreement with the NLO SM prediction 9.2^{+2.9}_{-2.4} fb. The measurement constrains the top quark Yukawa coupling strength parameter to be $|Y_t/Y_t^{SM}| < 2.1$ (95% CL).

⁷ SIRUNYAN 17AB based on 2.6 fb⁻¹ of data. A multivariate analysis is used to discriminate between $t\bar{t}t\bar{t}$ signal and $t\bar{t}$ background. A combination with a previous search (CMS, KHACHATRYAN 16BJ) in the same-sign dilepton channel gives an upper limit of 69 fb (95% CL), corresponding to 7.4 (SM prediction).

⁸ SIRUNYAN 17S based on 35.9 fb⁻¹. The limit is in agreement with the NLO SM prediction 9.2^{+2.9}_{-2.4} fb. Superseded by SIRUNYAN 18BU. The signal events are also used to constrain various new physics models.

$t\bar{t}W$ Production Cross Section in pp Collisions at $\sqrt{s} = 8$ TeV

VALUE (fb)	DOCUMENT ID	TECN	COMMENT
•••	We do not use the following data for averages, fits, limits, etc. •••		
170 ⁺⁹⁰ ₋₈₀ ± 70	¹ KHACHATRYAN...14N CMS	14N	$t\bar{t}W \rightarrow$ same sign dilepton + $\ell^+ \ell^- + \text{jets}$
	¹ Based on 19.5 fb ⁻¹ of data. The result is consistent with the SM prediction of $\sigma(t\bar{t}W) = 206+21-23 fb$.		

$t\bar{t}W$ Production Cross Section in pp Collisions at $\sqrt{s} = 13$ TeV

VALUE (pb)	DOCUMENT ID	TECN	COMMENT
•••	We do not use the following data for averages, fits, limits, etc. •••		
0.87 ± 0.13 ± 0.14	¹ AABOUD 19AR ATLS	19AR	2,3,4 ℓ + $\ell^+ \ell^- + \text{jets}$
0.77 ± 0.12 ± 0.13 -0.11 -0.12	² SIRUNYAN 18BS CMS	18BS	$t\bar{t}W \rightarrow$ same sign dilepton + $\ell^+ \ell^- + \text{jets}$
	¹ AABOUD 19AR based on 35.9 fb ⁻¹ of data. $t\bar{t}W$ and $t\bar{t}Z$ cross sections are simultaneously measured using a combined fit to the events divided into multiple regions. The result is consistent with the SM prediction at NLO 0.60 ^{+0.08} _{-0.07} pb. It is also used to constrain the Wilson coefficients for dimension-six operators which modify the $t\bar{t}Z$ vertex.		
	² Based on 35.9 fb ⁻¹ of proton-proton data taken at $\sqrt{s} = 13$ TeV. The result is consistent with the SM prediction and is used to constrain the Wilson coefficients for dimension-six operators describing new interactions. The result is consistent with the SM prediction at NLO 0.628 ± 0.082 pb.		

$t\bar{t}Z$ Production Cross Section in pp Collisions at $\sqrt{s} = 8$ TeV

VALUE (fb)	DOCUMENT ID	TECN	COMMENT
•••	We do not use the following data for averages, fits, limits, etc. •••		
200 ⁺⁸⁰ ₋₇₀ ± 40 -30	¹ KHACHATRYAN...14N CMS	14N	$t\bar{t}Z \rightarrow 3,4 \ell + \ell^+ \ell^- + \text{jets}$
	¹ Based on 19.5 fb ⁻¹ of data. The result is consistent with the SM prediction of $\sigma(t\bar{t}Z) = 197+22-25 fb$.		

$t\bar{t}Z$ Production Cross Section in pp Collisions at $\sqrt{s} = 13$ TeV

VALUE (pb)	DOCUMENT ID	TECN	COMMENT
•••	We do not use the following data for averages, fits, limits, etc. •••		
0.95 ± 0.08 ± 0.10	¹ AABOUD 19AR ATLS	19AR	2,3,4 ℓ + $\ell^+ \ell^- + \text{jets}$
0.99 ± 0.09 ± 0.12 -0.08 -0.10	² SIRUNYAN 18BS CMS	18BS	$t\bar{t}Z \rightarrow 3,4 \ell + \ell^+ \ell^- + \text{jets}$
	¹ AABOUD 19AR based on 35.9 fb ⁻¹ of data. $t\bar{t}W$ and $t\bar{t}Z$ cross sections are simultaneously measured using a combined fit to the events divided into multiple regions. The result is consistent with the SM prediction at NLO 0.88 ^{+0.09} _{-0.11} pb. It is also used to constrain the Wilson coefficients for dimension-six operators which modify the $t\bar{t}Z$ vertex.		
	² Based on 35.9 fb ⁻¹ of proton-proton data taken at $\sqrt{s} = 13$ TeV. The result is consistent with the SM prediction and is used to constrain the Wilson coefficients for dimension-six operators describing new interactions. The result is consistent with the SM prediction at NLO 0.839 ± 0.101 pb.		

$t\bar{t}\gamma$ Production Cross Section in pp Collisions at $\sqrt{s} = 13$ TeV

VALUE (pb)	DOCUMENT ID	TECN	COMMENT
•••	We do not use the following data for averages, fits, limits, etc. •••		
	¹ AABOUD 19AD ATLS	19AD	$pp \rightarrow t\bar{t}\gamma$
	¹ AABOUD 19AD measured fiducial inclusive and differential cross-sections for $pp \rightarrow t\bar{t}\gamma$ at 13 TeV with 36.1 fb ⁻¹ of data. The results are in agreement with the theoretical predictions.		

$f(Q_0)$: $t\bar{t}$ Fraction of Events with a Veto on Additional Central Jet Activity in pp Collisions at $\sqrt{s} = 7$ TeV

VALUE (%)	DOCUMENT ID	TECN	COMMENT
•••	We do not use the following data for averages, fits, limits, etc. •••		
80.0 ± 1.1 ± 1.6	¹ CHATRCHYAN 14AE CMS	14AE	$Q_0 = 75$ GeV ($ \eta < 2.4$)
92.0 ± 0.7 ± 0.8	¹ CHATRCHYAN 14AE CMS	14AE	$Q_0 = 150$ GeV ($ \eta < 2.4$)
98.0 ± 0.3 ± 0.3	¹ CHATRCHYAN 14AE CMS	14AE	$Q_0 = 300$ GeV ($ \eta < 2.4$)
56.4 ± 1.3 ± 2.6 -2.8	² AAD 12BL ATLS	12BL	$Q_0 = 25$ GeV ($ \eta < 2.1$)
84.7 ± 0.9 ± 1.0	² AAD 12BL ATLS	12BL	$Q_0 = 75$ GeV ($ \eta < 2.1$)
95.2 ^{+0.5} _{-0.6} ± 0.4	² AAD 12BL ATLS	12BL	$Q_0 = 150$ GeV ($ \eta < 2.1$)

¹ CHATRCHYAN 15 based on 5.0 fb⁻¹ of data. The $t\bar{t}$ events are selected in the dilepton and lepton + jets decay channels. For other values of Q_0 see Table 5.

² Based on 2.05 fb⁻¹ of data. The $t\bar{t}$ events are selected in the dilepton decay channel with two identified b -jets.

Quark Particle Listings

t

Fraction of $t\bar{t}$ + multi-jet Events in pp Collisions at $\sqrt{s} = 7$ TeV

VALUE	DOCUMENT ID	TECN	COMMENT
• • •	We do not use the following data for averages, fits, limits, etc. • • •		
0.332 ± 0.090	¹ AAD	15D ATLS	$\ell + \cancel{E}_T + n_j$ ($n=3$ to 8)
0.436 ± 0.098	² CHATRCHYAN14AE	CMS	$t\bar{t}(\ell\ell) + 0$ jet ($E_T > 30$ GeV)
0.232 ± 0.125	² CHATRCHYAN14AE	CMS	$t\bar{t}(\ell\ell) + 1$ jet ($E_T > 30$ GeV)
	² CHATRCHYAN14AE	CMS	$t\bar{t}(\ell\ell) + \geq 2$ jet ($E_T > 30$ GeV)

¹ Based on 4.6 fb⁻¹ of data. Fiducial $t\bar{t}$ production cross section is presented as a function of the jet multiplicity for up to eight jets with the jet p_T threshold of 25, 40, 60, and 80 GeV, and as a function of jet p_T up to the 5th jet. MC models can be discriminated by using data for high jet multiplicity and by p_T distributions of the leading and 5th jet.

² Based on 5.0 fb⁻¹ of data. Events with two oppositely charged leptons, large \cancel{E}_T and jets with at least 1 b -tag are used to measure the fraction of $t\bar{t}$ plus additional jets. The gap fraction ($n=0$ jet rate) as a function of the jet p_T and that of H_T , the scalar sum of the p_T 's of additional jets, is shown in Fig. 8.

$t\bar{t}$ Charge Asymmetry (A_C) in pp Collisions at $\sqrt{s} = 7$ TeV

$A_C = (N(\Delta|y| > 0) - N(\Delta|y| < 0)) / (N(\Delta|y| > 0) + N(\Delta|y| < 0))$ where $\Delta|y| = |y_t| - |y_{\bar{t}}|$ is the difference between the absolute values of the top and antitop rapidities and N is the number of events with $\Delta|y|$ positive or negative.

VALUE (%)	DOCUMENT ID	TECN	COMMENT
• • •	We do not use the following data for averages, fits, limits, etc. • • •		
0.5 ± 0.7 ± 0.6	¹ AABOUD	18AMLHC	ATLAS+CMS combination (lepton + jets)
2.1 ± 2.5 ± 1.7	² AAD	15AJ ATLS	$\ell\ell + \cancel{E}_T + \geq 2j$
0.6 ± 1.0	³ AAD	14I ATLS	$\ell + \cancel{E}_T + \geq 4j$ ($\geq 1b$)
-1.0 ± 1.7 ± 0.8	⁴ CHATRCHYAN14D	CMS	$\ell\ell + \cancel{E}_T + \geq 2j$ ($\geq 1b$)
-1.9 ± 2.8 ± 2.4	⁵ AAD	12BK ATLS	$\ell + \cancel{E}_T + \geq 4j$ ($\geq 1b$)
0.4 ± 1.0 ± 1.1	⁶ CHATRCHYAN12BB	CMS	$\ell + \cancel{E}_T + \geq 4j$ ($\geq 1b$)
-1.3 ± 2.8 ± 2.9 -3.1	⁷ CHATRCHYAN12Bs	CMS	$\ell + \cancel{E}_T + \geq 4j$ ($\geq 1b$)

¹ ATLAS and CMS combination based on the data of AAD 14I and CHATRCHYAN 12BB. It takes into account the correlations of the measurements and systematic errors. The result is in agreement with the SM prediction (NLO QCD + NLO EW).

² AAD 15AJ based on 4.6 fb⁻¹ of data. After kinematic reconstruction the top quark momenta are corrected for detector resolution and acceptance effects by unfolding, using parton level information of the MC generators. The lepton charge asymmetry is measured as $A_C^{\ell} = 0.024 \pm 0.015 \pm 0.009$. All the measurements are consistent with the SM predictions.

³ Based on 4.7 fb⁻¹ of data. The result is consistent with the SM prediction of $A_C = 0.0123 \pm 0.0005$. The asymmetry is 0.011 ± 0.018 if restricted to those events where $\beta_Z(t\bar{t}) > 0.6$, which is also consistent with the SM prediction of $0.020^{+0.006}_{-0.007}$.

⁴ Based on 5.0 fb⁻¹ of data. The lepton charge asymmetry is measured as $A_C^{\ell} = 0.009 \pm 0.0010 \pm 0.006$. A_C^{ℓ} dependences on $m_{T\bar{T}}$, $|y(t\bar{t})|$, and $p_T(t\bar{t})$ are given in Fig. 5. All measurements are consistent with the SM predictions.

⁵ Based on 1.04 fb⁻¹ of data. The result is consistent with $A_C = 0.006 \pm 0.002$ (MC at NLO). No significant dependence of A_C on $m_{T\bar{T}}$ is observed.

⁶ Based on 5.0 fb⁻¹ of data at 7 TeV.

⁷ Based on 1.09 fb⁻¹ of data. The result is consistent with the SM predictions.

$t\bar{t}$ Charge Asymmetry (A_C) in pp Collisions at $\sqrt{s} = 8$ TeV

VALUE (%)	DOCUMENT ID	TECN	COMMENT
• • •	We do not use the following data for averages, fits, limits, etc. • • •		
0.55 ± 0.23 ± 0.25	¹ AABOUD	18AMLHC	ATLAS+CMS combination (lepton + jets)
2.1 ± 1.6	² AAD	16AE ATLS	$\ell\ell + \cancel{E}_T + \geq 2j$
0.9 ± 0.5	³ AAD	16AZ ATLS	$\ell + \cancel{E}_T + \geq 4j$
4.2 ± 3.2	⁴ AAD	16T ATLS	$m_{T\bar{T}} > 0.75$ TeV, $ y_t - y_{\bar{t}} < 2$, $\ell + \cancel{E}_T + \text{jets}$
1.1 ± 1.1 ± 0.7	⁵ KHACHATRYAN16AD	CMS	$\ell\ell + \cancel{E}_T + \geq 2j$ ($\geq 1b$)
0.33 ± 0.26 ± 0.33	⁶ KHACHATRYAN16AH	CMS	$\ell + \cancel{E}_T + \geq 4j$ ($\geq 1b$)
0.10 ± 0.68 ± 0.37	⁷ KHACHATRYAN16T	CMS	$\ell + \cancel{E}_T + \geq 4j$ ($\geq 1b$)

¹ ATLAS and CMS combination based on the data of AAD 16AZ and KHACHATRYAN 16AH. It takes into account the correlations of the measurements and systematic errors. A combination of the differential measurements of the charge asymmetry is also presented. The results are in agreement with the SM prediction (NNLO QCD + NLO EW).

² AAD 16AE is based on 20.3 fb⁻¹ of data. After kinematic reconstruction, the top quark momenta are corrected for detector resolution and acceptance effects by unfolding, using parton level information of the MC generators. The lepton charge asymmetry is measured as $A_C^{\ell} = 0.008 \pm 0.006$. All the measurements are consistent with the SM predictions.

³ AAD 16AZ based on 20.3 fb⁻¹ of data. All the differential and inclusive measurements are statistically limited and consistent with the SM predictions.

⁴ AAD 16T based on 20.3 fb⁻¹ of data. Uses reconstruction techniques for the decay topology of highly boosted top quarks. The observed asymmetry is transformed by unfolding to a parton-level result in the shown fiducial region. The result is consistent with the NLO SM prediction.

⁵ KHACHATRYAN 16AD based on 19.5 fb⁻¹ of data. The lepton charge asymmetry is measured as $A_C^{\ell} = 0.003 \pm 0.006 \pm 0.003$. All the measurements are consistent with the SM predictions.

⁶ KHACHATRYAN 16AH based on 19.6 fb⁻¹ of data. The same data set as in KHACHATRYAN 16T is used. A template technique is used, which is sensitive to the charge anti-symmetric component of the $t\bar{t}$ rapidity distributions and statistically advantageous. The result is consistent with the SM predictions.

⁷ KHACHATRYAN 16T based on 19.7 fb⁻¹ of data. The same data set as in KHACHATRYAN 16AH is used. After kinematic reconstruction the top quark momenta are corrected for detector resolution and acceptance effects by unfolding, using parton level information of the MC generators. All the measurements are consistent with the SM predictions.

t -quark Polarization in $t\bar{t}$ Events in $p\bar{p}$ Collisions at $\sqrt{s} = 1.96$ TeV

VALUE	DOCUMENT ID	TECN	COMMENT
• • •	We do not use the following data for averages, fits, limits, etc. • • •		
0.070 ± 0.055	¹ ABAZOV	17 D0	$\ell + \cancel{E}_T + \geq 3j$ ($\geq 1b$)
-0.102 ± 0.061	² ABAZOV	17 D0	$\ell + \cancel{E}_T + \geq 3j$ ($\geq 1b$)
0.040 ± 0.035	³ ABAZOV	17 D0	$\ell + \cancel{E}_T + \geq 3j$ ($\geq 1b$)
0.113 ± 0.091 ± 0.019	⁴ ABAZOV	15K D0	A_{FB}^{ℓ} in $\ell\ell + \cancel{E}_T + \geq 2j$ ($\geq 1b$)

¹ ABAZOV 17 based on 9.7 fb⁻¹ of data. The value is top quark polarization times spin analyzing power in the beam basis. Combination with the result of ABAZOV 15K yields 0.081 ± 0.048 . This result together with the helicity polarization is shown in a 2-dimensional plot in Fig. 4. These results are consistent with the SM prediction.

² ABAZOV 17 based on 9.7 fb⁻¹ of data. The value is top quark polarization times spin analyzing power in the helicity basis. The result is consistent with the SM prediction. This result together with the beam polarization is shown in a 2-dimensional plot in Fig. 4.

³ ABAZOV 17 based on 9.7 fb⁻¹ of data. The value is top quark polarization times spin analyzing power in the transverse basis. The result is consistent with the SM prediction.

⁴ ABAZOV 15K based on 9.7 fb⁻¹ of data. The value is top quark polarization times spin analyzing power in the beam basis. The result is consistent with the SM prediction of -0.0019 ± 0.0005 .

t -quark Polarization in $t\bar{t}$ Events in pp Collisions at $\sqrt{s} = 7$ TeV

The double differential distribution in polar angles, θ_1 (θ_2) of the decay product of the top (anti-top) decay products, is parametrized as $(1/\sigma)d\sigma/(d\cos\theta_1 d\cos\theta_2) = (1/4)(1 + A_t \cos\theta_1 + A_{\bar{t}} \cos\theta_2 - C \cos\theta_1 \cos\theta_2)$. The charged lepton is used to tag t or \bar{t} . The coefficient A_t and $A_{\bar{t}}$ measure the average helicity of t and \bar{t} , respectively. $A_{CPC} = A_t = A_{\bar{t}}$ assumes CP conservation, whereas $A_{CPV} = A_t = -A_{\bar{t}}$ corresponds to maximal CP violation.

VALUE	DOCUMENT ID	TECN	COMMENT
• • •	We do not use the following data for averages, fits, limits, etc. • • •		
-0.035 ± 0.014 ± 0.037	¹ AAD	13BE ATLS	A_{CPC}
0.020 ± 0.016 ± 0.013 -0.017	¹ AAD	13BE ATLS	A_{CPV}

¹ Based on 4.7 fb⁻¹ of data using the final states containing one or two isolated electrons or muons and jets with at least one b -tag.

t -quark Polarization in $t\bar{t}$ Events in pp Collisions at $\sqrt{s} = 8$ TeV

A_t , $A_{\bar{t}}$, A_{CPC} , A_{CPV} , and A_C are defined in header texts in the subsections, just above.

VALUE	DOCUMENT ID	TECN	COMMENT
• • •	We do not use the following data for averages, fits, limits, etc. • • •		
-0.044 ± 0.038 ± 0.027	¹ AABOUD	17G ATLS	A_t
-0.064 ± 0.040 ± 0.027	¹ AABOUD	17G ATLS	$A_{\bar{t}}$
0.296 ± 0.093 ± 0.037	¹ AABOUD	17G ATLS	A_C
-0.022 ± 0.058	² KHACHATRYAN16AI	CMS	A_{CPC}
0.000 ± 0.016	² KHACHATRYAN16AI	CMS	A_{CPV}

¹ AABOUD 17G based on 20.2 fb⁻¹ of pp data, using events with two leptons and two or more jets with at least one b -tag. Determined from measurements of 15 top quark spin observables. The second error corresponds to a variation of m_t about 172.5 GeV by 0.7 GeV. The values are consistent with the NLO SM predictions.

² KHACHATRYAN 16AI based on 19.5 fb⁻¹ of pp data at $\sqrt{s} = 8$ TeV, using events with two leptons and two or more jets with at least one b -tag. Determined from the lepton angular distributions as a function of the $t\bar{t}$ -system kinematical variables.

t -quark Polarization in Single Top Events in pp Collisions at $\sqrt{s} = 8$ TeV

VALUE	CL%	DOCUMENT ID	TECN	COMMENT
• • •	We do not use the following data for averages, fits, limits, etc. • • •			
> 0.72	95	¹ AABOUD	17BB ATLS	$\alpha_{\ell} P$; t-channel
0.97 ± 0.05 ± 0.11		² AABOUD	17I ATLS	$\alpha_{\ell} P$; t-channel
0.25 ± 0.08 ± 0.14		³ AABOUD	17I ATLS	$(F_+ + F_-)P$; t-channel
0.26 ± 0.03 ± 0.10		⁴ KHACHATRYAN16B0	CMS	$(\alpha_{\mu} P)/2$; t-channel

¹ AABOUD 17BB based on 20.2 fb⁻¹ of pp data. Triple-differential decay rate of top quark is used to simultaneously determine five generalized Wtb couplings as well as the top polarization. α_{ℓ} denotes the spin analyzing power of charged lepton, and the spin axis of the top polarization P is taken along the spectator-quark momentum in the top rest frame. The value is compatible with the SM prediction of about 0.9.

² AABOUD 17I based on 20.2 fb⁻¹ of pp data. A cut-based analysis is used to discriminate between signal and backgrounds. α_{ℓ} denotes the spin analyzing power of charged lepton, and the spin axis of the top polarization P is taken along the spectator-quark momentum in the top rest frame. See this paper for a number of other asymmetries and measurements that are not included here.

³ AABOUD 17I based on 20.2 fb⁻¹ of pp data. A cut-based analysis is used to discriminate between signal and backgrounds. F_{\pm} denotes W helicity fraction, and the spin axis of the top polarization P is taken along the spectator-quark momentum in the top rest frame. See this paper for a number of other asymmetries and measurements that are not included here.

⁴ KHACHATRYAN 16B0 based on 19.7 fb⁻¹ of data. A high-purity sample with a muon is selected by a multivariate analysis. The value is the top spin asymmetry, given by one half of the spin analyzing power α_{μ} ($=1$ at LO of SM) times the top polarization, P , where the spin axis is defined as the direction of the untagged jet in the top rest frame. The value is compatible with the SM prediction of 0.44 with a 2.0 σ deviation.

$g\bar{g} \rightarrow t\bar{t}$ Fraction in $p\bar{p}$ Collisions at $\sqrt{s} = 1.96$ TeV

VALUE	CL%	DOCUMENT ID	TECN	COMMENT
• • •	We do not use the following data for averages, fits, limits, etc. • • •			
< 0.33	68	¹ AALTONEN	09F CDF	$t\bar{t}$ correlations
0.07 ± 0.14 ± 0.07		² AALTONEN	08AG CDF	low p_T number of tracks

¹ Based on 955 pb⁻¹. AALTONEN 09F used differences in the $t\bar{t}$ production angular distribution and polarization correlation to discriminate between $g\bar{g} \rightarrow t\bar{t}$ and $q\bar{q} \rightarrow t\bar{t}$ subprocesses. The combination with the result of AALTONEN 08AG yields $0.07^{+0.15}_{-0.07}$.

²Result is based on 0.96 fb^{-1} of data. The contribution of the subprocesses $gg \rightarrow t\bar{t}$ and $q\bar{q} \rightarrow t\bar{t}$ is distinguished by using the difference between quark and gluon initiated jets in the number of small p_T ($0.3 \text{ GeV} < p_T < 3 \text{ GeV}$) charged particles in the central region ($|\eta| < 1.1$).

A_{FB}^{ℓ} of $t\bar{t}$ in $p\bar{p}$ Collisions at $\sqrt{s} = 1.96 \text{ TeV}$

A_{FB}^{ℓ} = Forward-backward asymmetry.

VALUE (%)	DOCUMENT ID	TECN	COMMENT
• • • We do not use the following data for averages, fits, limits, etc. • • •			
$12.8 \pm 2.1 \pm 1.4$	1 AALTONEN	18 TEVA	PDF, D0 combination
$17.5 \pm 5.6 \pm 3.1$	2 ABAZOV	15K D0	A_{FB}^{ℓ} in $\ell\ell + \cancel{E}_T + \geq 2j$ ($\geq 1b$)
7.2 ± 6.0	3 AALTONEN	14F CDF	A_{FB}^{ℓ} in dilepton channel ($\ell\ell + \cancel{E}_T + \geq 2j$)
7.6 ± 8.2	3 AALTONEN	14F CDF	$A_{FB}^{\ell\ell}$ in dilepton channel ($\ell\ell + \cancel{E}_T + \geq 2j$)
$4.2 \pm 2.3^{+1.7}_{-2.0}$	4 ABAZOV	14G D0	A_{FB}^{ℓ} ($\ell + \cancel{E}_T + \geq 3j$ ($0.1 \geq 2b$))
10.6 ± 3.0	5 ABAZOV	14H D0	A_{FB}^{ℓ} ($\ell + \cancel{E}_T + \geq 3j$ ($\geq 1b$))
20.1 ± 6.7	6 AALTONEN	13AD CDF	a_1/a_0 in $\ell + \cancel{E}_T + \geq 4j$ ($\geq 1b$)
-0.2 ± 3.1	6 AALTONEN	13AD CDF	a_3, a_5, a_7 in $\ell + \cancel{E}_T + \geq 4j$ ($\geq 1b$)
16.4 ± 4.7	7 AALTONEN	13S CDF	$\ell + \cancel{E}_T + \geq 4$ jets ($\geq 1b$ -tag)
$9.4^{+3.2}_{-2.9}$	8 AALTONEN	13X CDF	$\ell + \cancel{E}_T + \geq 4$ jets (≥ 1 b-tag)
11.8 ± 3.2	9 ABAZOV	13A D0	$\ell\ell$ & $\ell +$ jets comb.
-11.6 ± 15.3	10 AALTONEN	11F CDF	$m_{t\bar{t}} < 450 \text{ GeV}$
47.5 ± 11.4	10 AALTONEN	11F CDF	$m_{t\bar{t}} > 450 \text{ GeV}$
19.6 ± 6.5	11 ABAZOV	11AH D0	$\ell + \cancel{E}_T + \geq 4$ jets ($\geq 1b$ -tag)
17 ± 8	12 AALTONEN	08AB CDF	$p\bar{p}$ frame
24 ± 14	12 AALTONEN	08AB CDF	$t\bar{t}$ frame
$12 \pm 8 \pm 1$	13 ABAZOV	08L D0	$\ell + \cancel{E}_T + \geq 4$ jets

1 AALTONEN 18 based on $9\text{--}10 \text{ fb}^{-1}$ of $p\bar{p}$ data at $\sqrt{s} = 1.96 \text{ TeV}$. The value is the asymmetry in the number of reconstructed $t\bar{t}$ events with rapidity $y_t > y_{\bar{t}}$ and those with $y_t < y_{\bar{t}}$. The combined fits to CDF and D0 single lepton and $\ell\ell$ asymmetries give $A_{FB}^{\ell} = 0.073 \pm 0.016 \pm 0.012$ and $A_{FB}^{\ell\ell} = 0.108 \pm 0.043 \pm 0.016$, respectively. The results are consistent with the SM predictions.

2 ABAZOV 15K based on 9.7 fb^{-1} of data. The result is consistent with the SM predictions. By combining with the previous D0 measurement in the $\ell +$ jet channel ABABOV 14H, $A_{FB}^{\ell} = 0.118 \pm 0.025 \pm 0.013$ is obtained.

3 AALTONEN 14F based on 9.1 fb^{-1} of data. A_{FB}^{ℓ} and $A_{FB}^{\ell\ell}$ denote, respectively, the asymmetries $(N(x>0) - N(x<0))/N_{tot}$ for $x = q\ell/q\bar{\ell}$ ($q\ell$ is the charge of ℓ) and $x = \eta_{\ell^+} - \eta_{\ell^-}$. Both results are consistent with the SM predictions. By combining with the previous CDF measurement in the $\ell +$ jet channel AALTONEN 13X, $A_{FB}^{\ell} = 0.098 \pm 0.028$ is obtained. The combined result is about two sigma larger than the SM prediction of $A_{FB}^{\ell} = 0.038 \pm 0.003$.

4 Based on 9.7 fb^{-1} of $p\bar{p}$ data at $\sqrt{s} = 1.96 \text{ TeV}$. The asymmetry is corrected for the production level for events with $|y_t| < 1.5$. Asymmetry as functions of $E_T(\ell)$ and $|y_t|$ are given in Figs. 7 and 8, respectively. Combination with the asymmetry measured in the dilepton channel [ABAZOV 13P] gives $A_{FB}^{\ell} = 4.2 \pm 2.0 \pm 1.4 \%$, in agreement with the SM prediction of 2.0%.

5 Based on 9.7 fb^{-1} of data of $p\bar{p}$ data at $\sqrt{s} = 1.96 \text{ TeV}$. The measured asymmetry is in agreement with the SM predictions of $8.8 \pm 0.9 \%$ [BERNREUTHER 12], which includes the EW effects. The dependences of the asymmetry on $|y(t) - y(\bar{t})|$ and $m_{t\bar{t}}$ are shown in Figs. 9 and 10, respectively.

6 Based on 9.4 fb^{-1} of data. Reported A_{FB}^{ℓ} values come from the determination of a_j coefficients of $d\sigma/d(\cos\theta_\ell) = \sum_i a_i p_i(\cos\theta_\ell)$ measurement. The result of $a_1/a_0 = (40 \pm 12)\%$ seems higher than the NLO SM prediction of $(15^{+7}_{-3})\%$.

7 Based on 9.4 fb^{-1} of data. The quoted result is the asymmetry at the parton level.

8 Based on 9.4 fb^{-1} of data. The observed asymmetry is to be compared with the SM prediction of $A_{FB}^{\ell} = 0.038 \pm 0.003$.

9 Based on 5.4 fb^{-1} of data. ABABOV 13A studied the dilepton channel of the $t\bar{t}$ events and measured the leptonic forward-backward asymmetry to be $A_{FB}^{\ell} = 5.8 \pm 5.1 \pm 1.3\%$, which is consistent with the SM (QCD+EW) prediction of $4.7 \pm 0.1\%$. The result is obtained after combining the measurement ($15.2 \pm 4.0\%$) in the $\ell +$ jets channel ABABOV 11AH. The top quark helicity is measured by using the neutrino weighting method to be consistent with zero in both dilepton and $\ell +$ jets channels.

10 Based on 5.3 fb^{-1} of data. The error is statistical and systematic combined. Events with lepton $+ \cancel{E}_T + \geq 4$ jets ($\geq 1b$) are used. AALTONEN 11F also measures the asymmetry as a function of the rapidity difference $|y_t - y_{\bar{t}}|$. The NLO QCD predictions [MCFM] are $(4.0 \pm 0.6)\%$ and $(8.8 \pm 1.3)\%$ for $m_{t\bar{t}} < 450$ and $> 450 \text{ GeV}$, respectively.

11 Based on 5.4 fb^{-1} of data. The error is statistical and systematic combined. The quoted asymmetry is obtained after unfolding to be compared with the MC@NLO prediction of $(5.0 \pm 0.1)\%$. No significant difference between the $m_{t\bar{t}} < 450$ and $> 450 \text{ GeV}$ data samples is found. A corrected asymmetry based on the lepton from a top quark decay of $(15.2 \pm 4.0)\%$ is measured to be compared to the MC@NLO prediction of $(2.1 \pm 0.1)\%$.

12 Result is based on 1.9 fb^{-1} of data. The FB asymmetry in the $t\bar{t}$ events has been measured in the $\ell +$ jets mode, where the lepton charge is used as the flavor tag. The asymmetry in the $p\bar{p}$ frame is defined in terms of $\cos(\theta)$ of hadronically decaying t -quark momentum, whereas that in the $t\bar{t}$ frame is defined in terms of the t and \bar{t} rapidity difference. The results are consistent ($\leq 2\sigma$) with the SM predictions.

13 Result is based on 0.9 fb^{-1} of data. The asymmetry in the number of $t\bar{t}$ events with $y_t > y_{\bar{t}}$ and those with $y_t < y_{\bar{t}}$ has been measured in the lepton $+$ jets final state. The observed value is consistent with the SM prediction of 0.8% by MC@NLO, and an upper bound on the $Z' \rightarrow t\bar{t}$ contribution for the SM Z -like couplings is given in Fig. 2 for $350 \text{ GeV} < m_{Z'} < 1 \text{ TeV}$.

t-Quark Electric Charge

VALUE	DOCUMENT ID	TECN	COMMENT
$0.64 \pm 0.02 \pm 0.08$	1 AAD	13AY ATLAS	$\ell + \cancel{E}_T + \geq 4$ jets ($\geq 1b$)
• • • We do not use the following data for averages, fits, limits, etc. • • •			
	2 ABABOV	14D D0	$\ell + \cancel{E}_T + \geq 4$ jets ($\geq 2b$)
	3 AALTONEN	13J CDF	$p\bar{p}$ at 1.96 TeV
	4 AALTONEN	10S CDF	Repl. by AALTONEN 13J
	5 ABABOV	07C D0	fraction of $ q = 4e/3$ pair

1 AAD 13AY result is based on 2.05 fb^{-1} of pp data at $\sqrt{s} = 7 \text{ TeV}$, the result is obtained by reconstructing $t\bar{t}$ events in the lepton $+$ jets final state, where b -jet charges are tagged by the jet-charge algorithm. This measurement excludes the charge $-4/3$ assignment to the top quark at more than 8 standard deviations.

2 ABABOV 14D result is based on 5.3 fb^{-1} of $p\bar{p}$ data at $\sqrt{s} = 1.96 \text{ TeV}$. The electric charge of $b - W$ system in $t\bar{t}$ candidate events is measured from the charges of the leptons from W decay and in b jets. Under the assumption that the $b - W$ system consists of the sum of the top quark and the charge $-4/3$ quark $b'(-4/3)$ of the same mass, the top quark fraction is found to be $f = 0.88 \pm 0.13$ (stat) ± 0.11 (syst), or the upper bound for the $b'(-4/3)$ contamination of $1 - f < 0.46$ (95% CL).

3 AALTONEN 13J excludes the charge $-4/3$ assignment to the top quark at 99% CL, using 5.6 fb^{-1} of data in $p\bar{p}$ collisions at $\sqrt{s} = 1.96 \text{ TeV}$. Result is obtained by reconstructing $t\bar{t}$ events in the lepton $+$ jets final state, where b -jet charges are tagged by the jet-charge algorithm.

4 AALTONEN 10S excludes the charge $-4/3$ assignment for the top quark [CHANG 99] at 95%CL, using 2.7 fb^{-1} of data in $p\bar{p}$ collisions at $\sqrt{s} = 1.96 \text{ TeV}$. Result is obtained by reconstructing $t\bar{t}$ events in the lepton $+$ jets final state, where b -jet charges are tagged by the SLT (soft lepton tag) algorithm.

5 ABABOV 07C reports an upper limit $\rho < 0.80$ (90% CL) on the fraction ρ of exotic quark pairs $Q\bar{Q}$ with electric charge $|q| = 4e/3$ in $t\bar{t}$ candidate events with high p_T lepton, missing E_T and ≥ 4 jets. The result is obtained by measuring the fraction of events in which the quark pair decays into $W^- + b$ and $W^+ + \bar{b}$, where b and \bar{b} jets are discriminated by using the charge and momenta of tracks within the jet cones. The maximum CL at which the model of CHANG 99 can be excluded is 92%. Based on 370 pb^{-1} of data at $\sqrt{s} = 1.96 \text{ TeV}$.

t-Quark REFERENCES

AAD	20B	PL B800 135082	G. Aad et al.	(ATLAS Collab.)
SIRUNYAN	20D	PL B800 135042	A.M. Sirunyan et al.	(CMS Collab.)
ABABOV	19AC	EPJ C79 290	M. Aaboud et al.	(ATLAS Collab.)
ABABOV	19AD	EPJ C79 382	M. Aaboud et al.	(ATLAS Collab.)
ABABOV	19AP	PR D99 052009	M. Aaboud et al.	(ATLAS Collab.)
ABABOV	19AR	PR D99 072009	M. Aaboud et al.	(ATLAS Collab.)
ABABOV	19R	JHEP 1905 088	M. Aaboud et al.	(ATLAS and CMS Collab.)
ABABOV	19S	JHEP 1905 123	M. Aaboud et al.	(ATLAS Collab.)
AAD	19G	JHEP 1911 150	G. Aad et al.	(ATLAS Collab.)
SIRUNYAN	19AP	EPJ C79 313	A.M. Sirunyan et al.	(CMS Collab.)
SIRUNYAN	19AR	EPJ C79 368	A.M. Sirunyan et al.	(CMS Collab.)
SIRUNYAN	19BF	PRL 122 132003	A.M. Sirunyan et al.	(CMS Collab.)
SIRUNYAN	19BX	PR D100 072002	A.M. Sirunyan et al.	(CMS Collab.)
SIRUNYAN	19BY	PR D100 072007	A.M. Sirunyan et al.	(CMS Collab.)
SIRUNYAN	19CN	JHEP 1911 082	A.M. Sirunyan et al.	(CMS Collab.)
SIRUNYAN	19P	JHEP 1902 149	A.M. Sirunyan et al.	(CMS Collab.)
SIRUNYAN	19R	JHEP 1903 026	A.M. Sirunyan et al.	(CMS Collab.)
ABABOV	18AE	PL B780 557	M. Aaboud et al.	(ATLAS Collab.)
ABABOV	18AM	JHEP 1804 033	M. Aaboud et al.	(ATLAS and CMS Collab.)
ABABOV	18AT	JHEP 1807 176	M. Aaboud et al.	(ATLAS Collab.)
ABABOV	18AZ	EPJ C78 129	M. Aaboud et al.	(ATLAS Collab.)
ABABOV	18BH	EPJ C78 487	M. Aaboud et al.	(ATLAS Collab.)
ABABOV	18BK	PL B784 173	M. Aaboud et al.	(ATLAS Collab.)
ABABOV	18BW	JHEP 1809 139	M. Aaboud et al.	(ATLAS Collab.)
ABABOV	18CE	JHEP 1812 039	M. Aaboud et al.	(ATLAS Collab.)
ABABOV	18H	JHEP 1801 063	M. Aaboud et al.	(ATLAS Collab.)
ABABOV	18X	PR D98 032002	M. Aaboud et al.	(ATLAS Collab.)
AALTONEN	18	PRL 120 042001	T. Aaltonen et al.	(CDF and D0 Collab.)
SIRUNYAN	18AQ	JHEP 1803 115	A.M. Sirunyan et al.	(CMS Collab.)
SIRUNYAN	18BC	JHEP 1806 102	A.M. Sirunyan et al.	(CMS Collab.)
SIRUNYAN	18BD	JHEP 1806 101	A.M. Sirunyan et al.	(CMS Collab.)
SIRUNYAN	18BS	JHEP 1808 011	A.M. Sirunyan et al.	(CMS Collab.)
SIRUNYAN	18BU	EPJ C78 140	A.M. Sirunyan et al.	(CMS Collab.)
SIRUNYAN	18DE	EPJ C78 891	A.M. Sirunyan et al.	(CMS Collab.)
SIRUNYAN	18DL	JHEP 1810 117	A.M. Sirunyan et al.	(CMS Collab.)
SIRUNYAN	18L	PRL 120 231801	A.M. Sirunyan et al.	(CMS Collab.)
SIRUNYAN	18Z	PL B779 358	A.M. Sirunyan et al.	(CMS Collab.)
ABABOV	17AH	JHEP 1709 118	M. Aaboud et al.	(ATLAS Collab.)
ABABOV	17AV	JHEP 1710 129	M. Aaboud et al.	(ATLAS Collab.)
ABABOV	17BB	JHEP 1712 017	M. Aaboud et al.	(ATLAS Collab.)
ABABOV	17BC	EPJ C77 804	M. Aaboud et al.	(ATLAS Collab.)
ABABOV	17G	JHEP 1703 113	M. Aaboud et al.	(ATLAS Collab.)
ABABOV	17H	JHEP 1704 086	M. Aaboud et al.	(ATLAS Collab.)
ABABOV	17I	JHEP 1704 124	M. Aaboud et al.	(ATLAS Collab.)
ABABOV	17T	EPJ C77 531	M. Aaboud et al.	(ATLAS Collab.)
ABABOV	17Z	PR D95 072003	M. Aaboud et al.	(ATLAS Collab.)
ABABOV	17	PR D95 011101	V.M. Abazov et al.	(D0 Collab.)
ABABOV	17B	PR D95 112004	V.M. Abazov et al.	(D0 Collab.)
CHATRACHYAN	17	PL B770 50	S. Chatrchyan et al.	(CMS Collab.)
KHACHATRYAN	17B	EPJ C77 15	V. Khachatryan et al.	(CMS Collab.)
KHACHATRYAN	17G	JHEP 1702 028	V. Khachatryan et al.	(CMS Collab.)
KHACHATRYAN	17I	JHEP 1702 079	V. Khachatryan et al.	(CMS Collab.)
KHACHATRYAN	17N	EPJ C77 172	V. Khachatryan et al.	(CMS Collab.)
SIRUNYAN	17AA	PL B772 752	A.M. Sirunyan et al.	(CMS Collab.)
SIRUNYAN	17AB	PL B772 336	A.M. Sirunyan et al.	(CMS Collab.)
SIRUNYAN	17E	JHEP 1707 003	A.M. Sirunyan et al.	(CMS Collab.)
SIRUNYAN	17L	EPJ C77 354	A.M. Sirunyan et al.	(CMS Collab.)
SIRUNYAN	17N	EPJ C77 467	A.M. Sirunyan et al.	(CMS Collab.)
SIRUNYAN	17O	PR D96 032002	A.M. Sirunyan et al.	(CMS Collab.)
SIRUNYAN	17S	EPJ C77 578	A.M. Sirunyan et al.	(CMS Collab.)
SIRUNYAN	17W	JHEP 1709 051	A.M. Sirunyan et al.	(CMS Collab.)
ABABOV	16R	PL B761 136	M. Aaboud et al.	(ATLAS Collab.)
ABABOV	16T	PL B761 350	M. Aaboud et al.	(ATLAS Collab.)
AAD	16AE	PR D96 032006	G. Aad et al.	(ATLAS Collab.)
AAD	16AK	JHEP 1604 023	G. Aad et al.	(ATLAS Collab.)
AAD	16AS	EPJ C76 55	G. Aad et al.	(ATLAS Collab.)
AAD	16AZ	EPJ C76 87	G. Aad et al.	(ATLAS Collab.)
AAD	16B	JHEP 1601 064	G. Aad et al.	(ATLAS Collab.)
AAD	16BK	EPJ C76 642	G. Aad et al.	(ATLAS Collab.)
AAD	16D	EPJ C76 12	G. Aad et al.	(ATLAS Collab.)
AAD	16T	PL B756 52	G. Aad et al.	(ATLAS Collab.)
AAD	16U	PL B756 228	G. Aad et al.	(ATLAS Collab.)

See key on page 999

Quark Particle Listings

t, b' (Fourth Generation) Quark

ABAZOV	06U	PR D74 092005	V.M. Abazov et al.	(DO Collab.)	> 611
ABAZOV	06X	PR D74 112004	V.M. Abazov et al.	(DO Collab.)	> 372
ABULENCIA	06D	PRL 96 022004	A. Abulencia et al.	(CDF Collab.)	> 361
Also		PR D73 032003	A. Abulencia et al.	(CDF Collab.)	
Also		PR D73 092002	A. Abulencia et al.	(CDF Collab.)	
ABULENCIA	06G	PRL 96 152002	A. Abulencia et al.	(CDF Collab.)	> 338
Also		PR D74 032009	A. Abulencia et al.	(CDF Collab.)	> 380-430
ABULENCIA	06R	PL B639 172	A. Abulencia et al.	(CDF Collab.)	> 268
ABULENCIA	06U	PR D73 111303	A. Abulencia et al.	(CDF Collab.)	> 199
ABULENCIA	06V	PR D73 112006	A. Abulencia et al.	(CDF Collab.)	> 148
ABULENCIA	06Z	PRL 97 082004	A. Abulencia et al.	(CDF Collab.)	> 96
ABULENCIA, A	06C	PRL 96 202002	A. Abulencia et al.	(CDF Collab.)	> 128
ABULENCIA, A	06E	PR D74 072005	A. Abulencia et al.	(DO Collab.)	> 75
ABULENCIA, A	06F	PR D74 072006	A. Abulencia et al.	(DO Collab.)	> 85
ABAZOV	05	PL B606 25	V.M. Abazov et al.	(DO Collab.)	> 72
ABAZOV	05G	PL B617 1	V.M. Abazov et al.	(DO Collab.)	> 54
ABAZOV	05L	PR D72 011104	V.M. Abazov et al.	(DO Collab.)	> 43
ABAZOV	05P	PL B622 265	V.M. Abazov et al.	(DO Collab.)	> 34
Also		PL B517 282	V.M. Abazov et al.	(DO Collab.)	
Also		PR D53 031101	B. Abbott et al.	(DO Collab.)	
Also		PR D75 092007	V.M. Abazov et al.	(DO Collab.)	
ABAZOV	05Q	PL B626 35	V.M. Abazov et al.	(DO Collab.)	
ABAZOV	05R	PL B626 55	V.M. Abazov et al.	(DO Collab.)	
ABAZOV	05X	PL B626 45	V.M. Abazov et al.	(DO Collab.)	
ACOSTA	05A	PRL 95 102002	D. Acosta et al.	(CDF Collab.)	
ACOSTA	05D	PR D71 031101	D. Acosta et al.	(CDF Collab.)	
ACOSTA	05N	PR D71 121005	D. Acosta et al.	(CDF Collab.)	
ACOSTA	05S	PR D72 032002	D. Acosta et al.	(CDF Collab.)	
ACOSTA	05T	PR D72 052003	D. Acosta et al.	(CDF Collab.)	
ACOSTA	05U	PR D71 072005	D. Acosta et al.	(CDF Collab.)	
ACOSTA	05V	PR D71 052003	D. Acosta et al.	(CDF Collab.)	
ABAZOV	04G	NAT 429 638	V.M. Abazov et al.	(DO Collab.)	
ABDALLAH	04C	PL B590 21	J. Abdallah et al.	(DELPHI Collab.)	
ACOSTA	04H	PR D69 052003	D. Acosta et al.	(CDF Collab.)	
ACOSTA	04I	PRL 93 142001	D. Acosta et al.	(CDF Collab.)	
AKTAS	04	EPJ C33 9	A. Aktas et al.	(H1 Collab.)	
ABAZOV	03A	PR D67 012004	V.M. Abazov et al.	(DO Collab.)	
CHEKANOV	03	PL B559 153	S. Chekanov et al.	(ZEUS Collab.)	
ACHARD	02J	PL B549 290	P. Achard et al.	(L3 Collab.)	
ACOSTA	02	PR D65 091102	D. Acosta et al.	(CDF Collab.)	
HEISTER	02Q	PL B543 173	A. Heister et al.	(ALEPH Collab.)	
ABBIEINDI	01T	PL B521 181	G. Abbiendi et al.	(OPAL Collab.)	
AFFOLDER	01	PR D63 032003	T. Affolder et al.	(CDF Collab.)	
AFFOLDER	01A	PR D64 032002	T. Affolder et al.	(CDF Collab.)	
AFFOLDER	01C	PRL 86 3233	T. Affolder et al.	(CDF Collab.)	
AFFOLDER	00B	PRL 84 214	T. Affolder et al.	(CDF Collab.)	
BARATE	00S	PL B494 33	S. Barate et al.	(ALEPH Collab.)	
ABBOTT	99G	PR D60 052001	B. Abbott et al.	(DO Collab.)	
ABE	99B	PRL 82 271	F. ABE et al.	(CDF Collab.)	
Also		PRL 82 2808 (erratum)	F. ABE et al.	(CDF Collab.)	
CHANG	99	PR D59 091503	D. Chang, W. Chang, E. Ma		
ABBOTT	98D	PRL 80 2063	B. Abbott et al.	(DO Collab.)	
ABBOTT	98F	PR D58 052001	B. Abbott et al.	(DO Collab.)	
ABE	98E	PRL 80 2767	F. ABE et al.	(CDF Collab.)	
ABE	98F	PRL 80 2779	F. ABE et al.	(CDF Collab.)	
ABE	98G	PRL 80 2525	F. ABE et al.	(CDF Collab.)	
BHAT	98B	JUMP A13 5113	P.C. Bhat, H.B. Prosper, S.S. Snyder		
ABACHI	97E	PRL 79 1197	S. Abachi et al.	(DO Collab.)	
ABE	97R	PRL 79 1992	F. ABE et al.	(CDF Collab.)	
ABE	97V	PRL 79 3585	F. ABE et al.	(CDF Collab.)	
PDG	96	PL D54 1	R. M. Barnett et al.	(PDG Collab.)	
ABACHI	95	PRL 74 2632	S. Abachi et al.	(DO Collab.)	
ABE	95F	PRL 74 2626	F. ABE et al.	(CDF Collab.)	
ABE	94E	PR D50 2966	F. ABE et al.	(CDF Collab.)	
Also		PRL 73 225	F. ABE et al.	(CDF Collab.)	

b' (4^{th} Generation) Quark, Searches for

b' ($-1/3$)-quark/hadron mass limits in $p\bar{p}$ and pp collisions

VALUE (GeV)	CL%	DOCUMENT ID	TECN	COMMENT
>1130	95	1 SIRUNYAN	19AQ CMS	$B(b' \rightarrow Zb) = 1$
>1230	95	2 SIRUNYAN	19BWCMS	$B(b' \rightarrow Wt) = 1$
>1350	95	3 AABOUD	18AW ATLS	$B(b' \rightarrow Wt) = 1$
>1000	95	4 AABOUD	18CE ATLS	$\geq 2\ell + \cancel{E}_T + \geq 1bj$
> 950	95	5 AABOUD	18CL ATLS	Wt, Zb, hb modes
>1010	95	6,7 AABOUD	18CP ATLS	2,3 ℓ , singlet model
>1140	95	5,8 AABOUD	18CP ATLS	2,3 ℓ , doublet model
>1220	95	9,10 AABOUD	18CR ATLS	singlet <i>b'</i> . ATLAS Combination
>1370	95	9,11 AABOUD	18CR ATLS	<i>b'</i> in a weak isospin doublet (<i>t', b'</i>). ATLAS combination.
> 910	95	12 SIRUNYAN	18BM CMS	Wt, Zb, hb modes
> 845	95	13 SIRUNYAN	18Q CMS	$B(b' \rightarrow Wu) = 1$
> 730	95	14 SIRUNYAN	17AU CMS	
> 880	95	15 KHACHATRYAN	16AN CMS	$B(b' \rightarrow Wt) = 1$
> 620	95	16 AAD	15BY ATLS	Wt, Zb, hb modes
> 730	95	17 AAD	15BY ATLS	$B(b' \rightarrow Wt) = 1$
> 810	95	18 AAD	15Z ATLS	
> 755	95	19 AAD	14AZ ATLS	$B(b' \rightarrow Wt) = 1$
> 675	95	20 CHATRCHYAN	13I CMS	$B(b' \rightarrow Wt) = 1$
> 190	95	21 ABAZOV	08X D0	$c\tau = 200\text{mm}$
> 190	95	22 ACOSTA	03 CDF	quasi-stable <i>b'</i>
<350, 580-635, >700	95	23 AAD	15AR ATLS	$B(b' \rightarrow Hb) = 1$
> 690	95	24 AAD	15CN ATLS	$B(b' \rightarrow Wq) = 1 (q=u)$
> 480	95	25 AAD	12AT ATLS	$B(b' \rightarrow Wt) = 1$
> 400	95	26 AAD	12AU ATLS	$B(b' \rightarrow Zb) = 1$
> 350	95	27 AAD	12BC ATLS	$B(b' \rightarrow Wq) = 1 (q=u, c)$
> 450	95	28 AAD	12BE ATLS	$B(b' \rightarrow Wt) = 1$
> 685	95	29 CHATRCHYAN	12BH CMS	$m_{t'} = m_{b'}$

• • • We do not use the following data for averages, fits, limits, etc. • • •

- 30 CHATRCHYAN12X CMS $B(b' \rightarrow Wt) = 1$
 - 31 AALTONEN 11J CDF $b' \rightarrow Wt$
 - 32 CHATRCHYAN11L CMS Repl. by CHATRCHYAN 12X
 - 33 AALTONEN 10H CDF $b' \rightarrow Wt$
 - 34 FLACCO 10 RVUE $m_{b'} > m_{t'}$
 - 35,36 AALTONEN 07C CDF $B(b' \rightarrow Zb) = 1$
 - 37 AFFOLDER 00 CDF NC: $b' \rightarrow Zb$
 - 38 ABE 98N CDF NC: $b' \rightarrow Zb + \text{vertex}$
 - 39 ABACHI 97D D0 NC: $b' \rightarrow b\gamma$
 - 40 ABACHI 95F D0 $\ell\ell + \text{jets}, \ell + \text{jets}$
 - 41 MUKHOPAD... 93 RVUE NC: $b' \rightarrow b\ell\ell$
 - 42 ABE 92 CDF CC: $\ell\ell$
 - 43 ABE 90B CDF CC: $e + \mu$
 - 44 AKESSON 90 UA2 CC: $e + \text{jets} + \cancel{E}_T$
 - 45 ALBAJAR 90B UA1 CC: $\mu + \text{jets}$
 - 46 ALBAJAR 88 UA1 CC: $e \text{ or } \mu + \text{jets}$
- 1 SIRUNYAN 19AQ based on 35.9 fb^{-1} of pp data at $\sqrt{s} = 13 \text{ TeV}$. Pair production of vector-like b' is searched for with one b' decaying into Zb and the other b' decaying into Wt, Zb, hb . Events with an opposite-sign lepton pair consistent with coming from Z and jets are used. Mass limits are obtained for a variety of branching ratios of b' .
 - 2 SIRUNYAN 19BW based on 35.9 fb^{-1} of pp data at $\sqrt{s} = 13 \text{ TeV}$. The limit is for the pair-produced vector-like b' using all-hadronic final state. The analysis is made for the Zb, Wt, hb modes and mass limits are obtained for a variety of branching ratios.
 - 3 AABOUD 18AW based on 36.1 fb^{-1} of pp data at $\sqrt{s} = 13 \text{ TeV}$. The limit is for the pair-produced vector-like b' using lepton-plus-jets final state. The search is also sensitive to the decays into Zb and Hb final states.
 - 4 AABOUD 18CE based on 36.1 fb^{-1} of proton-proton data taken at $\sqrt{s} = 13 \text{ TeV}$. Events including a same-sign lepton pair are used. The limit is for a singlet model, assuming the branching ratios of b' into Zb, Wt and Hb as predicted by the model.
 - 5 AABOUD 18CL, AABOUD 18CP based on 36.1 fb^{-1} of pp data at $\sqrt{s} = 13 \text{ TeV}$. The limit is for the pair-produced vector-like b' using all-hadronic final state. The analysis is particularly powerful for the $b' \rightarrow hb$ mode. Assuming the pure decay only in this mode sets a limit $m_{b'} > 1010 \text{ GeV}$.
 - 6 AABOUD 18CP based on 36.1 fb^{-1} of pp data at $\sqrt{s} = 13 \text{ TeV}$. Pair and single production of vector-like b' are searched for with at least one b' decaying into Zb . In the case of $B(b' \rightarrow Zb) = 1$, the limit is $m_{b'} > 1220 \text{ GeV}$.
 - 7 The limit is for the singlet model, assuming that the branching ratios into Wt, Zb, hb add up to one.
 - 8 The limit is for the doublet model, assuming that the branching ratios into Wt, Zb, hb add up to one.
 - 9 AABOUD 18CR based on 36.1 fb^{-1} of pp data at $\sqrt{s} = 13 \text{ TeV}$. A combination of searches for the pair-produced vector-like b' in various decay channels ($b' \rightarrow Wt, Zb, hb$). Also a model-independent limit is obtained as $m_{b'} > 1.03 \text{ TeV}$, assuming that the branching ratios into Zb, Wt , and hb add up to one.
 - 10 The limit is for the singlet b' .
 - 11 The limit is for b' in a weak isospin doublet (t', b') and $|V_{t'b}| \ll |V_{tb}|$. For a b' in a doublet with a charge $-4/3$ vector-like quark, the limit $m_{b'} > 1.14 \text{ TeV}$ is obtained.
 - 12 SIRUNYAN 18BM based on 35.9 fb^{-1} of pp data at $\sqrt{s} = 13 \text{ TeV}$. The limit is for the pair-produced vector-like b' . Three channels (single lepton, same-charge 2 leptons, or at least 3 leptons) are considered for various branching fraction combinations. Assuming $B(tW) = 1$, the limit is 1240 GeV and for $B(bZ) = 1$ it is 960 GeV .
 - 13 SIRUNYAN 18Q based on 19.7 fb^{-1} of pp data at $\sqrt{s} = 8 \text{ TeV}$. The limit is for the pair-produced vector-like b' that couple only to light quarks. Upper cross section limits on the single production of a b' and constraints for other decay channels (Zq and Hq) are also given in the paper.
 - 14 SIRUNYAN 17AU based on $2.3\text{-}2.6 \text{ fb}^{-1}$ of pp data at $\sqrt{s} = 13 \text{ TeV}$. Limit on pair-produced singlet vector-like b' using one lepton and several jets. The mass bound is given for a b' transforming as a singlet under the electroweak symmetry group, assumed to decay through W, Z or Higgs boson (which decays to jets) and to a third generation quark.
 - 15 KHACHATRYAN 16AN based on 19.7 fb^{-1} of pp data at $\sqrt{s} = 8 \text{ TeV}$. Limit on pair-produced vector-like b' using 1, 2, and ≥ 2 leptons as well as fully hadronic final states. Other limits depending on the branching fractions to tW, bZ , and bH are given in Table IX.
 - 16 AAD 15BY based on 20.3 fb^{-1} of pp data at $\sqrt{s} = 8 \text{ TeV}$. Limit on pair-produced vector-like b' assuming the branching fractions to W, Z , and h modes of the singlet model. Used events containing $\geq 2\ell + \cancel{E}_T + \geq 2j (\geq 1b)$ and including a same-sign lepton pair.
 - 17 AAD 15BY based on 20.3 fb^{-1} of pp data at $\sqrt{s} = 8 \text{ TeV}$. Limit on pair-produced chiral b' -quark. Used events containing $\geq 2\ell + \cancel{E}_T + \geq 2j (\geq 1b)$ and including a same-sign lepton pair.
 - 18 AAD 15Z based on 20.3 fb^{-1} of pp data at $\sqrt{s} = 8 \text{ TeV}$. Used events with $\ell + \cancel{E}_T + \geq 6j (\geq 1b)$ and at least one pair of jets from weak boson decay, primarily designed to select the signature $b'\bar{b}' \rightarrow WW\bar{t}\bar{t}$. This is a limit on pair-produced vector-like b' . The lower mass limit is 640 GeV for a vector-like singlet b' .
 - 19 Based on 20.3 fb^{-1} of pp data at $\sqrt{s} = 8 \text{ TeV}$. No significant excess over SM expectation is found in the search for pair production or single production of b' in the events with dilepton from a high $p_T Z$ and additional jets ($\geq 1b$ -tag). If instead of $B(b' \rightarrow Wt) = 1$ an electroweak singlet with $B(b' \rightarrow Wt) \sim 0.45$ is assumed, the limit reduces to 685 GeV .
 - 20 Based on 5.0 fb^{-1} of pp data at $\sqrt{s} = 7 \text{ TeV}$. CHATRCHYAN 13I looked for events with one isolated electron or muon, large \cancel{E}_T , and at least four jets with large transverse momenta, where one jet is likely to originate from the decay of a bottom quark.
 - 21 Result is based on 1.1 fb^{-1} of data. No signal is found for the search of long-lived particles which decay into final states with two electrons or photons, and upper bound on the cross section times branching fraction is obtained for $2 < c\tau < 7000 \text{ mm}$; see Fig. 3. 95% CL excluded region of b' lifetime and mass is shown in Fig. 4.

Quark Particle Listings

b' (Fourth Generation) Quark

- ²² ACOSTA 03 looked for long-lived fourth generation quarks in the data sample of 90 pb⁻¹ of $\sqrt{s}=1.8$ TeV $p\bar{p}$ collisions by using the muon-like penetration and anomalously high ionization energy loss signature. The corresponding lower mass bound for the charge (2/3)e quark (t') is 220 GeV. The t' bound is higher than the b' bound because t' is more likely to produce charged hadrons than b' . The 95% CL upper bounds for the production cross sections are given in their Fig. 3.
- ²³ AAD 15AR based on 20.3 fb⁻¹ of pp data at $\sqrt{s}=8$ TeV. Used lepton-plus-jets final state. See Fig. 24 for mass limits in the plane of $B(b' \rightarrow Wt)$ vs. $B(b' \rightarrow Hb)$ from $b'\bar{b}' \rightarrow Hb + X$ searches.
- ²⁴ AAD 15CN based on 20.3 fb⁻¹ of pp data at $\sqrt{s}=8$ TeV. Limit on pair-production of chiral b' -quark. Used events with $\ell + E_T + \geq 4j$ (non- b -tagged). Limits on a heavy vector-like quark, which decays into Wq, Zq, hq , are presented in the plane $B(Q \rightarrow Wq)$ vs. $B(Q \rightarrow hq)$ in Fig. 12.
- ²⁵ Based on 1.04 fb⁻¹ of pp data at $\sqrt{s}=7$ TeV. No signal is found for the search of heavy quark pair production that decay into W and a t quark in the events with a high p_T isolated lepton, large E_T , and at least 6 jets in which one, two or more dijets are from W .
- ²⁶ Based on 2.0 fb⁻¹ of pp data at $\sqrt{s}=7$ TeV. No $b' \rightarrow Zb$ invariant mass peak is found in the search of heavy quark pair production that decay into Z and a b quark in events with $Z \rightarrow e^+e^-$ and at least one b -jet. The lower mass limit is 358 GeV for a vector-like singlet b' mixing solely with the third SM generation.
- ²⁷ Based on 1.04 fb⁻¹ of pp data at $\sqrt{s}=7$ TeV. No signal is found for the search of heavy quark pair production that decay into W and a quark in the events with dileptons, large E_T , and ≥ 2 jets.
- ²⁸ Based on 1.04 fb⁻¹ of pp data at $\sqrt{s}=7$ TeV. AAD 12BE looked for events with two isolated like-sign leptons and at least 2 jets, large E_T and $H_T > 350$ GeV.
- ²⁹ Based on 5 fb⁻¹ of pp data at $\sqrt{s}=7$ TeV. CHATRCHYAN 12BH searched for QCD and EW production of single and pair of degenerate 4th generation quarks that decay to bW or tW . Absence of signal in events with one lepton, same-sign dileptons or tripletons gives the bound. With a mass difference of 25 GeV/ c^2 between $m_{t'}$ and $m_{b'}$, the corresponding limit shifts by about ± 20 GeV/ c^2 .
- ³⁰ Based on 4.9 fb⁻¹ of pp data at $\sqrt{s}=7$ TeV. CHATRCHYAN 12X looked for events with tripletons or same-sign dileptons and at least one b jet.
- ³¹ Based on 4.8 fb⁻¹ of data in $p\bar{p}$ collisions at 1.96 TeV. AALTONEN 11J looked for events with $\ell + E_T + \geq 5j$ (≥ 1 b or c). No signal is observed and the bound $\sigma(b'\bar{b}') < 30$ fb for $m_{b'} > 375$ GeV is found for $B(b' \rightarrow Wt) = 1$.
- ³² Based on 34 pb⁻¹ of data in pp collisions at 7 TeV. CHATRCHYAN 11L looked for multi-jet events with tripletons or same-sign dileptons. No excess above the SM background excludes $m_{b'}$ between 255 and 361 GeV at 95% CL for $B(b' \rightarrow Wt) = 1$.
- ³³ Based on 2.7 fb⁻¹ of data in $p\bar{p}$ collisions at $\sqrt{s}=1.96$ TeV. AALTONEN 10H looked for pair production of heavy quarks which decay into tW^- or tW^+ , in events with same sign dileptons (e or μ), several jets and large missing E_T . The result is obtained for b' which decays into tW^- . For the charge 5/3 quark ($T_{5/3}$) which decays into tW^+ , $m_{T_{5/3}} > 365$ GeV (95% CL) is found when it has the charge -1/3 partner B of the same mass.
- ³⁴ FLACCO 10 result is obtained from AALTONEN 10H result of $m_{b'} > 338$ GeV, by relaxing the condition $B(b' \rightarrow Wt) = 100\%$ when $m_{b'} > m_{t'}$.
- ³⁵ Result is based on 1.06 fb⁻¹ of data. No excess from the SM Z +jet events is found when Z decays into e or $\mu\mu$. The $m_{b'}$ bound is found by comparing the resulting upper bound on $\sigma(b'\bar{b}') [1 - (1 - B(b' \rightarrow Zb))^2]$ and the LO estimate of the b' pair production cross section shown in Fig. 38 of the article.
- ³⁶ HUANG 08 reexamined the b' mass lower bound of 268 GeV obtained in AALTONEN 07c that assumes $B(b' \rightarrow Zb) = 1$, which does not hold for $m_{b'} > 255$ GeV. The lower mass bound is given in the plane of $\sin^2(\theta_{tb'})$ and $m_{b'}$.
- ³⁷ AFFOLDER 00 looked for b' that decays into $b+Z$. The signal searched for is $bbZZ$ events where one Z decays into e^+e^- or $\mu^+\mu^-$ and the other Z decays hadronically. The bound assumes $B(b' \rightarrow Zb) = 100\%$. Between 100 GeV and 199 GeV, the 95%CL upper bound on $\sigma(b' \rightarrow \bar{b}') \times B^2(b' \rightarrow Zb)$ is also given (see their Fig. 2).
- ³⁸ ABE 98n looked for $Z \rightarrow e^+e^-$ decays with displaced vertices. Quoted limit assumes $B(b' \rightarrow Zb) = 1$ and $c\tau_{b'} = 1$ cm. The limit is lower than m_{Z+m_b} (~ 96 GeV) if $c\tau > 22$ cm or $c\tau < 0.009$ cm. See their Fig. 4.
- ³⁹ ABACHI 97D searched for b' that decays mainly via FCNC. They obtained 95%CL upper bounds on $B(b'\bar{b}' \rightarrow \gamma + 3 \text{ jets})$ and $B(b'\bar{b}' \rightarrow 2\gamma + 2 \text{ jets})$, which can be interpreted as the lower mass bound $m_{b'} > m_{Z+m_b}$.
- ⁴⁰ ABACHI 95F bound on the top-quark also applies to b' and t' quarks that decay predominantly into W . See FROGGATT 97.
- ⁴¹ MUKHOPADHYAYA 93 analyze CDF dilepton data of ABE 92g in terms of a new quark decaying via flavor-changing neutral current. The above limit assumes $B(b' \rightarrow b\ell^+\ell^-) = 1\%$. For an exotic quark decaying only via virtual Z [$B(b\ell^+\ell^-) = 3\%$], the limit is 85 GeV.
- ⁴² ABE 92 dilepton analysis limit of >85 GeV at CL=95% also applies to b' quarks, as discussed in ABE 90b.
- ⁴³ ABE 90b exclude the region 28–72 GeV.
- ⁴⁴ AKESSON 90 searched for events having an electron with $p_T > 12$ GeV, missing momentum > 15 GeV, and a jet with $E_T > 10$ GeV, $|\eta| < 2.2$, and excluded $m_{b'}$ between 30 and 69 GeV.
- ⁴⁵ For the reduction of the limit due to non-charged-current decay modes, see Fig. 19 of ALBAJAR 90b.
- ⁴⁶ ALBAJAR 88 study events at $E_{cm} = 546$ and 630 GeV with a muon or isolated electron, accompanied by one or more jets and find agreement with Monte Carlo predictions for the production of charm and bottom, without the need for a new quark. The lower mass limit is obtained by using a conservative estimate for the $b'\bar{b}'$ production cross section and by assuming that it cannot be produced in W decays. The value quoted here is revised using the full $O(\alpha_s^3)$ cross section of ALTARELLI 88.

$b'(-1/3)$ mass limits from single production in $p\bar{p}$ and pp collisions

VALUE (GeV)	CL%	DOCUMENT ID	TECN	COMMENT
>1500	95	¹ AAD	16AH ATLS	$g b \rightarrow b' \rightarrow t W, B(b' \rightarrow t W)=1$
>1390	95	² KHACHATRY...16i	CMS	$g b \rightarrow b' \rightarrow t W, B(b' \rightarrow t W)=1$
>1430	95	³ KHACHATRY...16i	CMS	$g b \rightarrow b' \rightarrow t W, B(b' \rightarrow t W)=1$
>1530	95	⁴ KHACHATRY...16i	CMS	$g b \rightarrow b' \rightarrow t W, B(b' \rightarrow t W)=1$
> 693	95	⁵ ABAZOV	11F D0	$q u \rightarrow q' b' \rightarrow q'(Wu)$ $\bar{\kappa}_{ub'}=1, B(b' \rightarrow Wu)=1$
> 430	95	⁵ ABAZOV	11F D0	$q d \rightarrow q' b' \rightarrow q(Zd)$ $\bar{\kappa}_{db'}=\sqrt{2}, B(b' \rightarrow Zd)=1$
		⁶ SIRUNYAN	19AI CMS	$b Z / t W \rightarrow b' \rightarrow t W$

- • • We do not use the following data for averages, fits, limits, etc. • • •
- ¹ AAD 16AH based on 20.3 fb⁻¹ of data in pp collisions at 8 TeV. No significant excess over SM expectation is found in the search for a vector-like b' in the single-lepton and dilepton channels (ℓ or $\ell\ell$) + 1,2,3 j ($\geq 1b$). The model assumes that the b' has the excited quark couplings.
- ² Based on 19.7 fb⁻¹ of data in pp collisions at 8 TeV. Limit on left-handed b' assuming 100% decay to tW and using all-hadronic, lepton + jets, and dilepton final states.
- ³ Based on 19.7 fb⁻¹ of data in pp collisions at 8 TeV. Limit on right-handed b' assuming 100% decay to tW and using all-hadronic, lepton + jets, and dilepton final states.
- ⁴ Based on 19.7 fb⁻¹ of data in pp collisions at 8 TeV. Limit on vector-like b' assuming 100% decay to tW and using all-hadronic, lepton+jets, and dilepton final states.
- ⁵ Based on 5.4 fb⁻¹ of data in $p\bar{p}$ collisions at 1.96 TeV. ABAZOV 11F looked for single production of b' via the W or Z coupling to the first generation up or down quarks, respectively. Model independent cross section limits for the single production processes $p\bar{p} \rightarrow b'q \rightarrow Wuq$, and $p\bar{p} \rightarrow b'q \rightarrow Zdq$ are given in Figs. 3 and 4, respectively, and the mass limits are obtained for the model of ATRE 09 with degenerate bi-doublets of vector-like quarks.
- ⁶ SIRUNYAN 19AI based on 35.9 fb⁻¹ of pp data at $\sqrt{s}=13$ TeV. Exclusion limits are set on the product of the production cross section and branching fraction for the $b'(-1/3) + b$ and $b'(-1/3) + t$ modes as a function of the vector-like quark mass in Figs. 7 and 8 and in Tab. 2 for relative vector-like quark widths between 1 and 30% for left- and right-handed vector-like quark couplings. No significant deviation from the SM prediction is observed.

MASS LIMITS for b' (4th Generation) Quark or Hadron in e^+e^- Collisions

Search for hadrons containing a fourth-generation $-1/3$ quark denoted b' .

The last column specifies the assumption for the decay mode (CC denotes the conventional charged-current decay) and the event signature which is looked for.

VALUE (GeV)	CL%	DOCUMENT ID	TECN	COMMENT
>46.0	95	¹ DECAMP	90F ALEP	any decay
• • • We do not use the following data for averages, fits, limits, etc. • • •				
none 96–103	95	² ABDALLAH	07 DLPH	$b' \rightarrow bZ, cW$
		³ ADRIANI	93G L3	Quarkonium track
>44.7	95	ADRIANI	93M L3	$\Gamma(Z)$
>45	95	ABREU	91F DLPH	$\Gamma(Z)$
none 19.4–28.2	95	ABE	90D VNS	Any decay; event shape
>45.0	95	ABREU	90D DLPH	$B(C C) = 1$; event shape
>44.5	95	⁴ ABREU	90D DLPH	$b' \rightarrow cH^-, H^- \rightarrow \bar{c}s, \tau^- \nu$
>40.5	95	⁵ ABREU	90D DLPH	$\Gamma(Z \rightarrow \text{hadrons})$
>28.3	95	ADACHI	90 TOPZ	$B(FCNC)=100\%$; isol. γ or 4 jets
>41.4	95	⁶ AKRAWY	90B OPAL	Any decay; acoplanarity
>45.2	95	⁶ AKRAWY	90B OPAL	$B(C C) = 1$; acoplanarity
>46	95	⁷ AKRAWY	90J OPAL	$b' \rightarrow \gamma + \text{any}$
>27.5	95	⁸ ABE	89E VNS	$B(C C) = 1$; μ, e
none 11.4–27.3	95	⁹ ABE	89G VNS	$B(b' \rightarrow b\gamma) > 10\%$; isolated γ
>44.7	95	¹⁰ ABRAMS	89C MRK2	$B(C C) = 100\%$; isol. track
>42.7	95	¹⁰ ABRAMS	89C MRK2	$B(bg) = 100\%$; event shape
>42.0	95	¹⁰ ABRAMS	89C MRK2	Any decay; event shape
>28.4	95	^{11,12} ADACHI	89C TOPZ	$B(C C) = 1$; μ
>28.8	95	¹³ ENO	89 AMY	$B(C C) \geq 90\%$; μ, e
>27.2	95	^{13,14} ENO	89 AMY	any decay; event shape
>29.0	95	¹³ ENO	89 AMY	$B(b' \rightarrow b\gamma) \geq 85\%$; event shape
>24.4	95	¹⁵ IGARASHI	88 AMY	μ, e
>23.8	95	¹⁶ SAGAWA	88 AMY	event shape
>22.7	95	¹⁷ ADEVA	86 MRKJ	μ
>21	95	¹⁸ ALTHOFF	84C TASS	R , event shape
>19	95	¹⁹ ALTHOFF	84I TASS	Aplanarity

- ¹ DECAMP 90F looked for isolated charged particles, for isolated photons, and for four-jet final states. The modes $b' \rightarrow bg$ for $B(b' \rightarrow bg) > 65\%$ $b' \rightarrow b\gamma$ for $B(b' \rightarrow b\gamma) > 5\%$ are excluded. Charged Higgs decay were not discussed.
- ² ABDALLAH 07 searched for b' pair production at $E_{cm}=196\text{--}209$ GeV, with 420 pb⁻¹. No signal leads to the 95% CL upper limits on $B(b' \rightarrow bZ)$ and $B(b' \rightarrow cW)$ for $m_{b'} = 96$ to 103 GeV.
- ³ ADRIANI 93g search for vector quarkonium states near Z and give limit on quarkonium- Z mixing parameter $\delta m^2 < (10\text{--}30)$ GeV² (95%CL) for the mass 88–94.5 GeV. Using

See key on page 999

Quark Particle Listings

b' (Fourth Generation) Quark, t' (Fourth Generation) Quark

Richardson potential, a $1S(b'\bar{b}')$ state is excluded for the mass range 87.7–94.7 GeV. This range depends on the potential choice.

- 4 ABREU 90d assumed $m_{H^-} < m_{b'}$ – 3 GeV.
- 5 Superseded by ABREU 91f.
- 6 AKRAWY 90b search was restricted to data near the Z peak at $E_{cm} = 91.26$ GeV at LEP. The excluded region is between 23.6 and 41.4 GeV if no H^\pm decays exist. For charged Higgs decays the excluded regions are between $(m_{H^+} + 1.5 \text{ GeV})$ and 45.5 GeV.
- 7 AKRAWY 90j search for isolated photons in hadronic Z decay and derive $B(Z \rightarrow b'\bar{b}') \cdot B(b' \rightarrow \gamma X) / B(Z \rightarrow \text{hadrons}) < 2.2 \times 10^{-3}$. Mass limit assumes $B(b' \rightarrow \gamma X) > 10\%$.
- 8 ABE 89e search at $E_{cm} = 56\text{--}57$ GeV at TRISTAN for multihadron events with a spherical shape (using thrust and acoplanarity) or containing isolated leptons.
- 9 ABE 89c search was at $E_{cm} = 55\text{--}60.8$ GeV at TRISTAN.
- 10 If the photonic decay mode is large ($B(b' \rightarrow b\gamma) > 25\%$), the ABRAMS 89c limit is 45.4 GeV. The limit for Higgs decay ($b' \rightarrow cH^\pm, H^\pm \rightarrow \bar{\nu}S$) is 45.2 GeV.
- 11 ADACHI 89c search was at $E_{cm} = 56.5\text{--}60.8$ GeV at TRISTAN using multi-hadron events accompanying muons.
- 12 ADACHI 89c also gives limits for any mixture of CC and bg decays.
- 13 ENO 89 search at $E_{cm} = 50\text{--}60.8$ GeV at TRISTAN.
- 14 ENO 89 considers arbitrary mixture of the charged current, bg, and $b\gamma$ decays.
- 15 IGARASHI 88 searches for leptons in low-thrust events and gives $\Delta R(b') < 0.26$ (95% CL) assuming charged current decay, which translates to $m_{b'} > 24.4$ GeV.
- 16 SAGAWA 88 set limit $\sigma(\text{top}) < 6.1$ pb at CL=95% for top-flavored hadron production from event shape analyses at $E_{cm} = 52$ GeV. By using the quark parton model cross-section formula near threshold, the above limit leads to lower mass bounds of 23.8 GeV for charge $-1/3$ quarks.
- 17 ADEVA 86 give 95%CL upper bound on an excess of the normalized cross section, ΔR , as a function of the minimum c.m. energy (see their figure 3). Production of a pair of $1/3$ charge quarks is excluded up to $E_{cm} = 45.4$ GeV.
- 18 ALTHOFF 84c narrow state search sets limit $\Gamma(e^+e^-B)/\text{hadrons} < 2.4$ keV CL = 95% and heavy charge $1/3$ quark pair production $m > 21$ GeV, CL = 95%.
- 19 ALTHOFF 84i exclude heavy quark pair production for $7 < m < 19$ GeV ($1/3$ charge) using aplanarity distributions (CL = 95%).

REFERENCES FOR Searches for (Fourth Generation) b' Quark

SIRUNYAN	19A1	EPL C79 90	A.M. Sirunyan et al.	(CMS Collab.)
SIRUNYAN	19AQ	EPL C79 364	A.M. Sirunyan et al.	(CMS Collab.)
SIRUNYAN	19BW	PR D100 072001	A.M. Sirunyan et al.	(CMS Collab.)
AABOUD	18AW	JHEP 1808 048	M. Aaboud et al.	(ATLAS Collab.)
AABOUD	18CE	JHEP 1812 039	M. Aaboud et al.	(ATLAS Collab.)
AABOUD	18CL	PR D98 092005	M. Aaboud et al.	(ATLAS Collab.)
AABOUD	18CP	PR D98 112010	M. Aaboud et al.	(ATLAS Collab.)
AABOUD	18CR	PRL 121 211871	M. Aaboud et al.	(ATLAS Collab.)
SIRUNYAN	18BM	JHEP 1808 177	A.M. Sirunyan et al.	(CMS Collab.)
SIRUNYAN	18Q	PR D97 072008	A.M. Sirunyan et al.	(CMS Collab.)
SIRUNYAN	17AU	JHEP 1711 085	A.M. Sirunyan et al.	(CMS Collab.)
AAD	16AH	JHEP 1602 110	G. Aad et al.	(ATLAS Collab.)
KHACHATRYAN	16AN	PR D93 112009	V. Khachatryan et al.	(CMS Collab.)
KHACHATRYAN	16I	JHEP 1601 166	V. Khachatryan et al.	(CMS Collab.)
AAD	15AR	JHEP 1508 105	G. Aad et al.	(ATLAS Collab.)
AAD	15BY	JHEP 1510 150	G. Aad et al.	(ATLAS Collab.)
AAD	15CN	PR D92 112007	G. Aad et al.	(ATLAS Collab.)
AAD	15Z	PR D91 112011	G. Aad et al.	(ATLAS Collab.)
AAD	14AZ	JHEP 1411 104	G. Aad et al.	(ATLAS Collab.)
CHATRCHYAN	13I	JHEP 1301 154	S. Chatrchyan et al.	(CMS Collab.)
AAD	12AT	PRL 109 032001	G. Aad et al.	(ATLAS Collab.)
AAD	12AU	PRL 109 071801	G. Aad et al.	(ATLAS Collab.)
AAD	12BC	PR D86 012007	G. Aad et al.	(ATLAS Collab.)
AAD	12BE	JHEP 1204 069	G. Aad et al.	(ATLAS Collab.)
CHATRCHYAN	12BH	PR D86 112003	S. Chatrchyan et al.	(CMS Collab.)
CHATRCHYAN	12X	JHEP 1205 123	S. Chatrchyan et al.	(CMS Collab.)
AALTONEN	11J	PRL 106 141803	T. Aaltonen et al.	(CDF Collab.)
ABAZOV	11F	PRL 106 081801	V.M. Abazov et al.	(D0 Collab.)
CHATRCHYAN	11L	PL B701 204	S. Chatrchyan et al.	(CMS Collab.)
AALTONEN	10H	PRL 104 091801	T. Aaltonen et al.	(CDF Collab.)
FLACCO	10	PRL 105 111801	C.J. Flacco et al.	(UCI, HAIF)
ATRE	09	PR D79 054018	A. Atre et al.	(DO Collab.)
ABAZOV	08X	PRL 101 111802	V.M. Abazov et al.	(DO Collab.)
HUANG	08	PR D77 037302	F.Q. Huang, M. Sher	(UVA, WILL)
AALTONEN	07C	PR D76 072006	T. Aaltonen et al.	(CDF Collab.)
ABDALLAH	07	EPL C50 507	F. Abdallah et al.	(DELPHI Collab.)
ACOSTA	03	PRL 90 131801	D. Acosta et al.	(CDF Collab.)
AFFOLDER	00	PRL 84 835	A. Affolder et al.	(CDF Collab.)
ABE	98N	PR D58 051102	F. Abe et al.	(CDF Collab.)
ABACHI	97D	PRL 78 3818	S. Abachi et al.	(D0 Collab.)
FROGGATT	97	ZPHY C73 333	C.D. Froggatt, D.J. Smith, H.B. Nielsen	(GLAS+)
ABACHI	95F	PR D52 4877	S. Abachi et al.	(D0 Collab.)
ADRIANI	93G	PL B313 326	O. Adriani et al.	(L3 Collab.)
ADRIANI	93M	PRPL 236 1	O. Adriani et al.	(L3 Collab.)
MUKHOPADHYAY	92	PR D48 2105	B. Mukhopadhyaya, D.P. Roy	(TATA)
ABE	92	PRL 68 447	F. Abe et al.	(CDF Collab.)
Also		PR D45 3921	F. Abe et al.	(CDF Collab.)
ABE	92G	PR D45 3921	F. Abe et al.	(CDF Collab.)
ABREU	91F	NP B367 511	P. Abreu et al.	(DELPHI Collab.)
ABE	90B	PRL 64 147	F. Abe et al.	(CDF Collab.)
ABE	90D	PL B234 382	K. Abe et al.	(VENUS Collab.)
ABREU	90D	PL B242 536	P. Abreu et al.	(DELPHI Collab.)
ADACHI	90	PL B234 197	I. Adachi et al.	(TOPAZ Collab.)
AKESSON	90	ZPHY C46 179	T. Akesson et al.	(UA2 Collab.)
AKRAWY	90B	PL B236 364	M.Z. Akrawy et al.	(OPAL Collab.)
AKRAWY	90J	PL B246 285	M.Z. Akrawy et al.	(OPAL Collab.)
ALBAJAR	90B	ZPHY C48 1	C. Albajar et al.	(UA1 Collab.)
DECAMP	90F	PL B236 511	D. Decamp et al.	(ALEPH Collab.)
ABE	89E	PR D39 3524	K. Abe et al.	(VENUS Collab.)
ABE	89G	PRL 63 1776	K. Abe et al.	(VENUS Collab.)
ABRAMS	89C	PRL 63 2447	G.S. Abrams et al.	(Mark II Collab.)
ADACHI	89C	PL B229 427	I. Adachi et al.	(TOPAZ Collab.)
ENO	89	PRL 63 1910	S. Eno et al.	(AMY Collab.)
ALBAJAR	88	ZPHY C37 505	C. Albajar et al.	(UA1 Collab.)
ALTARELLI	88	NP B308 724	G. Altarelli et al.	(CERN, ROMA, ETH)
IGARASHI	88	PRL 60 2359	S. Igarashi et al.	(AMY Collab.)
SAGAWA	88	PR 60 83	H. Sagawa et al.	(AMY Collab.)
ADEVA	86	PR D34 681	B. Adeva et al.	(Mark-J Collab.)
ALTHOFF	84C	PL 138B 441	M. Althoff et al.	(TASSO Collab.)
ALTHOFF	84I	ZPHY C22 307	M. Althoff et al.	(TASSO Collab.)

t' (4th Generation) Quark, Searches for

$t'(2/3)$ -quark/hadron mass limits in $p\bar{p}$ and pp collisions

VALUE (GeV)	CL%	DOCUMENT ID	TECN	COMMENT
>1280	95	1 SIRUNYAN	19AQ CMS	$B(t' \rightarrow Zt) = 1$
>1370	95	2 SIRUNYAN	19BW CMS	$B(t' \rightarrow ht) = 1$
> 980	95	3 AABOUD	18CE ATLS	$\geq 2\ell + \cancel{E}_T + \geq 1bj$
>1010	95	4 AABOUD	18CL ATLS	$B(t' \rightarrow ht) = 1$
>1030	95	5,6 AABOUD	18CP ATLS	2,3 ℓ , singlet model
>1210	95	5,7 AABOUD	18CP ATLS	2,3 ℓ , doublet model
>1310	95	8,9 AABOUD	18CR ATLS	singlet t' . ATLAS combination
>1370	95	8,10 AABOUD	18CR ATLS	t' in a weak isospin doublet (t', b'). ATLAS combination.
>1140	95	11 SIRUNYAN	18BM CMS	Wb, Zt, ht modes
> 845	95	12 SIRUNYAN	18Q CMS	$B(t' \rightarrow Wq) = 1$ ($q=d,s$)
>1295	95	13 SIRUNYAN	18W CMS	$B(t' \rightarrow Wb) = 1$
>1160	95	14 AABOUD	17L ATLS	$B(t' \rightarrow Zt) = 1$
> 860	95	15 SIRUNYAN	17AU CMS	
> 770	95	16 AAD	15AR ATLS	$B(t' \rightarrow Wb) = 1$
> 590	95	17 AAD	15BY ATLS	Wb, Zt, ht modes
> 745	95	18 KHACHATRYAN...15AI	CMS	$B(t' \rightarrow ht) = 1$
> 735	95	19 AAD	14AZ ATLS	$B(b' \rightarrow Wt) = 1$
> 700	95	20 CHATRCHYAN14A	CMS	$B(t' \rightarrow Wb) = 1$
> 706	95	20 CHATRCHYAN14A	CMS	$B(t' \rightarrow Zt) = 1$
> 782	95	20 CHATRCHYAN14A	CMS	$B(t' \rightarrow ht) = 1$
> 350	95	21 AAD	12BC ATLS	$B(t' \rightarrow Wq)=1$ ($q=d,s,b$)
> 420	95	22 AAD	12C ATLS	$t' \rightarrow Xt$ ($m_X < 140$ GeV)
> 685	95	23 CHATRCHYAN12BH	CMS	$m_{b'} = m_{t'}$
> 557	95	24 CHATRCHYAN12P	CMS	$t'^{\pm} \bar{\nu} b' W^{\mp} \bar{\nu} \rightarrow b\ell^{\pm} \nu \bar{\nu} \ell^{\mp} \bar{\nu}$

• • • We do not use the following data for averages, fits, limits, etc. • • •

- > 656
 95 | 25 AAD | 13F ATLS | $B(t' \rightarrow Wb) = 1$ |
 - > 625
 95 | 26 CHATRCHYAN13I | CMS | $B(t' \rightarrow Zt) = 1$ |
 - > 404
 95 | 27 AAD | 12AR ATLS | $B(t' \rightarrow Wb) = 1$ |
 - > 570
 95 | 28 CHATRCHYAN12BC | CMS | $t'\bar{t}' \rightarrow W^+ b W^- \bar{b}$ |
 - > 400
 95 | 29 AALTONEN | 11AH CDF | $t' \rightarrow Xt$ ($m_X < 70$ GeV) |
 - > 358
 95 | 30 AALTONEN | 11AL CDF | $t' \rightarrow Wb$ |
 - > 340
 95 | 30 AALTONEN | 11AL CDF | $t' \rightarrow Wq$ ($q=d,s,b$) |
 - > 360
 95 | 31 AALTONEN | 11O CDF | $t' \rightarrow Xt$ ($m_X < 100$ GeV) |
 - > 285
 95 | 32 ABAZOV | 11Q D0 | $t' \rightarrow Wq$ ($q=d,s,b$) |
 - > 256
 95 | 33,34 AALTONEN | 08H CDF | $t' \rightarrow Wq$ |
- 1 SIRUNYAN 19AQ based on 35.9 fb⁻¹ of pp data at $\sqrt{s} = 13$ TeV. Pair production of vector-like t' is searched for with one t' decaying into Zt and the other t' decaying into Wb, Zt, ht. Events with an opposite-sign lepton pair consistent with coming from Z and jets are used. Mass limits are obtained for a variety of branching ratios of t' .
 - 2 SIRUNYAN 19BW based on 35.9 fb⁻¹ of pp data at $\sqrt{s} = 13$ TeV. The limit is for the pair-produced vector-like t' using all-hadronic final state. The analysis is made for the Wb, Zt, ht modes and mass limits are obtained for a variety of branching ratios.
 - 3 AABOUD 18CE based on 36.1 fb⁻¹ of proton-proton data taken at $\sqrt{s} = 13$ TeV. Events including a same-sign lepton pair are used. The limit is for a singlet model, assuming the branching ratios of t' into Zt, Wb and ht as predicted by the model.
 - 4 AABOUD 18CL based on 36.1 fb⁻¹ of pp data at $\sqrt{s} = 13$ TeV. The limit is for the pair-produced vector-like t' using all-hadronic final state. The analysis is also made for the Wb, Zt, ht modes and mass limits are obtained for a variety of branching ratios.
 - 5 AABOUD 18CP based on 36.1 fb⁻¹ of pp data at $\sqrt{s} = 13$ TeV. Pair and single production of vector-like t' are searched for with at least one t' decaying into Zt. In the case of $B(t' \rightarrow Zt) = 1$, the limit is $m_{t'} > 1340$ GeV.
 - 6 The limit is for the singlet model, assuming that the branching ratios into Zt, Wb, and ht add up to one.
 - 7 The limit is for the doublet model, assuming that the branching ratios into Zt, Wb, and ht add up to one.
 - 8 AABOUD 18CR based on 36.1 fb⁻¹ of pp data at $\sqrt{s} = 13$ TeV. A combination of searches for the pair-produced vector-like t' in various decay channels ($t' \rightarrow Wb, Zt, ht$). Also a model-independent limit is obtained as $m_{t'} > 1.31$ TeV, assuming that the branching ratios into Zt, Wb and ht add up to one.
 - 9 The limit is for the singlet t' .
 - 10 The limit is for t' in a weak isospin doublet (t', b') and $|V_{tb'}| \ll |V_{t'b}|$.
 - 11 SIRUNYAN 18BM based on 35.9 fb⁻¹ of pp data at $\sqrt{s} = 13$ TeV. The limit is for the pair-produced vector-like t' . Three channels (single lepton, same-charge 2 leptons, or at least 3 leptons) are considered for various branching fraction combinations. Assuming $B(t'H) = 1$, the limit is 1270 GeV and for $B(t'Z) = 1$ it is 1300 GeV.
 - 12 SIRUNYAN 18Q based on 19.7 fb⁻¹ of pp data at $\sqrt{s} = 8$ TeV. The limit is for the pair-produced vector-like t' that couple only to light quarks. Constraints for other decay channels (Zq and Hq) are also given in the paper.
 - 13 SIRUNYAN 18W based on 35.8 fb⁻¹ of pp data at $\sqrt{s} = 13$ TeV. The limit is for the vector-like t' pair-produced by strong interaction using lepton-plus-jets mode and assuming that $B(t' \rightarrow Wb)$ is 100% product of the production cross section and branching fraction to Wb for any new pair-produced heavy quark decaying to this channel as a narrow resonance.
 - 14 AABOUD 17L based on 36.1 fb⁻¹ of pp data at $\sqrt{s} = 13$ TeV. No signal is found in the search for heavy quark pair production that decay into Zt followed by $Z \rightarrow \nu\nu$ in

Quark Particle Listings

t' (Fourth Generation) Quark

- the events with one lepton, large E_T , and ≥ 4 jets. The lower mass limit 0.87 (1.05) TeV is obtained for the singlet (doublet) model with other possible decay modes.
- SIRUNYAN 17AU based on 2.3-2.6 fb⁻¹ of pp data at $\sqrt{s} = 13$ TeV. Limit on pair-produced singlet vector-like t' using one lepton and several jets. The mass bound is given for a t' transforming as a singlet under the electroweak symmetry group, assumed to decay through W , Z or Higgs boson (which decays to jets) and to a third generation quark. For a doublet, the limit is >830 GeV. Other limits are also given in the paper.
 - AAD 15AR based on 20.3 fb⁻¹ of pp data at $\sqrt{s} = 8$ TeV. Used lepton-plus-jets final state. See Fig. 20 for mass limits in the plane of $B(t' \rightarrow Ht)$ vs. $B(t' \rightarrow Wb)$ from a combination of $t't' \rightarrow Wb + X$ and $t't' \rightarrow Ht + X$ searches. Any branching ratio scenario is excluded for mass below 715 GeV.
 - AAD 15BY based on 20.3 fb⁻¹ of pp data at $\sqrt{s} = 8$ TeV. Limit on pair-produced vector-like t' assuming the branching fractions to W , Z , and h modes of the singlet model. Used events containing $\geq 2\ell + E_T + \geq 2j$ (≥ 1 b) and including a same-sign lepton pair.
 - KHACHATRYAN 15AI based on 19.7 fb⁻¹ of pp data at $\sqrt{s} = 8$ TeV. The search exploits all-hadronic final states by tagging boosted Higgs boson using jet substructure and b -tagging.
 - Based on 20.3 fb⁻¹ of pp data at $\sqrt{s} = 8$ TeV. No significant excess over SM expectation is found in the search for pair production or single production of t' in the events with dilepton from a high p_T Z and additional jets (≥ 1 b -tag). If instead of $B(b' \rightarrow Wt)$ is 1 an electroweak singlet with $B(b' \rightarrow Wt) \sim 0.45$ is assumed, the limit reduces to 685 GeV.
 - Based on 19.5 fb⁻¹ of pp data at $\sqrt{s} = 8$ TeV. The t' quark is pair produced and is assumed to decay into three different final states of bW , tZ , and th . The search is carried out using events with at least one isolated lepton.
 - Based on 1.04 fb⁻¹ of pp data at $\sqrt{s} = 7$ TeV. No signal is found for the search of heavy quark pair production that decay into W and a quark in the events with dileptons, large E_T , and ≥ 2 jets.
 - Based on 1.04 fb⁻¹ of data in pp collisions at 7 TeV. AAD 12C looked for $t't'$ production followed by t' decaying into a top quark and X , an invisible particle, in a final state with an isolated high- p_T lepton, four or more jets, and a large missing transverse energy. No excess over the SM $t\bar{t}$ production gives the upper limit on $t't'$ production cross section as a function of $m_{t'}$ and m_X . The result is obtained for $B(t' \rightarrow Wt) = 1$.
 - Based on 5 fb⁻¹ of pp data at $\sqrt{s} = 7$ TeV. CHATRCHYAN 12BH searched for QCD and EW production of single and pair of degenerate 4th generation quarks that decay to Wb or Wt . Absence of signal in events with one lepton, same-sign dileptons or tripletons gives the bound. With a mass difference of 25 GeV/ c^2 between $m_{t'}$ and $m_{b'}$, the corresponding limit shifts by about ± 20 GeV/ c^2 .
 - Based on 5.0 fb⁻¹ of pp data at $\sqrt{s} = 7$ TeV. CHATRCHYAN 12P looked for $t't'$ production events with two isolated high p_T leptons, large E_T , and 2 high p_T jets with b -tag. The absence of signal above the SM background gives the limit for $B(t' \rightarrow Wb) = 1$.
 - Based on 4.7 fb⁻¹ of pp data at $\sqrt{s} = 7$ TeV. No signal is found for the search of heavy quark pair production that decay into W and a b quark in the events with a high p_T isolated lepton, large E_T , and at least 3 jets (≥ 1 b -tag). Vector-like quark of charge $2/3$ with $400 < m_{t'} < 550$ GeV and $B(t' \rightarrow Wb) > 0.63$ is excluded at 95% CL.
 - Based on 5.0 fb⁻¹ of pp data at $\sqrt{s} = 7$ TeV. CHATRCHYAN 13I looked for events with one isolated electron or muon, large E_T , and at least four jets with large transverse momenta, where one jet is likely to originate from the decay of a bottom quark.
 - Based on 1.04 fb⁻¹ of pp data at $\sqrt{s} = 7$ TeV. No signal is found in the search for pair produced heavy quarks that decay into W boson and a b quark in the events with a high p_T isolated lepton, large E_T and at least 3 jets (≥ 1 b -tag).
 - Based on 5.0 fb⁻¹ of pp data at $\sqrt{s} = 7$ TeV. CHATRCHYAN 12Bc looked for $t't'$ production events with a single isolated high p_T lepton, large E_T and at least 4 high p_T jets with a b -tag. The absence of signal above the SM background gives the limit for $B(t' \rightarrow Wb) = 1$.
 - Based on 5.7 fb⁻¹ of data in $p\bar{p}$ collisions at 1.96 TeV. AALTONEN 11AH looked for $t't'$ production followed by t' decaying into a top quark and X , an invisible particle, in the all hadronic decay mode of $t\bar{t}$. No excess over the SM $t\bar{t}$ production gives the upper limit on $t't'$ production cross section as a function of $m_{t'}$ and m_X . The result is obtained for $B(t' \rightarrow Xt) = 1$.
 - Based on 5.6 fb⁻¹ of data in $p\bar{p}$ collisions at 1.96 TeV. AALTONEN 11AL looked for $\ell + \geq 4j$ events and set upper limits on $\sigma(t't')$ as functions of $m_{t'}$.
 - Based on 4.8 fb⁻¹ of data in $p\bar{p}$ collisions at 1.96 TeV. AALTONEN 11I looked for $t't'$ production signal when t' decays into a top quark and X , an invisible particle, in $\ell + E_T + jets$ channel. No excess over the SM $t\bar{t}$ production gives the upper limit on $t't'$ production cross section as a function of $m_{t'}$ and m_X . The result is obtained for $B(t' \rightarrow Xt) = 1$.
 - Based on 5.3 fb⁻¹ of data in $p\bar{p}$ collisions at 1.96 TeV. ABAZOV 11Q looked for $\ell + E_T + \geq 4j$ events and set upper limits on $\sigma(t't')$ as functions of $m_{t'}$.
 - Searches for pair production of a new heavy top-like quark t' decaying to a W boson and another quark by fitting the observed spectrum of total transverse energy and reconstructed t' mass in the lepton + jets events.
 - HUANG 08 reexamined the t' mass lower bound of 256 GeV obtained in AALTONEN 08H that assumes $B(b' \rightarrow qZ) = 1$ for $q = u, c$ which does not hold when $m_{b'} < m_{t'} - m_W$ or the mixing $\sin^2(\theta_{bt'})$ is so tiny that the decay occurs outside of the vertex detector. Fig. 1 gives that lower bound on $m_{t'}$ in the plane of $\sin^2(\theta_{bt'})$ and $m_{b'}$.

$t'(5/3)$ -quark/hadron mass limits in $p\bar{p}$ and pp collisions

VALUE (GeV)	CL%	DOCUMENT ID	TECN	COMMENT
>1330	95	1 SIRUNYAN	19T CMS	$t'_R(5/3) \rightarrow tW^+$
>1300	95	1 SIRUNYAN	19T CMS	$t'_L(5/3) \rightarrow tW^+$
>1350	95	2 AABOUD	18AW ATLS	$t'(5/3) \rightarrow tW^+$

>1190	95	3 AABOUD	18CE ATLS	$\geq 2\ell + E_T + \geq 1bj$
>1020	95	4 SIRUNYAN	17J CMS	$t'_R(5/3) \rightarrow tW^+$
> 990	95	4 SIRUNYAN	17J CMS	$t'_L(5/3) \rightarrow tW^+$
> 750	95	5 AAD	15BY ATLS	$t'(5/3) \rightarrow tW^+$
> 840	95	6 AAD	15Z ATLS	$t'(5/3) \rightarrow tW^+$
> 800	95	7 CHATRCHYAN	14T CMS	$t'(5/3) \rightarrow tW^+$

- SIRUNYAN 19T based on 35.9 fb⁻¹ of pp data at $\sqrt{s} = 13$ TeV. Signals are searched in the final states of $t't'$ pair production, with same-sign leptons (which come from a t' decay) or a single lepton (which comes from a W out of $4Ws$), along with jets, and no excess over the SM expectation is found.
- AABOUD 18AW based on 36.1 fb⁻¹ of pp data at $\sqrt{s} = 13$ TeV. Limit on $t'(5/3)$ in pair production assuming its coupling to Wt is equal to one. Lepton-plus-jets final state is used, characterized by $\ell + E_T + jets$ (≥ 1 b -tagged).
- AABOUD 18CE based on 36.1 fb⁻¹ of proton-proton data taken at $\sqrt{s} = 13$ TeV. Events including a same-sign lepton pair are used. The limit is for the pair-produced vector-like t' . With single t' production included, assuming $t'tW$ coupling of one, the limit is $m_{t'} > 1.6$ TeV.
- SIRUNYAN 17J based on 2.3 fb⁻¹ of pp data at $\sqrt{s} = 13$ TeV. Signals are searched in the final states of $t't'$ pair production, with same-sign leptons (which come from a t' decay) or a single lepton (which comes from a W out of $4Ws$), along with jets, and no excess over the SM expectation is found.
- AAD 15BY based on 20.3 fb⁻¹ of pp data at $\sqrt{s} = 8$ TeV. Limit on $t'(5/3)$ in pair and single production assuming its coupling to Wt is equal to one. Used events containing $\geq 2\ell + E_T + \geq 2j$ (≥ 1 b) and including a same-sign lepton pair.
- AAD 15Z based on 20.3 fb⁻¹ of pp data at $\sqrt{s} = 8$ TeV. Used events with $\ell + E_T + \geq 6j$ (≥ 1 b) and at least one pair of jets from weak boson decay, sensitive to the final state $b\bar{b}W^+W^-W^+W^-$.
- CHATRCHYAN 14T based on 19.5 fb⁻¹ of pp data at $\sqrt{s} = 8$ TeV. Non-observation of anomaly in H_T distribution in the same-sign dilepton events leads to the limit when pair produced $t'(5/3)$ quark decays exclusively into t and W^+ , resulting in the final state with $b\bar{b}W^+W^-W^+W^-$.

$t'(2/3)$ mass limits from single production in $p\bar{p}$ and pp collisions

VALUE (GeV)	CL%	DOCUMENT ID	TECN	COMMENT
>950	95	1 AAD	16AV ATLS	$qg \rightarrow q't'b, B(t' \rightarrow Wb)=0.5$
>403	95	2 ABAZOV	11F D0	$qd \rightarrow q't' \rightarrow q'(Wd)$ $\bar{\kappa}_{dt'}=1, B(t' \rightarrow Wd)=1$
>551	95	2 ABAZOV	11F D0	$qu \rightarrow q't' \rightarrow q(Zu)$ $\bar{\kappa}_{ut'}=\sqrt{2}, B(t' \rightarrow Zu)=1$

- AAD 16AV based on 20.3 fb⁻¹ of pp data at $\sqrt{s} = 8$ TeV. No significant excess over SM expectation is found in the search for a fully reconstructed vector-like t' in the mode $\ell + E_T + \geq 2j$ (≥ 1 b). A veto on massive large-radius jets is used to reject the $t\bar{t}$ background.
- Based on 5.4 fb⁻¹ of data in $p\bar{p}$ collisions at 1.96 TeV. ABAZOV 11F looked for single production of t' via the Z or E coupling to the first generation up or down quarks, respectively. Model independent cross section limits for the single production processes $p\bar{p} \rightarrow t'q \rightarrow (Wd)q$, and $p\bar{p} \rightarrow t'q \rightarrow (Zd)q$ are given in Figs. 3 and 4, respectively, and the mass limits are obtained for the model of ATRE 09 with degenerate bi-doublets of vector-like quarks.

$t'(5/3)$ mass limits from single production in $p\bar{p}$ and pp collisions

VALUE (GeV)	DOCUMENT ID	TECN	COMMENT
•••	1 SIRUNYAN	19AI CMS	$tW \rightarrow t'(5/3) \rightarrow tW$

- SIRUNYAN 19AI based on 35.9 fb⁻¹ of pp data at $\sqrt{s} = 13$ TeV. Exclusion limits are set on the product of the production cross section and branching fraction for the $b'(-1/3) + t$ and $t'(5/3) + t$ modes as a function of the vector-like quark mass in Fig. 8 and Tab. 2 for relative vector-like quark widths between 1 and 30% for left- and right-handed vector-like quark couplings. No significant deviation from the SM prediction is observed.

REFERENCES FOR Searches for (Fourth Generation) t' Quark

SIRUNYAN	19AI	EPJ C79 90	A.M. Sirunyan et al.	(CMS Collab.)
SIRUNYAN	19AQ	EPJ C79 364	A.M. Sirunyan et al.	(CMS Collab.)
SIRUNYAN	19BW	PR D100 072001	A.M. Sirunyan et al.	(CMS Collab.)
SIRUNYAN	19T	JHEP 1903 082	A.M. Sirunyan et al.	(CMS Collab.)
AABOUD	18AW	JHEP 1808 048	M. Aaboud et al.	(ATLAS Collab.)
AABOUD	18CE	JHEP 1812 039	M. Aaboud et al.	(ATLAS Collab.)
AABOUD	18CL	PR D98 092005	M. Aaboud et al.	(ATLAS Collab.)
AABOUD	18CP	PR D98 112010	M. Aaboud et al.	(ATLAS Collab.)
AABOUD	18CR	PRL 121 211801	M. Aaboud et al.	(ATLAS Collab.)
SIRUNYAN	18BM	JHEP 1808 177	A.M. Sirunyan et al.	(CMS Collab.)
SIRUNYAN	18L	PR D97 072008	A.M. Sirunyan et al.	(CMS Collab.)
SIRUNYAN	18W	PL B779 82	A.M. Sirunyan et al.	(CMS Collab.)
AABOUD	17L	JHEP 1708 052	M. Aaboud et al.	(ATLAS Collab.)
SIRUNYAN	17AJ	JHEP 1711 085	A.M. Sirunyan et al.	(CMS Collab.)
SIRUNYAN	17J	JHEP 1708 073	A.M. Sirunyan et al.	(CMS Collab.)
AAD	16AV	EPJ C76 442	G. Aad et al.	(ATLAS Collab.)
AAD	15AR	JHEP 1508 105	G. Aad et al.	(ATLAS Collab.)
AAD	15BY	JHEP 1510 150	G. Aad et al.	(ATLAS Collab.)
AAD	15Z	PR D91 112011	G. Aad et al.	(ATLAS Collab.)
KHACHATRYAN	15AI	JHEP 1506 080	V. Khachatryan et al.	(CMS Collab.)
AAD	14AZ	JHEP 1411 104	G. Aad et al.	(ATLAS Collab.)
CHATRCHYAN	14A	PL B729 149	S. Chatrchyan et al.	(CMS Collab.)
CHATRCHYAN	14T	PRL 112 171801	S. Chatrchyan et al.	(CMS Collab.)
AAD	13F	PL B718 1284	G. Aad et al.	(ATLAS Collab.)
CHATRCHYAN	13I	JHEP 1301 154	S. Chatrchyan et al.	(CMS Collab.)
AAD	12AR	PRL 108 261802	G. Aad et al.	(ATLAS Collab.)
AAD	12BC	PR D86 012007	G. Aad et al.	(ATLAS Collab.)
AAD	12C	PRL 108 041805	G. Aad et al.	(ATLAS Collab.)
CHATRCHYAN	12Bc	PL B718 307	S. Chatrchyan et al.	(CMS Collab.)

CHATRCHYAN	12BH	PR	D86	112003	S. Chatrchyan et al.	(CMS Collab.)
CHATRCHYAN	12P	PL	B716	103	S. Chatrchyan et al.	(CMS Collab.)
AALTONEN	11AH	PRL	107	191803	T. Aaltonen et al.	(CDF Collab.)
AALTONEN	11AL	PRL	107	261801	T. Aaltonen et al.	(CDF Collab.)
AALTONEN	11O	PRL	106	191801	T. Aaltonen et al.	(CDF Collab.)
ABAZOV	11F	PRL	106	081801	V.M. Abazov et al.	(DO Collab.)
ABAZOV	11Q	PRL	107	082001	V.M. Abazov et al.	(DO Collab.)
ATRE	09	PR	D79	054018	A. Atre et al.	(CDF Collab.)
AALTONEN	08H	PRL	100	161803	T. Aaltonen et al.	(CDF Collab.)
HUANG	08	PR	D77	037302	P.Q. Hung, M. Sher	(UVA, WILL)

Free Quark Searches

FREE QUARK SEARCHES

The basis for much of the theory of particle scattering and hadron spectroscopy is the construction of the hadrons from a set of fractionally charged constituents (quarks). A central element of Quantum Chromodynamics is that quarks cannot be observed as free particles but are confined to mesons and baryons. Experiments have produced no evidence for free quarks.

This compilation is only a guide to the literature, since the quoted experimental limits are often only indicative. Reviews can be found in Refs. 1-4.

References

1. M.L. Perl, E.R. Lee, and D. Lomba, Mod. Phys. Lett. **A19**, 2595 (2004).
2. P.F. Smith, Ann. Rev. Nucl. and Part. Sci. **39**, 73 (1989).
3. L. Lyons, Phys. Reports **129**, 225 (1985).
4. M. Marinelli and G. Morpurgo, Phys. Reports **85**, 161 (1982).

Quark Production Cross Section — Accelerator Searches

X-SECT (cm ²)	CHG (e/3)	MASS (GeV)	ENERGY (GeV)	BEAM	EVTS	DOCUMENT ID	TECN
<1.7-2.3E-39	±2	100-600	7000	pp	0	¹ CHATRCHYAN13AR	CMS
<14.5.4E-39	±1	100-600	7000	pp	0	¹ CHATRCHYAN13AR	CMS
<1.3E-36	±2	45-84	130-172	e ⁺ e ⁻	0	ABREU 97D	DLPH
<2.E-35	+2	250	1800	p \bar{p}	0	² ABE 92J	CDF
<1.E-35	+4	250	1800	p \bar{p}	0	² ABE 92J	CDF
<3.8E-28		14.5A	²⁸ Si-Pb		0	³ HE 91	PLAS
<3.2E-28		14.5A	²⁸ Si-Cu		0	³ HE 91	PLAS
<1.E-40	±1,2	<10		p,ν,ν̄	0	BERGSMA 84B	CHRM
<1.E-36	±1,2	<9	200	μ	0	AUBERT 83C	SPEC
<2.E-10	±2,4	1-3	200	p	0	⁴ BUSSIÈRE 80	CNTR
<5.E-38	+1,2	>5	300	p	0	^{5,6} STEVENSON 79	CNTR
<1.E-33	±1	<20	52	pp	0	BASILE 78	SPEC
<9.E-39	±1,2	<6	400	p	0	⁵ ANTREASIAN 77	SPEC
<8.E-35	+1,2	<20	52	pp	0	⁷ FABJAN 75	CNTR
<5.E-38	-1,2	4-9	200	p	0	NASH 74	CNTR
<1.E-32	+2,4	4-24	52	pp	0	ALPER 73	SPEC
<5.E-31	+1,2,4	<12	300	p	0	LEIPUNER 73	CNTR
<6.E-34	±1,2	<13	52	pp	0	BOTT 72	CNTR
<1.E-36	-4	4	70	p	0	ANTIPOV 71	CNTR
<1.E-35	±1,2	2	28	p	0	⁸ ALLABY 69B	CNTR
<4.E-37	-2	<5	70	p	0	⁴ ANTIPOV 69	CNTR
<3.E-37	-1,2	2-5	70	p	0	⁸ ANTIPOV 69B	CNTR
<1.E-35	+1,2	<7	30	p	0	DORFAN 65	CNTR
<2.E-35	-2	<2.5-5	30	p	0	⁹ FRANZINI 65B	CNTR
<5.E-35	+1,2	<2.2	21	p	0	BINGHAM 64	HLBC
<1.E-32	+1,2	<4.0	28	p	0	BLUM 64	HBC
<1.E-35	+1,2	<2.5	31	p	0	⁹ HAGOPIAN 64	HBC
<1.E-34	+1	<2	28	p	0	LEIPUNER 64	CNTR
<1.E-33	+1,2	<2.4	24	p	0	MORRISON 64	HBC

¹ CHATRCHYAN 13AR limits assume pair-produced long-lived spin-1/2 particles neutral under SU(3)_C and SU(2)_L.
² ABE 92J flux limits decrease as the mass increases from 50 to 500 GeV.
³ HE 91 limits are for charges of the form N±1/3 from 23/3 to 38/3.
⁴ Hadronic or leptonic quarks.
⁵ Cross section cm²/GeV².
⁶ 3 × 10⁻⁵ < lifetime < 1 × 10⁻³ s.
⁷ Includes BOTT 72 results.
⁸ Assumes isotropic cm production.
⁹ Cross section inferred from flux.

Quark Differential Production Cross Section — Accelerator Searches

X-SECT (cm ² sr ⁻¹ GeV ⁻¹)	CHG (e/3)	MASS (GeV)	ENERGY (GeV)	BEAM	EVTS	DOCUMENT ID	TECN
<4.E-36	-2,4	1.5-6	70	p	0	BALDIN 76	CNTR
<2.E-33	±4	5-20	52	pp	0	ALBROW 75	SPEC
<5.E-34	<7	7-15	44	pp	0	JOVANOV...	75 CNTR
<5.E-35			20	γ	0	¹ GALIK 74	CNTR
<9.E-35	-1,2		200	p	0	NASH 74	CNTR
<4.E-36	-4	2.3-2.7	70	p	0	ANTIPOV 71	CNTR
<3.E-35	±1,2	<2.7	27	p	0	ALLABY 69B	CNTR
<7.E-38	-1,2	<2.5	70	p	0	ANTIPOV 69B	CNTR

¹ Cross section in cm²/sr/equivalent quanta.

Quark Flux — Accelerator Searches

The definition of FLUX depends on the experiment

- (a) is the ratio of measured free quarks to predicted free quarks if there is no "confinement."
- (b) is the probability of fractional charge on nuclear fragments. Energy is in GeV/nucleon.
- (c) is the 90%CL upper limit on fractionally-charged particles produced per interaction.
- (d) is quarks per collision.
- (e) is inclusive quark-production cross-section ratio to σ(e⁺e⁻ → μ⁺μ⁻).
- (f) is quark flux per charged particle.
- (g) is the flux per ν-event.
- (h) is quark yield per π⁻ yield.
- (i) is 2-body exclusive quark-production cross-section ratio to σ(e⁺e⁻ → μ⁺μ⁻).

FLUX	CHG (e/3)	MASS (GeV)	ENERGY (GeV)	BEAM	EVTS	DOCUMENT ID	TECN	
<1.6E-3	b	see note		200	³² S-Pb	¹ HUENTRUP 96	PLAS	
<6.2E-4	b	see note		10.6	³² S-Pb	¹ HUENTRUP 96	PLAS	
<0.94E-4	e	±2	2-30	88-94	e ⁺ e ⁻	AKERS 95R	OPAL	
<1.7E-4	e	±2	30-40	88-94	e ⁺ e ⁻	AKERS 95R	OPAL	
<3.6E-4	e	±4	5-30	88-94	e ⁺ e ⁻	AKERS 95R	OPAL	
<1.9E-4	e	±4	30-45	88-94	e ⁺ e ⁻	AKERS 95R	OPAL	
<2.E-3	e	+1	5-40	88-94	e ⁺ e ⁻	² BUSKULIC 93C	ALEP	
<6.E-4	e	+2	5-30	88-94	e ⁺ e ⁻	² BUSKULIC 93C	ALEP	
<1.2E-3	e	+4	15-40	88-94	e ⁺ e ⁻	² BUSKULIC 93C	ALEP	
<3.6E-4	i	+4	5.0-10.2	88-94	e ⁺ e ⁻	BUSKULIC 93C	ALEP	
<3.6E-4	i	+4	16.5-26.0	88-94	e ⁺ e ⁻	BUSKULIC 93C	ALEP	
<6.9E-4	i	+4	26.0-33.3	88-94	e ⁺ e ⁻	BUSKULIC 93C	ALEP	
<9.1E-4	i	+4	33.3-38.6	88-94	e ⁺ e ⁻	BUSKULIC 93C	ALEP	
<1.1E-3	i	+4	38.6-44.9	88-94	e ⁺ e ⁻	BUSKULIC 93C	ALEP	
<1.6E-4	b	see note		see note		³ CECCHINI 93	PLAS	
	b	4,5,7,8	2.1A	¹⁶ O	0,20,6	⁴ GHOSH 92	EMUL	
<6.4E-5	g	1		ν,ν̄	1	⁵ BASILE 91	CNTR	
<3.7E-5	g	2		ν,ν̄	0	⁵ BASILE 91	CNTR	
<3.9E-5	g	1		ν,ν̄	1	⁶ BASILE 91	CNTR	
<2.8E-5	g	2		ν,ν̄	0	⁶ BASILE 91	CNTR	
<1.9E-4	c		14.5A	²⁸ Si-Pb	0	⁷ HE 91	PLAS	
<3.9E-4	c		14.5A	²⁸ Si-Cu	0	⁷ HE 91	PLAS	
<1.E-9	c	±1,2,4	14.5A	¹⁶ O-Ar	0	MATIS 91	MDRP	
<5.1E-10	c	±1,2,4	14.5A	¹⁶ O-Hg	0	MATIS 91	MDRP	
<8.1E-9	c	±1,2,4	14.5A	Si-Hg	0	MATIS 91	MDRP	
<1.7E-6	c	±1,2,4	60A	¹⁶ O-Hg	0	MATIS 91	MDRP	
<3.5E-7	c	±1,2,4	200A	¹⁶ O-Hg	0	MATIS 91	MDRP	
<1.3E-6	c	±1,2,4	200A	S-Hg	0	MATIS 91	MDRP	
<5E-2	e	2	19-27	52-60	e ⁺ e ⁻	ADACHI 90C	TOPZ	
<5E-2	e	4	<24	52-60	e ⁺ e ⁻	ADACHI 90C	TOPZ	
<1.E-4	e	+2	<3.5	10	e ⁺ e ⁻	BOWCOCK 89B	CLEO	
<1.E-6	d	±1,2	60	¹⁶ O-Hg	0	ALLOWAY 89	MDRP	
<3.5E-7	d	±1,2	200	¹⁶ O-Hg	0	ALLOWAY 89	MDRP	
<1.3E-6	d	±1,2	200	S-Hg	0	ALLOWAY 89	MDRP	
<1.2E-10	d	±1	1	800	p-Hg	MATIS 89	MDRP	
<1.1E-10	d	±2	1	800	p-Hg	MATIS 89	MDRP	
<1.2E-10	d	±1	1	800	p-N ₂	MATIS 89	MDRP	
<7.7E-11	d	±2	1	800	p-N ₂	MATIS 89	MDRP	
<6.E-9	h	-5	0.9-2.3	12	p	0	NAKAMURA 89	SPEC
<5.E-5	g	1,2	<0.5		ν,ν̄d	0	ALLASIA 88	BEC
<3.E-4	b	See note	14.5	¹⁶ O-Pb	0	⁸ HOFFMANN 88	PLAS	
<2.E-4	b	See note	200	¹⁶ O-Pb	0	⁹ HOFFMANN 88	PLAS	
<8E-5	b	19,20,22,23	200A			GERBIER 87	PLAS	
<2.E-4	a	±1,2	<300	320	p \bar{p}	0	LYONS 87	MLEV
<1.E-9	c	±1,2,4,5	14.5	¹⁶ O-Hg	0	SHAW 87	MDRP	
<3.E-3	d	-1,2,3,4,6	<5	2	Si-Si	¹⁰ ABACHI 86C	CNTR	
<1.E-4	e	±1,2,4	<4	10	e ⁺ e ⁻	ALBRECHT 85G	ARG	
<6.E-5	b	±1,2	1	540	p \bar{p}	0	BANNER 85	UA2
<5.E-3	e	-4	1-8	29	e ⁺ e ⁻	0	AIHARA 84	TPC
<1.E-2	e	±1,2	1-13	29	e ⁺ e ⁻	0	AIHARA 84B	TPC
<2.E-4	b	±1	72	⁴⁰ Ar	0	¹¹ BARWICK 84	CNTR	
<1.E-4	e	±2	<0.4	1.4	e ⁺ e ⁻	0	BONDAR 84	OLYA
<5.E-1	e	±1,2	<13	29	e ⁺ e ⁻	0	GURYAN 84	CNTR

Quark Particle Listings

Free Quark Searches

<3.E-3	b	±1,2	<2	540	$p\bar{p}$	0	BANNER	83	CNTR
<1.E-4	b	±1,2		106	^{56}Fe	0	LINDGREN	83	CNTR
<3.E-3	b	> ± 0.1		74	^{40}Ar	0	11 PRICE	83	PLAS
<1.E-2	e	±1,2	<14	29	e^+e^-	0	MARINI	82B	CNTR
<8.E-2	e	±1,2	<12	29	e^+e^-	0	ROSS	82	CNTR
<3.E-4	e	±2	1.8-2	7	e^+e^-	0	WEISS	81	MRK2
<5.E-2	e	+1,2,4,5	2-12	27	e^+e^-	0	BARTEL	80	JADE
<2.E-5	g	1,2			ν	0	5,6 BASILE	80	CNTR
<3.E-10	f	±2,4	1-3	200	p	0	12 BOZZOLI	79	CNTR
<6.E-11	f	±1	<21	52	pp	0	BASILE	78	SPEC
<5.E-3	g				ν_μ	0	BASILE	78B	CNTR
<2.E-9	f	±1	<26	62	pp	0	BASILE	77	SPEC
<7.E-10	f	+1,2	<20	52	p	0	13 FABJAN	75	CNTR
		+1,2	>4.5	γ	0	5,6 GALIK	74	CNTR	
		+1,2	>1.5	12	e^-	0	5,6 BELLAMY	68	CNTR
		+1,2	>0.9	γ	0	6 BATHOW	67	CNTR	
		+1,2	>0.9	6	γ	0	6 FOSS	67	CNTR

- HUENTRUP 96 quote 95% CL limits for production of fragments with charge differing by as much as $\pm 1/3$ (in units of e) for charge $6 \leq Z \leq 10$.
- BUSKULIC 93c limits for inclusive quark production are more conservative if the ALEPH hadronic fragmentation function is assumed.
- CECCHINI 93 limit at 90%CL for $23/3 \leq Z \leq 40/3$, for 16A GeV O, 14.5A Si, and 200A S incident on Cu target. Other limits are 2.3×10^{-4} for $17/3 \leq Z \leq 20/3$ and 1.2×10^{-4} for $20/3 \leq Z \leq 23/3$.
- GHOSH 92 reports measurement of spallation fragment charge based on ionization in emulsion. Out of 650 measured tracks, 2 were consistent with charge $5e/3$, and 4 with $7e/3$.
- Hadronic quark.
- Leptonic quark.
- HE 91 limits are for charges of the form $N \pm 1/3$ from $23/3$ to $38/3$, and correspond to cross-section limits of $380\mu\text{b}$ (Pb) and $320\mu\text{b}$ (Cu).
- The limits apply to projectile fragment charges of 17, 19, 20, 22, 23 in units of $e/3$.
- The limits apply to projectile fragment charges of 16, 17, 19, 20, 22, 23 in units of $e/3$.
- Flux limits and mass range depend on charge.
- Bound to nuclei.
- Quark lifetimes $> 1 \times 10^{-8}$ s.
- One candidate $m < 0.17$ GeV.

Quark Flux — Cosmic Ray Searches

Shielding values followed with an asterisk indicate altitude in km. Shielding values not followed with an asterisk indicate sea level in kg/cm^2 .

FLUX ($\text{cm}^{-2}\text{sr}^{-1}\text{s}^{-1}$)	CHG (e/3)	MASS (GeV)	SHIELDING	DOCUMENT ID	TECN
< 1.E-8	±1/6-1/10			1 AGNESE 15	CDMS
< 9.2E-15	±1		3800	2 AMBROSIO 00c	MCRO
<2.1E-15	±1			MORI 91	KAM2
<2.3E-15	±2			MORI 91	KAM2
<2.E-10	±1,2		0.3	WADA 88	CNTR
	±4		0.3	3 WADA 88	CNTR
	±4		0.3	4 WADA 86	CNTR
<1.E-12	±2,3/2		-70.	5 KAWAGOE 84B	PLAS
<9.E-10	±1,2		0.3	WADA 84B	CNTR
<4.E-9	±4		0.3	WADA 84B	CNTR
<2.E-12	±1,2,3		-0.3 *	MASHIMO 83	CNTR
<3.E-10	±1,2		0.3	MARINI 82	CNTR
<2.E-11	±1,2			MASHIMO 82	CNTR
<8.E-10	±1,2		0.3	5 NAPOLITANO 82	CNTR
				6 YOCK 78	CNTR
<1.E-9				7 BRIATORE 76	ELEC
<2.E-11	+1			8 HAZEN 75	CC
<2.E-10	+1,2			KRISOR 75	CNTR
<1.E-7	+1,2			8,9 CLARK 74B	CC
<3.E-10	+1	>20		KIFUNE 74	CNTR
<8.E-11	+1			8 ASHTON 73	CNTR
<2.E-8	+1,2			HICKS 73B	CNTR
<5.E-10	+4		2.8 *	BEAUCHAMP 72	CNTR
<1.E-10	+1,2			8 BOHM 72B	CNTR
<1.E-10	+1,2		2.8 *	COX 72	ELEC
<3.E-10	+2			CROUCH 72	CNTR
<3.E-8			7	7 DARDO 72	CNTR
<4.E-9	+1			8 EVANS 72	CC
<2.E-9		>10		7 TONWAR 72	CNTR
<2.E-10	+1		2.8 *	CHIN 71	CNTR
<3.E-10	+1,2			8 CLARK 71B	CC
<1.E-10	+1,2			8 HAZEN 71	CC
<5.E-10	+1,2		3.5 *	BOSIA 70	CNTR
	+1,2	<6.5		8 CHU 70	HLBC
<2.E-9	+1			FAISSNER 70B	CNTR
<2.E-10	+1,2		0.8 *	KRIDER 70	CNTR
<5.E-11	+2			CAIRNS 69	CC
<8.E-10	+1,2	<10		FUKUSHIMA 69	CNTR
	+2			8,10 MCCUSKER 69	CC
<1.E-10		>5	1.7,3.6	7 BJORNBOE 68	CNTR
<1.E-8	±1,2,4		6.3,2 *	5 BRIATORE 68	CNTR
<3.E-8		>2		FRANZINI 68	CNTR
<9.E-11	±1,2			GARMIRE 68	CNTR

<4.E-10		±1		HANAYAMA 68	CNTR	
<3.E-8		>15		KASHA 68	OSPK	
<2.E-10		+2		KASHA 68B	CNTR	
<2.E-10		+4		KASHA 68c	CNTR	
<2.E-10		+2		6 BARTON 67	CNTR	
<2.E-7		+4	0.008,0.5 *	BUHLER 67	CNTR	
<5.E-10		1,2	0.008,0.5 *	BUHLER 67B	CNTR	
<4.E-10		+1,2		GOMEZ 67	CNTR	
<2.E-9		+2		KASHA 67	CNTR	
<2.E-10		+2	220	BARTON 66	CNTR	
<2.E-9		+1,2	0.5 *	BUHLER 66	CNTR	
<3.E-9		+1,2		KASHA 66	CNTR	
<2.E-9		+1,2		LAMB 66	CNTR	
<2.E-8		+1,2	>7	2.8 *	DELISE 65	CNTR
<5.E-8		+2	>2.5	0.5 *	MASSAM 65	CNTR
<2.E-8		+1		2.5 *	BOWEN 64	CNTR
<2.E-7		+1		0.8	SUNYAR 64	CNTR

- See AGNESE 15 Fig.6 for limits on vertical density as function of charge extending to $|q|/e < 1/10$.
- AMBROSIO 00c limit is below 11×10^{-15} for $0.25 < q/e < 0.5$, and is changing rapidly near $q/e=2/3$, where it is 2×10^{-14} .
- Distribution in celestial sphere was described as anisotropic.
- With telescope axis at zenith angle 40° to the south.
- Leptonic quarks.
- Lifetime $> 10^{-8}$ s; charge $\pm 0.70, 0.68, 0.42$; and mass $> 4.4, 4.8, \text{ and } 20$ GeV, respectively.
- Time delayed air shower search.
- Prompt air shower search.
- Also $e/4$ and $e/6$ charges.
- No events in subsequent experiments.

Quark Density — Matter Searches

QUARKS/ NUCLEON	CHG (e/3)	MASS (GeV)	MATERIAL/METHOD	EVTS	DOCUMENT ID
<1.17E-22			silicone oil drops	0	1 LEE 02
<4.71E-22			silicone oil drops	1	2 HALYO 00
<4.7E-21	±1,2		silicone oil drops	0	MAR 96
<8.E-22	+2		Si/infrared photoionization	0	PERERA 93
<5.E-27	±1,2		sea water/levitation	0	HOMER 92
<4.E-20	±1,2		meteorites/mag. levitation	0	JONES 89
<1.E-19	±1,2		various/spectrometer	0	MILNER 87
<5.E-22	±1,2		W/levitation	0	SMITH 87
<3.E-20	+1,2		org liq/droplet tower	0	VAN POLEN 87
<6.E-20	-1,2		org liq/droplet tower	0	VAN POLEN 87
<3.E-21	±1		Hg drops-untreated	0	SAVAGE 86
<3.E-22	±1,2		levitated niobium	0	SMITH 86
<2.E-26	±1,2		^4He /levitation	0	SMITH 86B
<2.E-20	>±1	0.2-250	niobium+tungs/ion	0	MILNER 85
<1.E-21	±1		levitated niobium	0	SMITH 85
	+1,2	<100	niobium/mass spec	0	KUTSCHERA 84
<5.E-22			levitated steel	0	MARINELLI 84
<9.E-20	± <13		water/oil drop	0	JOYCE 83
<2.E-21	> ± 1/2		levitated steel	0	LIEBOWITZ 83
<1.E-19	±1,2		photo ion spec	0	VANDESTEEG 83
<2.E-20			mercury/oil drop	0	3 HODGES 81
1.E-20	+1		levitated niobium	4	4 LARUE 81
1.E-20	-1		levitated niobium	4	4 LARUE 81
<1.E-21			levitated steel	0	MARINELLI 80B
<6.E-16			helium/mass spec	0	BOYD 79
1.E-20	+1		levitated niobium	2	4 LARUE 79
<4.E-28			earth+/ion beam	0	OGOROD... 79
<5.E-15	+1		tungs./mass spec	0	BOYD 78
<5.E-16	+3	<1.7	hydrogen/mass spec	0	BOYD 78B
<1.E-21	±2,4		water/ion beam	0	LUND 78
<6.E-15	>1/2		levitated tungsten	0	PUTT 78
<1.E-22			metals/mass spec	0	SCHIFFER 78
<5.E-15			levitated tungsten ox	0	BLAND 77
<3.E-21			levitated iron	0	GALLINARO 77
2.E-21	-1		levitated niobium	1	4 LARUE 77
4.E-21	+1		levitated niobium	2	4 LARUE 77
<1.E-13	+3	<7.7	hydrogen/mass spec	0	MULLER 77
<5.E-27			water+/ion beam	0	OGOROD... 77
<1.E-21			lunar+/ion spec	0	STEVENS 76
<1.E-15	+1	<60	oxygen+/ion spec	0	ELBERT 70
<5.E-19			levitated graphite	0	MORPURGO 70
<5.E-23			water+/atom beam	0	COOK 69
<1.E-17	±1,2		levitated graphite	0	BRAGINSK 68
<1.E-17			water+/uv spec	0	RANK 68
<3.E-19	±1		levitated iron	0	STOVER 67
<1.E-10			sun/uv spec	0	5 BENNETT 66
<1.E-17	+1,2		meteorites+/ion beam	0	CHUPKA 66
<1.E-16	±1		levitated graphite	0	GALLINARO 66
<1.E-22			argon/electrometer	0	HILLAS 59
	-2		levitated oil	0	MILLIKAN 10

1 95% CL limit for fractional charge particles with $0.18e \leq |Q_{residual}| \leq 0.82e$ in total of 70.1 mg of silicone oil.

See key on page 999

Quark Particle Listings

Free Quark Searches

- ² 95% CL limit for particles with fractional charge $|Q_{residual}| > 0.16e$ in total of 17.4 mg of silicone oil.
- ³ Also set limits for $Q = \pm e/6$.
- ⁴ Note that in PHILLIPS 88 these authors report a subtle magnetic effect which could account for the apparent fractional charges.
- ⁵ Limit inferred by JONES 77b.

REFERENCES FOR Free Quark Searches

AGNESE 15 PRL 114 111302	R. Agnese <i>et al.</i>	(CDMS Collab.)
CHATRCHYAN 13AR PR D87 092008	S. Chattrchyan <i>et al.</i>	(CMS Collab.)
LEE 02 PR D66 012002	I.T. Lee <i>et al.</i>	
AMBROSIO 00C PR D62 052003	M. Ambrosio <i>et al.</i>	(MACRO Collab.)
HALYO 00 PRL 84 2576	V. Haljo <i>et al.</i>	
ABREU 97D PL B396 315	P. Abreu <i>et al.</i>	(DELPHI Collab.)
HUENSTRUP 96 PR C53 358	G. Huenstrup <i>et al.</i>	(SIEG)
MAR 96 PR D53 6017	N.M. Mar <i>et al.</i>	(SLAC, SCHA, LANL, UCI)
AKERS 95R ZPHY C67 203	R. Akers <i>et al.</i>	(OPAL Collab.)
BUSKULIC 93C PL B303 198	D. Buskulic <i>et al.</i>	(ALEPH Collab.)
CECCHINI 93 ASP 1 369	S. Cecchini <i>et al.</i>	
PERERA 93 PRL 70 1053	A.G.U. Perera <i>et al.</i>	(PITT)
ABE 92J PR D46 1889	F. Abe <i>et al.</i>	(CDF Collab.)
GHOSH 92 NC 105A 99	D. Ghosh <i>et al.</i>	(JADA, BANGB)
HOMER 92 ZPHY C55 549	G.J. Homer <i>et al.</i>	(RAL, SHMP, LOQM)
BASILE 91 NC 104A 405	M. Basile <i>et al.</i>	(BGNA, INFN, CERN, PLRM+)
HE 91 PR C44 1672	Y.B. He, P.B. Price	(UCB)
MATIS 91 NP A525 513	H.S. Matis <i>et al.</i>	(LBL, SFSU, UCI+)
MORI 91 PR D43 2843	M. Mori <i>et al.</i>	(Kamikande II Collab.)
ADACHI 90C PL B244 352	I. Adachi <i>et al.</i>	(TOPAZ Collab.)
BOWCOCK 89B PR D40 263	T.J.V. Bowcock <i>et al.</i>	(CLEO Collab.)
CALLOWAY 89 PR B232 549	D. Calloway <i>et al.</i>	(SFSU, UCI, LBL+)
JONES 89 ZPHY C43 349	W.G. Jones <i>et al.</i>	(LOIC, RAL)
MATIS 89 PR D39 1851	H.S. Matis <i>et al.</i>	(LBL, SFSU, UCI+)
NAKAMURA 89 PR D39 1261	T.T. Nakamura <i>et al.</i>	(KYOT, TMT C)
ALLASIA 88 PR D37 219	D. Allasia <i>et al.</i>	(WA25 Collab.)
HOFFMANN 88 PL B200 583	A. Hofmann <i>et al.</i>	(SIEG, USF)
PHILLIPS 88 NIM A264 125	J.D. Phillips, W.M. Fairbank, J. Navarro	(STAN)
WADA 88 NC 11C 229	T. Wada, Y. Yamashita, I. Yamamoto	(OKAY)
GERBIER 87 PRL 59 2535	G. Gerbier <i>et al.</i>	(UCB, CERN)
LYONS 87 ZPHY C36 363	L. Lyons <i>et al.</i>	(OXF, RAL, LOIC)
MILNER 87 PR D36 37	R.E. Milner <i>et al.</i>	(CIT)
SHAW 87 PR D36 3533	G.L. Shaw <i>et al.</i>	(UCI, LBL, LANL, SFSU)
SMITH 87 PL B197 447	P.F. Smith <i>et al.</i>	(RAL, LOIC)
VANPOLEN 87 PR D36 1983	J. van Polen, R.T. Hagstrom, G. Hirsch	(ANL+)
ABACHI 86C PR D33 2733	S. Abachi <i>et al.</i>	(UCLA, LBL, UCD)
SAVAGE 86 PL 167B 481	M.L. Savage <i>et al.</i>	(SFSU)
SMITH 86 PL B171 129	P.F. Smith <i>et al.</i>	(RAL, LOIC)
SMITH 86B PL B181 407	P.F. Smith <i>et al.</i>	(RAL, LOIC)
WADA 86 NC 9C 358	T. Wada	(OKAY)
ALBRECHT 85G PL 156B 134	T. Albrecht <i>et al.</i>	(ARGUS Collab.)
BANNER 85 PL 156B 129	M. Banner <i>et al.</i>	(UA2 Collab.)
MILNER 85 PRL 54 1472	R.E. Milner <i>et al.</i>	(CIT)
SMITH 85 PL 153B 188	P.F. Smith <i>et al.</i>	(RAL, LOIC)
AIHARA 84 PRL 52 168	H. Aihara <i>et al.</i>	(TPC Collab.)
AIHARA 84B PRL 52 2332	H. Aihara <i>et al.</i>	(TPC Collab.)
BARWICK 84 PR D30 691	S.W. Barwick, J.A. Musser, J.D. Stevenson	(UCB)
BERGSWA 84B ZPHY C24 217	F. Bergswa <i>et al.</i>	(CHARM Collab.)
BONDAR 84 JETPL 40 1265	A.E. Bondar <i>et al.</i>	(NOVO)
Translated from ZETF 60 44		
GURYN 84 PL 139B 313	W. Guryin <i>et al.</i>	(FRAS, LBL, NWES, STAN+)
KAWAGOE 84B LNC 41 604	K. Kawagoe <i>et al.</i>	(TOKY)
KUTSCHERA 84 PR D29 791	W. Kutschera <i>et al.</i>	(ANL, FNAL)
MARINELLI 84 PL 137B 439	M. Marinelli, G. Morpurgo	(GENO)
WADA 84B LNC 40 329	T. Wada, Y. Yamashita, I. Yamamoto	(OKAY)
AUBERT 83C PL 133B 461	J.J. Aubert <i>et al.</i>	(EMC Collab.)
BANNER 83 PL 121B 187	M. Banner <i>et al.</i>	(UA2 Collab.)
JOYCE 83 PRL 51 731	D.C. Joyce <i>et al.</i>	(SFSU)
LIEBOWITZ 83 PRL 50 1640	D. Liebowitz, M. Binder, K.O.H. Ziock	(UVA)
LINDGREN 83 PRL 51 1521	M.A. Lindgren <i>et al.</i>	(SFSU, UCR, UCI+)
MASHIMO 83 PL 128B 327	T. Mashimo <i>et al.</i>	(ICEPP)
PRICE 83 PRL 50 566	P.B. Price <i>et al.</i>	(UCB)
VANDESTEEG 83 PRL 50 1234	M.J.H. van de Steeg, H.V.H.M. Jongbloets, P. Wyder	
MARINI 82 PR D26 1777	A. Marini <i>et al.</i>	(FRAS, LBL, NWES, STAN+)
MARINI 82B PR 48 1649	A. Marini <i>et al.</i>	(FRAS, LBL, NWES, STAN+)
MASHIMO 82 JPSJ 51 3067	T. Mashimo, K. Kawagoe, M. Koshiba	(INUS)
NAPOLITANO 80 PR D25 2837	J. Napolitano <i>et al.</i>	(STAN, FRAS, LBL+)
ROSS 82 PL 118B 199	M.C. Ross <i>et al.</i>	(FRAS, LBL, NWES, STAN+)
HODGES 81 PRL 47 1651	C.L. Hodges <i>et al.</i>	(UCR, SFSU)
LARUE 81 PRL 46 967	G.S. Larue, J.D. Phillips, W.M. Fairbank	(STAN)
WEISS 81 PL 301B 439	J.M. Weiss <i>et al.</i>	(SLAC, LBL, UCB)
BARTL 80 ZPHY C6 295	W. Bartel <i>et al.</i>	(JADE Collab.)
BASILE 80 LNC 29 251	M. Basile <i>et al.</i>	(BGNA, CERN, FRAS, ROMA+)
BUSSIERE 80 NP B174 1	A. Bussiere <i>et al.</i>	(BGNA, SACL, LAPP)
MARINELLI 80B PL 94B 433	M. Marinelli, G. Morpurgo	(GENO)
Also PL 94B 427	M. Marinelli, G. Morpurgo	(GENO)
BOYD 79 PRL 43 1288	R.N. Boyd <i>et al.</i>	(OSU)
BOZZOLI 79 NP B159 363	W. Bozzoli <i>et al.</i>	(BGNA, LAPP, SACL+)
LARUE 79 PRL 42 142	G.S. Larue, W.M. Fairbank, J.D. Phillips	(STAN)
OGOROD... 79 JETP 49 953	D.D. Ogorodnikov, I.M. Samoilo, A.M. Solntsev	
Also 18B1		
STEVENSON 79 PR D20 82	M.L. Stevenson	(LBL)
BASILE 78 NC 45A 171	M. Basile <i>et al.</i>	(CERN, BGNA)
BASILE 78B NC 45A 281	M. Basile <i>et al.</i>	(CERN, BGNA)
BOYD 78 PRL 40 216	R.N. Boyd <i>et al.</i>	(ROCH)
BOYD 78B PL 72B 484	R.N. Boyd <i>et al.</i>	(ROCH)
LUND 78 R 25 75	T. Lund, R. Brandt, Y. Fares	(MARB)
PUTT 78 PR D17 1466	G.D. Putt, P.C.M. Yock	(AUCK)

SCHIFFER 78 PR D17 2241	J.P. Schiffer <i>et al.</i>	(CHIC, ANL)
YOCK 78 PR D18 641	P.C.M. Yock	(AUCK)
ANTREASIAN 77 PRL 39 513	D. Antreasian <i>et al.</i>	(EFI, PRIN)
BASILE 77 NC 40A 41	M. Basile <i>et al.</i>	(CERN, BGNA)
BLAND 77 PRL 39 369	R.W. Bland <i>et al.</i>	(SFSU)
GALLINARO 77 PRL 38 1255	G. Gallinaro, M. Marinelli, G. Morpurgo	(GENO)
JONES 77B RMP 49 717	L.W. Jones	
LARUE 77 PRL 38 1011	G.S. Larue, W.M. Fairbank, A.F. Hebard	(STAN)
MULLER 77 SCI 196 821	R.A. Muller <i>et al.</i>	(LBL)
OGOROD... 77 JETP 45 857	D.D. Ogorodnikov, I.M. Samoilo, A.M. Solntsev	
Also 1633		
BALDIN 76 SJNP 22 264	B.Y. Baldin <i>et al.</i>	(JINR)
Also 2512		
BRIATORE 76 NC 31A 553	L. Briatore <i>et al.</i>	(LCGT, FRAS, FREIB)
STEVENS 76 PR D14 716	C.M. Stevens, J.P. Schiffer, W. Chupka	(ANL)
ALBROW 75 NP B37 189	M.G. Albrow <i>et al.</i>	(CERN, DARE, FOM+)
FABIAN 75 NP B101 349	C.W. Fabjan <i>et al.</i>	(CERN, MPIM)
HAZEN 75 NP B95 189	W.E. Hazen <i>et al.</i>	(MICH, LEED)
JOVANOVICH... 75 PL 56B 105	J.V. Jovanovich <i>et al.</i>	(MANI, AACH, CERN+)
KRISOR 75 NC 27A 132	K. Krisor	(AACH3)
CLARK 74B PR D10 2721	A.F. Clark <i>et al.</i>	(LLL)
GALIK 74 PR D9 1856	R.S. Galik <i>et al.</i>	(SLAC, FNAL)
KIFUNE 74 JPSJ 36 629	T. Kifune <i>et al.</i>	
NASH 74 PRL 32 858	T. Nash <i>et al.</i>	(FNAL, CORN, NYU)
ALPER 73 PL 46B 265	B. Alper <i>et al.</i>	(CERN, LVP, LUND, BOHR+)
ASHTON 73 JP 46 577	F. Ashton <i>et al.</i>	(DURH)
HICKS 73B NC 14A 65	R.B. Hicks, R.W. Flint, S. Standil	(MANI)
LEIPUNER 73 PRL 31 1226	L.B. Leipuner <i>et al.</i>	(BNL, YALE)
BEAUCHAMP 72 PR D6 1211	W.T. Beauchamp <i>et al.</i>	(ARIZ)
BOHM 72B PRL 28 326	A. Bohm <i>et al.</i>	(AACH)
BOTT 72 PL 40B 693	M. Bott-Bodenhausen <i>et al.</i>	(CERN, MPIM)
COX 72 PR D6 1203	A.J. Cox <i>et al.</i>	(ARIZ)
CROUCH 72 PR D5 2667	M.F. Crouch, K. Mori, G.R. Smith	(CASE)
DARDO 72 NC 9A 319	M. Dardo <i>et al.</i>	(TORI)
EVANS 72 PRSE A70 143	G.R. Evans <i>et al.</i>	(EDIN, LEED)
TOWNAR 72 JP A5 569	S.C. Townar, S. Narayan, B.V. Sreekantan	(TATA)
ANTIPOV 71 NP B29 374	Y.M. Antipov <i>et al.</i>	(SERP)
CHIN 71 NC 2A 419	S. Chin <i>et al.</i>	(OSAK)
CLARK 71B PRL 27 51	A.F. Clark <i>et al.</i>	(LLL, LBL)
HAZEN 71 PRL 26 582	W.E. Hazen	(MICH)
BOSIA 70 NC 66A 167	G.F. Bosia, L. Briatore	(TORI)
CHU 70 PRL 24 917	W.T. Chu <i>et al.</i>	(OSU, ROSE, KANS)
Also 2550		
ELBERT 70 NP B20 217	J.W. Elbert <i>et al.</i>	(ANL)
FAISSNER 70B PRL 24 1357	H. Faissner <i>et al.</i>	(WISC)
KRIDER 70 PR D1 835	E.P. Krider, T. Bowen, R.M. Kalbach	(AACH3)
MORPURGO 70 NIM 79 95	G. Morpurgo, G. Gallinaro, G. Palmieri	(ARIZ)
ALLABY 69B NC 64A 75	J.V. Allaby <i>et al.</i>	(GENO)
ANTIPOV 69 NP 29B 245	Y.M. Antipov <i>et al.</i>	(CERN)
ANTIPOV 69B PL 30B 576	Y.M. Antipov <i>et al.</i>	(SERP)
CAIRNS 69 PR 186 1394	I. Cairns	(SYDN)
COOK 69 PR 188 2092	D.D. Cook <i>et al.</i>	(ILL)
FUKUSHIMA 69 PR 178 2058	Y. Fukushima <i>et al.</i>	(TOKY)
MCCUSKER 69 PRL 23 658	G.B. McCusker, I. Cairns	(SYDN)
BELLAMY 68 PR 166 1391	J.H. Bellamy <i>et al.</i>	(STAN, SLAC)
BJORNBØE 68 NC B53 241	J. Bjornboe <i>et al.</i>	(BOHR, TATA, BERN+)
BRAGINSKY 68 JETP 27 51	V.B. Braginsky <i>et al.</i>	(MOSU)
Also 91		
BRIATORE 68 Translated from ZETF 54 91	L. Briatore <i>et al.</i>	(TORI, CERN, BGNA)
FRANZINI 68 PRL 21 1013	P. Franzini, S. Shulman	(COLU)
GARMIRE 68 PR 166 1280	G. Garmire, C. Leong, V. Sreekantan	(MIT)
HANAYAMA 68 CJP 46 5734	Y. Hanayama <i>et al.</i>	(OSAK)
KASHA 68 PR 172 1297	H. Kasha, R.J. Stefanski	(BNL, YALE)
KASHA 68B PRL 20 217	H. Kasha <i>et al.</i>	(BNL, YALE)
KASHA 68C CJP 46 5730	H. Kasha <i>et al.</i>	(BNL, YALE)
RANK 68 PR 176 1635	D. Rank	(MICH)
BARTON 67 PRSL 90 87	J.C. Barton	(NPOL)
BATHOW 67 PL 25B 163	G. Bathow <i>et al.</i>	(DESY)
BUHLER 67 NC 49A 209	A. Buhler-Broglin <i>et al.</i>	(CERN, BGNA)
BUHLER 67B NC 51A 837	A. Buhler-Broglin <i>et al.</i>	(CERN, BGNA+)
FOSS 67 PL 25B 166	J. Foss <i>et al.</i>	(MIT)
GOMEZ 67 PRL 18 1022	R. Gomez <i>et al.</i>	(CIT)
KASHA 67 PR 154 1263	H. Kasha <i>et al.</i>	(BNL, YALE)
STOVER 67 PR 164 1599	R.W. Stover, T.J. Moran, J.W. Trischka	(SYRA)
BARTON 66 PL 21 360	J.C. Barton, C.T. Stockel	(NPOL)
BENNETT 66 PRL 17 1196	W.R. Bennett	(YALE)
BUHLER 66 NC 45A 520	A. Buhler-Broglin <i>et al.</i>	(CERN, BGNA+)
CHUPKA 66 PRL 17 60	W.A. Chupka, J.P. Schiffer, C.M. Stevens	(ANL)
GALLINARO 66 PL 23 609	G. Gallinaro, G. Morpurgo	(GENO)
KASHA 66 PR 150 1440	H. Kasha, L.B. Leipuner, R.K. Adair	(BNL, YALE)
LAMB 66 PRL 17 1068	R.C. Lamb <i>et al.</i>	(ANL)
DELISE 65 PR 140 8458	D.E. Lise, T. Bowen	(ARIZ)
DORFAN 65 PRL 14 999	D.E. Dorfman <i>et al.</i>	(COLU)
FRANZINI 65B PRL 14 196	P. Franzini <i>et al.</i>	(BNL, COLU)
MASSAM 65 NC 40A 589	T. Massam, T. Muller, A. Zichichi	(CERN)
BINGHAM 64 PL 9 201	H.H. Bingham <i>et al.</i>	(CERN, EPOL)
BLUM 64 PRL 13 353A	W. Blum <i>et al.</i>	(CERN)
BOWEN 64 PRL 13 728	T. Bowen <i>et al.</i>	(ARIZ)
HAGOPIAN 64 PRL 13 280	V. Hagopian <i>et al.</i>	(PENN, BNL)
LEIPUNER 64 PRL 12 423	L.B. Leipuner <i>et al.</i>	(BNL, YALE)
MORRISON 64 PR 9 199	D.R.O. Morrison	(CERN)
SUNYAR 64 PR 136 B1157	A.W. Sunyar, A.Z. Schwarzschild, P.I. Connors	(BNL)
HILLAS 59 NAT 184 B92	A.M. Hillas, T.E. Cranshaw	(AERE)
MILLIKAN 10 Phil Mag 19 209	R.A. Millikan	(CHIC)

OTHER RELATED PAPERS

LYONS 85 PRPL C129 225	L. Lyons	(OXF)
MARINELLI 82 PRPL 85 161	M. Marinelli, G. Morpurgo	(GENO)

LIGHT UNFLAVORED MESONS ($S = C = B = 0$)

- π^\pm 1209
- π^0 1212
- η 1214
- $f_0(500)$ aka σ ; was $f_0(600)$ 1219
- $\rho(770)$ 1221
- $\omega(782)$ 1228
- $\eta'(958)$ 1233
- $f_0(980)$ 1239
- $a_0(980)$ 1242
- $\phi(1020)$ 1243
- $h_1(1170)$ 1250
- $b_1(1235)$ 1251
- $a_1(1260)$ 1252
- $f_2(1270)$ 1254
- $f_1(1285)$ 1257
- $\eta(1295)$ 1260
- $\pi(1300)$ 1261
- $a_2(1320)$ 1262
- $f_0(1370)$ 1265
- $\pi_1(1400)$ 1268
- $\eta(1405)$ 1269
- $h_1(1415)$ was $h_1(1380)$ 1272
- $a_1(1420)$ 1272
- $f_1(1420)$ 1272
- $\omega(1420)$ 1274
- $f_2(1430)$ 1275
- $a_0(1450)$ 1275
- $\rho(1450)$ 1276
- $\eta(1475)$ 1281
- $f_0(1500)$ 1282
- $f_1(1510)$ 1285
- $f_2'(1525)$ 1286
- $f_2(1565)$ 1289
- $\rho(1570)$ 1290
- $h_1(1595)$ 1291
- $\pi_1(1600)$ 1291
- $a_1(1640)$ 1292
- $f_2(1640)$ 1293
- $\eta_2(1645)$ 1293
- $\omega(1650)$ 1293
- $\omega_3(1670)$ 1295
- $\pi_2(1670)$ 1295
- $\phi(1680)$ 1297
- $\rho_3(1690)$ 1299
- $\rho(1700)$ 1302
- $a_2(1700)$ 1307
- $f_0(1710)$ 1308
- $\eta(1760)$ 1310
- $\pi(1800)$ 1311
- $f_2(1810)$ 1312
- $X(1835)$ 1313
- $\phi_3(1850)$ 1314
- $\eta_2(1870)$ 1315
- $\pi_2(1880)$ 1315
- $\rho(1900)$ 1315
- $f_2(1910)$ 1316
- $a_0(1950)$ 1317
- $f_2(1950)$ 1317
- $a_4(1970)$ was $a_4(2040)$ 1318
- $\rho_3(1990)$ 1319
- $\pi_2(2005)$ 1319
- $f_2(2010)$ 1320

• Indicates the particle is in the Meson Summary Table

- $f_0(2020)$ 1320
- $f_4(2050)$ 1321
- $\pi_2(2100)$ 1322
- $f_0(2100)$ 1322
- $f_2(2150)$ 1323
- $\rho(2150)$ 1324
- $\phi(2170)$ 1325
- $f_0(2200)$ 1326
- $f_J(2220)$ 1326
- $\eta(2225)$ 1327
- $\rho_3(2250)$ 1328
- $f_2(2300)$ 1328
- $f_4(2300)$ 1329
- $f_0(2330)$ 1329
- $f_2(2340)$ 1330
- $\rho_5(2350)$ 1330
- $f_6(2510)$ 1331

OTHER LIGHT UNFLAVORED ($S = C = B = 0$)

- Further States 1332

STRANGE MESONS ($S = \pm 1, C = B = 0$)

- K^\pm 1337
- K^0 1353
- K_S^0 1354
- K_L^0 1358
- $K_0^*(700)$ aka κ ; was $K_0^*(800)$ 1373
- $K^*(892)$ 1374
- $K_1(1270)$ 1376
- $K_1(1400)$ 1378
- $K^*(1410)$ 1379
- $K_0^*(1430)$ 1379
- $K_2^*(1430)$ 1380
- $K(1460)$ 1383
- $K_2(1580)$ 1383
- $K(1630)$ 1383
- $K_1(1650)$ 1383
- $K^*(1680)$ 1384
- $K_2(1770)$ 1384
- $K_3^*(1780)$ 1385
- $K_2(1820)$ 1386
- $K(1830)$ 1387
- $K_0^*(1950)$ 1387
- $K_2^*(1980)$ 1387
- $K_4^*(2045)$ 1388
- $K_2(2250)$ 1388
- $K_3(2320)$ 1388
- $K_5^*(2380)$ 1389
- $K_4(2500)$ 1389
- $K(3100)$ 1389

CHARMED MESONS ($C = \pm 1$)

- D^\pm 1391
- D^0 1406
- $D^*(2007)^0$ 1438
- $D^*(2010)^\pm$ 1439
- $D_0^*(2300)^0$ was $D_0^*(2400)^0$ 1440
- $D_0^*(2300)^\pm$ was $D_0^*(2400)^\pm$ 1441
- $D_1(2420)^0$ 1441
- $D_1(2420)^\pm$ 1442
- $D_1(2430)^0$ 1443
- $D_2^*(2460)^0$ 1443
- $D_2^*(2460)^\pm$ 1444

(Continued on the next page)

$D(2550)^0$	1445	• $\chi_{c2}(3930)$ was $\chi_{c2}(2P)$	1761
$D_J^*(2600)$ was $D(2600)$	1445	$X(3940)$	1762
$D^*(2640)^\pm$	1446	• $X(4020)^\pm$	1763
$D(2740)^0$	1446	• $\psi(4040)$	1763
$D_3^*(2750)$	1446	$X(4050)^\pm$	1765
$D(3000)^0$	1447	$X(4055)^\pm$	1766
CHARMED, STRANGE MESONS ($C = S = \pm 1$)			
• D_s^\pm	1448	$X(4100)^\pm$	1766
• $D_s^{*\pm}$	1458	• $\chi_{c1}(4140)$ was $X(4140)$	1767
• $D_{s0}^*(2317)^\pm$	1459	• $\psi(4160)$	1767
• $D_{s1}(2460)^\pm$	1460	$X(4160)$	1770
• $D_{s1}^*(2536)^\pm$	1461	$Z_c(4200)$ was $X(4200)^\pm$	1770
• $D_{s2}^*(2573)$	1463	• $\psi(4230)$ aka $Y(4230)$; was $X(4230)$	1770
• $D_{s1}^*(2700)^\pm$	1463	$R_{c0}(4240)$ was $X(4240)^\pm$	1772
$D_{s1}^*(2860)^\pm$	1464	$X(4250)^\pm$	1772
$D_{s3}^*(2860)^\pm$	1464	• $\psi(4260)$ aka $Y(4260)$; was $X(4260)$	1772
$D_{sJ}(3040)^\pm$	1464	• $\chi_{c1}(4274)$ was $X(4274)$	1775
BOTTOM MESONS ($B = \pm 1$)			
• B^\pm	1466	$X(4350)$	1775
• B^0	1529	• $\psi(4360)$ aka $Y(4360)$; was $X(4360)$	1776
• B^\pm/B^0 ADMIXTURE	1603	$\psi(4390)$ was $X(4390)$	1777
• $B^\pm/B^0/B_s^0/b$ -baryon ADMIXTURE	1625	• $\psi(4415)$	1777
V_{cb} and V_{ub} CKM Matrix Elements	1633	• $Z_c(4430)$ was $X(4430)^\pm$	1779
• B^*	1634	$\chi_{c0}(4500)$ was $X(4500)$	1779
• $B_1(5721)^+$	1635	• $\psi(4660)$ aka $Y(4660)$; was $X(4660)$	1780
• $B_1(5721)^0$	1635	$\chi_{c0}(4700)$ was $X(4700)$	1781
$B_J^*(5732)$ aka B^{**}	1635	$b\bar{b}$ MESONS	
• $B_2^*(5747)^+$	1636	• $\eta_b(1S)$	1783
• $B_2^*(5747)^0$	1636	• $\Upsilon(1S)$	1784
$B_J(5840)^+$	1637	• $\chi_{b0}(1P)$	1790
$B_J(5840)^0$	1637	• $\chi_{b1}(1P)$	1792
• $B_J(5970)^+$	1638	• $h_b(1P)$	1794
• $B_J(5970)^0$	1638	• $\chi_{b2}(1P)$	1794
BOTTOM, STRANGE MESONS ($B = \pm 1, S = \mp 1$)			
• B_s^0	1640	$\eta_b(2S)$	1796
• B_s^*	1661	• $\Upsilon(2S)$	1796
$X(5568)^\pm$	1662	• $\Upsilon_2(1D)$ was $\Upsilon(1D)$	1801
• $B_{s1}(5830)^0$	1662	• $\chi_{b0}(2P)$	1802
• $B_{s2}^*(5840)^0$	1663	• $\chi_{b1}(2P)$	1803
$B_{sJ}^*(5850)$	1663	$h_b(2P)$	1806
BOTTOM, CHARMED MESONS ($B = C = \pm 1$)			
• B_c^+	1664	• $\chi_{b2}(2P)$	1806
$B_c(2S)^\pm$	1667	• $\Upsilon(3S)$	1808
$c\bar{c}$ MESONS			
• $\eta_c(1S)$	1668	• $\chi_{b1}(3P)$	1812
• $J/\psi(1S)$	1676	• $\chi_{b2}(3P)$	1812
• $\chi_{c0}(1P)$	1699	• $\Upsilon(4S)$ aka $\Upsilon(10580)$	1812
• $\chi_{c1}(1P)$	1709	• $Z_b(10610)$ was $X(10610)$	1814
• $h_c(1P)$	1718	• $Z_b(10650)$ was $X(10650)^\pm$	1816
• $\chi_{c2}(1P)$	1719	$\Upsilon(10753)$	1817
• $\eta_c(2S)$	1730	• $\Upsilon(10860)$	1817
• $\psi(2S)$	1733	• $\Upsilon(11020)$	1820
• $\psi(3770)$	1749	Notes in the Listings	
• $\psi_2(3823)$ was $\psi(3823)$, $X(3823)$	1756	$\rho(770)$	1221
• $\psi_3(3842)$	1756	$\rho(1450)$ and the $\rho(1700)$ (rev.)	1302
$\chi_{c0}(3860)$	1757	Charged kaon mass	1337
• $\chi_{c1}(3872)$ aka $X(3872)$	1757	Dalitz plot parameters for $K \rightarrow 3\pi$ decays	1345
• $Z_c(3900)$ was $X(3900)$	1759	$K_{\ell 3}^\pm$ and $K_{\ell 3}^0$ form factors	1347
• $X(3915)$ was $\chi_{c0}(3915)$	1761	CP -violation in $K_S \rightarrow 3\pi$	1357
• Indicates the particle is in the Meson Summary Table		Heavy Flavor Averaging Group (rev.)	1465
		Charmonium system	1668
		Branching ratios of $\psi(2S)$ and $\chi_{c0,1,2}$ (rev.)	1698
		Bottomonium system	1782
		Width determination of the Υ states	1782

(Continued on next page.)

Related Reviews in Volume 1

61. Form factors for rad. pion & kaon decays (rev.)	762
62. Scalar mesons below 2 GeV (rev.)	764
63. Pseudoscalar and pseudovector mesons	771
in the 1400 MeV region (rev.)	
64. Rare kaon decays (rev.)	774
65. CPT invariance tests in neutral kaon decay (rev.)	779
66. V_{ud} , V_{us} , Cabibbo angle, and CKM unitarity (rev.)	781
67. CP -violation in K_L decays	784
68. Review of multibody charm analyses (rev.)	788
69. $D^0-\bar{D}^0$ mixing (rev.)	792
70. D_s^+ branching fractions (rev.)	801
71. Leptonic decays of charged pseudoscalar mesons (rev.)	803
72. Production and decay of b -flavored hadrons (rev.)	814
73. Polarization in B decays (rev.)	824
74. $B^0-\bar{B}^0$ mixing (rev.)	828
75. Semileptonic B decays, V_{cb} and V_{ub} (rev.)	835
76. CKM angles from B hadrons, Determination of (new)	849
77. Spectroscopy of mesons containing two heavy quarks (rev.)	854
78. Non- $q\bar{q}$ mesons (rev.)	861

LIGHT UNFLAVORED MESONS
(S = C = B = 0)

For $I = 1$ (π, ρ, ω): $u\bar{d}, (u\bar{u}-d\bar{d})/\sqrt{2}, d\bar{u}$;
for $I = 0$ ($\eta, \eta', \eta(541), \omega, \phi, f, f'$): $c_1(u\bar{u} + d\bar{d}) + c_2(s\bar{s})$

π^\pm

$$J^G(J^P) = 1^-(0^-)$$

We have omitted some results that have been superseded by later experiments. The omitted results may be found in our 1988 edition Physics Letters **B204** 1 (1988).

π^\pm MASS

The most accurate charged pion mass measurements are based upon x-ray wavelength measurements for transitions in π^- -mesonic atoms. The observed line is the blend of three components, corresponding to different K-shell occupancies. JECKELMANN 94 revisits the occupancy question, with the conclusion that two sets of occupancy ratios, resulting in two different pion masses (Solutions A and B), are equally probable. We choose the higher Solution B since only this solution is consistent with a positive mass-squared for the muon neutrino, given the precise muon momentum measurements now available (DAUM 91, ASSAMAGAN 94, and ASSAMAGAN 96) for the decay of pions at rest. Earlier mass determinations with π^- -mesonic atoms may have used incorrect K-shell screening corrections.

Measurements with an error of > 0.005 MeV have been omitted from this Listing.

VALUE (MeV)	DOCUMENT ID	TECN	CHG	COMMENT
139.57039 ± 0.00018 OUR FIT	Error includes scale factor of 1.8.			
139.57039 ± 0.00017 OUR AVERAGE	Error includes scale factor of 1.6. See the ideogram below.			
139.57021 ± 0.00014	¹ DAUM 19	SPEC		$\pi^+ \rightarrow \mu^+ \nu_\mu$
139.57077 ± 0.00018	² TRASSINELLI 16	CNTR		X-ray transitions in pionic N2
139.57071 ± 0.00053	³ LENZ 98	CNTR	-	pionic N2-atoms gas target
139.56995 ± 0.00035	⁴ JECKELMANN 94	CNTR	-	π^- atom, Soln. B
• • • We do not use the following data for averages, fits, limits, etc. • • •				
139.57022 ± 0.00014	⁵ ASSAMAGAN 96	SPEC	+	$\pi^+ \rightarrow \mu^+ \nu_\mu$
139.56782 ± 0.00037	⁶ JECKELMANN 94	CNTR	-	π^- atom, Soln. A
139.56996 ± 0.00067	⁷ DAUM 91	SPEC	+	$\pi^+ \rightarrow \mu^+ \nu$
139.56752 ± 0.00037	⁸ JECKELMANN 86B	CNTR	-	Mesonic atoms
139.5704 ± 0.0011	⁷ ABELA 84	SPEC	+	See DAUM 91
139.5664 ± 0.0009	⁹ LU 80	CNTR	-	Mesonic atoms
139.5686 ± 0.0020	^{9,10} CARTER 76	CNTR	-	Mesonic atoms
139.5660 ± 0.0024	^{9,10} MARUSHEN... 76	CNTR	-	Mesonic atoms

¹ DAUM 19 value is based on their previous (1991+1996) measurements of the μ^+ momentum of 29.79200 ± 0.00011 MeV for π^+ decay at rest. It also uses $m_\mu = 105.6583745 \pm 0.0000024$ MeV, and assumes conservatively $m_{\nu_\mu} = 2.0 \pm 2.0$ MeV. It is the most precise charged pion mass determination.

² TRASSINELLI 16 use the muonic oxygen line for online energy calibration of the pionic line.

³ LENZ 98 result does not suffer K-electron configuration uncertainties as does JECKELMANN 94.

⁴ JECKELMANN 94 Solution B (dominant 2-electron K-shell occupancy), chosen for consistency with positive $m_{\nu_\mu}^2$.

⁵ ASSAMAGAN 96 measures the μ^+ momentum p_μ in $\pi^+ \rightarrow \mu^+ \nu_\mu$ decay at rest to be 29.79200 ± 0.00011 MeV/c. Combined with the μ^+ mass and the assumption $m_{\nu_\mu} = 0$, this gives the π^+ mass above; if $m_{\nu_\mu} > 0$, m_{π^+} given above is a lower limit. Combined instead with m_μ and (assuming CPT) the π^- mass of JECKELMANN 94, p_μ gives an upper limit on m_{ν_μ} (see the ν_μ).

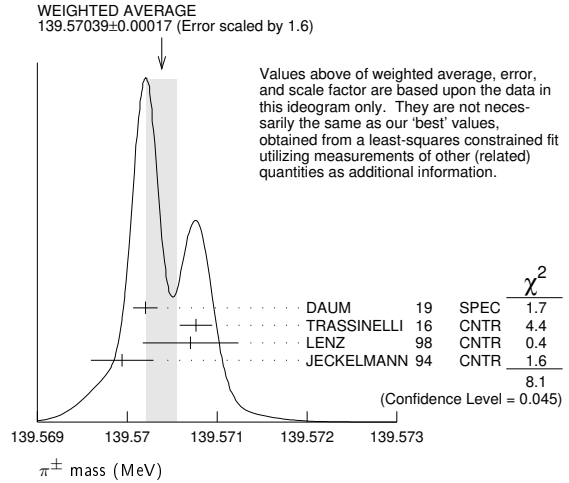
⁶ JECKELMANN 94 Solution A (small 2-electron K-shell occupancy) in combination with either the DAUM 91 or ASSAMAGAN 94 pion decay muon momentum measurement yields a significantly negative $m_{\nu_\mu}^2$. It is accordingly not used in our fits.

⁷ The DAUM 91 value includes the ABELA 84 result. The value is based on a measurement of the μ^+ momentum for π^+ decay at rest, $p_\mu = 29.79179 \pm 0.00053$ MeV, uses $m_\mu = 105.658389 \pm 0.000034$ MeV, and assumes that $m_{\nu_\mu} = 0$. The last assumption means that in fact the value is a lower limit.

⁸ JECKELMANN 86B gives $m_\pi/m_e = 273.12677(71)$. We use $m_e = 0.51099906(15)$ MeV from COHEN 87. The authors note that two solutions for the probability distribution of K-shell occupancy fit equally well, and use other data to choose the lower of the two possible π^\pm masses.

⁹ These values are scaled with a new wavelength-energy conversion factor $V\lambda = 1.23984244(37) \times 10^{-6}$ eV m from COHEN 87. The LU 80 screening correction relies upon a theoretical calculation of inner-shell refilling rates.

¹⁰ This MARUSHENKO 76 value used at the authors' request to use the accepted set of calibration γ energies. Error increased from 0.0017 MeV to include QED calculation error of 0.0017 MeV (12 ppm).



$m_{\pi^+} - m_{\mu^+}$

Measurements with an error > 0.05 MeV have been omitted from this Listing.

VALUE (MeV)	EVTS	DOCUMENT ID	TECN	CHG	COMMENT
• • • We do not use the following data for averages, fits, limits, etc. • • •					
33.91157 ± 0.00067		¹ DAUM 91	SPEC	+	$\pi^+ \rightarrow \mu^+ \nu$
33.9111 ± 0.0011		ABELA 84	SPEC		See DAUM 91
33.925 ± 0.025		BOOTH 70	CNTR	+	Magnetic spect.
33.881 ± 0.035	145	HYMAN 67	HEBC	+	K^- He

¹ The DAUM 91 value assumes that $m_{\nu_\mu} = 0$ and uses our $m_\mu = 105.658389 \pm 0.000034$ MeV.

$(m_{\pi^+} - m_{\pi^-}) / m_{\text{average}}$

A test of CPT invariance.

VALUE (units 10^{-4})	DOCUMENT ID	TECN
2 ± 5	AYRES 71	CNTR

π^\pm MEAN LIFE

Measurements with an error $> 0.02 \times 10^{-8}$ s have been omitted.

VALUE (10^{-8} s)	DOCUMENT ID	TECN	CHG	COMMENT
2.6033 ± 0.0005 OUR AVERAGE	Error includes scale factor of 1.2.			
2.60361 ± 0.0005 2	¹ KOPTEV 95	SPEC	+	Surface μ^+ 's
2.60231 ± 0.0005 0 ± 0.00084	NUMAO 95	SPEC	+	Surface μ^+ 's
2.609 ± 0.008	DUNAITSEV 73	CNTR	+	
2.602 ± 0.004	AYRES 71	CNTR	±	
2.604 ± 0.005	NORDBERG 67	CNTR	+	
2.602 ± 0.004	ECKHAUSE 65	CNTR	+	
• • • We do not use the following data for averages, fits, limits, etc. • • •				
2.640 ± 0.008	² KINSEY 66	CNTR	+	

¹ KOPTEV 95 combines the statistical and systematic errors; the statistical error dominates.

² Systematic errors in the calibration of this experiment are discussed by NORDBERG 67.

$(\tau_{\pi^+} - \tau_{\pi^-}) / \tau_{\text{average}}$

A test of CPT invariance.

VALUE (units 10^{-4})	DOCUMENT ID	TECN
5.5 ± 7.1	AYRES 71	CNTR
• • • We do not use the following data for averages, fits, limits, etc. • • •		
-14 ± 29	PETRUKHIN 68	CNTR
40 ± 70	BARDON 66	CNTR
23 ± 40	¹ LOBKOWICZ 66	CNTR

¹ This is the most conservative value given by LOBKOWICZ 66.

π ELECTRIC POLARIZABILITY α_π

See HOLSTEIN 14 for a general review on hadron polarizability.

VALUE (10^{-4} fm ³)	EVTS	DOCUMENT ID	TECN	COMMENT
2.0 ± 0.6 ± 0.7	63k	¹ ADOLPH 15A	SPEC	$\pi^- \gamma \rightarrow \pi^- \gamma$ Compton scatt.

¹ Value is derived assuming $\alpha_\pi = -\beta_\pi$.

Meson Particle Listings

π^\pm

π^\pm DECAY MODES

π^- modes are charge conjugates of the modes below.

For decay limits to particles which are not established, see the section on Searches for Axions and Other Very Light Bosons.

Mode	Fraction (Γ_i/Γ)	Confidence level
Γ_1 $\mu^+ \nu_\mu$	[a] (99.98770 ± 0.00004) %	
Γ_2 $\mu^+ \nu_\mu \gamma$	[b] (2.00 ± 0.25) × 10 ⁻⁴	
Γ_3 $e^+ \nu_e$	[a] (1.230 ± 0.004) × 10 ⁻⁴	
Γ_4 $e^+ \nu_e \gamma$	[b] (7.39 ± 0.05) × 10 ⁻⁷	
Γ_5 $e^+ \nu_e \pi^0$	(1.036 ± 0.006) × 10 ⁻⁸	
Γ_6 $e^+ \nu_e e^+ e^-$	(3.2 ± 0.5) × 10 ⁻⁹	
Γ_7 $e^+ \nu_e \nu \bar{\nu}$	< 5 × 10 ⁻⁶	90%

Lepton Family number (LF) or Lepton number (L) violating modes

Γ_8 $\mu^+ \bar{\nu}_e$	L	[c] < 1.5	× 10 ⁻³	90%
Γ_9 $\mu^+ \nu_e$	LF	[c] < 8.0	× 10 ⁻³	90%
Γ_{10} $\mu^- e^+ e^+ \nu$	LF	< 1.6	× 10 ⁻⁶	90%

[a] Measurements of $\Gamma(e^+ \nu_e)/\Gamma(\mu^+ \nu_\mu)$ always include decays with γ 's, and measurements of $\Gamma(e^+ \nu_e \gamma)$ and $\Gamma(\mu^+ \nu_\mu \gamma)$ never include low-energy γ 's. Therefore, since no clean separation is possible, we consider the modes with γ 's to be subreactions of the modes without them, and let $[\Gamma(e^+ \nu_e) + \Gamma(\mu^+ \nu_\mu)]/\Gamma_{\text{total}} = 100\%$.

[b] See the Particle Listings below for the energy limits used in this measurement; low-energy γ 's are not included.

[c] Derived from an analysis of neutrino-oscillation experiments.

π^\pm BRANCHING RATIOS

$\Gamma(e^+ \nu_e)/\Gamma_{\text{total}}$	Γ_3/Γ
See note [a] in the list of π^+ decay modes just above, and see also the next block of data. See also the note on "Decay Constants of Charged Pseudoscalar Mesons" in the D_s^+ Listings.	

VALUE (units 10 ⁻⁴)	DOCUMENT ID
1.230 ± 0.004 OUR EVALUATION	

$[\Gamma(e^+ \nu_e) + \Gamma(e^+ \nu_e \gamma)]/[\Gamma(\mu^+ \nu_\mu) + \Gamma(\mu^+ \nu_\mu \gamma)]$	$(\Gamma_3 + \Gamma_4)/(\Gamma_1 + \Gamma_2)$
See note [a] in the list of π^+ decay modes above. See NUMAO 92 for a discussion of $e-\mu$ universality. See also the note on "Decay Constants of Charged Pseudoscalar Mesons" in the D_s^+ Listings.	

VALUE (units 10 ⁻⁴)	EVTS	DOCUMENT ID	TECN	CHG	COMMENT
1.2327 ± 0.0023 OUR AVERAGE					
1.2344 ± 0.0023 ± 0.0019	400k	AGUILAR-AR...15	CNTR	+	Stopping π^+
1.2346 ± 0.0035 ± 0.0036	120k	CZAPEK	93	CALO	Stopping π^+
1.2265 ± 0.0034 ± 0.0044	190k	BRITTON	92	CNTR	Stopping π^+
1.218 ± 0.014	32k	BRYMAN	86	CNTR	Stopping π^+
••• We do not use the following data for averages, fits, limits, etc. •••					
1.273 ± 0.028	11k	¹ DICAPUA	64	CNTR	
1.21 ± 0.07		ANDERSON	60	SPEC	

¹DICAPUA 64 has been updated using the current mean life.

$\Gamma(\mu^+ \nu_\mu \gamma)/\Gamma_{\text{total}}$	Γ_2/Γ					
Note that measurements here do not cover the full kinematic range.						
VALUE (units 10 ⁻⁴)	EVTS	DOCUMENT ID	TECN	CHG	COMMENT	
2.0 ± 0.24 ± 0.08		¹ BRESSI	98	CALO	+	Stopping π^+
••• We do not use the following data for averages, fits, limits, etc. •••						
1.24 ± 0.25	26	CASTAGNOLI	58	EMUL		$KE_\mu < 3.38$ MeV
¹ BRESSI 98 result is given for $E_\gamma > 1$ MeV only. Result agrees with QED expectation, 2.283×10^{-4} and does not confirm discrepancy of earlier experiment CASTAGNOLI 58.						

$\Gamma(e^+ \nu_e \gamma)/\Gamma_{\text{total}}$	Γ_4/Γ				
The very different values reflect the very different kinematic ranges covered (bigger range, bigger value). And none of them covers the whole kinematic range.					
VALUE (units 10 ⁻⁸)	EVTS	DOCUMENT ID	TECN	COMMENT	
73.86 ± 0.54	65k	¹ BYCHKOV	09	PIBE	$e^+ \nu_\gamma$ at rest
••• We do not use the following data for averages, fits, limits, etc. •••					
16.1 ± 2.3		² BOLOTOV	90b	SPEC	17 GeV $\pi^- \rightarrow e^- \bar{\nu}_e \gamma$
5.6 ± 0.7	226	³ STETZ	78	SPEC	$P_e > 56$ MeV/c
3.0	143	DEPOMMIER	63b	CNTR	(KE) $e^+ \gamma > 48$ MeV

¹This BYCHKOV 09 value is for $E_\gamma > 10$ MeV and $\Theta_{e+\gamma} > 40^\circ$.

²BOLOTOV 90b is for $E_\gamma > 21$ MeV, $E_e > 70 - 0.8 E_\gamma$.

³STETZ 78 is for an $e^- \gamma$ opening angle $> 132^\circ$. Obtains 3.7 when using same cutoffs as DEPOMMIER 63b.

$\Gamma(e^+ \nu_e \pi^0)/\Gamma_{\text{total}}$ Γ_5/Γ

VALUE (units 10 ⁻⁸)	EVTS	DOCUMENT ID	TECN	CHG	COMMENT	
1.036 ± 0.006 OUR AVERAGE						
1.036 ± 0.006	64k	^{1,2} POCANIC	04	PIBE	+	π decay at rest
1.026 ± 0.039	1224	³ MCFARLANE	85	CNTR	+	Decay in flight
1.00 ^{+0.08} _{-0.10}	332	DEPOMMIER	68	CNTR	+	
1.07 ± 0.21	38	⁴ BACASTOW	65	OSPK	+	
1.10 ± 0.26		⁴ BERTRAM	65	OSPK	+	
1.1 ± 0.2	43	⁴ DUNAITSEV	65	CNTR	+	
0.97 ± 0.20	36	⁴ BARTLETT	64	OSPK	+	
••• We do not use the following data for averages, fits, limits, etc. •••						
1.15 ± 0.22	52	⁴ DEPOMMIER	63	CNTR	+	See DEPOMMIER 68

¹POCANIC 04 normalizes to $e^+ \nu_e$ decays, using the PDG 2004 value $B(\pi^+ \rightarrow e^+ \nu_e) = (1.230 \pm 0.004) \times 10^{-4}$. We add their statistical (0.004×10^{-8}) , systematic (0.004×10^{-8}) and systematic error due to the uncertainty of $B(\pi^+ \rightarrow e^+ \nu_e)$ (0.003×10^{-8}) in quadrature.

²This result can be used to calculate V_{ud} from pion beta decay: $V_{ud}^{PIBETA} = 0.9728 \pm 0.0030$.

³MCFARLANE 85 combines a measured rate $(0.394 \pm 0.015)/s$ with 1982 PDG mean life.

⁴DEPOMMIER 68 says the result of DEPOMMIER 63 is at least 10% too large because of a systematic error in the π^0 detection efficiency, and that this may be true of all the previous measurements (also V. Soergel, private communication, 1972).

$\Gamma(e^+ \nu_e e^+ e^-)/\Gamma(\mu^+ \nu_\mu)$ Γ_6/Γ_1

VALUE (units 10 ⁻³)	CL%	EVTS	DOCUMENT ID	TECN	COMMENT	
3.2 ± 0.5 ± 0.2		98	EGLI	89	SPEC	Uses $R_{P_{CAC}} = 0.068 \pm 0.004$

••• We do not use the following data for averages, fits, limits, etc. •••

0.46 ± 0.16 ± 0.07	7	¹ BARANOV	92	SPEC	Stopped π^+
< 4.8	90	KORENCHE...	76b	SPEC	
< 34	90	KORENCHE...	71	OSPK	

¹This measurement by BARANOV 92 is of the structure-dependent part of the decay. The value depends on values assumed for ratios of form factors.

$\Gamma(e^+ \nu_e \nu \bar{\nu})/\Gamma_{\text{total}}$ Γ_7/Γ

VALUE (units 10 ⁻⁶)	CL%	DOCUMENT ID	TECN	
< 5	90	PICCIOTTO	88	SPEC

$\Gamma(\mu^+ \bar{\nu}_e)/\Gamma_{\text{total}}$ Γ_8/Γ

Forbidden by total lepton number conservation. See the note on "Decay Constants of Charged Pseudoscalar Mesons" in the D_s^+ Listings.

VALUE (units 10 ⁻³)	CL%	DOCUMENT ID	TECN	COMMENT	
< 1.5	90	¹ COOPER	82	HLBC	Wideband ν beam
¹ COOPER 82 limit on $\bar{\nu}_e$ observation is here interpreted as a limit on lepton number violation.					

$\Gamma(\mu^+ \nu_e)/\Gamma_{\text{total}}$ Γ_9/Γ

Forbidden by lepton family number conservation.

VALUE (units 10 ⁻³)	CL%	DOCUMENT ID	TECN	COMMENT	
< 8.0	90	¹ COOPER	82	HLBC	Wideband ν beam
¹ COOPER 82 limit on ν_e observation is here interpreted as a limit on lepton family number violation.					

$\Gamma(\mu^- e^+ e^+ \nu)/\Gamma_{\text{total}}$ Γ_{10}/Γ

Forbidden by lepton family number conservation.

VALUE (units 10 ⁻⁶)	CL%	DOCUMENT ID	TECN	CHG	
< 1.6	90	BARANOV	91b	SPEC	+
••• We do not use the following data for averages, fits, limits, etc. •••					
< 7.7	90	KORENCHE...	87	SPEC	+

π^\pm — POLARIZATION OF EMITTED μ^\pm

$\pi^\pm \rightarrow \mu^\pm \nu$
Tests the Lorentz structure of leptonic charged weak interactions.

VALUE	CL%	DOCUMENT ID	TECN	CHG	COMMENT
••• We do not use the following data for averages, fits, limits, etc. •••					
< (-0.9959)	90	¹ FETSCHER	84	RVUE	+
-0.99 ± 0.16		² ABELA	83	SPEC	- μ X-rays
¹ FETSCHER 84 uses only the measurement of CARR 83.					
² Sign of measurement reversed in ABELA 83 to compare with μ^+ measurements.					

See the related review(s):
[Form Factors for Radiative Pion and Kaon Decays](#)

π^\pm FORM FACTORS

F_V , VECTOR FORM FACTOR					
VALUE	EVTS	DOCUMENT ID	TECN	COMMENT	
0.0254 ± 0.0017 OUR AVERAGE					
0.0258 ± 0.0017	65k	¹ BYCHKOV	09	PIBE	$e^+ \nu_\gamma$ at rest
0.014 ± 0.009		² BOLOTOV	90b	SPEC	17 GeV $\pi^- \rightarrow e^- \bar{\nu}_e \gamma$
0.023 ^{+0.015} _{-0.013}	98	EGLI	89	SPEC	$\pi^+ \rightarrow e^+ \nu_e e^+ e^-$

¹The BYCHKOV 09 F_A and F_V results are highly (anti-)correlated: $F_A + 1.0286 F_V = 0.03853 \pm 0.00014$.

²BOLOTOV 90b only determines the absolute value.

F_A , AXIAL-VECTOR FORM FACTOR

VALUE	EVTS	DOCUMENT ID	TECN	COMMENT
0.0119 ± 0.0001	65k	1,2 BYCHKOV	09 PIBE	$e^+ \nu_\gamma$ at rest
••• We do not use the following data for averages, fits, limits, etc. •••				
0.0115 ± 0.0004	41k	1,3 FRLEZ	04 PIBE	$\pi^+ \rightarrow e^+ \nu_\gamma$ at rest
0.0106 ± 0.0060		1,4 BOLOTOV	90B SPEC	17 GeV $\pi^- \rightarrow e^- \bar{\nu}_e \gamma$
0.021 $\pm^{+0.011}_{-0.013}$	98	EGLI	89 SPEC	$\pi^+ \rightarrow e^+ \nu_e e^+ e^-$
0.0135 ± 0.0016		1,4 BAY	86 SPEC	$\pi^+ \rightarrow e^+ \nu_\gamma$
0.006 ± 0.003		1,4 PIILONEN	86 SPEC	$\pi^+ \rightarrow e^+ \nu_\gamma$
0.011 ± 0.003		1,4,5 STETZ	78 SPEC	$\pi^+ \rightarrow e^+ \nu_\gamma$

- These values come from fixing the vector form factor at the CVC prediction, $F_V = 0.0259 \pm 0.0005$.
- When F_V is released, the BYCHKOV 09 F_A is 0.0117 ± 0.0017 , and F_A and F_V results are highly (anti-)correlated: $F_A + 1.0286 F_V = 0.03853 \pm 0.00014$.
- The sign of $\gamma = F_A / F_V$ is determined to be positive.
- Only the absolute value of F_A is determined.
- The result of STETZ 78 has a two-fold ambiguity. We take the solution compatible with later determinations.

VECTOR FORM FACTOR SLOPE PARAMETER a

This is a in $F_V(q^2) = F_V(0) (1 + a q^2)$

VALUE	EVTS	DOCUMENT ID	TECN	COMMENT
0.10 ± 0.06	65k	BYCHKOV	09 PIBE	$e^+ \nu_\gamma$ at rest

R , SECOND AXIAL-VECTOR FORM FACTOR

VALUE	EVTS	DOCUMENT ID	TECN	COMMENT
0.059 + 0.009 - 0.008	98	EGLI	89 SPEC	$\pi^+ \rightarrow e^+ \nu_e e^+ e^-$

π^\pm CHARGE RADIUS

The charge radius of the pion $\sqrt{\langle r_\pi^2 \rangle}$ is defined in relation to the form factor of the pion electromagnetic vertex, called vector form factor VFF, F_V^+ . The VFF is a function of the squared four-momentum transfer t , or of the squared c.m. energy s , depending on the channel in which the photon exchange takes place. In both cases, it is related to the slope of the VFF at zero, namely

$$\langle r_\pi^2 \rangle = 6 \frac{dF_V^+(q)}{dq} (q=0) \text{ where } q = t, s.$$

The quantity cannot be measured directly. It can be extracted from the cross sections of three processes: pion electroproduction, $eN \rightarrow eN\pi$, and pion electron scattering $e\pi \rightarrow e\pi$, for the t channel, and positron electron annihilation into two charged pions, $e^+e^- \rightarrow \pi^+\pi^-$, for the s channel. We encode all measurements, but we do not use electroproduction data in averaging because the extraction of the pion radius involves, in this case, theoretical uncertainties that cannot be controlled at the needed level of accuracy. In case of analyses based on the same data set, as ANANTHANARAYAN 17 and COLANGELO 19, which cannot be averaged, we combine the results into a common value, with the uncertainty range chosen to cover both analyses. Note that for consistency the form factor needs to be defined in both channels with the vacuum polarisation removed. For details see COLANGELO 19 or Appendix B of ANANTHANARAYAN 16a.

VALUE (fm)	DOCUMENT ID	TECN	COMMENT
0.659 ± 0.004 OUR AVERAGE			
0.656 ± 0.005	1 PDG	19 FIT	
0.65 ± 0.05 ± 0.06	ESCHRICH	01 CNTR	$\pi e \rightarrow \pi e$
0.663 ± 0.006	AMENDOLIA	86 CNTR	$\pi e \rightarrow \pi e$
0.663 ± 0.023	DALLY	82 CNTR	$\pi e \rightarrow \pi e$
••• We do not use the following data for averages, fits, limits, etc. •••			
0.655 ± 0.004	2 COLANGELO	19 FIT	Fit existing data
0.657 ± 0.003	3 ANANTHANA..17	FIT	Fit existing data
0.6603 ± 0.0005 ± 0.0004	4 HANHART	17 FIT	Fit existing data
0.740 ± 0.031	5 LIESENFELD	99 CNTR	$ep \rightarrow e\pi^+ n$
0.661 ± 0.012	6 BIJNENS	98 CNTR	χ PT extraction
0.660 ± 0.024	AMENDOLIA	84 CNTR	$\pi e \rightarrow \pi e$
0.711 ± 0.009 ± 0.016	5 BEBEK	78 CNTR	$eN \rightarrow e\pi N$
0.678 ± 0.004 ± 0.008	7 QUENZER	78 CNTR	$e^+e^- \rightarrow \pi^+\pi^-$
0.78 $\pm^{+0.09}_{-0.10}$	ADYLOV	77 CNTR	$\pi e \rightarrow \pi e$
0.74 $\pm^{+0.11}_{-0.13}$	BARDIN	77 CNTR	$ep \rightarrow e\pi^+ n$
0.56 ± 0.04	DALLY	77 CNTR	$\pi e \rightarrow \pi e$

- This value combines the measurements of ANANTHANARAYAN 17 and COLANGELO 19 which are based on the same data set. The uncertainty range is chosen to cover both results.
- COLANGELO 19 fit existing F_V data, using an extended Omnes dispersive representation. This analysis is based on the same data set of ANANTHANARAYAN 17. Accordingly, they cannot be averaged. We combine the results into a common value, with the uncertainty range chosen to cover the uncertainty ranges of both analyses.
- ANANTHANARAYAN 17 fit existing F_V data, using a mixed phase-modulus dispersive representation. This analysis is based on the same data set of COLANGELO 19. Accordingly, they cannot be averaged. We combine the results into a common value, with the uncertainty range chosen to cover the uncertainty ranges of both analyses.
- According to the authors the uncertainty could be underestimated. The value quoted omits the BaBar data AUBERT 09.
- The extractions could contain an additional theoretical uncertainty which cannot be sufficiently quantified.

⁶ BIJNENS 98 fits existing data.

⁷ The extraction is based on a parametrization that does not have correct analytic properties.

π^\pm REFERENCES

We have omitted some papers that have been superseded by later experiments. The omitted papers may be found in our 1988 edition Physics Letters **B204** 1 (1988).

COLANGELO 19	JHEP 1902 006	G. Colangelo, M. Hoferichter, P. Stoffer	(PSI)
DAUM 19	PL B796 11	M. Daum, R. Frosch, P.-R. Kettle	(PSI)
PDG 19	RPP 2019 at pdg.lbl.gov	M. Tanabashi et al.	(PDG Collab.)
ANANTHANA..17	PRL 119 132002	B. Ananthanarayan, I. Caprini, D. Das	
HANHART 17	EPJ C77 98	C. Hanhart et al.	
ANANTHANA..16a	PR D93 116007	B. Ananthanarayan et al.	
TRASSINELLI 16	PL B759 583	M. Trassinelli et al.	
ADOLPH 15a	PRL 114 062002	C. Adolph et al.	(COMPASS Collab.)
AGUILAR-AREVALO 15	PRL 115 071801	A. Aguilar-Arevalo et al.	(PIENU Collab.)
HOLSTEIN 14	ARNPS 64 51	B. Holstein, S. Scherer	(MASA, IANZ)
AUBERT 09	PR D79 011102	B. Aubert et al.	(BABAR Collab.)
BYCHKOV 09	PRL 103 051802	M. Bychkov et al.	(PSI PIBETA Collab.)
FRLEZ 04	PRL 93 181804	E. Frlez et al.	(PSI PIBETA Collab.)
POCANIC 04	PRL 93 181803	D. Pocanic et al.	(PSI PIBETA Collab.)
ESCHRICH 01	PL B522 233	I. Eschrich et al.	(FNAL SELEX Collab.)
LIESENFELD 99	PL B468 20	A. Liesenfeld et al.	
BIJNENS 98	JHEP 9805 014	J. Bijnens et al.	
BRESSI 98	NP B513 555	G. Bressi et al.	
LENZ 98	PL B416 60	S. Lenz et al.	
ASSAMAGAN 96	PR D53 6055	K.A. Assamagan et al.	(PSI, ZURI, VILL+)
KOPTEV 95	JETPL 61 877	V.P. Koptev et al.	(PNPI)
	Translated from ZETFP 61 865		
NUMAO 95	PR D52 4855	T. Numao et al.	(TRIU, BRCO)
ASSAMAGAN 94	PL B335 231	K.A. Assamagan et al.	(PSI, ZURI, VILL+)
JECKELMANN 94	PL B335 326	B. Jeckelmann, P.F.A. Goudsmit, H.J. Lesli	(WABRN+)
CZAPEK 93	PRL 70 17	G. Czapek et al.	(BERN, VILL)
BARANOV 92	SJNP 55 1644	V.A. Baranov et al.	(JINR)
	Translated from YAF 55 2940.		
BRITTON 92	PRL 68 3000	D.L. Britton et al.	(TRIU, CARL)
Also	PR D49 28	D.L. Britton et al.	(TRIU, CARL)
NUMAO 92B	MPL A7 3357	T. Numao	(TRIU)
BARANOV 91B	SJNP 54 790	V.A. Baranov et al.	(JINR)
	Translated from YAF 54 1298.		
DAUM 91	PL B265 425	M. Daum et al.	(VILL)
BOLOTOV 90B	PL B243 308	V.N. Bolotov et al.	(INRM)
EGLI 89	PL B222 533	S. Egli et al.	(SINDRUM Collab.)
Also	PL B175 97	S. Egli et al.	(AACH3, ETH, SIN, ZURI)
PDG 88	PL B204 1	G.P. Yost et al.	(LBL+)
PICCIOTTO 88	PR D37 1131	C.E. Picciotto et al.	(TRIU, CNRC)
COHEN 87	RMP 59 1121	E.R. Cohen, B.N. Taylor	(RISC, NBS)
KORENCHEN... 87	SJNP 46 192	S.M. Korenchenko et al.	(JINR)
	Translated from YAF 46 313.		
AMENDOLIA 86	NP B277 168	S.R. Amendolia et al.	(CERN NA7 Collab.)
BAY 86	PL B174 445	A. Bay et al.	(LAUS, ZURI)
BRYMAN 86	PR D33 1211	D.A. Bryman et al.	(TRIU, CNRC)
Also	PRL 50 7	D.A. Bryman et al.	(TRIU, CNRC)
JECKELMANN 86B	NP A457 709	B. Jeckelmann et al.	(ETH, FRIB)
Also	PRL 55 1444	B. Jeckelmann et al.	(ETH, FRIB)
PIILONEN 86	PRL 57 1402	L.E. Piilonen et al.	(LANL, TEMP, CHIC)
MCFARLANE 85	PR D32 547	W.K. McFarlane et al.	(TEMP, LANL)
ABELA 84	PL 146B 431	R. Abela et al.	(SIN)
Also	PL 74B 126	M. Daum et al.	(SIN)
Also	PR D20 2692	M. Daum et al.	(SIN)
AMENDOLIA 84	PL 146B 116	S.R. Amendolia et al.	(CERN NA7 Collab.)
FETSCHER 84	PL 140B 117	W. Fetscher	(ETH)
ABELA 83	NP A395 413	R. Abela et al.	(BASL, KARLK, KARLE)
CARR 83	PRL 51 627	J. Carr et al.	(LBL, NWES, TRIU)
COOPER 82	PL 112B 97	A.M. Cooper et al.	(RL)
DALLY 82	PRL 48 375	E.B. Dally et al.	
LU 80	PRL 45 1066	C.L. Lu et al.	(YALE, COLU, JHU)
BEBEK 78	PR D17 1693	C.J. Bebek et al.	
QUENZER 78	PL 76B 512	A. Quenzer et al.	(LAO)
STETZ 78	NP B138 285	A.W. Stetz et al.	(LBL, UCLA)
ADYLOV 77	NP B128 461	G.T. Adylov et al.	
BARDIN 77	NP B120 45	G. Bardin et al.	
DALLY 77	PRL 39 1176	E.B. Dally et al.	
CARTER 76	PRL 37 1380	A.L. Carter et al.	(CARL, CNRC, CHIC+)
KORENCHEN... 76B	JETP 44 35	S.M. Korenchenko et al.	(JINR)
	Translated from ZETF 71 67		
MARUSHEN... 76	JETPL 23 72	V.I. Marushenko et al.	(PNPI)
Also	Translated from ZETF 23 80.		
Also	Private Comm.	R.E. Shafer	(FNAL)
Also	Private Comm.	A. Smirnov	(PNPI)
DUNAITSEV 73	SJNP 16 292	A.F. Dunaitsev et al.	(SERP)
	Translated from YAF 16 524.		
AYRES 71	PR D3 1051	D.S. Ayres et al.	(LRL, UCSB)
Also	PR 157 1288	D.S. Ayres et al.	(LRL)
Also	PRL 21 261	D.S. Ayres et al.	(LRL, UCSB)
Also	Thesis UCLR 18369	D.S. Ayres	(LRL)
Also	PRL 23 1267	A.J. Greenberg et al.	(LRL, UCSB)
KORENCHEN... 71	SJNP 13 189	S.M. Korenchenko et al.	(JINR)
	Translated from YAF 13 339.		
BOOTH 70	PL 32B 723	P.S.L. Booth et al.	(LIVP)
DEPOMMIER 68	NP B4 189	P. Depommier et al.	(CNRS)
PETRIUKHIN 68	JINR P1 3862	P. Petriukhin et al.	(JINR)
HYMAN 67	PL 25B 376	L.G. Hyman et al.	(ANL, CMU, NWES)
NORDBERG 67	PL 24B 594	M.E. Nordberg, F. Lobkowicz, R.L. Burman	(ROCH)
BARDON 66	PRL 16 775	M. Bardon et al.	(COLU)
KINSEY 66	PR 144 1132	K.F. Kinsey, F. Lobkowicz, M.E. Nordberg	(ROCH)
LOBKOWICZ 66	PRL 17 548	F. Lobkowicz et al.	(ROCH, BNL)
BACASTOW 65	PR 139 B407	R.B. Bacastow et al.	(LRL, SLAC)
BERTRAM 65	PR 139 B617	W.K. Bertram et al.	(MICH, CMU)
DUNAITSEV 65	JETP 20 58	A.F. Dunaitsev et al.	(JINR)
	Translated from ZETF 47 84.		
ECKHAUSE 65	PL 19 348	M. Eckhause et al.	(WILL)
BARTLETT 64	PR 136 B1452	D. Bartlett et al.	(COLU)
DICAPUA 64	PR 133 B1333	M. di Capua et al.	(COLU)
Also	Private Comm.	L. Pondrom	(WISC)
DEPOMMIER 63	PL 5 61	P. Depommier et al.	(CERN)
DEPOMMIER 63B	PL 7 285	P. Depommier et al.	(CERN)
ANDERSON 60	PR 119 2050	H.L. Anderson et al.	(EFI)
CASTAGNOLI 58	PR 112 1779	C. Castagnoli, M. Muchnik	(ROMA)

Meson Particle Listings

π^0



$$I^G(J^{PC}) = 1^-(0^{-+})$$

We have omitted some results that have been superseded by later experiments. The omitted results may be found in our 1988 edition Physics Letters **B204** 1 (1988).

π^0 MASS

The value is calculated from m_{π^\pm} and $(m_{\pi^\pm} - m_{\pi^0})$. See also the notes under the π^\pm Mass Listings.

VALUE (MeV)	DOCUMENT ID
134.9768 ± 0.0005 OUR FIT	Error includes scale factor of 1.1.

$m_{\pi^\pm} - m_{\pi^0}$

Measurements with an error > 0.01 MeV have been omitted.

VALUE (MeV)	DOCUMENT ID	TECN	COMMENT
4.5936 ± 0.0005 OUR FIT			
4.5936 ± 0.0005 OUR AVERAGE			
4.59364 ± 0.00048	CRAWFORD 91	CNTR	$\pi^- p \rightarrow \pi^0 n, n$ TOF
4.5930 ± 0.0013	CRAWFORD 86	CNTR	$\pi^- p \rightarrow \pi^0 n, n$ TOF
• • •	We do not use the following data for averages, fits, limits, etc. • • •		
4.59366 ± 0.00048	CRAWFORD 88B	CNTR	See CRAWFORD 91
4.6034 ± 0.0052	VASILEVSKY 66	CNTR	
4.6056 ± 0.0055	CZIRR 63	CNTR	

π^0 MEAN LIFE

Most experiments measure the π^0 width which we convert to a lifetime. ATHERTON 85 is the only direct measurement of the π^0 lifetime. Our average based only on indirect measurement yields $(8.30 \pm 0.19) \times 10^{-17}$ s. The two Primakoff measurements from 1970 have been excluded from our average because they suffered model-related systematics unknown at the time. More information on the π^0 lifetime can be found in BERNSTEIN 13.

VALUE (10^{-17} s)	EVTS	DOCUMENT ID	TECN	COMMENT
8.32 ± 0.15 ± 0.18 OUR AVERAGE		Error includes scale factor of 1.2.		
8.5 ± 1.1	1182	¹ LARIN	11	PRMX Primakoff effect
8.4 ± 0.5 ± 0.5		² BYCHKOV	09	PIBE $\pi^+ \rightarrow e^+ \nu \gamma$ at rest
8.97 ± 0.22 ± 0.17		³ WILLIAMS	88	CBAL $e^+ e^- \rightarrow e^+ e^- \pi^0$
8.2 ± 0.4		ATHERTON	85	CNTR Direct measurement
• • •	We do not use the following data for averages, fits, limits, etc. • • •			
5.6 ± 0.6		BELLETTINI	70	CNTR Primakoff effect
9 ± 0.68		KRYSHKIN	70	CNTR Primakoff effect
7.3 ± 1.1		BELLETTINI	65B	CNTR Primakoff effect

¹LARIN 11 reported $\Gamma(\pi^0 \rightarrow \gamma\gamma) = 7.82 \pm 0.14 \pm 0.17$ eV which we converted to mean life $\tau = \hbar/\Gamma(\text{total})$.
²BYCHKOV 09 obtains this using the conserved-vector-current relation between the vector form factor F_V and the π^0 lifetime.
³WILLIAMS 88 gives $\Gamma(\gamma\gamma) = 7.7 \pm 0.5 \pm 0.5$ eV. We give here $\tau = \hbar/\Gamma(\text{total})$.
⁴BROWMAN 74 gives a π^0 width $\Gamma = 8.02 \pm 0.42$ eV. The mean life is \hbar/Γ .

π^0 DECAY MODES

For decay limits to particles which are not established, see the appropriate Search sections (A^0 (axion) and Other Light Boson (X^0) Searches, etc.).

Mode	Fraction (Γ_i/Γ)	Scale factor/ Confidence level
Γ_1 2γ	$(98.823 \pm 0.034) \%$	S=1.5
Γ_2 $e^+ e^- \gamma$	$(1.174 \pm 0.035) \%$	S=1.5
Γ_3 γ positronium	$(1.82 \pm 0.29) \times 10^{-9}$	
Γ_4 $e^+ e^+ e^- e^-$	$(3.34 \pm 0.16) \times 10^{-5}$	
Γ_5 $e^+ e^-$	$(4.64 \pm 0.33) \times 10^{-8}$	
Γ_6 4γ	$< 2 \times 10^{-8}$	CL=90%
Γ_7 $\nu\bar{\nu}$	$[a] < 2.7 \times 10^{-7}$	CL=90%
Γ_8 $\nu_e \bar{\nu}_e$	$< 1.7 \times 10^{-6}$	CL=90%
Γ_9 $\nu_\mu \bar{\nu}_\mu$	$< 1.6 \times 10^{-6}$	CL=90%
Γ_{10} $\nu_\tau \bar{\nu}_\tau$	$< 2.1 \times 10^{-6}$	CL=90%
Γ_{11} $\gamma\nu\bar{\nu}$	$< 1.9 \times 10^{-7}$	CL=90%

Charge conjugation (C) or Lepton Family number (LF) violating modes

Γ_{12} 3γ	C	$< 3.1 \times 10^{-8}$	CL=90%
Γ_{13} $\mu^+ e^-$	LF	$< 3.8 \times 10^{-10}$	CL=90%
Γ_{14} $\mu^- e^+$	LF	$< 3.4 \times 10^{-9}$	CL=90%
Γ_{15} $\mu^+ e^- + \mu^- e^+$	LF	$< 3.6 \times 10^{-10}$	CL=90%

[a] Astrophysical and cosmological arguments give limits of order 10^{-13} .

CONSTRAINED FIT INFORMATION

An overall fit to 2 branching ratios uses 6 measurements and one constraint to determine 3 parameters. The overall fit has a $\chi^2 = 4.6$ for 4 degrees of freedom.

The following *off-diagonal* array elements are the correlation coefficients $\langle \delta x_i \delta x_j \rangle / (\delta x_i \delta x_j)$, in percent, from the fit to the branching fractions, $x_i \equiv \Gamma_i / \Gamma_{\text{total}}$. The fit constrains the x_i whose labels appear in this array to sum to one.

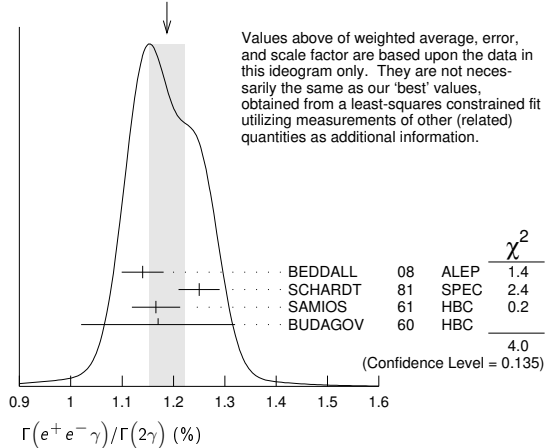
x_2	-100	
x_4	0	-1
	x_1	x_2

π^0 BRANCHING RATIOS

$\Gamma(e^+ e^- \gamma) / \Gamma(2\gamma)$	VALUE (%)	EVTS	DOCUMENT ID	TECN	COMMENT	Γ_2/Γ_1
1.188 ± 0.035 OUR FIT			Error includes scale factor of 1.5.			
1.188 ± 0.034 OUR AVERAGE			Error includes scale factor of 1.4. See the ideogram below.			
	1.140 ± 0.024 ± 0.033	12.5k	¹ BEDDALL	08	ALEP	$e^+ e^- \rightarrow Z \rightarrow \text{hadrons}$
	1.25 ± 0.04		SCHARDT	81	SPEC	$\pi^- p \rightarrow n\pi^0$
	1.166 ± 0.047	3071	² SAMIOS	61	HBC	$\pi^- p \rightarrow n\pi^0$
	1.17 ± 0.15	27	BUDAGOV	60	HBC	
• • •	We do not use the following data for averages, fits, limits, etc. • • •					
	1.1559 ± 0.0047 ± 0.0106	60k	³ ABOUZAID	19	KTEV	$K_L \rightarrow 3\pi^0$ in flight
	1.196		JOSEPH	60	THEO	QED calculation

¹BEDDALL 08 value is obtained from ALEPH archived data.
²SAMIOS 61 value uses a Panofsky ratio = 1.62.
³ABOUZAID 19 measured a value of $(0.3920 \pm 0.0016 \pm 0.0036) \%$ from 1999 KTEV data in $K_L \rightarrow 3\pi^0 \rightarrow 5\gamma e^+ e^-$ decays, normalised to $K_L \rightarrow 3\pi^0$, for $m(ee) > 15$ MeV and then extrapolated it to the full $m(ee)$ range using the Mikaelian and Smith predictions for the mass spectrum.

WEIGHTED AVERAGE
1.188 ± 0.034 (Error scaled by 1.4)



$\Gamma(\gamma$ positronium) $)/\Gamma(2\gamma)$

VALUE (units 10^{-9})	EVTS	DOCUMENT ID	TECN	COMMENT	Γ_3/Γ_1
1.84 ± 0.29	277	AFANASYEV	90	CNTR	pC 70 GeV

$\Gamma(e^+ e^+ e^- e^-) / \Gamma(2\gamma)$

VALUE (units 10^{-5})	EVTS	DOCUMENT ID	TECN	COMMENT	Γ_4/Γ_1
3.38 ± 0.16 OUR FIT					
3.38 ± 0.16 OUR AVERAGE					
3.46 ± 0.19	30.5k	¹ ABOUZAID	08D	KTEV	$K_L^0 \rightarrow \pi^0 \pi^0 \pi_{DD}^0$
3.18 ± 0.30	146	² SAMIOS	62B	HBC	

¹This ABOUZAID 08D value includes all radiative final states. The error includes both statistical and systematic errors. The correlation between the Dalitz-pair planes gives a direct measurement of the π^0 parity. The $\pi^0 2\gamma^*$ form factor is measured and limits are placed on a scalar contribution to the decay.
²SAMIOS 62B value uses a Panofsky ratio = 1.62.

$\Gamma(e^+ e^-) / \Gamma_{\text{total}}$

Experimental results are listed; branching ratios corrected for radiative effects are given in the footnotes. BERMAN 60 found $B(\pi^0 \rightarrow e^+ e^-) \geq 4.69 \times 10^{-8}$ via an exact QED calculation.

VALUE (units 10^{-8})	EVTS	DOCUMENT ID	TECN	CHG	COMMENT	Γ_5/Γ
6.46 ± 0.33 OUR AVERAGE						
6.44 ± 0.25 ± 0.22	794	¹ ABOUZAID	07	KTEV	$K_L^0 \rightarrow 3\pi^0$ in flight	
6.9 ± 2.3 ± 0.6	21	² DESHPANDE	93	SPEC	$K^+ \rightarrow \pi^+ \pi^0$	
7.6 $^{+2.9}_{-2.8}$ ± 0.5	8	³ MCFARLAND	93	SPEC	$K_L^0 \rightarrow 3\pi^0$ in flight	

See key on page 999

Meson Particle Listings

π^0

••• We do not use the following data for averages, fits, limits, etc. •••
6.09 ± 0.40 ± 0.24 275 4 ALAVI-HARATI 99c SPEC 0 Repl. by ABOUZAIID 07

1 ABOUZAIID 07 result is for $m_{e^+e^-}/m_{\pi^0} > 0.95$. With radiative corrections the result becomes $(7.48 ± 0.29 ± 0.25) × 10^{-8}$.

2 The DESHPANDE 93 result with bremsstrahlung radiative corrections is $(8.0 ± 2.6 ± 0.6) × 10^{-8}$.

3 The MCFARLAND 93 result is for $B[\pi^0 → e^+e^-, (m_{e^+e^-}/m_{\pi^0})^2 > 0.95]$. With radiative corrections it becomes $(8.8_{-3.2}^{+4.5} ± 0.6) × 10^{-8}$.

4 ALAVI-HARATI 99c quote result for $B[\pi^0 → e^+e^-, (m_{e^+e^-}/m_{\pi^0})^2 > 0.95]$ to minimize radiative contributions from $\pi^0 → e^+e^-\gamma$. After radiative corrections they obtain $(7.04 ± 0.46 ± 0.28) × 10^{-8}$.

$\Gamma(e^+e^-)/\Gamma(2\gamma)$ Γ_5/Γ_1

Table with columns: VALUE (units 10^-7), CL%, EVTS, DOCUMENT ID, TECN, COMMENT. Rows include NIEBUHR 89, ZEPHAT 87, FRANK 83, MISCHKE 82, FISCHER 78B.

$\Gamma(4\gamma)/\Gamma_{total}$ Γ_6/Γ

Table with columns: VALUE (units 10^-8), CL%, EVTS, DOCUMENT ID, TECN, COMMENT. Rows include MCDONOUGH 88, BOLOTOV 86c, AUERBACH 80.

$\Gamma(\nu\bar{\nu})/\Gamma_{total}$ Γ_7/Γ

The astrophysical and cosmological limits are many orders of magnitude lower, but we use the best laboratory limit for the Summary Tables.

Table with columns: VALUE (units 10^-6), CL%, DOCUMENT ID, TECN, COMMENT. Rows include ARTAMONOV 05A, ATIYA 91, LAM 91, NATALE 91, DORENBOS... 88, HERCZEG 81.

1 This limit applies to all possible $\nu\nu'$ states as well as to other massless, weakly interacting states.
2 LAM 91 considers the production of right-handed neutrinos produced from the cosmic thermal background at the temperature of about the pion mass through the reaction $\gamma\gamma → \pi^0 → \nu\bar{\nu}$.
3 NATALE 91 considers the excess energy-loss rate from SN1987A if the process $\gamma\gamma → \pi^0 → \nu\bar{\nu}$ occurs, permitted if the neutrinos have a right-handed component.

$\Gamma(\nu_e\bar{\nu}_e)/\Gamma_{total}$ Γ_8/Γ

Table with columns: VALUE (units 10^-6), CL%, DOCUMENT ID, TECN, COMMENT. Rows include DORENBOS... 88, HOFFMAN 88.

$\Gamma(\nu_\mu\bar{\nu}_\mu)/\Gamma_{total}$ Γ_9/Γ

Table with columns: VALUE (units 10^-6), CL%, EVTS, DOCUMENT ID, TECN, COMMENT. Rows include AUERBACH 04, HOFFMAN 88, DORENBOS... 88.

$\Gamma(\nu_\tau\bar{\nu}_\tau)/\Gamma_{total}$ Γ_{10}/Γ

Table with columns: VALUE (units 10^-6), CL%, DOCUMENT ID, TECN, COMMENT. Rows include HOFFMAN 88, DORENBOS... 88.

$\Gamma(\gamma\nu\bar{\nu})/\Gamma_{total}$ Γ_{11}/Γ

Table with columns: VALUE, CL%, DOCUMENT ID, TECN, COMMENT. Rows include CORTINA-GIL 19, ATIYA 92.

$\Gamma(3\gamma)/\Gamma_{total}$ Γ_{12}/Γ

Table with columns: VALUE (units 10^-8), CL%, EVTS, DOCUMENT ID, TECN, COMMENT. Rows include MCDONOUGH 88, HIGHLAND 80, AUERBACH 78, DUCLOS 65, KUTIN 65.

$\Gamma(\mu^+e^-)/\Gamma_{total}$ Γ_{13}/Γ

Table with columns: VALUE (units 10^-9), CL%, EVTS, DOCUMENT ID, TECN, COMMENT. Rows include APPEL 00, LEE 90, CAMPAGNARI 88.

$\Gamma(\mu^-e^+)/\Gamma_{total}$ Γ_{14}/Γ

Table with columns: VALUE (units 10^-9), CL%, EVTS, DOCUMENT ID, TECN, COMMENT. Rows include APPEL 00B, B865.

$[\Gamma(\mu^+e^-) + \Gamma(\mu^-e^+)]/\Gamma_{total}$ Γ_{15}/Γ

Table with columns: VALUE (units 10^-9), CL%, DOCUMENT ID, TECN, COMMENT. Rows include ABOUZAIID 08c, KROLAK 94, HERCZEG 84, BRYMAN 82.

π^0 ELECTROMAGNETIC FORM FACTOR

The amplitude for the process $\pi^0 → e^+e^-\gamma$ contains a form factor F(x) at the $\pi^0\gamma\gamma$ vertex, where $x = [m_{e^+e^-}/m_{\pi^0}]^2$. The parameter a in the linear expansion F(x) = 1 + ax is listed below.

All the measurements except that of BEHREND 91 are in the time-like region of momentum transfer.

LINEAR COEFFICIENT OF π^0 ELECTROMAGNETIC FORM FACTOR

Table with columns: VALUE (units 10^-2), EVTS, DOCUMENT ID, TECN, COMMENT. Rows include LAZZERONI 17, FARZANPAY 92, MEIJERDREES 92B, BEHREND 91, FONVIEILLE 89, TUPPER 83, FISCHER 78, DEVONS 69, KOBRACK 61, SAMIOS 61.

1 BEHREND 91 estimates that their systematic error is of the same order of magnitude as their statistical error, and so we have included a systematic error of this magnitude.
2 TUPPER 83 is a theoretical analysis of FISCHER 78 including 2-photon exchange in the corrections.
3 The FISCHER 78 error is statistical only. The result without radiation corrections is +0.05 ± 0.03.

π^0 REFERENCES

We have omitted some papers that have been superseded by later experiments. The omitted papers may be found in our 1988 edition Physics Letters B204 1 (1988).

ABOUZAIID 19 PR D100 032003 (KTeV Collab.)
CORTINA-GIL 19 JHEP 1905 182 (NA62 Collab.)
LAZZERONI 17 PL B7 69 38 (NA62 Collab.)
BERNSTEIN 13 RMP 85 49 (AMET, MIT)
LARIN 11 PRL 106 162303 (PrimEx Collab.)
BYCHKOV 09 PRL 103 051802 (PSI PIBETA Collab.)
ABOUZAIID 08C PRL 100 131803 (FNAL KTeV Collab.)
ABOUZAIID 08D PRL 100 182001 (FNAL KTeV Collab.)
BEDDALL 08 EPJ C54 365 (UGAZ)
ABOUZAIID 07 PR D75 012004 (KTeV Collab.)
ARTAMONOV 05A PR D72 091102 (BNL E949 Collab.)
AUERBACH 04 PRL 92 091801 (LSND Collab.)
APPEL 00 PRL 85 2450 (BNL 865 Collab.)
Also Thesis, Yale Univ. D.R. Bergman
Also Thesis, Univ. Zurich S. Pistak
APPEL 00B PRL 85 2877 R. Appel et al. (BNL 865 Collab.)

Meson Particle Listings

 π^0, η

ALAVI-HARATI	99C	PRL 83 922	A. Alavi-Harati et al.	(FNAL KTeV Collab.)
KROLAK	94	PL B320 407	P. Krolak et al.	(EFI, UCLA, COLO, ELMT+)
DESHPANDE	93	PRL 71 27	A. Deshpande et al.	(BNL E851 Collab.)
MCFARLAND	93	PRL 71 31	K.S. McFarland et al.	(EFI, UCLA, COLO+)
ATIYA	92	PRL 69 733	M.S. Atiya et al.	(BNL, LANL, PRIN+)
FARZANPAY	92	PL B278 413	F. Farzanpay et al.	(ORST, TRIU, BRCO+)
MEUERDREES	92B	PR D45 1439	R. Meijer Drees et al.	(PSI SINDRUM-I Collab.)
ATIYA	91	PRL 66 2189	M.S. Atiya et al.	(BNL, LANL, PRIN+)
BEHREND	91	ZPHY C49 401	H.J. Behrend et al.	(CELLO Collab.)
CRAWFORD	91	PR D43 46	J.F. Crawford et al.	(VILL, UVA)
LAM	91	PR D44 3345	W.P. Lam, K.W. Ng	(AST)
NATALE	91	PL B258 227	A.A. Natale	(SPIFT)
AFANASYEV	90	PL B236 116	L.G. Afanasyev et al.	(JINR, MOSU, SERP)
Also		SJNP 51 664	L.G. Afanasyev et al.	(JINR)
		Translated from YAF 51 1040.		
LEE	90	PRL 64 165	A.M. Lee et al.	(BNL, FNAL, VILL, WASH+)
FONVIEILLE	89	PL B233 65	H. Fonvieuille et al.	(CLER, LYON, SAACL)
NIEBUHR	89	PR D40 2796	C. Niebuhr et al.	(SINDRUM Collab.)
CAMPAGNARI	88	PRL 61 2062	C. Campagnari et al.	(BNL, FNAL, PSI+)
CRAWFORD	88B	PL B213 391	J.F. Crawford et al.	(PSI, UVA)
DORENBOS...	88	ZPHY C40 497	J. Dorenbosch et al.	(CHARM Collab.)
HOFFMAN	88	PL B208 149	C.M. Hoffman	(LANL)
MCDONOUGH	88	PR D38 2121	J.M. McDonough et al.	(TEMP, LANL, CHIC)
PDG	88	PL B204 1	G.P. Yost et al.	(LBL+)
WILLIAMS	88	PR D38 1365	D.A. Williams et al.	(Crystal Ball Collab.)
ZEPHAT	87	JP G13 1375	A.G. Zephath et al.	(OMICRON Collab.)
BOLOTOV	86C	JETPL 43 520	V.N. Bolotov et al.	(INRM)
		Translated from ZETFP 43 405.		
CRAWFORD	86	PRL 56 1043	J.F. Crawford et al.	(SIN, UVA)
ATHERTON	85	PL 158B 81	H.W. Atherton et al.	(CERN, ISU, LUND+)
HERCZEG	84	PR D29 1954	P. Herczeg, C.M. Hoffman	(LANL)
FRANK	83	PR D28 423	J.S. Frank et al.	(LANL, ARZS)
TUPPER	83	PR D28 2905	G.B. Tupper, T.R. Grose, M.A. Samuel	(OKSU)
BRYMAN	82	PR D26 2538	D.A. Bryman	(TRIU)
MISCHKE	82	PRL 48 1153	R.E. Mischke et al.	(LANL, ARZS)
HERCZEG	81	PL 100B 347	P. Herczeg, C.M. Hoffman	(LANL)
SCHARDT	81	PR D23 639	M.A. Schardt et al.	(ARZS, LANL)
AUERBACH	80	PL 90B 317	L.B. Auerbach et al.	(TEMP, LASL)
HIGHLAND	80	PRL 44 628	V.L. Highland et al.	(TEMP, LASL)
AUERBACH	78	PRL 41 275	L.B. Auerbach et al.	(TEMP, LASL)
FISCHER	78	PL 73B 359	J. Fischer et al.	(GEVA, SAACL)
FISCHER	78B	PL 73B 364	J. Fischer et al.	(GEVA, SAACL)
BROWMAN	74	PRL 33 1400	A. Browman et al.	(CORN, BING)
BELLETTINI	70	NC 66A 243	G. Bellettini et al.	(PISA, BONN)
KRYSHKIN	70	JETP 30 1037	V.I. Kryshkin, A.G. Sterligov, Y.P. Usov	(TMSK)
		Translated from ZETFP 57 1917.		
DEVONS	69	PR 184 1356	S. Devons et al.	(COLU, ROMA)
VASILEVSKY	66	PL 23 281	I.M. Vasilevsky et al.	(JINR)
BELLETTINI	65B	NC 40A 1139	G. Bellettini et al.	(PISA, FIRZ)
DUCLLOS	65	PL 19 253	J. Duclos et al.	(CERN, HEID)
KUTIN	65	JETPL 2 243	V.M. Kutjin, V.I. Petrukhin, Y.D. Prokoshkin	(JINR)
		Translated from ZETFP 2 387.		
CZIRR	63	PR 130 341	J.B. Czirr	(LRL)
SAMIOS	62B	PR 126 1844	N.P. Samios et al.	(COLU, BNL)
KOBRAK	61	NC 20 1115	H. Kobrak	(EFI)
SAMIOS	61	PR 121 275	N.P. Samios	(COLU, BNL)
BERMAN	60	NC 38 1192	S. Berman, D. Geffen	(JINR)
BUDAGOV	60	JETP 11 755	Y.A. Budagov et al.	(JINR)
		Translated from ZETFP 38 1047.		
JOSEPH	60	NC 16 997	D.W. Joseph	(EFI)

 η

$$I^G(J^{PC}) = 0^+(0^{-+})$$

We have omitted some results that have been superseded by later experiments. The omitted results may be found in our 1988 edition Physics Letters **B204** (1988).

 η MASS

Recent measurements resolve the obvious inconsistency in previous η mass measurements in favor of the higher value first reported by NA48 (LA1 02). We use only precise measurements consistent with this higher mass value for our η mass average.

VALUE (MeV)	EVTS	DOCUMENT ID	TECN	COMMENT
547.862 ± 0.017 OUR AVERAGE				
547.865 ± 0.031 ± 0.062		NIKOLAEV 14	CRYB	$\gamma p \rightarrow p \eta$
547.873 ± 0.005 ± 0.027	1M	GOSLAWSKI 12	SPEC	$d p \rightarrow {}^3\text{He} \eta$
547.874 ± 0.007 ± 0.029		AMBROSINO 07B	KLOE	$e^+ e^- \rightarrow \phi \rightarrow \eta \gamma$
547.785 ± 0.017 ± 0.057	16k	MILLER 07	CLEO	$\psi(2S) \rightarrow J/\psi \eta$
547.843 ± 0.030 ± 0.041	1134	LAI 02	NA48	$\eta \rightarrow 3\pi^0$
• • • We do not use the following data for averages, fits, limits, etc. • • •				
547.311 ± 0.028 ± 0.032		¹ ABDEL-BARY 05	SPEC	$d p \rightarrow {}^3\text{He} \eta$
547.12 ± 0.06 ± 0.25		KRUSCHE 95D	SPEC	$\gamma p \rightarrow \eta p$, threshold
547.30 ± 0.15		PLOUIN 92	SPEC	$d p \rightarrow {}^3\text{He} \eta$
547.45 ± 0.25		DUANE 74	SPEC	$\pi^- p \rightarrow n$ neutrals
548.2 ± 0.65		FOSTER 65c	HBC	
549.0 ± 0.7	148	FOELSCH 64	HBC	
548.0 ± 1.0	91	ALFF-... 62	HBC	
549.0 ± 1.2	53	BASTIEN 62	HBC	

¹ ABDEL-BARY 05 disagrees significantly with recent measurements of similar or better precision. See comment in the header.

 η WIDTH

This is the partial decay rate $\Gamma(\eta \rightarrow \gamma \gamma)$ divided by the fitted branching fraction for that mode. See the note at the start of the $\Gamma(2\gamma)$ data block, next below.

VALUE (keV)	DOCUMENT ID
1.31 ± 0.05 OUR FIT	

 η DECAY MODES

Mode	Fraction (Γ_i/Γ)	Scale factor/ Confidence level
Neutral modes		
Γ_1 neutral modes	(72.12 ± 0.34) %	S=1.2
Γ_2 2γ	(39.41 ± 0.20) %	S=1.1
Γ_3 $3\pi^0$	(32.68 ± 0.23) %	S=1.1
Γ_4 $\pi^0 2\gamma$	(2.56 ± 0.22) × 10 ⁻⁴	
Γ_5 $2\pi^0 2\gamma$	< 1.2 × 10 ⁻³	CL=90%
Γ_6 4γ	< 2.8 × 10 ⁻⁴	CL=90%
Γ_7 invisible	< 1.0 × 10 ⁻⁴	CL=90%
Charged modes		
Γ_8 charged modes	(27.89 ± 0.29) %	S=1.2
Γ_9 $\pi^+ \pi^- \pi^0$	(22.92 ± 0.28) %	S=1.2
Γ_{10} $\pi^+ \pi^- \gamma$	(4.22 ± 0.08) %	S=1.1
Γ_{11} $e^+ e^- \gamma$	(6.9 ± 0.4) × 10 ⁻³	S=1.3
Γ_{12} $\mu^+ \mu^- \gamma$	(3.1 ± 0.4) × 10 ⁻⁴	
Γ_{13} $e^+ e^-$	< 7 × 10 ⁻⁷	CL=90%
Γ_{14} $\mu^+ \mu^-$	(5.8 ± 0.8) × 10 ⁻⁶	
Γ_{15} $2e^+ 2e^-$	(2.40 ± 0.22) × 10 ⁻⁵	
Γ_{16} $\pi^+ \pi^- e^+ e^- (\gamma)$	(2.68 ± 0.11) × 10 ⁻⁴	
Γ_{17} $e^+ e^- \mu^+ \mu^-$	< 1.6 × 10 ⁻⁴	CL=90%
Γ_{18} $2\mu^+ 2\mu^-$	< 3.6 × 10 ⁻⁴	CL=90%
Γ_{19} $\mu^+ \mu^- \pi^+ \pi^-$	< 3.6 × 10 ⁻⁴	CL=90%
Γ_{20} $\pi^+ e^- \bar{\nu}_e + c.c.$	< 1.7 × 10 ⁻⁴	CL=90%
Γ_{21} $\pi^+ \pi^- 2\gamma$	< 2.1 × 10 ⁻³	
Γ_{22} $\pi^0 \pi^- \pi^0 \gamma$	< 5 × 10 ⁻⁴	CL=90%
Γ_{23} $\pi^0 \mu^+ \mu^- \gamma$	< 3 × 10 ⁻⁶	CL=90%

**Charge conjugation (C), Parity (P),
Charge conjugation × Parity (CP), or
Lepton Family number (LF) violating modes**

Γ_{24} $\pi^0 \gamma$	C	[a] < 9 × 10 ⁻⁵	CL=90%
Γ_{25} $\pi^+ \pi^-$	P, CP	< 1.3 × 10 ⁻⁵	CL=90%
Γ_{26} $2\pi^0$	P, CP	< 3.5 × 10 ⁻⁴	CL=90%
Γ_{27} $2\pi^0 \gamma$	C	< 5 × 10 ⁻⁴	CL=90%
Γ_{28} $3\pi^0 \gamma$	C	< 6 × 10 ⁻⁵	CL=90%
Γ_{29} 3γ	C	< 1.6 × 10 ⁻⁵	CL=90%
Γ_{30} $4\pi^0$	P, CP	< 6.9 × 10 ⁻⁷	CL=90%
Γ_{31} $\pi^0 e^+ e^-$	C	[b] < 8 × 10 ⁻⁶	CL=90%
Γ_{32} $\pi^0 \mu^+ \mu^-$	C	[b] < 5 × 10 ⁻⁶	CL=90%
Γ_{33} $\mu^+ e^- + \mu^- e^+$	LF	< 6 × 10 ⁻⁶	CL=90%

[a] Forbidden by angular momentum conservation.

[b] C parity forbids this to occur as a single-photon process.

CONSTRAINED FIT INFORMATION

An overall fit to 2 decay rate and 19 branching ratios uses 50 measurements and one constraint to determine 9 parameters. The overall fit has a $\chi^2 = 43.8$ for 42 degrees of freedom.

The following *off-diagonal* array elements are the correlation coefficients $\langle \delta x_i \delta x_j \rangle / (\delta x_i \delta x_j)$, in percent, from the fit to the branching fractions, $x_i \equiv \Gamma_i / \Gamma_{\text{total}}$. The fit constrains the x_i whose labels appear in this array to sum to one.

x_3	24								
x_4	4	1							
x_9	-73	-80	-4						
x_{10}	-56	-60	-3	61					
x_{11}	-5	-5	0	-6	-4				
x_{12}	-1	0	0	-1	0	0			
x_{16}	0	0	0	0	0	0	0		
Γ	-14	-3	-32	11	8	1	0	0	0
	x_2	x_3	x_4	x_9	x_{10}	x_{11}	x_{12}	x_{16}	

Mode	Rate (keV)	Scale factor
Γ_2 2γ	0.515 ± 0.018	
Γ_3 $3\pi^0$	0.427 ± 0.015	
Γ_4 $\pi^0 2\gamma$	(3.34 ± 0.28) × 10 ⁻⁴	
Γ_9 $\pi^+ \pi^- \pi^0$	0.299 ± 0.011	
Γ_{10} $\pi^+ \pi^- \gamma$	0.0551 ± 0.0022	
Γ_{11} $e^+ e^- \gamma$	0.0090 ± 0.0006	1.2

See key on page 999

Meson Particle Listings

η

Γ_{12}	$\mu^+ \mu^- \gamma$	(4.1 ± 0.5) × 10 ⁻⁴
Γ_{16}	$\pi^+ \pi^- e^+ e^- (\gamma)$	(3.50 ± 0.19) × 10 ⁻⁴

η DECAY RATES

$\Gamma(2\gamma)$ Γ_2
 See the table immediately above giving the fitted decay rates. Following the advice of NEFKENS 02, we have removed the Primakoff-effect measurement from the average. See also the "Note on the Decay Width $\Gamma(\eta \rightarrow \gamma\gamma)$," in our 1994 edition, Phys. Rev. D50, 1 August 1994, Part I, p. 1451, for a discussion of the various measurements.

VALUE (keV)	EVTs	DOCUMENT ID	TECN	COMMENT
0.515 ± 0.018 OUR FIT				
0.516 ± 0.018 OUR AVERAGE				
0.520 ± 0.020 ± 0.013		BABUSCI 13A	KLOE	$e^+ e^- \rightarrow e^+ e^- \eta$
0.51 ± 0.12 ± 0.05	36	BARU 90	MD1	$e^+ e^- \rightarrow e^+ e^- \eta$
0.490 ± 0.010 ± 0.048	2287	ROE 90	ASP	$e^+ e^- \rightarrow e^+ e^- \eta$
0.514 ± 0.017 ± 0.035	1295	WILLIAMS 88	CBAL	$e^+ e^- \rightarrow e^+ e^- \eta$
0.53 ± 0.04 ± 0.04		BARTEL 85E	JADE	$e^+ e^- \rightarrow e^+ e^- \eta$
• • • We do not use the following data for averages, fits, limits, etc. • • •				
0.476 ± 0.062		¹ RODRIGUES 08	CNTR	Reanalysis
0.64 ± 0.14 ± 0.13		AIHARA 86	TPC	$e^+ e^- \rightarrow e^+ e^- \eta$
0.56 ± 0.16	56	WEINSTEIN 83	CBAL	$e^+ e^- \rightarrow e^+ e^- \eta$
0.324 ± 0.046		BROWMAN 74B	CNTR	Primakoff effect
1.00 ± 0.22		² BEMPORAD 67	CNTR	Primakoff effect

¹RODRIGUES 08 uses a more sophisticated calculation for the inelastic background due to incoherent photoproduction to reanalyze the η photoproduction data on Be and Cu at 9 GeV from BROWMAN 74B. This brings the value of $\Gamma(\eta \rightarrow 2\gamma)$ in line with direct measurements of the width. The error here is only statistical.

²BEMPORAD 67 gives $\Gamma(2\gamma) = 1.21 \pm 0.26$ keV assuming $\Gamma(2\gamma)/\Gamma(\text{total}) = 0.314$. Bemporad private communication gives $\Gamma(2\gamma)^2/\Gamma(\text{total}) = 0.380 \pm 0.083$. We evaluate this using $\Gamma(2\gamma)/\Gamma(\text{total}) = 0.38 \pm 0.01$. Not included in average because the uncertainty resulting from the separation of the coulomb and nuclear amplitudes has apparently been underestimated.

VALUE (eV)	EVTs	DOCUMENT ID	TECN	COMMENT
0.334 ± 0.028 OUR FIT				
0.33 ± 0.03	1200	NEFKENS 14	CRYB	$\gamma p \rightarrow \eta p$

η BRANCHING RATIOS

Neutral modes

$\Gamma(\text{neutral modes})/\Gamma_{\text{total}}$	$\Gamma_1/\Gamma = (\Gamma_2 + \Gamma_3 + \Gamma_4)/\Gamma$
0.721 ± 0.0034 OUR FIT	Error includes scale factor of 1.2.
0.705 ± 0.008	16k BASILE 71D CNTR MM spectrometer
• • • We do not use the following data for averages, fits, limits, etc. • • •	
0.79 ± 0.08	BUNIATOV 67 OSPK

$\Gamma(2\gamma)/\Gamma_{\text{total}}$	Γ_2/Γ
39.41 ± 0.20 OUR FIT	Error includes scale factor of 1.1.
39.49 ± 0.17 ± 0.30	65k ABEGG 96 SPEC $pd \rightarrow {}^3\text{He}\eta$
• • • We do not use the following data for averages, fits, limits, etc. • • •	
38.45 ± 0.40 ± 0.36	14k ¹ LOPEZ 07 CLEO $\psi(2S) \rightarrow J/\psi\eta$

¹Not independent of other results listed for LOPEZ 07. Assuming decays of $\eta \rightarrow \gamma\gamma$, $3\pi^0$, $\pi^+\pi^-\pi^0$, $\pi^+\pi^-\gamma$, and $e^+e^-\gamma$ account for all η decays within a contribution of 0.3% to the systematic error.

$\Gamma(2\gamma)/\Gamma(\text{neutral modes})$	$\Gamma_2/\Gamma_1 = \Gamma_2/(\Gamma_2 + \Gamma_3 + \Gamma_4)$
0.5465 ± 0.0019 OUR FIT	
0.548 ± 0.023 OUR AVERAGE	Error includes scale factor of 1.5.
0.535 ± 0.018	BUTTRAM 70 OSPK
0.59 ± 0.033	BUNIATOV 67 OSPK
• • • We do not use the following data for averages, fits, limits, etc. • • •	
0.52 ± 0.09	88 ABROSIMOV 80 HLBC
0.60 ± 0.14	113 KENDALL 74 OSPK
0.57 ± 0.09	STRUGALSKI 71 HLBC
0.579 ± 0.052	FELDMAN 67 OSPK
0.416 ± 0.044	DIGUGNO 66 CNTR Error doubled
0.44 ± 0.07	GRUNHAUS 66 OSPK
0.39 ± 0.06	¹ JONES 66 CNTR

¹This result from combining cross sections from two different experiments.

$\Gamma(3\pi^0)/\Gamma_{\text{total}}$	Γ_3/Γ
32.68 ± 0.23 OUR FIT	Error includes scale factor of 1.1.
• • • We do not use the following data for averages, fits, limits, etc. • • •	
34.03 ± 0.56 ± 0.49	1821 ¹ LOPEZ 07 CLEO $\psi(2S) \rightarrow J/\psi\eta$

¹Not independent of other results listed for LOPEZ 07. Assuming decays of $\eta \rightarrow \gamma\gamma$, $3\pi^0$, $\pi^+\pi^-\pi^0$, $\pi^+\pi^-\gamma$, and $e^+e^-\gamma$ account for all η decays within a contribution of 0.3% to the systematic error.

$\Gamma(3\pi^0)/\Gamma(\text{neutral modes})$	$\Gamma_3/\Gamma_1 = \Gamma_3/(\Gamma_2 + \Gamma_3 + \Gamma_4)$
0.4531 ± 0.0019 OUR FIT	
0.439 ± 0.024	BUTTRAM 70 OSPK
• • • We do not use the following data for averages, fits, limits, etc. • • •	
0.44 ± 0.08	75 ABROSIMOV 80 HLBC
0.32 ± 0.09	STRUGALSKI 71 HLBC
0.41 ± 0.033	BUNIATOV 67 OSPK Not indep. of $\Gamma(2\gamma)/\Gamma(\text{neutral modes})$
0.177 ± 0.035	FELDMAN 67 OSPK
0.209 ± 0.054	DIGUGNO 66 CNTR Error doubled
0.29 ± 0.10	GRUNHAUS 66 OSPK

$\Gamma(3\pi^0)/\Gamma(2\gamma)$	Γ_3/Γ_2
0.829 ± 0.006 OUR FIT	
0.829 ± 0.007 OUR AVERAGE	
0.884 ± 0.022 ± 0.019	1821 LOPEZ 07 CLEO $\psi(2S) \rightarrow J/\psi\eta$
0.817 ± 0.012 ± 0.032	17.4k ¹ AKHMETSHIN 05 CMD2 $e^+e^- \rightarrow \phi \rightarrow \eta\gamma$
0.826 ± 0.024	ACHASOV 00D SND $e^+e^- \rightarrow \phi \rightarrow \eta\gamma$
0.832 ± 0.005 ± 0.012	KRUSCHE 95D SPEC $\gamma p \rightarrow \eta p$, threshold
0.841 ± 0.034	AMSLER 93 CBAR $\bar{p}p \rightarrow \pi^+\pi^-\eta$ at rest
0.822 ± 0.009	ALDE 84 GAM2
• • • We do not use the following data for averages, fits, limits, etc. • • •	
0.796 ± 0.016 ± 0.016	ACHASOV 00 SND See ACHASOV 00D
0.91 ± 0.14	COX 70B HBC
0.75 ± 0.09	DEVONS 70 OSPK
0.88 ± 0.16	BALTAY 67D DBC
1.1 ± 0.2	CENCE 67 OSPK
1.25 ± 0.39	BACCI 63 CNTR Inverse BR reported

¹Uses result from AKHMETSHIN 01b.

$\Gamma(\pi^0 2\gamma)/\Gamma_{\text{total}}$	Γ_4/Γ
Early results are summarized in the review by LANDSBERG 85.	
2.56 ± 0.22 OUR FIT	
2.21 ± 0.24 ± 0.47	≈ 500 ¹ PRAKHOV 08 CRYB $\pi^- p \rightarrow \eta n$ ≈ threshold
• • • We do not use the following data for averages, fits, limits, etc. • • •	
3.5 ± 0.7 ± 0.6	1.6k ^{2,3} PRAKHOV 05 CRYB See PRAKHOV 08
<8.4	90 7 ACHASOV 01D SND $e^+e^- \rightarrow \phi \rightarrow \eta\gamma$
<30	90 0 DAVYDOV 81 GAM2 $\pi^- p \rightarrow \eta n$

¹PRAKHOV 08 is a reanalysis of the data of PRAKHOV 05, using for the first time the invariant-mass spectrum of the two photons.

²Normalized using $\Gamma(\eta \rightarrow 2\gamma)/\Gamma = 0.3943 \pm 0.0026$.

³This measurement and the independent analysis of the same data by KNECHT 04 both imply a lower value of $\Gamma(\pi^0 2\gamma)$ than the one obtained by ALDE 84 from $\Gamma(\pi^0 2\gamma)/\Gamma(2\gamma)$.

$\Gamma(\pi^0 2\gamma)/\Gamma(2\gamma)$	Γ_4/Γ_2
0.65 ± 0.06 OUR FIT	
1.8 ± 0.4	ALDE 84 GAM2 0
• • • We do not use the following data for averages, fits, limits, etc. • • •	
2.5 ± 0.6	70 BINON 82 GAM2 See ALDE 84

$\Gamma(\pi^0 2\gamma)/\Gamma(3\pi^0)$	Γ_4/Γ_3
7.8 ± 0.7 OUR FIT	
• • • We do not use the following data for averages, fits, limits, etc. • • •	
8.3 ± 2.8 ± 1.4	¹ KNECHT 04 CRYB $\pi^- p \rightarrow \eta n$
¹ Independent analysis of same data as PRAKHOV 05.	

$\Gamma(2\pi^0 2\gamma)/\Gamma_{\text{total}}$	Γ_5/Γ
<1.2 × 10⁻³	90 ¹ NEFKENS 05A CRYB $p(720 \text{ MeV}/c) \pi^- \rightarrow n\eta$
• • • We do not use the following data for averages, fits, limits, etc. • • •	
<4.0 × 10 ⁻³	90 BLIK 07 GAM4 $\pi^- p \rightarrow \eta n$
¹ Measurement is done in limited $\gamma\gamma$ energy range.	

$\Gamma(4\gamma)/\Gamma_{\text{total}}$	Γ_6/Γ
<2.8 × 10⁻⁴	90 BLIK 07 GAM4 $\pi^- p \rightarrow \eta n$

$\Gamma(\text{invisible})/\Gamma(2\gamma)$	Γ_7/Γ_2
<2.6 × 10⁻⁴	90 ¹ ABLIKIM 13 BES3 $J/\psi \rightarrow \phi\eta$
• • • We do not use the following data for averages, fits, limits, etc. • • •	
<1.65 × 10 ⁻³	90 ² ABLIKIM 06Q BES2 $J/\psi \rightarrow \phi\eta$
¹ Based on 225M J/ψ decays.	
² Based on 58M J/ψ decays.	

Meson Particle Listings

 η

Charged modes

 $\Gamma(\pi^+\pi^-\pi^0)/\Gamma_{\text{total}}$ Γ_9/Γ

VALUE (units 10^{-2})	EVTS	DOCUMENT ID	TECN	COMMENT
22.92±0.28 OUR FIT				Error includes scale factor of 1.2.

- • • We do not use the following data for averages, fits, limits, etc. • • •

22.60±0.35±0.29	3915	¹ LOPEZ	07	CLEO $\psi(2S) \rightarrow J/\psi\eta$
-----------------	------	--------------------	----	--

¹ Not independent of other results listed for LOPEZ 07. Assuming decays of $\eta \rightarrow \gamma\gamma$, $3\pi^0$, $\pi^+\pi^-\pi^0$, $\pi^+\pi^-\gamma$, and $e^+e^-\gamma$ account for all η decays within a contribution of 0.3% to the systematic error.

 $\Gamma(\text{neutral modes})/\Gamma(\pi^+\pi^-\pi^0)$ $\Gamma_1/\Gamma_9 = (\Gamma_2+\Gamma_3+\Gamma_4)/\Gamma_9$

VALUE	EVTS	DOCUMENT ID	TECN	COMMENT
3.15±0.05 OUR FIT				Error includes scale factor of 1.2.
3.26±0.30 OUR AVERAGE				

2.54±1.89	74	KENDALL	74	OSPK
3.4 ±1.1	29	AGUILAR-...	72B	HBC
2.83±0.80	70	¹ BLOODW...	72B	HBC
3.6 ±0.6	244	FLATTE	67B	HBC
2.89±0.56		ALFF-...	66	HBC
3.6 ±0.8	50	KRAEMER	64	DBC
3.8 ±1.1		PAULI	64	DBC

¹ Error increased from published value 0.5 by Bloodworth (private communication).

 $\Gamma(2\gamma)/\Gamma(\pi^+\pi^-\pi^0)$ Γ_2/Γ_9

VALUE	EVTS	DOCUMENT ID	TECN	COMMENT
1.720±0.028 OUR FIT				Error includes scale factor of 1.2.
1.70 ±0.04 OUR AVERAGE				

1.704±0.032±0.026	3915	¹ LOPEZ	07	CLEO $\psi(2S) \rightarrow J/\psi\eta$
1.61 ±0.14		ABLIKIM	06E	BES2 $e^+e^- \rightarrow J/\psi \rightarrow \eta\gamma$
1.78 ±0.10 ±0.13	1077	AMSLER	95	CBAR $\bar{p}p \rightarrow \pi^+\pi^-\eta$ at rest
1.72 ±0.25	401	BAGLIN	69	HLBC
1.61 ±0.39		FOSTER	65	HBC

¹ LOPEZ 07 reports $\Gamma(\eta \rightarrow \pi^+\pi^-\pi^0) / \Gamma(\eta \rightarrow 2\gamma) = \Gamma_9/\Gamma_2 = 0.587 \pm 0.011 \pm 0.009$.

 $\Gamma(3\pi^0)/\Gamma(\pi^+\pi^-\pi^0)$ Γ_3/Γ_9

VALUE	EVTS	DOCUMENT ID	TECN	COMMENT
1.426±0.026 OUR FIT				Error includes scale factor of 1.2.
1.48 ±0.05 OUR AVERAGE				

1.46 ±0.03 ±0.09		ACHASOV	06A	SND $e^+e^- \rightarrow \eta\gamma$
1.52 ±0.04 ±0.08	23k	¹ AKHMETSHIN	01B	CMD2 $e^+e^- \rightarrow \phi \rightarrow \eta\gamma$
1.44 ±0.09 ±0.10	1627	AMSLER	95	CBAR $\bar{p}p \rightarrow \pi^+\pi^-\eta$ at rest
1.50 ^{+0.15} _{-0.29}	199	BAGLIN	69	HLBC
1.47 ^{+0.20} _{-0.17}		BULLOCK	68	HLBC
• • • We do not use the following data for averages, fits, limits, etc. • • •				
1.3 ±0.4		BAGLIN	67B	HLBC
0.90 ±0.24		FOSTER	65	HBC
2.0 ±1.0		FOELSCH	64	HBC
0.83 ±0.32		CRAWFORD	63	HBC

¹ AKHMETSHIN 01B uses results from AKHMETSHIN 99F.

 $\Gamma(\pi^+\pi^-\pi^0)/[\Gamma(2\gamma) + \Gamma(3\pi^0)]$ $\Gamma_9/(\Gamma_2+\Gamma_3)$

VALUE	DOCUMENT ID	TECN	COMMENT
0.318 ±0.005 OUR FIT			Error includes scale factor of 1.2.
0.304 ±0.012	ACHASOV	00D	SND $e^+e^- \rightarrow \phi \rightarrow \eta\gamma$

- • • We do not use the following data for averages, fits, limits, etc. • • •

0.3141±0.0081±0.0058	ACHASOV	00B	SND See ACHASOV 00D
----------------------	---------	-----	---------------------

 $\Gamma(\pi^+\pi^-\gamma)/\Gamma_{\text{total}}$ Γ_{10}/Γ

VALUE (units 10^{-2})	EVTS	DOCUMENT ID	TECN	COMMENT
4.22±0.08 OUR FIT				Error includes scale factor of 1.1.

- • • We do not use the following data for averages, fits, limits, etc. • • •

3.96±0.14±0.14	859	¹ LOPEZ	07	CLEO $\psi(2S) \rightarrow J/\psi\eta$
----------------	-----	--------------------	----	--

¹ Not independent of other results listed for LOPEZ 07. Assuming decays of $\eta \rightarrow \gamma\gamma$, $3\pi^0$, $\pi^+\pi^-\pi^0$, $\pi^+\pi^-\gamma$, and $e^+e^-\gamma$ account for all η decays within a contribution of 0.3% to the systematic error.

 $\Gamma(\pi^+\pi^-\gamma)/\Gamma(\pi^+\pi^-\pi^0)$ Γ_{10}/Γ_9

VALUE	EVTS	DOCUMENT ID	TECN	COMMENT
0.1842±0.0027 OUR FIT				Error includes scale factor of 1.1.
0.1847±0.0030 OUR AVERAGE				

0.1856±0.0005±0.0028	200k	BABUSCI	13	KLOE $e^+e^- \rightarrow \phi \rightarrow \eta\gamma$
0.175 ±0.007 ±0.006	859	LOPEZ	07	CLEO $\psi(2S) \rightarrow J/\psi\eta$
• • • We do not use the following data for averages, fits, limits, etc. • • •				
0.209 ±0.004	18k	THALER	73	ASPK
0.201 ±0.006	7250	GORMLEY	70	ASPK
0.28 ±0.04		BALTAY	67B	DBC
0.25 ±0.035		LITCHEFIELD	67	DBC
0.30 ±0.06		CRAWFORD	66	HBC
0.196 ±0.041		FOSTER	65c	HBC

 $\Gamma(e^+e^-\gamma)/\Gamma_{\text{total}}$ Γ_{11}/Γ

VALUE (units 10^{-3})	EVTS	DOCUMENT ID	TECN	COMMENT
6.9 ±0.4 OUR FIT				Error includes scale factor of 1.3.
6.7 ±0.5 OUR AVERAGE				Error includes scale factor of 1.2.

6.6 ±0.4 ±0.4	1345	BERGHAUSER	11	SPEC $\gamma p \rightarrow p\eta$
7.8 ±0.5 ±0.8	435 ± 31	BERLOWSKI	08	WASA $pd \rightarrow {}^3\text{He}\eta$
5.15±0.62±0.74	283	ACHASOV	01B	SND $e^+e^- \rightarrow \phi \rightarrow \eta\gamma$
7.10±0.64±0.46	323	AKHMETSHIN	01	CMD2 $e^+e^- \rightarrow \phi \rightarrow \eta\gamma$
• • • We do not use the following data for averages, fits, limits, etc. • • •				
9.4 ±0.7 ±0.5	172	¹ LOPEZ	07	CLEO $\psi(2S) \rightarrow J/\psi\eta$

¹ Not independent of other results listed for LOPEZ 07. Assuming decays of $\eta \rightarrow \gamma\gamma$, $3\pi^0$, $\pi^+\pi^-\pi^0$, $\pi^+\pi^-\gamma$, and $e^+e^-\gamma$ account for all η decays within a contribution of 0.3% to the systematic error.

 $\Gamma(e^+e^-\gamma)/\Gamma(\pi^+\pi^-\gamma)$ Γ_{11}/Γ_{10}

VALUE	EVTS	DOCUMENT ID	TECN	COMMENT
0.163±0.011 OUR FIT				Error includes scale factor of 1.2.
0.237±0.021±0.015	172	LOPEZ	07	CLEO $\psi(2S) \rightarrow J/\psi\eta$

 $\Gamma(e^+e^-\gamma)/\Gamma(\pi^+\pi^-\pi^0)$ Γ_{11}/Γ_9

VALUE (units 10^{-2})	EVTS	DOCUMENT ID	TECN	COMMENT
3.00±0.19 OUR FIT				Error includes scale factor of 1.3.
2.1 ±0.5	80	JANE	75B	OSPK See the erratum

 $\Gamma(\text{neutral modes})/[\Gamma(\pi^+\pi^-\pi^0) + \Gamma(\pi^+\pi^-\gamma) + \Gamma(e^+e^-\gamma)]$ $\Gamma_1/(\Gamma_9+\Gamma_{10}+\Gamma_{11}) = (\Gamma_2+\Gamma_3+\Gamma_4)/(\Gamma_9+\Gamma_{10}+\Gamma_{11})$

VALUE	EVTS	DOCUMENT ID	TECN	COMMENT
2.59±0.04 OUR FIT				Error includes scale factor of 1.2.
2.64±0.23		BALTAY	67B	DBC

- • • We do not use the following data for averages, fits, limits, etc. • • •

4.5 ±1.0	280	¹ JAMES	66	HBC
3.20±1.26	53	¹ BASTIEN	62	HBC
2.5 ±1.0	10	¹ PICKUP	62	HBC

¹ These experiments are not used in the averages as they do not separate clearly $\eta \rightarrow \pi^+\pi^-\pi^0$ and $\eta \rightarrow \pi^+\pi^-\gamma$ from each other. The reported values thus probably contain some unknown fraction of $\eta \rightarrow \pi^+\pi^-\gamma$.

 $\Gamma(2\gamma)/[\Gamma(\pi^+\pi^-\pi^0) + \Gamma(\pi^+\pi^-\gamma) + \Gamma(e^+e^-\gamma)]$ $\Gamma_2/(\Gamma_9+\Gamma_{10}+\Gamma_{11})$

VALUE	EVTS	DOCUMENT ID	TECN	COMMENT
1.417±0.023 OUR FIT				Error includes scale factor of 1.2.
1.1 ±0.4 OUR AVERAGE				

1.51 ±0.93	75	KENDALL	74	OSPK
0.99 ±0.48		CRAWFORD	63	HBC

 $\Gamma(\mu^+\mu^-\gamma)/\Gamma_{\text{total}}$ Γ_{12}/Γ

VALUE (units 10^{-4})	EVTS	DOCUMENT ID	TECN	COMMENT
3.1±0.4 OUR FIT				
3.1±0.4	600	DZHELADIN	80	SPEC $\pi^-p \rightarrow \eta n$

- • • We do not use the following data for averages, fits, limits, etc. • • •

1.5±0.75	100	BUSHNIN	78	SPEC See DZHELADIN 80
----------	-----	---------	----	-----------------------

 $\Gamma(e^+e^-)/\Gamma_{\text{total}}$ Γ_{13}/Γ

VALUE	CL%	DOCUMENT ID	TECN	COMMENT
<7 × 10⁻⁷	90	ACHASOV	18B	CNTR Inverse reaction $e^+e^- \rightarrow \eta$

- • • We do not use the following data for averages, fits, limits, etc. • • •

<2.3 × 10 ⁻⁶	90	AGAKISHIEV	14	$pp \rightarrow \eta + X$
<5.6 × 10 ⁻⁶	90	¹ AGAKISHIEV	12A	SPEC $pp \rightarrow \eta + X$
<2.7 × 10 ⁻⁵	90	BERLOWSKI	08	WASA $pd \rightarrow {}^3\text{He}\eta$
<0.77 × 10 ⁻⁴	90	BROWDER	97B	CLE2 $e^+e^- \simeq 10.5$ GeV
<2 × 10 ⁻⁴	90	WHITE	96	SPEC $pd \rightarrow \eta^3\text{He}$
<3 × 10 ⁻⁴	90	DAVIES	74	RVUE Uses ESTEN 67

¹ AGAKISHIEV 12A uses a data sample of 3.5 GeV proton beam collisions on liquid hydrogen target collected by the HADES detector.

 $\Gamma(\mu^+\mu^-)/\Gamma_{\text{total}}$ Γ_{14}/Γ

VALUE (units 10^{-6})	CL%	EVTS	DOCUMENT ID	TECN	COMMENT
5.8±0.8 OUR AVERAGE					

5.7±0.7±0.5	114	ABEGG	94	SPEC $pd \rightarrow \eta^3\text{He}$
6.5±2.1	27	DZHELADIN	80B	SPEC $\pi^-p \rightarrow \eta n$
• • • We do not use the following data for averages, fits, limits, etc. • • •				

5.6 ^{+0.6} _{-0.7} ±0.5	100	KESSLER	93	SPEC See ABEGG 94
--	-----	---------	----	-------------------

< 20	95	0	WEHMANN	68	OSPK
------	----	---	---------	----	------

 $\Gamma(\mu^+\mu^-)/\Gamma(2\gamma)$ Γ_{14}/Γ_2

VALUE (units 10^{-5})	DOCUMENT ID	TECN	COMMENT
• • • We do not use the following data for averages, fits, limits, etc. • • •			
5.9±2.2	HYAMS	69	OSPK

$\Gamma(2e^+2e^-)/\Gamma_{\text{total}}$ Γ_{15}/Γ

VALUE (units 10^{-5})	CL%	EVTS	DOCUMENT ID	TECN	COMMENT
$2.4 \pm 0.2 \pm 0.1$		362	¹ AMBROSINO 11B	KLOE	$e^+e^- \rightarrow \phi \rightarrow \eta\gamma$

• • • We do not use the following data for averages, fits, limits, etc. • • •

<9.7	90		BERLOWSKI 08	WASA	$pd \rightarrow {}^3\text{He} \eta$
<6.9	90		AKHMETSHIN 01	CMD2	$e^+e^- \rightarrow \phi \rightarrow \eta\gamma$

¹ This measurement is fully inclusive (includes " $2e^+2e^- \gamma$ " channel).

 $\Gamma(\pi^+\pi^-e^+e^- \gamma)/\Gamma_{\text{total}}$ Γ_{16}/Γ

VALUE (units 10^{-4})	EVTS	DOCUMENT ID	TECN	COMMENT
2.68 ± 0.11 OUR FIT				

$2.68 \pm 0.09 \pm 0.07$	1555 \pm 52	¹ AMBROSINO 09B	KLOE	$e^+e^- \rightarrow \phi \rightarrow \eta\gamma$
--------------------------	---------------	----------------------------	------	--

• • • We do not use the following data for averages, fits, limits, etc. • • •

$4.3 \pm 2.0 \pm 0.4$	16	BERLOWSKI 08	WASA	$pd \rightarrow {}^3\text{He} \eta$
$4.3 \pm 1.3 \pm 0.4$	16	BARGHOLTZ 07	CNTR	See BERLOWSKI 08
$3.7 \pm 2.5 \pm 0.3$	4	AKHMETSHIN 01	CMD2	$e^+e^- \rightarrow \phi \rightarrow \eta\gamma$

¹ This AMBROSINO 09B value includes radiative events.

 $\Gamma(e^+e^-\mu^+\mu^-)/\Gamma_{\text{total}}$ Γ_{17}/Γ

VALUE	CL%	DOCUMENT ID	TECN	COMMENT
$<1.6 \times 10^{-4}$	90	BERLOWSKI 08	WASA	$pd \rightarrow {}^3\text{He} \eta$

 $\Gamma(2\mu^+2\mu^-)/\Gamma_{\text{total}}$ Γ_{18}/Γ

VALUE	CL%	DOCUMENT ID	TECN	COMMENT
$<3.6 \times 10^{-4}$	90	BERLOWSKI 08	WASA	$pd \rightarrow {}^3\text{He} \eta$

 $\Gamma(\mu^+\mu^-\pi^+\pi^-)/\Gamma_{\text{total}}$ Γ_{19}/Γ

VALUE	CL%	DOCUMENT ID	TECN	COMMENT
$<3.6 \times 10^{-4}$	90	BERLOWSKI 08	WASA	$pd \rightarrow {}^3\text{He} \eta$

 $\Gamma(\pi^+e^-\nu_e + c.c.)/\Gamma(\pi^+\pi^-\pi^0)$ Γ_{20}/Γ_9

VALUE	CL%	DOCUMENT ID	TECN	COMMENT
$<7.3 \times 10^{-4}$	90	ABLIKIM 13G	BES3	$J/\psi \rightarrow \phi \eta$

 $\Gamma(\pi^+\pi^-2\gamma)/\Gamma(\pi^+\pi^-\pi^0)$ Γ_{21}/Γ_9

VALUE	CL%	DOCUMENT ID	TECN	COMMENT
$<9 \times 10^{-3}$		PRICE 67	HBC	

• • • We do not use the following data for averages, fits, limits, etc. • • •

$<16 \times 10^{-3}$	95	BALTAY 67B	DBC	
----------------------	----	------------	-----	--

 $\Gamma(\pi^+\pi^-\pi^0\gamma)/\Gamma(\pi^+\pi^-\pi^0)$ Γ_{22}/Γ_9

VALUE	CL%	EVTS	DOCUMENT ID	TECN	COMMENT
$<0.24 \times 10^{-2}$	90	0	THALER 73	ASPK	

• • • We do not use the following data for averages, fits, limits, etc. • • •

$<1.7 \times 10^{-2}$	90	ARNOLD 68	HLBC	
$<1.6 \times 10^{-2}$	95	BALTAY 67B	DBC	
$<7.0 \times 10^{-2}$		FLATTE 67	HBC	
$<0.9 \times 10^{-2}$		PRICE 67	HBC	

 $\Gamma(\pi^0\mu^+\mu^- \gamma)/\Gamma_{\text{total}}$ Γ_{23}/Γ

VALUE	CL%	DOCUMENT ID	TECN	COMMENT
$<3 \times 10^{-6}$	90	DZHELYADIN 81	SPEC	$\pi^- p \rightarrow \eta n$

Forbidden modes $\Gamma(\pi^0\gamma)/\Gamma_{\text{total}}$ Γ_{24}/Γ

Forbidden by angular momentum conservation.

VALUE	CL%	DOCUMENT ID	TECN	COMMENT
$<9 \times 10^{-5}$	90	NEFKENS 05A	CRYB	$p(720 \text{ MeV}/c) \pi^- \rightarrow n \eta$

 $\Gamma(\pi^+\pi^-)/\Gamma_{\text{total}}$ Γ_{25}/Γ

Forbidden by P and CP invariance.

VALUE	CL%	EVTS	DOCUMENT ID	TECN	COMMENT
$<1.3 \times 10^{-5}$	90	16M	AMBROSINO 05A	KLOE	$e^+e^- \rightarrow \phi \rightarrow \eta\gamma$

• • • We do not use the following data for averages, fits, limits, etc. • • •

$<5.3 \times 10^{-17}$			¹ ZHEVLAKOV 19	THEO	from nEDM limits
$<1.6 \times 10^{-5}$	90	25M	AAIJ 17D	LHCB	in $D \rightarrow \pi\pi\pi$ decays
$<3.9 \times 10^{-4}$	90	225M	ABLIKIM 11G	BES3	$e^+e^- \rightarrow J/\psi \rightarrow \eta\gamma$
$<3.3 \times 10^{-4}$	90		AKHMETSHIN 99B	CMD2	$e^+e^- \rightarrow \phi \rightarrow \eta\gamma$
$<9 \times 10^{-4}$	90		AKHMETSHIN 97C	CMD2	See AKHMETSHIN 99B
$<15 \times 10^{-4}$	0		THALER 73	ASPK	

¹ ZHEVLAKOV 19 derives the value from the experimental limits of nEDM by a calculation using an effective Lagrangian.

 $\Gamma(2\pi^0)/\Gamma_{\text{total}}$ Γ_{26}/Γ

Forbidden by P and CP invariance.

VALUE	CL%	EVTS	DOCUMENT ID	TECN	COMMENT
$<3.5 \times 10^{-4}$	90		BLIK 07	GAM4	$\pi^- p \rightarrow \eta n$

• • • We do not use the following data for averages, fits, limits, etc. • • •

$<2.7 \times 10^{-17}$			¹ ZHEVLAKOV 19	THEO	from nEDM limits
$<6.9 \times 10^{-4}$	90	225M	ABLIKIM 11G	BES3	$e^+e^- \rightarrow J/\psi \rightarrow \eta\gamma$
$<4.3 \times 10^{-4}$	90		AKHMETSHIN 99C	CMD2	$e^+e^- \rightarrow \phi \rightarrow \eta\gamma$
$<6 \times 10^{-4}$	90		² ACHASOV 98	SND	$e^+e^- \rightarrow \phi \rightarrow \eta\gamma$

¹ ZHEVLAKOV 19 derives the value from the experimental limits of nEDM by a calculation using an effective Lagrangian.

² ACHASOV 98 observes one event in a $\pm 3\sigma$ region around the η mass, while a Monte Carlo calculation gives 10 ± 5 events. The limit here is the Poisson upper limit for one observed event and no background.

 $\Gamma(2\pi^0\gamma)/\Gamma_{\text{total}}$ Γ_{27}/Γ

Forbidden by C invariance.

VALUE	CL%	DOCUMENT ID	TECN	CHG	COMMENT
$<5 \times 10^{-4}$	90	NEFKENS 05	CRYB 0		$p(720 \text{ MeV}/c) \pi^- \rightarrow n \eta$

• • • We do not use the following data for averages, fits, limits, etc. • • •

$<17 \times 10^{-4}$	90	BLIK 07	GAM4		$\pi^- p \rightarrow \eta n$
----------------------	----	---------	------	--	------------------------------

 $\Gamma(3\pi^0\gamma)/\Gamma_{\text{total}}$ Γ_{28}/Γ

Forbidden by C invariance.

VALUE	CL%	DOCUMENT ID	TECN	CHG	COMMENT
$<6 \times 10^{-5}$	90	NEFKENS 05	CRYB 0		$p(720 \text{ MeV}/c) \pi^- \rightarrow n \eta$

• • • We do not use the following data for averages, fits, limits, etc. • • •

$<24 \times 10^{-5}$	90	BLIK 07	GAM4		$\pi^- p \rightarrow \eta n$
----------------------	----	---------	------	--	------------------------------

 $\Gamma(3\gamma)/\Gamma_{\text{total}}$ Γ_{29}/Γ

Forbidden by C invariance.

VALUE	CL%	DOCUMENT ID	TECN	CHG	COMMENT
$<16 \times 10^{-5}$	90	BLIK 07	GAM4		$\pi^- p \rightarrow \eta n$
$<4 \times 10^{-5}$	90	NEFKENS 05A	CRYB		$p(720 \text{ MeV}/c) \pi^- \rightarrow n \eta$

• • • We do not use the following data for averages, fits, limits, etc. • • •

 $\Gamma(3\gamma)/\Gamma(2\gamma)$ Γ_{29}/Γ_2

VALUE	CL%	DOCUMENT ID	TECN	CHG	COMMENT
$<1.2 \times 10^{-3}$	95	ALDE 84	GAM2 0		

 $\Gamma(3\gamma)/\Gamma(3\pi^0)$ Γ_{29}/Γ_3

VALUE	CL%	DOCUMENT ID	TECN	COMMENT
$<4.9 \times 10^{-5}$	90	ALOISIO 04	KLOE	$\phi \rightarrow \eta\gamma$

 $\Gamma(4\pi^0)/\Gamma_{\text{total}}$ Γ_{30}/Γ

Forbidden by P and CP invariance.

VALUE	CL%	DOCUMENT ID	TECN	COMMENT
$<6.9 \times 10^{-7}$	90	PRAKHOV 00	CRYB	$\pi^- p \rightarrow n \eta$, 720 MeV/c

• • • We do not use the following data for averages, fits, limits, etc. • • •

$<200 \times 10^{-7}$	90	BLIK 07	GAM4	$\pi^- p \rightarrow \eta n$
-----------------------	----	---------	------	------------------------------

 $\Gamma(\pi^0 e^+ e^-)/\Gamma_{\text{total}}$ Γ_{31}/Γ

C parity forbids this to occur as a single-photon process.

VALUE	CL%	DOCUMENT ID	TECN	COMMENT
$<7.5 \times 10^{-6}$	90	ADLARSON 18C	WASA	$pd \rightarrow \eta {}^3\text{He}$

• • • We do not use the following data for averages, fits, limits, etc. • • •

$<1.6 \times 10^{-4}$	90	MARTYNOV 76	HLBC	
$<8.4 \times 10^{-4}$	90	BAZIN 68	DBC	
$<70 \times 10^{-4}$		RITTENBERG 65	HBC	

 $\Gamma(\pi^0 e^+ e^-)/\Gamma(\pi^+\pi^-\pi^0)$ Γ_{31}/Γ_9

C parity forbids this to occur as a single-photon process.

VALUE	CL%	DOCUMENT ID	TECN	COMMENT
$<3.28 \times 10^{-5}$	90	ADLARSON 18C	WASA	$pd \rightarrow \eta {}^3\text{He}$

• • • We do not use the following data for averages, fits, limits, etc. • • •

$<1.9 \times 10^{-4}$	90	JANE 75	OSPK	
$<42 \times 10^{-4}$	90	BAGLIN 67	HLBC	
$<16 \times 10^{-4}$	90	BILLING 67	HLBC	
$<77 \times 10^{-4}$		FOSTER 65B	HBC	
$<110 \times 10^{-4}$		PRICE 65	HBC	

 $\Gamma(\pi^0\mu^+\mu^-)/\Gamma_{\text{total}}$ Γ_{32}/Γ

C parity forbids this to occur as a single-photon process.

VALUE	CL%	DOCUMENT ID	TECN	COMMENT
$<5 \times 10^{-6}$	90	DZHELYADIN 81	SPEC	$\pi^- p \rightarrow \eta n$

• • • We do not use the following data for averages, fits, limits, etc. • • •

$<500 \times 10^{-6}$		WEHMANN 68	OSPK	
-----------------------	--	------------	------	--

 $[\Gamma(\mu^+e^-) + \Gamma(\mu^-e^+)]/\Gamma_{\text{total}}$ Γ_{33}/Γ

Forbidden by lepton family number conservation.

VALUE	CL%	DOCUMENT ID	TECN	COMMENT
$<6 \times 10^{-6}$	90	WHITE 96	SPEC	$pd \rightarrow \eta {}^3\text{He}$

Meson Particle Listings

η

η C-NONCONSERVING DECAY PARAMETERS

$\pi^+\pi^-\pi^0$ LEFT-RIGHT ASYMMETRY PARAMETER

Measurements with an error $> 1.0 \times 10^{-2}$ have been omitted.

VALUE (units 10^{-2})	EVTS	DOCUMENT ID	TECN
--------------------------	------	-------------	------

**0.09 ± 0.11
 -0.12 OUR AVERAGE**

$+0.09 \pm 0.10 \pm 0.09$ -0.14	1.34M	AMBROSINO 08D	KLOE
--------------------------------------	-------	---------------	------

0.28 ± 0.26	165k	JANE 74	OSPK
-----------------	------	---------	------

-0.05 ± 0.22	220k	LAYTER 72	ASPK
------------------	------	-----------	------

• • • We do not use the following data for averages, fits, limits, etc. • • •

1.5 ± 0.5	37k	¹ GORMLEY 68c	ASPK
---------------	-----	--------------------------	------

¹The GORMLEY 68c asymmetry is probably due to unmeasured $(\mathbf{E} \times \mathbf{B})$ spark chamber effects. New experiments with $(\mathbf{E} \times \mathbf{B})$ controls don't observe an asymmetry.

$\pi^+\pi^-\pi^0$ SEXTANT ASYMMETRY PARAMETER

Measurements with an error $> 2.0 \times 10^{-2}$ have been omitted.

VALUE (units 10^{-2})	EVTS	DOCUMENT ID	TECN
--------------------------	------	-------------	------

**0.12 ± 0.10
 -0.11 OUR AVERAGE**

$+0.08 \pm 0.10 \pm 0.08$ -0.13	1.34M	AMBROSINO 08D	KLOE
--------------------------------------	-------	---------------	------

0.20 ± 0.25	165k	JANE 74	OSPK
-----------------	------	---------	------

0.10 ± 0.22	220k	LAYTER 72	ASPK
-----------------	------	-----------	------

0.5 ± 0.5	37k	GORMLEY 68c	WIRE
---------------	-----	-------------	------

$\pi^+\pi^-\pi^0$ QUADRANT ASYMMETRY PARAMETER

VALUE (units 10^{-2})	EVTS	DOCUMENT ID	TECN
--------------------------	------	-------------	------

-0.09 ± 0.09 OUR AVERAGE

$-0.05 \pm 0.10 \pm 0.03$ -0.05	1.34M	AMBROSINO 08D	KLOE
--------------------------------------	-------	---------------	------

-0.30 ± 0.25	165k	JANE 74	OSPK
------------------	------	---------	------

-0.07 ± 0.22	220k	LAYTER 72	ASPK
------------------	------	-----------	------

$\pi^+\pi^-\gamma$ LEFT-RIGHT ASYMMETRY PARAMETER

Measurements with an error $> 2.0 \times 10^{-2}$ have been omitted.

VALUE (units 10^{-2})	EVTS	DOCUMENT ID	TECN
--------------------------	------	-------------	------

0.9 ± 0.4 OUR AVERAGE

1.2 ± 0.6	35k	JANE 74B	OSPK
---------------	-----	----------	------

0.5 ± 0.6	36k	THALER 72	ASPK
---------------	-----	-----------	------

1.22 ± 1.56	7257	GORMLEY 70	ASPK
-----------------	------	------------	------

$\pi^+\pi^-\gamma$ PARAMETER β (D -wave)

Sensitive to a D -wave contribution: $dN/d\cos\theta = \sin^2\theta (1 + \beta \cos^2\theta)$.

VALUE	EVTS	DOCUMENT ID	TECN
-------	------	-------------	------

-0.02 ± 0.07 OUR AVERAGE Error includes scale factor of 1.3.

0.11 ± 0.11	35k	JANE 74B	OSPK
-----------------	-----	----------	------

-0.060 ± 0.065	7250	GORMLEY 70	WIRE
--------------------	------	------------	------

• • • We do not use the following data for averages, fits, limits, etc. • • •

0.12 ± 0.06	¹ THALER 72	ASPK
-----------------	------------------------	------

¹The authors don't believe this indicates D -wave because the dependence of β on the γ energy is inconsistent with the theoretical prediction. A $\cos^2\theta$ dependence can also come from P - and F -wave interference.

η CP-NONCONSERVING DECAY PARAMETER

$\pi^+\pi^-e^+e^-$ DECAY-PLANE ASYMMETRY PARAMETER A_ϕ

In the η rest frame, the total momentum of the e^+e^- pair is equal and opposite to that of the $\pi^+\pi^-$ pair. Let \hat{z} be the unit vector along the momentum of the e^+e^- pair; let \hat{n}_{ee} and $\hat{n}_{\pi\pi}$ be the unit vectors normal to the e^+e^- and $\pi^+\pi^-$ planes; and let ϕ be the angle between the two normals. Then

$$\sin\phi \cos\phi = [(\hat{n}_{ee} \times \hat{n}_{\pi\pi}) \cdot \hat{z}] (\hat{n}_{ee} \cdot \hat{n}_{\pi\pi}),$$

and

$$A_\phi \equiv \frac{N_{\sin\phi \cos\phi > 0} - N_{\sin\phi \cos\phi < 0}}{N_{\sin\phi \cos\phi > 0} + N_{\sin\phi \cos\phi < 0}}$$

VALUE (units 10^{-2})	EVTS	DOCUMENT ID	TECN	COMMENT
--------------------------	------	-------------	------	---------

$-0.6 \pm 2.5 \pm 1.8$ 1555 \pm 52 AMBROSINO 09B KLOE $e^+e^- \rightarrow \phi \rightarrow \eta\gamma$

ENERGY DEPENDENCE OF $\eta \rightarrow 3\pi$ DALITZ PLOTS

PARAMETERS FOR $\eta \rightarrow \pi^+\pi^-\pi^0$

See the "Note on η Decay Parameters," page 1454, in our 1994 edition (Physical Review D50 1173 (1994)). The following experiments fit to one or more of the coefficients a, b, c, d, e, f for g for $|\text{matrix element}|^2 = 1 + ay + by^2 + cx + dx^2 + xy + fy^3 + gx^2y$.

VALUE	EVTS	DOCUMENT ID	TECN	COMMENT
-------	------	-------------	------	---------

• • • We do not use the following data for averages, fits, limits, etc. • • •

4.7M	¹ ANASTASI 16A	KLOE	$e^+e^- \rightarrow \phi \rightarrow \eta\gamma$
------	---------------------------	------	--

79k	ABLIKIM 15G	BES3	$e^+e^- \rightarrow J/\psi \rightarrow \gamma\eta$
-----	-------------	------	--

174k	ADLARSON 14A	WASA	$pd \rightarrow \eta^3\text{He}$
------	--------------	------	----------------------------------

1.34M	AMBROSINO 08D	KLOE	
-------	---------------	------	--

3230	² ABELE 98D	CBAR	$\bar{p}p \rightarrow \pi^0\pi^0\eta$ at rest
------	------------------------	------	---

1077	³ AMSLER 95	CBAR	$\bar{p}p \rightarrow \pi^+\pi^-\eta$ at rest
------	------------------------	------	---

81k	LAYTER 73	ASPK	
-----	-----------	------	--

220k	LAYTER 72	ASPK	
------	-----------	------	--

1138	CARPENTER 70	HBC
349	DANBURG 70	DBC
7250	GORMLEY 70	WIRE
526	BAGLIN 69	HLBC
7170	CNOPS 68	OSPK
37k	GORMLEY 68c	WIRE
1300	CLPWY 66	HBC
705	LARRIBE 66	HBC

¹ANASTASI 16A measure the Dalitz parameters a, b, d, f , and g . This is the first measurement of g .

²ABELE 98D obtains $a = -1.22 \pm 0.07$ and $b = 0.22 \pm 0.11$ when c (or d) is fixed at 0.06.

³AMSLER 95 fits to $(1+ay+by^2)$ and obtains $a = -0.94 \pm 0.15$ and $b = 0.11 \pm 0.27$.

α PARAMETER FOR $\eta \rightarrow 3\pi^0$

See the "Note on η Decay Parameters" in our 1994 edition, Phys. Rev. D50, 1 August 1994, Part I, p. 1454. The value here is of α in $|\text{matrix element}|^2 = 1 + 2\alpha z$.

VALUE	EVTS	DOCUMENT ID	TECN	COMMENT
-------	------	-------------	------	---------

-0.0288 ± 0.0012 OUR AVERAGE Error includes scale factor of 1.1.

$-0.0265 \pm 0.0010 \pm 0.0009$	7M	PRAKHOV 18	CRYB	$\gamma\rho \rightarrow \rho\eta$
---------------------------------	----	------------	------	-----------------------------------

$-0.055 \pm 0.014 \pm 0.004$	33k	ABLIKIM 15G	BES3	$e^+e^- \rightarrow J/\psi \rightarrow \gamma\eta$
------------------------------	-----	-------------	------	--

$-0.0301 \pm 0.0035 \pm 0.0022$ -0.0035	512k	AMBROSINO 10A	KLOE	$e^+e^- \rightarrow \phi \rightarrow \eta\gamma$
--	------	---------------	------	--

$-0.027 \pm 0.008 \pm 0.005$	120k	¹ ADOLPH 09	WASA	$pp \rightarrow \rho\rho\eta$
------------------------------	------	------------------------	------	-------------------------------

$-0.0322 \pm 0.0012 \pm 0.0022$	3M	² PRAKHOV 09	CRYB	$\gamma\rho \rightarrow \rho\eta$
---------------------------------	----	-------------------------	------	-----------------------------------

$-0.032 \pm 0.002 \pm 0.002$	1.8M	² UNVERZAGT 09	CRYB	$\gamma\rho \rightarrow \rho\eta$
------------------------------	------	---------------------------	------	-----------------------------------

$-0.026 \pm 0.010 \pm 0.010$	75k	BASHKANOV 07	WASA	$pp \rightarrow \rho\rho\eta$
------------------------------	-----	--------------	------	-------------------------------

$-0.010 \pm 0.021 \pm 0.010$	12k	ACHASOV 01c	SND	$e^+e^- \rightarrow \phi \rightarrow \eta\gamma$
------------------------------	-----	-------------	-----	--

-0.031 ± 0.004	1M	TIPPENS 01	CRYB	$\pi^-\rho \rightarrow \eta\eta$, 720 MeV
--------------------	----	------------	------	--

$-0.052 \pm 0.017 \pm 0.010$	98k	ABELE 98c	CBAR	$\bar{p}p \rightarrow 5\pi^0$
------------------------------	-----	-----------	------	-------------------------------

-0.022 ± 0.023	50k	ALDE 84	GAM2	
--------------------	-----	---------	------	--

• • • We do not use the following data for averages, fits, limits, etc. • • •

$-0.038 \pm 0.003 \pm 0.012$ -0.008	1.34M	³ AMBROSINO 08D	KLOE	
--	-------	----------------------------	------	--

-0.32 ± 0.37	192	BAGLIN 70	HLBC	
------------------	-----	-----------	------	--

¹This ADOLPH 09 result is independent of the BASHKANOV 07 result.

²The PRAKHOV 09 and UNVERZAGT 09 results are independent.

³This AMBROSINO 08D value is an indirect result using $\eta \rightarrow \pi^+\pi^0\pi^-$ events and a rescattering matrix that mixes isospin decay amplitudes.

PARAMETER Λ IN $\eta \rightarrow \ell^+\ell^-\gamma$ DECAY

In the pole approximation the electromagnetic transition form factor for a resonance of mass M is given by the expression:

$$|F|^2 = (1 - M_\ell^2/\Lambda^2)^{-2},$$

where for the parameter Λ vector dominance predicts $\Lambda \approx 0.770$ GeV.

VALUE (GeV/c ²)	EVTS	DOCUMENT ID	TECN	COMMENT
-----------------------------	------	-------------	------	---------

0.716 ± 0.011 OUR AVERAGE

0.712 ± 0.020	¹ ADLARSON 17B	A2MM	$\gamma\rho \rightarrow \eta\rho$
-------------------	---------------------------	------	-----------------------------------

$0.7191 \pm 0.0125 \pm 0.0093$	² ARNALDI 16	NA60	400 GeV p - A collisions
--------------------------------	-------------------------	------	------------------------------

$0.716 \pm 0.031 \pm 0.009$	³ ARNALDI 09	NA60	158A In-In collisions
-----------------------------	-------------------------	------	-----------------------

0.72 ± 0.09	600	DZHELYADIN 80	SPEC $\pi^-\rho \rightarrow \eta n, \eta \rightarrow \gamma\mu^+\mu^-$
-----------------	-----	---------------	--

¹ADLARSON 17B reports $\Lambda^{-2}(\eta \rightarrow \gamma e^+e^-) = 1.97 \pm 0.11$ (GeV/c²)⁻² which we converted to the quoted Λ value and uncertainty (total=statistical plus systematic).

²ARNALDI 16 reports $\Lambda^{-2}(\eta \rightarrow \gamma\mu^+\mu^-) = 1.934 \pm 0.067 \pm 0.050$ (GeV/c²)⁻² which we converted to the quoted Λ value.

³ARNALDI 09 reports $\Lambda^{-2}(\eta \rightarrow \gamma\mu^+\mu^-) = 1.95 \pm 0.17 \pm 0.05$ (GeV/c²)⁻² which we converted to the quoted Λ value.

η REFERENCES

ZHEVLAKOV 19	PR D99 031703	A.S. Zhevlakov et al.	(TMSK, MANZ, TUBIN+)
ACHASOV 18B	PR D98 052007	M.N. Achasov et al.	(SND Collab.)
ADLARSON 18C	PL B784 378	P. Adlarson et al.	(WASA-at-COSY Collab.)
PRAKHOV 18	PR C97 065203	S. Prakhov et al.	(A2 Collab. at MAMI)
AJAJ 17D	PL B764 233	R. Ajaj et al.	(LHCb Collab.)
ADLARSON 17B	PR C95 035208	P. Adlarson et al.	(A2 Collab. at MAMI)
ANASTASI 16A	JHEP 1605 019	A. Anastasi et al.	(KLOE-2 Collab.)
ARNALDI 16A	PL B757 437	R. Arnaldi et al.	(NA60 Collab.)
ABLIKIM 15G	PR D92 012014	M. Ablikim et al.	(BESIII Collab.)
ADLARSON 14A	PR C90 045207	P. Adlarson et al.	(WASA-at-COSY Collab.)
AGAKISHIEV 14	PL B731 265	G. Agakishiev et al.	(HADES Collab.)
NEFKENS 14	PR C90 025206	B.M.K. Nefkens et al.	(A2 Collab. at MAMI)
NIKOLAEV 14	EPJ A50 58	A. Nikolaev et al.	(MAM-B, MAINZ, BONN)
ABLIKIM 13	PR D87 012009	M. Ablikim et al.	(BESIII Collab.)
ABLIKIM 13G	PR D87 032006	M. Ablikim et al.	(BESIII Collab.)
BABUSCI 13	PL B718 910	D. Babusci et al.	(KLOE/KLOE-2 Collab.)
BABUSCI 13A	JHEP 1301 119	D. Babusci et al.	(KLOE-2 Collab.)
AGAKISHIEV 12A	EPJ A48 64	G. Agakishiev et al.	(HADES Collab.)
GOSLAWSKI 12	PR D85 112011	P. Goslawski et al.	(COSY-ANKE Collab.)
ABLIKIM 11B	PR D84 032006	M. Ablikim et al.	(BESIII Collab.)
AMBROSINO 11G	PL B702 324	F. Ambrosino et al.	(KLOE Collab.)
BERGHAUSER 11	PL B701 562	H. Berghäuser et al.	(GIES, UCLA, GUTE)
AMBROSINO 10A	PL B694 16	F. Ambrosino et al.	(KLOE Collab.)
ADOLPH 09B	PL B677 24	C. Adolph et al.	(WASA-at-COSY Collab.)
AMBROSINO 09B	PL B675 283	F. Ambrosino et al.	(KLOE Collab.)
ARNALDI 09	PL B677 260	R. Arnaldi et al.	(NA60 Collab.)
PRAKHOV 09	PR C79 035204	S. Prakhov et al.	(MAMI-C Crystal Ball Collab.)
UNVERZAGT 09	EPJ A39 169	M. Unverzagt et al.	(MAMI-B Crystal Ball Collab.)
AMBROSINO 08D	JHEP 0805 006	F. Ambrosino et al.	(DAPHNE KLOE Collab.)
BERLOWSKI 08	PR D77 032004	M. Berlowski et al.	(CELSIUS/WASA Collab.)
PRAKHOV 08	PR C78 015206	S. Prakhov et al.	(BNL Crystal Ball Collab.)
RODRIGUES 08	PRL 101 012301	T.E. Rodrigues et al.	(USP, FESP, UNESP+)
AMBROSINO 07B	JHEP 0712 073	F. Ambrosino et al.	(KLOE Collab.)
BARGHOLTZ 07	PL B644 299	Chr. Bargholtz et al.	(CELSIUS/WASA Collab.)
BASHKANOV 07	PR C76 048201	M. Bashkanov et al.	(CELSIUS/WASA Collab.)
BLIK 07	PAN 70 693	A.M. Blük et al.	(GAMS Collab.)

Translated from YAF 70 724.

See key on page 999

Meson Particle Listings

$\eta, f_0(500)$

Table listing meson particles with columns for name, PDG code, and references. Includes entries for LOPEZ, MILLER, ABLIKIM, etc., up to FLATTE.

Table listing meson particles with columns for name, PDG code, and references. Includes entries for FLATTE, LITCHFIELD, PRICE, etc., up to PICKUP.

$f_0(500)$

$I(G^{JPC}) = 0^+(0^{++})$

also known as σ ; was $f_0(600)$ See the related review(s): Scalar Mesons below 2 GeV

$f_0(500)$ T-MATRIX POLE \sqrt{s}

Note that $\Gamma \approx 2 \text{Im}(\sqrt{s_{\text{pole}}})$.

Table with columns: VALUE (MeV), DOCUMENT ID, TECN, COMMENT. Contains numerical values and references for the f0(500) pole position.

1 S-matrix pole; 8595 events. 2 Applying the chiral unitary approach at NLO to the K_{e4} data of BATLEY 10 and $\pi N \rightarrow \pi \pi N$ data of HYAMS 73, GRAYER 74, and PROTOPESCU 73.

Downloaded from https://academic.oup.com/ptep/article/2020/8/083C01/5891211 by guest on 20 August 2020

Meson Particle Listings

 $f_0(500)$

- ³ Uses the K_{e4} data of BATLEY 10c and the $\pi N \rightarrow \pi\pi N$ data of HYAMS 73, GRAYER 74, and PROTOPOESCU 73.
- ⁴ Analytic continuation using Roy equations.
- ⁵ Analytic continuation using GKPY equations.
- ⁶ Using Roy equations.
- ⁷ Average of three variants of the analytic K-matrix model. Uses the K_{e4} data of BATLEY 08a and the $\pi N \rightarrow \pi\pi N$ data of HYAMS 73 and GRAYER 74.
- ⁸ Average of the analyses of three data sets in the K-matrix model. Uses the data of BATLEY 08a, HYAMS 73, and GRAYER 74, partially of COHEN 80 or ETKIN 82b.
- ⁹ From the K_{e4} data of BATLEY 08a and $\pi N \rightarrow \pi\pi N$ data of HYAMS 73.
- ¹⁰ From the K_{e4} data of BATLEY 08a and $\pi N \rightarrow \pi\pi N$ data of PROTOPOESCU 73, GRAYER 74, and ESTABROOKS 74.
- ¹¹ From a mean of three different $f_0(500)$ parameterizations. Uses 40k events.
- ¹² From an isobar model using 2.6k events.
- ¹³ Reanalysis of ABLIKIM 04a, PISLAK 01, and HYAMS 73 data.
- ¹⁴ Using the N/D method.
- ¹⁵ From the solution of the Roy equation (ROY 71) for the isoscalar S-wave and using a phase-shift analysis of HYAMS 73 and PROTOPOESCU 73 data.
- ¹⁶ Reanalysis of the data from PROTOPOESCU 73, ESTABROOKS 74, GRAYER 74, ROSSELET 77, PISLAK 03, and AKHMETSHIN 04.
- ¹⁷ From a mean of six different analyses and $f_0(500)$ parameterizations.
- ¹⁸ Using data on $\psi(2S) \rightarrow J/\psi\pi\pi$ from BAI 00E and on $\Upsilon(nS) \rightarrow \Upsilon(mS)\pi\pi$ from BUTLER 94b and ALEXANDER 98.
- ¹⁹ Reanalysis of data from PROTOPOESCU 73, ESTABROOKS 74, GRAYER 74, and COHEN 80 in the unitarized ChPT model.
- ²⁰ From a combined analysis of HYAMS 73, AUGUSTIN 89, AITALA 01b, and PISLAK 01.
- ²¹ A similar analysis (KOMADA 01) finds $(580^{+79}_{-30}) - i(190^{+107}_{-49})$ MeV.
- ²² Coupled channel reanalysis of BATON 70, BENSINGER 71, BAILLON 72, HYAMS 73, HYAMS 75, ROSSELET 77, COHEN 80, and ETKIN 82b using the uniformizing variable.
- ²³ Using the inverse amplitude method and data of ESTABROOKS 73, GRAYER 74, and PROTOPOESCU 73.
- ²⁴ Reanalysis of data from HYAMS 73, GRAYER 74, SRINIVASAN 75, and ROSSELET 77 using the interfering amplitude method.
- ²⁵ Average and spread of 4 variants ("up" and "down") of KAMINSKI 97b 3-channel model.
- ²⁶ Uses data from BEIER 72b, OCHS 73, HYAMS 73, GRAYER 74, ROSSELET 77, CASON 83, ASTON 88, and ARMSTRONG 91b. Coupled channel analysis with flavor symmetry and all light two-pseudoscalars systems.
- ²⁷ Demonstrates explicitly that $f_0(500)$ and $f_0(1370)$ are two different poles.
- ²⁸ Analysis of data from FALVARD 88.
- ²⁹ Analysis of data from OCHS 73, ESTABROOKS 75, ROSSELET 77, and MUKHIN 80.
- ³⁰ Analysis of data from OCHS 73, GRAYER 74, and ROSSELET 77.
- ³¹ Coupled-channel analysis using data from PROTOPOESCU 73, HYAMS 73, HYAMS 75, GRAYER 74, ESTABROOKS 74, ESTABROOKS 75, FROGGATT 77, CORDEN 79, BISWAS 81.
- ³² Analysis of data from APEL 72c, GRAYER 74, CASON 76, PAWLICKI 77. Includes spread and errors of 4 solutions.
- ³³ Analysis of data from BATON 70, BENSINGER 71, COLTON 71, BAILLON 72, PROTOPOESCU 73, and WALKER 67.

 $f_0(500)$ BREIT-WIGNER MASS OR K-MATRIX POLE PARAMETERS

VALUE (MeV)	DOCUMENT ID	TECN	COMMENT
(400-550) OUR ESTIMATE			
513±32	³⁴ MURAMATSU 02	CLEO	$e^+e^- \approx 10$ GeV
$478^{+24}_{-23} \pm 17$	AITALA 01b	E791	$D^+ \rightarrow \pi^-\pi^+\pi^+$
563^{+58}_{-29}	³⁵ ISHIDA 01		$\Upsilon(3S) \rightarrow \Upsilon\pi\pi$
555	³⁶ ASNER 00	CLE2	$\tau^- \rightarrow \pi^-\pi^0\pi^0\nu_\tau$
540±36	ISHIDA 00b		$p\bar{p} \rightarrow \pi^0\pi^0\pi^0$
750±4	ALEKSEEV 99	SPEC	$1.78\pi^-\rho_{\text{polar}} \rightarrow \pi^-\pi^+n$
744±5	ALEKSEEV 98	SPEC	$1.78\pi^-\rho_{\text{polar}} \rightarrow \pi^-\pi^+n$
759±5	³⁷ TROYAN 98		$5.2np \rightarrow n\rho\pi^+\pi^-$
780±30	ALDE 97	GAM2	$450pp \rightarrow pp\rho^0\pi^0$
585±20	³⁸ ISHIDA 97		$\pi\pi \rightarrow \pi\pi$
761±12	³⁹ SVEC 96	RVUE	$6-17\pi N_{\text{polar}} \rightarrow \pi^+\pi^-N$
~ 860	40,41 TORNQVIST 96	RVUE	$\pi\pi \rightarrow \pi\pi, K\bar{K}, K\pi, \eta\pi$
1165±50	42,43 ANISOVICH 95	RVUE	$\pi^-p \rightarrow \pi^0\pi^0n, \bar{p}p \rightarrow \pi^0\pi^0\pi^0, \pi^0\pi^0\eta, \pi^0\eta\eta$
~ 1000	44 ACHASOV 94	RVUE	$\pi\pi \rightarrow \pi\pi$
414±20	³⁹ AUGUSTIN 89	DM2	

- ³⁴ Statistical uncertainty only.
- ³⁵ A similar analysis (KOMADA 01) finds 526^{+48}_{-37} MeV.
- ³⁶ From the best fit of the Dalitz plot.
- ³⁷ 6σ effect, no PWA.
- ³⁸ Reanalysis of data from HYAMS 73, GRAYER 74, SRINIVASAN 75, and ROSSELET 77 using the interfering amplitude method.
- ³⁹ Breit-Wigner fit to S-wave intensity measured in $\pi N \rightarrow \pi^-\pi^+N$ on polarized targets. The fit does not include $f_0(980)$.
- ⁴⁰ Uses data from ASTON 88, OCHS 73, HYAMS 73, ARMSTRONG 91b, GRAYER 74, CASON 83, ROSSELET 77, and BEIER 72b. Coupled channel analysis with flavor symmetry and all light two-pseudoscalars systems.
- ⁴¹ Also observed by ASNER 00 in $\tau^- \rightarrow \pi^-\pi^0\pi^0\nu_\tau$ decays.
- ⁴² Uses $\pi^0\pi^0$ data from ANISOVICH 94, AMSLER 94d, and ALDE 95b, $\pi^+\pi^-$ data from OCHS 73, GRAYER 74 and ROSSELET 77, and $\eta\eta$ data from ANISOVICH 94.
- ⁴³ The pole is on Sheet III. Demonstrates explicitly that $f_0(500)$ and $f_0(1370)$ are two different poles.

- ⁴⁴ Analysis of data from OCHS 73, ESTABROOKS 75, ROSSELET 77, and MUKHIN 80.

 $f_0(500)$ BREIT-WIGNER WIDTH

VALUE (MeV)	DOCUMENT ID	TECN	COMMENT
(400-700) OUR ESTIMATE			
• • •	We do not use the following data for averages, fits, limits, etc. • • •		
335±67	⁴⁵ MURAMATSU 02	CLEO	$e^+e^- \approx 10$ GeV
$324^{+42}_{-40} \pm 21$	AITALA 01b	E791	$D^+ \rightarrow \pi^-\pi^+\pi^+$
372^{+229}_{-95}	⁴⁶ ISHIDA 01		$\Upsilon(3S) \rightarrow \Upsilon\pi\pi$
540	⁴⁷ ASNER 00	CLE2	$\tau^- \rightarrow \pi^-\pi^0\pi^0\nu_\tau$
372±80	ISHIDA 00b		$p\bar{p} \rightarrow \pi^0\pi^0\pi^0$
119±13	ALEKSEEV 99	SPEC	$1.78\pi^-\rho_{\text{polar}} \rightarrow \pi^-\pi^+n$
77±22	ALEKSEEV 98	SPEC	$1.78\pi^-\rho_{\text{polar}} \rightarrow \pi^-\pi^+n$
35±12	⁴⁸ TROYAN 98		$5.2np \rightarrow n\rho\pi^+\pi^-$
780±60	ALDE 97	GAM2	$450pp \rightarrow pp\rho^0\pi^0$
385±70	⁴⁹ ISHIDA 97		$\pi\pi \rightarrow \pi\pi$
290±54	⁵⁰ SVEC 96	RVUE	$6-17\pi N_{\text{polar}} \rightarrow \pi^+\pi^-N$
~ 880	51,52 TORNQVIST 96	RVUE	$\pi\pi \rightarrow \pi\pi, K\bar{K}, K\pi, \eta\pi$
460±40	53,54 ANISOVICH 95	RVUE	$\pi^-p \rightarrow \pi^0\pi^0n, \bar{p}p \rightarrow \pi^0\pi^0\pi^0, \pi^0\pi^0\eta, \pi^0\eta\eta$
~ 3200	55 ACHASOV 94	RVUE	$\pi\pi \rightarrow \pi\pi$
494±58	⁵⁰ AUGUSTIN 89	DM2	

- ⁴⁵ Statistical uncertainty only.
- ⁴⁶ A similar analysis (KOMADA 01) finds 301^{+145}_{-100} MeV.
- ⁴⁷ From the best fit of the Dalitz plot.
- ⁴⁸ 6σ effect, no PWA.
- ⁴⁹ Reanalysis of data from HYAMS 73, GRAYER 74, SRINIVASAN 75, and ROSSELET 77 using the interfering amplitude method.
- ⁵⁰ Breit-Wigner fit to S-wave intensity measured in $\pi N \rightarrow \pi^-\pi^+N$ on polarized targets. The fit does not include $f_0(980)$.
- ⁵¹ Uses data from ASTON 88, OCHS 73, HYAMS 73, ARMSTRONG 91b, GRAYER 74, CASON 83, ROSSELET 77, and BEIER 72b. Coupled channel analysis with flavor symmetry and all light two-pseudoscalars systems.
- ⁵² Also observed by ASNER 00 in $\tau^- \rightarrow \pi^-\pi^0\pi^0\nu_\tau$ decays.
- ⁵³ Uses $\pi^0\pi^0$ data from ANISOVICH 94, AMSLER 94d, and ALDE 95b, $\pi^+\pi^-$ data from OCHS 73, GRAYER 74 and ROSSELET 77, and $\eta\eta$ data from ANISOVICH 94.
- ⁵⁴ The pole is on Sheet III. Demonstrates explicitly that $f_0(500)$ and $f_0(1370)$ are two different poles.
- ⁵⁵ Analysis of data from OCHS 73, ESTABROOKS 75, ROSSELET 77, and MUKHIN 80.

 $f_0(500)$ DECAY MODES

Mode	Fraction (Γ_i/Γ)
Γ_1 $\pi\pi$	seen
Γ_2 $\gamma\gamma$	seen

 $f_0(500)$ PARTIAL WIDTHS

$\Gamma(\gamma\gamma)$	VALUE (keV)	DOCUMENT ID	TECN	COMMENT	Γ_2
• • •	We do not use the following data for averages, fits, limits, etc. • • •				
2.05±0.21	⁵⁶ DAI 14A	RVUE	Compilation		
1.7±0.4	⁵⁷ HOFERICHTER11	RVUE	Compilation		
3.08±0.82	⁵⁸ MENNESSIER 11	RVUE	Compilation		
2.08±0.2 $^{+0.07}_{-0.04}$	⁵⁹ MOUSSALLAM11	RVUE	Compilation		
2.08	⁶⁰ MAO 09	RVUE	Compilation		
1.2±0.4	⁶¹ BERNABEU 08	RVUE			
3.9±0.6	⁵⁸ MENNESSIER 08	RVUE			
1.8±0.4	⁶² OLLER 08	RVUE	Compilation		
1.68±0.15	^{62,63} OLLER 08a	RVUE	Compilation		
3.1±0.5	^{64,65} PENNINGTON 08	RVUE	Compilation		
2.4±0.4	^{65,66} PENNINGTON 08	RVUE	Compilation		
4.1±0.3	⁶⁷ PENNINGTON 06	RVUE			
3.8±1.5	^{68,69} BOGLIONE 99	RVUE			
5.4±2.3	⁶⁸ MORGAN 90	RVUE			
10±6	COURAU 86	DM1			

- ⁵⁶ Using dispersive analysis with phases from GARCIA-MARTIN 11a and BUETTNER 04 as input.
- ⁵⁷ Using Roy-Steiner equations with $\pi\pi$ phase shifts from an update of COLANGELO 01 and from GARCIA-MARTIN 11a.
- ⁵⁸ Using an analytic K-matrix model.
- ⁵⁹ Using dispersion integral with phase input from Roy equations and data from MARSISKE 90, BOYER 90, BEHREND 92, UEHARA 08a, and MORI 07.
- ⁶⁰ Used dispersion theory. The value quoted used the $f_0(500)$ pole position of $457 - i276$ MeV.
- ⁶¹ Using p, n polarizabilities from PDG 06 and fitting to $\pi\pi$ phase motion from GARCIA-MARTIN 07 and σ -poles from GARCIA-MARTIN 07 and CAPRINI 06.
- ⁶² Using twice-subtracted dispersion integrals.
- ⁶³ Supersedes OLLER 08.
- ⁶⁴ Solution A (preferred solution based on χ^2 -analysis).

- 65 Dispersion theory based amplitude analysis of BOYER 90, MARSISKE 90, BEHREND 92, and MORI 07.
- 66 Solution B (worse than solution A; still acceptable when systematic uncertainties are included).
- 67 Using unitarity and the σ pole position from CAPRINI 06.
- 68 This width could equally well be assigned to the $f_0(1370)$. The authors analyse data from BOYER 90 and MARSISKE 90 and report strong correlation with $\gamma\gamma$ width of $f_2(1270)$.
- 69 Supersedes MORGAN 90.

$f_0(500)$ REFERENCES

ABLIKIM 17	PRL 118 012001	M. Ablikim <i>et al.</i>	(BESIII Collab.)
DAI 14A	PR D90 036004	L.-Y. Dai, M.R. Pennington	(CEBAF)
ALBALADEJO 12	PR D86 034003	M. Albaladejo, J.A. Oller	(MURC)
GARCIA-MAR... 11	PRL 107 072001	R. Garcia-Martin <i>et al.</i>	(MADR, CRAC)
GARCIA-MAR... 11A	PR D83 074004	R. Garcia-Martin <i>et al.</i>	(MADR, CRAC)
HOFERICHTER 11	EPJ C71 1743	M. Hofelicher, D.R. Phillips, C. Schat	(BONN+)
MENNESSIER 11	PL B696 40	G. Mennessier, S. Narison, X.-G. Wang	
MOUSSALLAM 11	EPJ C71 1814	B. Moussallam	
BATLEY 10	PL B686 101	J.R. Batley <i>et al.</i>	(CERN NA48/2 Collab.)
BATLEY 10C	EPJ C70 635	J.R. Batley <i>et al.</i>	(CERN NA48/2 Collab.)
MENNESSIER 10	PL B688 59	G. Mennessier, S. Narison, X.-G. Wang	
MAO 09	PR D79 116008	Y. Mao <i>et al.</i>	
BATLEY 08A	EPJ C54 411	J.R. Batley <i>et al.</i>	(CERN NA48/2 Collab.)
BERNABEU 08	PRL 100 241804	J. Bernabeu, J. Prades	(IFIC, GRAN)
CAPRINI 08	PR D77 114019	I. Caprini	
MENNESSIER 08	PL B665 205	G. Mennessier, S. Narison, W. Ochs	
OLLER 08	PL B659 201	J.A. Oller, L. Roca, C. Schat	(MURC, UBA)
OLLER 08A	EPJ A37 15	J.A. Oller, L. Roca	(MURC)
PENNINGTON 08	EPJ C56 1	M.R. Pennington <i>et al.</i>	
UEHARA 08A	PR D78 052004	S. Uehara <i>et al.</i>	(BELLE Collab.)
ABLIKIM 07A	PL B645 19	M. Ablikim <i>et al.</i>	(BES Collab.)
BONVICINI 07	PR D76 012001	G. Bonvicini <i>et al.</i>	(CLEO Collab.)
BUGG 07A	JP G34 151	D.V. Bugg <i>et al.</i>	
GARCIA-MAR... 07	PR D76 074034	R. Garcia-Martin, J.R. Pelaez, F.J. Yndurain	
MORI 07	PR D75 051101	T. Mori <i>et al.</i>	(BELLE Collab.)
ANISOVICH 06	JMP A21 3615	V.V. Anisovich	
CAPRINI 06	PRL 96 132001	I. Caprini, G. Colangelo, H. Leutwyler	(BCIP+)
PDG 06	JP G33 17	W.-M. Yao <i>et al.</i>	(PDG Collab.)
PENNINGTON 06	PRL 97 011601	M.R. Pennington	
ZHOU 05	JHEP 0502 043	Z.Y. Zhou <i>et al.</i>	
ABLIKIM 04A	PL B598 149	M. Ablikim <i>et al.</i>	(BES Collab.)
AKHMETSHIN 04	PL B578 285	R.R. Akhmetshin <i>et al.</i>	(Novosibirsk CMD-2 Collab.)
BUETTIKER 04	EPJ C33 409	P. Buettiker, S. Descotes-Genon, B. Moussallam	
GALLEGOS 04	PR D69 074033	A. Gallegos <i>et al.</i>	
PELAEZ 04A	MPL A19 2879	J.R. Pelaez	
BUGG 03	PL B572 1	D.V. Bugg	
PISLAK 03	PR D67 072004	S. Pislak <i>et al.</i>	(BNL E865 Collab.)
Also	PR D81 11903E	S. Pislak <i>et al.</i>	(BNL E865 Collab.)
MURAMATSU 02	PRL 89 051802	H. Muramatsu <i>et al.</i>	(CLEO Collab.)
Also	PRL 90 059901 (errata)	H. Muramatsu <i>et al.</i>	(CLEO Collab.)
AITALA 01B	PR D67 072004	E.M. Aitala <i>et al.</i>	(FNAL E791 Collab.)
BLACK 01	PR D64 014031	D. Black <i>et al.</i>	
COLANGELO 01	NP B603 125	G. Colangelo, J. Gasser, H. Leutwyler	
ISHIDA 01	PL B518 47	M. Ishida <i>et al.</i>	
KOMADA 01	PL B508 31	T. Komada <i>et al.</i>	
PISLAK 01	PRL 87 221801	S. Pislak <i>et al.</i>	(BNL E865 Collab.)
Also	PR D67 072004	S. Pislak <i>et al.</i>	(BNL E865 Collab.)
Also	PRL 105 019901E	S. Pislak <i>et al.</i>	(BNL E865 Collab.)
SUROVTSOV 01	PR D63 054024	S.S. Surovtsov, D. Krupa, M. Nagy	
ASNER 00	PR D61 012002	D.H. Asner <i>et al.</i>	(CLEO Collab.)
BAI 00E	PR D62 032002	J. Bai <i>et al.</i>	(BES Collab.)
ISHIDA 00B	PTP 104 203	M. Ishida <i>et al.</i>	
ALEKSEEV 99	NP B541 3	I.G. Alekseev <i>et al.</i>	
BOGLIONE 99	EPJ C9 11	M. Boglione, M.R. Pennington	
HANNAH 99	PR D60 017502	T. Hannah	
KAMINSKI 99	EPJ C9 141	R. Kaminski, L. Lesniak, B. Loiseau	(CRAC, PARIN)
OLLER 99	PR D60 099906 (erratum)	J.A. Oller <i>et al.</i>	
OLLER 99B	NP A652 407 (erratum)	J.A. Oller, E. Oset	
OLLER 99C	PR D60 074023	J.A. Oller, E. Oset	
ALEKSEEV 98	PAN 61 174	I.G. Alekseev <i>et al.</i>	
ALEXANDER 98	PR D58 052004	V.V. Alexander <i>et al.</i>	(CLEO Collab.)
ANISOVICH 98B	SFU 41 419	V.V. Anisovich <i>et al.</i>	
Translated from UFN 168	481.		
LOCHER 98	EPJ C4 317	M.P. Locher <i>et al.</i>	(PSI)
TROYAN 98	JINRRC 5-91 33	Yu. Troyan <i>et al.</i>	
ALDE 97	PL B397 350	D.M. Alde <i>et al.</i>	(GAMS Collab.)
DOBADO 97	PR D56 3057	A. Dobado, J.R. Pelaez	
ISHIDA 97	PTP 98 1005	S. Ishida <i>et al.</i>	(TOKY, MIYA, KEP)
KAMINSKI 97B	PL B413 130	R. Kaminski, L. Lesniak, B. Loiseau	(CRAC, IPN)
Also	PTP 95 745	S. Ishida <i>et al.</i>	(TOKY, MIYA, KEP)
SVEC 96	PR D53 2343	M. Svec	(MCGI)
TORNQVIST 96	PRL 76 1575	N.A. Tornqvist, M. Roos	(HEL5)
ALDE 95B	ZPHY C66 375	D.M. Alde <i>et al.</i>	(GAMS Collab.)
ANISOVICH 95	PL B355 363	V.V. Anisovich <i>et al.</i>	(PNPI, SERP)
JANSEN 95	PR D52 2690	G. Jansen <i>et al.</i>	(STON, ADLD, JULI)
ACHASOV 94	PR D49 5779	N.N. Achasov, G.N. Shestakov	(NOVM)
AMSLER 94D	PL B333 277	C. Amisler <i>et al.</i>	(Crystal Barrel Collab.)
ANISOVICH 94	PL B323 233	V.V. Anisovich <i>et al.</i>	(Crystal Barrel Collab.)
BUTLER 94B	PR D49 40	F. Butler <i>et al.</i>	(CLEO Collab.)
KAMINSKI 94	PR D50 3145	R. Kaminski, L. Lesniak, J.P. Maillet	(CRAC+)
ZOU 94B	PR D50 3150	B.S. Zou, D.V. Bugg	(CLEO, IJUP)
ZOU 93	PR D48 3348	B.S. Zou, D.V. Bugg	(CLEO)
BEHREND 92	ZPHY C56 381	H.J. Behrend	(CELLO Collab.)
ARMSTRONG 91B	ZPHY C52 389	T.A. Armstrong <i>et al.</i>	(ATHU, BARI, BIRM+)
BOYER 90	PR D42 1350	J. Boyer <i>et al.</i>	(Mark II Collab.)
MARSISKE 90	PR D41 3324	H. Marsiske <i>et al.</i>	(Crystal Ball Collab.)
MORGAN 90	ZPHY C48 623	D. Morgan, M.R. Pennington	(RAL, DURH)
AUGUSTIN 89	NP B320 1	J.E. Augustin, G. Cosme	(DM2 Collab.)
ASTON 88	NP B296 493	D. Aston <i>et al.</i>	(SLAC, NAGO, CINC, INUS)
FALVARD 88	PR D38 2706	A. Falvard <i>et al.</i>	(CLER, FRAS, LALO+)
COURAU 86	NP B271 1	A. Courau <i>et al.</i>	(CLER, LALO)
VANBEVEREN 86	ZPHY C30 615	E. van Beveren <i>et al.</i>	(Nijm, BIEL)
CASON 83	PR D28 1584	N.M. Cason <i>et al.</i>	(NDAM, ANL)
ETKIN 82B	PR D25 1784	A. Etkin <i>et al.</i>	(BNL, CUNY, TUFTS, VAND)
BISWAS 81	PRL 47 1378	N.N. Biswas <i>et al.</i>	(NDAM, ANL)
COHEN 80	PR D22 2595	D. Cohen <i>et al.</i>	(ANL) IJUP
MUKHIN 80	JETPL 32 601	K.N. Mukhin <i>et al.</i>	(KIAE)
Translated from ZETFP 32	616.		
CORDEN 79	NP B157 250	M.J. Corden <i>et al.</i>	(BIRM, RHEL, TELA+) JP
ESTABROOKS 79	PR D19 2678	P. Estabrooks	(CARL)
FROGGATT 77	NP B129 89	C.D. Froggatt, J.L. Petersen	(GLAS, IJUP)
PAWLIKI 77	PR D15 3196	A.J. Pawlik <i>et al.</i>	(ANL) IJUP
ROSSELET 77	PR D15 574	L. Rosset <i>et al.</i>	(GEVA, SAEL)
CASON 76	PRL 36 1485	N.M. Cason <i>et al.</i>	(NDAM, ANL) IJUP
ESTABROOKS 75	NP B95 322	P.G. Estabrooks, A.D. Martin	(DURH)
HYAMS 75	NP B100 205	B.D. Hyams <i>et al.</i>	(CERN, MPIM)

SRINIVASAN 75	PR D12 681	V. Srinivasan <i>et al.</i>	(NDAM, ANL)
ESTABROOKS 74	NP B79 301	P.G. Estabrooks, A.D. Martin	(DURH)
GRAYER 74	NP B75 189	G. Grayer <i>et al.</i>	(CERN, MPIM)
ESTABROOKS 73	Tallahassee	P.G. Estabrooks <i>et al.</i>	(CERN, MPIM)
HYAMS 73	NP B64 134	B.D. Hyams <i>et al.</i>	(CERN, MPIM)
OCHS 73	Thesis	W. Ochs	(MPIM, MUNI)
PROTOPOPO... 73	PR D7 1279	S.D. Protopopescu <i>et al.</i>	(LBL)
APEL 72C	PL 41B 542	W.D. Apel <i>et al.</i>	(KARLK, KARLE, PISA)
BAILLON 72	PL 38B 555	P.H. Bailion <i>et al.</i>	(SLAC)
BASDEVANT 72	PL 41B 178	J.L. Basdevant, C.D. Froggatt, J.L. Petersen	(CERN)
BEIER 72B	PRL 29 511	E.W. Beier <i>et al.</i>	(PENN)
BENSINGER 71	PL 36B 134	J.R. Bensingher <i>et al.</i>	(WISC)
COLTON 71	PR D3 2028	E.P. Colton <i>et al.</i>	(LBL, FNAL, UCLA+)
ROY 71	PL 36B 353	S.M. Roy	
BATON 70	PL 33B 528	J.P. Baton, G. Laurens, J. Reigner	(SACL)
WALKER 67	RMP 39 695	W.D. Walker	(WISC)

$\rho(770)$

$$I^G(J^{PC}) = 1^{+}(1^{-})$$

THE $\rho(770)$

Updated September 2019 by S. Eidelman (Novosibirsk) and G. Venanzoni (Pisa).

The determination of the parameters of the $\rho(770)$ is beset with many difficulties because of its large width. In physical region fits, the line shape does not correspond to a relativistic Breit-Wigner function with a P -wave width, but requires some additional shape parameter. This dependence on parameterization was demonstrated long ago [1]. Bose-Einstein correlations are another source of shifts in the $\rho(770)$ line shape, particularly in multiparticle final-state systems [2].

The same model dependence afflicts any other source of resonance parameters, such as the energy dependence of the phase shift δ_1^+ , or the pole position. It is, therefore, not surprising that a study of $\rho(770)$ dominance in the decays of the η and η' reveals the need for specific dynamical effects, in addition to the $\rho(770)$ pole [3,4].

The cleanest determination of the $\rho(770)$ mass and width comes from e^+e^- annihilation and τ -lepton decays. Analysis of ALEPH [5] showed that the charged $\rho(770)$ parameters measured from τ -lepton decays are consistent with those of the neutral one determined from e^+e^- data [6]. This conclusion is qualitatively supported by the later studies of CLEO [7] and Belle [8]. However, comparison of the two-pion mass spectrum in τ decays from OPAL [9], CLEO [7], and ALEPH [10,11], and the $e^+e^- \rightarrow \pi^+\pi^-$ cross section from CMD-2 [12,13], showed significant discrepancies between the two shapes which can be as high as 10% above the ρ meson [14,15]. This discrepancy remains after measurements of the two-pion cross section in e^+e^- annihilation at KLOE [16,17,18,19], SND [20,21], BaBar [22] and, more recently BESIII [23]. The effect is not accounted for by isospin breaking [24,25,26,27], but the accuracy of its calculation may be overestimated [28,29].

This problem seems to be solved after a recent analysis in [30] which showed that after correcting the τ data for the missing $\rho - \gamma$ mixing contribution, besides the other known isospin symmetry violating corrections, the $\pi\pi$ I=1 part of the hadronic vacuum polarization contribution to the muon $g - 2$ is fully compatible between τ based and e^+e^- based evaluations. The global fit of the whole set of the ρ , ω , and ϕ decays, taking into account mixing effects in the hidden local symmetry model, also showed consistency of the data on τ decays to two pions and e^+e^- annihilation [31,32]. However, because

Meson Particle Listings

 $\rho(770)$

of the progress in e^+e^- data, the τ input is now less precise and less reliable due to additional theoretical uncertainties [33] decreasing importance of τ versus e^+e^- comparison for the determination of $\rho(770)$ parameters and other applications, like, e.g., calculations of hadronic vacuum polarization.

References

- J. Pisut and M. Roos, Nucl. Phys. **B6**, 325 (1968).
- G.D. Lafferty, Z. Phys. **C60**, 659 (1993).
- A. Abele *et al.*, Phys. Lett. **B402**, 195 (1997).
- M. Benayoun *et al.*, Eur. Phys. J. **C31**, 525 (2003).
- R. Barate *et al.*, Z. Phys. **C76**, 15 (1997).
- L.M. Barkov *et al.*, Nucl. Phys. **B256**, 365 (1985).
- S. Anderson *et al.*, Phys. Rev. **D61**, 112002 (2000).
- M. Fujikawa *et al.*, Phys. Rev. **D78**, 072006 (2008).
- K. Ackerstaff *et al.*, Eur. Phys. J. **C7**, 571 (1999).
- M. Davier *et al.*, Nucl. Phys. (Proc. Supp.) **B123**, 47 (2003).
- S. Schael *et al.*, Phys. Reports **421**, 191 (2005).
- R.R. Akhmetshin *et al.*, Phys. Lett. **B527**, 161 (2002).
- R.R. Akhmetshin *et al.*, Phys. Lett. **B578**, 285 (2004).
- M. Davier *et al.*, Eur. Phys. J. **C27**, 497 (2003).
- M. Davier *et al.*, Eur. Phys. J. **C31**, 503 (2003).
- A. Aloisio *et al.*, Phys. Lett. **B606**, 12 (2005).
- F. Ambrosino *et al.*, Phys. Lett. **B670**, 285 (2009).
- F. Ambrosino *et al.*, Phys. Lett. **B700**, 102 (2011).
- D. Babusci *et al.*, Phys. Lett. **B720**, 336 (2013).
- M.N. Achasov *et al.*, Sov. Phys. JETP **101**, 1053 (2005).
- M.N. Achasov *et al.*, Sov. Phys. JETP **103**, 380 (2006).
- B. Aubert *et al.*, Phys. Rev. Lett. **103**, 231801 (2009).
- M. Ablikim *et al.*, Phys. Lett. **B753**, 629 (2016).
- R. Alemany *et al.*, Eur. Phys. J. **C2**, 123 (1998).
- H. Czyz and J.J. Kuhn, Eur. Phys. J. **C18**, 497 (2001).
- V. Cirigliano *et al.*, Phys. Lett. **B513**, 361 (2001).
- V. Cirigliano *et al.*, Eur. Phys. J. **C23**, 121 (2002).
- K. Maltman and C.E. Wolfe, Phys. Rev. **D73**, 013004 (2006).
- C.E. Wolfe and K. Maltman, Phys. Rev. **D80**, 114024 (2009).
- F. Jegerlehner and R. Szafron, Eur. Phys. J. **C71**, 1632 (2011).
- M. Benayoun *et al.*, Eur. Phys. J. **C72**, 1848 (2012).
- M. Benayoun *et al.*, Eur. Phys. J. **C73**, 2453 (2013).
- M. Davier *et al.*, Eur. Phys. J. **C77**, 827 (2017).

 $\rho(770)$ MASS

We no longer list S -wave Breit-Wigner fits, or data with high combinatorial background.

NEUTRAL ONLY, e^+e^-

VALUE (MeV)	EVTS	DOCUMENT ID	TECN	COMMENT
775.26 ± 0.25 OUR AVERAGE				
775.02 ± 0.35		¹ LEES	12g	BABR $e^+e^- \rightarrow \pi^+\pi^-\gamma$
775.97 ± 0.46 ± 0.70	900k	² AKHMETSHIN 07		$e^+e^- \rightarrow \pi^+\pi^-$
774.6 ± 0.4 ± 0.5	800k	^{3,4} ACHASOV	06	SND $e^+e^- \rightarrow \pi^+\pi^-$
775.65 ± 0.64 ± 0.50	114k	^{5,6} AKHMETSHIN 04	CMD2	$e^+e^- \rightarrow \pi^+\pi^-$
775.9 ± 0.5 ± 0.5	1.98M	⁷ ALOISIO	03	KLOE $1.02 e^+e^- \rightarrow \pi^+\pi^-\pi^0$
775.8 ± 0.9 ± 2.0	500k	⁷ ACHASOV	02	SND $1.02 e^+e^- \rightarrow \pi^+\pi^-\pi^0$
775.9 ± 1.1		⁸ BARKOV	85	OLYA $e^+e^- \rightarrow \pi^+\pi^-$

••• We do not use the following data for averages, fits, limits, etc. •••

763.49 ± 0.53		⁹ BARTOS	17	RVUE $e^+e^- \rightarrow \pi^+\pi^-$
758.23 ± 0.46		¹⁰ BARTOS	17A	RVUE $e^+e^- \rightarrow \pi^+\pi^-$
775.8 ± 0.5 ± 0.3	1.98M	¹¹ ALOISIO	03	KLOE $1.02 e^+e^- \rightarrow \pi^+\pi^-\pi^0$
775.9 ± 0.6 ± 0.5	1.98M	¹² ALOISIO	03	KLOE $1.02 e^+e^- \rightarrow \pi^+\pi^-\pi^0$
775.0 ± 0.6 ± 1.1	500k	¹³ ACHASOV	02	SND $1.02 e^+e^- \rightarrow \pi^+\pi^-\pi^0$
775.1 ± 0.7 ± 5.3		¹⁴ BENAYOUN	98	RVUE $e^+e^- \rightarrow \pi^+\pi^-$, $\mu^+\mu^-$
770.5 ± 1.9 ± 5.1		¹⁵ GARDNER	98	RVUE $0.28-0.92 e^+e^- \rightarrow \pi^+\pi^-$
764.1 ± 0.7		¹⁶ O'CONNELL	97	RVUE $e^+e^- \rightarrow \pi^+\pi^-$
757.5 ± 1.5		¹⁷ BERNICHA	94	RVUE $e^+e^- \rightarrow \pi^+\pi^-$
768 ± 1		¹⁸ GESHKEN...	89	RVUE $e^+e^- \rightarrow \pi^+\pi^-$

¹ Using the GOUNARIS 68 parametrization with the complex phase of the ρ - ω interference and leaving the masses and widths of the $\rho(1450)$, $\rho(1700)$, and $\rho(2150)$ resonances as free parameters of the fit.

² A combined fit of AKHMETSHIN 07, AULCHENKO 06, and AULCHENKO 05.

³ Supersedes ACHASOV 05A.

⁴ A fit of the SND data from 400 to 1000 MeV using parameters of the $\rho(1450)$ and $\rho(1700)$ from a fit of the data of BARKOV 85, BISELLO 89 and ANDERSON 00A.

⁵ Using the GOUNARIS 68 parametrization with the complex phase of the ρ - ω interference.

⁶ Update of AKHMETSHIN 02.

⁷ Assuming $m_{\rho^+} = m_{\rho^-} = m_{\rho^0}$, $\Gamma_{\rho^+} = \Gamma_{\rho^-}$.

⁸ From the GOUNARIS 68 parametrization of the pion form factor.

⁹ Applies the Unitary & Analytic Model of the pion electromagnetic form factor of DUBNICKA 10 to analyze the data of LEES 12g and ABLIKIM 16c.

¹⁰ Applies the Unitary & Analytic Model of the pion electromagnetic form factor of DUBNICKA 10 to analyze the data of ACHASOV 06, AKHMETSHIN 07, AUBERT 09as, and AMBROSINO 11a.

¹¹ Assuming $m_{\rho^+} = m_{\rho^-} = m_{\rho^0}$, $\Gamma_{\rho^+} = \Gamma_{\rho^-} = \Gamma_{\rho^0}$.

¹² Without limitations on masses and widths.

¹³ Assuming $m_{\rho^0} = m_{\rho^\pm}$, $g_{\rho^0\pi\pi} = g_{\rho^\pm\pi\pi}$.

¹⁴ Using the data of BARKOV 85 in the hidden local symmetry model.

¹⁵ From the fit to $e^+e^- \rightarrow \pi^+\pi^-$ data from the compilations of HEYN 81 and BARKOV 85, including the GOUNARIS 68 parametrization of the pion form factor.

¹⁶ A fit of BARKOV 85 data assuming the direct $\omega\pi\pi$ coupling.

¹⁷ Applying the S-matrix formalism to the BARKOV 85 data.

¹⁸ Includes BARKOV 85 data. Model-dependent width definition.

CHARGED ONLY, τ DECAYS and e^+e^-

VALUE (MeV)	EVTS	DOCUMENT ID	TECN	CHG	COMMENT
775.11 ± 0.34 OUR AVERAGE					
774.6 ± 0.2 ± 0.5	5.4M	^{1,2} FUJIKAWA	08	BELL ±	$\tau^- \rightarrow \pi^- \pi^0 \nu_\tau$
775.5 ± 0.7		^{2,3} SCHAELE	05c	ALEP	$\tau^- \rightarrow \pi^- \pi^0 \nu_\tau$
775.5 ± 0.5 ± 0.4	1.98M	⁴ ALOISIO	03	KLOE	$1.02 e^+e^- \rightarrow \pi^+\pi^-\pi^0$
775.1 ± 1.1 ± 0.5	87k	^{5,6} ANDERSON	00A	CLE2	$\tau^- \rightarrow \pi^- \pi^0 \nu_\tau$
761.60 ± 0.95		⁷ BARTOS	17A	RVUE	$\tau^- \rightarrow \pi^- \pi^0 \nu_\tau$
774.8 ± 0.6 ± 0.4	1.98M	⁸ ALOISIO	03	KLOE -	$1.02 e^+e^- \rightarrow \pi^+\pi^-\pi^0$
776.3 ± 0.6 ± 0.7	1.98M	⁸ ALOISIO	03	KLOE +	$1.02 e^+e^- \rightarrow \pi^+\pi^-\pi^0$
773.9 ± 2.0 ± 0.3		⁹ SANZ-CILLERO	03	RVUE	$\tau^- \rightarrow \pi^- \pi^0 \nu_\tau$
774.5 ± 0.7 ± 1.5	500k	⁴ ACHASOV	02	SND ±	$1.02 e^+e^- \rightarrow \pi^+\pi^-\pi^0$
775.1 ± 0.5		¹⁰ PICH	01	RVUE	$\tau^- \rightarrow \pi^- \pi^0 \nu_\tau$

••• We do not use the following data for averages, fits, limits, etc. •••

¹ $|F_\pi(0)|^2$ fixed to 1.

² From the GOUNARIS 68 parametrization of the pion form factor.

³ The error combines statistical and systematic uncertainties. Supersedes BARATE 97M.

⁴ Assuming $m_{\rho^+} = m_{\rho^-} = m_{\rho^0}$, $\Gamma_{\rho^+} = \Gamma_{\rho^-}$.

⁵ $\rho(1700)$ mass and width fixed at 1700 MeV and 235 MeV respectively.

⁶ From the GOUNARIS 68 parametrization of the pion form factor. The second error is a model error taking into account different parametrizations of the pion form factor.

⁷ Applies the Unitary & Analytic Model of the pion electromagnetic form factor of DUBNICKA 10 to analyze the data of FUJIKAWA 08.

⁸ Without limitations on masses and widths.

⁹ Using the data of BARATE 97M and the effective chiral Lagrangian.

¹⁰ From a fit of the model-independent parameterization of the pion form factor to the data of BARATE 97M.

MIXED CHARGES, OTHER REACTIONS

VALUE (MeV)	EVTS	DOCUMENT ID	TECN	CHG	COMMENT
763.0 ± 0.3 ± 1.2	600k	¹ ABELE	99e	CBAR	$0 \pm 0.0 \bar{p}p \rightarrow \pi^+\pi^-\pi^0$

¹ Assuming the equality of ρ^+ and ρ^- masses and widths.

CHARGED ONLY, HADROPRODUCED

VALUE (MeV)	EVTS	DOCUMENT ID	TECN	CHG	COMMENT
766.5 ± 1.1 OUR AVERAGE					
763.7 ± 3.2		ABELE	97	CBAR	$\bar{p}n \rightarrow \pi^- \pi^0 \pi^0$
768 ± 9		AGUILAR...	91	EHS	400 pp
767 ± 3	2935	¹ CAPRARO	87	SPEC -	200 $\pi^- \text{Cu} \rightarrow \pi^- \pi^0 \text{Cu}$
761 ± 5	967	¹ CAPRARO	87	SPEC -	200 $\pi^- \text{Pb} \rightarrow \pi^- \pi^0 \text{Pb}$
771 ± 4		HUSTON	86	SPEC +	202 $\pi^+ \text{A} \rightarrow \pi^+ \pi^0 \text{A}$
766 ± 7	6500	² BYERLY	73	OSPK -	5 $\pi^- p$

See key on page 999

Meson Particle Listings

$\rho(770)$

766.8±1.5	9650	³ PISUT	68	RVUE	-	1.7-3.2 π^-p , $t < 10$
767 ± 6	900	¹ EISNER	67	HBC	-	4.2 π^-p , $t < 10$

- ¹ Mass errors enlarged by us to Γ/\sqrt{N} ; see the note with the $K^*(892)$ mass.
- ² Phase shift analysis. Systematic errors added corresponding to spread of different fits.
- ³ From fit of 3-parameter relativistic P-wave Breit-Wigner to total mass distribution. Includes BATON 68, MILLER 67b, ALFF-STEINBERGER 66, HAGOPIAN 66, HAGOPIAN 66b, JACOBS 66b, JAMES 66, WEST 66, BLIEDEN 65 and CARMONY 64.

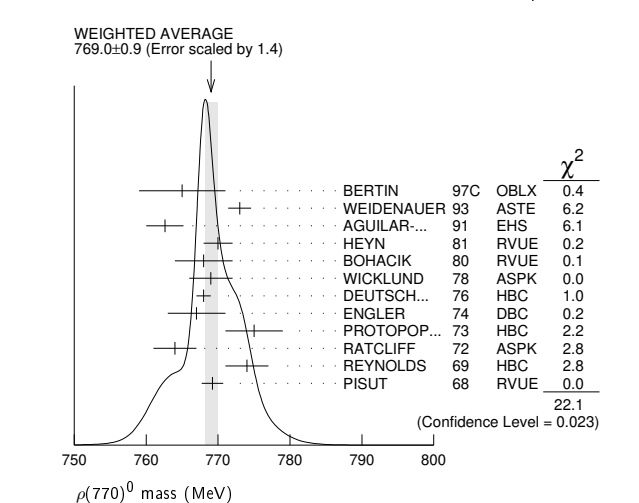
NEUTRAL ONLY, PHOTOPRODUCED

VALUE (MeV)	EVTs	DOCUMENT ID	TECN	COMMENT
769.0± 1.0 OUR AVERAGE				
771 ± 2 $^{+2}_{-1}$	63.5k	¹ ABRAMOWICZ12	ZEUS	$e p \rightarrow e \pi^+ \pi^- p$
770 ± 2 ± 1	79k	² BREITWEG	98B ZEUS	50-100 γp
767.6± 2.7		BARTALUCCI 78	CNTR	$\gamma p \rightarrow e^+ e^- p$
775 ± 5		GLADDING 73	CNTR	2.9-4.7 γp
767 ± 4	1930	BALLAM 72	HBC	2.8 γp
770 ± 4	2430	BALLAM 72	HBC	4.7 γp
765 ± 10		ALVENSLEB...	70	CNTR γA , $t < 0.01$
767.7± 1.9	140k	BIGGS 70	CNTR	<4.1 $\gamma C \rightarrow \pi^+ \pi^- C$
765 ± 5	4000	ASBURY 67b	CNTR	$\gamma + Pb$

- • • We do not use the following data for averages, fits, limits, etc. • • •
- 771 ± 2
 79k | ³BREITWEG | 98B ZEUS | 50-100 γp |- ¹ Using the KUHN 90 parametrization of the pion form factor, neglecting $\rho-\omega$ interference.
- ² From the parametrization according to SOEDING 66.
- ³ From the parametrization according to ROSS 66.

NEUTRAL ONLY, OTHER REACTIONS

VALUE (MeV)	EVTs	DOCUMENT ID	TECN	COMMENT
769.0 ± 0.9 OUR AVERAGE				Error includes scale factor of 1.4. See the ideogram below.
765 ± 6		BERTIN 97c	OBLX	0.0 $\bar{p} p \rightarrow \pi^+ \pi^- \pi^0$
773 ± 1.6		WEIDENAUER 93	ASTE	$\bar{p} p \rightarrow \pi^+ \pi^- \omega$
762.6 ± 2.6		AGUILAR...	91	EHS 400 pp
770 ± 2		¹ HEYN	81	RVUE Pion form factor
768 ± 4		^{2,3} BOHACIK	80	RVUE
769 ± 3		⁴ WICKLUND	78	ASPK 3,4,6 $\pi^\pm N$
768 ± 1	76k	DEUTSCH...	76	HBC 16 $\pi^+ p$
767 ± 4	4100	ENGLER 74	DBC	6 $\pi^+ n \rightarrow \pi^+ \pi^- p$
775 ± 4	32k	² PROTOPOP...	73	HBC 7.1 $\pi^+ p$, $t < 0.4$
764 ± 3	6.8k	⁵ RATCLIFF	72	ASPK 15 $\pi^- p$, $t < 0.3$
774 ± 3	1.7k	REYNOLDS 69	HBC	2.26 $\pi^- p$
769.2 ± 1.5	13.3k	⁶ PISUT	68	RVUE 1.7-3.2 $\pi^- p$, $t < 10$



- ⁶ Includes MALAMUD 69, ARMENISE 68, BACON 67, HUWE 67, MILLER 67b, ALFF-STEINBERGER 66, HAGOPIAN 66, HAGOPIAN 66b, JACOBS 66b, JAMES 66, WEST 66, GOLDBABER 64, ABOLINS 63.
- ⁷ From a fit to $\pi^+ \pi^-$ mass using $\rho(770)$ (parametrized with the Gounaris-Sakurai approach), $\omega(782)$, and box anomaly components.
- ⁸ From a fit to $\pi^+ \pi^-$ mass using $\rho(770)$ (parametrized with the Gounaris-Sakurai approach), $\omega(782)$, and $\rho(1450)$ components.
- ⁹ Breit-Wigner mass from a phase-shift analysis of HYAMS 73 and PROTOPOESCU 73 data.
- ¹⁰ Using relativistic Breit-Wigner and taking into account $\rho-\omega$ interference.
- ¹¹ Systematic errors not evaluated.
- ¹² Systematic effects not studied.
- ¹³ From fit of 3-parameter relativistic Breit-Wigner to helicity-zero part of P-wave intensity. CHABAUD 83 includes data of GRAYER 74.
- ¹⁴ Mass errors enlarged by us to Γ/\sqrt{N} ; see the note with the $K^*(892)$ mass.
- ¹⁵ Of HYAMS 68 six parametrizations, this is theoretically soundest. MR

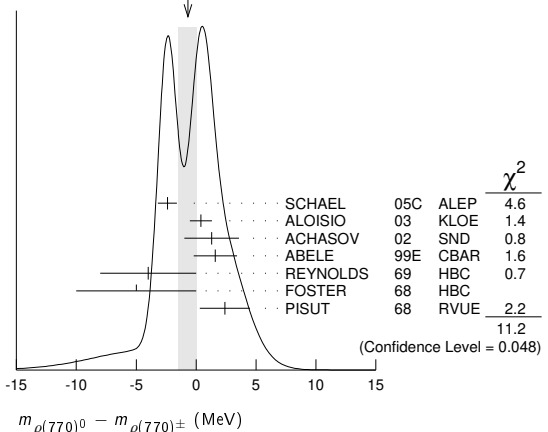
$m_{\rho(770)^0} - m_{\rho(770)^\pm}$

VALUE (MeV)	EVTs	DOCUMENT ID	TECN	CHG.	COMMENT
-0.7 ± 0.8 OUR AVERAGE					Error includes scale factor of 1.5. See the ideogram below.
-2.4 ± 0.8		¹ SCHAEEL	05c	ALEP	$\tau^- \rightarrow \pi^- \pi^0 \nu_\tau$
0.4 ± 0.7 ± 0.6	1.98M	² ALOISIO	03	KLOE	1.02 $e^+ e^- \rightarrow \pi^+ \pi^- \pi^0$
1.3 ± 1.1 ± 2.0	500k	² ACHASOV	02	SND	1.02 $e^+ e^- \rightarrow \pi^+ \pi^- \pi^0$
1.6 ± 0.6 ± 1.7	600k	ABELE	99E	CBAR ± 0	0.0 $\bar{p} p \rightarrow \pi^+ \pi^- \pi^0$
-4 ± 4	3000	³ REYNOLDS	69	HBC	-0 2.26 $\pi^- p$
-5 ± 5	3600	³ FOSTER	68	HBC	± 0.0 $\bar{p} p$
2.4 ± 2.1	22950	⁴ PISUT	68	RVUE	$\pi N \rightarrow \rho N$

- • • We do not use the following data for averages, fits, limits, etc. • • •
- 3.37 ± 1.06
 | ⁵BARTOS | 17A | RVUE | $e^+ e^- \rightarrow \pi^+ \pi^-$, $\tau^- \rightarrow \pi^- \pi^0 \nu_\tau$ |- ¹ From the combined fit of the τ^- data from ANDERSON 00a and SCHAEEL 05c and $e^+ e^-$ data from the compilation of BARKOV 85, AKHMETSHIN 04, and ALOISIO 05. Supersedes BARATE 97M.
- ² Assuming $m_{\rho^+} = m_{\rho^-}$, $\Gamma_{\rho^+} = \Gamma_{\rho^-}$.
- ³ From quoted masses of charged and neutral modes.
- ⁴ Includes MALAMUD 69, ARMENISE 68, BATON 68, BACON 67, HUWE 67, MILLER 67b, ALFF-STEINBERGER 66, HAGOPIAN 66, HAGOPIAN 66b, JACOBS 66b, JAMES 66, WEST 66, BLIEDEN 65, CARMONY 64, GOLDBABER 64, ABOLINS 63.
- ⁵ Applies the Unitary & Analytic Model of the pion electromagnetic form factor of DUBNICKA 10 to analyze the data of ACHASOV 06, AKHMETSHIN 07, AUBERT 09a, AMBROSINO 11a, and FUJIKAWA 08.

WEIGHTED AVERAGE

-0.7±0.8 (Error scaled by 1.5)



$m_{\rho(770)^+} - m_{\rho(770)^-}$

VALUE (MeV)	EVTs	DOCUMENT ID	TECN	COMMENT
1.5 ± 0.8 ± 0.7	1.98M	¹ ALOISIO	03	KLOE 1.02 $e^+ e^- \rightarrow \pi^+ \pi^- \pi^0$

- • • We do not use the following data for averages, fits, limits, etc. • • •
- ¹ Without limitations on masses and widths.

$\rho(770)$ RANGE PARAMETER

The range parameter R enters an energy-dependent correction to the width, of the form $(1 + q_r^2 R^2) / (1 + q^2 R^2)$, where q is the momentum of one of the pions in the $\pi\pi$ rest system. At resonance, $q = q_r$.

- ¹ HEYN 81 includes all spacelike and timelike F_π values until 1978.
- ² From pole extrapolation.
- ³ From phase shift analysis of GRAYER 74 data.
- ⁴ Phase shift analysis. Systematic errors added corresponding to spread of different fits.
- ⁵ Published values contain misprints. Corrected by private communication RATCLIFF 74.

Meson Particle Listings

$\rho(770)$

VALUE (GeV ⁻¹)	DOCUMENT ID	TECN	CHG	COMMENT
5.3^{+0.9}_{-0.7}	¹ CHABAUD	83	ASPK	0 17 $\pi^- \rho$ polarized

¹ The old PISUT 68 value, properly corrected, was 3.2 ± 0.6.

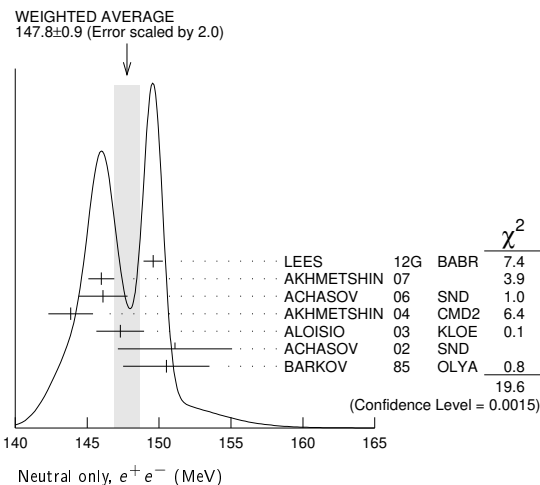
$\rho(770)$ WIDTH

We no longer list S-wave Breit-Wigner fits, or data with high combinatorial background.

NEUTRAL ONLY, e^+e^-

VALUE (MeV)	EVTS	DOCUMENT ID	TECN	COMMENT
147.8 ± 0.9 OUR AVERAGE				Error includes scale factor of 2.0. See the ideogram below.
149.59 ± 0.67		¹ LEES	12G	BABR $e^+e^- \rightarrow \pi^+\pi^-\gamma$
145.98 ± 0.75 ± 0.50	900k	² AKHMETSHIN	07	$e^+e^- \rightarrow \pi^+\pi^-$
146.1 ± 0.8 ± 1.5	800k	^{3,4} ACHASOV	06	SND $e^+e^- \rightarrow \pi^+\pi^-$
143.85 ± 1.33 ± 0.80	114k	^{5,6} AKHMETSHIN	04	CMD2 $e^+e^- \rightarrow \pi^+\pi^-$
147.3 ± 1.5 ± 0.7	1.98M	⁷ ALOISIO	03	KLOE 1.02 $e^+e^- \rightarrow \pi^+\pi^-$
151.1 ± 2.6 ± 3.0	500k	⁷ ACHASOV	02	SND 1.02 $e^+e^- \rightarrow \pi^+\pi^-$
150.5 ± 3.0		⁸ BARKOV	85	OLYA $e^+e^- \rightarrow \pi^+\pi^-$
144.06 ± 0.85		⁹ BARTOS	17	RVUE $e^+e^- \rightarrow \pi^+\pi^-$
144.56 ± 0.80		¹⁰ BARTOS	17A	RVUE $e^+e^- \rightarrow \pi^+\pi^-$
143.9 ± 1.3 ± 1.1	1.98M	¹¹ ALOISIO	03	KLOE 1.02 $e^+e^- \rightarrow \pi^+\pi^-$
147.4 ± 1.5 ± 0.7	1.98M	¹² ALOISIO	03	KLOE 1.02 $e^+e^- \rightarrow \pi^+\pi^-$
149.8 ± 2.2 ± 2.0	500k	¹³ ACHASOV	02	SND 1.02 $e^+e^- \rightarrow \pi^+\pi^-$
147.9 ± 1.5 ± 7.5		¹⁴ BENAYOUN	98	RVUE $e^+e^- \rightarrow \pi^+\pi^-$
153.5 ± 1.3 ± 4.6		¹⁵ GARDNER	98	RVUE 0.28-0.92 $e^+e^- \rightarrow \mu^+\mu^-$
145.0 ± 1.7		¹⁶ O'CONNELL	97	RVUE $e^+e^- \rightarrow \pi^+\pi^-$
142.5 ± 3.5		¹⁷ BERNICHA	94	RVUE $e^+e^- \rightarrow \pi^+\pi^-$
138 ± 1		¹⁸ GESHKEN...	89	RVUE $e^+e^- \rightarrow \pi^+\pi^-$

- Using the GOUNARIS 68 parametrization with the complex phase of the ρ - ω interference and leaving the masses and widths of the $\rho(1450)$, $\rho(1700)$, and $\rho(2150)$ resonances as free parameters of the fit.
- A combined fit of AKHMETSHIN 07, AULCHENKO 06, and AULCHENKO 05.
- Supersedes ACHASOV 05A.
- A fit of the SND data from 400 to 1000 MeV using parameters of the $\rho(1450)$ and $\rho(1700)$ from a fit of the data of BARKOV 85, BISELLO 89 and ANDERSON 00A.
- Using the GOUNARIS 68 parametrization with the complex phase of the ρ - ω interference.
- From a fit in the energy range 0.61 to 0.96 GeV. Update of AKHMETSHIN 02.
- Assuming $m_{\rho^+} = m_{\rho^-}$, $\Gamma_{\rho^+} = \Gamma_{\rho^-}$.
- From the GOUNARIS 68 parametrization of the pion form factor.
- Applies the Unitary & Analytic Model of the pion electromagnetic form factor of DUBNICKA 10 to analyze the data of LEES 12G and ABLIKIM 16C.
- Applies the Unitary & Analytic Model of the pion electromagnetic form factor of DUBNICKA 10 to analyze the data of ACHASOV 06, AKHMETSHIN 07, AUBERT 09as, and AMBROSINO 11A.
- Assuming $m_{\rho^+} = m_{\rho^-} = m_{\rho^0}$, $\Gamma_{\rho^+} = \Gamma_{\rho^-} = \Gamma_{\rho^0}$.
- Without limitations on masses and widths.
- Assuming $m_{\rho^0} = m_{\rho^{\pm}}$, $g_{\rho^0\pi\pi} = g_{\rho^{\pm}\pi\pi}$.
- Using the data of BARKOV 85 in the hidden local symmetry model.
- From the fit to $e^+e^- \rightarrow \pi^+\pi^-$ data from the compilations of HEYN 81 and BARKOV 85, including the GOUNARIS 68 parametrization of the pion form factor.
- A fit of BARKOV 85 data assuming the direct $\omega\pi\pi$ coupling.
- Applying the S-matrix formalism to the BARKOV 85 data.
- Includes BARKOV 85 data. Model-dependent width definition.



CHARGED ONLY, τ DECAYS and e^+e^-

VALUE (MeV)	EVTS	DOCUMENT ID	TECN	CHG	COMMENT
149.1 ± 0.8 OUR FIT					
149.1 ± 0.8 OUR AVERAGE					
148.1 ± 0.4 ± 1.7	5.4M	^{1,2} FUJIKAWA	08	BELL ±	$\tau^- \rightarrow \pi^- \pi^0 \nu_\tau$
149.0 ± 1.2		^{2,3} SCHAEEL	05c	ALEP	$\tau^- \rightarrow \pi^- \pi^0 \nu_\tau$
149.9 ± 2.3 ± 2.0	500k	⁴ ACHASOV	02	SND ±	1.02 $e^+e^- \rightarrow \pi^+\pi^- \pi^0$
150.4 ± 1.4 ± 1.4	87k	^{5,6} ANDERSON	00A	CLE2	$\tau^- \rightarrow \pi^- \pi^0 \nu_\tau$
139.90 ± 0.46		⁷ BARTOS	17A	RVUE	$\tau^- \rightarrow \pi^- \pi^0 \nu_\tau$
143.7 ± 1.3 ± 1.2	1.98M	⁴ ALOISIO	03	KLOE ±	1.02 $e^+e^- \rightarrow \pi^+\pi^- \pi^0$
142.9 ± 1.3 ± 1.4	1.98M	⁸ ALOISIO	03	KLOE -	1.02 $e^+e^- \rightarrow \pi^+\pi^- \pi^0$
144.7 ± 1.4 ± 1.2	1.98M	⁸ ALOISIO	03	KLOE +	1.02 $e^+e^- \rightarrow \pi^+\pi^- \pi^0$
150.2 ± 2.0 ± 0.7 ± 1.6		⁹ SANZ-CILLERO	03	RVUE	$\tau^- \rightarrow \pi^- \pi^0 \nu_\tau$
150.9 ± 2.2 ± 2.0	500k	¹⁰ ACHASOV	02	SND	1.02 $e^+e^- \rightarrow \pi^+\pi^- \pi^0$

- • • We do not use the following data for averages, fits, limits, etc. • • •
- ¹ $|F_\pi(0)|^2$ fixed to 1.
- ² From the GOUNARIS 68 parametrization of the pion form factor.
- ³ The error combines statistical and systematic uncertainties. Supersedes BARATE 97M.
- ⁴ Assuming $m_{\rho^+} = m_{\rho^-}$, $\Gamma_{\rho^+} = \Gamma_{\rho^-}$.
- ⁵ $\rho(1700)$ mass and width fixed at 1700 MeV and 235 MeV respectively.
- ⁶ From the GOUNARIS 68 parametrization of the pion form factor. The second error is a model error taking into account different parametrizations of the pion form factor.
- ⁷ Applies the Unitary & Analytic Model of the pion electromagnetic form factor of DUBNICKA 10 to analyze the data of FUJIKAWA 08.
- ⁸ Without limitations on masses and widths.
- ⁹ Using the data of BARATE 97M and the effective chiral Lagrangian.
- ¹⁰ Assuming $m_{\rho^0} = m_{\rho^{\pm}}$, $g_{\rho^0\pi\pi} = g_{\rho^{\pm}\pi\pi}$.

MIXED CHARGES, OTHER REACTIONS

VALUE (MeV)	EVTS	DOCUMENT ID	TECN	CHG	COMMENT
149.5 ± 1.3	600k	¹ ABELE	99E	CBAR	0 ± 0.0 $\bar{p}p \rightarrow \pi^+\pi^-\pi^0$

¹ Assuming the equality of ρ^+ and ρ^- masses and widths.

CHARGED ONLY, HADROPRODUCED

VALUE (MeV)	EVTS	DOCUMENT ID	TECN	CHG	COMMENT
150.2 ± 2.4 OUR FIT					
150.2 ± 2.4 OUR AVERAGE					
152.8 ± 4.3		ABELE	97	CBAR	$\bar{p}n \rightarrow \pi^-\pi^0\pi^0$
155 ± 11	2.9k	¹ CAPRARO	87	SPEC -	200 π^- Cu $\rightarrow \pi^-\pi^0$ Cu
154 ± 20	967	¹ CAPRARO	87	SPEC -	200 π^- Pb $\rightarrow \pi^-\pi^0$ Pb
150 ± 5		HUSTON	86	SPEC +	202 π^+ A $\rightarrow \pi^+\pi^0$ A
146 ± 12	6.5k	² BYERLY	73	OSPK	5 π^- p
148.2 ± 4.1	9.6k	³ PISUT	68	RVUE	1.7-3.2 π^- p, $t < 10$
146 ± 13	900	EISNER	67	HBC	4.2 π^- p, $t < 10$
137.0 ± 0.4		⁴ ABLIKIM	17	BES3	$J/\psi \rightarrow \gamma 3\pi$

- • • We do not use the following data for averages, fits, limits, etc. • • •
- ¹ Width errors enlarged by us to $4\Gamma/\sqrt{N}$; see the note with the $K^*(892)$ mass.
- ² Phase shift analysis. Systematic errors added corresponding to spread of different fits.
- ³ From fit of 3-parameter relativistic P-wave Breit-Wigner to total mass distribution. Includes BATON 68, MILLER 67B, ALFF-STEINBERGER 66, HAGOPIAN 66, HAGOPIAN 66B, JACOBS 66B, JAMES 66, WEST 66, BLIEDEN 65 and CARMONY 64.
- ⁴ S-matrix pole at a fixed ρ meson mass of 775.49 MeV.

NEUTRAL ONLY, PHOTOPRODUCED

VALUE (MeV)	EVTS	DOCUMENT ID	TECN	COMMENT
151.7 ± 2.6 OUR AVERAGE				
155 ± 5 ± 2	63.5k	¹ ABRAMOWICZ12	ZEUS	$ep \rightarrow e\pi^+\pi^-p$
146 ± 3 ± 13	79k	² BREITWEG	98B	ZEUS 50-100 γ p
150.9 ± 3.0		BARTALUCCI	78	CNTR $\gamma p \rightarrow e^+e^-p$
138 ± 3	79k	³ BREITWEG	98B	ZEUS 50-100 γ p
147 ± 11		GLADDING	73	CNTR 2.9-4.7 γ p
155 ± 12	2430	BALLAM	72	HBC 4.7 γ p
145 ± 13	1930	BALLAM	72	HBC 2.8 γ p
140 ± 5		ALVENSLEB...	70	CNTR γ A, $t < 0.01$
146.1 ± 2.9	140k	BIGGS	70	CNTR $< 4.1 \gamma$ C $\rightarrow \pi^+\pi^-$ C
160 ± 10		LANZEROTTI	68	CNTR γ p
130 ± 5	4000	ASBURY	67B	CNTR $\gamma +$ Pb

- ¹ Using the KUHN 90 parametrization of the pion form factor, neglecting ρ - ω interference.
- ² From the parametrization according to SOEDING 66.
- ³ From the parametrization according to ROSS 66.

NEUTRAL ONLY, OTHER REACTIONS

VALUE (MeV)	EVTS	DOCUMENT ID	TECN	COMMENT
150.9 ± 1.7 OUR AVERAGE				Error includes scale factor of 1.1.
122 ± 20		BERTIN	97c	OBLX 0.0 $\bar{p}p \rightarrow \pi^+\pi^-\pi^0$
145.7 ± 5.3		WEIDENAUER	93	ASTE $\bar{p}p \rightarrow \pi^+\pi^-\omega$
144.9 ± 3.7		DUBNICKA	89	RVUE π form factor
148 ± 6		^{1,2} BOHACIK	80	RVUE
152 ± 9		³ WICKLUND	78	ASPK 3.4, 6 $\pi^\pm p$ N
154 ± 2	76k	DEUTSCH...	76	HBC 16 π^+ p
157 ± 8	6.8k	⁴ RATCLIFF	72	ASPK 15 π^- p, $t < 0.3$
143 ± 8	1.7k	REYNOLDS	69	HBC 2.26 π^- p

••• We do not use the following data for averages, fits, limits, etc. •••

150.85 ± 0.55 ± 0.67	970k	⁵ ABLIKIM	18c	BES3	$\eta'(958) \rightarrow \gamma \pi^+ \pi^-$
150.18 ± 0.55 ± 0.65	970k	⁶ ABLIKIM	18c	BES3	$\eta(958) \rightarrow \gamma \pi^+ \pi^-$
147.0 ± 2.5	600k	⁷ ABELE	99E	CBAR	$0.0 \bar{p} p \rightarrow \pi^+ \pi^- \pi^0$
146 ± 3	4.9k	⁸ ADAMS	97	E665	$470 \mu p \rightarrow \mu X B$
160.0 + 4.1 - 4.0		⁹ CHABAUD	83	ASPK	$17 \pi^- p$ polarized
155 ± 1		¹⁰ HEYN	81	RVUE	π form factor
148.0 ± 1.3		^{1,2} LANG	79	RVUE	
146 ± 14	4.1k	ENGLER	74	DBC	$6 \pi^+ n \rightarrow \pi^+ \pi^- p$
143 ± 13		² ESTABROOKS	74	RVUE	$17 \pi^- p \rightarrow \pi^+ \pi^- n$
160 ± 10	32k	¹ PROTOPOP...	73	HBC	$7.1 \pi^+ p, t < 0.4$
145 ± 12	2.2k	^{3,11} HYAMS	68	OSPK	$11.2 \pi^- p$
163 ± 15	13.3k	¹² PISUT	68	RVUE	$1.7-3.2 \pi^- p, t < 1.0$

- ¹ From pole extrapolation.
- ² From phase shift analysis of GRAYER 74 data.
- ³ Width errors enlarged by us to $4\Gamma/\sqrt{N}$; see the note with the $K^*(892)$ mass.
- ⁴ Published values contain misprints. Corrected by private communication RATCLIFF 74.
- ⁵ From a fit to $\pi^+ \pi^-$ mass using $\rho(770)$ (parametrized with the Gounaris-Sakurai approach), $\omega(782)$, and box anomaly components.
- ⁶ From a fit to $\pi^+ \pi^-$ mass using $\rho(770)$ (parametrized with the Gounaris-Sakurai approach), $\omega(782)$, and $\rho(1450)$ components.
- ⁷ Using relativistic Breit-Wigner and taking into account ρ - ω interference.
- ⁸ Systematic errors not evaluated.
- ⁹ From fit of 3-parameter relativistic Breit-Wigner to helicity-zero part of P -wave intensity. CHABAUD 83 includes data of GRAYER 74.
- ¹⁰ HEYN 81 includes all spacelike and timelike F_π values until 1978.
- ¹¹ Of HYAMS 68 six parametrizations this is theoretically soundest. MR
- ¹² Includes MALAMUD 69, ARMENISE 68, BACON 67, HUWE 67, MILLER 67b, ALFF-STEINBERGER 66, HAGOPIAN 66, HAGOPIAN 66a, JACOBS 66a, JAMES 66, WEST 66, GOLDHABER 64, ABOLINS 63.

$\Gamma_{\rho(770)^0} - \Gamma_{\rho(770)^\pm}$		DOCUMENT ID	TECN	COMMENT
VALUE (MeV)	EVTs			
0.3 ± 1.3 OUR AVERAGE		Error includes scale factor of 1.4.		
-0.2 ± 1.0		¹ SCHAEEL	05c	ALEP $\tau^- \rightarrow \pi^- \pi^0 \nu_\tau$
3.6 ± 1.8 ± 1.7 1.98M		² ALOISIO	03	KLOE $1.02 e^+ e^- \rightarrow \pi^+ \pi^- \pi^0$

- We do not use the following data for averages, fits, limits, etc. •••
- 4.66 ± 0.85 ³ BARTOS 17A RVUE $e^+ e^- \rightarrow \pi^+ \pi^-, \tau^- \rightarrow \pi^- \pi^0 \nu_\tau$
- ¹ From the combined fit of the τ^- data from ANDERSON 00a and SCHAEEL 05c and $e^+ e^-$ data from the compilation of BARKOV 85, AKHMETSHIN 04, and ALOISIO 05. Supersedes BARATE 97m.
- ² Assuming $m_{\rho^+} = m_{\rho^-}, \Gamma_{\rho^+} = \Gamma_{\rho^-}$.
- ³ Applies the Unitary & Analytic Model of the pion electromagnetic form factor of DUBNICKA 10 to analyze the data of ACHASOV 06, AKHMETSHIN 07, AUBERT 09as, AMBROSINO 11a, and FUJIKAWA 08.

$\Gamma_{\rho(770)^+} - \Gamma_{\rho(770)^-}$		DOCUMENT ID	TECN	COMMENT
VALUE	EVTs			
1.8 ± 2.0 ± 0.5	1.98M	¹ ALOISIO	03	KLOE $1.02 e^+ e^- \rightarrow \pi^+ \pi^- \pi^0$

¹ Without limitations on masses and widths.

$\rho(770)$ DECAY MODES

Mode	Fraction (Γ_i/Γ)	Scale factor/ Confidence level
$\Gamma_1 \pi \pi$	~ 100	%
$\rho(770)^\pm$ decays		
$\Gamma_2 \pi^\pm \pi^0$	~ 100	%
$\Gamma_3 \pi^\pm \gamma$	(4.5 ± 0.5)	$\times 10^{-4}$ S=2.2
$\Gamma_4 \pi^\pm \eta$	< 6	$\times 10^{-3}$ CL=84%
$\Gamma_5 \pi^\pm \pi^+ \pi^- \pi^0$	< 2.0	$\times 10^{-3}$ CL=84%
$\rho(770)^0$ decays		
$\Gamma_6 \pi^+ \pi^-$	~ 100	%
$\Gamma_7 \pi^+ \pi^- \gamma$	(9.9 ± 1.6)	$\times 10^{-3}$ S=1.4
$\Gamma_8 \pi^0 \gamma$	(4.7 ± 0.6)	$\times 10^{-4}$
$\Gamma_9 \eta \gamma$	(3.00 ± 0.21)	$\times 10^{-4}$
$\Gamma_{10} \pi^0 \pi^0 \gamma$	(4.5 ± 0.8)	$\times 10^{-5}$
$\Gamma_{11} \mu^+ \mu^-$	[a]	(4.55 ± 0.28) $\times 10^{-5}$
$\Gamma_{12} e^+ e^-$	[a]	(4.72 ± 0.05) $\times 10^{-5}$
$\Gamma_{13} \pi^+ \pi^- \pi^0$	(1.01 + 0.54 - 0.36 ± 0.34)	$\times 10^{-4}$
$\Gamma_{14} \pi^+ \pi^- \pi^+ \pi^-$	(1.8 ± 0.9)	$\times 10^{-5}$
$\Gamma_{15} \pi^+ \pi^- \pi^0 \pi^0$	(1.6 ± 0.8)	$\times 10^{-5}$
$\Gamma_{16} \pi^0 e^+ e^-$	< 1.2	$\times 10^{-5}$ CL=90%
$\Gamma_{17} \eta e^+ e^-$		

[a] The $\omega\rho$ interference is then due to $\omega\rho$ mixing only, and is expected to be small. If $e\mu$ universality holds, $\Gamma(\rho^0 \rightarrow \mu^+ \mu^-) = \Gamma(\rho^0 \rightarrow e^+ e^-) \times 0.99785$.

CONSTRAINED FIT INFORMATION

An overall fit to the total width and a partial width uses 10 measurements and one constraint to determine 3 parameters. The overall fit has a $\chi^2 = 10.7$ for 8 degrees of freedom.

The following *off-diagonal* array elements are the correlation coefficients $\langle \delta p_i \delta p_j \rangle / (\delta p_i \cdot \delta p_j)$, in percent, from the fit to parameters p_i , including the branching fractions, $x_i \equiv \Gamma_i / \Gamma_{\text{total}}$. The fit constrains the x_i whose labels appear in this array to sum to one.

x_3	-100
Γ	$\begin{matrix} 15 & -15 \\ x_2 & x_3 \end{matrix}$

Mode	Rate (MeV)	Scale factor
$\Gamma_2 \pi^\pm \pi^0$	150.2 ± 2.4	
$\Gamma_3 \pi^\pm \gamma$	0.068 ± 0.007	2.3

CONSTRAINED FIT INFORMATION

An overall fit to the total width, a partial width, and 7 branching ratios uses 22 measurements and one constraint to determine 9 parameters. The overall fit has a $\chi^2 = 9.5$ for 14 degrees of freedom.

The following *off-diagonal* array elements are the correlation coefficients $\langle \delta p_i \delta p_j \rangle / (\delta p_i \cdot \delta p_j)$, in percent, from the fit to parameters p_i , including the branching fractions, $x_i \equiv \Gamma_i / \Gamma_{\text{total}}$. The fit constrains the x_i whose labels appear in this array to sum to one.

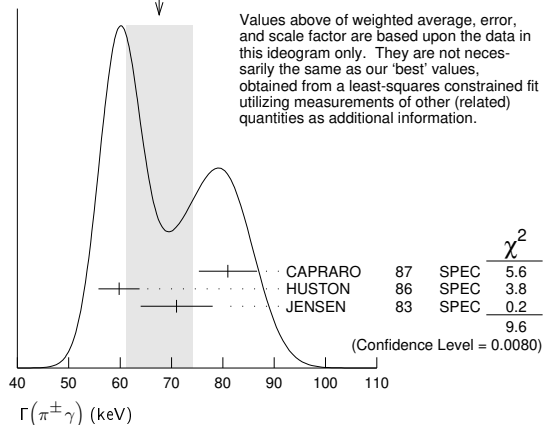
x_7	-100						
x_8	-4	0					
x_9	-1	0	1				
x_{10}	-1	0	0	0			
x_{11}	2	-3	0	0	0		
x_{12}	0	0	-8	-9	0	0	
x_{14}	-1	0	0	0	0	0	0
Γ	0	0	4	5	0	0	-54

Mode	Rate (MeV)	Scale factor
$\Gamma_6 \pi^+ \pi^-$	147.5 ± 0.9	
$\Gamma_7 \pi^+ \pi^- \gamma$	1.48 ± 0.24	
$\Gamma_8 \pi^0 \gamma$	0.070 ± 0.009	1.4
$\Gamma_9 \eta \gamma$	0.0447 ± 0.0032	
$\Gamma_{10} \pi^0 \pi^0 \gamma$	0.0066 ± 0.0012	
$\Gamma_{11} \mu^+ \mu^-$	[a]	0.0068 ± 0.0004
$\Gamma_{12} e^+ e^-$	[a]	0.00704 ± 0.00006
$\Gamma_{14} \pi^+ \pi^- \pi^+ \pi^-$	0.0027 ± 0.0014	

$\rho(770)$ PARTIAL WIDTHS

$\Gamma(\pi^\pm \gamma)$		DOCUMENT ID	TECN	CHG	COMMENT
VALUE (keV)					
68 ± 7 OUR FIT		Error includes scale factor of 2.3.			
68 ± 7 OUR AVERAGE		Error includes scale factor of 2.2. See the ideogram below.			
81 ± 4 ± 4		CAPRARO	87	SPEC	- 200 $\pi^- A \rightarrow \pi^- \pi^0 A$
59.8 ± 4.0		HUSTON	86	SPEC	+ 202 $\pi^+ A \rightarrow \pi^+ \pi^0 A$
71 ± 7		JENSEN	83	SPEC	- 156-260 $\pi^- A \rightarrow \pi^- \pi^0 A$

WEIGHTED AVERAGE
68 ± 7 (Error scaled by 2.2)



Meson Particle Listings

$\rho(770)$

$\Gamma(\pi^0\gamma)$ G8

VALUE (keV)	EVTS	DOCUMENT ID	TECN	COMMENT
77 ± 17 ± 11	36500	¹ ACHASOV 03	SND	0.60–0.97 $e^+e^- \rightarrow \pi^0\gamma$
121 ± 31		DOLINSKY 89	ND	$e^+e^- \rightarrow \pi^0\gamma$

¹ Using $\Gamma_{total} = 147.9 \pm 1.3$ MeV and $B(\rho \rightarrow \pi^0\gamma)$ from ACHASOV 03.

$\Gamma(\eta\gamma)$ G9

VALUE (keV)	DOCUMENT ID	TECN	COMMENT
62 ± 17	¹ DOLINSKY 89	ND	$e^+e^- \rightarrow \eta\gamma$

¹ Solution corresponding to constructive ω - ρ interference.

$\Gamma(e^+e^-)$ G12

VALUE (keV)	EVTS	DOCUMENT ID	TECN	COMMENT
7.04 ± 0.06 OUR FIT				
7.04 ± 0.06 OUR AVERAGE				
7.048 ± 0.057 ± 0.050	900k	¹ AKHMETSHIN 07	SND	$e^+e^- \rightarrow \pi^+\pi^-$
7.06 ± 0.11 ± 0.05	114k	^{2,3} AKHMETSHIN 04	CMD2	$e^+e^- \rightarrow \pi^+\pi^-$
6.77 ± 0.10 ± 0.30		BARKOV 85	OLYA	$e^+e^- \rightarrow \pi^+\pi^-$
7.12 ± 0.02 ± 0.11	800k	⁴ ACHASOV 06	SND	$e^+e^- \rightarrow \pi^+\pi^-$
6.3 ± 0.1		⁵ BENAYOUN 98	RVUE	$e^+e^- \rightarrow \pi^+\pi^-$, $\mu^+\mu^-$

¹ A combined fit of AKHMETSHIN 07, AULCHENKO 06, and AULCHENKO 05.
² Using the GOUNARIS 68 parametrization with the complex phase of the ρ - ω interference.
³ From a fit in the energy range 0.61 to 0.96 GeV. Update of AKHMETSHIN 02.
⁴ Supersedes ACHASOV 05A.
⁵ Using the data of BARKOV 85 in the hidden local symmetry model.

$\Gamma(\pi^+\pi^-\pi^+\pi^-)$ G14

VALUE (keV)	EVTS	DOCUMENT ID	TECN	COMMENT
2.8 ± 1.4 ± 0.5	153	AKHMETSHIN 00	CMD2	0.6–0.97 $e^+e^- \rightarrow \pi^+\pi^-\pi^+\pi^-$

$\rho(770) \Gamma(e^+e^-)\Gamma(i)/\Gamma^2(total)$

$\Gamma(e^+e^-)/\Gamma_{total} \times \Gamma(\pi^+\pi^-)/\Gamma_{total}$ G12/G × G6/G

VALUE (units 10 ⁻⁵)	EVTS	DOCUMENT ID	TECN	COMMENT
4.876 ± 0.023 ± 0.064	800k	^{1,2} ACHASOV 06	SND	$e^+e^- \rightarrow \pi^+\pi^-$
4.72 ± 0.02		³ BENAYOUN 10	RVUE	0.4–1.05 e^+e^-

¹ Supersedes ACHASOV 05A.
² A fit of the SND data from 400 to 1000 MeV using parameters of the $\rho(1450)$ and $\rho(1700)$ from a fit of the data of BARKOV 85, BISELLO 89 and ANDERSON 00A.
³ A simultaneous fit of $e^+e^- \rightarrow \pi^+\pi^-$, $\pi^+\pi^-\pi^0$, $\pi^0\gamma$, $\eta\gamma$ data.

$\Gamma(e^+e^-)/\Gamma_{total} \times \Gamma(\eta\gamma)/\Gamma_{total}$ G12/G × G9/G

VALUE (units 10 ⁻⁸)	EVTS	DOCUMENT ID	TECN	COMMENT
1.42 ± 0.10 OUR FIT				
1.45 ± 0.12 OUR AVERAGE				
1.32 ± 0.14 ± 0.08	33k	¹ ACHASOV 07B	SND	0.6–1.38 $e^+e^- \rightarrow \eta\gamma$
1.50 ± 0.65 ± 0.09	17.4k	² AKHMETSHIN 05	CMD2	0.60–1.38 $e^+e^- \rightarrow \eta\gamma$
1.61 ± 0.20 ± 0.11	23k	^{3,4} AKHMETSHIN 01B	CMD2	$e^+e^- \rightarrow \eta\gamma$
1.85 ± 0.49		⁵ DOLINSKY 89	ND	$e^+e^- \rightarrow \eta\gamma$
1.05 ± 0.02		⁶ BENAYOUN 10	RVUE	0.4–1.05 e^+e^-

¹ From a combined fit of $\sigma(e^+e^- \rightarrow \eta\gamma)$ with $\eta \rightarrow 3\pi^0$ and $\eta \rightarrow \pi^+\pi^-\pi^0$, and fixing $B(\eta \rightarrow 3\pi^0) / B(\eta \rightarrow \pi^+\pi^-\pi^0) = 1.44 \pm 0.04$. Recalculated by us from the cross section at the peak. Supersedes ACHASOV 00D and ACHASOV 06A.
² From the $\eta \rightarrow 2\gamma$ decay and using $B(\eta \rightarrow \gamma\gamma) = 39.43 \pm 0.26\%$.
³ From the $\eta \rightarrow 3\pi^0$ decay and using $B(\eta \rightarrow 3\pi^0) = (32.24 \pm 0.29) \times 10^{-2}$.
⁴ The combined fit from 600 to 1380 MeV taking into account $\rho(770)$, $\omega(782)$, $\phi(1020)$, and $\rho(1450)$ (mass and width fixed at 1450 MeV and 310 MeV respectively).
⁵ Recalculated by us from the cross section in the peak.
⁶ A simultaneous fit of $e^+e^- \rightarrow \pi^+\pi^-$, $\pi^+\pi^-\pi^0$, $\pi^0\gamma$, $\eta\gamma$ data.

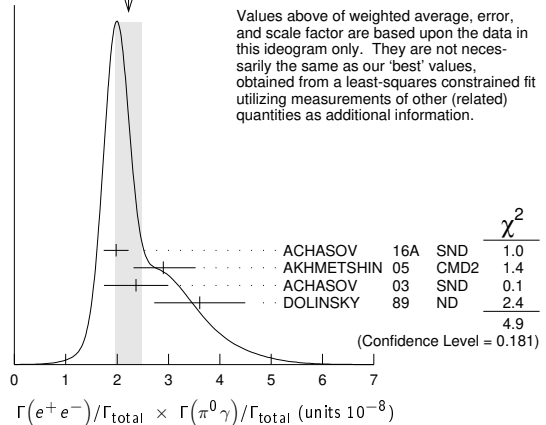
$\Gamma(e^+e^-)/\Gamma_{total} \times \Gamma(\pi^0\gamma)/\Gamma_{total}$ G12/G × G8/G

VALUE (units 10 ⁻⁸)	EVTS	DOCUMENT ID	TECN	COMMENT
2.22 ± 0.29 OUR FIT				Error includes scale factor of 1.4.
2.22 ± 0.26 OUR AVERAGE				Error includes scale factor of 1.3. See the ideogram below.
1.98 ± 0.22 ± 0.10		¹ ACHASOV 16A	SND	0.60–1.38 $e^+e^- \rightarrow \pi^0\gamma$
2.90 +0.60 -0.55 ± 0.18	18k	AKHMETSHIN 05	CMD2	0.60–1.38 $e^+e^- \rightarrow \pi^0\gamma$
2.37 ± 0.53 ± 0.33	36k	² ACHASOV 03	SND	0.60–0.97 $e^+e^- \rightarrow \pi^0\gamma$
3.61 ± 0.74 ± 0.49	10k	³ DOLINSKY 89	ND	$e^+e^- \rightarrow \pi^0\gamma$
1.875 ± 0.026		⁴ BENAYOUN 10	RVUE	0.4–1.05 e^+e^-

¹ From the VMD model with the $\rho(770)$, $\omega(782)$, $\phi(1020)$ resonances, and an additional resonance describing the total contribution of the $\rho(1450)$ and $\omega(1420)$ states. Supersedes ACHASOV 03.

² Using $\sigma_{\phi \rightarrow \pi^0\gamma}$ from ACHASOV 00 and $m_{\rho} = 775.97$ MeV in the model with the energy-independent phase of ρ - ω interference equal to $(-10.2 \pm 7.0)^\circ$.
³ Recalculated by us from the cross section in the peak.
⁴ A simultaneous fit of $e^+e^- \rightarrow \pi^+\pi^-$, $\pi^+\pi^-\pi^0$, $\pi^0\gamma$, $\eta\gamma$ data.

WEIGHTED AVERAGE
2.22±0.26 (Error scaled by 1.3)



Values above of weighted average, error, and scale factor are based upon the data in this ideogram only. They are not necessarily the same as our 'best' values, obtained from a least-squares constrained fit utilizing measurements of other (related) quantities as additional information.

$\Gamma(e^+e^-)/\Gamma_{total} \times \Gamma(\pi^+\pi^-\pi^0)/\Gamma_{total}$ G12/G × G13/G

VALUE (units 10 ⁻⁹)	EVTS	DOCUMENT ID	TECN	COMMENT
0.903 ± 0.076		¹ BENAYOUN 10	RVUE	0.4–1.05 e^+e^-
4.58 +2.46 -1.64 ± 1.56	1.2M	² ACHASOV 03D	RVUE	0.44–2.00 $e^+e^- \rightarrow \pi^+\pi^-\pi^0$

¹ A simultaneous fit of $e^+e^- \rightarrow \pi^+\pi^-$, $\pi^+\pi^-\pi^0$, $\pi^0\gamma$, $\eta\gamma$ data.
² Statistical significance is less than 3 σ .

$\rho(770)$ BRANCHING RATIOS

$\Gamma(\pi^\pm\eta)/\Gamma(\pi\pi)$ G4/G1

VALUE (units 10 ⁻⁴)	CL%	DOCUMENT ID	TECN	CHG	COMMENT
<60	84	FERBEL 66	HBC	±	$\pi^\pm p$ above 2.5

$\Gamma(\pi^\pm\pi^+\pi^-\pi^0)/\Gamma(\pi\pi)$ G5/G1

VALUE (units 10 ⁻⁴)	CL%	DOCUMENT ID	TECN	CHG	COMMENT
<20	84	FERBEL 66	HBC	±	$\pi^\pm p$ above 2.5
35 ± 40		JAMES 66	HBC	+	2.1 $\pi^+ p$

$\Gamma(\pi^+\pi^-\gamma)/\Gamma_{total}$ G7/G

VALUE	CL%	DOCUMENT ID	TECN	COMMENT
0.0099 ± 0.0016 OUR FIT				
0.0099 ± 0.0016				
0.0111 ± 0.0014		² VASSERMAN 88	ND	$e^+e^- \rightarrow \pi^+\pi^-\gamma$
<0.005	90	³ VASSERMAN 88	ND	$e^+e^- \rightarrow \pi^+\pi^-\gamma$

¹ Bremsstrahlung from a decay pion and for photon energy above 50 MeV.
² Superseded by DOLINSKY 91.
³ Structure radiation due to quark rearrangement in the decay.

$\Gamma(\pi^0\gamma)/\Gamma_{total}$ G8/G

VALUE (units 10 ⁻⁴)	EVTS	DOCUMENT ID	TECN	COMMENT
4.20 ± 0.52		¹ ACHASOV 16A	SND	0.60–1.38 $e^+e^- \rightarrow \pi^0\gamma$
6.21 +1.28 -1.18 ± 0.39	18k	^{2,3} AKHMETSHIN 05	CMD2	0.60–1.38 $e^+e^- \rightarrow \pi^0\gamma$
5.22 ± 1.17 ± 0.75	36k	^{3,4} ACHASOV 03	SND	0.60–0.97 $e^+e^- \rightarrow \pi^0\gamma$
6.8 ± 1.7		⁵ BENAYOUN 96	RVUE	0.54–1.04 $e^+e^- \rightarrow \pi^0\gamma$
7.9 ± 2.0		³ DOLINSKY 89	ND	$e^+e^- \rightarrow \pi^0\gamma$

¹ Using $B(\rho \rightarrow e^+e^-)$ from PDG 15. Supersedes ACHASOV 03.
² Using $B(\rho \rightarrow e^+e^-) = (4.67 \pm 0.09) \times 10^{-5}$.
³ Not independent of the corresponding $\Gamma(e^+e^-) \times \Gamma(\pi^0\gamma)/\Gamma_{total}^2$.
⁴ Using $B(\rho \rightarrow e^+e^-) = (4.54 \pm 0.10) \times 10^{-5}$.
⁵ Reanalysis of DRUZHININ 84, DOLINSKY 89, and DOLINSKY 91 taking into account a triangle anomaly contribution.

$\Gamma(\eta\gamma)/\Gamma_{total}$ G9/G

VALUE (units 10 ⁻⁴)	EVTS	DOCUMENT ID	TECN	CHG	COMMENT
3.00 ± 0.21 OUR FIT					
2.90 ± 0.32 OUR AVERAGE					
2.79 ± 0.34 ± 0.03	33k	¹ ACHASOV 07B	SND	0.6–1.38 $e^+e^- \rightarrow \eta\gamma$	
3.6 ± 0.9		² ANDREWS 77	CNTR	0 6.7–10 γ Cu	

• • • We do not use the following data for averages, fits, limits, etc. • • •

3.21 ± 1.39 ± 0.20	17.4k	3,4	AKH METSHIN 05	CMD2	0.60-1.38	$e^+e^- \rightarrow \eta\gamma$
3.39 ± 0.42 ± 0.23		2,5,6	AKH METSHIN 01B	CMD2		$e^+e^- \rightarrow \eta\gamma$
1.9 $^{+0.6}_{-0.8}$		7	BENAYOUN	96 RVUE	0.54-1.04	$e^+e^- \rightarrow \eta\gamma$
4.0 ± 1.1		2,4	DOLINSKY	89 ND		$e^+e^- \rightarrow \eta\gamma$

¹ACHASOV 07B reports $[\Gamma(\rho(770) \rightarrow \eta\gamma)/\Gamma_{\text{total}}] \times [B(\rho(770) \rightarrow e^+e^-)] = (1.32 \pm 0.14 \pm 0.08) \times 10^{-8}$ which we divide by our best value $B(\rho(770) \rightarrow e^+e^-) = (4.72 \pm 0.05) \times 10^{-5}$. Our first error is their experiment's error and our second error is the systematic error from using our best value. Supersedes ACHASOV 00D and ACHASOV 06A.

²Solution corresponding to constructive ρ - ω interference.

³Using $B(\rho \rightarrow e^+e^-) = (4.67 \pm 0.09) \times 10^{-5}$ and $B(\eta \rightarrow \gamma\gamma) = 39.43 \pm 0.26\%$.

⁴Not independent of the corresponding $\Gamma(e^+e^-) \times \Gamma(\eta\gamma)/\Gamma_{\text{total}}^2$.

⁵The combined fit from 600 to 1380 MeV taking into account $\rho(770)$, $\omega(782)$, $\phi(1020)$, and $\rho(1450)$ (mass and width fixed at 1450 MeV and 310 MeV respectively).

⁶Using $B(\rho \rightarrow e^+e^-) = (4.75 \pm 0.10) \times 10^{-5}$ from AKHMETSHIN 02 and $B(\eta \rightarrow 3\pi^0) = (32.24 \pm 0.29) \times 10^{-2}$.

⁷Reanalysis of DRUZHININ 84, DOLINSKY 89, and DOLINSKY 91 taking into account a triangle anomaly contribution. Constructive ρ - ω interference solution.

$\Gamma(\pi^0\pi^0\gamma)/\Gamma_{\text{total}}$ Γ_{10}/Γ

VALUE (units 10^{-5})	EVTS	DOCUMENT ID	TECN	COMMENT
4.5 ± 0.8 OUR FIT				
4.5 $^{+0.9}_{-0.8}$ OUR AVERAGE				

5.2 $^{+1.5}_{-1.3} \pm 0.6$	190	¹ AKHMETSHIN 04B	CMD2	0.6-0.97	$e^+e^- \rightarrow \pi^0\pi^0\gamma$
4.1 $^{+1.0}_{-0.9} \pm 0.3$	295	² ACHASOV 02F	SND	0.36-0.97	$e^+e^- \rightarrow \pi^0\pi^0\gamma$

• • • We do not use the following data for averages, fits, limits, etc. • • •

4.8 $^{+3.4}_{-1.8} \pm 0.5$	63	³ ACHASOV 00G	SND		$e^+e^- \rightarrow \pi^0\pi^0\gamma$
------------------------------	----	--------------------------	-----	--	---------------------------------------

¹This branching ratio includes the conventional VMD mechanism $\rho \rightarrow \omega\pi^0$, $\omega \rightarrow \pi^0\gamma$, and the new decay mode $\rho \rightarrow f_0(500)\gamma$, $f_0(500) \rightarrow \pi^0\pi^0$ with a branching ratio $(2.0 \pm 1.1 \pm 0.3) \times 10^{-5}$ differing from zero by 2.0 standard deviations.

²This branching ratio includes the conventional VMD mechanism $\rho \rightarrow \omega\pi^0$, $\omega \rightarrow \pi^0\gamma$ and the new decay mode $\rho \rightarrow f_0(500)\gamma$, $f_0(500) \rightarrow \pi^0\pi^0$ with a branching ratio $(1.9 \pm 0.9 \pm 0.4) \times 10^{-5}$ differing from zero by 2.4 standard deviations. Supersedes ACHASOV 00G.

³Superseded by ACHASOV 02F.

$\Gamma(\mu^+\mu^-)/\Gamma(\pi^+\pi^-)$ Γ_{11}/Γ_6

VALUE (units 10^{-5})	DOCUMENT ID	TECN	COMMENT
4.60 ± 0.28 OUR FIT			
4.6 ± 0.2 ± 0.2	ANTIPOV 89	SIGM	$\pi^- \text{Cu} \rightarrow \mu^+\mu^- \pi^- \text{Cu}$

• • • We do not use the following data for averages, fits, limits, etc. • • •

8.2 $^{+1.6}_{-3.6}$	¹ ROTHWELL 69	CNTR	Photoproduction
5.6 ± 1.5	² WEHMANN 69	OSPK	12 $\pi^- \text{C}$, Fe
9.7 $^{+3.1}_{-3.3}$	3,4 HYAMS 67	OSPK	11 $\pi^- \text{Li}$, H

¹Possibly large ρ - ω interference leads us to increase the minus error.

²Result contains 11 ± 11% correction using SU(3) for central value. The error on the correction takes account of possible ρ - ω interference and the upper limit agrees with the upper limit of $\omega \rightarrow \mu^+\mu^-$ from this experiment.

³But he even enlarges his error to take residual ω contamination into account. Since his value is high, seems the other experiments also can't have too many ω 's. But maybe Hyams has additional μ 's from $\rho \rightarrow \pi\pi$, decaying π 's.

⁴HYAMS 67's mass resolution is 20 MeV. The ω region was excluded.

$\Gamma(e^+e^-)/\Gamma(\pi\pi)$ Γ_{12}/Γ_1

VALUE (units 10^{-4})	DOCUMENT ID	TECN	COMMENT
0.40 ± 0.05	^{1,2} BENAKSAS 72	OSPK	$e^+e^- \rightarrow \pi^+\pi^-$

• • • We do not use the following data for averages, fits, limits, etc. • • •

¹The ρ' contribution is not taken into account.

²Barkov excludes Auslender and Benaksas for large statistical and systematic errors.

$\Gamma(\pi^+\pi^-\pi^0)/\Gamma_{\text{total}}$ Γ_{13}/Γ

VALUE (units 10^{-4})	CL%	EVTS	DOCUMENT ID	TECN	COMMENT
1.01 $^{+0.54}_{-0.36} \pm 0.34$	1.2M	¹ ACHASOV 03D	RVUE	0.44-2.00	$e^+e^- \rightarrow \pi^+\pi^-\pi^0$
<1.2	90	VASSERMAN 88B	ND		$e^+e^- \rightarrow \pi^+\pi^-\pi^0$

• • • We do not use the following data for averages, fits, limits, etc. • • •

¹Statistical significance is less than 3 σ .

$\Gamma(\pi^+\pi^-\pi^0)/\Gamma(\pi\pi)$ Γ_{13}/Γ_1

VALUE	CL%	DOCUMENT ID	TECN	CHG	COMMENT
~0.01		BRAMON 86	RVUE	0	$J/\psi \rightarrow \omega\pi^0$
<0.01	84	¹ ABRAMS 71	HBC	0	3.7 $\pi^+\pi^-$

• • • We do not use the following data for averages, fits, limits, etc. • • •

¹Model dependent, assumes $l = 1, 2, \text{ or } 3$ for the 3π system.

$\Gamma(\pi^+\pi^-\pi^+\pi^-)/\Gamma_{\text{total}}$ Γ_{14}/Γ

VALUE (units 10^{-5})	CL%	EVTS	DOCUMENT ID	TECN	COMMENT
1.8 ± 0.9 OUR FIT					
1.8 ± 0.9 ± 0.3	153	AKHMETSHIN 00	CMD2	0.6-0.97	$e^+e^- \rightarrow \pi^+\pi^-\pi^+\pi^-$
<20	90	KURDADZE 88	OLYA		$e^+e^- \rightarrow \pi^+\pi^-\pi^+\pi^-$

• • • We do not use the following data for averages, fits, limits, etc. • • •

$\Gamma(\pi^+\pi^-\pi^+\pi^-)/\Gamma(\pi\pi)$ Γ_{14}/Γ_1

VALUE (units 10^{-4})	CL%	DOCUMENT ID	TECN	CHG	COMMENT
<15	90	ERBE 69	HBC	0	2.5-5.8 $\gamma\rho$
<20		CHUNG 68	HBC	0	3.2,4.2 $\pi^- \rho$
<20	90	HUSON 68	HLBC	0	16.0 $\pi^- \rho$
<80		JAMES 66	HBC	0	2.1 $\pi^+ \rho$

• • • We do not use the following data for averages, fits, limits, etc. • • •

$\Gamma(\pi^+\pi^-\pi^0\pi^0)/\Gamma_{\text{total}}$ Γ_{15}/Γ

VALUE (units 10^{-5})	CL%	DOCUMENT ID	TECN	COMMENT
1.60 ± 0.74 ± 0.18		¹ ACHASOV 09A	SND	$e^+e^- \rightarrow \pi^+\pi^-\pi^0\pi^0$
<4	90	AULCHENKO 87C	ND	$e^+e^- \rightarrow \pi^+\pi^-\pi^0\pi^0$
<20	90	KURDADZE 86	OLYA	$e^+e^- \rightarrow \pi^+\pi^-\pi^0\pi^0$

• • • We do not use the following data for averages, fits, limits, etc. • • •

¹Assuming no interference between the ρ and ω contributions.

$\Gamma(\pi^0e^+e^-)/\Gamma_{\text{total}}$ Γ_{16}/Γ

VALUE (units 10^{-5})	CL%	DOCUMENT ID	TECN	COMMENT
<1.2	90	ACHASOV 08	SND	0.36-0.97 $e^+e^- \rightarrow \pi^0e^+e^-$
<1.6		AKHMETSHIN 05A	CMD2	0.72-0.84 e^+e^-

• • • We do not use the following data for averages, fits, limits, etc. • • •

$\Gamma(\eta e^+e^-)/\Gamma_{\text{total}}$ Γ_{17}/Γ

VALUE (units 10^{-5})	DOCUMENT ID	TECN	COMMENT
<0.7	AKHMETSHIN 05A	CMD2	0.72-0.84 e^+e^-

• • • We do not use the following data for averages, fits, limits, etc. • • •

$\rho(770)$ REFERENCES

ABLIKIM 18C	PRL 120 242003	M. Ablikim et al.	(BESIII Collab.)
ABLIKIM 17	PRL 118 012001	M. Ablikim et al.	(BESIII Collab.)
BARTOS 17	PR D96 113004	E. Bartos et al.	
BARTOS 17A	IJMP A32 1750154	E. Bartos et al.	
ABLIKIM 16C	PL B753 629	M. Ablikim et al.	(BESIII Collab.)
ACHASOV 16A	PR D93 092001	M.N. Achasov et al.	(SND Collab.)
PDG 15	RPP 2015 at pdg.lbl.gov		(PDG Collab.)
ABRAMOWICZ 12	EPJ C72 1869	H. Abramowicz et al.	(ZEUS Collab.)
LEES 12G	PR D86 032013	J.P. Lees et al.	(BABAR Collab.)
AMBROSINO 11A	PL B700 102	F. Ambrosino et al.	(KLOE Collab.)
BENAYOUN 10	EPJ C65 211	M. Benayoun et al.	
DUBNICKA 10	APS 60 1	S. Dubnicka, A.Z. Dubnickova	
ACHASOV 09A	JETP 109 379	M.N. Achasov et al.	(SND Collab.)
	Translated from ZETF 136 442.		
AUBERT 09AS	PRL 103 231801	B. Aubert et al.	(BABAR Collab.)
ACHASOV 08	JETP 107 61	M.N. Achasov et al.	(SND Collab.)
	Translated from ZETF 134 80.		
FUJIKAWA 08	PR D78 072006	M. Fujikawa et al.	(BELLE Collab.)
ACHASOV 07B	PR D76 077101	M.N. Achasov et al.	(SND Collab.)
AKHMETSHIN 07	PL B648 28	R.R. Akhmetshin et al.	(Novosibirsk CMD-2 Collab.)
ACHASOV 06	JETP 103 380	M.N. Achasov et al.	(Novosibirsk SND Collab.)
	Translated from ZETF 130 437.		
ACHASOV 06A	PR D74 014016	M.N. Achasov et al.	(SND Collab.)
AULCHENKO 06	JETPL 84 413	V.M. Aulchenko et al.	(Novosibirsk CMD-2 Collab.)
	Translated from ZETFP 84 491.		
ACHASOV 05A	JETP 101 1053	M.N. Achasov et al.	(Novosibirsk SND Collab.)
	Translated from ZETF 128 1201.		
AKHMETSHIN 05	PL B605 26	R.R. Akhmetshin et al.	(Novosibirsk CMD-2 Collab.)
AKHMETSHIN 05A	PL B613 29	R.R. Akhmetshin et al.	(Novosibirsk CMD-2 Collab.)
ALOISIO 05	PL B606 12	A. Aloisio et al.	(KLOE Collab.)
AULCHENKO 05	JETPL 82 743	V.M. Aulchenko et al.	(Novosibirsk CMD-2 Collab.)
	Translated from ZETFP 82 841.		
SCHAEF 05C	PRPL 421 131	S. Schaefer et al.	(ALEPH Collab.)
AKHMETSHIN 04	PL B578 285	R.R. Akhmetshin et al.	(Novosibirsk CMD-2 Collab.)
AKHMETSHIN 04B	PL B580 119	R.R. Akhmetshin et al.	(Novosibirsk CMD-2 Collab.)
ACHASOV 03	PL B559 171	M.N. Achasov et al.	(Novosibirsk SND Collab.)
ACHASOV 03D	PR D68 052006	M.N. Achasov et al.	(Novosibirsk SND Collab.)
ALOISIO 03	PL B561 55	A. Aloisio et al.	(KLOE Collab.)
SANZ-CILLERO 03	EPJ C27 587	J.J. Sanz-Cillero, A. Pich	
ACHASOV 02	PR D65 032002	M.N. Achasov et al.	(Novosibirsk SND Collab.)
ACHASOV 02F	PL B537 201	M.N. Achasov et al.	(Novosibirsk SND Collab.)
AKHMETSHIN 02	PL B527 161	R.R. Akhmetshin et al.	(Novosibirsk CMD-2 Collab.)
AKHMETSHIN 01B	PL B509 217	R.R. Akhmetshin et al.	(Novosibirsk CMD-2 Collab.)
COLANGELLO 01	NP B603 125	G. Colangelo, J. Gasser, H. Leytwyler	
PICH 01	PR D63 093005	A. Pich, J. Portoles	
ACHASOV 00D	EPJ C12 25	M.N. Achasov et al.	(Novosibirsk SND Collab.)
ACHASOV 00D	JETPL 72 282	M.N. Achasov et al.	(Novosibirsk SND Collab.)
	Translated from ZETFP 72 411.		
ACHASOV 00G	JETPL 71 355	M.N. Achasov et al.	(Novosibirsk SND Collab.)
	Translated from ZETFP 71 519.		
AKHMETSHIN 00	PL B475 190	R.R. Akhmetshin et al.	(Novosibirsk CMD-2 Collab.)
ANDERSON 00A	PR D61 112002	S. Anderson et al.	(CLEO Collab.)
ABELE 99E	PL B469 270	A. Abele et al.	(Crystal Barrel Collab.)
BENAYOUN 98	EPJ C2 269	M. Benayoun et al.	(IPNP, NOVO, ADL+)
BREITWEG 98B	EPJ C2 247	J. Breitweg et al.	(ZEUS Collab.)
GARDNER 98	PR D57 2716	S. Gardner, H.B. O'Connell	
	Also PR D62 019903 (err.)	S. Gardner, H.B. O'Connell	
ABELE 97	PL B391 191	A. Abele et al.	(Crystal Barrel Collab.)
ADAMS 97	ZPHY C74 237	M.R. Adams et al.	(E665 Collab.)
BARATE 97M	ZPHY C76 15	R. Barate et al.	(ALEPH Collab.)
BERTIN 97C	PL B408 476	A. Bertin et al.	(OBELIX Collab.)
BOGOLYUB... 97	PAN 60 46	M.Y. Bogolyubsky et al.	(MOSU, SERP)
	Translated from YAF 60 53.		

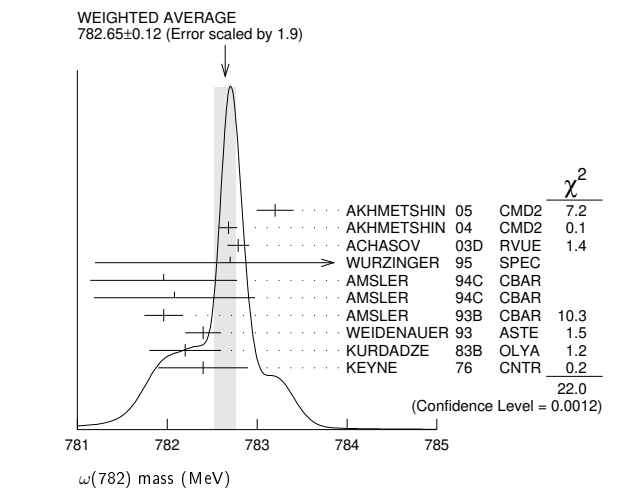
Meson Particle Listings

$\rho(770), \omega(782)$

O'CONNELL	97	NP A623 559	H.B. O'Connell et al.	(ADDL)
BENAYOUN	96	ZPHY C72 221	M. Benayoun et al.	(INPN, NOVO)
BERNICHIA	94	PR D50 445	A. Bernichia, G. Lopez Castro, J. Pesticau	(LOUV+)
WEIDENAUER	93	ZPHY C59 387	P. Weidenauer et al.	(ASTERIX Collab.)
AGUILAR...	91	ZPHY C50 405	M. Aguilar-Benitez et al.	(LEBC-EHS Collab.)
DOLINSKY	91	PRPL 202 99	S.I. Dolinsky et al.	(NOVO)
KUHN	90	ZPHY C48 445	J.H. Kuhn et al.	(MPIM)
ANTIPOV	89	ZPHY C42 185	Y.M. Antipov et al.	(SERP, JINR, BGNA+)
BISELLO	89	PR B220 321	D. Bisello et al.	(DM2 Collab.)
DOLINSKY	89	ZPHY C42 511	S.I. Dolinsky et al.	(NOVO)
DUBNICKA	89	JP G15 1349	S.V. Dubnicka et al.	(JINR, SLOV)
GESHKEN	89	ZPHY C45 351	B.V. Geshkenbein	(ITEP)
KURDADZE	88	JETPL 47 512	L.M. Kurdadze et al.	(NOVO)
VASSERMAN	88	SJNP 47 1035	I.B. Vasserman et al.	(NOVO)
VASSERMAN	88B	SJNP 48 480	I.B. Vasserman et al.	(NOVO)
AULCHENKO	87C	IYF 87-90 Preprint	V.M. Aulchenko et al.	(NOVO)
CAPRARO	87	NP B288 659	L. Capraro et al.	(CLER, FRAS, MILA+)
BRAMON	86	PL B173 97	A. Bramon, J. Casulleras	(BARC)
HUSTON	86	PR D33 3199	J. Huston et al.	(ROCH, FNAL, MINN)
KURDADZE	86	JETPL 43 843	L.M. Kurdadze et al.	(NOVO)
BARKOV	85	NP B256 365	L.M. Barkov et al.	(NOVO)
DRUZHININ	84	PL 144B 136	V.P. Druzhinin et al.	(NOVO)
CHABAUD	83	NP B223 1	V. Chabaud et al.	(CERN, CRAC, MPIM)
JENSEN	83	PR D27 26	T. Jensen et al.	(ROCH, FNAL, MINN)
HEYN	81	ZPHY C7 169	M.F. Heyn, C.B. Lang	(GRAZ)
BOHACIK	80	PR D21 1342	J. Bohacik, H. Kuhnelt	(SLOW, WIEN)
LANG	79	PR D19 956	C.B. Lang, A. Mas-Parreda	(GRAZ)
BARTALUCCI	78	NC 44A 567	S. Bartalucci et al.	(DESY, FRAS)
WICKLUND	78	PR D17 1197	A.B. Wicklund et al.	(ARL)
ANDREWS	77	PRL 38 1197	D.E. Andrews et al.	(ROCH)
DEUTSCH...	76	NP B103 426	M. Deuschmann et al.	(AACH3, BERL, BONN+)
ENGLER	74	PR D10 2070	A. Engler et al.	(CMU, CASE)
ESTABROOKS	74	NP B79 301	P.G. Estabrooks, A.D. Martin	(DURH)
GRAYER	74	NP B75 189	G. Grayer et al.	(CERN, MPIM)
RAT CLIFF	74	Private Comm.		
BYERLY	73	PR D7 637	W.L. Byerly et al.	(MICH)
GLADDING	73	PR D8 3721	G.E. Gladding et al.	(HARV)
HYAMS	73	NP B64 134	B.D. Hyams et al.	(CERN, MPIM)
PROTOPESCU...	73	PR D7 1279	S.D. Protopopescu et al.	(LBL)
BALLAM	72	PR D5 545	J. Ballam et al.	(SLAC, LBL, TUFTS)
BENAKSAS	72	PL 39B 289	J. Benaksas et al.	(ORSAY)
JACOBS	72	PR D6 1291	L.D. Jacobs	(SACL)
RAT CLIFF	72	PL 38B 345	B.N. Ratcliff et al.	(SLAC)
ABRAMS	71	PR D4 653	G.S. Abrams et al.	(LBL)
ALVENSLEB...	70	PRL 24 786	H. Alvensleben et al.	(DESY)
BIGGS	70	PRL 24 1197	P.J. Biggs et al.	(DARE)
ERBE	69	PR 188 2060	R. Erbe et al.	(German Bubble Chamber Collab.)
MALAMUD	69	Argonne Conf. 93	E.I. Malamud, P.E. Schlein	(UCLA)
REYNOLDS	69	PR 184 1424	B.G. Reynolds et al.	(FSU)
ROTHWELL	69	PRL 23 1521	P.L. Rothwell et al.	(NEAS)
WEHMANN	69	PR 178 2095	A.A. Wehmann et al.	(HARV, CASE, SLAC+)
ARMENISE	68	NC 54A 939	N. Armenise et al.	(BARI, BGNA, FIRZ+)
BATON	68	PR 176 1574	J.P. Baton, G. Laurens	(SACL)
CHUNG	68	PR 165 1491	S.U. Chung et al.	(LRL)
FOSTER	68	NP B6 107	M. Foster et al.	(CERN, CDEF)
GOUNARIS	68	PRL 21 244	G.J. Gounaris, J.J. Sakurai	(ORSAY, MILA, UCLA)
HUSON	68	PL 28B 208	R. Huson et al.	(CERN, MPIM)
HYAMS	68	NP B7 1	B.D. Hyams et al.	(CERN, MPIM)
LANZEROTTI	68	PR 166 1365	L.J. Lanzerotti et al.	(HARV)
PISUT	68	NP B6 325	J. Pisut, M. Roos	(CERN)
ASBURY	67B	PRL 19 865	J.G. Asbury et al.	(DESY, COLU)
BACON	67	PR 157 1263	T.C. Bacon et al.	(BNL)
EISNER	67	PR 164 1639	R.L. Eisner et al.	(PURD)
HUWE	67	PL 24B 252	D.O. Huwe et al.	(COLU)
HYAMS	67	PL 24B 634	B.D. Hyams et al.	(CERN, MPIM)
MILLER	67B	PR 153 1423	D.H. Miller et al.	(PURD)
ALFF-...	66	PR 145 1072	C. Alff-Steinberger et al.	(COLU, RUTG)
FERBEL	66	PL 21 111	T. Ferbel	(ROCH)
HAGOPIAN	66	PR 145 1128	V. Hagopian et al.	(PENN, SACL)
HAGOPIAN	66B	PR 152 1183	V. Hagopian, Y.L. Pan	(PENN, LRL)
JACOBS	66B	UCRL 16877	L.D. Jacobs	(LRL)
JAMES	66	PR 142 896	F.E. James, H.L. Kraybill	(YALE, BNL)
ROSS	66	PR 149 1172	M. Ross, L. Stodolsky	
SOEDING	66	PL B19 702	P. Soeding	
WEST	66	PR 149 1089	E. West et al.	(WISC)
BLIEDEN	65	PL 19 444	H.R. Blieden et al.	(CERN MMS Collab.)
CARMONY	64	PRL 12 254	D.D. Carmony et al.	(UCB)
GOLDBERGER	64	PRL 12 336	G. Goldhaber et al.	(LRL, UCB)
ABOLINS	63	PRL 11 381	M.A. Abolins et al.	(UCSD)

782.7 ± 0.9	535	VANAPEL...	78	HBC	7.2 $\bar{p}p \rightarrow \bar{p}p\omega$
783.5 ± 0.8	2100	GESSAROLI	77	HBC	11 $\pi^- p \rightarrow \omega n$
782.5 ± 0.8	418	AGUILAR...	72B	HBC	3.9, 4.6 $K^- p$
783.4 ± 1.0	248	BIZZARRI	71	HBC	0.0 $\rho\bar{p} \rightarrow K^+ K^- \omega$
781.0 ± 0.6	510	BIZZARRI	71	HBC	0.0 $\rho\bar{p} \rightarrow K_1^+ K_1^- \omega$
783.7 ± 1.0	3583	COYNE	71	HBC	3.7 $\pi^+ p \rightarrow \rho\pi^+\pi^+\pi^-\pi^0$
784.1 ± 1.2	750	ABRAMOVI...	70	HBC	3.9 $\pi^- p$
783.2 ± 1.6	9	BIGGS	70B	CNTR	<4.1 $\gamma C \rightarrow \pi^+\pi^- C$
782.4 ± 0.5	2400	BIZZARRI	69	HBC	0.0 $\bar{p}p$

- Update of AKHMETSIN 00c.
- From the combined fit of ANTONELLI 92, ACHASOV 01e, ACHASOV 02e, and ACHASOV 03d data on the $\pi^+\pi^-\pi^0$ and ANTONELLI 92 on the $\omega\pi^+\pi^-$ final states. Supersedes ACHASOV 99e and ACHASOV 02e.
- From the $\eta \rightarrow \gamma\gamma$ decay.
- From the $\eta \rightarrow 3\pi^0$ decay.
- Observed by threshold-crossing technique. Mass resolution = 4.8 MeV FWHM.
- From the $\rho-\omega$ interference in the $\pi^+\pi^-$ mass spectrum using the Breit-Wigner for the ω and leaving its mass and width as free parameters of the fit.
- Systematic uncertainties underestimated.
- From best-resolution sample of COYNE 71.
- From $\omega-\rho$ interference in the $\pi^+\pi^-$ mass spectrum assuming ω width 12.6 MeV.



VALUE (MeV)	EVTS	DOCUMENT ID	TECN	COMMENT
8.49 ± 0.08 OUR AVERAGE				
8.68 ± 0.23 ± 0.10	11200	1 AKHMETSIN 04	CMD2	$e^+e^- \rightarrow \pi^+\pi^-\pi^0$
8.68 ± 0.04 ± 0.15	1.2M	2 ACHASOV 03D	RVUE	0.44-2.00 $e^+e^- \rightarrow \pi^+\pi^-\pi^0$
8.2 ± 0.3	19500	WURZINGER 95	SPEC	1.33 $p d \rightarrow {}^3\text{He}\omega$
8.4 ± 0.1		3 AULCHENKO 87	ND	$e^+e^- \rightarrow \pi^+\pi^-\pi^0$
8.30 ± 0.40		BARKOV 87	CMD	$e^+e^- \rightarrow \pi^+\pi^-\pi^0$
9.8 ± 0.9	1488	KURDADZE 83B	OLYA	$e^+e^- \rightarrow \pi^+\pi^-\pi^0$
9.0 ± 0.8	433	CORDIER 80	DM1	$e^+e^- \rightarrow \pi^+\pi^-\pi^0$
9.1 ± 0.8	451	BENAKSAS 72B	OSP K	$e^+e^- \rightarrow \pi^+\pi^-\pi^0$
8.13 ± 0.45		4 LEES 12G	BABR	$e^+e^- \rightarrow \pi^+\pi^-\gamma$
12 ± 2	1430	COOPER 78B	HBC	0.7-0.8 $\bar{p}p \rightarrow 5\pi$
9.4 ± 2.5	2100	GESSAROLI 77	HBC	11 $\pi^- p \rightarrow \omega n$
10.22 ± 0.43	20000	5 KEYNE 76	CNTR	$\pi^- p \rightarrow \omega n$
13.3 ± 2	418	AGUILAR...	72B	HBC 3.9, 4.6 $K^- p$
10.5 ± 1.5		BORENSTEIN 72	HBC	2.18 $K^- p$
7.70 ± 0.9 ± 1.15	940	BROWN 72	MMS	2.5 $\pi^- p \rightarrow nMM$
10.3 ± 1.4	510	BIZZARRI 71	HBC	0.0 $\rho\bar{p} \rightarrow K_1^+ K_1^- \omega$
12.8 ± 3.0	248	BIZZARRI 71	HBC	0.0 $\rho\bar{p} \rightarrow K^+ K^- \omega$
9.5 ± 1.0	3583	COYNE 71	HBC	3.7 $\pi^+ p \rightarrow \rho\pi^+\pi^+\pi^-\pi^0$

- • • We do not use the following data for averages, fits, limits, etc. • • •
- 1 Update of AKHMETSIN 00c.
- 2 From the combined fit of ANTONELLI 92, ACHASOV 01e, ACHASOV 02e, and ACHASOV 03d data on the $\pi^+\pi^-\pi^0$ and ANTONELLI 92 on the $\omega\pi^+\pi^-$ final states. Supersedes ACHASOV 99e and ACHASOV 02e.
- 3 Relativistic Breit-Wigner includes radiative corrections.
- 4 From the $\rho-\omega$ interference in the $\pi^+\pi^-$ mass spectrum using the Breit-Wigner for the ω and leaving its mass and width as free parameters of the fit.
- 5 Observed by threshold-crossing technique. Mass resolution = 4.8 MeV FWHM.

$\omega(782)$

$$J^{PC} = 0^{-}(1^{-}-)$$

$\omega(782)$ MASS

VALUE (MeV)	EVTS	DOCUMENT ID	TECN	COMMENT
782.65 ± 0.12 OUR AVERAGE				Error includes scale factor of 1.9. See the ideogram below.
783.20 ± 0.13 ± 0.16	18680	AKHMETSIN 05	CMD2	0.60-1.38 $e^+e^- \rightarrow \pi^0\gamma$
782.68 ± 0.09 ± 0.04	11200	1 AKHMETSIN 04	CMD2	$e^+e^- \rightarrow \pi^+\pi^-\pi^0$
782.79 ± 0.08 ± 0.09	1.2M	2 ACHASOV 03D	RVUE	0.44-2.00 $e^+e^- \rightarrow \pi^+\pi^-\pi^0$
782.7 ± 0.1 ± 1.5	19500	WURZINGER 95	SPEC	1.33 $p d \rightarrow {}^3\text{He}\omega$
781.96 ± 0.17 ± 0.80	11k	3 AMSLER 94C	CBAR	0.0 $\bar{p}p \rightarrow \omega\eta\pi^0$
782.08 ± 0.36 ± 0.82	3463	4 AMSLER 94C	CBAR	0.0 $\bar{p}p \rightarrow \omega\eta\pi^0$
781.96 ± 0.13 ± 0.17	15k	AMSLER 93B	CBAR	0.0 $\bar{p}p \rightarrow \omega\pi^0\pi^0$
782.4 ± 0.2	270k	WEIDENAUER 93	ASTE	$\bar{p}p \rightarrow 2\pi^+2\pi^-\pi^0$
782.2 ± 0.4	1488	KURDADZE 83B	OLYA	$e^+e^- \rightarrow \pi^+\pi^-\pi^0$
782.4 ± 0.5	7000	5 KEYNE 76	CNTR	$\pi^- p \rightarrow \omega n$
• • • We do not use the following data for averages, fits, limits, etc. • • •				
781.91 ± 0.24		6 LEES 12G	BABR	$e^+e^- \rightarrow \pi^+\pi^-\gamma$
781.78 ± 0.10		7 BARKOV 87	CMD	$e^+e^- \rightarrow \pi^+\pi^-\pi^0$
783.3 ± 0.4	433	CORDIER 80	DM1	$e^+e^- \rightarrow \pi^+\pi^-\pi^0$
782.5 ± 0.8	33260	ROOS 80	RVUE	0.0-3.6 $\bar{p}p$
782.6 ± 0.8	3000	BENKHERI 79	OMEG	9-12 $\pi^\pm p$
781.8 ± 0.6	1430	COOPER 78B	HBC	0.7-0.8 $\bar{p}p \rightarrow 5\pi$

$\omega(782)$ DECAY MODES

Mode	Fraction (Γ_i/Γ)	Scale factor/ Confidence level
$\Gamma_1 \pi^+ \pi^- \pi^0$	(89.3 ± 0.6) %	
$\Gamma_2 \pi^0 \gamma$	(8.40 ± 0.22) %	S=1.8
$\Gamma_3 \pi^+ \pi^-$	(1.53 ± 0.06) %	
Γ_4 neutrals (excluding $\pi^0 \gamma$)	(7 ⁺⁷ / ₋₄) × 10 ⁻³	S=1.1
$\Gamma_5 \eta \gamma$	(4.5 ± 0.4) × 10 ⁻⁴	S=1.1
$\Gamma_6 \pi^0 e^+ e^-$	(7.7 ± 0.6) × 10 ⁻⁴	
$\Gamma_7 \pi^0 \mu^+ \mu^-$	(1.34 ± 0.18) × 10 ⁻⁴	S=1.5
$\Gamma_8 \eta e^+ e^-$		
$\Gamma_9 e^+ e^-$	(7.36 ± 0.15) × 10 ⁻⁵	S=1.5
$\Gamma_{10} \pi^+ \pi^- \pi^0 \pi^0$	< 2 × 10 ⁻⁴	CL=90%
$\Gamma_{11} \pi^+ \pi^- \gamma$	< 3.6 × 10 ⁻³	CL=95%
$\Gamma_{12} \pi^+ \pi^- \pi^+ \pi^-$	< 1 × 10 ⁻³	CL=90%
$\Gamma_{13} \pi^0 \pi^0 \gamma$	(6.7 ± 1.1) × 10 ⁻⁵	
$\Gamma_{14} \eta \pi^0 \gamma$	< 3.3 × 10 ⁻⁵	CL=90%
$\Gamma_{15} \mu^+ \mu^-$	(7.4 ± 1.8) × 10 ⁻⁵	
$\Gamma_{16} 3\gamma$	< 1.9 × 10 ⁻⁴	CL=95%

Charge conjugation (C) violating modes

$\Gamma_{17} \eta \pi^0$	C	< 2.2 × 10 ⁻⁴	CL=90%
$\Gamma_{18} 2\pi^0$	C	< 2.2 × 10 ⁻⁴	CL=90%
$\Gamma_{19} 3\pi^0$	C	< 2.3 × 10 ⁻⁴	CL=90%
Γ_{20} invisible		< 7 × 10 ⁻⁵	CL=90%

CONSTRAINED FIT INFORMATION

An overall fit to 15 branching ratios uses 55 measurements and one constraint to determine 10 parameters. The overall fit has a $\chi^2 = 57.0$ for 46 degrees of freedom.

The following off-diagonal array elements are the correlation coefficients $\langle \delta x_i \delta x_j \rangle / (\delta x_i \delta x_j)$, in percent, from the fit to the branching fractions, $x_i \equiv \Gamma_i/\Gamma_{total}$. The fit constrains the x_i whose labels appear in this array to sum to one.

x_2	28								
x_3	-9	-3							
x_4	-95	-55	0						
x_5	7	15	-1	-12					
x_6	-1	0	0	0	0				
x_7	0	0	0	0	0	0			
x_9	-35	-70	3	52	-22	0	0		
x_{13}	1	3	0	-2	0	0	0	-2	
x_{15}	0	0	0	0	0	0	0	0	0
	x_1	x_2	x_3	x_4	x_5	x_6	x_7	x_9	x_{13}

$\omega(782)$ PARTIAL WIDTHS

$\Gamma(\pi^0 \gamma)$	VALUE (keV)	EVTS	DOCUMENT ID	TECN	COMMENT
	880 ± 5.0	7815	¹ ACHASOV	13	SND 1.05-2.00 $e^+ e^- \rightarrow \pi^0 \pi^0 \gamma$
	788 ± 12 ± 27	36500	² ACHASOV	03	SND 0.60-0.97 $e^+ e^- \rightarrow \pi^0 \gamma$
	764 ± 5.1	10625	DOLINSKY	89	ND $e^+ e^- \rightarrow \pi^0 \gamma$

¹ Systematic uncertainty not estimated.
² Using $\Gamma_\omega = 8.44 \pm 0.09$ MeV and $B(\omega \rightarrow \pi^0 \gamma)$ from ACHASOV 03.

$\Gamma(\eta \gamma)$	VALUE (keV)	DOCUMENT ID	TECN	COMMENT
	6.1 ± 2.5	¹ DOLINSKY	89	ND $e^+ e^- \rightarrow \eta \gamma$

¹ Using $\Gamma_\omega = 8.4 \pm 0.1$ MeV and $B(\omega \rightarrow \eta \gamma)$ from DOLINSKY 89.

$\Gamma(e^+ e^-)$	VALUE (keV)	EVTS	DOCUMENT ID	TECN	COMMENT
0.60 ± 0.02 OUR EVALUATION					
	0.591 ± 0.015	11200	^{1,2} AKHMETSHIN	04	CMD2 $e^+ e^- \rightarrow \pi^+ \pi^- \pi^0$
	0.653 ± 0.003 ± 0.021	1.2M	³ ACHASOV	03D	RVUE 0.44-2.00 $e^+ e^- \rightarrow \pi^+ \pi^- \pi^0 \gamma$
	0.600 ± 0.031	10625	DOLINSKY	89	ND $e^+ e^- \rightarrow \pi^0 \gamma$

¹ Using $B(\omega \rightarrow \pi^+ \pi^- \pi^0) = 0.891 \pm 0.007$ and $\Gamma_{total} = 8.44 \pm 0.09$ MeV.
² Update of AKHMETSHIN 00c.
³ Using ACHASOV 03, ACHASOV 03D and $B(\omega \rightarrow \pi^+ \pi^-) = (1.70 \pm 0.28)\%$.

$\omega(782) \Gamma(e^+ e^-) \Gamma(i)/\Gamma^2(\text{total})$

$\Gamma(e^+ e^-)/\Gamma_{total} \times \Gamma(\pi^+ \pi^- \pi^0)/\Gamma_{total}$	VALUE (units 10 ⁻⁵)	EVTS	DOCUMENT ID	TECN	COMMENT
6.56 ± 0.12 OUR FIT					Error includes scale factor of 1.6.
6.38 ± 0.10 OUR AVERAGE					Error includes scale factor of 1.1.
	6.24 ± 0.11 ± 0.08	11.2k	¹ AKHMETSHIN	04	CMD2 $e^+ e^- \rightarrow \pi^+ \pi^- \pi^0$
	6.70 ± 0.06 ± 0.27		AUBERT,B	04N	BABR 10.6 $e^+ e^- \rightarrow \pi^+ \pi^- \pi^0 \gamma$
	6.74 ± 0.04 ± 0.24	1.2M	^{2,3} ACHASOV	03D	RVUE 0.44-2.00 $e^+ e^- \rightarrow \pi^+ \pi^- \pi^0 \gamma$
	6.37 ± 0.35		² DOLINSKY	89	ND $e^+ e^- \rightarrow \pi^+ \pi^- \pi^0$
	6.45 ± 0.24		² BARKOV	87	CMD $e^+ e^- \rightarrow \pi^+ \pi^- \pi^0$
	5.79 ± 0.42	1488	² KURDADZE	83B	OLYA $e^+ e^- \rightarrow \pi^+ \pi^- \pi^0$
	5.89 ± 0.54	433	² CORDIER	80	DM1 $e^+ e^- \rightarrow \pi^+ \pi^- \pi^0$
	7.54 ± 0.84	451	² BENAKSAS	72B	OSPK $e^+ e^- \rightarrow \pi^+ \pi^- \pi^0$
	6.20 ± 0.13		⁴ BENAYOUN	10	RVUE 0.4-1.05 $e^+ e^-$

$\Gamma(e^+ e^-)/\Gamma_{total} \times \Gamma(\pi^0 \gamma)/\Gamma_{total}$	VALUE (units 10 ⁻⁶)	EVTS	DOCUMENT ID	TECN	COMMENT
6.18 ± 0.11 OUR FIT					Error includes scale factor of 1.6.
6.37 ± 0.09 OUR AVERAGE					
	6.336 ± 0.056 ± 0.089		¹ ACHASOV	16A	SND 0.60-1.38 $e^+ e^- \rightarrow \pi^0 \gamma$
	6.47 ± 0.14 ± 0.39	18k	AKHMETSHIN	05	CMD2 0.60-1.38 $e^+ e^- \rightarrow \pi^0 \gamma$
	6.50 ± 0.11 ± 0.20	36k	² ACHASOV	03	SND 0.60-0.97 $e^+ e^- \rightarrow \pi^0 \gamma$
	6.34 ± 0.21 ± 0.21	10k	³ DOLINSKY	89	ND $e^+ e^- \rightarrow \pi^0 \gamma$
	6.80 ± 0.13		⁴ BENAYOUN	10	RVUE 0.4-1.05 $e^+ e^-$

¹ From the VMD model with the interfering $\rho(770)$, $\omega(782)$, $\phi(1020)$, and an additional resonance describing the total contribution of the $\rho(1450)$ and $\omega(1420)$ states. Supersedes ACHASOV 03.
² Using $\sigma_{\phi \rightarrow \pi^0 \gamma}$ from ACHASOV 00 and $m_\omega = 782.57$ MeV in the model with the energy-independent phase of ρ - ω interference equal to $(-10.2 \pm 7.0)^\circ$.
³ Recalculated by us from the cross section in the peak.
⁴ A simultaneous fit of $e^+ e^- \rightarrow \pi^+ \pi^-, \pi^+ \pi^- \pi^0, \pi^0 \gamma, \eta \gamma$ data.

$\Gamma(e^+ e^-)/\Gamma_{total} \times \Gamma(\pi^+ \pi^-)/\Gamma_{total}$	VALUE (units 10 ⁻⁶)	EVTS	DOCUMENT ID	TECN	COMMENT
1.225 ± 0.058 ± 0.041		800k	¹ ACHASOV	06	SND $e^+ e^- \rightarrow \pi^+ \pi^-$
	1.166 ± 0.036		² BENAYOUN	13	RVUE 0.4-1.05 $e^+ e^-$
	1.05 ± 0.08		³ DAVIER	13	RVUE $e^+ e^- \rightarrow \pi^+ \pi^- (\gamma)$

¹ Supersedes ACHASOV 05A.
² A simultaneous fit to $e^+ e^- \rightarrow \pi^+ \pi^-, \pi^+ \pi^- \pi^0, \pi^0 \gamma, \eta \gamma, K\bar{K}$, and $\tau^- \rightarrow \pi^- \pi^0 \nu_\tau$ data. Supersedes BENAYOUN 10.
³ From $e^+ e^- \rightarrow \pi^+ \pi^- (\gamma)$ data of LEES 12G.

$\Gamma(e^+ e^-)/\Gamma_{total} \times \Gamma(\eta \gamma)/\Gamma_{total}$	VALUE (units 10 ⁻⁸)	EVTS	DOCUMENT ID	TECN	COMMENT
3.32 ± 0.28 OUR FIT					Error includes scale factor of 1.1.
3.18 ± 0.28 OUR AVERAGE					
	3.10 ± 0.31 ± 0.11	33k	¹ ACHASOV	07B	SND 0.6-1.38 $e^+ e^- \rightarrow \eta \gamma$
	3.17 ± 1.85 ± 0.21	17.4k	² AKHMETSHIN	05	CMD2 0.60-1.38 $e^+ e^- \rightarrow \eta \gamma$
	3.41 ± 0.52 ± 0.21	23k	^{3,4} AKHMETSHIN	01B	CMD2 $e^+ e^- \rightarrow \eta \gamma$
	4.50 ± 0.10		⁵ BENAYOUN	10	RVUE 0.4-1.05 $e^+ e^-$

¹ From a combined fit of $\sigma(e^+ e^- \rightarrow \eta \gamma)$ with $\eta \rightarrow 3\pi^0$ and $\eta \rightarrow \pi^+ \pi^- \pi^0$, and fixing $B(\eta \rightarrow 3\pi^0) / B(\eta \rightarrow \pi^+ \pi^- \pi^0) = 1.44 \pm 0.04$. Recalculated by us from the cross section at the peak. Supersedes ACHASOV 00D and ACHASOV 06A.
² From the $\eta \rightarrow 2\gamma$ decay and using $B(\eta \rightarrow \gamma \gamma) = 39.43 \pm 0.26\%$.
³ From the $\eta \rightarrow 3\pi^0$ decay and using $B(\eta \rightarrow 3\pi^0) = (32.24 \pm 0.29) \times 10^{-2}$.
⁴ The combined fit from 600 to 1380 MeV taking into account $\rho(770)$, $\omega(782)$, $\phi(1020)$, and $\rho(1450)$ (mass and width fixed at 1450 MeV and 310 MeV respectively).
⁵ A simultaneous fit of $e^+ e^- \rightarrow \pi^+ \pi^-, \pi^+ \pi^- \pi^0, \pi^0 \gamma, \eta \gamma$ data.

$\Gamma(e^+ e^-)/\Gamma_{total} \times \Gamma(\mu^+ \mu^-)/\Gamma_{total}$	VALUE (units 10 ⁻³)	EVTS	DOCUMENT ID	TECN	COMMENT
4.3 ± 1.8 ± 2.2		4.5M	¹ ANASTASI	17	KLOE $e^+ e^- \rightarrow \mu^+ \mu^- \gamma$

¹ From a fit of the real part of the vacuum polarization by a sum of the leptonic and hadronic contributions, where the hadronic contribution is parametrized as a sum of Breit-Wigner resonances $\omega(782)$, $\phi(1020)$ and using a GOUNARIS 68 parametrization for the $\rho(770)$, and a non-resonant term.

Meson Particle Listings

$\omega(782)$

$\omega(782)$ BRANCHING RATIOS

$\Gamma(\pi^+\pi^-\pi^0)/\Gamma_{total}$ Γ_1/Γ
 NIECKNIG 12 describes final-state interactions between the three pions in a dispersive framework using data on the $\pi\pi$ P-wave scattering phase shift.

VALUE	EVTS	DOCUMENT ID	TECN	COMMENT
0.9024 ± 0.0019		1 AMBROSINO 08G	KLOE	1.0-1.03 $e^+e^- \rightarrow \pi^+\pi^-\pi^0, 2\pi^0\gamma$
0.8965 ± 0.0016 ± 0.0048	1.2M	2,3 ACHASOV 03D	RVUE	0.44-2.00 $e^+e^- \rightarrow \pi^+\pi^-\pi^0, 2\pi^0\gamma$
0.880 ± 0.020 ± 0.032	11200	3,4 AKHMETSHIN 00C	CMD2	$e^+e^- \rightarrow \pi^+\pi^-\pi^0$
0.8942 ± 0.0062		3 DOLINSKY 89	ND	$e^+e^- \rightarrow \pi^+\pi^-\pi^0$

1 Not independent of $\Gamma(\pi^0\gamma)/\Gamma(\pi^+\pi^-\pi^0)$ from AMBROSINO 08G.
 2 Using ACHASOV 03, ACHASOV 03D and $B(\omega \rightarrow \pi^+\pi^-) = (1.70 \pm 0.28)\%$.
 3 Not independent of the corresponding $\Gamma(e^+e^-) \times \Gamma(\pi^+\pi^-\pi^0)/\Gamma_{total}^2$.
 4 Using $\Gamma(e^+e^-) = 0.60 \pm 0.02$ keV.

$\Gamma(\pi^0\gamma)/\Gamma_{total}$ Γ_2/Γ
 VALUE (units 10^{-2}) EVTS DOCUMENT ID TECN COMMENT

VALUE (units 10^{-2})	EVTS	DOCUMENT ID	TECN	COMMENT
8.88 ± 0.18		1 ACHASOV 16A	SND	0.60-1.38 $e^+e^- \rightarrow \pi^0\gamma$
8.09 ± 0.14		2 AMBROSINO 08G	KLOE	$e^+e^- \rightarrow \pi^+\pi^-\pi^0, 2\pi^0\gamma$
9.06 ± 0.20 ± 0.57	18k	3,4 AKHMETSHIN 05	CMD2	0.60-1.38 $e^+e^- \rightarrow \pi^0\gamma$
9.34 ± 0.15 ± 0.31	36k	4 ACHASOV 03	SND	0.60-0.97 $e^+e^- \rightarrow \pi^0\gamma$
8.65 ± 0.16 ± 0.42	1.2M	5,6 ACHASOV 03D	RVUE	0.44-2.00 $e^+e^- \rightarrow \pi^+\pi^-\pi^0, 2\pi^0\gamma$
8.39 ± 0.24	9k	7 BENAYOUN 96	RVUE	$e^+e^- \rightarrow \pi^0\gamma$
8.88 ± 0.62	10k	4 DOLINSKY 89	ND	$e^+e^- \rightarrow \pi^0\gamma$

1 Using $B(\omega \rightarrow e^+e^-)$ from PDG 15. Supersedes ACHASOV 03.
 2 Not independent of $\Gamma(\pi^0\gamma)/\Gamma(\pi^+\pi^-\pi^0)$ from AMBROSINO 08G.
 3 Using $B(\omega \rightarrow e^+e^-) = (7.14 \pm 0.13) \times 10^{-5}$.
 4 Not independent of the corresponding $\Gamma(e^+e^-) \times \Gamma(\pi^0\gamma)/\Gamma_{total}^2$.
 5 Using ACHASOV 03, ACHASOV 03D and $B(\omega \rightarrow \pi^+\pi^-) = (1.70 \pm 0.28)\%$.
 6 Not independent of the corresponding $\Gamma(e^+e^-) \times \Gamma(\pi^+\pi^-\pi^0)/\Gamma_{total}^2$.
 7 Reanalysis of DRUZHININ 84, DOLINSKY 89, DOLINSKY 91 taking into account the triangle anomaly contributions.

$\Gamma(\pi^0\gamma)/\Gamma(\pi^+\pi^-\pi^0)$ Γ_2/Γ_1
 VALUE (units 10^{-2}) DOCUMENT ID TECN COMMENT

VALUE (units 10^{-2})	DOCUMENT ID	TECN	COMMENT
9.41 ± 0.23 OUR FIT	Error includes scale factor of 2.0.		
9.05 ± 0.27 OUR AVERAGE	Error includes scale factor of 1.8.		
8.97 ± 0.16	AMBROSINO 08G	KLOE	$e^+e^- \rightarrow \pi^+\pi^-\pi^0, 2\pi^0\gamma$
9.94 ± 0.36 ± 0.38	1 AULCHENKO 00A	SND	$e^+e^- \rightarrow \pi^+\pi^-\pi^0, 2\pi^0\gamma$
8.4 ± 1.3	KEYNE 76	CNTR	$\pi^-p \rightarrow \omega n$
10.9 ± 2.5	BENAKSAS 72C	OSPK	$e^+e^- \rightarrow \pi^0\gamma$
8.1 ± 2.0	BALDIN 71	HLBC	2.9 π^+p
13 ± 4	JACQUET 69B	HLBC	2.05 $\pi^+p \rightarrow \pi^+p\omega$

• • • We do not use the following data for averages, fits, limits, etc. • • •
 9.7 ± 0.2 ± 0.5 2,3 ACHASOV 03D RVUE 0.44-2.00 $e^+e^- \rightarrow \pi^+\pi^-\pi^0$
 9.9 ± 0.7 2 DOLINSKY 89 ND $e^+e^- \rightarrow \pi^0\gamma$

1 From $\sigma_0^{\omega\pi^0} \rightarrow \pi^0\pi^0\gamma(m_\phi)/\omega\pi^0 \rightarrow \pi^+\pi^-\pi^0(m_\phi)$ with a phase-space correction factor of 1/1.023.
 2 Not independent of the corresponding $\Gamma(e^+e^-) \times \Gamma(\pi^0\gamma)/\Gamma_{total}^2$.
 3 Using ACHASOV 03. Based on 1.2M events.

$\Gamma(\pi^+\pi^-)/\Gamma_{total}$ Γ_3/Γ
 See also $\Gamma(\pi^+\pi^-)/\Gamma(\pi^+\pi^-\pi^0)$.
 VALUE (units 10^{-2}) EVTS DOCUMENT ID TECN COMMENT

VALUE (units 10^{-2})	EVTS	DOCUMENT ID	TECN	COMMENT
1.53 ± 0.06 OUR FIT				
1.51 ± 0.07 OUR AVERAGE	Error includes scale factor of 1.1.			
1.52 ± 0.08		1 HANHART 18	RVUE	$e^+e^- \rightarrow \pi^+\pi^-$
1.46 ± 0.12 ± 0.02	900k	2 AKHMETSHIN 07		$e^+e^- \rightarrow \pi^+\pi^-$
1.30 ± 0.24 ± 0.05	11.2k	3 AKHMETSHIN 04	CMD2	$e^+e^- \rightarrow \pi^+\pi^-$
2.38 ± 1.77 ± 0.90 ± 0.18	5.4k	4 ACHASOV 02E	SND	1.1-1.38 $e^+e^- \rightarrow \pi^+\pi^-$
2.3 ± 0.5		BARKOV 85	OLYA	$e^+e^- \rightarrow \pi^+\pi^-$
1.6 +0.9 -0.7		QUENZER 78	DM1	$e^+e^- \rightarrow \pi^+\pi^-$
3.6 ± 1.9		BENAKSAS 72	OSPK	$e^+e^- \rightarrow \pi^+\pi^-$

• • • We do not use the following data for averages, fits, limits, etc. • • •
 1.29 ± 0.22 ± 0.03 970k 5,6 ABLIKIM 18C BES3 $\eta'(958) \rightarrow \gamma\pi^+\pi^-$
 1.28 ± 0.22 ± 0.03 970k 7,8 ABLIKIM 18C BES3 $\eta'(958) \rightarrow \gamma\pi^+\pi^-$
 1.75 ± 0.11 4.5M 9 ACHASOV 05A SND $e^+e^- \rightarrow \pi^+\pi^-$
 2.01 ± 0.29 10 BENAYOUN 03 RVUE $e^+e^- \rightarrow \pi^+\pi^-$
 1.9 ± 0.3 11 GARDNER 99 RVUE $e^+e^- \rightarrow \pi^+\pi^-$
 2.3 ± 0.4 12 BENAYOUN 98 RVUE $e^+e^- \rightarrow \pi^+\pi^-, \mu^+\mu^-$
 1.0 ± 0.11 13 WICKLUND 78 ASPK 3,4,6 $\pi^\pm N$
 1.22 ± 0.30 ALVENSLEB... 71C CNTR Photoproduction
 1.3 +1.2 -0.9 MOFFEIT 71 HBC 2.8,4,7 γp
 0.80 ± 0.28 -0.20 14 BIGGS 70B CNTR 4.2 $\gamma C \rightarrow \pi^+\pi^- C$

1 Dispersive analysis. Value extracted from average of data from AUBERT 09As, AKHMETSHIN 07, ACHASOV 06, AMBROSINO 11A, BABUSCI 13D, ABLIKIM 16b normalised by PDG evaluation for $\Gamma(\omega \rightarrow e^+e^-)$.

2 A combined fit of AKHMETSHIN 07, AULCHENKO 06, and AULCHENKO 05.
 3 Update of AKHMETSHIN 02.
 4 From the $m_{\pi^+\pi^-}$ spectrum taking into account the interference of the $\rho\pi$ and $\omega\pi$ amplitudes.
 5 From a fit to $\pi^+\pi^-$ mass using $\rho(770)$ (parametrized with the Gounaris-Sakurai approach), $\omega(782)$, and box anomaly components.
 6 ABLIKIM 18c reports $[\Gamma(\omega(782) \rightarrow \pi^+\pi^-)/\Gamma_{total}] \times [B(\eta'(958) \rightarrow \omega\gamma)] = (3.25 \pm 0.21 \pm 0.52) \times 10^{-4}$ which we divide by our best value $B(\eta'(958) \rightarrow \omega\gamma) = (2.52 \pm 0.07) \times 10^{-2}$. Our first error is their experiment's error and our second error is the systematic error from using our best value.
 7 From a fit to $\pi^+\pi^-$ mass using $\rho(770)$ (parametrized with the Gounaris-Sakurai approach), $\omega(782)$, and $\rho(1450)$ components.
 8 ABLIKIM 18c reports $[\Gamma(\omega(782) \rightarrow \pi^+\pi^-)/\Gamma_{total}] \times [B(\eta'(958) \rightarrow \omega\gamma)] = (3.22 \pm 0.21 \pm 0.52) \times 10^{-4}$ which we divide by our best value $B(\eta'(958) \rightarrow \omega\gamma) = (2.52 \pm 0.07) \times 10^{-2}$. Our first error is their experiment's error and our second error is the systematic error from using our best value.
 9 Using $\Gamma(\omega \rightarrow e^+e^-)$ from the 2004 Edition of this Review (PDG 04).
 10 Using the data of AKHMETSHIN 02 in the hidden local symmetry model.
 11 Using the data of BARKOV 85.
 12 Using the data of BARKOV 85 in the hidden local symmetry model.
 13 From a model-dependent analysis assuming complete coherence.
 14 Re-evaluated under $\Gamma(\pi^+\pi^-)/\Gamma(\pi^+\pi^-\pi^0)$ by BEHREND 71 using more accurate $\omega \rightarrow \rho$ photoproduction cross-section ratio.

$\Gamma(\pi^+\pi^-)/\Gamma(\pi^+\pi^-\pi^0)$ Γ_3/Γ_1
 See also $\Gamma(\pi^+\pi^-)/\Gamma_{total}$.

VALUE	DOCUMENT ID	TECN	COMMENT
0.0171 ± 0.0007 OUR FIT			
0.026 ± 0.005 OUR AVERAGE			
0.021 +0.028 -0.009	1,2 RATCLIFF 72	ASPK	15 $\pi^-p \rightarrow n2\pi$
0.028 ± 0.006	1 BEHREND 71	ASPK	Photoproduction
0.022 ± 0.009 -0.01	3 ROOS 70	RVUE	

1 The fitted width of these data is 160 MeV in agreement with present average, thus the ω contribution is overestimated. Assuming ρ width 145 MeV.
 2 Significant interference effect observed. NB of $\omega \rightarrow 3\pi$ comes from an extrapolation.
 3 ROOS 70 combines ABRAMOVICH 70 and BIZZARRI 70.

$\Gamma(\pi^+\pi^-)/\Gamma(\pi^0\gamma)$ Γ_3/Γ_2
 VALUE EVTS DOCUMENT ID TECN COMMENT

VALUE	EVTS	DOCUMENT ID	TECN	COMMENT
0.20 ± 0.04	1.98M	1 ALOISIO 03	KLOE	1.02 $e^+e^- \rightarrow \pi^+\pi^-\pi^0$

1 Using the data of ALOISIO 02D.

$\Gamma(\text{neutrals})/\Gamma_{total}$ $(\Gamma_2+\Gamma_4)/\Gamma$
 VALUE EVTS DOCUMENT ID TECN COMMENT

VALUE	EVTS	DOCUMENT ID	TECN	COMMENT
0.091 ± 0.006 OUR FIT				
0.081 ± 0.011 OUR AVERAGE				
0.075 ± 0.025		BIZZARRI 71	HBC	0.0 $\rho\bar{p}$
0.079 ± 0.019		DEINET 69B	OSPK	1.5 π^-p
0.084 ± 0.015		BOLLINI 68C	CNTR	2.1 π^-p

• • • We do not use the following data for averages, fits, limits, etc. • • •
 0.073 ± 0.018 42 BASILE 72B CNTR 1.67 π^-p

$\Gamma(\text{neutrals})/\Gamma(\pi^+\pi^-\pi^0)$ $(\Gamma_2+\Gamma_4)/\Gamma_1$
 VALUE EVTS DOCUMENT ID TECN COMMENT

VALUE	EVTS	DOCUMENT ID	TECN	COMMENT
0.102 ± 0.008 OUR FIT				
0.103 +0.011 -0.010 OUR AVERAGE				
0.15 ± 0.04	46	AGUILAR... 72B	HBC	3.9,4.6 K^-p
0.10 ± 0.03	19	BARASH 67B	HBC	0.0 $\bar{p}p$
0.134 ± 0.026	850	DIUGNO 66B	CNTR	1.4 π^-p
0.097 ± 0.016	348	FLATTE 66	HBC	1.4 - 1.7 $K^-p \rightarrow \Lambda MM$
0.06 +0.05 -0.02		JAMES 66	HBC	2.1 π^+p
0.08 ± 0.03	35	KRAEMER 64	DBC	1.2 π^+d
0.11 ± 0.02	20	BUSCHBECK 63	HBC	1.5 K^-p

• • • We do not use the following data for averages, fits, limits, etc. • • •

VALUE	CL%	DOCUMENT ID	TECN	COMMENT
0.78 ± 0.07		1 DAKIN 72	OSPK	1.4 $\pi^-p \rightarrow nMM$
>0.81	90	DEINET 69B	OSPK	

1 Error statistical only. Authors obtain good fit also assuming $\pi^0\gamma$ as the only neutral decay.

$\Gamma(\text{neutrals})/\Gamma(\text{charged particles})$ $(\Gamma_2+\Gamma_4)/(\Gamma_1+\Gamma_3)$
 VALUE DOCUMENT ID TECN COMMENT

VALUE	DOCUMENT ID	TECN	COMMENT
0.100 ± 0.008 OUR FIT			
0.124 ± 0.021	FELDMAN 67C	OSPK	1.2 π^-p

$\Gamma(\eta\gamma)/\Gamma_{total}$		Γ_5/Γ	
VALUE (units 10^{-4})	EVTS	DOCUMENT ID	TECN COMMENT
4.5 ± 0.4 OUR FIT		Error includes scale factor of 1.1.	
6.3 ± 1.3 OUR AVERAGE		Error includes scale factor of 1.2.	
6.6 ± 1.7		¹ ABELE 97E	CBAR 0.0 $p\bar{p} \rightarrow 5\gamma$
8.3 ± 2.1		ALDE 93	GAM2 38 $\pi^- p \rightarrow \omega n$
3.0 $^{+2.5}_{-1.8}$		² ANDREWS 77	CNTR 6.7-10 γCu

• • • We do not use the following data for averages, fits, limits, etc. • • •

4.2 ± 0.4 ± 0.1 33k ³ ACHASOV 07B SND 0.6-1.38 $e^+e^- \rightarrow \eta\gamma$

4.44 $^{+2.59}_{-1.83} \pm 0.28$ 17.4k ^{4,5} AKHMETSHIN 05 CMD2 0.60-1.38 $e^+e^- \rightarrow \eta\gamma$

5.10 ± 0.72 ± 0.34 23k ⁶ AKHMETSHIN 01B CMD2 $e^+e^- \rightarrow \eta\gamma$

0.7 to 5.5 ⁷ CASE 00 CBAR 0.0 $p\bar{p} \rightarrow \eta\eta\gamma$

6.56 $^{+2.41}_{-2.55}$ 3525 ^{2,8} BENAYOUN 96 RVUE $e^+e^- \rightarrow \eta\gamma$

7.3 ± 2.9 ^{2,4} DOLINSKY 89 ND $e^+e^- \rightarrow \eta\gamma$

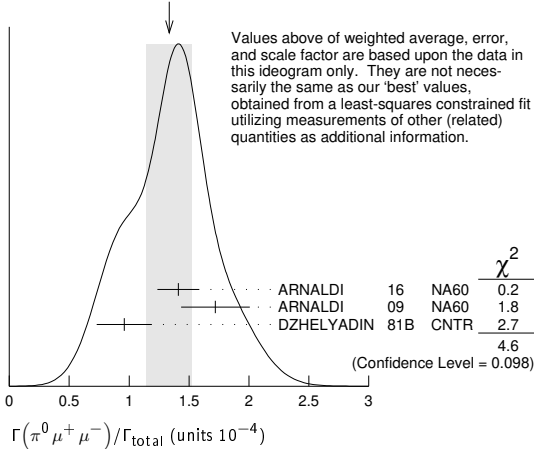
¹ No flat $\eta\eta\gamma$ background assumed.
² Solution corresponding to constructive $\omega\rho$ interference.
³ ACHASOV 07B reports $[\Gamma(\omega(782) \rightarrow \eta\gamma)/\Gamma_{total}] \times [B(\omega(782) \rightarrow e^+e^-)] = (3.10 \pm 0.31 \pm 0.11) \times 10^{-8}$ which we divide by our best value $B(\omega(782) \rightarrow e^+e^-) = (7.36 \pm 0.15) \times 10^{-5}$. Our first error is their experiment's error and our second error is the systematic error from using our best value. Supersedes ACHASOV 00D and ACHASOV 06A.
⁴ Not independent of the corresponding $\Gamma(e^+e^-) \times \Gamma(\eta\gamma)/\Gamma_{total}^2$.
⁵ Using $B(\omega \rightarrow e^+e^-) = (7.14 \pm 0.13) \times 10^{-5}$ and $B(\eta \rightarrow \gamma\gamma) = 39.43 \pm 0.26\%$.
⁶ Using $B(\omega \rightarrow e^+e^-) = (7.07 \pm 0.19) \times 10^{-5}$ and using $B(\eta \rightarrow 3\pi^0) = (32.24 \pm 0.29) \times 10^{-2}$. Solution corresponding to constructive $\omega\rho$ interference. The combined fit from 600 to 1380 MeV taking into account $\rho(770)$, $\omega(782)$, $\phi(1020)$, and $\rho(1450)$ (mass and width fixed at 1450 MeV and 310 MeV respectively). Not independent of the corresponding $\Gamma(e^+e^-) \times \Gamma(\eta\gamma)/\Gamma_{total}^2$.
⁷ Depending on the degree of coherence with the flat $\eta\eta\gamma$ background and using $B(\omega \rightarrow \pi^0\gamma) = (8.5 \pm 0.5) \times 10^{-2}$.
⁸ Reanalysis of DRUZHININ 84, DOLINSKY 89, DOLINSKY 91 taking into account the triangle anomaly contributions.

$\Gamma(\eta\gamma)/\Gamma(\pi^0\gamma)$		Γ_5/Γ_2	
VALUE	DOCUMENT ID	TECN	COMMENT
• • • We do not use the following data for averages, fits, limits, etc. • • •			
0.0098 ± 0.0024	¹ ALDE 93	GAM2	38 $\pi^- p \rightarrow \omega n$
0.0082 ± 0.0033	² DOLINSKY 89	ND	$e^+e^- \rightarrow \eta\gamma$
0.010 ± 0.045	APEL 72B	OSPK	4-8 $\pi^- p \rightarrow n3\gamma$

$\Gamma(\pi^0 e^+ e^-)/\Gamma_{total}$		Γ_6/Γ	
VALUE (units 10^{-4})	EVTS	DOCUMENT ID	TECN COMMENT
7.7 ± 0.6 OUR FIT			
7.7 ± 0.6 OUR AVERAGE			
7.61 ± 0.53 ± 0.64		ACHASOV 08	SND 0.36-0.97 $e^+e^- \rightarrow \pi^0 e^+ e^-$
8.19 ± 0.71 ± 0.62		AKHMETSHIN 05A	CMD2 0.72-0.84 e^+e^-
5.9 ± 1.9	43	DOLINSKY 88	ND $e^+e^- \rightarrow \pi^0 e^+ e^-$

$\Gamma(\pi^0 \mu^+ \mu^-)/\Gamma_{total}$		Γ_7/Γ	
VALUE (units 10^{-4})	EVTS	DOCUMENT ID	TECN COMMENT
1.34 ± 0.18 OUR FIT		Error includes scale factor of 1.5.	
1.34 ± 0.19 OUR AVERAGE		Error includes scale factor of 1.5. See the ideogram below.	
1.41 ± 0.09 ± 0.15		ARNALDI 16	NA60 400 GeV (p-A) collisions
1.72 ± 0.25 ± 0.14	3k	ARNALDI 09	NA60 158A In-In collisions
0.96 ± 0.23		DZHELJADIN 81B	CNTR 25-33 $\pi^- p \rightarrow \omega n$

WEIGHTED AVERAGE
 1.34 ± 0.19 (Error scaled by 1.5)



$\Gamma(\eta e^+ e^-)/\Gamma_{total}$		Γ_8/Γ	
VALUE (units 10^{-5})	DOCUMENT ID	TECN	COMMENT
• • • We do not use the following data for averages, fits, limits, etc. • • •			
< 1.1	AKHMETSHIN 05A	CMD2	0.72-0.84 e^+e^-

$\Gamma(e^+ e^-)/\Gamma_{total}$		Γ_9/Γ	
VALUE (units 10^{-4})	EVTS	DOCUMENT ID	TECN COMMENT
0.736 ± 0.015 OUR FIT		Error includes scale factor of 1.5.	
• • • We do not use the following data for averages, fits, limits, etc. • • •			
0.700 ± 0.016	11200	^{1,2} AKHMETSHIN 04	CMD2 $e^+e^- \rightarrow \pi^+ \pi^- \pi^0$
0.752 ± 0.004 ± 0.024	1.2M	^{2,3} ACHASOV 03D	RVUE 0.44-2.00 $e^+e^- \rightarrow \pi^+ \pi^- \pi^0$
0.714 ± 0.036		² DOLINSKY 89	ND $e^+e^- \rightarrow \pi^+ \pi^- \pi^0$
0.72 ± 0.03		² BARKOV 87	CMD $e^+e^- \rightarrow \pi^+ \pi^- \pi^0$
0.64 ± 0.04	1488	² KURDADZE 83B	OLYA $e^+e^- \rightarrow \pi^+ \pi^- \pi^0$
0.675 ± 0.069	433	² CORDIER 80	DM1 $e^+e^- \rightarrow \pi^+ \pi^- \pi^0$
0.83 ± 0.10	451	² BENA KSAS 72B	OSPK $e^+e^- \rightarrow \pi^+ \pi^- \pi^0$
0.77 ± 0.06		⁴ AUGUSTIN 69D	OSPK $e^+e^- \rightarrow \pi^+ \pi^- \pi^0$
0.65 ± 0.13	33	⁵ ASTVACAT... 68	OSPK Assume SU(3)+mixing

¹ Using $B(\omega \rightarrow \pi^+ \pi^- \pi^0) = 0.891 \pm 0.007$. Update of AKHMETSHIN 00c.
² Not independent of the corresponding $\Gamma(e^+e^-) \times \Gamma(\pi^+ \pi^- \pi^0)/\Gamma_{total}^2$.
³ Using ACHASOV 03, ACHASOV 03D and $B(\omega \rightarrow \pi^+ \pi^-) = (1.70 \pm 0.28)\%$.
⁴ Rescaled by us to correspond to ω width 8.4 MeV. Systematic errors underestimated.
⁵ Not resolved from ρ decay. Error statistical only.

$\Gamma(\pi^+ \pi^- \pi^0)/\Gamma_{total}$		Γ_{10}/Γ	
VALUE (units 10^{-4})	CL%	DOCUMENT ID	TECN COMMENT
< 2	90	ACHASOV 09A	SND $e^+e^- \rightarrow \pi^+ \pi^- \pi^0 \pi^0$
• • • We do not use the following data for averages, fits, limits, etc. • • •			
< 200	90	KURDADZE 86	OLYA $e^+e^- \rightarrow \pi^+ \pi^- \pi^0 \pi^0$

$\Gamma(\pi^+ \pi^- \gamma)/\Gamma_{total}$		Γ_{11}/Γ	
VALUE	CL%	DOCUMENT ID	TECN COMMENT
< 0.0036	95	WEIDENAUER 90	ASTE $p\bar{p} \rightarrow \pi^+ \pi^- \pi^+ \pi^- \gamma$
• • • We do not use the following data for averages, fits, limits, etc. • • •			
< 0.004	95	BITYUKOV 88B	SPEC 32 $\pi^- p \rightarrow \pi^+ \pi^- \gamma X$

$\Gamma(\pi^+ \pi^- \gamma)/\Gamma(\pi^+ \pi^- \pi^0)$		Γ_{11}/Γ_1	
VALUE	CL%	DOCUMENT ID	TECN COMMENT
• • • We do not use the following data for averages, fits, limits, etc. • • •			
< 0.066	90	KALBFLEISCH 75	HBC 2.18 $K^- p \rightarrow \Lambda \pi^+ \pi^- \gamma$
< 0.05	90	FLATTE 66	HBC 1.2-1.7 $K^- p \rightarrow \Lambda \pi^+ \pi^- \gamma$

$\Gamma(\pi^+ \pi^- \pi^+ \pi^-)/\Gamma_{total}$		Γ_{12}/Γ	
VALUE	CL%	DOCUMENT ID	TECN COMMENT
< 1 × 10 ⁻³	90	KURDADZE 88	OLYA $e^+e^- \rightarrow \pi^+ \pi^- \pi^+ \pi^-$

$\Gamma(\pi^0 \pi^0 \gamma)/\Gamma_{total}$		Γ_{13}/Γ	
VALUE (units 10^{-5})	EVTS	DOCUMENT ID	TECN COMMENT
6.7 ± 1.1 OUR FIT			
6.5 ± 1.2 OUR AVERAGE			
6.4 $^{+2.4}_{-2.0} \pm 0.8$	190	¹ AKHMETSHIN 04B	CMD2 0.6-0.97 $e^+e^- \rightarrow \pi^0 \pi^0 \gamma$
6.6 $^{+1.4}_{-1.3} \pm 0.6$	295	ACHASOV 02F	SND 0.36-0.97 $e^+e^- \rightarrow \pi^0 \pi^0 \gamma$
• • • We do not use the following data for averages, fits, limits, etc. • • •			
11.8 $^{+2.1}_{-1.9} \pm 1.4$	190	² AKHMETSHIN 04B	CMD2 0.6-0.97 $e^+e^- \rightarrow \pi^0 \pi^0 \gamma$
7.8 ± 2.7 ± 2.0	63	^{1,3} ACHASOV 00G	SND $e^+e^- \rightarrow \pi^0 \pi^0 \gamma$
12.7 ± 2.3 ± 2.5	63	^{2,3} ACHASOV 00G	SND $e^+e^- \rightarrow \pi^0 \pi^0 \gamma$

¹ In the model assuming the $\rho \rightarrow \pi^0 \pi^0 \gamma$ decay via the $\omega\pi$ and $f_0(500)\gamma$ mechanisms.
² In the model assuming the $\rho \rightarrow \pi^0 \pi^0 \gamma$ decay via the $\omega\pi$ mechanism only.
³ Superseded by ACHASOV 02F.

$\Gamma(\pi^0 \pi^0 \gamma)/\Gamma(\pi^0 \gamma)$		Γ_{13}/Γ_2		
VALUE (units 10^{-4})	CL%	EVTS	DOCUMENT ID	TECN COMMENT
7.9 ± 1.3 OUR FIT				
8.5 ± 2.9				
• • • We do not use the following data for averages, fits, limits, etc. • • •				
< 50	90		DOLINSKY 89	ND $e^+e^- \rightarrow \pi^0 \pi^0 \gamma$
< 1800	95		KEYNE 76	CNTR $\pi^- p \rightarrow \omega n$
< 1500	90		BENA KSAS 72C	OSPK e^+e^-
< 1400			BALDIN 71	HLBC 2.9 $\pi^+ p$
< 1000	90		BARMIN 64	HLBC 1.3-2.8 $\pi^- p$

Meson Particle Listings

 $\omega(782)$ $\Gamma(\pi^0\pi^0\gamma)/\Gamma(\text{neutrals})$

VALUE	CL%	DOCUMENT ID	TECN	COMMENT
0.22±0.07		¹ DAKIN	72	OSPK 1.4 $\pi^- p \rightarrow nMM$
<0.19	90	DEINET	69B	OSPK

¹ See $\Gamma(\pi^0\gamma)/\Gamma(\text{neutrals})$.

 $\Gamma(\eta\pi^0\gamma)/\Gamma_{\text{total}}$

VALUE (units 10^{-5})	CL%	DOCUMENT ID	TECN	COMMENT
<3.3	90	AKHMETSHIN 04B	CMD2	$0.6-0.97 e^+e^- \rightarrow \eta\pi^0\gamma$

 $\Gamma(\mu^+\mu^-)/\Gamma_{\text{total}}$

VALUE (units 10^{-5})	EVTS	DOCUMENT ID	TECN	COMMENT
7.4±1.8 OUR FIT				
7.4±1.8 OUR AVERAGE				
6.6±1.4±1.7	4.5M	¹ ANASTASI	17	KLOE $e^+e^- \rightarrow \mu^+\mu^-\gamma$
9.0±2.9±1.1	18	HEISTER	02C	ALEP $Z \rightarrow \mu^+\mu^- + X$

¹ Assuming lepton universality in the decay $\omega \rightarrow \ell^+\ell^-$ and correcting for different phase space between electron and muon final states.

 $\Gamma(\mu^+\mu^-)/\Gamma(\pi^+\pi^-\pi^0)$

VALUE (units 10^{-3})	CL%	DOCUMENT ID	TECN	COMMENT
<0.2	90	WILSON	69	OSPK 1.2 $\pi^- C \rightarrow Fe$
<1.7	74	FLATTE	66	HBC 1.2 - 1.7 $K^- p \rightarrow \Lambda\mu^+\mu^-$
<1.2		BARBARO...	65	HBC 2.7 $K^- p$

 $\Gamma(\pi^0\mu^+\mu^-)/\Gamma(\mu^+\mu^-)$

VALUE	EVTS	DOCUMENT ID	TECN	COMMENT
1.2±0.6	30	¹ DZHELYADIN	79	CNTR 25-33 $\pi^- p$

¹ Superseded by DZHELYADIN 81B result above.

 $\Gamma(3\gamma)/\Gamma_{\text{total}}$

VALUE (units 10^{-4})	CL%	DOCUMENT ID	TECN	COMMENT
<1.9	95	¹ ABELE	97E	CBAR 0.0 $\bar{p}p \rightarrow 5\gamma$
<2	90	¹ PROKOSHKIN	95	GAM2 38 $\pi^- p \rightarrow 3\gamma n$

¹ From direct 3γ decay search.

 $\Gamma(\eta\pi^0)/\Gamma_{\text{total}}$

VALUE	CL%	DOCUMENT ID	TECN	COMMENT
<0.001	90	ALDE	94B	GAM2 38 $\pi^- p \rightarrow \eta\pi^0 n$

 $[\Gamma(\eta\gamma) + \Gamma(\eta\pi^0)]/\Gamma(\pi^+\pi^-\pi^0)$

VALUE	CL%	DOCUMENT ID	TECN	COMMENT
<0.016	90	¹ FLATTE	66	HBC 1.2 - 1.7 $K^- p \rightarrow \Lambda\pi^+\pi^- MM$
<0.045	95	JACQUET	69B	HLBC 2.05 $\pi^+ p \rightarrow \pi^+ p \omega$

¹ Restated by us using $B(\eta \rightarrow \text{charged modes}) = 29.2\%$.

 $\Gamma(\eta\pi^0)/\Gamma(\pi^0\gamma)$

VALUE (units 10^{-3})	CL%	DOCUMENT ID	TECN	COMMENT
<2.6	90	¹ STAROSTIN	09	CRYM $\gamma p \rightarrow \eta\pi^0 p$

¹ STAROSTIN 09 reports $[\Gamma(\omega(782) \rightarrow \eta\pi^0)/\Gamma(\omega(782) \rightarrow \pi^0\gamma)] \times [B(\eta \rightarrow 2\gamma)] < 1.01 \times 10^{-3}$ which we divide by our best value $B(\eta \rightarrow 2\gamma) = 39.41 \times 10^{-2}$.

 $\Gamma(2\pi^0)/\Gamma(\pi^0\gamma)$

VALUE (units 10^{-3})	CL%	DOCUMENT ID	TECN	COMMENT
<2.59	90	STAROSTIN	09	CRYM $\gamma p \rightarrow 2\pi^0 p$

 $\Gamma(3\pi^0)/\Gamma_{\text{total}}$

VALUE	CL%	DOCUMENT ID	TECN	COMMENT
<3 × 10 ⁻⁴	90	PROKOSHKIN	95	GAM2 38 $\pi^- p \rightarrow 3\pi^0 n$

 $\Gamma(3\pi^0)/\Gamma(\pi^0\gamma)$

VALUE (units 10^{-3})	CL%	DOCUMENT ID	TECN	COMMENT
<2.72	90	STAROSTIN	09	CRYM $\gamma p \rightarrow 3\pi^0 p$

 $\Gamma(3\pi^0)/\Gamma(\pi^+\pi^-\pi^0)$

VALUE	CL%	DOCUMENT ID	TECN	COMMENT
<0.009	90	BARBERIS	01	450 $p p \rightarrow p_f 3\pi^0 p_s$

 $\Gamma(\text{invisible})/\Gamma(\pi^+\pi^-\pi^0)$

VALUE	CL%	DOCUMENT ID	TECN	COMMENT
<8.1 × 10 ⁻⁵	90	ABLIKIM	18s	BES3 $J/\psi \rightarrow \omega\eta \rightarrow \omega\pi^+\pi^-\pi^0$

PARAMETER Λ IN $\omega \rightarrow \pi^0\ell^+\ell^-$ DECAY

In the pole approximation the electromagnetic transition form factor for a resonance of mass M is given by the expression:

$$|F|^2 = (1 - M^2/\Lambda^2)^{-2},$$

where for the parameter Λ vector dominance predicts $\Lambda = M_p \approx 0.770$ GeV. The ARNALDI 09 measurement is in obvious conflict with this expectation. Note that for $\eta \rightarrow \gamma\mu^+\mu^-$ decay ARNALDI 09 and DZHELYADIN 80 obtain the value of Λ consistent with vector dominance.

PARAMETER Λ IN $\omega \rightarrow \pi^0\mu^+\mu^-$ DECAY

VALUE (GeV)	EVTS	DOCUMENT ID	TECN	COMMENT
0.670 ± 0.006 OUR AVERAGE				
0.6707 ± 0.0039 ± 0.0056		¹ ARNALDI	16	NA60 400 GeV (p -A) collisions
0.668 ± 0.009 ± 0.003	3k	² ARNALDI	09	NA60 158A In-In collisions
0.65 ± 0.03		DZHELYADIN	81B	CNTR 25-33 $\pi^- p \rightarrow \omega n$

¹ ARNALDI 16 reports $\Lambda^{-2}(\omega) = 2.223 \pm 0.026 \pm 0.037$ GeV⁻² which we converted to the quoted Λ value.

² ARNALDI 09 reports $\Lambda^{-2}(\omega) = 2.24 \pm 0.06 \pm 0.02$ GeV⁻² which we converted to the quoted Λ value.

PARAMETER Λ IN $\omega \rightarrow \pi^0e^+e^-$ DECAY

VALUE (GeV)	EVTS	DOCUMENT ID	TECN	COMMENT
0.709 ± 0.037	1.1k	¹ ADLARSON	17B	A2MM $\gamma p \rightarrow \omega p$
		¹ ADLARSON	17B	reports $\Lambda^{-2}(\omega\pi^0) = 1.99 \pm 0.21$ GeV ⁻² that we converted to the quoted Λ value.

ENERGY DEPENDENCE OF $\omega \rightarrow \pi^+\pi^-\pi^0$ DALITZ PLOT

The following experiments fit to one or more of the coefficients α, β, γ for $|matrix element|^2 \propto P(1 + 2\alpha Z + 2\beta Z^2 \sin(3\phi) + 2\gamma Z^2 + O(Z^5/2))$ where P is the P -wave phase-space factor and Z, ϕ are kinematical variables as defined in ADLARSON 17.

VALUE	EVTS	DOCUMENT ID	TECN	COMMENT
0.133 ± 0.008 OUR AVERAGE				
0.1321 ± 0.0067 ± 0.0046	260k	¹ ABLIKIM	18AD	BES3 $J/\psi \rightarrow \omega\eta$
0.147 ± 0.036	44k	ADLARSON	17	WASA α in $p d \rightarrow {}^3\text{He} \omega, p p \rightarrow p p \omega$

¹ Keeping a term linear in Z only. A fit with the terms proportional to Z and $Z^3/2$ gives $\alpha = 0.133 \pm 0.041$ and $\beta = 0.037 \pm 0.054$.

 $\omega(782)$ REFERENCES

ABLIKIM	18AD	PR D98 112007	M. Ablikim et al.	(BESIII Collab.)
ABLIKIM	18C	PRL 120 242003	M. Ablikim et al.	(BESIII Collab.)
ABLIKIM	18S	PR D98 032001	M. Ablikim et al.	(BESIII Collab.)
HANHART	18	EPJ C78 450	C. Hanhart et al.	
ADLARSON	17	PL B770 418	P. Adlarson et al.	(WASA-at-COSY Collab.)
ADLARSON	17B	PR C95 035208	P. Adlarson et al.	(A2 Collab. at MAMI)
ANASTASI	17	PL B767 485	A. Anastasi et al.	(KLOE-2 Collab.)
ABLIKIM	16B	PL B753 103	M. Ablikim et al.	(BESIII Collab.)
ACHASOV	16A	PR D93 092001	M.N. Achasov et al.	(SND Collab.)
ARNALDI	16	PL B757 437	R. Arnaldi et al.	(NA60 Collab.)
PDG	15	RPP 2015 at pub.lnl.gov		(PDG Collab.)
ACHASOV	13	PR D88 054013	M.N. Achasov et al.	(SND Collab.)
BABUSCI	13D	PL B720 336	D. Babusci et al.	(CATA, CALB, BARI)
BENAYOUN	13	EPJ C73 2453	M. Benayoun, P. David, L. DelBuono (PARIN, BERLIN+)	
DAVIER	13	EPJ C73 2597	M. Davier et al.	
LEES	12G	PR D86 032013	J.P. Lees et al.	(BABAR Collab.)
NIECKNIG	12	EPJ C72 2014	F. Niecknig, B. Kubis, S.P. Schneider	(BONN)
AMBROSINO	11A	PL B700 102	F. Ambrosino et al.	(KLOE Collab.)
BENAYOUN	10	EPJ C65 211	M. Benayoun et al.	
ACHASOV	09A	JETP 109 379	M.N. Achasov et al.	(SND Collab.)
ARNALDI	09	PL B677 260	R. Arnaldi et al.	(NA60 Collab.)
AUBERT	09AS	PRL 103 231801	B. Aubert et al.	(BABAR Collab.)
STAROSTIN	09	PR C79 065201	A. Starostin et al.	(Crystal Ball Collab. at MAMI)
ACHASOV	08	JETP 107 61	M.N. Achasov et al.	(SND Collab.)
ACHASOV	08G	PL B669 223	F. Ambrosino et al.	(KLOE Collab.)
ACHASOV	07B	PR D76 077101	M.N. Achasov et al.	(SND Collab.)
AKHMETSHIN	07	PL B648 28	R.R. Akhmetshin et al.	(Novosibirsk CMD-2 Collab.)
ACHASOV	06	JETP 103 380	M.N. Achasov et al.	(Novosibirsk CMD-2 Collab.)
ACHASOV	06A	Translated from ZETP 130 437.		
ACHASOV	06A	PR D74 014016	M.N. Achasov et al.	(SND Collab.)
AULCHENKO	06	JETPL 84 413	V.M. Aulchenko et al.	(Novosibirsk CMD-2 Collab.)
ACHASOV	05A	JETP 101 1053	M.N. Achasov et al.	(Novosibirsk SND Collab.)
ACHMETSHIN	05	PL B605 26	R.R. Akhmetshin et al.	(Novosibirsk CMD-2 Collab.)
AKHMETSHIN	05A	PL B613 29	R.R. Akhmetshin et al.	(Novosibirsk CMD-2 Collab.)
AULCHENKO	05	JETPL 82 743	V.M. Aulchenko et al.	(Novosibirsk CMD-2 Collab.)
		Translated from ZETFP 82 841.		

See key on page 999

Meson Particle Listings

$\omega(782), \eta'(958)$

$\eta'(958)$

$I^G(J^{PC}) = 0^+(0^{-+})$

$\eta'(958)$ MASS

Table with columns: VALUE (MeV), EVTS, DOCUMENT ID, TECN, COMMENT. Includes 'OUR AVERAGE' and various experimental data points.

• • • We do not use the following data for averages, fits, limits, etc. • • •
1 Using all η' decays.
2 Systematic uncertainty not estimated.
3 Using η' decays into neutrals. Not independent of the other listed BASILE 71 η' mass measurement.

$\eta'(958)$ WIDTH

Table with columns: VALUE (MeV), EVTS, DOCUMENT ID, TECN, CHG, COMMENT. Includes 'OUR FIT' and 'OUR AVERAGE'.

• • • We do not use the following data for averages, fits, limits, etc. • • •

$\eta'(958)$ DECAY MODES

Table with columns: Mode, Fraction (Γ_i/Γ), Confidence level. Lists various decay channels like $\pi^+\pi^-\eta$, $\rho^0\gamma$, $\pi^+\pi^-\pi^0$, etc.

Main table listing experimental data for $\eta'(958)$. Columns include author names, experiment codes, and publication details.

Meson Particle Listings

$\eta'(958)$

Charge conjugation (C), Parity (P), Lepton family number (LF) violating modes				
Γ_{31}	$\pi^+\pi^-$	P,CP	< 1.8	$\times 10^{-5}$ 90%
Γ_{32}	$\pi^0\pi^0$	P,CP	< 4	$\times 10^{-4}$ 90%
Γ_{33}	$\pi^0e^+e^-$	C	$[a] < 1.4$	$\times 10^{-3}$ 90%
Γ_{34}	ηe^+e^-	C	$[a] < 2.4$	$\times 10^{-3}$ 90%
Γ_{35}	3γ	C	< 1.0	$\times 10^{-4}$ 90%
Γ_{36}	$\mu^+\mu^-\pi^0$	C	$[a] < 6.0$	$\times 10^{-5}$ 90%
Γ_{37}	$\mu^+\mu^-\eta$	C	$[a] < 1.5$	$\times 10^{-5}$ 90%
Γ_{38}	$e\mu$	LF	< 4.7	$\times 10^{-4}$ 90%

[a] C parity forbids this to occur as a single-photon process.

CONSTRAINED FIT INFORMATION

An overall fit to the total width, a partial width, 2 combinations of partial widths obtained from integrated cross section, and 19 branching ratios uses 51 measurements and one constraint to determine 9 parameters. The overall fit has a $\chi^2 = 69.4$ for 43 degrees of freedom.

The following off-diagonal array elements are the correlation coefficients $\langle \delta p_i \delta p_j \rangle / (\delta p_i \delta p_j)$, in percent, from the fit to parameters p_i , including the branching fractions, $x_i \equiv \Gamma_i / \Gamma_{total}$. The fit constrains the x_i whose labels appear in this array to sum to one.

x_2	-24								
x_4	-74	-42							
x_5	-7	-6	-2						
x_7	-11	-7	9	-1					
x_8	-17	-9	19	0	2				
x_{11}	-1	-1	-1	0	0	0			
x_{22}	-9	-7	-7	-1	-2	-2	0		
Γ	11	-10	-1	1	-40	0	0	2	
	x_1	x_2	x_4	x_5	x_7	x_8	x_{11}	x_{22}	

Mode	Rate (MeV)
Γ_1 $\pi^+\pi^-\eta$	0.0799 ± 0.0029
Γ_2 $\rho^0\gamma$ (including non-resonant $\pi^+\pi^-\gamma$)	0.0554 ± 0.0019
Γ_4 $\pi^0\pi^0\eta$	0.0421 ± 0.0017
Γ_5 $\omega\gamma$	0.00474 ± 0.00020
Γ_7 $\gamma\gamma$	0.00434 ± 0.00013
Γ_8 $3\pi^0$	(4.7 ± 0.4) × 10 ⁻⁴
Γ_{11} $\pi^+\pi^-\pi^0$	(6.8 ± 0.4) × 10 ⁻⁴
Γ_{22} $\pi^+\pi^-e^+e^-$	(4.4 ± 2.3 / -1.8) × 10 ⁻⁴

$\eta'(958)$ PARTIAL WIDTHS

$\Gamma(\gamma\gamma)$	Γ_7			
VALUE (keV)	EVTs	DOCUMENT ID	TECN	COMMENT
4.34 ± 0.14 OUR FIT				
4.28 ± 0.19 OUR AVERAGE				
4.17 ± 0.10 ± 0.27	2000	¹ ACCIARRI	98Q L3	$e^+e^- \rightarrow e^+e^-\pi^+\pi^-\gamma$
4.53 ± 0.29 ± 0.51	266	KARCH	92 CBAL	$e^+e^- \rightarrow e^+e^-\eta\pi^0\pi^0$
3.61 ± 0.13 ± 0.48		² BEHREND	91 CELL	$e^+e^- \rightarrow e^+e^-\eta'(958)$
4.6 ± 1.1 ± 0.6	23	BARU	90 MD1	$e^+e^- \rightarrow e^+e^-\pi^+\pi^-\gamma$
4.57 ± 0.25 ± 0.44		BUTLER	90 MRK2	$e^+e^- \rightarrow e^+e^-\eta'(958)$
5.08 ± 0.24 ± 0.71	547	³ ROE	90 ASP	$e^+e^- \rightarrow e^+e^-2\gamma$
3.8 ± 0.7 ± 0.6	34	AIHARA	88c TPC	$e^+e^- \rightarrow e^+e^-\eta\pi^+\pi^-$
4.9 ± 0.5 ± 0.5	136	⁴ WILLIAMS	88 CBAL	$e^+e^- \rightarrow e^+e^-2\gamma$
••• We do not use the following data for averages, fits, limits, etc. •••				
4.7 ± 0.6 ± 0.9	143	⁵ GIDAL	87 MRK2	$e^+e^- \rightarrow e^+e^-\eta\pi^+\pi^-$
4.0 ± 0.9		⁶ BARTEL	85E JADE	$e^+e^- \rightarrow e^+e^-2\gamma$

¹ No non-resonant $\pi^+\pi^-$ contribution found.
² Reevaluated by us using $B(\eta' \rightarrow \rho(770)\gamma) = (30.2 \pm 1.3)\%$.
³ Reevaluated by us using $B(\eta' \rightarrow \gamma\gamma) = (2.11 \pm 0.13)\%$.
⁴ Reevaluated by us using $B(\eta' \rightarrow \gamma\gamma) = (2.11 \pm 0.13)\%$.
⁵ Superseded by BUTLER 90.
⁶ Systematic error not evaluated.

$\Gamma(e^+e^-)$	Γ_{29}			
VALUE (eV)	CL%	DOCUMENT ID	TECN	COMMENT
< 1.1 × 10⁻³	90	^{1,2} ACHASOV	15 SND	$0.958 e^+e^- \rightarrow \pi^+\pi^-\eta$
••• We do not use the following data for averages, fits, limits, etc. •••				
< 2.0 × 10 ⁻³	90	² ACHASOV	15 SND	$0.958 e^+e^- \rightarrow \pi^+\pi^-\eta$
< 2.4 × 10 ⁻³	90	² AKHMETSHIN	15 CMD3	$0.958 e^+e^- \rightarrow \pi^+\pi^-\eta$

¹ Combining data of ACHASOV 15 and AKHMETSHIN 15.
² Using η and η' branching fractions from PDG 14.

$\eta'(958) \Gamma(i)\Gamma(\gamma\gamma)/\Gamma(total)$

This combination of a partial width with the partial width into $\gamma\gamma$ and with the total width is obtained from the integrated cross section into channel(i) in the $\gamma\gamma$ annihilation.

$\Gamma(\gamma\gamma) \times \Gamma(\rho^0\gamma$ (including non-resonant $\pi^+\pi^-\gamma$))/ Γ_{total}	$\Gamma_7\Gamma_2/\Gamma$			
VALUE (keV)	EVTs	DOCUMENT ID	TECN	COMMENT
1.28 ± 0.04 OUR FIT				
1.26 ± 0.07 OUR AVERAGE				Error includes scale factor of 1.2.
1.09 ± 0.04 ± 0.13		BEHREND	91 CELL	$e^+e^- \rightarrow e^+e^-\rho(770)^0\gamma$
1.35 ± 0.09 ± 0.21		AIHARA	87 TPC	$e^+e^- \rightarrow e^+e^-\rho\gamma$
1.13 ± 0.04 ± 0.13	867	ALBRECHT	87B ARG	$e^+e^- \rightarrow e^+e^-\rho\gamma$
1.53 ± 0.09 ± 0.21		ALTHOFF	84E TASS	$e^+e^- \rightarrow e^+e^-\rho\gamma$
1.14 ± 0.08 ± 0.11	243	BERGER	84B PLUT	$e^+e^- \rightarrow e^+e^-\rho\gamma$
1.73 ± 0.34 ± 0.35	95	JENNI	83 MRK2	$e^+e^- \rightarrow e^+e^-\rho\gamma$
1.49 ± 0.13 ± 0.027	213	BARTEL	82B JADE	$e^+e^- \rightarrow e^+e^-\rho\gamma$
••• We do not use the following data for averages, fits, limits, etc. •••				
1.85 ± 0.31 ± 0.24	43	BEHREND	82c CELL	$e^+e^- \rightarrow e^+e^-\rho\gamma$

$\Gamma(\gamma\gamma) \times \Gamma(\pi^0\pi^0\eta)/\Gamma_{total}$	$\Gamma_7\Gamma_4/\Gamma$			
VALUE (keV)	EVTs	DOCUMENT ID	TECN	COMMENT
0.97 ± 0.04 OUR FIT				Error includes scale factor of 1.1.
0.92 ± 0.06 ± 0.11		¹ KARCH	92 CBAL	$e^+e^- \rightarrow e^+e^-\eta\pi^0\pi^0$
••• We do not use the following data for averages, fits, limits, etc. •••				
0.95 ± 0.05 ± 0.08		² KARCH	90 CBAL	$e^+e^- \rightarrow e^+e^-\eta\pi^0\pi^0$
1.00 ± 0.08 ± 0.10		^{2,3} ANTREASYAN	87 CBAL	$e^+e^- \rightarrow e^+e^-\eta\pi^0\pi^0$
¹ Reevaluated by us using $B(\eta \rightarrow \gamma\gamma) = (39.21 \pm 0.34)\%$. Supersedes ANTREASYAN 87 and KARCH 90.				
² Superseded by KARCH 92.				
³ Using $BR(\eta \rightarrow 2\gamma) = (38.9 \pm 0.5)\%$.				

$\eta'(958) \Gamma(i)\Gamma(e^+e^-)/\Gamma(total)$

$\Gamma(\pi^+\pi^-\eta) \times \Gamma(e^+e^-)/\Gamma_{total}$	$\Gamma_1\Gamma_{29}/\Gamma$			
VALUE (10 ⁻³ eV)	CL%	DOCUMENT ID	TECN	COMMENT
< 1.0	90	¹ AKHMETSHIN	15 CMD3	$0.958 e^+e^- \rightarrow \pi^+\pi^-\eta$
¹ AKHMETSHIN 15 reports $[\Gamma(\eta'(958) \rightarrow \pi^+\pi^-\eta) \times \Gamma(\eta'(958) \rightarrow e^+e^-)]/\Gamma_{total} \times [B(\eta \rightarrow 2\gamma)] < 4.1 \times 10^{-4}$ eV which we divide by our best value $B(\eta \rightarrow 2\gamma) = 39.41 \times 10^{-2}$.				

$\eta'(958)$ BRANCHING RATIOS

$\Gamma(\pi^+\pi^-\eta)/\Gamma_{total}$	Γ_1/Γ			
VALUE (units 10 ⁻²)	EVTs	DOCUMENT ID	TECN	COMMENT
42.5 ± 0.5 OUR FIT				Error includes scale factor of 1.1.
41.24 ± 0.08 ± 1.24	312k	ABLIKIM	19T BES	$J/\psi \rightarrow \gamma\eta'$
••• We do not use the following data for averages, fits, limits, etc. •••				
42.4 ± 1.1 ± 0.4	1.2k	¹ PEDLAR	09 CLEO	$J/\psi \rightarrow \gamma\eta'$
¹ Not independent of other η' branching fractions and ratios in PEDLAR 09.				

$\Gamma(\pi^+\pi^-\eta$ (charged decay))/ Γ_{total}	0.2789 Γ_1/Γ			
VALUE	EVTs	DOCUMENT ID	TECN	COMMENT
0.1185 ± 0.0015 OUR FIT				Error includes scale factor of 1.1.
••• We do not use the following data for averages, fits, limits, etc. •••				
0.123 ± 0.014	107	RITTENBERG	69 HBC	$1.7-2.7 K^-p$
0.10 ± 0.04	10	LONDON	66 HBC	$2.24 K^-p \rightarrow \Lambda 2\pi^+\pi^-\pi^0$
0.07 ± 0.04	7	BADIER	65B HBC	$3 K^-p$

$\Gamma(\pi^+\pi^-\eta$ (neutral decay))/ Γ_{total}	0.7212 Γ_1/Γ			
VALUE	EVTs	DOCUMENT ID	TECN	COMMENT
0.306 ± 0.004 OUR FIT				Error includes scale factor of 1.1.
••• We do not use the following data for averages, fits, limits, etc. •••				
0.314 ± 0.026	281	RITTENBERG	69 HBC	$1.7-2.7 K^-p$

$\Gamma(\rho^0\gamma$ (including non-resonant $\pi^+\pi^-\gamma$))/ Γ_{total}	Γ_2/Γ			
VALUE (units 10 ⁻²)	EVTs	DOCUMENT ID	TECN	COMMENT
29.5 ± 0.4 OUR FIT				Error includes scale factor of 1.1.
29.90 ± 0.03 ± 0.55	913k	ABLIKIM	19T BES	$J/\psi \rightarrow \gamma\eta'$
••• We do not use the following data for averages, fits, limits, etc. •••				
28.7 ± 0.7 ± 0.4	0.2k	¹ PEDLAR	09 CLEO	$J/\psi \rightarrow \gamma\eta'$
32.9 ± 3.3	298	RITTENBERG	69 HBC	$1.7-2.7 K^-p$
20 ± 10	20	LONDON	66 HBC	$2.24 K^-p \rightarrow \Lambda \pi^+\pi^-\gamma$
34 ± 9	35	BADIER	65B HBC	$3 K^-p$
¹ Not independent of other η' branching fractions and ratios in PEDLAR 09.				

$\Gamma(\rho^0\gamma)/\Gamma_{total}$	Γ_3/Γ			
VALUE (%)	EVTs	DOCUMENT ID	TECN	COMMENT
••• We do not use the following data for averages, fits, limits, etc. •••				
33.34 ± 0.06 ± 1.60	970k	¹ ABLIKIM	18c BES3	$\eta'(958) \rightarrow \gamma\pi^+\pi^-$
34.43 ± 0.52 ± 1.97	970k	² ABLIKIM	18c BES3	$\eta'(958) \rightarrow \gamma\pi^+\pi^-$
¹ From a fit to $\pi^+\pi^-$ mass using $\rho(770)$, $\omega(782)$, and box anomaly components.				
² From a fit to $\pi^+\pi^-$ mass using $\rho(770)$, $\omega(782)$, and $\rho(1450)$ components.				

$\Gamma(\rho^0 \gamma (\text{including non-resonant } \pi^+ \pi^- \gamma))/\Gamma(\pi^+ \pi^- \eta)$ Γ_2/Γ_1

VALUE	DOCUMENT ID	TECN	COMMENT
0.694 ± 0.014 OUR FIT			Error includes scale factor of 1.1.
0.683 ± 0.020 OUR AVERAGE			
0.677 ± 0.024 ± 0.011	PEDLAR	09 CLE3	$J/\psi \rightarrow \eta' \gamma$
0.69 ± 0.03	ABLIKIM	06E BES2	$J/\psi \rightarrow \eta' \gamma$

$\Gamma(\rho^0 \gamma (\text{including non-resonant } \pi^+ \pi^- \gamma))/\Gamma(\pi^+ \pi^- \eta (\text{neutral decay}))$ $\Gamma_2/0.714\Gamma_1$

VALUE	EVTS	DOCUMENT ID	TECN	COMMENT
0.972 ± 0.020 OUR FIT				Error includes scale factor of 1.1.
0.97 ± 0.09 OUR AVERAGE				
0.70 ± 0.22		AMSLER	04B CBAR	$0 \bar{p} p \rightarrow \pi^+ \pi^- \eta$
1.07 ± 0.17		BELADIDZE	92c VES	$36 \pi^- \text{Be} \rightarrow \pi^- \eta' \eta \text{Be}$
0.92 ± 0.14	473	DANBURG	73 HBC	$2.2 K^- p \rightarrow \Lambda X^0$
1.11 ± 0.18	192	JACOBS	73 HBC	$2.9 K^- p \rightarrow \Lambda X^0$

$\Gamma(\pi^0 \pi^0 \eta)/\Gamma_{\text{total}}$ Γ_4/Γ

VALUE (units 10^{-2})	EVTS	DOCUMENT ID	TECN	COMMENT
22.4 ± 0.6 OUR FIT				Error includes scale factor of 1.1.
21.36 ± 0.10 ± 0.92				
	52k	ABLIKIM	19T BES	$J/\psi \rightarrow \gamma \eta'$
••• We do not use the following data for averages, fits, limits, etc. •••				
23.5 ± 1.3 ± 0.4	3.2k	¹ PEDLAR	09 CLEO	$J/\psi \rightarrow \gamma \eta'$

¹ Not independent of other η' branching fractions and ratios in PEDLAR 09.

$\Gamma(\pi^0 \pi^0 \eta (3\pi^0 \text{ decay}))/\Gamma_{\text{total}}$ $0.321\Gamma_4/\Gamma$

VALUE	EVTS	DOCUMENT ID	TECN	COMMENT
0.0718 ± 0.0018 OUR FIT				Error includes scale factor of 1.1.
••• We do not use the following data for averages, fits, limits, etc. •••				
0.11 ± 0.06	4	BENSINGER	70 DBC	$2.2 \pi^+ d$

$\Gamma(\pi^0 \pi^0 \eta)/\Gamma(\pi^+ \pi^- \eta)$ Γ_4/Γ_1

VALUE	DOCUMENT ID	TECN	COMMENT
0.527 ± 0.019 OUR FIT			Error includes scale factor of 1.1.
0.555 ± 0.043 ± 0.013			
	PEDLAR	09 CLE3	$J/\psi \rightarrow \eta' \gamma$

$\Gamma(\rho^0 \gamma (\text{including non-resonant } \pi^+ \pi^- \gamma))/\Gamma(\pi \pi \eta)$ $\Gamma_2/(\Gamma_1 + \Gamma_4)$

VALUE	DOCUMENT ID	TECN	COMMENT
0.454 ± 0.009 OUR FIT			Error includes scale factor of 1.1.
0.43 ± 0.02 ± 0.02			
••• We do not use the following data for averages, fits, limits, etc. •••			
0.31 ± 0.15	DAVIS	68 HBC	$5.5 K^- p$

$\Gamma(\omega \gamma)/\Gamma_{\text{total}}$ Γ_5/Γ

VALUE (units 10^{-2})	EVTS	DOCUMENT ID	TECN	COMMENT
2.52 ± 0.07 OUR FIT				
2.50 ± 0.07 OUR AVERAGE				
2.489 ± 0.018 ± 0.074	23k	ABLIKIM	19T BES	$J/\psi \rightarrow \gamma \eta'$
2.55 ± 0.03 ± 0.16	33.2k	¹ ABLIKIM	15AD BES3	$J/\psi \rightarrow \eta' \gamma$
••• We do not use the following data for averages, fits, limits, etc. •••				
2.34 ± 0.30 ± 0.04	70	² PEDLAR	09 CLEO	$J/\psi \rightarrow \gamma \eta'$

¹ Using $B(J/\psi \rightarrow \eta' \gamma) = (5.15 \pm 0.16) \times 10^{-3}$ and $B(\omega \rightarrow \pi^+ \pi^- \pi^0) = (89.2 \pm 0.7)\%$.
² Not independent of other η' branching fractions and ratios in PEDLAR 09.

$\Gamma(\omega \gamma)/\Gamma(\pi^+ \pi^- \eta)$ Γ_5/Γ_1

VALUE	EVTS	DOCUMENT ID	TECN	COMMENT
0.0593 ± 0.0018 OUR FIT				Error includes scale factor of 1.1.
0.055 ± 0.007 ± 0.001				
••• We do not use the following data for averages, fits, limits, etc. •••				
0.068 ± 0.013	68	ZANFINO	77 ASPK	$8.4 \pi^- p$

$\Gamma(\omega \gamma)/\Gamma(\pi^0 \pi^0 \eta)$ Γ_5/Γ_4

VALUE	DOCUMENT ID	TECN	COMMENT
0.113 ± 0.004 OUR FIT			
0.147 ± 0.016			
	ALDE	87B GAM2	$38 \pi^- p \rightarrow n 4 \gamma$

$\Gamma(\omega e^+ e^-)/\Gamma(\omega \gamma)$ Γ_6/Γ_5

VALUE (units 10^{-3})	DOCUMENT ID	TECN	COMMENT
••• We do not use the following data for averages, fits, limits, etc. •••			
7.71 ± 1.34 ± 0.54	¹ ABLIKIM	15AD BES3	$J/\psi \rightarrow \eta' \gamma$

¹ Obtained from other ABLIKIM 15AD measurements with common systematics taken into account.

$\Gamma(\omega e^+ e^-)/\Gamma_{\text{total}}$ Γ_6/Γ

VALUE (units 10^{-4})	EVTS	DOCUMENT ID	TECN	COMMENT
1.97 ± 0.34 ± 0.17				
	66	¹ ABLIKIM	15AD BES3	$J/\psi \rightarrow \eta' \gamma$

¹ Using $B(J/\psi \rightarrow \eta' \gamma) = (5.15 \pm 0.16) \times 10^{-3}$ and $B(\omega \rightarrow \pi^+ \pi^- \pi^0) = (89.2 \pm 0.7)\%$.

$\Gamma(\rho^0 \gamma (\text{including non-resonant } \pi^+ \pi^- \gamma))/[\Gamma(\pi^+ \pi^- \eta) + \Gamma(\pi^0 \pi^0 \eta) + \Gamma(\omega \gamma)]$ $\Gamma_2/(\Gamma_1 + \Gamma_4 + \Gamma_5)$

VALUE	DOCUMENT ID	TECN	COMMENT
0.437 ± 0.008 OUR FIT			Error includes scale factor of 1.1.
••• We do not use the following data for averages, fits, limits, etc. •••			
0.25 ± 0.14	DAUBER	64 HBC	$1.95 K^- p$

$[\Gamma(\pi^0 \pi^0 \eta (\text{charged decay})) + \Gamma(\omega (\text{charged decay}) \gamma)]/\Gamma_{\text{total}}$ $(0.286\Gamma_4 + 0.89\Gamma_5)/\Gamma$

VALUE	EVTS	DOCUMENT ID	TECN	COMMENT
0.0864 ± 0.0017 OUR FIT				Error includes scale factor of 1.1.
••• We do not use the following data for averages, fits, limits, etc. •••				
0.045 ± 0.029	42	RITTENBERG	69 HBC	$1.7\text{--}2.7 K^- p$

$\Gamma(\pi^+ \pi^- \text{ neutrals})/\Gamma_{\text{total}}$ $(0.714\Gamma_1 + 0.286\Gamma_4 + 0.89\Gamma_5)/\Gamma$

VALUE	EVTS	DOCUMENT ID	TECN	COMMENT
0.3897 ± 0.0028 OUR FIT				Error includes scale factor of 1.1.
••• We do not use the following data for averages, fits, limits, etc. •••				
0.4 ± 0.1	39	LONDON	66 HBC	$2.24 K^- p \rightarrow \Lambda \pi^+ \pi^- \text{ neutrals}$
0.35 ± 0.06	33	BADIER	65B HBC	$3 K^- p$

$\Gamma(\gamma \gamma)/\Gamma_{\text{total}}$ Γ_7/Γ

VALUE (units 10^{-2})	EVTS	DOCUMENT ID	TECN	COMMENT
2.307 ± 0.035 OUR FIT				Error includes scale factor of 1.1.
2.31 ± 0.06 OUR AVERAGE				Error includes scale factor of 1.8.
2.331 ± 0.012 ± 0.035	71k	ABLIKIM	19T BES	$J/\psi \rightarrow \gamma \eta'$
1.99 + ^{0.31} - ^{0.27} ± 0.07	114	¹ WICHT	08 BELL	$B^\pm \rightarrow K^\pm \gamma \gamma$
2.00 ± 0.18		² STANTON	80 SPEC	$8.45 \pi^- p \rightarrow n \pi^+ \pi^- 2 \gamma$
••• We do not use the following data for averages, fits, limits, etc. •••				
2.25 ± 0.16 ± 0.03	0.3k	³ PEDLAR	09 CLEO	$J/\psi \rightarrow \gamma \eta'$
1.8 ± 0.2	6000	⁴ APEL	79 NICE	$15\text{--}40 \pi^- p \rightarrow n 2 \gamma$
2.5 ± 0.7		DUANE	74 MMS	$\pi^- p \rightarrow n \text{MM}$
1.71 ± 0.33	68	DALPIAZ	72 CNTR	$1.6 \pi^- p \rightarrow n X^0$
2.0 + ^{0.8} - ^{0.6}	31	HARVEY	71 OSPK	$3.65 \pi^- p \rightarrow n X^0$

¹ WICHT 08 reports $[\Gamma(\eta'(958) \rightarrow \gamma \gamma)/\Gamma_{\text{total}}] \times [B(B^+ \rightarrow \eta' K^+)] = (1.40^{+0.16+0.15}_{-0.15-0.12}) \times 10^{-6}$ which we divide by our best value $B(B^+ \rightarrow \eta' K^+) = (7.04 \pm 0.25) \times 10^{-5}$. Our first error is their experiment's error and our second error is the systematic error from using our best value.

² Includes APEL 79 result.

³ Not independent of other η' branching fractions and ratios in PEDLAR 09.

⁴ Data is included in STANTON 80 evaluation.

$\Gamma(\gamma \gamma)/\Gamma(\pi^+ \pi^- \eta)$ Γ_7/Γ_1

VALUE	DOCUMENT ID	TECN	COMMENT
0.0543 ± 0.0012 OUR FIT			Error includes scale factor of 1.1.
0.053 ± 0.004 ± 0.001			
	PEDLAR	09 CLE3	$J/\psi \rightarrow \eta' \gamma$

$\Gamma(\gamma \gamma)/\Gamma(\rho^0 \gamma (\text{including non-resonant } \pi^+ \pi^- \gamma))$ Γ_7/Γ_2

VALUE	DOCUMENT ID	TECN	COMMENT
0.0783 ± 0.0016 OUR FIT			Error includes scale factor of 1.1.
0.080 ± 0.008			
	ABLIKIM	06E BES2	$J/\psi \rightarrow \eta' \gamma$

$\Gamma(\gamma \gamma)/\Gamma(\pi^0 \pi^0 \eta)$ Γ_7/Γ_4

VALUE	DOCUMENT ID	TECN	COMMENT
0.1031 ± 0.0028 OUR FIT			Error includes scale factor of 1.9.
0.105 ± 0.010 OUR AVERAGE			
0.091 ± 0.009	AMSLER	93 CBAR	$0.0 \bar{p} p$
0.112 ± 0.002 ± 0.006	ALDE	87B GAM2	$38 \pi^- p \rightarrow n 2 \gamma$

$\Gamma(\gamma \gamma)/\Gamma(\pi^0 \pi^0 \eta (\text{neutral decay}))$ $\Gamma_7/0.714\Gamma_4$

VALUE	EVTS	DOCUMENT ID	TECN	COMMENT
0.144 ± 0.004 OUR FIT				
••• We do not use the following data for averages, fits, limits, etc. •••				
0.188 ± 0.058	16	APEL	72 OSPK	$3.8 \pi^- p \rightarrow n X^0$

$\Gamma(\text{neutrals})/\Gamma_{\text{total}}$ $(0.714\Gamma_4 + 0.09\Gamma_5 + \Gamma_7)/\Gamma$

VALUE	EVTS	DOCUMENT ID	TECN	COMMENT
0.185 ± 0.004 OUR FIT				Error includes scale factor of 1.1.
••• We do not use the following data for averages, fits, limits, etc. •••				
0.185 ± 0.022	535	BASILE	71 CNTR	$1.6 \pi^- p \rightarrow n X^0$
0.189 ± 0.026	123	RITTENBERG	69 HBC	$1.7\text{--}2.7 K^- p$

$\Gamma(3\pi^0)/\Gamma_{\text{total}}$ Γ_8/Γ

VALUE (units 10^{-3})	EVTS	DOCUMENT ID	TECN	COMMENT
2.50 ± 0.17 OUR FIT				
3.57 ± 0.26 OUR AVERAGE				
3.522 ± 0.082 ± 0.254	2015	ABLIKIM	17 BES3	$J/\psi \rightarrow \gamma(3\pi^0)$
4.79 ± 0.59 ± 1.14	183	¹ ABLIKIM	15P BES3	$J/\psi \rightarrow K^+ K^- 3\pi$
••• We do not use the following data for averages, fits, limits, etc. •••				
3.56 ± 0.22 ± 0.34	309	² ABLIKIM	12E BES3	$J/\psi \rightarrow \gamma(3\pi^0)$

¹ We have added all systematic uncertainties in quadrature to a single value.

² Superseded by ABLIKIM 17.

$\Gamma(3\pi^0)/\Gamma(\pi^0 \pi^0 \eta)$ Γ_8/Γ_4

VALUE (units 10^{-4})	EVTS	DOCUMENT ID	TECN	COMMENT
112 ± 8 OUR FIT				
78 ± 10 OUR AVERAGE				
86 ± 19	235	BLIK	08 GAMS	$32 \pi^- p \rightarrow \eta' n$
74 ± 15		ALDE	87B GAM2	$38 \pi^- p \rightarrow n 6 \gamma$
75 ± 18		BINON	84 GAM2	$30\text{--}40 \pi^- p \rightarrow n 6 \gamma$

Meson Particle Listings

 $\eta'(958)$

$\Gamma(\mu^+\mu^-\gamma)/\Gamma(\gamma\gamma)$		Γ_9/Γ_7	
VALUE (units 10^{-3})	EVTS	DOCUMENT ID	TECN COMMENT
4.9 ± 1.2	33	VIKTOROV	80 CNTR 25,33 $\pi^- p \rightarrow 2\mu\gamma$

$\Gamma(\pi^+\pi^-\mu^+\mu^-)/\Gamma_{total}$		Γ_{10}/Γ	
VALUE (units 10^{-4})	CL%	DOCUMENT ID	TECN COMMENT
• • • We do not use the following data for averages, fits, limits, etc. • • •			
<0.29	90	¹ ABLIKIM	130 BES3 $J/\psi \rightarrow \gamma\eta'$
<2.4	90	² NAIK	09 CLEO $J/\psi \rightarrow \gamma\eta'$

¹ Using $\Gamma_2/\Gamma = (29.3 \pm 0.6)\%$ from PDG 12.

² Not independent of measured value of Γ_{10}/Γ_1 from NAIK 09.

$\Gamma(\pi^+\pi^-\mu^+\mu^-)/\Gamma(\pi^+\pi^-\eta)$		Γ_{10}/Γ_1	
VALUE (units 10^{-3})	CL%	DOCUMENT ID	TECN COMMENT
<0.5	90	¹ NAIK	09 CLEO $J/\psi \rightarrow \gamma\eta'$

¹ NAIK 09 reports $[\Gamma(\eta'(958) \rightarrow \pi^+\pi^-\mu^+\mu^-)/\Gamma(\eta'(958) \rightarrow \pi^+\pi^-\eta)] / [B(\eta \rightarrow 2\gamma)] < 1.3 \times 10^{-3}$ which we multiply by our best value $B(\eta \rightarrow 2\gamma) = 39.41 \times 10^{-2}$.

$\Gamma(\pi^+\pi^-\mu^+\mu^-)/\Gamma(\rho^0\gamma(\text{including non-resonant } \pi^+\pi^-\gamma))$		Γ_{10}/Γ_2	
VALUE (units 10^{-4})	CL%	DOCUMENT ID	TECN COMMENT
<1.0	90	ABLIKIM	130 BES3 $J/\psi \rightarrow \gamma\eta'$

$\Gamma(\pi^+\pi^-\pi^0)/\Gamma_{total}$		Γ_{11}/Γ	
VALUE (units 10^{-3})	EVTS	DOCUMENT ID	TECN COMMENT
3.61 ± 0.18 OUR FIT			
3.61 ± 0.18 OUR AVERAGE			
3.591 ± 0.054 ± 0.174	6067	ABLIKIM	17 BES3 $J/\psi \rightarrow \gamma(\pi^+\pi^-\pi^0)$
4.28 ± 0.49 ± 1.11	78	¹ ABLIKIM	15P BES3 $J/\psi \rightarrow K^+K^-3\pi$
3.7 ^{+1.1} _{-0.9} ± 0.4		² NAIK	09 CLEO $J/\psi \rightarrow \gamma\eta'$

$\Gamma(\pi^+\pi^-\pi^0)/\Gamma_{total}$		Γ_{11}/Γ	
VALUE (units 10^{-3})	EVTS	DOCUMENT ID	TECN COMMENT
3.61 ± 0.18 OUR FIT			
3.61 ± 0.18 OUR AVERAGE			
3.591 ± 0.054 ± 0.174	6067	ABLIKIM	17 BES3 $J/\psi \rightarrow \gamma(\pi^+\pi^-\pi^0)$
4.28 ± 0.49 ± 1.11	78	¹ ABLIKIM	15P BES3 $J/\psi \rightarrow K^+K^-3\pi$
3.7 ^{+1.1} _{-0.9} ± 0.4		² NAIK	09 CLEO $J/\psi \rightarrow \gamma\eta'$

$\Gamma(\pi^+\pi^-\pi^0)/\Gamma_{total}$		Γ_{11}/Γ	
VALUE (units 10^{-3})	EVTS	DOCUMENT ID	TECN COMMENT
3.61 ± 0.18 OUR FIT			
3.61 ± 0.18 OUR AVERAGE			
3.591 ± 0.054 ± 0.174	6067	ABLIKIM	17 BES3 $J/\psi \rightarrow \gamma(\pi^+\pi^-\pi^0)$
4.28 ± 0.49 ± 1.11	78	¹ ABLIKIM	15P BES3 $J/\psi \rightarrow K^+K^-3\pi$
3.7 ^{+1.1} _{-0.9} ± 0.4		² NAIK	09 CLEO $J/\psi \rightarrow \gamma\eta'$

• • • We do not use the following data for averages, fits, limits, etc. • • •

¹ We have added all systematic uncertainties in quadrature to a single value.

² Not independent of measured value of Γ_{11}/Γ_1 from NAIK 09.

³ Superseded by ABLIKIM 17.

$\Gamma((\pi^+\pi^-\pi^0) \text{ S-wave})/\Gamma_{total}$		Γ_{12}/Γ	
VALUE (units 10^{-4})	EVTS	DOCUMENT ID	TECN COMMENT
37.63 ± 0.77 ± 5.00	6580	¹ ABLIKIM	17 BES3 $J/\psi \rightarrow \gamma(\pi^+\pi^-\pi^0)$

¹ We have added all systematic uncertainties in quadrature.

$\Gamma(\pi^+\pi^-\rho^\pm)/\Gamma_{total}$		Γ_{13}/Γ	
VALUE (units 10^{-4})	EVTS	DOCUMENT ID	TECN COMMENT
7.44 ± 0.60 ± 2.23	1231	¹ ABLIKIM	17 BES3 $J/\psi \rightarrow \gamma(\pi^+\pi^-\rho^\pm)$

¹ We have added all systematic uncertainties in quadrature.

$\Gamma(\pi^+\pi^-\pi^0)/\Gamma(\pi^+\pi^-\eta)$		Γ_{11}/Γ_1	
VALUE (units 10^{-3})	EVTS	DOCUMENT ID	TECN COMMENT
8.5 ± 0.4 OUR FIT			Error includes scale factor of 1.1.
8.28 ^{+2.49}_{-2.12} ± 0.04	20	¹ NAIK	09 CLEO $J/\psi \rightarrow \gamma\eta'$

¹ NAIK 09 reports $[\Gamma(\eta'(958) \rightarrow \pi^+\pi^-\pi^0)/\Gamma(\eta'(958) \rightarrow \pi^+\pi^-\eta)] / [B(\eta \rightarrow 2\gamma)] = (21 ⁺⁶₋₅ ± 2) × 10⁻³ which we multiply by our best value $B(\eta \rightarrow 2\gamma) = (39.41 ± 0.20) × 10^{-2}$. Our first error is their experiment's error and our second error is the systematic error from using our best value.$

$\Gamma(\pi^0\rho^0)/\Gamma_{total}$		Γ_{14}/Γ	
VALUE	CL%	DOCUMENT ID	TECN COMMENT
<0.04	90	RITTENBERG	65 HBC 2.7 K^-p

$\Gamma(2(\pi^+\pi^-))/\Gamma_{total}$		Γ_{15}/Γ	
VALUE (units 10^{-3})	CL% EVTS	DOCUMENT ID	TECN COMMENT
8.4 ± 0.9 ± 0.1	199	¹ ABLIKIM	14M BES3 $J/\psi \rightarrow \gamma\eta'$

$\Gamma(2(\pi^+\pi^-))/\Gamma_{total}$		Γ_{15}/Γ	
VALUE (units 10^{-3})	CL% EVTS	DOCUMENT ID	TECN COMMENT
8.4 ± 0.9 ± 0.1	199	¹ ABLIKIM	14M BES3 $J/\psi \rightarrow \gamma\eta'$
< 24	90	² NAIK	09 CLEO $J/\psi \rightarrow \gamma\eta'$
<1000	90	RITTENBERG	69 HBC 1.7-2.7 K^-p

¹ ABLIKIM 14M reports $[\Gamma(\eta'(958) \rightarrow 2(\pi^+\pi^-))/\Gamma_{total}] × [B(J/\psi(1S) \rightarrow \gamma\eta'(958))] = (4.40 ± 0.35 ± 0.30) × 10^{-7}$ which we divide by our best value $B(J/\psi(1S) \rightarrow \gamma\eta'(958)) = (5.25 ± 0.07) × 10^{-3}$. Our first error is their experiment's error and our second error is the systematic error from using our best value.

² Not independent of measured value of Γ_{15}/Γ_1 from NAIK 09.

$\Gamma(2(\pi^+\pi^-))/\Gamma(\pi^+\pi^-\eta)$		Γ_{15}/Γ_1	
VALUE (units 10^{-3})	CL%	DOCUMENT ID	TECN COMMENT
<0.6	90	¹ NAIK	09 CLEO $J/\psi \rightarrow \gamma\eta'$

¹ NAIK 09 reports $[\Gamma(\eta'(958) \rightarrow 2(\pi^+\pi^-))/\Gamma(\eta'(958) \rightarrow \pi^+\pi^-\eta)] / [B(\eta \rightarrow 2\gamma)] < 1.4 × 10^{-3}$ which we multiply by our best value $B(\eta \rightarrow 2\gamma) = 39.41 × 10^{-2}$.

$\Gamma(\pi^+\pi^-\pi^0)/\Gamma_{total}$		Γ_{16}/Γ	
VALUE (units 10^{-4})	CL% EVTS	DOCUMENT ID	TECN COMMENT
1.79 ± 0.38 ± 0.02	84	¹ ABLIKIM	14M BES3 $J/\psi \rightarrow \gamma\eta'$

• • • We do not use the following data for averages, fits, limits, etc. • • •

¹ ABLIKIM 14M reports $[\Gamma(\eta'(958) \rightarrow \pi^+\pi^-\pi^0)/\Gamma_{total}] × [B(J/\psi(1S) \rightarrow \gamma\eta'(958))] = (9.38 ± 1.79 ± 0.89) × 10^{-7}$ which we divide by our best value $B(J/\psi(1S) \rightarrow \gamma\eta'(958)) = (5.25 ± 0.07) × 10^{-3}$. Our first error is their experiment's error and our second error is the systematic error from using our best value.

² Not independent of measured value of Γ_{16}/Γ_1 from NAIK 09.

$\Gamma(\pi^+\pi^-\pi^0)/\Gamma(\pi^+\pi^-\eta)$		Γ_{16}/Γ_1	
VALUE (units 10^{-3})	CL%	DOCUMENT ID	TECN COMMENT
<6	90	¹ NAIK	09 CLEO $J/\psi \rightarrow \gamma\eta'$

¹ NAIK 09 reports $[\Gamma(\eta'(958) \rightarrow \pi^+\pi^-\pi^0)/\Gamma(\eta'(958) \rightarrow \pi^+\pi^-\eta)] / [B(\eta \rightarrow 2\gamma)] < 15 × 10^{-3}$ which we multiply by our best value $B(\eta \rightarrow 2\gamma) = 39.41 × 10^{-2}$.

$\Gamma(2(\pi^+\pi^-) \text{ neutrals})/\Gamma_{total}$		Γ_{17}/Γ	
VALUE	CL%	DOCUMENT ID	TECN COMMENT
<0.01	95	DANBURG	73 HBC 2.2 $K^-p \rightarrow \Lambda X^0$

• • • We do not use the following data for averages, fits, limits, etc. • • •

<0.01

$\Gamma(2(\pi^+\pi^-)\pi^0)/\Gamma_{total}$		Γ_{18}/Γ	
VALUE	CL%	DOCUMENT ID	TECN COMMENT
<0.002	90	¹ NAIK	09 CLEO $J/\psi \rightarrow \gamma\eta'$
<0.01	90	RITTENBERG	69 HBC 1.7-2.7 K^-p

• • • We do not use the following data for averages, fits, limits, etc. • • •

<0.002

<0.01

¹ Not independent of measured value of Γ_{18}/Γ_1 from NAIK 09.

$\Gamma(2(\pi^+\pi^-)\pi^0)/\Gamma(\pi^+\pi^-\eta)$		Γ_{18}/Γ_1	
VALUE (units 10^{-3})	CL%	DOCUMENT ID	TECN COMMENT
<4	90	¹ NAIK	09 CLEO $J/\psi \rightarrow \gamma\eta'$

¹ NAIK 09 reports $[\Gamma(\eta'(958) \rightarrow 2(\pi^+\pi^-)\pi^0)/\Gamma(\eta'(958) \rightarrow \pi^+\pi^-\eta)] / [B(\eta \rightarrow 2\gamma)] < 11 × 10^{-3}$ which we multiply by our best value $B(\eta \rightarrow 2\gamma) = 39.41 × 10^{-2}$.

$\Gamma(2(\pi^+\pi^-)2\pi^0)/\Gamma_{total}$		Γ_{19}/Γ	
VALUE	CL%	DOCUMENT ID	TECN COMMENT
<0.01	95	KALBFLEISCH	64B HBC $K^-p \rightarrow \Lambda 2(\pi^+\pi^-)+MM$

• • • We do not use the following data for averages, fits, limits, etc. • • •

<0.01

<0.01

$\Gamma(3(\pi^+\pi^-))/\Gamma_{total}$		Γ_{20}/Γ	
VALUE (units 10^{-5})	CL%	DOCUMENT ID	TECN COMMENT
< 3.1	90	¹ ABLIKIM	13U BES3 $J/\psi \rightarrow \gamma 3(\pi^+\pi^-)$

• • • We do not use the following data for averages, fits, limits, etc. • • •

< 53

<500

¹ Using $B(J/\psi \rightarrow \gamma\eta'(958)) = (5.16 ± 0.15) × 10^{-3}$.

² Not independent of measured value of Γ_{20}/Γ_1 from NAIK 09.

$\Gamma(3(\pi^+\pi^-))/\Gamma(\pi^+\pi^-\eta)$		Γ_{20}/Γ_1	
VALUE (units 10^{-3})	CL%	DOCUMENT ID	TECN COMMENT
<1.2	90	¹ NAIK	09 CLEO $J/\psi \rightarrow \gamma\eta'$

¹ NAIK 09 reports $[\Gamma(\eta'(958) \rightarrow 3(\pi^+\pi^-))/\Gamma(\eta'(958) \rightarrow \pi^+\pi^-\eta)] / [B(\eta \rightarrow 2\gamma)] < 3.0 × 10^{-3}$ which we multiply by our best value $B(\eta \rightarrow 2\gamma) = 39.41 × 10^{-2}$.

$\Gamma(K^\pm\pi^\mp)/\Gamma(\rho^0\gamma(\text{including non-resonant } \pi^+\pi^-\gamma))$		Γ_{21}/Γ_2	
VALUE	CL%	DOCUMENT ID	TECN COMMENT
<1.3 × 10⁻⁴	90	ABLIKIM	16M BES3 $e^+e^- \rightarrow J/\psi \rightarrow \text{hadrons}$

$\Gamma(\pi^+\pi^-\pi^0)/\Gamma_{total}$		Γ_{22}/Γ	
VALUE (units 10^{-3})	CL% EVTS	DOCUMENT ID	TECN COMMENT
2.4 ^{+1.3}_{-0.9} OUR FIT			
2.11 ± 0.12 ± 0.14	429	¹ ABLIKIM	130 BES3 $J/\psi \rightarrow \gamma\eta'$
2.5 ^{+1.2} _{-0.9} ± 0.5		² NAIK	09 CLEO $J/\psi \rightarrow \gamma\eta'$

• • • We do not use the following data for averages, fits, limits, etc. • • •

<6

<6

¹ Using $\Gamma_2/\Gamma = (29.3 ± 0.6)\%$ from PDG 12.

² Not independent of measured value of Γ_{22}/Γ_1 from NAIK 09.

See key on page 999

Meson Particle Listings

$\eta'(958)$

$\Gamma(\pi^+\pi^-e^+e^-)/\Gamma(\pi^+\pi^-\eta)$		Γ_{22}/Γ_1	
VALUE (units 10^{-3})	EVTS	DOCUMENT ID	TECN COMMENT

5.5 $\pm_{-2.3}^{+3.0}$ OUR FIT

5.52 $\pm_{-2.30}^{+3.00} \pm 0.03$ 8 1 NAIK 09 CLEO $J/\psi \rightarrow \gamma\eta'$

¹ NAIK 09 reports $[\Gamma(\eta'(958) \rightarrow \pi^+\pi^-e^+e^-)/\Gamma(\eta'(958) \rightarrow \pi^+\pi^-\eta)] / [B(\eta \rightarrow 2\gamma)] = (14_{-5}^{+7} \pm 3) \times 10^{-3}$ which we multiply by our best value $B(\eta \rightarrow 2\gamma) = (39.41 \pm 0.20) \times 10^{-2}$. Our first error is their experiment's error and our second error is the systematic error from using our best value.

$\Gamma(\pi^+\pi^-e^+e^-)/\Gamma(\rho^0\gamma(\text{including non-resonant } \pi^+\pi^-\gamma))$		Γ_{22}/Γ_2	
VALUE (units 10^{-3})	EVTS	DOCUMENT ID	TECN COMMENT

7.2 $\pm 0.4 \pm 0.5$ 429 ABLIKIM 130 BES3 $J/\psi \rightarrow \gamma\eta'$

$\Gamma(\pi^+e^-\nu_e + c.c.)/\Gamma(\pi^+\pi^-\eta)$		Γ_{23}/Γ_1	
VALUE (units 10^{-4})	CL%	DOCUMENT ID	TECN COMMENT

<5.0 90 ABLIKIM 13G BES3 $J/\psi \rightarrow \phi\eta'$

$\Gamma(\gamma e^+e^-)/\Gamma_{\text{total}}$		Γ_{24}/Γ	
VALUE (units 10^{-3})	CL%	DOCUMENT ID	TECN COMMENT

• • • We do not use the following data for averages, fits, limits, etc. • • •

<0.9 90 BRIERE 00 CLEO 10.6 e^+e^-

$\Gamma(\gamma e^+e^-)/\Gamma(\gamma\gamma)$		Γ_{24}/Γ_7	
VALUE (units 10^{-2})	EVTS	DOCUMENT ID	TECN COMMENT

2.13 $\pm 0.09 \pm 0.07$ 864 ABLIKIM 150 BES3 $J/\psi \rightarrow \gamma e^+e^-$

$\Gamma(\pi^0\gamma\gamma)/\Gamma_{\text{total}}$		Γ_{25}/Γ	
VALUE (units 10^{-3})	EVTS	DOCUMENT ID	TECN COMMENT

3.20 $\pm 0.07 \pm 0.23$ 3.4k ABLIKIM 17T BES3 $J/\psi \rightarrow \gamma\eta'$

$\Gamma(\pi^0\gamma\gamma(\text{non resonant}))/\Gamma_{\text{total}}$		Γ_{26}/Γ	
VALUE (units 10^{-4})	EVTS	DOCUMENT ID	TECN COMMENT

6.16 $\pm 0.64 \pm 0.67$ 655 ABLIKIM 17T BES3 $J/\psi \rightarrow \gamma\eta'$

$\Gamma(\pi^0\gamma\gamma)/\Gamma(\pi^0\pi^0\eta)$		Γ_{25}/Γ_4	
VALUE (units 10^{-4})	CL%	DOCUMENT ID	TECN COMMENT

<37 90 ALDE 87B GAM2 38 $\pi^-\rho \rightarrow n4\gamma$

$\Gamma(\eta\gamma\gamma)/\Gamma_{\text{total}}$		Γ_{27}/Γ	
VALUE	CL%	DOCUMENT ID	TECN COMMENT

<1.33 $\times 10^{-4}$ 90 ABLIKIM 19AW BES3 $J/\psi \rightarrow \gamma\eta' \rightarrow \gamma\gamma\gamma 2\gamma$

$\Gamma(4\pi^0)/\Gamma_{\text{total}}$		Γ_{28}/Γ	
VALUE	CL%	DOCUMENT ID	TECN COMMENT

<3.2 $\times 10^{-4}$ 90 DONSKOV 14 GAM4 32.5 $\pi^-\rho \rightarrow \eta' n$

$\Gamma(4\pi^0)/\Gamma(\pi^0\pi^0\eta)$		Γ_{28}/Γ_4	
VALUE (units 10^{-4})	CL%	DOCUMENT ID	TECN COMMENT

• • • We do not use the following data for averages, fits, limits, etc. • • •

<23 90 ALDE 87B GAM2 38 $\pi^-\rho \rightarrow n8\gamma$

$\Gamma(e^+e^-)/\Gamma_{\text{total}}$		Γ_{29}/Γ	
VALUE	CL%	DOCUMENT ID	TECN COMMENT

< 5.6 $\times 10^{-9}$ 90 1 ACHASOV 15 SND 0.958 $e^+e^- \rightarrow \pi\pi\eta$

• • • We do not use the following data for averages, fits, limits, etc. • • •

<12 $\times 10^{-9}$ 90 2 AKHMETSHIN 15 CMD3 0.958 $e^+e^- \rightarrow \pi^+\pi^-\eta$

< 2.1 $\times 10^{-7}$ 90 VOROBYEV 88 ND $e^+e^- \rightarrow \pi^+\pi^-\eta$

¹ Combining data of ACHASOV 15 and AKHMETSHIN 15 and using $\Gamma(\eta') = 0.198 \pm 0.009$ MeV.

² Using $\Gamma_{\eta'(958)} = 198 \pm 9$ keV, $B(\eta'(958) \rightarrow \pi^+\pi^-\eta) = (42.9 \pm 0.7)\%$, and $B(\eta \rightarrow \gamma\gamma) = (39.41 \pm 0.20)\%$.

$\Gamma(\text{invisible})/\Gamma_{\text{total}}$		Γ_{30}/Γ	
VALUE (units 10^{-4})	CL%	DOCUMENT ID	TECN COMMENT

• • • We do not use the following data for averages, fits, limits, etc. • • •

<9.5 90 1 NAIK 09 CLEO $J/\psi \rightarrow \gamma\eta'$

¹ Not independent of measured value of Γ_{30}/Γ_1 from NAIK 09.

$\Gamma(\text{invisible})/\Gamma(\gamma\gamma)$		Γ_{30}/Γ_7	
VALUE (units 10^{-2})	CL%	DOCUMENT ID	TECN COMMENT

<2.4 90 ABLIKIM 13 BES3 $J/\psi \rightarrow \phi\eta'$

• • • We do not use the following data for averages, fits, limits, etc. • • •

<6.69 90 ABLIKIM 06Q BES $J/\psi \rightarrow \phi\eta'$

$\Gamma(\text{invisible})/\Gamma(\pi^+\pi^-\eta)$		Γ_{30}/Γ_1	
VALUE (units 10^{-3})	CL%	DOCUMENT ID	TECN COMMENT

• • • We do not use the following data for averages, fits, limits, etc. • • •

<2.1 90 1 NAIK 09 CLEO $J/\psi \rightarrow \gamma\eta'$

¹ NAIK 09 reports $[\Gamma(\eta'(958) \rightarrow \text{invisible})/\Gamma(\eta'(958) \rightarrow \pi^+\pi^-\eta)] / [B(\eta \rightarrow 2\gamma)] < 5.4 \times 10^{-3}$ which we multiply by our best value $B(\eta \rightarrow 2\gamma) = 39.41 \times 10^{-2}$.

$\Gamma(\pi^+\pi^-)/\Gamma_{\text{total}}$		Γ_{31}/Γ	
VALUE (units 10^{-4})	CL%	DOCUMENT ID	TECN COMMENT

< 0.18 90 1 AAIJ 17D LHCB $D_{(s)}^+ \rightarrow \pi^+\pi^-\pi^+$

• • • We do not use the following data for averages, fits, limits, etc. • • •

< 0.5 90 2 ABLIKIM 11G BES3 $J/\psi \rightarrow \gamma\pi^+\pi^-$

< 29 90 3 MORI 07A BELL $\gamma\gamma \rightarrow \pi^+\pi^-$

< 3.3 90 4 MORI 07A BELL $\gamma\gamma \rightarrow \pi^+\pi^-$

<800 95 DANBURG 73 HBC 2.2 $K^-\rho \rightarrow \Lambda X^0$

<200 90 RITTENBERG 69 HBC 1.7-2.7 $K^-\rho$

¹ Using branching fractions of $D_{(s)}^+$ decays from PDG 15.

² ABLIKIM 11G reports $[\Gamma(\eta'(958) \rightarrow \pi^+\pi^-)/\Gamma_{\text{total}}] \times [B(J/\psi(1S) \rightarrow \gamma\eta'(958))] < 2.84 \times 10^{-7}$ which we divide by our best value $B(J/\psi(1S) \rightarrow \gamma\eta'(958)) = 5.25 \times 10^{-3}$.

³ Taking into account interference with the $\gamma\gamma \rightarrow \pi^+\pi^-$ continuum.

⁴ Without interference with the $\gamma\gamma \rightarrow \pi^+\pi^-$ continuum.

$\Gamma(\pi^0\pi^0)/\Gamma_{\text{total}}$		Γ_{32}/Γ	
VALUE	CL%	DOCUMENT ID	TECN COMMENT

<4 $\times 10^{-4}$ 90 1 ABLIKIM 11G BES3 $J/\psi \rightarrow \gamma\pi^0\pi^0$

¹ ABLIKIM 11G reports $[\Gamma(\eta'(958) \rightarrow \pi^+\pi^-)/\Gamma_{\text{total}}] \times [B(J/\psi(1S) \rightarrow \gamma\eta'(958))] < 2.84 \times 10^{-7}$ which we divide by our best value $B(J/\psi(1S) \rightarrow \gamma\eta'(958)) = 5.25 \times 10^{-3}$.

$\Gamma(\pi^0\pi^0)/\Gamma(\pi^0\pi^0\eta)$		Γ_{32}/Γ_4	
VALUE (units 10^{-4})	CL%	DOCUMENT ID	TECN COMMENT

<45 90 ALDE 87B GAM2 38 $\pi^-\rho \rightarrow n4\gamma$

$\Gamma(\pi^0e^+e^-)/\Gamma_{\text{total}}$		Γ_{33}/Γ	
VALUE (units 10^{-3})	CL%	DOCUMENT ID	TECN COMMENT

< 1.4 90 BRIERE 00 CLEO 10.6 e^+e^-

• • • We do not use the following data for averages, fits, limits, etc. • • •

<13 90 RITTENBERG 65 HBC 2.7 $K^-\rho$

$\Gamma(\eta e^+e^-)/\Gamma_{\text{total}}$		Γ_{34}/Γ	
VALUE (units 10^{-3})	CL%	DOCUMENT ID	TECN COMMENT

< 2.4 90 BRIERE 00 CLEO 10.6 e^+e^-

• • • We do not use the following data for averages, fits, limits, etc. • • •

<11 90 RITTENBERG 65 HBC 2.7 $K^-\rho$

$\Gamma(3\gamma)/\Gamma(\pi^0\pi^0\eta)$		Γ_{35}/Γ_4	
VALUE (units 10^{-4})	CL%	DOCUMENT ID	TECN COMMENT

<4.6 90 ALDE 87B GAM2 38 $\pi^-\rho \rightarrow n3\gamma$

$\Gamma(\mu^+\mu^-)/\Gamma_{\text{total}}$		Γ_{36}/Γ	
VALUE (units 10^{-9})	CL%	DOCUMENT ID	TECN COMMENT

<6.0 90 DZHELADIN 81 CNTR 30 $\pi^-\rho \rightarrow \eta' n$

$\Gamma(\mu^+\mu^-\eta)/\Gamma_{\text{total}}$		Γ_{37}/Γ	
VALUE (units 10^{-5})	CL%	DOCUMENT ID	TECN COMMENT

<1.5 90 DZHELADIN 81 CNTR 30 $\pi^-\rho \rightarrow \eta' n$

$\Gamma(e\mu)/\Gamma_{\text{total}}$		Γ_{38}/Γ	
VALUE (units 10^{-4})	CL%	DOCUMENT ID	TECN COMMENT

<4.7 90 BRIERE 00 CLEO 10.6 e^+e^-

$\eta'(958) \rightarrow \eta\pi\pi$ DECAY PARAMETERS

$$|\text{MATRIX ELEMENT}|^2 = |1 + \alpha Y|^2 + CX + DX^2$$

X and Y are Dalitz variables; α is complex and C , and D are real-valued. Parameters C and D are not necessarily equal to c and d , respectively, in the generalized parameterization following this one. May be different for $\eta'(958) \rightarrow \eta\pi^+\pi^-$ and $\eta'(958) \rightarrow \eta\pi^0\pi^0$ decays. Because of different initial assumptions and strong correlations of the parameters we do not average the parameters in the section below.

Re(α) decay parameter

VALUE	EVTS	DOCUMENT ID	TECN COMMENT
-------	------	-------------	--------------

• • • We do not use the following data for averages, fits, limits, etc. • • •

-0.034 $\pm 0.002 \pm 0.002$ 351k ABLIKIM 18 BES3 $\eta' \rightarrow \eta\pi^+\pi^-$

-0.054 $\pm 0.004 \pm 0.001$ 56k ABLIKIM 18 BES3 $\eta' \rightarrow \eta\pi^0\pi^0$

Meson Particle Listings

 $\eta'(958)$

$-0.033 \pm 0.005 \pm 0.003$	44k	1	ABLIKIM	11	BES3	$J/\psi \rightarrow \gamma \eta \pi^+ \pi^-$
$-0.072 \pm 0.012 \pm 0.006$	7k	2	AMELIN	05A	VES	$28 \pi^- A \rightarrow \eta \pi^+ \pi^- \pi^- A^*$
$-0.021 \pm 0.018 \pm 0.017$	6.7k	3	BRIERE	00	CLEO	$10.6 e^+ e^- \rightarrow \eta \pi^+ \pi^- X$
$-0.058 \pm 0.013 \pm 0.003$	5.4k	4	ALDE	86	GAM2	$38 \pi^- p \rightarrow n \eta \pi^0 \pi^0$
-0.08 ± 0.03		4.5	KALBFLEISCH	74	RVUE	$\eta' \rightarrow \eta \pi^+ \pi^-$

¹ See ABLIKIM 11 for the full correlation matrix.

² Superseded by DOROFEEV 07, which found this parameterization unacceptable. See below.

³ Assuming $\text{Im}(\alpha) = 0$, $C = 0$, and $D = 0$.

⁴ Assuming $C = 0$.

⁵ From the data of DAUBER 64, RITTENBERG 69, AGUILAR-BENITEZ 72B, JACOBS 73, and DANBURG 73.

 $\text{Im}(\alpha)$ decay parameter

VALUE	EVTS	DOCUMENT ID	TECN	COMMENT	
$0.000 \pm 0.019 \pm 0.001$	351k	ABLIKIM	18	BES3 $\eta' \rightarrow \eta \pi^+ \pi^-$	
$0.000 \pm 0.038 \pm 0.002$	56k	ABLIKIM	18	BES3 $\eta' \rightarrow \eta \pi^0 \pi^0$	
$0.000 \pm 0.049 \pm 0.001$	44k	1	ABLIKIM	11	BES3 $J/\psi \rightarrow \gamma \eta \pi^+ \pi^-$
$0.0 \pm 0.1 \pm 0.0$	7k	2	AMELIN	05A	VES $28 \pi^- A \rightarrow \eta \pi^+ \pi^- \pi^- A^*$
$-0.00 \pm 0.13 \pm 0.00$	5.4k	3	ALDE	86	GAM2 $38 \pi^- p \rightarrow n \eta \pi^0 \pi^0$
0.0 ± 0.3		3.4	KALBFLEISCH	74	RVUE $\eta' \rightarrow \eta \pi^+ \pi^-$

¹ See ABLIKIM 11 for the full correlation matrix.

² Superseded by DOROFEEV 07, which found this parameterization unacceptable. See below.

³ Assuming $C = 0$.

⁴ From the data of DAUBER 64, RITTENBERG 69, AGUILAR-BENITEZ 72B, JACOBS 73, and DANBURG 73.

C decay parameter

VALUE	EVTS	DOCUMENT ID	TECN	COMMENT	
$0.0027 \pm 0.0024 \pm 0.0015$	351k	ABLIKIM	18	BES3 $\eta' \rightarrow \eta \pi^+ \pi^-$	
$0.018 \pm 0.009 \pm 0.003$	44k	1	ABLIKIM	11	BES3 $J/\psi \rightarrow \gamma \eta \pi^+ \pi^-$
$0.020 \pm 0.018 \pm 0.004$	7k	2	AMELIN	05A	VES $28 \pi^- A \rightarrow \eta \pi^+ \pi^- \pi^- A^*$

¹ See ABLIKIM 11 for the full correlation matrix.

² Superseded by DOROFEEV 07, which found this parameterization unacceptable. See below.

D decay parameter

VALUE	EVTS	DOCUMENT ID	TECN	COMMENT	
$-0.053 \pm 0.004 \pm 0.004$	351k	ABLIKIM	18	BES3 $\eta' \rightarrow \eta \pi^+ \pi^-$	
$-0.061 \pm 0.009 \pm 0.005$	56k	ABLIKIM	18	BES3 $\eta' \rightarrow \eta \pi^0 \pi^0$	
$-0.059 \pm 0.012 \pm 0.004$	44k	1	ABLIKIM	11	BES3 $J/\psi \rightarrow \gamma \eta \pi^+ \pi^-$
$-0.066 \pm 0.030 \pm 0.015$	7k	2	AMELIN	05A	VES $28 \pi^- A \rightarrow \eta \pi^+ \pi^- \pi^- A^*$
$0.00 \pm 0.03 \pm 0.00$	5.4k	3	ALDE	86	GAM2 $38 \pi^- p \rightarrow n \eta \pi^0 \pi^0$
0		3.4	KALBFLEISCH	74	RVUE $\eta' \rightarrow \eta \pi^+ \pi^-$

¹ See ABLIKIM 11 for the full correlation matrix.

² Superseded by DOROFEEV 07, which found this parameterization unacceptable. See below.

³ Assuming $C = 0$.

⁴ From the data of DAUBER 64, RITTENBERG 69, AGUILAR-BENITEZ 72B, JACOBS 73, and DANBURG 73.

 $\eta'(958) \rightarrow \eta \pi \pi$ DECAY PARAMETERS

$$|\text{MATRIX ELEMENT}|^2 \propto 1 + a Y + b Y^2 + c X + d X^2$$

X and Y are Dalitz variables and a , b , c , and d are real-valued parameters. May be different for $\eta'(958) \rightarrow \eta \pi^+ \pi^-$ and $\eta'(958) \rightarrow \eta \pi^0 \pi^0$ decays. We do not average measurements in the section below because parameter values from each experiment are strongly correlated.

a decay parameter

VALUE	EVTS	DOCUMENT ID	TECN	COMMENT	
$-0.056 \pm 0.004 \pm 0.002$	351k	ABLIKIM	18	BES3 $\eta' \rightarrow \eta \pi^+ \pi^-$	
$-0.087 \pm 0.009 \pm 0.006$	56k	ABLIKIM	18	BES3 $\eta' \rightarrow \eta \pi^0 \pi^0$	
$-0.074 \pm 0.008 \pm 0.006$	124k	ADLARSON	18A	A2MM $\eta' \rightarrow \eta \pi^0 \pi^0$	
$-0.072 \pm 0.007 \pm 0.008$		1	GONZALEZ-S...	18A	RVUE $\eta' \rightarrow \eta \pi^0 \pi^0$
$-0.047 \pm 0.011 \pm 0.003$	44k	2	ABLIKIM	11	BES3 $J/\psi \rightarrow \gamma \eta \pi^+ \pi^-$
$-0.066 \pm 0.016 \pm 0.003$	15k	3	BLIK	09	GAM4 $32.5 \pi^- p \rightarrow \eta' n$
$-0.127 \pm 0.016 \pm 0.008$	20k	4	DOROFEEV	07	VES $27 \pi^- p \rightarrow \eta' n$

¹ Theoretical analysis of ADLARSON 18A using resonance chiral perturbation theory to one loop.

² See ABLIKIM 11 for the full correlation matrix.

³ From $\eta' \rightarrow \eta \pi^0 \pi^0$ decay.

⁴ From $\eta' \rightarrow \eta \pi^+ \pi^-$ decay.

b decay parameter

VALUE	EVTS	DOCUMENT ID	TECN	COMMENT	
$-0.049 \pm 0.006 \pm 0.006$	351k	ABLIKIM	18	BES3 $\eta' \rightarrow \eta \pi^+ \pi^-$	
$-0.073 \pm 0.014 \pm 0.005$	56k	ABLIKIM	18	BES3 $\eta' \rightarrow \eta \pi^0 \pi^0$	
$-0.063 \pm 0.014 \pm 0.005$	124k	ADLARSON	18A	A2MM $\eta' \rightarrow \eta \pi^0 \pi^0$	
$-0.052 \pm 0.001 \pm 0.002$		1	GONZALEZ-S...	18A	RVUE $\eta' \rightarrow \eta \pi^0 \pi^0$
$-0.069 \pm 0.019 \pm 0.009$	44k	2	ABLIKIM	11	BES3 $J/\psi \rightarrow \gamma \eta \pi^+ \pi^-$
$-0.063 \pm 0.028 \pm 0.004$	15k	3	BLIK	09	GAM4 $32.5 \pi^- p \rightarrow \eta' n$
$-0.106 \pm 0.028 \pm 0.014$	20k	4	DOROFEEV	07	VES $27 \pi^- p \rightarrow \eta' n$

¹ Theoretical analysis of ADLARSON 18A using resonance chiral perturbation theory to one loop.

² See ABLIKIM 11 for the full correlation matrix.

³ From $\eta' \rightarrow \eta \pi^0 \pi^0$ decay.

⁴ From $\eta' \rightarrow \eta \pi^+ \pi^-$ decay.

c decay parameter

VALUE	EVTS	DOCUMENT ID	TECN	COMMENT	
$0.0027 \pm 0.0024 \pm 0.0018$	351k	ABLIKIM	18	BES3 $\eta' \rightarrow \eta \pi^+ \pi^-$	
$0.019 \pm 0.011 \pm 0.003$	44k	1	ABLIKIM	11	BES3 $J/\psi \rightarrow \gamma \eta \pi^+ \pi^-$
$-0.107 \pm 0.096 \pm 0.003$	15k	2	BLIK	09	GAM4 $32.5 \pi^- p \rightarrow \eta' n$
$0.015 \pm 0.011 \pm 0.014$	20k	3	DOROFEEV	07	VES $27 \pi^- p \rightarrow \eta' n$

¹ See ABLIKIM 11 for the full correlation matrix.

² From $\eta' \rightarrow \eta \pi^0 \pi^0$ decay.

³ From $\eta' \rightarrow \eta \pi^+ \pi^-$ decay.

d decay parameter

VALUE	EVTS	DOCUMENT ID	TECN	COMMENT	
$-0.063 \pm 0.004 \pm 0.003$	351k	ABLIKIM	18	BES3 $\eta' \rightarrow \eta \pi^+ \pi^-$	
$-0.074 \pm 0.009 \pm 0.004$	56k	ABLIKIM	18	BES3 $\eta' \rightarrow \eta \pi^0 \pi^0$	
$-0.050 \pm 0.009 \pm 0.005$	124k	ADLARSON	18A	A2MM $\eta' \rightarrow \eta \pi^0 \pi^0$	
$-0.051 \pm 0.008 \pm 0.006$		1	GONZALEZ-S...	18A	RVUE $\eta' \rightarrow \eta \pi^0 \pi^0$
$-0.073 \pm 0.012 \pm 0.003$	44k	2	ABLIKIM	11	BES3 $J/\psi \rightarrow \gamma \eta \pi^+ \pi^-$
$0.018 \pm 0.078 \pm 0.006$	15k	3	BLIK	09	GAM4 $32.5 \pi^- p \rightarrow \eta' n$
$-0.082 \pm 0.017 \pm 0.008$	20k	4	DOROFEEV	07	VES $27 \pi^- p \rightarrow \eta' n$

¹ Theoretical analysis of ADLARSON 18A using resonance chiral perturbation theory to one loop.

² See ABLIKIM 11 for the full correlation matrix.

³ From $\eta' \rightarrow \eta \pi^0 \pi^0$ decay. If $c \equiv 0$ from Bose-Einstein symmetry, $d = -0.067 \pm 0.020 \pm 0.003$.

⁴ From $\eta' \rightarrow \eta \pi^+ \pi^-$ decay.

 **$\eta'(958)$ β PARAMETER
|MATRIX ELEMENT|^2 = (1 + 2 β Z)**

See the "Note on η Decay Parameters" in our 1994 edition Physical Review D50 1173 (1994), p. 1454.

 β decay parameter

VALUE	EVTS	DOCUMENT ID	TECN	COMMENT
-0.61 ± 0.08 OUR AVERAGE				Error includes scale factor of 1.2.
$-0.640 \pm 0.046 \pm 0.047$	1.8k	ABLIKIM	15G	BES3 $J/\psi \rightarrow \gamma (\pi^0 \pi^0 \pi^0)$
-0.59 ± 0.18	235	BLIK	08	GAMS $32 \pi^- p \rightarrow \eta' n$
-0.1 ± 0.3		ALDE	87B	GAM2 $38 \pi^- p \rightarrow n 3\pi^0$

 $\eta'(958)$ C-NONCONSERVING DECAY PARAMETER

See the note on η decay parameters in the Stable Particle Particle Listings for definition of this parameter.

DECAY ASYMMETRY PARAMETER FOR $\pi^+ \pi^- \gamma$

VALUE	EVTS	DOCUMENT ID	TECN	COMMENT
-0.03 ± 0.04 OUR AVERAGE				
-0.019 ± 0.056		AIHARA	87	TPC $2\gamma \rightarrow \pi^+ \pi^- \gamma$
-0.069 ± 0.078	295	GRIGORIAN	75	STRC $2.1 \pi^- p$
0.00 ± 0.10	103	KALBFLEISCH	75	HBC $2.18 K^- p \rightarrow \Lambda \pi^+ \pi^- \gamma$

• • • We do not use the following data for averages, fits, limits, etc. • • •

0.07 \pm 0.08 152 RITTENBERG 65 HBC 2.1-2.7 $K^- p$

 $\eta'(958) \rightarrow \gamma \ell^+ \ell^-$ TRANSITION FORM FACTOR SLOPE

Related to the effective virtual meson mass Λ , via slope $\approx \Lambda^{-2}$. See e.g. LANDSBERG 85, eq. (3.8), for a detailed definition.

VALUE (GeV ⁻²)	EVTS	DOCUMENT ID	TECN	COMMENT	
1.62 ± 0.17 OUR AVERAGE					
$1.60 \pm 0.17 \pm 0.08$	864	1	ABLIKIM	15G	BES3 $J/\psi \rightarrow \gamma e^+ e^-$
1.7 ± 0.4	33	1	VIKTOROV	80	$25,33 \pi^- p \rightarrow 2\mu \gamma$

¹ In the single-pole Ansatz where slope = $1/(\Lambda^2 + \gamma^2)$ with Λ , γ being a Breit-Wigner mass, width for the effective contributing vector meson.

$\eta'(958)$ REFERENCES

... We do not use the following data for averages, fits, limits, etc. ...

Table of references for η'(958) meson, listing author names, publication details, and collaboration names.

Table of references for f0(980) meson, listing author names, publication details, and collaboration names.

f0(980) I^G(J^PC) = 0+(0++)

See the review on "Scalar Mesons below 2 GeV."

f0(980) MASS

Table with columns: VALUE (MeV), EVTS, DOCUMENT ID, TECN, COMMENT. Row 1: 990 ± 20 OUR ESTIMATE

Meson Particle Listings

$f_0(980)$

974 ± 4	42 GIDAL	81 MRK2	$J/\psi \rightarrow \pi^+ \pi^- X$
975	43 ACHASOV	80 RVUE	
986 ± 10	42 AGUILAR...	78 HBC	$0.7 \bar{p} p \rightarrow K_S^0 K_S^0$
969 ± 5	42 LEEPER	77 ASPK	$2-2.4 \pi^- p \rightarrow \pi^+ \pi^- n, K^+ K^- n$
987 ± 7	42 BINNIE	73 CNTR	$\pi^- p \rightarrow nMM$
1012 ± 6	44 GRAYER	73 ASPK	$17 \pi^- p \rightarrow \pi^+ \pi^- n$
1007 ± 20	44 HYAMS	73 ASPK	$17 \pi^- p \rightarrow \pi^+ \pi^- n$
997 ± 6	44 PROTOPOP...	73 HBC	$7 \pi^+ p \rightarrow \pi^+ p \pi^+ \pi^-$

- From the $D^\pm \rightarrow K^\pm K^+ K^-$ Dalitz plot fit with the Triple-M amplitude in the multi-meson model of AOUDE 18.
- Quoted number refers to real part of pole position.
- Analytic continuation using Roy equations. Uses the K_{e4} data of BATLEY 10c and the $\pi N \rightarrow \pi \pi N$ data of HYAMS 73, GRAYER 74, and PROTOPODESCU 73.
- Analytic continuation using GKPY equations. Uses the K_{e4} data of BATLEY 10c and the $\pi N \rightarrow \pi \pi N$ data of HYAMS 73, GRAYER 74, and PROTOPODESCU 73.
- Pole position. Used Roy equations.
- Average of the analyses of three data sets in the K-matrix model. Uses the data of BATLEY 08a, HYAMS 73, and GRAYER 74, partially of COHEN 80 or ETKIN 82b.
- On sheet II in a 2-pole solution. The other pole is found on sheet III at (850–100i) MeV
- Using a relativistic Breit-Wigner function and taking into account the finite D_S mass.
- Breit-Wigner mass. Using finite width corrections according to FLATTE 76 and ACHASOV 05, and the ratio $g_{f_0} K K / g_{f_0} \pi \pi = 0$.
- In the kaon-loop fit.
- In the no-structure fit.
- Systematic errors not estimated.
- FLATTE 76 parameterization. $g_{f_0} \pi \pi = 329 \pm 96$ MeV/c² assuming $g_{f_0} K \bar{K} / g_{f_0} \pi \pi = 2$.
- Breit-Wigner mass. Using finite width corrections according to FLATTE 76 and ACHASOV 05, and the ratio $g_{f_0} K K / g_{f_0} \pi \pi = 4.21 \pm 0.25 \pm 0.21$ from ABLIKIM 05.
- In the kaon-loop fit following formalism of ACHASOV 89.
- In the no-structure fit assuming a direct coupling of ϕ to $f_0 \gamma$.
- FLATTE 76 parameterization. Supersedes GARMASH 05.
- FLATTE 76 parameterization. $g_{f_0} K \bar{K} / g_{f_0} \pi \pi = 4.21 \pm 0.25 \pm 0.21$.
- K-matrix pole from combined analysis of $\pi^- p \rightarrow \pi^0 \pi^0 n, \pi^- p \rightarrow K \bar{K} n, \pi^+ \pi^- \rightarrow \pi^+ \pi^-, \bar{p} p \rightarrow \pi^0 \pi^0 \pi^0, \pi^0 \eta n, \pi^0 \pi^0 \eta, \pi^+ \pi^- \pi^0, K^+ K^- \pi^0, K_S^0 K_S^0 \pi^0, K^+ K_S^0 \pi^-$ at rest, $\bar{p} n \rightarrow \pi^- \pi^- \pi^+, K_S^0 K^- \pi^0, K_S^0 K_S^0 \pi^-$ at rest.
- From the negative interference with the $f_0(500)$ meson of AITALA 01b using the ACHASOV 89 parameterization for the $f_0(980)$, a Breit-Wigner for the $f_0(500)$, and ACHASOV 01f for the $\rho \pi$ contribution.
- Coupled-channel Breit-Wigner, couplings $g_\pi = 0.09 \pm 0.01 \pm 0.01, g_K = 0.02 \pm 0.04 \pm 0.03$.
- Supersedes ACHASOV 98i. Using the model of ACHASOV 89.
- Supersedes ACHASOV 98i.
- In the "narrow resonance" approximation.
- Assuming $\Gamma(f_0) = 40$ MeV.
- From a narrow pole fit taking into account $f_0(980)$ and $f_0(1200)$ intermediate mechanisms.
- From the combined fit of the photon spectra in the reactions $e^+ e^- \rightarrow \pi^+ \pi^- \gamma, \pi^0 \pi^0 \gamma$.
- Supersedes BARBERIS 99 and BARBERIS 99b
- T-matrix pole.
- From invariant mass fit.
- On sheet II in a 2 pole solution. The other pole is found on sheet III at (1039–93i) MeV.
- On sheet II in a 2 pole solution. The other pole is found on sheet III at (963–29i) MeV.
- Reanalysis of data from HYAMS 73, GRAYER 74, SRINIVASAN 75, and ROSSELET 77 using the interfering amplitude method.
- At high $|t|$.
- At low $|t|$.
- On sheet II in a 4-pole solution, the other poles are found on sheet III at (953–55i) MeV and on sheet IV at (938–35i) MeV.
- Combined fit of ALDE 95b, ANISOVICH 94, AMSLER 94d.
- On sheet II in a 2 pole solution. The other pole is found on sheet III at (996–103i) MeV.
- From sheet II pole position.
- On sheet II in a 2 pole solution. The other pole is found on sheet III at (797–185i) MeV and can be interpreted as a shadow pole.
- On sheet II in a 2 pole solution. The other pole is found on sheet III at (978–28i) MeV.
- From coupled channel analysis.
- Coupled channel analysis with finite width corrections.
- Included in AGUILAR-BENITEZ 78 fit.

$f_0(980)$ WIDTH

Width determination very model dependent. Peak width in $\pi \pi$ is about 50 MeV, but decay width can be much larger.

VALUE (MeV)	EVS	DOCUMENT ID	TECN	COMMENT
10 to 100 OUR ESTIMATE				
• • • We do not use the following data for averages, fits, limits, etc. • • •				
15.3 ± 4.7	424	ABLIKIM 15P	BES3	$J/\psi \rightarrow K^+ K^- 3\pi$
9.5 ± 1.1	706	ABLIKIM 12E	BES3	$J/\psi \rightarrow \gamma 3\pi$
42 ± 20 – 16		1,2 GARCIA-MAR..11	RVUE	Compilation
50 ± 20 – 12		2,3 GARCIA-MAR..11	RVUE	Compilation
48 ± 22 – 6		4 MOUSSALLAM11	RVUE	Compilation

36 ± 22	5 MENNESSIER 10	RVUE	Compilation
70 ± 20 – 32	6 ANISOVICH 09	RVUE	$0.0 \bar{p} p, \pi N$
91 ± 30 – 22 ± 3	44 7 ECKLUND 09	CLEO	$4.17 e^+ e^- \rightarrow D_S^- D_S^{*+} + c.c.$
66.9 ± 2.2 + 17.6 – 12.5	8 UEHARA 08A	BELL	$10.6 e^+ e^- \rightarrow e^+ e^- \pi^0 \pi^0$
65 ± 13	262 ± 30 9 AUBERT 07AK	BABR	$10.6 e^+ e^- \rightarrow \phi \pi^+ \pi^- \gamma$
81 ± 21	54 ± 9 9 AUBERT 07AK	BABR	$10.6 e^+ e^- \rightarrow \phi \pi^0 \pi^0 \gamma$
51.3 ± 20.8 + 13.2 – 17.7 – 3.8	10 MORI 07	BELL	$10.6 e^+ e^- \rightarrow e^+ e^- \pi^+ \pi^-$
61 ± 9 + 14 – 8	2584 11 GARMASH 05	BELL	$B^+ \rightarrow K^+ \pi^+ \pi^-$
64 ± 16	12 ANISOVICH 03	RVUE	
121 ± 23	TIKHOIMIROV 03	SPEC	$40.0 \pi^- C \rightarrow K_S^0 K_S^0 K_L^0 X$
~ 70	13 BRAMON 02	RVUE	$1.02 e^+ e^- \rightarrow \pi^0 \pi^0 \gamma$
44 ± 2 ± 2	848 14 AITALA 01A	E791	$D_S^+ \rightarrow \pi^- \pi^+ \pi^+$
201 ± 28	419 15 ACHASOV 00H	SND	$e^+ e^- \rightarrow \pi^0 \pi^0 \gamma$
122 ± 13	419 16,17 ACHASOV 00H	SND	$e^+ e^- \rightarrow \pi^0 \pi^0 \gamma$
56 ± 20	18 AKHMETSHIN 99C	CMD2	$e^+ e^- \rightarrow \pi^0 \pi^0 \gamma$
65 ± 20	BARBERIS 99	OMEG	$450 pp \rightarrow \rho_S \rho f K^+ K^-$
80 ± 10	BARBERIS 99B	OMEG	$450 pp \rightarrow \rho_S \rho f \pi^+ \pi^-$
80 ± 10	BARBERIS 99C	OMEG	$450 pp \rightarrow \rho_S \rho f \pi^0 \pi^0$
48 ± 12 ± 8	19 BARBERIS 99D	OMEG	$450 pp \rightarrow K^+ K^-, \pi^+ \pi^-$
65 ± 25	BELLAZZINI 99	GAM4	$450 pp \rightarrow \rho p \pi^0 \pi^0$
71 ± 14	20 KAMINSKI 99	RVUE	$\pi \pi \rightarrow \pi \pi, K \bar{K}, \sigma \sigma$
~ 28	20 OLLER 99	RVUE	$\pi \pi \rightarrow \pi \pi, K \bar{K}$
~ 25	20 OLLER 99B	RVUE	$\pi \pi \rightarrow \pi \pi, K \bar{K}$
~ 14	20 OLLER 99C	RVUE	$\pi \pi \rightarrow \pi \pi, K \bar{K}, \eta \eta$
70 ± 20	ALDE 98	GAM4	
86 ± 16	20 ANISOVICH 98B	RVUE	Compilation
54	21 LOCHER 98	RVUE	$\pi \pi \rightarrow \pi \pi, K \bar{K}$
69 ± 15	22 ALDE 97	GAM2	$450 pp \rightarrow \rho p \pi^0 \pi^0$
38 ± 20	23 BERTIN 97C	OBLX	$0.0 \bar{p} p \rightarrow \pi^+ \pi^- \pi^0$
~ 100	24 SHIDA 96	RVUE	$\pi \pi \rightarrow \pi \pi, K \bar{K}$
34	TORNQVIST 96	RVUE	$\pi \pi \rightarrow \pi \pi, K \bar{K}, K \pi, \eta \pi$
48 ± 10	3k 25 ALDE 95B	GAM2	$38 \pi^- p \rightarrow \pi^0 \pi^0 n$
95 ± 20	10k 26 ALDE 95B	GAM2	$38 \pi^- p \rightarrow \pi^0 \pi^0 n$
26 ± 10	AMSLER 95B	CBAR	$0.0 \bar{p} p \rightarrow 3\pi^0$
~ 112	27 AMSLER 95D	CBAR	$0.0 \bar{p} p \rightarrow \pi^0 \pi^0 \pi^0, \pi^0 \eta \eta, \pi^0 \pi^0 \eta$
80 ± 12	28 ANISOVICH 95	RVUE	
30	JANSEN 95	RVUE	$\pi \pi \rightarrow \pi \pi, K \bar{K}$
74	29 BUGG 94	RVUE	$\bar{p} p \rightarrow \eta 2\pi^0$
29 ± 2	30 KAMINSKI 94	RVUE	$\pi \pi \rightarrow \pi \pi, K \bar{K}$
46	31 ZOU 94B	RVUE	
48 ± 12	32 MORGAN 93	RVUE	$\pi \pi(K \bar{K}) \rightarrow \pi \pi(K \bar{K}), J/\psi \rightarrow \phi \pi \pi(K \bar{K}), D_S \rightarrow \pi(\pi \pi)$
37.4 ± 10.6	22 AGUILAR... 91	EHS	$400 pp$
72 ± 8	33 ARMSTRONG 91	OMEG	$300 pp \rightarrow \rho p \pi, \rho p K \bar{K}$
110 ± 30	BREAKSTONE 90	SFM	$pp \rightarrow \rho p \pi^+ \pi^-$
29 ± 13	22 ABACHI 86B	HRS	$e^+ e^- \rightarrow \pi^+ \pi^- X$
120 ± 281 ± 20	ETKIN 82B	MPS	$23 \pi^- p \rightarrow n 2 K_S^0$
28 ± 10	33 GIDAL 81	MRK2	$J/\psi \rightarrow \pi^+ \pi^- X$
70 to 300	34 ACHASOV 80	RVUE	
100 ± 80	35 AGUILAR... 78	HBC	$0.7 \bar{p} p \rightarrow K_S^0 K_S^0$
30 ± 8	33 LEEPER 77	ASPK	$2-2.4 \pi^- p \rightarrow \pi^+ \pi^- n, K^+ K^- n$
48 ± 14	33 BINNIE 73	CNTR	$\pi^- p \rightarrow nMM$
32 ± 10	36 GRAYER 73	ASPK	$17 \pi^- p \rightarrow \pi^+ \pi^- n$
30 ± 10	36 HYAMS 73	ASPK	$17 \pi^- p \rightarrow \pi^+ \pi^- n$
54 ± 16	36 PROTOPOP... 73	HBC	$7 \pi^+ p \rightarrow \pi^+ p \pi^+ \pi^-$

- Analytic continuation using Roy equations. Uses the K_{e4} data of BATLEY 10c and the $\pi N \rightarrow \pi \pi N$ data of HYAMS 73, GRAYER 74, and PROTOPODESCU 73.
- Quoted number refers to twice imaginary part of pole position.
- Analytic continuation using GKPY equations. Uses the K_{e4} data of BATLEY 10c and the $\pi N \rightarrow \pi \pi N$ data of HYAMS 73, GRAYER 74, and PROTOPODESCU 73.
- Pole position. Used Roy equations.
- Average of the analyses of three data sets in the K-matrix model. Uses the data of BATLEY 08a, HYAMS 73, and GRAYER 74, partially of COHEN 80 or ETKIN 82b.
- On sheet II in a 2-pole solution. The other pole is found on sheet III at (850–100i) MeV
- Using a relativistic Breit-Wigner function and taking into account the finite D_S mass.
- Breit-Wigner $\pi \pi$ width. Using finite width corrections according to FLATTE 76 and ACHASOV 05, and the ratio $g_{f_0} K K / g_{f_0} \pi \pi = 0$.
- Systematic errors not estimated.

See key on page 999

Meson Particle Listings
f_0(980)

- 10 Breit-Wigner pi-pi width. Using finite width corrections according to FLATTE 76 and ACHASOV 05, and the ratio g_f0 K K / g_f0 pi pi = 4.21 +/- 0.25 +/- 0.21 from ABLIKIM 05.
11 Breit-Wigner, solution 1, PWA ambiguous.
12 K-matrix pole from combined analysis of pi-p rho -> pi^0 pi^0 n, pi-p rho -> K Kbar n, pi+ pi- -> pi+ pi-, p pbar -> pi^0 pi^0 pi^0, pi^0 eta eta, pi^0 pi^0 eta, pi+ pi- pi^0, K+ K- pi^0, K_S^0 K_S^0 pi^0, K+ K_S^0 pi- at rest, p n -> pi- pi- pi+, K_S^0 K- pi^0, K_S^0 K_S^0 pi- at rest.
13 Using the data of AKHMETSHIN 99c, ACHASOV 00H, and ALOISIO 02D.
14 Breit-Wigner width.
15 Supersedes ACHASOV 98i. Using the model of ACHASOV 89.
16 Supersedes ACHASOV 98i.
17 In the "narrow resonance" approximation.
18 From the combined fit of the photon spectra in the reactions e+ e- -> pi+ pi- gamma, pi^0 pi^0 gamma.
19 Supersedes BARBERIS 99 and BARBERIS 99b
20 T-matrix pole.
21 On sheet II in a 2 pole solution. The other pole is found on sheet III at (1039-93i) MeV.
22 From invariant mass fit.
23 On sheet II in a 2 pole solution. The other pole is found on sheet III at (963-29i) MeV.
24 Reanalysis of data from HYAMS 73, GRAYER 74, SRINIVASAN 75, and ROSSELET 77 using the interfering amplitude method.
25 At high |t|.
26 At low |t|.
27 On sheet II in a 4-pole solution, the other poles are found on sheet III at (953-55i) MeV and on sheet IV at (938-35i) MeV.
28 Combined fit of ALDE 95B, ANISOVICH 94,
29 On sheet II in a 2 pole solution. The other pole is found on sheet III at (996-103i) MeV.
30 From sheet II pole position.
31 On sheet II in a 2 pole solution. The other pole is found on sheet III at (797-185i) MeV and can be interpreted as a shadow pole.
32 On sheet II in a 2 pole solution. The other pole is found on sheet III at (978-28i) MeV.
33 From coupled channel analysis.
34 Coupled channel analysis with finite width corrections.
35 From coupled channel fit to the HYAMS 73 and PROTOPODESCU 73 data. With a simultaneous fit to the pi-pi phase-shifts, inelasticity and to the K_S^0 K_S^0 invariant mass.
36 Included in AGUILAR-BENITEZ 78 fit.

f_0(980) DECAY MODES

Table with 3 columns: Mode, Fraction (Gamma_i / Gamma), and a column for the mode label (Gamma_1 to Gamma_4). Rows include pi pi, K Kbar, gamma gamma, and e+ e-.

f_0(980) PARTIAL WIDTHS

Table with 5 columns: Gamma(gamma), VALUE (keV), DOCUMENT ID, TECN, COMMENT, and Gamma_3. Includes 'OUR AVERAGE' and various experimental data points with footnotes 1-13.

Gamma(e+ e-) table with columns: VALUE (eV), CL%, DOCUMENT ID, TECN, COMMENT, and Gamma_4. Shows a value of <8.4 at 90% CL.

f_0(980) BRANCHING RATIOS

Gamma(pi pi) / [Gamma(pi pi) + Gamma(K Kbar)] table with columns: VALUE, EVTS, DOCUMENT ID, TECN, COMMENT, and Gamma_1 / (Gamma_1 + Gamma_2). Includes a note: 'We do not use the following data for averages, fits, limits, etc.' and a list of references.

f_0(980) REFERENCES

List of references for f_0(980) decays, branching ratios, and partial widths, including authors like AAIJ, ALOUISIO, ANISOVICH, etc., and journals like JHEP, PR, PRL, etc.

Meson Particle Listings

$f_0(980)$, $a_0(980)$

MARSISKE	90	PR D41 3324	H. Marsiske et al.	(Crystal Ball Collab.)
MORGAN	90	ZPHY C48 623	D. Morgan, M.R. Pennington	(RAL, DURH)
OEST	90	ZPHY C47 343	T. Oest et al.	(JADE Collab.)
ACHASOV	89	NP B315 465	N.N. Achasov, V.N. Ivanchenko	
AUGUSTIN	89	NP B320 1	J.E. Augustin, G. Cosme	(DM2 Collab.)
VOROBYEV	88	SJNP 48 273	P.V. Vorobiev et al.	(NOVO)
ABACHI	86B	PRL 57 1990	S. Abachi et al.	(PURD, ANL, IND, MICH+)
ETKIN	82B	PR D25 1786	A. Etkin et al.	(BNL, CUNY, TUFTS, VAND)
GIDAL	81	PL 107B 153	G. Gidal et al.	(SLAC, LBL)
ACHASOV	80	SJNP 32 566	N.N. Achasov, S.A. Devyanin, G.N. Shestakov	(NOVM)
COHEN	80	PR D22 2595	D. Cohen et al.	(ANL) IJP
LOVERRE	80	ZPHY C6 187	P.F. Loverre et al.	(CERN, CDEF, MADR+)
AGUILAR...	78	NP B140 73	M. Aguilar-Benitez et al.	(MADR, BOMB+)
CASON	78	PRL 41 271	N.M. Cason et al.	(NDAM, ANL)
LEEPER	77	PR D16 2054	R.J. Leeper et al.	(ISU)
ROSSELET	77	PR D15 574	L. Rosselet et al.	(GEVA, SAUCL)
FLATTE	76	PL 63B 224	S.M. Flatte	(CERN)
WETZEL	76	NP B115 208	W. Wetzel et al.	(ETH, CERN, LOIC)
SRINIVASAN	75	PR D12 681	V. Srinivasan et al.	(NDAM, ANL)
GRAYER	74	NP B75 189	G. Grayer et al.	(CERN, MPIM)
BINNIE	73	PRL 31 1534	D.M. Binnie et al.	(CERN, SHMP)
GRAYER	73	Tallahassee	G. Grayer et al.	(CERN, MPIM)
HYAMS	73	NP B64 134	B.D. Hyams et al.	(CERN, MPIM)
PROTOPOP...	73	PR D7 1279	S.D. Protopopescu et al.	(LBL)

$a_0(980)$

$$J^G(J^{PC}) = 1^-(0^{++})$$

See the review on "Scalar Mesons below 2 GeV."

$a_0(980)$ MASS

VALUE (MeV)	DOCUMENT ID
980 ± 20 OUR ESTIMATE	Mass determination very model dependent

$\eta\pi$ FINAL STATE ONLY

VALUE (MeV)	EVTS	DOCUMENT ID	TECN	CHG	COMMENT
• • • We do not use the following data for averages, fits, limits, etc. • • •					
982.5 ± 1.6 ± 1.1	16.9k	¹ AMBROSINO	09F	KLOE	1.02 e ⁺ e ⁻ → ηπ ⁰ γ
986 ± 4		ANISOVICH	09	RVUE	0.0 $\bar{p}p$, πN
982.3 ± 0.6 ± 3.1 - 0.7 - 4.7		² UEHARA	09A	BELL	γγ → π ⁰ η
987.4 ± 1.0 ± 3.0		^{3,4} BUGG	08A	RVUE 0	$\bar{p}p$ → π ⁰ π ⁰ η
989.1 ± 1.0 ± 3.0		^{4,5} BUGG	08A	RVUE 0	$\bar{p}p$ → π ⁰ π ⁰ η
985 ± 4 ± 6	318	ACHARD	02B	L3	183-209 e ⁺ e ⁻ → e ⁺ e ⁻ ηπ ⁺ π ⁻
995 ± 5.2 - 10	36	⁶ ACHASOV	00F	SND	e ⁺ e ⁻ → ηπ ⁰ γ
994 ± 3.3 + 8	36	⁷ ACHASOV	00F	SND	e ⁺ e ⁻ → ηπ ⁰ γ
975 ± 7		BARBERIS	00H		450 pp → p _f ηπ ⁰ p _s
988 ± 8		BARBERIS	00H		450 pp → Δ _f ⁺ ηπ ⁻ p _s
~ 1055		⁸ OLLER	99	RVUE	ηπ, K \bar{K}
~ 1009.2		⁸ OLLER	99B	RVUE	ππ → ππ, K \bar{K}
993.1 ± 2.1		⁹ TEIGE	99	B852	18.3 π ⁻ p → ηπ ⁺ π ⁻ n
988 ± 6		⁸ ANISOVICH	98B	RVUE	Compilation
987		TORNQVIST	96	RVUE	ππ → ππ, K \bar{K} , Kπ, ηπ
991		JANSSEN	95	RVUE	ηπ → ηπ, K \bar{K} , Kπ, ηπ
984.45 ± 1.23 ± 0.34		AMSLER	94C	CBAR	0.0 $\bar{p}p$ → ωηπ ⁰
982 ± 2		¹⁰ AMSLER	92	CBAR	0.0 $\bar{p}p$ → ηηπ ⁰
984 ± 4	1040	¹⁰ ARMSTRONG	91B	OMEG ±	300 pp → ppηπ ⁺ π ⁻
976 ± 6		ATKINSON	84E	OMEG ±	25-55 γp → ηπn
986 ± 3	500	¹¹ EVANGELIS...	81	OMEG ±	12 π ⁻ p → ηπ ⁺ π ⁻ π ⁻ p
990 ± 7	145	¹¹ GURTU	79	HBC ±	4.2 K ⁻ p → Λη2π
980 ± 11	47	CONFORTO	78	OSPK -	4.5 π ⁻ p → pX ⁻
978 ± 16	50	CORDEN	78	OMEG ±	12-15 π ⁻ p → nη2π
977 ± 7		GRASSLER	77	HBC -	16 π ⁺ p → pη3π
989 ± 4	70	WELLS	75	HBC -	3.1-6 K ⁻ p → Λη2π
972 ± 10	150	DEFOIX	72	HBC ±	0.7 $\bar{p}p$ → 7π
970 ± 15	20	BARNES	69C	HBC -	4-5 K ⁻ p → Λη2π
980 ± 10		CAMPBELL	69	DBC ±	2.7 π ⁺ d
980 ± 10	15	MILLER	69B	HBC -	4.5 K ⁻ N → ηπΛ
980 ± 10	30	AMMAR	68	HBC ±	5.5 K ⁻ p → Λη2π

¹ Using the model of ACHASOV 89 and ACHASOV 03b.
² From a fit with the S-wave amplitude including two interfering Breit-Wigners plus a background term.
³ Parameterizes couplings to $\bar{K}K$, πη, and πη'.
⁴ Using AMSLER 94d and ABELE 98.
⁵ From the T-matrix pole on sheet II.
⁶ Using the model of ACHASOV 89. Supersedes ACHASOV 98b.
⁷ Using the model of JAFFE 77. Supersedes ACHASOV 98b.
⁸ T-matrix pole.
⁹ Breit-Wigner fit, average between $a_0^±$ and a_0^0 . The fit favors a slightly heavier $a_0^±$.
¹⁰ From a single Breit-Wigner fit.
¹¹ From f₁(1285) decay.

$K\bar{K}$ ONLY

VALUE (MeV)	EVTS	DOCUMENT ID	TECN	COMMENT
• • • We do not use the following data for averages, fits, limits, etc. • • •				
947.7 ^{+5.5} _{-5.0} ± 6.6		¹ AAIJ	19H	LHCB pp → D [±] X
925 ± 5 ± 8	190k	² AAIJ	16N	LHCB D ⁰ → K _S ⁰ K [±] π [∓]
~ 1053		³ OLLER	99C	RVUE ππ → ππ, K \bar{K}
982 ± 3		⁴ ABELE	98	CBAR 0.0 $\bar{p}p$ → K _L ⁰ K [±] π [∓]
975 ± 15		BERTIN	98B	OBLX 0.0 $\bar{p}p$ → K _L ⁰ K [±] π [∓]
976 ± 6	316	DEBILLY	80	HBC 1.2-2 $\bar{p}p$ → f ₁ (1285)ω
1016 ± 10	100	⁵ ASTIER	67	HBC 0.0 $\bar{p}p$
1003.3 ± 7.0	143	⁶ ROSENFELD	65	RVUE

¹ From the D[±] → K[±]K⁺K⁻ Dalitz plot fit with the Triple-M amplitude in the multi-meson model of AOUE 18.
² Using a two-channel resonance parametrization with couplings fixed to ABELE 98.
³ T-matrix pole.
⁴ T-matrix pole on sheet II, the pole on sheet III is at 1006-i49 MeV.
⁵ ASTIER 67 includes data of BARLOW 67, CONFORTO 67, ARMENTEROS 65.
⁶ Plus systematic errors.

$a_0(980)$ WIDTH

VALUE (MeV)	EVTS	DOCUMENT ID	TECN	CHG	COMMENT
50 to 100 OUR ESTIMATE Width determination very model dependent. Peak width in ηπ is about 60 MeV, but decay width can be much larger.					

• • • We do not use the following data for averages, fits, limits, etc. • • •					
75.6 ± 1.6 ± 17.4 - 10.0		¹ UEHARA	09A	BELL	γγ → π ⁰ η
80.2 ± 3.8 ± 5.4		² BUGG	08A	RVUE 0	$\bar{p}p$ → π ⁰ π ⁰ η
50 ± 13 ± 4	318	ACHARD	02B	L3	183-209 e ⁺ e ⁻ → e ⁺ e ⁻ ηπ ⁺ π ⁻
72 ± 16		BARBERIS	00H		450 pp → p _f ηπ ⁰ p _s
61 ± 19		BARBERIS	00H		450 pp → Δ _f ⁺ ηπ ⁻ p _s
~ 42		³ OLLER	99	RVUE	ηπ, K \bar{K}
~ 112		³ OLLER	99B	RVUE	ππ → ηπ, K \bar{K}
71 ± 7		TEIGE	99	B852	18.3 π ⁻ p → ηπ ⁺ π ⁻ n
92 ± 20		³ ANISOVICH	98B	RVUE	Compilation
65 ± 10		⁴ BERTIN	98B	OBLX ±	0.0 $\bar{p}p$ → K [±] K _S ⁰ π [∓]
~ 100		TORNQVIST	96	RVUE	ππ → ππ, K \bar{K} , Kπ, ηπ
202		JANSSEN	95	RVUE	ηπ → ηπ, K \bar{K} , Kπ, ηπ
54.12 ± 0.34 ± 0.12		AMSLER	94C	CBAR	0.0 $\bar{p}p$ → ωηπ ⁰
54 ± 10		⁵ AMSLER	92	CBAR	0.0 $\bar{p}p$ → ηηπ ⁰
95 ± 14	1040	⁵ ARMSTRONG	91B	OMEG ±	300 pp → ppηπ ⁺ π ⁻
62 ± 15	500	⁶ EVANGELIS...	81	OMEG ±	12 π ⁻ p → ηπ ⁺ π ⁻ π ⁻ p
60 ± 20	145	⁶ GURTU	79	HBC ±	4.2 K ⁻ p → Λη2π
60 ± 50 + 30	47	CONFORTO	78	OSPK -	4.5 π ⁻ p → pX ⁻
86.0 ± 60.0 - 50.0	50	CORDEN	78	OMEG ±	12-15 π ⁻ p → nη2π
44 ± 22		GRASSLER	77	HBC -	16 π ⁺ p → pη3π
80 to 300		⁷ FLATTE	76	RVUE -	4.2 K ⁻ p → Λη2π
16.0 ± 25.0 + 16.0	70	WELLS	75	HBC -	3.1-6 K ⁻ p → Λη2π
30 ± 5	150	DEFOIX	72	HBC ±	0.7 $\bar{p}p$ → 7π
40 ± 15		CAMPBELL	69	DBC ±	2.7 π ⁺ d
60 ± 30	15	MILLER	69B	HBC -	4.5 K ⁻ N → ηπΛ
80 ± 30	30	AMMAR	68	HBC ±	5.5 K ⁻ p → Λη2π

¹ From a fit with the S-wave amplitude including two interfering Breit-Wigners plus a background term.
² From the T-matrix pole on sheet II, using AMSLER 94d and ABELE 98.
³ T-matrix pole.
⁴ The ηπ width.
⁵ From a single Breit-Wigner fit.
⁶ From f₁(1285) decay.
⁷ Using a two-channel resonance parametrization of GAY 76b data.

$K\bar{K}$ ONLY

VALUE (MeV)	EVTS	DOCUMENT ID	TECN	CHG	COMMENT
92 ± 8		¹ ABELE	98	CBAR	0.0 $\bar{p}p$ → K _L ⁰ K [±] π [∓]
~ 24		² OLLER	99C	RVUE	ππ → ππ, K \bar{K}
~ 25	100	³ ASTIER	67	HBC ±	
57 ± 13	143	⁴ ROSENFELD	65	RVUE ±	

¹ T-matrix pole on sheet II, the pole on sheet III is at 1006-i49 MeV.
² T-matrix pole.
³ ASTIER 67 includes data of BARLOW 67, CONFORTO 67, ARMENTEROS 65.
⁴ Plus systematic errors.

a₀(980), ϕ(1020)

a₀(980) DECAY MODES

Table with 3 columns: Mode, Fraction (Γ_i/Γ), and entries for modes 1-5 including ηπ, K K-bar, ρπ, γγ, and e+e-.

a₀(980) PARTIAL WIDTHS

Table for Γ(γγ) with columns VALUE (keV), DOCUMENT ID, TECN, and COMMENT. Includes a note about data usage and a reference to AMSLER 98 RVUE.

a₀(980) Γ(η)Γ(γγ)/Γ(total)

Table for Γ(ηπ) × Γ(γγ)/Γtotal with columns VALUE (keV), EVTS, DOCUMENT ID, TECN, COMMENT, and Γ1Γ4/Γ. Includes OUR AVERAGE and specific data points.

Table for Γ(ηπ) × Γ(e+e-)/Γtotal with columns VALUE (eV), CL%, DOCUMENT ID, TECN, COMMENT, and Γ1Γ5/Γ. Includes OUR AVERAGE and specific data points.

a₀(980) BRANCHING RATIOS

Table for Γ(K K-bar)/Γ(ηπ) with columns VALUE, DOCUMENT ID, TECN, CHG, COMMENT, and Γ2/Γ1. Includes OUR AVERAGE and various data points.

Table for Γ(ρπ)/Γ(ηπ) with columns VALUE, CL%, DOCUMENT ID, TECN, CHG, COMMENT, and Γ3/Γ1. Includes OUR AVERAGE and specific data points.

• • • We do not use the following data for averages, fits, limits, etc. • • •

1 Coupled channel analysis of π+π-π0, K+K-π0, and K±KSπ±.
2 Using π0π0η from AMSLER 94D.
3 From the decay of f1(1285).
4 This is a ratio of couplings.
5 A ratio of couplings, using AMSLER 94D and ABELE 98. Supersedes BUGG 94.

a₀(980) REFERENCES

List of references for a0(980) including authors like AAIJ, AOUDE, AMBROSINO, ANISOVICH, UEHARA, BUGG, ACHASOV, BARGIOTTI, ACHARD, ACHASOV, BARBERIS, OLLER, TEIGE, ABELE, ACHASOV, AMSLER, ANISOVICH, BARBERIS, BERTIN, TORNOVIST, JANSSEN, AMSLER, and AMSLER with their respective journal and year information.

Continuation of references for a0(980) and phi(1020) including authors like BUGG, AMSLER, ARMSTRONG, OEST, ACHASOV, VOROBYEV, ANTREASYAN, ATKINSON, EVANGELISTA, DEBILLY, GURTU, CONFORTO, CORDEN, GRASSLER, JAFFE, FLATTE, GAY, WELLS, DEFOIX, AMMAR, BARNES, CAMPBELL, MILLER, AMMAR, ASTIER, BARLOW, CONFORTO, ARMENTEROS, ROSENFELD, D.V. Bugg et al., C. Amisler et al., T.A. Armstrong et al., T. Oest et al., N.N. Achasov, V.N. Ivanchenko, P.V. Vorobiev et al., D. Antreasyan et al., M. Atkinson et al., C. Evangelista et al., L. de Billy et al., A. Gurto et al., B. Conforto et al., M.J. Corden et al., H. Grassler et al., R. Jaffe, S.M. Flatte, J.B. Gay et al., J. Wells et al., C. Defoix et al., R. Ammar et al., V.E. Barnes et al., J.H. Campbell et al., D.H. Miller et al., W.L. Yen et al., R. Ammar et al., A. Astier et al., J. Barlow et al., G. Conforto et al., R. Armenteros et al., A.H. Rosenfeld, (Crystal Barrel Collab.), (ATHU, BARI, BIRM+), (JADE Collab.), (NOVO), (Crystal Ball Collab.), (BOHN, CERN, GLAS+), (BARI, BONN, CERN+), (CURIN, LAUS, NEUC+), (CERN, ZEEM, NIJM, OXF), (RHEL, TNT0, CHIC+), (BIRM, RHEL, TELA+), (AACH3, BERL, BONN+), (MIT), (CERN), (CERN, AMST, NIJM) JP, (OXF), (CDEF, CERN), (KANS, NWES, ANL, WISC), (BNL, SYRA), (PURD), (PURD), (PURD), (NWES, ANL), (CDEF, CERN, IRAD), (CERN, CDEF, IRAD, LIVP), (CERN, CDEF, IPNP+), (CERN, CDEF), (LRL).

ϕ(1020)

I(GJPC) = 0-(1--)

ϕ(1020) MASS

Table for ϕ(1020) MASS with columns VALUE (MeV), EVTS, DOCUMENT ID, TECN, COMMENT. Includes OUR AVERAGE and various data points for decays like K+K-, KS0KS0, K+K-γ, etc.

• • • We do not use the following data for averages, fits, limits, etc. • • •

Meson Particle Listings

$\phi(1020)$

1019.4 ± 0.7		BINNIE	73B	CNTR	$\pi^- p \rightarrow \phi n$
1019.6 ± 0.5	120	¹³ AGUILAR-...	72B	HBC	3.9,4.6 $K^- p \rightarrow \Lambda K^+ K^-$
1019.9 ± 0.5	100	¹³ AGUILAR-...	72B	HBC	3.9,4.6 $K^- p \rightarrow K^- p K^+ K^-$
1020.4 ± 0.5	131	COLLEY	72	HBC	10 $K^+ p \rightarrow K^+ p \phi$
1019.9 ± 0.3	410	STOTTLE...	71	HBC	2.9 $K^- p \rightarrow \Sigma / \Lambda K \bar{K}$

- ¹ Average of KOZYREV 16 and KOZYREV 18 values taking into account the correlated uncertainties. Supersedes individual KOZYREV 16 and KOZYREV 18 results.
- ² Using a vector meson dominance model with contribution from $\phi(1020)$ and higher mass excitations of $\rho(770)$, $\omega(782)$, and $\phi(1020)$.
- ³ Using a phenomenological model based on KUHN 90 with a sum of Breit-Wigner resonances for $\rho(770)$, $\omega(782)$, $\phi(1020)$ and their higher mass excitations.
- ⁴ Update of AKHMETSHIN 99b
- ⁵ From the combined fit assuming that the total $\phi(1020)$ production cross section is saturated by those of $K^+ K^-$, $K_S K_L$, $\pi^+ \pi^- \pi^0$, and $\eta \gamma$ decays modes and using ACHASOV 00b for the $\eta \gamma$ decay mode.
- ⁶ Using a total width of 4.43 ± 0.05 MeV. Systematic uncertainty included.
- ⁷ Using a total width of 4.43 ± 0.05 MeV.
- ⁸ PELLINEN 82 review includes AKERLOF 77, DAUM 81, BALDI 77, AYRES 74, DE-GROOT 74.
- ⁹ From the $D^\pm \rightarrow K^\pm K^+ K^-$ Dalitz plot fit with the Triple-M amplitude in the multi-meson model of AOUDE 18.
- ¹⁰ Strongly correlated with AKHMETSHIN 04.
- ¹¹ Systematic errors not evaluated.
- ¹² Weighted and scaled average of 12 measurements of DIJKSTRA 86.
- ¹³ Mass errors enlarged by us to Γ/\sqrt{N} ; see the note with the $K^*(892)$ mass.

$\phi(1020)$ WIDTH

VALUE (MeV)	EVTS	DOCUMENT ID	TECN	COMMENT
4.249 ± 0.013 OUR AVERAGE		Error includes scale factor of 1.1.		
4.245 ± 0.013	2.3M	¹ KOZYREV	18	CMD3 $e^+ e^- \rightarrow K^+ K^-$, $K_S^0 K_L^0$
4.205 ± 0.103 ± 0.067	28k	² LEES	14H	BABR $e^+ e^- \rightarrow K_S^0 K_L^0 \gamma$
4.29 ± 0.04 ± 0.07		³ LEES	13Q	BABR $e^+ e^- \rightarrow K^+ K^- \gamma$
4.30 ± 0.06 ± 0.17	105k	AKHMETSHIN 06	CMD2	0.98-1.06 $e^+ e^- \rightarrow \pi^+ \pi^- \pi^0$
4.280 ± 0.033 ± 0.025	272k	⁴ AKHMETSHIN 04	CMD2	$e^+ e^- \rightarrow K_S^0 K_L^0$
4.21 ± 0.04	1900k	⁵ ACHASOV	01E	SND $e^+ e^- \rightarrow K^+ K^-$, $K_S K_L$, $\pi^+ \pi^- \pi^0$
4.44 ± 0.09	55 600	AKHMETSHIN 95	CMD2	$e^+ e^- \rightarrow$ hadrons
4.5 ± 0.7	1500	ARENTON	82	AEMS 11.8 polar. $pp \rightarrow K K$
4.2 ± 0.6	766	⁶ IVANOV	81	OLYA 1-1.4 $e^+ e^- \rightarrow K^+ K^-$
4.3 ± 0.6		⁶ CORDIER	80	DMI $e^+ e^- \rightarrow \pi^+ \pi^- \pi^0$
4.36 ± 0.29	3681	⁶ BUKIN	78C	OLYA $e^+ e^- \rightarrow$ hadrons
4.4 ± 0.6	984	⁶ BESCH	74	CNTR $2 \gamma p \rightarrow p K^+ K^-$
4.67 ± 0.72	681	⁶ BALAKIN	71	OSPK $e^+ e^- \rightarrow$ hadrons
4.09 ± 0.29		BIZOT	70	OSPK $e^+ e^- \rightarrow$ hadrons
• • • We do not use the following data for averages, fits, limits, etc. • • •				
4.249 ± 0.015	1.7M	KOZYREV	18	CMD3 $e^+ e^- \rightarrow K^+ K^-$
4.240 ± 0.017	610k	KOZYREV	16	CMD3 $e^+ e^- \rightarrow K_S^0 K_L^0$
4.37 ± 0.02		LEES	13F	BABR $D^+ \rightarrow K^+ K^- \pi^+$
4.24 ± 0.02 ± 0.03	542k	⁷ AKHMETSHIN 08	CMD2	1.02 $e^+ e^- \rightarrow K^+ K^-$
4.28 ± 0.13	12540	⁸ AUBERT,B	05J	BABR $D^0 \rightarrow \bar{K}^0 K^+ K^-$
4.45 ± 0.06	271k	DIJKSTRA	86	SPEC 100 π^- Be
3.6 ± 0.8	337	⁶ COOPER	78B	HBC 0.7-0.8 $\bar{p} p \rightarrow K_S^0 K_L^0 \pi^+ \pi^-$
4.5 ± 0.50	1300	^{6,8} AKERLOF	77	SPEC 400 pA $\rightarrow K^+ K^- X$
4.5 ± 0.8	500	^{6,8} AYRES	74	ASPK 3-6 $\pi^- p \rightarrow K^+ K^- n$, $K^- p \rightarrow K^+ K^- \Lambda / \Sigma^0$
3.81 ± 0.37		COSME	74B	OSPK $e^+ e^- \rightarrow K_L^0 K_S^0$
3.8 ± 0.7	454	⁶ BORENSTEIN	72	HBC 2.18 $K^- p \rightarrow K \bar{K} n$

- ¹ Average of KOZYREV 16 and KOZYREV 18 values taking into account the correlated uncertainties. Supersedes individual KOZYREV 16 and KOZYREV 18 results.
- ² Using a vector meson dominance model with contribution from $\phi(1020)$ and higher mass excitations of $\rho(770)$, $\omega(782)$, and $\phi(1020)$.
- ³ Using a phenomenological model based on KUHN 90 with a sum of Breit-Wigner resonances for $\rho(770)$, $\omega(782)$, $\phi(1020)$ and their higher mass excitations.
- ⁴ Update of AKHMETSHIN 99b
- ⁵ From the combined fit assuming that the total $\phi(1020)$ production cross section is saturated by those of $K^+ K^-$, $K_S K_L$, $\pi^+ \pi^- \pi^0$, and $\eta \gamma$ decays modes and using ACHASOV 00b for the $\eta \gamma$ decay mode.
- ⁶ Width errors enlarged by us to $4\Gamma/\sqrt{N}$; see the note with the $K^*(892)$ mass.
- ⁷ Strongly correlated with AKHMETSHIN 04.
- ⁸ Systematic errors not evaluated.

$\phi(1020)$ DECAY MODES

Mode	Fraction (Γ_i/Γ)	Scale factor/Confidence level
Γ_1 $K^+ K^-$	(49.2 ± 0.5) %	S=1.3
Γ_2 $K_L^0 K_S^0$	(34.0 ± 0.4) %	S=1.3

Γ_3 $\rho \pi^+ + \pi^+ \pi^- \pi^0$	(15.24 ± 0.33) %	S=1.2
Γ_4 $\rho \pi$		
Γ_5 $\pi^+ \pi^- \pi^0$		
Γ_6 $\eta \gamma$	(1.303 ± 0.025) %	S=1.2
Γ_7 $\pi^0 \gamma$	(1.30 ± 0.05) × 10 ⁻³	
Γ_8 $\ell^+ \ell^-$	—	
Γ_9 $e^+ e^-$	(2.973 ± 0.034) × 10 ⁻⁴	S=1.3
Γ_{10} $\mu^+ \mu^-$	(2.86 ± 0.19) × 10 ⁻⁴	
Γ_{11} $\eta e^+ e^-$	(1.08 ± 0.04) × 10 ⁻⁴	
Γ_{12} $\pi^+ \pi^-$	(7.3 ± 1.3) × 10 ⁻⁵	
Γ_{13} $\omega \pi^0$	(4.7 ± 0.5) × 10 ⁻⁵	
Γ_{14} $\omega \gamma$	< 5 %	CL=84%
Γ_{15} $\rho \gamma$	< 1.2 × 10 ⁻⁵	CL=90%
Γ_{16} $\pi^+ \pi^- \gamma$	(4.1 ± 1.3) × 10 ⁻⁵	
Γ_{17} $f_0(980) \gamma$	(3.22 ± 0.19) × 10 ⁻⁴	S=1.1
Γ_{18} $\pi^0 \pi^0 \gamma$	(1.12 ± 0.06) × 10 ⁻⁴	
Γ_{19} $\pi^+ \pi^- \pi^+ \pi^-$	(3.9 ± 2.8) × 10 ⁻⁶	
Γ_{20} $\pi^+ \pi^+ \pi^- \pi^- \pi^0$	< 4.6 × 10 ⁻⁶	CL=90%
Γ_{21} $\pi^0 e^+ e^-$	(1.33 ± 0.07) × 10 ⁻⁵	
Γ_{22} $\pi^0 \eta \gamma$	(7.27 ± 0.30) × 10 ⁻⁵	S=1.5
Γ_{23} $a_0(980) \gamma$	(7.6 ± 0.6) × 10 ⁻⁵	
Γ_{24} $K^0 \bar{K}^0 \gamma$	< 1.9 × 10 ⁻⁸	CL=90%
Γ_{25} $\eta'(958) \gamma$	(6.22 ± 0.21) × 10 ⁻⁵	
Γ_{26} $\eta \pi^0 \pi^0 \gamma$	< 2 × 10 ⁻⁵	CL=90%
Γ_{27} $\mu^+ \mu^- \gamma$	(1.4 ± 0.5) × 10 ⁻⁵	
Γ_{28} $\rho \gamma \gamma$	< 1.2 × 10 ⁻⁴	CL=90%
Γ_{29} $\eta \pi^+ \pi^-$	< 1.8 × 10 ⁻⁵	CL=90%
Γ_{30} $\eta \mu^+ \mu^-$	< 9.4 × 10 ⁻⁶	CL=90%
Γ_{31} $\eta U \rightarrow \eta e^+ e^-$	< 1 × 10 ⁻⁶	CL=90%
Γ_{32} invisible	< 1.7 × 10 ⁻⁴	CL=90%

Lepton Family number (LF) violating modes

Γ_{33} $e^\pm \mu^\mp$	LF < 2	× 10 ⁻⁶	CL=90%
-------------------------------	--------	--------------------	--------

CONSTRAINED FIT INFORMATION

An overall fit to 30 branching ratios uses 82 measurements and one constraint to determine 14 parameters. The overall fit has a $\chi^2 = 63.7$ for 69 degrees of freedom.

The following *off-diagonal* array elements are the correlation coefficients $\langle \delta x_i \delta x_j \rangle / (\delta x_i \delta x_j)$, in percent, from the fit to the branching fractions, $x_i \equiv \Gamma_i / \Gamma_{\text{total}}$. The fit constrains the x_i whose labels appear in this array to sum to one.

x_2	-78																			
x_3	-59	-4																		
x_6	-23	19	6																	
x_7	-15	14	4	10																
x_9	54	-52	-17	-38	-27															
x_{10}	-7	7	2	5	3	-13														
x_{12}	-3	3	1	2	2	-6	1													
x_{13}	-5	4	1	3	2	-8	1	1												
x_{17}	0	0	0	0	0	0	0	0	0											
x_{18}	-11	10	3	19	5	-20	2	1	2	0										
x_{19}	-1	1	0	1	0	-2	0	0	0	0	0									
x_{23}	0	0	0	0	0	0	0	0	0	0	0	0								
x_{25}	-8	6	2	33	3	-12	2	1	1	0										
	x_1	x_2	x_3	x_6	x_7	x_9	x_{10}	x_{12}	x_{13}	x_{17}										
x_{19}	0																			
x_{23}	0	0																		
x_{25}	6	0	0																	
	x_{18}	x_{19}	x_{23}																	

$\phi(1020)$ PARTIAL WIDTHS

$\Gamma(\eta \gamma)$	VALUE (keV)	DOCUMENT ID	TECN	COMMENT
-----------------------	-------------	-------------	------	---------

- • • We do not use the following data for averages, fits, limits, etc. • • •
- 58.9 ± 0.5 ± 2.4 ACHASOV 00 SND $e^+ e^- \rightarrow \eta \gamma$

$\Gamma(\pi^0\gamma)$ Γ_7

VALUE (keV)	DOCUMENT ID	TECN	COMMENT
5.40 ± 0.16 ^{+0.43} _{-0.40}	ACHASOV 00	SND	$e^+e^- \rightarrow \pi^0\gamma$

• • • We do not use the following data for averages, fits, limits, etc. • • •

$\Gamma(e^+e^-)$ Γ_8

VALUE (keV)	DOCUMENT ID	TECN	COMMENT
1.320 ± 0.017 ± 0.015	1 AMBROSINO 05	KLOE	$1.02 e^+e^- \rightarrow \mu^+\mu^-$

1 Weighted average of Γ_{ee} and $\sqrt{\Gamma_{ee}\Gamma_{\mu\mu}}$ from AMBROSINO 05 assuming lepton universality.

$\Gamma(e^+e^-)$ Γ_9

VALUE (keV)	DOCUMENT ID	TECN	COMMENT
1.27 ± 0.04 OUR EVALUATION			
1.251 ± 0.021 OUR AVERAGE			Error includes scale factor of 1.1.
1.235 ± 0.006 ± 0.022	1 AKHMETSHIN 11	CMD2	$1.02 e^+e^- \rightarrow \phi$
1.32 ± 0.05 ± 0.03	2 AMBROSINO 05	KLOE	$1.02 e^+e^- \rightarrow e^+\mu^-$
1.28 ± 0.05	AKHMETSHIN 95	CMD2	$1.02 e^+e^- \rightarrow \phi$

1 Combined analysis of the CMD-2 data on $\phi \rightarrow K^+K^-, K_S^0 K_L^0, \pi^+\pi^-\pi^0, \eta\gamma$ assuming that the sum of their branching fractions is 0.99741 ± 0.00007.
2 From forward-backward asymmetry and using $\Gamma_{total} = 4.26 \pm 0.05$ MeV from the 2004 edition of this Review.

$(\Gamma(e^+e^-) \times \Gamma(\mu^+\mu^-))^{1/2}$ $(\Gamma_9\Gamma_{10})^{1/2}$

VALUE (keV)	DOCUMENT ID	TECN	COMMENT
1.320 ± 0.018 ± 0.017	AMBROSINO 05	KLOE	$1.02 e^+e^- \rightarrow \mu^+\mu^-$

$\phi(1020) \Gamma(i)\Gamma(e^+e^-)/\Gamma(total)$

$\Gamma(K^+K^-) \times \Gamma(e^+e^-)/\Gamma total$ $\Gamma_1\Gamma_9/\Gamma$

VALUE (keV)	EVTS	DOCUMENT ID	TECN	COMMENT
0.6340 ± 0.0070 ± 0.0039		1 LEES 13Q	BABR	$e^+e^- \rightarrow K^+K^-\gamma$
0.669 ± 0.001 ± 0.023	1.7M	KOZYREV 18	CMD3	$e^+e^- \rightarrow K^+K^-$

• • • We do not use the following data for averages, fits, limits, etc. • • •

1 Using a phenomenological model based on KUHN 90 with a sum of Breit-Wigner resonances for $\rho(770), \omega(782), \phi(1020)$ and their higher mass excitations. The first error combines statistical and systematic uncertainties. The second one is due to the parametrization of the charged kaon form factor and mass calibration.

$\Gamma(K_L^0 K_S^0) \times \Gamma(e^+e^-)/\Gamma total$ $\Gamma_2\Gamma_9/\Gamma$

VALUE (keV)	EVTS	DOCUMENT ID	TECN	COMMENT
0.4200 ± 0.0033 ± 0.0123	28k	1 LEES 14H	BABR	$e^+e^- \rightarrow K_S^0 K_L^0 \gamma$

1 Using a vector meson dominance model with contribution from $\phi(1020)$ and higher mass excitations of $\rho(770), \omega(782),$ and $\phi(1020)$.

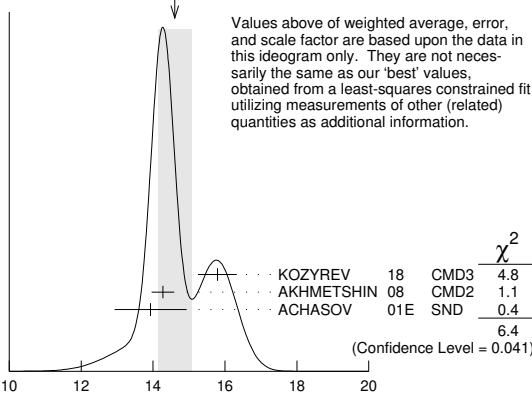
$\phi(1020) \Gamma(i)\Gamma(e^+e^-)/\Gamma^2(total)$

$\Gamma(K^+K^-)/\Gamma total \times \Gamma(e^+e^-)/\Gamma total$ $\Gamma_1/\Gamma \times \Gamma_9/\Gamma$

VALUE (units 10 ⁻⁹)	EVTS	DOCUMENT ID	TECN	COMMENT
14.63 ± 0.29 OUR FIT				Error includes scale factor of 1.5.
14.6 ± 0.5 OUR AVERAGE				Error includes scale factor of 1.8. See the ideogram below.
15.789 ± 0.541	1.7M	KOZYREV 18	CMD3	$e^+e^- \rightarrow K^+K^-$
14.27 ± 0.05 ± 0.31	542k	AKHMETSHIN 08	CMD2	$1.02 e^+e^- \rightarrow K^+K^-$
13.93 ± 0.14 ± 0.99	1000k	1 ACHASOV 01E	SND	$e^+e^- \rightarrow K^+K^-, K_S K_L, \pi^+\pi^-\pi^0$

1 From the combined fit assuming that the total $\phi(1020)$ production cross section is saturated by those of $K^+K^-, K_S K_L, \pi^+\pi^-\pi^0,$ and $\eta\gamma$ decays modes and using ACHASOV 00b for the $\eta\gamma$ decay mode.

WEIGHTED AVERAGE
14.6 ± 0.5 (Error scaled by 1.8)



$\Gamma(K_L^0 K_S^0)/\Gamma total \times \Gamma(e^+e^-)/\Gamma total$ $\Gamma_2/\Gamma \times \Gamma_9/\Gamma$

VALUE (units 10 ⁻⁹)	EVTS	DOCUMENT ID	TECN	COMMENT
10.13 ± 0.12 OUR FIT				Error includes scale factor of 1.1.
10.07 ± 0.13 OUR AVERAGE				
10.078 ± 0.223	610k	1 KOZYREV 16	CMD3	$e^+e^- \rightarrow K_S^0 K_L^0$
10.01 ± 0.04 ± 0.17	272k	2 AKHMETSHIN 04	CMD2	$e^+e^- \rightarrow K_L^0 K_S^0$
10.27 ± 0.07 ± 0.34	500k	3 ACHASOV 01E	SND	$e^+e^- \rightarrow K^+K^-, K_S K_L, \pi^+\pi^-\pi^0$

1 KOZYREV 16 also reports $\Gamma(e^+e^-) B(\phi \rightarrow K_S^0 K_L^0) = (0.428 \pm 0.001 \pm 0.009)$ keV.
2 Update of AKHMETSHIN 99d
3 From the combined fit assuming that the total $\phi(1020)$ production cross section is saturated by those of $K^+K^-, K_S K_L, \pi^+\pi^-\pi^0,$ and $\eta\gamma$ decays modes and using ACHASOV 00b for the $\eta\gamma$ decay mode.

$[\Gamma(\rho\pi) + \Gamma(\pi^+\pi^-\pi^0)]/\Gamma total \times \Gamma(e^+e^-)/\Gamma total$ $\Gamma_3/\Gamma \times \Gamma_9/\Gamma$

VALUE (units 10 ⁻⁵)	EVTS	DOCUMENT ID	TECN	COMMENT
4.53 ± 0.10 OUR FIT				Error includes scale factor of 1.1.
4.46 ± 0.12 OUR AVERAGE				
4.51 ± 0.16 ± 0.11	105k	AKHMETSHIN 06	CMD2	$0.98-1.06 e^+e^- \rightarrow \pi^+\pi^-\pi^0$
4.30 ± 0.08 ± 0.21		AUBERT,B 04N	BABR	$10.6 e^+e^- \rightarrow \pi^+\pi^-\pi^0\gamma$
4.665 ± 0.042 ± 0.261	400k	1 ACHASOV 01E	SND	$e^+e^- \rightarrow K^+K^-, K_S K_L, \pi^+\pi^-\pi^0$
4.35 ± 0.27 ± 0.08	11169	2 AKHMETSHIN 98	CMD2	$e^+e^- \rightarrow \pi^+\pi^-\pi^0$

• • • We do not use the following data for averages, fits, limits, etc. • • •

4.38 ± 0.12 BENAYOUN 10 RVUE 0.4-1.05 e^+e^-

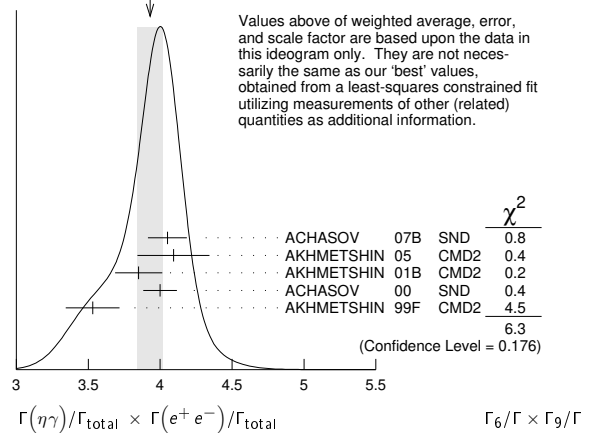
1 From the combined fit assuming that the total $\phi(1020)$ production cross section is saturated by those of $K^+K^-, K_S K_L, \pi^+\pi^-\pi^0,$ and $\eta\gamma$ decays modes and using ACHASOV 00b for the $\eta\gamma$ decay mode.
2 Recalculated by us from the cross section in the peak.

$\Gamma(\eta\gamma)/\Gamma total \times \Gamma(e^+e^-)/\Gamma total$ $\Gamma_6/\Gamma \times \Gamma_9/\Gamma$

VALUE (units 10 ⁻⁶)	EVTS	DOCUMENT ID	TECN	COMMENT
3.87 ± 0.07 OUR FIT				Error includes scale factor of 1.2.
3.93 ± 0.09 OUR AVERAGE				Error includes scale factor of 1.3. See the ideogram below.
4.050 ± 0.067 ± 0.118	33k	1 ACHASOV 07B	SND	$0.6-1.38 e^+e^- \rightarrow \eta\gamma$
4.093 ± 0.040 ± 0.247	17.4k	2 AKHMETSHIN 05	CMD2	$0.60-1.38 e^+e^- \rightarrow \eta\gamma$
3.850 ± 0.041 ± 0.159	23k	3,4 AKHMETSHIN 01B	CMD2	$e^+e^- \rightarrow \eta\gamma$
4.00 ± 0.04 ± 0.11		5 ACHASOV 00	SND	$e^+e^- \rightarrow \eta\gamma$
3.53 ± 0.08 ± 0.17	2200	6,7 AKHMETSHIN 99F	CMD2	$e^+e^- \rightarrow \eta\gamma$
4.19 ± 0.06		8 BENAYOUN 10	RVUE	$0.4-1.05 e^+e^-$

1 From a combined fit of $\sigma(e^+e^- \rightarrow \eta\gamma)$ with $\eta \rightarrow 3\pi^0$ and $\eta \rightarrow \pi^+\pi^-\pi^0$, and fixing $B(\eta \rightarrow 3\pi^0) / B(\eta \rightarrow \pi^+\pi^-\pi^0) = 1.44 \pm 0.04$. Recalculated by us from the cross section at the peak. Supersedes ACHASOV 00d and ACHASOV 06a.
2 From the $\eta \rightarrow 2\gamma$ decay and using $B(\eta \rightarrow \gamma\gamma) = 39.43 \pm 0.26\%$.
3 From the $\eta \rightarrow 3\pi^0$ decay and using $B(\eta \rightarrow 3\pi^0) = (32.24 \pm 0.29) \times 10^{-2}$.
4 The combined fit from 600 to 1380 MeV taking into account $\rho(770), \omega(782), \phi(1020),$ and $\rho(1450)$ (mass and width fixed at 1450 MeV and 310 MeV respectively).
5 From the $\eta \rightarrow 2\gamma$ decay and using $B(\eta \rightarrow 2\gamma) = (39.21 \pm 0.34) \times 10^{-2}$.
6 Recalculated by the authors from the cross section in the peak.
7 From the $\eta \rightarrow \pi^+\pi^-\pi^0$ decay and using $B(\eta \rightarrow \pi^+\pi^-\pi^0) = (23.1 \pm 0.5) \times 10^{-2}$.
8 A simultaneous fit of $e^+e^- \rightarrow \pi^+\pi^-, \pi^+\pi^-\pi^0, \pi^0\gamma, \eta\gamma$ data.

WEIGHTED AVERAGE
3.93 ± 0.09 (Error scaled by 1.3)



Meson Particle Listings

$\phi(1020)$

$$\Gamma(\pi^0\gamma)/\Gamma_{\text{total}} \times \Gamma(e^+e^-)/\Gamma_{\text{total}} \quad \Gamma_7/\Gamma \times \Gamma_9/\Gamma$$

VALUE (units 10^{-7})	EVTS	DOCUMENT ID	TECN	COMMENT
3.88 ± 0.14 OUR FIT				
3.87 ± 0.15 OUR AVERAGE				
4.04 ± 0.09 ± 0.19		¹ ACHASOV 16A	SND	0.60-1.38 $e^+e^- \rightarrow \pi^0\gamma$
3.75 ± 0.11 ± 0.29	18k	AKHMETSHIN 05	CMD2	0.60-1.38 $e^+e^- \rightarrow \pi^0\gamma$
3.67 ± 0.10 ± 0.27		² ACHASOV 00	SND	$e^+e^- \rightarrow \pi^0\gamma$
4.29 ± 0.11		³ BENAYOUN 10	RVUE	0.4-1.05 e^+e^-

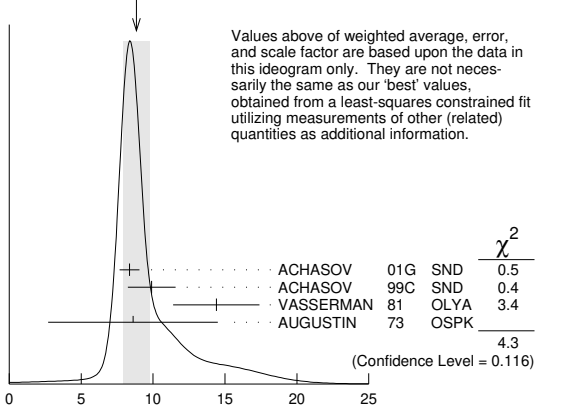
• • • We do not use the following data for averages, fits, limits, etc. • • •
¹ From the VMD model with the interfering $\rho(770)$, $\omega(782)$, $\phi(1020)$ resonances, and an additional resonance describing the total contribution of the $\rho(1450)$ and $\omega(1420)$ states. Supersedes ACHASOV 00.
² From the $\pi^0 \rightarrow 2\gamma$ decay and using $B(\pi^0 \rightarrow 2\gamma) = (98.798 \pm 0.032) \times 10^{-2}$.
³ A simultaneous fit of $e^+e^- \rightarrow \pi^+\pi^-, \pi^+\pi^-\pi^0, \pi^0\gamma, \eta\gamma$ data.

$$\Gamma(\mu^+\mu^-)/\Gamma_{\text{total}} \times \Gamma(e^+e^-)/\Gamma_{\text{total}} \quad \Gamma_{10}/\Gamma \times \Gamma_9/\Gamma$$

VALUE (units 10^{-8})	DOCUMENT ID	TECN	COMMENT
8.5 $^{+0.5}_{-0.6}$ OUR FIT			
8.8 ± 0.9 OUR AVERAGE			Error includes scale factor of 1.5. See the ideogram below.
8.36 ± 0.59 ± 0.37	ACHASOV 01G	SND	$e^+e^- \rightarrow \mu^+\mu^-$
9.9 ± 1.4 ± 0.9	¹ ACHASOV 99C	SND	$e^+e^- \rightarrow \mu^+\mu^-$
14.4 ± 3.0	² VASSERMAN 81	OLYA	$e^+e^- \rightarrow \mu^+\mu^-$
8.6 ± 5.9	² AUGUSTIN 73	OSPK	$e^+e^- \rightarrow \mu^+\mu^-$

¹ Recalculated by the authors from the cross section in the peak.
² Recalculated by us from the cross section in the peak.

WEIGHTED AVERAGE
8.8 ± 0.9 (Error scaled by 1.5)



Values above of weighted average, error, and scale factor are based upon the data in this ideogram only. They are not necessarily the same as our 'best' values, obtained from a least-squares constrained fit utilizing measurements of other (related) quantities as additional information.

$$\Gamma(\mu^+\mu^-)/\Gamma_{\text{total}} \times \Gamma(e^+e^-)/\Gamma_{\text{total}} \quad \Gamma_{10}/\Gamma \times \Gamma_9/\Gamma$$

$$\Gamma(\pi^+\pi^-)/\Gamma_{\text{total}} \times \Gamma(e^+e^-)/\Gamma_{\text{total}} \quad \Gamma_{12}/\Gamma \times \Gamma_9/\Gamma$$

VALUE (units 10^{-8})	DOCUMENT ID	TECN	COMMENT
2.2 ± 0.4 OUR FIT			
2.2 ± 0.4 OUR AVERAGE			
2.1 ± 0.3 ± 0.3	¹ ACHASOV 00C	SND	$e^+e^- \rightarrow \pi^+\pi^-$
1.95 $^{+1.15}_{-0.87}$	² GOLUBEV 86	ND	$e^+e^- \rightarrow \pi^+\pi^-$
6.01 $^{+3.19}_{-2.51}$	² VASSERMAN 81	OLYA	$e^+e^- \rightarrow \pi^+\pi^-$
3.31 ± 0.99	³ BENAYOUN 13	RVUE	0.4-1.05 e^+e^-

• • • We do not use the following data for averages, fits, limits, etc. • • •
¹ Recalculated by the authors from the cross section in the peak.
² Recalculated by us from the cross section in the peak.
³ A simultaneous fit to $e^+e^- \rightarrow \pi^+\pi^-, \pi^+\pi^-\pi^0, \pi^0\gamma, \eta\gamma, K\bar{K}$, and $\tau^- \rightarrow \pi^-\pi^0\nu_\tau$ data.

$$\Gamma(\omega\pi^0)/\Gamma_{\text{total}} \times \Gamma(e^+e^-)/\Gamma_{\text{total}} \quad \Gamma_{13}/\Gamma \times \Gamma_9/\Gamma$$

VALUE (units 10^{-8})	DOCUMENT ID	TECN	COMMENT
1.40 ± 0.15 OUR FIT			
1.37 ± 0.17 ± 0.01	^{1,2} AMBROSINO 08G	KLOE	$e^+e^- \rightarrow \pi^+\pi^-\pi^0, 2\pi^0\gamma$

¹ Recalculated by the authors from the cross section at the peak.
² AMBROSINO 08G reports $[\Gamma(\phi(1020) \rightarrow \omega\pi^0)/\Gamma_{\text{total}} \times \Gamma(\phi(1020) \rightarrow e^+e^-)/\Gamma_{\text{total}}] \times [B(\omega(782) \rightarrow \pi^+\pi^-\pi^0)] = (1.22 \pm 0.13 \pm 0.08) \times 10^{-8}$ which we divide by our best value $B(\omega(782) \rightarrow \pi^+\pi^-\pi^0) = (89.3 \pm 0.6) \times 10^{-2}$. Our first error is their experiment's error and our second error is the systematic error from using our best value.

$$\Gamma(\pi^0\pi^0\gamma)/\Gamma_{\text{total}} \times \Gamma(e^+e^-)/\Gamma_{\text{total}} \quad \Gamma_{18}/\Gamma \times \Gamma_9/\Gamma$$

VALUE (units 10^{-8})	DOCUMENT ID	TECN	COMMENT
3.34 ± 0.17 OUR FIT			
3.33 $^{+0.04}_{-0.09} \pm 0.19$	¹ AMBROSINO 07	KLOE	$e^+e^- \rightarrow \pi^0\pi^0\gamma$

¹ Calculated by the authors from the cross section at the peak.

$$\Gamma(\pi^+\pi^-\pi^+\pi^-)/\Gamma_{\text{total}} \times \Gamma(e^+e^-)/\Gamma_{\text{total}} \quad \Gamma_{19}/\Gamma \times \Gamma_9/\Gamma$$

VALUE (units 10^{-9})	EVTS	DOCUMENT ID	TECN	COMMENT
1.2 $^{+0.8}_{-0.7}$ OUR FIT				
1.17 ± 0.52 ± 0.64	3285	¹ AKHMETSHIN 00E	CMD2	$e^+e^- \rightarrow \pi^+\pi^-\pi^+\pi^-$

¹ Recalculated by the authors from the cross section in the peak.

$\phi(1020)$ BRANCHING RATIOS

$$\Gamma(K^+K^-)/\Gamma_{\text{total}} \quad \Gamma_1/\Gamma$$

VALUE	EVTS	DOCUMENT ID	TECN	COMMENT
0.492 ± 0.005 OUR FIT				Error includes scale factor of 1.3.
0.493 ± 0.010 OUR AVERAGE				
0.492 ± 0.012	2913	AKHMETSHIN 95	CMD2	$e^+e^- \rightarrow K^+K^-$
0.44 ± 0.05	321	KALBFLEISCH 76	HBC	2.18 $K^-p \rightarrow \Lambda K^+K^-$
0.49 ± 0.06	270	DEGROOT 74	HBC	4.2 $K^-p \rightarrow \Lambda\phi$
0.540 ± 0.034	565	BALAKIN 71	OSPK	$e^+e^- \rightarrow K^+K^-$
0.48 ± 0.04	252	LINDSEY 66	HBC	2.1-2.7 $K^-p \rightarrow \Lambda K^+K^-$

• • • We do not use the following data for averages, fits, limits, etc. • • •
¹ AKHMETSHIN 11 CMD2 1.02 $e^+e^- \rightarrow K^+K^-$
² ACHASOV 01E SND $e^+e^- \rightarrow K^+K^-, K_S^0 K_L^0, \pi^+\pi^-\pi^0$

¹ Combined analysis of the CMD-2 data on $\phi \rightarrow K^+K^-, K_L^0 K_S^0, \pi^+\pi^-\pi^0, \eta\gamma$ assuming that the sum of their branching fractions is 0.99741 ± 0.00007 .
² Using $B(\phi \rightarrow e^+e^-) = (2.93 \pm 0.14) \times 10^{-4}$.

$$\Gamma(K_L^0 K_S^0)/\Gamma_{\text{total}} \quad \Gamma_2/\Gamma$$

VALUE	EVTS	DOCUMENT ID	TECN	COMMENT
0.340 ± 0.004 OUR FIT				Error includes scale factor of 1.3.
0.331 ± 0.009 OUR AVERAGE				
0.335 ± 0.010	40644	AKHMETSHIN 95	CMD2	$e^+e^- \rightarrow K_L^0 K_S^0$
0.326 ± 0.035		DOLINSKY 91	ND	$e^+e^- \rightarrow K_L^0 K_S^0$
0.310 ± 0.024		DRUZHININ 84	ND	$e^+e^- \rightarrow K_L^0 K_S^0$
0.336 ± 0.002 ± 0.006		¹ AKHMETSHIN 11	CMD2	1.02 $e^+e^- \rightarrow K_S^0 K_L^0$
0.351 ± 0.013	500k	² ACHASOV 01E	SND	$e^+e^- \rightarrow K^+K^-, K_S^0 K_L^0, \pi^+\pi^-\pi^0$
0.27 ± 0.03	133	KALBFLEISCH 76	HBC	2.18 $K^-p \rightarrow \Lambda K_L^0 K_S^0$
0.257 ± 0.030	95	³ BALAKIN 71	OSPK	$e^+e^- \rightarrow K_L^0 K_S^0$
0.40 ± 0.04	167	LINDSEY 66	HBC	2.1-2.7 $K^-p \rightarrow \Lambda K_L^0 K_S^0$

• • • We do not use the following data for averages, fits, limits, etc. • • •
¹ Combined analysis of the CMD-2 data on $\phi \rightarrow K^+K^-, K_L^0 K_S^0, \pi^+\pi^-\pi^0, \eta\gamma$ assuming that the sum of their branching fractions is 0.99741 ± 0.00007 .
² Using $B(\phi \rightarrow e^+e^-) = (2.93 \pm 0.14) \times 10^{-4}$.
³ Balakin error increased by Paul.

$$\Gamma(K_L^0 K_S^0)/\Gamma(K^+K^-) \quad \Gamma_2/\Gamma_1$$

VALUE	EVTS	DOCUMENT ID	TECN	COMMENT
0.690 ± 0.015 OUR FIT				Error includes scale factor of 1.3.
0.740 ± 0.031 OUR AVERAGE				
0.70 ± 0.06	2732	BUKIN 78c	OLYA	$e^+e^- \rightarrow K_L^0 K_S^0$
0.82 ± 0.08		LOSTY 78	HBC	4.2 $K^-p \rightarrow \phi$ hyperon
0.71 ± 0.05		LAVEN 77	HBC	10 $K^-p \rightarrow K^+K^- \Lambda$
0.71 ± 0.08		LYONS 77	HBC	3-4 $K^-p \rightarrow \Lambda\phi$
0.89 ± 0.10	144	AGUILAR-...	72B	HBC 3.9,4.6 K^-p
0.638 ± 0.022	2.3M	¹ KOZYREV 18	CMD3	$e^+e^- \rightarrow K_L^0 K_S^0, K^+K^-$
0.68 ± 0.03		² AKHMETSHIN 95	CMD2	$e^+e^- \rightarrow K_L^0 K_S^0, K^+K^-$

¹ The prediction taking into account phase-space difference, radiative corrections, isospin breaking, and the Sommerfeld-Gamow-Sakharov factor gives 0.630.
² Theoretical analysis of BRAMON 00 taking into account phase-space difference, electromagnetic radiative corrections, as well as isospin breaking, predicts 0.62. FLOREZ-BAEZ 08 predicts 0.63 considering also structure-dependent radiative corrections. FISCHBACH 02 calculates additional corrections caused by the close threshold and predicts 0.68. See also BENAYOUN 01 and DUBYNSKIY 07. BENAYOUN 12 obtains 0.71 ± 0.01 in the HLS model.

$$\Gamma(K_L^0 K_S^0)/\Gamma(K\bar{K}) \quad \Gamma_2/(\Gamma_1 + \Gamma_2)$$

VALUE	EVTS	DOCUMENT ID	TECN	COMMENT
0.408 ± 0.005 OUR FIT				Error includes scale factor of 1.3.
0.45 ± 0.04 OUR AVERAGE				
0.44 ± 0.07		¹ LONDON 66	HBC	2.24 $K^-p \rightarrow \Lambda K\bar{K}$
0.48 ± 0.07	52	BADIER 65B	HBC	3 K^-p
0.40 ± 0.10	34	SCHLEIN 63	HBC	1.95 $K^-p \rightarrow \Lambda K\bar{K}$

¹ This is probably not affected by their controversial background subtraction; the value is from their numbers of $K_1 K_2$ vs K^+K^- events.

$$[\Gamma(\rho\pi) + \Gamma(\pi^+\pi^-\pi^0)]/\Gamma_{\text{total}} \quad \Gamma_3/\Gamma$$

VALUE	EVTS	DOCUMENT ID	TECN	COMMENT
0.1524 ± 0.0033 OUR FIT				Error includes scale factor of 1.2.
0.151 ± 0.009 OUR AVERAGE				Error includes scale factor of 1.7.
0.161 ± 0.008	11761	AKHMETSHIN 95	CMD2	$e^+e^- \rightarrow \pi^+\pi^-\pi^0$
0.143 ± 0.007		DOLINSKY 91	ND	$e^+e^- \rightarrow \pi^+\pi^-\pi^0$

Meson Particle Listings

$\phi(1020)$

• • • We do not use the following data for averages, fits, limits, etc. • • •

0.155 ± 0.002 ± 0.005	1	AKHMETSHIN 11	CMD2	1.02	$e^+e^- \rightarrow \pi^+\pi^-\pi^0$
0.159 ± 0.008	400k	2	ACHASOV 01E	SND	$e^+e^- \rightarrow K^+K^-, K_S^0 K_L^0, \pi^+\pi^-\pi^0$
0.145 ± 0.009 ± 0.003	11169	3	AKHMETSHIN 98	CMD2	$e^+e^- \rightarrow \pi^+\pi^-\pi^0$
0.139 ± 0.007		4	PARROUR 76B	OSPK	e^+e^-

1 Combined analysis of the CMD-2 data on $\phi \rightarrow K^+K^-, K_S^0 K_L^0, \pi^+\pi^-\pi^0, \eta\gamma$ assuming that the sum of their branching fractions is 0.99741 ± 0.00007 .
 2 Using $B(\phi \rightarrow e^+e^-) = (2.93 \pm 0.14) \times 10^{-4}$.
 3 Using $B(\phi \rightarrow e^+e^-) = (2.99 \pm 0.08) \times 10^{-4}$.
 4 Using $\Gamma(\phi) = 4.1$ MeV. If interference between the $\rho\pi$ and 3π modes is neglected, the fraction of the $\rho\pi$ is more than 80% at the 90% confidence level.

$\frac{\Gamma(\rho\pi) + \Gamma(\pi^+\pi^-\pi^0)}{\Gamma(K^+K^-)}$ Γ_3/Γ_1

VALUE	EVTs	DOCUMENT ID	TECN	COMMENT
0.310 ± 0.009 OUR FIT				Error includes scale factor of 1.2.
0.28 ± 0.09	34	AGUILAR-...	72B	HBC 3,9,4,6 $K^-\rho$

$\frac{\Gamma(\rho\pi) + \Gamma(\pi^+\pi^-\pi^0)}{\Gamma(K^0\bar{K}^0)}$ $\Gamma_3/(\Gamma_1+\Gamma_2)$

VALUE	DOCUMENT ID	TECN	COMMENT
0.183 ± 0.005 OUR FIT			Error includes scale factor of 1.2.
0.24 ± 0.04 OUR AVERAGE			
0.237 ± 0.039	CERRADA 77B	HBC	4.2 $K^-\rho \rightarrow \Lambda 3\pi$
0.30 ± 0.15	LONDON 66	HBC	2.24 $K^-\rho \rightarrow \Lambda \pi^+\pi^-\pi^0$

$\frac{\Gamma(\rho\pi) + \Gamma(\pi^+\pi^-\pi^0)}{\Gamma(K_S^0 K_L^0)}$ Γ_3/Γ_2

VALUE	EVTs	DOCUMENT ID	TECN	COMMENT
0.448 ± 0.011 OUR FIT				Error includes scale factor of 1.1.
0.51 ± 0.05 OUR AVERAGE				
0.56 ± 0.07	3681	BUKIN 78c	OLYA	$e^+e^- \rightarrow K_L^0 K_S^0, \pi^+\pi^-\pi^0$
0.47 ± 0.06	516	COSME 74	OSPK	$e^+e^- \rightarrow \pi^+\pi^-\pi^0$

$\Gamma(\pi^+\pi^-\pi^0)/\Gamma_{total}$ Γ_5/Γ

VALUE	CL%	EVTs	DOCUMENT ID	TECN	COMMENT
• • • We do not use the following data for averages, fits, limits, etc. • • •					
≈ 0.0087		1.98M	1,2	ALOISIO 03	KLOE 1.02 $e^+e^- \rightarrow \pi^+\pi^-\pi^0$
< 0.0006		90	3	ACHASOV 02	SND 1.02 $e^+e^- \rightarrow \pi^+\pi^-\pi^0$
< 0.23		90	3	CORDIER 80	DM1 $e^+e^- \rightarrow \pi^+\pi^-\pi^0$
< 0.20		90	3	PARROUR 76B	OSPK $e^+e^- \rightarrow \pi^+\pi^-\pi^0$

1 From a fit without limitations on charged and neutral ρ masses and widths.
 2 Adding the direct and $\omega\pi$ contributions and considering the interference between the $\rho\pi$ and $\pi^+\pi^-\pi^0$.
 3 Neglecting the interference between the $\rho\pi$ and $\pi^+\pi^-\pi^0$.

$\Gamma(\eta\gamma)/\Gamma_{total}$ Γ_6/Γ

VALUE (units 10^{-2})	EVTs	DOCUMENT ID	TECN	COMMENT
1.303 ± 0.025 OUR FIT				Error includes scale factor of 1.2.
1.26 ± 0.04 OUR AVERAGE				
1.246 ± 0.025 ± 0.057	10k	1	ACHASOV 98F	SND $e^+e^- \rightarrow 7\gamma$
1.18 ± 0.11	279	2	AKH METSHIN 95	CMD2 $e^+e^- \rightarrow \pi^+\pi^-\gamma$
1.30 ± 0.06		3	DRUZHININ 84	ND $e^+e^- \rightarrow 3\gamma$
1.4 ± 0.2		4	DRUZHININ 84	ND $e^+e^- \rightarrow 6\gamma$
0.88 ± 0.20	290		KURDADZE 83c	OLYA $e^+e^- \rightarrow 3\gamma$
1.35 ± 0.29			ANDREWS 77	CNTR 6.7-10 γ Cu
1.5 ± 0.4	54	3	COSME 76	OSPK e^+e^-

• • • We do not use the following data for averages, fits, limits, etc. • • •

1.38 ± 0.02 ± 0.02		5	AKH METSHIN 11	CMD2 1.02 $e^+e^- \rightarrow \eta\gamma$
1.36 ± 0.05 ± 0.02	33k	6	ACHASOV 07B	SND 0.6-1.38 $e^+e^- \rightarrow \eta\gamma$
1.373 ± 0.014 ± 0.085	17.4k	7,8	AKH METSHIN 05	CMD2 0.60-1.38 $e^+e^- \rightarrow \eta\gamma$
1.287 ± 0.013 ± 0.063		9,10	AKH METSHIN 01B	CMD2 $e^+e^- \rightarrow \eta\gamma$
1.338 ± 0.012 ± 0.052		11	ACHASOV 00	SND $e^+e^- \rightarrow \eta\gamma$
1.18 ± 0.03 ± 0.06	2200	12	AKH METSHIN 99F	CMD2 $e^+e^- \rightarrow \eta\gamma$
1.21 ± 0.07		13	BENAYOUN 96	RVUE 0.54-1.04 $e^+e^- \rightarrow \eta\gamma$

1 Using $B(\phi \rightarrow e^+e^-) = (2.99 \pm 0.08) \times 10^{-4}$ and $B(\eta \rightarrow 3\pi^0) = (32.2 \pm 0.4) \times 10^{-2}$.
 2 From $\pi^+\pi^-\pi^0$ decay mode of η .
 3 From 2γ decay mode of η .
 4 From $3\pi^0$ decay mode of η .
 5 Combined analysis of the CMD-2 data on $\phi \rightarrow K^+K^-, K_S^0 K_L^0, \pi^+\pi^-\pi^0, \eta\gamma$ assuming that the sum of their branching fractions is 0.99741 ± 0.00007 .
 6 ACHASOV 07B reports $[\Gamma(\phi(1020) \rightarrow \eta\gamma)/\Gamma_{total}] \times [B(\phi(1020) \rightarrow e^+e^-)] = (4.050 \pm 0.067 \pm 0.118) \times 10^{-6}$ which we divide by our best value $B(\phi(1020) \rightarrow e^+e^-) = (2.973 \pm 0.034) \times 10^{-4}$. Our first error is their experiment's error and our second error is the systematic error from using our best value. Supersedes ACHASOV 00b and ACHASOV 06a.
 7 Using $B(\phi \rightarrow e^+e^-) = (2.98 \pm 0.04) \times 10^{-4}$ and $B(\eta \rightarrow \gamma\gamma) = 39.43 \pm 0.26\%$.
 8 Not independent of the corresponding $\Gamma(e^+e^-) \times \Gamma(\eta\gamma)/\Gamma_{total}^2$.
 9 Using $B(\phi \rightarrow e^+e^-) = (2.99 \pm 0.08) \times 10^{-4}$ and $B(\eta \rightarrow 3\pi^0) = (32.24 \pm 0.29) \times 10^{-2}$.
 10 The combined fit from 600 to 1380 MeV taking into account $\rho(770), \omega(782), \phi(1020)$, and $\rho(1450)$ (mass and width fixed at 1450 MeV and 310 MeV respectively).
 11 From the $\eta \rightarrow 2\gamma$ decay and using $B(\phi \rightarrow e^+e^-) = (2.99 \pm 0.08) \times 10^{-4}$.
 12 From $\pi^+\pi^-\pi^0$ decay mode of η and using $B(\phi \rightarrow e^+e^-) = (2.99 \pm 0.08) \times 10^{-4}$.
 13 Reanalysis of DRUZHININ 84, DOLINSKY 89, and DOLINSKY 91 taking into account a triangle anomaly contribution.

$\Gamma(\pi^0\gamma)/\Gamma_{total}$ Γ_7/Γ

VALUE (units 10^{-3})	EVTs	DOCUMENT ID	TECN	COMMENT
1.30 ± 0.05 OUR FIT				
1.31 ± 0.13 OUR AVERAGE				
1.30 ± 0.13		DRUZHININ 84	ND	$e^+e^- \rightarrow 3\gamma$
1.4 ± 0.5	32	COSME 76	OSPK	e^+e^-

• • • We do not use the following data for averages, fits, limits, etc. • • •

1.367 ± 0.072	1	ACHASOV 16A	SND	0.60-1.38 $e^+e^- \rightarrow \pi^0\gamma$
1.258 ± 0.037 ± 0.077	18k	2,3	AKHMETSHIN 05	CMD2 0.60-1.38 $e^+e^- \rightarrow \pi^0\gamma$
1.226 ± 0.036 ± 0.096		4	ACHASOV 00	SND $e^+e^- \rightarrow \pi^0\gamma$
1.26 ± 0.17		5	BENAYOUN 96	RVUE 0.54-1.04 $e^+e^- \rightarrow \pi^0\gamma$

1 Using $B(\phi \rightarrow e^+e^-)$ from PDG 15. Supersedes ACHASOV 00.
 2 Using $B(\phi \rightarrow e^+e^-) = (2.98 \pm 0.04) \times 10^{-4}$.
 3 Not independent of the corresponding $\Gamma(e^+e^-) \times \Gamma(\pi^0\gamma)/\Gamma_{total}^2$.
 4 From the $\pi^0 \rightarrow 2\gamma$ decay and using $B(\phi \rightarrow e^+e^-) = (2.99 \pm 0.08) \times 10^{-4}$.
 5 Reanalysis of DRUZHININ 84, DOLINSKY 89, and DOLINSKY 91 taking into account a triangle anomaly contribution.

$\Gamma(\eta\gamma)/\Gamma(\pi^0\gamma)$ Γ_6/Γ_7

VALUE	DOCUMENT ID	TECN	COMMENT
• • • We do not use the following data for averages, fits, limits, etc. • • •			
10.9 ± 0.3 ± 0.7	ACHASOV 00	SND	$e^+e^- \rightarrow \eta\gamma, \pi^0\gamma$

$\Gamma(e^+e^-)/\Gamma_{total}$ Γ_9/Γ

VALUE (units 10^{-4})	EVTs	DOCUMENT ID	TECN	COMMENT
2.973 ± 0.034 OUR FIT				Error includes scale factor of 1.3.
2.98 ± 0.07 OUR AVERAGE				Error includes scale factor of 1.1.
2.93 ± 0.14	1900k	1	ACHASOV 01E	SND $e^+e^- \rightarrow K^+K^-, K_S^0 K_L^0, \pi^+\pi^-\pi^0$
2.88 ± 0.09	55600		AKHMETSHIN 95	CMD2 $e^+e^- \rightarrow$ hadrons
3.00 ± 0.21	3681		BUKIN 78c	OLYA $e^+e^- \rightarrow$ hadrons
3.10 ± 0.14		2	PARROUR 76	OSPK e^+e^-
3.3 ± 0.3			COSME 74	OSPK $e^+e^- \rightarrow$ hadrons
2.81 ± 0.25	681		BALAKIN 71	OSPK $e^+e^- \rightarrow$ hadrons
3.50 ± 0.27			CHATELUS 71	OSPK e^+e^-

1 From the combined fit assuming that the total $\phi(1020)$ production cross section is saturated by those of $K^+K^-, K_S^0 K_L^0, \pi^+\pi^-\pi^0$, and $\eta\gamma$ decays modes and using ACHASOV 00b for the $\eta\gamma$ decay mode.
 2 Using total width 4.2 MeV. They detect 3π mode and observe significant interference with ω tail. This is accounted for in the result quoted above.

$\Gamma(\mu^+\mu^-)/\Gamma_{total}$ Γ_{10}/Γ

VALUE (units 10^{-4})	DOCUMENT ID	TECN	COMMENT
2.86 ± 0.19 OUR FIT			
2.5 ± 0.4 OUR AVERAGE			
2.69 ± 0.46	1	HAYES 71	CNTR 8.3,9.8 $\gamma C \rightarrow \mu^+\mu^- X$
2.17 ± 0.60	1	EARLES 70	CNTR 6.0 $\gamma C \rightarrow \mu^+\mu^- X$

• • • We do not use the following data for averages, fits, limits, etc. • • •

2.87 ± 0.20 ± 0.14	2	ACHASOV 01g	SND $e^+e^- \rightarrow \mu^+\mu^-$
3.30 ± 0.45 ± 0.32	3	ACHASOV 99c	SND $e^+e^- \rightarrow \mu^+\mu^-$
4.83 ± 1.02	4	VASSERMAN 81	OLYA $e^+e^- \rightarrow \mu^+\mu^-$
2.87 ± 1.98	4	AUGUSTIN 73	OSPK $e^+e^- \rightarrow \mu^+\mu^-$

1 Neglecting interference between resonance and continuum.
 2 Using $B(\phi \rightarrow e^+e^-) = (2.91 \pm 0.07) \times 10^{-4}$.
 3 Using $B(\phi \rightarrow e^+e^-) = (2.99 \pm 0.08) \times 10^{-4}$.
 4 Recalculated by us using $B(\phi \rightarrow e^+e^-) = (2.99 \pm 0.08) \times 10^{-4}$.

$\Gamma(\eta e^+e^-)/\Gamma_{total}$ Γ_{11}/Γ

VALUE (units 10^{-4})	EVTs	DOCUMENT ID	TECN	COMMENT
1.08 ± 0.007 OUR AVERAGE				
1.075 ± 0.007 ± 0.038	30k	1	BABUSCI 15	KLOE 1.02 $e^+e^- \rightarrow \eta e^+e^-$
1.19 ± 0.19 ± 0.12	213	2	ACHASOV 01B	SND $e^+e^- \rightarrow \eta e^+e^-$
1.14 ± 0.10 ± 0.06	355	3	AKHMETSHIN 01	CMD2 $e^+e^- \rightarrow \eta e^+e^-$

• • • We do not use the following data for averages, fits, limits, etc. • • •

1.13 ± 0.14 ± 0.07	183	4	AKHMETSHIN 01	CMD2 $e^+e^- \rightarrow \eta e^+e^-$
1.21 ± 0.14 ± 0.09	130	5	AKHMETSHIN 01	CMD2 $e^+e^- \rightarrow \eta e^+e^-$
1.04 ± 0.20 ± 0.08	42	6	AKHMETSHIN 01	CMD2 $e^+e^- \rightarrow \eta e^+e^-$
1.3 ± 0.8	7		GOLUBEV 85	ND $e^+e^- \rightarrow \eta e^+e^-$

1 Using $B(\eta \rightarrow 3\pi^0) = (32.57 \pm 0.23)\%$ from PDG 12.
 2 Using $B(\eta \rightarrow \gamma\gamma) = (39.25 \pm 0.32)\%$, $B(\phi \rightarrow \eta\gamma) = (1.26 \pm 0.06)\%$, and $B(\phi \rightarrow e^+e^-) = (3.00 \pm 0.06) \times 10^{-4}$.
 3 The average of the branching ratios separately obtained from the $\eta \rightarrow \gamma\gamma, 3\pi^0, \pi^+\pi^-\pi^0$ decays.
 4 From $\eta \rightarrow \gamma\gamma$ decays and using $B(\eta \rightarrow \gamma\gamma) = (39.33 \pm 0.25) \times 10^{-2}$, $B(\eta \rightarrow \pi^+\pi^-\gamma) = (4.75 \pm 11) \times 10^{-2}$, and $B(\phi \rightarrow \eta\gamma) = (1.297 \pm 0.033) \times 10^{-2}$.
 5 From $\eta \rightarrow 3\pi^0$ decays and using $B(\pi^0 \rightarrow \gamma\gamma) = (98.798 \pm 0.033) \times 10^{-2}$, $B(\eta \rightarrow 3\pi^0) = (32.24 \pm 0.29) \times 10^{-2}$, $B(\eta \rightarrow \pi^+\pi^-\gamma) = (4.75 \pm 0.11) \times 10^{-2}$, and $B(\phi \rightarrow \eta\gamma) = (1.297 \pm 0.033) \times 10^{-2}$.
 6 From $\eta \rightarrow \pi^+\pi^-\pi^0$ decays and using $B(\pi^0 \rightarrow \gamma\gamma) = (98.798 \pm 0.033) \times 10^{-2}$, $B(\pi^0 \rightarrow e^+e^-) = (1.198 \pm 0.032) \times 10^{-2}$, $B(\eta \rightarrow \pi^+\pi^-\pi^0) = (23.0 \pm 0.4) \times 10^{-2}$, $B(\phi \rightarrow \pi^+\pi^-\pi^0) = (15.5 \pm 0.6) \times 10^{-2}$, and $B(\phi \rightarrow \eta\gamma) = (1.297 \pm 0.033) \times 10^{-2}$.

Meson Particle Listings

$\phi(1020)$

$\Gamma(\pi^+\pi^-)/\Gamma_{total}$ Γ_{12}/Γ

VALUE (units 10^{-4})	CL%	DOCUMENT ID	TECN	COMMENT
$0.71 \pm 0.11 \pm 0.09$		¹ ACHASOV	00c	SND $e^+e^- \rightarrow \pi^+\pi^-$
$0.65_{-0.29}^{+0.38}$		¹ GOLUBEV	86	ND $e^+e^- \rightarrow \pi^+\pi^-$
$2.01_{-0.84}^{+1.07}$		¹ VASSERMAN	81	OLYA $e^+e^- \rightarrow \pi^+\pi^-$
<6.6	95	BUKIN	78B	OLYA $e^+e^- \rightarrow \pi^+\pi^-$
<2.7	95	ALVENSLEB...	72	CNTR 6.7 $\gamma C \rightarrow C\pi^+\pi^-$

¹ Using $B(\phi \rightarrow e^+e^-) = (2.99 \pm 0.08) \times 10^{-4}$.

$\Gamma(\omega\pi^0)/\Gamma_{total}$ Γ_{13}/Γ

VALUE (units 10^{-5})	DOCUMENT ID	TECN	COMMENT
4.7 ± 0.5 OUR FIT			
$5.2_{-1.1}^{+1.3}$	^{1,2} AULCHENKO	00A	SND $e^+e^- \rightarrow \pi^+\pi^-\pi^0\pi^0$
4.4 ± 0.6	³ AMBROSINO	08G	KLOE $e^+e^- \rightarrow \pi^+\pi^-\pi^0, 2\pi^0\gamma$
~ 5.4	⁴ ACHASOV	00E	SND $e^+e^- \rightarrow \pi^0\pi^0\gamma$
$5.5_{-1.4}^{+1.6} \pm 0.3$	^{2,5} AULCHENKO	00A	SND $e^+e^- \rightarrow \pi^+\pi^-\pi^0\pi^0$
$4.8_{-1.7}^{+1.9} \pm 0.8$	⁴ ACHASOV	99	SND $e^+e^- \rightarrow \pi^+\pi^-\pi^0\pi^0$

¹ Using the 1996 and 1998 data.
² (2.3 \pm 0.3)% correction for other decay modes of the $\omega(782)$ applied.
³ Not independent of the corresponding $\Gamma(\omega\pi^0) \times \Gamma(e^+e^-) / \Gamma^2(total)$.
⁴ Using the 1996 data.
⁵ Using the 1998 data.

$\Gamma(\omega\gamma)/\Gamma_{total}$ Γ_{14}/Γ

VALUE	CL%	DOCUMENT ID	TECN	COMMENT
< 0.05	84	LINDSEY	66	HBC 2.1-2.7 $K^-p \rightarrow \Lambda\pi^+\pi^-$ neutrals

$\Gamma(\rho\gamma)/\Gamma_{total}$ Γ_{15}/Γ

VALUE (units 10^{-4})	CL%	DOCUMENT ID	TECN	COMMENT
< 0.12	90	¹ AKHMETSHIN	99B	CMD2 $e^+e^- \rightarrow \pi^+\pi^-\gamma$
< 7	90	AKHMETSHIN	97c	CMD2 $e^+e^- \rightarrow \pi^+\pi^-\gamma$
<200	84	LINDSEY	66	HBC 2.1-2.7 $K^-p \rightarrow \Lambda\pi^+\pi^-$ neutrals

¹ Supersedes AKHMETSHIN 97c.

$\Gamma(\pi^+\pi^-\gamma)/\Gamma_{total}$ Γ_{16}/Γ

VALUE (units 10^{-4})	CL%	EVTS	DOCUMENT ID	TECN	COMMENT
$0.41 \pm 0.12 \pm 0.04$		30175	¹ AKHMETSHIN	99B	CMD2 $e^+e^- \rightarrow \pi^+\pi^-\gamma$
< 0.3	90		² AKHMETSHIN	97c	CMD2 $e^+e^- \rightarrow \pi^+\pi^-\gamma$
<600	90		KALBFLEISCH	75	HBC 2.18 $K^-p \rightarrow \Lambda\pi^+\pi^-$ neutrals
< 70	90		COSME	74	OSPK $e^+e^- \rightarrow \pi^+\pi^-\gamma$
<400	90		LINDSEY	65	HBC 2.1-2.7 $K^-p \rightarrow \Lambda\pi^+\pi^-$ neutrals

¹ For $E_\gamma > 20$ MeV and assuming that $B(\phi(1020) \rightarrow f_0(980)\gamma)$ is negligible. Supersedes AKHMETSHIN 97c.
² For $E_\gamma > 20$ MeV and assuming that $B(\phi(1020) \rightarrow f_0(980)\gamma)$ is negligible.

$\Gamma(f_0(980)\gamma)/\Gamma_{total}$ Γ_{17}/Γ

VALUE (units 10^{-4})	CL%	EVTS	DOCUMENT ID	TECN	COMMENT
3.22 ± 0.19 OUR FIT					Error includes scale factor of 1.1.
3.21 ± 0.19 OUR AVERAGE					
$3.21_{-0.09}^{+0.03} \pm 0.18$			¹ AMBROSINO	07	KLOE $e^+e^- \rightarrow \pi^0\pi^0\gamma$
$2.90 \pm 0.21 \pm 1.54$			² AKHMETSHIN	99c	CMD2 $e^+e^- \rightarrow \pi^+\pi^-\gamma, \pi^0\pi^0\gamma$
4.47 ± 0.21		2438	³ ALOISIO	02D	KLOE $e^+e^- \rightarrow \pi^0\pi^0\gamma$
$3.5 \pm 0.3_{-0.5}^{+1.3}$		419	^{4,5} ACHASOV	00H	SND $e^+e^- \rightarrow \pi^0\pi^0\gamma$
$1.93 \pm 0.46 \pm 0.50$		27188	⁶ AKHMETSHIN	99B	CMD2 $e^+e^- \rightarrow \pi^+\pi^-\gamma$
$3.05 \pm 0.25 \pm 0.72$		268	⁷ AKHMETSHIN	99c	CMD2 $e^+e^- \rightarrow \pi^0\pi^0\gamma$
1.5 ± 0.5		268	⁸ AKHMETSHIN	99c	CMD2 $e^+e^- \rightarrow \pi^0\pi^0\gamma$
$3.42 \pm 0.30 \pm 0.36$		164	⁴ ACHASOV	98i	SND $e^+e^- \rightarrow 5\gamma$
< 1	90		⁹ AKHMETSHIN	97c	CMD2 $e^+e^- \rightarrow \pi^+\pi^-\gamma$
< 7	90		¹⁰ AKHMETSHIN	97c	CMD2 $e^+e^- \rightarrow \pi^+\pi^-\gamma$
< 20	90		DRUZHNININ	87	ND $e^+e^- \rightarrow \pi^0\pi^0\gamma$

¹ Obtained by the authors taking into account the $\pi^+\pi^-$ decay mode. Includes a component due to $\pi\pi$ production via the $f_0(500)$ meson. Supersedes ALOISIO 02D.
² From the combined fit of the photon spectra in the reactions $e^+e^- \rightarrow \pi^+\pi^-\gamma, \pi^0\pi^0\gamma$.
³ From the negative interference with the $f_0(500)$ meson of AITALA 01B using the ACHASOV 89 parameterization for the $f_0(980)$, a Breit-Wigner for the $f_0(500)$, and ACHASOV 01F for the $\rho\pi$ contribution. Superseded by AMBROSINO 07.
⁴ Assuming that the $\pi^0\pi^0\gamma$ final state is completely determined by the $f_0\gamma$ mechanism, neglecting the decay $B(\phi \rightarrow K\bar{K}\gamma)$ and using $B(f_0 \rightarrow \pi^+\pi^-) = 2B(f_0 \rightarrow \pi^0\pi^0)$.

⁵ Using the value $B(\phi \rightarrow \eta\gamma) = (1.338 \pm 0.053) \times 10^{-2}$.
⁶ For $E_\gamma > 20$ MeV. Supersedes AKHMETSHIN 97c.
⁷ Neglecting other intermediate mechanisms ($\rho\pi, \sigma\gamma$).
⁸ A narrow pole fit taking into account $f_0(980)$ and $f_0(1200)$ intermediate mechanisms.
⁹ For destructive interference with the Bremsstrahlung process
¹⁰ For constructive interference with the Bremsstrahlung process

$\Gamma(f_0(980)\gamma)/\Gamma(\eta\gamma)$ Γ_{17}/Γ_6

VALUE (units 10^{-2})	EVTS	DOCUMENT ID	TECN	COMMENT
$2.47_{-0.16}^{+0.15}$ OUR FIT				Error includes scale factor of 1.1.
$2.6 \pm 0.2_{-0.8}^{+0.8}$	419	¹ ACHASOV	00H	SND $e^+e^- \rightarrow \pi^0\pi^0\gamma$

¹ Assuming that the $\pi^0\pi^0\gamma$ final state is completely determined by the $f_0\gamma$ mechanism, neglecting the decay $B(\phi \rightarrow K\bar{K}\gamma)$ and using $B(f_0 \rightarrow \pi^+\pi^-) = 2B(f_0 \rightarrow \pi^0\pi^0)$.

$\Gamma(\pi^0\pi^0\gamma)/\Gamma_{total}$ Γ_{18}/Γ

VALUE (units 10^{-4})	CL%	EVTS	DOCUMENT ID	TECN	COMMENT
1.07 ± 0.06 OUR AVERAGE					
$1.07_{-0.06}^{+0.01} +0.06$			¹ AMBROSINO	07	KLOE $e^+e^- \rightarrow \pi^0\pi^0\gamma$
$1.08 \pm 0.17 \pm 0.09$		268	AKHMETSHIN	99c	CMD2 $e^+e^- \rightarrow \pi^0\pi^0\gamma$
$1.09 \pm 0.03 \pm 0.05$		2438	ALOISIO	02D	KLOE $e^+e^- \rightarrow \pi^0\pi^0\gamma$
$1.158 \pm 0.093 \pm 0.052$		419	^{2,3} ACHASOV	00H	SND $e^+e^- \rightarrow \pi^0\pi^0\gamma$
<10	90		DRUZHNININ	87	ND $e^+e^- \rightarrow 5\gamma$

¹ Supersedes ALOISIO 02D.
² Using the value $B(\phi \rightarrow \eta\gamma) = (1.338 \pm 0.053) \times 10^{-2}$.
³ Supersedes ACHASOV 98i. Excluding $\omega\pi^0$.

$\Gamma(\pi^0\pi^0\gamma)/\Gamma(\eta\gamma)$ Γ_{18}/Γ_6

VALUE (units 10^{-2})	EVTS	DOCUMENT ID	TECN	COMMENT
0.86 ± 0.04 OUR FIT				
$0.865 \pm 0.070 \pm 0.017$	419	¹ ACHASOV	00H	SND $e^+e^- \rightarrow \pi^0\pi^0\gamma$
$0.90 \pm 0.08 \pm 0.07$	164	ACHASOV	98i	SND $e^+e^- \rightarrow 5\gamma$

¹ Supersedes ACHASOV 98i. Excluding $\omega\pi^0$.

$\Gamma(\pi^+\pi^-\pi^+\pi^-)/\Gamma_{total}$ Γ_{19}/Γ

VALUE (units 10^{-6})	CL%	EVTS	DOCUMENT ID	TECN	COMMENT
$6.5 \pm 2.7 \pm 1.6$		6.8k	¹ AKHMETSHIN	17	CMD3 $e^+e^- \rightarrow \pi^+\pi^-\pi^+\pi^-$
$3.93 \pm 1.74 \pm 2.14$		3.3k	AKHMETSHIN	00E	CMD2 $e^+e^- \rightarrow \pi^+\pi^-\pi^+\pi^-$
< 870	90		CORDIER	79	WIRE $e^+e^- \rightarrow \pi^+\pi^-\pi^+\pi^-$

¹ Using the cross section at the ϕ meson peak $\sigma(\phi) = 4172 \pm 42$ nb, the nonresonant cross section $\sigma(0) = 1.263 \pm 0.027$ nb and $\text{Re}(Z) = 0.146 \pm 0.030, \text{Im}(Z) = -0.002 \pm 0.024$ for the complex amplitude of the $\phi \rightarrow \pi^+\pi^-\pi^+\pi^-$ transition.

$\Gamma(\pi^+\pi^+\pi^-\pi^-)/\Gamma_{total}$ Γ_{20}/Γ

VALUE (units 10^{-6})	CL%	DOCUMENT ID	TECN	COMMENT
< 4.6	90	AKHMETSHIN	00E	CMD2 $e^+e^- \rightarrow \pi^+\pi^-\pi^+\pi^-$
<150	95	BARKOV	88	CMD $e^+e^- \rightarrow \pi^+\pi^-\pi^+\pi^-$

¹ We do not use the following data for averages, fits, limits, etc. ●●●

$\Gamma(\pi^0 e^+ e^-)/\Gamma_{total}$ Γ_{21}/Γ

VALUE (units 10^{-5})	CL%	EVTS	DOCUMENT ID	TECN	COMMENT
$1.33_{-0.10}^{+0.07}$ OUR AVERAGE					
$1.35 \pm 0.05_{-0.10}^{+0.05}$		9.5k	¹ ANASTASI	16B	KLOE $e^+e^- \rightarrow \pi^0 e^+ e^-$
$1.01 \pm 0.28 \pm 0.29$		52	² ACHASOV	02D	SND $e^+e^- \rightarrow \pi^0 e^+ e^-$
$1.22 \pm 0.34 \pm 0.21$		46	³ AKHMETSHIN	01c	CMD2 $e^+e^- \rightarrow \pi^0 e^+ e^-$
<12	90		DOLINSKY	88	ND $e^+e^- \rightarrow \pi^0 e^+ e^-$

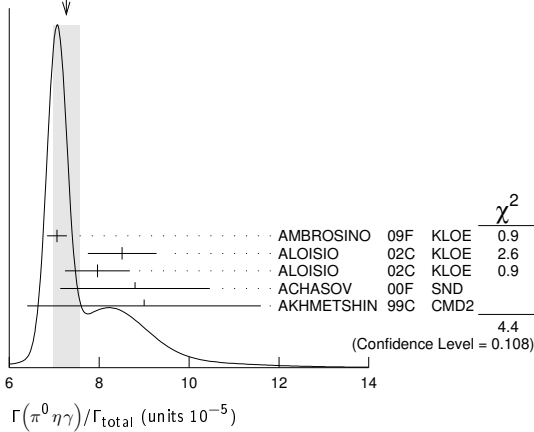
¹ Using $B(\pi^0 \rightarrow \gamma\gamma)$ from the 2014 Edition of this Review (PDG 14).
² Using various branching ratios from the 2000 Edition of this Review (PDG 00).
³ Using $B(\pi^0 \rightarrow \gamma\gamma) = 0.98798 \pm 0.00032, B(\phi \rightarrow \eta\gamma) = (1.297 \pm 0.033) \times 10^{-2}$, and $B(\eta \rightarrow \pi^+\pi^-\gamma) = (4.75 \pm 0.11) \times 10^{-2}$.

$\Gamma(\pi^0\eta\gamma)/\Gamma_{total}$ Γ_{22}/Γ

VALUE (units 10^{-5})	CL%	EVTS	DOCUMENT ID	TECN	COMMENT
7.27 ± 0.30 OUR AVERAGE					Error includes scale factor of 1.5. See the ideogram below.
7.06 ± 0.22		16.9k	¹ AMBROSINO	09F	KLOE 1.02 $e^+e^- \rightarrow \eta\pi^0\gamma$
$8.51 \pm 0.51 \pm 0.57$		607	² ALOISIO	02c	KLOE $e^+e^- \rightarrow \eta\pi^0\gamma$
$7.96 \pm 0.60 \pm 0.40$		197	³ ALOISIO	02c	KLOE $e^+e^- \rightarrow \eta\pi^0\gamma$
$8.8 \pm 1.4 \pm 0.9$		36	⁴ ACHASOV	00F	SND $e^+e^- \rightarrow \eta\pi^0\gamma$
$9.0 \pm 2.4 \pm 1.0$		80	AKHMETSHIN	99c	CMD2 $e^+e^- \rightarrow \eta\pi^0\gamma$
$7.01 \pm 0.10 \pm 0.20$		13.3k	^{2,5} AMBROSINO	09F	KLOE 1.02 $e^+e^- \rightarrow \eta\pi^0\gamma$
$7.12 \pm 0.13 \pm 0.22$		3.6k	^{3,6} AMBROSINO	09F	KLOE 1.02 $e^+e^- \rightarrow \eta\pi^0\gamma$
$8.3 \pm 2.3 \pm 1.2$		20	ACHASOV	98B	SND $e^+e^- \rightarrow 5\gamma$
<250	90		DOLINSKY	91	ND $e^+e^- \rightarrow \pi^0\eta\gamma$

¹ We do not use the following data for averages, fits, limits, etc. ●●●

WEIGHTED AVERAGE
7.27±0.30 (Error scaled by 1.5)



- 1 Combined results of $\eta \rightarrow \gamma\gamma$ and $\eta \rightarrow \pi^+\pi^-\pi^0$ decay modes measurements.
- 2 From the decay mode $\eta \rightarrow \gamma\gamma$.
- 3 From the decay mode $\eta \rightarrow \pi^+\pi^-\pi^0$.
- 4 Supersedes ACHASOV 98B.
- 5 Using $B(\phi \rightarrow \eta\gamma) = (1.304 \pm 0.025)\%$, $B(\eta \rightarrow 3\pi^0) = (32.56 \pm 0.23)\%$, and $B(\eta \rightarrow \gamma\gamma) = (39.31 \pm 0.20)\%$.
- 6 Using $B(\phi \rightarrow \eta\gamma) = (1.304 \pm 0.025)\%$, $B(\eta \rightarrow 3\pi^0) = (32.56 \pm 0.23)\%$, and $B(\eta \rightarrow \pi^+\pi^-\pi^0) = (22.73 \pm 0.28)\%$.

$\Gamma(a_0(980)\gamma)/\Gamma_{total}$		Γ_{23}/Γ		
VALUE (units 10^{-5})	CL%	DOCUMENT ID	TECN	COMMENT
7.6±0.6 OUR FIT				
7.6±0.6 OUR AVERAGE				
7.4±0.7		1 ALOISIO 02c	KLOE	$e^+e^- \rightarrow \eta\pi^0\gamma$
8.8±1.7	36	2 ACHASOV 00f	SND	$e^+e^- \rightarrow \eta\pi^0\gamma$
••• We do not use the following data for averages, fits, limits, etc. •••				
11 ± 2		3 GOKALP 02	RVUE	$e^+e^- \rightarrow \eta\pi^0\gamma$
<500	90	DOLINSKY 91	ND	$e^+e^- \rightarrow \pi^0\eta\gamma$
1 Using $M_{a_0(980)}=984.8$ MeV and assuming $a_0(980)\gamma$ dominance.				
2 Assuming $a_0(980)\gamma$ dominance in the $\eta\pi^0\gamma$ final state.				
3 Using data of ACHASOV 00f.				

$\Gamma(f_0(980)\gamma)/\Gamma(a_0(980)\gamma)$		Γ_{17}/Γ_{23}		
VALUE	CL%	DOCUMENT ID	TECN	COMMENT
6.1±0.6		1 ALOISIO 02c	KLOE	$e^+e^- \rightarrow \eta\pi^0\gamma$
1 Using results of ALOISIO 02d and assuming that $f_0(980)$ decays into $\pi\pi$ only and $a_0(980)$ into $\eta\pi$ only.				

$\Gamma(K^0\bar{K}^0\gamma)/\Gamma_{total}$		Γ_{24}/Γ		
VALUE	CL%	DOCUMENT ID	TECN	COMMENT
<1.9 × 10⁻⁸	90	AMBROSINO 09c	KLOE	$e^+e^- \rightarrow K_S^0 K_S^0 \gamma$

$\Gamma(\eta'(958)\gamma)/\Gamma_{total}$		Γ_{25}/Γ		
VALUE (units 10^{-5})	CL%	DOCUMENT ID	TECN	COMMENT
6.22±0.21 OUR FIT				
6.22±0.30 OUR AVERAGE				
6.22±0.27±0.12	3407	1 AMBROSINO 07a	KLOE	$1.02 e^+e^- \rightarrow \pi^+\pi^-\pi^0\gamma$
6.7 ± _{-2.4} ±0.8	12	2 AULCHENKO 03b	SND	$e^+e^- \rightarrow \eta'\gamma$
••• We do not use the following data for averages, fits, limits, etc. •••				
6.7 ± _{-4.2} ±1.5	7	AULCHENKO 03b	SND	$e^+e^- \rightarrow \gamma\gamma$
6.10±0.61±0.43	120	3 ALOISIO 02e	KLOE	$1.02 e^+e^- \rightarrow \pi^+\pi^-\pi^0\gamma$
8.2 ± _{-1.9} ±1.1	21	4 AKHMETSHIN 00b	CMD2	$e^+e^- \rightarrow \pi^+\pi^-\pi^0\gamma$
4.9 ± _{-1.8} ±0.6	9	5 AKHMETSHIN 00f	CMD2	$e^+e^- \rightarrow \pi^+\pi^-\pi^+\pi^-\pi^0\gamma$
6.4 ±1.6	30	6 AKHMETSHIN 00f	CMD2	$e^+e^- \rightarrow \eta'(958)\gamma$
6.7 ± _{-2.9} ±1.0	5	7 AULCHENKO 99	SND	$e^+e^- \rightarrow \pi^+\pi^-\pi^0\gamma$
<11	90	AULCHENKO 98	SND	$e^+e^- \rightarrow \gamma\gamma$
12 ± ₋₅ ±2	6	4 AKHMETSHIN 97b	CMD2	$e^+e^- \rightarrow \pi^+\pi^-\pi^0\gamma$
<41	90	DRUZHININ 87	ND	$e^+e^- \rightarrow \gamma\eta\pi^+\pi^-$

- 1 AMBROSINO 07a reports $[\Gamma(\phi(1020) \rightarrow \eta'(958)\gamma)/\Gamma_{total}] / [B(\phi(1020) \rightarrow \eta\gamma)] = (4.77 \pm 0.09 \pm 0.19) \times 10^{-3}$ which we multiply by our best value $B(\phi(1020) \rightarrow \eta\gamma) = (1.303 \pm 0.025) \times 10^{-2}$. Our first error is their experiment's error and our second error is the systematic error from using our best value.
- 2 Averaging AULCHENKO 03b with AULCHENKO 99.
- 3 Using $B(\phi \rightarrow \eta\gamma) = (1.297 \pm 0.033)\%$.

- 4 Using the value $B(\phi \rightarrow \eta\gamma) = (1.26 \pm 0.06) \times 10^{-2}$.
- 5 Using $B(\phi \rightarrow K_L^0 K_S^0) = (33.8 \pm 0.6)\%$.
- 6 Averaging AKHMETSHIN 00b with AKHMETSHIN 00f.
- 7 Using the value $B(\eta' \rightarrow \eta\pi^+\pi^-) = (43.7 \pm 1.5) \times 10^{-2}$ and $B(\eta \rightarrow \gamma\gamma) = (39.25 \pm 0.31) \times 10^{-2}$.

$\Gamma(\eta'(958)\gamma)/\Gamma(K_L^0 K_S^0)$		Γ_{25}/Γ_2		
VALUE (units 10^{-4})	EVTS	DOCUMENT ID	TECN	COMMENT
1.83±0.06 OUR FIT				
1.46 ±_{-0.54} ±0.18	9	1 AKHMETSHIN 00f	CMD2	$e^+e^- \rightarrow \pi^+\pi^-\pi^+\pi^- \geq 2\gamma$

- 1 Using various branching ratios of $K_S^0, K_L^0, \eta, \eta'$ from the 2000 edition (The European Physical Journal **C15** 1 (2000)) of this Review.

$\Gamma(\eta'(958)\gamma)/\Gamma(\eta\gamma)$		Γ_{25}/Γ_6		
VALUE (units 10^{-3})	EVTS	DOCUMENT ID	TECN	COMMENT
4.77±0.15 OUR FIT				
4.78±0.20 OUR AVERAGE				
4.77±0.09±0.19	3407	AMBROSINO 07a	KLOE	$1.02 e^+e^- \rightarrow \pi^+\pi^-\pi^0\gamma$
4.70±0.47±0.31	120	1 ALOISIO 02e	KLOE	$1.02 e^+e^- \rightarrow \pi^+\pi^-\pi^0\gamma$
6.5 ± _{-1.5} ±0.8	21	AKHMETSHIN 00b	CMD2	$e^+e^- \rightarrow \pi^+\pi^-\pi^0\gamma$
••• We do not use the following data for averages, fits, limits, etc. •••				
9.5 ± _{-4.0} ±1.4	6	2 AKHMETSHIN 97b	CMD2	$e^+e^- \rightarrow \pi^+\pi^-\pi^0\gamma$

- 1 From the decay mode $\eta' \rightarrow \eta\pi^+\pi^-, \eta \rightarrow \gamma\gamma$.
- 2 Superseded by AKHMETSHIN 00b.

$\Gamma(\eta\pi^0\pi^0\gamma)/\Gamma_{total}$		Γ_{26}/Γ		
VALUE (units 10^{-5})	CL%	DOCUMENT ID	TECN	COMMENT
<2	90	AULCHENKO 98	SND	$e^+e^- \rightarrow \gamma\gamma$

$\Gamma(\mu^+\mu^-\gamma)/\Gamma_{total}$		Γ_{27}/Γ		
VALUE (units 10^{-5})	EVTS	DOCUMENT ID	TECN	COMMENT
1.43±0.45 ±0.14	27188	1 AKHMETSHIN 99b	CMD2	$e^+e^- \rightarrow \mu^+\mu^-\gamma$
••• We do not use the following data for averages, fits, limits, etc. •••				
2.3 ±1.0	824 ± 33	2 AKHMETSHIN 97c	CMD2	$e^+e^- \rightarrow \mu^+\mu^-\gamma$
1 For $E_\gamma > 20$ MeV. Supersedes AKHMETSHIN 97c.				
2 For $E_\gamma > 20$ MeV.				

$\Gamma(\rho\gamma\gamma)/\Gamma_{total}$		Γ_{28}/Γ		
VALUE (units 10^{-4})	CL%	DOCUMENT ID	TECN	COMMENT
<1.2	90	AULCHENKO 08	CMD2	$\phi \rightarrow \pi^+\pi^-\gamma\gamma$
••• We do not use the following data for averages, fits, limits, etc. •••				
<5	90	AKHMETSHIN 98	CMD2	$e^+e^- \rightarrow \pi^+\pi^-\gamma\gamma$

$\Gamma(\eta\pi^+\pi^-)/\Gamma_{total}$		Γ_{29}/Γ		
VALUE (units 10^{-5})	CL%	DOCUMENT ID	TECN	COMMENT
< 1.8	90	AKHMETSHIN 00e	CMD2	$e^+e^- \rightarrow \pi^+\pi^-\pi^+\pi^-\pi^0$
••• We do not use the following data for averages, fits, limits, etc. •••				
< 6.1	90	AULCHENKO 08	CMD2	$\phi \rightarrow \eta\pi^+\pi^-$
<30	90	AKHMETSHIN 98	CMD2	$e^+e^- \rightarrow \pi^+\pi^-\gamma\gamma$

$\Gamma(\eta\mu^+\mu^-)/\Gamma_{total}$		Γ_{30}/Γ		
VALUE (units 10^{-6})	CL%	DOCUMENT ID	TECN	COMMENT
<9.4	90	AKHMETSHIN 01	CMD2	$e^+e^- \rightarrow \eta e^+e^-$

$\Gamma(\eta U \rightarrow \eta e^+e^-)/\Gamma_{total}$		Γ_{31}/Γ		
VALUE	CL%	DOCUMENT ID	TECN	COMMENT
<1 × 10⁻⁶	90	1 BABUSCI 13b	KLOE	$1.02 e^+e^- \rightarrow \eta e^+e^-$
1 For a narrow vector U with mass between 5 and 470 MeV, from the combined analysis of $\eta \rightarrow \pi^+\pi^-\pi^0$ and $\eta \rightarrow \pi^0\pi^0\pi^0$ from ARCHILLI 12. Measured 90% CL limits as a function of m_U range from 2.2×10^{-8} to 10^{-6} .				

$\Gamma(\text{invisible})/\Gamma(K^+K^-)$		Γ_{32}/Γ_1		
VALUE	CL%	DOCUMENT ID	TECN	COMMENT
<3.4 × 10⁻⁴	90	ABLIKIM 18s	BES3	$J/\psi \rightarrow \phi\eta \rightarrow \phi\pi^+\pi^-\pi^0$

Lepton Family number (LF) violating modes

$\Gamma(e^\pm\mu^\mp)/\Gamma_{total}$		Γ_{33}/Γ		
VALUE	CL%	DOCUMENT ID	TECN	COMMENT
<2 × 10⁻⁶	90	ACHASOV 10a	SND	$e^+e^- \rightarrow e^\pm\mu^\mp$

$\pi^+\pi^-\pi^0 / \rho\pi$ AMPLITUDE RATIO a_1 IN DECAY OF $\phi \rightarrow \pi^+\pi^-\pi^0$

NIECKNIG 12 describes final-state interactions between the three pions in a dispersive framework using data on the $\pi\pi$ P-wave scattering phase shift.

See key on page 999

Meson Particle Listings

$h_1(1170), b_1(1235)$

••• We do not use the following data for averages, fits, limits, etc. •••

1168 ± 4	ANDO	92	SPEC	8 $\pi^- p \rightarrow \pi^+ \pi^- \pi^0 n$
1190 ± 60	2 DANKOWY...	81	SPEC	0 8 $\pi p \rightarrow 3\pi n$

¹ Average and spread of values using 2 variants of the model of BOWLER 75.
² Uses the model of BOWLER 75.

$h_1(1170)$ WIDTH

VALUE (MeV)	DOCUMENT ID	TECN	CHG	COMMENT
375 ± 6 ± 34	³ ANDO	92	SPEC	8 $\pi^- p \rightarrow \pi^+ \pi^- \pi^0 n$
345 ± 6	ANDO	92	SPEC	8 $\pi^- p \rightarrow \pi^+ \pi^- \pi^0 n$
320 ± 50	⁴ DANKOWY...	81	SPEC	0 8 $\pi p \rightarrow 3\pi n$

³ Average and spread of values using 2 variants of the model of BOWLER 75.
⁴ Uses the model of BOWLER 75.

$h_1(1170)$ DECAY MODES

Mode	Fraction (Γ_i/Γ)
Γ_1 $\rho\pi$	seen

$h_1(1170)$ BRANCHING RATIOS

$\Gamma(\rho\pi)/\Gamma_{total}$	DOCUMENT ID	TECN	COMMENT	Γ_1/Γ
••• We do not use the following data for averages, fits, limits, etc. •••				
seen	ANDO	92	SPEC	8 $\pi^- p \rightarrow \pi^+ \pi^- \pi^0 n$
seen	ATKINSON	84	OMEG	20-70 $\gamma p \rightarrow \pi^+ \pi^- \pi^0 p$
seen	DANKOWY...	81	SPEC	8 $\pi p \rightarrow 3\pi n$

$h_1(1170)$ REFERENCES

ANDO	92	PL B291 496	A. Ando et al.	(KEK, KYOT, NIRS, SAGA+)
ATKINSON	84	NP B231 15	M. Atkinson et al.	(BONN, CERN, GLAS+)
DANKOWY...	81	PRL 46 580	J.A. Dankowych et al.	(TNT, BNL, CARL+)
BOWLER	75	NP B97 227	M.G. Bowler et al.	(OXFPP, DARE)

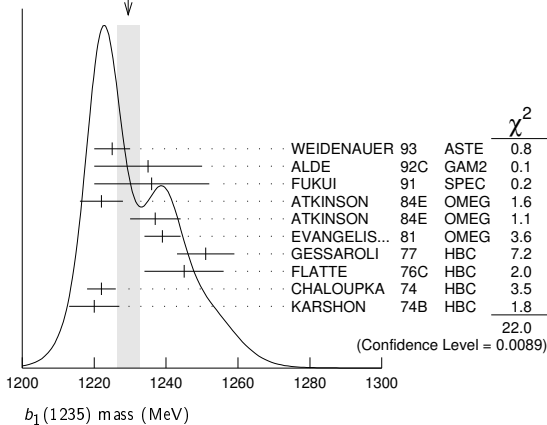
$b_1(1235)$

$$I^G(J^{PC}) = 1^+(1^{+-})$$

$b_1(1235)$ MASS

VALUE (MeV)	EVTs	DOCUMENT ID	TECN	CHG	COMMENT
1229.5 ± 3.2 OUR AVERAGE					Error includes scale factor of 1.6. See the ideogram below.
1225 ± 5		WEIDENAUER 93	ASTE		$\bar{p}p \rightarrow 2\pi^+ 2\pi^- \pi^0$
1235 ± 15		ALDE 92c	GAM2		38,100 $\pi^- p \rightarrow \omega \pi^0 n$
1236 ± 16		FUKUI 91	SPEC		8.95 $\pi^- p \rightarrow \omega \pi^0 n$
1222 ± 6		ATKINSON 84E	OMEG ±		25-55 $\gamma p \rightarrow \omega \pi X$
1237 ± 7		ATKINSON 84E	OMEG 0		25-55 $\gamma p \rightarrow \omega \pi X$
1239 ± 5		EVANGELIS... 81	OMEG -		12 $\pi^- p \rightarrow \omega \pi p$
1251 ± 8	450	GESSAROLI 77	HBC -		11 $\pi^- p \rightarrow \pi^- \omega p$
1245 ± 11	890	FLATTE 76c	HBC -		4.2 $K^- p \rightarrow \pi^- \omega \Sigma^+$
1222 ± 4	1400	CHALOUKKA 74	HBC -		3.9 $\pi^- p$
1220 ± 7	600	KARSHON 74B	HBC +		4.9 $\pi^+ p$
••• We do not use the following data for averages, fits, limits, etc. •••					
1190 ± 10		AUGUSTIN 89	DM2 ±		$e^+ e^- \rightarrow 5\pi$
1213 ± 5		ATKINSON 84c	OMEG 0		20-70 γp
1271 ± 11		COLLICK 84	SPEC +		200 $\pi^+ Z \rightarrow Z \pi \omega$

WEIGHTED AVERAGE
1229.5 ± 3.2 (Error scaled by 1.6)



$b_1(1235)$ WIDTH

VALUE (MeV)	EVTs	DOCUMENT ID	TECN	CHG	COMMENT
142 ± 9 OUR AVERAGE					Error includes scale factor of 1.2.
113 ± 12		WEIDENAUER 93	ASTE		$\bar{p}p \rightarrow 2\pi^+ 2\pi^- \pi^0$
160 ± 30		ALDE 92c	GAM2		38,100 $\pi^- p \rightarrow \omega \pi^0 n$
151 ± 31		FUKUI 91	SPEC		8.95 $\pi^- p \rightarrow \omega \pi^0 n$
170 ± 15		EVANGELIS... 81	OMEG -		12 $\pi^- p \rightarrow \omega \pi p$
170 ± 50	225	BALTAY 78B	HBC +		15 $\pi^+ p \rightarrow p 4\pi$
155 ± 32	450	GESSAROLI 77	HBC -		11 $\pi^- p \rightarrow \pi^- \omega p$
182 ± 45	890	FLATTE 76c	HBC -		4.2 $K^- p \rightarrow \pi^- \omega \Sigma^+$
135 ± 20	1400	CHALOUKKA 74	HBC -		3.9 $\pi^- p$
156 ± 22	600	KARSHON 74B	HBC +		4.9 $\pi^+ p$
••• We do not use the following data for averages, fits, limits, etc. •••					
210 ± 19		AUGUSTIN 89	DM2 ±		$e^+ e^- \rightarrow 5\pi$
231 ± 14		ATKINSON 84c	OMEG 0		20-70 γp
232 ± 29		COLLICK 84	SPEC +		200 $\pi^+ Z \rightarrow Z \pi \omega$

$b_1(1235)$ DECAY MODES

Mode	Fraction (Γ_i/Γ)	Confidence level
Γ_1 $\omega\pi$	seen	
Γ_2 $\pi^\pm \gamma$	(D/S amplitude ratio = 0.277 ± 0.027)	
Γ_3 $\eta\rho$	seen	
Γ_4 $\pi^+ \pi^+ \pi^- \pi^0$	< 50 %	84%
Γ_5 $K^*(892)^\pm K^\mp$	seen	
Γ_6 $(K\bar{K})^\pm \pi^0$	< 8 %	90%
Γ_7 $K_S^0 K_L^0 \pi^\pm$	< 6 %	90%
Γ_8 $K_S^0 K_S^0 \pi^\pm$	< 2 %	90%
Γ_9 $\phi\pi$	< 1.5 %	84%

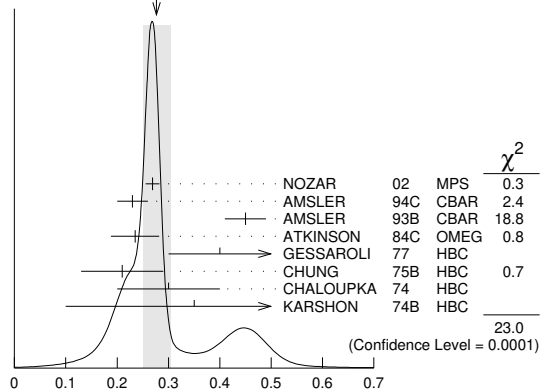
$b_1(1235)$ PARTIAL WIDTHS

$\Gamma(\pi^\pm \gamma)$	DOCUMENT ID	TECN	CHG	COMMENT
230 ± 60	COLLICK 84	SPEC	+	200 $\pi^+ Z \rightarrow Z \pi \omega$

$b_1(1235)$ D-wave/S-wave AMPLITUDE RATIO IN DECAY OF $b_1(1235) \rightarrow \omega\pi$

VALUE	EVTs	DOCUMENT ID	TECN	CHG	COMMENT
0.277 ± 0.027 OUR AVERAGE					Error includes scale factor of 2.4. See the ideogram below.
0.269 ± 0.009 ± 0.010		NOZAR 02	MPS -		18 $\pi^- p \rightarrow \omega \pi^- p$
0.23 ± 0.03		AMSLER 94c	CBAR		0.0 $\bar{p}p \rightarrow \omega \eta \pi^0$
0.45 ± 0.04		AMSLER 93B	CBAR		0.0 $\bar{p}p \rightarrow \omega \pi^0 \pi^0$
0.235 ± 0.047		ATKINSON 84c	OMEG		20-70 γp
0.4 + 0.1 - 0.1		GESSAROLI 77	HBC -		11 $\pi^- p \rightarrow \pi^- \omega p$
0.21 ± 0.08		CHUNG 75B	HBC +		7.1 $\pi^+ p$
0.3 ± 0.1		CHALOUKKA 74	HBC -		3.9-7.5 $\pi^- p$
0.35 ± 0.25	600	KARSHON 74B	HBC +		4.9 $\pi^+ p$

WEIGHTED AVERAGE
0.277 ± 0.027 (Error scaled by 2.4)



$b_1(1235)$ D-wave/S-wave amplitude ratio in decay of $b_1(1235) \rightarrow \omega\pi$

$b_1(1235)$ D-wave/S-wave AMPLITUDE PHASE DIFFERENCE IN DECAY OF $b_1(1235) \rightarrow \omega\pi$

VALUE (°)	DOCUMENT ID	TECN	CHG	COMMENT
10.5 ± 2.4 ± 3.9	NOZAR 02	MPS	-	18 $\pi^- p \rightarrow \omega \pi^- p$

Meson Particle Listings

$b_1(1235), a_1(1260)$

$b_1(1235)$ BRANCHING RATIOS

$\Gamma(\eta\rho)/\Gamma(\omega\pi)$		Γ_3/Γ_1	
VALUE	DOCUMENT ID	TECN	COMMENT
<0.10	ATKINSON	84D	OMEG 20-70 γp
$\Gamma(\pi^+\pi^-\pi^0)/\Gamma(\omega\pi)$		Γ_4/Γ_1	
VALUE	DOCUMENT ID	TECN	CHG
<0.5	ABOLINS	63	HBC + 3.5 $\pi^+ p$
$\Gamma(K^*(892)^\pm K^\mp)/\Gamma_{total}$		Γ_5/Γ	
VALUE	DOCUMENT ID	TECN	COMMENT
seen	1 ABLIKIM	10E	BES2 $J/\psi \rightarrow K^\pm K_S^0 \pi^+ \pi^0$
1 From a fit including ten additional resonances and energy-independent Breit-Wigner width.			
$\Gamma((K\bar{K})^\pm \pi^0)/\Gamma(\omega\pi)$		Γ_6/Γ_1	
VALUE	DOCUMENT ID	TECN	CHG
<0.08	BALTAY	67	HBC \pm 0.0 $\bar{p} p$
$\Gamma(K_S^0 K_L^0 \pi^\pm)/\Gamma(\omega\pi)$		Γ_7/Γ_1	
VALUE	DOCUMENT ID	TECN	CHG
<0.06	BALTAY	67	HBC \pm 0.0 $\bar{p} p$
$\Gamma(K_S^0 K_S^0 \pi^\pm)/\Gamma(\omega\pi)$		Γ_8/Γ_1	
VALUE	DOCUMENT ID	TECN	CHG
<0.02	BALTAY	67	HBC \pm 0.0 $\bar{p} p$
$\Gamma(\phi\pi)/\Gamma(\omega\pi)$		Γ_9/Γ_1	
VALUE	DOCUMENT ID	TECN	CHG
<0.004	VIKTOROV	96	SPEC 0 32.5 $\pi^- p \rightarrow K^+ K^- \pi^0 n$
••• We do not use the following data for averages, fits, limits, etc. •••			
<0.04	BIZZARRI	69	HBC \pm 0.0 $\bar{p} p$
<0.015	DAHL	67	HBC 1.6-4.2 $\pi^- p$

$b_1(1235)$ REFERENCES

ABLIKIM	10E	PL B693 88	M. Ablikim et al.	(BES II Collab.)
NOZAR	02	PL B541 35	M. Nozar et al.	
VIKTOROV	96	PAN 59 1184	V.A. Viktorov et al.	(SERP)
Translated from YAF 59 1239.				
AMSLER	94C	PL B327 425	C. Amstler et al.	(Crystal Barrel Collab.)
AMSLER	93B	PL B311 362	C. Amstler et al.	(Crystal Barrel Collab.)
WEIDENAUER	93	ZPHY C59 387	P. Weidenauer et al.	(ASTERIX Collab.)
ALDE	92C	ZPHY C54 553	D.M. Alde et al.	(BELG, SERP, KEK, LANL+)
FUKUI	91	PL B257 241	S. Fukui et al.	(SUGI, NAGO, KEK, KYOT+)
AUGUSTIN	89	NP B320 1	J.E. Augustin, G. Cosme	(DM2 Collab.)
ATKINSON	84C	NP B243 1	M. Atkinson et al.	(BONN, CERN, GLAS+ JP)
ATKINSON	84D	NP B242 269	M. Atkinson et al.	(BONN, CERN, GLAS+)
ATKINSON	84E	PL 138B 459	M. Atkinson et al.	(BONN, CERN, GLAS+)
COLLICK	84	PRL 53 2374	B. Collick et al.	(MINN, ROCH, FNAL)
EVANGELISTA...	81	NP B178 197	C. Evangelista et al.	(BARI, BONN, CERN+)
BALTAY	78B	PR D17 62	C. Baltay et al.	(COLU, BING)
GESSAROLI	77	NP B126 382	R. Gessaroli et al.	(BGN, FIRZ, GENO+ JP)
FLATTE	76C	PL 64B 225	S.M. Flatte et al.	(CERN, AMST, NIJH+ JP)
CHUNG	75B	PR D11 2426	S.U. Chung et al.	(BNL, LBL, UCSC JP)
CHALOUPIKA	74	PL 51B 407	V. Chaloupka et al.	(CERN JP)
KARSHON	74B	PR D10 3608	U. Karshon et al.	(REHO JP)
BIZZARRI	69	NP B14 169	R. Bizzarri et al.	(CERN, CDEF)
BALTAY	67	PRL 18 93	C. Baltay et al.	(COLU)
DAHL	67	PR 163 1377	O.L. Dahl et al.	(LRL)
ABOLINS	63	PRL 11 381	M.A. Abolins et al.	(UCSD)

$a_1(1260)$

$$I^G(J^{PC}) = 1^-(1^{++})$$

See also our review under the $a_1(1260)$ in PDG 06, Journal of Physics **G33** 1 (2006).

$a_1(1260)$ MASS

VALUE (MeV)	EVTS	DOCUMENT ID	TECN	COMMENT
1230 \pm 40	OUR ESTIMATE			
1299 \pm 12	46M	1 AGHASYAN	18B	COMP 190 $\pi^- p \rightarrow \pi^- \pi^+ \pi^- p$
••• We do not use the following data for averages, fits, limits, etc. •••				
1195.05 \pm 1.05 \pm 6.33	894k	AAIJ	18A1	LHCB $D^0 \rightarrow K\bar{\pi} \pi^\pm \pi^\pm \pi^\mp$
1209 \pm 4 \pm 12		2 MIKHASENKO	18	RVUE $\tau^- \rightarrow \pi^- \pi^+ \pi^- \nu_\tau$
1225 \pm 9 \pm 20	7k	3 DARGENT	17	RVUE $D^0 \rightarrow \pi^- \pi^+ \pi^- \pi^+$
1255 \pm 6 \pm 7	420k	4 ALEKSEEV	10	COMP 190 $\pi^- P_b \rightarrow \pi^- \pi^- \pi^+ P_b'$
1243 \pm 12 \pm 20		5 AUBERT	07AU	BABR 10.6 $e^+ e^- \rightarrow \rho^0 \pi^\pm \pi^\mp \gamma$
1230-1270	6360	6 LINK	07A	FOCS $D^0 \rightarrow \pi^- \pi^+ \pi^- \pi^+$
1203 \pm 3		7 GOMEZ-DUM...	04	RVUE $\tau^+ \rightarrow \pi^+ \pi^+ \pi^- \nu_\tau$
1330 \pm 24	90k	SALVINI	04	OBLX $\bar{p} p \rightarrow 2\pi^+ 2\pi^-$
1331 \pm 10 \pm 3	37k	8 ASNER	00	CLE2 10.6 $e^+ e^- \rightarrow \tau^+ \tau^-$
1255 \pm 7 \pm 6	5904	9 ABREU	98G	DLPH $e^+ e^-$
1207 \pm 5 \pm 8	5904	10 ABREU	98G	DLPH $e^+ e^-$
1196 \pm 4 \pm 5	5904	11,12 ABREU	98G	DLPH $e^+ e^-$

1240 \pm 10		BARBERIS	98B	450 $p p \rightarrow p_f \pi^+ \pi^- \pi^0 p_S$
1262 \pm 9 \pm 7	9,13	ACKERSTAFF	97R	OPAL $E_{cm}^{ee} = 88-94, \tau \rightarrow 3\pi\nu$
1210 \pm 7 \pm 2	10,13	ACKERSTAFF	97R	OPAL $E_{cm}^{ee} = 88-94, \tau \rightarrow 3\pi\nu$
1211 \pm 7 \pm 50		10 ALBRECHT	93C	ARG $\tau^+ \rightarrow \pi^+ \pi^+ \pi^- \nu$
1121 \pm 8		14 ANDO	92	SPEC $8 \pi^- p \rightarrow \pi^+ \pi^- \pi^0 n$
1242 \pm 37		15 IVANOV	91	RVUE $\tau \rightarrow \pi^+ \pi^+ \pi^- \nu$
1260 \pm 14		16 IVANOV	91	RVUE $\tau \rightarrow \pi^+ \pi^+ \pi^- \nu$
1250 \pm 9		17 IVANOV	91	RVUE $\tau \rightarrow \pi^+ \pi^+ \pi^- \nu$
1208 \pm 15		ARMSTRONG	90	OMEG 300.0 $p p \rightarrow p p \pi^+ \pi^- \pi^0$
1220 \pm 15		18 ISGUR	89	RVUE $\tau^+ \rightarrow \pi^+ \pi^+ \pi^- \nu$
1260 \pm 25		19 BOWLER	88	RVUE $\tau^+ \rightarrow \pi^+ \pi^+ \pi^- \nu$
1166 \pm 18 \pm 11		BAND	87	MAC $\tau^+ \rightarrow \pi^+ \pi^+ \pi^- \nu$
1164 \pm 41 \pm 23		BAND	87	MAC $\tau^+ \rightarrow \pi^+ \pi^0 \pi^0 \nu$
1250 \pm 40		18 TORNVIST	87	RVUE
1046 \pm 11		ALBRECHT	86B	ARG $\tau^+ \rightarrow \pi^+ \pi^+ \pi^- \nu$
1056 \pm 20 \pm 15		RUCKSTUHL	86	DLCO $\tau^+ \rightarrow \pi^+ \pi^+ \pi^- \nu$
1194 \pm 14 \pm 10		SCHMIDKE	86	MRK2 $\tau^+ \rightarrow \pi^+ \pi^+ \pi^- \nu$
1255 \pm 23		BELLINI	85	SPEC 40 $\pi^- A \rightarrow \pi^- \pi^+ \pi^- A$
1240 \pm 80		20 DANKOWY...	81	SPEC 8.45 $\pi^- p \rightarrow n 3\pi$
1280 \pm 30		20 DAUM	81B	CNTR 63,94 $\pi^- p \rightarrow p 3\pi$
1041 \pm 13		21 GAVILLET	77	HBC 4.2 $K^- p \rightarrow \Sigma 3\pi$

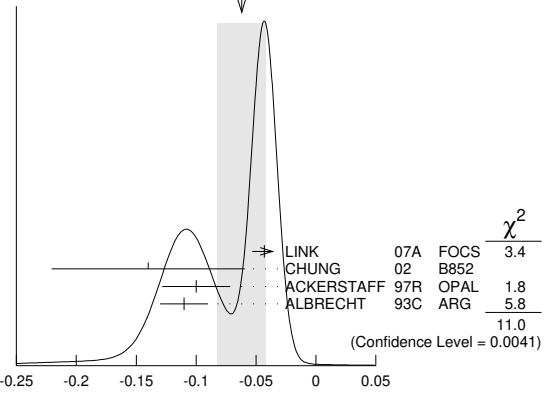
- Statistical error negligible.
- From the pole position. Using an amplitude analysis based on approximate three-body unitary of τ data from SCHAEEL 05c.
- Reanalysis of CLEO data using Breit-Wigner parameterization.
- Superseded by AGHASYAN 2018B.
- The $\rho^\pm \pi^\mp$ state can be also due to the $\pi(1300)$.
- Using the Breit-Wigner parameterization; strong correlation between mass and width.
- Using the data of BARATE 98R.
- From a fit to the 3π mass spectrum including the $K\bar{K}^*(892)$ threshold.
- Uses the model of KUHN 90.
- Uses the model of ISGUR 89.
- Includes the effect of a possible a_1' state.
- Uses the model of FEINDT 90.
- Supersedes AKERS 95P.
- Average and spread of values using 2 variants of the model of BOWLER 75.
- Reanalysis of RUCKSTUHL 86.
- Reanalysis of SCHMIDKE 86.
- Reanalysis of ALBRECHT 86B.
- From a combined reanalysis of ALBRECHT 86B, SCHMIDKE 86, and RUCKSTUHL 86.
- From a combined reanalysis of ALBRECHT 86B and DAUM 81B.
- Uses the model of BOWLER 75.
- Produced in K^- backward scattering.

$a_1(1260)$ WIDTH

VALUE (MeV)	EVTS	DOCUMENT ID	TECN	COMMENT
250 to 600	OUR ESTIMATE			
420 \pm 35	OUR AVERAGE			
430 \pm 80	46M	1 AGHASYAN	18B	COMP 190 $\pi^- p \rightarrow \pi^- \pi^+ \pi^- p$
430 \pm 24 \pm 31		DARGENT	17	RVUE $D^0 \rightarrow \pi^- \pi^+ \pi^- \pi^+$
422.01 \pm 2.10 \pm 12.72	894k	AAIJ	18A1	LHCB $D^0 \rightarrow K\bar{\pi} \pi^\pm \pi^\pm \pi^\mp$
576 \pm 11 \pm 89	20	2 MIKHASENKO	18	RVUE $\tau^- \rightarrow \pi^- \pi^+ \pi^- \nu_\tau$
367 \pm 9 \pm 28	420k	3 ALEKSEEV	10	COMP 190 $\pi^- P_b \rightarrow \pi^- \pi^- \pi^+ P_b'$
410 \pm 31 \pm 30		4 AUBERT	07AU	BABR 10.6 $e^+ e^- \rightarrow \rho^0 \pi^\pm \pi^\mp \gamma$
520-680	6360	5 LINK	07A	FOCS $D^0 \rightarrow \pi^- \pi^+ \pi^- \pi^+$
480 \pm 20		6 GOMEZ-DUM...	04	RVUE $\tau^+ \rightarrow \pi^+ \pi^+ \pi^- \nu_\tau$
580 \pm 41	90k	SALVINI	04	OBLX $\bar{p} p \rightarrow 2\pi^+ 2\pi^-$
460 \pm 85	205	7 DRUTSKOY	02	BELL $B \rightarrow D^{(*)} K^- K^{*0}$
814 \pm 36 \pm 13	37k	8 ASNER	00	CLE2 10.6 $e^+ e^- \rightarrow \tau^+ \tau^-$
450 \pm 50	22k	9 AKHMETSHIN	99E	CMD2 1.05-1.38 $e^+ e^- \rightarrow \pi^+ \pi^- \pi^0 \pi^0$
570 \pm 10		10 BONDAR	99	RVUE $e^+ e^- \rightarrow 4\pi, \tau \rightarrow 3\pi\nu_\tau$
587 \pm 27 \pm 21	5904	11 ABREU	98G	DLPH $e^+ e^-$
478 \pm 3 \pm 15	5904	12 ABREU	98G	DLPH $e^+ e^-$
425 \pm 14 \pm 8	5904	13,14 ABREU	98G	DLPH $e^+ e^-$
400 \pm 35		BARBERIS	98B	450 $p p \rightarrow p_f \pi^+ \pi^- \pi^0 p_S$
621 \pm 32 \pm 58		11,15 ACKERSTAFF	97R	OPAL $E_{cm}^{ee} = 88-94, \tau \rightarrow 3\pi\nu$
457 \pm 15 \pm 17		12,15 ACKERSTAFF	97R	OPAL $E_{cm}^{ee} = 88-94, \tau \rightarrow 3\pi\nu$
446 \pm 21 \pm 140	0	12 ALBRECHT	93C	ARG $\tau^+ \rightarrow \pi^+ \pi^+ \pi^- \nu$

239	± 11		ANDO	92	SPEC	$8 \pi^- \rho \rightarrow \pi^+ \pi^- \pi^0 n$
266	$\pm 13 \pm 4$	16	ANDO	92	SPEC	$8 \pi^- \rho \rightarrow \pi^+ \pi^- \pi^0 n$
465	$+228$ -143		IVANOV	91	RVUE	$\tau \rightarrow \pi^+ \pi^+ \pi^- \nu$
298	$+40$ -34		IVANOV	91	RVUE	$\tau \rightarrow \pi^+ \pi^+ \pi^- \nu$
488	± 32		IVANOV	91	RVUE	$\tau \rightarrow \pi^+ \pi^+ \pi^- \nu$
430	± 50		ARMSTRONG	90	OMEG	$300.0 \rho \rho \rightarrow \rho \rho \pi^+ \pi^- \pi^0$
420	± 40	20	ISGUR	89	RVUE	$\tau^+ \rightarrow \pi^+ \pi^+ \pi^- \nu$
396	± 43	21	BOWLER	88	RVUE	
405	$\pm 75 \pm 25$		BAND	87	MAC	$\tau^+ \rightarrow \pi^+ \pi^+ \pi^- \nu$
419	$\pm 108 \pm 57$		BAND	87	MAC	$\tau^+ \rightarrow \pi^+ \pi^0 \pi^0 \nu$
521	± 27		ALBRECHT	86B	ARG	$\tau^+ \rightarrow \pi^+ \pi^+ \pi^- \nu$
476	$+132$ -120	± 54	RUCKSTUHL	86	DLCO	$\tau^+ \rightarrow \pi^+ \pi^+ \pi^- \nu$
462	$\pm 56 \pm 30$		SCHMIDKE	86	MRK2	$\tau^+ \rightarrow \pi^+ \pi^+ \pi^- \nu$
292	± 40		BELLINI	85	SPEC	$40 \pi^- A \rightarrow \pi^- \pi^+ \pi^- A$
380	± 100	22	DANKOWY...	81	SPEC	$8.45 \pi^- \rho \rightarrow n 3\pi$
300	± 50	22	DAUM	81B	CNTR	$63.94 \pi^- \rho \rightarrow \rho 3\pi$
230	± 50	23	GAVILLET	77	HBC	$4.2 K^- \rho \rightarrow \Sigma 3\pi$

WEIGHTED AVERAGE
-0.062±0.020 (Error scaled by 2.3)



D-wave/S-wave AMPLITUDE RATIO IN DECAY OF $a_1(1260) \rightarrow \rho \pi$

- 1 Deck-type background not subtracted.
- 2 Uses the model of ISGUR 89.
- 3 Supersedes AKERS 95P.

- 1 Statistical error negligible.
- 2 From the pole position. Using an amplitude analysis based on approximate three-body unitary of τ data from SCHAEEL 05c.
- 3 Superseded by AGHASYAN 2018B.
- 4 The $\rho^\pm \pi^\mp$ state can be also due to the $\pi(1300)$.
- 5 Using the Breit-Wigner parameterization; strong correlation between mass and width.
- 6 Using the data of BARATE 98R.
- 7 From a fit of the $K^- K^*0$ distribution assuming $m_{a_1} = 1230$ MeV and purely resonant production of the $K^- K^*0$ system.
- 8 From a fit to the 3π mass spectrum including the $K \bar{K}^*(892)$ threshold.
- 9 Using the $a_1(1260)$ mass of 1230 MeV.
- 10 From AKHMETSHIN 99E and ASNER 00 data using the $a_1(1260)$ mass of 1230 MeV.
- 11 Uses the model of KUHN 90.
- 12 Uses the model of ISGUR 89.
- 13 Includes the effect of a possible a_1' state.
- 14 Uses the model of FEINDT 90.
- 15 Supersedes AKERS 95P.
- 16 Average and spread of values using 2 variants of the model of BOWLER 75.
- 17 Reanalysis of RUCKSTUHL 86.
- 18 Reanalysis of SCHMIDKE 86.
- 19 Reanalysis of ALBRECHT 86B.
- 20 From a combined reanalysis of ALBRECHT 86B, SCHMIDKE 86, and RUCKSTUHL 86.
- 21 From a combined reanalysis of ALBRECHT 86B and DAUM 81B.
- 22 Uses the model of BOWLER 75.
- 23 Produced in K^- backward scattering.

$a_1(1260)$ DECAY MODES

Mode	Fraction (Γ_i/Γ)
Γ_1 3π	seen
Γ_2 $(\rho\pi)S$ -wave, $\rho \rightarrow \pi\pi$	seen
Γ_3 $(\rho\pi)D$ -wave, $\rho \rightarrow \pi\pi$	seen
Γ_4 $(\rho(1450)\pi)S$ -wave, $\rho \rightarrow \pi\pi$	seen
Γ_5 $(\rho(1450)\pi)D$ -wave, $\rho \rightarrow \pi\pi$	seen
Γ_6 $f_0(500)\pi, f_0 \rightarrow \pi\pi$	seen
Γ_7 $f_0(980)\pi, f_0 \rightarrow \pi\pi$	not seen
Γ_8 $f_0(1370)\pi, f_0 \rightarrow \pi\pi$	seen
Γ_9 $f_2(1270)\pi, f_2 \rightarrow \pi\pi$	seen
Γ_{10} $\pi^+ \pi^- \pi^0$	seen
Γ_{11} $\pi^0 \pi^0 \pi^0$	not seen
Γ_{12} $K K \pi$	seen
Γ_{13} $K^*(892) K$	seen
Γ_{14} $\pi \gamma$	seen

$a_1(1260)$ PARTIAL WIDTHS

$\Gamma(\pi\gamma)$	VALUE (keV)	DOCUMENT ID	TECN	COMMENT	Γ_{14}
	640 ± 246	ZIELINSKI	84c	SPEC	200 $\pi^+ Z \rightarrow Z 3\pi$

D-wave/S-wave AMPLITUDE RATIO IN DECAY OF $a_1(1260) \rightarrow \rho \pi$

VALUE	DOCUMENT ID	TECN	COMMENT
-0.062±0.020 OUR AVERAGE	Error includes scale factor of 2.3. See the ideogram below.		
-0.043±0.009±0.005	LINK	07A	FOCS $D^0 \rightarrow \pi^- \pi^+ \pi^- \pi^+$
-0.14±0.04±0.07	1 CHUNG	02	B852 $18.3 \pi^- \rho \rightarrow \pi^+ \pi^- \pi^- \nu$
-0.10±0.02±0.02	2,3 ACKERSTAFF	97R	OPAL $E_{cm}^{ee} = 88-94, \tau \rightarrow 3\pi \nu$
-0.11±0.02	2 ALBRECHT	93C	ARG $\tau^+ \rightarrow \pi^+ \pi^+ \pi^- \nu$

$a_1(1260)$ BRANCHING RATIOS

$\Gamma((\rho\pi)S$ -wave, $\rho \rightarrow \pi\pi)/\Gamma_{total}$	VALUE (units 10^{-2})	EVTS	DOCUMENT ID	TECN	COMMENT	Γ_2/Γ
••• We do not use the following data for averages, fits, limits, etc. •••						
60.19	37k	1	ASNER	00	CLE2 $10.6 e^+ e^- \rightarrow \tau^+ \tau^-$ $\tau^- \rightarrow \pi^- \pi^0 \pi^0 \nu_\tau$	

$\Gamma((\rho\pi)D$ -wave, $\rho \rightarrow \pi\pi)/\Gamma_{total}$	VALUE (units 10^{-2})	EVTS	DOCUMENT ID	TECN	COMMENT	Γ_3/Γ
••• We do not use the following data for averages, fits, limits, etc. •••						
$1.30 \pm 0.60 \pm 0.22$	37k	1	ASNER	00	CLE2 $10.6 e^+ e^- \rightarrow \tau^+ \tau^-$ $\tau^- \rightarrow \pi^- \pi^0 \pi^0 \nu_\tau$	

$\Gamma((\rho(1450)\pi)S$ -wave, $\rho \rightarrow \pi\pi)/\Gamma_{total}$	VALUE (units 10^{-2})	EVTS	DOCUMENT ID	TECN	COMMENT	Γ_4/Γ
••• We do not use the following data for averages, fits, limits, etc. •••						
$0.56 \pm 0.84 \pm 0.32$	37k	1,2	ASNER	00	CLE2 $10.6 e^+ e^- \rightarrow \tau^+ \tau^-$ $\tau^- \rightarrow \pi^- \pi^0 \pi^0 \nu_\tau$	

$\Gamma((\rho(1450)\pi)D$ -wave, $\rho \rightarrow \pi\pi)/\Gamma_{total}$	VALUE (units 10^{-2})	EVTS	DOCUMENT ID	TECN	COMMENT	Γ_5/Γ
••• We do not use the following data for averages, fits, limits, etc. •••						
$2.04 \pm 1.20 \pm 0.28$	37k	1,2	ASNER	00	CLE2 $10.6 e^+ e^- \rightarrow \tau^+ \tau^-$ $\tau^- \rightarrow \pi^- \pi^0 \pi^0 \nu_\tau$	

$\Gamma(f_0(500)\pi, f_0 \rightarrow \pi\pi)/\Gamma_{total}$	VALUE (units 10^{-2})	EVTS	DOCUMENT ID	TECN	COMMENT	Γ_6/Γ
••• We do not use the following data for averages, fits, limits, etc. •••						
seen			CHUNG	02	B852 $18.3 \pi^- \rho \rightarrow \pi^+ \pi^- \pi^- \nu$	
$18.76 \pm 4.29 \pm 1.48$	37k	1,3	ASNER	00	CLE2 $10.6 e^+ e^- \rightarrow \tau^+ \tau^-$ $\tau^- \rightarrow \pi^- \pi^0 \pi^0 \nu_\tau$	

$\Gamma(f_0(500)\pi, f_0 \rightarrow \pi\pi)/\Gamma((\rho\pi)S$ -wave, $\rho \rightarrow \pi\pi)$	VALUE	EVTS	DOCUMENT ID	TECN	COMMENT	Γ_6/Γ_2
••• We do not use the following data for averages, fits, limits, etc. •••						
0.06 ± 0.05	90k		SALVINI	04	OBLX $\bar{p} p \rightarrow 2\pi^+ 2\pi^-$	
~ 0.3	28k		AKHMETSHIN 99E	CMD2	$1.05-1.38 e^+ e^- \rightarrow \pi^+ \pi^- \pi^+ \pi^-$	
0.003 ± 0.003		4	LONGACRE	82	RVUE	

$\Gamma(f_0(980)\pi, f_0 \rightarrow \pi\pi)/\Gamma_{total}$	VALUE (units 10^{-2})	EVTS	DOCUMENT ID	TECN	COMMENT	Γ_7/Γ
••• We do not use the following data for averages, fits, limits, etc. •••						
not seen	37k		ASNER	00	CLE2 $10.6 e^+ e^- \rightarrow \tau^+ \tau^-$ $\tau^- \rightarrow \pi^- \pi^0 \pi^0 \nu_\tau$	

$\Gamma(f_0(1370)\pi, f_0 \rightarrow \pi\pi)/\Gamma_{total}$	VALUE (units 10^{-2})	EVTS	DOCUMENT ID	TECN	COMMENT	Γ_8/Γ
••• We do not use the following data for averages, fits, limits, etc. •••						
$7.40 \pm 2.71 \pm 1.26$	37k	1,5	ASNER	00	CLE2 $10.6 e^+ e^- \rightarrow \tau^+ \tau^-$ $\tau^- \rightarrow \pi^- \pi^0 \pi^0 \nu_\tau$	

Meson Particle Listings

$a_1(1260)$, $f_2(1270)$

$\Gamma(f_2(1270)\pi, f_2 \rightarrow \pi\pi)/\Gamma_{total}$ Γ_9/Γ

VALUE (units 10^{-2})	EVTS	DOCUMENT ID	TECN	COMMENT
••• We do not use the following data for averages, fits, limits, etc. •••				
$1.19 \pm 0.49 \pm 0.17$	37k	^{1,6} ASNER	00	CLE2 $10.6 e^+ e^- \rightarrow \tau^+ \tau^-$, $\tau^- \rightarrow \pi^- \pi^0 \pi^0 \nu_\tau$

$\Gamma(\pi^+ \pi^- \pi^0)/\Gamma_{total}$ Γ_{10}/Γ

VALUE	DOCUMENT ID	COMMENT
seen	BARBERIS 98B	450 $pp \rightarrow p_f \pi^+ \pi^- \pi^0 p_S$

$\Gamma(\pi^0 \pi^0 \pi^0)/\Gamma(\pi^+ \pi^- \pi^0)$ Γ_{11}/Γ_{10}

VALUE	CL%	DOCUMENT ID	COMMENT
••• We do not use the following data for averages, fits, limits, etc. •••			
<0.008	90	⁷ BARBERIS 01	450 $pp \rightarrow p_f 3\pi^0 p_S$

$\Gamma(K^*(892)K)/\Gamma_{total}$ Γ_{13}/Γ

VALUE (units 10^{-2})	EVTS	DOCUMENT ID	TECN	COMMENT
••• We do not use the following data for averages, fits, limits, etc. •••				
2.2 ± 0.5	2255	⁸ COAN	04	CLEO $\tau^- \rightarrow K^- \pi^- K^+ \nu_\tau$
8 to 15	205	⁹ DRUTSKOY	02	BELL $B \rightarrow D^{(*)} K^- K^+ 0$
$3.3 \pm 0.5 \pm 0.1$	37k	¹⁰ ASNER	00	CLE2 $10.6 e^+ e^- \rightarrow \tau^+ \tau^-$, $\tau^- \rightarrow \pi^- \pi^0 \pi^0 \nu_\tau$
2.6 ± 0.3		¹¹ BARATE	99R	ALEP $\tau \rightarrow K \bar{K} \pi \nu_\tau$

- ¹ From a fit to the Dalitz plot.
- ² Assuming for $\rho(1450)$ mass and width of 1370 and 386 MeV respectively.
- ³ Assuming for $f_0(500)$ (σ) mass and width of 860 and 880 MeV respectively.
- ⁴ Uses multichannel Aitchison-Bowler model (BOWLER 75). Uses data from GAVILLET 77, DAUM 80, and DANKOWYCH 81.
- ⁵ Assuming for $f_0(1370)$ mass and width of 1186 and 350 MeV respectively.
- ⁶ Assuming for $f_2(1270)$ mass and width of 1275 and 185 MeV respectively.
- ⁷ Inconsistent with observations of $\sigma\pi$, $f_0(1370)\pi$, and $f_2(1270)\pi$ decay modes.
- ⁸ Using structure functions from KUHN 92 and DECKER 93A and B ($\tau^- \rightarrow K^- \pi^- K^+ \nu_\tau$) = (0.155 \pm 0.006 \pm 0.009)% from BRIERE 03.
- ⁹ From a comparison to ALAM 94 assuming purely resonant production of the $K^- K^+ 0$ system.
- ¹⁰ From a fit to the 3π mass spectrum including the $K \bar{K}^*(892)$ threshold.
- ¹¹ Assuming $a_1(1260)$ dominance and taking B($\tau \rightarrow a_1(1260)\nu_\tau$) from BUSKULIC 96.

$a_1(1260)$ REFERENCES

AJAJ	18AI	EPJ C78 443	R. Ajaj et al.	(LHCb Collab.)
AGHAYAN	18B	PR D98 092003	M. Aghasyan et al.	(COMPASS Collab.)
MIKHASENKO	18	PR D98 096021	M. Mikhaseenko et al.	(JPAC Collab.)
DARGENT	17	JHEP 1705 143	P. Dargent et al.	(HEID, BRIS)
ALEKSEEV	10	PRL 104 241803	M.G. Alekshev et al.	(COMPASS Collab.)
AUBERT	07AU	PR D76 092005	B. Aubert et al.	(BABAR Collab.)
LINK	07A	PR D75 052003	J.M. Link et al.	(FNAL FOCUS Collab.)
PDG	06	JP G33 1	W.-M. Yao et al.	(PDG Collab.)
SCHAEEL	05C	PRPL 421 191	S. Schaeel et al.	(ALEPH Collab.)
COAN	04	PRL 92 232001	T.E. Coan et al.	(CLEO Collab.)
GOMEZ-DUMM...	04	PR D69 073002	D. Gomez Dumm, A. Pich, J. Portoles	
SALVINI	04	EPJ C35 21	P. Salvini et al.	(OBELIX Collab.)
BRIERE	03	PRL 90 181802	R. A. Briere et al.	(CLEO Collab.)
CHUNG	02	PR D65 072001	S.U. Chung et al.	(BNL E852 Collab.)
DRUTSKOY	02	PL B542 171	A. Drutskoy et al.	(BELLE Collab.)
BARBERIS	01	PL B507 14	D. Barberis et al.	
ASNER	00	PR D61 012002	D.M. Asner et al.	(CLEO Collab.)
AKHMETSHIN	99E	PL B466 392	R.R. Akhmetshin et al.	(Novosibirsk CMD-2 Collab.)
BARATE	99R	EPJ C11 599	R. Barate et al.	(ALEPH Collab.)
BONDAR	99	PL B466 403	A.E. Bondar et al.	(Novosibirsk CMD-2 Collab.)
ABREU	98G	PL B426 411	P. Abreu et al.	(DELPHI Collab.)
BARATE	98R	EPJ C4 409	R. Barate et al.	(ALEPH Collab.)
BARBERIS	98B	PL B422 399	D. Barberis et al.	(WA 102 Collab.)
ACKERSTAFF	97R	ZPHY C75 593	K. Ackerstaff et al.	(OPAL Collab.)
BUSKULIC	96	ZPHY C70 579	D. Buskulic et al.	(ALEPH Collab.)
AKERS	95P	ZPHY C67 45	R. Akers et al.	(OPAL Collab.)
ALAM	94	PR D50 43	M.S. Alam et al.	(CLEO Collab.)
ALBRECHT	93C	ZPHY C58 61	H. Albrecht et al.	(ARGUS Collab.)
DECKER	93A	ZPHY C58 445	R. Decker et al.	
ANDO	92	PL B291 496	A. Ando et al.	(KEK, KYOT, NIRS, SAGA+)
KUHN	92	ZPHY C56 661	H. Kuhn, E. Mirkes	
IVANOV	91	ZPHY C49 563	Y.P. Ivanov, A.A. Osipov, M.K. Volkov	(JINR)
ARMSTRONG	90	ZPHY C48 213	T.A. Armstrong, M. Benayoun, W. Beusch	(WA76 Coll.)
FEINDT	90	ZPHY C48 681	M. Feindt	(HAMB)
KUHN	90	ZPHY C48 445	J.H. Kuhn et al.	(MPIM)
ISGUR	89	PR D39 1357	N. Isgur, C. Morningstar, C. Reader	(TNT0)
BOWLER	88	PL B209 99	M.G. Bowler	(OXF)
BAND	87	PL B198 287	H.R. Band et al.	(MAC Collab.)
TORNQVIST	87	ZPHY C36 695	N.A. Tornqvist	(HELS)
ALBRECHT	86B	ZPHY C33 7	H. Albrecht et al.	(ARGUS Collab.)
RUCKSTUHL	86	PRL 56 2132	W. Ruckstuhl et al.	(DELCO Collab.)
SCHMIDKE	86	PRL 57 527	W.B. Schmidke et al.	(Mark II Collab.)
BELLINI	85	SJNP 41 781	D. Bellini et al.	
		Translated from YAF 41 1223.		
ZIELINSKI	84C	PRL 52 1195	M. Zielinski et al.	(ROCH, MINN, FNAL)
LONGACRE	82	PR D26 82	R.S. Longacre	(BNL)
DANKOWYCH...	81	NP B198 269	J.A. Dankowych et al.	(TNT0, BNL, CARL+)
DAUM	81B	NP B182 269	C. Daum et al.	(AMST, CERN, CRAC, MPIM+)
DAUM	80	PL B9B 281	C. Daum et al.	(AMST, CERN, CRAC, MPIM+)
GAVILLET	77	PL 69B 119	P. Gavillet et al.	(AMST, CERN, NUM+)
BOWLER	75	NP B97 227	M.G. Bowler et al.	(OXFTE, DARE)

$f_2(1270)$ MASS

VALUE (MeV)	EVTS	DOCUMENT ID	TECN	COMMENT
1275.5 \pm 0.8 OUR AVERAGE				
$1275.8 \pm 1.0 \pm 0.4$		¹ BOGOLYUB...	13	SPEC $7\pi^+(K^+,p)A \rightarrow n\gamma + X$
$1262 \pm \frac{1}{2} \pm 8$		² ABLIKIM	06v	BES2 $e^+ e^- \rightarrow J/\psi \rightarrow \gamma\pi^+\pi^-$

1275 \pm 15		ABLIKIM	05	BES2 $J/\psi \rightarrow \phi\pi^+\pi^-$
1283 \pm 5		ALDE	98	GAM4 $100 \pi^- p \rightarrow \pi^0 \pi^0 n$
1278 \pm 5		³ BERTIN	97c	OBLX $0.0 \bar{p} p \rightarrow \pi^+ \pi^- \pi^0$
1272 \pm 8	200k	PROKOSHKIN	94	GAM2 $38 \pi^- p \rightarrow \pi^0 \pi^0 n$
1269.7 \pm 5.2	5730	AUGUSTIN	89	DM2 $e^+ e^- \rightarrow 5\pi$
1283 \pm 8	400	⁴ ALDE	87	GAM4 $100 \pi^- p \rightarrow 4\pi^0 n$
1274 \pm 5		⁴ AUGUSTIN	87	DM2 $J/\psi \rightarrow \gamma\pi^+\pi^-$
1283 \pm 6		⁵ LONGACRE	86	MPS $22 \pi^- p \rightarrow n2K_S^0$
1276 \pm 7		COURAU	84	DLCO $e^+ e^- \rightarrow e^+ e^- \pi^+ \pi^-$
1273.3 \pm 2.3		⁶ CHABAUD	83	ASP K $17 \pi^- p$ polarized
1280 \pm 4		⁷ CASON	82	STRC $8 \pi^+ p \rightarrow \Delta^{++} \pi^0 \pi^0$
1281 \pm 7	11600	GIDAL	81	MRK2 J/ψ decay
1282 \pm 5		⁸ CORDEN	79	OMEG $12-15 \pi^- p \rightarrow n2\pi$
1269 \pm 4	10k	APEL	75	NICE $40 \pi^- p \rightarrow n2\pi^0$
1272 \pm 4	4600	ENGLER	74	DBC $6 \pi^+ n \rightarrow \pi^+ \pi^- p$
1277 \pm 4	5300	FLATTE	71	HBC $7.0 \pi^+ p$
1273 \pm 8		⁴ STUNTEBECK	70	HBC $8 \pi^- p, 5.4 \pi^+ d$
1265 \pm 8		BOESEBECK	68	HBC $8 \pi^+ p$

••• We do not use the following data for averages, fits, limits, etc. •••				
$1259 \pm 4 \pm 4$	1.7k	^{9,10} DOBBS	15	$J/\psi \rightarrow \gamma\pi^+\pi^-$
$1267 \pm 4 \pm 3$	1.5k	^{9,10} DOBBS	15	$\psi(2S) \rightarrow \gamma\pi^+\pi^-$
1270 ± 8		¹¹ ANISOVICH	09	RVUE $0.0 \bar{p} p, \pi N$
1277 ± 6	870	¹² SCHEGELSKY	06A	RVUE $\gamma\gamma \rightarrow K_S^0 K_S^0$
1251 ± 10		TIKHOMIROV	03	SPEC $40.0 \pi^- C \rightarrow K_S^0 K_S^0 K_L^0 X$
1260 ± 10		¹³ ALDE	97	GAM2 $450 pp \rightarrow p p \pi^0 \pi^0$
1278 ± 6		¹³ GRYGOREV	96	SPEC $40 \pi^- N \rightarrow K_S^0 K_S^0 X$
1262 ± 11		AGUILAR...	91	EHS $400 pp$
1275 ± 10		AKER	91	CBAR $0.0 \bar{p} p \rightarrow 3\pi^0$
1220 ± 10		BREAKSTONE	90	SFM $pp \rightarrow p p \pi^+ \pi^-$
1288 ± 12		ABACHI	86B	HRS $e^+ e^- \rightarrow \pi^+ \pi^- X$
1284 ± 30	3k	BINON	83	GAM2 $38 \pi^- p \rightarrow n2\eta$
1280 ± 20	3k	APEL	82	CNTR $25 \pi^- p \rightarrow n2\pi^0$
1284 ± 10	16000	DEUTSCH...	76	HBC $16 \pi^+ p$
1258 ± 10	600	TAKAHASHI	72	HBC $8 \pi^- p \rightarrow n2\pi$
1275 ± 13		ARMENISE	70	HBC $9 \pi^+ n \rightarrow p\pi^+\pi^-$
1261 ± 5	1960	⁴ ARMENISE	68	DBC $5.1 \pi^+ n \rightarrow p\pi^+ MM^-$
1270 ± 10	360	⁴ ARMENISE	68	DBC $5.1 \pi^+ n \rightarrow p\pi^0 MM$
1268 ± 6		¹⁴ JOHNSON	68	HBC $3.7-4.2 \pi^- p$

- ¹ Averaged over six nuclear targets, no statistically significant dependence on target nucleus observed.
- ² Breit-Wigner mass.
- ³ T-matrix pole.
- ⁴ Mass errors enlarged by us to Γ/\sqrt{N} ; see the note with the $K^*(892)$ mass.
- ⁵ From a partial-wave analysis of data using a K-matrix formalism with 5 poles.
- ⁶ From an energy-independent partial-wave analysis.
- ⁷ From an amplitude analysis of the reaction $\pi^+ \pi^- \rightarrow 2\pi^0$.
- ⁸ From an amplitude analysis of $\pi^+ \pi^- \rightarrow \pi^+ \pi^-$ scattering data.
- ⁹ Using CLEO-c data but not authored by the CLEO Collaboration.
- ¹⁰ From a fit to a Breit-Wigner line shape with fixed $\Gamma = 185$ MeV.
- ¹¹ 4-poles, 5-channel K matrix fit.
- ¹² From analysis of L3 data at 91 and 183-209 GeV.
- ¹³ Systematic uncertainties not estimated.
- ¹⁴ JOHNSON 68 includes BONDAR 63, LEE 64, DERADO 65, EISNER 67.

$f_2(1270)$ WIDTH

VALUE (MeV)	EVTS	DOCUMENT ID	TECN	COMMENT
186.7 \pm 2.2 OUR FIT Error includes scale factor of 1.4.				
185.9 \pm 2.8 OUR AVERAGE Error includes scale factor of 1.6. See the ideogram below.				

$190.3 \pm 1.9 \pm 1.8$		¹ BOGOLYUB...	13	SPEC $7\pi^+(K^+,p)A \rightarrow n\gamma + X$
$175 \pm 4 \pm 10$		² ABLIKIM	06v	BES2 $e^+ e^- \rightarrow J/\psi \rightarrow \gamma\pi^+\pi^-$
190 \pm 20		ABLIKIM	05	BES2 $J/\psi \rightarrow \phi\pi^+\pi^-$
171 \pm 10		ALDE	98	GAM4 $100 \pi^- p \rightarrow \pi^0 \pi^0 n$
204 \pm 20		³ BERTIN	97c	OBLX $0.0 \bar{p} p \rightarrow \pi^+ \pi^- \pi^0$
192 \pm 5	200k	PROKOSHKIN	94	GAM2 $38 \pi^- p \rightarrow \pi^0 \pi^0 n$
180 \pm 24		AGUILAR...	91	EHS $400 pp$
186 \pm 9	5730	⁴ AUGUSTIN	89	DM2 $e^+ e^- \rightarrow 5\pi$
150 \pm 30	400	⁴ ALDE	87	GAM4 $100 \pi^- p \rightarrow 4\pi^0 n$
$186 \pm \frac{9}{2}$		⁵ LONGACRE	86	MPS $22 \pi^- p \rightarrow n2K_S^0$
$179.2 \pm \frac{6.9}{6.6}$		⁶ CHABAUD	83	ASP K $17 \pi^- p$ polarized
160 ± 11		DENNEY	83	LASS $10 \pi^+ N$

$f_2(1270)$

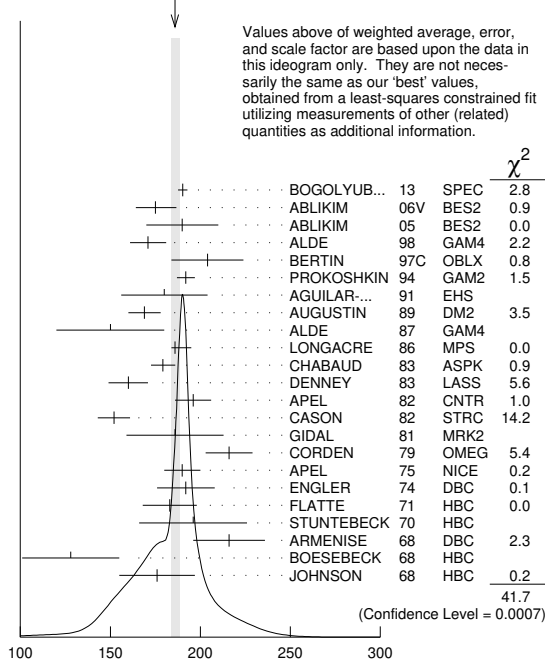
 $I^G(J^{PC}) = 0^+(2^{++})$

$f_2(1270)$

196 ±10	3k	APEL	82	CNTR	25	$\pi^- p \rightarrow n2\pi^0$
152 ± 9		7 CASON	82	STRC	8	$\pi^+ p \rightarrow \Delta^{++}\pi^0\pi^0$
186 ±27	11600	GIDAL	81	MRK2		J/ψ decay
216 ±13		8 CORDEN	79	OMEG	12-15	$\pi^- p \rightarrow n2\pi$
190 ±10	10k	APEL	75	NICE	40	$\pi^- p \rightarrow n2\pi^0$
192 ±16	4600	ENGLER	74	DBC	6	$\pi^+ n \rightarrow \pi^+\pi^-p$
183 ±15	5300	FLATTE	71	HBC	7	$\pi^+ p \rightarrow \Delta^{++}f_2$
196 ±30		4 STUNTEBECK	70	HBC	8	$\pi^- p, 5.4 \pi^+ d$
216 ±20	1960	4 ARMENISE	68	DBC	5.1	$\pi^+ n \rightarrow p\pi^+MM^-$
128 ±27		4 BOESEBECK	68	HBC	8	$\pi^+ p$
176 ±21		4,9 JOHNSON	68	HBC	3.7-4.2	$\pi^- p$
194 ±36		10 ANISOVICH	09	RVUE	0.0	$\bar{p}p, \pi N$
195 ±15	870	11 SCHEGELSKY	06A	RVUE	$\gamma\gamma \rightarrow K_S^0 K_S^0$	
121 ±26		TIKHOMIROV	03	SPEC	40.0	$\pi^- C \rightarrow K_S^0 K_S^0 K_L^0 X$
187 ±20		12 ALDE	97	GAM2	45.0	$pp \rightarrow p p \pi^0 \pi^0$
184 ±10		12 GRYGOREV	96	SPEC	40	$\pi^- N \rightarrow K_S^0 K_S^0 X$
200 ±10		AKER	91	CBAR	0.0	$\bar{p}p \rightarrow 3\pi^0$
240 ±40	3k	BINON	83	GAM2	38	$\pi^- p \rightarrow n2\eta$
187 ±30	650	4 ANTIPOV	77	CIBS	25	$\pi^- p \rightarrow p3\pi$
225 ±38	16000	DEUTSCH...	76	HBC	16	$\pi^+ p$
166 ±28	600	4 TAKAHASHI	72	HBC	8	$\pi^- p \rightarrow n2\pi$
173 ±53		4 ARMENISE	70	HBC	9	$\pi^+ n \rightarrow p\pi^+\pi^-$

- 1 Averaged over six nuclear targets, no statistically significant dependence on target nucleus observed.
- 2 Breit-Wigner width
- 3 T-matrix pole.
- 4 Width errors enlarged by us to $4\Gamma/\sqrt{N}$; see the note with the $K^*(892)$ mass.
- 5 From a partial-wave analysis of data using a K-matrix formalism with 5 poles.
- 6 From an energy-independent partial-wave analysis.
- 7 From an amplitude analysis of the reaction $\pi^+\pi^- \rightarrow 2\pi^0$.
- 8 From an amplitude analysis of $\pi^+\pi^- \rightarrow \pi^+\pi^-$ scattering data.
- 9 JOHNSON 68 includes BONDAR 63, LEE 64, DERADO 65, EISNER 67.
- 10 4-poles, 5-channel K matrix fit.
- 11 From analysis of L3 data at 91 and 183-209 GeV.
- 12 Systematic uncertainties not estimated.

WEIGHTED AVERAGE
185.9±2.8-2.1 (Error scaled by 1.6)



Values above of weighted average, error, and scale factor are based upon the data in this ideogram only. They are not necessarily the same as our 'best' values, obtained from a least-squares constrained fit utilizing measurements of other (related) quantities as additional information.

$f_2(1270)$ width (MeV)

$f_2(1270)$ DECAY MODES

Mode	Fraction (Γ_i/Γ)	Scale factor/Confidence level
Γ_1 $\pi\pi$	(84.2 \pm 2.9 $-$ 0.9) %	S=1.1
Γ_2 $\pi^+\pi^-2\pi^0$	(7.7 \pm 1.1 $-$ 3.2) %	S=1.2
Γ_3 $K\bar{K}$	(4.6 \pm 0.5 $-$ 0.4) %	S=2.7
Γ_4 $2\pi^+2\pi^-$	(2.8 \pm 0.4) %	S=1.2

Γ_5 $\eta\eta$	(4.0 \pm 0.8) $\times 10^{-3}$	S=2.1
Γ_6 $4\pi^0$	(3.0 \pm 1.0) $\times 10^{-3}$	
Γ_7 $\gamma\gamma$	(1.42 \pm 0.24) $\times 10^{-5}$	S=1.4
Γ_8 $\eta\pi\pi$	< 8 $\times 10^{-3}$	CL=95%
Γ_9 $K^0 K^- \pi^+ + c.c.$	< 3.4 $\times 10^{-3}$	CL=95%
Γ_{10} $e^+ e^-$	< 6 $\times 10^{-10}$	CL=90%

CONSTRAINED FIT INFORMATION

An overall fit to the total width, 4 partial widths, a combination of partial widths obtained from integrated cross sections, and 6 branching ratios uses 45 measurements and one constraint to determine 8 parameters. The overall fit has a $\chi^2 = 83.0$ for 38 degrees of freedom.

The following off-diagonal array elements are the correlation coefficients $\langle \delta p_i \delta p_j \rangle / (\delta p_i \delta p_j)$, in percent, from the fit to parameters p_i , including the branching fractions, $x_i \equiv \Gamma_i/\Gamma_{total}$. The fit constrains the x_i whose labels appear in this array to sum to one.

x_2	-90						
x_3	10	-39					
x_4	10	-38	1				
x_5	1	-6	0	0			
x_6	0	-7	0	0	0		
x_7	3	1	-15	0	0	0	
Γ	-71	65	-10	-7	-1	0	-6
	x_1	x_2	x_3	x_4	x_5	x_6	x_7

Mode	Rate (MeV)	Scale factor
Γ_1 $\pi\pi$	157.2 \pm 4.0 $-$ 1.1	
Γ_2 $\pi^+\pi^-2\pi^0$	14.4 \pm 2.1 $-$ 6.0	1.2
Γ_3 $K\bar{K}$	8.5 \pm 0.8	2.8
Γ_4 $2\pi^+2\pi^-$	5.2 \pm 0.7	1.2
Γ_5 $\eta\eta$	0.75 \pm 0.14	2.1
Γ_6 $4\pi^0$	0.56 \pm 0.19	
Γ_7 $\gamma\gamma$	0.0026 \pm 0.0005	1.4

$f_2(1270)$ PARTIAL WIDTHS

$\Gamma(\pi\pi)$	VALUE (MeV)	EVTS	DOCUMENT ID	TECN	COMMENT	Γ_1	
157.2 \pm 4.0 $-$ 1.1 OUR FIT							
157.0 \pm 6.0			1 LONGACRE	86	MPS	22 $\pi^- p \rightarrow n2K_S^0$	
••• We do not use the following data for averages, fits, limits, etc. •••							
152 \pm 8		870	2 SCHEGELSKY	06A	RVUE	$\gamma\gamma \rightarrow K_S^0 K_S^0$	
$\Gamma(K\bar{K})$	VALUE (MeV)	EVTS	DOCUMENT ID	TECN	COMMENT	Γ_3	
8.5 \pm 0.8 OUR FIT					Error includes scale factor of 2.8.		
9.0 \pm 0.7 $-$ 0.3			1 LONGACRE	86	MPS	22 $\pi^- p \rightarrow n2K_S^0$	
••• We do not use the following data for averages, fits, limits, etc. •••							
7.5 \pm 2.0		870	2 SCHEGELSKY	06A	RVUE	$\gamma\gamma \rightarrow K_S^0 K_S^0$	
$\Gamma(\eta\eta)$	VALUE (MeV)	EVTS	DOCUMENT ID	TECN	COMMENT	Γ_5	
0.75 \pm 0.14 OUR FIT					Error includes scale factor of 2.1.		
1.0 \pm 0.1			1 LONGACRE	86	MPS	22 $\pi^- p \rightarrow n2K_S^0$	
••• We do not use the following data for averages, fits, limits, etc. •••							
1.8 \pm 0.4		870	2 SCHEGELSKY	06A	RVUE	$\gamma\gamma \rightarrow K_S^0 K_S^0$	

$\Gamma(\gamma\gamma)$ Γ_7
The value of this width depends on the theoretical model used. Unitary approaches with scalars typically (with exception of PENNINGTON 08) give values clustering around 2.6 keV; without an S-wave contribution, values are systematically higher (typically around 3 keV).

VALUE (keV)	EVTS	DOCUMENT ID	TECN	COMMENT		
2.6 \pm 0.5 OUR FIT				Error includes scale factor of 1.4.		
2.93 \pm 0.40		3 DAI	14A	RVUE	Compilation	
••• We do not use the following data for averages, fits, limits, etc. •••						
3.14 \pm 0.20		4,5 PENNINGTON	08	RVUE	Compilation	
3.82 \pm 0.30		5,6 PENNINGTON	08	RVUE	Compilation	
2.55 \pm 0.15	870	2 SCHEGELSKY	06A	RVUE	$\gamma\gamma \rightarrow K_S^0 K_S^0$	
2.84 \pm 0.35		BOGLIONE	99	RVUE	$\gamma\gamma \rightarrow \pi^+\pi^-, \pi^0\pi^0$	
2.93 \pm 0.23 \pm 0.32		7 YABUKI	95	VNS		
2.58 \pm 0.13 \pm 0.36 $-$ 0.27		8 BEHREND	92	CELL	$e^+e^- \rightarrow e^+e^-\pi^+\pi^-$	

Meson Particle Listings

 $f_2(1270)$

3.10 ± 0.35 ± 0.35		⁹ BLINOV	92	MD1	$e^+e^- \rightarrow e^+e^-\pi^+\pi^-$
2.27 ± 0.47 ± 0.11		ADACHI	90D	TOPZ	$e^+e^- \rightarrow e^+e^-\pi^+\pi^-$
3.15 ± 0.04 ± 0.39		BOYER	90	MRK2	$e^+e^- \rightarrow e^+e^-\pi^+\pi^-$
3.19 ± 0.16 ^{+0.29} _{-0.28}		MARSISKE	90	CBAL	$e^+e^- \rightarrow e^+e^-\pi^0\pi^0$
2.35 ± 0.65		MORGAN	90	RVUE	$\gamma\gamma \rightarrow \pi^+\pi^-, \pi^0\pi^0$
3.19 ± 0.09 ^{+0.22} _{-0.38}	2177	OEST	90	JADE	$e^+e^- \rightarrow e^+e^-\pi^0\pi^0$
3.2 ± 0.1 ± 0.4		¹¹ AIHARA	86B	TPC	$e^+e^- \rightarrow e^+e^-\pi^+\pi^-$
2.5 ± 0.1 ± 0.5		BEHREND	84B	CELL	$e^+e^- \rightarrow e^+e^-\pi^+\pi^-$
2.85 ± 0.25 ± 0.5		¹² BERGER	84	PLUT	$e^+e^- \rightarrow e^+e^-2\pi^+$
2.70 ± 0.05 ± 0.20		COURAU	84	DLCO	$e^+e^- \rightarrow e^+e^-\pi^+\pi^-$
2.5 ± 0.13 ± 0.38		¹³ SMITH	84C	MRK2	$e^+e^- \rightarrow e^+e^-\pi^+\pi^-$
2.7 ± 0.2 ± 0.6		EDWARDS	82F	CBAL	$e^+e^- \rightarrow e^+e^-2\pi^0$
2.9 ^{+0.6} _{-0.4} ± 0.6		¹⁴ EDWARDS	82F	CBAL	$e^+e^- \rightarrow e^+e^-2\pi^0$
3.2 ± 0.2 ± 0.6		BRANDELIK	81B	TASS	$e^+e^- \rightarrow e^+e^-\pi^+\pi^-$
3.6 ± 0.3 ± 0.5		ROUSSARIE	81	MRK2	$e^+e^- \rightarrow e^+e^-\pi^+\pi^-$
2.3 ± 0.8		¹⁵ BERGER	80B	PLUT	e^+e^-

$\Gamma(e^+e^-)$		Γ_{10}			
VALUE (eV)	CL%	DOCUMENT ID	TECN	COMMENT	
<0.11	90	ACHASOV	00K	SND $e^+e^- \rightarrow \pi^0\pi^0$	
• • • We do not use the following data for averages, fits, limits, etc. • • •					
<1.7	90	VOROBYEV	88	ND $e^+e^- \rightarrow \pi^0\pi^0$	

- From a partial-wave analysis of data using a K-matrix formalism with 5 poles.
- From analysis of L3 data at 91 and 183–209 GeV and using SU(3) relations.
- Based on a K-matrix analysis of BELLE data from MORI 07, UEHARA 08a, UEHARA 09 and UEHARA 13. The width is derived for the pole on the third sheet which is closest to the physical axis. Supersedes PENNINGTON 08.
- Solution A (preferred solution based on χ^2 -analysis).
- Dispersion theory based amplitude analysis of BOYER 90, MARSISKE 90, BEHREND 92, and MORI 07.
- Solution B (worse than solution A; still acceptable when systematic uncertainties are included).
- With a narrow scalar state around 1220 MeV.
- Using a unitarized model with a 300–500 keV wide scalar at 1100 MeV.
- Using the unitarized model of LYTH 85.
- Error includes spread of different solutions. Data of MARK2 and CRYSTAL BALL used in the analysis. Authors report strong correlations with $\gamma\gamma$ width of $f_0(1370)$: $\Gamma(f_2) + 1/4 \Gamma(f_0) = 3.6 \pm 0.3$ KeV.
- Radiative corrections modify the partial widths; for instance the COURAU 84 value becomes 2.66 ± 0.21 in the calculation of LANDRO 86.
- Using the MENNESSIER 83 model.
- Superseded by BOYER 90.
- If helicity = 2 assumption is not made.
- Using mass, width and $B(f_2(1270) \rightarrow 2\pi)$ from PDG 78.

 $f_2(1270) \Gamma(i)\Gamma(\gamma\gamma)/\Gamma(\text{total})$

$\Gamma(K\bar{K}) \times \Gamma(\gamma\gamma)/\Gamma_{\text{total}}$		$\Gamma_3\Gamma_7/\Gamma$			
VALUE (keV)	CL%	DOCUMENT ID	TECN	COMMENT	
0.121 ± 0.020 OUR FIT		Error includes scale factor of 1.3.			
0.091 ± 0.007 ± 0.027		¹ ALBRECHT	90G	ARG $e^+e^- \rightarrow e^+e^-K^+K^-$	
• • • We do not use the following data for averages, fits, limits, etc. • • •					
0.104 ± 0.007 ± 0.072		² ALBRECHT	90G	ARG $e^+e^- \rightarrow e^+e^-K^+K^-$	
¹ Using an incoherent background.					
² Using a coherent background.					

$\Gamma(\eta) \times \Gamma(\gamma\gamma)/\Gamma_{\text{total}}$		$\Gamma_5\Gamma_7/\Gamma$			
VALUE (eV)	CL%	DOCUMENT ID	TECN	COMMENT	
11.5 ^{+1.8+4.5}_{-2.0-3.7}		¹ UEHARA	10A	BELL $10.6 e^+e^- \rightarrow e^+e^-\eta\eta$	
¹ Including interference with the $f_2'(1525)$ (parameters fixed to the values from the 2008 edition of this review, PDG 08) and $f_0(\Upsilon)$.					

Helicity-0/Helicity-2 RATIO IN $\gamma\gamma \rightarrow f_2(1270) \rightarrow \pi\pi$

VALUE (units 10^{-2})	DOCUMENT ID	TECN	COMMENT
3.7 ± 0.3 ^{+15.9}_{-2.9}	UEHARA	08A	BELL $10.6 e^+e^- \rightarrow e^+e^-\pi^0\pi^0$
• • • We do not use the following data for averages, fits, limits, etc. • • •			
9.5 ± 1.8	¹ DAI	14A	RVUE Compilation
13	^{2,3} PENNINGTON	08	RVUE Compilation
26	^{3,4} PENNINGTON	08	RVUE Compilation

- Based on a K-matrix analysis of BELLE data from MORI 07, UEHARA 08a, UEHARA 09 and UEHARA 13. The width is derived for the pole on the third sheet which is closest to the physical axis.
- Solution A (preferred solution based on χ^2 -analysis).
- Dispersion theory based amplitude analysis of BOYER 90, MARSISKE 90, BEHREND 92, and MORI 07.
- Solution B (worse than solution A; still acceptable when systematic uncertainties are included).

 $f_2(1270)$ BRANCHING RATIOS

$\Gamma(\pi\pi)/\Gamma_{\text{total}}$		Γ_1/Γ			
VALUE	EVTS	DOCUMENT ID	TECN	COMMENT	
0.842 ± 0.029 OUR FIT		Error includes scale factor of 1.1.			
0.837 ± 0.020 OUR AVERAGE					
0.849 ± 0.025		CHABAUD	83	ASPK $17 \pi^-\pi^0$ polarized	
0.85 ± 0.05	250	BEAUPRE	71	HBC $8 \pi^+\pi^0 \rightarrow \Delta^{++}f_2$	
0.8 ± 0.04	600	OH	70	HBC $1.26 \pi^-\pi^0 \rightarrow \pi^+\pi^-\pi^0$	

$\Gamma(\pi^+\pi^-2\pi^0)/\Gamma(\pi\pi)$		Γ_2/Γ_1			
VALUE	EVTS	DOCUMENT ID	TECN	COMMENT	
Should be twice $\Gamma(2\pi^+2\pi^-)/\Gamma(\pi\pi)$ if decay is $\rho\rho$. (See ASCOLI 68D.)					
0.091 ^{+0.014}_{-0.040} OUR FIT		Error includes scale factor of 1.2.			
0.15 ± 0.06	600	EISENBERG	74	HBC $4.9 \pi^+\pi^0 \rightarrow \Delta^{++}f_2$	
• • • We do not use the following data for averages, fits, limits, etc. • • •					
0.07		EMMS	75D	DBC $4 \pi^+\pi^0 \rightarrow \rho f_2$	

$\Gamma(K\bar{K})/\Gamma(\pi\pi)$		Γ_3/Γ_1			
VALUE	EVTS	DOCUMENT ID	TECN	COMMENT	
We average only experiments which either take into account $f_2(1270)$ - $a_2(1320)$ interference explicitly or demonstrate that $a_2(1320)$ production is negligible.					
0.054 ± 0.005 OUR FIT		Error includes scale factor of 2.7.			
0.041 ± 0.004 OUR AVERAGE					
0.045 ± 0.01		¹ BARGIOTTI	03	OBLX $\bar{p}p$	
0.037 ^{+0.008} _{-0.021}		ETKIN	82B	MPS $23 \pi^-\pi^0 \rightarrow n2K_S^0$	
0.045 ± 0.009		CHABAUD	81	ASPK $17 \pi^-\pi^0$ polarized	
0.039 ± 0.008		LOVERRE	80	HBC $4 \pi^-\pi^0 \rightarrow K\bar{K}N$	
• • • We do not use the following data for averages, fits, limits, etc. • • •					
0.052 ± 0.025		ABLIKIM	04E	BES2 $J/\psi \rightarrow \omega K^+K^-$	
0.036 ± 0.005		² COSTA	80	OMEG $1-2.2 \pi^-\pi^0 \rightarrow K^+K^-\pi^0$	
0.030 ± 0.005		³ MARTIN	79	RVUE	
0.027 ± 0.009		⁴ POLYCHRO...	79	STRC $7 \pi^-\pi^0 \rightarrow n2K_S^0$	
0.025 ± 0.015		EMMS	75D	DBC $4 \pi^+\pi^0 \rightarrow \rho f_2$	
0.031 ± 0.012	20	ADERHOLZ	69	HBC $8 \pi^+\pi^0 \rightarrow K^+K^-\pi^+\pi^0$	

$\Gamma(2\pi^+2\pi^-)/\Gamma(\pi\pi)$		Γ_4/Γ_1			
VALUE	EVTS	DOCUMENT ID	TECN	COMMENT	
0.033 ± 0.005 OUR FIT		Error includes scale factor of 1.2.			
0.033 ± 0.004 OUR AVERAGE		Error includes scale factor of 1.1.			
0.024 ± 0.006	160	EMMS	75D	DBC $4 \pi^+\pi^0 \rightarrow \rho f_2$	
0.051 ± 0.025	70	EISENBERG	74	HBC $4.9 \pi^+\pi^0 \rightarrow \Delta^{++}f_2$	
0.043 ^{+0.007} _{-0.011}	285	LOUIE	74	HBC $3.9 \pi^-\pi^0 \rightarrow \rho f_2$	
0.037 ± 0.007	154	ANDERSON	73	DBC $6 \pi^+\pi^0 \rightarrow \rho f_2$	
0.047 ± 0.013		OH	70	HBC $1.26 \pi^-\pi^0 \rightarrow \pi^+\pi^-\pi^0$	

$\Gamma(\eta\eta)/\Gamma_{\text{total}}$		Γ_5/Γ			
VALUE (units 10^{-3})	CL%	DOCUMENT ID	TECN	COMMENT	
4.0 ± 0.8 OUR FIT		Error includes scale factor of 2.1.			
2.9 ± 0.5 OUR AVERAGE					
2.7 ± 0.7		BINON	05	GAMS $33 \pi^-\pi^0 \rightarrow \eta\eta\eta$	
2.8 ± 0.7		ALDE	86D	GAM4 $100 \pi^-\pi^0 \rightarrow 2\eta\eta$	
5.2 ± 1.7		BINON	83	GAM2 $38 \pi^-\pi^0 \rightarrow 2\eta\eta$	

$\Gamma(\eta\eta)/\Gamma(\pi\pi)$		Γ_5/Γ_1			
VALUE	CL%	DOCUMENT ID	TECN	COMMENT	
0.003 ± 0.001		BARBERIS	00E	450 $\rho\rho \rightarrow \rho f_2 \eta \eta \rho_S$	
• • • We do not use the following data for averages, fits, limits, etc. • • •					
<0.05	95	EDWARDS	82F	CBAL $e^+e^- \rightarrow e^+e^-2\eta$	
<0.016	95	EMMS	75D	DBC $4 \pi^+\pi^0 \rightarrow \rho f_2$	
<0.09	95	EISENBERG	74	HBC $4.9 \pi^+\pi^0 \rightarrow \Delta^{++}f_2$	

$\Gamma(4\pi^0)/\Gamma_{\text{total}}$		Γ_6/Γ			
VALUE	EVTS	DOCUMENT ID	TECN	COMMENT	
0.0030 ± 0.0010 OUR FIT		Error includes scale factor of 1.1.			
0.003 ± 0.001	400 ± 50	ALDE	87	GAM4 $100 \pi^-\pi^0 \rightarrow 4\pi^0 n$	

$\Gamma(\gamma\gamma)/\Gamma_{\text{total}}$		Γ_7/Γ			
VALUE (units 10^{-5})	CL%	DOCUMENT ID	TECN	COMMENT	
• • • We do not use the following data for averages, fits, limits, etc. • • •					
1.57 ± 0.01 ^{+1.39} _{-0.14}		UEHARA	08A	BELL $10.6 e^+e^- \rightarrow e^+e^-\pi^0\pi^0$	

$\Gamma(\eta\pi\pi)/\Gamma(\pi\pi)$		Γ_8/Γ_1			
VALUE	CL%	DOCUMENT ID	TECN	COMMENT	
<0.010	95	EMMS	75D	DBC $4 \pi^+\pi^0 \rightarrow \rho f_2$	

See key on page 999

Meson Particle Listings

$f_2(1270)$, $f_1(1285)$

$\Gamma(K^0 K^- \pi^+ + c.c.)/\Gamma(\pi\pi)$		Γ_9/Γ_1	
VALUE	CL%	DOCUMENT ID	TECN COMMENT
<0.004	95	EMMS	75D DBC $4\pi^+ n \rightarrow p f_2$

$\Gamma(e^+ e^-)/\Gamma_{total}$		Γ_{10}/Γ	
VALUE (units 10^{-10})	CL%	DOCUMENT ID	TECN COMMENT
<6	90	ACHASOV	00k SND $e^+ e^- \rightarrow \pi^0 \pi^0$

¹ Coupled channel analysis of $\pi^+ \pi^- \pi^0$, $K^+ K^- \pi^0$, and $K^\pm K_S^0 \pi^\mp$.
² Re-evaluated by CHABAUD 83.
³ Includes PAWLICKI 77 data.
⁴ Takes into account the $f_2(1270)$ - $f_2(1252)$ interference.

$f_2(1270)$ REFERENCES

DOBBS	15	PR D91 052006	S. Dobbs et al.	(NWES)
DAI	14A	PR D90 036004	L.-Y. Dai, M.R. Pennington	(CEBAF)
BOGOLYUB...	13	PAN 76 1324	M.Yu. Bogolyubsky et al.	(HYPERON-M Collab.)
UEHARA	13	PTEP 2013 123C01	S. Uehara et al.	(BELLE Collab.)
UEHARA	10A	PR D92 114031	S. Uehara et al.	(BELLE Collab.)
ANISOVICH	09	UJP A24 2481	V.V. Anisovich, A.V. Sarantsev	
UEHARA	09	PR D79 052009	S. Uehara et al.	(BELLE Collab.)
PDG	08	PL B667 1	C. Amisler et al.	(PDG Collab.)
PENNINGTON	08	EPJ C56 1	M.R. Pennington et al.	
UEHARA	08A	PR D78 052004	S. Uehara et al.	(BELLE Collab.)
MORI	07	PR D75 051101	T. Mori et al.	(BELLE Collab.)
ABLIKIM	06V	PL B642 441	M. Ablikim et al.	(BES Collab.)
SCHGELSKEY	06A	EPJ A27 207	V.A. Schegelsky et al.	
ABLIKIM	05	PL B607 243	M. Ablikim et al.	(BES Collab.)
BINON	05	PAN 68 960	F. Binon et al.	
ABLIKIM	04E	PL B603 138	M. Ablikim et al.	(BES Collab.)
BARGIOTTI	03	EPJ C26 371	M. Bargiotti et al.	(OBELIX Collab.)
TIKHOMIROV	03	PAN 66 828	G.D. Tikhomirov et al.	
ACHASOV	00K	PL B492 8	M.N. Achasov et al.	(Novosibirsk SND Collab.)
BARBERIS	00E	PL B479 59	D. Barberis et al.	(WA 102 Collab.)
BOGLIONE	99	EPJ C9 11	M. Boglione, M.R. Pennington	
ALDE	98	EPJ A3 361	D. Alde et al.	(GAM4 Collab.)
ALDE		PAN 62 405	D. Alde et al.	(GAMS Collab.)
ALDE	97	PL B397 350	D.M. Alde et al.	(GAMS Collab.)
BERTIN	97C	PL B408 476	A. Bertin et al.	(OBELIX Collab.)
GRYGOREV	96	PAN 59 2105	V.K. Grigoriev, O.N. Baloshin, B.P. Barkov	(ITEP)
YABUKI	95	JPS J 64 435	F. Yabuki et al.	(VENUS Collab.)
PROKOSHIN	94	PD 39 420	Y.D. Prokoshin, A.A. Kondashov	(SERP)
BEHREND	92	ZPHY C56 381	H.J. Behrend et al.	(CELLO Collab.)
BLINOV	92	ZPHY C53 33	A.E. Blinov et al.	(NOVO)
AGUILAR...	91	ZPHY C50 405	M. Aguilar-Benitez et al.	(LEBC-EHS Collab.)
AKER	91	PL B260 249	E. Aker et al.	(Crystal Barrel Collab.)
ADACHI	90D	PL B234 185	I. Adachi et al.	(TOPAZ Collab.)
ALBRECHT	90G	ZPHY C48 183	H. Albrecht et al.	(ARGUS Collab.)
BOYER	90	PR D42 1350	M. Boyer et al.	(Mark II Collab.)
BREASTONE	90	ZPHY C48 569	A.M. Breakstone et al.	(ISU, BGNA, CERN+)
MARSIKSE	90	PR D41 3324	H. Marsiske et al.	(Crystal Ball Collab.)
MORGAN	90	ZPHY C48 623	D. Morgan, M.R. Pennington	(RAL, DURH)
OEST	90	ZPHY C47 343	T. Oest et al.	(JADE Collab.)
AUGUSTIN	89	NP B320 1	J.E. Augustin, G. Cosme	(DM2 Collab.)
VOROBYEV	88	SJNP 48 273	P.V. Vorobyev et al.	(NOVO)
ALDE	87	PL B198 286	D.M. Alde et al.	(LANL, BRUX, SERP, LAPP)
AUGUSTIN	87	ZPHY C36 369	J.E. Augustin et al.	(LALO, CLER, FRAS+)
ABACHI	86B	PRL 57 1990	J.F. Abachi et al.	(PURD, ANL, IND, MICH+)
AIHARA	86B	PRL 57 404	H. Aihara et al.	(TPC-2γ Collab.)
ALDE	86D	NP B269 485	D.M. Alde et al.	(BELG, LAPP, SERP, CERN+)
LANDRO	86	PL B172 445	M. Landro, K.J. Mork, H.A. Olsen	(CUNY+)
LONGACRE	86	PL B177 223	R.S. Longacre et al.	(BNL, BRAN, UTR+)
LYTH	85	JP G11 459	D.L. Lyth	
BEHREND	84B	ZPHY C23 223	H.J. Behrend et al.	(CELLO Collab.)
BERGER	84	ZPHY C26 199	C. Berger et al.	(PLUTO Collab.)
COURAU	84	PL 147B 227	A. Courau et al.	(CIT, SLAC)
SMITH	84C	PR D30 851	J.R. Smith et al.	(SLAC, LBL, HARV)
BINON	83	NC 78A 313	F.G. Binon et al.	(BELG, LAPP, SERP+)
CHABAUD	83	SJNP 38 561	F.G. Binon et al.	(BELG, LAPP, SERP+)
DENNEY	83	NP B223 1	V. Chabaud et al.	(CERN, CRAC, MPIM)
MENNESSIER	83	PR D28 2726	D.L. Denney et al.	(IOWA, MICH)
APEL	82	ZPHY C16 241	G. Mennessier	(MONP)
CASON	82	NP B201 197	W.D. Apel et al.	(KARLK, KARLE, PISA, SERP+)
EDWARDS	82F	PRL 48 1316	N.M. Cason et al.	(NDAM, ANL)
ETKIN	82B	PL 110B 82	C. Edwards et al.	(CIT, HARV, PRIN+)
BRANDELK	81B	PR D25 1786	A. Etkin et al.	(BNL, CUNY, TUFTS, VAND)
CHABAUD	81	ZPHY C10 117	R. Brandelik et al.	(TASSO Collab.)
GIDAL	81	APP B12 575	V. Chabaud et al.	(CERN, CRAC, MPIM)
ROUSSARIE	81	PL 107B 153	G. Gidal et al.	(SLAC, LBL)
BERGER	80B	PL 105B 304	A. Roussarie et al.	(SLAC, LBL)
COSTA	80	NP B175 402	C. Berger et al.	(PLUTO Collab.)
LOVERRE	80	NP B175 402	G. Costa et al.	(BARI, BONN, CERN, GLAS+)
CORDEN	79	ZPHY C6 187	P.F. Loverre et al.	(CERN, CDF, MADR+)
MARTIN	79	NP B157 250	M.J. Corden et al.	(BIRM, RHEL, TELA+)
POLYCHRO...	79	NP B158 520	A.D. Martin, E.N. Ozmutlu	(DURH)
PDG	78	PR D19 1317	V.A. Polychronakos et al.	(NDAM, ANL)
ANTIPOV	77	PL 75B 1	C. Brifman et al.	
PAWLICKI	77	NP B119 45	Y.M. Antipov et al.	(SERP, GEVA)
DEUTSCH...	76	NP B103 426	A.J. Pawlicki et al.	(ANL)
APEL	75	NP B96 155	M. Deuschmann et al.	(AACH3, BERL, BONN+)
EMMS	75D	NP B96 155	W.D. Apel et al.	(KARLK, KARLE, PISA, SERP+)
EISENBERG	74	NP B96 155	M.J. Emms et al.	(BIRM, DURH, RHEL)
ENGLER	74	PL 52B 239	Y. Eisenberg et al.	(REHO)
LOUIE	74	PR D10 2070	A. Engler et al.	(CMU, CASE)
ANDERSON	73	PL 48B 385	J. Louie et al.	(SACL, CERN)
TAKAHASHI	72	PRL 31 562	J.C. Anderson et al.	(CMU, CASE)
BEAUPRE	71	PR D6 1266	K. Takahashi et al.	(TOHOK, PENN, NDAM+)
FLATTE	71	NP B28 77	J.V. Beaupre et al.	(AACH, BERL, CERN)
ARMENISE	70	PL 34B 551	S.M. Flatte et al.	(LBL)
OH	70	LNC 4 199	N. Armenise et al.	(BARI, BGNA, FIRZ)
STUNTEBECK	70	PR D1 2494	B.Y. Oh et al.	(WISC, TNTO) JP
ADERHOLZ	69	PL 32B 391	P.H. Stuntebeck et al.	(NDAM)
ARMENISE	69	NP B11 259	M. Aderholz et al.	(AACH3, BERL, CERN+)
ASCOLI	68D	NC 54A 999	N. Armenise et al.	(BARI, BGNA, FIRZ+)
BOESEBECK	68	PRL 21 1712	G. Ascoli et al.	(ILL)
BOESEBECK	68	NP B4 501	K. Boesebeck et al.	(AACH, BERL, CERN)

JOHNSON	68	PR 176 1651	P.B. Johnson et al.	(NDAM, PURD, SLAC)
EISNER	67	PR 164 1699	R.L. Eisner et al.	(PURD)
DERADO	65	PRL 14 872	I. Derado et al.	(NDAM)
LEE	64	PRL 12 342	Y.Y. Lee et al.	(MICH)
BONDAR	63	PL 5 153	L. Bondar et al.	(AACH, BIRM, BONN, DESY+)

$f_1(1285)$

$$J^G(J^{PC}) = 0^+(1^+)$$

$f_1(1285)$ MASS

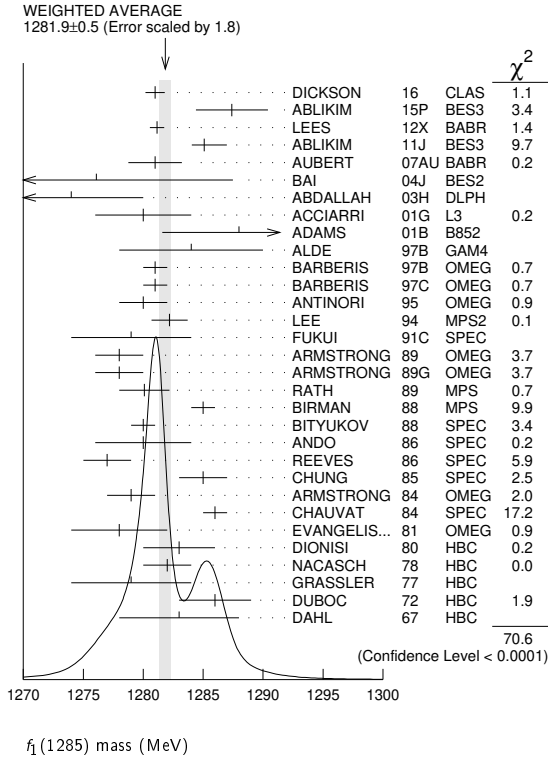
VALUE (MeV)	EVTS	DOCUMENT ID	TECN	COMMENT
1281.9 ± 0.5	OUR AVERAGE	Error includes scale factor of 1.8. See the ideogram below.		
1281.0 ± 0.8		DICKSON	16 CLAS	2.55 $\gamma p \rightarrow \eta \pi^+ \pi^- p$
1287.4 ± 3.0	87	ABLIKIM	15P BES3	$J/\psi \rightarrow K^+ K^- 3\pi$
1281.16 ± 0.39 ± 0.45		1 LEES	12X BABR	$\tau^- \rightarrow \pi^- f_1(1285) \nu_\tau$
1285.1 ± 1.0 ± 1.6 ± 0.3		2 ABLIKIM	11J BES3	$J/\psi \rightarrow \omega(\eta \pi^+ \pi^-)$
1281 ± 2 ± 1		AUBERT	07AU BABR	10.6 $e^+ e^- \rightarrow f_1(1285) \pi^+ \pi^- \gamma$
1276.1 ± 8.1 ± 8.0	203	BAI	04J BES2	$J/\psi \rightarrow \gamma \gamma \pi^+ \pi^-$
1274 ± 6	237	ABDALLAH	03H DLPH	91.2 $e^+ e^- \rightarrow K_S^0 K^\pm \pi^\mp + X$
1280 ± 4		ACCIARRI	01G L3	
1288 ± 4 ± 5	20k	ADAMS	01B B852	18 GeV $\pi^- p \rightarrow K^+ K^- \pi^0 n$
1284 ± 6	1400	ALDE	97B GAM4	100 $\pi^- p \rightarrow \eta \pi^0 \pi^0 n$
1281 ± 1		BARBERIS	97B OMEG	450 $pp \rightarrow pp2(\pi^+ \pi^-)$
1281 ± 1		BARBERIS	97C OMEG	450 $pp \rightarrow ppK_S^0 K^\pm \pi^\mp$
1280 ± 2		3 AN TINORI	95 OMEG	300,450 $pp \rightarrow pp2(\pi^+ \pi^-)$
1282.2 ± 1.5		LEE	94 MPS2	18 $\pi^- p \rightarrow K^+ \bar{K}^0 2\pi^- p$
1279 ± 5		FUKUI	91C SPEC	8.95 $\pi^- p \rightarrow \eta \pi^+ \pi^- n$
1278 ± 2	140	ARMSTRONG	89 OMEG	300 $pp \rightarrow K \bar{K} \pi pp$
1278 ± 2		ARMSTRONG	89G OMEG	85 $\pi^+ p \rightarrow 4\pi pp, pp \rightarrow 4\pi pp$
1280.1 ± 2.1	60	RATH	89 MPS	21.4 $\pi^- p \rightarrow K_S^0 K_S^0 \pi^0 n$
1285 ± 1	4750	4 BIRMAN	88 MPS	8 $\pi^- p \rightarrow K^+ \bar{K}^0 \pi^- n$
1280 ± 1	504	BITYUKOV	88 SPEC	32.5 $\pi^- p \rightarrow K^+ K^- \pi^0 n$
1280 ± 4		ANDO	86 SPEC	8 $\pi^- p \rightarrow \eta \pi^+ \pi^- n$
1277 ± 2	420	REEVES	86 SPEC	6.6 $p\bar{p} \rightarrow K K \pi X$
1285 ± 2		CHUNG	85 SPEC	8 $\pi^- p \rightarrow N K \bar{K} \pi$
1279 ± 2	604	ARMSTRONG	84 OMEG	85 $\pi^+ p \rightarrow K \bar{K} \pi pp, pp \rightarrow K \bar{K} \pi pp$
1286 ± 1		CHAUVAT	84 SPEC	ISR 31.5 pp
1278 ± 4		EVANGELIS...	81 OMEG	12 $\pi^- p \rightarrow \eta \pi^+ \pi^- \pi^- p$
1283 ± 3	103	DIONISI	80 HBC	4 $\pi^- p \rightarrow K \bar{K} \pi n$
1282 ± 2	320	NACASCH	78 HBC	0.7, 0.76 $p\bar{p} \rightarrow K \bar{K} 3\pi$
1279 ± 5	210	GRASSLER	77 HBC	16 $\pi^+ p$
1286 ± 3	180	DUBOC	72 HBC	1.2 $p\bar{p} \rightarrow 2K4\pi$
1283 ± 5		DAHL	67 HBC	1.6-4.2 $\pi^- p$
1289.3 ± 2.8	234	ABLIKIM	19BA BES3	$e^+ e^- \rightarrow \psi(2S)$
1284.2 ± 2.2		5 AAIJ	14V LHCB	$\bar{B}^0(s) \rightarrow J/\psi 2(\pi^+ \pi^-)$
1281.9 ± 9		5 SOSA	99 SPEC	$pp \rightarrow P_{slow} (K_S^0 K^+ \pi^-) p_{fast}$
1282.8 ± 0.6		5 SOSA	99 SPEC	$pp \rightarrow P_{slow} (K_S^0 K^- \pi^+) p_{fast}$
1270 ± 10		AMELIN	95 YES	37 $\pi^- N \rightarrow \pi^- \pi^+ \pi^- \gamma N$
1280 ± 2		ABATZIS	94 OMEG	450 $pp \rightarrow pp2(\pi^+ \pi^-)$
1282 ± 4		ARMSTRONG	93C E760	$p\bar{p} \rightarrow \pi^0 \eta \eta \rightarrow 6\gamma$
1270 ± 6 ± 10		ARMSTRONG	92C OMEG	300 $pp \rightarrow pp\pi^+ \pi^- \gamma$
1281 ± 1		ARMSTRONG	89E OMEG	300 $pp \rightarrow pp2(\pi^+ \pi^-)$
1279 ± 6 ± 10	16	BECKER	87 MRK3	$e^+ e^- \rightarrow \phi K \bar{K} \pi$
1286 ± 9		GIDAL	87 MRK2	$e^+ e^- \rightarrow \eta \pi^+ \pi^-$
1287 ± 5	353	BITYUKOV	84B SPEC	32 $\pi^- p \rightarrow K^+ K^- \pi^0 n$
~1279		6 TORNQVIST	82B RVUE	
1275 ± 6	31	BROMBERG	80 SPEC	100 $\pi^- p \rightarrow K \bar{K} \pi X$
1288 ± 9	200	GURTU	79 HBC	4.2 $K^- p \rightarrow n \eta 2\pi$
~1275.0	46	7 STANTON	79 CNTR	8.5 $\pi^- p \rightarrow n2\gamma 2\pi$
1271 ± 10	34	CORDEN	78 OMEG	12-15 $\pi^- p \rightarrow K^+ K^- \pi n$
1295 ± 12	85	CORDEN	78 OMEG	12-15 $\pi^- p \rightarrow n5\pi$
1292 ± 10	150	DEFOIX	72 HBC	0.7 $p\bar{p} \rightarrow 7\pi$
1280 ± 3	500	8 THUN	72 MMS	13.4 $\pi^- p$
1303 ± 8		BARDAVIN...	71 HBC	8 $\pi^+ p \rightarrow p6\pi$
1283 ± 6		BOESEBECK	71 HBC	16.0 $\pi p \rightarrow p5\pi$
1270 ± 10		CAMPBELL	69 DBC	2.7 $\pi^+ d$
1285 ± 7		LORSTAD	69 HBC	0.7 $p\bar{p}$, 4,5-body
1290 ± 7		D'ANDLAU	68 HBC	1.2 $p\bar{p}$, 5-6 body

¹ Using the $2\pi^+ 2\pi^-$ and $\pi^+ \pi^- \eta$ modes of $f_1(1285)$ decay.

Meson Particle Listings

$f_1(1285)$

- ²The selected process is $J/\psi \rightarrow \omega a_0(980)\pi$.
- ³Supersedes ABATZIS 94, ARMSTRONG 89E.
- ⁴From partial wave analysis of $K^+ \bar{K}^0 \pi^-$ system.
- ⁵No systematic error given.
- ⁶From a unitarized quark-model calculation.
- ⁷From phase shift analysis of $\eta\pi^+ \pi^-$ system.
- ⁸Seen in the missing mass spectrum.



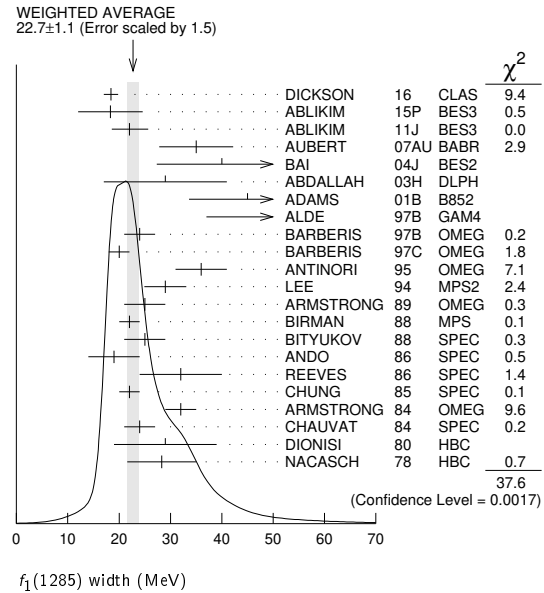
$f_1(1285)$ WIDTH

Only experiments giving width error less than 20 MeV are kept for averaging.

VALUE (MeV)	EVTS	DOCUMENT ID	TECN	COMMENT
22.7 ± 1.1 OUR AVERAGE		Error includes scale factor of 1.5. See the ideogram below.		
18.4 ± 1.4		DICKSON 16 CLAS	2.55 $\gamma p \rightarrow \eta\pi^+ \pi^- p$	
18.3 ± 6.3	87	ABLIKIM 15P BES3	$J/\psi \rightarrow K^+ K^- 3\pi$	
22.0 ± 3.1 ± 2.0 / 1.5		1 ABLIKIM 11J BES3	$J/\psi \rightarrow \omega(\eta\pi^+ \pi^-)$	
35 ± 6 ± 4		AUBERT 07AU BABR	10.6 $e^+ e^- \rightarrow f_1(1285)\pi^+ \pi^- \gamma$	
40.0 ± 8.6 ± 9.3	203	BAI 04J BES2	$J/\psi \rightarrow \gamma\gamma\pi^+ \pi^-$	
29 ± 12	237	ABDALLAH 03H DLPH	91.2 $e^+ e^- \rightarrow K_S^0 K^\pm \pi^\mp + X$	
45 ± 9 ± 7	20k	ADAMS 01B B852	18 GeV $\pi^- p \rightarrow K^+ K^- \pi^0 n$	
55 ± 18	1400	ALDE 97B GAM4	100 $\pi^- p \rightarrow \eta\pi^0 \pi^0 n$	
24 ± 3		BARBERIS 97B OMEG	450 $pp \rightarrow pp2(\pi^+ \pi^-)$	
20 ± 2		BARBERIS 97C OMEG	450 $pp \rightarrow ppK_S^0 K^\pm \pi^\mp$	
36 ± 5		2 ANTINORI 95 OMEG	300,450 $pp \rightarrow pp2(\pi^+ \pi^-)$	
29.0 ± 4.1		LEE 94 MPS2	18 $\pi^- p \rightarrow K^+ \bar{K}^0 2\pi^- p$	
25 ± 4	140	ARMSTRONG 89 OMEG	300 $pp \rightarrow K \bar{K} \pi pp$	
22 ± 2	4750	3 BIRMAN 88 MPS	8 $\pi^- p \rightarrow K^+ \bar{K}^0 \pi^- n$	
25 ± 4	504	BITYUKOV 88 SPEC	32.5 $\pi^- p \rightarrow K^+ K^- \pi^0 n$	
19 ± 5		ANDO 86 SPEC	8 $\pi^- p \rightarrow \eta\pi^+ \pi^- n$	
32 ± 8	420	REEVES 86 SPEC	6.6 $p\bar{p} \rightarrow K K \pi X$	
22 ± 2		CHUNG 85 SPEC	8 $\pi^- p \rightarrow N K \bar{K} \pi$	
32 ± 3	604	ARMSTRONG 84 OMEG	85 $\pi^+ p \rightarrow K \bar{K} \pi \pi p$, $pp \rightarrow K \bar{K} \pi pp$	
24 ± 3		CHAUVAT 84 SPEC	ISR 31.5 pp	
29 ± 10	103	DIONISI 80 HBC	4 $\pi^- p \rightarrow K \bar{K} \pi n$	
28.3 ± 6.7	320	NACASCH 78 HBC	0.7, 0.76 $p\bar{p} \rightarrow K \bar{K} 3\pi$	
• • • We do not use the following data for averages, fits, limits, etc. • • •				
17.1 ± 3.4	234	ABLIKIM 19BA BES3	$e^+ e^- \rightarrow \psi(2S)$	
32.4 ± 5.8		4 AAIJ 14Y LHCB	$\bar{B}^0(s) \rightarrow J/\psi 2(\pi^+ \pi^-)$	
18.2 ± 1.2		4 SOSA 99 SPEC	$pp \rightarrow p_{slow} (K_S^0 K^+ \pi^-)$ P_{fast}	

19.4 ± 1.5		4 SOSA 99 SPEC	$pp \rightarrow p_{slow} (K_S^0 K^- \pi^+)$ P_{fast}
40 ± 5		ABATZIS 94 OMEG	450 $pp \rightarrow pp2(\pi^+ \pi^-)$
31 ± 5		ARMSTRONG 89E OMEG	300 $pp \rightarrow pp2(\pi^+ \pi^-)$
41 ± 12		ARMSTRONG 89G OMEG	85 $\pi^+ p \rightarrow 4\pi\pi p$, $pp \rightarrow 4\pi pp$
17.9 ± 10.9	60	RATH 89 MPS	21.4 $\pi^- p \rightarrow K_S^0 K_S^0 \pi^0 n$
14 +20 / -14 ± 10	16	BECKER 87 MRK3	$e^+ e^- \rightarrow \phi K \bar{K} \pi$
26 ± 12		EVANGELIS... 81 OMEG	12 $\pi^- p \rightarrow \eta\pi^+ \pi^- \pi^- p$
25 ± 15	200	GURTU 79 HBC	4.2 $K^- p \rightarrow \eta\eta 2\pi$
~ 10		5 STANTON 79 CNTR	8.5 $\pi^- p \rightarrow n2\gamma 2\pi$
24 ± 18	210	GRASSLER 77 HBC	16 $\pi^+ p$
28 ± 5	150	6 DEFOIX 72 HBC	0.7 $p\bar{p} \rightarrow 7\pi$
46 ± 9	180	DUBOC 72 HBC	1.2 $p\bar{p} \rightarrow 2K 4\pi$
37 ± 5	500	7 THUN 72 MMS	13.4 $\pi^- p$
10 ± 10		BOESEBECK 71 HBC	16.0 $\pi p \rightarrow p5\pi$
30 ± 15		CAMPBELL 69 DBC	2.7 $\pi^+ d$
60 ± 15		6 LORSTAD 69 HBC	0.7 $p\bar{p}$, 4,5-body
35 ± 10		6 DAHL 67 HBC	1.6-4.2 $\pi^- p$

- ¹The selected process is $J/\psi \rightarrow \omega a_0(980)\pi$.
- ²Supersedes ABATZIS 94, ARMSTRONG 89E.
- ³From partial wave analysis of $K^+ \bar{K}^0 \pi^-$ system.
- ⁴No systematic error given.
- ⁵From phase shift analysis of $\eta\pi^+ \pi^-$ system.
- ⁶Resolution is not unfolded.
- ⁷Seen in the missing mass spectrum.



$f_1(1285)$ DECAY MODES

Mode	Fraction (Γ_i/Γ)	Scale factor/ Confidence level
Γ_1 4π	(32.7 ± 1.9) %	S=1.2
Γ_2 $\pi^0 \pi^0 \pi^+ \pi^-$	(21.8 ± 1.3) %	S=1.2
Γ_3 $2\pi^+ 2\pi^-$	(10.9 ± 0.6) %	S=1.2
Γ_4 $\rho^0 \pi^+ \pi^-$	(10.9 ± 0.6) %	S=1.2
Γ_5 $\rho^0 \rho^0$	seen	
Γ_6 $4\pi^0$	< 7 × 10 ⁻⁴	CL=90%
Γ_7 $\eta\pi^+ \pi^-$	(35 ± 15) %	
Γ_8 $\eta\pi\pi$	(52.2 ± 2.0) %	S=1.2
Γ_9 $a_0(980)\pi$ [ignoring $a_0(980) \rightarrow K \bar{K}$]	(38 ± 4) %	
Γ_{10} $\eta\pi\pi$ [excluding $a_0(980)\pi$]	(14 ± 4) %	
Γ_{11} $K \bar{K} \pi$	(9.0 ± 0.4) %	S=1.1
Γ_{12} $K \bar{K}^*(892)$	not seen	
Γ_{13} $\pi^+ \pi^- \pi^0$	(3.0 ± 0.9) × 10 ⁻³	
Γ_{14} $\rho^\pm \pi^\mp$	< 3.1 × 10 ⁻³	CL=95%
Γ_{15} $\gamma\rho^0$	(6.1 ± 1.0) %	S=1.7
Γ_{16} $\phi\gamma$	(7.4 ± 2.6) × 10 ⁻⁴	
Γ_{17} $e^+ e^-$	< 9.4 × 10 ⁻⁹	CL=90%
Γ_{18} $\gamma\gamma^*$		
Γ_{19} $\gamma\gamma$		

See key on page 999

Meson Particle Listings

 $f_1(1285)$

CONSTRAINED FIT INFORMATION

An overall fit to 6 branching ratios uses 18 measurements and one constraint to determine 5 parameters. The overall fit has a $\chi^2 = 24.0$ for 14 degrees of freedom.

The following *off-diagonal* array elements are the correlation coefficients $\langle \delta x_i \delta x_j \rangle / (\delta x_i \delta x_j)$, in percent, from the fit to the branching fractions, $x_i \equiv \Gamma_i / \Gamma_{\text{total}}$. The fit constrains the x_i whose labels appear in this array to sum to one.

x_9	-30			
x_{10}	-12	-88		
x_{11}	22	-10	-4	
x_{15}	-25	-7	-3	-27
	x_1	x_9	x_{10}	x_{11}

 $f_1(1285) \Gamma(i) \Gamma(\gamma\gamma) / \Gamma(\text{total})$

$\Gamma(\eta\pi\pi) \times \Gamma(\gamma\gamma) / \Gamma_{\text{total}}$		$\Gamma_8 \Gamma_{19} / \Gamma = (\Gamma_9 + \Gamma_{10}) \Gamma_{19} / \Gamma$			
VALUE (keV)	CL%	DOCUMENT ID	TECN	COMMENT	
<0.62	95	GIDAL	87	MRK2	$e^+e^- \rightarrow e^+e^-\eta\pi^+\pi^-$

$\Gamma(\eta\pi\pi) \times \Gamma(\gamma\gamma^*) / \Gamma_{\text{total}}$		$\Gamma_8 \Gamma_{18} / \Gamma = (\Gamma_9 + \Gamma_{10}) \Gamma_{18} / \Gamma$			
VALUE (keV)	EVTS	DOCUMENT ID	TECN	COMMENT	
1.4 ± 0.4 OUR AVERAGE		Error includes scale factor of 1.4.			
1.18 ± 0.25 ± 0.20	26	^{1,2} AIHARA	88B	TPC	$e^+e^- \rightarrow e^+e^-\eta\pi^+\pi^-$
2.30 ± 0.61 ± 0.42		^{1,3} GIDAL	87	MRK2	$e^+e^- \rightarrow e^+e^-\eta\pi^+\pi^-$
••• We do not use the following data for averages, fits, limits, etc. •••					
1.8 ± 0.3 ± 0.3	420	⁴ ACHARD	02B	L3	183–209 $e^+e^- \rightarrow e^+e^-\eta\pi^+\pi^-$

¹ Assuming a ρ -pole form factor.

² Published value multiplied by $\eta\pi\pi$ branching ratio 0.49.

³ Published value divided by 2 and multiplied by the $\eta\pi\pi$ branching ratio 0.49.

⁴ Published value multiplied by the $\eta\pi\pi$ branching ratio 0.52.

 $f_1(1285)$ BRANCHING RATIOS

$\Gamma(K\bar{K}\pi) / \Gamma(4\pi)$		Γ_{11} / Γ_1			
VALUE	DOCUMENT ID	TECN	COMMENT		
0.274 ± 0.017 OUR FIT	Error includes scale factor of 1.4.				
0.271 ± 0.016 OUR AVERAGE	Error includes scale factor of 1.2.				
0.265 ± 0.014	¹ BARBERIS	97c	OMEG	450 $pp \rightarrow p\rho K_S^0 K^\pm \pi^\mp$	
0.28 ± 0.05	² ARMSTRONG	89E	OMEG	300 $pp \rightarrow p\rho f_1(1285)$	
0.37 ± 0.03 ± 0.05	³ ARMSTRONG	89G	OMEG	85 $\pi p \rightarrow 4\pi X$	
••• We do not use the following data for averages, fits, limits, etc. •••					
	¹ Using $2(\pi^+\pi^-)$ data from BARBERIS 97b.				
	² Assuming $\rho\pi\pi$ and $a_0(980)\pi$ intermediate states.				
	³ 4π consistent with being entirely $\rho\pi\pi$.				

$\Gamma(\pi^0\pi^0\pi^+\pi^-) / \Gamma_{\text{total}}$		$\Gamma_2 / \Gamma = \frac{2}{3} \Gamma_1 / \Gamma$			
VALUE	DOCUMENT ID	TECN	COMMENT		
0.218 ± 0.013 OUR FIT	Error includes scale factor of 1.2.				

$\Gamma(2\pi^+2\pi^-) / \Gamma_{\text{total}}$		$\Gamma_3 / \Gamma = \frac{1}{3} \Gamma_1 / \Gamma$			
VALUE	DOCUMENT ID	TECN	COMMENT		
0.109 ± 0.006 OUR FIT	Error includes scale factor of 1.2.				

$\Gamma(\rho^0\pi^+\pi^-) / \Gamma_{\text{total}}$		$\Gamma_4 / \Gamma = \frac{1}{3} \Gamma_1 / \Gamma$			
VALUE	DOCUMENT ID	TECN	COMMENT		
0.109 ± 0.006 OUR FIT	Error includes scale factor of 1.2.				

$\Gamma(\rho^0\pi^+\pi^-) / \Gamma(2\pi^+2\pi^-)$		Γ_4 / Γ_3			
VALUE	DOCUMENT ID	TECN	COMMENT		
••• We do not use the following data for averages, fits, limits, etc. •••					
1.0 ± 0.4	GRASSLER	77	HBC	16 GeV	$\pi^\pm p$

$\Gamma(\rho^0\rho^0) / \Gamma_{\text{total}}$		Γ_5 / Γ			
VALUE	DOCUMENT ID	TECN	COMMENT		
seen	BARBERIS	00c	450 $pp \rightarrow p_f 4\pi p_5$		

$\Gamma(4\pi^0) / \Gamma_{\text{total}}$		Γ_6 / Γ			
VALUE (units 10^{-4})	CL%	DOCUMENT ID	TECN	COMMENT	
<7	90	ALDE	87	GAM4	100 $\pi^- p \rightarrow 4\pi^0 n$

$\Gamma(\pi^+\pi^-\pi^0) / \Gamma(\eta\pi^+\pi^-)$		Γ_{13} / Γ_7			
VALUE (%)	EVTS	DOCUMENT ID	TECN	COMMENT	
0.86 ± 0.16 ± 0.20	2.3k	¹ DOROFEEV	11	VES	$\pi^- N \rightarrow \pi^- f_1(1285) N$

¹ Value obtained selecting the region corresponding to $f_0(980)$ in the $\pi^+\pi^-$ mass spectrum.

$\Gamma(\eta\pi\pi) / \Gamma_{\text{total}}$		$\Gamma_8 / \Gamma = (\Gamma_9 + \Gamma_{10}) / \Gamma$			
VALUE	DOCUMENT ID	TECN	COMMENT		
0.522 ± 0.020 OUR FIT	Error includes scale factor of 1.2.				

 $\Gamma(4\pi) / \Gamma(\eta\pi\pi)$

VALUE	DOCUMENT ID	TECN	COMMENT
0.63 ± 0.06 OUR FIT	Error includes scale factor of 1.3.		
0.41 ± 0.14 OUR AVERAGE			
0.37 ± 0.11 ± 0.11	BOLTON	92	MRK3 $J/\psi \rightarrow \gamma f_1(1285)$
0.64 ± 0.40	GURTU	79	HBC 4.2 $K^- p$
••• We do not use the following data for averages, fits, limits, etc. •••			
0.93 ± 0.30	¹ GRASSLER	77	HBC 16 $\pi^\mp p$
¹ Assuming $\rho\pi\pi$ and $a_0(980)\pi$ intermediate states.			

 $\Gamma(2\pi^+2\pi^-) / \Gamma(\eta\pi\pi)$

VALUE	DOCUMENT ID	TECN	COMMENT
0.28 ± 0.02 ± 0.02	¹ LEES	12x	BABR $\tau^- \rightarrow \pi^- f_1(1285) \nu_\tau$
¹ Assuming $B(f_1(1285) \rightarrow \pi\pi\eta) = 3/2 B(f_1(1285) \rightarrow \pi^+\pi^-\eta)$.			

 $\Gamma(a_0(980)\pi \text{ [ignoring } a_0(980) \rightarrow K\bar{K}]) / \Gamma(\eta\pi\pi)$

VALUE	CL%	DOCUMENT ID	TECN	COMMENT
0.72 ± 0.08 OUR FIT				
0.72 ± 0.07 OUR AVERAGE				
0.74 ± 0.02 ± 0.09		DICKSON	16	CLAS $\gamma p \rightarrow f_1(1285) p$
0.72 ± 0.15		GURTU	79	HBC 4.2 $K^- p$
0.6 $\begin{smallmatrix} +0.3 \\ -0.2 \end{smallmatrix}$		CORDEN	78	OMEG 12–15 $\pi^- p$
••• We do not use the following data for averages, fits, limits, etc. •••				
>0.69	95	ACHARD	02B	L3 183–209 $e^+e^- \rightarrow e^+e^-\eta\pi^+\pi^-$
0.28 ± 0.07		ALDE	97B	GAM4 100 $\pi^- p \rightarrow \eta\pi^0\pi^0 n$
1.0 ± 0.3		GRASSLER	77	HBC 16 $\pi^\mp p$

 $\Gamma(K\bar{K}\pi) / \Gamma(\eta\pi\pi)$

VALUE	DOCUMENT ID	TECN	COMMENT
0.172 ± 0.012 OUR FIT	Error includes scale factor of 1.1.		
0.176 ± 0.012 OUR AVERAGE			
0.216 ± 0.010 ± 0.031	DICKSON	16	CLAS $\gamma p \rightarrow f_1(1285) p$
0.166 ± 0.01 ± 0.008	BARBERIS	98c	OMEG 450 $pp \rightarrow p_f f_1(1285) p_S$
0.42 ± 0.15	GURTU	79	HBC 4.2 $K^- p$
0.5 ± 0.2	¹ CORDEN	78	OMEG 12–15 $\pi^- p$
0.20 ± 0.08	² DEFOIX	72	HBC 0.7 $\bar{p} p \rightarrow 7\pi$
0.16 ± 0.08	CAMPBELL	69	DBC 2.7 $\pi^+ d$

¹ CORDEN 78 assumes low-mass $\eta\pi\pi$ region is dominantly 1^{++} . See BARBERIS 98c and MANAK 00a for discussion.

² $K\bar{K}$ system characterized by the $l = 1$ threshold enhancement. (See under $a_0(980)$).

 $\Gamma(K\bar{K}^*(892)) / \Gamma_{\text{total}}$

VALUE	DOCUMENT ID	TECN	COMMENT
not seen	NACASCH	78	HBC 0.7, 0.76 $\bar{p} p \rightarrow K\bar{K}^* 3\pi$
••• We do not use the following data for averages, fits, limits, etc. •••			
seen	¹ ACHARD	07	L3 183–209 $e^+e^- \rightarrow e^+e^-K_S^0 K^\pm \pi^\mp$
¹ A clear signal of 19.8 ± 4.4 events observed at high Q^2 .			

 $\Gamma(\pi^+\pi^-\pi^0) / \Gamma_{\text{total}}$

VALUE (%)	EVTS	DOCUMENT ID	TECN	COMMENT
0.30 ± 0.055 ± 0.074	2.3k	¹ DOROFEEV	11	VES $\pi^- N \rightarrow \pi^- f_1(1285) N$
¹ Value obtained selecting the region corresponding to $f_0(980)$ in the $\pi^+\pi^-$ mass spectrum. The systematic error includes the uncertainty on the partial width $f_1 \rightarrow \eta\pi\pi$ obtained from PDG 10 data.				

 $\Gamma(\rho^\pm\pi^\mp) / \Gamma_{\text{total}}$

VALUE (%)	CL%	DOCUMENT ID	TECN	COMMENT
<0.31	95	DOROFEEV	11	VES $\pi^- N \rightarrow \pi^- f_1(1285) N$

 $\Gamma(\gamma\rho^0) / \Gamma_{\text{total}}$

VALUE (units 10^{-2})	CL%	DOCUMENT ID	TECN	COMMENT
6.1 ± 1.0 OUR FIT		Error includes scale factor of 1.7.		
••• We do not use the following data for averages, fits, limits, etc. •••				
2.8 ± 0.7 ± 0.6		¹ AMELIN	95	VES 37 $\pi^- N \rightarrow \pi^- \pi^+ \pi^- \gamma N$
<5	95	BITYUKOV	91B	SPEC 32 $\pi^- p \rightarrow \pi^+ \pi^- \gamma n$
¹ Not an independent measurement.				

 $\Gamma(\gamma\rho^0) / \Gamma(2\pi^+2\pi^-)$

VALUE	DOCUMENT ID	TECN	COMMENT
0.55 ± 0.10 OUR FIT	Error includes scale factor of 1.5.		
0.45 ± 0.18	¹ COFFMAN	90	MRK3 $J/\psi \rightarrow \gamma\gamma\pi^+\pi^-$
¹ Using $B(J/\psi \rightarrow \gamma f_1(1285) \rightarrow \gamma\gamma\rho^0) = 0.25 \times 10^{-4}$ and $B(J/\psi \rightarrow \gamma f_1(1285) \rightarrow \gamma 2\pi^+ 2\pi^-) = 0.55 \times 10^{-4}$ given by MIR 88.			

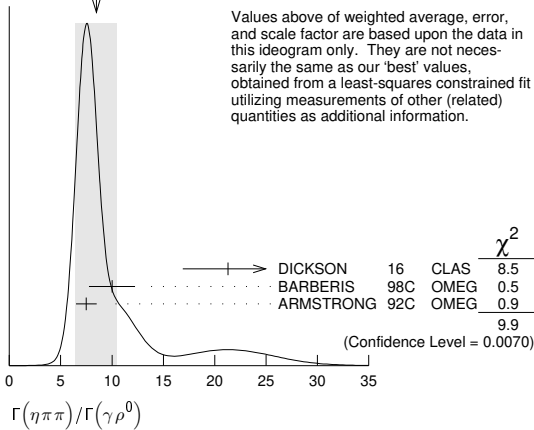
 $\Gamma(\eta\pi\pi) / \Gamma(\gamma\rho^0)$

VALUE	DOCUMENT ID	TECN	COMMENT
8.6 ± 1.6 OUR FIT	Error includes scale factor of 1.9.		
8.5 ± 2.0 OUR AVERAGE	Error includes scale factor of 2.2. See the ideogram below.		
21.3 ± 4.4	DICKSON	16	CLAS $\gamma p \rightarrow f_1(1285) p$
10.0 ± 1.0 ± 2.0	BARBERIS	98c	OMEG 450 $pp \rightarrow p_f f_1(1285) p_S$
7.5 ± 1.0	¹ ARMSTRONG	92c	OMEG 300 $pp \rightarrow pp\pi^+\pi^-\gamma, pp\eta\pi^+\pi^-$
¹ Published value multiplied by 1.5.			

Meson Particle Listings

$f_1(1285), \eta(1295)$

WEIGHTED AVERAGE
8.5±2.0 (Error scaled by 2.2)



$\Gamma(\gamma\rho^0)/\Gamma(K\bar{K}\pi)$ Γ_{15}/Γ_{11}

VALUE	CL%	DOCUMENT ID	TECN	COMMENT
••• We do not use the following data for averages, fits, limits, etc. •••				
>0.035	90	¹ COFFMAN 90	MRK3	$J/\psi \rightarrow \gamma\gamma\pi^+\pi^-$
¹ Using $B(J/\psi \rightarrow \gamma f_1(1285) \rightarrow \gamma\gamma\rho^0) = 0.25 \times 10^{-4}$ and $B(J/\psi \rightarrow \gamma f_1(1285) \rightarrow \gamma K\bar{K}\pi) < 0.72 \times 10^{-3}$.				

$\Gamma(\phi\gamma)/\Gamma(K\bar{K}\pi)$ Γ_{16}/Γ_{11}

VALUE (units 10^{-2})	CL%	EVTS	DOCUMENT ID	TECN	COMMENT
0.82±0.21±0.20		19	BITYUKOV 88	SPEC	$32.5 \pi^- \rho \rightarrow K^+ K^- \pi^0 n$
••• We do not use the following data for averages, fits, limits, etc. •••					
<0.50	95		BARBERIS 98c	OMEG	$450 p\rho \rightarrow p f_1(1285) \rho_S$
<0.93	95		AMELIN 95	VES	$37 \pi^- N \rightarrow \pi^- \pi^+ \pi^- \gamma N$

$\Gamma(e^+e^-)/\Gamma_{total}$ Γ_{17}/Γ

VALUE	CL%	DOCUMENT ID	TECN	COMMENT
<9.4 × 10⁻⁹	90	¹ ACHASOV 20	SND	$e^+e^- \rightarrow \eta\pi^0\pi^0$
¹ ACHASOV 20 reports two candidate events corresponding to a significance of 2.5 σ and the branching fraction of $(5.1^{+3.7}_{-2.7}) \times 10^{-9}$.				

$f_1(1285)$ REFERENCES

ACHASOV 20	PL B800 135074	M.N. Achasov et al.	(SND Collab.)
ABLIKIM 19BA	PR D100 092003	M. Ablikim et al.	(BESIII Collab.)
DICKSON 16	PR C93 065202	R. Dickson et al.	(JLab CLAS Collab.)
ABLIKIM 15P	PR D92 012007	M. Ablikim et al.	(BESIII Collab.)
AAJ 14Y	PRL 112 091802	R. Aaij et al.	(LHCb Collab.)
LEES 12X	PR D86 092010	J.P. Lees et al.	(BABAR Collab.)
ABLIKIM 11J	PRL 107 182001	M. Ablikim et al.	(BESIII Collab.)
DOROFEEV 11	EPJ A47 48	V. Dorofeev et al.	(SERP, MIPT)
PDG 10	JP G37 075021	K. Nakamura et al.	(PDG Collab.)
ACHARD 07	JHEP 0703 018	P. Achard et al.	(L3 Collab.)
AUBERT 07AU	PR D76 092005	B. Aubert et al.	(BABAR Collab.)
BAI 04J	PL B594 47	J.Z. Bai et al.	(BES Collab.)
ABDALLAH 03H	PL B569 129	J. Abdallah et al.	(DELPHI Collab.)
ACHARD 02B	PL B526 269	P. Achard et al.	(L3 Collab.)
ACCIARRI 01G	PL B501 1	M. Acciarri et al.	(L3 Collab.)
ADAMS 01B	PL B516 264	G.S. Adams et al.	(BNL E852 Collab.)
BARBERIS 00C	PL B471 440	D. Barberis et al.	(WA 102 Collab.)
MANAK 00A	PR D62 012003	J.J. Manak et al.	(BNL E852 Collab.)
SOSA 99	PRL 83 913	M. Sosa et al.	
BARBERIS 95C	PL B440 225	D. Barberis et al.	(WA 102 Collab.)
ALDE 97B	PAN 60 386	D. Alde et al.	(GAMS Collab.)
Translated from YAF 60 458.			
BARBERIS 97B	PL B413 217	D. Barberis et al.	(WA 102 Collab.)
BARBERIS 97C	PL B413 225	D. Barberis et al.	(WA 102 Collab.)
AMELIN 95	ZPHY C66 71	D.V. Amelin et al.	(VES Collab.)
ANTINORI 95	PL B353 589	F. Antinori et al.	(ATHU, BARI, BIRM+)
ABATZIS 94	PL B324 509	S. Abatzis et al.	(ATHU, BARI, BIRM+)
LEE 94	PL B323 227	M. Lee et al.	(BNL, IND, KYUIN, MASD+)
ARMSTRONG 93C	PL B307 394	T.A. Armstrong et al.	(FNAL, FERR, GENO+)
ARMSTRONG 92C	ZPHY C54 371	T.A. Armstrong et al.	(ATHU, BARI, BIRM+)
BOLTON 92	PL B278 495	T. Bolton et al.	(Mark III Collab.)
BITYUKOV 91B	SJNP 54 318	S.I. Bityukov et al.	(SERP)
Translated from YAF 54 529.			
FUKUI 91C	PL B267 293	S. Fukui et al.	(SUGI, NAGO, KEK, KYOT+)
COFFMAN 90	PR D41 1410	D.M. Coffman et al.	(Mark III Collab.)
ARMSTRONG 89	PL B221 216	T.A. Armstrong et al.	(CERN, CDEF, BIRM+)
ARMSTRONG 89E	PL B228 536	T.A. Armstrong, M. Benayoun	(ATHU, BARI, BIRM+)
ARMSTRONG 89G	ZPHY C43 55	T.A. Armstrong et al.	(CERN, BIRM, BARI+)
RATH 89	PR D40 693	M.G. Rath et al.	(NDAM, BRAN, BNL, CUNY+)
AIHARA 88B	PL B209 107	H. Aihara et al.	(TPC-2 γ Collab.)
BIRMAN 88	PRL 61 1557	A. Birman et al.	(BNL, FSU, IND, MASD)JP
BITYUKOV 88	PL B203 327	S.I. Bityukov et al.	(SERP)
MIR 88	Photon-Photon 88, 126	R. Mir	(Mark III Collab.)
Conference			
ALDE 87	PL B198 286	D.M. Alde et al.	(LANL, BRUX, SERP, LAPP)
BECKER 87	PRL 59 186	J.J. Becker et al.	(Mark III Collab.)
GIDAL 87	PRL 59 2012	G. Gidal et al.	(LBL, SLAC, HARV)
ANDO 86	PRL 57 1296	A. Ando et al.	(KEK, KYOT, NIRS, SAGA+)JP

REEVES 86	PR D34 1960	D.F. Reeves et al.	(FLOR, BNL, IND+)JP
CHUNG 85	PRL 55 779	S.U. Chung et al.	(BNL, FLOR, IND+)JP
ARMSTRONG 84	PL 146B 273	T.A. Armstrong et al.	(ATHU, BARI, BIRM+)JP
BITYUKOV 84B	PL 144B 133	S.I. Bityukov et al.	(SERP)
CHAUVAT 84	PL 148B 382	P. Chauvat et al.	(CERN, CLER, UCLA+)
TORNQVIST 82B	NP B203 268	N.A. Tornqvist	(HELS)
EVANGELIS... 81	NP B178 197	C. Evangelista et al.	(BARI, BONN, CERN+)
BROMBERG 80	PR D22 1513	C.M. Bromberg et al.	(CIT, FNAL, ILLC+)
DIONISI 80	NP B169 1	C. Dionisi et al.	(CERN, MADR, CDEF+)
GURTU 79	NP B151 181	A. Gurto et al.	(CERN, ZEEM, NIJM, OXF)
STANTON 79	PRL 42 346	N.R. Stanton et al.	(OSU, CARL, MCGI+)
CORDEN 78	NP B144 253	M.J. Corden et al.	(BIRM, RHEL, TELA+)
NACASCH 78	NP B135 203	R. Nacasch et al.	(PARIS, MADR, CERN)
GRASSLER 77	NP B121 189	H. Grassler et al.	(AACH3, BERL, BONN+)
DEFOIX 72	NP B44 125	C. Defoix et al.	(CDEF, CERN)
DUBOC 72	NP B46 429	J. Duboc et al.	(PARIS, LIVP)
THUN 72	PRL 28 1733	R. Thun et al.	(STON, NEAS)
BARDADIN... 71	PR D4 2711	M. Bardadin-Otwinowska et al.	(WARSA)
BOESEBECK 71	PL 34B 659	K. Boesebeck	(AACH, BERL, BONN, CERN, CRAC+)
CAMPBELL 69	PRL 22 1204	J.H. Campbell et al.	(RURD)
LORSTAD 69	NP B14 63	B. Lorstad et al.	(CDEF, CERN)JP
D'ANDLAU 68	NP B5 693	C. d'Andlau et al.	(CDEF, CERN, IRAD+)JP
DAHL 67	PR 163 1377	O.I. Dahl et al.	(LRL)JP

$\eta(1295)$

$$J^G(J^{PC}) = 0^+(0^{-+})$$

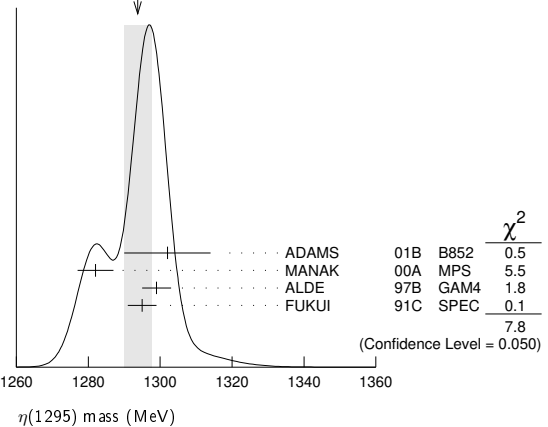
See the review on "Pseudoscalar and pseudovector mesons in the 1400 MeV region."

$\eta(1295)$ MASS

VALUE (MeV)	EVTS	DOCUMENT ID	TECN	COMMENT
1294±4 OUR AVERAGE	Error	includes scale factor of 1.6. See the ideogram below.		
1302±9±8	20k	ADAMS	01B B852	18 GeV $\pi^- \rho \rightarrow K^+ K^- \pi^0 n$
1282±5	9082	MANAK	00A MPS	18 $\pi^- \rho \rightarrow \eta\pi^+\pi^- n$
1299±4	2100	ALDE	97B GAM4	100 $\pi^- \rho \rightarrow \eta\pi^0\pi^0 n$
1295±4		FUKUI	91c SPEC	8.95 $\pi^- \rho \rightarrow \eta\pi^+\pi^- n$

••• We do not use the following data for averages, fits, limits, etc. •••
1264±8 ¹AUGUSTIN 90 DM2 $J/\psi \rightarrow \gamma\eta\pi^+\pi^-$
~ 1275 STANTON 79 CNTR 8.4 $\pi^- \rho \rightarrow n\eta 2\pi$

WEIGHTED AVERAGE
1294±4 (Error scaled by 1.6)



¹ PWA analysis of AUGUSTIN 92 assigns 0^{-+} quantum numbers to this state rather than 1^{++} as before.

$\eta(1295)$ WIDTH

VALUE (MeV)	EVTS	DOCUMENT ID	TECN	COMMENT
55±5 OUR AVERAGE				
57±23±21	20k	ADAMS	01B B852	18 GeV $\pi^- \rho \rightarrow K^+ K^- \pi^0 n$
66±13	9082	MANAK	00A MPS	18 $\pi^- \rho \rightarrow \eta\pi^+\pi^- n$
53±6		FUKUI	91c SPEC	8.95 $\pi^- \rho \rightarrow \eta\pi^+\pi^- n$

••• We do not use the following data for averages, fits, limits, etc. •••
<40±20 2100 ALDE 97B GAM4 100 $\pi^- \rho \rightarrow \eta\pi^0\pi^0 n$
44±20 ²AUGUSTIN 90 DM2 $J/\psi \rightarrow \gamma\eta\pi^+\pi^-$
~ 70 STANTON 79 CNTR 8.4 $\pi^- \rho \rightarrow n\eta 2\pi$

² PWA analysis of AUGUSTIN 92 assigns 0^{-+} quantum numbers to this state rather than 1^{++} as before.

$\eta(1295)$ DECAY MODES

Table with 3 columns: Mode, Fraction (Γ_i/Γ), and values for various decay channels like $\eta\pi^+\pi^-$, $a_0(980)\pi$, $\gamma\gamma$, $\eta\pi^0\pi^0$, $\eta(\pi\pi)s$ -wave, $\sigma\eta$, and $K\bar{K}\pi$.

$\eta(1295) \Gamma(i)\Gamma(\gamma\gamma)/\Gamma(\text{total})$

Table for $\Gamma(\eta\pi^+\pi^-) \times \Gamma(\gamma\gamma)/\Gamma(\text{total})$ with columns: VALUE (keV), CL%, DOCUMENT ID, TECN, COMMENT. Value: <0.066.

••• We do not use the following data for averages, fits, limits, etc. •••

Table with 5 columns: VALUE, CL%, DOCUMENT ID, TECN, COMMENT. Values: <0.6, 90, AIHARA 88c TPC, 449±39±47, 268±50.

Table with 5 columns: VALUE, CL%, DOCUMENT ID, TECN, COMMENT. Value: <0.3, ANTREASANYAN 87 CBAL.

Table for $\Gamma(K\bar{K}\pi) \times \Gamma(\gamma\gamma)/\Gamma(\text{total})$ with columns: VALUE (keV), CL%, DOCUMENT ID, TECN, COMMENT. Value: <0.014.

••• We do not use the following data for averages, fits, limits, etc. •••

Table with 5 columns: VALUE, CL%, DOCUMENT ID, TECN, COMMENT. Value: <0.014, 90, AHOHE 3,4.

³ Using $\eta(1295)$ mass and width 1294 MeV and 55 MeV, respectively.

⁴ Assuming three-body phase-space decay to $K_S^0 K^\pm \pi^\mp$.

$\eta(1295)$ BRANCHING RATIOS

Table for $\Gamma(a_0(980)\pi)/\Gamma(\text{total})$ with columns: VALUE, DOCUMENT ID, TECN, COMMENT, Γ_2/Γ . Value: not seen.

••• We do not use the following data for averages, fits, limits, etc. •••

Table with 5 columns: VALUE, DOCUMENT ID, TECN, COMMENT, Γ_2/Γ . Value: seen, BIRMAN 88 MPS.

Table with 5 columns: VALUE, DOCUMENT ID, TECN, COMMENT, Γ_2/Γ . Value: large, ANDO 86 SPEC.

Table for $\Gamma(a_0(980)\pi)/\Gamma(\eta\pi^0\pi^0)$ with columns: VALUE, DOCUMENT ID, TECN, COMMENT, Γ_2/Γ_4 . Value: 0.65±0.10.

⁵ Assuming that $a_0(980)$ decays only to $\eta\pi$.

Table for $\Gamma(\eta(\pi\pi)s\text{-wave})/\Gamma(\eta\pi^0\pi^0)$ with columns: VALUE, DOCUMENT ID, TECN, COMMENT, Γ_5/Γ_4 . Value: 0.35±0.10.

Table for $\Gamma(a_0(980)\pi)/\Gamma(\sigma\eta)$ with columns: VALUE, EVTS, DOCUMENT ID, TECN, COMMENT, Γ_2/Γ_6 . Value: 0.48±0.22.

$\eta(1295)$ REFERENCES

Reference list for $\eta(1295)$ with columns: NAME, ID, PUBLICATION, AUTHOR, COLLAB.

$\pi(1300)$

$I^G(J^{PC}) = 1^-(0^{-+})$

$\pi(1300)$ MASS

Table for $\pi(1300)$ MASS with columns: VALUE (MeV), EVTS, DOCUMENT ID, TECN, COMMENT.

••• We do not use the following data for averages, fits, limits, etc. •••

Table with 5 columns: VALUE, CL%, DOCUMENT ID, TECN, COMMENT. Values: 1128±26±70, 1345±8±10, 1200±40, 1343±15±24.

Table with 5 columns: VALUE, DOCUMENT ID, TECN, COMMENT. Values: 1375±40, 1275±15, ~1114, 1190±30, 1240±30, 1273±50, 1342±20, ~1400.

¹ From analysis of L3 data at 183–209 GeV. ² Uses multichannel Aitchison-Bowler model (BOWLER 75). Uses data from DAUM 80 and DANKOWYCH 81.

$\pi(1300)$ WIDTH

Table for $\pi(1300)$ WIDTH with columns: VALUE (MeV), EVTS, DOCUMENT ID, TECN, COMMENT.

••• We do not use the following data for averages, fits, limits, etc. •••

Table with 5 columns: VALUE, CL%, DOCUMENT ID, TECN, COMMENT. Values: 314±39±66, 260±20±30, 470±120, 449±39±47, 268±50.

Table with 5 columns: VALUE, CL%, DOCUMENT ID, TECN, COMMENT. Values: 218±100, ~340, 440±80, 360±120, 580±100.

Table with 5 columns: VALUE, CL%, DOCUMENT ID, TECN, COMMENT. Values: 220±70, ~600.

³ From analysis of L3 data at 183–209 GeV. ⁴ Uses multichannel Aitchison-Bowler model (BOWLER 75). Uses data from DAUM 80 and DANKOWYCH 81.

$\pi(1300)$ DECAY MODES

Table with 3 columns: Mode, Fraction (Γ_i/Γ), and values for $\rho\pi$, $\pi(\pi\pi)s$ -wave, and $\gamma\gamma$.

$\pi(1300) \Gamma(i)\Gamma(\gamma\gamma)/\Gamma(\text{total})$

Table for $\Gamma(\rho\pi) \times \Gamma(\gamma\gamma)/\Gamma(\text{total})$ with columns: VALUE (keV), CL%, DOCUMENT ID, TECN, COMMENT. Value: <0.085.

••• We do not use the following data for averages, fits, limits, etc. •••

Table with 5 columns: VALUE, CL%, DOCUMENT ID, TECN, COMMENT. Values: <0.8, <0.54.

⁵ From analysis of L3 data at 183–209 GeV.

$\pi(1300)$ BRANCHING RATIOS

Table for $\Gamma(\pi(\pi\pi)s\text{-wave})/\Gamma(\rho\pi)$ with columns: VALUE, CL%, EVTS, DOCUMENT ID, TECN, COMMENT, Γ_2/Γ_1 .

••• We do not use the following data for averages, fits, limits, etc. •••

Table with 5 columns: VALUE, CL%, DOCUMENT ID, TECN, COMMENT, Γ_2/Γ_1 . Values: 2.2±0.4, <0.15, 2.12.

⁶ Uses multichannel Aitchison-Bowler model (BOWLER 75). Uses data from DAUM 80 and DANKOWYCH 81.

$\pi(1300)$ REFERENCES

Reference list for $\pi(1300)$ with columns: NAME, ID, PUBLICATION, AUTHOR, COLLAB.

Meson Particle Listings

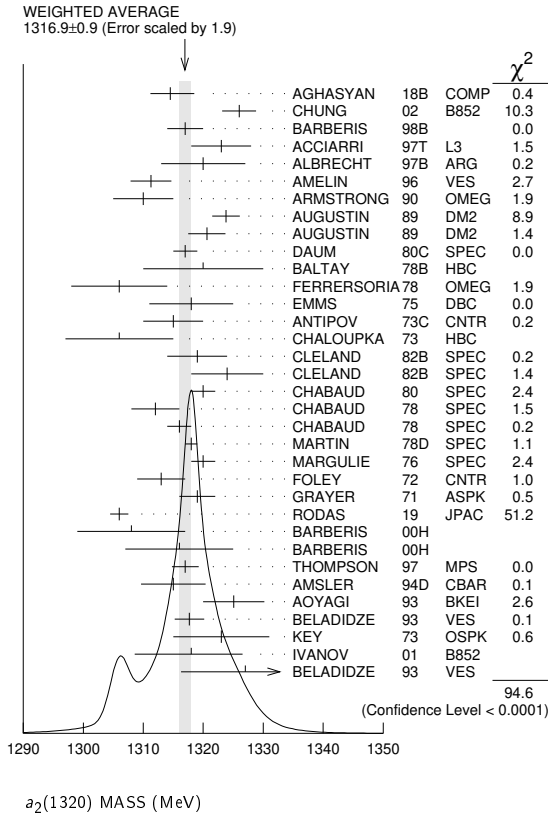
$a_2(1320)$

$a_2(1320)$

$$J^G(J^{PC}) = 1^-(2^{++})$$

$a_2(1320)$ MASS

VALUE (MeV) DOCUMENT ID
1316.9 ± 0.9 OUR AVERAGE Includes data from the 4 datablocks that follow this one. Error includes scale factor of 1.9. See the ideogram below.



3π MODE

VALUE (MeV) EVTS DOCUMENT ID TECN CHG COMMENT
 The data in this block is included in the average printed for a previous datablock.

1318.6 ± 1.3 OUR AVERAGE Error includes scale factor of 1.4. See the ideogram below.

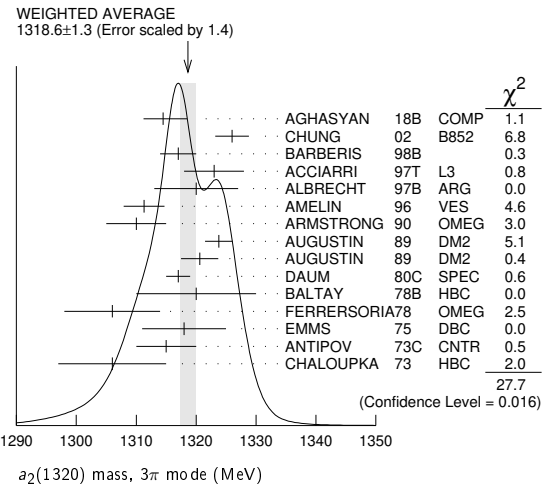
1314.5 ± 4.0 3.3	46M	¹ AGHASYAN	18B	COMP	190 $\pi^- p \rightarrow \pi^- \pi^+ \pi^- p$
1326 ± 2 ± 2		CHUNG	02	B852	18.3 $\pi^- p \rightarrow \pi^+ \pi^- \pi^- p$
1317 ± 3		BARBERIS	98B		45.0 $p p \rightarrow \rho_f \pi^+ \pi^- \pi^0 p_s$
1323 ± 4 ± 3		ACCIARRI	97T	L3	$e^+ e^- \rightarrow \pi^+ \pi^- \pi^0$
1320 ± 7		ALBRECHT	97B	ARG	$e^+ e^- \rightarrow \pi^+ \pi^- \pi^0$
1311.3 ± 1.6 ± 3.0	72.4k	AMELIN	96	VES	36 $\pi^- p \rightarrow \pi^+ \pi^- \pi^0 n$
1310 ± 5		ARMSTRONG	90	OMEG 0	300.0 $p p \rightarrow \rho \pi^+ \pi^- \pi^0$
1323.8 ± 2.3	4022	AUGUSTIN	89	DM2 ±	$J/\psi \rightarrow \rho^\pm a_2^\mp$
1320.6 ± 3.1	3562	AUGUSTIN	89	DM2 0	$J/\psi \rightarrow \rho^0 a_2^0$
1317 ± 2	25k	² DAUM	80C	SPEC	63,94 $\pi^- p \rightarrow 3\pi p$
1320 ± 10	1097	² BALTAY	78B	HBC +0	15 $\pi^+ p \rightarrow \rho 4\pi$
1306 ± 8		FERRERSORIA	78	OMEG -	9 $\pi^- p \rightarrow \rho 3\pi$
1318 ± 7	1.6k	² EMMS	75	DBC 0	4 $\pi^+ n \rightarrow \rho(3\pi)^0$
1315 ± 5		² ANTIPOV	73C	CNTR -	25,40 $\pi^- p \rightarrow \rho \eta \pi^-$
1306 ± 9	1580	CHALOUKPA	73	HBC -	3.9 $\pi^- p$

••• We do not use the following data for averages, fits, limits, etc. •••

1321 ± 1 ± 0 -7	420k	³ ALEKSEEV	10	COMP	190 $\pi^- p \rightarrow \pi^- \pi^+ \pi^+ p b'$
1300 ± 2 ± 4	18k	⁴ SCHEGELSKY	06	RVUE 0	$\gamma \gamma \rightarrow \pi^+ \pi^- \pi^0$
1305 ± 14		CONDO	93	SHF	$\gamma p \rightarrow n \pi^+ \pi^+ \pi^-$
1310 ± 2		² EVANGELIS...	81	OMEG -	12 $\pi^- p \rightarrow 3\pi p$
1343 ± 11	490	BALTAY	78B	HBC 0	15 $\pi^+ p \rightarrow \Delta 3\pi$

1309 ± 5	5k	BINNIE	71	MMS -	$\pi^- p$ near a_2 thresh-old
1299 ± 6	28k	BOWEN	71	MMS -	5 $\pi^- p$
1300 ± 6	24k	BOWEN	71	MMS +	5 $\pi^+ p$
1309 ± 4	17k	BOWEN	71	MMS -	7 $\pi^- p$
1306 ± 4	941	ALSTON...	70	HBC +	7.0 $\pi^+ p \rightarrow 3\pi p$

- 1 Statistical error negligible.
- 2 From a fit to $J^P = 2^+ \rho \pi$ partial wave.
- 3 Superseded by AGHASYAN 2018B.
- 4 From analysis of L3 data at 183-209 GeV.



$K\bar{K}$ MODE

VALUE (MeV) EVTS DOCUMENT ID TECN CHG COMMENT
 The data in this block is included in the average printed for a previous datablock.

1318.1 ± 0.7 OUR AVERAGE

1319 ± 5	4700	^{1,2} CLELAND	82B	SPEC +	50 $\pi^+ p \rightarrow K_S^0 K^+ p$
1324 ± 6	5200	^{1,2} CLELAND	82B	SPEC -	50 $\pi^- p \rightarrow K_S^0 K^- p$
1320 ± 2	4000	CHABAUD	80	SPEC -	17 $\pi^- A \rightarrow K_S^0 K^- A$
1312 ± 4	11000	CHABAUD	78	SPEC -	9.8 $\pi^- p \rightarrow K^- K_S^0 p$
1316 ± 2	4730	CHABAUD	78	SPEC -	18.8 $\pi^- p \rightarrow K^- K_S^0 p$
1318 ± 1		^{1,3} MARTIN	78D	SPEC -	10 $\pi^- p \rightarrow K_S^0 K^- p$
1320 ± 2	2724	MARGULIE	76	SPEC -	23 $\pi^- p \rightarrow K^- K_S^0 p$
1313 ± 4	730	FOLEY	72	CNTR -	20.3 $\pi^- p \rightarrow K^- K_S^0 p$
1319 ± 3	1500	³ GRAYER	71	ASPK -	17.2 $\pi^- p \rightarrow K^- K_S^0 p$

••• We do not use the following data for averages, fits, limits, etc. •••

1304 ± 10	870	⁴ SCHEGELSKY	06A	RVUE 0	$\gamma \gamma \rightarrow K_S^0 K_S^0$
1330 ± 11	1000	^{1,2} CLELAND	82B	SPEC +	30 $\pi^+ p \rightarrow K_S^0 K^+ p$
1324 ± 5	350	HYAMS	78	ASPK +	12.7 $\pi^+ p \rightarrow K^+ K_S^0 p$

- 1 From a fit to $J^P = 2^+$ partial wave.
- 2 Number of events evaluated by us.
- 3 Systematic error in mass scale subtracted.
- 4 From analysis of L3 data at 91 and 183-209 GeV.

$\eta \pi$ MODE

VALUE (MeV) EVTS DOCUMENT ID TECN CHG COMMENT
 The data in this block is included in the average printed for a previous datablock.

1312.2 ± 2.8 OUR AVERAGE Error includes scale factor of 2.6. See the ideogram below.

1306.0 ± 0.8 ± 1.3		¹ RODAS	19	JPAC	191 $\pi^- p \rightarrow \eta^{(\prime)} \pi^- p$
1308 ± 9		BARBERIS	00H		45.0 $p p \rightarrow \rho_f \eta \pi^0 p_s$
1316 ± 9		BARBERIS	00H		45.0 $p p \rightarrow \Delta_f^+ \eta \pi^- p_s$
1317 ± 1 ± 2		THOMPSON	97	MPS	18 $\pi^- p \rightarrow \eta \pi^- p$
1315 ± 5 ± 2		² AMSLER	94D	CBAR	0.0 $\bar{p} p \rightarrow \pi^0 \pi^0 \eta$
1325.1 ± 5.1		AOYAGI	93	BKEI	$\pi^- p \rightarrow \eta \pi^- p$
1317.7 ± 1.4 ± 2.0		BELADIDZE	93	VES	37 $\pi^- N \rightarrow \eta \pi^- N$
1323 ± 8	1000	³ KEY	73	OSPK -	6 $\pi^- p \rightarrow \rho \pi^- \eta$

••• We do not use the following data for averages, fits, limits, etc. •••

1307 ± 1 ± 6		⁴ JACKURA	18	JPAC	$\pi^- p \rightarrow \eta \pi^- p$
1315 ± 12		⁵ ADOLPH	15	COMP	191 $\pi^- p \rightarrow \eta^{(\prime)} \pi^- p$
1309 ± 4		ANISOVICH	09	RVUE	$\bar{p} p, \pi N$
1324 ± 5		ARMSTRONG	93C	E760 0	$\bar{p} p \rightarrow \pi^0 \eta \eta \rightarrow 6\gamma$
1336.2 ± 1.7	2561	DELFOSE	81	SPEC +	$\pi^\pm p \rightarrow \rho \pi^\pm \eta$
1330.7 ± 2.4	1653	DELFOSE	81	SPEC -	$\pi^\pm p \rightarrow \rho \pi^\pm \eta$
1324 ± 8	6200	^{3,6} CONFORTO	73	OSPK -	6 $\pi^- p \rightarrow p \pi^- \eta$

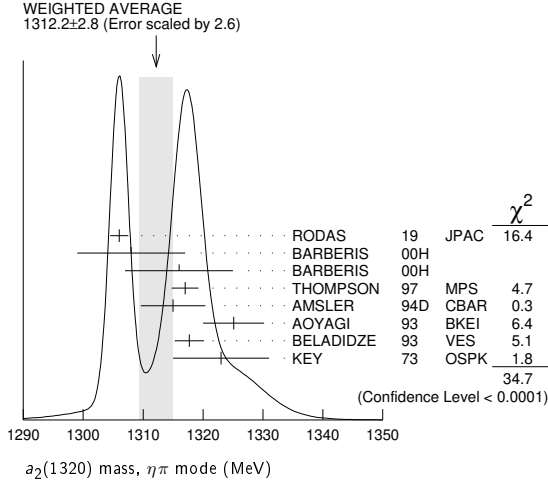
- 1 The coupled-channel analysis of both the $\eta \pi$ and $\eta' \pi$ systems using ADOLPH 15data. The mass is extracted from the T-matrix pole.
- 2 The systematic error of 2 MeV corresponds to the spread of solutions.
- 3 Error includes 5 MeV systematic mass-scale error.
- 6 From analysis of L3 data at 183-209 GeV.

See key on page 999

Meson Particle Listings

$a_2(1320)$

- ⁴ Superseded by RODAS 19.
- ⁵ ADOLPH 15 value is derived from a Breit-Wigner fit with mass-dependent width taking the $\eta\pi$ and $\rho\pi$ channels into account.
- ⁶ Missing mass with enriched MMS = $\eta\pi^-$, $\eta = 2\gamma$.



η/π MODE

VALUE (MeV)	DOCUMENT ID	TECN	COMMENT
-------------	-------------	------	---------

The data in this block is included in the average printed for a previous datablock.

1322 ± 7 OUR AVERAGE

1318 ± 8 ⁺³ ₋₅	IVANOV	01	B852	18 $\pi^- p \rightarrow \eta' \pi^- p$
1327.0 ± 10.7	BELADIDZE	93	VES	37 $\pi^- N \rightarrow \eta' \pi^- N$

$a_2(1320)$ WIDTH

3 π MODE

VALUE (MeV)	EVTS	DOCUMENT ID	TECN	CHG	COMMENT
-------------	------	-------------	------	-----	---------

105.0⁺ ± 1.7 OUR AVERAGE

106.6 ⁺ ± 3.4 _{-7.0}	46M	¹ AGHASYAN	18B	COMP	190 $\pi^- p \rightarrow \pi^- \pi^+ \pi^- p$
108 ± 3 ± 15		CHUNG	02	B852	18.3 $\pi^- p \rightarrow \pi^+ \pi^- \pi^- p$
120 ± 10		BARBERIS	98B		450 $\rho p \rightarrow \rho_f \pi^+ \pi^- \pi^0 \rho_S$
105 ± 10 ± 11		ACCIARRI	97T	L3	$e^+ e^- \rightarrow \pi^+ \pi^- \pi^0$
120 ± 10		ALBRECHT	97B	ARG	$e^+ e^- \rightarrow \pi^+ \pi^- \pi^0$
103.0 ± 6.0 ± 3.3	72.4k	AMELIN	96	VES	36 $\pi^- p \rightarrow \pi^+ \pi^- \pi^0 n$
120 ± 10		ARMSTRONG	90	OMEG 0	300.0 $\rho p \rightarrow \rho p \pi^+ \pi^- \pi^0$
107.0 ± 9.7	4022	AUGUSTIN	89	DM2 ±	$J/\psi \rightarrow \rho^\pm a_2^\mp$
118.5 ± 12.5	3562	AUGUSTIN	89	DM2 0	$J/\psi \rightarrow \rho^0 a_2^0$
97 ± 5		² EVANGELIS...	81	OMEG -	12 $\pi^- p \rightarrow 3\pi p$
96 ± 9	25k	² DAUM	80C	SPEC -	63,94 $\pi^- p \rightarrow 3\pi p$
110 ± 15	1097	² BALTAY	78B	HBC +0	15 $\pi^+ p \rightarrow p4\pi$
112 ± 18	1.6k	² EMMS	75	DBC 0	4 $\pi^+ n \rightarrow \rho(3\pi)^0$
122 ± 14	1.2k	^{2,3} WAGNER	75	HBC 0	7 $\pi^+ p \rightarrow \Delta^{++}(3\pi)^0$
115 ± 15		² ANTIPOV	73C	CNTR -	25,40 $\pi^- p \rightarrow \rho\eta\pi^-$
99 ± 15	1580	CHALOUPKA	73	HBC -	3.9 $\pi^- p$
105 ± 5	28k	BOWEN	71	MMS -	5 $\pi^- p$
99 ± 5	24k	BOWEN	71	MMS +	5 $\pi^+ p$
103 ± 5	17k	BOWEN	71	MMS -	7 $\pi^- p$

- • • We do not use the following data for averages, fits, limits, etc. • • •
- 110 ± 2 ⁺²₋₁₅ 420k ⁴ ALEKSEEV 10 COMP 190 $\pi^- Pb \rightarrow \pi^- \pi^- \pi^+ Pb'$
- 117 ± 6 ± 20 18k ⁵ SCHEGELSKY 06 RVUE 0 $\gamma\gamma \rightarrow \pi^+ \pi^- \pi^0$
- 120 ± 40 CONDO 93 SHF $\gamma p \rightarrow n\pi^+ \pi^+ \pi^-$
- 115 ± 14 490 BALTAY 78B HBC 0 15 $\pi^+ p \rightarrow \Delta 3\pi$
- 72 ± 16 5k BINNIE 71 MMS - $\pi^- p$ near a_2 thresh-old
- 79 ± 12 941 ALSTON... 70 HBC + 7.0 $\pi^+ p \rightarrow 3\pi p$

¹ Statistical error negligible.
² From a fit to $J^P = 2^+ \rho\pi$ partial wave.
³ Width errors enlarged by us to $4\Gamma/\sqrt{N}$; see the note with the $K^*(892)$ mass.
⁴ Superseded by AGHASYAN 2018B.
⁵ From analysis of L3 data at 183–209 GeV.

$K\bar{K}$ AND $\eta\pi$ MODES

VALUE (MeV)	DOCUMENT ID
-------------	-------------

107 ± 5 OUR ESTIMATE

112.5 ± 1.2 OUR AVERAGE Includes data from the 2 datablocks that follow this one.

$K\bar{K}$ MODE

VALUE (MeV)	EVTS	DOCUMENT ID	TECN	CHG	COMMENT
-------------	------	-------------	------	-----	---------

The data in this block is included in the average printed for a previous datablock.

109.8 ± 2.4 OUR AVERAGE

112 ± 20	4700	^{1,2} CLELAND	82B	SPEC +	50 $\pi^+ p \rightarrow K_S^0 K^+ p$
120 ± 25	5200	^{1,2} CLELAND	82B	SPEC -	50 $\pi^- p \rightarrow K_S^0 K^- p$
106 ± 4	4000	CHABAUD	80	SPEC -	17 $\pi^- A \rightarrow K_S^0 K^- A$
126 ± 11	11000	CHABAUD	78	SPEC -	9.8 $\pi^- p \rightarrow K^- K_S^0 p$
101 ± 8	4730	CHABAUD	78	SPEC -	18.8 $\pi^- p \rightarrow K^- K_S^0 p$
113 ± 4		^{1,3} MARTIN	78D	SPEC -	10 $\pi^- p \rightarrow K_S^0 K^- p$
105 ± 8	2724	³ MARGULIE	76	SPEC -	23 $\pi^- p \rightarrow K^- K_S^0 p$
113 ± 19	730	FOLEY	72	CNTR -	20.3 $\pi^- p \rightarrow K^- K_S^0 p$
123 ± 13	1500	³ GRAYER	71	ASPK -	17.2 $\pi^- p \rightarrow K^- K_S^0 p$
• • •		We do not use the following data for averages, fits, limits, etc. • • •			
120 ± 15	870	⁴ SCHEGELSKY	06A	RVUE 0	$\gamma\gamma \rightarrow K_S^0 K_S^0$
121 ± 51	1000	^{1,2} CLELAND	82B	SPEC +	30 $\pi^+ p \rightarrow K_S^0 K^+ p$
110 ± 18	350	HYAMS	78	ASPK +	12.7 $\pi^+ p \rightarrow K^+ K_S^0 p$

¹ From a fit to $J^P = 2^+$ partial wave.
² Number of events evaluated by us.
³ Width errors enlarged by us to $4\Gamma/\sqrt{N}$; see the note with the $K^*(892)$ mass.
⁴ From analysis of L3 data at 91 and 183–209 GeV.

$\eta\pi$ MODE

VALUE (MeV)	EVTS	DOCUMENT ID	TECN	CHG	COMMENT
-------------	------	-------------	------	-----	---------

The data in this block is included in the average printed for a previous datablock.

113.4 ± 1.3 OUR AVERAGE

114.4 ± 1.6 ± 0.0		¹ RODAS	19	JPAC	191 $\pi^- p \rightarrow \eta^{(\prime)} \pi^- p$
115 ± 20		BARBERIS	00H		450 $\rho p \rightarrow \rho_f \eta \pi^0 \rho_S$
112 ± 14		BARBERIS	00H		450 $\rho p \rightarrow \Delta_f^{++} \eta \pi^- \rho_S$
112 ± 3 ± 2		² AMSLER	94D	CBAR	0.0 $\bar{p} p \rightarrow \pi^0 \pi^0 \eta$
103 ± 6 ± 3		BELADIDZE	93	VES	37 $\pi^- N \rightarrow \eta \pi^- N$
112.2 ± 5.7	2561	DELFOSSÉ	81	SPEC +	$\pi^\pm p \rightarrow \rho \pi^\pm \eta$
116.6 ± 7.7	1653	DELFOSSÉ	81	SPEC -	$\pi^\pm p \rightarrow \rho \pi^\pm \eta$
108 ± 9	1000	KEY	73	OSPK -	6 $\pi^- p \rightarrow \rho \pi^- \eta$
• • •		We do not use the following data for averages, fits, limits, etc. • • •			
112 ± 1 ± 8		³ JACKURA	18	JPAC	$\pi^- p \rightarrow \eta \pi^- p$
119 ± 14		⁴ ADOLPH	15	COMP	191 $\pi^- p \rightarrow \eta^{(\prime)} \pi^- p$
110 ± 4		ANISOVICH	09	RVUE	$\bar{p} p, \pi N$
127 ± 2 ± 2		⁵ THOMPSON	97	MPS	18 $\pi^- p \rightarrow \eta \pi^- p$
118 ± 10		ARMSTRONG	93C	E760 0	$\bar{p} p \rightarrow \pi^0 \eta \eta \rightarrow 6\gamma$
104 ± 9	6200	⁶ CONFORTO	73	OSPK -	6 $\pi^- p \rightarrow \rho M M^-$

¹ The coupled-channel analysis of both the $\eta\pi$ and $\eta'\pi$ systems using ADOLPH 15 data. The width is extracted from the T-matrix pole.
² The systematic error of 2 MeV corresponds to the spread of solutions.
³ Superseded by RODAS 19.
⁴ ADOLPH 15 value is derived from a Breit-Wigner fit with mass-dependent width taking the $\eta\pi$ and $\rho\pi$ channels into account.
⁵ Resolution is not unfolded.
⁶ Missing mass with enriched MMS = $\eta\pi^-$, $\eta = 2\gamma$.

η/π MODE

VALUE (MeV)	DOCUMENT ID	TECN	COMMENT
-------------	-------------	------	---------

119 ± 25 OUR AVERAGE

140 ± 35 ± 20	IVANOV	01	B852	18 $\pi^- p \rightarrow \eta' \pi^- p$
106 ± 32	BELADIDZE	93	VES	37 $\pi^- N \rightarrow \eta' \pi^- N$

$a_2(1320)$ DECAY MODES

Mode	Fraction (Γ_i/Γ)	Scale factor/Confidence level
Γ_1 3 π	(70.1 ± 2.7) %	S=1.2
Γ_2 $\rho(770)\pi$		
Γ_3 $f_2(1270)\pi$		
Γ_4 $\rho(1450)\pi$		
Γ_5 $\eta\pi$	(14.5 ± 1.2) %	
Γ_6 $\omega\pi\pi$	(10.6 ± 3.2) %	S=1.3
Γ_7 $K\bar{K}$	(4.9 ± 0.8) %	
Γ_8 $\eta'(958)\pi$	(5.5 ± 0.9) × 10 ⁻³	
Γ_9 $\pi^\pm\gamma$	(2.91 ± 0.27) × 10 ⁻³	
Γ_{10} $\gamma\gamma$	(9.4 ± 0.7) × 10 ⁻⁶	
Γ_{11} e^+e^-	< 5 × 10 ⁻⁹	CL=90%

Meson Particle Listings

$a_2(1320)$

CONSTRAINED FIT INFORMATION

An overall fit to 5 branching ratios uses 18 measurements and one constraint to determine 4 parameters. The overall fit has a $\chi^2 = 9.3$ for 15 degrees of freedom.

The following *off-diagonal* array elements are the correlation coefficients $\langle \delta x_i \delta x_j \rangle / (\delta x_i \delta x_j)$, in percent, from the fit to the branching fractions, $x_i \equiv \Gamma_i / \Gamma_{\text{total}}$. The fit constrains the x_i whose labels appear in this array to sum to one.

x_5	10		
x_6	-89	-46	
x_7	-1	-2	-24
	x_1	x_5	x_6

$a_2(1320)$ PARTIAL WIDTHS

$\Gamma(\eta\pi)$	Γ_5				
VALUE (MeV)	EVTS	DOCUMENT ID	TECN	CHG	COMMENT
••• We do not use the following data for averages, fits, limits, etc. •••					
18.5 ± 3.0	870	¹ SCHEGELSKY 06A	RVUE	0	$\gamma\gamma \rightarrow K_S^0 K_S^0$
¹ From analysis of L3 data at 91 and 183–209 GeV, using $\Gamma(a_2(1320) \rightarrow \gamma\gamma) = 0.91$ keV and SU(3) relations.					

$\Gamma(K\bar{K})$	Γ_7				
VALUE (MeV)	EVTS	DOCUMENT ID	TECN	CHG	COMMENT
••• We do not use the following data for averages, fits, limits, etc. •••					
7.0 $^{+2.0}_{-1.5}$	870	¹ SCHEGELSKY 06A	RVUE	0	$\gamma\gamma \rightarrow K^0 \bar{K}_S^0$
¹ From analysis of L3 data at 91 and 183–209 GeV, using $\Gamma(a_2(1320) \rightarrow \gamma\gamma) = 0.91$ keV and SU(3) relations.					

$\Gamma(\pi^\pm\gamma)$	Γ_9				
VALUE (keV)	EVTS	DOCUMENT ID	TECN	CHG	COMMENT
311 ± 25 OUR AVERAGE					
358 ± 6 ± 42		¹ ADOLPH 14	COMP	-	190 $\pi^- \text{Pb} \rightarrow \pi^+ \pi^- \pi^- \text{Pb}'$
284 ± 25 ± 25	7.1k	MOLCHANOV 01	SELX		600 $\pi^- \text{A} \rightarrow \pi^+ \pi^- \pi^- \text{A}$
295 ± 60		CIHANGIR 82	SPEC	+	200 $\pi^+ \text{A}$
••• We do not use the following data for averages, fits, limits, etc. •••					
461 ± 110		² MAY 77	SPEC	±	9.7 γA
¹ Primakoff reaction using $a_2(1320) \rightarrow 3\pi$ branching ratio of 70.1%.					
² Assuming one-pion exchange.					

$\Gamma(\gamma\gamma)$	Γ_{10}				
VALUE (keV)	EVTS	DOCUMENT ID	TECN	CHG	COMMENT
1.00 ± 0.06 OUR AVERAGE					
0.98 ± 0.05 ± 0.09		ACCIARRI 97T	L3		$e^+e^- \rightarrow e^+e^- \pi^+ \pi^- \pi^0$
0.96 ± 0.03 ± 0.13		ALBRECHT 97b	ARG		$e^+e^- \rightarrow e^+e^- \pi^+ \pi^- \pi^0$
1.26 ± 0.26 ± 0.18	36	BARU 90	MD1		$e^+e^- \rightarrow e^+e^- \pi^+ \pi^- \pi^0$
1.00 ± 0.07 ± 0.15	415	BEHREND 90c	CELL	0	$e^+e^- \rightarrow e^+e^- \pi^+ \pi^- \pi^0$
1.03 ± 0.13 ± 0.21		BUTLER 90	MRK2		$e^+e^- \rightarrow e^+e^- \pi^+ \pi^- \pi^0$
1.01 ± 0.14 ± 0.22	85	OEST 90	JADE		$e^+e^- \rightarrow e^+e^- \pi^0 \eta$
0.90 ± 0.27 ± 0.15	56	¹ ALTHOFF 86	TASS	0	$e^+e^- \rightarrow e^+e^- 3\pi$
1.14 ± 0.20 ± 0.26		² ANTREASYSAN 86	CBAL	0	$e^+e^- \rightarrow e^+e^- \pi^0 \eta$
1.06 ± 0.18 ± 0.19		BERGER 84c	PLUT	0	$e^+e^- \rightarrow e^+e^- 3\pi$
••• We do not use the following data for averages, fits, limits, etc. •••					
0.81 ± 0.19 $^{+0.42}_{-0.11}$	35	¹ BEHREND 82c	CELL	0	$e^+e^- \rightarrow e^+e^- 3\pi$
0.77 ± 0.18 ± 0.27	22	² EDWARDS 82f	CBAL	0	$e^+e^- \rightarrow e^+e^- \pi^0 \eta$
¹ From $\rho\pi$ decay mode.					
² From $\eta\pi^0$ decay mode.					

$\Gamma(e^+e^-)$	Γ_{11}			
VALUE (eV)	CL%	DOCUMENT ID	TECN	COMMENT
< 0.56	90	ACHASOV 00k	SND	$e^+e^- \rightarrow \pi^0 \pi^0$
••• We do not use the following data for averages, fits, limits, etc. •••				
< 25	90	VOROBYEV 88	ND	$e^+e^- \rightarrow \pi^0 \eta$

$a_2(1320)$ $\Gamma(i)\Gamma(\gamma\gamma)/\Gamma(\text{total})$

$\Gamma(3\pi) \times \Gamma(\gamma\gamma)/\Gamma_{\text{total}}$	$\Gamma_1\Gamma_{10}/\Gamma$			
VALUE (keV)	EVTS	DOCUMENT ID	TECN	COMMENT
••• We do not use the following data for averages, fits, limits, etc. •••				
0.65 ± 0.02 ± 0.02	18k	¹ SCHEGELSKY 06	RVUE	$\gamma\gamma \rightarrow \pi^+ \pi^- \pi^0$
¹ From analysis of L3 data at 183–209 GeV.				

$\Gamma(\eta\pi) \times \Gamma(\gamma\gamma)/\Gamma_{\text{total}}$	$\Gamma_5\Gamma_{10}/\Gamma$		
VALUE (keV)	DOCUMENT ID	TECN	COMMENT
••• We do not use the following data for averages, fits, limits, etc. •••			
0.145 $^{+0.097}_{-0.034}$	¹ UEHARA 09A	BELL	$e^+e^- \rightarrow e^+e^- \eta \pi^0$
¹ From the D_2 -wave. The fraction of the D_0 -wave is $3.4^{+2.3\%}_{-1.1\%}$.			

$\Gamma(K\bar{K}) \times \Gamma(\gamma\gamma)/\Gamma_{\text{total}}$	$\Gamma_7\Gamma_{10}/\Gamma$		
VALUE (keV)	DOCUMENT ID	TECN	COMMENT
0.126 ± 0.007 ± 0.028	¹ ALBRECHT 90G	ARG	$e^+e^- \rightarrow e^+e^- K^+ K^-$
••• We do not use the following data for averages, fits, limits, etc. •••			
0.081 ± 0.006 ± 0.027	² ALBRECHT 90G	ARG	$e^+e^- \rightarrow e^+e^- K^+ K^-$
¹ Using an incoherent background.			
² Using a coherent background.			

$a_2(1320)$ BRANCHING RATIOS

$[\Gamma(\rho(1270)\pi) + \Gamma(\rho(1450)\pi)] / \Gamma(\rho(770)\pi)$	$(\Gamma_3 + \Gamma_4) / \Gamma_2$				
VALUE	CL%	DOCUMENT ID	TECN	CHG	COMMENT
< 0.12	90	ABRAMOVI... 70B	HBC	-	3.93 $\pi^- p$

$\Gamma(\rho(770)\pi) / \Gamma(\rho(1270)\pi)$	Γ_2 / Γ_3			
VALUE	EVTS	DOCUMENT ID	TECN	COMMENT
16.5 $^{+1.2}_{-2.4}$	46M	¹ AGHASYAN 18B	COMP	190 $\pi^- p \rightarrow \pi^- \pi^+ \pi^- p$
¹ Statistical error negligible.				

$\Gamma(\eta\pi) / \Gamma(3\pi)$	Γ_5 / Γ_1				
VALUE	EVTS	DOCUMENT ID	TECN	CHG	COMMENT
0.207 ± 0.018 OUR FIT					
0.213 ± 0.020 OUR AVERAGE					
0.18 ± 0.05		FORINO 76	HBC		11 $\pi^- p$
0.22 ± 0.05	52	ANTIPOV 73	CNTR	-	40 $\pi^- p$
0.211 ± 0.044	149	CHALOUKPA 73	HBC	-	3.9 $\pi^- p$
0.246 ± 0.042	167	ALSTON-... 71	HBC	+	7.0 $\pi^+ p$
0.25 ± 0.09	15	BOECKMANN 70	HBC	+	5.0 $\pi^+ p$
0.23 ± 0.08	22	ASCOLI 68	HBC	-	5 $\pi^- p$
0.12 ± 0.08		CHUNG 68	HBC	-	3.2 $\pi^- p$
0.22 ± 0.09		CONTE 67	HBC	-	11.0 $\pi^- p$

$\Gamma(\omega\pi\pi) / \Gamma(3\pi)$	Γ_6 / Γ_1				
VALUE	EVTS	DOCUMENT ID	TECN	CHG	COMMENT
0.15 ± 0.05 OUR FIT					Error includes scale factor of 1.3.
0.15 ± 0.05 OUR AVERAGE					Error includes scale factor of 1.3. See the ideogram below.
0.28 ± 0.09	60	DIAZ 74	DBC	0	6 $\pi^+ n$
0.18 ± 0.08		¹ KARSHON 74	HBC		Avg. of above two
0.10 ± 0.05	279	² CHALOUKPA 73	HBC	-	3.9 $\pi^- p$
••• We do not use the following data for averages, fits, limits, etc. •••					
0.29 ± 0.08	140	¹ KARSHON 74	HBC	+	4.9 $\pi^+ p$
0.10 ± 0.04	60	¹ KARSHON 74	HBC	+	4.9 $\pi^+ p$
0.19 ± 0.08		DEFOIX 73	HBC	0	0.7 $\bar{p} p$
¹ KARSHON 74 suggest an additional $l = 0$ state strongly coupled to $\omega\pi\pi$ which could explain discrepancies in branching ratios and masses. We use a central value and a systematic spread.					
² Decays to $b_1(1040)\pi$, $b_1 \rightarrow \omega\pi$. Error increased to account for possible systematic errors of complicated analysis.					



Meson Particle Listings
a₂(1320), f₀(1370)

Γ(KK̄)/Γ(3π) Γ₇/Γ₁

Table with columns: VALUE, EVTS, DOCUMENT ID, TECN, CHG, COMMENT. Includes data for 0.070 ± 0.012 OUR FIT and 0.078 ± 0.017. Lists authors like BERTIN, CHALOUKPA, ALSTON-... and their respective document IDs and techniques.

Γ(KK̄)/Γ(ηπ) Γ₇/Γ₅

Table with columns: VALUE, DOCUMENT ID, TECN, COMMENT. Includes data for 0.08 ± 0.02. Lists authors like BERTIN and document ID 98B.

Γ(ηπ)/[Γ(3π) + Γ(ηπ) + Γ(KK̄)] Γ₅/[Γ₁ + Γ₅ + Γ₇]

Table with columns: VALUE, EVTS, DOCUMENT ID, TECN, CHG, COMMENT. Includes data for 0.162 ± 0.012 OUR FIT and 0.140 ± 0.028 OUR AVERAGE. Lists authors like ESPIGAT, BARNHAM.

Γ(KK̄)/[Γ(3π) + Γ(ηπ) + Γ(KK̄)] Γ₇/[Γ₁ + Γ₅ + Γ₇]

Table with columns: VALUE, EVTS, DOCUMENT ID, TECN, CHG, COMMENT. Includes data for 0.054 ± 0.009 OUR FIT and 0.048 ± 0.012 OUR AVERAGE. Lists authors like TOET, DAMERI, BARNHAM, ESPIGAT, etc.

Γ(η'(958)π)/Γ_{total} Γ₈/Γ

Table with columns: VALUE, CL%, DOCUMENT ID, TECN, CHG, COMMENT. Includes data for <0.006 and <0.02. Lists authors like ALDE, BARNHAM, BOESEBECK.

Γ(η'(958)π)/Γ(3π) Γ₈/Γ₁

Table with columns: VALUE, CL%, DOCUMENT ID, TECN, CHG, COMMENT. Includes data for <0.011 and <0.04. Lists authors like EISENSTEIN, ALSTON-..., BARNHAM, BOECKMANN.

Γ(η'(958)π)/Γ(ηπ) Γ₈/Γ₅

Table with columns: VALUE, DOCUMENT ID, TECN, COMMENT. Includes data for 0.038 ± 0.005 OUR AVERAGE. Lists authors like ADOLPH, ABELE, BELADIDZE, BOECKMANN, ASCOLI, BOESEBECK, CHUNG, CONTE.

Γ(π±π±)/Γ_{total} Γ₉/Γ

Table with columns: VALUE, DOCUMENT ID, TECN, COMMENT. Includes data for 0.005 ± 0.005. Lists authors like EISENBERG.

Γ(e+e-)/Γ_{total} Γ₁₁/Γ

Table with columns: VALUE (units 10^-9), CL%, DOCUMENT ID, TECN, COMMENT. Includes data for <6. Lists authors like ACHASOV.

a₂(1320) REFERENCES

List of references for a₂(1320) and f₀(1370) decays. Includes authors like Rodas, Aghasyan, Jackura, Adolph, etc., and their respective document IDs and techniques.

f₀(1370)

I_G(J^{PC}) = 0⁺(0⁺ +)

See the review on "Scalar Mesons below 2 GeV" and a note on "Non-q \bar{q} Candidates" in PDG 06, Journal of Physics G33 1 (2006).

f₀(1370) T-MATRIX POLE POSITION

Note that Γ ≈ 2 Im(√s_{pole}).

Table with columns: VALUE (MeV), DOCUMENT ID, TECN, COMMENT. Includes data for (1290 ± 50) - i(170 ± 20) and other pole positions. Lists authors like ANISOVICH, BARGIOTTI, BARBERIS, KAMINSKI, ANISOVICH, BARBERIS.

Downloaded from https://academic.oup.com/ptep/article/2020/8/083C01/5891211 by guest on 20 August 2020

Meson Particle Listings

 $f_0(1370)$

(1548 ± 40) - i(560 ± 40)	BERTIN	97c	OBLX	0.0 $\bar{p}p \rightarrow \pi^+ \pi^- \pi^0$
(1380 ± 40) - i(180 ± 25)	ABELE	96b	CBAR	0.0 $\bar{p}p \rightarrow \pi^0 K_L^0 K_L^0$
(1300 ± 15) - i(115 ± 8)	BUGG	96	RVUE	
(1330 ± 50) - i(150 ± 40)	⁵ AMSLER	95b	CBAR	$\bar{p}p \rightarrow 3\pi^0$
(1360 ± 35) - i(150-300)	⁵ AMSLER	95c	CBAR	$\bar{p}p \rightarrow \pi^0 \eta \eta$
(1390 ± 30) - i(190 ± 40)	⁶ AMSLER	95d	CBAR	$\bar{p}p \rightarrow 3\pi^0, \pi^0 \eta \eta,$ $\pi^0 \pi^0 \eta$
1346 - i249	^{7,8} JANSSEN	95	RVUE	$\pi \pi \rightarrow \pi \pi, K \bar{K}$
1214 - i168	^{8,9} TORNQVIST	95	RVUE	$\pi \pi \rightarrow \pi \pi, K \bar{K}, K \pi,$ $\eta \pi$
1364 - i139	AMSLER	94d	CBAR	$\bar{p}p \rightarrow \pi^0 \pi^0 \eta$
(1365 ⁺²⁰ ₋₅₅) - i(134 ± 35)	ANISOVICH	94	CBAR	$\bar{p}p \rightarrow 3\pi^0, \pi^0 \eta \eta$
(1340 ± 40) - i(127 ⁺³⁰ ₋₂₀)	¹⁰ BUGG	94	RVUE	$\bar{p}p \rightarrow 3\pi^0, \eta \eta \pi^0,$ $\eta \pi^0 \pi^0$
(1430 ± 5) - i(73 ± 13)	¹¹ KAMINSKI	94	RVUE	$\pi \pi \rightarrow \pi \pi, K \bar{K}$
1420 - i220	¹² AU	87	RVUE	$\pi \pi \rightarrow \pi \pi, K \bar{K}$

- ¹ Another pole is found at $(1510 \pm 130) - i(800^{+100}_{-150})$ MeV.
² Coupled channel analysis of $\pi^+ \pi^- \pi^0, K^+ K^- \pi^0,$ and $K^\pm K_S^0 \pi^\mp$.
³ Average between $\pi^+ \pi^- 2\pi^0$ and $2(\pi^+ \pi^-)$.
⁴ T-matrix pole on sheet ---.
⁵ Supersedes ANISOVICH 94.
⁶ Coupled-channel analysis of $\bar{p}p \rightarrow 3\pi^0, \pi^0 \eta \eta,$ and $\pi^0 \pi^0 \eta$ on sheet IV. Demonstrates explicitly that $f_0(500)$ and $f_0(1370)$ are two different poles.
⁷ Analysis of data from FALVARD 88.
⁸ The pole is on Sheet III. Demonstrates explicitly that $f_0(500)$ and $f_0(1370)$ are two different poles.
⁹ Uses data from BEIER 72b, OCHS 73, HYAMS 73, GRAY 74, ROSSELET 77, CASON 83, ASTON 88, and ARMSTRONG 91b. Coupled channel analysis with flavor symmetry and all light two-pseudoscalars systems.
¹⁰ Reanalysis of ANISOVICH 94 data.
¹¹ T-matrix pole on sheet III.
¹² Analysis of data from OCHS 73, GRAY 74, BECKER 79, and CASON 83.

 $f_0(1370)$ BREIT-WIGNER MASS OR K-MATRIX POLE PARAMETER

VALUE (MeV)	DOCUMENT ID
1200 to 1500 OUR ESTIMATE	
$\pi\pi$ MODE	
VALUE (MeV)	EVTS DOCUMENT ID TECN COMMENT
1400 ± 40	¹ AUBERT 09L BABR $B^\pm \rightarrow \pi^\pm \pi^\pm \pi^\mp$
1470 ⁺⁶ ₋₇ ⁺⁷² ₋₂₅₅	² UEHARA 08A BELL $10.6 e^+ e^- \rightarrow e^+ e^- \pi^0 \pi^0$
1259 ± 55	2.6k BONVICINI 07 CLEO $D^+ \rightarrow \pi^- \pi^+ \pi^+$
1309 ± 1 ± 15	³ BUGG 07A RVUE $0.0 p\bar{p} \rightarrow 3\pi^0$
1449 ± 13	4.3k ⁴ GARMASH 06 BELL $B^+ \rightarrow K^+ \pi^+ \pi^-$
1350 ± 50	ABLIKIM 05 BES2 $J/\psi \rightarrow \phi \pi^+ \pi^-$
1265 ± 30 ⁺²⁰ ₋₃₅	ABLIKIM 05Q BES2 $\psi(2S) \rightarrow \gamma \pi^+ \pi^- K^+ K^-$
1434 ± 18 ± 9	848 AITALA 01A E791 $D_s^+ \rightarrow \pi^- \pi^+ \pi^+$
1308 ± 10	BARBERIS 99B OMEG $450 pp \rightarrow p_S p_f \pi^+ \pi^-$
1315 ± 50	BELLAZZINI 99 GAM4 $450 pp \rightarrow p p \pi^0 \pi^0$
1315 ± 30	ALDE 98 GAM4 $100 \pi^- p \rightarrow \pi^0 \pi^0 n$
1280 ± 55	BERTIN 98 OBLX $0.05-0.405 \bar{p}p \rightarrow \pi^+ \pi^+ \pi^-$
1186	^{5,6} TORNQVIST 95 RVUE $\pi \pi \rightarrow \pi \pi, K \bar{K}, K \pi, \eta \pi$
1472 ± 12	ARMSTRONG 91 OMEG $300 pp \rightarrow p p \pi \pi, p p K \bar{K}$
1275 ± 20	BREAKSTONE 90 SFM $62 pp \rightarrow p p \pi^+ \pi^-$
1420 ± 20	AKESSON 86 SPEC $63 pp \rightarrow p p \pi^+ \pi^-$
1256	FROGGATT 77 RVUE $\pi^+ \pi^-$ channel

- ¹ Breit-Wigner mass.
² Breit-Wigner mass. May also be the $f_0(1500)$.
³ Reanalysis of ABELE 96c data.
⁴ Also observed by GARMASH 07 in $B^0 \rightarrow K_S^0 \pi^+ \pi^-$ decays. Supersedes GARMASH 05.
⁵ Uses data from BEIER 72b, OCHS 73, HYAMS 73, GRAY 74, ROSSELET 77, CASON 83, ASTON 88, and ARMSTRONG 91b. Coupled channel analysis with flavor symmetry and all light two-pseudoscalars systems.
⁶ Also observed by ASNER 00 in $\tau^- \rightarrow \pi^- \pi^0 \pi^0 \nu_\tau$ decays

 $K\bar{K}$ MODE

VALUE (MeV)	EVTS DOCUMENT ID TECN COMMENT
1422 ± 15 ± 28	¹ AAIJ 19H LHCB $pp \rightarrow D^\pm X$
1360 ± 31 ± 28	4.30 ^{2,3} DOBBS 15 $J/\psi \rightarrow \gamma K^+ K^-$
1350 ± 48 ± 15	1.68 ^{2,3} DOBBS 15 $\psi(2S) \rightarrow \gamma K^+ K^-$
1440 ± 6	VLADIMIRSK...06 SPEC $40 \pi^- p \rightarrow K_S^0 K_S^0 n$
1391 ± 10	TIKHOMIROV 03 SPEC $40.0 \pi^- C \rightarrow K_S^0 K_S^0 K_L^0 X$
1440 ± 50	BOLONKIN 88 SPEC $40 \pi^- p \rightarrow K_S^0 K_S^0 n$
1463 ± 9	ETKIN 82B MPS $23 \pi^- p \rightarrow n 2K_S^0$
1425 ± 15	WICKLUND 80 SPEC $6 \pi N \rightarrow K^+ K^- N$
~ 1300	POLYCHRO... 79 STRC $7 \pi^- p \rightarrow n 2K_S^0$

- ¹ From the $D^\pm \rightarrow K^\pm K^+ K^-$ Dalitz plot fit with the isobar model A.
² Using CLEO-c data but not authorized by the CLEO Collaboration.
³ From a fit to a Breit-Wigner line shape with fixed $\Gamma = 346$ MeV.

 4π MODE $2(\pi\pi)_S + \rho\rho$

VALUE (MeV)	EVTS DOCUMENT ID TECN COMMENT
1395 ± 40	ABELE 01 CBAR $0.0 \bar{p}d \rightarrow \pi^- 4\pi^0 p$
1374 ± 38	AMSLER 94 CBAR $0.0 \bar{p}p \rightarrow \pi^+ \pi^- 3\pi^0$
1345 ± 12	ADAMO 93 OBLX $\bar{p}p \rightarrow 3\pi^+ 2\pi^-$
1386 ± 30	GASPERO 93 DBC $0.0 \bar{p}n \rightarrow 2\pi^+ 3\pi^-$
~ 1410	5751 ¹ BETTINI 66 DBC $0.0 \bar{p}n \rightarrow 2\pi^+ 3\pi^-$
¹ $\rho\rho$ dominant.	

 $\eta\eta$ MODE

VALUE (MeV)	DOCUMENT ID TECN COMMENT
1262 ⁺⁵¹ ₋₇₈ ⁺⁸² ₋₁₀₃	¹ UEHARA 10A BELL $10.6 e^+ e^- \rightarrow e^+ e^- \eta \eta$
1430	AMSLER 92 CBAR $0.0 \bar{p}p \rightarrow \pi^0 \eta \eta$
1220 ± 40	ALDE 86D GAM4 $100 \pi^- p \rightarrow n 2\eta$

- ¹ Breit-Wigner mass. May also be the $f_0(1500)$.

COUPLED CHANNEL MODE

VALUE (MeV)	DOCUMENT ID TECN COMMENT
1330.2 ^{+5.9} _{-6.5} ± 5.1	¹ AAIJ 19H LHCB $pp \rightarrow D^\pm X$
1306 ± 20	² ANISOVICH 03 RVUE
¹ From the $D^\pm \rightarrow K^\pm K^+ K^-$ Dalitz plot fit with the Triple-M amplitude in the multi-meson model of AOUDE 18. ² K-matrix pole from combined analysis of $\pi^- p \rightarrow \pi^0 \pi^0 n, \pi^- p \rightarrow K \bar{K} n, \pi^+ \pi^- \rightarrow \pi^+ \pi^-, \bar{p}p \rightarrow \pi^0 \pi^0 \pi^0, \pi^0 \eta \eta, \pi^0 \pi^0 \eta, \pi^+ \pi^- \pi^0, K^+ K^- \pi^0, K_S^0 K_S^0 \pi^0, K^+ K_S^0 \pi^-$ at rest, $\bar{p}n \rightarrow \pi^- \pi^- \pi^+, K_S^0 K^- \pi^0, K_S^0 K_S^0 \pi^-$ at rest.	

 $f_0(1370)$ BREIT-WIGNER WIDTH

VALUE (MeV)	DOCUMENT ID
200 to 500 OUR ESTIMATE	
$\pi\pi$ MODE	
VALUE (MeV)	EVTS DOCUMENT ID TECN COMMENT
300 ± 80	¹ AUBERT 09L BABR $B^\pm \rightarrow \pi^\pm \pi^\pm \pi^\mp$
90 ⁺² ₋₁ ⁺⁵⁰ ₋₂₂	² UEHARA 08A BELL $10.6 e^+ e^- \rightarrow e^+ e^- \pi^0 \pi^0$
298 ± 21	2.6k BONVICINI 07 CLEO $D^+ \rightarrow \pi^- \pi^+ \pi^+$
126 ± 25	4286 ³ GARMASH 06 BELL $B^+ \rightarrow K^+ \pi^+ \pi^-$
265 ± 40	ABLIKIM 05 BES2 $J/\psi \rightarrow \phi \pi^+ \pi^-$
350 ± 100 ⁺¹⁰⁵ ₋₆₀	ABLIKIM 05Q BES2 $\psi(2S) \rightarrow \gamma \pi^+ \pi^- K^+ K^-$
173 ± 32 ± 6	848 AITALA 01A E791 $D_s^+ \rightarrow \pi^- \pi^+ \pi^+$
222 ± 20	BARBERIS 99B OMEG $450 pp \rightarrow p_S p_f \pi^+ \pi^-$
255 ± 60	BELLAZZINI 99 GAM4 $450 pp \rightarrow p p \pi^0 \pi^0$
190 ± 50	ALDE 98 GAM4 $100 \pi^- p \rightarrow \pi^0 \pi^0 n$
323 ± 13	BERTIN 98 OBLX $0.05-0.405 \bar{p}p \rightarrow \pi^+ \pi^+ \pi^-$
350	^{4,5} TORNQVIST 95 RVUE $\pi \pi \rightarrow \pi \pi, K \bar{K}, K \pi, \eta \pi$
195 ± 33	ARMSTRONG 91 OMEG $300 pp \rightarrow p p \pi \pi, p p K \bar{K}$
285 ± 60	BREAKSTONE 90 SFM $62 pp \rightarrow p p \pi^+ \pi^-$
460 ± 50	AKESSON 86 SPEC $63 pp \rightarrow p p \pi^+ \pi^-$
~ 400	⁶ FROGGATT 77 RVUE $\pi^+ \pi^-$ channel

- ¹ The systematic errors are not reported.
² Breit-Wigner width. May also be the $f_0(1500)$.
³ Also observed by GARMASH 07 in $B^0 \rightarrow K_S^0 \pi^+ \pi^-$ decays. Supersedes GARMASH 05.
⁴ Uses data from BEIER 72b, OCHS 73, HYAMS 73, GRAY 74, ROSSELET 77, CASON 83, ASTON 88, and ARMSTRONG 91b. Coupled channel analysis with flavor symmetry and all light two-pseudoscalars systems.
⁵ Also observed by ASNER 00 in $\tau^- \rightarrow \pi^- \pi^0 \pi^0 \nu_\tau$ decays
⁶ Width defined as distance between 45 and 135° phase shift.

 $K\bar{K}$ MODE

VALUE (MeV)	DOCUMENT ID TECN COMMENT
324 ± 38 ± 42	¹ AAIJ 19H LHCB $pp \rightarrow D^\pm X$
121 ± 15	VLADIMIRSK...06 SPEC $40 \pi^- p \rightarrow K_S^0 K_S^0 n$
55 ± 26	TIKHOMIROV 03 SPEC $40.0 \pi^- C \rightarrow K_S^0 K_S^0 K_L^0 X$
250 ± 80	BOLONKIN 88 SPEC $40 \pi^- p \rightarrow K_S^0 K_S^0 n$
118 ⁺¹³⁸ ₋₁₆	ETKIN 82B MPS $23 \pi^- p \rightarrow n 2K_S^0$
160 ± 30	WICKLUND 80 SPEC $6 \pi N \rightarrow K^+ K^- N$
~ 150	POLYCHRO... 79 STRC $7 \pi^- p \rightarrow n 2K_S^0$

- ¹ From the $D^\pm \rightarrow K^\pm K^+ K^-$ Dalitz plot fit with the isobar model A.

 4π MODE $2(\pi\pi)_S + \rho\rho$

VALUE (MeV)	EVTS DOCUMENT ID TECN COMMENT
275 ± 55	ABELE 01 CBAR $0.0 \bar{p}d \rightarrow \pi^- 4\pi^0 p$

375 ± 61	AMSLER	94	CBAR	0.0	$\bar{p}p \rightarrow \pi^+ \pi^- 3\pi^0$	
398 ± 26	ADAMO	93	OBLX		$\bar{p}p \rightarrow 3\pi^+ 2\pi^-$	
310 ± 50	GASPERO	93	DBC	0.0	$\bar{p}n \rightarrow 2\pi^+ 3\pi^-$	
~ 90	5751	¹ BETTINI	66	DBC	0.0	$\bar{p}n \rightarrow 2\pi^+ 3\pi^-$

¹ $\rho\rho$ dominant.

$\eta\eta$ MODE

VALUE (MeV)	DOCUMENT ID	TECN	COMMENT
• • •	We do not use the following data for averages, fits, limits, etc. • • •		
484 +246 +246 -170 -263	¹ UEHARA	10A	BELL 10.6 $e^+e^- \rightarrow e^+e^-\eta\eta$
250	AMSLER	92	CBAR 0.0 $\bar{p}p \rightarrow \pi^0\eta\eta$
320 ± 40	ALDE	86D	GAM4 100 $\pi^-\rho \rightarrow n2\eta$

¹ Breit-Wigner width. May also be the $f_0(1500)$.

COUPLED CHANNEL MODE

VALUE (MeV)	DOCUMENT ID	TECN	COMMENT
• • •	We do not use the following data for averages, fits, limits, etc. • • •		
147 +30 -50	¹ ANISOVICH	03	RVUE

¹ K-matrix pole from combined analysis of $\pi^-\rho \rightarrow \pi^0\pi^0n$, $\pi^-\rho \rightarrow K\bar{K}n$, $\pi^+\pi^- \rightarrow \pi^+\pi^-\pi^0$, $\bar{p}p \rightarrow \pi^0\pi^0\pi^0$, $\pi^0\eta\eta$, $\pi^0\pi^0\eta$, $\pi^+\pi^-\pi^0$, $K^+K^-\pi^0$, $K_S^0K_S^0\pi^0$, $K^+K_S^0\pi^-$ at rest, $\bar{p}n \rightarrow \pi^-\pi^-\pi^+$, $K_S^0K^-\pi^0$, $K_S^0K_S^0\pi^-$ at rest.

f₀(1370) DECAY MODES

Mode	Fraction (Γ_i/Γ)
Γ_1 $\pi\pi$	seen
Γ_2 4π	seen
Γ_3 $4\pi^0$	seen
Γ_4 $2\pi^+2\pi^-$	seen
Γ_5 $\pi^+\pi^-2\pi^0$	seen
Γ_6 $\rho\rho$	seen
Γ_7 $2(\pi\pi)_{S\text{-wave}}$	seen
Γ_8 $\pi(1300)\pi$	seen
Γ_9 $a_1(1260)\pi$	seen
Γ_{10} $\eta\eta$	seen
Γ_{11} $K\bar{K}$	seen
Γ_{12} $K\bar{K}n\pi$	not seen
Γ_{13} 6π	not seen
Γ_{14} $\omega\omega$	not seen
Γ_{15} $\gamma\gamma$	seen
Γ_{16} e^+e^-	not seen

f₀(1370) PARTIAL WIDTHS

$\Gamma(\gamma\gamma)$	Γ_{15}
See $\gamma\gamma$ widths under $f_0(500)$ and MORGAN 90.	

$\Gamma(e^+e^-)$	Γ_{16}			
VALUE (eV)	CL%	DOCUMENT ID	TECN	COMMENT
<20	90	VOROBYEV	88	ND $e^+e^- \rightarrow \pi^0\pi^0$

f₀(1370) $\Gamma(i)\Gamma(\gamma\gamma)/\Gamma(\text{total})$

$\Gamma(\eta\eta) \times \Gamma(\gamma\gamma)/\Gamma_{\text{total}}$	$\Gamma_{10}\Gamma_{15}/\Gamma$		
VALUE (eV)	DOCUMENT ID	TECN	COMMENT
• • •	We do not use the following data for averages, fits, limits, etc. • • •		
121 +133 +169 -53 -106	¹ UEHARA	10A	BELL 10.6 $e^+e^- \rightarrow e^+e^-\eta\eta$

¹ Including interference with the $f_2'(1525)$ (parameters fixed to the values from the 2008 edition of this review, PDG 08) and $f_2(1270)$. May also be the $f_0(1500)$.

f₀(1370) BRANCHING RATIOS

$\Gamma(\pi\pi)/\Gamma_{\text{total}}$	Γ_1/Γ			
VALUE	CL%	DOCUMENT ID	TECN	COMMENT
• • •	We do not use the following data for averages, fits, limits, etc. • • •			
<0.10	95	OCHS	13	RVUE
0.26 ± 0.09		BUGG	96	RVUE
<0.15		¹ AMSLER	94	CBAR $\bar{p}p \rightarrow \pi^+\pi^-3\pi^0$
<0.06		GASPERO	93	DBC 0.0 $\bar{p}n \rightarrow \text{hadrons}$

¹ Using AMSLER 95B ($3\pi^0$).

$\Gamma(4\pi)/\Gamma_{\text{total}}$	$\Gamma_2/\Gamma = (\Gamma_3+\Gamma_4+\Gamma_5)/\Gamma$		
VALUE	DOCUMENT ID	TECN	COMMENT
• • •	We do not use the following data for averages, fits, limits, etc. • • •		
>0.72	GASPERO	93	DBC 0.0 $\bar{p}n \rightarrow \text{hadrons}$

$\Gamma(4\pi^0)/\Gamma(4\pi)$	Γ_3/Γ_2		
VALUE	DOCUMENT ID	TECN	COMMENT
• • •	We do not use the following data for averages, fits, limits, etc. • • •		
seen	ABELE	96	CBAR 0.0 $\bar{p}p \rightarrow 5\pi^0$
0.068 ± 0.005	¹ GASPERO	93	DBC 0.0 $\bar{p}n \rightarrow \text{hadrons}$

¹ Model-dependent evaluation.

$\Gamma(2\pi^+2\pi^-)/\Gamma(4\pi)$	$\Gamma_4/\Gamma_2 = \Gamma_4/(\Gamma_3+\Gamma_4+\Gamma_5)$		
VALUE	DOCUMENT ID	TECN	COMMENT
• • •	We do not use the following data for averages, fits, limits, etc. • • •		
0.420 ± 0.014	¹ GASPERO	93	DBC 0.0 $\bar{p}n \rightarrow 2\pi^+3\pi^-$

¹ Model-dependent evaluation.

$\Gamma(\pi^+\pi^-2\pi^0)/\Gamma(4\pi)$	$\Gamma_5/\Gamma_2 = \Gamma_5/(\Gamma_3+\Gamma_4+\Gamma_5)$		
VALUE	DOCUMENT ID	TECN	COMMENT
• • •	We do not use the following data for averages, fits, limits, etc. • • •		
0.512 ± 0.019	¹ GASPERO	93	DBC 0.0 $\bar{p}n \rightarrow \text{hadrons}$

¹ Model-dependent evaluation.

$\Gamma(\rho\rho)/\Gamma(4\pi)$	Γ_6/Γ_2		
VALUE	DOCUMENT ID	TECN	COMMENT
• • •	We do not use the following data for averages, fits, limits, etc. • • •		
0.26 ± 0.07	ABELE	01B	CBAR 0.0 $\bar{p}d \rightarrow 5\pi\rho$

$\Gamma(2(\pi\pi)_{S\text{-wave}})/\Gamma(\pi\pi)$	Γ_7/Γ_1		
VALUE	DOCUMENT ID	TECN	COMMENT
• • •	We do not use the following data for averages, fits, limits, etc. • • •		
5.6 ± 2.6	¹ ABELE	01	CBAR 0.0 $\bar{p}d \rightarrow \pi^-4\pi^0\rho$

¹ From the combined data of ABELE 96 and ABELE 96C.

$\Gamma(2(\pi\pi)_{S\text{-wave}})/\Gamma(4\pi)$	Γ_7/Γ_2		
VALUE	DOCUMENT ID	TECN	COMMENT
• • •	We do not use the following data for averages, fits, limits, etc. • • •		
0.51 ± 0.09	ABELE	01B	CBAR 0.0 $\bar{p}d \rightarrow 5\pi\rho$

$\Gamma(\rho\rho)/\Gamma(2(\pi\pi)_{S\text{-wave}})$	Γ_6/Γ_7		
VALUE	DOCUMENT ID	TECN	COMMENT
• • •	We do not use the following data for averages, fits, limits, etc. • • •		
large	BARBERIS	00c	450 $\rho\rho \rightarrow \rho_f 4\pi\rho_S$
1.6 ± 0.2	AMSLER	94	CBAR $\bar{p}p \rightarrow \pi^+\pi^-3\pi^0$
~ 0.65	GASPERO	93	DBC 0.0 $\bar{p}n \rightarrow \text{hadrons}$

$\Gamma(\pi(1300)\pi)/\Gamma(4\pi)$	Γ_8/Γ_2		
VALUE	DOCUMENT ID	TECN	COMMENT
• • •	We do not use the following data for averages, fits, limits, etc. • • •		
0.17 ± 0.06	ABELE	01B	CBAR 0.0 $\bar{p}d \rightarrow 5\pi\rho$

$\Gamma(a_1(1260)\pi)/\Gamma(4\pi)$	Γ_9/Γ_2		
VALUE	DOCUMENT ID	TECN	COMMENT
• • •	We do not use the following data for averages, fits, limits, etc. • • •		
0.06 ± 0.02	ABELE	01B	CBAR 0.0 $\bar{p}d \rightarrow 5\pi\rho$

$\Gamma(\eta\eta)/\Gamma(4\pi)$	$\Gamma_{10}/\Gamma_2 = \Gamma_{10}/(\Gamma_3+\Gamma_4+\Gamma_5)$		
VALUE	DOCUMENT ID	TECN	COMMENT
• • •	We do not use the following data for averages, fits, limits, etc. • • •		
(28 ± 11) × 10 ⁻³	¹ ANISOVICH	02D	SPEC Combined fit
(4.7 ± 2.0) × 10 ⁻³	BARBERIS	00e	450 $\rho\rho \rightarrow \rho_f\eta\eta\rho_S$

¹ From a combined K-matrix analysis of Crystal Barrel (0. $\rho\bar{p} \rightarrow \pi^0\pi^0\pi^0$, $\pi^0\eta\eta$, $\pi^0\pi^0\eta$), GAMS ($\pi\rho \rightarrow \pi^0\pi^0n$, $\eta\eta n$, $\eta\eta'n$), and BNL ($\pi\rho \rightarrow K\bar{K}n$) data.

$\Gamma(K\bar{K})/\Gamma_{\text{total}}$	Γ_{11}/Γ		
VALUE	DOCUMENT ID	TECN	COMMENT
• • •	We do not use the following data for averages, fits, limits, etc. • • •		
0.35 ± 0.13	BUGG	96	RVUE

$\Gamma(K\bar{K}n\pi)/\Gamma(\pi\pi)$	Γ_{11}/Γ_1		
VALUE	DOCUMENT ID	TECN	COMMENT
• • •	We do not use the following data for averages, fits, limits, etc. • • •		
0.08 ± 0.08	ABLIKIM	05	BES2 $J/\psi \rightarrow \phi\pi^+\pi^-, \phi K^+K^-$
0.91 ± 0.20	¹ BARGIOTTI	03	OBLX $\bar{p}p$
0.12 ± 0.06	² ANISOVICH	02D	SPEC Combined fit
0.46 ± 0.15 ± 0.11	BARBERIS	99D	OMEG 450 $\rho\rho \rightarrow K^+K^-, \pi^+\pi^-$

¹ Coupled channel analysis of $\pi^+\pi^-\pi^0$, $K^+K^-\pi^0$, and $K_S^0K_S^0\pi^\mp$.
² From a combined K-matrix analysis of Crystal Barrel (0. $\rho\bar{p} \rightarrow \pi^0\pi^0\pi^0$, $\pi^0\eta\eta$, $\pi^0\pi^0\eta$), GAMS ($\pi\rho \rightarrow \pi^0\pi^0n$, $\eta\eta n$, $\eta\eta'n$), and BNL ($\pi\rho \rightarrow K\bar{K}n$) data.

$\Gamma(K\bar{K}n\pi)/\Gamma_{\text{total}}$	Γ_{12}/Γ		
VALUE	DOCUMENT ID	TECN	COMMENT
• • •	We do not use the following data for averages, fits, limits, etc. • • •		
<0.03	GASPERO	93	DBC 0.0 $\bar{p}n \rightarrow \text{hadrons}$

Meson Particle Listings

$f_0(1370), \pi_1(1400)$

$\Gamma(6\pi)/\Gamma_{total}$	DOCUMENT ID	TECN	COMMENT	Γ_{13}/Γ
VALUE				
••• We do not use the following data for averages, fits, limits, etc. •••				
<0.22	GASPERO 93	DBC	0.0 $\bar{p}n \rightarrow$ hadrons	

$\Gamma(\omega\omega)/\Gamma_{total}$	DOCUMENT ID	TECN	COMMENT	Γ_{14}/Γ
VALUE				
••• We do not use the following data for averages, fits, limits, etc. •••				
<0.13	GASPERO 93	DBC	0.0 $\bar{p}n \rightarrow$ hadrons	

$f_0(1370)$ REFERENCES

AAJ 19H	JHEP 1904 063	R. Aaij et al.	(LHCb Collab.)
AOUDE 18	PR D98 056021	R.T. Aoude et al.	
DOBBS 15	PR D91 052006	S. Dobbs et al.	(NWES)
OCHS 13	JP G40 043001	W. Ochs	
UEHARA 10A	PR D82 114031	S. Uehara et al.	(BELLE Collab.)
ANISOVICH 09	IMP A24 2481	V.V. Anisovich, A.V. Sarantsev	
AUBERT 09L	PR D79 072006	B. Aubert et al.	(BABAR Collab.)
PDG 08	PL B667 1	C. Amisler et al.	(PDG Collab.)
UEHARA 08A	PR D78 052004	S. Uehara et al.	(BELLE Collab.)
BONVICINI 07	PR D76 012001	G. Bonvicini et al.	(CLEO Collab.)
BUGG 07A	JP G34 151	D.V. Bugg et al.	
GARMASH 07	PR D75 012006	A. Garmash et al.	(BELLE Collab.)
GARMASH 06	PRL 96 251803	A. Garmash et al.	(BELLE Collab.)
PDG 06	JP G33 1	W.-M. Yao et al.	(PDG Collab.)
VLADIMIRSK... 06	PAN 69 493	V.V. Vladimirov et al.	(ITEP, Moscow)
ABLIKIM 05	Translated from YAF 69 515.	M. Ablikim et al.	(BES Collab.)
ABLIKIM 05Q	PR D72 092002	M. Ablikim et al.	(BES Collab.)
GARMASH 05	PR D71 092003	A. Garmash et al.	(BELLE Collab.)
ANISOVICH 03	EPJ A16 229	V.V. Anisovich et al.	
BARGIOTTI 03	EPJ C26 371	M. Bargiotti et al.	(OBELIX Collab.)
TIKHOMIROV 03	PAN 66 828	G.D. Tikhomirov et al.	
ANISOVICH 02D	Translated from YAF 66 860.	V.V. Anisovich et al.	
ABELE 01	EPJ C19 667	A. Abele et al.	(Crystal Barrel Collab.)
ABELE 01B	EPJ C21 261	A. Abele et al.	(Crystal Barrel Collab.)
AITALA 01A	PRL 86 765	E.M. Aitala et al.	(FNAL E791 Collab.)
ASNER 00	PR D61 012002	D.M. Asner et al.	(CLEO Collab.)
BARBERIS 00C	PL B471 440	D. Barberis et al.	(WA 102 Collab.)
BARBERIS 00E	PL B479 59	D. Barberis et al.	(WA 102 Collab.)
BARBERIS 99B	PL B453 316	D. Barberis et al.	(Omega Expt.)
BARBERIS 99D	PL B462 462	D. Barberis et al.	(Omega Expt.)
BELLAZZINI 99	PL B467 296	R. Bellazzini et al.	
KAMINSKI 99	EPJ C9 141	R. Kaminski, L. Lesniak, B. Loiseau	(CRAC, PARIN)
ALDE 98	EPJ A3 361	D. Alde et al.	(GAM4 Collab.)
Also	PAN 62 405	D. Alde et al.	(GAMS Collab.)
ANISOVICH 98B	Translated from YAF 62 446.	V.V. Anisovich et al.	
SPU 41 419	Translated from UFN 168 481.	V.V. Anisovich et al.	
BERTIN 98	PR D57 95	A. Bertin et al.	(OBELIX Collab.)
BARBERIS 97B	PL B413 217	D. Barberis et al.	(WA 102 Collab.)
BERTIN 97C	PL B408 476	A. Bertin et al.	(OBELIX Collab.)
ABELE 96	PL B380 453	A. Abele et al.	(Crystal Barrel Collab.)
ABELE 96B	PL B385 425	A. Abele et al.	(Crystal Barrel Collab.)
ABELE 96C	NP A609 562	A. Abele et al.	(Crystal Barrel Collab.)
BUGG 96	NP B471 59	D.V. Bugg, A.V. Sarantsev, B.S. Zou	(LOQM, PNPI)
AMSLER 95B	PL B342 433	C. Amisler et al.	(Crystal Barrel Collab.)
AMSLER 95C	PL B353 571	C. Amisler et al.	(Crystal Barrel Collab.)
AMSLER 95D	PL B355 425	C. Amisler et al.	(Crystal Barrel Collab.)
JANSSEN 95	PR D92 2690	G. Janssen et al.	(STON, ADLD, JULI)
TORNVIST 95	ZPHY C68 647	N.A. Tornqvist	(HELS)
AMSLER 94	PL B322 431	C. Amisler et al.	(Crystal Barrel Collab.)
AMSLER 94D	PL B333 277	C. Amisler et al.	(Crystal Barrel Collab.)
ANISOVICH 94	PL B323 233	V.V. Anisovich et al.	(Crystal Barrel Collab.)
BUGG 94	PR D50 4412	D.V. Bugg et al.	(LOQM)
KAMINSKI 94	PR D50 3145	R. Kaminski, L. Lesniak, J.P. Maillet	(CRAC+)
ADAMO 93	NP A558 13C	A. Adamo et al.	(OBELIX Collab.)
GASPERO 93	NP A562 407	M. Gaspero	(ROMAI) JPC
AMSLER 92	PL B291 347	C. Amisler et al.	(Crystal Barrel Collab.)
ARMSTRONG 91	ZPHY C51 351	T.A. Armstrong et al.	(ATHU, BARI, BIRM+)
ARMSTRONG 91B	ZPHY C52 389	T.A. Armstrong et al.	(ATHU, BARI, BIRM+)
BREAKSTONE 90	ZPHY C48 569	A.M. Breakstone et al.	(ISU, BGN, CERN+)
MORGAN 90	ZPHY C48 623	D. Morgan, M.R. Pennington	(RAL, DURH)
ASTON 88	NP B296 493	D. Aston et al.	(SLAC, NAGO, CINC, INUS)
BOLONKIN 88	NP B309 426	B.V. Bolonkin et al.	(ITEP, SERP)
FALVARD 88	PR D38 2706	A. Falvard et al.	(CLER, FRAS, LALO+)
VOROBYEV 88	SJNP 48 273	P.V. Vorobiev et al.	(NOVO)
Translated from YAF 48 436.			
AU 87	PR D35 1633	K.L. Au, D. Morgan, M.R. Pennington	(DURH, RAL)
AKESSON 86	NP B264 154	T. Akesson et al.	(Axial Field Spec. Collab.)
ALDE 86D	NP B269 485	D.M. Alde et al.	(BELG, LAPP, SERP, CERN+)
CASON 83	PR D28 1586	N.M. Cason et al.	(NDAM, ANL)
ETKIN 82B	D25 1786	A. Etkin et al.	(BNL, CUNY, TUFTS, VAND)
WICKLUND 80	PRL 45 1469	A.B. Wicklund et al.	(ANL)
BECKER 79	NP B151 46	H. Becker et al.	(MPIM, CERN, ZEEM, CRAC)
POLYCHRO... 79	PR D19 1317	V.A. Polychronakos et al.	(NDAM, ANL)
FROGGATT 77	NP B129 89	C.D. Froggatt, J.L. Petersen	(GLAS, NORD)
ROSSELET 77	PR D15 574	L. Rosselet et al.	(GEVA, SAEL)
GRAYER 74	NP B75 189	G. Grayer et al.	(CERN, MPIM)
HYAMS 73	NP B64 134	B.D. Hyams et al.	(CERN, MPIM)
OCHS 73	Thesis	W. Ochs	(MPIM, MUNI)
BEIER 72B	PRL 29 511	E.W. Beier et al.	(PENN)
BETTINI 66	NC 42A 695	A. Bettini et al.	(PADO, PISA)

$\pi_1(1400)$

$$J^G(J^{PC}) = 1^-(1^-+)$$

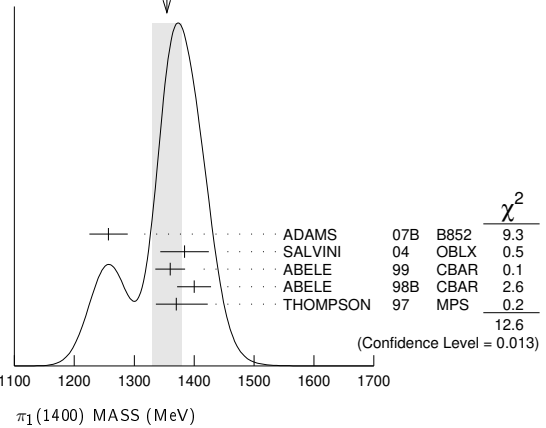
See the review on "Non- $q\bar{q}$ Mesons" and a note in PDG 06, Journal of Physics **G33** 1 (2006).

$\pi_1(1400)$ MASS

VALUE (MeV)	EVTS	DOCUMENT ID	TECN	CHG	COMMENT
1354 ± 25	OUR AVERAGE	Error includes scale factor of 1.8. See the ideogram below.			
1257 ± 20 ± 25	23.5k	ADAMS	07b	B852	18 $\pi^- p \rightarrow \eta\pi^0 n$

1384 ± 20 ± 35	90k	SALVINI	04	OBLX	$\bar{p}p \rightarrow 2\pi^+ 2\pi^-$
1360 ± 25		ABELE	99	CBAR	0.0 $\bar{p}p \rightarrow \pi^0 \pi^0 \eta$
1400 ± 20 ± 20		ABELE	98b	CBAR	0.0 $\bar{p}n \rightarrow \pi^- \pi^0 \eta$
1370 ± 16	$^{+50}_{-30}$	¹ THOMPSON	97	MPS	18 $\pi^- p \rightarrow \eta\pi^- p$
••• We do not use the following data for averages, fits, limits, etc. •••					
1323.1 ± 4.6		² AOYAGI	93	BKEI	$\pi^- p \rightarrow \eta\pi^- p$
1406 ± 20		³ ALDE	88b	GAM4 0	100 $\pi^- p \rightarrow \eta\pi^0 n$
¹ Natural parity exchange, questioned by DZIERBA 03.					
² Unnatural parity exchange.					
³ Seen in the P_0 -wave intensity of the $\eta\pi^0$ system, unnatural parity exchange.					

WEIGHTED AVERAGE
1354±25 (Error scaled by 1.8)



$\pi_1(1400)$ WIDTH

VALUE (MeV)	EVTS	DOCUMENT ID	TECN	CHG	COMMENT
330 ± 35	OUR AVERAGE				
354 ± 64 ± 58	23.5k	ADAMS	07b	B852	18 $\pi^- p \rightarrow \eta\pi^0 n$
378 ± 50 ± 50	90k	SALVINI	04	OBLX	$\bar{p}p \rightarrow 2\pi^+ 2\pi^-$
220 ± 90		ABELE	99	CBAR	0.0 $\bar{p}p \rightarrow \pi^0 \pi^0 \eta$
310 ± 50	$^{+50}_{-30}$	ABELE	98b	CBAR	0.0 $\bar{p}n \rightarrow \pi^- \pi^0 \eta$
385 ± 40	$^{+65}_{-105}$	⁴ THOMPSON	97	MPS	18 $\pi^- p \rightarrow \eta\pi^- p$
••• We do not use the following data for averages, fits, limits, etc. •••					
143.2 ± 12.5		⁵ AOYAGI	93	BKEI	$\pi^- p \rightarrow \eta\pi^- p$
180 ± 20		⁶ ALDE	88b	GAM4 0	100 $\pi^- p \rightarrow \eta\pi^0 n$
⁴ Resolution is not unfolded, natural parity exchange, questioned by DZIERBA 03.					
⁵ Unnatural parity exchange.					
⁶ Seen in the P_0 -wave intensity of the $\eta\pi^0$ system, unnatural parity exchange.					

$\pi_1(1400)$ DECAY MODES

Mode	Fraction (Γ_i/Γ)
$\Gamma_1 \eta\pi^0$	seen
$\Gamma_2 \eta\pi^-$	seen
$\Gamma_3 \eta'\pi$	
$\Gamma_4 \rho(770)\pi$	not seen

$\pi_1(1400)$ BRANCHING RATIOS

$\Gamma(\eta\pi^0)/\Gamma_{total}$	DOCUMENT ID	TECN	CHG	COMMENT	Γ_1/Γ
VALUE					
••• We do not use the following data for averages, fits, limits, etc. •••					
not seen	PROKOSHKIN 95b	GAM4		100 $\pi^- p \rightarrow \eta\pi^0 n$	
not seen	⁷ BUGG	94	RVUE	$\bar{p}p \rightarrow \eta 2\pi^0$	
not seen	⁸ APEL	81	NICE 0	40 $\pi^- p \rightarrow \eta\pi^0 n$	
⁷ Using Crystal Barrel data.					
⁸ A general fit allowing S, D, and P waves (including m=0) is not done because of limited statistics.					

$\Gamma(\eta\pi^-)/\Gamma_{total}$	DOCUMENT ID	TECN	COMMENT	Γ_2/Γ
VALUE				
••• We do not use the following data for averages, fits, limits, etc. •••				
possibly seen	BELADIDZE 93	VES	37 $\pi^- N \rightarrow \eta\pi^- N$	

See key on page 999

Meson Particle Listings

$\pi_1(1400), \eta(1405)$

$\Gamma(\eta'/\pi)/\Gamma(\eta\pi^0)$

VALUE	CL%	DOCUMENT ID	TECN	COMMENT
<0.80	95	BOUTEMEUR 90	GAM4	100 $\pi^- \rho \rightarrow 4\gamma n$

$\Gamma(\rho(770)\pi)/\Gamma_{total}$

VALUE	DOCUMENT ID	TECN	COMMENT
not seen	AGHASYAN 18B	COMP	190 $\pi^- \rho \rightarrow \pi^- \pi^+ \pi^- \rho$

Γ_3/Γ_1

- 2 From fit to the $a_0(980)\pi^0$ partial wave.
- 3 Best fit with a single Breit Wigner.
- 4 Superseded by AMSLER 04B.

$\pi_1(1400)$ REFERENCES

AGHASYAN 18B	PR D98 092003	M. Aghasyan et al.	(COMPASS Collab.)
ADAMS 07B	PL B657 27	G.S. Adams et al.	(BNL E852 Collab.)
PDG 06	JP G33 1	W.-M. Yao et al.	(PDG Collab.)
SALVINI 04	EPJ C35 21	P. Salvini et al.	(OBELIX Collab.)
DZIERBA 03	PR D67 094015	A.R. Dzierba et al.	
ABELE 99	PL B446 349	A. Abele et al.	(Crystal Barrel Collab.)
ABELE 98B	PL B423 175	A. Abele et al.	(Crystal Barrel Collab.)
THOMPSON 97	PL R 79 1630	D.R. Thompson et al.	(BNL E852 Collab.)
PROKOSHKIN 95B	PAN 58 606	Y.D. Prokoshkin, S.A. Sadovsky	(SERP)
BUGG 94	PR D50 4412	D.V. Bugg et al.	(LOQM)
AOYAGI 93	PL B314 246	H. Aoyagi et al.	(BKEI Collab.)
BEHADIDZE 93	PL B313 276	G.M. Behadidze et al.	(VES Collab.)
BOUTEMEUR 90	Hadron 89 Conf. p 119	M. BoutemEUR, M. Poulet	(SERP, BELG, LANL)
ALDE 88B	PL B205 397	D.M. Alde et al.	(SERP, BELG, LANL, LAPP)
APEL 81	NP B193 269	W.D. Apel et al.	(SERP, CERN)

$\eta(1405)$

$I^G(JPC) = 0^+(0^-+)$

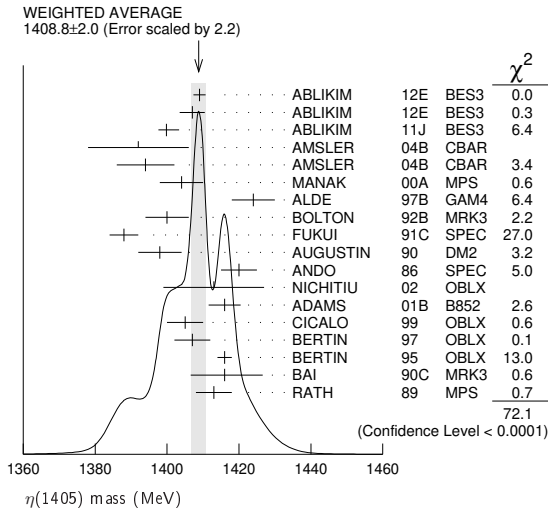
See also the $\eta(1475)$.

See the related review(s):

Pseudoscalar and Pseudovector Mesons in the 1400 MeV Region

$\eta(1405)$ MASS

1408.8 ± 2.0 OUR AVERAGE Includes data from the 2 datablocks that follow this one. Error includes scale factor of 2.2. See the ideogram below.



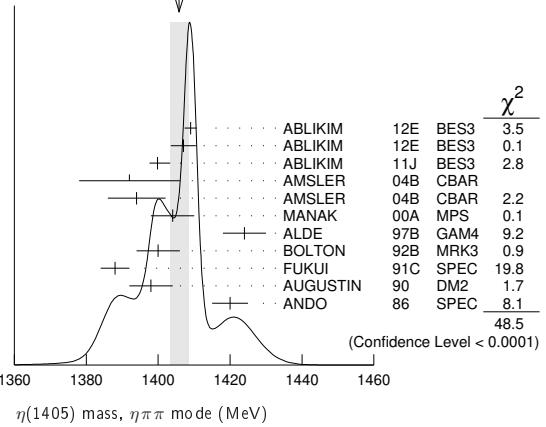
$\eta\pi\pi$ MODE

The data in this block is included in the average printed for a previous datablock.

VALUE (MeV)	EVTS	DOCUMENT ID	TECN	COMMENT
1405.8 ± 2.6 OUR AVERAGE				Error includes scale factor of 2.3. See the ideogram below.
1409.0 ± 1.7	743	ABLIKIM 12E BES3		$J/\psi \rightarrow \gamma(\pi^+ \pi^- \pi^0)$
1407.0 ± 3.5	198	ABLIKIM 12E BES3		$J/\psi \rightarrow \gamma(\pi^0 \pi^0 \pi^0)$
1399.8 ± 2.2 ^{+2.8} _{-0.1}		1 ABLIKIM 11J BES3		$J/\psi \rightarrow \omega(\eta\pi^+ \pi^-)$
1392 ± 14	900 ± 375	AMSLER 04B CBAR		$0 \bar{p}p \rightarrow \pi^+ \pi^- \pi^+ \pi^- \eta$
1394 ± 8	6.6 ± 2.0k	AMSLER 04B CBAR		$0 \bar{p}p \rightarrow \pi^+ \pi^- \pi^0 \pi^0 \eta$
1404 ± 6	9082	MANAK 00A MPS		$18 \pi^- p \rightarrow \eta\pi^+ \pi^- n$
1424 ± 6	2200	ALDE 97B GAM4		$100 \pi^- p \rightarrow \eta\pi^0 \pi^0 n$
1400 ± 6		2 BOLTON 92B MRK3		$J/\psi \rightarrow \gamma\eta\pi^+ \pi^-$
1388 ± 4		FUKUI 91C SPEC		$8.95 \pi^- p \rightarrow \eta\pi^+ \pi^- n$
1398 ± 6	261	3 AUGUSTIN 90 DM2		$J/\psi \rightarrow \gamma\eta\pi^+ \pi^-$
1420 ± 5		ANDO 86 SPEC		$8 \pi^- p \rightarrow \eta\pi^+ \pi^- n$
1404.0 ± 11.0	195	ABLIKIM 19B/BES3		$e^+ e^- \rightarrow \psi(2S)$
1385 ± 7		BAI 99 BES		$J/\psi \rightarrow \gamma\eta\pi^+ \pi^-$
1409 ± 3		4 AMSLER 95F CBAR		$0 \bar{p}p \rightarrow \pi^+ \pi^- \pi^0 \pi^0 \eta$

1 The selected process is $J/\psi \rightarrow \omega a_0(980)\pi$.

WEIGHTED AVERAGE
1405.8 ± 2.6 (Error scaled by 2.3)



$K\bar{K}\pi$ MODE ($a_0(980)\pi$ or direct $K\bar{K}\pi$)

The data in this block is included in the average printed for a previous datablock.

VALUE (MeV)	EVTS	DOCUMENT ID	TECN	COMMENT
1413.9 ± 1.7 OUR AVERAGE				Error includes scale factor of 1.1.
1413 ± 14	3651	1 NICHITIU 02 OBLX		$0 \bar{p}p \rightarrow K^+ K^- \pi^+ \pi^- \pi^0$
1416 ± 4 ± 2	20k	ADAMS 01B B852		$18 \text{ GeV } \pi^- p \rightarrow K^+ K^- \pi^0 n$
1405 ± 5		2 CICALO 99 OBLX		$0 \bar{p}p \rightarrow K^\pm K_S^0 \pi^\mp \pi^+ \pi^-$
1407 ± 5		2 BERTIN 97 OBLX		$0 \bar{p}p \rightarrow K^\pm(K^0) \pi^\mp \pi^+ \pi^-$
1416 ± 2		2 BERTIN 95 OBLX		$0 \bar{p}p \rightarrow K\bar{K}\pi\pi$
1416 ± 8 ⁺⁷ ₋₅	700	3 BAI 90C MRK3		$J/\psi \rightarrow \gamma K_S^0 K^\pm \pi^\mp$
1413 ± 5		3 RATH 89 MPS		$21.4 \pi^- p \rightarrow n K_S^0 K^\pm \pi^0$
1459 ± 5		4 AUGUSTIN 92 DM2		$J/\psi \rightarrow \gamma K\bar{K}\pi$

- 1 Decaying dominantly directly to $K^+ K^- \pi^0$.
- 2 Decaying into $(K\bar{K})_S \pi$, $(K\pi)_S \bar{K}$, and $a_0(980)\pi$.
- 3 From fit to the $a_0(980)\pi^0$ partial wave. Cannot rule out a $a_0(980)\pi^{1^+}$ partial wave.
- 4 Excluded from averaging because averaging would be meaningless.

$\pi\pi\gamma$ MODE

The data in this block is included in the average printed for a previous datablock.

VALUE (MeV)	EVTS	DOCUMENT ID	TECN	COMMENT
1403 ± 17 OUR AVERAGE				Error includes scale factor of 1.8.
1390 ± 12	235 ± 91	AMSLER 04B CBAR		$0 \bar{p}p \rightarrow \pi^+ \pi^- \pi^+ \pi^- \eta$
1424 ± 10 ± 11	547	BAI 04J BES2		$J/\psi \rightarrow \gamma\gamma\pi^+ \pi^-$
1401 ± 18		1,2 AUGUSTIN 90 DM2		$J/\psi \rightarrow \pi^+ \pi^- \gamma\gamma$
1432 ± 8		2 COFFMAN 90 MRK3		$J/\psi \rightarrow \pi^+ \pi^- 2\gamma$

1 Best fit with a single Breit Wigner.

2 This peak in the $\gamma\rho$ channel may not be related to the $\eta(1405)$.

4 π MODE

The data in this block is included in the average printed for a previous datablock.

VALUE (MeV)	EVTS	DOCUMENT ID	TECN	COMMENT
1420 ± 20		BUGG 95 MRK3		$J/\psi \rightarrow \gamma\pi^+ \pi^- \pi^+ \pi^-$
1489 ± 12	3270	1 BISELLO 89B DM2		$J/\psi \rightarrow 4\pi\gamma$

1 Estimated by us from various fits.

$K\bar{K}\pi$ MODE (unresolved)

The data in this block is included in the average printed for a previous datablock.

VALUE (MeV)	EVTS	DOCUMENT ID	TECN	COMMENT
1452.7 ± 3.3	191	1,2 ABLIKIM 13M BES3		$\psi(2S) \rightarrow \omega K\bar{K}\pi$
1437.6 ± 3.2	249 ± 35	1,2 ABLIKIM 08E BES2		$J/\psi \rightarrow \omega K_S^0 K^+ \pi^- + c.c.$
1445.9 ± 5.7	62 ± 18	1,2 ABLIKIM 08E BES2		$J/\psi \rightarrow \omega K^+ K^- \pi^0$
1442 ± 10	410	1 BAI 98C BES		$J/\psi \rightarrow \gamma K^+ K^- \pi^0$
1445 ± 8	693	1 AUGUSTIN 90 DM2		$J/\psi \rightarrow \gamma K_S^0 K^\pm \pi^\mp$
1433 ± 8	296	1 AUGUSTIN 90 DM2		$J/\psi \rightarrow \gamma K^+ K^- \pi^-$
1413 ± 8	500	1 DUCH 89 ASTE		$\bar{p}p \rightarrow \pi^+ \pi^- K^\pm \pi^\mp K^0$
1453 ± 7	170	1 RATH 89 MPS		$21.4 \pi^- p \rightarrow K_S^0 K^\pm \pi^0 n$
1419 ± 1	8800	1 BIRMAN 88 MPS		$8 \pi^- p \rightarrow K^+ \bar{K}^0 \pi^- n$
1424 ± 3	620	1 REEVES 86 SPEC		$6.6 \bar{p}p \rightarrow K\bar{K}\pi X$
1421 ± 2		1 CHUNG 85 SPEC		$8 \pi^- p \rightarrow K\bar{K}\pi n$
1440 ± 20	174	1 EDWARDS 82E CBAL		$J/\psi \rightarrow \gamma K^+ K^- \pi^0$

Meson Particle Listings

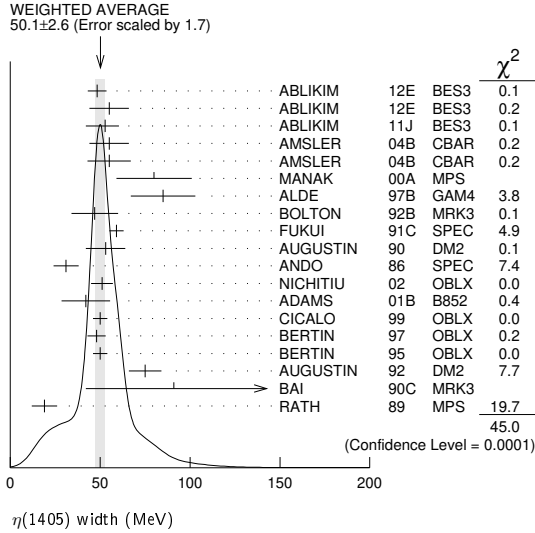
$\eta(1405)$

1440	$+10$ -15	1	SCHARRE	80	MRK2	$J/\psi \rightarrow \gamma K_S^0 K^\pm \pi^\mp$	
1425	± 7	800	1,3	BAILLON	67	HBC	$0 \bar{p} p \rightarrow K \bar{K} \pi \pi \pi$

- ¹ These experiments identify only one pseudoscalar in the 1400–1500 range. Data could also refer to $\eta(1475)$.
- ² Systematic uncertainty not evaluated.
- ³ From best fit of 0^-+ partial wave, 50% $K^*(892)K$, 50% $a_0(980)\pi$.

$\eta(1405)$ WIDTH

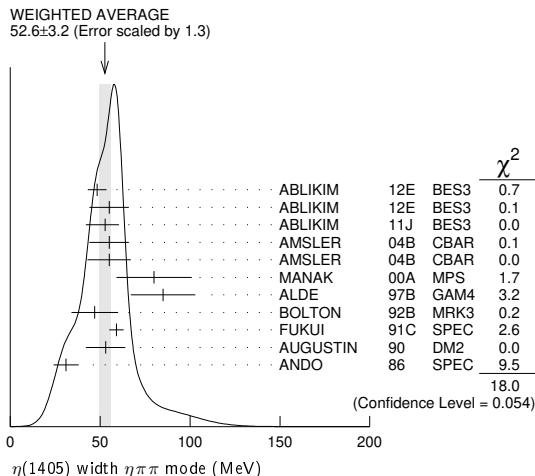
50.1 ± 2.6 OUR AVERAGE Includes data from the 2 datablocks that follow this one. Error includes scale factor of 1.7. See the ideogram below.



$\eta\pi\pi$ MODE

52.6 ± 3.2 OUR AVERAGE Error includes scale factor of 1.3. See the ideogram below.

VALUE (MeV)	EVTS	DOCUMENT ID	TECN	COMMENT
48.3 ± 5.2	743	ABLIKIM 12E BES3		$J/\psi \rightarrow \gamma(\pi^+ \pi^- \pi^0)$
55.0 ± 11.0	198	ABLIKIM 12E BES3		$J/\psi \rightarrow \gamma(\pi^0 \pi^0 \pi^0)$
52.8 ± 7.6 ^{+0.1} _{-7.6}		1 ABLIKIM 11J BES3		$J/\psi \rightarrow \omega(\eta\pi^+ \pi^-)$
55 ± 11	900	AMSLER 04B CBAR		$0 \bar{p} p \rightarrow \pi^+ \pi^- \pi^+ \pi^- \eta$
55 ± 12	6.6k	AMSLER 04B CBAR		$0 \bar{p} p \rightarrow \pi^+ \pi^- \pi^0 \pi^0 \gamma$
80 ± 21	9.0k	MANAK 00A MPS		$18 \pi^- p \rightarrow \eta\pi^+ \pi^- n$
85 ± 18	2.2k	ALDE 97B GAM4		$100 \pi^- p \rightarrow \eta\pi^0 \pi^0 n$
47 ± 13		2 BOLTON 92B MRK3		$J/\psi \rightarrow \gamma\eta\pi^+ \pi^-$
59 ± 4		FUKUI 91C SPEC		$8.95 \pi^- p \rightarrow \eta\pi^+ \pi^- n$
53 ± 11		3 AUGUSTIN 90 DM2		$J/\psi \rightarrow \gamma\eta\pi^+ \pi^-$
31 ± 7		ANDO 86 SPEC		$8 \pi^- p \rightarrow \eta\pi^+ \pi^- n$
••• We do not use the following data for averages, fits, limits, etc. •••				
79.0 ± 16.0	195	ABLIKIM 19BA BES3		$e^+ e^- \rightarrow \psi(2S)$
86 ± 10		4 AMSLER 95F CBAR		$0 \bar{p} p \rightarrow \pi^+ \pi^- \pi^0 \pi^0 \eta$



- ¹ The selected process is $J/\psi \rightarrow \omega a_0(980)\pi$.
- ² From fit to the $a_0(980)\pi 0^-+$ partial wave.

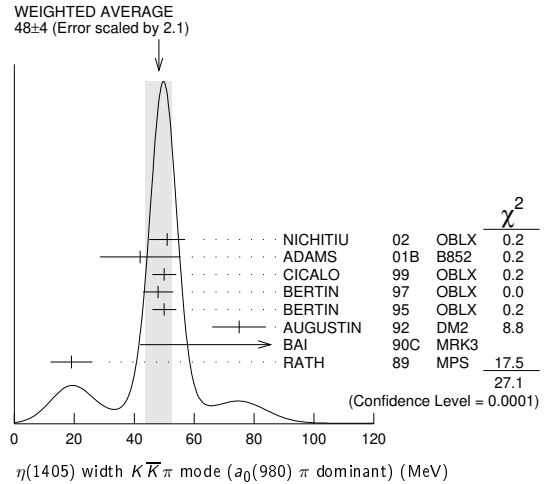
- ³ From $\eta\pi^+ \pi^-$ mass distribution - mainly $a_0(980)\pi$ - no spin-parity determination available.
- ⁴ Superseded by AMSLER 04B.

$K\bar{K}\pi$ MODE ($a_0(980)\pi$ or direct $K\bar{K}\pi$)

48 ± 4 OUR AVERAGE Error includes scale factor of 2.1. See the ideogram below.

VALUE (MeV)	EVTS	DOCUMENT ID	TECN	COMMENT
51 ± 6	3651	1 NICHITIU 02 OBLX		$0 \bar{p} p \rightarrow K^+ K^- \pi^+ \pi^- \pi^0$
42 ± 10 ± 9	20k	ADAMS 01B B852		$18 \text{ GeV } \pi^- p \rightarrow K^+ K^- \pi^0 n$
50 ± 4		CICALO 99 OBLX		$0 \bar{p} p \rightarrow K^\pm K_S^0 \pi^\mp \pi^+ \pi^-$
48 ± 5		2 BERTIN 97 OBLX		$0.0 \bar{p} p \rightarrow K^\pm (K^0) \pi^\mp \pi^+ \pi^-$
50 ± 4		2 BERTIN 95 OBLX		$0 \bar{p} p \rightarrow K \bar{K} \pi \pi \pi$
75 ± 9		AUGUSTIN 92 DM2		$J/\psi \rightarrow \gamma K \bar{K} \pi$
91 ⁺⁶⁷ ₋₃₁ ± 15 ⁺³⁸		3 BAI 90C MRK3		$J/\psi \rightarrow \gamma K_S^0 K^\pm \pi^\mp$
19 ± 7		3 RATH 89 MPS		$21.4 \pi^- p \rightarrow n K_S^0 K_S^0 \pi^0$

- ¹ Decaying dominantly directly to $K^+ K^- \pi^0$.
- ² Decaying into $(K\bar{K})_S \pi$, $(K\pi)_S \bar{K}$, and $a_0(980)\pi$.
- ³ From fit to the $a_0(980)\pi 0^-+$ partial wave, but $a_0(980)\pi 1^++$ cannot be excluded.



$\pi\pi\gamma$ MODE

89 ± 17 OUR AVERAGE Error includes scale factor of 1.7.

VALUE (MeV)	EVTS	DOCUMENT ID	TECN	COMMENT
64 ± 18	235 ± 91	AMSLER 04B CBAR		$0 \bar{p} p \rightarrow \pi^+ \pi^- \pi^+ \pi^- \gamma$
101.0 ± 8.8 ± 8.8	547	BAI 04J BES2		$J/\psi \rightarrow \gamma\gamma\pi^+ \pi^-$
••• We do not use the following data for averages, fits, limits, etc. •••				
174 ± 44		AUGUSTIN 90 DM2		$J/\psi \rightarrow \pi^+ \pi^- \gamma\gamma$
90 ± 26		1 COFFMAN 90 MRK3		$J/\psi \rightarrow \pi^+ \pi^- 2\gamma$

- ¹ This peak in the $\gamma\rho$ channel may not be related to the $\eta(1405)$.

4 π MODE

144 ± 13

VALUE (MeV)	EVTS	DOCUMENT ID	TECN	COMMENT
160 ± 30		BUGG 95 MRK3		$J/\psi \rightarrow \gamma\pi^+ \pi^- \pi^+ \pi^-$
144 ± 13	3270	1 BISELLO 89B DM2		$J/\psi \rightarrow 4\pi\gamma$

- ¹ Estimated by us from various fits.

$K\bar{K}\pi$ MODE (unresolved)

48 ± 4 OUR AVERAGE Error includes scale factor of 2.1. See the ideogram below.

VALUE (MeV)	EVTS	DOCUMENT ID	TECN	COMMENT
45.9 ± 8.2	191	1,2 ABLIKIM 13M BES3		$\psi(2S) \rightarrow \omega K K \pi$
48.9 ± 9.0	249 ± 35	1,2 ABLIKIM 08E BES2		$J/\psi \rightarrow \omega K_S^0 K^+ \pi^- + c.c.$
34.2 ± 18.5	62 ± 18	1,2 ABLIKIM 08E BES2		$J/\psi \rightarrow \omega K^+ K^- \pi^0$
93 ± 14	296	1 AUGUSTIN 90 DM2		$J/\psi \rightarrow \gamma K^+ K^- \pi^0$
105 ± 10	693	1 AUGUSTIN 90 DM2		$J/\psi \rightarrow \gamma K_S^0 K^\pm \pi^\mp$
62 ± 16	500	1 DUCH 89 ASTE		$\bar{p} p \rightarrow K \bar{K} \pi \pi \pi$
100 ± 11	170	1 RATH 89 MPS		$21.4 \pi^- p \rightarrow K_S^0 K_S^0 \pi^0 n$
66 ± 2	8800	1 BIRMAN 88 MPS		$8 \pi^- p \rightarrow K^+ \bar{K}^0 \pi^- n$
60 ± 10	620	1 REEVES 86 SPEC		$6.6 \text{ GeV } \bar{p} p \rightarrow K K \pi X$
60 ± 10		1 CHUNG 85 SPEC		$8 \pi^- p \rightarrow K \bar{K} \pi n$
55 ⁺²⁰ ₋₃₀ ± 10	174	1 EDWARDS 82E CBAL		$J/\psi \rightarrow \gamma K^+ K^- \pi^0$
50 ± 20		1 SCHARRE 80 MRK2		$J/\psi \rightarrow \gamma K_S^0 K^\pm \pi^\mp$
80 ± 10	800	1,3 BAILLON 67 HBC		$0 \bar{p} p \rightarrow K \bar{K} \pi \pi \pi$

- ¹ These experiments identify only one pseudoscalar in the 1400–1500 range. Data could also refer to $\eta(1475)$.
- ² Systematic uncertainty not evaluated.
- ³ From best fit to 0^-+ partial wave, 50% $K^*(892)K$, 50% $a_0(980)\pi$.

$\eta(1405)$ DECAY MODES

Mode	Fraction (Γ_i/Γ)	Confidence level
Γ_1 $K\bar{K}\pi$	seen	
Γ_2 $\eta\pi\pi$	seen	
Γ_3 $a_0(980)\pi$	seen	
Γ_4 $\eta(\pi\pi)$ s-wave	seen	
Γ_5 $f_0(980)\pi^0 \rightarrow \pi^+\pi^-\pi^0$	not seen	
Γ_6 $f_0(980)\eta$	seen	
Γ_7 4π	seen	
Γ_8 $\rho\rho$	<58 %	99.85%
Γ_9 $\gamma\gamma$		
Γ_{10} $\rho^0\gamma$	seen	
Γ_{11} $\phi\gamma$		
Γ_{12} $K^*(892)K$	seen	

$\eta(1405)$ $\Gamma(\eta)\Gamma(\gamma\gamma)/\Gamma(\text{total})$

$\Gamma(K\bar{K}\pi) \times \Gamma(\gamma\gamma)/\Gamma_{\text{total}}$ $\Gamma_1\Gamma_9/\Gamma$

VALUE (keV)	CL%	DOCUMENT ID	TECN	COMMENT
<0.035	90	1,2 AHOHE	05	CLE2 10.6 $e^+e^- \rightarrow e^+e^-K_S^0K^\pm\pi^\mp$

• • • We do not use the following data for averages, fits, limits, etc. • • •
¹ Using $\eta(1405)$ mass and width 1410 MeV and 51 MeV, respectively.
² Assuming three-body phase-space decay to $K_S^0K^\pm\pi^\mp$.

$\Gamma(\eta\pi\pi) \times \Gamma(\gamma\gamma)/\Gamma_{\text{total}}$ $\Gamma_2\Gamma_9/\Gamma$

VALUE (keV)	CL%	DOCUMENT ID	TECN	COMMENT
<0.095	95	ACCIARRI	01G L3	183-202 $e^+e^- \rightarrow e^+e^-\eta\pi^+\pi^-$

$\Gamma(\rho^0\gamma) \times \Gamma(\gamma\gamma)/\Gamma_{\text{total}}$ $\Gamma_{10}\Gamma_9/\Gamma$

VALUE (keV)	CL%	DOCUMENT ID	TECN	COMMENT
<1.5	95	ALTHOFF	84E TASS	$e^+e^- \rightarrow e^+e^-\pi^+\pi^-\gamma$

$\eta(1405)$ BRANCHING RATIOS

$\Gamma(\eta\pi\pi)/\Gamma(K\bar{K}\pi)$ Γ_2/Γ_1

VALUE	CL%	DOCUMENT ID	TECN	COMMENT
1.09 ± 0.48		¹ AMSLER	04B CBAR	$0\bar{p}p \rightarrow \pi^+\pi^-\pi^+\pi^-\eta$

• • • We do not use the following data for averages, fits, limits, etc. • • •
<0.5 90 EDWARDS 83B CBAL $J/\psi \rightarrow \eta\pi\pi\gamma$
<1.1 90 SCHARRE 80 MRK2 $J/\psi \rightarrow \eta\pi\pi\gamma$
<1.5 95 FOSTER 68B HBC 0.0 $\bar{p}p$

¹ Using the data of BAILLON 67 on $\bar{p}p \rightarrow K\bar{K}\pi$.

$\Gamma(\rho^0\gamma)/\Gamma(\eta\pi\pi)$ Γ_{10}/Γ_2

VALUE	DOCUMENT ID	TECN	COMMENT
0.111 ± 0.064	AMSLER	04B CBAR	$0\bar{p}p$

$\Gamma(a_0(980)\pi)/\Gamma(K\bar{K}\pi)$ Γ_3/Γ_1

VALUE	EVTS	DOCUMENT ID	TECN	COMMENT
~0.15		¹ BERTIN	95 OBLX	$0\bar{p}p \rightarrow K\bar{K}\pi\pi\pi$
~0.8	500	¹ DUCH	89 ASTE	$\bar{p}p \rightarrow \pi^+\pi^-\pi^\pm\pi^\mp K^0$
~0.75		¹ REEVES	86 SPEC	$6.6\bar{p}p \rightarrow K\bar{K}\pi X$

¹ Assuming that the $a_0(980)$ decays only into $K\bar{K}$.

$\Gamma(a_0(980)\pi)/\Gamma(\eta\pi\pi)$ Γ_3/Γ_2

VALUE	EVTS	DOCUMENT ID	TECN	COMMENT
0.29 ± 0.10		ABELE	98E CBAR	$0\bar{p}p \rightarrow \eta\pi^0\pi^0\pi^0$
0.19 ± 0.04	2200	¹ ALDE	97B GAM4	$100\pi^-\bar{p} \rightarrow \eta\pi^0\pi^0\eta$
0.56 ± 0.04 ± 0.03		¹ AMSLER	95F CBAR	$0\bar{p}p \rightarrow \pi^+\pi^-\pi^0\pi^0\eta$

¹ Assuming that the $a_0(980)$ decays only into $\eta\pi$.

$\Gamma(a_0(980)\pi)/\Gamma(\eta\pi\pi)$ s-wave Γ_3/Γ_4

VALUE	EVTS	DOCUMENT ID	TECN	COMMENT
0.91 ± 0.12		ANISOVICH	01A SPEC	$0.0\bar{p}p \rightarrow \eta\pi^+\pi^-\pi^+\pi^-$
0.15 ± 0.04	9082	¹ MANAK	00A MPS	$18\pi^-\bar{p} \rightarrow \eta\pi^+\pi^-n$
0.70 ± 0.12 ± 0.20		² BAI	99 BES	$J/\psi \rightarrow \gamma\eta\pi^+\pi^-$

¹ Statistical error only.
² Assuming that the $a_0(980)$ decays only into $\eta\pi$.

$\Gamma(\rho^0\gamma)/\Gamma(K\bar{K}\pi)$ Γ_{10}/Γ_1

VALUE	DOCUMENT ID	TECN	COMMENT
0.0152 ± 0.0038	¹ COFFMAN	90 MRK3	$J/\psi \rightarrow \gamma\gamma\pi^+\pi^-$

¹ Using $B(J/\psi \rightarrow \gamma\eta(1405) \rightarrow \gamma K\bar{K}\pi) = 4.2 \times 10^{-3}$ and $B(J/\psi \rightarrow \gamma\eta(1405) \rightarrow \gamma\gamma\rho^0) = 6.4 \times 10^{-5}$.

$\Gamma(\gamma\gamma)/\Gamma(K\bar{K}\pi)$ Γ_9/Γ_1

VALUE	CL%	DOCUMENT ID	TECN	COMMENT
<1.78 × 10 ⁻³	90	¹ ABLIKIM	180 BES3	$\psi(2S) \rightarrow \pi^+\pi^-\gamma\gamma\gamma$

¹ Using results from BAI 00d.

$\Gamma(\eta(\pi\pi)$ s-wave $\Gamma(\eta\pi\pi)$ Γ_4/Γ_2

VALUE	EVTS	DOCUMENT ID	TECN	COMMENT
0.81 ± 0.04	2200	ALDE	97B GAM4	$100\pi^-\bar{p} \rightarrow \eta\pi^0\pi^0n$

• • • We do not use the following data for averages, fits, limits, etc. • • •

$\Gamma(f_0(980)\eta)/\Gamma(\eta\pi\pi)$ Γ_6/Γ_2

VALUE	DOCUMENT ID	TECN	COMMENT
0.32 ± 0.07	¹ ANISOVICH	00 SPEC	$0.9-1.2\bar{p}p \rightarrow \eta 3\pi^0$

¹ Using preliminary Crystal Barrel data.

$\Gamma(f_0(980)\pi^0 \rightarrow \pi^+\pi^-\pi^0)/\Gamma_{\text{total}}$ Γ_5/Γ

VALUE	DOCUMENT ID	TECN	COMMENT
not seen	¹ ABLIKIM	17A BES3	$\psi(2S) \rightarrow \gamma\pi^+\pi^-\pi^0$

¹ ABLIKIM 17A reports $B(\psi(2S) \rightarrow \gamma\eta(1405) \rightarrow \gamma f_0(980)\pi^0 \rightarrow \gamma\pi^+\pi^-\pi^0) < 5.0 \times 10^{-7}$.

$\Gamma(\rho\rho)/\Gamma_{\text{total}}$ Γ_8/Γ

VALUE	CL%	DOCUMENT ID	TECN	COMMENT
<0.58	99.85	1,2 AMSLER	04B CBAR	$0\bar{p}p$

¹ Assuming that the $\eta(1405)$ decays are saturated by the $\pi\pi\eta$, $K\bar{K}\pi$ and $\rho\rho$ modes.
² Using the data of BAILLON 67 on $\bar{p}p \rightarrow K\bar{K}\pi$.

$\Gamma(K^*(892)K)/\Gamma(a_0(980)\pi)$ Γ_{12}/Γ_3

VALUE	DOCUMENT ID	TECN	COMMENT
0.084 ± 0.024	¹ ADAMS	01B B852	$18\text{ GeV } \pi^-\bar{p} \rightarrow K^+K^-\pi^0n$

¹ Statistical error only.

$\Gamma(\phi\gamma)/\Gamma(\rho^0\gamma)$ Γ_{11}/Γ_{10}

VALUE	CL%	DOCUMENT ID	TECN	COMMENT
0.09 ± 0.03		¹ ABLIKIM	181 BES3	$J/\psi \rightarrow \gamma\gamma\phi(1020)$
0.13 ± 0.04		² ABLIKIM	181 BES3	$J/\psi \rightarrow \gamma\gamma\phi(1020)$
<0.77	95	³ BAI	04J BES2	$J/\psi \rightarrow \gamma\gamma K^+K^-$

¹ Constructive interference between $X(1835)$ and $\eta(1405)/\eta(1475)$ decays to $\gamma\phi$ is assumed. Also see $\eta(1475)$. ABLIKIM 181 reports the inverse as 11.10 ± 3.5 .
² Destructive interference between $X(1835)$ and $\eta(1405)/\eta(1475)$ decays to $\gamma\phi$ is assumed. Also see $\eta(1475)$. ABLIKIM 181 reports the inverse as 7.53 ± 2.49 .
³ Calculated by us from $B(J/\psi \rightarrow \eta(1405)\gamma \rightarrow \phi\gamma\gamma) < 0.82 \times 10^{-4}$ and $B(J/\psi \rightarrow \eta(1405)\gamma \rightarrow \rho^0\gamma\gamma) = (1.07 \pm 0.17 \pm 0.11) \times 10^{-4}$.

$\eta(1405)$ REFERENCES

ABLIKIM	198A	PR D100 092003	M. Ablikim et al.	(BESIII Collab.)
ABLIKIM	181	PR D97 051101	M. Ablikim et al.	(BESIII Collab.)
ABLIKIM	180	PR D97 072014	M. Ablikim et al.	(BESIII Collab.)
ABLIKIM	17A1	PR D96 112008	M. Ablikim et al.	(BESIII Collab.)
ABLIKIM	13M	PR D87 092006	M. Ablikim et al.	(BESIII Collab.)
ABLIKIM	11E	PRL 108 182001	M. Ablikim et al.	(BESIII Collab.)
ABLIKIM	12J	PRL 107 182001	M. Ablikim et al.	(BESIII Collab.)
ABLIKIM	08E	PR D77 032005	M. Ablikim et al.	(BES Collab.)
ABLIKIM	01B	PR D71 072001	R. Ahohe et al.	(CLEO Collab.)
AMSLER	04B	EPJ C33 23	C. Amisler et al.	(Crystal Barrel Collab.)
BAI	04J	PL B594 47	J.Z. Bai et al.	(BES Collab.)
NICHITIU	02	PL B545 261	F. Nichitiu et al.	(OBELIX Collab.)
ACCIARRI	01G	PL B501 1	M. Acciarrri et al.	(L3 Collab.)
ADAMS	01B	PL B516 264	G.S. Adams et al.	(BNL E852 Collab.)
ANISOVICH	01	NP A490 567	A.V. Anisovich et al.	
ANISOVICH	00	PL B472 168	A.V. Anisovich et al.	
BAI	00D	PL B476 25	J.Z. Bai et al.	(BES Collab.)
MANAK	00A	PR D62 012003	J.J. Manak et al.	(BNL E852 Collab.)
BAI	99	PL B446 356	J.Z. Bai et al.	(BES Collab.)
CICALO	99	PL B462 453	C. Cicalo et al.	(OBELIX Collab.)
ABELE	98E	NP B514 45	A. Abele et al.	(Crystal Barrel Collab.)
BAI	98C	PL B440 217	J.Z. Bai et al.	(BES Collab.)
ALDE	97B	PAN 60 386	D. Alde et al.	(GAMS Collab.)
Transferred from YAF 60 458.				
BERTIN	97	PL B400 226	Bertin et al.	(OBELIX Collab.)
AMSLER	95F	PL B358 389	C. Amisler et al.	(Crystal Barrel Collab.)
BERTIN	95	PL B361 187	A. Bertin et al.	(OBELIX Collab.)
BUGG	95	PL B353 378	D.V. Bugg et al.	(LOQM, PNPI, WASH)
AUGUSTIN	92	PR D46 1951	J.E. Augustin, G. Cosme	(DM2 Collab.)
BOLTON	92B	PRL 69 1328	T. Bolton et al.	(Mark III Collab.)
FUKUI	91C	PL B267 293	S. Fukui et al.	(SUGI, NAGO, KEK, KYOT+)
AUGUSTIN	90	PR D42 10	J.E. Augustin et al.	(DM2 Collab.)
BAI	90C	PRL 65 2507	Z. Bai et al.	(Mark III Collab.)
COFFMAN	90	PR D41 1410	D.M. Coffman et al.	(Mark III Collab.)
BISELLO	89B	PR D39 701	G. Bisello et al.	(DM2 Collab.)
DUCH	89	ZPHY C45 223	K.D. Duch et al.	(ASTERIX Collab.) JP
RATH	89	PR D40 693	M.G. Rath et al.	(NDAM, BRAN, BNL, CUNY+)
BIRMAN	88	PRL 61 1557	A. Birman et al.	(BNL, FSU, IND, MASD) JP
ANDO	86	PRL 57 1296	A. Ando et al.	(KEK, KYOT, NIRS, SAGA+) JP
REEVES	86	PR D34 1960	D.F. Reeves et al.	(FLOR, BNL, IND+) JP
CHUNG	85	PRL 55 779	S.U. Chung et al.	(BNL, FLOR, IND+) JP
ALTHOFF	84E	PL 147B 487	M. Althoff et al.	(TASSO Collab.)
EDWARDS	83B	PRL 51 859	C. Edwards et al.	(CIT, HARV, PRIN+)
EDWARDS	82E	PRL 49 253	C. Edwards et al.	(CIT, HARV, PRIN+)
Also				
SCHARRE	80	PL 97B 329	D.L. Scharre et al.	(SLAC, LBL)
FOSTER	68B	NP B8 174	M. Foster et al.	(CERN, CDEF)
BAILLON	67	NC 50A 393	P.H. Baillon et al.	(CERN, CDEF, IRAD)

Meson Particle Listings

$h_1(1415)$, $a_1(1420)$, $f_1(1420)$

$h_1(1415)$

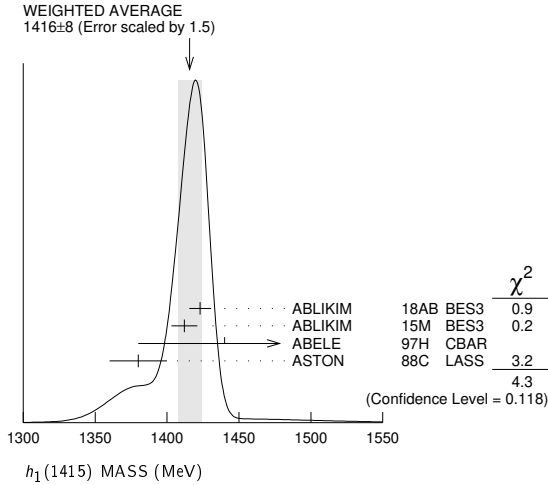
$$J^{PC} = 0^-(1^+ -)$$

was $h_1(1380)$

$h_1(1415)$ MASS

VALUE (MeV)	EVTS	DOCUMENT ID	TECN	COMMENT
1416 ± 8	OUR AVERAGE	Error includes scale factor of 1.5. See the ideogram below.		
1423 ± 2.1 ± 7.3	2.2k	¹ ABLIKIM	18AB BES3	$J/\psi \rightarrow \eta' h_1 \rightarrow \eta' K^* \bar{K}$
1412 ± 4 ± 8		¹ ABLIKIM	15M BES3	$\psi(2S) \rightarrow \gamma \chi_{c1,2} \rightarrow \gamma \phi(h_1 \rightarrow K^* \bar{K})$
1440 ± 60		ABELE	97H CBAR	$\bar{p} p \rightarrow K_L^0 K_S^0 \pi^0 \pi^0$
1380 ± 20		ASTON	88C LASS	11 $K^- p \rightarrow K_S^0 K^\pm \pi^\mp \Lambda$

¹ Final states $K^+ K^- \pi^0$ and $K_S^0 K^\pm \pi^\mp$.



$h_1(1415)$ WIDTH

VALUE (MeV)	EVTS	DOCUMENT ID	TECN	COMMENT
90 ± 15	OUR AVERAGE	Error includes scale factor of 1.1.		
90.3 ± 9.8 ± 17.5	2.2k	¹ ABLIKIM	18AB BES3	$J/\psi \rightarrow \eta' h_1 \rightarrow \eta' K^* \bar{K}$
84 ± 12 ± 40		¹ ABLIKIM	15M BES3	$\psi(2S) \rightarrow \gamma \chi_{c1,2} \rightarrow \gamma \phi(h_1 \rightarrow K^* \bar{K})$
170 ± 80		ABELE	97H CBAR	$\bar{p} p \rightarrow K_L^0 K_S^0 \pi^0 \pi^0$
80 ± 30		ASTON	88C LASS	11 $K^- p \rightarrow K_S^0 K^\pm \pi^\mp \Lambda$

¹ Final states $K^+ K^- \pi^0$ and $K_S^0 K^\pm \pi^\mp$.

$h_1(1415)$ DECAY MODES

Mode	Fraction (Γ_i/Γ)
Γ_1 $K \bar{K}^*(892) + c.c.$	seen

$h_1(1415)$ REFERENCES

ABLIKIM	18AB PR D98 072005	M. Ablikim <i>et al.</i>	(BESIII Collab.)
ABLIKIM	15M PR D91 112008	M. Ablikim <i>et al.</i>	(BESIII Collab.)
ABELE	97H PL B415 280	A. Abele <i>et al.</i>	(Crystal Barrel Collab.)
ASTON	88C PL B201 573	D. Aston <i>et al.</i>	(SLAC, NAGO, CIN, INUS)

$a_1(1420)$

$$J^{PC} = 1^-(1^+ +)$$

OMITTED FROM SUMMARY TABLE

$a_1(1420)$ MASS

VALUE (MeV)	EVTS	DOCUMENT ID	TECN	COMMENT
1411 ± 4	OUR AVERAGE	Error includes scale factor of 1.1.		
1414 ± 15	46M	¹ AGHASYAN	18B COMP	190 $\pi^- p \rightarrow \pi^- \pi^+ \pi^- p$
1414 ± 15		^{2,3} ADOLPH	15C COMP	190 $\pi^- p \rightarrow \pi^- \pi^+ \pi^- p$

• • • We do not use the following data for averages, fits, limits, etc. • • •

¹ Statistical error negligible.
² Using the isobar model and partial-wave analysis with 88 waves.
³ Superseded by AGHASYAN 2018B.

$a_1(1420)$ WIDTH

VALUE (MeV)	EVTS	DOCUMENT ID	TECN	COMMENT
161 ± 11	OUR AVERAGE	Error includes scale factor of 1.1.		
161 ± 14	46M	¹ AGHASYAN	18B COMP	190 $\pi^- p \rightarrow \pi^- \pi^+ \pi^- p$
153 ± 8		^{2,3} ADOLPH	15C COMP	190 $\pi^- p \rightarrow \pi^- \pi^+ \pi^- p$

• • • We do not use the following data for averages, fits, limits, etc. • • •

¹ Statistical error negligible.
² Using the isobar model and partial-wave analysis with 88 waves.
³ Superseded by AGHASYAN 2018B.

$a_1(1420)$ DECAY MODES

Mode	Fraction (Γ_i/Γ)
Γ_1 $f_0(980) \pi$	seen

$a_1(1420)$ BRANCHING RATIOS

$\Gamma(f_0(980) \pi) / \Gamma_{total}$	Fraction (Γ_i/Γ)
seen	OUR AVERAGE
seen	¹ ADOLPH 15C COMP 190 $\pi^- p \rightarrow \pi^- \pi^+ \pi^- p$

¹ Using the isobar model and partial-wave analysis with 88 waves.

$a_1(1420)$ REFERENCES

AGHASYAN	18B PR D98 092003	M. Aghasyan <i>et al.</i>	(COMPASS Collab.)
ADOLPH	15C PRL 115 082001	C. Adolph <i>et al.</i>	(COMPASS Collab.)

$f_1(1420)$

$$J^{PC} = 0^+(1^+ +)$$

See the review on "Pseudoscalar and Pseudovector Mesons in the 1400 MeV Region."

$f_1(1420)$ MASS

VALUE (MeV)	EVTS	DOCUMENT ID	TECN	COMMENT
1426.3 ± 0.9	OUR AVERAGE	Error includes scale factor of 1.1.		
1434 ± 5 ± 5	133	¹ AACHARD	07 L3	183-209 $e^+ e^- \rightarrow K_S^0 K^\pm \pi^\mp$
1426 ± 6	711	ABDALLAH	03H DLPH	91.2 $e^+ e^- \rightarrow K_S^0 K^\pm \pi^\mp + X$
1420 ± 14	3651	NICHITIU	02 OBLX	0 $\bar{p} p \rightarrow K^+ K^- \pi^+ \pi^- \pi^0$
1428 ± 4 ± 2	20k	ADAMS	01B B852	18 GeV $\pi^- p \rightarrow K^+ K^- \pi^0 n$
1426 ± 1		BARBERIS	97C OMEG	450 $pp \rightarrow pp K_S^0 K^\pm \pi^\mp$
1425 ± 8		BERTIN	97 OBLX	0.0 $\bar{p} p \rightarrow K^\pm (K^0) \pi^\mp \pi^+ \pi^-$
1430 ± 4		² ARMSTRONG	92E OMEG	85,300 $\pi^+ p, pp \rightarrow \pi^+ p, pp (K \bar{K} \pi)$
1462 ± 20		³ AUGUSTIN	92 DM2	$J/\psi \rightarrow \gamma K \bar{K} \pi$
1443 ± 7 ± 3	1100	BAI	90C MRK3	$J/\psi \rightarrow \gamma K_S^0 K^\pm \pi^\mp$
1425 ± 10	17	BEHREND	89 CELL	$\gamma \gamma \rightarrow K_S^0 K^\pm \pi^\mp$
1442 ± 5 ± 10	111	BECKER	87 MRK3	$e^+ e^-, \omega K \bar{K} \pi$
1423 ± 4		GIDAL	87B MRK2	$e^+ e^- \rightarrow e^+ e^- K \bar{K} \pi$
1417 ± 13	13	AIHARA	86C TPC	$e^+ e^- \rightarrow e^+ e^- K \bar{K} \pi$
1422 ± 3		CHAUVAT	84 SPEC	ISR 31.5 pp
1440 ± 10		⁴ BROMBERG	80 SPEC	100 $\pi^- p \rightarrow K \bar{K} \pi X$
1426 ± 6	221	DIONISI	80 HBC	4 $\pi^- p \rightarrow K \bar{K} \pi n$
1420 ± 20		DAHL	87 HBC	1.6-4.2 $\pi^- p$
1430.8 ± 0.9		⁵ SOSA	99 SPEC	$pp \rightarrow p_{slow} (K_S^0 K^+ \pi^-) p_{fast}$
1433.4 ± 0.8		⁵ SOSA	99 SPEC	$pp \rightarrow p_{slow} (K_S^0 K^- \pi^+) p_{fast}$
1435 ± 9		PROKOSHKIN	97B GAM4	100 $\pi^- p \rightarrow \eta \pi^0 \pi^0 n$
1429 ± 3	389	ARMSTRONG	89 OMEG	300 $pp \rightarrow K \bar{K} \pi pp$
1425 ± 2	1520	ARMSTRONG	84 OMEG	85 $\pi^+ p, pp \rightarrow (\pi^+, p) (K \bar{K} \pi) p$
~ 1420		BITYUKOV	84 SPEC	32 $K^- p \rightarrow K^+ K^- \pi^0 \gamma$

• • • We do not use the following data for averages, fits, limits, etc. • • •

¹ From a fit with a width fixed at 55 MeV.
² This result supersedes ARMSTRONG 84, ARMSTRONG 89.
³ From fit to the $K^*(892) K 1^+ +$ partial wave.
⁴ Mass error increased to account for $a_0(980)$ mass cut uncertainties.
⁵ No systematic error given.

f₁(1420) WIDTH

Table with columns: VALUE (MeV), EVTS, DOCUMENT ID, TECN, COMMENT. Includes sub-sections for Γ(ππρ)/Γ(KK̄π) and Γ(ηππ)/Γ(KK̄π). Contains data for various experiments like ABDALLAH, NICHITIU, ADAMS, BARBERIS, BERTIN, ARMSTRONG, AUGUSTIN, BAI, BEHREND, BECKER, AIHARA, CHAUVAT, BROMBERG, DIONISI, DAHL, SOSA, PROKOSHKIN, and BITYUKOV.

f₁(1420) DECAY MODES

Table with columns: Mode, Fraction (Γ_i/Γ). Lists decay modes like K̄K̄π, K̄K*(892)+ c.c., ηππ, a₀(980)π, ππρ, 4π, ρ⁰γ, and φγ.

f₁(1420) Γ(i)Γ(γγ)/Γ(total)

Table with columns: Γ(KK̄π) × Γ(γγ*)/Γ_{total}, VALUE (keV), CL%, EVTS, DOCUMENT ID, TECN, COMMENT. Includes sub-sections for Γ(KK̄π) × Γ(γγ*)/Γ_{total} and Γ(KK̄*(892)+ c.c.)/Γ(KK̄π).

f₁(1420) BRANCHING RATIOS

Table with columns: Γ(KK̄*(892)+ c.c.)/Γ(KK̄π), VALUE, DOCUMENT ID, TECN, COMMENT. Includes sub-sections for Γ(KK̄*(892)+ c.c.)/Γ(KK̄π) and Γ₂/Γ₁.

Γ(ππρ)/Γ(KK̄π)

Table with columns: VALUE, CL%, DOCUMENT ID, TECN, COMMENT. Includes sub-sections for Γ(ππρ)/Γ(KK̄π) and Γ₅/Γ₁.

Γ(ηππ)/Γ(KK̄π)

Table with columns: VALUE, CL%, DOCUMENT ID, TECN, COMMENT. Includes sub-sections for Γ(ηππ)/Γ(KK̄π) and Γ₃/Γ₁.

Γ(a₀(980)π)/Γ(ηππ)

Table with columns: VALUE, CL%, DOCUMENT ID, TECN, COMMENT. Includes sub-sections for Γ(a₀(980)π)/Γ(ηππ) and Γ₄/Γ₃.

Γ(4π)/Γ(KK̄*(892)+ c.c.)

Table with columns: VALUE, CL%, DOCUMENT ID, TECN, COMMENT. Includes sub-sections for Γ(4π)/Γ(KK̄*(892)+ c.c.) and Γ₆/Γ₂.

Γ(KK̄π)/[Γ(KK̄*(892)+ c.c.) + Γ(a₀(980)π)]

Table with columns: VALUE, DOCUMENT ID, TECN, COMMENT. Includes sub-sections for Γ(KK̄π)/[Γ(KK̄*(892)+ c.c.) + Γ(a₀(980)π)] and Γ₁/(Γ₂+Γ₄).

Γ(a₀(980)π)/Γ(KK̄*(892)+ c.c.)

Table with columns: VALUE, CL%, DOCUMENT ID, TECN, COMMENT. Includes sub-sections for Γ(a₀(980)π)/Γ(KK̄*(892)+ c.c.) and Γ₄/Γ₂.

Γ(4π)/Γ(KK̄π)

Table with columns: VALUE, CL%, DOCUMENT ID, TECN, COMMENT. Includes sub-sections for Γ(4π)/Γ(KK̄π) and Γ₆/Γ₁.

Γ(ρ⁰γ)/Γ_{total}

Table with columns: VALUE, CL%, DOCUMENT ID, TECN, COMMENT. Includes sub-sections for Γ(ρ⁰γ)/Γ_{total} and Γ₇/Γ.

Γ(ρ⁰γ)/Γ(KK̄π)

Table with columns: VALUE, CL%, DOCUMENT ID, TECN, COMMENT. Includes sub-sections for Γ(ρ⁰γ)/Γ(KK̄π) and Γ₇/Γ₁.

Γ(φγ)/Γ(KK̄π)

Table with columns: VALUE, DOCUMENT ID, TECN, COMMENT. Includes sub-sections for Γ(φγ)/Γ(KK̄π) and Γ₈/Γ₁.

f₁(1420) REFERENCES

Table with columns: AUTHOR, YEAR, JOURNAL, COLLAB. Lists references for f₁(1420) from various experiments and collaborations.

Meson Particle Listings

 $f_1(1420), \omega(1420)$

CHAUVAT	84	PL 148B 382	P. Chauvat <i>et al.</i>	(CERN, CLER, UCLA+)
JENNI	83	PR D27 1031	P. Jenni <i>et al.</i>	(SLAC, LBL)
BROMBERG	80	PR D22 1513	C.M. Bromberg <i>et al.</i>	(CIT, FNAL, ILLC+)
DIONISI	80	NP B169 1	C. Dionisi <i>et al.</i>	(CERN, MADR, CDEF+)
CORDEN	78	NP B144 253	M.J. Corden <i>et al.</i>	(BIRM, RHEL, TELA+)
DEFOIX	72	NP B44 125	C. Defoix <i>et al.</i>	(CDEF, CERN)
DAHL	67	PR 163 1377	O.L. Dahl <i>et al.</i>	(LRL) IJP
Also		PRL 14 1074	D.H. Miller <i>et al.</i>	(LRL, UCB)

 $\omega(1420)$

$$I^G(J^{PC}) = 0^-(1^{--})$$

See also the $\omega(1650)$ particle listing.

 $\omega(1420)$ MASS

VALUE (MeV)	EVTs	DOCUMENT ID	TECN	COMMENT
1410 ± 60 OUR ESTIMATE				
• • • We do not use the following data for averages, fits, limits, etc. • • •				
1418 ± 30 ± 10	824	¹ AKHMETSHIN 17A	CMD3	1.4–2.0 $e^+e^- \rightarrow \omega\eta$
1470 ± 50	13.1k	² AULCHENKO 15A	SND	1.05–1.80 $e^+e^- \rightarrow \pi^+\pi^-\pi^0$
1382 ± 23 ± 70		AUBERT	07AU BABR	10.6 $e^+e^- \rightarrow \omega\pi^+\pi^-\gamma$
1350 ± 20 ± 20		AUBERT,B	04N BABR	10.6 $e^+e^- \rightarrow \pi^+\pi^-\pi^0\gamma$
1400 ± 50 ± 130	1.2M	³ ACHASOV	03D RVUE	0.44–2.00 $e^+e^- \rightarrow \pi^+\pi^-\pi^0\gamma$
1450 ± 10		⁴ HENNER	02 RVUE	1.2–2.0 $e^+e^- \rightarrow \rho\pi, \omega\pi\pi$
1373 ± 70	177	⁵ AKHMETSHIN 00D	CMD2	1.2–1.38 $e^+e^- \rightarrow \omega\pi^+\pi^-$
1370 ± 25	5095	ANISOVICH	00H SPEC	0.0 $p\bar{p} \rightarrow \omega\pi^0\pi^0\pi^0$
1400 ⁺¹⁰⁰ ₋₂₀₀		⁶ ACHASOV	98H RVUE	$e^+e^- \rightarrow \pi^+\pi^-\pi^0$
~ 1400		⁷ ACHASOV	98H RVUE	$e^+e^- \rightarrow \omega\pi^+\pi^-$
~ 1460		⁸ ACHASOV	98H RVUE	$e^+e^- \rightarrow K^+K^-$
1440 ± 70		⁹ CLEGG	94 RVUE	
1419 ± 31	315	¹⁰ ANTONELLI	92 DM2	1.34–2.4 $e^+e^- \rightarrow \rho\pi$

- From a fit of the interfering $\omega(1420)$ and $\omega(1650)$ with a relative phase of π and other parameters floating.
- From a fit with contributions from $\omega(782)$, $\phi(1020)$, $\omega(1420)$, and $\omega(1650)$.
- From the combined fit of ANTONELLI 92, ACHASOV 01E, ACHASOV 02E, and ACHASOV 03D data on the $\pi^+\pi^-\pi^0$ and ANTONELLI 92 on the $\omega\pi^+\pi^-$ final states. Supersedes ACHASOV 99E and ACHASOV 02E.
- Using results of CORDIER 81 and preliminary data of DOLINSKY 91 and ANTONELLI 92.
- Using the data of AKHMETSHIN 00D and ANTONELLI 92. The $\rho\pi$ dominance for the energy dependence of the $\omega(1420)$ and $\omega(1650)$ width assumed.
- Using data from BARKOV 87, DOLINSKY 91, and ANTONELLI 92.
- Using the data from ANTONELLI 92.
- Using the data from IVANOV 81 and BISELLO 88b.
- From a fit to two Breit-Wigner functions and using the data of DOLINSKY 91 and ANTONELLI 92.
- From a fit to two Breit-Wigner functions interfering between them and with the ω, ϕ tails with fixed (+, -, +) phases.

 $\omega(1420)$ WIDTH

VALUE (MeV)	EVTs	DOCUMENT ID	TECN	COMMENT
290 ± 190 OUR ESTIMATE				
• • • We do not use the following data for averages, fits, limits, etc. • • •				
104 ± 35 ± 10	824	¹ AKHMETSHIN 17A	CMD3	1.4–2.0 $e^+e^- \rightarrow \omega\eta$
880 ± 170	13.1k	² AULCHENKO 15A	SND	1.05–1.80 $e^+e^- \rightarrow \pi^+\pi^-\pi^0$
480 ± 180		³ ACHASOV	10D SND	1.075–2.0 $e^+e^- \rightarrow \pi^0\gamma$
130 ± 50 ± 100		AUBERT	07AU BABR	10.6 $e^+e^- \rightarrow \omega\pi^+\pi^-\gamma$
450 ± 70 ± 70		AUBERT,B	04N BABR	10.6 $e^+e^- \rightarrow \pi^+\pi^-\pi^0\gamma$
870 ⁺⁵⁰⁰ ₋₃₀₀ ± 450	1.2M	⁴ ACHASOV	03D RVUE	0.44–2.00 $e^+e^- \rightarrow \pi^+\pi^-\pi^0\gamma$
199 ± 15		⁵ HENNER	02 RVUE	1.2–2.0 $e^+e^- \rightarrow \rho\pi, \omega\pi\pi$
188 ± 45	177	⁶ AKHMETSHIN 00D	CMD2	1.2–1.38 $e^+e^- \rightarrow \omega\pi^+\pi^-$
360 ⁺¹⁰⁰ ₋₆₀	5095	ANISOVICH	00H SPEC	0.0 $p\bar{p} \rightarrow \omega\pi^0\pi^0\pi^0$
240 ± 70		⁷ CLEGG	94 RVUE	
174 ± 59	315	⁸ ANTONELLI	92 DM2	1.34–2.4 $e^+e^- \rightarrow \rho\pi$

- From a fit of the interfering $\omega(1420)$ and $\omega(1650)$ with a relative phase of π and other parameters floating.
- From a fit with contributions from $\omega(782)$, $\phi(1020)$, $\omega(1420)$, and $\omega(1650)$.
- From a fit of a VMD model with two effective resonances with masses of 1450 MeV and 1700 MeV to describe the excited vector states $\omega(1420)$, $\rho(1450)$, $\omega(1650)$, and $\rho(1700)$. Systematic errors not evaluated.
- From the combined fit of ANTONELLI 92, ACHASOV 01E, ACHASOV 02E, and ACHASOV 03D data on the $\pi^+\pi^-\pi^0$ and ANTONELLI 92 on the $\omega\pi^+\pi^-$ final states. Supersedes ACHASOV 99E and ACHASOV 02E.
- Using results of CORDIER 81 and preliminary data of DOLINSKY 91 and ANTONELLI 92.
- Using the data of AKHMETSHIN 00D and ANTONELLI 92. The $\rho\pi$ dominance for the energy dependence of the $\omega(1420)$ and $\omega(1650)$ width assumed.
- From a fit to two Breit-Wigner functions and using the data of DOLINSKY 91 and ANTONELLI 92.
- From a fit to two Breit-Wigner functions interfering between them and with the ω, ϕ tails with fixed (+, -, +) phases.

 $\omega(1420)$ DECAY MODES

Mode	Fraction (Γ_i/Γ)
Γ_1 $\rho\pi$	seen
Γ_2 $\omega\pi\pi$	seen
Γ_3 $\omega\eta$	
Γ_4 $b_1(1235)\pi$	seen
Γ_5 e^+e^-	seen
Γ_6 $\pi^0\gamma$	

 $\omega(1420)$ $\Gamma(i)\Gamma(e^+e^-)/\Gamma^2(\text{total})$

$\Gamma(\rho\pi)/\Gamma_{\text{total}} \times \Gamma(e^+e^-)/\Gamma_{\text{total}}$	$\Gamma_1/\Gamma \times \Gamma_5/\Gamma$			
VALUE (units 10^{-6})	EVTs	DOCUMENT ID	TECN	COMMENT
• • • We do not use the following data for averages, fits, limits, etc. • • •				
0.73 ± 0.08	13.1k	¹ AULCHENKO 15A	SND	1.05–1.80 $e^+e^- \rightarrow \pi^+\pi^-\pi^0$
0.82 ± 0.05 ± 0.06		AUBERT,B	04N BABR	10.6 $e^+e^- \rightarrow \pi^+\pi^-\pi^0\gamma$
0.65 ± 0.13 ± 0.21	1.2M	^{2,3} ACHASOV	03D RVUE	0.44–2.00 $e^+e^- \rightarrow \pi^+\pi^-\pi^0\gamma$
0.625 ± 0.160		^{4,5} CLEGG	94 RVUE	
0.466 ± 0.178		^{6,7} ANTONELLI	92 DM2	1.34–2.4 $e^+e^- \rightarrow \rho\pi$

- From a fit with contributions from $\omega(782)$, $\phi(1020)$, $\omega(1420)$, and $\omega(1650)$.
- Calculated by us from the cross section at the peak.
- From the combined fit of ANTONELLI 92, ACHASOV 01E, ACHASOV 02E, and ACHASOV 03D data on the $\pi^+\pi^-\pi^0$ and ANTONELLI 92 on the $\omega\pi^+\pi^-$ final states. Supersedes ACHASOV 99E and ACHASOV 02E.
- From a fit to two Breit-Wigner functions and using the data of DOLINSKY 91 and ANTONELLI 92.
- From the partial and leptonic width given by the authors.
- From a fit to two Breit-Wigner functions interfering between them and with the ω, ϕ tails with fixed (+, -, +) phases.
- From the product of the leptonic width and partial branching ratio given by the authors.

 $\Gamma(\omega\pi\pi)/\Gamma_{\text{total}} \times \Gamma(e^+e^-)/\Gamma_{\text{total}}$ $\Gamma_2/\Gamma \times \Gamma_5/\Gamma$

VALUE (units 10^{-8})	DOCUMENT ID	TECN	COMMENT
• • • We do not use the following data for averages, fits, limits, etc. • • •			
19.7 ± 5.7	AUBERT	07AU BABR	10.6 $e^+e^- \rightarrow \omega\pi^+\pi^-\gamma$
1.9 ± 1.9	¹ AKHMETSHIN 00D	CMD2	1.2–2.4 $e^+e^- \rightarrow \omega\pi^+\pi^-$

- Using the data of AKHMETSHIN 00D and ANTONELLI 92. The $\rho\pi$ dominance for the energy dependence of the $\omega(1420)$ and $\omega(1650)$ width assumed.

 $\Gamma(\omega\eta)/\Gamma_{\text{total}} \times \Gamma(e^+e^-)/\Gamma_{\text{total}}$ $\Gamma_3/\Gamma \times \Gamma_5/\Gamma$

VALUE (units 10^{-8})	EVTs	DOCUMENT ID	TECN	COMMENT
• • • We do not use the following data for averages, fits, limits, etc. • • •				
2.1 ^{+1.0} _{-0.8}		ACHASOV	19 SND	$e^+e^- \rightarrow \pi^+\pi^-\pi^0\eta$
5.0 ± 2.6 ± 0.3	824	¹ AKHMETSHIN 17A	CMD3	1.4–2.0 $e^+e^- \rightarrow \omega\eta$
1.6 ^{+0.9} _{-0.7}	898	² ACHASOV	16B SND	1.34–2.00 $e^+e^- \rightarrow \omega\eta$

- From a fit of the interfering $\omega(1420)$ and $\omega(1650)$ with a relative phase of π and other parameters floating. From an alternative fit $\Gamma(\omega(1420) \rightarrow \omega\eta)/\Gamma_{\text{total}} \times \Gamma(\omega(1420) \rightarrow e^+e^-) = 5.3 \pm 1.6$ eV.
- From a fit with contributions from $\omega(1420)$, $\omega(1650)$, and $\phi(1680)$. The mass and the width of $\omega(1420)$ are fixed to the 2014 edition (PDG 14) of this review.

 $\Gamma(\pi^0\gamma)/\Gamma_{\text{total}} \times \Gamma(e^+e^-)/\Gamma_{\text{total}}$ $\Gamma_6/\Gamma \times \Gamma_5/\Gamma$

VALUE (units 10^{-8})	DOCUMENT ID	TECN	COMMENT
• • • We do not use the following data for averages, fits, limits, etc. • • •			
0.23 ± 0.14	¹ ACHASOV	10D SND	1.075–2.0 $e^+e^- \rightarrow \pi^0\gamma$
2.03 ^{+0.70} _{-0.75}	² AKHMETSHIN 05	CMD2	0.60–1.38 $e^+e^- \rightarrow \pi^0\gamma$

- From a fit of a VMD model with two effective resonances with masses of 1450 MeV and 1700 MeV to describe the excited vector states $\omega(1420)$, $\rho(1450)$, $\omega(1650)$, and $\rho(1700)$. Systematic errors not evaluated.
- Using 1420 MeV and 220 MeV for the $\omega(1420)$ mass and width.

 $\omega(1420)$ BRANCHING RATIOS

$\Gamma(\omega\pi\pi)/\Gamma_{\text{total}}$	Γ_2/Γ		
VALUE	DOCUMENT ID	TECN	COMMENT

- • • We do not use the following data for averages, fits, limits, etc. • • •
- 0.301 ± 0.029
- possibly seen
- ¹ HENNER 02 RVUE 1.2–2.0 $e^+e^- \rightarrow \rho\pi, \omega\pi\pi$
- AKHMETSHIN 00D CMD2 $e^+e^- \rightarrow \omega\pi^+\pi^-$

$\Gamma(\omega\pi\pi)/\Gamma(b_1(1235)\pi)$	Γ_2/Γ_4			
VALUE	EVTs	DOCUMENT ID	TECN	COMMENT

- • • We do not use the following data for averages, fits, limits, etc. • • •
- 0.60 ± 0.16
- 5095
- ANISOVICH 00H SPEC 0.0 $p\bar{p} \rightarrow \omega\pi^0\pi^0\pi^0$

See key on page 999

Meson Particle Listings

$\omega(1420)$, $f_2(1430)$, $a_0(1450)$

$\Gamma(\rho\pi)/\Gamma_{total}$		Γ_1/Γ		
VALUE	DOCUMENT ID	TECN	COMMENT	
••• We do not use the following data for averages, fits, limits, etc. •••				
0.699 ± 0.029	¹ HENNER	02	RVUE $1.2-2.0 e^+ e^- \rightarrow \rho\pi, \omega\pi\pi$	
$\Gamma(e^+e^-)/\Gamma_{total}$		Γ_5/Γ		
VALUE (units 10^{-7})	EVTS	DOCUMENT ID	TECN	COMMENT
••• We do not use the following data for averages, fits, limits, etc. •••				
~ 6.6	1.2M	^{2,3} ACHASOV	03d	RVUE $0.44-2.00 e^+ e^- \rightarrow \pi^+\pi^-\pi^0$
23 ± 1		¹ HENNER	02	RVUE $1.2-2.0 e^+ e^- \rightarrow \rho\pi, \omega\pi\pi$
¹ Assuming that the $\omega(1420)$ decays into $\rho\pi$ and $\omega\pi\pi$ only.				
² Calculated by us from the cross section at the peak.				
³ Assuming that the $\omega(1420)$ decays into $\rho\pi$ only.				

$\omega(1420)$ REFERENCES

ACHASOV	19	PR D99 112004	M.N. Achasov et al.	(SND Collab.)
AKHMETSHIN	17A	PL B773 150	R.R. Akhmetshin et al.	(CMD-3 Collab.)
ACHASOV	16B	PR D94 092002	M.N. Achasov et al.	(SND Collab.)
AULCHENKO	15A	JETP 121 27	V.M. Aulchenko et al.	(SND Collab.)
Translated from ZETF 148 34.				
PDG	14	CP C38 070001	K. Olive et al.	(PDG Collab.)
ACHASOV	10D	PR D98 112001	M.N. Achasov et al.	(SND Collab.)
AUBERT	07AU	PR D76 092005	B. Aubert et al.	(BABAR Collab.)
AKHMETSHIN	05	PL B605 26	R.R. Akhmetshin et al.	(Novosibirsk CMD-2 Collab.)
AUBERT.B	04N	PR D70 072004	B. Aubert et al.	(BABAR Collab.)
ACHASOV	03D	PR D68 052006	M.N. Achasov et al.	(Novosibirsk SND Collab.)
ACHASOV	02E	PR D66 032001	M.N. Achasov et al.	(Novosibirsk SND Collab.)
HENNER	02	EPL C26 3	V.K. Henner et al.	
ACHASOV	01E	PR D63 072002	M.N. Achasov et al.	(Novosibirsk SND Collab.)
AKHMETSHIN	00D	PL B489 125	R.R. Akhmetshin et al.	(Novosibirsk CMD-2 Collab.)
ANISOVICH	00H	PL B485 341	A.V. Anisovich et al.	
ACHASOV	99E	PL B462 365	M.N. Achasov et al.	(Novosibirsk SND Collab.)
ACHASOV	98H	PR D57 4334	N.N. Achasov, A.A. Kozhevnikov	
CLEGG	94	ZPHY C62 455	A.B. Clegg, A. Donnachie	(LANC, MCHS)
ANTONELLI	92	ZPHY C56 15	A. Antonelli et al.	(DM2 Collab.)
DOLINSKY	91	PRPL 202 99	S.I. Dolinsky et al.	(NOVO)
BISELLO	88B	ZPHY C39 13	D. Bisello et al.	(PADO, CLER, FRAS+) (NOVO)
BARKOV	87	JETPL 46 164	L.M. Barkov et al.	(NOVO)
Translated from ZETFP 46 132.				
CORDIER	81	PL 106B 155	A. Cordier et al.	(ORSAY)
IVANOV	81	PL 107B 297	P.M. Ivanov et al.	(NOVO)

$f_2(1430)$ $I^G(J^{PC}) = 0^+(2^{++})$

OMITTED FROM SUMMARY TABLE
This entry lists nearby peaks observed in the D wave of the $K\bar{K}$ and $\pi^+\pi^-$ systems. Needs confirmation.

$f_2(1430)$ MASS

VALUE (MeV)	DOCUMENT ID	TECN	COMMENT
≈ 1430 OUR ESTIMATE			
••• We do not use the following data for averages, fits, limits, etc. •••			
1453 ± 4	¹ VLADIMIRSK..01	SPEC	$40 \pi^- p \rightarrow K_S^0 K_S^0 n$
1421 ± 5	AUGUSTIN	87	DM2 $J/\psi \rightarrow \gamma\pi^+\pi^-$
1480 ± 5.0	AKESSON	86	SPEC $pp \rightarrow pp\pi^+\pi^-$
1436^{+26}_{-16}	DAUM	84	CNTR $17-18 \pi^- p \rightarrow K^+ K^- n$
1412 ± 3	DAUM	84	CNTR $63 \pi^- p \rightarrow K_S^0 K_S^0 n, K^+ K^- n$
1439^{+5}_{-6}	² BEUSCH	67	OSPK $5,7,12 \pi^- p \rightarrow K_S^0 K_S^0 n$
¹ $J^{PC} = 0^{++}$ or 2^{++} .			
² Not seen by WETZEL 76.			

$f_2(1430)$ WIDTH

VALUE (MeV)	DOCUMENT ID	TECN	COMMENT
••• We do not use the following data for averages, fits, limits, etc. •••			
13 ± 5	³ VLADIMIRSK..01	SPEC	$40 \pi^- p \rightarrow K_S^0 K_S^0 n$
30 ± 9	AUGUSTIN	87	DM2 $J/\psi \rightarrow \gamma\pi^+\pi^-$
150 ± 5.0	AKESSON	86	SPEC $pp \rightarrow pp\pi^+\pi^-$
81^{+56}_{-29}	DAUM	84	CNTR $17-18 \pi^- p \rightarrow K^+ K^- n$
14 ± 6	DAUM	84	CNTR $63 \pi^- p \rightarrow K_S^0 K_S^0 n, K^+ K^- n$
43^{+17}_{-18}	⁴ BEUSCH	67	OSPK $5,7,12 \pi^- p \rightarrow K_S^0 K_S^0 n$
³ $J^{PC} = 0^{++}$ or 2^{++} .			
⁴ Not seen by WETZEL 76.			

$f_2(1430)$ DECAY MODES

Mode	
Γ_1	$K\bar{K}$
Γ_2	$\pi\pi$

$f_2(1430)$ REFERENCES

VLADIMIRSK..01	PAN 64 1895	V.V. Vladimirov et al.
Translated from YAF 64 1979.		
AUGUSTIN	87	ZPHY C36 369
AKESSON	86	NP B264 154
DAUM	84	ZPHY C23 339
WETZEL	76	NP B115 208
BEUSCH	67	PL 25B 357
J.E. Augustin et al. (LALO, CLER, FRAS+)		
T. Akesson et al. (Axial Field Spec. Collab.)		
C. Daum et al. (AMST, CERN, CRAC, MPIM+)		
W. Wetzel et al. (ETH, CERN, LOIC)		
W. Beusch et al. (ETH, CERN)		

$a_0(1450)$ $I^G(J^{PC}) = 1^-(0^{++})$

See the review on "Scalar Mesons below 2 GeV."

$a_0(1450)$ MASS

VALUE (MeV)	EVTS	DOCUMENT ID	TECN	COMMENT
1474 ± 19 OUR AVERAGE				
1480 ± 30		ABELE	98	CBAR $0.0 \bar{p}p \rightarrow K_S^0 K^\pm \pi^\mp$
1470 ± 25		¹ AMSLER	95D	CBAR $0.0 \bar{p}p \rightarrow \pi^0 \pi^0 \pi^0, \pi^0 \eta, \pi^0 \pi^0 \eta$
••• We do not use the following data for averages, fits, limits, etc. •••				
$1458 \pm 14 \pm 15$	190k	² AAIJ	16N	LHCB $D^0 \rightarrow K_S^0 K^\pm \pi^\mp$
1515 ± 30		³ ANISOVICH	09	RVUE $0.0 \bar{p}p, \pi N$
$1316.8^{+0.7+24.7}_{-1.0-4.6}$		⁴ UEHARA	09A	BELL $\gamma\gamma \rightarrow \pi^0 \eta$
$1432 \pm 13 \pm 25$		⁵ BUGG	08A	RVUE $\bar{p}p$
1477 ± 10	80k	⁶ UMAN	06	E835 $5.2 \bar{p}p \rightarrow \eta\eta\pi^0$
1441^{+40}_{-15}	35280	³ BAKER	03	SPEC $\bar{p}p \rightarrow \omega\pi^+\pi^-\pi^0$
1303 ± 16		⁷ BARGIOTTI	03	OBLX $\bar{p}p$
1296 ± 10		⁸ AMSLER	02	CBAR $0.9 \bar{p}p \rightarrow \pi^0 \pi^0 \eta$
1565 ± 30		⁹ ANISOVICH	98B	RVUE Compilation
1290 ± 10		⁸ BERTIN	98B	OBLX $0.0 \bar{p}p \rightarrow K^\pm K_S \pi^\mp$
1450 ± 40		AMSLER	94D	CBAR $0.0 \bar{p}p \rightarrow \pi^0 \pi^0 \eta$
1410 ± 25		ETKIN	82C	MPS $23 \pi^- p \rightarrow n2K_S^0$
~ 1300		MARTIN	78	SPEC $10 K^\pm p \rightarrow K_S^0 \pi p$
1255 ± 5		¹⁰ CASON	76	
¹ Coupled-channel analysis of AMSLER 95B, AMSLER 95c, and AMSLER 94D.				
² Using a model with Gaussian constraints to the PDG averaged values.				
³ From the pole position.				
⁴ May be a different state.				
⁵ Using data from AMSLER 94D, ABLE 98, and BAKER 03. Supersedes BUGG 94.				
⁶ Statistical error only.				
⁷ Coupled channel analysis of $\pi^+\pi^-\pi^0, K^+K^-\pi^0$, and $K^\pm K_S^0 \pi^\mp$.				
⁸ T-matrix pole.				
⁹ Not confirmed by BUGG 08A.				
¹⁰ Isospin 0 not excluded.				

$a_0(1450)$ WIDTH

VALUE (MeV)	EVTS	DOCUMENT ID	TECN	COMMENT
265 ± 13 OUR AVERAGE				
265 ± 15		ABELE	98	CBAR $0.0 \bar{p}p \rightarrow K_S^0 K^\pm \pi^\mp$
265 ± 30		¹ AMSLER	95D	CBAR $0.0 \bar{p}p \rightarrow \pi^0 \pi^0 \pi^0, \pi^0 \eta, \pi^0 \pi^0 \eta$
••• We do not use the following data for averages, fits, limits, etc. •••				
$282 \pm 12 \pm 13$	190k	² AAIJ	16N	LHCB $D^0 \rightarrow K_S^0 K^\pm \pi^\mp$
230 ± 36		³ ANISOVICH	09	RVUE $0.0 \bar{p}p, \pi N$
$65.0^{+2.1+99.1}_{-5.4-32.6}$		⁴ UEHARA	09A	BELL $\gamma\gamma \rightarrow \pi^0 \eta$
$196 \pm 10 \pm 10$		⁵ BUGG	08A	RVUE $\bar{p}p$
267 ± 11	80k	⁶ UMAN	06	E835 $5.2 \bar{p}p \rightarrow \eta\eta\pi^0$
110 ± 14	35280	³ BAKER	03	SPEC $\bar{p}p \rightarrow \omega\pi^+\pi^-\pi^0$
92 ± 16		⁷ BARGIOTTI	03	OBLX $\bar{p}p$
81 ± 21		⁸ AMSLER	02	CBAR $0.9 \bar{p}p \rightarrow \pi^0 \pi^0 \eta$
292 ± 40		⁹ ANISOVICH	98B	RVUE Compilation
80 ± 5		⁸ BERTIN	98B	OBLX $0.0 \bar{p}p \rightarrow K^\pm K_S \pi^\mp$
270 ± 40		AMSLER	94D	CBAR $0.0 \bar{p}p \rightarrow \pi^0 \pi^0 \eta$
230 ± 30		ETKIN	82C	MPS $23 \pi^- p \rightarrow n2K_S^0$
~ 250		MARTIN	78	SPEC $10 K^\pm p \rightarrow K_S^0 \pi p$
79 ± 10		¹⁰ CASON	76	
¹ Coupled-channel analysis of AMSLER 95B, AMSLER 95c, and AMSLER 94D.				
² Using a model with Gaussian constraints to the PDG averaged values.				
³ From the pole position.				
⁴ May be a different state.				
⁵ Using data from AMSLER 94D, ABLE 98, and BAKER 03. Supersedes BUGG 94.				
⁶ Statistical error only.				
⁷ Coupled channel analysis of $\pi^+\pi^-\pi^0, K^+K^-\pi^0$, and $K^\pm K_S^0 \pi^\mp$.				
⁸ T-matrix pole.				
⁹ Not confirmed by BUGG 08A.				
¹⁰ Isospin 0 not excluded.				

Meson Particle Listings

 $a_0(1450)$, $\rho(1450)$ $a_0(1450)$ DECAY MODES

Mode	Fraction (Γ_i/Γ)
Γ_1 $\pi\eta$	0.093 ± 0.020
Γ_2 $\pi\eta'(958)$	0.033 ± 0.017
Γ_3 $K\bar{K}$	0.082 ± 0.028
Γ_4 $\omega\pi\pi$	DEFINED AS 1
Γ_5 $a_0(980)\pi\pi$	seen
Γ_6 $\gamma\gamma$	seen

 $a_0(1450)$ $\Gamma(i)\Gamma(\gamma\gamma)/\Gamma(\text{total})$

$\Gamma(\pi\eta) \times \Gamma(\gamma\gamma)/\Gamma_{\text{total}}$	DOCUMENT ID	TECN	COMMENT	$\Gamma_1\Gamma_6/\Gamma$
VALUE (eV)				
$432 \pm 6 \pm_{256}^{+1073}$	¹ UEHARA	09A	BELL	$\gamma\gamma \rightarrow \pi^0\eta$
¹ May be a different state.				

 $a_0(1450)$ BRANCHING RATIOS

$\Gamma(\pi\eta'(958))/\Gamma(\pi\eta)$	DOCUMENT ID	TECN	COMMENT	Γ_2/Γ_1
VALUE				
0.35 ± 0.16	¹ ABELE	98	CBAR	$0.0 \bar{p}p \rightarrow K_L^0 K^\pm \pi^\mp$
••• We do not use the following data for averages, fits, limits, etc. •••				
0.43 ± 0.19	ABELE	97c	CBAR	$0.0 \bar{p}p \rightarrow \pi^0 \pi^0 \eta'$
¹ Using $\pi^0\eta$ from AMSLER 94d.				

$\Gamma(K\bar{K})/\Gamma(\pi\eta)$	DOCUMENT ID	TECN	COMMENT	Γ_3/Γ_1
VALUE				
0.88 ± 0.23	¹ ABELE	98	CBAR	$0.0 \bar{p}p \rightarrow K_L^0 K^\pm \pi^\mp$
¹ Using $\pi^0\eta$ from AMSLER 94d.				

$\Gamma(\omega\pi\pi)/\Gamma(\pi\eta)$	DOCUMENT ID	TECN	COMMENT	Γ_4/Γ_1
VALUE				
10.7 ± 2.3	¹ BAKER	03	SPEC	$\bar{p}p \rightarrow \omega\pi^+\pi^-\pi^0$
¹ Using results on $\bar{p}p \rightarrow a_0(1450)^0\pi^0$, $a_0(1450) \rightarrow \eta\pi^0$ from ABELE 96c and assuming the $\omega\rho$ mechanism for the $\omega\pi\pi$ state.				

$\Gamma(a_0(980)\pi\pi)/\Gamma_{\text{total}}$	DOCUMENT ID	TECN	COMMENT	Γ_5/Γ
VALUE				
seen	BUGG	08A	RVUE	$\bar{p}p$

$\Gamma(a_0(980)\pi\pi)/\Gamma(\pi\eta)$	DOCUMENT ID	TECN	CHG	COMMENT	Γ_5/Γ_1
VALUE					
≤ 4.3	ANISOVICH	01	RVUE	0	$\bar{p}p \rightarrow \eta 2\pi^+ 2\pi^-$
••• We do not use the following data for averages, fits, limits, etc. •••					

$\Gamma(\gamma\gamma)/\Gamma_{\text{total}}$	DOCUMENT ID	TECN	COMMENT	Γ_6/Γ
VALUE				
seen	¹ UEHARA	09A	BELL	$\gamma\gamma \rightarrow \pi^0\eta$
¹ May be a different state.				

 $a_0(1450)$ REFERENCES

AJJ	16N	PR D93 052018	R. Ajai et al.	(LHCb Collab.)
ANISOVICH	09	JMP A24 2481	V.V. Anisovich, A.V. Sarantsev	
UEHARA	09A	PR D80 032001	S. Uehara et al.	(BELLE Collab.)
BUGG	08A	PR D78 074023	D.V. Bugg	(LOQM)
UMAN	06	PR D73 052009	I. Uman et al.	(FNAL E835)
BAKER	03	PL B563 140	C.A. Baker et al.	
BARGIOTTI	03	EPJ C26 371	M. Bargiotti et al.	(OBELIX Collab.)
AMSLER	02	EPJ C23 29	C. Amisler et al.	
ANISOVICH	01	NP A690 567	A.V. Anisovich et al.	
ABELE	98	PR D57 3860	A. Abele et al.	(Crystal Barrel Collab.)
ANISOVICH	98B	SPU 411 419	V.V. Anisovich et al.	
		Translated from UFN 168 481.		
BERTIN	98B	PL B434 180	A. Bertin et al.	(OBELIX Collab.)
ABELE	97C	PL B404 179	A. Abele et al.	(Crystal Barrel Collab.)
ABELE	96C	NP A609 562	A. Abele et al.	(Crystal Barrel Collab.)
AMSLER	95B	PL B342 433	C. Amisler et al.	(Crystal Barrel Collab.)
AMSLER	95C	PL B353 571	C. Amisler et al.	(Crystal Barrel Collab.)
AMSLER	95D	PL B355 425	C. Amisler et al.	(Crystal Barrel Collab.)
AMSLER	94D	PL B333 277	C. Amisler et al.	(Crystal Barrel Collab.)
BUGG	94	PR D50 4412	D.V. Bugg et al.	(LOQM)
ETKIN	82C	NP D25 2446	A. Etkin et al.	(BNL, CUNY, TUFTS, VAND)
MARTIN	78	NP B134 392	A.D. Martin et al.	(DURH, GEVA)
CASON	76	PRL 36 1465	N.M. Cason et al.	(NDAM, ANL)

 $\rho(1450)$

$$I^G(J^{PC}) = 1^+(1^-)$$

THE $\rho(1450)$ AND THE $\rho(1700)$

Updated September 2019 by S. Eidelman (Novosibirsk), C. Hanhart (Juelich) and G. Venanzoni (Pisa).

In our 1988 edition, we replaced the $\rho(1600)$ entry with two new ones, the $\rho(1450)$ and the $\rho(1700)$, because there was emerging evidence that the 1600-MeV region actually contains two ρ -like resonances. Erkal [1] had pointed out this possibility with a theoretical analysis on the consistency of 2π and 4π electromagnetic form factors and the $\pi\pi$ scattering length. Donnachie [2], with a full analysis of data on the 2π and 4π final states in e^+e^- annihilation and photoproduction reactions, had also argued that in order to obtain a consistent picture, two resonances were necessary. The existence of $\rho(1450)$ was supported by the analysis of $\eta\rho^0$ mass spectra obtained in photoproduction and e^+e^- annihilation [3], as well as that of $e^+e^- \rightarrow \omega\pi$ [4].

The analysis of [2] was further extended by [5,6] to include new data on 4π -systems produced in e^+e^- annihilation, and in τ -decays (τ decays to 4π , and e^+e^- annihilation to 4π can be related by the Conserved Vector Current assumption). These systems were successfully analyzed using interfering contributions from two ρ -like states, and from the tail of the $\rho(770)$ decaying into two-body states. While specific conclusions on $\rho(1450) \rightarrow 4\pi$ were obtained, little could be said about the $\rho(1700)$.

Independent evidence for two 1^- states is provided by [7] in 4π electroproduction at $\langle Q^2 \rangle = 1$ (GeV/c)², and by [8] in a high-statistics sample of the $\eta\pi\pi$ system in π^-p charge exchange.

This scenario with two overlapping resonances is supported by other data. Bisello [9] measured the pion form factor in the interval 1.35–2.4 GeV, and observed a deep minimum around 1.6 GeV. The best fit was obtained with the hypothesis of ρ -like resonances at 1420 and 1770 MeV, with widths of about 250 MeV. Antonelli [10] found that the $e^+e^- \rightarrow \eta\pi^+\pi^-$ cross section is better fitted with two fully interfering Breit-Wigners, with parameters in fair agreement with those of [2] and [9]. These results can be considered as a confirmation of the $\rho(1450)$.

Decisive evidence for the $\pi\pi$ decay mode of both $\rho(1450)$ and $\rho(1700)$ comes from $\bar{p}p$ annihilation at rest [11]. It has been shown that these resonances also possess a $K\bar{K}$ decay mode [12–14]. High-statistics studies of the decays $\tau \rightarrow \pi\pi\nu_\tau$ [15,16], and $\tau \rightarrow 4\pi\nu_\tau$ [17] also require the $\rho(1450)$, but are not sensitive to the $\rho(1700)$, because it is too close to the τ mass. A recent very-high-statistics study of the $\tau \rightarrow \pi\pi\nu_\tau$ decay performed at Belle [18] reports the first observation of both $\rho(1450)$ and $\rho(1700)$ in τ decays. A clear picture of the two $\pi^+\pi^-$ resonances interfering with the $\rho(770)$ in e^+e^- annihilation was also reported by BaBar using the ISR method [19].

The structure of these ρ states is not yet completely clear. Barnes [20] and Close [21] claim that $\rho(1450)$ has a mass

consistent with radial $2S$, but its decays show characteristics of hybrids, and suggest that this state may be a $2S$ -hybrid mixture. Donnachie [22] argues that hybrid states could have a 4π decay mode dominated by the $a_1\pi$. Such behavior has been observed by [23] in $e^+e^- \rightarrow 4\pi$ in the energy range 1.05–1.38 GeV, and by [17] in $\tau \rightarrow 4\pi$ decays. CLEO [24] and Belle [25] observe the $\rho(1450) \rightarrow \omega\pi$ decay mode in B -meson decays, however, do not find $\rho(1700) \rightarrow \omega\pi^0$. A similar conclusion is made by [26,27], who studied the process $e^+e^- \rightarrow \omega\pi^0$ and do not observe a statistically significant signal of the $\rho(1700)$. Various decay modes of the $\rho(1450)$ and $\rho(1700)$ are observed in $\bar{p}n$ and $\bar{p}p$ annihilation [28,29], but no definite conclusions can be drawn. More data should be collected to clarify the nature of the ρ states, particularly in the energy range above 1.6 GeV.

We now list under a separate entry the $\rho(1570)$, the $\phi\pi$ state with $J^{PC} = 1^{--}$ earlier observed by [30] (referred to as $C(1480)$) and recently confirmed by [31]. While [32] shows that it may be a threshold effect, [5] and [33] suggest two independent vector states with this decay mode. The $C(1480)$ has not been seen in the $\bar{p}p$ [34] and e^+e^- [35,36] experiments. However, the sensitivity of the two latter is an order of magnitude lower than that of [31]. Note that [31] can not exclude that their observation is due to an OZI-suppressed decay mode of the $\rho(1700)$.

Several observations on the $\omega\pi$ system in the 1200-MeV region [37–43] may be interpreted in terms of either $J^P = 1^-$ $\rho(770) \rightarrow \omega\pi$ production [44], or $J^P = 1^+$ $b_1(1235)$ production [42,43]. We argue that no special entry for a $\rho(1250)$ is needed. The LASS amplitude analysis [45] showing evidence for $\rho(1270)$ is preliminary and needs confirmation. For completeness, the relevant observations are listed under the $\rho(1450)$.

Recently [46] reported a very broad 1^{--} resonance-like K^+K^- state in $J/\psi \rightarrow K^+K^-\pi^0$ decays. Its pole position corresponds to mass of 1576 MeV and width of 818 MeV. [47–49] suggest its exotic structure (molecular or multiquark), while [50] and [51] explain it by the interference between the $\rho(1450)$ and $\rho(1700)$. The latter statement is qualitatively supported by BaBar [52] and SND [53]. We quote [46] as $X(1575)$ in the section “Further States.”

Evidence for ρ -like mesons decaying into 6π states was first noted by [54] in the analysis of 6π mass spectra from e^+e^- annihilation [55,56] and diffractive photoproduction [57]. Clegg [54] argued that two states at about 2.1 and 1.8 GeV exist: while the former is a candidate for the $\rho(2150)$, the latter could be a manifestation of the $\rho(1700)$ distorted by threshold effects. BaBar reported observations of the new decay modes of the $\rho(2150)$ in the channels $\eta'(958)\pi^+\pi^-$ and $f_1(1285)\pi^+\pi^-$ [58]. The relativistic quark model [59] predicts the 2^3D_1 state with $J^{PC} = 1^{--}$ at 2.15 GeV which can be identified with the $\rho(2150)$.

We no longer list under a separate particle $\rho(1900)$ various observations of irregular behavior of the cross sections near the $N\bar{N}$ threshold. Dips of various width around 1.9

GeV were reported by the E687 Collaboration (a narrow one in the $3\pi^+3\pi^-$ diffractive photoproduction [60,61]), by the FENICE experiment (a narrow structure in the R value [62]), by BaBar in ISR (a narrow structure in the $e^+e^- \rightarrow \phi\pi$ final state [63], but much broader in $e^+e^- \rightarrow 3\pi^+3\pi^-$ and $e^+e^- \rightarrow 2(\pi^+\pi^-\pi^0)$ [64]), by CMD-3 (also a rather broad dip in $e^+e^- \rightarrow 3\pi^+3\pi^-$ [65]). A dedicated scan of the $N\bar{N}$ -threshold region by CMD-3 confirms this effect in the $e^+e^- \rightarrow 3\pi^+3\pi^-$ and $e^+e^- \rightarrow K^+K^-\pi^+\pi^-$ final states, but does not see it in the cross section of $e^+e^- \rightarrow 2\pi^+2\pi^-$ [66]. Most probably, these structures emerge as a threshold effect due to the opening of the $N\bar{N}$ channel [67,68,69].

References

1. C. Erkal, Z. Phys. **C31**, 615 (1986).
2. A. Donnachie and H. Mirzaie, Z. Phys. **C33**, 407 (1987).
3. A. Donnachie and A.B. Clegg, Z. Phys. **C34**, 257 (1987).
4. A. Donnachie and A.B. Clegg, Z. Phys. **C51**, 689 (1991).
5. A.B. Clegg and A. Donnachie, Z. Phys. **C40**, 313 (1988).
6. A.B. Clegg and A. Donnachie, Z. Phys. **C62**, 455 (1994).
7. T.J. Killian *et al.*, Phys. Rev. **D21**, 3005 (1980).
8. S. Fukui *et al.*, Phys. Lett. **B202**, 441 (1988).
9. D. Bisello *et al.*, Phys. Lett. **B220**, 321 (1989).
10. A. Antonelli *et al.*, Phys. Lett. **B212**, 133 (1988).
11. A. Abele *et al.*, Phys. Lett. **B391**, 191 (1997).
12. A. Abele *et al.*, Phys. Rev. **D57**, 3860 (1998).
13. A. Bertin *et al.*, Phys. Lett. **B434**, 180 (1998).
14. A. Abele *et al.*, Phys. Lett. **B468**, 178 (1999).
15. R. Barate *et al.*, Z. Phys. **C76**, 15 (1997).
16. S. Anderson, Phys. Rev. **D61**, 112002 (2000).
17. K.W. Edwards *et al.*, Phys. Rev. **D61**, 072003 (2000).
18. M. Fujikawa *et al.*, Phys. Rev. **D78**, 072006 (2008).
19. J.P. Lees *et al.*, Phys. Rev. **D86**, 032013 (2012).
20. T. Barnes *et al.*, Phys. Rev. **D55**, 4157 (1997).
21. F.E. Close *et al.*, Phys. Rev. **D56**, 1584 (1997).
22. A. Donnachie and Yu.S. Kalashnikova, Phys. Rev. **D60**, 114011 (1999).
23. R.R. Akhmetshin *et al.*, Phys. Lett. **B466**, 392 (1999).
24. J.P. Alexander *et al.*, Phys. Rev. **D64**, 092001 (2001).
25. D. Matvienko *et al.*, Phys. Rev. **D92**, 012013 (2015).
26. R.R. Akhmetshin *et al.*, Phys. Lett. **B562**, 173 (2003).
27. M.N. Achasov *et al.*, Phys. Rev. **D94**, 112001 (2016).
28. A. Abele *et al.*, Eur. Phys. J. **C21**, 261 (2001).
29. M. Bargiotti *et al.*, Phys. Lett. **B561**, 233 (2003).
30. S.I. Bityukov *et al.*, Phys. Lett. **B188**, 383 (1987).
31. B. Aubert *et al.*, Phys. Rev. **D77**, 092002 (2008).
32. N.N. Achasov and G.N. Shestakov, Phys. Atom. Nucl. **59**, 1262 (1996).
33. L.G. Landsberg, Sov. J. Nucl. Phys. **55**, 1051 (1992).
34. A. Abele *et al.*, Phys. Lett. **B415**, 280 (1997).
35. V.M. Aulchenko *et al.*, Sov. Phys. JETP Lett. **45**, 145 (1987).
36. D. Bisello *et al.*, Z. Phys. **C52**, 227 (1991).
37. P. Frenkiel *et al.*, Nucl. Phys. **B47**, 61 (1972).
38. G. Cosme *et al.*, Phys. Lett. **B63**, 352 (1976).

Meson Particle Listings

 $\rho(1450)$

39. D.P. Barber *et al.*, Z. Phys. **C4**, 169 (1980).
 40. D. Aston, Phys. Lett. **B92**, 211 (1980).
 41. M. Atkinson *et al.*, Nucl. Phys. **B243**, 1 (1984).
 42. J.E. Brau *et al.*, Phys. Rev. **D37**, 2379 (1988).
 43. C. Amsler *et al.*, Phys. Lett. **B311**, 362 (1993).
 44. J. Layssac and F.M. Renard, Nuovo Cimento **6A**, 134 (1971).
 45. D. Aston *et al.*, Nucl. Phys. (Proc. Supp.) **B21**, 105 (1991).
 46. M. Ablikim *et al.*, Phys. Rev. Lett. **97**, 142002 (2006).
 47. G.-J. Ding and M.-L. Yan, Phys. Lett. **B643**, 33 (2006).
 48. F.K. Guo *et al.*, Nucl. Phys. **A773**, 78 (2006).
 49. A. Zhang *et al.*, Phys. Rev. **D76**, 036004 (2007).
 50. B.A. Li, Phys. Rev. **D76**, 094016 (2007).
 51. X. Liu *et al.*, Phys. Rev. **D75**, 074017 (2007).
 52. J.P. Lees *et al.*, Phys. Rev. **D88**, 032013 (2013).
 53. M.N. Achasov *et al.*, Phys. Rev. **D94**, 112006 (2016).
 54. A.B. Clegg and A. Donnachie, Z. Phys. **C45**, 677 (1990).
 55. D. Bisello *et al.*, Phys. Lett. **107B**, 145 (1981).
 56. A. Castro *et al.*, LAL-88-58(1988).
 57. M. Atkinson *et al.*, Z. Phys. **C29**, 333 (1985).
 58. B. Aubert *et al.*, Phys. Rev. **D76**, 092005 (2007).
 59. S. Godfrey and N. Isgur, Phys. Rev. **D32**, 189 (1985).
 60. P.L. Frabetti *et al.*, Phys. Lett. **B514**, 240 (2001).
 61. P.L. Frabetti *et al.*, Phys. Lett. **B578**, 290 (2004).
 62. A. Antonelli *et al.*, Phys. Lett. **B365**, 427 (1996).
 63. B. Aubert *et al.*, Phys. Rev. **D77**, 092002 (2008).
 64. B. Aubert *et al.*, Phys. Rev. **D73**, 052003 (2006).
 65. R.R. Akhmetshin *et al.*, Phys. Lett. **B723**, 83 (2013).
 66. R.R. Akhmetshin *et al.*, Phys. Lett. **B794**, 64 (2019).
 67. A. Obrazovsky and S. Serednyakov, Sov. Phys. JETP Lett. **99**, 315 (2014).
 68. J. Heidenauer *et al.*, Phys. Rev. **D92**, 054032 (2015).
 69. A.I. Milstein and S.G. Salmikov, Nucl. Phys. **A977**, 60 (2018).

 $\rho(1450)$ MASS $\rho(1450)$ MASS

VALUE (MeV)	DOCUMENT ID
1465 ± 25 OUR ESTIMATE	This is only an educated guess; the error given is larger than the error on the average of the published values.

 $\eta\rho^0$ MODE

VALUE (MeV)	EVTS	DOCUMENT ID	TECN	COMMENT
1500 ± 10	7.4k	¹ ACHASOV 18	SND	$1.22-2.00 e^+e^- \rightarrow \eta\pi^+\pi^-$
1497 ± 14		² AKHMETSHIN 01B	CMD2	$e^+e^- \rightarrow \eta\gamma$
1421 ± 15		³ AKHMETSHIN 00D	CMD2	$e^+e^- \rightarrow \eta\pi^+\pi^-$
1470 ± 20		ANTONELLI 88	DM2	$e^+e^- \rightarrow \eta\pi^+\pi^-$
1446 ± 10		FUKUI 88	SPEC	$8.95 \pi^-p \rightarrow \eta\pi^+\pi^-n$

¹ From the combined fit of AULCHENKO 15 and ACHASOV 18 in the model with the interfering $\rho(1450)$, $\rho(1700)$ and $\rho(2150)$ with the parameters of the $\rho(1450)$ and $\rho(1700)$ floating and the mass and width of the $\rho(2150)$ fixed at 2155 MeV and 320 MeV, respectively. The phases of the resonances are π , 0 and π , respectively.

² Using the data of AKHMETSHIN 01B on $e^+e^- \rightarrow \eta\gamma$, AKHMETSHIN 00D and ANTONELLI 88 on $e^+e^- \rightarrow \eta\pi^+\pi^-$.

³ Using the data of ANTONELLI 88, DOLINSKY 91, and AKHMETSHIN 00D. The energy-independent width of the $\rho(1450)$ and $\rho(1700)$ mesons assumed.

 $\omega\pi$ MODE

VALUE (MeV)	EVTS	DOCUMENT ID	TECN	COMMENT
1510 ± 7	10.2k	¹ ACHASOV 16D	SND	$1.05-2.00 e^+e^- \rightarrow \pi^0\pi^0\gamma$
$1544 \pm 22 \pm 11$	821	² MATVIENKO 15	BELL	$\bar{B}^0 \rightarrow D^{*+}\omega\pi^-$

1491 ± 19	7815	³ ACHASOV 13	SND	$1.05-2.00 e^+e^- \rightarrow \pi^0\pi^0\gamma$
$1582 \pm 17 \pm 25$	2382	⁴ AKHMETSHIN 03B	CMD2	$e^+e^- \rightarrow \pi^0\pi^0\gamma$
$1349 \pm 25 \pm 10$	341	⁵ ALEXANDER 01B	CLE2	$B \rightarrow D^{(*)}\omega\pi^-$
1523 ± 10		⁶ EDWARDS 00A	CLE2	$\tau^- \rightarrow \omega\pi^- \nu_\tau$
1463 ± 25		⁷ CLEGG 94	RVUE	
1250		⁸ ASTON 80C	OMEG	$20-70 \gamma\rho \rightarrow \omega\pi^0\rho$
1290 ± 40		⁸ BARBER 80C	SPEC	$3-5 \gamma\rho \rightarrow \omega\pi^0\rho$

¹ From a phenomenological model based on vector meson dominance with interfering $\rho(770)$, $\rho(1450)$, and $\rho(1700)$. The $\rho(1700)$ mass and width are fixed at 1720 MeV and 250 MeV, respectively. Systematic uncertainties not estimated. Supersedes ACHASOV 13.

² Using Breit-Wigner parameterization of the $\rho(1450)$ and assuming equal probabilities of the $\rho(1450) \rightarrow \pi\pi$ and $\rho(1450) \rightarrow \omega\pi$ decays.

³ From a phenomenological model based on vector meson dominance with the interfering $\rho(1450)$ and $\rho(1700)$ and their widths fixed at 400 and 250 MeV, respectively. Systematic uncertainty not estimated.

⁴ Using the data of AKHMETSHIN 03B and BISELLO 91B assuming the $\omega\pi^0$ and $\pi^+\pi^-$ mass dependence of the total width. $\rho(1700)$ mass and width fixed at 1700 MeV and 240 MeV, respectively.

⁵ Using Breit-Wigner parameterization of the $\rho(1450)$ and assuming the $\omega\pi^-$ mass dependence for the total width.

⁶ Mass-independent width parameterization. $\rho(1700)$ mass and width fixed at 1700 MeV and 235 MeV respectively.

⁷ Using data from BISELLO 91B, DOLINSKY 86 and ALBRECHT 87L.

⁸ Not separated from $b_1(1235)$, not pure $J^P = 1^-$ effect.

 4π MODE

VALUE (MeV)	DOCUMENT ID	TECN	COMMENT
1435 ± 40	ABELE 01B	CBAR	$0.0 \bar{p}n \rightarrow 2\pi^-2\pi^0\pi^+$
1350 ± 50	ACHASOV 97	RVUE	$e^+e^- \rightarrow 2(\pi^+\pi^-)$
1449 ± 4	¹ ARMSTRONG 89E	OMEG	$300 p\rho \rightarrow p\rho 2(\pi^+\pi^-)$

¹ Not clear whether this observation has $I=1$ or 0.

 $\pi\pi$ MODE

VALUE (MeV)	EVTS	DOCUMENT ID	TECN	COMMENT
1326.35 ± 3.46		¹ BARTOS 17	RVUE	$e^+e^- \rightarrow \pi^+\pi^-$
1342.31 ± 46.62		² BARTOS 17A	RVUE	$e^+e^- \rightarrow \pi^+\pi^-$
1373.83 ± 11.37		³ BARTOS 17A	RVUE	$\tau^- \rightarrow \pi^- \pi^0 \nu_\tau$
1429 ± 41	20K	⁴ LEES 17C	BABR	$J/\psi \rightarrow \pi^+\pi^-\pi^0$
1350 ± 20	± 20 -30 63.5k	⁵ ABRAMOWICZ12	ZEUS	$e\rho \rightarrow e\pi^+\pi^-p$
1493 ± 15		⁶ LEES 12G	BABR	$e^+e^- \rightarrow \pi^+\pi^-\gamma$
1446 ± 7	± 28 5.4M	^{7,8} FUJIKAWA 08	BELL	$\tau^- \rightarrow \pi^- \pi^0 \nu_\tau$
1328 ± 15		⁹ SCHAEEL 05C	ALEP	$\tau^- \rightarrow \pi^- \pi^0 \nu_\tau$
1406 ± 15	87k	^{7,10} ANDERSON 00A	CLE2	$\tau^- \rightarrow \pi^- \pi^0 \nu_\tau$
~ 1368		¹¹ ABELE 99C	CBAR	$0.0 \bar{p}d \rightarrow \pi^+\pi^-\pi^-\rho$
1348 ± 33		BERTIN 98	OBLX	$0.05-0.405 \bar{p}p \rightarrow \pi^+\pi^-$
1411 ± 14		¹² ABELE 97	CBAR	$\bar{p}n \rightarrow \pi^-\pi^0\pi^0$
1370 ± 90 -70		ACHASOV 97	RVUE	$e^+e^- \rightarrow \pi^+\pi^-$
1359 ± 40		¹⁰ BERTIN 97C	OBLX	$0.0 \bar{p}p \rightarrow \pi^+\pi^-\pi^0$
1282 ± 37		BERTIN 97D	OBLX	$0.05 \bar{p}p \rightarrow 2\pi^+2\pi^-$
1424 ± 25		BISELLO 89	DM2	$e^+e^- \rightarrow \pi^+\pi^-$
1265.5 ± 75.3		DUBNICKA 89	RVUE	$e^+e^- \rightarrow \pi^+\pi^-$
1292 ± 17		¹³ KURDADZE 83	OLYA	$0.64-1.4 e^+e^- \rightarrow \pi^+\pi^-$

¹ Applies the Unitary & Analytic Model of the pion electromagnetic form factor of DUBNICKA 10 to analyze the data of LEES 12G and ABLIKIM 16C.

² Applies the Unitary & Analytic Model of the pion electromagnetic form factor of DUBNICKA 10 to analyze the data of ACHASOV 06, AKHMETSHIN 07, AUBERT 09As, and AMBROSINO 11A.

³ Applies the Unitary & Analytic Model of the pion electromagnetic form factor of DUBNICKA 10 to analyze the data of FUJIKAWA 08.

⁴ From a Dalitz plot analysis in an isobar model with $\rho(1450)$ and $\rho(1700)$ masses and widths floating.

⁵ Using the KUHN 90 parametrization of the pion form factor, neglecting $\rho-\omega$ interference.

⁶ Using the GOUNARIS 68 parametrization of the pion form factor leaving the masses and widths of the $\rho(1450)$, $\rho(1700)$, and $\rho(2150)$ resonances as free parameters of the fit.

⁷ From the GOUNARIS 68 parametrization of the pion form factor.

⁸ $|F_{\pi^0}(0)|^2$ fixed to 1.

⁹ From the combined fit of the τ^- data from ANDERSON 00A and SCHAEEL 05C and e^+e^- data from the compilation of BARKOV 85, AKHMETSHIN 04, and AL OISIO 05. $\rho(1700)$ mass and width fixed at 1713 MeV and 235 MeV, respectively. Supersedes BARATE 97M.

¹⁰ $\rho(1700)$ mass and width fixed at 1700 MeV and 235 MeV, respectively.

¹¹ $\rho(1700)$ mass and width fixed at 1780 MeV and 275 MeV respectively.

¹² T-matrix pole.

¹³ Using for $\rho(1700)$ mass and width 1600 ± 20 and 300 ± 10 MeV respectively.

 $K\bar{K}$ MODE

VALUE (MeV)	EVTS	DOCUMENT ID	TECN	CHG	COMMENT
$1208 \pm 8 \pm 9$	190k	¹ AAIJ 16N	LHCB		$D^0 \rightarrow K_S^0 K^{\pm}\pi^{\mp}$
1422.8 ± 6.5	27k	² ABELE 99D	CBAR	\pm	$0.0 \bar{p}p \rightarrow K^+ K^- \pi^0$

¹ Using the GOUNARIS 68 parameterization with fixed width.

² K-matrix pole. Isospin not determined, could be $\omega(1420)$.

ρ(1450)

K⁺K⁰(892) + c.c. MODE

Table with columns: VALUE (MeV), DOCUMENT ID, TECN, COMMENT. Row 1: 1505 ± 19 ± 7, AUBERT, 08s, BABR, 10.6 e+ e- -> K+ K0(892) gamma

m_ρ(1450)^0 - m_ρ(1450)^±

Table with columns: VALUE (MeV), DOCUMENT ID, TECN, COMMENT. Row 1: -31.53 ± 47.99, 1 BARTOS, 17A, RVUE, e+ e- -> pi+ pi-, tau- -> pi- pi0 nu_tau

1 Applies the Unitary & Analytic Model of the pion electromagnetic form factor of DUB-NICKA 10 to analyze the data of ACHASOV 06, AKHMETSHIN 07, AUBERT 09As, AMBROSINO 11A, and FUJIKAWA 08.

ρ(1450) WIDTH

ρ(1450) WIDTH

Table with columns: VALUE (MeV), DOCUMENT ID, TECN, COMMENT. Row 1: 400 ± 60 OUR ESTIMATE, This is only an educated guess; the error given is larger than the error on the average of the published values.

1 From a fit of a VMD model with two effective resonances with masses of 1450 MeV and 1700 MeV to describe the excited vector states ω(1420), ρ(1450), ω(1650), and ρ(1700). Systematic errors not evaluated.

ηπ^0 MODE

Table with columns: VALUE (MeV), EVTS, DOCUMENT ID, TECN, COMMENT. Rows include ACHASOV 18, AKHMETSHIN 01B, AKHMETSHIN 00D, ANTONELLI 88, FUKUI 88.

1 From the combined fit of AULCHENKO 15 and ACHASOV 18 in the model with the interfering ρ(1450), ρ(1700) and ρ(2150) with the parameters of the ρ(1450) and ρ(1700) floating and the mass and width of the ρ(2150) fixed at 2155 MeV and 320 MeV, respectively. The phases of the resonances are π, 0 and π, respectively.

ωπ MODE

Table with columns: VALUE (MeV), EVTS, DOCUMENT ID, TECN, COMMENT. Rows include ACHASOV 16D, MATVIENKO 15, AKHMETSHIN 03B, ALEXANDER 01B, EDWARDS 00A, CLEGG 94, ASTON 80C, BARBER 80C.

1 From a phenomenological model based on vector meson dominance with interfering ρ(770), ρ(1450), and ρ(1700). The ρ(1700) mass and width are fixed at 1720 MeV and 250 MeV, respectively. Systematic uncertainties not estimated. Supersedes ACHASOV 13.

4π MODE

Table with columns: VALUE (MeV), DOCUMENT ID, TECN, COMMENT. Row 1: 325 ± 100, ABELE, 01B, CBAR, 0.0 p-bar n -> 2 pi- 2 pi0 pi+

ππ MODE

Table with columns: VALUE (MeV), EVTS, DOCUMENT ID, TECN, COMMENT. Rows include BARTOS 17, BARTOS 17A, BARTOS 17A, LEES 17C.

Table with columns: VALUE, DOCUMENT ID, TECN, COMMENT. Rows include ABRAMOWICZ12, LEES, FUJIKAWA, SCHAEEL, ANDERSON, ABELE, BERTIN, ABELE, BERTIN, BERTIN, BISELLO, DUBNICKA, KURDADZE.

1 Applies the Unitary & Analytic Model of the pion electromagnetic form factor of DUB-NICKA 10 to analyze the data of LEES 12G and ABLIKIM 16c. 2 Applies the Unitary & Analytic Model of the pion electromagnetic form factor of DUB-NICKA 10 to analyze the data of ACHASOV 06, AKHMETSHIN 07, AUBERT 09As, and AMBROSINO 11A.

K⁺K⁰ MODE

Table with columns: VALUE (MeV), EVTS, DOCUMENT ID, TECN, CHG, COMMENT. Rows include AAIJ, ABELE.

1 Using the GOUNARIS 68 parameterization with fixed mass. 2 K-matrix pole. Isospin not determined, could be ω(1420).

K⁺K⁰(892) + c.c. MODE

Table with columns: VALUE (MeV), DOCUMENT ID, TECN, COMMENT. Row 1: 418 ± 25 ± 4, AUBERT, 08s, BABR, 10.6 e+ e- -> K+ K0(892) gamma

Γ_ρ(1450)^0 - Γ_ρ(1450)^±

Table with columns: VALUE (MeV), DOCUMENT ID, TECN, COMMENT. Row 1: 151.30 ± 140.42, 1 BARTOS, 17A, RVUE, e+ e- -> pi+ pi-, tau- -> pi- pi0 nu_tau

1 Applies the Unitary & Analytic Model of the pion electromagnetic form factor of DUB-NICKA 10 to analyze the data of ACHASOV 06, AKHMETSHIN 07, AUBERT 09As, AMBROSINO 11A, and FUJIKAWA 08.

ρ(1450) DECAY MODES

Table with columns: Mode, Fraction (Γ_i/Γ). Rows include pi pi, pi+ pi-, 4 pi, omega pi, a1(1260) pi, h1(1170) pi, pi(1300) pi, rho rho, rho(pi pi) s-wave, e+ e-, eta rho, a2(1320) pi, K+ K-, K+ K-, K+ K-(892) + c.c., pi0 gamma, eta gamma, f0(500) gamma, f0(980) gamma, f0(1370) gamma, f2(1270) gamma.

Meson Particle Listings

 $\rho(1450)$

$\rho(1450) \Gamma(i) \Gamma(e^+ e^-) / \Gamma(\text{total})$				
$\Gamma(\pi\pi) \times \Gamma(e^+ e^-) / \Gamma(\text{total})$	$\Gamma_{11} \Gamma_{10} / \Gamma$			
VALUE (keV)	DOCUMENT ID	TECN	COMMENT	
0.12	¹ DIEKMAN 88	RVUE	$e^+ e^- \rightarrow \pi^+ \pi^-$	
$0.027^{+0.015}_{-0.010}$	² KURDADZE 83	OLYA	$0.64-1.4 e^+ e^- \rightarrow \pi^+ \pi^-$	
¹ Using total width = 235 MeV.				
² Using for $\rho(1700)$ mass and width 1600 ± 20 and 300 ± 10 MeV respectively.				

$\Gamma(\eta\rho) \times \Gamma(e^+ e^-) / \Gamma(\text{total})$				
VALUE (eV)	DOCUMENT ID	TECN	COMMENT	$\Gamma_{11} \Gamma_{10} / \Gamma$
$210 \pm 24 \pm 10$	¹ LEES 18	BABR	$e^+ e^- \rightarrow \eta \pi^+ \pi^-$	
74 ± 20	² AKHMETSHIN 00D	CMD2	$e^+ e^- \rightarrow \eta \pi^+ \pi^-$	
91 ± 19	ANTONELLI 88	DM2	$e^+ e^- \rightarrow \eta \pi^+ \pi^-$	
¹ Includes non-resonant contribution. The selected fit model includes three ρ excited states. Model uncertainty is 20%.				
² Using the data of ANTONELLI 88, DOLINSKY 91, and AKHMETSHIN 00D. The energy-independent width of the $\rho(1450)$ and $\rho(1700)$ mesons assumed.				

$\Gamma(\eta\gamma) \times \Gamma(e^+ e^-) / \Gamma(\text{total})$				
VALUE (eV)	DOCUMENT ID	TECN	COMMENT	$\Gamma_{17} \Gamma_{10} / \Gamma$
<16.4	¹ AKHMETSHIN 05	CMD2	$0.60-1.38 e^+ e^- \rightarrow \eta\gamma$	
$2.2 \pm 0.5 \pm 0.3$	² AKHMETSHIN 01B	CMD2	$e^+ e^- \rightarrow \eta\gamma$	
¹ From 2γ decay mode of η using 1465 MeV and 310 MeV for the $\rho(1450)$ mass and width. Recalculated by us.				
² Using the data of AKHMETSHIN 01B on $e^+ e^- \rightarrow \eta\gamma$, AKHMETSHIN 00D and ANTONELLI 88 on $e^+ e^- \rightarrow \eta \pi^+ \pi^-$. Recalculated by us using width of 226 MeV.				

$\Gamma(K\bar{K}^*(892) + \text{c.c.}) \times \Gamma(e^+ e^-) / \Gamma(\text{total})$				
VALUE (eV)	DOCUMENT ID	TECN	COMMENT	$\Gamma_{15} \Gamma_{10} / \Gamma$
$127 \pm 15 \pm 6$	AUBERT 08s	BABR	$10.6 e^+ e^- \rightarrow K\bar{K}^*(892)\gamma$	

$\rho(1450) \Gamma(i) / \Gamma(\text{total}) \times \Gamma(e^+ e^-) / \Gamma(\text{total})$				
$\Gamma(\omega\pi) / \Gamma(\text{total}) \times \Gamma(e^+ e^-) / \Gamma(\text{total})$				
VALUE (units 10^{-6})	EVTS	DOCUMENT ID	TECN	COMMENT
2.1 ± 0.4	10.2k	¹ ACHASOV 16D	SND	$1.05-2.00 e^+ e^- \rightarrow \pi^0 \pi^0 \gamma$
5.3 ± 0.4	7815	² ACHASOV 13	SND	$1.05-2.00 e^+ e^- \rightarrow \pi^0 \pi^0 \gamma$
¹ From a phenomenological model based on vector meson dominance with interfering $\rho(770)$, $\rho(1450)$, and $\rho(1700)$. The $\rho(1700)$ mass and width are fixed at 1720 MeV and 250 MeV, respectively. Systematic uncertainties not estimated. Supersedes ACHASOV 13.				
² From a phenomenological model based on vector meson dominance with the interfering $\rho(1450)$ and $\rho(1700)$ and their widths fixed at 400 and 250 MeV, respectively. Systematic uncertainty not estimated.				

$\Gamma(\eta\rho) / \Gamma(\text{total}) \times \Gamma(e^+ e^-) / \Gamma(\text{total})$				
VALUE (units 10^{-7})	EVTS	DOCUMENT ID	TECN	COMMENT
7.3 ± 0.3	7.4k	¹ ACHASOV 18	SND	$1.22-2.00 e^+ e^- \rightarrow \eta \pi^+ \pi^-$
$4.3^{+1.1}_{-0.9} \pm 0.2$	4.9k	² AULCHENKO 15	SND	$1.22-2.00 e^+ e^- \rightarrow \eta \pi^+ \pi^-$
¹ From the combined fit of AULCHENKO 15 and ACHASOV 18 in the model with the interfering $\rho(1450)$, $\rho(1700)$ and $\rho(2150)$ with the parameters of the $\rho(1450)$ and $\rho(1700)$ floating and the mass and width of the $\rho(2150)$ fixed at 2155 MeV and 320 MeV, respectively. The phases of the resonances are π , 0 and π , respectively.				
² From a fit to the $e^+ e^- \rightarrow \eta \pi^+ \pi^-$ cross section with vector meson dominance model including $\rho(770)$, $\rho(1450)$, and $\rho(1700)$ decaying exclusively via $\eta\rho(770)$. Masses and widths of vector states are fixed to PDG 14. Coupling constants are assumed to be real.				

$\Gamma(\rho(500)\gamma) / \Gamma(\text{total}) \times \Gamma(e^+ e^-) / \Gamma(\text{total})$				
VALUE (units 10^{-9})	CL%	DOCUMENT ID	TECN	COMMENT
<4.0	90	ACHASOV 11	SND	$e^+ e^- \rightarrow \pi^0 \pi^0 \gamma$

$\Gamma(\pi^0\gamma) / \Gamma(\text{total}) \times \Gamma(e^+ e^-) / \Gamma(\text{total})$				
VALUE (units 10^{-9})	DOCUMENT ID	TECN	COMMENT	$\Gamma_{16} \Gamma_{10} / \Gamma$
2.3 ± 1.4	¹ ACHASOV 10D	SND	$1.075-2.0 e^+ e^- \rightarrow \pi^0 \gamma$	
¹ From a fit of a VMD model with two effective resonances with masses of 1450 MeV and 1700 MeV to describe the excited vector states $\omega(1420)$, $\rho(1450)$, $\omega(1650)$, and $\rho(1700)$. Systematic errors not evaluated.				

$\Gamma(\rho(980)\gamma) / \Gamma(\text{total}) \times \Gamma(e^+ e^-) / \Gamma(\text{total})$				
VALUE (units 10^{-9})	CL%	DOCUMENT ID	TECN	COMMENT
<2.6	90	ACHASOV 11	SND	$e^+ e^- \rightarrow \pi^0 \pi^0 \gamma$

$\Gamma(\rho(1370)\gamma) / \Gamma(\text{total}) \times \Gamma(e^+ e^-) / \Gamma(\text{total})$				
VALUE (units 10^{-9})	CL%	DOCUMENT ID	TECN	COMMENT
<3.5	90	ACHASOV 11	SND	$e^+ e^- \rightarrow \pi^0 \pi^0 \gamma$

$\Gamma(\rho(1270)\gamma) / \Gamma(\text{total}) \times \Gamma(e^+ e^-) / \Gamma(\text{total})$				
VALUE (units 10^{-9})	CL%	DOCUMENT ID	TECN	COMMENT
<0.8	90	¹ ACHASOV 11	SND	$e^+ e^- \rightarrow \pi^0 \pi^0 \gamma$
¹ Using Breit-Wigner parametrization of the $\rho(1450)$ with mass and width of 1465 MeV and 400 MeV, respectively.				

 $\rho(1450)$ BRANCHING RATIOS

$\Gamma(\pi\pi) / \Gamma(4\pi)$				
VALUE	DOCUMENT ID	TECN	COMMENT	Γ_1 / Γ_3
0.37 ± 0.10	^{1,2} ABELE 01B	CBAR	$0.0 \bar{p}n \rightarrow 5\pi$	
¹ $\omega\pi$ not included.				
² Using ABELE 97.				

$\Gamma(K^+ K^-) / \Gamma(\pi^+ \pi^-)$				
VALUE (%)	EVTS	DOCUMENT ID	TECN	COMMENT
$30.7 \pm 8.4 \pm 8.2$	20K	¹ LEES 17C	BABR	$J/\psi \rightarrow h^+ h^- \pi^0$
¹ From Dalitz plot analyses in isobar models.				

$\Gamma(\omega\pi) / \Gamma(\text{total})$				
VALUE	EVTS	DOCUMENT ID	TECN	COMMENT
seen	821	¹ MATVIENKO 15	BELL	$\bar{B}^0 \rightarrow D^{*+} \omega \pi^-$
seen	1.6k	ACHASOV 12	SND	$e^+ e^- \rightarrow \pi^0 \pi^0 \gamma$
~ 0.21		CLEGG 94	RVUE	
¹ Using Breit-Wigner parameterization of the $\rho(1450)$ and assuming equal probabilities of the $\rho(1450) \rightarrow \pi\pi$ and $\rho(1450) \rightarrow \omega\pi$ decays.				

$\Gamma(\pi\pi) / \Gamma(\omega\pi)$				
VALUE	DOCUMENT ID	TECN	COMMENT	Γ_1 / Γ_4
~ 0.32	CLEGG 94	RVUE		

$\Gamma(\omega\pi) / \Gamma(4\pi)$				
VALUE	DOCUMENT ID	TECN	COMMENT	Γ_4 / Γ_3
<0.14	CLEGG 88	RVUE		

$\Gamma(a_1(1260)\pi) / \Gamma(4\pi)$				
VALUE	DOCUMENT ID	TECN	COMMENT	Γ_5 / Γ_3
0.27 ± 0.08	¹ ABELE 01B	CBAR	$0.0 \bar{p}n \rightarrow 5\pi$	
¹ $\omega\pi$ not included.				

$\Gamma(h_1(1170)\pi) / \Gamma(4\pi)$				
VALUE	DOCUMENT ID	TECN	COMMENT	Γ_6 / Γ_3
0.08 ± 0.04	¹ ABELE 01B	CBAR	$0.0 \bar{p}n \rightarrow 5\pi$	
¹ $\omega\pi$ not included.				

$\Gamma(\rho(1300)\pi) / \Gamma(4\pi)$				
VALUE	DOCUMENT ID	TECN	COMMENT	Γ_7 / Γ_3
0.37 ± 0.13	¹ ABELE 01B	CBAR	$0.0 \bar{p}n \rightarrow 5\pi$	
¹ $\omega\pi$ not included.				

$\Gamma(\rho\rho) / \Gamma(4\pi)$				
VALUE	DOCUMENT ID	TECN	COMMENT	Γ_8 / Γ_3
0.11 ± 0.05	¹ ABELE 01B	CBAR	$0.0 \bar{p}n \rightarrow 5\pi$	
¹ $\omega\pi$ not included.				

$\Gamma(\rho(\pi\pi)s\text{-wave}) / \Gamma(4\pi)$				
VALUE	DOCUMENT ID	TECN	COMMENT	Γ_9 / Γ_3
0.17 ± 0.09	¹ ABELE 01B	CBAR	$0.0 \bar{p}n \rightarrow 5\pi$	
¹ $\omega\pi$ not included.				

$\Gamma(\eta\rho) / \Gamma(\text{total})$				
VALUE	EVTS	DOCUMENT ID	TECN	COMMENT
seen	35	¹ ACHASOV 14	SND	$1.15-2.00 e^+ e^- \rightarrow \eta\gamma$
<0.04		DONNACHIE 87B	RVUE	
¹ From a phenomenological model based on vector meson dominance with $\rho(1450)$ and $\phi(1680)$ masses and widths from the PDG 12.				

See key on page 999

Meson Particle Listings

$\rho(1450)$, $\eta(1475)$

$\Gamma(\eta\rho)/\Gamma(\omega\rho)$ Γ_{11}/Γ_4

VALUE	DOCUMENT ID	TECN	COMMENT
0.081 ± 0.020	^{1,2} AULCHENKO 15	SND	1.22–2.00 $e^+e^- \rightarrow \eta\pi^+\pi^-$
~0.24	³ DONNACHIE 91	RVUE	
>2	FUKUI 91	SPEC	8.95 $\pi^-p \rightarrow \omega\pi^0n$

¹ From a fit to the $e^+e^- \rightarrow \eta\pi^+\pi^-$ cross section with vector meson dominance model including $\rho(770)$, $\rho(1450)$, and $\rho(1700)$ decaying exclusively via $\eta\rho(770)$. Masses and widths of vector states are fixed to PDG 14. Coupling constants are assumed to be real.
² Reports the inverse of the quoted value as 12.3 ± 3.1 .
³ Using data from BISELLO 91b, DOLINSKY 86 and ALBRECHT 87L.

$\Gamma(\pi\pi)/\Gamma(\eta\rho)$ Γ_1/Γ_{11}

VALUE	DOCUMENT ID	TECN	COMMENT
1.3 ± 0.4	¹ AULCHENKO 15	SND	1.22–2.00 $e^+e^- \rightarrow \eta\pi^+\pi^-$

¹ From a fit to the $e^+e^- \rightarrow \eta\pi^+\pi^-$ cross section with vector meson dominance model including $\rho(770)$, $\rho(1450)$, and $\rho(1700)$ decaying exclusively via $\eta\rho(770)$. Masses and widths of vector states are fixed to PDG 14. Coupling constants are assumed to be real.

$\Gamma(a_2(1320)\pi)/\Gamma_{total}$ Γ_{12}/Γ

VALUE	DOCUMENT ID	TECN	COMMENT
not seen	AMELIN 00	VES	37 $\pi^-p \rightarrow \eta\pi^+\pi^-n$

$\Gamma(K\bar{K})/\Gamma(\omega\rho)$ Γ_{13}/Γ_4

VALUE	DOCUMENT ID	TECN	COMMENT
<0.08	¹ DONNACHIE 91	RVUE	

¹ Using data from BISELLO 91b, DOLINSKY 86 and ALBRECHT 87L.

$\Gamma(K\bar{K}^*(892) + c.c.)/\Gamma_{total}$ Γ_{15}/Γ

VALUE	DOCUMENT ID	TECN	COMMENT
possibly seen	COAN 04	CLEO	$\tau^- \rightarrow K^-\pi^-K^+\nu_\tau$

$\Gamma(\eta\gamma)/\Gamma_{total}$ Γ_{17}/Γ

VALUE	EVTS	DOCUMENT ID	TECN	COMMENT
seen	35	¹ ACHASOV 14	SND	1.15–2.00 $e^+e^- \rightarrow \eta\gamma$

¹ From a phenomenological model based on vector meson dominance with $\rho(1450)$ and $\phi(1680)$ masses and widths from the PDG 12.

$\rho(1450)$ REFERENCES

ACHASOV 18	PR D97 012008	M.N. Achasov et al.	(SND Collab.)
LEES 18	PR D97 052007	J.P. Lees et al.	(BABAR Collab.)
BARTOS 17	PR D96 113004	E. Bartos et al.	
BARTOS 17A	JUMP A32 1750154	E. Bartos et al.	
LEES 17C	PR D95 072007	J.P. Lees et al.	(BABAR Collab.)
AALI 16N	PR D93 052018	R. Aaij et al.	(LHCb Collab.)
ABLIKIM 16C	PL B753 629	M. Ablikim et al.	(BESIII Collab.)
ACHASOV 16D	PR D94 112001	M.N. Achasov et al.	(SND Collab.)
AULCHENKO 15	PR D91 052013	V.M. Aulchenko et al.	(SND Collab.)
MATVIENKO 15	PR D92 012013	D. Matvienko et al.	(BELLE Collab.)
ACHASOV 14	PR D90 032002	M.N. Achasov et al.	(SND Collab.)
PDG 14	CP C38 070001	K. Olive et al.	(PDG Collab.)
ACHASOV 13	PR D88 054013	M.N. Achasov et al.	(SND Collab.)
ABRAMOWICZ 12	EPJ C72 1849	H. Abramowicz et al.	(ZEUS Collab.)
ACHASOV 12	JETPL 94 734	M.N. Achasov et al.	
LEES 12G	PR D86 032013	J.P. Lees et al.	(BABAR Collab.)
PDG 12	PR D86 010001	J. Beringer et al.	(PDG Collab.)
ACHASOV 11	JETP 113 75	M.N. Achasov et al.	(SND Collab.)
AMBROSINO 11A	PL B700 102	F. Ambrosino et al.	(KLOE Collab.)
ACHASOV 10D	PR D98 112001	M.N. Achasov et al.	(SND Collab.)
DUBNICKA 10	APS 60 1	S. Dubnicka, A.Z. Dubnickova	
AUBERT 09AS	PRL 103 231801	B. Aubert et al.	(BABAR Collab.)
AUBERT 08S	PR D77 092002	B. Aubert et al.	(BABAR Collab.)
FUJIKAWA 08	PR D78 072006	M. Fujikawa et al.	(BELLE Collab.)
AKHMETSHIN 07	PL B648 28	R.R. Akhmetshin et al.	(Novosibirsk CMD-2 Collab.)
ACHASOV 06	JETP 103 380	M.N. Achasov et al.	(Novosibirsk SND Collab.)
AKHMETSHIN 05	Translated from ZETFP 130 437.	R.R. Akhmetshin et al.	(Novosibirsk CMD-2 Collab.)
ALOISIO 05	PL B606 12	A. Aloisio et al.	(KLOE Collab.)
SCHAEEL 05C	PRPL 421 191	S. Schaeel et al.	(ALEPH Collab.)
AKHMETSHIN 04	PL B578 285	R.R. Akhmetshin et al.	(Novosibirsk CMD-2 Collab.)
COAN 04	PRL 92 232001	T.E. Coan et al.	(CLEO Collab.)
AKHMETSHIN 03B	PL B562 173	R.R. Akhmetshin et al.	(Novosibirsk CMD-2 Collab.)
ABELE 01B	EPJ C21 261	A. Abele et al.	(Crystal Barrel Collab.)
AKHMETSHIN 01B	PL B509 217	R.R. Akhmetshin et al.	(Novosibirsk CMD-2 Collab.)
ALEXANDER 01B	PR D64 092001	J.P. Alexander et al.	(CLEO Collab.)
AKHMETSHIN 00D	PL B489 125	R.R. Akhmetshin et al.	(Novosibirsk CMD-2 Collab.)
AMELIN 00	NP A668 83	D. Amelin et al.	(VES Collab.)
ANDERSON 00A	PR D61 112002	S. Anderson et al.	(CLEO Collab.)
EDWARDS 00A	PR D61 072003	K.W. Edwards et al.	(CLEO Collab.)
ABELE 99C	PL B450 275	A. Abele et al.	(Crystal Barrel Collab.)
ABELE 99D	PL B468 178	A. Abele et al.	(Crystal Barrel Collab.)
BERTIN 98	PR D57 55	A. Bertin et al.	(OBELIX Collab.)
ABELE 97	PL B391 191	A. Abele et al.	(Crystal Barrel Collab.)
ACHASOV 97	PR D55 2663	M.N. Achasov et al.	(NOVM)
BARATE 97M	ZPHY C76 15	R. Barate et al.	(ALEPH Collab.)
BERTIN 97C	PL B408 476	A. Bertin et al.	(OBELIX Collab.)
BERTIN 97D	PL B414 220	A. Bertin et al.	(OBELIX Collab.)
CLEGG 94	ZPHY C62 455	A.B. Clegg, A. Donnachie	(LANC, MCHS)
BISELLO 91B	NPBPS 821 111	D. Bisello	(DM2 Collab.)

DOLINSKY 91	PRPL 202 99	S.I. Dolinsky et al.	(NOVO)
DONNACHIE 91	ZPHY C51 689	A. Donnachie, A.B. Clegg	(MCHS, LANC)
FUKUI 91	PL B257 241	S. Fukui et al.	(SUGI, NAGO, KEK, KYOT+)
KUHN 90	ZPHY C48 445	J.H. Kuhn et al.	(M2M)
ARMSTRONG 89E	PL B228 536	T.A. Armstrong, M. Benayoun	(ATHU, BARI, BIRM+)
BISELLO 89	PL B220 321	D. Bisello et al.	(DM2 Collab.)
DUBNICKA 89	JP G15 1349	S. Dubnicka et al.	(JINR, SLOV)
ANTONELLI 88	PL B212 133	A. Antonelli et al.	(DM2 Collab.)
CLEGG 88	ZPHY C40 313	A.B. Clegg, A. Donnachie	(MCHS, LANC)
DIKMAN 88	PRPL 159 99	B. Diekmann	(BOHN)
FUKUI 88	PL B202 441	S. Fukui et al.	(SUGI, NAGO, KEK, KYOT+)
ALBRECHT 87L	PL B185 223	H. Albrecht et al.	(ARGUS Collab.)
DONNACHIE 87B	ZPHY C34 257	A. Donnachie, A.B. Clegg	(MCHS, LANC)
DOLINSKY 86	PL B174 453	S.I. Dolinsky et al.	(NOVO)
BARKOV 85	NP B256 365	L.M. Barkov et al.	(NOVO)
KURDADZE 83	JETPL 37 733	L.M. Kurdadze et al.	(NOVO)
ASTON 80C	PL 92B 211	D. Aston	(BOHN, CERN, EPOL, GLAS, LANC+)
BARBER 80C	ZPHY C4 169	D.P. Barber et al.	(DARE, LANC, SHEP)
GOUNARIS 68	PRL 21 244	G.J. Gounaris, J.J. Sakurai	

$\eta(1475)$

$$J^{PC} = 0^+(0^-+)$$

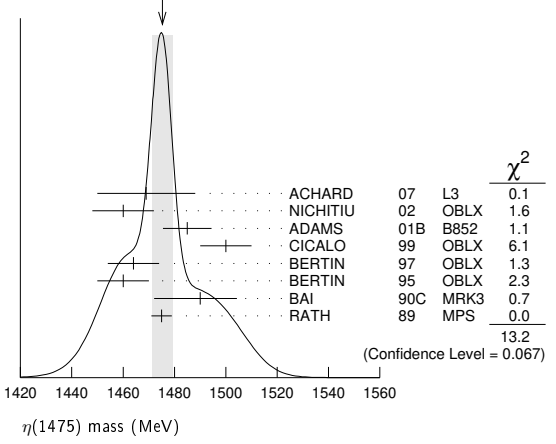
See the $\eta(1405)$ and the related review on "Pseudoscalar and Pseudovector Mesons in the 1400 MeV Region."

$\eta(1475)$ MASS

VALUE (MeV)	EVTS	DOCUMENT ID	TECN	COMMENT
1475 ± 4 OUR AVERAGE		Error includes scale factor of 1.4. See the ideogram below.		
1469 ± 14 ± 13	74	ACHARD 07	L3	183–209 $e^+e^- \rightarrow e^+e^-K_S^0K^\pm\pi^\mp$
1460 ± 12	3651	NICHITIU 02	OBLX	0 $\bar{p}p \rightarrow K^+K^-\pi^+\pi^-\pi^0$
1485 ± 8 ± 5	20k	ADAMS 01B	B852	18 GeV $\pi^-p \rightarrow K^+K^-\pi^0n$
1500 ± 10		CICALO 99	OBLX	0 $\bar{p}p \rightarrow K^\pm K_S^0\pi^\mp\pi^+\pi^-$
1464 ± 10		BERTIN 97	OBLX	0 $\bar{p}p \rightarrow K^\pm(K^0)\pi^\mp\pi^+\pi^-$
1460 ± 10		BERTIN 95	OBLX	0 $\bar{p}p \rightarrow K\bar{K}\pi\pi\pi$
1490 ⁺¹⁴ ₋₈ ⁺³ ₋₁₆	1100	BAI 90C	MRK3	$J/\psi \rightarrow \gamma K_S^0 K^\pm\pi^\mp$
1475 ± 4		RATH 89	MPS	21.4 $\pi^-p \rightarrow nK_S^0 K_S^0\pi^0$
1477 ± 7 ± 13		¹ ABLIKIM 18i	BES3	$J/\psi \rightarrow \gamma\gamma\phi(1020)$
1565 ± 8 ⁺⁰ ₋₆₃		² ABLIKIM 15T	BES3	$J/\psi \rightarrow \gamma K_S^0 K_S^0\eta$
1421 ± 14		AUGUSTIN 92	DM2	$J/\psi \rightarrow \gamma K\bar{K}\pi$

¹ From a fit to $\gamma\phi$ invariant mass. Angular analysis consistent with $J^{PC} = 0^-+$. Other J^{PC} not excluded.
² Could also be the $\eta(1405)$.

WEIGHTED AVERAGE 1475 ± 4 (Error scaled by 1.4)



$\eta(1475)$ WIDTH

VALUE (MeV)	EVTS	DOCUMENT ID	TECN	COMMENT
90 ± 9 OUR AVERAGE		Error includes scale factor of 1.6. See the ideogram below.		
67 ± 18 ± 7	74	ACHARD 07	L3	183–209 $e^+e^- \rightarrow e^+e^-K_S^0K^\pm\pi^\mp$
120 ± 15	3651	NICHITIU 02	OBLX	0 $\bar{p}p \rightarrow K^+K^-\pi^+\pi^-\pi^0$
98 ± 18 ± 3	20k	ADAMS 01B	B852	18 GeV $\pi^-p \rightarrow K^+K^-\pi^0n$
100 ± 20		CICALO 99	OBLX	0 $\bar{p}p \rightarrow K^\pm K_S^0\pi^\mp\pi^+\pi^-$
105 ± 15		BERTIN 97	OBLX	0.0 $\bar{p}p \rightarrow K^\pm(K^0)\pi^\mp\pi^+\pi^-$
105 ± 15		BERTIN 95	OBLX	0 $\bar{p}p \rightarrow K\bar{K}\pi\pi\pi$
54 ⁺³⁷ ₋₂₁ ⁺¹³ ₋₂₄		BAI 90C	MRK3	$J/\psi \rightarrow \gamma K_S^0 K^\pm\pi^\mp$
51 ± 13		RATH 89	MPS	21.4 $\pi^-p \rightarrow nK_S^0 K_S^0\pi^0$

Meson Particle Listings

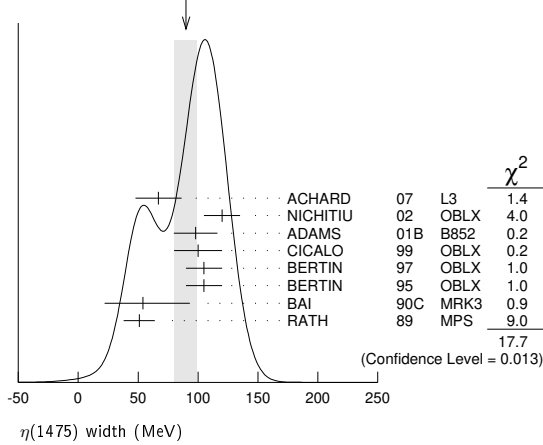
$\eta(1475)$, $f_0(1500)$

• • • We do not use the following data for averages, fits, limits, etc. • • •

$118 \pm 22 \pm 17$	¹ ABLIKIM	18i	BES3	$J/\psi \rightarrow \gamma\gamma\phi(1020)$
$45^{+14}_{-13} - 28$	² ABLIKIM	15T	BES3	$J/\psi \rightarrow \gamma K_S^0 K_S^0 \eta$
63 ± 18	AUGUSTIN	92	DM2	$J/\psi \rightarrow \gamma K \bar{K} \pi$

¹ From a fit to $\gamma\phi$ invariant mass. Angular analysis consistent with $J^{PC} = 0^{-+}$. Other J^{PC} not excluded.
² Could also be the $\eta(1405)$.

WEIGHTED AVERAGE
 90 ± 9 (Error scaled by 1.6)



$\eta(1475)$ DECAY MODES

Mode	Fraction (Γ_i/Γ)
Γ_1 $K \bar{K} \pi$	seen
Γ_2 $K \bar{K}^*(892) + c.c.$	seen
Γ_3 $a_0(980)\pi$	seen
Γ_4 $\gamma\gamma$	seen
Γ_5 $K_S^0 K_S^0 \eta$	possibly seen
Γ_6 $\gamma\phi(1020)$	possibly seen

$\eta(1475)$ $\Gamma(i)\Gamma(\gamma\gamma)/\Gamma(\text{total})$

VALUE (keV)	CL%	EVTS	DOCUMENT ID	TECN	COMMENT	$\Gamma_1\Gamma_4/\Gamma$	
$0.23 \pm 0.05 \pm 0.05$		74	¹ ACHARD	07	L3	$183-209 e^+e^- \rightarrow e^+e^- K_S^0 K_S^0 K^\pm \pi^\mp$	

• • • We do not use the following data for averages, fits, limits, etc. • • •
 < 0.089 90 ^{2,3} AHOHE 05 CLE2 $10.6 e^+e^- \rightarrow e^+e^- K_S^0 K_S^0 K^\pm \pi^\mp$

¹ Supersedes ACCIARRI 01G. Using $B(K_S^0 \rightarrow \pi^+ \pi^-) = 0.6895$.
² Using $\eta(1475)$ mass of 1481 MeV and width of 48 MeV. The upper limit increases to 0.140 keV if the world average value, 87 MeV, of the width is used.
³ Assuming three-body phase-space decay to $K_S^0 K^\pm \pi^\mp$.

$\eta(1475)$ BRANCHING RATIOS

VALUE	DOCUMENT ID	TECN	COMMENT	Γ_2/Γ_1
-------	-------------	------	---------	---------------------

• • • We do not use the following data for averages, fits, limits, etc. • • •
 0.50 ± 0.10 ¹ BAILLON 67 HBC $0.0 \bar{p}p \rightarrow K \bar{K} \pi \pi$

¹ Data could also refer to $\eta(1405)$.

VALUE	CL%	DOCUMENT ID	TECN	COMMENT	$\Gamma_2/(\Gamma_2+\Gamma_3)$
-------	-----	-------------	------	---------	--------------------------------

• • • We do not use the following data for averages, fits, limits, etc. • • •
 < 0.25 90 EDWARDS 82E CBAL $J/\psi \rightarrow K^+ K^- \pi^0 \gamma$

VALUE	CL%	DOCUMENT ID	TECN	COMMENT	Γ_4/Γ_1
-------	-----	-------------	------	---------	---------------------

$< 1.27 \times 10^{-3}$ 90 ¹ ABLIKIM 18o BES3 $\psi(2S) \rightarrow \pi^+ \pi^- \gamma \gamma$

¹ Using results from BAI 00D.

VALUE	DOCUMENT ID	TECN	COMMENT	Γ_6/Γ
-------	-------------	------	---------	-------------------

possibly seen ¹ ABLIKIM 18i BES3 $J/\psi \rightarrow \gamma\gamma\phi(1020)$

¹ Seen as a peak in $\gamma\phi$ invariant mass. Angular analysis consistent with $J^{PC} = 0^{-+}$. Other J^{PC} not excluded. Also see $\eta(1405)$.

$\eta(1475)$ REFERENCES

ABLIKIM	18i	PR D97 051101	M. Ablikim et al.	(BESIII Collab.)
ABLIKIM	18o	PR D97 072014	M. Ablikim et al.	(BESIII Collab.)
ABLIKIM	15T	PRL 115 091803	M. Ablikim et al.	(BESIII Collab.)
ACHARD	07	JHEP 0703 018	P. Achard et al.	(L3 Collab.)
AHOHE	05	PR D71 072001	R. Ahohe et al.	(CLEO Collab.)
NICHITIU	02	PL B545 261	F. Nichitiu et al.	(OBELIX Collab.)
ACCIARRI	01G	PL B501 1	M. Acciarri et al.	(L3 Collab.)
ADAMS	01B	PL B516 264	G.S. Adams et al.	(BNL E852 Collab.)
BAI	00D	PL B476 25	J.Z. Bai et al.	(BES Collab.)
CICALO	99	PL B462 453	C. Cicalo et al.	(OBELIX Collab.)
BERTIN	97	PL B400 226	A. Bertin et al.	(OBELIX Collab.)
BERTIN	95	PL B361 187	A. Bertin et al.	(OBELIX Collab.)
AUGUSTIN	92	PR D46 1951	J.E. Augustin, G. Cosme	(DM2 Collab.)
BAI	90C	PRL 65 2507	Z. Bai et al.	(Mark III Collab.)
RATH	89	PR D40 693	M.G. Rath et al.	(NDAM, BRAN, BNL, CUNY+)
EDWARDS	82E	PRL 49 259	C. Edwards et al.	(CIT, HARV, PRIN+)
BAILLON	67	NC 50A 393	P.H. Baillon et al.	(CERN, CDEF, IRAD)

$f_0(1500)$

$$J^G(J^{PC}) = 0^+(0^{++})$$

See the reviews on "Scalar Mesons below 2 GeV" and on "Non- $q\bar{q}$ Mesons".

$f_0(1500)$ MASS

VALUE (MeV)	EVTS	DOCUMENT ID	TECN	COMMENT
1506 ± 6	OUR AVERAGE			Error includes scale factor of 1.4. See the ideogram below.
1515 ± 12		¹ BARBERIS	00A	$450 pp \rightarrow p_f \eta \eta p_S$
1511 ± 9		^{1,2} BARBERIS	00C	$450 pp \rightarrow p_f 4\pi p_S$
1510 ± 8		¹ BARBERIS	00E	$450 pp \rightarrow p_f \eta \eta p_S$
1522 ± 25		¹ BERTIN	98	OBLX $0.05-0.405 \bar{p}p \rightarrow \pi^+ \pi^+ \pi^-$
1449 ± 20		¹ BERTIN	97C	OBLX $0.0 \bar{p}p \rightarrow \pi^+ \pi^- \pi^0$
1500 ± 10		³ AMSLER	95D	CBAR $0.0 \bar{p}p \rightarrow \pi^0 \pi^0 \pi^0, \pi^0 \eta \eta, \pi^0 \pi^0 \eta$

• • • We do not use the following data for averages, fits, limits, etc. • • •
 1465 ± 18 ⁴ ROPERTZ 18 RVUE $\bar{B}_s^0 \rightarrow J/\psi(\pi^+ \pi^- / K^+ K^-)$

1447 $\pm 16 \pm 13$	163	^{5,6} DOBBS	15	$J/\psi \rightarrow \gamma \pi^+ \pi^-$
1442 $\pm 9 \pm 4$	261	^{5,6} DOBBS	15	$\psi(2S) \rightarrow \gamma \pi^+ \pi^-$
1460.9 ± 2.9		⁷ AAIJ	14BR	LHCB $\bar{B}_s^0 \rightarrow J/\psi \pi^+ \pi^-$
1468 $^{+14}_{-15} \pm 23$	$^{+74}_{-74}$	⁸ ABLIKIM	13N	BES3 $e^+e^- \rightarrow J/\psi \rightarrow \gamma \eta \eta$
1486 ± 10		¹ ANISOVICH	09	RVUE $0.0 \bar{p}p, \pi N$
1470 ± 60	568	⁹ KLEMP	08	E791 $D_s^+ \rightarrow \pi^- \pi^+ \pi^+$
1470 $^{+6}_{-7} \pm 72$	$^{+255}_{-255}$	¹⁰ UEHARA	08A	BELL $10.6 e^+e^- \rightarrow e^+e^- \pi^0 \pi^0$
1466 $\pm 6 \pm 20$		¹¹ ABLIKIM	06V	BES2 $e^+e^- \rightarrow J/\psi \rightarrow \gamma \pi^+ \pi^-$
1495 ± 4		AMSLER	06	CBAR $0.9 \bar{p}p \rightarrow K^+ K^- \pi^0$
1539 ± 20	9.9k	AUBERT	06O	BABR $B^+ \rightarrow K^+ K^+ K^-$
1473 ± 5	80k	^{11,12} UMAN	06	E835 $5.2 \bar{p}p \rightarrow \eta \eta \pi^0$
1478 ± 6		VLADIMIRSK...	06	SPEC $40 \pi^- p \rightarrow K_S^0 K_S^0 n$
1493 ± 7		¹¹ BINON	05	GAMS $33 \pi^- p \rightarrow \eta \eta n$
1524 ± 14	1400	¹³ GARMASH	05	BELL $B^+ \rightarrow K^+ K^+ K^-$
1489 $^{+8}_{-4}$		¹⁴ ANISOVICH	03	RVUE
1490 ± 30		¹¹ ABELE	01	CBAR $0.0 \bar{p}d \rightarrow \pi^- 4\pi^0 p$
1497 ± 10		¹¹ BARBERIS	99	OMEG $450 pp \rightarrow p_S p_f K^+ K^-$
1502 ± 10		¹¹ BARBERIS	99B	OMEG $450 pp \rightarrow p_S p_f \pi^+ \pi^-$
1502 $\pm 12 \pm 10$		¹⁵ BARBERIS	99D	OMEG $450 pp \rightarrow K^+ K^-$
1530 ± 45		¹¹ BELLAZZINI	99	GAM4 $450 pp \rightarrow pp \pi^0 \pi^0$
1505 ± 18		¹¹ FRENCH	99	$300 pp \rightarrow p_f(K^+ K^-) p_S$
1447 ± 27		¹⁶ KAMINSKI	99	RVUE $\pi\pi \rightarrow \pi\pi, K\bar{K}, \sigma\sigma$
1580 ± 80		¹¹ ALDE	98	GAM4 $100 \pi^- p \rightarrow \pi^0 \pi^0 n$
1499 ± 8		¹ ANISOVICH	98B	RVUE Compilation
~ 1520		REYES	98	SPEC $800 pp \rightarrow p_S p_f K_S^0 K_S^0$
1510 ± 20		¹ BARBERIS	97B	OMEG $450 pp \rightarrow pp 2(\pi^+ \pi^-)$
~ 1475		FRABETTI	97D	E687 $D_s^\pm \rightarrow \pi^\mp \pi^\pm \pi^\pm$
~ 1505		ABELE	96	CBAR $0.0 \bar{p}p \rightarrow 5\pi^0$
1515 ± 20		ABELE	96B	CBAR $0.0 \bar{p}p \rightarrow \pi^0 K_L^0 K_L^0$
1500 ± 8		¹ ABELE	96C	RVUE Compilation
1460 ± 20	120	¹¹ AMELIN	96B	VES $37 \pi^- A \rightarrow \eta \eta \pi^- A$
1500 ± 8		BUGG	96	RVUE
1500 ± 15		¹⁷ AMSLER	95B	CBAR $0.0 \bar{p}p \rightarrow 3\pi^0$
1505 ± 15		¹⁸ AMSLER	95C	CBAR $0.0 \bar{p}p \rightarrow \eta \eta \pi^0$
1445 ± 5		¹⁹ ANTINORI	95	OMEG $300,450 pp \rightarrow pp 2(\pi^+ \pi^-)$
1497 ± 30		¹¹ ANTINORI	95	OMEG $300,450 pp \rightarrow pp \pi^+ \pi^-$
~ 1505		BUGG	95	MRK3 $J/\psi \rightarrow \gamma \pi^+ \pi^- \pi^+ \pi^-$
1446 ± 5		¹¹ ABATZIS	94	OMEG $450 pp \rightarrow pp 2(\pi^+ \pi^-)$
1545 ± 25		¹¹ AMSLER	94E	CBAR $0.0 \bar{p}p \rightarrow \pi^0 \eta \eta'$
1520 ± 25		^{1,20} ANISOVICH	94	CBAR $0.0 \bar{p}p \rightarrow 3\pi^0, \pi^0 \eta \eta$
1505 ± 20		^{1,21} BUGG	94	RVUE $\bar{p}p \rightarrow 3\pi^0, \eta \eta \pi^0, \eta \pi^0 \pi^0$

See key on page 999

Meson Particle Listings

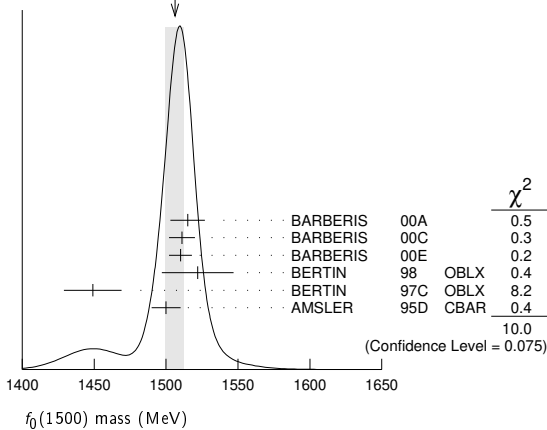
$f_0(1500)$

1560 ± 25	11 AMSLER	92 CBAR	0.0 $\bar{p}p \rightarrow \pi^0 \eta \eta$
1550 ± 45 ± 30	11 BELADIDZE	92c VES	36 $\pi^- \text{Be} \rightarrow \pi^- \eta' \eta \text{Be}$
1449 ± 4	11 ARMSTRONG	89E OMEG	300 $pp \rightarrow pp 2(\pi^+ \pi^-)$
1610 ± 20	11 ALDE	88 GAM4	300 $\pi^- N \rightarrow \pi^- N 2\eta$
~ 1525	ASTON	88D LASS	11 $K^- p \rightarrow K_S^0 K_S^0 \Lambda$
1570 ± 20	600 11 ALDE	87 GAM4	100 $\pi^- p \rightarrow 4\pi^0 n$
1575 ± 45	22 ALDE	86D GAM4	100 $\pi^- p \rightarrow 2\eta n$
1568 ± 33	11 BINON	84c GAM2	38 $\pi^- p \rightarrow \eta \eta' n$
1592 ± 25	11 BINON	83 GAM2	38 $\pi^- p \rightarrow 2\eta n$
1525 ± 5	11 GRAY	83 DBC	0.0 $\bar{p}N \rightarrow 3\pi$

108 ± 9	80k 8,9 UMAN	06 E835	5.2 $\bar{p}p \rightarrow \eta \eta \pi^0$
119 ± 10	VLADIMIRSK...	06 SPEC	40 $\pi^- p \rightarrow K_S^0 K_S^0 n$
90 ± 15	8 BINON	05 GAMS	33 $\pi^- p \rightarrow \eta \eta n$
136 ± 23	10 GARMASH	05 BELL	$B^+ \rightarrow K^+ K^+ K^-$
102 ± 10	11 ANISOVICH	03 RVUE	
140 ± 40	8 ABELE	01 CBAR	0.0 $\bar{p}d \rightarrow \pi^- 4\pi^0 p$
104 ± 25	8 BARBERIS	99 OMEG	450 $pp \rightarrow p_S p_f K^+ K^-$
131 ± 15	8 BARBERIS	99B OMEG	450 $pp \rightarrow p_S p_f \pi^+ \pi^-$
98 ± 18 ± 16	12 BARBERIS	99D OMEG	450 $pp \rightarrow K^+ K^-, \pi^+ \pi^-$
160 ± 50	8 BELLAZZINI	99 GAM4	450 $pp \rightarrow p p \pi^0 \pi^0$
100 ± 33	8 FRENCH	99	300 $pp \rightarrow p_f(K^+ K^-) p_S$
108 ± 46	13 KAMINSKI	99 RVUE	$\pi \pi \rightarrow \pi \pi, K \bar{K}, \sigma \sigma$
280 ± 100	8 ALDE	98 GAM4	100 $\pi^- p \rightarrow \pi^0 \pi^0 n$
130 ± 20	1 ANISOVICH	98B RVUE	Compilation
120 ± 35	1 BARBERIS	97B OMEG	450 $pp \rightarrow p p 2(\pi^+ \pi^-)$
~ 100	FRABETTI	97D E687	$D_S^\pm \rightarrow \pi^\mp \pi^\pm \pi^\pm$
~ 169	ABELE	96 CBAR	0.0 $\bar{p}p \rightarrow 5\pi^0$
105 ± 15	ABELE	96B CBAR	0.0 $\bar{p}p \rightarrow \pi^0 K_L^0 K_L^0$
100 ± 30	120 8 AMELIN	96B VES	37 $\pi^- A \rightarrow \eta \eta \pi^- A$
132 ± 15	BUGG	96 RVUE	
120 ± 25	14 AMSLER	95B CBAR	0.0 $\bar{p}p \rightarrow 3\pi^0$
120 ± 30	15 AMSLER	95C CBAR	0.0 $\bar{p}p \rightarrow \eta \eta \pi^0$
65 ± 10	16 AN TINORI	95 OMEG	300,450 $pp \rightarrow p p 2(\pi^+ \pi^-)$
199 ± 30	8 AN TINORI	95 OMEG	300,450 $pp \rightarrow p p \pi^+ \pi^-$
56 ± 12	8 ABATZIS	94 OMEG	450 $pp \rightarrow p p 2(\pi^+ \pi^-)$
100 ± 40	8 AMSLER	94E CBAR	0.0 $\bar{p}p \rightarrow \pi^0 \eta \eta'$
148 ± 20	1,17 ANISOVICH	94 CBAR	0.0 $\bar{p}p \rightarrow 3\pi^0, \pi^0 \eta \eta$
150 ± 20	1,18 BUGG	94 RVUE	$\bar{p}p \rightarrow 3\pi^0, \eta \eta \pi^0, \eta \pi^0 \pi^0$
245 ± 50	8 AMSLER	92 CBAR	0.0 $\bar{p}p \rightarrow \pi^0 \eta \eta$
153 ± 67 ± 50	8 BELADIDZE	92c VES	36 $\pi^- \text{Be} \rightarrow \pi^- \eta' \eta \text{Be}$
78 ± 18	8 ARMSTRONG	89E OMEG	300 $pp \rightarrow p p 2(\pi^+ \pi^-)$
170 ± 40	8 ALDE	88 GAM4	300 $\pi^- N \rightarrow \pi^- N 2\eta$
150 ± 20	600 8 ALDE	87 GAM4	100 $\pi^- p \rightarrow 4\pi^0 n$
265 ± 65	19 ALDE	86D GAM4	100 $\pi^- p \rightarrow 2\eta n$
260 ± 60	8 BINON	84c GAM2	38 $\pi^- p \rightarrow \eta \eta' n$
210 ± 40	8 BINON	83 GAM2	38 $\pi^- p \rightarrow 2\eta n$
101 ± 13	8 GRAY	83 DBC	0.0 $\bar{p}N \rightarrow 3\pi$

- T-matrix pole.
- Average between $\pi^+ \pi^- 2\pi^0$ and $2(\pi^+ \pi^-)$.
- T-matrix pole. Coupled-channel analysis of AMSLER 95B, AMSLER 95c, and AMSLER 94d.
- T-matrix pole of 3 channel unitary model fit to data from AAIJ 14BR and AAIJ 17V extracted using Pade approximants.
- Using CLEO-c data but not authored by the CLEO Collaboration.
- From a fit to a Breit-Wigner line shape with fixed $\Gamma = 109$ MeV.
- Solution 1, statistical error only.
- From partial wave analysis including all possible combinations of $0^{++}, 2^{++}$, and 4^{++} resonances.
- Reanalysis of AITALA 01A data. This state could also be $f_0(1370)$.
- Breit-Wigner mass. May also be the $f_0(1370)$.
- Breit-Wigner mass.
- Statistical error only.
- Breit-Wigner, solution 1, PWA ambiguous.
- K-matrix pole from combined analysis of $\pi^- p \rightarrow \pi^0 \pi^0 n, \pi^- p \rightarrow K \bar{K} n, \pi^+ \pi^- \rightarrow \pi^+ \pi^-, \bar{p}p \rightarrow \pi^0 \pi^0 \pi^0, \pi^0 \eta \eta, \pi^0 \pi^0 \eta, \pi^+ \pi^- \pi^0, K^+ K^- \pi^0, K_S^0 K_S^0 \pi^0, K^+ K_S^0 \pi^-$ at rest, $\bar{p}n \rightarrow \pi^- \pi^- \pi^+, K_S^0 K^- \pi^0, K_S^0 K_S^0 \pi^-$ at rest.
- Supersedes BARBERIS 99 and BARBERIS 99b.
- T-matrix pole on sheet --+.
- T-matrix pole, supersedes ANISOVICH 94.
- T-matrix pole, supersedes ANISOVICH 94 and AMSLER 92.
- Supersedes ABATZIS 94, ARMSTRONG 89E. Breit-Wigner mass.
- From a simultaneous analysis of the annihilations $\bar{p}p \rightarrow 3\pi^0, \pi^0 \eta \eta$.
- Reanalysis of ANISOVICH 94 data.
- From central value and spread of two solutions. Breit-Wigner mass.

WEIGHTED AVERAGE
1506±6 (Error scaled by 1.4)



- T-matrix pole.
- Average between $\pi^+ \pi^- 2\pi^0$ and $2(\pi^+ \pi^-)$.
- T-matrix pole. Coupled-channel analysis of AMSLER 95B, AMSLER 95c, and AMSLER 94d.
- T-matrix pole of 3 channel unitary model fit to data from AAIJ 14BR and AAIJ 17V extracted using Pade approximants.
- Solution 1, statistical error only.
- From partial wave analysis including all possible combinations of $0^{++}, 2^{++}$, and 4^{++} resonances.
- Breit-Wigner width. May also be the $f_0(1370)$.
- Breit-Wigner width.
- Statistical error only.
- Breit-Wigner, solution 1, PWA ambiguous.
- K-matrix pole from combined analysis of $\pi^- p \rightarrow \pi^0 \pi^0 n, \pi^- p \rightarrow K \bar{K} n, \pi^+ \pi^- \rightarrow \pi^+ \pi^-, \bar{p}p \rightarrow \pi^0 \pi^0 \pi^0, \pi^0 \eta \eta, \pi^0 \pi^0 \eta, \pi^+ \pi^- \pi^0, K^+ K^- \pi^0, K_S^0 K_S^0 \pi^0, K^+ K_S^0 \pi^-$ at rest, $\bar{p}n \rightarrow \pi^- \pi^- \pi^+, K_S^0 K^- \pi^0, K_S^0 K_S^0 \pi^-$ at rest.
- Supersedes BARBERIS 99 and BARBERIS 99b.
- T-matrix pole on sheet --+.
- T-matrix pole, supersedes ANISOVICH 94.
- T-matrix pole, supersedes ANISOVICH 94 and AMSLER 92.
- Supersedes ABATZIS 94, ARMSTRONG 89E. Breit-Wigner mass.
- From a simultaneous analysis of the annihilations $\bar{p}p \rightarrow 3\pi^0, \pi^0 \eta \eta$.
- Reanalysis of ANISOVICH 94 data.
- From central value and spread of two solutions. Breit-Wigner mass.

$f_0(1500)$ WIDTH

VALUE (MeV)	EVTS	DOCUMENT ID	TECN	COMMENT
112 ± 9 OUR AVERAGE				
110 ± 24		1 BARBERIS 00A		450 $pp \rightarrow p_f \eta \eta p_S$
102 ± 18		1,2 BARBERIS 00C		450 $pp \rightarrow p_f 4\pi p_S$
110 ± 16		1 BARBERIS 00E		450 $pp \rightarrow p_f \eta \eta p_S$
108 ± 33		1 BERTIN 98 OBLX		0.05-0.405 $\bar{p}p \rightarrow \pi^+ \pi^+ \pi^-$
114 ± 30		1 BERTIN 97C OBLX		0.0 $\bar{p}p \rightarrow \pi^+ \pi^- \pi^0$
154 ± 30		3 AMSLER 95D CBAR		0.0 $\bar{p}p \rightarrow \pi^0 \pi^0 \pi^0, \pi^0 \eta \eta, \pi^0 \pi^0 \eta$
• • • We do not use the following data for averages, fits, limits, etc. • • •				
100 ± 18		4 ROPERTZ 18 RVUE		$\bar{B}_s^0 \rightarrow J/\psi(\pi^+ \pi^- / K^+ K^-)$
124 ± 7		5 AAIJ 14BR LHCB		$\bar{B}_s^0 \rightarrow J/\psi \pi^+ \pi^-$
136 ± 41 ± 28 26 ± 100	5.5k	6 ABLIKIM 13N BES3		$e^+ e^- \rightarrow J/\psi \rightarrow \gamma \eta \eta$
114 ± 10		1 ANISOVICH 09 RVUE		0.0 $\bar{p}p, \pi N$
90 ± 2 ± 50 1 ± 22		7 UEHARA 08A BELL		10.6 $e^+ e^- \rightarrow e^+ e^- \pi^0 \pi^0$
108 ± 14 ± 25		8 ABLIKIM 06V BES2		$e^+ e^- \rightarrow J/\psi \rightarrow \gamma \pi^+ \pi^-$
121 ± 8		AMSLER 06 CBAR		0.9 $\bar{p}p \rightarrow K^+ K^- \pi^0$
257 ± 33	9.9k	AUBERT 06o BABR		$B^+ \rightarrow K^+ K^+ K^-$

$f_0(1500)$ DECAY MODES

Mode	Fraction (Γ_i/Γ)	Scale factor
Γ_1 $\pi \pi$	(34.5 ± 2.2) %	1.2
Γ_2 $\pi^+ \pi^-$	seen	
Γ_3 $2\pi^0$	seen	
Γ_4 4π	(48.9 ± 3.3) %	1.2
Γ_5 $4\pi^0$	seen	
Γ_6 $2\pi^+ 2\pi^-$	seen	
Γ_7 $2(\pi\pi)S$ -wave	seen	
Γ_8 $\rho\rho$	seen	
Γ_9 $\pi(1300)\pi$	seen	
Γ_{10} $a_1(1260)\pi$	seen	
Γ_{11} $\eta\eta$	(6.0 ± 0.9) %	1.1
Γ_{12} $\eta\eta'(958)$	(2.2 ± 0.8) %	1.4
Γ_{13} $K\bar{K}$	(8.5 ± 1.0) %	1.1
Γ_{14} $\gamma\gamma$	not seen	

Meson Particle Listings

 $f_0(1500)$

CONSTRAINED FIT INFORMATION

An overall fit to 6 branching ratios uses 10 measurements and one constraint to determine 5 parameters. The overall fit has a $\chi^2 = 5.6$ for 6 degrees of freedom.

The following *off-diagonal* array elements are the correlation coefficients $\langle \delta x_i \delta x_j \rangle / (\delta x_i \delta x_j)$, in percent, from the fit to the branching fractions, $x_i \equiv \Gamma_i / \Gamma_{\text{total}}$. The fit constrains the x_i whose labels appear in this array to sum to one.

x_4	-88				
x_{11}	27	-56			
x_{12}	3	-32	26		
x_{13}	43	-64	20	2	
	x_1	x_4	x_{11}	x_{12}	

 $f_0(1500) \Gamma(i) \Gamma(\gamma\gamma) / \Gamma(\text{total})$

$\Gamma(\pi\pi) \times \Gamma(\gamma\gamma) / \Gamma_{\text{total}}$	CL%	DOCUMENT ID	TECN	COMMENT	Γ_{14} / Γ
••• We do not use the following data for averages, fits, limits, etc. •••					
$33^{+12}_{-6} + 1809_{-21}$		¹ UEHARA	08A BELL	$10.6 e^+ e^- \rightarrow e^+ e^- \pi^0 \pi^0$	
not seen		ACCIARRI	01H L3	$\gamma\gamma \rightarrow K_S^0 K_S^0, E_{\text{cm}}^{\text{res}} = 91, 183-209 \text{ GeV}$	
<460	95	BARATE	00E ALEP	$\gamma\gamma \rightarrow \pi^+ \pi^-$	
¹ May also be the $f_0(1370)$. Multiplied by us by 3 to obtain the $\pi\pi$ value.					

 $f_0(1500)$ BRANCHING RATIOS

$\Gamma(\pi\pi) / \Gamma_{\text{total}}$	DOCUMENT ID	TECN	COMMENT	Γ_1 / Γ
••• We do not use the following data for averages, fits, limits, etc. •••				
0.454 ± 0.104	BUGG	96	RVUE	

$\Gamma(\pi^+ \pi^-) / \Gamma_{\text{total}}$	DOCUMENT ID	TECN	COMMENT	Γ_2 / Γ
seen	BERTIN	98	OBLX	$0.05-0.405 \bar{p}p \rightarrow \pi^+ \pi^+ \pi^-$
••• We do not use the following data for averages, fits, limits, etc. •••				
possibly seen	FRABETTI	97D	E687	$D_S^\pm \rightarrow \pi^\mp \pi^\pm \pi^\pm$

$\Gamma(4\pi) / \Gamma(\pi\pi)$	DOCUMENT ID	TECN	COMMENT	Γ_4 / Γ_1
1.42 ± 0.18 OUR FIT	Error includes scale factor of 1.2.			
1.42 ± 0.18 OUR AVERAGE	Error includes scale factor of 1.2.			
1.37 ± 0.16	BARBERIS	00D	$450 pp \rightarrow p_f 4\pi p_S$	
2.1 ± 0.6	¹ AMSLER	98	RVUE	
••• We do not use the following data for averages, fits, limits, etc. •••				
2.1 ± 0.2	² ANISOVICH	02D	SPEC	Combined fit
3.4 ± 0.8	¹ ABELE	96	CBAR	$0.0 \bar{p}p \rightarrow 5\pi^0$
¹ Excluding $\rho\rho$ contribution to 4π .				
² From a combined K-matrix analysis of Crystal Barrel ($0. \bar{p}p \rightarrow \pi^0 \pi^0 \pi^0, \pi^0 \eta \eta, \pi^0 \pi^0 \eta$), GAMS ($\pi p \rightarrow \pi^0 \pi^0 n, \eta \eta n, \eta \eta' n$), and BNL ($\pi p \rightarrow K \bar{K} n$) data.				

$\Gamma(2(\pi\pi)_{s\text{-wave}}) / \Gamma(\pi\pi)$	DOCUMENT ID	TECN	COMMENT	Γ_7 / Γ_1
••• We do not use the following data for averages, fits, limits, etc. •••				
0.42 ± 0.26	¹ ABELE	01	CBAR	$0.0 \bar{p}d \rightarrow \pi^- 4\pi^0 p$
¹ From the combined data of ABELE 96 and ABELE 96c.				

$\Gamma(2(\pi\pi)_{s\text{-wave}}) / \Gamma(4\pi)$	DOCUMENT ID	TECN	COMMENT	Γ_7 / Γ_4
••• We do not use the following data for averages, fits, limits, etc. •••				
0.26 ± 0.07	ABELE	01B	CBAR	$0.0 \bar{p}d \rightarrow 5\pi p$

$\Gamma(\rho\rho) / \Gamma(4\pi)$	DOCUMENT ID	TECN	COMMENT	Γ_8 / Γ_4
••• We do not use the following data for averages, fits, limits, etc. •••				
0.13 ± 0.08	ABELE	01B	CBAR	$0.0 \bar{p}d \rightarrow 5\pi p$

$\Gamma(\rho\rho) / \Gamma(2(\pi\pi)_{s\text{-wave}})$	DOCUMENT ID	COMMENT	Γ_8 / Γ_7
2.87 ± 0.34 OUR AVERAGE	Error includes scale factor of 1.1.		
3.3 ± 0.5	BARBERIS	00c $450 pp \rightarrow p_f \pi^+ \pi^- 2\pi^0 p_S$	
2.6 ± 0.4	BARBERIS	00c $450 pp \rightarrow p_f 2(\pi^+ \pi^-) p_S$	

$\Gamma(\pi(1300)\pi) / \Gamma(4\pi)$	DOCUMENT ID	TECN	COMMENT	Γ_9 / Γ_4
••• We do not use the following data for averages, fits, limits, etc. •••				
0.50 ± 0.25	ABELE	01B	CBAR	$0.0 \bar{p}d \rightarrow 5\pi p$

$\Gamma(a_1(1260)\pi) / \Gamma(4\pi)$	DOCUMENT ID	TECN	COMMENT	Γ_{10} / Γ_4
••• We do not use the following data for averages, fits, limits, etc. •••				
0.12 ± 0.05	ABELE	01B	CBAR	$0.0 \bar{p}d \rightarrow 5\pi p$

$\Gamma(\eta\eta) / \Gamma_{\text{total}}$	DOCUMENT ID	TECN	COMMENT	Γ_{11} / Γ
••• We do not use the following data for averages, fits, limits, etc. •••				
large	ALDE	88	GAM4	$300 \pi^- N \rightarrow \eta \eta \pi^- N$
large	BINON	83	GAM2	$38 \pi^- p \rightarrow 2\eta n$

$\Gamma(\eta\eta) / \Gamma(\pi\pi)$	DOCUMENT ID	TECN	COMMENT	Γ_{11} / Γ_1
0.173 ± 0.024 OUR FIT	Error includes scale factor of 1.1.			
0.175 ± 0.027 OUR AVERAGE				
0.18 ± 0.03	BARBERIS	00E	$450 pp \rightarrow p_f \eta \eta p_S$	
0.157 ± 0.060	¹ AMSLER	95D	CBAR	$0.0 \bar{p}p \rightarrow \pi^0 \pi^0 \pi^0, \pi^0 \eta \eta, \pi^0 \pi^0 \eta$
••• We do not use the following data for averages, fits, limits, etc. •••				
0.080 ± 0.033	AMSLER	02	CBAR	$0.9 \bar{p}p \rightarrow \pi^0 \eta \eta, \pi^0 \pi^0 \pi^0$
0.11 ± 0.03	² ANISOVICH	02D	SPEC	Combined fit
0.078 ± 0.013	³ ABELE	96c	RVUE	Compilation
0.230 ± 0.097	⁴ AMSLER	95c	CBAR	$0.0 \bar{p}p \rightarrow \eta \eta \pi^0$
¹ Coupled-channel analysis of AMSLER 95B, AMSLER 95c, and AMSLER 94D.				
² From a combined K-matrix analysis of Crystal Barrel ($0. \bar{p}p \rightarrow \pi^0 \pi^0 \pi^0, \pi^0 \eta \eta, \pi^0 \pi^0 \eta$), GAMS ($\pi p \rightarrow \pi^0 \pi^0 n, \eta \eta n, \eta \eta' n$), and BNL ($\pi p \rightarrow K \bar{K} n$) data.				
³ 2π width determined to be $60 \pm 12 \text{ MeV}$.				
⁴ Using AMSLER 95B ($3\pi^0$).				

$\Gamma(4\pi^0) / \Gamma(\eta\eta)$	DOCUMENT ID	TECN	COMMENT	Γ_5 / Γ_{11}
••• We do not use the following data for averages, fits, limits, etc. •••				
0.8 ± 0.3	ALDE	87	GAM4	$100 \pi^- p \rightarrow 4\pi^0 n$

$\Gamma(\eta\eta'(958)) / \Gamma(\pi\pi)$	DOCUMENT ID	TECN	COMMENT	Γ_{12} / Γ_1
0.064 ± 0.022 OUR FIT	Error includes scale factor of 1.4.			
0.095 ± 0.026	BARBERIS	00A	$450 pp \rightarrow p_f \eta \eta p_S$	
••• We do not use the following data for averages, fits, limits, etc. •••				
0.005 ± 0.003	¹ ANISOVICH	02D	SPEC	Combined fit
¹ From a combined K-matrix analysis of Crystal Barrel ($0. \bar{p}p \rightarrow \pi^0 \pi^0 \pi^0, \pi^0 \eta \eta, \pi^0 \pi^0 \eta$), GAMS ($\pi p \rightarrow \pi^0 \pi^0 n, \eta \eta n, \eta \eta' n$), and BNL ($\pi p \rightarrow K \bar{K} n$) data.				

$\Gamma(\eta\eta'(958)) / \Gamma(\eta\eta)$	DOCUMENT ID	TECN	COMMENT	$\Gamma_{12} / \Gamma_{11}$
0.37 ± 0.13 OUR FIT	Error includes scale factor of 1.5.			
0.29 ± 0.10	¹ AMSLER	95c	CBAR	$0.0 \bar{p}p \rightarrow \eta \eta \pi^0$
••• We do not use the following data for averages, fits, limits, etc. •••				
0.05 ± 0.03	² ANISOVICH	02D	SPEC	Combined fit
0.84 ± 0.23	ABELE	96c	RVUE	Compilation
2.7 ± 0.8	BINON	84c	GAM2	$38 \pi^- p \rightarrow \eta \eta' n$
¹ Using AMSLER 94E ($\eta \eta' \pi^0$).				
² From a combined K-matrix analysis of Crystal Barrel ($0. \bar{p}p \rightarrow \pi^0 \pi^0 \pi^0, \pi^0 \eta \eta, \pi^0 \pi^0 \eta$), GAMS ($\pi p \rightarrow \pi^0 \pi^0 n, \eta \eta n, \eta \eta' n$), and BNL ($\pi p \rightarrow K \bar{K} n$) data.				

$\Gamma(K\bar{K}) / \Gamma_{\text{total}}$	DOCUMENT ID	TECN	COMMENT	Γ_{13} / Γ
••• We do not use the following data for averages, fits, limits, etc. •••				
0.044 ± 0.021	BUGG	96	RVUE	

$\Gamma(K\bar{K}) / \Gamma(\pi\pi)$	DOCUMENT ID	TECN	COMMENT	Γ_{13} / Γ_1
0.246 ± 0.025 OUR FIT	Error includes scale factor of 1.1.			
0.236 ± 0.026 OUR AVERAGE				
0.25 ± 0.03	¹ BARGIOTTI	03	OBLX	$\bar{p}p$
0.19 ± 0.07	² ABELE	98	CBAR	$0.0 \bar{p}p \rightarrow K_L^0 K^\pm \pi^\mp$
0.20 ± 0.08	³ ABELE	96B	CBAR	$0.0 \bar{p}p \rightarrow \pi^0 K_L^0 K_L^0$
••• We do not use the following data for averages, fits, limits, etc. •••				
0.16 ± 0.05	⁴ ANISOVICH	02D	SPEC	Combined fit
$0.33 \pm 0.03 \pm 0.07$	BARBERIS	99D	OMEG	$450 pp \rightarrow K^+ K^-, \pi^+ \pi^-$
¹ Coupled channel analysis of $\pi^+ \pi^- \pi^0, K^+ K^- \pi^0$, and $K^\pm K_S^0 \pi^\mp$.				
² Using $\pi^0 \pi^0$ from AMSLER 95B.				
³ Using AMSLER 95B ($3\pi^0$), AMSLER 94C ($2\pi^0 \eta$) and SU(3).				
⁴ From a combined K-matrix analysis of Crystal Barrel ($0. \bar{p}p \rightarrow \pi^0 \pi^0 \pi^0, \pi^0 \eta \eta, \pi^0 \pi^0 \eta$), GAMS ($\pi p \rightarrow \pi^0 \pi^0 n, \eta \eta n, \eta \eta' n$), and BNL ($\pi p \rightarrow K \bar{K} n$) data.				

$\Gamma(K\bar{K}) / \Gamma(\eta\eta)$	CL%	DOCUMENT ID	TECN	COMMENT	$\Gamma_{13} / \Gamma_{11}$
1.43 ± 0.24 OUR FIT	Error includes scale factor of 1.1.				
1.85 ± 0.41		BARBERIS	00E	$450 pp \rightarrow p_f \eta \eta p_S$	
••• We do not use the following data for averages, fits, limits, etc. •••					
1.5 ± 0.6		¹ ANISOVICH	02D	SPEC	Combined fit
<0.4	90	² PROKOSHKIN	91	GAM4	$300 \pi^- p \rightarrow \pi^- \rho \eta \eta$

See key on page 999

Meson Particle Listings

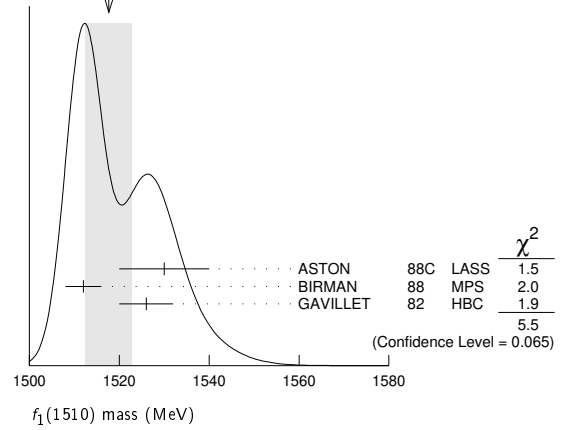
$f_0(1500)$, $f_1(1510)$

<0.6 ³ BINON 83 GAM2 38 $\pi^- p \rightarrow 2\eta n$
¹ From a combined K-matrix analysis of Crystal Barrel ($0. p\bar{p} \rightarrow \pi^0 \pi^0 \pi^0, \pi^0 \eta \eta, \pi^0 \pi^0 \eta$), GAMS ($\pi p \rightarrow \pi^0 \pi^0 n, \eta \eta n, \eta \eta' n$), and BNL ($\pi p \rightarrow K\bar{K}n$) data.
² Combining results of GAM4 with those of WA76 on $K\bar{K}$ central production.
³ Using ETKIN 82b and COHEN 80.

$f_0(1500)$ REFERENCES

ROPERTZ 18	EPJ C78 1000	S. Ropertz, C. Hanhart, B. Kubis	(BONN, JULI)
AAJ 17V	JHEP 1708 037	R. Aaij <i>et al.</i>	(LHCb Collab.)
DOBBS 15	PR D91 052006	S. Dobbs <i>et al.</i>	(NWES)
AAJ 14BR	PR D89 092006	R. Aaij <i>et al.</i>	(LHCb Collab.)
ABLIKIM 13N	PR D87 092009	Ablikim M. <i>et al.</i>	(BESIII Collab.)
ANISOVICH 09	IJMP A24 2481	V.V. Anisovich, A.V. Sarantsev	(BONN+)
KLEMPF 08	EPJ C55 39	E. Klempf, M. Matveev, A.V. Sarantsev	(BELLE Collab.)
UEHARA 08A	PR D78 092004	S. Uehara <i>et al.</i>	(BES Collab.)
ABLIKIM 06V	PL B642 441	M. Ablikim <i>et al.</i>	(CBAR Collab.)
AMSLER 06P	PL B639 165	C. Amstler <i>et al.</i>	(BABAR Collab.)
AUBERT 06O	PR D74 032003	B. Aubert <i>et al.</i>	(FNAL E835)
UMAN 06	PR D73 052009	I. Uman <i>et al.</i>	(ITEP, Moscow)
VLADIMIRSK... 06	PAN 69 493	V.V. Vladimirovsky <i>et al.</i>	(ITEP, Moscow)
Translated from YAF 69 515.			
BINON 05	PAN 68 960	F. Binon <i>et al.</i>	(Crystal Barrel Collab.)
Translated from YAF 68 938.			
GARMASH 05	PR D71 092003	A. Garmash <i>et al.</i>	(BELLE Collab.)
ANISOVICH 03	EPJ A16 229	V.V. Anisovich <i>et al.</i>	(OBELIX Collab.)
BARGIOTTI 03	EPJ C26 371	M. Bargiotti <i>et al.</i>	(OBELIX Collab.)
AMSLER 02	EPJ C23 29	C. Amstler <i>et al.</i>	(OBELIX Collab.)
ANISOVICH 02D	PAN 65 1545	V.V. Anisovich <i>et al.</i>	(OBELIX Collab.)
Translated from YAF 65 1583.			
ABELE 01	EPJ C19 667	A. Abele <i>et al.</i>	(Crystal Barrel Collab.)
ABELE 01B	EPJ C21 261	A. Abele <i>et al.</i>	(Crystal Barrel Collab.)
ACCIARRI 01H	PL B501 173	M. Acciari <i>et al.</i>	(L3 Collab.)
AITALA 01A	PRL 86 765	E.M. Aitala <i>et al.</i>	(FNAL E791 Collab.)
BARATE 00E	PL B472 189	R. Barate <i>et al.</i>	(ALEPH Collab.)
BARBERIS 00A	PL B471 429	D. Barberis <i>et al.</i>	(WA 102 Collab.)
BARBERIS 00C	PL B471 440	D. Barberis <i>et al.</i>	(WA 102 Collab.)
BARBERIS 00D	PL B474 423	D. Barberis <i>et al.</i>	(WA 102 Collab.)
BARBERIS 00E	PL B479 59	D. Barberis <i>et al.</i>	(WA 102 Collab.)
BARBERIS 99	PL B453 305	D. Barberis <i>et al.</i>	(Omega Expt.)
BARBERIS 99B	PL B453 316	D. Barberis <i>et al.</i>	(Omega Expt.)
BARBERIS 99D	PL B462 462	D. Barberis <i>et al.</i>	(Omega Expt.)
BELLAZZINI 99	PL B467 296	R. Bellazzini <i>et al.</i>	(WA76 Collab.)
FRENCH 99	PL B460 213	B. French <i>et al.</i>	(WA76 Collab.)
KAMINSKI 99	EPJ C9 141	R. Kaminski, L. Lesniak, B. Loiseau	(CRAC, PARIN)
ABELE 98	PR D57 3860	A. Abele <i>et al.</i>	(Crystal Barrel Collab.)
ALDE 98	EPJ A3 361	D. Alde <i>et al.</i>	(GAM4 Collab.)
Also	PAN 62 405	D. Alde <i>et al.</i>	(GAMS Collab.)
Translated from YAF 62 446.			
AMSLER 98	RMP 70 1293	C. Amstler	(GAMS Collab.)
ANISOVICH 98B	SPU 41 419	V.V. Anisovich <i>et al.</i>	(GAMS Collab.)
Translated from UFN 168 481.			
BERTIN 98	PR D57 55	A. Bertin <i>et al.</i>	(OBELIX Collab.)
REYES 98	PRL 81 4079	M.A. Reyes <i>et al.</i>	(OBELIX Collab.)
BARBERIS 97B	PL B413 217	D. Barberis <i>et al.</i>	(WA 102 Collab.)
BERTIN 97C	PL B408 476	A. Bertin <i>et al.</i>	(OBELIX Collab.)
FRABETTI 97D	PL B407 79	P.L. Frabetti <i>et al.</i>	(FNAL E687 Collab.)
ABELE 96	PL B380 453	A. Abele <i>et al.</i>	(Crystal Barrel Collab.)
ABELE 96B	PL B385 425	A. Abele <i>et al.</i>	(Crystal Barrel Collab.)
ABELE 96C	NP A609 562	A. Abele <i>et al.</i>	(Crystal Barrel Collab.)
AMELIN 96B	PAN 59 976	D.V. Amelin <i>et al.</i>	(SERP, TBIL)
Translated from YAF 59 1021.			
BUGG 96	NP B471 59	D.V. Bugg, A.V. Sarantsev, B.S. Zou	(LOQM, PNPI)
AMSLER 95B	PL B342 433	C. Amstler <i>et al.</i>	(Crystal Barrel Collab.)
AMSLER 95C	PL B353 571	C. Amstler <i>et al.</i>	(Crystal Barrel Collab.)
AMSLER 95D	PL B355 425	C. Amstler <i>et al.</i>	(Crystal Barrel Collab.)
ANTINORI 95	PL B353 589	F. Antinori <i>et al.</i>	(ATHU, BARI, BIRM+)
BUGG 95	PL B353 378	D.V. Bugg <i>et al.</i>	(LOQM, PNPI, WASH)
ABATZIS 94	PL B324 509	S. Abatzis <i>et al.</i>	(ATHU, BARI, BIRM+)
AMSLER 94C	PL B327 425	C. Amstler <i>et al.</i>	(Crystal Barrel Collab.)
AMSLER 94D	PL B333 277	C. Amstler <i>et al.</i>	(Crystal Barrel Collab.)
AMSLER 94E	PL B340 259	C. Amstler <i>et al.</i>	(Crystal Barrel Collab.)
ANISOVICH 94	PL B323 233	V.V. Anisovich <i>et al.</i>	(Crystal Barrel Collab.)
BUGG 94	PR D50 4412	D.V. Bugg <i>et al.</i>	(LOQM)
AMSLER 92	PL B291 347	C. Amstler <i>et al.</i>	(Crystal Barrel Collab.)
BELADIDZE 92C	SJNP 55 1535	G.M. Beladidze, S.I. Bityukov, G.V. Borisov	(SERP+)
Translated from YAF 55 2748.			
PROKOSHKIN 91	SPD 36 155	Y.D. Prokoshkin	(GAM2 and GAM4 Collab.)
Translated from DANS 316 900.			
ARMSTRONG 89E	PL B228 536	T.A. Armstrong, M. Benayoun	(ATHU, BARI, BIRM+)
ALDE 88	PL B201 160	D.M. Alde <i>et al.</i>	(SERP, BELG, LANL, LAPP+)
ASTON 88D	NP B301 525	D. Aston <i>et al.</i>	(SLAC, NAGO, CIN, INUS)
ALDE 87	PL B198 286	D.M. Alde <i>et al.</i>	(LANL, BRUX, SERP, LAPP)
ALDE 86D	NP B269 485	D.M. Alde <i>et al.</i>	(BELG, LAPP, SERP, CERN+)
BINON 84C	NC 80A 363	F.G. Binon <i>et al.</i>	(BELG, LAPP, SERP+)
BINON 83	NC 78A 313	F.G. Binon <i>et al.</i>	(BELG, LAPP, SERP+)
Also	SJNP 38 561	F.G. Binon <i>et al.</i>	(BELG, LAPP, SERP+)
Translated from YAF 38 934.			
GRAY 83	PR D27 307	L. Gray <i>et al.</i>	(SYRA)
ETKIN 82B	PR D25 1786	A. Etkin <i>et al.</i>	(BNL, CUNY, TUFTS, VAND)
COHEN 80	PR D22 2595	D. Cohen <i>et al.</i>	(ANL)

WEIGHTED AVERAGE
1518±5 (Error scaled by 1.7)

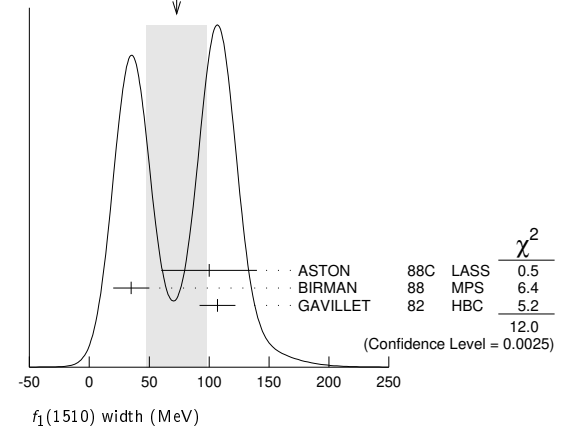


$f_1(1510)$ WIDTH

VALUE (MeV)	EVTs	DOCUMENT ID	TECN	COMMENT
73±25 OUR AVERAGE	Error	includes scale factor of 2.5. See the ideogram below.		
100±40	600	ASTON	88C LASS	11 $K^- p \rightarrow K_S^0 K^\pm \pi^\mp \Lambda$
35±15	271	BIRMAN	88 MPS	8 $\pi^- p \rightarrow K^+ \bar{K}^0 \pi^- n$
107±15	271	GAVILLET	82 HBC	4.2 $K^- p \rightarrow \Lambda K K \pi$

³ From partial wave analysis of $K^+ \bar{K}^0 \pi^-$ state.

WEIGHTED AVERAGE
73±25 (Error scaled by 2.5)



$f_1(1510)$ DECAY MODES

Mode	Fraction (Γ_i/Γ)
Γ_1 $K\bar{K}^*(892) + c.c.$	seen
Γ_2 $\pi^+ \pi^- \eta'$	seen

$f_1(1510)$ BRANCHING RATIOS

$\Gamma(\pi^+ \pi^- \eta')/\Gamma_{total}$	Γ_2/Γ
seen	230
	ABL IKIM 11c BES3 $J/\psi \rightarrow \gamma \pi^+ \pi^- \eta'$

$f_1(1510)$ REFERENCES

ABLIKIM 11C	PRL 106 072002	M. Ablikim <i>et al.</i>	(BESIII Collab.)
BAUER 93B	PR D48 3976	D.A. Bauer <i>et al.</i>	(SLAC)
AIHARA 88C	PR D38 1	H. Aihara <i>et al.</i>	(TPC-2 γ Collab.)
ASTON 88C	PL B201 573	D. Aston <i>et al.</i>	(SLAC, NAGO, CIN, INUS) JIP
BIRMAN 88P	PRL 61 1557	A. Birman <i>et al.</i>	(BNL, FSU, IND, MASD) JIP
GAVILLET 82	ZPHY C16 119	P. Gavillet <i>et al.</i>	(CERN, CDEF, PADO+)

$f_1(1510)$

$$J^G(J^{PC}) = 0^+(1^{++})$$

OMITTED FROM SUMMARY TABLE
See the minireview under $\eta(1405)$.

$f_1(1510)$ MASS

VALUE (MeV)	EVTs	DOCUMENT ID	TECN	COMMENT
1518±5 OUR AVERAGE	Error	includes scale factor of 1.7. See the ideogram below.		
1530±10		ASTON	88C LASS	11 $K^- p \rightarrow K_S^0 K^\pm \pi^\mp \Lambda$
1512±4	600	BIRMAN	88 MPS	8 $\pi^- p \rightarrow K^+ \bar{K}^0 \pi^- n$
1526±6	271	GAVILLET	82 HBC	4.2 $K^- p \rightarrow \Lambda K K \pi$
••• We do not use the following data for averages, fits, limits, etc. •••				
~1525	2	BAUER	93B	$\gamma \gamma^* \rightarrow \pi^+ \pi^- \pi^0 \pi^0$

¹ From partial wave analysis of $K^+ \bar{K}^0 \pi^-$ state.

² Not seen by AIHARA 88C in the $K_S^0 K^\pm \pi^\mp$ final state.

Meson Particle Listings

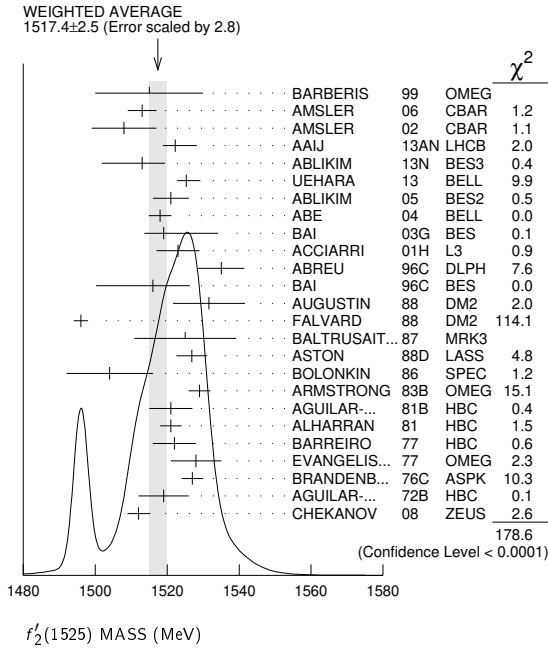
$f_2'(1525)$

$f_2'(1525)$

$$J^G(J^{PC}) = 0^+(2^{++})$$

$f_2'(1525)$ MASS

1517.4 ± 2.5 OUR AVERAGE Includes data from the 6 datablocks that follow this one. Error includes scale factor of 2.8. See the ideogram below.



PRODUCED BY PION BEAM

The data in this block is included in the average printed for a previous datablock.

• • • We do not use the following data for averages, fits, limits, etc. • • •

VALUE (MeV)	EVTs	DOCUMENT ID	TECN	COMMENT
1521 ± 13		TIKHOMIROV 03 SPEC	40.0	$\pi^- C \rightarrow K_S^0 K_S^0 K_L^0 X$
1547 \pm $\frac{+10}{-2}$	1	LONGACRE 86 MPS	22	$\pi^- p \rightarrow K_S^0 K_S^0 n$
1496 \pm $\frac{+9}{-8}$	2	CHABAUD 81 ASPK	6	$\pi^- p \rightarrow K^+ K^- n$
1497 \pm $\frac{+8}{-9}$		CHABAUD 81 ASPK	18.4	$\pi^- p \rightarrow K^+ K^- n$
1492 ± 29		GORLICH 80 ASPK	17	$\pi^- p$ polarized $\rightarrow K^+ K^- n$
1502 ± 25	3	CORDEN 79 OMEG	12-15	$\pi^- p \rightarrow \pi^+ \pi^- n$
1480	14	CRENNELL 66 HBC	6.0	$\pi^- p \rightarrow K_S^0 K_S^0 n$

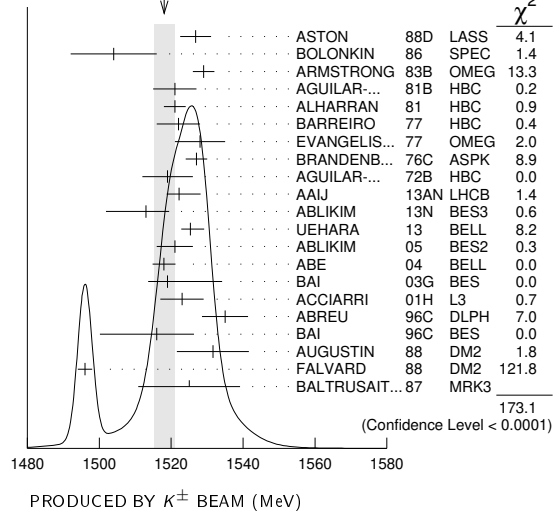
PRODUCED BY K^\pm BEAM

The data in this block is included in the average printed for a previous datablock.

1518.1 ± 2.8 OUR AVERAGE Includes data from the datablock that follows this one. Error includes scale factor of 3.0. See the ideogram below.

VALUE (MeV)	EVTs	DOCUMENT ID	TECN	COMMENT
1526.8 ± 4.3		ASTON 88D LASS	11	$K^- p \rightarrow K_S^0 K_S^0 \Lambda$
1504 ± 12		BOLONKIN 86 SPEC	40	$K^- p \rightarrow K_S^0 K_S^0 Y$
1529 ± 3		ARMSTRONG 83B OMEG	18.5	$K^- p \rightarrow K^- K^+ \Lambda$
1521 ± 6	650	AGUILAR... 81B HBC	4.2	$K^- p \rightarrow \Lambda K^+ K^-$
1521 ± 3	572	ALHARRAN 81 HBC	8.25	$K^- p \rightarrow \Lambda K \bar{K}$
1522 ± 6	123	BARREIRO 77 HBC	4.15	$K^- p \rightarrow \Lambda K_S^0 K_S^0$
1528 ± 7	166	EVANGELIS... 77 OMEG	10	$K^- p \rightarrow K^+ K^- (\Lambda, \Sigma)$
1527 ± 3	120	BRANDENB... 76C ASPK	13	$K^- p \rightarrow K^+ K^- (\Lambda, \Sigma)$
1519 ± 7	100	AGUILAR... 72B HBC	3.9, 4.6	$K^- p \rightarrow K \bar{K} (\Lambda, \Sigma)$
• • • We do not use the following data for averages, fits, limits, etc. • • •				
1514 ± 8	61	BINON 07 GAMS	32.5	$K^- p \rightarrow \eta \eta (\Lambda / \Sigma^0)$
1513 ± 10	4	BARKOV 99 SPEC	40	$K^- p \rightarrow K_S^0 K_S^0 y$

WEIGHTED AVERAGE
1518.1 ± 2.8 (Error scaled by 3.0)



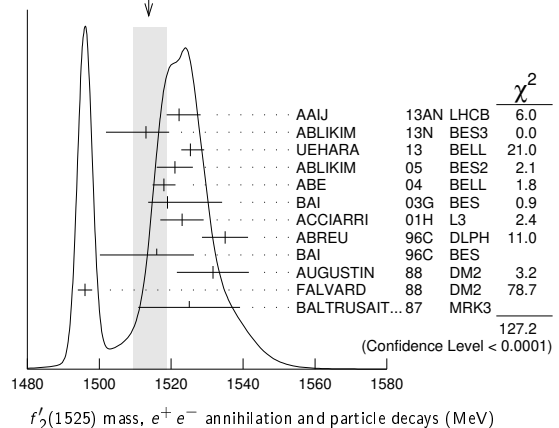
PRODUCED IN e^+e^- ANNIHILATION AND PARTICLE DECAYS

The data in this block is included in the average printed for a previous datablock.

1514 \pm $\frac{+5}{-4}$ OUR AVERAGE Error includes scale factor of 3.8. See the ideogram below.

VALUE (MeV)	EVTs	DOCUMENT ID	TECN	COMMENT
1522.2 ± 2.8 \pm $\frac{+5.3}{-2.0}$		AAIJ 13AN LHCB	$\bar{B}_S^0 \rightarrow J/\psi K^+ K^-$	
1513 ± 5 \pm $\frac{+4}{-10}$	5.5k	5 ABLIKIM 13N BES3	$e^+ e^- \rightarrow J/\psi \rightarrow \gamma \eta \eta$	
1525.3 \pm $\frac{+1.2}{-1.4}$ \pm $\frac{+3.7}{-2.1}$		UEHARA 13 BELL	$\gamma \gamma \rightarrow K_S^0 K_S^0$	
1521 ± 5		ABLIKIM 05 BES2	$J/\psi \rightarrow \phi K^+ K^-$	
1518 ± 1 ± 3		ABE 04 BELL	$10.6 e^+ e^- \rightarrow e^+ e^- K^+ K^-$	
1519 ± 2 \pm $\frac{+15}{-5}$		BAI 03G BES	$J/\psi \rightarrow \gamma K \bar{K}$	
1523 ± 6	331	6 ACCIARRI 01H L3	$91, 183-209 e^+ e^- \rightarrow e^+ e^- K_S^0 K_S^0$	
1535 ± 5 ± 4		ABREU 96C DLPH	$Z^0 \rightarrow K^+ K^- + X$	
1516 ± 5 \pm $\frac{+9}{-15}$		BAI 96C BES	$J/\psi \rightarrow \gamma K^+ K^-$	
1531.6 ± 10.0		AUGUSTIN 88 DM2	$J/\psi \rightarrow \gamma K^+ K^-$	
1496 ± 2		7 FALVARD 88 DM2	$J/\psi \rightarrow \phi K^+ K^-$	
1525 ± 10 ± 10		BALTRUSAIT... 87 MRK3	$J/\psi \rightarrow \gamma K^+ K^-$	
• • • We do not use the following data for averages, fits, limits, etc. • • •				
1532 ± 3 ± 6	644	8,9 DOBBS 15	$J/\psi \rightarrow \gamma K^+ K^-$	
1557 ± 9 ± 3	113	8,9 DOBBS 15	$\psi(2S) \rightarrow \gamma K^+ K^-$	
1526 ± 7	29	10 LEES 14H BABR	$e^+ e^- \rightarrow K_S^0 K_S^0 K^+ K^- \gamma$	
1523 ± 5	870	11 SCHEGELSKY 06A RVUE	$\gamma \gamma \rightarrow K_S^0 K_S^0$	
1515 ± 5		12 FALVARD 88 DM2	$J/\psi \rightarrow \phi K^+ K^-$	

WEIGHTED AVERAGE
1514 ± 5.4 (Error scaled by 3.8)



PRODUCED IN $\bar{p}p$ ANNIHILATION

VALUE (MeV)	DOCUMENT ID	TECN	COMMENT
-------------	-------------	------	---------

The data in this block is included in the average printed for a previous datablock.

1512 ± 4 OUR AVERAGE

1513 ± 4	AMSLER 06	CBAR	0.9 $\bar{p}p \rightarrow K^+ K^- \pi^0$
1508 ± 9	13 AMSLER 02	CBAR	0.9 $\bar{p}p \rightarrow \pi^0 \eta \eta, \pi^0 \pi^0 \pi^0$
• • •	We do not use the following data for averages, fits, limits, etc. • • •		
1530 ± 12	14 ANISOVICH 09	RVUE	0.0 $\bar{p}p, \pi N$

CENTRAL PRODUCTION

VALUE (MeV)	DOCUMENT ID	TECN	COMMENT
-------------	-------------	------	---------

The data in this block is included in the average printed for a previous datablock.

1515 ± 15

BARBERIS 99	OMEG	450 $pp \rightarrow p_S p_f K^+ K^-$
-------------	------	--------------------------------------

PRODUCED IN $e p$ COLLISIONS

VALUE (MeV)	EVTS	DOCUMENT ID	TECN	COMMENT
-------------	------	-------------	------	---------

The data in this block is included in the average printed for a previous datablock.

1512 ± 3^{+1.4}_{-0.5}

15	CHEKANOV 08	ZEUS	$e p \rightarrow K_S^0 K_S^0 X$
----	-------------	------	---------------------------------

• • • We do not use the following data for averages, fits, limits, etc. • • •

1537 ⁺⁹ ₋₈	84	16 CHEKANOV 04	ZEUS $e p \rightarrow K_S^0 K_S^0 X$
----------------------------------	----	----------------	--------------------------------------

- 1 From a partial-wave analysis of data using a K-matrix formalism with 5 poles.
- 2 CHABAUD 81 is a reanalysis of PAWLICKI 77 data.
- 3 From an amplitude analysis where the $f_2'(1525)$ width and elasticity are in complete disagreement with the values obtained from $K\bar{K}$ channel, making the solution dubious.
- 4 Systematic errors not estimated.
- 5 From partial wave analysis including all possible combinations of $0^{++}, 2^{++}$, and 4^{++} resonances.
- 6 Supersedes ACCIARRI 95j.
- 7 From an analysis including interference with $f_0(1710)$.
- 8 Using CLEO-c data but not authored by the CLEO Collaboration.
- 9 From a fit to a Breit-Wigner line shape with fixed $\Gamma = 73$ MeV.
- 10 From a fit to a Breit-Wigner line shape plus a second-order polynomial function. Systematic errors not evaluated.
- 11 From analysis of L3 data at 91 and 183–209 GeV.
- 12 From an analysis ignoring interference with $f_0(1710)$.
- 13 T-matrix pole.
- 14 4-poles, 5-channel K matrix fit.
- 15 In the SU(3) based model with a specific interference pattern of the $f_2(1270), a_2^0(1320)$, and $f_2'(1525)$ mesons incoherently added to the $f_0(1710)$ and non-resonant background.
- 16 Systematic errors not estimated.

$f_2'(1525)$ WIDTH

VALUE (MeV)	DOCUMENT ID	COMMENT
86 ± 5 OUR FIT		Error includes scale factor of 2.2.
86.9^{+2.3}_{-2.1}	PDG 18	Average of width measurements

PRODUCED BY PION BEAM

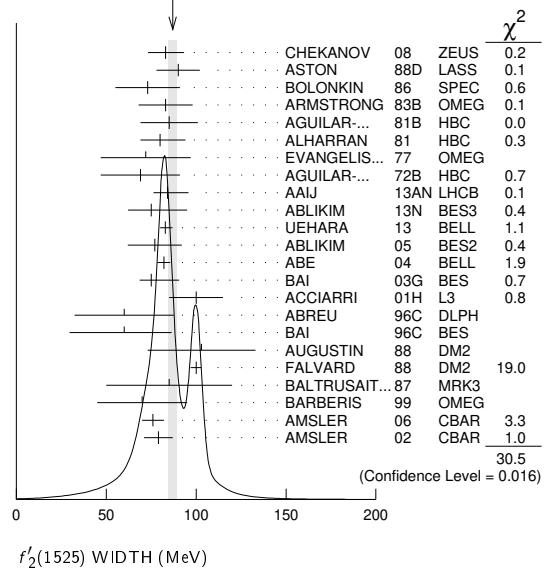
VALUE (MeV)	DOCUMENT ID	TECN	COMMENT
-------------	-------------	------	---------

86.9^{+2.3}_{-2.1} OUR AVERAGE Includes data from the 5 datablocks that follow this one. Error includes scale factor of 1.4. See the ideogram below.

• • • We do not use the following data for averages, fits, limits, etc. • • •

102 ± 4.2	TIKHOMIROV 03	SPEC	40.0 $\pi^- C \rightarrow K_S^0 K_S^0 K_L^0 X$
108 ⁺⁵ ₋₂	17 LONGACRE 86	MPS	22 $\pi^- p \rightarrow K_S^0 K_S^0 n$
69 ⁺²² ₋₁₆	18 CHABAUD 81	ASPK	6 $\pi^- p \rightarrow K^+ K^- n$
137 ⁺²³ ₋₂₁	CHABAUD 81	ASPK	18.4 $\pi^- p \rightarrow K^+ K^- n$
150 ⁺⁸³ ₋₅₀	GORLICH 80	ASPK	17 $\pi^- p$ polarized $\rightarrow K^+ K^- n$
165 ± 4.2	19 CORDEN 79	OMEG	12–15 $\pi^- p \rightarrow \pi^+ \pi^- n$
92 ⁺³⁹ ₋₂₂	20 POLYCHRO... 79	STRC	7 $\pi^- p \rightarrow n K_S^0 K_S^0$

WEIGHTED AVERAGE
86.9+2.3-2.1 (Error scaled by 1.4)



PRODUCED BY K^\pm BEAM

VALUE (MeV)	EVTS	DOCUMENT ID	TECN	COMMENT
-------------	------	-------------	------	---------

The data in this block is included in the average printed for a previous datablock.

82 ± 6 OUR AVERAGE

90 ± 12	ASTON 88D	LASS	11 $K^- p \rightarrow K_S^0 K_S^0 \Lambda$
73 ± 18	BOLONKIN 86	SPEC	40 $K^- p \rightarrow K_S^0 K_S^0 Y$
83 ± 15	ARMSTRONG 83B	OMEG	18.5 $K^- p \rightarrow K^- K^+ \Lambda$
85 ± 16	650 AGUILAR... 81B	HBC	4.2 $K^- p \rightarrow \Lambda K^+ K^-$
80 ⁺¹⁴ ₋₁₁	572 ALHARRAN 81	HBC	8.25 $K^- p \rightarrow \Lambda K\bar{K}$
72 ± 25	166 EVANGELIS... 77	OMEG	10 $K^- p \rightarrow K^+ K^- (\Lambda, \Sigma)$
69 ± 22	100 AGUILAR... 72B	HBC	3.9, 4.6 $K^- p \rightarrow K\bar{K} (\Lambda, \Sigma)$
• • •	We do not use the following data for averages, fits, limits, etc. • • •		
92 ⁺²⁵ ₋₁₆	61 BINON 07	GAMS	32.5 $K^- p \rightarrow \eta \eta (\Lambda / \Sigma^0)$
75 ± 20	21 BARKOV 99	SPEC	40 $K^- p \rightarrow K_S^0 K_S^0 y$
62 ⁺¹⁹ ₋₁₄	123 BARREIRO 77	HBC	4.15 $K^- p \rightarrow \Lambda K_S^0 K_S^0$
61 ± 8	120 BRANDENB... 76C	ASPK	13 $K^- p \rightarrow K^+ K^- (\Lambda, \Sigma)$

PRODUCED IN $e^+ e^-$ ANNIHILATION AND PARTICLE DECAYS

VALUE (MeV)	EVTS	DOCUMENT ID	TECN	COMMENT
-------------	------	-------------	------	---------

The data in this block is included in the average printed for a previous datablock.

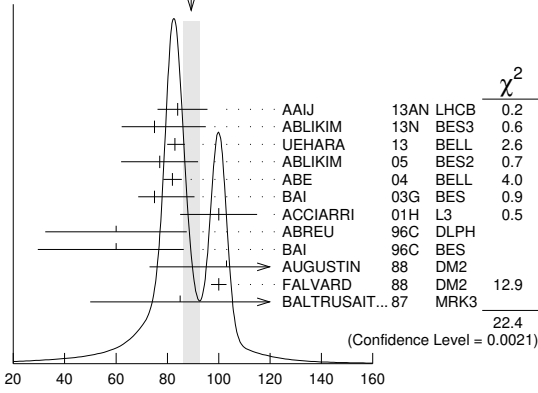
89.2^{+3.4}_{-3.0} OUR AVERAGE Error includes scale factor of 1.8. See the ideogram below.

84 ± 6 ⁺¹⁰ ₋₅	AAIJ 13AN	LHCB	$\bar{B}_S^0 \rightarrow J/\psi K^+ K^-$
75 ⁺¹² ₋₁₀ ⁺¹⁶ ₋₈	5.5k 22	ABLIKIM 13N	BES3 $e^+ e^- \rightarrow J/\psi \rightarrow \gamma \eta \eta$
82.9 ^{+2.1} _{-2.2} ^{+3.3} _{-2.0}	UEHARA 13	BELL	$\gamma \gamma \rightarrow K_S^0 K_S^0$
77 ± 15	ABLIKIM 05	BES2	$J/\psi \rightarrow \phi K^+ K^-$
82 ± 2 ± 3	ABE 04	BELL	10.6 $e^+ e^- \rightarrow e^+ e^- K^+ K^-$
75 ± 4 ⁺¹⁵ ₋₅	BAI 03G	BES	$J/\psi \rightarrow \gamma K\bar{K}$
100 ± 15	331 23	ACCIARRI 01H	L3 91, 183–209 $e^+ e^- \rightarrow e^+ e^- K_S^0 K_S^0$
60 ± 20 ± 19	ABREU 96C	DLPH	$Z^0 \rightarrow K^+ K^- + X$
60 ± 23 ⁺¹³ ₋₂₀	BAI 96C	BES	$J/\psi \rightarrow \gamma K^+ K^-$
103 ± 30	AUGUSTIN 88	DM2	$J/\psi \rightarrow \gamma K^+ K^-$
100 ± 3	24 FALVARD 88	DM2	$J/\psi \rightarrow \phi K^+ K^-$
85 ± 35	BALTRUSAIT... 87	MRK3	$J/\psi \rightarrow \gamma K^+ K^-$
• • •	We do not use the following data for averages, fits, limits, etc. • • •		
37 ± 12	29	25 LEES 14H	BABR $e^+ e^- \rightarrow K_S^0 K_S^0 K^+ K^- \gamma$
104 ± 10	870	26 SCHEGELSKY 06A	RVUE $\gamma \gamma \rightarrow K_S^0 K_S^0$
62 ± 10	27 FALVARD 88	DM2	$J/\psi \rightarrow \phi K^+ K^-$

Meson Particle Listings

$f'_2(1525)$

WEIGHTED AVERAGE
89.2±3.4-3.0 (Error scaled by 1.8)



$f'_2(1525)$ width, e^+e^- annihilation and particle decays (MeV)

PRODUCED IN $\bar{p}p$ ANNIHILATION

VALUE (MeV)	DOCUMENT ID	TECN	COMMENT
The data in this block is included in the average printed for a previous datablock.			
77 ± 5 OUR AVERAGE			
76 ± 6	AMSLER	06	CBAR 0.9 $\bar{p}p \rightarrow K^+ K^- \pi^0$
79 ± 8	AMSLER	02	CBAR 0.9 $\bar{p}p \rightarrow \pi^0 \eta \eta, \pi^0 \pi^0 \pi^0$
• • • We do not use the following data for averages, fits, limits, etc. • • •			
128 ± 20	ANISOVICH	09	RVUE 0.0 $\bar{p}p, \pi N$

CENTRAL PRODUCTION

VALUE (MeV)	DOCUMENT ID	TECN	COMMENT
The data in this block is included in the average printed for a previous datablock.			
70 ± 25	BARBERIS	99	OMEG 450 $pp \rightarrow p_S p_f K^+ K^-$

PRODUCED IN $e p$ COLLISIONS

VALUE (MeV)	EVTS	DOCUMENT ID	TECN	COMMENT	
The data in this block is included in the average printed for a previous datablock.					
83 ± 9⁺⁵₋₄	30	CHEKANOV	08	ZEUS $e p \rightarrow K_S^0 K_S^0 X$	
• • • We do not use the following data for averages, fits, limits, etc. • • •					
50 ± 34 ₋₂₂	84	31	CHEKANOV	04	ZEUS $e p \rightarrow K_S^0 K_S^0 X$
17 From a partial-wave analysis of data using a K-matrix formalism with 5 poles.					
18 CHABAUD 81 is a reanalysis of PAWLICKI 77 data.					
19 From an amplitude analysis where the $f'_2(1525)$ width and elasticity are in complete disagreement with the values obtained from $K\bar{K}$ channel, making the solution dubious.					
20 From a fit to the D with $f_2(1270)$ - $f'_2(1525)$ interference. Mass fixed at 1516 MeV.					
21 Systematic errors not estimated.					
22 From partial wave analysis including all possible combinations of $0^{++}, 2^{++},$ and 4^{++} resonances.					
23 Supersedes ACCIARRI 95J.					
24 From an analysis including interference with $f_0(1710)$.					
25 From a fit to a Breit-Wigner line shape plus a second-order polynomial function. Systematic errors not evaluated.					
26 From analysis of L3 data at 91 and 183–209 GeV.					
27 From an analysis ignoring interference with $f_0(1710)$.					
28 T-matrix pole.					
29 4-poles, 5-channel K matrix fit.					
30 In the SU(3) based model with a specific interference pattern of the $f_2(1270)$, $a_2^0(1320)$, and $f'_2(1525)$ mesons incoherently added to the $f_0(1710)$ and non-resonant background.					
31 Systematic errors not estimated.					

$f'_2(1525)$ DECAY MODES

Mode	Fraction (Γ_i/Γ)	Scale factor
Γ_1 $K\bar{K}$	(87.6 ± 2.2) %	1.1
Γ_2 $\eta\eta$	(11.6 ± 2.2) %	1.1
Γ_3 $\pi\pi$	(8.3 ± 1.6) × 10 ⁻³	
Γ_4 $K\bar{K}^*(892) + c.c.$		
Γ_5 $\pi K\bar{K}$		
Γ_6 $\pi\pi\eta$		
Γ_7 $\pi^+ \pi^+ \pi^- \pi^-$		
Γ_8 $\gamma\gamma$	(9.5 ± 1.1) × 10 ⁻⁷	1.1

CONSTRAINED FIT INFORMATION

An overall fit to the total width, 2 partial widths, a combination of partial widths obtained from integrated cross sections, and 3 branching ratios uses 17 measurements and one constraint to determine 5 parameters. The overall fit has a $\chi^2 = 18.2$ for 13 degrees of freedom.

The following *off-diagonal* array elements are the correlation coefficients $\langle \delta p_i \delta p_j \rangle / (\delta p_i \delta p_j)$, in percent, from the fit to parameters p_i , including the branching fractions, $x_i \equiv \Gamma_i / \Gamma_{\text{total}}$. The fit constrains the x_i whose labels appear in this array to sum to one.

x_2	-100			
x_3	-6	-1		
x_8	-19	19	1	
Γ	-4	4	0	-44
	x_1	x_2	x_3	x_8

Mode	Rate (MeV)	Scale factor
Γ_1 $K\bar{K}$	75 ± 4	1.8
Γ_2 $\eta\eta$	9.9 ± 1.9	1.1
Γ_3 $\pi\pi$	0.71 ± 0.14	1.1
Γ_8 $\gamma\gamma$	(8.2 ± 0.9) × 10 ⁻⁵	

$f'_2(1525)$ PARTIAL WIDTHS

$\Gamma(K\bar{K})$	VALUE (MeV)	DOCUMENT ID	TECN	COMMENT	Γ_1
75 ± 4 OUR FIT	Error includes scale factor of 1.8.				
63⁺⁶₋₅	32	LONGACRE	86	MPS	22 $\pi^- p \rightarrow K_S^0 K_S^0 n$

$\Gamma(\eta\eta)$	VALUE (MeV)	EVTS	DOCUMENT ID	TECN	COMMENT	Γ_2
9.9 ± 1.9 OUR FIT	Error includes scale factor of 1.1.					
• • • We do not use the following data for averages, fits, limits, etc. • • •						
5.0 ± 0.8	870	33	SCHEGELSKY	06A	RVUE $\gamma\gamma \rightarrow K_S^0 K_S^0$	
24 ⁺³ ₋₁	32	LONGACRE	86	MPS	22 $\pi^- p \rightarrow K_S^0 K_S^0 n$	

$\Gamma(\pi\pi)$	VALUE (MeV)	EVTS	DOCUMENT ID	TECN	COMMENT	Γ_3
0.71 ± 0.14 OUR FIT	Error includes scale factor of 1.1.					
1.4^{+1.0}_{-0.5}	32	LONGACRE	86	MPS	22 $\pi^- p \rightarrow K_S^0 K_S^0 n$	
• • • We do not use the following data for averages, fits, limits, etc. • • •						
0.2 ^{+1.0} _{-0.2}	870	33	SCHEGELSKY	06A	RVUE $\gamma\gamma \rightarrow K_S^0 K_S^0$	

$\Gamma(\gamma\gamma)$	VALUE (keV)	EVTS	DOCUMENT ID	TECN	COMMENT	Γ_8
0.082 ± 0.009 OUR FIT						
• • • We do not use the following data for averages, fits, limits, etc. • • •						
0.13 ± 0.03	870	33	SCHEGELSKY	06A	RVUE $\gamma\gamma \rightarrow K_S^0 K_S^0$	
32 From a partial-wave analysis of data using a K-matrix formalism with 5 poles.						
33 From analysis of L3 data at 91 and 183–209 GeV, using $\Gamma(f'_2(1525) \rightarrow K\bar{K}) = 68$ MeV and SU(3) relations.						

$f'_2(1525)$ $\Gamma(i)\Gamma(\gamma\gamma)/\Gamma(\text{total})$

$\Gamma(K\bar{K}) \times \Gamma(\gamma\gamma)/\Gamma_{\text{total}}$	VALUE (keV)	EVTS	DOCUMENT ID	TECN	COMMENT	$\Gamma_1\Gamma_8/\Gamma$
0.072 ± 0.007 OUR FIT						
0.072 ± 0.007 OUR AVERAGE						
0.048 ^{+0.067} _{-0.008} ^{+0.108} _{-0.012}	UEHARA	13	BELL		$\gamma\gamma \rightarrow K_S^0 K_S^0$	
0.0564 ± 0.0048 ± 0.0116	ABE	04	BELL		10.6 $e^+e^- \rightarrow e^+e^- K^+ K^-$	
0.076 ± 0.006 ± 0.011	331	34	ACCIARRI	01H	L3 $e^+e^- \rightarrow e^+e^- K_S^0 K_S^0$	
0.067 ± 0.008 ± 0.015	35	ALBRECHT	90G	ARG	$e^+e^- \rightarrow e^+e^- K^+ K^-$	
0.11 ^{+0.03} _{-0.02} ± 0.02	BEHREND	89C	CELL		$e^+e^- \rightarrow e^+e^- K_S^0 K_S^0$	
0.10 ^{+0.04} _{-0.03} ± 0.03 ^{+0.03} _{-0.02}	BERGER	88	PLUT		$e^+e^- \rightarrow e^+e^- K_S^0 K_S^0$	
0.12 ± 0.07 ± 0.04	35	AIHARA	86B	TPC	$e^+e^- \rightarrow e^+e^- K^+ K^-$	
0.11 ± 0.02 ± 0.04	35	ALTHOFF	83	TASS	$e^+e^- \rightarrow e^+e^- K\bar{K}$	
• • • We do not use the following data for averages, fits, limits, etc. • • •						
0.0314 ± 0.0050 ± 0.0077	36	ALBRECHT	90G	ARG	$e^+e^- \rightarrow e^+e^- K^+ K^-$	
34 Supersedes ACCIARRI 95J. From analysis of L3 data at 91 and 183–209 GeV,						
35 Using an incoherent background.						
36 Using a coherent background.						

f'_2(1525), f_2(1565)

f'_2(1525) BRANCHING RATIOS

Table with columns: Gamma(eta)/Gamma_total, DOCUMENT ID, TECN, COMMENT, Gamma/Gamma. Includes data for UEHARA 10A BELL and PROKOSHKIN 91 GAM4.

37 Combining results of GAM4 with those of WA76 on K-Kbar central production and results of CBAL, MRK3 and DM2 on J/psi -> gamma eta.

Gamma(eta)/Gamma(K-Kbar)

Table with columns: VALUE, CL%, EVTS, DOCUMENT ID, TECN, COMMENT, Gamma/Gamma. Includes data for BINON 07 GAMS and PROKOSHKIN 91 GAM4.

38 Using the compilation of the cross sections for f'_2(1525) production in K-p collisions from ASTON 88D.

39 Combining results of GAM4 with those of WA76 on K-Kbar central production and results of CBAL, MRK3 and DM2 on J/psi -> gamma eta.

Gamma(pi pi)/Gamma_total

Table with columns: VALUE, CL%, DOCUMENT ID, TECN, COMMENT, Gamma/Gamma. Includes data for COSTA 80 OMEG and GORLICH 80 ASPK.

40 Assuming that the f'_2(1525) is produced by an one-pion exchange production mechanism.

41 MARTIN 79 uses the PAWLICKI 77 data with different input value of the f'_2(1525) -> K-Kbar branching ratio.

Gamma(pi pi)/Gamma(K-Kbar)

Table with columns: VALUE, CL%, DOCUMENT ID, TECN, COMMENT, Gamma/Gamma. Includes data for AUGUSTIN 87 DM2.

[Gamma(K-Kbar*(892)+c.c.) + Gamma(pi K-Kbar)]/Gamma(K-Kbar)

Table with columns: VALUE, CL%, DOCUMENT ID, TECN, COMMENT, Gamma/Gamma. Includes data for AGUILAR... 72B HBC and AMMAR 67 HBC.

Gamma(pi pi eta)/Gamma(K-Kbar)

Table with columns: VALUE, CL%, DOCUMENT ID, TECN, COMMENT, Gamma/Gamma. Includes data for AGUILAR... 72B HBC and AMMAR 67 HBC.

Gamma(pi+ pi+ pi- pi-)/Gamma(K-Kbar)

Table with columns: VALUE, CL%, DOCUMENT ID, TECN, COMMENT, Gamma/Gamma. Includes data for AGUILAR... 72B HBC.

Large table listing various meson decays and production experiments with columns for experiment name, document ID, and comment.

f_2(1565)

I^G(J^PC) = 0^+(2^+ +)

OMITTED FROM SUMMARY TABLE

Seen mostly in antineutron-nucleon annihilation. Needs confirmation in other channels.

f_2(1565) MASS

Table with columns: VALUE (MeV), DOCUMENT ID, TECN, COMMENT. Includes data for AMSLER 02 CBAR and BERTIN 98 OBLX.

- 1 T-matrix pole.
2 On sheet II in a two-pole solution.
3 Supersedes the omega state of BELADIDZE 92B earlier assigned to the f_2(1640).
4 Breit-Wigner width.
5 T-matrix pole, large coupling to rho rho and omega omega, could be f_2(1640).
6 Coupled-channel analysis of AMSLER 95B, AMSLER 95C, and AMSLER 94D.
7 From a simultaneous analysis of the annihilations p-bar p -> 3 pi^0, pi^0 eta including AKER 91 data.
8 J^P not determined, could be partly f_0(1500).
9 J^P not determined.
10 Superseded by AMSLER 95B.

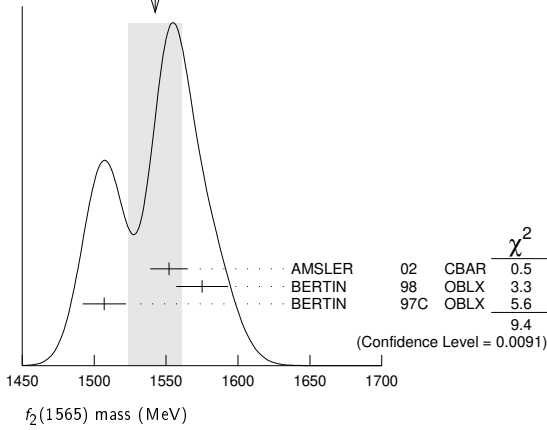
f'_2(1525) REFERENCES

List of references for f'_2(1525) including PDG, DOBBS, LEES, AALI, ABLIKIM, UEHARA, ANISOVICH, CHEKANOV, BINON, AMSLER, SCHEGELSKY, ABLIKIM, ABE, CHEKANOV, BAI, TIKHOMIROV, and others.

Meson Particle Listings

$f_2(1565), \rho(1570)$

WEIGHTED AVERAGE
1542±19 (Error scaled by 2.2)



$f_2(1565)$ WIDTH

VALUE (MeV)	DOCUMENT ID	TECN	COMMENT
122± 13 OUR AVERAGE			
113± 23	11 AMSLER	02 CBAR	0.9 $\bar{p}p \rightarrow \pi^0 \eta \eta, \pi^0 \pi^0 \pi^0$
119± 24	11 BERTIN	98 OBLX	0.05-0.405 $\bar{p}p \rightarrow \pi^+ \pi^+ \pi^-$
130± 20	11 BERTIN	97C OBLX	0.0 $\bar{p}p \rightarrow \pi^+ \pi^- \pi^0$
••• We do not use the following data for averages, fits, limits, etc. •••			
280± 40	12 ANISOVICH	09 RVUE	0.0 $\bar{p}p, \pi N$
140± 11	13,14 AMELIN	06 VES	36 $\pi^- p \rightarrow \omega \omega n$
130± 20±40	14 AMELIN	00 VES	37 $\pi^- p \rightarrow \eta \pi^+ \pi^- n$
180± 60	15 ABELE	96C RVUE	Compilation
~142	16 AMSLER	95D CBAR	0.0 $\bar{p}p \rightarrow \pi^0 \pi^0 \pi^0, \pi^0 \eta \eta, \pi^0 \pi^0 \eta$
263±101	BALOSHIN	95 SPEC	40 $\pi^- C \rightarrow K_S^0 K_S^0 X$
166± 80 20	17 ANISOVICH	94 CBAR	0.0 $\bar{p}p \rightarrow 3\pi^0, \eta \eta \pi^0$
130± 10	18 ADAMO	93 OBLX	$\bar{p}p \rightarrow \pi^+ \pi^+ \pi^-$
148± 27	19 ARMSTRONG	93C E760	$\bar{p}p \rightarrow \pi^0 \eta \eta \rightarrow 6\gamma$
103± 15	19 ARMSTRONG	93D E760	$\bar{p}p \rightarrow 3\pi^0 \rightarrow 6\gamma$
111± 10	19 ARMSTRONG	93D E760	$\bar{p}p \rightarrow \eta \pi^0 \pi^0 \rightarrow 6\gamma$
~206	20 WEIDENAUER	93 ASTE	0.0 $\bar{p}N \rightarrow 3\pi^- 2\pi^+$
132± 37	19 ADAMO	92 OBLX	$\bar{p}p \rightarrow \pi^+ \pi^+ \pi^-$
120± 10	21 AKER	91 CBAR	0.0 $\bar{p}p \rightarrow 3\pi^0$
170± 40	MAY	90 ASTE	0.0 $\bar{p}p \rightarrow \pi^+ \pi^- \pi^0$
116± 9	BRIDGES	86C DBC	0.0 $\bar{p}N \rightarrow 3\pi^- 2\pi^+$

- 11 T-matrix pole.
- 12 On sheet II in a two-pole solution.
- 13 Supersedes the $\omega\omega$ state of BELADIDZE 92b earlier assigned to the $f_2(1640)$.
- 14 Breit-Wigner width.
- 15 T-matrix pole, large coupling to $\rho\rho$ and $\omega\omega$, could be $f_2(1640)$.
- 16 Coupled-channel analysis of AMSLER 95b, AMSLER 95c, and AMSLER 94d.
- 17 From a simultaneous analysis of the annihilations $\bar{p}p \rightarrow 3\pi^0, \pi^0 \eta \eta$ including AKER 91 data.
- 18 Supersedes ADAMO 92.
- 19 J^P not determined, could be partly $f_0(1500)$.
- 20 J^P not determined.
- 21 Superseded by AMSLER 95b.

$f_2(1565)$ DECAY MODES

Mode	Fraction (Γ_i/Γ)
Γ_1 $\pi\pi$	seen
Γ_2 $\pi^+ \pi^-$	seen
Γ_3 $\pi^0 \pi^0$	seen
Γ_4 $\rho^0 \rho^0$	seen
Γ_5 $2\pi^+ 2\pi^-$	seen
Γ_6 $\eta\eta$	seen
Γ_7 $\omega\omega$	seen
Γ_8 $K\bar{K}$	seen
Γ_9 $\gamma\gamma$	seen

$f_2(1565)$ PARTIAL WIDTHS

$\Gamma(\eta\eta)$	VALUE (MeV)	EVTS	DOCUMENT ID	TECN	COMMENT
••• We do not use the following data for averages, fits, limits, etc. •••					
	1.2±0.3	870	22 SCHEGELSKY 06A	RVUE	$\gamma\gamma \rightarrow K_S^0 K_S^0$

$\Gamma(K\bar{K})$

VALUE (MeV)	EVTS	DOCUMENT ID	TECN	COMMENT
••• We do not use the following data for averages, fits, limits, etc. •••				
2.0±1.0	870	22 SCHEGELSKY 06A	RVUE	$\gamma\gamma \rightarrow K_S^0 K_S^0$

$\Gamma(\gamma\gamma)$

VALUE (MeV)	EVTS	DOCUMENT ID	TECN	COMMENT
••• We do not use the following data for averages, fits, limits, etc. •••				
0.70±0.14	870	22 SCHEGELSKY 06A	RVUE	$\gamma\gamma \rightarrow K_S^0 K_S^0$
22 From analysis of L3 data at 91 and 183-209 GeV, using $f_2(1565)$ mass of 1570 MeV, width of 160 MeV, $\Gamma(\pi\pi) = 25$ MeV, and SU(3) relations.				

$f_2(1565)$ BRANCHING RATIOS

$\Gamma(\pi\pi)/\Gamma_{total}$	VALUE	DOCUMENT ID	TECN	COMMENT
••• We do not use the following data for averages, fits, limits, etc. •••				
seen		BAKER	99B SPEC	0 $\bar{p}p \rightarrow \omega\omega\pi^0$

$\Gamma(\pi^+ \pi^-)/\Gamma_{total}$	VALUE	DOCUMENT ID	TECN	COMMENT
••• We do not use the following data for averages, fits, limits, etc. •••				
seen		BERTIN	98 OBLX	0.05-0.405 $\bar{p}p \rightarrow \pi^+ \pi^+ \pi^-$
not seen		23 ANISOVICH	94B RVUE	$\bar{p}p \rightarrow \pi^+ \pi^- \pi^0$
seen		MAY	89 ASTE	$\bar{p}p \rightarrow \pi^+ \pi^- \pi^0$
23 ANISOVICH 94b is from a reanalysis of MAY 90.				

$\Gamma(\pi^0 \pi^0)/\Gamma_{total}$	VALUE	DOCUMENT ID	TECN	COMMENT
••• We do not use the following data for averages, fits, limits, etc. •••				
seen		BERTIN	98 OBLX	0.05-0.405 $\bar{p}p \rightarrow \pi^+ \pi^+ \pi^-$
not seen		23 ANISOVICH	94B RVUE	$\bar{p}p \rightarrow \pi^+ \pi^- \pi^0$
seen		MAY	89 ASTE	$\bar{p}p \rightarrow \pi^+ \pi^- \pi^0$
23 ANISOVICH 94b is from a reanalysis of MAY 90.				

$\Gamma(\pi^0 \pi^0)/\Gamma_{total}$	VALUE	DOCUMENT ID	TECN	COMMENT
••• We do not use the following data for averages, fits, limits, etc. •••				
seen		AMSLER	95B CBAR	0.0 $\bar{p}p \rightarrow 3\pi^0$

$\Gamma(\pi^+ \pi^-)/\Gamma(\rho^0 \rho^0)$	VALUE	DOCUMENT ID	TECN	COMMENT
••• We do not use the following data for averages, fits, limits, etc. •••				
0.042±0.013		BRIDGES	86B DBC	$\bar{p}N \rightarrow 3\pi^- 2\pi^+$

$\Gamma(\eta\eta)/\Gamma(\pi^0 \pi^0)$	VALUE	DOCUMENT ID	TECN	COMMENT
••• We do not use the following data for averages, fits, limits, etc. •••				
0.024±0.005±0.012		24 ARMSTRONG	93C E760	$\bar{p}p \rightarrow \pi^0 \eta \eta \rightarrow 6\gamma$
24 J^P not determined, could be partly $f_0(1500)$.				

$\Gamma(\omega\omega)/\Gamma_{total}$	VALUE	DOCUMENT ID	TECN	COMMENT
••• We do not use the following data for averages, fits, limits, etc. •••				
seen		BAKER	99B SPEC	0 $\bar{p}p \rightarrow \omega\omega\pi^0$

$f_2(1565)$ REFERENCES

ANISOVICH 09	IJMP A24 2481	V.V. Anisovich, A.V. Sarantsev
AMELIN 06	PAN 69 690	D.V. Amelin et al.
	Translated from YAF 69 715.	(VES Collab.)
SCHEGELSKY 06A	EPJ A27 207	V.A. Schegelsky et al.
AMSLER 02	EPJ C23 29	C. Amisler et al.
AMELIN 00	NP A668 83	D. Amelin et al.
BAKER 99B	PL B467 147	C.A. Baker et al.
BERTIN 98	PR D57 55	A. Bertin et al.
BERTIN 97C	PL B408 476	A. Bertin et al.
ABELE 96C	NP A609 562	A. Abele et al.
AMSLER 95B	PL B342 433	C. Amisler et al.
AMSLER 95C	PL B353 571	C. Amisler et al.
AMSLER 95D	PL B355 425	C. Amisler et al.
BALOSHIN 95	PAN 58 46	O.M. Baloshin et al.
	Translated from YAF 58 50.	(ITEP)
AMSLER 94D	PL B333 277	C. Amisler et al.
ANISOVICH 94	PL B323 233	V.V. Anisovich et al.
ANISOVICH 94B	PR D50 1972	V.V. Anisovich et al.
ADAMO 93C	NP A558 13C	A. Adamo et al.
ARMSTRONG 93C	PL B307 394	T.A. Armstrong et al.
ARMSTRONG 93D	PL B307 399	T.A. Armstrong et al.
WEIDENAUER 93	ZPHY C59 387	P. Weidenauer et al.
ADAMO 92	PL B287 368	A. Adamo et al.
BELADIDZE 92B	ZPHY C54 367	G.M. Beladidze et al.
AKER 91	PL B260 249	E. Aker et al.
MAY 90	ZPHY C46 203	B. May et al.
MAY 89	PL B225 450	B. May et al.
BRIDGES 86B	PRL 56 215	D.L. Bridges et al.
BRIDGES 86C	PRL 57 1534	D.L. Bridges et al.

$\rho(1570)$

$$I^G(J^{PC}) = 1^+(1^{- -})$$

OMITTED FROM SUMMARY TABLE

May be an OZI-violating decay mode of $\rho(1700)$. See our mini-review under the $\rho(1700)$.

See key on page 999

Meson Particle Listings

$\rho(1570)$, $h_1(1595)$, $\pi_1(1600)$

$\rho(1570)$ MASS

VALUE (MeV)	EVTS	DOCUMENT ID	TECN	COMMENT
1570 ± 36 ± 62	54	¹ AUBERT 08s	BABR	10.6 e ⁺ e ⁻ → $\phi\pi^0\gamma$
1480 ± 40		² BITYUKOV 87	SPEC	32.5 π^-p → $\phi\pi^0n$

¹ From the fit with two resonances.
² Systematic errors not estimated.

$\rho(1570)$ WIDTH

VALUE (MeV)	EVTS	DOCUMENT ID	TECN	COMMENT
144 ± 75 ± 43	54	³ AUBERT 08s	BABR	10.6 e ⁺ e ⁻ → $\phi\pi^0\gamma$
130 ± 60		⁴ BITYUKOV 87	SPEC	32.5 π^-p → $\phi\pi^0n$

³ From the fit with two resonances.
⁴ Systematic errors not estimated.

$\rho(1570)$ DECAY MODES

Mode	Fraction (Γ_i/Γ)
Γ_1 e ⁺ e ⁻	
Γ_2 $\phi\pi$	not seen
Γ_3 $\omega\pi$	

$\rho(1570)$ $\Gamma(i)\Gamma(e^+e^-)/\Gamma(\text{total})$

$\Gamma(\phi\pi) \times \Gamma(e^+e^-)/\Gamma_{\text{total}}$	CL%	EVTS	DOCUMENT ID	TECN	COMMENT	Γ_2/Γ_1
3.5 ± 0.9 ± 0.3		54	⁵ AUBERT 08s	BABR	10.6 e ⁺ e ⁻ → $\phi\pi^0\gamma$	
<70	90		⁶ AULCHENKO 87b	ND	e ⁺ e ⁻ → $K_S^0 K_L^0 \pi^0$	

⁵ From the fit with two resonances.
⁶ Using mass and width of BITYUKOV 87.

$\rho(1570)$ BRANCHING RATIOS

$\Gamma(\phi\pi)/\Gamma_{\text{total}}$	DOCUMENT ID	TECN	COMMENT	Γ_2/Γ
not seen	ABELE 97H	CBAR	$\bar{p}p$ → $K_L^0 K_S^0 \pi^0 \pi^0$	
<0.01	⁷ DONNACHIE 91	RVUE		

⁷ Using data from BISELLO 91b, DOLINSKY 86, and ALBRECHT 87L.

$\Gamma(\phi\pi)/\Gamma(\omega\pi)$	CL%	DOCUMENT ID	TECN	COMMENT	Γ_2/Γ_3
>0.5	95	BITYUKOV 87	SPEC	32.5 π^-p → $\phi\pi^0n$	

$\rho(1570)$ REFERENCES

AUBERT 08s	PR D77 092002	B. Aubert et al.	(BABAR Collab.)
ABELE 97H	PL B415 280	A. Abele et al.	(Crystal Barrel Collab.)
BISELLO 91b	NPBPS B21 111	D. Bisello	(DM2 Collab.)
DONNACHIE 91	ZPHY C51 689	A. Donnachie, A.B. Clegg	(MCHS, LANC)
ALBRECHT 87L	PL B185 223	H. Albrecht et al.	(ARGUS Collab.)
AULCHENKO 87b	JETPL 45 145	V.M. Aulchenko et al.	(NOVO)
BITYUKOV 87	Translated from ZETFP 45 118	S.I. Bityukov et al.	(SERP)
DOLINSKY 86	PL B174 453	S.I. Dolinsky et al.	(NOVO)

$h_1(1595)$

$$I^G(J^{PC}) = 0^-(1^{+-})$$

OMITTED FROM SUMMARY TABLE

Seen in a partial-wave analysis of the $\omega\eta$ system produced in the reaction $\pi^-p \rightarrow \omega\eta n$ at 18 GeV/c.

$h_1(1595)$ MASS

VALUE (MeV)	DOCUMENT ID	TECN	COMMENT
1594 ± 15 ± 10 ± 60	EUGENIO 01	SPEC	18 π^-p → $\omega\eta n$

$h_1(1595)$ WIDTH

VALUE (MeV)	DOCUMENT ID	TECN	COMMENT
384 ± 60 ± 70 ± 100	EUGENIO 01	SPEC	18 π^-p → $\omega\eta n$

$h_1(1595)$ DECAY MODES

Mode	Fraction (Γ_i/Γ)
Γ_1 $\omega\eta$	seen

$h_1(1595)$ REFERENCES

EUGENIO 01	PL B497 190	P. Eugenio et al.
------------	-------------	-------------------

$\pi_1(1600)$

$$I^G(J^{PC}) = 1^-(1^{-+})$$

See the review on "Non- $q\bar{q}$ Mesons" and a note in PDG 06, Journal of Physics **G33** 1 (2006).

$\pi_1(1600)$ MASS

VALUE (MeV)	EVTS	DOCUMENT ID	TECN	COMMENT
1660 ± 15 ± 11 OUR AVERAGE				Error includes scale factor of 1.2.
1564 ± 24 ± 86		¹ RODAS 19	JPAC	191 π^-p → $\eta^{(\prime)}\pi^-p$
1600 ± 110 ± 60	46M	² AGHASYAN 18B	COMP	190 π^-p → $\pi^-\pi^+\pi^-p$
1664 ± 8 ± 10	145k	³ LU 05	B852	18 π^-p → $\omega\pi^-\pi^0p$
1709 ± 24 ± 41	69k	⁴ KUHN 04	B852	18 π^-p → $\eta\pi^+\pi^-\pi^-p$
1597 ± 10 ± 45 ± 10		⁴ IVANOV 01	B852	18 π^-p → $\eta'\pi^-p$
1660 ± 10 ± 0 ± 64	420k	⁵ ALEKSEEV 10	COMP	190 π^-Pb → $\pi^-\pi^-\pi^+Pb'$
1593 ± 8 ± 29 ± 47		^{4,6} ADAMS 98B	B852	18.3 π^-p → $\pi^+\pi^-\pi^-p$

••• We do not use the following data for averages, fits, limits, etc. •••

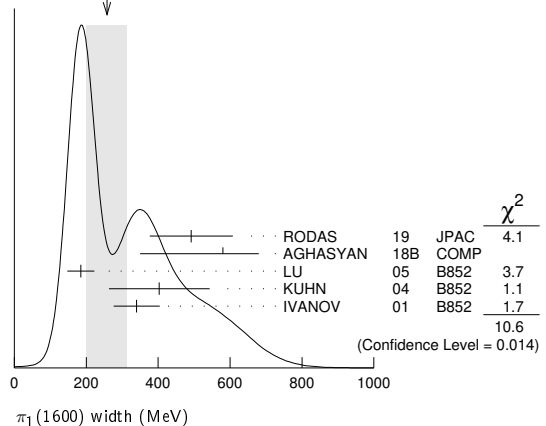
- The coupled-channel analysis of both the $\eta\pi$ and $\eta'\pi$ systems using ADOLPH 15data. The mass is extracted from the T-matrix pole.
- Statistical error negligible.
- May be a different state: natural and unnatural parity exchanges.
- Natural parity exchange.
- Superseded by AGHASYAN 2018B.
- Superseded by DZIERBA 06 excluding this state in a more refined PWA analysis, with 2.6 M events of $\pi^-p \rightarrow \pi^-\pi^-\pi^+p$ and 3 M events of $\pi^-p \rightarrow \pi^-\pi^0\pi^0p$ of E852 data.

$\pi_1(1600)$ WIDTH

VALUE (MeV)	EVTS	DOCUMENT ID	TECN	COMMENT
257 ± 60 OUR AVERAGE				Error includes scale factor of 1.9. See the ideogram below.
492 ± 54 ± 102		¹ RODAS 19	JPAC	191 π^-p → $\eta^{(\prime)}\pi^-p$
580 ± 100 ± 230	46M	² AGHASYAN 18B	COMP	190 π^-p → $\pi^-\pi^+\pi^-p$
185 ± 25 ± 28	145k	³ LU 05	B852	18 π^-p → $\omega\pi^-\pi^0p$
403 ± 80 ± 115	69k	⁴ KUHN 04	B852	18 π^-p → $\eta\pi^+\pi^-\pi^-p$
340 ± 40 ± 50		⁴ IVANOV 01	B852	18 π^-p → $\eta'\pi^-p$
269 ± 21 ± 42 ± 64	420k	⁵ ALEKSEEV 10	COMP	190 π^-Pb → $\pi^-\pi^-\pi^+Pb'$
168 ± 20 ± 150 ± 12		^{4,6} ADAMS 98B	B852	18.3 π^-p → $\pi^+\pi^-\pi^-p$

••• We do not use the following data for averages, fits, limits, etc. •••

WEIGHTED AVERAGE
257±60 (Error scaled by 1.9)



- The coupled-channel analysis of both the $\eta\pi$ and $\eta'\pi$ systems using ADOLPH 15data. The width is extracted from the T-matrix pole.
- Statistical error negligible.
- May be a different state: natural and unnatural parity exchanges.

Meson Particle Listings

$\pi_1(1600)$, $a_1(1640)$

⁴ Natural parity exchange.
⁵ Superseded by AGHASYAN 2018B.
⁶ Superseded by DZIERBA 06 excluding this state in a more refined PWA analysis, with 2.6 M events of $\pi^- p \rightarrow \pi^- \pi^- \pi^+ p$ and 3 M events of $\pi^- p \rightarrow \pi^- \pi^0 \pi^0 p$ of E852 data.

$\pi_1(1600)$ DECAY MODES

Mode	Fraction (Γ_i/Γ)
Γ_1 $\pi \pi \pi$	seen
Γ_2 $\rho^0 \pi^-$	seen
Γ_3 $f_2(1270) \pi^-$	not seen
Γ_4 $b_1(1235) \pi$	seen
Γ_5 $\eta'(958) \pi^-$	seen
Γ_6 $f_1(1285) \pi$	seen

$\pi_1(1600)$ BRANCHING RATIOS

$\Gamma(\rho^0 \pi^-)/\Gamma_{total}$	VALUE	DOCUMENT ID	TECN	COMMENT	Γ_2/Γ
seen		ALEKSEEV	10	COMP 190 $\pi^- p b \rightarrow \pi^- \pi^- \pi^+ p b'$	
not seen		NOZAR	09	CLAS $\gamma p \rightarrow 2\pi^+ \pi^- n$	
not seen		¹ DZIERBA	06	B852 18 $\pi^- p$	

¹ From the PWA analysis of 2.6 M $\pi^- p \rightarrow \pi^- \pi^- \pi^+ p$ and 3 M events of $\pi^- p \rightarrow \pi^- \pi^0 \pi^0 p$ of E852 data. Supersedes ADAMS 98B.

$\Gamma(f_2(1270) \pi^-)/\Gamma_{total}$	VALUE	DOCUMENT ID	TECN	COMMENT	Γ_3/Γ
not seen		¹ DZIERBA	06	B852 18 $\pi^- p$	

¹ From the PWA analysis of 2.6 M $\pi^- p \rightarrow \pi^- \pi^- \pi^+ p$ and 3 M events of $\pi^- p \rightarrow \pi^- \pi^0 \pi^0 p$ of E852 data. Supersedes CHUNG 02.

$\Gamma(b_1(1235) \pi)/\Gamma_{total}$	VALUE	EVTS	DOCUMENT ID	TECN	COMMENT	Γ_4/Γ
seen		35280	¹ BAKER	03	SPEC $\bar{p} p \rightarrow \omega \pi^+ \pi^- \pi^0$	
seen		145k	LU	05	B852 18 $\pi^- p \rightarrow \omega \pi^- \pi^0 p$	

¹ $B((b_1 \pi)_{D-wave})/B((b_1 \pi)_{S-wave}) = 0.3 \pm 0.1$.

$\Gamma(\eta'(958) \pi^-)/\Gamma_{total}$	VALUE	DOCUMENT ID	TECN	COMMENT	Γ_5/Γ
seen		IVANOV	01	B852 18 $\pi^- p \rightarrow \eta' \pi^- p$	

$\Gamma(f_1(1285) \pi)/\Gamma(\eta'(958) \pi^-)$	VALUE	EVTS	DOCUMENT ID	TECN	COMMENT	Γ_6/Γ_5
3.80 ± 0.78		69k	¹ KUHN	04	B852 18 $\pi^- p \rightarrow \eta \pi^+ \pi^- \pi^- p$	

¹ Using $\eta'(958)$ π data from IVANOV 01.

$\pi_1(1600)$ REFERENCES

RODAS	19	PRL 122 042002	A. Rodas et al.	(JPAC Collab.)
AGHASYAN	18B	PR D98 092003	M. Aghasyan et al.	(COMPASS Collab.)
ADOLPH	15	PL B740 303	M. Adolph et al.	(COMPASS Collab.)
ALEKSEEV	10	PRL 104 241803	M.G. Alekseev et al.	(COMPASS Collab.)
NOZAR	09	PRL 102 102002	M. Nozar et al.	(JLab CLAS Collab.)
DZIERBA	06	PR D73 072001	A.R. Dzierba et al.	(BNL E852 Collab.)
PDG	06	JP G33 1	W.-M. Yao et al.	(PDG Collab.)
LU	05	PRL 94 032002	M. Lu et al.	(BNL E852 Collab.)
KUHN	04	PL B595 109	J. Kuhn et al.	(BNL E852 Collab.)
BAKER	03	PL B563 140	C.A. Baker et al.	(BNL E852 Collab.)
CHUNG	02	PR D65 072001	S.U. Chung et al.	(BNL E852 Collab.)
IVANOV	01	PRL 86 3977	E.I. Ivanov et al.	(BNL E852 Collab.)
ADAMS	98B	PRL 81 9760	G.S. Adams et al.	(BNL E852 Collab.)

$a_1(1640)$ $I^G(J^{PC}) = 1^-(1^{++})$

Possibly seen in the study of the hadronic structure in decay $\tau \rightarrow 3\pi\nu_\tau$ (ABREU 98G and ASNER 00).

$a_1(1640)$ MASS

VALUE (MeV)	EVTS	DOCUMENT ID	TECN	COMMENT
1655 ± 16 OUR AVERAGE		Error includes scale factor of 1.2.		
1700 ± 35	46M	¹ AGHASYAN	18B	COMP 190 $\pi^- p \rightarrow \pi^- \pi^+ \pi^- p$
1691 ± 18 ± 30		DARGENT	17	RVUE $D^0 \rightarrow \pi^- \pi^+ \pi^- \pi^+$
1630 ± 20	35k	² BAKER	03	SPEC $\bar{p} p \rightarrow \omega \pi^+ \pi^- \pi^0$
1714 ± 9 ± 36		CHUNG	02	B852 18.3 $\pi^- p \rightarrow \pi^+ \pi^- \pi^- p$
1640 ± 12 ± 30		BAKER	99	SPEC 1.94 $\bar{p} p \rightarrow 4\pi^0$

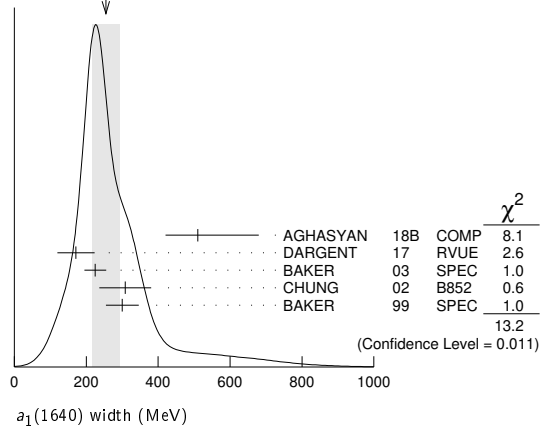
• • • We do not use the following data for averages, fits, limits, etc. • • •
 170 ± 90 BELLINI 85 SPEC 40 $\pi^- A \rightarrow \pi^- \pi^+ \pi^- A$
¹ Statistical error negligible.
² Using the $a_1(1260)$ mass and width results of BOWLER 88.

$a_1(1640)$ WIDTH

VALUE (MeV)	EVTS	DOCUMENT ID	TECN	COMMENT
254 ± 40 OUR AVERAGE		Error includes scale factor of 1.8. See the ideogram below.		
510 ⁺¹⁷⁰ ₋₉₀	46M	¹ AGHASYAN	18B	COMP 190 $\pi^- p \rightarrow \pi^- \pi^+ \pi^- p$
171 ± 33 ± 40		DARGENT	17	RVUE $D^0 \rightarrow \pi^- \pi^+ \pi^- \pi^+$
225 ± 30	35k	² BAKER	03	SPEC $\bar{p} p \rightarrow \omega \pi^+ \pi^- \pi^0$
308 ± 37 ± 62		CHUNG	02	B852 18.3 $\pi^- p \rightarrow \pi^+ \pi^- \pi^- p$
300 ± 22 ± 40		BAKER	99	SPEC 1.94 $\bar{p} p \rightarrow 4\pi^0$
300 ± 100		BELLINI	85	SPEC 40 $\pi^- A \rightarrow \pi^- \pi^+ \pi^- A$

• • • We do not use the following data for averages, fits, limits, etc. • • •
¹ Statistical error negligible.
² Using the $a_1(1260)$ mass and width results of BOWLER 88.

WEIGHTED AVERAGE
 254 ± 40 (Error scaled by 1.8)



$a_1(1640)$ DECAY MODES

Mode	Fraction (Γ_i/Γ)
Γ_1 $\pi \pi \pi$	seen
Γ_2 $f_2(1270) \pi$	seen
Γ_3 $\sigma \pi$	seen
Γ_4 $\rho \pi S$ -wave	seen
Γ_5 $\rho \pi D$ -wave	seen
Γ_6 $\omega \pi \pi$	seen
Γ_7 $f_1(1285) \pi$	seen
Γ_8 $a_1(1260) \eta$	not seen

$a_1(1640)$ BRANCHING RATIOS

$\Gamma(f_2(1270) \pi)/\Gamma(\sigma \pi)$	VALUE	DOCUMENT ID	TECN	COMMENT	Γ_2/Γ_3
0.24 ± 0.07		BAKER	99	SPEC 1.94 $\bar{p} p \rightarrow 4\pi^0$	

$\Gamma(\rho \pi D\text{-wave})/\Gamma_{total}$	VALUE	DOCUMENT ID	TECN	COMMENT	Γ_5/Γ
seen		CHUNG	02	B852 18.3 $\pi^- p \rightarrow \pi^+ \pi^- \pi^- p$	
seen		AMELIN	95B	VES 36 $\pi^- A \rightarrow \pi^+ \pi^- \pi^- A$	

$\Gamma(\omega \pi \pi)/\Gamma_{total}$	VALUE	EVTS	DOCUMENT ID	TECN	COMMENT	Γ_6/Γ
seen		35280	¹ BAKER	03	SPEC $\bar{p} p \rightarrow \omega \pi^+ \pi^- \pi^0$	

¹ Assuming the $\omega \rho$ mechanism for the $\omega \pi \pi$ state.

$\Gamma(f_1(1285) \pi)/\Gamma_{total}$	VALUE	DOCUMENT ID	TECN	COMMENT	Γ_7/Γ
not seen		KUHN	04	B852 18 $\pi^- p \rightarrow \eta \pi^+ \pi^- \pi^- p$	
seen		LEE	94	MPS2 18 $\pi^- p \rightarrow K^+ \bar{K}^0 \pi^- \pi^- p$	

See key on page 999

Meson Particle Listings

$a_1(1640), f_2(1640), \eta_2(1645), \omega(1650)$

$\Gamma(a_1(1260)\eta)/\Gamma_{total}$				Γ_8/Γ
VALUE	DOCUMENT ID	TECN	COMMENT	
not seen	KUHN	04	B852	$18 \pi^- p \rightarrow \eta \pi^+ \pi^- \pi^- p$

$a_1(1640)$ REFERENCES

NAME	PR	YEAR	DOC	TECN	COMMENT
AGHASYAN	18B	PR D98 092003	M. Aghasyan et al.		(COMPASS Collab.)
DARGENT	17	JHEP 1705 143	P. d'Argent et al.		(HEID, BRIS)
KUHN	04	PL B595 109	J. Kuhn et al.		(BNL E852 Collab.)
BAKER	03	PL B563 140	C.A. Baker et al.		
CHUNG	02	PR D65 072001	S.U. Chung et al.		(BNL E852 Collab.)
ASNER	00	PR D61 012002	D.M. Asner et al.		(CLEO Collab.)
BAKER	99	PL B449 114	C.A. Baker et al.		
ABREU	98G	PL B426 411	P. Abreu et al.		(DELPHI Collab.)
AMELIN	95B	PL B356 595	D.V. Amelin et al.		(SERP, TBIL)
LEE	94	PL B323 227	J.H. Lee et al.		(BNL, IND, KYUN, MASD+)
BOWLER	88	PL B209 99	M.G. Bowler		(OXF)
BELLINI	85	SJNP 41 781	D. Bellini et al.		
Translated from YAF 41 1223.					

$f_2(1640)$	$I^G(J^{PC}) = 0^+(2^{++})$
OMITTED FROM SUMMARY TABLE	

$f_2(1640)$ MASS

VALUE (MeV)	DOCUMENT ID	TECN	COMMENT
1639 ± 6 OUR AVERAGE	Error includes scale factor of 1.2.		
1620 ± 16	BUGG	95	MRK3 $J/\psi \rightarrow \gamma \pi^+ \pi^- \pi^+ \pi^-$
1647 ± 7	ADAMO	92	OBLX $\bar{p} p \rightarrow 3\pi^+ 2\pi^-$
1635 ± 7	ALDE	90	GAM2 $38 \pi^- p \rightarrow \omega \omega n$
• • • We do not use the following data for averages, fits, limits, etc. • • •			
1640 ± 5	AMSLER	06	CBAR $0.9 \bar{p} p \rightarrow K^+ K^- \pi^0$
1659 ± 6	VLADIMIRSK..06	SPEC	$40 \pi^- p \rightarrow K_S^0 K_S^0 n$
1643 ± 7	¹ ALDE	89B	GAM2 $38 \pi^- p \rightarrow \omega \omega n$
¹ Superseded by ALDE 90.			

$f_2(1640)$ WIDTH

VALUE (MeV)	CL%	DOCUMENT ID	TECN	COMMENT
99⁺⁶⁰₋₄₀ OUR AVERAGE	Error includes scale factor of 2.9.			
140 ⁺⁶⁰ ₋₂₀		BUGG	95	MRK3 $J/\psi \rightarrow \gamma \pi^+ \pi^- \pi^+ \pi^-$
58 ± 20		ADAMO	92	OBLX $\bar{p} p \rightarrow 3\pi^+ 2\pi^-$
• • • We do not use the following data for averages, fits, limits, etc. • • •				
44 ± 9		AMSLER	06	CBAR $0.9 \bar{p} p \rightarrow K^+ K^- \pi^0$
152 ± 18		VLADIMIRSK..06	SPEC	$40 \pi^- p \rightarrow K_S^0 K_S^0 n$
< 70	90	ALDE	90	GAM2 $38 \pi^- p \rightarrow \omega \omega n$

$f_2(1640)$ DECAY MODES

Mode	Fraction (Γ_i/Γ)
Γ_1 $\omega \omega$	seen
Γ_2 4π	seen
Γ_3 $K\bar{K}$	seen

$f_2(1640)$ BRANCHING RATIOS

$\Gamma(K\bar{K})/\Gamma_{total}$	Γ_3/Γ
seen	seen
	AMSLER 06 CBAR $0.9 \bar{p} p \rightarrow K^+ K^- \pi^0$

$f_2(1640)$ REFERENCES

NAME	PL	YEAR	DOC	TECN	COMMENT
AMSLER	06	PL B639 165	C. Anisler et al.		(CBAR Collab.)
VLADIMIRSK..06	06	PAN 69 433	V.V. Vladimirov et al.		(ITEP, Moscow)
Translated from YAF 69 515.					
BUGG	95	PL B353 378	D.V. Bugg et al.		(LOQM, PNPI, WASH)JP
ADAMO	92	PL B287 368	A. Adamo et al.		(OBELIX Collab.)
ALDE	90	PL B241 600	D.M. Alde et al.		(SERP, BELG, LANL, LAPP+)
ALDE	89B	PL B216 451	D.M. Alde et al.		(SERP, BELG, LANL, LAPP+)IGJPC

$\eta_2(1645)$	$I^G(J^{PC}) = 0^+(2^{-+})$
----------------	-----------------------------

$\eta_2(1645)$ MASS

VALUE (MeV)	DOCUMENT ID	TECN	CHG	COMMENT
1617 ± 5 OUR AVERAGE				
1613 ± 8	BARBERIS	00B		$450 pp \rightarrow p_f \eta \pi^+ \pi^- p_S$
1617 ± 8	BARBERIS	00C		$450 pp \rightarrow p_f 4\pi p_S$
1620 ± 20	BARBERIS	97B	OMEG	$450 pp \rightarrow pp 2(\pi^+ \pi^-)$
1645 ± 14 ± 15	ADOMEIT	96	CBAR 0	$1.94 \bar{p} p \rightarrow \eta 3\pi^0$

• • • We do not use the following data for averages, fits, limits, etc. • • •
 1645 ± 6 ± 20 ANISOVICH 00E SPEC 0.9-1.94 $\bar{p} p \rightarrow \eta 3\pi^0$

$\eta_2(1645)$ WIDTH

VALUE (MeV)	DOCUMENT ID	TECN	CHG	COMMENT
181 ± 11 OUR AVERAGE				
185 ± 17	BARBERIS	00B		$450 pp \rightarrow p_f \eta \pi^+ \pi^- p_S$
177 ± 18	BARBERIS	00C		$450 pp \rightarrow p_f 4\pi p_S$
180 ± 25	BARBERIS	97B	OMEG	$450 pp \rightarrow pp 2(\pi^+ \pi^-)$
180 ⁺⁴⁰ ₋₂₁ ± 25	ADOMEIT	96	CBAR 0	$1.94 \bar{p} p \rightarrow \eta 3\pi^0$
• • • We do not use the following data for averages, fits, limits, etc. • • •				
200 ± 25	ANISOVICH	00E	SPEC	$0.9-1.94 \bar{p} p \rightarrow \eta 3\pi^0$

$\eta_2(1645)$ DECAY MODES

Mode	Fraction (Γ_i/Γ)
Γ_1 $a_2(1320)\pi$	seen
Γ_2 $K\bar{K}\pi$	seen
Γ_3 $K^*\bar{K}$	seen
Γ_4 $\eta \pi^+ \pi^-$	seen
Γ_5 $a_0(980)\pi$	seen
Γ_6 $f_2(1270)\eta$	not seen

$\eta_2(1645)$ BRANCHING RATIOS

$\Gamma(K\bar{K}\pi)/\Gamma(a_2(1320)\pi)$	Γ_2/Γ_1
0.07 ± 0.03	¹ BARBERIS 97C OMEG $450 pp \rightarrow pp K\bar{K}\pi$
¹ Using $2(\pi^+ \pi^-)$ data from BARBERIS 97B.	

$\Gamma(a_2(1320)\pi)/\Gamma(a_0(980)\pi)$

VALUE	DOCUMENT ID	TECN	COMMENT
13.1 ± 2.3 OUR AVERAGE			
13.5 ± 4.6	² ANISOVICH 11	SPEC	$0.9-1.94 p\bar{p}$
13.0 ± 2.7	BARBERIS 00B		$450 pp \rightarrow p_f \eta \pi^+ \pi^- p_S$
² Reanalysis of ADOMEIT 96 and ANISOVICH 00E.			

$\Gamma(f_2(1270)\eta)/\Gamma_{total}$

VALUE	DOCUMENT ID	COMMENT
not seen	BARBERIS 00B	$450 pp \rightarrow p_f \eta \pi^+ \pi^- p_S$

$\eta_2(1645)$ REFERENCES

NAME	PL	YEAR	DOC	TECN	COMMENT
ANISOVICH	11	EPL C71 1511	A.V. Anisovich et al.		(LOQM, RAL, PNPI)
ANISOVICH	00E	PL B477 19	A.V. Anisovich et al.		
BARBERIS	00B	PL B471 435	D. Barberis et al.		(WA 102 Collab.)
BARBERIS	00C	PL B471 440	D. Barberis et al.		(WA 102 Collab.)
BARBERIS	97B	PL B413 217	D. Barberis et al.		(WA 102 Collab.)
BARBERIS	97C	PL B413 225	D. Barberis et al.		(WA 102 Collab.)
ADOMEIT	96	ZPHY C71 227	J. Adomeit et al.		(Crystal Barrel Collab.)

$\omega(1650)$	$I^G(J^{PC}) = 0^-(1^{-+})$
See also the $\omega(1420)$ particle listing.	

$\omega(1650)$ MASS

VALUE (MeV)	EVTS	DOCUMENT ID	TECN	COMMENT
1670 ± 30 OUR ESTIMATE				
1651 ± 3 ⁺¹⁶ ₋₆	183k	¹ ABLIKIM 19AQ BES		$J/\psi \rightarrow K^+ K^- \pi^0$
1673 ± 6 ⁺⁷ ₋₇		ACHASOV 19	SND	$e^+ e^- \rightarrow \pi^+ \pi^- \pi^0 \eta$
1671 ± 6 ± 10	824	² AKHMETSHIN 17A	CMD3	$1.4-2.0 e^+ e^- \rightarrow \omega \eta$
1660 ± 10	898	³ ACHASOV 16B	SND	$1.34-2.00 e^+ e^- \rightarrow \omega \eta$
1680 ± 10	13.1k	⁴ AULCHENKO 15A	SND	$1.05-1.80 e^+ e^- \rightarrow \pi^+ \pi^- \pi^0$
1667 ± 13 ± 6		AUBERT 07AU BABR		$10.6 e^+ e^- \rightarrow \omega \pi^+ \pi^- \gamma$
1645 ± 8	13	AUBERT 06D BABR		$10.6 e^+ e^- \rightarrow \omega \eta \gamma$
1660 ± 10 ± 2		AUBERT,B 04N BABR		$10.6 e^+ e^- \rightarrow \pi^+ \pi^- \pi^0 \gamma$
1770 ± 50 ± 60	1.2M	⁵ ACHASOV 03D	RVUE	$0.44-2.00 e^+ e^- \rightarrow \pi^+ \pi^- \pi^0$
1619 ± 5		⁶ HENNER 02	RVUE	$1.2-2.0 e^+ e^- \rightarrow \rho \pi,$ $\omega \pi \pi$
1700 ± 20		EUGENIO 01	SPEC	$18 \pi^- p \rightarrow \omega \eta n$
1705 ± 26	612	⁷ AKHMETSHIN 00D	CMD2	$e^+ e^- \rightarrow \omega \pi^+ \pi^-$
1820 ⁺¹⁹⁰ ₋₁₅₀		⁸ ACHASOV 98H	RVUE	$e^+ e^- \rightarrow \pi^+ \pi^- \pi^0$
1840 ⁺¹⁰⁰ ₋₇₀		⁹ ACHASOV 98H	RVUE	$e^+ e^- \rightarrow \omega \pi^+ \pi^-$

Meson Particle Listings

 $\omega(1650)$

1780^{+170}_{-300}	10	ACHASOV	98H	RVUE	$e^+e^- \rightarrow K^+K^-$
~ 2100	11	ACHASOV	98H	RVUE	$e^+e^- \rightarrow K_S^0 K^\pm \pi^\mp$
1606 ± 9	12	CLEGG	94	RVUE	
1662 ± 13	750	13 ANTONELLI	92	DM2	$1.34-2.4e^+e^- \rightarrow \rho\pi,$
1670 ± 20		ATKINSON	83B	OMEG	$20-70 \gamma\rho \rightarrow 3\pi X$
1657 ± 13		CORDIER	81	DM1	$e^+e^- \rightarrow \omega 2\pi$
1679 ± 34	21	ESPOSITO	80	FRAM	$e^+e^- \rightarrow 3\pi$
1652 ± 17		COSME	79	OSPK	$e^+e^- \rightarrow 3\pi$

¹ Could also be $\rho(1700)$. Branching ratio $J/\psi \rightarrow X \pi^0 \rightarrow K^+K^-\pi^0 = (5.3 \pm 0.3^{+0.6}_{-0.5}) \times 10^{-5}$.

² From a fit of the interfering $\omega(1420)$ and $\omega(1650)$ with a relative phase of π and other parameters floating.

³ From a fit with contributions from $\omega(1420)$, $\omega(1650)$, and $\phi(1680)$.

⁴ From a fit with contributions from $\omega(782)$, $\phi(1020)$, $\omega(1420)$, and $\omega(1650)$.

⁵ From the combined fit of ANTONELLI 92, ACHASOV 01E, ACHASOV 02E, and ACHASOV 03D data on the $\pi^+\pi^-\pi^0$ and ANTONELLI 92 on the $\omega\pi^+\pi^-$ final states. Supersedes ACHASOV 99E and ACHASOV 02E.

⁶ Using results of CORDIER 81 and preliminary data of DOLINSKY 91 and ANTONELLI 92.

⁷ Using the data of AKHMETSHIN 00D and ANTONELLI 92. The $\rho\pi$ dominance for the energy dependence of the $\omega(1420)$ and $\omega(1650)$ width assumed.

⁸ Using data from BARKOV 87, DOLINSKY 91, and ANTONELLI 92.

⁹ Using the data from ANTONELLI 92.

¹⁰ Using the data from IVANOV 81 and BISELLO 88B.

¹¹ Using the data from BISELLO 91c.

¹² From a fit to two Breit-Wigner functions and using the data of DOLINSKY 91 and ANTONELLI 92.

¹³ From the combined fit of the $\rho\pi$ and $\omega\pi\pi$ final states.

 $\omega(1650)$ WIDTH

VALUE (MeV)	EVTs	DOCUMENT ID	TECN	COMMENT
315 \pm 35 OUR ESTIMATE				

• • • We do not use the following data for averages, fits, limits, etc. • • •

$194 \pm 8^{+15}_{-7}$	183k	1	ABLIKIM	19AQ	BES	$J/\psi \rightarrow K^+K^-\pi^0$
95 ± 11			ACHASOV	19	SND	$e^+e^- \rightarrow \pi^+\pi^-\pi^0\eta$
$113 \pm 9 \pm 10$	824	2	AKHMETSHIN	17A	CMD3	$1.4-2.0 e^+e^- \rightarrow \omega\eta$
110 ± 20	898	3	ACHASOV	16B	SND	$1.34-2.00 e^+e^- \rightarrow \omega\eta$
310 ± 30	13.1k	4	AULCHENKO	15A	SND	$1.05-1.80 e^+e^- \rightarrow \omega\eta$
$222 \pm 25 \pm 20$			AUBERT	07AU	BABR	$10.6 e^+e^- \rightarrow \omega\pi^+\pi^-\gamma$
114 ± 14	13		AUBERT	06D	BABR	$10.6 e^+e^- \rightarrow \omega\eta\eta$
$230 \pm 30 \pm 20$			AUBERT,B	04N	BABR	$10.6 e^+e^- \rightarrow \pi^+\pi^-\pi^0\gamma$
$490^{+200}_{-150} \pm 130$	1.2M	5	ACHASOV	03D	RVUE	$0.44-2.00 e^+e^- \rightarrow \pi^+\pi^-\pi^0$
250 ± 14		6	HENNER	02	RVUE	$1.2-2.0 e^+e^- \rightarrow \rho\pi, \omega\pi\pi$
250 ± 50			EUGENIO	01	SPEC	$18 \pi^-\rho \rightarrow \omega\eta\eta$
370 ± 25	612	7	AKHMETSHIN	00D	CMD2	$e^+e^- \rightarrow \omega\pi^+\pi^-$
113 ± 20		8	CLEGG	94	RVUE	
280 ± 24	750	9	ANTONELLI	92	DM2	$1.34-2.4e^+e^- \rightarrow \rho\pi, \omega\pi\pi$
160 ± 20			ATKINSON	83B	OMEG	$20-70 \gamma\rho \rightarrow 3\pi X$
136 ± 46			CORDIER	81	DM1	$e^+e^- \rightarrow \omega 2\pi$
99 ± 49	21		ESPOSITO	80	FRAM	$e^+e^- \rightarrow 3\pi$
42 ± 17			COSME	79	OSPK	$e^+e^- \rightarrow 3\pi$

¹ Could also be $\rho(1700)$. Branching ratio $J/\psi \rightarrow X \pi^0 \rightarrow K^+K^-\pi^0 = (5.3 \pm 0.3^{+0.6}_{-0.5}) \times 10^{-5}$.

² From a fit of the interfering $\omega(1420)$ and $\omega(1650)$ with a relative phase of π and other parameters floating.

³ From a fit with contributions from $\omega(1420)$, $\omega(1650)$, and $\phi(1680)$.

⁴ From a fit with contributions from $\omega(782)$, $\phi(1020)$, $\omega(1420)$, and $\omega(1650)$.

⁵ From the combined fit of ANTONELLI 92, ACHASOV 01E, ACHASOV 02E, and ACHASOV 03D data on the $\pi^+\pi^-\pi^0$ and ANTONELLI 92 on the $\omega\pi^+\pi^-$ final states. Supersedes ACHASOV 99E and ACHASOV 02E.

⁶ Using results of CORDIER 81 and preliminary data of DOLINSKY 91 and ANTONELLI 92.

⁷ Using the data of AKHMETSHIN 00D and ANTONELLI 92. The $\rho\pi$ dominance for the energy dependence of the $\omega(1420)$ and $\omega(1650)$ width assumed.

⁸ From a fit to two Breit-Wigner functions and using the data of DOLINSKY 91 and ANTONELLI 92.

⁹ From the combined fit of the $\rho\pi$ and $\omega\pi\pi$ final states.

 $\omega(1650)$ DECAY MODES

Mode	Fraction (Γ_i/Γ)
Γ_1 $\rho\pi$	seen
Γ_2 $\omega\pi\pi$	seen
Γ_3 $\omega\eta$	seen
Γ_4 e^+e^-	seen
Γ_5 $\pi^0\gamma$	not seen

 $\omega(1650)$ $\Gamma(\rho\pi)/\Gamma^2(\text{total})$

$\Gamma(\rho\pi)/\Gamma_{\text{total}}$	$\times \Gamma(e^+e^-)/\Gamma_{\text{total}}$	$\Gamma_1/\Gamma \times \Gamma_4/\Gamma$
---	---	--

VALUE (units 10^{-6})	EVTs	DOCUMENT ID	TECN	COMMENT		
1.56 ± 0.23	13.1k	1	AULCHENKO	15A	SND	$1.05-1.80 e^+e^- \rightarrow \pi^+\pi^-\pi^0$
$1.3 \pm 0.1 \pm 0.1$			AUBERT,B	04N	BABR	$10.6 e^+e^- \rightarrow \pi^+\pi^-\pi^0\gamma$
$1.2^{+0.4}_{-0.1} \pm 0.8$	1.2M	2,3	ACHASOV	03D	RVUE	$0.44-2.00 e^+e^- \rightarrow \pi^+\pi^-\pi^0$
0.921 ± 0.230		4,5	CLEGG	94	RVUE	
0.479 ± 0.050	750	6,7	ANTONELLI	92	DM2	$1.34-2.4e^+e^- \rightarrow \rho\pi,$

¹ From a fit with contributions from $\omega(782)$, $\phi(1020)$, $\omega(1420)$, and $\omega(1650)$.

² Calculated by us from the cross section at the peak.

³ From the combined fit of ANTONELLI 92, ACHASOV 01E, ACHASOV 02E, and ACHASOV 03D data on the $\pi^+\pi^-\pi^0$ and ANTONELLI 92 on the $\omega\pi^+\pi^-$ final states. Supersedes ACHASOV 99E and ACHASOV 02E.

⁴ From a fit to two Breit-Wigner functions and using the data of DOLINSKY 91 and ANTONELLI 92.

⁵ From the partial and leptonic width given by the authors.

⁶ From the combined fit of the $\rho\pi$ and $\omega\pi\pi$ final states.

⁷ From the product of the leptonic width and partial branching ratio given by the authors.

$\Gamma(\omega\pi\pi)/\Gamma_{\text{total}}$	$\times \Gamma(e^+e^-)/\Gamma_{\text{total}}$	$\Gamma_2/\Gamma \times \Gamma_4/\Gamma$
--	---	--

VALUE (units 10^{-7})	EVTs	DOCUMENT ID	TECN	COMMENT		
7.0 ± 0.5			AUBERT	07AU	BABR	$10.6 e^+e^- \rightarrow \omega\pi^+\pi^-\gamma$
$4.1 \pm 0.9 \pm 1.3$	1.2M	1,2	ACHASOV	03D	RVUE	$0.44-2.00 e^+e^- \rightarrow \pi^+\pi^-\pi^0$
5.40 ± 0.95		3	AKHMETSHIN	00D	CMD2	$1.2-1.38 e^+e^- \rightarrow \omega\pi^+\pi^-$
3.18 ± 0.80		4,5	CLEGG	94	RVUE	
6.07 ± 0.61	750	6,7	ANTONELLI	92	DM2	$1.34-2.4 e^+e^- \rightarrow \rho\pi, \omega\pi\pi$

¹ Calculated by us from the cross section at the peak.

² From the combined fit of ANTONELLI 92, ACHASOV 01E, ACHASOV 02E, and ACHASOV 03D data on the $\pi^+\pi^-\pi^0$ and ANTONELLI 92 on the $\omega\pi^+\pi^-$ final states. Supersedes ACHASOV 99E and ACHASOV 02E.

³ Using the data of AKHMETSHIN 00D and ANTONELLI 92. The $\rho\pi$ dominance for the energy dependence of the $\omega(1420)$ and $\omega(1650)$ width assumed.

⁴ From a fit to two Breit-Wigner functions and using the data of DOLINSKY 91 and ANTONELLI 92.

⁵ From the partial and leptonic width given by the authors.

⁶ From the combined fit of the $\rho\pi$ and $\omega\pi\pi$ final states.

⁷ From the product of the leptonic width and partial branching ratio given by the authors.

$\Gamma(\omega\eta)/\Gamma_{\text{total}}$	$\times \Gamma(e^+e^-)/\Gamma_{\text{total}}$	$\Gamma_3/\Gamma \times \Gamma_4/\Gamma$
--	---	--

VALUE (units 10^{-7})	EVTs	DOCUMENT ID	TECN	COMMENT		
$5.62^{+0.45}_{-0.42}$			ACHASOV	19	SND	$e^+e^- \rightarrow \pi^+\pi^-\pi^0\eta$
$4.5 \pm 0.3 \pm 0.3$	824	1	AKHMETSHIN	17A	CMD3	$1.4-2.0 e^+e^- \rightarrow \omega\eta$
4.4 ± 0.5	898	2	ACHASOV	16B	SND	$1.34-2.00 e^+e^- \rightarrow \omega\eta$
5.7 ± 0.6	13		AUBERT	06D	BABR	$10.6 e^+e^- \rightarrow \omega\eta\eta$
< 60 at 90% CL		3	AKHMETSHIN	03B	CMD2	$e^+e^- \rightarrow \eta\pi^0\gamma$

¹ From a fit of the interfering $\omega(1420)$ and $\omega(1650)$ with a relative phase of π and other parameters floating. From an alternative fit $\Gamma(\omega(1650) \rightarrow \omega\eta)/\Gamma_{\text{total}} \times \Gamma(\omega(1650) \rightarrow e^+e^-) = 51 \pm 3$ eV.

² From a fit with contributions from $\omega(1420)$, $\omega(1650)$, and $\phi(1680)$.

³ $\omega(1650)$ mass and width fixed at 1700 MeV and 250 MeV, respectively.

 $\omega(1650)$ BRANCHING RATIOS

$\Gamma(\rho\pi)/\Gamma_{\text{total}}$	Γ_1/Γ
---	-------------------

VALUE	EVTs	DOCUMENT ID	TECN	COMMENT		
~ 0.65	1.2M	1	ACHASOV	03D	RVUE	$0.44-2.00 e^+e^- \rightarrow \pi^+\pi^-\pi^0$
0.380 ± 0.014		2	HENNER	02	RVUE	$1.2-2.0 e^+e^- \rightarrow \rho\pi, \omega\pi\pi$
						¹ From the combined fit of ANTONELLI 92, ACHASOV 01E, ACHASOV 02E, and ACHASOV 03D data on the $\pi^+\pi^-\pi^0$ and ANTONELLI 92 on the $\omega\pi^+\pi^-$ final states. Supersedes ACHASOV 99E and ACHASOV 02E.
						² Assuming that the $\omega(1650)$ decays into $\rho\pi$ and $\omega\pi\pi$ only.

$\Gamma(\omega\pi\pi)/\Gamma_{\text{total}}$	Γ_2/Γ
--	-------------------

VALUE	EVTs	DOCUMENT ID	TECN	COMMENT		
~ 0.35	1.2M	1	ACHASOV	03D	RVUE	$0.44-2.00 e^+e^- \rightarrow \pi^+\pi^-\pi^0$
0.620 ± 0.014		2	HENNER	02	RVUE	$1.2-2.0 e^+e^- \rightarrow \rho\pi, \omega\pi\pi$
						¹ From the combined fit of ANTONELLI 92, ACHASOV 01E, ACHASOV 02E, and ACHASOV 03D data on the $\pi^+\pi^-\pi^0$ and ANTONELLI 92 on the $\omega\pi^+\pi^-$ final states. Supersedes ACHASOV 99E and ACHASOV 02E.
						² Assuming that the $\omega(1650)$ decays into $\rho\pi$ and $\omega\pi\pi$ only.

See key on page 999

Meson Particle Listings

$\omega(1650), \omega_3(1670), \pi_2(1670)$

$\Gamma(e^+e^-)/\Gamma_{total}$					Γ_4/Γ
VALUE (units 10^{-7})	EVTS	DOCUMENT ID	TECN	COMMENT	
••• We do not use the following data for averages, fits, limits, etc. •••					
~ 18	1.2M	^{1,2} ACHASOV	03d	RVUE	$0.44-2.00 e^+e^- \rightarrow \pi^+\pi^-\pi^0$
32 ± 1		² HENNER	02	RVUE	$1.2-2.0 e^+e^- \rightarrow \rho\pi, \omega\pi\pi$
¹ Calculated by us from the cross section at the peak.					
² Assuming that the $\omega(1650)$ decays into $\rho\pi$ and $\omega\pi\pi$ only.					

$\Gamma(\pi^0\gamma)/\Gamma_{total}$					Γ_5/Γ
VALUE	EVTS	DOCUMENT ID	TECN	COMMENT	
not seen		¹ ACHASOV	10D	SND	$1.075-2.0 e^+e^- \rightarrow \pi^0\gamma$
¹ From a fit of a VMD model with two effective resonances with masses of 1450 MeV and 1700 MeV to describe the excited vector states $\omega(1420), \rho(1450), \omega(1650)$, and $\rho(1700)$. The width of the highest mass effective resonance is fixed at 315 MeV.					

$\omega(1650)$ REFERENCES

ABLIKIM	19AQ	PR D100 032004	M. Ablikim et al.	(BESIII Collab.)
ACHASOV	19	PR D99 112004	M.N. Achasov et al.	(SND Collab.)
AKHMETSHIN	17A	PL B773 150	R.R. Akhmetshin et al.	(CMD-3 Collab.)
ACHASOV	16B	PR D94 092002	M.N. Achasov et al.	(SND Collab.)
AULCHENKO	15A	JETP 121 27	V.M. Aulchenko et al.	(SND Collab.)
Translated from ZETF 148 34.				
ACHASOV	10D	PR D98 112001	M.N. Achasov et al.	(SND Collab.)
AUBERT	07AU	PR D76 092005	B. Aubert et al.	(BABAR Collab.)
AUBERT	06D	PR D73 052003	B. Aubert et al.	(BABAR Collab.)
AUBERT.B	04N	PR D70 072004	B. Aubert et al.	(BABAR Collab.)
ACHASOV	03D	PR D68 052006	M.N. Achasov et al.	(Novosibirsk SND Collab.)
AKHMETSHIN	03B	PL B562 173	R.R. Akhmetshin et al.	(Novosibirsk CMD-2 Collab.)
ACHASOV	02E	PR D66 032001	M.N. Achasov et al.	(Novosibirsk SND Collab.)
HENNER	02	EPJ C26 3	V.K. Henner et al.	
ACHASOV	01E	PR D63 072002	M.N. Achasov et al.	(Novosibirsk SND Collab.)
EUGENIO	01	PL B497 190	P. Eugenio et al.	
AKHMETSHIN	00D	PL B489 125	R.R. Akhmetshin et al.	(Novosibirsk CMD-2 Collab.)
ACHASOV	99E	PL B462 365	M.N. Achasov et al.	(Novosibirsk SND Collab.)
ACHASOV	98H	PR D57 4334	N.N. Achasov, A.A. Kozhevnikov	
CLEGG	94	ZPHY C62 455	A.B. Clegg, A. Donnachie	(LANC, MCHS)
ANTONELLI	92	ZPHY C56 15	A. Antonelli et al.	(DM2 Collab.)
BISELLO	91C	ZPHY C52 227	D. Bisello et al.	(DM2 Collab.)
DOLINSKY	91	PRPL 202 99	S.I. Dolinsky et al.	(NOVO)
BISELLO	88B	ZPHY C39 13	D. Bisello et al.	(PADO, CLER, FRAS+)
BARKOV	87	JETPL 46 164	L.M. Barkov et al.	(NOVO)
Translated from ZETFP 46 132.				
ATKINSON	83B	PL 127B 132	M. Atkinson et al.	(BONN, CERN, GLAS+)
CORDIER	81	PL 106B 155	A. Cordier et al.	(ORSAY)
IVANOV	81	PL 107B 297	P.M. Ivanov et al.	(NOVO)
ESPOSITO	80	LCN 28 195	G. Esposito et al.	(FRAS, NAPL, PADO+)
COSME	79	NP B152 215	G. Cosme et al.	(IPN)

$\omega_3(1670)$

$$I^G(J^{PC}) = 0^-(3^{--})$$

$\omega_3(1670)$ MASS

VALUE (MeV)	EVTS	DOCUMENT ID	TECN	COMMENT
1667 ± 4 OUR AVERAGE				
$1665.3 \pm 5.2 \pm 4.5$	23400	AMELIN	96	VES
1685 ± 20	60	BAUBILLIER	79	HBC
1673 ± 12	430	^{1,2} BALTAY	78E	HBC
1650 ± 12		CORDEN	78B	OMEG
1669 ± 11	600	² WAGNER	75	HBC
1678 ± 14	500	DIAZ	74	DBC
1660 ± 13	200	DIAZ	74	DBC
1679 ± 17	200	MATTHEWS	71D	DBC
1670 ± 20		KENYON	69	DBC
••• We do not use the following data for averages, fits, limits, etc. •••				
~ 1700	110	¹ CERRADA	77B	HBC
1695 ± 20		BARNES	69B	HBC
1636 ± 20		ARMENISE	68B	DBC
¹ Phase rotation seen for $J^P = 3^- \rho\pi$ wave.				
² From a fit to $I(J^P) = 0(3^-) \rho\pi$ partial wave.				

$\omega_3(1670)$ WIDTH

VALUE (MeV)	EVTS	DOCUMENT ID	TECN	COMMENT
168 ± 10 OUR AVERAGE				
$149 \pm 19 \pm 7$	23400	AMELIN	96	VES
160 ± 80	60	³ BAUBILLIER	79	HBC
173 ± 16	430	^{4,5} BALTAY	78E	HBC
253 ± 39		CORDEN	78B	OMEG
173 ± 28	600	^{3,5} WAGNER	75	HBC
167 ± 40	500	DIAZ	74	DBC
122 ± 39	200	DIAZ	74	DBC
155 ± 40	200	³ MATTHEWS	71D	DBC
••• We do not use the following data for averages, fits, limits, etc. •••				
90 ± 20		BARNES	69B	HBC
100 ± 40		KENYON	69	DBC
112 ± 60		ARMENISE	68B	DBC
³ Width errors enlarged by us to $4\Gamma/\sqrt{N}$; see the note with the $K^*(892)$ mass.				
⁴ Phase rotation seen for $J^P = 3^- \rho\pi$ wave.				
⁵ From a fit to $I(J^P) = 0(3^-) \rho\pi$ partial wave.				

$\omega_3(1670)$ DECAY MODES

Mode	Fraction (Γ_i/Γ)
Γ_1 $\rho\pi$	seen
Γ_2 $\omega\pi\pi$	seen
Γ_3 $b_1(1235)\pi$	possibly seen

$\omega_3(1670)$ BRANCHING RATIOS

$\Gamma(\omega\pi\pi)/\Gamma(\rho\pi)$					Γ_2/Γ_1
VALUE	EVTS	DOCUMENT ID	TECN	COMMENT	
••• We do not use the following data for averages, fits, limits, etc. •••					
0.71 ± 0.27	100	DIAZ	74	DBC	$6\pi^+n \rightarrow p5\pi^0$
$\Gamma(b_1(1235)\pi)/\Gamma(\rho\pi)$					Γ_3/Γ_1
VALUE	CL%	DOCUMENT ID	TECN	COMMENT	
possibly seen		DIAZ	74	DBC	$6\pi^+n \rightarrow p5\pi^0$
$\Gamma(b_1(1235)\pi)/\Gamma(\omega\pi\pi)$					Γ_3/Γ_2
VALUE	CL%	DOCUMENT ID	TECN	COMMENT	
••• We do not use the following data for averages, fits, limits, etc. •••					
>0.75	68	BAUBILLIER	79	HBC	$8.2 K^-p$ backward

$\omega_3(1670)$ REFERENCES

AMELIN	96	ZPHY C70 71	D.V. Amelin et al.	(SERP, TBIL)
BAUBILLIER	79	PL 89B 131	M. Baubillier et al.	(BIRM, CERN, GLAS+)
BALTAY	78E	PR L 40 87	C. Baltay, C.V. Cautis, M. Kaelin	(COLU)JP
CORDEN	78B	NP B138 235	M.J. Corden et al.	(BIRM, RHEL, TELA+)
CERRADA	77B	NP B126 241	M. Cerrada et al.	(AMST, CERN, NIJUM+JP)
WAGNER	75	PL 58B 201	F. Wagner, M. Tabak, D.M. Chew	(LBL)JP
DIAZ	74	PR L 32 260	J. Diaz et al.	(CASE, CMU)
MATTHEWS	71D	PR D3 2561	J.A.J. Matthews et al.	(TNT0, WISC)
BARNES	69B	PR L 23 142	V.E. Barnes et al.	(BNL)
KENYON	69	PR L 23 146	I.R. Kenyon et al.	(BNL, UCND, ORNL)
ARMENISE	68B	PL 26B 336	N. Armenise et al.	(BARI, BGNA, FIRZ+)

$\pi_2(1670)$

$$I^G(J^{PC}) = 1^-(2^{-+})$$

$\pi_2(1670)$ MASS

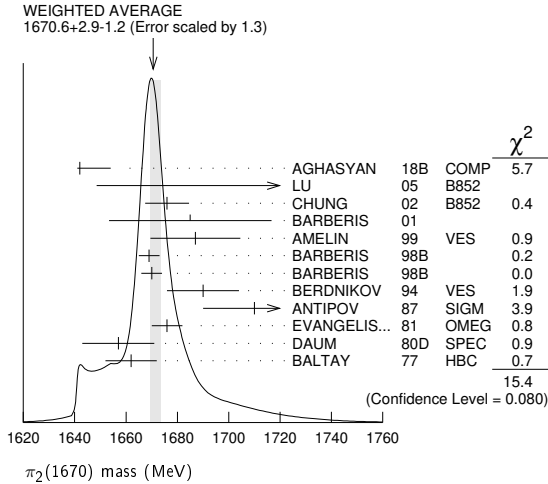
VALUE (MeV)	EVTS	DOCUMENT ID	TECN	CHG	COMMENT
1670.6 ± 2.9 OUR AVERAGE					Error includes scale factor of 1.3. See the ideogram below.
1642 ± 12	46M	¹ AGHASYAN	18B	COMP	$190 \pi^-p \rightarrow \pi^-\pi^+\pi^-\rho$
$1749 \pm 10 \pm 100$	145k	LU	05	B852	$18 \pi^-p \rightarrow \omega\pi^-\pi^0\rho$
$1676 \pm 3 \pm 8$		² CHUNG	02	B852	$18.3 \pi^-p \rightarrow \pi^+\pi^-\pi^-\rho$
$1685 \pm 10 \pm 30$		BARBERIS	01		$450 p\rho \rightarrow p_f 3\pi^0 p_s$
$1687 \pm 9 \pm 15$		AMELIN	99	VES	$37 \pi^-A \rightarrow \omega\pi^-\pi^0 A^*$
1669 ± 4		BARBERIS	98B		$450 p\rho \rightarrow p_f \rho\pi p_s$
1670 ± 4		BARBERIS	98B		$450 p\rho \rightarrow p_f f_2(1270)\pi p_s$
1690 ± 14		³ BERDNIKOV	94	VES	$37 \pi^-A \rightarrow K^+K^-\pi^-A$
1710 ± 20	700	ANTIPOV	87	SIGM	$50 \pi^-Cu \rightarrow \mu^+\mu^-\pi^-Cu$
1676 ± 6		³ EVANGELIS...	81	OMEG	$12 \pi^-p \rightarrow 3\pi\rho$
1657 ± 14		^{3,4} DAUM	80D	SPEC	$63-94 \pi\rho \rightarrow 3\pi X$
1662 ± 10	2000	³ BALTAY	77	HBC	$15 \pi^+p \rightarrow \rho 3\pi$
••• We do not use the following data for averages, fits, limits, etc. •••					
$1658 \pm 3 \pm 24$	420k	⁵ ALEKSEEV	10	COMP	$190 \pi^-Pb \rightarrow \pi^-\pi^-\pi^+\pi^+Pb'$
1730 ± 20		⁶ AMELIN	95B	VES	$36 \pi^-A \rightarrow \pi^+\pi^-\pi^-A$
$1742 \pm 31 \pm 49$		ANTREAS YAN	90	CBAL	$e^+e^- \rightarrow e^+e^-\pi^0\pi^0\pi^0$
1624 ± 21		² BELLINI	85	SPEC	$40 \pi^-A \rightarrow \pi^-\pi^+\pi^-A$
1622 ± 35		⁷ BELLINI	85	SPEC	$40 \pi^-A \rightarrow \pi^-\pi^+\pi^-A$
1693 ± 28		⁸ BELLINI	85	SPEC	$40 \pi^-A \rightarrow \pi^-\pi^+\pi^-A$
1710 ± 20		⁹ DAUM	81B	SPEC	$63,94 \pi^-p$
1660 ± 10		³ ASCOLI	73	HBC	$5-25 \pi^-p \rightarrow \rho 2\pi$

¹ Statistical error negligible.
² From $f_2(1270)\pi$ decay.
³ From a fit to $J^P = 2^-S$ -wave $f_2(1270)\pi$ partial wave.
⁴ Clear phase rotation seen in $2^-S, 2^-P, 2^-D$ waves. We quote central value and spread of single-resonance fits to three channels.
⁵ Superseded by AGHASYAN 2018B.
⁶ J^{PC} ambiguous.

Meson Particle Listings

$\pi_2(1670)$

⁷ From $\rho\pi$ decay.
⁸ From $\sigma\pi$ decay.
⁹ From a two-resonance fit to four 2^-0^+ waves. This should not be averaged with all the single resonance fits.



$\pi_2(1670)$ WIDTH

VALUE (MeV)	EVTS	DOCUMENT ID	TECN	CHG	COMMENT
258⁺⁸₋₉	OUR AVERAGE	Error includes scale factor of 1.2.			
311 ⁺¹² ₋₂₃	46M	¹⁰ AGHASYAN	18B	COMP	190 $\pi^- p \rightarrow \pi^- \pi^+ \pi^- p$
408 ⁺⁶⁰ ± 250	145k	LU	05	B852	18 $\pi^- p \rightarrow \omega \pi^- \pi^0 p$
254 ⁺³ ± 31		¹¹ CHUNG	02	B852	18.3 $\pi^- p \rightarrow \pi^+ \pi^- \pi^- p$
265 ⁺³⁰ ± 40		BARBERIS	01		450 $\rho p \rightarrow \rho_f 3\pi^0 p_s$
168 ⁺⁴³ ± 53		AMELIN	99	VES	37 $\pi^- A \rightarrow \omega \pi^- \pi^0 A^*$
268 ⁺¹⁵		BARBERIS	98B		450 $\rho p \rightarrow \rho_f \rho \pi p_s$
256 ⁺¹⁵		BARBERIS	98B		450 $\rho p \rightarrow \rho_f f_2(1270) \pi p_s$
190 ⁺⁵⁰		¹² BERDNIKOV	94	VES	37 $\pi^- A \rightarrow K^+ K^- \pi^- A$
170 ⁺⁸⁰	700	ANTIPOV	87	SIGM	50 $\pi^- Cu \rightarrow \mu^+ \mu^- \pi^- Cu$
260 ⁺²⁰		¹² EVANGELIS...	81	OMEG	12 $\pi^- p \rightarrow 3\pi p$
219 ⁺²⁰		^{12,13} DAUM	80D	SPEC	63-94 $\pi p \rightarrow 3\pi X$
285 ⁺⁶⁰	2000	¹² BALTAY	77	HBC	15 $\pi^+ p \rightarrow \rho 3\pi$
••• We do not use the following data for averages, fits, limits, etc. •••					
271 ⁺⁹ ± 22	420k	¹⁴ ALEKSEEV	10	COMP	190 $\pi^- Pb \rightarrow \pi^- \pi^- \pi^+ Pb'$
310 ⁺²⁰		¹⁵ AMELIN	95B	VES	36 $\pi^- A \rightarrow \pi^+ \pi^- \pi^- A$
236 ⁺⁴⁹ ± 36		ANTREASYAN	90	CBAL	$e^+ e^- \rightarrow \pi^0 \pi^0 \pi^0$
304 ⁺²²		¹¹ BELLINI	85	SPEC	40 $\pi^- A \rightarrow \pi^- \pi^+ \pi^- A$
404 ⁺¹⁰⁸		¹⁶ BELLINI	85	SPEC	40 $\pi^- A \rightarrow \pi^- \pi^+ \pi^- A$
330 ⁺⁹⁰		¹⁷ BELLINI	85	SPEC	40 $\pi^- A \rightarrow \pi^- \pi^+ \pi^- A$
312 ⁺⁵⁰		¹⁸ DAUM	81B	SPEC	63,94 $\pi^- p$
270 ⁺⁶⁰		¹² ASCOLI	73	HBC	5-25 $\pi^- p \rightarrow \rho \pi_2$

¹⁰ Statistical error negligible.
¹¹ From $f_2(1270)\pi$ decay.
¹² From a fit to $J^P = 2^- 2^- f_2(1270)\pi$ partial wave.
¹³ Clear phase rotation seen in $2^-S, 2^-P, 2^-D$ waves. We quote central value and spread of single-resonance fits to three channels.
¹⁴ Superseded by AGHASYAN 2018B.
¹⁵ J^PC ambiguous.
¹⁶ From $\rho\pi$ decay.
¹⁷ From $\sigma\pi$ decay.
¹⁸ From a two-resonance fit to four 2^-0^+ waves. This should not be averaged with all the single resonance fits.

$\pi_2(1670)$ DECAY MODES

Mode	Fraction (Γ_i/Γ)	Confidence level
Γ_1 3π	(95.8 ± 1.4) %	
Γ_2 $\pi^+ \pi^- \pi^0$		
Γ_3 $\pi^0 \pi^0 \pi^0$		
Γ_4 $f_2(1270)\pi$	(56.3 ± 3.2) %	
Γ_5 $\rho\pi$	(31 ± 4) %	

Γ_6 $\sigma\pi$	(10 ± 4) %	
Γ_7 $\pi(\pi\pi)_S$ -wave	(8.7 ± 3.4) %	
Γ_8 $\pi^+ \pi^+ \pi^-$	(53 ± 4) %	
Γ_9 $K\bar{K}^*(892) + c.c.$	(4.2 ± 1.4) %	
Γ_{10} $\omega\rho$	(2.7 ± 1.1) %	
Γ_{11} $\pi^\pm \gamma$	(7.0 ± 1.2) × 10 ⁻⁴	
Γ_{12} $\gamma\gamma$	< 2.8 × 10 ⁻⁷	90%
Γ_{13} $\eta\pi$	< 5 %	
Γ_{14} $\pi^\pm 2\pi^+ 2\pi^-$	< 5 %	
Γ_{15} $\rho(1450)\pi$	< 3.6 × 10 ⁻³	97.7%
Γ_{16} $b_1(1235)\pi$	< 1.9 × 10 ⁻³	97.7%
Γ_{17} $\eta 3\pi$		
Γ_{18} $f_1(1285)\pi$	possibly seen	
Γ_{19} $a_2(1320)\pi$	not seen	

CONSTRAINED FIT INFORMATION

An overall fit to 4 branching ratios uses 6 measurements and one constraint to determine 4 parameters. The overall fit has a $\chi^2 = 1.9$ for 3 degrees of freedom.

The following off-diagonal array elements are the correlation coefficients $\langle \delta x_i \delta x_j \rangle / (\delta x_i \delta x_j)$, in percent, from the fit to the branching fractions, $x_i \equiv \Gamma_i/\Gamma_{total}$. The fit constrains the x_i whose labels appear in this array to sum to one.

x_5	-53		
x_7	-29	-59	
x_9	-8	-21	-9
	x_4	x_5	x_7

$\pi_2(1670)$ PARTIAL WIDTHS

$\Gamma(\pi^\pm \gamma)$	VALUE (keV)	DOCUMENT ID	TECN	CHG	COMMENT	Γ_{11}	
181 ± 11 ± 27		¹⁹ ADOLPH	14	COMP	190 $\pi^- Pb \rightarrow \pi^+ \pi^- \pi^- Pb'$		
¹⁹ Primakoff reaction. Assumes incoherent $f_2(1270)\pi$ contribution to 3π final state and uses $B(\pi_2(1670) \rightarrow f_2\pi) = 56\%$.							
$\Gamma(\gamma\gamma)$	VALUE (keV)	CL%	DOCUMENT ID	TECN	CHG	COMMENT	Γ_{12}
<0.072	90		²⁰ ACCIARRI	97T	L3	$e^+ e^- \rightarrow e^+ e^- \pi^+ \pi^- \pi^0$	
••• We do not use the following data for averages, fits, limits, etc. •••							
<0.19	90		²⁰ ALBRECHT	97B	ARG	$e^+ e^- \rightarrow e^+ e^- \pi^+ \pi^- \pi^0$	
1.41 ± 0.23 ± 0.28			ANTREASYAN	90	CBAL	0 $e^+ e^- \rightarrow e^+ e^- \pi^0 \pi^0 \pi^0$	
0.8 ± 0.3 ± 0.12			²¹ BEHREND	90c	CELL	0 $e^+ e^- \rightarrow e^+ e^- \pi^+ \pi^- \pi^0$	
1.3 ± 0.3 ± 0.2			²² BEHREND	90c	CELL	0 $e^+ e^- \rightarrow e^+ e^- \pi^+ \pi^- \pi^0$	
²⁰ Decaying into $f_2(1270)\pi$ and $\rho\pi$.							
²¹ Constructive interference between $f_2(1270)\pi, \rho\pi$ and background.							
²² Incoherent Ansatz.							

$\pi_2(1670)$ $\Gamma(i)\Gamma(\gamma\gamma)/\Gamma(total)$

$\Gamma(\pi^+ \pi^- \pi^0) \times \Gamma(\gamma\gamma)/\Gamma_{total}$	VALUE (keV)	CL%	DOCUMENT ID	TECN	COMMENT	$\Gamma_2 \Gamma_{12}/\Gamma$
<0.1	95		²³ SCHEGELSKY	06	RVUE $\gamma\gamma \rightarrow \pi^+ \pi^- \pi^0$	
²³ From analysis of L3 data at 183-209 GeV.						

$\pi_2(1670)$ BRANCHING RATIOS

$\Gamma(3\pi)/\Gamma_{total}$	VALUE	DOCUMENT ID	TECN	COMMENT	$\Gamma_1/\Gamma = (\Gamma_4 + \Gamma_5 + \Gamma_7)/\Gamma$
0.958 ± 0.014 OUR FIT					
$\Gamma(\pi^0 \pi^0 \pi^0)/\Gamma(\pi^+ \pi^- \pi^0)$	VALUE	DOCUMENT ID	COMMENT	Γ_3/Γ_2	
0.29 ± 0.03 ± 0.05		BARBERIS	01 450 $\rho p \rightarrow \rho_f 3\pi^0 p_s$		
$\Gamma(\rho\pi)/0.565\Gamma(f_2(1270)\pi)$	VALUE	DOCUMENT ID	TECN	COMMENT	$\Gamma_5/0.565\Gamma_4$
(With $f_2(1270) \rightarrow \pi^+ \pi^-$.)					
0.97 ± 0.09 OUR AVERAGE		Error includes scale factor of 1.9.			
0.76 ± 0.07 ± 0.10		CHUNG	02	B852	18.3 $\pi^- p \rightarrow \pi^+ \pi^- \pi^- p$
1.01 ± 0.05		BARBERIS	98B		450 $\rho p \rightarrow \rho_f \pi^+ \pi^- \pi^0 p_s$
$\Gamma(\sigma\pi)/\Gamma(f_2(1270)\pi)$	VALUE	DOCUMENT ID	TECN	COMMENT	Γ_6/Γ_4
0.17 ± 0.02 ± 0.07		CHUNG	02	B852	18.3 $\pi^- p \rightarrow \pi^+ \pi^- \pi^- p$

See key on page 999

Meson Particle Listings

$\pi_2(1670)$, $\phi(1680)$

••• We do not use the following data for averages, fits, limits, etc. •••
 0.24±0.10 24,25 BAKER 99 SPEC 1.94 $\bar{p}p \rightarrow 4\pi^0$

$\frac{1}{2}\Gamma(\rho\pi)/\Gamma(\pi^\pm\pi^+\pi^-)$ $\frac{1}{2}\Gamma_5/\Gamma_8 = \frac{1}{2}\Gamma_5/(0.565\Gamma_4 + \frac{1}{2}\Gamma_5 + 0.624\Gamma_7)$

VALUE	DOCUMENT ID	TECN	CHG	COMMENT
0.29±0.04 OUR FIT				
0.29±0.05	26 DAUM	81B	SPEC	63,94 π^-p
••• We do not use the following data for averages, fits, limits, etc. •••				
<0.3	BARTSCH	68	HBC	+ 8 $\pi^+p \rightarrow 3\pi p$

0.565 $\Gamma(f_2(1270)\pi)/\Gamma(\pi^\pm\pi^+\pi^-)$

0.565 $\Gamma_4/\Gamma_8 = 0.565\Gamma_4/(0.565\Gamma_4 + \frac{1}{2}\Gamma_5 + 0.624\Gamma_7)$

(With $f_2(1270) \rightarrow \pi^+\pi^-$.)

VALUE	DOCUMENT ID	TECN	CHG	COMMENT
0.604±0.035 OUR FIT				
0.60 ±0.05 OUR AVERAGE	Error includes scale factor of 1.3.			
0.61 ±0.04	26 DAUM	81B	SPEC	63,94 π^-p
0.76 $\pm_{-0.34}^{+0.24}$	ARMENISE	69	DBC	+ 5.1 $\pi^+d \rightarrow d3\pi$
0.35 ±0.20	BALTAY	68	HBC	+ 7-8.5 π^+p
••• We do not use the following data for averages, fits, limits, etc. •••				
0.59	BARTSCH	68	HBC	+ 8 $\pi^+p \rightarrow 3\pi p$

0.624 $\Gamma(\pi(\pi\pi)s\text{-wave})/\Gamma(\pi^\pm\pi^+\pi^-)$

0.624 $\Gamma_7/\Gamma_8 = 0.624\Gamma_7/(0.565\Gamma_4 + \frac{1}{2}\Gamma_5 + 0.624\Gamma_7)$

(With $(\pi\pi)_{S\text{-wave}} \rightarrow \pi^+\pi^-$.)

VALUE	DOCUMENT ID	TECN	CHG	COMMENT
0.10±0.04 OUR FIT				
0.10±0.05	26 DAUM	81B	SPEC	63,94 π^-p

$\Gamma(K\bar{K}^*(892) + c.c.)/\Gamma(f_2(1270)\pi)$ Γ_9/Γ_4

VALUE	DOCUMENT ID	TECN	CHG	COMMENT
0.075±0.025 OUR FIT				
0.075±0.025	27 ARMSTRONG	82B	OMEG	- 16 $\pi^-p \rightarrow K^+K^-\pi^-p$

$\Gamma(\omega\rho)/\Gamma_{\text{total}}$ Γ_{10}/Γ

VALUE	DOCUMENT ID	TECN	COMMENT
0.027±0.004±0.010	28 AMELIN	99	VES 37 $\pi^-A \rightarrow \omega\pi^-\pi^0A^*$

$\Gamma(\eta\pi)/\Gamma(\pi^\pm\pi^+\pi^-)$ $\Gamma_{13}/\Gamma_8 = \Gamma_{13}/(0.565\Gamma_4 + \frac{1}{2}\Gamma_5 + 0.624\Gamma_7)$

(All η decays.)

VALUE	DOCUMENT ID	TECN	CHG	COMMENT
<0.09	BALTAY	68	HBC	+ 7-8.5 π^+p
••• We do not use the following data for averages, fits, limits, etc. •••				
<0.10	CRENNELL	70	HBC	- 6 $\pi^-p \rightarrow f_2\pi^-N$

$\Gamma(\pi^\pm 2\pi^+ 2\pi^-)/\Gamma(\pi^\pm\pi^+\pi^-)$ $\Gamma_{14}/\Gamma_8 = \Gamma_{14}/(0.565\Gamma_4 + \frac{1}{2}\Gamma_5 + 0.624\Gamma_7)$

VALUE	DOCUMENT ID	TECN	CHG	COMMENT
<0.10	CRENNELL	70	HBC	- 6 $\pi^-p \rightarrow f_2\pi^-N$
••• We do not use the following data for averages, fits, limits, etc. •••				
<0.1	BALTAY	68	HBC	+ 7,8.5 π^+p

$\Gamma(\rho(1450)\pi)/\Gamma_{\text{total}}$ Γ_{15}/Γ

VALUE	CL%	DOCUMENT ID	TECN	COMMENT
<0.0036	97.7	AMELIN	99	VES 37 $\pi^-A \rightarrow \omega\pi^-\pi^0A^*$

$\Gamma(b_1(1235)\pi)/\Gamma_{\text{total}}$ Γ_{16}/Γ

VALUE	CL%	DOCUMENT ID	TECN	COMMENT
<0.0019	97.7	AMELIN	99	VES 37 $\pi^-A \rightarrow \omega\pi^-\pi^0A^*$

$\Gamma(f_1(1285)\pi)/\Gamma_{\text{total}}$ Γ_{18}/Γ

VALUE	EVTS	DOCUMENT ID	TECN	COMMENT
possibly seen	69k	KUHN	04	B852 18 $\pi^-p \rightarrow \eta\pi^+\pi^-\pi^-p$

$\Gamma(a_2(1320)\pi)/\Gamma_{\text{total}}$ Γ_{19}/Γ

VALUE	EVTS	DOCUMENT ID	TECN	COMMENT
not seen	69k	KUHN	04	B852 18 $\pi^-p \rightarrow \eta\pi^+\pi^-\pi^-p$

D-wave/S-wave RATIO FOR $\pi_2(1670) \rightarrow f_2(1270)\pi$

VALUE	DOCUMENT ID	TECN	COMMENT
-0.18±0.06	24 BAKER	99	SPEC 1.94 $\bar{p}p \rightarrow 4\pi^0$
••• We do not use the following data for averages, fits, limits, etc. •••			
0.22±0.10	26 DAUM	81B	SPEC 63,94 π^-p

F-wave/P-wave RATIO FOR $\pi_2(1670) \rightarrow \rho\pi$

VALUE	DOCUMENT ID	TECN	COMMENT
-0.72±0.07±0.14	CHUNG	02	B852 18.3 $\pi^-p \rightarrow \pi^+\pi^-\pi^-p$
24	Using preliminary CBAR data.		
25	With the $\sigma\pi$ in $L=2$ and the $f_2(1270)\pi$ in $L=0$.		
26	From a two-resonance fit to four 2^-0^+ waves.		
27	From a partial-wave analysis of $K^+K^-\pi^-$ system.		
28	Normalized to the $B(\pi_2(1670) \rightarrow f_2\pi)$.		

$\pi_2(1670)$ REFERENCES

AGHASYAN	18B	PR D98 092003	M. Aghasyan <i>et al.</i>	(COMPASS Collab.)
ADOLPH	14	EPJ A50 79	C. Adolph <i>et al.</i>	(COMPASS Collab.)
ALEKSEEV	10	PRL 104 241803	M.G. Alekseev <i>et al.</i>	(COMPASS Collab.)
SCHEGELSKY	06	EPJ A27 199	V.A. Schegelsky <i>et al.</i>	
LU	05	PRL 94 032002	M. Lu <i>et al.</i>	(BNL E852 Collab.)
KUHN	04	PL B595 109	J. Kuhn <i>et al.</i>	(BNL E852 Collab.)
CHUNG	02	PR D65 072001	S.U. Chung <i>et al.</i>	(BNL E852 Collab.)
BARBERIS	01	PL B507 14	D. Barberis <i>et al.</i>	
AMELIN	99	PAN 62 445	D.V. Amelin <i>et al.</i>	(VES Collab.)
		Translated from YAF 62 487.		
BAKER	99	PL B449 114	C.A. Baker <i>et al.</i>	
BARBERIS	98B	PL B422 399	D. Barberis <i>et al.</i>	(WA 102 Collab.)
ACCIARRI	97T	PL B413 147	M. Acciarri <i>et al.</i>	(L3 Collab.)
ALBRECHT	97B	ZPHY C74 469	H. Albrecht <i>et al.</i>	(ARGUS Collab.)
AMELIN	95B	PL B356 595	D.V. Amelin <i>et al.</i>	(SERP, TBIL)
BERDNIKOV	94	PL B337 219	E.B. Berdnikov <i>et al.</i>	(SERP, TBIL)
ANTREASYAN	90	ZPHY C48 561	D. Antreasyan <i>et al.</i>	(Crystal Ball Collab.)
BEHREND	90C	ZPHY C46 583	H.J. Behrend <i>et al.</i>	(CELLO Collab.)
ANTIPOV	87	EPL 4 403	Y.M. Antipov <i>et al.</i>	(SERP, JINR, INRM+)
BELLINI	85	SJNP 41 781	D. Bellini <i>et al.</i>	
		Translated from YAF 41 1223.		
ARMSTRONG	82B	NP B202 1	T.A. Armstrong, B. Baccari	(AACH3, BARI, BONN+)
DAUM	81B	NP B182 269	C. Daum <i>et al.</i>	(AMST, CERN, CRAC, MPIM+)
EVANGELISTA	81	NP B178 197	C. Evangelista <i>et al.</i>	(BARI, BONN, CERN+)
		Also NP B186 594		
DAUM	80D	PL 898 285	C. Daum <i>et al.</i>	(AMST, CERN, CRAC, MPIM+), JP
BALTAY	77	PRL 39 591	C. Baltay, C.V. Curtis, M. Katelkar	(COLU) JP
ASCOLI	73	PR D7 669	G. Ascoli	(ILL, TNTO, GENO, HAMB, MILA+), JP
CRENNELL	70	PRL 24 781	D.J. Crennell <i>et al.</i>	(BNL)
ARMENISE	69	LNC 2 501	N. Armenise <i>et al.</i>	(BARI, BGNA, FIRZ)
BALTAY	68	PRL 20 887	C. Baltay <i>et al.</i>	(COLU, ROCH, RUTG, YALE) I
BARTSCH	68	NP B7 345	J. Bartsch <i>et al.</i>	(AACH, BERL, CERN) JP

$\phi(1680)$

$$I^G(J^{PC}) = 0^-(1^{--})$$

$\phi(1680)$ MASS

e^+e^- PRODUCTION

VALUE (MeV)	EVTS	DOCUMENT ID	TECN	COMMENT
1680±20 OUR ESTIMATE				
••• We do not use the following data for averages, fits, limits, etc. •••				
1641 \pm_{-18}^{+24}		ACHASOV	19	SND $e^+e^- \rightarrow \pi^+\pi^-\pi^0\eta$
1667 ± 5 ± 11	3k	1 IVANOV	19A	CMD3 1.59-2.007 $e^+e^- \rightarrow K^+K^-\eta$
1700 ± 23	2k	2 ACHASOV	18A	SND 1.3-2.0 $e^+e^- \rightarrow K_S^0 K_L^0 \pi^0$
1674 ± 12 ± 6	6.2k	3 LEES	14H	BABR $e^+e^- \rightarrow K_S^0 K_L^0 \gamma$
1733 ± 10 ± 10		4 LEES	12F	BABR 10.6 $e^+e^- \rightarrow \phi\pi^+\pi^-\gamma$
1689 ± 7 ± 10	4.8k	5 SHEN	09	BELL 10.6 $e^+e^- \rightarrow K^+K^-\pi^+\pi^-\gamma$
1709 ± 20 ± 43		6 AUBERT	08s	BABR 10.6 $e^+e^- \rightarrow$ hadrons
1623 ± 20	948	7 AKHMETSHIN	03	CMD2 1.05-1.38 $e^+e^- \rightarrow K_L^0 K_S^0$
~ 1500		8 ACHASOV	98H	RVUE $e^+e^- \rightarrow \pi^+\pi^-\pi^0, \omega\pi^+\pi^-, K^+K^-$
~ 1900		9 ACHASOV	98H	RVUE $e^+e^- \rightarrow K_S^0 K^\pm\pi^\mp$
1700 ± 20		10 CLEGG	94	RVUE $e^+e^- \rightarrow K^+K^-, K_S^0 K\pi$
1657 ± 27	367	BISELLO	91c	DM2 $e^+e^- \rightarrow K_S^0 K^\pm\pi^\mp$
1655 ± 17		11 BISELLO	88B	DM2 $e^+e^- \rightarrow K^+K^-$
1680 ± 10		12 BUON	82	DM1 $e^+e^- \rightarrow$ hadrons
1677 ± 12		13 MANE	82	DM1 $e^+e^- \rightarrow K_S^0 K\pi$

1 From a fit with coherent interference of the $\phi(1680)$ with a non-resonant contribution.
 2 Assuming the $K\bar{K}^*(892) + c.c.$ dynamics. Systematic uncertainties not estimated.
 3 Using a vector meson dominance model with contribution from $\phi(1020)$, $\phi(1680)$, and higher mass excitations of $\rho(770)$ and $\omega(782)$.
 4 Using events with $\pi\pi$ invariant mass less than 0.85 GeV.
 5 From a fit with two incoherent Breit-Wigners.
 6 From the simultaneous fit to the $K\bar{K}^*(892) + c.c.$ and $\phi\eta$ data from AUBERT 08s using the results of AUBERT 07AK.
 7 From the combined fit of AKHMETSHIN 03 and MANE 81 also including ρ, ω , and ϕ . Neither isospin nor flavor structure known.
 8 Using data from IVANOV 81, BARKOV 87, BISELLO 88b, DOLINSKY 91, and ANTONELLI 92.
 9 Using the data from BISELLO 91c.
 10 Using BISELLO 88b and MANE 82 data.
 11 From global fit including ρ, ω, ϕ and $\rho(1700)$ assume mass 1570 MeV and width 510 MeV for ρ radial excitation.
 12 From global fit of ρ, ω, ϕ and their radial excitations to channels $\omega\pi^+\pi^-, K^+K^-, K_S^0 K_L^0, K_S^0 K^\pm\pi^\mp$. Assume mass 1570 MeV and width 510 MeV for ρ radial excitations, mass 1570 and width 500 MeV for ω radial excitation.
 13 Fit to one channel only, neglecting interference with $\omega, \rho(1700)$.

Meson Particle Listings

$\phi(1680)$

PHOTOPRODUCTION

VALUE (MeV)	DOCUMENT ID	TECN	COMMENT
••• We do not use the following data for averages, fits, limits, etc. •••			
1753 ± 3	¹ LINK 02k	FOCS	20-160 $\gamma p \rightarrow K^+ K^- p$
1726 ± 22	¹ BUSENITZ 89	TPS	$\gamma p \rightarrow K^+ K^- X$
1760 ± 20	¹ ATKINSON 85c	OMEG	20-70 $\gamma p \rightarrow K^+ K^- X$
1690 ± 10	¹ ASTON 81f	OMEG	25-70 $\gamma p \rightarrow K^+ K^- X$

¹ We list here a state decaying into $K^+ K^-$ possibly different from $\phi(1680)$.

$p\bar{p}$ ANNIHILATION

VALUE (MeV)	DOCUMENT ID	TECN	COMMENT
••• We do not use the following data for averages, fits, limits, etc. •••			
1700 ± 8	¹ AMSLER 06	CBAR	0.9 $\bar{p} p \rightarrow K^+ K^- \pi^0$

¹ Could also be $\rho(1700)$.

$\phi(1680)$ WIDTH

e^+e^- PRODUCTION

VALUE (MeV)	EVTS	DOCUMENT ID	TECN	COMMENT
150 ± 50 OUR ESTIMATE This is only an educated guess; the error given is larger than the error on the average of the published values.				
••• We do not use the following data for averages, fits, limits, etc. •••				
103 + ²⁶ / ₋₂₄		ACHASOV 19	SND	$e^+e^- \rightarrow \pi^+ \pi^- \pi^0 \eta$
176 ± 23 ± 38	3k	¹ IVANOV 19A	CMD3	1.59-2.007 $e^+e^- \rightarrow K^+ K^- \eta$
300 ± 50	2k	² ACHASOV 18A	SND	1.3-2.0 $e^+e^- \rightarrow K_S^0 K_L^0 \pi^0$
165 ± 38 ± 70	6.2k	³ LEES 14H	BABR	$e^+e^- \rightarrow K_S^0 K_L^0 \gamma$
300 ± 15 ± 37		⁴ LEES 12F	BABR	10.6 $e^+e^- \rightarrow \phi \pi^+ \pi^- \gamma$
211 ± 14 ± 19	4.8k	⁵ SHEN 09	BELL	10.6 $e^+e^- \rightarrow K^+ K^- \pi^+ \pi^- \gamma$
322 ± 77 ± 160		⁶ AUBERT 08s	BABR	10.6 $e^+e^- \rightarrow$ hadrons
139 ± 60	948	⁷ AKHMETSHIN 03	CMD2	1.05-1.38 $e^+e^- \rightarrow K_L^0 K_S^0$
300 ± 60		⁸ CLEGG 94	RVUE	$e^+e^- \rightarrow K^+ K^-, K_S^0 K \pi$
146 ± 55	367	⁹ BISELLO 91c	DM2	$e^+e^- \rightarrow K_S^0 K^\pm \pi^\mp$
207 ± 45		⁹ BISELLO 88b	DM2	$e^+e^- \rightarrow K^+ K^-$
185 ± 22		¹⁰ BUON 82	DM1	$e^+e^- \rightarrow$ hadrons
102 ± 36		¹¹ MANE 82	DM1	$e^+e^- \rightarrow K_S^0 K \pi$

¹ From a fit with coherent interference of the $\phi(1680)$ with a non-resonant contribution.
² Assuming the $K \bar{K}^*(892) + c.c.$ dynamics. Systematic uncertainties not estimated.
³ Using a vector meson dominance model with contribution from $\phi(1020)$, $\phi(1680)$, and higher mass excitations of $\rho(770)$ and $\omega(782)$.
⁴ Using events with $\pi\pi$ invariant mass less than 0.85 GeV.
⁵ From a fit with two incoherent Breit-Wigners.
⁶ From the simultaneous fit to the $K \bar{K}^*(892) + c.c.$ and $\phi\eta$ data from AUBERT 08s using the results of AUBERT 07AK.
⁷ From the combined fit of AKHMETSHIN 03 and MANE 81 also including ρ, ω , and ϕ . Neither isospin nor flavor structure known.
⁸ Using BISELLO 88b and MANE 82 data.
⁹ From global fit including ρ, ω, ϕ and $\rho(1700)$
¹⁰ From global fit of ρ, ω, ϕ and their radial excitations to channels $\omega\pi^+\pi^-, K^+K^-, K_S^0 K_L^0, K_S^0 K^\pm \pi^\mp$. Assume mass 1570 MeV and width 510 MeV for ρ radial excitations, mass 1570 and width 500 MeV for ω radial excitation.
¹¹ Fit to one channel only, neglecting interference with $\omega, \rho(1700)$.

PHOTOPRODUCTION

VALUE (MeV)	DOCUMENT ID	TECN	COMMENT
••• We do not use the following data for averages, fits, limits, etc. •••			
122 ± 63	¹ LINK 02k	FOCS	20-160 $\gamma p \rightarrow K^+ K^- p$
121 ± 47	¹ BUSENITZ 89	TPS	$\gamma p \rightarrow K^+ K^- X$
80 ± 40	¹ ATKINSON 85c	OMEG	20-70 $\gamma p \rightarrow K^+ K^- X$
100 ± 40	¹ ASTON 81f	OMEG	25-70 $\gamma p \rightarrow K^+ K^- X$

¹ We list here a state decaying into $K^+ K^-$ possibly different from $\phi(1680)$.

$p\bar{p}$ ANNIHILATION

VALUE (MeV)	DOCUMENT ID	TECN	COMMENT
••• We do not use the following data for averages, fits, limits, etc. •••			
143 ± 24	¹ AMSLER 06	CBAR	0.9 $\bar{p} p \rightarrow K^+ K^- \pi^0$

¹ Could also be $\rho(1700)$.

$\phi(1680)$ DECAY MODES

Mode	Fraction (Γ_i/Γ)
Γ_1 $K \bar{K}^*(892) + c.c.$	seen
Γ_2 $K_S^0 K \pi$	seen
Γ_3 $K \bar{K}$	seen
Γ_4 $K_L^0 K_S^0$	
Γ_5 $e^+ e^-$	seen
Γ_6 $\omega \pi \pi$	not seen
Γ_7 $\phi \pi \pi$	
Γ_8 $K^+ K^- \pi^+ \pi^-$	seen
Γ_9 $\eta \phi$	seen
Γ_{10} $K^+ K^- \eta$	
Γ_{11} $\eta \gamma$	seen
Γ_{12} $K^+ K^- \pi^0$	

$\phi(1680) \Gamma(i)\Gamma(e^+e^-)/\Gamma(\text{total})$

This combination of a partial width with the partial width into e^+e^- and with the total width is obtained from the integrated cross section into channel (i) in e^+e^- annihilation. We list only data that have not been used to determine the partial width $\Gamma(i)$ or the branching ratio $\Gamma(i)/\text{total}$.

VALUE (eV)	EVTS	DOCUMENT ID	TECN	COMMENT
••• We do not use the following data for averages, fits, limits, etc. •••				
14.3 ± 2.4 ± 6.2	6.2k	¹ LEES	14H	BABR $e^+e^- \rightarrow K_S^0 K_L^0 \gamma$

¹ Using a vector meson dominance model with contribution from $\phi(1020)$, $\phi(1680)$, and higher mass excitations of $\rho(770)$ and $\omega(782)$.

VALUE (10^{-2} keV)	DOCUMENT ID	TECN	COMMENT
••• We do not use the following data for averages, fits, limits, etc. •••			
4.2 ± 0.2 ± 0.3	LEES	12F	BABR 10.6 $e^+e^- \rightarrow \phi \pi^+ \pi^- \gamma$

VALUE (eV)	EVTS	DOCUMENT ID	TECN	COMMENT
••• We do not use the following data for averages, fits, limits, etc. •••				
94 ± 13 ± 15	3k	¹ IVANOV 19A	CMD3	1.59-2.007 $e^+e^- \rightarrow K^+ K^- \eta$

¹ From a fit with coherent interference of the $\phi(1680)$ with a non-resonant contribution.

$\phi(1680) \Gamma(i)\Gamma(e^+e^-)/\Gamma^2(\text{total})$

This combination of a branching ratio into channel (i) and branching ratio into e^+e^- is directly measured and obtained from the cross section at the peak. We list only data that have not been used to determine the branching ratio into (i) or e^+e^- .

VALUE (units 10^{-6})	EVTS	DOCUMENT ID	TECN	COMMENT
••• We do not use the following data for averages, fits, limits, etc. •••				
0.131 ± 0.059	948	¹ AKHMETSHIN 03	CMD2	1.05-1.38 $e^+e^- \rightarrow K_L^0 K_S^0$

¹ From the combined fit of AKHMETSHIN 03 and MANE 81 also including ρ, ω , and ϕ . Neither isospin nor flavor structure known. Recalculated by us.

VALUE (units 10^{-6})	EVTS	DOCUMENT ID	TECN	COMMENT
••• We do not use the following data for averages, fits, limits, etc. •••				
1.15 ± 0.16 ± 0.01		¹ AUBERT 08s	BABR	10.6 $e^+e^- \rightarrow K \bar{K}^*(892) \gamma + c.c.$

¹ From the simultaneous fit to the $K \bar{K}^*(892) + c.c.$ and $\phi\eta$ data from AUBERT 08s using the results of AUBERT 07AK.
² Recalculated by us with the published value of $B(K \bar{K}^*(892) + c.c.) \times \Gamma(e^+e^-)$.

VALUE (units 10^{-7})	EVTS	DOCUMENT ID	TECN	COMMENT
••• We do not use the following data for averages, fits, limits, etc. •••				
1.86 ± 0.14 ± 0.21	4.8k	¹ SHEN 09	BELL	10.6 $e^+e^- \rightarrow K^+ K^- \pi^+ \pi^- \gamma$

¹ Multiplied by 3/2 to take into account the $\phi\pi^0\pi^0$ mode. Using $B(\phi \rightarrow K^+ K^-) = (49.2 \pm 0.6)\%$.

VALUE (units 10^{-7})	EVTS	DOCUMENT ID	TECN	COMMENT
••• We do not use the following data for averages, fits, limits, etc. •••				
5.64 + ^{1.74} / _{-1.80}		ACHASOV 19	SND	$e^+e^- \rightarrow \pi^+ \pi^- \pi^0 \eta$

¹ From a fit with coherent interference of the $\phi(1680)$ with a non-resonant contribution.
² From the simultaneous fit to the $K \bar{K}^*(892) + c.c.$ and $\phi\eta$ data from AUBERT 08s using the results of AUBERT 07AK.

$\phi(1680)$ BRANCHING RATIOS

VALUE	DOCUMENT ID	TECN	COMMENT
••• We do not use the following data for averages, fits, limits, etc. •••			
dominant	MANE 82	DM1	$e^+e^- \rightarrow K_S^0 K^\pm \pi^\mp$

VALUE	DOCUMENT ID	TECN	COMMENT
••• We do not use the following data for averages, fits, limits, etc. •••			
0.07 ± 0.01	BUON 82	DM1	e^+e^-

$\Gamma(\omega\pi\pi)/\Gamma(K\bar{K}^*(892) + c.c.)$				Γ_6/Γ_1
VALUE	DOCUMENT ID	TECN	COMMENT	
<0.10	BUON	82	DM1	e^+e^-

$\Gamma(\eta\phi)/\Gamma_{total}$				Γ_9/Γ	
VALUE	EVTS	DOCUMENT ID	TECN	COMMENT	
seen	35	¹ ACHASOV	14	SND	$1.15-2.00 e^+e^- \rightarrow \eta\gamma$

¹ From a phenomenological model based on vector meson dominance with $\rho(1450)$ and $\phi(1680)$ masses and widths from the PDG 12.

$\Gamma(\eta\phi)/\Gamma(K\bar{K}^*(892) + c.c.)$				Γ_9/Γ_1
VALUE	DOCUMENT ID	TECN	COMMENT	
≈ 0.37	¹ AUBERT	08s	BABR	$10.6 e^+e^- \rightarrow \text{hadrons}$

$\Gamma(\eta\gamma)/\Gamma_{total}$				Γ_{11}/Γ	
VALUE	EVTS	DOCUMENT ID	TECN	COMMENT	
seen	35	¹ ACHASOV	14	SND	$1.15-2.00 e^+e^- \rightarrow \eta\gamma$

¹ From a phenomenological model based on vector meson dominance with $\rho(1450)$ and $\phi(1680)$ masses and widths from the PDG 12.

$\phi(1680)$ REFERENCES

ACHASOV	19	PR D99 112004	M.N. Achasov et al.	(SND Collab.)
IVANOV	19A	PL B798 134946	V.L. Ivanov et al.	(CMD-3 Collab.)
ACHASOV	18A	PR D97 032011	M.N. Achasov et al.	(SND Collab.)
ACHASOV	14	PR D90 032002	M.N. Achasov et al.	(SND Collab.)
LEES	14H	PR D89 092002	J.P. Lees et al.	(BABAR Collab.)
LEES	12F	PR D86 012008	J.P. Lees et al.	(BABAR Collab.)
PDG	12	PR D86 010001	J. Beringer et al.	(PDG Collab.)
SHEN	09	PR D80 031101	C.P. Shen et al.	(BELLE Collab.)
AUBERT	08S	PR D77 092002	B. Aubert et al.	(BABAR Collab.)
AUBERT	07AK	PR D76 012008	B. Aubert et al.	(BABAR Collab.)
AMSLER	06	PL B639 165	C. Amisler et al.	(CBAR Collab.)
AKHMETSHIN	03	PL B551 27	R.R. Akhmetshin et al.	(Novosibirsk CMD-2 Collab.)
Also		PAN 65 1222	E.V. Anashkin, V.M. Aulchenko, R.R. Akhmetshin	
LINK	02K	PL B545 50	J.M. Link et al.	(FNAL FOCUS Collab.)
ACHASOV	98H	PR D57 4334	M.N. Achasov, A.A. Kozhevnikov	
CLEGG	94	ZPHY C62 455	A.B. Clegg, A. Donnachie	(LANC, MCHS)
ANTONELLI	92	ZPHY C56 15	A. Antonelli et al.	(DM2 Collab.)
BISELLO	91C	ZPHY C52 227	D. Bisello et al.	(DM2 Collab.)
DOLINSKY	91	PRPL 202 99	S.I. Dolinsky et al.	(NOVO)
BUSENITZ	89	PR D40 1	J.K. Busenitz et al.	(ILL, FNAL)
BISELLO	88B	ZPHY C39 13	D. Bisello et al.	(PADO, CLER, FRAS+)
BARKOV	87	JETPL 46 164	L.M. Barkov et al.	(NOVO)
ATKINSON	85C	ZPHY C27 233	M. Atkinson et al.	(BONN, CERN, GLAS+)
BUON	82	PL 118B 221	J. Buon et al.	(LALO, MONP)
MANE	82	PL 112B 178	F. Mane et al.	(LALO)
ASTON	81F	PL 104B 231	D. Aston	(BONN, CERN, EPOL, GLAS, LANC+)
IVANOV	81	PL 107B 297	P.M. Ivanov et al.	(NOVO)
MANE	81	PL 99B 261	F. Mane et al.	(ORSAY)

$\rho_3(1690)$

$$I^G(J^{PC}) = 1^+(3^{--})$$

$\rho_3(1690)$ MASS

VALUE (MeV)	DOCUMENT ID
1688.8 ± 2.1 OUR AVERAGE	Includes data from the 5 datablocks that follow this one.

2π MODE					
VALUE (MeV)	EVTS	DOCUMENT ID	TECN	CHG	COMMENT

The data in this block is included in the average printed for a previous datablock.

1686 ± 4 OUR AVERAGE					
1677 ± 14		EVANGELIS...	81	OMEG -	$12 \pi^- \rho \rightarrow 2\pi\rho$
1679 ± 11	476	BALTAY	78B	HBC 0	$15 \pi^+ \rho \rightarrow \pi^+ \pi^- n$
1678 ± 12	175	¹ ANTIPOV	77	CIBS 0	$25 \pi^- \rho \rightarrow \rho 3\pi$
1690 ± 7	600	¹ ENGLER	74	DBC 0	$6 \pi^+ n \rightarrow \pi^+ \pi^- p$
1693 ± 8		² GRAY	74	ASPK 0	$17 \pi^- \rho \rightarrow \pi^+ \pi^- n$
1678 ± 12		MATTHEWS	71c	DBC 0	$7 \pi^+ n$
$\bullet \bullet \bullet$ We do not use the following data for averages, fits, limits, etc. $\bullet \bullet \bullet$					
1734 ± 10		³ CORDEN	79	OMEG	$12-15 \pi^- \rho \rightarrow n2\pi$
1692 ± 12		^{2,4} ESTABROOKS	75	RVUE	$17 \pi^- \rho \rightarrow \pi^+ \pi^- n$
1737 ± 23		ARMENISE	70	DBC 0	$9 \pi^+ n$
1650 ± 35	122	BARTSCH	70B	HBC +	$8 \pi^+ \rho \rightarrow N2\pi$
1687 ± 21		STUNTEBECK	70	HDBC 0	$8 \pi^- \rho, 5.4 \pi^+ d$
1683 ± 13		ARMENISE	68	DBC 0	$5.1 \pi^+ d$
1670 ± 30		GOLDBERG	65	HBC 0	$6 \pi^+ d, 8 \pi^- p$

¹ Mass errors enlarged by us to Γ/\sqrt{N} ; see the note with the $K^*(892)$ mass.
² Uses same data as HYAMS 75.
³ From a phase shift solution containing a $f_2'(1525)$ width two times larger than the $K\bar{K}$ result.
⁴ From phase-shift analysis. Error takes account of spread of different phase-shift solutions.

$K\bar{K}$ AND $K\bar{K}\pi$ MODES					
VALUE (MeV)	EVTS	DOCUMENT ID	TECN	CHG	COMMENT

The data in this block is included in the average printed for a previous datablock.

1696 ± 4 OUR AVERAGE					
1699 ± 5		ALPER	80	CNTR 0	$62 \pi^- \rho \rightarrow K^+ K^- n$
1698 ± 12	6k	^{5,6} MARTIN	78D	SPEC	$10 \pi \rho \rightarrow K_S^0 K^- \rho$
1692 ± 6		BLUM	75	ASPK 0	$18.4 \pi^- \rho \rightarrow nK^+ K^-$
1690 ± 16		ADERHOLZ	69	HBC +	$8 \pi^+ \rho \rightarrow K\bar{K}\pi$
$\bullet \bullet \bullet$ We do not use the following data for averages, fits, limits, etc. $\bullet \bullet \bullet$					
1694 ± 8		⁷ COSTA	80	OMEG	$10 \pi^- \rho \rightarrow K^+ K^- n$
$\bullet \bullet \bullet$ We do not use the following data for averages, fits, limits, etc. $\bullet \bullet \bullet$					
⁵ From a fit to $J^P = 3^-$ partial wave. ⁶ Systematic error on mass scale subtracted. ⁷ They cannot distinguish between $\rho_3(1690)$ and $\omega_3(1670)$.					

$(4\pi)^\pm$ MODE					
VALUE (MeV)	EVTS	DOCUMENT ID	TECN	CHG	COMMENT

The data in this block is included in the average printed for a previous datablock.

1686 ± 5 OUR AVERAGE					
1694 ± 6		⁸ EVANGELIS...	81	OMEG -	$12 \pi^- \rho \rightarrow p4\pi$
1665 ± 15	177	BALTAY	78B	HBC +	$15 \pi^+ \rho \rightarrow p4\pi$
1670 ± 10		THOMPSON	74	HBC +	$13 \pi^+ \rho$
1687 ± 20		CASON	73	HBC -	$8,18.5 \pi^- \rho$
1685 ± 14		⁹ CASON	73	HBC -	$8,18.5 \pi^- \rho$
1680 ± 40	144	BARTSCH	70B	HBC +	$8 \pi^+ \rho \rightarrow N4\pi$
1689 ± 20	102	⁹ BARTSCH	70B	HBC +	$8 \pi^+ \rho \rightarrow N2\rho$
1705 ± 21		CASO	70	HBC -	$11.2 \pi^- \rho \rightarrow n\rho 2\pi$
$\bullet \bullet \bullet$ We do not use the following data for averages, fits, limits, etc. $\bullet \bullet \bullet$					
1718 ± 10		¹⁰ EVANGELIS...	81	OMEG -	$12 \pi^- \rho \rightarrow p4\pi$
1673 ± 9		¹¹ EVANGELIS...	81	OMEG -	$12 \pi^- \rho \rightarrow p4\pi$
1733 ± 9	66	⁹ KLIGER	74	HBC -	$4.5 \pi^- \rho \rightarrow p4\pi$
1630 ± 15		HOLMES	72	HBC +	$10-12 K^+ \rho$
1720 ± 15		BALTAY	68	HBC +	$7, 8.5 \pi^+ \rho$

⁸ From $\rho^- \rho^0$ mode, not independent of the other two EVANGELISTA 81 entries.
⁹ From $\rho^\pm \rho^0$ mode.
¹⁰ From $a_2(1320)^- \pi^0$ mode, not independent of the other two EVANGELISTA 81 entries.
¹¹ From $a_2(1320)^0 \pi^-$ mode, not independent of the other two EVANGELISTA 81 entries.

$\omega\pi$ MODE					
VALUE (MeV)	EVTS	DOCUMENT ID	TECN	CHG	COMMENT

The data in this block is included in the average printed for a previous datablock.

1681 ± 7 OUR AVERAGE					
1670 ± 25		¹² ALDE	95	GAM2	$38 \pi^- \rho \rightarrow \omega\pi^0 n$
1690 ± 15		EVANGELIS...	81	OMEG -	$12 \pi^- \rho \rightarrow \omega\pi\rho$
1666 ± 14		GESSAROLI	77	HBC	$11 \pi^- \rho \rightarrow \omega\pi\rho$
1686 ± 9		THOMPSON	74	HBC +	$13 \pi^+ \rho$
$\bullet \bullet \bullet$ We do not use the following data for averages, fits, limits, etc. $\bullet \bullet \bullet$					
1654 ± 24		BARNHAM	70	HBC +	$10 K^+ \rho \rightarrow \omega\pi X$
¹² Supersedes ALDE 92c.					

$\eta\pi^+ \pi^-$ MODE					
(For difficulties with MMS experiments, see the $a_2(1320)$ mini-review in the 1973 edition.)					
VALUE (MeV)	EVTS	DOCUMENT ID	TECN	CHG	COMMENT

The data in this block is included in the average printed for a previous datablock.

1682 ± 12 OUR AVERAGE					
1685 ± 10 ± 20		AMELIN	00	VES	$37 \pi^- \rho \rightarrow \eta\pi^+ \pi^- n$
1680 ± 15		FUKUI	88	SPEC 0	$8.95 \pi^- \rho \rightarrow \eta\pi^+ \pi^- n$
$\bullet \bullet \bullet$ We do not use the following data for averages, fits, limits, etc. $\bullet \bullet \bullet$					
1700 ± 47		¹³ ANDERSON	69	MMS -	$16 \pi^- \rho$ backward
1632 ± 15		^{13,14} FOCACCI	66	MMS -	$7-12 \pi^- \rho \rightarrow pMM$
1700 ± 15		^{13,14} FOCACCI	66	MMS -	$7-12 \pi^- \rho \rightarrow pMM$
1748 ± 15		^{13,14} FOCACCI	66	MMS -	$7-12 \pi^- \rho \rightarrow pMM$

¹³ Seen in 2.5-3 GeV/c $\bar{p}p$. $2\pi^+ 2\pi^-$, with 0, 1, $2\pi^+ \pi^-$ pairs in ρ band not seen by OREN 74 (2.3 GeV/c $\bar{p}p$) with more statistics. (Jan. 1976)
¹⁴ Not seen by BOWEN 72.

$\rho_3(1690)$ WIDTH

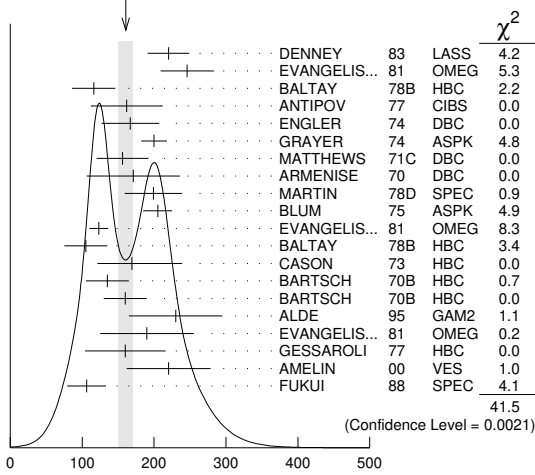
$2\pi, K\bar{K},$ AND $K\bar{K}\pi$ MODES					
VALUE (MeV)	EVTS	DOCUMENT ID	TECN	CHG	COMMENT

161 ± 10 OUR AVERAGE Includes data from the 5 datablocks that follow this one. Error includes scale factor of 1.5. See the ideogram below.

Meson Particle Listings

$\rho_3(1690)$

WEIGHTED AVERAGE
161±10 (Error scaled by 1.5)



$\rho_3(1690)$ width, 2π , $K\bar{K}$, and $K\bar{K}\pi$ modes (MeV)

2π MODE

VALUE (MeV)	EVTs	DOCUMENT ID	TECN	CHG	COMMENT
-------------	------	-------------	------	-----	---------

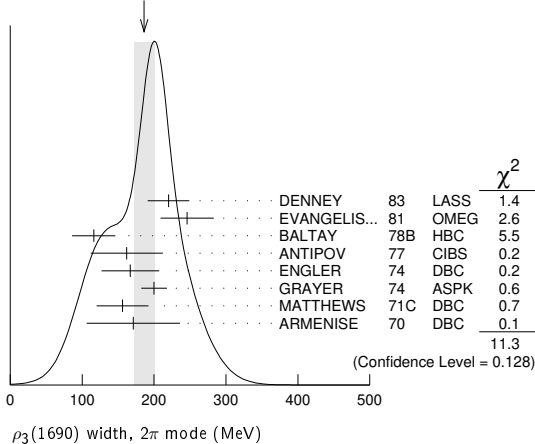
The data in this block is included in the average printed for a previous datablock.

186±14 OUR AVERAGE Error includes scale factor of 1.3. See the ideogram below.

220±29		DENNEY	83	LASS	10 $\pi^+ N$
246±37		EVANGELIS...	81	OMEG	12 $\pi^- p \rightarrow 2\pi p$
116±30	476	BALTAY	78B	HBC	15 $\pi^+ p \rightarrow \pi^+ \pi^- n$
162±5.0	175	15 ANTIPOV	77	CIBS	0 25 $\pi^- p \rightarrow p3\pi$
167±4.0	600	ENGLER	74	DBC	0 6 $\pi^+ n \rightarrow \pi^+ \pi^- p$
200±18		16 GRAYER	74	ASPK	0 17 $\pi^- p \rightarrow \pi^+ \pi^- n$
156±36		MATTHEWS	71C	DBC	0 7 $\pi^+ n$
171±65		ARMENISE	70	DBC	0 9 $\pi^+ d$
••• We do not use the following data for averages, fits, limits, etc. •••					
322±35		17 CORDEN	79	OMEG	12-15 $\pi^- p \rightarrow n2\pi$
240±30		16,18 ESTABROOKS	75	RVUE	17 $\pi^- p \rightarrow \pi^+ \pi^- n$
180±30	122	BARTSCH	70B	HBC	+ 8 $\pi^+ p \rightarrow N2\pi$
267±72		STUNTEBECK	70	HDDB	0 8 $\pi^- p, 5.4 \pi^+ d$
188±49		ARMENISE	68	DBC	0 5.1 $\pi^+ d$
180±40		GOLDBERG	65	HBC	0 6 $\pi^+ d, 8 \pi^- p$

15 Width errors enlarged by us to $4\Gamma/\sqrt{N}$; see the note with the $K^*(892)$ mass.
 16 Uses same data as HYAMS 75 and BECKER 79.
 17 From a phase shift solution containing a $f_2'(1525)$ width two times larger than the $K\bar{K}$ result.
 18 From phase-shift analysis. Error takes account of spread of different phase-shift solutions.

WEIGHTED AVERAGE
186±14 (Error scaled by 1.3)



$\rho_3(1690)$ width, 2π mode (MeV)

$K\bar{K}$ AND $K\bar{K}\pi$ MODES

VALUE (MeV)	EVTs	DOCUMENT ID	TECN	CHG	COMMENT
-------------	------	-------------	------	-----	---------

The data in this block is included in the average printed for a previous datablock.

204±18 OUR AVERAGE

199±40	6000	19 MARTIN	78D	SPEC	10 $\pi p \rightarrow K_S^0 K^- p$
205±20		BLUM	75	ASPK	0 18.4 $\pi^- p \rightarrow nK^+ K^-$

••• We do not use the following data for averages, fits, limits, etc. •••

219±4		ALPER	80	CNTR	0 62 $\pi^- p \rightarrow K^+ K^- n$
186±11		20 COSTA	80	OMEG	10 $\pi^- p \rightarrow K^+ K^- n$
112±60		ADERHOLZ	69	HBC	+ 8 $\pi^+ p \rightarrow K\bar{K}\pi$

19 From a fit to $J^P = 3^-$ partial wave.
 20 They cannot distinguish between $\rho_3(1690)$ and $\omega_3(1670)$.

(4π) $^\pm$ MODE

VALUE (MeV)	EVTs	DOCUMENT ID	TECN	CHG	COMMENT
-------------	------	-------------	------	-----	---------

The data in this block is included in the average printed for a previous datablock.

129±10 OUR AVERAGE

123±13		21 EVANGELIS...	81	OMEG	- 12 $\pi^- p \rightarrow p4\pi$
105±30	177	BALTAY	78B	HBC	+ 15 $\pi^+ p \rightarrow p4\pi$
169±70		CASON	73	HBC	- 8,18.5 $\pi^- p$
135±30	144	BARTSCH	70B	HBC	+ 8 $\pi^+ p \rightarrow N4\pi$
160±30	102	BARTSCH	70B	HBC	+ 8 $\pi^+ p \rightarrow N2\rho$

••• We do not use the following data for averages, fits, limits, etc. •••

230±28		22 EVANGELIS...	81	OMEG	- 12 $\pi^- p \rightarrow p4\pi$
184±33		23 EVANGELIS...	81	OMEG	- 12 $\pi^- p \rightarrow p4\pi$
150	66	24 KLIGER	74	HBC	- 4.5 $\pi^- p \rightarrow p4\pi$
106±25		THOMPSON	74	HBC	+ 13 $\pi^+ p$
125±83		24 CASON	73	HBC	- 8,18.5 $\pi^- p$
130±30		HOLMES	72	HBC	+ 10-12 $K^+ p$
180±30	90	24 BARTSCH	70B	HBC	+ 8 $\pi^+ p \rightarrow Na_2\pi$
100±35		BALTAY	68	HBC	+ 7, 8.5 $\pi^+ p$

21 From $\rho^- \rho^0$ mode, not independent of the other two EVANGELISTA 81 entries.
 22 From $a_2(1320) \pi^0$ mode, not independent of the other two EVANGELISTA 81 entries.
 23 From $a_2(1320) \pi^-$ mode, not independent of the other two EVANGELISTA 81 entries.
 24 From $\rho^\pm \rho^0$ mode.

$\omega\pi$ MODE

VALUE (MeV)	DOCUMENT ID	TECN	CHG	COMMENT
-------------	-------------	------	-----	---------

The data in this block is included in the average printed for a previous datablock.

190±40 OUR AVERAGE

230±65	25	ALDE	95	GAM2	38 $\pi^- p \rightarrow \omega\pi^0 n$
190±65		EVANGELIS...	81	OMEG	- 12 $\pi^- p \rightarrow \omega\pi p$
160±56		GESSAROLI	77	HBC	11 $\pi^- p \rightarrow \omega\pi p$
••• We do not use the following data for averages, fits, limits, etc. •••					
89±25		THOMPSON	74	HBC	+ 13 $\pi^+ p$
130±73		BARNHAM	70	HBC	+ 10 $K^+ p \rightarrow \omega\pi X$

25 Supersedes ALDE 92c.

$\eta\pi^+\pi^-$ MODE

(For difficulties with MMS experiments, see the $a_2(1320)$ mini-review in the 1973 edition.)

VALUE (MeV)	DOCUMENT ID	TECN	CHG	COMMENT
-------------	-------------	------	-----	---------

The data in this block is included in the average printed for a previous datablock.

126±40 OUR AVERAGE Error includes scale factor of 1.8.

220±30±50		AMELIN	00	VES	37 $\pi^- p \rightarrow \eta\pi^+\pi^- n$
106±27		FUKUI	88	SPEC	0 8.95 $\pi^- p \rightarrow \eta\pi^+\pi^- n$
••• We do not use the following data for averages, fits, limits, etc. •••					
195		26 ANDERSON	69	MMS	- 16 $\pi^- p$ backward
< 21	26,27	FOCACCI	66	MMS	- 7-12 $\pi^- p \rightarrow pMM$
< 30	26,27	FOCACCI	66	MMS	- 7-12 $\pi^- p \rightarrow pMM$
< 38	26,27	FOCACCI	66	MMS	- 7-12 $\pi^- p \rightarrow pMM$

26 Seen in 2.5-3 GeV/c $\bar{p}p$. $2\pi^+2\pi^-$, with 0, 1, 2 $\pi^+\pi^-$ pairs in ρ^0 band not seen by OREN 74 (2.3 GeV/c $\bar{p}p$) with more statistics. (Jan. 1979)
 27 Not seen by BOWEN 72.

$\rho_3(1690)$ DECAY MODES

Mode	Fraction (Γ_i/Γ)	Scale factor
Γ_1 4π	(71.1 ± 1.9) %	
Γ_2 $\pi^\pm \pi^+ \pi^- \pi^0$	(67 ± 22) %	
Γ_3 $\omega\pi$	(16 ± 6) %	
Γ_4 $\pi\pi$	(23.6 ± 1.3) %	
Γ_5 $K\bar{K}\pi$	(3.8 ± 1.2) %	
Γ_6 $K\bar{K}$	(1.58 ± 0.26) %	1.2
Γ_7 $\eta\pi^+\pi^-$	seen	
Γ_8 $\rho(770)\eta$	seen	
Γ_9 $\pi\pi\rho$	seen	
Γ_{10} $a_2(1320)\pi$	seen	
Γ_{11} $\rho\rho$	seen	
Γ_{12} $\phi\pi$		
Γ_{13} $\eta\pi$		
Γ_{14} $\pi^\pm 2\pi^+ 2\pi^- \pi^0$		

CONSTRAINED FIT INFORMATION

An overall fit to 5 branching ratios uses 10 measurements and one constraint to determine 4 parameters. The overall fit has a $\chi^2 = 14.7$ for 7 degrees of freedom.

The following *off-diagonal* array elements are the correlation coefficients $\langle \delta x_i \delta x_j \rangle / (\delta x_i \delta x_j)$, in percent, from the fit to the branching fractions, $x_i \equiv \Gamma_i / \Gamma_{\text{total}}$. The fit constrains the x_i whose labels appear in this array to sum to one.

x_4	-77		
x_5	-74	17	
x_6	-15	2	0
	x_1	x_4	x_5

$\rho_3(1690)$ BRANCHING RATIOS

$\Gamma(\pi\pi) / \Gamma_{\text{total}}$	DOCUMENT ID	TECN	CHG	COMMENT	Γ_4 / Γ
0.236 ± 0.013 OUR FIT					
0.243 ± 0.013 OUR AVERAGE					

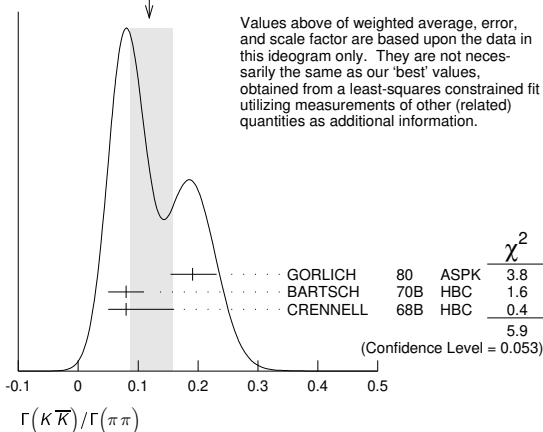
0.259 ^{+0.018} _{-0.019}	BECKER	79	ASPK	0	17 $\pi^- \rho$ polarized
0.23 ± 0.02	CORDEN	79	OMEG		12-15 $\pi^- \rho \rightarrow n2\pi$
0.22 ± 0.04	²⁸ MATTHEWS	71c	HDBC	0	7 $\pi^+ n \rightarrow \pi^- \rho$
• • • We do not use the following data for averages, fits, limits, etc. • • •					
0.245 ± 0.006	²⁹ ESTABROOKS	75	RVUE		17 $\pi^- \rho \rightarrow \pi^+ \pi^- n$
²⁸ One-pion-exchange model used in this estimation.					
²⁹ From phase-shift analysis of HYAMS 75 data.					

$\Gamma(\pi\pi) / \Gamma(\pi^+ \pi^+ \pi^- \pi^0)$	DOCUMENT ID	TECN	CHG	COMMENT	Γ_4 / Γ_2
0.35 ± 0.11	CASON	73	HBC	-	8,18.5 $\pi^- \rho$
• • • We do not use the following data for averages, fits, limits, etc. • • •					
<0.2	HOLMES	72	HBC	+	10-12 $K^+ \rho$
<0.12	BALLAM	71b	HBC	-	16 $\pi^- \rho$

$\Gamma(\pi\pi) / \Gamma(4\pi)$	DOCUMENT ID	TECN	CHG	COMMENT	Γ_4 / Γ_1
0.332 ± 0.026 OUR FIT	Error includes scale factor of 1.1.				
0.30 ± 0.10	BALTAY	78b	HBC	0	15 $\pi^+ \rho \rightarrow p4\pi$

$\Gamma(K\bar{K}) / \Gamma(\pi\pi)$	DOCUMENT ID	TECN	CHG	COMMENT	Γ_6 / Γ_4
0.067 ± 0.011 OUR FIT	Error includes scale factor of 1.2.				
0.118 ± 0.040 0.032 OUR AVERAGE	Error includes scale factor of 1.7. See the ideogram below.				
0.191 ^{+0.040} _{-0.037}	GORLICH	80	ASPK	0	17,18 $\pi^- \rho$ polarized
0.08 ± 0.03	BARTSCH	70b	HBC	+	8 $\pi^+ \rho$
0.08 ± 0.08 -0.03	CRENNELL	68b	HBC		6.0 $\pi^- \rho$

WEIGHTED AVERAGE
0.118±0.040-0.032 (Error scaled by 1.7)



$\Gamma(K\bar{K}\pi) / \Gamma(\pi\pi)$	DOCUMENT ID	TECN	CHG	COMMENT	Γ_5 / Γ_4
0.16 ± 0.05 OUR FIT					
0.16 ± 0.05	³⁰ BARTSCH	70b	HBC	+	8 $\pi^+ \rho$

³⁰ Increased by us to correspond to $B(\rho_3(1690) \rightarrow \pi\pi) = 0.24$.

$[\Gamma(\pi\pi\rho) + \Gamma(a_2(1320)\pi) + \Gamma(\rho\rho)] / \Gamma(\pi^+ \pi^+ \pi^- \pi^0)$	DOCUMENT ID	TECN	CHG	COMMENT	$(\Gamma_9 + \Gamma_{10} + \Gamma_{11}) / \Gamma_2$
0.94 ± 0.09 OUR AVERAGE					
0.96 ± 0.21	BALTAY	78b	HBC	+	15 $\pi^+ \rho \rightarrow p4\pi$
0.88 ± 0.15	BALLAM	71b	HBC	-	16 $\pi^- \rho$
1 ± 0.15	BARTSCH	70b	HBC	+	8 $\pi^+ \rho$
consistent with 1					
	CASO	68	HBC	-	11 $\pi^- \rho$

$\Gamma(\rho\rho) / \Gamma(\pi^+ \pi^+ \pi^- \pi^0)$	DOCUMENT ID	TECN	CHG	COMMENT	Γ_{11} / Γ_2
0.12 ± 0.11	BALTAY	78b	HBC	+	15 $\pi^+ \rho \rightarrow p4\pi$
0.56	KLIGER	74	HBC	-	4.5 $\pi^- \rho \rightarrow p4\pi$
0.13 ± 0.09	³¹ THOMPSON	74	HBC	+	13 $\pi^+ \rho$
0.7 ± 0.15	BARTSCH	70b	HBC	+	8 $\pi^+ \rho$
³¹ $\rho\rho$ and $a_2(1320)\pi$ modes are indistinguishable.					

$\Gamma(\rho\rho) / [\Gamma(\pi\pi\rho) + \Gamma(a_2(1320)\pi) + \Gamma(\rho\rho)]$	DOCUMENT ID	TECN	CHG	COMMENT	$\Gamma_{11} / (\Gamma_9 + \Gamma_{10} + \Gamma_{11})$
0.48 ± 0.16	CASO	68	HBC	-	11 $\pi^- \rho$

$\Gamma(a_2(1320)\pi) / \Gamma(\pi^+ \pi^+ \pi^- \pi^0)$	DOCUMENT ID	TECN	CHG	COMMENT	Γ_{10} / Γ_2
0.66 ± 0.08	BALTAY	78b	HBC	+	15 $\pi^+ \rho \rightarrow p4\pi$
0.36 ± 0.14	³² THOMPSON	74	HBC	+	13 $\pi^+ \rho$
not seen	CASON	73	HBC	-	8,18.5 $\pi^- \rho$
0.6 ± 0.15	BARTSCH	70b	HBC	+	8 $\pi^+ \rho$
0.6	BALTAY	68	HBC	+	7,8.5 $\pi^+ \rho$
³² $\rho\rho$ and $a_2(1320)\pi$ modes are indistinguishable.					

$\Gamma(\omega\pi) / \Gamma(\pi^+ \pi^+ \pi^- \pi^0)$	DOCUMENT ID	TECN	CHG	COMMENT	Γ_3 / Γ_2	
0.23 ± 0.05 OUR AVERAGE	Error includes scale factor of 1.2.					
0.33 ± 0.07	THOMPSON	74	HBC	+	13 $\pi^+ \rho$	
0.12 ± 0.07	BALLAM	71b	HBC	-	16 $\pi^- \rho$	
0.25 ± 0.10	BALTAY	68	HBC	+	7,8.5 $\pi^+ \rho$	
0.25 ± 0.10	JOHNSTON	68	HBC	-	7.0 $\pi^- \rho$	
• • • We do not use the following data for averages, fits, limits, etc. • • •						
<0.11	95	BALTAY	78b	HBC	+	15 $\pi^+ \rho \rightarrow p4\pi$
<0.09	KLIGER	74	HBC	-	4.5 $\pi^- \rho \rightarrow p4\pi$	

$\Gamma(\phi\pi) / \Gamma(\pi^+ \pi^+ \pi^- \pi^0)$	DOCUMENT ID	TECN	CHG	COMMENT	Γ_{12} / Γ_2
<0.11	BALTAY	68	HBC	+	7,8.5 $\pi^+ \rho$

$\Gamma(\pi^+ 2\pi^+ 2\pi^- \pi^0) / \Gamma(\pi^+ \pi^+ \pi^- \pi^0)$	DOCUMENT ID	TECN	CHG	COMMENT	Γ_{14} / Γ_2
<0.15	BALTAY	68	HBC	+	7,8.5 $\pi^+ \rho$

$\Gamma(\eta\pi) / \Gamma(\pi^+ \pi^+ \pi^- \pi^0)$	DOCUMENT ID	TECN	CHG	COMMENT	Γ_{13} / Γ_2
<0.02	THOMPSON	74	HBC	+	13 $\pi^+ \rho$

$\Gamma(K\bar{K}) / \Gamma_{\text{total}}$	DOCUMENT ID	TECN	CHG	COMMENT	Γ_6 / Γ
0.0158 ± 0.0026 OUR FIT	Error includes scale factor of 1.2.				
0.0130 ± 0.0024 OUR AVERAGE					
0.013 ± 0.003	COSTA	80	OMEG	0	10 $\pi^- \rho \rightarrow K^+ K^- n$
0.013 ± 0.004	³³ MARTIN	78b	SPEC	-	10 $\pi \rho \rightarrow K_S^0 K^- \rho$
³³ From $(\Gamma_4 \Gamma_6)^{1/2} = 0.056 \pm 0.034$ assuming $B(\rho_3(1690) \rightarrow \pi\pi) = 0.24$.					

$\Gamma(\omega\pi) / [\Gamma(\omega\pi) + \Gamma(\rho\rho)]$	DOCUMENT ID	TECN	CHG	COMMENT	$\Gamma_3 / (\Gamma_3 + \Gamma_{11})$
0.22 ± 0.08	CASON	73	HBC	-	8,18.5 $\pi^- \rho$

$\Gamma(\eta\pi^+ \pi^-) / \Gamma_{\text{total}}$	DOCUMENT ID	TECN	COMMENT	Γ_7 / Γ
seen	FUKUI	88	SPEC	8.95 $\pi^- \rho \rightarrow \eta\pi^+ \pi^- n$

$\Gamma(a_2(1320)\pi) / \Gamma(\rho(770)\eta)$	DOCUMENT ID	TECN	COMMENT	Γ_{10} / Γ_8
5.5 ± 2.0	AMELIN	00	VES	37 $\pi^- \rho \rightarrow \eta\pi^+ \pi^- n$

Meson Particle Listings

 $\rho_3(1690)$, $\rho(1700)$ $\rho_3(1690)$ REFERENCES

AMELIN	00	NP A668 83	D. Amelin et al.	(VES Collab.)
ALDE	95	ZPHY C66 379	D.M. Alde et al.	(GAMS Collab.) JP
ALDE	92C	ZPHY C54 553	D.M. Alde et al.	(BELG, SERP, KEK, LANL+)
FUKUI	88	PL B202 441	S. Fukui et al.	(SUGI, NAGO, KEK, KYOT+)
DENNEY	83	PR D28 2726	D.L. Denney et al.	(IOWA, MICH)
EVANGELIS...	81	NP B178 197	C. Evangelista et al.	(BARI, BONN, CERN+)
ALPER	80	PL 94B 422	B. Alper et al.	(AMST, CERN, CRAC, MPIM+)
COSTA	80	NP B175 402	G. Costa et al.	(BARI, BONN, CERN, GLAS+)
GÖRGLICH	80	NP B174 16	L. Gorlich et al.	(CRAC, MPIM, CERN+)
BECKER	79	NP B151 46	H. Becker et al.	(MPIM, CERN, ZEEM, CRAC)
CORDEN	79	NP B157 250	M.J. Corden et al.	(BIRM, RHEL, TEHA+)
BALTAY	78B	PR D17 62	C. Baltay et al.	(COLU, BING)
MARTIN	78B	NP B140 158	A.D. Martin et al.	(DURH, GEVA)
MARTIN	78D	PL 74B 417	A.D. Martin et al.	(DURH, GEVA)
ANTIPOV	77	NP B119 45	Y.M. Antipov et al.	(SERP, GEVA)
GESSAROLI	77	NP B126 382	R. Gessaroli et al.	(BGNA, FIRZ, GENO+)
BLUM	75	PL 57B 403	W. Blum et al.	(CERN, MPIM) JP
ESTABROOKS	75	NP B95 322	P.G. Estabrooks, A.D. Martin	(DURH)
HYAMS	75	NP B100 205	B.D. Hyams et al.	(CERN, MPIM)
ENGLER	74	PR D10 2070	A. Engler et al.	(CMU, CASE)
GRAVER	74	NP B75 189	G. Grayer et al.	(CERN, MPIM)
KLIGER	74	SJNP 19 428	G.K. Kliger et al.	(ITEP)
Translated from YAF 19 839.				
OREN	74	NP B71 189	Y. Oren et al.	(ANL, OXF)
THOMPSON	74	NP B69 220	G. Thompson et al.	(PURD)
CASON	73	PR D7 1971	N.M. Cason et al.	(NDAM)
BOWEN	72	PRL 29 890	D.R. Bowen et al.	(NEAS, STON)
HOLMES	72	PR D6 3336	R. Holmes et al.	(ROCH)
BALLAM	71B	PR D3 2606	J. Ballam et al.	(SLAC)
MATTHEWS	71C	NP B33 1	J.A.J. Matthews et al.	(TNTO, WISC) JP
ARMENISE	70	LNC 4 199	N. Armenise et al.	(BARI, BGNA, FIRZ)
BARNHAM	70	PRL 24 1083	K.W.J. Barnham et al.	(BIRM)
BARTSCH	70B	NP B22 109	J. Bartsch et al.	(AACH, BERL, CERN)
CASO	70	LNC 3 707	C. Caso et al.	(GENO, HAMB, MILA, SAACL)
STUNTEBECK	70	PL 32B 391	P.H. Stuntebeck et al.	(NDAM)
ADERHOLZ	69	NP B11 259	M. Aderholz et al.	(AACH3, BERL, CERN+)
ANDERSON	69	PRL 22 1390	E.W. Anderson et al.	(BNL, CMU)
ARMENISE	68	NC 54A 999	N. Armenise et al.	(BARI, BGNA, FIRZ+)
BALTAY	68	PRL 20 887	C. Baltay et al.	(COLU, ROCH, RUTG, YALE)
CASO	68	NC 54A 983	C. Caso et al.	(GENO, HAMB, MILA, SAACL)
CRENNELL	68B	PL 28B 136	D.J. Crennell et al.	(BNL)
JOHNSTON	68	PRL 20 1414	T.F. Johnston et al.	(TNTO, WISC) JP
FOCACCI	66	PRL 17 890	M.N. Focacci et al.	(CERN)
GOLDBERG	65	PL 17 354	M. Goldberg et al.	(CERN, EPOL, ORSAY+)

 $\rho(1700)$

$$J^G(J^{PC}) = 1^+(1^{--})$$

THE $\rho(1450)$ AND THE $\rho(1700)$

Updated September 2019 by S. Eidelman (Novosibirsk), C. Hanhart (Juelich) and G. Venanzoni (Pisa).

In our 1988 edition, we replaced the $\rho(1600)$ entry with two new ones, the $\rho(1450)$ and the $\rho(1700)$, because there was emerging evidence that the 1600-MeV region actually contains two ρ -like resonances. Erkal [1] had pointed out this possibility with a theoretical analysis on the consistency of 2π and 4π electromagnetic form factors and the $\pi\pi$ scattering length. Donnachie [2], with a full analysis of data on the 2π and 4π final states in e^+e^- annihilation and photoproduction reactions, had also argued that in order to obtain a consistent picture, two resonances were necessary. The existence of $\rho(1450)$ was supported by the analysis of $\eta\rho^0$ mass spectra obtained in photoproduction and e^+e^- annihilation [3], as well as that of $e^+e^- \rightarrow \omega\pi$ [4].

The analysis of [2] was further extended by [5,6] to include new data on 4π -systems produced in e^+e^- annihilation, and in τ -decays (τ decays to 4π , and e^+e^- annihilation to 4π can be related by the Conserved Vector Current assumption). These systems were successfully analyzed using interfering contributions from two ρ -like states, and from the tail of the $\rho(770)$ decaying into two-body states. While specific conclusions on $\rho(1450) \rightarrow 4\pi$ were obtained, little could be said about the $\rho(1700)$.

Independent evidence for two 1^- states is provided by [7] in 4π electroproduction at $\langle Q^2 \rangle = 1$ (GeV/c)², and by [8] in a high-statistics sample of the $\eta\pi\pi$ system in π^-p charge exchange.

This scenario with two overlapping resonances is supported by other data. Bisello [9] measured the pion form factor in the interval 1.35–2.4 GeV, and observed a deep minimum around 1.6 GeV. The best fit was obtained with the hypothesis of ρ -like resonances at 1420 and 1770 MeV, with widths of about 250 MeV. Antonelli [10] found that the $e^+e^- \rightarrow \eta\pi^+\pi^-$ cross section is better fitted with two fully interfering Breit-Wigners, with parameters in fair agreement with those of [2] and [9]. These results can be considered as a confirmation of the $\rho(1450)$.

Decisive evidence for the $\pi\pi$ decay mode of both $\rho(1450)$ and $\rho(1700)$ comes from $\bar{p}p$ annihilation at rest [11]. It has been shown that these resonances also possess a $K\bar{K}$ decay mode [12–14]. High-statistics studies of the decays $\tau \rightarrow \pi\pi\nu_\tau$ [15,16], and $\tau \rightarrow 4\pi\nu_\tau$ [17] also require the $\rho(1450)$, but are not sensitive to the $\rho(1700)$, because it is too close to the τ mass. A recent very-high-statistics study of the $\tau \rightarrow \pi\pi\nu_\tau$ decay performed at Belle [18] reports the first observation of both $\rho(1450)$ and $\rho(1700)$ in τ decays. A clear picture of the two $\pi^+\pi^-$ resonances interfering with the $\rho(770)$ in e^+e^- annihilation was also reported by BaBar using the ISR method [19].

The structure of these ρ states is not yet completely clear. Barnes [20] and Close [21] claim that $\rho(1450)$ has a mass consistent with radial $2S$, but its decays show characteristics of hybrids, and suggest that this state may be a $2S$ -hybrid mixture. Donnachie [22] argues that hybrid states could have a 4π decay mode dominated by the $a_1\pi$. Such behavior has been observed by [23] in $e^+e^- \rightarrow 4\pi$ in the energy range 1.05–1.38 GeV, and by [17] in $\tau \rightarrow 4\pi$ decays. CLEO [24] and Belle [25] observe the $\rho(1450) \rightarrow \omega\pi$ decay mode in B -meson decays, however, do not find $\rho(1700) \rightarrow \omega\pi^0$. A similar conclusion is made by [26,27], who studied the process $e^+e^- \rightarrow \omega\pi^0$ and do not observe a statistically significant signal of the $\rho(1700)$. Various decay modes of the $\rho(1450)$ and $\rho(1700)$ are observed in $\bar{p}n$ and $\bar{p}p$ annihilation [28,29], but no definite conclusions can be drawn. More data should be collected to clarify the nature of the ρ states, particularly in the energy range above 1.6 GeV.

We now list under a separate entry the $\rho(1570)$, the $\phi\pi$ state with $J^{PC} = 1^{--}$ earlier observed by [30] (referred to as $C(1480)$) and recently confirmed by [31]. While [32] shows that it may be a threshold effect, [5] and [33] suggest two independent vector states with this decay mode. The $C(1480)$ has not been seen in the $\bar{p}p$ [34] and e^+e^- [35,36] experiments. However, the sensitivity of the two latter is an order of magnitude lower than that of [31]. Note that [31] can not exclude that their observation is due to an OZI-suppressed decay mode of the $\rho(1700)$.

Several observations on the $\omega\pi$ system in the 1200-MeV region [37–43] may be interpreted in terms of either $J^P = 1^- \rho(770) \rightarrow \omega\pi$ production [44], or $J^P = 1^+ b_1(1235)$ production [42,43]. We argue that no special entry for a $\rho(1250)$ is needed. The LASS amplitude analysis [45] showing evidence for $\rho(1270)$ is preliminary and needs confirmation.

For completeness, the relevant observations are listed under the $\rho(1450)$.

Recently [46] reported a very broad 1^{--} resonance-like K^+K^- state in $J/\psi \rightarrow K^+K^-\pi^0$ decays. Its pole position corresponds to mass of 1576 MeV and width of 818 MeV. [47–49] suggest its exotic structure (molecular or multiquark), while [50] and [51] explain it by the interference between the $\rho(1450)$ and $\rho(1700)$. The latter statement is qualitatively supported by BaBar [52] and SND [53]. We quote [46] as $X(1575)$ in the section “Further States.”

Evidence for ρ -like mesons decaying into 6π states was first noted by [54] in the analysis of 6π mass spectra from e^+e^- annihilation [55,56] and diffractive photoproduction [57]. Clegg [54] argued that two states at about 2.1 and 1.8 GeV exist: while the former is a candidate for the $\rho(2150)$, the latter could be a manifestation of the $\rho(1700)$ distorted by threshold effects. BaBar reported observations of the new decay modes of the $\rho(2150)$ in the channels $\eta'(958)\pi^+\pi^-$ and $f_1(1285)\pi^+\pi^-$ [58]. The relativistic quark model [59] predicts the 2^3D_1 state with $J^{PC} = 1^{--}$ at 2.15 GeV which can be identified with the $\rho(2150)$.

We no longer list under a separate particle $\rho(1900)$ various observations of irregular behavior of the cross sections near the $N\bar{N}$ threshold. Dips of various width around 1.9 GeV were reported by the E687 Collaboration (a narrow one in the $3\pi^+3\pi^-$ diffractive photoproduction [60,61]), by the FENICE experiment (a narrow structure in the R value [62]), by BaBar in ISR (a narrow structure in $e^+e^- \rightarrow \phi\pi$ final state [63], but much broader in $e^+e^- \rightarrow 3\pi^+3\pi^-$ and $e^+e^- \rightarrow 2(\pi^+\pi^-\pi^0)$ [64]), by CMD-3 (also a rather broad dip in $e^+e^- \rightarrow 3\pi^+3\pi^-$ [65]). A dedicated scan of the $N\bar{N}$ -threshold region by CMD-3 confirms this effect in the $e^+e^- \rightarrow 3\pi^+3\pi^-$ and $e^+e^- \rightarrow K^+K^-\pi^+\pi^-$ final states, but does not see it in the cross section of $e^+e^- \rightarrow 2\pi^+2\pi^-$ [66]. Most probably, these structures emerge as a threshold effect due to the opening of the $N\bar{N}$ channel [67,68,69].

References

1. C. Erkal, Z. Phys. **C31**, 615 (1986).
2. A. Donnachie and H. Mirzaie, Z. Phys. **C33**, 407 (1987).
3. A. Donnachie and A.B. Clegg, Z. Phys. **C34**, 257 (1987).
4. A. Donnachie and A.B. Clegg, Z. Phys. **C51**, 689 (1991).
5. A.B. Clegg and A. Donnachie, Z. Phys. **C40**, 313 (1988).
6. A.B. Clegg and A. Donnachie, Z. Phys. **C62**, 455 (1994).
7. T.J. Killian *et al.*, Phys. Rev. **D21**, 3005 (1980).
8. S. Fukui *et al.*, Phys. Lett. **B202**, 441 (1988).
9. D. Bisello *et al.*, Phys. Lett. **B220**, 321 (1989).
10. A. Antonelli *et al.*, Phys. Lett. **B212**, 133 (1988).
11. A. Abele *et al.*, Phys. Lett. **B391**, 191 (1997).
12. A. Abele *et al.*, Phys. Rev. **D57**, 3860 (1998).
13. A. Bertin *et al.*, Phys. Lett. **B434**, 180 (1998).
14. A. Abele *et al.*, Phys. Lett. **B468**, 178 (1999).
15. R. Barate *et al.*, Z. Phys. **C76**, 15 (1997).
16. S. Anderson, Phys. Rev. **D61**, 112002 (2000).
17. K.W. Edwards *et al.*, Phys. Rev. **D61**, 072003 (2000).
18. M. Fujikawa *et al.*, Phys. Rev. **D78**, 072006 (2008).
19. J.P. Lees *et al.*, Phys. Rev. **D86**, 032013 (2012).
20. T. Barnes *et al.*, Phys. Rev. **D55**, 4157 (1997).
21. F.E. Close *et al.*, Phys. Rev. **D56**, 1584 (1997).
22. A. Donnachie and Yu.S. Kalashnikova, Phys. Rev. **D60**, 114011 (1999).
23. R.R. Akhmetshin *et al.*, Phys. Lett. **B466**, 392 (1999).
24. J.P. Alexander *et al.*, Phys. Rev. **D64**, 092001 (2001).
25. D. Matvienko *et al.*, Phys. Rev. **D92**, 012013 (2015).
26. R.R. Akhmetshin *et al.*, Phys. Lett. **B562**, 173 (2003).
27. M.N. Achasov *et al.*, Phys. Rev. **D94**, 112001 (2016).
28. A. Abele *et al.*, Eur. Phys. J. **C21**, 261 (2001).
29. M. Bargiotti *et al.*, Phys. Lett. **B561**, 233 (2003).
30. S.I. Bityukov *et al.*, Phys. Lett. **B188**, 383 (1987).
31. B. Aubert *et al.*, Phys. Rev. **D77**, 092002 (2008).
32. N.N. Achasov and G.N. Shestakov, Phys. Atom. Nucl. **59**, 1262 (1996).
33. L.G. Landsberg, Sov. J. Nucl. Phys. **55**, 1051 (1992).
34. A. Abele *et al.*, Phys. Lett. **B415**, 280 (1997).
35. V.M. Aulchenko *et al.*, Sov. Phys. JETP Lett. **45**, 145 (1987).
36. D. Bisello *et al.*, Z. Phys. **C52**, 227 (1991).
37. P. Frenkiel *et al.*, Nucl. Phys. **B47**, 61 (1972).
38. G. Cosme *et al.*, Phys. Lett. **B63**, 352 (1976).
39. D.P. Barber *et al.*, Z. Phys. **C4**, 169 (1980).
40. D. Aston, Phys. Lett. **B92**, 211 (1980).
41. M. Atkinson *et al.*, Nucl. Phys. **B243**, 1 (1984).
42. J.E. Brau *et al.*, Phys. Rev. **D37**, 2379 (1988).
43. C. Amsler *et al.*, Phys. Lett. **B311**, 362 (1993).
44. J. Layssac and F.M. Renard, Nuovo Cimento **6A**, 134 (1971).
45. D. Aston *et al.*, Nucl. Phys. (Proc. Supp.) **B21**, 105 (1991).
46. M. Ablikim *et al.*, Phys. Rev. Lett. **97**, 142002 (2006).
47. G.-J. Ding and M.-L. Yan, Phys. Lett. **B643**, 33 (2006).
48. F.K. Guo *et al.*, Nucl. Phys. **A773**, 78 (2006).
49. A. Zhang *et al.*, Phys. Rev. **D76**, 036004 (2007).
50. B.A. Li, Phys. Rev. **D76**, 094016 (2007).
51. X. Liu *et al.*, Phys. Rev. **D75**, 074017 (2007).
52. J.P. Lees *et al.*, Phys. Rev. **D88**, 032013 (2013).
53. M.N. Achasov *et al.*, Phys. Rev. **D94**, 112006 (2016).
54. A.B. Clegg and A. Donnachie, Z. Phys. **C45**, 677 (1990).
55. D. Bisello *et al.*, Phys. Lett. **107B**, 145 (1981).
56. A. Castro *et al.*, LAL-88-58(1988).
57. M. Atkinson *et al.*, Z. Phys. **C29**, 333 (1985).
58. B. Aubert *et al.*, Phys. Rev. **D76**, 092005 (2007).
59. S. Godfrey and N. Isgur, Phys. Rev. **D32**, 189 (1985).
60. P.L. Frabetti *et al.*, Phys. Lett. **B514**, 240 (2001).
61. P.L. Frabetti *et al.*, Phys. Lett. **B578**, 290 (2004).
62. A. Antonelli *et al.*, Phys. Lett. **B365**, 427 (1996).
63. B. Aubert *et al.*, Phys. Rev. **D77**, 092002 (2008).
64. B. Aubert *et al.*, Phys. Rev. **D73**, 052003 (2006).
65. R.R. Akhmetshin *et al.*, Phys. Lett. **B723**, 83 (2013).
66. R.R. Akhmetshin *et al.*, Phys. Lett. **B794**, 64 (2019).

Meson Particle Listings

 $\rho(1700)$

67. A. Obrazovsky and S. Serebnyakov, Sov. Phys. JETP Lett. **99**, 315 (2014).
68. J. Heidenauer *et al.*, Phys. Rev. **D92**, 054032 (2015).
69. A.I. Milstein and S.G. Salmikov, Nucl. Phys. **A977**, 60 (2018).

 $\rho(1700)$ MASS $\eta\rho^0$ AND $\pi^+\pi^-$ MODES

VALUE (MeV)	DOCUMENT ID
1720 ± 20 OUR ESTIMATE	

 $\eta\rho^0$ MODE

VALUE (MeV)	EVTs	DOCUMENT ID	TECN	COMMENT
The data in this block is included in the average printed for a previous datablock.				

• • • We do not use the following data for averages, fits, limits, etc. • • •

1840 ± 10	7.4k	¹ ACHASOV	18	SND	$1.22-2.00 e^+e^- \rightarrow \eta\pi^+\pi^-$
1740 ± 20		ANTONELLI	88	DM2	$e^+e^- \rightarrow \eta\pi^+\pi^-$
1701 ± 15		² FUKUI	88	SPEC	$8.95 \pi^-p \rightarrow \eta\pi^+\pi^-n$

¹ From the combined fit of AULCHENKO 15 and ACHASOV 18 in the model with the interfering $\rho(1450)$, $\rho(1700)$ and $\rho(2150)$ with the parameters of the $\rho(1450)$ and $\rho(1700)$ floating and the mass and width of the $\rho(2150)$ fixed at 2155 MeV and 320 MeV, respectively. The phases of the resonances are π , 0 and π , respectively.

² Assuming $\rho^+ f_0(1370)$ decay mode interferes with $a_1(1260)^+\pi$ background. From a two Breit-Wigner fit.

 $\pi\pi$ MODE

VALUE (MeV)	EVTs	DOCUMENT ID	TECN	COMMENT
The data in this block is included in the average printed for a previous datablock.				

• • • We do not use the following data for averages, fits, limits, etc. • • •

1770.54 ± 5.49		¹ BARTOS	17	RVUE	$e^+e^- \rightarrow \pi^+\pi^-$
1718.50 ± 65.44		² BARTOS	17A	RVUE	$e^+e^- \rightarrow \pi^+\pi^-$
1766.80 ± 52.36		³ BARTOS	17A	RVUE	$\tau^- \rightarrow \pi^-\pi^0\nu_\tau$
1644 ± 36	20K	⁴ LEES	17c	BABR	$J/\psi \rightarrow \pi^+\pi^-\pi^0$
1780 ± 20	$+15$ -20	⁵ ABRAMOWICZ12	ZEUS	$e\rho \rightarrow e\pi^+\pi^-p$	
1861 ± 17		⁶ LEES	12G	BABR	$e^+e^- \rightarrow \pi^+\pi^-\gamma$
1728 ± 17	± 89	^{7,8} FUJIKAWA	08	BELL	$\tau^- \rightarrow \pi^-\pi^0\nu_\tau$
1780 ± 37 -29		⁹ ABELE	97	CBAR	$\bar{p}n \rightarrow \pi^-\pi^0\pi^0$
1719 ± 15		⁹ BERTIN	97c	OBLX	$0.0 \bar{p}p \rightarrow \pi^+\pi^-\pi^0$
1730 ± 30		CLEGG	94	RVUE	$e^+e^- \rightarrow \pi^+\pi^-$
1768 ± 21		BISELLO	89	DM2	$e^+e^- \rightarrow \pi^+\pi^-$
1745.7 ± 91.9		DUBNICKA	89	RVUE	$e^+e^- \rightarrow \pi^+\pi^-$
1546 ± 26		GESHKEN...	89	RVUE	
1650		¹⁰ ERKAL	85	RVUE	$20-70 \gamma\rho \rightarrow \gamma\pi$
1550 ± 70		ABE	84B	HYBR	$20 \gamma\rho \rightarrow \pi^+\pi^-p$
1590 ± 20		¹¹ ASTON	80	OMEG	$20-70 \gamma\rho \rightarrow p2\pi$
1600 ± 10		¹² ATIYA	79B	SPEC	$50 \gamma C \rightarrow C2\pi$
1598 ± 24 -22		BECKER	79	ASPK	$17 \pi^-p$ polarized
1659 ± 25		¹⁰ LANG	79	RVUE	
1575		¹⁰ MARTIN	78c	RVUE	$17 \pi^-p \rightarrow \pi^+\pi^-n$
1610 ± 30		¹⁰ FROGGATT	77	RVUE	$17 \pi^-p \rightarrow \pi^+\pi^-n$
1590 ± 20		¹³ HYAMS	73	ASPK	$17 \pi^-p \rightarrow \pi^+\pi^-n$

¹ Applies the Unitary & Analytic Model of the pion electromagnetic form factor of DUBNICKA 10 to analyze the data of LEES 12G and ABLIKIM 16c.

² Applies the Unitary & Analytic Model of the pion electromagnetic form factor of DUBNICKA 10 to analyze the data of ACHASOV 06, AKHMETSHIN 07, AUBERT 09as, and AMBROSINO 11A.

³ Applies the Unitary & Analytic Model of the pion electromagnetic form factor of DUBNICKA 10 to analyze the data of FUJIKAWA 08.

⁴ From a Dalitz plot analysis in an isobar model with $\rho(1450)$ and $\rho(1700)$ masses and widths floating.

⁵ Using the KUHN 90 parametrization of the pion form factor, neglecting $\rho-\omega$ interference.

⁶ Using the GOUNARIS 68 parametrization of the pion form factor leaving the masses and widths of the $\rho(1450)$, $\rho(1700)$, and $\rho(2150)$ resonances as free parameters of the fit.

⁷ $|F_\pi(0)|^2$ fixed to 1.

⁸ From the GOUNARIS 68 parametrization of the pion form factor.

⁹ T-matrix pole.

¹⁰ From phase shift analysis of HYAMS 73 data.

¹¹ Simple relativistic Breit-Wigner fit with constant width.

¹² An additional 40 MeV uncertainty in both the mass and width is present due to the choice of the background shape.

¹³ Included in BECKER 79 analysis.

 $\pi\omega$ MODE

VALUE (MeV)	EVTs	DOCUMENT ID	TECN	COMMENT
• • • We do not use the following data for averages, fits, limits, etc. • • •				

1708 ± 41	7815	¹ ACHASOV	13	SND	$1.05-2.00 e^+e^- \rightarrow \pi^0\pi^0\gamma$
1550 ± 1620		² ACHASOV	00i	SND	$e^+e^- \rightarrow \pi^0\pi^0\gamma$

1580 to 1710	³ ACHASOV	00i	SND	$e^+e^- \rightarrow \pi^0\pi^0\gamma$
1710 ± 90	ACHASOV	97	RVUE	$e^+e^- \rightarrow \omega\pi^0$

¹ From a phenomenological model based on vector meson dominance with the interfering $\rho(1450)$ and $\rho(1700)$ and their widths fixed at 400 and 250 MeV, respectively. Systematic uncertainty not estimated.

² Taking into account both $\rho(1450)$ and $\rho(1700)$ contributions. Using the data of ACHASOV 00i on $e^+e^- \rightarrow \omega\pi^0$ and of EDWARDS 00A on $\tau^- \rightarrow \omega\pi^-\nu_\tau$. $\rho(1450)$ mass and width fixed at 1400 MeV and 500 MeV respectively.

³ Taking into account the $\rho(1700)$ contribution only. Using the data of ACHASOV 00i on $e^+e^- \rightarrow \omega\pi^0$ and of EDWARDS 00A on $\tau^- \rightarrow \omega\pi^-\nu_\tau$.

 $K\bar{K}$ MODE

VALUE (MeV)	EVTs	DOCUMENT ID	TECN	CHG	COMMENT
• • • We do not use the following data for averages, fits, limits, etc. • • •					

$1541 \pm 12 \pm 33$	190k	¹ AAIJ	16N	LHCB	$D^0 \rightarrow K_S^0 K^\pm \pi^\mp$
1740.8 ± 22.2	27k	² ABELE	99D	CBAR	$\pm 0.0 \bar{p}p \rightarrow K^+K^-\pi^0$
1582 ± 36	1600	CLELAND	82B	SPEC	$\pm 5.0 \pi p \rightarrow K_S^0 K^\pm p$

¹ Using the GOUNARIS 68 parameterization with a fixed width. Value is average using different $K\pi$ S-wave parameterizations in fit.

² K-matrix pole. Isospin not determined, could be $\omega(1650)$ or $\phi(1680)$.

 $2(\pi^+\pi^-)$ MODE

VALUE (MeV)	EVTs	DOCUMENT ID	TECN	COMMENT
• • • We do not use the following data for averages, fits, limits, etc. • • •				

1851 ± 27 -24		ACHASOV	97	RVUE	$e^+e^- \rightarrow 2(\pi^+\pi^-)$
1570 ± 20		¹ CORDIER	82	DM1	$e^+e^- \rightarrow 2(\pi^+\pi^-)$
1520 ± 30		² ASTON	81E	OMEG	$20-70 \gamma\rho \rightarrow p4\pi$
1654 ± 25		³ DIBIANCA	81	DBC	$\pi^+d \rightarrow p\rho 2(\pi^+\pi^-)$
1666 ± 39		¹ BACCI	80	FRAG	$e^+e^- \rightarrow 2(\pi^+\pi^-)$
1780	34	KILLIAN	80	SPEC	$11 e^-p \rightarrow 2(\pi^+\pi^-)$
1500		⁴ ATIYA	79B	SPEC	$50 \gamma C \rightarrow C4\pi^\pm$
1570 ± 60	65	⁵ ALEXANDER	75	HBC	$7.5 \gamma\rho \rightarrow p4\pi$
1550 ± 60		² CONVERSI	74	OSPK	$e^+e^- \rightarrow 2(\pi^+\pi^-)$
1550 ± 50	160	SCHACHT	74	STRC	$5.5-9 \gamma\rho \rightarrow p4\pi$
1450 ± 100	340	SCHACHT	74	STRC	$9-18 \gamma\rho \rightarrow p4\pi$
1430 ± 50	400	BINGHAM	72B	HBC	$9.3 \gamma\rho \rightarrow p4\pi$

¹ Simple relativistic Breit-Wigner fit with model dependent width.

² Simple relativistic Breit-Wigner fit with constant width.

³ One peak fit result.

⁴ Parameters roughly estimated, not from a fit.

⁵ Skew mass distribution compensated by Ross-Stodolsky factor.

 $\pi^+\pi^-\pi^0\pi^0$ MODE

VALUE (MeV)	DOCUMENT ID	TECN	COMMENT
• • • We do not use the following data for averages, fits, limits, etc. • • •			

1660 ± 30	AT KINSON	85B	OMEG	$20-70 \gamma\rho$
---------------	-----------	-----	------	--------------------

 $3(\pi^+\pi^-)$ AND $2(\pi^+\pi^-\pi^0)$ MODES

VALUE (MeV)	DOCUMENT ID	TECN	COMMENT
• • • We do not use the following data for averages, fits, limits, etc. • • •			

1730 ± 34	¹ FRABETTI	04	E687	$\gamma\rho \rightarrow 3\pi^+3\pi^-p$
1783 ± 15	CLEGG	90	RVUE	$e^+e^- \rightarrow 3(\pi^+\pi^-)2(\pi^+\pi^-\pi^0)$

¹ From a fit with two resonances with the JACOB 72 continuum.

 $m_{\rho(1700)^0} - m_{\rho(1700)^\pm}$

VALUE (MeV)	DOCUMENT ID	TECN	COMMENT
• • • We do not use the following data for averages, fits, limits, etc. • • •			

-48.30 ± 83.81	¹ BARTOS	17A	RVUE	$e^+e^- \rightarrow \pi^+\pi^-$, $\tau^- \rightarrow \pi^-\pi^0\nu_\tau$
--------------------	---------------------	-----	------	--

¹ Applies the Unitary & Analytic Model of the pion electromagnetic form factor of DUBNICKA 10 to analyze the data of ACHASOV 06, AKHMETSHIN 07, AUBERT 09as, AMBROSINO 11A, and FUJIKAWA 08.

 $\rho(1700)$ WIDTH $\eta\rho^0$ AND $\pi^+\pi^-$ MODES

VALUE (MeV)	DOCUMENT ID
250 ± 100 OUR ESTIMATE	

 $\eta\rho^0$ MODE

VALUE (MeV)	EVTs	DOCUMENT ID	TECN	COMMENT
The data in this block is included in the average printed for a previous datablock.				

• • • We do not use the following data for averages, fits, limits, etc. • • •

132 ± 40	7.4k	¹ ACHASOV	18	SND	$1.22-2.00 e^+e^- \rightarrow \eta\pi^+\pi^-$
150 ± 30		ANTONELLI	88	DM2	$e^+e^- \rightarrow \eta\pi^+\pi^-$
282 ± 44		² FUKUI	88	SPEC	$8.95 \pi^-p \rightarrow \eta\pi^+\pi^-n$

¹ From the combined fit of AULCHENKO 15 and ACHASOV 18 in the model with the interfering $\rho(1450)$, $\rho(1700)$ and $\rho(2150)$ with the parameters of the $\rho(1450)$ and $\rho(1700)$ floating and the mass and width of the $\rho(2150)$ fixed at 2155 MeV and 320 MeV, respectively. The phases of the resonances are π , 0 and π , respectively.

² Assuming $\rho^+ f_0(1370)$ decay mode interferes with $a_1(1260)^+\pi$ background. From a two Breit-Wigner fit.

$\pi\pi$ MODE

VALUE (MeV)	EVTS	DOCUMENT ID	TECN	COMMENT
-------------	------	-------------	------	---------

The data in this block is included in the average printed for a previous datablock.

• • • We do not use the following data for averages, fits, limits, etc. • • •				
268.98 ± 11.40		¹ BARTOS 17	RVUE	$e^+e^- \rightarrow \pi^+\pi^-$
489.58 ± 16.95		² BARTOS 17A	RVUE	$e^+e^- \rightarrow \pi^+\pi^-$
414.71 ± 119.48		³ BARTOS 17A	RVUE	$\tau^- \rightarrow \pi^-\pi^0\nu_\tau$
109 ± 19	20K	⁴ LEES 17C	BABR	$J/\psi \rightarrow \pi^+\pi^-\pi^0$
310 ± 30	$^{+25}_{-35}$ 63.5k	⁵ ABRAMOWICZ12	ZEUS	$e\rho \rightarrow e\pi^+\pi^-p$
316 ± 26		⁶ LEES 12G	BABR	$e^+e^- \rightarrow \pi^+\pi^-\gamma$
164 ± 21	$^{+89}_{-26}$ 5.4M	^{7,8} FUJIKAWA 08	BELL	$\tau^- \rightarrow \pi^-\pi^0\nu_\tau$
275 ± 45		⁹ ABELE 97	CBAR	$\bar{p}n \rightarrow \pi^-\pi^0\pi^0$
310 ± 40		⁹ BERTIN 97C	OBLX	$0.0\bar{p}p \rightarrow \pi^+\pi^-\pi^0$
400 ± 100		⁹ CLEGG 94	RVUE	$e^+e^- \rightarrow \pi^+\pi^-$
224 ± 22		⁹ BISELLO 89	DM2	$e^+e^- \rightarrow \pi^+\pi^-$
242.5 ± 163.0		⁹ DUBNICKA 89	RVUE	$e^+e^- \rightarrow \pi^+\pi^-$
620 ± 60		⁹ GESHKEN... 89	RVUE	$e^+e^- \rightarrow \pi^+\pi^-$
<315		¹⁰ ERKAL 85	RVUE	20-70 $\gamma\rho \rightarrow \gamma\pi$
280 ± 30	$^{+30}_{-80}$	¹⁰ ABE 84B	HYBR	20 $\gamma\rho \rightarrow \pi^+\pi^-p$
230 ± 80		¹¹ ASTON 80	OMEG	20-70 $\gamma\rho \rightarrow p2\pi$
283 ± 14		¹² ATIYA 79B	SPEC	50 $\gamma C \rightarrow C2\pi$
175 ± 98	$^{-53}$	¹² BECKER 79	ASPK	17 π^-p polarized
232 ± 34		¹⁰ LANG 79	RVUE	
340		¹⁰ MARTIN 78C	RVUE	17 $\pi^-p \rightarrow \pi^+\pi^-n$
300 ± 100		¹⁰ FROGGATT 77	RVUE	17 $\pi^-p \rightarrow \pi^+\pi^-n$
180 ± 50		¹³ HYAMS 73	ASPK	17 $\pi^-p \rightarrow \pi^+\pi^-n$

- Applies the Unitary & Analytic Model of the pion electromagnetic form factor of DUBNICKA 10 to analyze the data of LEES 12G and ABLIKIM 16c.
- Applies the Unitary & Analytic Model of the pion electromagnetic form factor of DUBNICKA 10 to analyze the data of ACHASOV 06, AKHMETSIN 07, AUBERT 09as, and AMBROSINO 11a.
- Applies the Unitary & Analytic Model of the pion electromagnetic form factor of DUBNICKA 10 to analyze the data of FUJIKAWA 08.
- From a Dalitz plot analysis in an isobar model with $\rho(1450)$ and $\rho(1700)$ masses and widths floating.
- Using the KUHN 90 parametrization of the pion form factor, neglecting $\rho-\omega$ interference.
- Using the GOUNARIS 68 parametrization of the pion form factor leaving the masses and widths of the $\rho(1450)$, $\rho(1700)$, and $\rho(2150)$ resonances as free parameters of the fit.
- $|F_\pi(0)|^2$ fixed to 1.
- From the GOUNARIS 68 parametrization of the pion form factor.
- T-matrix pole.
- From phase shift analysis of HYAMS 73 data.
- Simple relativistic Breit-Wigner fit with constant width.
- An additional 40 MeV uncertainty in both the mass and width is present due to the choice of the background shape.
- Included in BECKER 79 analysis.

$K\bar{K}$ MODE

VALUE (MeV)	EVTS	DOCUMENT ID	TECN	CHG	COMMENT
-------------	------	-------------	------	-----	---------

• • • We do not use the following data for averages, fits, limits, etc. • • •					
187.2 ± 26.7	27k	¹ ABELE 99D	CBAR	±	0.0 $\bar{p}p \rightarrow K^+K^-\pi^0$
265 ± 120	1600	CLELAND 82B	SPEC	±	5.0 $\pi p \rightarrow K_S^0 K^\pm p$

¹ K-matrix pole. Isospin not determined, could be $\omega(1650)$ or $\phi(1680)$.

$2(\pi^+\pi^-)$ MODE

VALUE (MeV)	EVTS	DOCUMENT ID	TECN	COMMENT
-------------	------	-------------	------	---------

• • • We do not use the following data for averages, fits, limits, etc. • • •				
510 ± 40		¹ CORDIER 82	DM1	$e^+e^- \rightarrow 2(\pi^+\pi^-)$
400 ± 50		² ASTON 81E	OMEG	20-70 $\gamma\rho \rightarrow p4\pi$
400 ± 146		³ DIBIANCA 81	DBC	$\pi^+d \rightarrow pp2(\pi^+\pi^-)$
700 ± 160		¹ BACCI 80	FRAG	$e^+e^- \rightarrow 2(\pi^+\pi^-)$
100	34	KILLIAN 80	SPEC	11 $e^-p \rightarrow 2(\pi^+\pi^-)$
600		⁴ ATIYA 79B	SPEC	50 $\gamma C \rightarrow C4\pi^\pm$
340 ± 160	65	ALEXANDER 75	HBC	7.5 $\gamma\rho \rightarrow p4\pi$
360 ± 100		² CONVERSI 74	OSPK	$e^+e^- \rightarrow 2(\pi^+\pi^-)$
400 ± 120	160	⁶ SCHACHT 74	STRC	5.5-9 $\gamma\rho \rightarrow p4\pi$
850 ± 200	340	⁶ SCHACHT 74	STRC	9-18 $\gamma\rho \rightarrow p4\pi$
650 ± 100	400	BINGHAM 72B	HBC	9.3 $\gamma\rho \rightarrow p4\pi$

- Simple relativistic Breit-Wigner fit with model-dependent width.
- Simple relativistic Breit-Wigner fit with constant width.
- One peak fit result.
- Parameters roughly estimated, not from a fit.
- Skew mass distribution compensated by Ross-Stodolsky factor.
- Width errors enlarged by us to $4\Gamma/\sqrt{N}$; see the note with the $K^*(892)$ mass.

$\pi^+\pi^-\pi^0\pi^0$ MODE

VALUE (MeV)	DOCUMENT ID	TECN	COMMENT
-------------	-------------	------	---------

• • • We do not use the following data for averages, fits, limits, etc. • • •			
300 ± 50	ATKINSON 85B	OMEG	20-70 $\gamma\rho$

$\omega\pi^0$ MODE

VALUE (MeV)	DOCUMENT ID	TECN	COMMENT
-------------	-------------	------	---------

• • • We do not use the following data for averages, fits, limits, etc. • • •			
350 to 580	¹ ACHASOV 00i	SND	$e^+e^- \rightarrow \pi^0\pi^0\gamma$
490 to 1040	² ACHASOV 00i	SND	$e^+e^- \rightarrow \pi^0\pi^0\gamma$

- Taking into account both $\rho(1450)$ and $\rho(1700)$ contributions. Using the data of ACHASOV 00i on $e^+e^- \rightarrow \omega\pi^0$ and of EDWARDS 00a on $\tau^- \rightarrow \omega\pi^-\nu_\tau$. $\rho(1450)$ mass and width fixed at 1400 MeV and 500 MeV respectively.
- Taking into account the $\rho(1700)$ contribution only. Using the data of ACHASOV 00i on $e^+e^- \rightarrow \omega\pi^0$ and of EDWARDS 00a on $\tau^- \rightarrow \omega\pi^-\nu_\tau$.

$3(\pi^+\pi^-)$ AND $2(\pi^+\pi^-\pi^0)$ MODES

VALUE (MeV)	DOCUMENT ID	TECN	COMMENT
-------------	-------------	------	---------

• • • We do not use the following data for averages, fits, limits, etc. • • •			
315 ± 100	¹ FRABETTI 04	E687	$\gamma\rho \rightarrow 3\pi^+3\pi^-p$
285 ± 20	CLEGG 90	RVUE	$e^+e^- \rightarrow 3(\pi^+\pi^-)2(\pi^+\pi^-\pi^0)$

¹ From a fit with two resonances with the JACOB 72 continuum.

$\Gamma_{\rho(1700)^0} - \Gamma_{\rho(1700)^\pm}$

VALUE (MeV)	DOCUMENT ID	TECN	COMMENT
-------------	-------------	------	---------

• • • We do not use the following data for averages, fits, limits, etc. • • •			
74.87 ± 120.67	¹ BARTOS 17A	RVUE	$e^+e^- \rightarrow \pi^+\pi^-\tau^+ \rightarrow \pi^-\pi^0\nu_\tau$

¹ Applies the Unitary & Analytic Model of the pion electromagnetic form factor of DUBNICKA 10 to analyze the data of ACHASOV 06, AKHMETSIN 07, AUBERT 09as, AMBROSINO 11a, and FUJIKAWA 08.

$\rho(1700)$ DECAY MODES

Mode	Fraction (Γ_i/Γ)
Γ_1 4π	
Γ_2 $2(\pi^+\pi^-)$	seen
Γ_3 $\rho\pi\pi$	seen
Γ_4 $\rho^0\pi^+\pi^-$	seen
Γ_5 $\rho^0\pi^0\pi^0$	
Γ_6 $\rho^\pm\pi^\mp\pi^0$	seen
Γ_7 $a_1(1260)\pi$	seen
Γ_8 $h_1(1170)\pi$	seen
Γ_9 $\pi(1300)\pi$	seen
Γ_{10} $\rho\rho$	seen
Γ_{11} $\pi^+\pi^-$	seen
Γ_{12} $\pi\pi$	seen
Γ_{13} $K\bar{K}^*(892) + c.c.$	seen
Γ_{14} $\eta\rho$	seen
Γ_{15} $a_2(1320)\pi$	not seen
Γ_{16} $K\bar{K}$	seen
Γ_{17} e^+e^-	seen
Γ_{18} $\pi^0\omega$	seen
Γ_{19} $\pi^0\gamma$	not seen

$\rho(1700) \Gamma(i)\Gamma(e^+e^-)/\Gamma(\text{total})$

This combination of a partial width with the partial width into e^+e^- and with the total width is obtained from the cross-section into channel in e^+e^- annihilation.

$\Gamma(2(\pi^+\pi^-)) \times \Gamma(e^+e^-)/\Gamma_{\text{total}}$ $\Gamma_2\Gamma_{17}/\Gamma$

VALUE (keV)	DOCUMENT ID	TECN	COMMENT
-------------	-------------	------	---------

• • • We do not use the following data for averages, fits, limits, etc. • • •			
2.6 ± 0.2	DEL COURT 81B	DM1	$e^+e^- \rightarrow 2(\pi^+\pi^-)$
2.83 ± 0.42	BACCI 80	FRAG	$e^+e^- \rightarrow 2(\pi^+\pi^-)$

$\Gamma(\pi^+\pi^-) \times \Gamma(e^+e^-)/\Gamma_{\text{total}}$ $\Gamma_{11}\Gamma_{17}/\Gamma$

VALUE (keV)	DOCUMENT ID	TECN	COMMENT
-------------	-------------	------	---------

• • • We do not use the following data for averages, fits, limits, etc. • • •			
0.13	¹ DIEKMAN 88	RVUE	$e^+e^- \rightarrow \pi^+\pi^-$
0.029 $^{+0.016}_{-0.012}$	KURDADZE 83	OLYA	0.64-1.4 $e^+e^- \rightarrow \pi^+\pi^-$

¹ Using total width = 220 MeV.

$\Gamma(K\bar{K}^*(892) + c.c.) \times \Gamma(e^+e^-)/\Gamma_{\text{total}}$ $\Gamma_{13}\Gamma_{17}/\Gamma$

VALUE (keV)	DOCUMENT ID	TECN	COMMENT
-------------	-------------	------	---------

• • • We do not use the following data for averages, fits, limits, etc. • • •			
0.305 ± 0.071	¹ BIZOT 80	DM1	e^+e^-

¹ Model dependent.

Meson Particle Listings

 $\rho(1700)$ $\Gamma(\eta\rho) \times \Gamma(e^+e^-)/\Gamma_{\text{total}}$ $\Gamma_{14}\Gamma_{17}/\Gamma$

VALUE (keV)	DOCUMENT ID	TECN	COMMENT
••• We do not use the following data for averages, fits, limits, etc. •••			
$84 \pm 26 \pm 4$	¹ LEES 18	BABR	$e^+e^- \rightarrow \eta\pi^+\pi^-$
7 ± 3	ANTONELLI 88	DM2	$e^+e^- \rightarrow \eta\pi^+\pi^-$
¹ Includes non-resonant contribution. The selected fit model includes three ρ excited states. Model uncertainty is 80%.			

 $\Gamma(K\bar{K}) \times \Gamma(e^+e^-)/\Gamma_{\text{total}}$ $\Gamma_{16}\Gamma_{17}/\Gamma$

VALUE (keV)	DOCUMENT ID	TECN	COMMENT
••• We do not use the following data for averages, fits, limits, etc. •••			
0.035 ± 0.029	¹ BIZOT 80	DM1	e^+e^-
¹ Model dependent.			

 $\Gamma(\rho\pi\pi) \times \Gamma(e^+e^-)/\Gamma_{\text{total}}$ $\Gamma_3\Gamma_{17}/\Gamma$

VALUE (keV)	DOCUMENT ID	TECN	COMMENT
••• We do not use the following data for averages, fits, limits, etc. •••			
3.510 ± 0.090	¹ BIZOT 80	DM1	e^+e^-
¹ Model dependent.			

 $\rho(1700) \Gamma(i)/\Gamma(\text{total}) \times \Gamma(e^+e^-)/\Gamma(\text{total})$ $\Gamma(\pi^0\omega)/\Gamma_{\text{total}} \times \Gamma(e^+e^-)/\Gamma_{\text{total}}$ $\Gamma_{18}/\Gamma \times \Gamma_{17}/\Gamma$

VALUE (units 10^{-8})	EVTS	DOCUMENT ID	TECN	COMMENT
••• We do not use the following data for averages, fits, limits, etc. •••				
0.09 ± 0.05	10.2k	¹ ACHASOV 16d	SND	$1.05-2.00 e^+e^- \rightarrow \pi^0\pi^0\gamma$
1.7 ± 0.4	7815	² ACHASOV 13	SND	$1.05-2.00 e^+e^- \rightarrow \pi^0\pi^0\gamma$
¹ From a phenomenological model based on vector meson dominance with interfering $\rho(700)$, $\rho(1450)$, and $\rho(1700)$. The $\rho(1700)$ mass and width are fixed at 1720 MeV and 250 MeV, respectively. Systematic uncertainty not estimated. Supersedes ACHASOV 13.				
² From a phenomenological model based on vector meson dominance with the interfering $\rho(1450)$ and $\rho(1700)$ and their widths fixed at 400 and 250 MeV, respectively. Systematic uncertainty not estimated.				

 $\Gamma(\eta\rho)/\Gamma_{\text{total}} \times \Gamma(e^+e^-)/\Gamma_{\text{total}}$ $\Gamma_{14}/\Gamma \times \Gamma_{17}/\Gamma$

VALUE (units 10^{-8})	EVTS	DOCUMENT ID	TECN	COMMENT
••• We do not use the following data for averages, fits, limits, etc. •••				
$8.3^{+3.8}_{-3.1}$	7.4k	¹ ACHASOV 18	SND	$1.22-2.00 e^+e^- \rightarrow \eta\pi^+\pi^-$
¹ From the combined fit of AULCHENKO 15 and ACHASOV 18 in the model with the interfering $\rho(1450)$, $\rho(1700)$ and $\rho(2150)$ with the parameters of the $\rho(1450)$ and $\rho(1700)$ floating and the mass and width of the $\rho(2150)$ fixed at 2155 MeV and 320 MeV, respectively. The phases of the resonances are π , 0 and π , respectively.				

 $\rho(1700)$ BRANCHING RATIOS $\Gamma(\rho\pi\pi)/\Gamma(4\pi)$ Γ_3/Γ_1

VALUE	DOCUMENT ID	TECN	COMMENT
••• We do not use the following data for averages, fits, limits, etc. •••			
0.28 ± 0.06	¹ ABELE 01B	CBAR	$0.0 \bar{p}n \rightarrow 5\pi$
¹ $\omega\pi$ not included.			

 $\Gamma(\rho^0\pi^+\pi^-)/\Gamma(2(\pi^+\pi^-))$ Γ_4/Γ_2

VALUE	EVTS	DOCUMENT ID	TECN	COMMENT
••• We do not use the following data for averages, fits, limits, etc. •••				
~ 1.0		DEL COURT 81B	DM1	$e^+e^- \rightarrow 2(\pi^+\pi^-)$
0.7 ± 0.1	500	SCHACHT 74	STRC	$5.5-18 \gamma\rho \rightarrow p4\pi$
0.80		¹ BINGHAM 72B	HBC	$9.3 \gamma\rho \rightarrow p4\pi$
¹ The $\pi\pi$ system is in S-wave.				

 $\Gamma(\rho^0\pi^0\pi^0)/\Gamma(\rho^\pm\pi^\mp\pi^0)$ Γ_5/Γ_6

VALUE	DOCUMENT ID	TECN	CHG	COMMENT
••• We do not use the following data for averages, fits, limits, etc. •••				
<0.10	ATKINSON 85B	OMEG		$20-70 \gamma\rho$
<0.15	ATKINSON 82	OMEG 0		$20-70 \gamma\rho \rightarrow p4\pi$

 $\Gamma(a_1(1260)\pi)/\Gamma(4\pi)$ Γ_7/Γ_1

VALUE	DOCUMENT ID	TECN	COMMENT
••• We do not use the following data for averages, fits, limits, etc. •••			
0.16 ± 0.05	¹ ABELE 01B	CBAR	$0.0 \bar{p}n \rightarrow 5\pi$
¹ $\omega\pi$ not included.			

 $\Gamma(h_1(1170)\pi)/\Gamma(4\pi)$ Γ_8/Γ_1

VALUE	DOCUMENT ID	TECN	COMMENT
••• We do not use the following data for averages, fits, limits, etc. •••			
0.17 ± 0.06	¹ ABELE 01B	CBAR	$0.0 \bar{p}n \rightarrow 5\pi$
¹ $\omega\pi$ not included.			

 $\Gamma(\pi(1300)\pi)/\Gamma(4\pi)$ Γ_9/Γ_1

VALUE	DOCUMENT ID	TECN	COMMENT
••• We do not use the following data for averages, fits, limits, etc. •••			
0.30 ± 0.10	¹ ABELE 01B	CBAR	$0.0 \bar{p}n \rightarrow 5\pi$
¹ $\omega\pi$ not included.			

 $\Gamma(\rho\rho)/\Gamma(4\pi)$ Γ_{10}/Γ_1

VALUE	DOCUMENT ID	TECN	COMMENT
••• We do not use the following data for averages, fits, limits, etc. •••			
0.09 ± 0.03	¹ ABELE 01B	CBAR	$0.0 \bar{p}n \rightarrow 5\pi$
¹ $\omega\pi$ not included.			

 $\Gamma(\pi^+\pi^-)/\Gamma_{\text{total}}$ Γ_{11}/Γ

VALUE	DOCUMENT ID	TECN	COMMENT
••• We do not use the following data for averages, fits, limits, etc. •••			
$0.287^{+0.043}_{-0.042}$	BECKER 79	ASPK	$17 \pi^- p$ polarized
0.15 to 0.30	¹ MARTIN 78C	RVUE	$17 \pi^- p \rightarrow \pi^+\pi^- n$
<0.20	² COSTA... 77B	RVUE	$e^+e^- \rightarrow 2\pi, 4\pi$
0.30 ± 0.05	¹ FROGGATT 77	RVUE	$17 \pi^- p \rightarrow \pi^+\pi^- n$
<0.15	³ EISENBERG 73	HBC	$5 \pi^+ p \rightarrow \Delta^{++} 2\pi$
0.25 ± 0.05	⁴ HYAMS 73	ASPK	$17 \pi^- p \rightarrow \pi^+\pi^- n$
¹ From phase shift analysis of HYAMS 73 data.			
² Estimate using unitarity, time reversal invariance, Breit-Wigner.			
³ Estimated using one-pion-exchange model.			
⁴ Included in BECKER 79 analysis.			

 $\Gamma(\pi^+\pi^-)/\Gamma(2(\pi^+\pi^-))$ Γ_{11}/Γ_2

VALUE	DOCUMENT ID	TECN	COMMENT
••• We do not use the following data for averages, fits, limits, etc. •••			
0.13 ± 0.05	ASTON 80	OMEG	$20-70 \gamma\rho \rightarrow p2\pi$
<0.14	¹ DAVIER 73	STRC	$6-18 \gamma\rho \rightarrow p4\pi$
<0.2	² BINGHAM 72B	HBC	$9.3 \gamma\rho \rightarrow p2\pi$
¹ Upper limit is estimate.			
² 2σ upper limit.			

 $\Gamma(\pi\pi)/\Gamma(4\pi)$ Γ_{12}/Γ_1

VALUE	DOCUMENT ID	TECN	COMMENT
••• We do not use the following data for averages, fits, limits, etc. •••			
0.16 ± 0.04	^{1,2} ABELE 01B	CBAR	$0.0 \bar{p}n \rightarrow 5\pi$
¹ Using ABELE 97.			
² $\omega\pi$ not included.			

 $\Gamma(K\bar{K}^*(892) + \text{c.c.})/\Gamma_{\text{total}}$ Γ_{13}/Γ

VALUE	DOCUMENT ID	TECN	COMMENT
••• We do not use the following data for averages, fits, limits, etc. •••			
possibly seen	COAN 04	CLEO	$\tau^- \rightarrow K^-\pi^- K^+ \nu_\tau$

 $\Gamma(K\bar{K}^*(892) + \text{c.c.})/\Gamma(2(\pi^+\pi^-))$ Γ_{13}/Γ_2

VALUE	DOCUMENT ID	TECN	COMMENT
••• We do not use the following data for averages, fits, limits, etc. •••			
0.15 ± 0.03	¹ DELCOURT 81B	DM1	$e^+e^- \rightarrow \bar{K} K \pi$
¹ Assuming $\rho(1700)$ and ω radial excitations to be degenerate in mass.			

 $\Gamma(\eta\rho)/\Gamma_{\text{total}}$ Γ_{14}/Γ

VALUE	CL%	DOCUMENT ID	TECN	COMMENT
••• We do not use the following data for averages, fits, limits, etc. •••				
possibly seen		AKHMETSHIN 00D	CMD2	$e^+e^- \rightarrow \eta\pi^+\pi^-$
<0.04		DONNACHIE 87B	RVUE	
<0.02	58	ATKINSON 86B	OMEG	$20-70 \gamma\rho$

 $\Gamma(\eta\rho)/\Gamma(2(\pi^+\pi^-))$ Γ_{14}/Γ_2

VALUE	DOCUMENT ID	TECN	COMMENT
••• We do not use the following data for averages, fits, limits, etc. •••			
0.123 ± 0.027	DEL COURT 82	DM1	$e^+e^- \rightarrow \pi^+\pi^- \text{MM}$
~ 0.1	ASTON 80	OMEG	$20-70 \gamma\rho$

 $\Gamma(\pi^+\pi^- \text{ neutrals})/\Gamma(2(\pi^+\pi^-))$ $(\Gamma_5 + \Gamma_6 + 0.714\Gamma_{14})/\Gamma_2$

VALUE	DOCUMENT ID	TECN	COMMENT
••• We do not use the following data for averages, fits, limits, etc. •••			
2.6 ± 0.4	¹ BALLAM 74	HBC	$9.3 \gamma\rho$
¹ Upper limit. Background not subtracted.			

 $\Gamma(a_2(1320)\pi)/\Gamma_{\text{total}}$ Γ_{15}/Γ

VALUE	DOCUMENT ID	TECN	COMMENT
••• We do not use the following data for averages, fits, limits, etc. •••			
not seen	AMELIN 00	VES	$37 \pi^- p \rightarrow \eta\pi^+\pi^- n$

See key on page 999

Meson Particle Listings

$\rho(1700), a_2(1700)$

$\Gamma(K\bar{K})/\Gamma(2\pi^+\pi^-)$ Γ_{16}/Γ_2

Table with columns: VALUE, CL%, DOCUMENT ID, TECN, CHG, COMMENT. Contains data for DELCOURT and BINGHAM experiments.

$\Gamma(K\bar{K})/\Gamma(K\bar{K}^*(892)+c.c.)$ Γ_{16}/Γ_{13}

Table with columns: VALUE, DOCUMENT ID, TECN, COMMENT. Contains data for BUON experiment.

$\Gamma(\pi^0\omega)/\Gamma_{total}$ Γ_{18}/Γ

Table with columns: VALUE, EVTS, DOCUMENT ID, TECN, COMMENT. Contains data for MATVIENKO, ACHASOV, AKHMETSHIN, and ACHASOV experiments.

$\Gamma(\pi^0\gamma)/\Gamma_{total}$ Γ_{19}/Γ

Table with columns: VALUE, DOCUMENT ID, TECN, COMMENT. Contains data for ACHASOV experiment.

$\rho(1700)$ REFERENCES

Large reference table listing authors, document IDs, and technical details for various experiments related to the rho(1700) meson.

$a_2(1700)$

$J^{PC} = 1^-(2^+)$

$a_2(1700)$ MASS

Table with columns: VALUE (MeV), EVTS, DOCUMENT ID, TECN, COMMENT. Lists mass measurements from experiments like RODAS, AMSLER, AGHASYAN, JACKURA, ABLIKIM, ANISOVICH, SCHEGELSKY, UMAN, LU, ABE, ACCIARRI, ABELE, and GRYGOREV.

1 The coupled-channel analysis of both the $\eta\pi$ and $\eta'\pi$ systems using ADOLPH 15data. The mass is extracted from the T-matrix pole.
2 T-matrix pole.
3 Statistical error negligible.
4 Breit-Wigner mass.
5 Superseded by RODAS 19.
6 From analysis of L3 data at 183-209 GeV.
7 Statistical error only.
8 Spin 2 dominant, isospin not determined, could also be $I=1$.
9 Possibly two $J^P = 2^+$ resonances with isospins 0 and 1.

$a_2(1700)$ WIDTH

Table with columns: VALUE (MeV), EVTS, DOCUMENT ID, TECN, COMMENT. Lists width measurements from experiments like RODAS, AMSLER, AGHASYAN, JACKURA, ABLIKIM, ANISOVICH, SCHEGELSKY, UMAN, LU, ABE, ACCIARRI, and ABELE.

1 The coupled-channel analysis of both the $\eta\pi$ and $\eta'\pi$ systems using ADOLPH 15data. The width is extracted from the T-matrix pole.
2 T-matrix pole.
3 Statistical error negligible.
4 Breit-Wigner width.
5 Superseded by RODAS 19.
6 From analysis of L3 data at 183-209 GeV.
7 Statistical error only.
8 Spin 2 dominant, isospin not determined, could also be $I=1$.

$a_2(1700)$ DECAY MODES

Table with columns: Mode, Fraction (Γ_i/Γ). Lists decay modes like $\eta\pi$, $\gamma\gamma$, $\rho\pi$, $f_2(1270)\pi$, $K\bar{K}$, $\omega\pi^-\pi^0$, and $\omega\rho$.

$a_2(1700)$ PARTIAL WIDTHS

Table with columns: VALUE (MeV), EVTS, DOCUMENT ID, TECN, COMMENT. Lists partial width measurement for $\gamma\gamma \rightarrow K_S^0 K_S^0$ from SCHEGELSKY.

Meson Particle Listings

$a_2(1700)$, $f_0(1710)$

$\Gamma(\gamma\gamma)$					Γ_2
VALUE (keV)	EVTS	DOCUMENT ID	TECN	COMMENT	
0.30±0.05	870	¹ SCHEGELSKY 06A	RVUE	$\gamma\gamma \rightarrow K_S^0 K_S^0$	

$\Gamma(K\bar{K})$					Γ_5
VALUE (MeV)	EVTS	DOCUMENT ID	TECN	COMMENT	
5.0±3.0	870	¹ SCHEGELSKY 06A	RVUE	$\gamma\gamma \rightarrow K_S^0 K_S^0$	

¹ From analysis of L3 data at 91 and 183–209 GeV, using $a_2(1700)$ mass of 1730 MeV and width of 340 MeV, and SU(3) relations.

$a_2(1700) \Gamma(i)\Gamma(\gamma\gamma)/\Gamma(\text{total})$

$[\Gamma(\rho\pi) + \Gamma(f_2(1270)\pi)] \times \Gamma(\gamma\gamma)/\Gamma_{\text{total}}$					$(\Gamma_3 + \Gamma_4)\Gamma_2/\Gamma$
VALUE (keV)	EVTS	DOCUMENT ID	TECN	COMMENT	
0.29±0.04±0.02		ACCIARRI 97T	L3	$\gamma\gamma \rightarrow \pi^+\pi^-\pi^0$	

••• We do not use the following data for averages, fits, limits, etc. •••

0.37 ^{+0.12} _{-0.08} ±0.10	18k	¹ SCHEGELSKY 06	RVUE	$\gamma\gamma \rightarrow \pi^+\pi^-\pi^0$	
--	-----	----------------------------	------	--	--

$\Gamma(K\bar{K}) \times \Gamma(\gamma\gamma)/\Gamma_{\text{total}}$					Γ_5/Γ
VALUE (eV)	DOCUMENT ID	TECN	COMMENT		

••• We do not use the following data for averages, fits, limits, etc. •••

20.6±4.2±4.6	² ABE 04	BELL	10.6	$e^+e^- \rightarrow e^+e^-K^+K^-$	
49±11±13	³ ACCIARRI 01H	L3		$\gamma\gamma \rightarrow K_S^0 K_S^0, E_{\text{cm}}^e = 91, 183\text{--}209 \text{ GeV}$	

¹ From analysis of L3 data at 183–209 GeV.

² Assuming spin 2.

³ Spin 2 dominant, isospin not determined, could also be $I=1$.

$a_2(1700)$ BRANCHING RATIOS

$\Gamma(\rho\pi)/\Gamma(f_2(1270)\pi)$					Γ_3/Γ_4
VALUE	EVTS	DOCUMENT ID	TECN	COMMENT	

••• We do not use the following data for averages, fits, limits, etc. •••

3.4±0.4±0.1	18k	¹ SCHEGELSKY 06	RVUE	$\gamma\gamma \rightarrow \pi^+\pi^-\pi^0$	
-------------	-----	----------------------------	------	--	--

¹ From analysis of L3 data at 183–209 GeV.

$a_2(1700)$ REFERENCES

RODAS 19	PRL 122 042002	A. Rodas et al.	(JPAC Collab.)
AGHASYAN 18B	PR D98 092003	M. Aghasyan et al.	(COMPASS Collab.)
JACKURA 18	PL B779 464	A. Jackura et al.	(JPAC and COMPASS Collab.)
ABLIKIM 17K	PR D95 032002	M. Ablikim et al.	(BESIII Collab.)
ADOLPH 15	PL B740 303	M. Adolph et al.	(COMPASS Collab.)
ANISOVICH 09	JUMP A24 2481	V.V. Anisovich, A.V. Sarantsev	
SCHEGELSKY 06	EPJ A27 199	V.A. Schegelsky et al.	
SCHEGELSKY 06A	EPJ A27 207	V.A. Schegelsky et al.	
UMAN 06	PR D73 052009	I. Uman et al.	(FNAL E835)
LU 05	PR L94 032002	M. Lu et al.	(BNL E852 Collab.)
ABE 04	EPJ C32 323	K. Abe et al.	(BELLE Collab.)
AMSLER 02	EPJ C23 29	C. Amisler et al.	
ACCIARRI 01H	PL B501 173	M. Acciarri et al.	(L3 Collab.)
ABELE 99B	EPJ C8 67	A. Abele et al.	(Crystal Barrel Collab.)
GRYGOREV 99	PAN 62 470	V.K. Grygorev et al.	
ACCIARRI 97T	PL B413 147	M. Acciarri et al.	(L3 Collab.)

••• We do not use the following data for averages, fits, limits, etc. •••

1744±7±5	381	^{6,7} DOBBS 15	$J/\psi \rightarrow \gamma\pi^+\pi^-$
1705±11±5	237	^{6,7} DOBBS 15	$\psi(2S) \rightarrow \gamma\pi^+\pi^-$
1706±4±5	1.0k	^{6,7} DOBBS 15	$J/\psi \rightarrow \gamma K^+K^-$
1690±8±3	349	^{6,7} DOBBS 15	$\psi(2S) \rightarrow \gamma K^+K^-$
1750±13		AMSLER 06	CBAR $1.64 \bar{p}p \rightarrow K^+K^-\pi^0$
1747±5	80k	4.8 UMAN 06	E835 $5.2 \bar{p}p \rightarrow \eta\eta\pi^0$
1776±15		VLADIMIRSK..06	SPEC $40 \pi^-p \rightarrow K_S^0 K_S^0 n$
1790 ⁺⁴⁰ ₋₃₀		9 ABLIKIM 05	BES2 $J/\psi \rightarrow \phi\pi^+\pi^-$
1760±15	⁺¹⁵ ₋₁₀	9 ABLIKIM 05Q	BES2 $\psi(2S) \rightarrow \gamma\pi^+\pi^-K^+K^-$
1670±20		4 BINON 05	GAMS $33 \pi^-p \rightarrow \eta\eta n$
1732±15		10 ANISOVICH 03	RVUE
1682±16		TIKHOMIROV 03	SPEC $40.0 \pi^-C \rightarrow K_S^0 K_S^0 K_S^0 X$
1670±26	3.6k	11 NICHITIU 02	OBLX $0 \bar{p}p \rightarrow K^+K^-\pi^+\pi^-$
1698±18		12 BARBERIS 00E	$450 \bar{p}p \rightarrow p_f \eta \eta p_S^0$
1770±12		13 ANISOVICH 99B	SPEC $0.6\text{--}1.2 \bar{p}p \rightarrow \eta\eta\pi^0$
1730±15		BARBERIS 99	OMEG $450 \bar{p}p \rightarrow p_S p_f K^+K^-$
1750±20		BARBERIS 99B	OMEG $450 \bar{p}p \rightarrow p_S p_f \pi^+\pi^-$
1710±12±11		14 BARBERIS 99D	OMEG $450 \bar{p}p \rightarrow K^+K^-, \pi^+\pi^-$
1750±30		15 ANISOVICH 98B	RVUE Compilation
1720±39		BAI 98H	BES $J/\psi \rightarrow \gamma\pi^0\pi^0$
1775±1.5	57	16 BARKOV 98	$\pi^-p \rightarrow K_S^0 K_S^0 n$
1690±11		17 ARBEU 96C	DLPH $Z^0 \rightarrow K^+K^-+X$
1696±5	⁺⁹ ₋₃₄	18 BAI 96C	BES $J/\psi \rightarrow \gamma K^+K^-$
1781±8	⁺¹⁰ ₋₃₁	BAI 96C	BES $J/\psi \rightarrow \gamma K^+K^-$
1768±14		BALOSHIN 95	SPEC $40 \pi^-C \rightarrow K_S^0 K_S^0 X$
1750±15		19 BUGG 95	MRK3 $J/\psi \rightarrow \gamma\pi^+\pi^-\pi^+\pi^-$
1620±16		18 BUGG 95	MRK3 $J/\psi \rightarrow \gamma\pi^+\pi^-\pi^+\pi^-$
1748±10		20 ARMSTRONG 93C	E760 $\bar{p}p \rightarrow \pi^0\eta\eta \rightarrow 6\gamma$
~175.0		BREAKSTONE 93	SFM $\bar{p}p \rightarrow \bar{p}p\pi^-\pi^+\pi^-$
1744±15		21 ALDE 92D	GAM2 $38 \pi^-p \rightarrow \eta\eta n$
1713±10		22 ARMSTRONG 89D	OMEG $300 \bar{p}p \rightarrow \bar{p}p K^+K^-$
1706±10		22 ARMSTRONG 89D	OMEG $300 \bar{p}p \rightarrow \bar{p}p K_S^0 K_S^0$
1707±10		AUGUSTIN 88	DM2 $J/\psi \rightarrow \gamma K^+K^-, K_S^0 K_S^0$
1700±15		18 BOLONKIN 88	SPEC $40 \pi^-p \rightarrow K_S^0 K_S^0 n$
1720±60		BOLONKIN 88	SPEC $40 \pi^-p \rightarrow K_S^0 K_S^0 n$
1638±10		23 FALVARD 88	DM2 $J/\psi \rightarrow \phi K^+K^-, K_S^0 K_S^0$
1690±4		24 FALVARD 88	DM2 $J/\psi \rightarrow \phi K^+K^-, K_S^0 K_S^0$
1698±15		20 AUGUSTIN 87	DM2 $J/\psi \rightarrow \gamma\pi^+\pi^-$
1720±10±10		18 BALTRUSAIT..87	MRK3 $J/\psi \rightarrow \gamma K^+K^-$
1755±8		25 ALDE 86C	GAM2 $38 \pi^-p \rightarrow n2\eta$
1730 ⁺² ₋₁₀		26 LONGACRE 86	RVUE $22 \pi^-p \rightarrow n2K_S^0$
1742±15		20 WILLIAMS 84	MP SF $200 \pi^-N \rightarrow 2K_S^0 X$
1670±50		BLOOM 83	CBAL $J/\psi \rightarrow \gamma 2\eta$
1650±50		BURKE 82	MRK2 $J/\psi \rightarrow \gamma 2\rho$
1640±50		27,28 EDWARDS 82D	CBAL $J/\psi \rightarrow \gamma 2\eta$
1730±10±20		29 ETKIN 82C	MPS $23 \pi^-p \rightarrow n2K_S^0$

¹ From partial wave analysis including all possible combinations of 0^{++} , 2^{++} , and 4^{++} resonances.

² Spin 0 favored over spin 2.

³ In the SU(3) based model with a specific interference pattern of the $f_2(1270)$, $a_2^0(1320)$, and $f_2'(1525)$ mesons incoherently added to the $f_0(1710)$ and non-resonant background.

⁴ Breit-Wigner mass.

⁵ $J^P = 0^+$, supersedes by ARMSTRONG 89D.

⁶ Using CLEO-c data but not authored by the CLEO Collaboration.

⁷ From a fit to a Breit-Wigner line shape with fixed $\Gamma = 135$ MeV.

⁸ Systematic errors not estimated.

⁹ This state may be different from $f_0(1710)$, see CLOSE 05.

¹⁰ K-matrix pole, assuming $J^P = 0^+$, from combined analysis of $\pi^-p \rightarrow \pi^0\pi^0 n$, $\pi^-p \rightarrow K\bar{K}n$, $\pi^+\pi^- \rightarrow \pi^+\pi^-$, $\bar{p}p \rightarrow \pi^0\pi^0\pi^0$, $\pi^0\eta\eta$, $\pi^0\pi^0\eta$, $\pi^+\pi^-\pi^0$, $K^+K^-\pi^0$, $K_S^0 K_S^0 \pi^0$, $K^+K_S^0 \pi^-$ at rest, $\bar{p}n \rightarrow \pi^-\pi^-\pi^+$, $K_S^0 K^- \pi^0$, $K_S^0 K_S^0 \pi^-$ at rest.

¹¹ Decaying to $f_0(1370)\pi\pi$.

¹² T-matrix pole.

¹³ Not seen by AMSLER 02.

¹⁴ Supersedes BARBERIS 99 and BARBERIS 99B.

¹⁵ T-matrix pole, assuming $J^P = 0^+$

¹⁶ No J^{PC} determination.

¹⁷ No J^{PC} determination, width not determined.

¹⁸ $J^P = 2^+$.

¹⁹ From a fit to the 0^+ partial wave.

²⁰ No J^{PC} determination.

²¹ ALDE 92D combines all the GAMS-2000 data.

²² $J^P = 2^+$, superseded by FRENCH 99.

²³ From an analysis ignoring interference with $f_2'(1525)$.

²⁴ From an analysis including interference with $f_2'(1525)$.

²⁵ Superseded by ALDE 92D.

²⁶ Uses MRK3 data. From a partial-wave analysis of data using a K-matrix formalism with 5 poles, but assuming spin 2. Fit with constrained inelasticity.

²⁷ $J^P = 2^+$ preferred.

²⁸ From fit neglecting nearby $f_2'(1525)$. Replaced by BLOOM 83.

$f_0(1710)$

$$I^G(J^{PC}) = 0^+(0^{++})$$

See the review on "Non- $q\bar{q}$ Mesons."

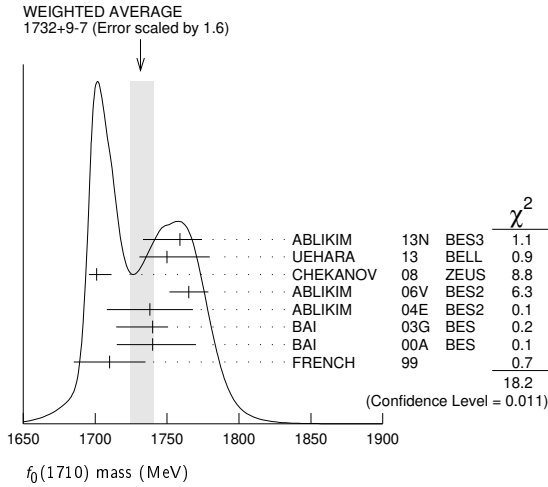
$f_0(1710)$ MASS

OUR EVALUATION below is based on T-matrix poles from BARBERIS 00E and BARBERIS 99D.

VALUE (MeV)	EVTS	DOCUMENT ID	TECN	COMMENT
1704±12				OUR EVALUATION
1732⁺⁹₋₇				OUR AVERAGE Error includes scale factor of 1.6. See the ideogram below.
1759±6	⁺¹⁴ ₋₂₅	5.5k	¹ ABLIKIM 13N	BES3 $e^+e^- \rightarrow J/\psi \rightarrow \gamma\eta\eta$
1750 ⁺⁶ ₋₇	⁺²⁹ ₋₁₈		² UEHARA 13	BELL $\gamma\gamma \rightarrow K_S^0 K_S^0$
1701±5	⁺⁹ ₋₂	4k	³ CHEKANOV 08	ZEUS $e p \rightarrow K_S^0 K_S^0 X$
1765 ⁺⁴ ₋₃	±13		⁴ ABLIKIM 06V	BES2 $e^+e^- \rightarrow J/\psi \rightarrow \gamma\pi^+\pi^-$
1738±30			ABLIKIM 04E	BES2 $J/\psi \rightarrow \omega K^+K^-$
1740±4	⁺¹⁰ ₋₂₅		BAI 03G	BES $J/\psi \rightarrow \gamma K\bar{K}$
1740 ⁺³⁰ ₋₂₅			BAI 00A	BES $J/\psi \rightarrow \gamma(\pi^+\pi^-\pi^+\pi^-)$
1710±25			⁵ FRENCH 99	$300 \bar{p}p \rightarrow p_f(K^+K^-)p_S$

$f_0(1710)$

²⁹ Superseded by LONGACRE 86.



$f_0(1710)$ WIDTH

OUR EVALUATION below is based on T-matrix poles from BARBERIS 00E and BARBERIS 99B.

VALUE (MeV)	EVTs	DOCUMENT ID	TECN	COMMENT
123 ± 18	OUR EVALUATION			
147 ± 12	OUR AVERAGE	Error includes scale factor of 1.2.		
172 ± 10	5.5k	1 ABLIKIM	13N BES3	$e^+e^- \rightarrow J/\psi \rightarrow \gamma\eta\eta$
139 ± 11		2 UEHARA	13 BELL	$\gamma\gamma \rightarrow K_S^0 K_S^0$
100 ± 24	4k	3 CHEKANOV	08 ZEUS	$ep \rightarrow K_S^0 K_S^0 X$
145 ± 8	±69	4 ABLIKIM	06V BES2	$e^+e^- \rightarrow J/\psi \rightarrow \gamma\pi^+\pi^-$
125 ± 20		ABLIKIM	04E BES2	$J/\psi \rightarrow \omega K^+K^-$
166 ± 5	+15	BAI	03G BES	$J/\psi \rightarrow \gamma K\bar{K}$
120 ± 50	-40	BAI	00A BES	$J/\psi \rightarrow \gamma(\pi^+\pi^-\pi^+\pi^-)$
105 ± 34		5 FRENCH	99	$300 pp \rightarrow p_f(K^+K^-)p_s$
••• We do not use the following data for averages, fits, limits, etc. •••				
148 ± 40		AMSLER	06 CBAR	$1.64 \bar{p}p \rightarrow K^+K^-\pi^0$
188 ± 13	80k	4,6 UMAN	06 E835	$5.2 \bar{p}p \rightarrow \eta\eta\pi^0$
250 ± 30		VLADIMIRSK..06	SPEC	$40 \pi^-\pi^0 \rightarrow K_S^0 K_S^0 n$
270 ± 60		7 ABLIKIM	05 BES2	$J/\psi \rightarrow \phi\pi^+\pi^-$
125 ± 25	+10	4 ABLIKIM	05Q BES2	$\psi(2S) \rightarrow \gamma\pi^+\pi^-K^+K^-$
260 ± 50		4 BINON	05 GAMS	$33 \pi^-\pi^0 \rightarrow \eta\eta n$
144 ± 30		8,9 ANISOVICH	03 RVUE	
320 ± 50		9,10 ANISOVICH	03 RVUE	
102 ± 26		TIKHOMIROV	03 SPEC	$40.0 \pi^-\pi^0 \rightarrow K_S^0 K_S^0 K_S^0 X$
267 ± 44	3651	11 NICHITIU	02 OBLX	$0 \bar{p}p \rightarrow K^+K^-\pi^+\pi^0$
120 ± 26		12 BARBERIS	00E	$450 pp \rightarrow p_f\eta\eta p_s$
220 ± 40		13,14 ANISOVICH	99B SPEC	$0.6-1.2 p\bar{p} \rightarrow \eta\eta\pi^0$
100 ± 25		BARBERIS	99 OMEG	$450 pp \rightarrow p_s p_f K^+K^-$
160 ± 30		BARBERIS	99B OMEG	$450 pp \rightarrow p_s p_f \pi^+\pi^-$
126 ± 16	±18	12,15 BARBERIS	99D OMEG	$450 pp \rightarrow K^+K^-, \pi^+\pi^-$
250 ± 140		16 ANISOVICH	98B	Compilation
30 ± 7	57	17 BARKOV	98	$\pi^-\pi^0 \rightarrow K_S^0 K_S^0 n$
103 ± 18	+30	18 BAI	96c BES	$J/\psi \rightarrow \gamma K^+K^-$
85 ± 24	+22	BAI	96c BES	$J/\psi \rightarrow \gamma K^+K^-$
56 ± 19		BALOSHIN	95 SPEC	$40 \pi^-\pi^0 \rightarrow K_S^0 K_S^0 X$
160 ± 40		19 BUGG	95 MRK3	$J/\psi \rightarrow \gamma\pi^+\pi^-\pi^+\pi^-$
160 ± 60		BUGG	95 MRK3	$J/\psi \rightarrow \gamma\pi^+\pi^-\pi^+\pi^-$
264 ± 25		20 ARMSTRONG	93c E760	$\bar{p}p \rightarrow \pi^0\eta\eta \rightarrow 6\gamma$
200 to 300		BREAKSTONE	93 SFM	$pp \rightarrow pp\pi^+\pi^-\pi^+\pi^-$
< 80 90% CL		21 ALDE	92D GAM2	$38 \pi^-\pi^0 \rightarrow \eta\eta N^*$
181 ± 30		22 ARMSTRONG	89D OMEG	$300 pp \rightarrow ppK^+K^-$
104 ± 30		22 ARMSTRONG	89D OMEG	$300 pp \rightarrow ppK_S^0 K_S^0$
166.4 ± 33.2		AUGUSTIN	88 DM2	$J/\psi \rightarrow \gamma K^+K^-, K_S^0 K_S^0$
30 ± 20		18 BOLONKIN	88 SPEC	$40 \pi^-\pi^0 \rightarrow K_S^0 K_S^0 n$
350 ± 150		BOLONKIN	88 SPEC	$40 \pi^-\pi^0 \rightarrow K_S^0 K_S^0 n$
148 ± 17		23 FALVARD	88 DM2	$J/\psi \rightarrow \phi K^+K^-, K_S^0 K_S^0$

184 ± 6	24 FALVARD	88 DM2	$J/\psi \rightarrow \phi K^+K^-, K_S^0 K_S^0$
136 ± 28	20 AUGUSTIN	87 DM2	$J/\psi \rightarrow \gamma\pi^+\pi^-$
130 ± 20	18 BALTRUSAIT..87	MRK3	$J/\psi \rightarrow \gamma K^+K^-$
122 ± 74	25 LONGACRE	86 RVUE	$22 \pi^-\pi^0 \rightarrow n2K_S^0$
15			
57 ± 38	26 WILLIAMS	84 MP5F	$200 \pi^-\pi^0 \rightarrow 2K_S^0 X$
160 ± 80	BLOOM	83 CBAL	$J/\psi \rightarrow \gamma 2\eta$
200 ± 100	BURKE	82 MRK2	$J/\psi \rightarrow \gamma 2\rho$
220 ± 100	27,28 EDWARDS	82D CBAL	$J/\psi \rightarrow \gamma 2\eta$
70			
200 ± 156	29 ETKIN	82B MPS	$23 \pi^-\pi^0 \rightarrow n2K_S^0$
9			

- From partial wave analysis including all possible combinations of 0^{++} , 2^{++} , and 4^{++} resonances.
- Spin 0 favored over spin 2.
- In the SU(3) based model with a specific interference pattern of the $f_2(1270)$, $\rho_2^0(1320)$, and $f_2'(1525)$ mesons incoherently added to the $f_0(1710)$ and non-resonant background.
- Breit-Wigner width.
- $J^P = 0^+$, superseded by ARMSTRONG 89D.
- Systematic errors not estimated.
- This state may be different from $f_0(1710)$, see CLOSE 05.
- (Solution I)
- K-matrix pole, assuming $J^P = 0^+$, from combined analysis of $\pi^-\pi^0 \rightarrow \pi^0\pi^0 n$, $\pi^-\pi^0 \rightarrow K\bar{K}n$, $\pi^+\pi^-\pi^0 \rightarrow \pi^+\pi^-\pi^0$, $\bar{p}p \rightarrow \pi^0\pi^0\pi^0$, $\pi^0\eta\eta$, $\pi^0\pi^0\eta$, $\pi^+\pi^-\pi^0$, $K^+K^-\pi^0$, $K_S^0 K_S^0 \pi^0$, $K^+K_S^0 \pi^-$ at rest, $\bar{p}n \rightarrow \pi^-\pi^-\pi^+$, $K_S^0 K^-\pi^0$, $K_S^0 K_S^0 \pi^-$ at rest.
- (Solution I)
- Decaying to $f_0(1370)\pi\pi$.
- T-matrix pole.
- $J^P = 0^+$.
- Not seen by AMSLER 02.
- Supersedes BARBERIS 99 and BARBERIS 99B.
- T-matrix pole, assuming $J^P = 0^+$
- No J^{PC} determination.
- $J^P = 2^+$.
- From a fit to the 0^+ partial wave.
- No J^{PC} determination.
- ALDE 92d combines all the GAMS-2000 data.
- $J^P = 2^+$, (0^+ excluded).
- From an analysis ignoring interference with $f_2'(1525)$.
- From an analysis including interference with $f_2'(1525)$.
- Uses MRK3 data. From a partial-wave analysis of data using a K-matrix formalism with 5 poles, but assuming spin 2. Fit with constrained inelasticity.
- No J^{PC} determination.
- $J^P = 2^+$ preferred.
- From fit neglecting nearby $f_2'(1525)$. Replaced by BLOOM 83.
- From an amplitude analysis of the $K_S^0 K_S^0$ system, superseded by LONGACRE 86.

$f_0(1710)$ DECAY MODES

Mode	Fraction (Γ_i/Γ)
Γ_1 $K\bar{K}$	seen
Γ_2 $\eta\eta$	seen
Γ_3 $\pi\pi$	seen
Γ_4 $\gamma\gamma$	seen
Γ_5 $\omega\omega$	seen

$f_0(1710)$ $\Gamma(i)\Gamma(\gamma\gamma)/\Gamma(\text{total})$

VALUE (eV)	CL%	DOCUMENT ID	TECN	COMMENT	$\Gamma_1\Gamma_4/\Gamma$
12 ± 3 + 227		UEHARA	13 BELL	$\gamma\gamma \rightarrow K_S^0 K_S^0$	
-2 - 8					

VALUE (eV)	CL%	DOCUMENT ID	TECN	COMMENT
<480	95	ALBRECHT	90G ARG	$\gamma\gamma \rightarrow K^+K^-$
<110	95	1 BEHREND	89C CELL	$\gamma\gamma \rightarrow K_S^0 K_S^0$
<280	95	1 ALTHOFF	85B TASS	$\gamma\gamma \rightarrow K\bar{K}\pi$

1 Assuming helicity 2.

VALUE (keV)	CL%	DOCUMENT ID	TECN	COMMENT	$\Gamma_3\Gamma_4/\Gamma$
<0.82	95	1 BARATE	00E ALEP	$\gamma\gamma \rightarrow \pi^+\pi^-$	

1 Assuming spin 0.

$f_0(1710)$ BRANCHING RATIOS

VALUE	EVTs	DOCUMENT ID	TECN	COMMENT	Γ_1/Γ
seen	1004	1 DOBBS	15	$J/\psi \rightarrow \gamma K^+K^-$	
seen	349	1 DOBBS	15	$\psi(2S) \rightarrow \gamma K^+K^-$	
0.36 ± 0.12		ALBALADEJO	88 RVUE		
0.38 ± 0.09		2 LONGACRE	86 MPS	$22 \pi^-\pi^0 \rightarrow n2K_S^0$	
0.19					

- Using CLEO-c data but not authored by the CLEO Collaboration.
- From a partial-wave analysis of data using a K-matrix formalism with 5 poles, but assuming spin 2. Fit with constrained inelasticity.

Meson Particle Listings

$f_0(1710), \eta(1760)$

$\Gamma(\eta\eta)/\Gamma_{total}$ Γ_2/Γ

VALUE	DOCUMENT ID	TECN
0.22 ± 0.12	ALBALADEJO 08	RVUE
0.18 ^{+0.03} _{-0.13}	¹ LONGACRE 86	RVUE

¹ From a partial-wave analysis of data using a K-matrix formalism with 5 poles, but assuming spin 2. Fit with constrained inelasticity.

$\Gamma(\pi\pi)/\Gamma_{total}$ Γ_3/Γ

VALUE	EVTs	DOCUMENT ID	TECN	COMMENT
seen	381	¹ DOBBS 15		$J/\psi \rightarrow \gamma\pi^+\pi^-$
seen	237	¹ DOBBS 15		$\psi(2S) \rightarrow \gamma\pi^+\pi^-$
not seen		AMSLER 02	CBAR	$0.9\bar{p}p \rightarrow \pi^0\eta\eta, \pi^0\pi^0\pi^0$
0.039 ^{+0.002} _{-0.024}		² LONGACRE 86	RVUE	

¹ Using CLEO-c data but not authored by the CLEO Collaboration.
² From a partial-wave analysis of data using a K-matrix formalism with 5 poles, but assuming spin 2. Fit with constrained inelasticity.

$\Gamma(\pi\pi)/\Gamma(K\bar{K})$ Γ_3/Γ_1

VALUE	CL%	DOCUMENT ID	TECN	COMMENT
0.23 ± 0.05	OUR AVERAGE			Error includes scale factor of 1.2.
0.64 ± 0.27 ± 0.18		LEES 18A	BABR	$\Upsilon(1S) \rightarrow \gamma\pi^+\pi^-, \gamma K^+K^-$
0.41 ^{+0.11} _{-0.17}		ABLIKIM 06V	BES2	$e^+e^- \rightarrow J/\psi \rightarrow \gamma\pi^+\pi^-$
0.2 ± 0.024 ± 0.036		BARBERIS 99D	OMEG 450	$pp \rightarrow K^+K^-, \pi^+\pi^-$
0.39 ± 0.14		ARMSTRONG 91	OMEG 300	$pp \rightarrow \rho\rho\pi\pi, \rho\rho K\bar{K}$
0.32 ± 0.14		ALBALADEJO 08	RVUE	
< 0.11	95	¹ ABLIKIM 04E	BES2	$J/\psi \rightarrow \omega K^+K^-$
5.8 ^{+9.1} _{-5.5}		² ANISOVICH 02D	SPEC	Combined fit

¹ Using data from ABLIKIM 04a.
² From a combined K-matrix analysis of Crystal Barrel ($0. p\bar{p} \rightarrow \pi^0\pi^0\pi^0, \pi^0\eta\eta, \pi^0\pi^0\eta$), GAMS ($\pi\rho \rightarrow \pi^0\pi^0n, \eta\eta n, \eta\eta' n$), and BNL ($\pi\rho \rightarrow K\bar{K}n$) data.

$\Gamma(\eta\eta)/\Gamma(K\bar{K})$ Γ_2/Γ_1

VALUE	CL%	DOCUMENT ID	TECN	COMMENT
0.48 ± 0.15		BARBERIS 00E		450 $pp \rightarrow \rho f \eta \eta \rho_s$
0.46 ^{+0.70} _{-0.38}		¹ ANISOVICH 02D	SPEC	Combined fit
< 0.02	90	² PROKOSHKIN 91	GA24	300 $\pi^-p \rightarrow \pi^- \rho \eta \eta$

¹ From a combined K-matrix analysis of Crystal Barrel ($0. p\bar{p} \rightarrow \pi^0\pi^0\pi^0, \pi^0\eta\eta, \pi^0\pi^0\eta$), GAMS ($\pi\rho \rightarrow \pi^0\pi^0n, \eta\eta n, \eta\eta' n$), and BNL ($\pi\rho \rightarrow K\bar{K}n$) data.
² Combining results of GAM4 with those of ARMSTRONG 89D.

$\Gamma(\omega\omega)/\Gamma_{total}$ Γ_5/Γ

VALUE	EVTs	DOCUMENT ID	TECN	COMMENT
seen	180	ABLIKIM 06H	BES	$J/\psi \rightarrow \gamma\omega\omega$

$f_0(1710)$ REFERENCES

LEES 18A	PR D97 112006	J.P. Lees et al.	(BABAR Collab.)
DOBBS 15	PR D91 052006	S. Dobbs et al.	(NWES)
ABLIKIM 13N	PR D87 092009	Ablikim M. et al.	(BESIII Collab.)
UEHARA 13	PTEP 2013 123C01	S. Uehara et al.	(BELLE Collab.)
ALBALADEJO 08	PRL 101 252002	M. Albaladejo, J.A. Oller	
CHEKANOV 08	PRL 101 112003	S. Chekanov et al.	(ZEUS Collab.)
ABLIKIM 06H	PR D73 112007	M. Ablikim et al.	(BES Collab.)
ABLIKIM 06V	PL B642 441	M. Ablikim et al.	(BES Collab.)
AMSLER 06	PL B639 165	C. Amstler et al.	(CBAR Collab.)
UMAN 06	PR D73 052009	I. Uman et al.	(FNAL E835)
VLADIMIRSK... 06	PAN 69 493	V.V. Vladimirov et al.	(ITEP, Moscow)
ABLIKIM 05	PL B607 243	M. Ablikim et al.	(BES Collab.)
ABLIKIM 05Q	PR D72 092002	M. Ablikim et al.	(BES Collab.)
BINON 05	PAN 68 960	F. Binon et al.	
CLOSE 05	PR D71 094022	F.E. Close, Q. Zhao	
ABLIKIM 04A	PL B598 149	M. Ablikim et al.	(BES Collab.)
ABLIKIM 04E	PL B603 138	M. Ablikim et al.	(BES Collab.)
ANISOVICH 03	EPJ A16 229	V.V. Anisovich et al.	
BAI 03G	PR D68 052003	J.Z. Bai et al.	(BES Collab.)
TIKHOMIROV 03	PAN 66 828	G.D. Tikhomirov et al.	
AMSLER 02	EPJ C23 29	C. Amstler et al.	
ANISOVICH 02D	PAN 65 1545	V.V. Anisovich et al.	
NICHITIU 02	PL B545 261	F. Nichitiu et al.	(OBELIX Collab.)
BAI 00A	PL B472 207	J.Z. Bai et al.	(BES Collab.)
BARATE 00E	PL B472 189	R. Barate et al.	(ALEPH Collab.)
BARBERIS 00E	PL B479 59	D. Barberis et al.	(WA 102 Collab.)
ANISOVICH 99B	PL B449 154	A.V. Anisovich et al.	
BARBERIS 99	PL B453 305	D. Barberis et al.	(Omega Expt.)
BARBERIS 99B	PL B453 316	D. Barberis et al.	(Omega Expt.)
BARBERIS 99D	PL B462 462	D. Barberis et al.	(Omega Expt.)
FRENCH 99	PL B460 213	B. French et al.	(WA76 Collab.)
ANISOVICH 98B	SFU 41 419	V.V. Anisovich et al.	
BAI 98H	PRL 81 1179	J.Z. Bai et al.	(BES Collab.)
BARKOV 98	JETPL 68 764	B.P. Barkov et al.	
ABREU 96C	PL B379 309	P. Abreu et al.	(DELPHI Collab.)
BAI 96C	PRL 77 3959	J.Z. Bai et al.	(BES Collab.)
BALOSHIN 95	PAN 58 46	O.N. Baloshin et al.	(ITEP)
	Translated from YAF 58 50.		

BUGG 95	PL B353 378	D.V. Bugg et al.	(LOQM, PNPI, WASH)
ARMSTRONG 93C	PL B307 394	T.A. Armstrong et al.	(FNAL, FERR, GENO+)
BREAKSTONE 93	ZPHY C58 251	A.M. Breakstone et al.	(IOWA, CERN, DORT+)
ALDE 92D	PL B284 457	D.M. Alde et al.	(GAM2 Collab.)
	Also SJNP 54 451	D.M. Alde et al.	(GAM2 Collab.)
	Translated from YAF 54 745.		
ARMSTRONG 91	ZPHY C51 351	T.A. Armstrong et al.	(ATHU, BARI, BIRM+)
PROKOSHKIN 91	SPD 36 155	Y.D. Prokoshkin	(GAM2 and GAM4 Collab.)
	Translated from DANS 316 900.		
ALBRECHT 90G	ZPHY C48 183	H. Albrecht et al.	(ARGUS Collab.)
ARMSTRONG 89D	PL B227 186	T.A. Armstrong, M. Benayoun	(ATHU, BARI, BIRM+)
BEHREND 89C	ZPHY C43 91	H.J. Behrend et al.	(CELLO Collab.)
AUGUSTIN 88	PRL 60 2238	J.E. Augustin et al.	(DM2 Collab.)
BOLONKIN 88	NP B309 426	B.V. Bolonkin et al.	(ITEP, SERP)
FALVARD 88	PR D38 2706	A. Falvard et al.	(CLER, FRAS, LALO+)
AUGUSTIN 87	ZPHY C36 369	J.E. Augustin et al.	(LALO, CLER, FRAS+)
BALTRUSAITIS... 87	PR D35 2077	R.M. Baltrusaitis et al.	(Mark III Collab.)
ALDE 86C	PL B182 105	D.M. Alde et al.	(SERP, BELG, LAM, LAPP)
LONGACRE 86	PL B177 223	R.S. Longacre et al.	(BNL, BRAN, CUNY+)
ALTHOFF 85B	ZPHY C29 189	M. Althoff et al.	(TASSO Collab.)
WILLIAMS 84	PR D30 877	E.G.H. Williams et al.	(VAND, NDAM, TUFTS+)
BLOOM 83	ARNS 33 143	E.D. Bloom, C. Peck	(SLAC, CIT)
BURKE 82	PRL 49 632	D.L. Burke et al.	(LBL, SLAC)
EDWARDS 82D	PRL 48 458	C. Edwards et al.	(CIT, HARV, PRIN+)
ETKIN 82B	PR D25 1786	A. Etkin et al.	(BNL, CUNY, TUFTS, VAND)
ETKIN 82C	PR D25 2446	A. Etkin et al.	(BNL, CUNY, TUFTS, VAND)

$\eta(1760)$ $I^G(J^{PC}) = 0^+(0^-+)$

OMITTED FROM SUMMARY TABLE
 Seen by DM2 in the $\rho\rho$ system (BISELLO 89B). Structure in this region has been reported before in the same system (BALTRUSAITIS 86B) and in the $\omega\omega$ system (BALTRUSAITIS 85C, BISELLO 87).

$\eta(1760)$ MASS

VALUE (MeV)	EVTs	DOCUMENT ID	TECN	COMMENT
1751 ± 15	OUR AVERAGE			
1768 ⁺²⁴ ₋₂₅ ± 10	465	¹ ZHANG 12A	BELL	$e^+e^- \rightarrow e^+e^-\eta'/\pi^+\pi^-$
1744 ± 10 ± 15	1045	² ABLIKIM 06H	BES	$J/\psi \rightarrow \gamma\omega\omega$
1703 ⁺¹² ₋₁₁ ± 2		³ ZHANG 12A	BELL	$e^+e^- \rightarrow e^+e^-\eta'/\pi^+\pi^-$
1760 ± 11	320	⁴ BISELLO 89B	DM2	$J/\psi \rightarrow 4\pi\gamma$

¹ From a single-resonance fit.
² From a partial wave analysis including $\eta(1760), f_0(1710), f_2(1640),$ and $f_2(1910)$.
³ From a two-resonance fit.
⁴ Estimated by us from various fits. Systematic uncertainties not estimated.

$\eta(1760)$ WIDTH

VALUE (MeV)	EVTs	DOCUMENT ID	TECN	COMMENT
240 ± 30	OUR AVERAGE			
224 ⁺⁶² ₋₅₆ ± 25	465	⁵ ZHANG 12A	BELL	$e^+e^- \rightarrow e^+e^-\eta'/\pi^+\pi^-$
244 ⁺²⁴ ₋₂₁ ± 25	1045	⁶ ABLIKIM 06H	BES	$J/\psi \rightarrow \gamma\omega\omega$
42 ⁺³⁶ ₋₂₂ ± 15		⁷ ZHANG 12A	BELL	$e^+e^- \rightarrow e^+e^-\eta'/\pi^+\pi^-$
60 ± 16	320	⁸ BISELLO 89B	DM2	$J/\psi \rightarrow 4\pi\gamma$

⁵ From a single-resonance fit.
⁶ From a partial wave analysis including $\eta(1760), f_0(1710), f_2(1640),$ and $f_2(1910)$.
⁷ From a two-resonance fit.
⁸ Estimated by us from various fits. Systematic uncertainties not estimated.

$\eta(1760)$ DECAY MODES

Mode	Fraction (Γ_i/Γ)
Γ_1	4π
Γ_2	$2\pi^+2\pi^-$
Γ_3	$\pi^+\pi^-\pi^0$
Γ_4	$\rho^0\rho^0$
Γ_5	$\rho^+\rho^-$
Γ_6	$\omega\omega$
Γ_7	$\eta'\pi^+\pi^-$
Γ_8	$\gamma\gamma$

$\eta(1760)$ $\Gamma(i)\Gamma(\gamma)/\Gamma_{total}$

VALUE (eV)	EVTs	DOCUMENT ID	TECN	COMMENT
28.2^{+7.9}_{-7.5} ± 3.7	465	⁹ ZHANG 12A	BELL	$e^+e^- \rightarrow e^+e^-\eta'/\pi^+\pi^-$

See key on page 999

Meson Particle Listings

$\eta(1760), \pi(1800)$

- • • We do not use the following data for averages, fits, limits, etc. • • •
 - $3.0^{+2.0}_{-1.2} \pm 0.8$ 52 ¹⁰ ZHANG 12A BELL $e^+e^- \rightarrow e^+e^- \eta' \pi^+ \pi^-$
 - $18^{+13}_{-10} \pm 5$ 315 ¹¹ ZHANG 12A BELL $e^+e^- \rightarrow e^+e^- \eta' \pi^+ \pi^-$
- ⁹ From a single-resonance fit.
¹⁰ From a two-resonance fit. For constructive interference with the X(1835).
¹¹ From a two-resonance fit. For destructive interference with the X(1835).

$\eta(1760)$ BRANCHING RATIOS

$\Gamma(2\pi^+2\pi^-)/\Gamma_{total}$		Γ_2/Γ		
VALUE	DOCUMENT ID	TECN	COMMENT	
seen	BISELLO 89B	DM2	$J/\psi \rightarrow \gamma 2\pi^+ 2\pi^-$	
$\Gamma(\pi^+ \pi^- 2\pi^0)/\Gamma_{total}$		Γ_3/Γ		
VALUE	DOCUMENT ID	TECN	COMMENT	
seen	BISELLO 89B	DM2	$J/\psi \rightarrow \gamma \pi^+ \pi^- 2\pi^0$	
$\Gamma(\rho^0 \rho^0)/\Gamma_{total}$		Γ_4/Γ		
VALUE	DOCUMENT ID	TECN	COMMENT	
seen	BISELLO 89B	DM2	$J/\psi \rightarrow \gamma \rho^0 \rho^0$	
seen	BALTRUSAIT...86	MRK3	$J/\psi \rightarrow \gamma \rho^0 \rho^0$	
$\Gamma(\rho^+ \rho^-)/\Gamma_{total}$		Γ_5/Γ		
VALUE	DOCUMENT ID	TECN	COMMENT	
seen	BISELLO 89B	DM2	$J/\psi \rightarrow \gamma \rho^+ \rho^-$	
seen	BALTRUSAIT...86	MRK3	$J/\psi \rightarrow \gamma \rho^+ \rho^-$	
$\Gamma(\omega\omega)/\Gamma_{total}$		Γ_6/Γ		
VALUE	DOCUMENT ID	TECN	COMMENT	
seen	BISELLO 87	DM2	$J/\psi \rightarrow \gamma \omega\omega$	
seen	BALTRUSAIT...85C	MRK3	$J/\psi \rightarrow \gamma \omega\omega$	
$\Gamma(\gamma\gamma)/\Gamma(\omega\omega)$		Γ_8/Γ_6		
VALUE	CL%	DOCUMENT ID	TECN	COMMENT
$<2.48 \times 10^{-3}$	90	¹² ABLIKIM 180	BES3	$\psi(2S) \rightarrow \pi^+ \pi^- \gamma \gamma \gamma$

¹² Using results from ABLIKIM 06H.

$\eta(1760)$ REFERENCES

ABLIKIM 180	PR D97 072014	M. Ablikim et al.	(BESIII Collab.)
ZHANG 12A	PR D86 052002	C.C. Zhang et al.	(BELLE Collab.)
ABLIKIM 06H	PR D73 112007	M. Ablikim et al.	(BES Collab.)
BISELLO 89B	PR D39 701	G. Busetto et al.	(DM2 Collab.)
BISELLO 87	PL B192 239	D. Bisello et al.	(PADO, CLER, FRAS+)
BALTRUSAIT...86	PR D33 629	R.M. Baltrusaitis et al.	(Mark III Collab.)
BALTRUSAIT...86B	PR D33 1222	R.M. Baltrusaitis et al.	(Mark III Collab.)
BALTRUSAIT...85C	PRL 55 1723	R.M. Baltrusaitis et al.	(CIT, UCSC+)

$\pi(1800)$

$$J^G(J^{PC}) = 1^-(0^{-+})$$

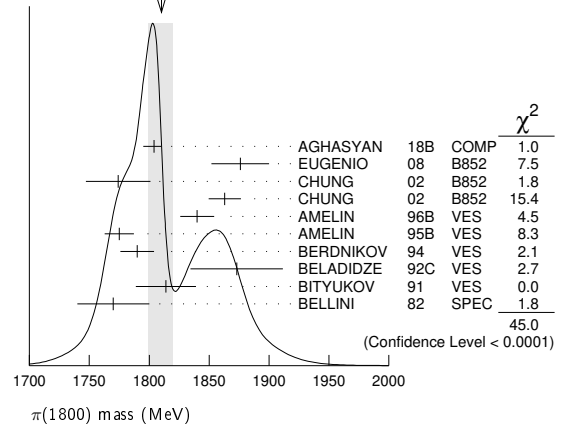
See the review on "Non- $q\bar{q}$ Mesons."

$\pi(1800)$ MASS

VALUE (MeV)	EVTS	DOCUMENT ID	TECN	CHG	COMMENT
1810^{+9}_{-11}		OUR AVERAGE Error includes scale factor of 2.2. See the ideogram below.			
1804^{+6}_{-9}	46M	⁸ AGHASYAN 18B	COMP		$190 \pi^- p \rightarrow \pi^- \pi^+ \pi^- p$
$1876 \pm 18 \pm 16$	4k	⁹ EUGENIO 08	B852	-	$18 \pi^- p \rightarrow \eta \eta \pi^- p$
$1774 \pm 18 \pm 20$		¹⁰ CHUNG 02	B852		$18.3 \pi^- p \rightarrow \pi^+ \pi^- \pi^- p$
$1863 \pm 9 \pm 10$		¹¹ CHUNG 02	B852		$18.3 \pi^- p \rightarrow \pi^+ \pi^- \pi^- p$
$1840 \pm 10 \pm 10$	1.2k	AMELIN 96B	VES	-	$37 \pi^- A \rightarrow \eta \eta \pi^- A$
$1775 \pm 7 \pm 10$		¹² AMELIN 95B	VES	-	$36 \pi^- A \rightarrow \pi^+ \pi^- \pi^- A$
1790 ± 14		¹³ BERDNIKOV 94	VES	-	$37 \pi^- A \rightarrow K^+ K^- \pi^- A$
$1873 \pm 33 \pm 20$		BELADIDZE 92C	VES	-	$36 \pi^- Be \rightarrow \pi^- \eta' \eta Be$
$1814 \pm 10 \pm 23$	426	BITYUKOV 91	VES	-	$36 \pi^- C \rightarrow \pi^- \eta \eta C$
1770 ± 30	1.1k	BELLINI 82	SPEC	-	$40 \pi^- A \rightarrow 3\pi A$
$1785 \pm 9^{+12}_{-6}$	420k	¹⁴ ALEKSEEV 10	COMP		$190 \pi^- Pb \rightarrow \pi^- \pi^- \pi^+ Pb'$
$1737 \pm 5 \pm 15$		AMELIN 99	VES		$37 \pi^- A \rightarrow \omega \pi^- \pi^0 A^*$

- • • We do not use the following data for averages, fits, limits, etc. • • •
- ¹ Statistical error negligible.
- ² From a single-pole fit.
- ³ In the $f_0(980) \pi$ wave.
- ⁴ In the $f_0(500) \pi$ wave.
- ⁵ From a fit to $J^{PC} = 0^{-+} f_0(980) \pi, f_0(1370) \pi$ waves.
- ⁶ From a fit to $J^{PC} = 0^{-+} K_0^*(1430) K^-$ and $f_0(980) \pi^-$ waves.
- ⁷ Superseded by AGHASYAN 2018B.

WEIGHTED AVERAGE
1810+9-11 (Error scaled by 2.2)



$\pi(1800)$ WIDTH

VALUE (MeV)	EVTS	DOCUMENT ID	TECN	CHG	COMMENT
215^{+8}_{-11}		OUR AVERAGE			
220^{+8}_{-11}	46M	⁸ AGHASYAN 18B	COMP		$190 \pi^- p \rightarrow \pi^- \pi^+ \pi^- p$
$221 \pm 26 \pm 38$	4k	⁹ EUGENIO 08	B852	-	$18 \pi^- p \rightarrow \eta \eta \pi^- p$
$223 \pm 48 \pm 50$		¹⁰ CHUNG 02	B852		$18.3 \pi^- p \rightarrow \pi^+ \pi^- \pi^- p$
$191 \pm 21 \pm 20$		¹¹ CHUNG 02	B852		$18.3 \pi^- p \rightarrow \pi^+ \pi^- \pi^- p$
$210 \pm 30 \pm 30$	1.2k	AMELIN 96B	VES	-	$37 \pi^- A \rightarrow \eta \eta \pi^- A$
$190 \pm 15 \pm 15$		¹² AMELIN 95B	VES	-	$36 \pi^- A \rightarrow \pi^+ \pi^- \pi^- A$
210 ± 70		¹³ BERDNIKOV 94	VES	-	$37 \pi^- A \rightarrow K^+ K^- \pi^- A$
$225 \pm 35 \pm 20$		BELADIDZE 92C	VES	-	$36 \pi^- Be \rightarrow \pi^- \eta' \eta Be$
$205 \pm 18 \pm 32$	426	BITYUKOV 91	VES	-	$36 \pi^- C \rightarrow \pi^- \eta \eta C$
310 ± 50	1.1k	BELLINI 82	SPEC	-	$40 \pi^- A \rightarrow 3\pi A$
$208 \pm 22^{+21}_{-37}$	420k	¹⁴ ALEKSEEV 10	COMP		$190 \pi^- Pb \rightarrow \pi^- \pi^- \pi^+ Pb'$
$259 \pm 19 \pm 6$		AMELIN 99	VES		$37 \pi^- A \rightarrow \omega \pi^- \pi^0 A^*$

- • • We do not use the following data for averages, fits, limits, etc. • • •
- ⁸ Statistical error negligible.
- ⁹ From a single-pole fit.
- ¹⁰ In the $f_0(980) \pi$ wave.
- ¹¹ In the $f_0(500) \pi$ wave.
- ¹² From a fit to $J^{PC} = 0^{-+} f_0(980) \pi, f_0(1370) \pi$ waves.
- ¹³ From a fit to $J^{PC} = 0^{-+} K_0^*(1430) K^-$ and $f_0(980) \pi^-$ waves.
- ¹⁴ Superseded by AGHASYAN 2018B.

$\pi(1800)$ DECAY MODES

Mode	Fraction (Γ_i/Γ)
$\Gamma_1 \pi^+ \pi^- \pi^-$	seen
$\Gamma_2 f_0(500) \pi^-$	seen
$\Gamma_3 f_0(980) \pi^-$	seen
$\Gamma_4 f_0(1370) \pi^-$	seen
$\Gamma_5 f_0(1500) \pi^-$	not seen
$\Gamma_6 \rho \pi^-$	not seen
$\Gamma_7 \eta \eta \pi^-$	seen
$\Gamma_8 a_0(980) \eta$	seen
$\Gamma_9 a_2(1320) \eta$	not seen
$\Gamma_{10} f_2'(1270) \pi$	not seen
$\Gamma_{11} f_0(1370) \pi^-$	not seen
$\Gamma_{12} f_0(1500) \pi^-$	seen
$\Gamma_{13} \eta \eta' (958) \pi^-$	seen
$\Gamma_{14} K_0^*(1430) K^-$	seen
$\Gamma_{15} K^*(892) K^-$	not seen

$\pi(1800)$ BRANCHING RATIOS

$\Gamma(f_0(980) \pi^-)/\Gamma(f_0(500) \pi^-)$		Γ_3/Γ_2	
VALUE	DOCUMENT ID	TECN	COMMENT
$0.44 \pm 0.08 \pm 0.38$	¹⁵ CHUNG 02	B852	$18.3 \pi^- p \rightarrow \pi^+ \pi^- \pi^- p$

Meson Particle Listings

$\pi(1800)$, $f_2(1810)$

$\Gamma(f_0(980)\pi^-)/\Gamma(f_0(1370)\pi^-)$ Γ_3/Γ_4

VALUE	DOCUMENT ID	TECN	CHG	COMMENT
1.7 ± 1.3	16 AMELIN	95B	VES	- $36 \pi^- A \rightarrow \pi^+ \pi^- \pi^- A$

$\Gamma(f_0(1370)\pi^-)/\Gamma_{total}$ Γ_4/Γ

VALUE	DOCUMENT ID	TECN	CHG	COMMENT
seen	BELLINI	82	SPEC	- $40 \pi^- A \rightarrow 3\pi A$

$\Gamma(f_0(1500)\pi^-)/\Gamma_{total}$ Γ_5/Γ

VALUE	DOCUMENT ID	TECN	COMMENT
not seen	CHUNG	02	B852 $18.3 \pi^- p \rightarrow \pi^+ \pi^- \pi^- p$

$\Gamma(\rho\pi^-)/\Gamma_{total}$ Γ_6/Γ

VALUE	DOCUMENT ID	TECN	CHG	COMMENT
not seen	BELLINI	82	SPEC	- $40 \pi^- A \rightarrow 3\pi A$

$\Gamma(\rho\pi^-)/\Gamma(f_0(980)\pi^-)$ Γ_6/Γ_3

VALUE	CL%	DOCUMENT ID	TECN	CHG	COMMENT
<0.25		CHUNG	02	B852	$18.3 \pi^- p \rightarrow \pi^+ \pi^- \pi^- p$
<0.14	90	AMELIN	95B	VES	- $36 \pi^- A \rightarrow \pi^+ \pi^- \pi^- A$

$\Gamma(\eta\eta\pi^-)/\Gamma(\pi^+ \pi^- \pi^-)$ Γ_7/Γ_1

VALUE	EVTs	DOCUMENT ID	TECN	CHG	COMMENT
0.5 ± 0.1	1200	16 AMELIN	96B	VES	- $37 \pi^- A \rightarrow \eta\eta\pi^- A$

$\Gamma(a_2(1320)\eta)/\Gamma_{total}$ Γ_9/Γ

VALUE	DOCUMENT ID	TECN	COMMENT
not seen	EUGENIO	08	B852 $18 \pi^- p \rightarrow \eta\eta\pi^- p$

$\Gamma(f_2(1270)\pi)/\Gamma_{total}$ Γ_{10}/Γ

VALUE	DOCUMENT ID	TECN	COMMENT
not seen	EUGENIO	08	B852 $18 \pi^- p \rightarrow \eta\eta\pi^- p$

$\Gamma(f_0(1370)\pi^-)/\Gamma_{total}$ Γ_{11}/Γ

VALUE	DOCUMENT ID	TECN	COMMENT
not seen	EUGENIO	08	B852 $18 \pi^- p \rightarrow \eta\eta\pi^- p$

$\Gamma(f_0(1500)\pi^-)/\Gamma(a_0(980)\eta)$ Γ_{12}/Γ_8

VALUE	EVTs	DOCUMENT ID	TECN	CHG	COMMENT
0.48 ± 0.17	4k	16,17 EUGENIO	08	B852	- $18 \pi^- p \rightarrow \eta\eta\pi^- p$
0.030 ± 0.014		16 ANISOVICH	01B	SPEC	0 $0.6-1.94 p\bar{p} \rightarrow \eta\eta\pi^0 \pi^0$
0.08 ± 0.03	1200	16,18 AMELIN	96B	VES	- $37 \pi^- A \rightarrow \eta\eta\pi^- A$

$\Gamma(\eta\eta'(958)\pi^-)/\Gamma(\eta\eta\pi^-)$ Γ_{13}/Γ_7

VALUE	EVTs	DOCUMENT ID	TECN	CHG	COMMENT
0.29 ± 0.07		16 BELADIDZE	92C	VES	- $36 \pi^- Be \rightarrow \pi^- \eta' \eta Be$
0.3 ± 0.1	426 ± 57	16 BITYUKOV	91	VES	- $36 \pi^- C \rightarrow \pi^- \eta\eta C$

$\Gamma(K_0^*(1430)K^-)/\Gamma_{total}$ Γ_{14}/Γ

VALUE	DOCUMENT ID	TECN	CHG	COMMENT
seen	BERDNIKOV	94	VES	- $37 \pi^- A \rightarrow K^+ K^- \pi^- A$

$\Gamma(K^*(892)K^-)/\Gamma_{total}$ Γ_{15}/Γ

VALUE	DOCUMENT ID	TECN	CHG	COMMENT
not seen	BERDNIKOV	94	VES	- $37 \pi^- A \rightarrow K^+ K^- \pi^- A$

15 Assuming that $f_0(980)$ decays only to $\pi\pi$.
 16 Systematic errors not estimated.
 17 From a single-pole fit.
 18 Assuming that $f_0(1500)$ decays only to $\eta\eta$ and $a_0(980)$ decays only to $\eta\pi$.

$\pi(1800)$ REFERENCES

AGHASYAN	18B	PR D98 092003	M. Aghasyan et al.	(COMPASS Collab.)
ALEKSEEV	10	PRL 104 241803	M.G. Alekseev et al.	(COMPASS Collab.)
EUGENIO	08	PL B660 466	P. Eugenio et al.	(BNL E852 Collab.)
CHUNG	02	PR D65 072001	S.U. Chung et al.	(BNL E852 Collab.)
ANISOVICH	01B	PL B500 222	A.V. Anisovich et al.	(BNL E852 Collab.)
AMELIN	99	PAN 62 445	D.V. Amelin et al.	(VES Collab.)
AMELIN	96B	PAN 59 976	D.V. Amelin et al.	(SERP, TBIL)IGJPC
AMELIN	95B	PL B356 595	D.V. Amelin et al.	(SERP, TBIL)
BERDNIKOV	94	PL B337 219	E.B. Berdnikov et al.	(SERP, TBIL)
BELADIDZE	92C	SJMP 55 1535	G.M. Beladidze, S.I. Bityukov, G.V. Borisov	(SERP+)
BITYUKOV	91	PL B248 137	S.I. Bityukov et al.	(SERP, TBIL)
BELLINI	82	PRL 48 1697	G. Bellini et al.	(MILA, BGNA, JINR)

$f_2(1810)$

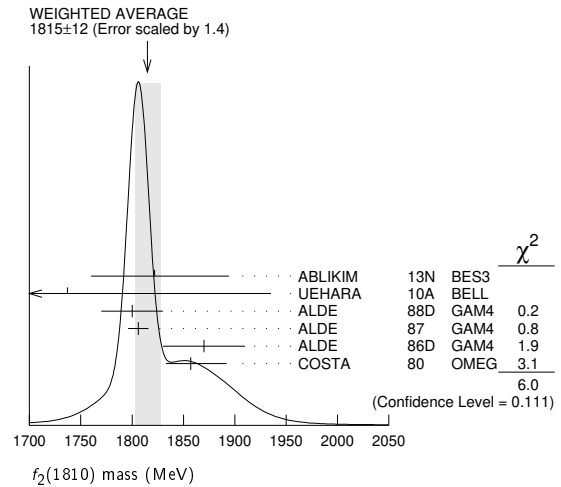
$$I^G(J^{PC}) = 0^+(2^{++})$$

OMITTED FROM SUMMARY TABLE
Needs confirmation.

$f_2(1810)$ MASS

VALUE (MeV)	EVTs	DOCUMENT ID	TECN	COMMENT
1815 ± 12 OUR AVERAGE				Error includes scale factor of 1.4. See the ideogram below.
$1822^{+29}_{-24} +^{66}_{-57}$	5.5k	1 ABLIKIM	13N	BES3 $e^+ e^- \rightarrow J/\psi \rightarrow \gamma\eta\eta$
$1737 \pm 9^{+198}_{-65}$		2 UEHARA	10A	BELL $10.6 e^+ e^- \rightarrow e^+ e^- \eta\eta$
1800 ± 30	40	ALDE	88D	GAM4 $300 \pi^- p \rightarrow \pi^- p 4\pi^0$
1806 ± 10	1600	ALDE	87	GAM4 $100 \pi^- p \rightarrow 4\pi^0 n$
1870 ± 40		3 ALDE	86D	GAM4 $100 \pi^- p \rightarrow \eta\eta n$
1857^{+35}_{-24}		4 COSTA	80	OMEG $10 \pi^- p \rightarrow K^+ K^- n$
1858^{+18}_{-71}		5 LONGACRE	86	RVUE Compilation
1799 ± 15		6 CASON	82	STRC $8 \pi^+ p \rightarrow \Delta^{++} \pi^0 \pi^0$

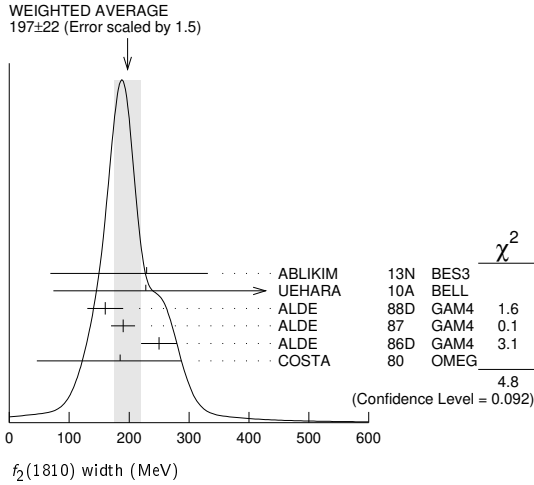
1 From partial wave analysis including all possible combinations of 0^{++} , 2^{++} , and 4^{++} resonances.
 2 Breit-Wigner mass. Could also be the $f_2(1910)$.
 3 Seen in only one solution.
 4 Error increased by spread of two solutions. Included in LONGACRE 86 global analysis.
 5 From a partial-wave analysis of data using a K-matrix formalism with 5 poles. Includes compilation of several other experiments.
 6 From an amplitude analysis of the reaction $\pi^+ \pi^- \rightarrow 2\pi^0$. The resonance in the $2\pi^0$ final state is not confirmed by PROKOSHKIN 97.



$f_2(1810)$ WIDTH

VALUE (MeV)	EVTs	DOCUMENT ID	TECN	COMMENT
197 ± 22 OUR AVERAGE				Error includes scale factor of 1.5. See the ideogram below.
$229^{+52}_{-42} +^{88}_{-155}$	5.5k	7 ABLIKIM	13N	BES3 $e^+ e^- \rightarrow J/\psi \rightarrow \gamma\eta\eta$
$228^{+21}_{-20} +^{234}_{-153}$		8 UEHARA	10A	BELL $10.6 e^+ e^- \rightarrow e^+ e^- \eta\eta$
160 ± 30	40	ALDE	88D	GAM4 $300 \pi^- p \rightarrow \pi^- p 4\pi^0$
190 ± 20	1600	ALDE	87	GAM4 $100 \pi^- p \rightarrow 4\pi^0 n$
250 ± 30		9 ALDE	86D	GAM4 $100 \pi^- p \rightarrow \eta\eta n$
185^{+102}_{-139}		10 COSTA	80	OMEG $10 \pi^- p \rightarrow K^+ K^- n$

11 LONGACRE 86 RVUE Compilation
 12 CASON 82 STRC $8 \pi^+ p \rightarrow \Delta^{++} \pi^0 \pi^0$
 7 From partial wave analysis including all possible combinations of 0^{++} , 2^{++} , and 4^{++} resonances.
 8 Breit-Wigner width. Could also be the $f_2(1910)$.
 9 Seen in only one solution.
 10 Error increased by spread of two solutions. Included in LONGACRE 86 global analysis.
 11 From a partial-wave analysis of data using a K-matrix formalism with 5 poles. Includes compilation of several other experiments.
 12 From an amplitude analysis of the reaction $\pi^+ \pi^- \rightarrow 2\pi^0$. The resonance in the $2\pi^0$ final state is not confirmed by PROKOSHKIN 97.



$f_2(1810)$ REFERENCES

ABLIKIM	13N	PR D87 092009	Ablikim <i>et al.</i>	(BESIII Collab.)
UEHARA	10A	PR D82 114031	S. Uehara <i>et al.</i>	(BELLE Collab.)
PDG	08	PL B667 1	C. Amsler <i>et al.</i>	(PDG Collab.)
AMSLER	02	EPJ C23 29	C. Amsler <i>et al.</i>	
PROKOSHKIN	97	PD 42 117	Y.D. Prokoshkin <i>et al.</i>	(SERP)
		Translated from DANS 353 323.		
ALDE	88D	SJNP 47 810	D.M. Alde <i>et al.</i>	(SERP, BELG, LANL, LAPP+)
		Translated from YAF 47 1273.		
ALDE	87	PL B198 286	D.M. Alde <i>et al.</i>	(LANL, BRUX, SERP, LAPP)
ALDE	86D	NP B269 485	D.M. Alde <i>et al.</i>	(BELG, LAPP, SERP, CERN+)
LONGACRE	86	PL B177 223	R.S. Longacre <i>et al.</i>	(BNL, BRAN, CUNY+)
CASON	82	PRL 48 1316	N.M. Cason <i>et al.</i>	(NDAM, ANL)
COSTA	80	NP B175 402	G. Costa <i>et al.</i>	(BARI, BONN, CERN, GLAS+)

$X(1835)$

$$J^G(J^{PC}) = ?(0^{-+})$$

OMITTED FROM SUMMARY TABLE

Could be a superposition of two states, one with small width appearing as threshold enhancement in $p\bar{p}$, the other one with a larger width. For the former ABLIKIM 12D determine $J^{PC} = 0^{-+}$.

$X(1835)$ MASS

VALUE (MeV)	EVTS	DOCUMENT ID	TECN	COMMENT
1826.5 \pm 13.0	3.4	OUR AVERAGE		
1825.3 \pm 2.4 $^{+17.3}_{-2.4}$		1 ABLIKIM	16J	BES3 $J/\psi \rightarrow \gamma\pi^+\pi^-\eta'$
1844 \pm 9 $^{+16}_{-25}$		ABLIKIM	15T	BES3 $J/\psi \rightarrow \gamma K_S^0 K_S^0 \eta$
1839 \pm 26 \pm 26		2 ABLIKIM	18I	BES3 $J/\psi \rightarrow \gamma\gamma\phi(1020)$
1909.5 \pm 15.9 $^{+9.4}_{-27.5}$		3 ABLIKIM	16J	BES3 $J/\psi \rightarrow \gamma\pi^+\pi^-\eta'$
1842.2 \pm 4.2 $^{+7.1}_{-2.6}$	0.6k	ABLIKIM	13U	BES3 $J/\psi \rightarrow \gamma 3(\pi^+\pi^-)$
1832 $^{+19}_{-5} \pm$ 26		4 ABLIKIM	12D	BES3 $J/\psi \rightarrow \gamma p\bar{p}$
1836.5 \pm 3.0 $^{+5.6}_{-2.1}$	4265	5 ABLIKIM	11C	BES3 $J/\psi \rightarrow \gamma\pi^+\pi^-\eta'$
1877.3 \pm 6.3 $^{+3.4}_{-7.4}$		6 ABLIKIM	11J	BES3 $J/\psi \rightarrow \omega(\eta\pi^+\pi^-)$
1837 $^{+10}_{-12} \pm$ 9 $^{+9}_{-7}$	231	7,8 ALEXANDER	10	CLEO $J/\psi \rightarrow \gamma p\bar{p}$
1833.7 \pm 6.1 \pm 2.7	264	ABLIKIM	05R	BES2 $J/\psi \rightarrow \gamma\pi^+\pi^-\eta'$
1831 \pm 7		8,9 ABLIKIM	05R	BES2 $J/\psi \rightarrow \gamma p\bar{p}$
1859 $^{+3}_{-10} \pm$ 5 $^{+5}_{-25}$		8 BAI	03F	BES2 $J/\psi \rightarrow \gamma p\bar{p}$

- From a fit of the measured $\pi^+\pi^-\eta'$ lineshape that accounts for the abrupt distortion observed at the $p\bar{p}$ threshold through interference with a second previously unseen narrow resonance near 1870 MeV. The fit uses Breit-Wigner functions for the signal shapes and includes known backgrounds and contributors.
- From a fit to $\gamma\phi$ invariant mass. Angular analysis consistent with $J^{PC} = 0^{-+}$. Other J^{PC} not excluded.
- Pole mass from a fit of the measured $\pi^+\pi^-\eta'$ lineshape to a Flatte formula that accounts for the abrupt distortion observed at the $p\bar{p}$ threshold; the fit also includes known backgrounds and contributors, as well as an *ad hoc* Breit-Wigner function ($M \approx 1919$ MeV; $\Gamma \approx 51$ MeV) that is required for a good fit.
- From the fit including final state interaction effects in isospin 0 S-wave according to SIBIRTSSEV 05A. Supersedes ABLIKIM 10G.
- From a fit of the $\pi^+\pi^-\eta'$ mass distribution to a combination of $\gamma f_1(1510)$, $\gamma X(1835)$, and two unconfirmed states $\gamma X(2120)$, and $\gamma X(2370)$, for $M(p\bar{p}) < 2.8$ GeV, and accounting for backgrounds from non- η' events and $J/\psi \rightarrow \pi^0\pi^+\pi^-\eta'$.
- The selected process is $J/\psi \rightarrow \omega a_0(980)\pi$. This state may be due also to $\eta_2(1870)$ or to a combination of $X(1835)$ and $\eta_2(1870)$.
- From a fit of the $p\bar{p}$ mass distribution to a combination of $\gamma X(1835)$, γR with $M(R) = 2100$ MeV and $\Gamma(R) = 160$ MeV, and $\gamma p\bar{p}$ phase space, for $M(p\bar{p}) < 2.85$ GeV.
- Evidence for a threshold enhancement in the $p\bar{p}$ mass spectrum was also reported by ABE 02k, AUBERT, B 05L, and WANG 05A in $B^+ \rightarrow p\bar{p}K^+$, WANG 05A in $B^0 \rightarrow p\bar{p}K_S^0$, ABE 02w in $\bar{B}^0 \rightarrow p\bar{p}D^0$, DEL-AMO-SANCHEZ 12 in $B \rightarrow D(D^*)p\bar{p}(\pi)$, and WEI 08 in $B^+ \rightarrow p\bar{p}\pi^+$ decays. Not seen by ATHAR 06 in $\Upsilon(1S) \rightarrow p\bar{p}\gamma$.
- From the fit including final state interaction effects in isospin 0 S-wave according to SIBIRTSSEV 05A. Systematic errors not estimated.

$X(1835)$ WIDTH

VALUE (MeV)	CL%	EVTS	DOCUMENT ID	TECN	COMMENT
242 $^{+14}_{-15}$			OUR AVERAGE		
245.2 \pm 13.1 $^{+4.6}_{-9.6}$			1 ABLIKIM	16J	BES3 $J/\psi \rightarrow \gamma\pi^+\pi^-\eta'$
192 $^{+20}_{-17} \pm$ 62 $^{+62}_{-43}$			ABLIKIM	15T	BES3 $J/\psi \rightarrow \gamma K_S^0 K_S^0 \eta$
175 \pm 5.7 \pm 25			2 ABLIKIM	18I	BES3 $J/\psi \rightarrow \gamma\gamma\phi(1020)$
273.5 \pm 21.4 $^{+6.1}_{-64.0}$			3 ABLIKIM	16J	BES3 $J/\psi \rightarrow \gamma\pi^+\pi^-\eta'$
83 \pm 14 \pm 11	0.6k		ABLIKIM	13U	BES3 $J/\psi \rightarrow \gamma 3(\pi^+\pi^-)$
< 76	90		4 ABLIKIM	12D	BES3 $J/\psi \rightarrow \gamma p\bar{p}$

$f_2(1810)$ DECAY MODES

Mode	Fraction (Γ_i/Γ)
Γ_1 $\pi\pi$	
Γ_2 $\eta\eta$	seen
Γ_3 $4\pi^0$	seen
Γ_4 K^+K^-	
Γ_5 $\gamma\gamma$	seen

$f_2(1810)$ $\Gamma(\eta)/\Gamma(\text{total})$

$\Gamma(\eta\eta) \times \Gamma(\gamma\gamma)/\Gamma_{\text{total}}$	DOCUMENT ID	TECN	COMMENT
5.2 \pm 0.9 $^{+37.3}_{-4.5}$	13 UEHARA	10A	BELL 10.6 $e^+e^- \rightarrow e^+e^-\eta\eta$

¹³Including interference with the $f_2'(1525)$ (parameters fixed to the values from the 2008 edition of this review, PDG 08) and $f_2(1270)$. May also be the $f_0(1500)$.

$f_2(1810)$ BRANCHING RATIOS

$\Gamma(\pi\pi)/\Gamma_{\text{total}}$	DOCUMENT ID	TECN	COMMENT
not seen	AMSLER 02	CBAR	0.9 $p\bar{p} \rightarrow \pi^0\eta\eta, \pi^0\pi^0\pi^0$
not seen	PROKOSHKIN 97	GAM2	38 $\pi^-p \rightarrow \pi^0\pi^0n$
0.21 $^{+0.02}_{-0.03}$	14 LONGACRE 86	RVUE	Compilation
0.44 \pm 0.03	15 CASON 82	STRC	8 $\pi^+p \rightarrow \Delta^+\pi^0\pi^0$

¹⁴From a partial-wave analysis of data using a K-matrix formalism with 5 poles. Includes compilation of several other experiments.

¹⁵Included in LONGACRE 86 global analysis.

$\Gamma(\eta\eta)/\Gamma_{\text{total}}$	DOCUMENT ID	TECN	COMMENT
seen	ABLIKIM 13N	BES3	PWA of $J/\psi \rightarrow \gamma\eta\eta$
0.008 \pm 0.028 $^{+0.028}_{-0.003}$	16 LONGACRE 86	RVUE	Compilation

¹⁶From a partial-wave analysis of data using a K-matrix formalism with 5 poles. Includes compilation of several other experiments.

$\Gamma(\pi\pi)/\Gamma(4\pi^0)$	DOCUMENT ID	TECN	COMMENT
< 0.75	ALDE 87	GAM4	100 $\pi^-p \rightarrow 4\pi^0n$

$\Gamma(4\pi^0)/\Gamma(\eta\eta)$	DOCUMENT ID	TECN	COMMENT
0.8 \pm 0.3	ALDE 87	GAM4	100 $\pi^-p \rightarrow 4\pi^0n$

$\Gamma(K^+K^-)/\Gamma_{\text{total}}$	DOCUMENT ID	TECN	COMMENT
0.003 \pm 0.019 $^{+0.019}_{-0.002}$	17 LONGACRE 86	RVUE	Compilation
seen	COSTA 80	OMEG	10 $\pi^-p \rightarrow K^+K^-n$

¹⁷From a partial-wave analysis of data using a K-matrix formalism with 5 poles. Includes compilation of several other experiments.

Meson Particle Listings

X(1835), $\phi_3(1850)$

190 ± 9 ⁺³⁸ / ₋₃₆	4265	⁵ ABLIKIM	11c	BES3	$J/\psi \rightarrow \gamma\pi^+\pi^-\eta'$
57 ± 12 ⁺¹⁹ / ₋₄		⁶ ABLIKIM	11j	BES3	$J/\psi \rightarrow \omega(\eta\pi^+\pi^-)$
0 ⁺⁴⁴ / ₋₀	231	^{7,8} ALEXANDER	10	CLEO	$J/\psi \rightarrow \gamma\rho\bar{p}$
67.7 ± 20.3 ± 7.7	264	⁹ ABLIKIM	05R	BES2	$J/\psi \rightarrow \gamma\pi^+\pi^-\eta'$
< 153	90	^{8,9} ABLIKIM	05R	BES2	$J/\psi \rightarrow \gamma\rho\bar{p}$
< 30		⁸ BAI	03F	BES2	$J/\psi \rightarrow \gamma\rho\bar{p}$

- From a fit of the measured $\pi^+\pi^-\eta'$ lineshape that accounts for the abrupt distortion observed at the $p\bar{p}$ threshold through interference with a second previously unseen narrow resonance near 1870 MeV. The fit uses Breit-Wigner functions for the signal shapes and includes known backgrounds and contributors.
- From a fit to $\gamma\phi$ invariant mass. Angular analysis consistent with $J^{PC} = 0^{-+}$. Other J^{PC} not excluded.
- Pole width from a fit of the measured $\pi^+\pi^-\eta'$ lineshape to a Flatté formula that accounts for the abrupt distortion observed at the $p\bar{p}$ threshold; the fit also includes known backgrounds and contributors, as well as an *ad hoc* Breit-Wigner function ($M \approx 1919$ MeV; $\Gamma \approx 51$ MeV) that is required for a good fit.
- From the fit including final state interaction effects in isospin 0 S-wave according to SIBIRTSSEV 05A. Supersedes ABLIKIM 10G.
- From a fit of the $\pi^+\pi^-\eta'$ mass distribution to a combination of $\gamma f_1(1510)$, $\gamma X(1835)$, and two unconfirmed states $\gamma X(2120)$, and $\gamma X(2370)$, for $M(p\bar{p}) < 2.8$ GeV, and accounting for backgrounds from non- η' events and $J/\psi \rightarrow \pi^0\pi^+\pi^-\eta'$.
- The selected process is $J/\psi \rightarrow \omega\pi_0(980)\pi$. This state may be due also to $\eta_2(1870)$ or to a combination of $X(1835)$ and $\eta_2(1870)$.
- From a fit of the $p\bar{p}$ mass distribution to a combination of $\gamma X(1835)$, γR with $M(R) = 2100$ MeV and $\Gamma(R) = 160$ MeV, and $\gamma p\bar{p}$ phase space, for $M(p\bar{p}) < 2.85$ GeV.
- Evidence for a threshold enhancement in the $p\bar{p}$ mass spectrum was also reported by ABE 02K, AUBERT,B 05L, and WANG 05A in $B^+ \rightarrow p\bar{p}K^+$, WANG 05A in $B^0 \rightarrow p\bar{p}K_S^0$, ABE 02W in $\bar{B}^0 \rightarrow p\bar{p}D^0$, DEL-AMO-SANCHEZ 12 in $B \rightarrow D(D^*)p\bar{p}(\pi)$, and WEI 08 in $B^+ \rightarrow p\bar{p}\pi^+$ decays. Not seen by ATHAR 06 in $\Upsilon(1S) \rightarrow p\bar{p}\gamma$.
- From the fit including final state interaction effects in isospin 0 S-wave according to SIBIRTSSEV 05A. Systematic errors not estimated.

X(1835) DECAY MODES

Mode	Fraction (Γ_i/Γ)
Γ_1 $p\bar{p}$	seen
Γ_2 $\eta'\pi^+\pi^-$	seen
Γ_3 $\gamma\gamma$	
Γ_4 $K_S^0 K_S^0 \eta$	seen
Γ_5 $\gamma\phi(1020)$	possibly seen
Γ_6 $3(\pi^+\pi^-)$	seen

X(1835) $\Gamma(i)\Gamma(\gamma\gamma)/\Gamma(\text{total})$

$\Gamma(\eta'\pi^+\pi^-) \times \Gamma(\gamma\gamma)/\Gamma_{\text{total}}$	$\Gamma_2/\Gamma_3/\Gamma$
VALUE (eV)	CL% DOCUMENT ID TECN COMMENT
••• We do not use the following data for averages, fits, limits, etc. •••	
<35.6	90 ¹ ZHANG 12A BELL $e^+e^- \rightarrow e^+e^-\eta'\pi^+\pi^-$
<83	90 ² ZHANG 12A BELL $e^+e^- \rightarrow e^+e^-\eta'\pi^+\pi^-$

- From a two-resonance fit and constructive interference of the $\eta(1760)$ and $X(1835)$, a significance of 2.8 σ .
- From a two-resonance fit and destructive interference of the $\eta(1760)$ and $X(1835)$, a significance of 2.8 σ .

X(1835) BRANCHING RATIOS

$\Gamma(p\bar{p})/\Gamma(\eta'\pi^+\pi^-)$	Γ_1/Γ_2
VALUE	DOCUMENT ID TECN COMMENT
••• We do not use the following data for averages, fits, limits, etc. •••	
0.333	ABLIKIM 05R BES2 $J/\psi \rightarrow \gamma\pi^+\pi^-\eta'$

$\Gamma(\eta'\pi^+\pi^-)/\Gamma(K_S^0 K_S^0 \eta)$	Γ_2/Γ_4
VALUE	DOCUMENT ID TECN COMMENT
••• We do not use the following data for averages, fits, limits, etc. •••	
6.7 ± 1.8	¹ ABLIKIM 15T BES3 $J/\psi \rightarrow \gamma K_S^0 K_S^0 \eta$

¹ Using results from ABLIKIM 05R.

$\Gamma(\eta'\pi^+\pi^-)/\Gamma_{\text{total}}$	Γ_2/Γ
VALUE	DOCUMENT ID TECN COMMENT
seen	¹ ABLIKIM 16j BES3 $J/\psi \rightarrow \gamma\pi^+\pi^-\eta'$

¹ ABLIKIM 16j quotes $B(J/\psi \rightarrow \gamma X(1835)) \times B(X(1835) \rightarrow \pi^+\pi^-\eta') = (3.93 \pm 0.38^{+0.31}_{-0.84}) \times 10^{-4}$ from a fit of the measured $\pi^+\pi^-\eta'$ lineshape that accounts for the abrupt distortion observed at the $p\bar{p}$ threshold with a Flatté formula in addition to known backgrounds and contributors, as well as an *ad hoc* Breit-Wigner ($M \approx 1919$ MeV; $\Gamma \approx 51$ MeV) that is required for a good fit. Another explanation for the distortion provided by ABLIKIM 16j is that a second resonance near 1870 MeV interferes with the $X(1835)$; fits to this possibility yield product branching fraction values compatible with that shown within the respective systematic uncertainties.

$\Gamma(\gamma\phi(1020))/\Gamma_{\text{total}}$	Γ_5/Γ
VALUE	DOCUMENT ID TECN COMMENT
possibly seen	¹ ABLIKIM 18i BES3 $J/\psi \rightarrow \gamma\gamma\phi(1020)$

¹ Seen as a peak in $\gamma\phi$ invariant mass. Angular analysis consistent with $J^{PC} = 0^{-+}$. Other J^{PC} not excluded.

$\Gamma(\gamma\gamma)/\Gamma(\eta'\pi^+\pi^-)$	Γ_3/Γ_2
VALUE	CL% DOCUMENT ID TECN COMMENT
<9.80 × 10 ⁻³	90 ¹ ABLIKIM 18o BES3 $\psi(2S) \rightarrow \pi^+\pi^-\gamma\gamma$

¹ Using results from ABLIKIM 16j.

$\Gamma(3(\pi^+\pi^-))/\Gamma_{\text{total}}$	Γ_6/Γ
VALUE	EVTS DOCUMENT ID TECN COMMENT
seen	0.6k ABLIKIM 13u BES3 $J/\psi \rightarrow \gamma 3(\pi^+\pi^-)$

X(1835) REFERENCES

ABLIKIM 18i	PR D97 051101	M. Ablíkım et al.	(BESIII Collab.)
ABLIKIM 18o	PR D97 072014	M. Ablíkım et al.	(BESIII Collab.)
ABLIKIM 16j	PRL 117 042002	M. Ablíkım et al.	(BESIII Collab.)
ABLIKIM 15T	PRL 115 091803	M. Ablíkım et al.	(BESIII Collab.)
ABLIKIM 13u	PR D88 091502	M. Ablíkım et al.	(BESIII Collab.)
ABLIKIM 12D	PRL 108 112003	M. Ablíkım et al.	(BESIII Collab.) JPC
DEL-AMO-SA...	PR D85 092017	P. del Amo Sanchez et al.	(BABAR Collab.)
ZHANG 12A	PR D86 052002	C.C. Zhang et al.	(BELLE Collab.)
ABLIKIM 11C	PRL 106 072002	M. Ablíkım et al.	(BESIII Collab.)
ABLIKIM 11J	PRL 107 182001	M. Ablíkım et al.	(BESIII Collab.)
ABLIKIM 10G	CP C34 421	M. Ablíkım et al.	(BESIII Collab.)
ALEXANDER 10	PR D82 092002	J.P. Alexander et al.	(CLEO Collab.)
WEI 08	PL B659 80	J.-T. Wei et al.	(BELLE Collab.)
ATHAR 06	PR D73 032001	S.B. Athar et al.	(CLEO Collab.)
ABLIKIM 05R	PRL 95 292001	M. Ablíkım et al.	(BES Collab.)
AUBERT,B 05L	PR D72 051101	B. Aubert et al.	(BABAR Collab.)
SIBIRTSSEV 05A	PR D71 054010	A. Sibirtsev, J. Haidenbauer	
WANG 05A	PL B617 141	M.-Z. Wang et al.	(BELLE Collab.)
BAI 03F	PRL 91 022001	J.Z. Bai et al.	(BES II Collab.)
ABE 02K	PRL 88 181803	K. Abe et al.	(BELLE Collab.)
ABE 02W	PRL 89 151802	K. Abe et al.	(BELLE Collab.)

$\phi_3(1850)$

$$I^G(J^{PC}) = 0^-(3^{-})$$

$\phi_3(1850)$ MASS

VALUE (MeV)	EVTS	DOCUMENT ID	TECN	COMMENT
1854 ± 7	OUR AVERAGE			
1855 ± 10		ASTON	88E LASS	11 $K^-p \rightarrow K^-K^+\Lambda$, $K_S^0 K^\pm \pi^\mp \Lambda$
1870 ⁺³⁰ / ₋₂₀	430	ARMSTRONG 82	OMEG	18.5 $K^-p \rightarrow K^-K^+\Lambda$
1850 ± 10	123	ALHARRAN 81B	HBC	8.25 $K^-p \rightarrow K\bar{K}\Lambda$

$\phi_3(1850)$ WIDTH

VALUE (MeV)	EVTS	DOCUMENT ID	TECN	COMMENT
87 ⁺²⁸/₋₂₃	OUR AVERAGE			Error includes scale factor of 1.2.
64 ± 31		ASTON	88E LASS	11 $K^-p \rightarrow K^-K^+\Lambda$, $K_S^0 K^\pm \pi^\mp \Lambda$
160 ⁺⁹⁰ / ₋₅₀	430	ARMSTRONG 82	OMEG	18.5 $K^-p \rightarrow K^-K^+\Lambda$
80 ⁺⁴⁰ / ₋₃₀	123	ALHARRAN 81B	HBC	8.25 $K^-p \rightarrow K\bar{K}\Lambda$

$\phi_3(1850)$ DECAY MODES

Mode	Fraction (Γ_i/Γ)
Γ_1 $K\bar{K}$	seen
Γ_2 $K\bar{K}^*(892) + \text{c.c.}$	seen

$\phi_3(1850)$ BRANCHING RATIOS

$\Gamma(K\bar{K}^*(892) + \text{c.c.})/\Gamma(K\bar{K})$	Γ_2/Γ_1
VALUE	DOCUMENT ID TECN COMMENT
0.55 ^{+0.85}/_{-0.45}	ASTON 88E LASS 11 $K^-p \rightarrow K^-K^+\Lambda$, $K_S^0 K^\pm \pi^\mp \Lambda$

••• We do not use the following data for averages, fits, limits, etc. •••

0.8 ± 0.4	ALHARRAN 81B HBC 8.25 $K^-p \rightarrow K\bar{K}\pi\Lambda$
-----------	---

$\phi_3(1850)$ REFERENCES

ASTON 88E	PL B208 324	D. Aston et al.	(SLAC, NAGO, CINC, INUS)IGJPC
ARMSTRONG 82	PL 110B 77	T.A. Armstrong et al.	(BARI, BIRM, CERN+)JP
ALHARRAN 81B	PL 101B 357	S. Al-Harran et al.	(BIRM, CERN, GLAS+)

See key on page 999

Meson Particle Listings

$\eta_2(1870), \pi_2(1880), \rho(1900)$

$\eta_2(1870)$ $I^G(J^{PC}) = 0^+(2^-)$

$\eta_2(1870)$ MASS

VALUE (MeV)	EVTS	DOCUMENT ID	TECN	COMMENT
1842 ± 8	8	OUR AVERAGE		
1835 ± 12		BARBERIS	00B	450 $pp \rightarrow \rho_f \eta \pi^+ \pi^- \rho_S$
1844 ± 13		BARBERIS	00C	450 $pp \rightarrow \rho_f 4 \pi \rho_S$
1840 ± 25		BARBERIS	97B	OMEG 450 $pp \rightarrow \rho p 2(\pi^+ \pi^-)$
1875 ± 20 ± 35		ADOMEIT	96	CBAR 1.94 $\bar{p}p \rightarrow \eta 3\pi^0$
1881 ± 32 ± 40	26	KARCH	92	CBAL $e^+ e^- \rightarrow e^+ e^- \eta \pi^0 \pi^0$
• • • We do not use the following data for averages, fits, limits, etc. • • •				
1860 ± 5 ± 15		ANISOVICH	00E	SPEC 0.9-1.94 $\bar{p}p \rightarrow \eta 3\pi^0$
1840 ± 15		BAI	99	BES $J/\psi \rightarrow \gamma \eta \pi^+ \pi^-$

$\eta_2(1870)$ WIDTH

VALUE (MeV)	EVTS	DOCUMENT ID	TECN	COMMENT
225 ± 14	OUR AVERAGE			
235 ± 22		BARBERIS	00B	450 $pp \rightarrow \rho_f \eta \pi^+ \pi^- \rho_S$
228 ± 23		BARBERIS	00C	450 $pp \rightarrow \rho_f 4 \pi \rho_S$
200 ± 40		BARBERIS	97B	OMEG 450 $pp \rightarrow \rho p 2(\pi^+ \pi^-)$
200 ± 25 ± 45		ADOMEIT	96	CBAR 1.94 $\bar{p}p \rightarrow \eta 3\pi^0$
221 ± 92 ± 44	26	KARCH	92	CBAL $e^+ e^- \rightarrow e^+ e^- \eta \pi^0 \pi^0$
• • • We do not use the following data for averages, fits, limits, etc. • • •				
250 ± 25 ± 50	-35	ANISOVICH	00E	SPEC 0.9-1.94 $\bar{p}p \rightarrow \eta 3\pi^0$
170 ± 40		BAI	99	BES $J/\psi \rightarrow \gamma \eta \pi^+ \pi^-$

$\eta_2(1870)$ DECAY MODES

Mode	Fraction (Γ_i/Γ)
Γ_1 $\eta \pi \pi$	
Γ_2 $a_2(1320) \pi$	
Γ_3 $f_2(1270) \eta$	
Γ_4 $a_0(980) \pi$	
Γ_5 $\gamma \gamma$	seen

$\eta_2(1870)$ BRANCHING RATIOS

$\Gamma(a_2(1320)\pi)/\Gamma(f_2(1270)\eta)$ Γ_2/Γ_3

VALUE	DOCUMENT ID	TECN	COMMENT
1.7 ± 0.4	OUR AVERAGE		
1.60 ± 0.40	¹ ANISOVICH	11	SPEC 0.9-1.94 $p\bar{p}$
20.4 ± 6.6	BARBERIS	00B	450 $pp \rightarrow \rho_f \eta \pi^+ \pi^- \rho_S$
4.1 ± 2.3	ADOMEIT	96	CBAR 1.94 $\bar{p}p \rightarrow \eta 3\pi^0$
¹ Reanalysis of ADOMEIT 96 and ANISOVICH 00E.			

$\Gamma(a_2(1320)\pi)/\Gamma(a_0(980)\pi)$ Γ_2/Γ_4

VALUE	DOCUMENT ID	COMMENT
32.6 ± 12.6	BARBERIS	00B 450 $pp \rightarrow \rho_f \eta \pi^+ \pi^- \rho_S$

$\Gamma(a_0(980)\pi)/\Gamma(f_2(1270)\eta)$ Γ_4/Γ_3

VALUE	DOCUMENT ID	TECN	COMMENT
0.48 ± 0.45	¹ ANISOVICH	11	SPEC 0.9-1.94 $p\bar{p}$
¹ Reanalysis of ADOMEIT 96 and ANISOVICH 00E.			

$\Gamma(\gamma\gamma)/\Gamma_{total}$ Γ_5/Γ

VALUE	DOCUMENT ID	TECN	COMMENT
seen	KARCH	92	CBAL $e^+ e^- \rightarrow e^+ e^- \eta \pi^0 \pi^0$

$\eta_2(1870)$ REFERENCES

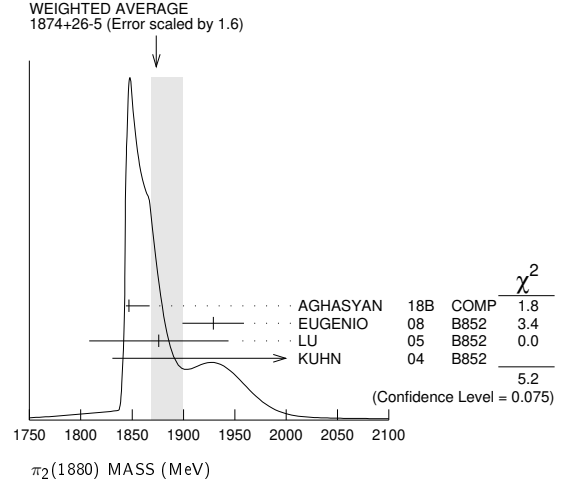
ANISOVICH	11	EPJ C71 1511	A.V. Anisovich et al.	(LOQM, RAL, PNPI)
ANISOVICH	00E	PL B477 19	A.V. Anisovich et al.	
BARBERIS	00B	PL B471 435	D. Barberis et al.	(WA 102 Collab.)
BARBERIS	00C	PL B471 440	D. Barberis et al.	(WA 102 Collab.)
BAI	99	PL B446 356	J.Z. Bai et al.	(BES Collab.)
BARBERIS	97B	PL B413 217	D. Barberis et al.	(WA 102 Collab.)
ADOMEIT	96	ZPHY C71 227	J. Adomeit et al.	(Crystal Barrel Collab.)
KARCH	92	ZPHY C54 33	K. Karch et al.	(Crystal Ball Collab.)

$\pi_2(1880)$ $I^G(J^{PC}) = 1^-(2^-)$

$\pi_2(1880)$ MASS

VALUE (MeV)	EVTS	DOCUMENT ID	TECN	CHG	COMMENT
1874 ± 26	5	OUR AVERAGE			
1847 ± 20	46M	¹ AGHASYAN	18B	COMP	190 $\pi^- p \rightarrow \pi^- \pi^+ \pi^- p$
1929 ± 24 ± 18	4k	EUGENIO	08	B852	- 18 $\pi^- p \rightarrow \eta \eta \pi^- p$
1876 ± 11 ± 67	145k	LU	05	B852	- 18 $\pi^- p \rightarrow \omega \pi^- \pi^0 p$
2003 ± 88 ± 148	69k	KUHN	04	B852	- 18 $\pi^- p \rightarrow \eta \pi^+ \pi^- \pi^- p$

• • • We do not use the following data for averages, fits, limits, etc. • • •
 1880 ± 20 ANISOVICH 01B SPEC 0 0.6-1.94 $\bar{p}p \rightarrow \eta \eta \pi^0 \pi^0$
¹ Statistical error negligible.



$\pi_2(1880)$ WIDTH

VALUE (MeV)	EVTS	DOCUMENT ID	TECN	CHG	COMMENT
237 ± 33	30	OUR AVERAGE			
Error includes scale factor of 1.2.					
246 ± 28	46M	² AGHASYAN	18B	COMP	190 $\pi^- p \rightarrow \pi^- \pi^+ \pi^- p$
323 ± 87 ± 43	4k	EUGENIO	08	B852	- 18 $\pi^- p \rightarrow \eta \eta \pi^- p$
146 ± 17 ± 62	145k	LU	05	B852	- 18 $\pi^- p \rightarrow \omega \pi^- \pi^0 p$
306 ± 132 ± 121	69k	KUHN	04	B852	- 18 $\pi^- p \rightarrow \eta \pi^+ \pi^- \pi^- p$
• • • We do not use the following data for averages, fits, limits, etc. • • •					
255 ± 45		ANISOVICH	01B	SPEC	0 0.6-1.94 $\bar{p}p \rightarrow \eta \eta \pi^0 \pi^0$
² Statistical error negligible.					

$\pi_2(1880)$ DECAY MODES

Mode
Γ_1 $\eta \eta \pi^-$
Γ_2 $a_0(980) \eta$
Γ_3 $a_2(1320) \eta$
Γ_4 $f_0(1500) \pi$
Γ_5 $f_1(1285) \pi$
Γ_6 $\omega \pi^- \pi^0$

$\Gamma(a_2(1320)\eta)/\Gamma(f_1(1285)\pi)$ Γ_3/Γ_5

VALUE	EVTS	DOCUMENT ID	TECN	CHG	COMMENT
22.7 ± 7.3	69k	KUHN	04	B852	- 18 $\pi^- p \rightarrow \eta \pi^+ \pi^- \pi^- p$

$\Gamma(f_0(1500)\pi)/\Gamma(a_0(980)\eta)$ Γ_4/Γ_2

VALUE	DOCUMENT ID	TECN	CHG	COMMENT
0.28 ± 0.20	³ ANISOVICH	01B	SPEC	0 0.6-1.94 $\bar{p}p \rightarrow \eta \eta \pi^0 \pi^0$
-0.15				
³ Systematic errors not estimated.				

$\pi_2(1880)$ REFERENCES

AGHASYAN	18B	PR D98 092003	M. Aghasyan et al.	(COMPASS Collab.)
EUGENIO	08	PL B660 466	P. Eugenio et al.	(BNL E852 Collab.)
LU	05	PRL 94 032002	M. Lu et al.	(BNL E852 Collab.)
KUHN	04	PL B595 109	J. Kuhn et al.	(BNL E852 Collab.)
ANISOVICH	01B	PL B500 222	A.V. Anisovich et al.	

$\rho(1900)$ $I^G(J^{PC}) = 1^+(1^-)$

OMITTED FROM SUMMARY TABLE
 See our mini-review under the $\rho(1700)$.

Downloaded from https://academic.oup.com/ptep/article/2020/8/083C01/5891211 by guest on 20 August 2020

Meson Particle Listings

$\rho(1900)$, $f_2(1910)$

$\rho(1900)$ MASS

VALUE (MeV)	EVTs	DOCUMENT ID	TECN	COMMENT
• • • We do not use the following data for averages, fits, limits, etc. • • •				
1909 ± 17 ± 25	54	¹ AUBERT	08s BABR	10.6 e ⁺ e ⁻ → φπ ⁰ γ
1880 ± 30		AUBERT	06d BABR	10.6 e ⁺ e ⁻ → 3π ⁺ 3π ⁻ γ
1860 ± 20		AUBERT	06d BABR	10.6 e ⁺ e ⁻ → 2(π ⁺ π ⁻ π ⁰)γ
1910 ± 10	2,3	FRABETTI	04 E687	γp → 3π ⁺ 3π ⁻ p
1870 ± 10		ANTONELLI	96 SPEC	e ⁺ e ⁻ → hadrons

¹ From the fit with two resonances.
² From a fit with two resonances with the JACOB 72 continuum.
³ Supersedes FRABETTI 01.

$\rho(1900)$ WIDTH

VALUE (MeV)	EVTs	DOCUMENT ID	TECN	COMMENT
• • • We do not use the following data for averages, fits, limits, etc. • • •				
48 ± 17 ± 2	54	⁴ AUBERT	08s BABR	10.6 e ⁺ e ⁻ → φπ ⁰ γ
130 ± 30		AUBERT	06d BABR	10.6 e ⁺ e ⁻ → 3π ⁺ 3π ⁻ γ
160 ± 20		AUBERT	06d BABR	10.6 e ⁺ e ⁻ → 2(π ⁺ π ⁻ π ⁰)γ
37 ± 13	5,6	FRABETTI	04 E687	γp → 3π ⁺ 3π ⁻ p
10 ± 5		ANTONELLI	96 SPEC	e ⁺ e ⁻ → hadrons

⁴ From the fit with two resonances.
⁵ From a fit with two resonances with the JACOB 72 continuum.
⁶ Supersedes FRABETTI 01.

$\rho(1900)$ $\Gamma(\pi)\Gamma(e^+e^-)/\Gamma^2(\text{total})$

VALUE (units 10 ⁻⁸)	EVTs	DOCUMENT ID	TECN	COMMENT
• • • We do not use the following data for averages, fits, limits, etc. • • •				
4.2 ± 1.2 ± 0.8	54	⁷ AUBERT	08s BABR	10.6 e ⁺ e ⁻ → φπ ⁰ γ

⁷ From the fit with two resonances.

$\rho(1900)$ DECAY MODES

Mode	Fraction (Γ_i/Γ)
Γ_1 6π	seen
Γ_2 3π ⁺ 3π ⁻	seen
Γ_3 2π ⁺ 2π ⁻ 2π ⁰	
Γ_4 φπ	
Γ_5 hadrons	seen
Γ_6 e ⁺ e ⁻	seen
Γ_7 $\bar{N}N$	not seen

$\rho(1900)$ BRANCHING RATIOS

VALUE	EVTs	DOCUMENT ID	TECN	COMMENT
seen	8k	AKHMETSHIN 13	CMD3	e ⁺ e ⁻ → 3π ⁺ 3π ⁻
not seen		AGNELLO 02	OBLX	$\bar{n}p \rightarrow 3\pi^+ 2\pi^- \pi^0$
seen		FRABETTI 01	E687	γp → 3π ⁺ 3π ⁻ p
seen		ANTONELLI 96	SPEC	e ⁺ e ⁻ → hadrons

$\rho(1900)$ REFERENCES

AKHMETSHIN 13	PL B723 82	R.R. Akhmetshin et al.	(CMD-3 Collab.)
AUBERT 08s	PR D77 092002	B. Aubert et al.	(BABAR Collab.)
AUBERT 06d	PR D73 052003	B. Aubert et al.	(BABAR Collab.)
FRABETTI 04	PL B578 290	P.L. Frabetti et al.	(FNAL E687 Collab.)
AGNELLO 02	PL B527 39	M. Agnello et al.	(OBELIX Collab.)
FRABETTI 01	PL B514 240	P.L. Frabetti et al.	(FNAL E687 Collab.)
ANTONELLI 96	PL B365 427	A. Antonelli et al.	(FENICE Collab.)
JACOB 72	PR D5 1847	M. Jacob, R. Slansky	

$f_2(1910)$

$$J^{PC} = 0^+(2^{++})$$

OMITTED FROM SUMMARY TABLE

We list here three different peaks with close masses and widths seen in the mass distributions of ωω, ηη', and K⁺K⁻ final states. ALDE 91B argues that they are of different nature.

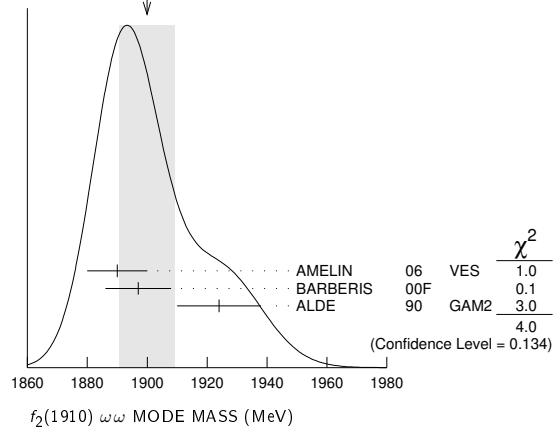
$f_2(1910)$ MASS

$f_2(1910)$ ωω MODE

VALUE (MeV)	DOCUMENT ID	TECN	COMMENT
1900 ± 9 OUR AVERAGE Error includes scale factor of 1.4. See the ideogram below.			
1890 ± 10	¹ AMELIN	06 VES	36 π ⁻ p → ωωn
1897 ± 11	BARBERIS	00F	450 pp → p _f ωωp _s
1924 ± 14	ALDE	90 GAM2	38 π ⁻ p → ωωn

¹ Supersedes BELADIDZE 92b.

WEIGHTED AVERAGE
1900±9 (Error scaled by 1.4)



$f_2(1910)$ ηη' MODE

VALUE (MeV)	DOCUMENT ID	TECN	COMMENT
1934 ± 16			
	¹ BARBERIS	00A	450 pp → p _f ηη'p _s
1934 ± 20	² ANISOVICH	00J	SPEC
1911 ± 10	ALDE	91B	GAM2 38 π ⁻ p → ηη'n

¹ Also compatible with J^{PC}=1⁻⁺.
² Combined fit with ηη, ππ, and ηππ.

$f_2(1910)$ K⁺K⁻ MODE

VALUE (MeV)	DOCUMENT ID	TECN	COMMENT
• • • We do not use the following data for averages, fits, limits, etc. • • •			
1941 ± 18	¹ AMSLER	06	CBAR 1.64 $\bar{p}p \rightarrow K^+K^-\pi^0$

¹ Tentative, could be f₂(1950).

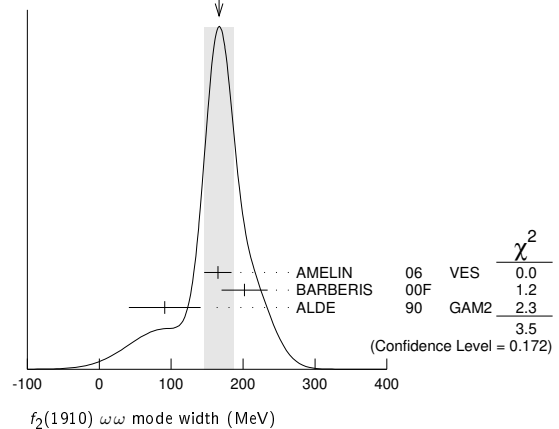
$f_2(1910)$ WIDTH

$f_2(1910)$ ωω MODE

VALUE (MeV)	DOCUMENT ID	TECN	COMMENT
167 ± 21 OUR AVERAGE Error includes scale factor of 1.3. See the ideogram below.			
165 ± 19	¹ AMELIN	06	VES 36 π ⁻ p → ωωn
202 ± 32	BARBERIS	00F	450 pp → p _f ωωp _s
91 ± 50	ALDE	90	GAM2 38 π ⁻ p → ωωn

¹ Supersedes BELADIDZE 92b.

WEIGHTED AVERAGE
167±21 (Error scaled by 1.3)



$f_2(1910)$ ηη' MODE

VALUE (MeV)	DOCUMENT ID	TECN	COMMENT
141 ± 41			
	¹ BARBERIS	00A	450 pp → p _f ηη'p _s
271 ± 25	² ANISOVICH	00J	SPEC
90 ± 35	ALDE	91B	GAM2 38 π ⁻ p → ηη'n

¹ Also compatible with J^{PC}=1⁻⁺.
² Combined fit with ηη, ππ, and ηππ.

See key on page 999

Meson Particle Listings

$f_2(1910)$, $a_0(1950)$, $f_2(1950)$

$f_2(1910) K^+ K^-$ MODE

VALUE (MeV)	DOCUMENT ID	TECN	COMMENT
120 ± 40	AMSLER 06	CBAR	1.64 $\bar{p}p \rightarrow K^+ K^- \pi^0$

$f_2(1910)$ DECAY MODES

Mode	Fraction (Γ_i/Γ)
$\Gamma_1 \pi^0 \pi^0$	
$\Gamma_2 K^+ K^-$	seen
$\Gamma_3 K_S^0 K_S^0$	
$\Gamma_4 \eta \eta$	seen
$\Gamma_5 \omega \omega$	seen
$\Gamma_6 \eta \eta'$	seen
$\Gamma_7 \eta' \eta'$	
$\Gamma_8 \rho \rho$	seen
$\Gamma_9 a_2(1320) \pi$	seen
$\Gamma_{10} f_2(1270) \eta$	seen

$f_2(1910)$ BRANCHING RATIOS

$\Gamma(K^+ K^-)/\Gamma_{total}$	DOCUMENT ID	TECN	COMMENT	Γ_2/Γ
seen	¹ AMSLER 06	CBAR	1.64 $\bar{p}p \rightarrow K^+ K^- \pi^0$	

¹ Tentative, could be $f_2(1950)$.

$\Gamma(\pi^0 \pi^0)/\Gamma(\eta \eta')$	DOCUMENT ID	TECN	COMMENT	Γ_1/Γ_6
<0.1	ALDE 89	GAM2	$38 \pi^- p \rightarrow \eta \eta' n$	

$\Gamma(K_S^0 K_S^0)/\Gamma(\eta \eta')$	DOCUMENT ID	TECN	COMMENT	Γ_3/Γ_6
<0.066	BALOSHIN 86	SPEC	$40 \pi p \rightarrow K_S^0 K_S^0 n$	

$\Gamma(\eta \eta)/\Gamma(\eta \eta')$	DOCUMENT ID	TECN	COMMENT	Γ_4/Γ_6
<0.05	ALDE 91B	GAM2	$38 \pi^- p \rightarrow \eta \eta' n$	

$\Gamma(\omega \omega)/\Gamma(\eta \eta')$	DOCUMENT ID	COMMENT	Γ_5/Γ_6
2.6 ± 0.6	BARBERIS 00F	450 $p p \rightarrow p_f \omega p_S$	

$\Gamma(\eta' \eta')/\Gamma_{total}$	DOCUMENT ID	TECN	COMMENT	Γ_7/Γ
probably not seen possibly seen	BARBERIS 00A BELADIDZE 92D	00A VES	450 $p p \rightarrow p_f \eta' \eta' p_S$ $37 \pi^- p \rightarrow \eta' \eta' n$	

$\Gamma(\rho \rho)/\Gamma(\omega \omega)$	DOCUMENT ID	COMMENT	Γ_8/Γ_5
2.6 ± 0.4	BARBERIS 00F	450 $p p \rightarrow p_f \omega p_S$	

$\Gamma(f_2(1270) \eta)/\Gamma(a_2(1320) \pi)$	DOCUMENT ID	TECN	COMMENT	Γ_{10}/Γ_9
0.09 ± 0.05	¹ ANISOVICH 11	SPEC	0.9-1.94 $p \bar{p}$	

¹ Reanalysis of ADOMEIT 96 and ANISOVICH 00E.

$f_2(1910)$ REFERENCES

ANISOVICH 11	EPJ C71 1511	A.V. Anisovich et al.	(LOQM, RAL, PNPI)
AMELIN 06	PAN 69 690	D.V. Amelin et al.	(VES Collab.)
AMSLER 06	PL B639 165	C. Amstler et al.	(CBAR Collab.)
ANISOVICH 00E	PL B477 19	A.V. Anisovich et al.	
ANISOVICH 00J	PL B491 47	A.V. Anisovich et al.	(RAL, LOQM, PNPI+)
BARBERIS 00A	PL B471 429	D. Barberis et al.	(WA 102 Collab.)
BARBERIS 00F	PL B484 198	D. Barberis et al.	(WA 102 Collab.)
ADOMEIT 96	ZPHY C71 227	J. Adomeit et al.	(Crystal Barrel Collab.)
BELADIDZE 92B	ZPHY C54 367	G.M. Beladidze et al.	(VES Collab.)
BELADIDZE 92D	ZPHY C57 13	G.M. Beladidze et al.	(VES Collab.)
ALDE 91B	SJNP 54 455	D.M. Alde et al.	(SERP, BELG, LANL, LAPP+)
Also	Translated from YAF 54 751.		
ALDE 90	PL B276 375	D.M. Alde et al.	(BELG, SERP, KEK, LANL+)
ALDE 89	PL B241 600	D.M. Alde et al.	(SERP, BELG, LANL, LAPP+)
Also	PL B216 447	D.M. Alde et al.	(SERP, BELG, LANL, LAPP)
Also	SJNP 48 1035	D.M. Alde et al.	(BELG, SERP, LANL, LAPP)
Also	Translated from YAF 48 1724.		
BALOSHIN 86	SJNP 43 959	O.N. Baloshin et al.	(ITEP)
Also	Translated from YAF 43 1487.		

$a_0(1950)$

$$I^G(J^{PC}) = 1^-(0^{++})$$

OMITTED FROM SUMMARY TABLE

Needs confirmation. Seen in $\gamma \gamma \rightarrow \eta_c(1S) \rightarrow K \bar{K} \pi$ by LEES 16A with significance 2.5 σ in $K_S^0 K^\pm \pi^\mp$ and 4.2 σ in $K^+ K^- \pi^0$.

$a_0(1950)$ MASS

VALUE (MeV)	EVTS	DOCUMENT ID	TECN	COMMENT
1931 ± 14 ± 22	12k	^{1,2} LEES	16A	BABR $\gamma \gamma \rightarrow \eta_c(1S) \rightarrow K \bar{K} \pi$
1949 ± 32 ± 76	8k	¹ LEES	16A	BABR $\gamma \gamma \rightarrow \eta_c(1S) \rightarrow K_S^0 K^\pm \pi^\mp$
1927 ± 15 ± 23	4k	¹ LEES	16A	BABR $\gamma \gamma \rightarrow \eta_c(1S) \rightarrow K^+ K^- \pi^0$

¹ From a model-independent partial wave analysis fit to a relativistic Breit-Wigner function with a floating width.
² Weighted average of the $K_S^0 K^\pm$ and $K^+ K^-$ decay modes.

$a_0(1950)$ WIDTH

VALUE (MeV)	EVTS	DOCUMENT ID	TECN	COMMENT
271 ± 22 ± 29	12k	^{1,2} LEES	16A	BABR $\gamma \gamma \rightarrow \eta_c(1S) \rightarrow K \bar{K} \pi$
265 ± 36 ± 110	8k	¹ LEES	16A	BABR $\gamma \gamma \rightarrow \eta_c(1S) \rightarrow K_S^0 K^\pm \pi^\mp$
274 ± 28 ± 30	4k	¹ LEES	16A	BABR $\gamma \gamma \rightarrow \eta_c(1S) \rightarrow K^+ K^- \pi^0$

¹ From a model-independent partial wave analysis fit to a relativistic Breit-Wigner function with a floating mass.
² Weighted average of the $K_S^0 K^\pm$ and $K^+ K^-$ decay modes.

$a_0(1950)$ DECAY MODES

Mode	Fraction (Γ_i/Γ)
$\Gamma_1 K \bar{K}$	seen

$a_0(1950)$ BRANCHING RATIOS

$\Gamma(K \bar{K})/\Gamma_{total}$	DOCUMENT ID	TECN	COMMENT	Γ_1/Γ
seen	LEES 12k	¹ LEES	16A	BABR $\gamma \gamma \rightarrow \eta_c(1S) \rightarrow K \bar{K} \pi$

¹ From a model-independent partial wave analysis.

$a_0(1950)$ REFERENCES

LEES 16A PR D93 012005 J.P. Lees et al. (BABAR Collab.)

$f_2(1950)$

$$I^G(J^{PC}) = 0^+(2^{++})$$

$f_2(1950)$ MASS

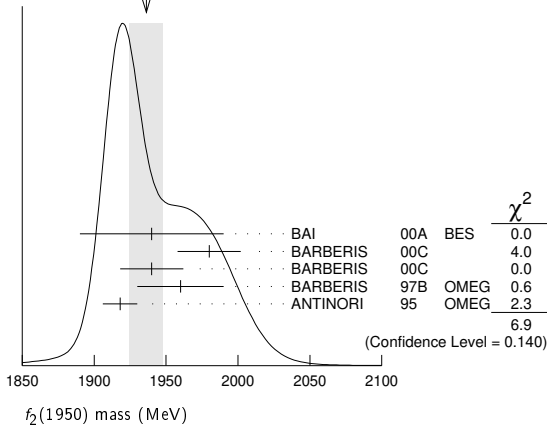
VALUE (MeV)	DOCUMENT ID	TECN	COMMENT
1936 ± 12 OUR AVERAGE			Error includes scale factor of 1.3. See the ideogram below.
1940 ± 50	BAI 00A	BES	$J/\psi \rightarrow \gamma(\pi^+ \pi^- \pi^+ \pi^-)$
1980 ± 22	¹ BARBERIS 00C		450 $p p \rightarrow p p 4 \pi$
1940 ± 22	² BARBERIS 00C		450 $p p \rightarrow p p 2 \pi 2 \pi^0$
1960 ± 30	BARBERIS 97B	OMEG	450 $p p \rightarrow p p 2(\pi^+ \pi^-)$
1918 ± 12	ANTINORI 95	OMEG	300,450 $p p \rightarrow p p 2(\pi^+ \pi^-)$
2038 ⁺¹³⁺¹² ₋₁₁₋₇₃	³ UEHARA 09	BELL	10.6 $e^+ e^- \rightarrow e^+ e^- \pi^0 \pi^0$
1930 ± 25	⁴ BINON 05	GAMS	33 $\pi^- p \rightarrow \eta \eta n$
1980 ± 2 ± 14	ABE 04	BELL	10.6 $e^+ e^- \rightarrow e^+ e^- K^+ K^-$
1867 ± 46	⁵ AMSLER 02	CBAR	0.9 $\bar{p} p \rightarrow \pi^0 \eta \eta, \pi^0 \pi^0 \pi^0$
2010 ± 25	ANISOVICH 00J	SPEC	
1980 ± 50	ANISOVICH 99B	SPEC	1.35-1.94 $p \bar{p} \rightarrow \eta \eta \pi^0$
~ 1990	⁶ OAKDEN 94	RVUE	0.36-1.55 $p \bar{p} \rightarrow \pi \pi$
1950 ± 15	⁷ ASTON 91	LASS	11 $K^- p \rightarrow \Lambda K \bar{K} \pi \pi$

- Decaying into $\pi^+ \pi^- 2 \pi^0$.
- Decaying into $2(\pi^+ \pi^-)$.
- Taking into account $f_4(2050)$.
- First solution, PWA is ambiguous.
- T-matrix pole.
- From solution B of amplitude analysis of data on $p \bar{p} \rightarrow \pi \pi$. See however KLOET 96 who fit $\pi^+ \pi^-$ only and find waves only up to $J = 3$ to be important but not significantly resonant.
- Cannot determine spin to be 2.

Meson Particle Listings

$f_2(1950)$, $a_4(1970)$

WEIGHTED AVERAGE
1936±12 (Error scaled by 1.3)



$f_2(1950)$ WIDTH

VALUE (MeV)	DOCUMENT ID	TECN	COMMENT
464 ± 24 OUR AVERAGE			
380 ⁺¹²⁰ ₋₉₀	BAI	00A	BES $J/\psi \rightarrow \gamma(\pi^+\pi^-\pi^+\pi^-)$
520 ± 50	⁸ BARBERIS	00c	450 $pp \rightarrow pp4\pi$
485 ± 55	⁹ BARBERIS	00c	450 $pp \rightarrow pp4\pi$
460 ± 40	BARBERIS	97B	OMEG 450 $pp \rightarrow pp2(\pi^+\pi^-)$
390 ± 60	ANTINORI	95	OMEG 300,450 $pp \rightarrow pp2(\pi^+\pi^-)$
441 ⁺²⁷⁺²⁸ ₋₂₅₋₁₉₂	¹⁰ UEHARA	09	BELL 10.6 $e^+e^- \rightarrow e^+e^-\pi^0\pi^0$
450 ± 50	¹¹ BINON	05	GAMS 33 $\pi^-p \rightarrow \eta\eta n$
297 ± 12 ± 6	ABE	04	BELL 10.6 $e^+e^- \rightarrow e^+e^-K^+K^-$
385 ± 58	¹² AMSLER	02	CBAR 0.9 $\bar{p}p \rightarrow \pi^0\eta\eta, \pi^0\pi^0\pi^0$
495 ± 35	ANISOVICH	00j	SPEC
500 ± 100	ANISOVICH	99B	SPEC 1.35-1.94 $\bar{p}p \rightarrow \eta\eta\pi^0$
~100	¹³ OAKDEN	94	RVUE 0.36-1.55 $\bar{p}p \rightarrow \pi\pi$
25 ± 50	¹⁴ ASTON	91	LASS 11 $K^-p \rightarrow \Lambda K\bar{K}\pi\pi$

- • • We do not use the following data for averages, fits, limits, etc. • • •
- ⁸ Decaying into $\pi^+\pi^-\pi^0$.
- ⁹ Decaying into $2(\pi^+\pi^-)$.
- ¹⁰ Taking into account $f_4(2050)$.
- ¹¹ First solution, PWA is ambiguous.
- ¹² T-matrix pole.
- ¹³ From solution B of amplitude analysis of data on $\bar{p}p \rightarrow \pi\pi$. See however KLOET 96 who fit $\pi^+\pi^-$ only and find waves only up to $J = 3$ to be important but not significantly resonant.
- ¹⁴ Cannot determine spin to be 2.

$f_2(1950)$ DECAY MODES

Mode	Fraction (Γ_i/Γ)
Γ_1 $K^*(892)\bar{K}^*(892)$	seen
Γ_2 $\pi\pi$	
Γ_3 $\pi^+\pi^-$	seen
Γ_4 $\pi^0\pi^0$	seen
Γ_5 4π	seen
Γ_6 $\pi^+\pi^-\pi^+\pi^-$	
Γ_7 $a_2(1320)\pi$	
Γ_8 $f_2(1270)\pi\pi$	
Γ_9 $\eta\eta$	seen
Γ_{10} $K\bar{K}$	seen
Γ_{11} $\gamma\gamma$	seen
Γ_{12} $\rho\bar{\rho}$	seen

$f_2(1950)$ $\Gamma(i)\Gamma(\gamma\gamma)/\Gamma(\text{total})$

VALUE (eV)	DOCUMENT ID	TECN	COMMENT	$\Gamma_{10}\Gamma_{11}/\Gamma$
122 ± 4 ± 26	¹⁵ ABE	04	BELL 10.6 $e^+e^- \rightarrow e^+e^-K^+K^-$	

• • • We do not use the following data for averages, fits, limits, etc. • • •

¹⁵ Assuming spin 2.

$\Gamma(\pi\pi) \times \Gamma(\gamma\gamma)/\Gamma_{\text{total}}$ $\Gamma_2\Gamma_{11}/\Gamma$

VALUE	DOCUMENT ID	TECN	COMMENT
• • • We do not use the following data for averages, fits, limits, etc. • • •			
162 ⁺⁶⁹⁺¹¹³⁷ ₋₄₂₋₂₀₄	¹⁶ UEHARA	09	BELL 10.6 $e^+e^- \rightarrow e^+e^-\pi^0\pi^0$

¹⁶ Taking into account $f_4(2050)$.

$f_2(1950)$ BRANCHING RATIOS

$\Gamma(K^*(892)\bar{K}^*(892))/\Gamma_{\text{total}}$	Γ_1/Γ
seen	ASTON 91 LASS 0 11 $K^-p \rightarrow \Lambda K\bar{K}\pi\pi$

$\Gamma(a_2(1320)\pi)/\Gamma_{\text{total}}$ Γ_7/Γ

VALUE	DOCUMENT ID	TECN	COMMENT
• • • We do not use the following data for averages, fits, limits, etc. • • •			
not seen	BARBERIS	00B	450 $pp \rightarrow p_f\eta\pi^+\pi^-\rho_S$
not seen	BARBERIS	00C	450 $pp \rightarrow p_f4\pi\rho_S$
possibly seen	BARBERIS	97B	OMEG 450 $pp \rightarrow pp2(\pi^+\pi^-)$

$\Gamma(\eta\eta)/\Gamma(4\pi)$ Γ_9/Γ_5

VALUE	CL%	DOCUMENT ID	COMMENT
• • • We do not use the following data for averages, fits, limits, etc. • • •			
<5.0 × 10 ⁻³	90	BARBERIS	00E 450 $pp \rightarrow p_f\eta\eta\rho_S$

$\Gamma(\eta\eta)/\Gamma(\pi^+\pi^-)$ Γ_9/Γ_3

VALUE	DOCUMENT ID	TECN	COMMENT
0.14 ± 0.05	AMSLER	02	CBAR 0.9 $\bar{p}p \rightarrow \pi^0\eta\eta, \pi^0\pi^0\pi^0$

$\Gamma(\rho\bar{\rho})/\Gamma_{\text{total}}$ Γ_{12}/Γ

VALUE	EVTS	DOCUMENT ID	TECN	COMMENT
seen	111	ALEXANDER	10	CLEO $\psi(2S) \rightarrow \gamma\rho\bar{\rho}$

$f_2(1950)$ REFERENCES

ALEXANDER 10	PR D82 092002	J.P. Alexander et al.	(CLEO Collab.)
UEHARA 09	PR D79 052009	S. Uehara et al.	(BELLE Collab.)
BINON 05	PAN 68 960	F. Binon et al.	
	Translated from YAF 68 998.		
ABE 04	EPJ C32 323	K. Abe et al.	(BELLE Collab.)
AMSLER 02	EPJ C23 29	C. Amisler et al.	
ANISOVICH 00J	PL B491 47	A.V. Anisovich et al.	(RAL, LOQM, FNPI+)
BAI 00A	PL B472 207	J.Z. Bai et al.	(BES Collab.)
BARBERIS 00B	PL B471 435	D. Barberis et al.	(WA 102 Collab.)
BARBERIS 00C	PL B471 440	D. Barberis et al.	(WA 102 Collab.)
BARBERIS 00E	PL B479 59	D. Barberis et al.	(WA 102 Collab.)
ANISOVICH 99B	PL B449 154	A.V. Anisovich et al.	
BARBERIS 97B	PL B413 217	D. Barberis et al.	(WA 102 Collab.)
KLOET 96	PR D53 6120	W.M. Kloet, F. Myhrer	(RUTG, NORD)
ANTINORI 95	PL B353 589	F. Antinori et al.	(ATHU, BARI, BIRM+JP)
OAKDEN 94	NP A574 731	M.N. Oakden, M.R. Pennington	(DURH)
ASTON 91	NPBS B21 5	D. Aston et al.	(LASS Collab.)

$a_4(1970)$

$$I^G(J^{PC}) = 1^-(4^{++})$$

was $a_4(2040)$

$a_4(1970)$ MASS

VALUE (MeV)	EVTS	DOCUMENT ID	TECN	CHG	COMMENT
1967 ± 16 OUR AVERAGE		Error includes scale factor of 2.1. See the ideogram below.			
1935 ⁺¹¹ ₋₁₃	46M	¹ AGHASYAN	18B	COMP	190 $\pi^-p \rightarrow \pi^-\pi^+\pi^-\rho$
1900 ⁺⁸⁰ ₋₂₀		ADOLPH	15	COMP	191 $\pi^-p \rightarrow \eta^{(\prime)}\pi^-\rho$
1985 ± 10 ± 13	145k	LU	05	B852	18 $\pi^-p \rightarrow \omega\pi^-\pi^0\rho$
1996 ± 25 ± 43		CHUNG	02	B852	18.3 $\pi^-p \rightarrow 3\pi\rho$
2000 ± 40 ⁺⁶⁰ ₋₂₀		IVANOV	01	B852	18 $\pi^-p \rightarrow \eta'\pi^-\rho$
2010 ± 20		² DONSKOV	96	GAM2 0	38 $\pi^-p \rightarrow \eta\pi^0 n$
2040 ± 30		³ CLELAND	82B	SPEC ±	50 $\pi\rho \rightarrow K_S^0 K^\pm\rho$
• • • We do not use the following data for averages, fits, limits, etc. • • •					
1885 ± 13 ⁺⁵⁰ ₋₂	420k	⁴ ALEKSEEV	10	COMP	190 $\pi^-\rho \rightarrow \pi^-\pi^-\pi^+\rho$
2004 ± 6	80k	⁵ UMAN	06	E835	5.2 $\bar{p}p \rightarrow \eta\eta\pi^0$
2005 ± 25 ₋₄₅		⁶ ANISOVICH	01F	SPEC	2.0 $\bar{p}p \rightarrow 3\pi^0, \pi^0\eta, \pi^0\eta'$
1944 ± 8 ± 50		⁷ AMELIN	99	VES	37 $\pi^-A \rightarrow \omega\pi^-\pi^0 A^*$
1903 ± 10		⁸ BALDI	78	SPEC	10 $\pi^-p \rightarrow \rho K_S^0 K^-$
2030 ± 50		⁹ CORDEN	78c	OMEG 0	15 $\pi^-p \rightarrow 3\pi n$

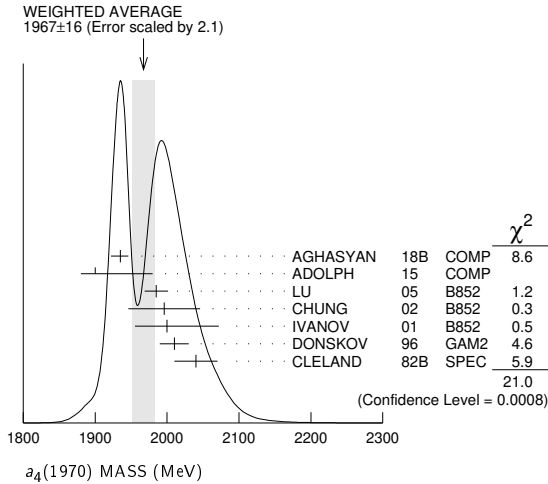
- ¹ Statistical error negligible.
- ² From a simultaneous fit to the G_+ and G_0 wave intensities.
- ³ From an amplitude analysis.
- ⁴ Superseded by AGHASYAN 2018B.
- ⁵ Statistical error only.
- ⁶ From the combined analysis of ANISOVICH 99c, ANISOVICH 99e, and ANISOVICH 01F.

See key on page 999

Meson Particle Listings

$a_4(1970), \rho_3(1990), \pi_2(2005)$

⁷ May be a different state.
⁸ From a fit to the Y_8^0 moment. Limited by phase space.
⁹ $J^P = 4^+$ is favored, though $J^P = 2^+$ cannot be excluded.



$a_4(1970)$ WIDTH

VALUE (MeV)	EVTS	DOCUMENT ID	TECN	CHG	COMMENT
$324 \pm \frac{15}{18}$ OUR AVERAGE					
$333 \pm \frac{16}{21}$	46M	¹ AGHASYAN	18B	COMP	$190 \pi^- p \rightarrow \pi^- \pi^+ \pi^- p$
$300 \pm \frac{80}{100}$		ADOLPH	15	COMP	$191 \pi^- p \rightarrow \eta^{(\prime)} \pi^- p$
$231 \pm \frac{30 \pm 46}{81 \pm 85}$	145k	LU	05	B852	$18 \pi^- p \rightarrow \omega \pi^- \pi^0 p$
$298 \pm \frac{81 \pm 85}{50}$		CHUNG	02	B852	$18.3 \pi^- p \rightarrow 3\pi p$
$350 \pm \frac{100 \pm 70}{50}$		IVANOV	01	B852	$18 \pi^- p \rightarrow \eta' \pi^- p$
370 ± 80		² DONSKOV	96	GAM2 0	$38 \pi^- p \rightarrow \eta \pi^0 n$
380 ± 150		³ CLELAND	82B	SPEC ±	$50 \pi^- p \rightarrow K_S^0 K^\pm p$
• • • We do not use the following data for averages, fits, limits, etc. • • •					
$294 \pm \frac{25 \pm 46}{19}$	420k	⁴ ALEKSEEV	10	COMP	$190 \pi^- p \rightarrow \pi^- \pi^- \pi^+ P b'$
401 ± 16	80k	⁵ UMAN	06	E835	$5.2 \bar{p} p \rightarrow \eta \eta \pi^0$
180 ± 30		⁶ ANISOVICH	01F	SPEC	$2.0 \bar{p} p \rightarrow 3\pi^0, \pi^0 \eta, \pi^0 \eta'$
$324 \pm 26 \pm 75$		⁷ AMELIN	99	VES	$37 \pi^- A \rightarrow \omega \pi^- \pi^0 A^*$
166 ± 43		⁸ BALDI	78	SPEC -	$10 \pi^- p \rightarrow \rho K_S^0 K^-$
510 ± 200		⁹ CORDEN	78C	OMEG 0	$15 \pi^- p \rightarrow 3\pi n$

¹ Statistical error negligible.
² From a simultaneous fit to the G_+ and G_0 wave intensities.
³ From an amplitude analysis.
⁴ Superseded by AGHASYAN 2018B.
⁵ Statistical error only.
⁶ From the combined analysis of ANISOVICH 99C, ANISOVICH 99E, and ANISOVICH 01F.
⁷ May be a different state.
⁸ From a fit to the Y_8^0 moment. Limited by phase space.
⁹ $J^P = 4^+$ is favored, though $J^P = 2^+$ cannot be excluded.

$a_4(1970)$ DECAY MODES

Mode	Fraction (Γ_i/Γ)
Γ_1 $K\bar{K}$	seen
Γ_2 $\pi^+ \pi^- \pi^0$	seen
Γ_3 $\rho\pi$	seen
Γ_4 $f_2(1270)\pi$	seen
Γ_5 $\omega \pi^- \pi^0$	seen
Γ_6 $\omega\rho$	seen
Γ_7 $\eta\pi$	seen
Γ_8 $\eta'(958)\pi$	seen

$a_4(1970)$ BRANCHING RATIOS

$\Gamma(K\bar{K})/\Gamma_{total}$	Γ_1/Γ			
VALUE	DOCUMENT ID	TECN	CHG	COMMENT
seen	BALDI	78	SPEC ±	$10 \pi^- p \rightarrow K_S^0 K^- p$
$\Gamma(\pi^+ \pi^- \pi^0)/\Gamma_{total}$	Γ_2/Γ			
VALUE	DOCUMENT ID	TECN	CHG	COMMENT
seen	CORDEN	78C	OMEG 0	$15 \pi^- p \rightarrow 3\pi n$

$\Gamma(\rho\pi)/\Gamma(f_2(1270)\pi)$

VALUE	EVTS	DOCUMENT ID	TECN	COMMENT
$1.7 \pm \frac{0.9}{0.8}$ OUR AVERAGE				Error includes scale factor of 3.7.
$2.9 \pm \frac{0.6}{0.4}$	46M	¹ AGHASYAN	18B	COMP $190 \pi^- p \rightarrow \pi^- \pi^+ \pi^- p$
$1.1 \pm 0.2 \pm 0.2$		CHUNG	02	B852 $18.3 \pi^- p \rightarrow 3\pi p$
¹ Statistical error negligible.				

$\Gamma(\eta\pi)/\Gamma_{total}$

VALUE	DOCUMENT ID	TECN	CHG	COMMENT
seen	DONSKOV	96	GAM2 0	$38 \pi^- p \rightarrow \eta \pi^0 n$

$\Gamma(\eta'(958)\pi)/\Gamma(\eta\pi)$

VALUE	DOCUMENT ID	TECN	COMMENT
0.23 ± 0.07	ADOLPH	15	COMP $191 \pi^- p \rightarrow \eta^{(\prime)} \pi^- p$

$\Gamma(\omega\rho)/\Gamma_{total}$

VALUE	EVTS	DOCUMENT ID	TECN	COMMENT
seen	145k	LU	05	B852 $18 \pi^- p \rightarrow \omega \pi^- \pi^0 p$

$a_4(1970)$ REFERENCES

AGHASYAN	18B	PR D98 092003	M. Aghasyan et al.	(COMPASS Collab.)
ADOLPH	15	PL B740 303	M. Adolph et al.	(COMPASS Collab.)
ALEKSEEV	10	PRL 104 241803	M.G. Aleksev et al.	(COMPASS Collab.)
UMAN	06	PR D73 052009	I. Uman et al.	(FNAL E835)
LU	05	PRL 94 032002	M. Lu et al.	(BNL E852 Collab.)
CHUNG	02	PR D65 072001	S.U. Chung et al.	(BNL E852 Collab.)
ANISOVICH	01F	PL B517 261	A.V. Anisovich et al.	
IVANOV	01	PRL 86 3977	E.I. Ivanov et al.	(BNL E852 Collab.)
AMELIN	99	PAN 62 445	D.V. Amelin et al.	(VES Collab.)
Translated from YAF 62 487.				
ANISOVICH	99C	PL B452 173	A.V. Anisovich et al.	
ANISOVICH	99E	PL B452 187	A.V. Anisovich et al.	
DONSKOV	96	PAN 59 982	S.V. Donskov et al.	(GAMS Collab.) IJGPC
Translated from YAF 59 1027.				
CLELAND	82B	NP B208 228	W.E. Cleland et al.	(DURH, GEVA, LAUS+)
BALDI	78	PL 74B 413	R. Baldi et al.	(GEVA) JP
CORDEN	78C	NP B136 77	M.J. Corden et al.	(BIRM, RHEL, TELA+) JP

$\rho_3(1990)$

$$I^G(J^{PC}) = 1^+(3^{--})$$

OMITTED FROM SUMMARY TABLE

$\rho_3(1990)$ MASS

VALUE (MeV)	DOCUMENT ID	TECN	COMMENT
• • • We do not use the following data for averages, fits, limits, etc. • • •			
1982 ± 14	¹ ANISOVICH	02	SPEC $0.6-1.9 p\bar{p} \rightarrow \omega \pi^0, \omega \eta \pi^0, \pi^+ \pi^-$
~ 2007	HASAN	94	RVUE $\bar{p} p \rightarrow \pi \pi$
¹ From the combined analysis of ANISOVICH 00J, ANISOVICH 01D, ANISOVICH 01E, and ANISOVICH 02.			

$\rho_3(1990)$ WIDTH

VALUE (MeV)	DOCUMENT ID	TECN	COMMENT
• • • We do not use the following data for averages, fits, limits, etc. • • •			
188 ± 24	² ANISOVICH	02	SPEC $0.6-1.9 p\bar{p} \rightarrow \omega \pi^0, \omega \eta \pi^0, \pi^+ \pi^-$
~ 287	HASAN	94	RVUE $\bar{p} p \rightarrow \pi \pi$
² From the combined analysis of ANISOVICH 00J, ANISOVICH 01D, ANISOVICH 01E, and ANISOVICH 02.			

$\rho_3(1990)$ REFERENCES

ANISOVICH	02	PL B542 8	A.V. Anisovich et al.
ANISOVICH	01D	PL B508 6	A.V. Anisovich et al.
ANISOVICH	01E	PL B513 281	A.V. Anisovich et al.
ANISOVICH	00J	PL B491 47	A.V. Anisovich et al.
HASAN	94	PL B334 215	A. Hasan, D.V. Bugg

$\pi_2(2005)$

$$I^G(J^{PC}) = 1^-(2^{-+})$$

OMITTED FROM SUMMARY TABLE

$\pi_2(2005)$ MASS

VALUE (MeV)	EVTS	DOCUMENT ID	TECN	COMMENT
$1963 \pm \frac{17}{27}$ OUR AVERAGE				
$1962 \pm \frac{17}{29}$	46M	¹ AGHASYAN	18B	COMP $190 \pi^- p \rightarrow \pi^- \pi^+ \pi^- p$
$1974 \pm 14 \pm 83$	145k	LU	05	B852 $18 \pi^- p \rightarrow \omega \pi^- \pi^0 p$
2005 ± 15		ANISOVICH	01F	SPEC $2.0 \bar{p} p \rightarrow 3\pi^0, \pi^0 \eta, \pi^0 \eta'$
¹ Statistical uncertainty negligible.				

Meson Particle Listings

 $\pi_2(2005)$, $f_2(2010)$, $f_0(2020)$ $\pi_2(2005)$ WIDTH

VALUE (MeV)	EVTS	DOCUMENT ID	TECN	COMMENT
370^{+16}_{-120}	46M	¹ AGHASYAN	18B COMP	$190 \pi^- p \rightarrow \pi^- \pi^+ \pi^- p$
$341 \pm 61 \pm 139$	145k	LU	05 B852	$18 \pi^- p \rightarrow \omega \pi^- \pi^0 p$
••• We do not use the following data for averages, fits, limits, etc. •••				
200 ± 40		ANISOVICH	01F SPEC	$2.0 \bar{p} p \rightarrow 3\pi^0, \pi^0 \eta, \pi^0 \eta'$
¹ Statistical uncertainty negligible.				

 $\pi_2(2005)$ DECAY MODES

Mode	Fraction (Γ_i/Γ)
$\Gamma_1 \pi^- \pi^+ \pi^-$	seen
$\Gamma_2 \omega \pi^0 \pi^-$	seen

 $\pi_2(2005)$ BRANCHING RATIOS

$\Gamma(\pi^- \pi^+ \pi^-)/\Gamma_{\text{total}}$	Γ_1/Γ		
VALUE	DOCUMENT ID	TECN	COMMENT
seen	AGHASYAN	18B COMP	$190 \pi^- p \rightarrow \pi^- \pi^+ \pi^- p$
$\Gamma(\omega \pi^0 \pi^-)/\Gamma_{\text{total}}$	Γ_2/Γ		
VALUE	DOCUMENT ID	TECN	COMMENT
seen	LU	05 B852	$18 \pi^- p \rightarrow \omega \pi^- \pi^0 p$

 $\pi_2(2005)$ REFERENCES

AGHASYAN	18B	PR D98 092003	M. Aghasyan et al.	(COMPASS Collab.)
LU	05	PRL 94 032002	M. Lu et al.	(BNL E852 Collab.)
ANISOVICH	01F	PL B517 261	A.V. Anisovich et al.	

 $f_2(2010)$

$$J^G(J^{PC}) = 0^+(2^{++})$$

 $f_2(2010)$ MASS

VALUE (MeV)	DOCUMENT ID	TECN	COMMENT
2011^{+62}_{-76}	¹ ETKIN	88 MPS	$22 \pi^- p \rightarrow \phi \phi n$
••• We do not use the following data for averages, fits, limits, etc. •••			
2005 ± 12	VLADIMIRSK...06	SPEC	$40 \pi^- p \rightarrow K_S^0 K_S^0 n$
1980 ± 20	² BOLONKIN	88 SPEC	$40 \pi^- p \rightarrow K_S^0 K_S^0 n$
2050^{+90}_{-50}	ETKIN	85 MPS	$22 \pi^- p \rightarrow 2\phi n$
2120^{+20}_{-120}	LINDENBAUM	84 RVUE	
2160 ± 50	ETKIN	82 MPS	$22 \pi^- p \rightarrow 2\phi n$

¹Includes data of ETKIN 85. The percentage of the resonance going into $\phi \phi 2^{++} S_2$, D_2 , and D_0 is 98^{+1}_{-3} , 0^{+1}_{-0} , and 2^{+2}_{-1} , respectively.

²Statistically very weak, only 1.4 s.d.

 $f_2(2010)$ WIDTH

VALUE (MeV)	DOCUMENT ID	TECN	COMMENT
202^{+67}_{-62}	³ ETKIN	88 MPS	$22 \pi^- p \rightarrow \phi \phi n$
••• We do not use the following data for averages, fits, limits, etc. •••			
209 ± 32	VLADIMIRSK...06	SPEC	$40 \pi^- p \rightarrow K_S^0 K_S^0 n$
145 ± 50	⁴ BOLONKIN	88 SPEC	$40 \pi^- p \rightarrow K_S^0 K_S^0 n$
200^{+160}_{-50}	ETKIN	85 MPS	$22 \pi^- p \rightarrow 2\phi n$
300^{+150}_{-50}	LINDENBAUM	84 RVUE	
310 ± 70	ETKIN	82 MPS	$22 \pi^- p \rightarrow 2\phi n$

³Includes data of ETKIN 85.

⁴Statistically very weak, only 1.4 s.d.

 $f_2(2010)$ DECAY MODES

Mode	Fraction (Γ_i/Γ)
$\Gamma_1 \phi \phi$	seen
$\Gamma_2 K \bar{K}$	seen

 $f_2(2010)$ BRANCHING RATIOS

$\Gamma(K \bar{K})/\Gamma_{\text{total}}$	Γ_2/Γ		
VALUE	DOCUMENT ID	TECN	COMMENT
seen	VLADIMIRSK...06	SPEC	$40 \pi^- p \rightarrow K_S^0 K_S^0 n$

 $f_0(2010)$ REFERENCES

VLADIMIRSK...06	PAN 69 493	V.V. Vladimirov et al.	(ITEP, Moscow)
	Translated from YAF 69 515.		
BOLONKIN	88 NP B309 426	B.V. Bolonkin et al.	(ITEP, SERP)
ETKIN	88 PL B201 568	A. Etkin et al.	(BNL, CUNY)
ETKIN	85 PL 165B 217	A. Etkin et al.	(BNL, CUNY)
LINDENBAUM	84 CNPP 13 285	S.J. Lindenbaum	(CUNY)
ETKIN	82 PRL 49 1620	A. Etkin et al.	(BNL, CUNY)
Also	Brighton Conf. 351	S.J. Lindenbaum	(BNL, CUNY)

 $f_0(2020)$

$$J^G(J^{PC}) = 0^+(0^{++})$$

OMITTED FROM SUMMARY TABLE

Needs confirmation.

 $f_0(2020)$ MASS

VALUE (MeV)	EVTS	DOCUMENT ID	TECN	COMMENT
1992 ± 16		^{1,2} BARBERIS	00C	$450 pp \rightarrow p_f 4\pi p_s$
••• We do not use the following data for averages, fits, limits, etc. •••				
1910 ± 50		³ ROPERTZ	18 RVUE	$\bar{B}_s^0 \rightarrow J/\psi(\pi^+ \pi^- / K^+ K^-)$
2037 ± 8	80k	⁴ UMAN	06 E835	$5.2 \bar{p} p \rightarrow \eta \eta \pi^0$
2040 ± 38		ANISOVICH	00J SPEC	
2010 ± 60		ALDE	98 GAM4	$100 \pi^- p \rightarrow \pi^0 \pi^0 n$
2020 ± 35		BARBERIS	97B OMEG	$450 pp \rightarrow p p 2(\pi^+ \pi^-)$

¹Average between $\pi^+ \pi^- 2\pi^0$ and $2(\pi^+ \pi^-)$.

²T-matrix pole.

³T-matrix pole of 3 channel unitary model fit to data from AAIJ 14Br and AAIJ 17v extracted using Pade approximants.

⁴Statistical error only.

 $f_0(2020)$ WIDTH

VALUE (MeV)	EVTS	DOCUMENT ID	TECN	COMMENT
442 ± 60		^{1,2} BARBERIS	00C	$450 pp \rightarrow p_f 4\pi p_s$
••• We do not use the following data for averages, fits, limits, etc. •••				
400 ± 80		³ ROPERTZ	18 RVUE	$\bar{B}_s^0 \rightarrow J/\psi(\pi^+ \pi^- / K^+ K^-)$
296 ± 17	80k	⁴ UMAN	06 E835	$5.2 \bar{p} p \rightarrow \eta \eta \pi^0$
405 ± 40		ANISOVICH	00J SPEC	
240 ± 100		ALDE	98 GAM4	$100 \pi^- p \rightarrow \pi^0 \pi^0 n$
410 ± 50		BARBERIS	97B OMEG	$450 pp \rightarrow p p 2(\pi^+ \pi^-)$

¹Average between $\pi^+ \pi^- 2\pi^0$ and $2(\pi^+ \pi^-)$.

²T-matrix pole.

³T-matrix pole of 3 channel unitary model fit to data from AAIJ 14Br and AAIJ 17v extracted using Pade approximants.

⁴Statistical error only.

 $f_0(2020)$ DECAY MODES

Mode	Fraction (Γ_i/Γ)
$\Gamma_1 \rho \pi \pi$	seen
$\Gamma_2 \pi^0 \pi^0$	seen
$\Gamma_3 \rho \rho$	seen
$\Gamma_4 \omega \omega$	seen
$\Gamma_5 \eta \eta$	seen

 $f_0(2020)$ BRANCHING RATIOS

$\Gamma(\rho \rho)/\Gamma(\omega \omega)$	Γ_3/Γ_4		
VALUE	DOCUMENT ID	TECN	COMMENT
~3	BARBERIS	00F	$450 pp \rightarrow p_f \omega \omega p_s$
$\Gamma(\eta \eta)/\Gamma_{\text{total}}$	Γ_5/Γ		
VALUE	DOCUMENT ID	TECN	COMMENT
seen	UMAN	06 E835	$5.2 \bar{p} p \rightarrow \eta \eta \pi^0$

 $f_0(2020)$ REFERENCES

ROPERTZ	18	EPJ C78 1000	S. Ropertz, C. Hanhart, B. Kubis	(BONN, JULI)
AAIJ	17V	JHEP 1708 037	R. Aaij et al.	(LHCb Collab.)
AAIJ	14BR	PR D89 092006	R. Aaij et al.	(LHCb Collab.)
UMAN	06	PR D73 052009	L. Uman et al.	(FNAL E835)
ANISOVICH	00J	PL B491 47	A.V. Anisovich et al.	(RAL, LOQM, PNPI+)
BARBERIS	00C	PL B471 440	D. Barberis et al.	(WA 102 Collab.)
BARBERIS	00F	PL B484 198	D. Barberis et al.	(WA 102 Collab.)
ALDE	98	EPJ A3 361	D. Alde et al.	(GAM4 Collab.)
Also	PAN	62 405	D. Alde et al.	(GAMS Collab.)
BARBERIS	97B	PL B413 217	D. Barberis et al.	(WA 102 Collab.)
		Translated from YAF 62 446.		

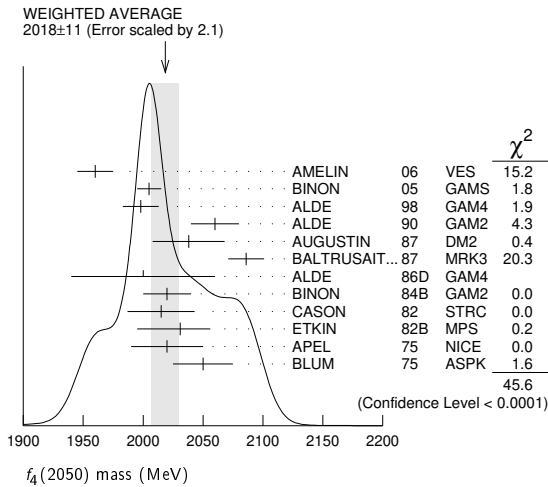
$f_4(2050)$

$I^G(J^{PC}) = 0^+(4^{++})$

$f_4(2050)$ MASS

VALUE (MeV)	EVTs	DOCUMENT ID	TECN	COMMENT
2018 ± 11	OUR AVERAGE	Error includes scale factor of 2.1. See the ideogram below.		
1960 ± 15		AMELIN 06	VES	$36 \pi^- p \rightarrow \omega \omega n$
2005 ± 10		BINON 05	GAMS	$33 \pi^- p \rightarrow \eta \eta n$
1998 ± 15		ALDE 98	GAM4	$100 \pi^- p \rightarrow \pi^0 \pi^0 n$
2060 ± 20		ALDE 90	GAM2	$38 \pi^- p \rightarrow \omega \omega n$
2038 ± 30		AUGUSTIN 87	DM2	$J/\psi \rightarrow \gamma \pi^+ \pi^-$
2086 ± 15		BALTRUSAIT... 87	MRK3	$J/\psi \rightarrow \gamma \pi^+ \pi^-$
2000 ± 60		ALDE 86D	GAM4	$100 \pi^- p \rightarrow n 2 \eta$
2020 ± 20	40k	BINON 84B	GAM2	$38 \pi^- p \rightarrow n 2 \pi^0$
2015 ± 28		CASON 82	STRC	$8 \pi^+ p \rightarrow \Delta^{++} \pi^0 \pi^0$
2031 ⁺²⁵ ₋₃₆		ETKIN 82B	MPS	$23 \pi^- p \rightarrow n 2 K^0_S$
2020 ± 30	700	APEL 75	NICE	$40 \pi^- p \rightarrow n 2 \pi^0$
2050 ± 25		BLUM 75	ASPK	$18.4 \pi^- p \rightarrow n K^+ K^-$
1966 ± 25		ANISOVICH 09	RVUE	$0.0 \bar{p} p, \pi N$
1885 ⁺¹⁴⁺²¹⁸ ₋₁₃₋₂₅		UEHARA 09	BELL	$10.6 e^+ e^- \rightarrow e^+ e^- \pi^0 \pi^0$
2018 ± 6		ANISOVICH 00j	SPEC	$2.0 \bar{p} p \rightarrow \eta \pi^0 \pi^0, \pi^0 \pi^0, \eta \eta, \eta \eta', \pi \pi$
~ 2000		MARTIN 98	RVUE	$N \bar{N} \rightarrow \pi \pi$
~ 2010		MARTIN 97	RVUE	$N \bar{N} \rightarrow \pi \pi$
~ 2040		OAKDEN 94	RVUE	$0.36-1.55 \bar{p} p \rightarrow \pi \pi$
~ 1990		OAKDEN 94	RVUE	$0.36-1.55 \bar{p} p \rightarrow \pi \pi$
1978 ± 5		ALPER 80	CNTR	$62 \pi^- p \rightarrow K^+ K^- n$
2040 ± 10		ROZANSKA 80	SPRK	$18 \pi^- p \rightarrow p \bar{p} n$
1935 ± 13		CORDEN 79	OMEG	$12-15 \pi^- p \rightarrow n 2 \pi$
1988 ± 7		EVANGELIS... 79B	OMEG	$10 \pi^- p \rightarrow K^+ K^- n$
1922 ± 14		ANTIPOV 77	CIBS	$25 \pi^- p \rightarrow p 3 \pi$

- 1 From the first PWA solution.
- 2 From a partial-wave analysis of the data.
- 3 From an amplitude analysis of the reaction $\pi^+ \pi^- \rightarrow 2 \pi^0$.
- 4 K matrix pole.
- 5 Taking into account the $f_2(1950)$. Helicity-2 production favored.
- 6 Energy-dependent analysis.
- 7 Single energy analysis.
- 8 From solution A of amplitude analysis of data on $\bar{p} p \rightarrow \pi \pi$. See however KLOET 96 who fit $\pi^+ \pi^-$ only and find waves only up to $J = 3$ to be important but not significantly resonant.
- 9 From solution B of amplitude analysis of data on $\bar{p} p \rightarrow \pi \pi$. See however KLOET 96 who fit $\pi^+ \pi^-$ only and find waves only up to $J = 3$ to be important but not significantly resonant.
- 10 $I(J^{PC}) = 0(4^+)$ from amplitude analysis assuming one-pion exchange.
- 11 Width errors enlarged by us to $4\Gamma/\sqrt{N}$; see the note with the $K^*(892)$ mass.



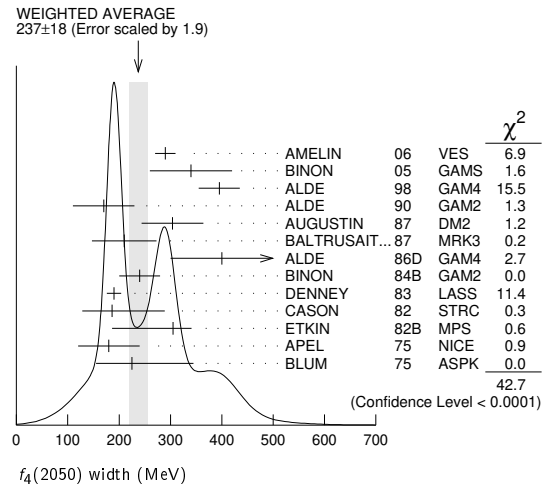
$f_4(2050)$ WIDTH

VALUE (MeV)	EVTs	DOCUMENT ID	TECN	COMMENT
237 ± 18	OUR AVERAGE	Error includes scale factor of 1.9. See the ideogram below.		
290 ± 20		AMELIN 06	VES	$36 \pi^- p \rightarrow \omega \omega n$
340 ± 80		BINON 05	GAMS	$33 \pi^- p \rightarrow \eta \eta n$
395 ± 40		ALDE 98	GAM4	$100 \pi^- p \rightarrow \pi^0 \pi^0 n$
170 ± 60		ALDE 90	GAM2	$38 \pi^- p \rightarrow \omega \omega n$
304 ± 60		AUGUSTIN 87	DM2	$J/\psi \rightarrow \gamma \pi^+ \pi^-$
210 ± 63		BALTRUSAIT... 87	MRK3	$J/\psi \rightarrow \gamma \pi^+ \pi^-$

400 ± 100		ALDE 86D	GAM4	$100 \pi^- p \rightarrow n 2 \eta$
240 ± 40	40k	BINON 13	GAM2	$38 \pi^- p \rightarrow n 2 \pi^0$
190 ± 14		DENNEY 83	LASS	$10 \pi^+ n/\pi^+ p$
186 ⁺¹⁰³ ₋₅₈		CASON 14	STRC	$8 \pi^+ p \rightarrow \Delta^{++} \pi^0 \pi^0$
305 ⁺³⁶ ₋₁₁₉		ETKIN 82B	MPS	$23 \pi^- p \rightarrow n 2 K^0_S$
180 ± 60	700	APEL 75	NICE	$40 \pi^- p \rightarrow n 2 \pi^0$
225 ⁺¹²⁰ ₋₇₀		BLUM 75	ASPK	$18.4 \pi^- p \rightarrow n K^+ K^-$

- • • We do not use the following data for averages, fits, limits, etc. • • •
- 260 ± 40
- 453 ± 20⁺³¹₋₁₂₉
- 182 ± 7
- ~ 170
- ~ 200
- ~ 60
- ~ 80
- 243 ± 16
- 140 ± 15
- 263 ± 57
- 100 ± 28
- 107 ± 56

- 12 From the first PWA solution.
- 13 From a partial-wave analysis of the data.
- 14 From an amplitude analysis of the reaction $\pi^+ \pi^- \rightarrow 2 \pi^0$.
- 15 K matrix pole.
- 16 Taking into account the $f_2(1950)$. Helicity-2 production favored.
- 17 Energy-dependent analysis.
- 18 Single energy analysis.
- 19 From solution A of amplitude analysis of data on $\bar{p} p \rightarrow \pi \pi$. See however KLOET 96 who fit $\pi^+ \pi^-$ only and find waves only up to $J = 3$ to be important but not significantly resonant.
- 20 From solution B of amplitude analysis of data on $\bar{p} p \rightarrow \pi \pi$. See however KLOET 96 who fit $\pi^+ \pi^-$ only and find waves only up to $J = 3$ to be important but not significantly resonant.
- 21 $I(J^{PC}) = 0(4^+)$ from amplitude analysis assuming one-pion exchange.
- 22 Width errors enlarged by us to $4\Gamma/\sqrt{N}$; see the note with the $K^*(892)$ mass.



$f_4(2050)$ DECAY MODES

Mode	Fraction (Γ_i/Γ)
Γ_1 $\omega \omega$	seen
Γ_2 $\pi \pi$	(17.0 ± 1.5) %
Γ_3 $K \bar{K}$	(6.8 ^{+3.4} _{-1.8}) × 10 ⁻³
Γ_4 $\eta \eta$	(2.1 ± 0.8) × 10 ⁻³
Γ_5 $4 \pi^0$	< 1.2 %
Γ_6 $\gamma \gamma$	
Γ_7 $a_2(1320) \pi$	seen

$f_4(2050)$ $\Gamma(i)\Gamma(\gamma\gamma)/\Gamma(\text{total})$

$\Gamma(K \bar{K}) \times \Gamma(\gamma\gamma)/\Gamma_{\text{total}}$	CL%	DOCUMENT ID	TECN	COMMENT	$\Gamma_3 \Gamma_6 / \Gamma$
< 0.29	95	ALTHOFF 85B	TASS	$\gamma \gamma \rightarrow K \bar{K} \pi$	

- • • We do not use the following data for averages, fits, limits, etc. • • •

Meson Particle Listings

$f_4(2050)$, $\pi_2(2100)$, $f_0(2100)$

$\Gamma(\pi\pi) \times \Gamma(\gamma\gamma)/\Gamma_{\text{total}}$			$\Gamma_2\Gamma_6/\Gamma$		
VALUE (eV)	CL%	EVTs	DOCUMENT ID	TECN	COMMENT
• • • We do not use the following data for averages, fits, limits, etc. • • •					
23.1 ^{+3.6+70.5} _{-3.3-15.6}			23 UEHARA	09 BELL	10.6 $e^+e^- \rightarrow e^+e^-\pi^0\pi^0$
<1100	95	13 ± 4	OEST	90 JADE	$e^+e^- \rightarrow e^+e^-\pi^0\pi^0$

²³ Taking into account the $f_2(1950)$. Helicity-2 production favored.

$f_4(2050)$ BRANCHING RATIOS

$\Gamma(\omega\omega)/\Gamma_{\text{total}}$	Γ_1/Γ		
VALUE	DOCUMENT ID	TECN	COMMENT
seen	AMELIN	06 VES	$36 \pi^- p \rightarrow \omega\omega n$
• • • We do not use the following data for averages, fits, limits, etc. • • •			
not seen	BARBERIS	00F	$450 pp \rightarrow p_f\omega p_S$

$\Gamma(\omega\omega)/\Gamma(\pi\pi)$	Γ_1/Γ_2		
VALUE	DOCUMENT ID	TECN	COMMENT
1.5 ± 0.3	ALDE	90 GAM2	$38 \pi^- p \rightarrow \omega\omega n$

$\Gamma(\pi\pi)/\Gamma_{\text{total}}$	Γ_2/Γ		
VALUE	DOCUMENT ID	TECN	COMMENT
0.170 ± 0.015 OUR AVERAGE			
0.18 ± 0.03	24 BINON	83C GAM2	$38 \pi^- p \rightarrow n4\gamma$
0.16 ± 0.03	24 CASON	82 STRC	$8 \pi^+ p \rightarrow \Delta^{++}\pi^0\pi^0$
0.17 ± 0.02	24 CORDEN	79 OMEG	$12-15 \pi^- p \rightarrow n2\pi$

²⁴ Assuming one pion exchange.

$\Gamma(K\bar{K})/\Gamma(\pi\pi)$	Γ_3/Γ_2		
VALUE	DOCUMENT ID	TECN	COMMENT
0.04 ^{+0.02} _{-0.01}	ETKIN	82B MPS	$23 \pi^- p \rightarrow n2K_S^0$

$\Gamma(\eta\eta)/\Gamma_{\text{total}}$	Γ_4/Γ		
VALUE (units 10 ⁻³)	DOCUMENT ID	TECN	COMMENT
2.1 ± 0.8	ALDE	86D GAM4	$100 \pi^- p \rightarrow n4\gamma$

$\Gamma(4\pi^0)/\Gamma_{\text{total}}$	Γ_5/Γ		
VALUE	DOCUMENT ID	TECN	COMMENT
<0.012	ALDE	87 GAM4	$100 \pi^- p \rightarrow 4\pi^0 n$

$\Gamma(a_2(1320)\pi)/\Gamma_{\text{total}}$	Γ_7/Γ		
VALUE	DOCUMENT ID	TECN	COMMENT
seen	AMELIN	00 VES	$37 \pi^- p \rightarrow \eta\pi^+\pi^- n$

$f_4(2050)$ REFERENCES

ANISOVICH	09	IJMP A24 2481	V.V. Anisovich, A.V. Sarantsev	
UEHARA	09	PR D79 052009	S. Uehara et al.	(BELLE Collab.)
AMELIN	06	PAN 69 690	D.V. Amelin et al.	(VES Collab.)
		Translated from YAF 69 715.		
BINON	05	PAN 68 960	F. Binon et al.	
		Translated from YAF 68 998.		
AMELIN	00	NP A668 83	D. Amelin et al.	(VES Collab.)
ANISOVICH	00J	PL B491 47	A.V. Anisovich et al.	(RAL, LOQM, PNPI+)
BARBERIS	00F	PL B484 198	D. Barberis et al.	(WA 102 Collab.)
ALDE	98	EPJ A3 361	D. Alde et al.	(GAM4 Collab.)
		PAN 62 405	D. Alde et al.	(GAMS Collab.)
		Also Translated from YAF 62 446.		
MARTIN	98	PR C57 3492	B.R. Martin et al.	
MARTIN	97	PR C56 1114	B.R. Martin, G.C. Oades	(LOUC, AARH)
KLOET	96	PR D53 6120	W.M. Kloet, F. Myhrer	(RUTG, NORD)
OAKDEN	94	NP A574 731	M.N. Oakden, M.R. Pennington	(DURH)
ALDE	90	PL B241 600	D.M. Alde et al.	(SERP, BELG, LANL, LAPP+)
OEST	90	ZPHY C47 343	T. Oest et al.	(JADE Collab.)
ALDE	87	PL B198 286	D.M. Alde et al.	(LANL, BRUX, SERP, LAPP)
AUGUSTIN	87	ZPHY C36 369	J.E. Augustin et al.	(LALO, CLER, FRAS+)
BALTUSAITIS	87	PR D35 2077	R.M. Baltusaitis et al.	(Mark III Collab.)
ALDE	86D	NP B269 485	D.M. Alde et al.	(MPIM, CERN)
ALTHOFF	85B	ZPHY C29 189	M. Althoff et al.	(TASSO Collab.)
BINON	84B	LNC 39 41	F.G. Binon et al.	(SERP, BELG, LAPP)
BINON	83C	SJNP 38 723	F.G. Binon et al.	(SERP, BRUX+)
		Translated from YAF 38 1199.		
DENNEY	83	PR D28 2726	D.L. Denney et al.	(IOWA, MICH)
CASON	82	PRL 48 1316	N.M. Cason et al.	(NDAM, ANL)
ETKIN	82B	PR D25 1786	A. Etkin et al.	(BNL, CUNY, TUFTS, VAND)
ALPER	80	PL 94B 422	B. Alper et al.	(AMST, CERN, CRAC, MPIM+)
ROZANSKA	80	NP B162 505	M. Rozanska et al.	(MPIM, CERN)
CORDEN	79	NP B157 250	M.J. Corden et al.	(BIRM, RHEL, TEHA+)
EVANGELIS...	79B	NP B154 381	C. Evangelista et al.	(BARI, BONN, CERN+)
ANTIPOV	77	NP B119 45	Y.M. Antipov et al.	(SERP, GEVA)
APEL	75	PL 57B 398	W.D. Apel et al.	(KARLK, KARLE, PISA, SERP+)
BLUM	75	PL 57B 403	W. Blum et al.	(CERN, MPIM)

$\pi_2(2100)$

$$I^G(J^{PC}) = 1^-(2^-+)$$

OMITTED FROM SUMMARY TABLE
Needs confirmation.

$\pi_2(2100)$ MASS

VALUE (MeV)	DOCUMENT ID	TECN	COMMENT
2090 ± 29 OUR AVERAGE			
2090 ± 30	¹ AMELIN	95B VES	$36 \pi^- A \rightarrow \pi^+\pi^-\pi^- A$
2100 ± 150	² DAUM	81B CNTR	$63,94 \pi^- p \rightarrow 3\pi X$

¹ From a fit to $J^{PC} = 2^-+ f_2(1270)\pi, (\pi\pi)_S\pi$ waves.
² From a two-resonance fit to four 2^-0+ waves.

$\pi_2(2100)$ WIDTH

VALUE (MeV)	DOCUMENT ID	TECN	COMMENT
625 ± 50 OUR AVERAGE			Error includes scale factor of 1.2.
520 ± 100	³ AMELIN	95B VES	$36 \pi^- A \rightarrow \pi^+\pi^-\pi^- A$
651 ± 50	⁴ DAUM	81B CNTR	$63,94 \pi^- p \rightarrow 3\pi X$

³ From a fit to $J^{PC} = 2^-+ f_2(1270)\pi, (\pi\pi)_S\pi$ waves.
⁴ From a two-resonance fit to four 2^-0+ waves.

$\pi_2(2100)$ DECAY MODES

Mode	Fraction (Γ_i/Γ)
Γ_1 3π	seen
Γ_2 $\rho\pi$	seen
Γ_3 $f_2(1270)\pi$	seen
Γ_4 $(\pi\pi)_S\pi$	seen

$\pi_2(2100)$ BRANCHING RATIOS

$\Gamma(\rho\pi)/\Gamma(3\pi)$	Γ_2/Γ_1		
VALUE	DOCUMENT ID	TECN	COMMENT
0.19 ± 0.05	⁵ DAUM	81B CNTR	$63,94 \pi^- p$

$\Gamma(f_2(1270)\pi)/\Gamma(3\pi)$	Γ_3/Γ_1		
VALUE	DOCUMENT ID	TECN	COMMENT
0.36 ± 0.09	⁵ DAUM	81B CNTR	$63,94 \pi^- p$

$\Gamma((\pi\pi)_S\pi)/\Gamma(3\pi)$	Γ_4/Γ_1		
VALUE	DOCUMENT ID	TECN	COMMENT
0.45 ± 0.07	⁵ DAUM	81B CNTR	$63,94 \pi^- p$

D-wave/S-wave RATIO FOR $\pi_2(2100) \rightarrow f_2(1270)\pi$	Γ_2/Γ_1		
VALUE	DOCUMENT ID	TECN	COMMENT
0.39 ± 0.23	⁵ DAUM	81B CNTR	$63,94 \pi^- p$

⁵ From a two-resonance fit to four 2^-0+ waves.

$\pi_2(2100)$ REFERENCES

AMELIN	95B	PL B356 595	D.V. Amelin et al.	(SERP, TBIL)
DAUM	81B	NP B182 269	C. Daum et al.	(AMST, CERN, CRAC, MPIM+)

$f_0(2100)$

$$I^G(J^{PC}) = 0^+(0^{++})$$

OMITTED FROM SUMMARY TABLE
Needs confirmation.

$f_0(2100)$ MASS

VALUE (MeV)	EVTs	DOCUMENT ID	TECN	COMMENT
2086⁺²⁰₋₂₄ OUR AVERAGE				
2081 ± 13 ⁺²⁴ ₋₃₆	5.5k	¹ ABLIKIM	13N BES3	$e^+e^- \rightarrow J/\psi \rightarrow \gamma\eta\eta$
2090 ± 30		BAI	00A BES	$J/\psi \rightarrow \gamma(\pi^+\pi^-\pi^+\pi^-)$
• • • We do not use the following data for averages, fits, limits, etc. • • •				
2090 ± 10 ± 6	529	^{2,3} DOBBS	15	$J/\psi \rightarrow \gamma\pi^+\pi^-$
2099 ± 17 ± 8	283	^{2,3} DOBBS	15	$\psi(2S) \rightarrow \gamma\pi^+\pi^-$
2105 ± 8	80k	⁴ UMAN	06 E835	$5.2 \bar{p}p \rightarrow \eta\eta\pi^0$
2102 ± 13		⁵ ANISOVICH	00J SPEC	$2.0 \bar{p}p \rightarrow \eta\pi^0\pi^0, \pi^0\pi^0, \eta\eta, \eta\eta', \pi^+\pi^-$
2105 ± 10		ANISOVICH	99K SPEC	$0.6-1.94 \bar{p}p \rightarrow \eta\eta, \eta\eta'$
~2104		BUGG	95	$J/\psi \rightarrow \gamma\pi^+\pi^-\pi^+\pi^-$
~2122		HASAN	94 RVUE	$\bar{p}p \rightarrow \pi\pi$

¹ From partial wave analysis including all possible combinations of $0^{++}, 2^{++},$ and 4^{++} resonances.
² Using CLEO-c data but not authored by the CLEO Collaboration.
³ From a fit to a Breit-Wigner line shape with fixed $\Gamma = 209$ MeV.
⁴ Statistical error only.
⁵ Includes the data of ANISOVICH 00B indicating to exotic decay pattern.

See key on page 999

Meson Particle Listings

$f_0(2100)$, $f_2(2150)$

$f_0(2100)$ WIDTH

VALUE (MeV)	EVTS	DOCUMENT ID	TECN	COMMENT
284⁺⁶⁰₋₃₂ OUR AVERAGE				
273 ⁺²⁷ ₋₂₄ ⁺⁷⁰ ₋₂₃	5.5k	⁶ ABLIKIM	13N BES3	$e^+e^- \rightarrow J/\psi \rightarrow \gamma\eta\eta$
330 \pm 100		BAI	00A BES	$J/\psi \rightarrow \gamma(\pi^+\pi^-\pi^+\pi^-)$
••• We do not use the following data for averages, fits, limits, etc. •••				
236 \pm 14	80k	⁷ UMAN	06 E835	$5.2 \bar{p}p \rightarrow \eta\eta\pi^0$
211 \pm 29		⁸ ANISOVICH	00J SPEC	$2.0 \bar{p}p \rightarrow \eta\pi^0\pi^0, \pi^0\pi^0,$ $\eta\eta, \eta\eta', \pi^+\pi^-$
200 \pm 25		ANISOVICH	99K SPEC	$0.6-1.94 \bar{p}p \rightarrow \eta\eta, \eta\eta'$
\sim 203		BUGG	95	$J/\psi \rightarrow \gamma\pi^+\pi^-\pi^+\pi^-$
\sim 273		HASAN	94 RVUE	$\bar{p}p \rightarrow \pi\pi$
⁶ From partial wave analysis including all possible combinations of 0^{++} , 2^{++} , and 4^{++} resonances.				
⁷ Statistical error only.				
⁸ Includes the data of ANISOVICH 00B indicating to exotic decay pattern.				

$f_0(2100)$ REFERENCES

DOBBS	15	PR D91 052006	S. Dobbs <i>et al.</i>	(NWES)
ABLIKIM	13N	PR D87 092009	Ablikim M. <i>et al.</i>	(BESIII Collab.)
UMAN	06	PR D73 052009	I. Uman <i>et al.</i>	(FNAL E835)
ANISOVICH	00B	NP A662 319	A.V. Anisovich <i>et al.</i>	
ANISOVICH	00J	PL B491 47	A.V. Anisovich <i>et al.</i>	(RAL, LOQM, PNPI+)
BAI	00A	PL B472 207	J.Z. Bai <i>et al.</i>	(BES Collab.)
ANISOVICH	99K	PL B468 309	A.V. Anisovich <i>et al.</i>	
BUGG	95	PL B353 378	D.V. Bugg <i>et al.</i>	(LOQM, PNPI, WASH)
HASAN	94	PL B334 215	A. Hasan, D.V. Bugg	(LOQM)

$f_2(2150)$

$$I^G(J^{PC}) = 0^+(2^{++})$$

OMITTED FROM SUMMARY TABLE
This entry was previously called T_0 .

$f_2(2150)$ MASS

$f_2(2150)$ MASS, COMBINED MODES (MeV)

VALUE (MeV)	EVTS	DOCUMENT ID	TECN	COMMENT
2157\pm12 OUR AVERAGE				Includes data from the datablock that follows this one.
••• We do not use the following data for averages, fits, limits, etc. •••				
2170 \pm 6	80k	¹ UMAN	06 E835	$5.2 \bar{p}p \rightarrow \eta\eta\pi^0$
¹ Statistical error only.				
$\eta\eta$ MODE				
VALUE (MeV)		DOCUMENT ID	TECN	COMMENT
The data in this block is included in the average printed for a previous datablock.				

2157 \pm 12 OUR AVERAGE

2151 \pm 16		BARBERIS	00E	$450 \bar{p}p \rightarrow p_f \eta \eta p_S$
2175 \pm 20		PROKOSHKIN	95D GAM4	$300 \pi^- N \rightarrow \pi^- N 2\eta,$ $450 \bar{p}p \rightarrow p p 2\eta$
2130 \pm 35		SINGOVSKI	94 GAM4	$450 \bar{p}p \rightarrow p p 2\eta$
••• We do not use the following data for averages, fits, limits, etc. •••				
2140 \pm 30		² ABELE	99B CBAR	$1.94 \bar{p}p \rightarrow \pi^0 \eta \eta$
2104 \pm 20		³ ARMSTRONG	93C E760	$\bar{p}p \rightarrow \pi^0 \eta \eta \rightarrow 6\gamma$
² Spin not determined.				
³ No J^{PC} determination.				

$\eta\pi\pi$ MODE

VALUE (MeV)	DOCUMENT ID	TECN	CHG	COMMENT
••• We do not use the following data for averages, fits, limits, etc. •••				
2135 \pm 20 \pm 45	⁴ ADOMEIT	96 CBAR	0	$1.94 \bar{p}p \rightarrow \eta 3\pi^0$
⁴ ANISOVICH 00E recommends to withdraw ADOMEIT 96 that assumed a single $J^P = 2^+$ resonance.				

$\bar{p}p \rightarrow \pi\pi$

VALUE (MeV)	DOCUMENT ID	TECN	COMMENT
••• We do not use the following data for averages, fits, limits, etc. •••			
\sim 2090	⁵ OAKDEN	94 RVUE	$0.36-1.55 \bar{p}p \rightarrow \pi\pi$
\sim 2120	⁶ OAKDEN	94 RVUE	$0.36-1.55 \bar{p}p \rightarrow \pi\pi$
\sim 2170	⁷ MARTIN	80B RVUE	
\sim 2150	⁷ MARTIN	80C RVUE	
\sim 2150	⁸ DULUDE	78B OSPK	$1-2 \bar{p}p \rightarrow \pi^0\pi^0$
⁵ OAKDEN 94 makes an amplitude analysis of LEAR data on $\bar{p}p \rightarrow \pi\pi$ using a method based on Barrelet zeros. This is solution A. The amplitude analysis of HASAN 94 includes earlier data as well, and assume that the data can be parametrized in terms of towers of nearly degenerate resonances on the leading Regge trajectory. See also KLOET 96 and MARTIN 97 who make related analyses.			
⁶ From solution B of amplitude analysis of data on $\bar{p}p \rightarrow \pi\pi$.			

⁷ $I(J^P) = 0(2^+)$ from simultaneous analysis of $p\bar{p} \rightarrow \pi^-\pi^+$ and $\pi^0\pi^0$.
⁸ $I^G(J^P) = 0^+(2^+)$ from partial-wave amplitude analysis.

S-CHANNEL $\bar{p}p, \bar{N}N$ or $\bar{K}K$

VALUE (MeV)	DOCUMENT ID	TECN	CHG	COMMENT
••• We do not use the following data for averages, fits, limits, etc. •••				
2139 ⁺⁸ ₋₉	⁹ EVANGELIS...	97 SPEC		$0.6-2.4 \bar{p}p \rightarrow K_S^0 K_S^0$
\sim 2190	⁹ CUTTS	78B CNTR		$0.97-3 \bar{p}p \rightarrow \bar{N}N$
2155 \pm 15	^{9,10} COUPLAND	77 CNTR	0	$0.7-2.4 \bar{p}p \rightarrow \bar{p}p$
2193 \pm 2	^{9,11} ALSPECTOR	73 CNTR		$\bar{p}p$ S channel
⁹ Isospins 0 and 1 not separated.				
¹⁰ From a fit to the total elastic cross section.				
¹¹ Referred to as T or T region by ALSPECTOR 73.				

$K\bar{K}$ MODE

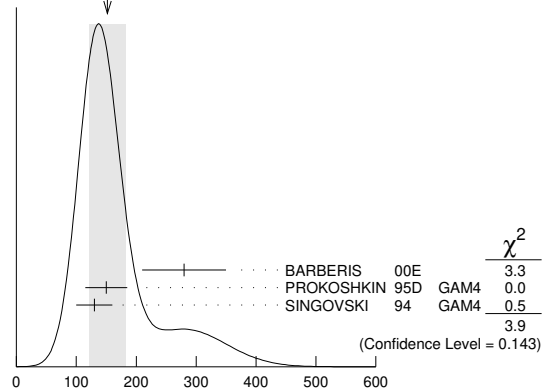
VALUE (MeV)	DOCUMENT ID	TECN	COMMENT
••• We do not use the following data for averages, fits, limits, etc. •••			
2200 \pm 13	VLADIMIRSK..06	SPEC	$40 \pi^- p \rightarrow K_S^0 K_S^0 n$
2150 \pm 20	ABLIKIM	04E BES2	$J/\psi \rightarrow \omega K^+ K^-$
2130 \pm 35	BARBERIS	99 OMEG	$450 \bar{p}p \rightarrow \rho_S \rho_f K^+ K^-$

$f_2(2150)$ WIDTH

$f_2(2150)$ WIDTH, COMBINED MODES (MeV)

VALUE (MeV)	EVTS	DOCUMENT ID	TECN	COMMENT
152\pm30 OUR AVERAGE				Includes data from the datablock that follows this one. Error includes scale factor of 1.4. See the ideogram below.
••• We do not use the following data for averages, fits, limits, etc. •••				
182 \pm 11	80k	¹² UMAN	06 E835	$5.2 \bar{p}p \rightarrow \eta\eta\pi^0$
¹² Statistical error only.				

WEIGHTED AVERAGE
152 \pm 30 (Error scaled by 1.4)



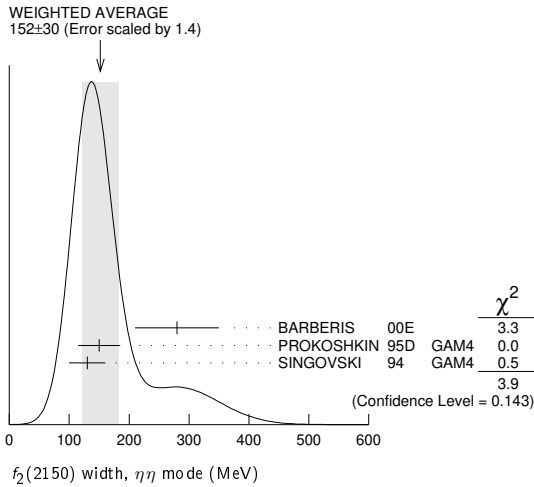
$f_2(2150)$ width, combined modes (MeV)

$\eta\eta$ MODE

VALUE (MeV)	DOCUMENT ID	TECN	COMMENT
The data in this block is included in the average printed for a previous datablock.			
152\pm30 OUR AVERAGE Error includes scale factor of 1.4. See the ideogram below.			
280 \pm 70	BARBERIS	00E	$450 \bar{p}p \rightarrow p_f \eta \eta p_S$
150 \pm 35	PROKOSHKIN	95D GAM4	$300 \pi^- N \rightarrow \pi^- N 2\eta,$ $450 \bar{p}p \rightarrow p p 2\eta$
130 \pm 30	SINGOVSKI	94 GAM4	$450 \bar{p}p \rightarrow p p 2\eta$
••• We do not use the following data for averages, fits, limits, etc. •••			
310 \pm 50	¹³ ABELE	99B CBAR	$1.94 \bar{p}p \rightarrow \pi^0 \eta \eta$
203 \pm 10	¹⁴ ARMSTRONG	93C E760	$\bar{p}p \rightarrow \pi^0 \eta \eta \rightarrow 6\gamma$
¹³ Spin not determined.			
¹⁴ No J^{PC} determination.			

Meson Particle Listings

$f_2(2150), \rho(2150)$



$\eta\pi\pi$ MODE

VALUE (MeV)	DOCUMENT ID	TECN	CHG	COMMENT
$250 \pm 25 \pm 45$	¹⁵ ADOMEIT	96	CBAR	0 $1.94 \bar{p}p \rightarrow \eta 3\pi^0$

¹⁵ ANISOVICH 00E recommends to withdraw ADOMEIT 96 that assumed a single $J^P = 2^+$ resonance.

$\bar{p}p \rightarrow \pi\pi$

VALUE (MeV)	DOCUMENT ID	TECN	COMMENT
250 OUR ESTIMATE			
$0.36 - 1.55$	¹⁶ OAKDEN	94	RVUE $\bar{p}p \rightarrow \pi\pi$
~ 250	¹⁷ MARTIN	80B	RVUE
~ 250	¹⁷ MARTIN	80C	RVUE
~ 250	¹⁸ DULUDE	78B	OSPK $1-2 \bar{p}p \rightarrow \pi^0\pi^0$

¹⁶ See however KLOET 96 who fit $\pi^+\pi^-$ only and find waves only up to $J = 3$ to be important but not significantly resonant.
¹⁷ $I(J^P) = 0(2^+)$ from simultaneous analysis of $p\bar{p} \rightarrow \pi^-\pi^+$ and $\pi^0\pi^0$.
¹⁸ $I^G(J^P) = 0^+(2^+)$ from partial-wave amplitude analysis.

S-CHANNEL $\bar{p}p, \bar{N}N$ or $\bar{K}K$

VALUE (MeV)	DOCUMENT ID	TECN	CHG	COMMENT
56^{+31}_{-16}	¹⁹ EVANGELIS...	97	SPEC	$0.6-2.4 \bar{p}p \rightarrow K_S^0 K_S^0$
135 ± 75	^{20,21} COUPLAND	77	CNTR	0 $0.7-2.4 \bar{p}p \rightarrow \bar{p}p$
98 ± 8	²¹ ALSPECTOR	73	CNTR	$\bar{p}p$ S channel

¹⁹ Isospin 0 and 2 not separated.
²⁰ From a fit to the total elastic cross section.
²¹ Isospins 0 and 1 not separated.

$K\bar{K}$ MODE

VALUE (MeV)	DOCUMENT ID	TECN	COMMENT
91 ± 62	VLADIMIRSK...06	SPEC	$40 \pi^-\rho \rightarrow K_S^0 K_S^0 n$
150 ± 30	ABLIKIM	04E	BES2 $J/\psi \rightarrow \omega K^+ K^-$
270 ± 50	BARBERIS	99	OMEG $450 pp \rightarrow p_S p_f K^+ K^-$

$f_2(2150)$ DECAY MODES

Mode	Fraction (Γ_i/Γ)
Γ_1 $\pi\pi$	
Γ_2 $\eta\eta$	seen
Γ_3 $K\bar{K}$	seen
Γ_4 $f_2(1270)\eta$	seen
Γ_5 $a_2(1320)\pi$	seen
Γ_6 $\rho\bar{\rho}$	seen

$f_2(2150)$ BRANCHING RATIOS

$\Gamma(K\bar{K})/\Gamma(\eta\eta)$	CL%	DOCUMENT ID	TECN	COMMENT	Γ_3/Γ_2
1.28 ± 0.23		BARBERIS	00E	$450 pp \rightarrow p_f \eta \eta p_S$	

• • • We do not use the following data for averages, fits, limits, etc. • • •

VALUE	CL%	DOCUMENT ID	TECN	COMMENT
< 0.1	95	²² PROKOSHKIN 95D	GAM4	$300 \pi^- N \rightarrow \pi^- N 2\eta, 450 pp \rightarrow p p 2\eta$

²² Using data from ARMSTRONG 89D.

$\Gamma(\pi\pi)/\Gamma(\eta\eta)$

VALUE	CL%	DOCUMENT ID	TECN	COMMENT	Γ_1/Γ_2
< 0.33	95	²³ PROKOSHKIN 95D	GAM4	$300 \pi^- N \rightarrow \pi^- N 2\eta, 450 pp \rightarrow p p 2\eta$	

²³ Derived from a $\pi^0\pi^0/\eta\eta$ limit.

$\Gamma(f_2(1270)\eta)/\Gamma(a_2(1320)\pi)$

VALUE	DOCUMENT ID	TECN	COMMENT	Γ_4/Γ_5
0.79 ± 0.11	²⁴ ADOMEIT	96	CBAR $1.94 \bar{p}p \rightarrow \eta 3\pi^0$	

²⁴ Using $B(a_2(1320) \rightarrow \eta\pi) = 0.145$

$\Gamma(\rho\bar{\rho})/\Gamma_{total}$

VALUE	EVTS	DOCUMENT ID	TECN	COMMENT	Γ_6/Γ
seen	73	ALEXANDER	10	CLEO $\psi(2S) \rightarrow \gamma\rho\bar{\rho}$	

$f_2(2150)$ REFERENCES

ALEXANDER 10	PR D82 092002	J.P. Alexander et al.	(CLEO Collab.)
UMAN 06	PR D73 052009	I. Uman et al.	(FNAL E835)
VLADIMIRSK...06	PAN 69 493	V.V. Vladimirov et al.	(ITEP, Moscow)
ABLIKIM 04E	PL B603 138	M. Ablikim et al.	(BES Collab.)
ANISOVICH 00E	PL B477 19	A.V. Anisovich et al.	(WA 102 Collab.)
BARBERIS 00E	PL B479 59	D. Barberis et al.	(Crystal Barrel Collab.)
ABELE 99B	EPJ C8 67	A. Abele et al.	(Omega Expt.)
BARBERIS 99B	PL B453 305	D. Barberis et al.	(LEAR Collab.)
EVANGELIS... 97	PR D56 3803	C. Evangelista et al.	(LOUC, AARRH)
MARTIN 97	PR C56 1114	B.R. Martin, G.C. Oades	(Crystal Barrel Collab.)
ADOMEIT 96	ZPHY C71 227	J. Adomeit et al.	(RUTG, NORD)
KLOET 96	PR D53 6120	W.M. Kloet, F. Myhrer	(SERP)IGJPC
PROKOSHKIN 95D	PD 40 495	Y.D. Prokoshkin	
HASAN 94	PL B334 215	A. Hasan, D.V. Bugg	(LOQM)
OAKDEN 94	NP A574 731	M.N. Oakden, M.R. Pennington	(DURH)
SINGOVSKI 94	NC A107 1911	A.V. Singovsky	(SERP)
ARMSTRONG 89D	PL B307 394	T.A. Armstrong et al.	(FNAL, FERR, GENO+)
ARMSTRONG 89D	PL B227 186	T.A. Armstrong, M. Benayoun	(ATHU, BARI, BIRM+)
MARTIN 80B	NP B176 355	B.R. Martin, D. Morgan	(LOUC, RHEL)JP
MARTIN 80C	NP B169 216	A.D. Martin, M.R. Pennington	(DURH)JP
CUTTS 78B	PR D17 16	D. Cutts et al.	(STON, WISC)
DULUDE 78B	PL 79B 335	R.S. Dulude et al.	(BROW, MIT, BARI)JP
COUPLAND 77	PL 71B 460	M. Coupland et al.	(LOQM, RHEL)
ALSPECTOR 73	PRL 30 511	J. Alspector et al.	(RUTG, UPNJ)

$\rho(2150)$

$$I^G(J^PC) = 1^+(1^-)$$

OMITTED FROM SUMMARY TABLE

This entry was previously called $T_1(2190)$. See our mini-review under the $\rho(1700)$.

$\rho(2150)$ MASS

e^+e^- PRODUCED

VALUE (MeV)	DOCUMENT ID	TECN	COMMENT
2201 ± 19	¹ LEES	20	BABR $e^+e^- \rightarrow K^+ K^- \gamma$
$2227 \pm 9 \pm 9$	² LEES	20	RVUE $e^+e^- \rightarrow K^+ K^-$
$2039 \pm 8^{+36}_{-18}$	³ ABLIKIM	19AQ	BES $J/\psi \rightarrow K^+ K^- \pi^0$
$2239.2 \pm 7.1 \pm 11.3$	⁴ ABLIKIM	19L	BES3 $e^+e^- \rightarrow K^+ K^-$
2254 ± 22	⁵ LEES	12G	BABR $e^+e^- \rightarrow \pi^+ \pi^- \gamma$
$2150 \pm 40 \pm 50$	AUBERT	07AU	BABR $10.6 e^+e^- \rightarrow f_1(1285) \pi^+ \pi^- \gamma$
1990	AUBERT	07AU	BABR $10.6 e^+e^- \rightarrow \eta' \pi^+ \pi^- \gamma$
2153 ± 37	BIAGINI	91	RVUE $e^+e^- \rightarrow \pi^+ \pi^-, K^+ K^-$
2110 ± 50	⁶ CLEGG	90	RVUE $e^+e^- \rightarrow 3(\pi^+ \pi^-), 2(\pi^+ \pi^- \pi^0)$

¹ From the fit to the BABAR data of LEES 13Q assuming a coherent sum of a single Breit-Wigner resonance and a nonresonant contribution. The resonance significance is 3.5σ .
² From the fit to the BABAR data of LEES 13Q and BESIII data of ABLIKIM 19L assuming a coherent sum of a single Breit-Wigner resonance and a nonresonant contribution.
³ Could also be another state. Seen in J/ψ decay with branching ratio $J/\psi \rightarrow X \pi^0 \rightarrow K^+ K^- \pi^0 = (6.7 \pm 1.1^{+2.2}_{-1.8}) \times 10^{-6}$.
⁴ The observed structure can be due to both the $\phi(2170)$ and $\rho(2150)$.
⁵ Using the GOUNARIS 68 parametrization of the pion form factor leaving the masses and widths of the $\rho(1450)$, $\rho(1700)$, and $\rho(2150)$ resonances as free parameters of the fit.
⁶ Includes ATKINSON 85.

$\bar{p}p \rightarrow \pi\pi$

VALUE (MeV)	DOCUMENT ID	TECN	COMMENT
~ 2191	HASAN	94	RVUE $\bar{p}p \rightarrow \pi\pi$
~ 2070	¹ OAKDEN	94	RVUE $0.36-1.55 \bar{p}p \rightarrow \pi\pi$
~ 2170	² MARTIN	80B	RVUE
~ 2100	² MARTIN	80C	RVUE

¹ See however KLOET 96 who fit $\pi^+\pi^-$ only and find waves only up to $J = 3$ to be important but not significantly resonant.
² $I(J^P) = 1(1^-)$ from simultaneous analysis of $p\bar{p} \rightarrow \pi^-\pi^+$ and $\pi^0\pi^0$.

See key on page 999

Meson Particle Listings

$\rho(2150), \phi(2170)$

S-CHANNEL $\bar{N}N$

Table with columns: VALUE (MeV), DOCUMENT ID, TECN, COMMENT. Lists experimental data for S-channel NN decays.

Footnotes for S-channel NN section, including references to ANISOVICH, CUTTS, COUPLAND, ALSPECTOR, and ABRAMS.

$\pi^- p \rightarrow \omega \pi^0 n$

Table with columns: VALUE (MeV), DOCUMENT ID, TECN, COMMENT. Lists data for pi-p to omega pi0 n decays.

$\rho(2150)$ WIDTH

e^+e^- PRODUCED

Table with columns: VALUE (MeV), DOCUMENT ID, TECN, COMMENT. Lists e+e- production data for rho(2150).

Footnotes for rho(2150) width section, discussing Breit-Wigner resonance and nonresonant contributions.

$\bar{p}p \rightarrow \pi\pi$

Table with columns: VALUE (MeV), DOCUMENT ID, TECN, COMMENT. Lists p-bar p to pi pi decays.

Footnotes for p-bar p to pi pi section, including KLOET and MARTIN references.

S-CHANNEL $\bar{N}N$

Table with columns: VALUE (MeV), DOCUMENT ID, TECN, COMMENT. Lists S-channel NN decays.

Footnotes for S-channel NN section, including references to ANISOVICH, COUPLAND, ALSPECTOR, and ABRAMS.

$\pi^- p \rightarrow \omega \pi^0 n$

Table with columns: VALUE (MeV), DOCUMENT ID, TECN, COMMENT. Lists pi-p to omega pi0 n decays.

$\rho(2150)$ DECAY MODES

Table with columns: Mode, Fraction (Gamma_i/Gamma). Lists decay modes and their relative fractions for rho(2150).

$\rho(2150) \Gamma(i)\Gamma(e^+e^-)/\Gamma^2(\text{total})$

Table with columns: VALUE (units 10^-7), DOCUMENT ID, TECN, COMMENT. Lists branching ratios for rho(2150) to pi+ pi-.

Footnote for rho(2150) pi+ pi- branching ratio, calculated by us from the reported value of cross section.

Table with columns: VALUE (units 10^-8), DOCUMENT ID, TECN, COMMENT. Lists branching ratios for rho(2150) to eta' pi+ pi-.

Footnote for rho(2150) eta' pi+ pi- branching ratio, calculated by us from the reported value of cross section.

$\rho(2150)$ REFERENCES

List of references for rho(2150) decays, including works by Lees, ABLIKIM, LEES, AUBERT, ANISOVICH, HASAN, OAKDEN, ALDE, BIAGINI, CLEGG, ATKINSON, MARTIN, CUTTS, COUPLAND, PEASLEE, ALSPECTOR, ABRAMS, COOPER, and GOUNARIS.

$\phi(2170)$

J^PC = 0^-(1^-)

$\phi(2170)$ MASS

Table with columns: VALUE (MeV), EVTS, DOCUMENT ID, TECN, COMMENT. Lists mass measurements for phi(2170).

Footnotes for phi(2170) mass section, including references to ABLIKIM, SHEN, AUBERT, and BE.

Footnotes for phi(2170) mass section, including references to SHEN, AUBERT, and BE.

Meson Particle Listings

 $\phi(2170)$, $f_0(2200)$, $f_j(2220)$ $\phi(2170)$ WIDTH

VALUE (MeV)	EVTS	DOCUMENT ID	TECN	COMMENT
125 ± 65 OUR EVALUATION				
• • • We do not use the following data for averages, fits, limits, etc. • • •				
104 ± 24 ± 12	95	ABLIKIM	19I	BES3 $e^+e^- \rightarrow \eta\phi f_0(980)$
139.8 ± 12.3 ± 20.6		¹ ABLIKIM	19L	BES3 $e^+e^- \rightarrow K^+K^-$
104 ± 15 ± 15	471	ABLIKIM	15H	BES3 $J/\psi \rightarrow \eta\phi\pi^+\pi^-$
77 ± 15 ± 10		^{2,3} LEES	12F	BABR $10.6 e^+e^- \rightarrow \phi\pi^+\pi^-\gamma$
192 ± 23 ± $\frac{25}{-61}$	4.8k	⁴ SHEN	09	BELL $10.6 e^+e^- \rightarrow K^+K^-\pi^+\pi^-\gamma$
65 ± 23 ± 17	52	ABLIKIM	08F	BES $J/\psi \rightarrow \eta\phi f_0(980)$
61 ± 50 ± 13	483	AUBERT	08S	BABR $10.6 e^+e^- \rightarrow \phi\eta\gamma$
71 ± 21	116	⁵ AUBERT	07AK	BABR $10.6 e^+e^- \rightarrow K^+K^-\pi^+\pi^-\gamma$
102 ± 27	149	⁵ AUBERT	07AK	BABR $10.6 e^+e^- \rightarrow K^+K^-\pi^0\pi^0\gamma$
58 ± 16 ± 20	201	^{3,6} AUBERT,BE	06D	BABR $10.6 e^+e^- \rightarrow K^+K^-\pi\pi\gamma$

¹ The observed structure can be due to both the $\phi(2170)$ and $\rho(2150)$.

² Fit includes interference with the $\phi(1680)$.

³ From the $\phi f_0(980)$ component.

⁴ From a fit with two incoherent Breit-Wigners.

⁵ From the $K^+K^-f_0(980)$ component.

⁶ Superseded by LEES 12F.

 $\phi(2170)$ DECAY MODES

Mode	Fraction (Γ_i/Γ)
Γ_1 e^+e^-	seen
Γ_2 $\phi\eta$	
Γ_3 $\phi\pi\pi$	
Γ_4 $\phi f_0(980)$	seen
Γ_5 $K^+K^-\pi^+\pi^-$	
Γ_6 $K^+K^-f_0(980) \rightarrow K^+K^-\pi^+\pi^-$	seen
Γ_7 $K^+K^-\pi^0\pi^0$	
Γ_8 $K^+K^-f_0(980) \rightarrow K^+K^-\pi^0\pi^0$	seen
Γ_9 $K^*0 K^\pm\pi^\mp$	not seen
Γ_{10} $K^*(892)^0 \bar{K}^*(892)^0$	not seen

 $\phi(2170)$ $\Gamma(i)\Gamma(e^+e^-)/\Gamma(\text{total})$

$\Gamma(\phi\eta) \times \Gamma(e^+e^-)/\Gamma_{\text{total}}$	$\Gamma_2\Gamma_1/\Gamma$			
VALUE (eV)	EVTS	DOCUMENT ID	TECN	COMMENT
• • • We do not use the following data for averages, fits, limits, etc. • • •				
1.7 ± 0.7 ± 1.3	483	AUBERT	08S	BABR $10.6 e^+e^- \rightarrow \phi\eta\gamma$

$\Gamma(\phi f_0(980)) \times \Gamma(e^+e^-)/\Gamma_{\text{total}}$	$\Gamma_4\Gamma_1/\Gamma$			
VALUE (eV)	EVTS	DOCUMENT ID	TECN	COMMENT
2.3 ± 0.3 ± 0.3		^{1,2} LEES	12F	BABR $10.6 e^+e^- \rightarrow \phi\pi^+\pi^-\gamma$
• • • We do not use the following data for averages, fits, limits, etc. • • •				
2.5 ± 0.8 ± 0.4	201	^{2,3} AUBERT,BE	06D	BABR $10.6 e^+e^- \rightarrow K^+K^-\pi\pi\gamma$

¹ From a fit with constructive interference with the $\phi(1680)$. In a fit with destructive interference, the value is larger by a factor of 1.2.

² From the $\phi f_0(980)$ component.

³ Superseded by LEES 12F.

 $\phi(2170)$ $\Gamma(i)\Gamma(e^+e^-)/\Gamma^2(\text{total})$

$\Gamma(\phi\pi\pi)/\Gamma_{\text{total}} \times \Gamma(e^+e^-)/\Gamma_{\text{total}}$	$\Gamma_3/\Gamma \times \Gamma_1/\Gamma$			
VALUE (units 10^{-7})	EVTS	DOCUMENT ID	TECN	COMMENT
• • • We do not use the following data for averages, fits, limits, etc. • • •				
1.65 ± 0.15 ± 0.18	4.8k	¹ SHEN	09	BELL $10.6 e^+e^- \rightarrow K^+K^-\pi^+\pi^-\gamma$
¹ Multiplied by 3/2 to take into account the $\phi\pi^0\pi^0$ mode. Using $B(\phi \rightarrow K^+K^-) = (49.2 \pm 0.6)\%$.				

 $\phi(2170)$ BRANCHING RATIOS

$\Gamma(K^+K^-f_0(980) \rightarrow K^+K^-\pi^+\pi^-)/\Gamma_{\text{total}}$	Γ_6/Γ		
VALUE	DOCUMENT ID	TECN	COMMENT
seen	AUBERT	07AK	BABR $10.6 e^+e^- \rightarrow K^+K^-\pi^+\pi^-\gamma$
$\Gamma(K^+K^-f_0(980) \rightarrow K^+K^-\pi^0\pi^0)/\Gamma_{\text{total}}$	Γ_8/Γ		
VALUE	DOCUMENT ID	TECN	COMMENT
seen	AUBERT	07AK	BABR $10.6 e^+e^- \rightarrow K^+K^-\pi^0\pi^0\gamma$
$\Gamma(K^*0 K^\pm\pi^\mp)/\Gamma_{\text{total}}$	Γ_9/Γ		
VALUE	DOCUMENT ID	TECN	COMMENT
not seen	AUBERT	07AK	BABR $10.6 \text{ GeV } e^+e^-$

 $\Gamma(K^*(892)^0 \bar{K}^*(892)^0)/\Gamma_{\text{total}}$

VALUE	DOCUMENT ID	TECN	COMMENT	Γ_{10}/Γ
not seen	ABLIKIM	10c	BES2 $J/\psi \rightarrow \eta K^+\pi^- K^-\pi^+$	

 $\phi(2170)$ REFERENCES

ABLIKIM	19I	PR D99 012014	M. Ablikim <i>et al.</i>	(BESIII Collab.)
ABLIKIM	19L	PR D99 032001	M. Ablikim <i>et al.</i>	(BESIII Collab.)
ABLIKIM	15H	PR D91 052017	M. Ablikim <i>et al.</i>	(BESIII Collab.)
LEES	12F	PR D86 012008	J.P. Lees <i>et al.</i>	(BABAR Collab.)
ABLIKIM	10C	PL B685 27	M. Ablikim <i>et al.</i>	(BES II Collab.)
SHEN	09	PR D80 031101	C.P. Shen <i>et al.</i>	(BELLE Collab.)
ABLIKIM	08F	PRL 100 102003	M. Ablikim <i>et al.</i>	(BES Collab.)
AUBERT	08S	PR D77 092002	B. Aubert <i>et al.</i>	(BABAR Collab.)
AUBERT	07AK	PR D76 012008	B. Aubert <i>et al.</i>	(BABAR Collab.)
AUBERT,BE	06D	PR D74 091103	B. Aubert <i>et al.</i>	(BABAR Collab.)

 $f_0(2200)$

$$J^G(J^{PC}) = 0^+(0^{++})$$

OMITTED FROM SUMMARY TABLE

Seen in $K_S^0 K_S^0$ (AUGUSTIN 88), K^+K^- (ABLIKIM 05Q) and $\eta\eta$ (BINON 05) system. Not seen in $\mathcal{T}(1S)$ radiative decays (BARU 89).

 $f_0(2200)$ MASS

VALUE (MeV)	EVTS	DOCUMENT ID	TECN	COMMENT
2187 ± 14 OUR AVERAGE				
2170 ± 20 ± $\frac{10}{-15}$		ABLIKIM	05Q	BES2 $\psi(2S) \rightarrow \gamma\pi^+\pi^-K^+K^-$
2197 ± 17		¹ AUGUSTIN	88	DM2 $J/\psi \rightarrow \gamma K_S^0 K_S^0$
• • • We do not use the following data for averages, fits, limits, etc. • • •				
2206 ± 12 ± 8	381	^{2,3} DOBBS	15	$J/\psi \rightarrow \gamma K^+K^-$
2188 ± 17 ± 16	203	^{2,3} DOBBS	15	$\psi(2S) \rightarrow \gamma K^+K^-$
2210 ± 50		⁴ BINON	05	GAMS $33 \pi^- \rho \rightarrow \eta\eta\eta$
~ 2122		HASAN	94	RVUE $\bar{p}p \rightarrow \pi\pi$
~ 2321		HASAN	94	RVUE $\bar{p}p \rightarrow \pi\pi$

¹ Cannot determine spin to be 0.

² Using CLEO-c data but not authored by the CLEO Collaboration.

³ From a fit to a Breit-Wigner line shape with fixed $\Gamma = 238$ MeV.

⁴ First solution, PWA is ambiguous.

 $f_0(2200)$ WIDTH

VALUE (MeV)	DOCUMENT ID	TECN	COMMENT
207 ± 40 OUR AVERAGE			
220 ± 60 ± $\frac{40}{-45}$	ABLIKIM	05Q	BES2 $\psi(2S) \rightarrow \gamma\pi^+\pi^-K^+K^-$
201 ± 51	⁵ AUGUSTIN	88	DM2 $J/\psi \rightarrow \gamma K_S^0 K_S^0$
• • • We do not use the following data for averages, fits, limits, etc. • • •			
380 ± 90	⁶ BINON	05	GAMS $33 \pi^- \rho \rightarrow \eta\eta\eta$
~ 273	HASAN	94	RVUE $\bar{p}p \rightarrow \pi\pi$
~ 223	HASAN	94	RVUE $\bar{p}p \rightarrow \pi\pi$
⁵ Cannot determine spin to be 0.			
⁶ First solution, PWA is ambiguous.			

 $f_0(2200)$ REFERENCES

DOBBS	15	PR D91 052006	S. Dobbs <i>et al.</i>	(NWES)
ABLIKIM	05Q	PR D72 092002	M. Ablikim <i>et al.</i>	(BES Collab.)
BINON	05	PAN 68 960	F. Binon <i>et al.</i>	
		Translated from YAF 68 998.		
HASAN	94	PL B334 215	A. Hasan, D.V. Bugg	(LOQM)
BARU	89	ZPHY C42 505	S.E. Baru <i>et al.</i>	(NOVO)
AUGUSTIN	88	PRL 60 2238	J.E. Augustin <i>et al.</i>	(DM2 Collab.)

 $f_j(2220)$

$$J^G(J^{PC}) = 0^+(2^{++} \text{ or } 4^{++})$$

OMITTED FROM SUMMARY TABLE

Needs confirmation. See our mini-review in the 2004 edition of this Review, PDG 04.

 $f_j(2220)$ MASS

VALUE (MeV)	EVTS	DOCUMENT ID	TECN	COMMENT
2231.1 ± 3.5 OUR AVERAGE				
2235 ± 4 ± 6	74	BAI	96B	BES $e^+e^- \rightarrow J/\psi \rightarrow \gamma\pi^+\pi^-$
2230 ± $\frac{6}{-7}$ ± 16	46	BAI	96B	BES $e^+e^- \rightarrow J/\psi \rightarrow \gamma K^+K^-$
2232 ± $\frac{8}{-7}$ ± 15	23	BAI	96B	BES $e^+e^- \rightarrow J/\psi \rightarrow \gamma K_S^0 K_S^0$
2235 ± 4 ± 5	32	BAI	96B	BES $e^+e^- \rightarrow J/\psi \rightarrow \gamma\rho\bar{\rho}$
2209 ± $\frac{17}{-15}$ ± 10		ASTON	88F	LASS $11 K^- \rho \rightarrow K^+K^-A$
2230 ± 20		BOLONKIN	88	SPEC $40 \pi^- \rho \rightarrow K_S^0 K_S^0 n$
2220 ± 10	41	¹ ALDE	86B	GA24 $38-100 \pi \rho \rightarrow n\eta\eta'$
2230 ± 6 ± 14	93	BALTRUSAIT...86D	MRK3	$e^+e^- \rightarrow \gamma K^+K^-$
2232 ± 7 ± 7	23	BALTRUSAIT...86D	MRK3	$e^+e^- \rightarrow \gamma K_S^0 K_S^0$

••• We do not use the following data for averages, fits, limits, etc. •••
2223.9 ± 2.5 2 VLADIMIRSK...08 SPEC 40 π⁻ p → K_S⁰ K_S⁰ n + mπ⁰
2246 ± 36 BAI 98H BES J/ψ → γ π⁰ π⁰
1 ALDE 86B uses data from both the GAMS-2000 and GAMS-4000 detectors.
2 J^{PC} = 2⁺ +. Systematic uncertainties not evaluated

f_j(2220) WIDTH

Table with columns: VALUE (MeV), CL%, EVTS, DOCUMENT ID, TECN, COMMENT. Includes entries for OUR AVERAGE and various decay channels like π⁺π⁻, K⁺K⁻, ρ⁺ρ⁻, etc.

f_j(2220) DECAY MODES

Table with columns: Mode, Fraction (Γ_j/Γ). Lists decay modes like ππ, π⁺π⁻, K⁺K⁻, ρ⁺ρ⁻, γγ, ηη'(958), φφ, ηη.

f_j(2220) Γ(i)Γ(γγ)/Γ(total)

Table with columns: VALUE (eV), CL%, DOCUMENT ID, TECN, COMMENT. Includes entry for ACCIARRI 01H L3.

••• We do not use the following data for averages, fits, limits, etc. •••
< 5.6 1 GODANG 97 CLE2 γγ → K_S⁰ K_S⁰
< 86 95 1 ALBRECHT 90G ARG γγ → K⁺ K⁻
<1000 95 2 ALTHOFF 85B TASS γγ, K⁺ K⁻ π

Table with columns: VALUE (eV), CL%, DOCUMENT ID, TECN, COMMENT. Includes entry for ALAM 98C CLE2.

f_j(2220) Γ(i)Γ(ρρ)/Γ²(total)

Table with columns: VALUE (units 10⁻⁵), CL%, DOCUMENT ID, TECN, COMMENT. Includes entry for AMSLER 01 CBAR.

••• We do not use the following data for averages, fits, limits, etc. •••
<(11-42) 99 2 HASAN 96 SPEC 1.35-1.55 ρρ → π⁺ π⁻

Table with columns: VALUE (units 10⁻⁵), CL%, DOCUMENT ID, TECN, COMMENT. Includes entry for EVANGELIS... 98 SPEC.

Table with columns: VALUE (units 10⁻⁵), CL%, DOCUMENT ID, TECN, COMMENT. Includes entry for AMSLER 01 CBAR.

1 For J^P = 2⁺ in the mass range 2222-2240 MeV and the total width between 10 and 20 MeV.
2 For J^P = 2⁺ and J^P = 4⁺ in the mass range 2220-2245 MeV and the total width of 15 MeV.
3 For J^P = 2⁺, the mass of 2235 MeV and the total width of 15 MeV.

f_j(2220) BRANCHING RATIOS

Table with columns: Γ(ππ)/Γ_{total}, VALUE, DOCUMENT ID, COMMENT, Γ₁/Γ. Includes entries for DOBBS 15.

Table with columns: Γ(K⁺K⁻)/Γ_{total}, VALUE, DOCUMENT ID, COMMENT, Γ₃/Γ. Includes entries for DOBBS 15.

Table with columns: Γ(ππ)/Γ(K⁺K⁻), VALUE, DOCUMENT ID, TECN, COMMENT, Γ₁/Γ₃. Includes entry for BAI 96B BES.

Table with columns: Γ(ρρ)/Γ_{total}, VALUE (units 10⁻⁴), CL%, DOCUMENT ID, TECN, COMMENT, Γ₄/Γ. Includes entries for AUBERT, WANG, EVANGELIS..., BARNES, BARDIN, SCULLI.

1 Assuming Γ < 30 MeV.
2 Assuming Γ ~ 20 MeV, J^P = 2⁺ and B(f_j(2220) → K⁺K⁻) = 100%.
3 Assuming Γ = 30-35 MeV, J^P = 2⁺ and B(f_j(2220) → K⁺K⁻) = 100%.

Table with columns: Γ(ρρ)/Γ(K⁺K⁻), VALUE, DOCUMENT ID, TECN, COMMENT, Γ₄/Γ₃. Includes entry for BAI 96B BES.

f_j(2220) REFERENCES

DOBBS 15 PR D91 052006 S. Dobbs et al. (NWES)
VLADIMIRSK... 08 PAN 71 2129 V.V. Vladimirov et al. (ITEP)
AUBERT 07AV PR D76 092004 B. Aubert et al. (BABAR Collab.)
WANG 05A PL B617 141 M.-Z. Wang et al. (BELLE Collab.)
PDG 04 PL B592 1 S. Eidelman et al. (PDG Collab.)
ACCIARRI 01H PL B501 173 M. Acciari et al. (L3 Collab.)
AMSLER 01 PL B520 175 C. Amisler et al. (Crystal Barrel Collab.)
ALAM 98C PRL 81 3328 M.S. Alam et al. (CLEO Collab.)
BAI 98H PRL 81 1179 J.Z. Bai et al. (BES Collab.)
EVANGELIS... 98 PR D57 6370 C. Evangelista et al. (JETSET Collab.)
EVANGELIS... 97 PR D56 3803 C. Evangelista et al. (LEAR Collab.)
GODANG 97 PRL 79 3829 R. Godang et al. (CLEO Collab.)
BAI 96B PRL 76 3502 J.Z. Bai et al. (BES Collab.)
HASAN 96 PL B388 376 A. Hasan, D.V. Bugg (BRUN, LOQM)
BARNES 93 PL B309 469 P.D. Barnes et al. (PS185 Collab.)
ALBRECHT 90G ZPHY C48 183 H. Albrecht et al. (ARGUS Collab.)
ASTON 88F PL B215 199 D. Aston et al. (SLAC, NAGO, CIN, INUS, JP)
BOLONKIN 88 NP B309 426 B.V. Bolonkin et al. (ITEP, SERP)
ALDE 87C SJNP 45 255 D. Alde et al.
BARDIN 87 PL B195 292 G. Bardin et al. (SACL, FERR, CERN, PADO+)
SCULLI 87 PRL 58 1715 J. Sculli et al. (NYU, BNL)
ALDE 86B PL B177 120 D.M. Alde et al. (SERP, BELG, LANL, LAPP)
BALTRUSAITIS... 86D PRL 56 107 R.M. Baltrusaitis (CIT, UCSC, ILL, SLAC+)
ALTHOFF 85B ZPHY C29 189 M. Althoff et al. (TASSO Collab.)

OTHER RELATED PAPERS

DEL-AMO-SA... 100 PRL 105 172001 P. del Amo Sanchez et al. (BABAR Collab.)

η(2225) Γ^G(J^{PC}) = 0⁺(0⁻ +)

OMITTED FROM SUMMARY TABLE
Seen in J/ψ → γφφ. Possibly seen in B → φφK by LEES 11A.

η(2225) MASS

Table with columns: VALUE (MeV), EVTS, DOCUMENT ID, TECN, COMMENT. Includes entries for OUR AVERAGE and ABLIKIM 16N BES3, ABLIKIM 08I BES, BAI 90B MRK3, BAI 90B MRK3.

••• We do not use the following data for averages, fits, limits, etc. •••
~ 2220 BISELLO 86B DM2 J/ψ → γK⁺ K⁻ K⁺ K⁻
1 From a partial wave analysis of J/ψ → γφφ that also finds significant signals for for η(2100), 0⁻ + phase space, f₀(2100), f₂(2010), f₂(2300), f₂(2340), and a previously unseen 0⁻ + state X(2500) (M = 2470⁺¹⁵ +101⁻¹⁹ -23 MeV, Γ = 230⁺⁶⁴ +56⁻³⁵ -33 MeV).

Meson Particle Listings

 $\eta(2225)$, $\rho_3(2250)$, $f_2(2300)$ $\eta(2225)$ WIDTH

VALUE (MeV)	EVTS	DOCUMENT ID	TECN	CHG	COMMENT
185 ± 40	20	OUR AVERAGE			
185 ± 12+43 14-17		¹ ABLIKIM	16N	BES3	$J/\psi \rightarrow \gamma K^+ K^- K^+ K^-$
190 ± 30+50 40	196 ± 19	ABLIKIM	08I	BES	$J/\psi \rightarrow \gamma K^+ K^- K_S^0 K_L^0$
150 ± 300 60 ± 60		BAI	90B	MRK3	$J/\psi \rightarrow \gamma K^+ K^- K^+ K^-$
••• We do not use the following data for averages, fits, limits, etc. •••					
~ 80		BISELLO	86B	DM2	$J/\psi \rightarrow \gamma K^+ K^- K^+ K^-$

¹ From a partial wave analysis of $J/\psi \rightarrow \gamma \phi \phi$ that also finds significant signals for $\eta(2100)$, 0^{-+} phase space, $f_0(2100)$, $f_2(2010)$, $f_2(2300)$, $f_2(2340)$, and a previously unseen 0^{-+} state $X(2500)$ ($M = 2470^{+15+101}_{-19-23}$ MeV, $\Gamma = 230^{+64+56}_{-35-33}$ MeV).

 $\eta(2225)$ REFERENCES

ABLIKIM	16N	PR D93 112011	M. Ablikim	(BESIII Collab.)
LEES	11A	PR D84 012001	J.P. Lees et al.	(BABAR Collab.)
ABLIKIM	08I	PL B662 330	M. Ablikim et al.	(BES Collab.)
BAI	90B	PRL 65 1309	Z. Bai et al.	(Mark III Collab.)
BISELLO	86B	PL B179 294	D. Bisello et al.	(DM2 Collab.)

 $\rho_3(2250)$

$$I^G(J^{PC}) = 1^+(3^{--})$$

OMITTED FROM SUMMARY TABLE

Contains results mostly from formation experiments. For further production experiments see the Further States entry. See also $\rho(2150)$, $f_2(2150)$, $f_4(2300)$, $\rho_5(2350)$.

 $\rho_3(2250)$ MASS $\bar{p}p \rightarrow \pi\pi$ or $K\bar{K}$

VALUE (MeV)	DOCUMENT ID	TECN	CHG	COMMENT
••• We do not use the following data for averages, fits, limits, etc. •••				
~ 2232	HASAN	94	RVUE	$\bar{p}p \rightarrow \pi\pi$
~ 2090	¹ OAKDEN	94	RVUE	0.36-1.55 $\bar{p}p \rightarrow \pi\pi$
~ 2250	² MARTIN	80B	RVUE	
~ 2300	² MARTIN	80C	RVUE	
~ 2140	³ CARTER	78B	CNTR 0	0.7-2.4 $\bar{p}p \rightarrow K^- K^+$
~ 2150	⁴ CARTER	77	CNTR 0	0.7-2.4 $\bar{p}p \rightarrow \pi\pi$

¹ See however KLOET 96 who fit $\pi^+\pi^-$ only and find waves only up to $J = 3$ to be important but not significantly resonant.

² $I(J^{PC}) = 1(3^-)$ from simultaneous analysis of $p\bar{p} \rightarrow \pi^-\pi^+$ and $\pi^0\pi^0$.

³ $I = 0, 1$. $J^P = 3^-$ from Barrelet-zero analysis.

⁴ $I(J^{PC}) = 1(3^-)$ from amplitude analysis.

S-CHANNEL $\bar{N}N$

VALUE (MeV)	DOCUMENT ID	TECN	CHG	COMMENT
••• We do not use the following data for averages, fits, limits, etc. •••				
2260 ± 20	⁵ ANISOVICH	02	SPEC	0.6-1.9 $p\bar{p} \rightarrow \omega\pi^0$, $\omega\eta\pi^0, \pi^+\pi^-$
~ 2190	⁶ CUTTS	78B	CNTR	0.97-3 $\bar{p}p \rightarrow \bar{N}N$
2155 ± 15	^{6,7} COUPLAND	77	CNTR 0	0.7-2.4 $\bar{p}p \rightarrow \bar{p}p$
2193 ± 2	^{6,8} ALSPECTOR	73	CNTR	$\bar{p}p$ S channel
2190 ± 10	⁹ ABRAMS	70	CNTR	S channel $\bar{p}N$

⁵ From the combined analysis of ANISOVICH 00J, ANISOVICH 01D, ANISOVICH 01E, and ANISOVICH 02.

⁶ Isospins 0 and 1 not separated.

⁷ From a fit to the total elastic cross section.

⁸ Referred to as T or T' region by ALSPECTOR 73.

⁹ Seen as bump in $I = 1$ state. See also COOPER 68. PEASLEE 75 confirm $\bar{p}p$ results of ABRAMS 70, no narrow structure.

 $\pi^-p \rightarrow \eta\pi\pi$

VALUE (MeV)	DOCUMENT ID	TECN	CHG	COMMENT
••• We do not use the following data for averages, fits, limits, etc. •••				
2290 ± 20 ± 30	AMELIN	00	VES	37 $\pi^-p \rightarrow \eta\pi^+\pi^-n$

 $\rho_3(2250)$ WIDTH $\bar{p}p \rightarrow \pi\pi$ or $K\bar{K}$

VALUE (MeV)	DOCUMENT ID	TECN	CHG	COMMENT
••• We do not use the following data for averages, fits, limits, etc. •••				
~ 220	HASAN	94	RVUE	$\bar{p}p \rightarrow \pi\pi$
~ 60	¹⁰ OAKDEN	94	RVUE	0.36-1.55 $\bar{p}p \rightarrow \pi\pi$
~ 250	¹¹ MARTIN	80B	RVUE	
~ 200	¹¹ MARTIN	80C	RVUE	
~ 150	¹² CARTER	78B	CNTR 0	0.7-2.4 $\bar{p}p \rightarrow K^- K^+$
~ 200	¹³ CARTER	77	CNTR 0	0.7-2.4 $\bar{p}p \rightarrow \pi\pi$

¹⁰ See however KLOET 96 who fit $\pi^+\pi^-$ only and find waves only up to $J = 3$ to be important but not significantly resonant.

¹¹ $I(J^{PC}) = 1(3^-)$ from simultaneous analysis of $p\bar{p} \rightarrow \pi^-\pi^+$ and $\pi^0\pi^0$.

¹² $I = 0, 1$. $J^P = 3^-$ from Barrelet-zero analysis.

¹³ $I(J^{PC}) = 1(3^-)$ from amplitude analysis.

S-CHANNEL $\bar{N}N$

VALUE (MeV)	DOCUMENT ID	TECN	CHG	COMMENT
••• We do not use the following data for averages, fits, limits, etc. •••				
160 ± 25	¹⁴ ANISOVICH	02	SPEC	0.6-1.9 $p\bar{p} \rightarrow \omega\pi^0$, $\omega\eta\pi^0, \pi^+\pi^-$
135 ± 75	^{15,16} COUPLAND	77	CNTR 0	0.7-2.4 $\bar{p}p \rightarrow \bar{p}p$
98 ± 8	¹⁶ ALSPECTOR	73	CNTR	$\bar{p}p$ S channel
~ 85	¹⁷ ABRAMS	70	CNTR	S channel $\bar{p}N$

¹⁴ From the combined analysis of ANISOVICH 00J, ANISOVICH 01D, ANISOVICH 01E, and ANISOVICH 02.

¹⁵ From a fit to the total elastic cross section.

¹⁶ Isospins 0 and 1 not separated.

¹⁷ Seen as bump in $I = 1$ state. See also COOPER 68. PEASLEE 75 confirm $\bar{p}p$ results of ABRAMS 70, no narrow structure.

 $\pi^-p \rightarrow \eta\pi\pi$

VALUE (MeV)	DOCUMENT ID	TECN	CHG	COMMENT
••• We do not use the following data for averages, fits, limits, etc. •••				
230 ± 50 ± 80	AMELIN	00	VES	37 $\pi^-p \rightarrow \eta\pi^+\pi^-n$

 $\rho_3(2250)$ REFERENCES

ANISOVICH	02	PL B542 8	A.V. Anisovich et al.	
ANISOVICH	01D	PL B508 6	A.V. Anisovich et al.	
ANISOVICH	01E	PL B513 281	A.V. Anisovich et al.	
AMELIN	00	NP A668 83	D. Amelin et al.	(VES Collab.)
ANISOVICH	00J	PL B491 47	A.V. Anisovich et al.	(RAL, LOQM, FNPI+)
KLOET	96	PR D53 6120	W.M. Kloet, F. Myhrer	(RUTG, IORD)
HASAN	94	PL B334 215	A. Hasan, D.V. Bugg	(LOQM)
OAKDEN	94	NP A574 731	M.N. Oakden, M.R. Pennington	(DURH)
MARTIN	80B	NP B176 355	B.R. Martin, D. Morgan	(LOUC, RHEL)JP
MARTIN	80C	NP B169 216	A.D. Martin, M.R. Pennington	(DURH)JP
CARTER	78B	NP B141 467	A.A. Carter	(LOQM)
CUTTS	78B	PR D17 16	D. Cutts et al.	(STON, WISC)
CARTER	77	PL 67B 117	A.A. Carter et al.	(LOQM, RHEL)JP
COUPLAND	77	PL 71B 460	M. Coupland et al.	(LOQM, RHEL)
PEASLEE	75	PL 57B 189	D.C. Peaslee et al.	(CANB, BARI, BROW+)
ALSPECTOR	73	PRL 30 511	J. Alspector et al.	(RUTG, UPJN)
ABRAMS	70	PR D1 1917	R.J. Abrams et al.	(BNL)
COOPER	68	PRL 20 1059	W.A. Cooper et al.	(ANL)

 $f_2(2300)$

$$I^G(J^{PC}) = 0^+(2^{++})$$

 $f_2(2300)$ MASS

VALUE (MeV)	DOCUMENT ID	TECN	CHG	COMMENT
2297 ± 28	¹ ETKIN	88	MPS	22 $\pi^-p \rightarrow \phi\phi n$
••• We do not use the following data for averages, fits, limits, etc. •••				
2243 ± 7+3 6-29	² UEHARA	13	BELL	$\gamma\gamma \rightarrow K_S^0 K_S^0$
2270 ± 12	VLADIMIRSK..06	SPEC	40	$\pi^-p \rightarrow K_S^0 K_S^0 n$
2327 ± 9 ± 6	ABE	04	BELL	10.6 $e^+e^- \rightarrow e^+e^- K^+ K^-$
2231 ± 10	BOOTH	86	OMEG	85 $\pi^-Be \rightarrow 2\phi Be$
2220 ± 90 20	LINDENBAUM	84	RVUE	
2320 ± 40	ETKIN	82	MPS	22 $\pi^-p \rightarrow 2\phi n$

¹ Includes data of ETKIN 85. The percentage of the resonance going into $\phi\phi 2^{++} S_2$, D_2 , and D_0 is 6^{+15}_{-5} , 25^{+18}_{-14} , and 69^{+16}_{-27} , respectively.

² Spin 2 preferred, tentatively assigned to $f_2(2300)$.

 $f_2(2300)$ WIDTH

VALUE (MeV)	DOCUMENT ID	TECN	CHG	COMMENT
149 ± 41	³ ETKIN	88	MPS	22 $\pi^-p \rightarrow \phi\phi n$
••• We do not use the following data for averages, fits, limits, etc. •••				
145 ± 12+27 -34	⁴ UEHARA	13	BELL	$\gamma\gamma \rightarrow K_S^0 K_S^0$
90 ± 29	VLADIMIRSK..06	SPEC	40	$\pi^-p \rightarrow K_S^0 K_S^0 n$
275 ± 36 ± 20	ABE	04	BELL	10.6 $e^+e^- \rightarrow e^+e^- K^+ K^-$
133 ± 50	BOOTH	86	OMEG	85 $\pi^-Be \rightarrow 2\phi Be$
200 ± 50	LINDENBAUM	84	RVUE	
220 ± 70	ETKIN	82	MPS	22 $\pi^-p \rightarrow 2\phi n$

³ Includes data of ETKIN 85.

⁴ Spin 2 preferred, tentatively assigned to $f_2(2300)$.

 $f_2(2300)$ DECAY MODES

Mode	Fraction (Γ_i/Γ)
Γ_1 $\phi\phi$	seen
Γ_2 $K\bar{K}$	seen
Γ_3 $\gamma\gamma$	seen

See key on page 999

Meson Particle Listings

$f_2(2300)$, $f_4(2300)$, $f_0(2330)$

$f_2(2300) \Gamma(i)\Gamma(\gamma\gamma)/\Gamma(\text{total})$

$\Gamma(K\bar{K}) \times \Gamma(\gamma\gamma)/\Gamma_{\text{total}}$	DOCUMENT ID	TECN	COMMENT	$\Gamma_2\Gamma_3/\Gamma$
$3.2^{+0.5+1.3}_{-0.4-2.2}$	UEHARA	13	BELL $\gamma\gamma \rightarrow K_S^0 K_S^0$	
$44 \pm 6 \pm 12$	⁵ ABE	04	BELL $10.6 e^+ e^- \rightarrow e^+ e^- K^+ K^-$	

⁵ Assuming spin 2.

$f_2(2300)$ REFERENCES

UEHARA 13	PTEP 2013 123C01	S. Uehara <i>et al.</i>	(BELLE Collab.)
VLADIMIRSK... 06	PAN 69 493	V.V. Vladimirovsky <i>et al.</i>	(ITEP, Moscow)
ABE 04	Translated from YAF 69 515	K. Abe <i>et al.</i>	(BELLE Collab.)
ETKIN 88	EPJ C32 323	A. Etkin <i>et al.</i>	(BNL, CUNY)
BOOTH 86	PL B201 568	P.S.L. Booth <i>et al.</i>	(LIVP, GLAS, CERN)
ETKIN 85	NP B273 677	A. Etkin <i>et al.</i>	(BNL, CUNY)
LINDENBAUM 84	PL 165B 217	S.J. Lindenbaum	(CUNY)
ETKIN 82	CNPP 13 285	A. Etkin <i>et al.</i>	(BNL, CUNY)
	PRL 49 1620		

$f_4(2300)$

$$I^G(J^{PC}) = 0^+(4^{++})$$

OMITTED FROM SUMMARY TABLE

This entry was previously called $U_0(2350)$. Contains results mostly from formation experiments. For further production experiments see the Further States entry. See also $\rho(2150)$, $f_2(2150)$, $\rho_3(2250)$, $\rho_5(2350)$.

$f_4(2300)$ MASS

$\bar{p}p \rightarrow \pi\pi$ or $\bar{K}K$

VALUE (MeV)	DOCUMENT ID	TECN	COMMENT
~ 2314	HASAN 94	RVUE	$\bar{p}p \rightarrow \pi\pi$
~ 2300	¹ MARTIN 80B	RVUE	
~ 2300	¹ MARTIN 80C	RVUE	
~ 2340	² CARTER 78B	CNTR	$0.7-2.4 \bar{p}p \rightarrow K^- K^+$
~ 2330	DULUDE 78B	OSPK	$1-2 \bar{p}p \rightarrow \pi^0 \pi^0$
~ 2310	³ CARTER 77	CNTR	$0.7-2.4 \bar{p}p \rightarrow \pi\pi$

¹ $I(J^P) = 0(4^+)$ from simultaneous analysis of $p\bar{p} \rightarrow \pi^- \pi^+$ and $\pi^0 \pi^0$.
² $I(J^P) = 0(4^+)$ from Barrelet-zero analysis.
³ $I(J^P) = 0(4^+)$ from amplitude analysis.

S-CHANNEL $\bar{p}p$ or $\bar{N}N$

VALUE (MeV)	DOCUMENT ID	TECN	COMMENT
2283 ± 17	⁴ ANISOVICH 00J	SPEC	
~ 2380	⁵ CUTTS 78B	CNTR	$0.97-3 \bar{p}p \rightarrow \bar{N}N$
2345 ± 15	^{5,6} COUPLAND 77	CNTR	$0.7-2.4 \bar{p}p \rightarrow \bar{p}p$
2359 ± 2	^{5,7} ALSPECTOR 73	CNTR	$\bar{p}p$ S channel
2375 ± 10	ABRAMS 70	CNTR	S channel $\bar{N}N$

⁴ From the combined analysis of ANISOVICH 99c and ANISOVICH 99f on $\bar{p}p \rightarrow \eta\pi^0 \pi^0$, $\pi^0 \pi^0$, $\eta\eta$, $\eta\eta'$, $\pi^+ \pi^-$.
⁵ Isospins 0 and 1 not separated.
⁶ From a fit to the total elastic cross section.
⁷ Referred to as U or U region by ALSPECTOR 73.

$\pi^- p \rightarrow \eta\pi\pi n$

VALUE (MeV)	DOCUMENT ID	TECN	COMMENT
$2330 \pm 20 \pm 40$	AMELIN 00	VES	$37 \pi^- p \rightarrow \eta\pi^+ \pi^- n$

pp CENTRAL PRODUCTION

VALUE (MeV)	DOCUMENT ID	COMMENT
2320 ± 60 OUR ESTIMATE		
2332 ± 15	BARBERIS 00F	$450 pp \rightarrow p_f \omega p_S$

$f_4(2300)$ WIDTH

$\bar{p}p \rightarrow \pi\pi$ or $\bar{K}K$

VALUE (MeV)	DOCUMENT ID	TECN	COMMENT
~ 278	HASAN 94	RVUE	$\bar{p}p \rightarrow \pi\pi$
~ 200	⁸ MARTIN 80C	RVUE	
~ 150	⁹ CARTER 78B	CNTR	$0.7-2.4 \bar{p}p \rightarrow K^- K^+$
~ 210	¹⁰ CARTER 77	CNTR	$0.7-2.4 \bar{p}p \rightarrow \pi\pi$

⁸ $I(J^P) = 0(4^+)$ from simultaneous analysis of $p\bar{p} \rightarrow \pi^- \pi^+$ and $\pi^0 \pi^0$.
⁹ $I(J^P) = 0(4^+)$ from Barrelet-zero analysis.
¹⁰ $I(J^P) = 0(4^+)$ from amplitude analysis.

S-CHANNEL $\bar{p}p$ or $\bar{N}N$

VALUE (MeV)	DOCUMENT ID	TECN	COMMENT
310 ± 25	¹¹ ANISOVICH 00J	SPEC	
135^{+150}_{-65}	^{12,13} COUPLAND 77	CNTR	$0.7-2.4 \bar{p}p \rightarrow \bar{p}p$
165^{+18}_{-8}	¹³ ALSPECTOR 73	CNTR	$\bar{p}p$ S channel
~ 190	ABRAMS 70	CNTR	S channel $\bar{N}N$

¹¹ From the combined analysis of ANISOVICH 99c and ANISOVICH 99f on $\bar{p}p \rightarrow \eta\pi^0 \pi^0$, $\pi^0 \pi^0$, $\eta\eta$, $\eta\eta'$, $\pi^+ \pi^-$.
¹² From a fit to the total elastic cross section.
¹³ Isospins 0 and 1 not separated.

$\pi^- p \rightarrow \eta\pi\pi n$

VALUE (MeV)	DOCUMENT ID	TECN	COMMENT
$235 \pm 50 \pm 40$	AMELIN 00	VES	$37 \pi^- p \rightarrow \eta\pi^+ \pi^- n$

pp CENTRAL PRODUCTION

VALUE (MeV)	DOCUMENT ID	COMMENT
250 ± 80 OUR ESTIMATE		
260 ± 57	BARBERIS 00F	$450 pp \rightarrow p_f \omega p_S$

$f_4(2300)$ DECAY MODES

Mode	Fraction (Γ_i/Γ)
Γ_1 $\rho\rho$	seen
Γ_2 $\omega\omega$	seen
Γ_3 $\eta\pi\pi$	seen
Γ_4 $\pi\pi$	seen
Γ_5 $K\bar{K}$	seen
Γ_6 $\bar{N}N$	seen

$f_4(2300)$ BRANCHING RATIOS

$\Gamma(\rho\rho)/\Gamma(\omega\omega)$	DOCUMENT ID	COMMENT	Γ_1/Γ_2
2.8 ± 0.5	BARBERIS 00F	$450 pp \rightarrow p_f \omega p_S$	

$f_4(2300)$ REFERENCES

AMELIN 00	NP A668 83	D. Amelin <i>et al.</i>	(VES Collab.)
ANISOVICH 00J	PL B491 47	A.V. Anisovich <i>et al.</i>	(RAL, LOQM, PNPI+)
BARBERIS 00F	PL B484 198	D. Barberis <i>et al.</i>	(WA 102 Collab.)
ANISOVICH 99C	PL B452 173	A.V. Anisovich <i>et al.</i>	
ANISOVICH 99F	NP A551 253	A.V. Anisovich <i>et al.</i>	(LOQM)
HASAN 94	PL B334 215	A. Hasan, D.V. Bugg	(LOUQ, RHEL) JP
MARTIN 80B	NP B176 355	B.R. Martin, D. Morgan	(DURH) JP
MARTIN 80C	NP B169 216	A.D. Martin, M.R. Pennington	(DURH) JP
CARTER 78B	NP B141 467	A.A. Carter	(LOQM)
CUTTS 78B	PR D17 16	D. Cutts <i>et al.</i>	(STON, WISC)
DULUDE 78B	PL 79B 335	R.S. Dulude <i>et al.</i>	(BROW, MIT, BARI) JP
CARTER 77	PL 67B 117	A.A. Carter <i>et al.</i>	(DURH) JP
COUPLAND 77	PL 71B 460	M. Coupland <i>et al.</i>	(LOQM, RHEL)
ALSPECTOR 73	PRL 30 511	J. Alspector <i>et al.</i>	(RUTG, UPNJ)
ABRAMS 70	PR D1 1917	R.J. Abrams <i>et al.</i>	(BNL)

$f_0(2330)$

$$I^G(J^{PC}) = 0^+(0^{++})$$

OMITTED FROM SUMMARY TABLE

$f_0(2330)$ MASS

VALUE (MeV)	DOCUMENT ID	TECN	COMMENT
2314 ± 25	¹ BUGG 04A	RVUE	
2337 ± 14	ANISOVICH 00J	SPEC	$2.0 \bar{p}p \rightarrow \pi\pi, \eta\eta$
~ 2321	HASAN 94	RVUE	$\bar{p}p \rightarrow \pi\pi$

¹ Partial wave analysis of the data on $p\bar{p} \rightarrow \bar{\Lambda}\Lambda$ from BARNES 00.

$f_0(2330)$ WIDTH

VALUE (MeV)	DOCUMENT ID	TECN	COMMENT
144 ± 20	² BUGG 04A	RVUE	
217 ± 33	ANISOVICH 00J	SPEC	$2.0 \bar{p}p \rightarrow \pi\pi, \eta\eta$
~ 223	HASAN 94	RVUE	$\bar{p}p \rightarrow \pi\pi$

² Partial wave analysis of the data on $p\bar{p} \rightarrow \bar{\Lambda}\Lambda$ from BARNES 00.

$f_0(2330)$ REFERENCES

BUGG 04A	EPJ C36 161	D.V. Bugg	
ANISOVICH 00J	PL B491 47	A.V. Anisovich <i>et al.</i>	(RAL, LOQM, PNPI+)
BARNES 00	PR C62 055203	P.D. Barnes <i>et al.</i>	
HASAN 94	PL B334 215	A. Hasan, D.V. Bugg	(LOQM)

Meson Particle Listings

$f_2(2340)$, $\rho_5(2350)$

$f_2(2340)$

$$I^G(J^{PC}) = 0^+(2^{++})$$

$f_2(2340)$ MASS

VALUE (MeV)	EVTS	DOCUMENT ID	TECN	COMMENT
2345 ± 50 OUR AVERAGE				
2362 ± 31 +140 -30 -63	5.5k	1 ABLIKIM	13N BES3	$e^+e^- \rightarrow J/\psi \rightarrow \gamma\eta\eta$
2339 ± 55		2 ETKIN	88 MPS	$22 \pi^- p \rightarrow \phi\phi n$
••• We do not use the following data for averages, fits, limits, etc. •••				
2350 ± 7	80k	3 UMAN	06 E835	$5.2 \bar{p}p \rightarrow \eta\eta\pi^0$
2392 ± 10		BOOTH	86 OMEG	$85 \pi^- Be \rightarrow 2\phi Be$
2360 ± 20		LINDENBAUM	84 RVUE	

1 From partial wave analysis including all possible combinations of 0^{++} , 2^{++} , and 4^{++} resonances.
 2 Includes data of ETKIN 85. The percentage of the resonance going into $\phi\phi 2^{++} S_2$, D_2 , and D_0 is 37 ± 19 , 4 ± 12 , and 59 ± 21 , respectively.
 3 Statistical error only.

$f_2(2340)$ WIDTH

VALUE (MeV)	EVTS	DOCUMENT ID	TECN	COMMENT
322 ± 70 OUR AVERAGE				
334 ± 62 +165 -54 -100	5.5k	4 ABLIKIM	13N BES3	$e^+e^- \rightarrow J/\psi \rightarrow \gamma\eta\eta$
319 ± 81 -69		5 ETKIN	88 MPS	$22 \pi^- p \rightarrow \phi\phi n$
••• We do not use the following data for averages, fits, limits, etc. •••				
218 ± 16	80k	6 UMAN	06 E835	$5.2 \bar{p}p \rightarrow \eta\eta\pi^0$
198 ± 50		BOOTH	86 OMEG	$85 \pi^- Be \rightarrow 2\phi Be$
150 ± 150 -50		LINDENBAUM	84 RVUE	

4 From partial wave analysis including all possible combinations of 0^{++} , 2^{++} , and 4^{++} resonances.
 5 Includes data of ETKIN 85.
 6 Statistical error only.

$f_2(2340)$ DECAY MODES

Mode	Fraction (Γ_i/Γ)
Γ_1 $\phi\phi$	seen
Γ_2 $\eta\eta$	seen

$f_2(2340)$ BRANCHING RATIOS

$\Gamma(\eta\eta)/\Gamma_{total}$	DOCUMENT ID	TECN	COMMENT	Γ_2/Γ
seen	UMAN	06 E835	$5.2 \bar{p}p \rightarrow \eta\eta\pi^0$	

$f_2(2340)$ REFERENCES

ABLIKIM	13N	PR D87 092009	Ablikim M. et al.	(BESIII Collab.)
UMAN	06	PR D73 052009	I. Uman et al.	(FNAL E835)
ETKIN	88	PL B201 568	A. Etkin et al.	(BNL, CUNY)
BOOTH	86	NP B273 677	P.S.L. Booth et al.	(LIVP, GLAS, CERN)
ETKIN	85	PL 165B 217	A. Etkin et al.	(BNL, CUNY)
LINDENBAUM	84	CNPP 13 285	S.J. Lindenbaum	(CUNY)

$\rho_5(2350)$

$$I^G(J^{PC}) = 1^+(5^{--})$$

OMITTED FROM SUMMARY TABLE
 This entry was previously called $U_1(2400)$. See also $\rho(2150)$, $f_2(2150)$, $\rho_3(2250)$, $f_4(2300)$.

$\rho_5(2350)$ MASS

VALUE (MeV)	DOCUMENT ID	TECN	COMMENT	
$\pi^- p \rightarrow \omega\pi^0 n$				
2330 ± 35	ALDE	95 GAM2	$38 \pi^- p \rightarrow \omega\pi^0 n$	
$\bar{p}p \rightarrow \pi\pi$ or $\bar{K}K$				
VALUE (MeV)	DOCUMENT ID	TECN	CHG	COMMENT
••• We do not use the following data for averages, fits, limits, etc. •••				
~ 2303	HASAN	94 RVUE		$\bar{p}p \rightarrow \pi\pi$
~ 2300	1 MARTIN	80B RVUE		
~ 2250	1 MARTIN	80C RVUE		
~ 2500	2 CARTER	78B CNTR 0	0.7-2.4	$\bar{p}p \rightarrow K^- K^+$
~ 2480	3 CARTER	77 CNTR 0	0.7-2.4	$\bar{p}p \rightarrow \pi\pi$

S-CHANNEL $\bar{N}N$

VALUE (MeV)	DOCUMENT ID	TECN	CHG	COMMENT
••• We do not use the following data for averages, fits, limits, etc. •••				
2300 ± 45	4 ANISOVICH	02 SPEC		$0.6-1.9 \bar{p}p \rightarrow \omega\pi^0$, $\omega\eta\pi^0, \pi^+\pi^-$
2295 ± 30	ANISOVICH	00J SPEC		
~ 2380	5 CUTTS	78B CNTR		$0.97-3 \bar{p}p \rightarrow \bar{N}N$
2345 ± 15	5,6 COUPLAND	77 CNTR 0		$0.7-2.4 \bar{p}p \rightarrow \bar{p}p$
2359 ± 2	5,7 ALSPECTOR	73 CNTR		$\bar{p}p$ S channel
2350 ± 10	8 ABRAMS	70 CNTR		S channel $\bar{N}N$
2360 ± 25	9 OH	70B HDBC -0		$\bar{p}(p n), K^* K 2\pi$

$\pi^- p \rightarrow K^+ K^- n$

VALUE (MeV)	DOCUMENT ID	TECN	CHG	COMMENT
••• We do not use the following data for averages, fits, limits, etc. •••				
2307 ± 6	ALPER	80 CNTR 0		$62 \pi^- p \rightarrow K^+ K^- n$
1 $I(J^P) = 1(5^-)$ from simultaneous analysis of $p\bar{p} \rightarrow \pi^- \pi^+$ and $\pi^0 \pi^0$. 2 $I = 0(1); J^P = 5^-$ from Barrelet-zero analysis. 3 $I(J^P) = 1(5^-)$ from amplitude analysis. 4 From the combined analysis of ANISOVICH 00J, ANISOVICH 01D, ANISOVICH 01E, and ANISOVICH 02. 5 Isospins 0 and 1 not separated. 6 From a fit to the total elastic cross section. 7 Referred to as U or U region by ALSPECTOR 73. 8 For $I = 1 \bar{N}N$. 9 No evidence for this bump seen in the $\bar{p}p$ data of CHAPMAN 71B. Narrow state not confirmed by OH 73 with more data.				

$\rho_5(2350)$ WIDTH

VALUE (MeV)	DOCUMENT ID	TECN	COMMENT
$\pi^- p \rightarrow \omega\pi^0 n$			
400 ± 100	ALDE	95 GAM2	$38 \pi^- p \rightarrow \omega\pi^0 n$

$\bar{p}p \rightarrow \pi\pi$ or $\bar{K}K$

VALUE (MeV)	DOCUMENT ID	TECN	CHG	COMMENT
••• We do not use the following data for averages, fits, limits, etc. •••				
~ 169	HASAN	94 RVUE		$\bar{p}p \rightarrow \pi\pi$
~ 250	10 MARTIN	80B RVUE		
~ 300	10 MARTIN	80C RVUE		
~ 150	11 CARTER	78B CNTR 0	0.7-2.4	$\bar{p}p \rightarrow K^- K^+$
~ 210	12 CARTER	77 CNTR 0	0.7-2.4	$\bar{p}p \rightarrow \pi\pi$

S-CHANNEL $\bar{N}N$

VALUE (MeV)	DOCUMENT ID	TECN	CHG	COMMENT
••• We do not use the following data for averages, fits, limits, etc. •••				
260 ± 75	13 ANISOVICH	02 SPEC		$0.6-1.9 \bar{p}p \rightarrow \omega\pi^0$, $\omega\eta\pi^0, \pi^+\pi^-$
235 ± 65 -40	ANISOVICH	00J SPEC		
135 ± 150 -65	14,15 COUPLAND	77 CNTR 0		$0.7-2.4 \bar{p}p \rightarrow \bar{p}p$
165 ± 18 -8	15 ALSPECTOR	73 CNTR		$\bar{p}p$ S channel
< 60	16 OH	70B HDBC -0		$\bar{p}(p n), K^* K 2\pi$
~ 140	ABRAMS	67C CNTR		S channel $\bar{p}N$

$\pi^- p \rightarrow K^+ K^- n$

VALUE (MeV)	DOCUMENT ID	TECN	CHG	COMMENT
••• We do not use the following data for averages, fits, limits, etc. •••				
245 ± 20	ALPER	80 CNTR 0		$62 \pi^- p \rightarrow K^+ K^- n$
10 $I(J^P) = 1(5^-)$ from simultaneous analysis of $p\bar{p} \rightarrow \pi^- \pi^+$ and $\pi^0 \pi^0$. 11 $I = 0(1); J^P = 5^-$ from Barrelet-zero analysis. 12 $I(J^P) = 1(5^-)$ from amplitude analysis. 13 From the combined analysis of ANISOVICH 00J, ANISOVICH 01D, ANISOVICH 01E, and ANISOVICH 02. 14 From a fit to the total elastic cross section. 15 Isospins 0 and 1 not separated. 16 No evidence for this bump seen in the $\bar{p}p$ data of CHAPMAN 71B. Narrow state not confirmed by OH 73 with more data.				

$\rho_5(2350)$ REFERENCES

ANISOVICH	02	PL B542 8	A.V. Anisovich et al.	
ANISOVICH	01D	PL B508 6	A.V. Anisovich et al.	
ANISOVICH	01E	PL B513 281	A.V. Anisovich et al.	
ANISOVICH	00J	PL B491 47	A.V. Anisovich et al.	(RAL, LOQM, PNPI+)
ALDE	95	ZPHY C66 379	D.H. Alde et al.	(GAMS Collab) JP
HASAN	94	PL B334 215	A. Hasan et al.	(LOQM)
ALPER	80	PL 94B 422	B. Alper et al.	(AMST, CERN, CRAC, MPIM+)
MARTIN	80B	NP B176 355	B.R. Martin, D. Morgan	(LOUC, RHEL) JP
MARTIN	80C	NP B169 216	A.D. Martin, M.R. Pennington	(DURH) JP
CARTER	78B	NP B141 467	A.A. Carter	(LOQM)
CUTTS	78B	PR D17 16	D. Cutts et al.	(STON, WISC)
CARTER	77	PL 67B 117	A.A. Carter et al.	(LOQM, RHEL) JP
COUPLAND	77	PL 71B 460	M. Coupland et al.	(LOQM, RHEL)
ALSPECTOR	73	PRL 30 511	J. Alspector et al.	(RUTG, UPNJ)
OH	73	NP B51 57	B.Y. Oh et al.	(MSU)
CHAPMAN	71B	PR D1 1275	J.W. Chapman et al.	(MICH)
ABRAMS	70	PR D1 1917	R.J. Abrams et al.	(BNL)
OH	70B	PRL 24 1257	B.Y. Oh et al.	(MSU)
ABRAMS	67C	PRL 18 1209	R.J. Abrams et al.	(BNL)

See key on page 999

Meson Particle Listings

$f_6(2510)$

$f_6(2510)$

$$I^G(J^{PC}) = 0^+(6^{++})$$

OMITTED FROM SUMMARY TABLE
Needs confirmation.

$f_6(2510)$ MASS

VALUE (MeV)	DOCUMENT ID	TECN	COMMENT
2465 ± 50 OUR AVERAGE	Error includes scale factor of 2.1.		
2420 ± 30	ALDE 98	GAM4	100 $\pi^- p \rightarrow \pi^0 \pi^0 n$
2510 ± 30	BINON 84B	GAM2	38 $\pi^- p \rightarrow n 2\pi^0$
• • • We do not use the following data for averages, fits, limits, etc. • • •			
2485 ± 40	¹ ANISOVICH 00J	SPEC	1.92–2.41 $p\bar{p}$
¹ From the combined analysis of ANISOVICH 99c, ANISOVICH 99f, ANISOVICH 99j, ANISOVICH 99k, and ANISOVICH 00b.			

$f_6(2510)$ WIDTH

VALUE (MeV)	DOCUMENT ID	TECN	COMMENT
255 ± 40 OUR AVERAGE			
270 ± 60	ALDE 98	GAM4	100 $\pi^- p \rightarrow \pi^0 \pi^0 n$
240 ± 60	BINON 84B	GAM2	38 $\pi^- p \rightarrow n 2\pi^0$
• • • We do not use the following data for averages, fits, limits, etc. • • •			
410 ± 90	² ANISOVICH 00J	SPEC	1.92–2.41 $p\bar{p}$
² From the combined analysis of ANISOVICH 99c, ANISOVICH 99f, ANISOVICH 99j, ANISOVICH 99k, and ANISOVICH 00b.			

$f_6(2510)$ DECAY MODES

Mode	Fraction (Γ_i/Γ)
$\Gamma_1 \pi\pi$	(6.0 ± 1.0) %

$f_6(2510)$ BRANCHING RATIOS

$\Gamma(\pi\pi)/\Gamma_{total}$	DOCUMENT ID	TECN	COMMENT	Γ_1/Γ
0.06 ± 0.01	³ BINON 83C	GAM2	38 $\pi^- p \rightarrow n 4\gamma$	
³ Assuming one pion exchange and using data of BOLOTOV 74.				

$f_6(2510)$ REFERENCES

ANISOVICH 00B	NP A662 319	A.V. Anisovich <i>et al.</i>	
ANISOVICH 00J	PL B491 47	A.V. Anisovich <i>et al.</i>	(RAL, LOQM, PNPI+)
ANISOVICH 99C	PL B452 173	A.V. Anisovich <i>et al.</i>	
ANISOVICH 99F	NP A651 253	A.V. Anisovich <i>et al.</i>	
ANISOVICH 99J	PL B471 271	A.V. Anisovich <i>et al.</i>	
ANISOVICH 99K	PL B468 309	A.V. Anisovich <i>et al.</i>	
ALDE 98	EPJ A3 361	D. Alde <i>et al.</i>	(GAM4 Collab.)
Also	PAN 62 405	D. Alde <i>et al.</i>	(GAMS Collab.)
	Translated from YAF 62 446.		
BINON 84B	LNC 39 41	F.G. Binon <i>et al.</i>	(SERP, BELG, LAPP)JP
BINON 83C	SJNP 38 723	F.G. Binon <i>et al.</i>	(SERP, BRUX+)
	Translated from YAF 38 1199.		
BOLOTOV 74	PL 52B 489	V.N. Bolotov <i>et al.</i>	(SERP)

Meson Particle Listings

Further States

OTHER LIGHT MESONS

Further States

OMITTED FROM SUMMARY TABLE

This section contains states observed by a single group or states poorly established that thus need confirmation.

QUANTUM NUMBERS, MASSES, WIDTHS, AND BRANCHING RATIOS

X(360) $I^G(J^{PC}) = ??(??^+)$

MASS (MeV)	WIDTH (MeV)	EVTs	DOCUMENT ID	TECN	COMMENT
360 ± 7 ± 9	64 ± 18	2.3k	¹ ABRAAMYAN 09	CNTR	2.75 dC → γγX

¹ Not seen in pC → γγX at 5.5 GeV/c.

X(1070) $I^G(J^{PC}) = ??(0^{++})$

MASS (MeV)	WIDTH (MeV)	DOCUMENT ID	COMMENT
1072 ± 1	3.5 ± 0.5	² VLADIMIRSK...08	40 π ⁻ p → K _S ⁰ K _S ⁰ n + mπ ⁰

² Supersedes GRIGOR'EV 05.

X(1110) $I^G(J^{PC}) = 0^+(\text{even}^+)$

MASS (MeV)	WIDTH (MeV)	DOCUMENT ID	TECN	COMMENT
1107 ± 4	111 ± 8 ± 15	DAFTARI 87	DBC	0. $\bar{p}n \rightarrow \rho^-\pi^+\pi^-$

η₂(1200-1600) $I^G(J^{PC}) = 0^+(0^{++})$

MASS (MeV)	WIDTH (MeV)	DOCUMENT ID	TECN	COMMENT
1323 ± 8	237 ± 20	VLADIMIRSK...06	SPEC	40 π ⁻ p → K _S ⁰ K _S ⁰ n
1480 ⁺¹⁰⁰ ₋₁₅₀	1030 ⁺⁸⁰ ₋₁₇₀	³ ANISOVICH 03	SPEC	
1530 ⁺⁹⁰ ₋₂₅₀	560 ± 40	⁴ ANISOVICH 03	SPEC	

³ K-matrix pole from combined analysis of π⁻p → π⁰π⁰n, π⁻p → K \bar{K} n, π⁺π⁻ → π⁺π⁻, $\bar{p}p \rightarrow \pi^0\pi^0\pi^0, \pi^0\eta\eta, \pi^0\pi^0\eta, \pi^+\pi^-\pi^0, K^+K^-\pi^0, K_S^0K_S^0\pi^0, K^+K_S^0\pi^0$ at rest, $\bar{p}n \rightarrow \pi^-\pi^-\pi^+, K_S^0K^-\pi^0, K_S^0K_S^0\pi^0$ at rest.

⁴ K-matrix pole from combined analysis of π⁻p → π⁰π⁰n, π⁻p → K \bar{K} n, $\bar{p}p \rightarrow \pi^0\pi^0\pi^0, \pi^0\eta\eta, \pi^0\pi^0\eta$ at rest.

X(1420) $I^G(J^{PC}) = 2^+(0^{++})$

MASS (MeV)	WIDTH (MeV)	DOCUMENT ID	TECN	COMMENT
1420 ± 20	160 ± 10	FILIPPI 00	OBLX	0 $\bar{p}p \rightarrow \pi^+\pi^+\pi^-$

X(1545) $I^G(J^{PC}) = ??(??^+)$

MASS (MeV)	WIDTH (MeV)	DOCUMENT ID	COMMENT
1545 ± 3	6.0 ± 2.5	⁵ VLADIMIRSK...08	40 π ⁻ p → K _S ⁰ K _S ⁰ n + mπ ⁰

⁵ Supersedes VLADIMIRSKII 00.

X(1575) $I^G(J^{PC}) = ??(1^{--})$

MASS (MeV)	WIDTH (MeV)	DOCUMENT ID	TECN	COMMENT
1576 ⁺⁴⁹⁺⁹⁸ ₋₅₅₋₉₁	818 ⁺²²⁺⁶⁴ ₋₂₃₋₁₃₃	⁶ ABLIKIM 06s	BES	J/ψ → K ⁺ K ⁻ π ⁰

⁶ A broad peak observed at K⁺K⁻ invariant mass. Mass and width above are its pole position. The observed branching ratio is B(J/ψ → Xπ⁰) B(X → K⁺K⁻) = (8.5 ± 0.6^{+2.7}_{-3.6}) × 10⁻⁴.

X(1600) $I^G(J^{PC}) = 2^+(2^{++})$

MASS (MeV)	WIDTH (MeV)	DOCUMENT ID	TECN	COMMENT
1600 ± 100	400 ± 200	⁷ ALBRECHT 91F	ARG	10.2 e ⁺ e ⁻ → e ⁺ e ⁻ 2(π ⁺ π ⁻)

⁷ Our estimate.

X(1650) $I^G(J^{PC}) = 0^-(??^-)$

MASS (MeV)	WIDTH (MeV)	EVTs	DOCUMENT ID	TECN	COMMENT
1652 ± 7	<50	100	PROKOSHKIN 96	GAM2	32,38 πp → ωηn

X(1730) $I^G(J^{PC}) = ??(??^+)$

MASS (MeV)	WIDTH (MeV)	EVTs	DOCUMENT ID	TECN	COMMENT
1731.0 ± 1.2 ± 2.0	3.2 ± 0.8 ± 1.3	58	VLADIMIRSK...07	SPEC	40 π ⁻ p → K _S ⁰ K _S ⁰ X

X(1750) $I^G(J^{PC}) = ??(1^{--})$

MASS (MeV)	WIDTH (MeV)	DOCUMENT ID	TECN	COMMENT
1753.5 ± 1.5 ± 2.3	122.2 ± 6.2 ± 8.0	LINK 02k	FOCS	20-160 γp → K ⁺ K ⁻ π ⁰

B(X(1750) → K*(892)⁰K⁰ → K[±]π[∓]K_S⁰)/B(X(1750) → K⁺K⁻)

VALUE	CL%	DOCUMENT ID	TECN
<0.065	90	LINK	02k FOCS

B(X(1750) → K*(892)[±]K[∓] → K_S⁰π[±]K[∓])/B(X(1750) → K⁺K⁻)

VALUE	CL%	DOCUMENT ID	TECN
<0.183	90	LINK	02k FOCS

η₂(1750) $I^G(J^{PC}) = 0^+(2^{++})$

MASS (MeV)	WIDTH (MeV)	EVTs	DOCUMENT ID	TECN	COMMENT
1755 ± 10	67 ± 12	870	⁸ SCHEGELSKY 06A	RVUE	γγ → K _S ⁰ K _S ⁰

Γ(K \bar{K})

VALUE (MeV)	EVTs	DOCUMENT ID	TECN	COMMENT
17 ± 5	870	⁹ SCHEGELSKY 06A	RVUE	γγ → K _S ⁰ K _S ⁰

Γ(γγ)

VALUE (MeV)	EVTs	DOCUMENT ID	TECN	COMMENT
0.13 ± 0.04	870	⁹ SCHEGELSKY 06A	RVUE	γγ → K _S ⁰ K _S ⁰

Γ(ππ)

VALUE (MeV)	EVTs	DOCUMENT ID	TECN	COMMENT
1.3 ± 1.0	870	⁹ SCHEGELSKY 06A	RVUE	γγ → K _S ⁰ K _S ⁰

Γ(ηη)

VALUE (MeV)	EVTs	DOCUMENT ID	TECN	COMMENT
2.0 ± 0.5	870	⁹ SCHEGELSKY 06A	RVUE	γγ → K _S ⁰ K _S ⁰

⁸ From analysis of L3 data at 91 and 183-209 GeV.
⁹ From analysis of L3 data at 91 and 183-209 GeV and using SU(3) relations.

X(1775) $I^G(J^{PC}) = 1^-(??^-)$

MASS (MeV)	WIDTH (MeV)	DOCUMENT ID	TECN	COMMENT
1763 ± 20	192 ± 60	CONDO 91	SHF	γp → (pπ ⁺)(π ⁺ π ⁻ π ⁻)
1787 ± 18	118 ± 60	CONDO 91	SHF	γp → nπ ⁺ π ⁺ π ⁻

η₂(1800) $I^G(J^{PC}) = 0^+(0^{++})$

MASS (MeV)	WIDTH (MeV)	DOCUMENT ID	TECN	COMMENT
1795 ± 7 ⁺²³ ₋₂₀	95 ± 10 ⁺⁷⁸ ₋₈₂	ABLIKIM 13J	BES3	J/ψ → γωφ
1812 ⁺¹⁹ ₋₂₆ ± 18	105 ± 20 ± 28	¹⁰ ABLIKIM 06J	BES2	J/ψ → γωφ

¹⁰ Not seen by LIU 09 in B[±] → K[±]ωφ.

X(1850 - 3100) $I^G(J^{PC}) = ??(1^{--})$

Γ(e ⁺ e ⁻)/B(X → hadrons) (eV)	CL%	DOCUMENT ID	TECN	COMMENT
<120	90	¹¹ ANASHIN 11	KEDR	e ⁺ e ⁻ → hadrons

¹¹ This limit is center-of-mass energy dependent. We quote the most stringent one.

X(1855) $I^G(J^{PC}) = ??(??^?)$

MASS (MeV)	WIDTH (MeV)	DOCUMENT ID	TECN	COMMENT
1856.6 ± 5	20 ± 5	BRIDGES 86D	SPEC	0. $\bar{p}d \rightarrow \pi\pi N$

X(1870) $I^G(J^{PC}) = ??(2^{??})$

MASS (MeV)	WIDTH (MeV)	DOCUMENT ID	TECN	COMMENT
1870 ± 40	250 ± 30	ALDE 86D	GAM4	100 π ⁻ p → 2ηX

a₃(1875) $I^G(J^{PC}) = 1^-(3^{++})$

MASS (MeV)	WIDTH (MeV)	DOCUMENT ID	TECN	COMMENT
1874 ± 43 ± 96	385 ± 121 ± 114	CHUNG 02	B852	18.3 π ⁻ p → π ⁺ π ⁻ π ⁻ p

B(a₃(1875) → f₂(1270)π)/B(a₃(1875) → ρπ)

VALUE	DOCUMENT ID	TECN	COMMENT
0.8 ± 0.2	¹² CHUNG 02	B852	18.3 π ⁻ p → π ⁺ π ⁻ π ⁻ p

¹² Using the observable fractions of 50.0% ρπ, 56.5% f₂π, and 11.8% ρ₃π.

B(a₃(1875) → ρ₃(1690)π)/B(a₃(1875) → ρπ)

VALUE	DOCUMENT ID	TECN	COMMENT
0.9 ± 0.3	¹³ CHUNG 02	B852	18.3 π ⁻ p → π ⁺ π ⁻ π ⁻ p

¹³ Using the observable fractions of 50.0% ρπ, 56.5% f₂π, and 11.8% ρ₃π.

a₁(1930) $I^G(J^{PC}) = 1^-(1^{++})$

MASS (MeV)	WIDTH (MeV)	DOCUMENT ID	TECN	COMMENT
1930 ⁺³⁰ ₋₇₀	155 ± 45	ANISOVICH 01F	SPEC	2.0 $\bar{p}p \rightarrow 3\pi^0, \pi^0\eta, \pi^0\eta'$

See key on page 999

Meson Particle Listings

Further States

X(1935) $I^G(J^{PC}) = 1^+(1^{-?})$

MASS (MeV)	WIDTH (MeV)	DOCUMENT ID	TECN	COMMENT
1935 ± 20	215 ± 30	EVANGELIS... 79	OMEG	10,16 $\pi^- p \rightarrow \bar{p} p n$

$\rho_2(1940)$ $I^G(J^{PC}) = 1^+(2^{-})$

MASS (MeV)	WIDTH (MeV)	DOCUMENT ID	TECN	COMMENT
1940 ± 40	155 ± 40	14 ANISOVICH	02	SPEC 0.6-1.9 $p\bar{p} \rightarrow \omega\pi^0, \omega\eta\pi^0, \pi^+\pi^-$

¹⁴From the combined analysis of ANISOVICH 00J, ANISOVICH 01D, ANISOVICH 01E, and ANISOVICH 02.

$\omega_3(1945)$ $I^G(J^{PC}) = 0^-(3^{-})$

MASS (MeV)	WIDTH (MeV)	DOCUMENT ID	TECN	COMMENT
1945 ± 20	115 ± 22	15 ANISOVICH	02B	SPEC 0.6-1.9 $p\bar{p} \rightarrow \omega\eta, \omega\pi^0\pi^0$

¹⁵From the combined analysis of ANISOVICH 00D, ANISOVICH 01C, and ANISOVICH 02B.

$a_2(1950)$ $I^G(J^{PC}) = 1^-(2^{++})$

MASS (MeV)	WIDTH (MeV)	DOCUMENT ID	TECN	COMMENT
1950 ⁺³⁰ ₋₇₀	180 ⁺³⁰ ₋₇₀	16 ANISOVICH	01F	SPEC 1.96-2.41 $\bar{p}p$

¹⁶From the combined analysis of ANISOVICH 99C, ANISOVICH 99E, and ANISOVICH 01F.

$\omega(1960)$ $I^G(J^{PC}) = 0^-(1^{-})$

MASS (MeV)	WIDTH (MeV)	DOCUMENT ID	TECN	COMMENT
1960 ± 25	195 ± 60	17 ANISOVICH	02B	SPEC 0.6-1.9 $p\bar{p} \rightarrow \omega\eta, \omega\pi^0\pi^0$

¹⁷From the combined analysis of ANISOVICH 00D, ANISOVICH 01C, and ANISOVICH 02B.

$b_1(1960)$ $I^G(J^{PC}) = 1^+(1^{+-})$

MASS (MeV)	WIDTH (MeV)	DOCUMENT ID	TECN	COMMENT
1960 ± 35	230 ± 50	18 ANISOVICH	02	SPEC 0.6-1.9 $p\bar{p} \rightarrow \omega\pi^0, \omega\eta\pi^0, \pi^+\pi^-$

¹⁸From the combined analysis of ANISOVICH 00J, ANISOVICH 01D, ANISOVICH 01E, and ANISOVICH 02.

$h_1(1965)$ $I^G(J^{PC}) = 0^-(1^{+-})$

MASS (MeV)	WIDTH (MeV)	DOCUMENT ID	TECN	COMMENT
1965 ± 45	345 ± 75	19 ANISOVICH	02B	SPEC 0.6-1.9 $p\bar{p} \rightarrow \omega\eta, \omega\pi^0\pi^0$

¹⁹From the combined analysis of ANISOVICH 00D, ANISOVICH 01C, and ANISOVICH 02B.

$f_1(1970)$ $I^G(J^{PC}) = 0^+(1^{++})$

MASS (MeV)	WIDTH (MeV)	DOCUMENT ID	TECN	COMMENT
1971 ± 15	240 ± 45	ANISOVICH	00J	SPEC

X(1970) $I^G(J^{PC}) = ?^?(???)$

MASS (MeV)	WIDTH (MeV)	DOCUMENT ID	TECN	COMMENT
1970 ± 10	40 ± 20	CHLIAPNIK... 80	HBC	32 $K^+ p \rightarrow 2K_S^0 2\pi X$

X(1975) $I^G(J^{PC}) = ?^?(???)$

MASS (MeV)	WIDTH (MeV)	EVTS	DOCUMENT ID	TECN	COMMENT
1973 ± 15	80	30	CASO	70	HBC 11.2 $\pi^- p \rightarrow \rho 2\pi$

$\omega_2(1975)$ $I^G(J^{PC}) = 0^-(2^{-})$

MASS (MeV)	WIDTH (MeV)	DOCUMENT ID	TECN	COMMENT
1975 ± 20	175 ± 25	20 ANISOVICH	02B	SPEC 0.6-1.9 $p\bar{p} \rightarrow \omega\eta, \omega\pi^0\pi^0$

²⁰From the combined analysis of ANISOVICH 00D, ANISOVICH 01C, and ANISOVICH 02B.

$a_2(1990)$ $I^G(J^{PC}) = 1^-(2^{++})$

MASS (MeV)	WIDTH (MeV)	EVTS	DOCUMENT ID	TECN	COMMENT
2050 ± 10 ± 40	190 ± 22 ± 100	18k	21 SCHEGELSKY	06	RVUE $\gamma\gamma \rightarrow \pi^+\pi^-\pi^0$
2003 ± 10 ± 19	249 ± 23 ± 32		LU	05	B852 18 $\pi^- p \rightarrow \omega\pi^-\pi^0\pi^0$

²¹From analysis of L3 data at 183-209 GeV.

$\Gamma(\gamma\gamma) \Gamma(\pi^+\pi^-\pi^0) / \Gamma(\text{total})$

VALUE (keV)	EVTS	DOCUMENT ID	TECN	COMMENT
0.11 ± 0.04 ± 0.05	18k	22 SCHEGELSKY	06	RVUE $\gamma\gamma \rightarrow \pi^+\pi^-\pi^0$

²²From analysis of L3 data at 183-209 GeV.

$\rho(2000)$ $I^G(J^{PC}) = 1^+(1^{-})$

MASS (MeV)	WIDTH (MeV)	DOCUMENT ID	TECN	COMMENT
2000 ± 30	260 ± 45	23 BUGG	04C	RVUE Compilation
~ 1988	~ 244	HASAN	94	RVUE $\bar{p}p \rightarrow \pi\pi$

²³From the combined analysis of ANISOVICH 00J, ANISOVICH 01D, ANISOVICH 01E, and ANISOVICH 02.

$f_2(2000)$ $I^G(J^{PC}) = 0^+(2^{++})$

MASS (MeV)	WIDTH (MeV)	DOCUMENT ID	TECN	COMMENT
2001 ± 10	312 ± 32	ANISOVICH	00J	SPEC
~ 1996	~ 134	HASAN	94	RVUE $\bar{p}p \rightarrow \pi\pi$

X(2000) $I^G(J^{PC}) = 1^-(?^{?+})$

MASS (MeV)	WIDTH (MeV)	DOCUMENT ID	TECN	CHG	COMMENT
1964 ± 35	225 ± 50	24 ARMSTRONG	93D	E760	$\bar{p}p \rightarrow 3\pi^0 \rightarrow 6\gamma$
~ 2100	~ 500	24 ANTIPOV	77	CIBS	- 25 $\pi^- p \rightarrow \rho\pi^- \rho_3$
2214 ± 15	355 ± 21	25 BALTAY	77	HBC	0 15 $\pi^- p \rightarrow \Delta^{++} 3\pi$
2080 ± 40	340 ± 80	KALELKAR	75	HBC	+ 15 $\pi^+ p \rightarrow \rho\pi^+ \rho_3$

²⁴Cannot determine spin to be 3.

²⁵BALTAY 77 favors $J^P = ,3^+$.

X(2000) $I^G(J^{PC}) = ?^?(4^{++})$

MASS (MeV)	WIDTH (MeV)	DOCUMENT ID	TECN	COMMENT
1998 ± 3 ± 5	<15	VLADIMIRSK...03	SPEC	$\pi^- p \rightarrow K_S^0 K_S^0 M M$

$\eta(2010)$ $I^G(J^{PC}) = 0^+(0^{-})$

MASS (MeV)	WIDTH (MeV)	DOCUMENT ID	TECN	COMMENT
2010 ⁺³⁵ ₋₆₀	270 ± 60	ANISOVICH	00J	SPEC

$\pi_1(2015)$ $I^G(J^{PC}) = 1^-(1^{-})$

MASS (MeV)	WIDTH (MeV)	EVTS	DOCUMENT ID	TECN	COMMENT
2014 ± 20 ± 16	230 ± 32 ± 73	145k	LU	05	B852 18 $\pi^- p \rightarrow \omega\pi^-\pi^0 p$
2001 ± 30 ± 92	333 ± 52 ± 49	69k	KUHN	04	B852 18 $\pi^- p \rightarrow \eta\pi^+\pi^-\pi^- p$

$a_0(2020)$ $I^G(J^{PC}) = 1^-(0^{++})$

MASS (MeV)	WIDTH (MeV)	DOCUMENT ID	TECN	COMMENT
2025 ± 30	330 ± 75	ANISOVICH	99C	SPEC

X(2020) $I^G(J^{PC}) = ?^?(???)$

MASS (MeV)	WIDTH (MeV)	DOCUMENT ID	TECN	COMMENT
2015 ± 3	10 ± 4	FERRER	99	RVUE $\pi p \rightarrow p\rho\bar{p}\pi(\pi)$

$h_3(2025)$ $I^G(J^{PC}) = 0^-(3^{+-})$

MASS (MeV)	WIDTH (MeV)	DOCUMENT ID	TECN	COMMENT
2025 ± 20	145 ± 30	26 ANISOVICH	02B	SPEC 0.6-1.9 $p\bar{p} \rightarrow \omega\eta, \omega\pi^0\pi^0$

²⁶From the combined analysis of ANISOVICH 00D, ANISOVICH 01C, and ANISOVICH 02B.

$b_3(2030)$ $I^G(J^{PC}) = 1^+(3^{+-})$

MASS (MeV)	WIDTH (MeV)	DOCUMENT ID	TECN	COMMENT
2032 ± 12	117 ± 11	27 ANISOVICH	02	SPEC 0.6-1.9 $p\bar{p} \rightarrow \omega\pi^0, \omega\eta\pi^0, \pi^+\pi^-$

²⁷From the combined analysis of ANISOVICH 00J, ANISOVICH 01D, ANISOVICH 01E, and ANISOVICH 02.

$a_2(2030)$ $I^G(J^{PC}) = 1^-(2^{++})$

MASS (MeV)	WIDTH (MeV)	DOCUMENT ID	TECN	COMMENT
2030 ± 20	205 ± 30	28 ANISOVICH	01F	SPEC 1.96-2.41 $\bar{p}p$

²⁸From the combined analysis of ANISOVICH 99C, ANISOVICH 99E, and ANISOVICH 01F.

$a_3(2030)$ $I^G(J^{PC}) = 1^-(3^{++})$

MASS (MeV)	WIDTH (MeV)	DOCUMENT ID	TECN	COMMENT
2031 ± 12	150 ± 18	29 ANISOVICH	01F	SPEC 1.96-2.41 $\bar{p}p$

²⁹From the combined analysis of ANISOVICH 99C, ANISOVICH 99E, and ANISOVICH 01F.

$\eta_2(2030)$ $I^G(J^{PC}) = 0^+(2^{-})$

MASS (MeV)	WIDTH (MeV)	DOCUMENT ID	TECN	COMMENT
2030 ± 5 ± 15	205 ± 10 ± 15	ANISOVICH	00E	SPEC

Meson Particle Listings

Further States

B($a_2\pi$)$_L=0$/B($a_2\pi$)$_L=2$				
VALUE	DOCUMENT ID	TECN	COMMENT	
0.05±0.03	30 ANISOVICH	11	SPEC	0.9–1.94 $\rho\bar{p}$

³⁰ Reanalysis of ADOMEIT 96 and ANISOVICH 00E.

B($a_0\pi$)/B($a_2\pi$)$_L=2$				
VALUE	DOCUMENT ID	TECN	COMMENT	
0.10±0.08	31 ANISOVICH	11	SPEC	0.9–1.94 $\rho\bar{p}$

³¹ Reanalysis of ADOMEIT 96 and ANISOVICH 00E.

B($f_2\eta$)/B($a_2\pi$)$_L=2$				
VALUE	DOCUMENT ID	TECN	COMMENT	
0.13±0.06	32 ANISOVICH	11	SPEC	0.9–1.94 $\rho\bar{p}$

³² Reanalysis of ADOMEIT 96 and ANISOVICH 00E.

$f_3(2050)$ $I^G(J^{PC}) = 0^+(3^{++})$				
MASS (MeV)	WIDTH (MeV)	DOCUMENT ID	TECN	COMMENT
2048±8	213±34	ANISOVICH	00J	SPEC 2.0 $\rho\bar{p} \rightarrow \eta\pi^0\pi^0$

$f_0(2060)$ $I^G(J^{PC}) = 0^+(0^{++})$				
MASS (MeV)	WIDTH (MeV)	DOCUMENT ID	TECN	COMMENT
~2050	~120	33 OAKDEN	94	RVUE 0.36–1.55 $\bar{p}p \rightarrow \pi\pi$
~2060	~50	33 OAKDEN	94	RVUE 0.36–1.55 $\bar{p}p \rightarrow \pi\pi$

³³ See SEMENOV 99 and KLOET 96.

$\pi(2070)$ $I^G(J^{PC}) = 1^-(0^{-+})$				
MASS (MeV)	WIDTH (MeV)	DOCUMENT ID	TECN	COMMENT
2070±35	310 $^{+100}_{-50}$	ANISOVICH	01F	SPEC 2.0 $\bar{p}p \rightarrow 3\pi^0, \pi^0\eta, \pi^0\eta'$

$X(2075)$ $I^G(J^{PC}) = ?^?(???)$				
MASS (MeV)	WIDTH (MeV)	DOCUMENT ID	TECN	COMMENT
2075±12±5	90±35±9	34 ABLIKIM	04J	BES2 $J/\psi \rightarrow K^-\rho\bar{\Lambda}$

³⁴ From a fit in the region $M_{\rho\bar{\Lambda}} - M_{\rho} - M_{\Lambda} < 150$ MeV. S-wave in the $\rho\bar{\Lambda}$ system preferred. A similar near-threshold enhancement in the $\rho\bar{\Lambda}$ system is observed in $B^+ \rightarrow \rho\bar{\Lambda}\bar{D}^0$ by CHEN 11F.

$X(2080)$ $I^G(J^{PC}) = ?^?(???)$				
MASS (MeV)	WIDTH (MeV)	DOCUMENT ID	TECN	COMMENT
2080±10	110±20	KREYMER	80	STRC 13 $\pi^-d \rightarrow \rho\bar{p}n(n_S)$

$X(2080)$ $I^G(J^{PC}) = ?^?(3^{-2})$				
MASS (MeV)	WIDTH (MeV)	DOCUMENT ID	TECN	COMMENT
2080±10	190±15	ROZANSKA	80	SPRK 18 $\pi^-p \rightarrow \rho\bar{p}n$

$a_1(2095)$ $I^G(J^{PC}) = 1^-(1^{++})$					
MASS (MeV)	WIDTH (MeV)	EVT S	DOCUMENT ID	TECN	COMMENT
2096±17±12±1	451±41±81	69k	KUHN	04	B852 18 $\pi^-p \rightarrow \eta\pi^+\pi^-\pi^-p$

B($a_1(2095) \rightarrow f_1(1285)\pi$) / B($a_1(2095) \rightarrow a_1(1260)$)				
VALUE	EVT S	DOCUMENT ID	TECN	COMMENT
3.18±0.64	69k	KUHN	04	B852 18 $\pi^-p \rightarrow \eta\pi^+\pi^-\pi^-p$

$\eta(2100)$ $I^G(J^{PC}) = 0^+(0^{-+})$					
MASS (MeV)	WIDTH (MeV)	EVT S	DOCUMENT ID	TECN	COMMENT
2050 $^{+30+75}_{-24-26}$	250 $^{+36+181}_{-30-164}$	35	ABLIKIM	16N	BES3 $J/\psi \rightarrow \gamma K^+$
2103±50	187±75	586	36 BISELLO	89B	DM2 $J/\psi \rightarrow 4\pi\gamma$

³⁵ From a partial wave analysis of $J/\psi \rightarrow \gamma\phi\phi$, for which the primary signal is $\eta(2225) \rightarrow \phi\phi$, and that also finds significant signals for for 0^{-+} phase space, $f_0(2100)$, $f_2(2010)$, $f_2(2300)$, $f_2(2340)$, and a previously unseen 0^{-+} state $X(2500)$ ($M = 2470^{+15+101}_{-19-23}$ MeV, $\Gamma = 230^{+64+56}_{-35-33}$ MeV).

³⁶ ASTON 81B sees no peak, has 850 events in Ajinenko+Barth bins. ARESTOV 80 sees no peak.

$X(2100)$ $I^G(J^{PC}) = ?^?(0^{??})$				
MASS (MeV)	WIDTH (MeV)	DOCUMENT ID	TECN	COMMENT
2100±40	250±40	ALDE	86D	GAM4 100 $\pi^-p \rightarrow 2\eta X$

$X(2110)$ $I^G(J^{PC}) = 1^+(3^{-2})$				
MASS (MeV)	WIDTH (MeV)	DOCUMENT ID	TECN	COMMENT
2110±10	330±20	EVANGELIS...	79	OMEG 10,16 $\pi^-p \rightarrow \bar{p}pn$

$f_2(2140)$ $I^G(J^{PC}) = 0^+(2^{++})$					
MASS (MeV)	WIDTH (MeV)	EVT S	DOCUMENT ID	TECN	COMMENT
2141±12	49±28	389	GREEN	86	MPSF 400 $pA \rightarrow 4KX$

$X(2150)$ $I^G(J^{PC}) = ?^?(2^{+?})$					
MASS (MeV)	WIDTH (MeV)	DOCUMENT ID	TECN	COMMENT	
2150±10	260±10	ROZANSKA	80	SPRK	18 $\pi^-p \rightarrow \rho\bar{p}n$

$a_2(2175)$ $I^G(J^{PC}) = 1^-(2^{++})$					
MASS (MeV)	WIDTH (MeV)	DOCUMENT ID	TECN	COMMENT	
2175±40	310 $^{+90}_{-45}$	ANISOVICH	01F	SPEC	2.0 $\bar{p}p \rightarrow 3\pi^0, \pi^0\eta, \pi^0\eta'$

$\eta(2190)$ $I^G(J^{PC}) = 0^+(0^{-+})$					
MASS (MeV)	WIDTH (MeV)	DOCUMENT ID	TECN	COMMENT	
2190±50	850±100	BUGG	99	BES	

$\omega_2(2195)$ $I^G(J^{PC}) = 0^-(2^{-+})$					
MASS (MeV)	WIDTH (MeV)	DOCUMENT ID	TECN	COMMENT	
2195±30	225±40	37 ANISOVICH	02B	SPEC	0.6–1.9 $\rho\bar{p} \rightarrow \omega\eta, \omega\pi^0\pi^0$

³⁷ From the combined analysis of A NISOVICH 00D, ANISOVICH 01C, and ANISOVICH 02B.

$\omega(2205)$ $I^G(J^{PC}) = 0^-(1^{-+})$					
MASS (MeV)	WIDTH (MeV)	DOCUMENT ID	TECN	COMMENT	
2205±30	350±90	38 ANISOVICH	02B	SPEC	0.6–1.9 $\rho\bar{p} \rightarrow \omega\eta, \omega\pi^0\pi^0$

³⁸ From the combined analysis of A NISOVICH 00D, ANISOVICH 01C, and ANISOVICH 02B.

$X(2210)$ $I^G(J^{PC}) = ?^?(???)$					
MASS (MeV)	WIDTH (MeV)	DOCUMENT ID	TECN	COMMENT	
2210 $^{+79}_{-21}$	203 $^{+437}_{-87}$	EVANGELIS...	79B	OMEG	10 $\pi^-p \rightarrow K^+K^-n$

$X(2210)$ $I^G(J^{PC}) = ?^?(???)$					
MASS (MeV)	WIDTH (MeV)	DOCUMENT ID	TECN	COMMENT	
2207±22	130	CASO	70	HBC	11.2 π^-p

$h_1(2215)$ $I^G(J^{PC}) = 0^-(1^{+-})$					
MASS (MeV)	WIDTH (MeV)	DOCUMENT ID	TECN	COMMENT	
2215±40	325±55	39 ANISOVICH	02B	SPEC	0.6–1.9 $\rho\bar{p} \rightarrow \omega\eta, \omega\pi^0\pi^0$

³⁹ From the combined analysis of A NISOVICH 00D, ANISOVICH 01C, and ANISOVICH 02B.

$\rho_2(2225)$ $I^G(J^{PC}) = 1^+(2^{-+})$					
MASS (MeV)	WIDTH (MeV)	DOCUMENT ID	TECN	COMMENT	
2225±35	335 $^{+100}_{-50}$	40 ANISOVICH	02	SPEC	0.6–1.9 $\rho\bar{p} \rightarrow \omega\pi^0, \omega\eta\pi^0, \pi^+\pi^-$

⁴⁰ From the combined analysis of ANISOVICH 00J, ANISOVICH 01D, ANISOVICH 01E, and ANISOVICH 02.

$\rho_4(2230)$ $I^G(J^{PC}) = 1^+(4^{-+})$					
MASS (MeV)	WIDTH (MeV)	DOCUMENT ID	TECN	COMMENT	
2230±25	210±30	41 ANISOVICH	02	SPEC	0.6–1.9 $\rho\bar{p} \rightarrow \omega\pi^0, \omega\eta\pi^0, \pi^+\pi^-$

⁴¹ From the combined analysis of ANISOVICH 00J, ANISOVICH 01D, ANISOVICH 01E, and ANISOVICH 02.

$b_1(2240)$ $I^G(J^{PC}) = 1^+(1^{+-})$					
MASS (MeV)	WIDTH (MeV)	DOCUMENT ID	TECN	COMMENT	
2240±35	320±85	42 ANISOVICH	02	SPEC	0.6–1.9 $\rho\bar{p} \rightarrow \omega\pi^0, \omega\eta\pi^0, \pi^+\pi^-$

⁴² From the combined analysis of ANISOVICH 00J, ANISOVICH 01D, ANISOVICH 01E, and ANISOVICH 02.

$f_2(2240)$ $I^G(J^{PC}) = 0^+(2^{++})$					
MASS (MeV)	WIDTH (MeV)	DOCUMENT ID	TECN	COMMENT	
2240±15	241±30	43 ANISOVICH	00J	SPEC	1.92–2.41 $\rho\bar{p}$

••• We do not use the following data for averages, fits, limits, etc. •••

~2226 ~226 HASAN 94 RVUE $\rho\bar{p} \rightarrow \pi\pi$

⁴³ From the combined analysis of ANISOVICH 99C, ANISOVICH 99F, ANISOVICH 99J, ANISOVICH 99K, and ANISOVICH 00B. See also ANISOVICH 12.

$b_3(2245)$ $I^G(J^{PC}) = 1^+(3^+ -)$				
MASS (MeV)	WIDTH (MeV)	DOCUMENT ID	TECN	COMMENT
2245 ± 50	320 ± 70	44 BUGG	04c	RVUE

⁴⁴ From the combined analysis of ANISOVICH 00j, ANISOVICH 01d, ANISOVICH 01e, and ANISOVICH 02.

$\eta_2(2250)$ $I^G(J^{PC}) = 0^+(2^- +)$				
MASS (MeV)	WIDTH (MeV)	DOCUMENT ID	TECN	COMMENT
2248 ± 20	280 ± 20	ANISOVICH	00i	SPEC
2267 ± 14	290 ± 50	ANISOVICH	00j	SPEC

$\pi_4(2250)$ $I^G(J^{PC}) = 1^-(4^- +)$				
MASS (MeV)	WIDTH (MeV)	DOCUMENT ID	TECN	COMMENT
2250 ± 15	215 ± 25	ANISOVICH	01f	SPEC 2.0 $\bar{p}p \rightarrow 3\pi^0, \pi^0\eta, \pi^0\eta'$

$\omega_4(2250)$ $I^G(J^{PC}) = 0^-(4^- -)$				
MASS (MeV)	WIDTH (MeV)	DOCUMENT ID	TECN	COMMENT
2250 ± 30	150 ± 50	45 ANISOVICH	02b	SPEC 0.6-1.9 $p\bar{p} \rightarrow \omega\eta, \omega\pi^0\pi^0$

⁴⁵ From the combined analysis of ANISOVICH 00b, ANISOVICH 01c, and ANISOVICH 02b.

$\omega_5(2250)$ $I^G(J^{PC}) = 0^-(5^- -)$				
MASS (MeV)	WIDTH (MeV)	DOCUMENT ID	TECN	COMMENT
2250 ± 70	320 ± 95	46 BUGG	04	RVUE

⁴⁶ From the combined analysis of ANISOVICH 00b, ANISOVICH 01c, and ANISOVICH 02b.

$\omega_3(2255)$ $I^G(J^{PC}) = 0^-(3^- -)$				
MASS (MeV)	WIDTH (MeV)	DOCUMENT ID	TECN	COMMENT
2255 ± 15	175 ± 30	47 ANISOVICH	02b	SPEC 0.6-1.9 $p\bar{p} \rightarrow \omega\eta, \omega\pi^0\pi^0$

⁴⁷ From the combined analysis of ANISOVICH 00b, ANISOVICH 01c, and ANISOVICH 02b.

$a_4(2255)$ $I^G(J^{PC}) = 1^-(4^+ +)$				
MASS (MeV)	WIDTH (MeV)	DOCUMENT ID	TECN	COMMENT
2237 ± 5	291 ± 12	UMAN	06	E835 5.2 $\bar{p}p \rightarrow \eta\eta\pi^0$
2255 ± 40	330 ⁺¹¹⁰ ₋₅₀	48 ANISOVICH	01f	SPEC 1.96-2.41 $\bar{p}p$

⁴⁸ From the combined analysis of ANISOVICH 99c, ANISOVICH 99e, and ANISOVICH 01f.

$a_2(2255)$ $I^G(J^{PC}) = 1^-(2^+ +)$				
MASS (MeV)	WIDTH (MeV)	DOCUMENT ID	TECN	COMMENT
2255 ± 20	230 ± 15	49 ANISOVICH	01g	SPEC 1.96-2.41 $\bar{p}p$

⁴⁹ From the combined analysis of ANISOVICH 99c, ANISOVICH 99e, ANISOVICH 01f, and ANISOVICH 01g.

$X(2260)$ $I^G(J^{PC}) = 0^+(4^+?)$				
MASS (MeV)	WIDTH (MeV)	DOCUMENT ID	TECN	COMMENT
2260 ± 20	400 ± 100	EVANGELIS...	79	OMEG 10,16 $\pi^-p \rightarrow \bar{p}pn$

$\rho(2270)$ $I^G(J^{PC}) = 1^+(1^- -)$				
MASS (MeV)	WIDTH (MeV)	DOCUMENT ID	TECN	COMMENT
2265 ± 40	325 ± 80	50 ANISOVICH	02	SPEC 0.6-1.9 $p\bar{p} \rightarrow \omega\pi^0, \omega\eta\pi^0, \pi^+\pi^-$

2280 ± 50 440 ± 110 ATKINSON 85 OMEG 20-70 $\gamma p \rightarrow p\omega\pi^+\pi^-\pi^0$

⁵⁰ From the combined analysis of ANISOVICH 00j, ANISOVICH 01d, ANISOVICH 01e, and ANISOVICH 02.

$a_1(2270)$ $I^G(J^{PC}) = 1^-(1^+ +)$				
MASS (MeV)	WIDTH (MeV)	DOCUMENT ID	TECN	COMMENT
2270 ⁺⁵⁵ ₋₄₀	305 ⁺⁷⁰ ₋₄₀	ANISOVICH	01f	SPEC 2.0 $\bar{p}p \rightarrow 3\pi^0, \pi^0\eta, \pi^0\eta'$

$h_3(2275)$ $I^G(J^{PC}) = 0^-(3^+ -)$				
MASS (MeV)	WIDTH (MeV)	DOCUMENT ID	TECN	COMMENT
2275 ± 25	190 ± 45	51 ANISOVICH	02b	SPEC 0.6-1.9 $p\bar{p} \rightarrow \omega\eta, \omega\pi^0\pi^0$

⁵¹ From the combined analysis of ANISOVICH 00b, ANISOVICH 01c, and ANISOVICH 02b.

$a_3(2275)$ $I^G(J^{PC}) = 1^-(3^+ +)$				
MASS (MeV)	WIDTH (MeV)	DOCUMENT ID	TECN	COMMENT
2275 ± 35	350 ⁺¹⁰⁰ ₋₅₀	52 ANISOVICH	01g	SPEC 1.96-2.41 $\bar{p}p$

⁵² From the combined analysis of ANISOVICH 99c, ANISOVICH 99e, ANISOVICH 01f, and ANISOVICH 01g.

$\pi_2(2285)$ $I^G(J^{PC}) = 1^-(2^- +)$				
MASS (MeV)	WIDTH (MeV)	DOCUMENT ID	TECN	COMMENT
2285 ± 20 ± 25	250 ± 20 ± 25	53 ANISOVICH	11	SPEC 0.9-1.94 $p\bar{p}$

⁵³ Reanalysis of ADOMEIT 96 and ANISOVICH 00e.

$\omega_3(2285)$ $I^G(J^{PC}) = 0^-(3^- -)$				
MASS (MeV)	WIDTH (MeV)	DOCUMENT ID	TECN	COMMENT
2278 ± 28	224 ± 50	54 BUGG	04a	RVUE
2285 ± 60	230 ± 40	55 ANISOVICH	02b	SPEC 0.6-1.9 $p\bar{p} \rightarrow \omega\eta, \omega\pi^0\pi^0$

⁵⁴ Partial wave analysis of the data on $p\bar{p} \rightarrow \bar{\Lambda}\Lambda$ from BARNES 00.

⁵⁵ From the combined analysis of ANISOVICH 00b, ANISOVICH 01c, and ANISOVICH 02b.

$\omega(2290)$ $I^G(J^{PC}) = 0^-(1^- -)$				
MASS (MeV)	WIDTH (MeV)	DOCUMENT ID	TECN	COMMENT
2290 ± 20	275 ± 35	56 BUGG	04a	RVUE

⁵⁶ Partial wave analysis of the data on $p\bar{p} \rightarrow \bar{\Lambda}\Lambda$ from BARNES 00.

$f_2(2295)$ $I^G(J^{PC}) = 0^+(2^+ +)$				
MASS (MeV)	WIDTH (MeV)	DOCUMENT ID	TECN	COMMENT
2293 ± 13	216 ± 37	57 ANISOVICH	00j	SPEC 1.92-2.41 $p\bar{p}$

⁵⁷ From the combined analysis of ANISOVICH 99c, ANISOVICH 99f, ANISOVICH 99j, ANISOVICH 99k, and ANISOVICH 00b. See also ANISOVICH 12.

$f_3(2300)$ $I^G(J^{PC}) = 0^+(3^+ +)$				
MASS (MeV)	WIDTH (MeV)	DOCUMENT ID	TECN	COMMENT
2334 ± 25	200 ± 20	58 BUGG	04a	RVUE

⁵⁸ Partial wave analysis of the data on $p\bar{p} \rightarrow \bar{\Lambda}\Lambda$ from BARNES 00.

$f_1(2310)$ $I^G(J^{PC}) = 0^+(1^+ +)$				
MASS (MeV)	WIDTH (MeV)	DOCUMENT ID	TECN	COMMENT
2310 ± 60	255 ± 70	ANISOVICH	00j	SPEC

$\eta(2320)$ $I^G(J^{PC}) = 0^+(0^- +)$				
MASS (MeV)	WIDTH (MeV)	DOCUMENT ID	TECN	COMMENT
2320 ± 15	230 ± 35	59 ANISOVICH	00m	SPEC

⁵⁹ From the combined analysis of $\bar{p}p \rightarrow \eta\eta\eta$ from ANISOVICH 00m and $\bar{p}p \rightarrow \eta\pi^0\pi^0$ from ANISOVICH 00j.

$\eta_4(2330)$ $I^G(J^{PC}) = 0^+(4^- +)$				
MASS (MeV)	WIDTH (MeV)	DOCUMENT ID	TECN	COMMENT
2328 ± 38	240 ± 90	ANISOVICH	00j	SPEC 2.0 $p\bar{p} \rightarrow \eta\pi^0\pi^0$

$\omega(2330)$ $I^G(J^{PC}) = 0^-(1^- -)$				
MASS (MeV)	WIDTH (MeV)	DOCUMENT ID	TECN	COMMENT
2330 ± 30	435 ± 75	ATKINSON	88	OMEG 25-50 $\gamma p \rightarrow \rho^\pm \rho^0 \pi^\mp$

$X(2340)$ $I^G(J^{PC}) = ?(???)$					
MASS (MeV)	WIDTH (MeV)	EVTS	DOCUMENT ID	TECN	COMMENT
2340 ± 20	180 ± 60	126	60 BALTAY	75	HBC 15 $\pi^+p \rightarrow p_5\pi$

⁶⁰ Dominant decay into $\rho^0\rho^0\pi^+$. BALTAY 78 finds confirmation in $2\pi^+\pi^-2\pi^0$ events which contain $\rho^+\rho^0\pi^0$ and $2\rho^+\pi^-$.

$\pi(2360)$ $I^G(J^{PC}) = 1^-(0^- +)$				
MASS (MeV)	WIDTH (MeV)	DOCUMENT ID	TECN	COMMENT
2360 ± 25	300 ⁺¹⁰⁰ ₋₅₀	ANISOVICH	01f	SPEC 2.0 $\bar{p}p \rightarrow 3\pi^0, \pi^0\eta, \pi^0\eta'$

$X(2360)$ $I^G(J^{PC}) = ?(4^+?)$				
MASS (MeV)	WIDTH (MeV)	DOCUMENT ID	TECN	COMMENT
2360 ± 10	430 ± 30	ROZANSKA	80	SPRK 18 $\pi^-p \rightarrow p\bar{p}\eta$

$X(2440)$ $I^G(J^{PC}) = ?(5^-?)$				
MASS (MeV)	WIDTH (MeV)	DOCUMENT ID	TECN	COMMENT
2440 ± 10	310 ± 20	ROZANSKA	80	SPRK 18 $\pi^-p \rightarrow p\bar{p}\eta$

$a_6(2450)$ $I^G(J^{PC}) = 1^-(6^+ +)$				
MASS (MeV)	WIDTH (MeV)	DOCUMENT ID	TECN	COMMENT
2450 ± 130	400 ± 250	CLELAND	82b	SPEC 50 $\pi p \rightarrow K_S^0 K^\pm p$

$X(2540)$ $I^G(J^{PC}) = 0^+(0^+ +)$				
MASS (MeV)	WIDTH (MeV)	DOCUMENT ID	TECN	COMMENT
2539 ± 14 ⁺³⁸ ₋₁₄	274 ⁺⁷⁷⁺¹²⁶ ₋₆₁₋₁₆₃	UEHARA	13	BELL $\gamma\gamma \rightarrow K_S^0 K_S^0$

Meson Particle Listings

Further States

$\Gamma(\gamma\gamma) \times \mathbf{B}(K\bar{K})$				
VALUE (eV)	DOCUMENT ID	TECN	COMMENT	
40^{+9+17}_{-7-40}	UEHARA	13	BELL	$\gamma\gamma \rightarrow K_S^0 K_S^0$

$X(2632) \quad I^G(J^{PC}) = ?^?(?^{??})$				
MASS (MeV)	WIDTH (MeV)	DOCUMENT ID	TECN	COMMENT
2635.2 ± 3.3		61 EVDOKIMOV	04	SELX $X(2632) \rightarrow D_S^+ \eta$
2631.6 ± 2.1	< 17	62 EVDOKIMOV	04	SELX $X(2632) \rightarrow D_S^0 K^+$
61 From a mass difference to D_S^+ of 666.9 ± 3.3 MeV.				
62 From a mass difference to D_S^0 of 767.0 ± 2.0 MeV.				

$\mathbf{B}(X(2632) \rightarrow D^0 K^+) / \mathbf{B}(X(2632) \rightarrow D_S^+ \eta)$				
VALUE	DOCUMENT ID	TECN		
0.14 ± 0.06	63 EVDOKIMOV	04	SELX	
63 Possible interpretation of this decay pattern is discussed by YASUI 07.				

$X(2680) \quad I^G(J^{PC}) = ?^?(?^{??})$				
MASS (MeV)	WIDTH (MeV)	DOCUMENT ID	TECN	COMMENT
2676 ± 27	150	CASO	70	HBC $11.2 \pi^- p \rightarrow \rho^- \pi^+ \pi^- p$

$X(2710) \quad I^G(J^{PC}) = ?^?(6^{+?})$				
MASS (MeV)	WIDTH (MeV)	DOCUMENT ID	TECN	COMMENT
2710 ± 20	170 ± 40	ROZANSKA	80	SPRK $18 \pi^- p \rightarrow p \bar{p} n$

$X(2750) \quad I^G(J^{PC}) = ?^?(7^{-?})$				
MASS (MeV)	WIDTH (MeV)	DOCUMENT ID	TECN	COMMENT
2747 ± 32	195 ± 75	DENNEY	83	LASS $10 \pi^+ p \rightarrow K^+ K^- \pi^+ p$

$f_6(3100) \quad I^G(J^{PC}) = 0^+(6^{++})$				
MASS (MeV)	WIDTH (MeV)	DOCUMENT ID	TECN	COMMENT
3100 ± 100	700 ± 130	BINON	05	GAMS $33 \pi^- p \rightarrow \eta \eta n$

$X(3250) \quad I^G(J^{PC}) = ?^?(?^{??})$ 3-Body Decays				
MASS (MeV)	WIDTH (MeV)	DOCUMENT ID	TECN	COMMENT
$3250 \pm 8 \pm 20$	45 ± 18	ALEEV	93	BIS2 $X(3250) \rightarrow \Lambda \bar{p} K^+$
$3265 \pm 7 \pm 20$	40 ± 18	ALEEV	93	BIS2 $X(3250) \rightarrow \bar{\Lambda} p K^-$

$X(3250) \quad I^G(J^{PC}) = ?^?(?^{??})$ 4-Body Decays				
MASS (MeV)	WIDTH (MeV)	DOCUMENT ID	TECN	COMMENT
$3245 \pm 8 \pm 20$	25 ± 11	ALEEV	93	BIS2 $X(3250) \rightarrow \Lambda \bar{p} K^+ \pi^\pm$
$3250 \pm 9 \pm 20$	50 ± 20	ALEEV	93	BIS2 $X(3250) \rightarrow \bar{\Lambda} p K^- \pi^\mp$
$3270 \pm 8 \pm 20$	25 ± 11	ALEEV	93	BIS2 $X(3250) \rightarrow K_S^0 p \bar{p} K^\pm$

$X(3350) \quad I^G(J^{PC}) = ?^?(?^{??})$				
MASS (MeV)	WIDTH (MeV)	EVTS	DOCUMENT ID	TECN COMMENT
$3350^{+10}_{-20} \pm 20$	$70^{+40}_{-30} \pm 40$	50 ± 10	64 GABYSHEV	06A BELL $B^- \rightarrow \Lambda_c^+ \bar{p} \pi^-$
64 A similar enhancement in the $\Lambda_c^+ \bar{p}$ final state is also reported by BABAR collaboration in AUBERT 10H.				

REFERENCES for Further States

ABLIKIM	16N	PR D93 112011	M. Ablikim	(BESIII Collab.)
ABLIKIM	13J	PR D87 032008	M. Ablikim et al.	(BESIII Collab.)
UEHARA	13	PTEP 2013 123C01	S. Uehara et al.	(BELLE Collab.)
ANISOVICH	12	PR D85 014001	A.V. Anisovich et al.	
ANASHIN	11	PL B703 543	V.V. Anashin et al.	(KEDR Collab.)

ANISOVICH	11	EPJ C71 1511	A.V. Anisovich et al.	(LOQM, RAL, PNPI)
CHEN	11F	PR D84 071501	P. Chen et al.	(BELLE Collab.)
AUBERT	10H	PR D82 031102	B. Aubert et al.	(BABAR Collab.)
ABRAAMYAN	09	PR C80 034001	Kh.U. Abraamyan et al.	
LIU	09	PR D79 071102	C. Liu et al.	(BELLE Collab.)
VLADIMIRSK...	08	PAN 71 2129	V.V. Vladimirsky et al.	(ITEP)
VLADIMIRSK...	07	PAN 70 1706	V.V. Vladimirsky et al.	
YASUI	07	PR D76 034009	S. Yasui, M. Oka	
ABLIKIM	06J	PRL 96 162002	M. Ablikim et al.	(BES Collab.)
ABLIKIM	06S	PRL 97 142002	M. Ablikim et al.	(BES Collab.)
GABYSHEV	06A	PRL 97 242001	N. Gabyshev et al.	(BELLE Collab.)
SCHEGELSKY	06A	EPJ A27 199	V.A. Schegelsky et al.	
SCHEGELSKY	06A	EPJ A27 207	V.A. Schegelsky et al.	
UMAN	06	PR D73 052009	I. Uman et al.	(FNAL E835)
VLADIMIRSK...	06	PAN 69 493	V.V. Vladimirsky et al.	(ITEP, Moscow)
BINON	05	PAN 68 960	F. Binon et al.	
GRIGOR'EV	05	PAN 68 1271	V.K. Grigor'ev et al.	(ITEP)
LU	05	PRL 94 032002	M. Lu et al.	(BNL E852 Collab.)
ABLIKIM	04J	PRL 93 112002	M. Ablikim et al.	(BES Collab.)
BUGG	04	PL B595 556 (err.)	D.V. Bugg	
BUGG	04A	EPJ C36 161	D.V. Bugg	
BUGG	04C	PRPL 397 257	D.V. Bugg	
EVDOKIMOV	04	PRL 93 242001	A.V. Evdokimov et al.	(SELEX Collab.)
KUHN	04	PL B595 109	J. Kuhn et al.	(BNL E852 Collab.)
ANISOVICH	03	EPJ A16 229	V.V. Anisovich et al.	
VLADIMIRSK...	03	PAN 66 700	V.V. Vladimirsky et al.	
ANISOVICH	02	PL B542 8	A.V. Anisovich et al.	
ANISOVICH	02B	PL B542 19	A.V. Anisovich et al.	
CHUNG	02	PR D65 072001	S.U. Chung et al.	(BNL E852 Collab.)
LINK	02K	PL B545 50	J.M. Link et al.	(FNAL FOCUS Collab.)
ANISOVICH	01C	PL B507 23	A.V. Anisovich et al.	
ANISOVICH	01D	PL B508 6	A.V. Anisovich et al.	
ANISOVICH	01E	PL B513 281	A.V. Anisovich et al.	
ANISOVICH	01F	PL B517 261	A.V. Anisovich et al.	
ANISOVICH	01G	PL B517 273	A.V. Anisovich et al.	
ANISOVICH	00B	NP A662 319	A.V. Anisovich et al.	
ANISOVICH	00D	PL B476 15	A.V. Anisovich et al.	
ANISOVICH	00E	PL B477 19	A.V. Anisovich et al.	
ANISOVICH	00J	PL B491 40	A.V. Anisovich et al.	
ANISOVICH	00I	PL B491 47	A.V. Anisovich et al.	(RAL, LOQM, PNPI+)
ANISOVICH	00M	PL B496 145	A.V. Anisovich et al.	
BARNES	00	PR C62 055203	P.D. Barnes et al.	
FILIPPI	00	PL B495 284	A. Filippi et al.	(OBELIX Experiment)
VLADIMIRSK...	00	JETPL 72 486	V.V. Vladimirskii et al.	
ANISOVICH	99C	PL B452 173	A.V. Anisovich et al.	
ANISOVICH	99E	PL B452 187	A.V. Anisovich et al.	
ANISOVICH	99F	NP A651 253	A.V. Anisovich et al.	
ANISOVICH	99J	PL B471 271	A.V. Anisovich et al.	
ANISOVICH	99K	PL B468 309	A.V. Anisovich et al.	
BUGG	99	PL B458 511	D.V. Bugg et al.	
FERRER	99	EPJ C10 249	A. Ferrer et al.	
SEMENOV	99	SFU 42 847	S.V. Semenov	
ADOMEIT	96	ZPHY C71 227	J. Adomeit et al.	(Crystal Barrel Collab.)
KLOET	96	PR D53 6120	W.M. Kloet, F. Myhrer	(RUTG, NORD)
PROKOSHKIN	96	PD 41 247	Y.D. Prokoshkin, V.D. Samoilenko	(SERP)
HASAN	94	PL B334 215	A. Hasan, D.V. Bugg	(LOQM)
OAKDEN	94	NP A574 731	M.N. Oakden, M.R. Pennington	(DURH)
ALEEV	93	PAN 56 1358	A.N. Aleev et al.	(BIS-2 Collab.)
ARMSTRONG	93D	PL B307 399	T.A. Armstrong et al.	(FNAL, FERR, GENO+)
ALBRECHT	91F	ZPHY C50 1	H. Albrecht et al.	(ARGUS Collab.)
CONDO	91	PR D43 2787	G.T. Condo et al.	(SLAC Hybrid Collab.)
BISELLO	89B	PR D39 701	G. Busetto et al.	(DM2 Collab.)
ATKINSON	88	ZPHY C38 635	M. Atkinson et al.	(BONN, CERN, GLAS+)
DAFTARI	87	PRL 58 859	I.K. Daftari et al.	(SYRA)
ALDE	86D	NP B269 485	D.M. Alde et al.	(BELG, LAPP, SERP, CERN+)
BRIDGES	86D	PL B180 313	D.L. Bridges et al.	(SYRA, BNL, CASE+)
GREEN	86	PRL 56 1639	D.R. Green et al.	(FNAL, ARIZ, FSU+)
ATKINSON	85	ZPHY C29 333	M. Atkinson et al.	(BONN, CERN, GLAS+)
DENNEY	83	PR D28 2726	D.L. Denney et al.	(IOWA, MICH)
CLELAND	82B	NP B208 228	W.E. Cleland et al.	(DURH, GEVA, LAUS+)
ASTON	81B	NP B189 205	D. Aston et al.	(BONN, CERN, EPOL, GLAS+)
ARESTOV	80	IHEP 80-165	Y.I. Arestov et al.	(SERP)
CHLIAPNIK...	80	ZPHY C3 285	P.V. Chliapnikov et al.	(SERP, BRUX, MONS)
KREYMER	80	PR D22 36	A.E. Kreymer et al.	(IND, PURD, SLAC+)
ROZANSKA	80	NP B162 505	M. Rozanska et al.	(MPIM, CERN)
EVANGELIS...	79	NP B153 253	C. Evangelista et al.	(BARI, BONN, CERN+)
EVANGELIS...	79B	NP B154 381	C. Evangelista et al.	(BARI, BONN, CERN+)
BALTAY	78	PR D17 52	C. Baltay et al.	(COLU, BING)
ANTIPOV	77	NP B119 45	Y.M. Antipov et al.	(SERP, GEVA)
BALTAY	77	PRL 39 591	C. Baltay, C.V. Cautis, M. Kaelkar	(COLU)
BALTAY	75	PRL 35 891	C. Baltay et al.	(COLU, BING)
KALELKAR	75	Thesis Nevis 207	M.S. Kaelkar	(COLU)
CASO	70	LNC 3 707	C. Caso et al.	(GENO, HAMB, MILA, SACL)

STRANGE MESONS
($S = \pm 1, C = B = 0$)
 $K^+ = u\bar{s}, K^0 = d\bar{s}, \bar{K}^0 = \bar{d}s, K^- = \bar{u}s$, similarly for K^{*} 's

K^\pm $I(J^P) = \frac{1}{2}(0^-)$

CHARGED KAON MASS

Revised 1994 by T.G. Trippe (LBNL).

The average of the six charged kaon mass measurements which we use in the Particle Listings is

$$m_{K^\pm} = 493.677 \pm 0.013 \text{ MeV } (S = 2.4), \quad (1)$$

where the error has been increased by the scale factor S . The large scale factor indicates a serious disagreement between different input data. The average before scaling the error is

$$m_{K^\pm} = 493.677 \pm 0.005 \text{ MeV }, \quad (2)$$

$$\chi^2 = 22.9 \text{ for } 5 \text{ D.F.}, \text{ Prob. } = 0.04\%,$$

where the high χ^2 and correspondingly low χ^2 probability further quantify the disagreement.

The main disagreement is between the two most recent and precise results,

$$m_{K^\pm} = 493.696 \pm 0.007 \text{ MeV} \quad \text{DENISOV 91}$$

$$m_{K^\pm} = 493.636 \pm 0.011 \text{ MeV } (S = 1.5) \quad \text{GALL 88}$$

$$\text{Average} = 493.679 \pm 0.006 \text{ MeV}$$

$$\chi^2 = 21.2 \text{ for } 1 \text{ D.F.}, \text{ Prob. } = 0.0004\%, \quad (3)$$

both of which are measurements of x-ray energies from kaonic atoms. Comparing the average in Eq. (3) with the overall average in Eq. (2), it is clear that DENISOV 91 and GALL 88 dominate the overall average, and that their disagreement is responsible for most of the high χ^2 .

The GALL 88 measurement was made using four different kaonic atom transitions, $K^- \text{Pb } (9 \rightarrow 8)$, $K^- \text{Pb } (11 \rightarrow 10)$, $K^- \text{W } (9 \rightarrow 8)$, and $K^- \text{W } (11 \rightarrow 10)$. The m_{K^\pm} values they obtain from each of these transitions is shown in the Particle Listings and in Fig. 1. Their $K^- \text{Pb } (9 \rightarrow 8)$ m_{K^\pm} is below and somewhat inconsistent with their other three transitions. The average of their four measurements is

$$m_{K^\pm} = 493.636 \pm 0.007,$$

$$\chi^2 = 7.0 \text{ for } 3 \text{ D.F.}, \text{ Prob. } = 7.2\%. \quad (4)$$

This is a low but acceptable χ^2 probability so, to be conservative, GALL 88 scaled up the error on their average by $S=1.5$ to obtain their published error ± 0.011 shown in Eq. (3) above and used in the Particle Listings average.

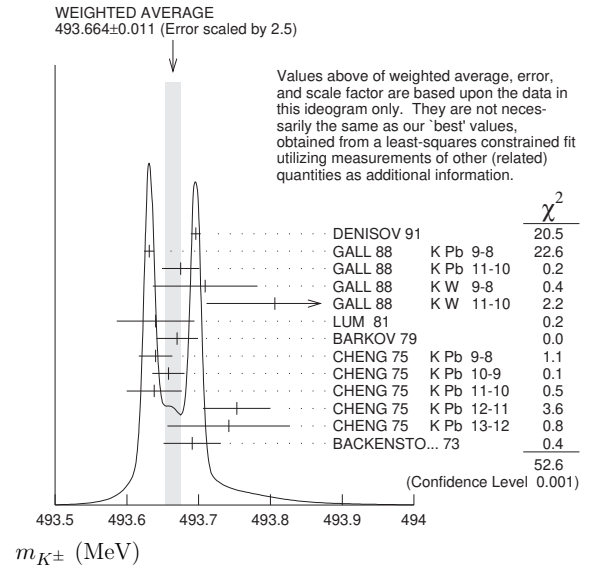


Figure 1: Ideogram of m_{K^\pm} mass measurements. GALL 88 and CHENG 75 measurements are shown separately for each transition they measured.

The ideogram in Fig. 1 shows that the DENISOV 91 measurement and the GALL 88 $K^- \text{Pb } (9 \rightarrow 8)$ measurement yield two well-separated peaks. One might suspect the GALL 88 $K^- \text{Pb } (9 \rightarrow 8)$ measurement since it is responsible both for the internal inconsistency in the GALL 88 measurements and the disagreement with DENISOV 91.

To see if the disagreement could result from a systematic problem with the $K^- \text{Pb } (9 \rightarrow 8)$ transition, we have separated the CHENG 75 data, which also used $K^- \text{Pb}$, into its separate transitions. Figure 1 shows that the CHENG 75 and GALL 88 $K^- \text{Pb } (9 \rightarrow 8)$ values are consistent, suggesting the possibility of a common effect such as contaminant nuclear γ rays near the $K^- \text{Pb } (9 \rightarrow 8)$ transition energy, although the CHENG 75 errors are too large to make a strong conclusion. The average of all 13 measurements has a χ^2 of 52.6 as shown in Fig. 1 and the first line of Table 1, yielding an unacceptable χ^2 probability of 0.00005%. The second line of Table 1 excludes both the GALL 88 and CHENG 75 measurements of the $K^- \text{Pb } (9 \rightarrow 8)$ transition and yields a χ^2 probability of 43%. The third [fourth] line of Table 1 excludes only the GALL 88 $K^- \text{Pb } (9 \rightarrow 8)$ [DENISOV 91] measurement and yields a χ^2 probability of 20% [8.6%]. Table 1 shows that removing both measurements of the $K^- \text{Pb } (9 \rightarrow 8)$ transition produces the most consistent set of data, but that excluding only the GALL 88 $K^- \text{Pb } (9 \rightarrow 8)$ transition or DENISOV 91 also produces acceptable probabilities.

Meson Particle Listings

 K^\pm **Table 1:** m_{K^\pm} averages for some combinations of Fig. 1 data.

m_{K^\pm} (MeV)	χ^2	D.F.	Prob. (%)	Measurements used
493.664 ± 0.004	52.6	12	0.00005	all 13 measurements
493.690 ± 0.006	10.1	10	43	no K^- Pb(9→8)
493.687 ± 0.006	14.6	11	20	no GALL 88 K^- Pb(9→8)
493.642 ± 0.006	17.8	11	8.6	no DENISOV 91

Yu.M. Ivanov, representing DENISOV 91, has estimated corrections needed for the older experiments because of improved ^{192}Ir and ^{198}Au calibration γ -ray energies. He estimates that CHENG 75 and BACKENSTOSS 73 m_{K^\pm} values could be raised by about 15 keV and 22 keV, respectively. With these estimated corrections, Table 1 becomes Table 2. The last line of Table 2 shows that if such corrections are assumed, then GALL 88 K^- Pb (9 → 8) is inconsistent with the rest of the data even when DENISOV 91 is excluded. Yu.M. Ivanov warns that these are rough estimates. Accordingly, we do not use Table 2 to reject the GALL 88 K^- Pb (9 → 8) transition, but we note that a future reanalysis of the CHENG 75 data could be useful because it might provide supporting evidence for such a rejection.

Table 2: m_{K^\pm} averages for some combinations of Fig. 1 data after raising CHENG 75 and BACKENSTOSS 73 values by 0.015 and 0.022 MeV respectively.

m_{K^\pm} (MeV)	χ^2	D.F.	Prob. (%)	Measurements used
493.666 ± 0.004	53.9	12	0.00003	all 13 measurements
493.693 ± 0.006	9.0	10	53	no K^- Pb(9→8)
493.690 ± 0.006	11.5	11	40	no GALL 88 K^- Pb(9→8)
493.645 ± 0.006	23.0	11	1.8	no DENISOV 91

The GALL 88 measurement uses a Ge semiconductor spectrometer which has a resolution of about 1 keV, so they run the risk of some contaminant nuclear γ rays. Studies of γ rays following stopped π^- and Σ^- absorption in nuclei (unpublished) do not show any evidence for contaminants according to GALL 88 spokesperson, B.L. Roberts. The DENISOV 91 measurement uses a crystal diffraction spectrometer with a resolution of 6.3 eV for radiation at 22.1 keV to measure the 4f-3d transition in K^- ^{12}C . The high resolution and the light nucleus reduce the probability for overlap by contaminant γ rays, compared with the measurement of GALL 88. The DENISOV 91 measurement is supported by their high-precision measurement of the 4d-2p transition energy in π^- ^{12}C , which is good agreement with the calculated energy.

While we suspect that the GALL 88 K^- Pb (9 → 8) measurements could be the problem, we are unable to find clear grounds for rejecting it. Therefore, we retain their measurement in the average and accept the large scale factor until further information can be obtained from new measurements and/or from reanalysis of GALL 88 and CHENG 75 data.

We thank B.L. Roberts (Boston Univ.) and Yu.M. Ivanov (Petersburg Nuclear Physics Inst.) for their extensive help in understanding this problem.

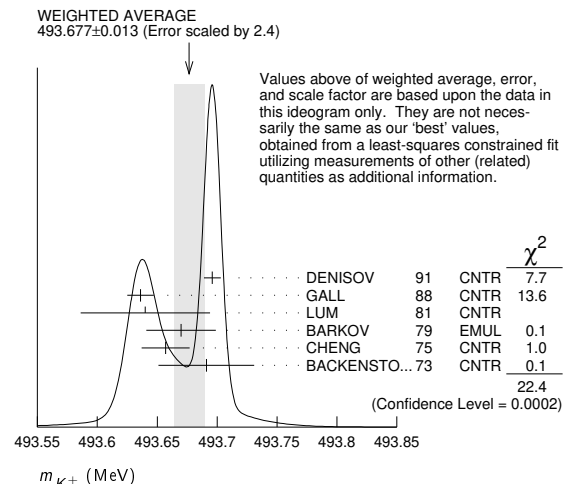
 K^\pm MASS

VALUE (MeV)	DOCUMENT ID	TECN	CHG	COMMENT
493.677 ± 0.016 OUR FIT	Error includes scale factor of 2.8.			
493.677 ± 0.013 OUR AVERAGE	Error includes scale factor of 2.4. See the ideogram below.			
493.696 ± 0.007	¹ DENISOV	91	CNTR	— Kaonic atoms
493.636 ± 0.011	² GALL	88	CNTR	— Kaonic atoms
493.640 ± 0.054	LUM	81	CNTR	— Kaonic atoms
493.670 ± 0.029	BARKOV	79	EMUL	± $e^+ e^- \rightarrow K^+ K^-$
493.657 ± 0.020	² CHENG	75	CNTR	— Kaonic atoms
493.691 ± 0.040	BACKENSTO...73	CNTR	—	Kaonic atoms
• • • We do not use the following data for averages, fits, limits, etc. • • •				
493.631 ± 0.007	GALL	88	CNTR	— K^- Pb (9 → 8)
493.675 ± 0.026	GALL	88	CNTR	— K^- Pb (11 → 10)
493.709 ± 0.073	GALL	88	CNTR	— K^- W (9 → 8)
493.806 ± 0.095	GALL	88	CNTR	— K^- W (11 → 10)
$493.640 \pm 0.022 \pm 0.008$	³ CHENG	75	CNTR	— K^- Pb (9 → 8)
$493.658 \pm 0.019 \pm 0.012$	³ CHENG	75	CNTR	— K^- Pb (10 → 9)
$493.638 \pm 0.035 \pm 0.016$	³ CHENG	75	CNTR	— K^- Pb (11 → 10)
$493.753 \pm 0.042 \pm 0.021$	³ CHENG	75	CNTR	— K^- Pb (12 → 11)
$493.742 \pm 0.081 \pm 0.027$	³ CHENG	75	CNTR	— K^- Pb (13 → 12)

¹ Error increased from 0.0059 based on the error analysis in IVANOV 92.

² This value is the authors' combination of all of the separate transitions listed for this paper.

³ The CHENG 75 values for separate transitions were calculated from their Table 7 transition energies. The first error includes a 20% systematic error in the noncircular contaminant shift. The second error is due to a ± 5 eV uncertainty in the theoretical transition energies.

 $m_{K^+} - m_{K^-}$

Test of CPT.

VALUE (MeV)	EVTS	DOCUMENT ID	TECN	CHG
-0.032 ± 0.090	1.5M	¹ FORD	72	ASPK ±

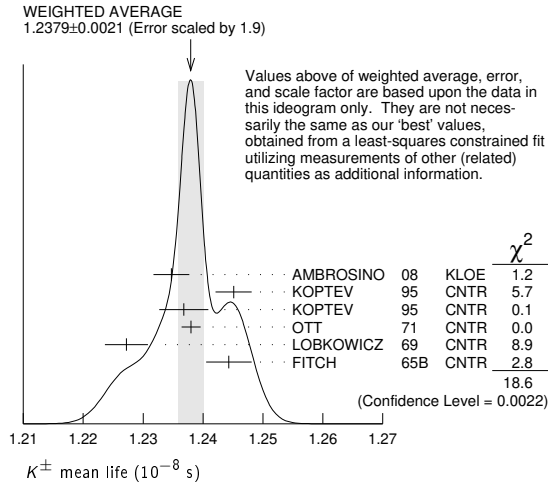
¹ FORD 72 uses $m_{\pi^+} - m_{\pi^-} = +28 \pm 70$ keV.

 K^\pm MEAN LIFE

VALUE (10^{-8} s)	EVTS	DOCUMENT ID	TECN	CHG	COMMENT
1.2380 ± 0.0020 OUR FIT	Error includes scale factor of 1.8.				
1.2379 ± 0.0021 OUR AVERAGE	Error includes scale factor of 1.9. See the ideogram below.				
1.2347 ± 0.0030	15M	¹ AMBROSINO	08	KLOE ±	$\phi \rightarrow K^+ K^-$
1.2451 ± 0.0030	250k	KOPTEV	95	CNTR	K at rest, U target
1.2368 ± 0.0041	150k	KOPTEV	95	CNTR	K at rest, Cu target
1.2380 ± 0.0016	3M	OTT	71	CNTR	K at rest
1.2272 ± 0.0036		LOBKOWICZ	69	CNTR	K in flight
1.2443 ± 0.0038		FITCH	65B	CNTR	K at rest
• • • We do not use the following data for averages, fits, limits, etc. • • •					
1.2415 ± 0.0024	400k	² KOPTEV	95	CNTR	K at rest
1.221 ± 0.011		FORD	67	CNTR	±
1.231 ± 0.011		BOYARSKI	62	CNTR	±

¹ Result obtained by averaging the decay length and decay time analyses taking correlations into account.

² KOPTEV 95 report this weighted average of their U-target and Cu-target results, where they have weighted by $1/\sigma$ rather than $1/\sigma^2$.



$$\frac{(\tau_{K^+} - \tau_{K^-})}{\tau_{\text{average}}}$$

This quantity is a measure of CPT invariance in weak interactions.

VALUE (%)	DOCUMENT ID	TECN
0.10 ± 0.09 OUR AVERAGE	Error includes scale factor of 1.2.	
-0.4 ± 0.4	AMBROSINO 08	KLOE
0.090 ± 0.078	LOBKOWICZ 69	CNTR
0.47 ± 0.30	FORD 67	CNTR

See the related review(s):
Rare Kaon Decays

K^\pm DECAY MODES

K^- modes are charge conjugates of the modes below.

Mode	Fraction (Γ_i/Γ)	Scale factor/ Confidence level
Leptonic and semileptonic modes		
Γ_1 $e^+ \nu_e$	$(1.582 \pm 0.007) \times 10^{-5}$	
Γ_2 $\mu^+ \nu_\mu$	$(63.56 \pm 0.11) \%$	S=1.2
Γ_3 $\pi^0 e^+ \nu_e$	$(5.07 \pm 0.04) \%$	S=2.1
Called K_{e3}^+ .		
Γ_4 $\pi^0 \mu^+ \nu_\mu$	$(3.352 \pm 0.033) \%$	S=1.9
Called $K_{\mu 3}^+$.		
Γ_5 $\pi^0 \pi^0 e^+ \nu_e$	$(2.55 \pm 0.04) \times 10^{-5}$	S=1.1
Γ_6 $\pi^+ \pi^- e^+ \nu_e$	$(4.247 \pm 0.024) \times 10^{-5}$	
Γ_7 $\pi^+ \pi^- \mu^+ \nu_\mu$	$(1.4 \pm 0.9) \times 10^{-5}$	
Γ_8 $\pi^0 \pi^0 \pi^0 e^+ \nu_e$	$< 3.5 \times 10^{-6}$	CL=90%
Hadronic modes		
Γ_9 $\pi^+ \pi^0$	$(20.67 \pm 0.08) \%$	S=1.2
Γ_{10} $\pi^+ \pi^0 \pi^0$	$(1.760 \pm 0.023) \%$	S=1.1
Γ_{11} $\pi^+ \pi^+ \pi^-$	$(5.583 \pm 0.024) \%$	
Leptonic and semileptonic modes with photons		
Γ_{12} $\mu^+ \nu_\mu \gamma$	[a,b] $(6.2 \pm 0.8) \times 10^{-3}$	
Γ_{13} $\mu^+ \nu_\mu \gamma$ (SD ⁺)	[c,d] $(1.33 \pm 0.22) \times 10^{-5}$	
Γ_{14} $\mu^+ \nu_\mu \gamma$ (SD ⁺ INT)	[c,d] $< 2.7 \times 10^{-5}$	CL=90%
Γ_{15} $\mu^+ \nu_\mu \gamma$ (SD ⁻ + SD ⁻ INT)	[c,d] $< 2.6 \times 10^{-4}$	CL=90%
Γ_{16} $e^+ \nu_e \gamma$	$(9.4 \pm 0.4) \times 10^{-6}$	
Γ_{17} $\pi^0 e^+ \nu_e \gamma$	[a,b] $(2.56 \pm 0.16) \times 10^{-4}$	
Γ_{18} $\pi^0 e^+ \nu_e \gamma$ (SD)	[c,d] $< 5.3 \times 10^{-5}$	CL=90%
Γ_{19} $\pi^0 \mu^+ \nu_\mu \gamma$	[a,b] $(1.25 \pm 0.25) \times 10^{-5}$	
Γ_{20} $\pi^0 \pi^0 e^+ \nu_e \gamma$	$< 5 \times 10^{-6}$	CL=90%
Hadronic modes with photons or $\ell\bar{\ell}$ pairs		
Γ_{21} $\pi^+ \pi^0 \gamma$ (INT)	$(-4.2 \pm 0.9) \times 10^{-6}$	
Γ_{22} $\pi^+ \pi^0 \gamma$ (DE)	[a,e] $(6.0 \pm 0.4) \times 10^{-6}$	
Γ_{23} $\pi^+ \pi^0 e^+ e^-$	$(4.24 \pm 0.14) \times 10^{-6}$	
Γ_{24} $\pi^+ \pi^0 \pi^0 \gamma$	[a,b] $(7.6 \pm 6.0 / -3.0) \times 10^{-6}$	
Γ_{25} $\pi^+ \pi^+ \pi^- \gamma$	[a,b] $(7.1 \pm 0.5) \times 10^{-6}$	

Γ_{26} $\pi^+ \gamma \gamma$	[a] $(1.01 \pm 0.06) \times 10^{-6}$	
Γ_{27} $\pi^+ 3\gamma$	[a] $< 1.0 \times 10^{-4}$	CL=90%
Γ_{28} $\pi^+ e^+ e^- \gamma$	$(1.19 \pm 0.13) \times 10^{-8}$	

Leptonic modes with $\ell\bar{\ell}$ pairs

Γ_{29} $e^+ \nu_e \nu \bar{\nu}$	$< 6 \times 10^{-5}$	CL=90%
Γ_{30} $\mu^+ \nu_\mu \nu \bar{\nu}$	$< 2.4 \times 10^{-6}$	CL=90%
Γ_{31} $e^+ \nu_e e^+ e^-$	$(2.48 \pm 0.20) \times 10^{-8}$	
Γ_{32} $\mu^+ \nu_\mu e^+ e^-$	$(7.06 \pm 0.31) \times 10^{-8}$	
Γ_{33} $e^+ \nu_e \mu^+ \mu^-$	$(1.7 \pm 0.5) \times 10^{-8}$	
Γ_{34} $\mu^+ \nu_\mu \mu^+ \mu^-$	$< 4.1 \times 10^{-7}$	CL=90%

Lepton family number (LF), Lepton number (L), $\Delta S = \Delta Q$ (SQ) violating modes, or $\Delta S = 1$ weak neutral current (S1) modes

Γ_{35} $\pi^+ \pi^+ e^- \bar{\nu}_e$	SQ	$< 1.3 \times 10^{-8}$	CL=90%
Γ_{36} $\pi^+ \pi^+ \mu^- \bar{\nu}_\mu$	SQ	$< 3.0 \times 10^{-6}$	CL=95%
Γ_{37} $\pi^+ e^+ e^-$	S1	$(3.00 \pm 0.09) \times 10^{-7}$	
Γ_{38} $\pi^+ \mu^+ \mu^-$	S1	$(9.4 \pm 0.6) \times 10^{-8}$	S=2.6
Γ_{39} $\pi^+ \nu \bar{\nu}$	S1	$(1.7 \pm 1.1) \times 10^{-10}$	
Γ_{40} $\pi^+ \pi^0 \nu \bar{\nu}$	S1	$< 4.3 \times 10^{-5}$	CL=90%
Γ_{41} $\mu^- \nu e^+ e^+$	LF	$< 2.1 \times 10^{-8}$	CL=90%
Γ_{42} $\mu^+ \nu_e$	LF	[f] $< 4 \times 10^{-3}$	CL=90%
Γ_{43} $\pi^+ \mu^+ e^-$	LF	$< 1.3 \times 10^{-11}$	CL=90%
Γ_{44} $\pi^+ \mu^- e^+$	LF	$< 5.2 \times 10^{-10}$	CL=90%
Γ_{45} $\pi^- \mu^+ e^+$	L	$< 5.0 \times 10^{-10}$	CL=90%
Γ_{46} $\pi^- e^+ e^+$	L	$< 2.2 \times 10^{-10}$	CL=90%
Γ_{47} $\pi^- \mu^+ \mu^+$	L	$< 4.2 \times 10^{-11}$	CL=90%
Γ_{48} $\mu^+ \bar{\nu}_e$	L	[f] $< 3.3 \times 10^{-3}$	CL=90%
Γ_{49} $\pi^0 e^+ \bar{\nu}_e$	L	$< 3 \times 10^{-3}$	CL=90%
Γ_{50} $\pi^+ \gamma$	[g] $< 2.3 \times 10^{-9}$	CL=90%	

- [a] See the Particle Listings below for the energy limits used in this measurement.
- [b] Most of this radiative mode, the low-momentum γ part, is also included in the parent mode listed without γ 's.
- [c] Structure-dependent part.
- [d] See the review on "Form Factors for Radiative Pion and Kaon Decays" for definitions and details.
- [e] Direct-emission branching fraction.
- [f] Derived from an analysis of neutrino-oscillation experiments.
- [g] Violates angular-momentum conservation.

CONSTRAINED FIT INFORMATION

An overall fit to the mean life, a decay rate, and 15 branching ratios uses 35 measurements and one constraint to determine 8 parameters. The overall fit has a $\chi^2 = 53.4$ for 28 degrees of freedom.

The following *off-diagonal* array elements are the correlation coefficients $\langle \delta p_i \delta p_j \rangle / (\delta p_i \delta p_j)$, in percent, from the fit to parameters p_i , including the branching fractions, $x_i \equiv \Gamma_i / \Gamma_{\text{total}}$. The fit constrains the x_i whose labels appear in this array to sum to one.

x_3	-66						
x_4	-64	90					
x_5	-12	-5	-5				
x_9	-67	0	-1	-6			
x_{10}	-13	-6	-5	91	-6		
x_{11}	-14	-6	-6	2	-7	2	
Γ	3	1	1	0	2	0	
	x_2	x_3	x_4	x_5	x_9	x_{10}	x_{11}

Mode	Rate (10^8 s^{-1})	Scale factor
Γ_2 $\mu^+ \nu_\mu$	0.5134 ± 0.0012	1.5
Γ_3 $\pi^0 e^+ \nu_e$	0.0410 ± 0.0004	2.1
Called K_{e3}^+ .		
Γ_4 $\pi^0 \mu^+ \nu_\mu$	0.02707 ± 0.00027	1.9
Called $K_{\mu 3}^+$.		
Γ_5 $\pi^0 \pi^0 e^+ \nu_e$	$(2.059 \pm 0.029) \times 10^{-5}$	1.1
Γ_9 $\pi^+ \pi^0$	0.1670 ± 0.0007	1.3
Γ_{10} $\pi^+ \pi^0 \pi^0$	0.01421 ± 0.00018	1.1
Γ_{11} $\pi^+ \pi^+ \pi^-$	0.04510 ± 0.00019	

Meson Particle Listings

K^\pm

K^\pm DECAY RATES

$\Gamma(\mu^+ \nu_\mu)$		Γ_2	
VALUE (10^6 s^{-1})	DOCUMENT ID	TECN	CHG
51.34 ± 0.12 OUR FIT	Error includes scale factor of 1.5.		
• • • We do not use the following data for averages, fits, limits, etc. • • •			
51.2 ± 0.8	FORD	67	CNTR ±

$\Gamma(\pi^+ \pi^+ \pi^-)$		Γ_{11}		
VALUE (10^6 s^{-1})	EVTS	DOCUMENT ID	TECN	CHG
4.510 ± 0.019 OUR FIT	Error includes scale factor of 1.5.			
4.511 ± 0.024	1 FORD 70 ASPK			
• • • We do not use the following data for averages, fits, limits, etc. • • •				
4.529 ± 0.032	3.2M	1 FORD	70 ASPK	
4.496 ± 0.030		1 FORD	67 CNTR ±	
1 First FORD 70 value is second FORD 70 combined with FORD 67.				

K^+ BRANCHING RATIOS

Leptonic and semileptonic modes

$\Gamma(e^+ \nu_e)/\Gamma(\mu^+ \nu_\mu)$		Γ_1/Γ_2		
VALUE (units 10^{-5})	EVTS	DOCUMENT ID	TECN	CHG
2.488 ± 0.009 OUR AVERAGE	Error includes scale factor of 1.5.			
2.488 ± 0.007 ± 0.007	150k	1 LAZZERONI	13 NA62 ±	
2.493 ± 0.025 ± 0.019	13.8k	2 AMBROSINO	09E KLOE ±	
• • • We do not use the following data for averages, fits, limits, etc. • • •				
2.487 ± 0.011 ± 0.007	60k	3 LAZZERONI	11 NA62 +	
2.51 ± 0.15	404	HEINTZE	76 SPEC +	
2.37 ± 0.17	534	HEARD	75B SPEC +	
2.42 ± 0.42	112	CLARK	72 OSPK +	
1 LAZZERONI 13 uses full data sample collected from 2007 to 2008. This ratio is defined to be fully inclusive, including internal-bremsstrahlung.				
2 The ratio is defined to include internal-bremsstrahlung, ignoring direct-emission contributions. AMBROSINO 09E determined the ratio from the measurement of $\Gamma(K \rightarrow e \nu(\gamma), E_\gamma < 10 \text{ MeV}) / \Gamma(K \rightarrow \mu \nu(\gamma))$. 89.8% of $K \rightarrow e \nu(\gamma)$ events had $E_\gamma < 10 \text{ MeV}$.				
3 This ratio is defined to be fully inclusive, including internal-bremsstrahlung.				

$\Gamma(\mu^+ \nu_\mu)/\Gamma_{\text{total}}$		Γ_2/Γ			
VALUE (units 10^{-2})	EVTS	DOCUMENT ID	TECN	CHG	COMMENT
63.56 ± 0.11 OUR FIT	Error includes scale factor of 1.2.				
63.60 ± 0.16 OUR AVERAGE					
63.66 ± 0.09 ± 0.15	865k	1 AMBROSINO	06A KLOE +		
63.24 ± 0.44	62k	CHIANG	72 OSPK +	1.84 GeV/c K^+	
1 Fully inclusive. Used tagged kaons from ϕ decays.					

$\Gamma(\pi^0 e^+ \nu_e)/\Gamma_{\text{total}}$		Γ_3/Γ			
VALUE (units 10^{-2})	EVTS	DOCUMENT ID	TECN	CHG	COMMENT
5.07 ± 0.04 OUR FIT	Error includes scale factor of 2.1.				
4.94 ± 0.05 OUR AVERAGE					
4.965 ± 0.038 ± 0.037		1 AMBROSINO	08A KLOE ±		
4.86 ± 0.10	3516	CHIANG	72 OSPK +	1.84 GeV/c K^+	
• • • We do not use the following data for averages, fits, limits, etc. • • •					
4.7 ± 0.3	429	SHAKLEE	64 HLBC +		
5.0 ± 0.5		ROE	61 HLBC +		
1 Depends on K^+ lifetime τ . AMBROSINO 08A uses PDG 06 value of $\tau = (1.2385 \pm 0.0024) \times 10^{-8}$ sec. The correlation between K_{e3}^+ and $K_{\mu 3}^+$ branching fraction measurements is 62.7%.					

$\Gamma(\pi^0 e^+ \nu_e)/\Gamma(\mu^+ \nu_\mu)$		Γ_3/Γ_2		
VALUE	EVTS	DOCUMENT ID	TECN	CHG
0.0798 ± 0.0008 OUR FIT	Error includes scale factor of 1.9.			
• • • We do not use the following data for averages, fits, limits, etc. • • •				
0.069 ± 0.006	350	ZELLER	69 ASPK +	
0.0775 ± 0.0033	960	BOTTERILL	68C ASPK +	
0.069 ± 0.006	561	GARLAND	68 OSPK +	
0.0791 ± 0.0054	295	1 AUERBACH	67 OSPK +	
1 AUERBACH 67 changed from 0.0797 ± 0.0054. See comment with ratio $\Gamma(\pi^0 \mu^+ \nu_\mu)/\Gamma(\mu^+ \nu_\mu)$. The value 0.0785 ± 0.0025 given in AUERBACH 67 is an average of AUERBACH 67 $\Gamma(\pi^0 e^+ \nu_e)/\Gamma(\mu^+ \nu_\mu)$ and CESTER 66 $\Gamma(\pi^0 e^+ \nu_e)/[\Gamma(\mu^+ \nu_\mu) + \Gamma(\pi^+ \pi^0)]$.				

$\Gamma(\pi^0 e^+ \nu_e)/[\Gamma(\mu^+ \nu_\mu) + \Gamma(\pi^+ \pi^0)]$		$\Gamma_3/(\Gamma_2 + \Gamma_0)$		
VALUE (units 10^{-2})	EVTS	DOCUMENT ID	TECN	CHG
6.02 ± 0.06 OUR FIT	Error includes scale factor of 2.1.			
6.02 ± 0.15 OUR AVERAGE				
6.16 ± 0.22	5110	ESCHSTRUTH	68 OSPK +	
5.89 ± 0.21	1679	CESTER	66 OSPK +	

• • • We do not use the following data for averages, fits, limits, etc. • • •
 5.92 ± 0.65 ¹ WEISSENBERG... 76 SPEC +
¹ Value calculated from WEISSENBERG 76 ($\pi^0 e \nu$), ($\mu \nu$), and ($\pi \pi^0$) values to eliminate dependence on our 1974 ($\pi 2\pi^0$) and ($\pi \pi^+ \pi^-$) fractions.

$\Gamma(\pi^0 e^+ \nu_e)/[\Gamma(\pi^0 \mu^+ \nu_\mu) + \Gamma(\pi^+ \pi^0) + \Gamma(\pi^+ \pi^0 \pi^0)]$		$\Gamma_3/(\Gamma_4 + \Gamma_9 + \Gamma_{10})$		
VALUE	EVTS	DOCUMENT ID	TECN	CHG
0.1967 ± 0.0016 OUR FIT	Error includes scale factor of 2.5.			
0.1962 ± 0.0008 ± 0.0035	71k	SHER	03 B865 +	

$\Gamma(\pi^0 e^+ \nu_e)/\Gamma(\pi^+ \pi^0)$		Γ_3/Γ_9			
VALUE	EVTS	DOCUMENT ID	TECN	CHG	COMMENT
0.2454 ± 0.0023 OUR FIT	Error includes scale factor of 2.6.				
0.2467 ± 0.0011 OUR AVERAGE	Error includes scale factor of 1.1.				
0.2423 ± 0.0015 ± 0.0037	31k	UVAROV	14 ISTR -	ISTR +	
0.2470 ± 0.0009 ± 0.0004	87k	BATLEY	07A NA48 ±		
• • • We do not use the following data for averages, fits, limits, etc. • • •					
0.221 ± 0.012	786	1 LUCAS	73B HBC -	Dalitz pairs only	
1 LUCAS 73B gives $N(K_{e3}) = 786 \pm 3.1\%$, $N(2\pi) = 3564 \pm 3.1\%$. We use these values to obtain quoted result.					

$\Gamma(\pi^0 e^+ \nu_e)/\Gamma(\pi^+ \pi^+ \pi^-)$		Γ_3/Γ_{11}		
VALUE	EVTS	DOCUMENT ID	TECN	CHG
0.908 ± 0.009 OUR FIT	Error includes scale factor of 1.6.			
• • • We do not use the following data for averages, fits, limits, etc. • • •				
0.867 ± 0.027	2768	BARMIN	87 XEBC +	
0.856 ± 0.040	2827	BRAUN	75 HLBC +	
0.850 ± 0.019	4385	1 HAIDT	71 HLBC +	
0.846 ± 0.021	4385	1 EICHTEN	68 HLBC +	
0.94 ± 0.09	854	BELLOTTI	67B HLBC	
0.90 ± 0.06	230	BORREANI	64 HBC +	
1 HAIDT 71 is a reanalysis of EICHTEN 68. Not included in average because of large discrepancy in $\Gamma(\pi^0 \mu^+ \nu)/\Gamma(\pi^0 e^+ \nu)$ with more precise results.				

$\Gamma(\pi^0 \mu^+ \nu_\mu)/\Gamma_{\text{total}}$		Γ_4/Γ			
VALUE (units 10^{-2})	EVTS	DOCUMENT ID	TECN	CHG	COMMENT
3.352 ± 0.033 OUR FIT	Error includes scale factor of 1.9.				
3.24 ± 0.04 OUR AVERAGE					
3.233 ± 0.029 ± 0.026		1 AMBROSINO	08A KLOE ±		
3.33 ± 0.16	2345	CHIANG	72 OSPK +	1.84 GeV/c K^+	
• • • We do not use the following data for averages, fits, limits, etc. • • •					
2.8 ± 0.4		2 TAYLOR	59 EMUL +		
1 Depends on K^+ lifetime τ . AMBROSINO 08A uses PDG 06 value of $\tau = (1.2385 \pm 0.0024) \times 10^{-8}$ sec. The correlation between K_{e3}^+ and $K_{\mu 3}^+$ branching fraction measurements is 62.7%.					
2 Earlier experiments not averaged.					

$\Gamma(\pi^0 \mu^+ \nu_\mu)/\Gamma(\mu^+ \nu_\mu)$		Γ_4/Γ_2		
VALUE	EVTS	DOCUMENT ID	TECN	CHG
0.0527 ± 0.0006 OUR FIT	Error includes scale factor of 1.8.			
• • • We do not use the following data for averages, fits, limits, etc. • • •				
0.054 ± 0.009	240	ZELLER	69 ASPK +	
0.0480 ± 0.0037	424	1 GARLAND	68 OSPK +	
0.0486 ± 0.0040	307	2 AUERBACH	67 OSPK +	
1 GARLAND 68 changed from 0.055 ± 0.004 in agreement with μ -spectrum calculation of GAILLARD 70 appendix B. L.G.Pondrom, (private communication 73).				
2 AUERBACH 67 changed from 0.0602 ± 0.0046 by erratum which brings the μ -spectrum calculation into agreement with GAILLARD 70 appendix B.				

$\Gamma(\pi^0 \mu^+ \nu_\mu)/\Gamma(\pi^0 e^+ \nu_e)$		Γ_4/Γ_3			
VALUE	EVTS	DOCUMENT ID	TECN	CHG	COMMENT
0.6608 ± 0.0029 OUR FIT	Error includes scale factor of 1.1.				
0.6618 ± 0.0027 OUR AVERAGE					
0.663 ± 0.003 ± 0.001	77k	BATLEY	07A NA48 ±		
0.671 ± 0.007 ± 0.008	24k	HORIE	01 SPEC		
0.670 ± 0.014		1 HEINTZE	77 SPEC +		
0.667 ± 0.017	5601	BOTTERILL	68B ASPK +		
• • • We use the following data for averages but not for fits. • • •					
0.6511 ± 0.0064		2 AMBROSINO	08A KLOE ±		
• • • We do not use the following data for averages, fits, limits, etc. • • •					
0.608 ± 0.014	1585	3 BRAUN	75 HLBC +		
0.705 ± 0.063	554	4 LUCAS	73B HBC -	Dalitz pairs only	
0.698 ± 0.025	3480	5 CHIANG	72 OSPK +	1.84 GeV/c K^+	
0.596 ± 0.025		6 HAIDT	71 HLBC +		
0.604 ± 0.022	1398	6 EICHTEN	68 HLBC		
0.703 ± 0.056	1509	CALLAHAN	66B HLBC		
1 HEINTZE 77 value from fit to λ_0 . Assumes μ -e universality.					
2 Not used in the fit. This result enters the fit via correlation of K_{e3}^+ and $K_{\mu 3}^+$ branching fraction measurements of AMBROSINO 08A.					
3 BRAUN 75 value is from form factor fit. Assumes μ -e universality.					
4 LUCAS 73B gives $N(K_{\mu 3}) = 554 \pm 7.6\%$, $N(K_{e3}) = 786 \pm 3.1\%$. We divide.					
5 CHIANG 72 $\Gamma(\pi^0 \mu^+ \nu_\mu)/\Gamma(\pi^0 e^+ \nu_e)$ is statistically independent of CHIANG 72 $\Gamma(\pi^0 \mu^+ \nu_\mu)/\Gamma_{\text{total}}$ and $\Gamma(\pi^0 e^+ \nu_e)/\Gamma_{\text{total}}$.					
6 HAIDT 71 is a reanalysis of EICHTEN 68. Not included in average because of large discrepancy with more precise results.					

$[\Gamma(\pi^0 \mu^+ \nu_\mu) + \Gamma(\pi^+ \pi^0)]/\Gamma_{\text{total}}$ ($\Gamma_4 + \Gamma_9$)/ Γ
We combine these two modes for experiments measuring them in xenon bubble chamber because of difficulties of separating them there.

VALUE (units 10^{-2})	EVTS	DOCUMENT ID	TECN	CHG
24.02 ± 0.08 OUR FIT				Error includes scale factor of 1.2.
• • • We do not use the following data for averages, fits, limits, etc. • • •				
25.4 ± 0.9	886	SHAKLEE	64	HLBC +
23.4 ± 1.1		ROE	61	HLBC +

$\Gamma(\pi^0 \mu^+ \nu_\mu)/\Gamma(\pi^+ \pi^0)$ Γ_4/Γ_9
VALUE (units 10^{-2}) EVTS DOCUMENT ID TECN CHG
0.1637 ± 0.0006 ± 0.0003 77k BATLEY 07A NA48 ±

$\Gamma(\pi^0 \mu^+ \nu_\mu)/\Gamma(\pi^+ \pi^+ \pi^-)$ Γ_4/Γ_{11}
VALUE (units 10^{-3}) EVTS DOCUMENT ID TECN CHG COMMENT
0.600 ± 0.007 OUR FIT Error includes scale factor of 1.6.
• • • We do not use the following data for averages, fits, limits, etc. • • •
0.503 ± 0.019 1505 1 HAIDT 71 HLBC +
0.510 ± 0.017 1505 1 EICHTEN 68 HLBC +
0.63 ± 0.07 2845 2 BISI 65B BC + HBC+HLBC

¹HAIDT 71 is a reanalysis of EICHTEN 68. Not included in average because of large discrepancy in $\Gamma(\pi^0 \mu^+ \nu)/\Gamma(\pi^0 e^+ \nu)$ with more precise results.
²Error enlarged for background problems. See GAILLARD 70.

$\Gamma(\pi^0 \pi^0 e^+ \nu_e)/\Gamma_{\text{total}}$ Γ_5/Γ
VALUE (units 10^{-5}) EVTS DOCUMENT ID TECN CHG
2.55 ± 0.04 OUR FIT Error includes scale factor of 1.1.
2.54 ± 0.89 10 BARMIN 88B HLBC +

$\Gamma(\pi^0 \pi^0 e^+ \nu_e)/\Gamma(\pi^+ \pi^0 \pi^0)$ Γ_5/Γ_{10}
VALUE (units 10^{-3}) EVTS DOCUMENT ID TECN CHG
1.449 ± 0.008 OUR FIT
1.449 ± 0.006 ± 0.006 65.2k 1 BATLEY 14A NA48 ±

¹Data collected in 2003–2004. This leads to the scalar form factor $(1 + \delta_{EM}) f_5 = 6.079 \pm 0.012 \pm 0.027 \pm 0.046$ where the last error is due to the normalizing decay mode uncertainty.

$\Gamma(\pi^0 \pi^0 e^+ \nu_e)/\Gamma(\pi^0 e^+ \nu_e)$ Γ_5/Γ_3
VALUE (units 10^{-4}) EVTS DOCUMENT ID TECN CHG
5.03 ± 0.09 OUR FIT Error includes scale factor of 1.2.
4.1 ± 1.0 OUR AVERAGE
-0.7
4.2 ± 1.0 25 BOLOTOV 86B CALO -
-0.9
3.8 ± 5.0 2 LJUNG 73 HLBC +
-1.2

$\Gamma(\pi^+ \pi^- e^+ \nu_e)/\Gamma(\pi^+ \pi^+ \pi^-)$ Γ_6/Γ_{11}
VALUE (units 10^{-4}) EVTS DOCUMENT ID TECN CHG
7.606 ± 0.029 OUR AVERAGE
7.615 ± 0.008 ± 0.028 1.1M 1 BATLEY 12 NA48 ±
7.35 ± 0.01 ± 0.19 388k 2 PISLAK 01 B865
7.21 ± 0.32 30k ROSSELET 77 SPEC +
• • • We do not use the following data for averages, fits, limits, etc. • • •
7.36 ± 0.68 500 BOURQUIN 71 ASPK
7.0 ± 0.9 106 SCHWEINB... 71 HLBC +
5.83 ± 0.63 269 ELY 69 HLBC +

¹BATLEY 12 uses data collected in 2003–2004. The result is inclusive of $K^{\pm} \rightarrow \pi^+ \pi^- e^+ \nu \gamma$ decays. Using PDG 12 value for $\Gamma(\pi^+ \pi^- \pi^+)/\Gamma = (5.59 \pm 0.04) \times 10^{-2}$. BATLEY 12 obtains $B(\pi^+ \pi^- e \nu) = (4.257 \pm 0.004 \pm 0.035) \times 10^{-5}$ where the syst. error is dominated by the error on the normalization mode.

²PISLAK 01 reports $\Gamma(\pi^+ \pi^- e^+ \nu_e)/\Gamma_{\text{total}} = (4.109 \pm 0.008 \pm 0.110) \times 10^{-5}$ using the PDG 00 value $\Gamma(\pi^+ \pi^+ \pi^-)/\Gamma_{\text{total}} = (5.59 \pm 0.05) \times 10^{-2}$. We divide by the PDG value and unfold its error from the systematic error. PISLAK 03 and PISLAK 10A give additional details on the branching ratio measurement and give improved errors on the S-wave $\pi\pi$ scattering length: $a_0^0 = 0.235 \pm 0.013$ and $a_0^2 = -0.0410 \pm 0.0027$.

$\Gamma(\pi^+ \pi^- \mu^+ \nu_\mu)/\Gamma_{\text{total}}$ Γ_7/Γ
VALUE (units 10^{-5}) EVTS DOCUMENT ID TECN CHG
• • • We do not use the following data for averages, fits, limits, etc. • • •
0.77 ± 0.54 1 CLINE 65 FBC +
-0.50

$\Gamma(\pi^+ \pi^- \mu^+ \nu_\mu)/\Gamma(\pi^+ \pi^+ \pi^-)$ Γ_7/Γ_{11}
VALUE (units 10^{-4}) EVTS DOCUMENT ID TECN CHG
2.57 ± 1.55 7 BISI 67 DBC +
• • • We do not use the following data for averages, fits, limits, etc. • • •
~ 2.5 1 GREINER 64 EMUL +

$\Gamma(\pi^0 \pi^0 e^+ \nu_e)/\Gamma_{\text{total}}$ Γ_8/Γ
VALUE (units 10^{-6}) CL% EVTS DOCUMENT ID TECN CHG
<3.5 90 0 BOLOTOV 88 SPEC -
• • • We do not use the following data for averages, fits, limits, etc. • • •
<9 90 0 BARMIN 92 XEBC +

Hadronic modes

$\Gamma(\pi^+ \pi^0)/\Gamma_{\text{total}}$ Γ_9/Γ
VALUE (units 10^{-2}) EVTS DOCUMENT ID TECN CHG COMMENT
20.67 ± 0.08 OUR FIT Error includes scale factor of 1.2.
20.70 ± 0.16 OUR AVERAGE Error includes scale factor of 1.8.

20.65 ± 0.05 ± 0.08 1.4M 1 AMBROSINO 08E KLOE + $\phi \rightarrow K^+ K^-$
21.18 ± 0.28 16k CHIANG 72 OSPK + 1.84 GeV/c K^+
• • • We do not use the following data for averages, fits, limits, etc. • • •
21.0 ± 0.6 CALLAHAN 65 HLBC See Γ_9/Γ_{11}
¹Fully inclusive of final-state radiation. The branching ratio is evaluated using K^+ lifetime, $\tau = 12.385$ ns.

$\Gamma(\pi^+ \pi^0)/\Gamma(\pi^+ \pi^+ \pi^-)$ Γ_9/Γ_{11}
VALUE (units 10^{-2}) EVTS DOCUMENT ID TECN CHG
3.702 ± 0.022 OUR FIT Error includes scale factor of 1.1.
• • • We do not use the following data for averages, fits, limits, etc. • • •
3.96 ± 0.15 1045 CALLAHAN 66 FBC +

$\Gamma(\pi^+ \pi^0)/\Gamma(\mu^+ \nu_\mu)$ Γ_9/Γ_2
VALUE EVTS DOCUMENT ID TECN CHG COMMENT
0.3252 ± 0.0016 OUR FIT Error includes scale factor of 1.2.
0.3325 ± 0.0032 OUR AVERAGE
0.3329 ± 0.0047 ± 0.0010 45k USHER 92 SPEC + $p\bar{p}$ at rest
0.3355 ± 0.0057 1 WEISSENBE... 76 SPEC +
0.3277 ± 0.0065 4517 2 AUERBACH 67 OSPK +
• • • We do not use the following data for averages, fits, limits, etc. • • •
0.328 ± 0.005 25k 1 WEISSENBE... 74 STRC +
0.305 ± 0.018 1600 ZELLER 69 ASPK +

¹WEISSENBERG 76 revises WEISSENBERG 74.
²AUERBACH 67 changed from 0.3253 ± 0.0065. See comment with ratio $\Gamma(\pi^0 \mu^+ \nu_\mu)/\Gamma(\mu^+ \nu_\mu)$.

$\Gamma(\pi^+ \pi^0 \pi^0)/\Gamma_{\text{total}}$ Γ_{10}/Γ
VALUE (units 10^{-2}) EVTS DOCUMENT ID TECN CHG COMMENT
1.760 ± 0.023 OUR FIT Error includes scale factor of 1.1.
1.775 ± 0.028 OUR AVERAGE Error includes scale factor of 1.2.
1.763 ± 0.013 ± 0.022 ALOISIO 04A KLOE ±
1.84 ± 0.06 1307 CHIANG 72 OSPK + 1.84 GeV/c K^+
• • • We do not use the following data for averages, fits, limits, etc. • • •
1.53 ± 0.11 198 1 PANDOULAS 70 EMUL +
1.8 ± 0.2 108 SHAKLEE 64 HLBC +
1.7 ± 0.2 ROE 61 HLBC +
1.5 ± 0.2 2 TAYLOR 59 EMUL +

¹Includes events of TAYLOR 59.
²Earlier experiments not averaged.

$\Gamma(\pi^+ \pi^0 \pi^0)/\Gamma(\pi^+ \pi^0)$ Γ_{10}/Γ_9
VALUE EVTS DOCUMENT ID TECN CHG COMMENT
0.0851 ± 0.0012 OUR FIT Error includes scale factor of 1.1.
• • • We do not use the following data for averages, fits, limits, etc. • • •
0.081 ± 0.005 574 1 LUCAS 73B HBC - Dalitz pairs only
¹LUCAS 73B gives $N(\pi^2 \pi^0) = 574 \pm 5.9\%$, $N(2\pi) = 3564 \pm 3.1\%$. We quote $0.5N(\pi^2 \pi^0)/N(2\pi)$ where 0.5 is because only Dalitz pair π^0 s were used.

$\Gamma(\pi^+ \pi^0 \pi^0)/\Gamma(\pi^+ \pi^+ \pi^-)$ Γ_{10}/Γ_{11}
VALUE EVTS DOCUMENT ID TECN CHG COMMENT
0.315 ± 0.004 OUR FIT Error includes scale factor of 1.1.
0.303 ± 0.009 2027 BISI 65 BC + HBC+HLBC
• • • We do not use the following data for averages, fits, limits, etc. • • •
0.393 ± 0.099 17 YOUNG 65 EMUL +

$\Gamma(\pi^+ \pi^+ \pi^-)/\Gamma_{\text{total}}$ Γ_{11}/Γ
VALUE (units 10^{-2}) EVTS DOCUMENT ID TECN CHG COMMENT
5.583 ± 0.024 OUR FIT
5.565 ± 0.031 ± 0.025 68k 1 BABUSCI 14B KLOE +
• • • We do not use the following data for averages, fits, limits, etc. • • •
5.56 ± 0.20 2330 2 CHIANG 72 OSPK + 1.84 GeV/c K^+
5.34 ± 0.21 693 3 PANDOULAS 70 EMUL +
5.71 ± 0.15 DEMARCO 65 HBC
6.0 ± 0.4 YOUNG 65 EMUL +
5.54 ± 0.12 2332 CALLAHAN 64 HLBC +
5.1 ± 0.2 540 SHAKLEE 64 HLBC +
5.7 ± 0.3 ROE 61 HLBC +

¹Inclusive of final-state radiation. Result obtained from averaging two branching ratios: one from a sample with $K^- \rightarrow \mu \nu(\gamma)$ tagging and another with $K^- \rightarrow \pi^- \pi^0(\gamma)$ tagging.

²Value is not independent of CHIANG 72 $\Gamma(\mu^+ \nu_\mu)/\Gamma_{\text{total}}$, $\Gamma(\pi^+ \pi^0)/\Gamma_{\text{total}}$, $\Gamma(\pi^+ \pi^0 \pi^0)/\Gamma_{\text{total}}$, $\Gamma(\pi^0 \mu^+ \nu_\mu)/\Gamma_{\text{total}}$, and $\Gamma(\pi^0 e^+ \nu_e)/\Gamma_{\text{total}}$.

³Includes events of TAYLOR 59.

Meson Particle Listings

K^\pm

Leptonic and semileptonic modes with photons

$\Gamma(\mu^+ \nu_\mu \gamma)/\Gamma_{\text{total}}$						Γ_{12}/Γ
VALUE (units 10^{-3})	EVTS	DOCUMENT ID	TECN	CHG	COMMENT	
6.2 ± 0.8 OUR AVERAGE						
6.6 ± 1.5		1,2 DEMIDOV	90	XEBC	$P(\mu) < 231.5 \text{ MeV}/c$	
6.0 ± 0.9		BARMIN	88	HLBC +	$P(\mu) < 231.5 \text{ MeV}/c$	
• • • We do not use the following data for averages, fits, limits, etc. • • •						
3.5 ± 0.8		2,3 DEMIDOV	90	XEBC	$E(\gamma) > 20 \text{ MeV}$	
3.2 ± 0.5	57	4 BARMIN	88	HLBC +	$E(\gamma) > 20 \text{ MeV}$	
5.4 ± 0.3		5 AKIBA	85	SPEC	$P(\mu) < 231.5 \text{ MeV}/c$	

¹ $P(\mu)$ cut given in DEMIDOV 90 paper, 235.1 MeV/c, is a misprint according to authors (private communication).
² DEMIDOV 90 quotes only inner bremsstrahlung (IB) part.
³ Not independent of above DEMIDOV 90 value. Cuts differ.
⁴ Not independent of above BARMIN 88 value. Cuts differ.
⁵ Assumes μ - e universality and uses constraints from $K \rightarrow e \nu \gamma$.

$\Gamma(\mu^+ \nu_\mu \gamma(SD^+))/\Gamma_{\text{total}}$						Γ_{13}/Γ
VALUE (units 10^{-5})	CL%	EVTS	DOCUMENT ID	TECN	CHG	COMMENT
1.33 ± 0.12 ± 0.18						
	25	88	1 ADLER	00B	B787	
• • • We do not use the following data for averages, fits, limits, etc. • • •						
<3.0	90		AKIBA	85	SPEC	

¹ ADLER 00B obtains the branching ratio by extrapolating the measurement in the kinematic region $E_\mu > 137 \text{ MeV}$, $E_\gamma > 90 \text{ MeV}$ to the full SD^+ phase-space. Also reports $|F_V + F_A| = 0.165 \pm 0.007 \pm 0.011$ and $-0.04 < F_V - F_A < 0.24$ at 90% CL.

$\Gamma(\mu^+ \nu_\mu \gamma(SD^+INT))/\Gamma_{\text{total}}$						Γ_{14}/Γ
VALUE (units 10^{-5})	CL%	EVTS	DOCUMENT ID	TECN	CHG	COMMENT
<2.7						
	90		AKIBA	85	SPEC	

Interference term between internal Bremsstrahlung and SD^+ term. See the "Note on $\pi^\pm \rightarrow \ell^\pm \nu_\ell \gamma$ and $K^\pm \rightarrow \ell^\pm \nu_\ell \gamma$ Form Factors" in the π^\pm section of the Particle Data Listings above.

$\Gamma(\mu^+ \nu_\mu \gamma(SD^- + SD^-INT))/\Gamma_{\text{total}}$						Γ_{15}/Γ
VALUE (units 10^{-4})	CL%	EVTS	DOCUMENT ID	TECN	CHG	COMMENT
<2.6						
	90		1 AKIBA	85	SPEC	

¹ Assumes μ - e universality and uses constraints from $K \rightarrow e \nu \gamma$.

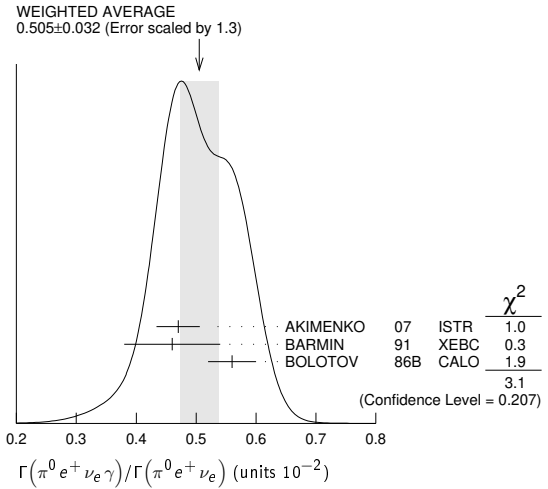
$\Gamma(e^+ \nu_e \gamma)/\Gamma(\mu^+ \nu_\mu)$						Γ_{16}/Γ_2
VALUE (units 10^{-5})	EVTS	DOCUMENT ID	TECN	CHG	COMMENT	
1.483 ± 0.066 ± 0.013						
	1.4K	1 AMBROSINO	09E	KLOE	$\pm E_\gamma$ in 10–250 MeV, $p_e > 200 \text{ MeV}/c$	

¹ AMBROSINO 09E measured the differential width $dR_\gamma/dE_\gamma = (1/\Gamma(K \rightarrow \mu \nu)) (d\Gamma(K \rightarrow e \nu \gamma)/dE_\gamma)$. Result obtained by integrating the differential width over E_γ from 10 to 250 MeV.

$\Gamma(\pi^0 e^+ \nu_e \gamma)/\Gamma(\pi^0 e^+ \nu_e)$						Γ_{17}/Γ_3
VALUE (units 10^{-2})	EVTS	DOCUMENT ID	TECN	CHG	COMMENT	
0.505 ± 0.032 OUR AVERAGE						
0.47 ± 0.02 ± 0.03	4476	1 AKIMENKO	07	ISTR	$E_\gamma > 10 \text{ MeV}$, $0.6 < \cos(\theta_{e\gamma}) < 0.9$	
0.46 ± 0.08	82	2 BARMIN	91	XEBC	$E_\gamma > 10 \text{ MeV}$, $0.6 < \cos(\theta_{e\gamma}) < 0.9$	
0.56 ± 0.04	192	3 BOLOTOV	86B	CALO	$E_\gamma > 10 \text{ MeV}$	
• • • We do not use the following data for averages, fits, limits, etc. • • •						
1.81 ± 0.03 ± 0.07	4476	1 AKIMENKO	07	ISTR	$E_\gamma > 10 \text{ MeV}$, $\theta_{e\gamma} > 10^\circ$	
0.63 ± 0.02 ± 0.03	4476	1 AKIMENKO	07	ISTR	$E_\gamma > 30 \text{ MeV}$, $\theta_{e\gamma} > 20^\circ$	
1.51 ± 0.25	82	2 BARMIN	91	XEBC	$E_\gamma > 10 \text{ MeV}$, $\cos(\theta_{e\gamma}) < 0.98$	
0.48 ± 0.20	16	4 LJUNG	73	HLBC +	$E_\gamma > 30 \text{ MeV}$	
0.22 +0.15 -0.10		4 LJUNG	73	HLBC +	$E_\gamma > 30 \text{ MeV}$	
0.76 ± 0.28	13	5 ROMANO	71	HLBC	$E_\gamma > 10 \text{ MeV}$	
0.53 ± 0.22		5 ROMANO	71	HLBC +	$E_\gamma > 30 \text{ MeV}$	
1.2 ± 0.8		BELLOTTI	67	HLBC	$E_\gamma > 30 \text{ MeV}$	

¹ AKIMENKO 07 provides values for three kinematic regions. For averaging, we use value with $E_\gamma > 10 \text{ MeV}$ and $0.6 < \cos(\theta_{e\gamma}) < 0.9$.
² BARMIN 91 quotes branching ratio $\Gamma(K \rightarrow e \pi^0 \nu \gamma)/\Gamma_{\text{all}}$. The measured normalization is $[\Gamma(K \rightarrow e \pi^0 \nu) + \Gamma(K \rightarrow \pi^+ \pi^+ \pi^-)]$. For comparison with other experiments we use $\Gamma(K \rightarrow e \pi^0 \nu)/\Gamma_{\text{all}} = 0.0482$ to calculate the values quoted here.
³ $\cos(\theta_{e\gamma})$ between 0.6 and 0.9.
⁴ First LJUNG 73 value is for $\cos(\theta_{e\gamma}) < 0.9$, second value is for $\cos(\theta_{e\gamma})$ between 0.6 and 0.9 for comparison with ROMANO 71.

⁵ Both ROMANO 71 values are for $\cos(\theta_{e\gamma})$ between 0.6 and 0.9. Second value is for comparison with second LJUNG 73 value. We use lowest E_γ cut for Summary Table value. See ROMANO 71 for E_γ dependence.



$\Gamma(\pi^0 e^+ \nu_e \gamma(SD))/\Gamma_{\text{total}}$						Γ_{18}/Γ
VALUE (units 10^{-5})	CL%	EVTS	DOCUMENT ID	TECN	CHG	COMMENT
<5.3						
	90		BOLOTOV	86B	CALO	

$\Gamma(\pi^0 \mu^+ \nu_\mu \gamma)/\Gamma_{\text{total}}$						Γ_{19}/Γ
VALUE (units 10^{-5})	CL%	EVTS	DOCUMENT ID	TECN	CHG	COMMENT
1.25 ± 0.25 OUR AVERAGE						
1.10 ± 0.32 ± 0.05		23	1 ADLER	10	B787	$30 < E_\gamma < 60 \text{ MeV}$
1.46 ± 0.22 ± 0.32		153	2 TCHIKILEV	07	ISTR	$30 < E_\gamma < 60 \text{ MeV}$
• • • We do not use the following data for averages, fits, limits, etc. • • •						
2.4 ± 0.5 ± 0.6		125	SHIMIZU	06	K470 +	$E_\gamma > 30 \text{ MeV}$; $\theta_{\mu\gamma} > 20^\circ$
<6.1	90	0	LJUNG	73	HLBC +	$E(\gamma) > 30 \text{ MeV}$

¹ Value obtained from $B(K^+ \rightarrow \pi^0 \mu^+ \nu_\mu \gamma) = (2.51 \pm 0.74 \pm 0.12) \times 10^{-5}$ obtained in the kinematic region $E_\gamma > 20 \text{ MeV}$, and then theoretical $K_{\mu 3\gamma}$ spectrum has been used. Also $B(K^+ \rightarrow \pi^0 \mu^+ \nu_\mu \gamma) = (1.58 \pm 0.46 \pm 0.08) \times 10^{-5}$, for $E_\gamma > 30 \text{ MeV}$ and $\theta_{\mu\gamma} > 20^\circ$, was determined.
² Obtained from measuring $B(K_{\mu 3\gamma}) / B(K_{\mu 3})$ and using PDG 02 value $B(K_{\mu 3}) = 3.27\%$. $B(K_{\mu 3\gamma}) = (8.82 \pm 0.94 \pm 0.86) \times 10^{-5}$ is obtained for $5 \text{ MeV} < E_\gamma < 30 \text{ MeV}$.

$\Gamma(\pi^0 \pi^0 e^+ \nu_e \gamma)/\Gamma_{\text{total}}$						Γ_{20}/Γ
VALUE (units 10^{-6})	CL%	EVTS	DOCUMENT ID	TECN	CHG	COMMENT
<5						
	90	0	BARMIN	92	XEBC +	$E_\gamma > 10 \text{ MeV}$

Hadronic modes with photons

$\Gamma(\pi^+ \pi^0 \gamma(INT))/\Gamma_{\text{total}}$						Γ_{21}/Γ
VALUE (units 10^{-6})	CL%	EVTS	DOCUMENT ID	TECN	CHG	COMMENT
-4.24 ± 0.63 ± 0.70						
	600k		1 BATLEY	10A	NA48 ±	T_{π^+} 0–80 MeV

The $K^+ \rightarrow \pi^+ \pi^0 \gamma$ differential decay rate can be described in terms of T_{π^+} , the charged pion kinetic energy, and $W^2 = (P_K \cdot P_\gamma)(P_{\pi^+} \cdot P_\gamma) / (m_K m_{\pi^+})^2$; then we can write $d^2\Gamma(K^+ \rightarrow \pi^+ \pi^0 \gamma) / (dT_{\pi^+} dW^2) = d^2\Gamma(K^+ \rightarrow \pi^+ \pi^0 \gamma)_{IB} / (dT_{\pi^+} dW^2) [1 + 2 \cos(\phi + \delta_1^+ - \delta_0^0) m_\pi^2 m_K^2 W^2 X_E + m_\pi^4 m_K^4 (X_E^2 + X_M^2) W^4]$. The IB differential and total branching ratios are expressed in terms of the non-radiative experimental width $\Gamma(K^+ \rightarrow \pi^+ \pi^0)$ by Low's theorem. Using PDG 10 $B(K^+ \rightarrow \pi^+ \pi^0) = 0.2066 \pm 0.0008$, one obtains respectively $B(K^+ \rightarrow \pi^+ \pi^0 \gamma)_{IB} (55 < T_{\pi^+} < 90 \text{ MeV}) = 2.55 \times 10^{-4}$ and $B(K^+ \rightarrow \pi^+ \pi^0 \gamma)_{IB} (0 < T_{\pi^+} < 80 \text{ MeV}) = 1.80 \times 10^{-4}$. Fitting respectively the piece proportional to W^2 and the piece proportional to W^4 , the interference contribution (INT), proportional to X_E , and the direct contribution (DE) proportional to $X_E^2 + X_M^2$ are extracted.

$\Gamma(\pi^+ \pi^0 \gamma(DE))/\Gamma_{\text{total}}$						Γ_{22}/Γ
VALUE (units 10^{-6})	CL%	EVTS	DOCUMENT ID	TECN	CHG	COMMENT
5.99 ± 0.27 ± 0.25						
	600k		1 BATLEY	10A	NA48 ±	T_{π^+} 0–80 MeV

Direct emission (DE) part of $\Gamma(\pi^+ \pi^0 \gamma)/\Gamma_{\text{total}}$, assuming that interference (INT) component is zero.

••• We do not use the following data for averages, fits, limits, etc. •••

3.8 ± 0.8 ± 0.7	10k	ALIEV	06	K470	+	T_{π^+}	55–90 MeV
3.7 ± 3.9 ± 1.0	930	UVAROV	06	ISTR	–	T_{π^-}	55–90 MeV
3.2 ± 1.3 ± 1.0	4k	ALIEV	03	K470	+	T_{π^+}	55–90 MeV
6.1 ± 2.5 ± 1.9	4k	ALIEV	03	K470	+	T_{π^+}	full range
4.7 ± 0.8 ± 0.3	20k	ADLER	00c	B787	+	T_{π^+}	55–90 MeV
20.5 ± 4.6	+3.9	BOLOTOV	87	WIRE	–	T_{π^-}	55–90 MeV
–2.3	–2.3						
15.6 ± 3.5 ± 5.0		ABRAMS	72	ASPK	±	T_{π^\pm}	55–90 MeV

¹ The cut on the photon energy implies $W^2 > 0.2$. BATLEY 10a obtains the INT and DE fractional branchings with respect to IB from a simultaneous kinematical fit of INT and DE and then we use the PDG 10 value for $B(K^+ \rightarrow \pi^+ \pi^0) = 20.66 \pm 0.08$ to determine the IB. The INT and DE correlation coefficients -0.93 . Assuming constant electric and magnetic amplitudes, X_E and X_M , these INT and DE values imply $X_E = -24 \pm 6 \text{ GeV}^{-4}$ and $X_M = -254 \pm 9 \text{ GeV}^{-4}$.

² ADLER 00c measures the INT component to be $(-0.4 \pm 1.6)\%$ of the inner bremsstrahlung (IB) component.

$\Gamma(\pi^+ \pi^0 \pi^0 \gamma) / \Gamma(\pi^+ \pi^0 \pi^0)$ $\Gamma_{24} / \Gamma_{10}$

VALUE (units 10^{-4})	DOCUMENT ID	TECN	CHG	COMMENT	
4.3 ± 3.2	BOLOTOV	85	SPEC	–	$E(\gamma) > 10 \text{ MeV}$
–1.7					

$\Gamma(\pi^+ \pi^+ \pi^- \gamma) / \Gamma_{\text{total}}$ Γ_{25} / Γ

VALUE (units 10^{-4})	EVTS	DOCUMENT ID	TECN	CHG	COMMENT	
0.071 ± 0.005 OUR AVERAGE						
0.071 ± 0.005	450	SHAPKIN	19	OKA	+	$E(\gamma) > 30 \text{ MeV}$
1.10 ± 0.48	7	BARMIN	89	XEBC		$E(\gamma) > 5 \text{ MeV}$
1.0 ± 0.4		STAMER	65	EMUL	+	$E(\gamma) > 11 \text{ MeV}$

$\Gamma(\pi^+ \pi^0 e^+ e^-) / \Gamma_{\text{total}}$ Γ_{23} / Γ

VALUE (units 10^{-6})	EVTS	DOCUMENT ID	TECN
4.24 ± 0.14	4.9K	¹ BATLEY	19 NA48

¹ BATLEY 19 result is obtained from an exposure of 1.7×10^{11} charged kaon decays recorded in 2003–2004. The study of the kinematic space shows evidence for a structure dependent contribution consistent with predictions from chiral perturbation theory.

$\Gamma(\pi^+ \gamma \gamma) / \Gamma_{\text{total}}$ Γ_{26} / Γ

VALUE (units 10^{-7})	CL%	EVTS	DOCUMENT ID	TECN	CHG	COMMENT
10.1 ± 0.6 OUR AVERAGE						
10.03 ± 0.51 ± 0.24	215	¹ LAZZERONI	14 NA62	±		
11 ± 3 ± 1	31	² KITCHING	97 B787	+		

••• We do not use the following data for averages, fits, limits, etc. •••

9.10 ± 0.72 ± 0.22	149	³ BATLEY	14 NA48	±		
< 0.083	90	⁴ ARTAMONOV	05 B949	+	$P_{\pi^-} > 213 \text{ MeV}/c$	
< 10	90	0 ATIYA	90b B787	+	$T_{\pi^-} 117\text{--}127 \text{ MeV}$	
< 84	90	0 ASANO	82 CNTR	+	$T_{\pi^-} 117\text{--}127 \text{ MeV}$	
< 420 ± 520	0	0 ABRAMS	77 SPEC	+	$T_{\pi^-} < 92 \text{ MeV}$	
< 350	90	0 LJUNG	73 HLBC	+	6–102, 114–127 MeV	
< 500	90	0 KLEMS	71 OSPK	+	$T_{\pi^-} < 117 \text{ MeV}$	
–100 ± 600		0 CHEN	68 OSPK	+	$T_{\pi^-} 60\text{--}90 \text{ MeV}$	

¹ LAZZERONI 14 combines NA62 and NA48/2 results. The result for the full kinematic range is extrapolated from the model-independent branching fraction $(9.65 \pm 0.61 \pm 0.14) \times 10^{-7}$ for $(m_{\gamma\gamma}/m_K)^2 > 0.2$. The measured ChPT parameter $\tilde{c} = 1.86 \pm 0.25$.

² KITCHING 97 is extrapolated from their model-independent branching fraction $(6.0 \pm 1.5 \pm 0.7) \times 10^{-7}$ for $100 \text{ MeV}/c < P_{\pi^+} < 180 \text{ MeV}/c$ using Chiral Perturbation Theory.

³ BATLEY 14 uses data collected in 2003 and 2004. Branching ratio is obtained by determining the parameter $\tilde{c} = 1.41 \pm 0.38 \pm 0.11$ and integrating the $O(p^6)$ chiral spectrum. A model independent value for the branching ratio is also obtained $(8.77 \pm 0.87 \pm 0.17) \times 10^{-7}$ for kinematic range $(m_{\gamma\gamma}/m_K)^2 > 0.2$.

⁴ ARTAMONOV 05 limit assumes ChPT with $\tilde{c} = 1.8$ with unitarity corrections. With $\tilde{c} = 1.6$ and no unitarity corrections they obtain $< 2.3 \times 10^{-8}$ at 90% CL. This partial branching ratio is predicted to be 6.10×10^{-9} and 0.49×10^{-9} for the cases with and without unitarity correction.

$\Gamma(\pi^+ 3\gamma) / \Gamma_{\text{total}}$ Γ_{27} / Γ

VALUE (units 10^{-4})	CL%	DOCUMENT ID	TECN	CHG	COMMENT	
< 1.0	90	ASANO	82	CNTR	+	$T(\pi) 117\text{--}127 \text{ MeV}$

••• We do not use the following data for averages, fits, limits, etc. •••

< 3.0	90	KLEMS	71	OSPK	+	$T(\pi) > 117 \text{ MeV}$
-------	----	-------	----	------	---	----------------------------

$\Gamma(\pi^+ e^+ e^- \gamma) / \Gamma_{\text{total}}$ Γ_{28} / Γ

VALUE (units 10^{-8})	EVTS	DOCUMENT ID	TECN	COMMENT
1.19 ± 0.12 ± 0.04	113	¹ BATLEY	08 NA48	$m_{ee\gamma} > 260 \text{ MeV}$

¹ BATLEY 08 also reports the Chiral Perturbation Theory parameter $\tilde{c} = 0.9 \pm 0.45$ obtained using the shape of the $e^+ e^- \gamma$ invariant mass spectrum. By extrapolating the theoretical amplitude to $m_{ee\gamma} < 260 \text{ MeV}$, it obtains the inclusive $B(K^+ \rightarrow \pi^+ e^+ e^- \gamma) = (1.29 \pm 0.13 \pm 0.03) \times 10^{-8}$, where the first error is the combined statistical and systematic errors and the second error is from the uncertainty in \tilde{c} .

Leptonic modes with $\ell\bar{\ell}$ pairs

$\Gamma(e^+ \nu_e \nu \bar{\nu}) / \Gamma(e^+ \nu_e)$ Γ_{29} / Γ_1

VALUE	CL%	EVTS	DOCUMENT ID	TECN	CHG	
< 3.8	90	0	HEINTZE	79	SPEC	+

$\Gamma(\mu^+ \nu_\mu \nu \bar{\nu}) / \Gamma_{\text{total}}$ Γ_{30} / Γ

VALUE	CL%	DOCUMENT ID	TECN	CHG
< 2.4 × 10⁻⁶	90	¹ ARTA MONOV	16 B949	+
••• We do not use the following data for averages, fits, limits, etc. •••				
< 6.0 × 10 ⁻⁶	90	² PANG	73 CNTR	+

¹ ARTAMONOV 16 assumes Standard model μ spectrum. The search is performed in the muon momentum region between 130 and 175 MeV/c.

² PANG 73 assumes μ spectrum from $\nu\text{-}\nu$ interaction of BARDIN 70.

$\Gamma(e^+ \nu_e e^+ e^-) / \Gamma_{\text{total}}$ Γ_{31} / Γ

VALUE (units 10^{-8})	EVTS	DOCUMENT ID	TECN	CHG	COMMENT	
2.48 ± 0.14 ± 0.14	410	POBLAGUEV	02 B865	+	$m_{ee} > 150 \text{ MeV}$	
••• We do not use the following data for averages, fits, limits, etc. •••						
20 ± 20	4	DIAMANT...	76	SPEC	+	$m_{e^+e^-} > 140 \text{ MeV}$

$\Gamma(\mu^+ \nu_\mu e^+ e^-) / \Gamma_{\text{total}}$ Γ_{32} / Γ

VALUE (units 10^{-8})	EVTS	DOCUMENT ID	TECN	CHG	COMMENT	
7.06 ± 0.16 ± 0.26	2.7k	POBLAGUEV	02 B865	+	$m_{ee} > 145 \text{ MeV}$	
••• We do not use the following data for averages, fits, limits, etc. •••						
100 ± 30	14	DIAMANT...	76	SPEC	+	$m_{e^+e^-} > 140 \text{ MeV}$

$\Gamma(e^+ \nu_e \mu^+ \mu^-) / \Gamma_{\text{total}}$ Γ_{33} / Γ

VALUE (units 10^{-8})	CL%	DOCUMENT ID	TECN
1.72 ± 0.45		MA	06 B865
••• We do not use the following data for averages, fits, limits, etc. •••			
< 50	90	ADLER	98 B787

$\Gamma(\mu^+ \nu_\mu \mu^+ \mu^-) / \Gamma_{\text{total}}$ Γ_{34} / Γ

VALUE (units 10^{-7})	CL%	DOCUMENT ID	TECN	CHG
< 4.1	90	ATIYA	89 B787	+

Lepton Family number (LF), Lepton number (L), $\Delta S = \Delta Q$ (SQ) violating modes, or $\Delta S = 1$ weak neutral current (S1) modes

$\Gamma(\pi^+ \pi^+ e^- \bar{\nu}_e) / \Gamma_{\text{total}}$ Γ_{35} / Γ

VALUE (units 10^{-7})	CL%	EVTS	DOCUMENT ID	TECN	CHG	
< 9.0	95	0	SCHWEINB...	71	HLBC	+
< 6.9	95	0	ELY	69	HLBC	+
< 20.	95	0	BIRGE	65	FBC	+

$\Gamma(\pi^+ \pi^+ e^- \bar{\nu}_e) / \Gamma(\pi^+ \pi^- e^+ \nu_e)$ Γ_{35} / Γ_6

VALUE (units 10^{-4})	CL%	EVTS	DOCUMENT ID	TECN
< 3	90	3	¹ BLOCH	76 SPEC
••• We do not use the following data for averages, fits, limits, etc. •••				
< 130.	95	0	BOURQUIN	71 ASPK

¹ BLOCH 76 quotes 3.6×10^{-4} at CL = 95%, we convert.

$\Gamma(\pi^+ \pi^+ \mu^- \bar{\nu}_\mu) / \Gamma_{\text{total}}$ Γ_{36} / Γ

VALUE (units 10^{-6})	CL%	EVTS	DOCUMENT ID	TECN	CHG	
< 3.0	95	0	BIRGE	65	FBC	+

$\Gamma(\pi^+ e^+ e^-) / \Gamma_{\text{total}}$ Γ_{37} / Γ

VALUE (units 10^{-7})	EVTS	DOCUMENT ID	TECN	CHG
3.00 ± 0.09 OUR AVERAGE				
3.11 ± 0.04 ± 0.12	7253	¹ BATLEY	09 NA48	±
2.94 ± 0.05 ± 0.14	10300	² APPEL	99 SPEC	+
2.75 ± 0.23 ± 0.13	500	³ ALLIEGRO	92 SPEC	+
2.7 ± 0.5	41	⁴ BLOCH	75 SPEC	+

¹ Value extrapolated from a measurement in the region $z = (m_{ee}/m_K)^2 > 0.08$. BATLEY 09 also evaluated the shape of the form factor using four different theoretical models.

² APPEL 99 establishes vector nature of this decay and determines form factor $f(z) = f_0(1 + \delta Z)$, $Z = M_{ee}^2/m_K^2$, $\delta = 2.14 \pm 0.13 \pm 0.15$.

³ ALLIEGRO 92 assumes a vector interaction with a form factor given by $\lambda = 0.105 \pm 0.035 \pm 0.015$ and a correlation coefficient of -0.82 .

⁴ BLOCH 75 assumes a vector interaction.

Meson Particle Listings

K^\pm

$\Gamma(\pi^+ \mu^+ \mu^-)/\Gamma_{total}$ Γ_{38}/Γ
 Test for $\Delta S = 1$ weak neutral current. Allowed by higher-order electroweak interactions.

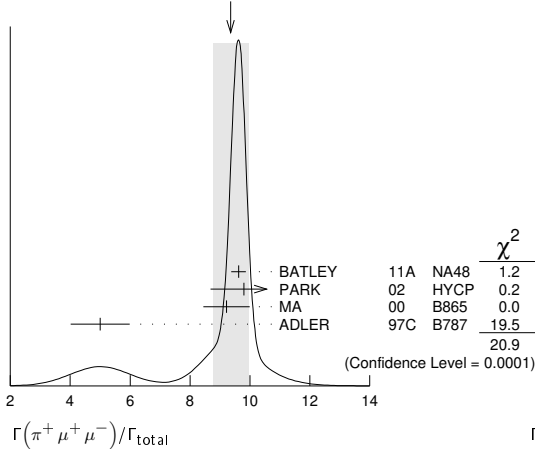
VALUE (units 10^{-8})	CL%	EVTS	DOCUMENT ID	TECN	CHG	COMMENT
9.4 ± 0.6	OUR AVERAGE					Error includes scale factor of 2.6. See the ideogram below.
9.62 ± 0.21 ± 0.13		3120	¹ BATLEY	11A NA48	±	2003-04 data
9.8 ± 1.0 ± 0.5		110	² PARK	02 HYCP	±	
9.22 ± 0.60 ± 0.49		402	³ MA	00 B865	+	
5.0 ± 0.4 ± 0.9		207	⁴ ADLER	97c B787	+	

• • • We do not use the following data for averages, fits, limits, etc. • • •

9.7 ± 1.2 ± 0.4		65	PARK	02 HYCP	+	
10.0 ± 1.9 ± 0.7		35	PARK	02 HYCP	-	
<23		90	ATIYA	89 B787	+	

- ¹ BATLEY 11A also studies the form factor $f(z)$ dependence of the decay, described via single photon exchange: i) assuming a linear form factor, $f(z) = f_0(1 + \delta z)$, $z = (M_{\mu\mu}/m_K)^2$, finding $f_0 = 0.470 \pm 0.040$ and $\delta = 3.11 \pm 0.57$ and ii) assuming a linear form factor including π - π rescattering, $W_{\pi\pi}$, as in DAMBROSIO 98A, finding $f(z) = G_F m_K^2 (a_+ + b_+ z) + W_{\pi\pi}(z)$, $a_+ = -0.575 \pm 0.039$, $b_+ = -0.813 \pm 0.145$.
- ² PARK 02 “±” result comes from combining $K^+ \rightarrow \pi^+ \mu^+ \mu^-$ and $K^- \rightarrow \pi^- \mu^+ \mu^-$, assuming CP is conserved.
- ³ MA 00 establishes vector nature of this decay and determines form factor $f(z) = f_0(1 + \delta z)$, $z = (M_{\mu\mu}/m_K)^2$, $\delta = 2.45_{-0.95}^{+1.30}$.
- ⁴ ADLER 97c gives systematic error 0.7×10^{-8} and theoretical uncertainty 0.6×10^{-8} , which we combine in quadrature to obtain our second error.

WEIGHTED AVERAGE
9.4±0.6 (Error scaled by 2.6)



$\Gamma(\pi^+ \nu \mu)/\Gamma_{total}$ Γ_{39}/Γ
 Test for $\Delta S = 1$ weak neutral current. Allowed by higher-order electroweak interactions. Branching ratio values are extrapolated from the momentum or energy regions shown in the comments assuming Standard Model phase space except for those labeled “Scalar” or “Tensor” to indicate the assumed non-Standard-Model interaction.

VALUE (units 10^{-9})	CL%	EVTS	DOCUMENT ID	TECN	CHG	COMMENT
0.173 ± 0.115 -0.105		7	¹ ARTAMONOV 08	B949	+	$140 < P_\pi < 199$ MeV, $211 < P_\pi < 229$ MeV
< 1.1	90	1	² CORTINA-GIL 19B	NA62	+	decay-in-flight
$0.789_{-0.510}^{+0.926}$		3	³ ARTAMONOV 08	B949	+	$140 < P_\pi < 199$ MeV
< 2.2	90	1	⁴ ADLER	04 B787	+	$211 < P_\pi < 229$ MeV
< 2.7	90		ADLER	04 B787	+	Scalar
< 1.8	90		ADLER	04 B787	+	Tensor
$0.147_{-0.089}^{+0.130}$		3	⁵ ANISIMOVSK...04	B949	+	$211 < P_\pi < 229$ MeV
$0.157_{-0.082}^{+0.175}$		2	ADLER	02 B787	+	$P_\pi > 211$ MeV/c
< 4.2	90	1	ADLER	02c B787	+	$140 < P_\pi < 195$ MeV
< 4.7	90		ADLER	02c B787	+	Scalar
< 2.5	90		ADLER	02c B787	+	Tensor
$0.15_{-0.12}^{+0.34}$		1	ADLER	00 B787		In ADLER 02
$0.42_{-0.35}^{+0.97}$		1	ADLER	97 B787		
< 2.4	90		ADLER	96 B787		
< 7.5	90		ATIYA	93 B787	+	$T(\pi)$ 115-127 MeV
< 5.2	90		ATIYA	93 B787	+	
< 17	90	0	ATIYA	93B B787	+	$T(\pi)$ 60-100 MeV
< 34	90		ATIYA	90 B787	+	
<140	90		ASANO	81B CNTR	+	$T(\pi)$ 116-127 MeV

- ¹ Value obtained combining ANISIMOVSKY 04, ADLER 04, and the present ARTAMONOV 08 results.
- ² Based on a sample of 1.21×10^{11} K^+ decays collected in 2016. One signal candidate is observed while the expected background is 0.152 events. The single-event-sensitivity is estimated to be 3.15×10^{-10} .

- ³ Observed 3 events with an estimated background of $0.93 \pm 0.17_{-0.24}^{+0.32}$. Signal-to-background ratio for each of these 3 events is 0.20, 0.42, and 0.47.
- ⁴ Value obtained combining the previous result ADLER 02c with 1 event and the present result with 0 events to obtain an expected background 1.22 ± 0.24 events and 1 event observed.
- ⁵ Value obtained combining the previous E787 result ADLER 02 with 2 events and the present E949 with 1 event. The additional event has a signal-to-background ratio 0.9. Superseded by ARTAMONOV 08.
- ⁶ Superseded by ADLER 04.
- ⁷ Combining ATIYA 93 and ATIYA 93B results. Superseded by ADLER 96.

$\Gamma(\pi^+ \pi^0 \nu \mu)/\Gamma_{total}$ Γ_{40}/Γ
 Test for $\Delta S = 1$ weak neutral current. Allowed by higher-order electroweak interactions.

VALUE (units 10^{-5})	CL%	DOCUMENT ID	TECN
<4.3	90	¹ ADLER	01 SPEC

- ¹ Search region defined by $90 \text{ MeV} < c < P_{\pi^+} < 188 \text{ MeV}/c$ and $135 \text{ MeV} < E_{\pi^0} < 180 \text{ MeV}$.

$\Gamma(\mu^- \nu e^+ e^+)/\Gamma(\pi^+ \pi^- e^+ \nu_e)$ Γ_{41}/Γ_6
 Test of lepton family number conservation.

VALUE (units 10^{-3})	CL%	EVTS	DOCUMENT ID	TECN	CHG
<0.5	90	0	¹ DIAMANT-...	76	SPEC +

- ¹ DIAMANT-BERGER 76 quotes this result times our 1975 $\pi^+ \pi^- e \nu$ BR ratio.

$\Gamma(\mu^+ \nu_e)/\Gamma_{total}$ Γ_{42}/Γ
 Forbidden by lepton family number conservation.

VALUE	CL%	EVTS	DOCUMENT ID	TECN	COMMENT
<0.004	90	0	¹ LYONS	81	HLBC 200 GeV K^+ narrow band ν beam

- • • We do not use the following data for averages, fits, limits, etc. • • •
- | | | | | | |
|--------|----|--|---------------------|----|--------------------------|
| <0.012 | 90 | | ¹ COOPER | 82 | HLBC Wideband ν beam |
|--------|----|--|---------------------|----|--------------------------|
- ¹ COOPER 82 and LYONS 81 limits on ν_e observation are here interpreted as limits on lepton family number violation in the absence of mixing.

$\Gamma(\pi^+ \mu^+ e^-)/\Gamma_{total}$ Γ_{43}/Γ
 Test of lepton family number conservation.

VALUE (units 10^{-10})	CL%	DOCUMENT ID	TECN	CHG
<0.13	90	¹ SHER	05 RVUE	+
<0.21	90	SHER	05 B865	+
<0.39	90	APPEL	00 B865	+
<2.1	90	LEE	90 SPEC	+

- ¹ This result combines SHER 05 1998 data, APPEL 00 1996 data, and data from BERGMAN 97 and PISLAK 97 theses, all from BNL-E865, with LEE 90 BNL-E777 data.

$\Gamma(\pi^+ \mu^- e^+)/\Gamma_{total}$ Γ_{44}/Γ
 Test of lepton family number conservation.

VALUE (units 10^{-10})	CL%	EVTS	DOCUMENT ID	TECN	CHG
< 5.2	90	0	APPEL	00B B865	+

• • • We do not use the following data for averages, fits, limits, etc. • • •

<70	90	0	¹ DIAMANT-...	76	SPEC +
-----	----	---	--------------------------	----	--------

- ¹ Measurement actually applies to the sum of the $\pi^+ \mu^- e^+$ and $\pi^- \mu^+ e^+$ modes.

$\Gamma(\pi^- \mu^+ e^+)/\Gamma_{total}$ Γ_{45}/Γ
 Test of total lepton number conservation.

VALUE (units 10^{-10})	CL%	EVTS	DOCUMENT ID	TECN	CHG
< 5.0	90	0	APPEL	00B B865	+

• • • We do not use the following data for averages, fits, limits, etc. • • •

<70	90	0	¹ DIAMANT-...	76	SPEC +
-----	----	---	--------------------------	----	--------

- ¹ Measurement actually applies to the sum of the $\pi^+ \mu^- e^+$ and $\pi^- \mu^+ e^+$ modes.

$\Gamma(\pi^- e^+ e^+)/\Gamma_{total}$ Γ_{46}/Γ
 Test of total lepton number conservation.

VALUE	CL%	DOCUMENT ID	TECN	CHG	COMMENT
<2.2 × 10⁻¹⁰	90	¹ CORTINA-GIL 19A	NA 62	+	decay-in-flight

• • • We do not use the following data for averages, fits, limits, etc. • • •

<6.4 × 10 ⁻¹⁰	90	APPEL	00B B865	+	
<9.2 × 10 ⁻⁹	90	DIAMANT-...	76	SPEC	+
<1.5 × 10 ⁻⁵		CHANG	68	HBC	-

- ¹ CORTINA-GIL 19A results are obtained with 2017 data.

$\Gamma(\pi^- \mu^+ \mu^+)/\Gamma_{total}$ Γ_{47}/Γ
 Forbidden by total lepton number conservation.

VALUE	CL%	DOCUMENT ID	TECN	CHG	COMMENT
<4.2 × 10⁻¹¹	90	¹ CORTINA-GIL 19A	NA 62	+	decay-in-flight

• • • We do not use the following data for averages, fits, limits, etc. • • •

<8.6 × 10 ⁻¹¹	90	² BATLEY	17	NA 48	±
<1.1 × 10 ⁻⁹	90	BATLEY	11A	NA 48	±
<3.0 × 10 ⁻⁹	90	APPEL	00B	B865	+
<1.5 × 10 ⁻⁴	90	³ LITTEMBERG	92	HBC	

- ¹ CORTINA-GIL 19A results are obtained with 2017 data.
- ² BATLEY 17 result is based on data taken in 2003 to 2004. Limits for two-body resonance X in $K^\pm \rightarrow \pi \mu \mu$ decays are also reported.
- ³ LITTEMBERG 92 is from retroactive data analysis of CHANG 68 bubble chamber data.

$\Gamma(\mu^+ \bar{\nu}_e) / \Gamma_{total}$ Γ_{48} / Γ
 Forbidden by total lepton number conservation.

VALUE (units 10^{-3})	CL%	DOCUMENT ID	TECN	COMMENT
<3.3	90	¹ COOPER 82	HLBC	Wideband ν beam

¹ COOPER 82 limit on $\bar{\nu}_e$ observation is here interpreted as a limit on lepton number violation in the absence of mixing.

$\Gamma(\pi^0 e^+ \bar{\nu}_e) / \Gamma_{total}$ Γ_{49} / Γ
 Forbidden by total lepton number conservation.

VALUE	CL%	DOCUMENT ID	TECN	COMMENT
<0.003	90	¹ COOPER 82	HLBC	Wideband ν beam

¹ COOPER 82 limit on $\bar{\nu}_e$ observation is here interpreted as a limit on lepton number violation in the absence of mixing.

$\Gamma(\pi^+ \gamma) / \Gamma_{total}$ Γ_{50} / Γ
 Violates angular momentum conservation and gauge invariance. Current interest in this decay is as a search for non-commutative space-time effects as discussed in ARTAMONOV 05 and for exotic physics such as a vacuum expectation value of a new vector field, non-local Superstring effects, or departures from Lorentz invariance, as discussed in ADLER 02b.

VALUE (units 10^{-3})	CL%	DOCUMENT ID	TECN	CHG
< 2.3	90	ARTAMONOV 05	B949	+
• • • We do not use the following data for averages, fits, limits, etc. • • •				
< 360	90	ADLER 02b	B787	+
<1400	90	ASANO 82	CNTR	+
<4000	90	¹ KLEMS 71	OSPK	+

¹ Test of model of Selleri, Nuovo Cimento **60A** 291 (1969).

CPT VIOLATION TESTS IN K^\pm DECAYS

$$\Delta = (\Gamma(K^+) - \Gamma(K^-)) / (\Gamma(K^+) + \Gamma(K^-))$$

$\Delta(K^\pm \rightarrow \mu^\pm \nu_\mu)$ RATE DIFFERENCE/SUM

VALUE (%)	DOCUMENT ID	TECN
-0.27 ± 0.21	FORD 67	CNTR

$\Delta(K^\pm \rightarrow \pi^\pm \pi^0)$ RATE DIFFERENCE/SUM

VALUE (%)	DOCUMENT ID	TECN
0.4 ± 0.6	HERZO 69	OSPK

CP VIOLATION TESTS IN K^\pm DECAYS

$$\Delta = (\Gamma(K^+) - \Gamma(K^-)) / (\Gamma(K^+) + \Gamma(K^-))$$

$\Delta(K^\pm \rightarrow \pi^\pm e^+ e^-)$ RATE DIFFERENCE/SUM

VALUE (units 10^{-2})	DOCUMENT ID	TECN
-2.2 ± 1.5 ± 0.6	¹ BATLEY 09	NA48

¹ This implies an upper limit of 2.1×10^{-2} at 90% CL.

$\Delta(K^\pm \rightarrow \pi^\pm \mu^+ \mu^-)$ RATE DIFFERENCE/SUM

VALUE	DOCUMENT ID	TECN
0.010 ± 0.023 OUR AVERAGE		
0.011 ± 0.023	¹ BATLEY 09	NA48
-0.02 ± 0.11 ± 0.04	PARK 02	HYCP

¹ This corresponds to the asymmetry upper limit of $< 2.9 \times 10^{-2}$ at 90% CL.

$\Delta(K^\pm \rightarrow \pi^\pm \pi^0 \gamma)$ RATE DIFFERENCE/SUM

VALUE (units 10^{-3})	EVTS	DOCUMENT ID	TECN	CHG	COMMENT
0.0 ± 1.2 OUR AVERAGE					
0.0 ± 1.0 ± 0.6	1M	¹ BATLEY 10a	NA48		
4 ± 29	2461	SMITH 76	WIRE	±	E_π 55-90 MeV
5 ± 20	4000	ABRAMS 73b	ASPK	±	E_π 51-100 MeV

¹ This value implies the upper bound for this asymmetry 1.5×10^{-3} at 90% CL.

$\Delta(K^\pm \rightarrow \pi^\pm \pi^+ \pi^-)$ RATE DIFFERENCE/SUM

VALUE (%)	EVTS	DOCUMENT ID	TECN	CHG
0.04 ± 0.06		¹ FORD 70	ASPK	
• • • We do not use the following data for averages, fits, limits, etc. • • •				
-0.01 ± 0.08		² SMITH 73	ASPK	±
0.05 ± 0.07	3.2M	¹ FORD 70	ASPK	
-0.25 ± 0.45		FLETCHER 67	OSPK	
-0.02 ± 0.11		¹ FORD 67	CNTR	

¹ First FORD 70 value is second FORD 70 combined with FORD 67.
² SMITH 73 value of $K^\pm \rightarrow \pi^\pm \pi^+ \pi^-$ rate difference is derived from SMITH 73 value of $K^\pm \rightarrow \pi^\pm 2\pi^0$ rate difference.

$\Delta(K^\pm \rightarrow \pi^\pm \pi^0 \pi^0)$ RATE DIFFERENCE/SUM

VALUE (%)	EVTS	DOCUMENT ID	TECN	CHG
-0.02 ± 0.28 OUR AVERAGE				
0.04 ± 0.29		SMITH 73	ASPK	±
-0.6 ± 0.9	1802	HERZO 69	OSPK	

T VIOLATION TESTS IN K^+ AND K^- DECAYS

P_T in $K^+ \rightarrow \pi^0 \mu^+ \nu_\mu$

T-violating muon polarization. Sensitive to new sources of CP violation beyond the Standard Model.

VALUE (units 10^{-3})	EVTS	DOCUMENT ID	TECN	CHG
-1.7 ± 2.3 ± 1.1		¹ ABE 04f	K246	+
• • • We do not use the following data for averages, fits, limits, etc. • • •				
-4.2 ± 4.9 ± 0.9	3.9M	ABE 99s	K246	+

¹ Includes three sets of data: 96-97 (ABE 99s), 98, and 99-00 totaling about three times the ABE 99s data sample. Corresponds to $P_T < 5.0 \times 10^{-3}$ at 90% CL.

P_T in $K^+ \rightarrow \mu^+ \nu_\mu \gamma$

T-violating muon polarization. Sensitive to new sources of CP violation beyond the Standard Model.

VALUE (units 10^{-2})	EVTS	DOCUMENT ID	TECN	CHG
-0.64 ± 1.85 ± 0.10	114k	¹ ANISIMOVSK...03	K246	+

¹ Muons stopped and polarization measured from decay to positrons.

$\text{Im}(\xi)$ in $K^+ \rightarrow \pi^0 \mu^+ \nu_\mu$ DECAY (from transverse μ pol.)

Test of T reversal invariance.

VALUE	EVTS	DOCUMENT ID	TECN	CHG	COMMENT
-0.006 ± 0.008 OUR AVERAGE					
-0.0053 ± 0.0071 ± 0.0036		¹ ABE 04f	K246	+	
-0.016 ± 0.025	20M	CAMPBELL 81	CNTR	+	Pol.
• • • We do not use the following data for averages, fits, limits, etc. • • •					
-0.013 ± 0.016 ± 0.003	3.9M	ABE 99s	CNTR	+	$\rho_T K^+$ at rest

¹ Includes three sets of data: 96-97 (ABE 99s), 98, and 99-00 totaling about three times the ABE 99s data sample. Corresponds to $\text{Im}(\xi) < 0.016$ at 90% CL.

DALITZ PLOT PARAMETERS FOR $K \rightarrow 3\pi$ DECAYS

Revised 1999 by T.G. Trippe (LBNL).

The Dalitz plot distribution for $K^\pm \rightarrow \pi^\pm \pi^\pm \pi^\mp$, $K^\pm \rightarrow \pi^0 \pi^0 \pi^\pm$, and $K_L^0 \rightarrow \pi^+ \pi^- \pi^0$ can be parameterized by a series expansion such as that introduced by Weinberg [1]. We use the form

$$\begin{aligned}
 |M|^2 \propto & 1 + g \frac{(s_3 - s_0)}{m_{\pi^+}^2} + h \left[\frac{s_3 - s_0}{m_{\pi^+}^2} \right]^2 \\
 & + j \frac{(s_2 - s_1)}{m_{\pi^+}^2} + k \left[\frac{s_2 - s_1}{m_{\pi^+}^2} \right]^2 \\
 & + f \frac{(s_2 - s_1)(s_3 - s_0)}{m_{\pi^+}^2 m_{\pi^+}^2} + \dots, \quad (1)
 \end{aligned}$$

where $m_{\pi^+}^2$ has been introduced to make the coefficients g , h , j , and k dimensionless, and

$$\begin{aligned}
 s_i &= (P_K - P_i)^2 = (m_K - m_i)^2 - 2m_K T_i, \quad i = 1, 2, 3, \\
 s_0 &= \frac{1}{3} \sum_i s_i = \frac{1}{3} (m_K^2 + m_1^2 + m_2^2 + m_3^2).
 \end{aligned}$$

Here the P_i are four-vectors, m_i and T_i are the mass and kinetic energy of the i^{th} pion, and the index 3 is used for the odd pion.

The coefficient g is a measure of the slope in the variable s_3 (or T_3) of the Dalitz plot, while h and k measure the quadratic dependence on s_3 and $(s_2 - s_1)$, respectively. The coefficient j is related to the asymmetry of the plot and must be zero if CP invariance holds. Note also that if CP is good, g , h , and k must be the same for $K^+ \rightarrow \pi^+ \pi^+ \pi^-$ as for $K^- \rightarrow \pi^- \pi^- \pi^+$.

Since different experiments use different forms for $|M|^2$, in order to compare the experiments we have converted to g , h , j , and k whatever coefficients have been measured. Where such conversions have been done, the measured coefficient a_y , a_t , a_u , or a_v is given in the comment at the right. For definitions of

Meson Particle Listings

 K^\pm

these coefficients, details of this conversion, and discussion of the data, see the April 1982 version of this note [2].

References

1. S. Weinberg, Phys. Rev. Lett. **4**, 87 (1960).
2. Particle Data Group, Phys. Lett. **111B**, 69 (1982).

ENERGY DEPENDENCE OF K^\pm DALITZ PLOT

$$|\text{matrix element}|^2 = 1 + gu + hu^2 + kv^2$$

where $u = (s_3 - s_0) / m_\pi^2$ and $v = (s_2 - s_1) / m_\pi^2$

LINEAR COEFFICIENT g FOR $K^\pm \rightarrow \pi^\pm \pi^+ \pi^-$

Some experiments use Dalitz variables x and y . In the comments we give $a_y =$ coefficient of y term. See note above on "Dalitz Plot Parameters for $K \rightarrow 3\pi$ Decays." For discussion of the conversion of a_y to g , see the earlier version of the same note in the Review published in Physics Letters **111B** 70 (1982).

VALUE	EVTS	DOCUMENT ID	TECN	CHG	COMMENT
-0.21134 ± 0.00017	471M	¹ BATLEY	07B	NA48	±
•••	We do not use the following data for averages, fits, limits, etc. •••				
-0.2221 ± 0.0065	225k	DEVAUX	77	SPEC	+ $a_y = .2814 \pm .0082$
-0.199 ± 0.008	81k	² LUCAS	73	HBC	- $a_y = 0.252 \pm 0.011$
-0.2157 ± 0.0028	750k	FORD	72	ASPK	+ $a_y = .2734 \pm .0035$
-0.2186 ± 0.0028	750k	FORD	72	ASPK	- $a_y = .2770 \pm .0035$
-0.200 ± 0.009	39819	³ HOFFMASTER	72	HLBC	+
-0.196 ± 0.012	17898	⁴ GRAUMAN	70	HLBC	+ $a_y = 0.228 \pm 0.030$
-0.193 ± 0.010	50919	MAST	69	HBC	- $a_y = 0.244 \pm 0.013$
-0.218 ± 0.016	9994	⁵ BUTLER	68	HBC	+ $a_y = 0.277 \pm 0.020$
-0.190 ± 0.023	5778	^{5,6} MOSCOSO	68	HBC	- $a_y = 0.242 \pm 0.029$
-0.22 ± 0.024	5428	^{5,6} ZINCHENKO	67	HBC	+ $a_y = 0.28 \pm 0.03$
-0.220 ± 0.035	1347	⁷ FERRO-LUZZI	61	HBC	- $a_y = 0.28 \pm 0.045$

¹ Final state strong interaction and radiative corrections not included in the fit.

² Quadratic dependence is required by K_L^0 experiments.

³ HOFFMASTER 72 includes GRAUMAN 70 data.

⁴ Emulsion data added — all events included by HOFFMASTER 72.

⁵ Experiments with large errors not included in average.

⁶ Also includes DBC events.

⁷ No radiative corrections included.

QUADRATIC COEFFICIENT h FOR $K^\pm \rightarrow \pi^\pm \pi^+ \pi^-$

VALUE (units 10^{-2})	EVTS	DOCUMENT ID	TECN	CHG	
1.848 ± 0.040	471M	¹ BATLEY	07B	NA48	±
•••	We do not use the following data for averages, fits, limits, etc. •••				
-0.06 ± 1.43	225k	DEVAUX	77	SPEC	+
1.87 ± 0.62	750k	FORD	72	ASPK	+
1.25 ± 0.62	750k	FORD	72	ASPK	-
-0.9 ± 1.4	39819	HOFFMASTER	72	HLBC	+
-0.1 ± 1.2	50919	MAST	69	HBC	-

¹ Final state strong interaction and radiative corrections not included in the fit.

QUADRATIC COEFFICIENT k FOR $K^\pm \rightarrow \pi^\pm \pi^+ \pi^-$

VALUE (units 10^{-3})	EVTS	DOCUMENT ID	TECN	CHG	
-4.63 ± 0.14	471M	¹ BATLEY	07B	NA48	±
•••	We do not use the following data for averages, fits, limits, etc. •••				
-20.5 ± 3.9	225k	DEVAUX	77	SPEC	+
-7.5 ± 1.9	750k	FORD	72	ASPK	+
-8.3 ± 1.9	750k	FORD	72	ASPK	-
-10.5 ± 4.5	39819	HOFFMASTER	72	HLBC	+
-14 ± 12	50919	MAST	69	HBC	-

¹ Final state strong interaction and radiative corrections not included in the fit.

 $(g_+ - g_-) / (g_+ + g_-)$ FOR $K^\pm \rightarrow \pi^\pm \pi^+ \pi^-$

This is a CP violating asymmetry between linear coefficients g_+ for $K^+ \rightarrow \pi^+ \pi^+ \pi^-$ decay and g_- for $K^- \rightarrow \pi^- \pi^+ \pi^-$ decay.

VALUE (units 10^{-4})	EVTS	DOCUMENT ID	TECN
-1.5 ± 1.5 ± 1.6	3.1G	¹ BATLEY	07E NA48
•••	We do not use the following data for averages, fits, limits, etc. •••		
1.7 ± 2.1 ± 2.0	1.7G	² BATLEY	06 NA48
-70.0 ± 53	3.2M	FORD	70 ASPK

¹ BATLEY 07E includes data from BATLEY 06. Uses quadratic parametrization and value $g_+ + g_- = 2g$ from BATLEY 07B. This measurement neglects any possible charge asymmetries in higher order slope parameters h or k .

² This measurement neglects any possible charge asymmetries in higher order slope parameters h or k .

LINEAR COEFFICIENT g FOR $K^\pm \rightarrow \pi^\pm \pi^0 \pi^0$

Unless otherwise stated, all experiments include terms quadratic in $(s_3 - s_0) / m_\pi^2$. See note above on "Dalitz Plot Parameters for $K \rightarrow 3\pi$ Decays."

See BATUSOV 98 for a discussion of the discrepancy between their result and others, especially BOLOTOV 86. At this time we have no way to resolve the discrepancy so we depend on the large scale factor as a warning.

VALUE	EVTS	DOCUMENT ID	TECN	CHG	COMMENT
0.626 ± 0.007 OUR AVERAGE					
0.6259 ± 0.0043 ± 0.0093	493k	AKOPDZHAN..05B	TNF	±	
0.627 ± 0.004 ± 0.010	252k	^{1,2} AJINENKO	03B	ISTR	-
•••	We do not use the following data for averages, fits, limits, etc. •••				
0.736 ± 0.014 ± 0.012	33k	BATUSOV	98	SPEC	+
0.582 ± 0.021	43k	BOLOTOV	86	CALO	-
0.670 ± 0.054	3263	BRAUN	76B	HLBC	+
0.630 ± 0.038	5635	SHEAFF	75	HLBC	+
0.510 ± 0.060	27k	SMITH	75	WIRE	+
0.67 ± 0.06	1365	AUBERT	72	HLBC	+
0.544 ± 0.048	4048	DAVISON	69	HLBC	+

¹ Measured using in-flight decays of the 25 GeV negative secondary beam.

² They form new world averages $g_- = (0.617 \pm 0.018)$ and $g_+ = (0.684 \pm 0.033)$ which give $\Delta g_{\pi^0} = 0.051 \pm 0.028$.

QUADRATIC COEFFICIENT h FOR $K^\pm \rightarrow \pi^\pm \pi^0 \pi^0$

VALUE	EVTS	DOCUMENT ID	TECN	CHG	COMMENT
0.052 ± 0.008 OUR AVERAGE					
0.0551 ± 0.0044 ± 0.0086	493k	AKOPDZHAN..05B	TNF	±	
0.046 ± 0.004 ± 0.012	252k	¹ AJINENKO	03B	ISTR	-
•••	We do not use the following data for averages, fits, limits, etc. •••				
0.128 ± 0.015 ± 0.024	33k	BATUSOV	98	SPEC	+
0.037 ± 0.024	43k	BOLOTOV	86	CALO	-
0.152 ± 0.082	3263	BRAUN	76B	HLBC	+
0.041 ± 0.030	5635	SHEAFF	75	HLBC	+
0.009 ± 0.040	27k	SMITH	75	WIRE	+
-0.01 ± 0.08	1365	AUBERT	72	HLBC	+
0.026 ± 0.050	4048	DAVISON	69	HLBC	+

¹ Measured using in-flight decays of the 25 GeV negative secondary beam.

QUADRATIC COEFFICIENT k FOR $K^\pm \rightarrow \pi^\pm \pi^0 \pi^0$

VALUE	EVTS	DOCUMENT ID	TECN	CHG	
0.0054 ± 0.0035 OUR AVERAGE					
0.0082 ± 0.0011 ± 0.0014	493k	AKOPDZHAN..05B	TNF	±	
0.001 ± 0.001 ± 0.002	252k	¹ AJINENKO	03B	ISTR	-
•••	We do not use the following data for averages, fits, limits, etc. •••				
0.0197 ± 0.0045 ± 0.0029	33k	BATUSOV	98	SPEC	+

¹ Measured using in-flight decays of the 25 GeV negative secondary beam.

 $(g_+ - g_-) / (g_+ + g_-)$ FOR $K^\pm \rightarrow \pi^\pm \pi^0 \pi^0$

A nonzero value for this quantity indicates CP violation.

VALUE (units 10^{-4})	EVTS	DOCUMENT ID	TECN
1.8 ± 1.8 OUR AVERAGE			
1.8 ± 1.7 ± 0.6	91.3M	¹ BATLEY	07E NA48
2 ± 18 ± 5	619k	² AKOPDZHAN..05	TNF
•••	We do not use the following data for averages, fits, limits, etc. •••		
1.8 ± 2.2 ± 1.3	47M	³ BATLEY	06A NA48

¹ BATLEY 07E includes data from BATLEY 06A. Uses quadratic parametrization and PDG 06 value $g = 0.626 \pm 0.007$ to obtain $g_+ - g_- = (2.2 \pm 2.1 \pm 0.7) \times 10^{-4}$. Neglects any possible charge asymmetries in higher order slope parameters h or k .

² Asymmetry obtained assuming that $g_+ + g_- = 2 \times 0.652$ (PDG 02) and that asymmetries in h and k are zero.

³ Linear and quadratic slopes from PDG 04 are used. Any possible charge asymmetries in higher order slope parameters h or k are neglected.

ALTERNATIVE PARAMETRIZATIONS OF $K^\pm \rightarrow \pi^\pm \pi^0 \pi^0$ DALITZ PLOT

The following functional form for the matrix element suggested by $\pi\pi$ rescattering in $K^+ \rightarrow \pi^+ \pi^+ \pi^0 \rightarrow \pi^+ \pi^0 \pi^0$ is used for this fit (CABIBBO 04A, CABIBBO 05): Matrix element = $M_0 + M_1$ where $M_0 = 1 + (1/2)g_0 u + (1/2)h' u^2 + (1/2)k_0 v^2$ with $u = (s_3 - s_0) / (m_{\pi^+})^2$, $v = (s_2 - s_1) / (m_{\pi^+})^2$ and where M_1 takes into account the non-analytic piece due to $\pi\pi$ rescattering amplitudes a_0 and a_2 ; The parameters g_0 and h' are related to the parameters g and h of the matrix element squared given in the previous section by the approximations $g_0 \sim g^{PDG}$ and $h' \sim h^{PDG} - (g/2)^2$ and $k_0 \sim k^{PDG}$.

In addition, we also consider the effective field theory framework of COLANGELO 06A and BISSEGGER 09 to extract g_{BB} and h'_{BB} .

LINEAR COEFFICIENT g_0 FOR $K^\pm \rightarrow \pi^\pm \pi^0 \pi^0$

VALUE	EVTS	DOCUMENT ID	TECN	CHG	
0.6525 ± 0.0009 ± 0.0033	60M	¹ BATLEY	09A	NA48	±
•••	We do not use the following data for averages, fits, limits, etc. •••				
0.645 ± 0.004 ± 0.009	23M	² BATLEY	06B	NA48	±

¹ This fit is obtained with the CABIBBO 05 matrix element in the $2\pi^0$ invariant mass squared range $0.074094 < m_{2\pi^0}^2 < 0.104244 \text{ GeV}^2$. Electromagnetic corrections and CHPT constraints for $\pi\pi$ phase shifts (a_0 and a_2) have been used. Also measured ($a_0 - a_2$) $m_{\pi^+} = 0.2646 \pm 0.0021 \pm 0.0023$, where k_0 was kept fixed in the fit at -0.0099 .

² Superseded by BATLEY 09A. This fit is obtained with the CABIBBO 05 matrix element in the $2\pi^0$ invariant mass squared range $0.074 \text{ GeV}^2 < m_{2\pi^0}^2 < 0.097 \text{ GeV}^2$, assuming $k = 0$ (no term proportional to $(s_2 - s_1)^2$) and excluding the kinematic region around the cusp ($m_{2\pi^0}^2 = (2m_{\pi^+})^2 \pm 0.000525 \text{ GeV}^2$). Also $\pi\pi$ phase shifts a_0 and a_2 are measured: ($a_0 - a_2$) $m_{\pi^+} = 0.268 \pm 0.010 \pm 0.004 \pm 0.013$ (external) and $a_2 m_{\pi^+} = -0.041 \pm 0.022 \pm 0.014$.

QUADRATIC COEFFICIENT h' FOR $K^\pm \rightarrow \pi^\pm \pi^0 \pi^0$

VALUE	EVTS	DOCUMENT ID	TECN	CHG
$-0.0433 \pm 0.0008 \pm 0.0026$	60M	¹ BATLEY	09A NA48	\pm

••• We do not use the following data for averages, fits, limits, etc. •••

$-0.047 \pm 0.012 \pm 0.011$	23M	² BATLEY	06B NA48	\pm
------------------------------	-----	---------------------	----------	-------

¹This fit is obtained with the CABIBBO 05 matrix element in the $2\pi^0$ invariant mass squared range $0.074094 < m_{2\pi^0}^2 < 0.104244 \text{ GeV}^2$. Electromagnetic corrections and CHPT constraints for $\pi\pi$ phase shifts (a_0 and a_2) have been used. Also measured $(a_0 - a_2) m_{\pi^+} = 0.2646 \pm 0.0021 \pm 0.0023$, where k_0 was kept fixed in the fit at -0.0099 .

²Superseded by BATLEY 09A. This fit is obtained with the CABIBBO 05 matrix element in the $2\pi^0$ invariant mass squared range $0.074 \text{ GeV}^2 < m_{2\pi^0}^2 < 0.097 \text{ GeV}^2$, assuming $k = 0$ (no term proportional to $(s_2 - s_1)^2$) and excluding the kinematic region around the cusp ($m_{2\pi^0}^2 = (2m_{\pi^+})^2 \pm 0.000525 \text{ GeV}^2$). Also $\pi\pi$ phase shifts a_0 and a_2 are measured: $(a_0 - a_2) m_{\pi^+} = 0.268 \pm 0.010 \pm 0.004 \pm 0.013(\text{external})$ and $a_2 m_{\pi^+} = -0.041 \pm 0.022 \pm 0.014$.

QUADRATIC COEFFICIENT k_0 FOR $K^\pm \rightarrow \pi^\pm \pi^0 \pi^0$

VALUE	EVTS	DOCUMENT ID	TECN	CHG
$0.0095 \pm 0.00017 \pm 0.00048$	60M	¹ BATLEY	09A NA48	\pm

¹Assumed $a_2 m_{\pi^+} = -0.0044$ in the fit.

LINEAR COEFFICIENT g_{BB} FOR $K^\pm \rightarrow \pi^\pm \pi^0 \pi^0$

VALUE	EVTS	DOCUMENT ID	TECN	CHG
$0.6219 \pm 0.0009 \pm 0.0033$	60M	¹ BATLEY	09A NA48	\pm

¹This fit is obtained using parametrizations of COLANGELO 06A and BISSEGGER 09 in the $2\pi^0$ invariant mass squared range $0.074094 < m_{2\pi^0}^2 < 0.104244 \text{ GeV}^2$. Electromagnetic corrections and CHPT constraints for $\pi\pi$ phase shifts (a_0 and a_2) have been used. Also measured $(a_0 - a_2) m_{\pi^+} = 0.2633 \pm 0.0024 \pm 0.0024$, where k_0 was kept fixed in the fit at 0.0085.

QUADRATIC COEFFICIENT h'_{BB} FOR $K^\pm \rightarrow \pi^\pm \pi^0 \pi^0$

VALUE	EVTS	DOCUMENT ID	TECN	CHG
$-0.0520 \pm 0.0009 \pm 0.0026$	60M	¹ BATLEY	09A NA48	\pm

¹This fit is obtained using parametrizations of COLANGELO 06A and BISSEGGER 09 in the $2\pi^0$ invariant mass squared range $0.074094 < m_{2\pi^0}^2 < 0.104244 \text{ GeV}^2$. Electromagnetic corrections and CHPT constraints for $\pi\pi$ phase shifts (a_0 and a_2) have been used. Also measured $(a_0 - a_2) m_{\pi^+} = 0.2633 \pm 0.0024 \pm 0.0024$, where k_0 was kept fixed in the fit at 0.0085.

 $K_{\ell 3}^\pm$ AND $K_{\ell 3}^0$ FORM FACTORS

Updated September 2013 by T.G. Trippe (LBNL) and C.-J. Lin (LBNL).

Assuming that only the vector current contributes to $K \rightarrow \pi \ell \nu$ decays, we write the matrix element as

$$M \propto f_+(t) [(P_K + P_\pi)_\mu \bar{\ell} \gamma_\mu (1 + \gamma_5) \nu] + f_-(t) [m_\ell \bar{\ell} (1 + \gamma_5) \nu], \quad (1)$$

where P_K and P_π are the four-momenta of the K and π mesons, m_ℓ is the lepton mass, and f_+ and f_- are dimensionless form factors which can depend only on $t = (P_K - P_\pi)^2$, the square of the four-momentum transfer to the leptons. If time-reversal invariance holds, f_+ and f_- are relatively real. $K_{\mu 3}$ experiments, discussed immediately below, measure f_+ and f_- , while $K_{e 3}$ experiments, discussed further below, are sensitive only to f_+ because the small electron mass makes the f_- term negligible.

$K_{\mu 3}$ Experiments. Analyses of $K_{\mu 3}$ data frequently assume a linear dependence of f_+ and f_- on t , i.e.,

$$f_\pm(t) = f_\pm(0) [1 + \lambda_\pm(t/m_{\pi^+}^2)]. \quad (2)$$

Most $K_{\mu 3}$ data are adequately described by Eq. (2) for f_+ and a constant f_- (i.e., $\lambda_- = 0$).

Two commonly used equivalent parametrizations:

(1) λ_+ , $\xi(0)$ parametrization. Older analyses of $K_{\mu 3}$ data often introduce the ratio of the two form factors

$$\xi(t) = f_-(t)/f_+(t). \quad (3)$$

The $K_{\mu 3}$ decay distribution is then described by the two parameters λ_+ and $\xi(0)$ (assuming time reversal invariance and $\lambda_- = 0$).

(2) λ_+ , λ_0 parametrization. More recent $K_{\mu 3}$ analyses have parametrized in terms of the form factors f_+ and f_0 , which are associated with vector and scalar exchange, respectively, to the lepton pair. f_0 is related to f_+ and f_- by

$$f_0(t) = f_+(t) + [t/(m_K^2 - m_\pi^2)] f_-(t). \quad (4)$$

Here $f_0(0)$ must equal $f_+(0)$ unless $f_-(t)$ diverges at $t = 0$. The earlier assumption that f_+ is linear in t and f_- is constant leads to f_0 linear in t :

$$f_0(t) = f_0(0) [1 + \lambda_0(t/m_{\pi^+}^2)]. \quad (5)$$

With the assumption that $f_0(0) = f_+(0)$, the two parametrizations, $(\lambda_+, \xi(0))$ and (λ_+, λ_0) are equivalent as long as correlation information is retained. (λ_+, λ_0) correlations tend to be less strong than $(\lambda_+, \xi(0))$ correlations.

Since the 2006 edition of the *Review* [4], we no longer quote results in the $(\lambda_+, \xi(0))$ parametrization. We have removed many older low statistics results from the Listings. See the 2004 version of this note [5] for these older results, and the 1982 version [6] for additional discussion of the $K_{\mu 3}^0$ parameters, correlations, and conversion between parametrizations.

Quadratic Parametrization. More recent high-statistics experiments have included a quadratic term in the expansion of $f_+(t)$,

$$f_+(t) = f_+(0) \left[1 + \lambda'_+(t/m_{\pi^+}^2) + \frac{\lambda''_+}{2}(t/m_{\pi^+}^2)^2 \right]. \quad (6)$$

If there is a non-vanishing quadratic term, then λ_+ of Eq. (2) represents the average slope, which is then different from λ'_+ . Our convention is to include the factor $\frac{1}{2}$ in the quadratic term, and to use m_{π^+} even for $K_{e 3}^+$ and $K_{\mu 3}^+$ decays. We have converted other's parametrizations to match our conventions, as noted in the beginning of the " $K_{\ell 3}^\pm$ and $K_{\ell 3}^0$ Form Factors" sections of the Listings.

Pole Parametrization. The pole model describes the t -dependence of $f_+(t)$ and $f_0(t)$ in terms of the exchange of the lightest vector and scalar K^* mesons with masses M_v and M_s , respectively:

$$f_+(t) = f_+(0) \left[\frac{M_v^2}{M_v^2 - t} \right], \quad f_0(t) = f_0(0) \left[\frac{M_s^2}{M_s^2 - t} \right]. \quad (7)$$

Dispersive Parametrization. This approach [7,8] uses dispersive techniques and the known low-energy $K\pi$ phases to parametrize the vector and scalar form factors:

$$f_+(t) = f_+(0) \exp \left[\frac{t}{m_\pi^2} (\Lambda_+ + H(t)) \right]; \quad (8)$$

$$f_0(t) = f_+(0) \exp \left[\frac{t}{(m_K^2 - m_\pi^2)} (\ln[C] - G(t)) \right], \quad (9)$$

where Λ_+ is the slope of the vector form factor, and $\ln[C] = \ln[f_0(m_K^2 - m_\pi^2)]$ is the logarithm of the scalar form factor at

Meson Particle Listings

K^\pm

the Callan-Treiman point. The functions $H(t)$ and $G(t)$ are dispersive integrals.

K_{e3} Experiments. Analysis of K_{e3} data is simpler than that of $K_{\mu 3}$ because the second term of the matrix element assuming a pure vector current [Eq. (1) above] can be neglected. Here f_+ can be assumed to be linear in t , in which case the linear coefficient λ_+ of Eq. (2) is determined, or quadratic, in which case the linear coefficient λ'_+ and quadratic coefficient λ''_+ of Eq. (6) are determined.

If we remove the assumption of a pure vector current, then the matrix element for the decay, in addition to the terms in Eq. (1), would contain

$$+2m_K f_S \bar{\ell}(1 + \gamma_5)\nu + (2f_T/m_K)(P_K)_\lambda(P_\pi)_\mu \bar{\ell}\sigma_{\lambda\mu}(1 + \gamma_5)\nu, \quad (10)$$

where f_S is the scalar form factor, and f_T is the tensor form factor. In the case of the K_{e3} decays where the f_- term can be neglected, experiments have yielded limits on $|f_S/f_+|$ and $|f_T/f_+|$.

Fits for K_{e3} Form Factors. For K_{e3} data, we determine best values for the three parametrizations: linear (λ_+), quadratic (λ'_+ , λ''_+) and pole (M_v). For $K_{\mu 3}$ data, we determine best values for the three parametrizations: linear (λ_+ , λ_0), quadratic (λ'_+ , λ''_+ , λ_0) and pole (M_v , M_s). We then assume $\mu - e$ universality so that we can combine K_{e3} and $K_{\mu 3}$ data, and again determine best values for the three parametrizations: linear (λ_+ , λ_0), quadratic (λ'_+ , λ''_+ , λ_0), and pole (M_v , M_s). When there is more than one parameter, fits are done including input correlations. Simple averages suffice in the two K_{e3} cases where there is only one parameter: linear (λ_+) and pole (M_v).

Both KTeV and KLOE see an improvement in the quality of their fits relative to linear fits when a quadratic term is introduced, as well as when the pole parametrization is used. The quadratic parametrization has the disadvantage that the quadratic parameter λ''_+ is highly correlated with the linear parameter λ'_+ , in the neighborhood of 95%, and that neither parameter is very well determined. The pole fit has the same number of parameters as the linear fit, but yields slightly better fit probabilities, so that it would be advisable for all experiments to include the pole parametrization as one of their choices [9].

The “Kaon Particle Listings” show the results with and without assuming $\mu - e$ universality. The “Meson Summary Tables” show all of the results assuming $\mu - e$ universality, but most results not assuming $\mu - e$ universality are given only in the Listings.

References

1. L.M. Chounet, J.M. Gaillard, and M.K. Gaillard, Phys. Reports **4C**, 199 (1972).
2. H.W. Fearing, E. Fischbach, and J. Smith, Phys. Rev. **D2**, 542 (1970).
3. N. Cabibbo and A. Maksymowicz, Phys. Lett. **9**, 352 (1964).
4. W.-M. Yao *et al.*, Particle Data Group, J. Phys. **G33**, 1 (2006).

5. S. Eidelman *et al.*, Particle Data Group, Phys. Lett. **B592**, 1 (2004).
6. M. Roos *et al.*, Particle Data Group, Phys. Lett. **111B**, 73 (1982).
7. V. Bernard *et al.*, Phys. Lett. **B638**, 48 (2006).
8. A. Lai *et al.*, Phys. Lett. **B647**, 341 (2007), and references therein.
9. We thank P. Franzini (Rome U. and Frascati) for useful discussions on this point.

K_{e3}^\pm FORM FACTORS

In the form factor comments, the following symbols are used.

f_+ and f_- are form factors for the vector matrix element.

f_S and f_T refer to the scalar and tensor term.

$f_0 = f_+ + f_- t/(m_{K^+}^2 - m_{\pi^0}^2)$.

$t =$ momentum transfer to the π .

λ_+ and λ_0 are the linear expansion coefficients of f_+ and f_0 :

$f_+(t) = f_+(0) (1 + \lambda_+ t/m_{\pi^+}^2)$

For quadratic expansion

$f_+(t) = f_+(0) (1 + \lambda'_+ t/m_{\pi^+}^2 + \frac{\lambda''_+}{2} t^2/m_{\pi^+}^4)$

as used by KTeV. If there is a non-vanishing quadratic term, then λ_+ represents an average slope, which is then different from λ'_+ .

NA48/2 and OKA quadratic expansion coefficients are converted with $\lambda'_+{}^{PDG} = \lambda'_+{}^{NA48/2}$ and $\lambda''_+{}^{PDG} = 2 \lambda''_+{}^{NA48/2}$

$\lambda'_+{}^{PDG} = (\frac{m_{\pi^+}}{m_{\pi^0}})^2 \lambda'_+{}^{OKA}$ and

$\lambda''_+{}^{PDG} = 2 (\frac{m_{\pi^+}}{m_{\pi^0}})^4 \lambda''_+{}^{OKA}$

OKA linear expansion coefficients are converted with $\lambda_+{}^{PDG} = (\frac{m_{\pi^+}}{m_{\pi^0}})^2 \lambda_+{}^{OKA}$ and $\lambda_0{}^{PDG} = (\frac{m_{\pi^+}}{m_{\pi^0}})^2 \lambda_0{}^{OKA}$

The pole parametrization is

$f_+(t) = f_+(0) (\frac{M_V^2}{M_V^2 - t})$

$f_0(t) = f_0(0) (\frac{M_S^2}{M_S^2 - t})$

where M_V and M_S are the vector and scalar pole masses.

The following abbreviations are used:

DP = Dalitz plot analysis.

PI = π spectrum analysis.

MU = μ spectrum analysis.

POL = μ polarization analysis.

BR = $K_{\mu 3}^\pm/K_{e3}^\pm$ branching ratio analysis.

E = positron or electron spectrum analysis.

RC = radiative corrections.

For previous λ'_+ and λ''_+ parametrizations used by NA48 (e.g. LAI 07A) and ISTRA (e.g. YUSHCHENKO 04B) see PDG 18.

λ_+ (LINEAR ENERGY DEPENDENCE OF f_+ IN K_{e3}^\pm DECAY)

These results are for a linear expansion only. See the next section for fits including a quadratic term. For radiative correction of the K_{e3}^\pm Dalitz plot, see GINSBERG 67, BECHERRAWY 70, CIRIGLIANO 02, CIRIGLIANO 04, and ANDRE 07. Results labeled OUR FIT are discussed in the review “ K_{e3}^\pm and $K_{\mu 3}^0$ Form Factors” above. For earlier, lower statistics results, see the 2004 edition of this review, Physics Letters **B592** 1 (2004).

VALUE (units 10^{-2})	EVTs	DOCUMENT ID	TECN	CHG	COMMENT
2.959 ± 0.025 OUR FIT	Assuming $\mu - e$ universality				
2.956 ± 0.025 OUR AVERAGE					
2.95 ± 0.022 ± 0.018	5.25M	YUSHCHENKO 18	OKA	+	
3.044 ± 0.083 ± 0.074	1.1M	AKOPDZANOV 09	TNF	±	
2.966 ± 0.050 ± 0.034	919k	¹ YUSHCHENKO 04B	ISTR	-	DP
2.78 ± 0.26 ± 0.30	41k	SHIMIZU	00	SPEC	+
2.84 ± 0.27 ± 0.20	32k	² AKIMENKO 91	SPEC		PI, no RC
2.9 ± 0.4	62k	³ BOLOTOV 88	SPEC		PI, no RC
3.06 ± 0.09 ± 0.06	550k	^{1,4} AJINENKO 03c	ISTR	-	DP
2.93 ± 0.15 ± 0.2	130k	⁴ AJINENKO 02	SPEC		DP

• • • We do not use the following data for averages, fits, limits, etc. • • •

¹ Rescaled to agree with our conventions as noted above.

² AKIMENKO 91 state that radiative corrections would raise λ_+ by 0.0013.

³ BOLOTOV 88 state radiative corrections of GINSBERG 67 would raise λ_+ by 0.002.

⁴ Superseded by YUSHCHENKO 04B.

λ_+ (LINEAR ENERGY DEPENDENCE OF f_+ IN K_{e3}^\pm DECAY)

Results labeled OUR FIT are discussed in the review " K_{e3}^\pm and $K_{\mu 3}^0$ Form Factors" above. For earlier, lower statistics results, see the 2004 edition of this review, Physics Letters **B592** 1 (2004).

VALUE (units 10^{-2})	EVTS	DOCUMENT ID	TECN	CHG	COMMENT
2.959 ± 0.025 OUR FIT					Assuming $\mu-e$ universality
3.09 ± 0.25 OUR FIT					Error includes scale factor of 1.5. Not assuming $\mu-e$ universality
2.96 ± 0.14 ± 0.10	540k	¹ YUSHCHENKO04	ISTR	-	DP
• • •					We do not use the following data for averages, fits, limits, etc. • • •
3.21 ± 0.45	112k	² AJINENKO	03	ISTR	- DP

¹ Rescaled to agree with our conventions as noted above.
² Superseded by YUSHCHENKO 04.

λ_0 (LINEAR ENERGY DEPENDENCE OF f_0 IN K_{e3}^\pm DECAY)

Results labeled OUR FIT are discussed in the review " K_{e3}^\pm and $K_{\mu 3}^0$ Form Factors" above. For earlier, lower statistics results, see the 2004 edition of this review, Physics Letters **B592** 1 (2004).

VALUE (units 10^{-2})	$d\lambda_0/d\lambda_+$	EVTS	DOCUMENT ID	TECN	CHG	COMMENT
1.76 ± 0.25 OUR FIT						Error includes scale factor of 2.7. Assuming $\mu-e$ universality
1.73 ± 0.27 OUR FIT						Error includes scale factor of 2.6. Not assuming $\mu-e$ universality
1.420 ± 0.114 ± 0.107		2.3M	¹ BATLEY	18	NA48	±
1.96 ± 0.12 ± 0.06	-0.348	540k	² YUSHCHENKO04	ISTR	-	DP
• • •						We do not use the following data for averages, fits, limits, etc. • • •
2.09 ± 0.45	-0.46	112k	³ AJINENKO	03	ISTR	- DP
1.9 ± 0.64		24k	⁴ HORIE	01	SPEC	+ BR
1.9 ± 1.0	+0.03	55k	⁵ HEINTZE	77	SPEC	+ BR

¹ Data collected in 2004 by NA48/2. Obtained from a fit with a quadratic vector form factor. Correlation coefficient with linear slope is 0.511, with quadratic slope is -0.513. $\chi^2/NDF = 409.9/381$. BATLEY 18 also performed a combined K_{e3}^\pm and $K_{\mu 3}^\pm$ fit assuming $\mu-e$ universality and obtained $(14.47 \pm 0.63 \pm 1.17) \times 10^{-3}$.
² Rescaled to agree with our conventions as noted above.
³ Superseded by YUSHCHENKO 04.
⁴ HORIE 01 assumes $\mu-e$ universality in K_{e3}^\pm decay and uses SHIMIZU 00 value $\lambda = 0.0278 \pm 0.0040$ from K_{e3}^\pm decay.
⁵ HEINTZE 77 uses $\lambda_+ = 0.029 \pm 0.003$. $d\lambda_0/d\lambda_+$ estimated by us.

λ'_+ (LINEAR K_{e3}^\pm FORM FACTOR FROM QUADRATIC FIT)

VALUE (units 10^{-2})	EVTS	DOCUMENT ID	TECN	CHG	COMMENT
2.59 ± 0.04 OUR AVERAGE					
2.426 ± 0.078 ± 0.130	4.4M	¹ BATLEY	18	NA48	±
2.611 ± 0.035 ± 0.028	5.25M	YUSHCHENKO18	OKA	+	
2.485 ± 0.163 ± 0.034	919k	^{2,3} YUSHCHENKO04B	ISTR	-	DP
• • •					We do not use the following data for averages, fits, limits, etc. • • •
3.07 ± 0.21	550k	^{2,4} AJINENKO	03c	ISTR	- DP

¹ Data collected in 2004 by NA48/2. Correlation coefficient with quadratic slope is -0.929. $\chi^2/NDF = 569.1/687$. BATLEY 18 also performed a combined K_{e3}^\pm and $K_{\mu 3}^\pm$ fit assuming $\mu-e$ universality and obtained $(24.24 \pm 0.75 \pm 1.3) \times 10^{-3}$.
² Rescaled to agree with our conventions as noted above.
³ YUSHCHENKO 04B λ'_+ and λ''_+ are strongly correlated with coefficient $\rho(\lambda'_+, \lambda''_+) = -0.95$.
⁴ Superseded by YUSHCHENKO 04B.

λ''_+ (QUADRATIC K_{e3}^\pm FORM FACTOR)

VALUE (units 10^{-2})	EVTS	DOCUMENT ID	TECN	CHG	COMMENT
0.186 ± 0.021 OUR AVERAGE					
0.164 ± 0.030 ± 0.039	4.4M	¹ BATLEY	18	NA48	±
0.191 ± 0.019 ± 0.014	5.25M	YUSHCHENKO18	OKA	+	
0.192 ± 0.062 ± 0.071	919k	^{2,3} YUSHCHENKO04B	ISTR	-	DP
• • •					We do not use the following data for averages, fits, limits, etc. • • •
-0.5 ± 0.7 ± 1.5	550k	^{2,4} AJINENKO	03c	ISTR	- DP

¹ Data collected in 2004 by NA48/2. Correlation coefficient with quadratic slope is -0.929. $\chi^2/NDF = 569.1/687$. BATLEY 18 also performed a combined K_{e3}^\pm and $K_{\mu 3}^\pm$ fit assuming $\mu-e$ universality and obtained $(1.67 \pm 0.29 \pm 0.41) \times 10^{-3}$.
² Rescaled to agree with our conventions as noted above.
³ YUSHCHENKO 04B λ'_+ and λ''_+ are strongly correlated with coefficient $\rho(\lambda'_+, \lambda''_+) = -0.95$.
⁴ Superseded by YUSHCHENKO 04B.

λ'_+ (LINEAR $K_{\mu 3}^\pm$ FORM FACTOR FROM QUADRATIC FIT)

VALUE (units 10^{-3})	EVTS	DOCUMENT ID	TECN	CHG	COMMENT
24.27 ± 2.88 ± 2.89	2.3M	¹ BATLEY	18	NA48	±

¹ Data collected in 2004 by NA48/2. Correlation coefficient with quadratic slope is -0.974, with scalar slope is 0.511. $\chi^2/NDF = 409.9/381$. BATLEY 18 also performed a combined K_{e3}^\pm and $K_{\mu 3}^\pm$ fit assuming $\mu-e$ universality and obtained $(24.24 \pm 0.75 \pm 1.3) \times 10^{-3}$.

λ''_+ (QUADRATIC $K_{\mu 3}^\pm$ FORM FACTOR)

VALUE (units 10^{-3})	EVTS	DOCUMENT ID	TECN	CHG	
1.83 ± 1.05 ± 1.09	2.3M	¹ BATLEY	18	NA48	±

¹ Data collected in 2004 by NA48/2. Correlation coefficient with linear slope is -0.974, with scalar slope is 0.513. $\chi^2/NDF = 409.9/381$. BATLEY 18 also performed a combined K_{e3}^\pm and $K_{\mu 3}^\pm$ fit assuming $\mu-e$ universality and obtained $(1.67 \pm 0.29 \pm 0.41) \times 10^{-3}$.

M_V (VECTOR POLE MASS FOR K_{e3}^\pm DECAY)

See the review on K_{13}^\pm and K_{13}^0 Form Factors for details.

VALUE (MeV)	EVTS	DOCUMENT ID	TECN	CHG	
890.3 ± 2.8 OUR AVERAGE					
885.2 ± 3.3 ± 7.2	4.4M	¹ BATLEY	18	NA48	±
891 ± 3	5.25M	² YUSHCHENKO18	OKA	+	

¹ Data collected in 2004 by NA48/2. $\chi^2/NDF = 568.9/688$. BATLEY 18 also performed a combined K_{e3}^\pm and $K_{\mu 3}^\pm$ fit assuming $\mu-e$ universality and obtained $884.4 \pm 3.1 \pm 6.7$ MeV.
² Assumed no scalar or tensor contributions to the form factor.

M_V (VECTOR POLE MASS FOR $K_{\mu 3}^\pm$ DECAY)

VALUE (MeV)	EVTS	DOCUMENT ID	TECN	CHG	
878.4 ± 8.8 ± 8.3	2.3M	¹ BATLEY	18	NA48	±

¹ Data collected in 2004 by NA48/2. $\chi^2/NDF = 409.9/382$. BATLEY 18 also performed a combined K_{e3}^\pm and $K_{\mu 3}^\pm$ fit assuming $\mu-e$ universality and obtained $884.4 \pm 3.1 \pm 6.7$ MeV.

M_S (SCALAR POLE MASS FOR K_{e3}^\pm DECAY)

VALUE (MeV)	EVTS	DOCUMENT ID	TECN	CHG	
1214.8 ± 23.5 ± 49.2	2.3M	¹ BATLEY	18	NA48	±

¹ Data collected in 2004 by NA48/2. $\chi^2/NDF = 409.9/382$. BATLEY 18 also performed a combined K_{e3}^\pm and $K_{\mu 3}^\pm$ fit assuming $\mu-e$ universality and obtained $1208.3 \pm 21.2 \pm 47.5$ MeV.

A_+ (DISPERSIVE VECTOR FORM FACTOR IN K_{e3}^\pm DECAY)

See the review on K_{13}^\pm and K_{13}^0 Form Factors for details.

VALUE (units 10^{-2})	EVTS	DOCUMENT ID	TECN	CHG	
2.460 ± 0.017 OUR AVERAGE					
2.494 ± 0.021 ± 0.064	4.4M	¹ BATLEY	18	NA48	±
2.458 ± 0.018	5.25M	² YUSHCHENKO18	OKA	+	

¹ Data collected in 2004 by NA48/2. $\chi^2/NDF = 569.0/688$. BATLEY 18 also performed a combined K_{e3}^\pm and $K_{\mu 3}^\pm$ fit assuming $\mu-e$ universality and obtained $(24.99 \pm 0.20 \pm 0.62) \times 10^{-3}$.
² Assumed no scalar or tensor contributions to the form factor.

A_+ (DISPERSIVE VECTOR FORM FACTOR IN $K_{\mu 3}^\pm$ DECAY)

VALUE (units 10^{-3})	EVTS	DOCUMENT ID	TECN	CHG	
25.36 ± 0.58 ± 0.72	2.3M	¹ BATLEY	18	NA48	±

¹ Data collected in 2004 by NA48/2. $\chi^2/NDF = 410.3/382$. BATLEY 18 also performed a combined K_{e3}^\pm and $K_{\mu 3}^\pm$ fit assuming $\mu-e$ universality and obtained $(24.99 \pm 0.20 \pm 0.62) \times 10^{-3}$.

$\ln(C)$ (DISPERSIVE SCALAR FORM FACTOR IN K_{e3}^\pm decays)

VALUE (units 10^{-3})	EVTS	DOCUMENT ID	TECN	CHG	
182.17 ± 6.31 ± 14.45	2.3M	¹ BATLEY	18	NA48	±

¹ Data collected in 2004 by NA48/2. Combined fit with dispersive vector form factor $A_+ = 25.36 \pm 0.58 \pm 0.72$. Correlation coefficient is 0.104. $\chi^2/NDF = 410.3/382$. BATLEY 18 also performed a combined K_{e3}^\pm and $K_{\mu 3}^\pm$ fit assuming $\mu-e$ universality and obtained $(183.65 \pm 5.92 \pm 14.25) \times 10^{-3}$.

$|f_S/f_+|$ FOR K_{e3}^\pm DECAY

Ratio of scalar to f_+ couplings.

VALUE (units 10^{-2})	CL%	EVTS	DOCUMENT ID	TECN	CHG	COMMENT
-0.08 ± 0.34 ± 0.40 OUR AVERAGE						
0.01 ± 0.38 ± 0.46		5.25M	YUSHCHENKO18	OKA	+	$\lambda'_+, \lambda''_+, f_S$ fit
-0.37 ± 0.66 ± 0.41		919k	YUSHCHENKO04B	ISTR	-	$\lambda'_+, \lambda''_+, f_S$ fit
0.2 ± 2.6 ± 1.4		41k	SHIMIZU	00	SPEC	λ_+, f_S, f_T fit
• • •						We do not use the following data for averages, fits, limits, etc. • • •
0.2 ± 2.0 ± 2.2 ± 0.3		550k	¹ AJINENKO	03c	ISTR	- λ_+, f_S, f_T fit
-1.9 ± 2.5 ± 1.6		130k	¹ AJINENKO	02	SPEC	λ_+, f_S fit
7.0 ± 1.6 ± 1.6		32k	AKIMENKO	91	SPEC	$\lambda_+, f_S, f_T, \phi$ fit
0 ± 10		2827	² BRAUN	75	HLBC	+
< 13		4017	CHIANG	72	OSPK	+
14 ± 3 ± 4		2707	² STEINER	71	HLBC	+
< 23		90	BOTTERILL	68c	ASPK	

Meson Particle Listings

 K^\pm

< 18	90	BELLOTTI	67B	HLBC
< 30	95	KALMUS	67	HLBC +

- ¹ Superseded by YUSHCHENKO 04b.
² Statistical errors only.

 $|f_T/f_+|$ FOR K_{e3}^\pm DECAYRatio of tensor to f_+ couplings.

VALUE (units 10^{-2})	EVTS	DOCUMENT ID	TECN	CHG	COMMENT
-1.2 ± 1.3					OUR AVERAGE
-1.24 ± 1.6	5.25M	YUSHCHENKO18	OKA	+	$\lambda'_+, \lambda''_+, f_T$ fit
$-1.2 \pm 2.1 \pm 1.1$	919k	YUSHCHENKO04B	ISTR	-	$\lambda'_+, \lambda''_+, f_T$ fit
$1 \pm 14 \pm 9$	41k	SHIMIZU	00	SPEC	λ_+, f_S, f_T fit
••• We do not use the following data for averages, fits, limits, etc. •••					
2.1 ± 6.4	550k	1 AJJENKO	03c	ISTR	λ_+, f_S, f_T fit
-4.5 ± 6.0	130k	1 AJJENKO	02	SPEC	λ_+, f_T fit
53 ± 9	32k	AKIMENKO	91	SPEC	$\lambda_+, f_S, f_T, \phi$ fit

- ¹ Superseded by YUSHCHENKO 04b.

 f_S/f_+ FOR $K_{\mu 3}^\pm$ DECAYRatio of scalar to f_+ couplings.

VALUE (units 10^{-2})	EVTS	DOCUMENT ID	TECN	CHG	COMMENT
$0.17 \pm 0.14 \pm 0.54$	540k	1 YUSHCHENKO04	ISTR	-	DP
••• We do not use the following data for averages, fits, limits, etc. •••					
$0.4 \pm 0.5 \pm 0.5$	112k	2 AJJENKO	03	ISTR	DP

- ¹ The second error is the theoretical error from the uncertainty in the chiral perturbation theory prediction for λ_0 , ± 0.0053 , combined in quadrature with the systematic error ± 0.0009 .

- ² The second error is the theoretical error from the uncertainty in the chiral perturbation theory prediction for λ_0 . Superseded by YUSHCHENKO 04.

 f_T/f_+ FOR $K_{\mu 3}^\pm$ DECAYRatio of tensor to f_+ couplings.

VALUE (units 10^{-2})	EVTS	DOCUMENT ID	TECN	CHG	COMMENT
$-0.07 \pm 0.71 \pm 0.20$	540k	YUSHCHENKO04	ISTR	-	DP
••• We do not use the following data for averages, fits, limits, etc. •••					
$-2.1 \pm 2.8 \pm 1.4$	112k	1 AJJENKO	03	ISTR	DP
2 ± 12	1585	BRAUN	75	HLBC	

- ¹ The second error is the theoretical error from the uncertainty in the chiral perturbation theory prediction for λ_0 . Superseded by YUSHCHENKO 04.

 K_{24}^\pm FORM FACTORS

Based on the parametrizations of AMOROS 99, the K_{24}^\pm form factors can be expressed as

$$F_S = f_S + f'_S q^2 + f''_S q^4 + f'_e S_e / 4m_\pi^2$$

$$F_P = f_P$$

$$G_P = g_P + g'_P q^2$$

$$H_P = h_P$$

where $q^2 = (S_\pi / 4m_\pi^2) - 1$, S_π is the invariant mass squared of the dipion, and S_e is the invariant mass squared of the dilepton.

 f_S FOR $K^\pm \rightarrow \pi^+ \pi^- e^\pm \nu$ DECAY

VALUE	EVTS	DOCUMENT ID	TECN	CHG
5.712 ± 0.032				
OUR AVERAGE				
$5.705 \pm 0.003 \pm 0.035$	1.1M	1 BATLEY	12	NA48 ±
$5.75 \pm 0.02 \pm 0.08$	400k	2 PISLAK	03	B865 +

- ¹ BATLEY 12 uses data collected in 2003–2004. The result is obtained from a measurement of $\Gamma(\pi^+ \pi^- e \nu) / \Gamma(\pi^+ \pi^- \pi^+) / \Gamma(\pi^+ \pi^- \pi^+) / \Gamma = (5.59 \pm 0.04) \times 10^{-2}$.

- ² Radiative corrections included. Using Roy equations and not including isospin breaking, PISLAK 03 obtains the following $\pi\pi$ scattering lengths $a_0^0 = 0.228 \pm 0.012 \pm 0.004 - 0.012$ (theor.) and $a_0^2 = -0.0365 \pm 0.0023 \pm 0.0008 - 0.0026$ (theor.).

 f'_S/f_S FOR $K^\pm \rightarrow \pi^+ \pi^- e^\pm \nu$ DECAY

VALUE (units 10^{-2})	EVTS	DOCUMENT ID	TECN	CHG
$15.2 \pm 0.7 \pm 0.5$	1.13M	1 BATLEY	10c	NA48 ±
••• We do not use the following data for averages, fits, limits, etc. •••				
$17.2 \pm 0.9 \pm 0.6$	670k	2 BATLEY	08A	NA48 ±

- ¹ Radiative corrections included. Using Roy equations and including isospin breaking, BATLEY 10c obtains the following scattering lengths $a_0^0 = 0.2220 \pm 0.0128 \pm 0.0050 \pm 0.0037$ (theor.), $a_0^2 = -0.0432 \pm 0.0086 \pm 0.0034 \pm 0.0028$ (theor.). The correlation with $f''_S/f_S = -0.954$ and with $f'_e/f_S = 0.080$. Supersedes BATLEY 08A.

- ² Radiative corrections included. Using Roy equations and not including isospin breaking, BATLEY 08A obtains the following $\pi\pi$ scattering length $a_0^0 = 0.233 \pm 0.016 \pm 0.007$ $a_0^2 = -0.0471 \pm 0.011 \pm 0.004$.

 f''_S/f_S FOR $K^\pm \rightarrow \pi^+ \pi^- e^\pm \nu$ DECAY

VALUE (units 10^{-2})	EVTS	DOCUMENT ID	TECN	CHG
$-7.3 \pm 0.7 \pm 0.6$	1.13M	1 BATLEY	10c	NA48 ±
••• We do not use the following data for averages, fits, limits, etc. •••				
$-9.0 \pm 0.9 \pm 0.7$	670k	2 BATLEY	08A	NA48 ±

- ¹ Radiative corrections included. Using Roy equations and including isospin breaking, BATLEY 10c obtains the following scattering lengths $a_0^0 = 0.2220 \pm 0.0128 \pm 0.0050 \pm 0.0037$ (theor.), $a_0^2 = -0.0432 \pm 0.0086 \pm 0.0034 \pm 0.0028$ (theor.). The correlation with $f'_S/f_S = -0.954$ and with $f'_e/f_S = 0.019$. Supersedes BATLEY 08A.

- ² Radiative corrections included. Using Roy equations and not including isospin breaking, BATLEY 08A obtains the following $\pi\pi$ scattering length $a_0^0 = 0.233 \pm 0.016 \pm 0.007$ $a_0^2 = -0.0471 \pm 0.011 \pm 0.004$.

 f'_e/f_S FOR $K^\pm \rightarrow \pi^+ \pi^- e^\pm \nu$ DECAY

VALUE (units 10^{-2})	EVTS	DOCUMENT ID	TECN	CHG
$6.8 \pm 0.6 \pm 0.7$	1.13M	1 BATLEY	10c	NA48 ±
••• We do not use the following data for averages, fits, limits, etc. •••				
$8.1 \pm 0.8 \pm 0.9$	670k	2 BATLEY	08A	NA48 ±

- ¹ Radiative corrections included. Using Roy equations and including isospin breaking, BATLEY 10c obtains the following scattering lengths $a_0^0 = 0.2220 \pm 0.0128 \pm 0.0050 \pm 0.0037$ (theor.), $a_0^2 = -0.0432 \pm 0.0086 \pm 0.0034 \pm 0.0028$ (theor.). The correlation with $f'_S/f_S = 0.080$ and with $f''_S/f_S = 0.019$. Supersedes BATLEY 08A.

- ² Radiative corrections included. Using Roy equations and not including isospin breaking, BATLEY 08A obtains the following $\pi\pi$ scattering length $a_0^0 = 0.233 \pm 0.016 \pm 0.007$ $a_0^2 = -0.0471 \pm 0.011 \pm 0.004$.

 f_P/f_S FOR $K^\pm \rightarrow \pi^+ \pi^- e^\pm \nu$ DECAY

VALUE (units 10^{-2})	EVTS	DOCUMENT ID	TECN	CHG
$-4.8 \pm 0.3 \pm 0.4$	1.13M	1 BATLEY	10c	NA48 ±
••• We do not use the following data for averages, fits, limits, etc. •••				
$-4.8 \pm 0.4 \pm 0.4$	670k	2 BATLEY	08A	NA48 ±

- ¹ Radiative corrections included. Using Roy equations and including isospin breaking, BATLEY 10c obtains the following scattering lengths $a_0^0 = 0.2220 \pm 0.0128 \pm 0.0050 \pm 0.0037$ (theor.), $a_0^2 = -0.0432 \pm 0.0086 \pm 0.0034 \pm 0.0028$ (theor.). Supersedes BATLEY 08A.

- ² Radiative corrections included. Using Roy equations and not including isospin breaking, BATLEY 08A obtains the following $\pi\pi$ scattering length $a_0^0 = 0.233 \pm 0.016 \pm 0.007$ $a_0^2 = -0.0471 \pm 0.011 \pm 0.004$.

 g_P/f_S FOR $K^\pm \rightarrow \pi^+ \pi^- e^\pm \nu$ DECAY

VALUE (units 10^{-2})	EVTS	DOCUMENT ID	TECN	CHG
$86.8 \pm 1.0 \pm 1.0$	1.13M	1 BATLEY	10c	NA48 ±
••• We do not use the following data for averages, fits, limits, etc. •••				
$87.3 \pm 1.3 \pm 1.2$	670k	2 BATLEY	08A	NA48 ±
$80.9 \pm 0.9 \pm 1.2$	400k	3 PISLAK	03	B865 ±

- ¹ Radiative corrections included. Using Roy equations and including isospin breaking, BATLEY 10c obtains the following scattering lengths $a_0^0 = 0.2220 \pm 0.0128 \pm 0.0050 \pm 0.0037$ (theor.), $a_0^2 = -0.0432 \pm 0.0086 \pm 0.0034 \pm 0.0028$ (theor.). Supersedes BATLEY 08A. The correlation with $g'_P/f_S = -0.914$. Supersedes BATLEY 08A.

- ² Radiative corrections included. Using Roy equations and not including isospin breaking, BATLEY 08A obtains the following $\pi\pi$ scattering length $a_0^0 = 0.233 \pm 0.016 \pm 0.007$ $a_0^2 = -0.0471 \pm 0.011 \pm 0.004$.

- ³ Radiative corrections included. Using Roy equations PISLAK 03 obtains the following scattering lengths $a_0^0 = 0.203 \pm 0.033 \pm 0.004$, $a_0^2 = -0.055 \pm 0.023 \pm 0.003$.

 g'_P/f_S FOR $K^\pm \rightarrow \pi^+ \pi^- e^\pm \nu$ DECAY

VALUE (units 10^{-2})	EVTS	DOCUMENT ID	TECN	CHG
$8.9 \pm 1.7 \pm 1.3$	1.13M	1 BATLEY	10c	NA48 ±
••• We do not use the following data for averages, fits, limits, etc. •••				
$8.1 \pm 2.2 \pm 1.5$	670k	2 BATLEY	08A	NA48 ±
$12.0 \pm 1.9 \pm 0.7$	400k	3 PISLAK	03	B865 ±

- ¹ Radiative corrections included. Using Roy equations and including isospin breaking, BATLEY 10c obtains the following scattering lengths $a_0^0 = 0.2220 \pm 0.0128 \pm 0.0050 \pm 0.0037$ (theor.), $a_0^2 = -0.0432 \pm 0.0086 \pm 0.0034 \pm 0.0028$ (theor.). The correlation with $g_P/f_S = -0.914$. Supersedes BATLEY 08A.

- ² Radiative corrections included. Using Roy equations and not including isospin breaking, BATLEY 08A obtains the following $\pi\pi$ scattering length $a_0^0 = 0.233 \pm 0.016 \pm 0.007$ $a_0^2 = -0.0471 \pm 0.011 \pm 0.004$.

- ³ Radiative corrections included. Using Roy equations PISLAK 03 obtains the following scattering lengths $a_0^0 = 0.203 \pm 0.033 \pm 0.004$, $a_0^2 = -0.055 \pm 0.023 \pm 0.003$.

 h_P/f_S FOR $K^\pm \rightarrow \pi^+ \pi^- e^\pm \nu$ DECAY

VALUE (units 10^{-2})	EVTS	DOCUMENT ID	TECN	CHG
$-39.8 \pm 1.5 \pm 0.8$	1.13M	1 BATLEY	10c	NA48 ±

• • • We do not use the following data for averages, fits, limits, etc. • • •

-41.1 ± 1.9 ± 0.8	670k	² BATLEY	08A	NA48	±
-51.3 ± 3.3 ± 3.5	400k	³ PISLAK	03	B865	±

¹ Radiative corrections included. Using Roy equations and including isospin breaking, BATLEY 10c obtains the following scattering lengths $a_0^0 = 0.2220 \pm 0.0128 \pm 0.0050 \pm 0.0037$ (theor.), $a_0^2 = -0.0432 \pm 0.0086 \pm 0.0034 \pm 0.0028$ (theor.). Supersedes BATLEY 08A.

² Radiative corrections included. Using Roy equations and not including isospin breaking, BATLEY 08A obtains the following $\pi\pi$ scattering length $a_0^0 = 0.233 \pm 0.016 \pm 0.007$, $a_0^2 = -0.0471 \pm 0.011 \pm 0.004$.

³ Radiative corrections included. Using Roy equations PISLAK 03 obtains the following scattering lengths $a_0^0 = 0.203 \pm 0.033 \pm 0.004$, $a_0^2 = -0.055 \pm 0.023 \pm 0.003$.

DECAY FORM FACTOR FOR $K^\pm \rightarrow \pi^0 \pi^0 e^\pm \nu$
Given in BOLOTOV 86b, BARMIN 88b, and SHIMIZU 04.

$K^\pm \rightarrow \ell^\pm \nu \gamma$ FORM FACTORS

For definitions of the axial-vector F_A and vector F_V form factor, see the "Note on $\pi^\pm \rightarrow \ell^\pm \nu \gamma$ and $K^\pm \rightarrow \ell^\pm \nu \gamma$ Form Factors" in the π^\pm section. In the kaon literature, often different definitions $a_K = F_A/m_K$ and $v_K = F_V/m_K$ are used.

$F_A + F_V$, SUM OF AXIAL-VECTOR AND VECTOR FORM FACTOR FOR $K \rightarrow e\nu e\gamma$

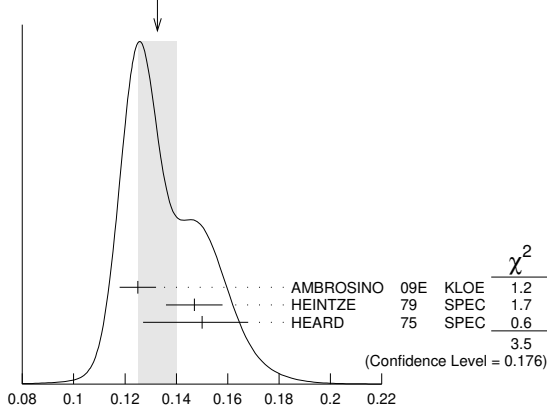
VALUE	EVTS	DOCUMENT ID	TECN	COMMENT
0.133 ± 0.008 OUR AVERAGE		Error includes scale factor of 1.3.		See the ideogram below.
0.125 ± 0.007 ± 0.001	1.4K	¹ AMBROSINO	09E	KLOE E_γ in 10–250 MeV, $p_e > 200$ MeV/c
0.147 ± 0.011	51	² HEINTZE	79	SPEC
0.150 ± 0.018 -0.023	56	³ HEARD	75	SPEC

¹ AMBROSINO 09E measures the absolute value $|F_A + F_V|$ which is parametrized as $|F_A + F_V| = F_V (1 + \lambda(1-x)) + F_A$, $x = 2E_\gamma/m_K$. ($F_A + F_V$) and λ are fit parameters. The fitted value of $\lambda = 0.38 \pm 0.20 \pm 0.02$ with a correlation of -0.93 between ($F_A + F_V$) and λ .

² HEINTZE 79 quotes absolute value of $|F_A + F_V| \sin\theta_c$. We use $\sin\theta_c = V_{us} = 0.2205$.

³ HEARD 75 quotes absolute value of $|F_A + F_V| \sin\theta_c$. We use $\sin\theta_c = V_{us} = 0.2205$.

WEIGHTED AVERAGE
0.133 ± 0.008 (Error scaled by 1.3)



$F_A + F_V$, SUM OF AXIAL-VECTOR AND VECTOR FORM FACTOR FOR $K \rightarrow e\nu e\gamma$

$F_A + F_V$, SUM OF AXIAL-VECTOR AND VECTOR FORM FACTOR FOR $K \rightarrow \mu\nu\mu\gamma$

VALUE	CL%	EVTS	DOCUMENT ID	TECN	CHG
0.165 ± 0.007 ± 0.011		2588	¹ ADLER	00B	B787 +
-1.2 to 1.1	90		DEMIDOV	90	XEBC
< 0.23	90		¹ AKIBA	85	SPEC

¹ Quotes absolute value. Sign not determined.

$F_A - F_V$, DIFFERENCE OF AXIAL-VECTOR AND VECTOR FORM FACTOR FOR $K \rightarrow e\nu e\gamma$

VALUE	CL%	DOCUMENT ID	TECN	
< 0.49		¹ HEINTZE	79	SPEC

¹ HEINTZE 79 quotes $|F_A - F_V| < \sqrt{11} |F_A + F_V|$.

$F_A - F_V$, DIFFERENCE OF AXIAL-VECTOR AND VECTOR FORM FACTOR FOR $K \rightarrow \mu\nu\mu\gamma$

VALUE	CL%	EVTS	DOCUMENT ID	TECN	CHG
-0.153 ± 0.033 OUR AVERAGE			Error includes scale factor of 1.1.		
-0.134 ± 0.021 ± 0.027	95K		KRAVTSOV	19	OKA +
-0.21 ± 0.06	22K		DUK	11	ISTR -

• • • We do not use the following data for averages, fits, limits, etc. • • •

-0.24 to 0.04	90	2588	ADLER	00B	B787 +
-2.2 to 0.6	90		DEMIDOV	90	XEBC
-2.5 to 0.3	90		AKIBA	85	SPEC

K^\pm CHARGE RADIUS

VALUE (fm)	DOCUMENT ID	COMMENT
0.560 ± 0.031 OUR AVERAGE		
0.580 ± 0.040	AMENDOLIA 86B	$Ke \rightarrow Ke$
0.530 ± 0.050	DALLY 80	$Ke \rightarrow Ke$
0.620 ± 0.037	BLATNIK 79	VMD + dispersion relations

• • • We do not use the following data for averages, fits, limits, etc. • • •

K^+ LONGITUDINAL POLARIZATION OF EMITTED μ^+

VALUE	CL%	DOCUMENT ID	TECN	CHG	COMMENT
< -0.990	90	¹ AOKI	94	SPEC	+
< -0.990	90	IMAZATO	92	SPEC	+
-0.970 ± 0.047		² YAMANAKA	86	SPEC	+
-1.0 ± 0.1		² CUTTS	69	SPRK	+
-0.96 ± 0.12		² COOMBES	57	CNTR	+

¹ AOKI 94 measures $\xi P_\mu = -0.9996 \pm 0.0030 \pm 0.0048$. The above limit is obtained by summing the statistical and systematic errors in quadrature, normalizing to the physically significant region ($|\xi P_\mu| < 1$) and assuming that $\xi=1$, its maximum value.

² Assumes $\xi=1$.

FORWARD-BACKWARD ASYMMETRY IN K^\pm DECAYS

$$A_{FB}(K^\pm_{\pi\mu\mu}) = \frac{\Gamma(\cos(\theta_{K\mu}) > 0) - \Gamma(\cos(\theta_{K\mu}) < 0)}{\Gamma(\cos(\theta_{K\mu}) > 0) + \Gamma(\cos(\theta_{K\mu}) < 0)}$$

VALUE	CL%	DOCUMENT ID	TECN	
< 2.3 × 10⁻²	90	¹ BATLEY	11A	NA48

¹ BATLEY 11A gives a corresponding value of the asymmetry $A_{FB} = (-2.4 \pm 1.8) \times 10^{-2}$.

K^\pm REFERENCES

BATLEY	19	PL B788 552	J.R. Batley et al.	(NA48/2 Collab.)
CORTINA-GIL	19A	PL B797 134794	E. Cortina Gil et al.	(NA62 Collab.)
CORTINA-GIL	19B	PL B791 156	E. Cortina Gil et al.	(NA62 Collab.)
KRAVTSOV	19	EPJ C79 635	V.I. Kravtsov et al.	(OKA Collab.)
SHAPKIN	19	EPJ C79 296	M.M. Shapkin et al.	(OKA Collab.)
BATLEY	18	JHEP 1810 150	J.R. Batley et al.	(NA48/2 Collab.)
PDG	18	PR D98 030001	M. Tanabashi et al.	(PDG Collab.)
YUSHCHENKO	18	JETPL 107 139	G.P. Yushchenko et al.	(OKA Collab.)
BATLEY	17	PL B769 67	J.R. Batley et al.	(NA48/2 Collab.)
ARTAMONOV	16	PR D94 032012	A.V. Artamonov et al.	(BNL E949 Collab.)
BABUSCI	14B	PL B738 128	D. Babusci et al.	(KLOE and KLOE-2 Collab.)
BATLEY	14	PL B730 141	J.R. Batley et al.	(CERN NA48/2 Collab.)
BATLEY	14A	JHEP 1408 159	J.R. Batley et al.	(CERN NA48/2 Collab.)
LAZZERONI	14	PL B732 65	C. Lazzeroni et al.	(CERN NA62 Collab.)
UVAROV	14	PAN 77 725	V.A. Uvarov et al.	(ISTRA+ Collab.)
LAZZERONI	13	PL B719 326	C. Lazzeroni et al.	(CERN NA62 Collab.)
BATLEY	12	PL B715 105	J.R. Batley et al.	(CERN NA48/2 Collab.)
PDG	12	PR D86 010001	J. Beringer et al.	(PDG Collab.)
BATLEY	11A	PL B697 107	J.R. Batley et al.	(CERN NA48/2 Collab.)
DUK	11	PL B695 59	V.A. Duk et al.	(ISTRA+ Collab.)
LAZZERONI	11	PL B698 105	C. Lazzeroni et al.	(CERN NA62 Collab.)
ADLER	10	PR D81 092001	S. Adler et al.	(BNL E787 Collab.)
BATLEY	10A	EPJ C68 75	J.R. Batley et al.	(CERN NA48/2 Collab.)
BATLEY	10C	EPJ C70 635	J.R. Batley et al.	(CERN NA48/2 Collab.)
PDG	10	JP G37 075021	K. Nakamura et al.	(PDG Collab.)
PISLAK	10A	PRL 105 019901E	S. Pislak et al.	(BNL E865 Collab.)
AKOPDZHANOV	09	PAN 71 2074	G.A. Akopdzhanov et al.	(IHEP Collab.)
AMBROSINO	09E	EPJ C64 627	F. Ambrosino et al.	(KLOE Collab.)
Also		EPJ C65 703 (err.)	F. Ambrosino et al.	(KLOE Collab.)
BATLEY	09	PL B677 246	J.R. Batley et al.	(CERN NA48/2 Collab.)
BATLEY	09A	EPJ C64 589	J.R. Batley et al.	(CERN NA48/2 Collab.)
BISSEGER	09	NP B806 178	M. Bissegger et al.	(KLOE Collab.)
AMBROSINO	08B	JHEP 0801 073	F. Ambrosino et al.	(KLOE Collab.)
AMBROSINO	08A	JHEP 0802 098	F. Ambrosino et al.	(KLOE Collab.)
AMBROSINO	08E	PL B666 305	F. Ambrosino et al.	(KLOE Collab.)
ARTAMONOV	08	PRL 101 191802	A.V. Artamonov et al.	(BNL E949 Collab.)
Also		PR D79 092004	A.V. Artamonov et al.	(BNL E949 Collab.)
BATLEY	08	PL B659 493	J.R. Batley et al.	(CERN NA48/2 Collab.)
BATLEY	08A	EPJ C54 411	J.R. Batley et al.	(CERN NA48/2 Collab.)
AKIMENKO	07	PAN 70 702	S.A. Akimenko et al.	(ISTRA+ Collab.)
ANDRE	07	ANP 322 2518	T. Andre	(EFI Collab.)
BATLEY	07A	EPJ C50 329	J.R. Batley et al.	(CERN NA48/2 Collab.)
Also		EPJ C52 1021 (err.)	J.R. Batley et al.	(CERN NA48/2 Collab.)
BATLEY	07B	PL B649 349	J.R. Batley et al.	(CERN NA48/2 Collab.)
BATLEY	07E	EPJ C52 875	J.R. Batley et al.	(CERN NA48/2 Collab.)
LAI	07A	PL B647 341	A. Lai et al.	(CERN NA48 Collab.)
TCHIKILEV	07	PAN 70 29	O.G. Tchikilev et al.	(ISTRA+ Collab.)
ALIEV	06	EPJ C46 61	M.A. Aliev et al.	(KEK E470 Collab.)
AMBROSINO	06A	PL B632 76	F. Ambrosino et al.	(KLOE Collab.)
BATLEY	06	PL B634 474	J.R. Batley et al.	(CERN NA48/2 Collab.)
BATLEY	06A	PL B638 22	J.R. Batley et al.	(CERN NA48/2 Collab.)
Also		PL B640 297 (err.)	J.R. Batley et al.	(CERN NA48/2 Collab.)
BATLEY	06B	PL B633 173	J.R. Batley et al.	(CERN NA48/2 Collab.)
COLANGELO	06A	PL B638 187	G. Colangelo et al.	(CERN NA48/2 Collab.)
MA	06	PR D73 137101	H. Ma et al.	(BNL E865 Collab.)
PDG	06	JP G33 1	W.-M. Yao et al.	(PDG Collab.)
SHIMIZU	06	PL B633 190	S. Shimizu et al.	(KEK E470 Collab.)
UVAROV	06	PAN 69 26	V.A. Uvarov et al.	(ISTRA+ Collab.)
AKOPDZHANOV	05	EPJ C40 343	G.A. Akopdzhanov et al.	(IHEP Collab.)
Also		PAN 68 948	G.A. Akopdzhanov et al.	(IHEP Collab.)
AKOPDZHANOV	05B	JETPL 82 675	G.A. Akopdzhanov et al.	(IHEP Collab.)
Translated from YAF 68 966.				
Translated from ZETFP 82 771.				

Meson Particle Listings

 K^{\pm}

ARTAMONOV	05	PL B623 192	A.V. Artamonov et al.	(BNL E949 Collab.)	BRAUN	76B	LNCL 17 521	H.M. Braun et al.	(AACH3, BARI, BELG+)
CABIBBO	05	JHEP 0503 021	N. Cabibbo, G. Isidori	(CERN, ROMAI, FRAS)	DIAMANT-...	76	PL 62B 485	A.M. Diamant-Berger et al.	(SACL, GEVA)
SHER	05	PR D72 012005	A. Sher et al.	(BNL E865 Collab.)	HEINTZE	76	PL 60B 302	J. Heintze et al.	(HEIP)
ABE	04F	PRL 93 131601	M. ABE et al.	(KEK E246 Collab.)	SMITH	76	NP B109 173	K.M. Smith et al.	(GLAS, LIVP, OXF+)
Also		PR D73 072005	M. ABE et al.	(KEK E246 Collab.)	WEISSENBE...	76	NP B115 55	A.O. Weissenberg et al.	(ITEP, LEBD)
ADLER	04	PR D70 037102	S. Adler et al.	(BNL E787 Collab.)	BLOCH	75	PL 56B 201	P. Bloch et al.	(SACL, GEVA)
ALOSIO	04A	PL B597 139	A. Aloisio et al.	(KLOE Collab.)	BRAUN	75	NP B89 210	H.M. Braun et al.	(AACH3, BARI, BRUX+)
ANISIMOVSK...	04	PRL 93 031801	V.V. Anisimovskiy et al.	(BNL E949 Collab.)	CHENG	75	NP A254 381	S.C. Cheng et al.	(COLU, YALE)
Also		PR D77 052003	S. Adler et al.	(BNL E949 Collab.)	HEARD	75	PL 55B 324	K.S. Heard et al.	(CERN, HEIDH)
CABIBBO	04A	PRL 93 121801	N. Cabibbo	(CERN, ROMAI)	HEARD	75B	PL 55B 327	K.S. Heard et al.	(CERN, HEIDH)
CIRIGLIANO	04	EPJ C35 53	V. Cirigliano, H. Neufeld, H. Pichl	(CIT, VALE+)	SHEAFF	75	PR D12 2570	M. Sheaff et al.	(WISC)
PDG	04	PL B592 1	S. Edelmann et al.	(PDG Collab.)	SMITH	75	NP B91 45	K.M. Smith et al.	(GLAS, LIVP, OXF+)
SHIMIZU	04	PR D70 037101	S. Shimizu et al.	(KEK E470 Collab.)	WEISSENBE...	74	PL 48B 474	A.O. Weissenberg et al.	(ITEP, LEBD)
YUSHCHENKO	04	PL B581 31	O.P. Yushchenko et al.	(INRM, INRM)	ABRAMS	73B	PRL 30 500	R.J. Abrams et al.	(BNL)
YUSHCHENKO	04B	PL B589 111	O.P. Yushchenko et al.	(INRM)	BACKENSTOS...	73	PL 43B 431	G. Backenstoss et al.	(CERN, KARLK, KARLE+)
AJINENKO	03	PAN 66 105	I.V. Ajinenko et al.	(IHEP, INRM)	LJUNG	73	PR D8 1307	D. Ljung, D. Cline	(WISC)
Also		Translated from YAF 66 107	I.V. Ajinenko et al.	(IHEP, INRM)	Also		PRL 28 523	D. Ljung	(WISC)
AJINENKO	03B	PL B567 159	I.V. Ajinenko et al.	(IHEP, INRM)	Also		PRL 28 527	D. Cline, D. Ljung	(WISC)
AJINENKO	03C	PL B574 14	I.V. Ajinenko et al.	(IHEP, INRM)	Also		PRL 28 526	C. Camerini et al.	(WISC)
ALIEV	03	PL B554 7	M.A. Aliev et al.	(KEK E470 Collab.)	LUCAS	73B	PR D8 719	P.W. Lucas, H.D. Taft, W.J. Willis	(YALE)
ANISIMOVSK...	03	PL B562 166	V.V. Anisimovskiy et al.	(BNL E865 Collab.)	LUCAS	73B	PR D8 727	P.W. Lucas, H.D. Taft, W.J. Willis	(YALE)
PISLAK	03	PR D67 072004	S. Pislak et al.	(BNL E865 Collab.)	PANG	73	PR D8 1989	C.Y. Pang et al.	(EFI, ARIZ, LBL)
Also		PR D81 119903E	S. Pislak et al.	(BNL E865 Collab.)	Also		PL 40B 699	G.D. Cable et al.	(EFI, LBL)
SHER	03	PRL 91 261802	A. Sher et al.	(BNL E865 Collab.)	SMITH	73	NP B60 411	K.M. Smith et al.	(GLAS, LIVP, OXF+)
ADLER	02	PRL 88 041803	S. Adler et al.	(BNL E787 Collab.)	ABRAMS	72	PRL 29 1118	R.J. Abrams et al.	(BNL)
ADLER	02B	PR D65 052009	S. Adler et al.	(BNL E787 Collab.)	AUBERT	72	NC 12A 509	H. Aubert et al.	(ORSAY, BRUX, EPOL)
ADLER	02C	PL B537 211	S. Adler et al.	(BNL E787 Collab.)	CHIANG	72	PR D6 1254	I.H. Chiang et al.	(ROCH, WISC)
AJINENKO	02	PAN 65 2064	I.V. Ajinenko et al.	(IHEP, INRM)	CLARK	72	PRL 29 1274	A.R. Clark et al.	(BNL)
Also		Translated from YAF 65 2125	I.V. Ajinenko et al.	(IHEP, INRM)	FORD	72	PL 38B 335	W.T. Ford et al.	(PRIN)
CIRIGLIANO	02	EPJ C23 121	V. Cirigliano et al.	(VIEN, VALE, MARS)	HOFMMASTER	72	NP B36 1	S. Hofmester et al.	(STEV, SETO, LEHI)
PARK	02	PRL 88 111801	H.K. Park et al.	(FNAL HyperCP Collab.)	BOURQUIN	71	PL 36B 615	M.H. Bourquin et al.	(GEVA, SACL)
PDG	02	PR D66 010001	K. Hagiwara et al.	(PDG Collab.)	HAIDT	71	PR D3 10	D. Haidt et al.	(AACH, BARI, CERN, EPOL, NIJM+)
POBLAGUEV	02	PRL 89 061803	A.A. Poblaguev et al.	(BNL 865 Collab.)	Also		PL 29B 691	D. Haidt et al.	(AACH, BARI, CERN, EPOL+)
ADLER	01	PR D63 032004	S. Adler et al.	(BNL E787 Collab.)	KLEMS	71	PR D4 66	J.H. Klems, R.H. Hildebrand, R. Stiening	(CHIC+)
HORIE	01	PL B513 311	K. Horie et al.	(KEK E426 Collab.)	Also		PRL 24 1086	J.H. Klems, R.H. Hildebrand, R. Stiening	(LRL+)
PISLAK	01	PRL 87 221801	S. Pislak et al.	(BNL E865 Collab.)	Also		PRL 25 473	J.H. Klems, R.H. Hildebrand, R. Stiening	(LRL+)
Also		PR D67 072004	S. Pislak et al.	(BNL E865 Collab.)	OTT	71	PR D3 52	R.J. Ott, T.W. Pritchard	(LOQM)
Also		PRL 105 019901E	S. Pislak et al.	(BNL E865 Collab.)	ROMANO	71	PL 36B 525	F. Romano et al.	(BARI, CERN, ORSAY)
ADLER	00	PRL 84 3768	S. Adler et al.	(BNL E787 Collab.)	SCHWEINBER...	71	PL 36B 246	W. Schweinberger	(AACH, BELG, CERN, NIJM+)
ADLER	00B	PRL 85 2256	S. Adler et al.	(BNL E787 Collab.)	STEINER	71	PL 36B 521	H.J. Steiner et al.	(AACH, BARI, CERN, EPOL, ORSAY+)
ADLER	00C	PRL 85 4856	S. Adler et al.	(BNL E787 Collab.)	BARDIN	70	PL 32B 121	D.V. Bardin, S.N. Bilenky, B.M. Pontecorvo	(JINR)
APPEL	00	PRL 85 2450	R. Appel et al.	(BNL 865 Collab.)	BECHERRAWY	70	PR D1 1452	T. Becherawy	(ROCH)
Also		Thesis, Yale Univ.	D.R. Bergman	(BNL 865 Collab.)	FORD	70	PR D25 1370	W.T. Ford et al.	(PRIN)
Also		Thesis, Univ. Zurich	S. Pislak	(BNL 865 Collab.)	GALLARD	70	CERN 70-14	J.M. Gallard, L.M. Chounet	(CERN, ORSAY)
APPEL	00B	PRL 85 2877	R. Appel et al.	(BNL 865 Collab.)	GRAUMAN	70	PR D1 1277	J. Grauman et al.	(STEV, SETO, LEHI)
MA	00	PRL 84 2580	H. Ma et al.	(BNL 865 Collab.)	Also		PRL 23 737	J.U. Grauman et al.	(STEV, SETO, LEHI)
PDG	00	EPJ C15 1	D.E. Groom et al.	(PDG Collab.)	PANDOUHAS	70	PR D2 1205	D. Pandoulas et al.	(STEV, SETO)
SHIMIZU	00	PL B495 33	S. Shimizu et al.	(KEK E246 Collab.)	CUTTS	69	PR 184 1380	D. Cutts et al.	(LRL, MIT)
ABE	99S	PRL 83 4293	M. ABE et al.	(KEK E246 Collab.)	Also		PRL 20 955	D. Cutts et al.	(LRL, MIT)
AMOROS	99	JP G25 1607	G. Amoros, J. Bijnens	(LUND, HELS)	DAVISON	69	PR 180 1333	D.C. Davison et al.	(UCR)
APPEL	99	PRL 83 4482	R. Appel et al.	(BNL 865 Collab.)	ELY	69	PR 180 1319	R.P.J. Ely et al.	(LOUC, WISC, LBL)
ADLER	98	PR D58 012003	S. Adler et al.	(BNL E787 Collab.)	HERZO	69	PR 186 1403	D. Herzo et al.	(ILL)
BATUSOV	98	NP B516 3	V.Y. Batusov et al.	(BNL E787 Collab.)	LOBKOWICZ	69	PR 185 1676	F. Lobkowicz et al.	(ROCH, BNL)
DAMBROSIO	98A	JHEP 9808 004	G. D'Ambrósio et al.	(BNL E787 Collab.)	Also		PRL 17 548	F. Lobkowicz et al.	(ROCH, BNL)
ADLER	97	PRL 79 2204	S. Adler et al.	(BNL E787 Collab.)	MAST	69	PR 183 1200	T.S. Mast et al.	(LRL)
ADLER	97C	PRL 79 4756	S. Adler et al.	(BNL E787 Collab.)	SELLER	69	NC 60A 291	F. Selleri	(UCLA, LBL)
BERGMAN	97	Thesis, Yale Univ.	D.R. Bergman	(BNL E787 Collab.)	ZELLER	69	PR 182 1420	M.E. Zeller et al.	(UCLA, LBL)
KITCHING	97	PRL 79 4079	P. Kitching et al.	(BNL E787 Collab.)	BOTTERILL	68B	PRL 21 766	D.R. Botterill et al.	(OXF)
PISLAK	97	Thesis, Univ. Zurich	S. Pislak	(BNL E787 Collab.)	BOTTERILL	68C	PR 174 1661	D.R. Botterill et al.	(OXF)
ADLER	96	PRL 76 1421	S. Adler et al.	(BNL E787 Collab.)	BUTLER	68	UCRL 18420	W.D. Butler et al.	(LRL, MIT)
KOPTEV	95	JETPL 61 877	V.P. Koptev et al.	(PNPI)	CHANG	68	PRL 20 510	C.Y. Chang et al.	(UMD, RUTG)
Also		Translated from ZETFP 61 865	M. Aoki et al.	(INUS, KEK, TOKMS)	CHEN	68	PR 20 73	M. Chen et al.	(LRL, MIT)
AOKI	94	PR D50 69	M. Aoki et al.	(BNL E787 Collab.)	EICHEN	68	PR 27B 586	T. Eichten et al.	(AACH, BARI, CERN, EPOL, ORSAY+)
ATYA	93	PRL 70 2521	M.S. Atiya et al.	(BNL E787 Collab.)	ESCHTRUTH	68	PR 165 1487	E. Eschtruth et al.	(PRIN, PENN)
Also		PRL 71 305 (erratum)	M.S. Atiya et al.	(BNL E787 Collab.)	GARLAND	68	PR 167 1225	R. Garland et al.	(COLU, RUTG, WISC)
ATYA	93B	PR D48 1	M.S. Atiya et al.	(BNL E787 Collab.)	MOSCOSO	68	Thesis	L. Moscoso	(ORSAY)
ALLIEGRO	92	PRL 68 278	C. Alliegro et al.	(BNL, FNAL, PSI+)	AUERBACH	67	PR 155 1505	L.B. Auerbach et al.	(PENN, PRIN)
BARMIN	92	SJNP 55 547	V.V. Barmin et al.	(ITEP)	Also		PR D9 3216	L.B. Auerbach	(PENN, PRIN)
Also		Translated from YAF 55 976	J. Imazato et al.	(KEK, INUS, TOKY+)	BELLOTTI	67B	Heidelberg Conf.	E. Bellotti, A. Pullia	(MILA)
IMAZATO	92	PRL 69 877	J. Imazato et al.	(KEK, INUS, TOKY+)	BELLOTTI	67B	NC 52A 1287	E. Bellotti, E. Fiorini, A. Pullia	(MILA)
IVANOV	92	THESIS	Yu.M. Ivanov	(PNPI)	Also		PL 20 690	E. Bellotti et al.	(MILA)
LITTENBERG	92	PRL 68 443	L.S. Littenberg, R.E. Shrock	(BNL, STON)	BISI	67	PR 25B 572	V. Bisi et al.	(TORI)
USHER	92	PR D45 3961	T. Usher et al.	(UCI)	FLETCHER	67	PRL 19 98 08	C.F. Fletcher et al.	(ILL)
AKIMENKO	91	PL B259 225	S.A. Akimenko et al.	(SERP, JINR, Tbil+)	FORD	67	PRL 18 1214	W.T. Ford et al.	(PRIN)
BARMIN	91	SJNP 53 606	V.V. Barmin et al.	(ITEP)	GINSBURG	67	PR 162 1570	E.S. Ginsburg	(MAB5)
DENISOV	91	JETPL 54 558	A.S. Denisov et al.	(PNPI)	KALMUS	67	PR 159 1187	G.E. Kalmus, A. Kernan	(LRL)
Also		Translated from ZETFP 54 557	Yu.M. Ivanov	(PNPI)	ZINCHENKO	67	Thesis Rutgers	A.I. Zinchenko	(RUTG)
ATYA	90	PRL 64 21	M.S. Atiya et al.	(BNL E787 Collab.)	CALLAHAN	66	NC 44A 90	A.C. Callahan	(WISC)
ATYA	90B	PRL 65 1188	M.S. Atiya et al.	(BNL E787 Collab.)	CALLAHAN	66B	PR 150 1153	A.C. Callahan et al.	(WISC, LRL, UCR+)
DEMIDOV	90	SJNP 52 1006	V.S. Demidov et al.	(ITEP)	CESTER	66	PL 21 343	R. Cester et al.	(PPA)
Also		Translated from YAF 52 1595	A.M. Lee et al.	(BNL, FNAL, VILL, WASH+)	See footnote 1 in AUERBACH 67.			L.B. Auerbach et al.	(PENN, PRIN)
LEE	90	PRL 64 165	A.M. Lee et al.	(BNL E787 Collab.)	Also		PR 155 1505	L.B. Auerbach et al.	(PENN, PRIN)
ATYA	89	PRL 63 2177	M.S. Atiya et al.	(BNL E787 Collab.)	BIRGE	65	PR 139 B1600	R.W. Birge et al.	(LRL, WISC)
BARMIN	89	SJNP 50 421	V.V. Barmin et al.	(ITEP)	BISI	65	NC 35 768	V. Bisi et al.	(TORI)
Also		Translated from YAF 50 679	V.V. Barmin et al.	(ITEP)	BISI	65B	PR 139 B1068	V. Bisi et al.	(TORI)
BARMIN	88	SJNP 47 643	V.V. Barmin et al.	(ITEP)	CALLAHAN	65	PRL 15 129	A. Callahan, D. Cline	(WISC)
Also		Translated from YAF 47 1011	V.V. Barmin et al.	(ITEP)	CLINE	65	PL 15 293	D. Cline, W.F. Fry	(WISC)
BARMIN	88B	SJNP 48 1032	V.V. Barmin et al.	(ITEP)	DEMARCO	65	PR 140 B1430	A. de Marco, C. Grosse, G. Rinaudo	(TORI, CERN)
BOLOTOV	88	Translated from YAF 48 1749	V.N. Bolotov et al.	(ASCI)	FITCH	65B	PR 140 B1088	V.L. Fitch, C.A. Quarles, H.C. Wilkins	(PRIN+)
BOLOTOV	88	JETPL 47 7	V.N. Bolotov et al.	(ASCI)	STAMER	65	PR 138 B440	P. Stamer et al.	(STEV)
GALL	88	PR 160 186	K.P. Gall et al.	(BOST, MIT, WILL, CIT+)	YOUNG	65	Thesis UCRL 16362	P.S. Young	(LRL)
BARMIN	87	SJNP 45 62	V.V. Barmin et al.	(ITEP)	Also		PR 16 1464	G. Borreani, G. Rinaudo, A.E. Werbrouck	(TORI)
BOLOTOV	87	SJNP 45 1023	V.V. Barmin et al.	(ITEP)	BORREANI	64	PL 12 123	G. Borreani, G. Rinaudo, A.E. Werbrouck	(TORI)
BOLOTOV	87	SJNP 45 1652	V.N. Bolotov et al.	(INRM)	CALLAHAN	64	PR 136 B1463	A. Callahan, R. March, R. Stark	(WISC)
AMENDOLIA	86B	PL B178 435	S.R. Amendolia et al.	(CERN NA7 Collab.)	GREINER	64	PRL 13 284	D.E. Greiner, W.Z. Osborne, W.H. Barkas	(LRL)
BOLOTOV	86	SJNP 44 73	V.N. Bolotov et al.	(INRM)	SHAKLEE	64	PR 136 B1423	F.S. Shaklee et al.	(MICH)
Also		Translated from YAF 44 117	V.N. Bolotov et al.	(INRM)	BOYARSKI	62	PR 128 2398	A.M. Boyarski et al.	(MIT)
BOLOTOV	86B	SJNP 44 68	V.N. Bolotov et al.	(INRM)	FERRO-LUZZI	61	NC 22 1087	M. Ferro-Luzzi et al.	(LRL)
Also		Translated from YAF 44 108	V.N. Bolotov et al.	(INRM)	ROE	61	PRL 7 346	B.P. Roe et al.	(MICH, LRL)
YAMANAKA	86	PR D34 95	T. Yamana et al.	(KEK, TOKY)	TAYLOR	59	PR 114 359	S. Taylor et al.	(COLU)
Also		PRL 52 329	R.S. Hayano et al.	(TOKY, KEK)	COOMBES	57	PR 108 1348	C.A. Coombes et al.	(LBL)
AKIBA	85	PR D32 2911	Y. Akiba et al.	(TOKY, TINT, TSUK, KEK)					
BOLOTOV	85	JETPL 42 481	V.N. Bolotov et al.	(INRM)					
Also		Translated from ZETFP 42 390	Y. Asano et al.	(KEK, TOKY, INUS, OSAK)	LITTENBERG	93	ARNPS 43 729	L.S. Littenberg, G. Valencia	(BNL, FNAL)
ASANO	82	PL 113B 195	Y. Asano et al.	(KEK, TOKY, INUS, OSAK)	Also		Rare and Radiative Kaon Decays		
COOPER	82	PL 112B 97	A.M. Cooper et al.	(RL)	RITCHIE	93	RMP 65 1149	J.L. Ritchie, S.G. Wojcicki	
PDG	82B	PL 111B 70	M. Roos et al.	(HELS, CIT, CERN)	BATTISTON	92	PRPL 214 293	R. Battiston et al.	(PGIA, CERN, TRSTT)
ASANO	81B	PL 107B 159	Y. Asano et al.	(KEK, TOKY, INUS, OSAK)	Also		Status and Perspectives of K Decay Physics		
CAMPBELL	81	PRL 47 1032	M.K. Campbell et al.	(YALE, BNL)	BRYMAN	89	IJMP A4 79	D.A. Bryman	(TRIU)
Also		PR D27 1056	S.R. Blatt et al.	(YALE, BNL)	Also		Rare Kaon Decays		
LUM	81	PR D23 2522	G.K. Lum et al.	(LBL, NBS+)	CHOUNET	72	PRPL 4C 199	L.M. Chounet, J.M. Gaillard, M.K. Gaillard	(ORSAY+)
LYONS	81	ZPHY C10 215	L. Lyons, C. Althajar, G. Myatt	(OXF)	FEARING	70	PR D2 542	H.W. Fearing, E. Fischbach, J. Smith	(STON, BOHR)
DALLY	80	PRL 45 232	E.B. Dally et al.	(UCLA+)	HAIDT	69B	PL 29B 696	D. Haidt et al.	(AACH, BARI, CERN, EPOL+)
BARKOV	79	NP B148 53	L.M. Barkov et al.	(NOVO, KIAE)	CRONIN	68B	Vienna Conf. 241	J.W. Cronin	(PRIN)
BLATNIK	79	LNCL 24 39	S. Blatnik, J. Stahov, C.B. Lang	(TUZL, GRAZ)	Willis	67	Heidelberg Conf. 273	W.J. Willis	(YALE)
HEINTZE	79	NP B149 365	J. Heintze et al.	(HEIDP, CERN)	Also		Rapporteur talk.		
ABRAMS	77	PR D15 22	R.J. Abrams et al.	(BNL)	CABIBBO	66	Berkeley Conf.		

See key on page 999

Meson Particle Listings

K^\pm, K^0

Also	PL 11 360	N. Cabibbo, A. Maksymowicz	(CERN)
Also	PL 14 72	N. Cabibbo, A. Maksymowicz	(CERN)
BIRGE	63 PRL 11 35	R.W. Birge et al.	(LRL, WISC, BARI)
BLOCK	62B CERN Conf. 371	M.M. Block, L. Lendinara, L. Monari	(NWES, BGNA)
BRENE	61 NP 22 553	N. Brene, L. Egardt, B. Qvist	(NORD)



$$I(J^P) = \frac{1}{2}(0^-)$$

K⁰ MASS

VALUE (MeV)	EVTS	DOCUMENT ID	TECN	COMMENT
497.611 ± 0.013 OUR FIT	Error includes scale factor of 1.2.			
497.611 ± 0.013 OUR AVERAGE	Error includes scale factor of 1.2.			
497.607 ± 0.007 ± 0.015	261k	¹ TOMARADZE 14		$\psi(2S) \rightarrow K_S^0 X$
497.583 ± 0.005 ± 0.020	35k	AMBROSINO 07B	KLOE	$e^+e^- \rightarrow K_L^0 K_S^0$
497.625 ± 0.001 ± 0.031	655k	LAI 02	NA48	K^0 beam
497.661 ± 0.033	3713	BARKOV 87B	CMD	$e^+e^- \rightarrow K_L^0 K_S^0$
497.742 ± 0.085	780	BARKOV 85B	CMD	$e^+e^- \rightarrow K_L^0 K_S^0$
• • • We do not use the following data for averages, fits, limits, etc. • • •				
497.44 ± 0.50		FITCH 67	OSP K	
498.9 ± 0.5	4500	BALTAY 66	HBC	K^0 from $\bar{p}p$
497.44 ± 0.33	2223	KIM 65B	HBC	K^0 from $\bar{p}p$
498.1 ± 0.4		CHRISTENS... 64	OSP K	

¹ Obtained by analyzing CLEO-c data but not authored by the CLEO Collaboration.

m_{K⁰} - m_{K[±]}

VALUE (MeV)	EVTS	DOCUMENT ID	TECN	CHG	COMMENT
3.934 ± 0.020 OUR FIT	Error includes scale factor of 1.6.				
• • • We do not use the following data for averages, fits, limits, etc. • • •					
3.95 ± 0.21	417	HILL 68B	DBC	+	$K^+d \rightarrow K^0 pp$
3.90 ± 0.25	9	BURNSTEIN 65	HBC	-	
3.71 ± 0.35	7	KIM 65B	HBC	-	$K^-p \rightarrow n\bar{K}^0$
5.4 ± 1.1		CRAWFORD 59	HBC	+	
3.9 ± 0.6		ROSENFELD 59	HBC	-	

K⁰ MEAN SQUARE CHARGE RADIUS

VALUE (fm ²)	EVTS	DOCUMENT ID	TECN	COMMENT
-0.077 ± 0.010 OUR AVERAGE				
-0.077 ± 0.007 ± 0.011	5037	ABOUZAID 06	KTEV	$K_L^0 \rightarrow \pi^+\pi^-\pi^+e^-$
-0.090 ± 0.021		LAI 03C	NA48	$K_L^0 \rightarrow \pi^+\pi^-\pi^+e^-$
-0.054 ± 0.026		MOLZON 78		K_S^0 regen. by electrons
• • • We do not use the following data for averages, fits, limits, etc. • • •				
-0.087 ± 0.046		BLATNIK 79		VMD + dispersion relations
-0.050 ± 0.130		FOETH 69B		K_S^0 regen. by electrons

T-VIOLATION PARAMETER IN K⁰-K⁰ MIXING

The asymmetry $A_T = \frac{\Gamma(\bar{K}^0 \rightarrow K^0) - \Gamma(K^0 \rightarrow \bar{K}^0)}{\Gamma(\bar{K}^0 \rightarrow K^0) + \Gamma(K^0 \rightarrow \bar{K}^0)}$ must vanish if T invariance holds.

ASYMMETRY A_T IN K⁰-K⁰ MIXING

VALUE (units 10 ⁻³)	EVTS	DOCUMENT ID	TECN
6.6 ± 1.3 ± 1.0	640k	¹ ANGELOPOULOS... 98E	CPLR

¹ ANGELOPOULOS 98E measures the asymmetry $A_T = [\Gamma(\bar{K}^0_{t=0} \rightarrow e^+\pi^-\nu_{t=\tau}) - \Gamma(K^0_{t=0} \rightarrow e^-\pi^+\nu_{t=\tau})] / [\Gamma(\bar{K}^0_{t=0} \rightarrow e^+\pi^-\nu_{t=\tau}) + \Gamma(K^0_{t=0} \rightarrow e^-\pi^+\nu_{t=\tau})]$ as a function of the neutral-kaon eigentime τ . The initial strangeness of the neutral kaon is tagged by the charge of the accompanying charged kaon in the reactions $p\bar{p} \rightarrow K^-\pi^+K^0$ and $p\bar{p} \rightarrow K^+\pi^-K^0$. The strangeness at the time of the decay is tagged by the lepton charge. The reported result is the average value of A_T over the interval $1\tau_S < \tau < 20\tau_S$. From this value of A_T ANGELOPOULOS 01B, assuming CP T invariance in the $e\pi\nu$ decay amplitude, determine the T -violating as $\Delta S = \Delta S$ conserving parameter (for its definition, see Review below) $4\text{Re}(\epsilon) = (6.2 \pm 1.4 \pm 1.0) \times 10^{-3}$.

See the related review(s):

[CPT Invariance Tests in Neutral Kaon Decay](#)

CP-VIOLATION PARAMETERS

Re(ε)

VALUE (units 10 ⁻³)	DOCUMENT ID	TECN
1.596 ± 0.013	¹ AMBROSINO 06H	KLOE
• • • We do not use the following data for averages, fits, limits, etc. • • •		
1.664 ± 0.010	² LAI 05A	NA48

¹ AMBROSINO 06H uses Bell-Steinberger relations with the following measurements: $B(K_L^0 \rightarrow \pi^+\pi^-)$ in AMBROSINO 06F, $B(K_S^0 \rightarrow \pi^0\pi^0\pi^0)$ in AMBROSINO 05B, the K_S^0 -semileptonic charge asymmetry in AMBROSINO 06E, and K^0 -semileptonic results in ANGELOPOULOS 98F.

² LAI 05A values are obtained through unitarity (Bell-Steinberger relations), improving determination of η_{000} and combining other data from PDG 04 and APOSTOLAKIS 99B.

CPT-VIOLATION PARAMETERS

In K^0 - \bar{K}^0 mixing, if CP -violating interactions include a T conserving part then

$$|K_S\rangle = [|K_1\rangle + (\epsilon + \delta)|K_2\rangle] / \sqrt{1 + |\epsilon + \delta|^2}$$

$$|K_L\rangle = [|K_2\rangle + (\epsilon - \delta)|K_1\rangle] / \sqrt{1 + |\epsilon - \delta|^2}$$

where

$$|K_1\rangle = [|K^0\rangle + |\bar{K}^0\rangle] / \sqrt{2}$$

$$|K_2\rangle = [|K^0\rangle - |\bar{K}^0\rangle] / \sqrt{2}$$

and

$$|\bar{K}^0\rangle = CP|K^0\rangle.$$

The parameter δ specifies the CP -violating part.

Estimates of δ are given below assuming the validity of the $\Delta S = \Delta Q$ rule. See also THOMSON 95 for a test of CP -symmetry conservation in K^0 decays using the Bell-Steinberger relation.

REAL PART OF δ

A nonzero value violates CP T invariance.

VALUE (units 10 ⁻⁴)	EVTS	DOCUMENT ID	TECN	COMMENT
2.51 ± 2.25		¹ ABOUZAID 11	KTEV	
• • • We do not use the following data for averages, fits, limits, etc. • • •				
2.3 ± 2.7		² AMBROSINO 06H	KLOE	
2.4 ± 2.8		³ APOSTOLA... 99B	RVUE	
2.9 ± 2.6 ± 0.6	1.3M	⁴ ANGELOPOULOS... 98F	CPLR	
180 ± 200	6481	⁵ DEMIDOV 95		$K_{\ell 3}$ reanalysis

- ¹ ABOUZAID 11 uses Bell-Steinberger relations.
- ² AMBROSINO 06H uses Bell-Steinberger relations with the following measurements: $B(K^0 \rightarrow \pi^+\pi^-)$ in AMBROSINO 06F, $B(K_S^0 \rightarrow \pi^0\pi^0\pi^0)$ in AMBROSINO 05B, the K_S^0 -semileptonic charge asymmetry in AMBROSINO 06E, and K^0 -semileptonic results in ANGELOPOULOS 98F.
- ³ APOSTOLAKIS 99B assumes only unitarity and combines CPLEAR and other results.
- ⁴ ANGELOPOULOS 98F use $\Delta S = \Delta Q$. If $\Delta S = \Delta Q$ is not assumed, they find $\text{Re}\delta = (3.0 \pm 3.3 \pm 0.6) \times 10^{-4}$.
- ⁵ DEMIDOV 95 reanalyzes data from HART 73 and NIEBERGALL 74.

IMAGINARY PART OF δ

A nonzero value violates CP T invariance.

VALUE (units 10 ⁻⁵)	EVTS	DOCUMENT ID	TECN	COMMENT
-1.5 ± 1.6		¹ ABOUZAID 11	KTEV	
• • • We do not use the following data for averages, fits, limits, etc. • • •				
0.4 ± 2.1		² AMBROSINO 06H	KLOE	
-0.2 ± 2.0		³ LAI 05A	NA48	
2.4 ± 5.0		⁴ APOSTOLA... 99B	RVUE	
-90 ± 290 ± 100	1.3M	⁵ ANGELOPOULOS... 98F	CPLR	
2100 ± 3700	6481	⁶ DEMIDOV 95		$K_{\ell 3}$ reanalysis

- ¹ ABOUZAID 11 uses Bell-Steinberger relations.
- ² AMBROSINO 06H uses Bell-Steinberger relations with the following measurements: $B(K_L^0 \rightarrow \pi^+\pi^-)$ in AMBROSINO 06F, $B(K_S^0 \rightarrow \pi^0\pi^0\pi^0)$ in AMBROSINO 05B, the K^0 -semileptonic charge asymmetry in AMBROSINO 06E, and K^0 -semileptonic results in ANGELOPOULOS 98F.
- ³ LAI 05A values are obtained through unitarity (Bell-Steinberger relations), improving determination of η_{000} and combining other data from PDG 04 and APOSTOLAKIS 99B.
- ⁴ APOSTOLAKIS 99B assumes only unitarity and combines CPLEAR and other results.
- ⁵ If $\Delta S = \Delta Q$ is not assumed, ANGELOPOULOS 98F finds $\text{Im}\delta = (-15 \pm 23 \pm 3) \times 10^{-3}$.
- ⁶ DEMIDOV 95 reanalyzes data from HART 73 and NIEBERGALL 74.

Re(y)

A non-zero value would violate CP T invariance in $\Delta S = \Delta Q$ amplitude. $\text{Re}(y)$ is the following combination of K_{e3} decay amplitudes:

$$\text{Re}(y) = \text{Re} \left(\frac{A(\bar{K}^0 \rightarrow e^-\pi^+\nu_e) - A(K^0 \rightarrow e^+\pi^-\nu_e)}{A(\bar{K}^0 \rightarrow e^-\pi^+\nu_e) + A(K^0 \rightarrow e^+\pi^-\nu_e)} \right)$$

VALUE (units 10 ⁻³)	EVTS	DOCUMENT ID	TECN
0.4 ± 2.5	13k	¹ AMBROSINO 06E	KLOE
• • • We do not use the following data for averages, fits, limits, etc. • • •			
0.3 ± 3.1		² APOSTOLA... 99B	CPLR

- ¹ They use the PDG 04 for the K_L^0 semileptonic charge asymmetry and PDG 04 (CP review, CP NOT ASSUMED) for $\text{Re}(\epsilon)$.
- ² Constrained by Bell-Steinberger (or unitarity) relation.

Re(x₋)

A non-zero value would violate CP T invariance in decay amplitudes with $\Delta S \neq \Delta Q$. x_- , used here to define $\text{Re}(x_-)$, and x_+ , used below in the $\Delta S = \Delta Q$ section are the following combinations of K_{e3} decay amplitudes:

$$x_- = \frac{1}{2} \left(\frac{A(\bar{K}^0 \rightarrow \pi^-\pi^+\nu_e) + A(K^0 \rightarrow \pi^+\pi^-\nu_e)}{A(K^0 \rightarrow \pi^-\pi^+\nu_e)} + \frac{A(K^0 \rightarrow \pi^+\pi^-\nu_e)}{A(K^0 \rightarrow \pi^+\pi^-\nu_e)} \right)$$

VALUE (units 10 ⁻³)	EVTS	DOCUMENT ID	TECN	COMMENT
-2.9 ± 2.0		¹ AMBROSINO 06H	KLOE	

Meson Particle Listings

K^0, K_S^0

••• We do not use the following data for averages, fits, limits, etc. •••

- 0.8 ± 2.5 13k 2 AMBROSINO 06E KLOE
- 0.5 ± 3.0 3 APOSTOLA... 99B CPLR Strangeness tagged
- 2 ± 13 ± 3 650k ANGELOPO... 98F CPLR Strangeness tagged

- 1 AMBROSINO 06H uses Bell-Steinberger relations with the following measurements: $B(K_L^0 \rightarrow \pi^+ \pi^-)$ in AMBROSINO 06F, $B(K_S^0 \rightarrow \pi^0 \pi^0 \pi^0)$ in AMBROSINO 05B, the K_S^0 -semileptonic charge asymmetry in AMBROSINO 06E, and K^0 -semileptonic results in ANGELOPOULOS 98F.
- 2 Uses PDG 04 for the K_L^0 semileptonic charge asymmetry and $\text{Re}(\delta)$ from CPLEAR, ANGELOPOULOS 98F.
- 3 Constrained by Bell-Steinberger (or unitarity) relation.

$$|m_{K^0} - m_{\bar{K}^0}| / m_{\text{average}}$$

A test of CPT invariance. "Our Evaluation" is described in the "Tests of Conservation Laws" section. It assumes CPT invariance in the decay and neglects some contributions from decay channels other than $\pi\pi$.

VALUE	CL%	DOCUMENT ID	TECN
$<6 \times 10^{-19}$	90	PDG	12

••• We do not use the following data for averages, fits, limits, etc. •••

- $(-3 \pm 4) \times 10^{-18}$ 1 ANGELOPO... 99B RVUE
- 1 ANGELOPOULOS 99B assumes only unitarity and combines CPLEAR and other results.

$$(\Gamma_{K^0} - \Gamma_{\bar{K}^0}) / m_{\text{average}}$$

A test of CPT invariance.

VALUE	DOCUMENT ID	TECN
$(7.8 \pm 8.4) \times 10^{-18}$	1 ANGELOPO... 99B RVUE	

- 1 ANGELOPOULOS 99B assumes only unitarity and combines CPLEAR with other results. Correlated with $(m_{K^0} - m_{\bar{K}^0}) / m_{\text{average}}$ with a correlation coefficient of -0.95 .

TESTS OF $\Delta S = \Delta Q$ RULE

$\text{Re}(x_+)$

A non-zero value would violate the $\Delta S = \Delta Q$ rule in CPT conserving transitions. x_+ is defined above in the $\text{Re}(x_-)$ section.

VALUE (units 10^{-3})	EVTS	DOCUMENT ID	TECN
-0.9 ± 3.0 OUR AVERAGE			

- 2 ± 10 1 BATLEY 07D NA48
- 0.5 ± 3.6 13k 2 AMBROSINO 06E KLOE
- 1.8 ± 6.1 3 ANGELOPO... 98D CPLR

- 1 Result obtained from the measurement $\Gamma(K_S^0 \rightarrow \pi e \nu) / \Gamma(K_L^0 \rightarrow \pi e \nu) = 0.993 \pm 0.34$, neglecting possible CPT non-invariance and using PDG 06 values of $B(K_L^0 \rightarrow \pi e \nu) = 0.4053 \pm 0.0015$, $\tau_L = (5.114 \pm 0.021) \times 10^{-8}$ s and $\tau_S = (0.8958 \pm 0.0005) \times 10^{-10}$ s.
- 2 $\text{Re}(x_+)$ can be shown to be equal to the following combination of rates:

$$\text{Re}(x_+) = \frac{1}{2} \frac{\Gamma(K_S^0 \rightarrow \pi e \nu) - \Gamma(K_L^0 \rightarrow \pi e \nu)}{\Gamma(K_S^0 \rightarrow \pi e \nu) + \Gamma(K_L^0 \rightarrow \pi e \nu)}$$

- which is valid up to first order in terms violating CPT and/or the $\Delta S = \Delta Q$ rule.
- 3 Obtained neglecting CPT violating amplitudes.

K^0 REFERENCES

TOMARADZE 14 PR D89 031501	A. Tomaradze et al.	(NWES, WAYN)
PDG 12 PR D86 010001	J. Berlinger et al.	(PDG Collab.)
ABOUZAID 11 PR D83 092001	E. Abouzaid et al.	(FNAL KTeV Collab.)
AMBROSINO 07B JHEP 0712 073	F. Ambrosino et al.	(KLOE Collab.)
BATLEY 07D PL B653 145	J.R. Batley et al.	(CERN NA48 Collab.)
ABOUZAID 06 PRL 96 101801	E. Abouzaid et al.	(KTeV Collab.)
AMBROSINO 06E PL B636 173	F. Ambrosino et al.	(KLOE Collab.)
AMBROSINO 06F PL B638 140	F. Ambrosino et al.	(KLOE Collab.)
AMBROSINO 06H JHEP 0612 011	F. Ambrosino et al.	(KLOE Collab.)
PDG 06 JP G33 1	W.-M. Yao et al.	(PDG Collab.)
AMBROSINO 05B PL B619 61	F. Ambrosino et al.	(KLOE Collab.)
LAI 05A PL B610 165	A. Lai et al.	(CERN NA48 Collab.)
PDG 04 PL B592 1	S. Eidelman et al.	(PDG Collab.)
LAI 03C EPJ C30 33	A. Lai et al.	(CERN NA48 Collab.)
LAI 02 PL B533 196	A. Lai et al.	(CERN NA48 Collab.)
ANGELOPO... 01B EPJ C22 55	A. Angelopoulos et al.	(CLEAR Collab.)
ANGELOPO... 99B PL B471 332	A. Angelopoulos et al.	(CLEAR Collab.)
APOSTOLA... 99B PL B456 297	A. Apostolakis et al.	(CLEAR Collab.)
ANGELOPO... 98D PL B444 38	A. Angelopoulos et al.	(CLEAR Collab.)
Also EPJ C22 55	A. Angelopoulos et al.	(CLEAR Collab.)
ANGELOPO... 98E PL B444 43	A. Angelopoulos et al.	(CLEAR Collab.)
ANGELOPO... 98F PL B444 52	A. Angelopoulos et al.	(CLEAR Collab.)
Also EPJ C22 55	A. Angelopoulos et al.	(CLEAR Collab.)
DEMIDOV 95 PAN 58 968	V. Demidov, K. Gusev, E. Shabalina	(ITEP)
From YAF 58 1041		
THOMSON 95 PR D51 1412	G.B. Thomson, Y. Zou	(RUTG)
BARKOV 87B SJNP 46 630	L.M. Barkov et al.	(NOVO)
Translated from YAF 46 1088.		
BARKOV 85B JETPL 42 138	L.M. Barkov et al.	(NOVO)
Translated from ZETFP 42 113.		
BLATNIK 79 LNC 24 39	S. Blatnik, J. Stahov, C.B. Lang	(TUZL, GRAZ)
MOLZON 78 PRL 41 1213	W.R. Molzon et al.	(EFI+)
NIEBERGALL 74 PL 49B 103	F. Niebergall et al.	(CERN, ORSAY, VIEN)
HART 73 NP B66 317	J.C. Hart et al.	(CAVE, RHUL)
FOETH 69B PL 30B 276	H. Foeth et al.	(AACH, CERN, TORI)
HILL 68B PR 168 1534	D.G. Hill et al.	(BNL, CMU)
FITCH 67 PR 164 1711	V.L. Fitch et al.	(PRIN)
BALTAY 66 PR 142 932	C. Baltay et al.	(YALE, BNL)
BURNSTEIN 65 PR 138 B895	R.A. Burnstein, H.A. Rubin	(UMD)
KIM 65B PR 140 B1334	J.K. Kim, L. Kirsch, D. Miller	(COLU)
CHRISTENS... 64 PRL 13 138	J.H. Christenson et al.	(PRIN)
CRAWFORD 59 PRL 2 112	F.S. Crawford et al.	(LRL)
ROSENFELD 59 PRL 2 110	A.H. Rosenfeld, F.T. Solmitz, R.D. Tripp	(LRL)



$$I(J^P) = \frac{1}{2}(0^-)$$

K_S^0 MEAN LIFE

For earlier measurements, beginning with BOLDT 58B, see our 1986 edition, Physics Letters **170B** 130 (1986).

OUR FIT is described in the note on " CP violation in K_L decays" in the K^0 Particle Listings. The result labeled "OUR FIT Assuming CP^T " ["OUR FIT Not assuming CP^T "] includes all measurements except those with the comment "Not assuming CP^T " ["Assuming CP^T "]. Measurements with neither comment do not assume CPT and enter both fits.

VALUE (10^{-10} s)	EVTS	DOCUMENT ID	TECN	COMMENT
0.8954 ± 0.0004 OUR FIT				Error includes scale factor of 1.1. Assuming CP^T
0.89564 ± 0.00033 OUR FIT				Not assuming CP^T
0.89589 ± 0.00070		1,2 ABOUZAID 11	KTEV	Not assuming CP^T
0.89623 ± 0.00047		1,3 ABOUZAID 11	KTEV	Assuming CP^T
0.89562 ± 0.00029 ± 0.00043	20M	4 AMBROSINO 11	KLOE	Not assuming CP^T
0.89598 ± 0.00048 ± 0.00051	16M	LAI 02c	NA48	
0.8971 ± 0.0021		BERTANZA 97	NA31	
0.8941 ± 0.0014 ± 0.0009		SCHWINGEN... 95	E773	Assuming CP^T
0.8929 ± 0.0016		GIBBONS 93	E731	Assuming CP^T
••• We do not use the following data for averages, fits, limits, etc. •••				
0.8965 ± 0.0007		5 ALAVI-HARATI 03	KTEV	Assuming CP^T
0.8958 ± 0.0013		6 ALAVI-HARATI 03	KTEV	Not assuming CP^T
0.8920 ± 0.0044	214k	GROSSMAN 87	SPEC	
0.905 ± 0.007		7 ARONSON 82B	SPEC	
0.881 ± 0.009	26k	ARONSON 76	SPEC	
0.8926 ± 0.0032 ± 0.0002		8 CARITHERS 75	SPEC	
0.8937 ± 0.0048	6M	GEWENGER 74B	ASP K	
0.8958 ± 0.0045	50k	9 SKJEGGEST... 72	HBC	
0.856 ± 0.008	19994	10 DONALD 68B	HBC	
0.872 ± 0.009	20000	9,10 HILL 68	DBC	

- 1 The two ABOUZAID 11 values use the same full KTeV dataset from 1996, 1997, and 1999. The first enters the "assuming CP^T " fit and the second enters the "not assuming CP^T " fit.
- 2 ABOUZAID 11 fit has Δm , τ_S , ϕ_e , $\text{Re}(\epsilon'/\epsilon)$, and $\text{Im}(\epsilon'/\epsilon)$ as free parameters. See $\text{Im}(\epsilon'/\epsilon)$ in the " K_L^0 CP violation" section for correlation information.
- 3 ABOUZAID 11 fit has Δm and τ_S free but constrains ϕ_e to the Superweak value, i.e. assumes CP^T . This τ_S value is correlated with their $\Delta m = m_{K_L^0} - m_{K_S^0}$ measurement in the K_L^0 listings. The correlation coefficient $\rho(\tau_S, \Delta m) = -0.670$.
- 4 Fit to the proper time distribution.
- 5 This ALAVI-HARATI 03 fit has Δm and τ_S free but constrains ϕ_{+-} to the Superweak value, i.e. assumes CP^T . This τ_S value is correlated with their $\Delta m = m_{K_L^0} - m_{K_S^0}$ measurement in the K_L^0 listings. The correlation coefficient $\rho(\tau_S, \Delta m) = -0.396$. Superseded by ABOUZAID 11.
- 6 This ALAVI-HARATI 03 fit has Δm , ϕ_{+-} , and τ_{K_S} free. See ϕ_{+-} in the " K_L CP violation" section for correlation information. Superseded by ABOUZAID 11.
- 7 ARONSON 82 find that K_S^0 mean life may depend on the kaon energy.
- 8 CARITHERS 75 measures the Δm dependence of the total decay rate (inverse mean life) to be $\Gamma(K_S^0) = [(1.122 \pm 0.004) + 0.16(\Delta m - 0.5348)/\Delta m] 10^{10} / \text{s}$, or, in terms of mean life, CARITHERS 75 measures $\tau_S = (0.8913 \pm 0.0032) - 0.238 [\Delta m - 0.5348] (10^{-10} \text{ s})$. We have adjusted the measurement to use our best values of $(\Delta m = 0.5293 \pm 0.0009) (10^{10} \text{ h s}^{-1})$. Our first error is their experiment's error and our second error is the systematic error from using our best values.
- 9 HILL 68 has been changed by the authors from the published value (0.865 ± 0.009) because of a correction in the shift due to η_{+-} . SKJEGGESTAD 72 and HILL 68 give detailed discussions of systematics encountered in this type of experiment.
- 10 Pre-1971 experiments are excluded from the average because of disagreement with later more precise experiments.

K_S^0 DECAY MODES

Mode	Fraction (Γ_i/Γ)	Scale factor/ Confidence level
Hadronic modes		
Γ_1 $\pi^0 \pi^0$	(30.69 ± 0.05) %	
Γ_2 $\pi^+ \pi^-$	(69.20 ± 0.05) %	
Γ_3 $\pi^+ \pi^- \pi^0$	(3.5 ± 1.1 / -0.9) × 10 ⁻⁷	
Modes with photons or $\ell\bar{\ell}$ pairs		
Γ_4 $\pi^+ \pi^- \gamma$	[a,b] (1.79 ± 0.05) × 10 ⁻³	
Γ_5 $\pi^+ \pi^- e^+ e^-$	(4.79 ± 0.15) × 10 ⁻⁵	
Γ_6 $\pi^0 \gamma \gamma$	[a] (4.9 ± 1.8) × 10 ⁻⁸	
Γ_7 $\gamma \gamma$	(2.63 ± 0.17) × 10 ⁻⁶	S=3.0
Semileptonic modes		
Γ_8 $\pi^\pm e^\mp \nu_e$	[c] (7.04 ± 0.08) × 10 ⁻⁴	
Γ_9 $\pi^\pm \mu^\mp \nu_\mu$	[c,d] (4.69 ± 0.05) × 10 ⁻⁴	

CP violating (CP) and ΔS = 1 weak neutral current (S1) modes

Table with 5 columns: Index, Mode, CP, Value, CL. Rows include Γ10, Γ11, Γ12, Γ13, Γ14 with various decay modes like μ+μ-, e+e-, π0e+e-, π0μ+μ-.

- [a] See the Particle Listings below for the energy limits used in this measurement.
[b] Most of this radiative mode, the low-momentum γ part, is also included in the parent mode listed without γ's.
[c] The value is for the sum of the charge states or particle/antiparticle states indicated.
[d] Not a measurement. Calculated as 0.666·B(π±e∓νe).

CONSTRAINED FIT INFORMATION

An overall fit to 4 branching ratios uses 5 measurements and one constraint to determine 4 parameters. The overall fit has a χ2 = 0.1 for 2 degrees of freedom.

The following off-diagonal array elements are the correlation coefficients (δxiδxj)/(δxiδxj), in percent, from the fit to the branching fractions, xi ≡ Γi/Γtotal. The fit constrains the xi whose labels appear in this array to sum to one.

Correlation matrix table with x1, x2, x8 on both axes and values like -100, -6, 3, -6, 3, 100.

K_S⁰ DECAY RATES

Table for Γ(π±e∓νe) with columns: VALUE, EVTS, DOCUMENT ID, TECN, COMMENT.

- We do not use the following data for averages, fits, limits, etc.
8.1 ± 1.6 75 1 AKHMETSHIN 99 CMD2 Tagged K_S⁰ using φ → K_L⁰K_S⁰
7.50 ± 0.08 2 PDG 98
seen BURGUN 72 HBC K+p → K⁰ρπ+
9.3 ± 2.5 AUBERT 65 HLBC ΔS=ΔQ, CP cons. not assumed

1 AKHMETSHIN 99 is from a measured branching ratio B(K_S⁰ → πeνe) = (7.2 ± 1.4) × 10⁻⁴ and τ_{K_S⁰} = (0.8934 ± 0.0008) × 10⁻¹⁰ s. Not independent of measured branching ratio.
2 PDG 98 from K_L⁰ measurements, assuming that ΔS=ΔQ in K⁰ decay so that Γ(K_S⁰ → π±e∓νe) = Γ(K_L⁰ → π±e∓νe).

Table for Γ(π±μ∓νμ) with columns: VALUE, DOCUMENT ID.

- We do not use the following data for averages, fits, limits, etc.
5.25 ± 0.07 1 PDG 98
1 PDG 98 from K_L⁰ measurements, assuming that ΔS=ΔQ in K⁰ decay so that Γ(K_S⁰ → π±μ∓νμ) = Γ(K_L⁰ → π±μ∓νμ).

K_S⁰ BRANCHING RATIOS

Hadronic modes

Table for Γ(π0π0)/Γtotal with columns: VALUE, EVTS, DOCUMENT ID, TECN.

- We do not use the following data for averages, fits, limits, etc.
0.335 ± 0.014 1066 BROWN 63 HLBC
0.288 ± 0.021 198 CHRETIEN 63 HLBC
0.30 ± 0.035 BROWN 61 HLBC

Table for Γ(π+π-)/Γtotal with columns: VALUE, EVTS, DOCUMENT ID, TECN, COMMENT.

- We do not use the following data for averages, fits, limits, etc.
0.670 ± 0.010 3447 DOYLE 69 HBC π-ρ → ΛK⁰

Table for Γ(π+π-)/Γ(π0π0) with columns: VALUE, EVTS, DOCUMENT ID, TECN, COMMENT.

- 2.255 ± 0.005 OUR FIT
2.2549 ± 0.0054 1 AMBROSINO 06c KLOE

- We do not use the following data for averages, fits, limits, etc.
2.2555 ± 0.0012 ± 0.0054 2 AMBROSINO 06c KLOE
2.236 ± 0.003 ± 0.015 766k 2 ALOISIO 02b KLOE
2.11 ± 0.09 1315 EVERHART 76 WIRE π-ρ → ΛK⁰
2.169 ± 0.094 16k COWELL 74 OSPK π-ρ → ΛK⁰
2.16 ± 0.08 4799 HILL 73 DBC K+d → K⁰ρρ
2.22 ± 0.10 3068 3 ALITTI 72 HBC K+p → π+ρK⁰
2.22 ± 0.08 6380 MORSE 72b DBC K+n → K⁰ρ
2.10 ± 0.11 701 4 NAGY 72 HLBC K+n → K⁰ρ
2.22 ± 0.095 6150 5 BALTAY 71 HBC Kρ → K⁰neutrals
2.282 ± 0.043 7944 6 MOFFETT 70 OSPK K+n → K⁰ρ
2.12 ± 0.17 267 4 BOZOKI 69 HLBC
2.285 ± 0.055 3016 6 GOBBI 69 OSPK K+n → K⁰ρ
2.10 ± 0.06 3700 MORFIN 69 HLBC K+n → K⁰ρ

1 This result combines AMBROSINO 06c KLOE 2001-02 data with ALOISIO 02b KLOE 2000 data. K_S⁰ → π+π- fully inclusive.
2 Includes radiative decays π+π-γ.
3 The directly measured quantity is K_S⁰ → π+π-/all K⁰ = 0.345 ± 0.005.
4 NAGY 72 is a final result which includes BOZOKI 69.
5 The directly measured quantity is K_S⁰ → π+π-/all π⁰ = 0.345 ± 0.005.
6 MOFFETT 70 is a final result which includes GOBBI 69.

Table for Γ(π+π-π0)/Γtotal with columns: VALUE, EVTS, DOCUMENT ID, TECN, COMMENT.

- 3.5 ± 1.1 OUR AVERAGE
4.7 ± 1.7 ± 1.7 ± 1.5 1 BATLEY 05 NA48
2.5 ± 1.3 ± 0.5 ± 1.0 ± 0.6 500k 2 ADLER 97b CPLR
4.8 ± 2.2 ± 1.1 3 ZOU 96 E621

- We do not use the following data for averages, fits, limits, etc.
4.1 ± 2.5 ± 0.5 ± 1.9 ± 0.6 4 ADLER 96e CPLR Sup. by ADLER 97b
3.9 ± 5.4 ± 0.9 ± 1.8 ± 0.7 5 THOMSON 94 E621 Sup. by ZOU 96

1 BATLEY 05 is obtained by measuring the interference parameters in K_S⁰, K_L⁰ → π+π-π0. Re(λ) = 0.038 ± 0.008 ± 0.006 and Im(λ) = -0.013 ± 0.005 ± 0.004; the correlation coeff. between Re(λ) and Im(λ) is 0.66 (statistical only).
2 ADLER 97b find the CP-conserving parameters Re(λ) = (28 ± 7 ± 3) × 10⁻³, Im(λ) = (-10 ± 8 ± 2) × 10⁻³. They estimate B(K_S⁰ → π+π-π0) from Re(λ) and the K_L⁰ decay parameters. See also ANGELOPOULOS 98c.
3 ZOU 96 is from the the measured quantities |ρ+-0| = 0.039 ± 0.009 ± 0.005 and φρ = (-9 ± 18)°.
4 ADLER 96e is from the measured quantities Re(λ) = 0.036 ± 0.010 ± 0.002 ± 0.003 and Im(λ) consistent with zero. Note that the quantity λ is the same as ρ+-0 used in other footnotes.
5 THOMSON 94 calculates this branching ratio from their measurements |ρ+-0| = 0.035 ± 0.019 ± 0.004 and φρ = (-59 ± 48)° where |ρ+-0|e^{iφρ} = A(K_S⁰ → π+π-π0, l = 2)/A(K_L⁰ → π+π-π0).

Modes with photons or ℓℓ pairs

Table for Γ(π+π-γ)/Γ(π+π-) with columns: VALUE, EVTS, DOCUMENT ID, TECN, COMMENT.

- 2.59 ± 0.08 OUR AVERAGE
2.56 ± 0.09 1286 RAMBERG 93 E731 pγ > 50 MeV/c
2.68 ± 0.15 1 TAUREG 76 SPEC pγ > 50 MeV/c
••• We do not use the following data for averages, fits, limits, etc.
7.10 ± 0.22 3723 RAMBERG 93 E731 pγ > 20 MeV/c
3.0 ± 0.6 29 2 BOBISUT 74 HLBC pγ > 40 MeV/c
2.8 ± 0.6 3 BURGUN 73 HBC pγ > 50 MeV/c

1 TAUREG 76 find direct emission contribution < 0.06, CL = 90%.
2 BOBISUT 74 not included in average because pγ cut differs. Estimates direct emission contribution to be 0.5 or less, CL = 95%.
3 BURGUN 73 estimates that direct emission contribution is 0.3 ± 0.6.

Table for Γ(π+π-e+e-)/Γtotal with columns: VALUE, EVTS, DOCUMENT ID, TECN, COMMENT.

- 4.79 ± 0.15 OUR AVERAGE
4.83 ± 0.11 ± 0.14 23k 1 BATLEY 11 NA48 2002 data
4.69 ± 0.30 676 2 LAI 03c NA48 1998+1999 data
••• We do not use the following data for averages, fits, limits, etc.
4.71 ± 0.23 ± 0.22 620 2,3 LAI 03c NA48 1999 data
4.5 ± 0.7 ± 0.4 56 LAI 00b NA48 1998 data

1 BATLEY 11 reports [Γ(K_S⁰ → π+π-e+e-)/Γtotal] / [B(K_L⁰ → π+π-π0)] / [B(π0 → e+e-γ)] = (3.28 ± 0.06 ± 0.04) × 10⁻² which we multiply by our best values B(K_L⁰ → π+π-π0) = (12.54 ± 0.05) × 10⁻², B(π0 → e+e-γ) = (1.174 ± 0.035) × 10⁻². Our first error is their experiment's error and our second error is the systematic error from using our best values. Also a limit on the absolute value of the interference between bremsstrahlung and E1 transition is given : < 4 × 10⁻⁷ at 90% CL.
2 Uses normalization BR(K_L⁰ → π+π-π0)*BR(π0 → e+e-) = (1.505 ± 0.047) × 10⁻³ from our 2000 Edition.
3 Second error is 0.16(syst) ± 0.15(norm) combined in quadrature.

Meson Particle Listings

 K_S^0 $\Gamma(\pi^0\gamma\gamma)/\Gamma_{\text{total}}$ Γ_6/Γ

VALUE (units 10^{-8})	CL%	EVTS	DOCUMENT ID	TECN	COMMENT
$4.9 \pm 1.6 \pm 0.9$		17	¹ LAI	04 NA48	$m_{\gamma\gamma}^2/m_K^2 > 0.2$

• • • We do not use the following data for averages, fits, limits, etc. • • •

<33	90		LAI	03B NA48	$m_{\gamma\gamma}^2/m_K^2 > 0.2$
-----	----	--	-----	----------	----------------------------------

¹ Spectrum also measured and found consistent with the one generated by a constant matrix element.

 $\Gamma(\gamma\gamma)/\Gamma_{\text{total}}$ Γ_7/Γ

VALUE (units 10^{-6})	CL%	EVTS	DOCUMENT ID	TECN	COMMENT
2.63 ± 0.17 OUR AVERAGE					Error includes scale factor of 3.0.

2.26 ± 0.12 ± 0.06	711		¹ AMBROSINO	08c KLOE	$\phi \rightarrow K_S^0 K_L^0$
--------------------	-----	--	------------------------	----------	--------------------------------

2.713 ± 0.063 ± 0.005	7.5k		² LAI	03 NA48	
-----------------------	------	--	------------------	---------	--

• • • We do not use the following data for averages, fits, limits, etc. • • •

2.58 ± 0.36 ± 0.22	149		LAI	00 NA48	
--------------------	-----	--	-----	---------	--

2.2 ± 1.1	16		³ BARR	95B NA31	
-----------	----	--	-------------------	----------	--

2.4 ± 0.9	35		⁴ BARR	95B NA31	
-----------	----	--	-------------------	----------	--

< 13	90		BALATS	89 SPEC	
------	----	--	--------	---------	--

2.4 ± 1.2	19		BURKHARDT	87 NA31	
-----------	----	--	-----------	---------	--

<133	90		BARMIN	86B XEBC	
------	----	--	--------	----------	--

¹ AMBROSINO 08c reports $(2.26 \pm 0.12 \pm 0.06) \times 10^{-6}$ from a measurement of $[\Gamma(K_S^0 \rightarrow \gamma\gamma)/\Gamma_{\text{total}}] \times [B(K_S^0 \rightarrow \pi^0\pi^0)]$ assuming $B(K_S^0 \rightarrow \pi^0\pi^0) = (30.69 \pm 0.05) \times 10^{-2}$.

² LAI 03 reports $[\Gamma(K_S^0 \rightarrow \gamma\gamma)/\Gamma_{\text{total}}] / [B(K_S^0 \rightarrow \pi^0\pi^0)] = (8.84 \pm 0.18 \pm 0.10) \times 10^{-6}$

which we multiply by our best value $B(K_S^0 \rightarrow \pi^0\pi^0) = (30.69 \pm 0.05) \times 10^{-2}$. Our first error is their experiment's error and our second error is the systematic error from using our best value.

³ BARR 95B result is calculated using $B(K_L \rightarrow \gamma\gamma) = (5.86 \pm 0.17) \times 10^{-4}$.

⁴ BARR 95B quotes this as the combined BARR 95B + BURKHARDT 87 result after rescaling BURKHARDT 87 to use same branching ratios and lifetimes as BARR 95B.

Semileptonic modes

 $\Gamma(\pi^\pm e^\mp \nu_e)/\Gamma_{\text{total}}$ Γ_8/Γ

VALUE (units 10^{-4})	CL%	EVTS	DOCUMENT ID	TECN	COMMENT
7.04 ± 0.08 OUR FIT					

7.04 ± 0.08 OUR AVERAGE					
---	--	--	--	--	--

7.046 ± 0.18 ± 0.16			¹ BATLEY	07D NA48	$K^0(\overline{K}^0)(t) \rightarrow \pi e \nu$
---------------------	--	--	---------------------	----------	--

6.91 ± 0.34 ± 0.15	624		² ALOISIO	02 KLOE	Tagged K_S^0 using $\phi \rightarrow K_L^0 K_S^0$
--------------------	-----	--	----------------------	---------	---

• • • We use the following data for averages but not for fits. • • •

7.05 ± 0.09	13k		³ AMBROSINO	06E KLOE	Not fitted
-------------	-----	--	------------------------	----------	------------

• • • We do not use the following data for averages, fits, limits, etc. • • •

7.2 ± 1.4	75		AKHMETSHIN	99 CMD2	Tagged K_S^0 using $\phi \rightarrow K_L^0 K_S^0$
-----------	----	--	------------	---------	---

¹ Reconstructed from $K^0(\overline{K}^0)(t) \rightarrow \pi e \nu$ distributions using PDG values of $B(K_L^0 \rightarrow \pi e \nu) = 0.4053 \pm 0.0015$, $\tau_L = (5.114 \pm 0.021) \times 10^{-8}$ s and $\tau_S = (0.8958 \pm 0.0005) \times 10^{-10}$ s.

² Uses the PDG 00 value for $B(K_S^0 \rightarrow \pi^+\pi^-)$.

³ Obtained by imposing $\sum_i B(K_S^0 \rightarrow i) = 1$, where i runs over all the four branching ratios $\pi^+\pi^-$, $\pi^0\pi^0$, $\pi e \nu$, and $\pi \mu \nu$. Input value of $B(K_S^0 \rightarrow \pi^+\pi^-) / B(K_S^0 \rightarrow \pi^0\pi^0)$ from AMBROSINO 06c is used. To derive $\Gamma(K_S^0 \rightarrow \pi^+\mu\nu) / \Gamma(K_S^0 \rightarrow \pi^+e\nu)$, lepton universality is assumed, radiative corrections from ANDRE 07 are used, and phase space integrals are taken from KTeV, ALEXOPOULOS 04A. This branching fraction enters our fit via their $\Gamma(\pi^\pm e^\mp \nu_e) / \Gamma(\pi^+\pi^-)$ branching ratio measurement.

 $\Gamma(\pi^\pm \mu^\mp \nu_\mu)/\Gamma_{\text{total}}$ Γ_9/Γ

The PDG 06 value below has not been measured but is computed to be 0.666 times the $K_S \rightarrow \pi^\pm e^\mp \nu_e$ branching fraction. It is included in the fit that constrains the four branching ratios $\pi^+\pi^-$, $\pi^0\pi^0$, $\pi e \nu$, and $\pi \mu \nu$ to sum to 1. This treatment, used by AMBROSINO 06E, is preferable to our previous practice of constraining the $\pi^+\pi^-$ and $\pi^0\pi^0$ modes to sum to 1. The 0.666 factor is obtained from AMBROSINO 06E and assumes lepton universality, radiative corrections from ANDRE 07, and phase space integrals from KTeV, ALEXOPOULOS 04A.

VALUE (units 10^{-4})	DOCUMENT ID	COMMENT
4.69 ± 0.06 OUR FIT		

$4.691 \pm 0.001 \pm 0.056$	¹ PDG	06 calculated from $\pi^\pm e^\mp \nu_e$
---	------------------	--

¹ The PDG 06 value is computed to be $B_{\text{PDG06}}(\pi\mu\nu) = 0.666 B_{\text{FIT}}(\pi e\nu)$. The first error specifies the arbitrarily small error, 0.001×10^{-4} , on $B_{\text{PDG06}}(\pi\mu\nu)$ for fixed $B_{\text{FIT}}(\pi e\nu)$. The second error is that due to the uncertainty in $B_{\text{FIT}}(\pi e\nu)$.

 $\Gamma(\pi^\pm e^\mp \nu_e)/\Gamma(\pi^+\pi^-)$ Γ_8/Γ_2

VALUE (units 10^{-4})	EVTS	DOCUMENT ID	TECN
10.18 ± 0.12 OUR FIT			

$10.19 \pm 0.11 \pm 0.07$	13k	AMBROSINO	06E KLOE
---	-----	-----------	----------

CP violating (CP) and $\Delta S = 1$ weak neutral current (S1) modes $\Gamma(3\pi^0)/\Gamma_{\text{total}}$ Γ_{10}/Γ

Violates CP conservation.

VALUE (units 10^{-7})	CL%	EVTS	DOCUMENT ID	TECN	COMMENT
< 0.26	90	590M	¹ BABUSCI	13c KLOE	$\phi \rightarrow K_L^0 K_S^0$

• • • We do not use the following data for averages, fits, limits, etc. • • •

< 1.2	90	37.8M	AMBROSINO	05B KLOE
-------	----	-------	-----------	----------

< 7.4	90	4.9M	² LAI	05A NA48
-------	----	------	------------------	----------

<140	90	7M	ACHASOV	99D SND
------	----	----	---------	---------

<190	90	17300	³ ANGELOPO...	98B CPLR
------	----	-------	--------------------------	----------

<370	90		BARMIN	83 HLBC
------	----	--	--------	---------

¹ BABUSCI 13c uses 1.7 fb^{-1} of data of $\phi \rightarrow K_L^0 K_S^0$ decays with K_L^0 interaction in the calorimeter, collected from 2004 to 2005. No candidate events were found in the data with an expected background of $0.04_{-0.03}^{+0.15}$ events. Upper limit is obtained by normalizing to $K_S^0 \rightarrow 2\pi^0$ decays.

² LAI 05A value is obtained from their bound on $|\eta_{000}|$ (not assuming CP T) and $B(K_L^0 \rightarrow 3\pi^0) = 0.211 \pm 0.003$, and PDG 04 values for K_L^0 and K_S^0 lifetimes. If CP T is assumed then $B(K_S^0 \rightarrow 3\pi^0)_{\text{CPT}} < 2.3 \times 10^{-7}$ at 90% CL

³ ANGELOPOULOS 98B is from $\text{Im}(\eta_{000}) = -0.05 \pm 0.12 \pm 0.05$, assuming $\text{Re}(\eta_{000}) = \text{Re}(\epsilon) = 1.635 \times 10^{-3}$ and using the value $B(K_L^0 \rightarrow \pi^0\pi^0\pi^0) = 0.2112 \pm 0.0027$.

 $\Gamma(\mu^+\mu^-)/\Gamma_{\text{total}}$ Γ_{11}/Γ

Test for $\Delta S = 1$ weak neutral current. Allowed by first-order weak interaction combined with electromagnetic interaction.

VALUE	CL%	DOCUMENT ID	TECN
$< 8 \times 10^{-10}$	90	¹ AAIJ	17BQ LHCB

• • • We do not use the following data for averages, fits, limits, etc. • • •

< 9×10^{-9}	90	² AAIJ	13G LHCB
----------------------	----	-------------------	----------

< 3.2×10^{-7}	90	GJESDAL	73 ASPK
------------------------	----	---------	---------

< 7×10^{-6}	90	HYAMS	69B OSPK
----------------------	----	-------	----------

¹ AAIJ 17BQ uses 3.0 fb^{-1} of pp collisions at $\sqrt{s} = 7$ and 8 TeV. The result utilizes the normalization mode branching fraction $B(K_S^0 \rightarrow \pi^+\pi^-) = (69.20 \pm 0.05) \times 10^{-2}$ from PDG 16. Supersedes AAIJ 13G.

² AAIJ 13G uses 1.0 fb^{-1} of pp collisions at $\sqrt{s} = 7$ TeV. They obtained $B(K_S^0 \rightarrow \mu^+\mu^-) < 11 \times 10^{-9}$ at 95% C.L.

 $\Gamma(e^+e^-)/\Gamma_{\text{total}}$ Γ_{12}/Γ

Test for $\Delta S = 1$ weak neutral current. Allowed by first-order weak interaction combined with electromagnetic interaction.

VALUE (units 10^{-7})	CL%	DOCUMENT ID	TECN	COMMENT
< 0.09	90	¹ AMBROSINO	09A KLOE	$e^+e^- \rightarrow \phi \rightarrow K_S^0 K_L^0$

• • • We do not use the following data for averages, fits, limits, etc. • • •

< 1.4	90	ANGELOPO...	97 CPLR
-------	----	-------------	---------

< 28	90	BLICK	94 CNTR	Hyperon facility
------	----	-------	---------	------------------

<100	90	BARMIN	86 XEBC
------	----	--------	---------

¹ AMBROSINO 09A reports $< 0.09 \times 10^{-7}$ from a measurement of $[\Gamma(K_S^0 \rightarrow e^+e^-) / \Gamma_{\text{total}}] / [B(K_S^0 \rightarrow \pi^+\pi^-)]$ assuming $B(K_S^0 \rightarrow \pi^+\pi^-) = (69.20 \pm 0.05) \times 10^{-2}$.

 $\Gamma(\pi^0 e^+ e^-)/\Gamma_{\text{total}}$ Γ_{13}/Γ

Test for $\Delta S = 1$ weak neutral current. Allowed by first-order weak interaction combined with electromagnetic interaction.

VALUE (units 10^{-9})	CL%	EVTS	DOCUMENT ID	TECN	COMMENT
$3.0_{-1.2}^{+1.5} \pm 0.2$		7	¹ BATLEY	03 NA48	$m_{ee} > 0.165 \text{ GeV}$

• • • We do not use the following data for averages, fits, limits, etc. • • •

< 140	90	LAI	01 NA48
-------	----	-----	---------

< 1100	90	0	BARR	93B NA31
--------	----	---	------	----------

< 45000	90		GIBBONS	88 E731
---------	----	--	---------	---------

¹ BATLEY 03 extrapolate also to the full kinematical region using a constant form factor and a vector matrix element. The resulting branching ratio is $(5.8_{-2.4}^{+2.9}) \times 10^{-9}$.

 $\Gamma(\pi^0 \mu^+ \mu^-)/\Gamma_{\text{total}}$ Γ_{14}/Γ

Test for $\Delta S = 1$ weak neutral current. Allowed by first-order weak interaction combined with electromagnetic interaction.

VALUE (units 10^{-9})	EVTS	DOCUMENT ID	TECN	COMMENT
$2.9_{-1.2}^{+1.5} \pm 0.2$	6	¹ BATLEY	04A NA48	NA48/1 K_S^0 beam

¹ Background estimate is $0.22_{-0.11}^{+0.18}$ events. Branching ratio assumes a vector matrix element and unit form factor.

 K_S^0 FORM FACTORS

For discussion, see note on $K_{\ell 3}$ form factors in the K^\pm section of the Particle Listings above. Because the semileptonic branching fraction is smaller in K_S^0 than K_L^0 by the ratio of the mean lives, the K_S^0 semileptonic form factor has so far been measured only in the K_{e3} mode using the linear expansion $f_+(t) = f_+(0) (1 + \lambda_+ t / m_{\pi^+}^2)$, which gives the vector form factor $f_+(t)$ relative to its value at $t = 0$.

 λ_+ (LINEAR ENERGY DEPENDENCE OF f_+ IN K_{e3} DECAY)

VALUE (units 10^{-2})	EVTS	DOCUMENT ID	TECN
3.39 ± 0.41	15k	AMBROSINO	06E KLOE

CP VIOLATION IN $K_S \rightarrow 3\pi$

Written 1996 by T. Nakada (Paul Scherrer Institute) and L. Wolfenstein (Carnegie-Mellon University).

The possible final states for the decay $K^0 \rightarrow \pi^+\pi^-\pi^0$ have isospin $I = 0, 1, 2$, and 3 . The $I = 0$ and $I = 2$ states have $CP = +1$ and K_S can decay into them without violating CP symmetry, but they are expected to be strongly suppressed by centrifugal barrier effects. The $I = 1$ and $I = 3$ states, which have no centrifugal barrier, have $CP = -1$ so that the K_S decay to these requires CP violation.

In order to see CP violation in $K_S \rightarrow \pi^+\pi^-\pi^0$, it is necessary to observe the interference between K_S and K_L decay, which determines the amplitude ratio

$$\eta_{+-0} = \frac{A(K_S \rightarrow \pi^+\pi^-\pi^0)}{A(K_L \rightarrow \pi^+\pi^-\pi^0)} \quad (1)$$

If η_{+-0} is obtained from an integration over the whole Dalitz plot, there is no contribution from the $I = 0$ and $I = 2$ final states and a nonzero value of η_{+-0} is entirely due to CP violation.

Only $I = 1$ and $I = 3$ states, which are $CP = -1$, are allowed for $K^0 \rightarrow \pi^0\pi^0\pi^0$ decays and the decay of K_S into $3\pi^0$ is an unambiguous sign of CP violation. Similarly to η_{+-0} , η_{000} is defined as

$$\eta_{000} = \frac{A(K_S \rightarrow \pi^0\pi^0\pi^0)}{A(K_L \rightarrow \pi^0\pi^0\pi^0)} \quad (2)$$

If one assumes that CPT invariance holds and that there are no transitions to $I = 3$ (or to nonsymmetric $I = 1$ states), it can be shown that

$$\eta_{+-0} = \eta_{000} = \epsilon + i \frac{\text{Im } a_1}{\text{Re } a_1} \quad (3)$$

With the Wu-Yang phase convention, a_1 is the weak decay amplitude for K^0 into $I = 1$ final states; ϵ is determined from CP violation in $K_L \rightarrow 2\pi$ decays. The real parts of η_{+-0} and η_{000} are equal to $\text{Re}(\epsilon)$. Since currently-known upper limits on $|\eta_{+-0}|$ and $|\eta_{000}|$ are much larger than $|\epsilon|$, they can be interpreted as upper limits on $\text{Im}(\eta_{+-0})$ and $\text{Im}(\eta_{000})$ and so as limits on the CP -violating phase of the decay amplitude a_1 .

CP-VIOLATION PARAMETERS IN K_S^0 DECAY

$$A_S = [\Gamma(K_S^0 \rightarrow \pi^- e^+ \nu_e) - \Gamma(K_S^0 \rightarrow \pi^+ e^- \bar{\nu}_e)] / \text{SUM}$$

Such asymmetry violates CP . If CPT is assumed then $A_S = 2 \text{Re}(\epsilon)$.

VALUE (units 10^{-3})	EVTS	DOCUMENT ID	TECN
-3.8 ± 5.0 ± 2.6	83K	¹ ANASTASI 18A	KLOE
••• We do not use the following data for averages, fits, limits, etc. •••			
1.5 ± 9.6 ± 2.9	13k	AMBROSINO 06E	KLOE

¹ ANASTASI 18A result is a combination of the new measurement and AMBROSINO 06E. The new ANASTASI 18A measurement using data collected from 2004–2005, which corresponds to an integrated luminosity of 1.63 fb^{-1} is $A_S = (-4.9 \pm 5.7 \pm 2.6) \times 10^{-3}$.

PARAMETERS FOR $K_S^0 \rightarrow 3\pi$ DECAY

$$\text{Im}(\eta_{+-0})^2 = \Gamma(K_S^0 \rightarrow \pi^+\pi^-\pi^0, CP\text{-violating}) / \Gamma(K_L^0 \rightarrow \pi^+\pi^-\pi^0)$$

CPT assumed valid (i.e. $\text{Re}(\eta_{+-0}) \simeq 0$).

VALUE	CL%	EVTS	DOCUMENT ID	TECN
••• We do not use the following data for averages, fits, limits, etc. •••				
<0.23	90	601	¹ BARMIN 85	HLBC
<0.12	90	384	METCALF 72	ASPK

¹ BARMIN 85 find $\text{Re}(\eta_{+-0}) = (0.05 \pm 0.17)$ and $\text{Im}(\eta_{+-0}) = (0.15 \pm 0.33)$. Includes events of BALDO-CEOLIN 75.

$$\text{Im}(\eta_{+-0}) = \text{Im}(A(K_S^0 \rightarrow \pi^+\pi^-\pi^0, CP\text{-violating}) / A(K_L^0 \rightarrow \pi^+\pi^-\pi^0))$$

VALUE	CL%	EVTS	DOCUMENT ID	TECN	COMMENT
-0.002 ± 0.009 ± 0.002 - 0.001		500k	¹ ADLER	97B	CPLR
••• We do not use the following data for averages, fits, limits, etc. •••					
-0.002 ± 0.018 ± 0.003		137k	² ADLER	96D	CPLR Sup. by ADLER 97B
-0.015 ± 0.017 ± 0.025		272k	³ ZOU	94	SPEC
¹ ADLER 97B also find $\text{Re}(\eta_{+-0}) = -0.002 \pm 0.007 \pm 0.004 - 0.001$. See also ANGELOPOU-LOS 98C.					
² The ADLER 96D fit also yields $\text{Re}(\eta_{+-0}) = 0.006 \pm 0.013 \pm 0.001$ with a correlation +0.66 between real and imaginary parts. Their results correspond to $ \eta_{+-0} < 0.037$ with 90% CL.					
³ ZOU 94 use theoretical constraint $\text{Re}(\eta_{+-0}) = \text{Re}(\epsilon) = 0.0016$. Without this constraint they find $\text{Im}(\eta_{+-0}) = 0.019 \pm 0.061$ and $\text{Re}(\eta_{+-0}) = 0.019 \pm 0.027$.					

$$\text{Im}(\eta_{000})^2 = \Gamma(K_S^0 \rightarrow 3\pi^0) / \Gamma(K_L^0 \rightarrow 3\pi^0)$$

CPT assumed valid (i.e. $\text{Re}(\eta_{000}) \simeq 0$). This limit determines branching ratio $\Gamma(3\pi^0)/\Gamma_{\text{total}}$ above.

VALUE	CL%	EVTS	DOCUMENT ID	TECN	COMMENT
••• We do not use the following data for averages, fits, limits, etc. •••					
<0.1	90	632	¹ BARMIN 83	HLBC	
<0.28	90		² GJESDAL 74B	SPEC	Indirect meas.
¹ BARMIN 83 find $\text{Re}(\eta_{000}) = (-0.08 \pm 0.18)$ and $\text{Im}(\eta_{000}) = (-0.05 \pm 0.27)$. Assuming CPT invariance they obtain the limit quoted above.					
² GJESDAL 74B uses $K_{2\pi}$, $K_{\mu 3}$, and K_{e3} decay results, unitarity, and CPT . Calculates $ \langle \eta_{000} \rangle = 0.26 \pm 0.20$. We convert to upper limit.					

$$\text{Im}(\eta_{000}) = \text{Im}(A(K_S^0 \rightarrow \pi^0\pi^0\pi^0) / A(K_L^0 \rightarrow \pi^0\pi^0\pi^0))$$

$K_S^0 \rightarrow \pi^0\pi^0\pi^0$ violates CP conservation, in contrast to $K_S^0 \rightarrow \pi^+\pi^-\pi^0$ which has a CP -conserving part.

VALUE	CL%	EVTS	DOCUMENT ID	TECN	COMMENT
-0.001 ± 0.016 OUR AVERAGE					
0.000 ± 0.009 ± 0.013		4.9M	¹ LAI	05A NA48	Assumes CPT
-0.05 ± 0.12 ± 0.05		17300	² ANGELOPOU...	98B	CPLR Assumes CPT
¹ LAI 05A assumes $\text{Re}(\eta_{000}) = \text{Re}(\epsilon) = 1.66 \times 10^{-3}$. The equivalent limit is $ \eta_{000} _{CPT} < 0.025$ at 90% CL. Without assuming CPT invariance, they obtain $\text{Re}(\eta_{000}) = -0.002 \pm 0.011 \pm 0.015$ and $\text{Im}(\eta_{000}) = -0.003 \pm 0.013 \pm 0.017$ with a statistical correlation coefficient of 0.77 and an overall correlation coefficient of 0.57 between imaginary and real part. The equivalent limit is $ \eta_{000} < 0.045$ at 90% CL.					
² ANGELOPOULOS 98B assumes $\text{Re}(\eta_{000}) = \text{Re}(\epsilon) = 1.635 \times 10^{-3}$. Without assuming CPT invariance, they obtain $\text{Re}(\eta_{000}) = 0.18 \pm 0.14 \pm 0.06$ and $\text{Im}(\eta_{000}) = 0.15 \pm 0.20 \pm 0.03$.					

$$|\eta_{000}| = |A(K_S^0 \rightarrow 3\pi^0) / A(K_L^0 \rightarrow 3\pi^0)|$$

A non-zero value violates CP invariance.

VALUE	CL%	EVTS	DOCUMENT ID	TECN	COMMENT
<0.0088		90 590M	BABUSCI	13C	KLOE
••• We do not use the following data for averages, fits, limits, etc. •••					
<0.018	90	37.8M	AMBROSINO 05B	KLOE	
<0.045	90	4.9M	LAI	05A	NA48

DECAY-PLANE ASYMMETRY IN $\pi^+\pi^-e^+e^-$ DECAYS

This is the CP -violating asymmetry

$$A = \frac{N_{\sin\phi\cos\phi>0.0} - N_{\sin\phi\cos\phi<0.0}}{N_{\sin\phi\cos\phi>0.0} + N_{\sin\phi\cos\phi<0.0}}$$

where ϕ is the angle between the e^+e^- and $\pi^+\pi^-$ planes in the K_S^0 rest frame.

$$CP \text{ asymmetry } A \text{ in } K_S^0 \rightarrow \pi^+\pi^-e^+e^-$$

VALUE (%)	DOCUMENT ID	TECN	COMMENT
-0.4 ± 0.8 OUR AVERAGE			
-0.4 ± 0.8	¹ BATLEY	11 NA48	2002 data
-1.1 ± 4.1	LAI	03C NA48	1998+1999 data
••• We do not use the following data for averages, fits, limits, etc. •••			
0.5 ± 4.0 ± 1.6	LAI	03C NA48	1999 data
¹ The result is used to set the limit $A < 1.5\%$ at 90% C.L.			

K_S^0 REFERENCES

ANASTASI 18A	JHEP 1809 021	A. Anastasi et al.	(KLOE-2 Collab.)
AJAI 17BQ	EPJ C77 678	R. Ajai et al.	(LHCb Collab.)
PDG 16	CP C40 100001	C. Patrignani et al.	(PDG Collab.)
AJAI 13G	JHEP 1301 090	R. Ajai et al.	(LHCb Collab.)
BABUSCI 13C	PL B723 54	D. Babusci et al.	(KLOE-2 Collab.)
ABOUZAID 11	PR D83 092001	E. Abouzaid et al.	(FNAL KTeV Collab.)
AMBROSINO 11	EPJ C71 1604	F. Ambrosino et al.	(KLOE Collab.)
BATLEY 11	PL B694 301	J.R. Batley et al.	(CERN NA48/1 Collab.)
AMBROSINO 09A	PL B672 203	F. Ambrosino et al.	(KLOE Collab.)
AMBROSINO 08C	JHEP 0805 051	F. Ambrosino et al.	(KLOE Collab.)
ANDRE 07	ANP 322 2518	T. Andre	(EFT)
BATLEY 07D	PL B653 145	J.R. Batley et al.	(CERN NA48 Collab.)
AMBROSINO 06C	EPJ C48 767	F. Ambrosino et al.	(KLOE Collab.)
AMBROSINO 06E	PL B636 173	F. Ambrosino et al.	(KLOE Collab.)
PDG 06	JP G33 1	W.-M. Yao et al.	(PDG Collab.)
AMBROSINO 05B	PL B619 61	F. Ambrosino et al.	(KLOE Collab.)
BATLEY 05	PL B630 31	J.R. Batley et al.	(NA48 Collab.)
LAI 05A	PL B610 165	A. Lai et al.	(CERN NA48 Collab.)
ALEXOPOU... 04A	PR D70 092007	T. Alexopoulos et al.	(FNAL KTeV Collab.)
BATLEY 04A	PL B599 197	J.R. Batley et al.	(NA48 Collab.)
LAI 04	PL B578 276	A. Lai et al.	(CERN NA48 Collab.)

Meson Particle Listings

K_S^0, K_L^0

PDG	Code	Label	Reference	Collaboration
ALAVI-HARATI	03	PL B592 1	S. Eidelman et al.	(PDG Collab.)
Also		PR D67 012005	A. Alavi-Harati et al.	(FNAL KTeV Collab.)
BATLEY	03	PL B576 43	A. Alavi-Harati et al.	(FNAL KTeV Collab.)
LAI	03	PL B551 7	J.R. Batley et al.	(CERN NA48 Collab.)
LAI	03B	PL B556 105	A. Lai et al.	(CERN NA48 Collab.)
LAI	03C	EPJ C30 33	A. Lai et al.	(CERN NA48 Collab.)
ALOSIO	02	PL B535 37	A. Aloisio et al.	(KLOE Collab.)
ALOSIO	02B	PL B538 21	A. Aloisio et al.	(KLOE Collab.)
LAI	02C	PL B537 28	A. Lai et al.	(CERN NA48 Collab.)
LAI	01	PL B514 253	A. Lai et al.	(CERN NA48 Collab.)
LAI	00	PL B493 29	A. Lai et al.	(CERN NA48 Collab.)
LAI	00B	PL B496 137	A. Lai et al.	(CERN NA48 Collab.)
PDG	00	EPJ C15 1	D.E. Groom et al.	(PDG Collab.)
ACHASOV	99D	PL B459 674	M.N. Achasov et al.	(Novosibirsk CMD-2 Collab.)
AKHMETSHIN	99D	PL B456 90	R.R. Akhmetshin et al.	(Novosibirsk CMD-2 Collab.)
ANGELOPOU...	98B	PL B425 391	A. Angelopoulos et al.	(CLEAR Collab.)
ANGELOPOU...	98C	EPJ C5 389	A. Angelopoulos et al.	(CLEAR Collab.)
PDG	98	EPJ C3 1	C. Caso et al.	(PDG Collab.)
ADLER	97B	PL B407 193	R. Adler et al.	(CLEAR Collab.)
ANGELOPOU...	97	PL B413 232	A. Angelopoulos et al.	(CLEAR Collab.)
BERTANZA	97	ZPHY C73 629	L. Bertanza et al.	(PISA, CERN, EDIN, MANZ, ORSAY+)
ADLER	96D	PL B370 167	R. Adler et al.	(CLEAR Collab.)
ADLER	96E	PL B374 313	R. Adler et al.	(CLEAR Collab.)
ZOU	96	PL B369 362	Y. Zou et al.	(RUTG, MINN, MICH)
BARR	95B	PL B351 579	G.D. Barr et al.	(CERN, EDIN, MANZ, LALO+)
SCHWINGEN...	95	PRL 74 4376	B. Schwinger et al.	(EFL, CHIC+)
BLICK	94	PL B334 234	A.M. Blick et al.	(SERP, JINR)
THOMSON	94	PL B337 411	G.B. Thomson et al.	(RUTG, MINN, MICH)
ZOU	94	PL B329 519	Y. Zou et al.	(RUTG, MINN, MICH)
BARB	93B	PL B304 381	G.D. Barr et al.	(CERN, EDIN, MANZ, LALO+)
GIBBONS	93	PRL 70 1159	L.K. Gibbons et al.	(FNAL E731 Collab.)
Also		PR D55 1625	L.K. Gibbons et al.	(FNAL E731 Collab.)
RAMBERG	93	PRL 70 2525	E. Ramberg et al.	(FNAL E731 Collab.)
BALATS	89	SJNP 49 828	M.Y. Balats et al.	(ITEP)
GIBBONS	88	PRL 61 2661	L.K. Gibbons et al.	(FNAL E731 Collab.)
BURKHARDT	87	PL B199 139	H. Burkhardt et al.	(CERN, EDIN, MANZ+)
GROSSMAN	87	PRL 59 18	N. Grossman et al.	(MINN, MICH, RUTG)
BARMIN	86	SJNP 44 422	V.V. Barmin et al.	(ITEP)
Translated from YAF	44	965	V.V. Barmin et al.	(ITEP, PADO)
BARMIN	86B	NC 96A 159	M. Aguilar-Benitez et al.	(CERN, CIT+)
PDG	86B	PL 170B 130	V.V. Barmin et al.	(ITEP, PADO)
BARMIN	85	NC 85A 67	V.V. Barmin et al.	(ITEP)
Also		SJNP 41 759	V.V. Barmin et al.	(ITEP)
Translated from YAF	41	1187	V.V. Barmin et al.	(ITEP, PADO)
BARMIN	83	PL 129B 129	V.V. Barmin et al.	(ITEP, PADO)
Also		SJNP 39 269	V.V. Barmin et al.	(ITEP, PADO)
Translated from YAF	39	428	V.V. Barmin et al.	(BNL, CHIC, STAN+)
ARONSON	82	PRL 48 1078	S.H. Aronson et al.	(BNL, CHIC, PURD)
ARONSON	82B	PRL 48 1306	S.H. Aronson et al.	(PURD, BNL, CHIC)
Also		PL 116B 73	E. Fischbach et al.	(BNL, CHIC, PURD)
Also		PR D28 476	S.H. Aronson et al.	(BNL, CHIC, PURD)
Also		PR D28 159	S.H. Aronson et al.	(WIS C, EFL, UCSD+)
ARONSON	76	NC 32A 236	S.H. Aronson et al.	(PENN)
EVERHART	76	PR D14 661	G.C. Everhart et al.	(HEIDH, CERN, DORT)
TAUREG	76	PL 65B 92	H. Taureg et al.	(PADO, WIS C)
BALDO...	75	NC 25A 688	M. Baldo-Geolin et al.	(WIS C, EFL, UCSD+)
CARITHERS	75	PRL 34 1244	W.C.J. Carithers et al.	(COLU, NYU)
BOBISUT	74	LNC 11 646	F. Bobisut et al.	(PADO)
COWELL	74	PR D10 2083	P.L. Cowell et al.	(STON, COLU)
GEWENIGER	74B	PL 48B 487	C. Geweniger et al.	(CERN, HEIDH)
GJESDAL	74B	PL 52B 119	S. Gjesdal et al.	(CERN, HEIDH)
BURGUN	73	PL 46B 483	G. Burgun et al.	(SACL, CERN)
GJESDAL	73	PL 44B 217	S. Gjesdal et al.	(CERN, HEIDH)
HILL	73	PR D8 1290	D.G. Hill et al.	(BNL, CMU)
ALITTI	72	PL 39B 568	J. Alitti, E. Lesquoy, A. Muller	(SACL, CERN, OSLO)
BURGUN	72	NP B50 194	G. Burgun et al.	(CERN, IPN, WIEN)
METCALF	72	PL 40B 703	M. Metcalf et al.	(COLO, PRIN, UMD)
MORSE	72B	PRL 28 388	R. Morse et al.	(BUDA)
NAGY	72	NP B47 94	E. Nagy, F. Telbisz, G. Vesztegombi	(BUDA)
Also		PL 30B 498	G. Bozoki et al.	(OSLO, CERN, SACL)
SKJEGGESTAD	72	NP B48 343	O. Skjeggstad et al.	(COLU)
BALTAY	71	PRL 27 1678	C. Baltay et al.	(COLU)
Also		Thesis Nevis 187	W.A. Cooper	(ROCH)
MOFFETT	70	BAPS 15 512	R. Moffett et al.	(BUDA)
BOZOKI	69	PL 30B 498	G. Bozoki et al.	(LRL)
DOYLE	69	Thesis UCRL 18139	J.C. Doyle	(ROCH)
GOBBI	69	PRL 22 682	B. Gobbi et al.	(CERN, MPIM)
HYAMS	69B	PL 29B 521	B.D. Hyams et al.	(LIVP, CERN, INP+)
MORFIN	69	PRL 23 660	J.G. Morfin, D. Sinclair	(BNL, CMU)
DONALD	68B	PL 27B 58	R.A. Donald et al.	(EPOL, ORSAY)
HILL	68	PR 171 1418	D.G. Hill et al.	(LRL, MICH)
AUBERT	65	PL 17 59	B. Aubert et al.	(BRAN, BROW, HARV+)
BROWN	63	PR 130 769	J.L. Brown et al.	(MICH)
CHRETIEN	63	PR 131 2208	M. Chretien et al.	(MIT)
BROWN	61	NC 19 1155	J.L. Brown et al.	
BOLDT	58B	PRL 1 150	E. Boldt, D.O. Caldwell, Y. Pal	

OTHER RELATED PAPERS

LITTENBERG	93	ARNPS 43 729	L.S. Littenberg, G. Valencia	(BNL, FNAL)
Also		Rare and Radiative Kaon Decays		
BATTISTON	92	PRPL 214 293	R. Battiston et al.	(PGIA, CERN, TRSTT)
Also		Status and Perspectives of K Decay Physics		
TRILLING	65B	UCRL 16473	G.N. Trilling	(LRL)
Updated from 1965 Argonne Conference, page 115				
CRAWFORD	62	CERN Conf. 827	F.S. Crawford	(LRL)
FITCH	61	NC 22 1160	V.L. Fitch, P.A. Piroue, R.B. Perkins	(PRIN+)
GOOD	61	PR 124 1223	R.H. Good et al.	(LRL)
BIRGE	60	Rochester Conf. 601	R.W. Birge et al.	(LRL, WIS C)
MULLER	60	PRL 4 418	F. Muller et al.	(LRL, BNL)

K_L^0

$$I(J^P) = \frac{1}{2}(0^-)$$

$$m_{K_L^0} - m_{K_S^0}$$

For earlier measurements, beginning with GOOD 61 and FITCH 61, see our 1986 edition, Physics Letters **170B** 132 (1986).

OUR FIT is described in the note on "CP violation in K_L decays" in the K^0 Particle Listings. The result labeled "OUR FIT Assuming CPT" ["OUR FIT Not assuming CPT"] includes all measurements except those with the comment "Not assuming CPT" ["Assuming CPT"]. Measurements with neither comment do not assume CPT and enter both fits.

VALUE (10^{10} s^{-1})	DOCUMENT ID	TECN	COMMENT
0.5293 ± 0.0009 OUR FIT	Error includes scale factor of 1.3. Assuming CPT		
0.5289 ± 0.0010 OUR FIT	Not assuming CPT		
0.52797 ± 0.00195	1,2 ABOUZAIID 11	KTEV	Not assuming CPT
0.52699 ± 0.00123	1,3 ABOUZAIID 11	KTEV	Assuming CPT
0.5240 ± 0.0044 ± 0.0033	APOSTOLA... 99c	CPLR	$K^0 \rightarrow \pi^+ \pi^-$
0.5297 ± 0.0030 ± 0.0022	4 SCHWINGEN... 95	E773	20-160 GeV K beams
0.5286 ± 0.0028	5 GIBBONS 93	E731	Assuming CPT
0.5257 ± 0.0049 ± 0.0021	4 GIBBONS 93c	E731	Not assuming CPT
0.5340 ± 0.00255 ± 0.0015	6 GEWENIGER 74c	SPEC	Gap method
0.5334 ± 0.0040 ± 0.0015	6,7 GJESDAL 74	SPEC	Assuming CPT
0.5261 ± 0.0015	8 ALAVI-HARATI 03	KTEV	Assuming CPT
0.5288 ± 0.00043	9 ALAVI-HARATI 03	KTEV	Not assuming CPT
0.5343 ± 0.0063 ± 0.0025	10 ANGELOPO... 01	CPLR	
0.5295 ± 0.0020 ± 0.0003	11 ANGELOPO... 98D	CPLR	Assuming CPT
0.5307 ± 0.0013	12 ADLER 96C	RVUE	
0.5274 ± 0.0029 ± 0.0005	11 ADLER 95	CPLR	Sup. by ANGELOPOU-LOS 98D
0.482 ± 0.014	13 ARONSON 82B	SPEC	$E=30-110 \text{ GeV}$
0.534 ± 0.007	14 CARNEGIE 71	ASPK	Gap method
0.542 ± 0.006	14 ARONSON 70	ASPK	Gap method
0.542 ± 0.006	CULLEN 70	CNTR	

- • • We do not use the following data for averages, fits, limits, etc. • • •
- 1 The two ABOUZAIID 11 values use the same data. The first enters the "assuming CPT" fit and the second enters the "not assuming CPT" fit.
- 2 ABOUZAIID 11 fit has Δm , τ_S , ϕ_c , $\text{Re}(e'/\epsilon)$, and $\text{Im}(e'/\epsilon)$ as free parameters. See $\text{Im}(e'/\epsilon)$ in the " K_L^0 CP violation" section for correlation information.
- 3 ABOUZAIID 11 fit has Δm and τ_S free but constrains ϕ_c to the Superweak value, i.e. assumes CPT. See " K_S^0 Mean Life" section for correlation information.
- 4 Fits Δm and ϕ_{+-} simultaneously. GIBBONS 93c systematic error is from B. Winstein via private communication. 20-160 GeV K beams.
- 5 GIBBONS 93 value assume $\phi_{+-} = \phi_{00} = \phi_{SW} = (43.7 \pm 0.2)^\circ$, i.e. assumes CPT. 20-160 GeV K beams.
- 6 These two experiments have a common systematic error due to the uncertainty in the momentum scale, as pointed out in WAHL 89.
- 7 GJESDAL 74 uses charge asymmetry in K_{e3}^0 decays.
- 8 ALAVI-HARATI 03 fit Δm and $\tau_{K_S^0}$ simultaneously. ϕ_{+-} is constrained to the Superweak value, i.e. CPT is assumed. See " K_S^0 Mean Life" section for correlation information. Superseded by ABOUZAIID 11.
- 9 ALAVI-HARATI 03 fit Δm , ϕ_{+-} , and $\tau_{K_S^0}$ simultaneously. See ϕ_{+-} in the " K_L CP violation" section for correlation information. Superseded by ABOUZAIID 11.
- 10 ANGELOPOULOS 01 uses strong interactions strangeness tagging at two different times.
- 11 Uses K_{e3}^0 and K_{e3}^0 strangeness tagging at production and decay. Assumes CPT conservation on $\Delta S = -\Delta Q$ transitions.
- 12 ADLER 96c is the result of a fit which includes nearly the same data as entered into the "OUR FIT" value above.
- 13 ARONSON 82 find that Δm may depend on the kaon energy.
- 14 ARONSON 70 and CARNEGIE 71 use K_S^0 mean life = $(0.862 \pm 0.006) \times 10^{-10} \text{ s}$. We have not attempted to adjust these values for the subsequent change in the K_S^0 mean life or in η_{+-} .

K_L^0 MEAN LIFE

VALUE (10^{-8} s)	EVTS	DOCUMENT ID	TECN	COMMENT	
5.116 ± 0.021 OUR FIT	Error includes scale factor of 1.1.				
5.099 ± 0.021 OUR AVERAGE					
5.072 ± 0.011 ± 0.035	13M	1 AMBROSINO 06	KLOE	$\sum_i B_i = 1$	
5.092 ± 0.017 ± 0.025	15M	AMBROSINO 05c	KLOE		
5.154 ± 0.044	0.4M	VOSBURGH 72	CNTR		
• • • We do not use the following data for averages, fits, limits, etc. • • •					
5.15 ± 0.14		DEVLIN 67	CNTR		
1 AMBROSINO 06 uses $\phi \rightarrow K_L K_S$ with K_L tagged by $K_S \rightarrow \pi^+ \pi^-$. The four major K_L BR's are measured, the small remainder ($\pi^+ \pi^-, \pi^0 \pi^0, \gamma \gamma$) is taken from PDG 04. This KLOE K_L lifetime is obtained by imposing $\sum_i B_i = 1$. The correlation matrix among the four measured K_L BR's and this K_L lifetime is					
	K_{e3}	$K_{\mu 3}$	$3\pi^0$	$\pi^+ \pi^- \pi^0$	τ_{K_L}
	K_{e3}	1	-0.25	-0.56	-0.07
	$K_{\mu 3}$	1	-0.43	-0.20	0.33
	$3\pi^0$		1	-0.39	-0.21
	$\pi^+ \pi^- \pi^0$			1	-0.39
	τ_{K_L}				1

These correlations are taken into account in our fit. The average of this KLOE mean life measurement and the independent KLOE measurement in AMBROSINO 05c is $(5.084 \pm 0.023) \times 10^{-8} \text{ s}$.

K_L^0 DECAY MODES

Mode	Fraction (Γ_i/Γ)	Scale factor/Confidence level
Semileptonic modes		
$\Gamma_1 \pi^\pm e^\mp \nu_e$ Called K_{e3}^0 .	[a] (40.55 ± 0.11) %	S=1.7

Meson Particle Listings

K_L^0

²ALEXOPOULOS 04 constrains $\sum_i B_i = 0.9993$ for the six major K_L branching fractions. The correlations among these branching fractions are taken into account in our fit. The correlation matrix is

	K_{e3}	$K_{\mu 3}$	$3\pi^0$	$\pi^+\pi^-\pi^0$	$\pi^+\pi^-$	$\pi^0\pi^0$
K_{e3}	1					
$K_{\mu 3}$	0.15	1				
$3\pi^0$	-0.77	-0.62	1			
$\pi^+\pi^-\pi^0$	0.18	0.08	-0.54	1		
$\pi^+\pi^-$	0.28	0.22	-0.48	0.49	1	
$\pi^0\pi^0$	-0.72	-0.54	0.89	-0.46	-0.39	1

$\Gamma(\pi^\pm \mu^\mp \nu_\mu)/\Gamma_{total}$ Γ_2/Γ

VALUE	EVTS	DOCUMENT ID	TECN	COMMENT
0.2704 ± 0.0007 OUR FIT				Error includes scale factor of 1.1.
0.2700 ± 0.0008 OUR AVERAGE				
0.2698 ± 0.0005 ± 0.0015	13M	¹ AMBROSINO 06	KLOE	
0.2701 ± 0.0009		² ALEXOPOU... 04	KTEV	

¹There are correlations between these five KLOE measurements: $B(K_L \rightarrow \pi e \nu)$, $B(K_L \rightarrow \pi \mu \nu)$, $B(K_L \rightarrow 3\pi^0)$, $B(K_L \rightarrow \pi^+\pi^-\pi^0)$, and τ_{K_L} measured in AMBROSINO 06. See the footnote for the τ_{K_L} measurement for the correlation matrix.

²For correlations with other ALEXOPOULOS 04 measurements, see the footnote with their $B(K_L \rightarrow \pi e \nu)$ measurement.

$[\Gamma(\pi^\pm e^\mp \nu_e) + \Gamma(\pi^\pm \mu^\mp \nu_\mu)]/\Gamma_{total}$ $(\Gamma_1 + \Gamma_2)/\Gamma$

VALUE	DOCUMENT ID	TECN	COMMENT
0.6760 ± 0.0012 OUR FIT			Error includes scale factor of 1.6.

$\Gamma(\pi^\pm \mu^\mp \nu_\mu)/\Gamma(\pi^\pm e^\mp \nu_e)$ Γ_2/Γ_1

VALUE	EVTS	DOCUMENT ID	TECN	COMMENT
0.6669 ± 0.0027 OUR FIT				Error includes scale factor of 1.2.
0.666 ± 0.004 OUR AVERAGE				Error includes scale factor of 1.6.
• • • We use the following data for averages but not for fits. • • •				
0.6740 ± 0.0059	13M	¹ AMBROSINO 06	KLOE	Not in fit
0.6640 ± 0.0014 ± 0.0022	394K	² ALEXOPOU... 04	KTEV	Not in fit
• • • We do not use the following data for averages, fits, limits, etc. • • •				
0.702 ± 0.011	33k	CHO 80	HBC	
0.662 ± 0.037	10k	WILLIAMS 74	ASPK	
0.741 ± 0.044	6700	BRANDENB... 73	HBC	
0.662 ± 0.030	1309	EVANS 73	HLBC	
0.68 ± 0.08	3548	BASILE 70	OSPK	
0.71 ± 0.05	770	BUDAGOV 68	HLBC	

¹AMBROSINO 06 enters the fit via their separate measurements of these two modes.
²ALEXOPOULOS 04 enters the fit via their separate measurements of these two modes.

$\Gamma((\pi\mu\text{atom})\nu)/\Gamma(\pi^\pm \mu^\mp \nu_\mu)$ Γ_3/Γ_2

VALUE (units 10^{-7})	EVTS	DOCUMENT ID	TECN	COMMENT
3.90 ± 0.39	155	¹ ARONSON 86	SPEC	
• • • We do not use the following data for averages, fits, limits, etc. • • •				
seen	18	COOMBES 76	WIRE	

¹ARONSON 86 quote theoretical value of $(4.31 \pm 0.08) \times 10^{-7}$.

$\Gamma(\pi^0 \pi^\pm e^\mp \nu)/\Gamma_{total}$ Γ_4/Γ

VALUE (units 10^{-5})	CL%	EVTS	DOCUMENT ID	TECN	COMMENT
5.20 ± 0.11 OUR AVERAGE					
5.21 ± 0.07 ± 0.09		5402	BATLEY 04	NA48	
5.16 ± 0.20 ± 0.22		729	MAKOFF 93	E731	
• • • We do not use the following data for averages, fits, limits, etc. • • •					
6.2 ± 2.0		16	CARROLL 80c	SPEC	
< 220		90	¹ DONALDSON 74	SPEC	

¹DONALDSON 74 uses $K_L^0 \rightarrow \pi^+\pi^-\pi^0$ /(all K_L^0 decays) = 0.126.

$\Gamma(\pi^\pm e^\mp \nu e^+ e^-)/\Gamma(\pi^+\pi^-\pi^0)$ Γ_5/Γ_7

VALUE (units 10^{-5})	EVTS	DOCUMENT ID	TECN	COMMENT
10.02 ± 0.17 ± 0.29	19k	¹ ABOUZAIID 07c	KTEV	$M_{ee} > 5$ MeV, $E_{ee}^* > 30$ MeV

¹ E_{ee}^* is the energy of the e^+e^- pair in the kaon rest frame. ABOUZAIID 07c reports $[\Gamma(K_L^0 \rightarrow \pi^\pm e^\mp \nu e^+ e^-)/\Gamma(K_L^0 \rightarrow \pi^+\pi^-\pi^0)] / [B(\pi^0 \rightarrow e^+e^-\gamma)] = (8.54 \pm 0.07 \pm 0.13) \times 10^{-3}$ which we multiply by our best value $B(\pi^0 \rightarrow e^+e^-\gamma) = (1.174 \pm 0.035) \times 10^{-2}$. Our first error is their experiment's error and our second error is the systematic error from using our best value.

————— **Hadronic modes,** —————
 including Charge conjugation×Parity Violating (CPV) modes

$\Gamma(3\pi^0)/\Gamma_{total}$ Γ_6/Γ

VALUE	EVTS	DOCUMENT ID	TECN	COMMENT
0.1952 ± 0.0012 OUR FIT				Error includes scale factor of 1.6.
0.1969 ± 0.0026 OUR AVERAGE				Error includes scale factor of 2.0.
• • • We use the following data for averages but not for fits. • • •				
0.1997 ± 0.0003 ± 0.0019	13M	¹ AMBROSINO 06	KLOE	Not fitted
0.1945 ± 0.0018		¹ ALEXOPOU... 04	KTEV	Not fitted

¹We exclude these $B(K_L \rightarrow 3\pi^0)$ measurements from our fit because the authors have constrained K_L branching fractions to sum to one. It enters our fit via the other measurements from the experiment and their correlations, along with our constraint that the fitted branching fractions sum to one.

$\Gamma(3\pi^0)/\Gamma(\pi^\pm e^\mp \nu_e)$ Γ_6/Γ_1

VALUE	EVTS	DOCUMENT ID	TECN	COMMENT
0.481 ± 0.004 OUR FIT				Error includes scale factor of 1.8.
• • • We use the following data for averages but not for fits. • • •				
0.4782 ± 0.0014 ± 0.0053	209K	¹ ALEXOPOU... 04	KTEV	Not in fit
• • • We do not use the following data for averages, fits, limits, etc. • • •				
0.545 ± 0.004 ± 0.009	38k	KREUTZ 95	NA31	

¹This measurement enters the fit via their separate measurements of these two modes.

$\Gamma(3\pi^0)/[\Gamma(\pi^\pm e^\mp \nu_e) + \Gamma(\pi^\pm \mu^\mp \nu_\mu) + \Gamma(\pi^+\pi^-\pi^0)]$ $\Gamma_6/(\Gamma_1 + \Gamma_2 + \Gamma_7)$

VALUE	EVTS	DOCUMENT ID	TECN	COMMENT
0.2436 ± 0.0018 OUR FIT				Error includes scale factor of 1.6.
• • • We do not use the following data for averages, fits, limits, etc. • • •				
0.251 ± 0.014	549	BUDAGOV 68	HLBC	ORSAY measur.
0.277 ± 0.021	444	BUDAGOV 68	HLBC	Ecole polytec.meas
0.31 ± 0.07	29	KULYUKINA 68	CC	
0.24 ± 0.08	24	ANIKINA 64	CC	

$\Gamma(3\pi^0)/\Gamma(\pi^+\pi^-\pi^0)$ Γ_6/Γ_7

VALUE	EVTS	DOCUMENT ID	TECN	COMMENT
1.557 ± 0.012 OUR FIT				Error includes scale factor of 1.3.
• • • We use the following data for averages but not for fits. • • •				
1.582 ± 0.027	13M	¹ AMBROSINO 06	KLOE	Not in fit
• • • We do not use the following data for averages, fits, limits, etc. • • •				
1.611 ± 0.014 ± 0.034	28k	KREUTZ 95	NA31	
1.65 ± 0.07	883	BARMIN 72b	HLBC	Error statistical only
1.80 ± 0.13	1010	BUDAGOV 68	HLBC	
2.0 ± 0.6	188	ALEKSANYAN 64b	FBC	

¹AMBROSINO 06 enters the fit via their separate measurements of these two modes.

$\Gamma(\pi^+\pi^-\pi^0)/\Gamma_{total}$ Γ_7/Γ

VALUE	EVTS	DOCUMENT ID	TECN	COMMENT
0.1254 ± 0.0005 OUR FIT				
0.1255 ± 0.0006 OUR AVERAGE				
0.1263 ± 0.0004 ± 0.0011	13M	¹ AMBROSINO 06	KLOE	
0.1252 ± 0.0007		² ALEXOPOU... 04	KTEV	

¹There are correlations between these five KLOE measurements: $B(K_L \rightarrow \pi e \nu)$, $B(K_L \rightarrow \pi \mu \nu)$, $B(K_L \rightarrow 3\pi^0)$, $B(K_L \rightarrow \pi^+\pi^-\pi^0)$, and τ_{K_L} measured in AMBROSINO 06. See the footnote for the τ_{K_L} measurement for the correlation matrix.

²For correlations with other ALEXOPOULOS 04 measurements, see the footnote with their $B(K_L \rightarrow \pi e \nu)$ measurement.

$\Gamma(\pi^+\pi^-\pi^0)/\Gamma(\pi^\pm e^\mp \nu_e)$ Γ_7/Γ_1

VALUE	EVTS	DOCUMENT ID	TECN	COMMENT
0.3092 ± 0.0016 OUR FIT				Error includes scale factor of 1.1.
• • • We use the following data for averages but not for fits. • • •				
0.3078 ± 0.0005 ± 0.0017	799K	¹ ALEXOPOU... 04	KTEV	Not in fit
• • • We do not use the following data for averages, fits, limits, etc. • • •				
0.336 ± 0.003 ± 0.007	28k	KREUTZ 95	NA31	

¹This measurement enters the fit via their separate measurements for the two modes.

$\Gamma(\pi^+\pi^-\pi^0)/[\Gamma(\pi^\pm e^\mp \nu_e) + \Gamma(\pi^\pm \mu^\mp \nu_\mu) + \Gamma(\pi^+\pi^-\pi^0)]$ $\Gamma_7/(\Gamma_1 + \Gamma_2 + \Gamma_7)$

VALUE	EVTS	DOCUMENT ID	TECN	COMMENT
0.1565 ± 0.0006 OUR FIT				Error includes scale factor of 1.1.
• • • We do not use the following data for averages, fits, limits, etc. • • •				
0.163 ± 0.003	6499	CHO 77	HBC	
0.1605 ± 0.0038	1590	ALEXANDER 73b	HBC	
0.146 ± 0.004	3200	BRANDENB... 73	HBC	
0.159 ± 0.010	558	EVANS 73	HLBC	
0.167 ± 0.016	1402	KULYUKINA 68	CC	
0.161 ± 0.005		HOPKINS 67	HBC	
0.162 ± 0.015	126	HAWKINS 66	HBC	
0.159 ± 0.015	326	ASTBURY 65b	CC	
0.178 ± 0.017	566	GUIDONI 65	HBC	
0.144 ± 0.004	1729	HOPKINS 65	HBC	See HOPKINS 67

$\Gamma(\pi^+\pi^-)/\Gamma_{total}$ Γ_8/Γ

VALUE (units 10^{-3})	DOCUMENT ID	TECN	COMMENT
1.967 ± 0.010 OUR FIT			Error includes scale factor of 1.5.
1.975 ± 0.012	¹ ALEXOPOU... 04	KTEV	

¹For correlations with other ALEXOPOULOS 04 measurements, see the footnote with their $B(K_L \rightarrow \pi e \nu)$ measurement.

$\Gamma(\pi^+\pi^-)/\Gamma(\pi^\pm e^\mp \nu_e)$ Γ_8/Γ_1

VALUE (units 10^{-3})	EVTS	DOCUMENT ID	TECN	COMMENT
4.849 ± 0.020 OUR FIT				Error includes scale factor of 1.1.
4.840 ± 0.020 OUR AVERAGE				
4.826 ± 0.022 ± 0.016	47k	¹ LAI 07	NA48	
• • • We use the following data for averages but not for fits. • • •				
4.856 ± 0.017 ± 0.023	84k	² ALEXOPOU... 04	KTEV	Not in fit

¹The LAI 07 central value of 4.835×10^{-3} has been reduced by 0.19% to 4.826×10^{-3} to subtract the contribution from the direct emission mode $K_L^0 \rightarrow \pi^+\pi^-\gamma$ (DE).

²This measurement enters the fit via their separate measurements for the two modes.

$[\Gamma(\pi^+\pi^-) + \Gamma(\pi^+\pi^-\gamma(\text{DE}))]/\Gamma(\pi^\pm\mu^\mp\nu_\mu)$ $(\Gamma_8+\Gamma_{14})/\Gamma_2$

VALUE (units 10^{-3})	EVTS	DOCUMENT ID	TECN
7.38 ± 0.04 OUR FIT			Error includes scale factor of 1.4.
7.275 ± 0.042 ± 0.054	45k	¹ AMBROSINO 06F KLOE	

¹Fully inclusive. Taking $B(K_L^0 \rightarrow \pi\mu\nu)$ from KLOE, AMBROSINO 06, $B(K_L^0 \rightarrow \pi^+\pi^-\gamma(\text{DE})) = (1.963 \pm 0.012 \pm 0.017) \times 10^{-3}$ is obtained.

$\Gamma(\pi^+\pi^-)/[\Gamma(\pi^\pm e^\mp\nu_e) + \Gamma(\pi^\pm\mu^\mp\nu_\mu)]$ $\Gamma_8/(\Gamma_1+\Gamma_2)$

Violates CP conservation.

VALUE (units 10^{-3})	EVTS	DOCUMENT ID	TECN	COMMENT
2.909 ± 0.013 OUR FIT				Error includes scale factor of 1.3.

- • • We do not use the following data for averages, fits, limits, etc. • • •
- 3.13 ± 0.14 1687 COUPAL 85 SPEC $\eta_{+-} = 2.28 \pm 0.06$
- 3.04 ± 0.14 2703 DEVOE 77 SPEC $\eta_{+-} = 2.25 \pm 0.05$
- 2.51 ± 0.23 309 ¹DEBOUARD 67 OSPK $\eta_{+-} = 2.00 \pm 0.09$
- 2.35 ± 0.19 525 ¹FITCH 67 OSPK $\eta_{+-} = 1.94 \pm 0.08$

¹Old experiments excluded from fit. See subsection on η_{+-} in section on "PARAMETERS FOR $K_L^0 \rightarrow 2\pi$ DECAY" below for average η_{+-} of these experiments and for note on discrepancy.

$\Gamma(\pi^\pm e^\mp\nu_e)/\Gamma(2 \text{ tracks})$ $\Gamma_1/(\Gamma_1+\Gamma_2+0.03508\Gamma_6+\Gamma_7+\Gamma_8)$

$\Gamma(2 \text{ tracks}) = \Gamma(\pi^\pm e^\mp\nu_e) + \Gamma(\pi^\pm\mu^\mp\nu_\mu) + 0.03508 \Gamma(3\pi^0) + \Gamma(\pi^+\pi^-\pi^0) + \Gamma(\pi^+\pi^-)$ where 0.03508 is the fraction of $3\pi^0$ events with one Dalitz decay ($\pi^0 \rightarrow \gamma e^+e^-$).

VALUE	EVTS	DOCUMENT ID	TECN
0.5006 ± 0.0009 OUR FIT			Error includes scale factor of 1.3.
0.4978 ± 0.0035	6.8M	LAI 04B NA48	

$\Gamma(\pi^+\pi^-)/[\Gamma(\pi^\pm e^\mp\nu_e) + \Gamma(\pi^\pm\mu^\mp\nu_\mu) + \Gamma(\pi^+\pi^-\pi^0)]$ $\Gamma_8/(\Gamma_1+\Gamma_2+\Gamma_7)$

Violates CP conservation.

VALUE (units 10^{-3})	EVTS	DOCUMENT ID	TECN	COMMENT
2.454 ± 0.011 OUR FIT				Error includes scale factor of 1.3.

- • • We do not use the following data for averages, fits, limits, etc. • • •
 - 2.60 ± 0.07 4200 ¹MESSNER 73 ASPK $\eta_{+-} = 2.23 \pm 0.05$
- ¹From same data as $\Gamma(\pi^+\pi^-)/\Gamma(\pi^+\pi^-\pi^0)$ MESSNER 73, but with different normalization.

$\Gamma(\pi^+\pi^-)/\Gamma(\pi^+\pi^-\pi^0)$ Γ_8/Γ_7

Violates CP conservation.

VALUE (units 10^{-2})	EVTS	DOCUMENT ID	TECN	COMMENT
1.568 ± 0.010 OUR FIT				Error includes scale factor of 1.3.

- • • We do not use the following data for averages, fits, limits, etc. • • •
- 1.64 ± 0.04 4200 MESSNER 73 ASPK $\eta_{+-} = 2.23$

$\Gamma(\pi^0\pi^0)/\Gamma_{\text{total}}$ Γ_9/Γ

Violates CP conservation.

VALUE (units 10^{-3})	DOCUMENT ID	TECN
0.864 ± 0.006 OUR FIT		
0.865 ± 0.012	¹ ALEXOPOU... 04 KTEV	

¹For correlations with other ALEXOPOULOS 04 measurements, see the footnote with their $B(K_L \rightarrow \pi e \nu)$ measurement.

$\Gamma(\pi^0\pi^0)/\Gamma(\pi^+\pi^-)$ Γ_9/Γ_8

Violates CP conservation.

VALUE	DOCUMENT ID	TECN
0.4395 ± 0.0023 OUR FIT		
0.4390 ± 0.0012	ETAFIT 16	

$\Gamma(\pi^0\pi^0)/\Gamma(3\pi^0)$ Γ_9/Γ_6

Violates CP conservation.

VALUE (units 10^{-2})	EVTS	DOCUMENT ID	TECN	COMMENT
0.443 ± 0.004 OUR FIT				Error includes scale factor of 2.1.

- • • We use the following data for averages but not for fits. • • •
- 0.4446 ± 0.0016 ± 0.0019** 100K ¹ALEXOPOU... 04 KTEV Not in fit
- • • We do not use the following data for averages, fits, limits, etc. • • •
- 0.37 ± 0.08 29 BARMIN 70 HLBC $\eta_{00} = 2.02 \pm 0.23$
- 0.32 ± 0.15 30 BUDAGOV 70 HLBC $\eta_{00} = 1.9 \pm 0.5$
- 0.46 ± 0.11 57 BANNER 69 OSPK $\eta_{00} = 2.2 \pm 0.3$

¹This measurement enters the fit via their separate measurements for the two modes.

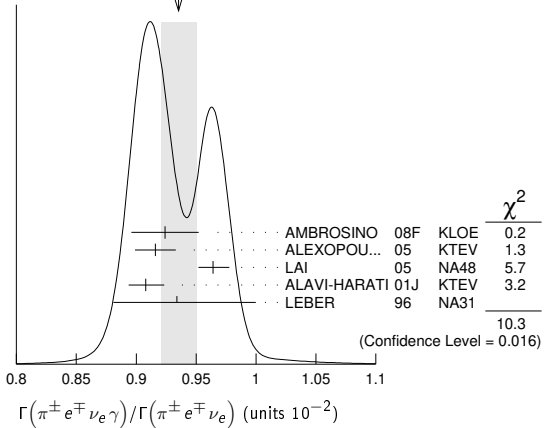
———— Semileptonic modes with photons ————

$\Gamma(\pi^\pm e^\mp\nu_e)/\Gamma(\pi^\pm e^\mp\nu_e)$ Γ_{10}/Γ_1

VALUE (units 10^{-2})	EVTS	DOCUMENT ID	TECN	COMMENT
0.935 ± 0.015 OUR AVERAGE				Error includes scale factor of 1.9. See the ideogram below.
0.924 ± 0.023 ± 0.016	9k	¹ AMBROSINO 08F KLOE		$E_\gamma^* > 30 \text{ MeV}, \theta_{e\gamma}^* > 20^\circ$
0.916 ± 0.017	4309	² ALEXOPOU... 05 KTEV		$E_\gamma^* > 30 \text{ MeV}, \theta_{e\gamma}^* > 20^\circ$
0.964 ± 0.008 ± $^{+0.011}_{-0.009}$	19K	LAI 05 NA48		$E_\gamma^* > 30 \text{ MeV}, \theta_{e\gamma}^* > 20^\circ$
0.908 ± 0.008 ± $^{+0.013}_{-0.012}$	15k	ALAVI-HARATI01J KTEV		$E_\gamma^* \geq 30 \text{ MeV}, \theta_{e\gamma}^* \geq 20^\circ$
0.934 ± 0.036 ± $^{+0.055}_{-0.039}$	1384	LEBER 96 NA31		$E_\gamma^* \geq 30 \text{ MeV}, \theta_{e\gamma}^* \geq 20^\circ$

¹Direct emission contribution measured $\langle X \rangle = -2.3 \pm 1.3 \pm 1.4$.
²Also measured cut $E_\gamma^* > 10 \text{ MeV}, \theta_{e\gamma}^* > 0^\circ$ 14221 evts: $\Gamma(\pi^\pm e^\mp\nu_e\gamma) / \Gamma(\pi^\pm e^\mp\nu_e) = (4.942 \pm 0.062)\%$.

WEIGHTED AVERAGE
0.935±0.015 (Error scaled by 1.9)



$\Gamma(\pi^\pm\mu^\mp\nu_\mu\gamma)/\Gamma(\pi^\pm\mu^\mp\nu_\mu)$ Γ_{11}/Γ_2

VALUE (units 10^{-3})	EVTS	DOCUMENT ID	TECN	COMMENT
2.09 ± 0.08 OUR AVERAGE				
2.09 ± 0.09		¹ ALEXOPOU... 05	KTEV	$E_\gamma^* > 30 \text{ MeV}$
2.08 ± 0.17 ± $^{+0.16}_{-0.21}$	252	BENDER 98	NA48	$E_\gamma^* \geq 30 \text{ MeV}$

¹Also measured cut $E_\gamma^* > 10 \text{ MeV}$, 1385 evts: $\Gamma(\pi^\pm\mu^\mp\nu_\mu\gamma) / \Gamma(\pi^\pm\mu^\mp\nu_\mu) = (0.530 \pm 0.014 \pm 0.012)\%$.

———— Hadronic modes with photons or $e\bar{e}$ pairs ————

$\Gamma(\pi^0\pi^0\gamma)/\Gamma_{\text{total}}$ Γ_{12}/Γ

VALUE (units 10^{-6})	CL%	DOCUMENT ID	TECN	COMMENT
< 0.243	90	ABOUZAID 08B KTEV		$K_L^0 \rightarrow \pi^0\pi_D^0\gamma, \pi_D^0 \rightarrow e\bar{e}\gamma$
• • • We do not use the following data for averages, fits, limits, etc. • • •				
< 5.6	90	BARR 94 NA31		
< 230	90	ROBERTS 94 E799		

$\Gamma(\pi^+\pi^-\gamma)/\Gamma(\pi^+\pi^-\pi^0)$ Γ_{13}/Γ_7

For earlier limits see our 1992 edition Physical Review D45 S1 (1992).

VALUE (units 10^{-4})	EVTS	DOCUMENT ID	TECN	COMMENT
• • • We do not use the following data for averages, fits, limits, etc. • • •				
1.23 ± 0.13	516	^{1,2} CARROLL 80B SPEC		$E_\gamma^* > 20 \text{ MeV}$
2.33 ± 0.23	546	^{1,3} CARROLL 80B SPEC		
3.56 ± 0.26	1062	^{1,4} CARROLL 80B SPEC		$E_\gamma^* > 20 \text{ MeV}$

¹CARROLL 80B quotes $B(\pi^+\pi^-\gamma)$ using normalization $B(\pi^+\pi^-\pi^0) = 0.1239$. We divide by this value to obtain their measured $\Gamma(\pi^+\pi^-\gamma) / \Gamma(\pi^+\pi^-\pi^0)$.

²Internal Bremsstrahlung component only.
³Direct γ emission component only.
⁴Both IB and DE components.

$\Gamma(\pi^+\pi^-\gamma)/\Gamma(\pi^+\pi^-)$ Γ_{13}/Γ_8

VALUE (units 10^{-2})	EVTS	DOCUMENT ID	TECN	COMMENT
2.11 ± 0.08 OUR FIT				Error includes scale factor of 2.9.
2.11 ± 0.08 OUR AVERAGE				Error includes scale factor of 2.9.
2.08 ± 0.02 ± 0.02	8669	¹ ALAVI-HARATI01B KTEV		$E_\gamma^* > 20 \text{ MeV}$
2.30 ± 0.07	3136	RAMBERG 93 E731		$E_\gamma^* > 20 \text{ MeV}$

¹ALAVI-HARATI 01B includes both Direct Emission (DE) and Inner Bremsstrahlung (IB) processes.

$\Gamma(\pi^+\pi^-\gamma(\text{DE}))/\Gamma(\pi^+\pi^-)$ Γ_{14}/Γ_{13}

These values assume that $\Gamma(K_L^0 \rightarrow \pi^+\pi^-\gamma) = \Gamma(K_L^0 \rightarrow \pi^+\pi^-\gamma(\text{DE})) + \Gamma(K_L^0 \rightarrow \pi^+\pi^-\gamma(\text{IB}))$, the sum of widths for the direct emission (DE) and inner bremsstrahlung (IE) processes, with no IB-DE interference. DE assumes a form factor as described in RAMBERG 93.

VALUE	EVTS	DOCUMENT ID	TECN	COMMENT
0.684 ± 0.009 OUR FIT				
0.684 ± 0.009 OUR AVERAGE				
0.689 ± 0.021	111k	ABOUZAID 06A KTEV		$E_\gamma^* > 20 \text{ MeV}$
0.683 ± 0.011	8669	ALAVI-HARATI01B KTEV		$E_\gamma^* > 20 \text{ MeV}$
0.685 ± 0.041	3136	RAMBERG 93 E731		$E_\gamma^* > 20 \text{ MeV}$

Meson Particle Listings

K_L^0

$\Gamma(\pi^0 2\gamma)/\Gamma_{\text{total}}$ Γ_{15}/Γ

VALUE (units 10^{-6})	CL%	EVTS	DOCUMENT ID	TECN	COMMENT
1.273 ± 0.033 OUR AVERAGE					
1.28 ± 0.06 ± 0.01		1.4k	¹ ABOUZAIID	08	KTEV
1.27 ± 0.04 ± 0.01		2.5k	² LAI	02b	NA48
• • • We do not use the following data for averages, fits, limits, etc. • • •					
1.68 ± 0.07 ± 0.08		884	³ ALAVI-HARATI	99b	KTEV
1.7 ± 0.2 ± 0.2		63	⁴ BARR	92	NA31
1.86 ± 0.60 ± 0.60		60	PAPADIMITR...	91	E731 $m_{\gamma\gamma} > 280$ MeV
<5.1		90	PAPADIMITR...	91	E731 $m_{\gamma\gamma} < 264$ MeV
2.1 ± 0.6		14	⁵ BARR	90c	NA31 $m_{\gamma\gamma} > 280$ MeV

¹ ABOUZAIID 08 reports $(1.29 \pm 0.03 \pm 0.05) \times 10^{-6}$ from a measurement of $[\Gamma(K_L^0 \rightarrow \pi^0 2\gamma)/\Gamma_{\text{total}}] / [B(K_L^0 \rightarrow \pi^0 \pi^0)]$ assuming $B(K_L^0 \rightarrow \pi^0 \pi^0) = (8.69 \pm 0.04) \times 10^{-4}$, which we rescale to our best value $B(K_L^0 \rightarrow \pi^0 \pi^0) = (8.64 \pm 0.06) \times 10^{-4}$. Our first error is their experiment's error and our second error is the systematic error from using our best value.
² LAI 02b reports $[\Gamma(K_L^0 \rightarrow \pi^0 2\gamma)/\Gamma_{\text{total}}] / [B(K_L^0 \rightarrow \pi^0 \pi^0)] = (1.467 \pm 0.032 \pm 0.032) \times 10^{-3}$ which we multiply by our best value $B(K_L^0 \rightarrow \pi^0 \pi^0) = (8.64 \pm 0.06) \times 10^{-4}$. Our first error is their experiment's error and our second error is the systematic error from using our best value. They also find that $B(\pi^0 2\gamma, m_{\gamma\gamma} < 110$ MeV) $< 0.6 \times 10^{-8}$ (90% CL).
³ ALAVI-HARATI 99b finds that $\Gamma(\pi^0 2\gamma, m_{\gamma\gamma} < 240$ MeV) / $\Gamma(\pi^0 2\gamma) = (17.3 \pm 1.3 \pm 1.5)\%$. Superseded by ABOUZAIID 08.
⁴ BARR 92 find that $\Gamma(\pi^0 2\gamma, m_{\gamma\gamma} < 240$ MeV) / $\Gamma(\pi^0 2\gamma) < 0.09$ (90% CL).
⁵ BARR 90c superseded by BARR 92.

$\Gamma(\pi^0 \gamma e^+ e^-)/\Gamma_{\text{total}}$ Γ_{16}/Γ

VALUE (units 10^{-8})	CL%	EVTS	DOCUMENT ID	TECN	COMMENT
1.62 ± 0.14 ± 0.09					
		125	¹ ABOUZAIID	07D	KTEV
• • • We do not use the following data for averages, fits, limits, etc. • • •					
2.34 ± 0.35 ± 0.13		44	ALAVI-HARATI	01E	KTEV
<71		90	MURAKAMI	99	SPEC

¹ ABOUZAIID 07D includes 1997 (ALAVI-HARATI 01E) and 1999 data. It measures the ratio of $B(K_L^0 \rightarrow \pi^0 \gamma e^+ e^-) / B(K_L^0 \rightarrow \pi^0 \pi^0_D)$, where π^0_D is the Dalitz decaying π^0 , and uses PDG 06 values $B(K_L^0 \rightarrow \pi^0 \pi^0) = (8.69 \pm 0.04) \times 10^{-4}$, and $B(\pi^0_D \rightarrow e^+ e^- \gamma) = (1.198 \pm 0.032) \times 10^{-2}$. Supersedes ALAVI-HARATI 01E result.

Other modes with photons or $\ell\bar{\ell}$ pairs

$\Gamma(2\gamma)/\Gamma_{\text{total}}$ Γ_{17}/Γ

VALUE (units 10^{-4})	EVTS	DOCUMENT ID	TECN	COMMENT
2.47 ± 0.04 OUR FIT Error includes scale factor of 1.1.				
• • • We do not use the following data for averages, fits, limits, etc. • • •				
4.54 ± 0.84		¹ BANNER	72b	OSPK
4.5 ± 1.0		ENSTROM	71	OSPK K_L^0 1.5–9 GeV/c
5.0 ± 1.0		² REPELLIN	71	OSPK
5.5 ± 1.1		90 KUNZ	68	OSPK Norm.to $3\pi(C+N)$

¹ This value uses $(\eta_{00}/\eta_{+-})^2 = 1.05 \pm 0.14$. In general, $\Gamma(2\gamma)/\Gamma_{\text{total}} = [(4.32 \pm 0.55) \times 10^{-4}] [(\eta_{00}/\eta_{+-})^2]$.
² Assumes regeneration amplitude in copper at 2 GeV is 22 mb. To evaluate for a given regeneration amplitude and error, multiply by (regeneration amplitude/22mb)².

$\Gamma(2\gamma)/\Gamma(3\pi^0)$ Γ_{17}/Γ_6

VALUE (units 10^{-3})	EVTS	DOCUMENT ID	TECN	COMMENT
2.802 ± 0.017 OUR FIT				
2.802 ± 0.018 OUR AVERAGE				
2.79 ± 0.02 ± 0.02	27k	ADINOLFI	03	KLOE
2.81 ± 0.01 ± 0.02		LAI	03	NA48
• • • We do not use the following data for averages, fits, limits, etc. • • •				
2.13 ± 0.43	28	BARMIN	71	HLBC
2.24 ± 0.28	115	BANNER	69	OSPK
2.5 ± 0.7	16	ARNOLD	68b	HLBC Vacuum decay

$\Gamma(2\gamma)/\Gamma(\pi^0 \pi^0)$ Γ_{17}/Γ_9

VALUE	EVTS	DOCUMENT ID	TECN	COMMENT
0.633 ± 0.006 OUR FIT Error includes scale factor of 1.4.				
0.632 ± 0.004 ± 0.008				
	110k	BURKHARDT	87	NA31

$\Gamma(3\gamma)/\Gamma_{\text{total}}$ Γ_{18}/Γ

VALUE	CL%	DOCUMENT ID	TECN	COMMENT
<7.4 × 10⁻⁸				
	90	¹ TUNG	11	K391
• • • We do not use the following data for averages, fits, limits, etc. • • •				
<2.4 × 10 ⁻⁷		² BARR	95c	NA31

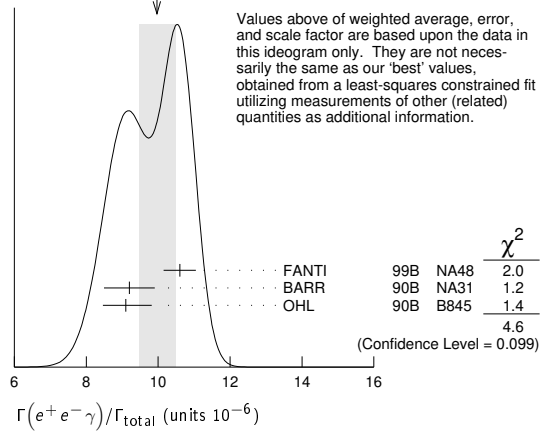
¹ TUNG 11 reports the result assuming parity violating interaction and using 2005 data (Run-II and III). Assuming parity conserving or phase space interaction, the 90% upper limits obtained are 7.5×10^{-8} and 8.6×10^{-8} , respectively.
² Assumes a phase-space decay distribution.

$\Gamma(e^+ e^- \gamma)/\Gamma_{\text{total}}$ Γ_{19}/Γ

VALUE (units 10^{-6})	EVTS	DOCUMENT ID	TECN	COMMENT
9.4 ± 0.4 OUR FIT Error includes scale factor of 2.0.				
10.0 ± 0.5 OUR AVERAGE Error includes scale factor of 1.5. See the ideogram below.				
10.6 ± 0.2 ± 0.4	6864	¹ FANTI	99b	NA48
9.2 ± 0.5 ± 0.5	1053	BARR	90b	NA31
9.1 ± 0.4 ^{+0.6} _{-0.5}	919	OHL	90b	B845

¹ For FANTI 99b, the ± 0.4 systematic error includes for uncertainties in the calculation, primarily uncertainties in the $\pi^0 \rightarrow e^+ e^- \gamma$ and $K_L^0 \rightarrow \pi^0 \pi^0$ branching ratios, evaluated using our 1999 Web edition values.

WEIGHTED AVERAGE
10.0 ± 0.5 (Error scaled by 1.5)



$\Gamma(e^+ e^- \gamma)/\Gamma(3\pi^0)$ Γ_{19}/Γ_6

VALUE (units 10^{-5})	EVTS	DOCUMENT ID	TECN	COMMENT
4.82 ± 0.21 OUR FIT Error includes scale factor of 2.0.				
4.63 ± 0.04 ± 0.13				
	83k	¹ ABOUZAIID	07b	KTEV

¹ ABOUZAIID 07b reports $[\Gamma(K_L^0 \rightarrow e^+ e^- \gamma)/\Gamma(K_L^0 \rightarrow 3\pi^0)] / [3\Gamma(\pi^0 \rightarrow 2\gamma)/\Gamma_{\text{total}} \times \Gamma(\pi^0 \rightarrow e^+ e^- \gamma)/\Gamma_{\text{total}}] = (1.3302 \pm 0.0046 \pm 0.0103) \times 10^{-3}$ which we multiply by our best value $3\Gamma(\pi^0 \rightarrow 2\gamma)/\Gamma_{\text{total}} \times \Gamma(\pi^0 \rightarrow e^+ e^- \gamma)/\Gamma_{\text{total}} = 0.0348 \pm 0.0010$. Our first error is their experiment's error and our second error is the systematic error from using our best value.

$\Gamma(\mu^+ \mu^- \gamma)/\Gamma_{\text{total}}$ Γ_{20}/Γ

VALUE (units 10^{-7})	EVTS	DOCUMENT ID	TECN	COMMENT
3.59 ± 0.11 OUR AVERAGE Error includes scale factor of 1.3.				
3.62 ± 0.04 ± 0.08	9100	ALAVI-HARATI	01G	KTEV
3.4 ± 0.6 ± 0.4	45	FANTI	97	NA48
3.23 ± 0.23 ± 0.19	197	SPENCER	95	E799

$\Gamma(e^+ e^- \gamma)/\Gamma_{\text{total}}$ Γ_{21}/Γ

VALUE (units 10^{-7})	EVTS	DOCUMENT ID	TECN	COMMENT
5.95 ± 0.33 OUR AVERAGE				
5.84 ± 0.15 ± 0.32	1543	ALAVI-HARATI	01F	KTEV $E_\gamma^* > 5$ MeV
8.0 ± 1.5 ^{+1.4} _{-1.2}	40	SETZU	98	NA31 $E_\gamma^* > 5$ MeV
6.5 ± 1.2 ± 0.6	58	NAKAYA	94	E799 $E_\gamma^* > 5$ MeV
6.6 ± 3.2		MORSE	92	B845 $E_\gamma^* > 5$ MeV

$\Gamma(\mu^+ \mu^- \gamma\gamma)/\Gamma_{\text{total}}$ Γ_{22}/Γ

VALUE (units 10^{-9})	EVTS	DOCUMENT ID	TECN	COMMENT
10.4^{+7.5}_{-5.9} ± 0.7				
	4	ALAVI-HARATI	00E	KTEV $m_{\gamma\gamma} \geq 1$ MeV/c ²

Charge conjugation × Parity (CP) or Lepton Family number (LF) violating modes, or $\Delta S = 1$ weak neutral current (S1) modes

$\Gamma(\mu^+ \mu^-)/\Gamma(\pi^+ \pi^-)$ Γ_{23}/Γ_8

Test for $\Delta S = 1$ weak neutral current. Allowed by higher-order electroweak interaction.

VALUE (units 10^{-6})	EVTS	DOCUMENT ID	TECN	COMMENT
3.48 ± 0.05 OUR AVERAGE				
3.474 ± 0.057	6210	AMBROSE	00	B871
3.87 ± 0.30	179	¹ AKAGI	95	SPEC
3.38 ± 0.17	707	HEINSON	95	B791

• • • We do not use the following data for averages, fits, limits, etc. • • •
 3.9 ± 0.3 ± 0.1 178 ² AKAGI 91b SPEC In AKAGI 95
 3.45 ± 0.18 ± 0.13 368 ³ HEINSON 91 SPEC In HEINSON 95
 4.1 ± 0.5 54 INAGAKI 89 SPEC In AKAGI 91b
 2.8 ± 0.3 ± 0.2 87 MATHIAZHA...89b SPEC In HEINSON 91

¹ AKAGI 95 gives this number multiplied by the PDG 1992 average for $\Gamma(K_L^0 \rightarrow \pi^+ \pi^-)/\Gamma_{\text{total}}$.

²AKAGI 91B give this number multiplied by the 1990 PDG average for $\Gamma(K_L^0 \rightarrow \pi^+ \pi^-)/\Gamma(\text{total})$.

³HEINSON 91 give $\Gamma(K_L^0 \rightarrow \mu\mu)/\Gamma_{\text{total}}$. We divide out the $\Gamma(K_L^0 \rightarrow \pi^+ \pi^-)/\Gamma_{\text{total}}$ PDG average which they used.

$\Gamma(e^+ e^-)/\Gamma_{\text{total}}$ Γ_{24}/Γ

Test for $\Delta S = 1$ weak neutral current. Allowed by higher-order electroweak interaction.

VALUE (units 10^{-7})	CL%	EVTS	DOCUMENT ID	TECN
0.087 ± 0.057 -0.041		4	AMBROSE 98	B871

• • • We do not use the following data for averages, fits, limits, etc. • • •

<1.6	90	1	AKAGI 95	SPEC
<0.41	90	0	¹ ARISAKA 93B	B791

¹ARISAKA 93B includes all events with <6 MeV radiated energy.

$\Gamma(\pi^+ \pi^- e^+ e^-)/\Gamma_{\text{total}}$ Γ_{25}/Γ

Test for $\Delta S = 1$ weak neutral current. Allowed by higher-order electroweak interaction.

VALUE (units 10^{-7})	CL%	EVTS	DOCUMENT ID	TECN	COMMENT
3.11 ± 0.19 OUR AVERAGE					
3.08 ± 0.09 ± 0.18		1125	¹ LAI 03c	03c	NA48
3.2 ± 0.6 ± 0.4		37	ADAMS 98		KTEV
4.4 ± 1.3 ± 0.5		13	TAKEUCHI 98		SPEC

• • • We do not use the following data for averages, fits, limits, etc. • • •

<4.6	90		NOMURA 97	SPEC	$m_{ee} > 4$ MeV
------	----	--	-----------	------	------------------

¹LAI 03c second error is 0.15(syst)±0.10(norm) combined in quadrature. The normalization uses $BR(K_L^0 \rightarrow \pi^+ \pi^- \pi^0) * BR(\pi^0 \rightarrow e^+ e^-) = (1.505 \pm 0.047) \times 10^{-3}$ from our 2000 Edition.

$\Gamma(\pi^0 \pi^0 e^+ e^-)/\Gamma_{\text{total}}$ Γ_{26}/Γ

Test for $\Delta S = 1$ weak neutral current. Allowed by higher-order electroweak interaction.

VALUE (units 10^{-9})	CL%	EVTS	DOCUMENT ID	TECN
<6.6	90	1	ALAVI-HARATI02c	E799

$\Gamma(\pi^0 \pi^0 \mu^+ \mu^-)/\Gamma_{\text{total}}$ Γ_{27}/Γ

Test for $\Delta S = 1$ weak neutral current. Allowed by higher-order electroweak interaction.

VALUE	CL%	DOCUMENT ID	TECN
<9.2 × 10⁻¹¹	90	¹ ABOUZAID 11A	E799

¹ABOUZAID 11A also reports $B(K_L^0 \rightarrow \pi^0 \pi^0 X^0 \rightarrow \pi^0 \pi^0 \mu^+ \mu^-) < 1.0 \times 10^{-10}$ at 90% C.L., where the X^0 is a possible new neutral boson that was reported by PARK 05 with a mass of 214.3 ± 0.5 MeV/ c^2 .

$\Gamma(\mu^+ \mu^- e^+ e^-)/\Gamma_{\text{total}}$ Γ_{28}/Γ

Test for $\Delta S = 1$ weak neutral current. Allowed by higher-order electroweak interaction.

VALUE (units 10^{-9})	CL%	EVTS	DOCUMENT ID	TECN	COMMENT
2.69 ± 0.27 OUR AVERAGE					
2.69 ± 0.24 ± 0.12		131	¹ ALAVI-HARATI 03B		KTEV
2.9 ^{+6.7} / _{-2.4}		1	GU 96		E799

• • • We do not use the following data for averages, fits, limits, etc. • • •

2.62 ± 0.40 ± 0.17	43	ALAVI-HARATI 01H	KTEV	Sup. by ALAVI-HARATI 03B
--------------------	----	------------------	------	--------------------------

<4900	90	BALATS 83	SPEC	
-------	----	-----------	------	--

¹ALAVI-HARATI 03B also measures the linear slope $\alpha = -1.59 \pm 0.37$.

$\Gamma(e^+ e^- e^+ e^-)/\Gamma_{\text{total}}$ Γ_{29}/Γ

Test for $\Delta S = 1$ weak neutral current. Allowed by higher-order electroweak interaction.

VALUE (units 10^{-8})	EVTS	DOCUMENT ID	TECN	COMMENT
3.56 ± 0.21 OUR AVERAGE				
3.30 ± 0.24 ± 0.25	200	¹ LAI 05B	05B	NA48
3.72 ± 0.18 ± 0.23	441	ALAVI-HARATI 01D		KTEV
3.96 ± 0.78 ± 0.32	27	GU 94		E799
3.07 ± 1.25 ± 0.26	6	VAGINS 93		B845

• • • We do not use the following data for averages, fits, limits, etc. • • •

6 ± 2 ± 1	18	² AKAGI 95	SPEC	$m_{ee} > 470$ MeV
7 ± 3 ± 2	6	² AKAGI 95	SPEC	$m_{ee} > 470$ MeV
10.4 ± 3.7 ± 1.1	8	³ BARR 95	NA31	
6 ± 2 ± 1	18	AKAGI 93	CNTR	Sup. by AKAGI 95
4 ± 3	2	BARR 91	NA31	Sup. by BARR 95

¹LAI 05B uses 1998 and 1999 data. Data are normalized to the observed events of $K_L^0 \rightarrow \pi^+ \pi^- \pi^0$ (π^0 into Dalitz pair) and PDG 04 values are used for $B(K_L^0 \rightarrow \pi^+ \pi^- \pi^0)$ and $B(\pi^0 \rightarrow e^+ e^- \gamma)$. The systematic error includes a normalization error of ±0.10.

²Values are for the total branching fraction, acceptance-corrected for the m_{ee} cuts shown.

³Distribution of angles between two $e^+ e^-$ pair planes favors $CP = -1$ for K_L^0 .

$\Gamma(\pi^0 \mu^+ \mu^-)/\Gamma_{\text{total}}$ Γ_{30}/Γ

Violates CP in leading order. Test for $\Delta S = 1$ weak neutral current. Allowed by higher-order electroweak interaction.

VALUE (units 10^{-9})	CL%	EVTS	DOCUMENT ID	TECN
<0.38	90		ALAVI-HARATI 00D	KTEV

• • • We do not use the following data for averages, fits, limits, etc. • • •

<5.1	90	0	HARRIS 93	E799
------	----	---	-----------	------

$\Gamma(\pi^0 e^+ e^-)/\Gamma_{\text{total}}$ Γ_{31}/Γ

Violates CP in leading order. Direct and indirect CP-violating contributions are expected to be comparable and to dominate the CP-conserving part. LAI 02B result suggests that CP-violation effects dominate. Test for $\Delta S = 1$ weak neutral current. Allowed by higher-order electroweak interaction.

VALUE (units 10^{-10})	CL%	EVTS	DOCUMENT ID	TECN	COMMENT
< 2.8	90		¹ ALAVI-HARATI 04A	KTEV	combined result

• • • We do not use the following data for averages, fits, limits, etc. • • •

< 3.5	90		ALAVI-HARATI 04A	KTEV	
0.0047 ^{+0.0022} / _{-0.0018}			² LAI	02B	NA48 CP-conserving part

< 5.1	90	2	ALAVI-HARATI 01	KTEV	
0.01 to 0.02			ALAVI-HARATI 99B	KTEV	CP-conserving part

< 43	90	0	HARRIS 93B	E799	
< 75	90	0	BARKER 90	E731	
< 55	90	0	OHL 90	B845	
< 400	90		BARR 88	NA31	
< 3200	90		JASTRZEM... 88	SPEC	

¹ Combined result of ALAVI-HARATI 04A 1999-2000 data set and ALAVI-HARATI 01 1997 data set.

² LAI 02B uses the absence of a signal in $K_L^0 \rightarrow \pi^0 \gamma \gamma$ with $m(\gamma\gamma) < m(\pi^0)$ and their a_V value to predict this value.

$\Gamma(\pi^0 \nu \bar{\nu})/\Gamma_{\text{total}}$ Γ_{32}/Γ

Violates CP in leading order. Test of direct CP violation since the indirect CP-violating and CP-conserving contributions are expected to be suppressed. Test of $\Delta S = 1$ weak neutral current.

VALUE (units 10^{-8})	CL%	DOCUMENT ID	TECN
< 0.30	90	¹ AHN 19	KOTO

• • • We do not use the following data for averages, fits, limits, etc. • • •

< 5.1	90	² AHN 17	KOTO
< 2.6	90	³ AHN 10	K391
< 6.7	90	⁴ AHN 08	K391
< 21	90	⁵ AHN 06	K391

< 59	90	ALAVI-HARATI 00	KTEV
------	----	-----------------	------

¹ AHN 19 result is based on data collected in 2015, which corresponds to 2.2×10^{19} protons on target. A single event sensitivity of $(1.30 \pm 0.01 \pm 0.14) \times 10^{-9}$ was achieved with no candidate events observed. An upper limit of $< 2.4 \times 10^{-9}$ at the 90% C.L. for the $K_L \rightarrow \pi^0 X^0$ decay was also set, where X^0 is an invisible particle with a mass of 135 MeV/ c^2 .

² AHN 17 result is based on the first 100 hours of physics running in 2013. One candidate event was observed with an expected background of 0.34 ± 0.16 events. An upper limit of $< 3.7 \times 10^{-8}$ at the 90% C.L. for the $K_L \rightarrow \pi^0 X^0$ decay was also set, where X^0 is an invisible particle with a mass of 135 MeV/ c^2 .

³ Obtained combining Run-2 (AHN 08) and Run-3 data.

⁴ Value obtained using data from February to April 2005.

⁵ Value obtained analyzing 10% of data of RUN 1 (performed in 2004).

$\Gamma(\pi^0 \pi^0 \nu \bar{\nu})/\Gamma_{\text{total}}$ Γ_{33}/Γ

VALUE	CL%	DOCUMENT ID	TECN
< 8.1 × 10⁻⁷	90	¹ OGATA 11	K391

• • • We do not use the following data for averages, fits, limits, etc. • • •

< 4.7 × 10 ⁻⁵	90	² NIX 07	K391
--------------------------	----	---------------------	------

¹ Using 2005 Run-I data. OGATA 11 also sets a limit on the $K_L^0 \rightarrow \pi^0 \pi^0 X \rightarrow$ invisible particles process: the limit on the branching fraction varied from 7.0×10^{-7} to 4.0×10^{-5} for the mass of X ranging from 50 to 200 MeV/ c^2 .

² Observed 1 event with expected background of 0.43 ± 0.35 events. NIX 07 also measured $B(K_L^0 \rightarrow \pi^0 \pi^0 P) < 1.2 \times 10^{-6}$ at 90% CL, where P is the pseudoscalar particle and $m_P < 100$ MeV.

$\Gamma(e^\pm \mu^\mp)/\Gamma_{\text{total}}$ Γ_{34}/Γ

Test of lepton family number conservation.

VALUE (units 10^{-11})	CL%	EVTS	DOCUMENT ID	TECN
< 0.47	90		AMBROSE 98B	B871

• • • We do not use the following data for averages, fits, limits, etc. • • •

< 9.4	90	0	AKAGI 95	SPEC
< 3.9	90	0	ARISA KA 93	B791
< 3.3	90	0	¹ ARISA KA 93	B791

¹ This is the combined result of ARISA KA 93 and MATHIAZHAGAN 89.

$\Gamma(e^\pm e^\pm \mu^\mp \mu^\mp)/\Gamma_{\text{total}}$ Γ_{35}/Γ

Test of lepton family number conservation.

VALUE (units 10^{-11})	CL%	EVTS	DOCUMENT ID	TECN	COMMENT
< 4.12	90	0	ALAVI-HARATI 03B	KTEV	

• • • We do not use the following data for averages, fits, limits, etc. • • •

< 12.3	90	0	¹ ALAVI-HARATI 01H	KTEV	Sup. by ALAVI-HARATI 03B
< 610	90	0	¹ GU 96	E799	

¹ Assuming uniform phase space distribution.

$\Gamma(\pi^0 \mu^\pm e^\mp)/\Gamma_{\text{total}}$ Γ_{36}/Γ

Test of lepton family number conservation.

VALUE (units 10^{-10})	CL%	DOCUMENT ID	TECN
< 0.76	90	ABOUZAID 08c	KTEV

• • • We do not use the following data for averages, fits, limits, etc. • • •

< 62	90	ARISA KA 98	E799
------	----	-------------	------

Meson Particle Listings

K_L^0

$\Gamma(\pi^0 \pi^0 \mu^\pm e^\mp) / \Gamma_{\text{total}}$ Γ_{37}/Γ
 Test of lepton family number conservation.

VALUE (units 10^{-10})	CL%	DOCUMENT ID	TECN
<1.7	90	ABOUZAID 08c	KTEV

See the related review(s):
 V_{ud}, V_{us} the Cabibbo Angle, and CKM Unitarity

ENERGY DEPENDENCE OF K_L^0 DALITZ PLOT

For discussion, see note on Dalitz plot parameters in the K^\pm section of the Particle Listings above. For definitions of $a_V, a_T, a_U,$ and $a_Y,$ see the earlier version of the same note in the 1982 edition of this Review published in Physics Letters **111B** 70 (1982).

$$|\text{matrix element}|^2 = 1 + gu + hu^2 + jv + kv^2 + fuv$$

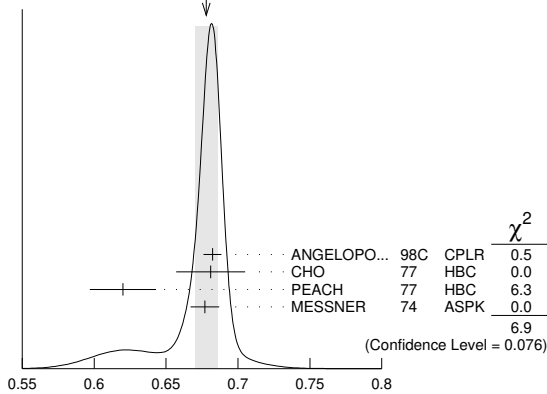
where $u = (s_3 - s_0) / m_\pi^2$ and $v = (s_2 - s_1) / m_\pi^2$

LINEAR COEFFICIENT g FOR $K_L^0 \rightarrow \pi^+ \pi^- \pi^0$

VALUE	EVTS	DOCUMENT ID	TECN	COMMENT
0.678 ± 0.008 OUR AVERAGE				Error includes scale factor of 1.5. See the ideogram below.
0.6823 ± 0.0044 ± 0.0044	500k	ANGELOPO... 98c	CPLR	
0.681 ± 0.024	6499	CHO 77	HBC	
0.620 ± 0.023	4709	PEACH 77	HBC	
0.677 ± 0.010	509k	MESSNER 74	ASPK	$a_Y = -0.917 \pm 0.013$
• • • We do not use the following data for averages, fits, limits, etc. • • •				
0.69 ± 0.07	192	¹ BALDO... 75	HLBC	
0.590 ± 0.022	56k	¹ BUCHANAN 75	SPEC	$a_U = -0.277 \pm 0.010$
0.619 ± 0.027	20k	^{1,2} BISI 74	ASPK	$a_T = -0.282 \pm 0.011$
0.612 ± 0.032		¹ ALEXANDER 73B	HBC	
0.73 ± 0.04	3200	¹ BRANDENB... 73	HBC	
0.608 ± 0.043	1486	¹ KRENZ 72	HLBC	$a_T = -0.277 \pm 0.018$
0.650 ± 0.012	29k	¹ ALBROW 70	ASPK	$a_Y = -0.858 \pm 0.015$
0.593 ± 0.022	36k	^{1,3} BUCHANAN 70	SPEC	$a_U = -0.278 \pm 0.010$
0.664 ± 0.056	4400	¹ SMITH 70	OSPK	$a_T = -0.306 \pm 0.024$
0.400 ± 0.045	2446	¹ BASILE 68B	OSPK	$a_T = -0.188 \pm 0.020$
0.649 ± 0.044	1350	¹ HOPKINS 67	HBC	$a_T = -0.294 \pm 0.018$
0.428 ± 0.055	1198	¹ NEFKENS 67	OSPK	$a_U = -0.204 \pm 0.025$

- Quadratic dependence required by some experiments. (See sections on "QUADRATIC COEFFICIENT h " and "QUADRATIC COEFFICIENT k " below.) Correlations prevent us from averaging results of fits not including $g, h,$ and k terms.
- BISI 74 value comes from quadratic fit with quad. term consistent with zero. g error is thus larger than if linear fit were used.
- BUCHANAN 70 result revised by BUCHANAN 75 to include radiative correlations and to use more reliable K_L^0 momentum spectrum of second experiment (had same beam).

WEIGHTED AVERAGE
 0.678±0.008 (Error scaled by 1.5)



QUADRATIC COEFFICIENT h FOR $K_L^0 \rightarrow \pi^+ \pi^- \pi^0$

See notes in section "LINEAR COEFFICIENT g FOR $K_L^0 \rightarrow \pi^+ \pi^- \pi^0$ |MATRIX ELEMENT|^2" above.

VALUE	EVTS	DOCUMENT ID	TECN
0.076 ± 0.006 OUR AVERAGE			
0.061 ± 0.004 ± 0.015	500k	ANGELOPO... 98c	CPLR
0.095 ± 0.032	6499	CHO 77	HBC
0.048 ± 0.036	4709	PEACH 77	HBC
0.079 ± 0.007	509k	MESSNER 74	ASPK
• • • We do not use the following data for averages, fits, limits, etc. • • •			
-0.011 ± 0.018	29k	¹ ALBROW 70	ASPK
0.043 ± 0.052	4400	¹ SMITH 70	OSPK

- Quadratic coefficients h and k required by some experiments. (See section on "QUADRATIC COEFFICIENT k " below.) Correlations prevent us from averaging results of fits not including $g, h,$ and k terms.

QUADRATIC COEFFICIENT k FOR $K_L^0 \rightarrow \pi^+ \pi^- \pi^0$

VALUE	EVTS	DOCUMENT ID	TECN
0.0099 ± 0.0015 OUR AVERAGE			
0.0104 ± 0.0017 ± 0.0024	500k	ANGELOPO... 98c	CPLR
0.024 ± 0.010	6499	CHO 77	HBC
-0.008 ± 0.012	4709	PEACH 77	HBC
0.0097 ± 0.0018	509k	MESSNER 74	ASPK

LINEAR COEFFICIENT j FOR $K_L^0 \rightarrow \pi^+ \pi^- \pi^0$ (CP-VIOLATING TERM)

Listed in CP-violation section below.

QUADRATIC COEFFICIENT f FOR $K_L^0 \rightarrow \pi^+ \pi^- \pi^0$ (CP-VIOLATING TERM)

Listed in CP-violation section below.

QUADRATIC COEFFICIENT h FOR $K_L^0 \rightarrow \pi^0 \pi^0 \pi^0$

We do not average measurements that do not account for the effect of final state rescattering.

VALUE (units 10^{-3})	EVTS	DOCUMENT ID	TECN
+0.59 ± 0.20 ± 1.16	68M	¹ ABOUZAID 08a	KTEV
• • • We do not use the following data for averages, fits, limits, etc. • • •			
-6.1 ± 0.9 ± 0.5	14.7M	² LAI 01B	NA48
-3.3 ± 1.1 ± 0.7	5M	^{2,3} SOMALWAR 92	E731

- Result obtained using C13pl model of CABIBBO 05 to include $\pi\pi$ rescattering effects. The systematic error includes an external error of 1.06×10^{-3} from the parametrization input of $(a_0 - a_2) m_{\pi^+} = 0.268 \pm 0.017$ from BATLEY 06b.
- LAI 01B and SOMALWAR 92 results do not include $\pi\pi$ final state rescattering effects.
- SOMALWAR 92 chose m_{π^+} as normalization to make it compatible with the Particle Data Group $K_L^0 \rightarrow \pi^+ \pi^- \pi^0$ definitions.

K_L^0 FORM FACTORS

For discussion, see note on form factors in the K^\pm section of the Particle Listings above.

In the form factor comments, the following symbols are used.

f_+ and f_- are form factors for the vector matrix element.

f_S and f_T refer to the scalar and tensor term.

$$f_0(t) = f_+(t) + f_-(t) t / (m_{K^0}^2 - m_{\pi^+}^2).$$

t = momentum transfer to the π .

λ_+ and λ_0 are the linear expansion coefficients of f_+ and f_0 :

$$f_+(t) = f_+(0) (1 + \lambda_+ t / m_{\pi^+}^2)$$

For quadratic expansion

$$f_+(t) = f_+(0) (1 + \lambda'_+ t / m_{\pi^+}^2 + \frac{\lambda''_+}{2} t^2 / m_{\pi^+}^4)$$

as used by KTeV. If there is a non-vanishing quadratic term, then λ_+ represents an average slope, which is then different from λ'_+ .

NA48 (K_{e3}) and ISTRA quadratic expansion coefficients are converted with

$$\lambda'_+ PDG = \lambda_+ NA48 \text{ and } \lambda''_+ PDG = 2 \lambda'_+ NA48$$

$$\lambda'_+ PDG = (\frac{m_{\pi^+}}{m_{\pi^0}})^2 \lambda_+ ISTRA \text{ and}$$

$$\lambda''_+ PDG = 2 (\frac{m_{\pi^+}}{m_{\pi^0}})^4 \lambda'_+ ISTRA$$

ISTRA linear expansion coefficients are converted with

$$\lambda_+ PDG = (\frac{m_{\pi^+}}{m_{\pi^0}})^2 \lambda_+ ISTRA \text{ and } \lambda_0 PDG = (\frac{m_{\pi^+}}{m_{\pi^0}})^2 \lambda_0 ISTRA$$

The pole parametrization is

$$f_+(t) = f_+(0) (\frac{M_V^2}{M_V^2 - t})$$

$$f_0(t) = f_0(0) (\frac{M_S^2}{M_S^2 - t})$$

where M_V and M_S are the vector and scalar pole masses.

The dispersive parametrization is

$$f_+(t) = f_+(0) \exp[\frac{t}{m_{\pi^+}^2} (\Lambda_+ + H(t))];$$

$$f_0(t) = f_0(0) \exp[\frac{t}{m_K^2 - m_{\pi^+}^2} (\ln[C] - G(t))],$$

where Λ_+ is the slope parameter and $\ln[C] = \ln[f_0(m_K^2 - m_{\pi^+}^2)]$

is the logarithm of the scalar form factor at the Callan-Treiman point.

$H(t)$ and $G(t)$ are dispersive integrals.

The following abbreviations are used:

DP = Dalitz plot analysis.

PI = π spectrum analysis.

MU = μ spectrum analysis.

POL = μ polarization analysis.

BR = $K_{\mu 3}^0 / K_{e 3}^0$ branching ratio analysis.

E = positron or electron spectrum analysis.

RC = radiative corrections.

λ_+ (LINEAR ENERGY DEPENDENCE OF f_+ IN K_{e3}^0 DECAY)

For radiative correction of K_{e3}^0 DP, see GINSBERG 67, BECHERRAWY 70, CIRIGLIANO 02, CIRIGLIANO 04, and ANDRE 07. Results labeled OUR FIT are discussed in the review “ K_{e3}^\pm and K_{e3}^0 Form Factors” in the K^\pm Listings. For earlier, lower statistics results, see the 2004 edition of this review, Physics Letters **B592** 1 (2004).

VALUE (units 10^{-2})	EVTS	DOCUMENT ID	TECN	COMMENT
2.82 ± 0.04 OUR FIT				Error includes scale factor of 1.1. Assuming μ -e universality
2.85 ± 0.04 OUR AVERAGE				
2.86 ± 0.05 ± 0.04	2M	AMBROSINO 06D	KLOE	
2.832 ± 0.037 ± 0.043	1.9M	ALEXOPOU... 04A	KTEV	PI, no $\mu = e$
2.88 ± 0.04 ± 0.11	5.6M	¹ LAI 04c	NA48	DP
• • • We do not use the following data for averages, fits, limits, etc. • • •				
2.84 ± 0.07 ± 0.13	5.6M	² LAI 04c	NA48	DP
2.45 ± 0.12 ± 0.22	366k	APOSTOLA... 00	CPLR	DP
3.06 ± 0.34	74k	BIRULEV 81	SPEC	DP
3.12 ± 0.25	500k	GJESDAL 76	SPEC	DP
2.70 ± 0.28	25k	BLUMENTHAL 75	SPEC	DP

¹ Results from linear fit and assuming only vector and axial couplings.
² Results from linear fit with $|f_S/f_+|$ and $|f_T/f_+|$ free.

λ_+ (LINEAR ENERGY DEPENDENCE OF f_+ IN $K_{\mu 3}^0$ DECAY)

Results labeled OUR FIT are discussed in the review “ K_{e3}^\pm and K_{e3}^0 Form Factors” in the K^\pm Listings. For earlier, lower statistics results, see the 2004 edition of this review, Physics Letters **B592** 1 (2004).

VALUE (units 10^{-2})	EVTS	DOCUMENT ID	TECN	COMMENT
2.82 ± 0.04 OUR FIT				Error includes scale factor of 1.1. Assuming μ -e universality
2.71 ± 0.10 OUR FIT				Error includes scale factor of 1.4. Not assuming μ -e universality
2.67 ± 0.06 ± 0.08	2.3M	¹ LAI 07A	NA48	DP
2.745 ± 0.088 ± 0.063	1.5M	ALEXOPOU... 04A	KTEV	DP, no $\mu = e$
2.813 ± 0.051	3.4M	ALEXOPOU... 04A	KTEV	PI, DP, $\mu = e$
3.0 ± 0.3	1.6M	DONALDSON 74B	SPEC	DP
• • • We do not use the following data for averages, fits, limits, etc. • • •				
4.27 ± 0.44	150k	BIRULEV 81	SPEC	DP

¹ LAI 07A gives a correlation -0.40 between their λ_0 and λ_+ measurements.

λ_0 (LINEAR ENERGY DEPENDENCE OF f_0 IN $K_{\mu 3}^0$ DECAY)

Wherever possible, we have converted the above values of $\xi(0)$ into values of λ_0 using the associated λ_+^H and $d\xi(0)/d\lambda_+$. Results labeled OUR FIT are discussed in the review “ K_{e3}^\pm and K_{e3}^0 Form Factors” in the K^\pm Listings. For earlier, lower statistics results, see the 2004 edition of this review, Physics Letters **B592** 1 (2004).

VALUE (units 10^{-2})	$d\lambda_0/d\lambda_+$	EVTS	DOCUMENT ID	TECN	COMMENT
1.38 ± 0.18 OUR FIT					Error includes scale factor of 2.2. Assuming μ -e universality
1.42 ± 0.23 OUR FIT					Error includes scale factor of 2.8. Not assuming μ -e universality
1.17 ± 0.07 ± 0.10		2.3M	¹ LAI 07A	NA48	DP
1.657 ± 0.125	-0.44	1.5M	² ALEXOPOU... 04A	KTEV	DP, no $\mu = e$
1.635 ± 0.121	-0.85	3.4M	³ ALEXOPOU... 04A	KTEV	PI, DP, $\mu = e$
+1.9 ± 0.4	-0.47	1.6M	⁴ DONALDSON 74B	SPEC	DP
• • • We do not use the following data for averages, fits, limits, etc. • • •					
3.41 ± 0.67	unknown	150k	⁵ BIRULEV 81	SPEC	DP

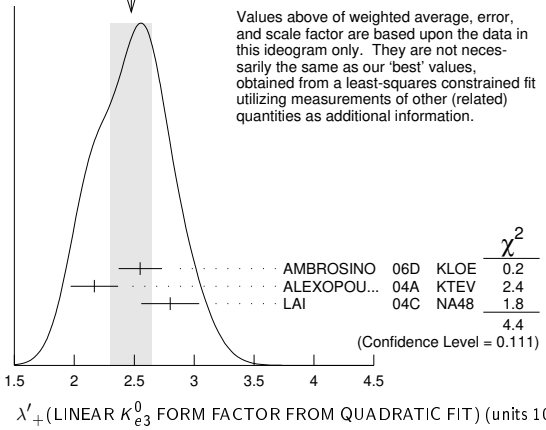
¹ LAI 07A gives a correlation -0.40 between their λ_0 and λ_+ measurements.
² ALEXOPOULOS 04A gives a correlation -0.38 between their λ_0 and λ_+ measurements.
³ ALEXOPOULOS 04A gives a correlation -0.36 between their λ_0 and λ_+ measurements.
⁴ DONALDSON 74B $d\lambda_0/d\lambda_+$ obtained from figure 18.
⁵ BIRULEV 81 gives $d\lambda_0/d\lambda_+ = -1.5$, giving an unreasonably narrow error ellipse which dominates all other results. We use $d\lambda_0/d\lambda_+ = 0$.

λ'_+ (LINEAR K_{e3}^0 FORM FACTOR FROM QUADRATIC FIT)

VALUE (units 10^{-2})	EVTS	DOCUMENT ID	TECN	COMMENT
2.40 ± 0.12 OUR FIT				Error includes scale factor of 1.2. Assuming μ -e universality
2.49 ± 0.13 OUR FIT				Error includes scale factor of 1.1. Not assuming μ -e universality
2.48 ± 0.17 OUR AVERAGE				Error includes scale factor of 1.5. See the ideogram below.
2.55 ± 0.15 ± 0.10	2M	¹ AMBROSINO 06D	KLOE	
2.167 ± 0.137 ± 0.143	1.9M	² ALEXOPOU... 04A	KTEV	PI, no $\mu = e$
2.80 ± 0.19 ± 0.15	5.6M	³ LAI 04c	NA48	DP

¹ We use AMBROSINO 06D result in the fit not assuming μ -e universality. This result enters the fit assuming μ -e universality via AMBROSINO 07C measurement of λ'_+ in $K_{\mu 3}$ decays. AMBROSINO 06D gives a correlation -0.95 between their λ'_+ and λ''_+ .
² ALEXOPOULOS 04A gives a correlation -0.97 between their λ'_+ and λ''_+ .
³ For LAI 04c we calculate a correlation -0.88 between their λ'_+ and λ''_+ .

WEIGHTED AVERAGE
2.48±0.17 (Error scaled by 1.5)



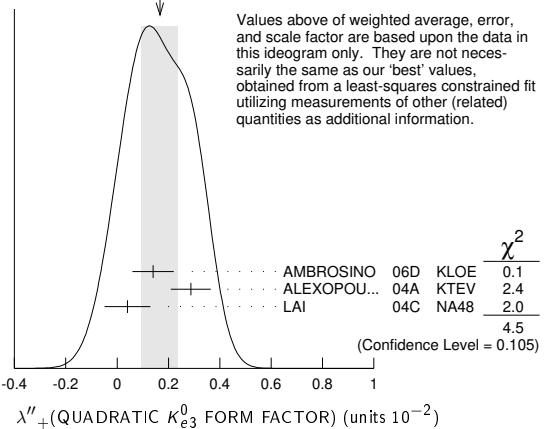
Values above of weighted average, error, and scale factor are based upon the data in this ideogram only. They are not necessarily the same as our 'best' values, obtained from a least-squares constrained fit utilizing measurements of other (related) quantities as additional information.

λ''_+ (QUADRATIC K_{e3}^0 FORM FACTOR)

VALUE (units 10^{-2})	EVTS	DOCUMENT ID	TECN	COMMENT
0.20 ± 0.05 OUR FIT				Error includes scale factor of 1.2. Assuming μ -e universality
0.16 ± 0.05 OUR FIT				Error includes scale factor of 1.1. Not assuming μ -e universality
0.17 ± 0.07 OUR AVERAGE				Error includes scale factor of 1.5. See the ideogram below.
0.14 ± 0.07 ± 0.04	2M	¹ AMBROSINO 06D	KLOE	
0.287 ± 0.057 ± 0.053	1.9M	² ALEXOPOU... 04A	KTEV	PI, no $\mu = e$
0.04 ± 0.08 ± 0.04	5.6M	^{3,4} LAI 04c	NA48	DP

¹ We use AMBROSINO 06D result in the fit not assuming μ -e universality. This result enters the fit assuming μ -e universality via AMBROSINO 07C measurement of λ''_+ in $K_{\mu 3}$ decays. AMBROSINO 06D gives a correlation -0.95 between their λ'_+ and λ''_+ .
² ALEXOPOULOS 04A gives a correlation -0.97 between their λ'_+ and λ''_+ .
³ Values doubled to agree with PDG conventions described above.
⁴ LAI 04c gives a correlation -0.88 between their λ'_+ and λ''_+ .

WEIGHTED AVERAGE
0.17±0.07 (Error scaled by 1.5)



Values above of weighted average, error, and scale factor are based upon the data in this ideogram only. They are not necessarily the same as our 'best' values, obtained from a least-squares constrained fit utilizing measurements of other (related) quantities as additional information.

λ'_+ (LINEAR $K_{\mu 3}^0$ FORM FACTOR FROM QUADRATIC FIT)

VALUE (units 10^{-2})	EVTS	DOCUMENT ID	TECN	COMMENT
2.40 ± 0.12 OUR FIT				Error includes scale factor of 1.2. Assuming μ -e universality
1.89 ± 0.24 OUR FIT				Not assuming μ -e universality
2.23 ± 0.98 ± 0.37	1.8M	¹ AMBROSINO 07C	KLOE	no $\mu = e$
2.56 ± 0.15 ± 0.09	3.8M	¹ AMBROSINO 07C	KLOE	$\mu = e$
2.05 ± 0.22 ± 0.24	2.3M	¹ LAI 07A	NA48	DP
1.703 ± 0.319 ± 0.177	1.5M	¹ ALEXOPOU... 04A	KTEV	DP, no $\mu = e$
2.064 ± 0.175	3.4M	¹ ALEXOPOU... 04A	KTEV	PI, DP, $\mu = e$

¹ See section λ_0 below for correlations.

λ''_+ (QUADRATIC $K_{\mu 3}^0$ FORM FACTOR)

VALUE (units 10^{-2})	EVTS	DOCUMENT ID	TECN	COMMENT
0.20 ± 0.05 OUR FIT				Error includes scale factor of 1.2. Assuming μ -e universality
0.37 ± 0.12 OUR FIT				Error includes scale factor of 1.3. Not assuming μ -e universality
0.48 ± 0.49 ± 0.16	1.8M	¹ AMBROSINO 07C	KLOE	no $\mu = e$
0.15 ± 0.07 ± 0.04	3.8M	¹ AMBROSINO 07C	KLOE	$\mu = e$
0.26 ± 0.09 ± 0.10	2.3M	¹ LAI 07A	NA48	DP
0.443 ± 0.131 ± 0.072	1.5M	¹ ALEXOPOU... 04A	KTEV	DP, no $\mu = e$
0.320 ± 0.069	3.4M	¹ ALEXOPOU... 04A	KTEV	PI, DP, $\mu = e$

¹ See section λ_0 below for correlations.

Meson Particle Listings

K_L^0

λ_0 (LINEAR f_0 $K_{\mu 3}^0$ FORM FACTOR FROM QUADRATIC FIT)

VALUE (units 10^{-2})	EVTS	DOCUMENT ID	TECN	COMMENT
1.16 ± 0.09 OUR FIT				Error includes scale factor of 1.2. Assuming μ -e universality
1.07 ± 0.14 OUR FIT				Error includes scale factor of 1.3. Not assuming μ -e universality
0.91 ± 0.59 ± 0.26	1.8M	¹ AMBROSINO 07c	KLOE	no $\mu = e$
1.54 ± 0.18 ± 0.13	3.8M	² AMBROSINO 07c	KLOE	$\mu = e$
0.95 ± 0.11 ± 0.08	2.3M	³ LAI 07A	NA48	DP
1.281 ± 0.136 ± 0.122	1.5M	⁴ ALEXOPOU... 04A	KTEV	DP, no $\mu = e$
1.372 ± 0.131	3.4M	⁵ ALEXOPOU... 04A	KTEV	PI, DP, $\mu = e$

¹ AMBROSINO 07c, not assuming μ -e universality, gives a correlation matrix

$$\begin{matrix} \chi'^2_+ & & \chi''_+ \\ \chi''_+ & -0.97 & 1 \\ \lambda_0 & 0.81 & -0.91 \end{matrix}$$

² AMBROSINO 07c, assuming μ -e universality, gives a correlation matrix

$$\begin{matrix} \chi'^2_+ & & \chi''_+ \\ \chi''_+ & -0.95 & 1 \\ \lambda_0 & 0.29 & -0.38 \end{matrix}$$

³ LAI 07A gives a correlation matrix

$$\begin{matrix} \chi'^2_+ & & \chi''_+ \\ \chi''_+ & -0.96 & 1 \\ \lambda_0 & 0.63 & -0.73 \end{matrix}$$

⁴ ALEXOPOULOS 04A, not assuming μ -e universality, gives a correlation matrix

$$\begin{matrix} \chi'^2_+ & & \chi''_+ & \lambda_0 \\ \chi''_+ & -0.96 & 1 & \\ \lambda_0 & 0.65 & -0.75 & 1 \end{matrix}$$

⁵ ALEXOPOULOS 04A, assuming μ -e universality, gives a correlation matrix

$$\begin{matrix} \chi'^2_+ & & \chi''_+ & \lambda_0 \\ \chi''_+ & -0.97 & 1 & \\ \lambda_0 & 0.34 & -0.44 & 1 \end{matrix}$$

M_V^e (POLE MASS FOR K_{e3}^0 DECAY)

VALUE (MeV)	EVTS	DOCUMENT ID	TECN	COMMENT
878 ± 6 OUR FIT				Error includes scale factor of 1.1. Assuming μ -e universality
875 ± 5 OUR AVERAGE				
870 ± 6 ± 7	2M	AMBROSINO 06D	KLOE	
881.03 ± 5.12 ± 4.94	1.9M	ALEXOPOU... 04A	KTEV	PI, no $\mu = e$
859 ± 18	5.6M	LAI 04C	NA48	

M_V^μ (POLE MASS FOR $K_{\mu 3}^0$ DECAY)

VALUE (MeV)	EVTS	DOCUMENT ID	TECN	COMMENT
878 ± 6 OUR FIT				Error includes scale factor of 1.1. Assuming μ -e universality
900 ± 21 OUR FIT				Error includes scale factor of 1.7. Not assuming μ -e universality
905 ± 9 ± 17	2.3M	¹ LAI 07A	NA48	DP
889.19 ± 12.81 ± 9.92	1.5M	¹ ALEXOPOU... 04A	KTEV	DP, no $\mu = e$
882.32 ± 6.54	3.4M	¹ ALEXOPOU... 04A	KTEV	PI, DP, $\mu = e$

¹ See section M_S^μ below for correlations.

M_S^μ (POLE MASS FOR $K_{\mu 3}^0$ DECAY)

VALUE (MeV)	EVTS	DOCUMENT ID	TECN	COMMENT
1252 ± 90 OUR FIT				Error includes scale factor of 2.6. Assuming μ -e universality
1222 ± 80 OUR FIT				Error includes scale factor of 2.3. Not assuming μ -e universality
1400 ± 46 ± 53	2.3M	¹ LAI 07A	NA48	DP
1167.14 ± 28.30 ± 31.04	1.5M	² ALEXOPOU... 04A	KTEV	PI, no $\mu = e$
1173.80 ± 39.47	3.4M	³ ALEXOPOU... 04A	KTEV	PI, DP, $\mu = e$

¹ LAI 07A gives a correlation -0.47 between their M_S^μ and M_V^μ measurements, not assuming μ -e universality.

² ALEXOPOULOS 04A gives a correlation -0.46 between their M_S^μ and M_V^μ measurements, not assuming μ -e universality.

³ ALEXOPOULOS 04A gives a correlation -0.40 between their M_S^μ and M_V^μ measurements, assuming μ -e universality.

Λ_+ (DISPERSIVE VECTOR FORM FACTOR FOR $K_{\mu 3}^0$ DECAY)

See the review on " K_{e3}^0 and $K_{\mu 3}^0$ Form Factors" for details of the dispersive parametrization.

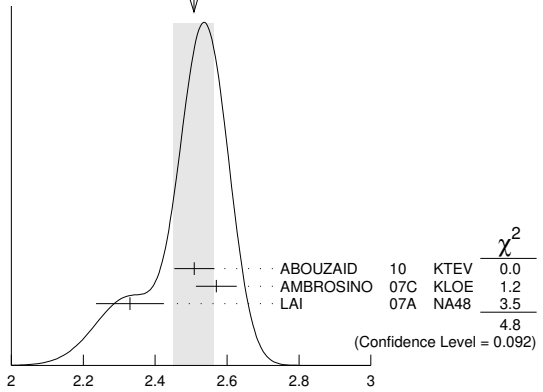
VALUE (units 10^{-2})	EVTS	DOCUMENT ID	TECN	COMMENT
2.51 ± 0.06 OUR AVERAGE				Error includes scale factor of 1.5. See the ideogram below.
2.509 ± 0.035 ± 0.043	3.4M	¹ ABOUZAID 10	KTEV	$\mu = e$
2.57 ± 0.04 ± 0.04	3.8M	² AMBROSINO 07c	KLOE	$\mu = e$
2.33 ± 0.05 ± 0.08	2.3M	³ LAI 07A	NA48	DP

¹ Obtained from a sample of 1.9 M K_{e3} and 1.5 M $K_{\mu 3}$. The correlation between Λ_+ and $\ln(C)$ is -0.269 .

² AMBROSINO 07c results include 2M K_{e3} events from AMBROSINO 06D. The correlation between Λ_+ and $\ln(C)$ is -0.26 .

³ LAI 07A gives a correlation -0.44 between their Λ_+ and $\ln(C)$ measurements.

WEIGHTED AVERAGE
2.51±0.06 (Error scaled by 1.5)



Λ_+ (DISPERSIVE VECTOR FORM FACTOR FOR $K_{\mu 3}^0$ DECAY) (units 10^{-2})

$\ln(C)$ (DISPERSIVE SCALAR FORM FACTOR FOR $K_{\mu 3}^0$ DECAY)

See the review on " K_{e3}^0 and $K_{\mu 3}^0$ Form Factors" for details of the dispersive parametrization.

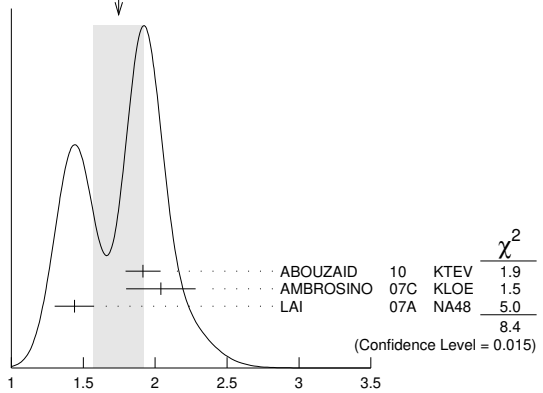
VALUE (units 10^{-1})	EVTS	DOCUMENT ID	TECN	COMMENT
1.75 ± 0.18 OUR AVERAGE				Error includes scale factor of 2.0. See the ideogram below.
1.915 ± 0.078 ± 0.094	3.4M	¹ ABOUZAID 10	KTEV	$\mu = e$
2.04 ± 0.19 ± 0.15	3.8M	² AMBROSINO 07c	KLOE	$\mu = e$
1.438 ± 0.080 ± 0.112	2.3M	³ LAI 07A	NA48	DP

¹ Obtained from a sample of 1.9 M K_{e3} and 1.5 M $K_{\mu 3}$. The correlation between Λ_+ and $\ln(C)$ is -0.269 .

² AMBROSINO 07c results include 2M K_{e3} events from AMBROSINO 06D. We convert (Λ_+, Λ_0) to $(\Lambda_+, \ln(C))$ parametrization using $\ln(C) = (\Lambda_0 \cdot 11.713 + 0.0398) \pm 0.0041$, where the error is due to theory parametrization of the form factor. The correlation between Λ_+ and $\ln(C)$ is -0.26 .

³ LAI 07A gives a correlation -0.44 between their Λ_+ and $\ln(C)$ measurements.

WEIGHTED AVERAGE
1.75±0.18 (Error scaled by 2.0)



$\ln(C)$ (DISPERSIVE SCALAR FORM FACTOR FOR $K_{\mu 3}^0$ DECAY) (units 10^{-1})

$a_1(t_0, Q^2)$ FORM FACTOR PARAMETER

See HILL 06 for a definition of this parameter.

VALUE	EVTS	DOCUMENT ID	TECN
1.023 ± 0.028 ± 0.029	2M	¹ ABOUZAID 06c	KTEV

¹ $Q^2 = 2 \text{ GeV}^2$, $t_0 = 0.49 (m_K - m_\pi)^2$. Correlation between a_1 and a_2 : $\rho_{12} = -0.064$.

$a_2(t_0, Q^2)$ FORM FACTOR PARAMETER

See HILL 06 for a definition of this parameter.

VALUE	EVTS	DOCUMENT ID	TECN
0.75 ± 1.58 ± 1.47	2M	¹ ABOUZAID 06c	KTEV

¹ $Q^2 = 2 \text{ GeV}^2$, $t_0 = 0.49 (m_K - m_\pi)^2$. Correlation between a_1 and a_2 : $\rho_{12} = -0.064$.

$|f_S/f_+|$ FOR K_{e3}^0 DECAY

Ratio of scalar to f_+ couplings.

VALUE (units 10^{-2})	CL%	EVTS	DOCUMENT ID	TECN	COMMENT
$1.5^{+0.7}_{-1.0} \pm 1.2$		5.6M	¹ LAI	04C	NA48
• • • We do not use the following data for averages, fits, limits, etc. • • •					
<9.5	95	18k	HILL	78	STRC
<7.	68	48k	BIRULEV	76	SPEC See also BIRULEV 81
<4.	68	25k	BLUMENTHAL75		SPEC

¹ Results from linear fit with $|f_S/f_+|$ and $|f_T/f_+|$ free.

$|f_T/f_+|$ FOR K_{e3}^0 DECAY

Ratio of tensor to f_+ couplings.

VALUE (units 10^{-2})	CL%	EVTS	DOCUMENT ID	TECN	COMMENT
$5^{+3}_{-4} \pm 3$		5.6M	¹ LAI	04C	NA48
• • • We do not use the following data for averages, fits, limits, etc. • • •					
<40.	95	18k	HILL	78	STRC
<34.	68	48k	BIRULEV	76	SPEC See also BIRULEV 81
<23.	68	25k	BLUMENTHAL75		SPEC

¹ Results from linear fit with $|f_S/f_+|$ and $|f_T/f_+|$ free.

$|f_T/f_+|$ FOR $K_{\mu 3}^0$ DECAY

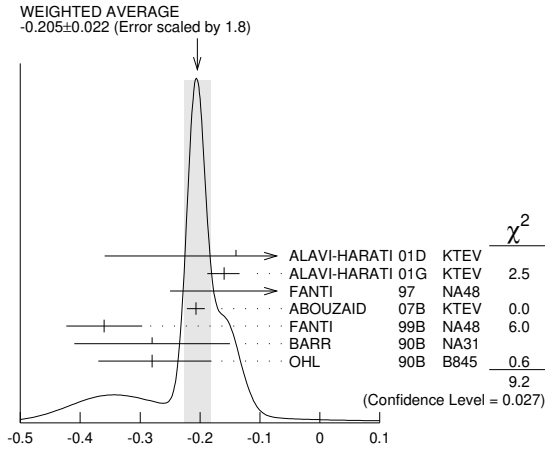
Ratio of tensor to f_+ couplings.

VALUE (units 10^{-2})	DOCUMENT ID	TECN
$12. \pm 12.$	BIRULEV 81	SPEC

α_{K^*} DECAY FORM FACTOR FOR $K_L \rightarrow \ell^+ \ell^- \gamma, K_L^0 \rightarrow \ell^+ \ell^- \ell^+ \ell^-$

Average of all α_{K^*} measurements (from each of three datablocks following this one) assuming lepton universality.

VALUE	DOCUMENT ID
-0.205 ± 0.022 OUR AVERAGE	Includes data from the 3 datablocks that follow this one. Error includes scale factor of 1.8. See the ideogram below.



α_{K^*} DECAY FORM FACTOR FOR $K_L \rightarrow \ell^+ \ell^- \gamma, K_L^0 \rightarrow \ell^+ \ell^- \ell^+ \ell^-$

α_{K^*} DECAY FORM FACTOR FOR $K_L \rightarrow e^+ e^- \gamma$

α_{K^*} is the constant in the model of BERGSTROM 83 which measures the relative strength of the vector-vector transition $K_L \rightarrow K^* \gamma$ with $K^* \rightarrow \rho, \omega, \phi \rightarrow \gamma^*$ and the pseudoscalar-pseudoscalar transition $K_L \rightarrow \pi, \eta, \eta' \rightarrow \gamma \gamma^*$.

VALUE	EVTS	DOCUMENT ID	TECN
-0.217 ± 0.034 OUR AVERAGE		Error includes scale factor of 2.4.	

$-0.207 \pm 0.012 \pm 0.009$	83k	¹ ABOUZAID	07B KTEV
$-0.36 \pm 0.06 \pm 0.02$	6864	FANTI	99B NA48
-0.28 ± 0.13		BARR	90B NA31
$-0.280^{+0.099}_{-0.090}$		OHL	90B B845

¹ ABOUZAID 07B measures $C \cdot \alpha_{K^*} = -0.517 \pm 0.030 \pm 0.022$. We assume $C = 2.5$, as in all other measurements.

α_{K^*} DECAY FORM FACTOR FOR $K_L \rightarrow \mu^+ \mu^- \gamma$

α_{K^*} is the constant in the model of BERGSTROM 83 described in the previous section.

VALUE	EVTS	DOCUMENT ID	TECN
-0.158 ± 0.027 OUR AVERAGE			

$-0.160^{+0.026}_{-0.028}$	9100	ALAVI-HARATI01G	KTEV
$-0.04^{+0.24}_{-0.21}$		FANTI	97 NA48

$\alpha_{K^*}^{\text{eff}}$ DECAY FORM FACTOR FOR $K_L \rightarrow e^+ e^- e^+ e^-$

$\alpha_{K^*}^{\text{eff}}$ is the parameter describing the relative strength of an intermediate pseudoscalar decay amplitude and a vector meson decay amplitude in the model of BERGSTROM 83. It takes into account both the radiative effects and the form factor. Since there are two $e^+ e^-$ pairs here compared with one in $e^+ e^- \gamma$ decays, a factorized expression is used for the $e^+ e^- e^+ e^-$ decay form factor.

VALUE	EVTS	DOCUMENT ID	TECN
$-0.14 \pm 0.16 \pm 0.15$	441	ALAVI-HARATI01D	KTEV

α_{DIP} DECAY FORM FACTOR FOR $K_L^0 \rightarrow \ell^+ \ell^- \gamma, K_L^0 \rightarrow \ell^+ \ell^- \ell^+ \ell^-$

Average of all α_{DIP} measurements (from each of three datablocks following this one) assuming lepton universality.

VALUE	DOCUMENT ID
-1.69 ± 0.08 OUR AVERAGE	Includes data from the 3 datablocks that follow this one. Error includes scale factor of 1.7.

α_{DIP} DECAY FORM FACTOR FOR $K_L^0 \rightarrow e^+ e^- \gamma$

α_{DIP} parameter in $K_L^0 \rightarrow \gamma^* \gamma^*$ form factor by DAMBROSIO 98, motivated by vector meson dominance and a proper short distance behavior.

VALUE	EVTS	DOCUMENT ID	TECN
$-1.729 \pm 0.043 \pm 0.028$	83k	ABOUZAID 07B	KTEV

α_{DIP} DECAY FORM FACTOR FOR $K_L^0 \rightarrow \mu^+ \mu^- \gamma$

α_{DIP} is a constant in the model of DAMBROSIO 98 described in the previous section. The data in this block is included in the average printed for a previous datablock.

-1.54 ± 0.10	9100	ALAVI-HARATI01G	KTEV
------------------	------	-----------------	------

α_{DIP} DECAY FORM FACTOR FOR $K_L^0 \rightarrow e^+ e^- \mu^+ \mu^-$

α_{DIP} is a constant in the model of DAMBROSIO 98 described in the previous section. The data in this block is included in the average printed for a previous datablock.

-1.59 ± 0.37	131	ALAVI-HARATI03B	KTEV
------------------	-----	-----------------	------

a_1/a_2 FORM FACTOR FOR M1 DIRECT EMISSION AMPLITUDE

Form factor = $\tilde{g}_{M1} [1 + \frac{a_1/a_2}{(M_p^2 - M_K^2) + 2M_K E_\gamma}]$ as described in ALAVI-HARATI 00b.

VALUE (GeV ²)	EVTS	DOCUMENT ID	TECN	COMMENT
-0.737 ± 0.014 OUR AVERAGE				
$-0.744 \pm 0.027 \pm 0.032$	5241	¹ ABOUZAID 06	KTEV	$\pi^+ \pi^- e^+ e^-$
$-0.738 \pm 0.007 \pm 0.018$	111k	² ABOUZAID 06A	KTEV	$\pi^+ \pi^+ \gamma$
$-0.81^{+0.07}_{-0.13} \pm 0.02$		³ LAI	03C	NA48 $\pi^+ \pi^- e^+ e^-$
$-0.737 \pm 0.026 \pm 0.022$		⁴ ALAVI-HARATI01B		$\pi^+ \pi^- \gamma$
$-0.720 \pm 0.028 \pm 0.009$	1766	⁵ ALAVI-HARATI00B	KTEV	$\pi^+ \pi^- e^+ e^-$

¹ ABOUZAID 06 also measured $|\tilde{g}_{M1}| = 1.11 \pm 0.14$.
² ABOUZAID 06A also measured $|\tilde{g}_{M1}| = 1.198 \pm 0.035 \pm 0.086$.
³ LAI 03c also measured $\tilde{g}_{M1} = 0.99^{+0.28}_{-0.27} \pm 0.07$.
⁴ ALAVI-HARATI 01B fit gives $\chi^2/\text{DOF} = 38.8/27$. Linear and quadratic fits give $\chi^2/\text{DOF} = 43.2/27$ and $37.6/26$ respectively.
⁵ ALAVI-HARATI 00B also measured $|\tilde{g}_{M1}| = 1.35^{+0.20}_{-0.17} \pm 0.04$.

\tilde{f}_S DECAY FORM FACTOR FOR $K_L^0 \rightarrow \pi^\pm \pi^0 e^\mp \nu_e$

VALUE	DOCUMENT ID	TECN
0.049 ± 0.011 OUR AVERAGE	Error includes scale factor of 1.7.	
$0.052 \pm 0.006 \pm 0.002$	BATLEY 04	NA48
$0.010 \pm 0.016 \pm 0.017$	MAKOFF 93	E731

\tilde{f}_P DECAY FORM FACTOR FOR $K_L^0 \rightarrow \pi^\pm \pi^0 e^\mp \nu_e$

VALUE	DOCUMENT ID	TECN
-0.052 ± 0.012 OUR AVERAGE		
$-0.051 \pm 0.011 \pm 0.005$	BATLEY 04	NA48
$-0.079 \pm 0.049 \pm 0.022$	MAKOFF 93	E731

λ_B DECAY FORM FACTOR FOR $K_L^0 \rightarrow \pi^\pm \pi^0 e^\mp \nu_e$

VALUE	DOCUMENT ID	TECN
0.085 ± 0.020 OUR AVERAGE		
$0.087 \pm 0.019 \pm 0.006$	BATLEY 04	NA48
$0.014 \pm 0.087 \pm 0.070$	MAKOFF 93	E731

\tilde{h} DECAY FORM FACTOR FOR $K_L^0 \rightarrow \pi^\pm \pi^0 e^\mp \nu_e$

VALUE	DOCUMENT ID	TECN
-0.30 ± 0.13 OUR AVERAGE		
$-0.32 \pm 0.12 \pm 0.07$	BATLEY 04	NA48
$-0.07 \pm 0.31 \pm 0.31$	MAKOFF 93	E731

L_3 CHIRAL PERT. THEO. PARAM. FOR $K_L^0 \rightarrow \pi^\pm \pi^0 e^\mp \nu_e$

VALUE (units 10^{-3})	DOCUMENT ID	TECN
-3.96 ± 0.28 OUR AVERAGE	Error includes scale factor of 1.6.	
-4.1 ± 0.2	BATLEY 04	NA48
-3.4 ± 0.4	¹ MAKOFF 93	E731

¹ MAKOFF 93 sign has been changed to negative to agree with the sign convention used in BATLEY 04.

Meson Particle Listings

K_L^0

a_V , VECTOR MESON EXCHANGE CONTRIBUTION

VALUE	EVTS	DOCUMENT ID	TECN	COMMENT
-0.43±0.06 OUR AVERAGE				Error includes scale factor of 1.5.
-0.31±0.05±0.07	1.4k	¹ ABOUZAID 08	KTEV	
-0.46±0.03±0.04		LAI 02B NA48	$K_L^0 \rightarrow \pi^0 2\gamma$	
-0.67±0.21±0.12		ALAVI-HARATI01E	KTEV $K_L^0 \rightarrow \pi^0 e^+ e^- \gamma$	
-0.72±0.05±0.06		² ALAVI-HARATI199B	KTEV $K_L^0 \rightarrow \pi^0 2\gamma$	

• • • We do not use the following data for averages, fits, limits, etc. • • •
¹ Using KTeV dataset collected in 1996, 1997, and 1999.
² Superseded by ABOUZAID 08.

See the related review(s):
 CP Violation in K_L^0 Decays

CP-VIOLATION PARAMETERS IN K_L^0 DECAYS

CHARGE ASYMMETRY IN K_{S3}^0 DECAYS

Such asymmetry violates CP. It is related to $\text{Re}(\epsilon)$.

$A_L =$ weighted average of $A_L(\mu)$ and $A_L(e)$

In previous editions and in the literature the symbol used for this asymmetry was δ_L^+ or δ . We use A_L for consistency with B^0 asymmetry notation and with recent K_S^0 notation.

VALUE (%)	EVTS	DOCUMENT ID	TECN	COMMENT
0.332±0.006 OUR AVERAGE				Includes data from the 2 datablocks that follow this one.
0.333±0.050	33M	WILLIAMS 73	ASPK $K_{\mu 3} + K_{e 3}$	

$A_L(\mu) = [\Gamma(\pi^- \mu^+ \nu_\mu) - \Gamma(\pi^+ \mu^- \bar{\nu}_\mu)]/\text{SUM}$

Only the combined value below is put into the Meson Summary Table.

VALUE (%)	EVTS	DOCUMENT ID	TECN
0.304±0.025 OUR AVERAGE			
0.313±0.029	15M	GEWENIGER 74	ASPK
0.278±0.051	7.7M	PICCIONI 72	ASPK

• • • We do not use the following data for averages, fits, limits, etc. • • •
 0.60 ±0.14 4.1M MCCARTHY 73 CNTR
 0.57 ±0.17 1M ¹ PACIOTTI 69 OSPK
 0.403±0.134 1M ¹ DORFAN 67 OSPK

¹ PACIOTTI 69 is a reanalysis of DORFAN 67 and is corrected for $\mu^+ \mu^-$ range difference in MCCARTHY 72.

$A_L(e) = [\Gamma(\pi^- e^+ \nu_e) - \Gamma(\pi^+ e^- \bar{\nu}_e)]/\text{SUM}$

Only the combined value below is put into the Meson Summary Table.

VALUE (%)	EVTS	DOCUMENT ID	TECN
0.334 ±0.007 OUR AVERAGE			
0.3322±0.0058±0.0047	298M	ALAVI-HARATI02	
0.341 ±0.018	34M	GEWENIGER 74	ASPK
0.318 ±0.038	40M	FITCH 73	ASPK
0.346 ±0.033	10M	MARX 70	CNTR

• • • We do not use the following data for averages, fits, limits, etc. • • •
 0.36 ±0.18 600k ASHFORD 72 ASPK
 0.246 ±0.059 10M ¹ SAAL 69 CNTR
 0.224 ±0.036 10M ¹ BENNETT 67 CNTR

¹ SAAL 69 is a reanalysis of BENNETT 67.

PARAMETERS FOR $K_L^0 \rightarrow 2\pi$ DECAY

$$\eta_{+-} = A(K_L^0 \rightarrow \pi^+ \pi^-) / A(K_S^0 \rightarrow \pi^+ \pi^-)$$

$$\eta_{00} = A(K_L^0 \rightarrow \pi^0 \pi^0) / A(K_S^0 \rightarrow \pi^0 \pi^0)$$

The fitted values of $|\eta_{+-}|$ and $|\eta_{00}|$ given below are the results of a fit to $|\eta_{+-}|$, $|\eta_{00}|$, $|\eta_{00}/\eta_{+-}|$, and $\text{Re}(\epsilon'/\epsilon)$. Independent information on $|\eta_{+-}|$ and $|\eta_{00}|$ can be obtained from the fitted values of the $K_L^0 \rightarrow \pi\pi$ and $K_S^0 \rightarrow \pi\pi$ branching ratios and the K_L^0 and K_S^0 lifetimes. This information is included as data in the $|\eta_{+-}|$ and $|\eta_{00}|$ sections with a Document ID "BRFIT." See the note "CP violation in K_L decays" above for details.

$|\eta_{00}| = |A(K_L^0 \rightarrow 2\pi^0) / A(K_S^0 \rightarrow 2\pi^0)|$

VALUE (units 10^{-3})	DOCUMENT ID	TECN	COMMENT
2.220±0.011 OUR FIT			Error includes scale factor of 1.8.
2.243±0.014	BRFIT 16		
• • • We do not use the following data for averages, fits, limits, etc. • • •			
2.47 ±0.31 ±0.24	ANGELOPO... 98	CPLR	
2.49 ±0.40	¹ ADLER 96B	CPLR	Sup. by ANGELOPOULOS 98
2.33 ±0.18	CHRISTENS... 79	ASPK	
2.71 ±0.37	² WOLFF 71	OSPK	Cu reg., 4γ 's
2.95 ±0.63	² CHOLLET 70	OSPK	Cu reg., 4γ 's

¹ Error is statistical only.

² CHOLLET 70 gives $|\eta_{00}| = (1.23 \pm 0.24) \times (\text{regeneration amplitude, 2 GeV/c Cu})/10000\text{mb}$. WOLFF 71 gives $|\eta_{00}| = (1.13 \pm 0.12) \times (\text{regeneration amplitude, 2 GeV/c Cu})/10000\text{mb}$. We compute both $|\eta_{00}|$ values for (regeneration amplitude, 2 GeV/c Cu) = $24 \pm 2\text{mb}$. This regeneration amplitude results from averaging over FAISSNER 69, extrapolated using optical-model calculations of Bohm et al., Physics Letters **27B** 594 (1968) and the data of BALATS 71. (From H. Faissner, private communication).

$|\eta_{+-}| = |A(K_L^0 \rightarrow \pi^+ \pi^-) / A(K_S^0 \rightarrow \pi^+ \pi^-)|$

VALUE (units 10^{-3})	EVTS	DOCUMENT ID	TECN	COMMENT
2.232±0.011 OUR FIT				Error includes scale factor of 1.8.
2.226±0.007		BRFIT 16		
• • • We do not use the following data for averages, fits, limits, etc. • • •				
2.223±0.012		¹ LAI 07	NA48	
2.219±0.013		² AMBROSINO 06F	KLOE	
2.228±0.010		³ ALEXOPOU... 04	KTEV	
2.286±0.023±0.026	70M	⁴ APOSTOLA... 99C	CPLR K^0, \bar{K}^0 asymmetry	
2.310±0.043±0.031		⁵ ADLER 95B	CPLR K^0, \bar{K}^0 asymmetry	
2.32 ±0.14 ±0.03	10 ⁵	ADLER 92B	CPLR K^0, \bar{K}^0 asymmetry	
2.30 ±0.035		GEWENIGER 74B	ASPK	

¹ Value obtained from the NA48 measurements of $\Gamma(K_L^0 \rightarrow \pi^+ \pi^-)/\Gamma(K_L^0 \rightarrow \pi^+ \nu_e)$ and $\tau_{K_S^0}$ and KLOE measurements of $B(K_S^0 \rightarrow \pi^+ \pi^-)$ and $\tau_{K_L^0}$. $\Gamma(K_L^0 \rightarrow \pi^+ \pi^-)$ is defined to include the inner bremsstrahlung component $\Gamma(K_L^0 \rightarrow \pi^+ \pi^- \gamma(\text{IB}))$ but exclude the direct emission component $B(K_S^0 \rightarrow \pi^+ \pi^- (\text{DE}))$. Their $|\eta_{+-}|$ value is not directly used in our fit, but enters the fit via their branching ratio and lifetime measurements.

² AMBROSINO 06F uses KLOE branching ratios and τ_L together with τ_S from PDG 04. Their $|\eta_{+-}|$ value is not directly used in our fit, but enters the fit via their branching ratio and lifetime measurements.

³ ALEXOPOULOS 04 $|\eta_{+-}|$ uses their $K_L^0 \rightarrow \pi\pi$ branching fractions, $\tau_S = (0.8963 \pm 0.0005) \times 10^{-10}$ s from the average of KTeV and NA48 τ_S measurements, and assumes that $\Gamma(K_S^0 \rightarrow \pi\ell\nu_\ell) = \Gamma(K_L^0 \rightarrow \pi\ell\nu_\ell)$ giving $B(K_S^0 \rightarrow \pi\ell\nu_\ell) = 0.118\%$. Their η_{+-} is not directly used in our fit, but enters our fit via their branching ratio measurements.

⁴ APOSTOLAKIS 99C report (2.264 ± 0.023 ± 0.026 + 9.1[$\tau_S - 0.8934$]) $\times 10^{-3}$. We evaluate for our 2006 best value $\tau_S = (0.8958 \pm 0.0005) \times 10^{-10}$ s.

⁵ ADLER 95B report (2.312 ± 0.043 ± 0.030 - 1[$\Delta m - 0.5274$] + 9.1[$\tau_S - 0.8926$]) $\times 10^{-3}$. We evaluate for our 1996 best values $\Delta m = (0.5304 \pm 0.0014) \times 10^{-10} \text{ns}^{-1}$ and $\tau_S = (0.8927 \pm 0.0009) \times 10^{-10}$ s. Superseded by APOSTOLAKIS 99C.

$|\epsilon| = (2|\eta_{+-}| + |\eta_{00}|)/3$

This expression is a very good approximation, good to about one part in 10^{-4} because of the small measured value of $\phi_{00} - \phi_{+-}$ and small theoretical ambiguities.

VALUE (units 10^{-3})	DOCUMENT ID
2.228±0.011 OUR FIT	Error includes scale factor of 1.8.

$|\eta_{00}/\eta_{+-}|$

VALUE	EVTS	DOCUMENT ID	TECN
0.9950±0.0007 OUR FIT			Error includes scale factor of 1.6.
0.9930±0.0020 OUR AVERAGE			
0.9931 ±0.0020		^{1,2} BARR 93D	NA31
0.9904 ±0.0084 ±0.0036		³ WOODS 88	E731
• • • We do not use the following data for averages, fits, limits, etc. • • •			
0.9939 ±0.0013 ±0.0015	1M	¹ BARR 93D	NA31
0.9899 ±0.0020 ±0.0025		¹ BURKHARDT 88	NA31

¹ This is the square root of the ratio R given by BURKHARDT 88 and BARR 93D.

² This is the combined results from BARR 93D and BURKHARDT 88, taking into account a common systematic uncertainty of 0.0014.

³ We calculate $|\eta_{00}/\eta_{+-}| = 1 - 3(\epsilon'/\epsilon)$ from WOODS 88 (ϵ'/ϵ) value.

$\text{Re}(\epsilon'/\epsilon) = (1 - |\eta_{00}/\eta_{+-}|)/3$

We have neglected terms of order $\omega \cdot \text{Re}(\epsilon'/\epsilon)$, where $\omega = \text{Re}(A_2)/\text{Re}(A_0) \approx 1/22$. If included, this correction would lower $\text{Re}(\epsilon'/\epsilon)$ by about 0.04×10^{-3} . See SOZZI 04.

VALUE (units 10^{-3})	DOCUMENT ID	TECN	COMMENT
1.66 ±0.23 OUR FIT			Error includes scale factor of 1.6.
1.68 ±0.20 OUR AVERAGE			Error includes scale factor of 1.4. See the ideogram below.
1.92 ±0.21	¹ ABOUZAID 11	KTEV	Assuming CPT
1.47 ±0.22	BATLEY 02	NA48	
0.74 ±0.52 ±0.29	GIBBONS 93B	E731	
• • • We use the following data for averages but not for fits. • • •			
2.3 ±0.65	^{2,3} BARR 93D	NA31	
• • • We do not use the following data for averages, fits, limits, etc. • • •			
2.110 ±0.343	^{1,4} ABOUZAID 11	KTEV	Not assuming CPT
2.07 ±0.28	ALAVI-HARATI03	KTEV	In ABOUZAID 11
1.53 ±0.26	LAI 01C	NA48	Incl. in BATLEY 02
2.80 ±0.30 ±0.28	ALAVI-HARATI99D	KTEV	In ALAVI-HARATI 03
1.85 ±0.45 ±0.58	FANTI 99C	NA48	In LAI 01C
2.0 ±0.7	⁵ BARR 93D	NA31	
-0.4 ±1.4 ±0.6	PATTERSON 90	E731	in GIBBONS 93B
3.3 ±1.1	⁵ BURKHARDT 88	NA31	
3.2 ±2.8 ±1.2	² WOODS 88	E731	

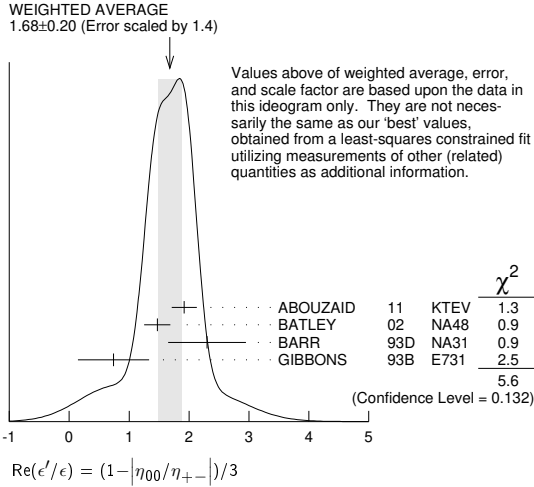
¹ The two ABOUZAID 11 values use the same data. The fits are performed with and without CPT invariance requirement.

See key on page 999

Meson Particle Listings

K_L^0

- ² These values are derived from $|\eta_{00}/\eta_{+-}|$ measurements. They enter the average in this section but enter the fit via the $|\eta_{00}/\eta_{+-}|$ only.
- ³ This is the combined results from BARR 93D and BURKHARDT 88, taking into account their common systematic uncertainty.
- ⁴ We use ABOUZAID 11 $\text{Re}(\epsilon'/\epsilon)$ value with *CPT* assumption in our fits for $|\eta_{+-}|$, $|\eta_{00}|$, and $\text{Re}(\epsilon'/\epsilon)$.
- ⁵ These values are derived from $|\eta_{00}/\eta_{+-}|$ measurements.



ϕ_{+-} , PHASE OF η_{+-}

The dependence of the phase on Δm and τ_S is given for each experiment in the comments below, where Δm is the $K_L^0 - K_S^0$ mass difference in units 10^{10}hs^{-1} and τ_S is the K_S mean life in units 10^{-10}s . We also give the regeneration phase ϕ_f in the comments below.

OUR FIT is described in the note on “*CP* violation in K_L decays” in the K_L^0 Particle Listings. Most experiments in this section are included in both the “Not Assuming *CPT*” and “Assuming *CPT*” fits. In the latter fit, they have little direct influence on ϕ_{+-} because their errors are large compared to that assuming *CPT*, but they influence Δm and τ_S through their dependencies on these parameters, which are given in the footnotes.

VALUE (°)	EVTs	DOCUMENT ID	TECN	COMMENT
43.51 ± 0.05 OUR FIT				Error includes scale factor of 1.2. Assuming <i>CPT</i>
43.4 ± 0.5 OUR FIT				Error includes scale factor of 1.2. Not assuming <i>CPT</i>
42.9 ± 0.6 ± 0.3	70M	¹ APOSTOLA... 99c	CPLR	$K^0 - \bar{K}^0$ asymmetry
42.9 ± 0.8 ± 0.2		^{2,3} SCHWINGENHEUER...95	E773	CH_{11} regenerator
41.4 ± 0.9 ± 0.2		^{3,4} GIBBONS 93	E731	B_4C regenerator
44.5 ± 1.6 ± 0.6		⁵ CAROSI 90	NA31	Vacuum regen.
43.3 ± 1.0 ± 0.5		⁶ GEWENIGER 74B	ASPK	Vacuum regen.
• • • We do not use the following data for averages, fits, limits, etc. • • •				
43.76 ± 0.64		⁷ ABOUZAID 11	KTEV	Not assuming <i>CPT</i>
44.12 ± 0.72 ± 1.20		⁸ ALAVI-HARATI03	KTEV	Not assuming <i>CPT</i>
42.5 ± 0.4 ± 0.3		^{9,10} ADLER 96C	RVUE	
43.4 ± 1.1 ± 0.3		¹¹ ADLER 95B	CPLR	$K^0 - \bar{K}^0$ asymmetry
42.3 ± 4.4 ± 1.4	100k	¹² ADLER 92B	CPLR	$K^0 - \bar{K}^0$ asymmetry
47.7 ± 2.0 ± 0.9		^{3,13} KARLSSON 90	E731	
44.3 ± 2.8 ± 0.2		¹⁴ CARITHERS 75	SPEC	C regenerator

- ¹ APOSTOLAKIS 99c measures $\phi_{+-} = (43.19 \pm 0.53 \pm 0.28) + 300 [\Delta m - 0.5301] (^\circ)$. We have adjusted the measurement to use our best values of $(\Delta m = 0.5293 \pm 0.0009) (10^{10} \text{hs}^{-1})$. Our first error is their experiment's error and our second error is the systematic error from using our best values.
- ² SCHWINGENHEUER 95 measures $\phi_{+-} = (43.53 \pm 0.76) + 173 [\Delta m - 0.5282] - 275 [\tau_S - 0.8926] (^\circ)$. We have adjusted the measurement to use our best values of $(\Delta m = 0.5293 \pm 0.0009) (10^{10} \text{hs}^{-1})$, $(\tau_S = 0.8954 \pm 0.0004) (10^{-10} \text{s})$. Our first error is their experiment's error and our second error is the systematic error from using our best values.
- ³ These experiments measure $\phi_{+-} - \phi_f$ and calculate the regeneration phase from the power law momentum dependence of the regeneration amplitude using analyticity and dispersion relations. SCHWINGENHEUER 95 [GIBBONS 93] includes a systematic error of $0.35^\circ [0.5^\circ]$ for uncertainties in their modeling of the regeneration amplitude.
- ⁴ GIBBONS 93 measures $\phi_{+-} = (42.21 \pm 0.9) + 189 [\Delta m - 0.5257] - 460 [\tau_S - 0.8922] (^\circ)$. We have adjusted the measurement to use our best values of $(\Delta m = 0.5293 \pm 0.0009) (10^{10} \text{hs}^{-1})$, $(\tau_S = 0.8954 \pm 0.0004) (10^{-10} \text{s})$. Our first error is their experiment's error and our second error is the systematic error from using our best values. This is actually reported in SCHWINGENHEUER 95, footnote 8. GIBBONS 93 reports $\phi_{+-} (42.2 \pm 1.4)^\circ$. They measure $\phi_{+-} - \phi_f$ and calculate the regeneration phase ϕ_f from the power law momentum dependence of the regeneration amplitude using analyticity. An error of 0.6° is included for possible uncertainties in the regeneration phase.
- ⁵ CAROSI 90 measures $\phi_{+-} = (46.9 \pm 1.4 \pm 0.7) + 579 [\Delta m - 0.5351] + 303 [\tau_S - 0.8922] (^\circ)$. We have adjusted the measurement to use our best values of $(\Delta m = 0.5293 \pm 0.0009) (10^{10} \text{hs}^{-1})$, $(\tau_S = 0.8954 \pm 0.0004) (10^{-10} \text{s})$. Our first error is their experiment's error and our second error is the systematic error from using our best values.

- ⁶ GEWENIGER 74B measures $\phi_{+-} = (49.4 \pm 1.0) + 565 [\Delta m - 0.540] (^\circ)$. We have adjusted the measurement to use our best values of $(\Delta m = 0.5293 \pm 0.0009) (10^{10} \text{hs}^{-1})$. Our first error is their experiment's error and our second error is the systematic error from using our best values.
- ⁷ Not independent of other phase parameters reported in ABOUZAID 11.
- ⁸ ALAVI-HARATI 03 ϕ_{+-} is correlated with their $\Delta m = m_{K_L^0} - m_{K_S^0}$ and τ_{K_S} measurements in the K_L^0 and K_S^0 sections respectively. The correlation coefficients are $\rho(\phi_{+-}, \Delta m) = +0.955$, $\rho(\phi_{+-}, \tau_S) = -0.871$, and $\rho(\tau_S, \Delta m) = -0.840$. *CPT* is not assumed. Uses scintillator Pb regenerator. Superseded by ABOUZAID 11.
- ⁹ ADLER 96C measures $\phi_{+-} = (43.82 \pm 0.41) + 339 [\Delta m - 0.5307] - 252 [\tau_S - 0.8922] (^\circ)$. We have adjusted the measurement to use our best values of $(\Delta m = 0.5293 \pm 0.0009) (10^{10} \text{hs}^{-1})$, $(\tau_S = 0.8954 \pm 0.0004) (10^{-10} \text{s})$. Our first error is their experiment's error and our second error is the systematic error from using our best values.
- ¹⁰ ADLER 96C is the result of a fit which includes nearly the same data as entered into the “OUR FIT” value in the 1996 edition of this Review (Physical Review **D54** 1 (1996)).
- ¹¹ ADLER 95B measures $\phi_{+-} = (42.7 \pm 0.9 \pm 0.6) + 316 [\Delta m - 0.5274] + 30 [\tau_S - 0.8926] (^\circ)$. We have adjusted the measurement to use our best values of $(\Delta m = 0.5293 \pm 0.0009) (10^{10} \text{hs}^{-1})$, $(\tau_S = 0.8954 \pm 0.0004) (10^{-10} \text{s})$. Our first error is their experiment's error and our second error is the systematic error from using our best values.
- ¹² ADLER 92B quote separately two systematic errors: ± 0.4 from their experiment and ± 1.0 degrees due to the uncertainty in the value of Δm .
- ¹³ KARLSSON 90 systematic error does not include regeneration phase uncertainty.
- ¹⁴ CARITHERS 75 measures $\phi_{+-} = (45.5 \pm 2.8) + 224 [\Delta m - 0.5348] (^\circ)$. We have adjusted the measurement to use our best values of $(\Delta m = 0.5293 \pm 0.0009) (10^{10} \text{hs}^{-1})$. Our first error is their experiment's error and our second error is the systematic error from using our best values. $\phi_f = -40.9 \pm 2.6^\circ$.

ϕ_{00} , PHASE OF η_{00}

See comment in ϕ_{+-} header above for treatment of Δm and τ_S dependence, as well as for the inclusion of data in both the “Assuming *CPT*” and “Not Assuming *CPT*” fits.

OUR FIT is described in the note on “*CP* violation in K_L decays” in the K_L^0 Particle Listings.

VALUE (°)	DOCUMENT ID	TECN	COMMENT
43.52 ± 0.05 OUR FIT			Error includes scale factor of 1.3. Assuming <i>CPT</i>
43.7 ± 0.6 OUR FIT			Error includes scale factor of 1.2. Not assuming <i>CPT</i>
44.5 ± 2.3 ± 0.5	¹ CAROSI 90	NA31	
• • • We do not use the following data for averages, fits, limits, etc. • • •			
44.06 ± 0.68	² ABOUZAID 11	KTEV	Not assuming <i>CPT</i>
41.7 ± 5.9 ± 0.2	³ ANGELOPOU... 98	CPLR	
50.8 ± 7.1 ± 1.7	⁴ ADLER 96B	CPLR	Sup. by ANGELOPOULOS 98
47.4 ± 1.4 ± 0.9	⁵ KARLSSON 90	E731	
¹ CAROSI 90 measures $\phi_{00} = (47.1 \pm 2.1 \pm 1.0) + 579 [\Delta m - 0.5351] + 252 [\tau_S - 0.8922] (^\circ)$. We have adjusted the measurement to use our best values of $(\Delta m = 0.5293 \pm 0.0009) (10^{10} \text{hs}^{-1})$, $(\tau_S = 0.8954 \pm 0.0004) (10^{-10} \text{s})$. Our first error is their experiment's error and our second error is the systematic error from using our best values.			
² Not independent of other phase parameters reported in ABOUZAID 11.			
³ ANGELOPOULOS 98 measures $\phi_{00} = (42.0 \pm 5.6 \pm 1.9) + 240 [\Delta m - 0.5307] (^\circ)$. We have adjusted the measurement to use our best values of $(\Delta m = 0.5293 \pm 0.0009) (10^{10} \text{hs}^{-1})$. Our first error is their experiment's error and our second error is the systematic error from using our best values. The τ_S dependence is negligible.			
⁴ ADLER 96B identified initial neutral kaon individually as being a K^0 or a \bar{K}^0 . The systematic uncertainty is $\pm 1.5^\circ$ combined in quadrature with $\pm 0.8^\circ$ due to Δm .			
⁵ KARLSSON 90 systematic error does not include regeneration phase uncertainty.			

$\phi_\epsilon = (2\phi_{+-} + \phi_{00})/3$

This expression is a very good approximation, good to about 10^{-3} degrees because of the small measured values of $\phi_{00} - \phi_{+-}$ and $\text{Re}(\epsilon'/\epsilon)$, and small theoretical ambiguities.

VALUE (°)	DOCUMENT ID	TECN	COMMENT
43.52 ± 0.05 OUR FIT			Error includes scale factor of 1.2. Assuming <i>CPT</i>
43.5 ± 0.5 OUR FIT			Error includes scale factor of 1.3. Not assuming <i>CPT</i>
43.5164 ± 0.0002 ± 0.0518	¹ SUPERWEAK 16		Assuming <i>CPT</i>
43.86 ± 0.63	² ABOUZAID 11	KTEV	Not assuming <i>CPT</i>
¹ SUPERWEAK 16 is a fake measurement used to impose the <i>CPT</i> or Superweak constraint $\phi_{+-} = \phi_{\text{SW}} = \tan^{-1} [2 \frac{\Delta m}{\hbar} (\frac{\tau_S \tau_L}{\tau_S - \tau_L})]$. This “measurement” is linearized using values near the PDG 04 edition values of Δm , τ_S and τ_L , and then adjusted to our current values as described in the following “measurement”. SUPERWEAK 16 measures $\phi_\epsilon = (43.50258 \pm 0.00021) + 54.1 [\Delta m - 0.5289] + 32.0 [\tau_S - 0.89564] (^\circ)$. We have adjusted the measurement to use our best values of $(\Delta m = 0.5293 \pm 0.0009) (10^{10} \text{hs}^{-1})$, $(\tau_S = 0.8954 \pm 0.0004) (10^{-10} \text{s})$. Our first error is their experiment's error and our second error is the systematic error from using our best values.			
² ABOUZAID 11 uses the full KTeV dataset collected in 1996, 1997, and 1999. See $\text{Im}(\epsilon'/\epsilon)$ section for correlation information.			

$\text{Im}(\epsilon'/\epsilon) = -(\phi_{00} - \phi_{+-})/3$

For small $|\epsilon'/\epsilon|$, $\text{Im}(\epsilon'/\epsilon)$ is related to the phases of η_{00} and η_{+-} by the above expression.

VALUE (°)	DOCUMENT ID	TECN	COMMENT
-0.002 ± 0.005 OUR FIT			Error includes scale factor of 1.7. Assuming <i>CPT</i>
-0.11 ± 0.11 OUR FIT			Not assuming <i>CPT</i>
-0.0985 ± 0.1157	¹ ABOUZAID 11	KTEV	Not assuming <i>CPT</i>
¹ ABOUZAID 11 uses the full KTeV dataset collected in 1996, 1997, and 1999. The fit has Δm , τ_S , ϕ_ϵ , $\text{Re}(\epsilon'/\epsilon)$, and $\text{Im}(\epsilon'/\epsilon)$ as free parameters. The reported value of $\text{Im}(\epsilon'/\epsilon) = (-17.20 \pm 20.20) \times 10^{-4}$ rad. The correlation coefficients are $\rho(\phi_\epsilon, \Delta m) = 0.828$, $\rho(\phi_\epsilon, \tau_S) = -0.765$, $\rho(\Delta m, \tau_S) = -0.858$, $\rho(\text{Im}(\epsilon'/\epsilon), \phi_\epsilon) = -0.041$, $\rho(\text{Im}(\epsilon'/\epsilon), \Delta m) = 0.026$, $\rho(\text{Im}(\epsilon'/\epsilon), \tau_S) = -0.010$.			

Meson Particle Listings

K_L^0

DECAY-PLANE ASYMMETRY IN $\pi^+\pi^-\pi^+\pi^-$ DECAYS

This is the CP -violating asymmetry

$$A = \frac{N_{\sin\phi\cos\phi>0.0} - N_{\sin\phi\cos\phi<0.0}}{N_{\sin\phi\cos\phi>0.0} + N_{\sin\phi\cos\phi<0.0}}$$

where ϕ is the angle between the e^+e^- and $\pi^+\pi^-$ planes in the K_L^0 rest frame.

CP ASYMMETRY A in $K_L^0 \rightarrow \pi^+\pi^-\pi^+\pi^-$

VALUE (%)	DOCUMENT ID	TECN
13.7 ± 1.5 OUR AVERAGE		
13.6 ± 1.4 ± 1.5	ABOUZAID 06	KTEV
14.2 ± 3.0 ± 1.9	LAI 03C	NA48
13.6 ± 2.5 ± 1.2	ALAVI-HARATI00B	KTEV

PARAMETERS FOR $e^+e^-\pi^+\pi^-$ DECAYS

These are the CP -violating parameters in the ϕ distribution, where ϕ is the angle between the planes of the two e^+e^- pairs in the kaon rest frame:

$$d\Gamma/d\phi \propto 1 + \beta_{CP} \cos(2\phi) + \gamma_{CP} \sin(2\phi)$$

where $\beta_{CP} = -0.20$ and $\gamma_{CP} = 0$ values correspond to no CP violation.

β_{CP} from $K_L^0 \rightarrow e^+e^-\pi^+\pi^-$

VALUE	EVTS	DOCUMENT ID	TECN	COMMENT
-0.19 ± 0.07 OUR AVERAGE				
-0.13 ± 0.10 ± 0.03	200	¹ LAI	05B	NA48
-0.23 ± 0.09 ± 0.02	441	ALAVI-HARATI01D	KTEV	$M_{ee} > 8 \text{ MeV}/c^2$

¹ LAI 05B obtains $\beta_{CP} = -0.13 \pm 0.10$ (stat) if $\gamma_{CP} = 0$ is assumed.

γ_{CP} from $K_L^0 \rightarrow e^+e^-\pi^+\pi^-$

VALUE	EVTS	DOCUMENT ID	TECN	COMMENT
0.01 ± 0.11 OUR AVERAGE				Error includes scale factor of 1.6.
+0.13 ± 0.10 ± 0.03	200	LAI	05B	NA48
-0.09 ± 0.09 ± 0.02	441	ALAVI-HARATI01D	KTEV	$M_{ee} > 8 \text{ MeV}/c^2$

CHARGE ASYMMETRY IN $\pi^+\pi^-\pi^0$ DECAYS

These are CP -violating charge-asymmetry parameters, defined at beginning of section "LINEAR COEFFICIENT g FOR $K_L^0 \rightarrow \pi^+\pi^-\pi^0$ " above. See also note on Dalitz plot parameters in K^\pm section and note on " CP violation in K_L decays" above.

LINEAR COEFFICIENT j FOR $K_L^0 \rightarrow \pi^+\pi^-\pi^0$

VALUE	EVTS	DOCUMENT ID	TECN
0.0012 ± 0.0008 OUR AVERAGE			
0.0010 ± 0.0024 ± 0.0030	500k	ANGELOPO...	98C CPLR
-0.001 ± 0.011	6499	CHO	77
0.001 ± 0.003	4709	PEACH	77
0.0013 ± 0.0009	3M	SCRIBANO	70
0.0 ± 0.017	4400	SMITH	70 OSPK
0.001 ± 0.004	238k	BLANPIED	68

QUADRATIC COEFFICIENT f FOR $K_L^0 \rightarrow \pi^+\pi^-\pi^0$

VALUE	EVTS	DOCUMENT ID	TECN
0.0045 ± 0.0024 ± 0.0059	500k	ANGELOPO...	98C CPLR

PARAMETERS for $K_L^0 \rightarrow \pi^+\pi^-\gamma$ DECAY

$$|\eta_{+-\gamma}| = |A(K_L^0 \rightarrow \pi^+\pi^-\gamma, CP \text{ violating})/A(K_S^0 \rightarrow \pi^+\pi^-\gamma)|$$

VALUE (units 10^{-3})	EVTS	DOCUMENT ID	TECN
2.35 ± 0.07 OUR AVERAGE			
2.359 ± 0.062 ± 0.040	9045	MATTHEWS 95	E773
2.15 ± 0.26 ± 0.20	3671	RAMBERG 93B	E731

$\phi_{+-\gamma}$ = phase of $\eta_{+-\gamma}$

VALUE (°)	EVTS	DOCUMENT ID	TECN
44 ± 4 OUR AVERAGE			
43.8 ± 3.5 ± 1.9	9045	MATTHEWS 95	E773
72 ± 23 ± 17	3671	RAMBERG 93B	E731

$|\epsilon'_{+-\gamma}|/\epsilon$ for $K_L^0 \rightarrow \pi^+\pi^-\gamma$

VALUE	CL%	EVTS	DOCUMENT ID	TECN
<0.3	90	3671	¹ RAMBERG 93B	E731

¹ RAMBERG 93B limit on $|\epsilon'_{+-\gamma}|/\epsilon$ assumes that any difference between η_{+-} and $\eta_{+-\gamma}$ is due to direct CP violation.

$|g_{E1}|$ for $K_L^0 \rightarrow \pi^+\pi^-\gamma$

This parameter is the amplitude of the direct emission of a CP violating E1 electric dipole photon.

VALUE	CL%	EVTS	DOCUMENT ID	TECN	COMMENT
<0.21	90	111k	ABOUZAID 06A	KTEV	$E_\gamma > 20 \text{ MeV}$

T VIOLATION TESTS IN K_L^0 DECAYS

$\text{Im}(\xi)$ in $K_{\mu 3}^0$ DECAY (from transverse μ pol.)

VALUE	EVTS	DOCUMENT ID	TECN	COMMENT
-0.007 ± 0.026 OUR AVERAGE				
0.009 ± 0.030	12M	MORSE	80	CNTR Polarization
0.35 ± 0.30	207k	¹ CLARK	77	SPEC POL, $t=0$
-0.085 ± 0.064	2.2M	² SANDWEISS	73	CNTR POL, $t=0$
-0.02 ± 0.08		LONGO	69	CNTR POL, $t=3.3$
-0.2 ± 0.6		ABRAMS	68B	OSPK Polarization
0.012 ± 0.026		SCHMIDT	79	CNTR Repl. by MORSE 80

• • • We do not use the following data for averages, fits, limits, etc. • • •

¹ CLARK 77 value has additional $\xi(0)$ dependence $+0.21\text{Re}[\xi(0)]$.
² SANDWEISS 73 value corrected from value quoted in their paper due to new value of $\text{Re}(\xi)$. See footnote 4 of SCHMIDT 79.

CPT-INVARIANCE TESTS IN K_L^0 DECAYS

PHASE DIFFERENCE $\phi_{00} - \phi_{+-}$

Test of CPT .

OUR FIT is described in the note on " CP violation in K_L decays" in the K_L^0 Particle Listings.

VALUE (°)	DOCUMENT ID	TECN	COMMENT
0.006 ± 0.014 OUR FIT			Error includes scale factor of 1.7. Assuming CPT
0.34 ± 0.32 OUR FIT			Not assuming CPT
0.006 ± 0.008	¹ SUPERWEAK 16		Assuming CPT
-0.30 ± 0.88	² SCHWINGEN...95		Combined E731, E773
0.30 ± 0.35	³ ABOUZAID 11	KTEV	Not assuming CPT
0.39 ± 0.22 ± 0.45	⁴ ALAVI-HARATI03	KTEV	
0.62 ± 0.71 ± 0.75	SCHWINGEN...95		E773
-1.6 ± 1.2	⁵ GIBBONS 93		E731
0.2 ± 2.6 ± 1.2	⁶ CAROSI 90		NA31
-0.3 ± 2.4 ± 1.2	KARLSSON 90		E731

- ¹ SUPERWEAK 16 is a fake experiment to constrain $\phi_{00} - \phi_{+-}$ to a small value as described in the note "CP violation in K_L decays."
- ² This SCHWINGENHEUER 95 values is the combined result of SCHWINGENHEUER 95 and GIBBONS 93, accounting for correlated systematic errors.
- ³ Not independent of other phase parameters reported in ABOUZAID 11.
- ⁴ ALAVI-HARATI 03 fit $\text{Re}(\epsilon'/\epsilon)$, $\text{Im}(\epsilon'/\epsilon)$, Δm , τ_S , and ϕ_{+-} simultaneously, not assuming CPT . Phase difference is obtained from $\phi_{00} - \phi_{+-} \approx -3\text{Im}(\epsilon'/\epsilon)$ for small $|\epsilon'/\epsilon|$. Superseded by ABOUZAID 11.
- ⁵ GIBBONS 93 give detailed dependence of systematic error on lifetime (see the section on the K_S^0 mean life) and mass difference (see the section on $m_{K_L^0} - m_{K_S^0}$).
- ⁶ CAROSI 90 is excluded from the fit because it is not independent of ϕ_{+-} and ϕ_{00} values.

PHASE DIFFERENCE $\phi_{+-} - \phi_{SW}$

Test of CPT . The Superweak phase $\phi_{SW} \equiv \tan^{-1}(2\Delta m/\Delta\Gamma)$ where $\Delta m = m_{K_L^0} - m_{K_S^0}$ and $\Delta\Gamma = \hbar(\tau_L - \tau_S)/(\tau_L\tau_S)$.

VALUE (°)	DOCUMENT ID	TECN
0.61 ± 0.62 ± 1.01	¹ ALAVI-HARATI03	KTEV

¹ ALAVI-HARATI 03 fit is the same as their ϕ_{+-} , τ_{K_S} , Δm fit, except that the parameter $\phi_{+-} - \phi_{SW}$ is used in place of ϕ .

$$\text{Re}(\frac{2}{3}\eta_{+-} + \frac{1}{3}\eta_{00}) - \frac{A_L}{A_S}$$

VALUE (units 10^{-6})	DOCUMENT ID	TECN	COMMENT
-3 ± 35	¹ ALAVI-HARATI02	E799	Uses A_L from K_{e3} decays

¹ ALAVI-HARATI 02 uses PDG 00 values of η_{+-} and η_{00} .

$\Delta S = \Delta Q$ IN K^0 DECAYS

The relative amount of $\Delta S \neq \Delta Q$ component present is measured by the parameter x , defined as

$$x = A(\bar{K}^0 \rightarrow \pi^-\ell^+\nu)/A(K^0 \rightarrow \pi^-\ell^+\nu)$$

We list $\text{Re}\{x\}$ and $\text{Im}\{x\}$ for K_{e3} and $K_{\mu 3}$ combined.

$$x = A(\bar{K}^0 \rightarrow \pi^-\ell^+\nu)/A(K^0 \rightarrow \pi^-\ell^+\nu) = A(\Delta S = -\Delta Q)/A(\Delta S = \Delta Q)$$

REAL PART OF x

VALUE	EVTS	DOCUMENT ID	TECN	COMMENT
-0.0018 ± 0.0041 ± 0.0045		ANGELOPO... 98D	CPLR	K_{e3} from K^0

• • • We do not use the following data for averages, fits, limits, etc. • • •

Table with columns for value, EVTS, DOCUMENT ID, TECN, and COMMENT. Contains data for various meson decays like pi- to K0 lambda, K+ to K0 p pi+, etc.

1 BURGUN 72 is a final result which includes BURGUN 71.
2 First GRAHAM 72 value is second GRAHAM 72 value combined with MANTSCH 72.
3 CHO 70 is analysis of unambiguous events in new data and HILL 67.
4 BENNETT 69 is a reanalysis of BENNETT 68.
5 BALDO-CEOLIN 65 gives x and theta converted by us to Re(x) and Im(x).
6 FRANZINI 65 gives x and theta for Re(x) and Im(x). See SCHMIDT 67.

IMAGINARY PART OF x

Assumes m_KL^0 - m_KS^0 positive. See Listings above.

Table with columns: VALUE, EVTS, DOCUMENT ID, TECN, COMMENT. Row 1: 0.0012 +/- 0.0019 +/- 0.0009, 640k, ANGELOPO... 01B, CPLR, K23 from K0

• • • We do not use the following data for averages, fits, limits, etc. • • •

Table with columns for value, EVTS, DOCUMENT ID, TECN, and COMMENT. Contains data for various meson decays like pi- to K0 lambda, K+ to K0 p pi+, etc.

1 Superseded by ANGELOPOULOS 01b.
2 BURGUN 72 is a final result which includes BURGUN 71.
3 First GRAHAM 72 value is second GRAHAM 72 value combined with MANTSCH 72.
4 Footnote 10 of HILL 67 should read +0.58, not -0.58 (private communication) CHO 70 is analysis of unambiguous events in new data and HILL 67.
5 BALDO-CEOLIN 65 gives x and theta converted by us to Re(x) and Im(x).
6 FRANZINI 65 gives x and theta for Re(x) and Im(x). See SCHMIDT 67.

KL^0 REFERENCES

Table with columns: AUTHOR, YEAR, DOCUMENT ID, AUTHOR, YEAR, DOCUMENT ID, AUTHOR, YEAR, DOCUMENT ID. Lists references for K0L.

Large table with columns: AUTHOR, YEAR, DOCUMENT ID, AUTHOR, YEAR, DOCUMENT ID, AUTHOR, YEAR, DOCUMENT ID. Lists references for various meson decays.

Meson Particle Listings

K^0_L

ARISAKA	93B	PRL 71 3910	K. Arisaka et al. (BNL E791 Collab.)	VOSBURGH	72	PR D6 1834	K.G. Vosburgh et al. (RUTG, MASA)
BARR	93D	PL B317 233	G.D. Barr et al. (CERN, EDIN, MANZ, LALO+)	Also		PRL 26 866	K.G. Vosburgh et al. (RUTG, MASA)
GIBBONS	93	PRL 70 1199	L.K. Gibbons et al. (FNAL E731 Collab.)	BALATS	71	SJNP 13 53	M.Y. Balats et al. (ITEP)
Also		PR D55 6625	L.K. Gibbons et al. (FNAL E731 Collab.)	Translated from YAF 13 93			
GIBBONS	93B	PRL 70 1203	L.K. Gibbons et al. (CHIC)	BARMIN	71	PL 35B 604	V.V. Barmin et al. (ITEP)
GIBBONS	93C	Thesis RX-1487	L.K. Gibbons et al. (FNAL E731 Collab.)	BURGIN	71	LNC 2 1169	G. Burgun et al. (SACL, CERN, OSLO)
Also		PR D55 6625	L.K. Gibbons et al. (EFU, UCLA, COLO+)	CARNEGIE	71	PR D4 1	G. Burgun et al. (PRIN)
HARRIS	93	PRL 71 3914	D.A. Harris et al. (EFU, UCLA, COLO+)	CHAN	71	Thesis LBL-350	J.H.S. Chan (LRL)
HARRIS	93B	PRL 71 3918	D.A. Harris et al. (FNAL E731 Collab.)	CHO	71	PR D3 1557	Y. Cho et al. (CMU, BNL, CASE)
MAKOFF	93	PRL 70 1591	G. Makoff et al. (FNAL E731 Collab.)	ENSTROM	71	PR D4 2629	J. Enstrom et al. (SLAC, STAN)
Also		PRL 75 2049 (erratum)	G. Makoff et al. (FNAL E731 Collab.)	Also		Thesis SLAC-0125	J.E. Enstrom (STAN)
RAMBERG	93	PRL 70 2525	E. Ramberg et al. (FNAL E731 Collab.)	JAMES	71	PL 35B 265	F. James et al. (CERN, SACL, OSLO)
RAMBERG	93B	PRL 70 2529	E.J. Ramberg et al. (FNAL E731 Collab.)	MEISNER	71	PR D3 59	G.W. Meisner et al. (MASA, BNL, YALE)
VAGINS	93	PRL 71 35	M.R. Vagins et al. (BNL E845 Collab.)	REPELLIN	71	PL 36B 603	J.P. Repellin et al. (ORSAY, CERN)
ADLER	92B	PL B286 180	R. Adler et al. (CLEAR Collab.)	WEBBER	71	PR D3 64	B.R. Webber et al. (LRL)
Also		SJNP 55 840	R. Adler et al. (CLEAR Collab.)	Also		PRL 21 498	B.R. Webber et al. (LRL)
BARR	92	PL B284 440	G.D. Barr et al. (CERN, EDIN, MANZ, LALO+)	Also		Thesis UCRL 19226	B.R. Webber (LRL)
MORSE	92	PR D45 36	W.M. Morse et al. (BNL, YALE, VASS)	WOLFF	71	PL 36B 517	B. Wolff et al. (ORSAY, CERN)
PDG	92	PR D45 51	K. Hikasa et al. (KEK, LBL, BOST+)	ALBROW	70	PL 33B 516	M.G. Albrow et al. (MCHS, DARE)
SOMALWAR	92	PRL 68 2580	S.V. Somalwar et al. (FNAL E731 Collab.)	ARONSON	70	PRL 25 1057	S.H. Aronson et al. (EFU, ILLC, SLAC)
AKAGI	91B	PRL 67 2618	T. Akagi et al. (TOHOK, TOKY, KYOT, KEK)	BARMIN	70	PL 33B 377	V.V. Barmin et al. (ITEP, JINR)
BARR	91	PL B259 389	G.D. Barr et al. (CERN, EDIN, MANZ, LALO+)	BASILE	70	PR D2 78	P. Basile et al. (SACL)
HEINSON	91	PR D44 1	A.P. Heinson et al. (UCI, UCLA, LANL+)	BECHERRAWY	70	PR D1 1452	T. Becherawy (ROCH)
PAPADIMITRI...	91	PR D44 573	V. Papadimitriou et al. (FNAL E731 Collab.)	BUCHANAN	70	PL 33B 623	C.D. Buchanan et al. (SLAC, JHU, UCLA)
BARKER	90	PR D41 3546	A.R. Barker et al. (FNAL E731 Collab.)	Also		Private Comm.	A.J. Cox
Also		PRL 61 2661	L.K. Gibbons et al. (FNAL E731 Collab.)	BUDAGOV	70	PR D2 815	I.A. Budagov et al. (CERN, ORSAY, EPOL)
BARR	90B	PL B240 283	G.D. Barr et al. (CERN, EDIN, MANZ, LALO+)	Also		PL 28B 215	I.A. Budagov et al. (CERN, ORSAY, EPOL)
BARR	90C	PL B242 523	G.D. Barr et al. (CERN, EDIN, MANZ, LALO+)	CHO	70	PR D1 3031	Y. Cho et al. (CMU, BNL, CASE)
CAROLI	90	PL B237 303	R. Carosi et al. (CERN, EDIN, MANZ, LALO+)	Also		PRL 19 668	D.G. Hill et al. (BNL, CHU)
KARLSSON	90	PRL 64 2976	M. Karlsson et al. (FNAL E731 Collab.)	CHOLLET	70	PL 31B 658	J.C. Chollet et al. (CERN)
OHL	90	PRL 68 2755	K.E. Ohi et al. (BNL E845 Collab.)	CULLEN	70	PL 37B 523	M. Cullen et al. (AACH, CERN, TORI)
OHL	90B	PRL 69 1407	K.E. Ohi et al. (BNL E845 Collab.)	MARX	70	PL 32B 219	J. Marx et al. (COLU, HARV, CERN)
PATTERSON	90	PRL 64 1491	J.R. Patterson et al. (FNAL E731 Collab.)	Also		Thesis Nevis 179	J. Marx (COLU)
INAGAKI	89	PR D40 1712	T. Inagaki et al. (KEK, TOKY, KYOT)	SCRIBANO	70	PL 32B 224	A. Scribano et al. (PISA, COLU, HARV)
MATHIAZHA...	89	PRL 63 2181	C. Mathiazhagan et al. (UCI, UCLA, LANL+)	SMITH	70	PL 32B 133	R.C. Smith et al. (UMD, BNL)
MATHIAZHA...	89B	PRL 63 2185	C. Mathiazhagan et al. (UCI, UCLA, LANL+)	WEBBER	70	PR D1 1967	B.R. Webber et al. (LRL)
WAHL	89	CERN-EP/89-86	H. Wahl (CERN)	Also		Thesis UCRL 19226	B.R. Webber (LRL)
BARR	88	PL B214 303	G.D. Barr et al. (CERN, EDIN, MANZ, LALO+)	BANNER	69	PR 188 2033	M. Banner et al. (PRIN)
BURKHARDT	88	PL B206 169	H. Burkhardt et al. (CERN, EDIN, MANZ+)	Also		PRL 21 1103	M. Banner et al. (PRIN)
JASTRZEM...	88	PRL 61 2300	E. Jastrzembski et al. (BNL, YALE)	Also		PRL 21 1107	J.W. Cronin, J.K. Liu, J.E. Pilcher (PRIN)
WOODS	88	PRL 60 1695	M. Woods et al. (FNAL E731 Collab.)	BENNETT	69	PL 29B 317	S. Bennett et al. (COLU, BNL)
BURKHARDT	87	PL B199 139	H. Burkhardt et al. (CERN, EDIN, MANZ+)	FAISSNER	69	PL 29B 204	H. Faissner et al. (AACH3, CERN, TORI)
ARONS ON	86	PR D33 3180	S.H. Aronson et al. (BNL, CHIC, STAN+)	LITTENBERG	69	PR 22 654	L.S. Littenberg et al. (UCSD)
Also		PRL 48 1078	S.H. Aronson et al. (BNL, CHIC, STAN+)	LONGO	69	PR 181 1808	M.J. Longo, K.K. Young, J.A. Helland (MICH, UCLA)
PDG	86C	PL 170B 132	M. Aguilar-Benitez et al. (CERN, CIT+)	PACIOTTI	69	Thesis UCRL 19446	M.A. Paciotti (LRL)
COUPL	85C	PRL 55 566	D.P. Coupl et al. (CHIC, SACL)	SAAL	69	Thesis	H.J. Saal (COLU)
BALATS	83	SJNP 38 556	M.Y. Balats et al. (ITEP)	ABRAMS	68B	PR 176 1603	R.J. Abrams et al. (ILL)
Translated from YAF 38 927				ARNOLD	68B	PL 28B 56	R.G. Arnold et al. (CERN, ORSAY)
BERGSTROM	83	PL 131B 229	L. Bergstrom, E. Masso, P. Singer (CERN)	BASILE	68B	PL 28B 58	P. Basile et al. (SACL)
ARONS ON	82	PRL 48 1078	S.H. Aronson et al. (BNL, CHIC, STAN+)	BENNETT	68	PL 27B 244	S. Bennett et al. (COLU, CERN)
ARONS ON	82B	PRL 48 1306	S.H. Aronson et al. (BNL, CHIC, PURD)	BLANPIED	68	PRL 21 1650	W.A. Blanpied et al. (CASE, HARV, MCGI)
Also		PL 116B 73	E. Fischbach et al. (PURD, BNL, CHIC)	BOHM	68B	PL 27B 534	I.A. Bohm et al. (CERN)
Also		PR D29 476	S.H. Aronson et al. (BNL, CHIC, PURD)	BUDAGOV	68	NC 27B 182	I.A. Budagov et al. (CERN, ORSAY, IPNP)
Also		PR D28 495	S.H. Aronson et al. (BNL, CHIC, PURD)	Also		PL 28B 215	I.A. Budagov et al. (CERN, ORSAY, EPOL)
PDG	82B	PL 111B 70	M. Roos et al. (HEL5, CIT, CERN)	JAMES	68	NP B8 365	F. James, H. Briand (IPNP, CERN)
BIRULEV	81	NP B182 1	V.K. Birulev et al. (JINR)	Also		PRL 21 257	J.A. Helland, M.J. Longo, K.K. Young (UCLA, MICH)
Also		SJNP 31 622	V.K. Birulev et al. (JINR)	KULYUKINA	68	JETP 26 20	L.A. Kulyukina et al. (JINR)
Translated from YAF 31 1204				Translated from ZETF 53 29			
CARROLL	80B	PRL 44 529	A.S. Carroll et al. (BNL, ROCH)	KUNZ	68	Thesis PU-68-46	P.F. Kunz (PRIN)
CARROLL	80C	PL 96B 407	A.S. Carroll et al. (BNL, ROCH)	BENNETT	67	PRL 19 993	S. Bennett et al. (COLU)
CHO	80	PR D22 2688	Y. Cho et al. (ANL, CMU)	DEBOUARD	67	NC 52A 662	X. de Bouard et al. (CERN)
MORSE	80	PR D21 1750	W.M. Morse et al. (BNL, YALE)	Also		PRL 18 58	X. de Bouard et al. (CERN, ORSAY, MFM)
CHRISTENS...	79	PRL 43 1209	J.H. Christensen et al. (BNL, NYU)	DEVLIN	67	PR 169 1045	T.J. Devlin et al. (PRIN, UMD)
SCHMIDT	79	PRL 43 556	M.P. Schmidt et al. (YALE, BNL)	G.A. Sayer et al. (UMD, PPA, PRIN)			
HILL	78	PL 73B 483	D.G. Hill et al. (BNL, SLAC, SBER)	DORFAN	67	PRL 19 987	D.E. Dorfman et al. (SLAC, LRL)
CHO	77	PR D15 587	Y. Cho et al. (ANL, CMU)	FELDMAN	67B	PR 155 1611	L. Feldman et al. (PENN)
CLARK	77	PR D15 553	A.R. Clark et al. (LBL)	FITCH	67	PR 164 1711	V.L. Fitch et al. (PRIN)
Also		Thesis LBL-4275	G. Shen (LBL)	GINSBERG	67	PR 162 1570	E.S. Ginsberg (MASB)
DEVOE	77	PR D16 565	R. Devoe et al. (FEU, ANL)	HILL	67	PRL 19 668	D.G. Hill et al. (BNL, CMU)
PEACH	77	NP B127 399	V.J. Peach et al. (BGNA, EDIN, GLAS+)	HOPKINS	67	PRL 19 185	H.W.K. Hopkins, T.C. Bacon, F.R. Eisler (BNL)
BIRULEV	76	SJNP 24 178	K.K. Birulev et al. (JINR)	NEFKENS	67	PR 157 1233	B.M.K. Nefkens et al. (ILL)
Translated from YAF 24 340				SCHMIDT	67	Thesis Nevis 160	P. Schmidt (COLU)
COOMBS	76	PRL 37 249	R.W. Coombs et al. (STAN, NYU)	BEHR	67	PL 22 540	L. Behr et al. (EPOL, MILA, PADO, ORSAY)
GJESDAL	76	NP B109 118	G. Gjesdal et al. (CERN, HEIDH)	HAWKINS	66	PL 21 238	C.J.B. Hawkins (YALE)
BALDO...	75	NC 25A 688	M. Baldo-Ceolin et al. (PADO, WIS C)	Also		PR 156 1444	C.J.B. Hawkins (YALE)
BLUMENTHAL	75	PRL 34 164	R.B. Blumenthal et al. (PENN, CHIC, TEMP)	ANDERSON	65	PRL 14 475	J.A. Anderson et al. (LRL, WISC)
BUCHANAN	75	PR D11 457	C.D. Buchanan et al. (UCLA, SLAC, JHU)	ASTBURY	65B	PL 18 175	P. Astbury et al. (CERN, ZURI)
CARITHERS	75	PRL 34 1244	W.C.J. Carithers et al. (COLU, NYU)	AUBERT	65	PL 17 59	B. Aubert et al. (EPOL, ORSAY)
SMITH	75B	Thesis UCSD unpub.	J.G. Smith (UCSD)	Also		PL 24B 75	J.P. Lowsy et al. (EPOL, ORSAY)
BISI	74	PL 50B 504	V. Bisi, M.I. Ferrero (TORI)	BALDO...	65	NC 38 684	M. Baldo-Ceolin et al. (PADO)
DONALDSON	74	Thesis SLAC-0184	G. Donaldson (SLAC)	FRANZINI	65	PR 140 B127	P. Franzini et al. (COLU, RUTG)
Also		PR D14 2839	G. Donaldson et al. (SLAC)	GUIDONI	65	Argonne Conf. 49	P. Guidoni et al. (BNL, YALE)
DONALDSON	74B	PR D9 2940	G. Donaldson et al. (SLAC, UCSC C)	HOPKINS	65	Argonne Conf. 49	H.W.K. Hopkins, T.C. Bacon, F. Eisler (VAN D+)
Also		PRL 31 337	G. Donaldson et al. (SLAC, UCSC C)	ALEKSANYAN	64B	Dubna Conf. 2 102	A.S. Aleksanyan et al. (YERE)
GEWENIGER	74	PL 48B 483	C. Geweniger et al. (CERN, HEIDH)	Also		JETP 19 1019	A.S. Aleksanyan et al. (LEBD, MPEI, YERE)
Also		Thesis CERN Int. 74-4	V. Luth (CERN)	Translated from ZETF 46 1504			
GEWENIGER	74B	PL 48B 487	C. Geweniger et al. (CERN, HEIDH)	ANIKINA	64	JETP 19 42	M.K. Anikina et al. (GEOR, JINR)
Also		PL 52B 119	S. Gjesdal et al. (CERN, HEIDH)	Translated from ZETF 46 59			
GEWENIGER	74C	PL 52B 108	C. Geweniger et al. (CERN, HEIDH)	FITCH	61	NC 22 1160	V.L. Fitch, P.A. Piroue, R.B. Perkins (PRIN+)
GJESDAL	74	PL 52B 113	S. Gjesdal et al. (CERN, HEIDH)	GOOD	61	PR 124 1223	R.H. Good et al. (LRL)
MESSNER	74	PRL 33 1458	R. Messner et al. (COLO, SLAC, UCSC)				
NIEBERGALL	74	PL 49B 103	F. Niebergall et al. (CERN, ORSAY, VIEN)				
WILLIAMS	74	PRL 33 240	H.H. Williams et al. (BNL, YALE)				
ALEXANDER	73B	NP B65 501	G. Alexander et al. (TELA, HEID)				
BRANDENB...	73	PR D8 1978	G.W. Brandenburg et al. (SLAC)				
EVANS	73	PR D7 36	G.R. Evans et al. (EDIN, CERN)				
Also		PRL 23 427	G.R. Evans et al. (EDIN, CERN)				
FACKLER	73	PRL 31 847	O. Fackler et al. (MIT)				
FITCH	73	PRL 31 1524	V.L. Fitch et al. (PRIN)				
Also		Thesis COO-3072-13	R.C. Webb (PRIN)				
HART	73	NP B66 317	J.C. Hart et al. (CAVE, RHEL)				
MALLARY	73	PR D7 1953	M.L. Mallary et al. (CIT)				
Also		PRL 25 1214	F.J. Scullin et al. (CIT)				
MCCARTHY	73	PR D7 687	R.L. McCarthy et al. (LBL)				
Also		PL 42B 291	R.L. McCarthy et al. (LBL)				
Also		Thesis LBL-550	R.L. McCarthy (LBL)				
MESSNER	73	PRL 30 876	R. Messner et al. (COLO, SLAC, UCSC)				
SANDWEISS	73	PRL 30 1002	J. Sandweiss et al. (YALE, ANL)				
WILLIAMS	73	PRL 31 1521	H.H. Williams et al. (BNL, YALE)				
ASHFORD	72	PL 38B 47	V.A. Ashford et al. (UCSD)				
BANNER	72B	PRL 29 237	M. Banner et al. (PRIN)				
BARMIN	72B	SJNP 15 638	V.V. Barmin et al. (ITEP)				
Translated from YAF 15 1152							
BURGUN	72	NP B50 194	G. Burgun et al. (SACL, CERN, OSLO)				
GRAHAM	72	NC 9A 166	F.F. Graham et al. (ILL, NEAS)				
JAMES	72	NP B49 1	F. James et al. (CERN, SACL, OSLO)				
KRENZ	72	LNC 4 213	W. Krenz et al. (AACH, CERN, EDIN)				
MANN	72	PR D6 137	W.A. Mann et al. (MASA, BNL, YALE)				
MANTSCH	72	NC 9A 160	P.M. Mantsch et al. (ILL, NEAS)				
MCCARTHY	72	PL 42B 291	R.L. McCarthy et al. (LBL)				
PICCIONI	72	PRL 29 1412	R. Piccioni et al. (SLAC)				
Also		PR D9 2939	R. Piccioni et al. (SLAC, UCSC, COLO)				

OTHER RELATED PAPERS

HAYAKAWA	73	PR D48 1150	M. Hayakawa, A.I. Sanda (NAGO)
"Searching for $T, CP, \Delta S = \Delta Q$ Rule Violations in the Neutral K Meson System: A Guide"			
LITTENBERG	93	ARNPS 43 729	L.S. Littenberg, G. Valencia (BNL, FNAL)
Rare and Radiative Kaon Decays			
RITCHIE	93	RMP 65 1149	J.L. Ritchie, S.G. Wojcicki (VAN D+)
"Rare K Decays"			

FIRESTONE 66B PRL 17 116 A. Firestone *et al.* (YALE, BNL)
 BEHR 65 Argonne Conf. 59 L. Behr *et al.* (EPOL, MILA, PADO)
 MESTVIRISH... 65 JINR P 2449 A.N. Mestvirishvili *et al.* (JINR)
 TRILLING 65B UCRL 16473 G.N. Trilling (LRL)
 Updated from 1965 Argonne Conference, page 115.
 JOVANOV... 63 BNL Conf. 42 J.V. Jovanovich *et al.* (BNL, UMD)

$K_0^*(700)$

$I(J^P) = \frac{1}{2}(0^+)$

also known as κ ; was $K_0^*(800)$

Needs confirmation. See the mini-review on scalar mesons under $f_0(500)$ (see the index for the page number).

$K_0^*(700)$ T-Matrix Pole \sqrt{s}

VALUE (MeV)	DOCUMENT ID	TECN	COMMENT
(630-730) - i (260-340) OUR EVALUATION			
• • • We do not use the following data for averages, fits, limits, etc. • • •			
$(670 \pm 18) - i (295 \pm 28)$	1 PELAEZ	17 RVUE	
$(764 \pm 63^{+71}_{-54}) - i (306 \pm 149^{+143}_{-85})$	2 ABLIKIM	11B BES2	1.3k $J/\psi \rightarrow K_S^0 K_S^0 \pi^+ \pi^-$
$(665 \pm 9) - i (268^{+21}_{-6})$	3 GUO	11B RVUE	
$(849 \pm 77^{+18}_{-14}) - i (256 \pm 40^{+46}_{-22})$	2 ABLIKIM	10E BES2	1.4k $J/\psi \rightarrow K^\pm K_S^0 \pi^\mp \pi^0$
$(663 \pm 8 \pm 34) - i (329 \pm 5 \pm 22)$	4 BUGG	10 RVUE	S-matrix pole
$(706.0 \pm 1.8 \pm 22.8) - i (319.4 \pm 2.2 \pm 20.2)$	5 BONVICINI	08A CLEO	141k $D^+ \rightarrow K^- \pi^+ \pi^+$
$(841 \pm 30^{+81}_{-73}) - i (309 \pm 45^{+48}_{-72})$	2 ABLIKIM	06C BES2	25k $J/\psi \rightarrow \bar{K}^*(892)^0 K^+ \pi^-$
$(750^{+30}_{-55}) - i (342 \pm 60)$	6 BUGG	06 RVUE	
$(658 \pm 13) - i (279 \pm 12)$	7 DESCOTES-G..06	RVUE	$\pi K \rightarrow \pi K$
$(757 \pm 33) - i (279 \pm 41)$	8 GUO	06 RVUE	
$(694 \pm 53) - i (303 \pm 30)$	9 ZHOU	06 RVUE	$K\rho \rightarrow K^- \pi^+ n$
$(754 \pm 22) - i (230 \pm 27)$	10 PELAEZ	04A RVUE	$K\rho \rightarrow K\rho$
$(594 \pm 79) - i (362 \pm 166)$	9 ZHENG	04 RVUE	$K^- \rho \rightarrow K^- \pi^+ n$
$(722 \pm 60) - i (386 \pm 50)$	9 BUGG	03 RVUE	11 $K^- \rho \rightarrow K^- \pi^+ n$
$(875 \pm 75) - i (335 \pm 110)$	11 ISHIDA	97B RVUE	11 $K^- \rho \rightarrow K^- \pi^+ n$
727 - i 263	12 VANBEVEREN	86 RVUE	

- 1 Extracted from Forward Dispersion Relations using sequences of Pade approximants .
- 2 Extracted from Breit-Wigner parameters.
- 3 Fit to scattering phase shifts using UChPT amplitudes with explicit resonances.
- 4 Supersedes BUGG 06. Combined analysis of ASTON 88, ABLIKIM 06c, AITALA 06, and LINK 09 using an s-dependent width with couplings to $K\pi$ and $K\eta'$, and the Adler zero near thresholds.
- 5 From a complex pole included in the fit. Using parameters from the model that fits data best.
- 6 Reanalysis of ASTON 88, AITALA 02, and ABLIKIM 06c using for the κ an s-dependent width with an Adler zero near threshold.
- 7 Using Roy-Steiner equations (ROY 71) consistent with unitarity, analyticity and crossing symmetry constraints.
- 8 From UChPT fitted to MERCER 71, BINGHAM 72 and ESTABROOKS 78. Amplitude shown to be consistent with data of ABLIKIM 06c.
- 9 Reanalysis of ASTON 88 data.
- 10 Reanalysis of data from LINGLIN 73, ESTABROOKS 78, and ASTON 88 using the Inverse Amplitude Method.
- 11 Reanalysis of ASTON 88 using interfering Breit-Wigner amplitudes. Extracted from Breit-Wigner parameters.
- 12 Unitarized Quark Model.

$K_0^*(700)$ Breit-Wigner Mass

VALUE (MeV)	EVTS	DOCUMENT ID	TECN	COMMENT
824 ± 30	OUR AVERAGE			
$826 \pm 49^{+49}_{-34}$	1.3k	1 ABLIKIM	11B BES2	$J/\psi \rightarrow K_S^0 K_S^0 \pi^+ \pi^-$
$810 \pm 68^{+15}_{-24}$	1.4k	2 ABLIKIM	10E BES2	$J/\psi \rightarrow K^\pm K_S^0 \pi^\mp \pi^0$
$878 \pm 23^{+64}_{-55}$	25k	3 ABLIKIM	06C BES2	$J/\psi \rightarrow \bar{K}^*(892)^0 K^+ \pi^-$
$797 \pm 19 \pm 43$	15k	4.5 AITALA	02 E791	$D^+ \rightarrow K^- \pi^+ \pi^+$
• • • We do not use the following data for averages, fits, limits, etc. • • •				
888.0 ± 1.9	141k	6 BONVICINI	08A CLEO	$D^+ \rightarrow K^- \pi^+ \pi^+$
$856 \pm 17 \pm 13$	54k	7 LINK	07B FOCS	$D^+ \rightarrow K^- \pi^+ \pi^+$
855 ± 15	0.6k	8 CAWLFIELD	06A CLEO	$D^0 \rightarrow K^+ K^- \pi^0$
905^{+65}_{-30}		9 ISHIDA	97B RVUE	11 $K^- \rho \rightarrow K^- \pi^+ n$

- 1 The Breit-Wigner parameters from a fit with seven intermediate resonances. The S-matrix pole position is $(764 \pm 63^{+71}_{-54}) - i (306 \pm 149^{+143}_{-85})$ MeV.
- 2 From a fit including ten additional resonances and energy-independent Breit-Wigner width.
- 3 A fit in the $K_0^*(700) + K^*(892) + K^*(1410)$ model with mass and width of the $K_0^*(700)$ from ABLIKIM 06c well describes the left slope of the $K_S^0 \pi^-$ invariant mass spectrum in $\tau^- \rightarrow K_S^0 \pi^- \nu_\tau$ decay studied by EPIFANOV 07. Averaged value from different parameterizations.

- 4 Not seen by KOPP 01 using 7070 events of $D^0 \rightarrow K^- \pi^+ \pi^0$. LINK 02e and LINK 05i show clear evidence for a constant non-resonant scalar amplitude rather than $K_0^*(700)$ in their high statistics analysis of $D^+ \rightarrow K^- \pi^+ \mu^+ \nu_\mu$.
- 5 AUBERT 07r does not find evidence for the charged $K_0^*(700)$ using 11k events of $D^0 \rightarrow K^- K^+ \pi^0$.
- 6 Using parameters from the model that fits data best.
- 7 A Breit-Wigner mass and width.
- 8 Breit-Wigner parameters. A significant S-wave can be also modeled as a non-resonant contribution.
- 9 Reanalysis of ASTON 88 using interfering Breit-Wigner amplitudes.

$K_0^*(700)$ Breit-Wigner Width

VALUE (MeV)	EVTS	DOCUMENT ID	TECN	COMMENT
478 ± 50	OUR AVERAGE			
$449 \pm 156^{+144}_{-81}$	1.3k	1 ABLIKIM	11B BES2	$J/\psi \rightarrow K_S^0 K_S^0 \pi^+ \pi^-$
$536 \pm 87^{+106}_{-47}$	1.4k	2 ABLIKIM	10E BES2	$J/\psi \rightarrow K^\pm K_S^0 \pi^\mp \pi^0$
$499 \pm 52 \pm 55^{+87}_{-87}$	25k	3 ABLIKIM	06C BES2	$J/\psi \rightarrow \bar{K}^*(892)^0 K^+ \pi^-$
$410 \pm 43 \pm 87$	15k	4.5 AITALA	02 E791	$D^+ \rightarrow K^- \pi^+ \pi^+$
• • • We do not use the following data for averages, fits, limits, etc. • • •				
550.4 ± 11.8	141k	6 BONVICINI	08A CLEO	$D^+ \rightarrow K^- \pi^+ \pi^+$
$464 \pm 28 \pm 22$	54k	7 LINK	07B FOCS	$D^+ \rightarrow K^- \pi^+ \pi^+$
251 ± 48	0.6k	8 CAWLFIELD	06A CLEO	$D^0 \rightarrow K^+ K^- \pi^0$
545^{+235}_{-110}		9 ISHIDA	97B RVUE	11 $K^- \rho \rightarrow K^- \pi^+ n$

- 1 The Breit-Wigner parameters from a fit with seven intermediate resonances. The S-matrix pole position is $(764 \pm 63^{+71}_{-54}) - i (306 \pm 149^{+143}_{-85})$ MeV.
- 2 From a fit including ten additional resonances and energy-independent Breit-Wigner width.
- 3 A fit in the $K_0^*(700) + K^*(892) + K^*(1410)$ model with mass and width of the $K_0^*(700)$ from ABLIKIM 06c well describes the left slope of the $K_S^0 \pi^-$ invariant mass spectrum in $\tau^- \rightarrow K_S^0 \pi^- \nu_\tau$ decay studied by EPIFANOV 07. Averaged value from different parameterizations.
- 4 Not seen by KOPP 01 using 7070 events of $D^0 \rightarrow K^- \pi^+ \pi^0$. LINK 02e and LINK 05i show clear evidence for a constant non-resonant scalar amplitude rather than $K_0^*(700)$ in their high statistics analysis of $D^+ \rightarrow K^- \pi^+ \mu^+ \nu_\mu$.
- 5 AUBERT 07r does not find evidence for the charged $K_0^*(700)$ using 11k events of $D^0 \rightarrow K^- K^+ \pi^0$.
- 6 Using parameters from the model that fits data best.
- 7 A Breit-Wigner mass and width.
- 8 Statistical error only. A fit to the Dalitz plot including the $K_0^*(700)^\pm, K^*(892)^\pm$, and ϕ resonances modeled as Breit-Wigners. A significant S-wave can be also modeled as a non-resonant contribution.
- 9 Reanalysis of ASTON 88 using interfering Breit-Wigner amplitudes.

$K_0^*(700)$ DECAY MODES

Mode	Fraction (Γ_i/Γ)
Γ_1 $K\pi$	100 %

$K_0^*(700)$ REFERENCES

PELAEZ 17	EPJ C77 91	J.R. Pelaez, A.Rodas, J.Ruiz de Elvira
ABLIKIM 11B	PL B698 183	M. Ablikim <i>et al.</i> (BES II Collab.)
GUO 11B	PR D84 034005	Z.-H. Guo, J.A. Oller
ABLIKIM 10E	PL B693 88	M. Ablikim <i>et al.</i> (BES II Collab.)
BUGG 10	PR D81 014002	D.V. Bugg (LOQM)
LINK 09	PL B681 14	J.M. Link <i>et al.</i> (FNAL FOCUS Collab.)
BONVICINI 08A	PR D78 052001	G. Bonvicini <i>et al.</i> (CLEO Collab.)
AUBERT 07T	PR D76 011102	B. Aubert <i>et al.</i> (BABAR Collab.)
EPIFANOV 07	PL B654 65	D. Epifanov <i>et al.</i> (BELLE Collab.)
LINK 07B	PL B653 1	J.M. Link <i>et al.</i> (FNAL FOCUS Collab.)
ABLIKIM 06C	PL B633 681	M. Ablikim <i>et al.</i> (BES Collab.)
AITALA 06	PR D73 032004	E.M. Aitala <i>et al.</i> (FNAL E791 Collab.)
Also	PR D74 059901 (errat.)	E.M. Aitala <i>et al.</i> (FNAL E791 Collab.)
BUGG 06	PL B632 471	D.V. Bugg (LOQM)
CAWLFIELD 06A	PR D74 031108	C. Cawfield <i>et al.</i> (CLEO Collab.)
DESCOTES-G..06	EPJ C48 553	S. Descotes-Genon, B. Moussallam
GUO 06	NP A773 78	F.K. Guo <i>et al.</i>
ZHOU 06	NP A775 212	Z.Y. Zhou, H.Q. Zheng
LINK 05I	PL B621 72	J.M. Link <i>et al.</i> (FNAL FOCUS Collab.)
PELAEZ 04A	MPL A19 2879	J.R. Pelaez
ZHENG 04	NP A733 235	H.Q. Zheng <i>et al.</i>
BUGG 03	PL B572 1	D.V. Bugg
AITALA 02	PRL 89 121801	E.M. Aitala <i>et al.</i> (FNAL E791 Collab.)
LINK 02E	PL B535 43	J.M. Link <i>et al.</i> (FNAL FOCUS Collab.)
KOPP 01	PR D63 092001	S. Kopp <i>et al.</i> (CLEO Collab.)
ISHIDA 97B	PTP 98 621	S. Ishida <i>et al.</i>
ASTON 88	NP B296 493	D. Aston <i>et al.</i> (SLAC, NAGO, CIN, INUS)
VANBEVEREN 86	ZPHY C30 615	E. van Beveren <i>et al.</i> (NUM, BIEL)
ESTABROOKS 78	NP B133 490	P.G. Estabrooks <i>et al.</i> (MCGI, CARL, DURH+)
LINGLIN 73	NP B55 408	D. Linglin (CERN)
BINGHAM 72	NP B41 1	H.H. Bingham <i>et al.</i> (International K^+ Collab.)
MERCER 71	NP B32 381	R. Mercer <i>et al.</i> (JHU)
ROY 71	PL 36B 353	S.M. Roy

Meson Particle Listings

$K^*(892)$

$K^*(892)$

$$I(J^P) = \frac{1}{2}(1^-)$$

$K^*(892)$ MASS

CHARGED ONLY, HADROPRODUCED

VALUE (MeV)	EVTS	DOCUMENT ID	TECN	CHG	COMMENT
891.66 ± 0.26	OUR AVERAGE				
892.6 ± 0.5	5840	BAUBILLIER 84B	HBC	-	8.25 $K^- p \rightarrow \bar{K}^0 \pi^- p$
888 ± 3		NAPIER 84	SPEC	+	200 $\pi^- p \rightarrow 2K_S^0 X$
891 ± 1		NAPIER 84	SPEC	-	200 $\pi^- p \rightarrow 2K_S^0 X$
891.7 ± 2.1	3700	BARTH 83	HBC	+	70 $K^+ p \rightarrow K_S^0 \pi^+ X$
891 ± 1	4100	TOAFF 81	HBC	-	6.5 $K^- p \rightarrow \bar{K}^0 \pi^- p$
892.8 ± 1.6		AJINENKO 80	HBC	+	32 $K^+ p \rightarrow K_S^0 \pi^+ X$
890.7 ± 0.9	1800	AGUILAR... 78B	HBC	±	0.76 $\bar{p} p \rightarrow K^\mp K_S^0 \pi^\pm$
886.6 ± 2.4	1225	BALAND 78	HBC	±	12 $\bar{p} p \rightarrow (K\pi)^\pm X$
891.7 ± 0.6	6706	COOPER 78	HBC	±	0.76 $\bar{p} p \rightarrow (K\pi)^\pm X$
891.9 ± 0.7	9000	1 PALER 75	HBC	-	14.3 $K^- p \rightarrow (K\pi)^- X$
892.2 ± 1.5	4404	AGUILAR... 71B	HBC	-	3.9,4.6 $K^- p \rightarrow (K\pi)^- p$
891 ± 2	1000	CRENNELL 69D	DBC	-	3.9 $K^- N \rightarrow K^0 \pi^- X$
890 ± 3.0	720	BARLOW 67	HBC	±	1.2 $\bar{p} p \rightarrow (K^0 \pi)^\pm K^\mp$
889 ± 3.0	600	BARLOW 67	HBC	±	1.2 $\bar{p} p \rightarrow (K^0 \pi)^\pm K\pi$
891 ± 2.3	620	2 DEBAERE 67B	HBC	±	3.5 $K^+ p \rightarrow K^0 \pi^+ p$
891.0 ± 1.2	1700	3 WOJCICKI 64	HBC	-	1.7 $K^- p \rightarrow \bar{K}^0 \pi^- p$

- • • We do not use the following data for averages, fits, limits, etc. • • •
- 893.6 ± 0.1 $^{+0.2}_{-0.3}$ 183k ABLIKIM 19AQ BES ± $J/\psi \rightarrow K^+ K^- \pi^0$
- 895.6 ± 0.8 4K 4 LEES 17C BABR $J/\psi \rightarrow K_S^0 K^\pm \pi^\mp$
- 893.2 ± 0.1 ± 1.0 190k 5 AAIJ 16N LHCB $D^0 \rightarrow K_S^0 K^\pm \pi^\mp$
- 893.5 ± 1.1 27k 6 ABELE 99D CBAR ± 0.0 $\bar{p} p \rightarrow K^+ K^- \pi^0$
- 890.4 ± 0.2 ± 0.5 80k 7 BIRD 89 LASS - 11 $K^- p \rightarrow \bar{K}^0 \pi^- p$
- 890.0 ± 2.3 800 2,3 CLELAND 82 SPEC + 30 $K^+ p \rightarrow K_S^0 \pi^+ p$
- 896.0 ± 1.1 3200 2,3 CLELAND 82 SPEC + 50 $K^+ p \rightarrow K_S^0 \pi^+ p$
- 893 ± 1 3600 2,3 CLELAND 82 SPEC - 50 $K^+ p \rightarrow K_S^0 \pi^- p$
- 896.0 ± 1.9 380 DELFOSSE 81 SPEC + 50 $K^\pm p \rightarrow K^\pm \pi^0 p$
- 886.0 ± 2.3 187 DELFOSSE 81 SPEC - 50 $K^\pm p \rightarrow K^\pm \pi^0 p$
- 894.2 ± 2.0 765 2 CLARK 73 HBC - 3.13 $K^- p \rightarrow \bar{K}^0 \pi^- p$
- 894.3 ± 1.5 1150 2,3 CLARK 73 HBC - 3.3 $K^- p \rightarrow \bar{K}^0 \pi^- p$
- 892.0 ± 2.6 341 2 SCHWEING...68 HBC - 5.5 $K^- p \rightarrow \bar{K}^0 \pi^- p$

CHARGED ONLY, PRODUCED IN τ LEPTON DECAYS

VALUE (MeV)	EVTS	DOCUMENT ID	TECN	COMMENT
895.47 ± 0.20 ± 0.74	53k	1 EPIFANOV 07	BELL	$\tau^- \rightarrow K_S^0 \pi^- \nu_\tau$
892.0 ± 0.5		2 BOITO 10	RVUE	$\tau^- \rightarrow K_S^0 \pi^- \nu_\tau$
892.0 ± 0.9		3,4 BOITO 09	RVUE	$\tau^- \rightarrow K_S^0 \pi^- \nu_\tau$
895.3 ± 0.2		4,5 JAMIN 08	RVUE	$\tau^- \rightarrow K_S^0 \pi^- \nu_\tau$
896.4 ± 0.9	12k	6 BONVICINI 02	CLEO	$\tau^- \rightarrow K^- \pi^0 \nu_\tau$
895 ± 2		7 BARATE 99R	ALEP	$\tau^- \rightarrow K^- \pi^0 \nu_\tau$

- 1 From a fit in the $K_S^0(700) + K^*(892) + K^*(1410)$ model.
- 2 From the pole position of the $K\pi$ vector form factor using EPIFANOV 07 and constraints from K_{f3} decays in ANTONELLI 10.
- 3 From the pole position of the $K\pi$ vector form factor in the complex s -plane and using EPIFANOV 07 data.
- 4 Systematic uncertainties not estimated.
- 5 Reanalysis of EPIFANOV 07 using resonance chiral theory.
- 6 Calculated by us from the shift by 4.7 ± 0.9 MeV (statistical uncertainty only) reported in BONVICINI 02 with respect to the world average value from PDG 00.
- 7 With mass and width of the $K^*(1410)$ fixed at 1412 MeV and 227 MeV, respectively.

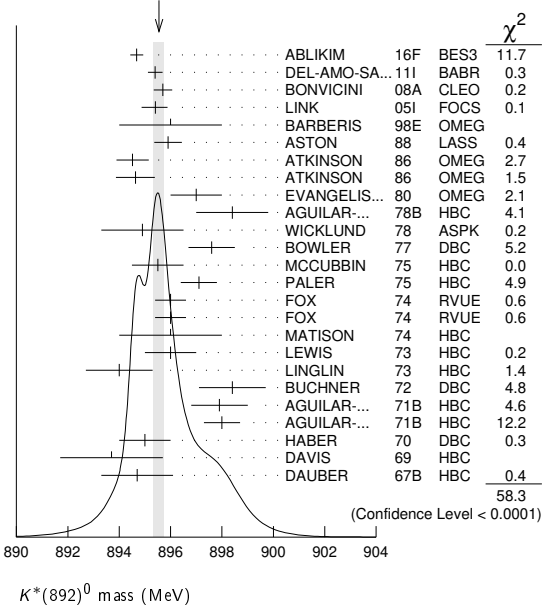
NEUTRAL ONLY

VALUE (MeV)	EVTS	DOCUMENT ID	TECN	COMMENT
895.55 ± 0.20	OUR AVERAGE			
894.68 ± 0.25 ± 0.05		1 ABLIKIM 16F	BES3	$D^+ \rightarrow K^- \pi^+ e^+ \nu_e$
895.4 ± 0.2 ± 0.2	243k	2 DEL-AMO-SA...11I	BABR	$D^+ \rightarrow K^- \pi^+ e^+ \nu_e$
895.7 ± 0.2 ± 0.3	141k	3 BONVICINI 08A	CLEO	$D^+ \rightarrow K^- \pi^+ \pi^+$
895.41 ± 0.32 $^{+0.35}_{-0.43}$	18k	4 LINK 05I	FOCS	$D^+ \rightarrow K^- \pi^+ \mu^+ \nu_\mu$
896 ± 2		BARBERIS 98E	OMEG	450 $pp \rightarrow p_f p_S K^* \bar{K}^*$
895.9 ± 0.5 ± 0.2		ASTON 88	LASS	11 $K^- p \rightarrow K^- \pi^+ n$
894.52 ± 0.63	25k	5 ATKINSON 86	OMEG	20-70 γp
894.63 ± 0.76	20k	5 ATKINSON 86	OMEG	20-70 γp
897 ± 1	28k	EVANGELIS... 80	OMEG	10 $\pi^- p \rightarrow K^+ \pi^- (\Lambda, \Sigma)$
898.4 ± 1.4	1180	AGUILAR... 78B	HBC	0.76 $\bar{p} p \rightarrow K^\mp K_S^0 \pi^\pm$

894.9 ± 1.6		WICKLUND 78	ASPK	3,4,6 $K^\pm N \rightarrow (K\pi)^0 N$
897.6 ± 0.9		BOWLER 77	DBC	5.4 $K^+ d \rightarrow K^+ \pi^- p p$
895.5 ± 1.0	3600	MCCUBBIN 75	HBC	3.6 $K^- p \rightarrow K^- \pi^+ n$
897.1 ± 0.7	22k	5 PALER 75	HBC	14.3 $K^- p \rightarrow (K\pi)^0 X$
896.0 ± 0.6	10k	FOX 74	RVUE	2 $K^- p \rightarrow K^- \pi^+ n$
896.0 ± 0.6		FOX 74	RVUE	2 $K^+ n \rightarrow K^+ \pi^- p$
896 ± 2		6 MATISON 74	HBC	12 $K^+ p \rightarrow K^+ \pi^- \Delta$
896 ± 1	3186	LEWIS 73	HBC	2.1-2.7 $K^+ p \rightarrow K\pi\pi p$
894.0 ± 1.3		6 LINGLIN 73	HBC	2-13 $K^+ p \rightarrow K^+ \pi^- \pi^+ p$
898.4 ± 1.3	1700	7 BUCHNER 72	DBC	4.6 $K^+ n \rightarrow K^+ \pi^- p$
897.9 ± 1.1	2934	7 AGUILAR... 71B	HBC	3.9,4.6 $K^- p \rightarrow K^- \pi^+ n$
898.0 ± 0.7	5362	7 AGUILAR... 71B	HBC	3.9,4.6 $K^- p \rightarrow K^- \pi^+ \pi^- p$
895 ± 1	4300	8 HABER 70	DBC	3 $K^- N \rightarrow K^- \pi^+ X$
893.7 ± 2.0	10k	DAVIS 69	HBC	12 $K^+ p \rightarrow K^+ \pi^- \pi^+ p$
894.7 ± 1.4	1040	7 DAUBER 67B	HBC	2.0 $K^- p \rightarrow K^- \pi^+ \pi^- p$
• • • We do not use the following data for averages, fits, limits, etc. • • •				
898.1 ± 1.0	4K	9 LEES 17C	BABR	$J/\psi \rightarrow K_S^0 K^\pm \pi^\mp$
895.53 ± 0.17		LEES 13F	BABR	$D^+ \rightarrow K^+ K^- \pi^+$
894.9 ± 0.5 ± 0.7	14.4k	10 MITCHELL 09A	CLEO	$D_S^+ \rightarrow K^+ K^- \pi^+$
896.2 ± 0.3	20k	11 AUBERT 07AK	BABR	10.6 $e^+ e^- \rightarrow K^{*0} K^\pm \pi^\mp \gamma$
900.7 ± 1.1	5900	BARTH 83	HBC	70 $K^+ p \rightarrow K^+ \pi^- X$

- 1 Taking also into account the $K_S^0(1430)^0$ and $K_S^0(1430)^0$.
- 2 Taking into account the $K^*(892)^0$, S -wave and P -wave ($K^*(1410)^0$).
- 3 From the isobar model with a complex pole for the κ .
- 4 Fit to $K\pi$ mass spectrum includes a non-resonant scalar component.
- 5 Inclusive reaction. Complicated background and phase-space effects.
- 6 From pole extrapolation.
- 7 Mass errors enlarged by us to Γ/\sqrt{N} . See note.
- 8 Number of events in peak reevaluated by us.
- 9 From a Dalitz plot analysis in an isobar model with charged and neutral $K^*(892)$ masses and widths floating.
- 10 This value comes from a fit with χ^2 of 178/117.
- 11 Systematic uncertainties not estimated.

WEIGHTED AVERAGE
895.55 ± 0.20 (Error scaled by 1.7)



$K^*(892)$ MASSES AND MASS DIFFERENCES

Unrealistically small errors have been reported by some experiments. We use simple “realistic” tests for the minimum errors on the determination of a mass and width from a sample of N events:

$$\delta_{\min}(m) = \frac{\Gamma}{\sqrt{N}}, \quad \delta_{\min}(\Gamma) = 4 \frac{\Gamma}{\sqrt{N}}. \quad (1)$$

We consistently increase unrealistic errors before averaging. For a detailed discussion, see the 1971 edition of this Note.

K*(892)

m_{K*(892)^0} - m_{K*(892)^±}

Table with columns: VALUE (MeV), EVTS, DOCUMENT ID, TECN, CHG, COMMENT. Includes data for AGUILAR-... and BARASH.

1 Number of events in peak reevaluated by us.

K*(892) RANGE PARAMETER

All from partial wave amplitude analyses.

Table with columns: VALUE (GeV^-1), EVTS, DOCUMENT ID, TECN, CHG, COMMENT. Includes data for DEL-AMO-SA.11i, LINK, ASTON, BIRD.

1 Taking into account the K*(892)^0, S-wave and P-wave (K*(1410)^0). 2 Fit to K pi mass spectrum includes a non-resonant scalar component.

K*(892) WIDTH

CHARGED ONLY, HADROPRODUCED

Table with columns: VALUE (MeV), EVTS, DOCUMENT ID, TECN, CHG, COMMENT. Includes data for BAUBILLIER, NAPIER, TOAFF, AJINENKO, AGUILAR-..., COOPER, PALER, CLARK, CLARK, AGUILAR-..., WOJCICKI.

• • • We do not use the following data for averages, fits, limits, etc. • • •

Table with columns: VALUE (MeV), EVTS, DOCUMENT ID, TECN, CHG, COMMENT. Includes data for ABLIKIM, LEES, AAIJ, ABELE, BIRD, BARTH, CLELAND, CLELAND, CLELAND, DELFOSSE, DELFOSSE.

1 Width errors enlarged by us to 4 x Gamma/sqrt(N); see note. 2 Inclusive reaction. Complicated background and phase-space effects. 3 Number of events in peak reevaluated by us. 4 From a Dalitz plot analysis in an isobar model with charged and neutral K*(892) masses and widths floating. 5 Average of fit results with different parametrizations for the K pi S-wave. 6 K-matrix pole. 7 From a partial wave amplitude analysis.

CHARGED ONLY, PRODUCED IN tau LEPTON DECAYS

Table with columns: VALUE (MeV), EVTS, DOCUMENT ID, TECN, COMMENT. Includes data for EPIFANOV, BOITO, BOITO, JAMIN, BARATE.

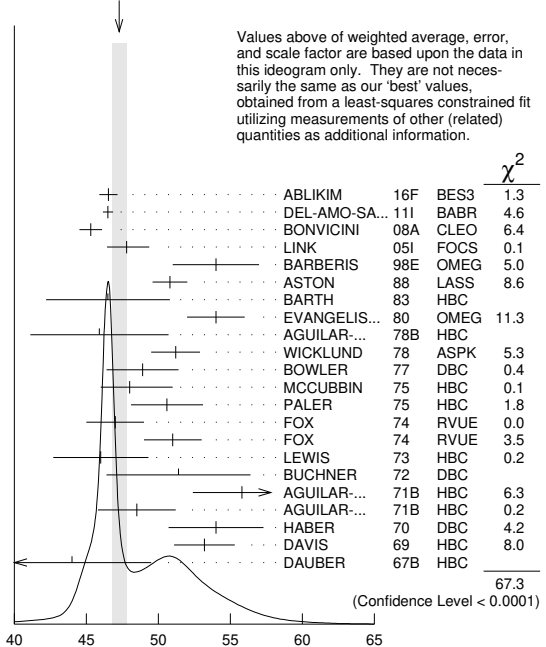
1 From a fit in the K_0^*(700) + K*(892) + K*(1410) model. 2 From the pole position of the K pi vector form factor using EPIFANOV 07 and constraints from K_1^0 decays in ANTONELLI 10. 3 From the pole position of the K pi vector form factor in the complex s-plane and using EPIFANOV 07 data. 4 Systematic uncertainties not estimated. 5 Reanalysis of EPIFANOV 07 using resonance chiral theory. 6 With mass and width of the K*(1410) fixed at 1412 MeV and 227 MeV, respectively.

NEUTRAL ONLY

Table with columns: VALUE (MeV), EVTS, DOCUMENT ID, TECN, COMMENT. Includes data for ABLIKIM, DEL-AMO-SA.11i, BONVICINI, LINK, BARBERIS, ASTON, BARTH, EVANGELIS..., AGUILAR-..., WICKLUND, BOWLER, MCCUBBIN, PALER, FOX, FOX, LEWIS, BUCHNER, AGUILAR-..., HABER, DAVIS, DAUBER.

1 Taking also into account the K_0^*(1430)^0 and K_2^*(1430)^0. 2 Taking into account the K*(892)^0, S-wave and P-wave (K*(1410)^0). 3 From the isobar model with a complex pole for the xi. 4 Fit to K pi mass spectrum includes a non-resonant scalar component. 5 Inclusive reaction. Complicated background and phase-space effects. 6 Width errors enlarged by us to 4 x Gamma/sqrt(N); see note. 7 Number of events in peak reevaluated by us. 8 From a Dalitz plot analysis in an isobar model with charged and neutral K*(892) masses and widths floating. 9 This value comes from a fit with chi^2 of 178/117. 10 Systematic uncertainties not estimated.

WEIGHTED AVERAGE 47.3±0.5 (Error scaled by 2.0)



NEUTRAL ONLY (MeV)

Meson Particle Listings

$K^*(892), K_1(1270)$

$K^*(892)$ DECAY MODES

Mode	Fraction (Γ_i/Γ)	Confidence level
Γ_1 $K\pi$	~ 100	%
Γ_2 $(K\pi)^\pm$	(99.901 ± 0.009)	%
Γ_3 $(K\pi)^0$	(99.754 ± 0.021)	%
Γ_4 $K^0\gamma$	$(2.46 \pm 0.21) \times 10^{-3}$	
Γ_5 $K^\pm\gamma$	$(9.9 \pm 0.9) \times 10^{-4}$	
Γ_6 $K\pi\pi$	< 7	$\times 10^{-4}$

CONSTRAINED FIT INFORMATION

An overall fit to the total width and a partial width uses 13 measurements and one constraint to determine 3 parameters. The overall fit has a $\chi^2 = 7.8$ for 11 degrees of freedom.

The following *off-diagonal* array elements are the correlation coefficients $\langle \delta p_i \delta p_j \rangle / (\delta p_i \delta p_j)$, in percent, from the fit to parameters p_i , including the branching fractions, $x_i \equiv \Gamma_i/\Gamma_{\text{total}}$. The fit constrains the x_i whose labels appear in this array to sum to one.

x_5	-100	
Γ	19	-19
		x_2 x_5

Mode	Rate (MeV)
Γ_2 $(K\pi)^\pm$	50.7 ± 0.9
Γ_5 $K^\pm\gamma$	0.050 ± 0.005

CONSTRAINED FIT INFORMATION

An overall fit to the total width and a partial width uses 23 measurements and one constraint to determine 3 parameters. The overall fit has a $\chi^2 = 68.4$ for 21 degrees of freedom.

The following *off-diagonal* array elements are the correlation coefficients $\langle \delta p_i \delta p_j \rangle / (\delta p_i \delta p_j)$, in percent, from the fit to parameters p_i , including the branching fractions, $x_i \equiv \Gamma_i/\Gamma_{\text{total}}$. The fit constrains the x_i whose labels appear in this array to sum to one.

x_4	-100	
Γ	12	-12
		x_3 x_4

Mode	Rate (MeV)	Scale factor
Γ_3 $(K\pi)^0$	47.2 ± 0.5	1.9
Γ_4 $K^0\gamma$	0.117 ± 0.010	

$K^*(892)$ PARTIAL WIDTHS

$\Gamma(K^0\gamma)$	VALUE (keV)	EVTS	DOCUMENT ID	TECN	CHG	COMMENT	Γ_4
116 ± 10 OUR FIT							
116.5 ± 9.9	584		CARLSMITH 86	SPEC	0	$K_L^0 A \rightarrow K_S^0 \pi^0 A$	

$\Gamma(K^\pm\gamma)$	VALUE (keV)	DOCUMENT ID	TECN	CHG	COMMENT	Γ_5
50 ± 5 OUR FIT						
50 ± 5 OUR AVERAGE						
48 ± 11		BERG 83	SPEC	-	156 $K^- A \rightarrow \bar{K} \pi A$	
51 ± 5		CHANDLEE 83	SPEC	+	200 $K^+ A \rightarrow K \pi A$	

$K^*(892)$ BRANCHING RATIOS

$\Gamma(K^0\gamma)/\Gamma_{\text{total}}$	VALUE (units 10^{-3})	DOCUMENT ID	TECN	CHG	COMMENT	Γ_4/Γ
2.46 ± 0.21 OUR FIT						
1.5 ± 0.7		CARITHERS 75B	CNTR	0	8-16 $\bar{K}^0 A$	

$\Gamma(K^\pm\gamma)/\Gamma_{\text{total}}$	VALUE (units 10^{-3})	CL%	DOCUMENT ID	TECN	CHG	COMMENT	Γ_5/Γ
0.99 ± 0.09 OUR FIT							
<1.6	95		BEMPORAD 73	CNTR	+	10-16 $K^+ A$	

$\Gamma(K\pi\pi)/\Gamma((K\pi)^\pm)$

VALUE	CL%	DOCUMENT ID	TECN	CHG	COMMENT	Γ_6/Γ_2
$< 7 \times 10^{-4}$	95	JONGEJANS 78	HBC		$4 K^- p \rightarrow p \bar{K}^0 2\pi$	
$< 20 \times 10^{-4}$		WOJCICKI 64	HBC	-	$1.7 K^- p \rightarrow \bar{K}^0 \pi^- p$	

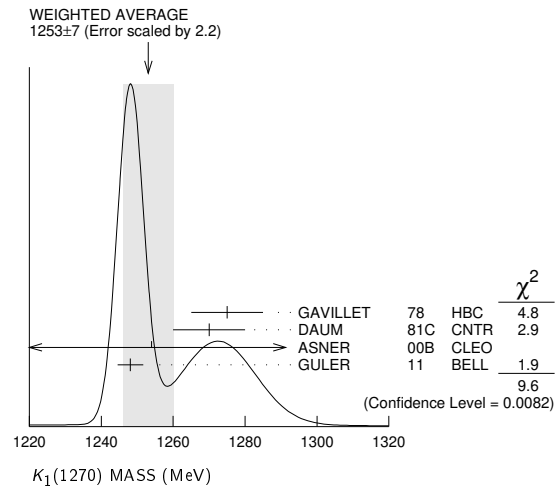
$K^*(892)$ REFERENCES

ABLIKIM 19AQ	PR D100 032004	M. Ablikim <i>et al.</i>	(BESIII Collab.)
LEES 17C	PR D95 072007	J.P. Lees <i>et al.</i>	(BABAR Collab.)
AAJ 16N	PR D93 052018	R. Aaij <i>et al.</i>	(LHCb Collab.)
ABLIKIM 16F	PR D94 032001	M. Ablikim <i>et al.</i>	(BESIII Collab.)
LEES 13F	PR D87 052010	J.P. Lees <i>et al.</i>	(BABAR Collab.)
DEL-AMO-SA... 11I	PR D83 072001	P. del Amo Sanchez <i>et al.</i>	(BABAR Collab.)
ANTONELLI 10	EPJ C69 399	M. Antonelli <i>et al.</i>	(FlaviaNet Working Group)
BOITO 10	JHEP 1009 031	D.R. Boito, R. Escribano, M. Jamin	(BARC)
BOITO 09	EPJ C59 821	D.R. Boito, R. Escribano, M. Jamin	(BARC)
MITCHELL 09A	PR D79 072008	R.E. Mitchell <i>et al.</i>	(CLEO Collab.)
BONVICINI 08A	PR D78 052001	G. Bonvicini <i>et al.</i>	(CLEO Collab.)
JAMIN 08	PL B664 78	M. Jamin, A. Pich, J. Portoles	(CLEO Collab.)
AUBERT 07AK	PR D76 012008	B. Aubert <i>et al.</i>	(BABAR Collab.)
EPIFANOV 07	PL B654 65	D. Epifanov <i>et al.</i>	(BELLE Collab.)
LINK 05I	PL B621 72	J.M. Link <i>et al.</i>	(FNAL FOCUS Collab.)
BONVICINI 02	PRL 88 111803	G. Bonvicini <i>et al.</i>	(CLEO Collab.)
PDG 00	EPJ C15 1	D.E. Groom <i>et al.</i>	(PDG Collab.)
ABELE 99D	PL B468 178	A. Abele <i>et al.</i>	(Crystal Barrel Collab.)
BARATE 99R	EPJ C11 599	R. Barate <i>et al.</i>	(ALEPH Collab.)
BARBERIS 98E	PL B436 204	D. Barberis <i>et al.</i>	(Omega Expt.)
BIRD 89	SLAC-332	P.F. Bird	(SLAC)
ASTON 88	NP B296 493	D. Aston <i>et al.</i>	(SLAC, NAGO, CIN, INUS)
ATKINSON 86	ZPHY C30 621	M. Atkinson <i>et al.</i>	(BONN, CERN, GLAS+)
CARLSMITH 86	PRL 56 18	D. Carlsmith <i>et al.</i>	(EFI, SACL)
BAUBILLIER 84B	ZPHY C26 37	M. Baubillier <i>et al.</i>	(BIRM, CERN, GLAS+)
NAPIER 84	PL B49B 514	A. Napier <i>et al.</i>	(TUFTS, ARIZ, FNAL, FLO+)
BARTH 83	NP B223 296	M. Barth <i>et al.</i>	(BRUX, CERN, GENO, MONS+)
BERG 83	Thesis UMI 83-21652	D.M. Berg	(ROCH)
CHANDLEE 83	PRL 51 168	C. Chandlee <i>et al.</i>	(ROCH, FNAL, MINN)
CLELAND 82	NP B208 189	W.E. Cleland <i>et al.</i>	(DURH, GEVA, LAUS+)
DELFOSE 81	NP B183 349	A. Delfosse <i>et al.</i>	(GEVA, LAUS)
TOAFF 81	PR D23 1500	S. Toaff <i>et al.</i>	(ANL, KANS)
AJINENKO 80	ZPHY C5 177	I.V. Ajinenko <i>et al.</i>	(SERP, BRUX, MONS+)
EVANGELIS... 80	NP B165 383	C. Evangelista <i>et al.</i>	(BARI, BONN, CERN+)
AGUILAR... 78B	NP B141 101	M. Aguilar-Benitez <i>et al.</i>	(MADR, TATA+)
BALAND 78	NP B140 220	J.F. Baland <i>et al.</i>	(MONS, BELG, CERN+)
COOPER 78	NP B136 365	A.M. Cooper <i>et al.</i>	(TATA, CERN, CDEF+)
JONGEJANS 78	NP B139 383	B. Jongejans <i>et al.</i>	(ZEEM, CERN, NIJN+)
WICKLUND 78	PR D17 1197	A.B. Wicklund <i>et al.</i>	(ANL)
BOWLER 77	NP B126 31	M.G. Bowler <i>et al.</i>	(OXF)
CARITHERS 75B	PRL 35 349	W.C.J. Carithers <i>et al.</i>	(ROCH, MCGI)
MCCUBBIN 75	NP B86 13	N.A. McCubbin, L. Lyons	(OXF)
PALER 75	NP B96 1	K. Paler <i>et al.</i>	(RHEL, SACL, EPOL)
FOX 74	NP B80 403	G.C. Fox, M.L. Griss	(CIT)
MATISON 74	PR D9 1872	M.J. Matison <i>et al.</i>	(LBL)
BEMPORAD 73	NP B51 1	C. Bemporad <i>et al.</i>	(CERN, ETH, LOIC)
CLARK 73	NP B54 432	A.G. Clark, L. Lyons, D. Radojicic	(OXF)
LEWIS 73	NP B40 283	PH. Lewis <i>et al.</i>	(LOWC, LOIC, CDEF)
LINGLIN 73	NP B55 408	D. Linglin	(CERN)
BUCHNER 72	NP B45 333	K. Buchner <i>et al.</i>	(MPIM, CERN, BRUX)
AGUILAR... 71B	PR D4 2583	M. Aguilar-Benitez, R.L. Eisner, J.B. Kinson	(BNL)
HABER 70	NP B17 289	B. Haber <i>et al.</i>	(REHO, SACL, BGNA, EPOL)
CRENNELL 69D	PRL 22 487	D.J. Crennell <i>et al.</i>	(BNL)
DAVIS 69	PRL 23 1071	P.J. Davis <i>et al.</i>	(LRL)
SCHWEING... 68	PR 166 1317	F. Schweingruber <i>et al.</i>	(ANL, NWES)
BARASH 67B	PR 156 1399	N. Barash <i>et al.</i>	(COLU)
BARLOW 67	NC 50A 701	J. Barlow <i>et al.</i>	(CERN, CDEF, IRAD, LVP)
DAUBER 67B	NP 153 1403	P.M. Dauber <i>et al.</i>	(UCLA)
DEBAERE 67B	NC 51A 401	W. de Baere <i>et al.</i>	(BRUX, CERN)
WOJCICKI 64	PR 135 B484	S.G. Wojcicki	(LRL)

$K_1(1270) \quad I(J^P) = \frac{1}{2}(1^+)$

$K_1(1270)$ MASS

VALUE (MeV) DOCUMENT ID
1253 ± 7 OUR AVERAGE Includes data from the 4 datablocks that follow this one. Error includes scale factor of 2.2. See the ideogram below.



See key on page 999

Meson Particle Listings

$K_1(1270)$

PRODUCED BY K^- , BACKWARD SCATTERING, HYPERON EXCHANGE

VALUE (MeV)	EVTS	DOCUMENT ID	TECN	CHG	COMMENT
The data in this block is included in the average printed for a previous datablock.					

1275 ± 10 700 GAVILLET 78 HBC + 4.2 $K^- p \rightarrow \Xi^-(K\pi\pi)^+$

PRODUCED BY K BEAMS

VALUE (MeV)	EVTS	DOCUMENT ID	TECN	CHG	COMMENT
The data in this block is included in the average printed for a previous datablock.					

1270 ± 10 1 DAUM 81c CNTR - 63 $K^- p \rightarrow K^- 2\pi$

••• We do not use the following data for averages, fits, limits, etc. •••

~ 1276	2	TORNQVIST	82B	RVUE	
~ 1300		VERGEEST	79	HBC	- 4.2 $K^- p \rightarrow (\bar{K}\pi\pi)^- p$
1289 ± 25	3	CARNEGIE	77	ASPK	± 13 $K^\pm p \rightarrow (K\pi\pi)^\pm p$
~ 1300		BRANDENB...	76	ASPK	± 13 $K^\pm p \rightarrow (K\pi\pi)^\pm p$
~ 1270		OTTER	76	HBC	- 10,14,16 $K^- p \rightarrow (\bar{K}\pi\pi)^- p$
1260		DAVIS	72	HBC	+ 12 $K^+ p$
1234 ± 12		FIRESTONE	72B	DBC	+ 12 $K^+ d$

¹ Well described in the chiral unitary approach of GENG 07 with two poles at 1195 and 1284 MeV and widths of 246 and 146 MeV, respectively.

² From a unitarized quark-model calculation.

³ From a model-dependent fit with Gaussian background to BRANDENBURG 76 data.

PRODUCED BY BEAMS OTHER THAN K MESONS

VALUE (MeV)	EVTS	DOCUMENT ID	TECN	CHG	COMMENT
The data in this block is included in the average printed for a previous datablock.					

1248.1 ± 3.3 ± 1.4 GULER 11 BELL $B^+ \rightarrow J/\psi K^+ \pi^+ \pi^-$

••• We do not use the following data for averages, fits, limits, etc. •••

1289.81 ± 0.56 ± 1.66	894k	AAIJ	18A1	LHCB	$D^0 \rightarrow K^+ \pi^\pm \pi^\pm \pi^\mp$
1279 ± 10	25k	1	ABLIIKIM	06c	BES2 $J/\psi \rightarrow \bar{K}^*(892)^0 K^+ \pi^-$
1294 ± 10	310	RODEBACK	81	HBC	$4 \pi^- p \rightarrow \Lambda K 2\pi$
1300	40	CRENNELL	72	HBC	$4.5 \pi^- p \rightarrow \Lambda K 2\pi$
1242 + 9 / - 10	2	ASTIER	69	HBC	$\bar{p} p$
1300	45	CRENNELL	67	HBC	$6 \pi^- p \rightarrow \Lambda K 2\pi$

¹ Systematic errors not estimated.

² This was called the C meson.

PRODUCED IN τ LEPTON DECAYS

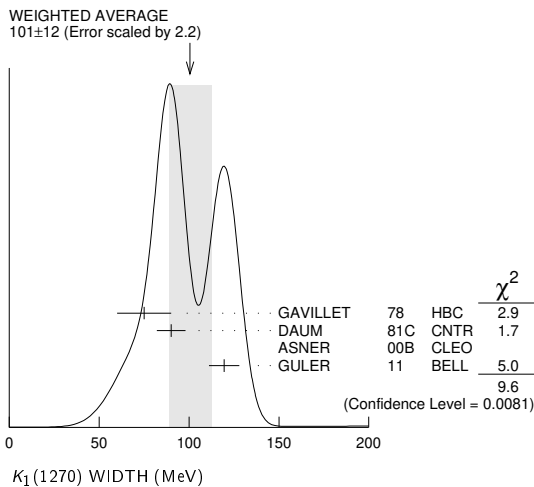
VALUE (MeV)	EVTS	DOCUMENT ID	TECN	CHG	COMMENT
The data in this block is included in the average printed for a previous datablock.					

1254 ± 33 ± 34 7k ASNER 00B CLEO ± $\tau^- \rightarrow K^- \pi^+ \pi^- \nu_\tau$

$K_1(1270)$ WIDTH

90 ± 20 OUR ESTIMATE This is only an educated guess; the error given is larger than the error on the average of the published values.

101 ± 12 OUR AVERAGE Includes data from the 4 datablocks that follow this one. Error includes scale factor of 2.2. See the ideogram below.



PRODUCED BY K^- , BACKWARD SCATTERING, HYPERON EXCHANGE

VALUE (MeV)	EVTS	DOCUMENT ID	TECN	CHG	COMMENT
The data in this block is included in the average printed for a previous datablock.					

75 ± 15 700 GAVILLET 78 HBC + 4.2 $K^- p \rightarrow \Xi^- K\pi\pi$

PRODUCED BY K BEAMS

VALUE (MeV)	EVTS	DOCUMENT ID	TECN	CHG	COMMENT
The data in this block is included in the average printed for a previous datablock.					

90 ± 8 1 DAUM 81c CNTR - 63 $K^- p \rightarrow K^- 2\pi$

••• We do not use the following data for averages, fits, limits, etc. •••

~ 150		VERGEEST	79	HBC	- 4.2 $K^- p \rightarrow (\bar{K}\pi\pi)^- p$
150 ± 71	2	CARNEGIE	77	ASPK	± 13 $K^\pm p \rightarrow (K\pi\pi)^\pm p$
~ 200		BRANDENB...	76	ASPK	± 13 $K^\pm p \rightarrow (K\pi\pi)^\pm p$
120		DAVIS	72	HBC	+ 12 $K^+ p$
188 ± 21		FIRESTONE	72B	DBC	+ 12 $K^+ d$

¹ Well described in the chiral unitary approach of GENG 07 with two poles at 1195 and 1284 MeV and widths of 246 and 146 MeV, respectively.

² From a model-dependent fit with Gaussian background to BRANDENBURG 76 data.

PRODUCED BY BEAMS OTHER THAN K MESONS

VALUE (MeV)	EVTS	DOCUMENT ID	TECN	CHG	COMMENT
The data in this block is included in the average printed for a previous datablock.					

119.5 ± 5.2 ± 6.7 GULER 11 BELL $B^+ \rightarrow J/\psi K^+ \pi^+ \pi^-$

••• We do not use the following data for averages, fits, limits, etc. •••

116.11 ± 1.65 ± 2.96	894k	AAIJ	18A1	LHCB	$D^0 \rightarrow K^+ \pi^\pm \pi^\pm \pi^\mp$
131 ± 21	25k	1	ABLIIKIM	06c	BES2 $J/\psi \rightarrow \bar{K}^*(892)^0 K^+ \pi^-$
66 ± 15	310	RODEBACK	81	HBC	$4 \pi^- p \rightarrow \Lambda K 2\pi$
60	40	CRENNELL	72	HBC	$4.5 \pi^- p \rightarrow \Lambda K 2\pi$
127 + 7 / - 25	2	ASTIER	69	HBC	$\bar{p} p$
60	45	CRENNELL	67	HBC	$6 \pi^- p \rightarrow \Lambda K 2\pi$

¹ Systematic errors not estimated.

PRODUCED IN τ LEPTON DECAYS

VALUE (MeV)	EVTS	DOCUMENT ID	TECN	CHG	COMMENT
The data in this block is included in the average printed for a previous datablock.					

260 + 90 / - 70 ± 80 7k ASNER 00B CLEO ± $\tau^- \rightarrow K^- \pi^+ \pi^- \nu_\tau$

$K_1(1270)$ DECAY MODES

Mode	Fraction (Γ_j/Γ)
Γ_1 $K \rho$	(42 ± 6) %
Γ_2 $K_0^*(1430)\pi$	(28 ± 4) %
Γ_3 $K^*(892)\pi$	(16 ± 5) %
Γ_4 $K\omega$	(11.0 ± 2.0) %
Γ_5 $K f_0(1370)$	(3.0 ± 2.0) %
Γ_6 γK^0	seen

$K_1(1270)$ PARTIAL WIDTHS

$\Gamma(K\rho)$ Γ_1

VALUE (MeV)	DOCUMENT ID	TECN	CHG	COMMENT
••• We do not use the following data for averages, fits, limits, etc. •••				

57 ± 5	MAZZUCATO	79	HBC	+ 4.2 $K^- p \rightarrow \Xi^- (K\pi\pi)^+$
75 ± 6	CARNEGIE	77B	ASPK	± 13 $K^\pm p \rightarrow (K\pi\pi)^\pm p$

$\Gamma(K_0^*(1430)\pi)$ Γ_2

VALUE (MeV)	DOCUMENT ID	TECN	CHG	COMMENT
••• We do not use the following data for averages, fits, limits, etc. •••				

26 ± 6	CARNEGIE	77B	ASPK	± 13 $K^\pm p \rightarrow (K\pi\pi)^\pm p$
--------	----------	-----	------	--

$\Gamma(K^*(892)\pi)$ Γ_3

VALUE (MeV)	DOCUMENT ID	TECN	CHG	COMMENT
••• We do not use the following data for averages, fits, limits, etc. •••				

14 ± 11	MAZZUCATO	79	HBC	+ 4.2 $K^- p \rightarrow \Xi^- (K\pi\pi)^+$
2 ± 2	CARNEGIE	77B	ASPK	± 13 $K^\pm p \rightarrow (K\pi\pi)^\pm p$

$\Gamma(K\omega)$ Γ_4

VALUE (MeV)	DOCUMENT ID	TECN	CHG	COMMENT
••• We do not use the following data for averages, fits, limits, etc. •••				

4 ± 4	MAZZUCATO	79	HBC	+ 4.2 $K^- p \rightarrow \Xi^- (K\pi\pi)^+$
24 ± 3	CARNEGIE	77B	ASPK	± 13 $K^\pm p \rightarrow (K\pi\pi)^\pm p$

$\Gamma(K f_0(1370))$ Γ_5

VALUE (MeV)	DOCUMENT ID	TECN	CHG	COMMENT
••• We do not use the following data for averages, fits, limits, etc. •••				

22 ± 5	CARNEGIE	77B	ASPK	± 13 $K^\pm p \rightarrow (K\pi\pi)^\pm p$
--------	----------	-----	------	--

$\Gamma(\gamma K^0)$ Γ_6

VALUE (keV)	DOCUMENT ID	TECN	COMMENT
73.2 ± 6.1 ± 28.3	ALAVI-HARATI02B	KTEV	$K + A \rightarrow K^* + A$

Meson Particle Listings

$K_1(1270), K_1(1400)$

$K_1(1270)$ BRANCHING RATIOS

$\Gamma(K\rho)/\Gamma_{total}$	VALUE	DOCUMENT ID	TECN	COMMENT	Γ_1/Γ
0.42 ± 0.06	1	DAUM	81c	CNTR	$63 K^- p \rightarrow K^- 2\pi p$
••• We do not use the following data for averages, fits, limits, etc. •••					
0.584 ± 0.043	2	GULER	11	BELL	$B^+ \rightarrow J/\psi K^+ \pi^+ \pi^-$
dominant		RODEBACK	81	HBC	$4 \pi^- p \rightarrow \Lambda K 2\pi$

$\Gamma(K_0^*(1430)\pi)/\Gamma_{total}$	VALUE	DOCUMENT ID	TECN	COMMENT	Γ_2/Γ
0.28 ± 0.04	1	DAUM	81c	CNTR	$63 K^- p \rightarrow K^- 2\pi p$
••• We do not use the following data for averages, fits, limits, etc. •••					
0.0201 ± 0.0064	2	GULER	11	BELL	$B^+ \rightarrow J/\psi K^+ \pi^+ \pi^-$

$\Gamma(K^*(892)\pi)/\Gamma_{total}$	VALUE	DOCUMENT ID	TECN	COMMENT	Γ_3/Γ
0.16 ± 0.05	1	DAUM	81c	CNTR	$63 K^- p \rightarrow K^- 2\pi p$
••• We do not use the following data for averages, fits, limits, etc. •••					
0.171 ± 0.023	2	GULER	11	BELL	$B^+ \rightarrow J/\psi K^+ \pi^+ \pi^-$

$\Gamma(K\omega)/\Gamma_{total}$	VALUE	DOCUMENT ID	TECN	COMMENT	Γ_4/Γ
0.11 ± 0.02	1	DAUM	81c	CNTR	$63 K^- p \rightarrow K^- 2\pi p$
••• We do not use the following data for averages, fits, limits, etc. •••					
0.225 ± 0.052	2	GULER	11	BELL	$B^+ \rightarrow J/\psi K^+ \pi^+ \pi^-$

$\Gamma(K\omega)/\Gamma(K\rho)$	VALUE	CL%	DOCUMENT ID	TECN	COMMENT	Γ_4/Γ_1
<0.30	95		RODEBACK	81	HBC	$4 \pi^- p \rightarrow \Lambda K 2\pi$
••• We do not use the following data for averages, fits, limits, etc. •••						

$\Gamma(K f_0(1370))/\Gamma_{total}$	VALUE	DOCUMENT ID	TECN	COMMENT	Γ_5/Γ
0.03 ± 0.02	1	DAUM	81c	CNTR	$63 K^- p \rightarrow K^- 2\pi p$

D-wave/S-wave RATIO FOR $K_1(1270) \rightarrow K^*(892)\pi$

VALUE	DOCUMENT ID	TECN	COMMENT
1.0 ± 0.7	1	DAUM	81c CNTR $63 K^- p \rightarrow K^- 2\pi p$

¹ Average from low and high t data.
² Assuming that decays are saturated by the $K\rho, K_0^*(1430)\pi, K^*(892)\pi, K\omega$ decay modes and neglecting interference between them. The values $B(\omega \rightarrow \pi^+\pi^-) = (1.53^{+0.11}_{-0.13})\%$ and $B(K_0^*(1430) \rightarrow K\pi) = (93 \pm 10)\%$ are used. Systematic uncertainties not estimated.

$K_1(1270)$ REFERENCES

AAIJ	18AI	EPJ C78 443	R. Aaij et al.	(LHCb Collab.)
GULER	11	PR D83 032005	H. Guler et al.	(BELLE Collab.)
GENG	07	PR D75 014017	L.S. Geng et al.	(BES Collab.)
ABLIKIM	06C	PL B633 681	M. Ablikim et al.	(FNAL KTeV Collab.)
ALAVI-HARATI	02B	PRL 89 072001	A. Alavi-Harati et al.	(CLEO Collab.)
ASNER	00B	PR D62 072006	D.M. Asner et al.	(CLEO Collab.)
TORNQVIST	82B	NP B203 268	N.A. Tornqvist	(HELS)
DAUM	81C	NP B187 1	C. Daum et al.	(AMST, CERN, CRAC, MPIM+)
RODEBACK	81	ZPHY C9 9	S. Rodeback et al.	(CERN, CDEF, MADR+)
MAZZUCATO	79	NP B156 532	M. Mazzucato et al.	(CERN, ZEEM, NIJM+)
VERGEEST	79	NP B158 265	J.S.M. Vergeest et al.	(NIJM, AMST, CERN+)
GAVILLET	78	PL 76B 517	P. Gavillet et al.	(AMST, CERN, NIJM+)
CARNEGIE	77	NP B127 509	R.K. Carnegie et al.	(SLAC)
CARNEGIE	77B	PL 68B 287	R.K. Carnegie et al.	(SLAC)
BRANDENB...	76	PRL 36 703	G.W. Brandenburg et al.	(SLAC) JP
OTTER	76	NP B106 77	G. Otter et al.	(AACH3, BERL, CERN, LOIC+)
CRENNELL	72	PR D6 1220	D.J. Crennell et al.	(BNL)
DAVIS	72	PR D5 2688	P.J. Davis et al.	(LBL)
FIRESTONE	72B	PR D5 505	A. Firestone et al.	(LBL)
ASTIER	69	NP B10 65	A. Astier et al.	(CDEF, CERN, IPNP, LIVP) JP
CRENNELL	67	PRL 19 44	D.J. Crennell et al.	(BNL) I

$K_1(1400)$

$$J(P) = \frac{1}{2}(1^+)$$

$K_1(1400)$ MASS

VALUE (MeV)	EVTs	DOCUMENT ID	TECN	CHG	COMMENT
1403 ± 7 OUR AVERAGE					
$1463 \pm 64 \pm 68$	7k	ASNER	00B	CLEO	$\tau^- \rightarrow K^- \pi^+ \pi^- \nu_\tau$
$1373 \pm 14 \pm 18$		1 ASTON	87	LASS	$0 11 K^- p \rightarrow \bar{K}^0 \pi^+ \pi^- n$
1392 ± 18		BAUBILLIER	82B	HBC	$0 8.25 K^- p \rightarrow K_S^0 \pi^+ \pi^- n$
1410 ± 25		DAUM	81C	CNTR	$- 63 K^- p \rightarrow K^- 2\pi p$
1415 ± 15		ETKIN	80	MPS	$0 6 K^- p \rightarrow \bar{K}^0 \pi^+ \pi^- n$
1404 ± 10		2 CARNEGIE	77	ASPK	$\pm 13 K^\pm p \rightarrow (K\pi\pi)^\pm p$

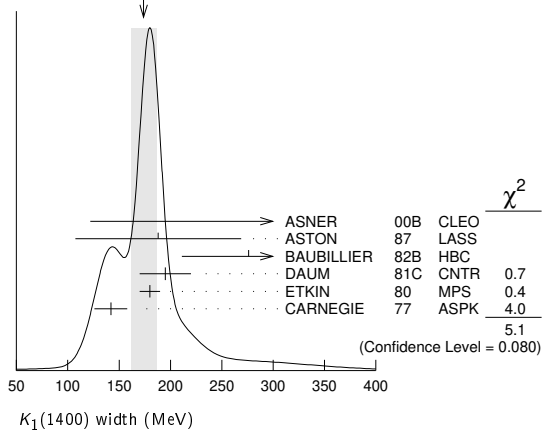
••• We do not use the following data for averages, fits, limits, etc. •••

1418 ± 8	25k	3 ABLIKIM	06c	BES2	$J/\psi \rightarrow \bar{K}^*(892)^0 K^+ \pi^-$
~ 1350		4 TORNQVIST	82B	RVUE	
~ 1400		VERGEEST	79	HBC	$- 4.2 K^- p \rightarrow (\bar{K}\pi\pi)^- p$
~ 1400		BRANDENB...	76	ASPK	$\pm 13 K^\pm p \rightarrow (K\pi\pi)^\pm p$
1420		DAVIS	72	HBC	$+ 12 K^+ p$
1368 ± 18		FIRESTONE	72B	DBC	$+ 12 K^+ d$
¹ From partial-wave analysis of $K^0 \pi^+ \pi^-$ system.					
² From a model-dependent fit with Gaussian background to BRANDENBURG 76 data.					
³ Systematic errors not estimated.					
⁴ From a unitarized quark-model calculation.					

$K_1(1400)$ WIDTH

VALUE (MeV)	EVTs	DOCUMENT ID	TECN	CHG	COMMENT
174 ± 13 OUR AVERAGE					Error includes scale factor of 1.6. See the ideogram below.
$300^{+370}_{-110} \pm 140$	7k	ASNER	00B	CLEO	$\pm \tau^- \rightarrow K^- \pi^+ \pi^- \nu_\tau$
$188 \pm 54 \pm 60$		5 ASTON	87	LASS	$0 11 K^- p \rightarrow \bar{K}^0 \pi^+ \pi^- n$
276 ± 65		BAUBILLIER	82B	HBC	$0 8.25 K^- p \rightarrow K_S^0 \pi^+ \pi^- n$
195 ± 25		DAUM	81C	CNTR	$- 63 K^- p \rightarrow K^- 2\pi p$
180 ± 10		ETKIN	80	MPS	$0 6 K^- p \rightarrow \bar{K}^0 \pi^+ \pi^- n$
142 ± 16		6 CARNEGIE	77	ASPK	$\pm 13 K^\pm p \rightarrow (K\pi\pi)^\pm p$
••• We do not use the following data for averages, fits, limits, etc. •••					
152 ± 16	25k	7 ABLIKIM	06c	BES2	$J/\psi \rightarrow \bar{K}^*(892)^0 K^+ \pi^-$
~ 200		VERGEEST	79	HBC	$- 4.2 K^- p \rightarrow (\bar{K}\pi\pi)^- p$
~ 160		BRANDENB...	76	ASPK	$\pm 13 K^\pm p \rightarrow (K\pi\pi)^\pm p$
80		DAVIS	72	HBC	$+ 12 K^+ p$
241 ± 30		FIRESTONE	72B	DBC	$+ 12 K^+ d$
⁵ From partial-wave analysis of $K^0 \pi^+ \pi^-$ system.					
⁶ From a model-dependent fit with Gaussian background to BRANDENBURG 76 data.					
⁷ Systematic errors not estimated.					

WEIGHTED AVERAGE
174±13 (Error scaled by 1.6)



$K_1(1400)$ DECAY MODES

Mode	Fraction (Γ_i/Γ)
$\Gamma_1 K^*(892)\pi$	$(94 \pm 6) \%$
$\Gamma_2 K\rho$	$(3.0 \pm 3.0) \%$
$\Gamma_3 K f_0(1370)$	$(2.0 \pm 2.0) \%$
$\Gamma_4 K\omega$	$(1.0 \pm 1.0) \%$
$\Gamma_5 K_0^*(1430)\pi$	not seen
$\Gamma_6 \gamma K^0$	seen

$K_1(1400)$ PARTIAL WIDTHS

$\Gamma(K^*(892)\pi)$	VALUE (MeV)	DOCUMENT ID	TECN	CHG	COMMENT	Γ_1
117 ± 10		CARNEGIE	77	ASPK	$\pm 13 K^\pm p \rightarrow (K\pi\pi)^\pm p$	

$\Gamma(K\rho)$	VALUE (MeV)	DOCUMENT ID	TECN	CHG	COMMENT	Γ_2
2 ± 1		CARNEGIE	77	ASPK	$\pm 13 K^\pm p \rightarrow (K\pi\pi)^\pm p$	

See key on page 999

Meson Particle Listings

$K_1(1400)$, $K^*(1410)$, $K_0^*(1430)$

$\Gamma(K\omega)$ Γ_4				
VALUE (MeV)	DOCUMENT ID	TECN	CHG	COMMENT
23±12	CARNEGIE	77	ASPK	± 13 $K^\pm p \rightarrow (K\pi\pi)^\pm p$

$\Gamma(\gamma K^0)$ Γ_6				
VALUE (keV)	DOCUMENT ID	TECN	CHG	COMMENT
280.8±23.2±40.4	ALAVI-HARATI02B	KTEV		$K + A \rightarrow K^* + A$

$K_1(1400)$ BRANCHING RATIOS

$\Gamma(K^*(892)\pi)/\Gamma_{total}$ Γ_1/Γ				
VALUE	DOCUMENT ID	TECN	CHG	COMMENT
0.94±0.06	⁸ DAUM	81c	CNTR	63 $K^- p \rightarrow K^- 2\pi p$

$\Gamma(K\rho)/\Gamma_{total}$ Γ_2/Γ				
VALUE	DOCUMENT ID	TECN	CHG	COMMENT
0.03±0.03	⁸ DAUM	81c	CNTR	63 $K^- p \rightarrow K^- 2\pi p$

$\Gamma(Kf_0(1370))/\Gamma_{total}$ Γ_3/Γ				
VALUE	DOCUMENT ID	TECN	CHG	COMMENT
0.02±0.02	⁸ DAUM	81c	CNTR	63 $K^- p \rightarrow K^- 2\pi p$

$\Gamma(K\omega)/\Gamma_{total}$ Γ_4/Γ				
VALUE	DOCUMENT ID	TECN	CHG	COMMENT
0.01±0.01	⁸ DAUM	81c	CNTR	63 $K^- p \rightarrow K^- 2\pi p$

$\Gamma(K_0^*(1430)\pi)/\Gamma_{total}$ Γ_5/Γ				
VALUE	DOCUMENT ID	TECN	CHG	COMMENT
not seen	⁸ DAUM	81c	CNTR	63 $K^- p \rightarrow K^- 2\pi p$

D-wave/S-wave RATIO FOR $K_1(1400) \rightarrow K^*(892)\pi$

VALUE	DOCUMENT ID	TECN	CHG	COMMENT
0.04±0.01	⁸ DAUM	81c	CNTR	63 $K^- p \rightarrow K^- 2\pi p$

⁸ Average from low and high t data.

$K_1(1400)$ REFERENCES

ABLIKIM	06C	PL B633 681	M. Ablikim et al.	(BES Collab.)
ALAVI-HARATI	02B	PRL 89 072001	A. Alavi-Harati et al.	(FNAL KTeV Collab.)
ASNER	00B	PR D62 072006	D.M. Asner et al.	(CLEO Collab.)
ASTON	87	NP B292 693	D. Aston et al.	(SLAC, NAGO, CINC, INUS)
BAUBILLIER	82B	NP B202 21	M. Baubillier et al.	(BIRM, CERN, GLAS+)
TORNQVIST	82B	NP B203 268	N.A. Tornqvist	(HELS)
DAUM	81C	NP B187 1	C. Daum et al.	(AMST, CERN, CRAC, MPIM+)
ETKIN	80	PR D22 42	A. Etkin et al.	(BNL, CUNY)JP
VERGEEST	79	NP B158 265	J.S.M. Vergeest et al.	(NUM, AMST, CERN+)
CARNEGIE	77	NP B127 509	R.K. Carnegie et al.	(SLAC)
BRANDENB...	76	PRL 36 703	G.W. Brandenburg et al.	(SLAC)JP
DAVIS	72	PR D5 2688	P.J. Davis et al.	(LBL)
FIRESTONE	72B	PR D9 505	A. Firestone et al.	(LBL)

$K^*(1410)$

$$I(J^P) = \frac{1}{2}(1^-)$$

$K^*(1410)$ MASS

VALUE (MeV)	EVTs	DOCUMENT ID	TECN	CHG	COMMENT
1414±15 OUR AVERAGE		Error includes scale factor of 1.3.			
1380±21±19		ASTON	88	LASS	0 11 $K^- p \rightarrow K^- \pi^+ n$
1420±7±10		ASTON	87	LASS	0 11 $K^- p \rightarrow \bar{K}^0 \pi^+ \pi^- n$
••• We do not use the following data for averages, fits, limits, etc. •••					
1437±8±16	190k	¹ AAIJ	16N	LHCB	$D^0 \rightarrow (K_S^0 \pi^\mp) K^\pm$
1426±8±24	190k	² AAIJ	16N	LHCB	$D^0 \rightarrow K_S^0(K^\pm \pi^\mp)$
1276 ⁺⁷² ₋₇₇		^{3,4} BOITO	09	RVUE	$\tau^- \rightarrow K_S^0 \pi^- \nu_\tau$
1367±54		BIRD	89	LASS	- 11 $K^- p \rightarrow \bar{K}^0 \pi^- p$
1474±25		BAUBILLIER	82B	HBC	0 8.25 $K^- p \rightarrow \bar{K}^0 2\pi n$
1500±30		ETKIN	80	MPS	0 6 $K^- p \rightarrow \bar{K}^0 \pi^+ \pi^- n$
¹ Using a parametrization for the $K\pi$ S-wave similar to ASTON 88 with fixed resonance width.					
² Using a $K\pi$ S-wave parametrization with resonant and non-resonant contributions.					
³ From the pole position of the $K\pi$ vector form factor in the complex s-plane and using EPIFANOV 07 data.					
⁴ Systematic uncertainties not estimated.					

$K^*(1410)$ WIDTH

VALUE (MeV)	EVTs	DOCUMENT ID	TECN	CHG	COMMENT
232±21 OUR AVERAGE		Error includes scale factor of 1.1.			
176±52±22		ASTON	88	LASS	0 11 $K^- p \rightarrow K^- \pi^+ n$
240±18±12		ASTON	87	LASS	0 11 $K^- p \rightarrow \bar{K}^0 \pi^+ \pi^- n$

••• We do not use the following data for averages, fits, limits, etc. •••

210±20±60	190k	¹ AAIJ	16N	LHCB	$D^0 \rightarrow (K_S^0 \pi^\mp) K^\pm$
270±20±40	190k	¹ AAIJ	16N	LHCB	$D^0 \rightarrow K_S^0(K^\pm \pi^\mp)$
198 ⁺⁶¹ ₋₈₇		^{2,3} BOITO	09	RVUE	$\tau^- \rightarrow K_S^0 \pi^- \nu_\tau$
114±101		BIRD	89	LASS	- 11 $K^- p \rightarrow \bar{K}^0 \pi^- p$
275±65		BAUBILLIER	82B	HBC	0 8.25 $K^- p \rightarrow \bar{K}^0 2\pi n$
500±100		ETKIN	80	MPS	0 6 $K^- p \rightarrow \bar{K}^0 \pi^+ \pi^- n$
¹ Using a $K\pi$ S-wave parametrization with resonant and non-resonant contributions.					
² From the pole position of the $K\pi$ vector form factor in the complex s-plane and using EPIFANOV 07 data.					
³ Systematic uncertainties not estimated.					

$K^*(1410)$ DECAY MODES

Mode	Fraction (Γ_i/Γ)	Confidence level
Γ_1 $K^*(892)\pi$	> 40 %	95%
Γ_2 $K\pi$	(6.6±1.3) %	
Γ_3 $K\rho$	< 7 %	95%
Γ_4 γK^0	< 2.3 × 10 ⁻⁴	90%

$K^*(1410)$ PARTIAL WIDTHS

$\Gamma(\gamma K^0)$ Γ_4				
VALUE (keV)	CL%	DOCUMENT ID	TECN	COMMENT
<52.9	90	ALAVI-HARATI02B	KTEV	$K + A \rightarrow K^* + A$

$K^*(1410)$ BRANCHING RATIOS

$\Gamma(K\rho)/\Gamma(K^*(892)\pi)$ Γ_3/Γ_1					
VALUE	CL%	DOCUMENT ID	TECN	CHG	COMMENT
<0.17	95	ASTON	84	LASS	0 11 $K^- p \rightarrow \bar{K}^0 2\pi n$

$\Gamma(K\pi)/\Gamma(K^*(892)\pi)$ Γ_2/Γ_1					
VALUE	CL%	DOCUMENT ID	TECN	CHG	COMMENT
<0.16	95	ASTON	84	LASS	0 11 $K^- p \rightarrow \bar{K}^0 2\pi n$

$\Gamma(K\pi)/\Gamma_{total}$ Γ_2/Γ				
VALUE	DOCUMENT ID	TECN	CHG	COMMENT
0.066±0.010±0.008	ASTON	88	LASS	0 11 $K^- p \rightarrow K^- \pi^+ n$

$K^*(1410)$ REFERENCES

AAIJ	16N	PR D93 052018	R. Aaij et al.	(LHCB Collab.)
BOITO	09	EPJ C9 821	D.R. Boito, R. Escobedo, M. Jamin	
EPIFANOV	07	PL B654 65	D. Epifanov et al.	(BELLE Collab.)
ALAVI-HARATI	02B	PRL 89 072001	A. Alavi-Harati et al.	(FNAL KTeV Collab.)
BIRD	89	SLAC-332	P.F. Bird	(SLAC)
ASTON	88	NP B296 493	D. Aston et al.	(SLAC, NAGO, CINC, INUS)
ASTON	87	NP B292 693	D. Aston et al.	(SLAC, NAGO, CINC, INUS)
ASTON	84	PL 149B 258	D. Aston et al.	(SLAC, CARL, OTTA)JP
BAUBILLIER	82B	NP B202 21	M. Baubillier et al.	(BIRM, CERN, GLAS+)
ETKIN	80	PR D22 42	A. Etkin et al.	(BNL, CUNY)JP

$K_0^*(1430)$

$$I(J^P) = \frac{1}{2}(0^+)$$

See our minireview in the 1994 edition and in this edition under the $f_0(500)$.

$K_0^*(1430)$ MASS

VALUE (MeV)	EVTs	DOCUMENT ID	TECN	COMMENT
1425±50 OUR ESTIMATE		••• We do not use the following data for averages, fits, limits, etc. •••		
1438 ± 8 ± 4	5.4k	¹ LEES	14E	BABR $\eta_c(1S) \rightarrow K^+ K^- \eta/\pi^0$
1427 ± 4 ± 13		² BUGG	10	RVUE S-matrix pole
1466.6±0.7±3.4	141k	³ BONVICINI	08A	CLEO $D^+ \rightarrow K^- \pi^+ \pi^+$
~ 1412		⁴ LINK	07	FOCS $D^+ \rightarrow K^- K^+ \pi^+$
1461.0±4.0±2.1	54k	⁵ LINK	07B	FOCS $D^+ \rightarrow K^- \pi^+ \pi^+$
1406 ± 29		⁶ BUGG	06	RVUE
1435 ± 6		⁷ ZHOU	06	RVUE $Kp \rightarrow K^- \pi^+ n$
1455 ± 20 ± 15		ABLIKIM	05Q	BES2 $\psi(2S) \rightarrow \gamma \pi^+ \pi^- K^+ K^-$
1456 ± 8		⁸ ZHENG	04	RVUE $K^- p \rightarrow K^- \pi^+ n$
~ 1419		⁹ BUGG	03	RVUE 11 $K^- p \rightarrow K^- \pi^+ n$
~ 1440		¹⁰ LI	03	RVUE 11 $K^- p \rightarrow K^- \pi^+ n$
1459 ± 9	15k	¹¹ AITALA	02	E791 $D^+ \rightarrow K^- \pi^+ \pi^+$
~ 1440		¹² JAMIN	00	RVUE $Kp \rightarrow Kp$
1436 ± 8		¹³ BARBERIS	98E	OMEG 450 pp → $p_f p_S K^+ K^- \pi^+ \pi^-$

Meson Particle Listings

$K_0^*(1430)$, $K_2^*(1430)$

1415 ±25 ~ 1450	⁹ ANISOVICH 97c	RVUE	11	$K^- p \rightarrow K^- \pi^+ n$
1412 ± 6	¹⁴ TORNQVIST 96	RVUE	$\pi\pi \rightarrow \pi\pi, K\bar{K}, K\pi$	
~ 1430	¹⁵ ASTON 88	LASS	11	$K^- p \rightarrow K^- \pi^+ n$
~ 1425	BAUBILLIER 84B	HBC	8.25	$K^- p \rightarrow \bar{K}^0 \pi^- p$
~ 1450.0	¹⁶ ESTABROOKS 78	ASPK	13	$K^\pm p \rightarrow K^\pm \pi^\pm (n, \Delta)$
	MARTIN 78	SPEC	10	$K^\pm p \rightarrow K_S^0 \pi p$

- Using both $\eta \rightarrow \gamma\gamma$ and $\eta \rightarrow \pi^+\pi^-\pi^0$. From a likelihood scan in the presence of several interfering scalar-meson resonances with fixed width $\Gamma(K_0^*(1430)) = 210$ MeV.
- S-matrix pole. Supersedes BUGG 06. Combined analysis of ASTON 88, ABLIKIM 06c, AITALA 06, and LINK 09 using an s-dependent width with couplings to $K\pi$ and $K\eta'$, and the Adler zero near thresholds.
- From the isobar model with a complex pole for the κ .
- From a non-parametric analysis.
- A Breit-Wigner mass and width.
- S-matrix pole. Reanalysis of ASTON 88, AITALA 02, and ABLIKIM 06c including the κ with an s-dependent width and an Adler zero near threshold.
- S-matrix pole. Using ASTON 88 and assuming $K_0^*(700)$, $K_0^*(1950)$.
- Using ASTON 88 and assuming $K_0^*(700)$.
- T-matrix pole. Reanalysis of ASTON 88 data.
- Breit-Wigner fit. Using ASTON 88.
- Assuming a low-mass scalar $K\pi$ resonance, $\kappa(700)$.
- T-matrix pole. Using data from ESTABROOKS 78 and ASTON 88.
- J^P not determined, could be $K_2^*(1430)$.
- T-matrix pole.
- Uses a model for the background, without this background they get a mass 1340 MeV, where the phase shift passes 90°.
- Mass defined by pole position. From elastic $K\pi$ partial-wave analysis.

$K_0^*(1430)$ WIDTH

VALUE (MeV)	EVTs	DOCUMENT ID	TECN	COMMENT
270 ±80	OUR ESTIMATE			
• • •	We do not use the following data for averages, fits, limits, etc. • • •			
210 ±20 ±12	5.4k	¹ LEES	14E	BABR $\eta_C(1S) \rightarrow K^+ K^- \eta/\pi^0$
270 ±10 ±40		² BUGG	10	RVUE S-matrix pole
174.2 ± 1.9 ± 3.2	141k	³ BONVICINI	08A	CLEO $D^+ \rightarrow K^- \pi^+ \pi^+$
~ 500		⁴ LINK	07	FOCS $D^+ \rightarrow K^- K^+ \pi^+$
177.0 ± 8.0 ± 3.4	54k	⁵ LINK	07B	FOCS $D^+ \rightarrow K^- \pi^+ \pi^+$
350 ±40		⁶ BUGG	06	RVUE
288 ±22		⁷ ZHOU	06	RVUE $Kp \rightarrow K^- \pi^+ n$
270 ±45 ⁺³⁰ / ₋₃₅		ABLIKIM	05Q	BES2 $\psi(2S) \rightarrow \gamma\pi^+\pi^- K^+ K^-$
217 ±31		⁸ ZHENG	04	RVUE $K^- p \rightarrow K^- \pi^+ n$
~ 316		⁹ BUGG	03	RVUE $11 K^- p \rightarrow K^- \pi^+ n$
~ 350		¹⁰ LI	03	RVUE $11 K^- p \rightarrow K^- \pi^+ n$
175 ±17	15k	¹¹ AITALA	02	E791 $D^+ \rightarrow K^- \pi^+ \pi^+$
~ 300		¹² JAMIN	00	RVUE $Kp \rightarrow Kp$
196 ±45		¹³ BARBERIS	98E	OMEG $450 pp \rightarrow p_f p_s K^+ K^- \pi^+ \pi^-$
330 ±50		⁹ ANISOVICH 97c	RVUE	11 $K^- p \rightarrow K^- \pi^+ n$
~ 320		¹⁴ TORNQVIST 96	RVUE	$\pi\pi \rightarrow \pi\pi, K\bar{K}, K\pi$
294 ±23		ASTON 88	LASS	11 $K^- p \rightarrow K^- \pi^+ n$
~ 200		BAUBILLIER 84B	HBC	8.25 $K^- p \rightarrow \bar{K}^0 \pi^- p$
200 to 300		¹⁵ ESTABROOKS 78	ASPK	13 $K^\pm p \rightarrow K^\pm \pi^\pm (n, \Delta)$

- Using both $\eta \rightarrow \gamma\gamma$ and $\eta \rightarrow \pi^+\pi^-\pi^0$. From a likelihood scan in the presence of several interfering scalar-meson resonances with fixed mass $M(K_0^*(1430)) = 1435$ MeV.
- S-matrix pole. Supersedes BUGG 06. Combined analysis of ASTON 88, ABLIKIM 06c, AITALA 06, and LINK 09 using an s-dependent width with couplings to $K\pi$ and $K\eta'$, and the Adler zero near thresholds.
- From the isobar model with a complex pole for the κ .
- From a non-parametric analysis.
- A Breit-Wigner mass and width.
- S-matrix pole. Reanalysis of ASTON 88, AITALA 02, and ABLIKIM 06c including the κ with an s-dependent width and an Adler zero near threshold.
- S-matrix pole. Using ASTON 88 and assuming $K_0^*(700)$, $K_0^*(1950)$.
- Using ASTON 88 and assuming $K_0^*(700)$.
- T-matrix pole. Reanalysis of ASTON 88 data.
- Breit-Wigner fit. Using ASTON 88.
- Assuming a low-mass scalar $K\pi$ resonance, $\kappa(700)$.
- T-matrix pole. Using data from ESTABROOKS 78 and ASTON 88.
- J^P not determined, could be $K_2^*(1430)$.
- T-matrix pole.
- From elastic $K\pi$ partial-wave analysis.

$K_0^*(1430)$ DECAY MODES

Mode	Fraction (Γ_i/Γ)
Γ_1 $K\pi$	(93 ±10) %
Γ_2 $K\eta$	(8.6 ± 2.7 / 3.4) %
Γ_3 $K\eta'(958)$	seen

$K_0^*(1430)$ BRANCHING RATIOS

$\Gamma(K\pi)/\Gamma_{total}$	DOCUMENT ID	TECN	CHG	COMMENT	Γ_1/Γ
0.93 ± 0.04 ± 0.09	ASTON	88	LASS	0	11 $K^- p \rightarrow K^- \pi^+ n$

$\Gamma(K\eta)/\Gamma(K\pi)$	EVTs	DOCUMENT ID	TECN	COMMENT	Γ_2/Γ_1
9.2 ± 2.5 ^{+1.0} / _{-2.5}	5.4k	¹ LEES	14E	BABR $\eta_C(1S) \rightarrow K^+ K^- \eta/\pi^0$	

¹ Using both $\eta \rightarrow \gamma\gamma$ and $\eta \rightarrow \pi^+\pi^-\pi^0$. From a Dalitz analysis in the presence of several interfering scalar-meson resonances.

$\Gamma(K\eta'(958))/\Gamma_{total}$	DOCUMENT ID	TECN	COMMENT	Γ_3/Γ
seen	ABLIKIM	14J	BES3	$\psi(2S) \rightarrow \gamma K^+ K^- \eta'(958)$

$K_0^*(1430)$ REFERENCES

ABLIKIM 14J	PR D89 074030	M. Ablikim <i>et al.</i>	(BESIII Collab.)
LEES 14E	PR D89 112004	J.P. Lees <i>et al.</i>	(BABAR Collab.)
BUGG 10	PR D81 014002	D.V. Bugg <i>et al.</i>	(LOQM)
LINK 09	PL B681 14	J.M. Link <i>et al.</i>	(FNAL FOCUS Collab.)
BONVICINI 08A	PR D78 052001	G. Bonvicini <i>et al.</i>	(CLEO Collab.)
LINK 07	PL B648 156	J.M. Link <i>et al.</i>	(FNAL FOCUS Collab.)
LINK 07B	PL B653 1	J.M. Link <i>et al.</i>	(FNAL FOCUS Collab.)
ABLIKIM 06C	PL B633 681	M. Ablikim <i>et al.</i>	(BES Collab.)
AITALA 06	PR D73 032004	E.M. Aitala <i>et al.</i>	(FNAL E791 Collab.)
Also	PR D74 059901 (errat.)	E.M. Aitala <i>et al.</i>	(FNAL E791 Collab.)
BUGG 06	PL B632 471	D.V. Bugg	(LOQM)
ZHOU 06	NP A775 212	Z.Y. Zhou, H.Q. Zheng	
ABLIKIM 05Q	PR D72 092002	M. Ablikim <i>et al.</i>	(BES Collab.)
ZHENG 04	NP A733 235	H.Q. Zheng <i>et al.</i>	
BUGG 03	PL B572 1	D.V. Bugg	
LI 03	PR D67 034025	L. Li, B. Zou, G. Li	
AITALA 02	PRL 89 121801	E.M. Aitala <i>et al.</i>	(FNAL E791 Collab.)
JAMIN 00	NP B587 331	M. Jamin <i>et al.</i>	
BARBERIS 98E	PL B436 204	D. Barberis <i>et al.</i>	(Omega Expt.)
ANISOVICH 97C	PL B413 137	A.V. Anisovich, A.V. Sarantsev	
TORNQVIST 96	PRL 76 1575	N.A. Tornqvist, M. Roos	(HELS)
ASTON 88	NP B296 493	D. Aston <i>et al.</i>	(SLAC, NAGO, CIN, INUS)
BAUBILLIER 84B	ZPHY C26 37	M. Baubillier <i>et al.</i>	(BIRM, CERN, GLAS+)
ESTABROOKS 78	NP B133 490	P.G. Estabrooks <i>et al.</i>	(MCGI, CARL, DURH+)
MARTIN 78	NP B134 392	A.D. Martin <i>et al.</i>	(DURH, GEVA)

$K_2^*(1430)$

$$J(J^P) = \frac{1}{2}(2^+)$$

We consider that phase-shift analyses provide more reliable determinations of the mass and width.

$K_2^*(1430)$ MASS

CHARGED ONLY, WITH FINAL STATE $K\pi$

VALUE (MeV)	EVTs	DOCUMENT ID	TECN	CHG	COMMENT
1427.3 ± 1.5	OUR AVERAGE				Error includes scale factor of 1.3. See the ideogram below.
1432.7 ± 0.7 ^{+2.2} / _{-2.3}	183k	ABLIKIM	19AQ	BES	$J/\psi \rightarrow K^+ K^- \pi^0$
1420 ± 4	1587	BAUBILLIER	84B	HBC	8.25 $K^- p \rightarrow \bar{K}^0 \pi^- p$
1436 ± 5.5	400	^{1,2} CLELAND	82	SPEC	+ 30 $K^+ p \rightarrow K_S^0 \pi^+ p$
1430 ± 3.2	1500	^{1,2} CLELAND	82	SPEC	+ 50 $K^+ p \rightarrow K_S^0 \pi^+ p$
1430 ± 3.2	1200	^{1,2} CLELAND	82	SPEC	- 50 $K^+ p \rightarrow K_S^0 \pi^- p$
1423 ± 5	935	TOAFF	81	HBC	6.5 $K^- p \rightarrow \bar{K}^0 \pi^- p$
1428.0 ± 4.6		³ MARTIN	78	SPEC	+ 10 $K^\pm p \rightarrow K_S^0 \pi p$
1423.8 ± 4.6		³ MARTIN	78	SPEC	- 10 $K^\pm p \rightarrow K_S^0 \pi p$
1420.0 ± 3.1	1400	AGUILAR...	71B	HBC	- 3.9, 4.6 $K^- p$
1425 ± 8.0	225	^{1,2} BARNHAM	71c	HBC	+ $K^+ p \rightarrow K^0 \pi^+ p$
1416 ± 10	220	CRENNELL	69D	DBC	- 3.9 $K^- N \rightarrow \bar{K}^0 \pi^- N$
1414 ± 13.0	60	¹ LIND	69	HBC	+ 9 $K^+ p \rightarrow K^0 \pi^+ p$
1427 ± 12	63	¹ SCHWEING...	68	HBC	+ 5.5 $K^- p \rightarrow \bar{K} \pi N$
1423 ± 11.0	39	¹ BASSANO	67	HBC	- 4.6-5.0 $K^- p \rightarrow \bar{K}^0 \pi^- p$

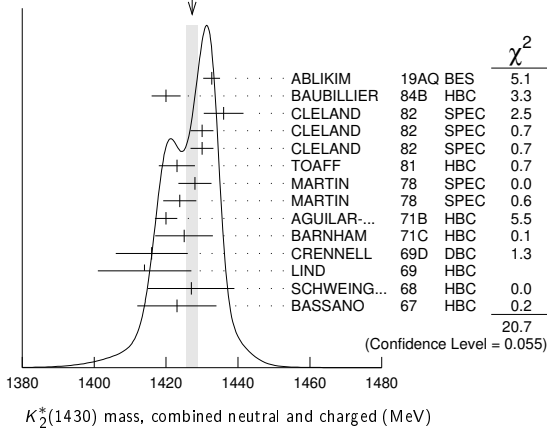
- • • We do not use the following data for averages, fits, limits, etc. • • •
- | | | | | | |
|----------------|-------------|-------------------|----|------|--|
| 1423.4 ± 2 ± 3 | 24809 ± 820 | ⁴ BIRD | 89 | LASS | - 11 $K^- p \rightarrow \bar{K}^0 \pi^- p$ |
|----------------|-------------|-------------------|----|------|--|

See key on page 999

Meson Particle Listings

$K_2^*(1430)$

WEIGHTED AVERAGE
1427.3±1.5 (Error scaled by 1.3)



NEUTRAL ONLY

VALUE (MeV)	EVTS	DOCUMENT ID	TECN	COMMENT
1432.4 ± 1.3 OUR AVERAGE				
1431.2 ± 1.8 ± 0.7	5	ASTON 88	LASS	11 $K^-p \rightarrow K^- \pi^+ n$
1434 ± 4 ± 6	5	ASTON 87	LASS	11 $K^-p \rightarrow \bar{K}^0 \pi^+ \pi^- n$
1433 ± 6 ± 10	5	ASTON 84B	LASS	11 $K^-p \rightarrow \bar{K}^0 2\pi n$
1471 ± 12	5	BAUBILLIER 82B	HBC	8.25 $K^-p \rightarrow N K_S^0 \pi \pi$
1428 ± 3	5	ASTON 81C	LASS	11 $K^-p \rightarrow K^- \pi^+ n$
1434 ± 2	5	ESTABROOKS 78	ASPK	13 $K^\pm p \rightarrow \rho K \pi$
1440 ± 10	5	BOWLER 77	DBC	5.5 $K^+ d \rightarrow K \pi p p$

• • • We do not use the following data for averages, fits, limits, etc. • • •

1428.5 ± 3.9	1786 ± 127	6	AUBERT 07AK BABR	10.6 $e^+ e^- \rightarrow K^{*0} K^\pm \pi^\mp \gamma$
1420 ± 7	300	8	HENDRICK 76 DBC	8.25 $K^+ N \rightarrow K^+ \pi N$
1421.6 ± 4.2	800	8	MCCUBBIN 75 HBC	3.6 $K^- p \rightarrow K^- \pi^+ n$
1420.1 ± 4.3	7	LINGLIN 73	HBC	2-13 $K^+ p \rightarrow K^+ \pi^- X$
1419.1 ± 3.7	1800	7	AGUILAR... 71B HBC	3.9, 4.6 $K^- p$
1416 ± 6	600	8	CORDS 71 DBC	9 $K^+ n \rightarrow K^+ \pi^- p$
1421.1 ± 2.6	2200	69	DAVIS 69 HBC	12 $K^+ p \rightarrow K^+ \pi^- X$

- Errors enlarged by us to Γ/\sqrt{N} ; see the note with the $K^*(892)$ mass.
- Number of events in peak re-evaluated by us.
- Systematic error added by us.
- From a partial wave amplitude analysis.
- From phase shift or partial-wave analysis.
- Systematic errors not estimated.
- From pole extrapolation, using world $K^+ p$ data summary tape.

$K_2^*(1430)$ WIDTH

CHARGED ONLY, WITH FINAL STATE $K\pi$

VALUE (MeV)	EVTS	DOCUMENT ID	TECN	CHG	COMMENT
100.0 ± 2.1 OUR FIT					
100.0 ± 2.2 OUR AVERAGE					Error includes scale factor of 1.1.
102.5 ± 1.6 ± 3.1 / -2.8	183k	ABLIKIM 19AQ BES	±		$J/\psi \rightarrow K^+ K^- \pi^0$
109 ± 22	400	8,9 CLELAND 82	SPEC	+	30 $K^+ p \rightarrow K_S^0 \pi^+ p$
114 ± 12.8	1500	8,9 CLELAND 82	SPEC	+	50 $K^+ p \rightarrow K_S^0 \pi^+ p$
113 ± 12.8	1200	8,9 CLELAND 82	SPEC	-	50 $K^+ p \rightarrow K_S^0 \pi^- p$
85 ± 16	935	TOAFF 81	HBC	-	6.5 $K^- p \rightarrow \bar{K}^0 \pi^- p$
96.5 ± 3.8		MARTIN 78	SPEC	+	10 $K^\pm p \rightarrow K_S^0 \pi p$
97.7 ± 4.0		MARTIN 78	SPEC	-	10 $K^\pm p \rightarrow K_S^0 \pi p$
94.7 ± 15.1 / -12.5	1400	AGUILAR... 71B	HBC	-	3.9, 4.6 $K^- p$
98 ± 4 ± 4	25k	10 BIRD 89	LASS	-	11 $K^- p \rightarrow \bar{K}^0 \pi^- p$

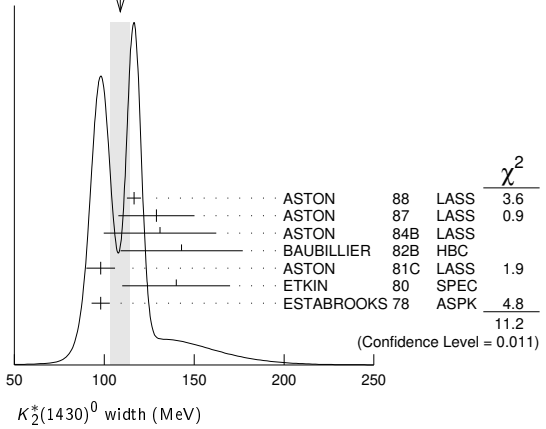
NEUTRAL ONLY

VALUE (MeV)	EVTS	DOCUMENT ID	TECN	COMMENT
109 ± 5 OUR AVERAGE				Error includes scale factor of 1.9. See the ideogram below.
116.5 ± 3.6 ± 1.7	11	ASTON 88	LASS	11 $K^- p \rightarrow K^- \pi^+ n$
129 ± 15 ± 15	11	ASTON 87	LASS	11 $K^- p \rightarrow \bar{K}^0 \pi^+ \pi^- n$
131 ± 24 ± 20	11	ASTON 84B	LASS	11 $K^- p \rightarrow \bar{K}^0 2\pi n$
143 ± 34	11	BAUBILLIER 82B	HBC	8.25 $K^- p \rightarrow N K_S^0 \pi \pi$
98 ± 8	11	ASTON 81C	LASS	11 $K^- p \rightarrow K^- \pi^+ n$
140 ± 30	11	ETKIN 80	SPEC	6 $K^- p \rightarrow \bar{K}^0 \pi^+ \pi^- n$
98 ± 5	11	ESTABROOKS 78	ASPK	13 $K^\pm p \rightarrow \rho K \pi$

• • • We do not use the following data for averages, fits, limits, etc. • • •

113.7 ± 9.2	1786 ± 127	12	AUBERT 07AK BABR	10.6 $e^+ e^- \rightarrow K^{*0} K^\pm \pi^\mp \gamma$
125 ± 29	300	8	HENDRICK 76 DBC	8.25 $K^+ N \rightarrow K^+ \pi N$
116 ± 18	800	8	MCCUBBIN 75 HBC	3.6 $K^- p \rightarrow K^- \pi^+ n$
61 ± 14	13	LINGLIN 73	HBC	2-13 $K^+ p \rightarrow K^+ \pi^- X$
116.6 ± 10.3 / -15.5	1800		AGUILAR... 71B HBC	3.9, 4.6 $K^- p$
144 ± 24.0	600	8	CORDS 71 DBC	9 $K^+ n \rightarrow K^+ \pi^- p$
101 ± 10	2200		DAVIS 69 HBC	12 $K^+ p \rightarrow K^+ \pi^- \pi^+ p$

WEIGHTED AVERAGE
109±5 (Error scaled by 1.9)



8 Errors enlarged by us to $4\Gamma/\sqrt{N}$; see the note with the $K^*(892)$ mass.

9 Number of events in peak re-evaluated by us.

10 From a partial wave amplitude analysis.

11 From phase shift or partial-wave analysis.

12 Systematic errors not estimated.

13 From pole extrapolation, using world $K^+ p$ data summary tape.

$K_2^*(1430)$ DECAY MODES

Mode	Fraction (Γ_i/Γ)	Scale factor / Confidence level
Γ_1 $K\pi$	(49.9 ± 1.2) %	
Γ_2 $K^*(892)\pi$	(24.7 ± 1.5) %	
Γ_3 $K^*(892)\pi\pi$	(13.4 ± 2.2) %	
Γ_4 $K\rho$	(8.7 ± 0.8) %	S=1.2
Γ_5 $K\omega$	(2.9 ± 0.8) %	
Γ_6 $K^+\gamma$	(2.4 ± 0.5) × 10 ⁻³	S=1.1
Γ_7 $K\eta$	(1.5 ± 3.4 / -1.0) × 10 ⁻³	S=1.3
Γ_8 $K\omega\pi$	< 7.2 × 10 ⁻⁴	CL=95%
Γ_9 $K^0\gamma$	< 9 × 10 ⁻⁴	CL=90%

CONSTRAINED FIT INFORMATION

An overall fit to the total width, a partial width, and 10 branching ratios uses 32 measurements and one constraint to determine 8 parameters. The overall fit has a $\chi^2 = 21.1$ for 25 degrees of freedom.

The following off-diagonal array elements are the correlation coefficients $\langle \delta p_i \delta p_j \rangle / (\delta p_i \delta p_j)$, in percent, from the fit to parameters p_i , including the branching fractions, $x_i \equiv \Gamma_i/\Gamma_{\text{total}}$. The fit constrains the x_i whose labels appear in this array to sum to one.

x_2	-9						
x_3	-40	-73					
x_4	-8	36	-52				
x_5	-11	-3	-26	-7			
x_6	-1	-1	-1	-1	0		
x_7	-4	-7	-5	-5	-2	0	
Γ	0	0	0	0	0	-10	0
	x_1	x_2	x_3	x_4	x_5	x_6	x_7

Meson Particle Listings

$K_2^*(1430)$

Mode	Rate (MeV)	Scale factor
Γ_1 $K\pi$	49.9 ± 1.6	
Γ_2 $K^*(892)\pi$	24.7 ± 1.6	
Γ_3 $K^*(892)\pi\pi$	13.5 ± 2.3	
Γ_4 $K\rho$	8.7 ± 0.8	1.2
Γ_5 $K\omega$	2.9 ± 0.8	
Γ_6 $K^+\gamma$	0.24 ± 0.05	1.1
Γ_7 $K\eta$	$0.15^{+0.34}_{-0.10}$	1.3

$K_2^*(1430)$ PARTIAL WIDTHS

$\Gamma(K^+\gamma)$						Γ_6
VALUE (keV)	DOCUMENT ID	TECN	CHG	COMMENT		
241 ± 50 OUR FIT	Error includes scale factor of 1.1.					
240 ± 45	CIHANGIR	82	SPEC	+	$200 K^+ Z \rightarrow Z K^+ \pi^0, Z K_S^0 \pi^+$	

$\Gamma(K^0\gamma)$						Γ_9
VALUE (keV)	CL%	DOCUMENT ID	TECN	CHG	COMMENT	
< 5.4	90	ALAVI-HARATI02B	KTEV		$K^+ A \rightarrow K^* + A$	
••• We do not use the following data for averages, fits, limits, etc. •••						
< 84	90	CARLSMITH	87	SPEC	0	$60\text{--}200 K_L^0 A \rightarrow K_S^0 \pi^0 A$

$K_2^*(1430)$ BRANCHING RATIOS

$\Gamma(K\pi)/\Gamma_{\text{total}}$						Γ_1/Γ
VALUE	DOCUMENT ID	TECN	CHG	COMMENT		
0.499 ± 0.012 OUR FIT						
0.488 ± 0.014 OUR AVERAGE						
$0.485 \pm 0.006 \pm 0.020$	¹⁴ ASTON	88	LASS	0	$11 K^- p \rightarrow K^- \pi^+ n$	
0.49 ± 0.02	¹⁴ ESTABROOKS	78	ASPK	\pm	$13 K^\pm p \rightarrow p K \pi$	

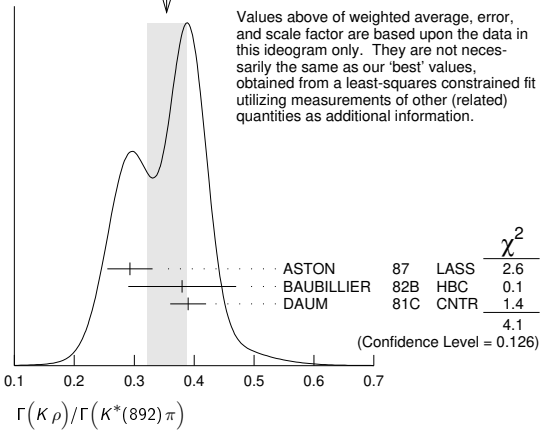
$\Gamma(K^*(892)\pi)/\Gamma(K\pi)$						Γ_2/Γ_1
VALUE	DOCUMENT ID	TECN	CHG	COMMENT		
0.496 ± 0.034 OUR FIT						
0.47 ± 0.04 OUR AVERAGE						
0.44 ± 0.09	ASTON	84B	LASS	0	$11 K^- p \rightarrow \bar{K}^0 2\pi n$	
0.62 ± 0.19	LAUSCHER	75	HBC	0	$10,16 K^- p \rightarrow K^- \pi^+ n$	
0.54 ± 0.16	DEHM	74	DBC	0	$4.6 K^+ N$	
0.47 ± 0.08	AGUILAR...	71B	HBC		$3.9, 4.6 K^- p$	
0.47 ± 0.10	BASSANO	67	HBC	-0	$4.6, 5.0 K^- p$	
0.45 ± 0.13	BADIER	65c	HBC	-	$3 K^- p$	

$\Gamma(K\omega)/\Gamma(K\pi)$						Γ_5/Γ_1
VALUE	DOCUMENT ID	TECN	CHG	COMMENT		
0.059 ± 0.017 OUR FIT						
0.070 ± 0.035 OUR AVERAGE						
0.05 ± 0.04	AGUILAR...	71B	HBC		$3.9, 4.6 K^- p$	
0.13 ± 0.07	BASSOMPIE...	69	HBC	0	$5 K^+ p$	

$\Gamma(K\rho)/\Gamma(K\pi)$						Γ_4/Γ_1
VALUE	DOCUMENT ID	TECN	CHG	COMMENT		
0.174 ± 0.017 OUR FIT	Error includes scale factor of 1.2.					
$0.150^{+0.029}_{-0.017}$ OUR AVERAGE						
0.18 ± 0.05	ASTON	84B	LASS	0	$11 K^- p \rightarrow \bar{K}^0 2\pi n$	
$0.02^{+0.10}_{-0.02}$	DEHM	74	DBC	0	$4.6 K^+ N$	
0.16 ± 0.05	AGUILAR...	71B	HBC		$3.9, 4.6 K^- p$	
0.14 ± 0.10	BASSANO	67	HBC	-0	$4.6, 5.0 K^- p$	
0.14 ± 0.07	BADIER	65c	HBC	-	$3 K^- p$	

$\Gamma(K\rho)/\Gamma(K^*(892)\pi)$						Γ_4/Γ_2
VALUE	DOCUMENT ID	TECN	CHG	COMMENT		
0.350 ± 0.031 OUR FIT	Error includes scale factor of 1.4.					
0.354 ± 0.033 OUR AVERAGE	Error includes scale factor of 1.4. See the ideogram below.					
$0.293 \pm 0.032 \pm 0.020$	ASTON	87	LASS	0	$11 K^- p \rightarrow \bar{K}^0 \pi^+ \pi^- n$	
0.38 ± 0.09	BAUBILLIER	82B	HBC	0	$8.25 K^- p \rightarrow N K_S^0 \pi \pi$	
0.39 ± 0.03	DAUM	81c	CNTR		$63 K^- p \rightarrow K^- 2\pi p$	

WEIGHTED AVERAGE
0.354±0.033 (Error scaled by 1.4)



$\Gamma(K\omega)/\Gamma(K^*(892)\pi)$						Γ_5/Γ_2
VALUE	DOCUMENT ID	TECN	CHG	COMMENT		
0.118 ± 0.034 OUR FIT						
0.10 ± 0.04	FIELD	67	HBC	-	$3.8 K^- p$	

$\Gamma(K\eta)/\Gamma(K^*(892)\pi)$						Γ_7/Γ_2
VALUE	DOCUMENT ID	TECN	CHG	COMMENT		
$0.006^{+0.014}_{-0.004}$ OUR FIT	Error includes scale factor of 1.2.					
0.07 ± 0.04	FIELD	67	HBC	-	$3.8 K^- p$	

$\Gamma(K\eta)/\Gamma(K\pi)$						Γ_7/Γ_1
VALUE	CL%	DOCUMENT ID	TECN	CHG	COMMENT	
$0.0030^{+0.0070}_{-0.0020}$ OUR FIT	Error includes scale factor of 1.3.					
0 ± 0.0056		¹⁵ ASTON	88B	LASS	-	$11 K^- p \rightarrow K^- \eta p$
••• We do not use the following data for averages, fits, limits, etc. •••						
< 0.04	95	AGUILAR...	71B	HBC		$3.9, 4.6 K^- p$
< 0.065		¹⁶ BASSOMPIE...	69	HBC		$5.0 K^+ p$
< 0.02		BISHOP	69	HBC		$3.5 K^+ p$

$\Gamma(K^*(892)\pi\pi)/\Gamma_{\text{total}}$						Γ_3/Γ
VALUE	DOCUMENT ID	TECN	CHG	COMMENT		
0.134 ± 0.022 OUR FIT						
0.12 ± 0.04	¹⁷ GOLDBERG	76	HBC	-	$3 K^- p \rightarrow p \bar{K}^0 \pi \pi$	

$\Gamma(K^*(892)\pi\pi)/\Gamma(K\pi)$						Γ_3/Γ_1
VALUE	DOCUMENT ID	TECN	CHG	COMMENT		
0.27 ± 0.05 OUR FIT						
0.21 ± 0.08	^{16,17} JONGEJANS	78	HBC	-	$4 K^- p \rightarrow p \bar{K}^0 \pi \pi$	

$\Gamma(K\omega\pi)/\Gamma_{\text{total}}$						Γ_8/Γ
VALUE (units 10^{-3})	CL%	EVTS	DOCUMENT ID	TECN	COMMENT	
< 0.72	95	0	JONGEJANS	78	HBC	$4 K^- p \rightarrow p \bar{K}^0 4\pi$

¹⁴ From phase shift analysis.
¹⁵ ASTON 88B quote < 0.0092 at CL=95%. We convert this to a central value and 1 sigma error in order to be able to use it in our constrained fit.
¹⁶ Restated by us.
¹⁷ Assuming $\pi\pi$ system has isospin 1, which is supported by the data.

$K_2^*(1430)$ REFERENCES

ABLIKIM	19AQ	PR D100 032004	M. Ablikim et al.	(BESIII Collab.)
AUBERT	07AK	PR D76 012008	B. Aubert et al.	(BABAR Collab.)
ALAVI-HARATI	02B	PRL 89 072001	A. Alavi-Harati et al.	(FNAL KTeV Collab.)
BIRD	89	SLAC-332	P.F. Bird	(SLAC)
ASTON	88	NP B296 493	D. Aston et al.	(SLAC, NAGO, CINC, INUS)
ASTON	88B	PL B201 169	D. Aston et al.	(SLAC, NAGO, CINC, INUS)
ASTON	87	NP B292 693	D. Aston et al.	(SLAC, NAGO, CINC, INUS)
CARLSMITH	87	PR D36 3502	D. Carlsmith et al.	(EFT, SAFL)
ASTON	84B	NP B247 261	D. Aston et al.	(SLAC, CARL, OTTA)
BAUBILLIER	84B	ZPHY C26 37	M. Baubillier et al.	(BIRM, CERN, GLAS+)
BAUBILLIER	82B	NP B202 21	M. Baubillier et al.	(BIRM, CERN, GLAS+)
CIHANGIR	82	PL 117B 123	S. Chhangir et al.	(FNAL, MINN, ROCH)
CLELAND	82	NP B208 189	W.E. Cleland et al.	(DURH, GEVA, LAUS+)
ASTON	81C	PL 106B 235	D. Aston et al.	(SLAC, CARL, OTTA) JP
DAUM	81C	NP B187 1	C. Daum et al.	(AMST, CERN, CRAC, MPIM+)
TOAFF	81	PR D23 1500	S. Toaff et al.	(ANL, KANS)
ETKIN	80	PR D22 42	A. Etkin et al.	(BNL, CUNY) JP
ESTABROOKS	78	NP B133 490	P.G. Estabrooks et al.	(MCGI, CARL, DURH+)
Also		PR D17 658	P.G. Estabrooks et al.	(MCGI, CARL, DURH+)
JONGEJANS	78	NP B139 383	R. Jongejans et al.	(ZEEM, CERN, NUM+)
MARTIN	78	NP B134 392	A.D. Martin et al.	(DURH, GEVA)
BOWLER	77	NP B126 31	M.G. Bowler et al.	(OXF)
GOLDBERG	76	LCN 17 253	J. Goldberg	(HAIF)

See key on page 999

Meson Particle Listings

$K_2^*(1430)$, $K(1460)$, $K_2(1580)$, $K(1630)$, $K_1(1650)$

HENDRICK	76	NP B112 189	K. Hendrickx et al.	(MONS, SACL, PARIS+)
LAUSCHER	75	NP B86 189	P. Lauscher et al.	(ABCLV Collab.) JP
MCCUBBIN	75	NP B86 13	N.A. McCubbin, L. Lyons	(OXF)
DEHM	74	NP B75 47	G. Dehm et al.	(MPIM, BRUX, MONS, CERN)
LINGLIN	73	NP B55 408	D. Linglin	(CERN)
AGUILAR...	71B	PR D4 2583	M. Aguilar-Benitez, R.L. Eisner, J.B. Kinson	(BNL)
BARNHAM	71C	NP B28 171	K.W.J. Barnham et al.	(BIRM, GLAS)
CORDS	71	PR D4 1974	D. Cords et al.	(PURD, UCD, IUPU)
BASSOMPIE...	69	NP B13 189	G. Bassompierre et al.	(CERN, BRUX) JP
BISHOP	69	NP B9 403	J.M. Bishop et al.	(WISC)
CRENNELL	69D	PRL 22 487	D.J. Crennell et al.	(BNL)
DAVIS	69	PRL 23 1071	P.J. Davis et al.	(LRL)
LIND	69	NP B14 1	V.G. Lind et al.	(LRL) JP
SCHWEING...	68	PR 166 1317	F. Schweingruber et al.	(ANL, NWES)
Also		Thesis	F.L. Schweingruber	(NWES, NWES)
BASSANO	67	PRL 19 968	D. Bassano et al.	(BNL, SYRA)
FIELD	67	PL 24B 638	J.H. Field et al.	(UCSD)
BADIER	65C	PL 19 612	J. Badier et al.	(EPOL, SACL, AMST)

$K(1460)$

$I(J^P) = \frac{1}{2}(0^-)$

OMITTED FROM SUMMARY TABLE
Observed in $K\pi\pi$ partial-wave analysis.

$K(1460)$ MASS

VALUE (MeV)	EVTS	DOCUMENT ID	TECN	CHG	COMMENT
••• We do not use the following data for averages, fits, limits, etc. •••					
1482.40 ± 3.58 ± 15.22	894k	AAIJ	18A1	LHCB	$D^0 \rightarrow K\bar{\pi} 2\pi^\pm \pi^\mp$
~ 1460	63	DAUM	81c	CNTR	$K^- p \rightarrow K^- 2\pi p$
~ 1400	13	¹ BRANDENB...	76B	ASPK	$K^\pm p \rightarrow K^\pm 2\pi p$
¹ Coupled mainly to $K f_0(1370)$. Decay into $K^*(892)\pi$ seen.					

$K(1460)$ WIDTH

VALUE (MeV)	EVTS	DOCUMENT ID	TECN	CHG	COMMENT
••• We do not use the following data for averages, fits, limits, etc. •••					
335.60 ± 6.20 ± 8.65	894k	AAIJ	18A1	LHCB	$D^0 \rightarrow K\bar{\pi} 2\pi^\pm \pi^\mp$
~ 260	63	DAUM	81c	CNTR	$K^- p \rightarrow K^- 2\pi p$
~ 250	15	¹ BRANDENB...	76B	ASPK	$K^\pm p \rightarrow K^\pm 2\pi p$
¹ Coupled mainly to $K f_0(1370)$. Decay into $K^*(892)\pi$ seen.					

$K(1460)$ DECAY MODES

Mode	Fraction (Γ_i/Γ)
Γ_1 $K^*(892)\pi$	seen
Γ_2 $K\rho$	seen
Γ_3 $K_0^0(1430)\pi$	seen

$K(1460)$ PARTIAL WIDTHS

$\Gamma(K^*(892)\pi)$	Γ_1		
VALUE (MeV)	DOCUMENT ID	TECN	COMMENT
••• We do not use the following data for averages, fits, limits, etc. •••			
~ 109	DAUM	81c	CNTR 63 $K^- p \rightarrow K^- 2\pi p$
$\Gamma(K\rho)$	Γ_2		
VALUE (MeV)	DOCUMENT ID	TECN	COMMENT
••• We do not use the following data for averages, fits, limits, etc. •••			
~ 34	DAUM	81c	CNTR 63 $K^- p \rightarrow K^- 2\pi p$
$\Gamma(K_0^0(1430)\pi)$	Γ_3		
VALUE (MeV)	DOCUMENT ID	TECN	COMMENT
••• We do not use the following data for averages, fits, limits, etc. •••			
~ 117	DAUM	81c	CNTR 63 $K^- p \rightarrow K^- 2\pi p$

$K(1460)$ REFERENCES

AAIJ	18A1	EPJ C78 443	R. Aaij et al.	(LHCb Collab.)
DAUM	81C	NP B187 1	C. Daum et al.	(AMST, CERN, CRAC, MPIM+)
BRANDENB...	76B	PRL 36 1239	G.W. Brandenburg et al.	(SLAC) JP

$K_2(1580)$

$I(J^P) = \frac{1}{2}(2^-)$

OMITTED FROM SUMMARY TABLE
Seen in partial-wave analysis of the $K^- \pi^+ \pi^-$ system. Needs confirmation.

$K_2(1580)$ MASS

VALUE (MeV)	DOCUMENT ID	CHG	COMMENT
••• We do not use the following data for averages, fits, limits, etc. •••			
~ 1580	OTTER	79	- 10,14,16 $K^- p$

$K_2(1580)$ WIDTH

VALUE (MeV)	DOCUMENT ID	CHG	COMMENT
••• We do not use the following data for averages, fits, limits, etc. •••			
~ 110	OTTER	79	- 10,14,16 $K^- p$

$K_2(1580)$ DECAY MODES

Mode	Fraction (Γ_i/Γ)
Γ_1 $K^*(892)\pi$	seen
Γ_2 $K_2^*(1430)\pi$	possibly seen

$K_2(1580)$ BRANCHING RATIOS

$\Gamma(K^*(892)\pi)/\Gamma_{total}$	Γ_1/Γ			
VALUE	DOCUMENT ID	TECN	CHG	COMMENT
seen	OTTER	79	HBC	- 10,14,16 $K^- p$
••• We do not use the following data for averages, fits, limits, etc. •••				
possibly seen	GULER	11	BELL	$B^+ \rightarrow J/\psi K^+ \pi^+ \pi^-$

$\Gamma(K_2^*(1430)\pi)/\Gamma_{total}$	Γ_2/Γ			
VALUE	DOCUMENT ID	TECN	CHG	COMMENT
possibly seen	OTTER	79	HBC	- 10,14,16 $K^- p$

$K_2(1580)$ REFERENCES

GULER	11	PR D83 032005	H. Guler et al.	(BELLE Collab.)
OTTER	79	NP B147 1	G. Otter et al.	(AACH3, BERL, CERN, LOIC+) JP

$K(1630)$

$I(J^P) = \frac{1}{2}(?^-)$

OMITTED FROM SUMMARY TABLE
Seen as a narrow peak, compatible with the experimental resolution, in the invariant mass of the $K_S^0 \pi^+ \pi^-$ system produced in $\pi^- p$ interactions at high momentum transfers.

$K(1630)$ MASS

VALUE (MeV)	EVTS	DOCUMENT ID	TECN	COMMENT
1629 ± 7	~ 75	KARNAUKHOV98	BC	16.0 $\pi^- p \rightarrow (K_S^0 \pi^+ \pi^-) X^+ \pi^- X^0$

$K(1630)$ WIDTH

VALUE (MeV)	EVTS	DOCUMENT ID	TECN	COMMENT
16 ± ¹⁹ / ₁₆	~ 75	¹ KARNAUKHOV98	BC	16.0 $\pi^- p \rightarrow (K_S^0 \pi^+ \pi^-) X^+ \pi^- X^0$
¹ Compatible with an experimental resolution of 14 ± 1 MeV.				

$K(1630)$ DECAY MODES

Mode
Γ_1 $K_S^0 \pi^+ \pi^-$

$K(1630)$ REFERENCES

KARNAUKHOV 98	PAN 61 203	V.M. Karnaukhov, C. Coca, V.I. Moroz
Translated from YAF 61 252.		

$K_1(1650)$

$I(J^P) = \frac{1}{2}(1^+)$

OMITTED FROM SUMMARY TABLE
This entry contains various peaks in strange meson systems ($K^+ \phi$, $K\pi\pi$) reported in partial-wave analysis in the 1600–1900 mass region.

$K_1(1650)$ MASS

VALUE (MeV)	EVTS	DOCUMENT ID	TECN	CHG	COMMENT
1672 ± 50 OUR AVERAGE					Error includes scale factor of 1.1.
1793 ± 59 ± ¹⁵³ / ₁₀₁	4289	¹ AAIJ	17c	LHCB	$B^+ \rightarrow J/\psi \phi K^+$
1650 ± 50		FRAME	86	OMEG +	13 $K^+ p \rightarrow \phi K^+ p$
••• We do not use the following data for averages, fits, limits, etc. •••					
~ 1840		ARMSTRONG	83	OMEG -	18.5 $K^- p \rightarrow 3K p$
~ 1800		DAUM	81c	CNTR -	63 $K^- p \rightarrow K^- 2\pi p$
¹ From an amplitude analysis of the decay $B^+ \rightarrow J/\psi \phi K^+$ with a significance of 7.6 σ .					

Meson Particle Listings

$K_1(1650)$, $K^*(1680)$, $K_2(1770)$

$K_1(1650)$ WIDTH

VALUE (MeV)	EVTS	DOCUMENT ID	TECN	CHG	COMMENT
158 ± 50 OUR AVERAGE					
365 ± 157 ⁺¹³⁸ ₋₂₁₅	4289	² AAIJ	17c	LHCB	$B^+ \rightarrow J/\psi \phi K^+$
150 ± 50		FRAME	86	OMEG +	13 $K^+ p \rightarrow \phi K^+ p$
• • • We do not use the following data for averages, fits, limits, etc. • • •					
~ 250		DAUM	81c	CNTR -	63 $K^- p \rightarrow K^- 2\pi p$
² From an amplitude analysis of the decay $B^+ \rightarrow J/\psi \phi K^+$ with a significance of 7.6 σ .					

$K_1(1650)$ DECAY MODES

Mode	Fraction (Γ_i/Γ)
Γ_1 $K \pi \pi$	
Γ_2 $K \phi$	

$K_1(1650)$ REFERENCES

AAIJ	17c	PRL 118 022003	R. Aaij et al.	(LHCb Collab.)
Also		PR D95 012002	R. Aaij et al.	(LHCb Collab.)
FRAME	86	NP B276 667	D. Frame et al.	(GLAS)
ARMSTRONG	83	NP B221 1	T.A. Armstrong et al.	(BARI, BIRM, CERN+)
DAUM	81c	NP B187 1	C. Daum et al.	(AMST, CERN, CRAC, MPIM+)

$K^*(1680)$

$$I(J^P) = \frac{1}{2}(1^-)$$

$K^*(1680)$ MASS

VALUE (MeV)	EVTS	DOCUMENT ID	TECN	CHG	COMMENT
1718 ± 18 OUR AVERAGE					
1722 ± 20 ⁺³³ ₋₁₀₉	4289	¹ AAIJ	17c	LHCB	$B^+ \rightarrow J/\psi \phi K^+$
1677 ± 10 ± 32		ASTON	88	LASS 0	11 $K^- p \rightarrow K^- \pi^+ n$
					$K^- p \rightarrow \bar{K}^0 \pi^+ n$
1735 ± 10 ± 20		ASTON	87	LASS 0	11 $K^- p \rightarrow \bar{K}^0 \pi^+ \pi^- n$
• • • We do not use the following data for averages, fits, limits, etc. • • •					
1678 ± 64		BIRD	89	LASS -	11 $K^- p \rightarrow \bar{K}^0 \pi^- p$
1800 ± 70		ETKIN	80	MPS 0	6 $K^- p \rightarrow \bar{K}^0 \pi^+ \pi^- n$
~ 1650		ESTABROOKS	78	ASPK 0	13 $K^\pm p \rightarrow K^\pm \pi^\pm n$
¹ From an amplitude analysis of the decay $B^+ \rightarrow J/\psi \phi K^+$ with a significance of 8.5 σ .					

$K^*(1680)$ WIDTH

VALUE (MeV)	EVTS	DOCUMENT ID	TECN	CHG	COMMENT
322 ± 110 OUR AVERAGE					
354 ± 75 ⁺¹⁴⁰ ₋₁₈₁	4289	² AAIJ	17c	LHCB	$B^+ \rightarrow J/\psi \phi K^+$
205 ± 16 ± 34		ASTON	88	LASS 0	11 $K^- p \rightarrow K^- \pi^+ n$
					$K^- p \rightarrow \bar{K}^0 \pi^+ \pi^- n$
423 ± 18 ± 30		ASTON	87	LASS 0	11 $K^- p \rightarrow \bar{K}^0 \pi^+ \pi^- n$
• • • We do not use the following data for averages, fits, limits, etc. • • •					
454 ± 270		BIRD	89	LASS -	11 $K^- p \rightarrow \bar{K}^0 \pi^- p$
170 ± 30		ETKIN	80	MPS 0	6 $K^- p \rightarrow \bar{K}^0 \pi^+ \pi^- n$
250 to 300		ESTABROOKS	78	ASPK 0	13 $K^\pm p \rightarrow K^\pm \pi^\pm n$
² From an amplitude analysis of the decay $B^+ \rightarrow J/\psi \phi K^+$ with a significance of 8.5 σ .					

$K^*(1680)$ DECAY MODES

Mode	Fraction (Γ_i/Γ)
Γ_1 $K \pi$	(38.7 ± 2.5) %
Γ_2 $K \rho$	(31.4 ^{+5.0} _{-2.1}) %
Γ_3 $K^*(892)\pi$	(29.9 ^{+2.2} _{-5.0}) %
Γ_4 $K \phi$	seen

CONSTRAINED FIT INFORMATION

An overall fit to 4 branching ratios uses 4 measurements and one constraint to determine 3 parameters. The overall fit has a $\chi^2 = 2.9$ for 2 degrees of freedom.

The following *off-diagonal* array elements are the correlation coefficients $\langle \delta x_i \delta x_j \rangle / (\delta x_i \delta x_j)$, in percent, from the fit to the branching fractions, $x_i \equiv \Gamma_i / \Gamma_{\text{total}}$. The fit constrains the x_i whose labels appear in this array to sum to one.

x_2	-36
x_3	-39 -72
	$x_1 \quad x_2$

$K^*(1680)$ BRANCHING RATIOS

$\Gamma(K\pi)/\Gamma_{\text{total}}$	DOCUMENT ID	TECN	CHG	COMMENT	Γ_1/Γ
0.387 ± 0.026 OUR FIT					
0.388 ± 0.014 ± 0.022	ASTON	88	LASS 0	11 $K^- p \rightarrow K^- \pi^+ n$	

$\Gamma(K\pi)/\Gamma(K^*(892)\pi)$	DOCUMENT ID	TECN	CHG	COMMENT	Γ_1/Γ_3
1.30^{+0.23}_{-0.14} OUR FIT					
2.8 ± 1.1	ASTON	84	LASS 0	11 $K^- p \rightarrow \bar{K}^0 2\pi n$	

$\Gamma(K\rho)/\Gamma(K\pi)$	DOCUMENT ID	TECN	CHG	COMMENT	Γ_2/Γ_1
0.81^{+0.14}_{-0.09} OUR FIT					
1.2 ± 0.4	ASTON	84	LASS 0	11 $K^- p \rightarrow \bar{K}^0 2\pi n$	

$\Gamma(K\rho)/\Gamma(K^*(892)\pi)$	DOCUMENT ID	TECN	CHG	COMMENT	Γ_2/Γ_3
1.05^{+0.27}_{-0.11} OUR FIT					
0.97 ± 0.09^{+0.30}_{-0.10}	ASTON	87	LASS 0	11 $K^- p \rightarrow \bar{K}^0 \pi^+ \pi^- n$	

$\Gamma(K\phi)/\Gamma_{\text{total}}$	EVTS	DOCUMENT ID	TECN	COMMENT	Γ_4/Γ
seen	4289	³ AAIJ	17c	LHCB $B^+ \rightarrow J/\psi \phi K^+$	
³ From an amplitude analysis of the decay $B^+ \rightarrow J/\psi \phi K^+$ with a significance of 8.5 σ .					

$K^*(1680)$ REFERENCES

AAIJ	17c	PRL 118 022003	R. Aaij et al.	(LHCb Collab.)
Also		PR D95 012002	R. Aaij et al.	(LHCb Collab.)
BIRD	89	SLAC-332	P.F. Bird	(SLAC)
ASTON	88	NP B296 493	D. Aston et al.	(SLAC, NAGO, CIN, INUS)
ASTON	87	NP B292 693	D. Aston et al.	(SLAC, NAGO, CIN, INUS)
ASTON	84	PL 149B 258	D. Aston et al.	(SLAC, CARL, OTTA) JP
ETKIN	80	PR D22 42	A. Etkin et al.	(BNL, CUNY) JP
ESTABROOKS	78	NP B133 490	P.G. Estabrooks et al.	(MCGI, CARL, DURH+) JP

$K_2(1770)$

$$I(J^P) = \frac{1}{2}(2^-)$$

See our mini-review in the 2004 edition of this Review, PDG 04.

$K_2(1770)$ MASS

VALUE (MeV)	EVTS	DOCUMENT ID	TECN	CHG	COMMENT
1773 ± 8 OUR AVERAGE					
1777 ± 35 ⁺¹²² ₋₇₇	4289	¹ AAIJ	17c	LHCB	$B^+ \rightarrow J/\psi \phi K^+$
1773 ± 8		² ASTON	93	LASS	11 $K^- p \rightarrow K^- \omega p$
• • • We do not use the following data for averages, fits, limits, etc. • • •					
1743 ± 15		TIKHOMIROV	03	SPEC	40.0 $\frac{\pi^- C}{K_S^0 K_S^0 K_L^0 X}$
1810 ± 20		FRAME	86	OMEG +	13 $K^+ p \rightarrow \phi K^+ p$
~ 1730		ARMSTRONG	83	OMEG -	18.5 $K^- p \rightarrow 3K p$
~ 1780		³ DAUM	81c	CNTR -	63 $K^- p \rightarrow K^- 2\pi p$
1710 ± 15	60	CHUNG	74	HBC -	7.3 $K^- p \rightarrow K^- \omega p$
1767 ± 6		BLIEDEN	72	MMS -	11-16 $K^- p$
1730 ± 20	306	⁴ FIRESTONE	72B	DBC +	12 $K^+ d$
1765 ± 40		⁵ COLLEY	71	HBC +	10 $K^+ p \rightarrow K_2 \pi N$
1740		DENEGRI	71	DBC -	12.6 $K^- d \rightarrow \bar{K} 2\pi d$
1745 ± 20		AGUILAR...	70c	HBC -	4.6 $K^- p$
1780 ± 15		BARTSCH	70c	HBC -	10.1 $K^- p$
1760 ± 15		LUDLAM	70	HBC -	12.6 $K^- p$

- From an amplitude analysis of the decay $B^+ \rightarrow J/\psi \phi K^+$ with a significance of 5.0 σ .
- From a partial wave analysis of the $K^- \omega$ system.
- From a partial wave analysis of the $K^- 2\pi$ system.
- Produced in conjunction with excited deuteron.
- Systematic errors added correspond to spread of different fits.

$K_2(1770)$ WIDTH

VALUE (MeV)	EVTS	DOCUMENT ID	TECN	CHG	COMMENT
186 ± 14 OUR AVERAGE					
217 ± 116 ⁺²²¹ ₋₁₅₄	4289	⁶ AAIJ	17c	LHCB	$B^+ \rightarrow J/\psi \phi K^+$
186 ± 14		⁷ ASTON	93	LASS	11 $K^- p \rightarrow K^- \omega p$

See key on page 999

Meson Particle Listings

$K_2(1770)$, $K_3^*(1780)$

• • • We do not use the following data for averages, fits, limits, etc. • • •

147 ± 70	TIKHOMIROV 03	SPEC	$40.0 \pi^- \bar{C} \rightarrow K_S^0 K_S^0 K_L^0 X$
140 ± 40	FRAME 86	OMEG +	$13 K^+ p \rightarrow \phi K^+ p$
~ 220	ARMSTRONG 83	OMEG -	$18.5 K^- p \rightarrow 3Kp$
~ 210	8 DAUM 81c	CNTR -	$63 K^- p \rightarrow K^- 2\pi p$
110 ± 50	60 CHUNG 74	HBC -	$7.3 K^- p \rightarrow K^- \omega p$
100 ± 26	BLIEDEN 72	MMS -	$11-16 K^- p$
210 ± 30	306 9 FIRESTONE 72B	DBC +	$12 K^+ d$
90 ± 70	10 COLLEY 71	HBC +	$10 K^+ p \rightarrow K 2\pi N$
130	DENEGRI 71	DBC -	$12.6 K^- d \rightarrow \bar{K} 2\pi d$
100 ± 50	AGUILAR... 70c	HBC -	$4.6 K^- p$
138 ± 40	BARTSCH 70c	HBC -	$10.1 K^- p$
50 ± 40	LUDLAM 70	HBC -	$12.6 K^- p$
20			

6 From an amplitude analysis of the decay $B^+ \rightarrow J/\psi \phi K^+$ with a significance of 5.0 σ .
 7 From a partial wave analysis of the $K^- \omega$ system.
 8 From a partial wave analysis of the $K^- 2\pi$ system.
 9 Produced in conjunction with excited deuteron.
 10 Systematic errors added correspond to spread of different fits.

$K_2(1770)$ DECAY MODES

Mode	Fraction (Γ_i/Γ)
Γ_1 $K \pi \pi$	
Γ_2 $K_2^*(1430) \pi$	seen
Γ_3 $K^*(892) \pi$	seen
Γ_4 $K f_2(1270)$	seen
Γ_5 $K f_0(980)$	
Γ_6 $K \phi$	seen
Γ_7 $K \omega$	seen

$K_2(1770)$ BRANCHING RATIOS

$\Gamma(K_2^*(1430)\pi)/\Gamma(K\pi\pi)$ Γ_2/Γ_1
 ($K_2^*(1430) \rightarrow K\pi$)

VALUE	DOCUMENT ID	TECN	CHG	COMMENT
~ 0.03	DAUM 81c	CNTR		$63 K^- p \rightarrow K^- 2\pi p$
~ 1.0	11 FIRESTONE 72B	DBC +		$12 K^+ d$
< 1.0	COLLEY 71	HBC		$10 K^+ p$
0.2 ± 0.2	AGUILAR... 70c	HBC -		$4.6 K^- p$
< 1.0	BARTSCH 70c	HBC -		$10.1 K^- p$
1.0	BARBARO... 69	HBC +		$12.0 K^+ p$

11 Produced in conjunction with excited deuteron.

$\Gamma(K^*(892)\pi)/\Gamma(K\pi\pi)$ Γ_3/Γ_1

VALUE	DOCUMENT ID	TECN	CHG	COMMENT
~ 0.23	DAUM 81c	CNTR		$63 K^- p \rightarrow K^- 2\pi p$

$\Gamma(K f_2(1270))/\Gamma(K\pi\pi)$ Γ_4/Γ_1
 ($f_2(1270) \rightarrow \pi\pi$)

VALUE	DOCUMENT ID	TECN	CHG	COMMENT
~ 0.74	DAUM 81c	CNTR		$63 K^- p \rightarrow K^- 2\pi p$

$\Gamma(K f_0(980))/\Gamma_{total}$ Γ_5/Γ

VALUE	DOCUMENT ID	TECN	CHG	COMMENT
possibly seen	TIKHOMIROV 03	SPEC		$40.0 \pi^- \bar{C} \rightarrow K_S^0 K_S^0 K_L^0 X$

$\Gamma(K\phi)/\Gamma_{total}$ Γ_6/Γ

VALUE	EVTS	DOCUMENT ID	TECN	CHG	COMMENT
seen	4289	12 AAJ 17c	LHCB		$B^+ \rightarrow J/\psi \phi K^+$
seen		ARMSTRONG 83	OMEG -		$18.5 K^- p \rightarrow K^- \phi N$

12 From an amplitude analysis of the decay $B^+ \rightarrow J/\psi \phi K^+$ with a significance of 5.0 σ .

$\Gamma(K\omega)/\Gamma_{total}$ Γ_7/Γ

VALUE	DOCUMENT ID	TECN	CHG	COMMENT
seen	OTTER 81	HBC	\pm	$8.25, 10, 16 K^\pm p$
seen	CHUNG 74	HBC	-	$7.3 K^- p \rightarrow K^- \omega p$

$K_2(1770)$ REFERENCES

AAJ 17c	PRL 118 022003	R. Aaij et al.	(LHCB Collab.)
Also	PR D95 012002	R. Aaij et al.	(LHCB Collab.)
PDG 04	PL B592 1	S. Eidelman et al.	(PDG Collab.)
TIKHOMIROV 03	PAN 66 828	G.D. Tikhomirov et al.	
	Translated from YAF 66 860.		
ASTON 93	PL B308 186	D. Aston et al.	(SLAC, NAGO, CINC, INUS)

FRAME 86	NP B276 667	D. Frame et al.	(GLAS)
ARMSTRONG 83	NP B221 1	T.A. Armstrong et al.	(BARI, BIRM, CERN+)
DAUM 81c	NP B187 1	C. Daum et al.	(AMST, CERN, CRAC, MPIM+)
OTTER 81	NP B181 1	G. Otter	(AACH3, BERL, LOIC, VIEN, BIRM+)
CHUNG 74	PL 51B 413	S.U. Chung et al.	(BNL)
BLIEDEN 72	PL 39B 668	H.R. Blieden et al.	(STON, NEAS)
FIRESTONE 72B	PR D5 505	A. Firestone et al.	(LBL)
COLLEY 71	NP B26 71	D.C. Colley et al.	(BIRM, GLAS)
DENEGRI 71	NP B28 13	D. Denegri et al.	(JHU) JP
AGUILAR... 70c	PRL 25 54	M. Aguilar-Benitez et al.	(BNL)
BARTSCH 70c	PL 33B 186	J. Bartsch et al.	(AACH, BERL, CERN+)
LUDLAM 70	PR D2 1234	T. Ludlam, J. Sandweiss, A.J. Slaughter	(YALE)
BARBARO... 69	PRL 22 1207	A. Barbaro-Galtieri et al.	(LRL)

$K_3^*(1780)$

$I(J^P) = \frac{1}{2}(3^-)$

$K_3^*(1780)$ MASS

VALUE (MeV)	EVTS	DOCUMENT ID	TECN	CHG	COMMENT
1776 ± 7 OUR AVERAGE		Error includes scale factor of 1.1.			
$1781 \pm 8 \pm 4$		1 ASTON 88	LASS	0	$11 K^- p \rightarrow K^- \pi^+ n$
$1740 \pm 14 \pm 15$		1 ASTON 87	LASS	0	$11 K^- p \rightarrow \bar{K}^0 \pi^+ \pi^- n$
1779 ± 11		2 BALDI 76	SPEC +		$10 K^+ p \rightarrow K^0 \pi^+ p$
1776 ± 26		3 BRANDENB... 76D	ASPK	0	$13 K^\pm p \rightarrow K^\pm \pi^\mp N$

• • • We do not use the following data for averages, fits, limits, etc. • • •

$1720 \pm 10 \pm 15$	6111	4 BIRD 89	LASS	-	$11 K^- p \rightarrow \bar{K}^0 \pi^- p$
1749 ± 10		ASTON 88B	LASS	-	$11 K^- p \rightarrow K^- \eta p$
1780 ± 9	300	BAUBILLIER 84B	HBC	-	$8.25 K^- p \rightarrow \bar{K}^0 \pi^- p$
1790 ± 15		BAUBILLIER 82B	HBC	0	$8.25 K^- p \rightarrow K_S^0 2\pi N$
1784 ± 9	2060	CLELAND 82	SPEC	\pm	$50 K^+ p \rightarrow K_S^0 \pi^\pm p$
1786 ± 15		5 ASTON 81D	LASS	0	$11 K^- p \rightarrow K^- \pi^+ n$
1762 ± 9	190	TOAFF 81	HBC	-	$6.5 K^- p \rightarrow \bar{K}^0 \pi^- p$
1850 ± 50		ETKIN 80	MPS	0	$6 K^- p \rightarrow \bar{K}^0 \pi^+ \pi^-$
1812 ± 28		BEUSCH 78	OMEG		$10 K^- p \rightarrow \bar{K}^0 \pi^+ \pi^-$
1786 ± 8		CHUNG 78	MPS	0	$6 K^- p \rightarrow \bar{K}^0 \pi^+ \pi^- n$

1 From energy-independent partial-wave analysis.
 2 From a fit to Y_6^2 moment. $J^P = 3^-$ found.
 3 Confirmed by phase shift analysis of ESTABROOKS 78, yields $J^P = 3^-$.
 4 From a partial wave amplitude analysis.
 5 From a fit to the Y_6^0 moment.

$K_3^*(1780)$ WIDTH

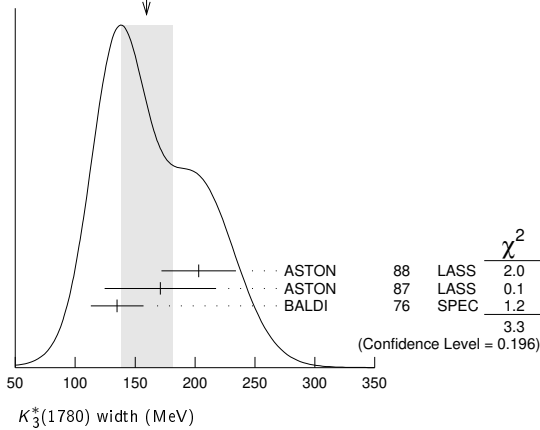
VALUE (MeV)	EVTS	DOCUMENT ID	TECN	CHG	COMMENT
159 ± 21 OUR AVERAGE		Error includes scale factor of 1.3. See the ideogram below.			
$203 \pm 30 \pm 8$		6 ASTON 88	LASS	0	$11 K^- p \rightarrow K^- \pi^+ n$
$171 \pm 42 \pm 20$		6 ASTON 87	LASS	0	$11 K^- p \rightarrow \bar{K}^0 \pi^+ \pi^- n$
135 ± 22		7 BALDI 76	SPEC +		$10 K^+ p \rightarrow K^0 \pi^+ p$
$187 \pm 31 \pm 20$	6111	8 BIRD 89	LASS	-	$11 K^- p \rightarrow \bar{K}^0 \pi^- p$
$193 \pm 51 \pm 37$		ASTON 88B	LASS	-	$11 K^- p \rightarrow K^- \eta p$
99 ± 30	300	BAUBILLIER 84B	HBC	-	$8.25 K^- p \rightarrow \bar{K}^0 \pi^- p$
~ 130		BAUBILLIER 82B	HBC	0	$8.25 K^- p \rightarrow K_S^0 2\pi N$
191 ± 24	2060	CLELAND 82	SPEC	\pm	$50 K^+ p \rightarrow K_S^0 \pi^\pm p$
225 ± 60		9 ASTON 81D	LASS	0	$11 K^- p \rightarrow K^- \pi^+ n$
~ 80	190	TOAFF 81	HBC	-	$6.5 K^- p \rightarrow \bar{K}^0 \pi^- p$
240 ± 50		ETKIN 80	MPS	0	$6 K^- p \rightarrow \bar{K}^0 \pi^+ \pi^-$
181 ± 44		10 BEUSCH 78	OMEG		$10 K^- p \rightarrow \bar{K}^0 \pi^+ \pi^-$
96 ± 31		CHUNG 78	MPS	0	$6 K^- p \rightarrow \bar{K}^0 \pi^+ \pi^- n$
270 ± 70		11 BRANDENB... 76D	ASPK	0	$13 K^\pm p \rightarrow K^\pm \pi^\mp N$

6 From energy-independent partial-wave analysis.
 7 From a fit to Y_6^2 moment. $J^P = 3^-$ found.
 8 From a partial wave amplitude analysis.
 9 From a fit to Y_6^0 moment.
 10 Errors enlarged by us to $4\Gamma/\sqrt{N}$; see the note with the $K^*(892)$ mass.
 11 ESTABROOKS 78 find that BRANDENBURG 76D data are consistent with 175 MeV width. Not averaged.

Meson Particle Listings

$K_3^*(1780)$, $K_2(1820)$

WEIGHTED AVERAGE
159±21 (Error scaled by 1.3)



$K_3^*(1780)$ REFERENCES

BIRD	89	SLAC-332	P.F. Bird	(SLAC)
ASTON	88	NP B296 493	D. Aston <i>et al.</i>	(SLAC, NAGO, CINC, INUS)
ASTON	88B	PL B201 169	D. Aston <i>et al.</i>	(SLAC, NAGO, CINC, INUS) JP
ASTON	87	NP B292 693	D. Aston <i>et al.</i>	(SLAC, NAGO, CINC, INUS)
ASTON	84B	NP B247 261	D. Aston <i>et al.</i>	(SLAC, CARL, OTTA)
BAUBILLIER	84B	ZPHY C26 37	M. Baubillier <i>et al.</i>	(BIRM, CERN, GLAS+)
BAUBILLIER	82B	NP B202 21	M. Baubillier <i>et al.</i>	(BIRM, CERN, GLAS+)
CLELAND	82	NP B208 189	W.E. Cleland <i>et al.</i>	(DURH, GEVA, LAUS+)
ASTON	81D	PL 99B 502	D. Aston <i>et al.</i>	(SLAC, CARL, OTTA) JP
TOAFF	81	PR D23 1500	S. Toaff <i>et al.</i>	(ANL, KANS)
ETKIN	80	PR D22 42	A. Etkin <i>et al.</i>	(BNL, CUNY) JP
BEUSCH	78	PL 74B 282	W. Beusch <i>et al.</i>	(CERN, AACH3, ETH) JP
CHUNG	78	PRL 40 355	S.U. Chung <i>et al.</i>	(BNL, BRAN, CUNY+) JP
ESTABROOKS	78	NP B133 490	P.G. Estabrooks <i>et al.</i>	(MCGI, CARL, DURH+) JP
Also		PR D17 658	P.G. Estabrooks <i>et al.</i>	(MCGI, CARL, DURH+)
BALDI	76	PL 63B 344	R. Baldi <i>et al.</i>	(GEVA) JP
BRANDENB...	76D	PL 60B 478	G.W. Brandenburg <i>et al.</i>	(SLAC) JP

$K_2(1820)$

$$I(J^P) = \frac{1}{2}(2^-)$$

See our mini-review in the 2004 edition of this *Review* (PDG 04) under $K_2(1770)$.

$K_2(1820)$ MASS

VALUE (MeV)	EVTS	DOCUMENT ID	TECN	COMMENT
1819±12 OUR AVERAGE				
1853±27 ⁺¹⁸ ₋₃₅	4289	¹ AAIJ	17c	LHCB $B^+ \rightarrow J/\psi \phi K^+$
1816±13		² ASTON	93	LASS $11K^-p \rightarrow K^- \omega p$
••• We do not use the following data for averages, fits, limits, etc. •••				
~ 1840		³ DAUM	81c	CNTR $63K^-p \rightarrow K^- 2\pi p$
¹ From an amplitude analysis of the decay $B^+ \rightarrow J/\psi \phi K^+$ with a significance of 3.0 σ .				
² From a partial wave analysis of the $K^- \omega$ system.				
³ From a partial wave analysis of the $K^- 2\pi$ system.				

$K_2(1820)$ WIDTH

VALUE (MeV)	EVTS	DOCUMENT ID	TECN	COMMENT
264±34 OUR AVERAGE				
167±58 ⁺⁸² ₋₇₂	4289	⁴ AAIJ	17c	LHCB $B^+ \rightarrow J/\psi \phi K^+$
276±35		⁵ ASTON	93	LASS $11K^-p \rightarrow K^- \omega p$
••• We do not use the following data for averages, fits, limits, etc. •••				
~ 230		⁶ DAUM	81c	CNTR $63K^-p \rightarrow K^- 2\pi p$
⁴ From an amplitude analysis of the decay $B^+ \rightarrow J/\psi \phi K^+$ with a significance of 3.0 σ .				
⁵ From a partial wave analysis of the $K^- \omega$ system.				
⁶ From a partial wave analysis of the $K^- 2\pi$ system.				

$K_2(1820)$ DECAY MODES

Mode	Fraction (Γ_i/Γ)
Γ_1 $K \pi \pi$	seen
Γ_2 $K_2^*(1430) \pi$	seen
Γ_3 $K^*(892) \pi$	seen
Γ_4 $K f_2(1270)$	seen
Γ_5 $K \omega$	seen
Γ_6 $K \phi$	seen

$K_2(1820)$ BRANCHING RATIOS

$\Gamma(K_2^*(1430)\pi)/\Gamma(K\pi\pi)$	Γ_2/Γ_1			
VALUE	DOCUMENT ID	TECN	COMMENT	
••• We do not use the following data for averages, fits, limits, etc. •••				
~ 0.77	DAUM	81c	CNTR $63K^-p \rightarrow \bar{K} 2\pi p$	
$\Gamma(K^*(892)\pi)/\Gamma(K\pi\pi)$	Γ_3/Γ_1			
VALUE	DOCUMENT ID	TECN	COMMENT	
••• We do not use the following data for averages, fits, limits, etc. •••				
~ 0.05	DAUM	81c	CNTR $63K^-p \rightarrow \bar{K} 2\pi p$	
$\Gamma(K f_2(1270))/\Gamma(K\pi\pi)$	Γ_4/Γ_1			
VALUE	DOCUMENT ID	TECN	COMMENT	
••• We do not use the following data for averages, fits, limits, etc. •••				
~ 0.18	DAUM	81c	CNTR $63K^-p \rightarrow \bar{K} 2\pi p$	
$\Gamma(K\phi)/\Gamma_{total}$	Γ_6/Γ			
VALUE	EVTS	DOCUMENT ID	TECN	COMMENT
seen	4289	⁷ AAIJ	17c	LHCB $B^+ \rightarrow J/\psi \phi K^+$
⁷ From an amplitude analysis of the decay $B^+ \rightarrow J/\psi \phi K^+$ with a significance of 3.0 σ .				

$K_3^*(1780)$ DECAY MODES

Mode	Fraction (Γ_i/Γ)	Confidence level
Γ_1 $K \rho$	(31 ± 9) %	
Γ_2 $K^*(892) \pi$	(20 ± 5) %	
Γ_3 $K \pi$	(18.8 ± 1.0) %	
Γ_4 $K \eta$	(30 ± 13) %	
Γ_5 $K_2^*(1430) \pi$	< 16 %	95%

CONSTRAINED FIT INFORMATION

An overall fit to 3 branching ratios uses 4 measurements and one constraint to determine 4 parameters. The overall fit has a $\chi^2 = 0.0$ for 1 degrees of freedom.

The following *off-diagonal* array elements are the correlation coefficients $\langle \delta x_i \delta x_j \rangle / (\delta x_i \delta x_j)$, in percent, from the fit to the branching fractions, $x_i \equiv \Gamma_i / \Gamma_{total}$. The fit constrains the x_i whose labels appear in this array to sum to one.

x_2	85		
x_3	18	21	
x_4	-98	-94	-27
	x_1	x_2	x_3

$K_3^*(1780)$ BRANCHING RATIOS

$\Gamma(K\rho)/\Gamma(K^*(892)\pi)$	Γ_1/Γ_2				
VALUE	DOCUMENT ID	TECN	CHG	COMMENT	
1.52±0.23 OUR FIT					
1.52±0.21±0.10	ASTON	87	LASS	0	
				11 $K^-p \rightarrow \bar{K}^0 \pi^+ \pi^- n$	
$\Gamma(K^*(892)\pi)/\Gamma(K\pi)$	Γ_2/Γ_3				
VALUE	DOCUMENT ID	TECN	CHG	COMMENT	
1.09±0.26 OUR FIT					
1.09±0.26	ASTON	84B	LASS	0	
				11 $K^-p \rightarrow \bar{K}^0 2\pi n$	
$\Gamma(K\pi)/\Gamma_{total}$	Γ_3/Γ				
VALUE	DOCUMENT ID	TECN	CHG	COMMENT	
0.188±0.010 OUR FIT					
0.188±0.010 OUR AVERAGE					
0.187±0.008±0.008	ASTON	88	LASS	0	
0.19±0.02	ESTABROOKS	78	ASPK	0	
				13 $K^\pm p \rightarrow K \pi N$	
$\Gamma(K\eta)/\Gamma(K\pi)$	Γ_4/Γ_3				
VALUE	DOCUMENT ID	TECN	CHG	COMMENT	
1.6 ± 0.7 OUR FIT					
••• We do not use the following data for averages, fits, limits, etc. •••					
0.41±0.050	¹² BIRD	89	LASS	-	
				11 $K^-p \rightarrow \bar{K}^0 \pi^- p$	
0.50±0.18	ASTON	88B	LASS	-	
				11 $K^-p \rightarrow K^- \eta p$	
¹² This result supersedes ASTON 88B.					
$\Gamma(K_2^*(1430)\pi)/\Gamma(K^*(892)\pi)$	Γ_5/Γ_2				
VALUE	CL%	DOCUMENT ID	TECN	CHG	COMMENT
<0.78	95	ASTON	87	LASS	0
					11 $K^-p \rightarrow \bar{K}^0 \pi^+ \pi^- n$

See key on page 999

Meson Particle Listings

$K_2(1820)$, $K(1830)$, $K_0^*(1950)$, $K_2^*(1980)$

$K_2(1820)$ REFERENCES

AAJ	17C	PRL 118 022003	R. Aaij et al.	(LHCb Collab.)
Also		PR D95 012002	R. Aaij et al.	(LHCb Collab.)
PDG	04	PL B592 1	S. Edelman et al.	(PDG Collab.)
ASTON	93	PL B308 186	D. Aston et al.	(SLAC, NAGO, CIN, INUS)
DAUM	81C	NP B187 1	C. Daum et al.	(AMST, CERN, CRAC, MPIM+)

$K(1830)$

$I(J^P) = \frac{1}{2}(0^-)$

OMITTED FROM SUMMARY TABLE
Seen in partial-wave analysis of $K\phi$ system. Needs confirmation.

$K(1830)$ MASS

VALUE (MeV)	EVTS	DOCUMENT ID	TECN	CHG	COMMENT
$1874 \pm 43 \pm_{-115}^{59}$	4289	¹ AAIJ	17c	LHCB	$B^+ \rightarrow J/\psi\phi K^+$
••• We do not use the following data for averages, fits, limits, etc. •••					
~ 1830		ARMSTRONG 83	OMEG	-	$18.5 K^- p \rightarrow 3Kp$
¹ From an amplitude analysis of the decay $B^+ \rightarrow J/\psi\phi K^+$ with a significance of 3.5 σ .					

$K(1830)$ WIDTH

VALUE (MeV)	EVTS	DOCUMENT ID	TECN	CHG	COMMENT
$168 \pm 90 \pm_{-104}^{280}$	4289	² AAIJ	17c	LHCB	$B^+ \rightarrow J/\psi\phi K^+$
••• We do not use the following data for averages, fits, limits, etc. •••					
~ 250		ARMSTRONG 83	OMEG	-	$18.5 K^- p \rightarrow 3Kp$
² From an amplitude analysis of the decay $B^+ \rightarrow J/\psi\phi K^+$ with a significance of 3.5 σ .					

$K(1830)$ DECAY MODES

Mode	Fraction (Γ_i/Γ)
$\Gamma_1 K\phi$	

$K(1830)$ REFERENCES

AAJ	17C	PRL 118 022003	R. Aaij et al.	(LHCb Collab.)
Also		PR D95 012002	R. Aaij et al.	(LHCb Collab.)
ARMSTRONG	83	NP B221 1	T.A. Armstrong et al.	(BARI, BIRM, CERN+)JP

$K_0^*(1950)$

$I(J^P) = \frac{1}{2}(0^+)$

OMITTED FROM SUMMARY TABLE
Seen in partial-wave analysis of the $K^- \pi^+$ system. Needs confirmation.

$K_0^*(1950)$ MASS

VALUE (MeV)	DOCUMENT ID	TECN	CHG	COMMENT
$1945 \pm 10 \pm 20$	¹ ASTON 88	LASS	0	$11 K^- p \rightarrow K^- \pi^+ n$
••• We do not use the following data for averages, fits, limits, etc. •••				
1917 ± 12	² ZHOU 06	RVUE		$Kp \rightarrow K^- \pi^+ n$
1820 ± 40	³ ANISOVICH 97c	RVUE		$11 K^- p \rightarrow K^- \pi^+ n$
¹ We take the central value of the two solutions and the larger error given.				
² S-matrix pole. Using ASTON 88 and assuming $K_0^*(700)$, $K_0^*(1430)$.				
³ T-matrix pole. Reanalysis of ASTON 88 data.				

$K_0^*(1950)$ WIDTH

VALUE (MeV)	DOCUMENT ID	TECN	CHG	COMMENT
$201 \pm 34 \pm 79$	⁴ ASTON 88	LASS	0	$11 K^- p \rightarrow K^- \pi^+ n$
••• We do not use the following data for averages, fits, limits, etc. •••				
145 ± 38	⁵ ZHOU 06	RVUE		$Kp \rightarrow K^- \pi^+ n$
250 ± 100	⁶ ANISOVICH 97c	RVUE		$11 K^- p \rightarrow K^- \pi^+ n$
⁴ We take the central value of the two solutions and the larger error given.				
⁵ S-matrix pole. Using ASTON 88 and assuming $K_0^*(700)$, $K_0^*(1430)$.				
⁶ T-matrix pole. Reanalysis of ASTON 88 data.				

$K_0^*(1950)$ DECAY MODES

Mode	Fraction (Γ_i/Γ)
$\Gamma_1 K^- \pi^+$	(52±14) %

$K_0^*(1950)$ BRANCHING RATIOS

$\Gamma(K^- \pi^+)/\Gamma_{total}$	DOCUMENT ID	TECN	CHG	COMMENT	Γ_1/Γ
$0.52 \pm 0.08 \pm 0.12$	⁷ ASTON 88	LASS	0	$11 K^- p \rightarrow K^- \pi^+ n$	
••• We do not use the following data for averages, fits, limits, etc. •••					
~ 0.60	⁸ ZHOU 06	RVUE		$Kp \rightarrow K^- \pi^+ n$	
⁷ We take the central value of the two solutions and the larger error given.					
⁸ S-matrix pole. Using ASTON 88 and assuming $K_0^*(700)$, $K_0^*(1430)$.					

$K_0^*(1950)$ REFERENCES

ZHOU	06	NP A775 212	Z.Y. Zhou, H.Q. Zheng	
ANISOVICH	97C	PL B413 137	A.V. Anisovich, A.V. Sarantsev	
ASTON	88	NP B296 493	D. Aston et al.	(SLAC, NAGO, CIN, INUS)

$K_2^*(1980)$

$I(J^P) = \frac{1}{2}(2^+)$

OMITTED FROM SUMMARY TABLE
Needs confirmation.

$K_2^*(1980)$ MASS

VALUE (MeV)	EVTS	DOCUMENT ID	TECN	CHG	COMMENT
1943 ± 50 OUR AVERAGE					Error includes scale factor of 2.2.
$1868 \pm 8 \pm_{-57}^{40}$	183k	ABLIKIM 19AQBES	±		$J/\psi \rightarrow K^+ K^- \pi^0$
$2073 \pm 94 \pm_{-240}^{245}$	4289	¹ AAIJ 17c	LHCB		$B^+ \rightarrow J/\psi\phi K^+$
$1973 \pm 8 \pm 25$		ASTON 87	LASS	0	$11 K^- p \rightarrow \bar{K}^0 \pi^+ \pi^- n$
••• We do not use the following data for averages, fits, limits, etc. •••					
2020 ± 20		TIKHOMIROV 03	SPEC		$40.0 \pi^- C \rightarrow K_S^0 K_S^0 K_L^0 X$
1978 ± 40	241	BIRD 89	LASS	-	$11 K^- p \rightarrow \bar{K}^0 \pi^- p$
¹ From an amplitude analysis of the decay $B^+ \rightarrow J/\psi\phi K^+$ with a significance of 5.4 σ .					

$K_2^*(1980)$ WIDTH

VALUE (MeV)	EVTS	DOCUMENT ID	TECN	CHG	COMMENT
$307 \pm_{-51}^{50}$ OUR AVERAGE					Error includes scale factor of 1.2.
$272 \pm 24 \pm_{-15}^{50}$	183k	ABLIKIM 19AQBES	±		$J/\psi \rightarrow K^+ K^- \pi^0$
$678 \pm 311 \pm_{-559}^{1153}$	4289	² AAIJ 17c	LHCB		$B^+ \rightarrow J/\psi\phi K^+$
$373 \pm 33 \pm 60$		ASTON 87	LASS	0	$11 K^- p \rightarrow \bar{K}^0 \pi^+ \pi^- n$
••• We do not use the following data for averages, fits, limits, etc. •••					
180 ± 70		TIKHOMIROV 03	SPEC		$40.0 \pi^- C \rightarrow K_S^0 K_S^0 K_L^0 X$
398 ± 47	241	BIRD 89	LASS	-	$11 K^- p \rightarrow \bar{K}^0 \pi^- p$
² From an amplitude analysis of the decay $B^+ \rightarrow J/\psi\phi K^+$ with a significance of 5.4 σ .					

$K_2^*(1980)$ DECAY MODES

Mode	Fraction (Γ_i/Γ)
$\Gamma_1 K^*(892)\pi$	possibly seen
$\Gamma_2 K\rho$	possibly seen
$\Gamma_3 K f_2(1270)$	possibly seen
$\Gamma_4 K\phi$	seen

$K_2^*(1980)$ BRANCHING RATIOS

$\Gamma(K^*(892)\pi)/\Gamma_{total}$	DOCUMENT ID	TECN	CHG	COMMENT	Γ_1/Γ
possibly seen	GULER 11	BELL		$B^+ \rightarrow J/\psi K^+ \pi^+ \pi^-$	
$\Gamma(K\rho)/\Gamma_{total}$	DOCUMENT ID	TECN	CHG	COMMENT	Γ_2/Γ
possibly seen	GULER 11	BELL		$B^+ \rightarrow J/\psi K^+ \pi^+ \pi^-$	
$\Gamma(K\rho)/\Gamma(K^*(892)\pi)$	DOCUMENT ID	TECN	CHG	COMMENT	Γ_2/Γ_1
$1.49 \pm 0.24 \pm 0.09$	ASTON 87	LASS	0	$11 K^- p \rightarrow \bar{K}^0 \pi^+ \pi^- n$	
$\Gamma(K f_2(1270))/\Gamma_{total}$	DOCUMENT ID	TECN	CHG	COMMENT	Γ_3/Γ
possibly seen	TIKHOMIROV 03	SPEC		$40.0 \pi^- C \rightarrow K_S^0 K_S^0 K_L^0 X$	
$\Gamma(K\phi)/\Gamma_{total}$	EVTS	DOCUMENT ID	TECN	COMMENT	Γ_4/Γ
seen	4289	³ AAIJ 17c	LHCB	$B^+ \rightarrow J/\psi\phi K^+$	
³ From an amplitude analysis of the decay $B^+ \rightarrow J/\psi\phi K^+$ with a significance of 5.4 σ .					

Meson Particle Listings

 $K_2^*(1980)$, $K_4^*(2045)$, $K_2(2250)$, $K_3(2320)$ $K_2^*(1980)$ REFERENCES

ABLIKIM	19AQ	PR D100 032004	M. Ablikim <i>et al.</i>	(BESIII Collab.)
AAU	17C	PRL 116 022003	R. Aaij <i>et al.</i>	(LHCb Collab.)
Albo		PR D95 012002	R. Aaij <i>et al.</i>	(LHCb Collab.)
GULER	11	PR D83 032005	H. Guler <i>et al.</i>	(BELLE Collab.)
TIKHOMIROV	03	PAN 66 828	G.D. Tikhomirov <i>et al.</i>	(BELLE Collab.)
		Translated from YAF 66 860.		
BIRD	89	SLAC-332	P.F. Bird	(SLAC)
ASTON	87	NP B292 693	D. Aston <i>et al.</i>	(SLAC, NAGO, CINC, INUS)

 $K_4^*(2045)$

$$I(J^P) = \frac{1}{2}(4^+)$$

 $K_4^*(2045)$ MASS

VALUE (MeV)	EVTS	DOCUMENT ID	TECN	CHG	COMMENT
2048\pm 9	8	OUR AVERAGE			Error includes scale factor of 1.1.
2090 \pm 9	11 \pm 29	183k	ABLIKIM	19AQ BES	\pm $J/\psi \rightarrow K^+ K^- \pi^0$
2062 \pm 14	13		¹ ASTON	86 LASS	0 $11 K^- p \rightarrow K^- \pi^+ n$
2039 \pm 10		400	^{2,3} CLELAND	82 SPEC	\pm $50 K^+ p \rightarrow K_S^0 \pi^\pm p$
2070 \pm 100		40	⁴ ASTON	81c LASS	0 $11 K^- p \rightarrow K^- \pi^+ n$
• • • We do not use the following data for averages, fits, limits, etc. • • •					
2079 \pm 7		431	TORRES	86 MPSF	400 pA \rightarrow 4KX
2088 \pm 20		650	BAUBILLIER	82 HBC	- 8.25 $K^- p \rightarrow K_S^0 \pi^- p$
2115 \pm 46		488	CARMONY	77 HBC	0 $9 K^+ d \rightarrow K^+ \pi^+ X$
¹ From a fit to all moments.					
² From a fit to 8 moments.					
³ Number of events evaluated by us.					
⁴ From energy-independent partial-wave analysis.					

 $K_4^*(2045)$ WIDTH

VALUE (MeV)	EVTS	DOCUMENT ID	TECN	CHG	COMMENT
199\pm 27	19	OUR AVERAGE			
201 \pm 19	19 \pm 57	183k	ABLIKIM	19AQ BES	\pm $J/\psi \rightarrow K^+ K^- \pi^0$
221 \pm 48	27		⁵ ASTON	86 LASS	0 $11 K^- p \rightarrow K^- \pi^+ n$
189 \pm 35		400	^{6,7} CLELAND	82 SPEC	\pm $50 K^+ p \rightarrow K_S^0 \pi^\pm p$
• • • We do not use the following data for averages, fits, limits, etc. • • •					
61 \pm 58		431	TORRES	86 MPSF	400 pA \rightarrow 4KX
170 \pm 100		650	BAUBILLIER	82 HBC	- 8.25 $K^- p \rightarrow K_S^0 \pi^- p$
240 \pm 500		100	⁸ ASTON	81c LASS	0 $11 K^- p \rightarrow K^- \pi^+ n$
300 \pm 200			CARMONY	77 HBC	0 $9 K^+ d \rightarrow K^+ \pi^+ X$
⁵ From a fit to all moments.					
⁶ From a fit to 8 moments.					
⁷ Number of events evaluated by us.					
⁸ From energy-independent partial-wave analysis.					

 $K_4^*(2045)$ DECAY MODES

Mode	Fraction (Γ_i/Γ)
Γ_1 $K\pi$	(9.9 \pm 1.2) %
Γ_2 $K^*(892)\pi\pi$	(9 \pm 5) %
Γ_3 $K^*(892)\pi\pi\pi$	(7 \pm 5) %
Γ_4 $\rho K\pi$	(5.7 \pm 3.2) %
Γ_5 $\omega K\pi$	(5.0 \pm 3.0) %
Γ_6 $\phi K\pi$	(2.8 \pm 1.4) %
Γ_7 $\phi K^*(892)$	(1.4 \pm 0.7) %

 $K_4^*(2045)$ BRANCHING RATIOS

$\Gamma(K\pi)/\Gamma_{\text{total}}$	Γ_1/Γ			
0.099\pm0.012				
VALUE	DOCUMENT ID	TECN	CHG	COMMENT
0.099 \pm 0.012	ASTON	88	LASS	0 $11 K^- p \rightarrow K^- \pi^+ n$
$\Gamma(K^*(892)\pi\pi)/\Gamma(K\pi)$	Γ_2/Γ_1			
0.89\pm0.53				
VALUE	DOCUMENT ID	TECN	CHG	COMMENT
0.89 \pm 0.53	BAUBILLIER	82	HBC	- 8.25 $K^- p \rightarrow \rho K_S^0 3\pi$
$\Gamma(K^*(892)\pi\pi\pi)/\Gamma(K\pi)$	Γ_3/Γ_1			
0.75\pm0.49				
VALUE	DOCUMENT ID	TECN	CHG	COMMENT
0.75 \pm 0.49	BAUBILLIER	82	HBC	- 8.25 $K^- p \rightarrow \rho K_S^0 3\pi$
$\Gamma(\rho K\pi)/\Gamma(K\pi)$	Γ_4/Γ_1			
0.58\pm0.32				
VALUE	DOCUMENT ID	TECN	CHG	COMMENT
0.58 \pm 0.32	BAUBILLIER	82	HBC	- 8.25 $K^- p \rightarrow \rho K_S^0 3\pi$

 $\Gamma(\omega K\pi)/\Gamma(K\pi)$

VALUE	DOCUMENT ID	TECN	CHG	COMMENT	Γ_5/Γ_1	
0.50\pm0.30	BAUBILLIER	82	HBC	-	8.25 $K^- p \rightarrow \rho K_S^0 3\pi$	

 $\Gamma(\phi K\pi)/\Gamma_{\text{total}}$

VALUE	DOCUMENT ID	TECN	COMMENT	Γ_6/Γ
0.028\pm0.014	⁹ TORRES	86	MPSF 400 pA \rightarrow 4KX	

 $\Gamma(\phi K^*(892))/\Gamma_{\text{total}}$

VALUE	DOCUMENT ID	TECN	COMMENT	Γ_7/Γ
0.014\pm0.007	⁹ TORRES	86	MPSF 400 pA \rightarrow 4KX	

⁹ Error determination is model dependent. $K_2^*(2045)$ REFERENCES

ABLIKIM	19AQ	PR D100 032004	M. Ablikim <i>et al.</i>	(BESIII Collab.)
ASTON	88	NP B296 493	D. Aston <i>et al.</i>	(SLAC, NAGO, CINC, INUS)
ASTON	86	PL B180 308	D. Aston <i>et al.</i>	(SLAC, NAGO, CINC, INUS)
TORRES	86	PR D34 707	S. Torres <i>et al.</i>	(VPI, ARIZ, FNAL, FSU+)
BAUBILLIER	82	PL 118B 447	M. Baubillier <i>et al.</i>	(BIRM, CERN, GLAS+)
CLELAND	82	NP B208 189	W.E. Cleland <i>et al.</i>	(DURH, GEVA, LAUS+)
ASTON	81C	PL 106B 235	D. Aston <i>et al.</i>	(SLAC, CARL, OTTA)JP
CARMONY	77	PR D16 1251	D.D. Carmony <i>et al.</i>	(PURD, UCD, IUPUI)

 $K_2(2250)$

$$I(J^P) = \frac{1}{2}(2^-)$$

OMITTED FROM SUMMARY TABLE

This entry contains various peaks in strange meson systems reported in the 2150–2260 MeV region, as well as enhancements seen in the antihyperon-nucleon system, either in the mass spectra or in the $J^P = 2^-$ wave.

 $K_2(2250)$ MASS

VALUE (MeV)	EVTS	DOCUMENT ID	TECN	CHG	COMMENT
2247\pm17	OUR AVERAGE				
2200 \pm 40		¹ ARMSTRONG	83c	OMEG	- 18 $K^- p \rightarrow \Lambda \bar{p} X$
2235 \pm 50		¹ BAUBILLIER	81	HBC	- 8 $K^- p \rightarrow \Lambda \bar{p} X$
2260 \pm 20		¹ CLELAND	81	SPEC	\pm 50 $K^+ p \rightarrow \Lambda \bar{p} X$
• • • We do not use the following data for averages, fits, limits, etc. • • •					
2280 \pm 20		TIKHOMIROV	03	SPEC	$40.0 \frac{\pi^- C}{K_S^0 K_S^0 K_L^0} X$
2147 \pm 4		37	CHLIAPNIK...	79	HBC + 32 $K^+ p \rightarrow \Lambda \bar{p} X$
2240 \pm 20		20	LISSAUER	70	HBC 9 $K^+ p$
¹ $J^P = 2^-$ from moments analysis.					

 $K_2(2250)$ WIDTH

VALUE (MeV)	EVTS	DOCUMENT ID	TECN	CHG	COMMENT
180\pm30	OUR AVERAGE				Error includes scale factor of 1.4.
150 \pm 30		² ARMSTRONG	83c	OMEG	- 18 $K^- p \rightarrow \Lambda \bar{p} X$
210 \pm 30		² CLELAND	81	SPEC	\pm 50 $K^+ p \rightarrow \Lambda \bar{p} X$
• • • We do not use the following data for averages, fits, limits, etc. • • •					
180 \pm 60		TIKHOMIROV	03	SPEC	$40.0 \frac{\pi^- C}{K_S^0 K_S^0 K_L^0} X$
\sim 200		² BAUBILLIER	81	HBC	- 8 $K^- p \rightarrow \Lambda \bar{p} X$
\sim 40		37	CHLIAPNIK...	79	HBC + 32 $K^+ p \rightarrow \Lambda \bar{p} X$
80 \pm 20		20	LISSAUER	70	HBC 9 $K^+ p$
² $J^P = 2^-$ from moments analysis.					

 $K_2(2250)$ DECAY MODES

Mode	Fraction (Γ_i/Γ)
Γ_1 $K\pi\pi$	
Γ_2 $K f_2(1270)$	
Γ_3 $K^*(892) f_0(980)$	
Γ_4 $\rho \bar{\Lambda}$	

 $K_2(2250)$ REFERENCES

TIKHOMIROV	03	PAN 66 828	G.D. Tikhomirov <i>et al.</i>	(BESIII Collab.)
ARMSTRONG	83C	NP B227 365	T.A. Armstrong <i>et al.</i>	(BIRM, CERN, GLAS+)
BAUBILLIER	81	NP B183 1	M. Baubillier <i>et al.</i>	(BIRM, CERN, GLAS+)
CLELAND	81	NP B184 1	W.E. Cleland <i>et al.</i>	(PITT, GEVA, LAUS+)
CHLIAPNIK...	79	NP B158 253	P.V. Chliapnikov <i>et al.</i>	(CERN, BELG, MONS)
LISSAUER	70	NP B18 491	D. Lissauer <i>et al.</i>	(LBL)

 $K_3(2320)$

$$I(J^P) = \frac{1}{2}(3^+)$$

OMITTED FROM SUMMARY TABLE

Seen in the $J^P = 3^+$ wave of the antihyperon-nucleon system. Needs confirmation.

See key on page 999

Meson Particle Listings

$K_3(2320)$, $K_5^*(2380)$, $K_4(2500)$, $K(3100)$

$K_3(2320)$ MASS

VALUE (MeV)	DOCUMENT ID	TECN	CHG	COMMENT
2324 ± 24 OUR AVERAGE				
2330 ± 40	¹ ARMSTRONG 83c	OMEG	-	18 $K^- p \rightarrow \Lambda \bar{p} X$
2320 ± 30	¹ CLELAND 81	SPEC	±	50 $K^+ p \rightarrow \Lambda \bar{p} X$
¹ $J^P = 3^+$ from moments analysis.				

$K_3(2320)$ WIDTH

VALUE (MeV)	DOCUMENT ID	TECN	CHG	COMMENT
150 ± 30				
	² ARMSTRONG 83c	OMEG	-	18 $K^- p \rightarrow \Lambda \bar{p} X$
• • • We do not use the following data for averages, fits, limits, etc. • • •				
~ 250	² CLELAND 81	SPEC	±	50 $K^+ p \rightarrow \Lambda \bar{p} X$
² $J^P = 3^+$ from moments analysis.				

$K_3(2320)$ DECAY MODES

Mode	Fraction (Γ_i/Γ)
Γ_1 $\rho \bar{\Lambda}$	(6.1 ± 1.2) %

$K_3(2320)$ REFERENCES

ARMSTRONG 83c	NP B227 365	T.A. Armstrong et al.	(BARI, BIRM, CERN+)
CLELAND 81	NP B184 1	W.E. Cleland et al.	(PITT, GEVA, LAUS+)

$K_5^*(2380)$

$I(J^P) = \frac{1}{2}(5^-)$

OMITTED FROM SUMMARY TABLE
Needs confirmation.

$K_5^*(2380)$ MASS

VALUE (MeV)	DOCUMENT ID	TECN	CHG	COMMENT
2382 ± 14 ± 19				
	¹ ASTON 86	LASS	0	11 $K^- p \rightarrow K^- \pi^+ n$
¹ From a fit to all the moments.				

$K_5^*(2380)$ WIDTH

VALUE (MeV)	DOCUMENT ID	TECN	CHG	COMMENT
178 ± 37 ± 32				
	² ASTON 86	LASS	0	11 $K^- p \rightarrow K^- \pi^+ n$
² From a fit to all the moments.				

$K_5^*(2380)$ DECAY MODES

Mode	Fraction (Γ_i/Γ)
Γ_1 $K \pi$	(6.1 ± 1.2) %

$K_5^*(2380)$ BRANCHING RATIOS

$\Gamma(K \pi)/\Gamma_{total}$	DOCUMENT ID	TECN	CHG	COMMENT	Γ_1/Γ
0.061 ± 0.012	ASTON 88	LASS	0	11 $K^- p \rightarrow K^- \pi^+ n$	

$K_5^*(2380)$ REFERENCES

ASTON 88	NP B296 493	D. Aston et al.	(SLAC, NAGO, CINC, INUS)
ASTON 86	PL B180 308	D. Aston et al.	(SLAC, NAGO, CINC, INUS)

$K_4(2500)$

$I(J^P) = \frac{1}{2}(4^-)$

OMITTED FROM SUMMARY TABLE
Needs confirmation.

$K_4(2500)$ MASS

VALUE (MeV)	DOCUMENT ID	TECN	CHG	COMMENT
2490 ± 20				
	¹ CLELAND 81	SPEC	±	50 $K^+ p \rightarrow \Lambda \bar{p}$
¹ $J^P = 4^-$ from moments analysis.				

$K_4(2500)$ WIDTH

VALUE (MeV)	DOCUMENT ID	TECN	CHG	COMMENT
• • • We do not use the following data for averages, fits, limits, etc. • • •				
~ 250	² CLELAND 81	SPEC	±	50 $K^+ p \rightarrow \Lambda \bar{p}$
² $J^P = 4^-$ from moments analysis.				

$K_4(2500)$ DECAY MODES

Mode	Fraction (Γ_i/Γ)
Γ_1 $\rho \bar{\Lambda}$	

$K_4(2500)$ REFERENCES

CLELAND 81	NP B184 1	W.E. Cleland et al.	(PITT, GEVA, LAUS+)
------------	-----------	---------------------	---------------------

$K(3100)$

$I^G(J^PC) = ?^?(?^{??})$

OMITTED FROM SUMMARY TABLE

Narrow peak observed in several ($\Lambda \bar{p}$ + pions) and ($\bar{\Lambda} p$ + pions) states in Σ^- Be reactions by BOURQUIN 86 and in $n p$ and $n A$ reactions by ALEEV 93. Not seen by BOEHNLEIN 91. If due to strong decays, this state has exotic quantum numbers ($B=0, Q=+1, S=-1$ for $\Lambda \bar{p} \pi^+ \pi^+$ and $I \geq 3/2$ for $\Lambda \bar{p} \pi^-$). Needs confirmation.

$K(3100)$ MASS

VALUE (MeV)	DOCUMENT ID	TECN	CHG	COMMENT
≈ 3100 OUR ESTIMATE				
3-BODY DECAYS				
3054 ± 11 OUR AVERAGE				
3060 ± 7 ± 20	¹ ALEEV 93	BIS2		$K(3100) \rightarrow \Lambda \bar{p} \pi^+$
3056 ± 7 ± 20	¹ ALEEV 93	BIS2		$K(3100) \rightarrow \bar{\Lambda} p \pi^-$
3055 ± 8 ± 20	¹ ALEEV 93	BIS2		$K(3100) \rightarrow \Lambda \bar{p} \pi^-$
3045 ± 8 ± 20	¹ ALEEV 93	BIS2		$K(3100) \rightarrow \bar{\Lambda} p \pi^+$

VALUE (MeV)	DOCUMENT ID	TECN	CHG	COMMENT
4-BODY DECAYS				
3059 ± 11 OUR AVERAGE				
3067 ± 6 ± 20	¹ ALEEV 93	BIS2		$K(3100) \rightarrow \Lambda \bar{p} \pi^+ \pi^+$
3060 ± 8 ± 20	¹ ALEEV 93	BIS2		$K(3100) \rightarrow \Lambda \bar{p} \pi^+ \pi^-$
3055 ± 7 ± 20	¹ ALEEV 93	BIS2		$K(3100) \rightarrow \bar{\Lambda} p \pi^- \pi^-$
3052 ± 8 ± 20	¹ ALEEV 93	BIS2		$K(3100) \rightarrow \bar{\Lambda} p \pi^- \pi^+$
• • • We do not use the following data for averages, fits, limits, etc. • • •				
3105 ± 30	BOURQUIN 86	SPEC		$K(3100) \rightarrow \Lambda \bar{p} \pi^+ \pi^+$
3115 ± 30	BOURQUIN 86	SPEC		$K(3100) \rightarrow \Lambda \bar{p} \pi^+ \pi^-$

VALUE (MeV)	DOCUMENT ID	TECN	CHG	COMMENT
5-BODY DECAYS				
• • • We do not use the following data for averages, fits, limits, etc. • • •				
3095 ± 30	BOURQUIN 86	SPEC		$K(3100) \rightarrow \Lambda \bar{p} \pi^+ \pi^+ \pi^-$
¹ Supersedes ALEEV 90.				

$K(3100)$ WIDTH

VALUE (MeV)	DOCUMENT ID	TECN	CHG	COMMENT
3-BODY DECAYS				
• • • We do not use the following data for averages, fits, limits, etc. • • •				
42 ± 16	² ALEEV 93	BIS2		$K(3100) \rightarrow \Lambda \bar{p} \pi^+$
36 ± 15	² ALEEV 93	BIS2		$K(3100) \rightarrow \bar{\Lambda} p \pi^-$
50 ± 18	² ALEEV 93	BIS2		$K(3100) \rightarrow \Lambda \bar{p} \pi^-$
30 ± 15	² ALEEV 93	BIS2		$K(3100) \rightarrow \bar{\Lambda} p \pi^+$

VALUE (MeV)	CL%	DOCUMENT ID	TECN	CHG	COMMENT
4-BODY DECAYS					
• • • We do not use the following data for averages, fits, limits, etc. • • •					
22 ± 8		² ALEEV 93	BIS2		$K(3100) \rightarrow \Lambda \bar{p} \pi^+ \pi^+$
28 ± 12		² ALEEV 93	BIS2		$K(3100) \rightarrow \Lambda \bar{p} \pi^+ \pi^-$
32 ± 15		² ALEEV 93	BIS2		$K(3100) \rightarrow \bar{\Lambda} p \pi^- \pi^-$
30 ± 15		² ALEEV 93	BIS2		$K(3100) \rightarrow \bar{\Lambda} p \pi^- \pi^+$
<30	90	BOURQUIN 86	SPEC		$K(3100) \rightarrow \Lambda \bar{p} \pi^+ \pi^+$
<80	90	BOURQUIN 86	SPEC		$K(3100) \rightarrow \Lambda \bar{p} \pi^+ \pi^-$

VALUE (MeV)	CL%	DOCUMENT ID	TECN	CHG	COMMENT
5-BODY DECAYS					
• • • We do not use the following data for averages, fits, limits, etc. • • •					
<30	90	BOURQUIN 86	SPEC		$K(3100) \rightarrow \Lambda \bar{p} \pi^+ \pi^+ \pi^-$
² Supersedes ALEEV 90.					

$K(3100)$ DECAY MODES

Mode	Fraction (Γ_i/Γ)
Γ_1 $K(3100)^0 \rightarrow \Lambda \bar{p} \pi^+$	
Γ_2 $K(3100)^{--} \rightarrow \bar{\Lambda} p \pi^-$	
Γ_3 $K(3100)^- \rightarrow \Lambda \bar{p} \pi^+ \pi^-$	

Meson Particle Listings

 $K(3100)$

Γ_4	$K(3100)^+ \rightarrow \Lambda \bar{p} \pi^+ \pi^+$
Γ_5	$K(3100)^0 \rightarrow \Lambda \bar{p} \pi^+ \pi^+ \pi^-$
Γ_6	$K(3100)^0 \rightarrow \Sigma(1385)^+ \bar{p}$

 $K(3100)$ REFERENCES

ALEEV	93	PAN 56 1358	A.N. Aleev <i>et al.</i>	(BIS-2 Collab.)
		Translated from YAF 56 100.		
BOEHNLEIN	91	NPBPS B21 174	A. Boehnlein <i>et al.</i>	(FLOR, BNL, IND+)
ALEEV	90	ZPHY C47 533	A.N. Aleev <i>et al.</i>	(BIS-2 Collab.)
BOURQUIN	86	PL B172 113	M.H. Bourquin <i>et al.</i>	(GEVA, RAL, HEIDP+)

$\Gamma(\Sigma(1385)^+ \bar{p})/\Gamma(\Lambda \bar{p} \pi^+)$					Γ_6/Γ_1
VALUE	CL%	DOCUMENT ID	TECN	COMMENT	
<0.04	90	ALEEV	93	BIS2	$K(3100)^0 \rightarrow \Sigma(1385)^+ \bar{p}$

CHARMED MESONS

($C = \pm 1$)

$D^+ = c\bar{d}, D^0 = c\bar{u}, \bar{D}^0 = \bar{c}u, D^- = \bar{c}d,$ similarly for D^{*s}

D^\pm

$$J(P) = \frac{1}{2}(0^-)$$

D^\pm MASS

The fit includes $D^\pm, D^0, D_S^\pm, D^{*0}, D^{*+}, D_S^{*0}, D_1(2420)^0, D_2^*(2460)^0,$ and $D_{S1}(2536)^\pm$ mass and mass difference measurements.

VALUE (MeV)	EVTS	DOCUMENT ID	TECN	COMMENT
1869.65 ± 0.05 OUR FIT				
1869.5 ± 0.4 OUR AVERAGE				
1869.53 ± 0.49 ± 0.20	110 ± 15	ANASHIN	10A	KEDR e^+e^- at $\psi(3770)$
1870.0 ± 0.5 ± 1.0	317	BARLAG	90c	ACCM π^- Cu 230 GeV
1869.4 ± 0.6		1 TRILLING	81	RVUE e^+e^- 3.77 GeV
• • • We do not use the following data for averages, fits, limits, etc. • • •				
1875 ± 10	9	ADAMOVICH	87	EMUL Photoproduction
1860 ± 16	6	ADAMOVICH	84	EMUL Photoproduction
1863 ± 4		DERRICK	84	HRS e^+e^- 29 GeV
1868.4 ± 0.5		1 SCHINDLER	81	MRK2 e^+e^- 3.77 GeV
1874 ± 5		GOLDHABER	77	MRK1 D^0, D^+ recoil spectra
1868.3 ± 0.9		1 PERUZZI	77	LGW e^+e^- 3.77 GeV
1874 ± 11		PICCOLO	77	MRK1 e^+e^- 4.03, 4.41 GeV
1876 ± 15	50	PERUZZI	76	MRK1 $K^\mp \pi^\pm \pi^\pm$

¹PERUZZI 77 and SCHINDLER 81 errors do not include the 0.13% uncertainty in the absolute SPEAR energy calibration. TRILLING 81 uses the high precision $J/\psi(1S)$ and $\psi(2S)$ measurements of ZHOLENTZ 80 to determine this uncertainty and combines the PERUZZI 77 and SCHINDLER 81 results to obtain the value quoted.

D^\pm MEAN LIFE

Measurements with an error $> 100 \times 10^{-15}$ s have been omitted from the Listings.

VALUE (10^{-15} s)	EVTS	DOCUMENT ID	TECN	COMMENT
1040 ± 7 OUR AVERAGE				
1039.4 ± 4.3 ± 7.0	110k	LINK	02F	FOCS γ nucleus, ≈ 180 GeV
1033.6 ± 22.1 ± 9.9 ± 12.7	3.7k	BONVICINI	99	CLEO $e^+e^- \approx \Upsilon(4S)$
1048 ± 15 ± 11	9k	FRABETTI	94D	E687 $D^+ \rightarrow K^- \pi^+ \pi^+$
• • • We do not use the following data for averages, fits, limits, etc. • • •				
1075 ± 40 ± 18	2.4k	FRABETTI	91	E687 γ Be, $D^+ \rightarrow K^- \pi^+ \pi^+$
1030 ± 80 ± 60	200	ALVAREZ	90	NA14 $\gamma, D^+ \rightarrow K^- \pi^+ \pi^+$
1050 ± 77 ± 72	317	1 BARLAG	90c	ACCM π^- Cu 230 GeV
1050 ± 80 ± 70	363	ALBRECHT	88i	ARG e^+e^- 10 GeV
1090 ± 30 ± 25	2.9k	RAAB	88	E691 Photoproduction

¹BARLAG 90c estimates the systematic error to be negligible.

D^\pm DECAY MODES

Most decay modes (other than the semileptonic modes) that involve a neutral K meson are now given as K_S^0 modes, not as \bar{K}^0 modes. Nearly always it is a K_S^0 that is measured, and interference between Cabibbo-allowed and doubly Cabibbo-suppressed modes can invalidate the assumption that $2\Gamma(K_S^0) = \Gamma(\bar{K}^0)$.

Mode	Fraction (Γ_i/Γ)	Scale factor/ Confidence level
------	--------------------------------	-----------------------------------

Inclusive modes

Γ_1	e^+ semileptonic	(16.07 ± 0.30) %	
Γ_2	μ^+ anything	(17.6 ± 3.2) %	
Γ_3	K^- anything	(25.7 ± 1.4) %	
Γ_4	\bar{K}^0 anything + K^0 anything	(61 ± 5) %	
Γ_5	K^+ anything	(5.9 ± 0.8) %	
Γ_6	$K^*(892)^-$ anything	(6 ± 5) %	
Γ_7	$\bar{K}^*(892)^0$ anything	(23 ± 5) %	
Γ_8	$K^*(892)^0$ anything	< 6.6 %	CL=90%
Γ_9	η anything	(6.3 ± 0.7) %	
Γ_{10}	η' anything	(1.04 ± 0.18) %	
Γ_{11}	ϕ anything	(1.12 ± 0.04) %	

Leptonic and semileptonic modes

Γ_{12}	$e^+ \nu_e$	< 8.8	$\times 10^{-6}$	CL=90%
Γ_{13}	$\gamma e^+ \nu_e$	< 3.0	$\times 10^{-5}$	CL=90%
Γ_{14}	$\mu^+ \nu_\mu$	(3.74 ± 0.17)	$\times 10^{-4}$	
Γ_{15}	$\tau^+ \nu_\tau$	(1.20 ± 0.27)	$\times 10^{-3}$	
Γ_{16}	$\bar{K}^0 e^+ \nu_e$	(8.73 ± 0.10) %		
Γ_{17}	$\bar{K}^0 \mu^+ \nu_\mu$	(8.76 ± 0.19) %		
Γ_{18}	$K^- \pi^+ e^+ \nu_e$	(4.02 ± 0.18) %		S=3.2
Γ_{19}	$\bar{K}^*(892)^0 e^+ \nu_e, \bar{K}^*(892)^0 \rightarrow K^- \pi^+$	(3.77 ± 0.17) %		
Γ_{20}	$(K^- \pi^+)_{[0.8-1.0]\text{GeV}} e^+ \nu_e$	(3.39 ± 0.09) %		
Γ_{21}	$(K^- \pi^+)_{S\text{-wave}} e^+ \nu_e$	(2.28 ± 0.11)	$\times 10^{-3}$	
Γ_{22}	$\bar{K}^*(1410)^0 e^+ \nu_e, \bar{K}^*(1410)^0 \rightarrow K^- \pi^+$	< 6	$\times 10^{-3}$	CL=90%
Γ_{23}	$\bar{K}_2^*(1430)^0 e^+ \nu_e, \bar{K}_2^*(1430)^0 \rightarrow K^- \pi^+$	< 5	$\times 10^{-4}$	CL=90%
Γ_{24}	$K^- \pi^+ e^+ \nu_e$ nonresonant	< 7	$\times 10^{-3}$	CL=90%
Γ_{25}	$\bar{K}^*(892)^0 e^+ \nu_e$	(5.40 ± 0.10) %		S=1.1
Γ_{26}	$K^- \pi^+ \mu^+ \nu_\mu$	(3.65 ± 0.34) %		
Γ_{27}	$\bar{K}^*(892)^0 \mu^+ \nu_\mu, \bar{K}^*(892)^0 \rightarrow K^- \pi^+$	(3.52 ± 0.10) %		
Γ_{28}	$K^- \pi^+ \mu^+ \nu_\mu$ nonresonant	(1.9 ± 0.5)	$\times 10^{-3}$	
Γ_{29}	$\bar{K}^*(892)^0 \mu^+ \nu_\mu$	(5.27 ± 0.15) %		
Γ_{30}	$K^- \pi^+ \pi^0 \mu^+ \nu_\mu$	< 1.5	$\times 10^{-3}$	CL=90%
Γ_{31}	$\bar{K}_1^0(1270)^0 e^+ \nu_e, \bar{K}_1^0 \rightarrow K^- \pi^+ \pi^0$	(1.06 ± 0.15)	$\times 10^{-3}$	
Γ_{32}	$\bar{K}_2^*(1430)^0 \mu^+ \nu_\mu$	< 2.3	$\times 10^{-4}$	CL=90%
Γ_{33}	$\bar{K}^*(1680)^0 \mu^+ \nu_\mu$	< 1.5	$\times 10^{-3}$	CL=90%
Γ_{34}	$\pi^0 e^+ \nu_e$	(3.72 ± 0.17)	$\times 10^{-3}$	S=2.0
Γ_{35}	$\pi^0 \mu^+ \nu_\mu$	(3.50 ± 0.15)	$\times 10^{-3}$	
Γ_{36}	$\eta e^+ \nu_e$	(1.11 ± 0.07)	$\times 10^{-3}$	
Γ_{37}	$\pi^- \pi^+ e^+ \nu_e$	(2.45 ± 0.10)	$\times 10^{-3}$	
Γ_{38}	$f_0(500)^0 e^+ \nu_e, f_0(500)^0 \rightarrow \pi^+ \pi^-$	(6.3 ± 0.5)	$\times 10^{-4}$	
Γ_{39}	$\rho^0 e^+ \nu_e$	(2.18 ± 0.17 ± 0.25)	$\times 10^{-3}$	
Γ_{40}	$\rho^0 \mu^+ \nu_\mu$	(2.4 ± 0.4)	$\times 10^{-3}$	
Γ_{41}	$\omega e^+ \nu_e$	(1.69 ± 0.11)	$\times 10^{-3}$	
Γ_{42}	$\eta'(958) e^+ \nu_e$	(2.0 ± 0.4)	$\times 10^{-4}$	
Γ_{43}	$a(980)^0 e^+ \nu_e, a(980)^0 \rightarrow \eta \pi^0$	(1.7 ± 0.8 ± 0.7)	$\times 10^{-4}$	
Γ_{44}	$\phi e^+ \nu_e$	< 1.3	$\times 10^{-5}$	CL=90%
Γ_{45}	$D^0 e^+ \nu_e$	< 1.0	$\times 10^{-4}$	CL=90%

Hadronic modes with a \bar{K} or $\bar{K}K\bar{K}$

Γ_{46}	$K_S^0 \pi^+$	(1.562 ± 0.031) %		S=1.7
Γ_{47}	$K_L^0 \pi^+$	(1.46 ± 0.05) %		
Γ_{48}	$K^- 2\pi^+$	[a] (9.38 ± 0.16) %		S=1.6
Γ_{49}	$(K^- \pi^+)_{S\text{-wave}} \pi^+$	(7.52 ± 0.17) %		
Γ_{50}	$\bar{K}_0^*(700)^0 \pi^+, \bar{K}_0^*(700) \rightarrow K^- \pi^+$			
Γ_{51}	$\bar{K}_0^*(1430)^0 \pi^+, \bar{K}_0^*(1430)^0 \rightarrow K^- \pi^+$	[b] (1.25 ± 0.06) %		
Γ_{52}	$\bar{K}^*(892)^0 \pi^+, \bar{K}^*(892)^0 \rightarrow K^- \pi^+$	(1.04 ± 0.12) %		
Γ_{53}	$\bar{K}^*(1410)^0 \pi^+, \bar{K}^{*0} \rightarrow$	not seen		
Γ_{54}	$\bar{K}_2^*(1430)^0 \pi^+, \bar{K}_2^*(1430)^0 \rightarrow K^- \pi^+$	[b] (2.3 ± 0.7)	$\times 10^{-4}$	
Γ_{55}	$\bar{K}^*(1680)^0 \pi^+, \bar{K}^*(1680)^0 \rightarrow K^- \pi^+$	[b] (2.2 ± 1.1)	$\times 10^{-4}$	
Γ_{56}	$K^- (2\pi^+)_{I=2}$	(1.45 ± 0.26) %		
Γ_{57}	$K^- 2\pi^+$ nonresonant			
Γ_{58}	$K_S^0 \pi^+ \pi^0$	[a] (7.36 ± 0.21) %		
Γ_{59}	$K_S^0 \rho^+$	(6.14 ± 0.60 ± 1.4)		
Γ_{60}	$K_S^0 \rho(1450)^+, \rho^+ \rightarrow \pi^+ \pi^0$	(1.5 ± 1.2)	$\times 10^{-3}$	
Γ_{61}	$\bar{K}^*(892)^0 \pi^+, \bar{K}^*(892)^0 \rightarrow K_S^0 \pi^0$	(2.64 ± 0.32)	$\times 10^{-3}$	
Γ_{62}	$\bar{K}_0^*(1430)^0 \pi^+, \bar{K}_0^*(1430)^0 \rightarrow K_S^0 \pi^0$	(2.7 ± 0.9)	$\times 10^{-3}$	
Γ_{63}	$\bar{K}_0^*(1680)^0 \pi^+, \bar{K}_0^*(1680)^0 \rightarrow K_S^0 \pi^0$	(10 ± 7 ± 10)	$\times 10^{-4}$	
Γ_{64}	$\bar{K}^0 \pi^+, \bar{K}^0 \rightarrow K_S^0 \pi^0$	(6 ± 5 ± 4)	$\times 10^{-3}$	

Meson Particle Listings

 D^{\pm}

Γ_{65}	$K_S^0 \pi^+ \pi^0$ nonresonant	$(3 \pm 4) \times 10^{-3}$	
Γ_{66}	$K_S^0 \pi^+ \pi^0$ nonresonant and $\bar{K}^0 \pi^+$	$(1.37 \pm_{-0.40}^{+0.21}) \%$	
Γ_{67}	$(K_S^0 \pi^0)_{S\text{-wave}} \pi^+$	$(1.27 \pm_{-0.33}^{+0.27}) \%$	
Γ_{68}	$K_S^0 \pi^+ \eta'(958)$	$(1.90 \pm 0.21) \times 10^{-3}$	
Γ_{69}	$K^- 2\pi^+ \pi^0$	[c] $(6.25 \pm 0.18) \%$	
Γ_{70}	$K_S^0 2\pi^+ \pi^-$	[c] $(3.10 \pm 0.09) \%$	
Γ_{71}	$K^- 3\pi^+ \pi^-$	[a] $(5.7 \pm 0.5) \times 10^{-3}$	S=1.1
Γ_{72}	$\bar{K}^*(892)^0 2\pi^+ \pi^-$, $\bar{K}^*(892)^0 \rightarrow K^- \pi^+$	$(1.2 \pm 0.4) \times 10^{-3}$	
Γ_{73}	$\bar{K}^*(892)^0 \rho^0 \pi^+$, $\bar{K}^*(892)^0 \rightarrow K^- \pi^+$	$(2.3 \pm 0.4) \times 10^{-3}$	
Γ_{74}	$\bar{K}^*(892)^0 a_1(1260)^+$	[d] $(9.3 \pm 1.9) \times 10^{-3}$	
Γ_{75}	$\bar{K}^*(892)^0 2\pi^+ \pi^-$ no- ρ , $\bar{K}^*(892)^0 \rightarrow K^- \pi^+$		
Γ_{76}	$K^- \rho^0 2\pi^+$	$(1.72 \pm 0.28) \times 10^{-3}$	
Γ_{77}	$K^- 3\pi^+ \pi^-$ nonresonant	$(4.0 \pm 2.9) \times 10^{-4}$	
Γ_{78}	$K^+ 2K_S^0$	$(2.54 \pm 0.13) \times 10^{-3}$	
Γ_{79}	$K^+ K^- K_S^0 \pi^+$	$(2.4 \pm 0.5) \times 10^{-4}$	

Pionic modes

Γ_{80}	$\pi^+ \pi^0$	$(1.247 \pm 0.033) \times 10^{-3}$	
Γ_{81}	$2\pi^+ \pi^-$	$(3.27 \pm 0.18) \times 10^{-3}$	
Γ_{82}	$\rho^0 \pi^+$	$(8.3 \pm 1.5) \times 10^{-4}$	
Γ_{83}	$\pi^+ (\pi^+ \pi^-)_{S\text{-wave}}$	$(1.83 \pm 0.16) \times 10^{-3}$	
Γ_{84}	$\sigma \pi^+$, $\sigma \rightarrow \pi^+ \pi^-$	$(1.38 \pm 0.12) \times 10^{-3}$	
Γ_{85}	$f_0(980) \pi^+$, $f_0(980) \rightarrow \pi^+ \pi^-$	$(1.56 \pm 0.33) \times 10^{-4}$	
Γ_{86}	$f_0(1370) \pi^+$, $f_0(1370) \rightarrow \pi^+ \pi^-$	$(8 \pm 4) \times 10^{-5}$	
Γ_{87}	$f_2(1270) \pi^+$, $f_2(1270) \rightarrow \pi^+ \pi^-$	$(5.0 \pm 0.9) \times 10^{-4}$	
Γ_{88}	$\rho(1450)^0 \pi^+$, $\rho(1450)^0 \rightarrow \pi^+ \pi^-$	$< 8 \times 10^{-5}$	CL=95%
Γ_{89}	$f_0(1500) \pi^+$, $f_0(1500) \rightarrow \pi^+ \pi^-$	$(1.1 \pm 0.4) \times 10^{-4}$	
Γ_{90}	$f_0(1710) \pi^+$, $f_0(1710) \rightarrow \pi^+ \pi^-$	$< 5 \times 10^{-5}$	CL=95%
Γ_{91}	$f_0(1790) \pi^+$, $f_0(1790) \rightarrow \pi^+ \pi^-$	$< 7 \times 10^{-5}$	CL=95%
Γ_{92}	$(\pi^+ \pi^+)_{S\text{-wave}} \pi^-$	$< 1.2 \times 10^{-4}$	CL=95%
Γ_{93}	$2\pi^+ \pi^-$ nonresonant	$< 1.1 \times 10^{-4}$	CL=95%
Γ_{94}	$\pi^+ 2\pi^0$	$(4.7 \pm 0.4) \times 10^{-3}$	
Γ_{95}	$2\pi^+ \pi^- \pi^0$	$(1.16 \pm 0.08) \%$	
Γ_{96}	$3\pi^+ 2\pi^-$	$(1.66 \pm 0.16) \times 10^{-3}$	S=1.1
Γ_{97}	$\eta \pi^+$	$(3.77 \pm 0.09) \times 10^{-3}$	
Γ_{98}	$\eta \pi^+ \pi^0$	$(1.38 \pm 0.35) \times 10^{-3}$	
Γ_{99}	$\omega \pi^+$	$(2.8 \pm 0.6) \times 10^{-4}$	
Γ_{100}	$\eta'(958) \pi^+$	$(4.97 \pm 0.19) \times 10^{-3}$	
Γ_{101}	$\eta'(958) \pi^+ \pi^0$	$(1.6 \pm 0.5) \times 10^{-3}$	

Hadronic modes with a $K\bar{K}$ pair

Γ_{102}	$K^+ K_S^0$	$(3.04 \pm 0.09) \times 10^{-3}$	S=2.2
Γ_{103}	$K_S^0 K^+$		
Γ_{104}	$K_S^0 K^+$	$(3.21 \pm 0.16) \times 10^{-3}$	
Γ_{105}	$K_S^0 K^+ \pi^0$	$(5.07 \pm 0.30) \times 10^{-3}$	
Γ_{106}	$K_S^0 K^+ \pi^0$	$(5.24 \pm 0.31) \times 10^{-3}$	
Γ_{107}	$K^+ K^- \pi^+$	[a] $(9.68 \pm 0.18) \times 10^{-3}$	
Γ_{108}	$\phi \pi^+$	$(5.70 \pm 0.14) \times 10^{-3}$	
Γ_{109}	$\phi \pi^+$, $\phi \rightarrow K^+ K^-$	$(2.69 \pm_{-0.08}^{+0.07}) \times 10^{-3}$	
Γ_{110}	$K^+ \bar{K}^*(892)^0$, $\bar{K}^*(892)^0 \rightarrow K^- \pi^+$	$(2.49 \pm_{-0.13}^{+0.08}) \times 10^{-3}$	
Γ_{111}	$K^+ \bar{K}_0^*(1430)^0$, $\bar{K}_0^*(1430)^0 \rightarrow$ $K^- \pi^+$	$(1.82 \pm 0.35) \times 10^{-3}$	
Γ_{112}	$K^+ \bar{K}_2^*(1430)^0$, $\bar{K}_2^* \rightarrow$ $K^- \pi^+$	$(1.6 \pm_{-0.8}^{+1.2}) \times 10^{-4}$	
Γ_{113}	$K^+ \bar{K}_0^*(700)$, $\bar{K}_0^* \rightarrow K^- \pi^+$	$(6.8 \pm_{-2.1}^{+3.5}) \times 10^{-4}$	
Γ_{114}	$a_0(1450)^0 \pi^+$, $a_0^0 \rightarrow K^+ K^-$	$(4.5 \pm_{-1.8}^{+7.0}) \times 10^{-4}$	
Γ_{115}	$\phi(1680) \pi^+$, $\phi \rightarrow K^+ K^-$	$(4.9 \pm_{-1.9}^{+4.0}) \times 10^{-5}$	
Γ_{116}	$K_S^0 K_S^0 \pi^+$	$(2.70 \pm 0.13) \times 10^{-3}$	

Γ_{117}	$K^+ K_S^0 \pi^+ \pi^-$	$(1.74 \pm 0.18) \times 10^{-3}$
Γ_{118}	$K_S^0 K^- 2\pi^+$	$(2.38 \pm 0.17) \times 10^{-3}$
Γ_{119}	$K^+ K^- 2\pi^+ \pi^-$	$(2.3 \pm 1.2) \times 10^{-4}$

A few poorly measured branching fractions:

Γ_{120}	$\phi \pi^+ \pi^0$	$(2.3 \pm 1.0) \%$	
Γ_{121}	$\phi \rho^+$	$< 1.5 \%$	CL=90%
Γ_{122}	$K^+ K^- \pi^+ \pi^0$ non- ϕ	$(1.5 \pm_{-0.6}^{+0.7}) \%$	
Γ_{123}	$K^*(892)^+ K_S^0$	$(1.7 \pm 0.8) \%$	

Doubly Cabibbo-suppressed modes

Γ_{124}	$K^+ \pi^0$	$(2.08 \pm 0.21) \times 10^{-4}$	S=1.4
Γ_{125}	$K^+ \eta$	$(1.25 \pm 0.16) \times 10^{-4}$	S=1.1
Γ_{126}	$K^+ \eta'(958)$	$(1.85 \pm 0.20) \times 10^{-4}$	
Γ_{127}	$K^+ \pi^+ \pi^-$	$(4.91 \pm 0.09) \times 10^{-4}$	
Γ_{128}	$K^+ \rho^0$	$(1.9 \pm 0.5) \times 10^{-4}$	
Γ_{129}	$K^*(892)^0 \pi^+$, $K^*(892)^0 \rightarrow$ $K^+ \pi^-$	$(2.3 \pm 0.4) \times 10^{-4}$	
Γ_{130}	$K^+ f_0(980)$, $f_0(980) \rightarrow$ $\pi^+ \pi^-$	$(4.4 \pm 2.6) \times 10^{-5}$	
Γ_{131}	$K_2^*(1430)^0 \pi^+$, $K_2^*(1430)^0 \rightarrow$ $K^+ \pi^-$	$(3.9 \pm 2.7) \times 10^{-5}$	
Γ_{132}	$K^+ \pi^+ \pi^-$ nonresonant	not seen	
Γ_{133}	$2K^+ K^-$	$(6.14 \pm 0.11) \times 10^{-5}$	
Γ_{134}	$\phi(1020)^0 K^+$	$< 2.1 \times 10^{-5}$	CL=90%
Γ_{135}	$K^+ \phi(1020)$, $\phi \rightarrow K^+ K^-$	$(4.4 \pm 0.6) \times 10^{-6}$	
Γ_{136}	$K^+ (K^+ K^-)_{S\text{-wave}}$	$(5.77 \pm 0.12) \times 10^{-5}$	

 $\Delta C = 1$ weak neutral current (CI) modes, or
Lepton Family number (LF) or Lepton number (L) violating modes

Γ_{137}	$\pi^+ e^+ e^-$	CI $< 1.1 \times 10^{-6}$	CL=90%
Γ_{138}	$\pi^+ \pi^0 e^+ e^-$	$< 1.4 \times 10^{-5}$	CL=90%
Γ_{139}	$\pi^+ \phi$, $\phi \rightarrow e^+ e^-$	[e] $(1.7 \pm_{-0.9}^{+1.4}) \times 10^{-6}$	
Γ_{140}	$\pi^+ \mu^+ \mu^-$	CI $< 7.3 \times 10^{-8}$	CL=90%
Γ_{141}	$\pi^+ \phi$, $\phi \rightarrow \mu^+ \mu^-$	[e] $(1.8 \pm 0.8) \times 10^{-6}$	
Γ_{142}	$\rho^+ \mu^+ \mu^-$	CI $< 5.6 \times 10^{-4}$	CL=90%
Γ_{143}	$K^+ e^+ e^-$	[f] $< 1.0 \times 10^{-6}$	CL=90%
Γ_{144}	$K^+ \pi^0 e^+ e^-$	$< 1.5 \times 10^{-5}$	CL=90%
Γ_{145}	$K_S^0 \pi^+ e^+ e^-$	$< 2.6 \times 10^{-5}$	CL=90%
Γ_{146}	$K_S^0 K^+ e^+ e^-$	$< 1.1 \times 10^{-5}$	CL=90%
Γ_{147}	$K^+ \mu^+ \mu^-$	[f] $< 4.3 \times 10^{-6}$	CL=90%
Γ_{148}	$\pi^+ e^+ \mu^-$	LF $< 2.9 \times 10^{-6}$	CL=90%
Γ_{149}	$\pi^+ e^- \mu^+$	LF $< 3.6 \times 10^{-6}$	CL=90%
Γ_{150}	$K^+ e^+ \mu^-$	LF $< 1.2 \times 10^{-6}$	CL=90%
Γ_{151}	$K^+ e^- \mu^+$	LF $< 2.8 \times 10^{-6}$	CL=90%
Γ_{152}	$\pi^- 2e^+$	L $< 1.1 \times 10^{-6}$	CL=90%
Γ_{153}	$\pi^- 2\mu^+$	L $< 2.2 \times 10^{-8}$	CL=90%
Γ_{154}	$\pi^- e^+ \mu^+$	L $< 2.0 \times 10^{-6}$	CL=90%
Γ_{155}	$\rho^- 2\mu^+$	L $< 5.6 \times 10^{-4}$	CL=90%
Γ_{156}	$K^- 2e^+$	L $< 9 \times 10^{-7}$	CL=90%
Γ_{157}	$K_S^0 \pi^- 2e^+$	$< 3.3 \times 10^{-6}$	CL=90%
Γ_{158}	$K^- \pi^0 2e^+$	$< 8.5 \times 10^{-6}$	CL=90%
Γ_{159}	$K^- 2\mu^+$	L $< 1.0 \times 10^{-5}$	CL=90%
Γ_{160}	$K^- e^+ \mu^+$	L $< 1.9 \times 10^{-6}$	CL=90%
Γ_{161}	$K^*(892)^- 2\mu^+$	L $< 8.5 \times 10^{-4}$	CL=90%

Γ_{162}	Unaccounted decay modes	$(63.3 \pm 0.4) \%$	S=1.3
----------------	-------------------------	---------------------	-------

[a] The branching fraction for this mode may differ from the sum of the submodes that contribute to it, due to interference effects. See the relevant papers.

[b] These subfractions of the $K^- 2\pi^+$ mode are uncertain: see the Particle Listings.

[c] Submodes of the $D^+ \rightarrow K^- 2\pi^+ \pi^0$ and $K_S^0 2\pi^+ \pi^-$ were studied by ANJOS 92C and COFFMAN 92B, but with at most 142 events for the first mode and 229 for the second – not enough for precise results. With nothing new for 18 years, we refer to our 2008 edition, Physics Letters **B667** 1 (2008), for those results.

[d] The unseen decay modes of the resonances are included.

[e] This is not a test for the $\Delta C=1$ weak neutral current, but leads to the $\pi^+ \ell^+ \ell^-$ final state.

[f] This mode is not a useful test for a $\Delta C=1$ weak neutral current because both quarks must change flavor in this decay.

CONSTRAINED FIT INFORMATION

An overall fit to 31 branching ratios uses 41 measurements and one constraint to determine 17 parameters. The overall fit has a chi-squared = 62.8 for 25 degrees of freedom.

The following off-diagonal array elements are the correlation coefficients $\langle \delta x_i \delta x_j \rangle / (\delta x_i \delta x_j)$, in percent, from the fit to the branching fractions, $x_i \equiv \Gamma_i / \Gamma_{\text{total}}$. The fit constrains the x_i whose labels appear in this array to sum to one.

Table with correlation coefficients for x18, x25, x29, x39, x46, x48, x71, x80, x96, x97, x100, x102, x124, x125, x126, x162, x17, x18, x25, x29, x39, x46, x48, x71, x80, x96, x97, x100, x102, x124, x125, x126.

D+ BRANCHING RATIOS

Some now-obsolete measurements have been omitted from these Listings.

c-quark decays

Gamma(c -> e+ anything) / Gamma(c -> anything)

For the Summary Table, we only use the average of e+ and mu+ measurements from Z0 -> c c-bar decays; see the second data block.

Table with columns VALUE, EVTS, DOCUMENT ID, TECN, COMMENT. Value: 0.103 ± 0.009 ± 0.009 / -0.008

1 ABBIENDI 99K uses the excess of right-sign over wrong-sign leptons opposite reconstructed D*(2010)+ -> D0 pi+ decays in Z0 -> c c-bar.

Gamma(c -> mu+ anything) / Gamma(c -> anything)

For the Summary Table, we only use the average of e+ and mu+ measurements from Z0 -> c c-bar decays; see the next data block.

Table with columns VALUE, EVTS, DOCUMENT ID, TECN, COMMENT. Value: 0.082 ± 0.005 OUR AVERAGE

••• We do not use the following data for averages, fits, limits, etc. •••

0.093 ± 0.009 ± 0.009 88 KAYIS-TOPAK.02 CHRS See KAYIS-TOPAKSU 05

0.089 ± 0.018 ± 0.025 BARTEL 85J JADE See BARTEL 87

1 ABBIENDI 99K uses the excess of right-sign over wrong-sign leptons opposite reconstructed D*(2010)+ -> D0 pi+ decays in Z0 -> c c-bar.

2 ALBRECHT 92F uses the excess of right-sign over wrong-sign leptons in a sample of events tagged by fully reconstructed D*(2010)+ -> D0 pi+ decays.

Gamma(c -> l+ anything) / Gamma(c -> anything)

This is an average (not a sum) of e+ and mu+ measurements.

Table with columns VALUE, EVTS, DOCUMENT ID, TECN, COMMENT. Value: 0.096 ± 0.004 OUR AVERAGE

1 ABREU 00o uses leptons opposite fully reconstructed D*(2010)+, D+, or D0 mesons.

2 ABBIENDI 99K uses the excess of right-sign over wrong-sign leptons opposite reconstructed D*(2010)+ -> D0 pi+ decays in Z0 -> c c-bar.

Gamma(c -> D*(2010)+ anything) / Gamma(c -> anything)

Table with columns VALUE, EVTS, DOCUMENT ID, TECN, COMMENT. Value: 0.255 ± 0.015 ± 0.008

1 ABREU 00o uses slow pions opposite fully reconstructed D*(2010)+, D+, or D0 mesons as a signal of D*(2010)- production.

Inclusive modes

Gamma(e+ semileptonic) / Gamma_total

Gamma_1 / Gamma

The sum of our K0 e+ nu_e, K*(892)0 e+ nu_e, pi0 e+ nu_e, eta e+ nu_e, rho0 e+ nu_e, and omega e+ nu_e branching fractions is 15.3 ± 0.3%.

Table with columns VALUE (%), EVTS, DOCUMENT ID, TECN, COMMENT. Value: 16.07 ± 0.30 OUR AVERAGE

16.13 ± 0.10 ± 0.29 26.2 ± 0.2k 1 ASNER 10 CLEO e+ e- at 3774 MeV

15.2 ± 0.9 ± 0.8 521 ± 32 ABLIKIM 07G BES2 e+ e- approx psi(3770)

16.13 ± 0.20 ± 0.33 8798 ± 105 2 ADAM 06A CLEO See ASNER 10

17.0 ± 1.9 ± 0.7 158 BALTRUSAIT...85B MRK3 e+ e- 3.77 GeV

1 Using the D+ and D0 lifetimes, ASNER 10 finds that the ratio of the D+ and D0 semileptonic widths is 0.985 ± 0.015 ± 0.024.

2 Using the D+ and D0 lifetimes, ADAM 06A finds that the ratio of the D+ and D0 inclusive e+ widths is 0.985 ± 0.028 ± 0.015, consistent with the isospin-invariance prediction of 1.

Gamma(mu+ anything) / Gamma_total

Gamma_2 / Gamma

Table with columns VALUE (%), EVTS, DOCUMENT ID, TECN, COMMENT. Value: 17.6 ± 2.7 ± 1.8

17.6 ± 2.7 ± 1.8 100 ± 12 1 ABLIKIM 08L BES2 e+ e- approx psi(3772)

1 ABLIKIM 08L finds the ratio of D+ -> mu+ X and D0 -> mu+ X branching fractions to be 2.59 ± 0.70 ± 0.25, in accord with the ratio of D+ and D0 lifetimes, 2.54 ± 0.02.

Gamma(K- anything) / Gamma_total

Gamma_3 / Gamma

Table with columns VALUE (%), EVTS, DOCUMENT ID, TECN, COMMENT. Value: 25.7 ± 1.4 OUR AVERAGE

24.7 ± 1.3 ± 1.2 631 ± 33 ABLIKIM 07G BES2 e+ e- approx psi(3770)

27.8 ± 3.6 BARLAG 92C ACCM pi- Cu 230 GeV

27.1 ± 2.3 ± 2.4 COFFMAN 91 MRK3 e+ e- 3.77 GeV

Gamma(K0 anything) + Gamma(K0 anything) / Gamma_total

Gamma_4 / Gamma

Table with columns VALUE (%), EVTS, DOCUMENT ID, TECN, COMMENT. Value: 61 ± 5 OUR AVERAGE

60.5 ± 5.5 ± 3.3 244 ± 22 ABLIKIM 06u BES2 e+ e- at 3773 MeV

61.2 ± 6.5 ± 4.3 COFFMAN 91 MRK3 e+ e- 3.77 GeV

Gamma(K+ anything) / Gamma_total

Gamma_5 / Gamma

Table with columns VALUE (%), EVTS, DOCUMENT ID, TECN, COMMENT. Value: 5.9 ± 0.8 OUR AVERAGE

6.1 ± 0.9 ± 0.4 189 ± 27 ABLIKIM 07G BES2 e+ e- approx psi(3770)

5.5 ± 1.3 ± 0.9 COFFMAN 91 MRK3 e+ e- 3.77 GeV

Gamma(K*(892)- anything) / Gamma_total

Gamma_6 / Gamma

Table with columns VALUE (%), EVTS, DOCUMENT ID, TECN, COMMENT. Value: 5.7 ± 5.2 ± 0.7

5.7 ± 5.2 ± 0.7 7.2 ± 6.5 ABLIKIM 06u BES2 e+ e- at 3773 MeV

Gamma(K*(892)0 anything) / Gamma_total

Gamma_7 / Gamma

Table with columns VALUE (%), EVTS, DOCUMENT ID, TECN, COMMENT. Value: 23.2 ± 4.5 ± 3.0

23.2 ± 4.5 ± 3.0 189 ± 36 ABLIKIM 05P BES e+ e- approx 3773 MeV

Gamma(K*(892)0 anything) / Gamma_total

Gamma_8 / Gamma

Table with columns VALUE (%), CL%, DOCUMENT ID, TECN, COMMENT. Value: <6.6

<6.6 90 ABLIKIM 05P BES e+ e- approx 3773 MeV

Gamma(eta anything) / Gamma_total

Gamma_9 / Gamma

This ratio includes eta particles from eta' decays.

Table with columns VALUE (%), EVTS, DOCUMENT ID, TECN, COMMENT. Value: 6.3 ± 0.5 ± 0.5

6.3 ± 0.5 ± 0.5 1972 ± 142 HUANG 06B CLEO e+ e- at psi(3770)

Gamma(eta' anything) / Gamma_total

Gamma_10 / Gamma

Table with columns VALUE (%), EVTS, DOCUMENT ID, TECN, COMMENT. Value: 1.04 ± 0.16 ± 0.09

1.04 ± 0.16 ± 0.09 82 ± 13 HUANG 06B CLEO e+ e- at psi(3770)

$\Gamma(K^- 2\pi^+ \text{ nonresonant})/\Gamma(K^- 2\pi^+)$ Γ_{57}/Γ_{48}
This is the "fit fraction" from the Dalitz-plot analysis. Later analyses find little need for this decay mode.

Table with columns: VALUE, DOCUMENT ID, TECN, COMMENT. Includes data from AITALA, FRABETTI, ANJOS, ADLER.

$\Gamma(K_S^0 \pi^+ \pi^0)/\Gamma_{\text{total}}$ Γ_{58}/Γ_{48}

Table with columns: VALUE (units 10⁻²), EVTS, DOCUMENT ID, TECN, COMMENT. Includes data from DOBBS, HE, ADLER.

$\Gamma(K_S^0 \pi^+ \pi^0)/\Gamma(K^- 2\pi^+)$ Γ_{58}/Γ_{48}

Table with columns: VALUE, DOCUMENT ID, TECN, COMMENT. Includes data from BONVICINI.

$\Gamma(K_S^0 \rho^+ \pi^0)/\Gamma(K_S^0 \pi^+ \pi^0)$ Γ_{59}/Γ_{58}

Table with columns: VALUE (units 10⁻²), DOCUMENT ID, TECN, COMMENT. Includes data from ABLIKIM.

$\Gamma(K_S^0 \rho(1450)^+, \rho^+ \to \pi^+ \pi^0)/\Gamma(K_S^0 \pi^+ \pi^0)$ Γ_{60}/Γ_{58}

Table with columns: VALUE (%), DOCUMENT ID, TECN, COMMENT. Includes data from ABLIKIM.

$\Gamma(\bar{K}^*(892)^0 \pi^+, \bar{K}^*(892)^0 \to K_S^0 \pi^+ \pi^0)/\Gamma(K_S^0 \pi^+ \pi^0)$ Γ_{61}/Γ_{58}

Table with columns: VALUE (units 10⁻²), DOCUMENT ID, TECN, COMMENT. Includes data from ABLIKIM.

$\Gamma(\bar{K}_0^*(1430)^0 \pi^+, \bar{K}_0^*(1430)^0 \to K_S^0 \pi^+ \pi^0)/\Gamma(K_S^0 \pi^+ \pi^0)$ Γ_{62}/Γ_{58}

Table with columns: VALUE (%), DOCUMENT ID, TECN, COMMENT. Includes data from ABLIKIM.

$\Gamma(\bar{K}_0^*(1680)^0 \pi^+, \bar{K}_0^*(1680)^0 \to K_S^0 \pi^+ \pi^0)/\Gamma(K_S^0 \pi^+ \pi^0)$ Γ_{63}/Γ_{58}

Table with columns: VALUE (%), DOCUMENT ID, TECN, COMMENT. Includes data from ABLIKIM.

$\Gamma(\bar{\pi}^0 \pi^+, \bar{\pi}^0 \to K_S^0 \pi^+ \pi^0)/\Gamma(K_S^0 \pi^+ \pi^0)$ Γ_{64}/Γ_{58}

Table with columns: VALUE (%), DOCUMENT ID, TECN, COMMENT. Includes data from ABLIKIM.

$\Gamma(K_S^0 \pi^+ \pi^0 \text{ nonresonant})/\Gamma(K_S^0 \pi^+ \pi^0)$ Γ_{65}/Γ_{58}

Table with columns: VALUE (units 10⁻²), DOCUMENT ID, TECN, COMMENT. Includes data from ABLIKIM.

$\Gamma(K_S^0 \pi^+ \pi^0 \text{ nonresonant and } \bar{\pi}^0 \pi^+)/\Gamma(K_S^0 \pi^+ \pi^0)$ Γ_{66}/Γ_{58}

Table with columns: VALUE (%), DOCUMENT ID, TECN, COMMENT. Includes data from ABLIKIM.

$\Gamma((K_S^0 \pi^+ \pi^0)_{S\text{-wave } \pi^+})/\Gamma(K_S^0 \pi^+ \pi^0)$ Γ_{67}/Γ_{58}

Table with columns: VALUE (%), DOCUMENT ID, TECN, COMMENT. Includes data from ABLIKIM.

$\Gamma(K_S^0 \pi^+ \eta(958))/\Gamma_{\text{total}}$ Γ_{68}/Γ_{48}

Table with columns: VALUE (units 10⁻³), EVTS, DOCUMENT ID, TECN, COMMENT. Includes data from ABLIKIM.

$\Gamma(K^- 2\pi^+ \pi^0)/\Gamma_{\text{total}}$ Γ_{69}/Γ_{48}

See our 2008 Review (Physics Letters B667 1 (2008)) for measurements of submodes of this mode.

Table with columns: VALUE (units 10⁻²), EVTS, DOCUMENT ID, TECN, COMMENT. Includes data from DOBBS, HE, COFFMAN, BALTRUSAITIS.

DOBBS 07 and HE 05 use single- and double-tagged events in an overall fit. DOBBS 07 supersedes HE 05.

$\Gamma(K^- 2\pi^+ \pi^0)/\Gamma(K^- 2\pi^+)$ Γ_{69}/Γ_{48}

Table with columns: VALUE, DOCUMENT ID, TECN, COMMENT. Includes data from BONVICINI.

$\Gamma(K_S^0 2\pi^+ \pi^-)/\Gamma_{\text{total}}$ Γ_{70}/Γ_{48}

See our 2008 Review (Physics Letters B667 1 (2008)) for measurements of submodes of this mode.

Table with columns: VALUE (units 10⁻²), EVTS, DOCUMENT ID, TECN, COMMENT. Includes data from DOBBS, HE, BARLAG.

DOBBS 07 and HE 05 use single- and double-tagged events in an overall fit. DOBBS 07 supersedes HE 05.

$\Gamma(K_S^0 2\pi^+ \pi^-)/\Gamma(K^- 2\pi^+)$ Γ_{70}/Γ_{48}

Table with columns: VALUE, DOCUMENT ID, TECN, COMMENT. Includes data from BONVICINI.

$\Gamma(K^- 3\pi^+ \pi^-)/\Gamma(K^- 2\pi^+)$ Γ_{71}/Γ_{48}

Table with columns: VALUE, EVTS, DOCUMENT ID, TECN, COMMENT. Includes data from LINK, FRABETTI, ANJOS.

$\Gamma(\bar{K}^*(892)^0 2\pi^+ \pi^-, \bar{K}^*(892)^0 \to K^- \pi^+)/\Gamma(K^- 3\pi^+ \pi^-)$ Γ_{72}/Γ_{71}

Table with columns: VALUE, DOCUMENT ID, TECN, COMMENT. Includes data from LINK.

$\Gamma(\bar{K}^*(892)^0 \rho^0 \pi^+, \bar{K}^*(892)^0 \to K^- \pi^+)/\Gamma(K^- 2\pi^+)$ Γ_{73}/Γ_{48}

Table with columns: VALUE, DOCUMENT ID, TECN, COMMENT. Includes data from FRABETTI.

$\Gamma(\bar{K}^*(892)^0 \rho^0 \pi^+, \bar{K}^*(892)^0 \to K^- \pi^+)/\Gamma(K^- 3\pi^+ \pi^-)$ Γ_{73}/Γ_{71}

Table with columns: VALUE, DOCUMENT ID, TECN, COMMENT. Includes data from LINK.

$\Gamma(\bar{K}^*(892)^0 a_1(1260)^+)/\Gamma(K^- 2\pi^+)$ Γ_{74}/Γ_{48}

Table with columns: VALUE, DOCUMENT ID, TECN, COMMENT. Includes data from LINK.

$\Gamma(\bar{K}^*(892)^0 2\pi^+ \pi^- \text{ no } \rho, \bar{K}^*(892)^0 \to K^- \pi^+)/\Gamma(K^- 2\pi^+)$ Γ_{75}/Γ_{48}

Table with columns: VALUE, DOCUMENT ID, TECN, COMMENT. Includes data from FRABETTI.

$\Gamma(K^- \rho^0 2\pi^+)/\Gamma(K^- 2\pi^+)$ Γ_{76}/Γ_{48}

Table with columns: VALUE, DOCUMENT ID, TECN, COMMENT. Includes data from FRABETTI.

$\Gamma(K^- \rho^0 2\pi^+)/\Gamma(K^- 3\pi^+ \pi^-)$ Γ_{76}/Γ_{71}

Table with columns: VALUE, DOCUMENT ID, TECN, COMMENT. Includes data from LINK.

$\Gamma(K^- 3\pi^+ \pi^- \text{ nonresonant})/\Gamma(K^- 3\pi^+ \pi^-)$ Γ_{77}/Γ_{71}

Table with columns: VALUE, CL%, DOCUMENT ID, TECN, COMMENT. Includes data from LINK.

Meson Particle Listings

D[±]

• • • We do not use the following data for averages, fits, limits, etc. • • •
 <0.026 90 FRABETTI 97c E687 γ Be, $\bar{E}_\gamma \approx 200$ GeV

$\Gamma(K^+ 2K_S^0)/\Gamma_{total}$ Γ_{78}/Γ

VALUE (units 10 ⁻⁴)	EVTS	DOCUMENT ID	TECN	COMMENT
25.4 ± 0.5 ± 1.2	3551	ABLIKIM	17A BES3	$e^+e^- \rightarrow \psi(3770)$

$\Gamma(K^+ 2K_S^0)/\Gamma(K^- 2\pi^+)$ Γ_{78}/Γ_{48}

VALUE	EVTS	DOCUMENT ID	TECN	COMMENT
0.035 ± 0.010 ± 0.005	39 ± 9	ALBRECHT	94i ARG	$e^+e^- \approx 10$ GeV
0.085 ± 0.018	70 ± 12	AMMAR	91 CLEO	$e^+e^- \approx 10.5$ GeV

• • • We do not use the following data for averages, fits, limits, etc. • • •

$\Gamma(\phi(1020)^0 K^+)/\Gamma_{total}$ Γ_{134}/Γ

VALUE	CL%	DOCUMENT ID	TECN	COMMENT
<2.1 × 10⁻⁵	90	ABLIKIM	19B1 BES3	e^+e^- at 3773 MeV

$\Gamma(K^+ K^- K_S^0 \pi^+)/\Gamma(K_S^0 2\pi^+ \pi^-)$ Γ_{79}/Γ_{70}

VALUE (units 10 ⁻³)	EVTS	DOCUMENT ID	TECN	COMMENT
7.7 ± 1.5 ± 0.9	35 ± 7	LINK	01c FOCS	γ nucleus, $\bar{E}_\gamma \approx 180$ GeV

Pionic modes

$\Gamma(\pi^+ \pi^0)/\Gamma_{total}$ Γ_{80}/Γ

VALUE (units 10 ⁻³)	EVTS	DOCUMENT ID	TECN	COMMENT
1.247 ± 0.033 OUR FIT				
1.259 ± 0.033 ± 0.023	10k	ABLIKIM	18w BES3	e^+e^- , 3773 MeV

$\Gamma(\pi^+ \pi^0)/\Gamma(K^- 2\pi^+)$ Γ_{80}/Γ_{48}

VALUE (units 10 ⁻²)	EVTS	DOCUMENT ID	TECN	COMMENT
1.33 ± 0.04 OUR FIT	Error includes scale factor of 1.1.			
1.31 ± 0.06 OUR AVERAGE				
1.29 ± 0.04 ± 0.05	2649 ± 76	MENDEZ	10 CLEO	e^+e^- at 3774 MeV
1.33 ± 0.11 ± 0.09	1229 ± 99	AUBERT,B	06f BABR	$e^+e^- \approx \Upsilon(4S)$
1.44 ± 0.19 ± 0.10	171 ± 22	ARMS	04 CLEO	$e^+e^- \approx 10$ GeV

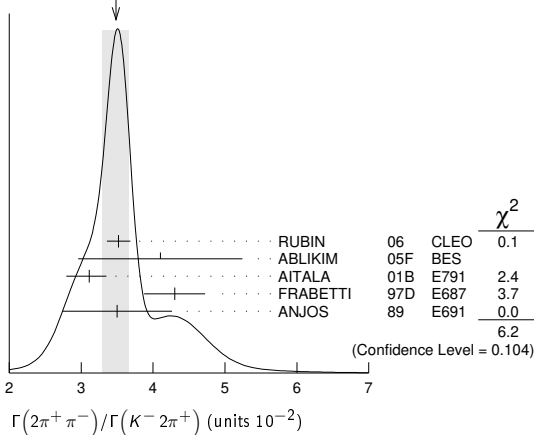
• • • We do not use the following data for averages, fits, limits, etc. • • •

1.33 ± 0.07 ± 0.06	914 ± 46	RUBIN	06 CLEO	See MENDEZ 10
--------------------	----------	-------	---------	---------------

$\Gamma(2\pi^+ \pi^-)/\Gamma(K^- 2\pi^+)$ Γ_{81}/Γ_{48}

VALUE (units 10 ⁻²)	EVTS	DOCUMENT ID	TECN	COMMENT
3.48 ± 0.19 OUR AVERAGE	Error includes scale factor of 1.4. See the ideogram below.			
3.52 ± 0.11 ± 0.12	3303 ± 95	RUBIN	06 CLEO	e^+e^- at $\psi(3770)$
4.1 ± 1.1 ± 0.3	85 ± 22	ABLIKIM	05f BES	$e^+e^- \approx \psi(3770)$
3.11 ± 0.18 ± 0.16 -0.26	1172	AITALA	01B E791	π^- nucleus, 500 GeV
4.3 ± 0.3 ± 0.3	236	FRABETTI	97D E687	γ Be ≈ 200 GeV
3.5 ± 0.7 ± 0.3	83	ANJOS	89 E691	Photoproduction

WEIGHTED AVERAGE
3.48 ± 0.19 (Error scaled by 1.4)

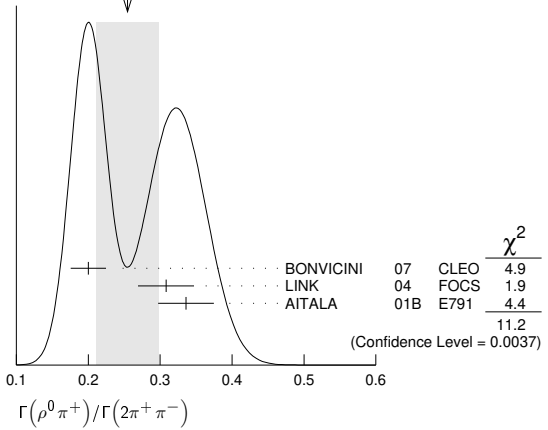


$\Gamma(\rho^0 \pi^+)/\Gamma(2\pi^+ \pi^-)$ Γ_{82}/Γ_{81}

This is the "fit fraction" from the Dalitz-plot analysis.

VALUE	DOCUMENT ID	TECN	COMMENT
0.25 ± 0.04 OUR AVERAGE	Error includes scale factor of 2.4. See the ideogram below.		
0.200 ± 0.023 ± 0.009	BONVICINI	07 CLEO	Dalitz fit, ≈ 2240 evts
0.3082 ± 0.0314 ± 0.0230	LINK	04 FOCS	Dalitz fit, 1527 ± 51 evts
0.336 ± 0.032 ± 0.022	AITALA	01B E791	Dalitz fit, 1172 evts

WEIGHTED AVERAGE
0.25 ± 0.04 (Error scaled by 2.4)



$\Gamma(\pi^+ (\pi^+ \pi^-)_{S\text{-wave}})/\Gamma(2\pi^+ \pi^-)$ Γ_{83}/Γ_{81}

This is the "fit fraction" from the Dalitz-plot analysis. See also the next three data blocks.

VALUE	DOCUMENT ID	TECN	COMMENT
0.5600 ± 0.0324 ± 0.0214	1 LINK	04 FOCS	Dalitz fit, 1527 ± 51 evts

¹ LINK 04 borrows a K-matrix parametrization from ANISOVICH 03 of the full $\pi-\pi$ S-wave isoscalar scattering amplitude to describe the $\pi^+ \pi^-$ S-wave component of the $\pi^+ \pi^+ \pi^-$ state. The fit fraction given above is a sum over five f_0 mesons, the $f_0(980)$, $f_0(1300)$, $f_0(1200-1600)$, $f_0(1500)$, and $f_0(1750)$. See LINK 04 for details and discussion.

$\Gamma(\sigma \pi^+, \sigma \rightarrow \pi^+ \pi^-)/\Gamma(2\pi^+ \pi^-)$ Γ_{84}/Γ_{81}

This is the "fit fraction" from the Dalitz-plot analysis.

VALUE	DOCUMENT ID	TECN	COMMENT
0.422 ± 0.027 OUR AVERAGE			
0.418 ± 0.014 ± 0.025	BONVICINI	07 CLEO	Dalitz fit, ≈ 2240 evts
0.463 ± 0.090 ± 0.021	AITALA	01B E791	Dalitz fit, 1172 evts

$\Gamma(f_0(980) \pi^+, f_0(980) \rightarrow \pi^+ \pi^-)/\Gamma(2\pi^+ \pi^-)$ Γ_{85}/Γ_{81}

This is the "fit fraction" from the Dalitz-plot analysis.

VALUE	DOCUMENT ID	TECN	COMMENT
0.048 ± 0.010 OUR AVERAGE	Error includes scale factor of 1.3.		
0.041 ± 0.009 ± 0.003	BONVICINI	07 CLEO	Dalitz fit, ≈ 2240 evts
0.062 ± 0.013 ± 0.004	AITALA	01B E791	Dalitz fit, 1172 evts

$\Gamma(f_0(1370) \pi^+, f_0(1370) \rightarrow \pi^+ \pi^-)/\Gamma(2\pi^+ \pi^-)$ Γ_{86}/Γ_{81}

This is the "fit fraction" from the Dalitz-plot analysis.

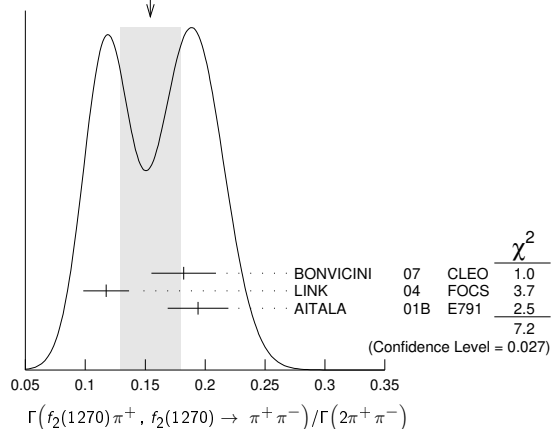
VALUE	DOCUMENT ID	TECN	COMMENT
0.024 ± 0.013 OUR AVERAGE			
0.026 ± 0.018 ± 0.006	BONVICINI	07 CLEO	Dalitz fit, ≈ 2240 evts
0.023 ± 0.015 ± 0.008	AITALA	01B E791	Dalitz fit, 1172 evts

$\Gamma(f_2(1270) \pi^+, f_2(1270) \rightarrow \pi^+ \pi^-)/\Gamma(2\pi^+ \pi^-)$ Γ_{87}/Γ_{81}

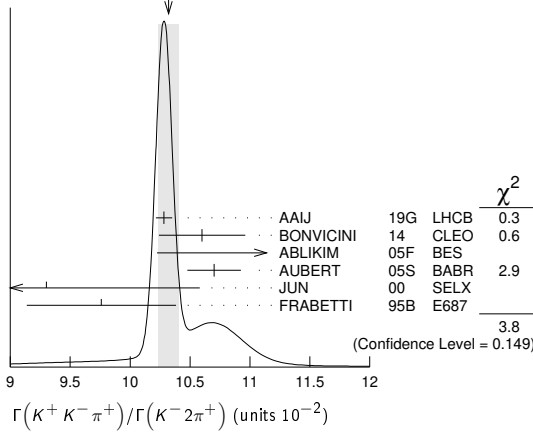
This is the "fit fraction" from the Dalitz-plot analysis.

VALUE	DOCUMENT ID	TECN	COMMENT
0.154 ± 0.025 OUR AVERAGE	Error includes scale factor of 1.9. See the ideogram below.		
0.182 ± 0.026 ± 0.007	BONVICINI	07 CLEO	Dalitz fit, ≈ 2240 evts
0.1174 ± 0.0190 ± 0.0029	LINK	04 FOCS	Dalitz fit, 1527 ± 51 evts
0.194 ± 0.025 ± 0.004	AITALA	01B E791	Dalitz fit, 1172 evts

WEIGHTED AVERAGE
0.154 ± 0.025 (Error scaled by 1.9)



Meson Particle Listings

 D^{\pm} WEIGHTED AVERAGE
10.32±0.09 (Error scaled by 1.4) $\Gamma(\phi\pi^+)/\Gamma_{\text{total}}$ Γ_{108}/Γ

VALUE (units 10^{-3})	EVTS	DOCUMENT ID	TECN	COMMENT
$5.70 \pm 0.05 \pm 0.13$	18k	ABLIKIM	19B1	BES3 e^+e^- at 3773 MeV

 $\Gamma(\phi\pi^+, \phi \rightarrow K^+K^-)/\Gamma(K^+K^-\pi^+)$ $\Gamma_{109}/\Gamma_{107}$

This is the "fit fraction" from the Dalitz-plot analysis.

VALUE (%)	DOCUMENT ID	TECN	COMMENT
$27.8 \pm 0.4 \pm 0.2$ -0.5	RUBIN	08	CLEO Dalitz fit, 19,458±163 evts

 $\Gamma(K^+\bar{K}^*(892)^0, \bar{K}^*(892)^0 \rightarrow K^-\pi^+)/\Gamma(K^+K^-\pi^+)$ $\Gamma_{110}/\Gamma_{107}$

This is the "fit fraction" from the Dalitz-plot analysis.

VALUE (%)	DOCUMENT ID	TECN	COMMENT
$25.7 \pm 0.5 \pm 0.4$ -1.2	RUBIN	08	CLEO Dalitz fit, 19,458±163 evts

 $\Gamma(K^+\bar{K}_0^*(1430)^0, \bar{K}_0^*(1430)^0 \rightarrow K^-\pi^+)/\Gamma(K^+K^-\pi^+)$ $\Gamma_{111}/\Gamma_{107}$

This is the "fit fraction" from the Dalitz-plot analysis.

VALUE (%)	DOCUMENT ID	TECN	COMMENT
$18.8 \pm 1.2 \pm 3.3$ -3.4	RUBIN	08	CLEO Dalitz fit, 19,458±163 evts

 $\Gamma(K^+\bar{K}_2^*(1430)^0, \bar{K}_2^*(1430)^0 \rightarrow K^-\pi^+)/\Gamma(K^+K^-\pi^+)$ $\Gamma_{112}/\Gamma_{107}$

This is the "fit fraction" from the Dalitz-plot analysis.

VALUE (%)	DOCUMENT ID	TECN	COMMENT
$17.0 \pm 3.5 \pm 1.8$	FRABETTI	95B	E687 Dalitz fit, 915 evts

 $\Gamma(K^+\bar{K}_0^*(700), \bar{K}_0^*(700) \rightarrow K^-\pi^+)/\Gamma(K^+K^-\pi^+)$ $\Gamma_{113}/\Gamma_{107}$

This is the "fit fraction" from the Dalitz-plot analysis.

VALUE (%)	DOCUMENT ID	TECN	COMMENT
$7.0 \pm 0.8 \pm 3.5$ -2.0	RUBIN	08	CLEO Dalitz fit, 19,458±163 evts

 $\Gamma(a_0(1450)^0\pi^+, a_0^0 \rightarrow K^+K^-)/\Gamma(K^+K^-\pi^+)$ $\Gamma_{114}/\Gamma_{107}$

This is the "fit fraction" from the Dalitz-plot analysis.

VALUE (%)	DOCUMENT ID	TECN	COMMENT
$4.6 \pm 0.6 \pm 7.2$ -1.8	RUBIN	08	CLEO Dalitz fit, 19,458±163 evts

 $\Gamma(\phi(1680)\pi^+, \phi \rightarrow K^+K^-)/\Gamma(K^+K^-\pi^+)$ $\Gamma_{115}/\Gamma_{107}$

This is the "fit fraction" from the Dalitz-plot analysis.

VALUE (%)	DOCUMENT ID	TECN	COMMENT
$0.51 \pm 0.11 \pm 0.37$ -0.16	RUBIN	08	CLEO Dalitz fit, 19,458±163 evts

 $\Gamma(K_S^0 K_S^0 \pi^+)/\Gamma_{\text{total}}$ Γ_{116}/Γ

This is the "fit fraction" from the Dalitz-plot analysis.

VALUE (units 10^{-4})	EVTS	DOCUMENT ID	TECN	COMMENT
$27.0 \pm 0.5 \pm 1.2$	4897	ABLIKIM	17A	BES3 $e^+e^- \rightarrow \psi(3770)$

 $\Gamma(K^+ K_S^0 \pi^-\pi^-)/\Gamma(K_S^0 2\pi^+\pi^-)$ Γ_{117}/Γ_{70}

This is the "fit fraction" from the Dalitz-plot analysis.

VALUE (units 10^{-2})	EVTS	DOCUMENT ID	TECN	COMMENT
$5.62 \pm 0.39 \pm 0.40$	469 ± 32	LINK	01c	FOCS γ nucleus, $\bar{E}_\gamma \approx 180$ GeV

 $\Gamma(K_S^0 K^- 2\pi^+)/\Gamma(K_S^0 2\pi^+\pi^-)$ Γ_{118}/Γ_{70}

This is the "fit fraction" from the Dalitz-plot analysis.

VALUE (units 10^{-2})	EVTS	DOCUMENT ID	TECN	COMMENT
$7.68 \pm 0.41 \pm 0.32$	670 ± 35	LINK	01c	FOCS γ nucleus, $\bar{E}_\gamma \approx 180$ GeV

 $\Gamma(K^+ K^- 2\pi^+\pi^-)/\Gamma(K^- 3\pi^+\pi^-)$ Γ_{119}/Γ_{71}

VALUE	EVTS	DOCUMENT ID	TECN	COMMENT
$0.040 \pm 0.009 \pm 0.019$	38	LINK	03D	FOCS γ A, $\bar{E}_\gamma \approx 180$ GeV

 $\Gamma(\phi\pi^+\pi^0)/\Gamma_{\text{total}}$ Γ_{120}/Γ Unseen decay modes of the ϕ are included.

VALUE	DOCUMENT ID	TECN	COMMENT
0.023 ± 0.010	¹ BARLAG	92c	ACCM π^- Cu 230 GeV

 $\Gamma(\phi\rho^+)/\Gamma(K^- 2\pi^+)$ Γ_{121}/Γ_{48} Unseen decay modes of the ϕ are included.

VALUE	CL%	DOCUMENT ID	TECN	COMMENT
<0.16	90	DAOUDI	92	CLEO $e^+e^- \approx 10.5$ GeV

 $\Gamma(K^+ K^- \pi^+\pi^0 \text{ non-}\phi)/\Gamma_{\text{total}}$ Γ_{122}/Γ

VALUE	DOCUMENT ID	TECN	COMMENT
0.015 ± 0.007 -0.006	¹ BARLAG	92c	ACCM π^- Cu 230 GeV

 $\Gamma(K^+ K^- \pi^+\pi^0 \text{ non-}\phi)/\Gamma(K^- 2\pi^+)$ Γ_{122}/Γ_{48} Unseen decay modes of the ϕ are included.

VALUE	CL%	DOCUMENT ID	TECN	COMMENT
<0.25	90	ANJOS	89E	E691 Photoproduction

 $\Gamma(K^* (892)^+ K_S^0)/\Gamma(K_S^0 \pi^+)$ Γ_{123}/Γ_{46} Unseen decay modes of the $K^*(892)^+$ are included.

VALUE	EVTS	DOCUMENT ID	TECN	COMMENT
$1.1 \pm 0.3 \pm 0.4$	67	FRABETTI	95	E687 γ Be $\bar{E}_\gamma \approx 200$ GeV

Doubly Cabibbo-suppressed modes

 $\Gamma(K^+\pi^0)/\Gamma_{\text{total}}$ Γ_{124}/Γ

VALUE (units 10^{-4})	EVTS	DOCUMENT ID	TECN	COMMENT
2.08 ± 0.21 OUR FIT				Error includes scale factor of 1.4.

 2.35 ± 0.20 OUR AVERAGE

VALUE	EVTS	DOCUMENT ID	TECN	COMMENT
$2.32 \pm 0.21 \pm 0.06$	1.8k	ABLIKIM	18w	BES3 e^+e^- , 3773 MeV

VALUE	EVTS	DOCUMENT ID	TECN	COMMENT
$2.52 \pm 0.47 \pm 0.26$	189 ± 37	AUBERT,B	06F	BABR $e^+e^- \approx \gamma(4S)$

 $2.28 \pm 0.36 \pm 0.17$ 148 ± 23 DYTMAN 06 CLEO See MENDEZ 10 $\Gamma(K^+\pi^0)/\Gamma(K^- 2\pi^+)$ Γ_{124}/Γ_{48}

VALUE (units 10^{-3})	EVTS	DOCUMENT ID	TECN	COMMENT
2.21 ± 0.23 OUR FIT				Error includes scale factor of 1.5.

VALUE	EVTS	DOCUMENT ID	TECN	COMMENT
$1.9 \pm 0.2 \pm 0.1$	343 ± 37	MENDEZ	10	CLEO e^+e^- at 3774 MeV

 $\Gamma(K^+\eta)/\Gamma_{\text{total}}$ Γ_{125}/Γ

VALUE (units 10^{-3})	EVTS	DOCUMENT ID	TECN	COMMENT
0.125 ± 0.016 OUR FIT				Error includes scale factor of 1.1.

VALUE	EVTS	DOCUMENT ID	TECN	COMMENT
$0.151 \pm 0.025 \pm 0.014$	439	ABLIKIM	18w	BES3 e^+e^- , 3773 MeV

 $\Gamma(K^+\eta)/\Gamma(\eta\pi^+)$ Γ_{125}/Γ_{97}

VALUE (%)	EVTS	DOCUMENT ID	TECN	COMMENT
3.3 ± 0.4 OUR FIT				Error includes scale factor of 1.1.

VALUE (%)	EVTS	DOCUMENT ID	TECN	COMMENT
$3.06 \pm 0.43 \pm 0.14$	166 ± 23	WON	11	BELL $e^+e^- \approx \gamma(4S)$

 $\Gamma(K^+\eta'(958))/\Gamma_{\text{total}}$ Γ_{126}/Γ

VALUE (units 10^{-3})	EVTS	DOCUMENT ID	TECN	COMMENT
0.185 ± 0.020 OUR FIT				

VALUE	EVTS	DOCUMENT ID	TECN	COMMENT
$0.164 \pm 0.051 \pm 0.024$	87	ABLIKIM	18w	BES3 e^+e^- , 3773 MeV

 $\Gamma(K^+\eta'(958))/\Gamma(\eta'(958)\pi^+)$ $\Gamma_{126}/\Gamma_{100}$

VALUE (%)	EVTS	DOCUMENT ID	TECN	COMMENT
3.7 ± 0.4 OUR FIT				

VALUE (%)	EVTS	DOCUMENT ID	TECN	COMMENT
$3.77 \pm 0.39 \pm 0.10$	180 ± 19	WON	11	BELL $e^+e^- \approx \gamma(4S)$

 $\Gamma(K^+\pi^+\pi^-)/\Gamma(K^- 2\pi^+)$ Γ_{127}/Γ_{48}

VALUE (units 10^{-3})	EVTS	DOCUMENT ID	TECN	COMMENT
5.238 ± 0.025 OUR AVERAGE				

VALUE	EVTS	DOCUMENT ID	TECN	COMMENT
$5.231 \pm 0.009 \pm 0.023$	795k	AAIJ	19G	LHCB $p\bar{p}$ at 8 TeV

VALUE	EVTS	DOCUMENT ID	TECN	COMMENT
$5.69 \pm 0.18 \pm 0.14$	2638 ± 84	KO	09	BELL e^+e^- at $\gamma(4S)$

VALUE	EVTS	DOCUMENT ID	TECN	COMMENT
$6.5 \pm 0.8 \pm 0.4$	189 ± 24	LINK	04F	FOCS γ A, $\bar{E}_\gamma \approx 180$ GeV

VALUE	EVTS	DOCUMENT ID	TECN	COMMENT
$7.7 \pm 1.7 \pm 0.8$	59 ± 13	AITALA	97c	E791 π^- A, 500 GeV

VALUE	EVTS	DOCUMENT ID	TECN	COMMENT
$7.2 \pm 2.3 \pm 1.7$	21	FRABETTI	95E	E687 γ Be, $\bar{E}_\gamma \approx 220$ GeV

 $\Gamma(K^+\rho^0)/\Gamma(K^+\pi^+\pi^-)$ $\Gamma_{128}/\Gamma_{127}$

This is the "fit fraction" from the Dalitz-plot analysis.

VALUE	DOCUMENT ID	TECN	COMMENT
0.39 ± 0.09 OUR AVERAGE			

VALUE	EVTS	DOCUMENT ID	TECN	COMMENT
$0.3943 \pm 0.0787 \pm 0.0815$		LINK	04F	FOCS Dalitz fit, 189 evts

VALUE	EVTS	DOCUMENT ID	TECN	COMMENT
$0.37 \pm 0.14 \pm 0.07$		AITALA	97c	E791 Dalitz fit, 59 evts

$\Gamma(K^*(892)^0 \pi^+, K^*(892)^0 \rightarrow K^+ \pi^-) / \Gamma(K^+ \pi^+ \pi^-)$ $\Gamma_{129} / \Gamma_{127}$
 This is the "fit fraction" from the Dalitz-plot analysis.

VALUE	DOCUMENT ID	TECN	COMMENT
0.47 ± 0.08 OUR AVERAGE			
0.5220 ± 0.0684 ± 0.0638	LINK	04F	FOCS Dalitz fit, 189 evts
0.35 ± 0.14 ± 0.01	AITALA	97c	E791 Dalitz fit, 59 evts

$\Gamma(K^+ f_0(980), f_0(980) \rightarrow \pi^+ \pi^-) / \Gamma(K^+ \pi^+ \pi^-)$ $\Gamma_{130} / \Gamma_{127}$
 This is the "fit fraction" from the Dalitz-plot analysis.

VALUE	DOCUMENT ID	TECN	COMMENT
0.0892 ± 0.0333 ± 0.0412	LINK	04F	FOCS Dalitz fit, 189 evts

$\Gamma(K_2^*(1430)^0 \pi^+, K_2^*(1430)^0 \rightarrow K^+ \pi^-) / \Gamma(K^+ \pi^+ \pi^-)$ $\Gamma_{131} / \Gamma_{127}$
 This is the "fit fraction" from the Dalitz-plot analysis.

VALUE	DOCUMENT ID	TECN	COMMENT
0.0803 ± 0.0372 ± 0.0391	LINK	04F	FOCS Dalitz fit, 189 evts

$\Gamma(K^+ \pi^+ \pi^- \text{ nonresonant}) / \Gamma(K^+ \pi^+ \pi^-)$ $\Gamma_{132} / \Gamma_{127}$
 This is the "fit fraction" from the Dalitz-plot analysis.

VALUE	DOCUMENT ID	TECN	COMMENT
0.36 ± 0.14 ± 0.07	1 AITALA	97c	E791 Dalitz fit, 59 evts

• • • We do not use the following data for averages, fits, limits, etc. • • •

1 LINK 04F, with three times as many events, finds no need for a nonresonant amplitude.

$\Gamma(2K^+ K^-) / \Gamma(K^- 2\pi^+)$ $\Gamma_{133} / \Gamma_{48}$

VALUE (units 10^{-4})	EVTS	DOCUMENT ID	TECN	COMMENT
6.54 ± 0.05 OUR AVERAGE				
6.541 ± 0.025 ± 0.042	134k	AAIJ	19G	LHCB pp at 8 TeV
9.49 ± 2.17 ± 0.22	65	1 LINK	02i	FOCS γ nucleus, \approx 180 GeV

1 LINK 02i finds little evidence for ϕK^+ or $f_0(980) K^+$ submodes.

$\Gamma(K^+ \phi(1020), \phi \rightarrow K^+ K^-) / \Gamma(2K^+ K^-)$ $\Gamma_{135} / \Gamma_{133}$

VALUE (%)	DOCUMENT ID	TECN	COMMENT
7.1 ± 0.9	1 AAJ	19H	LHCB pp at 8TeV

1 Fit fraction from a Dalitz plot analysis of $D^+ \rightarrow K^+ K^+ K^-$ decays. The last uncertainty is due to the amplitude model.

$\Gamma(K^+ (K^+ K^-)_{s\text{-wave}}) / \Gamma(2K^+ K^-)$ $\Gamma_{136} / \Gamma_{133}$

VALUE	DOCUMENT ID	TECN	COMMENT
0.94 ± 0.01	1 AAJ	19H	LHCB pp at 8TeV

1 Fit fraction from a Dalitz plot analysis of $D^+ \rightarrow K^+ K^+ K^-$ decays. The last uncertainty is due to the amplitude model.

Rare or forbidden modes

$\Gamma(\pi^+ e^+ e^-) / \Gamma_{\text{total}}$ Γ_{137} / Γ
 A test for the $\Delta C = 1$ weak neutral current. Allowed by higher-order electroweak interactions.

VALUE	CL%	DOCUMENT ID	TECN	COMMENT
<1.1 × 10⁻⁶	90	LEES	11G	BABR $e^+ e^- \approx \Upsilon(4S)$

• • • We do not use the following data for averages, fits, limits, etc. • • •

<5.9 × 10 ⁻⁶	90	1 RUBIN	10	CLEO $e^+ e^-$ at $\psi(3770)$
<7.4 × 10 ⁻⁶	90	HE	05A	CLEO See RUBIN 10
<5.2 × 10 ⁻⁵	90	AITALA	99G	E791 $\pi^- N$ 500 GeV
<1.1 × 10 ⁻⁴	90	FRABETTI	97B	E687 γ Be, $\overline{E}_\gamma \approx$ 220 GeV
<6.6 × 10 ⁻⁵	90	AITALA	96	E791 $\pi^- N$ 500 GeV
<2.5 × 10 ⁻³	90	WEIR	90B	MRK2 $e^+ e^-$ 29 GeV
<2.6 × 10 ⁻³	90	HAAS	88	CLEO $e^+ e^-$ 10 GeV

1 This RUBIN 10 limit is for the $e^+ e^-$ mass in the continuum away from the $\phi(1020)$. See the next data block.

$\Gamma(\pi^+ \pi^0 e^+ e^-) / \Gamma_{\text{total}}$ Γ_{138} / Γ

VALUE	CL%	DOCUMENT ID	TECN	COMMENT
<1.4 × 10⁻⁵	90	ABLIKIM	18P	BES3 $e^+ e^-$, 3773 MeV

$\Gamma(\pi^+ \phi, \phi \rightarrow e^+ e^-) / \Gamma_{\text{total}}$ Γ_{139} / Γ
 This is not a test for the $\Delta C = 1$ weak neutral current, but leads to the $\pi^+ e^+ e^-$ final state.

VALUE	EVTS	DOCUMENT ID	TECN	COMMENT
(1.7 ± 1.4 ± 0.1) × 10⁻⁶	4	1 RUBIN	10	CLEO $e^+ e^-$ at $\psi(3770)$

• • • We do not use the following data for averages, fits, limits, etc. • • •

(2.7 ± 3.6 ± 0.2) × 10 ⁻⁶	2	HE	05A	CLEO See RUBIN 10
--------------------------------------	---	----	-----	-------------------

1 This RUBIN 10 result is consistent with the known $D^+ \rightarrow \phi \pi^+$ and $\phi \rightarrow e^+ e^-$ fractions.

$\Gamma(\pi^+ \mu^+ \mu^-) / \Gamma_{\text{total}}$ Γ_{140} / Γ
 A test for the $\Delta C = 1$ weak neutral current. Allowed by higher-order electroweak interactions.

VALUE	CL%	DOCUMENT ID	TECN	COMMENT
<7.3 × 10⁻⁸	90	AAIJ	13Af	LHCB pp at 7 TeV

• • • We do not use the following data for averages, fits, limits, etc. • • •

<6.5 × 10 ⁻⁶	90	LEES	11G	BABR $e^+ e^- \approx \Upsilon(4S)$
<3.9 × 10 ⁻⁶	90	1 ABAZOV	08D	D0 $p\overline{p}$, $E_{\text{cm}} = 1.96$ TeV
<8.8 × 10 ⁻⁶	90	LINK	03F	FOCS γ A, $\overline{E}_\gamma \approx$ 180 GeV
<1.5 × 10 ⁻⁵	90	AITALA	99G	E791 $\pi^- N$ 500 GeV
<8.9 × 10 ⁻⁵	90	FRABETTI	97B	E687 γ Be, $\overline{E}_\gamma \approx$ 220 GeV
<1.8 × 10 ⁻⁵	90	AITALA	96	E791 $\pi^- N$ 500 GeV
<2.2 × 10 ⁻⁴	90	KODAMA	95	E653 π^- emulsion 600 GeV
<5.9 × 10 ⁻³	90	WEIR	90B	MRK2 $e^+ e^-$ 29 GeV
<2.9 × 10 ⁻³	90	HAAS	88	CLEO $e^+ e^-$ 10 GeV

1 This ABAZOV 08D limit is for the $\mu^+ \mu^-$ mass in the continuum away from the $\phi(1020)$. See the next data block.

$\Gamma(\pi^+ \phi, \phi \rightarrow \mu^+ \mu^-) / \Gamma_{\text{total}}$ Γ_{141} / Γ
 This is not a test for the $\Delta C = 1$ weak neutral current, but leads to the $\pi^+ \mu^+ \mu^-$ final state.

VALUE	DOCUMENT ID	TECN	COMMENT
(1.8 ± 0.5 ± 0.6) × 10⁻⁶	1 ABAZOV	08D	D0 $p\overline{p}$, $E_{\text{cm}} = 1.96$ TeV

1 This ABAZOV 08D value is consistent with the known $D^+ \rightarrow \phi \pi^+$ and $\phi \rightarrow \mu^+ \mu^-$ fractions.

$\Gamma(\rho^+ \mu^+ \mu^-) / \Gamma_{\text{total}}$ Γ_{142} / Γ
 A test for the $\Delta C = 1$ weak neutral current. Allowed by higher-order electroweak interactions.

VALUE	CL%	DOCUMENT ID	TECN	COMMENT
<5.6 × 10⁻⁴	90	KODAMA	95	E653 π^- emulsion 600 GeV

$\Gamma(K^+ e^+ e^-) / \Gamma_{\text{total}}$ Γ_{143} / Γ
 Both quarks would have to change flavor for this decay to occur.

VALUE	CL%	DOCUMENT ID	TECN	COMMENT
<1.0 × 10⁻⁶	90	LEES	11G	BABR $e^+ e^- \approx \Upsilon(4S)$

• • • We do not use the following data for averages, fits, limits, etc. • • •

<3.0 × 10 ⁻⁶	90	RUBIN	10	CLEO $e^+ e^-$ at $\psi(3770)$
<6.2 × 10 ⁻⁶	90	HE	05A	CLEO See RUBIN 10
<2.0 × 10 ⁻⁴	90	AITALA	99G	E791 $\pi^- N$ 500 GeV
<2.0 × 10 ⁻⁴	90	FRABETTI	97B	E687 γ Be, $\overline{E}_\gamma \approx$ 220 GeV
<4.8 × 10 ⁻³	90	WEIR	90B	MRK2 $e^+ e^-$ 29 GeV

$\Gamma(K^+ \pi^0 e^+ e^-) / \Gamma_{\text{total}}$ Γ_{144} / Γ

VALUE	CL%	DOCUMENT ID	TECN	COMMENT
<1.5 × 10⁻⁵	90	ABLIKIM	18P	BES3 $e^+ e^-$, 3773 MeV

$\Gamma(K_2^0 \pi^+ e^+ e^-) / \Gamma_{\text{total}}$ Γ_{145} / Γ

VALUE	CL%	DOCUMENT ID	TECN	COMMENT
<2.6 × 10⁻⁵	90	ABLIKIM	18P	BES3 $e^+ e^-$, 3773 MeV

$\Gamma(K_2^0 K^+ e^+ e^-) / \Gamma_{\text{total}}$ Γ_{146} / Γ

VALUE	CL%	DOCUMENT ID	TECN	COMMENT
<1.1 × 10⁻⁵	90	ABLIKIM	18P	BES3 $e^+ e^-$, 3773 MeV

$\Gamma(K^+ \mu^+ \mu^-) / \Gamma_{\text{total}}$ Γ_{147} / Γ
 Both quarks would have to change flavor for this decay to occur.

VALUE	CL%	DOCUMENT ID	TECN	COMMENT
<4.3 × 10⁻⁶	90	LEES	11G	BABR $e^+ e^- \approx \Upsilon(4S)$

• • • We do not use the following data for averages, fits, limits, etc. • • •

<9.2 × 10 ⁻⁶	90	LINK	03F	FOCS γ A, $\overline{E}_\gamma \approx$ 180 GeV
<4.4 × 10 ⁻⁵	90	AITALA	99G	E791 $\pi^- N$ 500 GeV
<9.7 × 10 ⁻⁵	90	FRABETTI	97B	E687 γ Be, $\overline{E}_\gamma \approx$ 220 GeV
<3.2 × 10 ⁻⁴	90	KODAMA	95	E653 π^- emulsion 600 GeV
<9.2 × 10 ⁻³	90	WEIR	90B	MRK2 $e^+ e^-$ 29 GeV

$\Gamma(\pi^+ e^+ \mu^-) / \Gamma_{\text{total}}$ Γ_{148} / Γ
 A test of lepton-family-number conservation.

VALUE	CL%	DOCUMENT ID	TECN	COMMENT
<2.9 × 10⁻⁶	90	LEES	11G	BABR $e^+ e^- \approx \Upsilon(4S)$

• • • We do not use the following data for averages, fits, limits, etc. • • •

<1.1 × 10 ⁻⁴	90	FRABETTI	97B	E687 γ Be, $\overline{E}_\gamma \approx$ 220 GeV
<3.3 × 10 ⁻³	90	WEIR	90B	MRK2 $e^+ e^-$ 29 GeV

$\Gamma(\pi^+ e^- \mu^+) / \Gamma_{\text{total}}$ Γ_{149} / Γ
 A test of lepton-family-number conservation.

VALUE	CL%	DOCUMENT ID	TECN	COMMENT
<3.6 × 10⁻⁶	90	LEES	11G	BABR $e^+ e^- \approx \Upsilon(4S)$

• • • We do not use the following data for averages, fits, limits, etc. • • •

<1.3 × 10 ⁻⁴	90	FRABETTI	97B	E687 γ Be, $\overline{E}_\gamma \approx$ 220 GeV
<3.3 × 10 ⁻³	90	WEIR	90B	MRK2 $e^+ e^-$ 29 GeV

$\Gamma(K^+ e^+ \mu^-) / \Gamma_{\text{total}}$ Γ_{150} / Γ
 A test of lepton-family-number conservation.

VALUE	CL%	DOCUMENT ID	TECN	COMMENT
<1.2 × 10⁻⁶	90	LEES	11G	BABR $e^+ e^- \approx \Upsilon(4S)$

• • • We do not use the following data for averages, fits, limits, etc. • • •

<1.3 × 10 ⁻⁴	90	FRABETTI	97B	E687 γ Be, $\overline{E}_\gamma \approx$ 220 GeV
<3.4 × 10 ⁻³	90	WEIR	90B	MRK2 $e^+ e^-$ 29 GeV

Meson Particle Listings

D^\pm

$\Gamma(K^+ e^- \mu^+)/\Gamma_{\text{total}}$ Γ_{151}/Γ

A test of lepton-family-number conservation.

VALUE	CL%	DOCUMENT ID	TECN	COMMENT
$<2.8 \times 10^{-6}$	90	LEES	11G	BABR $e^+ e^- \approx \Upsilon(4S)$
$<1.2 \times 10^{-4}$	90	FRABETTI	97B	E687 γ Be, $\bar{E}_\gamma \approx 220$ GeV
$<3.4 \times 10^{-3}$	90	WEIR	90B	MRK2 $e^+ e^-$ 29 GeV

••• We do not use the following data for averages, fits, limits, etc. •••

$\Gamma(\pi^- 2e^+)/\Gamma_{\text{total}}$ Γ_{152}/Γ

A test of lepton-number conservation.

VALUE	CL%	DOCUMENT ID	TECN	COMMENT
$<1.1 \times 10^{-6}$	90	RUBIN	10	CLEO $e^+ e^-$ at $\psi(3770)$
$<1.9 \times 10^{-6}$	90	LEES	11G	BABR $e^+ e^- \approx \Upsilon(4S)$
$<3.6 \times 10^{-6}$	90	HE	05A	CLEO See RUBIN 10
$<9.6 \times 10^{-5}$	90	AITALA	99G	E791 $\pi^- N$ 500 GeV
$<1.1 \times 10^{-4}$	90	FRABETTI	97B	E687 γ Be, $\bar{E}_\gamma \approx 220$ GeV
$<4.8 \times 10^{-3}$	90	WEIR	90B	MRK2 $e^+ e^-$ 29 GeV

••• We do not use the following data for averages, fits, limits, etc. •••

$\Gamma(\pi^- 2\mu^+)/\Gamma_{\text{total}}$ Γ_{153}/Γ

A test of lepton-number conservation.

VALUE	CL%	DOCUMENT ID	TECN	COMMENT
$<2.2 \times 10^{-8}$	90	AAIJ	13AF	LHCB pp at 7 TeV
$<2.0 \times 10^{-6}$	90	LEES	11G	BABR $e^+ e^- \approx \Upsilon(4S)$
$<4.8 \times 10^{-6}$	90	LINK	03F	FOCS γ A, $\bar{E}_\gamma \approx 180$ GeV
$<1.7 \times 10^{-5}$	90	AITALA	99G	E791 $\pi^- N$ 500 GeV
$<8.7 \times 10^{-5}$	90	FRABETTI	97B	E687 γ Be, $\bar{E}_\gamma \approx 220$ GeV
$<2.2 \times 10^{-4}$	90	KODAMA	95	E653 π^- emulsion 600 GeV
$<6.8 \times 10^{-3}$	90	WEIR	90B	MRK2 $e^+ e^-$ 29 GeV

••• We do not use the following data for averages, fits, limits, etc. •••

$\Gamma(\pi^- e^+ \mu^+)/\Gamma_{\text{total}}$ Γ_{154}/Γ

A test of lepton-number conservation.

VALUE	CL%	DOCUMENT ID	TECN	COMMENT
$<2.0 \times 10^{-6}$	90	LEES	11G	BABR $e^+ e^- \approx \Upsilon(4S)$
$<5.0 \times 10^{-5}$	90	AITALA	99G	E791 $\pi^- N$ 500 GeV
$<1.1 \times 10^{-4}$	90	FRABETTI	97B	E687 γ Be, $\bar{E}_\gamma \approx 220$ GeV
$<3.7 \times 10^{-3}$	90	WEIR	90B	MRK2 $e^+ e^-$ 29 GeV

••• We do not use the following data for averages, fits, limits, etc. •••

$\Gamma(\rho^- 2\mu^+)/\Gamma_{\text{total}}$ Γ_{155}/Γ

A test of lepton-number conservation.

VALUE	CL%	DOCUMENT ID	TECN	COMMENT
$<5.6 \times 10^{-4}$	90	KODAMA	95	E653 π^- emulsion 600 GeV

$\Gamma(K^- 2e^+)/\Gamma_{\text{total}}$ Γ_{156}/Γ

A test of lepton-number conservation.

VALUE	CL%	DOCUMENT ID	TECN	COMMENT
$<0.9 \times 10^{-6}$	90	LEES	11G	BABR $e^+ e^- \approx \Upsilon(4S)$
$<3.5 \times 10^{-6}$	90	RUBIN	10	CLEO $e^+ e^-$ at $\psi(3770)$
$<4.5 \times 10^{-6}$	90	HE	05A	CLEO See RUBIN 10
$<1.2 \times 10^{-4}$	90	FRABETTI	97B	E687 γ Be, $\bar{E}_\gamma \approx 220$ GeV
$<9.1 \times 10^{-3}$	90	WEIR	90B	MRK2 $e^+ e^-$ 29 GeV

••• We do not use the following data for averages, fits, limits, etc. •••

$\Gamma(K_S^0 \pi^- 2e^+)/\Gamma_{\text{total}}$ Γ_{157}/Γ

VALUE	CL%	DOCUMENT ID	TECN	COMMENT
$<3.3 \times 10^{-6}$	90	ABLIKIM	19AL	BES3 $e^+ e^-$ at 3773 MeV

$\Gamma(K^- \pi^0 2e^+)/\Gamma_{\text{total}}$ Γ_{158}/Γ

VALUE	CL%	DOCUMENT ID	TECN	COMMENT
$<8.5 \times 10^{-6}$	90	ABLIKIM	19AL	BES3 $e^+ e^-$ at 3773 MeV

$\Gamma(K^- 2\mu^+)/\Gamma_{\text{total}}$ Γ_{159}/Γ

A test of lepton-number conservation.

VALUE	CL%	DOCUMENT ID	TECN	COMMENT
$<10 \times 10^{-6}$	90	LEES	11G	BABR $e^+ e^- \approx \Upsilon(4S)$
$<1.3 \times 10^{-5}$	90	LINK	03F	FOCS γ A, $\bar{E}_\gamma \approx 180$ GeV
$<1.2 \times 10^{-4}$	90	FRABETTI	97B	E687 γ Be, $\bar{E}_\gamma \approx 220$ GeV
$<3.2 \times 10^{-4}$	90	KODAMA	95	E653 π^- emulsion 600 GeV
$<4.3 \times 10^{-3}$	90	WEIR	90B	MRK2 $e^+ e^-$ 29 GeV

••• We do not use the following data for averages, fits, limits, etc. •••

$\Gamma(K^- e^+ \mu^+)/\Gamma_{\text{total}}$ Γ_{160}/Γ

A test of lepton-number conservation.

VALUE	CL%	DOCUMENT ID	TECN	COMMENT
$<1.9 \times 10^{-6}$	90	LEES	11G	BABR $e^+ e^- \approx \Upsilon(4S)$
$<1.3 \times 10^{-4}$	90	FRABETTI	97B	E687 γ Be, $\bar{E}_\gamma \approx 220$ GeV
$<4.0 \times 10^{-3}$	90	WEIR	90B	MRK2 $e^+ e^-$ 29 GeV

••• We do not use the following data for averages, fits, limits, etc. •••

$\Gamma(K^*(892) - 2\mu^+)/\Gamma_{\text{total}}$ Γ_{161}/Γ

A test of lepton-number conservation.

VALUE	CL%	DOCUMENT ID	TECN	COMMENT
$<8.5 \times 10^{-4}$	90	KODAMA	95	E653 π^- emulsion 600 GeV

D^\pm CP-VIOLATING DECAY-RATE ASYMMETRIES

This is the difference between D^+ and D^- partial widths for the decay to state f , divided by the sum of the widths:
 $A_{CP}(f) = [\Gamma(D^+ \rightarrow f) - \Gamma(D^- \rightarrow \bar{f})] / [\Gamma(D^+ \rightarrow f) + \Gamma(D^- \rightarrow \bar{f})]$.

$A_{CP}(\mu^\pm \nu)$ in $D^+ \rightarrow \mu^+ \nu_\mu$, $D^- \rightarrow \mu^- \bar{\nu}_\mu$

VALUE (%)	DOCUMENT ID	TECN	COMMENT
$+8 \pm 8$	EISENSTEIN 08	CLEO	$e^+ e^-$ at $\psi(3770)$

$A_{CP}(K_L^0 e^\pm \nu)$ in $D^+ \rightarrow K_L^0 e^+ \nu_e$, $D^- \rightarrow K_L^0 e^- \bar{\nu}_e$

VALUE (%)	DOCUMENT ID	TECN	COMMENT
$-0.59 \pm 0.60 \pm 1.48$	ABLIKIM 15AF	BES3	$e^+ e^-$ 3773 MeV

$A_{CP}(K_S^0 \pi^\pm)$ in $D^\pm \rightarrow K_S^0 \pi^\pm$

VALUE (%)	EVTS	DOCUMENT ID	TECN	COMMENT
-0.41 ± 0.09	OUR AVERAGE			
$-1.1 \pm 0.6 \pm 0.2$		BONVICINI 14	CLEO	All CLEO-c runs
$-0.363 \pm 0.094 \pm 0.067$	1738k	¹ KO	12A	BELL $e^+ e^- \approx \Upsilon(nS)$
$-0.44 \pm 0.13 \pm 0.10$	807k	DEL-AMO-SA...	11H	BABR $e^+ e^- \approx \Upsilon(4S)$
$-1.6 \pm 1.5 \pm 0.9$	10.6k	² LINK	02B	FOCS γ nucleus, $\bar{E}_\gamma \approx 180$ GeV
$-0.71 \pm 0.19 \pm 0.20$		KO	10	BELL See KO 12A
$-1.3 \pm 0.7 \pm 0.3$	30k	MENDEZ	10	CLEO See BONVICINI 14
$-0.6 \pm 1.0 \pm 0.3$		DOBBS	07	CLEO See MENDEZ 10

••• We do not use the following data for averages, fits, limits, etc. •••

¹ KO 12A finds that after subtracting the contribution due to $K^0 - \bar{K}^0$ mixing, the CP asymmetry due to the change of charm is $(-0.024 \pm 0.094 \pm 0.067)\%$, consistent with zero.
² LINK 02B measures $N(D^+ \rightarrow K_S^0 \pi^+) / N(D^+ \rightarrow K^- \pi^+ \pi^+)$, the ratio of numbers of events observed, and similarly for the D^- .

$A_{CP}(K_L^0 K^\pm)$ in $D^\pm \rightarrow K_L^0 K^\pm$

VALUE (units 10^{-2})	EVTS	DOCUMENT ID	TECN	COMMENT
$-4.2 \pm 3.2 \pm 1.2$	650	ABLIKIM 19M	BES3	$e^+ e^-$ at 3773 MeV

$A_{CP}(K^\mp 2\pi^\pm)$ in $D^+ \rightarrow K^- 2\pi^+$, $D^- \rightarrow K^+ 2\pi^-$

VALUE (%)	EVTS	DOCUMENT ID	TECN	COMMENT
-0.18 ± 0.16	OUR AVERAGE			
$-0.16 \pm 0.15 \pm 0.09$	2.3M	ABAZOV	14L	D0 $p\bar{p}$, $\sqrt{s} = 1.96$ TeV
$-0.3 \pm 0.2 \pm 0.4$		BONVICINI 14	CLEO	All CLEO-c runs
$-0.1 \pm 0.4 \pm 0.9$	231k	MENDEZ	10	CLEO See BONVICINI 14
$-0.5 \pm 0.4 \pm 0.9$		DOBBS	07	CLEO See MENDEZ 10

••• We do not use the following data for averages, fits, limits, etc. •••

$A_{CP}(K^\mp \pi^\pm \pi^\pm \pi^0)$ in $D^+ \rightarrow K^- \pi^+ \pi^+ \pi^0$, $D^- \rightarrow K^+ \pi^- \pi^- \pi^0$

VALUE (%)	DOCUMENT ID	TECN	COMMENT
$-0.3 \pm 0.6 \pm 0.4$	BONVICINI 14	CLEO	All CLEO-c runs
$1.0 \pm 0.9 \pm 0.9$	DOBBS 07	CLEO	See BONVICINI 14

••• We do not use the following data for averages, fits, limits, etc. •••

$A_{CP}(K_S^0 \pi^\pm \pi^0)$ in $D^+ \rightarrow K_S^0 \pi^+ \pi^0$, $D^- \rightarrow K_S^0 \pi^- \pi^0$

VALUE (%)	DOCUMENT ID	TECN	COMMENT
$-0.1 \pm 0.7 \pm 0.2$	BONVICINI 14	CLEO	All CLEO-c runs
$0.3 \pm 0.9 \pm 0.3$	DOBBS 07	CLEO	See BONVICINI 14

••• We do not use the following data for averages, fits, limits, etc. •••

$A_{CP}(K_S^0 \pi^\pm \pi^+ \pi^-)$ in $D^+ \rightarrow K_S^0 \pi^+ \pi^+ \pi^-$, $D^- \rightarrow K_S^0 \pi^- \pi^- \pi^+$

VALUE (%)	DOCUMENT ID	TECN	COMMENT
$0.0 \pm 1.2 \pm 0.3$	BONVICINI 14	CLEO	All CLEO-c runs
$0.1 \pm 1.1 \pm 0.6$	DOBBS 07	CLEO	See BONVICINI 14

••• We do not use the following data for averages, fits, limits, etc. •••

$A_{CP}(\pi^\pm \pi^0)$ in $D^\pm \rightarrow \pi^\pm \pi^0$

VALUE (%)	EVTS	DOCUMENT ID	TECN	COMMENT
2.4 ± 1.2	OUR AVERAGE			
$2.31 \pm 1.24 \pm 0.23$	108k	BABU	18	BELL At/near $\Upsilon(4S)$, $\Upsilon(5S)$
$2.9 \pm 2.9 \pm 0.3$	2.6k	MENDEZ	10	CLEO $e^+ e^-$ at 3774 MeV

$A_{CP}(\pi^\pm \eta)$ in $D^\pm \rightarrow \pi^\pm \eta$

VALUE (%)	EVTS	DOCUMENT ID	TECN	COMMENT
1.0 ± 1.5	OUR AVERAGE			Error includes scale factor of 1.4.
$+1.74 \pm 1.13 \pm 0.19$		WON	11	BELL $e^+ e^- \approx \Upsilon(4S)$
$-2.0 \pm 2.3 \pm 0.3$	2.9k	MENDEZ	10	CLEO $e^+ e^-$ at 3774 MeV

$A_{CP}(\pi^\pm \eta'(958))$ in $D^\pm \rightarrow \pi^\pm \eta'(958)$

VALUE (%)	EVTS	DOCUMENT ID	TECN	COMMENT
-0.6 ± 0.7	OUR AVERAGE			
$-0.61 \pm 0.72 \pm 0.54$	63k	AAIJ	17AF	LHCB pp at 7, 8 TeV
$-0.12 \pm 1.12 \pm 0.17$		WON	11	BELL $e^+ e^- \approx \Upsilon(4S)$
$-4.0 \pm 3.4 \pm 0.3$	1.0k	MENDEZ	10	CLEO $e^+ e^-$ at 3774 MeV

See key on page 999

Meson Particle Listings

 D^\pm $A_{CP}(\bar{K}^0/K^0 K^\pm)$ in $D^+ \rightarrow \bar{K}^0 K^+$, $D^- \rightarrow K^0 K^-$

VALUE (%)	EVTS	DOCUMENT ID	TECN	COMMENT
-----------	------	-------------	------	---------

0.11 ± 0.17 OUR AVERAGE

0.03 ± 0.17 ± 0.14	1.0M	¹ AAIJ	14BD LHCb	pp at 7, 8 TeV
0.08 ± 0.28 ± 0.14	277k	KO	13 BELL	e^+e^- at $\Upsilon(4S)$
0.46 ± 0.36 ± 0.25	159k	LEES	13E BABR	e^+e^- at $\Upsilon(4S)$

¹ AAIJ 14BD reports its result as $A_{CP}(D^\pm \rightarrow K_S^0 \pi^\pm)$ with CP -violation effects in the $K^0 - \bar{K}^0$ system subtracted. It also measures $A_{CP}(D^\pm \rightarrow \bar{K}^0/K^0 K^\pm) + A_{CP}(D_S^\pm \rightarrow \bar{K}^0/K^0 \pi^\pm) = (0.41 \pm 0.49 \pm 0.26)\%$.

 $A_{CP}(K_S^0 K^\pm)$ in $D^\pm \rightarrow K_S^0 K^\pm$

VALUE (%)	EVTS	DOCUMENT ID	TECN	COMMENT
-----------	------	-------------	------	---------

-0.01 ± 0.07 OUR AVERAGE

-0.004 ± 0.061 ± 0.045	6M	AAIJ	19T LHCb	pp at 7, 8, 13 TeV
-1.8 ± 2.7 ± 1.6	780	ABLIKIM	19M BES3	e^+e^- at 3773 MeV
-0.25 ± 0.28 ± 0.14	277k	KO	13 BELL	e^+e^- at $\Upsilon(nS)$
0.13 ± 0.36 ± 0.25	159k	LEES	13E BABR	e^+e^- at $\Upsilon(4S)$
-0.2 ± 1.5 ± 0.9	5.2k	MENDEZ	10 CLEO	e^+e^- at 3774 MeV
7.1 ± 6.1 ± 1.2	949	¹ LINK	02B FOCS	γ nucleus, $\bar{E}_\gamma \approx 180$ GeV

• • • We do not use the following data for averages, fits, limits, etc. • • •

-0.16 ± 0.58 ± 0.25		KO	10 BELL	$e^+e^- \approx \Upsilon(4S)$
6.9 ± 6.0 ± 1.5	949	² LINK	02B FOCS	γ nucleus, $\bar{E}_\gamma \approx 180$ GeV

¹ LINK 02B measures $N(D^+ \rightarrow K_S^0 K^+)/N(D^+ \rightarrow K_S^0 \pi^+)$, the ratio of numbers of events observed, and similarly for the D^- .

² LINK 02B measures $N(D^+ \rightarrow K_S^0 K^+)/N(D^+ \rightarrow K^- \pi^+ \pi^+)$, the ratio of numbers of events observed, and similarly for the D^- .

 $A_{CP}(K_S^0 K^\pm \pi^0)$ in $D^\pm \rightarrow K_S^0 K^\pm \pi^0$

VALUE (units 10^{-2})	EVTS	DOCUMENT ID	TECN	COMMENT
--------------------------	------	-------------	------	---------

1.4 ± 3.7 ± 2.4	470	ABLIKIM	19M BES3	e^+e^- at 3773 MeV
------------------------	-----	---------	----------	----------------------

 $A_{CP}(K_L^0 K^\pm \pi^0)$ in $D^\pm \rightarrow K_L^0 K^\pm \pi^0$

VALUE (units 10^{-2})	EVTS	DOCUMENT ID	TECN	COMMENT
--------------------------	------	-------------	------	---------

-0.6 ± 4.1 ± 1.7	410	ABLIKIM	19M BES3	e^+e^- at 3773 MeV
-------------------------	-----	---------	----------	----------------------

 $A_{CP}(K^+ K^- \pi^\pm)$ in $D^\pm \rightarrow K^+ K^- \pi^\pm$

See also AAIJ 11G for a search for CP asymmetry in the $D^\pm \rightarrow K^+ K^- \pi^\pm$ Dalitz plots using 370k decays and four different binning schemes. No evidence for CP asymmetry was found.

VALUE (%)	EVTS	DOCUMENT ID	TECN	COMMENT
-----------	------	-------------	------	---------

0.37 ± 0.29 OUR AVERAGE

0.37 ± 0.30 ± 0.15	224k	¹ LEES	13F BABR	e^+e^- at $\Upsilon(4S)$
-0.03 ± 0.84 ± 0.29		RUBIN	08 CLEO	e^+e^- at 3774 MeV
1.4 ± 1.0 ± 0.8	43k	² AUBERT	05S BABR	e^+e^- at $\Upsilon(4S)$
0.6 ± 1.1 ± 0.5	14k	³ LINK	00B FOCS	
-1.4 ± 2.9		³ AITALA	97B E791	-0.062 $<A_{CP} <$ +0.034 (90% CL)
-3.1 ± 6.8		³ FRABETTI	94I E687	-0.14 $<A_{CP} <$ +0.081 (90% CL)

• • • We do not use the following data for averages, fits, limits, etc. • • •

-0.1 ± 0.9 ± 0.4		⁴ BONVICINI	14 CLEO	See RUBIN 08
-0.1 ± 1.5 ± 0.8		DOBBS	07 CLEO	See BONVICINI 14 and RUBIN 08

¹ This is the integrated CP asymmetry. LEES 13F also searches for CP asymmetries in four regions of the Dalitz plots (two of which are listed below); in comparisons of binned D^+ and D^- Dalitz plots; in parametrized fits to those plots, including 2-body submodes; and in comparisons of Legendre-polynomial distributions for the $K^+ K^-$ and $K^- \pi^+$ systems.

² AUBERT 05S measures $N(D^+ \rightarrow K^+ K^- \pi^+)/N(D_S^+ \rightarrow K^+ K^- \pi^+)$, the ratio of the numbers of events observed, and similarly for the D^- .

³ FRABETTI 94I, AITALA 98C, and LINK 00B measure $N(D^+ \rightarrow K^- K^+ \pi^+)/N(D^+ \rightarrow K^- \pi^+ \pi^+)$, the ratio of numbers of events observed, and similarly for the D^- .

⁴ RUBIN 08 performs a dedicated analysis of this decay mode on the same dataset, with slightly better precision. We therefore take it that BONVICINI 14 does not supersede RUBIN 08's A_{CP} result.

 $A_{CP}(K^\pm K^*0)$ in $D^+ \rightarrow K^+ \bar{K}^{*0}$, $D^- \rightarrow K^- K^{*0}$

VALUE (%)	EVTS	DOCUMENT ID	TECN	COMMENT
-----------	------	-------------	------	---------

-0.3 ± 0.4 OUR AVERAGE

-0.3 ± 0.4 ± 0.2	73k	¹ LEES	13F BABR	e^+e^- at $\Upsilon(4S)$
-0.4 ± 2.0 ± 0.6		RUBIN	08 CLEO	Fit-fraction asymmetry
+0.9 ± 1.7 ± 0.7	11k	² AUBERT	05S BABR	e^+e^- at $\Upsilon(4S)$
-1.0 ± 5.0		³ AITALA	97B E791	-0.092 $<A_{CP} <$ +0.072 (90% CL)
-12 ± 13		³ FRABETTI	94I E687	-0.33 $<A_{CP} <$ +0.094 (90% CL)

¹ This LEES 13F result is for the $K^\mp \pi^\pm$ mass-squared between 0.4 and 1.0 GeV^2 , and does not actually separate out the K^* .

² AUBERT 05S measures $N(D^+ \rightarrow K^+ \bar{K}^{*0})/N(D_S^+ \rightarrow K^+ K^- \pi^+)$, the ratio of the numbers of events observed, and similarly for the D^- .

³ FRABETTI 94I and AITALA 97B measure $N(D^+ \rightarrow K^+ \bar{K}^*(892)^0)/N(D^+ \rightarrow K^- \pi^+ \pi^+)$, the ratio of numbers of events observed, and similarly for the D^- .

 $A_{CP}(\phi \pi^\pm)$ in $D^\pm \rightarrow \phi \pi^\pm$

VALUE (%)	EVTS	DOCUMENT ID	TECN	COMMENT
-----------	------	-------------	------	---------

0.01 ± 0.09 OUR AVERAGE

0.003 ± 0.040 ± 0.029	55M	AAIJ	19T LHCb	pp at 7, 8, 13 TeV
-0.3 ± 0.3 ± 0.5	97k	¹ LEES	13F BABR	e^+e^- at $\Upsilon(4S)$
+0.51 ± 0.28 ± 0.05	237k	STARIC	12 BELL	Mainly at $\Upsilon(4S)$
-1.8 ± 1.6 ± 0.2 ± 0.4		RUBIN	08 CLEO	Fit-fraction asymmetry
+0.2 ± 1.5 ± 0.6	10k	² AUBERT	05S BABR	e^+e^- at $\Upsilon(4S)$
-2.8 ± 3.6		³ AITALA	97B E791	-0.087 $<A_{CP} <$ +0.031 (90% CL)
+6.6 ± 8.6		³ FRABETTI	94I E687	-0.075 $<A_{CP} <$ +0.21 (90% CL)

• • • We do not use the following data for averages, fits, limits, etc. • • •

-0.04 ± 0.14 ± 0.14	1.58M	⁴ AAIJ	13W LHCb	pp at 7 TeV
---------------------	-------	-------------------	----------	---------------

¹ This LEES 13F result is for the $K^+ K^-$ mass-squared less than 1.3 GeV^2 and the $K^\mp \pi^\pm$ mass-squared above 1.0 GeV^2 , and does not actually separate out the ϕ .

² AUBERT 05S measures $N(D^+ \rightarrow \phi \pi^+)/N(D_S^+ \rightarrow K^+ K^- \pi^+)$, the ratio of the numbers of events observed, and similarly for the D^- .

³ FRABETTI 94I and AITALA 97B measure $N(D^+ \rightarrow \phi \pi^+)/N(D^+ \rightarrow K^- \pi^+ \pi^+)$, the ratio of numbers of events observed, and similarly for the D^- .

⁴ See AAIJ 19T.

 $A_{CP}(K^\pm K_S^*(1430)^0)$ in $D^+ \rightarrow K^+ \bar{K}_S^{*0}(1430)^0$, $D^- \rightarrow K^- K_S^*(1430)^0$

VALUE (%)	DOCUMENT ID	TECN	COMMENT
-----------	-------------	------	---------

+8 ± 6 ± 4	RUBIN	08 CLEO	Fit-fraction asymmetry
-------------------	-------	---------	------------------------

 $A_{CP}(K^\pm K_2^*(1430)^0)$ in $D^+ \rightarrow K^+ \bar{K}_2^{*0}(1430)^0$, $D^- \rightarrow K^- K_2^*(1430)^0$

VALUE (%)	DOCUMENT ID	TECN	COMMENT
-----------	-------------	------	---------

+43 ± 19 ± 5	RUBIN	08 CLEO	Fit-fraction asymmetry
---------------------	-------	---------	------------------------

 $A_{CP}(K^\pm K_0^*(700))$ in $D^+ \rightarrow K^+ \bar{K}_0^{*0}(700)$, $D^- \rightarrow K^- K_0^*(700)$

VALUE (%)	DOCUMENT ID	TECN	COMMENT
-----------	-------------	------	---------

-12 ± 11 ± 14	RUBIN	08 CLEO	Fit-fraction asymmetry
----------------------	-------	---------	------------------------

 $A_{CP}(a_0(1450)^0 \pi^\pm)$ in $D^\pm \rightarrow a_0(1450)^0 \pi^\pm$

VALUE (%)	DOCUMENT ID	TECN	COMMENT
-----------	-------------	------	---------

-19 ± 12 ± 11	RUBIN	08 CLEO	Fit-fraction asymmetry
----------------------	-------	---------	------------------------

 $A_{CP}(\phi(1680) \pi^\pm)$ in $D^\pm \rightarrow \phi(1680) \pi^\pm$

VALUE (%)	DOCUMENT ID	TECN	COMMENT
-----------	-------------	------	---------

-9 ± 22 ± 14	RUBIN	08 CLEO	Fit-fraction asymmetry
---------------------	-------	---------	------------------------

 $A_{CP}(\pi^+ \pi^- \pi^\pm)$ in $D^\pm \rightarrow \pi^+ \pi^- \pi^\pm$

See also AAIJ 14C for a search for CP violation in $D^\pm \rightarrow \pi^+ \pi^- \pi^\pm$ Dalitz plots using model-independent binned and unbinned methods. No evidence was found.

VALUE (%)	DOCUMENT ID	TECN	COMMENT
-----------	-------------	------	---------

-1.7 ± 4.2	¹ AITALA	97B E791	-0.086 $<A_{CP} <$ +0.052 (90% CL)
-------------------	---------------------	----------	------------------------------------

¹ AITALA 97B measure $N(D^+ \rightarrow \pi^+ \pi^- \pi^+)/N(D^+ \rightarrow K^- \pi^+ \pi^+)$, the ratio of numbers of events observed, and similarly for the D^- .

 $A_{CP}(K_S^0 K^\pm \pi^+ \pi^-)$ in $D^\pm \rightarrow K_S^0 K^\pm \pi^+ \pi^-$

VALUE (%)	EVTS	DOCUMENT ID	TECN	COMMENT
-----------	------	-------------	------	---------

-4.2 ± 6.4 ± 2.2	523 ± 32	LINK	05E FOCS	γ A, $\bar{E}_\gamma \approx 180$ GeV
-------------------------	----------	------	----------	--

 $A_{CP}(K^\pm \pi^0)$ in $D^\pm \rightarrow K^\pm \pi^0$

VALUE (%)	EVTS	DOCUMENT ID	TECN	COMMENT
-----------	------	-------------	------	---------

-3.5 ± 10.7 ± 0.9	343 ± 37	MENDEZ	10 CLEO	e^+e^- at 3774 MeV
--------------------------	----------	--------	---------	----------------------

 $D^\pm \chi^2$ TESTS OF CP -VIOLATION (CPV)

We list model-independent searches for local CP violation in phase-space distributions of multi-body decays.

Most of these searches divide phase space (Dalitz plot for 3-body decays, five-dimensional equivalent for 4-body decays) into bins, and perform a χ^2 test comparing normalized yields N_i, \bar{N}_i in CP -conjugate bin pairs i : $\chi^2 = \sum_i (N_i - \alpha \bar{N}_i) / \sigma(N_i - \alpha \bar{N}_i)$. The factor $\alpha = (\sum_i N_i) / (\sum_i \bar{N}_i)$ removes the dependence on phase-space-integrated rate asymmetries. The result is used to obtain the probability (p-value) to obtain the measured χ^2 or larger under the assumption of CP conservation [AUBERT 08AO, BEDIAGA 09]. Alternative methods obtain p-values from other test variables based on unbinned analyses [WILLIAMS 11, AAIJ 14C]. Results can be combined using Fisher's method [MOSTELLER 48].

Local CPV in $D^\pm \rightarrow \pi^+ \pi^- \pi^\pm$

p-value (%)	EVTS	DOCUMENT ID	TECN	COMMENT
-------------	------	-------------	------	---------

78.1	3.1M	¹ AAIJ	14C LHCb	χ^2
-------------	------	-------------------	----------	----------

¹ AAIJ 14C uses binned and unbinned methods, and finds slightly better sensitivity with the former. We took the first value in the table of results for the binned method.

Meson Particle Listings

D^\pm

Local CPV in $D^\pm \rightarrow K^+ K^- \pi^\pm$

p-value (%)	EVTS	DOCUMENT ID	TECN	COMMENT
31 OUR EVALUATION				
72	224k	LEES	13F BABR	χ^2
12.7	370k	1 AAIJ	11G LHCB	χ^2

¹ AAIJ 11G publishes results for several binning schemes. We picked the first value in their table of results.

CP VIOLATING ASYMMETRIES OF P-ODD (T-ODD) MOMENTS

$A_{Tviol}(K_S^0 K^\pm \pi^\pm \pi^\mp)$ in $D^\pm \rightarrow K_S^0 K^\pm \pi^\pm \pi^\mp$

$C_T \equiv \bar{p}_{K^+} \cdot (\bar{p}_{\pi^+} \times \bar{p}_{\pi^-})$ is a parity-odd correlation of the K^+ , π^+ , and π^- momenta for the D^+ . $\bar{C}_T \equiv \bar{p}_{K^-} \cdot (\bar{p}_{\pi^-} \times \bar{p}_{\pi^+})$ is the corresponding quantity for the D^- . Then $A_T \equiv [\Gamma(C_T > 0) - \Gamma(C_T < 0)] / [\Gamma(C_T > 0) + \Gamma(C_T < 0)]$, and $\bar{A}_T \equiv [\Gamma(-\bar{C}_T > 0) - \Gamma(-\bar{C}_T < 0)] / [\Gamma(-\bar{C}_T > 0) + \Gamma(-\bar{C}_T < 0)]$, and $A_{Tviol} \equiv \frac{1}{2}(A_T - \bar{A}_T)$. C_T and \bar{C}_T are commonly referred to as T-odd moments, because they are odd under T reversal. However, the T-conjugate process $K_S^0 K^\pm \pi^\pm \pi^\mp \rightarrow D^\pm$ is not accessible, while the P-conjugate process is.

VALUE (units 10^{-3})	EVTS	DOCUMENT ID	TECN	COMMENT
$-12.0 \pm 10.0 \pm 4.6$	21.2 ± 0.4k	LEES	11E BABR	$e^+ e^- \approx \mathcal{T}(4S)$
••• We do not use the following data for averages, fits, limits, etc. •••				
23 $\pm 6.2 \pm 2.2$	523 ± 32	LINK	05E FOCS	$\gamma A, \bar{E}\gamma \approx 180$ GeV

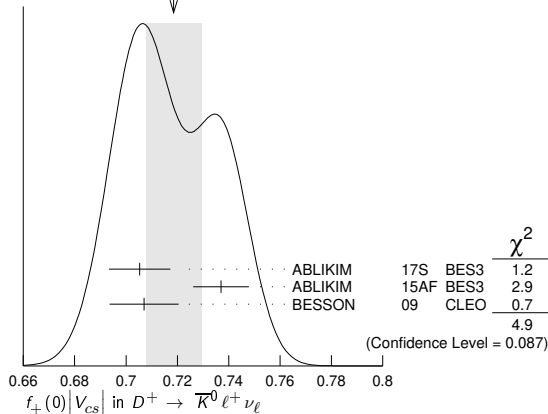
SEMILEPTONIC FORM FACTORS

$f_+(0)|V_{cs}|$ in $D^+ \rightarrow \bar{K}^0 \ell^+ \nu_\ell$

VALUE	EVTS	DOCUMENT ID	TECN	COMMENT
0.719 ± 0.011	OUR AVERAGE	Error includes scale factor of 1.6. See the ideogram below.		
0.7053 $\pm 0.0040 \pm 0.0112$		ABLIKIM	17s BES3	$K_S^0 e^+ \nu_e$ 2-parameter fit
0.737 $\pm 0.006 \pm 0.009$		1 ABLIKIM	15AF BES3	$K_L e^+ \nu_e$ 3-parameter fit
0.707 $\pm 0.010 \pm 0.009$		2 BESSON	09 CLEO	$K_S e^+ \nu_e$ 3-parameter fit

¹ ABLIKIM 15AF finds $0.728 \pm 0.006 \pm 0.011$ for a 2-parameter fit.
² BESSON 09 finds $0.716 \pm 0.007 \pm 0.009$ for a 2-parameter fit.

WEIGHTED AVERAGE
 0.719 ± 0.011 (Error scaled by 1.6)



$r_1 \equiv a_1/a_0$ in $D^+ \rightarrow \bar{K}^0 \ell^+ \nu_\ell$

VALUE	EVTS	DOCUMENT ID	TECN	COMMENT
-2.13 ± 0.14	OUR AVERAGE	Error includes scale factor of 1.5.		
$-2.18 \pm 0.14 \pm 0.05$		ABLIKIM	17s BES3	$K_S^0 e^+ \nu_e$ 2-parameter fit
$-2.23 \pm 0.42 \pm 0.53$	40k	1 ABLIKIM	15AF BES3	$K_L e^+ \nu_e$ 3-parameter fit
$-1.66 \pm 0.44 \pm 0.10$		2 BESSON	09 CLEO	$K_S e^+ \nu_e$ 3-parameter fit

¹ ABLIKIM 15AF finds $r_1 = -1.91 \pm 0.33 \pm 0.28$ for a 2-parameter fit.
² BESSON 09 finds $r_1 = -2.10 \pm 0.25 \pm 0.08$ for 2-parameter fit.

$r_2 \equiv a_2/a_0$ in $D^+ \rightarrow \bar{K}^0 \ell^+ \nu_\ell$

VALUE	EVTS	DOCUMENT ID	TECN	COMMENT
-3 ± 12	OUR AVERAGE	Error includes scale factor of 1.5.		
$+11 \pm 9 \pm 9$	40k	ABLIKIM	15AF BES3	$K_L e^+ \nu_e$ 3-parameter fit
$-14 \pm 11 \pm 1$		BESSON	09 CLEO	$K_S e^+ \nu_e$ 3-parameter fit

$f_+(0)|V_{cd}|$ in $D^+ \rightarrow \pi^0 \ell^+ \nu_\ell$

VALUE	EVTS	DOCUMENT ID	TECN	COMMENT
0.1407 ± 0.0025	OUR AVERAGE	Error includes scale factor of 1.5.		
$0.1400 \pm 0.0026 \pm 0.0007$		ABLIKIM	17s BES3	$\pi^0 e^+ \nu_e$ 2-parameter fit
$0.146 \pm 0.007 \pm 0.002$		BESSON	09 CLEO	$\pi^0 e^+ \nu_e$ 3-parameter fit

$r_1 \equiv a_1/a_0$ in $D^+ \rightarrow \pi^0 \ell^+ \nu_\ell$

VALUE	EVTS	DOCUMENT ID	TECN	COMMENT
-2.00 ± 0.13	OUR AVERAGE	Error includes scale factor of 1.5.		
$-2.01 \pm 0.13 \pm 0.02$		ABLIKIM	17s BES3	$\pi^0 e^+ \nu_e$ 2-parameter fit
$-1.37 \pm 0.88 \pm 0.24$		BESSON	09 CLEO	$\pi^0 e^+ \nu_e$ 3-parameter fit

$r_2 \equiv a_2/a_0$ in $D^+ \rightarrow \pi^0 \ell^+ \nu_\ell$

VALUE	EVTS	DOCUMENT ID	TECN	COMMENT
$-4 \pm 5 \pm 1$		BESSON	09 CLEO	$\pi^0 e^+ \nu_e$ 3-parameter fit

$f_+(0)|V_{cd}|$ in $D^+ \rightarrow \eta e^+ \nu_e$

VALUE (units 10^{-2})	EVTS	DOCUMENT ID	TECN	COMMENT
8.3 ± 0.5	OUR AVERAGE	Error includes scale factor of 1.9.		
$7.86 \pm 0.64 \pm 0.21$	373	ABLIKIM	18R BES3	z expansion
$8.6 \pm 0.6 \pm 0.1$		YELTON	11 CLEO	z expansion

$r_1 \equiv a_1/a_0$ in $D^+ \rightarrow \eta e^+ \nu_e$

VALUE (units 10^{-2})	EVTS	DOCUMENT ID	TECN	COMMENT
-5.3 ± 2.7	OUR AVERAGE	Error includes scale factor of 1.9.		
$-7.33 \pm 1.69 \pm 0.40$	373	ABLIKIM	18R BES3	z expansion
$-1.83 \pm 2.23 \pm 0.28$		YELTON	11 CLEO	z expansion

$r_V \equiv V(0)/A_1(0)$ in $D^+ \rightarrow \omega e^+ \nu_e$

VALUE	EVTS	DOCUMENT ID	TECN	COMMENT
$1.24 \pm 0.09 \pm 0.06$		ABLIKIM	15W BES3	$292 \text{ fb}^{-1}, 3773 \text{ MeV}$

$r_2 \equiv A_2(0)/A_1(0)$ in $D^+ \rightarrow \omega e^+ \nu_e$

VALUE	EVTS	DOCUMENT ID	TECN	COMMENT
$1.06 \pm 0.15 \pm 0.05$		ABLIKIM	15W BES3	$292 \text{ fb}^{-1}, 3773 \text{ MeV}$

$r_V \equiv V(0)/A_1(0)$ in $D^+, D^0 \rightarrow \rho e^+ \nu_e$

VALUE	EVTS	DOCUMENT ID	TECN	COMMENT
1.64 ± 0.10	OUR AVERAGE	Error includes scale factor of 1.2.		
$1.695 \pm 0.083 \pm 0.051$	2.5k	1 ABLIKIM	19c BES3	$e^+ e^-$ at 3773 MeV
$1.48 \pm 0.15 \pm 0.05$		1,2 DOBBS	13 CLEO	$e^+ e^-$ at $\psi(3770)$

¹ Uses both D^+ and D^0 events.
² Using PDG 10 values of V_{cd} and lifetimes, DOBBS 13 gets $A_1(0) = 0.56 \pm 0.01 \pm 0.02, A_2(0) = 0.47 \pm 0.06 \pm 0.04$, and $V(0) = 0.84 \pm 0.09 \pm 0.05$.

$r_2 \equiv A_2(0)/A_1(0)$ in $D^+, D^0 \rightarrow \rho e^+ \nu_e$

VALUE	EVTS	DOCUMENT ID	TECN	COMMENT
0.84 ± 0.06	OUR AVERAGE	Error includes scale factor of 1.2.		
$0.845 \pm 0.056 \pm 0.039$	2.5k	1 ABLIKIM	19c BES3	$e^+ e^-$ at 3773 MeV
$0.83 \pm 0.11 \pm 0.04$		1,2 DOBBS	13 CLEO	$e^+ e^-$ at $\psi(3770)$

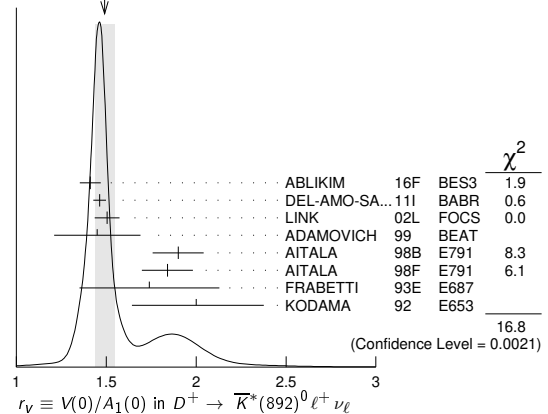
¹ Uses both D^+ and D^0 events.
² Using PDG 10 values of V_{cd} and lifetimes, DOBBS 13 gets $A_1(0) = 0.56 \pm 0.01 \pm 0.02, A_2(0) = 0.47 \pm 0.06 \pm 0.04$, and $V(0) = 0.84 \pm 0.09 \pm 0.05$.

$r_V \equiv V(0)/A_1(0)$ in $D^+ \rightarrow \bar{K}^*(892)^0 \ell^+ \nu_\ell$

See also BRIERE 10 for $\bar{K}^* \ell^+ \nu_\ell$ helicity-basis form-factor measurements.

VALUE	EVTS	DOCUMENT ID	TECN	COMMENT
1.49 ± 0.05	OUR AVERAGE	Error includes scale factor of 2.1. See the ideogram below.		
$1.411 \pm 0.058 \pm 0.007$	16.2k	ABLIKIM	16F BES3	$\bar{K}^*(892)^0 e^+ \nu_e$
$1.463 \pm 0.017 \pm 0.031$		1 DEL-AMO-SA...	11I BABR	
$1.504 \pm 0.057 \pm 0.039$	15k	2 LINK	02L FOCS	$\bar{K}^*(892)^0 \mu^+ \nu_\mu$
$1.45 \pm 0.23 \pm 0.07$	763	ADAMOVICH	99 BEAT	$\bar{K}^*(892)^0 \mu^+ \nu_\mu$
$1.90 \pm 0.11 \pm 0.09$	3000	3 AITALA	98B E791	$\bar{K}^*(892)^0 e^+ \nu_e$
$1.84 \pm 0.11 \pm 0.09$	3034	AITALA	98F E791	$\bar{K}^*(892)^0 \mu^+ \nu_\mu$
$1.74 \pm 0.27 \pm 0.28$	874	FRABETTI	93E E687	$\bar{K}^*(892)^0 \mu^+ \nu_\mu$
$2.00 \pm 0.34 \pm 0.16$	305	KODAMA	92 E653	$\bar{K}^*(892)^0 \mu^+ \nu_\mu$
••• We do not use the following data for averages, fits, limits, etc. •••				
$2.0 \pm 0.6 \pm 0.3$	183	ANJOS	90E E691	$\bar{K}^*(892)^0 e^+ \nu_e$

WEIGHTED AVERAGE
 1.49 ± 0.05 (Error scaled by 2.1)



¹ DEL-AMO-SANCHEZ 11I finds the pole mass $m_A = (2.63 \pm 0.10 \pm 0.13) \text{ GeV}$ (m_V is fixed at 2 GeV).

² LINK 02L includes the effects of interference with an S-wave background. This much improves the goodness of fit, but does not much shift the values of the form factors.

See key on page 999

Meson Particle Listings D±

3 This is slightly different from the AITALA 98B value: see ref. [5] in AITALA 98F.

r2 ≡ A2(0)/A1(0) in D+ → K*(892)0 e+ νe

See also BRIERE 10 for K* e+ νe helicity-basis form-factor measurements.

Table with columns: VALUE, EVTS, DOCUMENT ID, TECN, COMMENT. Contains data for various experiments like ABLIKIM, DEL-AMO-SA, ADAMOVICH, AITALA, FRABETTI, KODAMA.

• • • We do not use the following data for averages, fits, limits, etc. • • •

1 DEL-AMO-SANCHEZ 11i finds the pole mass mA = (2.63 ± 0.10 ± 0.13) GeV (mV is fixed at 2 GeV).

2 LINK 02L includes the effects of interference with an S-wave background. This much improves the goodness of fit, but does not much shift the values of the form factors.

r3 ≡ A3(0)/A1(0) in D+ → K*(892)0 e+ νe

See also BRIERE 10 for K* e+ νe helicity-basis form-factor measurements.

Table with columns: VALUE, EVTS, DOCUMENT ID, TECN, COMMENT. Contains data for AITALA 98F E791.

ΓL/ΓT in D+ → K*(892)0 e+ νe

See also BRIERE 10 for K* e+ νe helicity-basis form-factor measurements.

Table with columns: VALUE, EVTS, DOCUMENT ID, TECN, COMMENT. Contains data for ADAMOVICH, FRABETTI, KODAMA, ANJOS.

• • • We do not use the following data for averages, fits, limits, etc. • • •

Γ+/Γ- in D+ → K*(892)0 e+ νe

See also BRIERE 10 for K* e+ νe helicity-basis form-factor measurements.

Table with columns: VALUE, EVTS, DOCUMENT ID, TECN, COMMENT. Contains data for ADAMOVICH, KODAMA, ANJOS.

Amplitude analyses

D → Kπππ partial wave analyses

Amplitude analyses of D+ decays to a variety of 4-body kaon or pion final states, fitting simultaneously different partial wave components.

Table with columns: VALUE, DOCUMENT ID, TECN, COMMENT. Contains data for ABLIKIM 19aZ BES3 D+ → K0S π+ π+ π-.

D± REFERENCES

Large table listing references for D± mesons, including authors, document IDs, and techniques.

Large table listing references for D± mesons, including authors, document IDs, and techniques.

Downloaded from https://academic.oup.com/ptep/article/2020/8/083C01/5891211 by guest on 20 August 2020

Meson Particle Listings

D^\pm, D^0

Author	Year	Ref	Collab.
FRABETTI	94I	PR D50 2953	P.L. Frabetti et al. (FNAL E687 Collab.)
AKERIB	93	PRL 71 3070	D.S. Akerib et al. (CLEO Collab.)
ANJOS	93	PR D48 56	J.C. Anjos et al. (FNAL E691 Collab.)
FRABETTI	93E	PL B307 262	P.L. Frabetti et al. (FNAL E687 Collab.)
ALBRECHT	92F	PL B278 202	H. Albrecht et al. (ARGUS Collab.)
ANJOS	92C	PR D46 1941	J.C. Anjos et al. (FNAL E691 Collab.)
BARLAG	92C	ZPHY C55 383	S. Barlag et al. (ACCMOR Collab.)
Also		ZPHY C49 29	D.M. Coffman et al. (ACCMOR Collab.)
COFFMAN	92B	PR D45 2196	D.M. Coffman et al. (Mark III Collab.)
DAOUDI	92	PR D45 3965	M. Daoudi et al. (CLEO Collab.)
KODAMA	92	PL B274 246	K. Kodama et al. (FNAL E653 Collab.)
KODAMA	92C	PL B286 187	K. Kodama et al. (FNAL E653 Collab.)
ADAMOVICH	91	PL B268 142	M.I. Adamovich et al. (WA82 Collab.)
ALBRECHT	91	PL B255 634	H. Albrecht et al. (ARGUS Collab.)
ALVAREZ	91B	ZPHY C50 11	M.P. Alvarez et al. (CERN NA14/2 Collab.)
AMMAR	91	PR D44 3383	R. Ammar et al. (CLEO Collab.)
BAI	91	PRL 66 1011	Z. Bai et al. (Mark III Collab.)
COFFMAN	91	PL B263 135	D.M. Coffman et al. (Mark III Collab.)
FRABETTI	91	PL B263 584	P.L. Frabetti et al. (FNAL E687 Collab.)
ALVAREZ	90	ZPHY C47 539	M.P. Alvarez et al. (CERN NA14/2 Collab.)
ANJOS	90C	PR D41 2705	J.C. Anjos et al. (FNAL E691 Collab.)
ANJOS	90D	PR D42 2414	J.C. Anjos et al. (FNAL E691 Collab.)
ANJOS	90E	PRL 65 2630	J.C. Anjos et al. (FNAL E691 Collab.)
BARLAG	90C	ZPHY C46 563	S. Barlag et al. (ACCMOR Collab.)
WEIR	90B	PR D41 1384	A.J. Weir et al. (Mark II Collab.)
ANJOS	89	PRL 62 125	J.C. Anjos et al. (FNAL E691 Collab.)
ANJOS	89B	PRL 62 722	J.C. Anjos et al. (FNAL E691 Collab.)
ANJOS	89E	PL B223 267	J.C. Anjos et al. (FNAL E691 Collab.)
ADLER	88C	PRL 60 89	J. Adler et al. (Mark III Collab.)
ALBRECHT	88I	PL B210 267	H. Albrecht et al. (ARGUS Collab.)
HAAS	88	PRL 60 1614	P. Haas et al. (CLEO Collab.)
ONG	88	PRL 60 2587	R.A. Ong et al. (Mark II Collab.)
RAAB	88	PR D37 2391	J.R. Raab et al. (FNAL E691 Collab.)
ADAMOVICH	87	EPL 4 887	M.I. Adamovich et al. (Photon Emulsion Collab.)
ADLER	87	PL B196 107	J. Adler et al. (Mark III Collab.)
BARTEL	87	ZPHY C33 339	W. Bartel et al. (JADE Collab.)
BALTRUSAITIS	86E	PRL 56 2140	R.M. Baltrusaitis et al. (Mark III Collab.)
BALTRUSAITIS	85B	PRL 54 1976	R.M. Baltrusaitis et al. (Mark III Collab.)
BALTRUSAITIS	85E	PRL 55 150	R.M. Baltrusaitis et al. (Mark III Collab.)
BARTEL	85J	PL 163B 277	W. Bartel et al. (JADE Collab.)
ADAMOVICH	84	PL 140B 119	M.I. Adamovich et al. (CERN WA92 Collab.)
ALTHOFF	84G	ZPHY C22 219	M. Althoff et al. (TASSO Collab.)
DERRICK	84	PRL 53 1971	M. Derrick et al. (HRS Collab.)
SCHINDLER	81	PR D24 78	R.H. Schindler et al. (Mark II Collab.)
TRILLING	81	PRPL 75 57	G.H. Trilling et al. (LBL, UCJ)
ZHOLENTZ	80	PL 96B 214	A.A. Zholents et al. (NOVO)
Also		SJNP 34 814	A.A. Zholents et al. (NOVO)
Also		Translated from YAF 34 1471.	
GOLDBABER	77	PL 69B 503	G. Goldhaber et al. (Mark I Collab.)
PERUZZI	77	PRL 39 1301	I. Peruzzi et al. (LGV Collab.)
PICCOLO	77	PL 70B 240	M. Piccolo et al. (Mark I Collab.)
PERUZZI	76	PRL 37 569	I. Peruzzi et al. (Mark I Collab.)
MOSTELLER	48	Am.Stat. 3 No.5 30	R.A. Fisher, F. Mosteller

OTHER RELATED PAPERS

Author	Year	Ref	Collab.
RICHMAN	95	RMP 67 893	J.D. Richman, P.R. Burchat (UCSB, STAN)
ROSNER	95	CNPP 21 369	J. Rosner (CHIC)



$$I(J^P) = \frac{1}{2}(0^-)$$

D^0 MASS

The fit includes $D^\pm, D^0, D_S^\pm, D^{*\pm}, D^{*0}, D_S^{*\pm}, D_1(2420)^0, D_2^*(2460)^0$, and $D_{S1}(2536)^\pm$ mass and mass difference measurements.

Given the recent addition of much more precise measurements, we have omitted all those masses published up through 1990. See any Review before 2015 for those earlier results.

VALUE (MeV)	EVTS	DOCUMENT ID	TECN	COMMENT
1864.83 ± 0.05 OUR FIT				
1864.84 ± 0.05 OUR AVERAGE				
1864.845 ± 0.025 ± 0.057	63k	¹ TOMARADZE 14	LHCB	$D^0 \rightarrow K^- 2\pi^+ \pi^-$
1864.75 ± 0.15 ± 0.11		AAIJ 13v	LHCB	$D^0 \rightarrow K^+ 2K^- \pi^+$
1864.841 ± 0.048 ± 0.063	4.3k	² LEES 13s	BABR	e^+e^- at $\Upsilon(4S)$
1865.30 ± 0.33 ± 0.23	0.1k	ANASHIN 10A	KEDR	e^+e^- at $\psi(3770)$
1864.847 ± 0.150 ± 0.095	0.3k	CAWLFIELD 07	CLEO	$D^0 \rightarrow K_S^0 \phi$

¹ Obtained by analyzing CLEO-c data but not authored by the CLEO Collaboration. The largest source of error in the TOMARADZE 14 value is from the uncertainties in the K^- and K_S^0 masses. The systematic error given above is the addition in quadrature of $\pm 0.022 \pm 0.053$ MeV, where the second error is from those mass uncertainties.

² The largest source of error in the LEES 13s value is from the uncertainty of the K^+ mass. The quoted systematic error is in fact $\pm 0.043 + 3 (m_{K^+} - 493.677)$, in MeV.

$m_{D^\pm} - m_{D^0}$

The fit includes $D^\pm, D^0, D_S^\pm, D^{*\pm}, D^{*0}, D_S^{*\pm}, D_1(2420)^0, D_2^*(2460)^0$, and $D_{S1}(2536)^\pm$ mass and mass difference measurements.

VALUE (MeV)	DOCUMENT ID	TECN	COMMENT
4.822 ± 0.015 OUR FIT			
4.76 ± 0.12 ± 0.07	AAIJ 13v	LHCB	$D^+ \rightarrow K^+ K^- \pi^+$

D^0 MEAN LIFE

Measurements with an error $> 10 \times 10^{-15}$ s have been omitted from the average.

VALUE (10^{-15} s)	EVTS	DOCUMENT ID	TECN	COMMENT
410.1 ± 1.5 OUR AVERAGE				
409.6 ± 1.1 ± 1.5	210k	LINK 02F	FOCS	γ nucleus, ≈ 180 GeV
407.9 ± 6.0 ± 4.3	10k	KUSHNIR... 01	SELX	$K^- \pi^+, K^- \pi^+ \pi^+ \pi^-$
413 ± 3 ± 4	35k	AITALA 99E	E791	$K^- \pi^+$
408.5 ± 4.1 ± 3.5	25k	BONVICINI 99	CLE2	$e^+e^- \approx \Upsilon(4S)$
413 ± 4 ± 3	16k	FRABETTI 94D	E687	$K^- \pi^+, K^- \pi^+ \pi^+ \pi^-$
• • • We do not use the following data for averages, fits, limits, etc. • • •				
424 ± 11 ± 7	5118	FRABETTI 91	E687	$K^- \pi^+, K^- \pi^+ \pi^+ \pi^-$
417 ± 18 ± 15	890	ALVAREZ 90	NA14	$K^- \pi^+, K^- \pi^+ \pi^+ \pi^-$
388 +23 -21	641	¹ BARLAG 90c	ACCM	π^- Cu 230 GeV
480 ± 40 ± 30	776	ALBRECHT 88I	ARG	e^+e^- 10 GeV
422 ± 8 ± 10	4212	RAAB 88	E691	Photoproduction
420 ± 50	90	BARLAG 87B	ACCM	K^- and π^- 200 GeV

¹ BARLAG 90c estimate systematic error to be negligible.

See the related review(s):

$D^0 - \bar{D}^0$ Mixing

$$|m_{D_1^0} - m_{D_2^0}| = x \Gamma$$

The D_1^0 and D_2^0 are the mass eigenstates of the D^0 meson, as described in the note on " $D^0 - \bar{D}^0$ Mixing," above. The experiments usually present $x \equiv \Delta m / \Gamma$. Then $\Delta m = x \Gamma = x \hbar / \tau$.

"OUR EVALUATION" comes from CPV allowing averages provided by the Heavy Flavor Averaging Group, see the note on " $D^0 - \bar{D}^0$ Mixing."

VALUE ($10^{10} \tau s^{-1}$)	CL%	DOCUMENT ID	TECN	COMMENT
0.95 ± 0.41 OUR EVALUATION				
0.7 ± 0.4 OUR AVERAGE				Error includes scale factor of 1.4. See the ideogram below.
0.66 +0.41 -0.37		¹ AAIJ 19x	LHCB	$D^0 \rightarrow K_S^0 \pi^+ \pi^-$
		² AAIJ 18k	LHCB	pp at 7, 8, 13 TeV
		³ AAIJ 16v	LHCB	pp at 7 TeV
- 2.10 ± 1.29 ± 0.41		⁴ LEES 16B	BABR	e^+e^- , 10.6 GeV
3.7 ± 2.9 ± 1.5		⁵ KO 14	BELL	$e^+e^- \rightarrow \Upsilon(nS)$
		⁶ PENG 14	BELL	$e^+e^- \rightarrow \Upsilon(nS)$
1.37 ± 0.46 +0.18 -0.28		⁷ AALTONEN 13AE	CDF	$p\bar{p}$ at 1.96 TeV
		⁸ DEL-AMO-SA. 10D	BABR	e^+e^- , 10.6 GeV
0.39 ± 0.56 ± 0.35				
• • • We do not use the following data for averages, fits, limits, etc. • • •				
6.4 +1.4 -1.7 ± 1.0		⁹ AAIJ 17A0	LHCB	Repl. by AAIJ 18k
		¹⁰ AAIJ 13CE	LHCB	Repl. by AAIJ 17A0
		¹¹ AAIJ 13N	LHCB	Repl. by AAIJ 13CE
- 2 +7 -6		¹² AUBERT 09AN	BABR	e^+e^- at 10.58 GeV
1.98 ± 0.73 +0.32 -0.41		¹³ LOWREY 09	CLEO	e^+e^- at $\psi(3770)$
< 7	95	¹⁴ ZHANG 07B	BELL	Repl. by PENG 14
-11 to +22		¹⁵ ZHANG 06	BELL	e^+e^-
< 11	90	¹⁴ ASNER 05	CLEO	$e^+e^- \approx 10$ GeV
< 30	90	BITENC 05	BELL	
< 7	95	CAWLFIELD 05	CLEO	
< 2	95	LI 05A	BELL	See ZHANG 06
< 22	95	¹⁶ LINK 05H	FOCS	γ nucleus
< 23	95	AUBERT 04q	BABR	
< 11	95	¹⁵ AUBERT 03z	BABR	e^+e^- , 10.6 GeV
< 7	95	¹⁷ GODANG 00	CLE2	e^+e^-
< 32	90	^{18,19} AITALA 98	E791	π^- nucleus, 500 GeV
< 24	90	²⁰ AITALA 96c	E791	π^- nucleus, 500 GeV
< 21	90	^{19,21} ANJOS 88c	E691	Photoproduction

¹ AAIJ 19x D^0 come from D^{*+} and $\bar{B} \rightarrow D^0 \mu^- X$ decays (and c.c.) in pp collisions at 7 and 8 TeV. Measurement allows for CP violation (none seen).

² The result was established with D^0 from prompt and secondary D^* . Based on 5 fb⁻¹ of data collected at $\sqrt{s} = 7, 8, 13$ TeV. Assumes no CP violation. Reported $x'^2 = (3.9 \pm 2.7) \times 10^{-5}$ and $y' = (5.28 \pm 0.52) \times 10^{-3}$, where $x' = x \cos(\delta) + y \sin(\delta)$, $y' = y$.

³ Model-independent measurement of the charm mixing parameters in the decay $D^0 \rightarrow K_S^0 \pi^+ \pi^-$ using 1.0 fb⁻¹ of LHCB data at $\sqrt{s} = 7$ TeV.

⁴ Time-dependent amplitude analysis of $D^0 \rightarrow \pi^+ \pi^- \pi^0$.

⁵ Based on 976 fb⁻¹ of data collected at $Y(nS)$ resonances. Assumes no CP violation. Reported $x'^2 = (0.09 \pm 0.22) \times 10^{-3}$ and $y' = (4.6 \pm 3.4) \times 10^{-3}$, where $x' = x \cos(\delta) + y \sin(\delta)$, $y' = y \cos(\delta) - x \sin(\delta)$ and δ is the strong phase between $D^0 \rightarrow K^+ \pi^-$ and $\bar{D}^0 \rightarrow K^+ \pi^-$.

⁶ The time-dependent Dalitz-plot analysis of $D^0 \rightarrow K_S^0 \pi^+ \pi^-$ is employed. Decay-time information and interference on the Dalitz plot are used to distinguish doubly Cabibbo-suppressed decays from mixing and to measure the relative phase between $D^0 \rightarrow K^{*+} \pi^-$ and $\bar{D}^0 \rightarrow K^{*+} \pi^-$. This value allows CP violation and is sensitive to the sign of Δm .

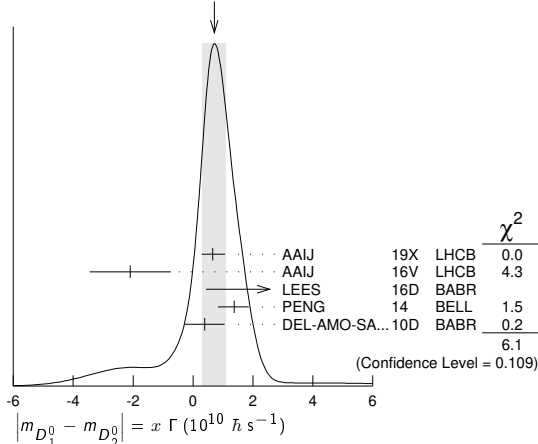
See key on page 999

Meson Particle Listings

D^0

- ⁷ Based on 9.6 fb^{-1} of data collected at the Tevatron. Assumes no CP violation. Reported $x'^2 = (0.08 \pm 0.18) \times 10^{-3}$ and $y' = (4.3 \pm 4.3) \times 10^{-3}$, where $x' = x \cos(\delta) + y \sin(\delta)$, $y' = y \cos(\delta) - x \sin(\delta)$ and δ is the strong phase between the $D^0 \rightarrow K^+ \pi^-$ and $\bar{D}^0 \rightarrow K^+ \pi^-$.
- ⁸ DEL-AMO-SANCHEZ 10D uses $540,800 \pm 800 K_S^0 \pi^+ \pi^-$ and $79,900 \pm 300 K_S^0 K^+ K^-$ events in a time-dependent amplitude analysis of the D^0 and \bar{D}^0 Dalitz plots. No evidence was found for CP violation, and the values here assume no such violation.
- ⁹ The result was established with D^0 from prompt and secondary D^* . Based on 3 fb^{-1} of data collected at $\sqrt{s} = 7, 8 \text{ TeV}$. Assumes no CP violation. Reported $x'^2 = (3.6 \pm 4.3) \times 10^{-5}$ and $y' = (5.23 \pm 0.84) \times 10^{-3}$, where $x' = x \cos(\delta) + y \sin(\delta)$, $y' = y \cos(\delta) - x \sin(\delta)$ and δ is the strong phase between the $D^0 \rightarrow K^+ \pi^-$ and $\bar{D}^0 \rightarrow K^+ \pi^-$.
- ¹⁰ Based on 3 fb^{-1} of data collected at $\sqrt{s} = 7, 8 \text{ TeV}$. Assumes no CP violation. Reported $x'^2 = (5.5 \pm 4.9) \times 10^{-4}$ and $y' = (4.8 \pm 1.0) \times 10^{-3}$, where $x' = x \cos(\delta) + y \sin(\delta)$, $y' = y \cos(\delta) - x \sin(\delta)$ and δ is the strong phase between the $D^0 \rightarrow K^+ \pi^-$ and $\bar{D}^0 \rightarrow K^+ \pi^-$.
- ¹¹ Based on 1 fb^{-1} of data collected at $\sqrt{s} = 7 \text{ TeV}$ in 2011. Assumes no CP violation. Reported $x'^2 = (-0.9 \pm 1.3) \times 10^{-4}$ and $y' = (7.2 \pm 2.4) \times 10^{-3}$, where $x' = x \cos(\delta) + y \sin(\delta)$, $y' = y \cos(\delta) - x \sin(\delta)$ and δ is the strong phase between the $D^0 \rightarrow K^+ \pi^-$ and $\bar{D}^0 \rightarrow K^+ \pi^-$.
- ¹² The AUBERT 09AN values are inferred from the branching ratio $\Gamma(D^0 \rightarrow K^+ \pi^- \pi^0) / \Gamma(D^0 \rightarrow K^+ \pi^- \pi^0)$ given near the end of this Listings. Mixing is distinguished from DCS decays using decay-time information. Interference between mixing and DCS is allowed. The phase between $D^0 \rightarrow K^+ \pi^- \pi^0$ and $\bar{D}^0 \rightarrow K^+ \pi^- \pi^0$ is assumed to be small. The width difference here is y'' , which is not the same as y_{CP} in the note on D^0 - \bar{D}^0 mixing.
- ¹³ LOWREY 09 uses quantum correlations in $e^+ e^- \rightarrow D^0 \bar{D}^0$ at the $\psi(3770)$. See below for coherence factors and average relative strong phases for both $D^0 \rightarrow K^+ \pi^- \pi^0$ and $D^0 \rightarrow K^+ \pi^- 2\pi^+$. A fit that includes external measurements of charm mixing parameters gets $\Delta m = (2.34 \pm 0.61) \times 10^{10} \text{ h s}^{-1}$.
- ¹⁴ The ASNER 05 and ZHANG 07b values are from the time-dependent Dalitz plot analysis of $D^0 \rightarrow K_S^0 \pi^+ \pi^-$. Decay-time information and interference on the Dalitz plot are used to distinguish doubly Cabibbo-suppressed decays from mixing and to measure the relative phase between $D^0 \rightarrow K^{*+} \pi^-$ and $\bar{D}^0 \rightarrow K^{*+} \pi^-$. This value allows CP violation and is sensitive to the sign of Δm .
- ¹⁵ The AUBERT 03Z, LI 05A, and ZHANG 06 limits are inferred from the D^0 - \bar{D}^0 mixing ratio $\Gamma(K^+ \pi^- \text{ (via } \bar{D}^0)) / \Gamma(K^+ \pi^- \text{ (via } D^0))$ given near the end of this D^0 Listings. Decay-time information is used to distinguish DCS decays from D^0 - \bar{D}^0 mixing. The limit allows interference between the DCS and mixing ratios, and also allows CP violation. The limit allows interference between the DCS and mixing ratios, and also allows CP violation. AUBERT 03Z assumes the strong phase between $D^0 \rightarrow K^+ \pi^-$ and $\bar{D}^0 \rightarrow K^+ \pi^-$ amplitudes is small; if an arbitrary phase is allowed, the limit degrades by 20%. The LI 05A and ZHANG 06 limits are valid for an arbitrary strong phase.
- ¹⁶ This LINK 05H limit is inferred from the D^0 - \bar{D}^0 mixing ratio $\Gamma(K^+ \pi^- \text{ (via } \bar{D}^0)) / \Gamma(K^+ \pi^- \text{ (via } D^0))$ given near the end of this D^0 Listings. Decay-time information is used to distinguish DCS decays from D^0 - \bar{D}^0 mixing. The limit allows interference between the DCS and mixing ratios, and also allows CP violation. The strong phase between $D^0 \rightarrow K^+ \pi^-$ and $\bar{D}^0 \rightarrow K^+ \pi^-$ is assumed to be small. If an arbitrary relative strong phase is allowed, the limit degrades by 25%.
- ¹⁷ This GODANG 00 limit is inferred from the D^0 - \bar{D}^0 mixing ratio $\Gamma(K^+ \pi^- \text{ (via } \bar{D}^0)) / \Gamma(K^+ \pi^- \text{ (via } D^0))$ given near the end of this D^0 Listings. Decay-time information is used to distinguish DCS decays from D^0 - \bar{D}^0 mixing. The limit allows interference between the DCS and mixing ratios, and also allows CP violation. The strong phase between $D^0 \rightarrow K^+ \pi^-$ and $\bar{D}^0 \rightarrow K^+ \pi^-$ is assumed to be small. If an arbitrary relative strong phase is allowed, the limit degrades by a factor of two.
- ¹⁸ AITALA 98 allows interference between the doubly Cabibbo-suppressed and mixing amplitudes, and also allows CP violation in this term, but assumes that $A_D = A_R = 0$. See the note on " D^0 - \bar{D}^0 Mixing," above.
- ¹⁹ This limit is inferred from R_M for $f = K^+ \pi^-$ and $f = K^+ \pi^- \pi^+ \pi^-$. See the note on " D^0 - \bar{D}^0 Mixing," above. Decay-time information is used to distinguish doubly Cabibbo-suppressed decays from D^0 - \bar{D}^0 mixing.
- ²⁰ This limit is inferred from R_M for $f = K^+ \ell^- \bar{\nu}_\ell$. See the note on " D^0 - \bar{D}^0 Mixing," above.
- ²¹ ANJOS 88c assumes that $y = 0$. See the note on " D^0 - \bar{D}^0 Mixing," above. Without this assumption, the limit degrades by about a factor of two.

WEIGHTED AVERAGE
 0.7 ± 0.4 (Error scaled by 1.4)



$$(\Gamma_{D_1^0} - \Gamma_{D_2^0}) / \Gamma = 2y$$

The D_1^0 and D_2^0 are the mass eigenstates of the D^0 meson, as described in the note on " D^0 - \bar{D}^0 Mixing," above.

Due to the strong phase difference between $D^0 \rightarrow K^+ \pi^-$ and $\bar{D}^0 \rightarrow K^+ \pi^-$, we exclude from the average those measurements of y' that are inferred from the D^0 - \bar{D}^0 mixing ratio $\Gamma(K^+ \pi^- \text{ via } \bar{D}^0) / \Gamma(K^+ \pi^-)$ given near the end of this D^0 Listings.

Some early results have been omitted. See our 2006 Review (Journal of Physics **G33** 1 (2006)).

"OUR EVALUATION" comes from CPV allowing averages provided by the Heavy Flavor Averaging Group, see the note on " D^0 - \bar{D}^0 Mixing."

VALUE (units 10^{-2})	EVTS	DOCUMENT ID	TECN	COMMENT
1.29 ± 0.14				OUR EVALUATION
1.10 ± 0.19				OUR AVERAGE
1.14 ± 0.26 ± 0.18				Error includes scale factor of 1.2.
1.48 ± 0.74	2.3M	1 AAIJ	19 LHCB	pp at 7, 8 TeV
		2 AAIJ	19X LHCB	$D^0 \rightarrow K_S^0 \pi^+ \pi^-$
		3 AAIJ	18K LHCB	pp at 7, 8, 13 TeV
0.06 ± 0.92 ± 0.26		4 AAIJ	16V LHCB	pp at 7 TeV
0.4 ± 1.8 ± 1.0		5 LEES	16D BABR	$e^+ e^- \rightarrow 10.6 \text{ GeV}$
2.22 ± 0.44 ± 0.18		6 STARIC	16 BELL	$e^+ e^- \rightarrow \Upsilon(1S)$
-4.0 ± 2.6 ± 1.4		7 ABLIKIM	15D BES3	$e^+ e^-$ at $\psi(3770)$
		8 KO	14 BELL	$e^+ e^- \rightarrow \Upsilon(1S)$
0.60 ± 0.30 ± 0.10		9 PENG	14 BELL	$e^+ e^- \rightarrow \Upsilon(1S)$
		10 AALTONEN	13AE CDF	$p\bar{p}$ at 1.96 TeV
1.44 ± 0.36 ± 0.24		11 LEES	13 BABR	$e^+ e^- \rightarrow \Upsilon(4S)$
0.55 ± 0.63 ± 0.41		12 AAIJ	12K LHCB	pp at 7 TeV
1.14 ± 0.40 ± 0.30		13 DEL-AMO-SA...	10D BABR	$e^+ e^- \rightarrow 10.6 \text{ GeV}$
0.22 ± 1.22 ± 1.04		14 ZUPANC	09 BELL	$e^+ e^- \approx \Upsilon(4S)$
-1.0 ± 2.0 ± 1.4	18k	15 ABE	02i BELL	$e^+ e^- \approx \Upsilon(4S)$
-2.4 ± 5.0 ± 2.8	3393	16 CSORNA	02 CLE2	$e^+ e^- \approx \Upsilon(4S)$
6.84 ± 2.78 ± 1.48	10k	15 LINK	00 FOCUS	γ nucleus
+1.6 ± 5.8 ± 2.1		15 AITALA	K9E E791	$K^- \pi^+, K^+ K^-$
••• We do not use the following data for averages, fits, limits, etc. •••				
		17 AAIJ	17A0 LHCB	Repl. by AAIJ 18k
		18 AAIJ	13CE LHCB	Repl. by AAIJ 17A0
		19 AAIJ	13N LHCB	Repl. by AAIJ 13CE
		20 AUBERT	09A1 BABR	See LEES 13
2.32 ± 0.44 ± 0.36		21 AUBERT	09AN BABR	$e^+ e^-$ at 10.58 GeV
-0.12 ± 1.10 ± 0.68				
1.4 ± 4.8 ± 5.4		22 LOWREY	09 CLEO	$e^+ e^-$ at $\psi(3770)$
1.70 ± 1.52	12.7 ± 0.3k	23 AALTONEN	08E CDF	$p\bar{p}$, $\sqrt{s} = 1.96 \text{ TeV}$
2.06 ± 0.66 ± 0.38		24 AUBERT	08U BABR	See AUBERT 09A1
1.94 ± 0.88 ± 0.62	4030 ± 90	23 AUBERT	07W BABR	$e^+ e^- \approx 10.6 \text{ GeV}$
2.62 ± 0.64 ± 0.50	160k	25 STARIC	07 BELL	Repl. by STARIC 16
0.74 ± 0.50 ± 0.20	534k	26 ZHANG	07B BELL	Repl. by PENG 14
-0.7 ± 4.9	4k ± 88	23,27 ZHANG	06 BELL	$e^+ e^-$
-3.0 ± 5.0 ± 1.6 ± 4.8 ± 0.8		26 ASNER	05 CLEO	$e^+ e^- \approx 10 \text{ GeV}$
-0.3 ± 5.7		23,27 LI	05A BELL	See ZHANG 06
-5.2 ± 18.4 ± 16.8		23,27 LINK	05H FOCUS	γ nucleus
1.6 ± 0.8 ± 1.0 ± 0.8	450k	28 AUBERT	03P BABR	See AUBERT 08U
1.6 ± 6.2 ± 12.8		23,27 AUBERT	03Z BABR	$e^+ e^- \rightarrow 10.6 \text{ GeV}$
-5.0 ± 2.8 ± 3.2 ± 0.6		23 GODANG	00 CLE2	$e^+ e^-$

- ¹ Based on 3 fb^{-1} of data collected at $\sqrt{s} = 7, 8 \text{ TeV}$. Measures the lifetime difference between $D^0 \rightarrow K^- K^+$ and $D^0 \rightarrow \pi^- \pi^+$ (CP even) decays and $D^0 \rightarrow K^- \pi^+$ (CP mixed) decays, or $y_{CP} = (\Gamma_{CP+} - \Gamma_{CP-}) / (\Gamma_{CP+} + \Gamma_{CP-})$. The D^0 mesons are required to originate from semimuonic decays of B mesons. We list $2y_{CP} = \Delta \Gamma / \Gamma$.
- ² AAIJ 19X D^0 come from D^{*+} and $\bar{B}^0 \rightarrow D^0 \mu^- X$ decays (and c.c.) in pp collisions at 7 and 8 TeV. Measurement allows for CP violation (none seen).
- ³ The result was established with D^0 from prompt and secondary D^* . Based on 5 fb^{-1} of data collected at $\sqrt{s} = 7, 8, 13 \text{ TeV}$. Assumes no CP violation. Reported $x'^2 = (3.9 \pm 2.7) \times 10^{-5}$ and $y' = (5.28 \pm 0.52) \times 10^{-3}$, where $x' = x \cos(\delta) + y \sin(\delta)$, $y' = y \cos(\delta) - x \sin(\delta)$ and δ is the strong phase between the $D^0 \rightarrow K^+ \pi^-$ and $\bar{D}^0 \rightarrow K^+ \pi^-$.
- ⁴ Model-independent measurement of the charm mixing parameters in the decay $D^0 \rightarrow K_S^0 \pi^+ \pi^-$ using 1.0 fb^{-1} of LHCb data at $\sqrt{s} = 7 \text{ TeV}$.
- ⁵ Time-dependent amplitude analysis of $D^0 \rightarrow \pi^+ \pi^- \pi^0$.
- ⁶ An improved measurement of $\bar{D}^0 - D^0$ mixing and a search for CP violation in D^0 decays to CP -even final states $K^+ K^-$ and $\pi^+ \pi^-$ using the final Belle data sample of 976 fb^{-1} .
- ⁷ ABLIKIM 15D uses quantum correlations in $e^+ e^- \rightarrow D^0 \bar{D}^0$ at the $\psi(3770)$.
- ⁸ Based on 976 fb^{-1} of data collected at $Y(1S)$ resonances. Assumes no CP violation. Reported $x'^2 = (0.09 \pm 0.22) \times 10^{-3}$ and $y' = (4.6 \pm 3.4) \times 10^{-3}$, where $x' = x \cos(\delta) + y \sin(\delta)$, $y' = y \cos(\delta) - x \sin(\delta)$ and δ is the strong phase between $D^0 \rightarrow K^+ \pi^-$ and $\bar{D}^0 \rightarrow K^+ \pi^-$.

Meson Particle Listings

D^0

- ⁹The time-dependent Dalitz-plot analysis of $D^0 \rightarrow K_S^0 \pi^+ \pi^-$ is employed. Decay-time information and interference on the Dalitz plot are used to distinguish doubly Cabibbo-suppressed decays from mixing and to measure the relative phase between $D^0 \rightarrow K^{*+} \pi^-$ and $\bar{D}^0 \rightarrow K^{*+} \pi^-$. This value allows CP violation and is sensitive to the sign of Δm .
- ¹⁰Based on 9.6 fb^{-1} of data collected at the Tevatron. Assumes no CP violation. Reported $x'^2 = (0.08 \pm 0.18) \times 10^{-3}$ and $y' = (4.3 \pm 4.3) \times 10^{-3}$, where $x' = x \cos(\delta) + y \sin(\delta)$, $y' = y \cos(\delta) - x \sin(\delta)$ and δ is the strong phase between the $D^0 \rightarrow K^+ \pi^-$ and $\bar{D}^0 \rightarrow K^+ \pi^-$.
- ¹¹Obtained $y_{CP} = (0.72 \pm 0.18 \pm 0.12)\%$ based on three effective D^0 lifetimes measured in $K^+ \pi^-$, $K^- K^+$, and $\pi^- \pi^+$. We list $2y_{CP} = \Delta\Gamma/\Gamma$.
- ¹²Compared the lifetimes of D^0 decay to the CP eigenstate $K^+ K^-$ with D^0 decay to $\pi^+ \pi^-$. The values here assume no CP violation.
- ¹³DEL-AMO-SANCHEZ 10b uses $540,800 \pm 800 K_S^0 \pi^+ \pi^-$ and $79,900 \pm 300 K_S^0 K^+ K^-$ events in a time-dependent amplitude analyses of the D^0 and \bar{D}^0 Dalitz plots. No evidence was found for CP violation, and the values here assume no such violation.
- ¹⁴ZUPANC 09 uses a method based on measuring the mean decay time of $D^0 \rightarrow K_S^0 K^+ K^-$ events for different $K^+ K^-$ mass intervals.
- ¹⁵LINK 00, AITALA 99E, and ABE 02i measure the lifetime difference between $D^0 \rightarrow K^- K^+$ (CP even) decays and $D^0 \rightarrow K^- \pi^+$ (CP mixed) decays, or $y_{CP} = [\Gamma(CP+) - \Gamma(CP-)] / [\Gamma(CP+) + \Gamma(CP-)]$. We list $2y_{CP} = \Delta\Gamma/\Gamma$.
- ¹⁶CSORNA 02 measures the lifetime difference between $D^0 \rightarrow K^- K^+$ and $\pi^- \pi^+$ (CP even) decays and $D^0 \rightarrow K^- \pi^+$ (CP mixed) decays, or $y_{CP} = [\Gamma(CP+) - \Gamma(CP-)] / [\Gamma(CP+) + \Gamma(CP-)]$. We list $2y_{CP} = \Delta\Gamma/\Gamma$.
- ¹⁷The result was established with D^0 from prompt and secondary D^* . Based on 3 fb^{-1} of data collected at $\sqrt{s} = 7, 8 \text{ TeV}$. Assumes no CP violation. Reported $x'^2 = (3.6 \pm 4.3) \times 10^{-5}$ and $y' = (5.23 \pm 0.84) \times 10^{-3}$, where $x' = x \cos(\delta) + y \sin(\delta)$, $y' = y \cos(\delta) - x \sin(\delta)$ and δ is the strong phase between the $D^0 \rightarrow K^+ \pi^-$ and $\bar{D}^0 \rightarrow K^+ \pi^-$.
- ¹⁸Based on 3 fb^{-1} of data collected at $\sqrt{s} = 7, 8 \text{ TeV}$. Assumes no CP violation. Reported $x'^2 = (5.5 \pm 4.9) \times 10^{-4}$ and $y' = (4.8 \pm 1.0) \times 10^{-3}$, where $x' = x \cos(\delta) + y \sin(\delta)$, $y' = y \cos(\delta) - x \sin(\delta)$ and δ is the strong phase between the $D^0 \rightarrow K^+ \pi^-$ and $\bar{D}^0 \rightarrow K^+ \pi^-$.
- ¹⁹Based on 1 fb^{-1} of data collected at $\sqrt{s} = 7 \text{ TeV}$ in 2011. Assumes no CP violation. Reported $x'^2 = (-0.9 \pm 1.3) \times 10^{-4}$ and $y' = (7.2 \pm 2.4) \times 10^{-3}$, where $x' = x \cos(\delta) + y \sin(\delta)$, $y' = y \cos(\delta) - x \sin(\delta)$ and δ is the strong phase between the $D^0 \rightarrow K^+ \pi^-$ and $\bar{D}^0 \rightarrow K^+ \pi^-$.
- ²⁰This combines the $y_{CP} = (\tau_{K\pi} / \tau_{KK}) - 1$ using untagged $K^- \pi^+$ and $K^- K^+$ events of AUBERT 09A1 with the disjoint y_{CP} using tagged $K^- \pi^+$, $K^- K^+$, and $\pi^- \pi^+$ events of AUBERT 08U.
- ²¹The AUBERT 09AN values are inferred from the branching ratio $\Gamma(D^0 \rightarrow K^+ \pi^- \pi^0)$ via $\bar{D}^0 / \Gamma(D^0 \rightarrow K^- \pi^+ \pi^0)$ given near the end of this Listings. Mixing is distinguished from DCS decays using decay-time information. Interference between mixing and DCS is allowed. The phase between $D^0 \rightarrow K^+ \pi^- \pi^0$ and $\bar{D}^0 \rightarrow K^+ \pi^- \pi^0$ is assumed to be small. The width difference here is y'' , which is not the same as y_{CP} in the note on $D^0 - \bar{D}^0$ mixing.
- ²²LOWREY 09 uses quantum correlations in $e^+ e^- \rightarrow D^0 \bar{D}^0$ at the $\psi(3770)$. See below for coherence factors and average relative strong phases for both $D^0 \rightarrow K^- \pi^+ \pi^0$ and $D^0 \rightarrow K^- \pi^- 2\pi^+$. A fit that includes external measurements of charm mixing parameters gets $2y = (1.62 \pm 0.32) \times 10^{-2}$.
- ²³The GODANG 00, AUBERT 03Z, LINK 05H, LI 05A, ZHANG 06, AUBERT 07W, and AALTONEN 08E limits are inferred from the $D^0 - \bar{D}^0$ mixing ratio $\Gamma(K^+ \pi^-)$ (via $\bar{D}^0) / \Gamma(K^- \pi^+)$ given near the end of this D^0 Listings. Decay-time information is used to distinguish DCS decays from $D^0 - \bar{D}^0$ mixing. The limits allow interference between the DCS and mixing ratios, and all except AUBERT 07W and AALTONEN 08E also allow CP violation. The phase between $D^0 \rightarrow K^+ \pi^-$ and $\bar{D}^0 \rightarrow K^+ \pi^-$ is assumed to be small. This is a measurement of y' and is not the same as the y_{CP} of our note above on " $D^0 - \bar{D}^0$ Mixing."
- ²⁴This value combines the results of AUBERT 08U and AUBERT 03P.
- ²⁵STARIC 07 compares the lifetimes of D^0 decay to the CP eigenstates $K^+ K^-$ and $\pi^+ \pi^-$ with D^0 decay to $K^- \pi^+$.
- ²⁶The ASNER 05 and ZHANG 07B values are from the time-dependent Dalitz-plot analysis of $D^0 \rightarrow K_S^0 \pi^+ \pi^-$. Decay-time information and interference on the Dalitz plot are used to distinguish doubly Cabibbo-suppressed decays from mixing and to measure the relative phase between $D^0 \rightarrow K^{*+} \pi^-$ and $\bar{D}^0 \rightarrow K^{*+} \pi^-$. This limit allows CP violation.
- ²⁷The ranges of AUBERT 03Z, LINK 05H, LI 05A, and ZHANG 06 measurements are for 95% confidence level.
- ²⁸AUBERT 03P measures $Y \equiv 2\tau^0 / (\tau^+ + \tau^-) - 1$, where τ^0 is the $D^0 \rightarrow K^- \pi^+$ (and $\bar{D}^0 \rightarrow K^+ \pi^-$) lifetime, and τ^+ and τ^- are the D^0 and \bar{D}^0 lifetimes to CP -even states (here $K^- K^+$ and $\pi^- \pi^+$). In the limit of CP conservation, $Y = Y \equiv \Delta\Gamma / 2\Gamma$ (we list $2y = \Delta\Gamma/\Gamma$). AUBERT 03P also uses $\tau^+ - \tau^-$ to get $\Delta Y = -0.008 \pm 0.006 \pm 0.002$.

$|q/p|$

The mass eigenstates D_1^0 and D_2^0 are related to the $C = \pm 1$ states by $|D_{1,2}^0\rangle = p|D^0\rangle + q|\bar{D}^0\rangle$. See the note on " $D^0 - \bar{D}^0$ Mixing" above.

"OUR EVALUATION" comes from CPV allowing averages provided by the Heavy Flavor Averaging Group. This would include as-yet-unpublished results, see the note on " $D^0 - \bar{D}^0$ Mixing."

VALUE	EVTS	DOCUMENT ID	TECN	COMMENT
$0.92^{+0.12}_{-0.09}$ OUR EVALUATION		HFAG fit; see the note on " $D^0 - \bar{D}^0$ Mixing."		
$0.97^{+0.14}_{-0.12}$ OUR AVERAGE				
$1.05^{+0.22}_{-0.17}$	2.3M	1 AAIJ	19X LHCb	$D^0 \rightarrow K_S^0 \pi^+ \pi^-$

$0.90^{+0.16+0.08}_{-0.15-0.06}$	2 AAIJ	18k LHCb	pp at 7, 8, 13 TeV
	3 PENG	14 BELL	$e^+ e^- \rightarrow \Upsilon(nS)$

• • • We do not use the following data for averages, fits, limits, etc. • • •

$0.86^{+0.30+0.10}_{-0.29-0.08}$	4 AAIJ	13CE LHCb	Repl. by AAIJ 18K
	5 ZHANG	07B BELL	Repl. by PENG 14

- ¹AAIJ 19X D^0 come from D^{*+} and $\bar{B} \rightarrow D^0 \mu^- X$ decays (and c.c.) in pp collisions at 7 and 8 TeV.
- ²Based on 5 fb^{-1} of data collected at $\sqrt{s} = 7, 8, 13 \text{ TeV}$. Allowing for CP violation, the direct CP violation in mixing is reported $1.00 < |q/p| < 1.35$ at the 68.3% CL for the $D^0 \rightarrow K^+ \pi^-$ and $\bar{D}^0 \rightarrow K^+ \pi^-$.
- ³The time-dependent Dalitz-plot analysis of $D^0 \rightarrow K_S^0 \pi^+ \pi^-$ is employed. Decay-time information and interference on the Dalitz plot are used to distinguish doubly Cabibbo-suppressed decays from mixing and to measure the relative phase between $D^0 \rightarrow K^{*+} \pi^-$ and $\bar{D}^0 \rightarrow K^{*+} \pi^-$. This value allows CP violation and is sensitive to the sign of Δm .
- ⁴Based on 3 fb^{-1} of data collected at $\sqrt{s} = 7, 8 \text{ TeV}$. Allowing for CP violation, the direct CP violation in mixing is reported $0.75 < |q/p| < 1.24$ at the 68.3% CL for the $D^0 \rightarrow K^+ \pi^-$ and $\bar{D}^0 \rightarrow K^+ \pi^-$.
- ⁵The phase of p/q is $(-14^{+16}_{-18} \pm 5)^\circ$. The ZHANG 07B value is from the time-dependent Dalitz-plot analysis of $D^0 \rightarrow K_S^0 \pi^+ \pi^-$. Decay-time information and interference on the Dalitz plot are used to distinguish doubly Cabibbo-suppressed decays from mixing and to measure the relative phase between $D^0 \rightarrow K^{*+} \pi^-$ and $\bar{D}^0 \rightarrow K^{*+} \pi^-$. This value allows CP violation.

A_Γ

A_Γ is the decay-rate asymmetry for CP -even final states $A_\Gamma = (\bar{\tau}_+ - \tau_+) / (\bar{\tau}_+ + \tau_+)$. See the note on " $D^0 - \bar{D}^0$ Mixing" above.

VALUE (units 10^{-3})	EVTS	DOCUMENT ID	TECN	COMMENT
-0.125 ± 0.526 OUR EVALUATION				
-0.31 ± 0.23 OUR AVERAGE				Error includes scale factor of 1.1.
$-0.44 \pm 0.23 \pm 0.06$	21M	1 AAIJ	20 LHCb	$D^0 \rightarrow K^+ K^-$
$0.25 \pm 0.43 \pm 0.07$	7M	2 AAIJ	20 LHCb	$D^0 \rightarrow \pi^+ \pi^-$
$-0.3 \pm 0.2 \pm 0.7$		3 STARIC	16 BELL	$e^+ e^- \rightarrow \Upsilon(nS)$
-1.2 ± 1.2	1.8M	4 AALTONEN	14Q CDF	$p\bar{p}$, $\sqrt{s} = 1.96 \text{ TeV}$
$0.9 \pm 2.6 \pm 0.6$	0.7M	LEES	13 BABR	$e^+ e^- \rightarrow \Upsilon(4S)$
$-5.9 \pm 5.9 \pm 2.1$		5 AAIJ	12k LHCb	pp at 7 TeV, 2010 data.
• • • We do not use the following data for averages, fits, limits, etc. • • •				
$-0.30 \pm 0.32 \pm 0.10$	9.6M	5 AAIJ	17AK LHCb	Repl. by AAIJ 20
$0.46 \pm 0.58 \pm 0.12$	3.0M	6 AAIJ	17AK LHCb	Repl. by AAIJ 20
$-1.34 \pm 0.77^{+0.26}_{-0.34}$	2.3M	7 AAIJ	15AA LHCb	Repl. by AAIJ 20
$-0.92 \pm 1.45^{+0.25}_{-0.33}$	0.8M	8 AAIJ	15AA LHCb	Repl. by AAIJ 20
$-0.35 \pm 0.62 \pm 0.12$		5 AAIJ	14AL LHCb	Repl. by AAIJ 17AK
$0.33 \pm 1.06 \pm 0.14$		6 AAIJ	14AL LHCb	Repl. by AAIJ 17AK
$2.6 \pm 3.6 \pm 0.8$		AUBERT	08U BABR	See LEES 13
$0.1 \pm 3.0 \pm 2.5$		STARIC	07 BELL	Repl. by STARIC 16
$8 \pm 6 \pm 2$		AUBERT	03P BABR	$e^+ e^- \approx \Upsilon(4S)$

- ¹Measured using $D^0 \rightarrow K^+ K^-$ decays, combines measurements with D^0 either from partially reconstructed semileptonic B hadron decays or from $D^{*+} \rightarrow D^0 \pi^+$.
- ²Measured using $D^0 \rightarrow \pi^+ \pi^-$ decays, combines measurements with D^0 either from partially reconstructed semileptonic B hadron decays or from $D^{*+} \rightarrow D^0 \pi^+$.
- ³An improved measurement of $\bar{D}^0 - D^0$ mixing and a search for CP violation in D^0 decays to CP -even final states $K^+ K^-$ and $\pi^+ \pi^-$ using the final Belle data sample of 976 fb^{-1} .
- ⁴Combined result from $D^0 \rightarrow K^+ K^-$ and $D^0 \rightarrow \pi^+ \pi^-$, with D^0 from $D^{*+} \rightarrow D^0 \pi^+$ (and cc).
- ⁵Measured using $D^{*+} \rightarrow D^0 \pi^+$, $D^0 \rightarrow K^+ K^-$ decays (and cc).
- ⁶Measured using $D^{*+} \rightarrow D^0 \pi^+$, $D^0 \rightarrow \pi^+ \pi^-$ decays (and cc).
- ⁷Measured using $D^0 \rightarrow K^+ K^-$ decays, with D^0 from partially reconstructed semileptonic B hadron decays.
- ⁸Measured using $D^0 \rightarrow \pi^+ \pi^-$ decays, with D^0 from partially reconstructed semileptonic B hadron decays.

$\phi_{K_S^0 \pi^+ \pi^-}$

Parametrizes CP violation in the interference between D^0 mixing and decay. The mass eigenstates D_1^0 and D_2^0 are related to the $C = \pm 1$ states by $|D_{1,2}^0\rangle = p|D^0\rangle + q|\bar{D}^0\rangle$. In the absence of CP violation in the decay, and using the usual phase convention where CP conservation implies q/p is real, $\phi_{K_S^0 \pi^+ \pi^-}$ is identical to the decay-mode-independent parameter $\phi = \arg(q/p)$.

VALUE	EVTS	DOCUMENT ID	TECN	COMMENT
$-0.09^{+0.10}_{-0.13}$ OUR AVERAGE				
$-0.09^{+0.11}_{-0.16}$	2.3M	1 AAIJ	19X LHCb	$D^0 \rightarrow K_S^0 \pi^+ \pi^-$
$-0.10 \pm 0.19 \pm 0.05^{+0.05}_{-0.07}$	1.2M	2 PENG	14 BELL	$e^+ e^-$ at $\Upsilon(4S, 5S)$

- ¹AAIJ 19X D^0 come from D^{*+} and $\bar{B} \rightarrow D^0 \mu^- X$ decays (and c.c.) in pp collisions at 7 and 8 TeV.
- ²The last uncertainty is due to the amplitude model.

cos δ

δ is the $D^0 \rightarrow K^+\pi^-$ relative strong phase.

VALUE	DOCUMENT ID	TECN	COMMENT
0.97 ± 0.11 OUR AVERAGE			
1.02 ± 0.11 ± 0.06	¹ ABLIKIM	14c	BES3 $e^+e^- \rightarrow D^0\bar{D}^0$, 3.77 GeV
0.81 ^{+0.22+0.07} _{-0.18-0.05}	² ASNER	12	CLEO $e^+e^- \rightarrow D^0\bar{D}^0$, 3.77 GeV
1.03 ^{+0.31} _{-0.17} ± 0.06	³ ASNER	08	CLEO Repl. by ASNER 12

- • • We do not use the following data for averages, fits, limits, etc. • • •
- ¹ Uses quantum correlations in $e^+e^- \rightarrow D^0\bar{D}^0$ at the $\psi(3770)$ to measure the asymmetry of the branching fraction of $D^0 \rightarrow K^-\pi^+$ in CP -odd and CP -even eigenstates to be $(12.7 \pm 1.3 \pm 0.7)\%$. A fit that includes external measurements of charm mixing parameters finds the value quoted above.
- ² Uses quantum correlations in $e^+e^- \rightarrow D^0\bar{D}^0$ at the $\psi(3770)$, where decay rates of CP -tagged $K\pi$ final states depend on the strong phases between the decays of $D^0 \rightarrow K^+\pi^-$ and $\bar{D}^0 \rightarrow K^+\pi^-$. The measurements obtained $\sin(\delta) = -0.01 \pm 0.41 \pm 0.04$ and $|\delta| = (10^{+28+13}_{-53-00})^\circ$ as well. A fit that includes external measurements of charm mixing parameters finds $\cos(\delta) = 1.15^{+0.19+0.00}_{-0.17-0.08}$, $\sin(\delta) = 0.56^{+0.32+0.21}_{-0.31-0.20}$, and $|\delta| = (18^{+11}_{-17})^\circ$.
- ³ ASNER 08 uses quantum correlations in $e^+e^- \rightarrow D^0\bar{D}^0$ at the $\psi(3770)$, where decay rates of CP -tagged $K\pi$ final states depend on $\cos \delta$ because of interfering amplitudes. The above measurement implies $|\delta| < 75^\circ$ with a confidence level of 95%. A fit that includes external measurements of charm mixing parameters finds $\cos \delta = 1.10 \pm 0.35 \pm 0.07$. See also the note on " $D^0-\bar{D}^0$ Mixing" p. 783 in our 2008 Review (PDG 08).

$D^0 \rightarrow K^-\pi^+\pi^0$ COHERENCE FACTOR $R_{K\pi\pi^0}$

See the note on ' $D^0-\bar{D}^0$ Mixing' for the definition. $R_{K\pi\pi^0}$ can have any value between 0 and 1. A value near 1 indicates the decay is dominated by a few intermediate states with limited interference.

VALUE	DOCUMENT ID	TECN	COMMENT
0.82 ± 0.06	1,2,3 EVANS	16	$e^+e^- \rightarrow D^0\bar{D}^0$ at $\psi(3770)$
0.82 ± 0.07	1,3 LIBBY	14	Repl. by EVANS 16
0.78 ^{+0.11} _{-0.25}	⁴ LOWREY	09	CLEO Repl. by LIBBY 14

- • • We do not use the following data for averages, fits, limits, etc. • • •
- ¹ Uses quantum correlations in $e^+e^- \rightarrow D^0\bar{D}^0$ at the $\psi(3770)$, where the decay rates of CP -tagged $K^-\pi^+\pi^0$ final states depend on $R_{K\pi\pi^0}$ and $\delta^{K\pi\pi^0}$.
- ² A combined fit with a recent LHCb $D^0\bar{D}^0$ mixing results in AAIJ 16f is also reported to be 0.81 ± 0.06 .
- ³ Obtained by analyzing CLEO-c data but not authored by the CLEO Collaboration.
- ⁴ LOWREY 09 uses quantum correlations in $e^+e^- \rightarrow D^0\bar{D}^0$ at the $\psi(3770)$, where the decay rates of CP -tagged $K^-\pi^+\pi^0$ final states depend on $R_{K\pi\pi^0}$ and $\delta^{K\pi\pi^0}$. A fit that includes external measurements of charm mixing parameters gets $R_{K\pi\pi^0} = 0.84 \pm 0.07$.

$D^0 \rightarrow K^-\pi^+\pi^0$ AVERAGE RELATIVE STRONG PHASE $\delta^{K\pi\pi^0}$

The quoted value of δ is based on the same sign CP phase of D^0 and \bar{D}^0 convention.

VALUE ($^\circ$)	DOCUMENT ID	TECN	COMMENT
199⁺¹³₋₁₄	1,2,3 EVANS	16	$e^+e^- \rightarrow D^0\bar{D}^0$ at $\psi(3770)$
164 ⁺²⁰ ₋₁₄	1,3 LIBBY	14	Repl. by EVANS 16
239 ⁺³² ₋₂₈	⁴ LOWREY	09	CLEO Repl. by LIBBY 14

- • • We do not use the following data for averages, fits, limits, etc. • • •
- ¹ Uses quantum correlations in $e^+e^- \rightarrow D^0\bar{D}^0$ at the $\psi(3770)$, where the decay rates of CP -tagged $K^-\pi^+\pi^0$ final states depend on $R_{K\pi\pi^0}$ and $\delta^{K\pi\pi^0}$.
- ² A combined fit with a recent LHCb $D^0\bar{D}^0$ mixing results in AAIJ 16f is also reported to be 198^{+14}_{-15} degree.
- ³ Obtained by analyzing CLEO-c data but not authored by the CLEO Collaboration.
- ⁴ LOWREY 09 uses quantum correlations in $e^+e^- \rightarrow D^0\bar{D}^0$ at the $\psi(3770)$, where the decay rates of CP -tagged $K^-\pi^+\pi^0$ final states depend on $R_{K\pi\pi^0}$ and $\delta^{K\pi\pi^0}$. A fit that includes external measurements of charm mixing parameters gets $\delta^{K\pi\pi^0} = (227^{+14}_{-17})^\circ$.

$D^0 \rightarrow K^-\pi^-2\pi^+$ COHERENCE FACTOR $R_{K3\pi}$

See the note on ' $D^0-\bar{D}^0$ Mixing' for the definition. $R_{K3\pi}$ can have any value between 0 and 1. A value near 1 indicates the decay is dominated by a few intermediate states with limited interference.

VALUE	EVTS	DOCUMENT ID	TECN	COMMENT
0.53^{+0.18}_{-0.21}	1,2,3	EVANS	16	$e^+e^- \rightarrow D^0\bar{D}^0$ at $\psi(3770)$, pp at 7,8 TeV
0.458 ± 0.010 ± 0.023	0.9M,3k	⁴ AAIJ	18A1	LHCb amplitude models
0.32 ^{+0.20} _{-0.28}	1,3	LIBBY	14	Repl. by EVANS 16
0.36 ^{+0.24} _{-0.30}	5	LOWREY	09	CLEO Repl. by LIBBY 14

- • • We do not use the following data for averages, fits, limits, etc. • • •
- ¹ Uses quantum correlations in $e^+e^- \rightarrow D^0\bar{D}^0$ at the $\psi(3770)$, where the decay rates of CP -tagged $K^-\pi^-2\pi^+$ final states depend on $R_{K3\pi}$ and $\delta^{K3\pi}$.
- ² A combined fit with a recent LHCb $D^0\bar{D}^0$ mixing results in AAIJ 16f is also reported, to be $0.43^{+0.17}_{-0.13}$.

- ³ Obtained by analyzing CLEO-c data but not authored by the CLEO Collaboration.
- ⁴ Calculated from amplitude models to $D^0 \rightarrow K^-\pi^-2\pi^+$ and $D^0 \rightarrow K^+\pi^+2\pi^-$ and cc. Reports $0.458 \pm 0.010 \pm 0.012 \pm 0.020$ value where the 3rd uncertainty is the model uncertainty. We combined both systematic uncertainties in quadrature. Because of the importance of model independence in the practical use of the coherence factor, we do not include model-derived results in the average.
- ⁵ LOWREY 09 uses quantum correlations in $e^+e^- \rightarrow D^0\bar{D}^0$ at the $\psi(3770)$, where the decay rates of CP -tagged $K^-\pi^-2\pi^+$ final states depend on $R_{K3\pi}$ and $\delta^{K3\pi}$. A fit that includes external measurements of charm mixing parameters gets $R_{K3\pi} = 0.33^{+0.26}_{-0.23}$.

$D^0 \rightarrow K^-\pi^-2\pi^+$ AVERAGE RELATIVE STRONG PHASE $\delta^{K3\pi}$

The quoted value of δ is based on the same sign CP phase of D^0 and \bar{D}^0 convention.

VALUE ($^\circ$)	DOCUMENT ID	TECN	COMMENT
125⁺²²₋₁₄	1,2,3	EVANS	16 $e^+e^- \rightarrow D^0\bar{D}^0$ at $\psi(3770)$
255 ⁺²¹ ₋₇₈	1,3	LIBBY	14 Repl. by EVANS 16
118 ⁺⁶² ₋₅₃	4	LOWREY	09 CLEO Repl. by LIBBY 14

- • • We do not use the following data for averages, fits, limits, etc. • • •
- ¹ Uses quantum correlations in $e^+e^- \rightarrow D^0\bar{D}^0$ at the $\psi(3770)$, where the decay rates of CP -tagged $K^-\pi^-2\pi^+$ final states depend on $R_{K3\pi}$ and $\delta^{K3\pi}$.
- ² A combined fit with a recent LHCb $D^0\bar{D}^0$ mixing results in AAIJ 16f is also reported to be $(128^{+28}_{-17})^\circ$.
- ³ Obtained by analyzing CLEO-c data but not authored by the CLEO Collaboration.
- ⁴ LOWREY 09 uses quantum correlations in $e^+e^- \rightarrow D^0\bar{D}^0$ at the $\psi(3770)$, where the decay rates of CP -tagged $K^-\pi^-2\pi^+$ final states depend on $R_{K3\pi}$ and $\delta^{K3\pi}$. A fit that includes external measurements of charm mixing parameters gets $\delta^{K3\pi} = (114^{+26}_{-23})^\circ$.

$D^0 \rightarrow K^-\pi^-2\pi^+$, $R_{K3\pi}$ ($y \cos\delta^{K3\pi} - x \sin\delta^{K3\pi}$)

VALUE (10^{-3}TeV^{-1})	EVTS	DOCUMENT ID	TECN	COMMENT
-3.0 ± 0.7	42.5k	¹ AAIJ	16f	LHCb pp at 7, 8 TeV

- ¹ From a time-dependent analysis of D mixing in $D^0 \rightarrow K^+\pi^-\pi^+$. This result uses external constraints on $R_M = 1/2(x^2 + y^2)$. Without such constraints, AAIJ 16f measure $(0.3 \pm 1.8) \times 10^{-3}$, with a large correlation coefficient to R_M .

$D^0 \rightarrow K_S^0 K^+\pi^-$ COHERENCE FACTOR $R_{K_S^0 K\pi}$

VALUE	DOCUMENT ID	TECN	COMMENT
0.70 ± 0.08	¹ INSLER	12	CLEO $e^+e^- \rightarrow D^0\bar{D}^0$ at 3.77 GeV

- ¹ Uses quantum correlations in $e^+e^- \rightarrow D^0\bar{D}^0$ at the $\psi(3770)$, where the signal side D decays to $K_S^0 K\pi$ and the tag-side D decays to $K\pi$, $K\pi\pi\pi$, $K\pi\pi^0$, and 10 additional CP -even, CP -odd, and mixed CP modes involving K_S^0 or K_L^0 .

$D^0 \rightarrow K_S^0 K^+\pi^-$ AVERAGE RELATIVE STRONG PHASE $\delta^{K_S^0 K\pi}$

The quoted value of δ is based on the same sign CP phase of D^0 and \bar{D}^0 convention.

VALUE ($^\circ$)	DOCUMENT ID	TECN	COMMENT
0.1 ± 15.7	¹ INSLER	12	CLEO $e^+e^- \rightarrow D^0\bar{D}^0$ at 3.77 GeV

- ¹ Uses quantum correlations in $e^+e^- \rightarrow D^0\bar{D}^0$ at the $\psi(3770)$, where the signal side D decays to $K_S^0 K\pi$ and the tag-side D decays to $K\pi$, $K\pi\pi\pi$, $K\pi\pi^0$, and 10 additional CP -even, CP -odd, and mixed CP modes involving K_S^0 or K_L^0 .

$D^0 \rightarrow K^* K$ COHERENCE FACTOR $R_{K^* K}$

VALUE	DOCUMENT ID	TECN	COMMENT
0.94 ± 0.12	¹ INSLER	12	CLEO $e^+e^- \rightarrow D^0\bar{D}^0$ at 3.77 GeV

- ¹ Uses quantum correlations in $e^+e^- \rightarrow D^0\bar{D}^0$ at the $\psi(3770)$, where the signal side D decays to $K_S^0 K\pi$ and the tag-side D decays to $K\pi$, $K\pi\pi\pi$, $K\pi\pi^0$, and 10 additional CP -even, CP -odd, and mixed CP modes involving K_S^0 or K_L^0 .

$D^0 \rightarrow K^* K$ AVERAGE RELATIVE STRONG PHASE $\delta^{K^* K}$

The quoted value of δ is based on the same sign CP phase of D^0 and \bar{D}^0 convention.

VALUE ($^\circ$)	DOCUMENT ID	TECN	COMMENT
-16.6 ± 18.4	¹ INSLER	12	CLEO $e^+e^- \rightarrow D^0\bar{D}^0$ at 3.77 GeV

- ¹ Uses quantum correlations in $e^+e^- \rightarrow D^0\bar{D}^0$ at the $\psi(3770)$, where the signal side D decays to $K_S^0 K\pi$ and the tag-side D decays to $K\pi$, $K\pi\pi\pi$, $K\pi\pi^0$, and 10 additional CP -even, CP -odd, and mixed CP modes involving K_S^0 or K_L^0 .

D^0 DECAY MODES

Most decay modes (other than the semileptonic modes) that involve a neutral K meson are now given as K_S^0 modes, not as \bar{K}^0 modes. Nearly always it is a K_S^0 that is measured, and interference between Cabibbo-allowed and doubly Cabibbo-suppressed modes can invalidate the assumption that $2\Gamma(K_S^0) = \Gamma(\bar{K}^0)$.

Mode	Fraction (Γ_i/Γ)	Scale factor/ Confidence level			
Topological modes					
Γ_1	0-prongs	[a] (15 ± 6) %			
Γ_2	2-prongs	(71 ± 6) %			
Γ_3	4-prongs	[b] (14.6 ± 0.5) %			
Γ_4	6-prongs	[c] (6.5 ± 1.3) × 10 ⁻⁴			
Inclusive modes					
Γ_5	e^+ anything	[d] (6.49 ± 0.11) %			
Γ_6	μ^+ anything	(6.8 ± 0.6) %			
Γ_7	K^- anything	(54.7 ± 2.8) %	S=1.3		
Γ_8	\bar{K}^0 anything + K^0 anything	(47 ± 4) %			
Γ_9	K^+ anything	(3.4 ± 0.4) %			
Γ_{10}	$K^*(892)^-$ anything	(15 ± 9) %			
Γ_{11}	$\bar{K}^*(892)^0$ anything	(9 ± 4) %			
Γ_{12}	$K^*(892)^+$ anything	< 3.6 %	CL=90%		
Γ_{13}	$K^*(892)^0$ anything	(2.8 ± 1.3) %			
Γ_{14}	η anything	(9.5 ± 0.9) %			
Γ_{15}	η' anything	(2.48 ± 0.27) %			
Γ_{16}	ϕ anything	(1.08 ± 0.04) %			
Γ_{17}	invisibles	< 9.4 × 10 ⁻⁵	CL=90%		
Semileptonic modes					
Γ_{18}	$K^- \ell^+ \nu_\ell$	(3.542 ± 0.035) %	S=1.3		
Γ_{19}	$K^- e^+ \nu_e$	(3.41 ± 0.04) %			
Γ_{20}	$K^- \mu^+ \nu_\mu$	(2.15 ± 0.16) %			
Γ_{21}	$K^*(892)^- e^+ \nu_e$	(1.89 ± 0.24) %			
Γ_{22}	$K^*(892)^- \mu^+ \nu_\mu$	(1.6 ± 1.3) %			
Γ_{23}	$K^- \pi^0 e^+ \nu_e$	(1.44 ± 0.04) %			
Γ_{24}	$\bar{K}^0 \pi^- e^+ \nu_e$	(7.9 ± 1.7) × 10 ⁻⁴			
Γ_{25}	$(\bar{K}^0 \pi^-)_{S\text{-wave}} e^+ \nu_e$	(2.8 ± 1.4) × 10 ⁻⁴			
Γ_{26}	$K^- \pi^+ \pi^- e^+ \nu_e$	(7.6 ± 4.0) × 10 ⁻⁴			
Γ_{27}	$K_1(1270)^- e^+ \nu_e$	< 1.3 × 10 ⁻³	CL=90%		
Γ_{28}	$K^- \pi^+ \pi^- \mu^+ \nu_\mu$	< 1.5 × 10 ⁻³	CL=90%		
Γ_{29}	$(\bar{K}^*(892) \pi^-) \mu^+ \nu_\mu$	(2.91 ± 0.04) × 10 ⁻³			
Γ_{30}	$\pi^- e^+ \nu_e$	(2.67 ± 0.12) × 10 ⁻³	S=1.3		
Γ_{31}	$\pi^- \mu^+ \nu_\mu$	(1.45 ± 0.07) × 10 ⁻³			
Γ_{32}	$\pi^- \pi^0 e^+ \nu_e$	(1.50 ± 0.12) × 10 ⁻³	S=1.9		
Γ_{33}	$\rho^- e^+ \nu_e$	(1.33 ± 0.34) × 10 ⁻⁴			
Γ_{34}	$a(980)^- e^+ \nu_e, a^- \rightarrow \eta \pi^-$	(3.950 ± 0.031) %	S=1.2		
Γ_{35}	$K^- \pi^+$	(1.240 ± 0.022) %			
Γ_{36}	$K_S^0 \pi^0$	(10.0 ± 0.7) × 10 ⁻³			
Γ_{37}	$K_L^0 \pi^0$	[e] (2.80 ± 0.18) %	S=1.1		
Γ_{38}	$K_S^0 \pi^+ \pi^-$	(6.3 ± 0.6) × 10 ⁻³			
Γ_{39}	$K_S^0 \rho^0$	(2.0 ± 0.6) × 10 ⁻⁴			
Γ_{40}	$K_S^0 \omega, \omega \rightarrow \pi^+ \pi^-$	(3.3 ± 0.8) × 10 ⁻³			
Γ_{41}	$K_S^0 (\pi^+ \pi^-)_{S\text{-wave}}$	(1.20 ± 0.40) × 10 ⁻³			
Γ_{42}	$K_S^0 f_0(980), f_0 \rightarrow \pi^+ \pi^-$	(2.8 ± 0.9) × 10 ⁻³			
Γ_{43}	$K_S^0 f_0(1370), f_0 \rightarrow \pi^+ \pi^-$	(9 ± 10) × 10 ⁻⁵			
Γ_{44}	$K_S^0 f_2(1270), f_2 \rightarrow \pi^+ \pi^-$	(1.64 ± 0.14) %			
Γ_{45}	$K^*(892)^- \pi^+, K^{*-} \rightarrow K_S^0 \pi^-$	(2.67 ± 0.40) × 10 ⁻³			
Γ_{46}	$K_2^*(1430)^- \pi^+, K_2^{*-} \rightarrow K_S^0 \pi^-$	(3.4 ± 1.9) × 10 ⁻⁴			
Γ_{47}	$K^*(1680)^- \pi^+, K^{*-} \rightarrow K_S^0 \pi^-$	(4.4 ± 3.5) × 10 ⁻⁴			
Γ_{48}	$K^*(892)^+ \pi^-, K^{*+} \rightarrow K_S^0 \pi^+$	[f] (1.13 ± 0.60) × 10 ⁻⁴			
Γ_{49}	$K_2^*(1430)^+ \pi^-, K_2^{*+} \rightarrow K_S^0 \pi^+$	[f] < 1.4 × 10 ⁻⁵	CL=95%		
Γ_{50}	$K^*(1430)^+ \pi^-, K^{*+} \rightarrow K_S^0 \pi^+$	[f] < 3.4 × 10 ⁻⁵	CL=95%		
Γ_{51}	$K_S^0 \pi^+ \pi^-$ nonresonant	(2.5 ± 6.0) × 10 ⁻⁴			
Γ_{52}	$K^- \pi^+ \pi^0$	[e] (14.4 ± 0.5) %	S=2.0		
Γ_{53}	$K^- \rho^+$	(11.3 ± 0.7) %			
Γ_{54}	$K^- \rho(1700)^+, \rho^+ \rightarrow \pi^+ \pi^0$	(8.2 ± 1.8) × 10 ⁻³			
Γ_{55}	$K^*(892)^- \pi^+, K^*(892)^- \rightarrow K^- \pi^0$	(2.31 ± 0.20) %			
Γ_{56}	$\bar{K}^*(892)^0 \pi^0, \bar{K}^*(892)^0 \rightarrow K^- \pi^+$	(1.95 ± 0.24) %			
Γ_{57}	$K_0^*(1430)^- \pi^+, K_0^{*-} \rightarrow K^- \pi^0$	(4.8 ± 2.2) × 10 ⁻³			
Γ_{58}	$\bar{K}_0^*(1430)^0 \pi^0, \bar{K}_0^{*0} \rightarrow K^- \pi^+$	(5.9 ± 5.0) × 10 ⁻³			
Γ_{59}	$K^*(1680)^- \pi^+, K^{*-} \rightarrow K^- \pi^0$	(1.9 ± 0.7) × 10 ⁻³			
Γ_{60}	$K^- \pi^+ \pi^0$ nonresonant	(1.15 ± 0.60) %			
Γ_{61}	$K_S^0 2\pi^0$	(9.1 ± 1.1) × 10 ⁻³	S=2.2		
Γ_{62}	$K_S^0 (2\pi^0)_{S\text{-wave}}$	(2.6 ± 0.7) × 10 ⁻³			
Γ_{63}	$\bar{K}^*(892)^0 \pi^0, \bar{K}^{*0} \rightarrow K_S^0 \pi^0$	(8.1 ± 0.7) × 10 ⁻³			
Γ_{64}	$\bar{K}^*(1430)^0 \pi^0, \bar{K}^{*0} \rightarrow K_S^0 \pi^0$	(4 ± 23) × 10 ⁻⁵			
Γ_{65}	$\bar{K}^*(1680)^0 \pi^0, \bar{K}^{*0} \rightarrow K_S^0 \pi^0$	(1.0 ± 0.4) × 10 ⁻³			
Γ_{66}	$K_S^0 f_2(1270), f_2 \rightarrow 2\pi^0$	(2.3 ± 1.1) × 10 ⁻⁴			
Γ_{67}	$2K_S^0, \text{one } K_S^0 \rightarrow 2\pi^0$	(3.2 ± 1.1) × 10 ⁻⁴			
Γ_{68}	$K_S^0 2\pi^0$ nonresonant				
Γ_{69}	$K^- 2\pi^+ \pi^-$	[e] (8.23 ± 0.14) %	S=1.1		
Γ_{70}	$K^- \pi^+ \rho^0$ total	(6.87 ± 0.31) %			
Γ_{71}	$K^- \pi^+ \rho^0 3\text{-body}$	(6.1 ± 1.6) × 10 ⁻³			
Γ_{72}	$\bar{K}^*(892)^0 \rho^0, \bar{K}^{*0} \rightarrow K^- \pi^+$	(1.01 ± 0.05) %			
Γ_{73}	$\bar{K}^*(892)^0 \rho^0$ transverse,	(1.2 ± 0.4) %			
Γ_{74}	$K^- a_1(1260)^+, a_1^+ \rightarrow \rho^0 \pi^+$	(4.33 ± 0.32) %			
Γ_{75}	$K_1(1270)^- \pi^+, K_1^- \rightarrow K^- \pi^+ \pi^-$ total,	(3.9 ± 0.4) × 10 ⁻³			
Γ_{76}	$\bar{K}^*(892)^0 \pi^+ \pi^-$ total,				
Γ_{77}	$\bar{K}^*(892)^0 \rightarrow K^- \pi^+$				
Γ_{78}	$\bar{K}^*(892)^0 \pi^+ \pi^- 3\text{-body}, \bar{K}^{*0} \rightarrow K^- \pi^+$	(6.6 ± 2.3) × 10 ⁻⁴			
Γ_{79}	$K_1(1270)^- \pi^+, K_1^- \rightarrow \bar{K}^*(892)^0 \pi^-, \bar{K}^{*0} \rightarrow K^- \pi^+$				
Γ_{80}	$K^- 2\pi^+ \pi^-$ nonresonant	(1.81 ± 0.07) %			
Γ_{81}	$K_S^0 \pi^+ \pi^- \pi^0$	[g] (5.2 ± 0.6) %			
Γ_{82}	$K_S^0 \eta, \eta \rightarrow \pi^+ \pi^- \pi^0$	(1.17 ± 0.03) × 10 ⁻³			
Γ_{83}	$K_S^0 \omega, \omega \rightarrow \pi^+ \pi^- \pi^0$	(9.9 ± 0.6) × 10 ⁻³			
Γ_{84}	$K^- \pi^+ 2\pi^0$	(8.86 ± 0.23) %			
Γ_{85}	$K^- 2\pi^+ \pi^- \pi^0$	(4.3 ± 0.4) %			
Γ_{86}	$\bar{K}^*(892)^0 \pi^+ \pi^- \pi^0, \bar{K}^{*0} \rightarrow K^- \pi^+$	(1.3 ± 0.6) %			
Γ_{87}	$K^- \pi^+ \omega, \omega \rightarrow \pi^+ \pi^- \pi^0$	(2.8 ± 0.5) %			
Γ_{88}	$\bar{K}^*(892)^0 \omega, \bar{K}^{*0} \rightarrow K^- \pi^+, \omega \rightarrow \pi^+ \pi^- \pi^0$	(6.5 ± 3.0) × 10 ⁻³			
Γ_{89}	$K_S^0 \eta \pi^0$	(5.7 ± 1.1) × 10 ⁻³			
Γ_{90}	$K_S^0 a_0(980), a_0 \rightarrow \eta \pi^0$	(6.8 ± 2.1) × 10 ⁻³			
Γ_{91}	$\bar{K}^*(892)^0 \eta, \bar{K}^{*0} \rightarrow K_S^0 \pi^0$	(1.7 ± 0.5) × 10 ⁻³			
Γ_{92}	$K_S^0 2\pi^+ 2\pi^-$	(2.66 ± 0.30) × 10 ⁻³			
Γ_{93}	$K_S^0 \rho^0 \pi^+ \pi^-, \text{no } K^*(892)^-$	(1.1 ± 0.7) × 10 ⁻³			
Γ_{94}	$K^*(892)^- 2\pi^+ \pi^-, K^*(892)^- \rightarrow K_S^0 \pi^-, \text{no } \rho^0$	(5 ± 7) × 10 ⁻⁴			
Γ_{95}	$K^*(892)^- \rho^0 \pi^+, K^*(892)^- \rightarrow K_S^0 \pi^-$	(1.6 ± 0.6) × 10 ⁻³			
Γ_{96}	$K_S^0 2\pi^+ 2\pi^-$ nonresonant	< 1.2 × 10 ⁻³	CL=90%		
Γ_{97}	$\bar{K}^0 \pi^+ \pi^- 2\pi^0 (\pi^0)$				
Γ_{98}	$K^- 3\pi^+ 2\pi^-$	(2.2 ± 0.6) × 10 ⁻⁴			
Fractions of some of the following modes with resonances have already appeared above as submodes of particular charged-particle modes. These nine modes below are all corrected for unseen decays of the resonances.					
Γ_{99}	$K_S^0 \eta$	(5.09 ± 0.13) × 10 ⁻³			
Γ_{100}	$K_S^0 \omega$	(1.11 ± 0.06) %			
Γ_{101}	$K_S^0 \eta'(958)$	(9.49 ± 0.32) × 10 ⁻³			
Γ_{102}	$\bar{K}^*(892)^0 \pi^+ \pi^- \pi^0$	(1.9 ± 0.9) %			
Γ_{103}	$\bar{K}^*(892)^0 \eta$				

Γ ₁₀₄	$K^- \pi^+ \omega$	(3.1 ± 0.6) %		Γ ₁₆₃	Resonant $(\pi^+ \pi^-) \pi^+ \pi^-$	(1.51 ± 0.12) × 10 ⁻³	
Γ ₁₀₅	$\bar{K}^*(892)^0 \omega$	(1.1 ± 0.5) %			3-body total		
Γ ₁₀₆	$K^- \pi^+ \eta'(958)$	(6.43 ± 0.34) × 10 ⁻³		Γ ₁₆₄	$\sigma \pi^+ \pi^-$	(6.2 ± 0.9) × 10 ⁻⁴	
Γ ₁₀₇	$K_S^0 \eta'(958) \pi^0$	(2.52 ± 0.27) × 10 ⁻³		Γ ₁₆₅	$\sigma \rho(770)^0$	(5.0 ± 2.5) × 10 ⁻⁴	
Γ ₁₀₈	$K^*(892)^0 \eta'(958)$	< 1.0 × 10 ⁻³	CL=90%	Γ ₁₆₆	$f_0(980) \pi^+ \pi^-$, $f_0 \rightarrow \pi^+ \pi^-$	(1.8 ± 0.5) × 10 ⁻⁴	
Hadronic modes with three K's							
Γ ₁₀₉	$K_S^0 K^+ K^-$	(4.42 ± 0.32) × 10 ⁻³		Γ ₁₆₇	$f_2(1270) \pi^+ \pi^-$, $f_2 \rightarrow \pi^+ \pi^-$	(3.7 ± 0.6) × 10 ⁻⁴	
Γ ₁₁₀	$K_S^0 a_0(980)^0$, $a_0^0 \rightarrow K^+ K^-$	(2.9 ± 0.4) × 10 ⁻³		Γ ₁₆₈	$2f_2(1270)$, $f_2 \rightarrow \pi^+ \pi^-$	(1.6 ± 1.8) × 10 ⁻⁴	
Γ ₁₁₁	$K^- a_0(980)^+$, $a_0^+ \rightarrow K^+ K_S^0$	(5.9 ± 1.8) × 10 ⁻⁴		Γ ₁₆₉	$f_0(1370) \sigma$, $f_0 \rightarrow \pi^+ \pi^-$	(1.6 ± 0.5) × 10 ⁻³	
Γ ₁₁₂	$K^+ a_0(980)^-$, $a_0^- \rightarrow K^- K_S^0$	< 1.1 × 10 ⁻⁴	CL=95%	Γ ₁₇₀	$\pi^+ \pi^- 2\pi^0$	(1.02 ± 0.09) %	
Γ ₁₁₃	$K_S^0 f_0(980)$, $f_0 \rightarrow K^+ K^-$	< 9 × 10 ⁻⁵	CL=95%	Γ ₁₇₁	$\eta \pi^0$	[h] (6.3 ± 0.6) × 10 ⁻⁴	S=1.1
Γ ₁₁₄	$K_S^0 \phi$, $\phi \rightarrow K^+ K^-$	(2.03 ± 0.15) × 10 ⁻³		Γ ₁₇₂	$\omega \pi^0$	[h] (1.17 ± 0.35) × 10 ⁻⁴	
Γ ₁₁₅	$K_S^0 f_0(1370)$, $f_0 \rightarrow K^+ K^-$	(1.7 ± 1.1) × 10 ⁻⁴		Γ ₁₇₃	$\omega \eta$	(1.98 ± 0.18) × 10 ⁻³	S=1.1
Γ ₁₁₆	$3K_S^0$	(7.5 ± 0.7) × 10 ⁻⁴	S=1.4	Γ ₁₇₄	$2\pi^+ 2\pi^- \pi^0$	(4.2 ± 0.5) × 10 ⁻³	
Γ ₁₁₇	$K^+ 2K^- \pi^+$	(2.25 ± 0.32) × 10 ⁻⁴		Γ ₁₇₅	$\eta \pi^+ \pi^-$	[h] (1.09 ± 0.16) × 10 ⁻³	
Γ ₁₁₈	$K^+ K^- \bar{K}^*(892)^0$, $\bar{K}^{*0} \rightarrow K^- \pi^+$	(4.5 ± 1.8) × 10 ⁻⁵		Γ ₁₇₆	$\omega \pi^+ \pi^-$	[h] (1.6 ± 0.5) × 10 ⁻³	
Γ ₁₁₉	$K^- \pi^+ \phi$, $\phi \rightarrow K^+ K^-$	(4.1 ± 1.7) × 10 ⁻⁵		Γ ₁₇₇	$\eta 2\pi^0$	(3.8 ± 1.3) × 10 ⁻⁴	
Γ ₁₂₀	$\phi \bar{K}^*(892)^0$, $\phi \rightarrow K^+ K^-$, $\bar{K}^{*0} \rightarrow K^- \pi^+$	(1.08 ± 0.21) × 10 ⁻⁴		Γ ₁₇₈	$3\pi^+ 3\pi^-$	(4.3 ± 1.2) × 10 ⁻⁴	
Γ ₁₂₁	$K^+ 2K^- \pi^+$ nonresonant	(3.4 ± 1.5) × 10 ⁻⁵		Γ ₁₇₉	$\eta'(958) \pi^0$	(9.2 ± 1.0) × 10 ⁻⁴	
Γ ₁₂₂	$2K_S^0 K^\pm \pi^\mp$	(5.9 ± 1.3) × 10 ⁻⁴		Γ ₁₈₀	$\eta'(958) \pi^+ \pi^-$	(4.5 ± 1.7) × 10 ⁻⁴	
Pionic modes							
Γ ₁₂₃	$\pi^+ \pi^-$	(1.45 ± 0.024) × 10 ⁻³	S=1.3	Γ ₁₈₁	2η	(2.11 ± 0.19) × 10 ⁻³	S=2.2
Γ ₁₂₄	$2\pi^0$	(8.26 ± 0.25) × 10 ⁻⁴		Γ ₁₈₂	$2\eta \pi^0$	(7.3 ± 2.2) × 10 ⁻⁴	
Γ ₁₂₅	$\pi^+ \pi^- \pi^0$	(1.49 ± 0.06) %	S=2.1	Γ ₁₈₃	3η	< 1.3 × 10 ⁻⁴	CL=90%
Γ ₁₂₆	$\rho^+ \pi^-$	(1.01 ± 0.04) %		Γ ₁₈₄	$\eta \eta'(958)$	(1.01 ± 0.19) × 10 ⁻³	
Γ ₁₂₇	$\rho^0 \pi^0$	(3.86 ± 0.23) × 10 ⁻³		Hadronic modes with a $K\bar{K}$ pair			
Γ ₁₂₈	$\rho^- \pi^+$	(5.15 ± 0.25) × 10 ⁻³		Γ ₁₈₅	$K^+ K^-$	(4.08 ± 0.06) × 10 ⁻³	S=1.6
Γ ₁₂₉	$\rho(1450)^+ \pi^-$, $\rho^+ \rightarrow \pi^+ \pi^0$	(1.6 ± 2.1) × 10 ⁻⁵		Γ ₁₈₆	$2K_S^0$	(1.41 ± 0.05) × 10 ⁻⁴	S=1.1
Γ ₁₃₀	$\rho(1450)^0 \pi^0$, $\rho^0 \rightarrow \pi^+ \pi^-$	(4.5 ± 2.0) × 10 ⁻⁵		Γ ₁₈₇	$K_S^0 K^- \pi^+$	(3.3 ± 0.5) × 10 ⁻³	S=1.1
Γ ₁₃₁	$\rho(1450)^- \pi^+$, $\rho^- \rightarrow \pi^- \pi^0$	(2.7 ± 0.4) × 10 ⁻⁴		Γ ₁₈₈	$\bar{K}^*(892)^0 K_S^0$, $\bar{K}^{*0} \rightarrow K^- \pi^+$	(8.2 ± 1.6) × 10 ⁻⁵	
Γ ₁₃₂	$\rho(1700)^+ \pi^-$, $\rho^+ \rightarrow \pi^+ \pi^0$	(6.1 ± 1.5) × 10 ⁻⁴		Γ ₁₈₉	$K^*(892)^+ K^-$, $K^{*+} \rightarrow K_S^0 \pi^+$	(1.89 ± 0.30) × 10 ⁻³	
Γ ₁₃₃	$\rho(1700)^0 \pi^0$, $\rho^0 \rightarrow \pi^+ \pi^-$	(7.4 ± 1.8) × 10 ⁻⁴		Γ ₁₉₀	$\bar{K}^*(1410)^0 K_S^0$, $\bar{K}^{*0} \rightarrow K^- \pi^+$	(1.3 ± 1.9) × 10 ⁻⁴	
Γ ₁₃₄	$\rho(1700)^- \pi^+$, $\rho^- \rightarrow \pi^- \pi^0$	(4.8 ± 1.1) × 10 ⁻⁴		Γ ₁₉₁	$K^*(1410)^+ K^-$, $K^{*+} \rightarrow K_S^0 \pi^+$	(3.2 ± 1.9) × 10 ⁻⁴	
Γ ₁₃₅	$f_0(980) \pi^0$, $f_0 \rightarrow \pi^+ \pi^-$	(3.7 ± 0.9) × 10 ⁻⁵		Γ ₁₉₂	$(K^- \pi^+)_{S\text{-wave}} K_S^0$	(6.0 ± 2.9) × 10 ⁻⁴	
Γ ₁₃₆	$f_0(500) \pi^0$, $f_0 \rightarrow \pi^+ \pi^-$	(1.22 ± 0.22) × 10 ⁻⁴		Γ ₁₉₃	$(K_S^0 \pi^+)_{S\text{-wave}} K^-$	(3.9 ± 1.0) × 10 ⁻⁴	
Γ ₁₃₇	$f_0(1370) \pi^0$, $f_0 \rightarrow \pi^+ \pi^-$	(5.5 ± 2.1) × 10 ⁻⁵		Γ ₁₉₄	$a_0(980)^- \pi^+$, $a_0^- \rightarrow K_S^0 K^-$	(1.3 ± 1.4) × 10 ⁻⁴	
Γ ₁₃₈	$f_0(1500) \pi^0$, $f_0 \rightarrow \pi^+ \pi^-$	(5.8 ± 1.6) × 10 ⁻⁵		Γ ₁₉₅	$a_0(1450)^- \pi^+$, $a_0^- \rightarrow K_S^0 K^-$	(2.5 ± 2.0) × 10 ⁻⁵	
Γ ₁₃₉	$f_0(1710) \pi^0$, $f_0 \rightarrow \pi^+ \pi^-$	(4.6 ± 1.6) × 10 ⁻⁵		Γ ₁₉₆	$a_2(1320)^- \pi^+$, $a_2^- \rightarrow K_S^0 K^-$	(5 ± 5) × 10 ⁻⁶	
Γ ₁₄₀	$f_2(1270) \pi^0$, $f_2 \rightarrow \pi^+ \pi^-$	(1.97 ± 0.21) × 10 ⁻⁴		Γ ₁₉₇	$\rho(1450)^- \pi^+$, $\rho^- \rightarrow K_S^0 K^-$	(4.6 ± 2.5) × 10 ⁻⁵	
Γ ₁₄₁	$\pi^+ \pi^- \pi^0$ nonresonant	(1.3 ± 0.4) × 10 ⁻⁴		Γ ₁₉₈	$K_S^0 K^+ \pi^-$	(2.17 ± 0.34) × 10 ⁻³	S=1.1
Γ ₁₄₂	$3\pi^0$	(2.0 ± 0.5) × 10 ⁻⁴		Γ ₁₉₉	$K^*(892)^0 K_S^0$, $K^{*0} \rightarrow K^+ \pi^-$	(1.12 ± 0.21) × 10 ⁻⁴	
Γ ₁₄₃	$2\pi^+ 2\pi^-$	(7.56 ± 0.20) × 10 ⁻³		Γ ₂₀₀	$K^*(892)^- K^+$, $K^{*-} \rightarrow K_S^0 \pi^-$	(6.2 ± 1.0) × 10 ⁻⁴	
Γ ₁₄₄	$a_1(1260)^+ \pi^-$, $a_1^+ \rightarrow 2\pi^+ \pi^-$ total	(4.54 ± 0.31) × 10 ⁻³		Γ ₂₀₁	$K^*(1410)^0 K_S^0$, $K^{*0} \rightarrow K^+ \pi^-$	(5 ± 8) × 10 ⁻⁵	
Γ ₁₄₅	$a_1(1260)^+ \pi^-$, $a_1^+ \rightarrow \rho^0 \pi^+ S\text{-wave}$	(3.14 ± 0.21) × 10 ⁻³		Γ ₂₀₂	$K^*(1410)^- K^+$, $K^{*-} \rightarrow K_S^0 \pi^-$	(2.6 ± 2.0) × 10 ⁻⁴	
Γ ₁₄₆	$a_1(1260)^+ \pi^-$, $a_1^+ \rightarrow \rho^0 \pi^+ D\text{-wave}$	(1.9 ± 0.5) × 10 ⁻⁴		Γ ₂₀₃	$(K^+ \pi^-)_{S\text{-wave}} K_S^0$	(3.7 ± 1.9) × 10 ⁻⁴	
Γ ₁₄₇	$a_1(1260)^+ \pi^-$, $a_1^+ \rightarrow \sigma \pi^+$	(6.4 ± 0.7) × 10 ⁻⁴		Γ ₂₀₄	$(K_S^0 \pi^-)_{S\text{-wave}} K^+$	(1.4 ± 0.6) × 10 ⁻⁴	
Γ ₁₄₈	$a_1(1260)^- \pi^+$, $a_1^- \rightarrow \rho^0 \pi^- S\text{-wave}$	(2.3 ± 0.9) × 10 ⁻⁴		Γ ₂₀₅	$a_0(980)^+ \pi^-$, $a_0^+ \rightarrow K_S^0 K^+$	(6 ± 4) × 10 ⁻⁴	
Γ ₁₄₉	$a_1(1260)^- \pi^+$, $a_1^- \rightarrow \sigma \pi^-$	(6.1 ± 3.4) × 10 ⁻⁵		Γ ₂₀₆	$a_0(1450)^+ \pi^-$, $a_0^+ \rightarrow K_S^0 K^+$	(3.2 ± 2.5) × 10 ⁻⁵	
Γ ₁₅₀	$\pi(1300)^+ \pi^-$, $\pi(1300)^+ \rightarrow \sigma \pi^+$	(5.1 ± 2.7) × 10 ⁻⁴		Γ ₂₀₇	$\rho(1700)^+ \pi^-$, $\rho^+ \rightarrow K_S^0 K^+$	(1.1 ± 0.6) × 10 ⁻⁵	
Γ ₁₅₁	$\pi(1300)^- \pi^+$, $\pi(1300)^- \rightarrow \sigma \pi^-$	(2.3 ± 2.2) × 10 ⁻⁴		Γ ₂₀₈	$K^+ K^- \pi^0$	(3.42 ± 0.14) × 10 ⁻³	
Γ ₁₅₂	$a_1(1640)^+ \pi^-$, $a_1^+ \rightarrow \rho^0 \pi^+ D\text{-wave}$	(3.2 ± 1.6) × 10 ⁻⁴		Γ ₂₀₉	$K^*(892)^+ K^-$, $K^*(892)^+ \rightarrow K^+ \pi^0$	(1.52 ± 0.07) × 10 ⁻³	
Γ ₁₅₃	$a_1(1640)^+ \pi^-$, $a_1^+ \rightarrow \sigma \pi^+$	(1.8 ± 1.4) × 10 ⁻⁴		Γ ₂₁₀	$K^*(892)^- K^+$, $K^*(892)^- \rightarrow K^- \pi^0$	(5.4 ± 0.4) × 10 ⁻⁴	
Γ ₁₅₄	$\pi_2(1670)^+ \pi^-$, $\pi_2^+ \rightarrow f_2(1270)^0 \pi^+$, $f_2^0 \rightarrow \pi^+ \pi^-$	(2.0 ± 0.9) × 10 ⁻⁴		Γ ₂₁₁	$(K^+ \pi^0)_{S\text{-wave}} K^-$	(2.43 ± 0.18) × 10 ⁻³	
Γ ₁₅₅	$\pi_2(1670)^+ \pi^-$, $\pi_2^+ \rightarrow \sigma \pi^+$	(2.6 ± 1.0) × 10 ⁻⁴		Γ ₂₁₂	$(K^- \pi^0)_{S\text{-wave}} K^+$	(1.3 ± 0.5) × 10 ⁻⁴	
Γ ₁₅₆	$2\rho^0$ total	(1.85 ± 0.13) × 10 ⁻³		Γ ₂₁₃	$f_0(980) \pi^0$, $f_0 \rightarrow K^+ K^-$	(3.6 ± 0.6) × 10 ⁻⁴	
Γ ₁₅₇	$2\rho^0$, parallel helicities	(8.3 ± 3.2) × 10 ⁻⁵		Γ ₂₁₄	$\phi \pi^0$, $\phi \rightarrow K^+ K^-$	(6.6 ± 0.4) × 10 ⁻⁴	
Γ ₁₅₈	$2\rho^0$, perpendicular helicities	(4.8 ± 0.6) × 10 ⁻⁴		Γ ₂₁₅	$K^+ K^- \pi^0$ nonresonant		
Γ ₁₅₉	$2\rho^0$, longitudinal helicities	(1.27 ± 0.10) × 10 ⁻³		Γ ₂₁₆	$2K_S^0 \pi^0$	< 5.9 × 10 ⁻⁴	
Γ ₁₆₀	$2\rho(770)^0$, S-wave	(1.8 ± 1.3) × 10 ⁻⁴		Γ ₂₁₇	$K^+ K^- \pi^+ \pi^-$	(2.47 ± 0.11) × 10 ⁻³	
Γ ₁₆₁	$2\rho(770)^0$, P-wave	(5.3 ± 1.3) × 10 ⁻⁴		Γ ₂₁₈	$\phi(\pi^+ \pi^-)_{S\text{-wave}}$, $\phi \rightarrow K^+ K^-$	(10 ± 5) × 10 ⁻⁵	
Γ ₁₆₂	$2\rho(770)^0$, D-wave	(6.2 ± 3.0) × 10 ⁻⁴					

Meson Particle Listings

 D^0

Γ_{219}	$(\phi\rho^0)_{S\text{-wave}}, \phi \rightarrow K^+K^-$	$(6.9 \pm 0.6) \times 10^{-4}$	
Γ_{220}	$(\phi\rho^0)_{P\text{-wave}}, \phi \rightarrow K^+K^-$	$(4.0 \pm 1.9) \times 10^{-5}$	
Γ_{221}	$(\phi\rho^0)_{D\text{-wave}}, \phi \rightarrow K^+K^-$	$(4.2 \pm 1.4) \times 10^{-5}$	
Γ_{222}	$K^*(892)^0 \bar{K}^*(892)^0, K^{*0} \rightarrow K^{\pm}\pi^{\mp}$		
Γ_{223}	$K^+K^-\rho^0$ 3-body		
Γ_{224}	$f_0(980)\pi^+\pi^-, f_0 \rightarrow K^+K^-$		
Γ_{225}	$(K^*(892)^0 \bar{K}^*(892)^0)_{S\text{-wave}}, K^{*0} \rightarrow K^{\pm}\pi^{\mp}$	$(2.24 \pm 0.13) \times 10^{-4}$	
Γ_{226}	$(K^*(892)^0 \bar{K}^*(892)^0)_{P\text{-wave}}, K^* \rightarrow K^{\pm}\pi^{\mp}$	$(1.20 \pm 0.08) \times 10^{-4}$	
Γ_{227}	$(K^*(892)^0 \bar{K}^*(892)^0)_{D\text{-wave}}, K^* \rightarrow K^{\pm}\pi^{\mp}$	$(4.7 \pm 0.4) \times 10^{-5}$	
Γ_{228}	$K^*(892)^0 K^{\mp}\pi^{\pm}$ 3-body, $K^{*0} \rightarrow K^{\pm}\pi^{\mp}$		
Γ_{229}	$K^*(892)^0 (K^-\pi^+)_{S\text{-wave}}$ 3-body, $K^{*0} \rightarrow K^+\pi^-$	$(1.4 \pm 0.6) \times 10^{-4}$	
Γ_{230}	$(K^-\pi^+)_{P\text{-wave}}, (K^+\pi^-)_{S\text{-wave}}$		
Γ_{231}	$K_1(1270)^{\pm} K^{\mp}, K_1^{\pm} \rightarrow K^{\pm}\pi^{\mp}\pi^{\mp}$		
Γ_{232}	$K_1(1270)^+ K^-, K_1^+ \rightarrow K^{*0}\pi^+$	$(1.4 \pm 0.9) \times 10^{-4}$	
Γ_{233}	$K_1(1270)^+ K^-, K_1^+ \rightarrow K^*(1430)^0\pi^+, K^{*0} \rightarrow K^+\pi^-$	$(1.5 \pm 0.5) \times 10^{-4}$	
Γ_{234}	$K_1(1270)^+ K^-, K_1^+ \rightarrow \rho^0 K^+$	$(2.2 \pm 0.6) \times 10^{-4}$	
Γ_{235}	$K_1(1270)^+ K^-, K_1^+ \rightarrow \omega(782)K^+, \omega \rightarrow \pi^+\pi^-$	$(1.5 \pm 1.2) \times 10^{-5}$	
Γ_{236}	$K_1(1270)^- K^+, K_1^- \rightarrow \bar{K}^{*0}\pi^-$		
Γ_{237}	$K_1(1270)^- K^+, K_1^- \rightarrow \rho^0 K^-$	$(1.3 \pm 0.4) \times 10^{-4}$	
Γ_{238}	$K_1(1400)^{\pm} K^{\mp}, K_1^{\pm} \rightarrow K^{\pm}\pi^{\mp}\pi^{\mp}$		
Γ_{239}	$K_1(1400)^+ K^-, K_1^+ \rightarrow K^*(892)^0\pi^+, K^{*0} \rightarrow K^+\pi^-$	$(4.6 \pm 0.4) \times 10^{-4}$	
Γ_{240}	$K^*(1410)^+ K^-, K^{*+} \rightarrow K^{*0}\pi^+$		
Γ_{241}	$K^*(1410)^- K^+, K^{*-} \rightarrow \bar{K}^{*0}\pi^-$	$(7.0 \pm 1.1) \times 10^{-5}$	
Γ_{242}	$K_1(1680)^+ K^-, K_1^+ \rightarrow K^{*0}\pi^+, K^{*0} \rightarrow K^+\pi^-$	$(8.9 \pm 3.2) \times 10^{-5}$	
Γ_{243}	$K^+K^-\pi^+\pi^-$ non-resonant	$(2.7 \pm 0.6) \times 10^{-4}$	
Γ_{244}	$2K_S^0\pi^+\pi^-$	$(1.22 \pm 0.23) \times 10^{-3}$	
Γ_{245}	$K_S^0 K^- 2\pi^+\pi^-$	$< 1.4 \times 10^{-4}$	CL=90%
Γ_{246}	$K^+K^-\pi^+\pi^-\pi^0$	$(3.1 \pm 2.0) \times 10^{-3}$	

Other $K\bar{K}X$ modes. They include all decay modes of the ϕ , η , and ω .

Γ_{247}	$\phi\pi^0$	$(1.17 \pm 0.04) \times 10^{-3}$	
Γ_{248}	$\phi\eta$	$(1.8 \pm 0.5) \times 10^{-4}$	
Γ_{249}	$\phi\omega$	$< 2.1 \times 10^{-3}$	CL=90%

Radiative modes

Γ_{250}	$\rho^0\gamma$	$(1.82 \pm 0.32) \times 10^{-5}$	
Γ_{251}	$\omega\gamma$	$< 2.4 \times 10^{-4}$	CL=90%
Γ_{252}	$\phi\gamma$	$(2.81 \pm 0.19) \times 10^{-5}$	
Γ_{253}	$\bar{K}^*(892)^0\gamma$	$(4.2 \pm 0.7) \times 10^{-4}$	

Doubly Cabibbo suppressed (DC) modes or $\Delta C = 2$ forbidden via mixing (C2M) modes

Γ_{254}	$K^+\ell^-\bar{\nu}_\ell$ via \bar{D}^0	$< 2.2 \times 10^{-5}$	CL=90%
Γ_{255}	K^+ or $K^*(892)^+$ $e^-\bar{\nu}_e$ via \bar{D}^0	$< 6 \times 10^{-5}$	CL=90%
Γ_{256}	$K^+\pi^-$	$(1.50 \pm 0.07) \times 10^{-4}$	S=3.0
Γ_{257}	$K^+\pi^-$ via DCS	$(1.364 \pm 0.026) \times 10^{-4}$	
Γ_{258}	$K^+\pi^-$ via \bar{D}^0	$< 1.6 \times 10^{-5}$	CL=95%
Γ_{259}	$K_S^0\pi^+\pi^-$ in $D^0 \rightarrow \bar{D}^0$	$< 1.8 \times 10^{-4}$	CL=95%
Γ_{260}	$K^*(892)^+\pi^-, K^{*+} \rightarrow K_S^0\pi^+$	$(1.13 \pm_{0.34}^{0.60}) \times 10^{-4}$	
Γ_{261}	$K_0^*(1430)^+\pi^-, K_0^{*+} \rightarrow K_S^0\pi^+$	$< 1.4 \times 10^{-5}$	
Γ_{262}	$K_2^*(1430)^+\pi^-, K_2^{*+} \rightarrow K_S^0\pi^+$	$< 3.4 \times 10^{-5}$	

Γ_{263}	$K^+\pi^-\pi^0$	DC	$(3.06 \pm 0.15) \times 10^{-4}$
Γ_{264}	$K^+\pi^-\pi^0$ via \bar{D}^0		$(7.6 \pm_{0.6}^{0.5}) \times 10^{-4}$
Γ_{265}	$K^+\pi^+2\pi^-$ via DCS		$(2.49 \pm 0.07) \times 10^{-4}$
Γ_{266}	$K^+\pi^+2\pi^-$	DC	$(2.65 \pm 0.06) \times 10^{-4}$
Γ_{267}	$K^+\pi^+2\pi^-$ via \bar{D}^0		$(7.9 \pm 3.0) \times 10^{-6}$
Γ_{268}	$K^+\pi^-$ or $K^+\pi^+2\pi^-$ via \bar{D}^0		
Γ_{269}	μ^- anything via \bar{D}^0	< 4	$\times 10^{-4}$ CL=90%

 $\Delta C = 1$ weak neutral current (CI) modes, Lepton Family number (LF) violating modes, Lepton (L) or Baryon (B) number violating modes

Γ_{270}	$\gamma\gamma$	CI	$< 8.5 \times 10^{-7}$	CL=90%
Γ_{271}	e^+e^-	CI	$< 7.9 \times 10^{-8}$	CL=90%
Γ_{272}	$\mu^+\mu^-$	CI	$< 6.2 \times 10^{-9}$	CL=90%
Γ_{273}	$\pi^0 e^+ e^-$	CI	$< 4 \times 10^{-6}$	CL=90%
Γ_{274}	$\pi^0 \mu^+ \mu^-$	CI	$< 1.8 \times 10^{-4}$	CL=90%
Γ_{275}	$\eta e^+ e^-$	CI	$< 3 \times 10^{-6}$	CL=90%
Γ_{276}	$\eta \mu^+ \mu^-$	CI	$< 5.3 \times 10^{-4}$	CL=90%
Γ_{277}	$\pi^+\pi^- e^+ e^-$	CI	$< 7 \times 10^{-6}$	CL=90%
Γ_{278}	$\rho^0 e^+ e^-$	CI	$< 1.0 \times 10^{-4}$	CL=90%
Γ_{279}	$\pi^+\pi^-\mu^+\mu^-$	CI	$(9.6 \pm 1.2) \times 10^{-7}$	
Γ_{280}	$\pi^+\pi^-\mu^+\mu^-$ (non-res)		$< 5.5 \times 10^{-7}$	CL=90%
Γ_{281}	$\rho^0 \mu^+ \mu^-$	CI	$< 2.2 \times 10^{-5}$	CL=90%
Γ_{282}	$\omega e^+ e^-$	CI	$< 6 \times 10^{-6}$	CL=90%
Γ_{283}	$\omega \mu^+ \mu^-$	CI	$< 8.3 \times 10^{-4}$	CL=90%
Γ_{284}	$K^-K^+ e^+ e^-$	CI	$< 1.1 \times 10^{-5}$	CL=90%
Γ_{285}	$\phi e^+ e^-$	CI	$< 5.2 \times 10^{-5}$	CL=90%
Γ_{286}	$K^-K^+ \mu^+ \mu^-$	CI	$(1.54 \pm 0.32) \times 10^{-7}$	
Γ_{287}	$K^-K^+ \mu^+ \mu^-$ (non-res)		$< 3.3 \times 10^{-5}$	CL=90%
Γ_{288}	$\phi \mu^+ \mu^-$	CI	$< 3.1 \times 10^{-5}$	CL=90%
Γ_{289}	$\bar{K}^0 e^+ e^-$	[j]	$< 2.4 \times 10^{-5}$	CL=90%
Γ_{290}	$\bar{K}^0 \mu^+ \mu^-$	[j]	$< 2.6 \times 10^{-4}$	CL=90%
Γ_{291}	$K^-\pi^+ e^+ e^-$			
Γ_{292}	$K^-\pi^+ e^+ e^-, 675 < m_{ee} < 875 \text{ MeV}$		$(4.0 \pm 0.5) \times 10^{-6}$	
Γ_{293}	$K^-\pi^+ e^+ e^-, 1.005 < m_{ee} < 1.035 \text{ GeV}$		$< 5 \times 10^{-7}$	CL=90%
Γ_{294}	$\bar{K}^*(892)^0 e^+ e^-$	[j]	$< 4.7 \times 10^{-5}$	CL=90%
Γ_{295}	$K^-\pi^+ \mu^+ \mu^-$	CI	$< 3.59 \times 10^{-4}$	CL=90%
Γ_{296}	$K^-\pi^+ \mu^+ \mu^-, 675 < m_{\mu\mu} < 875 \text{ MeV}$		$(4.2 \pm 0.4) \times 10^{-6}$	
Γ_{297}	$\bar{K}^*(892)^0 \mu^+ \mu^-$	[j]	$< 2.4 \times 10^{-5}$	CL=90%
Γ_{298}	$\pi^+\pi^-\pi^0 \mu^+ \mu^-$	CI	$< 8.1 \times 10^{-4}$	CL=90%
Γ_{299}	$\mu^{\pm} e^{\mp}$	LF	[j] $< 1.3 \times 10^{-8}$	CL=90%
Γ_{300}	$\pi^0 e^{\pm} \mu^{\mp}$	LF	[j] $< 8.6 \times 10^{-5}$	CL=90%
Γ_{301}	$\eta e^{\pm} \mu^{\mp}$	LF	[j] $< 1.0 \times 10^{-4}$	CL=90%
Γ_{302}	$\pi^+\pi^- e^{\pm} \mu^{\mp}$	LF	[j] $< 1.5 \times 10^{-5}$	CL=90%
Γ_{303}	$\rho^0 e^{\pm} \mu^{\mp}$	LF	[j] $< 4.9 \times 10^{-5}$	CL=90%
Γ_{304}	$\omega e^{\pm} \mu^{\mp}$	LF	[j] $< 1.2 \times 10^{-4}$	CL=90%
Γ_{305}	$K^-K^+ e^{\pm} \mu^{\mp}$	LF	[j] $< 1.8 \times 10^{-4}$	CL=90%
Γ_{306}	$\phi e^{\pm} \mu^{\mp}$	LF	[j] $< 3.4 \times 10^{-5}$	CL=90%
Γ_{307}	$\bar{K}^0 e^{\pm} \mu^{\mp}$	LF	[j] $< 1.0 \times 10^{-4}$	CL=90%
Γ_{308}	$K^-\pi^+ e^{\pm} \mu^{\mp}$	LF	[j] $< 5.53 \times 10^{-4}$	CL=90%
Γ_{309}	$\bar{K}^*(892)^0 e^{\pm} \mu^{\mp}$	LF	[j] $< 8.3 \times 10^{-5}$	CL=90%
Γ_{310}	$2\pi^- 2e^+ + \text{c.c.}$	L	$< 1.12 \times 10^{-4}$	CL=90%
Γ_{311}	$2\pi^- 2\mu^+ + \text{c.c.}$	L	$< 2.9 \times 10^{-5}$	CL=90%
Γ_{312}	$K^-\pi^- 2e^+ + \text{c.c.}$			
Γ_{313}	$K^-\pi^- 2e^+$		$< 2.8 \times 10^{-6}$	CL=90%
Γ_{314}	$K^-\pi^- 2\mu^+ + \text{c.c.}$	L	$< 3.9 \times 10^{-4}$	CL=90%
Γ_{315}	$2K^- 2e^+ + \text{c.c.}$	L	$< 1.52 \times 10^{-4}$	CL=90%
Γ_{316}	$2K^- 2\mu^+ + \text{c.c.}$	L	$< 9.4 \times 10^{-5}$	CL=90%
Γ_{317}	$\pi^-\pi^- e^+ \mu^+ + \text{c.c.}$	L	$< 7.9 \times 10^{-5}$	CL=90%
Γ_{318}	$K^-\pi^- e^+ \mu^+ + \text{c.c.}$	L	$< 2.18 \times 10^{-4}$	CL=90%
Γ_{319}	$2K^- e^+ \mu^+ + \text{c.c.}$	L	$< 5.7 \times 10^{-5}$	CL=90%
Γ_{320}	$p e^-$	L,B	[k] $< 1.0 \times 10^{-5}$	CL=90%
Γ_{321}	$\bar{p} e^+$	L,B	[l] $< 1.1 \times 10^{-5}$	CL=90%

Γ_{322}	Unaccounted decay modes	$(36.9 \pm 1.2) \%$	S=1.1
----------------	-------------------------	---------------------	-------

[a] This value is obtained by subtracting the branching fractions for 2-, 4- and 6-prongs from unity.

[b] This is the sum of our $K^-2\pi^+\pi^-$, $K^-2\pi^+\pi^-\pi^0$, $\bar{K}^0 2\pi^+ 2\pi^-$, $K^+ 2K^-\pi^+$, $2\pi^+ 2\pi^-$, $2\pi^+ 2\pi^-\pi^0$, $K^+K^-\pi^+\pi^-$, and $K^+K^-\pi^+\pi^-\pi^0$, branching fractions.

- [c] This is the sum of our $K^- 3\pi^+ 2\pi^-$ and $3\pi^+ 3\pi^-$ branching fractions.
- [d] The branching fractions for the $K^- e^+ \nu_e$, $K^*(892)^- e^+ \nu_e$, $\pi^- e^+ \nu_e$, and $\rho^- e^+ \nu_e$ modes add up to $6.17 \pm 0.17\%$.
- [e] The branching fraction for this mode may differ from the sum of the submodes that contribute to it, due to interference effects. See the relevant papers.
- [f] This is a doubly Cabibbo-suppressed mode.
- [g] Submodes of the $D^0 \rightarrow K_S^0 \pi^+ \pi^- \pi^0$ mode with a K^* and/or ρ were studied by COFFMAN 92B, but with only 140 events. With nothing new for 18 years, we refer to our 2008 edition, Physics Letters **B667** 1 (2008), for those results.
- [h] This branching fraction includes all the decay modes of the resonance in the final state.
- [i] This mode is not a useful test for a $\Delta C=1$ weak neutral current because both quarks must change flavor in this decay.
- [j] The value is for the sum of the charge states or particle/antiparticle states indicated.
- [k] This limit is for either D^0 or \bar{D}^0 to $p e^-$.
- [l] This limit is for either D^0 or \bar{D}^0 to $\bar{p} e^+$.

CONSTRAINED FIT INFORMATION

An overall fit to 64 branching ratios uses 126 measurements and one constraint to determine 32 parameters. The overall fit has a $\chi^2 = 141.9$ for 95 degrees of freedom.

The following *off-diagonal* array elements are the correlation coefficients $\langle \delta x_i \delta x_j \rangle / (\delta x_i \delta x_j)$, in percent, from the fit to the branching fractions, $x_i \equiv \Gamma_i / \Gamma_{total}$. The fit constrains the x_i whose labels appear in this array to sum to one.

x_{19}	0																			
x_{20}	6	0																		
x_{21}	0	0	0																	
x_{30}	0	0	0	0																
x_{31}	0	0	0	0	0															
x_{35}	0	4	0	1	5	0														
x_{36}	0	1	0	1	1	0	15													
x_{38}	0	0	0	14	0	0	5	8												
x_{53}	0	1	0	0	1	0	22	3	1											
x_{70}	0	2	0	0	2	0	46	7	2	10										
x_{81}	0	0	0	5	0	0	2	3	37	0										
x_{85}	0	0	0	0	0	0	8	1	0	2										
x_{99}	0	0	0	0	0	0	5	1	0	1										
x_{100}	0	0	0	1	0	0	0	0	4	0										
x_{101}	0	0	0	2	0	0	9	2	12	2										
x_{116}	0	0	0	3	0	0	1	2	21	0										
x_{123}	0	2	0	0	2	0	43	6	2	9										
x_{124}	0	0	0	0	0	0	7	1	0	2										
x_{125}	0	1	0	0	1	0	19	3	1	81										
x_{143}	0	1	0	0	1	0	30	5	2	7										
x_{171}	0	0	0	0	0	0	4	1	0	1										
x_{179}	0	0	0	0	0	0	4	1	0	1										
x_{181}	0	0	0	0	0	0	2	0	0	0										
x_{184}	0	0	0	0	0	0	2	0	0	0										
x_{185}	0	2	0	0	2	0	49	7	3	11										
x_{186}	0	0	0	1	0	0	7	47	4	2										
x_{187}	0	0	0	5	0	0	3	3	34	1										
x_{198}	0	0	0	5	0	0	3	3	34	1										
x_{252}	0	0	0	0	0	0	11	2	1	2										
x_{256}	0	1	0	0	1	0	16	3	1	4										
x_{322}	-48	-4	-6	-18	-1	-1	-24	-8	-39	-50										
	x_6	x_{19}	x_{20}	x_{21}	x_{30}	x_{31}	x_{35}	x_{36}	x_{38}	x_{53}										

x_{81}	1																				
x_{85}	12	0																			
x_{99}	3	0	0																		
x_{100}	0	12	0	0																	
x_{101}	4	4	1	0	1																
x_{116}	1	8	0	0	1	2															
x_{123}	20	1	3	2	0	4	0														
x_{124}	3	0	1	0	0	1	0	3													
x_{125}	9	0	2	1	0	2	0	8	1												
x_{143}	46	1	6	2	0	3	0	13	2	6											
x_{171}	2	0	0	0	0	0	0	2	0	1											
x_{179}	2	0	0	0	0	0	0	2	0	1											
x_{181}	1	0	0	0	0	0	0	1	0	0											
x_{184}	1	0	0	0	0	0	0	1	0	0											
x_{185}	22	1	4	3	0	4	1	21	3	9											
x_{186}	3	1	1	0	0	1	1	3	0	1											
x_{187}	1	13	0	0	2	4	7	1	0	0											
x_{198}	1	13	0	0	2	4	7	1	0	0											
x_{252}	5	0	1	1	0	1	0	5	1	2											
x_{256}	7	0	1	1	0	2	0	7	1	3											
x_{322}	-23	-57	-36	-2	-12	-9	-9	-10	-2	-42											
	x_{70}	x_{81}	x_{85}	x_{99}	x_{100}	x_{101}	x_{116}	x_{123}	x_{124}	x_{125}											

x_{171}	1																				
x_{179}	1	0																			
x_{181}	0	0	0																		
x_{184}	1	0	0	0																	
x_{185}	15	2	2	1	1																
x_{186}	2	0	0	0	0	3															
x_{187}	1	0	0	0	0	1	1														
x_{198}	1	0	0	0	0	1	1	100													
x_{252}	3	0	0	0	0	18	1	0	0												
x_{256}	5	1	1	0	0	9	1	0	0	2											
x_{322}	-13	-1	-2	-2	-2	-12	-4	-20	-19	-3											
	x_{143}	x_{171}	x_{179}	x_{181}	x_{184}	x_{185}	x_{186}	x_{187}	x_{198}	x_{252}											

x_{322}	-4																				
x_{256}																					

CONSTRAINED FIT INFORMATION

An overall fit to 3 branching ratios uses 3 measurements and one constraint to determine 4 parameters. The overall fit has a $\chi^2 = 0.0$ for 0 degrees of freedom.

The following *off-diagonal* array elements are the correlation coefficients $\langle \delta x_i \delta x_j \rangle / (\delta x_i \delta x_j)$, in percent, from the fit to the branching fractions, $x_i \equiv \Gamma_i / \Gamma_{total}$. The fit constrains the x_i whose labels appear in this array to sum to one.

x_2	-100																				
x_3	-46	39																			
x_4	0	0	0																		
	x_1	x_2	x_3																		

D^0 BRANCHING RATIOS

Some older now obsolete results have been omitted from these Listings.

Topological modes

$\Gamma(0\text{-prongs})/\Gamma_{total}$ Γ_1/Γ
This value is obtained by subtracting the branching fractions for 2-, 4-, and 6-prongs from unity.

VALUE	DOCUMENT ID
0.15 ± 0.06 OUR FIT	

$\Gamma(4\text{-prongs})/\Gamma(2\text{-prongs})$	Γ_3/Γ_2			
VALUE	EVTS	DOCUMENT ID	TECN	COMMENT
0.207 ± 0.016 OUR FIT				
$0.207 \pm 0.016 \pm 0.004$	226	ONENGUT	05	CHRS ν_μ emulsion, $\bar{E}_\nu \approx 27$ GeV

Meson Particle Listings

D^0

$\Gamma(4\text{-prongs})/\Gamma_{\text{total}}$ Γ_3/Γ
 This is the sum of our $K^-2\pi^+\pi^-$, $K^-2\pi^+\pi^-\pi^0$, $\bar{K}^02\pi^+2\pi^-$, $K^+2K^-\pi^+$, $2\pi^+2\pi^-$, $2\pi^+2\pi^-\pi^0$, $K^+K^-\pi^+\pi^-$, and $K^+K^-\pi^+\pi^-\pi^0$ branching fractions.

VALUE	DOCUMENT ID	TECN	COMMENT
0.146 ± 0.005 OUR FIT			
0.146 ± 0.005	PDG	19	

$\Gamma(6\text{-prongs})/\Gamma_{\text{total}}$ Γ_4/Γ
 This is the sum of our $K^-3\pi^+2\pi^-$ and $3\pi^+3\pi^-$ branching fractions.

VALUE (units 10^{-4})	DOCUMENT ID	TECN	COMMENT
6.5 ± 1.3 OUR FIT			
6.5 ± 1.3	PDG	19	

———— Inclusive modes ————

$\Gamma(e^+ \text{ anything})/\Gamma_{\text{total}}$ Γ_5/Γ
 The branching fractions for the $K^-e^+\nu_e$, $K^*(892)^-e^+\nu_e$, $\pi^-e^+\nu_e$, and $\rho^-e^+\nu_e$ modes add up to 6.17 ± 0.17 %.

VALUE (%)	EVTS	DOCUMENT ID	TECN	COMMENT
6.49 ± 0.11 OUR AVERAGE				
6.46 ± 0.09 ± 0.11	6584 ± 96	¹ ASNER	10 CLEO	e^+e^- at 3774 MeV
6.3 ± 0.7 ± 0.4	290 ± 32	ABLIKIM	07G BES2	$e^+e^- \approx \psi(3770)$
6.46 ± 0.17 ± 0.13	2246 ± 57	ADAM	06A CLEO	See ASNER 10
6.9 ± 0.3 ± 0.5	1670	ALBRECHT	96C ARG	$e^+e^- \approx 10$ GeV
6.64 ± 0.18 ± 0.29	4609	KUBOTA	96B CLE2	$e^+e^- \approx \Upsilon(4S)$

¹ Using the D^+ and D^0 lifetimes, ASNER 10 finds that the ratio of the D^+ and D^0 semileptonic widths is $0.985 \pm 0.015 \pm 0.024$.

$\Gamma(\mu^+ \text{ anything})/\Gamma_{\text{total}}$ Γ_6/Γ
6.8 ± 0.6 OUR FIT
6.4 ± 0.8 OUR AVERAGE

VALUE (%)	EVTS	DOCUMENT ID	TECN	COMMENT
6.8 ± 1.5 ± 0.8	79 ± 10	¹ ABLIKIM	08L BES2	$e^+e^- \approx \psi(3772)$
6.5 ± 1.2 ± 0.3	36	KAYIS-TOPAK.05	CHRS	ν_μ emulsion
6.0 ± 0.7 ± 1.2	310	ALBRECHT	96C ARG	$e^+e^- \approx 10$ GeV

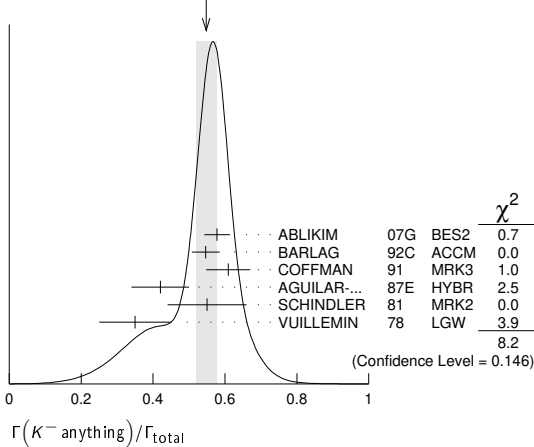
¹ ABLIKIM 08L finds the ratio of $D^+ \rightarrow \mu^+ X$ and $D^0 \rightarrow \mu^+ X$ branching fractions to be $2.59 \pm 0.70 \pm 0.25$, in accord with the ratio of D^+ and D^0 lifetimes, 2.54 ± 0.02 .

$\Gamma(K^- \text{ anything})/\Gamma_{\text{total}}$ Γ_7/Γ
0.547 ± 0.028 OUR AVERAGE Error includes scale factor of 1.3. See the ideogram below.

VALUE (%)	EVTS	DOCUMENT ID	TECN	COMMENT
0.578 ± 0.016 ± 0.032	2098 ± 59	ABLIKIM	07G BES2	$e^+e^- \approx \psi(3770)$
0.546 + 0.039 - 0.038		¹ BARLAG	92C ACCM	π^- Cu 230 GeV
0.609 ± 0.032 ± 0.052		COFFMAN	91 MRK3	e^+e^- 3.77 GeV
0.42 ± 0.08		AGUILAR...	87E HYBR	$\pi p, pp$ 360, 400 GeV
0.55 ± 0.11	121	SCHINDLER	81 MRK2	e^+e^- 3.771 GeV
0.35 ± 0.10	19	VUILLEMIN	78 LGW	e^+e^- 3.772 GeV

¹ BARLAG 92c computes the branching fraction using topological normalization.

WEIGHTED AVERAGE
0.547 ± 0.028 (Error scaled by 1.3)



$[\Gamma(K^0 \text{ anything}) + \Gamma(K^+ \text{ anything})]/\Gamma_{\text{total}}$ Γ_8/Γ
0.47 ± 0.04 OUR AVERAGE

VALUE (%)	EVTS	DOCUMENT ID	TECN	COMMENT
0.476 ± 0.048 ± 0.030	250 ± 25	ABLIKIM	06u BES2	e^+e^- at 3773 MeV
0.455 ± 0.050 ± 0.032		COFFMAN	91 MRK3	e^+e^- 3.77 GeV

$\Gamma(K^+ \text{ anything})/\Gamma_{\text{total}}$ Γ_9/Γ
0.034 ± 0.004 OUR AVERAGE

VALUE (%)	EVTS	DOCUMENT ID	TECN	COMMENT
0.035 ± 0.007 ± 0.003	119 ± 23	ABLIKIM	07G BES2	$e^+e^- \approx \psi(3770)$
0.034 + 0.007 - 0.005		¹ BARLAG	92c ACCM	π^- Cu 230 GeV
0.028 ± 0.009 ± 0.004		COFFMAN	91 MRK3	e^+e^- 3.77 GeV
0.03 + 0.05 - 0.02		AGUILAR...	87E HYBR	$\pi p, pp$ 360, 400 GeV
0.08 ± 0.03	25	SCHINDLER	81 MRK2	e^+e^- 3.771 GeV

¹ BARLAG 92c computes the branching fraction using topological normalization.

$\Gamma(K^*(892)^- \text{ anything})/\Gamma_{\text{total}}$ Γ_{10}/Γ
0.153 ± 0.083 ± 0.019

VALUE (%)	EVTS	DOCUMENT ID	TECN	COMMENT
0.153 ± 0.083 ± 0.019	28 ± 15	ABLIKIM	06u BES2	e^+e^- at 3773 MeV

$\Gamma(K^*(892)^0 \text{ anything})/\Gamma_{\text{total}}$ Γ_{11}/Γ
0.087 ± 0.040 ± 0.012

VALUE (%)	EVTS	DOCUMENT ID	TECN	COMMENT
0.087 ± 0.040 ± 0.012	96 ± 44	ABLIKIM	05P BES	$e^+e^- \approx 3773$ MeV

$\Gamma(K^*(892)^+ \text{ anything})/\Gamma_{\text{total}}$ Γ_{12}/Γ
< 0.036

VALUE (%)	CL%	DOCUMENT ID	TECN	COMMENT
< 0.036	90	ABLIKIM	06u BES2	e^+e^- at 3773 MeV

$\Gamma(K^*(892)^0 \text{ anything})/\Gamma_{\text{total}}$ Γ_{13}/Γ
0.028 ± 0.012 ± 0.004

VALUE (%)	EVTS	DOCUMENT ID	TECN	COMMENT
0.028 ± 0.012 ± 0.004	31 ± 12	ABLIKIM	05P BES	$e^+e^- \approx 3773$ MeV

$\Gamma(\eta \text{ anything})/\Gamma_{\text{total}}$ Γ_{14}/Γ
 This ratio includes η particles from η' decays.

VALUE (%)	EVTS	DOCUMENT ID	TECN	COMMENT
9.5 ± 0.4 ± 0.8	4463 ± 197	HUANG	06B CLEO	e^+e^- at $\psi(3770)$

$\Gamma(\eta' \text{ anything})/\Gamma_{\text{total}}$ Γ_{15}/Γ
2.48 ± 0.17 ± 0.21

VALUE (%)	EVTS	DOCUMENT ID	TECN	COMMENT
2.48 ± 0.17 ± 0.21	299 ± 21	HUANG	06B CLEO	e^+e^- at $\psi(3770)$

$\Gamma(\phi \text{ anything})/\Gamma_{\text{total}}$ Γ_{16}/Γ
1.08 ± 0.04 OUR AVERAGE

VALUE (%)	EVTS	DOCUMENT ID	TECN	COMMENT
1.091 ± 0.027 ± 0.035	4.1k	ABLIKIM	19AYBES3	e^+e^- at 3773 MeV
1.05 ± 0.08 ± 0.07	368 ± 24	HUANG	06B CLEO	e^+e^- at $\psi(3770)$
• • • We do not use the following data for averages, fits, limits, etc. • • •				
1.71 + 0.76 - 0.71 ± 0.17	9	BAI	00c BES	$e^+e^- \rightarrow D\bar{D}^*, D^*\bar{D}^*$

$\Gamma(\text{invisibles})/\Gamma_{\text{total}}$ Γ_{17}/Γ
< 9.4 × 10⁻⁵

VALUE (%)	CL%	DOCUMENT ID	TECN	COMMENT
< 9.4 × 10 ⁻⁵	90	LAI	17 BELL	e^+e^- at $\Upsilon(nS)$, n=4,5

———— Semileptonic modes ————

$\Gamma(K^- e^+ \nu_e)/\Gamma_{\text{total}}$ Γ_{19}/Γ
3.542 ± 0.035 OUR FIT Error includes scale factor of 1.3.
3.503 ± 0.029 OUR AVERAGE

VALUE (%)	EVTS	DOCUMENT ID	TECN	COMMENT
3.505 ± 0.014 ± 0.033	71k	¹ ABLIKIM	15x BES3	2.92 fb ⁻¹ , 3.773 GeV
3.50 ± 0.03 ± 0.04	14.1k	¹ BESSON	09 CLEO	e^+e^- at $\psi(3770)$
3.45 ± 0.10 ± 0.19	1.3k	² WIDHALM	06 BELL	$e^+e^- \approx \Upsilon(4S)$
3.82 ± 0.40 ± 0.27	104	ABLIKIM	04C BES	e^+e^- , 3.773 GeV
3.4 ± 0.5 ± 0.4	55	ADLER	89 MRK3	e^+e^- 3.77 GeV
• • • We do not use the following data for averages, fits, limits, etc. • • •				
3.56 ± 0.03 ± 0.09		³ DOBBS	08 CLEO	See BESSON 09
3.44 ± 0.10 ± 0.10	1.3k	COAN	05 CLEO	See DOBBS 08

¹ See the form-factor parameters near the end of this D^0 Listing.

² The $\pi^-e^+\nu_e$ and $K^-e^+\nu_e$ results of WIDHALM 06 give $|\frac{V_{cd}}{V_{cs}} \cdot \frac{f_+^\pi(0)}{f_+^K(0)}|^2 = 0.042 \pm 0.003 \pm 0.003$.

³ DOBBS 08 establishes $|\frac{V_{cd}}{V_{cs}} \cdot \frac{f_+^\pi(0)}{f_+^K(0)}| = 0.188 \pm 0.008 \pm 0.002$ from the D^+ and D^0 decays to $\bar{K}e^+\nu_e$ and $\pi e^+\nu_e$.

$\Gamma(K^- e^+ \nu_e)/\Gamma(K^- \pi^+)$ Γ_{19}/Γ_5
0.897 ± 0.011 OUR FIT Error includes scale factor of 1.4.
0.930 ± 0.013 OUR AVERAGE

VALUE (%)	EVTS	DOCUMENT ID	TECN	COMMENT
0.927 ± 0.007 ± 0.012	76k ± 323	¹ AUBERT	07Bg BABR	$e^+e^- \approx \Upsilon(4S)$
0.978 ± 0.027 ± 0.044	2510	² BEAN	93c CLE2	$e^+e^- \approx \Upsilon(4S)$
0.90 ± 0.06 ± 0.06	584	³ CRAWFORD	91B CLEO	$e^+e^- \approx 10.5$ GeV
0.91 ± 0.07 ± 0.11	250	⁴ ANJOS	89F E691	Photoproduction

¹ The event samples in this AUBERT 07Bg result include radiative photons. The $D^0 \rightarrow K^-e^+\nu_e$ form factor at $q^2 = 0$ is $f_+(0) = 0.727 \pm 0.007 \pm 0.005 \pm 0.007$.

See key on page 999

Meson Particle Listings

D^0

- ² BEAN 93c uses $K^- \mu^+ \nu_\mu$ as well as $K^- e^+ \nu_e$ events and makes a small phase-space adjustment to the number of the μ^+ events to use them as e^+ events. A pole mass of $2.00 \pm 0.12 \pm 0.18$ GeV/ c^2 is obtained from the q^2 dependence of the decay rate.
- ³ CRAWFORD 91B uses $K^- e^+ \nu_e$ and $K^- \mu^+ \nu_\mu$ candidates to measure a pole mass of $2.1^{+0.4+0.3}_{-0.2-0.2}$ GeV/ c^2 from the q^2 dependence of the decay rate.
- ⁴ ANJOS 89F measures a pole mass of $2.1^{+0.4}_{-0.2} \pm 0.2$ GeV/ c^2 from the q^2 dependence of the decay rate.

$\Gamma(K^- \mu^+ \nu_\mu)/\Gamma_{\text{total}}$		Γ_{20}/Γ		
VALUE (%)	EVTS	DOCUMENT ID	TECN	COMMENT
3.41 ± 0.04 OUR FIT				
3.41 ± 0.04 OUR AVERAGE				
3.413 ± 0.019 ± 0.035	47k	ABLIKIM	19B BES3	$e^+ e^-$, 3773 MeV
3.45 ± 0.10 ± 0.21	1249 ± 43	WIDHALM	06 BELL	$e^+ e^- \approx \gamma(4S)$

$\Gamma(K^- \mu^+ \nu_\mu)/\Gamma(\mu^+ \text{ anything})$		Γ_{20}/Γ_6		
VALUE (%)	EVTS	DOCUMENT ID	TECN	COMMENT
0.50 ± 0.04 OUR FIT				
0.472 ± 0.051 ± 0.040	232	KODAMA	94 E653	π^- emulsion 600 GeV
••• We do not use the following data for averages, fits, limits, etc. •••				
0.32 ± 0.05 ± 0.05	124	KODAMA	91 EMUL	pA 800 GeV

$\Gamma(K^- \mu^+ \nu_\mu)/\Gamma(K^- \pi^+)$		Γ_{20}/Γ_{35}		
VALUE (%)	EVTS	DOCUMENT ID	TECN	COMMENT
0.863 ± 0.012 OUR FIT				Error includes scale factor of 1.1.
0.84 ± 0.04 OUR AVERAGE				
0.852 ± 0.034 ± 0.028	1897	¹ FRABETTI	95G E687	γ Be $\bar{E}_\gamma = 220$ GeV
0.82 ± 0.13 ± 0.13	338	² FRABETTI	93I E687	γ Be $\bar{E}_\gamma = 221$ GeV
0.79 ± 0.08 ± 0.09	231	³ CRAWFORD	91B CLEO	$e^+ e^- \approx 10.5$ GeV

- ¹ FRABETTI 95c extracts the ratio of form factors $f_-(0)/f_+(0) = -1.3^{+3.6}_{-3.4} \pm 0.6$, and measures a pole mass of $1.87^{+0.11+0.07}_{-0.08-0.06}$ GeV/ c^2 from the q^2 dependence of the decay rate.
- ² FRABETTI 93i measures a pole mass of $2.1^{+0.7+0.7}_{-0.3-0.3}$ GeV/ c^2 from the q^2 dependence of the decay rate.
- ³ CRAWFORD 91B measures a pole mass of $2.00 \pm 0.12 \pm 0.18$ GeV/ c^2 dependence of the decay rate.

$\Gamma(K^*(892)^- e^+ \nu_e)/\Gamma_{\text{total}}$		Γ_{21}/Γ		
VALUE (%)	EVTS	DOCUMENT ID	TECN	COMMENT
Both decay modes of the $K^*(892)^-$ are included.				
2.15 ± 0.16 OUR FIT				
2.16 ± 0.15 ± 0.08	219 ± 16	¹ COAN	05 CLEO	$e^+ e^-$ at $\psi(3770)$
¹ COAN 05 uses both $K^- \pi^0$ and $K_S^0 \pi^-$ events.				

$\Gamma(K^*(892)^- e^+ \nu_e)/\Gamma(K^0 \pi^- e^+ \nu_e)$		Γ_{21}/Γ_{24}		
VALUE (units 10^{-2})	EVTS	DOCUMENT ID	TECN	COMMENT
94.52 ± 0.97 ± 0.62	3.1k	ABLIKIM	19G BES3	$K_S^0 \pi^- e^+ \nu_e$ events

$\Gamma(K^*(892)^- e^+ \nu_e)/\Gamma(K_S^0 \pi^- \pi^-)$		Γ_{21}/Γ_{38}		
VALUE (%)	EVTS	DOCUMENT ID	TECN	COMMENT
Unseen decay modes of the $K^*(892)^-$ are included.				
0.77 ± 0.07 OUR FIT				
0.76 ± 0.12 ± 0.06	152	¹ BEAN	93c CLE2	$e^+ e^- \approx \gamma(4S)$

- ¹ BEAN 93c uses $K^* \mu^+ \nu_\mu$ as well as $K^* e^+ \nu_e$ events and makes a small phase-space adjustment to the number of the μ^+ events to use them as e^+ events.

$\Gamma(K^*(892)^- \mu^+ \nu_\mu)/\Gamma(K_S^0 \pi^- \pi^-)$		Γ_{22}/Γ_{38}		
VALUE (%)	EVTS	DOCUMENT ID	TECN	COMMENT
Unseen decay modes of the $K^*(892)^-$ are included.				
0.674 ± 0.068 ± 0.026	175 ± 17	¹ LINK	05B FOCS	$\gamma A, \bar{E}_\gamma \approx 180$ GeV
¹ LINK 05B finds that in $D^0 \rightarrow \bar{K}^0 \pi^- \mu^+ \nu_\mu$ the $\bar{K}^0 \pi^-$ system is 6% in S-wave.				

$\Gamma(K^- \pi^0 e^+ \nu_e)/\Gamma_{\text{total}}$		Γ_{23}/Γ		
VALUE (%)	EVTS	DOCUMENT ID	TECN	COMMENT
0.016 ± 0.013 ± 0.002	4	¹ BAI	91 MRK3	$e^+ e^- \approx 3.77$ GeV

- ¹ BAI 91 finds that a fraction $0.79^{+0.15+0.09}_{-0.17-0.03}$ of combined D^+ and D^0 decays to $\bar{K} \pi e^+ \nu_e$ (24 events) are $\bar{K}^*(892) e^+ \nu_e$. BAI 91 uses 56 $K^- e^+ \nu_e$ events to measure a pole mass of $1.8 \pm 0.3 \pm 0.2$ GeV/ c^2 from the q^2 dependence of the decay rate.

$\Gamma(K^0 \pi^- e^+ \nu_e)/\Gamma_{\text{total}}$		Γ_{24}/Γ		
VALUE (%)	EVTS	DOCUMENT ID	TECN	COMMENT
1.44 ± 0.04 OUR AVERAGE				
1.434 ± 0.029 ± 0.032	3.1k	ABLIKIM	19G BES3	$e^+ e^-$ at 3773 MeV
2.61 ± 1.04 ± 0.28	9 ± 3	ABLIKIM	06O BES2	$e^+ e^-$ at 3773 MeV
2.8 ± 1.7 ± 0.3	6	¹ BAI	91 MRK3	$e^+ e^- \approx 3.77$ GeV

- ¹ BAI 91 finds that a fraction $0.79^{+0.15+0.09}_{-0.17-0.03}$ of combined D^+ and D^0 decays to $\bar{K} \pi e^+ \nu_e$ (24 events) are $\bar{K}^*(892) e^+ \nu_e$.

$\Gamma((\bar{K}^0 \pi^-) \text{ S-wave } e^+ \nu_e)/\Gamma(\bar{K}^0 \pi^- e^+ \nu_e)$		Γ_{25}/Γ_{24}		
VALUE (units 10^{-2})	EVTS	DOCUMENT ID	TECN	COMMENT
5.51 ± 0.97 ± 0.62	3.1k	ABLIKIM	19G BES3	$K_S^0 \pi^- e^+ \nu_e$ events

$\Gamma(K^- \pi^+ \pi^- e^+ \nu_e)/\Gamma_{\text{total}}$		Γ_{26}/Γ		
VALUE (units 10^{-4})	EVTS	DOCUMENT ID	TECN	COMMENT
2.8 ± 1.4 ± 0.3	8	ARTUSO	07A CLEO	$e^+ e^-$ at $\gamma(3770)$

$\Gamma(K_1(1270)^- e^+ \nu_e)/\Gamma_{\text{total}}$		Γ_{27}/Γ		
VALUE (units 10^{-4})	EVTS	DOCUMENT ID	TECN	COMMENT
7.6 ± 4.1 ± 0.9	8	¹ ARTUSO	07A CLEO	$e^+ e^-$ at $\gamma(3770)$

- ¹ This ARTUSO 07A result is corrected for all decay modes of the $K_1(1270)^-$.

$\Gamma(K^- \pi^+ \pi^- \mu^+ \nu_\mu)/\Gamma(K^- \mu^+ \nu_\mu)$		Γ_{28}/Γ_{20}		
VALUE (%)	CL%	DOCUMENT ID	TECN	COMMENT
<0.037	90	KODAMA	93B E653	π^- emulsion 600 GeV

$\Gamma((\bar{K}^*(892) \pi)^- \mu^+ \nu_\mu)/\Gamma(K^- \mu^+ \nu_\mu)$		Γ_{29}/Γ_{20}		
VALUE (%)	CL%	DOCUMENT ID	TECN	COMMENT
<0.043	90	¹ KODAMA	93B E653	π^- emulsion 600 GeV

- ¹ KODAMA 93B searched in $K^- \pi^+ \pi^- \mu^+ \nu_\mu$, but the limit includes other $(\bar{K}^*(892) \pi)^-$ charge states.

$\Gamma(\pi^- e^+ \nu_e)/\Gamma_{\text{total}}$		Γ_{30}/Γ		
VALUE (%)	EVTS	DOCUMENT ID	TECN	COMMENT
0.293 ± 0.004 OUR FIT				
0.293 ± 0.004 OUR AVERAGE				
0.295 ± 0.004 ± 0.003	6.3k	¹ ABLIKIM	15x BES3	2.92 fb $^{-1}$, 3.773 GeV
0.288 ± 0.008 ± 0.003	1.3k	¹ BESSON	09 CLEO	$e^+ e^-$ at $\psi(3770)$
0.279 ± 0.027 ± 0.016	126	² WIDHALM	06 BELL	$e^+ e^- \approx \gamma(4S)$

- We do not use the following data for averages, fits, limits, etc. •••
- 0.299 ± 0.011 ± 0.009 ³ DOBBS 08 CLEO See BESSON 09
- 0.262 ± 0.025 ± 0.008 117 COAN 05 CLEO See DOBBS 08

- ¹ See the form-factor parameters near the end of this D^0 Listing.

- ² The $\pi^- e^+ \nu_e$ and $K^- e^+ \nu_e$ results of WIDHALM 06 give $|\frac{V_{cd}}{V_{cs}} \cdot \frac{f_+^\pi(0)}{f_+^K(0)}|^2 = 0.042 \pm 0.003 \pm 0.003$.

- ³ DOBBS 08 establishes $|\frac{V_{cd}}{V_{cs}} \cdot \frac{f_+^\pi(0)}{f_+^K(0)}| = 0.188 \pm 0.008 \pm 0.002$ from the D^+ and D^0 decays to $\bar{K} e^+ \nu_e$ and $\pi e^+ \nu_e$.

$\Gamma(\pi^- e^+ \nu_e)/\Gamma(K^- e^+ \nu_e)$		Γ_{30}/Γ_{19}		
VALUE (%)	EVTS	DOCUMENT ID	TECN	COMMENT
0.0822 ± 0.0014 OUR FIT				Error includes scale factor of 1.1.
0.085 ± 0.007 OUR AVERAGE				
0.082 ± 0.006 ± 0.005		¹ HUANG	05 CLEO	$e^+ e^- \approx \gamma(4S)$
0.101 ± 0.020 ± 0.003	91	² FRABETTI	96B E687	γ Be, $\bar{E}_\gamma \approx 200$ GeV
0.103 ± 0.039 ± 0.013	87	³ BUTLER	95 CLE2	< 0.156 (90% CL)

- ¹ HUANG 05 uses both e and μ events, and makes a small correction to the μ events to make them effectively e events. This result gives $|\frac{V_{cd}}{V_{cs}} \cdot \frac{f_+^\pi(0)}{f_+^K(0)}|^2 = 0.038^{+0.006+0.005}_{-0.007-0.003}$.

- ² FRABETTI 96B uses both e and μ events, and makes a small correction to the μ events to make them effectively e events. This result gives $|\frac{V_{cd}}{V_{cs}} \cdot \frac{f_+^\pi(0)}{f_+^K(0)}|^2 = 0.050 \pm 0.011 \pm 0.002$.

- ³ BUTLER 95 has 87 ± 33 $\pi^- e^+ \nu_e$ events. The result gives $|\frac{V_{cd}}{V_{cs}} \cdot \frac{f_+^\pi(0)}{f_+^K(0)}|^2 = 0.052 \pm 0.020 \pm 0.007$.

$\Gamma(\pi^- e^+ \nu_e)/\Gamma(K^- \pi^+)$		Γ_{30}/Γ_{35}		
VALUE (units 10^{-2})	EVTS	DOCUMENT ID	TECN	COMMENT
7.37 ± 0.12 OUR FIT				Error includes scale factor of 1.1.
7.02 ± 0.17 ± 0.23	375k	¹ LEES	15F BABR	347 fb $^{-1}$, 10.58 GeV

- ¹ See the form-factor parameters near the end of the D^0 Listing.

$\Gamma(\pi^- \mu^+ \nu_\mu)/\Gamma_{\text{total}}$		Γ_{31}/Γ		
VALUE (%)	EVTS	DOCUMENT ID	TECN	COMMENT
0.267 ± 0.012 OUR FIT				Error includes scale factor of 1.3.
0.268 ± 0.012 OUR AVERAGE				Error includes scale factor of 1.2.
0.272 ± 0.008 ± 0.006	2.3k	ABLIKIM	18A BES3	$e^+ e^-$, 3773 MeV
0.231 ± 0.026 ± 0.019	106 ± 13	WIDHALM	06 BELL	$e^+ e^- \approx \gamma(4S)$

$\Gamma(\pi^- \mu^+ \nu_\mu)/\Gamma(K^- \mu^+ \nu_\mu)$		Γ_{31}/Γ_{20}		
VALUE (%)	EVTS	DOCUMENT ID	TECN	COMMENT
0.0784 ± 0.0035 OUR FIT				Error includes scale factor of 1.2.
0.074 ± 0.008 ± 0.007	288 ± 29	¹ LINK	05 FOCS	$\gamma A, \bar{E}_\gamma \approx 180$ GeV

- ¹ LINK 05 finds the form-factor ratio $|\frac{f_0^\pi(0)}{f_0^K(0)}|$ to be $0.85 \pm 0.04 \pm 0.04 \pm 0.01$.

Meson Particle Listings

 D^0

$\Gamma(\pi^- \pi^0 e^+ \nu_e)/\Gamma_{\text{total}}$		Γ_{32}/Γ		
VALUE (units 10^{-3})	EVTS	DOCUMENT ID	TECN	COMMENT
1.445 ± 0.058 ± 0.039	1.1k	¹ ABLIKIM	19c BES3	$e^+ e^-$ at 3773 MeV
¹ Seen 100% via $D^0 \rightarrow \rho(770)^- e^+ \nu_e$, and also reported as the branching fraction for $D^0 \rightarrow \rho(770)^- e^+ \nu_e$.				

$\Gamma(\rho^- e^+ \nu_e)/\Gamma_{\text{total}}$		Γ_{33}/Γ		
VALUE (units 10^{-3})	EVTS	DOCUMENT ID	TECN	COMMENT
1.50 ± 0.12 OUR AVERAGE		Error includes scale factor of 1.9.		
1.445 ± 0.058 ± 0.039	1.1k	¹ ABLIKIM	19c BES3	$e^+ e^-$ at 3773 MeV
1.77 ± 0.12 ± 0.10	305 ± 21	^{2,3} DOBBS	13 CLEO	$e^+ e^-$ at $\psi(3770)$
• • • We do not use the following data for averages, fits, limits, etc. • • •				
1.94 ± 0.39 ± 0.13	31 ± 6	COAN	05 CLEO	See DOBBS 13

¹ This result is the same as the one reported for $D^0 \rightarrow \pi^- \pi^0 e^+ \nu_e$ which ABLIKIM 19c found to proceed 100% via $D^0 \rightarrow \rho(770)^- e^+ \nu_e$.
² DOBBS 13 finds $\Gamma(D^0 \rightarrow \rho^- e^+ \nu_e) / 2 \Gamma(D^+ \rightarrow \rho^0 e^+ \nu_e) = 1.03 \pm 0.09^{+0.08}_{-0.02}$; isospin invariance predicts the ratio is 1.0.
³ See the D^+ Listings for $D \rightarrow \rho e^+ \nu_e$ form factors.

$\Gamma(a(980)^- e^+ \nu_e, a^- \rightarrow \eta \pi^-)/\Gamma_{\text{total}}$		Γ_{34}/Γ		
VALUE (units 10^{-4})	EVTS	DOCUMENT ID	TECN	COMMENT
1.33 ± 0.33 ± 0.29 ± 0.09	26	¹ ABLIKIM	18f BES3	$e^+ e^-$ at 3773 MeV
¹ Signal observed at 6.4 σ C.L.				

Hadronic modes with a single \bar{K}

$\Gamma(K^- \pi^+)/\Gamma_{\text{total}}$		Γ_{35}/Γ		
VALUE (%)	EVTS	DOCUMENT ID	TECN	COMMENT
3.950 ± 0.031 OUR FIT		Error includes scale factor of 1.2.		
3.909 ± 0.034 OUR AVERAGE				
3.883 ± 0.006 ± 0.051	0.5M	¹ ABLIKIM	18w BES3	$e^+ e^-$, 3773 MeV
3.934 ± 0.021 ± 0.061		BONVICINI	14 CLEO	All CLEO-c runs
4.007 ± 0.037 ± 0.072	33.8k	AUBERT	08L BABR	$e^+ e^-$ at $\Upsilon(4S)$
3.82 ± 0.07 ± 0.12		² ARTUSO	98 CLE2	CLEO average
3.90 ± 0.09 ± 0.12	5.4k	³ BARATE	97c ALEP	From Z decays
3.41 ± 0.12 ± 0.28	1.2k	³ ALBRECHT	94f ARG	$e^+ e^- \approx \Upsilon(4S)$
3.62 ± 0.34 ± 0.44		³ DECAMP	91J ALEP	From Z decays
• • • We do not use the following data for averages, fits, limits, etc. • • •				
3.891 ± 0.035 ± 0.069		⁴ DOBBS	07 CLEO	See BONVICINI 14
3.91 ± 0.08 ± 0.09	10.3k	⁴ HE	05 CLEO	See DOBBS 07
3.81 ± 0.15 ± 0.16	1.2k	⁵ ARTUSO	98 CLE2	$e^+ e^-$ at $\Upsilon(4S)$
3.69 ± 0.11 ± 0.16		⁶ COAN	98 CLE2	See ARTUSO 98
4.5 ± 0.6 ± 0.4		⁷ ALBRECHT	94 ARG	$e^+ e^- \approx \Upsilon(4S)$
3.95 ± 0.08 ± 0.17	4.2k	^{3,8} AKERIB	93 CLE2	See ARTUSO 98
4.5 ± 0.8 ± 0.5	5.6	³ ABACHI	88 HRS	$e^+ e^-$ 29 GeV
4.2 ± 0.4 ± 0.4	0.9k	ADLER	88c MRK3	$e^+ e^-$ 3.77 GeV
4.1 ± 0.6	0.3k	⁹ SCHINDLER	81 MRK2	$e^+ e^-$ 3.771 GeV
4.3 ± 1.0	130	¹⁰ PERUZZI	77 LGW	$e^+ e^-$ 3.77 GeV

¹ ABLIKIM 18w measured the combined $K^{\mp} \pi^{\pm}$ branching fraction to be 3.898%. We have subtracted off the doubly Cabibbo-suppressed branching fraction $B(D^0 \rightarrow K^+ \pi^-) = (1.50 \pm 0.07) \times 10^{-4}$, even though it is less than one-third of the uncertainty of the combined measurement, in order to treat this as a measurement of $B(D^0 \rightarrow K^- \pi^+)$.
² This combines the CLEO results of ARTUSO 98, COAN 98, and AKERIB 93.
³ ABACHI 88, DECAMP 91J, AKERIB 93, ALBRECHT 94f, and BARATE 97c use $D^*(2010)^+ \rightarrow D^0 \pi^+$ decays. The π^+ is both slow and of low p_T with respect to the event thrust axis or nearest jet ($\approx D^{*+}$ direction). The excess number of such π^+ 's over background gives the number of $D^*(2010)^+ \rightarrow D^0 \pi^+$ events, and the fraction with $D^0 \rightarrow K^- \pi^+$ gives the $D^0 \rightarrow K^- \pi^+$ branching fraction.
⁴ DOBBS 07 and HE 05 use single- and double-tagged events in an overall fit. DOBBS 07 supersedes HE 05.
⁵ ARTUSO 98, following ALBRECHT 94, uses D^0 mesons from $\bar{B}^0 \rightarrow D^*(2010)^+ X \ell^- \bar{\nu}_\ell$ decays. Our average uses the CLEO average of this value with the values of COAN 98 and AKERIB 93.
⁶ COAN 98 assumes that $\Gamma(B \rightarrow \bar{D} X \ell^+ \nu)/\Gamma(B \rightarrow X \ell^+ \nu) = 1.0 - 3|V_{ub}/V_{cb}|^2 - 0.010 \pm 0.005$, the last term accounting for $\bar{B} \rightarrow D_s^+ K X \ell^- \bar{\nu}$. COAN 98 is included in the CLEO average in ARTUSO 98.
⁷ ALBRECHT 94 uses D^0 mesons from $\bar{B}^0 \rightarrow D^{*+} \ell^- \bar{\nu}_\ell$ decays. This is a different set of events than used by ALBRECHT 94f.
⁸ This AKERIB 93 value includes radiative corrections; without them, the value is $0.0391 \pm 0.0008 \pm 0.0017$. AKERIB 93 is included in the CLEO average in ARTUSO 98.
⁹ SCHINDLER 81 (MARK-2) measures $\sigma(e^+ e^- \rightarrow \psi(3770)) \times$ branching fraction to be 0.24 ± 0.02 nb. We use the MARK-3 (ADLER 88c) value of $\sigma = 5.8 \pm 0.5 \pm 0.6$ nb.
¹⁰ PERUZZI 77 (MARK-1) measures $\sigma(e^+ e^- \rightarrow \psi(3770)) \times$ branching fraction to be 0.25 ± 0.05 nb. We use the MARK-3 (ADLER 88c) value of $\sigma = 5.8 \pm 0.5 \pm 0.6$ nb.

$\Gamma(K_S^0 \pi^0)/\Gamma_{\text{total}}$		Γ_{36}/Γ		
VALUE (%)	EVTS	DOCUMENT ID	TECN	COMMENT
1.240 ± 0.022 OUR FIT				
1.239 ± 0.006 ± 0.027	67k	ABLIKIM	18w BES3	$e^+ e^-$, 3773 MeV
• • • We do not use the following data for averages, fits, limits, etc. • • •				
1.240 ± 0.017 ± 0.056	614	HE	08 CLEO	See MENDEZ 10

$\Gamma(K_S^0 \pi^0)/[\Gamma(K^- \pi^+) + \Gamma(K^+ \pi^-)]$		$\Gamma_{36}/(\Gamma_{35} + \Gamma_{256})$		
VALUE (units 10^{-2})	EVTS	DOCUMENT ID	TECN	COMMENT
31.3 ± 0.6 OUR FIT				
30.4 ± 0.3 ± 0.9	20k	MENDEZ	10 CLEO	$e^+ e^-$ at 3774 MeV

$\Gamma(K_S^0 \pi^0)/\Gamma(K_S^0 \pi^+ \pi^-)$		Γ_{36}/Γ_{38}		
VALUE	EVTS	DOCUMENT ID	TECN	COMMENT
0.443 ± 0.028 OUR FIT				
0.44 ± 0.02 ± 0.05	1942 ± 64	PROCARIO	93B CLE2	$e^+ e^-$ 10.36–10.7 GeV
• • • We do not use the following data for averages, fits, limits, etc. • • •				
0.34 ± 0.04 ± 0.02	92	¹ ALBRECHT	92P ARG	$e^+ e^- \approx 10$ GeV
0.36 ± 0.04 ± 0.08	104	KINOSHITA	91 CLEO	$e^+ e^- \sim 10.7$ GeV

¹ This value is calculated from numbers in Table 1 of ALBRECHT 92p.

$\Gamma(K_L^0 \pi^0)/\Gamma_{\text{total}}$		Γ_{37}/Γ		
VALUE (%)	EVTS	DOCUMENT ID	TECN	COMMENT
0.998 ± 0.049 ± 0.048	1116	¹ HE	08 CLEO	$e^+ e^-$ at $\psi(3770)$

¹ The difference of HE 08 $D^0 \rightarrow K_S^0 \pi^0$ and $K_L^0 \pi^0$ branching fractions over the sum is $0.108 \pm 0.025 \pm 0.024$. This is consistent with U-spin symmetry and the Cabibbo angle.

$\Gamma(K_S^0 \pi^+ \pi^-)/\Gamma_{\text{total}}$		Γ_{38}/Γ		
VALUE (%)	EVTS	DOCUMENT ID	TECN	COMMENT
• • • We do not use the following data for averages, fits, limits, etc. • • •				
2.52 ± 0.20 ± 0.25	284 ± 22	¹ ALBRECHT	94f ARG	$e^+ e^- \approx \Upsilon(4S)$
3.2 ± 0.3 ± 0.5		ADLER	87 MRK3	$e^+ e^-$ 3.77 GeV
2.6 ± 0.8	32 ± 8	² SCHINDLER	81 MRK2	$e^+ e^-$ 3.771 GeV
4.0 ± 1.2	28	³ PERUZZI	77 LGW	$e^+ e^-$ 3.77 GeV

¹ See the footnote on the ALBRECHT 94f measurement of $\Gamma(K^- \pi^+)/\Gamma_{\text{total}}$ for the method used.

² SCHINDLER 81 (MARK-2) measures $\sigma(e^+ e^- \rightarrow \psi(3770)) \times$ branching fraction to be 0.30 ± 0.08 nb. We use the MARK-3 (ADLER 88c) value of $\sigma = 5.8 \pm 0.5 \pm 0.6$ nb.

³ PERUZZI 77 (MARK-1) measures $\sigma(e^+ e^- \rightarrow \psi(3770)) \times$ branching fraction to be 0.46 ± 0.12 nb. We use the MARK-3 (ADLER 88c) value of $\sigma = 5.8 \pm 0.5 \pm 0.6$ nb.

$\Gamma(K_S^0 \pi^+ \pi^-)/\Gamma(K^- \pi^+)$		Γ_{38}/Γ_{35}		
VALUE	EVTS	DOCUMENT ID	TECN	COMMENT
0.71 ± 0.05 OUR FIT		Error includes scale factor of 1.1.		
0.81 ± 0.05 ± 0.08	856 ± 35	FRABETTI	94J E687	γ Be $\bar{E}_\gamma = 220$ GeV
• • • We do not use the following data for averages, fits, limits, etc. • • •				
0.85 ± 0.40	35	AVERY	80 SPEC	$\gamma N \rightarrow D^{*+}$
1.4 ± 0.5	116	PICCOLO	77 MRK1	$e^+ e^-$ 4.03, 4.41 GeV

$\Gamma(K_S^0 \rho^0)/\Gamma(K_S^0 \pi^+ \pi^-)$		Γ_{39}/Γ_{38}		
VALUE	DOCUMENT ID	TECN	COMMENT	
This is the "fit fraction" from the Dalitz-plot analysis.				
0.224 ± 0.017 OUR AVERAGE		Error includes scale factor of 1.7.		
0.210 ± 0.016	¹ AUBERT	08AL BABR	Dalitz fit, ≈ 487 k evts	
0.264 ± 0.009 ± 0.010 ± 0.026	MURAMATSU	02 CLE2	Dalitz fit, 5299 evts	
• • • We do not use the following data for averages, fits, limits, etc. • • •				
0.267 ± 0.011 ± 0.009 ± 0.028	ASNER	04A CLEO	See MURAMATSU 02	
0.350 ± 0.028 ± 0.067	FRABETTI	94G E687	Dalitz fit, 597 evts	
0.227 ± 0.032 ± 0.009	ALBRECHT	93D ARG	Dalitz fit, 440 evts	
0.215 ± 0.051 ± 0.037	ANJOS	93 E691	γ Be 90–260 GeV	
0.20 ± 0.06 ± 0.03	FRABETTI	92B E687	γ Be, $\bar{E}_\gamma = 221$ GeV	
0.12 ± 0.01 ± 0.07	ADLER	87 MRK3	$e^+ e^-$ 3.77 GeV	

¹ The error on this AUBERT 08AL value includes both statistical and systematic uncertainties; the latter dominates.

$\Gamma(K_S^0 \omega, \omega \rightarrow \pi^+ \pi^-)/\Gamma(K_S^0 \pi^+ \pi^-)$		Γ_{40}/Γ_{38}		
VALUE	DOCUMENT ID	TECN	COMMENT	
0.0073 ± 0.0020 OUR AVERAGE				
0.009 ± 0.010	¹ AUBERT	08AL BABR	Dalitz fit, ≈ 487 k evts	
0.0072 ± 0.0018 ± 0.0010 ± 0.0009	MURAMATSU	02 CLE2	Dalitz fit, 5299 evts	
• • • We do not use the following data for averages, fits, limits, etc. • • •				
0.0081 ± 0.0019 ± 0.0018 ± 0.0010	ASNER	04A CLEO	See MURAMATSU 02	

¹ The error on this AUBERT 08AL value includes both statistical and systematic uncertainties; the latter dominates.

$\Gamma(K_S^0 \pi^+ \pi^-)_{S\text{-wave}}/\Gamma(K_S^0 \pi^+ \pi^-)$		Γ_{41}/Γ_{38}		
VALUE	DOCUMENT ID	TECN	COMMENT	
0.119 ± 0.026	¹ AUBERT	08AL BABR	Dalitz fit, ≈ 487 k evts	
• • • We do not use the following data for averages, fits, limits, etc. • • •				
0.0081 ± 0.0019 ± 0.0018 ± 0.0010	ASNER	04A CLEO	See MURAMATSU 02	

¹ The error on this AUBERT 08AL value includes both statistical and systematic uncertainties; the latter dominates.

$\Gamma(K_S^0 f_0(980), f_0 \rightarrow \pi^+ \pi^-)/\Gamma(K_S^0 \pi^+ \pi^-)$		Γ_{42}/Γ_{38}		
VALUE	DOCUMENT ID	TECN	COMMENT	
0.119 ± 0.026	¹ AUBERT	08AL BABR	Dalitz fit, ≈ 487 k evts	
• • • We do not use the following data for averages, fits, limits, etc. • • •				
0.0081 ± 0.0019 ± 0.0018 ± 0.0010	ASNER	04A CLEO	See MURAMATSU 02	

¹ The error on this AUBERT 08AL value includes both statistical and systematic uncertainties; the latter dominates.

$\Gamma(K_S^0 f_0(980), f_0 \rightarrow \pi^+ \pi^-)/\Gamma(K_S^0 \pi^+ \pi^-)$		Γ_{42}/Γ_{38}		
VALUE	DOCUMENT ID	TECN	COMMENT	
0.043 ± 0.005 ± 0.012 ± 0.006	MURAMATSU	02 CLE2	Dalitz fit, 5299 evts	

• • • We do not use the following data for averages, fits, limits, etc. • • •

0.042 ± 0.005 ^{+0.011} _{-0.005}	ASNER	04A	CLEO	See MURAMATSU 02
0.068 ± 0.016 ± 0.018	FRABETTI	94G	E687	Dalitz fit, 597 evts
0.046 ± 0.018 ± 0.006	ALBRECHT	93D	ARG	Dalitz fit, 440 evts

$\Gamma(K_S^0 f_0(1370), f_0 \rightarrow \pi^+ \pi^-) / \Gamma(K_S^0 \pi^+ \pi^-)$ $\Gamma_{43} / \Gamma_{38}$

This is the "fit fraction" from the Dalitz-plot analysis.

VALUE	DOCUMENT ID	TECN	COMMENT
0.099 ± 0.011^{+0.028} -0.044 OUR AVERAGE	MURAMATSU 02	CLE2	Dalitz fit, 5299 evts

• • • We do not use the following data for averages, fits, limits, etc. • • •

0.098 ± 0.014 ^{+0.026} _{-0.036}	ASNER	04A	CLEO	See MURAMATSU 02
0.077 ± 0.022 ± 0.031	FRABETTI	94G	E687	Dalitz fit, 597 evts
0.082 ± 0.028 ± 0.013	ALBRECHT	93D	ARG	Dalitz fit, 440 evts

$\Gamma(K_S^0 f_2(1270), f_2 \rightarrow \pi^+ \pi^-) / \Gamma(K_S^0 \pi^+ \pi^-)$ $\Gamma_{44} / \Gamma_{38}$

This is the "fit fraction" from the Dalitz-plot analysis.

VALUE	DOCUMENT ID	TECN	COMMENT
0.0032 ± 0.0035 -0.0022 OUR AVERAGE	MURAMATSU 02	CLE2	Dalitz fit, 5299 evts

0.006 ± 0.007	AUBERT	08AL	BABR	Dalitz fit, ≈ 487 k evts
0.0027 ± 0.0015 ^{+0.0037} _{-0.0017}	MURAMATSU 02	CLE2		Dalitz fit, 5299 evts

• • • We do not use the following data for averages, fits, limits, etc. • • •

0.0036 ± 0.0022 ^{+0.0032} _{-0.0019}	ASNER	04A	CLEO	See MURAMATSU 02
0.037 ± 0.014 ± 0.017	FRABETTI	94G	E687	Dalitz fit, 597 evts
0.050 ± 0.021 ± 0.008	ALBRECHT	93D	ARG	Dalitz fit, 440 evts

¹ The error on this AUBERT 08AL value includes both statistical and systematic uncertainties; the latter dominates.

$\Gamma(K^*(892)^- \pi^+, K^{*-} \rightarrow K_S^0 \pi^-) / \Gamma(K_S^0 \pi^+ \pi^-)$ $\Gamma_{45} / \Gamma_{38}$

This is the "fit fraction" from the Dalitz-plot analysis.

VALUE	DOCUMENT ID	TECN	COMMENT
0.588 ± 0.034 -0.050 OUR AVERAGE	MURAMATSU 02	CLE2	Dalitz fit, 5299 evts

0.557 ± 0.028	AUBERT	08AL	BABR	Dalitz fit, ≈ 487 k evts
0.657 ± 0.013 ^{+0.018} _{-0.040}	MURAMATSU 02	CLE2		Dalitz fit, 5299 evts

• • • We do not use the following data for averages, fits, limits, etc. • • •

0.663 ± 0.013 ^{+0.024} _{-0.043}	ASNER	04A	CLEO	See MURAMATSU 02
0.625 ± 0.036 ± 0.026	FRABETTI	94G	E687	Dalitz fit, 597 evts
0.718 ± 0.042 ± 0.030	ALBRECHT	93D	ARG	Dalitz fit, 440 evts
0.480 ± 0.097	ANJOS	93	E691	γ Be 90–260 GeV
0.56 ± 0.04 ± 0.05	ADLER	87	MRK3	$e^+ e^-$ 3.77 GeV

¹ The error on this AUBERT 08AL value includes both statistical and systematic uncertainties; the latter dominates.

$\Gamma(K_2^*(1430)^- \pi^+, K_2^{*-} \rightarrow K_S^0 \pi^-) / \Gamma(K_S^0 \pi^+ \pi^-)$ $\Gamma_{46} / \Gamma_{38}$

This is the "fit fraction" from the Dalitz-plot analysis.

VALUE	DOCUMENT ID	TECN	COMMENT
0.095 ± 0.014 -0.010 OUR AVERAGE	MURAMATSU 02	CLE2	Dalitz fit, 5299 evts

0.102 ± 0.015	AUBERT	08AL	BABR	Dalitz fit, ≈ 487 k evts
0.073 ± 0.007 ^{+0.031} _{-0.011}	MURAMATSU 02	CLE2		Dalitz fit, 5299 evts

• • • We do not use the following data for averages, fits, limits, etc. • • •

0.072 ± 0.007 ^{+0.014} _{-0.013}	ASNER	04A	CLEO	See MURAMATSU 02
0.109 ± 0.027 ± 0.029	FRABETTI	94G	E687	Dalitz fit, 597 evts
0.129 ± 0.034 ± 0.021	ALBRECHT	93D	ARG	Dalitz fit, 440 evts

¹ The error on this AUBERT 08AL value includes both statistical and systematic uncertainties; the latter dominates.

$\Gamma(K_2^*(1430)^- \pi^+, K_2^{*-} \rightarrow K_S^0 \pi^-) / \Gamma(K_S^0 \pi^+ \pi^-)$ $\Gamma_{47} / \Gamma_{38}$

This is the "fit fraction" from the Dalitz-plot analysis.

VALUE	DOCUMENT ID	TECN	COMMENT
0.0120 ± 0.0070 -0.0035 OUR AVERAGE	MURAMATSU 02	CLE2	Dalitz fit, 5299 evts

0.022 ± 0.016	AUBERT	08AL	BABR	Dalitz fit, ≈ 487 k evts
0.011 ± 0.002 ^{+0.007} _{-0.003}	MURAMATSU 02	CLE2		Dalitz fit, 5299 evts

• • • We do not use the following data for averages, fits, limits, etc. • • •

0.011 ± 0.002 ^{+0.005} _{-0.003}	ASNER	04A	CLEO	See MURAMATSU 02
---	-------	-----	------	------------------

¹ The error on this AUBERT 08AL value includes both statistical and systematic uncertainties; the latter dominates.

$\Gamma(K^*(1680)^- \pi^+, K^{*-} \rightarrow K_S^0 \pi^-) / \Gamma(K_S^0 \pi^+ \pi^-)$ $\Gamma_{48} / \Gamma_{38}$

This is the "fit fraction" from the Dalitz-plot analysis.

VALUE	DOCUMENT ID	TECN	COMMENT
0.016 ± 0.013 OUR AVERAGE	MURAMATSU 02	CLE2	Dalitz fit, 5299 evts

0.007 ± 0.019	AUBERT	08AL	BABR	Dalitz fit, ≈ 487 k evts
0.022 ± 0.004 ^{+0.018} _{-0.015}	MURAMATSU 02	CLE2		Dalitz fit, 5299 evts

• • • We do not use the following data for averages, fits, limits, etc. • • •

0.023 ± 0.005 ^{+0.007} _{-0.014}	ASNER	04A	CLEO	See MURAMATSU 02
---	-------	-----	------	------------------

¹ The error on this AUBERT 08AL value includes both statistical and systematic uncertainties; the latter dominates.

$\Gamma(K^*(892)^+ \pi^-, K^{*+} \rightarrow K_S^0 \pi^+) / \Gamma(K_S^0 \pi^+ \pi^-)$ $\Gamma_{49} / \Gamma_{38}$

This is the "fit fraction" from the Dalitz-plot analysis. This is a doubly Cabibbo-suppressed mode.

VALUE (units 10 ⁻³)	DOCUMENT ID	TECN	COMMENT
4.0 ± 2.0 OUR AVERAGE	MURAMATSU 02	CLE2	Dalitz fit, 5299 evts

4.6 ± 2.3	AUBERT	08AL	BABR	Dalitz fit, ≈ 487 k evts
3.4 ± 1.3 ^{+4.1} _{-0.4}	MURAMATSU 02	CLE2		Dalitz fit, 5299 evts

• • • We do not use the following data for averages, fits, limits, etc. • • •

3.4 ± 1.3 ^{+3.6} _{-0.5}	ASNER	04A	CLEO	See MURAMATSU 02
---	-------	-----	------	------------------

¹ The error on this AUBERT 08AL value includes both statistical and systematic uncertainties; the latter dominates.

$\Gamma(K_2^*(1430)^+ \pi^-, K_2^{*+} \rightarrow K_S^0 \pi^+) / \Gamma(K_S^0 \pi^+ \pi^-)$ $\Gamma_{50} / \Gamma_{38}$

This is the "fit fraction" from the Dalitz-plot analysis. This is a doubly Cabibbo-suppressed mode.

VALUE	CL%	DOCUMENT ID	TECN	COMMENT	
< 5 × 10⁻⁴	95	AUBERT	08AL	BABR	Dalitz fit, ≈ 487 k evts

$\Gamma(K_2^*(1430)^+ \pi^-, K_2^{*+} \rightarrow K_S^0 \pi^+) / \Gamma(K_S^0 \pi^+ \pi^-)$ $\Gamma_{51} / \Gamma_{38}$

This is the "fit fraction" from the Dalitz-plot analysis. This is a doubly Cabibbo-suppressed mode.

VALUE	CL%	DOCUMENT ID	TECN	COMMENT	
< 1.2 × 10⁻³	95	AUBERT	08AL	BABR	Dalitz fit, ≈ 487 k evts

$\Gamma(K_S^0 \pi^+ \pi^- \text{ nonresonant}) / \Gamma(K_S^0 \pi^+ \pi^-)$ $\Gamma_{52} / \Gamma_{38}$

This is the "fit fraction" from the Dalitz-plot analysis. Neither FRABETTI 94G nor ALBRECHT 93D (quoted in many of the earlier submodes of $K_S^0 \pi^+ \pi^-$) sees evidence for a nonresonant component.

VALUE	DOCUMENT ID	TECN	COMMENT
0.009 ± 0.004^{+0.020} -0.004	MURAMATSU 02	CLE2	Dalitz fit, 5299 evts

• • • We do not use the following data for averages, fits, limits, etc. • • •

0.007 ± 0.007 ^{+0.021} _{-0.006}	ASNER	04A	CLEO	See MURAMATSU 02
0.263 ± 0.024 ± 0.041	ANJOS	93	E691	γ Be 90–260 GeV
0.26 ± 0.08 ± 0.05	FRABETTI	92B	E687	γ Be, $E_{\gamma} = 221$ GeV
0.33 ± 0.05 ± 0.10	ADLER	87	MRK3	$e^+ e^-$ 3.77 GeV

$\Gamma(K^- \pi^+ \pi^0) / \Gamma_{\text{total}}$ Γ_{53} / Γ

VALUE (%)	EVTS	DOCUMENT ID	TECN	COMMENT
14.57 ± 0.12 ± 0.38	19k ± 150	DOBBS 07	CLEO	See BONVICINI 14
14.9 ± 0.3 ± 0.5	931	HE 05	CLEO	See DOBBS 07
13.3 ± 1.2 ± 1.3	37	ADLER 88C	MRK3	$e^+ e^-$ 3.77 GeV
11.7 ± 4.3		SCHINDLER 81	MRK2	$e^+ e^-$ 3.771 GeV

• • • We do not use the following data for averages, fits, limits, etc. • • •

14.57 ± 0.12 ± 0.38	DOBBS 07	07	CLEO	See BONVICINI 14
14.9 ± 0.3 ± 0.5	HE 05	05	CLEO	See DOBBS 07
13.3 ± 1.2 ± 1.3	ADLER 88C	88C	MRK3	$e^+ e^-$ 3.77 GeV
11.7 ± 4.3	SCHINDLER 81	81	MRK2	$e^+ e^-$ 3.771 GeV

¹ DOBBS 07 and HE 05 use single- and double-tagged events in an overall fit. DOBBS 07 supersedes HE 05.

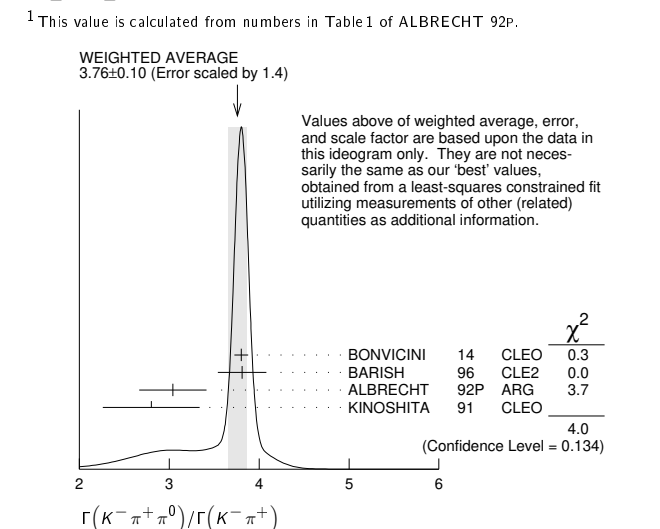
² SCHINDLER 81 (MARK-2) measures $\sigma(e^+ e^- \rightarrow \psi(3770)) \times$ branching fraction to be 0.68 ± 0.23 nb. We use the MARK-3 (ADLER 88C) value of $\sigma = 5.8 \pm 0.5 \pm 0.6$ nb.

$\Gamma(K^- \pi^+ \pi^0) / \Gamma(K^- \pi^+)$ $\Gamma_{53} / \Gamma_{35}$

This is the "fit fraction" from the Dalitz-plot analysis.

VALUE	EVTS	DOCUMENT ID	TECN	COMMENT
3.65 ± 0.13 OUR FIT				Error includes scale factor of 2.1.
3.76 ± 0.10 OUR AVERAGE				Error includes scale factor of 1.4. See the ideogram below.
3.802 ± 0.022 ± 0.073		BONVICINI 14	CLEO	All CLEO-c runs
3.81 ± 0.07 ± 0.26	10k	BARISH 96	CLE2	$e^+ e^- \approx \gamma(4S)$
3.04 ± 0.16 ± 0.34	931	ALBRECHT 92P	ARG	$e^+ e^- \approx 10$ GeV
2.8 ± 0.14 ± 0.52	1050	KINOSHITA 91	CLEO	$e^+ e^- \sim 10.7$ GeV

¹ This value is calculated from numbers in Table 1 of ALBRECHT 92P.



Meson Particle Listings

D^0

$\Gamma(K^- \rho^+) / \Gamma(K^- \pi^+ \pi^0)$ $\Gamma_{54} / \Gamma_{53}$

This is the "fit fraction" from the Dalitz-plot analysis.

VALUE	DOCUMENT ID	TECN	COMMENT
0.78 ± 0.04 OUR AVERAGE			
0.788 ± 0.019 ± 0.048	KOPP	01	CLE2 Dalitz fit, ≈ 7,000 evts
0.765 ± 0.041 ± 0.054	FRABETTI	94G	E687 Dalitz fit, 530 evts
• • • We do not use the following data for averages, fits, limits, etc. • • •			
0.647 ± 0.039 ± 0.150	ANJOS	93	E691 γ Be 90–260 GeV
0.81 ± 0.03 ± 0.06	ADLER	87	MRK3 $e^+ e^-$ 3.77 GeV

$\Gamma(K^- \rho(1700)^+ \rightarrow \pi^+ \pi^0) / \Gamma(K^- \pi^+ \pi^0)$ $\Gamma_{55} / \Gamma_{53}$

This is the "fit fraction" from the Dalitz-plot analysis.

VALUE	DOCUMENT ID	TECN	COMMENT
0.057 ± 0.008 ± 0.009	KOPP	01	CLE2 Dalitz fit, ≈ 7,000 evts

$\Gamma(K^*(892)^- \pi^+, K^*(892)^- \rightarrow K^- \pi^0) / \Gamma(K^- \pi^+ \pi^0)$ $\Gamma_{56} / \Gamma_{53}$

This is the "fit fraction" from the Dalitz-plot analysis.

VALUE	DOCUMENT ID	TECN	COMMENT
0.160 ± 0.025 OUR AVERAGE -0.013			
0.161 ± 0.007 ± 0.027 0.011	KOPP	01	CLE2 Dalitz fit, ≈ 7,000 evts
0.148 ± 0.028 ± 0.049	FRABETTI	94G	E687 Dalitz fit, 530 evts
• • • We do not use the following data for averages, fits, limits, etc. • • •			
0.084 ± 0.011 ± 0.012	ANJOS	93	E691 γ Be 90–260 GeV
0.12 ± 0.02 ± 0.03	ADLER	87	MRK3 $e^+ e^-$ 3.77 GeV

$\Gamma(K^*(892)^0 \pi^0, \bar{K}^*(892)^0 \rightarrow K^- \pi^+) / \Gamma(K^- \pi^+ \pi^0)$ $\Gamma_{57} / \Gamma_{53}$

This is the "fit fraction" from the Dalitz-plot analysis.

VALUE	DOCUMENT ID	TECN	COMMENT
0.135 ± 0.016 OUR AVERAGE			
0.127 ± 0.009 ± 0.016	KOPP	01	CLE2 Dalitz fit, ≈ 7,000 evts
0.165 ± 0.031 ± 0.015	FRABETTI	94G	E687 Dalitz fit, 530 evts
• • • We do not use the following data for averages, fits, limits, etc. • • •			
0.142 ± 0.018 ± 0.024	ANJOS	93	E691 γ Be 90–260 GeV
0.13 ± 0.02 ± 0.03	ADLER	87	MRK3 $e^+ e^-$ 3.77 GeV

$\Gamma(K_0^*(1430)^- \pi^+, K_0^*(1430)^- \rightarrow K^- \pi^0) / \Gamma(K^- \pi^+ \pi^0)$ $\Gamma_{58} / \Gamma_{53}$

This is the "fit fraction" from the Dalitz-plot analysis.

VALUE	DOCUMENT ID	TECN	COMMENT
0.033 ± 0.006 ± 0.014	KOPP	01	CLE2 Dalitz fit, ≈ 7,000 evts

$\Gamma(\bar{K}_0^*(1430)^0 \pi^0, \bar{K}_0^*(1430)^0 \rightarrow K^- \pi^+) / \Gamma(K^- \pi^+ \pi^0)$ $\Gamma_{59} / \Gamma_{53}$

This is the "fit fraction" from the Dalitz-plot analysis.

VALUE	DOCUMENT ID	TECN	COMMENT
0.041 ± 0.006 ± 0.032 -0.009	KOPP	01	CLE2 Dalitz fit, ≈ 7,000 evts

$\Gamma(K^*(1680)^- \pi^+, K^*(1680)^- \rightarrow K^- \pi^0) / \Gamma(K^- \pi^+ \pi^0)$ $\Gamma_{60} / \Gamma_{53}$

This is the "fit fraction" from the Dalitz-plot analysis.

VALUE	DOCUMENT ID	TECN	COMMENT
0.013 ± 0.003 ± 0.004	KOPP	01	CLE2 Dalitz fit, ≈ 7,000 evts

$\Gamma(K^- \pi^+ \pi^0 \text{ nonresonant}) / \Gamma(K^- \pi^+ \pi^0)$ $\Gamma_{61} / \Gamma_{53}$

This is the "fit fraction" from the Dalitz-plot analysis.

VALUE	EVTS	DOCUMENT ID	TECN	COMMENT
0.080 ± 0.040 OUR AVERAGE -0.014				
0.075 ± 0.009 ± 0.056 0.011		KOPP	01	CLE2 Dalitz fit, ≈ 7,000 evts
0.101 ± 0.033 ± 0.040		FRABETTI	94G	E687 Dalitz fit, 530 evts
• • • We do not use the following data for averages, fits, limits, etc. • • •				
0.036 ± 0.004 ± 0.018		ANJOS	93	E691 γ Be 90–260 GeV
0.09 ± 0.02 ± 0.04		ADLER	87	MRK3 $e^+ e^-$ 3.77 GeV
0.51 ± 0.22	21	SUMMERS	84	E691 Photoproduction

$\Gamma(K_S^0 2\pi^0) / \Gamma_{\text{total}}$ Γ_{62} / Γ

Error includes scale factor of 2.2.

VALUE (units 10^{-3})	EVTS	DOCUMENT ID	TECN	COMMENT
9.1 ± 1.1 OUR AVERAGE				
10.58 ± 0.38 ± 0.73	1259	LOWREY	11	CLEO $e^+ e^-$ ≈ 3.77 GeV
8.34 ± 0.45 ± 0.42		ASNER	08	CLEO $e^+ e^- \rightarrow D^0 \bar{D}^0$, 3.77 GeV

$\Gamma(K_S^0(2\pi^0)_S\text{-wave}) / \Gamma(K_S^0 2\pi^0)$ $\Gamma_{63} / \Gamma_{62}$

This is the "fit fraction" from the Dalitz-plot analysis.

VALUE (units 10^{-2})	DOCUMENT ID	TECN	COMMENT
28.9 ± 6.3 ± 3.1	LOWREY	11	CLEO Dalitz analysis, 1259 evts

$\Gamma(\bar{K}^*(892)^0 \pi^0, \bar{K}^*(892)^0 \rightarrow K_S^0 \pi^0) / \Gamma(K_S^0 2\pi^0)$ $\Gamma_{64} / \Gamma_{36}$

This is the "fit fraction" from the Dalitz-plot analysis.

VALUE (units 10^{-2})	DOCUMENT ID	TECN	COMMENT
65.6 ± 5.3 ± 2.5	LOWREY	11	CLEO Dalitz analysis, 1259 evts
• • • We do not use the following data for averages, fits, limits, etc. • • •			
55 ⁺¹³ ₋₁₀ ± 7	PROCARIO	93B	CLE2 Dalitz plot fit, 122 evts

$\Gamma(\bar{K}^*(1430)^0 \pi^0, \bar{K}^*(1430)^0 \rightarrow K_S^0 \pi^0) / \Gamma(K_S^0 2\pi^0)$ $\Gamma_{65} / \Gamma_{62}$

This is the "fit fraction" from the Dalitz-plot analysis.

VALUE (units 10^{-2})	DOCUMENT ID	TECN	COMMENT
0.49 ± 0.45 ± 2.51	LOWREY	11	CLEO Dalitz analysis, 1259 evts

$\Gamma(\bar{K}^*(1680)^0 \pi^0, \bar{K}^*(1680)^0 \rightarrow K_S^0 \pi^0) / \Gamma(K_S^0 2\pi^0)$ $\Gamma_{66} / \Gamma_{62}$

This is the "fit fraction" from the Dalitz-plot analysis.

VALUE (units 10^{-2})	DOCUMENT ID	TECN	COMMENT
11.2 ± 2.7 ± 2.5	LOWREY	11	CLEO Dalitz analysis, 1259 evts

$\Gamma(K_S^0 f_2(1270), f_2 \rightarrow 2\pi^0) / \Gamma(K_S^0 2\pi^0)$ $\Gamma_{67} / \Gamma_{62}$

This is the "fit fraction" from the Dalitz-plot analysis.

VALUE (units 10^{-2})	DOCUMENT ID	TECN	COMMENT
2.48 ± 0.91 ± 0.78	LOWREY	11	CLEO Dalitz analysis, 1259 evts

$\Gamma(2K_S^0, \text{one } K_S^0 \rightarrow 2\pi^0) / \Gamma(K_S^0 2\pi^0)$ $\Gamma_{68} / \Gamma_{62}$

This is the "fit fraction" from the Dalitz-plot analysis.

VALUE (units 10^{-2})	DOCUMENT ID	TECN	COMMENT
3.46 ± 0.92 ± 0.66	LOWREY	11	CLEO Dalitz analysis, 1259 evts

$\Gamma(K_S^0 2\pi^0 \text{ nonresonant}) / \Gamma(K_S^0 \pi^0)$ $\Gamma_{69} / \Gamma_{36}$

This is the "fit fraction" from the Dalitz-plot analysis.

VALUE	DOCUMENT ID	TECN	COMMENT
0.37 ± 0.08 ± 0.04	PROCARIO	93B	CLE2 Dalitz plot fit, 122 evts

$\Gamma(K^- 2\pi^+ \pi^-) / \Gamma_{\text{total}}$ Γ_{70} / Γ

This is the "fit fraction" from the Dalitz-plot analysis.

VALUE (%)	EVTS	DOCUMENT ID	TECN	COMMENT
• • • We do not use the following data for averages, fits, limits, etc. • • •				
8.30 ± 0.07 ± 0.20		1 DOBBS	07	CLEO See BONVICINI 14
8.3 ± 0.2 ± 0.3	15k	1 HE	05	CLEO See DOBBS 07
7.9 ± 1.5 ± 0.9		2 ALBRECHT	94	ARG $e^+ e^- \approx \Upsilon(4S)$
6.80 ± 0.27 ± 0.57	1.4k	3 ALBRECHT	94F	ARG $e^+ e^- \approx \Upsilon(4S)$
9.1 ± 0.8 ± 0.8		ADLER	88c	MRK3 $e^+ e^-$ 3.77 GeV
11.7 ± 2.5	185	4 SCHINDLER	81	MRK2 $e^+ e^-$ 3.771 GeV
6.2 ± 1.9	44	5 PERUZZI	77	LGW $e^+ e^-$ 3.77 GeV

¹ DOBBS 07 and HE 05 use single- and double-tagged events in an overall fit. DOBBS 07 supersedes HE 05.

² ALBRECHT 94 uses D^0 mesons from $\bar{B}^0 \rightarrow D^{*+} \ell^- \bar{\nu}_\ell$ decays. This is a different set of events than used by ALBRECHT 94F.

³ See the footnote on the ALBRECHT 94F measurement of $\Gamma(K^- \pi^+) / \Gamma_{\text{total}}$ for the method used.

⁴ SCHINDLER 81 (MARK-2) measures $\sigma(e^+ e^- \rightarrow \psi(3770)) \times$ branching fraction to be 0.68 ± 0.11 nb. We use the MARK-3 (ADLER 88c) value of $\sigma = 5.8 \pm 0.5 \pm 0.6$ nb.

⁵ PERUZZI 77 (MARK-1) measures $\sigma(e^+ e^- \rightarrow \psi(3770)) \times$ branching fraction to be 0.36 ± 0.10 nb. We use the MARK-3 (ADLER 88c) value of $\sigma = 5.8 \pm 0.5 \pm 0.6$ nb.

$\Gamma(K^- 2\pi^+ \pi^-) / \Gamma(K^- \pi^+)$ $\Gamma_{70} / \Gamma_{35}$

This is the "fit fraction" from the Dalitz-plot analysis.

VALUE	EVTS	DOCUMENT ID	TECN	COMMENT
2.083 ± 0.031 OUR FIT				
2.087 ± 0.032 OUR AVERAGE				
2.106 ± 0.013 ± 0.032		BONVICINI	14	CLEO All CLEO-c runs
1.94 ± 0.07 ^{+0.09} _{-0.11}		JUN	00	SELX Σ^- nucleus, 600 GeV
1.7 ± 0.2 ± 0.2	1745	ANJOS	92c	E691 γ Be 90–260 GeV
1.90 ± 0.25 ± 0.20	337	ALVAREZ	91B	NA14 Photoproduction
2.12 ± 0.16 ± 0.09		BORTOLETTO	088	CLEO $e^+ e^-$ 10.55 GeV
2.17 ± 0.28 ± 0.23		ALBRECHT	85F	ARG $e^+ e^-$ 10 GeV
• • • We do not use the following data for averages, fits, limits, etc. • • •				
2.0 ± 0.9	48	BAILEY	86	ACCM π^- Be fixed target
2.0 ± 1.0	10	BAILEY	83B	SPEC π^- Be $\rightarrow D^0$
2.2 ± 0.8	214	PICCOLO	77	MRK1 $e^+ e^-$ 4.03, 4.41 GeV

$\Gamma(K^- \pi^+ \pi^0 \text{ total}) / \Gamma(K^- 2\pi^+ \pi^-)$ $\Gamma_{71} / \Gamma_{70}$

This is the "fit fraction" from the Dalitz-plot analysis.

VALUE (units 10^{-2})	DOCUMENT ID	TECN	COMMENT
83.5 ± 3.5 OUR AVERAGE			
80 ± 3 ± 5	ANJOS	92c	E691 1745 $K^- 2\pi^+ \pi^-$ evts
85.5 ± 3.2 ± 3.0	COFFMAN	92B	MRK3 1281 ± 45 $K^- 2\pi^+ \pi^-$ evts

$\Gamma(K^- \pi^+ \rho^0 3\text{-body}) / \Gamma(K^- 2\pi^+ \pi^-)$ $\Gamma_{72} / \Gamma_{70}$

This is the "fit fraction" from the Dalitz-plot analysis.

VALUE (units 10^{-2})	EVTS	DOCUMENT ID	TECN	COMMENT
7.4 ± 2.0 OUR AVERAGE				
8.4 ± 1.1 ± 2.5	16k	ABLIKIM	17o	BES3 $D^0 \rightarrow K^- 2\pi^+ \pi^-$
5 ± 3 ± 2		ANJOS	92c	E691 1745 $K^- 2\pi^+ \pi^-$ evts
8.4 ± 2.2 ± 4.0		COFFMAN	92B	MRK3 1281 ± 45 $K^- 2\pi^+ \pi^-$ evts

$\Gamma(\bar{K}^*(892)^0 \rho^0, \bar{K}^*(892)^0 \rightarrow K^- \pi^+) / \Gamma(K^- 2\pi^+ \pi^-)$ $\Gamma_{73} / \Gamma_{70}$

This is the "fit fraction" from the Dalitz-plot analysis.

VALUE (units 10^{-2})	EVTS	DOCUMENT ID	TECN	COMMENT
12.3 ± 0.6 OUR AVERAGE				
12.3 ± 0.4 ± 0.5	16k	ABLIKIM	17o	BES3 $D^0 \rightarrow K^- 2\pi^+ \pi^-$
13 ± 2 ± 2		ANJOS	92c	E691 1745 $K^- 2\pi^+ \pi^-$ evts

$\Gamma(\bar{K}^*(892)^0 \rho^0 \text{ transverse}, \bar{K}^*(892)^0 \rightarrow K^- \pi^+) / \Gamma(K^- 2\pi^+ \pi^-)$ $\Gamma_{74} / \Gamma_{70}$

This is the "fit fraction" from the Dalitz-plot analysis.

VALUE	EVTS	DOCUMENT ID	TECN	COMMENT
0.142 ± 0.016 ± 0.05	1281	COFFMAN	92B	MRK3 $K^- 2\pi^+ \pi^-$ evts

$\Gamma(K^- a_1(1260)^+, a_1^+ \rightarrow \rho^0 \pi^+)/\Gamma(K^- 2\pi^+ \pi^-)$ Γ_{75}/Γ_{70}

VALUE (units 10 ⁻²)	EVTS	DOCUMENT ID	TECN	COMMENT
53 ± 4 OUR AVERAGE				
54.6 ± 2.8 ± 3.7	16k	ABLIKIM	17o	BES3 D ⁰ → K ⁻ 2π ⁺ π ⁻
47 ± 5 ± 10	1745	ANJOS	92c	E691 K ⁻ 2π ⁺ π ⁻ evts
49.2 ± 2.4 ± 8.0	1281	COFFMAN	92B	MRK3 K ⁻ 2π ⁺ π ⁻ evts

$\Gamma(K_1(1270)^- \pi^+, K_1^- \rightarrow K^- \pi^+ \pi^- \text{ total})/\Gamma(K^- 2\pi^+ \pi^-)$ Γ_{76}/Γ_{70}

VALUE (units 10 ⁻²)	EVTS	DOCUMENT ID	TECN	COMMENT
4.8 ± 0.4 OUR AVERAGE				
4.66 ± 0.05 ± 0.39 ± 0.24	891k	¹ AAIJ	18Al	LHCB D ⁰ → K ⁻ 2π ⁺ π ⁻
6.6 ± 1.9 ± 0.3	1281	COFFMAN	92B	MRK3 K ⁻ 2π ⁺ π ⁻ evts

¹The 3rd error is due to the uncertainty in the amplitude model composition.

$\Gamma(K_1(1270)^- \pi^+, K_1^- \rightarrow \bar{K}^*(892)^0 \pi^-, \bar{K}^{*0} \rightarrow K^- \pi^+)/\Gamma(K^- 2\pi^+ \pi^-)$ Γ_{79}/Γ_{70}

VALUE (units 10 ⁻²)	EVTS	DOCUMENT ID	TECN	COMMENT
0.8 ± 0.2 ± 0.2	16k	ABLIKIM	17o	BES3 D ⁰ → K ⁻ 2π ⁺ π ⁻

$\Gamma(K^- 2\pi^+ \pi^- \text{ nonresonant})/\Gamma(K^- 2\pi^+ \pi^-)$ Γ_{80}/Γ_{70}

VALUE (units 10 ⁻²)	EVTS	DOCUMENT ID	TECN	COMMENT
22.0 ± 0.8 OUR AVERAGE				
22.04 ± 0.28 ± 2.09 ± 1.51	891k	¹ AAIJ	18Al	LHCB D ⁰ → K ⁻ 2π ⁺ π ⁻
21.9 ± 0.6 ± 0.6	16k	² ABLIKIM	17o	BES3 D ⁰ → K ⁻ 2π ⁺ π ⁻
23 ± 2 ± 3	1.7k	ANJOS	92c	E691 D ⁰ → K ⁻ 2π ⁺ π ⁻
24.2 ± 2.5 ± 6.0	1.2k	COFFMAN	92B	MRK3 D ⁰ → K ⁻ 2π ⁺ π ⁻

¹The 3rd error is due to the uncertainty in the amplitude model composition.
²In addition to the 14 ABLIKIM 17o branching ratios we have listed, the paper gives 15 more ratios for mostly non-resonant modes. Four of the 15 have less than 2-standard-deviation significance. Here are some of the omitted modes, with S, P, V, A, and T for scalar, pseudo-scalar, vector, axial-vector, and tensor spin sub-structures: π⁺(K⁻ρ⁰)_P, π⁺(K⁻ρ⁰)_V, π⁺(K⁻*0 π⁻)_P, π⁺(K⁻*0 π⁻)_V, π⁺(π⁻(K⁻π⁺)_{S-wave})_A, (K⁻π⁺)_V(π⁺π⁻)_S, (K⁻π⁺)_T(π⁺π⁻)_S...

$\Gamma(K_S^0 \pi^+ \pi^- \pi^0)/\Gamma_{\text{total}}$ Γ_{81}/Γ

VALUE (%)	EVTS	DOCUMENT ID	TECN	COMMENT
5.2 ± 0.6 OUR FIT				
5.2 ± 1.1 ± 1.2	140	COFFMAN	92B	MRK3 e ⁺ e ⁻ 3.77 GeV
6.7 ± 1.6 ± 1.7		¹ BARLAG	92c	ACCM π ⁻ Cu 230 GeV

¹BARLAG 92c computes the branching fraction using topological normalization.

$\Gamma(K_S^0 \pi^+ \pi^- \pi^0)/\Gamma(K_S^0 \pi^+ \pi^-)$ Γ_{81}/Γ_{38}

Branching fractions for submodes of this mode with narrow resonances (the η, ω, η') are fairly well determined (see below). COFFMAN 92B gives fractions of K* and ρ submodes, but with only 140 ± 28 events above background could not determine them with much accuracy. We omit those measurements here; they are in our 2008 Review (Physics Letters **B667** 1 (2008)).

VALUE (%)	EVTS	DOCUMENT ID	TECN	COMMENT
1.85 ± 0.20 OUR FIT				
1.86 ± 0.23 OUR AVERAGE				
1.80 ± 0.20 ± 0.21	190	¹ ALBRECHT	92P	ARG e ⁺ e ⁻ ≈ 10 GeV
2.8 ± 0.8 ± 0.8	46	ANJOS	92c	E691 γ Be 90-260 GeV
1.85 ± 0.26 ± 0.30	158	KINOSHITA	91	CLEO e ⁺ e ⁻ ~ 10.7 GeV

¹This value is calculated from numbers in Table 1 of ALBRECHT 92P.

$\Gamma(K^- \pi^+ 2\pi^0)/\Gamma_{\text{total}}$ Γ_{84}/Γ

VALUE (%)	EVTS	DOCUMENT ID	TECN	COMMENT
8.86 ± 0.13 ± 0.19	6.1k	ABLIKIM	19Ak	BES3 e ⁺ e ⁻ at 3773 MeV
17.7 ± 2.9		¹ BARLAG	92c	ACCM π ⁻ Cu 230 GeV
14.9 ± 3.7 ± 3.0	24	² ADLER	88c	MRK3 e ⁺ e ⁻ 3.77 GeV
20.9 ± 7.4 ± 4.3	9	¹ AGUILAR-...	87F	HYBR π p, p p 360, 400 GeV

¹AGUILAR-BENITEZ 87F and BARLAG 92c compute the branching fraction using topological normalization. They do not distinguish the presence of a third π⁰, and thus are not included in the average.

²ADLER 88c uses an absolute normalization method finding this decay channel opposite a detected $\bar{D}^0 \rightarrow K^+ \pi^-$ in pure $D\bar{D}$ events.

$\Gamma(K^- 2\pi^+ \pi^- \pi^0)/\Gamma(K^- \pi^+)$ Γ_{85}/Γ_{35}

VALUE (%)	EVTS	DOCUMENT ID	TECN	COMMENT
1.09 ± 0.10 OUR FIT				
0.98 ± 0.11 ± 0.11	225	¹ ALBRECHT	92P	ARG e ⁺ e ⁻ ≈ 10 GeV

¹This value is calculated from numbers in Table 1 of ALBRECHT 92P.

$\Gamma(K^- 2\pi^+ \pi^- \pi^0)/\Gamma(K^- 2\pi^+ \pi^-)$ Γ_{85}/Γ_{70}

VALUE (%)	EVTS	DOCUMENT ID	TECN	COMMENT
0.52 ± 0.05 OUR FIT				
0.56 ± 0.07 OUR AVERAGE				
0.55 ± 0.07 ± 0.12 ± 0.09	167	KINOSHITA	91	CLEO e ⁺ e ⁻ ~ 10.7 GeV
0.57 ± 0.06 ± 0.05	180	ANJOS	90D	E691 Photoproduction

$\Gamma(K_S^0 \eta \pi^0)/\Gamma(K_S^0 \pi^0)$ Γ_{89}/Γ_{36}

VALUE (%)	EVTS	DOCUMENT ID	TECN	COMMENT
0.46 ± 0.07 ± 0.06	155 ± 22	¹ RUBIN	04	CLEO e ⁺ e ⁻ ≈ 10 GeV

¹The η here is detected in its γγ mode, but other η modes are included in the value given.

$\Gamma(K_S^0 a_0(980), a_0 \rightarrow \eta \pi^0)/\Gamma(K_S^0 \eta \pi^0)$ Γ_{90}/Γ_{89}

VALUE (%)	EVTS	DOCUMENT ID	TECN	COMMENT
1.19 ± 0.09 ± 0.26				
1.19 ± 0.09 ± 0.26	155	¹ RUBIN	04	CLEO Dalitz fit, 155 evts

This is the "fit fraction" from the Dalitz-plot analysis, with interference.
¹In addition to K_S⁰ a₀(980) and $\bar{K}^*(892)^0$ η modes, RUBIN 04 finds a fit fraction of 0.246 ± 0.092 ± 0.091 for other, undetermined modes.

$\Gamma(\bar{K}^*(892)^0 \eta, \bar{K}^{*0} \rightarrow K_S^0 \pi^0)/\Gamma(K_S^0 \eta \pi^0)$ Γ_{91}/Γ_{89}

VALUE (%)	EVTS	DOCUMENT ID	TECN	COMMENT
0.293 ± 0.062 ± 0.035				
0.293 ± 0.062 ± 0.035	155	¹ RUBIN	04	CLEO Dalitz fit, 155 evts

¹See the note on RUBIN 04 in the preceding data block.

$\Gamma(K_S^0 2\pi^+ 2\pi^-)/\Gamma(K_S^0 \pi^+ \pi^-)$ Γ_{92}/Γ_{38}

VALUE (%)	EVTS	DOCUMENT ID	TECN	COMMENT
0.095 ± 0.005 ± 0.007	1283 ± 57	LINK	04D	FOCS γ A, \bar{E}_γ ≈ 180 GeV
0.07 ± 0.02 ± 0.01	11	¹ ALBRECHT	92P	ARG e ⁺ e ⁻ ≈ 10 GeV
0.149 ± 0.026	56	ANMAR	91	CLEO e ⁺ e ⁻ ≈ 10.5 GeV
0.18 ± 0.07 ± 0.04	6	ANJOS	90D	E691 Photoproduction

¹This value is calculated from numbers in Table 1 of ALBRECHT 92P.

$\Gamma(K_S^0 \rho^0 \pi^+ \pi^-, \text{no } K^*(892)^-)/\Gamma(K_S^0 2\pi^+ 2\pi^-)$ Γ_{93}/Γ_{92}

VALUE (%)	EVTS	DOCUMENT ID	TECN	COMMENT
0.40 ± 0.24 ± 0.07				
0.40 ± 0.24 ± 0.07		LINK	04D	FOCS γ A, \bar{E}_γ ≈ 180 GeV

$\Gamma(K^*(892)^- 2\pi^+ \pi^-, K^*(892)^- \rightarrow K_S^0 \pi^-, \text{no } \rho^0)/\Gamma(K_S^0 2\pi^+ 2\pi^-)$ Γ_{94}/Γ_{92}

VALUE (%)	EVTS	DOCUMENT ID	TECN	COMMENT
0.17 ± 0.28 ± 0.02				
0.17 ± 0.28 ± 0.02		LINK	04D	FOCS γ A, \bar{E}_γ ≈ 180 GeV

$\Gamma(K^*(892)^- \rho^0 \pi^+, K^*(892)^- \rightarrow K_S^0 \pi^-)/\Gamma(K_S^0 2\pi^+ 2\pi^-)$ Γ_{95}/Γ_{92}

VALUE (%)	EVTS	DOCUMENT ID	TECN	COMMENT
0.60 ± 0.21 ± 0.09				
0.60 ± 0.21 ± 0.09		LINK	04D	FOCS γ A, \bar{E}_γ ≈ 180 GeV

$\Gamma(K_S^0 2\pi^+ 2\pi^- \text{ nonresonant})/\Gamma(K_S^0 2\pi^+ 2\pi^-)$ Γ_{96}/Γ_{92}

VALUE (%)	CL%	DOCUMENT ID	TECN	COMMENT
<0.46	90	LINK	04D	FOCS γ A, \bar{E}_γ ≈ 180 GeV

$\Gamma(K^- 3\pi^+ 2\pi^-)/\Gamma(K^- 2\pi^+ \pi^-)$ Γ_{98}/Γ_{70}

VALUE (units 10 ⁻³)	EVTS	DOCUMENT ID	TECN	COMMENT
2.70 ± 0.58 ± 0.38	48 ± 10	LINK	04B	FOCS γ A, \bar{E}_γ ≈ 180 GeV

$\Gamma(K_S^0 \eta)/\Gamma_{\text{total}}$ Γ_{99}/Γ

Unseen decay modes of the η are included.

VALUE (%)	EVTS	DOCUMENT ID	TECN	COMMENT
5.09 ± 0.13 OUR FIT				
5.13 ± 0.07 ± 0.12	9.5k	ABLIKIM	18w	BES3 e ⁺ e ⁻ , 3773 MeV
4.42 ± 0.15 ± 0.28		ASNER	08	CLEO See MENDEZ 10

$\Gamma(K_S^0 \eta)/[\Gamma(K^- \pi^+) + \Gamma(K^+ \pi^-)]$ $\Gamma_{99}/(\Gamma_{35} + \Gamma_{256})$

Unseen decay modes of the η are included.

VALUE (units 10 ⁻²)	EVTS	DOCUMENT ID	TECN	COMMENT
12.83 ± 0.33 OUR FIT				
12.3 ± 0.3 ± 0.7	2864 ± 65	MENDEZ	10	CLEO e ⁺ e ⁻ at 3774 MeV

$\Gamma(K_S^0 \eta)/\Gamma(K_S^0 \pi^0)$ Γ_{99}/Γ_{36}

Unseen decay modes of the η are included.

VALUE (%)	EVTS	DOCUMENT ID	TECN	COMMENT
0.32 ± 0.04 ± 0.03	225 ± 30	PROCARIO	93B	CLE2 η → γγ

$\Gamma(K_S^0 \eta)/\Gamma(K_S^0 \pi^+ \pi^-)$ Γ_{99}/Γ_{38}

Unseen decay modes of the η are included.

VALUE (%)	EVTS	DOCUMENT ID	TECN	COMMENT
0.14 ± 0.02 ± 0.02	80 ± 12	PROCARIO	93B	CLE2 η → π ⁺ π ⁻ π ⁰

$\Gamma(K_S^0 \omega)/\Gamma_{\text{total}}$ Γ_{100}/Γ

Unseen decay modes of the ω are included.

VALUE (%)	EVTS	DOCUMENT ID	TECN	COMMENT
1.11 ± 0.06 OUR FIT				
1.12 ± 0.04 ± 0.05				
1.12 ± 0.04 ± 0.05		ASNER	08	CLEO e ⁺ e ⁻ → D ⁰ \bar{D}^0 , 3.77 GeV

$\Gamma(K_S^0 \omega)/\Gamma(K^- \pi^+)$ Γ_{100}/Γ_{35}

Unseen decay modes of the ω are included.

VALUE (%)	EVTS	DOCUMENT ID	TECN	COMMENT
0.50 ± 0.18 ± 0.10				
0.50 ± 0.18 ± 0.10		ALBRECHT	89D	ARG e ⁺ e ⁻ 10 GeV

Meson Particle Listings

D^0

$\Gamma(K_S^0 \omega)/\Gamma(K_S^0 \pi^+ \pi^-)$ Γ_{100}/Γ_{38}

Unseen decay modes of the ω are included.

VALUE	EVTS	DOCUMENT ID	TECN	COMMENT
0.396 ± 0.032 OUR FIT				Error includes scale factor of 1.1.
0.33 ± 0.09 OUR AVERAGE				Error includes scale factor of 1.1.
0.29 ± 0.08 ± 0.05	16	¹ ALBRECHT 92P	ARG	$e^+ e^- \approx 10$ GeV
0.54 ± 0.14 ± 0.16	40	KINOSHITA 91	CLEO	$e^+ e^- \sim 10.7$ GeV

¹ This value is calculated from numbers in Table 1 of ALBRECHT 92P.

$\Gamma(K_S^0 \omega)/\Gamma(K_S^0 \pi^+ \pi^- \pi^0)$ Γ_{100}/Γ_{81}

Unseen decay modes of the ω are included.

VALUE	DOCUMENT ID	TECN	COMMENT
0.215 ± 0.026 OUR FIT			
0.220 ± 0.048 ± 0.0116	COFFMAN 92B	MRK3	1281 ± 45 $K^- 2\pi^+ \pi^-$ evts

$\Gamma(K_S^0 \eta(958))/\Gamma_{total}$ Γ_{101}/Γ

Unseen decay modes of the $\eta(958)$ are included.

VALUE (units 10^{-3})	EVTS	DOCUMENT ID	TECN	COMMENT
9.49 ± 0.32 OUR FIT				
9.49 ± 0.20 ± 0.36	3k	ABLIKIM 18W	BES3	$e^+ e^-$, 3773 MeV

$\Gamma(K_S^0 \eta(958))/[\Gamma(K^- \pi^+) + \Gamma(K^+ \pi^-)]$ $\Gamma_{101}/(\Gamma_{35} + \Gamma_{256})$

Unseen decay modes of the $\eta(958)$ are included.

VALUE (units 10^{-2})	EVTS	DOCUMENT ID	TECN	COMMENT
23.9 ± 0.8 OUR FIT				
24.3 ± 0.8 ± 1.1	1321 ± 42	MENDEZ 10	CLEO	$e^+ e^-$ at 3774 MeV

$\Gamma(K_S^0 \eta(958))/\Gamma(K_S^0 \pi^+ \pi^-)$ Γ_{101}/Γ_{38}

Unseen decay modes of the $\eta(958)$ are included.

VALUE	EVTS	DOCUMENT ID	TECN	COMMENT
0.339 ± 0.023 OUR FIT				
0.32 ± 0.04 OUR AVERAGE				
0.31 ± 0.02 ± 0.04	594	PROCARIO 93B	CLE2	$\eta' \rightarrow \eta \pi^+ \pi^-, \rho^0 \gamma$
0.37 ± 0.13 ± 0.06	18	¹ ALBRECHT 92P	ARG	$e^+ e^- \approx 10$ GeV

¹ This value is calculated from numbers in Table 1 of ALBRECHT 92P.

$\Gamma(\bar{K}^*(892)^0 \pi^+ \pi^- \pi^0)/\Gamma(K^- 2\pi^+ \pi^- \pi^0)$ Γ_{102}/Γ_{85}

Unseen decay modes of the $\bar{K}^*(892)^0$ are included.

VALUE	DOCUMENT ID	TECN	COMMENT
0.45 ± 0.15 ± 0.15	ANJOS 90D	E691	Photoproduction

$\Gamma(\bar{K}^*(892)^0 \eta)/\Gamma(K^- \pi^+)$ Γ_{103}/Γ_{35}

Unseen decay modes of the $\bar{K}^*(892)^0$ and η are included.

VALUE	EVTS	DOCUMENT ID	TECN	COMMENT
0.58 ± 0.19 ± 0.24 - 0.28	46	KINOSHITA 91	CLEO	$e^+ e^- \sim 10.7$ GeV

• • • We do not use the following data for averages, fits, limits, etc. • • •

$\Gamma(\bar{K}^*(892)^0 \eta)/\Gamma(K^- \pi^+ \pi^0)$ Γ_{103}/Γ_{53}

Unseen decay modes of the $\bar{K}^*(892)^0$ and η are included.

VALUE	EVTS	DOCUMENT ID	TECN	COMMENT
0.13 ± 0.02 ± 0.03	214	PROCARIO 93B	CLE2	$\bar{K}^{*0} \eta \rightarrow K^- \pi^+ / \gamma \gamma$

• • • We do not use the following data for averages, fits, limits, etc. • • •

$\Gamma(K^- \pi^+ \omega)/\Gamma(K^- \pi^+)$ Γ_{104}/Γ_{35}

Unseen decay modes of the ω are included.

VALUE	EVTS	DOCUMENT ID	TECN	COMMENT
0.78 ± 0.12 ± 0.10	99	¹ ALBRECHT 92P	ARG	$e^+ e^- \approx 10$ GeV

¹ This value is calculated from numbers in Table 1 of ALBRECHT 92P.

$\Gamma(\bar{K}^*(892)^0 \omega)/\Gamma(K^- \pi^+)$ Γ_{105}/Γ_{35}

Unseen decay modes of the $\bar{K}^*(892)^0$ and ω are included.

VALUE	EVTS	DOCUMENT ID	TECN	COMMENT
0.28 ± 0.11 ± 0.04	17	¹ ALBRECHT 92P	ARG	$e^+ e^- \approx 10$ GeV

¹ This value is calculated from numbers in Table 1 of ALBRECHT 92P.

$\Gamma(K^- \pi^+ \eta(958))/\Gamma_{total}$ Γ_{106}/Γ

Unseen decay modes of the $\eta(958)$ are included.

VALUE (units 10^{-3})	EVTS	DOCUMENT ID	TECN	COMMENT
6.43 ± 0.15 ± 0.31	2.5k	ABLIKIM 18Ac	BES3	$e^+ e^-$, 3773 MeV

$\Gamma(K^- \pi^+ \eta(958))/\Gamma(K^- 2\pi^+ \pi^-)$ Γ_{106}/Γ_{70}

Unseen decay modes of the $\eta(958)$ are included.

VALUE	EVTS	DOCUMENT ID	TECN	COMMENT
0.093 ± 0.014 ± 0.019	286	PROCARIO 93B	CLE2	$\eta' \rightarrow \eta \pi^+ \pi^-, \rho^0 \gamma$

$\Gamma(K_S^0 \eta(958) \pi^0)/\Gamma_{total}$ Γ_{107}/Γ

Unseen decay modes of the $\eta(958)$ are included.

VALUE (units 10^{-3})	EVTS	DOCUMENT ID	TECN	COMMENT
2.52 ± 0.22 ± 0.15	289	ABLIKIM 18Ac	BES3	$e^+ e^-$, 3773 MeV

$\Gamma(\bar{K}^*(892)^0 \eta(958))/\Gamma(K^- \pi^+ \eta(958))$ $\Gamma_{108}/\Gamma_{106}$

Unseen decay modes of the $\bar{K}^*(892)^0$ are included.

VALUE	CL%	DOCUMENT ID	TECN	COMMENT
<0.15	90	PROCARIO 93B	CLE2	

Hadronic modes with three K 's

$\Gamma(K_S^0 K^+ K^-)/\Gamma(K_S^0 \pi^+ \pi^-)$ Γ_{109}/Γ_{38}

VALUE	EVTS	DOCUMENT ID	TECN	COMMENT
0.158 ± 0.001 ± 0.005	14k ± 116	AUBERT,B 05J	BABR	$e^+ e^- \approx \Upsilon(4S)$
• • • We do not use the following data for averages, fits, limits, etc. • • •				
0.20 ± 0.05 ± 0.04	47	FRABETTI 92B	E687	γ Be, $\bar{E}_\gamma = 221$ GeV
0.170 ± 0.022	136	AMMAR 91	CLEO	$e^+ e^- \approx 10.5$ GeV
0.24 ± 0.08		BEBEK 86	CLEO	$e^+ e^-$ near $\Upsilon(4S)$
0.185 ± 0.055	52	ALBRECHT 85B	ARG	$e^+ e^- 10$ GeV

$\Gamma(K_S^0 a_0(980)^0, a_0^0 \rightarrow K^+ K^-)/\Gamma(K_S^0 K^+ K^-)$ $\Gamma_{110}/\Gamma_{109}$

This is the "fit fraction" from the Dalitz-plot analysis, with interference.

VALUE	DOCUMENT ID	TECN	COMMENT
0.664 ± 0.016 ± 0.070	AUBERT,B 05J	BABR	Dalitz fit, 12540 ± 112 evts

$\Gamma(K^- a_0(980)^+, a_0^+ \rightarrow K^+ K_S^0)/\Gamma(K_S^0 K^+ K^-)$ $\Gamma_{111}/\Gamma_{109}$

This is the "fit fraction" from the Dalitz-plot analysis, with interference.

VALUE	DOCUMENT ID	TECN	COMMENT
0.134 ± 0.011 ± 0.037	AUBERT,B 05J	BABR	Dalitz fit, 12540 ± 112 evts

$\Gamma(K^+ a_0(980)^-, a_0^- \rightarrow K^- K_S^0)/\Gamma(K_S^0 K^+ K^-)$ $\Gamma_{112}/\Gamma_{109}$

This is a doubly Cabibbo-suppressed mode.

VALUE	CL%	DOCUMENT ID	TECN	COMMENT
<0.025	95	AUBERT,B 05J	BABR	Dalitz fit, 12540 ± 112 evts

$\Gamma(K_S^0 f_0(980), f_0 \rightarrow K^+ K^-)/\Gamma(K_S^0 K^+ K^-)$ $\Gamma_{113}/\Gamma_{109}$

VALUE	CL%	DOCUMENT ID	TECN	COMMENT
<0.021	95	AUBERT,B 05J	BABR	Dalitz fit, 12540 ± 112 evts

$\Gamma(K_S^0 \phi, \phi \rightarrow K^+ K^-)/\Gamma(K_S^0 K^+ K^-)$ $\Gamma_{114}/\Gamma_{109}$

This is the "fit fraction" from the Dalitz-plot analysis, with interference.

VALUE	DOCUMENT ID	TECN	COMMENT
0.459 ± 0.007 ± 0.007	AUBERT,B 05J	BABR	Dalitz fit, 12540 ± 112 evts

$\Gamma(K_S^0 f_0(1370), f_0 \rightarrow K^+ K^-)/\Gamma(K_S^0 K^+ K^-)$ $\Gamma_{115}/\Gamma_{109}$

This is the "fit fraction" from the Dalitz-plot analysis, with interference.

VALUE	DOCUMENT ID	TECN	COMMENT
0.038 ± 0.007 ± 0.023	¹ AUBERT,B 05J	BABR	Dalitz fit, 12540 ± 112 evts

¹ AUBERT,B 05J calls the mode $K_S^0 f_0(1400)$, but insofar as it is seen here at all, it is certainly the same as $f_0(1370)$.

$\Gamma(3K_S^0)/\Gamma_{total}$ Γ_{116}/Γ

Unseen decay modes of the $\eta(958)$ are included.

VALUE (units 10^{-4})	EVTS	DOCUMENT ID	TECN	COMMENT
7.5 ± 0.7 OUR FIT				Error includes scale factor of 1.4.
7.21 ± 0.33 ± 0.44	597	ABLIKIM 17A	BES3	$e^+ e^- \rightarrow \psi(3770)$

$\Gamma(3K_S^0)/\Gamma(K_S^0 \pi^+ \pi^-)$ Γ_{116}/Γ_{38}

Unseen decay modes of the $\eta(958)$ are included.

VALUE (units 10^{-2})	EVTS	DOCUMENT ID	TECN	COMMENT
2.70 ± 0.26 OUR FIT				Error includes scale factor of 1.2.
3.2 ± 0.4 OUR AVERAGE				
3.58 ± 0.54 ± 0.52	170 ± 26	LINK 05A	FOCS	γ Be, $\bar{E}_\gamma \approx 180$ GeV
2.78 ± 0.38 ± 0.48	61	ASNER 96B	CLE2	$e^+ e^- \approx \Upsilon(4S)$
7.0 ± 2.4 ± 1.2	10 ± 3	FRABETTI 94J	E687	γ Be, $\bar{E}_\gamma = 220$ GeV
3.2 ± 1.0	22	AMMAR 91	CLEO	$e^+ e^- \approx 10.5$ GeV
3.4 ± 1.4 ± 1.0	5	ALBRECHT 90C	ARG	$e^+ e^- \approx 10$ GeV

$\Gamma(K^+ 2K^- \pi^+)/\Gamma(K^- 2\pi^+ \pi^-)$ Γ_{117}/Γ_{70}

VALUE	EVTS	DOCUMENT ID	TECN	COMMENT
0.0027 ± 0.0004 OUR AVERAGE				Error includes scale factor of 1.1.
0.00257 ± 0.00034 ± 0.00024	143	LINK 03G	FOCS	γ A, $\bar{E}_\gamma \approx 180$ GeV
0.0054 ± 0.0016 ± 0.0008	18	AITALA 01D	E791	π^- A, 500 GeV
0.0028 ± 0.0007 ± 0.0001	20	FRABETTI 95C	E687	γ Be, $\bar{E}_\gamma \approx 200$ GeV

$\Gamma(K^+ K^- \bar{K}^*(892)^0, \bar{K}^{*0} \rightarrow K^- \pi^+)/\Gamma(K^+ 2K^- \pi^+)$ $\Gamma_{118}/\Gamma_{117}$

VALUE	DOCUMENT ID	TECN	COMMENT
0.20 ± 0.07 ± 0.02	LINK 03G	FOCS	γ A, $\bar{E}_\gamma \approx 180$ GeV

$\Gamma(K^- \pi^+ \phi, \phi \rightarrow K^+ K^-)/\Gamma(K^+ 2K^- \pi^+)$ $\Gamma_{119}/\Gamma_{117}$

VALUE	DOCUMENT ID	TECN	COMMENT
0.18 ± 0.06 ± 0.04	LINK 03G	FOCS	γ A, $\bar{E}_\gamma \approx 180$ GeV

$\Gamma(\phi \bar{K}^*(892)^0, \phi \rightarrow K^+ K^-, \bar{K}^{*0} \rightarrow K^- \pi^+)/\Gamma(K^+ 2K^- \pi^+)$ $\Gamma_{120}/\Gamma_{117}$

VALUE	DOCUMENT ID	TECN	COMMENT
0.48 ± 0.06 ± 0.01	LINK 03G	FOCS	γ A, $\bar{E}_\gamma \approx 180$ GeV

$\Gamma(K^+ 2K^- \pi^+ \text{ nonresonant})/\Gamma(K^+ 2K^- \pi^+)$ $\Gamma_{121}/\Gamma_{117}$

VALUE	DOCUMENT ID	TECN	COMMENT
0.15 ± 0.06 ± 0.02	LINK 03G	FOCS	γ A, $\bar{E}_\gamma \approx 180$ GeV

$\Gamma(2K_S^0 K^\pm \pi^\mp) / \Gamma(K_S^0 \pi^+ \pi^-)$		$\Gamma_{122} / \Gamma_{38}$	
VALUE (units 10 ⁻²)	EVTS	DOCUMENT ID	TECN COMMENT
2.12 ± 0.38 ± 0.20	57 ± 10	LINK	05A FOCS γ Be, $\bar{E}_\gamma \approx 180$ GeV

Pionic modes

$\Gamma(\pi^+ \pi^-) / \Gamma_{total}$		Γ_{123} / Γ	
VALUE (units 10 ⁻³)	EVTS	DOCUMENT ID	TECN COMMENT
1.455 ± 0.024 OUR FIT	Error includes scale factor of 1.3.		
1.508 ± 0.018 ± 0.022	21k	ABLIKIM	18w BES3 $e^+ e^-$, 3773 MeV

$\Gamma(\pi^+ \pi^-) / \Gamma(K^- \pi^+)$		$\Gamma_{123} / \Gamma_{35}$	
VALUE (units 10 ⁻²)	EVTS	DOCUMENT ID	TECN COMMENT
3.68 ± 0.05 OUR FIT	Error includes scale factor of 1.3.		
3.59 ± 0.06 OUR AVERAGE			
3.594 ± 0.054 ± 0.040	7334 ± 97	ACOSTA	05c CDF $p\bar{p}$, $\sqrt{s} = 1.96$ TeV
3.53 ± 0.12 ± 0.06	3453	LINK	03 FOCS γ A, $\bar{E}_\gamma \approx 180$ GeV
3.51 ± 0.16 ± 0.17	710	CSORNA	02 CLE2 $e^+ e^- \approx \Upsilon(4S)$
4.0 ± 0.2 ± 0.3	2043	AITALA	98c E791 π^- A, 500 GeV
• • • We do not use the following data for averages, fits, limits, etc. • • •			
3.62 ± 0.10 ± 0.08	2085 ± 54	RUBIN	06 CLEO See MENDEZ 10
3.4 ± 0.7 ± 0.1	76 ± 15	ABLIKIM	05F BES $e^+ e^- \approx \psi(3770)$
4.3 ± 0.7 ± 0.3	177	FRABETTI	94c E687 γ Be $\bar{E}_\gamma = 220$ GeV
3.48 ± 0.30 ± 0.23	227	SELEN	93 CLE2 $e^+ e^- \approx \Upsilon(4S)$
5.5 ± 0.8 ± 0.5	120	ANJOS	91D E691 Photoproduction
5.0 ± 0.7 ± 0.5	110	ALEXANDER	90 CLEO $e^+ e^-$ 10.5–11 GeV

$\Gamma(\pi^+ \pi^-) / [\Gamma(K^- \pi^+) + \Gamma(K^+ \pi^-)]$		$\Gamma_{123} / (\Gamma_{35} + \Gamma_{256})$	
VALUE (units 10 ⁻²)	EVTS	DOCUMENT ID	TECN COMMENT
3.67 ± 0.05 OUR FIT	Error includes scale factor of 1.3.		
3.70 ± 0.06 ± 0.09	6210 ± 93	MENDEZ	10 CLEO $e^+ e^-$ at 3774 MeV

$\Gamma(2\pi^0) / \Gamma_{total}$		Γ_{124} / Γ	
VALUE (units 10 ⁻⁴)	EVTS	DOCUMENT ID	TECN COMMENT
8.26 ± 0.25 OUR FIT			
8.29 ± 0.30 OUR AVERAGE			
8.24 ± 0.21 ± 0.30	6k	ABLIKIM	15F BES3 $e^+ e^-$ at 3.773 GeV
8.4 ± 0.1 ± 0.5	26k	LEES	12L BABR $e^+ e^- \approx 10.58$ GeV

$\Gamma(2\pi^0) / \Gamma(K^- \pi^+)$		$\Gamma_{124} / \Gamma_{35}$	
VALUE (units 10 ⁻²)	EVTS	DOCUMENT ID	TECN COMMENT
• • • We do not use the following data for averages, fits, limits, etc. • • •			
2.05 ± 0.13 ± 0.16	499 ± 32	RUBIN	06 CLEO See MENDEZ 10
2.2 ± 0.4 ± 0.4	40	SELEN	93 CLE2 $e^+ e^- \rightarrow \Upsilon(4S)$

$\Gamma(2\pi^0) / [\Gamma(K^- \pi^+) + \Gamma(K^+ \pi^-)]$		$\Gamma_{124} / (\Gamma_{35} + \Gamma_{256})$	
VALUE (units 10 ⁻²)	EVTS	DOCUMENT ID	TECN COMMENT
2.08 ± 0.07 OUR FIT			
2.06 ± 0.07 ± 0.10	1567 ± 54	MENDEZ	10 CLEO $e^+ e^-$ at 3774 MeV

$\Gamma(\pi^+ \pi^- \pi^0) / \Gamma(K^- \pi^+)$		$\Gamma_{125} / \Gamma_{35}$	
VALUE (units 10 ⁻²)	EVTS	DOCUMENT ID	TECN COMMENT
37.7 ± 1.6 OUR FIT	Error includes scale factor of 2.2.		
34.4 ± 0.5 ± 1.2	11k ± 164	RUBIN	06 CLEO $e^+ e^-$ at $\psi(3770)$

$\Gamma(\pi^+ \pi^- \pi^0) / \Gamma(K^- \pi^+ \pi^0)$		$\Gamma_{125} / \Gamma_{53}$	
VALUE (units 10 ⁻²)	EVTS	DOCUMENT ID	TECN COMMENT
10.32 ± 0.25 OUR FIT	Error includes scale factor of 2.3.		
10.41 ± 0.23 OUR AVERAGE	Error includes scale factor of 2.0.		
10.12 ± 0.04 ± 0.18	123k ± 490	ARINSTEIN	08 BELL $e^+ e^- \approx \Upsilon(4S)$
10.59 ± 0.06 ± 0.13	60k ± 343	AUBERT,B	06x BABR $e^+ e^- \approx \Upsilon(4S)$

$\Gamma(\rho^+ \pi^-) / \Gamma(\pi^+ \pi^- \pi^0)$		$\Gamma_{126} / \Gamma_{125}$	
VALUE (units 10 ⁻²)	EVTS	DOCUMENT ID	TECN COMMENT
68.1 ± 0.6 OUR AVERAGE			
67.8 ± 0.0 ± 0.6		AUBERT	07Bj BABR Dalitz fit, 45k events
76.3 ± 1.9 ± 2.5		CRONIN-HEN..05	CLEO $e^+ e^- \approx 10$ GeV

This is the "fit fraction" from the Dalitz-plot analysis, with interference. See GASPERO 08 and BHATTACHARYA 10a for isospin decompositions of the $D^0 \rightarrow \pi^+ \pi^0 \pi^-$ Dalitz plot, both based on the amplitudes of AUBERT 07Bj. They quantify the conclusion that the final state is dominantly isospin 0.

$\Gamma(\rho^0 \pi^0) / \Gamma(\pi^+ \pi^- \pi^0)$		$\Gamma_{127} / \Gamma_{125}$	
VALUE (units 10 ⁻²)	EVTS	DOCUMENT ID	TECN COMMENT
25.9 ± 1.1 OUR AVERAGE			
26.2 ± 0.5 ± 1.1		AUBERT	07Bj BABR Dalitz fit, 45k events
24.4 ± 2.0 ± 2.1		CRONIN-HEN..05	CLEO $e^+ e^- \approx 10$ GeV

This is the "fit fraction" from the Dalitz-plot analysis, with interference.

$\Gamma(\rho^- \pi^+) / \Gamma(\pi^+ \pi^- \pi^0)$		$\Gamma_{128} / \Gamma_{125}$	
VALUE (units 10 ⁻²)	EVTS	DOCUMENT ID	TECN COMMENT
34.6 ± 0.8 OUR AVERAGE			
34.6 ± 0.8 ± 0.3		AUBERT	07Bj BABR Dalitz fit, 45k events
34.5 ± 2.4 ± 1.3		CRONIN-HEN..05	CLEO $e^+ e^- \approx 10$ GeV

This is the "fit fraction" from the Dalitz-plot analysis, with interference.

$\Gamma(\rho(1450)^+ \pi^-, \rho^+ \rightarrow \pi^+ \pi^0) / \Gamma(\pi^+ \pi^- \pi^0)$		$\Gamma_{129} / \Gamma_{125}$	
VALUE (units 10 ⁻²)	EVTS	DOCUMENT ID	TECN COMMENT
This is the "fit fraction" from the Dalitz-plot analysis.			
0.11 ± 0.07 ± 0.12		AUBERT	07Bj BABR Dalitz fit, 45k events

$\Gamma(\rho(1450)^0 \pi^0, \rho^0 \rightarrow \pi^+ \pi^-) / \Gamma(\pi^+ \pi^- \pi^0)$		$\Gamma_{130} / \Gamma_{125}$	
VALUE (units 10 ⁻²)	EVTS	DOCUMENT ID	TECN COMMENT
This is the "fit fraction" from the Dalitz-plot analysis.			
0.30 ± 0.11 ± 0.07		AUBERT	07Bj BABR Dalitz fit, 45k events

$\Gamma(\rho(1450)^- \pi^+, \rho^- \rightarrow \pi^- \pi^0) / \Gamma(\pi^+ \pi^- \pi^0)$		$\Gamma_{131} / \Gamma_{125}$	
VALUE (units 10 ⁻²)	EVTS	DOCUMENT ID	TECN COMMENT
This is the "fit fraction" from the Dalitz-plot analysis.			
1.79 ± 0.22 ± 0.12		AUBERT	07Bj BABR Dalitz fit, 45k events

$\Gamma(\rho(1700)^+ \pi^-, \rho^+ \rightarrow \pi^+ \pi^0) / \Gamma(\pi^+ \pi^- \pi^0)$		$\Gamma_{132} / \Gamma_{125}$	
VALUE (units 10 ⁻²)	EVTS	DOCUMENT ID	TECN COMMENT
This is the "fit fraction" from the Dalitz-plot analysis.			
4.1 ± 0.7 ± 0.7		AUBERT	07Bj BABR Dalitz fit, 45k events

$\Gamma(\rho(1700)^0 \pi^0, \rho^0 \rightarrow \pi^+ \pi^-) / \Gamma(\pi^+ \pi^- \pi^0)$		$\Gamma_{133} / \Gamma_{125}$	
VALUE (units 10 ⁻²)	EVTS	DOCUMENT ID	TECN COMMENT
This is the "fit fraction" from the Dalitz-plot analysis.			
5.0 ± 0.6 ± 1.0		AUBERT	07Bj BABR Dalitz fit, 45k events

$\Gamma(\rho(1700)^- \pi^+, \rho^- \rightarrow \pi^- \pi^0) / \Gamma(\pi^+ \pi^- \pi^0)$		$\Gamma_{134} / \Gamma_{125}$	
VALUE (units 10 ⁻²)	EVTS	DOCUMENT ID	TECN COMMENT
This is the "fit fraction" from the Dalitz-plot analysis.			
3.2 ± 0.4 ± 0.6		AUBERT	07Bj BABR Dalitz fit, 45k events

$\Gamma(f_0(980) \pi^0, f_0 \rightarrow \pi^+ \pi^-) / \Gamma(\pi^+ \pi^- \pi^0)$		$\Gamma_{135} / \Gamma_{125}$	
VALUE (units 10 ⁻²)	EVTS	DOCUMENT ID	TECN COMMENT
This is the "fit fraction" from the Dalitz-plot analysis.			
0.25 ± 0.04 ± 0.04		AUBERT	07Bj BABR Dalitz fit, 45k events

$\Gamma(f_0(500) \pi^0, f_0 \rightarrow \pi^+ \pi^-) / \Gamma(\pi^+ \pi^- \pi^0)$		$\Gamma_{136} / \Gamma_{125}$	
VALUE (units 10 ⁻²)	EVTS	DOCUMENT ID	TECN COMMENT
The $f_0(500)$ is the σ . This is the "fit fraction" from the Dalitz-plot analysis.			
0.82 ± 0.10 ± 0.10		AUBERT	07Bj BABR Dalitz fit, 45k events

$\Gamma(f_0(1370) \pi^0, f_0 \rightarrow \pi^+ \pi^-) / \Gamma(\pi^+ \pi^- \pi^0)$		$\Gamma_{137} / \Gamma_{125}$	
VALUE (units 10 ⁻²)	EVTS	DOCUMENT ID	TECN COMMENT
This is the "fit fraction" from the Dalitz-plot analysis.			
0.37 ± 0.11 ± 0.09		AUBERT	07Bj BABR Dalitz fit, 45k events

$\Gamma(f_0(1500) \pi^0, f_0 \rightarrow \pi^+ \pi^-) / \Gamma(\pi^+ \pi^- \pi^0)$		$\Gamma_{138} / \Gamma_{125}$	
VALUE (units 10 ⁻²)	EVTS	DOCUMENT ID	TECN COMMENT
This is the "fit fraction" from the Dalitz-plot analysis.			
0.39 ± 0.08 ± 0.07		AUBERT	07Bj BABR Dalitz fit, 45k events

$\Gamma(f_0(1710) \pi^0, f_0 \rightarrow \pi^+ \pi^-) / \Gamma(\pi^+ \pi^- \pi^0)$		$\Gamma_{139} / \Gamma_{125}$	
VALUE (units 10 ⁻²)	EVTS	DOCUMENT ID	TECN COMMENT
This is the "fit fraction" from the Dalitz-plot analysis.			
0.31 ± 0.07 ± 0.08		AUBERT	07Bj BABR Dalitz fit, 45k events

$\Gamma(f_2(1270) \pi^0, f_2 \rightarrow \pi^+ \pi^-) / \Gamma(\pi^+ \pi^- \pi^0)$		$\Gamma_{140} / \Gamma_{125}$	
VALUE (units 10 ⁻²)	EVTS	DOCUMENT ID	TECN COMMENT
This is the "fit fraction" from the Dalitz-plot analysis.			
1.32 ± 0.08 ± 0.10		AUBERT	07Bj BABR Dalitz fit, 45k events

$\Gamma(\pi^+ \pi^- \pi^0 \text{ nonresonant}) / \Gamma(\pi^+ \pi^- \pi^0)$		$\Gamma_{141} / \Gamma_{125}$	
VALUE (units 10 ⁻²)	EVTS	DOCUMENT ID	TECN COMMENT
This is the "fit fraction" from the Dalitz-plot analysis.			
0.84 ± 0.21 ± 0.12		AUBERT	07Bj BABR Dalitz fit, 45k events

$\Gamma(3\pi^0) / \Gamma_{total}$		Γ_{142} / Γ	
VALUE (units 10 ⁻⁴)	CL% EVTS	DOCUMENT ID	TECN COMMENT
2.0 ± 0.4 ± 0.3	60	1 ABLIKIM	18x BES3 $e^+ e^-$, 3773 MeV
• • • We do not use the following data for averages, fits, limits, etc. • • •			
<3.5	90	RUBIN	06 CLEO $e^+ e^-$ at $\psi(3770)$
1 Significance of signal reported by ABLIKIM 18x is 4.8 σ .			

$\Gamma(2\pi^+ 2\pi^-) / \Gamma(K^- \pi^+)$		$\Gamma_{143} / \Gamma_{35}$	
VALUE (units 10 ⁻²)	EVTS	DOCUMENT ID	TECN COMMENT
19.1 ± 0.5 OUR FIT			
19.1 ± 0.4 ± 0.6	7331 ± 130	RUBIN	06 CLEO $e^+ e^-$ at $\psi(3770)$

$\Gamma(2\pi^+ 2\pi^-) / \Gamma(K^- 2\pi^+ \pi^-)$		$\Gamma_{143} / \Gamma_{70}$	
VALUE (units 10 ⁻²)	EVTS	DOCUMENT ID	TECN COMMENT
9.19 ± 0.22 OUR FIT			
9.20 ± 0.26 OUR AVERAGE			
9.14 ± 0.18 ± 0.22	6360 ± 115	LINK	07A FOCS γ Be, $\bar{E}_\gamma \approx 180$ GeV
7.9 ± 1.8 ± 0.5	162	ABLIKIM	05F BES $e^+ e^- \approx \psi(3770)$
9.5 ± 0.7 ± 0.2	814	FRABETTI	95c E687 γ Be, $\bar{E}_\gamma \approx 200$ GeV
10.2 ± 1.3	345	AMMAR	91 CLEO $e^+ e^- \approx 10.5$ GeV

Meson Particle Listings

 D^0

• • • We do not use the following data for averages, fits, limits, etc. • • •

11.5 ± 2.3 ± 1.6	64	ADAMOVICH	92	OMEG	π^-	340	GeV
10.8 ± 2.4 ± 0.8	79	FRABETTI	92	E687	γ	Be	
9.6 ± 1.8 ± 0.7	66	ANJOS	91	E691	γ	Be	80–240 GeV

$\Gamma(a_1(1260)^+\pi^-, a_1^+ \rightarrow 2\pi^+\pi^- \text{ total})/\Gamma(2\pi^+2\pi^-)$ $\Gamma_{144}/\Gamma_{143}$

This is the fit fraction from the coherent amplitude analysis.

VALUE (units 10^{-2})	DOCUMENT ID	TECN	COMMENT
60.0 ± 3.0 ± 2.4	LINK	07A	FOCS 4-body fit, \approx 5.7k evts

$\Gamma(a_1(1260)^+\pi^-, a_1^+ \rightarrow \rho^0\pi^+ S\text{-wave})/\Gamma(2\pi^+2\pi^-)$ $\Gamma_{145}/\Gamma_{143}$

This is the fit fraction from the coherent amplitude analysis.

VALUE (units 10^{-2})	DOCUMENT ID	TECN	COMMENT
41.5 ± 2.5 OUR AVERAGE			
38.1 ± 2.3 ± 3.6	¹ DARGENT	17	4-body fit, 7.3k 4 π evts
43.3 ± 2.5 ± 1.9	LINK	07A	FOCS 4-body fit, \approx 5.7k evts

¹ Obtained by analyzing CLEO-c data but not authored by the CLEO Collaboration.

$\Gamma(a_1(1260)^+\pi^-, a_1^+ \rightarrow \rho^0\pi^+ D\text{-wave})/\Gamma(2\pi^+2\pi^-)$ $\Gamma_{146}/\Gamma_{143}$

This is the fit fraction from the coherent amplitude analysis.

VALUE (units 10^{-2})	DOCUMENT ID	TECN	COMMENT
2.5 ± 0.5 ± 0.4	¹ LINK	07A	FOCS 4-body fit, \approx 5.7k evts

¹ DARGENT 17 using 7.3k events find this contribution negligible.

$\Gamma(a_1(1260)^+\pi^-, a_1^+ \rightarrow \sigma\pi^+)/\Gamma(2\pi^+2\pi^-)$ $\Gamma_{147}/\Gamma_{143}$

This is the fit fraction from the coherent amplitude analysis.

VALUE (units 10^{-2})	DOCUMENT ID	TECN	COMMENT
8.4 ± 0.9 OUR AVERAGE			
10.2 ± 1.4 ± 3.3	¹ DARGENT	17	7.3k 4-body fit, 4 π evts
8.3 ± 0.7 ± 0.6	LINK	07A	FOCS 4-body fit, \approx 5.7k evts

¹ Obtained by analyzing CLEO-c data but not authored by the CLEO Collaboration.

$\Gamma(a_1(1260)^-\pi^+, a_1^- \rightarrow \rho^0\pi^- S\text{-wave})/\Gamma(2\pi^+2\pi^-)$ $\Gamma_{148}/\Gamma_{143}$

This is the fit fraction from a coherent amplitude analysis.

VALUE (units 10^{-2})	EVTS	DOCUMENT ID	COMMENT
3.1 ± 0.6 ± 1.0	7.3k	¹ DARGENT	17 4-body fit, 4 π evts

¹ Obtained by analyzing CLEO-c data but not authored by the CLEO Collaboration.

$\Gamma(a_1(1260)^-\pi^+, a_1^- \rightarrow \sigma\pi^-)/\Gamma(2\pi^+2\pi^-)$ $\Gamma_{149}/\Gamma_{143}$

This is the fit fraction from a coherent amplitude analysis.

VALUE (units 10^{-2})	EVTS	DOCUMENT ID	COMMENT
0.8 ± 0.2 ± 0.4	7.3k	¹ DARGENT	17 4-body fit, 4 π evts

¹ Obtained by analyzing CLEO-c data but not authored by the CLEO Collaboration.

$\Gamma(\pi(1300)^+\pi^-, \pi(1300)^+ \rightarrow \sigma\pi^+)/\Gamma(2\pi^+2\pi^-)$ $\Gamma_{150}/\Gamma_{143}$

This is the fit fraction from a coherent amplitude analysis.

VALUE (units 10^{-2})	EVTS	DOCUMENT ID	COMMENT
6.8 ± 0.9 ± 3.4	7.3k	¹ DARGENT	17 4-body fit, 4 π evts

¹ Obtained by analyzing CLEO-c data but not authored by the CLEO Collaboration.

$\Gamma(\pi(1300)^-\pi^+, \pi(1300)^- \rightarrow \sigma\pi^-)/\Gamma(2\pi^+2\pi^-)$ $\Gamma_{151}/\Gamma_{143}$

This is the fit fraction from a coherent amplitude analysis.

VALUE (units 10^{-2})	EVTS	DOCUMENT ID	COMMENT
3.0 ± 0.6 ± 2.8	7.3k	¹ DARGENT	17 4-body fit, 4 π evts

¹ Obtained by analyzing CLEO-c data but not authored by the CLEO Collaboration.

$\Gamma(a_1(1640)^+\pi^-, a_1^+ \rightarrow \rho^0\pi^+ D\text{-wave})/\Gamma(2\pi^+2\pi^-)$ $\Gamma_{152}/\Gamma_{143}$

This is the fit fraction from a coherent amplitude analysis.

VALUE (units 10^{-2})	EVTS	DOCUMENT ID	COMMENT
4.2 ± 0.6 ± 2.0	7.3k	^{1,2} DARGENT	17 4-body fit, 4 π evts

¹ Obtained by analyzing CLEO-c data but not authored by the CLEO Collaboration.
² 4-body fit, 4 π evts

$\Gamma(a_1(1640)^+\pi^-, a_1^+ \rightarrow \sigma\pi^+)/\Gamma(2\pi^+2\pi^-)$ $\Gamma_{153}/\Gamma_{143}$

This is the fit fraction from a coherent amplitude analysis.

VALUE (units 10^{-2})	EVTS	DOCUMENT ID	COMMENT
2.4 ± 0.7 ± 1.7	7.3k	¹ DARGENT	17 4-body fit, 4 π evts

¹ Obtained by analyzing CLEO-c data but not authored by the CLEO Collaboration.

$\Gamma(\pi_2(1670)^+\pi^-, \pi_2^+ \rightarrow f_2(1270)^0\pi^+, f_2^0 \rightarrow \pi^+\pi^-)/\Gamma(2\pi^+2\pi^-)$ $\Gamma_{154}/\Gamma_{143}$

This is the fit fraction from a coherent amplitude analysis.

VALUE (units 10^{-2})	EVTS	DOCUMENT ID	COMMENT
2.7 ± 0.6 ± 1.1	7.3k	¹ DARGENT	17 4-body fit, 4 π evts

¹ Obtained by analyzing CLEO-c data but not authored by the CLEO Collaboration.

$\Gamma(\pi_2(1670)^+\pi^-, \pi_2^+ \rightarrow \sigma\pi^+)/\Gamma(2\pi^+2\pi^-)$ $\Gamma_{155}/\Gamma_{143}$

This is the fit fraction from a coherent amplitude analysis.

VALUE (units 10^{-2})	EVTS	DOCUMENT ID	COMMENT
3.5 ± 0.6 ± 1.2	7.3k	¹ DARGENT	17 4-body fit, 4 π evts

¹ Obtained by analyzing CLEO-c data but not authored by the CLEO Collaboration.

$\Gamma(2\rho^0 \text{ total})/\Gamma(2\pi^+2\pi^-)$ $\Gamma_{156}/\Gamma_{143}$

This is the fit fraction from the coherent amplitude analysis.

VALUE (units 10^{-2})	DOCUMENT ID	TECN	COMMENT
24.5 ± 1.3 ± 1.0	LINK	07A	FOCS 4-body fit, \approx 5.7k evts

$\Gamma(2\rho^0, \text{ parallel helicities})/\Gamma(2\pi^+2\pi^-)$ $\Gamma_{157}/\Gamma_{143}$

This is the fit fraction from the coherent amplitude analysis.

VALUE (units 10^{-2})	DOCUMENT ID	TECN	COMMENT
1.1 ± 0.3 ± 0.3	LINK	07A	FOCS 4-body fit, \approx 5.7k evts

$\Gamma(2\rho^0, \text{ perpendicular helicities})/\Gamma(2\pi^+2\pi^-)$ $\Gamma_{158}/\Gamma_{143}$

This is the fit fraction from the coherent amplitude analysis.

VALUE (units 10^{-2})	DOCUMENT ID	TECN	COMMENT
6.4 ± 0.6 ± 0.5	LINK	07A	FOCS 4-body fit, \approx 5.7k evts

$\Gamma(2\rho^0, \text{ longitudinal helicities})/\Gamma(2\pi^+2\pi^-)$ $\Gamma_{159}/\Gamma_{143}$

This is the fit fraction from the coherent amplitude analysis.

VALUE (units 10^{-2})	DOCUMENT ID	TECN	COMMENT
16.8 ± 1.0 ± 0.8	LINK	07A	FOCS 4-body fit, \approx 5.7k evts

$\Gamma(2\rho(770)^0, S\text{-wave})/\Gamma(2\pi^+2\pi^-)$ $\Gamma_{160}/\Gamma_{143}$

This is the fit fraction from a coherent amplitude analysis.

VALUE (units 10^{-2})	EVTS	DOCUMENT ID	COMMENT
2.4 ± 0.7 ± 1.5	7.3k	¹ DARGENT	17 4-body fit, 4 π evts

¹ Obtained by analyzing CLEO-c data but not authored by the CLEO Collaboration.

$\Gamma(2\rho(770)^0, P\text{-wave})/\Gamma(2\pi^+2\pi^-)$ $\Gamma_{161}/\Gamma_{143}$

This is the fit fraction from a coherent amplitude analysis.

VALUE (units 10^{-2})	EVTS	DOCUMENT ID	COMMENT
7.0 ± 0.5 ± 1.6	7.3k	¹ DARGENT	17 4-body fit, 4 π evts

¹ Obtained by analyzing CLEO-c data but not authored by the CLEO Collaboration.

$\Gamma(2\rho(770)^0, D\text{-wave})/\Gamma(2\pi^+2\pi^-)$ $\Gamma_{162}/\Gamma_{143}$

This is the fit fraction from a coherent amplitude analysis.

VALUE (units 10^{-2})	EVTS	DOCUMENT ID	COMMENT
8.2 ± 1.0 ± 3.9	7.3k	¹ DARGENT	17 4-body fit, 4 π evts

¹ Obtained by analyzing CLEO-c data but not authored by the CLEO Collaboration.

$\Gamma(\text{Resonant } (\pi^+\pi^-)\pi^+\pi^- \text{ 3-body total})/\Gamma(2\pi^+2\pi^-)$ $\Gamma_{163}/\Gamma_{143}$

This is the fit fraction from the coherent amplitude analysis.

VALUE (units 10^{-2})	DOCUMENT ID	TECN	COMMENT
20.0 ± 1.2 ± 1.0	LINK	07A	FOCS 4-body fit, \approx 5.7k evts

$\Gamma(\sigma\pi^+\pi^-)/\Gamma(2\pi^+2\pi^-)$ $\Gamma_{164}/\Gamma_{143}$

This is the fit fraction from the coherent amplitude analysis.

VALUE (units 10^{-2})	DOCUMENT ID	TECN	COMMENT
8.2 ± 0.9 ± 0.7	LINK	07A	FOCS 4-body fit, \approx 5.7k evts

$\Gamma(\sigma\rho(770)^0)/\Gamma(2\pi^+2\pi^-)$ $\Gamma_{165}/\Gamma_{143}$

This is the fit fraction from a coherent amplitude analysis.

VALUE (units 10^{-2})	EVTS	DOCUMENT ID	COMMENT
6.6 ± 1.0 ± 3.2	7.3k	¹ DARGENT	17 4-body fit, 4 π evts

¹ Obtained by analyzing CLEO-c data but not authored by the CLEO Collaboration.

$\Gamma(f_0(1370)\sigma, f_0 \rightarrow \pi^+\pi^-)/\Gamma(2\pi^+2\pi^-)$ $\Gamma_{169}/\Gamma_{143}$

This is the fit fraction from a coherent amplitude analysis.

VALUE (units 10^{-2})	EVTS	DOCUMENT ID	COMMENT
21.2 ± 1.8 ± 6.7	7.3k	¹ DARGENT	17 4-body fit, 4 π evts

¹ Obtained by analyzing CLEO-c data but not authored by the CLEO Collaboration.

$\Gamma(f_0(980)\pi^+\pi^-, f_0 \rightarrow \pi^+\pi^-)/\Gamma(2\pi^+2\pi^-)$ $\Gamma_{166}/\Gamma_{143}$

This is the fit fraction from the coherent amplitude analysis.

VALUE (units 10^{-2})	DOCUMENT ID	TECN	COMMENT
2.4 ± 0.5 ± 0.4	LINK	07A	FOCS 4-body fit, \approx 5.7k evts

$\Gamma(f_2(1270)\pi^+\pi^-, f_2 \rightarrow \pi^+\pi^-)/\Gamma(2\pi^+2\pi^-)$ $\Gamma_{167}/\Gamma_{143}$

This is the fit fraction from the coherent amplitude analysis.

VALUE (units 10^{-2})	DOCUMENT ID	TECN	COMMENT
4.9 ± 0.6 ± 0.5	LINK	07A	FOCS 4-body fit, \approx 5.7k evts

$\Gamma(2f_2(1270), f_2 \rightarrow \pi^+\pi^-)/\Gamma(2\pi^+2\pi^-)$ $\Gamma_{168}/\Gamma_{143}$

This is the fit fraction from a coherent amplitude analysis.

VALUE (units 10^{-2})	EVTS	DOCUMENT ID	COMMENT
2.1 ± 0.5 ± 2.3	7.3k	¹ DARGENT	17 4-body fit, 4 π evts

¹ Obtained by analyzing CLEO-c data but not authored by the CLEO Collaboration.

$\Gamma(\pi^+\pi^-2\pi^0)/\Gamma(K^-\pi^+)$ Γ_{170}/Γ_{35}

VALUE (units 10^{-2})	EVTS	DOCUMENT ID	TECN	COMMENT
25.8 ± 1.5 ± 1.8	2724 ± 166	RUBIN	06	CLEO e^+e^- at $\psi(3770)$

$\Gamma(\eta\pi^0)/\Gamma_{\text{total}}$ Γ_{171}/Γ

Unseen decay modes of the η are included.

VALUE (units 10^{-4})	EVTS	DOCUMENT ID	TECN	COMMENT
6.3 ± 0.6 OUR FIT				Error includes scale factor of 1.1.
5.8 ± 0.5 ± 0.5	1.7k	ABLIKIM	18L	BES3 e^+e^- , 3773 MeV

• • • We do not use the following data for averages, fits, limits, etc. • • •
 6.5 ± 0.9 ± 0.4 75 ABLIKIM 16D BES3 See ABLIKIM 18L
 6.4 ± 1.0 ± 0.4 156 ± 24 ARTUSO 08 CLEO See MENDEZ 10

Γ(ηπ⁰)/Γ(K⁻π⁺) **Γ₁₇₁/Γ₃₅**
 Unseen decay modes of the η are included.

VALUE (units 10 ⁻²)	EVTS	DOCUMENT ID	TECN	COMMENT
1.47 ± 0.34 ± 0.11	62 ± 14	RUBIN	06	CLEO See ARTUSO 08

• • • We do not use the following data for averages, fits, limits, etc. • • •

Γ(ηπ⁰)/[Γ(K⁻π⁺) + Γ(K⁺π⁻)] **Γ₁₇₁/(Γ₃₅+Γ₂₅₆)**
 Unseen decay modes of the η are included.

VALUE (units 10 ⁻²)	EVTS	DOCUMENT ID	TECN	COMMENT
1.60 ± 0.14 OUR FIT	Error includes scale factor of 1.1.			
1.74 ± 0.15 ± 0.11	481 ± 40	MENDEZ	10	CLEO e ⁺ e ⁻ at 3774 MeV

Γ(ωπ⁰)/Γ_{total} **Γ₁₇₂/Γ**
 Unseen decay modes of the ω are included.

VALUE (units 10 ⁻⁴)	EVTS	DOCUMENT ID	TECN	COMMENT
1.17 ± 0.34 ± 0.07	45	ABLIKIM	16D	BES3 e ⁺ e ⁻ , 3773 MeV

Γ(2π⁺2π⁻π⁰)/Γ(K⁻π⁺) **Γ₁₇₄/Γ₃₅**

VALUE (units 10 ⁻²)	EVTS	DOCUMENT ID	TECN	COMMENT
10.7 ± 1.2 ± 0.5	1614 ± 171	RUBIN	06	CLEO e ⁺ e ⁻ at ψ(3770)

Γ(ηπ⁺π⁻)/Γ_{total} **Γ₁₇₅/Γ**
 Unseen decay modes of the η are included.

VALUE (units 10 ⁻⁴)	EVTS	DOCUMENT ID	TECN	COMMENT
10.9 ± 1.3 ± 0.9	257	ARTUSO	08	CLEO e ⁺ e ⁻ at ψ(3770)

Γ(η2π⁰)/Γ_{total} **Γ₁₇₇/Γ**

VALUE (units 10 ⁻⁴)	EVTS	DOCUMENT ID	TECN	COMMENT
3.8 ± 1.1 ± 0.7	42	ABLIKIM	18x	BES3 e ⁺ e ⁻ , 3773 MeV

¹ Significance of signal reported by ABLIKIM 18x is 3.8σ.

Γ(ωη)/Γ_{total} **Γ₁₇₃/Γ**

VALUE (units 10 ⁻³)	EVTS	DOCUMENT ID	TECN	COMMENT
1.98 ± 0.18 OUR AVERAGE	Error includes scale factor of 1.1.			
2.15 ± 0.17 ± 0.15	2.2k	ABLIKIM	18L	BES3 e ⁺ e ⁻ , 3773 MeV
1.78 ± 0.19 ± 0.15	600	SMITH	18	e ⁺ e ⁻ , 3773 MeV

¹ Obtained by analyzing CLEO-c data but not authored by the CLEO Collaboration.

Γ(ωπ⁺π⁻)/Γ(K⁻π⁺) **Γ₁₇₆/Γ₃₅**
 Unseen decay modes of the ω are included.

VALUE (units 10 ⁻²)	EVTS	DOCUMENT ID	TECN	COMMENT
4.1 ± 1.2 ± 0.4	472 ± 132	RUBIN	06	CLEO e ⁺ e ⁻ at ψ(3770)

Γ(3π⁺3π⁻)/Γ(K⁻2π⁺π⁻) **Γ₁₇₈/Γ₇₀**

VALUE (units 10 ⁻³)	EVTS	DOCUMENT ID	TECN	COMMENT
5.23 ± 0.59 ± 1.35	149 ± 17	LINK	04B	FOCS γA, E _γ ≈ 180 GeV

Γ(3π⁺3π⁻)/Γ(K⁻3π⁺2π⁻) **Γ₁₇₈/Γ₉₈**

VALUE	DOCUMENT ID	TECN	COMMENT
1.93 ± 0.47 ± 0.48	LINK	04B	FOCS γA, E _γ ≈ 180 GeV

¹ This LINK 04B result is not independent of other results in these Listings.

Γ(η'(958)π⁰)/Γ_{total} **Γ₁₇₉/Γ**
 Unseen decay modes of the η'(958) are included.

VALUE (units 10 ⁻⁴)	EVTS	DOCUMENT ID	TECN	COMMENT
9.2 ± 1.0 OUR FIT				
9.3 ± 1.1 ± 0.9	469 ± 56	ABLIKIM	18L	BES3 e ⁺ e ⁻ , 3773 MeV

• • • We do not use the following data for averages, fits, limits, etc. • • •

8.1 ± 1.5 ± 0.6	50 ± 9	ARTUSO	08	CLEO See MENDEZ 10
-----------------	--------	--------	----	--------------------

Γ(η'(958)π⁰)/[Γ(K⁻π⁺) + Γ(K⁺π⁻)] **Γ₁₇₉/(Γ₃₅+Γ₂₅₆)**
 Unseen decay modes of the η'(958) are included.

VALUE (units 10 ⁻²)	EVTS	DOCUMENT ID	TECN	COMMENT
2.32 ± 0.25 OUR FIT				
2.3 ± 0.3 ± 0.2	159 ± 19	MENDEZ	10	CLEO e ⁺ e ⁻ at 3774 MeV

Γ(η'(958)π⁺π⁻)/Γ_{total} **Γ₁₈₀/Γ**
 Unseen decay modes of the η'(958) are included.

VALUE (units 10 ⁻⁴)	EVTS	DOCUMENT ID	TECN	COMMENT
4.5 ± 1.6 ± 0.5	21 ± 8	ARTUSO	08	CLEO e ⁺ e ⁻ at ψ(3770)

Γ(2η)/Γ_{total} **Γ₁₈₁/Γ**
 Unseen decay modes of the η are included.

VALUE (units 10 ⁻⁴)	EVTS	DOCUMENT ID	TECN	COMMENT
21.1 ± 1.9 OUR FIT	Error includes scale factor of 2.2.			
22.0 ± 0.7 ± 0.6	3.4k	ABLIKIM	18L	BES3 e ⁺ e ⁻ , 3773 MeV

• • • We do not use the following data for averages, fits, limits, etc. • • •

16.7 ± 1.4 ± 1.3	255 ± 22	ARTUSO	08	CLEO See MENDEZ 10
------------------	----------	--------	----	--------------------

Γ(2η)/[Γ(K⁻π⁺) + Γ(K⁺π⁻)] **Γ₁₈₁/(Γ₃₅+Γ₂₅₆)**
 Unseen decay modes of the η are included.

VALUE (units 10 ⁻²)	EVTS	DOCUMENT ID	TECN	COMMENT
5.3 ± 0.5 OUR FIT	Error includes scale factor of 2.2.			
4.3 ± 0.3 ± 0.4	430 ± 29	MENDEZ	10	CLEO e ⁺ e ⁻ at 3774 MeV

Γ(2ηπ⁰)/Γ_{total} **Γ₁₈₂/Γ**

VALUE (units 10 ⁻⁴)	EVTS	DOCUMENT ID	TECN	COMMENT
7.3 ± 1.6 ± 1.5	27	ABLIKIM	18x	BES3 e ⁺ e ⁻ , 3773 MeV

¹ Significance of signal reported by ABLIKIM 18x is 5.5σ.

Γ(3η)/Γ_{total} **Γ₁₈₃/Γ**

VALUE	CL%	DOCUMENT ID	TECN	COMMENT
<1.3 × 10 ⁻⁴	90	ABLIKIM	18x	BES3 e ⁺ e ⁻ , 3773 MeV

Γ(ηη'(958))/Γ_{total} **Γ₁₈₄/Γ**
 Unseen decay modes of the η and η'(958) are included.

VALUE (units 10 ⁻⁴)	EVTS	DOCUMENT ID	TECN	COMMENT
10.1 ± 1.9 OUR FIT				
9.4 ± 2.5 ± 1.1	158 ± 41	ABLIKIM	18L	BES3 e ⁺ e ⁻ , 3773 MeV

• • • We do not use the following data for averages, fits, limits, etc. • • •

12.6 ± 2.5 ± 1.1	46 ± 9	ARTUSO	08	CLEO See MENDEZ 10
------------------	--------	--------	----	--------------------

Γ(ηη'(958))/[Γ(K⁻π⁺) + Γ(K⁺π⁻)] **Γ₁₈₄/(Γ₃₅+Γ₂₅₆)**
 Unseen decay modes of the η and η'(958) are included.

VALUE (units 10 ⁻²)	EVTS	DOCUMENT ID	TECN	COMMENT
2.5 ± 0.5 OUR FIT				
2.7 ± 0.6 ± 0.3	66 ± 15	MENDEZ	10	CLEO e ⁺ e ⁻ at 3774 MeV

Hadronic modes with a K⁺K⁻ pair

Γ(K⁺K⁻)/Γ_{total} **Γ₁₈₅/Γ**

VALUE (units 10 ⁻³)	EVTS	DOCUMENT ID	TECN	COMMENT
4.08 ± 0.06 OUR FIT	Error includes scale factor of 1.6.			
4.233 ± 0.021 ± 0.064	56k	ABLIKIM	18w	BES3 e ⁺ e ⁻ , 3773 MeV

• • • We do not use the following data for averages, fits, limits, etc. • • •

4.08 ± 0.08 ± 0.09	4.7k	BONVICINI	08	CLEO See MENDEZ 10
--------------------	------	-----------	----	--------------------

Γ(K⁺K⁻)/Γ(K⁻π⁺) **Γ₁₈₅/Γ₃₅**

VALUE	EVTS	DOCUMENT ID	TECN	COMMENT
0.1033 ± 0.0013 OUR FIT	Error includes scale factor of 1.6.			
0.1010 ± 0.0016 OUR AVERAGE	Error includes scale factor of 1.4. See the ideogram below.			

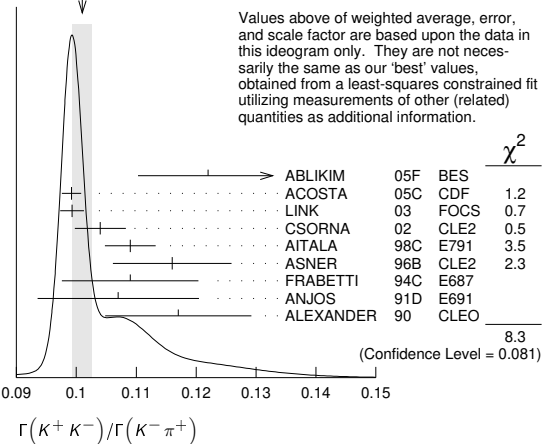
0.122 ± 0.011 ± 0.004	242 ± 20	ABLIKIM	05F	BES e ⁺ e ⁻ ≈ ψ(3770)
0.0992 ± 0.0011 ± 0.0012	16k ± 200	ACOSTA	05c	CDF p \bar{p} , √s=1.96 TeV
0.0993 ± 0.0014 ± 0.0014	11k	LINK	03	FOCS γ nucleus, E _γ ≈ 180 GeV

0.1040 ± 0.0033 ± 0.0027	1900	CSORNA	02	CLE2 e ⁺ e ⁻ ≈ γ(4S)
0.109 ± 0.003 ± 0.003	3317	AITALA	98c	E791 π ⁻ nucleus, 500 GeV
0.116 ± 0.007 ± 0.007	1102	ASNER	96B	CLE2 e ⁺ e ⁻ ≈ γ(4S)
0.109 ± 0.007 ± 0.009	581	FRABETTI	94c	E687 γBe E _γ = 220 GeV
0.107 ± 0.010 ± 0.009	193	ANJOS	91D	E691 Photoproduction
0.117 ± 0.010 ± 0.007	249	ALEXANDER	90	CLEO e ⁺ e ⁻ 10.5–11 GeV

• • • We do not use the following data for averages, fits, limits, etc. • • •

0.107 ± 0.029 ± 0.015	103	ADAMOVICH	92	OMEG π ⁻ 340 GeV
0.138 ± 0.027 ± 0.010	155	FRABETTI	92	E687 γBe
0.16 ± 0.05	34	ALVAREZ	91B	NA14 Photoproduction
0.10 ± 0.02 ± 0.01	131	ALBRECHT	90c	ARG e ⁺ e ⁻ ≈ 10 GeV
0.122 ± 0.018 ± 0.012	118	BALTRUSAITIS	85E	MRK3 e ⁺ e ⁻ 3.77 GeV
0.113 ± 0.030		ABRAMS	79D	MRK2 e ⁺ e ⁻ 3.77 GeV

WEIGHTED AVERAGE
 0.1010 ± 0.0016 (Error scaled by 1.4)



Meson Particle Listings

 D^0

$$\Gamma(K^+K^-)/[\Gamma(K^-\pi^+) + \Gamma(K^+\pi^-)] \quad \Gamma_{185}/(\Gamma_{35} + \Gamma_{256})$$

VALUE (units 10^{-2})	EVTS	DOCUMENT ID	TECN	COMMENT
10.29 ± 0.13 OUR FIT	Error includes scale factor of 1.6.			
10.41 ± 0.11 ± 0.12	13.8k	MENDEZ	10	CLEO e^+e^- at 3774 MeV

$$\Gamma(K^+K^-)/\Gamma(\pi^+\pi^-) \quad \Gamma_{185}/\Gamma_{123}$$

The unused results here are redundant with $\Gamma(K^+K^-)/\Gamma(K^-\pi^+) + \Gamma(\pi^+\pi^-)/\Gamma(K^-\pi^+)$ measurements by the same experiments.

VALUE	EVTS	DOCUMENT ID	TECN	COMMENT
• • • We do not use the following data for averages, fits, limits, etc. • • •				
2.760 ± 0.040 ± 0.034	7334	ACOSTA	05c	CDF $p\bar{p}$, $\sqrt{s}=1.96$ TeV
2.81 ± 0.10 ± 0.06		LINK	03	FOCS γ nucleus, $\bar{E}_\gamma \approx 180$ GeV
2.96 ± 0.16 ± 0.15	710	CSORNA	02	CLE2 $e^+e^- \approx \Upsilon(4S)$
2.75 ± 0.15 ± 0.16		AITALA	98c	E791 π^- nucleus, 500 GeV
2.53 ± 0.46 ± 0.19		FRABETTI	94c	E687 γ Be $\bar{E}_\gamma = 220$ GeV
2.23 ± 0.81 ± 0.46		ADAMOVICH	92	OMEG π^- 340 GeV
1.95 ± 0.34 ± 0.22		ANJOS	91d	E691 Photoproduction
2.5 ± 0.7		ALBRECHT	90c	ARG $e^+e^- \approx 10$ GeV
2.35 ± 0.37 ± 0.28		ALEXANDER	90	CLEO e^+e^- 10.5–11 GeV

$$\Gamma(2K_S^0)/\Gamma_{\text{total}} \quad \Gamma_{186}/\Gamma$$

VALUE (units 10^{-4})	EVTS	DOCUMENT ID	TECN	COMMENT
1.41 ± 0.05 OUR FIT	Error includes scale factor of 1.1.			
1.67 ± 0.11 ± 0.11	576	ABLIKIM	17A	BES3 $e^+e^- \rightarrow \psi(3770)$
• • • We do not use the following data for averages, fits, limits, etc. • • •				
1.46 ± 0.32 ± 0.09	68 ± 15	BONVICINI	08	CLEO See MENDEZ 10

$$\Gamma(2K_S^0)/[\Gamma(K^-\pi^+) + \Gamma(K^+\pi^-)] \quad \Gamma_{186}/(\Gamma_{35} + \Gamma_{256})$$

VALUE (units 10^{-2})	EVTS	DOCUMENT ID	TECN	COMMENT
0.357 ± 0.013 OUR FIT	Error includes scale factor of 1.1.			
0.41 ± 0.04 ± 0.02	215 ± 23	MENDEZ	10	CLEO e^+e^- at 3774 MeV

$$\Gamma(2K_S^0)/\Gamma(K_S^0\pi^+\pi^-) \quad \Gamma_{186}/\Gamma_{38}$$

This is the same as $\Gamma(K^0\bar{K}^0)/\Gamma(\bar{K}^0\pi^+\pi^-)$ because $D^0 \rightarrow K_S^0 K_L^0$ is forbidden by CP conservation.

VALUE (units 10^{-2})	EVTS	DOCUMENT ID	TECN	COMMENT
0.506 ± 0.034 OUR FIT				
1.20 ± 0.22 OUR AVERAGE				
1.44 ± 0.32 ± 0.16	79 ± 17	LINK	05A	FOCS γ Be, $\bar{E}_\gamma \approx 180$ GeV
1.01 ± 0.22 ± 0.16	26	ASNER	96B	CLE2 $e^+e^- \approx \Upsilon(4S)$
3.9 ± 1.3 ± 1.3	20 ± 7	FRABETTI	94J	E687 γ Be $\bar{E}_\gamma = 220$ GeV
• • • We do not use the following data for averages, fits, limits, etc. • • •				
2.1 $^{+1.1}_{-0.8}$ ± 0.2	5	ALEXANDER	90	CLEO e^+e^- 10.5–11 GeV

$$\Gamma(2K_S^0)/\Gamma(K_S^0\pi^0) \quad \Gamma_{186}/\Gamma_{36}$$

VALUE (units 10^{-2})	EVTS	DOCUMENT ID	TECN	COMMENT
1.14 ± 0.04 OUR FIT	Error includes scale factor of 1.1.			
1.101 ± 0.023 ± 0.030	4.8k	DASH	17	BELL At/near $\Upsilon(4S)$, $\Upsilon(5S)$

$$\Gamma(K_S^0 K^- \pi^+)/\Gamma(K^- \pi^+) \quad \Gamma_{187}/\Gamma_{35}$$

VALUE	DOCUMENT ID	TECN	COMMENT
0.084 ± 0.013 OUR FIT	Error includes scale factor of 1.1.		
0.08 ± 0.03	¹ ANJOS	91	E691 γ Be 80–240 GeV

¹ The factor 100 at the top of column 2 of Table I of ANJOS 91 should be omitted.

$$\Gamma(\phi\pi^0)/\Gamma_{\text{total}} \quad \Gamma_{247}/\Gamma$$

VALUE (units 10^{-3})	EVTS	DOCUMENT ID	TECN	COMMENT
1.168 ± 0.028 ± 0.028	3.3k	ABLIKIM	19B1	BES3 e^+e^- at 3773 MeV

$$\Gamma(\phi\eta)/\Gamma_{\text{total}} \quad \Gamma_{248}/\Gamma$$

VALUE (units 10^{-4})	EVTS	DOCUMENT ID	TECN	COMMENT
1.81 ± 0.46 ± 0.06	102	ABLIKIM	19B1	BES3 e^+e^- at 3773 MeV

$$\Gamma(K_S^0 K^- \pi^+)/\Gamma(K_S^0 \pi^+ \pi^-) \quad \Gamma_{187}/\Gamma_{38}$$

VALUE	EVTS	DOCUMENT ID	TECN	COMMENT
0.118 ± 0.017 OUR FIT	Error includes scale factor of 1.1.			
0.119 ± 0.021 OUR AVERAGE	Error includes scale factor of 1.3.			
0.108 ± 0.019	61	AMMAR	91	CLEO $e^+e^- \approx 10.5$ GeV
0.16 ± 0.03 ± 0.02	39	ALBRECHT	90c	ARG $e^+e^- \approx 10$ GeV

$$\Gamma(K^*(892)^0 K_S^0, \bar{K}^{*0} \rightarrow K^- \pi^+)/\Gamma(K_S^0 K^- \pi^+) \quad \Gamma_{188}/\Gamma_{187}$$

Fit fraction from Dalitz plot analyses. The fraction for the $K_S^0 \pi^+$ mass between 792 and 992 MeV is $0.370 \pm 0.003 \pm 0.012$.

VALUE (units 10^{-2})	EVTS	DOCUMENT ID	TECN	COMMENT
2.47 ± 0.15 ± 0.23	113k	¹ AAIJ	16N	LHCB Dalitz plot fit

¹ AAIJ 16N gives results for two S-wave parameterisations. We take the values from the model with LASS parametrization, and the difference as a systematic uncertainty.

$$\Gamma(K^*(892)^+ K^-, K^{*+} \rightarrow K_S^0 \pi^+)/\Gamma(K_S^0 K^- \pi^+) \quad \Gamma_{189}/\Gamma_{187}$$

Fit fraction from Dalitz plot analyses.

VALUE (units 10^{-2})	EVTS	DOCUMENT ID	TECN	COMMENT
56.9 ± 0.6 ± 1.1	113k	¹ AAIJ	16N	LHCB Dalitz plot fit

¹ AAIJ 16N gives results for two S-wave parameterisations. We take the values from the model with LASS parametrization, and the difference as a systematic uncertainty.

$$\Gamma(\bar{K}^*(1410)^0 K_S^0, \bar{K}^{*0} \rightarrow K^- \pi^+)/\Gamma(K_S^0 K^- \pi^+) \quad \Gamma_{190}/\Gamma_{187}$$

Fit fraction from Dalitz plot analyses.

VALUE (units 10^{-2})	EVTS	DOCUMENT ID	TECN	COMMENT
3.8 ± 0.5 ± 5.6	113k	¹ AAIJ	16N	LHCB Dalitz plot fit

¹ AAIJ 16N gives results for two S-wave parameterisations. We take the values from the model with LASS parametrization, and the difference as a uncertainty (which in this case dominates)

$$\Gamma(K^*(1410)^+ K^-, K^{*+} \rightarrow K_S^0 \pi^+)/\Gamma(K_S^0 K^- \pi^+) \quad \Gamma_{191}/\Gamma_{187}$$

Fit fraction from Dalitz plot analyses.

VALUE (units 10^{-2})	EVTS	DOCUMENT ID	TECN	COMMENT
9.6 ± 1.1 ± 5.4	113k	¹ AAIJ	16N	LHCB Dalitz plot fit

¹ AAIJ 16N gives results for two S-wave parameterisations. We take the values from the model with LASS parametrization, and the difference as a systematic uncertainty (which in this case dominates).

$$\Gamma((K^- \pi^+)_{S\text{-wave}} K_S^0)/\Gamma(K_S^0 K^- \pi^+) \quad \Gamma_{192}/\Gamma_{187}$$

Fit fraction from Dalitz plot analyses.

VALUE (units 10^{-2})	EVTS	DOCUMENT ID	TECN	COMMENT
18 ± 2 ± 8	113k	¹ AAIJ	16N	LHCB Dalitz plot fit

¹ AAIJ 16N gives results for two S-wave parameterisations. We take the values from the model with LASS parametrization, and the difference as a systematic uncertainty (which in this case dominates).

$$\Gamma((K_S^0 \pi^+)_{S\text{-wave}} K^-)/\Gamma(K_S^0 K^- \pi^+) \quad \Gamma_{193}/\Gamma_{187}$$

Fit fraction from Dalitz plot analyses.

VALUE (units 10^{-2})	EVTS	DOCUMENT ID	TECN	COMMENT
11.7 ± 1.0 ± 2.3	113k	¹ AAIJ	16N	LHCB Dalitz plot fit

¹ AAIJ 16N gives results for two S-wave parameterisations. We take the values from the model with LASS parametrization, and the difference as a systematic uncertainty.

$$\Gamma(a_0(980)^- \pi^+, a_0^- \rightarrow K_S^0 K^-)/\Gamma(K_S^0 K^- \pi^+) \quad \Gamma_{194}/\Gamma_{187}$$

Fit fraction from Dalitz plot analyses.

VALUE (units 10^{-2})	EVTS	DOCUMENT ID	TECN	COMMENT
4.0 ± 0.7 ± 4.1	113k	¹ AAIJ	16N	LHCB Dalitz plot fit

¹ AAIJ 16N gives results for two S-wave parameterisations. We take the values from the model with LASS parametrization, and the difference as a systematic uncertainty (which in this case dominates).

$$\Gamma(a_0(1450)^- \pi^+, a_0^- \rightarrow K_S^0 K^-)/\Gamma(K_S^0 K^- \pi^+) \quad \Gamma_{195}/\Gamma_{187}$$

Fit fraction from Dalitz plot analyses.

VALUE (units 10^{-2})	EVTS	DOCUMENT ID	TECN	COMMENT
0.74 ± 0.15 ± 0.57	113k	¹ AAIJ	16N	LHCB Dalitz plot fit

¹ AAIJ 16N gives results for two S-wave parameterisations. We take the values from the model with LASS parametrization, and the difference as a systematic uncertainty (which in this case dominates).

$$\Gamma(a_2(1320)^- \pi^+, a_2^- \rightarrow K_S^0 K^-)/\Gamma(K_S^0 K^- \pi^+) \quad \Gamma_{196}/\Gamma_{187}$$

Fit fraction from Dalitz plot analyses.

VALUE (units 10^{-2})	EVTS	DOCUMENT ID	TECN	COMMENT
0.15 ± 0.06 ± 0.14	113k	¹ AAIJ	16N	LHCB Dalitz plot fit

¹ AAIJ 16N gives results for two S-wave parameterisations. We take the values from the model with LASS parametrization, and the difference as a systematic uncertainty.

$$\Gamma(\rho(1450)^- \pi^+, \rho^- \rightarrow K_S^0 K^-)/\Gamma(K_S^0 K^- \pi^+) \quad \Gamma_{197}/\Gamma_{187}$$

Fit fraction from Dalitz plot analyses.

VALUE (units 10^{-2})	EVTS	DOCUMENT ID	TECN	COMMENT
1.4 ± 0.2 ± 0.7	113k	¹ AAIJ	16N	LHCB Dalitz plot fit

¹ AAIJ 16N gives results for two S-wave parameterisations. We take the values from the model with LASS parametrization, and the difference as a systematic uncertainty.

$$\Gamma(K_S^0 K^+ \pi^-)/\Gamma(K^- \pi^+) \quad \Gamma_{198}/\Gamma_{35}$$

VALUE	DOCUMENT ID	TECN	COMMENT
• • • We do not use the following data for averages, fits, limits, etc. • • •			
0.05 ± 0.025	¹ ANJOS	91	E691 γ Be 80–240 GeV

¹ The factor 100 at the top of column 2 of Table I of ANJOS 91 should be omitted.

$$\Gamma(K_S^0 K^+ \pi^-)/\Gamma(K_S^0 \pi^+ \pi^-) \quad \Gamma_{198}/\Gamma_{38}$$

VALUE	EVTS	DOCUMENT ID	TECN	COMMENT
0.098 ± 0.020	55	AMMAR	91	CLEO $e^+e^- \approx 10.5$ GeV

$$\Gamma(K_S^0 K^+ \pi^-)/\Gamma(K_S^0 K^- \pi^+) \quad \Gamma_{198}/\Gamma_{187}$$

VALUE	EVTS	DOCUMENT ID	TECN	COMMENT
0.654 ± 0.007 OUR FIT				
0.654 ± 0.007 OUR AVERAGE				
0.655 ± 0.004 ± 0.006	76k, 113k	AAIJ	16N	LHCB $p\bar{p}$ at 7, 8 TeV
0.592 ± 0.044 ± 0.018		INSLER	12	CLEO $e^+e^- \rightarrow D^0 \bar{D}^0$ at 3.77 GeV

$\Gamma(K^*(892)^0 K_S^0, K^{*0} \rightarrow K^+ \pi^-) / \Gamma(K^*(892)^0 K_S^0, \bar{K}^{*0} \rightarrow K^- \pi^+)$
Γ₁₉₉/Γ₁₈₈

VALUE	CL%	DOCUMENT ID	TECN	COMMENT
0.356 ± 0.034 ± 0.007		¹ INSLER 12	CLEO	$e^+ e^- \rightarrow D^0 \bar{D}^0$, 3.77 GeV
• • • We do not use the following data for averages, fits, limits, etc. • • •				
<0.010	90	AMMAR 91	CLEO	$e^+ e^- \approx 10.5$ GeV
¹ Uses quantum correlations in $e^+ e^- \rightarrow D^0 \bar{D}^0$ at the $\psi(3770)$, where the signal side D decays to $K_S^0 K \pi$ and the tag-side D decays to $K \pi, K \pi \pi, K \pi \pi^0$, and 10 additional CP-even, CP-odd, and mixed CP modes involving K_S^0 or K_L^0 .				

$\Gamma(K^*(892)^0 K_S^0, K^{*0} \rightarrow K^+ \pi^-) / \Gamma(K_S^0 K^+ \pi^-)$
Fit fraction from Dalitz plot analyses.
Γ₁₉₉/Γ₁₉₈

VALUE (units 10 ⁻²)	EVTS	DOCUMENT ID	TECN	COMMENT
5.17 ± 0.21 ± 0.47	76k	¹ AAIJ 16N	LHCB	Dalitz plot fit
¹ AAIJ 16N gives results for two S-wave parameterisations. We take the values from the model with LASS parametrization, and the difference as a systematic uncertainty.				

$\Gamma(K^*(892)^- K^+, K^{*-} \rightarrow K_S^0 \pi^-) / \Gamma(K_S^0 K^+ \pi^-)$
Fit fraction from Dalitz plot analyses.
Γ₂₀₀/Γ₁₉₈

VALUE (units 10 ⁻²)	EVTS	DOCUMENT ID	TECN	COMMENT
28.8 ± 0.4 ± 1.5	76k	¹ AAIJ 16N	LHCB	Dalitz plot fit
¹ AAIJ 16N gives results for two S-wave parameterisations. We take the values from the model with LASS parametrization, and the difference as a systematic uncertainty.				

$\Gamma(K^*(1410)^0 K_S^0, K^{*0} \rightarrow K^+ \pi^+) / \Gamma(K_S^0 K^+ \pi^-)$
Fit fraction from Dalitz plot analyses.
Γ₂₀₁/Γ₁₉₈

VALUE (units 10 ⁻²)	EVTS	DOCUMENT ID	TECN	COMMENT
2.2 ± 0.6 ± 3.7	76k	¹ AAIJ 16N	LHCB	Dalitz plot fit
¹ AAIJ 16N gives results for two S-wave parameterisations. We take the values from the model with LASS parametrization, and the difference as a systematic uncertainty (which in this case dominates).				

$\Gamma(K^*(1410)^- K^+, K^{*-} \rightarrow K_S^0 \pi^-) / \Gamma(K_S^0 K^+ \pi^-)$
Fit fraction from Dalitz plot analyses.
Γ₂₀₂/Γ₁₉₈

VALUE (units 10 ⁻²)	EVTS	DOCUMENT ID	TECN	COMMENT
11.9 ± 1.5 ± 9.1	76k	¹ AAIJ 16N	LHCB	Dalitz plot fit
¹ AAIJ 16N gives results for two S-wave parameterisations. We take the values from the model with LASS parametrization, and the difference as a systematic uncertainty (which in this case dominates).				

$\Gamma((K^+ \pi^-)_{S\text{-wave}} K_S^0) / \Gamma(K_S^0 K^+ \pi^-)$
Fit fraction from Dalitz plot analyses.
Γ₂₀₃/Γ₁₉₈

VALUE (units 10 ⁻²)	EVTS	DOCUMENT ID	TECN	COMMENT
17 ± 2 ± 8	76k	¹ AAIJ 16N	LHCB	Dalitz plot fit
¹ AAIJ 16N gives results for two S-wave parameterisations. We take the values from the model with LASS parametrization, and the difference as a systematic uncertainty.				

$\Gamma((K_S^0 \pi^-)_{S\text{-wave}} K^+) / \Gamma(K_S^0 K^+ \pi^-)$
Fit fraction from Dalitz plot analyses.
Γ₂₀₄/Γ₁₉₈

VALUE (units 10 ⁻²)	EVTS	DOCUMENT ID	TECN	COMMENT
6.3 ± 0.9 ± 2.3	76k	¹ AAIJ 16N	LHCB	Dalitz plot fit
¹ AAIJ 16N gives results for two S-wave parameterisations. We take the values from the model with LASS parametrization, and the difference as a systematic uncertainty.				

$\Gamma(a_0(980)^+ \pi^-, a_0^+ \rightarrow K_S^0 K^+) / \Gamma(K_S^0 K^+ \pi^-)$
Fit fraction from Dalitz plot analyses.
Γ₂₀₅/Γ₁₉₈

VALUE (units 10 ⁻²)	EVTS	DOCUMENT ID	TECN	COMMENT
26 ± 2 ± 18	76k	¹ AAIJ 16N	LHCB	Dalitz plot fit
¹ AAIJ 16N gives results for two S-wave parameterisations. We take the values from the model with LASS parametrization, and the difference as a systematic uncertainty (which in this case dominates).				

$\Gamma(a_0(1450)^+ \pi^-, a_0^+ \rightarrow K_S^0 K^+) / \Gamma(K_S^0 K^+ \pi^-)$
Fit fraction from Dalitz plot analyses.
Γ₂₀₆/Γ₁₉₈

VALUE (units 10 ⁻²)	EVTS	DOCUMENT ID	TECN	COMMENT
1.5 ± 0.3 ± 1.1	76k	¹ AAIJ 16N	LHCB	Dalitz plot fit
¹ AAIJ 16N gives results for two S-wave parameterisations. We take the values from the model with LASS parametrization, and the difference as a systematic uncertainty (which in this case dominates).				

$\Gamma(\rho(1700)^+ \pi^-, \rho^+ \rightarrow K_S^0 K^+) / \Gamma(K_S^0 K^+ \pi^-)$
Fit fraction from Dalitz plot analyses.
Γ₂₀₇/Γ₁₉₈

VALUE (units 10 ⁻²)	EVTS	DOCUMENT ID	TECN	COMMENT
0.53 ± 0.11 ± 0.23	76k	¹ AAIJ 16N	LHCB	Dalitz plot fit
¹ AAIJ 16N gives results for two S-wave parameterisations. We take the values from the model with LASS parametrization, and the difference as a systematic uncertainty.				

$\Gamma(K^+ K^- \pi^0) / \Gamma(K^- \pi^+ \pi^0)$
Γ₂₀₈/Γ₅₃

VALUE (units 10 ⁻²)	EVTS	DOCUMENT ID	TECN	COMMENT
2.37 ± 0.03 ± 0.04	11k ± 122	AUBERT,B	06x BABR	$e^+ e^- \approx \Upsilon(4S)$
• • • We do not use the following data for averages, fits, limits, etc. • • •				
0.95 ± 0.26	151	ASNER	96B CLE2	$e^+ e^- \approx \Upsilon(4S)$

$\Gamma(K^*(892)^+ K^-, K^*(892)^+ \rightarrow K^+ \pi^0) / \Gamma(K^+ K^- \pi^0)$
This is the "fit fraction" from the Dalitz-plot analysis with interference.
Γ₂₀₉/Γ₂₀₈

VALUE (units 10 ⁻²)	DOCUMENT ID	TECN	COMMENT
44.4 ± 0.8 ± 0.6	AUBERT 07T	BABR	Dalitz fit II, 11k evts
• • • We do not use the following data for averages, fits, limits, etc. • • •			
46.1 ± 3.1	¹ CAWLFIELD 06A	CLEO	Dalitz fit, 627 ± 30 evts
¹ The error on this CAWLFIELD 06A result is statistical only.			

$\Gamma(K^*(892)^- K^+, K^*(892)^- \rightarrow K^- \pi^0) / \Gamma(K^+ K^- \pi^0)$
This is the "fit fraction" from the Dalitz-plot analysis with interference.
Γ₂₁₀/Γ₂₀₈

VALUE (units 10 ⁻²)	DOCUMENT ID	TECN	COMMENT
15.9 ± 0.7 ± 0.6	AUBERT 07T	BABR	Dalitz fit II, 11k evts
• • • We do not use the following data for averages, fits, limits, etc. • • •			
12.3 ± 2.2	¹ CAWLFIELD 06A	CLEO	Dalitz fit, 627 ± 30 evts
¹ The error on this CAWLFIELD 06A result is statistical only.			

$\Gamma((K^+ \pi^0)_{S\text{-wave}} K^-) / \Gamma(K^+ K^- \pi^0)$
This is the "fit fraction" from the Dalitz-plot analysis with interference.
Γ₂₁₁/Γ₂₀₈

VALUE (units 10 ⁻²)	DOCUMENT ID	TECN	COMMENT
71.1 ± 3.7 ± 1.9	¹ AUBERT 07T	BABR	Dalitz fit II, 11k evts
¹ The only major difference between fits I and II in the AUBERT 07T analysis is in this mode, where the fit-I fraction is (16.3 ± 3.4 ± 2.1)%.			

$\Gamma((K^- \pi^0)_{S\text{-wave}} K^+) / \Gamma(K^+ K^- \pi^0)$
This is the "fit fraction" from the Dalitz-plot analysis with interference.
Γ₂₁₂/Γ₂₀₈

VALUE (units 10 ⁻²)	DOCUMENT ID	TECN	COMMENT
3.9 ± 0.9 ± 1.0	AUBERT 07T	BABR	Dalitz fit II, 11k evts

$\Gamma(f_0(980) \pi^0, f_0 \rightarrow K^+ K^-) / \Gamma(K^+ K^- \pi^0)$
This is the "fit fraction" from the Dalitz-plot analysis with interference.
Γ₂₁₃/Γ₂₀₈

VALUE (units 10 ⁻²)	DOCUMENT ID	TECN	COMMENT
10.5 ± 1.1 ± 1.2	¹ AUBERT 07T	BABR	Dalitz fit II, 11k evts
¹ When AUBERT 07T replace the $f_0(980) \pi^0$ mode with $a_0(980) \pi^0$, the fit fraction is a negligibly different (11.0 ± 1.5 ± 1.2)%.			

$\Gamma(\phi \pi^0, \phi \rightarrow K^+ K^-) / \Gamma(K^+ K^- \pi^0)$
This is the "fit fraction" from the Dalitz-plot analysis with interference.
Γ₂₁₄/Γ₂₀₈

VALUE (units 10 ⁻²)	DOCUMENT ID	TECN	COMMENT
19.4 ± 0.6 ± 0.5	AUBERT 07T	BABR	Dalitz fit II, 11k evts
• • • We do not use the following data for averages, fits, limits, etc. • • •			
14.9 ± 1.6	¹ CAWLFIELD 06A	CLEO	Dalitz fit, 627 ± 30 evts
¹ The error on this CAWLFIELD 06A result is statistical only.			

$\Gamma(K^+ K^- \pi^0 \text{ nonresonant}) / \Gamma(K^+ K^- \pi^0)$
This is the "fit fraction" from the Dalitz-plot analysis with interference.
Γ₂₁₅/Γ₂₀₈

VALUE	DOCUMENT ID	TECN	COMMENT
0.360 ± 0.037	¹ CAWLFIELD 06A	CLEO	Dalitz fit, 627 ± 30 evts
¹ The error is statistical only. CAWLFIELD 06A also fits the Dalitz plot replacing this flat nonresonant background with broad S-wave $\kappa^\pm \rightarrow K^\pm \pi^0$ resonances. There is no significant improvement in the fit, and $K^{*+} K^\mp$ and $\phi \pi^0$ results are not much changed.			

$\Gamma(2K_S^0 \pi^0) / \Gamma_{\text{total}}$
Γ₂₁₆/Γ

VALUE	DOCUMENT ID	TECN	COMMENT
<0.00059	ASNER 96B	CLE2	$e^+ e^- \approx \Upsilon(4S)$

$\Gamma(K^+ K^- \pi^+ \pi^-) / \Gamma(K^- 2\pi^+ \pi^-)$
Γ₂₁₇/Γ₇₀

VALUE (units 10 ⁻²)	EVTS	DOCUMENT ID	TECN	COMMENT
3.00 ± 0.13 OUR AVERAGE				
2.95 ± 0.11 ± 0.08	2669 ± 101	¹ LINK	05G FOCUS	$\gamma \text{Be}, \bar{E}_\gamma \approx 180$ GeV
3.13 ± 0.37 ± 0.36	136 ± 15	AITALA	98D E791	π^- nucleus, 500 GeV
3.5 ± 0.4 ± 0.2	244 ± 26	FRABETTI	95C E687	$\gamma \text{Be}, \bar{E}_\gamma \approx 200$ GeV
• • • We do not use the following data for averages, fits, limits, etc. • • •				
4.4 ± 1.8 ± 0.5	19 ± 8	ABLIKIM	05F BES	$e^+ e^- \approx \psi(3770)$
4.1 ± 0.7 ± 0.5	114 ± 20	ALBRECHT	94I ARG	$e^+ e^- \approx 10$ GeV
3.14 ± 1.0	89 ± 29	AMMAR	91 CLEO	$e^+ e^- \approx 10.5$ GeV
2.8 ^{+0.8} _{-0.7}		ANJOS	91 E691	γBe 80-240 GeV
¹ LINK 05G uses a smaller, cleaner subset of 1279 ± 48 events for the amplitude analysis that gives the results in the next data blocks.				

$\Gamma(\phi(\pi^+ \pi^-)_{S\text{-wave}}, \phi \rightarrow K^+ K^-) / \Gamma(K^+ K^- \pi^+ \pi^-)$
This is the fraction from a coherent amplitude analysis.
Γ₂₁₈/Γ₂₁₇

VALUE (units 10 ⁻²)	EVTS	DOCUMENT ID	TECN	COMMENT
4.0 ± 0.6 ± 2.1	3k	¹ DARGENT 17		4-body fit, $K K \pi \pi$ events
• • • We do not use the following data for averages, fits, limits, etc. • • •				
10.3 ± 1.0 ± 0.8	3k	² ARTUSO 12	CLEO	4-body fit, $K K \pi \pi$ events
1 ± 1	1.3k	LINK	05G FOCUS	4-body fit, $K K \pi \pi$ events

¹ Obtained by analyzing CLEO data but not authored by the CLEO Collaboration.
² See DARGENT 17

Meson Particle Listings

 D^0 $\Gamma((\phi\rho^0)_{S\text{-wave}}, \phi \rightarrow K^+K^-)/\Gamma(K^+K^-\pi^+\pi^-)$ $\Gamma_{219}/\Gamma_{217}$

This is the fraction from a coherent amplitude analysis.

VALUE (units 10^{-2})	EVTS	DOCUMENT ID	TECN	COMMENT
28.1 ± 1.3 ± 1.7	2.9k	^{1,2} DARGENT 17		4-body fit, $K K \pi \pi$ evts
• • • We do not use the following data for averages, fits, limits, etc. • • •				
38.3 ± 2.5 ± 3.8		^{1,3} ARTUSO 12	CLEO	Fitting 2959 evts.
29 ± 2 ± 1		LINK 05G	FOCS	Fits 1279 ± 48 evts.

¹ARTUSO 12 and DARGENT 17 use the same dataset, but ARTUSO 12 uses a formulation for the D-wave component that is in fact a mix of S- and D-wave, while DARGENT 17 uses a pure D-wave. This explains the discrepancy in their $\rho\phi$ S- and D-wave components.

²Obtained by analyzing CLEO data but not authored by the CLEO Collaboration.

³See DARGENT 17

 $\Gamma((\phi\rho^0)_{P\text{-wave}}, \phi \rightarrow K^+K^-)/\Gamma(K^+K^-\pi^+\pi^-)$ $\Gamma_{220}/\Gamma_{217}$

This is the fit fraction from a coherent amplitude analysis.

VALUE (units 10^{-2})	EVTS	DOCUMENT ID	TECN	COMMENT
1.6 ± 0.3 ± 0.7	2.9k	¹ DARGENT 17		4-body fit, $K K \pi \pi$ evts

¹Obtained by analyzing CLEO data but not authored by the CLEO Collaboration.

 $\Gamma((\phi\rho^0)_{D\text{-wave}}, \phi \rightarrow K^+K^-)/\Gamma(K^+K^-\pi^+\pi^-)$ $\Gamma_{221}/\Gamma_{217}$

VALUE (units 10^{-2})	EVTS	DOCUMENT ID	TECN	COMMENT
1.7 ± 0.4 ± 0.4	2.9k	^{1,2} DARGENT 17		4-body fit, $K K \pi \pi$ evts
• • • We do not use the following data for averages, fits, limits, etc. • • •				
3.4 ± 0.7 ± 0.6		^{1,3} ARTUSO 12	CLEO	Fitting 2959 evts.

¹ARTUSO 12 use a formulation for the D-wave component that is in fact a mix of S- and D-wave, while DARGENT 17 uses a pure D-wave.

²Obtained by analyzing CLEO data but not authored by the CLEO Collaboration.

³See DARGENT 17

 $\Gamma(K^*(892)^0 \bar{K}^*(892)^0, K^{*0} \rightarrow K^\pm \pi^\mp)/\Gamma(K^+K^-\pi^+\pi^-)$ $\Gamma_{222}/\Gamma_{217}$

This is the fraction from a coherent amplitude analysis.

VALUE (units 10^{-2})	DOCUMENT ID	TECN	COMMENT
3 ± 2 ± 1	LINK 05G	FOCS	Fits 1279 ± 48 evts.

 $\Gamma(K^+K^-\rho^0 \text{ 3-body})/\Gamma(K^+K^-\pi^+\pi^-)$ $\Gamma_{223}/\Gamma_{217}$

This is the fraction from a coherent amplitude analysis.

VALUE (units 10^{-2})	DOCUMENT ID	TECN	COMMENT
2 ± 2 ± 2	LINK 05G	FOCS	Fits 1279 ± 48 evts.

 $\Gamma(f_0(980)\pi^+\pi^-, f_0 \rightarrow K^+K^-)/\Gamma(K^+K^-\pi^+\pi^-)$ $\Gamma_{224}/\Gamma_{217}$

This is the fraction from a coherent amplitude analysis.

VALUE (units 10^{-2})	DOCUMENT ID	TECN	COMMENT
15 ± 3 ± 2	LINK 05G	FOCS	Fits 1279 ± 48 evts.

 $\Gamma((K^*(892)^0 \bar{K}^*(892)^0)_{S\text{-wave}}, K^{*0} \rightarrow K^\pm \pi^\mp)/\Gamma(K^+K^-\pi^+\pi^-)$ $\Gamma_{225}/\Gamma_{217}$

VALUE (units 10^{-2})	EVTS	DOCUMENT ID	TECN	COMMENT
9.06 ± 0.35 OUR AVERAGE				
9.18 ± 0.21 ± 0.28	163k	AAIJ 19c	LHCB	4-body fit, $K K \pi \pi$ evts
4.5 ± 0.8 ± 2.0	3k	¹ DARGENT 17		4-body fit, $K K \pi \pi$ evts
• • • We do not use the following data for averages, fits, limits, etc. • • •				
6.1 ± 0.8 ± 0.9	3k	² ARTUSO 12	CLEO	4-body fit, $K K \pi \pi$ evts

¹Obtained by analyzing CLEO data but not authored by the CLEO Collaboration.

²See DARGENT 17

 $\Gamma((K^*(892)^0 \bar{K}^*(892)^0)_{P\text{-wave}}, K^* \rightarrow K^\pm \pi^\mp)/\Gamma(K^+K^-\pi^+\pi^-)$ $\Gamma_{226}/\Gamma_{217}$

This is the fit fraction from a coherent amplitude analysis.

VALUE (units 10^{-2})	EVTS	DOCUMENT ID	TECN	COMMENT
4.87 ± 0.24 OUR AVERAGE				
4.90 ± 0.16 ± 0.18	163k	AAIJ 19c	LHCB	4-body fit, $K K \pi \pi$ evts
3.6 ± 0.7 ± 1.5	2.9k	¹ DARGENT 17		4-body fit, $K K \pi \pi$ evts
• • • We do not use the following data for averages, fits, limits, etc. • • •				
1.85 ± 0.09 ± 0.10	163k	AAIJ 19c	LHCB	4-body fit, $K K \pi \pi$ evts
4.0 ± 0.6 ± 0.7	2.9k	¹ DARGENT 17		4-body fit, $K K \pi \pi$ evts

¹Obtained by analyzing CLEO data but not authored by the CLEO Collaboration.

 $\Gamma((K^*(892)^0 \bar{K}^*(892)^0)_{D\text{-wave}}, K^* \rightarrow K^\pm \pi^\mp)/\Gamma(K^+K^-\pi^+\pi^-)$ $\Gamma_{227}/\Gamma_{217}$

This is the fit fraction from a coherent amplitude analysis.

VALUE (units 10^{-2})	EVTS	DOCUMENT ID	TECN	COMMENT
1.89 ± 0.13 OUR AVERAGE				
1.85 ± 0.09 ± 0.10	163k	AAIJ 19c	LHCB	4-body fit, $K K \pi \pi$ evts
4.0 ± 0.6 ± 0.7	2.9k	¹ DARGENT 17		4-body fit, $K K \pi \pi$ evts
• • • We do not use the following data for averages, fits, limits, etc. • • •				
11 ± 2 ± 1	LINK 05G	FOCS	Fits 1279 ± 48 evts.	

¹Obtained by analyzing CLEO data but not authored by the CLEO Collaboration.

 $\Gamma(K^*(892)^0 K^\mp \pi^\pm \text{ 3-body}, K^{*0} \rightarrow K^\pm \pi^\mp)/\Gamma(K^+K^-\pi^+\pi^-)$ $\Gamma_{228}/\Gamma_{217}$

This is the fraction from a coherent amplitude analysis.

VALUE (units 10^{-2})	EVTS	DOCUMENT ID	TECN	COMMENT
18.7 ± 1.5 OUR AVERAGE				
19.08 ± 0.60 ± 1.46	163k	AAIJ 19c	LHCB	4-body fit, $K K \pi \pi$ evts
12.4 ± 2.6 ± 6.3	2.9k	¹ DARGENT 17		4-body fit, $K K \pi \pi$ evts
• • • We do not use the following data for averages, fits, limits, etc. • • •				
22 ± 3 ± 4	LINK 05G	FOCS	Fits 1279 ± 48 evts.	

¹Obtained by analyzing CLEO data but not authored by the CLEO Collaboration.

 $\Gamma(K^*(892)^0 (K^-\pi^+)_{S\text{-wave}} \text{ 3-body}, K^{*0} \rightarrow K^+\pi^-)/\Gamma(K^+K^-\pi^+\pi^-)$ $\Gamma_{229}/\Gamma_{217}$

This is the fit fraction from a coherent amplitude analysis.

VALUE (units 10^{-2})	EVTS	DOCUMENT ID	TECN	COMMENT
5.8 ± 1.2 ± 2.1	2.9k	¹ DARGENT 17		4-body fit, $K K \pi \pi$ evts
• • • We do not use the following data for averages, fits, limits, etc. • • •				
10.9 ± 1.2 ± 1.7		¹ ARTUSO 12	CLEO	Fitting 2959 evts.

¹Obtained by analyzing CLEO data but not authored by the CLEO Collaboration.

 $\Gamma((K^-\pi^+)_{P\text{-wave}}, (K^+\pi^-)_{S\text{-wave}})/\Gamma(K^+K^-\pi^+\pi^-)$ $\Gamma_{230}/\Gamma_{217}$

VALUE (units 10^{-2})	DOCUMENT ID	TECN	COMMENT
• • • We do not use the following data for averages, fits, limits, etc. • • •			
33 ± 6 ± 4	¹ LINK 05G	FOCS	Fits 1279 ± 48 evts.

¹See DARGENT 17

 $\Gamma(K_1(1270)^\pm K^\mp, K_1^\pm \rightarrow K^\pm \pi^+ \pi^-)/\Gamma(K^+K^-\pi^+\pi^-)$ $\Gamma_{231}/\Gamma_{217}$

This is the fraction from a coherent amplitude analysis.

VALUE (units 10^{-2})	DOCUMENT ID	TECN	COMMENT
• • • We do not use the following data for averages, fits, limits, etc. • • •			
33 ± 6 ± 4	¹ LINK 05G	FOCS	Fits 1279 ± 48 evts.

¹This LINK 05G value includes $K_1(1270)^\pm \rightarrow \rho^0 K^\pm \rightarrow K_0^*(1430)^0 \pi^\pm$, and $K^*(892)^0 \pi^\pm$.

 $\Gamma(K_1(1270)^+ K^-, K_1^+ \rightarrow K^{*0} \pi^+)/\Gamma(K^+K^-\pi^+\pi^-)$ $\Gamma_{232}/\Gamma_{217}$

VALUE (units 10^{-2})	EVTS	DOCUMENT ID	TECN	COMMENT
5.5 ± 1.4 ± 3.4	3k	¹ DARGENT 17		4-body fit, $K K \pi \pi$ evts
• • • We do not use the following data for averages, fits, limits, etc. • • •				
7.3 ± 0.8 ± 1.9	3k	² ARTUSO 12	CLEO	4-body fit, $K K \pi \pi$ events

¹Obtained by analyzing CLEO data but not authored by the CLEO Collaboration.

²See DARGENT 17

 $\Gamma(K_1(1270)^+ K^-, K_1^+ \rightarrow K^*(1430)^0 \pi^+, K^{*0} \rightarrow K^+\pi^-)/\Gamma(K^+K^-\pi^+\pi^-)$ $\Gamma_{233}/\Gamma_{217}$

This is the fit fraction from a coherent amplitude analysis.

VALUE (units 10^{-2})	EVTS	DOCUMENT ID	TECN	COMMENT
6.1 ± 1.2 ± 1.8	2.9k	¹ DARGENT 17		4-body fit, $K K \pi \pi$ evts
• • • We do not use the following data for averages, fits, limits, etc. • • •				
4.7 ± 0.7 ± 0.8		² ARTUSO 12	CLEO	Fitting 2959 evts.

¹Obtained by analyzing CLEO data but not authored by the CLEO Collaboration.

²See DARGENT 17

 $\Gamma(K_1(1270)^+ K^-, K_1^+ \rightarrow \rho^0 K^+)/\Gamma(K^+K^-\pi^+\pi^-)$ $\Gamma_{234}/\Gamma_{217}$

VALUE (units 10^{-2})	EVTS	DOCUMENT ID	TECN	COMMENT
9.1 ± 1.5 ± 1.9	2.9k	¹ DARGENT 17		4-body fit, $K K \pi \pi$ evts
• • • We do not use the following data for averages, fits, limits, etc. • • •				
4.7 ± 0.7 ± 0.8		² ARTUSO 12	CLEO	Fitting 2959 evts.

¹Obtained by analyzing CLEO data but not authored by the CLEO Collaboration.

²See DARGENT 17

 $\Gamma(K_1(1270)^+ K^-, K_1^+ \rightarrow \omega(782)K^+, \omega \rightarrow \pi^+\pi^-)/\Gamma(K^+K^-\pi^+\pi^-)$ $\Gamma_{235}/\Gamma_{217}$

This is the fit fraction from a coherent amplitude analysis.

VALUE (units 10^{-2})	EVTS	DOCUMENT ID	TECN	COMMENT
0.6 ± 0.3 ± 0.4	2.9k	¹ DARGENT 17		4-body fit, $K K \pi \pi$ evts
• • • We do not use the following data for averages, fits, limits, etc. • • •				
0.9 ± 0.3 ± 0.4		¹ ARTUSO 12	CLEO	Fitting 2959 evts.

¹Obtained by analyzing CLEO data but not authored by the CLEO Collaboration.

 $\Gamma(K_1(1270)^- K^+, K_1^- \rightarrow \bar{K}^{*0} \pi^-)/\Gamma(K^+K^-\pi^+\pi^-)$ $\Gamma_{236}/\Gamma_{217}$

VALUE (units 10^{-2})	EVTS	DOCUMENT ID	TECN	COMMENT
• • • We do not use the following data for averages, fits, limits, etc. • • •				
0.9 ± 0.3 ± 0.4		¹ ARTUSO 12	CLEO	Fitting 2959 evts.

¹See DARGENT 17

 $\Gamma(K_1(1270)^- K^+, K_1^- \rightarrow \rho^0 K^-)/\Gamma(K^+K^-\pi^+\pi^-)$ $\Gamma_{237}/\Gamma_{217}$

VALUE (units 10^{-2})	EVTS	DOCUMENT ID	TECN	COMMENT
5.4 ± 0.7 ± 1.3	2.9k	¹ DARGENT 17		4-body fit, $K K \pi \pi$ evts
• • • We do not use the following data for averages, fits, limits, etc. • • •				
6.0 ± 0.8 ± 0.6		² ARTUSO 12	CLEO	Fitting 2959 evts.

¹Obtained by analyzing CLEO data but not authored by the CLEO Collaboration.

²See DARGENT 17

 $\Gamma(K_1(1400)^\pm K^\mp, K_1^\pm \rightarrow K^\pm \pi^+ \pi^-)/\Gamma(K^+K^-\pi^+\pi^-)$ $\Gamma_{238}/\Gamma_{217}$

This is the fraction from a coherent amplitude analysis.

VALUE (units 10^{-2})	DOCUMENT ID	TECN	COMMENT
• • • We do not use the following data for averages, fits, limits, etc. • • •			
22 ± 3 ± 4	LINK 05G	FOCS	Fits 1279 ± 48 evts.

 $\Gamma(K_1(1400)^+ K^-, K_1^+ \rightarrow K^*(892)^0 \pi^+, K^{*0} \rightarrow K^+\pi^-)/\Gamma(K^+K^-\pi^+\pi^-)$ $\Gamma_{239}/\Gamma_{217}$

This is the fit fraction from a coherent amplitude analysis.

VALUE (units 10^{-2})	EVTS	DOCUMENT ID	TECN	COMMENT
18.7 ± 1.5 OUR AVERAGE				
19.08 ± 0.60 ± 1.46	163k	AAIJ 19c	LHCB	4-body fit, $K K \pi \pi$ evts
12.4 ± 2.6 ± 6.3	2.9k	¹ DARGENT 17		4-body fit, $K K \pi \pi$ evts
• • • We do not use the following data for averages, fits, limits, etc. • • •				
22 ± 3 ± 4	LINK 05G	FOCS	Fits 1279 ± 48 evts.	

¹Obtained by analyzing CLEO data but not authored by the CLEO Collaboration.

See key on page 999

Meson Particle Listings

D^0

$\Gamma(K^*(1410)^+ K^-, K^{*+} \rightarrow K^{*0} \pi^+) / \Gamma(K^+ K^- \pi^+ \pi^-)$ $\Gamma_{240} / \Gamma_{217}$

VALUE (units 10^{-2})	EVTS	DOCUMENT ID	TECN	COMMENT
--------------------------	------	-------------	------	---------

• • • We do not use the following data for averages, fits, limits, etc. • • •
 4.2 ± 0.7 ± 0.8 ^{1,2} ARTUSO 12 CLEO Fitting 2959 evts.

¹ DARGENT 17 find $K^*(1410)^+ \pi^-$ and $K^*(1680)^+ \pi^-$, which both peak outside the $D^0 \rightarrow K K \pi \pi$ kinematic range, effectively indistinguishable; we list their result under $K^*(1680)^+ \pi^-$.
² See DARGENT 17

$\Gamma(K^*(1410)^- K^+, K^{*-} \rightarrow \bar{K}^{*0} \pi^-) / \Gamma(K^+ K^- \pi^+ \pi^-)$ $\Gamma_{241} / \Gamma_{217}$

VALUE (units 10^{-2})	EVTS	DOCUMENT ID	TECN	COMMENT
--------------------------	------	-------------	------	---------

2.82 ± 0.19 ± 0.39 163k AAJ 19c LHCb 4-body fit, $K K \pi \pi$ evts
 • • • We do not use the following data for averages, fits, limits, etc. • • •
 4.7 ± 0.7 ± 0.7 3k ¹ ARTUSO 12 CLEO 4-body fit, $K K \pi \pi$ evts
¹ See DARGENT 17.

$\Gamma(K_1(1680)^+ K^-, K_1^+ \rightarrow K^{*0} \pi^+, K^{*0} \rightarrow K^+ \pi^-) / \Gamma(K^+ K^- \pi^+ \pi^-)$ $\Gamma_{242} / \Gamma_{217}$

This is the fit fraction from a coherent amplitude analysis.

VALUE (units 10^{-2})	EVTS	DOCUMENT ID	TECN	COMMENT
--------------------------	------	-------------	------	---------

3.6 ± 0.8 ± 1.0 2.9k ^{1,2} DARGENT 17 4-body fit, $K K \pi \pi$ evts
¹ DARGENT 17 find $K^*(1410)^+ \pi^-$ and $K^*(1680)^+ \pi^-$, which both peak outside the $D^0 \rightarrow K K \pi \pi$ kinematic range, effectively indistinguishable.
² Obtained by analyzing CLEO data but not authored by the CLEO Collaboration.

$\Gamma(K^+ K^- \pi^+ \pi^- \text{ non-resonant}) / \Gamma(K^+ K^- \pi^+ \pi^-)$ $\Gamma_{243} / \Gamma_{217}$

This is the fit fraction from a coherent amplitude analysis.

VALUE (units 10^{-2})	EVTS	DOCUMENT ID	TECN	COMMENT
--------------------------	------	-------------	------	---------

11.1 ± 1.2 ± 2.2 2.9k ¹ DARGENT 17 4-body fit, $K K \pi \pi$ evts
¹ Obtained by analyzing CLEO data but not authored by the CLEO Collaboration.

$\Gamma(2K_S^0 \pi^+ \pi^-) / \Gamma(K_S^0 \pi^+ \pi^-)$ $\Gamma_{244} / \Gamma_{38}$

VALUE (units 10^{-2})	EVTS	DOCUMENT ID	TECN	COMMENT
--------------------------	------	-------------	------	---------

4.3 ± 0.8 OUR AVERAGE
 4.16 ± 0.70 ± 0.42 113 ± 21 LINK 05A FOCS γ Be, $\bar{E}_\gamma \approx 180$ GeV
 6.2 ± 2.0 ± 1.6 25 ALBRECHT 94i ARG $e^+ e^- \approx 10$ GeV

$\Gamma(K_S^0 K^- 2\pi^+ \pi^-) / \Gamma(K_S^0 2\pi^+ 2\pi^-)$ $\Gamma_{245} / \Gamma_{92}$

VALUE	CL%	DOCUMENT ID	TECN	COMMENT
-------	-----	-------------	------	---------

<0.054 90 LINK 04D FOCS γ A, $\bar{E}_\gamma \approx 180$ GeV

$\Gamma(K^+ K^- \pi^+ \pi^- \pi^0) / \Gamma_{\text{total}}$ Γ_{246} / Γ

VALUE	DOCUMENT ID	TECN	COMMENT
-------	-------------	------	---------

0.0031 ± 0.0020 ¹ BARLAG 92c ACCM π^- Cu 230 GeV
¹ BARLAG 92c computes the branching fraction using topological normalization.

$\Gamma(\phi \pi^0) / \Gamma(K^+ K^-)$ $\Gamma_{247} / \Gamma_{185}$

VALUE	EVTS	DOCUMENT ID	TECN	COMMENT
-------	------	-------------	------	---------

• • • We do not use the following data for averages, fits, limits, etc. • • •
 0.194 ± 0.006 ± 0.009 1254 TAJIMA 04 BELL $e^+ e^-$ at $\Upsilon(4S)$

$\Gamma(\phi \eta) / \Gamma(K^+ K^-)$ $\Gamma_{248} / \Gamma_{185}$

VALUE (units 10^{-2})	EVTS	DOCUMENT ID	TECN	COMMENT
--------------------------	------	-------------	------	---------

3.59 ± 1.14 ± 0.18 31 TAJIMA 04 BELL $e^+ e^-$ at $\Upsilon(4S)$

$\Gamma(\phi \omega) / \Gamma_{\text{total}}$ Γ_{249} / Γ

VALUE	CL%	DOCUMENT ID	TECN	COMMENT
-------	-----	-------------	------	---------

<0.0021 90 ALBRECHT 94i ARG $e^+ e^- \approx 10$ GeV

Radiative modes

$\Gamma(\rho^0 \gamma) / \Gamma(\pi^+ \pi^-)$ $\Gamma_{250} / \Gamma_{123}$

VALUE (units 10^{-2})	EVTS	DOCUMENT ID	TECN	COMMENT
--------------------------	------	-------------	------	---------

1.25 ± 0.21 ± 0.05 500 NANUT 17 BELL $e^+ e^-$ at $\Upsilon(nS)$, n=2,3,4,5

$\Gamma(\omega \gamma) / \Gamma_{\text{total}}$ Γ_{251} / Γ

VALUE	CL%	DOCUMENT ID	TECN	COMMENT
-------	-----	-------------	------	---------

<2.4 × 10⁻⁴ 90 ASNER 98 CLE2

$\Gamma(\phi \gamma) / \Gamma(K^- \pi^+)$ $\Gamma_{252} / \Gamma_{35}$

VALUE (units 10^{-4})	EVTS	DOCUMENT ID	TECN	COMMENT
--------------------------	------	-------------	------	---------

7.1 ± 0.5 OUR FIT
7.15 ± 0.78 ± 0.69 243 ± 25 AUBERT 08AZ BABR $e^+ e^- \approx 10.6$ GeV

$\Gamma(\phi \gamma) / \Gamma(K^+ K^-)$ $\Gamma_{252} / \Gamma_{185}$

VALUE (units 10^{-3})	EVTS	DOCUMENT ID	TECN	COMMENT
--------------------------	------	-------------	------	---------

6.9 ± 0.5 OUR FIT
6.88 ± 0.47 ± 0.21 524 NANUT 17 BELL $e^+ e^-$ at $\Upsilon(nS)$, n=2,3,4,5

• • • We do not use the following data for averages, fits, limits, etc. • • •

6.31 ^{+1.70+0.30} _{-1.48-0.36}	28	TAJIMA	04	BELL	See NANUT 17
--	----	--------	----	------	--------------

$\Gamma(\bar{K}^*(892)^0 \gamma) / \Gamma(K^- \pi^+)$ $\Gamma_{253} / \Gamma_{35}$

VALUE (units 10^{-3})	EVTS	DOCUMENT ID	TECN	COMMENT
--------------------------	------	-------------	------	---------

10.5 ± 1.7 OUR AVERAGE Error includes scale factor of 3.1.
 11.9 ± 0.5 ± 0.5 9.1k NANUT 17 BELL $e^+ e^-$ at $\Upsilon(nS)$, n=2,3,4,5
 8.43 ± 0.51 ± 0.70 2.2k AUBERT 08AZ BABR $e^+ e^- \approx 10.6$ GeV

Doubly Cabibbo-suppressed / Mixing modes

$\Gamma(K^+ K^- \nu_\ell \text{ via } \bar{D}^0) / \Gamma(K^- \ell^+ \nu_\ell)$ $\Gamma_{254} / \Gamma_{18}$

This is a limit on R_M without the complications of possible doubly Cabibbo-suppressed decays that occur when using hadronic modes. For the limits on $|m_1 - m_2|$ and $(\Gamma_1 - \Gamma_2) / \Gamma$ that come from the best mixing limit, see near the beginning of these D^0 Listings.

VALUE	CL%	DOCUMENT ID	TECN	COMMENT
-------	-----	-------------	------	---------

< 6.1 × 10⁻⁴ 90 ¹ BITENC 08 BELL $e^+ e^-$, 10.58 GeV

• • • We do not use the following data for averages, fits, limits, etc. • • •

< 50 × 10⁻⁴ 90 ² AITALA 96c E791 π^- nucleus, 500 GeV

¹ The BITENC 08 right-sign sample includes about 15% of $D^0 \rightarrow K^- \pi^0 \ell^+ \nu_\ell$ and other decays.
² AITALA 96c uses $D^{*+} \rightarrow D^0 \pi^+$ (and charge conjugate) decays to identify the charm at production and $D^0 \rightarrow K^- \ell^+ \nu_\ell$ (and charge conjugate) decays to identify the charm at decay.

$\Gamma(K^+ \alpha K^*(892)^+ e^- \nu_\ell \text{ via } \bar{D}^0) / [\Gamma(K^- e^+ \nu_\ell) + \Gamma(K^*(892)^- e^+ \nu_\ell)]$ $\Gamma_{255} / (\Gamma_{19} + \Gamma_{21})$

This is a limit on R_M without the complications of possible doubly Cabibbo-suppressed decays that occur when using hadronic modes. The experiments use $D^{*+} \rightarrow D^0 \pi^+$ (and charge conjugate) decays to identify the charm at production and the charge of the e to identify the charm at decay. These limits do not allow CP violation. For the limits on $|m_1 - m_2|$ and $(\Gamma_1 - \Gamma_2) / \Gamma$ that come from the best mixing limit, see near the beginning of these D^0 Listings.

VALUE	CL%	DOCUMENT ID	TECN	COMMENT
-------	-----	-------------	------	---------

<0.001 90 BITENC 05 BELL $e^+ e^- \approx 10.6$ GeV

• • • We do not use the following data for averages, fits, limits, etc. • • •

-0.0013 < R < +0.0012 90 AUBERT 07AB BABR $e^+ e^- \approx 10.58$ GeV

<0.0078 90 CAWLFIELD 05 CLEO $e^+ e^- \approx 10.6$ GeV

<0.0042 90 AUBERT,B 04Q BABR See AUBERT 07AB

$\Gamma(K^+ \pi^-) / \Gamma(K^- \pi^+)$ $\Gamma_{256} / \Gamma_{35}$

This is R , the time-integrated wrong-sign rate compared to the right-sign rate. See the note on " D^0 - \bar{D}^0 Mixing," near the start of the D^0 Listings.

The experiments here use the charge of the pion in $D^*(2010)^\pm \rightarrow (D^0 \text{ or } \bar{D}^0) \pi^\pm$ decay to tell whether a D^0 or a \bar{D}^0 was born. The $D^0 \rightarrow K^+ \pi^-$ decay can occur directly by doubly Cabibbo-suppressed (DCS) decay, or indirectly by $D^0 \rightarrow \bar{D}^0$ mixing followed by $\bar{D}^0 \rightarrow K^+ \pi^-$ decay. Some of the experiments can use the decay-time information to disentangle the two mechanisms. Here, we list the experimental branching ratio, which if there is no mixing is the DCS ratio. See the next data block for values of the DCS ratio R_D , and the following data block for limits on the mixing ratio R_M . See the section on CP -violating asymmetries near the end of this D^0 Listing for values of A_D , and the note on " D^0 - \bar{D}^0 Mixing" for limits on x' and y' .

Some early limits have been omitted from this Listing; see our 1998 edition (The European Physical Journal **C3** 1 (1998)) and our 2006 edition (Journal of Physics **G33** 1 (2006)).

VALUE (units 10^{-3})	EVTS	DOCUMENT ID	TECN	COMMENT
--------------------------	------	-------------	------	---------

3.79 ± 0.18 OUR FIT Error includes scale factor of 3.3.

3.79 ± 0.18 OUR AVERAGE Error includes scale factor of 3.3. See the ideogram below.

4.15 ± 0.10 12.7 ± 0.3k ¹ AALTONEN 08E CDF $p\bar{p}$, $\sqrt{s} = 1.96$ TeV

3.53 ± 0.08 ± 0.04 4030 ± 90 ² AUBERT 07W BABR $e^+ e^- \approx 10.6$ GeV

3.77 ± 0.08 ± 0.05 4024 ± 88 ¹ ZHANG 06 BELL $e^+ e^-$

• • • We do not use the following data for averages, fits, limits, etc. • • •

4.05 ± 0.21 ± 0.11 2.0 ± 0.1k ³ ABULENCIA 06x CDF See AALTONEN 08E

3.81 ± 0.17^{+0.08}_{-0.16} 845 ± 40 ² LI 05A BELL See ZHANG 06

4.29^{+0.63}_{-0.61} ± 0.27 234 ⁴ LINK 05H FOCS γ nucleus

3.57 ± 0.22 ± 0.27 ⁵ AUBERT 03Z BABR See AUBERT 07w

4.04 ± 0.85 ± 0.25 149 ⁶ LINK 01 FOCS γ nucleus

3.32^{+0.63}_{-0.65} ± 0.40 45 ¹ GODANG 00 CLE2 $e^+ e^-$

6.8^{+3.4}_{-3.3} ± 0.7 34 ² AITALA 98 E791 π^- nucl., 500 GeV

¹ GODANG 00, ZHANG 06, and AALTONEN 08E allow CP violation.

² AITALA 98, LI 05A, and AUBERT 07w assume no CP violation.

³ This ABULENCIA 06x result assumes no mixing.

⁴ This LINK 05H result assumes no mixing but allows CP violation. If neither mixing nor CP violation is allowed, $R = (4.29 \pm 0.63 \pm 0.28) \times 10^{-3}$.

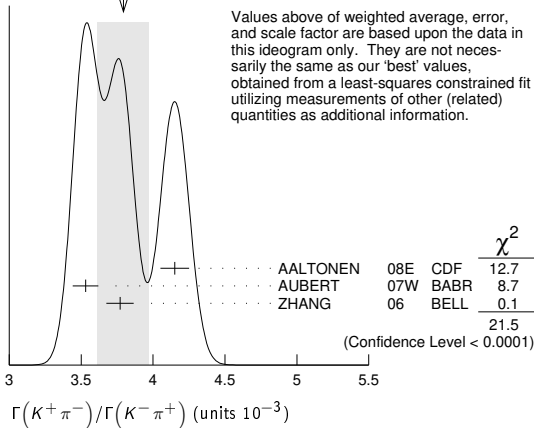
⁵ This AUBERT 03z result allows CP violation. If CP violation is not allowed, $R = 0.00359 \pm 0.00020 \pm 0.00027$.

⁶ This LINK 01 result assumes no mixing or CP violation.

Meson Particle Listings

D^0

WEIGHTED AVERAGE
3.79±0.18 (Error scaled by 3.3)



Values above of weighted average, error, and scale factor are based upon the data in this ideogram only. They are not necessarily the same as our 'best' values, obtained from a least-squares constrained fit utilizing measurements of other (related) quantities as additional information.

$\Gamma(K^+\pi^- \text{ via DCS})/\Gamma(K^-\pi^+)$

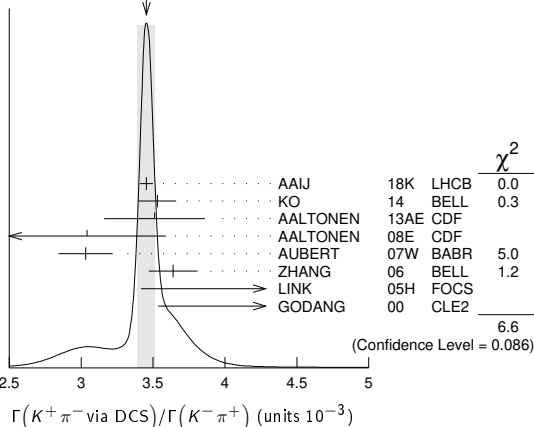
Γ_{257}/Γ_{35}

This is R_D , the doubly Cabibbo-suppressed ratio when mixing is allowed.

VALUE (units 10^{-3})	EVTS	DOCUMENT ID	TECN	COMMENT
3.45 ± 0.06 OUR AVERAGE				Error includes scale factor of 1.5. See the ideogram below.
3.454 ± 0.040 ± 0.020	722k	1 AAIJ	18K LHCB	pp at 7, 8, 13 TeV
3.53 ± 0.13		2 KO	14 BELL	$e^+e^- \rightarrow \Upsilon(nS)$
3.51 ± 0.35		3 AALTONEN	13AE CDF	$p\bar{p}$ at 1.96 TeV
3.04 ± 0.55	13k	AALTONEN	08E CDF	$p\bar{p}$, $\sqrt{s} = 1.96$ TeV
3.03 ± 0.16 ± 0.10	4.0k	4 AUBERT	07W BABR	$e^+e^- \approx 10.6$ GeV
3.64 ± 0.17	4.0k	5 ZHANG	06 BELL	e^+e^-
5.17 $^{+1.47}_{-1.58}$ ± 0.76	234	6 LINK	05H FOCS	γ nucleus
4.8 ± 1.2 ± 0.4	45	7 GODANG	00 CLE2	e^+e^-
••• We do not use the following data for averages, fits, limits, etc. •••				
3.533 ± 0.054	236k	8 AAIJ	17A0 LHCB	See AAIJ 18k
3.568 ± 0.066		9 AAIJ	13CE LHCB	pp at 7, 8 TeV
3.52 ± 0.15		10 AAIJ	13N LHCB	Repl. by AAIJ 13CE
2.87 ± 0.37	0.8k	LI	05A BELL	See ZHANG 06

- This AAIJ 18k value is for direct and indirect CP violation allowed. The value is the same if either one or the other is not allowed, but in each case the error then is $(0.028 \pm 0.014) \times 10^{-3}$.
- Based on 976 fb^{-1} of data collected at $\Upsilon(nS)$ resonances. Assumes no CP violation.
- Based on 9.6 fb^{-1} of data collected at the Tevatron. Assumes no CP violation.
- Result is the same whether or not CP violation is allowed.
- This ZHANG 06 assumes no CP violation.
- This LINK 05H result allows CP violation. Allowing mixing but not CP violation, $R_D = (3.81^{+1.67}_{-1.63} \pm 0.92) \times 10^{-3}$.
- This GODANG 00 result allows CP violation.
- The result was established with D^0 from prompt and secondary D^* assuming no CPV or no direct CPV .
- Based on 3 fb^{-1} of data collected at $\sqrt{s} = 7, 8$ TeV. Assumes no CP violation.
- Based on 1 fb^{-1} of data collected at $\sqrt{s} = 7$ TeV in 2011. Assumes no CP violation.

WEIGHTED AVERAGE
3.45±0.06 (Error scaled by 1.5)



$\Gamma(K^+\pi^- \text{ via } \bar{D}^0)/\Gamma(K^-\pi^+)$

Γ_{258}/Γ_{35}

This is R_M in the note on " $D^0-\bar{D}^0$ Mixing" near the start of the D^0 Listings. The experiments here (1) use the charge of the pion in $D^*(2010)^\pm \rightarrow (D^0 \text{ or } \bar{D}^0) \pi^\pm$ decay to tell whether a D^0 or a \bar{D}^0 was born; and (2) use the decay-time distribution to disentangle doubly Cabibbo-suppressed decay and mixing. For the limits on $|m_1 - m_2|$ and $(\Gamma_1 - \Gamma_2)/\Gamma$ that come from the best mixing limit, see near the beginning of these D^0 Listings.

VALUE	CL%	DOCUMENT ID	TECN	COMMENT
<0.00040	95	1 ZHANG	06 BELL	e^+e^-
••• We do not use the following data for averages, fits, limits, etc. •••				
<0.00046	95	2 LI	05A BELL	See ZHANG 06
<0.0063	95	3 LINK	05H FOCS	γ nucleus
<0.0013	95	4 AUBERT	03Z BABR	e^+e^- , 10.6 GeV
<0.00041	95	5 GODANG	00 CLE2	e^+e^-
<0.0092	95	6 BARATE	98W ALEP	e^+e^- at Z^0
<0.005	90	7 ANJOS	88c E691	Photoproduction

- This ZHANG 06 result allows CP violation, but the result does not change if CP violation is not allowed.
- This LI 05A result allows CP violation. The limit becomes < 0.00042 (95% CL) if CP violation is not allowed.
- LINK 05H obtains the same result whether or not CP violation is allowed.
- This AUBERT 03Z result allows CP violation and assumes that the strong phase between $D^0 \rightarrow K^+\pi^-$ and $\bar{D}^0 \rightarrow K^+\pi^-$ is small, and limits only $D^0 \rightarrow \bar{D}^0$ transitions via off-shell intermediate states. The limit on transitions via on-shell intermediate states is 0.0016.
- This GODANG 00 result allows CP violation and assumes that the strong phase between $D^0 \rightarrow K^+\pi^-$ and $\bar{D}^0 \rightarrow K^+\pi^-$ is small, and limits only $D^0 \rightarrow \bar{D}^0$ transitions via off-shell intermediate states. The limit on transitions via on-shell intermediate states is 0.0017.
- This BARATE 98W result assumes no interference between the DCS and mixing amplitudes ($\gamma = 0$ in the note on " $D^0-\bar{D}^0$ Mixing" near the start of the D^0 Listings). When interference is allowed, the limit degrades to 0.036 (95%CL).
- This ANJOS 88c result assumes no interference between the DCS and mixing amplitudes ($\gamma = 0$ in the note on " $D^0-\bar{D}^0$ Mixing" near the start of the D^0 Listings). When interference is allowed, the limit degrades to 0.019.

$\Gamma(K_S^0 \pi^+ \pi^- \text{ in } D^0 \rightarrow \bar{D}^0)/\Gamma(K_S^0 \pi^+ \pi^-)$

Γ_{259}/Γ_{38}

This is R_M in the note on " $D^0-\bar{D}^0$ Mixing" near the start of the D^0 Listings. The experiments here (1) use the charge of the pion in $D^*(2010)^\pm \rightarrow (D^0 \text{ or } \bar{D}^0) \pi^\pm$ decay to tell whether a D^0 or a \bar{D}^0 was born; and (2) use the decay-time distribution to disentangle doubly Cabibbo-suppressed decay and mixing. For the limits on $|m_1 - m_2|$ and $(\Gamma_1 - \Gamma_2)/\Gamma$ that come from the best mixing limit, see near the beginning of these D^0 Listings.

VALUE	CL%	DOCUMENT ID	TECN	COMMENT
<0.0063	95	1 ASNER	05 CLEO	$e^+e^- \approx 10$ GeV

- This ASNER 05 limit allows CP violation. If CP violation is not allowed, the limit is 0.0042 at 95% CL.

$\Gamma(K^+\pi^-\pi^0)/\Gamma(K^-\pi^+\pi^0)$

Γ_{263}/Γ_{53}

The experiments here use the charge of the pion in $D^*(2010)^\pm \rightarrow (D^0 \text{ or } \bar{D}^0) \pi^\pm$ decay to tell whether a D^0 or a \bar{D}^0 was born. The $D^0 \rightarrow K^+\pi^-\pi^0$ decay can occur directly by doubly Cabibbo-suppressed (DCS) decay, or indirectly by $D^0 \rightarrow \bar{D}^0$ mixing followed by $\bar{D}^0 \rightarrow K^+\pi^-\pi^0$ decay.

VALUE (units 10^{-3})	EVTS	DOCUMENT ID	TECN	COMMENT
2.12 ± 0.07 OUR AVERAGE				
2.01 ± 0.11		1 EVANS	16 CLEO	$e^+e^- \rightarrow D^0\bar{D}^0$ at $\psi(3770)$
2.14 ± 0.08 ± 0.08	763	2 AUBERT,B	06N BABR	$e^+e^- \approx \Upsilon(4S)$
2.29 ± 0.15 $^{+0.13}_{-0.09}$	1.9k	TIAN	05 BELL	$e^+e^- \approx \Upsilon(4S)$
4.3 $^{+1.1}_{-1.0}$ ± 0.7	38	BRANDENB...	01 CLE2	$e^+e^- \approx \Upsilon(4S)$

- A combined fit with a recent LHCb $D^0\bar{D}^0$ mixing results in AAIJ 16F is also reported to be $(2.00 \pm 0.11) \times 10^{-3}$.
- This AUBERT,B 06N result assumes no mixing.

$\Gamma(K^+\pi^-\pi^0 \text{ via } \bar{D}^0)/\Gamma(K^-\pi^+\pi^0)$

Γ_{264}/Γ_{53}

This is R_M in the note on " $D^0-\bar{D}^0$ Mixing" near the start of the D^0 Listings. The experiments here (1) use the charge of the pion in $D^*(2010)^\pm \rightarrow (D^0 \text{ or } \bar{D}^0) \pi^\pm$ decay to tell whether a D^0 or a \bar{D}^0 was born; and (2) use the decay-time distribution to disentangle doubly Cabibbo-suppressed decay and mixing. For the limits on $|m_1 - m_2|$ and $(\Gamma_1 - \Gamma_2)/\Gamma$ that come from the best mixing limit, see near the beginning of these D^0 Listings.

VALUE (units 10^{-3})	CL%	DOCUMENT ID	TECN	COMMENT
5.25 $^{+0.25}_{-0.31}$ ± 0.12		AUBERT	09AN BABR	e^+e^- at 10.58 GeV

- We do not use the following data for averages, fits, limits, etc. •••
- <0.54
- 95
- 1 AUBERT,B
- 06N BABR
- $e^+e^- \approx \Upsilon(4S)$
- This AUBERT,B 06N limit assumes no CP violation. The measured value corresponding to the limit is $(2.3^{+1.8}_{-1.4} \pm 0.4) \times 10^{-4}$. If CP violation is allowed, this becomes $(1.0^{+2.2}_{-0.7} \pm 0.3) \times 10^{-4}$.

$\Gamma(K^+\pi^+2\pi^- \text{ via DCS})/\Gamma(K^-2\pi^+\pi^-)$ Γ_{265}/Γ_{70}

VALUE (units 10 ⁻³)	EVTS	DOCUMENT ID	TECN	COMMENT
3.03 ± 0.07 OUR AVERAGE				
3.025 ± 0.077	42k,11M	¹ AAIJ	16F LHCb	pp at 7, 8 TeV
3.03 ± 0.13		² EVANS	16 CLEO	e ⁺ e ⁻ → D ⁰ \bar{D}^0 at $\psi(3770)$

- ¹This result uses external input on the mixing parameters x, y. Without this input, the result is (3.215 ± 0.136) × 10⁻³.
- ²A combined fit with a recent LHCb D⁰ \bar{D}^0 mixing results in AAJ 16F is also reported to be (3.01 ± 0.07) × 10⁻³.

$\Gamma(K^+\pi^+2\pi^-)/\Gamma(K^-2\pi^+\pi^-)$ Γ_{266}/Γ_{70}

The experiments here use the charge of the pion in D*(2010)[±] → (D⁰ or \bar{D}^0) π[±] decay to tell whether a D⁰ or a \bar{D}^0 was born. The D⁰ → K⁺π⁻π⁺π⁻ decay can occur directly by doubly Cabibbo-suppressed (DCS) decay, or indirectly by D⁰ → \bar{D}^0 mixing followed by \bar{D}^0 → K⁺π⁻π⁺π⁻ decay. Some of the experiments can use the decay-time information to disentangle the two mechanisms. Here, we list the experimental branching ratio, which if there is no mixing is the DCS ratio; in the next data block we give the limits on the mixing ratio.

Some early limits have been omitted from this Listing; see our 1998 edition (EPJ C3 1).

VALUE (units 10 ⁻³)	CL%	EVTS	DOCUMENT ID	TECN	COMMENT
3.22 ± 0.05 OUR AVERAGE					
3.22 ± 0.05		42k,11M	¹ AAIJ	16F LHCb	pp at 7, 8 TeV
3.24 ± 0.08 ± 0.07		3.3k	² WHITE	13 BELL	e ⁺ e ⁻ ≈ $\Upsilon(4S)$
4.4 $\pm_{-1.2}^{+1.3}$ ± 0.4		54	² DYTMAN	01 CLE2	e ⁺ e ⁻ ≈ $\Upsilon(4S)$
2.5 $\pm_{-3.4}^{+3.6}$ ± 0.3			³ AITALA	98 E791	π ⁻ nucl., 500 GeV

- • • We do not use the following data for averages, fits, limits, etc. • • •
- 3.20 ± 0.18 $\pm_{-0.13}^{+0.18}$ 1.7k ²TIAN 05 BELL See WHITE 13
- <18 90 ²AMMAR 91 CLEO e⁺e⁻ ≈ 10.5 GeV
- <18 90 ⁴ANJOS 88c E691 Photoproduction

- ¹AAIJ 16F result comes from time-dependent analysis that uses external input on the mixing parameters x, y. Without this input, the result is (3.29 ± 0.08) × 10⁻³.
- ²AMMAR 91 cannot and DYTMAN 01, TIAN 05 do not distinguish between doubly Cabibbo-suppressed decay and D⁰- \bar{D}^0 mixing.
- ³This AITALA 98 result assumes no D⁰- \bar{D}^0 mixing (R_M in the note on “D⁰- \bar{D}^0 Mixing”) it becomes -0.0020 $\pm_{-0.0106}^{+0.0117}$ ± 0.0035 when mixing is allowed and decay-time information is used to distinguish doubly Cabibbo-suppressed decays from mixing.
- ⁴ANJOS 88c uses decay-time information to distinguish doubly Cabibbo-suppressed (DCS) decays from D⁰- \bar{D}^0 mixing. However, the result assumes no interference between the DCS and mixing amplitudes (y' = 0 in the note on “D⁰- \bar{D}^0 Mixing” near the start of the D⁰ Listings). When interference is allowed, the limit degrades to 0.033.

$\Gamma(K^+\pi^+2\pi^- \text{ via } \bar{D}^0)/\Gamma(K^-2\pi^+\pi^-)$ Γ_{267}/Γ_{70}

This is a D⁰- \bar{D}^0 mixing limit. The experiments here (1) use the charge of the pion in D*(2010)[±] → (D⁰ or \bar{D}^0) π[±] decay to tell whether a D⁰ or a \bar{D}^0 was born; and (2) use the decay-time distribution to disentangle doubly Cabibbo-suppressed decay and mixing. For the limits on |m_{D₁⁰} - m_{D₂⁰}| and (Γ_{D₁⁰} - Γ_{D₂⁰})/Γ_{D₀} that come from the best mixing limit, see near the beginning of these D⁰ Listings.

VALUE (units 10 ⁻⁵)	CL%	DOCUMENT ID	TECN	COMMENT
9.6 ± 3.6		¹ AAIJ	16F LHCb	pp at 7, 8 TeV

- • • We do not use the following data for averages, fits, limits, etc. • • •
- <500 90 ²ANJOS 88c E691 Photoproduction
- ¹AAIJ 16F result comes from an unconstrained decay-time dependent fit to the wrong-sign to right-sign decay rates ratio as (x² + y²)/2.
- ²ANJOS 88c uses decay-time information to distinguish doubly Cabibbo-suppressed (DCS) decays from D⁰- \bar{D}^0 mixing. However, the result assumes no interference between the DCS and mixing amplitudes (y' = 0 in the note on “D⁰- \bar{D}^0 Mixing” near the start of the D⁰ Listings). When interference is allowed, the limit degrades to 0.007.

$\Gamma(K^+\pi^- \text{ or } K^+\pi^+2\pi^- \text{ via } \bar{D}^0)/\Gamma(K^-\pi^+ \text{ or } K^-2\pi^+\pi^-)$ Γ_{268}/Γ_{0}

This is a D⁰- \bar{D}^0 mixing limit. For the limits on |m_{D₁⁰} - m_{D₂⁰}| and (Γ_{D₀} - Γ_{D₂⁰})/Γ_{D₀} that come from the best mixing limit, see near the beginning of these D⁰ Listings.

VALUE	CL%	DOCUMENT ID	TECN	COMMENT
<0.0085	90	¹ AITALA	98 E791	π ⁻ nucleus, 500 GeV
<0.0037	90	² ANJOS	88c E691	Photoproduction

- • • We do not use the following data for averages, fits, limits, etc. • • •
- ¹AITALA 98 uses decay-time information to distinguish doubly Cabibbo-suppressed decays from D⁰- \bar{D}^0 mixing. The fit allows interference between the two amplitudes, and also allows CP violation in this term. The central value obtained is 0.0039 $\pm_{-0.0032}^{+0.0036}$ ± 0.0016. When interference is disallowed, the result becomes 0.0021 ± 0.0009 ± 0.0002.
- ²This combines results of ANJOS 88c on K⁺π⁻ and K⁺π⁺π⁺π⁻ (via \bar{D}^0) reported in the data block above (see footnotes there). It assumes no interference.

$\Gamma(\mu^- \text{ anything via } \bar{D}^0)/\Gamma(\mu^+ \text{ anything})$ Γ_{269}/Γ_6

This is a D⁰- \bar{D}^0 mixing limit. See the somewhat better limits above.

VALUE	CL%	DOCUMENT ID	TECN	COMMENT
<0.0056	90	LOUIS	86 SPEC	π ⁻ W 225 GeV
<0.012	90	BENVENUTI	85 CNTR	μC, 200 GeV
<0.044	90	BODEK	82 SPEC	π ⁻ , pFe → D ⁰

- • • We do not use the following data for averages, fits, limits, etc. • • •

Rare or forbidden modes

$\Gamma(\gamma\gamma)/\Gamma_{\text{total}}$ Γ_{270}/Γ

D⁰ → γγ is a flavor-changing neutral-current decay, forbidden in the Standard Model at the tree level.

VALUE	CL%	DOCUMENT ID	TECN	COMMENT
< 8.5 × 10⁻⁷	90	NISAR	16 BELL	e ⁺ e ⁻ at $\Upsilon(4S)$, $\Upsilon(5S)$
• • • We do not use the following data for averages, fits, limits, etc. • • •				
< 3.8 × 10 ⁻⁶	90	ABLIKIM	15F BES3	e ⁺ e ⁻ at 3.773 GeV
< 2.2 × 10 ⁻⁶	90	LEES	12L BABR	e ⁺ e ⁻ ≈ 10.58 GeV
< 29 × 10 ⁻⁶	90	COAN	03 CLE2	e ⁺ e ⁻ ≈ $\Upsilon(4S)$

$\Gamma(e^+e^-)/\Gamma_{\text{total}}$ Γ_{271}/Γ

A test for the ΔC = 1 weak neutral current. Allowed by first-order weak interaction combined with electromagnetic interaction.

VALUE	CL%	DOCUMENT ID	TECN	COMMENT
< 7.9 × 10⁻⁸	90	PETRIC	10 BELL	e ⁺ e ⁻ ≈ $\Upsilon(4S)$
• • • We do not use the following data for averages, fits, limits, etc. • • •				
< 1.7 × 10 ⁻⁷	90	LEES	12Q BABR	e ⁺ e ⁻ ≈ 10.58 GeV
< 1.2 × 10 ⁻⁶	90	AUBERT.B	04Y BABR	e ⁺ e ⁻ ≈ $\Upsilon(4S)$
< 8.19 × 10 ⁻⁶	90	PRIPSTEIN	00 E789	p nucleus, 800 GeV
< 6.2 × 10 ⁻⁶	90	AITALA	99G E791	π ⁻ N 500 GeV
< 1.3 × 10 ⁻⁵	90	FREYBERGER	96 CLE2	e ⁺ e ⁻ ≈ $\Upsilon(4S)$
< 1.3 × 10 ⁻⁴	90	ADLER	88 MRK3	e ⁺ e ⁻ 3.77 GeV
< 1.7 × 10 ⁻⁴	90	ALBRECHT	88G ARG	e ⁺ e ⁻ 10 GeV
< 2.2 × 10 ⁻⁴	90	HAAS	88 CLEO	e ⁺ e ⁻ 10 GeV

$\Gamma(\mu^+\mu^-)/\Gamma_{\text{total}}$ Γ_{272}/Γ

A test for the ΔC = 1 weak neutral current. Allowed by first-order weak interaction combined with electromagnetic interaction.

VALUE	CL%	DOCUMENT ID	TECN	COMMENT
< 6.2 × 10⁻⁹	90	AAIJ	13A LHCb	pp at 7 TeV
• • • We do not use the following data for averages, fits, limits, etc. • • •				
0.6–8.1 × 10 ⁻⁷	90	¹ LEES	12Q BABR	e ⁺ e ⁻ ≈ 10.58 GeV
< 2.1 × 10 ⁻⁷	90	AALTONEN	10X CDF	p \bar{p} , \sqrt{s} = 1.96 TeV
< 1.4 × 10 ⁻⁷	90	PETRIC	10 BELL	e ⁺ e ⁻ ≈ $\Upsilon(4S)$
< 2.0 × 10 ⁻⁶	90	ABT	04 HERB	pA, 920 GeV
< 1.3 × 10 ⁻⁶	90	AUBERT.B	04Y BABR	e ⁺ e ⁻ ≈ $\Upsilon(4S)$
< 2.5 × 10 ⁻⁶	90	ACOSTA	03F CDF	See AALTONEN 10X
< 1.56 × 10 ⁻⁵	90	PRIPSTEIN	00 E789	p nucleus, 800 GeV
< 5.2 × 10 ⁻⁶	90	AITALA	99G E791	π ⁻ N 500 GeV
< 4.1 × 10 ⁻⁶	90	ADAMOVIICH	97 BEAT	π ⁻ Cu, W 350 GeV
< 4.2 × 10 ⁻⁶	90	ALEXOPOU...	96 E771	p Si, 800 GeV
< 3.4 × 10 ⁻⁵	90	FREYBERGER	96 CLE2	e ⁺ e ⁻ ≈ $\Upsilon(4S)$
< 7.6 × 10 ⁻⁶	90	ADAMOVIICH	95 BEAT	See ADAMOVIICH 97
< 4.4 × 10 ⁻⁵	90	KODAMA	95 E653	π ⁻ emulsion 600 GeV
< 3.1 × 10 ⁻⁵	90	² MISHRA	94 E789	-4.1 ± 4.8 events
< 7.0 × 10 ⁻⁵	90	ALBRECHT	88G ARG	e ⁺ e ⁻ 10 GeV
< 1.1 × 10 ⁻⁵	90	LOUIS	86 SPEC	π ⁻ W 225 GeV
< 3.4 × 10 ⁻⁴	90	AUBERT	85 EMC	Deep inelast. μ ⁻ N

- ¹LEES 12Q gives a 2-sided range.
- ²Here MISHRA 94 uses “the statistical approach advocated by the PDG.” For an alternate approach, giving a limit of 9 × 10⁻⁶ at 90% confidence level, see the paper.

$\Gamma(\pi^0 e^+ e^-)/\Gamma_{\text{total}}$ Γ_{273}/Γ

A test for the ΔC = 1 weak neutral current. Allowed by higher-order electroweak interactions.

VALUE	CL%	DOCUMENT ID	TECN	COMMENT
< 4 × 10⁻⁶	90	ABLIKIM	18P BES3	e ⁺ e ⁻ , 3773 MeV
• • • We do not use the following data for averages, fits, limits, etc. • • •				
< 4.5 × 10 ⁻⁵	90	FREYBERGER	96 CLE2	e ⁺ e ⁻ ≈ $\Upsilon(4S)$

$\Gamma(\pi^0 \mu^+ \mu^-)/\Gamma_{\text{total}}$ Γ_{274}/Γ

A test for the ΔC=1 weak neutral current. Allowed by higher-order electroweak interactions.

VALUE	CL%	DOCUMENT ID	TECN	COMMENT
< 1.8 × 10⁻⁴	90	KODAMA	95 E653	π ⁻ emulsion 600 GeV
• • • We do not use the following data for averages, fits, limits, etc. • • •				
< 5.4 × 10 ⁻⁴	90	FREYBERGER	96 CLE2	e ⁺ e ⁻ ≈ $\Upsilon(4S)$

$\Gamma(\eta e^+ e^-)/\Gamma_{\text{total}}$ Γ_{275}/Γ

A test for the ΔC = 1 weak neutral current. Allowed by higher-order electroweak interactions.

VALUE	CL%	DOCUMENT ID	TECN	COMMENT
< 3 × 10⁻⁶	90	ABLIKIM	18P BES3	e ⁺ e ⁻ , 3773 MeV
• • • We do not use the following data for averages, fits, limits, etc. • • •				
< 1.1 × 10 ⁻⁴	90	FREYBERGER	96 CLE2	e ⁺ e ⁻ ≈ $\Upsilon(4S)$

$\Gamma(\eta \mu^+ \mu^-)/\Gamma_{\text{total}}$ Γ_{276}/Γ

A test for the ΔC = 1 weak neutral current. Allowed by higher-order electroweak interactions.

VALUE	CL%	DOCUMENT ID	TECN	COMMENT
< 5.3 × 10⁻⁴	90	FREYBERGER	96 CLE2	e ⁺ e ⁻ ≈ $\Upsilon(4S)$

Meson Particle Listings

 D^0 $\Gamma(\pi^+\pi^-\pi^+\pi^-)/\Gamma_{\text{total}}$ Γ_{277}/Γ

A test for the $\Delta C = 1$ weak neutral current. Allowed by higher-order electroweak interactions.

VALUE	CL%	DOCUMENT ID	TECN	COMMENT
$<7 \times 10^{-6}$	90	ABLIKIM 18P	BES3	e^+e^- , 3773 MeV
•••		We do not use the following data for averages, fits, limits, etc. •••		
$<3.73 \times 10^{-4}$	90	AITALA 01c	E791	π^- nucleus, 500 GeV

 $\Gamma(\rho^0 e^+ e^-)/\Gamma_{\text{total}}$ Γ_{278}/Γ

A test for the $\Delta C = 1$ weak neutral current. Allowed by higher-order electroweak interactions.

VALUE	CL%	DOCUMENT ID	TECN	COMMENT
$<1.0 \times 10^{-4}$	90	¹ FREYBERGER 96	CLE2	$e^+e^- \approx \Upsilon(4S)$
•••		We do not use the following data for averages, fits, limits, etc. •••		
$<1.24 \times 10^{-4}$	90	AITALA 01c	E791	π^- nucleus, 500 GeV
$<4.5 \times 10^{-4}$	90	HAAS 88	CLEO	e^+e^- 10 GeV

¹This FREYBERGER 96 limit is obtained using a phase-space model. The limit changes to $<1.8 \times 10^{-4}$ using a photon pole amplitude model.

 $\Gamma(\pi^+\pi^-\mu^+\mu^-)/\Gamma_{\text{total}}$ Γ_{279}/Γ

A test for the $\Delta C = 1$ weak neutral current. Allowed by higher-order electroweak interactions.

VALUE (units 10^{-7})	EVTS	DOCUMENT ID	TECN	COMMENT
$9.64 \pm 0.48 \pm 1.10$	561	¹ AAIJ	17Bg LHCb	pp at 8 TeV

¹The second AAJ17Bg error is the systematic 0.51×10^{-7} and normalization 0.97×10^{-7} mode errors added in quadrature.

 $\Gamma(\pi^+\pi^-\mu^+\mu^- \text{ (non-res)})/\Gamma_{\text{total}}$ Γ_{280}/Γ

A test for the $\Delta C = 1$ weak neutral current. Allowed by higher-order electroweak interactions.

VALUE	CL%	DOCUMENT ID	TECN	COMMENT
$<5.5 \times 10^{-7}$	90	¹ AAIJ	14B LHCb	pp at 7 TeV
•••		We do not use the following data for averages, fits, limits, etc. •••		
$<3.0 \times 10^{-5}$	90	AITALA 01c	E791	π^- nucleus, 500 GeV

¹AAIJ 14B measures this branching-fraction limit relative to the $\pi^+\pi^-\phi$, $\phi \rightarrow \mu^+\mu^-$ fraction. The above limit excludes the resonant ϕ , ω , and ρ regions, and then fills those gaps with a phase-space model.

 $\Gamma(\rho^0 \mu^+ \mu^-)/\Gamma_{\text{total}}$ Γ_{281}/Γ

A test for the $\Delta C = 1$ weak neutral current. Allowed by higher-order electroweak interactions.

VALUE	CL%	DOCUMENT ID	TECN	COMMENT
$<2.2 \times 10^{-5}$	90	AITALA 01c	E791	π^- nucleus, 500 GeV
•••		We do not use the following data for averages, fits, limits, etc. •••		
$<4.9 \times 10^{-4}$	90	¹ FREYBERGER 96	CLE2	$e^+e^- \approx \Upsilon(4S)$
$<2.3 \times 10^{-4}$	90	KODAMA 95	E653	π^- emulsion 600 GeV
$<8.1 \times 10^{-4}$	90	HAAS 88	CLEO	e^+e^- 10 GeV

¹This FREYBERGER 96 limit is obtained using a phase-space model. The limit changes to $<4.5 \times 10^{-4}$ using a photon pole amplitude model.

 $\Gamma(\omega e^+ e^-)/\Gamma_{\text{total}}$ Γ_{282}/Γ

A test for the $\Delta C = 1$ weak neutral current. Allowed by higher-order electroweak interactions.

VALUE	CL%	DOCUMENT ID	TECN	COMMENT
$<6 \times 10^{-6}$	90	ABLIKIM 18P	BES3	e^+e^- , 3773 MeV
•••		We do not use the following data for averages, fits, limits, etc. •••		
$<1.8 \times 10^{-4}$	90	¹ FREYBERGER 96	CLE2	$e^+e^- \approx \Upsilon(4S)$

¹This FREYBERGER 96 limit is obtained using a phase-space model. The limit changes to $<2.7 \times 10^{-4}$ using a photon pole amplitude model.

 $\Gamma(\omega \mu^+ \mu^-)/\Gamma_{\text{total}}$ Γ_{283}/Γ

A test for the $\Delta C = 1$ weak neutral current. Allowed by higher-order electroweak interactions.

VALUE	CL%	DOCUMENT ID	TECN	COMMENT
$<8.3 \times 10^{-4}$	90	¹ FREYBERGER 96	CLE2	$e^+e^- \approx \Upsilon(4S)$

¹This FREYBERGER 96 limit is obtained using a phase-space model. The limit changes to $<6.5 \times 10^{-4}$ using a photon pole amplitude model.

 $\Gamma(K^-K^+e^+e^-)/\Gamma_{\text{total}}$ Γ_{284}/Γ

A test for the $\Delta C = 1$ weak neutral current. Allowed by higher-order electroweak interactions.

VALUE	CL%	DOCUMENT ID	TECN	COMMENT
$<1.1 \times 10^{-5}$	90	ABLIKIM 18P	BES3	e^+e^- , 3773 MeV
•••		We do not use the following data for averages, fits, limits, etc. •••		
$<3.15 \times 10^{-4}$	90	AITALA 01c	E791	π^- nucleus, 500 GeV

 $\Gamma(K^- \pi^+ e^+ e^-, 675 < m_{ee} < 875 \text{ MeV})/\Gamma_{\text{total}}$ Γ_{292}/Γ

A test for the $\Delta C = 1$ weak neutral current. Allowed by higher-order electroweak interactions.

VALUE (units 10^{-6})	EVTS	DOCUMENT ID	TECN	COMMENT
$4.0 \pm 0.5 \pm 0.2 \pm 0.1$	68	^{1,2} LEES	19A BABR	e^+e^- near $\Upsilon(4S)$

¹Observation with 9.7 σ significance. The last uncertainty is due to the uncertainty on the branching fraction of the normalization mode, $D^0 \rightarrow K^- \pi^+ \pi^+ \pi^-$. The second uncertainty is other systematic and is dominated by the model parameterization.

²LEES 19A also sets an upper limit for non-resonant regions, where long-distance effects are expected to be small: $<3.1 \times 10^{-6}$ at 90% CL.

 $\Gamma(K^- \pi^+ e^+ e^-, 1.005 < m_{ee} < 1.035 \text{ GeV})/\Gamma_{\text{total}}$ Γ_{293}/Γ

A test for the $\Delta C = 1$ weak neutral current. Allowed by higher-order electroweak interactions.

VALUE	CL%	DOCUMENT ID	TECN	COMMENT
$<5 \times 10^{-7}$	90	¹ LEES	19A BABR	e^+e^- near $\Upsilon(4S)$

¹LEES 19A also sets an upper limit for non-resonant regions, where long-distance effects are expected to be small: $<3.1 \times 10^{-6}$ at 90% CL.

 $\Gamma(\phi e^+ e^-)/\Gamma_{\text{total}}$ Γ_{285}/Γ

A test for the $\Delta C = 1$ weak neutral current. Allowed by higher-order electroweak interactions.

VALUE	CL%	DOCUMENT ID	TECN	COMMENT
$<5.2 \times 10^{-5}$	90	¹ FREYBERGER 96	CLE2	$e^+e^- \approx \Upsilon(4S)$
•••		We do not use the following data for averages, fits, limits, etc. •••		
$<5.9 \times 10^{-5}$	90	AITALA 01c	E791	π^- nucleus, 500 GeV

¹This FREYBERGER 96 limit is obtained using a phase-space model. The limit changes to $<7.6 \times 10^{-5}$ using a photon pole amplitude model.

 $\Gamma(K^-K^+\mu^+\mu^-)/\Gamma_{\text{total}}$ Γ_{286}/Γ

A test for the $\Delta C = 1$ weak neutral current. Allowed by higher-order electroweak interactions.

VALUE (units 10^{-7})	EVTS	DOCUMENT ID	TECN	COMMENT
$1.54 \pm 0.27 \pm 0.18$	34	¹ AAIJ	17Bg LHCb	pp at 8 TeV

¹The second AAJ17Bg error is the systematic 0.09×10^{-7} and normalization 0.16×10^{-7} mode errors added in quadrature.

 $\Gamma(K^-K^+\mu^+\mu^- \text{ (non-res)})/\Gamma_{\text{total}}$ Γ_{287}/Γ

A test for the $\Delta C = 1$ weak neutral current. Allowed by higher-order electroweak interactions.

VALUE	CL%	DOCUMENT ID	TECN	COMMENT
$<3.3 \times 10^{-5}$	90	AITALA 01c	E791	π^- nucleus, 500 GeV

 $\Gamma(\phi \mu^+ \mu^-)/\Gamma_{\text{total}}$ Γ_{288}/Γ

A test for the $\Delta C = 1$ weak neutral current. Allowed by higher-order electroweak interactions.

VALUE	CL%	DOCUMENT ID	TECN	COMMENT
$<3.1 \times 10^{-5}$	90	AITALA 01c	E791	π^- nucleus, 500 GeV
•••		We do not use the following data for averages, fits, limits, etc. •••		
$<4.1 \times 10^{-4}$	90	¹ FREYBERGER 96	CLE2	$e^+e^- \approx \Upsilon(4S)$

¹This FREYBERGER 96 limit is obtained using a phase-space model. The limit changes to $<2.4 \times 10^{-4}$ using a photon pole amplitude model.

 $\Gamma(K^0 e^+ e^-)/\Gamma_{\text{total}}$ Γ_{289}/Γ

Not a useful test for $\Delta C = 1$ weak neutral current because both quarks must change flavor.

VALUE	CL%	DOCUMENT ID	TECN	COMMENT
$<2.4 \times 10^{-5}$	90	¹ ABLIKIM 18P	BES3	e^+e^- , 3773 MeV
•••		We do not use the following data for averages, fits, limits, etc. •••		
$<1.1 \times 10^{-4}$	90	FREYBERGER 96	CLE2	$e^+e^- \approx \Upsilon(4S)$
$<1.7 \times 10^{-3}$	90	ADLER 89c	MRK3	e^+e^- 3.77 GeV

¹ABLIKIM 18P report a 90% C.L. limit on $D^0 \rightarrow K_S^0 e^+ e^-$ of 1.2×10^{-5} which is here interpreted in terms of $D^0 \rightarrow \bar{K}^0 e^+ e^-$.

 $\Gamma(K^0 \mu^+ \mu^-)/\Gamma_{\text{total}}$ Γ_{290}/Γ

Not a useful test for $\Delta C = 1$ weak neutral current because both quarks must change flavor.

VALUE	CL%	DOCUMENT ID	TECN	COMMENT
$<2.6 \times 10^{-4}$	90	KODAMA 95	E653	π^- emulsion 600 GeV
•••		We do not use the following data for averages, fits, limits, etc. •••		
$<6.7 \times 10^{-4}$	90	FREYBERGER 96	CLE2	$e^+e^- \approx \Upsilon(4S)$

 $\Gamma(K^- \pi^+ e^+ e^-)/\Gamma_{\text{total}}$ Γ_{291}/Γ

A test for the $\Delta C = 1$ weak neutral current. Allowed by higher-order electroweak interactions.

VALUE	CL%	DOCUMENT ID	TECN	COMMENT
•••		We do not use the following data for averages, fits, limits, etc. •••		
$<4.1 \times 10^{-5}$	90	ABLIKIM 18P	BES3	see LEES 19A
$<3.85 \times 10^{-4}$	90	AITALA 01c	E791	π^- nucleus, 500 GeV

 $\Gamma(K^*(892)^0 e^+ e^-)/\Gamma_{\text{total}}$ Γ_{294}/Γ

Not a useful test for $\Delta C = 1$ weak neutral current because both quarks must change flavor.

VALUE	CL%	DOCUMENT ID	TECN	COMMENT
$<4.7 \times 10^{-5}$	90	AITALA 01c	E791	π^- nucleus, 500 GeV
•••		We do not use the following data for averages, fits, limits, etc. •••		
$<1.4 \times 10^{-4}$	90	¹ FREYBERGER 96	CLE2	$e^+e^- \approx \Upsilon(4S)$

¹This FREYBERGER 96 limit is obtained using a phase-space model. The limit changes to $<2.0 \times 10^{-4}$ using a photon pole amplitude model.

 $\Gamma(K^- \pi^+ \mu^+ \mu^-)/\Gamma_{\text{total}}$ Γ_{295}/Γ

A test for the $\Delta C = 1$ weak neutral current. Allowed by higher-order electroweak interactions.

VALUE	CL%	DOCUMENT ID	TECN	COMMENT
$<3.59 \times 10^{-4}$	90	AITALA 01c	E791	π^- nucleus, 500 GeV

$\Gamma(K^- \pi^+ \mu^+ \mu^-, 675 < m_{\mu\mu} < 875 \text{ MeV})/\Gamma_{\text{total}}$ Γ_{296}/Γ

VALUE (units 10^{-6})	EVTS	DOCUMENT ID	TECN	COMMENT
$4.17 \pm 0.12 \pm 0.40$	2.4k	¹ AAIJ	16i	LHCB pp at 8 TeV

¹ AAIJ 16i uses $B(D^0 \rightarrow K^- \pi^+ \pi^+ \pi^-) = (8.287 \pm 0.043 \pm 0.200) \times 10^{-2}$ value for the normalization mode.

$\Gamma(\bar{K}^*(892)^0 \mu^+ \mu^-)/\Gamma_{\text{total}}$ Γ_{297}/Γ

Not a useful test for $\Delta C=1$ weak neutral current because both quarks must change flavor.

VALUE	CL%	DOCUMENT ID	TECN	COMMENT
$< 2.4 \times 10^{-5}$	90	AITALA	01c	E791 π^- nucleus, 500 GeV
• • •				We do not use the following data for averages, fits, limits, etc. • • •
$< 1.18 \times 10^{-3}$	90	¹ FREYBERGER 96	CLE2	$e^+ e^- \approx \gamma(4S)$

¹ This FREYBERGER 96 limit is obtained using a phase-space model. The limit changes to $< 1.0 \times 10^{-3}$ using a photon pole amplitude model.

$\Gamma(\pi^+ \pi^- \pi^0 \mu^+ \mu^-)/\Gamma_{\text{total}}$ Γ_{298}/Γ

A test for the $\Delta C=1$ weak neutral current. Allowed by higher-order electroweak interactions.

VALUE	CL%	DOCUMENT ID	TECN	COMMENT
$< 8.1 \times 10^{-4}$	90	KODAMA	95	E653 π^- emulsion 600 GeV

$\Gamma(\mu^\pm e^\mp)/\Gamma_{\text{total}}$ Γ_{299}/Γ

A test of lepton family number conservation.

VALUE	CL%	DOCUMENT ID	TECN	COMMENT
$< 1.3 \times 10^{-8}$	90	AAIJ	16h	LHCB pp at 7, 8 GeV
• • •				We do not use the following data for averages, fits, limits, etc. • • •
$< 3.3 \times 10^{-7}$	90	LEES	12q	BABR $e^+ e^- \approx 10.58 \text{ GeV}$
$< 2.6 \times 10^{-7}$	90	PETRIC	10	BELL $e^+ e^- \approx \gamma(4S)$
$< 8.1 \times 10^{-7}$	90	AUBERT,B	04y	BABR $e^+ e^- \approx \gamma(4S)$
$< 1.72 \times 10^{-5}$	90	PRIPSTEIN	00	E789 p nucleus, 800 GeV
$< 8.1 \times 10^{-6}$	90	AITALA	99g	E791 $\pi^- N$ 500 GeV
$< 1.9 \times 10^{-5}$	90	¹ FREYBERGER 96	CLE2	$e^+ e^- \approx \gamma(4S)$
$< 1.0 \times 10^{-4}$	90	ALBRECHT	88g	ARG $e^+ e^-$ 10 GeV
$< 2.7 \times 10^{-4}$	90	HAAS	88	CLEO $e^+ e^-$ 10 GeV
$< 1.2 \times 10^{-4}$	90	BECKER	87c	MRK3 $e^+ e^-$ 3.77 GeV
$< 9 \times 10^{-4}$	90	PALKA	87	SIL1 200 GeV πp
$< 21 \times 10^{-4}$	90	² RILES	87	MRK2 $e^+ e^-$ 29 GeV

¹ This is the corrected result given in the erratum to FREYBERGER 96.
² RILES 87 assumes $B(D \rightarrow K \pi) = 3.0\%$ and has production model dependency.

$\Gamma(\pi^0 e^\pm \mu^\mp)/\Gamma_{\text{total}}$ Γ_{300}/Γ

A test of lepton family number conservation. The value is for the sum of the two charge states.

VALUE	CL%	DOCUMENT ID	TECN	COMMENT
$< 8.6 \times 10^{-5}$	90	FREYBERGER 96	CLE2	$e^+ e^- \approx \gamma(4S)$

$\Gamma(\eta e^\pm \mu^\mp)/\Gamma_{\text{total}}$ Γ_{301}/Γ

A test of lepton family number conservation. The value is for the sum of the two charge states.

VALUE	CL%	DOCUMENT ID	TECN	COMMENT
$< 1.0 \times 10^{-4}$	90	FREYBERGER 96	CLE2	$e^+ e^- \approx \gamma(4S)$

$\Gamma(\pi^+ \pi^- e^\pm \mu^\mp)/\Gamma_{\text{total}}$ Γ_{302}/Γ

A test of lepton family-number conservation. The value is for the sum of the two charge states.

VALUE	CL%	DOCUMENT ID	TECN	COMMENT
$< 1.5 \times 10^{-5}$	90	AITALA	01c	E791 π^- nucleus, 500 GeV

$\Gamma(\rho^0 e^\pm \mu^\mp)/\Gamma_{\text{total}}$ Γ_{303}/Γ

A test of lepton family number conservation. The value is for the sum of the two charge states.

VALUE	CL%	DOCUMENT ID	TECN	COMMENT
$< 4.9 \times 10^{-5}$	90	¹ FREYBERGER 96	CLE2	$e^+ e^- \approx \gamma(4S)$
• • •				We do not use the following data for averages, fits, limits, etc. • • •
$< 6.6 \times 10^{-5}$	90	AITALA	01c	E791 π^- nucleus, 500 GeV

¹ This FREYBERGER 96 limit is obtained using a phase-space model. The limit changes to $< 5.0 \times 10^{-5}$ using a photon pole amplitude model.

$\Gamma(\omega e^\pm \mu^\mp)/\Gamma_{\text{total}}$ Γ_{304}/Γ

A test of lepton family number conservation. The value is for the sum of the two charge states.

VALUE	CL%	DOCUMENT ID	TECN	COMMENT
$< 1.2 \times 10^{-4}$	90	¹ FREYBERGER 96	CLE2	$e^+ e^- \approx \gamma(4S)$

¹ This FREYBERGER 96 limit is obtained using a phase-space model. The same limit is obtained using a photon pole amplitude model.

$\Gamma(K^- K^+ e^\pm \mu^\mp)/\Gamma_{\text{total}}$ Γ_{305}/Γ

A test of lepton family-number conservation. The value is for the sum of the two charge states.

VALUE	CL%	DOCUMENT ID	TECN	COMMENT
$< 1.8 \times 10^{-4}$	90	AITALA	01c	E791 π^- nucleus, 500 GeV

$\Gamma(\phi e^\pm \mu^\mp)/\Gamma_{\text{total}}$ Γ_{306}/Γ

A test of lepton family number conservation. The value is for the sum of the two charge states.

VALUE	CL%	DOCUMENT ID	TECN	COMMENT
$< 3.4 \times 10^{-5}$	90	¹ FREYBERGER 96	CLE2	$e^+ e^- \approx \gamma(4S)$
• • •				We do not use the following data for averages, fits, limits, etc. • • •
$< 4.7 \times 10^{-5}$	90	AITALA	01c	E791 π^- nucleus, 500 GeV

¹ This FREYBERGER 96 limit is obtained using a phase-space model. The limit changes to $< 3.3 \times 10^{-5}$ using a photon pole amplitude model.

$\Gamma(\bar{K}^0 e^\pm \mu^\mp)/\Gamma_{\text{total}}$ Γ_{307}/Γ

A test of lepton family number conservation. The value is for the sum of the two charge states.

VALUE	CL%	DOCUMENT ID	TECN	COMMENT
$< 1.0 \times 10^{-4}$	90	FREYBERGER 96	CLE2	$e^+ e^- \approx \gamma(4S)$

$\Gamma(K^- \pi^+ e^\pm \mu^\mp)/\Gamma_{\text{total}}$ Γ_{308}/Γ

A test of lepton family-number conservation. The value is for the sum of the two charge states.

VALUE	CL%	DOCUMENT ID	TECN	COMMENT
$< 5.53 \times 10^{-4}$	90	AITALA	01c	E791 π^- nucleus, 500 GeV

$\Gamma(\bar{K}^*(892)^0 e^\pm \mu^\mp)/\Gamma_{\text{total}}$ Γ_{309}/Γ

A test of lepton family number conservation. The value is for the sum of the two charge states.

VALUE	CL%	DOCUMENT ID	TECN	COMMENT
$< 8.3 \times 10^{-5}$	90	AITALA	01c	E791 π^- nucleus, 500 GeV
• • •				We do not use the following data for averages, fits, limits, etc. • • •
$< 1.0 \times 10^{-4}$	90	¹ FREYBERGER 96	CLE2	$e^+ e^- \approx \gamma(4S)$

¹ This FREYBERGER 96 limit is obtained using a phase-space model. The same limit is obtained using a photon pole amplitude model.

$\Gamma(2\pi^- 2e^+ + c.c.)/\Gamma_{\text{total}}$ Γ_{310}/Γ

A test of lepton-number conservation. The value is for the sum of the two charge states.

VALUE	CL%	DOCUMENT ID	TECN	COMMENT
$< 1.12 \times 10^{-4}$	90	AITALA	01c	E791 π^- nucleus, 500 GeV

$\Gamma(2\pi^- 2\mu^+ + c.c.)/\Gamma_{\text{total}}$ Γ_{311}/Γ

A test of lepton-number conservation. The value is for the sum of the two charge states.

VALUE	CL%	DOCUMENT ID	TECN	COMMENT
$< 2.9 \times 10^{-5}$	90	AITALA	01c	E791 π^- nucleus, 500 GeV

$\Gamma(K^- \pi^- 2e^+ + c.c.)/\Gamma_{\text{total}}$ Γ_{312}/Γ

A test of lepton-number conservation. The value is for the sum of the two charge states.

VALUE	CL%	DOCUMENT ID	TECN	COMMENT
$< 2.06 \times 10^{-4}$	90	¹ AITALA	01c	E791 π^- nucleus, 500 GeV

¹ ABLIKIM 19AL find $\Gamma(D^0 \rightarrow K^- \pi^- 2e^+)/\Gamma(\text{total}) < 2.8 \times 10^{-6}$ at 90% CL (note their limit does not include decay to c.c. final state).

$\Gamma(K^- \pi^- 2e^+)/\Gamma_{\text{total}}$ Γ_{313}/Γ

VALUE	CL%	DOCUMENT ID	TECN	COMMENT
$< 2.8 \times 10^{-6}$	90	ABLIKIM	19AL	BES3 $e^+ e^-$ at 3773 MeV

$\Gamma(K^- \pi^- 2\mu^+ + c.c.)/\Gamma_{\text{total}}$ Γ_{314}/Γ

A test of lepton-number conservation. The value is for the sum of the two charge states.

VALUE	CL%	DOCUMENT ID	TECN	COMMENT
$< 3.9 \times 10^{-4}$	90	AITALA	01c	E791 π^- nucleus, 500 GeV

$\Gamma(2K^- 2e^+ + c.c.)/\Gamma_{\text{total}}$ Γ_{315}/Γ

A test of lepton-number conservation. The value is for the sum of the two charge states.

VALUE	CL%	DOCUMENT ID	TECN	COMMENT
$< 1.52 \times 10^{-4}$	90	AITALA	01c	E791 π^- nucleus, 500 GeV

$\Gamma(2K^- 2\mu^+ + c.c.)/\Gamma_{\text{total}}$ Γ_{316}/Γ

A test of lepton-number conservation. The value is for the sum of the two charge states.

VALUE	CL%	DOCUMENT ID	TECN	COMMENT
$< 9.4 \times 10^{-5}$	90	AITALA	01c	E791 π^- nucleus, 500 GeV

$\Gamma(\pi^- \pi^- e^+ \mu^+ + c.c.)/\Gamma_{\text{total}}$ Γ_{317}/Γ

A test of lepton-number conservation. The value is for the sum of the two charge states.

VALUE	CL%	DOCUMENT ID	TECN	COMMENT
$< 7.9 \times 10^{-5}$	90	AITALA	01c	E791 π^- nucleus, 500 GeV

$\Gamma(K^- \pi^- e^+ \mu^+ + c.c.)/\Gamma_{\text{total}}$ Γ_{318}/Γ

A test of lepton-number conservation. The value is for the sum of the two charge states.

VALUE	CL%	DOCUMENT ID	TECN	COMMENT
$< 2.18 \times 10^{-4}$	90	AITALA	01c	E791 π^- nucleus, 500 GeV

Meson Particle Listings

D^0

$\Gamma(2K^- e^+ \mu^+ + \text{c.c.})/\Gamma_{\text{total}}$ Γ_{319}/Γ
 A test of lepton-number conservation. The value is for the sum of the two charge states.

VALUE	CL%	DOCUMENT ID	TECN	COMMENT
$<5.7 \times 10^{-5}$	90	AITALA	01c	E791 π^- nucleus, 500 GeV

$\Gamma(p e^-)/\Gamma_{\text{total}}$ Γ_{320}/Γ
 A test of baryon- and lepton-number conservation.

VALUE	CL%	DOCUMENT ID	TECN	COMMENT
$<1.0 \times 10^{-5}$	90	1 RUBIN	09	CLEO $e^+ e^-$ at $\psi(3770)$

¹This RUBIN 09 limit is for either $D^0 \rightarrow p e^-$ or $\bar{D}^0 \rightarrow p e^-$ decay.

$\Gamma(\bar{p} e^+)/\Gamma_{\text{total}}$ Γ_{321}/Γ
 A test of baryon- and lepton-number conservation.

VALUE	CL%	DOCUMENT ID	TECN	COMMENT
$<1.1 \times 10^{-5}$	90	1 RUBIN	09	CLEO $e^+ e^-$ at $\psi(3770)$

¹This RUBIN 09 limit is for either $D^0 \rightarrow \bar{p} e^+$ or $\bar{D}^0 \rightarrow \bar{p} e^+$ decay.

D^0 CP-VIOLATING DECAY-RATE ASYMMETRIES

This is the difference between D^0 and \bar{D}^0 partial widths for the decay to state f , divided by the sum of the widths:
 $A_{CP}(f) = [\Gamma(D^0 \rightarrow f) - \Gamma(\bar{D}^0 \rightarrow \bar{f})] / [\Gamma(D^0 \rightarrow f) + \Gamma(\bar{D}^0 \rightarrow \bar{f})]$.

$A_{CP}(K^+ K^-)$ in $D^0, \bar{D}^0 \rightarrow K^+ K^-$

VALUE (%)	EVTS	DOCUMENT ID	TECN	COMMENT
-0.07 ± 0.11 OUR AVERAGE				
$0.04 \pm 0.12 \pm 0.10$	4.56M	AALJ	17M	LHCB pp 7, 8 TeV
$-0.24 \pm 0.22 \pm 0.09$	476k	1 AALTONEN	12B	CDF $p\bar{p}$, $\sqrt{s}=1.96$ TeV
$0.00 \pm 0.34 \pm 0.13$	129k	2 AUBERT	08M	BABR $e^+ e^- \approx 10.6$ GeV
$-0.43 \pm 0.30 \pm 0.11$	120k	3 STARIC	08	BELL $e^+ e^- \approx \Upsilon(4S)$
$+2.0 \pm 1.2 \pm 0.6$		4 ACOSTA	05c	CDF $p\bar{p}$, $\sqrt{s}=1.96$ TeV
$0.0 \pm 2.2 \pm 0.8$	3023	4 CSORNA	02	CLE2 $e^+ e^- \approx \Upsilon(4S)$
$-0.1 \pm 2.2 \pm 1.5$	3330	4 LINK	00B	FOCS
$-1.0 \pm 4.9 \pm 1.2$	609	4 AITALA	98c	E791 $-0.093 < A_{CP} < +0.073$ (90% CL)

- • • We do not use the following data for averages, fits, limits, etc. • • •
- $-0.06 \pm 0.15 \pm 0.10$ 1.8M 1 AALJ 14AK LHCB See AALJ 17M
- ¹See also " D^0 CP-violating asymmetry differences" at the end of the CP-violating asymmetries.
- ²AUBERT 08M uses corrected numbers of events directly, not ratios with $K^\mp \pi^\pm$ events.
- ³STARIC 08 uses $D^0 \rightarrow K^- \pi^+$ and $\bar{D}^0 \rightarrow K^+ \pi^-$ decays to correct for detector-induced asymmetries.
- ⁴AITALA 98c, LINK 00b, CSORNA 02, and ACOSTA 05c measure $N(D^0 \rightarrow K^+ K^-)/N(D^0 \rightarrow K^- \pi^+)$, the ratio of numbers of events observed, and similarly for the \bar{D}^0 .

$A_{CP}(K_S^0 K_S^0)$ in $D^0, \bar{D}^0 \rightarrow K_S^0 K_S^0$

VALUE (%)	EVTS	DOCUMENT ID	TECN	COMMENT
0.4 ± 1.4 OUR AVERAGE				
$2.3 \pm 2.8 \pm 0.9$	1.7k	AALJ	18AV	LHCB pp at 7, 8, 13 TeV
$-0.02 \pm 1.53 \pm 0.17$	5.4k	1 DASH	17	BELL At/near $\Upsilon(4S)$, $\Upsilon(5S)$
-23 ± 19	65	BONVICINI	01	CLE2 $e^+ e^- \approx 10.6$ GeV

- • • We do not use the following data for averages, fits, limits, etc. • • •
- $-2.9 \pm 5.2 \pm 2.2$ 630 AALJ 15AT LHCB see AALJ 18AV
- ¹The systematic uncertainty is dominated by the uncertainty on A_{CP} in the control channel $D^0 \rightarrow K_S^0 \pi^0$.

$A_{CP}(\pi^+ \pi^-)$ in $D^0, \bar{D}^0 \rightarrow \pi^+ \pi^-$

VALUE (%)	EVTS	DOCUMENT ID	TECN	COMMENT
0.13 ± 0.14 OUR AVERAGE				
$0.07 \pm 0.14 \pm 0.11$		1 AALJ	17M	LHCB pp 7, 8 TeV
$0.22 \pm 0.24 \pm 0.11$	215k	2 AALTONEN	12B	CDF $p\bar{p}$, $\sqrt{s}=1.96$ TeV
$-0.24 \pm 0.52 \pm 0.22$	63.7k	3 AUBERT	08M	BABR $e^+ e^- \approx 10.6$ GeV
$0.43 \pm 0.52 \pm 0.12$	51k	4 STARIC	08	BELL $e^+ e^- \approx \Upsilon(4S)$
$1.0 \pm 1.3 \pm 0.6$		5 ACOSTA	05c	CDF $p\bar{p}$, $\sqrt{s}=1.96$ TeV
$1.9 \pm 3.2 \pm 0.8$	1136	5 CSORNA	02	CLE2 $e^+ e^- \approx \Upsilon(4S)$
$4.8 \pm 3.9 \pm 2.5$	1177	5 LINK	00B	FOCS
$-4.9 \pm 7.8 \pm 3.0$	343	5 AITALA	98c	E791 $-0.186 < A_{CP} < +0.088$ (90% CL)

- • • We do not use the following data for averages, fits, limits, etc. • • •
- $-0.20 \pm 0.19 \pm 0.10$ 774k ^{2,6}AALJ 14AK LHCB See AALJ 17M
- ¹AALJ 17M value combines $\Delta A_{CP}(\pi\pi, KK)$ from AALJ 16d, $A_{CP}(KK)$ from AALJ 17M, and $A_{CP}(\pi\pi)$ from AALJ 14AK.
- ²See also " D^0 CP-violating asymmetry differences" at the end of the CP-violating asymmetries.
- ³AUBERT 08M uses corrected numbers of events directly, not ratios with $K^\mp \pi^\pm$ events.
- ⁴STARIC 08 uses $D^0 \rightarrow K^- \pi^+$ and $\bar{D}^0 \rightarrow K^+ \pi^-$ decays to correct for detector-induced asymmetries.
- ⁵AITALA 98c, LINK 00b, CSORNA 02, and ACOSTA 05c measure $N(D^0 \rightarrow \pi^+ \pi^-)/N(D^0 \rightarrow K^- \pi^+)$, the ratio of numbers of events observed, and similarly for the \bar{D}^0 .
- ⁶AALJ 14AK uses $\Delta A_{CP}(\pi\pi, KK)$ and $A_{CP}(KK)$ reported in the same paper.

$A_{CP}(\pi^0 \pi^0)$ in $D^0, \bar{D}^0 \rightarrow \pi^0 \pi^0$

VALUE (%)	EVTS	DOCUMENT ID	TECN	COMMENT
0.0 ± 0.6 OUR AVERAGE				
$-0.03 \pm 0.64 \pm 0.10$	34k	NISAR	14	BELL $e^+ e^-$ at/near Υ 's
0.1 ± 4.8	810	BONVICINI	01	CLE2 $e^+ e^- \approx 10.6$ GeV

$A_{CP}(\rho\gamma)$ in $D^0, \bar{D}^0 \rightarrow \rho\gamma$

VALUE (units 10^{-2})	DOCUMENT ID	TECN	COMMENT
$5.6 \pm 15.2 \pm 0.6$	NANUT	17	BELL $e^+ e^-$ at $\Upsilon(nS)$, $n=2,3,4,5$

$A_{CP}(\phi\gamma)$ in $D^0, \bar{D}^0 \rightarrow \phi\gamma$

VALUE (units 10^{-2})	DOCUMENT ID	TECN	COMMENT
$-9.4 \pm 6.6 \pm 0.1$	NANUT	17	BELL $e^+ e^-$ at $\Upsilon(nS)$, $n=2,3,4,5$

$A_{CP}(K^*(892)^0 \gamma)$ in $D^0, \bar{D}^0 \rightarrow K^*(892)^0 \gamma$

VALUE (units 10^{-2})	DOCUMENT ID	TECN	COMMENT
$-0.3 \pm 2.0 \pm 0.0$	NANUT	17	BELL $e^+ e^-$ at $\Upsilon(nS)$, $n=2,3,4,5$

$A_{CP}(\pi^+ \pi^- \pi^0)$ in $D^0, \bar{D}^0 \rightarrow \pi^+ \pi^- \pi^0$

VALUE (%)	EVTS	DOCUMENT ID	TECN	COMMENT
0.3 ± 0.4 OUR AVERAGE				
0.43 ± 1.30	123k±490	ARINSTEIN	08	BELL $e^+ e^- \approx \Upsilon(4S)$
$0.31 \pm 0.41 \pm 0.17$	80 ± .3k	1 AUBERT	08A0	BABR $e^+ e^- \approx 10.6$ GeV
$1 \pm \frac{+9}{-7} \pm 5$		CRONIN-HEN..05		CLEO $e^+ e^- \approx 10$ GeV

¹AUBERT 08A0 report their result using a different sign convention.

$A_{CP}(\rho(770)^+ \pi^- \rightarrow \pi^+ \pi^- \pi^0)$ in $D^0 \rightarrow \rho^+ \pi^-, \bar{D}^0 \rightarrow \rho^- \pi^+$

VALUE (%)	DOCUMENT ID	TECN	COMMENT
$+1.2 \pm 0.8 \pm 0.3$	AUBERT	08A0	BABR Table 1, -Col.5/2×Col.2

$A_{CP}(\rho(770)^0 \pi^0 \rightarrow \pi^+ \pi^- \pi^0)$ in $D^0, \bar{D}^0 \rightarrow \rho^0 \pi^0$

VALUE (%)	DOCUMENT ID	TECN	COMMENT
$-3.1 \pm 2.7 \pm 1.2$	AUBERT	08A0	BABR Table 1, -Col.5/2×Col.2

$A_{CP}(\rho(770)^- \pi^+ \rightarrow \pi^+ \pi^- \pi^0)$ in $D^0 \rightarrow \rho^- \pi^+, \bar{D}^0 \rightarrow \rho^+ \pi^-$

VALUE (%)	DOCUMENT ID	TECN	COMMENT
$-1.0 \pm 1.6 \pm 0.7$	AUBERT	08A0	BABR Table 1, -Col.5/2×Col.2

$A_{CP}(\rho(1450)^+ \pi^- \rightarrow \pi^+ \pi^- \pi^0)$ in $D^0 \rightarrow \rho(1450)^+ \pi^-, \bar{D}^0 \rightarrow \text{c.c.}$

VALUE (%)	DOCUMENT ID	TECN	COMMENT
$0 \pm 50 \pm 50$	AUBERT	08A0	BABR Table 1, -Col.5/2×Col.2

$A_{CP}(\rho(1450)^0 \pi^0 \rightarrow \pi^+ \pi^- \pi^0)$ in $D^0, \bar{D}^0 \rightarrow \rho(1450)^0 \pi^0$

VALUE (%)	DOCUMENT ID	TECN	COMMENT
$-17 \pm 33 \pm 17$	AUBERT	08A0	BABR Table 1, -Col.5/2×Col.2

$A_{CP}(\rho(1450)^- \pi^+ \rightarrow \pi^+ \pi^- \pi^0)$ in $D^0 \rightarrow \rho(1450)^- \pi^+, \bar{D}^0 \rightarrow \text{c.c.}$

VALUE (%)	DOCUMENT ID	TECN	COMMENT
$+6 \pm 8 \pm 3$	AUBERT	08A0	BABR Table 1, -Col.5/2×Col.2

$A_{CP}(\rho(1700)^+ \pi^- \rightarrow \pi^+ \pi^- \pi^0)$ in $D^0 \rightarrow \rho(1700)^+ \pi^-, \bar{D}^0 \rightarrow \text{c.c.}$

VALUE (%)	DOCUMENT ID	TECN	COMMENT
$-5 \pm 13 \pm 5$	AUBERT	08A0	BABR Table 1, -Col.5/2×Col.2

$A_{CP}(\rho(1700)^0 \pi^0 \rightarrow \pi^+ \pi^- \pi^0)$ in $D^0, \bar{D}^0 \rightarrow \rho(1700)^0 \pi^0$

VALUE (%)	DOCUMENT ID	TECN	COMMENT
$+13 \pm 8 \pm 3$	AUBERT	08A0	BABR Table 1, -Col.5/2×Col.2

$A_{CP}(\rho(1700)^- \pi^+ \rightarrow \pi^+ \pi^- \pi^0)$ in $D^0 \rightarrow \rho(1700)^- \pi^+, \bar{D}^0 \rightarrow \text{c.c.}$

VALUE (%)	DOCUMENT ID	TECN	COMMENT
$+8 \pm 10 \pm 5$	AUBERT	08A0	BABR Table 1, -Col.5/2×Col.2

$A_{CP}(f_0(980) \pi^0 \rightarrow \pi^+ \pi^- \pi^0)$ in $D^0, \bar{D}^0 \rightarrow f_0(980) \pi^0$

VALUE (%)	DOCUMENT ID	TECN	COMMENT
$0 \pm 25 \pm 25$	AUBERT	08A0	BABR Table 1, -Col.5/2×Col.2

$A_{CP}(f_0(1370) \pi^0 \rightarrow \pi^+ \pi^- \pi^0)$ in $D^0, \bar{D}^0 \rightarrow f_0(1370) \pi^0$

VALUE (%)	DOCUMENT ID	TECN	COMMENT
$+25 \pm 13 \pm 13$	AUBERT	08A0	BABR Table 1, -Col.5/2×Col.2

$A_{CP}(f_0(1500) \pi^0 \rightarrow \pi^+ \pi^- \pi^0)$ in $D^0, \bar{D}^0 \rightarrow f_0(1500) \pi^0$

VALUE (%)	DOCUMENT ID	TECN	COMMENT
$0 \pm 13 \pm 13$	AUBERT	08A0	BABR Table 1, -Col.5/2×Col.2

$A_{CP}(f_0(1710) \pi^0 \rightarrow \pi^+ \pi^- \pi^0)$ in $D^0, \bar{D}^0 \rightarrow f_0(1710) \pi^0$

VALUE (%)	DOCUMENT ID	TECN	COMMENT
$0 \pm 17 \pm 17$	AUBERT	08A0	BABR Table 1, -Col.5/2×Col.2

$A_{CP}(f_2(1270) \pi^0 \rightarrow \pi^+ \pi^- \pi^0)$ in $D^0, \bar{D}^0 \rightarrow f_2(1270) \pi^0$

VALUE (%)	DOCUMENT ID	TECN	COMMENT
$-4 \pm 4 \pm 4$	AUBERT	08A0	BABR Table 1, -Col.5/2×Col.2

See key on page 999

Meson Particle Listings

D^0

$A_{CP}(\sigma(400)\pi^0 \rightarrow \pi^+\pi^-\pi^0)$ in $D^0, \bar{D}^0 \rightarrow \sigma(400)\pi^0$

VALUE (%)	DOCUMENT ID	TECN	COMMENT
$+6 \pm 6 \pm 6$	AUBERT	08AO BABR	Table 1, -Col.5/2×Col.2

$A_{CP}(\text{nonresonant } \pi^+\pi^-\pi^0)$ in $D^0, \bar{D}^0 \rightarrow \text{nonresonant } \pi^+\pi^-\pi^0$

VALUE (%)	DOCUMENT ID	TECN	COMMENT
$-13 \pm 19 \pm 13$	AUBERT	08AO BABR	Table 1, -Col.5/2×Col.2

$A_{CP}(2\pi^+2\pi^-)$ in $D^0, \bar{D}^0 \rightarrow 2\pi^+2\pi^-$

VALUE (%)	EVTS	DOCUMENT ID	TECN	COMMENT
$0.54 \pm 1.04 \pm 0.51$	7.3k	1,2 DARGENT	17	e^+e^- at $\psi(3770)$

¹ Decay rate asymmetry integrated in decay time and across full 4π phase space.
² Obtained by analyzing CLEO-c data but not authored by the CLEO Collaboration.

$A_{CP}(a_1(1260)^+\pi^- \rightarrow 2\pi^+2\pi^-)$ in $D^0 \rightarrow a_1(1260)^+\pi^-, \bar{D}^0 \rightarrow \text{c.c.}$

VALUE (%)	EVTS	DOCUMENT ID	TECN	COMMENT
$4.7 \pm 2.6 \pm 4.9$	7.3k	¹ DARGENT	17	4-body fit, 4π evts

¹ Obtained by analyzing CLEO-c data but not authored by the CLEO Collaboration.

$A_{CP}(a_1(1260)^-\pi^+ \rightarrow 2\pi^+2\pi^-)$ in $D^0 \rightarrow a_1(1260)^-\pi^+, \bar{D}^0 \rightarrow \text{c.c.}$

VALUE (%)	EVTS	DOCUMENT ID	TECN	COMMENT
$13.7 \pm 13.8 \pm 11.4$	7.3k	¹ DARGENT	17	4-body fit, 4π evts

¹ Obtained by analyzing CLEO-c data but not authored by the CLEO Collaboration.

$A_{CP}(\pi(1300)^+\pi^- \rightarrow 2\pi^+2\pi^-)$ in $D^0 \rightarrow \pi(1300)^+\pi^-, \bar{D}^0 \rightarrow \text{c.c.}$

VALUE (%)	EVTS	DOCUMENT ID	TECN	COMMENT
$-1.6 \pm 12.9 \pm 6.7$	7.3k	¹ DARGENT	17	4-body fit, 4π evts

¹ Obtained by analyzing CLEO-c data but not authored by the CLEO Collaboration.

$A_{CP}(\pi(1300)^-\pi^+ \rightarrow 2\pi^+2\pi^-)$ in $D^0 \rightarrow \pi(1300)^-\pi^+, \bar{D}^0 \rightarrow \text{c.c.}$

VALUE (%)	EVTS	DOCUMENT ID	TECN	COMMENT
$-5.6 \pm 11.9 \pm 27.7$	7.3k	¹ DARGENT	17	4-body fit, 4π evts

¹ Obtained by analyzing CLEO-c data but not authored by the CLEO Collaboration.

$A_{CP}(a_1(1640)^+\pi^- \rightarrow 2\pi^+2\pi^-)$ in $D^0 \rightarrow a_1(1640)^+\pi^-, \bar{D}^0 \rightarrow \text{c.c.}$

VALUE (%)	EVTS	DOCUMENT ID	TECN	COMMENT
$8.6 \pm 17.8 \pm 19.3$	7.3k	¹ DARGENT	17	4-body fit, 4π evts

¹ Obtained by analyzing CLEO-c data but not authored by the CLEO Collaboration.

$A_{CP}(\pi_2(1670)^+\pi^- \rightarrow 2\pi^+2\pi^-)$ in $D^0 \rightarrow \pi_2(1670)^+\pi^-, \bar{D}^0 \rightarrow \text{c.c.}$

VALUE (%)	EVTS	DOCUMENT ID	TECN	COMMENT
$7.3 \pm 15.1 \pm 10.4$	7.3k	¹ DARGENT	17	4-body fit, 4π evts

¹ Obtained by analyzing CLEO-c data but not authored by the CLEO Collaboration.

$A_{CP}(\sigma f_0(1370) \rightarrow 2\pi^+2\pi^-)$ in $D^0, \bar{D}^0 \rightarrow \sigma f_0(1370)$

VALUE (%)	EVTS	DOCUMENT ID	TECN	COMMENT
$-14.6 \pm 16.5 \pm 9.4$	7.3k	¹ DARGENT	17	4-body fit, 4π evts

¹ Obtained by analyzing CLEO-c data but not authored by the CLEO Collaboration.

$A_{CP}(\sigma\rho(770)^0 \rightarrow 2\pi^+2\pi^-)$ in $D^0, \bar{D}^0 \rightarrow \sigma\rho(770)^0$

VALUE (%)	EVTS	DOCUMENT ID	TECN	COMMENT
$2.5 \pm 16.8 \pm 20.8$	7.3k	¹ DARGENT	17	4-body fit, 4π evts

¹ Obtained by analyzing CLEO-c data but not authored by the CLEO Collaboration.

$A_{CP}(2\rho(770)^0 \rightarrow 2\pi^+2\pi^-)$ in $D^0, \bar{D}^0 \rightarrow 2\rho(770)^0$

VALUE (%)	EVTS	DOCUMENT ID	TECN	COMMENT
$-5.6 \pm 5.0 \pm 2.9$	7.3k	¹ DARGENT	17	4-body fit, 4π evts

¹ Obtained by analyzing CLEO-c data but not authored by the CLEO Collaboration.

$A_{CP}(2f_2(1270) \rightarrow 2\pi^+2\pi^-)$ in $D^0, \bar{D}^0 \rightarrow 2f_2(1270)$

VALUE (%)	EVTS	DOCUMENT ID	TECN	COMMENT
$-28.3 \pm 12.3 \pm 20.9$	7.3k	¹ DARGENT	17	4-body fit, 4π evts

¹ Obtained by analyzing CLEO-c data but not authored by the CLEO Collaboration.

$A_{CP}(K^+K^-\pi^0)$ in $D^0, \bar{D}^0 \rightarrow K^+K^-\pi^0$

VALUE (%)	EVTS	DOCUMENT ID	TECN	COMMENT
$-1.00 \pm 1.67 \pm 0.25$	$11 \pm 0.11k$	AUBERT	08AO BABR	$e^+e^- \approx 10.6$ GeV

$A_{CP}(K^*(892)^+K^- \rightarrow K^+K^-\pi^0)$ in $D^0 \rightarrow K^*(892)^+K^-, \bar{D}^0 \rightarrow \text{c.c.}$

VALUE (%)	DOCUMENT ID	TECN	COMMENT
$-0.9 \pm 1.2 \pm 0.4$	¹ AUBERT	08AO BABR	Table 1, -Col.5/2×Col.2

¹ AUBERT 08AO report their result using a different sign convention.

$A_{CP}(K^*(1410)^+K^- \rightarrow K^+K^-\pi^0)$ in $D^0 \rightarrow K^*(1410)^+K^-, \bar{D}^0 \rightarrow \text{c.c.}$

VALUE (%)	DOCUMENT ID	TECN	COMMENT
$-21 \pm 23 \pm 8$	AUBERT	08AO BABR	Table 1, -Col.5/2×Col.2

$A_{CP}((K^+\pi^0)_{S\text{-wave}}K^- \rightarrow K^+K^-\pi^0)$ in $D^0 \rightarrow (K^+\pi^0)_S K^-, \bar{D}^0 \rightarrow \text{c.c.}$

VALUE (%)	DOCUMENT ID	TECN	COMMENT
$+7 \pm 15 \pm 3$	AUBERT	08AO BABR	Table 1, -Col.5/2×Col.2

$A_{CP}(\phi(1020)\pi^0 \rightarrow K^+K^-\pi^0)$ in $D^0, \bar{D}^0 \rightarrow \phi(1020)\pi^0$

VALUE (%)	DOCUMENT ID	TECN	COMMENT
$+1.1 \pm 2.1 \pm 0.5$	AUBERT	08AO BABR	Table 1, -Col.5/2×Col.2

$A_{CP}(f_0(980)\pi^0 \rightarrow K^+K^-\pi^0)$ in $D^0, \bar{D}^0 \rightarrow f_0(980)\pi^0$

VALUE (%)	DOCUMENT ID	TECN	COMMENT
$-3 \pm 19 \pm 1$	AUBERT	08AO BABR	Table 1, -Col.5/2×Col.2

$A_{CP}(a_0(980)^0\pi^0 \rightarrow K^+K^-\pi^0)$ in $D^0, \bar{D}^0 \rightarrow a_0(980)^0\pi^0$

VALUE (%)	DOCUMENT ID	TECN	COMMENT
$-5 \pm 16 \pm 2$	¹ AUBERT	08AO BABR	Table 1, -Col.5/2×Col.2

¹ This AUBERT 08AO value is obtained when the $a_0(980)^0$ replaces the $f_0(980)$ in the fit.

$A_{CP}(f'_2(1525)\pi^0 \rightarrow K^+K^-\pi^0)$ in $D^0, \bar{D}^0 \rightarrow f'_2(1525)\pi^0$

VALUE (%)	DOCUMENT ID	TECN	COMMENT
$0 \pm 50 \pm 150$	AUBERT	08AO BABR	Table 1, -Col.5/2×Col.2

$A_{CP}(K^*(892)^-K^+ \rightarrow K^+K^-\pi^0)$ in $D^0 \rightarrow K^*(892)^-K^+, \bar{D}^0 \rightarrow \text{c.c.}$

VALUE (%)	DOCUMENT ID	TECN	COMMENT
$-5 \pm 4 \pm 1$	AUBERT	08AO BABR	Table 1, -Col.5/2×Col.2

$A_{CP}(K^*(1410)^-K^+ \rightarrow K^+K^-\pi^0)$ in $D^0 \rightarrow K^*(1410)^-K^+, \bar{D}^0 \rightarrow \text{c.c.}$

VALUE (%)	DOCUMENT ID	TECN	COMMENT
$-17 \pm 28 \pm 7$	AUBERT	08AO BABR	Table 1, -Col.5/2×Col.2

$A_{CP}((K^-\pi^0)_{S\text{-wave}}K^+ \rightarrow K^+K^-\pi^0)$ in $D^0 \rightarrow (K^-\pi^0)_S K^+, \bar{D}^0 \rightarrow \text{c.c.}$

VALUE (%)	DOCUMENT ID	TECN	COMMENT
$-7 \pm 40 \pm 8$	AUBERT	08AO BABR	Table 1, -Col.5/2×Col.2

$A_{CP}(K_S^0\pi^0)$ in $D^0, \bar{D}^0 \rightarrow K_S^0\pi^0$

VALUE (%)	EVTS	DOCUMENT ID	TECN	COMMENT
-0.20 ± 0.17	OUR AVERAGE			
$-0.21 \pm 0.16 \pm 0.07$	467k	¹ NISAR	14	BELL e^+e^- at/near T^* 's
0.1 ± 1.3	9099	BONVICINI	01	CLE2 $e^+e^- \approx 10.6$ GeV
••• We do not use the following data for averages, fits, limits, etc. •••				
$-0.28 \pm 0.19 \pm 0.10$	326k	KO	11	BELL See NISAR 14
-1.8 ± 3.0		BARTELT	95	CLE2 See BONVICINI 01

¹ After subtracting CPV in $K^0 - \bar{K}^0$ mixing, NISAR 14 gets $A_{CP} = (+0.12 \pm 0.16 \pm 0.07)\%$.

$A_{CP}(K_S^0\eta)$ in $D^0, \bar{D}^0 \rightarrow K_S^0\eta$

VALUE (%)	EVTS	DOCUMENT ID	TECN	COMMENT
$+0.54 \pm 0.51 \pm 0.16$	46k	KO	11	BELL $e^+e^- \approx T(4S)$

$A_{CP}(K_S^0\eta')$ in $D^0, \bar{D}^0 \rightarrow K_S^0\eta'$

VALUE (%)	EVTS	DOCUMENT ID	TECN	COMMENT
$+0.98 \pm 0.67 \pm 0.14$	27k	KO	11	BELL $e^+e^- \approx T(4S)$

$A_{CP}(K_S^0\phi)$ in $D^0, \bar{D}^0 \rightarrow K_S^0\phi$

VALUE (%)	DOCUMENT ID	TECN	COMMENT
-2.8 ± 9.4	BARTELT	95	CLE2 $-18.2 < A_{CP} < +12.6\%$ (90%CL)

$A_{CP}(K^\mp\pi^\pm)$ in $D^0 \rightarrow K^-\pi^+, \bar{D}^0 \rightarrow K^+\pi^-$

VALUE (%)	EVTS	DOCUMENT ID	TECN	COMMENT
0.2 ± 0.5	OUR AVERAGE			
-0.01 ± 0.91		AAIJ	18k	LHCB pp at 7, 8, 13 TeV
$0.3 \pm 0.3 \pm 0.6$		BONVICINI	14	CLEO All CLEO-c runs
••• We do not use the following data for averages, fits, limits, etc. •••				
$+0.5 \pm 0.4 \pm 0.9$	150k	MENDEZ	10	CLEO See BONVICINI 14
$-0.4 \pm 0.5 \pm 0.9$		DOBBS	07	CLEO See BONVICINI 14

$A_{CP}(K^\pm\pi^\mp)$ in $D^0 \rightarrow K^+\pi^-, \bar{D}^0 \rightarrow K^-\pi^+$

VALUE (%)	EVTS	DOCUMENT ID	TECN	COMMENT
-0.9 ± 1.4	OUR AVERAGE			
-1.7 ± 1.6		^{1,2} AAJ	17AO	LHCB pp at 7, 8 TeV
$-2.1 \pm 5.2 \pm 1.5$	4.0k	AUBERT	07W	BABR $e^+e^- \approx 10.6$ GeV
$+2.3 \pm 4.7$	4.0k	³ ZHANG	06	BELL e^+e^-
$+18 \pm 14 \pm 4$		⁴ LINK	05H	FOCS γ nucleus
$+9.5 \pm 6.1 \pm 8.3$		⁵ AUBERT	03Z	BABR e^+e^- , 10.6 GeV
$+2 \pm 19$		⁶ GODANG	00	CLE2 e^+e^-
-20 ± 1	45			

••• We do not use the following data for averages, fits, limits, etc. •••

¹ AAIJ 13CE LHCB Repl. by AAJ 17AO
⁷ LI 05A BELL See ZHANG 06

¹ Based on 3 fb⁻¹ of data collected at $\sqrt{s} = 7, 8$ TeV. Allowing for CP violation, the direct CP-violation in mixing is reported for the $D^0 \rightarrow K^+\pi^-$ and $\bar{D}^0 \rightarrow K^-\pi^+$.

² The CPV is derived from $A_{CP} = (R_D^+ - R_D^-)/(R_D^+ + R_D^-)$.

³ This ZHANG 06 result allows mixing.

⁴ This LINK 05H result assumes no mixing. If mixing is allowed, it becomes $0.13^{+0.33}_{-0.25} \pm 0.10$.

⁵ This AUBERT 03Z limit assumes no mixing. If mixing is allowed, the 95% confidence-level interval is $(-2.8 < A_D < 4.9) \times 10^{-3}$.

⁶ This GODANG 00 result assumes no $D^0 - \bar{D}^0$ mixing and becomes $-0.43 < A_{CP} < +0.34$ at 95% CL. If mixing is allowed $A_{CP} = -0.01 \pm 0.16 \pm 0.01$.

⁷ This LI 05A result allows mixing.

Meson Particle Listings

 D^0 $A_{CP}(K^-\pi^+) \text{ in } D_{CP(\pm 1)} \rightarrow K^\mp \pi^\pm$

$$A_{CP}(K^-\pi^+) = [B(D_{CP(-)} \rightarrow K^-\pi^+ + \text{c.c.}) - B(D_{CP(+)} \rightarrow K^-\pi^+ + \text{c.c.})] / \text{Sum}$$

VALUE (%)	DOCUMENT ID	TECN	COMMENT
12.7 ± 1.3 ± 0.7	¹ ABLIKIM	14c	BES3 $e^+e^- \rightarrow D^0\bar{D}^0$, 3.77 GeV

¹ ABLIKIM 14c uses quantum correlations in $e^+e^- \rightarrow D^0\bar{D}^0$ at the $\psi(3770)$ to measure the asymmetry of the branching fraction of $D^0 \rightarrow K^-\pi^+$ in CP-odd and CP-even eigenstates. It then extracts the strong-phase difference $\delta_{K\pi}$.

 $A_{CP}(K^\mp \pi^\pm \pi^0) \text{ in } D^0 \rightarrow K^-\pi^+\pi^0, \bar{D}^0 \rightarrow K^+\pi^-\pi^0$

VALUE (%)	DOCUMENT ID	TECN	COMMENT
0.1 ± 0.5 OUR AVERAGE			

0.1 ± 0.3 ± 0.4	BONVICINI	14	CLEO All CLEO-c runs
-3.1 ± 8.6	¹ KOPP	01	CLE2 $e^+e^- \approx 10.6$ GeV

• • • We do not use the following data for averages, fits, limits, etc. • • •

0.2 ± 0.4 ± 0.8	DOBBS	07	CLEO See BONVICINI 14
-----------------	-------	----	-----------------------

¹ KOPP 01 fits separately the D^0 and \bar{D}^0 Dalitz plots and then calculates the integrated difference of normalized densities divided by the integrated sum.

 $A_{CP}(K^\pm \pi^\mp \pi^0) \text{ in } D^0 \rightarrow K^+\pi^-\pi^0, \bar{D}^0 \rightarrow K^-\pi^+\pi^0$

VALUE (%)	EVTS	DOCUMENT ID	TECN	COMMENT
0 ± 5 OUR AVERAGE				

-0.6 ± 5.3	1978 ± 104	TIAN	05	BELL $e^+e^- \approx 7(45)$
+9 ± ²⁵ ₋₂₂	38	BRANDENB...	01	CLE2 $e^+e^- \approx 7(45)$

 $A_{CP}(K_S^0 \pi^+ \pi^-) \text{ in } D^0, \bar{D}^0 \rightarrow K_S^0 \pi^+ \pi^-$

VALUE (%)	EVTS	DOCUMENT ID	TECN	COMMENT
-0.1 ± 0.8 OUR AVERAGE				

-0.05 ± 0.57 ± 0.54	350k	¹ AALTONEN	12AD	CDF
-0.9 ± 2.1 ± ^{1.6} _{-5.7}	4854	² ASNER	04A	CLEO $e^+e^- \approx 10$ GeV

¹ This is the overall result of AALTONEN 12AD. Following are the 15 CP fit-fraction asymmetries from the amplitude analysis of the D^0 and $\bar{D}^0 \rightarrow K_S^0 \pi^+ \pi^-$ Dalitz plots.

² This is the overall result of ASNER 04A; CP-violating limits are also given below for each of the 10 resonant submodes found in an amplitude analysis of the D^0 and $\bar{D}^0 \rightarrow K_S^0 \pi^+ \pi^-$ Dalitz plots.

 $A_{CP}(K^*(892)^\mp \pi^\pm \rightarrow K_S^0 \pi^+ \pi^-) \text{ in } D^0 \rightarrow K^* \pi^+, \bar{D}^0 \rightarrow K^* \pi^-$

VALUE (%)	DOCUMENT ID	TECN	COMMENT
+0.36 ± 0.33 ± 0.40	AALTONEN	12AD	CDF Dalitz fit, ~ 350k evts

• • • We do not use the following data for averages, fits, limits, etc. • • •

+2.5 ± 1.9 ± ^{3.3} _{-0.8}	ASNER	04A	CLEO Dalitz fit, 4854 evts
---	-------	-----	----------------------------

 $A_{CP}(K^*(892)^\pm \pi^\mp \rightarrow K_S^0 \pi^+ \pi^-) \text{ in } D^0 \rightarrow K^* \pi^-, \bar{D}^0 \rightarrow K^* \pi^+$

This is a doubly Cabibbo-suppressed mode.

VALUE (%)	DOCUMENT ID	TECN	COMMENT
+1.0 ± 5.7 ± 2.1	AALTONEN	12AD	CDF Dalitz fit, ~ 350k evts

• • • We do not use the following data for averages, fits, limits, etc. • • •

-21 ± 42 ± 28	ASNER	04A	CLEO Dalitz fit, 4854 evts
---------------	-------	-----	----------------------------

 $A_{CP}(K_S^0 \rho^0 \rightarrow K_S^0 \pi^+ \pi^-) \text{ in } D^0 \rightarrow \bar{K}^0 \rho^0, \bar{D}^0 \rightarrow K^0 \rho^0$

VALUE (%)	DOCUMENT ID	TECN	COMMENT
-0.05 ± 0.50 ± 0.08	AALTONEN	12AD	CDF Dalitz fit, ~ 350k evts

• • • We do not use the following data for averages, fits, limits, etc. • • •

+3.1 ± 3.8 ± ^{2.7} _{-2.2}	ASNER	04A	CLEO Dalitz fit, 4854 evts
---	-------	-----	----------------------------

 $A_{CP}(K_S^0 \omega \rightarrow K_S^0 \pi^+ \pi^-) \text{ in } D^0 \rightarrow \bar{K}^0 \omega, \bar{D}^0 \rightarrow K^0 \omega$

VALUE (%)	DOCUMENT ID	TECN	COMMENT
-12.6 ± 6.0 ± 2.6	AALTONEN	12AD	CDF Dalitz fit, ~ 350k evts

• • • We do not use the following data for averages, fits, limits, etc. • • •

-26 ± 24 ± ²² ₋₄	ASNER	04A	CLEO Dalitz fit, 4854 evts
--	-------	-----	----------------------------

 $A_{CP}(K_S^0 f_0(980) \rightarrow K_S^0 \pi^+ \pi^-) \text{ in } D^0 \rightarrow \bar{K}^0 f_0(980), \bar{D}^0 \rightarrow K^0 f_0(980)$

VALUE (%)	DOCUMENT ID	TECN	COMMENT
-0.4 ± 2.2 ± 1.6	AALTONEN	12AD	CDF Dalitz fit, ~ 350k evts

• • • We do not use the following data for averages, fits, limits, etc. • • •

-4.7 ± 11.0 ± ^{24.9} _{-8.8}	ASNER	04A	CLEO Dalitz fit, 4854 evts
---	-------	-----	----------------------------

 $A_{CP}(K_S^0 f_2(1270) \rightarrow K_S^0 \pi^+ \pi^-) \text{ in } D^0 \rightarrow \bar{K}^0 f_2(1270), \bar{D}^0 \rightarrow K^0 f_2(1270)$

VALUE (%)	DOCUMENT ID	TECN	COMMENT
-4.0 ± 3.4 ± 3.0	AALTONEN	12AD	CDF Dalitz fit, ~ 350k evts

• • • We do not use the following data for averages, fits, limits, etc. • • •

+34 ± 51 ± ³³ ₋₇₉	ASNER	04A	CLEO Dalitz fit, 4854 evts
---	-------	-----	----------------------------

 $A_{CP}(K_S^0 f_0(1370) \rightarrow K_S^0 \pi^+ \pi^-) \text{ in } D^0 \rightarrow \bar{K}^0 f_0(1370), \bar{D}^0 \rightarrow K^0 f_0(1370)$

VALUE (%)	DOCUMENT ID	TECN	COMMENT
-0.5 ± 4.6 ± 7.7	AALTONEN	12AD	CDF Dalitz fit, ~ 350k evts

• • • We do not use the following data for averages, fits, limits, etc. • • •

+18 ± 10 ± ¹³ ₋₂₂	ASNER	04A	CLEO Dalitz fit, 4854 evts
---	-------	-----	----------------------------

 $A_{CP}(K_S^0 \rho^0(1450) \text{ in } D^0 \rightarrow \bar{K}^0 \rho^0(1450), \bar{D}^0 \rightarrow K^0 \rho^0(1450)$

VALUE (%)	DOCUMENT ID	TECN	COMMENT
-4.1 ± 5.2 ± 8.1	AALTONEN	12AD	CDF Dalitz fit, ~ 350k evts

 $A_{CP}(K_S^0 f_0(600) \text{ in } D^0 \rightarrow \bar{K}^0 f_0(600), \bar{D}^0 \rightarrow K^0 f_0(600)$

VALUE (%)	DOCUMENT ID	TECN	COMMENT
-2.7 ± 2.7 ± 3.6	AALTONEN	12AD	CDF Dalitz fit, ~ 350k evts

 $A_{CP}(K^*(1410)^\mp \pi^\pm) \text{ in } D^0 \rightarrow K^*(1410)^-\pi^+, \bar{D}^0 \rightarrow K^*(1410)^+\pi^-$

VALUE (%)	DOCUMENT ID	TECN	COMMENT
-2.3 ± 5.7 ± 6.4	AALTONEN	12AD	CDF Dalitz fit, ~ 350k evts

 $A_{CP}(K_0^*(1430)^\mp \pi^\pm \rightarrow K_S^0 \pi^+ \pi^-) \text{ in } D^0 \rightarrow K_0^*(1430)^-\pi^+, \bar{D}^0 \rightarrow \text{c.c.}$

VALUE (%)	DOCUMENT ID	TECN	COMMENT
4.0 ± 2.4 ± 3.8	AALTONEN	12AD	CDF Dalitz fit, ~ 350k evts

• • • We do not use the following data for averages, fits, limits, etc. • • •

-0.2 ± 11.3 ± ^{8.8} _{-5.0}	ASNER	04A	CLEO Dalitz fit, 4854 evts
--	-------	-----	----------------------------

 $A_{CP}(K_0^*(1430)^\pm \pi^\mp) \text{ in } D^0 \rightarrow K_0^*(1430)^+\pi^-, \bar{D}^0 \rightarrow K_0^*(1430)^-\pi^+$

This is a doubly Cabibbo-suppressed mode.

VALUE (%)	DOCUMENT ID	TECN	COMMENT
+12 ± 11 ± 10	AALTONEN	12AD	CDF Dalitz fit, ~ 350k evts

 $A_{CP}(K_2^*(1430)^\mp \pi^\pm \rightarrow K_S^0 \pi^+ \pi^-) \text{ in } D^0 \rightarrow K_2^*(1430)^-\pi^+, \bar{D}^0 \rightarrow \text{c.c.}$

VALUE (%)	DOCUMENT ID	TECN	COMMENT
+2.9 ± 4.0 ± 4.1	AALTONEN	12AD	CDF Dalitz fit, ~ 350k evts

• • • We do not use the following data for averages, fits, limits, etc. • • •

-7 ± 25 ± ¹³ ₋₂₆	ASNER	04A	CLEO Dalitz fit, 4854 evts
--	-------	-----	----------------------------

 $A_{CP}(K_2^*(1430)^\pm \pi^\mp) \text{ in } D^0 \rightarrow K_2^*(1430)^+\pi^-, \bar{D}^0 \rightarrow K_2^*(1430)^-\pi^+$

This is a doubly Cabibbo-suppressed mode.

VALUE (%)	DOCUMENT ID	TECN	COMMENT
-10 ± 14 ± 29	AALTONEN	12AD	CDF Dalitz fit, ~ 350k evts

 $A_{CP}(K^*(1680)^\mp \pi^\pm \rightarrow K_S^0 \pi^+ \pi^-) \text{ in } D^0 \rightarrow K^*(1680)^-\pi^+, \bar{D}^0 \rightarrow \text{c.c.}$

VALUE (%)	DOCUMENT ID	TECN	COMMENT
-36 ± 19 ± ¹⁰₋₃₅	ASNER	04A	CLEO Dalitz fit, 4854 evts

• • • We do not use the following data for averages, fits, limits, etc. • • •

+0.7 ± 0.5 ± 0.9	DOBBS	07	CLEO See BONVICINI 14
------------------	-------	----	-----------------------

 $A_{CP}(K^-\pi^+\pi^+\pi^-) \text{ in } D^0 \rightarrow K^-\pi^+\pi^+\pi^-, \bar{D}^0 \rightarrow K^+\pi^-\pi^-\pi^+$

VALUE (%)	DOCUMENT ID	TECN	COMMENT
0.2 ± 0.3 ± 0.4	BONVICINI	14	CLEO All CLEO-c runs

• • • We do not use the following data for averages, fits, limits, etc. • • •

+0.7 ± 0.5 ± 0.9	DOBBS	07	CLEO See BONVICINI 14
------------------	-------	----	-----------------------

 $A_{CP}(K^\pm \pi^\mp \pi^+ \pi^-) \text{ in } D^0 \rightarrow K^+\pi^-\pi^+\pi^-, \bar{D}^0 \rightarrow K^-\pi^+\pi^+\pi^-$

VALUE (%)	EVTS	DOCUMENT ID	TECN	COMMENT
-1.8 ± 4.4	1721 ± 75	TIAN	05	BELL $e^+e^- \approx 7(45)$

 $A_{CP}(K^+K^-\pi^+\pi^-) \text{ in } D^0, \bar{D}^0 \rightarrow K^+K^-\pi^+\pi^-$

See also AAIJ 13BR for a search for CP violation in $D^0 \rightarrow K^+K^-\pi^+\pi^-$ in binned phase space. No evidence of CP violation was found.

VALUE (%)	EVTS	DOCUMENT ID	TECN	COMMENT
1.3 ± 1.7 OUR AVERAGE				

1.84 ± 1.74 ± 0.3	2.9k	¹ DARGENT	17	e^+e^-
-8.2 ± 5.6 ± 4.7	828 ± 46	LINK	05e	FOCS $\gamma A, \bar{E}\gamma \approx 180$ GeV

¹ Obtained by analyzing CLEO data but not authored by the CLEO Collaboration.

 $A_{CP}(K_1^*(1270)^+ K^- \rightarrow K^+ K^-\pi^+\pi^-) \text{ in } D^0 \rightarrow K_1^*(1270)^+ K^-, \bar{D}^0 \rightarrow \text{c.c.}$

Including the full $K_1^*(1270)^+$ phase space accessible in this decay chain, with its various resonance contributions.

VALUE (%)	EVTS	DOCUMENT ID	TECN	COMMENT
-2.3 ± 1.7 OUR AVERAGE				

-2.6 ± 1.7 ± 0.2	163k	AAIJ	19c	LHCb 4-body fit, $K K \pi \pi$ evts
25.3 ± 9.7 ± 12.7	2.9k	¹ DARGENT	17	4-body fit, $K K \pi \pi$ evts

¹ Obtained by analyzing CLEO data but not authored by the CLEO Collaboration.

 $A_{CP}(K_1^*(1270)^+ K^- \rightarrow K^{*0} \pi^+ K^-) \text{ in } D^0 \rightarrow K_1^*(1270)^+ K^-, \bar{D}^0 \rightarrow \text{c.c.}$

VALUE (%)	DOCUMENT ID	TECN	COMMENT
-0.7 ± 10.4	ARTUSO	12	CLEO Amplitude fit, 2959 evts.

 $A_{CP}(K_1^*(1270)^- K^+ \rightarrow \bar{K}^{*0} \pi^- K^+) \text{ in } D^0 \rightarrow K_1^*(1270)^- K^+, \bar{D}^0 \rightarrow \text{c.c.}$

VALUE (%)	DOCUMENT ID	TECN	COMMENT
-10.0 ± 31.5	ARTUSO	12	CLEO Amplitude fit, 2959 evts.

See key on page 999

Meson Particle Listings

D^0

$A_{CP}(K_1^*(1270)^- K^+ \rightarrow K^+ K^- \pi^+ \pi^-)$ in $D^0 \rightarrow K_1^*(1270)^- K^+, \bar{D}^0 \rightarrow$ c.c.

Including the full $K_1^*(1270)^-$ phase space accessible in this decay chain, with its various resonance contributions.

VALUE (%)	EVTS	DOCUMENT ID	TECN	COMMENT
1.7 ± 3.5 OUR AVERAGE				
3.3 ± 3.5 ± 0.5	163k	AAIJ	19c	LHCB 4-body fit, $K K \pi \pi$ evts
-50.4 ± 12.0 ± 16.1	2.9k	¹ DARGENT	17	4-body fit, $K K \pi \pi$ evts

¹ Obtained by analyzing CLEO data but not authored by the CLEO Collaboration.

$A_{CP}(K_1^*(1270)^+ K^- \rightarrow \rho^0 K^+ K^-)$ in $D^0 \rightarrow K_1^*(1270)^+ K^-, \bar{D}^0 \rightarrow$ c.c.

VALUE (%)	EVTS	DOCUMENT ID	TECN	COMMENT
-6.5 ± 16.9		ARTUSO	12	CLEO Amplitude fit, 2959 evts.

$A_{CP}(K_1^*(1270)^- K^+ \rightarrow \rho^0 K^- K^+)$ in $D^0 \rightarrow K_1^*(1270)^- K^+, \bar{D}^0 \rightarrow$ c.c.

VALUE (%)	EVTS	DOCUMENT ID	TECN	COMMENT
+9.6 ± 12.9		ARTUSO	12	CLEO Amplitude fit, 2959 evts.

$A_{CP}(K_1(1400)^+ K^- \rightarrow K^+ K^- \pi^+ \pi^-)$ in $D^0 \rightarrow K_1(1400)^+ K^-, \bar{D}^0 \rightarrow$ c.c.

Including the full $K_1(1400)^+$ phase space accessible in this decay chain, with its various resonance contributions.

VALUE (%)	EVTS	DOCUMENT ID	TECN	COMMENT
-4.4 ± 2.1 OUR AVERAGE				
-4.5 ± 2.1 ± 0.3	163k	AAIJ	19c	LHCB 4-body fit, $K K \pi \pi$ evts
9.2 ± 15.2 ± 20.3	2.9k	¹ DARGENT	17	4-body fit, $K K \pi \pi$ evts

¹ Obtained by analyzing CLEO data but not authored by the CLEO Collaboration.

$A_{CP}(K^*(1410)^+ K^- \rightarrow K^* \pi^+ K^-)$ in $D^0 \rightarrow K^*(1410)^+ K^-, \bar{D}^0 \rightarrow$ c.c.

VALUE (%)	EVTS	DOCUMENT ID	TECN	COMMENT
-20.0 ± 16.8		ARTUSO	12	CLEO Amplitude fit, 2959 evts.

$A_{CP}(K^*(1410)^- K^+ \rightarrow \bar{K}^{*0} \pi^- K^+)$ in $D^0 \rightarrow K^*(1410)^- K^+, \bar{D}^0 \rightarrow$ c.c.

VALUE (%)	EVTS	DOCUMENT ID	TECN	COMMENT
-1.1 ± 13.7		ARTUSO	12	CLEO Amplitude fit, 2959 evts.

$A_{CP}(K^*(1680)^+ K^- \rightarrow K^+ K^- \pi^+ \pi^-)$ in $D^0 \rightarrow K^*(1680)^+ K^-, \bar{D}^0 \rightarrow$ c.c.

Including the full $K^*(1680)^+$ phase space accessible in this decay chain, with its various resonance contributions.

VALUE (%)	EVTS	DOCUMENT ID	TECN	COMMENT
-17.1 ± 21.8 ± 18.5	2.9k	¹ DARGENT	17	4-body fit, $K K \pi \pi$ evts

¹ Obtained by analyzing CLEO data but not authored by the CLEO Collaboration.

$A_{CP}(K^{*0} \bar{K}^{*0})$ in $D^0, \bar{D}^0 \rightarrow K^{*0} \bar{K}^{*0}$

VALUE (%)	EVTS	DOCUMENT ID	TECN	COMMENT
-4.6 ± 9.0 ± 11.3	2.9k	¹ DARGENT	17	4-body fit, $K K \pi \pi$ evts

¹ Obtained by analyzing CLEO data but not authored by the CLEO Collaboration.

$A_{CP}(K^{*0} \bar{K}^{*0} S\text{-wave})$ in $D^0, \bar{D}^0 \rightarrow K^{*0} \bar{K}^{*0} S\text{-wave}$

VALUE (%)	EVTS	DOCUMENT ID	TECN	COMMENT
-3.9 ± 2.2 OUR AVERAGE				
-4.3 ± 2.2 ± 0.5	163k	AAIJ	19c	LHCB 4-body fit, $K K \pi \pi$ evts
+9.5 ± 13.5	3k	ARTUSO	12	CLEO 4-body fit, $K K \pi \pi$ evts

$A_{CP}(\phi \rho^0)$ in $D^0, \bar{D}^0 \rightarrow \phi \rho^0$

VALUE (%)	EVTS	DOCUMENT ID	TECN	COMMENT
1.5 ± 4.6 ± 8.0	2.9k	¹ DARGENT	17	4-body fit, $K K \pi \pi$ evts

¹ Obtained by analyzing CLEO data but not authored by the CLEO Collaboration.

$A_{CP}(\phi \rho^0 S\text{-wave})$ in $D^0, \bar{D}^0 \rightarrow \phi \rho^0 S\text{-wave}$

VALUE (%)	EVTS	DOCUMENT ID	TECN	COMMENT
-2.7 ± 5.3		ARTUSO	12	CLEO Amplitude fit, 2959 evts.

$A_{CP}(\phi \rho^0 D\text{-wave})$ in $D^0, \bar{D}^0 \rightarrow \phi \rho^0 D\text{-wave}$

VALUE (%)	EVTS	DOCUMENT ID	TECN	COMMENT
-37.1 ± 19.0		ARTUSO	12	CLEO Amplitude fit, 2959 evts.

$A_{CP}(\phi(\pi^+ \pi^-) S\text{-wave})$ in $D^0, \bar{D}^0 \rightarrow \phi(\pi^+ \pi^-) S\text{-wave}$

VALUE (%)	EVTS	DOCUMENT ID	TECN	COMMENT
6 ± 6 OUR AVERAGE				
5.8 ± 6.1 ± 0.8	163k	AAIJ	19c	LHCB 4-body fit, $K K \pi \pi$ evts
-4.0 ± 18.0 ± 44.6	3k	¹ DARGENT	17	4-body fit, $K K \pi \pi$ evts

• • • We do not use the following data for averages, fits, limits, etc. • • •

-8.6 ± 10.4	3k	² ARTUSO	12	CLEO 4-body fit, $K K \pi \pi$ evts
-------------	----	---------------------	----	-------------------------------------

¹ Obtained by analyzing CLEO data but not authored by the CLEO Collaboration.

² see DARGENT 17

$A_{CP}(K^*(892)^0 (K^- \pi^+) S\text{-wave})$ in $D^0, \bar{D}^0 \rightarrow K^*(892)^0 (K^- \pi^+) S\text{-wave}$

VALUE (%)	EVTS	DOCUMENT ID	TECN	COMMENT
-13.1 ± 17.9 ± 31.2	2.9k	¹ DARGENT	17	4-body fit, $K K \pi \pi$ evts

¹ Obtained by analyzing CLEO data but not authored by the CLEO Collaboration.

$A_{CP}(K^+ K^- \pi^+ \pi^- \text{ non-resonant})$ in $D^0, \bar{D}^0 \rightarrow K^+ K^- \pi^+ \pi^- \text{ non-resonant}$

VALUE (%)	DOCUMENT ID	TECN	COMMENT
+8.2 ± 10.9 ± 17.1	¹ DARGENT	17	4-body fit, 2.9k $K K \pi \pi$ evts

¹ Obtained by analyzing CLEO data but not authored by the CLEO Collaboration.

$A_{CP}((K^- \pi^+) P\text{-wave} (K^+ \pi^-) S\text{-wave})$ in $D^0 \rightarrow (K^- \pi^+) P\text{-wave} (K^+ \pi^-) S\text{-wave}, \bar{D}^0 \rightarrow$ c.c.

VALUE (%)	DOCUMENT ID	TECN	COMMENT
+2.7 ± 10.6	ARTUSO	12	CLEO Amplitude fit, 2959 evts.

$A_{CP}(K^+ K^- \mu^+ \mu^-)$ in $D^0, \bar{D}^0 \rightarrow K^+ K^- \mu^+ \mu^-$

VALUE (%)	EVTS	DOCUMENT ID	TECN	COMMENT
0 ± 11 ± 2	110	AAIJ	18i	LHCB pp at 7, 8, 13TeV

$A_{CP}(\pi^+ \pi^- \mu^+ \mu^-)$ in $D^0, \bar{D}^0 \rightarrow \pi^+ \pi^- \mu^+ \mu^-$

VALUE (%)	EVTS	DOCUMENT ID	TECN	COMMENT
4.9 ± 3.8 ± 0.7	1.1k	AAIJ	18i	LHCB pp at 7, 8, 13TeV

D^0 CP-EVEN FRACTIONS

The CP-even fraction F_{\pm} , defined for self-conjugate final states, like the coherence factor is useful for measuring the unitary triangle angle γ in $B \rightarrow DK$ decays. A purely CP-even state has $F_{\pm} = 1$, a CP-odd one has $F_{\pm} = 0$. For details, see NAYAK 15.

CP-even fraction in $D^0 \rightarrow \pi^+ \pi^- \pi^0$ decays

VALUE (%)	DOCUMENT ID	TECN	COMMENT
97.3 ± 1.7	MALDE	15	Uses CLEO data
• • • We do not use the following data for averages, fits, limits, etc. • • •			
96.8 ± 1.7 ± 0.6	NAYAK	15	see MALDE 15

CP-even fraction in $D^0 \rightarrow K^+ K^- \pi^0$ decays

VALUE (%)	DOCUMENT ID	TECN	COMMENT
73.2 ± 5.5	MALDE	15	Uses CLEO data
• • • We do not use the following data for averages, fits, limits, etc. • • •			
73.1 ± 5.8 ± 2.1	NAYAK	15	see MALDE 15

CP-even fraction in $D^0 \rightarrow \pi^+ \pi^- \pi^+ \pi^-$ decays

VALUE (%)	DOCUMENT ID	TECN	COMMENT
76.9 ± 2.1 ± 1.0	¹ HARNEW	18	Uses CLEO-c data
• • • We do not use the following data for averages, fits, limits, etc. • • •			
72.9 ± 0.9 ± 1.8	^{1,2} DARGENT	17	from amplitude model
73.7 ± 2.8	MALDE	15	CLEO amplitude model independent

¹ Obtained by analyzing CLEO-c data but not authored by the CLEO Collaboration.

² MALDE 15 and DARGENT 17 use different CLEO data sets, so in principle their results could be averaged. However, given the importance that model-independence has in the use of this value, we exclude the amplitude model-derived result from the average.

CP-even fraction in $D^0 \rightarrow K_S^0 \pi^+ \pi^- \pi^0$ decays

VALUE (%)	DOCUMENT ID	TECN	COMMENT
23.8 ± 1.2 ± 1.2	¹ RESMI	18	Uses CLEO-c data

¹ Obtained by analyzing CLEO-c data but not authored by the CLEO Collaboration.

CP-even fraction in $D^0 \rightarrow K^+ K^- \pi^+ \pi^-$ decays

VALUE (%)	DOCUMENT ID	TECN	COMMENT
75.3 ± 1.8 ± 3.9	¹ DARGENT	17	from amplitude model

¹ Obtained by analyzing CLEO data but not authored by the CLEO Collaboration.

D^0 CP-VIOLATING ASYMMETRY DIFFERENCES

$\Delta A_{CP} = A_{CP}(K^+ K^-) - A_{CP}(\pi^+ \pi^-)$

CP violation in these modes can come from the decay amplitudes (direct) and/or from mixing or interference of mixing and decay (indirect). The difference ΔA_{CP} is primarily sensitive to the direct component, and only retains a second-order dependence on the indirect component for measurements where the mean decay time of the $K^+ K^-$ and $\pi^+ \pi^-$ samples are not identical. The results below are averaged assuming the indirect component can be neglected.

VALUE (%)	EVTS	DOCUMENT ID	TECN	COMMENT
-0.154 ± 0.029	53M,17M	AAIJ	19d	LHCB Time-integrated

• • • We do not use the following data for averages, fits, limits, etc. • • •

-0.10 ± 0.08 ± 0.03	6.5M,2.2M	AAIJ	16d	LHCB See AAIJ 19d
0.14 ± 0.16 ± 0.08	2.2M,0.8M	AAIJ	14AK	LHCB See AAIJ 19d
0.49 ± 0.30 ± 0.14	0.56M,0.22M	AAIJ	13AD	LHCB See AAIJ 14AK
-0.82 ± 0.21 ± 0.11	1.4M,0.4M	AAIJ	12G	LHCB See AAIJ 16d
-0.46 ± 0.31 ± 0.12		AALTONEN	12B	CDF See AALTONEN 12o
-0.62 ± 0.21 ± 0.10		AALTONEN	12o	CDF Time-integrated
0.24 ± 0.62 ± 0.26		¹ AUBERT	08M	BABR Time-integrated
-0.86 ± 0.60 ± 0.07	120k	STARIC	08	BELL Time-integrated

¹ Calculated from the AUBERT 08M values of $A_{CP}(K^+ K^-)$ and $A_{CP}(\pi^+ \pi^-)$. The systematic error here combines the systematic errors in quadrature, and therefore somewhat over-estimates it.

Meson Particle Listings

D^0

D^0 TESTS OF LOCAL CP-VIOLATION (CPV)

We list model-independent searches for local CP violation in phase-space distributions of multi-body decays.

Most of these searches divide phase space (Dalitz plot for 3-body decays, five-dimensional equivalent for 4-body decays) into bins, and perform a χ^2 test comparing normalised yields N_i, \bar{N}_i in CP-conjugate bin pairs i : $\chi^2 = \sum_i (N_i - \alpha \bar{N}_i) / \sigma(N_i - \alpha \bar{N}_i)$. The factor $\alpha = (\sum_i N_i) / (\sum_i \bar{N}_i)$ removes the dependence on phase-space-integrated rate asymmetries. The result is used to obtain the probability (p-value) to obtain the measured χ^2 or larger under the assumption of CP conservation [AUBERT 08AO, BEDIAGA 09]. Alternative methods obtain p-values from other test variables based on unbinned analyses [WILLIAMS 11, AAIJ 14c]. Results can be combined using Fisher's method [MOSTELLER 48].

Local CPV in $D^0, \bar{D}^0 \rightarrow \pi^+ \pi^- \pi^0$

p-value (%)	EVTS	DOCUMENT ID	TECN	COMMENT
4.9 OUR EVALUATION				
2.6	566k	1 AAIJ	15A LHCb	unbinned method
32.8	82k	AUBERT	08AO BABR	χ^2

¹ Unusually, AAIJ 15A assigns an uncertainty on the p value of $\pm 0.5\%$. This results from limited test statistics.

Local CPV in $D^0, \bar{D}^0 \rightarrow \pi^+ \pi^- \pi^+ \pi^-$

p-value (%)	EVTS	DOCUMENT ID	TECN	COMMENT
0.6 \pm 0.2				
1.0M	1 AAIJ	17AE LHCb		unbinned, P-odd
4.6 \pm 0.5	1.0M	2,3 AAIJ	17AE LHCb	unbinned, P-even
41	330k	2,4 AAIJ	13BR LHCb	χ^2 , P-even

¹ This AAIJ 17AE value tests CP Violation in P-odd variables.
² This value tests CP Violation in P-even variables.
³ Not included in average as correlation to P-odd measurement using the same data is unclear.
⁴ See AAIJ 17AE.

Local CPV in $D^0, \bar{D}^0 \rightarrow K_S^0 \pi^+ \pi^-$

p-value (%)	EVTS	DOCUMENT ID	TECN	COMMENT
96	350k	AALTONEN	12AD CDF	χ^2

Local CPV in $D^0, \bar{D}^0 \rightarrow K^+ K^- \pi^0$

p-value (%)	EVTS	DOCUMENT ID	TECN	COMMENT
16.6	11k	AUBERT	08AO BABR	χ^2

Local CPV in $D^0, \bar{D}^0 \rightarrow K^+ K^- \pi^+ \pi^-$

p-value (%)	EVTS	DOCUMENT ID	TECN	COMMENT
9.1	57k	AAIJ	13BR LHCb	χ^2

CP VIOLATING ASYMMETRIES OF P-ODD (T-ODD) MOMENTS

The CP-sensitive P-odd (T-odd) correlation in D^0, \bar{D}^0 decays. The D^0 and \bar{D}^0 are distinguished by the charge of the parent D^* : $D^{*+} \rightarrow D^0 \pi^+$ and $D^{*-} \rightarrow \bar{D}^0 \pi^-$.

$A_{Tviol}(K^+ K^- \pi^+ \pi^-)$ in $D^0, \bar{D}^0 \rightarrow K^+ K^- \pi^+ \pi^-$

$C_T \equiv \vec{p}_{K^+} \cdot (\vec{p}_{\pi^+} \times \vec{p}_{\pi^-})$ is a parity-odd correlation of the K^+, π^+ , and π^- momenta (evaluated in the D^0 rest frame) for the D^0 . $\bar{C}_T \equiv \vec{p}_{K^-} \cdot (\vec{p}_{\pi^-} \times \vec{p}_{\pi^+})$ is the corresponding quantity for the \bar{D}^0 . Then $A_T \equiv [\Gamma(C_T > 0) - \Gamma(C_T < 0)] / [\Gamma(C_T > 0) + \Gamma(C_T < 0)]$, and $\bar{A}_T \equiv [\Gamma(-\bar{C}_T > 0) - \Gamma(-\bar{C}_T < 0)] / [\Gamma(-\bar{C}_T > 0) + \Gamma(-\bar{C}_T < 0)]$, and $A_{Tviol} \equiv \frac{1}{2}(A_T - \bar{A}_T)$. C_T and \bar{C}_T are commonly referred to as T-odd moments, because they are odd under T reversal. However, the T-conjugate process $K^+ K^- \pi^+ \pi^- \rightarrow D^0$ is not accessible, while the P-conjugate process is.

VALUE (units 10^{-3})	EVTS	DOCUMENT ID	TECN	COMMENT
2.9 \pm 2.2 OUR AVERAGE				
5.2 \pm 3.7 \pm 0.7	110k	1 KIM	19 BELL	$e^+ e^-$ at $\Upsilon(1S) - \Upsilon(6S)$
1.8 \pm 2.9 \pm 0.4	171k	AAIJ	14BC LHCb	$B \rightarrow D^0 \mu^- X$
1.0 \pm 5.1 \pm 4.4	47k	DEL-AMO-SA...10	BABR	$e^+ e^- \approx 10.6$ GeV
10 \pm 57 \pm 37	0.8k	LINK	05E FOCS	$\gamma A, \bar{E}_\gamma \approx 180$ GeV

¹ KIM 19 also study CP-violating asymmetries in several other kinematic variables. No evidence for CP violation is found in any of them.

$A_{Tviol}(K_S \pi^+ \pi^- \pi^0)$ in $D^0, \bar{D}^0 \rightarrow K_S \pi^+ \pi^- \pi^0$

VALUE (units 10^{-3})	EVTS	DOCUMENT ID	TECN	COMMENT
-0.28 \pm 1.38 \pm 0.23 \pm 0.76	745k	1 PRASANTH	17 BELL	$e^+ e^-$ at $\Upsilon(nS)$'s

¹ PRASANTH 17 also measures A_{Tviol} in sub-regions of the $D^0 \rightarrow K_S \pi^+ \pi^- \pi^0$ phase-space. No evidence of T violation is found.

D^0 CPT-VIOLATING DECAY-RATE ASYMMETRIES

$A_{CPT}(K^\mp \pi^\pm)$ in $D^0 \rightarrow K^- \pi^+, \bar{D}^0 \rightarrow K^+ \pi^-$

$A_{CPT}(t)$ is defined in terms of the time-dependent decay probabilities $P(D^0 \rightarrow K^- \pi^+)$ and $P(\bar{D}^0 \rightarrow K^+ \pi^-)$ by $A_{CPT}(t) = (P - \bar{P}) / (P + \bar{P})$. For small mixing parameters $x \equiv \Delta m / \Gamma$ and $y \equiv \Delta \Gamma / 2\Gamma$ (as is the case), and times t , $A_{CPT}(t)$ reduces to $[y \text{Re } \xi - x \text{Im } \xi] \Gamma t$, where ξ is the CPT-violating parameter.

The following is actually $y \text{Re } \xi - x \text{Im } \xi$.

VALUE	DOCUMENT ID	TECN	COMMENT
0.0083 \pm 0.0065 \pm 0.0041	LINK	03B FOCS	γ nucleus, $\bar{E}_\gamma \approx 180$ GeV

$D^0 \rightarrow K^*(892)^- \ell^+ \nu_\ell$ FORM FACTORS

$r_V \equiv V(0)/A_1(0)$ in $D^0 \rightarrow K^*(892)^- \ell^+ \nu_\ell$

VALUE	EVTS	DOCUMENT ID	TECN	COMMENT
1.46 \pm 0.07 OUR AVERAGE				
1.46 \pm 0.07 \pm 0.02	3k	ABLIKIM	19G BES3	$K^*(892)^- e^+ \nu_e$
1.71 \pm 0.68 \pm 0.34		LINK	05B FOCS	$K^*(892)^- \mu^+ \nu_\mu$

$r_2 \equiv A_2(0)/A_1(0)$ in $D^0 \rightarrow K^*(892)^- \ell^+ \nu_\ell$

VALUE	EVTS	DOCUMENT ID	TECN	COMMENT
0.68 \pm 0.06 OUR AVERAGE				
0.67 \pm 0.06 \pm 0.01	3k	ABLIKIM	19G BES3	$K^*(892)^- e^+ \nu_e$
0.91 \pm 0.37 \pm 0.10		LINK	05B FOCS	$K^*(892)^- \mu^+ \nu_\mu$

$D^0 \rightarrow K^- / \pi^- \ell^+ \nu_\ell$ FORM FACTORS

$f_+(0)$ in $D^0 \rightarrow K^- \ell^+ \nu_\ell$

VALUE	EVTS	DOCUMENT ID	TECN	COMMENT
0.736 \pm 0.004 OUR AVERAGE				
0.7368 \pm 0.0026 \pm 0.0036	71k	ABLIKIM	15X BES3	$\ell=e$, 2-parameter fit
0.727 \pm 0.007 \pm 0.009		AUBERT	07Bg BABR	$\ell=e$, 2-parameter fit

$f_+(0)|V_{cd}|$ in $D^0 \rightarrow K^- \ell^+ \nu_\ell$

VALUE	EVTS	DOCUMENT ID	TECN	COMMENT
0.7166 \pm 0.0030 OUR AVERAGE				
0.7133 \pm 0.0038 \pm 0.0029	47k	ABLIKIM	19B BES3	$\ell=\mu$, 2-parameter fit
0.7172 \pm 0.0025 \pm 0.0035	71k	1 ABLIKIM	15X BES3	$\ell=e$, 2-parameter fit
0.726 \pm 0.008 \pm 0.004		BESSION	09 CLEO	$\ell=e$, 3-parameter fit

¹ The 3-parameter fit yields 0.7195 \pm 0.0035 \pm 0.0041.

$r_1 \equiv a_1/a_0$ in $D^0 \rightarrow K^- \ell^+ \nu_\ell$

VALUE	EVTS	DOCUMENT ID	TECN	COMMENT
-2.40 \pm 0.16 OUR AVERAGE				
-2.33 \pm 0.16 \pm 0.08	71k	1 ABLIKIM	15X BES3	$\ell=e$, 3-parameter fit
-2.65 \pm 0.34 \pm 0.08		BESSION	09 CLEO	$\ell=e$, 3-parameter fit

¹ The 2-parameter fit yields -2.23 \pm 0.09 \pm 0.06.

$r_2 \equiv a_2/a_0$ in $D^0 \rightarrow K^- \ell^+ \nu_\ell$

VALUE	EVTS	DOCUMENT ID	TECN	COMMENT
5 \pm 4 OUR AVERAGE				
3.4 \pm 3.9 \pm 2.4	71k	ABLIKIM	15X BES3	$\ell=e$, 3-parameter fit
13 \pm 9 \pm 1		BESSION	09 CLEO	$\ell=e$, 3-parameter fit

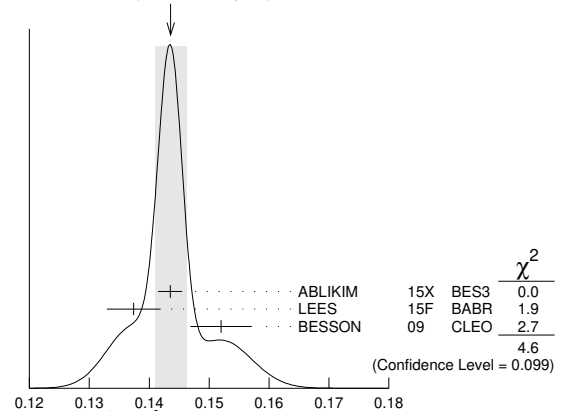
$f_+(0)$ in $D^0 \rightarrow \pi^- \ell^+ \nu_\ell$

VALUE	EVTS	DOCUMENT ID	TECN	COMMENT
0.6372 \pm 0.0080 \pm 0.0044				
0.6372 \pm 0.0080 \pm 0.0044	6.3k	ABLIKIM	15X BES3	$\ell=e$, 2-parameter fit

$f_+(0)|V_{cd}|$ in $D^0 \rightarrow \pi^- \ell^+ \nu_\ell$

VALUE	EVTS	DOCUMENT ID	TECN	COMMENT
0.1436 \pm 0.0026 OUR AVERAGE				
0.1435 \pm 0.0018 \pm 0.0009	6.3k	1 ABLIKIM	15X BES3	$\ell=e$, 2-parameter fit
0.1374 \pm 0.0038 \pm 0.0024	5.3k	2 LEES	15F BABR	$\ell=e$, 3-parameter fit
0.152 \pm 0.005 \pm 0.001		BESSION	09 CLEO	$\ell=e$, 3-parameter fit

WEIGHTED AVERAGE
0.1436 \pm 0.0026 (Error scaled by 1.5)



¹ The 3-parameter fit yields 0.1420 \pm 0.0024 \pm 0.0010.

See key on page 999

Meson Particle Listings

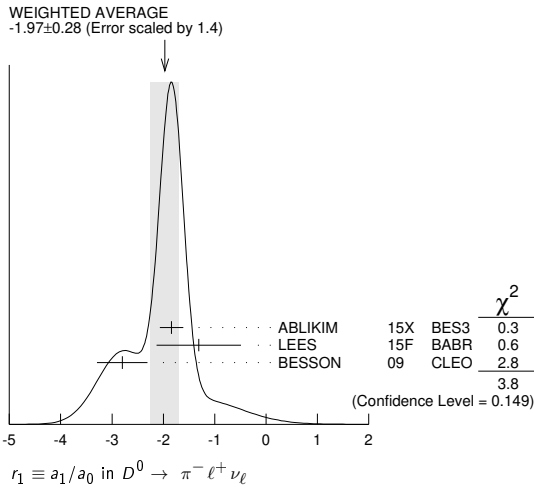
D^0

² LEES 15F reports a value $0.1374 \pm 0.0038 \pm 0.0022 \pm 0.0009$, where the last uncertainty is due to the uncertainties of the $D^0 \rightarrow K^- \pi^+$ branching fraction.

$r_1 \equiv a_1/a_0$ in $D^0 \rightarrow \pi^- \ell^+ \nu_\ell$

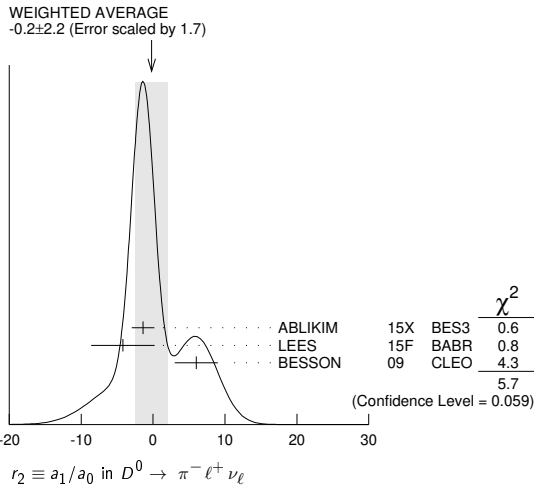
VALUE	EVTS	DOCUMENT ID	TECN	COMMENT
-1.97 ± 0.28 OUR AVERAGE				Error includes scale factor of 1.4. See the ideogram below.
$-1.84 \pm 0.22 \pm 0.07$	6.3k	¹ ABLIKIM	15X BES3	$\ell=e$, 3-parameter fit
$-1.31 \pm 0.70 \pm 0.43$	5.3k	LEES	15F BABR	$\ell=e$, 3-parameter fit
$-2.80 \pm 0.49 \pm 0.04$		BESSION	09 CLEO	$\ell=e$, 3-parameter fit

¹ The 2-parameter fit yields $-2.04 \pm 0.08 \pm 0.03$.



$r_2 \equiv a_1/a_0$ in $D^0 \rightarrow \pi^- \ell^+ \nu_\ell$

VALUE	EVTS	DOCUMENT ID	TECN	COMMENT
-0.2 ± 2.2 OUR AVERAGE				Error includes scale factor of 1.7. See the ideogram below.
$-1.4 \pm 1.5 \pm 0.5$	6.3k	ABLIKIM	15X BES3	$\ell=e$, 3-parameter fit
$-4.2 \pm 4.0 \pm 1.9$	5.3k	LEES	15F BABR	$\ell=e$, 3-parameter fit
$6 \pm 3 \pm 0$		BESSION	09 CLEO	$\ell=e$, 3-parameter fit



Amplitude analyses

$D \rightarrow K\pi\pi\pi, D \rightarrow KK\pi\pi$ partial wave analyses

Amplitude analyses of D^0 decays to a variety of 4-body kaon or pion final states, fitting simultaneously different partial wave components.

VALUE	DOCUMENT ID	TECN	COMMENT
¹ AAIJ	19c LHCb		$D^0 \rightarrow K^+ K^- \pi^+ \pi^-$
ABLIKIM	19AK BES3		$D^0 \rightarrow K^- \pi^+ \pi^0 \pi^0$
AAIJ	18AI LHCb		$D^0 \rightarrow K^- \pi^+ \pi^+ \pi^-$
ABLIKIM	17o BES3		$D^0 \rightarrow K^- \pi^+ \pi^+ \pi^-$

¹ AAIJ 19c also provides measurements of CP violation in $D^0 \rightarrow K^+ K^- \pi^+ \pi^-$, with results compatible with CP symmetry.

D^0 REFERENCES

AAIJ	20	PR D101 012005	R. Aaij et al.	(LHCb Collab.)
AAIJ	19	PRL 122 011802	R. Aaij et al.	(LHCb Collab.)
AAIJ	19C	JHEP 1902 126	R. Aaij et al.	(LHCb Collab.)
AAIJ	19D	PRL 122 211803	R. Aaij et al.	(LHCb Collab.)
AAIJ	19X	PRL 122 231802	R. Aaij et al.	(LHCb Collab.)
ABLIKIM	19AK	PR D99 092008	M. Ablikim et al.	(BESIII Collab.)
ABLIKIM	19AL	PR D99 112002	M. Ablikim et al.	(BESIII Collab.)
ABLIKIM	19AY	PR D100 072006	M. Ablikim et al.	(BESIII Collab.)
ABLIKIM	19B	PRL 122 011804	M. Ablikim et al.	(BESIII Collab.)
ABLIKIM	19BI	PL B798 135017	M. Ablikim et al.	(BESIII Collab.)
ABLIKIM	19C	PRL 122 062001	M. Ablikim et al.	(BESIII Collab.)
ABLIKIM	19G	PR D99 011103	M. Ablikim et al.	(BESIII Collab.)
KIM	19	PR D99 011104	J.B. Kim et al.	(BELLE Collab.)
LEES	19A	PRL 122 081802	J.P. Lees et al.	(BABAR Collab.)
PDG	19	RPP 2019 at pdg.lbl.gov	M. Tanabashi et al.	(PDG Collab.)
AAIJ	18AI	EPJ C78 443	R. Aaij et al.	(LHCb Collab.)
AAIJ	18AV	JHEP 1811 048	R. Aaij et al.	(LHCb Collab.)
AAIJ	18I	PRL 121 091801	R. Aaij et al.	(LHCb Collab.)
AAIJ	18K	PR D97 031101	R. Aaij et al.	(LHCb Collab.)
ABLIKIM	18AC	PR D98 092009	M. Ablikim et al.	(BESIII Collab.)
ABLIKIM	18AE	PRL 121 171803	M. Ablikim et al.	(BESIII Collab.)
ABLIKIM	18F	PRL 121 081802	M. Ablikim et al.	(BESIII Collab.)
ABLIKIM	18L	PR D97 052005	M. Ablikim et al.	(BESIII Collab.)
ABLIKIM	18P	PR D97 072015	M. Ablikim et al.	(BESIII Collab.)
ABLIKIM	18W	PR D97 072004	M. Ablikim et al.	(BESIII Collab.)
ABLIKIM	18X	PL B781 368	M. Ablikim et al.	(BESIII Collab.)
HARNEW	18	JHEP 1801 144	S. Harnew et al.	(BRIS, PNPL)
RESMI	18	JHEP 1801 082	P.K. Resmi et al.	(LHCb Collab.)
SMITH	18	PR D98 051101	M.J. Smith, D. Cinabro, P. Naik	(LTU, WAYN+)
AAIJ	17AE	PL B769 345	R. Aaij et al.	(LHCb Collab.)
AAIJ	17AK	PRL 118 261803	R. Aaij et al.	(LHCb Collab.)
AAIJ	17AO	PR D95 052004	R. Aaij et al.	(LHCb Collab.)
Also		PR D96 099907 (errata.)	R. Aaij et al.	(LHCb Collab.)
AAIJ	17BG	PRL 119 181805	R. Aaij et al.	(LHCb Collab.)
AAIJ	17M	PL B767 177	R. Aaij et al.	(LHCb Collab.)
ABLIKIM	17A	PL B765 231	M. Ablikim et al.	(BESIII Collab.)
ABLIKIM	17O	PR D95 072010	M. Ablikim et al.	(BESIII Collab.)
DARGENT	17	JHEP 1705 143	P. d'Argent et al.	(HEID, BRIS)
DASH	17	PRL 119 171801	N. Dash et al.	(BELLE Collab.)
LAI	17	PR D95 011102	Y.-T. Lai et al.	(BELLE Collab.)
MANUT	17	PRL 118 051801	T. Manut et al.	(BELLE Collab.)
PRASANTH	17	PR D95 091101	K. Prasant et al.	(BELLE Collab.)
AAIJ	16D	PRL 116 191601	R. Aaij et al.	(LHCb Collab.)
AAIJ	16F	PRL 116 241801	R. Aaij et al.	(LHCb Collab.)
AAIJ	16H	PL B754 167	R. Aaij et al.	(LHCb Collab.)
AAIJ	16I	PL B757 558	R. Aaij et al.	(LHCb Collab.)
AAIJ	16N	PR D93 052018	R. Aaij et al.	(LHCb Collab.)
AAIJ	16V	JHEP 1604 033	R. Aaij et al.	(LHCb Collab.)
ABLIKIM	16D	PRL 116 082001	M. Ablikim et al.	(BESIII Collab.)
EVANS	16	PL B757 520	T. Evans et al.	(OXF, BRIS, MADRA)
Also		PL B765 402 (errata.)	T. Evans et al.	(OXF, BRIS, MADRA)
LEES	16D	PR D93 051102	J.P. Lees et al.	(BABAR Collab.)
NISAR	16	PR D93 051102	N.K. Nisar et al.	(BELLE Collab.)
STARIC	16	PL B753 412	M. Staric et al.	(BELLE Collab.)
AAIJ	15A	PL B740 158	R. Aaij et al.	(LHCb Collab.)
AAIJ	15AA	JHEP 1504 043	R. Aaij et al.	(LHCb Collab.)
AAIJ	15AT	JHEP 1510 055	R. Aaij et al.	(LHCb Collab.)
ABLIKIM	15D	PL B744 339	M. Ablikim et al.	(BESIII Collab.)
ABLIKIM	15F	PR D91 112015	M. Ablikim et al.	(BESIII Collab.)
ABLIKIM	15X	PR D92 072012	M. Ablikim et al.	(BESIII Collab.)
LEES	15F	PR D91 052022	J.P. Lees et al.	(BABAR Collab.)
MALDE	15	PL B747 9	S. Malde et al.	(BRIS, CERN, MADRA, OXF+)
NAYAK	15	PL B740 1	M. Nayak et al.	(MADRA, OXF, CERN)
AAIJ	14AK	JHEP 1407 041	R. Aaij et al.	(LHCb Collab.)
AAIJ	14AL	PRL 112 041801	R. Aaij et al.	(LHCb Collab.)
AAIJ	14B	PL B728 234	R. Aaij et al.	(LHCb Collab.)
AAIJ	14BC	JHEP 1410 005	R. Aaij et al.	(LHCb Collab.)
AAIJ	14C	PL B728 585	R. Aaij et al.	(LHCb Collab.)
AALTONEN	14Q	PR D90 111103	T. Aaltonen et al.	(CDF Collab.)
ABLIKIM	14C	PL B734 227	M. Ablikim et al.	(BESIII Collab.)
BONVICINI	14	PR D89 072002	G. Bonvicini et al.	(CLEO Collab.)
KO	14	PRL 112 111801	B.R. Ko et al.	(BELLE Collab.)
LIBBY	14	PL B731 197	J. Libby et al.	(MADRA, OXF, PNL+)
NISAR	14	PRL 112 211601	N.K. Nisar et al.	(BELLE Collab.)
PENG	14	PR D89 091103	T. Peng et al.	(BELLE Collab.)
TOMARADZE	14	PR D89 031501	A. Tomaradze et al.	(NWES, WAYN)
AAIJ	13AD	PL B723 33	R. Aaij et al.	(LHCb Collab.)
AAIJ	13AI	PL B725 15	R. Aaij et al.	(LHCb Collab.)
AAIJ	13BR	PL B726 623	R. Aaij et al.	(LHCb Collab.)
AAIJ	13CE	PRL 111 251801	R. Aaij et al.	(LHCb Collab.)
AAIJ	13N	PRL 110 101802	R. Aaij et al.	(LHCb Collab.)
AAIJ	13V	JHEP 1306 065	R. Aaij et al.	(LHCb Collab.)
AALTONEN	13AE	PRL 111 231802	T. Aaltonen et al.	(CDF Collab.)
DOBBS	13	PRL 110 131802	S. Dobbs et al.	(CLEO Collab.)
LEES	13	PR D87 012004	J.P. Lees et al.	(BABAR Collab.)
LEES	13S	PR D88 071104	J.P. Lees et al.	(BABAR Collab.)
WHITE	13	PR D88 051101	E. White et al.	(BELLE Collab.)
AAIJ	12G	PRL 108 111602	R. Aaij et al.	(LHCb Collab.)
AAIJ	12K	JHEP 1204 129	R. Aaij et al.	(LHCb Collab.)
AALTONEN	12AB	PR D86 032007	T. Aaltonen et al.	(CDF Collab.)
AALTONEN	12B	PR D85 012009	T. Aaltonen et al.	(CDF Collab.)
AALTONEN	12O	PRL 109 111801	T. Aaltonen et al.	(CDF Collab.)
ARTUSO	12	PR D85 122002	M. Artuso et al.	(CLEO Collab.)
ASNER	12	PR D86 112001	D.M. Asner et al.	(CLEO Collab.)
INSLER	12	PR D85 092016	J. Insler et al.	(CLEO Collab.)
Also		PR D94 099005 (errata.)	J. Insler et al.	(CLEO Collab.)
LEES	12L	PR D85 091107	J.P. Lees et al.	(BABAR Collab.)
LEES	12Q	PR D86 032001	J.P. Lees et al.	(BABAR Collab.)
KO	11	PRL 106 211801	B.R. Ko et al.	(BELLE Collab.)
LOWREY	11	PR D84 092005	N. Lowrey et al.	(CLEO Collab.)
WILLIAMS	11	PR D84 054015	M. Williams	(LOIC)
AALTONEN	10X	PR D82 091105	T. Aaltonen et al.	(CDF Collab.)
ANASHIN	10A	PL B686 84	V.V. Anashin et al.	(VEPP-4M KEDR Collab.)
ASNER	10	PR D81 052007	D.M. Asner et al.	(CLEO Collab.)
BHATTACHARJEE	10A	PR D81 096008	B. Bhattacharya, C.-W. Chiang, J.L. Rosner	(CHIC+)
DEL-AMO-SA...	10	PR D81 111103	P. del Amo Sanchez et al.	(BABAR Collab.)
DEL-AMO-SA...	10D	PRL 105 081803	P. del Amo Sanchez et al.	(BABAR Collab.)
MENDEZ	10	PR D81 052013	H. Mendez et al.	(CLEO Collab.)
PETRIC	10	PR D81 091102	M. Petric et al.	(BELLE Collab.)
AUBERT	09AI	PR D80 071103	B. Aubert et al.	(BABAR Collab.)
AUBERT	09AM	PRL 103 211801	B. Aubert et al.	(BABAR Collab.)
BEDIAGA	09	PR D80 096006	I. Bediaga et al.	(CBPF, NDAM)
BESSION	09	PR D80 032005	D. Besson et al.	(CLEO Collab.)
Also		PR D79 052010	J.Y. Ge et al.	(CLEO Collab.)
LOWREY	09	PR D80 031105	N. Lowrey et al.	(CLEO Collab.)
RUBIN	09	PR D79 097101	P. Rubin et al.	(CLEO Collab.)
ZUPANC	09	PR D80 052006	A. Zupanc et al.	(BELLE Collab.)
AALTONEN	08E	PRL 100 121802	T. Aaltonen et al.	(CDF Collab.)
ABLIKIM	08L	PL B665 16	M. Ablikim et al.	(PL BESIII)
ARINSTEIN	08	PL B662 102	K. Arinstein et al.	(BELLE Collab.)

See key on page 999

Meson Particle Listings

$D^*(2007)^0, D^*(2010)^\pm$

$m_{D^*(2007)^0} - m_{D^0}$

The fit includes $D^\pm, D^0, D_s^\pm, D^{*\pm}, D^{*0}, D_1(2420)^0, D_2^*(2460)^0$, and $D_{s1}(2536)^\pm$ mass and mass difference measurements.

VALUE (MeV)	EVTS	DOCUMENT ID	TECN	COMMENT
142.014 ± 0.030 OUR FIT	Error	includes scale factor of 1.5.		
142.016 ± 0.030 OUR AVERAGE	Error	includes scale factor of 1.5.		
142.007 ± 0.015 ± 0.014	10K	² TOMARADZE 15	CLEO	$e^+e^- \rightarrow$ hadrons
142.2 ± 0.3 ± 0.2	145	ALBRECHT 95F	ARG	$e^+e^- \rightarrow$ hadrons
142.12 ± 0.05 ± 0.05	1176	BORTOLETTO92B	CLE2	$e^+e^- \rightarrow$ hadrons
• • •	We do not use the following data for averages, fits, limits, etc. • • •			
142.2 ± 2.0		SADROZINSKI 80	CBAL	$D^{*0} \rightarrow D^0\pi^0$
142.7 ± 1.7		³ GOLDHABER 77	MRK1	e^+e^-

² Obtained by analyzing CLEO-c data but not authored by the CLEO Collaboration. This value comes from the average of the results for two decay modes, $D^0 \rightarrow K^-\pi^+$ and $D^0 \rightarrow K^-\pi^+\pi^-\pi^+$.
³ From simultaneous fit to $D^*(2010)^+, D^*(2007)^0, D^+,$ and D^0 .

$D^*(2007)^0$ WIDTH

VALUE (MeV)	CL%	DOCUMENT ID	TECN	COMMENT
<2.1	90	⁴ ABACHI 88B	HRS	$D^{*0} \rightarrow D^+\pi^-$

⁴ Assuming $m_{D^{*0}} = 2007.2 \pm 2.1$ MeV/c².

$D^*(2007)^0$ DECAY MODES

$\bar{D}^*(2007)^0$ modes are charge conjugates of modes below.

Mode	Fraction (Γ_i/Γ)
Γ_1 $D^0\pi^0$	(64.7 ± 0.9) %
Γ_2 $D^0\gamma$	(35.3 ± 0.9) %

CONSTRAINED FIT INFORMATION

An overall fit to 2 branching ratios uses 5 measurements and one constraint to determine 2 parameters. The overall fit has a $\chi^2 = 2.5$ for 4 degrees of freedom.

The following off-diagonal array elements are the correlation coefficients $\langle \delta x_i \delta x_j \rangle / (\delta x_i \delta x_j)$, in percent, from the fit to the branching fractions, $x_i \equiv \Gamma_i/\Gamma_{\text{total}}$. The fit constrains the x_i whose labels appear in this array to sum to one.

$$x_2 \begin{vmatrix} -100 \\ x_1 \end{vmatrix}$$

$D^*(2007)^0$ BRANCHING RATIOS

$\Gamma(D^0\pi^0)/\Gamma(D^0\gamma)$	Γ_1/Γ_2	
1.83 ± 0.07 OUR FIT	Error	
1.85 ± 0.07 OUR AVERAGE	Error	
1.90 ± 0.07 ± 0.05	4.9k	
1.74 ± 0.02 ± 0.13		
ABLIKIM 15B BES3	10.6 $e^+e^- \rightarrow$ hadrons	
AUBERT,BE 05G BABR	10.6 $e^+e^- \rightarrow$ hadrons	
$\Gamma(D^0\pi^0)/\Gamma_{\text{total}}$	Γ_1/Γ	
0.647 ± 0.009 OUR FIT		
• • •	We do not use the following data for averages, fits, limits, etc. • • •	
0.655 ± 0.008 ± 0.005	3.2k	⁵ ABLIKIM 15B BES3 $e^+e^- \rightarrow$ hadrons
0.635 ± 0.003 ± 0.017	69k	⁵ AUBERT,BE 05G BABR 10.6 $e^+e^- \rightarrow$ hadrons
0.596 ± 0.035 ± 0.028	858	⁶ ALBRECHT 95F ARG $e^+e^- \rightarrow$ hadrons
0.636 ± 0.023 ± 0.033	1097	⁶ BUTLER 92 CLE2 $e^+e^- \rightarrow$ hadrons
$\Gamma(D^0\gamma)/\Gamma_{\text{total}}$	Γ_2/Γ	
0.353 ± 0.009 OUR FIT		
0.381 ± 0.029 OUR AVERAGE		
0.404 ± 0.035 ± 0.028	456	⁶ ALBRECHT 95F ARG $e^+e^- \rightarrow$ hadrons
0.364 ± 0.023 ± 0.033	621	⁶ BUTLER 92 CLE2 $e^+e^- \rightarrow$ hadrons
0.37 ± 0.08 ± 0.08		ADLER 88D MRK3 e^+e^-
• • •	We do not use the following data for averages, fits, limits, etc. • • •	
0.345 ± 0.008 ± 0.005	1.8k	⁵ ABLIKIM 15B BES3 $e^+e^- \rightarrow$ hadrons
0.365 ± 0.003 ± 0.017	68k	⁵ AUBERT,BE 05G BABR 10.6 $e^+e^- \rightarrow$ hadrons
0.47 ± 0.23		LOW 87 HRS 29 GeV e^+e^-
0.53 ± 0.13		BARTEL 85G JADE e^+e^- , hadrons
0.47 ± 0.12		COLES 82 MRK2 e^+e^-
0.45 ± 0.15		GOLDHABER 77 MRK1 e^+e^-

⁵ Derived from the ratio $\Gamma(D^0\pi^0)/\Gamma(D^0\gamma)$ assuming that the branching fractions of $D^{*0} \rightarrow D^0\pi^0$ and $D^{*0} \rightarrow D^0\gamma$ decays sum to 100%
⁶ The BUTLER 92 and ALBRECHT 95F branching ratios are not independent, they have been constrained by the authors to sum to 100%.

$D^*(2007)^0$ REFERENCES

ABLIKIM 15B PR D91 031101	M. Ablikim et al.	(BESIII Collab.)
TOMARADZE 15 PR D91 011102	A. Tomaradze et al.	(NWES)
AUBERT,BE 05G PR D72 091101	B. Aubert et al.	(BABAR Collab.)
ALBRECHT 95F ZPHY C66 63	H. Albrecht et al.	(ARGUS Collab.)
BORTOLETTO 92B PRL 69 2046	D. Bortoletto et al.	(CLEO Collab.)
BUTLER 92 PRL 69 2041	F. Butler et al.	(CLEO Collab.)
ABACHI 88B PL B212 533	S. Abachi et al.	(ANL, IND, MICH, PURD+)
ADLER 88D PL B208 152	J. Adler et al.	(Mark III Collab.)
LOW 87 PL B183 232	E.H. Low et al.	(HRS Collab.)
BARTEL 85G PL 161B 197	W. Bartel et al.	(JADE Collab.)
COLES 82 PR D26 2190	M.W. Coles et al.	(LBL, SLAC)
SADROZINSKI 80 Madison Conf. 681	H.F.W. Sadrozinski et al.	(PRIN, CIT+)
GOLDHABER 77 PL 69B 503	G. Goldhaber et al.	(Mark I Collab.)
NGUYEN 77 PRL 39 262	H.K. Nguyen et al.	(LBL, SLAC)

$D^*(2010)^\pm$

$I(J^P) = \frac{1}{2}(1^-)$
I, J, P need confirmation.

$D^*(2010)^\pm$ MASS

The fit includes $D^\pm, D^0, D_s^\pm, D^{*\pm}, D^{*0}, D_1(2420)^0, D_2^*(2460)^0$, and $D_{s1}(2536)^\pm$ mass and mass difference measurements.

VALUE (MeV)	DOCUMENT ID	TECN	CHG	COMMENT
2010.26 ± 0.05 OUR FIT				

• • • We do not use the following data for averages, fits, limits, etc. • • •
 2008 ± 3 ¹ GOLDHABER 77 MRK1 ± e^+e^-
 2008.6 ± 1.0 ² PERUZZI 77 LGW ± e^+e^-
¹ From simultaneous fit to $D^*(2010)^+, D^*(2007)^0, D^+,$ and D^0 ; not independent of FELDMAN 77B mass difference below.
² PERUZZI 77 mass not independent of FELDMAN 77B mass difference below and PERUZZI 77 D^0 mass value.

$m_{D^*(2010)^+} - m_{D^+}$

The fit includes $D^\pm, D^0, D_s^\pm, D^{*\pm}, D^{*0}, D_1(2420)^0, D_2^*(2460)^0$, and $D_{s1}(2536)^\pm$ mass and mass difference measurements.

VALUE (MeV)	EVTS	DOCUMENT ID	TECN	COMMENT
140.603 ± 0.015 OUR FIT				
140.602 ± 0.014 OUR AVERAGE				
140.6010 ± 0.0068 ± 0.0129	151k	LEES 17F BABR	$e^+e^- \rightarrow$ hadrons	
140.64 ± 0.08 ± 0.06	620	BORTOLETTO92B	CLE2 $e^+e^- \rightarrow$ hadrons	

$m_{D^*(2010)^+} - m_{D^0}$

The fit includes $D^\pm, D^0, D_s^\pm, D^{*\pm}, D^{*0}, D_1(2420)^0, D_2^*(2460)^0$, and $D_{s1}(2536)^\pm$ mass and mass difference measurements.

VALUE (MeV)	EVTS	DOCUMENT ID	TECN	COMMENT
145.4257 ± 0.0017 OUR FIT				
145.4258 ± 0.0020 OUR AVERAGE				Error includes scale factor of 1.2.
145.4259 ± 0.0004 ± 0.0017	312.8k	LEES 13x BABR	$D^{*\pm} \rightarrow D^0\pi^\pm \rightarrow (K\pi, K3\pi)\pi^\pm$	
145.412 ± 0.002 ± 0.012		ANASTASSOV 02 CLE2	$D^{*\pm} \rightarrow D^0\pi^\pm \rightarrow (K\pi)\pi^\pm$	
145.54 ± 0.08	611	³ ADINOLFI 99 BEAT	$D^{*\pm} \rightarrow D^0\pi^\pm$	
145.45 ± 0.02		³ BREITWEG 99 ZEUS	$D^{*\pm} \rightarrow D^0\pi^\pm \rightarrow (K\pi)\pi^\pm$	
145.42 ± 0.05		³ BREITWEG 99 ZEUS	$D^{*\pm} \rightarrow D^0\pi^\pm \rightarrow (K^-3\pi)\pi^\pm$	
145.5 ± 0.15	103	⁴ ADLOFF 97B H1	$D^{*\pm} \rightarrow D^0\pi^\pm$	
145.44 ± 0.08	152	⁴ BREITWEG 97 ZEUS	$D^{*\pm} \rightarrow D^0\pi^\pm$	
145.42 ± 0.11	199	⁴ BREITWEG 97 ZEUS	$D^{*0} \rightarrow K^-3\pi$ $D^{*\pm} \rightarrow D^0\pi^\pm$	
145.4 ± 0.2	48	⁴ DERRICK 95 ZEUS	$D^{*0} \rightarrow K^-3\pi$ $D^{*\pm} \rightarrow D^0\pi^\pm$	
145.39 ± 0.06 ± 0.03		BARLAG 92B ACCM	$\pi^- 230$ GeV	
145.5 ± 0.2	115	⁴ ALEXANDER 91B OPAL	$D^{*\pm} \rightarrow D^0\pi^\pm$	
145.30 ± 0.06		⁴ DECAMP 91J ALEP	$D^{*\pm} \rightarrow D^0\pi^\pm$	
145.40 ± 0.05 ± 0.10		ABACHI 88B HRS	$D^{*\pm} \rightarrow D^0\pi^\pm$	
145.46 ± 0.07 ± 0.03		ALBRECHT 85F ARG	$D^{*\pm} \rightarrow D^0\pi^\pm$	
145.5 ± 0.3	28	BAILEY 83 SPEC	$D^{*\pm} \rightarrow D^0\pi^\pm$	
145.5 ± 0.3	60	FITCH 81 SPEC	$\pi^- A$	
145.3 ± 0.5	30	FELDMAN 77B MRK1	$D^{*+} \rightarrow D^0\pi^+$	
• • •	We do not use the following data for averages, fits, limits, etc. • • •			
145.4256 ± 0.0006 ± 0.0017	138.5k	LEES 13x BABR	$D^{*\pm} \rightarrow D^0\pi^\pm \rightarrow (K^- \pi^+) \pi^\pm$	
145.4266 ± 0.0005 ± 0.0019	174.3k	LEES 13x BABR	$D^{*\pm} \rightarrow D^0\pi^\pm \rightarrow (K^- 2\pi^+ \pi^-) \pi^\pm$	
145.44 ± 0.09	122	⁴ BREITWEG 97B ZEUS	$D^{*\pm} \rightarrow D^0\pi^\pm$ $D^{*0} \rightarrow K^- \pi^+$	
145.8 ± 1.5	16	AHLEN 83 HRS	$D^{*+} \rightarrow D^0\pi^+$	
145.1 ± 1.8	12	BAILEY 83 SPEC	$D^{*+} \rightarrow D^0\pi^+$	

Meson Particle Listings

$D^*(2010)^\pm, D_0^*(2300)^0$

145.1	± 0.5	14	BAILEY	83	SPEC	$D^{*\pm} \rightarrow D^0 \pi^\pm$
145.5	± 0.5	14	YELTON	82	MRK2	$29 e^+ e^- \rightarrow K^- \pi^+$
~ 145.5			VERY	80	SPEC	γA
145.2	± 0.6	2	BLIETSCHAU	79	BEBC	νp

³Statistical errors only.
⁴Systematic error not evaluated.

$m_{D^*(2010)^+} - m_{D^*(2007)^0}$

VALUE (MeV)	DOCUMENT ID	TECN	COMMENT
2.6 ± 1.8	⁵ PERUZZI 77	LGW	$e^+ e^-$

• • • We do not use the following data for averages, fits, limits, etc. • • •
⁵ Not independent of FELDMAN 77B mass difference above, PERUZZI 77 D^0 mass, and GOLDHABER 77 $D^*(2007)^0$ mass.

$D^*(2010)^\pm$ WIDTH

VALUE (keV)	CL% EVTS	DOCUMENT ID	TECN	COMMENT
83.4 ± 1.8 ± 1.4	312.8k	⁶ LEES	13x	BABR $D^{*\pm} \rightarrow D^0 \pi^\pm \rightarrow (K \pi, K 3\pi) \pi^\pm$
96 ± 4 ± 22		⁶ ANASTASSOV 02	CLE2	$D^{*\pm} \rightarrow D^0 \pi^\pm \rightarrow (K \pi) \pi^\pm$
83.4 ± 1.7 ± 1.5	138.5k	⁶ LEES	13x	BABR $D^{*\pm} \rightarrow D^0 \pi^\pm \rightarrow (K^- \pi^+) \pi^\pm$
83.2 ± 1.5 ± 2.6	174.3k	⁶ LEES	13x	BABR $D^{*\pm} \rightarrow D^0 \pi^\pm \rightarrow (K^- 2\pi^+ \pi^-) \pi^\pm$
<131	90 110	BARLAG	92B	ACCM $\pi^- 230$ GeV

⁶ Ignoring the electromagnetic contribution from $D^{*\pm} \rightarrow D^\pm \gamma$.

$D^*(2010)^\pm$ DECAY MODES

$D^*(2010)^-$ modes are charge conjugates of the modes below.

Mode	Fraction (Γ_i/Γ)
Γ_1 $D^0 \pi^+$	(67.7 ± 0.5) %
Γ_2 $D^+ \pi^0$	(30.7 ± 0.5) %
Γ_3 $D^+ \gamma$	(1.6 ± 0.4) %

CONSTRAINED FIT INFORMATION

An overall fit to 3 branching ratios uses 6 measurements and one constraint to determine 3 parameters. The overall fit has a $\chi^2 = 0.3$ for 4 degrees of freedom.

The following *off-diagonal* array elements are the correlation coefficients $\langle \delta x_i \delta x_j \rangle / (\delta x_i \delta x_j)$, in percent, from the fit to the branching fractions, $x_i \equiv \Gamma_i/\Gamma_{\text{total}}$. The fit constrains the x_i whose labels appear in this array to sum to one.

x_2	-62	
x_3	-43	-44
	x_1	x_2

$D^*(2010)^+$ BRANCHING RATIOS

$\Gamma(D^0 \pi^+)/\Gamma_{\text{total}}$	DOCUMENT ID	TECN	COMMENT	Γ_1/Γ
0.677 ± 0.005 OUR FIT				
0.677 ± 0.006 OUR AVERAGE				
0.6759 ± 0.0029 ± 0.0064	^{7,8,9} BARTELT 98	CLE2	$e^+ e^-$	
0.688 ± 0.024 ± 0.013	ALBRECHT 95F	ARG	$e^+ e^- \rightarrow$ hadrons	
0.681 ± 0.010 ± 0.013	⁷ BUTLER 92	CLE2	$e^+ e^- \rightarrow$ hadrons	
• • • We do not use the following data for averages, fits, limits, etc. • • •				
0.57 ± 0.04 ± 0.04	ADLER 88D	MRK3	$e^+ e^-$	
0.44 ± 0.10	COLES 82	MRK2	$e^+ e^-$	
0.6 ± 0.15	⁹ GOLDHABER 77	MRK1	$e^+ e^-$	

$\Gamma(D^+ \pi^0)/\Gamma_{\text{total}}$	DOCUMENT ID	TECN	COMMENT	Γ_2/Γ
0.307 ± 0.005 OUR FIT				
0.3073 ± 0.0013 ± 0.0062	^{7,8,9} BARTELT 98	CLE2	$e^+ e^-$	
• • • We do not use the following data for averages, fits, limits, etc. • • •				
0.312 ± 0.011 ± 0.008	1404	ALBRECHT 95F	ARG $e^+ e^- \rightarrow$ hadrons	
0.308 ± 0.004 ± 0.008	410	⁷ BUTLER 92	CLE2 $e^+ e^- \rightarrow$ hadrons	
0.26 ± 0.02 ± 0.02	ADLER 88D	MRK3	$e^+ e^-$	
0.34 ± 0.07	COLES 82	MRK2	$e^+ e^-$	

$\Gamma(D^+ \gamma)/\Gamma_{\text{total}}$	CL% EVTS	DOCUMENT ID	TECN	COMMENT	Γ_3/Γ
0.016 ± 0.004 OUR FIT					
0.016 ± 0.005 OUR AVERAGE					
0.0168 ± 0.0042 ± 0.0029		^{7,8} BARTELT 98	CLE2	$e^+ e^-$	
0.011 ± 0.014 ± 0.016	12	⁷ BUTLER 92	CLE2	$e^+ e^- \rightarrow$ hadrons	
• • • We do not use the following data for averages, fits, limits, etc. • • •					
<0.052	90	ALBRECHT 95F	ARG	$e^+ e^- \rightarrow$ hadrons	
0.17 ± 0.05 ± 0.05		ADLER 88D	MRK3	$e^+ e^-$	
0.22 ± 0.12	10	COLES 82	MRK2	$e^+ e^-$	
⁷ The branching ratios are not independent, they have been constrained by the authors to sum to 100%.					
⁸ Systematic error includes theoretical error on the prediction of the ratio of hadronic modes.					
⁹ Assuming that isospin is conserved in the decay.					
¹⁰ Not independent of $\Gamma(D^0 \pi^+)/\Gamma_{\text{total}}$ and $\Gamma(D^+ \pi^0)/\Gamma_{\text{total}}$ measurement.					

$D^*(2010)^\pm$ REFERENCES

LEES 17F	PRL 119 202003	J.P. Lees <i>et al.</i>	(BABAR Collab.)
LEES 13X	PRL 111 111801	J.P. Lees <i>et al.</i>	(BABAR Collab.)
Also	PR D88 052003	J.P. Lees <i>et al.</i>	(BABAR Collab.)
Also	PR D88 079902 (err.)	J.P. Lees <i>et al.</i>	(BABAR Collab.)
ANASTASSOV 02	PR D65 032003	A. Anastassov <i>et al.</i>	(CLEO Collab.)
ADINOLFI 99	NP B547 3	M. Adinolfi <i>et al.</i>	(Belle Collab.)
BREITWEG 99	EPL C6 67	J. Breitweg <i>et al.</i>	(ZEUS Collab.)
BARTELT 98	PRL 80 3919	J. Bartelt <i>et al.</i>	(CLEO Collab.)
ADLOFF 97B	ZPHY C72 593	C. Adloff <i>et al.</i>	(HI Collab.)
BREITWEG 97	PL B401 192	J. Breitweg <i>et al.</i>	(ZEUS Collab.)
BREITWEG 97B	PL B407 402	J. Breitweg <i>et al.</i>	(ZEUS Collab.)
ALBRECHT 95F	ZPHY C66 63	H. Albrecht <i>et al.</i>	(ARGUS Collab.)
DERRICK 95	PL B349 225	M. Derrick <i>et al.</i>	(ZEUS Collab.)
BARLAG 92B	PL B278 480	S. Barlag <i>et al.</i>	(ACCMOR Collab.)
BORTOLETTO 92B	PRL 69 2046	D. Bortoletto <i>et al.</i>	(CLEO Collab.)
BUTLER 92	PRL 69 2041	F. Butler <i>et al.</i>	(CLEO Collab.)
ALEXANDER 91B	PL B262 341	G. Alexander <i>et al.</i>	(OPAL Collab.)
DECAMP 91J	PL B266 218	D. Decamp <i>et al.</i>	(ALEPH Collab.)
ABACHI 88B	PL B212 533	S. Abachi <i>et al.</i>	(ANL, IND, MICH, PURD+)
ADLER 88D	PL B208 152	J. Adler <i>et al.</i>	(ANL, IND, LBL+)
ALBRECHT 85F	PL 150B 235	H. Albrecht <i>et al.</i>	(ARGUS Collab.)
AHLEN 83	PRL 51 1147	S.P. Ahlen <i>et al.</i>	(ANL, IND, LBL+)
BAILEY 83	PL 132B 230	R. Bailey <i>et al.</i>	(AMST, BRIS, CERN, CRAC+)
COLES 82	PR D26 2190	M.W. Coles <i>et al.</i>	(LBL, SLAC)
YELTON 82	PRL 49 430	J.M. Yelton <i>et al.</i>	(SLAC, LBL, UCB+)
FITCH 81	PRL 46 761	V.L. Fitch <i>et al.</i>	(PRIN, SAcl, TORI+)
VERY 80	PRL 44 1309	P. Avery <i>et al.</i>	(ILL, FNAL, COLU)
BLIETSCHAU 79	PL B68 108	J. Blietschau <i>et al.</i>	(AACH3, BONN, CERN+)
FELDMAN 77B	PRL 38 1313	G.J. Feldman <i>et al.</i>	(Mark I Collab.)
GOLDHABER 77	PL 69B 503	G. Goldhaber <i>et al.</i>	(Mark I Collab.)
PERUZZI 77	PRL 39 1301	I. Peruzzi <i>et al.</i>	(LGW Collab.)

$D_0^*(2300)^0$

$$I(J^P) = \frac{1}{2}(0^+)$$

was $D_0^*(2400)^0$
 $J^P = 0^+$ assignment favored (ABE 04D).

$D_0^*(2300)^0$ MASS

VALUE (MeV)	EVTS	DOCUMENT ID	TECN	COMMENT
2300 ± 19 OUR AVERAGE				
2297 ± 8 ± 20	3.4k	AUBERT 09AB	BABR	$B^- \rightarrow D^+ \pi^- \pi^-$
2308 ± 17 ± 32		ABE 04D	BELL	$B^- \rightarrow D^+ \pi^- \pi^-$
• • • We do not use the following data for averages, fits, limits, etc. • • •				
2407 ± 21 ± 35	9.8k	¹ LINK 04A	FOCS	γA
¹ Possibly the feed-down from another state.				

$D_0^*(2300)^0$ WIDTH

VALUE (MeV)	EVTS	DOCUMENT ID	TECN	COMMENT
274 ± 40 OUR AVERAGE				
273 ± 12 ± 48	3.4k	AUBERT 09AB	BABR	$B^- \rightarrow D^+ \pi^- \pi^-$
276 ± 21 ± 63		ABE 04D	BELL	$B^- \rightarrow D^+ \pi^- \pi^-$
• • • We do not use the following data for averages, fits, limits, etc. • • •				
240 ± 55 ± 59	9.8k	² LINK 04A	FOCS	γA
² Possibly the feed-down from another state.				

$D_0^*(2300)^0$ DECAY MODES

Mode	Fraction (Γ_i/Γ)
Γ_1 $D^+ \pi^-$	seen

$D_0^*(2300)^0$ REFERENCES

AUBERT 09AB	PR D79 112004	B. Aubert <i>et al.</i>	(BABAR Collab.)
ABE 04D	PR D69 112002	K. Abe <i>et al.</i>	(BELLE Collab.)
LINK 04A	PL B586 11	J.M. Link <i>et al.</i>	(FOCUS Collab.)

See key on page 999

Meson Particle Listings

$D_0^*(2300)^\pm, D_1(2420)^0$

$D_0^*(2300)^\pm$

$I(J^P) = \frac{1}{2}(0^+)$

OMITTED FROM SUMMARY TABLE
was $D_0^*(2400)^\pm$
 J, P need confirmation.

$D_0^*(2300)^\pm$ MASS

VALUE (MeV)	EVTS	DOCUMENT ID	TECN	COMMENT
2349 ± 7 OUR AVERAGE				
2360 ± 15 ± 30		¹ AAIJ	15x LHCb	$B^0 \rightarrow \bar{D}^0 K^+ \pi^-$
2349 ± 6 ± 4		² AAIJ	15y LHCb	$B^0 \rightarrow \bar{D}^0 \pi^+ \pi^-$
• • • We do not use the following data for averages, fits, limits, etc. • • •				
2354 ± 7 ± 11		³ AAIJ	15y LHCb	$B^0 \rightarrow \bar{D}^0 \pi^+ \pi^-$
2403 ± 14 ± 35	18.8k	⁴ LINK	04A FOCS	γA
¹ From the Dalitz plot analysis including various K^* and D^{**} mesons as well as broad structures in the $K\pi$ S-wave and the $D\pi$ S- and P-waves.				
² Modeling the $\pi^+\pi^-$ S-wave with the isobar formalism.				
³ Modeling the $\pi^+\pi^-$ S-wave with the K-matrix formalism.				
⁴ Possibly the feed-down from another state.				

$D_0^*(2300)^\pm$ WIDTH

VALUE (MeV)	EVTS	DOCUMENT ID	TECN	COMMENT
221 ± 18 OUR AVERAGE				
255 ± 26 ± 51		¹ AAIJ	15x LHCb	$B^0 \rightarrow \bar{D}^0 K^+ \pi^-$
217 ± 13 ± 13		² AAIJ	15y LHCb	$B^0 \rightarrow \bar{D}^0 \pi^+ \pi^-$
• • • We do not use the following data for averages, fits, limits, etc. • • •				
230 ± 15 ± 21		³ AAIJ	15y LHCb	$B^0 \rightarrow \bar{D}^0 \pi^+ \pi^-$
283 ± 24 ± 34	18.8k	⁴ LINK	04A FOCS	γA
¹ From the Dalitz plot analysis including various K^* and D^{**} mesons as well as broad structures in the $K\pi$ S-wave and the $D\pi$ S- and P-waves.				
² Modeling the $\pi^+\pi^-$ S-wave with the isobar formalism.				
³ Modeling the $\pi^+\pi^-$ S-wave with the K-matrix formalism.				
⁴ Possibly the feed-down from another state.				

$D_0^*(2300)^\pm$ DECAY MODES

Mode	Fraction (Γ_i/Γ)
$\Gamma_1 D^0 \pi^+$	seen

$D_0^*(2300)^\pm$ REFERENCES

AAIJ	15X	PR D92 012012	R. Aaij <i>et al.</i>	(LHCb Collab.)
AAIJ	15Y	PR D92 032002	R. Aaij <i>et al.</i>	(LHCb Collab.)
LINK	04A	PL B586 11	J.M. Link <i>et al.</i>	(FOCUS Collab.)

$D_1(2420)^0$

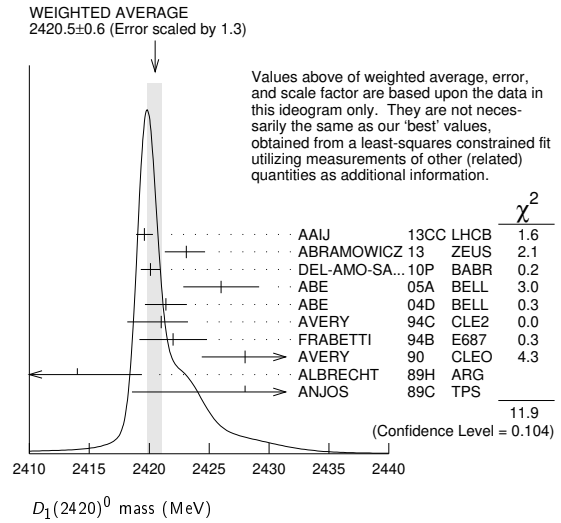
$I(J^P) = \frac{1}{2}(1^+)$

$D_1(2420)^0$ MASS

The fit includes $D^\pm, D^0, D_s^\pm, D^{*\pm}, D^{*0}, D_s^{*\pm}, D_1(2420)^0, D_2^*(2460)^0,$
and $D_{s1}(2536)^\pm$ mass and mass difference measurements.

VALUE (MeV)	EVTS	DOCUMENT ID	TECN	COMMENT
2420.8 ± 0.5 OUR FIT Error includes scale factor of 1.3.				
2420.5 ± 0.6 OUR AVERAGE Error includes scale factor of 1.3. See the ideogram below.				
2419.6 ± 0.1 ± 0.7	210k	AAIJ	13cc LHCb	$pp \rightarrow D^{*+} \pi^- X$
2423.1 ± 1.5 ± 0.4	2.7k	¹ ABRAMOWICZ13	ZEUS	$e^\pm p \rightarrow D^{(*)+} \pi^- X$
2420.1 ± 0.1 ± 0.8	103k	DEL-AMO-SA...10P	BABR	$e^+ e^- \rightarrow D^{*+} \pi^- X$
2426 ± 3 ± 1	151	ABE	05A BELL	$B^- \rightarrow D^0 \pi^+ \pi^- \pi^-$
2421.4 ± 1.5 ± 0.9		² ABE	04D BELL	$B^- \rightarrow D^{*+} \pi^- \pi^-$
2421 ± 1 ± 2	286	AVERY	94C CLE2	$e^+ e^- \rightarrow D^{*+} \pi^- X$
2422 ± 2 ± 2	51	FRABETTI	94B E687	$\gamma Be \rightarrow D^{*+} \pi^- X$
2428 ± 3 ± 2	279	AVERY	90 CLEO	$e^+ e^- \rightarrow D^{*+} \pi^- X$
2414 ± 2 ± 5	171	ALBRECHT	89H ARG	$e^+ e^- \rightarrow D^{*+} \pi^- X$
2428 ± 8 ± 5	171	ANJOS	89c TPS	$\gamma N \rightarrow D^{*+} \pi^- X$
• • • We do not use the following data for averages, fits, limits, etc. • • •				
2420.5 ± 2.1 ± 0.9	3110 ± 340	³ CHEKANOV	09 ZEUS	$e^\pm p \rightarrow D^{*+} \pi^- X$
2421.7 ± 0.7 ± 0.6	7.5k	ABULENCIA	06A CDF	$1900 p\bar{p} \rightarrow D^{*+} \pi^- X$
2425 ± 3	235	⁴ ABREU	98M DLPH	$e^+ e^-$
¹ From the combined fit of the $M(D^+ \pi^-)$ and $M(D^{*+} \pi^-)$ distributions. and A_{D_2} fixed to the theoretical prediction of -1.				
² Fit includes the contribution from $D_1^*(2430)^0$.				
³ Calculated using the mass difference $m(D_1^0) - m(D^{*+})_{PDG}$ reported below and $m(D^{*+})_{PDG} = 2010.27 \pm 0.17$ MeV. The 0.17 MeV uncertainty of the PDG mass value should be added to the experimental uncertainty of 0.9 MeV.				

⁴ No systematic error given.



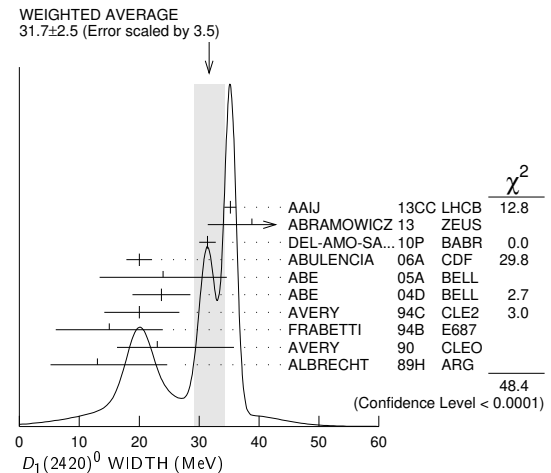
$m_{D_1^0} - m_{D^{*+}}$

The fit includes $D^\pm, D^0, D_s^\pm, D^{*\pm}, D^{*0}, D_s^{*\pm}, D_1(2420)^0, D_2^*(2460)^0,$
and $D_{s1}(2536)^\pm$ mass and mass difference measurements.

VALUE (MeV)	EVTS	DOCUMENT ID	TECN	COMMENT
410.6 ± 0.5 OUR FIT Error includes scale factor of 1.3.				
411.5 ± 0.8 OUR AVERAGE				
410.2 ± 2.1 ± 0.9	3110 ± 340	CHEKANOV	09 ZEUS	$e^\pm p \rightarrow D^{*+} \pi^- X$
411.7 ± 0.7 ± 0.4	7.5k	ABULENCIA	06A CDF	$1900 p\bar{p} \rightarrow D^{*+} \pi^- X$

$D_1(2420)^0$ WIDTH

VALUE (MeV)	EVTS	DOCUMENT ID	TECN	COMMENT
31.7 ± 2.5 OUR AVERAGE Error includes scale factor of 3.5. See the ideogram below.				
35.2 ± 0.4 ± 0.9	210k	AAIJ	13cc LHCb	$pp \rightarrow D^{*+} \pi^- X$
38.8 ± 5.0 ± 1.9	2.7k	¹ ABRAMOWICZ13	ZEUS	$e^\pm p \rightarrow D^{(*)+} \pi^- X$
31.4 ± 0.5 ± 1.3	103k	DEL-AMO-SA...10P	BABR	$e^+ e^- \rightarrow D^{*+} \pi^- X$
20.0 ± 1.7 ± 1.3	7.5k	ABULENCIA	06A CDF	$1900 p\bar{p} \rightarrow D^{*+} \pi^- X$
24 ± 7 ± 8	151	ABE	05A BELL	$B^- \rightarrow D^0 \pi^+ \pi^- \pi^-$
23.7 ± 2.7 ± 4.0		² ABE	04D BELL	$B^- \rightarrow D^{*+} \pi^- \pi^-$
20 ± 6 ± 3	286	AVERY	94C CLE2	$e^+ e^- \rightarrow D^{*+} \pi^- X$
15 ± 8 ± 4	51	FRABETTI	94B E687	$\gamma Be \rightarrow D^{*+} \pi^- X$
23 ± 8 ± 10	279	AVERY	90 CLEO	$e^+ e^- \rightarrow D^{*+} \pi^- X$
13 ± 6 ± 10	171	ALBRECHT	89H ARG	$e^+ e^- \rightarrow D^{*+} \pi^- X$
• • • We do not use the following data for averages, fits, limits, etc. • • •				
53.2 ± 7.2 ± 3.3	3110 ± 340	CHEKANOV	09 ZEUS	$e^\pm p \rightarrow D^{*+} \pi^- X$
58 ± 14 ± 10	171	ANJOS	89c TPS	$\gamma N \rightarrow D^{*+} \pi^- X$



¹ From the combined fit of the $M(D^+ \pi^-)$ and $M(D^{*+} \pi^-)$ distributions. and A_{D_2} fixed to the theoretical prediction of -1.

Meson Particle Listings

$D_1(2420)^0, D_1(2420)^\pm$

²Fit includes the contribution from $D_1^*(2430)^0$.

$D_1(2420)^0$ DECAY MODES

$\bar{D}_1(2420)^0$ modes are charge conjugates of modes below.

Mode	Fraction (Γ_i/Γ)
Γ_1 $D^*(2010)^+ \pi^-$	seen
Γ_2 $D^0 \pi^+ \pi^-$	seen
Γ_3 $D^0 \rho^0$	
Γ_4 $D^0 f_0(500)$	
Γ_5 $D_0^*(2300)^+ \pi^-$	
Γ_6 $D^+ \pi^-$	not seen
Γ_7 $D^{*0} \pi^+ \pi^-$	not seen

$D_1(2420)^0$ BRANCHING RATIOS

$\Gamma(D^*(2010)^+ \pi^-)/\Gamma_{\text{total}}$				Γ_1/Γ
VALUE	DOCUMENT ID	TECN	COMMENT	
seen	ACKERSTAFF 97W	OPAL	$e^+ e^- \rightarrow D^{*+} \pi^- X$	
seen	AVERY 90	CLEO	$e^+ e^- \rightarrow D^{*+} \pi^- X$	
seen	ALBRECHT 89H	ARG	$e^+ e^- \rightarrow D^* \pi^- X$	
seen	ANJOS 89c	TPS	$\gamma N \rightarrow D^{*+} \pi^- X$	

$\Gamma(D^+ \pi^-)/\Gamma(D^*(2010)^+ \pi^-)$				Γ_6/Γ_1
VALUE	CL%	DOCUMENT ID	TECN	COMMENT
<0.24	90	AVERY 90	CLEO	$e^+ e^- \rightarrow D^+ \pi^- X$

$D_1(2420)^0$ POLARIZATION AMPLITUDE A_{D_1}

A polarization amplitude A_{D_1} is a parameter that depends on the initial polarization of the D_1 and is sensitive to a possible S-wave contribution to its decay. For D_1 decays the helicity angle, θ_h , distribution varies like $1 + A_{D_1} \cos^2 \theta_h$, where θ_h is the angle in the D^* rest frame between the two pions emitted by the $D_1 \rightarrow D^* \pi$ and the $D^* \rightarrow D \pi$.

Unpolarized D_1 decaying purely via D-wave is predicted to give $A_{D_1} = 3$.

VALUE	EVTS	DOCUMENT ID	TECN	COMMENT
5.73 ± 0.25 OUR AVERAGE				
7.8 ^{+6.7} _{-2.7} ^{+4.6} _{-1.8}	2.7k	1 ABRAMOWICZ13	ZEUS	$e^\pm p \rightarrow D^{(*)+} \pi^- X$
5.72 ± 0.25	103k	DEL-AMO-SA..10P	BABR	$e^+ e^- \rightarrow D^{*+} \pi^- X$
5.9 ^{+3.0} _{-1.7} ^{+2.4} _{-1.0}		CHEKANOV 09	ZEUS	$e^\pm p \rightarrow D^{*+} \pi^- X$
• • • We do not use the following data for averages, fits, limits, etc. • • •				
3.30 ± 0.48	210k	2 AAIJ	13CC LHCb	$pp \rightarrow D^{*+} \pi^- X$
3.8 ± 0.6 ± 0.8		3 AUBERT	09Y BABR	$B^+ \rightarrow D_1^0 \ell^+ \nu_\ell$
2.74 ^{+1.40} _{-0.93}		4 AVERY	94c CLE2	$e^+ e^- \rightarrow D^{*+} \pi^- X$

¹ From the combined fit of the $M(D^+ \pi^-)$ and $M(D^{*+} \pi^-)$ distributions. and A_{D_2} fixed to the theoretical prediction of -1 . A pure D-wave not excluded although some S-wave mixing possible.
² Systematic uncertainty not estimated. Resonance parameters fixed.
³ Assuming $\Gamma(\Upsilon(4S) \rightarrow B^+ B^-) / \Gamma(\Upsilon(4S) \rightarrow B^0 \bar{B}^0) = 1.065 \pm 0.026$ and equal partial widths and helicity angle distributions for charged and neutral D_1 mesons.
⁴ Systematic uncertainties not estimated.

$D_1(2420)^0$ REFERENCES

AAIJ 13CC JHEP 1309 145	R. Aaij et al.	(LHCb Collab.)
ABRAMOWICZ 13 NP B866 229	H. Abramowicz et al.	(ZEUS Collab.)
DEL-AMO-SA..10P PR D82 111101	P. del Amo Sanchez et al.	(BABAR Collab.)
AUBERT 09Y PRL 103 051803	B. Aubert et al.	(BABAR Collab.)
CHEKANOV 09 EPJ C60 25	S. Chekanov et al.	(ZEUS Collab.)
ABUENCIA 06A PR D73 051104	A. Abulencia et al.	(CDF Collab.)
ABE 05A PRL 94 221805	K. Abe et al.	(BELLE Collab.)
ABE 04D PR D69 112002	K. Abe et al.	(BELLE Collab.)
ABREU 98M PL B426 231	P. Abreu et al.	(DELPHI Collab.)
ACKERSTAFF 97W ZPHY C76 425	K. Ackerstaff et al.	(OPAL Collab.)
AVERY 94C PL B331 236	P. Avery et al.	(CLEO Collab.)
FRABETTI 94B PRL 72 324	P.L. Frabetti et al.	(FNAL E687 Collab.)
AVERY 90 PR D41 774	P. Avery, D. Besson	(CLEO Collab.)
ALBRECHT 89H PL B232 398	H. Albrecht et al.	(ARGUS Collab.) JP
ANJOS 89C PRL 62 1717	J.C. Anjos et al.	(FNAL E691 Collab.)

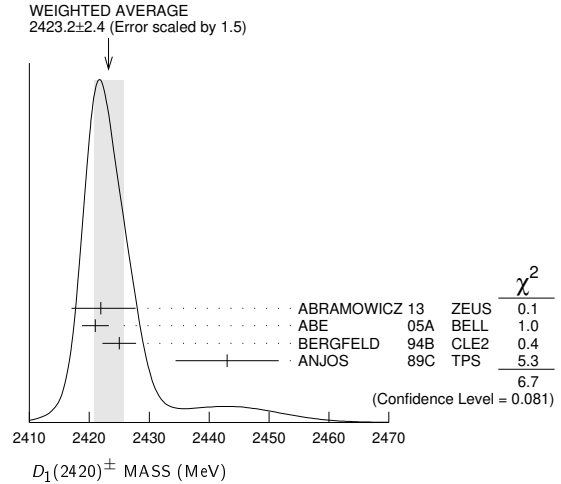
$D_1(2420)^\pm$ $I(J^P) = \frac{1}{2}(1^?)$
 I needs confirmation.

OMITTED FROM SUMMARY TABLE
 Seen in $D^*(2007)^0 \pi^+$. $J^P = 0^+$ ruled out.

$D_1(2420)^\pm$ MASS

VALUE (MeV)	EVTS	DOCUMENT ID	TECN	COMMENT
2423.2 ± 2.4 OUR AVERAGE				Error includes scale factor of 1.5. See the ideogram below.
2421.9 ± 4.7 ^{+3.4} _{-1.2}	759	1 ABRAMOWICZ13	ZEUS	$e^\pm p \rightarrow D^{(*)0} \pi^+ X$
2421 ± 2 ± 1	124	ABE	05A BELL	$\bar{B}^0 \rightarrow D^+ \pi^+ \pi^- \pi^-$
2425 ± 2 ± 2	146	BERGFELD	94B CLE2	$e^+ e^- \rightarrow D^{*0} \pi^+ X$
2443 ± 7 ± 5	190	ANJOS	89c TPS	$\gamma N \rightarrow D^0 \pi^+ X^0$

¹ From the fit of the $M(D^0 \pi^+)$ distribution. The widths of the D_1^+ and D_2^+ are fixed to 25 MeV and 37 MeV, and A_{D_1} and A_{D_2} are fixed to the theoretical predictions of 3 and -1 , respectively.



$m_{D_1^*(2420)^\pm} - m_{D_1^0(2420)^0}$

VALUE (MeV)	DOCUMENT ID	TECN	COMMENT
4 ⁺² ₋₃ ± 3	BERGFELD 94B	CLE2	$e^+ e^- \rightarrow \text{hadrons}$

$D_1(2420)^\pm$ WIDTH

VALUE (MeV)	EVTS	DOCUMENT ID	TECN	COMMENT
25 ± 6 OUR AVERAGE				
21 ± 5 ± 8	124	ABE	05A BELL	$\bar{B}^0 \rightarrow D^+ \pi^+ \pi^- \pi^-$
26 ⁺⁸ ₋₇ ± 4	146	BERGFELD	94B CLE2	$e^+ e^- \rightarrow D^{*0} \pi^+ X$
41 ± 19 ± 8	190	ANJOS	89c TPS	$\gamma N \rightarrow D^0 \pi^+ X^0$

$D_1(2420)^\pm$ DECAY MODES

$D_1^*(2420)^-$ modes are charge conjugates of modes below.

Mode	Fraction (Γ_i/Γ)
Γ_1 $D^*(2007)^0 \pi^+$	seen
Γ_2 $D^+ \pi^+ \pi^-$	seen
Γ_3 $D^+ \rho^0$	
Γ_4 $D^+ f_0(500)$	
Γ_5 $D_0^*(2300)^0 \pi^+$	
Γ_6 $D^0 \pi^+$	not seen
Γ_7 $D^{*+} \pi^+ \pi^-$	not seen

$D_1(2420)^\pm$ BRANCHING RATIOS

$\Gamma(D^*(2007)^0 \pi^+)/\Gamma_{\text{total}}$				Γ_1/Γ
VALUE	DOCUMENT ID	TECN	COMMENT	
seen	ANJOS 89c	TPS	$\gamma N \rightarrow D^0 \pi^+ X^0$	

$\Gamma(D^0 \pi^+)/\Gamma(D^*(2007)^0 \pi^+)$				Γ_6/Γ_1
VALUE	CL%	DOCUMENT ID	TECN	COMMENT
<0.18	90	BERGFELD 94B	CLE2	$e^+ e^- \rightarrow \text{hadrons}$

$D_1(2420)^\pm$ POLARIZATION AMPLITUDE A_{D_1}

A polarization amplitude A_{D_1} is a parameter that depends on the initial polarization of the D_1 and is sensitive to a possible S-wave contribution to its decay. For D_1 decays the helicity angle, θ_h , distribution varies like

See key on page 999

Meson Particle Listings

$D_1(2420)^\pm, D_1(2430)^0, D_2^*(2460)^0$

$1 + A_{D_1} \cos^2 \theta_h$, where θ_h is the angle in the D^* rest frame between the two pions emitted by the $D_1 \rightarrow D^* \pi$ and the $D^* \rightarrow D \pi$.

Unpolarized D_1 decaying purely via D -wave is predicted to give $A_{D_1} = 3$.

VALUE	DOCUMENT ID	TECN	COMMENT
$3.8 \pm 0.6 \pm 0.8$	² AUBERT	09Y	BABR $B^0 \rightarrow D_1^- \ell^+ \nu_\ell$
² Assuming $\Gamma(\Upsilon(4S) \rightarrow B^+ B^-) / \Gamma(\Upsilon(4S) \rightarrow B^0 \bar{B}^0) = 1.065 \pm 0.026$ and equal partial widths and helicity angle distributions for charged and neutral D_1 mesons.			

$D_1(2420)^\pm$ REFERENCES

ABRAMOWICZ 13	NP B866 229	H. Abramowicz et al.	(ZEUS Collab.)
AUBERT 09Y	PRL 103 051803	B. Aubert et al.	(BABAR Collab.)
ABE 05A	PRL 94 221805	K. Abe et al.	(BELLE Collab.)
BERGFELD 94B	PL B340 194	T. Bergfeld et al.	(CLEO Collab.)
ANJOS 89C	PRL 62 1717	J.C. Anjos et al.	(FNAL E691 Collab.)

$D_1(2430)^0$

$I(J^P) = \frac{1}{2}(1^+)$

OMITTED FROM SUMMARY TABLE

$J = 1^+$ assignment favored (ABE 04D).

$D_1(2430)^0$ MASS

VALUE (MeV)	DOCUMENT ID	TECN	COMMENT
$2427 \pm 26 \pm 25$	ABE	04D	BELL $B^- \rightarrow D^{*+} \pi^- \pi^-$
2477 ± 28	¹ AUBERT	06L	BABR $\bar{B}^0 \rightarrow D^{*+} \omega \pi^-$
¹ Systematic errors not estimated.			

$D_1(2430)^0$ WIDTH

VALUE (MeV)	DOCUMENT ID	TECN	COMMENT
$384_{-107}^{+107} \pm 74$	ABE	04D	BELL $B^- \rightarrow D^{*+} \pi^- \pi^-$
266 ± 97	² AUBERT	06L	BABR $\bar{B}^0 \rightarrow D^{*+} \omega \pi^-$
² Systematic errors not estimated.			

$D_1(2430)^0$ DECAY MODES

Mode	Fraction (Γ_i/Γ)
Γ_1 $D^*(2010)^+ \pi^-$	seen

$D_1(2430)^0$ REFERENCES

AUBERT 06L	PR D74 012001	B. Aubert et al.	(BABAR Collab.)
ABE 04D	PR D69 112002	K. Abe et al.	(BELLE Collab.)

$D_2^*(2460)^0$

$I(J^P) = \frac{1}{2}(2^+)$

$J^P = 2^+$ assignment strongly favored (ALBRECHT 89B, ALBRECHT 89H), natural parity confirmed by the helicity analysis (DEL-AMO-SANCHEZ 10P). AAIJ 13CC confirms $J^P = 2^+$ and natural parity.

$D_2^*(2460)^0$ MASS

The fit includes $D^\pm, D^0, D_s^\pm, D^{*+}, D^{*0}, D_s^{*+}, D_1(2420)^0, D_2^*(2460)^0$, and $D_{s1}(2536)^\pm$ mass and mass difference measurements.

VALUE (MeV)	EVTS	DOCUMENT ID	TECN	COMMENT
2460.7 ± 0.4 ± 1.2	OUR FIT	Error includes scale factor of 3.1.		
2460.56 ± 0.35	OUR AVERAGE	Error includes scale factor of 2.6. See the ideogram below.		
$2463.7 \pm 0.4 \pm 0.7$	28k	¹ AAIJ	16AH LHCB	$B^- \rightarrow D^+ \pi^- \pi^-$
$2460.4 \pm 0.4 \pm 1.2$	82k	AAIJ	13CC LHCB	$pp \rightarrow D^{*+} \pi^- X$
$2460.4 \pm 0.1 \pm 0.1$	675k	AAIJ	13CC LHCB	$pp \rightarrow D^+ \pi^- X$
$2462.5 \pm 2.4 \pm 1.3_{-1.1}^{+1.3}$	2.3k	² ABRAMOWICZ13	ZEUS	$e^\pm p \rightarrow D^*(*) \pi^- X$
$2462.2 \pm 0.1 \pm 0.8$	243k	DEL-AMO-SA...10P	BABR	$e^+ e^- \rightarrow D^+ \pi^- X$
$2460.4 \pm 1.2 \pm 2.2$	3.4k	AUBERT	09AB BABR	$B^- \rightarrow D^+ \pi^- \pi^-$
$2461.6 \pm 2.1 \pm 3.3$		³ ABE	04D BELL	$B^- \rightarrow D^+ \pi^- \pi^-$
$2464.5 \pm 1.1 \pm 1.9$	5.8k	³ LINK	04A FOCUS	γA
$2465 \pm 3 \pm 3$	486	AVERY	94C CLE2	$e^+ e^- \rightarrow D^+ \pi^- X$
$2453 \pm 3 \pm 2$	128	FRABETTI	94B E687	$\gamma Be \rightarrow D^+ \pi^- X$
$2461 \pm 3 \pm 1$	440	AVERY	90 CLEO	$e^+ e^- \rightarrow D^{*+} \pi^- X$
$2455 \pm 3 \pm 5$	337	ALBRECHT	89B ARG	$e^+ e^- \rightarrow D^+ \pi^- X$
$2459 \pm 3 \pm 2$	153	ANJOS	89C TPS	$\gamma N \rightarrow D^+ \pi^- X$

• • • We do not use the following data for averages, fits, limits, etc. • • •

$2469.1 \pm 3.7 \pm 1.2_{-1.3}^{+1.2}$	1.5k	⁴ CHEKANOV	09 ZEUS	$e^\pm p \rightarrow D^*(*) \pi^- X$
$2463.3 \pm 0.6 \pm 0.8$	20k	ABULENCIA	06A CDF	$1900 p\bar{p} \rightarrow D^+ \pi^- X$
2461 ± 6	126	⁵ ABREU	98M DLPH	$e^+ e^-$
2466 ± 7	1	ASRATYAN	95 BEBC	$53,40 \nu(\bar{\nu}) \rightarrow pX, dX$

¹ From the amplitude analysis in the model describing the $D^+ \pi^-$ wave together with virtual contributions from the $D^*(2007)^0$ and B^{*0} states, and components corresponding to the $D_2^*(2460)^0, D_1^*(2680)^0, D_3^*(2760)^0$, and $D_2^*(3000)^0$ resonances.

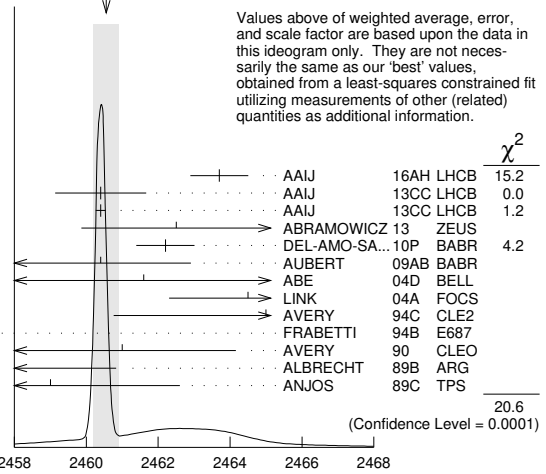
² From the combined fit of the $M(D^+ \pi^-)$ and $M(D^{*+} \pi^-)$ distributions. and A_{D_2} fixed to the theoretical prediction of -1 .

³ Fit includes the contribution from $D_0^*(2400)^0$.

⁴ Calculated using the mass difference $m(D_2^*(2460)^0) - m(D^{*+})_{PDG}$ reported below and $m(D^{*+})_{PDG} = 2010.27 \pm 0.17$ MeV. The 0.17 MeV uncertainty of the PDG mass value should be added to the experimental uncertainty of $+1.2$ MeV.

⁵ No systematic error given.

WEIGHTED AVERAGE
2460.56 ± 0.35 (Error scaled by 2.6)



$D_2^*(2460)^0$ mass (MeV)

$m_{D_2^{*0}} - m_{D^+}$

The fit includes $D^\pm, D^0, D_s^\pm, D^{*+}, D^{*0}, D_s^{*+}, D_1(2420)^0, D_2^*(2460)^0$, and $D_{s1}(2536)^\pm$ mass and mass difference measurements.

VALUE (MeV)	EVTS	DOCUMENT ID	TECN	COMMENT
591.0 ± 0.4	OUR FIT	Error includes scale factor of 2.9.		
593.9 ± 0.6 ± 0.5	20k	ABULENCIA	06A CDF	$1900 p\bar{p} \rightarrow D^+ \pi^- X$

$m_{D_2^{*0}} - m_{D^{*+}}$

The fit includes $D^\pm, D^0, D_s^\pm, D^{*+}, D^{*0}, D_s^{*+}, D_1(2420)^0, D_2^*(2460)^0$, and $D_{s1}(2536)^\pm$ mass and mass difference measurements.

VALUE (MeV)	EVTS	DOCUMENT ID	TECN	COMMENT
450.4 ± 0.4	OUR FIT	Error includes scale factor of 2.9.		
458.8 ± 3.7 ± 1.2_{-1.3}^{+1.2}	1560 ± 230	CHEKANOV	09 ZEUS	$e^\pm p \rightarrow D^*(*) \pi^- X$

$D_2^*(2460)^0$ WIDTH

VALUE (MeV)	EVTS	DOCUMENT ID	TECN	COMMENT
47.5 ± 1.1	OUR AVERAGE	Error includes scale factor of 1.8. See the ideogram below.		
$47.0 \pm 0.8 \pm 1.0$	28k	⁶ AAIJ	16AH LHCB	$B^- \rightarrow D^+ \pi^- \pi^-$
$43.2 \pm 1.2 \pm 3.0$	82k	AAIJ	13CC LHCB	$pp \rightarrow D^{*+} \pi^- X$
$45.6 \pm 0.4 \pm 1.1$	675k	AAIJ	13CC LHCB	$pp \rightarrow D^+ \pi^- X$
$46.6 \pm 8.1 \pm 5.9_{-3.8}^{+5.9}$	2.3k	⁷ ABRAMOWICZ13	ZEUS	$e^\pm p \rightarrow D^*(*) \pi^- X$
$50.5 \pm 0.6 \pm 0.7$	243k	DEL-AMO-SA...10P	BABR	$e^+ e^- \rightarrow D^+ \pi^- X$
$41.8 \pm 2.5 \pm 2.9$	3.4k	AUBERT	09AB BABR	$B^- \rightarrow D^+ \pi^- \pi^-$
$49.2 \pm 2.3 \pm 1.3$	20k	ABULENCIA	06A CDF	$1900 p\bar{p} \rightarrow D^+ \pi^- X$
$45.6 \pm 4.4 \pm 6.7$		⁸ ABE	04D BELL	$B^- \rightarrow D^+ \pi^- \pi^-$
$38.7 \pm 5.3 \pm 2.9$	5.8k	⁸ LINK	04A FOCUS	γA
$28 \pm 8_{-7}^{+8} \pm 6$	486	AVERY	94C CLE2	$e^+ e^- \rightarrow D^+ \pi^- X$
$25 \pm 10 \pm 5$	128	FRABETTI	94B E687	$\gamma Be \rightarrow D^+ \pi^- X$
$20 \pm 9 \pm 9_{-12}^{+9}$	440	AVERY	90 CLEO	$e^+ e^- \rightarrow D^{*+} \pi^- X$

Meson Particle Listings

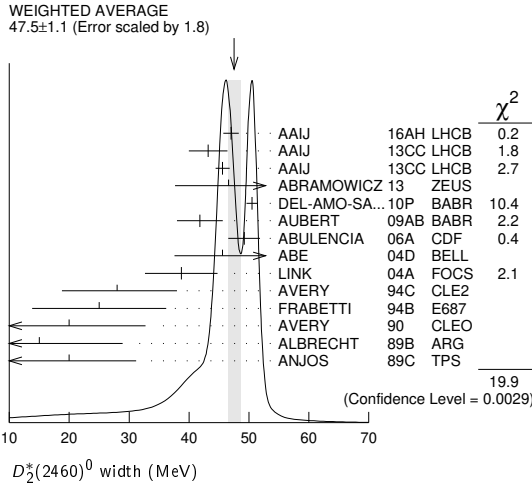
$D_2^*(2460)^0, D_2^*(2460)^\pm$

15	$+^{+13} -^{-10}$	$+^+5 -^{-10}$	337	ALBRECHT	89B	ARG	$e^+e^- \rightarrow D^+\pi^-X$
20	$\pm^{+10} \pm^+5$		153	ANJOS	89C	TPS	$\gamma N \rightarrow D^+\pi^-X$

⁶ From the amplitude analysis in the model describing the $D^+\pi^-$ wave together with virtual contributions from the $D^*(2007)^0$ and B^{*0} states, and components corresponding to the $D_2^*(2460)^0, D_1^*(2680)^0, D_3^*(2760)^0$, and $D_2^*(3000)^0$ resonances.

⁷ From the combined fit of the $M(D^+\pi^-)$ and $M(D^{*+}\pi^-)$ distributions. and A_{D_2} fixed to the theoretical prediction of -1 .

⁸ Fit includes the contribution from $D_0^*(2400)^0$.



$D_2^*(2460)^0$ DECAY MODES

$\bar{D}_2^*(2460)^0$ modes are charge conjugates of modes below.

Mode	Fraction (Γ_i/Γ)
Γ_1 $D^+\pi^-$	seen
Γ_2 $D^*(2010)^+\pi^-$	seen
Γ_3 $D^0\pi^+\pi^-$	not seen
Γ_4 $D^{*0}\pi^+\pi^-$	not seen

$D_2^*(2460)^0$ BRANCHING RATIOS

$\Gamma(D^+\pi^-)/\Gamma_{total}$	Γ_1/Γ
seen	3.4k
seen	337
seen	

$\Gamma(D^*(2010)^+\pi^-)/\Gamma_{total}$	Γ_2/Γ
seen	
seen	
seen	

$\Gamma(D^+\pi^-)/[\Gamma(D^+\pi^-) + \Gamma(D^*(2010)^+\pi^-)]$	$\Gamma_1/(\Gamma_1 + \Gamma_2)$
1.54 ± 0.15	OUR AVERAGE
1.4 ± 0.3 ± 0.3	2.3k
1.47 ± 0.03 ± 0.16	379k

Experiment	Value	EVTS	Document ID	TECN	Comment
9 ABRAMOWICZ13	ZEUS	$e^\pm p \rightarrow D^{(*)}\pi^-X$			
DEL-AMO-SA...10P	BABR	$e^+e^- \rightarrow D^{(*)}\pi^-X$			
CHEKANOV 09	ZEUS	$e^\pm p \rightarrow D^{(*)}\pi^-X$			
AVERY 94C	CLE2	$e^+e^- \rightarrow D^{*+}\pi^-X$			
AVERY 90	CLEO	$e^+e^- \rightarrow D^{*+}\pi^-X$			
ALBRECHT 89H	ARG	$e^+e^- \rightarrow D^*\pi^-X$			

••• We do not use the following data for averages, fits, limits, etc. •••

⁹ From the combined fit of the $M(D^+\pi^-)$ and $M(D^{*+}\pi^-)$ distributions. and A_{D_2} fixed to the theoretical prediction of -1 .

$\Gamma(D^+\pi^-)/[\Gamma(D^+\pi^-) + \Gamma(D^*(2010)^+\pi^-)]$	$\Gamma_1/(\Gamma_1 + \Gamma_2)$
0.62 ± 0.03 ± 0.02	8414
10 AUBERT 09Y	BABR $B^+ \rightarrow D_2^{*0} \ell^+ \nu_\ell$

¹⁰ Assuming $\Gamma(\Upsilon(4S) \rightarrow B^+B^-) / \Gamma(\Upsilon(4S) \rightarrow B^0\bar{B}^0) = 1.065 \pm 0.026$ and equal partial widths for charged and neutral D_2^* mesons.

$D_2^*(2460)^0$ POLARIZATION AMPLITUDE A_{D_2}

A polarization amplitude A_{D_2} is a parameter that depends on the initial polarization of the D_2 . For D_2 decays the helicity angle, θ_H , distribution varies like $1 + A_{D_2} \cos^2(\theta_H)$, where θ_H is the angle in the D^* rest frame between the two pions emitted by the $D_2 \rightarrow D^*\pi$ and $D^* \rightarrow D\pi$.

VALUE	EVTS	DOCUMENT ID	TECN	COMMENT
••• We do not use the following data for averages, fits, limits, etc. •••				
-1.16 ± 0.35	2.3k	11 ABRAMOWICZ13	ZEUS	$e^\pm p \rightarrow D^{(*)}\pi^-X$
consistent with -1	243k	DEL-AMO-SA...10P	BABR	$e^+e^- \rightarrow D^+\pi^-X$
$-0.74^{+0.49}_{-0.38}$		12 AVERY	94C CLE2	$e^+e^- \rightarrow D^{*+}\pi^-X$

¹¹ From the combined fit of the $M(D^+\pi^-)$ and $M(D^{*+}\pi^-)$ distributions.
¹² Systematic uncertainties not estimated.

$D_2^*(2460)^0$ REFERENCES

AAIJ	16AH	PR D94 072001	R. Aaij et al.	(LHCb Collab.)
AAIJ	13CC	JHEP 1309 145	R. Aaij et al.	(LHCb Collab.)
ABRAMOWICZ	13	NP B866 229	H. Abramowicz et al.	(ZEUS Collab.)
DEL-AMO-SA...	10P	PR D82 111101	P. del Amo Sanchez et al.	(BABAR Collab.)
AUBERT	09AB	PR D79 112004	B. Aubert et al.	(BABAR Collab.)
AUBERT	09Y	PRL 103 051803	B. Aubert et al.	(BABAR Collab.)
CHEKANOV	09	EPJ C60 25	S. Chekanov et al.	(ZEUS Collab.)
ABULENCIA	06A	PR D73 051104	A. Abulencia et al.	(CDF Collab.)
ABE	04D	PR D69 112002	K. Abe et al.	(BELLE Collab.)
LINK	04A	PL B586 11	J.M. Link et al.	(FOCUS Collab.)
ABREU	98M	PL B426 231	P. Abreu et al.	(DELPHI Collab.)
ACKERSTAFF	97W	ZPHY C76 425	K. Ackerstaff et al.	(OPAL Collab.)
ASRATYAN	95	ZPHY C68 43	A.E. Asratyan et al.	(BIRM, BELG, CERN+)
AVERY	94C	PL B331 236	P. Avery et al.	(CLEO Collab.)
FRABETTI	94B	PRL 72 324	P.L. Frabetti et al.	(FNAL E687 Collab.)
AVERY	90	PR D41 374	P. Avery, D. Besson	(CLEO Collab.)
ALBRECHT	89B	PL B221 422	H. Albrecht et al.	(ARGUS Collab.)
ALBRECHT	89H	PL B232 398	H. Albrecht et al.	(ARGUS Collab.)
ANJOS	89C	PRL 62 1717	J.C. Anjos et al.	(FNAL E691 Collab.)

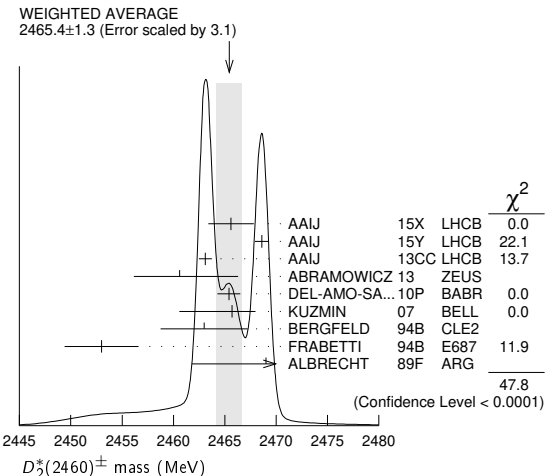
$D_2^*(2460)^\pm$

$$J(P) = \frac{1}{2}(2^+)$$

$J^P = 2^+$ assignment strongly favored (ALBRECHT 89B).

$D_2^*(2460)^\pm$ MASS

VALUE (MeV)	EVTS	DOCUMENT ID	TECN	COMMENT
2465.4 ± 1.3	OUR AVERAGE	Error includes scale factor of 3.1. See the ideogram below.		
2465.6 ± 1.8 ± 1.3		1 AAIJ	15X LHCB	$B^0 \rightarrow \bar{D}^0 K^+\pi^-$
2468.6 ± 0.6 ± 0.3		2 AAIJ	15Y LHCB	$B^0 \rightarrow \bar{D}^0 \pi^+\pi^-$
2463.1 ± 0.2 ± 0.6	342k	AAIJ	13CC LHCB	$pp \rightarrow D^0 \pi^+ X$
2460.6 ± 4.4 ± 3.6 ± 0.8	1371	3 ABRAMOWICZ13	ZEUS	$e^\pm p \rightarrow D^{(*)0} \pi^+ X$
2465.4 ± 0.2 ± 1.1	111k	4 DEL-AMO-SA...10P	BABR	$e^+e^- \rightarrow D^0 \pi^+ X$
2465.7 ± 1.8 ± 1.4 ± 0.8	2909	KUZMIN	07 BELL	$e^+e^- \rightarrow$ hadrons
2463 ± 3 ± 3	310	BERGFELD	94B CLE2	$e^+e^- \rightarrow D^0 \pi^+ X$
2453 ± 3 ± 2	185	FRABETTI	94B E687	$\gamma Be \rightarrow D^0 \pi^+ X$
2469 ± 4 ± 6		ALBRECHT	89F ARG	$e^+e^- \rightarrow D^0 \pi^+ X$
••• We do not use the following data for averages, fits, limits, etc. •••				
2468.1 ± 0.6 ± 0.5		5 AAIJ	15Y LHCB	$B^0 \rightarrow \bar{D}^0 \pi^+ \pi^-$
2467.6 ± 1.5 ± 0.8	3.5k	6 LINK	04A FOCUS	γA



¹ From the Dalitz plot analysis including various K^* and D^{**} mesons as well as broad structures in the $K\pi$ S-wave and the $D\pi$ S- and P-waves.
² Modeling the $\pi^+\pi^-$ S-wave with the isobar formalism.

See key on page 999

Meson Particle Listings

$D_2^*(2460)^\pm, D(2550)^0, D_J^*(2600)$

³ From the fit of the $M(D^0 \pi^+)$ distribution. The widths of the D_1^+ and D_2^{*+} are fixed to 25 MeV and 37 MeV, and A_{D_1} and A_{D_2} are fixed to the theoretical predictions of 3 and -1, respectively.

⁴ At a fixed width of 50.5 MeV.

⁵ Modeling the $\pi^+ \pi^-$ S-wave with the K-matrix formalism.

⁶ Fit includes the contribution from $D_0^*(2400)^\pm$. Not independent of the corresponding mass difference measurement, $(m_{D_2^*(2460)^\pm} - (m_{D_2^*(2460)^0})$.

$m_{D_2^*(2460)^\pm} - m_{D_2^*(2460)^0}$

VALUE (MeV)	DOCUMENT ID	TECN	COMMENT
2.4 ± 1.7 OUR AVERAGE			
3.1 ± 1.9 ± 0.9	LINK	04A	FOCS γA
- 2 ± 4 ± 4	BERGFELD	94B	CLE2 $e^+ e^- \rightarrow$ hadrons
0 ± 4	FRABETTI	94B	E687 $\gamma Be \rightarrow D \pi X$
14 ± 5 ± 8	ALBRECHT	89F	ARG $e^+ e^- \rightarrow D^0 \pi^+ X$

$D_2^*(2460)^\pm$ WIDTH

VALUE (MeV)	EVTS	DOCUMENT ID	TECN	COMMENT
46.7 ± 1.2 OUR AVERAGE				
46.0 ± 3.4 ± 3.2		1 AAIJ	15X	LHCB $B^0 \rightarrow \bar{D}^0 K^+ \pi^-$
47.3 ± 1.5 ± 0.7		2 AAIJ	15Y	LHCB $B^0 \rightarrow \bar{D}^0 \pi^+ \pi^-$
48.6 ± 1.3 ± 1.9	342k	AAIJ	13CC	LHCB $pp \rightarrow D^0 \pi^+ X$
49.7 ± 3.8 ± 6.4	2909	KUZMIN	07	BELL $e^+ e^- \rightarrow$ hadrons
34.1 ± 6.5 ± 4.2	3.5k	3 LINK	04A	FOCS γA
27 ⁺¹¹ ₋₈ ± 5	310	BERGFELD	94B	CLE2 $e^+ e^- \rightarrow D^0 \pi^+ X$
23 ± 9 ± 5	185	FRABETTI	94B	E687 $\gamma Be \rightarrow D^0 \pi^+ X$

• • • We do not use the following data for averages, fits, limits, etc. • • •
¹ From the Dalitz plot analysis including various K^* and D^{**} mesons as well as broad structures in the $K \pi$ S-wave and the $D \pi$ S- and P-waves.
² Modeling the $\pi^+ \pi^-$ S-wave with the isobar formalism.
³ Fit includes the contribution from $D_0^*(2400)^\pm$.
⁴ Modeling the $\pi^+ \pi^-$ S-wave with the K-matrix formalism.

$D_2^*(2460)^\pm$ DECAY MODES

$D_2^*(2460)^\pm$ modes are charge conjugates of modes below.

Mode	Fraction (Γ_i/Γ)
Γ_1 $D^0 \pi^+$	seen
Γ_2 $D^{*0} \pi^+$	seen
Γ_3 $D^+ \pi^+ \pi^-$	not seen
Γ_4 $D^{*+} \pi^+ \pi^-$	not seen

$D_2^*(2460)^\pm$ BRANCHING RATIOS

$\Gamma(D^0 \pi^+)/\Gamma_{total}$	Γ_1/Γ		
VALUE	DOCUMENT ID	TECN	COMMENT
seen	ALBRECHT	89F	ARG $e^+ e^- \rightarrow D^0 \pi^+ X$

$\Gamma(D^0 \pi^+)/\Gamma(D^{*0} \pi^+)$	Γ_1/Γ_2			
VALUE	DOCUMENT ID	TECN	COMMENT	
1.2 ± 0.4 OUR AVERAGE				
1.1 ± 0.4 ^{+0.3} _{-0.2}	1371	1 ABRAMOWICZ13	ZEUS $e^\pm p \rightarrow D^{(*)0} \pi^+ X$	
1.9 ± 1.1 ± 0.3		BERGFELD	94B	CLE2 $e^+ e^- \rightarrow$ hadrons

¹ From the fit of the $M(D^0 \pi^+)$ distribution. The widths of the D_1^+ and D_2^{*+} are fixed to 25 MeV and 37 MeV, and A_{D_1} and A_{D_2} are fixed to the theoretical predictions of 3 and -1, respectively.

$\Gamma(D^0 \pi^+)/[\Gamma(D^0 \pi^+) + \Gamma(D^{*0} \pi^+)]$	$\Gamma_1/(\Gamma_1 + \Gamma_2)$		
VALUE	DOCUMENT ID	TECN	COMMENT

• • • We do not use the following data for averages, fits, limits, etc. • • •
 0.62 ± 0.03 ± 0.02 3361 1 AUBERT 09Y BABR $\bar{B}^0 \rightarrow D_2^{*+} \ell^- \nu_\ell$
¹ Assuming $\Gamma(\Upsilon(4S) \rightarrow B^+ B^-) / \Gamma(\Upsilon(4S) \rightarrow B^0 \bar{B}^0) = 1.065 \pm 0.026$ and equal partial widths for charged and neutral D_2^* mesons.

$D_2^*(2460)^\pm$ REFERENCES

AAIJ	15X	PR D92 012012	R. Aaij et al.	(LHCb Collab.)
AAIJ	15Y	PR D92 032002	R. Aaij et al.	(LHCb Collab.)
AAIJ	13CC	JHEP 1309 145	R. Aaij et al.	(LHCb Collab.)
ABRAMOWICZ	13	NP B866 229	H. Abramowicz et al.	(ZEUS Collab.)
DEL-AMO-SA...	10P	PR D82 111101	P. del Amo Sanchez et al.	(BABAR Collab.)
AUBERT	09Y	PRL 103 051803	B. Aubert et al.	(BABAR Collab.)
KUZMIN	07	PR D76 012006	A. Kuzmin et al.	(BELLE Collab.)
LINK	04A	PL B586 11	J.M. Link et al.	(FOCUS Collab.)
BERGFELD	94B	PL B340 194	T. Bergfeld et al.	(CLEO Collab.)
FRABETTI	94B	PRL 72 324	P.L. Frabetti et al.	(FNAL E687 Collab.)
ALBRECHT	89B	PL B221 422	H. Albrecht et al.	(ARGUS Collab.)
ALBRECHT	89F	PL B231 208	H. Albrecht et al.	(ARGUS Collab.)

$D(2550)^0$

$I(J^P) = \frac{1}{2}(?)^?$

OMITTED FROM SUMMARY TABLE

Unnatural parity according to the helicity analysis of DEL-AMO-SANCHEZ 10P and AAIJ 13CC. DEL-AMO-SANCHEZ 10P suggests $J^P = 0^-$.

$D(2550)^0$ MASS

VALUE (MeV)	EVTS	DOCUMENT ID	TECN	COMMENT
2564 ± 20 OUR AVERAGE				Error includes scale factor of 3.9.
2579.5 ± 3.4 ± 5.5	60k	AAIJ	13cc	LHCB $pp \rightarrow D^{*+} \pi^- X$
2539.4 ± 4.5 ± 6.8	34k	DEL-AMO-SA...	10P	BABR $e^+ e^- \rightarrow D^{*+} \pi^- X$

$D(2550)^0$ WIDTH

VALUE (MeV)	EVTS	DOCUMENT ID	TECN	COMMENT
135 ± 17 OUR AVERAGE				
177.5 ± 17.8 ± 46.0	60k	AAIJ	13cc	LHCB $pp \rightarrow D^{*+} \pi^- X$
130 ± 12 ± 13	34k	DEL-AMO-SA...	10P	BABR $e^+ e^- \rightarrow D^{*+} \pi^- X$

$D(2550)^0$ DECAY MODES

Mode	Fraction (Γ_i/Γ)
Γ_1 $D^{*+} \pi^-$	seen

$D(2550)^0$ POLARIZATION AMPLITUDE A_{D_J}

A polarization amplitude A_{D_J} is a parameter that depends on the initial polarization of the D_J . For D_J decays the helicity angle, θ_H , distribution varies like $1 + A_{D_J} \cos^2(\theta_H)$, where θ_H is the angle in the D_J rest frame between the two pions emitted in the $D_J \rightarrow D^* \pi$ and $D^* \rightarrow D \pi$ decays.

VALUE	EVTS	DOCUMENT ID	TECN	COMMENT
• • • We do not use the following data for averages, fits, limits, etc. • • •				
4.2 ± 1.3	60k	1 AAIJ	13cc	LHCB $pp \rightarrow D^{*+} \pi^- X$

¹ Systematic uncertainty not estimated.

$D(2550)^0$ REFERENCES

AAIJ	13CC	JHEP 1309 145	R. Aaij et al.	(LHCb Collab.)
DEL-AMO-SA...	10P	PR D82 111101	P. del Amo Sanchez et al.	(BABAR Collab.)

$D_J^*(2600)$

$I(J^P) = \frac{1}{2}(?)^?$

OMITTED FROM SUMMARY TABLE

was $D(2600)$

J^P consistent with natural parity (DEL-AMO-SANCHEZ 10P, AAIJ 13CC).

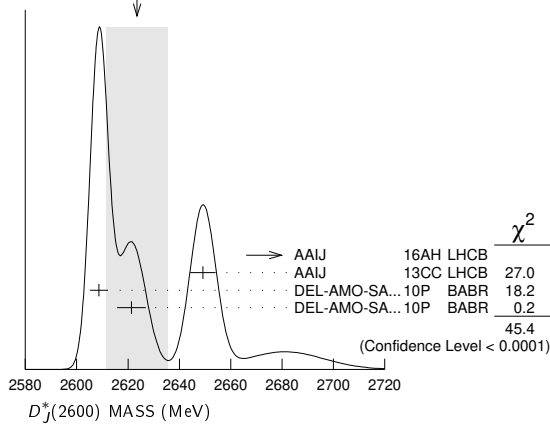
$D_J^*(2600)$ MASS

VALUE (MeV)	EVTS	DOCUMENT ID	TECN	CHG	COMMENT
2623 ± 12 OUR AVERAGE					Error includes scale factor of 4.8. See the ideogram below.
2681.1 ± 5.6 ± 14.0	28k	1 AAIJ	16AH	LHCB	$B^- \rightarrow D^+ \pi^- \pi^-$
2649.2 ± 3.5 ± 3.5	51k	AAIJ	13cc	LHCB	$pp \rightarrow D^{*+} \pi^- X$
2608.7 ± 2.4 ± 2.5	26k	DEL-AMO-SA...	10P	BABR 0	$e^+ e^- \rightarrow D^+ \pi^- X$
2621.3 ± 3.7 ± 4.2	13k	2 DEL-AMO-SA...	10P	BABR +	$e^+ e^- \rightarrow D^0 \pi^+ X$

¹ From the amplitude analysis in the model describing the $D^+ \pi^-$ wave together with virtual contributions from the $D^{*+}(2007)^0$ and B^{*0} states, and components corresponding to the $D_2^*(2460)^0$, $D_1^*(2680)^0$, $D_3^*(2760)^0$, and $D_2^*(3000)^0$ resonances.

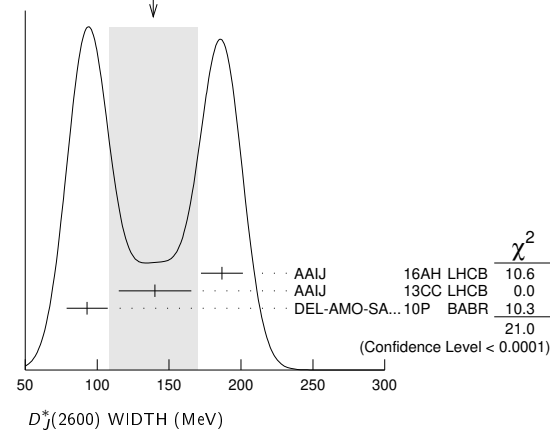
² At a fixed width of 93 MeV.

Meson Particle Listings

 $D_J^*(2600)$, $D^*(2640)^\pm$, $D(2740)^0$, $D_3^*(2750)$ WEIGHTED AVERAGE
2623±12 (Error scaled by 4.8) $D_J^*(2600)$ WIDTH

VALUE (MeV)	EVTS	DOCUMENT ID	TECN	COMMENT
139 ± 31	OUR AVERAGE	Error includes scale factor of 3.2. See the ideogram below.		
186.7 ± 8.5 ± 11.9	28k	³ AAIJ	16AH LHCb	$B^- \rightarrow D^+ \pi^- \pi^-$
140.2 ± 17.1 ± 18.6	51k	AAIJ	13cc LHCb	$pp \rightarrow D^{*+} \pi^- X$
93 ± 6 ± 13	26k	DEL-AMO-SA...10P	BABR	$e^+ e^- \rightarrow D^+ \pi^- X$

³From the amplitude analysis in the model describing the $D^+ \pi^-$ wave together with virtual contributions from the $D^*(2007)^0$ and B^*0 states, and components corresponding to the $D_2^*(2460)^0$, $D_1^*(2680)^0$, $D_3^*(2760)^0$, and $D_2^*(3000)^0$ resonances.

WEIGHTED AVERAGE
139±31 (Error scaled by 3.2) $D_J^*(2600)$ DECAY MODES

Mode	Fraction (Γ_i/Γ)
Γ_1 $D \pi$	seen
Γ_2 $D^+ \pi^-$	seen
Γ_3 $D^0 \pi^\pm$	seen
Γ_4 $D^* \pi$	seen
Γ_5 $D^{*+} \pi^-$	seen

 $D_J^*(2600)$ BRANCHING RATIOS

$\Gamma(D^+ \pi^-)/\Gamma(D^{*+} \pi^-)$	VALUE	EVTS	DOCUMENT ID	TECN	COMMENT	Γ_2/Γ_5
	0.32 ± 0.02 ± 0.09	76k	DEL-AMO-SA...10P	BABR	$e^+ e^- \rightarrow D^{(*)+} \pi^- X$	

 $D_J^*(2600)$ REFERENCES

AAIJ	16AH PR D94 072001	R. Aaij et al.	(LHCb Collab.)
AAIJ	13CC JHEP 1309 145	R. Aaij et al.	(LHCb Collab.)
DEL-AMO-SA...10P	PR D82 111101	P. del Amo Sanchez et al.	(BABAR Collab.)

 $D^*(2640)^\pm$

$I(J^P) = \frac{1}{2}(??)$

OMITTED FROM SUMMARY TABLE

Seen in Z decays by ABREU 98M. Not seen by ABBIENDI 01N and CHEKANOV 09. Needs confirmation.

 $D^*(2640)^\pm$ MASS

VALUE (MeV)	EVTS	DOCUMENT ID	TECN	COMMENT
2637 ± 2 ± 6	66 ± 14	ABREU	98M DLPH	$e^+ e^- \rightarrow D^{*+} \pi^+ \pi^- X$

 $D^*(2640)^\pm$ WIDTH

VALUE (MeV)	CL%	DOCUMENT ID	TECN	COMMENT
<15	95	ABREU	98M DLPH	$e^+ e^- \rightarrow D^{*+} \pi^+ \pi^- X$

 $D^*(2640)^+$ DECAY MODES

$D^*(2640)^-$ modes are charge conjugates of modes below.

Mode	Fraction (Γ_i/Γ)
Γ_1 $D^*(2010)^+ \pi^+ \pi^-$	seen

 $D^*(2640)^\pm$ REFERENCES

CHEKANOV	09	EPJ C60 25	S. Chekanov et al.	(ZEUS Collab.)
ABBIENDI	01N	EPJ C20 445	G. Abbiendi et al.	(OPAL Collab.)
ABREU	98M	PL B426 231	P. Abreu et al.	(DELPHI Collab.)

 $D(2740)^0$

$I(J^P) = \frac{1}{2}(??)$

OMITTED FROM SUMMARY TABLE

J^P consistent with unnatural parity (AAIJ 13CC).

 $D(2740)^0$ MASS

VALUE (MeV)	EVTS	DOCUMENT ID	TECN	COMMENT
2737.0 ± 3.5 ± 11.2	7.7k	AAIJ	13cc LHCb	$pp \rightarrow D^+ \pi^- X$

 $D(2740)^0$ WIDTH

VALUE (MeV)	EVTS	DOCUMENT ID	TECN	COMMENT
73.2 ± 13.4 ± 25.0	7.7k	AAIJ	13cc LHCb	$pp \rightarrow D^{*+} \pi^- X$

 $D(2740)^0$ DECAY MODES

Mode	Fraction (Γ_i/Γ)
Γ_1 $D^* \pi^-$	seen

 $D(2740)^0$ POLARIZATION AMPLITUDE A_{D_J}

A polarization amplitude A_{D_J} is a parameter that depends on the initial polarization of the D_J . For D_J decays the helicity angle, θ_H , distribution varies like $1 + A_{D_J} \cos^2(\theta_H)$, where θ_H is the angle in the D_J rest frame between the two pions emitted in the $D_J \rightarrow D^* \pi$ and $D^* \rightarrow D \pi$ decays.

VALUE	EVTS	DOCUMENT ID	TECN	COMMENT
• • • We do not use the following data for averages, fits, limits, etc. • • •				
3.1 ± 2.2	7.7k	¹ AAIJ	13cc LHCb	$pp \rightarrow D^{*+} \pi^- X$
				¹ Systematic uncertainty not estimated.

 $D(2740)^0$ REFERENCES

AAIJ	13CC JHEP 1309 145	R. Aaij et al.	(LHCb Collab.)
------	--------------------	----------------	----------------

 $D_3^*(2750)$

$I(J^P) = \frac{1}{2}(3^-)$

OMITTED FROM SUMMARY TABLE

J^P determined by AAIJ 15Y from the Dalitz plot analysis of $B^0 \rightarrow \bar{D}^0 \pi^+ \pi^-$ decays. J^P consistent with natural parity (AAIJ 13CC).

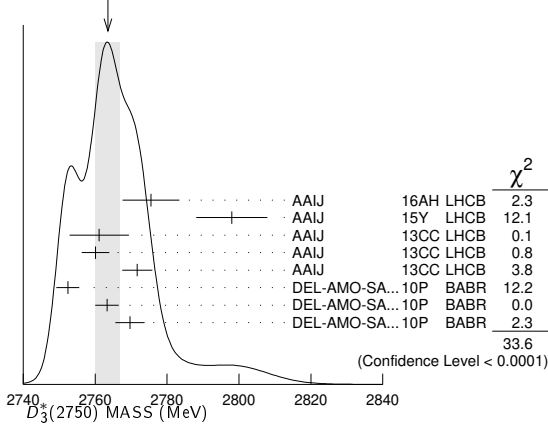
$D_3^*(2750)$, $D(3000)^0$

$D_3^*(2750)$ MASS

VALUE (MeV)	EVTS	DOCUMENT ID	TECN	CHG	COMMENT
2763.5 ± 3.4 OUR AVERAGE		Error includes scale factor of 2.2. See the ideogram below.			
2775.5 ± 4.5 ± 6.5	28k	¹ AAIJ	16AH	LHCB	$B^- \rightarrow D^+ \pi^- \pi^-$
2798 ± 7 ± 7		² AAIJ	15Y	LHCB	$B^0 \rightarrow \bar{D}^0 \pi^+ \pi^-$
2761.1 ± 5.1 ± 6.5	14k	AAIJ	13CC	LHCB 0	$pp \rightarrow D^{*+} \pi^- X$
2760.1 ± 1.1 ± 3.7	56k	AAIJ	13CC	LHCB 0	$pp \rightarrow D^+ \pi^- X$
2771.7 ± 1.7 ± 3.8	20k	AAIJ	13CC	LHCB +	$pp \rightarrow D^0 \pi^+ X$
2752.4 ± 1.7 ± 2.7	23.5k	³ DEL-AMO-SA...10P	BABR	0	$e^+ e^- \rightarrow D^{*+} \pi^- X$
2763.3 ± 2.3 ± 2.3	11.3k	³ DEL-AMO-SA...10P	BABR	0	$e^+ e^- \rightarrow D^+ \pi^- X$
2769.7 ± 3.8 ± 1.5	5.7k	^{3,4} DEL-AMO-SA...10P	BABR	+	$e^+ e^- \rightarrow D^0 \pi^+ X$
• • • We do not use the following data for averages, fits, limits, etc. • • •					
2802 ± 11 ± 10		⁵ AAIJ	15Y	LHCB	$B^0 \rightarrow \bar{D}^0 \pi^+ \pi^-$

- ¹ From the amplitude analysis in the model describing the $D^+ \pi^-$ wave together with virtual contributions from the $D^*(2007)^0$ and B^{*0} states, and components corresponding to the $D_2^*(2460)^0$, $D_1^*(2680)^0$, $D_3^*(2760)^0$, and $D_2^*(3000)^0$ resonances.
- ² Modeling the $\pi^+ \pi^-$ S-wave with the Isobar formalism.
- ³ The states observed in the $D^* \pi$ and $D \pi$ final states are not necessarily the same.
- ⁴ At a fixed width of 60.9 MeV.
- ⁵ Modeling the $\pi^+ \pi^-$ S-wave with the K-matrix formalism.

WEIGHTED AVERAGE
2763.5±3.4 (Error scaled by 2.2)



$D_3^*(2750)$ WIDTH

VALUE (MeV)	EVTS	DOCUMENT ID	TECN	CHG	COMMENT
66 ± 5 OUR AVERAGE					
95.3 ± 9.6 ± 34.0	28k	⁶ AAIJ	16AH	LHCB	$B^- \rightarrow D^+ \pi^- \pi^-$
105 ± 18 ± 24		⁷ AAIJ	15Y	LHCB	$B^0 \rightarrow \bar{D}^0 \pi^+ \pi^-$
74.4 ± 3.4 ± 37.0	14k	AAIJ	13CC	LHCB 0	$pp \rightarrow D^{*+} \pi^- X$
74.4 ± 3.4 ± 19.1	56k	AAIJ	13CC	LHCB 0	$pp \rightarrow D^+ \pi^- X$
66.7 ± 6.6 ± 10.5	20k	AAIJ	13CC	LHCB +	$pp \rightarrow D^0 \pi^+ X$
71 ± 6 ± 11	23.5k	⁸ DEL-AMO-SA...10P	BABR		$e^+ e^- \rightarrow D^{*+} \pi^- X$
60.9 ± 5.1 ± 3.6	11.3k	⁸ DEL-AMO-SA...10P	BABR		$e^+ e^- \rightarrow D^+ \pi^- X$
• • • We do not use the following data for averages, fits, limits, etc. • • •					
154 ± 27 ± 16		⁹ AAIJ	15Y	LHCB	$B^0 \rightarrow \bar{D}^0 \pi^+ \pi^-$

- ⁶ From the amplitude analysis in the model describing the $D^+ \pi^-$ wave together with virtual contributions from the $D^*(2007)^0$ and B^{*0} states, and components corresponding to the $D_2^*(2460)^0$, $D_1^*(2680)^0$, $D_3^*(2760)^0$, and $D_2^*(3000)^0$ resonances.
- ⁷ Modeling the $\pi^+ \pi^-$ S-wave with the Isobar formalism.
- ⁸ The states observed in the $D^* \pi$ and $D \pi$ final states are not necessarily the same.
- ⁹ Modeling the $\pi^+ \pi^-$ S-wave with the K-matrix formalism.

$D_3^*(2750)$ DECAY MODES

Mode	Fraction (Γ_i/Γ)
Γ_1 $D \pi$	seen
Γ_2 $D^+ \pi^-$	seen
Γ_3 $D^0 \pi^\pm$	seen
Γ_4 $D^* \pi$	seen
Γ_5 $D^{*+} \pi^-$	seen

$D_3^*(2750)$ BRANCHING RATIOS

$\Gamma(D^+ \pi^-)/\Gamma(D^{*+} \pi^-)$	VALUE	EVTS	DOCUMENT ID	TECN	COMMENT	Γ_2/Γ_5
	0.42 ± 0.05 ± 0.11	34.8k	¹⁰ DEL-AMO-SA...10P	BABR	$e^+ e^- \rightarrow D^{*+} \pi^- X$	

- ¹⁰ The states observed in the $D^* \pi$ and $D \pi$ final states are not necessarily the same.

$D_3^*(2750)$ POLARIZATION AMPLITUDE A_D

A polarization amplitude A_D is a parameter that depends on the initial polarization of the $D_3^*(2750)$. For $D_3^*(2750)$ decays the helicity angle, θ_H , distribution varies like $1 + A_D \cos(\theta_H)$, where θ_H is the angle in the D^* rest frame between the two pions emitted by the $D_3^*(2750) \rightarrow D^* \pi$ and $D^* \rightarrow D \pi$.

VALUE	EVTS	DOCUMENT ID	TECN	COMMENT
• • • We do not use the following data for averages, fits, limits, etc. • • •				
-0.33 ± 0.28	23.5k	¹¹ DEL-AMO-SA...10P	BABR	$e^+ e^- \rightarrow D^{*+} \pi^- X$
¹¹ Systematic uncertainties not estimated. The states observed in the $D^* \pi$ and $D \pi$ final states are not necessarily the same.				

$D_3^*(2750)$ REFERENCES

AAIJ 16AH PR D94 072001	R. Aaij et al.	(LHCb Collab.)
AAIJ 15Y PR D52 032002	R. Aaij et al.	(LHCb Collab.) JP
AAIJ 13CC JHEP 1309 145	R. Aaij et al.	(LHCb Collab.)
DEL-AMO-SA...10P PR D82 111101	P. del Amo Sanchez et al.	(BABAR Collab.)

$D(3000)^0$

$I(J^P) = \frac{1}{2}(??)$

OMITTED FROM SUMMARY TABLE

Both natural- and unnatural-parity components observed depending on the decay mode (AAIJ 13CC).

$D(3000)^0$ MASS

VALUE (MeV)	EVTS	DOCUMENT ID	TECN	COMMENT
3214 ± 29 ± 49	28k	¹ AAIJ	16AH	LHCB $B^- \rightarrow D^+ \pi^- \pi^-$
• • • We do not use the following data for averages, fits, limits, etc. • • •				
2971.8 ± 8.7	9.5k	^{2,3} AAIJ	13CC	LHCB $pp \rightarrow D^{*+} \pi^- X$
3008.1 ± 4.0	17.6k	^{2,4} AAIJ	13CC	LHCB $pp \rightarrow D^+ \pi^- X$

- ¹ From the amplitude analysis in the model describing the $D^+ \pi^-$ wave together with virtual contributions from the $D^*(2007)^0$ and B^{*0} states, and components corresponding to the $D_2^*(2460)^0$, $D_1^*(2680)^0$, $D_3^*(2760)^0$, and $D_2^*(3000)^0$ resonances.
- ² Systematic uncertainty not estimated.
- ³ Unnatural parity preferred.
- ⁴ Natural parity state. A state $D(3000)^+$ is possibly seen in $D^0 \pi^+$ final state.

$D(3000)^0$ WIDTH

VALUE (MeV)	EVTS	DOCUMENT ID	TECN	COMMENT
186 ± 38 ± 72	28k	⁵ AAIJ	16AH	LHCB $B^- \rightarrow D^+ \pi^- \pi^-$
• • • We do not use the following data for averages, fits, limits, etc. • • •				
188.1 ± 44.8	9.5k	^{6,7} AAIJ	13CC	LHCB $pp \rightarrow D^{*+} \pi^- X$
110.5 ± 11.5	17.6k	^{6,8} AAIJ	13CC	LHCB $pp \rightarrow D^+ \pi^- X$

- ⁵ From the amplitude analysis in the model describing the $D^+ \pi^-$ wave together with virtual contributions from the $D^*(2007)^0$ and B^{*0} states, and components corresponding to the $D_2^*(2460)^0$, $D_1^*(2680)^0$, $D_3^*(2760)^0$, and $D_2^*(3000)^0$ resonances.
- ⁶ Systematic uncertainty not estimated.
- ⁷ Unnatural parity preferred.
- ⁸ Natural parity state. A state $D(3000)^+$ is possibly seen in $D^0 \pi^+$ final state.

$D(3000)^0$ DECAY MODES

Mode	Fraction (Γ_i/Γ)
Γ_1 $D^{*+} \pi^-$	seen

$D(3000)^0$ POLARIZATION AMPLITUDE A_{D_J}

A polarization amplitude A_{D_J} is a parameter that depends on the initial polarization of the D_J . For D_J decays the helicity angle, θ_H , distribution varies like $1 + A_{D_J} \cos^2(\theta_H)$, where θ_H is the angle in the D_J rest frame between the two pions emitted in the $D_J \rightarrow D^* \pi$ and $D^* \rightarrow D \pi$ decays.

VALUE	EVTS	DOCUMENT ID	TECN	COMMENT
• • • We do not use the following data for averages, fits, limits, etc. • • •				
1.5 ± 0.9	9.5k	⁹ AAIJ	13CC	LHCB $pp \rightarrow D^{*+} \pi^- X$
⁹ Systematic uncertainty not estimated.				

$D(3000)^0$ REFERENCES

AAIJ 16AH PR D94 072001	R. Aaij et al.	(LHCb Collab.)
AAIJ 13CC JHEP 1309 145	R. Aaij et al.	(LHCb Collab.)

Meson Particle Listings

D_s^\pm

CHARMED, STRANGE MESONS ($C = S = \pm 1$)

$$D_s^+ = c\bar{s}, D_s^- = \bar{c}s, \text{ similarly for } D_s^{*\pm}$$

D_s^\pm

$$J(P) = 0(0^-)$$

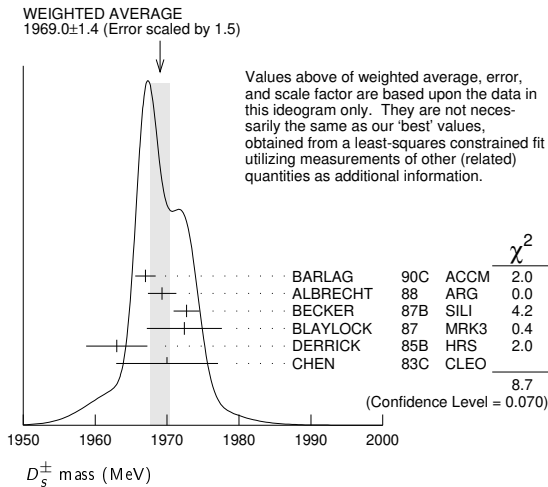
The angular distributions of the decays of the ϕ and $\bar{K}^*(892)^0$ in the $\phi\pi^+$ and $K^+\bar{K}^*(892)^0$ modes strongly indicate that the spin is zero. The parity given is that expected of a $c\bar{s}$ ground state.

D_s^\pm MASS

The fit includes $D_s^\pm, D^0, D_s^{*\pm}, D^{*0}, D_s^{*0}, D_1(2420)^0, D_2^*(2460)^0$, and $D_{s1}(2536)^\pm$ mass and mass difference measurements. Measurements of the D_s^\pm mass with an error greater than 10 MeV are omitted from the fit and average. A number of early measurements have been omitted altogether.

VALUE (MeV)	EVTS	DOCUMENT ID	TECN	COMMENT
1968.34 ± 0.07 OUR FIT				
1969.0 ± 1.4 OUR AVERAGE				Error includes scale factor of 1.5. See the ideogram below.
1967.0 ± 1.0 ± 1.0	54	BARLAG	90c	ACCM π^- Cu 230 GeV
1969.3 ± 1.4 ± 1.4		ALBRECHT	88	ARG e^+e^- 9.4–10.6 GeV
1972.7 ± 1.5 ± 1.0	21	BECKER	87B	SILI 200 GeV π, K, p
1972.4 ± 3.7 ± 3.7	27	BLAYLOCK	87	MRK3 e^+e^- 4.14 GeV
1963 ± 3 ± 3	30	DERRICK	85B	HRS e^+e^- 29 GeV
1970 ± 5 ± 5	104	CHEN	83c	CLEO e^+e^- 10.5 GeV
••• We do not use the following data for averages, fits, limits, etc. •••				
1968.3 ± 0.7 ± 0.7	290	¹ ANJOS	88	E691 Photoproduction
1980 ± 15	6	USHIDA	86	EMUL ν wideband
1973.6 ± 2.6 ± 3.0	163	ALBRECHT	85D	ARG e^+e^- 10 GeV
1948 ± 28 ± 10	65	AIHARA	84D	TPC e^+e^- 29 GeV
1975 ± 9 ± 10	49	ALTHOFF	84	TASS e^+e^- 14–25 GeV
1975 ± 4	3	BAILEY	84	ACCM hadron ⁺ Be → $\phi\pi^+ X$

¹ ANJOS 88 enters the fit via $m_{D_s^\pm} - m_{D^\pm}$ (see below).



$m_{D_s^\pm} - m_{D^\pm}$

The fit includes $D_s^\pm, D^0, D_s^{*\pm}, D^{*0}, D_s^{*0}, D_1(2420)^0, D_2^*(2460)^0$, and $D_{s1}(2536)^\pm$ mass and mass difference measurements.

VALUE (MeV)	EVTS	DOCUMENT ID	TECN	COMMENT
98.69 ± 0.05 OUR FIT				
98.69 ± 0.05 OUR AVERAGE				
98.68 ± 0.03 ± 0.04		AAIJ	13v	LHCB $D_s^+ \rightarrow K^+ K^- \pi^+$
99.41 ± 0.38 ± 0.21		ACOSTA	03D	CDF2 $\bar{p}p, \sqrt{s} = 1.96$ TeV
98.4 ± 0.1 ± 0.3	48k	AUBERT	02c	BABR $e^+e^- \approx \mathcal{T}(4S)$
99.5 ± 0.6 ± 0.3		BROWN	94	CLE2 $e^+e^- \approx \mathcal{T}(4S)$
98.5 ± 1.5	555	CHEN	89	CLEO e^+e^- 10.5 GeV
99.0 ± 0.8	290	ANJOS	88	E691 Photoproduction

D_s^\pm MEAN LIFE

Measurements with an error greater than 100×10^{-15} s or with fewer than 100 events have been omitted from the Listings.

VALUE (10^{-15} s)	EVTS	DOCUMENT ID	TECN	COMMENT
504 ± 4 OUR AVERAGE				Error includes scale factor of 1.2.
506.4 ± 3.0 ± 1.7 ± 1.7		¹ AAIJ	17AN	LHCB pp at 7, 8 TeV
507.4 ± 5.5 ± 5.1	13.6k	LINK	05J	FOCS $\phi\pi^+$ and $\bar{K}^{*0} K^+$
472.5 ± 17.2 ± 6.6	760	IORI	01	SELX 600 GeV Σ^-, π^-, p
518 ± 14 ± 7	1662	AITALA	99	E791 π^- nucleus, 500 GeV
486.3 ± 15.0 ± 4.9 ± 5.1	2167	² BONVICINI	99	CLE2 $e^+e^- \approx \mathcal{T}(4S)$
475 ± 20 ± 7	900	FRABETTI	93F	E687 γ Be, $\phi\pi^+$
500 ± 60 ± 30	104	FRABETTI	90	E687 γ Be, $\phi\pi^+$
470 ± 40 ± 20	228	RAAB	88	E691 Photoproduction

¹ This AAIJ 17AN value is derived from the difference between the D_s^- and D^- widths.

The 3rd uncertainty, $\pm 1.7 \times 10^{-15}$ s, arises from the uncertainty of the D^- width.

² BONVICINI 99 obtains 1.19 ± 0.04 for the ratio of D_s^\pm to D^0 lifetimes.

D_s^\pm DECAY MODES

Unless otherwise noted, the branching fractions for modes with a resonance in the final state include all the decay modes of the resonance. D_s^\pm modes are charge conjugates of the modes below.

Mode	Fraction (Γ_i/Γ)	Scale factor/ Confidence level
Inclusive modes		
Γ_1 e^+ semileptonic	[a] (6.5 ± 0.4) %	
Γ_2 π^+ anything	(119.3 ± 1.4) %	
Γ_3 π^- anything	(43.2 ± 0.9) %	
Γ_4 π^0 anything	(123 ± 7) %	
Γ_5 K^- anything	(18.7 ± 0.5) %	
Γ_6 K^+ anything	(28.9 ± 0.7) %	
Γ_7 K_S^0 anything	(19.0 ± 1.1) %	
Γ_8 η anything	[b] (29.9 ± 2.8) %	
Γ_9 ω anything	(6.1 ± 1.4) %	
Γ_{10} η' anything	[c] (10.3 ± 1.4) %	S=1.1
Γ_{11} $f_0(980)$ anything, $f_0 \rightarrow \pi^+\pi^-$	< 1.3 %	CL=90%
Γ_{12} ϕ anything	(15.7 ± 1.0) %	
Γ_{13} $K^+ K^-$ anything	(15.8 ± 0.7) %	
Γ_{14} $K_S^0 K^+$ anything	(5.8 ± 0.5) %	
Γ_{15} $K_S^0 K^-$ anything	(1.9 ± 0.4) %	
Γ_{16} $2K_S^0$ anything	(1.70 ± 0.32) %	
Γ_{17} $2K^+$ anything	< 2.6 × 10 ⁻³	CL=90%
Γ_{18} $2K^-$ anything	< 6 × 10 ⁻⁴	CL=90%
Leptonic and semileptonic modes		
Γ_{19} $e^+ \nu_e$	< 8.3 × 10 ⁻⁵	CL=90%
Γ_{20} $\mu^+ \nu_\mu$	(5.49 ± 0.16) × 10 ⁻³	
Γ_{21} $\tau^+ \nu_\tau$	(5.48 ± 0.23) %	
Γ_{22} $\gamma e^+ \nu_e$	< 1.3 × 10 ⁻⁴	CL=90%
Γ_{23} $K^+ K^- e^+ \nu_e$	—	
Γ_{24} $\phi e^+ \nu_e$	[d] (2.39 ± 0.16) %	S=1.3
Γ_{25} $\phi \mu^+ \nu_\mu$	(1.9 ± 0.5) %	
Γ_{26} $\eta e^+ \nu_e + \eta'(958) e^+ \nu_e$	[d] (3.03 ± 0.24) %	
Γ_{27} $\eta e^+ \nu_e$	[d] (2.32 ± 0.08) %	
Γ_{28} $\eta'(958) e^+ \nu_e$	[d] (8.0 ± 0.7) × 10 ⁻³	
Γ_{29} $\eta \mu^+ \nu_\mu$	(2.4 ± 0.5) %	
Γ_{30} $\eta'(958) \mu^+ \nu_\mu$	(1.1 ± 0.5) %	
Γ_{31} $\omega e^+ \nu_e$	[e] < 2.0 × 10 ⁻³	CL=90%
Γ_{32} $K^0 e^+ \nu_e$	(3.4 ± 0.4) × 10 ⁻³	
Γ_{33} $K^*(892)^0 e^+ \nu_e$	[d] (2.15 ± 0.28) × 10 ⁻³	S=1.1
Γ_{34} $f_0(980) e^+ \nu_e, f_0 \rightarrow \pi^+\pi^-$		
Hadronic modes with a $K\bar{K}$ pair		
Γ_{35} $K^+ K_S^0$	(1.46 ± 0.04) %	S=1.1
Γ_{36} $K^+ K^0$	(1.49 ± 0.06) %	
Γ_{37} $K^+ \bar{K}^0$	(2.95 ± 0.14) %	
Γ_{38} $K^+ K^- \pi^+$	[f] (5.39 ± 0.15) %	S=1.2
Γ_{39} $\phi\pi^+$	[d,g] (4.5 ± 0.4) %	
Γ_{40} $\phi\pi^+, \phi \rightarrow K^+ K^-$	[g] (2.24 ± 0.08) %	
Γ_{41} $K^+ \bar{K}^*(892)^0, \bar{K}^{*0} \rightarrow K^- \pi^+$	(2.58 ± 0.08) %	
Γ_{42} $f_0(980)\pi^+, f_0 \rightarrow K^+ K^-$	(1.14 ± 0.31) %	
Γ_{43} $f_0(1370)\pi^+, f_0 \rightarrow K^+ K^-$	(7 ± 5) × 10 ⁻⁴	
Γ_{44} $f_0(1710)\pi^+, f_0 \rightarrow K^+ K^-$	(6.6 ± 2.8) × 10 ⁻⁴	

Γ_{45}	$K^+ \bar{K}_0^*(1430)^0, \bar{K}_0^0 \rightarrow$	$(1.8 \pm 0.4) \times 10^{-3}$	
Γ_{46}	$K^+ K_S^0 \pi^+$	$(1.52 \pm 0.22) \%$	
Γ_{47}	$2K_S^0 \pi^+$	$(7.7 \pm 0.6) \times 10^{-3}$	
Γ_{48}	$K^0 \bar{K}^0 \pi^+$	—	
Γ_{49}	$K^*(892)^+ \bar{K}^0$	[d] $(5.4 \pm 1.2) \%$	
Γ_{50}	$K^+ K^- \pi^+ \pi^0$	$(6.2 \pm 0.6) \%$	S=1.1
Γ_{51}	$\phi \rho^+$	[d] $(8.4 \pm_{-2.3}^{+1.9}) \%$	
Γ_{52}	$K_S^0 K^- 2\pi^+$	$(1.65 \pm 0.10) \%$	
Γ_{53}	$K^*(892)^+ \bar{K}^*(892)^0$	[d] $(7.2 \pm 2.6) \%$	
Γ_{54}	$K^+ K_S^0 \pi^+ \pi^-$	$(9.9 \pm 0.8) \times 10^{-3}$	
Γ_{55}	$K^+ K^- 2\pi^+ \pi^-$	$(8.6 \pm 1.5) \times 10^{-3}$	
Γ_{56}	$\phi 2\pi^+ \pi^-$	[d] $(1.21 \pm 0.16) \%$	
Γ_{57}	$\phi \rho^0 \pi^+, \phi \rightarrow K^+ K^-$	$(6.5 \pm 1.3) \times 10^{-3}$	
Γ_{58}	$\phi a_1(1260)^+, \phi \rightarrow$ $K^+ K^-, a_1^+ \rightarrow$ $\rho^0 \pi^+$	$(7.4 \pm 1.2) \times 10^{-3}$	
Γ_{59}	$\phi 2\pi^+ \pi^-$ non- $\rho, \phi \rightarrow$ $K^+ K^-$	$(1.8 \pm 0.7) \times 10^{-3}$	
Γ_{60}	$K^+ K^- \rho^0 \pi^+$ non- ϕ	$< 2.6 \times 10^{-4}$	CL=90%
Γ_{61}	$K^+ K^- 2\pi^+ \pi^-$ nonresonant	$(9 \pm 7) \times 10^{-4}$	
Γ_{62}	$2K_S^0 2\pi^+ \pi^-$	$(8.4 \pm 3.5) \times 10^{-4}$	

Hadronic modes without K 's

Γ_{63}	$\pi^+ \pi^0$	$< 3.4 \times 10^{-4}$	CL=90%
Γ_{64}	$2\pi^+ \pi^-$	$(1.08 \pm 0.04) \%$	S=1.1
Γ_{65}	$\rho^0 \pi^+$	$(1.9 \pm 1.2) \times 10^{-4}$	
Γ_{66}	$\pi^+(\pi^+ \pi^-)_{S\text{-wave}}$	[h] $(9.0 \pm 0.4) \times 10^{-3}$	
Γ_{67}	$f_0(980) \pi^+, f_0 \rightarrow \pi^+ \pi^-$		
Γ_{68}	$f_0(1370) \pi^+, f_0 \rightarrow \pi^+ \pi^-$		
Γ_{69}	$f_0(1500) \pi^+, f_0 \rightarrow \pi^+ \pi^-$		
Γ_{70}	$f_2(1270) \pi^+, f_2 \rightarrow \pi^+ \pi^-$	$(1.09 \pm 0.20) \times 10^{-3}$	
Γ_{71}	$\rho(1450)^0 \pi^+, \rho^0 \rightarrow \pi^+ \pi^-$	$(3.0 \pm 1.9) \times 10^{-4}$	
Γ_{72}	$\pi^+ 2\pi^0$	$(6.5 \pm 1.3) \times 10^{-3}$	
Γ_{73}	$2\pi^+ \pi^- \pi^0$	—	
Γ_{74}	$\eta \pi^+$	[d] $(1.68 \pm 0.10) \%$	S=1.2
Γ_{75}	$\omega \pi^+$	[d] $(1.92 \pm 0.30) \times 10^{-3}$	
Γ_{76}	$3\pi^+ 2\pi^-$	$(7.9 \pm 0.8) \times 10^{-3}$	
Γ_{77}	$2\pi^+ \pi^- 2\pi^0$	—	
Γ_{78}	$\eta \rho^+$	[d] $(8.9 \pm 0.8) \%$	
Γ_{79}	$\eta \pi^+ \pi^0$	$(9.5 \pm 0.5) \%$	
Γ_{80}	$\eta(\pi^+ \pi^0)_{P\text{-wave}}$	$(5.1 \pm 3.1) \times 10^{-3}$	
Γ_{81}	$a_0(980)^+ \pi^0, a_0(980)^+ \rightarrow \eta \pi^+$	$(2.2 \pm 0.4) \%$	
Γ_{82}	$\omega \pi^+ \pi^0$	[d] $(2.8 \pm 0.7) \%$	
Γ_{83}	$3\pi^+ 2\pi^- \pi^0$	$(4.9 \pm 3.2) \%$	
Γ_{84}	$\omega 2\pi^+ \pi^-$	[d] $(1.6 \pm 0.5) \%$	
Γ_{85}	$\eta'(958) \pi^+$	[c,d] $(3.94 \pm 0.25) \%$	
Γ_{86}	$3\pi^+ 2\pi^- 2\pi^0$	—	
Γ_{87}	$\omega \eta \pi^+$	[d] $< 2.13 \%$	CL=90%
Γ_{88}	$\eta'(958) \rho^+$	[c,d] $(5.8 \pm 1.5) \%$	
Γ_{89}	$\eta'(958) \pi^+ \pi^0$	$(5.6 \pm 0.8) \%$	
Γ_{90}	$\eta'(958) \pi^+ \pi^0$ nonresonant	$< 5.1 \%$	CL=90%

Modes with one or three K 's

Γ_{91}	$K^+ \pi^0$	$(6.1 \pm 2.1) \times 10^{-4}$	
Γ_{92}	$K_S^0 \pi^+$	$(1.19 \pm 0.05) \times 10^{-3}$	
Γ_{93}	$K^+ \eta$	[d] $(1.72 \pm 0.34) \times 10^{-3}$	
Γ_{94}	$K^+ \omega$	[d] $(8.7 \pm 2.5) \times 10^{-4}$	
Γ_{95}	$K^+ \eta'(958)$	[d] $(1.7 \pm 0.5) \times 10^{-3}$	
Γ_{96}	$K^+ \pi^+ \pi^-$	$(6.5 \pm 0.4) \times 10^{-3}$	
Γ_{97}	$K^+ \rho^0$	$(2.5 \pm 0.4) \times 10^{-3}$	
Γ_{98}	$K^+ \rho(1450)^0, \rho^0 \rightarrow \pi^+ \pi^-$	$(6.9 \pm 2.4) \times 10^{-4}$	
Γ_{99}	$K^*(892)^0 \pi^+, K^{*0} \rightarrow K^+ \pi^-$	$(1.41 \pm 0.24) \times 10^{-3}$	
Γ_{100}	$K^*(1410)^0 \pi^+, K^{*0} \rightarrow$ $K^+ \pi^-$	$(1.23 \pm 0.28) \times 10^{-3}$	
Γ_{101}	$K^*(1430)^0 \pi^+, K^{*0} \rightarrow$ $K^+ \pi^-$	$(5.0 \pm 3.5) \times 10^{-4}$	
Γ_{102}	$K^+ \pi^+ \pi^-$ nonresonant	$(1.03 \pm 0.34) \times 10^{-3}$	
Γ_{103}	$K^0 \pi^+ \pi^0$	$(1.00 \pm 0.18) \%$	
Γ_{104}	$K_S^0 2\pi^+ \pi^-$	$(3.0 \pm 1.1) \times 10^{-3}$	
Γ_{105}	$K^+ \omega \pi^0$	[d] $< 8.2 \times 10^{-3}$	CL=90%
Γ_{106}	$K^+ \omega \pi^+ \pi^-$	[d] $< 5.4 \times 10^{-3}$	CL=90%
Γ_{107}	$K^+ \omega \eta$	[d] $< 7.9 \times 10^{-3}$	CL=90%
Γ_{108}	$2K^+ K^-$	$(2.16 \pm 0.20) \times 10^{-4}$	
Γ_{109}	$\phi K^+, \phi \rightarrow K^+ K^-$	$(8.8 \pm 2.0) \times 10^{-5}$	

Doubly Cabibbo-suppressed modes

Γ_{110}	$2K^+ \pi^-$	$(1.28 \pm 0.04) \times 10^{-4}$
Γ_{111}	$K^+ K^*(892)^0, K^{*0} \rightarrow$ $K^+ \pi^-$	$(6.0 \pm 3.4) \times 10^{-5}$

Baryon-antibaryon mode

Γ_{112}	$\rho \bar{\rho}$	$(1.22 \pm 0.11) \times 10^{-3}$	
Γ_{113}	$\rho \bar{\rho} e^+ \nu_e$	$< 2.0 \times 10^{-4}$	CL=90%

$\Delta C = 1$ weak neutral current (C1) modes, Lepton family number (LF), or Lepton number (L) violating modes

Γ_{114}	$\pi^+ e^+ e^-$	[j] $< 1.3 \times 10^{-5}$	CL=90%
Γ_{115}	$\pi^+ \phi, \phi \rightarrow e^+ e^-$	[j] $(6 \pm_{-4}^{+8}) \times 10^{-6}$	
Γ_{116}	$\pi^+ \mu^+ \mu^-$	[i] $< 4.1 \times 10^{-7}$	CL=90%
Γ_{117}	$K^+ e^+ e^-$	CI $< 3.7 \times 10^{-6}$	CL=90%
Γ_{118}	$K^+ \mu^+ \mu^-$	CI $< 2.1 \times 10^{-5}$	CL=90%
Γ_{119}	$K^*(892)^+ \mu^+ \mu^-$	CI $< 1.4 \times 10^{-3}$	CL=90%
Γ_{120}	$\pi^+ e^+ \mu^-$	LF $< 1.2 \times 10^{-5}$	CL=90%
Γ_{121}	$\pi^+ e^- \mu^+$	LF $< 2.0 \times 10^{-5}$	CL=90%
Γ_{122}	$K^+ e^- \mu^+$	LF $< 1.4 \times 10^{-5}$	CL=90%
Γ_{123}	$2K^+ e^- \mu^+$	LF $< 9.7 \times 10^{-6}$	CL=90%
Γ_{124}	$\pi^- 2e^+$	L $< 4.1 \times 10^{-6}$	CL=90%
Γ_{125}	$\pi^- 2\mu^+$	L $< 1.2 \times 10^{-7}$	CL=90%
Γ_{126}	$\pi^- e^+ \mu^+$	L $< 8.4 \times 10^{-6}$	CL=90%
Γ_{127}	$K^- 2e^+$	L $< 5.2 \times 10^{-6}$	CL=90%
Γ_{128}	$K^- 2\mu^+$	L $< 1.3 \times 10^{-5}$	CL=90%
Γ_{129}	$K^- e^+ \mu^+$	L $< 6.1 \times 10^{-6}$	CL=90%
Γ_{130}	$K^*(892)^- 2\mu^+$	L $< 1.4 \times 10^{-3}$	CL=90%

[a] This is the purely e^+ semileptonic branching fraction: the e^+ fraction from τ^+ decays has been subtracted off. The sum of our (non- τ) e^+ exclusive fractions — an $e^+ \nu_e$ with an $\eta, \eta', \phi, K^0,$ or K^{*0} — is $5.99 \pm 0.31 \%$.

[b] This fraction includes η from η' decays.

[c] The sum of our exclusive η' fractions — $\eta' e^+ \nu_e, \eta' \mu^+ \nu_\mu, \eta' \pi^+, \eta' \rho^+$, and $\eta' K^+$ — is $11.8 \pm 1.6 \%$.

[d] This branching fraction includes all the decay modes of the final-state resonance.

[e] A test for $u\bar{u}$ or $d\bar{d}$ content in the D_s^+ . Neither Cabibbo-favored nor Cabibbo-suppressed decays can contribute, and ω - ϕ mixing is an unlikely explanation for any fraction above about 2×10^{-4} .

[f] The branching fraction for this mode may differ from the sum of the submodes that contribute to it, due to interference effects. See the relevant papers.

[g] We decouple the $D_s^+ \rightarrow \phi \pi^+$ branching fraction obtained from mass projections (and used to get some of the other branching fractions) from the $D_s^+ \rightarrow \phi \pi^+, \phi \rightarrow K^+ K^-$ branching fraction obtained from the Dalitz-plot analysis of $D_s^+ \rightarrow K^+ K^- \pi^+$. That is, the ratio of these two branching fractions is not exactly the $\phi \rightarrow K^+ K^-$ branching fraction 0.491.

[h] This is the average of a model-independent and a K -matrix parametrization of the $\pi^+ \pi^-$ S -wave and is a sum over several f_0 mesons.

[i] This mode is not a useful test for a $\Delta C=1$ weak neutral current because both quarks must change flavor in this decay.

[j] This is *not* a test for the $\Delta C=1$ weak neutral current, but leads to the $\pi^+ \ell^+ \ell^-$ final state.

CONSTRAINED FIT INFORMATION

An overall fit to 13 branching ratios uses 18 measurements and one constraint to determine 10 parameters. The overall fit has a $\chi^2 = 6.8$ for 9 degrees of freedom.

The following *off-diagonal* array elements are the correlation coefficients $\langle \delta x_i \delta x_j \rangle / (\delta x_i \delta x_j)$, in percent, from the fit to the branching fractions, $x_i \equiv \Gamma_i / \Gamma_{\text{total}}$. The fit constrains the x_i whose labels appear in this array to sum to one.

Meson Particle Listings

D_s^\pm

X_{38}	51							
X_{50}	22	29						
X_{52}	28	30	11					
X_{54}	23	25	13	38				
X_{64}	34	50	19	19	17			
X_{74}	-7	-7	-15	1	-7	-7		
X_{75}	0	0	-1	0	0	0	4	
X_{96}	5	12	-6	7	1	3	16	1
	X_{35}	X_{38}	X_{50}	X_{52}	X_{54}	X_{64}	X_{74}	X_{75}

See the related review(s):

D_s^+ Branching Fractions

D_s^+ BRANCHING RATIOS

A number of older, now obsolete results have been omitted. They may be found in earlier editions.

Inclusive modes

$\Gamma(e^+ \text{ semileptonic})/\Gamma_{\text{total}}$ Γ_1/Γ
 This is the purely e^+ semileptonic branching fraction: the e^+ fraction from τ^+ decays has been subtracted off. The sum of our (non- τ) e^+ exclusive fractions — an $e^+ \nu_e$ with an η, η', ϕ, K^0 , or K^{*0} — is $5.99 \pm 0.31\%$.

VALUE (%)	EVTS	DOCUMENT ID	TECN	COMMENT
$6.52 \pm 0.39 \pm 0.15$	536 ± 29	1 ASNER	10	CLEO $e^+ e^-$ at 3774 MeV

¹ Using the D_s^+ and D^0 lifetimes, ASNER 10 finds that the ratio of the D_s^+ and D^0 semileptonic widths is $0.828 \pm 0.051 \pm 0.025$.

$\Gamma(\pi^+ \text{ anything})/\Gamma_{\text{total}}$ Γ_2/Γ
 Events with two π^+ 's count twice, etc. But π^+ 's from $K_S^0 \rightarrow \pi^+ \pi^-$ are not included.

VALUE (%)	DOCUMENT ID	TECN	COMMENT
$119.3 \pm 1.2 \pm 0.7$	DOBBS	09	CLEO $e^+ e^-$ at 4170 MeV

$\Gamma(\pi^- \text{ anything})/\Gamma_{\text{total}}$ Γ_3/Γ
 Events with two π^- 's count twice, etc. But π^- 's from $K_S^0 \rightarrow \pi^+ \pi^-$ are not included.

VALUE (%)	DOCUMENT ID	TECN	COMMENT
$43.2 \pm 0.9 \pm 0.3$	DOBBS	09	CLEO $e^+ e^-$ at 4170 MeV

$\Gamma(\pi^0 \text{ anything})/\Gamma_{\text{total}}$ Γ_4/Γ
 Events with two π^0 's count twice, etc. But π^0 's from $K_S^0 \rightarrow 2\pi^0$ are not included.

VALUE (%)	DOCUMENT ID	TECN	COMMENT
$123.4 \pm 3.8 \pm 5.3$	DOBBS	09	CLEO $e^+ e^-$ at 4170 MeV

$\Gamma(K^- \text{ anything})/\Gamma_{\text{total}}$ Γ_5/Γ

VALUE (%)	DOCUMENT ID	TECN	COMMENT
$18.7 \pm 0.5 \pm 0.2$	DOBBS	09	CLEO $e^+ e^-$ at 4170 MeV

$\Gamma(K^+ \text{ anything})/\Gamma_{\text{total}}$ Γ_6/Γ

VALUE (%)	DOCUMENT ID	TECN	COMMENT
$28.9 \pm 0.6 \pm 0.3$	DOBBS	09	CLEO $e^+ e^-$ at 4170 MeV

$\Gamma(K_S^0 \text{ anything})/\Gamma_{\text{total}}$ Γ_7/Γ

VALUE (%)	DOCUMENT ID	TECN	COMMENT
$19.0 \pm 1.0 \pm 0.4$	DOBBS	09	CLEO $e^+ e^-$ at 4170 MeV

$\Gamma(\eta \text{ anything})/\Gamma_{\text{total}}$ Γ_8/Γ
 This ratio includes η particles from η' decays.

VALUE (%)	EVTS	DOCUMENT ID	TECN	COMMENT
$29.9 \pm 2.2 \pm 1.7$		DOBBS	09	CLEO $e^+ e^-$ at 4170 MeV
$23.5 \pm 3.1 \pm 2.0$	674 ± 91	HUANG	06B	CLEO See DOBBS 09

• • • We do not use the following data for averages, fits, limits, etc. • • •

$\Gamma(\omega \text{ anything})/\Gamma_{\text{total}}$ Γ_9/Γ

VALUE (%)	DOCUMENT ID	TECN	COMMENT
$6.1 \pm 1.4 \pm 0.3$	DOBBS	09	CLEO $e^+ e^-$ at 4170 MeV

$\Gamma(\eta' \text{ anything})/\Gamma_{\text{total}}$ Γ_{10}/Γ

VALUE (%)	EVTS	DOCUMENT ID	TECN	COMMENT
10.3 ± 1.4 OUR AVERAGE	Error includes scale factor of 1.1.			
$8.8 \pm 1.8 \pm 0.5$	68	ABLIKIM	15z	BES3 482 pb^{-1} , 4009 MeV
$11.7 \pm 1.7 \pm 0.7$		DOBBS	09	CLEO $e^+ e^-$ at 4170 MeV
$8.7 \pm 1.9 \pm 0.8$	68	HUANG	06B	CLEO See DOBBS 09

• • • We do not use the following data for averages, fits, limits, etc. • • •

$\Gamma(f_0(980) \text{ anything}, f_0 \rightarrow \pi^+ \pi^-)/\Gamma_{\text{total}}$ Γ_{11}/Γ

VALUE (%)	CL%	DOCUMENT ID	TECN	COMMENT
<1.3	90	DOBBS	09	CLEO $e^+ e^-$ at 4170 MeV

$\Gamma(\phi \text{ anything})/\Gamma_{\text{total}}$ Γ_{12}/Γ

VALUE (%)	EVTS	DOCUMENT ID	TECN	COMMENT
$15.7 \pm 0.8 \pm 0.6$		DOBBS	09	CLEO $e^+ e^-$ at 4170 MeV
$16.1 \pm 1.2 \pm 1.1$	398 ± 27	HUANG	06B	CLEO See DOBBS 09

• • • We do not use the following data for averages, fits, limits, etc. • • •

$\Gamma(K^+ K^- \text{ anything})/\Gamma_{\text{total}}$ Γ_{13}/Γ

VALUE (%)	DOCUMENT ID	TECN	COMMENT
$15.8 \pm 0.6 \pm 0.3$	DOBBS	09	CLEO $e^+ e^-$ at 4170 MeV

$\Gamma(K_S^0 K^+ \text{ anything})/\Gamma_{\text{total}}$ Γ_{14}/Γ

VALUE (%)	DOCUMENT ID	TECN	COMMENT
$5.8 \pm 0.5 \pm 0.1$	DOBBS	09	CLEO $e^+ e^-$ at 4170 MeV

$\Gamma(K_S^0 K^- \text{ anything})/\Gamma_{\text{total}}$ Γ_{15}/Γ

VALUE (%)	DOCUMENT ID	TECN	COMMENT
$1.9 \pm 0.4 \pm 0.1$	DOBBS	09	CLEO $e^+ e^-$ at 4170 MeV

$\Gamma(2K_S^0 \text{ anything})/\Gamma_{\text{total}}$ Γ_{16}/Γ

VALUE (%)	DOCUMENT ID	TECN	COMMENT
$1.7 \pm 0.3 \pm 0.1$	DOBBS	09	CLEO $e^+ e^-$ at 4170 MeV

$\Gamma(2K^+ \text{ anything})/\Gamma_{\text{total}}$ Γ_{17}/Γ

VALUE (%)	CL%	DOCUMENT ID	TECN	COMMENT
<0.26	90	DOBBS	09	CLEO $e^+ e^-$ at 4170 MeV

$\Gamma(2K^- \text{ anything})/\Gamma_{\text{total}}$ Γ_{18}/Γ

VALUE (%)	CL%	DOCUMENT ID	TECN	COMMENT
<0.06	90	DOBBS	09	CLEO $e^+ e^-$ at 4170 MeV

Leptonic and semileptonic modes

See the related review(s):

Leptonic Decays of Charged Pseudoscalar Mesons

$\Gamma(e^+ \nu_e)/\Gamma_{\text{total}}$ Γ_{19}/Γ

VALUE	CL%	DOCUMENT ID	TECN	COMMENT
$<0.83 \times 10^{-4}$	90	¹ ZUPANC	13	BELL $e^+ e^-$ at $\Upsilon(4S), \Upsilon(5S)$

• • • We do not use the following data for averages, fits, limits, etc. • • •

$<2.3 \times 10^{-4}$	90	DEL-AMO-SA...10j	BABR	$e^+ e^-$, 10.58 GeV
$<1.2 \times 10^{-4}$	90	ALEXANDER	09	CLEO $e^+ e^-$ at 4170 MeV
$<1.3 \times 10^{-4}$	90	PEDLAR	07A	CLEO See ALEXANDER 09

¹ ZUPANC 13 also gives the limit as $<1.0 \times 10^{-4}$ at 95% CL.

$\Gamma(\mu^+ \nu_\mu)/\Gamma_{\text{total}}$ Γ_{20}/Γ
 See the note on "Decay Constants of Charged Pseudoscalar Mesons."

VALUE (units 10^{-3})	EVTS	DOCUMENT ID	TECN	COMMENT
5.49 ± 0.16 OUR AVERAGE				
$5.49 \pm 0.16 \pm 0.15$	1.1k	ABLIKIM	19E	BES3 $e^+ e^-$ at 4178 MeV
$4.95 \pm 0.67 \pm 0.26$	69	¹ ABLIKIM	16o	BES3 $e^+ e^-$ at 4.009 GeV
$5.31 \pm 0.28 \pm 0.20$	492 ± 26	² ZUPANC	13	BELL $e^+ e^-$ at $\Upsilon(4S), \Upsilon(5S)$

$6.02 \pm 0.38 \pm 0.34$ 275 ± 17 ³ DEL-AMO-SA...10j BABR $e^+ e^-$, 10.58 GeV
 $5.65 \pm 0.45 \pm 0.17$ 235 ± 14 ALEXANDER 09 CLEO $e^+ e^-$ at 4170 MeV

• • • We do not use the following data for averages, fits, limits, etc. • • •

$6.44 \pm 0.76 \pm 0.57$	169 ± 18	⁴ WIDHALM	08	BELL See ZUPANC 13
$5.94 \pm 0.66 \pm 0.31$	88	⁵ PEDLAR	07A	CLEO See ALEXANDER 09
$6.8 \pm 1.1 \pm 1.8$	553	⁶ HEISTER	02i	ALEP Z decays

¹ ABLIKIM 16o value is constrained by the Standard Model ratio of $\Gamma(D_s^+ \rightarrow \tau^+ \nu_\tau)/\Gamma(D_s^+ \rightarrow \mu^+ \nu_\mu) = 9.76$; the unconstrained value is $(0.517 \pm 0.075 \pm 0.021)\%$. The constrained value is used to obtain the decay constant, $f_{D_s^+} = (241.0 \pm 16.3 \pm 6.6)$ MeV.

² ZUPANC 13 uses both $\mu^+ \nu$ and $\tau^+ \nu$ events to get $f_{D_s} = (255.5 \pm 4.2 \pm 5.1)$ MeV.

³ DEL-AMO-SANCHEZ 10j uses $\mu^+ \nu_\mu$ and $\tau^+ \nu_\tau$ events together to get $f_{D_s} = (258.6 \pm 6.4 \pm 7.5)$ MeV.

⁴ WIDHALM 08 gets $f_{D_s} = (275 \pm 16 \pm 12)$ MeV from the branching fraction.

⁵ PEDLAR 07A also fits μ^+ and τ^+ events together and gets an effective $\mu^+ \nu_\mu$ branching fraction of $(6.38 \pm 0.59 \pm 0.33) \times 10^{-3}$.

⁶ This HEISTER 02i result is not actually an independent measurement of the absolute $\mu^+ \nu_\mu$ branching fraction, but is in fact based on our $\phi\pi^+$ branching fraction of $3.6 \pm 0.9\%$, so it cannot be included in our overall fit. HEISTER 02i combines its $D_s^+ \rightarrow \tau^+ \nu_\tau$ and $\mu^+ \nu_\mu$ branching fractions to get $f_{D_s} = (285 \pm 19 \pm 40)$ MeV.

$\Gamma(\mu^+ \nu_\mu)/\Gamma(\phi\pi^+)$ Γ_{20}/Γ_{39}
 See the note on "Decay Constants of Charged Pseudoscalar Mesons" above.

VALUE	EVTS	DOCUMENT ID	TECN	COMMENT
$0.143 \pm 0.018 \pm 0.006$	489 ± 55	¹ AUBERT	07v	BABR $e^+ e^- \approx \Upsilon(4S)$
$0.23 \pm 0.06 \pm 0.04$	18	² ALEXANDROV	00	BEAT π^- nucleus, 350 GeV

• • • We do not use the following data for averages, fits, limits, etc. • • •

- 0.173±0.023±0.035 182 ³ CHADHA 98 CLE2 $e^+e^- \approx \Upsilon(4S)$
 0.245±0.052±0.074 39 ⁴ ACOSTA 94 CLE2 See CHADHA 98
- ¹ AUBERT 07v gets $f_{D_s^+} = (283 \pm 17 \pm 16)$ MeV, using $\Gamma(D_s^+ \rightarrow \phi\pi^+)/\Gamma(\text{total}) = (4.71 \pm 0.46)\%$.
² ALEXANDROV 00 uses $f_D^2/f_{D_s}^2 = 0.82 \pm 0.09$ from a lattice-gauge-theory calculation to get the relative numbers of $D^+ \rightarrow \mu^+\nu_\mu$ and $D_s^+ \rightarrow \mu^+\nu_\mu$ events. The present result leads to $f_{D_s} = (323 \pm 44 \pm 36)$ MeV.
³ CHADHA 98 obtains $f_{D_s} = (280 \pm 19 \pm 28 \pm 34)$ MeV from this measurement, using $\Gamma(D_s^+ \rightarrow \phi\pi^+)/\Gamma(\text{total}) = 0.036 \pm 0.009$.
⁴ ACOSTA 94 obtains $f_{D_s} = (344 \pm 37 \pm 52 \pm 42)$ MeV from this measurement, using $\Gamma(D_s^+ \rightarrow \phi\pi^+)/\Gamma(\text{total}) = 0.037 \pm 0.009$.

$\Gamma(\tau^+\nu_\tau)/\Gamma_{\text{total}}$ **Γ_{21}/Γ**
 See the note on "Decay Constants of Charged Pseudoscalar Mesons" above.

VALUE (%)	EVTS	DOCUMENT ID	TECN	COMMENT
5.48±0.23 OUR AVERAGE				
4.83±0.65±0.26	33	¹ ABLIKIM	160 BES3	e^+e^- at 4.009 GeV
5.70±0.21± $^{+0.31}_{-0.30}$	2.2k	² ZUPANC	13 BELL	e^+e^- at $\Upsilon(4S)$, $\Upsilon(5S)$
4.96±0.37±0.57	748±53	³ DEL-AMO-SA..10j	BABR	$e^- \bar{\nu}_e \nu_\tau, \mu^- \bar{\nu}_\mu \nu_\tau$
6.42±0.81±0.18	126±16	⁴ ALEXANDER	09 CLEO	$\tau^+ \rightarrow \pi^+ \bar{\nu}_\tau$
5.52±0.57±0.21	155±17	⁴ NAIK	09A CLEO	$\tau^+ \rightarrow \rho^+ \bar{\nu}_\tau$
5.30±0.47±0.22	181±16	⁴ ONYISI	09 CLEO	$\tau^+ \rightarrow e^+ \nu_e \bar{\nu}_\tau$
••• We do not use the following data for averages, fits, limits, etc. •••				
6.17±0.71±0.34	102	⁵ ECKLUND	08 CLEO	See ONYISI 09
8.0 ±1.3 ±0.4	47	⁵ PEDLAR	07A CLEO	See ALEXANDER 09
5.79±0.77±1.84	881	⁶ HEISTER	02i ALEP	Z decays
7.0 ±2.1 ±2.0	22	⁷ ABBIENDI	01L OPAL	$D_s^{*+} \rightarrow \gamma D_s^+$ from Z's
7.4 ±2.8 ±2.4	16	⁸ ACCIARRI	97F L3	$D_s^{*+} \rightarrow \gamma D_s^+$ from Z's

- ¹ ABLIKIM 160 value is constrained by the Standard Model ratio of $\Gamma(D_s^+ \rightarrow \tau^+\nu_\tau)/\Gamma(D_s^+ \rightarrow \mu^+\nu_\mu) = 9.76$; the unconstrained value is $(3.28 \pm 1.83 \pm 0.37)\%$.
² ZUPANC 13 uses both $\mu^+\nu$ and $\tau^+\nu$ events to get $f_{D_s} = (255.5 \pm 4.2 \pm 5.1)$ MeV.
³ DEL-AMO-SANCHEZ 10j (with a small correction; see LEES 15d) uses $\mu^+\nu_\mu$ and $\tau^+\nu_\tau$ events together to get $f_{D_s} = (259.9 \pm 6.6 \pm 7.6)$ MeV.
⁴ ALEXANDER 09, NAIK 09A, and ONYISI 09 use different τ decay modes and are independent. The three papers combined give $f_{D_s} = (259.7 \pm 7.8 \pm 3.4)$ MeV.
⁵ ECKLUND 08 and PEDLAR 07A are independent: ECKLUND 08 uses $\tau^+ \rightarrow e^+\nu_e \bar{\nu}_\tau$ events, PEDLAR 07A uses $\tau^+ \rightarrow \pi^+ \bar{\nu}_\tau$ events.
⁶ HEISTER 02i combines its $D_s^+ \rightarrow \tau^+\nu_\tau$ and $\mu^+\nu_\mu$ branching fractions to get $f_{D_s} = (285 \pm 19 \pm 40)$ MeV.
⁷ This ABBIENDI 01L value gives a decay constant f_{D_s} of $(286 \pm 44 \pm 41)$ MeV.
⁸ The second ACCIARRI 97F error here combines in quadrature systematic (0.016) and normalization (0.018) errors. The branching fraction gives $f_{D_s} = (309 \pm 58 \pm 33 \pm 38)$ MeV.

$\Gamma(\tau^+\nu_\tau)/\Gamma(\mu^+\nu_\mu)$ **Γ_{21}/Γ_{20}**

VALUE	EVTS	DOCUMENT ID	TECN	COMMENT
••• We do not use the following data for averages, fits, limits, etc. •••				
10.73±0.69± $^{+0.56}_{-0.53}$	2.2k/492	¹ ZUPANC	13 BELL	e^+e^- at $\Upsilon(4S)$, $\Upsilon(5S)$
11.0 ±1.4 ±0.6	102	² ECKLUND	08 CLEO	See ONYISI 09
¹ This ZUPANC 13 ratio is not independent of the separate $\tau\nu$ and $\mu\nu$ fractions listed above. ² This ECKLUND 08 value also uses results from PEDLAR 07A, and it is not independent of other results in these Listings. Combined with earlier CLEO results, the decay constant f_{D_s} is $274 \pm 10 \pm 5$ MeV.				

$\Gamma(\gamma e^+\nu_e)/\Gamma_{\text{total}}$ **Γ_{22}/Γ**

VALUE	CL%	DOCUMENT ID	TECN	COMMENT
<1.3 × 10⁻⁴	90	ABLIKIM	19AD BES3	for $E_\gamma > 10$ MeV

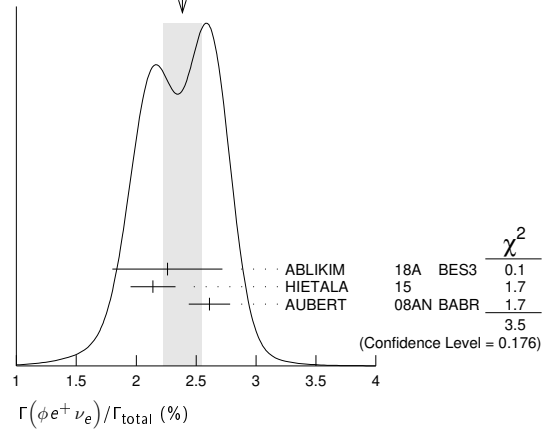
$\Gamma(K^+K^-e^+\nu_e)/\Gamma(K^+K^-\pi^+)$ **Γ_{23}/Γ_{38}**

VALUE	DOCUMENT ID	TECN	COMMENT
••• We do not use the following data for averages, fits, limits, etc. •••			
0.558±0.007±0.016	¹ AUBERT	08AN BABR	e^+e^- at $\Upsilon(4S)$
¹ This AUBERT 08AN ratio is only for the K^+K^- mass in the range 1.01–to–1.03 GeV in the numerator and 1.0095–to–1.0295 GeV in the denominator.			

$\Gamma(\phi e^+\nu_e)/\Gamma_{\text{total}}$ **Γ_{24}/Γ**
 See the end of the D_s^+ Listings for measurements of $D_s^+ \rightarrow \phi e^+\nu_e$ form factors. Unseen decay modes of the ϕ are included.

VALUE (%)	EVTS	DOCUMENT ID	TECN	COMMENT
2.39±0.16 OUR AVERAGE				Error includes scale factor of 1.3. See the ideogram below.
2.26±0.45±0.09	26	ABLIKIM	18A BES3	e^+e^- at 4.009 GeV
2.14±0.17±0.08	207	HIETALA	15	Uses CLEO data
2.61±0.03±0.17	25k	AUBERT	08AN BABR	e^+e^- at $\Upsilon(4S)$
••• We do not use the following data for averages, fits, limits, etc. •••				
2.36±0.23±0.13	106	ECKLUND	09 CLEO	See HIETALA 15
2.29±0.37±0.11	45	YELTON	09 CLEO	See ECKLUND 09

WEIGHTED AVERAGE
2.39±0.16 (Error scaled by 1.3)



$\Gamma(\phi e^+\nu_e)/\Gamma(\phi\pi^+)$ **Γ_{24}/Γ_{39}**
 As noted in the comment column, most of these measurements use $\phi\mu^+\nu_\mu$ events in addition to or instead of $\phi e^+\nu_e$ events.

VALUE	EVTS	DOCUMENT ID	TECN	COMMENT
••• We do not use the following data for averages, fits, limits, etc. •••				
0.540±0.033±0.048	793	LINK	02j FOCUS	Uses $\phi\mu^+\nu_\mu$
0.54 ±0.05 ±0.04	367	BUTLER	94 CLE2	Uses $\phi e^+\nu_e$ and $\phi\mu^+\nu_\mu$
0.58 ±0.17 ±0.07	97	FRABETTI	93c E687	Uses $\phi\mu^+\nu_\mu$
0.57 ±0.15 ±0.15	104	ALBRECHT	91 ARG	Uses $\phi e^+\nu_e$
0.49 ±0.10 ± $^{+0.10}_{-0.14}$	54	ALEXANDER	90b CLEO	Uses $\phi e^+\nu_e$ and $\phi\mu^+\nu_\mu$

$\Gamma(\phi\mu^+\nu_\mu)/\Gamma_{\text{total}}$ **Γ_{25}/Γ**

VALUE (%)	EVTS	DOCUMENT ID	TECN	COMMENT
1.94±0.53±0.09	22	ABLIKIM	18A BES3	e^+e^- at 4.009 GeV

$\Gamma(\eta e^+\nu_e)/\Gamma_{\text{total}}$ **Γ_{27}/Γ**
 Unseen decay modes of the η are included.

VALUE (%)	EVTS	DOCUMENT ID	TECN	COMMENT
2.32 ±0.08 OUR AVERAGE				
2.323±0.063±0.063	1.8k	ABLIKIM	19s BES3	e^+e^- at 4178 MeV
2.30 ±0.31 ±0.08	63	ABLIKIM	16T BES3	e^+e^- at 4.009 GeV
2.28 ±0.14 ±0.19	358	¹ HIETALA	15	Uses CLEO data
••• We do not use the following data for averages, fits, limits, etc. •••				
2.48 ±0.29 ±0.13	82	YELTON	09 CLEO	See HIETALA 15
¹ Obtained by analyzing CLEO-c data but not authored by the CLEO Collaboration.				

$\Gamma(\eta e^+\nu_e)/\Gamma(\phi e^+\nu_e)$ **Γ_{27}/Γ_{24}**
 Unseen decay modes of the η and the ϕ are included.

VALUE	EVTS	DOCUMENT ID	TECN	COMMENT
••• We do not use the following data for averages, fits, limits, etc. •••				
1.24±0.12±0.15	440	¹ BRANDENB...	95 CLE2	See HIETALA 15
¹ BRANDENBURG 95 uses both e^+ and μ^+ events and makes a phase-space adjustment to use the μ^+ events as e^+ events.				

$\Gamma(\eta'(958) e^+\nu_e)/\Gamma_{\text{total}}$ **Γ_{28}/Γ**
 Unseen decay modes of the $\eta'(958)$ are included.

VALUE (%)	EVTS	DOCUMENT ID	TECN	COMMENT
0.80 ±0.07 OUR AVERAGE				
0.824±0.073±0.027	261	ABLIKIM	19s BES3	e^+e^- at 4178 MeV
0.93 ±0.30 ±0.05	14	ABLIKIM	16T BES3	e^+e^- at 4009 MeV
0.68 ±0.15 ±0.06	20	¹ HIETALA	15	Uses CLEO data
••• We do not use the following data for averages, fits, limits, etc. •••				
0.91 ±0.33 ±0.05	7.5	YELTON	09 CLEO	See HIETALA 15
¹ Obtained by analyzing CLEO-c data but not authored by the CLEO Collaboration.				

$\Gamma(\eta'(958) e^+\nu_e)/\Gamma(\phi e^+\nu_e)$ **Γ_{28}/Γ_{24}**
 Unseen decay modes of the resonances are included.

VALUE	EVTS	DOCUMENT ID	TECN	COMMENT
••• We do not use the following data for averages, fits, limits, etc. •••				
0.43±0.11±0.07	29	¹ BRANDENB...	95 CLE2	See HIETALA 15
¹ BRANDENBURG 95 uses both e^+ and μ^+ events and makes a phase-space adjustment to use the μ^+ events as e^+ events.				

$[\Gamma(\eta e^+\nu_e) + \Gamma(\eta'(958) e^+\nu_e)]/\Gamma(\phi e^+\nu_e)$ **$\Gamma_{26}/\Gamma_{24} = (\Gamma_{27} + \Gamma_{28})/\Gamma_{24}$**
 Unseen decay modes of the resonances are included.

VALUE	DOCUMENT ID	TECN	COMMENT
••• We do not use the following data for averages, fits, limits, etc. •••			
1.67±0.17±0.17	¹ BRANDENB...	95 CLE2	See HIETALA 15
¹ This BRANDENBURG 95 data is redundant with data in previous blocks.			

Meson Particle Listings

D_s^\pm

$\Gamma(\eta\mu^+\nu_\mu)/\Gamma_{total}$	EVTS	DOCUMENT ID	TECN	COMMENT	Γ_{29}/Γ
2.42 ± 0.46 ± 0.11	44	ABLIKIM	18A	BES3	e^+e^- at 4.009 GeV

$\Gamma(\eta'(958)\mu^+\nu_\mu)/\Gamma_{total}$	EVTS	DOCUMENT ID	TECN	COMMENT	Γ_{30}/Γ
1.06 ± 0.54 ± 0.07	10	ABLIKIM	18A	BES3	e^+e^- at 4.009 GeV

$\Gamma(\omega e^+\nu_e)/\Gamma_{total}$	CL%	DOCUMENT ID	TECN	COMMENT	Γ_{31}/Γ
<0.20	90	MARTIN	11	CLEO	e^+e^- at 4170 MeV

A test for $u\bar{u}$ or $d\bar{d}$ content in the D_s^+ . Neither Cabibbo-favored nor Cabibbo-suppressed decays can contribute, and $\omega - \phi$ mixing is an unlikely explanation for any fraction above about 2×10^{-4} .

$\Gamma(K^0 e^+\nu_e)/\Gamma_{total}$	EVTS	DOCUMENT ID	TECN	COMMENT	Γ_{32}/Γ
0.34 ± 0.04 OUR AVERAGE					
0.325 ± 0.038 ± 0.016	117	¹ ABLIKIM	19D	BES3	e^+e^- at 4178 MeV
0.39 ± 0.08 ± 0.03	42	HIETALA	15		Uses CLEO data
• • • We do not use the following data for averages, fits, limits, etc. • • •					
0.37 ± 0.10 ± 0.02	14	YELTON	09	CLEO	See HIETALA 15
¹ K^0 reconstructed via $K^0 \rightarrow K_S^0 \rightarrow \pi^+\pi^-$ decays.					

$\Gamma(K^*(892)^0 e^+\nu_e)/\Gamma_{total}$	EVTS	DOCUMENT ID	TECN	COMMENT	Γ_{33}/Γ
0.215 ± 0.028 OUR AVERAGE					
0.237 ± 0.026 ± 0.020	155	ABLIKIM	19D	BES3	e^+e^- at 4178 MeV
0.18 ± 0.04 ± 0.01	32	¹ HIETALA	15		e^+e^- at 4.170 GeV
• • • We do not use the following data for averages, fits, limits, etc. • • •					
0.18 ± 0.07 ± 0.01	7.5	YELTON	09	CLEO	See HIETALA 15
¹ Uses CLEO data, but not authored by the CLEO collaboration					

$\Gamma(f_0(980) e^+\nu_e, f_0 \rightarrow \pi^+\pi^-)/\Gamma_{total}$	EVTS	DOCUMENT ID	TECN	COMMENT	Γ_{34}/Γ
0.13 ± 0.03 ± 0.01	42	¹ HIETALA	15		Uses CLEO data
0.20 ± 0.03 ± 0.01	44	ECKLUND	09	CLEO	See HIETALA 15
0.13 ± 0.04 ± 0.01	13	YELTON	09	CLEO	See ECKLUND 09
¹ HIETALA 15 uses a tighter cut on the reconstructed $\pi^+\pi^-$ mass (± 60 MeV around the f_0) than ECKLUND 09. It finds that applying the same tight cut to both analyses gives consistent results.					

Hadronic modes with a $K\bar{K}$ pair

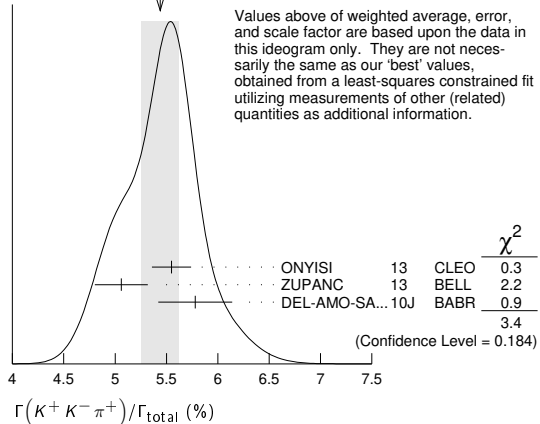
$\Gamma(K^+K_S^0)/\Gamma_{total}$	EVTS	DOCUMENT ID	TECN	COMMENT	Γ_{35}/Γ
1.46 ± 0.04 OUR FIT					
1.46 ± 0.05 OUR AVERAGE					
1.425 ± 0.038 ± 0.031	1.8k	ABLIKIM	19AMBES3		e^+e^- at 4178 MeV
1.52 ± 0.05 ± 0.03		ONYISI	13	CLEO	e^+e^- at 4.17 GeV
• • • We do not use the following data for averages, fits, limits, etc. • • •					
1.49 ± 0.07 ± 0.05		¹ ALEXANDER	08	CLEO	See ONYISI 13
¹ ALEXANDER 08 uses single- and double-tagged events in an overall fit.					

$\Gamma(K^+K_0^0)/\Gamma_{total}$	EVTS	DOCUMENT ID	TECN	COMMENT	Γ_{36}/Γ
1.485 ± 0.039 ± 0.046	2.3k	ABLIKIM	19AMBES3		e^+e^- at 4178 MeV

$\Gamma(K^+\bar{K}^0)/\Gamma_{total}$	EVTS	DOCUMENT ID	TECN	COMMENT	Γ_{37}/Γ
2.95 ± 0.11 ± 0.09	2.0k	¹ ZUPANC	13	BELL	e^+e^- at $\Upsilon(4S), \Upsilon(5S)$
¹ ZUPANC 13 finds the \bar{K}^0 from its missing-mass squared, not from $K_S^0 \rightarrow \pi^+\pi^-$.					
The DCS ($D_s^+ \rightarrow K^+K^0$) contribution to this fraction is estimated to be an order of magnitude below the statistical uncertainty.					

$\Gamma(K^+K^-\pi^+)/\Gamma_{total}$	EVTS	DOCUMENT ID	TECN	COMMENT	Γ_{38}/Γ
5.39 ± 0.15 OUR FIT					
5.44 ± 0.18 OUR AVERAGE					
5.55 ± 0.14 ± 0.13		ONYISI	13	CLEO	e^+e^- at 4.17 GeV
5.06 ± 0.15 ± 0.21	4.1k	ZUPANC	13	BELL	e^+e^- at $\Upsilon(4S), \Upsilon(5S)$
5.78 ± 0.20 ± 0.30		DEL-AMO-SA...10J	BABR		e^+e^- , 10.58 GeV
• • • We do not use the following data for averages, fits, limits, etc. • • •					
5.50 ± 0.23 ± 0.16		¹ ALEXANDER	08	CLEO	See ONYISI 13
¹ ALEXANDER 08 uses single- and double-tagged events in an overall fit.					

WEIGHTED AVERAGE
5.44 ± 0.18 (Error scaled by 1.3)



$\Gamma(\phi\pi^+)/\Gamma_{total}$	EVTS	DOCUMENT ID	TECN	COMMENT	Γ_{39}/Γ
4.5 ± 0.4 OUR AVERAGE					
4.62 ± 0.36 ± 0.51		¹ AUBERT	06N	BABR	e^+e^- at $\Upsilon(4S)$
4.81 ± 0.52 ± 0.38	212 ± 19	² AUBERT	05v	BABR	$e^+e^- \approx \Upsilon(4S)$
3.59 ± 0.77 ± 0.48		³ ARTUSO	96	CLE2	e^+e^- at $\Upsilon(4S)$
• • • We do not use the following data for averages, fits, limits, etc. • • •					
3.9 ^{+5.1 +1.8} _{-1.9 -1.1}		⁴ BAI	95c	BES	e^+e^- 4.03 GeV

The results here are model-independent. For earlier, model-dependent results, see our PDG 06 edition. We decouple the $D_s^+ \rightarrow \phi\pi^+$ branching fraction obtained from mass projections (and used to get some of the other branching fractions) from the $D_s^+ \rightarrow \phi\pi^+, \phi \rightarrow K^+K^-$ branching fraction obtained from the Dalitz-plot analysis of $D_s^+ \rightarrow K^+K^-\pi^+$. That is, the ratio of these two branching fractions is not exactly the $\phi \rightarrow K^+K^-$ branching fraction 0.491.

¹ This AUBERT 06N measurement uses $\bar{B}^0 \rightarrow D_s^{(*)-}D^{(*)+}$ and $B^- \rightarrow D_s^{(*)-}D^{(*)+}$ decays, including some from other papers. However, the result is independent of AUBERT 05v.

² AUBERT 05v uses the ratio of $B^0 \rightarrow D^{*-}D_s^{*+}$ events seen in two different ways, in both of which the $D^{*-} \rightarrow \bar{D}^0\pi^-$ decay is fully reconstructed: (1) The $D_s^{*+} \rightarrow D_s^+\gamma, D_s^+ \rightarrow \phi\pi^+$ decay is fully reconstructed. (2) The number of events in the D_s^+ peak in the missing mass spectrum against the $D^{*-}\gamma$ is measured.

³ ARTUSO 96 uses partially reconstructed $\bar{B}^0 \rightarrow D^{*+}D_s^{*-}$ decays to get a model-independent value for $\Gamma(D_s^- \rightarrow \phi\pi^-)/\Gamma(D^0 \rightarrow K^-\pi^+)$ of $0.92 \pm 0.20 \pm 0.11$.

⁴ BAI 95c uses $e^+e^- \rightarrow D_s^+D_s^-$ events in which one or both of the D_s^\pm are observed to obtain the first model-independent measurement of the $D_s^+ \rightarrow \phi\pi^+$ branching fraction, without assumptions about $\sigma(D_s^\pm)$. However, with only two "doubly-tagged" events, the statistical error is very large.

$\Gamma(\phi\pi^+, \phi \rightarrow K^+K^-)/\Gamma(K^+K^-\pi^+)$	EVTS	DOCUMENT ID	TECN	COMMENT	Γ_{40}/Γ_{38}
41.6 ± 0.8 OUR AVERAGE					
41.4 ± 0.8 ± 0.5		DEL-AMO-SA...11G	BABR		Dalitz fit, 96k ± 369 evts
42.2 ± 1.6 ± 0.3		MITCHELL	09A	CLEO	Dalitz fit, 12k evts
• • • We do not use the following data for averages, fits, limits, etc. • • •					
39.6 ± 3.3 ± 4.7		FRABETTI	95B	E687	Dalitz fit, 701 evts

$\Gamma(K^+\bar{K}^*(892)^0, \bar{K}^{*0} \rightarrow K^-\pi^+)/\Gamma(K^+K^-\pi^+)$	EVTS	DOCUMENT ID	TECN	COMMENT	Γ_{41}/Γ_{38}
47.8 ± 0.6 OUR AVERAGE					
47.9 ± 0.5 ± 0.5		DEL-AMO-SA...11G	BABR		Dalitz fit, 96k ± 369 evts
47.4 ± 1.5 ± 0.4		MITCHELL	09A	CLEO	Dalitz fit, 12k evts
• • • We do not use the following data for averages, fits, limits, etc. • • •					
47.8 ± 4.6 ± 4.0		FRABETTI	95B	E687	Dalitz fit, 701 evts

$\Gamma(f_0(980)\pi^+, f_0 \rightarrow K^+K^-)/\Gamma(K^+K^-\pi^+)$	EVTS	DOCUMENT ID	TECN	COMMENT	Γ_{42}/Γ_{38}
21 ± 6 OUR AVERAGE					
16.4 ± 0.7 ± 2.0		DEL-AMO-SA...11G	BABR		Dalitz fit, 96k ± 369 evts
28.2 ± 1.9 ± 1.8		MITCHELL	09A	CLEO	Dalitz fit, 12k evts
• • • We do not use the following data for averages, fits, limits, etc. • • •					
11.0 ± 3.5 ± 2.6		FRABETTI	95B	E687	Dalitz fit, 701 evts

$\Gamma(f_0(1370)\pi^+, f_0 \rightarrow K^+K^-)/\Gamma(K^+K^-\pi^+)$ Γ_{43}/Γ_{38}
 This is the "fit fraction" from the Dalitz-plot analysis.

VALUE (units 10^{-2})	DOCUMENT ID	TECN	COMMENT
1.3 ± 0.8 OUR AVERAGE	Error	includes scale factor of 3.9.	
1.1 ± 0.1 ± 0.2	DEL-AMO-SA...11G	BABR	Dalitz fit, 96k ± 369 evts
4.3 ± 0.6 ± 0.5	MITCHELL 09A	CLEO	Dalitz fit, 12k evts

$\Gamma(f_0(1710)\pi^+, f_0 \rightarrow K^+K^-)/\Gamma(K^+K^-\pi^+)$ Γ_{44}/Γ_{38}
 This is the "fit fraction" from the Dalitz-plot analysis.

VALUE (units 10^{-2})	DOCUMENT ID	TECN	COMMENT
1.2 ± 0.5 OUR AVERAGE	Error	includes scale factor of 3.8.	
1.1 ± 0.1 ± 0.1	DEL-AMO-SA...11G	BABR	Dalitz fit, 96k ± 369 evts
3.4 ± 0.5 ± 0.3	MITCHELL 09A	CLEO	Dalitz fit, 12k evts
• • • We do not use the following data for averages, fits, limits, etc. • • •			
3.4 ± 2.3 ± 3.5	FRABETTI 95B	E687	Dalitz fit, 701 evts

$\Gamma(K^+K_S^0(1430)^0, \bar{K}_S^0 \rightarrow K^-\pi^+)/\Gamma(K^+K^-\pi^+)$ Γ_{45}/Γ_{38}
 This is the "fit fraction" from the Dalitz-plot analysis.

VALUE (units 10^{-2})	DOCUMENT ID	TECN	COMMENT
3.4 ± 0.7 OUR AVERAGE	Error	includes scale factor of 1.2.	
2.4 ± 0.3 ± 1.0	DEL-AMO-SA...11G	BABR	Dalitz fit, 96k ± 369 evts
3.9 ± 0.5 ± 0.5	MITCHELL 09A	CLEO	Dalitz fit, 12k evts
• • • We do not use the following data for averages, fits, limits, etc. • • •			
9.3 ± 3.2 ± 3.2	FRABETTI 95B	E687	Dalitz fit, 701 evts

$\Gamma(K^+K_S^0\pi^0)/\Gamma_{total}$ Γ_{46}/Γ

VALUE (%)	DOCUMENT ID	TECN	COMMENT
1.52 ± 0.09 ± 0.20	ONYISI 13	CLEO	e^+e^- at 4.17 GeV

$\Gamma(2K_S^0\pi^+)/\Gamma_{total}$ Γ_{47}/Γ

VALUE (%)	DOCUMENT ID	TECN	COMMENT
0.77 ± 0.05 ± 0.03	ONYISI 13	CLEO	e^+e^- at 4.17 GeV

$\Gamma(K^*(892)+\bar{K}^0)/\Gamma(\phi\pi^+)$ Γ_{49}/Γ_{39}
 Unseen decay modes of the resonances are included.

VALUE	DOCUMENT ID	TECN	COMMENT
1.20 ± 0.21 ± 0.13	CHEN 89	CLEO	e^+e^- 10 GeV

$\Gamma(K^+K^-\pi^+\pi^0)/\Gamma_{total}$ Γ_{50}/Γ

VALUE (%)	DOCUMENT ID	TECN	COMMENT
6.2 ± 0.6 OUR FIT	Error	includes scale factor of 1.1.	
6.37 ± 0.21 ± 0.56	ONYISI 13	CLEO	e^+e^- at 4.17 GeV
• • • We do not use the following data for averages, fits, limits, etc. • • •			
5.65 ± 0.29 ± 0.40	¹ ALEXANDER 08	CLEO	See ONYISI 13
¹ ALEXANDER 08 uses single- and double-tagged events in an overall fit.			

$\Gamma(\phi\rho^+)/\Gamma(\phi\pi^+)$ Γ_{51}/Γ_{39}

VALUE	EVTS	DOCUMENT ID	TECN	COMMENT
1.86 ± 0.26 ± 0.29 ± 0.40	253	AVERY 92	CLE2	$e^+e^- \approx 10.5$ GeV

$\Gamma(K_S^0K^-2\pi^+)/\Gamma_{total}$ Γ_{52}/Γ

VALUE (%)	DOCUMENT ID	TECN	COMMENT
1.65 ± 0.10 OUR FIT			
1.69 ± 0.07 ± 0.08	ONYISI 13	CLEO	e^+e^- at 4.17 GeV
• • • We do not use the following data for averages, fits, limits, etc. • • •			
1.64 ± 0.10 ± 0.07	¹ ALEXANDER 08	CLEO	See ONYISI 13
¹ ALEXANDER 08 uses single- and double-tagged events in an overall fit.			

$\Gamma(K^*(892)+\bar{K}^*(892)^0)/\Gamma(\phi\pi^+)$ Γ_{53}/Γ_{39}
 Unseen decay modes of the resonances are included.

VALUE	DOCUMENT ID	TECN	COMMENT
1.6 ± 0.4 ± 0.4	ALBRECHT 92B	ARG	$e^+e^- \approx 10.4$ GeV

$\Gamma(K^+K_S^0\pi^+\pi^-)/\Gamma_{total}$ Γ_{54}/Γ

VALUE (%)	DOCUMENT ID	TECN	COMMENT
0.99 ± 0.08 OUR FIT			
1.03 ± 0.06 ± 0.08	ONYISI 13	CLEO	e^+e^- at 4.17 GeV

$\Gamma(K^+K_S^0\pi^+\pi^-)/\Gamma(K_S^0K^-2\pi^+)$ Γ_{54}/Γ_{52}

VALUE	EVTS	DOCUMENT ID	TECN	COMMENT
0.60 ± 0.05 OUR FIT				
0.586 ± 0.052 ± 0.043	476	LINK 01c	FOCS	$\gamma A, \bar{E}_\gamma \approx 180$ GeV

$\Gamma(K^+K^-2\pi^+\pi^-)/\Gamma(K^+K^-\pi^+)$ Γ_{55}/Γ_{38}

VALUE	EVTS	DOCUMENT ID	TECN	COMMENT
0.160 ± 0.027 OUR AVERAGE				
0.150 ± 0.019 ± 0.025	240	LINK 03D	FOCS	$\gamma A, \bar{E}_\gamma \approx 180$ GeV
0.188 ± 0.036 ± 0.040	75	FRABETTI 97c	E687	$\gamma Be, \bar{E}_\gamma \approx 200$ GeV

$\Gamma(\phi 2\pi^+\pi^-)/\Gamma(\phi\pi^+)$ Γ_{56}/Γ_{39}

VALUE	EVTS	DOCUMENT ID	TECN	COMMENT
0.269 ± 0.027 OUR AVERAGE				
0.249 ± 0.024 ± 0.021	136	LINK 03D	FOCS	$\gamma A, \bar{E}_\gamma \approx 180$ GeV
0.28 ± 0.06 ± 0.01	40	FRABETTI 97c	E687	$\gamma Be, \bar{E}_\gamma \approx 200$ GeV
0.58 ± 0.21 ± 0.10	21	FRABETTI 92	E687	γBe
0.42 ± 0.13 ± 0.07	19	ANJOS 88	E691	Photoproduction
1.11 ± 0.37 ± 0.28	62	ALBRECHT 85D	ARG	e^+e^- 10 GeV

$\Gamma(K^+K^-\rho^0\pi^+\text{non-}\phi)/\Gamma(K^+K^-2\pi^+\pi^-)$ Γ_{60}/Γ_{55}

VALUE	CL%	DOCUMENT ID	TECN	COMMENT
<0.03	90	LINK 03D	FOCS	$\gamma A, \bar{E}_\gamma \approx 180$ GeV

$\Gamma(\phi\rho^0\pi^+, \phi \rightarrow K^+K^-)/\Gamma(K^+K^-2\pi^+\pi^-)$ Γ_{57}/Γ_{55}

VALUE	DOCUMENT ID	TECN	COMMENT
0.75 ± 0.06 ± 0.04	LINK 03D	FOCS	$\gamma A, \bar{E}_\gamma \approx 180$ GeV

$\Gamma(\phi a_1(1260)^+, \phi \rightarrow K^+K^-, a_1^+ \rightarrow \rho^0\pi^+)/\Gamma(K^+K^-\pi^+)$ Γ_{58}/Γ_{38}

VALUE	DOCUMENT ID	TECN	COMMENT
0.137 ± 0.019 ± 0.011	LINK 03D	FOCS	$\gamma A, \bar{E}_\gamma \approx 180$ GeV

$\Gamma(K^+K^-2\pi^+\pi^-\text{nonresonant})/\Gamma(K^+K^-2\pi^+\pi^-)$ Γ_{61}/Γ_{55}

VALUE	DOCUMENT ID	TECN	COMMENT
0.10 ± 0.06 ± 0.05	LINK 03D	FOCS	$\gamma A, \bar{E}_\gamma \approx 180$ GeV

$\Gamma(\phi 2\pi^+\pi^-\text{non-}\rho, \phi \rightarrow K^+K^-)/\Gamma(K^+K^-2\pi^+\pi^-)$ Γ_{59}/Γ_{55}

VALUE	DOCUMENT ID	TECN	COMMENT
0.21 ± 0.05 ± 0.06	LINK 03D	FOCS	$\gamma A, \bar{E}_\gamma \approx 180$ GeV

$\Gamma(2K_S^0 2\pi^+\pi^-)/\Gamma(K_S^0K^-2\pi^+)$ Γ_{62}/Γ_{52}

VALUE	EVTS	DOCUMENT ID	TECN	COMMENT
0.051 ± 0.015 ± 0.015	37 ± 10	LINK 04D	FOCS	$\gamma A, \bar{E}_\gamma \approx 180$ GeV

Pionic modes

$\Gamma(\pi^+\pi^0)/\Gamma(K^+K_S^0)$ Γ_{63}/Γ_{35}

VALUE (units 10^{-2})	CL%	DOCUMENT ID	TECN	COMMENT
<2.3	90	MENDEZ 10	CLEO	e^+e^- at 4170 MeV
• • • We do not use the following data for averages, fits, limits, etc. • • •				
<4.1	90	ADAMS 07A	CLEO	See MENDEZ 10

$\Gamma(2\pi^+\pi^-)/\Gamma_{total}$ Γ_{64}/Γ

VALUE (%)	DOCUMENT ID	TECN	COMMENT
1.08 ± 0.04 OUR FIT	Error	includes scale factor of 1.1.	
1.11 ± 0.04 ± 0.04	ONYISI 13	CLEO	e^+e^- at 4.17 GeV
• • • We do not use the following data for averages, fits, limits, etc. • • •			
1.11 ± 0.07 ± 0.04	¹ ALEXANDER 08	CLEO	See ONYISI 13
¹ ALEXANDER 08 uses single- and double-tagged events in an overall fit.			

$\Gamma(2\pi^+\pi^-)/\Gamma(K^+K^-\pi^+)$ Γ_{64}/Γ_{38}

VALUE	EVTS	DOCUMENT ID	TECN	COMMENT
0.201 ± 0.007 OUR FIT				
0.199 ± 0.004 ± 0.009	$\approx 10.5k$	AUBERT 09o	BABR	$e^+e^- \approx 10.6$ GeV
• • • We do not use the following data for averages, fits, limits, etc. • • •				
0.265 ± 0.041 ± 0.031	98	FRABETTI 97D	E687	$\gamma Be \approx 200$ GeV

$\Gamma(\rho^0\pi^+)/\Gamma(2\pi^+\pi^-)$ Γ_{65}/Γ_{64}

VALUE	CL%	DOCUMENT ID	TECN	COMMENT
0.018 ± 0.005 ± 0.010		AUBERT 09o	BABR	Dalitz fit, $\approx 10.5k$ evts
• • • We do not use the following data for averages, fits, limits, etc. • • •				
not seen		LINK 04	FOCS	Dalitz fit, 1475 ± 50 evts
0.058 ± 0.023 ± 0.037		AITALA 01A	E791	Dalitz fit, 848 evts
<0.073	90	FRABETTI 97D	E687	$\gamma Be \approx 200$ GeV

$\Gamma(\pi^+(\pi^+\pi^-\text{s-wave})/\Gamma(2\pi^+\pi^-)$ Γ_{66}/Γ_{64}
 This is the "fit fraction" from the Dalitz-plot analysis. See also KLEMPF 08, which uses 568 $D_s^\pm \rightarrow 3\pi$ decays (over 280 background events) from FNAL E791 to study various parametrizations of the decay amplitudes. The emphasis there is more on S-wave $\pi\pi$ decay products — 20 different solutions are given — than on D_s^\pm fit fractions.

VALUE	DOCUMENT ID	TECN	COMMENT
0.833 ± 0.020 OUR AVERAGE			
0.830 ± 0.009 ± 0.019	¹ AUBERT 09o	BABR	Dalitz fit, $\approx 10.5k$ evts
0.8704 ± 0.0560 ± 0.0438	² LINK 04	FOCS	Dalitz fit, 1475 ± 50 evts
¹ AUBERT 09o gives the amplitude and phase of the $\pi^+\pi^-$ S-wave in 29 $\pi^+\pi^-$ invariant-mass bins.			
² LINK 04 borrows a K-matrix parametrization from ANISOVICH 03 of the full $\pi-\pi$ S-wave isoscalar scattering amplitude to describe the $\pi^+\pi^-$ S-wave component of the $\pi^+\pi^+\pi^-$ state. The fit fraction given above is a sum over five f_0 mesons, the $f_0(980)$, $f_0(1300)$, $f_0(1200-1600)$, $f_0(1500)$, and $f_0(1750)$. See LINK 04 for details and discussion.			

Meson Particle Listings

 D_S^\pm

$\Gamma(f_0(980)\pi^+, f_0 \rightarrow \pi^+\pi^-)/\Gamma(2\pi^+\pi^-)$ Γ_{67}/Γ_{64}
This is the "fit fraction" from the Dalitz-plot analysis. See above for the full $\pi^+(\pi^+\pi^-)_{S\text{-wave}}$ fit fraction.

VALUE	DOCUMENT ID	TECN	COMMENT
•••	We do not use the following data for averages, fits, limits, etc. •••		
$0.565 \pm 0.043 \pm 0.047$	AITALA	01A E791	Dalitz fit, 848 evts
$1.074 \pm 0.140 \pm 0.043$	FRABETTI	97D E687	γ Be ≈ 200 GeV

$\Gamma(f_0(1370)\pi^+, f_0 \rightarrow \pi^+\pi^-)/\Gamma(2\pi^+\pi^-)$ Γ_{68}/Γ_{64}
This is the "fit fraction" from the Dalitz-plot analysis. See above for the full $\pi^+(\pi^+\pi^-)_{S\text{-wave}}$ fit fraction.

VALUE	DOCUMENT ID	TECN	COMMENT
•••	We do not use the following data for averages, fits, limits, etc. •••		
$0.324 \pm 0.077 \pm 0.017$	AITALA	01A E791	Dalitz fit, 848 evts

$\Gamma(f_0(1500)\pi^+, f_0 \rightarrow \pi^+\pi^-)/\Gamma(2\pi^+\pi^-)$ Γ_{69}/Γ_{64}
This is the "fit fraction" from the Dalitz-plot analysis. See above for the full $\pi^+(\pi^+\pi^-)_{S\text{-wave}}$ fit fraction.

VALUE	DOCUMENT ID	TECN	COMMENT
•••	We do not use the following data for averages, fits, limits, etc. •••		
$0.274 \pm 0.114 \pm 0.019$	¹ FRABETTI	97D E687	γ Be ≈ 200 GeV
¹ FRABETTI 97D calls this mode $S(1475)\pi^+$, but finds the mass and width of this $S(1475)$ to be in excellent agreement with those of the $f_0(1500)$.			

$\Gamma(f_2(1270)\pi^+, f_2 \rightarrow \pi^+\pi^-)/\Gamma(2\pi^+\pi^-)$ Γ_{70}/Γ_{64}
This is the "fit fraction" from the Dalitz-plot analysis.

VALUE	DOCUMENT ID	TECN	COMMENT
0.101 ± 0.018 OUR AVERAGE			
$0.101 \pm 0.015 \pm 0.011$	AUBERT	09O BABR	Dalitz fit, $\approx 10.5k$ evts
$0.0974 \pm 0.0449 \pm 0.0294$	LINK	04 FOCUS	Dalitz fit, 1475 ± 50 evts
•••	We do not use the following data for averages, fits, limits, etc. •••		
$0.197 \pm 0.033 \pm 0.006$	AITALA	01A E791	Dalitz fit, 848 evts
$0.123 \pm 0.056 \pm 0.018$	FRABETTI	97D E687	γ Be ≈ 200 GeV

$\Gamma(\rho(1450)^0\pi^+, \rho^0 \rightarrow \pi^+\pi^-)/\Gamma(2\pi^+\pi^-)$ Γ_{71}/Γ_{64}
This is the "fit fraction" from the Dalitz-plot analysis.

VALUE	DOCUMENT ID	TECN	COMMENT
0.027 ± 0.018 OUR AVERAGE			
$0.023 \pm 0.008 \pm 0.017$	AUBERT	09O BABR	Dalitz fit, $\approx 10.5k$ evts
$0.0656 \pm 0.0343 \pm 0.0440$	LINK	04 FOCUS	Dalitz fit, 1475 ± 50 evts
•••	We do not use the following data for averages, fits, limits, etc. •••		
$0.044 \pm 0.021 \pm 0.002$	AITALA	01A E791	Dalitz fit, 848 evts

$\Gamma(\pi^+2\pi^0)/\Gamma_{\text{total}}$ Γ_{72}/Γ
Unseen decay modes of the η are included.

VALUE (%)	EVTS	DOCUMENT ID	TECN	COMMENT
$0.65 \pm 0.13 \pm 0.03$	72 ± 16	NAIK	09A CLEO	e^+e^- at 4170 MeV

$\Gamma(2\pi^+\pi^-\pi^0)/\Gamma(\phi\pi^+)$ Γ_{73}/Γ_{39}
Unseen decay modes of the resonances are included.

VALUE	CL%	DOCUMENT ID	TECN	COMMENT
•••	We do not use the following data for averages, fits, limits, etc. •••			
<3.3	90	ANJOS	89E E691	Photoproduction

$\Gamma(\eta\pi^+)/\Gamma_{\text{total}}$ Γ_{74}/Γ
Unseen decay modes of the η are included.

VALUE (%)	EVTS	DOCUMENT ID	TECN	COMMENT
1.68 ± 0.10 OUR FIT	Error includes scale factor of 1.2.			
1.71 ± 0.08 OUR AVERAGE				
$1.67 \pm 0.08 \pm 0.06$		ONYISI	13 CLEO	e^+e^- at 4.17 GeV
$1.82 \pm 0.14 \pm 0.07$	0.8k	ZUPANC	13 BELL	e^+e^- at $\Upsilon(4S), \Upsilon(5S)$
•••	We do not use the following data for averages, fits, limits, etc. •••			
$1.58 \pm 0.11 \pm 0.18$		¹ ALEXANDER	08 CLEO	See ONYISI 13
¹ ALEXANDER 08 uses single- and double-tagged events in an overall fit.				

$\Gamma(\eta\pi^+)/\Gamma(K^+K_S^0)$ Γ_{74}/Γ_{35}
Unseen decay modes of the η are included.

VALUE	EVTS	DOCUMENT ID	TECN	COMMENT
1.15 ± 0.08 OUR FIT	Error includes scale factor of 1.3.			
•••	We do not use the following data for averages, fits, limits, etc. •••			
$1.236 \pm 0.043 \pm 0.063$	2587 ± 89	MENDEZ	10 CLEO	See ONYISI 13

$\Gamma(\eta\pi^+)/\Gamma(\phi\pi^+)$ Γ_{74}/Γ_{39}
Unseen decay modes of the resonances are included.

VALUE	EVTS	DOCUMENT ID	TECN	COMMENT
•••	We do not use the following data for averages, fits, limits, etc. •••			
$0.48 \pm 0.03 \pm 0.04$	920	JESSOP	98 CLE2	$e^+e^- \approx \Upsilon(4S)$
$0.54 \pm 0.09 \pm 0.06$	165	ALEXANDER	92 CLE2	See JESSOP 98

$\Gamma(\omega\pi^+)/\Gamma_{\text{total}}$ Γ_{75}/Γ
Unseen decay modes of the ω are included.

VALUE (%)	EVTS	DOCUMENT ID	TECN	COMMENT
0.192 ± 0.030 OUR FIT				
0.181 ± 0.032 OUR AVERAGE				
$0.177 \pm 0.032 \pm 0.013$	65 ± 12	ABLIKIM	19AH BES3	e^+e^- at 4.178 GeV
$0.21 \pm 0.09 \pm 0.01$	6 ± 2.4	GE	09A CLEO	e^+e^- at 4170 MeV

$\Gamma(\omega\pi^+)/\Gamma(\eta\pi^+)$ Γ_{75}/Γ_{74}
Unseen decay modes of the resonances are included.

VALUE	DOCUMENT ID	TECN	COMMENT
0.114 ± 0.018 OUR FIT			
$0.16 \pm 0.04 \pm 0.03$	BALEST	97 CLE2	$e^+e^- \approx \Upsilon(4S)$

$\Gamma(3\pi^+2\pi^-)/\Gamma(K^+K^-\pi^+)$ Γ_{76}/Γ_{38}
Unseen decay modes of the resonances are included.

VALUE	EVTS	DOCUMENT ID	TECN	COMMENT
0.146 ± 0.014 OUR AVERAGE				
$0.145 \pm 0.011 \pm 0.010$	671	LINK	03D FOCUS	γ A, $\bar{E}_\gamma \approx 180$ GeV
$0.158 \pm 0.042 \pm 0.031$	37	FRABETTI	97C E687	γ Be, $\bar{E}_\gamma \approx 200$ GeV

$\Gamma(\eta\rho^+)/\Gamma_{\text{total}}$ Γ_{78}/Γ
Unseen decay modes of the η are included.

VALUE (%)	EVTS	DOCUMENT ID	TECN	COMMENT
$8.9 \pm 0.6 \pm 0.5$	328 ± 22	NAIK	09A CLEO	$\eta \rightarrow 2\gamma$

$\Gamma(\eta\rho^+)/\Gamma(\phi\pi^+)$ Γ_{78}/Γ_{39}
Unseen decay modes of the resonances are included.

VALUE	EVTS	DOCUMENT ID	TECN	COMMENT
•••	We do not use the following data for averages, fits, limits, etc. •••			
$2.98 \pm 0.20 \pm 0.39$	447	JESSOP	98 CLE2	$e^+e^- \approx \Upsilon(4S)$
$2.86 \pm 0.38 \pm 0.36$	217	AVERY	92 CLE2	See JESSOP 98

$\Gamma(\eta\rho^+)/\Gamma(\eta\pi^+\pi^0)$ Γ_{78}/Γ_{79}
Unseen decay modes of the resonances are included.

VALUE (units 10^{-2})	EVTS	DOCUMENT ID	TECN	COMMENT
$78.3 \pm 5.0 \pm 2.1$	1.2k	ABLIKIM	19BE BES3	$\eta\pi^+\pi^0$ amplitude analysis

$\Gamma(\eta\pi^+\pi^0)/\Gamma_{\text{total}}$ Γ_{79}/Γ
Unseen decay modes of the resonances are included.

VALUE (%)	EVTS	DOCUMENT ID	TECN	COMMENT
9.5 ± 0.5 OUR AVERAGE				
$9.50 \pm 0.28 \pm 0.41$	2.6k	ABLIKIM	19BE BES3	e^+e^- at 4.178 GeV
$9.2 \pm 0.4 \pm 1.1$		ONYISI	13 CLEO	e^+e^- at 4.17 GeV

$\Gamma(\eta(\pi^+\pi^0)_{\rho\text{-wave}})/\Gamma(\eta\pi^+\pi^0)$ Γ_{80}/Γ_{79}
Unseen decay modes of the resonances are included.

VALUE (units 10^{-2})	EVTS	DOCUMENT ID	TECN	COMMENT
$5.4 \pm 2.1 \pm 2.5$	1.2k	ABLIKIM	19BE BES3	$\eta\pi^+\pi^0$ amplitude analysis

$\Gamma(a_0(980)^+\pi^0, a_0(980)^+\pi^0 \rightarrow \eta\pi^+\pi^0)/\Gamma(\eta\pi^+\pi^0)$ Γ_{81}/Γ_{79}
Unseen decay modes of the resonances are included.

VALUE (units 10^{-2})	EVTS	DOCUMENT ID	TECN	COMMENT
$23.2 \pm 2.3 \pm 3.3$	1.2k	¹ ABLIKIM	19BE BES3	$\eta\pi^+\pi^0$ amplitude analysis
¹ Coherent sum of $D_S^+ \rightarrow a_0^+\pi^0 \rightarrow \eta\pi^+\pi^0$ and $D_S^+ \rightarrow a_0^0\pi^+ \rightarrow \eta\pi^+\pi^0$. ABLIKIM 19BE find $a_0(980)^0 - f(980)$ mixing effects negligibly small in this $D_S^+ \rightarrow \eta\pi^+\pi^0$ Dalitz plot analysis.				

$\Gamma(\omega\pi^+\pi^0)/\Gamma_{\text{total}}$ Γ_{82}/Γ
Unseen decay modes of the ω are included.

VALUE (%)	EVTS	DOCUMENT ID	TECN	COMMENT
$2.78 \pm 0.65 \pm 0.25$	34 ± 7.9	GE	09A CLEO	e^+e^- at 4170 MeV

$\Gamma(3\pi^+2\pi^-\pi^0)/\Gamma_{\text{total}}$ Γ_{83}/Γ
Unseen decay modes of the resonances are included.

VALUE	DOCUMENT ID	TECN	COMMENT
0.049 ± 0.033	BARLAG	92C ACCM	π^- 230 GeV
-0.030			

$\Gamma(\omega 2\pi^+\pi^-)/\Gamma_{\text{total}}$ Γ_{84}/Γ
Unseen decay modes of the ω are included.

VALUE (%)	EVTS	DOCUMENT ID	TECN	COMMENT
$1.58 \pm 0.45 \pm 0.09$	29 ± 8.2	GE	09A CLEO	e^+e^- at 4170 MeV

$\Gamma(\eta'(958)\pi^+)/\Gamma_{\text{total}}$ Γ_{85}/Γ
Unseen decay modes of the $\eta'(958)$ are included.

VALUE (%)	EVTS	DOCUMENT ID	TECN	COMMENT
$3.94 \pm 0.15 \pm 0.20$		ONYISI	13 CLEO	e^+e^- at 4.17 GeV
•••	We do not use the following data for averages, fits, limits, etc. •••			
$3.77 \pm 0.25 \pm 0.30$		¹ ALEXANDER	08 CLEO	See ONYISI 13
¹ ALEXANDER 08 uses single- and double-tagged events in an overall fit.				

$\Gamma(\eta'(958)\pi^+)/\Gamma(K^+K_S^0)$ Γ_{85}/Γ_{35}
Unseen decay modes of the $\eta'(958)$ are included.

VALUE	EVTS	DOCUMENT ID	TECN	COMMENT
•••	We do not use the following data for averages, fits, limits, etc. •••			
$2.654 \pm 0.088 \pm 0.139$	1436 ± 47	MENDEZ	10 CLEO	See ONYISI 13

$\Gamma(\eta'(958)\pi^+)/\Gamma(\phi\pi^+)$ Γ_{85}/Γ_{39}
Unseen decay modes of the resonances are included.

VALUE	EVTS	DOCUMENT ID	TECN	COMMENT
•••	We do not use the following data for averages, fits, limits, etc. •••			
$1.03 \pm 0.06 \pm 0.07$	537	JESSOP	98 CLE2	$e^+e^- \approx \Upsilon(4S)$
$1.20 \pm 0.15 \pm 0.11$	281	ALEXANDER	92 CLE2	See JESSOP 98
$2.5 \pm 1.0 \pm 1.5$	22	ALVAREZ	91 NA14	Photoproduction
$2.5 \pm 0.5 \pm 0.3$	215	ALBRECHT	90D ARG	$e^+e^- \approx 10.4$ GeV

$\Gamma(\omega\eta\pi^+)/\Gamma_{total}$ Γ_{87}/Γ
 Unseen decay modes of the ω and η are included.

VALUE	CL%	DOCUMENT ID	TECN	COMMENT
$<2.13 \times 10^{-2}$	90	GE	09A	CLEO e^+e^- at 4170 MeV

$\Gamma(\eta'(958)\rho^+)/\Gamma_{total}$ Γ_{88}/Γ

VALUE (%)	DOCUMENT ID	TECN	COMMENT
$5.8 \pm 1.4 \pm 0.4$	ABLKIM	15Z	BES3 482 pb^{-1} , 4009 MeV

$\Gamma(\eta'(958)\rho^+)/\Gamma(\phi\pi^+)$ Γ_{88}/Γ_{39}
 Unseen decay modes of the resonances are included.

VALUE	EVTs	DOCUMENT ID	TECN	COMMENT
$2.78 \pm 0.28 \pm 0.30$	137	¹ JESSOP	98	CLE2 $e^+e^- \approx \Upsilon(4S)$
$3.44 \pm 0.62^{+0.44}_{-0.46}$	68	AVERY	92	CLE2 See JESSOP 98

¹ This JESSOP 98 fraction, when combined with other η' fractions, greatly overshoots the inclusive η' fraction. See the measurement just above, which fits nicely.

$\Gamma(\eta'(958)\pi^+\pi^0)/\Gamma_{total}$ Γ_{89}/Γ

VALUE (%)	DOCUMENT ID	TECN	COMMENT
$5.6 \pm 0.5 \pm 0.6$	ONYISI	13	CLEO e^+e^- at 4.17 GeV

$\Gamma(\eta'(958)\pi^+\pi^0 \text{ nonresonant})/\Gamma_{total}$ Γ_{90}/Γ

VALUE	CL%	DOCUMENT ID	TECN	COMMENT
$<5.1 \times 10^{-2}$	90	ABLKIM	15Z	BES3 482 pb^{-1} , 4009 MeV

———— Modes with one or three K's ————

$\Gamma(K^+\pi^0)/\Gamma(K^+K_S^0)$ Γ_{91}/Γ_{35}

VALUE (units 10^{-2})	EVTs	DOCUMENT ID	TECN	COMMENT
$4.2 \pm 1.4 \pm 0.2$	202 ± 70	MENDEZ	10	CLEO e^+e^- at 4170 MeV

• • • We do not use the following data for averages, fits, limits, etc. • • •

$5.5 \pm 1.3 \pm 0.7$	141 ± 34	ADAMS	07A	CLEO See MENDEZ 10
-----------------------	--------------	-------	-----	--------------------

$\Gamma(K_S^0\pi^+)/\Gamma(K^+K_S^0)$ Γ_{92}/Γ_{35}

VALUE (units 10^{-2})	EVTs	DOCUMENT ID	TECN	COMMENT
8.12 ± 0.28 OUR AVERAGE				
$8.5 \pm 0.7 \pm 0.2$	393 ± 33	MENDEZ	10	CLEO e^+e^- at 4170 MeV
$8.03 \pm 0.24 \pm 0.19$	$17.6k \pm 481$	WON	09	BELL e^+e^- at $\Upsilon(4S)$
$10.4 \pm 2.4 \pm 1.4$	113 ± 26	LINK	08	FOCS $\gamma A, \bar{E}_\gamma \approx 180 \text{ GeV}$

• • • We do not use the following data for averages, fits, limits, etc. • • •

$8.2 \pm 0.9 \pm 0.2$	206 ± 22	ADAMS	07A	CLEO See MENDEZ 10
-----------------------	--------------	-------	-----	--------------------

$\Gamma(K^+\eta)/\Gamma(K^+K_S^0)$ Γ_{93}/Γ_{35}
 Unseen decay modes of the η are included.

VALUE (units 10^{-2})	EVTs	DOCUMENT ID	TECN	COMMENT
$11.8 \pm 2.2 \pm 0.6$	222 ± 41	MENDEZ	10	CLEO e^+e^- at 4170 MeV

$\Gamma(K^+\eta)/\Gamma(\eta\pi^+)$ Γ_{93}/Γ_{74}

VALUE (units 10^{-2})	EVTs	DOCUMENT ID	TECN	COMMENT
$8.9 \pm 1.5 \pm 0.4$	113 ± 18	ADAMS	07A	CLEO See MENDEZ 10

• • • We do not use the following data for averages, fits, limits, etc. • • •

$\Gamma(K^+\omega)/\Gamma_{total}$ Γ_{94}/Γ
 Unseen decay modes of the ω are included.

VALUE (units 10^{-4})	CL%	EVTs	DOCUMENT ID	TECN	COMMENT
$8.7 \pm 2.4 \pm 0.8$		29	¹ ABLKIM	19AH	BES3 e^+e^- at 4.178 GeV

• • • We do not use the following data for averages, fits, limits, etc. • • •

<24	90	GE	09A	CLEO e^+e^- at 4170 MeV
-------	----	----	-----	---------------------------

¹ Evidence for mode at 4.4 σ .

$\Gamma(K^+\eta(958))/\Gamma(K^+K_S^0)$ Γ_{95}/Γ_{35}
 Unseen decay modes of the $\eta(958)$ are included.

VALUE (units 10^{-2})	EVTs	DOCUMENT ID	TECN	COMMENT
$11.8 \pm 3.6 \pm 0.7$	56 ± 17	MENDEZ	10	CLEO e^+e^- at 4170 MeV

$\Gamma(K^+\eta(958))/\Gamma(\eta(958)\pi^+)$ Γ_{95}/Γ_{85}

VALUE (units 10^{-2})	EVTs	DOCUMENT ID	TECN	COMMENT
$4.2 \pm 1.3 \pm 0.3$	28 ± 9	ADAMS	07A	CLEO See MENDEZ 10

• • • We do not use the following data for averages, fits, limits, etc. • • •

$\Gamma(K^+\pi^+\pi^-)/\Gamma_{total}$ Γ_{96}/Γ

VALUE (%)	DOCUMENT ID	TECN	COMMENT
0.65 ± 0.04 OUR FIT			
$0.654 \pm 0.033 \pm 0.025$	ONYISI	13	CLEO e^+e^- at 4.17 GeV

• • • We do not use the following data for averages, fits, limits, etc. • • •

$0.69 \pm 0.05 \pm 0.03$	¹ ALEXANDER	08	CLEO See ONYISI 13
--------------------------	------------------------	----	--------------------

¹ ALEXANDER 08 uses single- and double-tagged events in an overall fit.

$\Gamma(K^+\pi^+\pi^-)/\Gamma(K^+K^-\pi^+)$ Γ_{96}/Γ_{38}

VALUE	EVTs	DOCUMENT ID	TECN	COMMENT
0.121 ± 0.008 OUR FIT				Error includes scale factor of 1.1.
$0.127 \pm 0.007 \pm 0.014$	567 ± 31	LINK	04F	FOCS $\gamma A, \bar{E}_\gamma \approx 180 \text{ GeV}$

$\Gamma(K^+\rho^0)/\Gamma(K^+\pi^+\pi^-)$ Γ_{97}/Γ_{96}
 This is the "fit fraction" from the Dalitz-plot analysis.

VALUE	DOCUMENT ID	TECN	COMMENT
$0.3883 \pm 0.0531 \pm 0.0261$	LINK	04F	FOCS Dalitz fit, 567 evts

$\Gamma(K^+\rho(1450)^0, \rho^0 \rightarrow \pi^+\pi^-)/\Gamma(K^+\pi^+\pi^-)$ Γ_{98}/Γ_{96}
 This is the "fit fraction" from the Dalitz-plot analysis.

VALUE	DOCUMENT ID	TECN	COMMENT
$0.1062 \pm 0.0351 \pm 0.0104$	LINK	04F	FOCS Dalitz fit, 567 evts

$\Gamma(K^*(892)^0\pi^+, K^*0 \rightarrow K^+\pi^-)/\Gamma(K^+\pi^+\pi^-)$ Γ_{99}/Γ_{96}
 This is the "fit fraction" from the Dalitz-plot analysis.

VALUE	DOCUMENT ID	TECN	COMMENT
$0.2164 \pm 0.0321 \pm 0.0114$	LINK	04F	FOCS Dalitz fit, 567 evts

$\Gamma(K^*(1410)^0\pi^+, K^*0 \rightarrow K^+\pi^-)/\Gamma(K^+\pi^+\pi^-)$ Γ_{100}/Γ_{96}
 This is the "fit fraction" from the Dalitz-plot analysis.

VALUE	DOCUMENT ID	TECN	COMMENT
$0.1882 \pm 0.0403 \pm 0.0122$	LINK	04F	FOCS Dalitz fit, 567 evts

$\Gamma(K^*(1430)^0\pi^+, K^*0 \rightarrow K^+\pi^-)/\Gamma(K^+\pi^+\pi^-)$ Γ_{101}/Γ_{96}
 This is the "fit fraction" from the Dalitz-plot analysis.

VALUE	DOCUMENT ID	TECN	COMMENT
$0.0765 \pm 0.0500 \pm 0.0170$	LINK	04F	FOCS Dalitz fit, 567 evts

$\Gamma(K^+\pi^+\pi^- \text{ nonresonant})/\Gamma(K^+\pi^+\pi^-)$ Γ_{102}/Γ_{96}
 This is the "fit fraction" from the Dalitz-plot analysis.

VALUE	DOCUMENT ID	TECN	COMMENT
$0.1588 \pm 0.0492 \pm 0.0153$	LINK	04F	FOCS Dalitz fit, 567 evts

$\Gamma(K^0\pi^+\pi^0)/\Gamma_{total}$ Γ_{103}/Γ

VALUE (%)	EVTs	DOCUMENT ID	TECN	COMMENT
$1.00 \pm 0.18 \pm 0.04$	44 ± 8	NAIK	09A	CLEO e^+e^- at 4170 MeV

$\Gamma(K_S^0 2\pi^+\pi^-)/\Gamma(K_S^0 K^- 2\pi^+)$ Γ_{104}/Γ_{52}

VALUE	EVTs	DOCUMENT ID	TECN	COMMENT
$0.18 \pm 0.04 \pm 0.05$	179 ± 36	LINK	08	FOCS $\gamma A, \bar{E}_\gamma \approx 180 \text{ GeV}$

$\Gamma(K^+\omega\pi^0)/\Gamma_{total}$ Γ_{105}/Γ
 Unseen decay modes of the ω are included.

VALUE (%)	CL%	DOCUMENT ID	TECN	COMMENT
<0.82	90	GE	09A	CLEO e^+e^- at 4170 MeV

$\Gamma(K^+\omega\pi^+\pi^-)/\Gamma_{total}$ Γ_{106}/Γ
 Unseen decay modes of the ω are included.

VALUE (%)	CL%	DOCUMENT ID	TECN	COMMENT
<0.54	90	GE	09A	CLEO e^+e^- at 4170 MeV

$\Gamma(K^+\omega\eta)/\Gamma_{total}$ Γ_{107}/Γ
 Unseen decay modes of the ω and η are included.

VALUE (%)	CL%	DOCUMENT ID	TECN	COMMENT
<0.79	90	GE	09A	CLEO e^+e^- at 4170 MeV

$\Gamma(K^+(K^+K^-))/\Gamma(K^+K^-\pi^+)$ Γ_{108}/Γ_{38}

VALUE (units 10^{-3})	EVTs	DOCUMENT ID	TECN	COMMENT
$4.0 \pm 0.3 \pm 0.2$	748 ± 60	DEL-AMO-SA..11g	BABR	$e^+e^- \approx \Upsilon(4S)$

• • • We do not use the following data for averages, fits, limits, etc. • • •

$8.95 \pm 2.12^{+2.24}_{-2.31}$	31	LINK	02i	FOCS $\gamma A, \approx 180 \text{ GeV}$
---------------------------------	----	------	-----	--

$\Gamma(\phi K^+, \phi \rightarrow K^+K^-)/\Gamma(2K^+K^-)$ $\Gamma_{109}/\Gamma_{108}$

VALUE	DOCUMENT ID	TECN	COMMENT
$0.41 \pm 0.08 \pm 0.03$	DEL-AMO-SA..11g	BABR	$e^+e^- \approx \Upsilon(4S)$

———— Doubly Cabibbo-suppressed modes ————

$\Gamma(2K^+\pi^-)/\Gamma(K^+K^-\pi^+)$ Γ_{110}/Γ_{38}

VALUE (units 10^{-3})	EVTs	DOCUMENT ID	TECN	COMMENT
2.371 ± 0.034 OUR AVERAGE				
$2.372 \pm 0.024 \pm 0.025$	67k	AAIJ	19g	LHCB pp at 8 TeV
$2.3 \pm 0.3 \pm 0.2$	356 ± 52	DEL-AMO-SA..11g	BABR	$e^+e^- \approx \Upsilon(4S)$
$2.29 \pm 0.28 \pm 0.12$	281 ± 34	KO	09	BELL e^+e^- at $\Upsilon(4S)$
$5.2 \pm 1.7 \pm 1.1$	27 ± 9	LINK	05k	FOCS $<0.78\sigma$, CL = 90%

$\Gamma(K^+K^*(892)^0, K^*0 \rightarrow K^+\pi^-)/\Gamma(2K^+\pi^-)$ $\Gamma_{111}/\Gamma_{110}$

VALUE	DOCUMENT ID	TECN	COMMENT
$0.47 \pm 0.22 \pm 0.15$	DEL-AMO-SA..11g	BABR	$e^+e^- \approx \Upsilon(4S)$

Meson Particle Listings

D_s^\pm

Baryon-antibaryon mode

$\Gamma(p\bar{p})/\Gamma_{total}$ Γ_{112}/Γ
This is the only baryonic mode allowed kinematically.

VALUE (units 10^{-3})	EVTS	DOCUMENT ID	TECN	COMMENT
1.22 ± 0.11 OUR AVERAGE				
$1.21 \pm 0.10 \pm 0.05$	193 ± 17	ABLIKIM	19oBES3	e^+e^- , $E_{cm} = 4178$ MeV
$1.30 \pm 0.36^{+0.12}_{-0.16}$	13.0 ± 3.6	ATHAR	08 CLEO	e^+e^- , $E_{cm} \approx 4170$ MeV

$\Gamma(p\bar{p}e^+\nu_e)/\Gamma_{total}$ Γ_{113}/Γ
This is the only baryonic mode allowed kinematically.

VALUE	CL%	DOCUMENT ID	TECN	COMMENT
$<2.0 \times 10^{-4}$	90	ABLIKIM	19bD BES3	e^+e^- at 4178 MeV

Rare or forbidden modes

$\Gamma(\pi^+e^+e^-)/\Gamma_{total}$ Γ_{114}/Γ
This mode is not a useful test for a $\Delta C=1$ weak neutral current because both quarks must change flavor in this decay.

VALUE	CL%	DOCUMENT ID	TECN	COMMENT
$<13 \times 10^{-6}$	90	LEES	11G BABR	$e^+e^- \approx \Upsilon(4S)$
$<2.2 \times 10^{-5}$	90	¹ RUBIN	10 CLEO	e^+e^- at 4170 MeV
$<27 \times 10^{-5}$	90	AITALA	99G E791	$\pi^- N$ 500 GeV

¹ This RUBIN 10 limit is for the e^+e^- mass in the continuum away from the $\phi(1020)$. See the next data block.

$\Gamma(\pi^+\phi, \phi \rightarrow e^+e^-)/\Gamma_{total}$ Γ_{115}/Γ

This is not a test for the $\Delta C = 1$ weak neutral current, but leads to the $\pi^+e^+e^-$ final state.

VALUE	EVTS	DOCUMENT ID	TECN	COMMENT
$(6^{+8}_{-4} \pm 1) \times 10^{-6}$	3	RUBIN	10 CLEO	e^+e^- at 4170 MeV

$\Gamma(\pi^+\mu^+\mu^-)/\Gamma_{total}$ Γ_{116}/Γ
This mode is not a useful test for a $\Delta C=1$ weak neutral current because both quarks must change flavor in this decay.

VALUE	CL%	DOCUMENT ID	TECN	COMMENT
$<4.1 \times 10^{-7}$	90	AAIJ	13AF LHCB	$p\bar{p}$ at 7 TeV
$<4.3 \times 10^{-5}$	90	LEES	11G BABR	$e^+e^- \approx \Upsilon(4S)$
$<2.6 \times 10^{-5}$	90	LINK	03F FOCS	γA , $\bar{E}_\gamma \approx 180$ GeV
$<1.4 \times 10^{-4}$	90	AITALA	99G E791	$\pi^- N$ 500 GeV
$<4.3 \times 10^{-4}$	90	KODAMA	95 E653	π^- emulsion 600 GeV

$\Gamma(K^+e^+e^-)/\Gamma_{total}$ Γ_{117}/Γ
A test for the $\Delta C=1$ weak neutral current. Allowed by higher-order electroweak interactions.

VALUE	CL%	DOCUMENT ID	TECN	COMMENT
$<3.7 \times 10^{-6}$	90	LEES	11G BABR	$e^+e^- \approx \Upsilon(4S)$
$<5.2 \times 10^{-5}$	90	RUBIN	10 CLEO	e^+e^- at 4170 MeV
$<1.6 \times 10^{-3}$	90	AITALA	99G E791	$\pi^- N$ 500 GeV

$\Gamma(K^+\mu^+\mu^-)/\Gamma_{total}$ Γ_{118}/Γ
A test for the $\Delta C=1$ weak neutral current. Allowed by higher-order electroweak interactions.

VALUE	CL%	DOCUMENT ID	TECN	COMMENT
$<21 \times 10^{-6}$	90	LEES	11G BABR	$e^+e^- \approx \Upsilon(4S)$
$<3.6 \times 10^{-5}$	90	LINK	03F FOCS	γA , $\bar{E}_\gamma \approx 180$ GeV
$<1.4 \times 10^{-4}$	90	AITALA	99G E791	$\pi^- N$ 500 GeV
$<5.9 \times 10^{-4}$	90	KODAMA	95 E653	π^- emulsion 600 GeV

$\Gamma(K^*(892)^+\mu^+\mu^-)/\Gamma_{total}$ Γ_{119}/Γ
A test for the $\Delta C=1$ weak neutral current. Allowed by higher-order electroweak interactions.

VALUE	CL%	DOCUMENT ID	TECN	COMMENT
$<1.4 \times 10^{-3}$	90	KODAMA	95 E653	π^- emulsion 600 GeV

$\Gamma(\pi^+e^+\mu^-)/\Gamma_{total}$ Γ_{120}/Γ
A test of lepton-family-number conservation.

VALUE	CL%	DOCUMENT ID	TECN	COMMENT
$<12 \times 10^{-6}$	90	LEES	11G BABR	$e^+e^- \approx \Upsilon(4S)$

$\Gamma(\pi^+e^+\mu^+)/\Gamma_{total}$ Γ_{121}/Γ
A test of lepton-family-number conservation.

VALUE	CL%	DOCUMENT ID	TECN	COMMENT
$<20 \times 10^{-6}$	90	LEES	11G BABR	$e^+e^- \approx \Upsilon(4S)$

$\Gamma(K^+e^+\mu^-)/\Gamma_{total}$ Γ_{122}/Γ
A test of lepton-family-number conservation.

VALUE	CL%	DOCUMENT ID	TECN	COMMENT
$<14 \times 10^{-6}$	90	LEES	11G BABR	$e^+e^- \approx \Upsilon(4S)$

$\Gamma(K^+e^-\mu^+)/\Gamma_{total}$ Γ_{123}/Γ

A test of lepton-family-number conservation.

VALUE	CL%	DOCUMENT ID	TECN	COMMENT
$<9.7 \times 10^{-6}$	90	LEES	11G BABR	$e^+e^- \approx \Upsilon(4S)$

$\Gamma(\pi^-2e^+)/\Gamma_{total}$ Γ_{124}/Γ

A test of lepton-number conservation.

VALUE	CL%	DOCUMENT ID	TECN	COMMENT
$<4.1 \times 10^{-6}$	90	LEES	11G BABR	$e^+e^- \approx \Upsilon(4S)$
$<1.4 \times 10^{-5}$	90	LEES	11G BABR	$e^+e^- \approx \Upsilon(4S)$
$<2.9 \times 10^{-5}$	90	LINK	03F FOCS	γA , $\bar{E}_\gamma \approx 180$ GeV
$<8.2 \times 10^{-5}$	90	AITALA	99G E791	$\pi^- N$ 500 GeV
$<69 \times 10^{-5}$	90	AITALA	99G E791	$\pi^- N$ 500 GeV

$\Gamma(\pi^-2\mu^+)/\Gamma_{total}$ Γ_{125}/Γ

A test of lepton-number conservation.

VALUE	CL%	DOCUMENT ID	TECN	COMMENT
$<1.2 \times 10^{-7}$	90	AAIJ	13AF LHCB	$p\bar{p}$ at 7 TeV
$<1.4 \times 10^{-5}$	90	LEES	11G BABR	$e^+e^- \approx \Upsilon(4S)$
$<2.9 \times 10^{-5}$	90	LINK	03F FOCS	γA , $\bar{E}_\gamma \approx 180$ GeV
$<8.2 \times 10^{-5}$	90	AITALA	99G E791	$\pi^- N$ 500 GeV
$<4.3 \times 10^{-4}$	90	KODAMA	95 E653	π^- emulsion 600 GeV

$\Gamma(\pi^-e^+\mu^+)/\Gamma_{total}$ Γ_{126}/Γ

A test of lepton-number conservation.

VALUE	CL%	DOCUMENT ID	TECN	COMMENT
$<8.4 \times 10^{-6}$	90	LEES	11G BABR	$e^+e^- \approx \Upsilon(4S)$
$<7.3 \times 10^{-4}$	90	AITALA	99G E791	$\pi^- N$ 500 GeV

$\Gamma(K^-2e^+)/\Gamma_{total}$ Γ_{127}/Γ

A test of lepton-number conservation.

VALUE	CL%	DOCUMENT ID	TECN	COMMENT
$<5.2 \times 10^{-6}$	90	LEES	11G BABR	$e^+e^- \approx \Upsilon(4S)$
$<1.7 \times 10^{-5}$	90	RUBIN	10 CLEO	e^+e^- at 4170 MeV
$<63 \times 10^{-5}$	90	AITALA	99G E791	$\pi^- N$ 500 GeV

$\Gamma(K^-2\mu^+)/\Gamma_{total}$ Γ_{128}/Γ

A test of lepton-number conservation.

VALUE	CL%	DOCUMENT ID	TECN	COMMENT
$<1.3 \times 10^{-5}$	90	LEES	11G BABR	$e^+e^- \approx \Upsilon(4S)$
$<1.3 \times 10^{-5}$	90	LINK	03F FOCS	γA , $\bar{E}_\gamma \approx 180$ GeV
$<1.8 \times 10^{-4}$	90	AITALA	99G E791	$\pi^- N$ 500 GeV
$<5.9 \times 10^{-4}$	90	KODAMA	95 E653	π^- emulsion 600 GeV

$\Gamma(K^-e^+\mu^+)/\Gamma_{total}$ Γ_{129}/Γ

A test of lepton-number conservation.

VALUE	CL%	DOCUMENT ID	TECN	COMMENT
$<6.1 \times 10^{-6}$	90	LEES	11G BABR	$e^+e^- \approx \Upsilon(4S)$
$<6.8 \times 10^{-4}$	90	AITALA	99G E791	$\pi^- N$ 500 GeV

$\Gamma(K^*(892)^-2\mu^+)/\Gamma_{total}$ Γ_{130}/Γ

A test of lepton-number conservation.

VALUE	CL%	DOCUMENT ID	TECN	COMMENT
$<1.4 \times 10^{-3}$	90	KODAMA	95 E653	π^- emulsion 600 GeV

$D_s^+ - D_s^-$ CP-VIOLATING DECAY-RATE ASYMMETRIES

This is the difference between D_s^+ and D_s^- partial widths for the decay to state f , divided by the sum of the widths:

$$A_{CP}(f) = [\Gamma(D_s^+ \rightarrow f) - \Gamma(D_s^- \rightarrow \bar{f})] / [\Gamma(D_s^+ \rightarrow f) + \Gamma(D_s^- \rightarrow \bar{f})]$$

$A_{CP}(\mu^\pm\nu)$ in $D_s^+ \rightarrow \mu^+\nu$, $D_s^- \rightarrow \mu^-\bar{\nu}_\mu$

VALUE (%)	DOCUMENT ID	TECN	COMMENT
4.8 ± 6.1	ALEXANDER 09	CLEO	e^+e^- at 4170 MeV

$A_{CP}(K^\pm K_S^0)$ in $D_s^\pm \rightarrow K^\pm K_S^0$

VALUE (%)	EVTS	DOCUMENT ID	TECN	COMMENT
0.09 ± 0.26 OUR AVERAGE				
$0.6 \pm 2.8 \pm 0.6$	1.8k	ABLIKIM	19AMBES3	e^+e^- at 4178 MeV
$-0.05 \pm 0.23 \pm 0.24$	288k	¹ LEES	13E BABR	e^+e^- at $\Upsilon(4S)$
$2.6 \pm 1.5 \pm 0.6$		ONYISI	13 CLEO	e^+e^- at 4.17 GeV
$0.12 \pm 0.36 \pm 0.22$		KO	10 BELL	$e^+e^- \approx \Upsilon(4S)$

$>>>$ We do not use the following data for averages, fits, limits, etc. $>>>$

VALUE (%)	TECN	COMMENT
$4.7 \pm 1.8 \pm 0.9$	4.0k	MELENZ 10 CLEO
$4.9 \pm 2.1 \pm 0.9$		ALEXANDER 08 CLEO

¹ LEES 13E finds that after subtracting the contribution due to $K^0 - \bar{K}^0$ mixing, the CP asymmetry is $(+0.28 \pm 0.23 \pm 0.24)\%$.

See key on page 999

Meson Particle Listings

D_s^\pm

$A_{CP}(K^\pm K_L^0)$ in $D_s^\pm \rightarrow K^\pm K_L^0$

VALUE (units 10^{-2})	EVTS	DOCUMENT ID	TECN	COMMENT
$-1.1 \pm 2.6 \pm 0.6$	2.3k	ABLIKIM	19AMBES3	$e^+ e^-$ at 4178 MeV

$A_{CP}(K^+ K^- \pi^\pm)$ in $D_s^\pm \rightarrow K^+ K^- \pi^\pm$

VALUE (%)	DOCUMENT ID	TECN	COMMENT
$-0.5 \pm 0.8 \pm 0.4$	ONYISI	13	CLEO $e^+ e^-$ at 4.17 GeV
••• We do not use the following data for averages, fits, limits, etc. •••			
$0.3 \pm 1.1 \pm 0.8$	ALEXANDER	08	CLEO See ONYISI 13

$A_{CP}(\phi \pi^\pm)$ in $D_s^\pm \rightarrow \phi \pi^\pm$

VALUE (%)	DOCUMENT ID	TECN	COMMENT
$-0.38 \pm 0.26 \pm 0.08$	ABAZOV	14B	D0 $p\bar{p}$ at 1.96 TeV

$A_{CP}(K^\pm K_S^0 \pi^0)$ in $D_s^\pm \rightarrow K^\pm K_S^0 \pi^0$

VALUE (%)	DOCUMENT ID	TECN	COMMENT
$-1.6 \pm 6.0 \pm 1.1$	ONYISI	13	CLEO $e^+ e^-$ at 4.17 GeV

$A_{CP}(2K_S^0 \pi^\pm)$ in $D_s^\pm \rightarrow 2K_S^0 \pi^\pm$

VALUE (%)	DOCUMENT ID	TECN	COMMENT
$3.1 \pm 5.2 \pm 0.6$	ONYISI	13	CLEO $e^+ e^-$ at 4.17 GeV

$A_{CP}(K^+ K^- \pi^\pm \pi^0)$ in $D_s^\pm \rightarrow K^+ K^- \pi^\pm \pi^0$

VALUE (%)	DOCUMENT ID	TECN	COMMENT
$0.0 \pm 2.7 \pm 1.2$	ONYISI	13	CLEO $e^+ e^-$ at 4.17 GeV
••• We do not use the following data for averages, fits, limits, etc. •••			
$-5.9 \pm 4.2 \pm 1.2$	ALEXANDER	08	CLEO See ONYISI 13

$A_{CP}(K^\pm K_S^0 \pi^+ \pi^-)$ in $D_s^\pm \rightarrow K^\pm K_S^0 \pi^+ \pi^-$

VALUE (%)	DOCUMENT ID	TECN	COMMENT
$-5.7 \pm 5.3 \pm 0.9$	ONYISI	13	CLEO $e^+ e^-$ at 4.17 GeV

$A_{CP}(K_S^0 K^\mp 2\pi^\pm)$ in $D_s^\pm \rightarrow K_S^0 K^\mp 2\pi^\pm$

VALUE (%)	DOCUMENT ID	TECN	COMMENT
$4.1 \pm 2.7 \pm 0.9$	ONYISI	13	CLEO $e^+ e^-$ at 4.17 GeV
••• We do not use the following data for averages, fits, limits, etc. •••			
$-0.7 \pm 3.6 \pm 1.1$	ALEXANDER	08	CLEO See ONYISI 13

$A_{CP}(\pi^+ \pi^- \pi^\pm)$ in $D_s^\pm \rightarrow \pi^+ \pi^- \pi^\pm$

VALUE (%)	DOCUMENT ID	TECN	COMMENT
$-0.7 \pm 3.0 \pm 0.6$	ONYISI	13	CLEO $e^+ e^-$ at 4.17 GeV
••• We do not use the following data for averages, fits, limits, etc. •••			
$2.0 \pm 4.6 \pm 0.7$	ALEXANDER	08	CLEO See ONYISI 13

$A_{CP}(\pi^\pm \eta)$ in $D_s^\pm \rightarrow \pi^\pm \eta$

VALUE (%)	EVTS	DOCUMENT ID	TECN	COMMENT
$1.1 \pm 3.0 \pm 0.8$		ONYISI	13	CLEO $e^+ e^-$ at 4.17 GeV
••• We do not use the following data for averages, fits, limits, etc. •••				
$-4.6 \pm 2.9 \pm 0.3$	2.5k	MENDEZ	10	CLEO See ONYISI 13
$-8.2 \pm 5.2 \pm 0.8$		ALEXANDER	08	CLEO See MENDEZ 10

$A_{CP}(\pi^\pm \eta')$ in $D_s^\pm \rightarrow \pi^\pm \eta'$

VALUE (%)	EVTS	DOCUMENT ID	TECN	COMMENT
-0.9 ± 0.5 OUR AVERAGE				
$-0.82 \pm 0.36 \pm 0.35$	152k	AAIJ	17AF	LHCB $p\bar{p}$ at 7, 8 TeV
$-2.2 \pm 2.2 \pm 0.6$		ONYISI	13	CLEO $e^+ e^-$ at 4.17 GeV
••• We do not use the following data for averages, fits, limits, etc. •••				
$-6.1 \pm 3.0 \pm 0.3$	1.4k	MENDEZ	10	CLEO See ONYISI 13
$-5.5 \pm 3.7 \pm 1.2$		ALEXANDER	08	CLEO See MENDEZ 10

$A_{CP}(\eta \pi^\pm \pi^0)$ in $D_s^\pm \rightarrow \eta \pi^\pm \pi^0$

VALUE (%)	DOCUMENT ID	TECN	COMMENT
$-0.5 \pm 3.9 \pm 2.0$	ONYISI	13	CLEO $e^+ e^-$ at 4.17 GeV

$A_{CP}(\eta' \pi^\pm \pi^0)$ in $D_s^\pm \rightarrow \eta' \pi^\pm \pi^0$

VALUE (%)	DOCUMENT ID	TECN	COMMENT
$-0.4 \pm 7.4 \pm 1.9$	ONYISI	13	CLEO $e^+ e^-$ at 4.17 GeV

$A_{CP}(K^\pm \pi^0)$ in $D_s^\pm \rightarrow K^\pm \pi^0$

VALUE (%)	EVTS	DOCUMENT ID	TECN	COMMENT
$-26.6 \pm 23.8 \pm 0.9$	202 ± 70	MENDEZ	10	CLEO $e^+ e^-$ at 4170 MeV
••• We do not use the following data for averages, fits, limits, etc. •••				
2 ± 29		ADAMS	07A	CLEO See MENDEZ 10

$A_{CP}(K^0/K^+ \pi^\pm)$ in $D_s^\pm \rightarrow K^0 \pi^+, D_s^- \rightarrow K^0 \pi^-$

VALUE (%)	EVTS	DOCUMENT ID	TECN	COMMENT
0.4 ± 0.5 OUR AVERAGE				
$0.38 \pm 0.46 \pm 0.17$	121k	¹ AAIJ	14BD	LHCB $p\bar{p}$ at 7, 8 TeV
$0.3 \pm 2.0 \pm 0.3$	14k	LEES	13E	BABR $e^+ e^-$ at $\Upsilon(4S)$
••• We do not use the following data for averages, fits, limits, etc. •••				
$0.61 \pm 0.83 \pm 0.14$	26k	AAIJ	13W	LHCB See AAJJ 14BD
¹ AAJJ 14BD reports its result as $A_{CP}(D_s^\pm \rightarrow K_S^0 K^\pm)$ with CP-violation effects in the $K^0 - \bar{K}^0$ system subtracted. It also measures $A_{CP}(D^\pm \rightarrow \bar{K}^0/K^0 K^\pm) + A_{CP}(D_s^\pm \rightarrow \bar{K}^0/K^0 \pi^\pm) = (0.41 \pm 0.49 \pm 0.26)\%$.				

$A_{CP}(K_S^0 \pi^\pm)$ in $D_s^\pm \rightarrow K_S^0 \pi^\pm$

VALUE (%)	EVTS	DOCUMENT ID	TECN	COMMENT
0.20 ± 0.18 OUR AVERAGE				
$0.16 \pm 0.17 \pm 0.05$	721k	AAIJ	19T	LHCB $p\bar{p}$ at 7, 8, 13 TeV
$0.6 \pm 2.0 \pm 0.3$	14k	LEES	13E	BABR $e^+ e^-$ at $\Upsilon(4S)$
$5.45 \pm 2.50 \pm 0.33$		KO	10	BELL $e^+ e^- \approx \Upsilon(4S)$
$16.3 \pm 7.3 \pm 0.3$	0.4k	MENDEZ	10	CLEO $e^+ e^-$ at 4170 MeV
••• We do not use the following data for averages, fits, limits, etc. •••				
27 ± 11		ADAMS	07A	CLEO See MENDEZ 10

$A_{CP}(K^\pm \pi^+ \pi^-)$ in $D_s^\pm \rightarrow K^\pm \pi^+ \pi^-$

VALUE (%)	DOCUMENT ID	TECN	COMMENT
$4.5 \pm 4.8 \pm 0.6$	ONYISI	13	CLEO $e^+ e^-$ at 4.17 GeV
••• We do not use the following data for averages, fits, limits, etc. •••			
$11.2 \pm 7.0 \pm 0.9$	ALEXANDER	08	CLEO See ONYISI 13

$A_{CP}(K^\pm \eta)$ in $D_s^\pm \rightarrow K^\pm \eta$

VALUE (%)	EVTS	DOCUMENT ID	TECN	COMMENT
$9.3 \pm 15.2 \pm 0.9$	222 ± 41	MENDEZ	10	CLEO $e^+ e^-$ at 4170 MeV
••• We do not use the following data for averages, fits, limits, etc. •••				
-20 ± 18		ADAMS	07A	CLEO See MENDEZ 10

$A_{CP}(K^\pm \eta'(958))$ in $D_s^\pm \rightarrow K^\pm \eta'(958)$

VALUE (%)	EVTS	DOCUMENT ID	TECN	COMMENT
$6.0 \pm 18.9 \pm 0.9$	56 ± 17	MENDEZ	10	CLEO $e^+ e^-$ at 4170 MeV
••• We do not use the following data for averages, fits, limits, etc. •••				
-17 ± 37		ADAMS	07A	CLEO See MENDEZ 10

CP VIOLATING ASYMMETRIES OF P-ODD (T-ODD) MOMENTS

$A_{Tviol}(K_S^0 K^\pm \pi^+ \pi^-)$ in $D_s^\pm \rightarrow K_S^0 K^\pm \pi^+ \pi^-$

$C_T \equiv \bar{p}_{K^+} \cdot (\bar{p}_{\pi^+} \times \bar{p}_{\pi^-})$ is a parity-odd correlation of the K^+ , π^+ , and π^- momenta for the D_s^+ . $\bar{C}_T \equiv \bar{p}_{K^-} \cdot (\bar{p}_{\pi^-} \times \bar{p}_{\pi^+})$ is the corresponding quantity for the D_s^- . Then
 $A_T \equiv [\Gamma(C_T > 0) - \Gamma(C_T < 0)] / [\Gamma(C_T > 0) + \Gamma(C_T < 0)]$, and
 $\bar{A}_T \equiv [\Gamma(-\bar{C}_T > 0) - \Gamma(-\bar{C}_T < 0)] / [\Gamma(-\bar{C}_T > 0) + \Gamma(-\bar{C}_T < 0)]$, and
 $A_{Tviol} \equiv \frac{1}{2}(A_T - \bar{A}_T)$. C_T and \bar{C}_T are commonly referred to as T -odd moments, because they are odd under T reversal. However, the T -conjugate process $K_S^0 K^\pm \pi^+ \pi^- \rightarrow D_s^\pm$ is not accessible, while the P -conjugate process is.

VALUE (units 10^{-3})	EVTS	DOCUMENT ID	TECN	COMMENT
$-13.6 \pm 7.7 \pm 3.4$	$29.8 \pm 0.3k$	LEES	11E	BABR $e^+ e^- \approx \Upsilon(4S)$
••• We do not use the following data for averages, fits, limits, etc. •••				
$-36 \pm 67 \pm 23$	508 ± 34	LINK	05E	FOCS γA , $\bar{E}_\gamma \approx 180$ GeV

D_s^\pm Semileptonic Form Factors and Decay Constants

$r_2 \equiv A_2(0)/A_1(0)$ in $D_s^\pm \rightarrow \phi \ell^+ \nu_\ell$

VALUE	EVTS	DOCUMENT ID	TECN	COMMENT
0.84 ± 0.11 OUR AVERAGE				Error includes scale factor of 2.4.
$0.816 \pm 0.036 \pm 0.030$	$25 \pm 0.5k$	¹ AUBERT	08AN	BABR $\phi e^+ \nu_e$
$0.713 \pm 0.202 \pm 0.284$	793	LINK	04C	FOCS $\phi \mu^+ \nu_\mu$
$1.57 \pm 0.25 \pm 0.19$	271	AITALA	99D	E791 $\phi e^+ \nu_e, \phi \mu^+ \nu_\mu$
$1.4 \pm 0.5 \pm 0.3$	308	AVERY	94B	CLE2 $\phi e^+ \nu_e$
$1.1 \pm 0.8 \pm 0.1$	90	FRABETTI	94F	E687 $\phi \mu^+ \nu_\mu$
$2.1 \pm 0.6 \pm 0.2$	19	KODAMA	93	E653 $\phi \mu^+ \nu_\mu$

¹ To compare with previous measurements, this AUBERT 08AN value is from a fit that fixes the pole masses at $m_A = 2.5$ GeV/c² and $m_V = 2.1$ GeV/c². A simultaneous fit to r_2 , r_V , r_0 (a significant s-wave contribution) and m_A , gives $r_2 = 0.763 \pm 0.071 \pm 0.065$.

See key on page 999

Meson Particle Listings

$D_s^{\pm}, D_{s0}^*(2317)^{\pm}$

$m_{D_s^{\pm}} - m_{D_s^0}$

The fit includes $D^{\pm}, D^0, D_s^{\pm}, D_s^{*0}, D_s^{*+}, D_1(2420)^0, D_2^*(2460)^0$, and $D_{s1}(2536)^{\pm}$ mass and mass difference measurements.

VALUE (MeV)	EVTS	DOCUMENT ID	TECN	COMMENT
143.8 ± 0.4 OUR FIT				
143.9 ± 0.4 OUR AVERAGE				
143.76 ± 0.39 ± 0.40		GRONBERG 95	CLE2	$e^+ e^-$
144.22 ± 0.47 ± 0.37		BROWN 94	CLE2	$e^+ e^-$
142.5 ± 0.8 ± 1.5		2 ALBRECHT 88	ARG	$e^+ e^- \rightarrow D_s^{\pm} \gamma X$
139.5 ± 8.3 ± 9.7	60	AIHARA 84D	TPC	$e^+ e^- \rightarrow$ hadrons
• • • We do not use the following data for averages, fits, limits, etc. • • •				
143.0 ± 18.0	8	ASRATYAN 85	HLBC	FNAL 15-ft, ν - 2 H
110 ± 46		BRANDELIK 79	DASP	$e^+ e^- \rightarrow D_s^{\pm} \gamma X$

²Result includes data of ALBRECHT 84b.

D_s^{\pm} WIDTH

VALUE (MeV)	CL%	DOCUMENT ID	TECN	COMMENT
< 1.9	90	GRONBERG 95	CLE2	$e^+ e^-$
< 4.5	90	ALBRECHT 88	ARG	$E_{cm}^{ee} = 10.2$ GeV
• • • We do not use the following data for averages, fits, limits, etc. • • •				
< 4.9	90	BROWN 94	CLE2	$e^+ e^-$
< 22	90	BLAYLOCK 87	MRK3	$e^+ e^- \rightarrow D_s^{\pm} \gamma X$

$D_s^{*\pm}$ DECAY MODES

D_s^{*-} modes are charge conjugates of the modes below.

Mode	Fraction (Γ_j/Γ)
$\Gamma_1 D_s^+ \gamma$	(93.5 ± 0.7) %
$\Gamma_2 D_s^+ \pi^0$	(5.8 ± 0.7) %
$\Gamma_3 D_s^+ e^+ e^-$	(6.7 ± 1.6) × 10 ⁻³

CONSTRAINED FIT INFORMATION

An overall fit to 2 branching ratios uses 3 measurements and one constraint to determine 3 parameters. The overall fit has a $\chi^2 = 0.0$ for 1 degrees of freedom.

The following *off-diagonal* array elements are the correlation coefficients $\langle \delta x_i \delta x_j \rangle / (\delta x_i \delta x_j)$, in percent, from the fit to the branching fractions, $x_i \equiv \Gamma_i / \Gamma_{total}$. The fit constrains the x_i whose labels appear in this array to sum to one.

x_2	-97	
x_3	-19	-4
	x_1	x_2

$D_s^{*\pm}$ BRANCHING RATIOS

$\Gamma(D_s^+ \gamma) / \Gamma_{total}$	Γ_1 / Γ
0.935 ± 0.007 OUR FIT	
• • • We do not use the following data for averages, fits, limits, etc. • • •	
seen	ASRATYAN 91 HLBC τ_{μ} Ne
seen	ALBRECHT 88 ARG $e^+ e^- \rightarrow D_s^{\pm} \gamma X$
seen	AIHARA 84D
seen	ALBRECHT 84b
seen	BRANDELIK 79

$\Gamma(D_s^+ \pi^0) / \Gamma(D_s^+ \gamma)$	Γ_2 / Γ_1
0.062 ± 0.008 OUR FIT	
0.062 ± 0.008 OUR AVERAGE	
0.062 ± 0.005 ± 0.006	AUBERT, BE 05G BABR 10.6 $e^+ e^- \rightarrow$ hadrons
0.062 ± 0.020 ± 0.022	GRONBERG 95 CLE2 $e^+ e^-$

$\Gamma(D_s^+ e^+ e^-) / \Gamma(D_s^+ \gamma)$	Γ_3 / Γ_1
7.2 ± 1.7 OUR FIT	
7.2 ± 1.3 ± 1.0	
38	CRONIN-HEN.12 CLEO 4.17 $e^+ e^- \rightarrow$ hadrons

D_s^{\pm} REFERENCES

CRONIN-HEN.12	PR D86 072005	D. Cronin-Hennessey et al.	(CLEO Collab.)
AUBERT, BE 05G	PR D72 091101	B. Aubert et al.	(BABAR Collab.)
GRONBERG 95	PRL 75 3232	J. Gronberg et al.	(CLEO Collab.)
BROWN 94	PR D50 1884	D. Brown et al.	(CLEO Collab.)
ASRATYAN 91	PL B257 525	A.E. Asratyan et al.	(ITEP, BELG, SAACL+)
ALBRECHT 88	PL B207 349	H. Albrecht et al.	(ARGUS Collab.)
BLAYLOCK 87	PRL 58 2171	G.T. Blaylock et al.	(Mark III Collab.)
ASRATYAN 85	PL 156B 441	A.E. Asratyan et al.	(ITEP, SERP)
AIHARA 84D	PRL 53 2465	H. Aihara et al.	(TPC Collab.)
ALBRECHT 84B	PL 146B 111	H. Albrecht et al.	(ARGUS Collab.)
BRANDELIK 79	PL 80B 412	R. Brandelik et al.	(DASP Collab.)

$D_{s0}^*(2317)^{\pm}$

$I(J^P) = 0(0^+)$
J, P need confirmation.

AUBERT 06P and CHOI 15A do not observe neutral and doubly charged partners of the $D_{s0}^*(2317)^{\pm}$.

$D_{s0}^*(2317)^{\pm}$ MASS

The fit includes $D^{\pm}, D^0, D_s^{\pm}, D_s^{*0}, D_s^{*+}, D_1(2420)^0, D_2^*(2460)^0$, and $D_{s1}(2536)^{\pm}$ mass and mass difference measurements.

VALUE (MeV)	EVTS	DOCUMENT ID	TECN	COMMENT
2317.8 ± 0.5 OUR FIT				
2318.0 ± 0.7 OUR AVERAGE				
2318.3 ± 1.2 ± 1.2	115	1 ABLIKIM 18J BES3		4.6 $e^+ e^- \rightarrow D_s^{*\pm} D_{s0}^*(2317)^{\mp}$
2319.6 ± 0.2 ± 1.4	3.1k	AUBERT 06P BABR		10.6 $e^+ e^- \rightarrow D_s^+ \pi^0 X$
2317.3 ± 0.4 ± 0.8	1.0k	2 AUBERT 04E BABR		10.6 $e^+ e^-$
• • • We do not use the following data for averages, fits, limits, etc. • • •				
2317.2 ± 1.3	88	3 AUBERT, B 04s BABR		$B \rightarrow D_{s0}^{(*)}(2317) + \bar{D}^{(*)}$
2317.2 ± 0.5 ± 0.9	761	4 MIKAMI 04 BELL		10.6 $e^+ e^-$
2316.8 ± 0.4 ± 3.0	1.2k	4,5 AUBERT 03G BABR		10.6 $e^+ e^-$
2317.6 ± 1.3	273	4,6 AUBERT 03G BABR		10.6 $e^+ e^-$
2319.8 ± 2.1 ± 2.0	24	4 KROKOVNY 03B BELL		10.6 $e^+ e^-$

¹ From a fit of the D_s^* recoil mass where the $D_{s0}^*(2317)$ signal is described with a Crystal Ball function convolved with a Gaussian function.

² Supersedes AUBERT 03G.

³ Systematic errors not evaluated.

⁴ Not independent of the corresponding $m_{D_{s0}^*(2317)} - m_{D_s^*}$.

⁵ From $D_s^+ \rightarrow K^+ K^- \pi^+$ decay.

⁶ From $D_s^+ \rightarrow K^+ K^- \pi^+ \pi^0$ decay.

$m_{D_{s0}^*(2317)^{\pm}} - m_{D_s^{\pm}}$

The fit includes $D^{\pm}, D^0, D_s^{\pm}, D_s^{*0}, D_s^{*+}, D_1(2420)^0, D_2^*(2460)^0$, and $D_{s1}(2536)^{\pm}$ mass and mass difference measurements.

VALUE (MeV)	EVTS	DOCUMENT ID	TECN	COMMENT
349.4 ± 0.5 OUR FIT				
349.2 ± 0.7 OUR AVERAGE				
348.7 ± 0.5 ± 0.7	761	MIKAMI 04 BELL		10.6 $e^+ e^-$
350.0 ± 1.2 ± 1.0	135	BESSION 03 CLE2		10.6 $e^+ e^-$
351.3 ± 2.1 ± 1.9	24	7 KROKOVNY 03B BELL		10.6 $e^+ e^-$
• • • We do not use the following data for averages, fits, limits, etc. • • •				
349.6 ± 0.4 ± 3.0	1267	8,9 AUBERT 03G BABR		10.6 $e^+ e^-$
350.2 ± 1.3	273	10,11 AUBERT 03G BABR		10.6 $e^+ e^-$
⁷ Recalculated by us using $m_{D_s^+} = 1968.5 \pm 0.6$ MeV.				
⁸ From $D_s^+ \rightarrow K^+ K^- \pi^+$ decay.				
⁹ Recalculated by us using $m_{D_s^+} = 1967.20 \pm 0.03$ MeV.				
¹⁰ From $D_s^+ \rightarrow K^+ K^- \pi^+ \pi^0$ decay.				
¹¹ Recalculated by us using $m_{D_s^+} = 1967.4 \pm 0.2$ MeV. Systematic errors not estimated.				

$D_{s0}^*(2317)^{\pm}$ WIDTH

VALUE (MeV)	CL%	EVTS	DOCUMENT ID	TECN	COMMENT
< 3.8	95	3180	AUBERT 06P BABR		10.6 $e^+ e^- \rightarrow D_s^+ \pi^0 X$
• • • We do not use the following data for averages, fits, limits, etc. • • •					
< 4.6	90	761	MIKAMI 04 BELL		10.6 $e^+ e^-$
< 10			AUBERT 03G BABR		10.6 $e^+ e^-$
< 7	90	135	BESSION 03 CLE2		10.6 $e^+ e^-$

Meson Particle Listings

$D_{s0}^*(2317)^\pm, D_{s1}(2460)^\pm$

$D_{s0}^*(2317)^\pm$ DECAY MODES

$D_{s0}^*(2317)^-$ modes are charge conjugates of modes below.

Mode	Fraction (Γ_i/Γ)	Confidence level
$\Gamma_1 D_s^+ \pi^0$	$(100^{+0}_{-20})\%$	
$\Gamma_2 D_s^+ \gamma$	$< 5\%$	90%
$\Gamma_3 D_s^*(2112)^+ \gamma$	$< 6\%$	90%
$\Gamma_4 D_s^+ \gamma \gamma$	$< 18\%$	95%
$\Gamma_5 D_s^*(2112)^+ \pi^0$	$< 11\%$	90%
$\Gamma_6 D_s^+ \pi^+ \pi^-$	$< 4 \times 10^{-3}$	90%
$\Gamma_7 D_s^+ \pi^0 \pi^0$	not seen	

$D_{s0}^*(2317)^\pm$ BRANCHING RATIOS

$\Gamma(D_s^+ \pi^0)/\Gamma_{\text{total}}$	Γ_1/Γ				
VALUE	EVTS	DOCUMENT ID	TECN	COMMENT	
$1.00^{+0.00+0.00}_{-0.14-0.14}$	47	ABL IKIM	18J	BES3	$4.6 e^+ e^- \rightarrow D_{s0}^{*\pm} D_{s0}^*(2317)^\mp$

• • • We do not use the following data for averages, fits, limits, etc. • • •
 seen 1.5k AUBERT 03G BABR $10.6 e^+ e^-$

$\Gamma(D_s^+ \gamma)/\Gamma(D_s^+ \pi^0)$	Γ_2/Γ_1				
VALUE	CL%	DOCUMENT ID	TECN	COMMENT	
< 0.05	90	MIKAMI	04	BELL	$10.6 e^+ e^-$

• • • We do not use the following data for averages, fits, limits, etc. • • •
 < 0.14 95 AUBERT 06P BABR $10.6 e^+ e^-$
 < 0.052 90 BESSON 03 CLE2 $10.6 e^+ e^-$

$\Gamma(D_s^*(2112)^+ \gamma)/\Gamma(D_s^+ \pi^0)$	Γ_3/Γ_1				
VALUE	CL%	DOCUMENT ID	TECN	COMMENT	
< 0.059	90	BESSON	03	CLE2	$10.6 e^+ e^-$

• • • We do not use the following data for averages, fits, limits, etc. • • •
 < 0.16 95 AUBERT 06P BABR $10.6 e^+ e^-$
 < 0.18 90 MIKAMI 04 BELL $10.6 e^+ e^-$

$\Gamma(D_s^+ \gamma \gamma)/\Gamma(D_s^+ \pi^0)$	Γ_4/Γ_1				
VALUE	CL%	DOCUMENT ID	TECN	COMMENT	
< 0.18	95	AUBERT	06P	BABR	$10.6 e^+ e^-$

• • • We do not use the following data for averages, fits, limits, etc. • • •
 not seen AUBERT 03G BABR $10.6 e^+ e^-$

$\Gamma(D_s^*(2112)^+ \pi^0)/\Gamma(D_s^+ \pi^0)$	Γ_5/Γ_1				
VALUE	CL%	DOCUMENT ID	TECN	COMMENT	
< 0.11	90	BESSON	03	CLE2	$10.6 e^+ e^-$

$\Gamma(D_s^+ \pi^+ \pi^-)/\Gamma(D_s^+ \pi^0)$	Γ_6/Γ_1				
VALUE	CL%	DOCUMENT ID	TECN	COMMENT	
< 0.004	90	MIKAMI	04	BELL	$10.6 e^+ e^-$

• • • We do not use the following data for averages, fits, limits, etc. • • •
 < 0.005 95 AUBERT 06P BABR $10.6 e^+ e^-$
 < 0.019 90 BESSON 03 CLE2 $10.6 e^+ e^-$

$\Gamma(D_s^+ \pi^0 \pi^0)/\Gamma(D_s^+ \pi^0)$	Γ_7/Γ_1				
VALUE	CL%	DOCUMENT ID	TECN	COMMENT	
< 0.25	95	AUBERT	06P	BABR	$10.6 e^+ e^-$

$D_{s0}^*(2317)^\pm$ REFERENCES

ABL IKIM	18J	PR D97 051103	M. Ablikim et al.	(BESIII Collab.)
CHOI	15A	PR D91 092011	S.-K. Choi et al.	(BELLE Collab.)
AUBERT	06P	PR D74 032007	B. Aubert et al.	(BABAR Collab.)
AUBERT	04E	PR D69 031101	B. Aubert et al.	(BABAR Collab.)
AUBERT,B	04S	PRL 93 181801	B. Aubert et al.	(BABAR Collab.)
MIKAMI	04	PRL 92 012002	Y. Mikami et al.	(BELLE Collab.)
AUBERT	03G	PRL 90 242001	B. Aubert et al.	(BABAR Collab.)
BESSON	03	PR D68 032002	D. Besson et al.	(CLEO Collab.)
KROKOVNY	03B	PRL 91 262002	P. Krokovny et al.	(BELLE Collab.)

$D_{s1}(2460)^\pm$

$I(J^P) = 0(1^+)$

$D_{s1}(2460)^\pm$ MASS

The fit includes $D^\pm, D^0, D_s^\pm, D^{*\pm}, D^{*0}, D_s^{*\pm}, D_1(2420)^0, D_2^*(2460)^0$, and $D_{s1}(2536)^\pm$ mass and mass difference measurements.

VALUE (MeV)	EVTS	DOCUMENT ID	TECN	COMMENT
2459.5 ± 0.6 OUR FIT		Error includes scale factor of 1.1.		
2459.6 ± 0.9 OUR AVERAGE		Error includes scale factor of 1.3.		
2460.1 ± 0.2 ± 0.8		1 AUBERT	06P	BABR $10.6 e^+ e^-$
2458.0 ± 1.0 ± 1.0	195	AUBERT	04E	BABR $10.6 e^+ e^-$
• • • We do not use the following data for averages, fits, limits, etc. • • •				
2459.5 ± 1.2 ± 3.7	920	AUBERT	06P	BABR $10.6 e^+ e^- \rightarrow D_s^+ \gamma X$
2458.6 ± 1.0 ± 2.5	560	AUBERT	06P	BABR $10.6 e^+ e^- \rightarrow D_s^+ \pi^0 \gamma X$
2460.2 ± 0.2 ± 0.8	123	AUBERT	06P	BABR $10.6 e^+ e^- \rightarrow D_s^+ \pi^+ \pi^- X$
2458.9 ± 1.5	112	2 AUBERT,B	04S	BABR $B \rightarrow D_{s1}(2460)^+ \bar{D}^{(*)}$
2461.1 ± 1.6	139	3 AUBERT,B	04S	BABR $B \rightarrow D_{s1}(2460)^+ \bar{D}^{(*)}$
2456.5 ± 1.3 ± 1.3	126	4,5 MIKAMI	04	BELL $10.6 e^+ e^-$
2459.5 ± 1.3 ± 2.0	152	6,7 MIKAMI	04	BELL $10.6 e^+ e^-$
2459.9 ± 0.9 ± 1.6	60	6,7 MIKAMI	04	BELL $10.6 e^+ e^-$
2459.2 ± 1.6 ± 2.0	57	KROKOVNY	03B	BELL $10.6 e^+ e^-$

- The average of the values obtained from the $D_s^+ \gamma, D_s^+ \pi^0 \gamma, D_s^+ \pi^+ \pi^-$ final state.
- Systematic errors not evaluated. From the decay to $D_s^+ \pi^0$.
- Systematic errors not evaluated. From the decay to $D_s^+ \gamma$.
- Not independent of the corresponding $m_{D_{s1}(2460)^\pm} - m_{D_s^{*\pm}}$.
- Using $m_{D_s^+} = 2112.4 \pm 0.7$ MeV.
- Not independent of the corresponding $m_{D_{s1}(2460)^\pm} - m_{D_s^\pm}$.
- Using $m_{D_s^+} = 1968.5 \pm 0.6$ MeV.

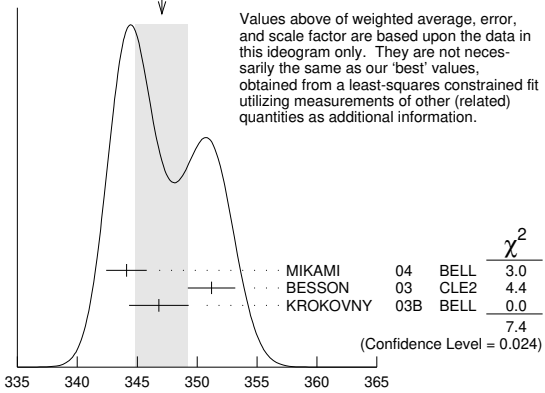
$m_{D_{s1}(2460)^\pm} - m_{D_s^{*\pm}}$

The fit includes $D^\pm, D^0, D_s^\pm, D^{*\pm}, D^{*0}, D_s^{*\pm}, D_1(2420)^0, D_2^*(2460)^0$, and $D_{s1}(2536)^\pm$ mass and mass difference measurements.

VALUE (MeV)	EVTS	DOCUMENT ID	TECN	COMMENT
347.3 ± 0.7 OUR FIT		Error includes scale factor of 1.2.		
347.1 ± 2.2 OUR AVERAGE		Error includes scale factor of 1.9. See the ideogram below.		
344.1 ± 1.3 ± 1.1	126	MIKAMI	04	BELL $10.6 e^+ e^-$
351.2 ± 1.7 ± 1.0	41	BESSON	03	CLE2 $10.6 e^+ e^-$
346.8 ± 1.6 ± 1.9	57	8 KROKOVNY	03B	BELL $10.6 e^+ e^-$

8 Recalculated by us using $m_{D_s^+} = 2112.4 \pm 0.7$ MeV.

WEIGHTED AVERAGE
 347.1 ± 2.2 (Error scaled by 1.9)



Values above of weighted average, error, and scale factor are based upon the data in this ideogram only. They are not necessarily the same as our 'best' values, obtained from a least-squares constrained fit utilizing measurements of other (related) quantities as additional information.

$m_{D_{s1}(2460)^\pm} - m_{D_s^\pm}$

The fit includes $D^\pm, D^0, D_s^\pm, D^{*\pm}, D^{*0}, D_s^{*\pm}, D_1(2420)^0, D_2^*(2460)^0$, and $D_{s1}(2536)^\pm$ mass and mass difference measurements.

VALUE (MeV)	EVTS	DOCUMENT ID	TECN	COMMENT
491.2 ± 0.6 OUR FIT		Error includes scale factor of 1.1.		
491.3 ± 1.4 OUR AVERAGE				
491.0 ± 1.3 ± 1.9	152	9 MIKAMI	04	BELL $10.6 e^+ e^-$
491.4 ± 0.9 ± 1.5	60	10 MIKAMI	04	BELL $10.6 e^+ e^-$

See key on page 999

Meson Particle Listings

$D_{s1}(2460)^{\pm}, D_{s1}(2536)^{\pm}$

⁹ From the decay to $D_s^+ \pi^- \gamma$.
¹⁰ From the decay to $D_s^+ \pi^+ \pi^-$.

$D_{s1}(2460)^{\pm}$ WIDTH

VALUE (MeV)	CL%	EVTS	DOCUMENT ID	TECN	COMMENT
< 3.5	95	123	AUBERT	06P BABR	$10.6 e^+ e^- \rightarrow D_s^+ \pi^+ \pi^- X$
••• We do not use the following data for averages, fits, limits, etc. •••					
< 6.3	95	560	AUBERT	06P BABR	$10.6 e^+ e^- \rightarrow D_s^+ \pi^0 \gamma X$
<10		195	AUBERT	04E BABR	$10.6 e^+ e^-$
< 5.5	90	126	MIKAMI	04 BELL	$10.6 e^+ e^-$
< 7	90	41	BESSION	03 CLE2	$10.6 e^+ e^-$

$D_{s1}(2460)^+$ DECAY MODES

$D_{s1}(2460)^-$ modes are charge conjugates of the modes below.

Mode	Fraction (Γ_i/Γ)	Scale factor/ Confidence level
$\Gamma_1 D_s^+ \pi^0$	$(48 \pm 11) \%$	
$\Gamma_2 D_s^+ \gamma$	$(18 \pm 4) \%$	
$\Gamma_3 D_s^+ \pi^+ \pi^-$	$(4.3 \pm 1.3) \%$	S=1.1
$\Gamma_4 D_s^+ \gamma$	< 8 %	CL=90%
$\Gamma_5 D_{s0}^+(2317)^+ \gamma$	$(3.7^{+5.0}_{-2.4}) \%$	
$\Gamma_6 D_s^+ \pi^0$		
$\Gamma_7 D_s^+ \pi^0 \pi^0$		
$\Gamma_8 D_s^+ \gamma \gamma$		

CONSTRAINED FIT INFORMATION

An overall fit to 7 branching ratios uses 8 measurements and one constraint to determine 5 parameters. The overall fit has a $\chi^2 = 3.4$ for 4 degrees of freedom.

The following off-diagonal array elements are the correlation coefficients $\langle \delta x_i \delta x_j \rangle / (\delta x_i \delta x_j)$, in percent, from the fit to the branching fractions, $x_i \equiv \Gamma_i/\Gamma_{\text{total}}$. The fit constrains the x_i whose labels appear in this array to sum to one.

x_2	80		
x_3	68	62	
x_5	-3	25	26
	x_1	x_2	x_3

$D_{s1}(2460)^{\pm}$ BRANCHING RATIOS

$\Gamma(D_s^+ \pi^0)/\Gamma_{\text{total}}$	Γ_1/Γ				
VALUE	CL%	EVTS	DOCUMENT ID	TECN	COMMENT
0.48 ± 0.11 OUR FIT					
$0.56 \pm 0.13 \pm 0.09$			¹¹ AUBERT	06N BABR	$B \rightarrow D_{s1}(2460)^- \bar{D}^{(*)}$

••• We do not use the following data for averages, fits, limits, etc. •••
seen 41 BESSION 03 CLE2 $10.6 e^+ e^-$

¹¹ Evaluated in AUBERT 06N including measurements from AUBERT,B 04s.

$\Gamma(D_s^+ \gamma)/\Gamma_{\text{total}}$	Γ_2/Γ				
VALUE	CL%	EVTS	DOCUMENT ID	TECN	COMMENT
0.18 ± 0.04 OUR FIT					
$0.16 \pm 0.04 \pm 0.03$			¹² AUBERT	06N BABR	$B \rightarrow D_{s1}(2460)^- \bar{D}^{(*)}$

¹² Evaluated in AUBERT 06N including measurements from AUBERT,B 04s.

$\Gamma(D_s^+ \gamma)/\Gamma(D_s^+ \pi^0)$	Γ_2/Γ_1				
VALUE	CL%	EVTS	DOCUMENT ID	TECN	COMMENT
0.38 ± 0.05 OUR FIT					
0.44 ± 0.09 OUR AVERAGE					
$0.55 \pm 0.13 \pm 0.08$		152	MIKAMI	04 BELL	$10.6 e^+ e^-$
$0.38 \pm 0.11 \pm 0.04$		38	KROKOVNY	03B BELL	$10.6 e^+ e^-$

••• We do not use the following data for averages, fits, limits, etc. •••
 $0.274 \pm 0.045 \pm 0.020$ 251 ¹³ AUBERT,B 04s BABR $B \rightarrow D_{s1}(2460)^+ \bar{D}^{(*)}$

< 0.49 90 BESSION 03 CLE2 $10.6 e^+ e^-$

¹³ Used by AUBERT 06N in their measurement of $B(D_s^{*-} \pi^0)$ and $B(D_s^- \gamma)$.

$\Gamma(D_s^+ \pi^+ \pi^-)/\Gamma(D_s^+ \pi^0)$	Γ_3/Γ_1				
VALUE	CL%	EVTS	DOCUMENT ID	TECN	COMMENT
0.090 ± 0.020 OUR FIT					Error includes scale factor of 1.2.
$0.14 \pm 0.04 \pm 0.02$		60	MIKAMI	04 BELL	$10.6 e^+ e^-$

••• We do not use the following data for averages, fits, limits, etc. •••
<0.08 90 BESSION 03 CLE2 $10.6 e^+ e^-$

$\Gamma(D_s^{*+} \gamma)/\Gamma(D_s^{*+} \pi^0)$	Γ_4/Γ_1			
VALUE	CL%	DOCUMENT ID	TECN	COMMENT
<0.16	90	BESSION 03 CLE2		$10.6 e^+ e^-$
••• We do not use the following data for averages, fits, limits, etc. •••				
<0.31	90	MIKAMI 04 BELL		$10.6 e^+ e^-$

$\Gamma(D_{s0}^+(2317)^+ \gamma)/\Gamma(D_s^{*+} \pi^0)$	Γ_5/Γ_1			
VALUE	CL%	DOCUMENT ID	TECN	COMMENT
<0.22	95	AUBERT 04E BABR		$10.6 e^+ e^-$
••• We do not use the following data for averages, fits, limits, etc. •••				
<0.58	90	BESSION 03 CLE2		$10.6 e^+ e^-$

$\Gamma(D_s^{*+} \pi^0)/[\Gamma(D_s^{*+} \pi^0) + \Gamma(D_{s0}^+(2317)^+ \gamma)]$	$\Gamma_1/(\Gamma_1 + \Gamma_5)$			
VALUE	CL%	DOCUMENT ID	TECN	COMMENT
0.93 ± 0.09 OUR FIT				
$0.97 \pm 0.09 \pm 0.05$		AUBERT 06P BABR		$10.6 e^+ e^-$

$\Gamma(D_s^+ \gamma)/[\Gamma(D_s^+ \pi^0) + \Gamma(D_{s0}^+(2317)^+ \gamma)]$	$\Gamma_2/(\Gamma_1 + \Gamma_5)$			
VALUE	CL%	DOCUMENT ID	TECN	COMMENT
0.35 ± 0.04 OUR FIT				
$0.337 \pm 0.036 \pm 0.038$		AUBERT 06P BABR		$10.6 e^+ e^-$

$\Gamma(D_s^+ \pi^+ \pi^-)/[\Gamma(D_s^+ \pi^0) + \Gamma(D_{s0}^+(2317)^+ \gamma)]$	$\Gamma_3/(\Gamma_1 + \Gamma_5)$			
VALUE	CL%	DOCUMENT ID	TECN	COMMENT
0.083 ± 0.017 OUR FIT				Error includes scale factor of 1.2.
$0.077 \pm 0.013 \pm 0.008$		AUBERT 06P BABR		$10.6 e^+ e^-$

$\Gamma(D_s^{*+} \gamma)/[\Gamma(D_s^{*+} \pi^0) + \Gamma(D_{s0}^+(2317)^+ \gamma)]$	$\Gamma_4/(\Gamma_1 + \Gamma_5)$			
VALUE	CL%	DOCUMENT ID	TECN	COMMENT
<0.24	95	AUBERT 06P BABR		$10.6 e^+ e^-$

$\Gamma(D_{s0}^+(2317)^+ \gamma)/[\Gamma(D_s^{*+} \pi^0) + \Gamma(D_{s0}^+(2317)^+ \gamma)]$	$\Gamma_5/(\Gamma_1 + \Gamma_5)$			
VALUE	CL%	DOCUMENT ID	TECN	COMMENT
<0.25	95	AUBERT 06P BABR		$10.6 e^+ e^-$

$\Gamma(D_s^+ \pi^0)/[\Gamma(D_s^+ \pi^0) + \Gamma(D_{s0}^+(2317)^+ \gamma)]$	$\Gamma_6/(\Gamma_1 + \Gamma_5)$			
VALUE	CL%	DOCUMENT ID	TECN	COMMENT
<0.042	95	AUBERT 06P BABR		$10.6 e^+ e^-$

$\Gamma(D_s^+ \pi^0 \pi^0)/[\Gamma(D_s^{*+} \pi^0) + \Gamma(D_{s0}^+(2317)^+ \gamma)]$	$\Gamma_7/(\Gamma_1 + \Gamma_5)$			
VALUE	CL%	DOCUMENT ID	TECN	COMMENT
<0.68	95	AUBERT 06P BABR		$10.6 e^+ e^-$

$\Gamma(D_s^+ \gamma \gamma)/[\Gamma(D_s^{*+} \pi^0) + \Gamma(D_{s0}^+(2317)^+ \gamma)]$	$\Gamma_8/(\Gamma_1 + \Gamma_5)$			
VALUE	CL%	DOCUMENT ID	TECN	COMMENT
<0.33	95	AUBERT 06P BABR		$10.6 e^+ e^-$

$D_{s1}(2460)^{\pm}$ REFERENCES

AUBERT 06N PR D74 031103	B. Aubert et al.	(BABAR Collab.)
AUBERT 06P PR D74 032007	B. Aubert et al.	(BABAR Collab.)
AUBERT 04E PR D69 031101	B. Aubert et al.	(BABAR Collab.)
AUBERT,B 04S PRL 93 181801	B. Aubert et al.	(BABAR Collab.)
MIKAMI 04 PRL 92 012002	Y. Mikami et al.	(BELLE Collab.)
BESSION 03 PR D68 032002	D. Besson et al.	(CLEO Collab.)
KROKOVNY 03B PRL 91 262002	P. Krokovny et al.	(BELLE Collab.)

$D_{s1}(2536)^{\pm}$

$I(J^P) = 0(1^+)$
 J, P need confirmation.

Seen in $D^*(2010)^+ K^0$, $D^*(2007)^0 K^+$, and $D_s^+ \pi^+ \pi^-$. Not seen in $D^+ K^0$ or $D^0 K^+$. $J^P = 1^+$ assignment strongly favored.

$D_{s1}(2536)^{\pm}$ MASS

The fit includes $D^{\pm}, D^0, D_s^{\pm}, D^{* \pm}, D^{*0}, D_s^{* \pm}, D_1(2420)^0, D_s^*(2460)^0$, and $D_{s1}(2536)^{\pm}$ mass and mass difference measurements.

VALUE (MeV)	CL%	EVTS	DOCUMENT ID	TECN	COMMENT
2535.11 ± 0.06 OUR FIT					
2535.21 ± 0.28 OUR AVERAGE					
$2537.7 \pm 0.5 \pm 3.1$	24		¹ ABLIKIM	19P BES3	$4.6 e^+ e^- \rightarrow D_s^+ \bar{D}^0 K^-$
$2535.7 \pm 0.6 \pm 0.5$	46		² ABAZOV	09G D0	$B_s^0 \rightarrow D_{s1}^- \mu^+ \nu_{\mu} X$
$2534.78 \pm 0.31 \pm 0.40$	182		AUBERT	08B BABR	$B \rightarrow \bar{D}^{(*)} D^* K$
$2534.6 \pm 0.3 \pm 0.7$	193		AUBERT	06P BABR	$10.6 e^+ e^- \rightarrow D_s^+ \pi^+ \pi^- X$
2535.3 ± 0.7	92		³ HEISTER	02B ALEP	$e^+ e^- \rightarrow D^{*+} K^0 X,$ $D^{*0} K^+ X$
2534.2 ± 1.2	9		ASRATYAN	94 BEBC	$\nu N \rightarrow D_s^* K^0 X, D^{*0} K^{\pm} X$
$2535 \pm 0.6 \pm 1$	75		FRABETTI	94B E687	$\gamma Be \rightarrow D^{*+} K^0 X,$ $D^{*0} K^+ X$
$2535.2 \pm 0.5 \pm 1.5$	28		ALBRECHT	92R ARG	$10.4 e^+ e^- \rightarrow D^{*0} K^+ X$
$2536.6 \pm 0.7 \pm 0.4$			AVERY	90 CLEO	$e^+ e^- \rightarrow D^{*+} K^0 X$
$2535.9 \pm 0.6 \pm 0.2$			ALBRECHT	89E ARG	$D_{s1}^* \rightarrow D^*(2010) K^0$

Meson Particle Listings

D_{s1}(2536)[±]

••• We do not use the following data for averages, fits, limits, etc. •••

2534.1 ± 0.6	116	4 AUSHEV	11	BELL	B → D _{s1} (2536) + D ^(*)
2535.08 ± 0.01 ± 0.15	8038	5 LEES	11B	BABR	10.6 e ⁺ e ⁻ → D ^(*) + K _S ⁰ X
2535.57 ^{+0.44} _{-0.41} ± 0.10	236	6 CHEKANOV	09	ZEUS	e [±] p → D ^(*) + K _S ⁰ X,
					D ^{(*)0} K ⁺ X
2535.3 ± 0.2 ± 0.5	134	7 ALEXANDER	93	CLE2	e ⁺ e ⁻ → D ^{(*)0} K ⁺ X
2534.8 ± 0.6 ± 0.6	44	8 ALEXANDER	93	CLE2	e ⁺ e ⁻ → D ^(*) + K ⁰ X
2535 ± 28		9 ASRATYAN	88	HLBC	νN → D _s γγX

1 From a fit of the D_s[±] recoil mass distribution with an incoherent sum of the S-wave and D-wave Breit-Wigner line shapes.
 2 Using the D^(*)(2010)[±] mass of 2010.0 ± 0.4 MeV from PDG 06.
 3 Calculated using m(D^(*)(2010)[±]) = 2010.0 ± 0.5 MeV, m(D^(*)(2007)⁰) = 2006.7 ± 0.5 MeV, and the mass difference below.
 4 Systematic uncertainties not evaluated.
 5 Calculated using the mass difference m(D_{s1}[±]) - m(D^(*))_{PDG} below and m(D^(*))_{PDG} = 2010.25 ± 0.14 MeV. Assuming S-wave decay of the D_{s1}(2536) to D^(*)+ K_S⁰, using a Breit-Wigner line shape corresponding to L=0.
 6 Calculated using the mass difference m(D_{s1}[±]) - m(D^(*))_{PDG} reported below and m(D^(*))_{PDG} = 2010.27 ± 0.17 MeV.
 7 Calculated using m(D^(*)(2007)⁰) = 2006.6 ± 0.5 MeV and the mass difference below.
 8 Calculated using m(D^(*)(2010)[±]) = 2010.1 ± 0.6 MeV and the mass difference below.
 9 Not seen in D^(*)K.

m_{D_{s1}(2536)±} - m_{D^(*)(2111)}

The fit includes D[±], D⁰, D_s[±], D^(*), D^{(*)0}, D₁(2420)⁰, D₂^(*)(2460)⁰, and D_{s1}(2536)[±] mass and mass difference measurements.

VALUE (MeV)	DOCUMENT ID	TECN	COMMENT
422.9 ± 0.4 OUR FIT			
424 ± 28	ASRATYAN 88	HLBC	D _s [±] γ

m_{D_{s1}(2536)±} - m_{D^(*)(2010)±}

The fit includes D[±], D⁰, D_s[±], D^(*), D^{(*)0}, D₁(2420)⁰, D₂^(*)(2460)⁰, and D_{s1}(2536)[±] mass and mass difference measurements.

VALUE (MeV)	EVTS	DOCUMENT ID	TECN	COMMENT
524.85 ± 0.04 OUR FIT				
524.84 ± 0.04 OUR AVERAGE				
524.83 ± 0.01 ± 0.04	8038	10 LEES	11B	BABR 10.6 e ⁺ e ⁻ → D ^(*) + K _S ⁰ X
525.30 ^{+0.44} _{-0.41} ± 0.10	236 ± 30	CHEKANOV 09	ZEUS	e [±] p → D ^(*) + K _S ⁰ X,
				D ^{(*)0} K ⁺ X
525.3 ± 0.6 ± 0.1	41	HEISTER 02B	ALEP	e ⁺ e ⁻ → D ^(*) + K ⁰ X
524.7 ± 0.6 ± 0.2	44	ALEXANDER 93	CLE2	e ⁺ e ⁻ → D ^(*) + K _S ⁰ X

¹⁰ Assuming S-wave decay of the D_{s1}(2536) to D^(*)+ K_S⁰, using a Breit-Wigner line shape corresponding to L=0.

m_{D_{s1}(2536)±} - m_{D^(*)(2007)0}

The fit includes D[±], D⁰, D_s[±], D^(*), D^{(*)0}, D₁(2420)⁰, D₂^(*)(2460)⁰, and D_{s1}(2536)[±] mass and mass difference measurements.

VALUE (MeV)	EVTS	DOCUMENT ID	TECN	COMMENT
528.26 ± 0.05 OUR FIT	Error includes scale factor of 1.2.			
528.68 ± 0.28 OUR AVERAGE				
528.7 ± 1.9 ± 0.5	51	HEISTER 02B	ALEP	e ⁺ e ⁻ → D ^{(*)0} K ⁺ X
527.3 ± 2.2	29	ACKERSTAFF 97W	OPAL	e ⁺ e ⁻ → D ^{(*)0} K ⁺ X
528.7 ± 0.2 ± 0.2	134	ALEXANDER 93	CLE2	e ⁺ e ⁻ → D ^{(*)0} K ⁺ X

D_{s1}(2536)[±] WIDTH

VALUE (MeV)	CL% EVTS	DOCUMENT ID	TECN	COMMENT
0.92 ± 0.05 OUR AVERAGE				
1.7 ± 1.2 ± 0.6	24	11 ABLIKIM	19P	BES3 4.6 e ⁺ e ⁻ → D _s [±] D ⁰ K ⁻
0.92 ± 0.03 ± 0.04	8038	12 LEES	11B	BABR 10.6 e ⁺ e ⁻ → D ^(*) + K _S ⁰ X

••• We do not use the following data for averages, fits, limits, etc. •••

< 2.5	95	193	AUBERT	06P	BABR 10.6 e ⁺ e ⁻ → D _s [±] π [±] π ⁻ X
< 3.2	90	75	FRABETTI	94B	E687 γBe → D ^(*) + π [±] X,
					D ^{(*)0} K ⁺ X + X
< 2.3	90	ALEXANDER	93	CLEO	e ⁺ e ⁻ → D ^{(*)0} K ⁺ X
< 3.9	90	ALBRECHT	92R	ARG	10.4 e ⁺ e ⁻ → D ^{(*)0} K ⁺ X
< 5.44	90	AVERY	90	CLEO	e ⁺ e ⁻ → D ^(*) + K ⁰ X
< 4.6	90	ALBRECHT	89E	ARG	D _{s1} [±] → D ^(*) (2010) K ⁰

11 From a fit of the D_s[±] recoil mass distribution with an incoherent sum of the S-wave and S-wave Breit-Wigner line shapes.
 12 Assuming S-wave decay of the D_{s1}(2536) to D^(*)+ K_S⁰, using a Breit-Wigner line shape corresponding to L=0.
 13 Systematic uncertainties not evaluated.

D_{s1}(2536)⁺ DECAY MODES

D_{s1}(2536)⁻ modes are charge conjugates of the modes below.

Mode	Fraction (Γ _i /Γ)	Confidence level
Γ ₁ D ^(*) (2010) ⁺ K ⁰	0.85 ± 0.12	
Γ ₂ (D ^(*) (2010) ⁺ K ⁰) _{S-wave}	0.61 ± 0.09	
Γ ₃ (D ^(*) (2010) ⁺ K ⁰) _{D-wave}		
Γ ₄ D ⁺ π ⁻ K ⁺	0.028 ± 0.005	
Γ ₅ D ^(*) (2007) ⁰ K ⁺	DEFINED AS 1	
Γ ₆ D ⁺ K ⁰	< 0.34	90%
Γ ₇ D ⁰ K ⁺	< 0.12	90%
Γ ₈ D _s ⁺ γ	possibly seen	
Γ ₉ D _s [±] π [±] π ⁻	seen	

D_{s1}(2536)⁺ BRANCHING RATIOS

Γ(D ^(*) (2007) ⁰ K ⁺)/Γ(D ^(*) (2010) ⁺ K ⁰)					Γ ₅ /Γ ₁
VALUE	EVTS	DOCUMENT ID	TECN	COMMENT	
1.18 ± 0.16 OUR AVERAGE					
0.88 ± 0.24 ± 0.08	116	AUSHEV	11	BELL B → D _{s1} (2536) + D ^(*)	
2.3 ± 0.6 ± 0.3	236 ± 30	CHEKANOV 09	ZEUS	e [±] p → D ^(*) + K _S ⁰ X,	
				D ^{(*)0} K ⁺ X	
1.32 ± 0.47 ± 0.23	92	14 HEISTER	02B	ALEP e ⁺ e ⁻ → D ^(*) + K ⁰ X,	
				D ^{(*)0} K ⁺ X	
1.9 ^{+1.1} _{-0.9} ± 0.4	35	14 ACKERSTAFF	97W	OPAL e ⁺ e ⁻ → D ^{(*)0} K ⁺ X,	
				D ^(*) + K ⁰ X	
1.1 ± 0.3		ALEXANDER 93	CLEO	e ⁺ e ⁻ → D ^{(*)0} K ⁺ X, D ^(*) + K ⁰ X	
1.4 ± 0.3 ± 0.2		15 ALBRECHT	92R	ARG 10.4 e ⁺ e ⁻ → D ^{(*)0} K ⁺ X, D ^(*) + K ⁰ X	

¹⁴ Ratio of the production rates measured in Z⁰ decays.
¹⁵ Evaluated by us from published inclusive cross-sections.

Γ((D ^(*) (2010) ⁺ K ⁰) _{S-wave})/Γ(D ^(*) (2010) ⁺ K ⁰)					Γ ₂ /Γ ₁
VALUE	EVTS	DOCUMENT ID	TECN	COMMENT	
0.72 ± 0.05 ± 0.01	5485	BALAGURA 08	BELL	10.6 e ⁺ e ⁻ → D ^(*) + K ⁰ X	

Γ(D ⁺ π ⁻ K ⁺)/Γ(D ^(*) (2010) ⁺ K ⁰)					Γ ₄ /Γ ₁
VALUE (units 10 ⁻²)	EVTS	DOCUMENT ID	TECN	COMMENT	
3.27 ± 0.18 ± 0.37	1264	BALAGURA 08	BELL	10.6 e ⁺ e ⁻ → D ⁺ π ⁻ K ⁺ X	

Γ(D ⁺ K ⁰)/Γ(D ^(*) (2010) ⁺ K ⁰)					Γ ₆ /Γ ₁
VALUE	CL%	DOCUMENT ID	TECN	COMMENT	
< 0.40	90	ALEXANDER 93	CLEO	e ⁺ e ⁻ → D ^(*) + K ⁰ X	

••• We do not use the following data for averages, fits, limits, etc. •••

< 0.43	90	ALBRECHT 89E	ARG	D _{s1} [*] → D ^(*) (2010) K ⁰
--------	----	--------------	-----	---

Γ(D ⁰ K ⁺)/Γ(D ^(*) (2007) ⁰ K ⁺)					Γ ₇ /Γ ₅
VALUE	CL%	DOCUMENT ID	TECN	COMMENT	
< 0.12	90	ALEXANDER 93	CLEO	e ⁺ e ⁻ → D ^{(*)0} K ⁺ X	

Γ(D _s ⁺ γ)/Γ _{total}					Γ ₈ /Γ
VALUE	DOCUMENT ID	TECN	COMMENT		
possibly seen	ASRATYAN 88	HLBC	νN → D _s γγX		

Γ(D _s ⁺ γ)/Γ(D ^(*) (2007) ⁰ K ⁺)					Γ ₈ /Γ ₅
VALUE	CL%	DOCUMENT ID	TECN	COMMENT	
< 0.42	90	ALEXANDER 93	CLEO	e ⁺ e ⁻ → D ^{(*)0} K ⁺ X	

Γ(D _s [±] π [±] π ⁻)/Γ _{total}					Γ ₉ /Γ
VALUE	DOCUMENT ID	TECN	COMMENT		
seen	AUBERT 06P	BABR	10.6 e ⁺ e ⁻ → D _s [±] π [±] π ⁻ X		

D_{s1}(2536)[±] REFERENCES

ABLIKIM 19P	CP C43 031001	M. Ablikim et al.	(BESIII Collab.)
AUSHEV 11	PR D83 051102	T. Aushev et al.	(BELLE Collab.)
LEES 11B	PR D83 072003	J.P. Lees et al.	(BABAR Collab.)
ABAZOV 09G	PRL 102 051801	V.M. Abazov et al.	(DO Collab.)
CHEKANOV 09	EPJ C60 25	S. Chekanov et al.	(ZEUS Collab.)
AUBERT 08B	PR D77 011102	B. Aubert et al.	(BABAR Collab.)
BALAGURA 08	PR D77 032001	V. Balagura et al.	(BELLE Collab.)
AUBERT 06P	PR D74 032007	B. Aubert et al.	(BABAR Collab.)
PDG 06	JP G33 1	W.-M. Yao et al.	(PDG Collab.)
HEISTER 02B	PL B526 34	A. Heister et al.	(ALEPH Collab.)
ACKERSTAFF 97W	ZPHY C76 425	K. Ackerstaff et al.	(OPAL Collab.)
ASRATYAN 94	ZPHY C61 563	A.E. Asratyan et al.	(BIRM, BELG, CERN+)
FRABETTI 94B	PRL 72 324	P.L. Frabetti et al.	(FNAL E687 Collab.)
ALEXANDER 93	PL B303 377	J. Alexander et al.	(CLEO Collab.)
ALBRECHT 92R	PL B297 425	H. Albrecht et al.	(ARGUS Collab.)
AVERY 90	PR D41 774	P. Avery, D. Besson	(CLEO Collab.)
ALBRECHT 89E	PL B230 162	H. Albrecht et al.	(ARGUS Collab.)
ASRATYAN 88	ZPHY C40 483	A.E. Asratyan et al.	(ITEP, SERP)

See key on page 999

Meson Particle Listings

$D_{s2}^*(2573)$, $D_{s1}^*(2700)^\pm$

$D_{s2}^*(2573)$

$$I(J^P) = 0(2^+)$$

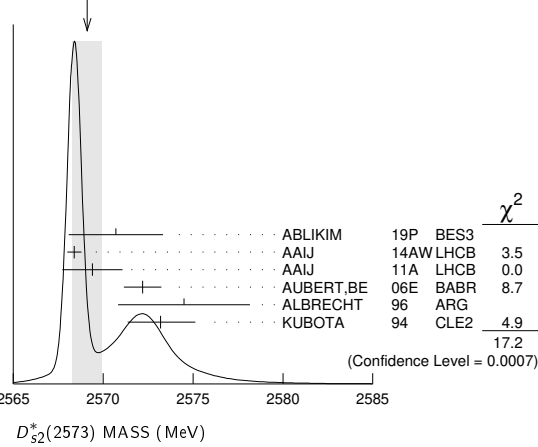
J^P is natural, width and decay modes consistent with 2^+ .
AAIJ 14AW confirms $J^P = 2^+$.

$D_{s2}^*(2573)$ MASS

VALUE (MeV)	EVTs	DOCUMENT ID	TECN	COMMENT
2569.1 ± 0.8	OUR AVERAGE	Error includes scale factor of 2.4. See the ideogram below.		
2570.7 ± 2.0 ± 1.7	62	¹ ABLIKIM 19P BES3	4.6	$e^+e^- \rightarrow D_s^+ \bar{D}^0 K^-$
2568.39 ± 0.29 ± 0.26		AAIJ 14AW LHCB	$B_s^0 \rightarrow \bar{D}^0 K^- \pi^+$	
2569.4 ± 1.6 ± 0.5	82	AAIJ 11A LHCB	$B_s \rightarrow D_{s2}^*(2573) \mu \bar{\nu} X$	
2572.2 ± 0.3 ± 1.0		AUBERT,BE 06E BABR	$e^+e^- \rightarrow DKX$	
2574.5 ± 0.3 ± 1.6		ALBRECHT 96 ARG	$e^+e^- \rightarrow D^0 K^+ X$	
2573.2 $^{+1.7}_{-1.6}$ ± 0.9	217	KUBOTA 94 CLE2	$e^+e^- \sim 10.5$ GeV	
••• We do not use the following data for averages, fits, limits, etc. •••				
2570.0 ± 4.3	25	² EVDOKIMOV 04 SELX	600	$\Sigma^- A \rightarrow D^0 K^+ X$
2568.6 ± 3.2	64	³ HEISTER 02B ALEP		$e^+e^- \rightarrow D^0 K^+ X$

¹ From a fit of the D_s^+ recoil mass distribution.
² Not independent of the mass difference below.
³ Calculated using $m_{D^0} = 1864.5 \pm 0.5$ MeV and the mass difference below.

WEIGHTED AVERAGE
2569.1±0.8 (Error scaled by 2.4)



$m_{D_{s2}^*(2573)} - m_{D^0}$

VALUE (MeV)	EVTs	DOCUMENT ID	TECN	COMMENT
704 ± 3 ± 1	64	HEISTER 02B ALEP		$e^+e^- \rightarrow D^0 K^+ X$
••• We do not use the following data for averages, fits, limits, etc. •••				
705.4 ± 4.3	25	¹ EVDOKIMOV 04 SELX	600	$\Sigma^- A \rightarrow D^0 K^+ X$

¹ Systematic errors not estimated.

$D_{s2}^*(2573)$ WIDTH

VALUE (MeV)	EVTs	DOCUMENT ID	TECN	COMMENT
16.9 ± 0.7	OUR AVERAGE			
17.2 ± 3.6 ± 1.1	62	¹ ABLIKIM 19P BES3	4.6	$e^+e^- \rightarrow D_s^+ \bar{D}^0 K^-$
16.9 ± 0.5 ± 0.6		AAIJ 14AW LHCB	$B_s^0 \rightarrow \bar{D}^0 K^- \pi^+$	
12.1 ± 4.5 ± 1.6	82	AAIJ 11A LHCB	$B_s \rightarrow D_{s2}^*(2573) \mu \bar{\nu} X$	
27.1 ± 0.6 ± 5.6		AUBERT,BE 06E BABR	$e^+e^- \rightarrow DKX$	
10.4 ± 8.3 ± 3.0		ALBRECHT 96 ARG	$e^+e^- \rightarrow D^0 K^+ X$	
16 $^{+5}_{-4}$ ± 3	217	KUBOTA 94 CLE2	$e^+e^- \sim 10.5$ GeV	
••• We do not use the following data for averages, fits, limits, etc. •••				
14 $^{+9}_{-6}$	25	² EVDOKIMOV 04 SELX	600	$\Sigma^- A \rightarrow D^0 K^+ X$

¹ From a fit of the D_s^+ recoil mass distribution.
² Systematic errors not estimated.

$D_{s2}^*(2573)^+$ DECAY MODES

$D_{s2}^*(2573)^-$ modes are charge conjugates of the modes below.

Mode	Fraction (Γ_i/Γ)
Γ_1 $D^0 K^+$	seen
Γ_2 $D^*(2007)^0 K^+$	not seen

$D_{s2}^*(2573)^+$ BRANCHING RATIOS

VALUE	EVTs	DOCUMENT ID	TECN	CHG	COMMENT	Γ_1/Γ
seen	217	KUBOTA 94 CLE2		\pm	$e^+e^- \sim 10.5$ GeV	

$\Gamma(D^*(2007)^0 K^+)/\Gamma(D^0 K^+)$

VALUE	CL%	DOCUMENT ID	TECN	CHG	COMMENT	Γ_2/Γ_1
< 0.33	90	KUBOTA 94 CLE2		$+$	$e^+e^- \sim 10.5$ GeV	

$D_{s2}^*(2573)$ REFERENCES

ABLIKIM 19P CP C43 031001	M. Ablikim et al.	(BESIII Collab.)
AAIJ 14AW PRL 113 162001	R. Aaij et al.	(LHCb Collab.) JP
AAIJ 11A PL B698 14	R. Aaij et al.	(LHCb Collab.)
AUBERT,BE 06E PRL 97 222001	B. Aubert et al.	(BABAR Collab.)
EVDOKIMOV 04 PRL 93 242001	A.V. Evdokimov et al.	(SELEX Collab.)
HEISTER 02B PL B526 34	A. Heister et al.	(ALEPH Collab.)
ALBRECHT 96 ZPHY C69 405	H. Albrecht et al.	(ARGUS Collab.)
KUBOTA 94 PRL 72 1972	Y. Kubota et al.	(CLEO Collab.)

$D_{s1}^*(2700)^\pm$

$$I(J^P) = 0(1^-)$$

$D_{s1}^*(2700)^+$ MASS

VALUE (MeV)	EVTs	DOCUMENT ID	TECN	COMMENT
2708.3 $^{+4.0}_{-3.4}$	OUR AVERAGE			
2699 $^{+14}_{-7}$		¹ LEES 15c BABR	$B \rightarrow D D^0 K^+$	
2709.2 ± 1.9 ± 4.5	52k	² AAIJ 12AU LHCB	$pp \rightarrow (DK)^+ X$ at 7 TeV	
2710 ± 2 $^{+12}_{-7}$	10.4k	³ AUBERT 09AR BABR	$e^+e^- \rightarrow D^{(*)} K X$	
2708 ± 9 $^{+11}_{-10}$	182	BRODZICKA 08 BELL	$B^+ \rightarrow D^0 \bar{D}^0 K^+$	
••• We do not use the following data for averages, fits, limits, etc. •••				
2694 ± 8 $^{+13}_{-3}$		LEES 15c BABR	$B^0 \rightarrow D^- D^0 K^+$	
2707 ± 8 ± 8		LEES 15c BABR	$B^+ \rightarrow \bar{D}^0 D^0 K^+$	
2688 ± 4 ± 3		⁴ AUBERT,BE 06E BABR	10.6 $e^+e^- \rightarrow DKX$	

¹ From a combined analysis of $B^0 \rightarrow D^- D^0 K^+$ and $B^+ \rightarrow \bar{D}^0 D^0 K^+$.
² From the combined fit of the $D^+ K_S^0$ and $D^0 K^+$ modes in the model including the $D_{s2}^*(2573)^+$, $D_{s1}^*(2700)^+$ and spin-0 $D_{s,J}^*(2860)^+$.
³ From simultaneous fits to the two DK mass spectra and to the total $D^* K$ mass spectrum.
⁴ Superseded by AUBERT 09AR.

$D_{s1}^*(2700)^+$ WIDTH

VALUE (MeV)	EVTs	DOCUMENT ID	TECN	COMMENT
120 ± 11	OUR AVERAGE			
127 $^{+24}_{-19}$		⁵ LEES 15c BABR	$B \rightarrow D D^0 K^+$	
115.8 ± 7.3 ± 12.1	52k	⁶ AAIJ 12AU LHCB	$pp \rightarrow (DK)^+ X$ at 7 TeV	
149 ± 7 $^{+39}_{-52}$	10.4k	⁷ AUBERT 09AR BABR	$e^+e^- \rightarrow D^{(*)} K X$	
108 ± 23 $^{+36}_{-31}$	182	BRODZICKA 08 BELL	$B^+ \rightarrow D^0 \bar{D}^0 K^+$	
••• We do not use the following data for averages, fits, limits, etc. •••				
145 ± 24 $^{+22}_{-14}$		LEES 15c BABR	$B^0 \rightarrow D^- D^0 K^+$	
113 ± 21 $^{+20}_{-16}$		LEES 15c BABR	$B^+ \rightarrow \bar{D}^0 D^0 K^+$	
112 ± 7 ± 36		⁸ AUBERT,BE 06E BABR	10.6 $e^+e^- \rightarrow DKX$	

⁵ From a combined analysis of $B^0 \rightarrow D^- D^0 K^+$ and $B^+ \rightarrow \bar{D}^0 D^0 K^+$.
⁶ From the combined fit of the $D^+ K_S^0$ and $D^0 K^+$ modes in the model including the $D_{s2}^*(2573)^+$, $D_{s1}^*(2700)^+$ and spin-0 $D_{s,J}^*(2860)^+$.
⁷ From simultaneous fits to the two DK mass spectra and to the total $D^* K$ mass spectrum.
⁸ Superseded by AUBERT 09AR.

$D_{s1}^*(2700)^\pm$ DECAY MODES

Mode
Γ_1 DK
Γ_2 $D^0 K^+$
Γ_3 $D^+ K_S^0$
Γ_4 $D^* K$
Γ_5 $D^{*0} K^+$
Γ_6 $D^{*+} K_S^0$

Meson Particle Listings

 $D_{s1}^*(2700)^\pm, D_{s1}^*(2860)^\pm, D_{s3}^*(2860)^\pm, D_{sJ}(3040)^\pm$
 $D_{s1}^*(2700)^\pm$ BRANCHING RATIOS

$\Gamma(D^*K)/\Gamma(DK)$	VALUE	EVTS	DOCUMENT ID	TECN	COMMENT	Γ_4/Γ_1
$0.91 \pm 0.13 \pm 0.12$	10.4k	9	AUBERT	09AR BABR	$e^+e^- \rightarrow D^{(*)}KX$	
⁹ From the average of the corresponding ratios with $D^{(*)0}K^+$ and $D^{(*)+}K_S^0$.						

$\Gamma(D^{*0}K^+)/\Gamma(D^0K^+)$	VALUE	EVTS	DOCUMENT ID	TECN	COMMENT	Γ_5/Γ_2
$0.88 \pm 0.14 \pm 0.14$	7716	10	AUBERT	09AR BABR	$e^+e^- \rightarrow D^{(*)}KX$	
¹⁰ From the $D^{*0}K^+$ and D^0K^+ , where $D^{*0} \rightarrow D^0\pi^0$.						

$\Gamma(D^{*+}K_S^0)/\Gamma(D^+K_S^0)$	VALUE	EVTS	DOCUMENT ID	TECN	COMMENT	Γ_6/Γ_3
$1.14 \pm 0.39 \pm 0.23$	2700	11	AUBERT	09AR BABR	$e^+e^- \rightarrow D^{(*)}KX$	
¹¹ From the $D^{*+}K_S^0$ and $D^+K_S^0$, where $D^{*+} \rightarrow D^+\pi^0$.						

 $D_{s1}^*(2700)^\pm$ REFERENCES

LEES	15C	PR D91 052002	J.P. Lees et al.	(BABAR Collab.)
AAIJ	12AU	JHEP 1210 151	R. Aaij et al.	(LHCb Collab.)
AUBERT	09AR	PR D80 092003	B. Aubert et al.	(BABAR Collab.)
BRODZICKA	08	PRL 100 092001	J. Brodzicka et al.	(BELLE Collab.)
AUBERT,BE	06E	PRL 97 222001	B. Aubert et al.	(BABAR Collab.)

 $D_{s1}^*(2860)^\pm \quad I(J^P) = 0(1^-)$

OMITTED FROM SUMMARY TABLE
 J^P consistent with 1^- from angular analysis of AAIJ 14AW. Observed by AUBERT,BE 06E and AUBERT 09AR in inclusive production of DK and D^*K in e^+e^- annihilation.

 $D_{s1}^*(2860)^+$ MASS

VALUE (MeV)	EVTS	DOCUMENT ID	TECN	COMMENT
$2859 \pm 12 \pm 24$		¹ AAIJ	14AW LHCb	$B_S^0 \rightarrow \bar{D}^0 K^- \pi^+$
••• We do not use the following data for averages, fits, limits, etc. •••				
$2866.1 \pm 1.0 \pm 6.3$	36k	^{2,3} AAIJ	12AU LHCb	$pp \rightarrow (DK)^+X$ at 7 TeV
$2862 \pm 2 \pm \frac{5}{2}$	3122	^{3,4} AUBERT	09AR BABR	$e^+e^- \rightarrow D^{(*)}KX$
$2856.6 \pm 1.5 \pm 5.0$		⁵ AUBERT,BE	06E BABR	$e^+e^- \rightarrow DKX$

- ¹ Separated from the spin-3 component $D_{s3}^*(2860)^-$ by a fit of the helicity angle of the $\bar{D}^0 K^-$ system, with a statistical significance of the spin-3 and spin-1 components in excess of 10σ .
² From the combined fit of the $D^+K_S^0$ and D^0K^+ modes in the model including the $D_{s2}^*(2573)^+$, $D_{s1}^*(2700)^+$ and spin-0 $D_{sJ}^*(2860)^+$.
³ Possible contribution from the $D_{s3}^*(2860)$ state.
⁴ From simultaneous fits to the two DK mass spectra and to the total D^*K mass spectrum.
⁵ Superseded by AUBERT 09AR.

 $D_{s1}^*(2860)^+$ WIDTH

VALUE (MeV)	EVTS	DOCUMENT ID	TECN	COMMENT
$159 \pm 23 \pm 77$		¹ AAIJ	14AW LHCb	$B_S^0 \rightarrow \bar{D}^0 K^- \pi^+$
••• We do not use the following data for averages, fits, limits, etc. •••				
$69.9 \pm 3.2 \pm 6.6$	36k	^{2,3} AAIJ	12AU LHCb	$pp \rightarrow (DK)^+X$ at 7 TeV
$48 \pm 3 \pm 6$	3122	^{3,4} AUBERT	09AR BABR	$e^+e^- \rightarrow D^{(*)}KX$
$47 \pm 7 \pm 10$		⁵ AUBERT,BE	06E BABR	$e^+e^- \rightarrow DKX$

- ¹ Separated from the spin-3 component $D_{s3}^*(2860)^-$ by a fit of the helicity angle of the $\bar{D}^0 K^-$ system, with a statistical significance of the spin-3 and spin-1 components in excess of 10σ .
² From the combined fit of the $D^+K_S^0$ and D^0K^+ modes in the model including the $D_{s2}^*(2573)^+$, $D_{s1}^*(2700)^+$ and spin-0 $D_{sJ}^*(2860)^+$.
³ Possible contribution from the $D_{s3}^*(2860)$ state.
⁴ From simultaneous fits to the two DK mass spectra and to the total D^*K mass spectrum.
⁵ Superseded by AUBERT 09AR.

 $D_{s1}^*(2860)^\pm$ DECAY MODES

Mode
Γ_1 DK
Γ_2 D^0K^+
Γ_3 $D^+K_S^0$
Γ_4 D^*K
Γ_5 $D^{*0}K^+$
Γ_6 $D^{*+}K_S^0$

 $D_{s1}^*(2860)^\pm$ BRANCHING RATIOS

$\Gamma(D^*K)/\Gamma(DK)$	VALUE	EVTS	DOCUMENT ID	TECN	COMMENT	Γ_4/Γ_1
$1.10 \pm 0.15 \pm 0.19$	3122	1	AUBERT	09AR BABR	$e^+e^- \rightarrow D^{(*)}KX$	
¹ From the average of the corresponding ratios with $D^{(*)0}K^+$ and $D^{(*)+}K_S^0$.						

$\Gamma(D^{*0}K^+)/\Gamma(D^0K^+)$	VALUE	EVTS	DOCUMENT ID	TECN	COMMENT	Γ_5/Γ_2
$1.04 \pm 0.17 \pm 0.20$	2241	1	AUBERT	09AR BABR	$e^+e^- \rightarrow D^{(*)}KX$	
¹ From the $D^{*0}K^+$ and D^0K^+ , where $D^{*0} \rightarrow D^0\pi^0$.						

$\Gamma(D^{*+}K_S^0)/\Gamma(D^+K_S^0)$	VALUE	EVTS	DOCUMENT ID	TECN	COMMENT	Γ_6/Γ_3
$1.38 \pm 0.35 \pm 0.49$	881	1	AUBERT	09AR BABR	$e^+e^- \rightarrow D^{(*)}KX$	
¹ From the $D^{*+}K_S^0$ and $D^+K_S^0$, where $D^{*+} \rightarrow D^+\pi^0$.						

 $D_{s1}^*(2860)^\pm$ REFERENCES

AAIJ	14AW	PRL 113 162001	R. Aaij et al.	(LHCb Collab.)JP
AAIJ	12AU	JHEP 1210 151	R. Aaij et al.	(LHCb Collab.)
AUBERT	09AR	PR D80 092003	B. Aubert et al.	(BABAR Collab.)
AUBERT,BE	06E	PRL 97 222001	B. Aubert et al.	(BABAR Collab.)

 $D_{s3}^*(2860)^\pm \quad I(J^P) = 0(3^-)$

OMITTED FROM SUMMARY TABLE
 J^P consistent with 3^- from angular analysis of AAIJ 14AW.

 $D_{s3}^*(2860)^+$ MASS

VALUE (MeV)	DOCUMENT ID	TECN	COMMENT
$2860.5 \pm 2.6 \pm 6.5$	¹ AAIJ	14AW LHCb	$B_S^0 \rightarrow \bar{D}^0 K^- \pi^+$
¹ Separated from the spin-1 component $D_{s1}^*(2860)^-$ by a fit of the helicity angle of the $\bar{D}^0 K^-$ system, with a statistical significance of the spin-3 and spin-1 components in excess of 10σ .			

 $D_{s3}^*(2860)^+$ WIDTH

VALUE (MeV)	DOCUMENT ID	TECN	COMMENT
$53 \pm 7 \pm 7$	¹ AAIJ	14AW LHCb	$B_S^0 \rightarrow \bar{D}^0 K^- \pi^+$
¹ Separated from the spin-1 component $D_{s1}^*(2860)^-$ by a fit of the helicity angle of the $\bar{D}^0 K^-$ system, with a statistical significance of the spin-3 and spin-1 components in excess of 10σ .			

 $D_{s3}^*(2860)^\pm$ REFERENCES

AAIJ	14AW	PRL 113 162001	R. Aaij et al.	(LHCb Collab.)JP
------	------	----------------	----------------	------------------

 $D_{sJ}(3040)^\pm \quad I(J^P) = 0(?^?)$

OMITTED FROM SUMMARY TABLE
 Observed by AUBERT 09AR in inclusive production of D^*K in e^+e^- annihilation.

 $D_{sJ}(3040)^+$ MASS

VALUE (MeV)	DOCUMENT ID	TECN	COMMENT
$3044 \pm 8 \pm \frac{30}{5}$	AUBERT	09AR BABR	$e^+e^- \rightarrow D^*KX$

 $D_{sJ}(3040)^+$ WIDTH

VALUE (MeV)	DOCUMENT ID	TECN	COMMENT
$239 \pm 35 \pm \frac{46}{42}$	AUBERT	09AR BABR	$e^+e^- \rightarrow D^*KX$

 $D_{sJ}(3040)^\pm$ DECAY MODES

Mode
Γ_1 D^*K
Γ_2 $D^{*0}K^+$
Γ_3 $D^{*+}K_S^0$

 $D_{sJ}(3040)^\pm$ REFERENCES

AUBERT	09AR	PR D80 092003	B. Aubert et al.	(BABAR Collab.)
--------	------	---------------	------------------	-----------------

BOTTOM MESONS**($B = \pm 1$)** $B^+ = u\bar{b}$, $B^0 = d\bar{b}$, $\bar{B}^0 = \bar{d}b$, $B^- = \bar{u}b$, similarly for B^{*s} **B-particle organization**

Many measurements of B decays involve admixtures of B hadrons. Previously we arbitrarily included such admixtures in the B^\pm section, but because of their importance we have created two new sections: “ B^\pm/B^0 Admixture” for $\Upsilon(4S)$ results and “ $B^\pm/B^0/B_s^0/b$ -baryon Admixture” for results at higher energies. Most inclusive decay branching fractions and χ_b at high energy are found in the Admixture sections. B^0/\bar{B}^0 mixing data are found in the B^0 section, while B_s^0/\bar{B}_s^0 mixing data and $B-\bar{B}$ mixing data for a B^0/B_s^0 admixture are found in the B_s^0 section. CP -violation data are found in the B^\pm , B^0 , and B^\pm/B^0 Admixture sections. b -baryons are found near the end of the Baryon section. Recently, we also created a new section: “ V_{cb} and V_{ub} CKM Matrix Elements.”

The organization of the B sections is now as follows, where bullets indicate particle sections and brackets indicate reviews.

[Production and Decay of *b*-flavored Hadrons]

[A Short Note on HFLAV Activities]

- B^\pm
 - mass, mean life
 - branching fractions
 - polarization in B^\pm decay
 - CP violation
- B^0
 - mass, mean life
 - branching fractions
 - [Polarization in B decay]
 - polarization in B^0 decay
 - [$B-\bar{B}$ Mixing]
 - B^0/\bar{B}^0 mixing
 - CP violation
- B^\pm/B^0 Admixture
 - branching fractions, CP violation
 - CP violation
- $B^\pm/B^0/B_s^0/b$ -baryon Admixture
 - mean life
 - production fractions
 - branching fractions
 - χ_b at high energy
 - production fractions in hadronic Z decay
- V_{cb} and V_{ub} CKM Matrix Elements
 - [Determination of V_{cb} and V_{ub}]
- B^*
 - mass
- $B_1(5721)^0$
 - mass
- $B_J^*(5732)$
 - mass, width
- $B_2(5747)^0$
 - mass
- B_s^0
 - mass, mean life
 - branching fractions
 - polarization in B_s^0 decay
 - B_s^0/\bar{B}_s^0 mixing
- B_s^*
 - mass
- $B_{s,J}^*(5850)$
 - mass, width
- B_c^\pm
 - mass, mean life
 - branching fractions

At the end of Baryon Listings:

- Λ_b
 - mass, mean life
 - branching fractions
- Σ_b^* , Σ_b^{*s}
 - mass
- Ξ_b^0 , Ξ_b^-
 - mean life
- Ω_b^-
 - mass, mean life
 - branching fractions
- b -baryon Admixture
 - mean life
 - branching fractions

See the related review(s):**Production and Decay of *b*-flavored Hadrons****HEAVY FLAVOR AVERAGING GROUP**

Revised August 2019 by U. Egede (Monash University) and A. Soffer (Tel Aviv University)

The Heavy Flavor Averaging Group (HFLAV)* is an international collaboration of physicists from experiments measuring properties of heavy flavored particles, *i.e.*, hadrons containing b and c quarks, and τ leptons. HFLAV calculates and publishes [1] world average values of quantities such as lifetimes, branching fractions, form factors, mixing parameters, and CP -violating asymmetries. Most parameters concern decays of B and D mesons, and many are related to elements of the Cabibbo-Kobayashi-Maskawa (CKM) quark mixing matrix [2], [3].

HFLAV was originally formed in 2002 to continue the activities of the LEP Heavy Flavor Steering group. Since its inception, a wide range of results have become available from increasingly larger data sets. Consequently, HFLAV has expanded to include seven subgroups:

- b -hadron lifetimes and oscillations, including parameters of CP violation in b mixing;
- decay-time-dependent CP violation in B decays, and angles of the CKM Unitarity Triangle;
- semileptonic decays of b -hadrons ($B \rightarrow X\ell\nu$, $\ell = e, \mu, \tau$), including determinations of the CKM matrix elements $|V_{cb}|$ and $|V_{ub}|$;
- b -hadron decays to hadronic final states containing c -quarks (open charm and charmonium);
- (rarer) b -hadron decays to final states not containing c -quarks, including fully hadronic, semileptonic ($B \rightarrow X\ell\ell, X\nu\bar{\nu}$), leptonic, and radiative decays;
- c -hadron physics including branching fractions, CP - and T -violating asymmetries, D^0/\bar{D}^0 mixing, semileptonic decays, and properties of excited D states and charm baryons;
- τ -lepton physics including branching fractions, tests of lepton universality, determination of the CKM matrix element $|V_{us}|$, and searches for lepton flavor violation.

* The group was originally referred to as “HFAG.” This acronym was changed to “HFLAV” in 2017.

Meson Particle Listings

b -flavored hadrons, B^\pm

Each subgroup has one or two conveners and typically a half-dozen members representing experiments that conduct measurements in that area. Most groups contain representatives from the BABAR, Belle, Belle II and LHCb experiments, and some groups have representatives from the ATLAS, BESIII, CLEO(c), CDF, CMS and D0 experiments. Members of HFLAV are appointed by their respective experimental collaborations. HFLAV has two co-leaders, who are appointed by the managements of Belle II and LHCb.

The averaging procedures used by HFLAV are similar to those of the PDG [4]. When calculating world averages, common parameters used for different input measurements are adjusted (rescaled) to common values. The confidence level of the fit is provided to indicate the consistency of the measurements included in the average. However, unlike the PDG, when obtaining a world average with a small confidence level (*i.e.*, a large χ^2 per degree of freedom), HFLAV does not usually scale the resulting uncertainty. Rather, the systematic uncertainties of the measurements are reviewed with experts from the experiments to understand the discrepancy. Unless inconsistencies among measurements are found, no correction is made to the calculated uncertainty. Close communication between representatives of the experiments and HFLAV members who perform averages helps ensure that measurement uncertainties, known correlations, and systematic effects are properly accounted for. If a special treatment is needed to calculate an average, or if an approximation used in an average calculation might not be sufficiently accurate (*e.g.*, assuming Gaussian uncertainties when the likelihood function is non-Gaussian), a note is included in the HFLAV publication and online documentation to describe this.

In general, HFLAV uses all publicly available results that have written documentation such as a journal publication, preprint, or conference note. These include preliminary results presented at conferences and workshops. However, preliminary results that remain unpublished for an extended period of time, or for which no publication is planned, are not included. A special subset of HFLAV averages are included in the PDG listings; for these averages, only measurements that are published or accepted for publication are used. The averages provided by HFLAV are listed by the PDG as “OUR EVALUATION” with a corresponding note.

All HFLAV averages and input measurements are documented in an approximately biennial journal paper or preprint; the most recent version is Ref. [1]. The latest results and plots are posted on an extensive set of webpages that are updated several times per year; these are available at

<https://hflav.web.cern.ch>.

References:

1. Y. Amhis *et al.* (Heavy Flavor Averaging Group) (2018), [arXiv:1909.12524], updated results and plots available at <https://hflav.web.cern.ch/>.
2. N. Cabibbo, Phys. Rev. Lett. **10**, 531 (1963).

3. M. Kobayashi and T. Maskawa, Prog. Theor. Phys. **49**, 652 (1973).
4. See Section 5 of the “Introduction” to this *Review*.

B^\pm

$$I(J^P) = \frac{1}{2}(0^-)$$

Quantum numbers not measured. Values shown are quark-model predictions.

See also the B^\pm/B^0 ADMIXTURE and $B^\pm/B^0/B_s^0/b$ -baryon ADMIXTURE sections.

B^\pm MASS

The fit uses m_{B^\pm} , ($m_{B^0} - m_{B^\pm}$), and m_{B^0} to determine m_{B^\pm} , m_{B^0} , and the mass difference.

VALUE (MeV)	EVTs	DOCUMENT ID	TECN	COMMENT
5279.34 ± 0.12 OUR FIT				
5279.25 ± 0.26 OUR AVERAGE				
5279.38 ± 0.11 ± 0.33		¹ AAIJ	12E	LHCB $p\bar{p}$ at 7 TeV
5279.10 ± 0.41 ± 0.36		² ACOSTA	06	CDF $p\bar{p}$ at 1.96 TeV
5279.1 ± 0.4 ± 0.4	526	³ CSORNA	00	CLE2 $e^+e^- \rightarrow \Upsilon(4S)$
5279.1 ± 1.7 ± 1.4	147	ABE	96B	CDF $p\bar{p}$ at 1.8 TeV
••• We do not use the following data for averages, fits, limits, etc. •••				
5278.8 ± 0.54 ± 2.0	362	ALAM	94	CLE2 $e^+e^- \rightarrow \Upsilon(4S)$
5278.3 ± 0.4 ± 2.0		BORTOLETTI	092	CLEO $e^+e^- \rightarrow \Upsilon(4S)$
5280.5 ± 1.0 ± 2.0		⁴ ALBRECHT	90J	ARG $e^+e^- \rightarrow \Upsilon(4S)$
5275.8 ± 1.3 ± 3.0	32	ALBRECHT	87C	ARG $e^+e^- \rightarrow \Upsilon(4S)$
5278.2 ± 1.8 ± 3.0	12	⁵ ALBRECHT	87D	ARG $e^+e^- \rightarrow \Upsilon(4S)$
5278.6 ± 0.8 ± 2.0		BEBEK	87	CLEO $e^+e^- \rightarrow \Upsilon(4S)$
¹ Uses $B^+ \rightarrow J/\psi K^+$ fully reconstructed decays.				
² Uses exclusively reconstructed final states containing a $J/\psi \rightarrow \mu^+\mu^-$ decays.				
³ CSORNA 00 uses fully reconstructed 526 $B^+ \rightarrow J/\psi(\ell) K^+$ events and invariant masses without beam constraint.				
⁴ ALBRECHT 90J assumes 10580 for $\Upsilon(4S)$ mass. Supersedes ALBRECHT 87C and ALBRECHT 87D.				
⁵ Found using fully reconstructed decays with $J/\psi(1S)$. ALBRECHT 87D assume $m_{\Upsilon(4S)} = 10577$ MeV.				

B^\pm MEAN LIFE

See $B^\pm/B^0/B_s^0/b$ -baryon ADMIXTURE section for data on B -hadron mean life averaged over species of bottom particles.

“OUR EVALUATION” is an average using rescaled values of the data listed below. The average and rescaling were performed by the Heavy Flavor Averaging Group (HFLAV) and are described at <https://hflav.web.cern.ch/>. The averaging/rescaling procedure takes into account correlations between the measurements and asymmetric lifetime errors.

VALUE (10^{-12} s)	EVTs	DOCUMENT ID	TECN	COMMENT
1.638 ± 0.004 OUR EVALUATION				
1.637 ± 0.004 ± 0.003		AAIJ	14E	LHCB $p\bar{p}$ at 7 TeV
1.639 ± 0.009 ± 0.009		¹ AALTONEN	11	CDF $p\bar{p}$ at 1.96 TeV
1.663 ± 0.023 ± 0.015		² AALTONEN	11B	CDF $p\bar{p}$ at 1.96 TeV
1.635 ± 0.011 ± 0.011		³ ABE	05B	BELL $e^+e^- \rightarrow \Upsilon(4S)$
1.624 ± 0.014 ± 0.018		⁴ ABDALLAH	04E	DLPH $e^+e^- \rightarrow Z$
1.636 ± 0.058 ± 0.025		⁵ ACOSTA	02C	CDF $p\bar{p}$ at 1.8 TeV
1.673 ± 0.032 ± 0.023		⁶ AUBERT	01F	BABR $e^+e^- \rightarrow \Upsilon(4S)$
1.648 ± 0.049 ± 0.035		⁷ BARATE	00R	ALEP $e^+e^- \rightarrow Z$
1.643 ± 0.037 ± 0.025		⁸ ABBIENDI	99J	OPAL $e^+e^- \rightarrow Z$
1.637 ± 0.058 $^{+0.045}_{-0.043}$		⁷ ABE	98Q	CDF $p\bar{p}$ at 1.8 TeV
1.66 ± 0.06 ± 0.03		⁸ ACCIARRI	98S	L3 $e^+e^- \rightarrow Z$
1.66 ± 0.06 ± 0.05		⁸ ABE	97J	SLD $e^+e^- \rightarrow Z$
1.58 $^{+0.21}_{-0.18}$ $^{+0.04}_{-0.03}$	94	⁵ BUSKULIC	96J	ALEP $e^+e^- \rightarrow Z$
1.61 ± 0.16 ± 0.12		^{7,9} ABREU	95Q	DLPH $e^+e^- \rightarrow Z$
1.72 ± 0.08 ± 0.06		¹⁰ ADAM	95	DLPH $e^+e^- \rightarrow Z$
1.52 ± 0.14 ± 0.09		⁷ AKERS	95T	OPAL $e^+e^- \rightarrow Z$
••• We do not use the following data for averages, fits, limits, etc. •••				
1.695 ± 0.026 ± 0.015		⁶ ABE	02H	BELL Repl. by ABE 05B
1.68 ± 0.07 ± 0.02		⁵ ABE	98B	CDF Repl. by ACOSTA 02C
1.56 ± 0.13 ± 0.06		⁷ ABE	96C	CDF Repl. by ABE 98Q
1.58 ± 0.09 ± 0.03		¹¹ BUSKULIC	96J	ALEP $e^+e^- \rightarrow Z$
1.58 ± 0.09 ± 0.04		⁷ BUSKULIC	96J	ALEP Repl. by BARATE 00R
1.70 ± 0.09		¹² ADAM	95	DLPH $e^+e^- \rightarrow Z$
1.61 ± 0.16 ± 0.05	148	⁵ ABE	94D	CDF Repl. by ABE 98B
1.30 $^{+0.33}_{-0.29}$ ± 0.16	92	⁷ ABREU	93D	DLPH Sup. by ABREU 95Q
1.56 ± 0.19 ± 0.13	134	¹⁰ ABREU	93G	DLPH Sup. by ADAM 95
1.51 $^{+0.30}_{-0.28}$ $^{+0.12}_{-0.14}$	59	⁷ ACTON	93C	OPAL Sup. by AKERS 95T
1.47 $^{+0.22}_{-0.19}$ $^{+0.15}_{-0.14}$	77	⁷ BUSKULIC	93D	ALEP Sup. by BUSKULIC 96J

- ¹ Measured mean life using fully reconstructed decays ($J/\psi K^{(*)}$).
- ² Measured using $B^- \rightarrow D^0 \pi^-$ with $D^0 \rightarrow K^- \pi^+$ events that were selected using a silicon vertex trigger.
- ³ Measurement performed using a combined fit of CP -violation, mixing and lifetimes.
- ⁴ Measurement performed using an inclusive reconstruction and B flavor identification technique.
- ⁵ Measured mean life using fully reconstructed decays.
- ⁶ Events are selected in which one B meson is fully reconstructed while the second B meson is reconstructed inclusively.
- ⁷ Data analyzed using $D/D^* \ell X$ event vertices.
- ⁸ Data analyzed using charge of secondary vertex.
- ⁹ ABREU 95q assumes $B(B^0 \rightarrow D^{*-} \ell^+ \nu_\ell) = 3.2 \pm 1.7\%$.
- ¹⁰ Data analyzed using vertex-charge technique to tag B charge.
- ¹¹ Combined result of $D/D^* \ell X$ analysis and fully reconstructed B analysis.
- ¹² Combined ABREU 95q and ADAM 95 result.

τ_{B^+}/τ_{B^-}	DOCUMENT ID	TECN	COMMENT
1.002 ± 0.004 ± 0.002	¹ AAIJ	14E	LHCB pp at 7 TeV

¹ Measured using $B^\pm \rightarrow J/\psi K^\pm$ decays.

B^+ DECAY MODES

B^- modes are charge conjugates of the modes below. Modes which do not identify the charge state of the B are listed in the B^\pm/B^0 ADMIXTURE section.

The branching fractions listed below assume 50% $B^0 \bar{B}^0$ and 50% $B^+ B^-$ production at the $\Upsilon(4S)$. We have attempted to bring older measurements up to date by rescaling their assumed $\Upsilon(4S)$ production ratio to 50:50 and their assumed D, D_s, D^* , and ψ branching ratios to current values whenever this would affect our averages and best limits significantly.

Indentation is used to indicate a subchannel of a previous reaction. All resonant subchannels have been corrected for resonance branching fractions to the final state so the sum of the subchannel branching fractions can exceed that of the final state.

For inclusive branching fractions, e.g., $B \rightarrow D^\pm X$, the values usually are multiplicities, not branching fractions. They can be greater than one.

Mode	Fraction (Γ_i/Γ)	Scale factor/ Confidence level
Semileptonic and leptonic modes		
Γ_1 $\ell^+ \nu_\ell X$	[a] (10.99 ± 0.28) %	
Γ_2 $e^+ \nu_e X_c$	(10.8 ± 0.4) %	
Γ_3 $D \ell^+ \nu_\ell X$	(9.7 ± 0.7) %	
Γ_4 $\bar{D}^0 \ell^+ \nu_\ell$	[a] (2.35 ± 0.09) %	
Γ_5 $\bar{D}^0 \tau^+ \nu_\tau$	(7.7 ± 2.5) × 10 ⁻³	
Γ_6 $\bar{D}^*(2007)^0 \ell^+ \nu_\ell$	[a] (5.66 ± 0.22) %	
Γ_7 $\bar{D}^*(2007)^0 \tau^+ \nu_\tau$	(1.88 ± 0.20) %	
Γ_8 $D^- \pi^+ \ell^+ \nu_\ell$	(4.4 ± 0.4) × 10 ⁻³	
Γ_9 $\bar{D}_0^*(2420)^0 \ell^+ \nu_\ell, \bar{D}_0^{*0} \rightarrow$	(2.5 ± 0.5) × 10 ⁻³	
Γ_{10} $D^- \pi^+ \nu_\ell, \bar{D}_2^*(2460)^0 \ell^+ \nu_\ell, \bar{D}_2^{*0} \rightarrow$	(1.53 ± 0.16) × 10 ⁻³	
Γ_{11} $D^*(n) \pi \ell^+ \nu_\ell (n \geq 1)$	(1.88 ± 0.25) %	
Γ_{12} $D^{*-} \pi^+ \ell^+ \nu_\ell$	(6.0 ± 0.4) × 10 ⁻³	
Γ_{13} $\bar{D}_1^*(2420)^0 \ell^+ \nu_\ell, \bar{D}_1^{*0} \rightarrow$	(3.03 ± 0.20) × 10 ⁻³	
Γ_{14} $D_1^{*-} \pi^+ \ell^+ \nu_\ell, \bar{D}_1^{*0} \rightarrow$	(2.7 ± 0.6) × 10 ⁻³	
Γ_{15} $\bar{D}_2^{*-} \pi^+ \ell^+ \nu_\ell, \bar{D}_2^{*0} \rightarrow$	(1.01 ± 0.24) × 10 ⁻³	S=2.0
Γ_{16} $\bar{D}^0 \pi^+ \pi^- \ell^+ \nu_\ell$	(1.7 ± 0.4) × 10 ⁻³	
Γ_{17} $\bar{D}^{*0} \pi^+ \pi^- \ell^+ \nu_\ell$	(8 ± 5) × 10 ⁻⁴	
Γ_{18} $D_s^{(*)-} K^+ \ell^+ \nu_\ell$	(6.1 ± 1.0) × 10 ⁻⁴	
Γ_{19} $D_s^- K^+ \ell^+ \nu_\ell$	(3.0 ± 1.4) × 10 ⁻⁴	
Γ_{20} $D_s^{*-} K^+ \ell^+ \nu_\ell$	(2.9 ± 1.9) × 10 ⁻⁴	
Γ_{21} $\pi^0 \ell^+ \nu_\ell$	(7.80 ± 0.27) × 10 ⁻⁵	
Γ_{22} $\pi^0 e^+ \nu_e$		
Γ_{23} $\eta \ell^+ \nu_\ell$	(3.9 ± 0.5) × 10 ⁻⁵	
Γ_{24} $\eta' \ell^+ \nu_\ell$	(2.3 ± 0.8) × 10 ⁻⁵	
Γ_{25} $\omega \ell^+ \nu_\ell$	[a] (1.19 ± 0.09) × 10 ⁻⁴	
Γ_{26} $\omega \mu^+ \nu_\mu$		
Γ_{27} $\rho^0 \ell^+ \nu_\ell$	[a] (1.58 ± 0.11) × 10 ⁻⁴	
Γ_{28} $p \bar{p} \ell^+ \nu_\ell$	(5.8 ± 2.6) × 10 ⁻⁶	
Γ_{29} $p \bar{p} \mu^+ \nu_\mu$	< 8.5 × 10 ⁻⁶	CL=90%

Γ_{30} $p \bar{p} e^+ \nu_e$	(8.2 ± 4.0) × 10 ⁻⁶	
Γ_{31} $e^+ \nu_e$	< 9.8 × 10 ⁻⁷	CL=90%
Γ_{32} $\mu^+ \nu_\mu$	2.90 × 10 ⁻⁰⁷ to 1.07 × 10 ⁻⁰⁶	CL=90%
Γ_{33} $\tau^+ \nu_\tau$	(1.09 ± 0.24) × 10 ⁻⁴	S=1.2
Γ_{34} $\ell^+ \nu_\ell \gamma$	< 3.0 × 10 ⁻⁶	CL=90%
Γ_{35} $e^+ \nu_e \gamma$	< 4.3 × 10 ⁻⁶	CL=90%
Γ_{36} $\mu^+ \nu_\mu \gamma$	< 3.4 × 10 ⁻⁶	CL=90%
Γ_{37} $\mu^+ \mu^- \mu^+ \nu_\mu$	< 1.6 × 10 ⁻⁸	CL=95%

Inclusive modes

Γ_{38} $D^0 X$	(8.6 ± 0.7) %
Γ_{39} $\bar{D}^0 X$	(79 ± 4) %
Γ_{40} $D^+ X$	(2.5 ± 0.5) %
Γ_{41} $D^- X$	(9.9 ± 1.2) %
Γ_{42} $D_s^+ X$	(7.9 ± 1.4) %
Γ_{43} $D_s^- X$	(1.10 ± 0.40) %
Γ_{44} $\Lambda_c^+ X$	(2.1 ± 0.9) %
Γ_{45} $\bar{\Lambda}_c^- X$	(2.8 ± 1.1) %
Γ_{46} $\bar{c} X$	(97 ± 4) %
Γ_{47} $c X$	(23.4 ± 2.2) %
Γ_{48} $c/\bar{c} X$	(120 ± 6) %

D, D^* , or D_s modes

Γ_{49} $\bar{D}^0 \pi^+$	(4.68 ± 0.13) × 10 ⁻³
Γ_{50} $D_{CP(+1)} \pi^+$	[b] (2.05 ± 0.18) × 10 ⁻³
Γ_{51} $D_{CP(-1)} \pi^+$	[b] (2.0 ± 0.4) × 10 ⁻³
Γ_{52} $\bar{D}^0 \rho^+$	(1.34 ± 0.18) %
Γ_{53} $\bar{D}^0 K^+$	(3.63 ± 0.12) × 10 ⁻⁴
Γ_{54} $D_{CP(+1)} K^+$	[b] (1.80 ± 0.07) × 10 ⁻⁴
Γ_{55} $D_{CP(-1)} K^+$	[b] (1.96 ± 0.18) × 10 ⁻⁴
Γ_{56} $D^0 K^+$	(3.57 ± 0.35) × 10 ⁻⁶
Γ_{57} $[K^- \pi^+]_D K^+$	[c] < 2.8 × 10 ⁻⁷
Γ_{58} $[K^+ \pi^-]_D K^+$	[c] < 1.5 × 10 ⁻⁵
Γ_{59} $[K^- \pi^+ \pi^0]_D K^+$	seen
Γ_{60} $[K^+ \pi^- \pi^0]_D K^+$	seen
Γ_{61} $[K^- \pi^+ \pi^+ \pi^-]_D K^+$	seen
Γ_{62} $[K^+ \pi^- \pi^+ \pi^-]_D K^+$	seen
Γ_{63} $[\pi^+ \pi^+ \pi^- \pi^-] K^+$	
Γ_{64} $[\pi^+ \pi^- \pi^+ \pi^-]_D K^*(892)^+$	
Γ_{65} $[K^- \pi^+]_D K^*(892)^+$	[c]
Γ_{66} $[K^+ \pi^-]_D K^*(892)^+$	[c]
Γ_{67} $[K^- \pi^+ \pi^- \pi^+]_D K^*(892)^+$	
Γ_{68} $[K^+ \pi^- \pi^+ \pi^-]_D K^*(892)^+$	
Γ_{69} $[K^- \pi^+]_D \pi^+$	[c] (6.3 ± 1.1) × 10 ⁻⁷
Γ_{70} $[K^+ \pi^-]_D \pi^+$	(1.78 ± 0.32) × 10 ⁻⁴
Γ_{71} $[K^- \pi^+ \pi^0]_D \pi^+$	seen
Γ_{72} $[K^+ \pi^- \pi^0]_D \pi^+$	seen
Γ_{73} $[K^- \pi^+ \pi^+ \pi^-]_D \pi^+$	seen
Γ_{74} $[K^+ \pi^- \pi^+ \pi^-]_D \pi^+$	seen
Γ_{75} $[K^- \pi^+]_{(D\pi)} \pi^+$	
Γ_{76} $[K^+ \pi^-]_{(D\pi)} \pi^+$	
Γ_{77} $[K^- \pi^+]_{(D\gamma)} \pi^+$	
Γ_{78} $[K^+ \pi^-]_{(D\gamma)} \pi^+$	
Γ_{79} $[K^- \pi^+]_{(D\pi)} K^+$	
Γ_{80} $[K^+ \pi^-]_{(D\pi)} K^+$	
Γ_{81} $[K^- \pi^+]_{(D\gamma)} K^+$	
Γ_{82} $[K^+ \pi^-]_{(D\gamma)} K^+$	
Γ_{83} $[\pi^+ \pi^- \pi^0]_D K^-$	(4.6 ± 0.9) × 10 ⁻⁶
Γ_{84} $[K_S^0 K^+ \pi^-]_D K^+$	seen
Γ_{85} $[K_S^0 K^- \pi^+]_D K^+$	seen
Γ_{86} $[K^*(892)^+ K^-]_D K^+$	seen
Γ_{87} $[K_S^0 K^- \pi^+]_D \pi^+$	seen
Γ_{88} $[K^*(892)^+ K^-]_D \pi^+$	seen
Γ_{89} $[K_S^0 K^+ \pi^-]_D \pi^+$	seen
Γ_{90} $[K^*(892)^- K^+]_D \pi^+$	seen
Γ_{91} $[K^+ K^- \pi^0]_D K^+$	
Γ_{92} $[K^+ K^- \pi^0]_D \pi^+$	
Γ_{93} $[\pi^+ \pi^- \pi^0]_D K^+$	
Γ_{94} $[\pi^+ \pi^- \pi^0]_D \pi^+$	
Γ_{95} $\bar{D}^0 K^*(892)^+$	(5.3 ± 0.4) × 10 ⁻⁴

Meson Particle Listings

B^\pm

Γ ₉₆	$D_{CP(-)} K^*(892)^+$	[b]	$(2.7 \pm 0.8) \times 10^{-4}$	Γ ₁₅₄	$\bar{D}_2^*(2462)^0 \pi^+$		$(1.8 \pm 0.5) \times 10^{-4}$
Γ ₉₇	$D_{CP(+)} K^*(892)^+$	[b]	$(6.2 \pm 0.7) \times 10^{-4}$		$\times B(\bar{D}_3^*(2462)^0 \rightarrow D^{*-} \pi^+)$		
Γ ₉₈	$D^0 K^*(892)^+$		$(3.1 \pm 1.6) \times 10^{-6}$	Γ ₁₅₅	$\bar{D}_1^*(2427)^0 \pi^+$		$(5.0 \pm 1.2) \times 10^{-4}$
Γ ₉₉	$\bar{D}^0 K^+ \pi^+ \pi^-$		$(5.2 \pm 2.1) \times 10^{-4}$		$\times B(\bar{D}_1^*(2427)^0 \rightarrow D^{*-} \pi^+)$		
Γ ₁₀₀	$[K^+ \pi^-]_D K^+ \pi^- \pi^+$			Γ ₁₅₆	$\bar{D}_1(2420)^0 \pi^+ \times B(\bar{D}_1^0 \rightarrow$	< 6	$\times 10^{-6}$ CL=90%
Γ ₁₀₁	$[K^- \pi^+]_D K^+ \pi^- \pi^+$				$\bar{D}^{*0} \pi^+ \pi^-)$		
Γ ₁₀₂	$D_{CP(+)} K^+ \pi^- \pi^+$			Γ ₁₅₇	$\bar{D}_1^*(2420)^0 \rho^+$	< 1.4	$\times 10^{-3}$ CL=90%
Γ ₁₀₃	$\bar{D}^0 K^+ \bar{K}^0$		$(5.5 \pm 1.6) \times 10^{-4}$	Γ ₁₅₈	$\bar{D}_2^*(2460)^0 \pi^+$	< 1.3	$\times 10^{-3}$ CL=90%
Γ ₁₀₄	$\bar{D}^0 K^+ \bar{K}^*(892)^0$		$(7.5 \pm 1.7) \times 10^{-4}$	Γ ₁₅₉	$\bar{D}_2^*(2460)^0 \pi^+ \times B(\bar{D}_2^{*0} \rightarrow$	< 2.2	$\times 10^{-5}$ CL=90%
Γ ₁₀₅	$\bar{D}^0 \pi^+ \pi^+ \pi^-$		$(5.6 \pm 2.1) \times 10^{-3}$		$\bar{D}^{*0} \pi^+ \pi^-)$		
Γ ₁₀₆	$[K^- \pi^+]_D \pi^+ \pi^- \pi^+$			Γ ₁₆₀	$\bar{D}_1^*(2680)^0 \pi^+, \bar{D}_1^*(2680)^0 \rightarrow$	$(8.4 \pm 2.1) \times 10^{-5}$	
Γ ₁₀₇	$\bar{D}^0 \pi^+ \pi^+ \pi^-$ nonresonant		$(5 \pm 4) \times 10^{-3}$		$D^- \pi^+$		
Γ ₁₀₈	$\bar{D}^0 \pi^+ \rho^0$		$(4.2 \pm 3.0) \times 10^{-3}$	Γ ₁₆₁	$\bar{D}_3^*(2760)^0 \pi^+,$	$(1.00 \pm 0.22) \times 10^{-5}$	
Γ ₁₀₉	$\bar{D}^0 a_1(1260)^+$		$(4 \pm 4) \times 10^{-3}$		$\bar{D}_3^*(2760)^0 \pi^+ \rightarrow D^- \pi^+$		
Γ ₁₁₀	$\bar{D}^0 \omega \pi^+$		$(4.1 \pm 0.9) \times 10^{-3}$	Γ ₁₆₂	$\bar{D}_2^*(3000)^0 \pi^+,$	$(2.0 \pm 1.4) \times 10^{-6}$	
Γ ₁₁₁	$D^*(2010)^- \pi^+ \pi^+$		$(1.35 \pm 0.22) \times 10^{-3}$		$\bar{D}_2^*(3000)^0 \pi^+ \rightarrow D^- \pi^+$		
Γ ₁₁₂	$D^*(2010)^- K^+ \pi^+$		$(8.2 \pm 1.4) \times 10^{-5}$	Γ ₁₆₃	$\bar{D}_2^*(2460)^0 \rho^+$	< 4.7	$\times 10^{-3}$ CL=90%
Γ ₁₁₃	$\bar{D}_1(2420)^0 \pi^+, \bar{D}_1^0 \rightarrow$		$(5.2 \pm 2.2) \times 10^{-4}$	Γ ₁₆₄	$\bar{D}^0 D_s^+$	$(9.0 \pm 0.9) \times 10^{-3}$	
	$D^*(2010)^- \pi^+$			Γ ₁₆₅	$D_{s0}^*(2317)^+ \bar{D}^0, D_{s0}^{*+} \rightarrow$	$(8.0 \pm \begin{matrix} 1.6 \\ -1.3 \end{matrix}) \times 10^{-4}$	
Γ ₁₁₄	$D^- \pi^+ \pi^+$		$(1.07 \pm 0.05) \times 10^{-3}$		$D_s^+ \pi^0$		
Γ ₁₁₅	$D^- K^+ \pi^+$		$(7.7 \pm 0.5) \times 10^{-5}$	Γ ₁₆₆	$D_{s0}(2317)^+ \bar{D}^0 \times$	< 7.6	$\times 10^{-4}$ CL=90%
Γ ₁₁₆	$D_0^*(2300)^0 K^+, D_0^{*0} \rightarrow$		$(6.1 \pm 2.4) \times 10^{-6}$		$B(D_{s0}(2317)^+ \rightarrow D_s^{*+} \gamma)$		
	$D^- \pi^+$			Γ ₁₆₇	$D_{s0}(2317)^+ \bar{D}^*(2007)^0 \times$	$(9 \pm 7) \times 10^{-4}$	
Γ ₁₁₇	$D_2^*(2460)^0 K^+, D_2^{*0} \rightarrow$		$(2.32 \pm 0.23) \times 10^{-5}$		$B(D_{s0}(2317)^+ \rightarrow D_s^+ \pi^0)$		
Γ ₁₁₈	$D_1^*(2760)^0 K^+, D_1^{*0} \rightarrow$		$(3.6 \pm 1.2) \times 10^{-6}$	Γ ₁₆₈	$D_{sJ}(2457)^+ \bar{D}^0$	$(3.1 \pm \begin{matrix} 1.0 \\ 0.9 \end{matrix}) \times 10^{-3}$	
	$D^- \pi^+$			Γ ₁₆₉	$D_{sJ}(2457)^+ \bar{D}^0 \times$	$(4.6 \pm \begin{matrix} 1.3 \\ -1.1 \end{matrix}) \times 10^{-4}$	
Γ ₁₁₉	$D^+ K^0$		< 2.9		$B(D_{sJ}(2457)^+ \rightarrow D_s^+ \gamma)$		
Γ ₁₂₀	$D^+ K^+ \pi^-$		$(5.6 \pm 1.1) \times 10^{-6}$	Γ ₁₇₀	$D_{sJ}(2457)^+ \bar{D}^0 \times$	< 2.2	$\times 10^{-4}$ CL=90%
Γ ₁₂₁	$D_2^*(2460)^0 K^+, D_2^{*0} \rightarrow$		< 6.3		$B(D_{sJ}(2457)^+ \rightarrow$		
	$D^+ \pi^-$		$\times 10^{-7}$ CL=90%		$D_s^+ \pi^+ \pi^-)$		
Γ ₁₂₂	$D^+ K^{*0}$		< 4.9	Γ ₁₇₁	$D_{sJ}(2457)^+ \bar{D}^0 \times$	< 2.7	$\times 10^{-4}$ CL=90%
Γ ₁₂₃	$D^+ \bar{K}^{*0}$		< 1.4		$B(D_{sJ}(2457)^+ \rightarrow D_s^+ \pi^0)$		
Γ ₁₂₄	$\bar{D}^*(2007)^0 \pi^+$		$(4.90 \pm 0.17) \times 10^{-3}$	Γ ₁₇₂	$D_{sJ}(2457)^+ \bar{D}^0 \times$	< 9.8	$\times 10^{-4}$ CL=90%
Γ ₁₂₅	$\bar{D}_{CP(+)}^0 \pi^+$	[d]	$(2.7 \pm 0.6) \times 10^{-3}$		$B(D_{sJ}(2457)^+ \rightarrow D_s^{*+} \gamma)$		
Γ ₁₂₆	$\bar{D}_{CP(-)}^0 \pi^+$	[d]	$(2.4 \pm 0.9) \times 10^{-3}$	Γ ₁₇₃	$D_{sJ}(2457)^+ \bar{D}^*(2007)^0$	$(1.20 \pm 0.30) \%$	
Γ ₁₂₇	$\bar{D}^*(2007)^0 \omega \pi^+$		$(4.5 \pm 1.2) \times 10^{-3}$	Γ ₁₇₄	$D_{sJ}(2457)^+ \bar{D}^*(2007)^0 \times$	$(1.4 \pm \begin{matrix} 0.7 \\ 0.6 \end{matrix}) \times 10^{-3}$	
Γ ₁₂₈	$\bar{D}^*(2007)^0 \rho^+$		$(9.8 \pm 1.7) \times 10^{-3}$		$B(D_{sJ}(2457)^+ \rightarrow D_s^+ \gamma)$		
Γ ₁₂₉	$\bar{D}^*(2007)^0 K^+$		$(3.97 \pm \begin{matrix} 0.31 \\ 0.28 \end{matrix}) \times 10^{-4}$	Γ ₁₇₅	$\bar{D}^0 D_{s1}(2536)^+ \times$	$(4.0 \pm 1.0) \times 10^{-4}$	
Γ ₁₃₀	$\bar{D}_{CP(+)}^0 K^+$	[d]	$(2.60 \pm 0.33) \times 10^{-4}$		$B(D_{s1}(2536)^+ \rightarrow$		
Γ ₁₃₁	$\bar{D}_{CP(-)}^0 K^+$	[d]	$(2.19 \pm 0.30) \times 10^{-4}$		$D^*(2007)^0 K^+ +$		
Γ ₁₃₂	$D^*(2007)^0 K^+$		$(7.8 \pm 2.2) \times 10^{-6}$		$D^*(2010)^+ K^0)$		
Γ ₁₃₃	$\bar{D}^*(2007)^0 K^*(892)^+$		$(8.1 \pm 1.4) \times 10^{-4}$	Γ ₁₇₆	$\bar{D}^0 D_{s1}(2536)^+ \times$	$(2.2 \pm 0.7) \times 10^{-4}$	
Γ ₁₃₄	$\bar{D}^*(2007)^0 K^+ \bar{K}^0$		< 1.06		$B(D_{s1}(2536)^+ \rightarrow$		
Γ ₁₃₅	$\bar{D}^*(2007)^0 K^+ \bar{K}^*(892)^0$		$(1.5 \pm 0.4) \times 10^{-3}$		$D^*(2007)^0 K^+)$		
Γ ₁₃₆	$\bar{D}^*(2007)^0 \pi^+ \pi^+ \pi^-$		$(1.03 \pm 0.12) \%$	Γ ₁₇₇	$\bar{D}^*(2007)^0 D_{s1}(2536)^+ \times$	$(5.5 \pm 1.6) \times 10^{-4}$	
Γ ₁₃₇	$\bar{D}^*(2007)^0 a_1(1260)^+$		$(1.9 \pm 0.5) \%$		$B(D_{s1}(2536)^+ \rightarrow$		
Γ ₁₃₈	$\bar{D}^*(2007)^0 \pi^- \pi^+ \pi^+ \pi^0$		$(1.8 \pm 0.4) \%$		$D^*(2007)^0 K^+)$		
Γ ₁₃₉	$\bar{D}^{*0} 3\pi^+ 2\pi^-$		$(5.7 \pm 1.2) \times 10^{-3}$	Γ ₁₇₈	$\bar{D}^0 D_{s1}(2536)^+ \times$	$(2.3 \pm 1.1) \times 10^{-4}$	
Γ ₁₄₀	$D^*(2010)^+ \pi^0$		< 3.6		$B(D_{s1}(2536)^+ \rightarrow D^{*+} K^0)$		
Γ ₁₄₁	$D^*(2010)^+ K^0$		< 9.0	Γ ₁₇₉	$\bar{D}^0 D_{sJ}(2700)^+ \times$	$(5.6 \pm 1.8) \times 10^{-4}$	S=1.7
Γ ₁₄₂	$D^*(2010)^- \pi^+ \pi^+ \pi^0$		$(1.5 \pm 0.7) \%$		$B(D_{sJ}(2700)^+ \rightarrow D^0 K^+)$		
Γ ₁₄₃	$D^*(2010)^- \pi^+ \pi^+ \pi^+ \pi^-$		$(2.6 \pm 0.4) \times 10^{-3}$	Γ ₁₈₀	$\bar{D}^{*0} D_{s1}(2536)^+, D_{s1}^+ \rightarrow$	$(3.9 \pm 2.6) \times 10^{-4}$	
Γ ₁₄₄	$\bar{D}^{*0} \pi^+$	[e]	$(5.7 \pm 1.2) \times 10^{-3}$		$D^{*+} K^0$		
Γ ₁₄₅	$\bar{D}_1^*(2420)^0 \pi^+$		$(1.5 \pm 0.6) \times 10^{-3}$		$\bar{D}^0 D_{sJ}(2573)^+, D_{sJ}^+ \rightarrow$	$(8 \pm 15) \times 10^{-6}$	
Γ ₁₄₆	$\bar{D}_1(2420)^0 \pi^+ \times B(\bar{D}_1^0 \rightarrow$		$(2.5 \pm \begin{matrix} 1.6 \\ 1.4 \end{matrix}) \times 10^{-4}$		$D^0 K^+$		
	$\bar{D}^0 \pi^+ \pi^-)$			Γ ₁₈₂	$\bar{D}^{*0} D_{sJ}(2573), D_{sJ}^+ \rightarrow D^0 K^+$	< 2	$\times 10^{-4}$ CL=90%
Γ ₁₄₇	$\bar{D}_1(2420)^0 \pi^+ \times B(\bar{D}_1^0 \rightarrow$		$(2.2 \pm 1.0) \times 10^{-4}$	Γ ₁₈₃	$\bar{D}^*(2007)^0 D_{sJ}(2573), D_{sJ}^+ \rightarrow$	< 5	$\times 10^{-4}$ CL=90%
	$\bar{D}^0 \pi^+ \pi^-$ (nonresonant))				$D^0 K^+$		
Γ ₁₄₈	$\bar{D}_2^*(2462)^0 \pi^+$		$(3.56 \pm 0.24) \times 10^{-4}$	Γ ₁₈₄	$\bar{D}^0 D_s^{*+}$	$(7.6 \pm 1.6) \times 10^{-3}$	
	$\times B(\bar{D}_3^*(2462)^0 \rightarrow D^- \pi^+)$			Γ ₁₈₅	$\bar{D}^*(2007)^0 D_s^+$	$(8.2 \pm 1.7) \times 10^{-3}$	
Γ ₁₄₉	$\bar{D}_2^*(2462)^0 \pi^+ \times B(\bar{D}_2^{*0} \rightarrow$		$(2.2 \pm 1.0) \times 10^{-4}$	Γ ₁₈₆	$\bar{D}^*(2007)^0 D_s^{*+}$	$(1.71 \pm 0.24) \%$	
	$\bar{D}^0 \pi^- \pi^+)$			Γ ₁₈₇	$D_s^{(*)+} \bar{D}^{*0}$	$(2.7 \pm 1.2) \%$	
Γ ₁₅₀	$\bar{D}_2^*(2462)^0 \pi^+ \times B(\bar{D}_2^{*0} \rightarrow$		< 1.7	Γ ₁₈₈	$\bar{D}^*(2007)^0 D^*(2010)^+$	$(8.1 \pm 1.7) \times 10^{-4}$	
	$\bar{D}^0 \pi^- \pi^+)$ (nonresonant))		$\times 10^{-4}$ CL=90%	Γ ₁₈₉	$\bar{D}^0 D^*(2010)^+ +$	< 1.30	$\%$ CL=90%
Γ ₁₅₁	$\bar{D}_2^*(2462)^0 \pi^+ \times B(\bar{D}_2^{*0} \rightarrow$		$(2.2 \pm 1.1) \times 10^{-4}$		$\bar{D}^*(2007)^0 D^+$		
	$D^*(2010)^- \pi^+)$			Γ ₁₉₀	$\bar{D}^0 D^*(2010)^+$	$(3.9 \pm 0.5) \times 10^{-4}$	
Γ ₁₅₂	$\bar{D}_0^*(2400)^0 \pi^+$		$(6.4 \pm 1.4) \times 10^{-4}$	Γ ₁₉₁	$\bar{D}^0 D^+$	$(3.8 \pm 0.4) \times 10^{-4}$	
	$\times B(\bar{D}_0^*(2400)^0 \rightarrow D^- \pi^+)$			Γ ₁₉₂	$\bar{D}^0 D + K^0$	$(1.55 \pm 0.21) \times 10^{-3}$	
Γ ₁₅₃	$\bar{D}_1(2421)^0 \pi^+$		$(6.8 \pm 1.5) \times 10^{-4}$	Γ ₁₉₃	$D^+ \bar{D}^*(2007)^0$	$(6.3 \pm 1.7) \times 10^{-4}$	
	$\times B(\bar{D}_1(2421)^0 \rightarrow D^{*-} \pi^+)$			Γ ₁₉₄	$\bar{D}^*(2007)^0 D^+ K^0$	$(2.1 \pm 0.5) \times 10^{-3}$	

Γ_{195}	$\bar{D}^0 D^*(2010)^+ K^0$	$(3.8 \pm 0.4) \times 10^{-3}$		Γ_{256}	$\chi_{c1}(3872) K^+, \chi_{c1} \rightarrow$	< 1.5	$\times 10^{-6}$ CL=90%
Γ_{196}	$\bar{D}^*(2007)^0 D^*(2010)^+ K^0$	$(9.2 \pm 1.2) \times 10^{-3}$			$\chi_{c1}(1P)\pi^+\pi^-$		
Γ_{197}	$\bar{D}^0 D^0 K^+$	$(1.45 \pm 0.33) \times 10^{-3}$	S=2.6	Γ_{257}	$\chi_{c1}(3872) K^+, \chi_{c1}(3872) \rightarrow$	< 8.1	$\times 10^{-6}$ CL=90%
Γ_{198}	$\bar{D}^*(2007)^0 D^0 K^+$	$(2.26 \pm 0.23) \times 10^{-3}$			$\chi_{c1}(1P)\pi^0$		
Γ_{199}	$\bar{D}^0 D^*(2007)^0 K^+$	$(6.3 \pm 0.5) \times 10^{-3}$		Γ_{258}	$X(3915) K^+$	< 2.8	$\times 10^{-4}$ CL=90%
Γ_{200}	$\bar{D}^*(2007)^0 D^*(2007)^0 K^+$	$(1.12 \pm 0.13) \%$		Γ_{259}	$X(3915)^0 K^+, X^0 \rightarrow \eta_c \eta$	< 4.7	$\times 10^{-5}$ CL=90%
Γ_{201}	$D^- D^+ K^+$	$(2.2 \pm 0.7) \times 10^{-4}$		Γ_{260}	$X(3915)^0 K^+, X^0 \rightarrow \eta_c \pi^0$	< 1.7	$\times 10^{-5}$ CL=90%
Γ_{202}	$D^- D^*(2010)^+ K^+$	$(6.3 \pm 1.1) \times 10^{-4}$		Γ_{261}	$X(4014)^0 K^+, X^0 \rightarrow \eta_c \eta$	< 3.9	$\times 10^{-5}$ CL=90%
Γ_{203}	$D^*(2010)^- D^+ K^+$	$(6.0 \pm 1.3) \times 10^{-4}$		Γ_{262}	$X(4014)^0 K^+, X^0 \rightarrow \eta_c \pi^0$	< 1.2	$\times 10^{-5}$ CL=90%
Γ_{204}	$D^*(2010)^- D^*(2010)^+ K^+$	$(1.32 \pm 0.18) \times 10^{-3}$		Γ_{263}	$Z_c(3900)^0 K^+, Z_c^0 \rightarrow$	< 4.7	$\times 10^{-5}$ CL=90%
Γ_{205}	$(\bar{D} + \bar{D}^*)(D + D^*) K$	$(4.05 \pm 0.30) \%$			$\eta_c \pi^+ \pi^-$		
Γ_{206}	$D_s^+ \pi^0$	$(1.6 \pm 0.5) \times 10^{-5}$		Γ_{264}	$X(4020)^0 K^+, X^0 \rightarrow \eta_c \pi^+ \pi^-$	< 1.6	$\times 10^{-5}$ CL=90%
Γ_{207}	$D_s^+ \pi^0$	< 2.6	$\times 10^{-4}$ CL=90%	Γ_{265}	$\chi_{c1}(3872) K^*(892)^+, \chi_{c1} \rightarrow$	< 4.8	$\times 10^{-6}$ CL=90%
Γ_{208}	$D_s^+ \eta$	< 4	$\times 10^{-4}$ CL=90%		$J/\psi \gamma$		
Γ_{209}	$D_s^+ \eta$	< 6	$\times 10^{-4}$ CL=90%	Γ_{266}	$\chi_{c1}(3872) K^*(892)^+, \chi_{c1} \rightarrow$	< 2.8	$\times 10^{-5}$ CL=90%
Γ_{210}	$D_s^+ \rho^0$	< 3.0	$\times 10^{-4}$ CL=90%		$\psi(2S) \gamma$		
Γ_{211}	$D_s^+ \rho^0$	< 4	$\times 10^{-4}$ CL=90%	Γ_{267}	$\chi_{c1}(3872)^+ K^0, \chi_{c1}^+ \rightarrow$	[f] < 6.1	$\times 10^{-6}$ CL=90%
Γ_{212}	$D_s^+ \omega$	< 4	$\times 10^{-4}$ CL=90%		$J/\psi(1S)\pi^+\pi^0$		
Γ_{213}	$D_s^+ \omega$	< 6	$\times 10^{-4}$ CL=90%	Γ_{268}	$\chi_{c1}(3872) K^0 \pi^+, \chi_{c1} \rightarrow$	$(1.06 \pm 0.31) \times 10^{-5}$	
Γ_{214}	$D_s^+ a_1(1260)^0$	< 1.8	$\times 10^{-3}$ CL=90%		$J/\psi(1S)\pi^+\pi^-$		
Γ_{215}	$D_s^+ a_1(1260)^0$	< 1.3	$\times 10^{-3}$ CL=90%	Γ_{269}	$Z_c(4430)^+ K^0, Z_c^+ \rightarrow J/\psi \pi^+$	< 1.5	$\times 10^{-5}$ CL=95%
Γ_{216}	$D_s^+ K^+ K^-$	$(7.2 \pm 1.1) \times 10^{-6}$		Γ_{270}	$Z_c(4430)^+ K^0, Z_c^+ \rightarrow$	< 4.7	$\times 10^{-5}$ CL=95%
Γ_{217}	$D_s^+ \phi$	< 4.2	$\times 10^{-7}$ CL=90%		$\psi(2S) \pi^+$		
Γ_{218}	$D_s^+ \phi$	< 1.2	$\times 10^{-5}$ CL=90%	Γ_{271}	$\psi(4260)^0 K^+, \psi^0 \rightarrow$	< 1.56	$\times 10^{-5}$ CL=95%
Γ_{219}	$D_s^+ \bar{K}^0$	< 8	$\times 10^{-4}$ CL=90%		$J/\psi \pi^+ \pi^-$		
Γ_{220}	$D_s^+ \bar{K}^0$	< 9	$\times 10^{-4}$ CL=90%	Γ_{272}	$X(3915) K^+, X \rightarrow J/\psi \gamma$	< 1.4	$\times 10^{-5}$ CL=90%
Γ_{221}	$D_s^+ \bar{K}^*(892)^0$	< 4.4	$\times 10^{-6}$ CL=90%	Γ_{273}	$X(3915) K^+, X \rightarrow \chi_{c1}(1P)\pi^0$	< 3.8	$\times 10^{-5}$ CL=90%
Γ_{222}	$D_s^+ K^{*0}$	< 3.5	$\times 10^{-6}$ CL=90%	Γ_{274}	$X(3930)^0 K^+, X^0 \rightarrow J/\psi \gamma$	< 2.5	$\times 10^{-6}$ CL=90%
Γ_{223}	$D_s^+ \bar{K}^*(892)^0$	< 3.5	$\times 10^{-4}$ CL=90%	Γ_{275}	$J/\psi(1S) K^+$	$(1.006 \pm 0.027) \times 10^{-3}$	
Γ_{224}	$D_s^+ \pi^+ K^+$	$(1.80 \pm 0.22) \times 10^{-4}$		Γ_{276}	$J/\psi(1S) K^0 \pi^+$	$(1.14 \pm 0.11) \times 10^{-3}$	
Γ_{225}	$D_s^+ \pi^+ K^+$	$(1.45 \pm 0.24) \times 10^{-4}$		Γ_{277}	$J/\psi(1S) K^+ \pi^+ \pi^-$	$(8.1 \pm 1.3) \times 10^{-4}$	S=2.5
Γ_{226}	$D_s^+ \pi^+ K^*(892)^+$	< 5	$\times 10^{-3}$ CL=90%	Γ_{278}	$J/\psi(1S) K^+ K^- K^+$	$(3.37 \pm 0.29) \times 10^{-5}$	
Γ_{227}	$D_s^+ \pi^+ K^*(892)^+$	< 7	$\times 10^{-3}$ CL=90%	Γ_{279}	$X(3915) K^+, X \rightarrow p \bar{p}$	< 7.1	$\times 10^{-8}$ CL=95%
Γ_{228}	$D_s^+ K^+ K^+$	$(9.7 \pm 2.1) \times 10^{-6}$		Γ_{280}	$J/\psi(1S) K^*(892)^+$	$(1.43 \pm 0.08) \times 10^{-3}$	
Γ_{229}	$D_s^+ K^+ K^+$	< 1.5	$\times 10^{-5}$ CL=90%	Γ_{281}	$J/\psi(1S) K(1270)^+$	$(1.8 \pm 0.5) \times 10^{-3}$	
				Γ_{282}	$J/\psi(1S) K(1400)^+$	< 5	$\times 10^{-4}$ CL=90%
				Γ_{283}	$J/\psi(1S) \eta K^+$	$(1.24 \pm 0.14) \times 10^{-4}$	
				Γ_{284}	$\chi_{c1-odd}(3872) K^+,$	< 3.8	$\times 10^{-6}$ CL=90%
					$\chi_{c1-odd} \rightarrow J/\psi \eta$		
				Γ_{285}	$\psi(4160) K^+, \psi \rightarrow J/\psi \eta$	< 7.4	$\times 10^{-6}$ CL=90%
				Γ_{286}	$J/\psi(1S) \eta' K^+$	< 8.8	$\times 10^{-5}$ CL=90%
				Γ_{287}	$J/\psi(1S) \phi K^+$	$(5.0 \pm 0.4) \times 10^{-5}$	
				Γ_{288}	$J/\psi(1S) K_1(1650), K_1 \rightarrow$	$(6 \pm 10) \times 10^{-6}$	
					ϕK^+		
				Γ_{289}	$J/\psi(1S) K^*(1680)^+, K^* \rightarrow$	$(3.4 \pm 1.9) \times 10^{-6}$	
					ϕK^+		
				Γ_{290}	$J/\psi(1S) K_2^*(1980), K_2^* \rightarrow$	$(1.5 \pm 0.9) \times 10^{-6}$	
					ϕK^+		
				Γ_{291}	$J/\psi(1S) K(1830)^+,$	$(1.3 \pm 1.3) \times 10^{-6}$	
					$K(1830)^+ \rightarrow \phi K^+$		
				Γ_{292}	$\chi_{c1}(4140) K^+, \chi_{c1} \rightarrow$	$(10 \pm 4) \times 10^{-6}$	
					$J/\psi(1S) \phi$		
				Γ_{293}	$\chi_{c1}(4274) K^+, \chi_{c1} \rightarrow$	$(3.6 \pm 2.2) \times 10^{-6}$	
					$J/\psi(1S) \phi$		
				Γ_{294}	$\chi_{c0}(4500) K^+, \chi_{c0}^0 \rightarrow$	$(3.3 \pm 2.1) \times 10^{-6}$	
					$J/\psi(1S) \phi$		
				Γ_{295}	$\chi_{c0}(4700) K^+, \chi_{c0}^0 \rightarrow$	$(6 \pm 5) \times 10^{-6}$	
					$J/\psi(1S) \phi$		
				Γ_{296}	$J/\psi(1S) \omega K^+$	$(3.20 \pm 0.60) \times 10^{-4}$	
					$\chi_{c1}(3872) K^+, \chi_{c1} \rightarrow J/\psi \omega$	$(6.0 \pm 2.2) \times 10^{-6}$	
				Γ_{297}	$X(3915) K^+, X \rightarrow J/\psi \omega$	$(3.0 \pm 0.9) \times 10^{-5}$	
				Γ_{298}	$J/\psi(1S) \pi^+$	$(3.87 \pm 0.11) \times 10^{-5}$	
				Γ_{299}	$J/\psi(1S) \pi^+ \pi^+ \pi^+ \pi^- \pi^-$	$(1.16 \pm 0.13) \times 10^{-5}$	
				Γ_{300}	$\psi(2S) \pi^+ \pi^+ \pi^-$	$(1.9 \pm 0.4) \times 10^{-5}$	
				Γ_{301}	$J/\psi(1S) \rho^+$	$(4.1 \pm 0.5) \times 10^{-5}$	S=1.4
				Γ_{302}	$J/\psi(1S) \pi^+ \pi^0$ nonresonant	< 7.3	$\times 10^{-6}$ CL=90%
				Γ_{303}	$J/\psi(1S) a_1(1260)^+$	< 1.2	$\times 10^{-3}$ CL=90%
				Γ_{304}	$J/\psi(1S) p \bar{p} \pi^+$	< 5.0	$\times 10^{-7}$ CL=90%
				Γ_{305}	$J/\psi(1S) p \bar{p}$	$(1.46 \pm 0.12) \times 10^{-5}$	
				Γ_{306}	$J/\psi(1S) \Sigma^0 p$	< 1.1	$\times 10^{-5}$ CL=90%
				Γ_{307}	$J/\psi(1S) D^+$	< 1.2	$\times 10^{-4}$ CL=90%
				Γ_{308}			

Meson Particle Listings

B^\pm

Γ ₃₀₉	$J/\psi(1S)\bar{D}^0\pi^+$	< 2.5	$\times 10^{-5}$	CL=90%
Γ ₃₁₀	$\psi(2S)\pi^+$	(2.44 ± 0.30)	$\times 10^{-5}$	
Γ ₃₁₁	$\psi(2S)K^+$	(6.19 ± 0.22)	$\times 10^{-4}$	
Γ ₃₁₂	$\psi(2S)K^*(892)^+$	(6.7 ± 1.4)	$\times 10^{-4}$	S=1.3
Γ ₃₁₃	$\psi(2S)K^0\pi^+$			
Γ ₃₁₄	$\psi(2S)K^+\pi^+\pi^-$	(4.3 ± 0.5)	$\times 10^{-4}$	
Γ ₃₁₅	$\psi(2S)\phi(1020)K^+$	(4.0 ± 0.7)	$\times 10^{-6}$	
Γ ₃₁₆	$\psi(3770)K^+$	(4.9 ± 1.3)	$\times 10^{-4}$	
Γ ₃₁₇	$\psi(3770)K^+, \psi \rightarrow D^0\bar{D}^0$	(1.5 ± 0.5)	$\times 10^{-4}$	S=1.4
Γ ₃₁₈	$\psi(3770)K^+, \psi \rightarrow D^+\bar{D}^-$	(9.4 ± 3.5)	$\times 10^{-5}$	
Γ ₃₁₉	$\psi(3770)K^+, \psi \rightarrow p\bar{p}$	< 2	$\times 10^{-7}$	CL=95%
Γ ₃₂₀	$\psi(4040)K^+$	< 1.3	$\times 10^{-4}$	CL=90%
Γ ₃₂₁	$\psi(4160)K^+$	(5.1 ± 2.7)	$\times 10^{-4}$	
Γ ₃₂₂	$\psi(4160)K^+, \psi \rightarrow \bar{D}^0D^0$	(8 ± 5)	$\times 10^{-5}$	
Γ ₃₂₃	$\chi_{c0}\pi^+, \chi_{c0} \rightarrow \pi^+\pi^-$	< 1	$\times 10^{-7}$	CL=90%
Γ ₃₂₄	$\chi_{c0}K^+$	(1.50 ± 0.15)	$\times 10^{-4}$	
Γ ₃₂₅	$\chi_{c0}K^*(892)^+$	< 2.1	$\times 10^{-4}$	CL=90%
Γ ₃₂₆	$\chi_{c1}(1P)\pi^+$	(2.2 ± 0.5)	$\times 10^{-5}$	
Γ ₃₂₇	$\chi_{c1}(1P)K^+$	(4.85 ± 0.33)	$\times 10^{-4}$	S=1.5
Γ ₃₂₈	$\chi_{c1}(1P)K^*(892)^+$	(3.0 ± 0.6)	$\times 10^{-4}$	S=1.1
Γ ₃₂₉	$\chi_{c1}(1P)K^0\pi^+$	(5.8 ± 0.4)	$\times 10^{-4}$	
Γ ₃₃₀	$\chi_{c1}(1P)K^+\pi^0$	(3.29 ± 0.35)	$\times 10^{-4}$	
Γ ₃₃₁	$\chi_{c1}(1P)K^+\pi^+\pi^-$	(3.74 ± 0.30)	$\times 10^{-4}$	
Γ ₃₃₂	$\chi_{c1}(2P)K^+, \chi_{c1}(2P) \rightarrow \pi^+\pi^-\chi_{c1}(1P)$	< 1.1	$\times 10^{-5}$	CL=90%
Γ ₃₃₃	$\chi_{c2}K^+$	(1.1 ± 0.4)	$\times 10^{-5}$	
Γ ₃₃₄	$\chi_{c2}K^+, \chi_{c2} \rightarrow p\bar{p}\pi^+\pi^-$	< 1.9	$\times 10^{-7}$	
Γ ₃₃₅	$\chi_{c2}K^*(892)^+$	< 1.2	$\times 10^{-4}$	CL=90%
Γ ₃₃₆	$\chi_{c2}K^0\pi^+$	(1.16 ± 0.25)	$\times 10^{-4}$	
Γ ₃₃₇	$\chi_{c2}K^+\pi^0$	< 6.2	$\times 10^{-5}$	CL=90%
Γ ₃₃₈	$\chi_{c2}K^+\pi^+\pi^-$	(1.34 ± 0.19)	$\times 10^{-4}$	
Γ ₃₃₉	$\chi_{c2}(3930)\pi^+, \chi_{c2} \rightarrow \pi^+\pi^-$	< 1	$\times 10^{-7}$	CL=90%
Γ ₃₄₀	$h_c(1P)K^+$	(3.7 ± 1.2)	$\times 10^{-5}$	
Γ ₃₄₁	$h_c(1P)K^+, h_c \rightarrow p\bar{p}$	< 6.4	$\times 10^{-8}$	CL=95%

K or K* modes

Γ ₃₄₂	$K^0\pi^+$	(2.37 ± 0.08)	$\times 10^{-5}$	
Γ ₃₄₃	$K^+\pi^0$	(1.29 ± 0.05)	$\times 10^{-5}$	
Γ ₃₄₄	$\eta'K^+$	(7.04 ± 0.25)	$\times 10^{-5}$	
Γ ₃₄₅	$\eta'K^*(892)^+$	(4.8 ± 1.8)	$\times 10^{-6}$	
Γ ₃₄₆	$\eta'K_0^*(1430)^+$	(5.2 ± 2.1)	$\times 10^{-6}$	
Γ ₃₄₇	$\eta'K_2^*(1430)^+$	(2.8 ± 0.5)	$\times 10^{-5}$	
Γ ₃₄₈	ηK^+	(2.4 ± 0.4)	$\times 10^{-6}$	S=1.7
Γ ₃₄₉	$\eta K^*(892)^+$	(1.93 ± 0.16)	$\times 10^{-5}$	
Γ ₃₅₀	$\eta K_0^*(1430)^+$	(1.8 ± 0.4)	$\times 10^{-5}$	
Γ ₃₅₁	$\eta K_2^*(1430)^+$	(9.1 ± 3.0)	$\times 10^{-6}$	
Γ ₃₅₂	$\eta(1295)K^+ \times B(\eta(1295) \rightarrow \eta\pi\pi)$	(2.9 ± 0.8)	$\times 10^{-6}$	
Γ ₃₅₃	$\eta(1405)K^+ \times B(\eta(1405) \rightarrow \eta\pi\pi)$	< 1.3	$\times 10^{-6}$	CL=90%
Γ ₃₅₄	$\eta(1405)K^+ \times B(\eta(1405) \rightarrow K^*K)$	< 1.2	$\times 10^{-6}$	CL=90%
Γ ₃₅₅	$\eta(1475)K^+ \times B(\eta(1475) \rightarrow K^*K)$	(1.38 ± 0.21)	$\times 10^{-5}$	
Γ ₃₅₆	$f_1(1285)K^+$	< 2.0	$\times 10^{-6}$	CL=90%
Γ ₃₅₇	$f_1(1420)K^+ \times B(f_1(1420) \rightarrow \eta\pi\pi)$	< 2.9	$\times 10^{-6}$	CL=90%
Γ ₃₅₈	$f_1(1420)K^+ \times B(f_1(1420) \rightarrow K^*K)$	< 4.1	$\times 10^{-6}$	CL=90%
Γ ₃₅₉	$\phi(1680)K^+ \times B(\phi(1680) \rightarrow K^*K)$	< 3.4	$\times 10^{-6}$	CL=90%
Γ ₃₆₀	$f_0(1500)K^+$	(3.7 ± 2.2)	$\times 10^{-6}$	
Γ ₃₆₁	ωK^+	(6.5 ± 0.4)	$\times 10^{-6}$	
Γ ₃₆₂	$\omega K^*(892)^+$	< 7.4	$\times 10^{-6}$	CL=90%
Γ ₃₆₃	$\omega(K\pi)_0^{*+}$	(2.8 ± 0.4)	$\times 10^{-5}$	
Γ ₃₆₄	$\omega K_0^*(1430)^+$	(2.4 ± 0.5)	$\times 10^{-5}$	
Γ ₃₆₅	$\omega K_2^*(1430)^+$	(2.1 ± 0.4)	$\times 10^{-5}$	
Γ ₃₆₆	$a_0(980)^+K^0 \times B(a_0(980)^+ \rightarrow \eta\pi^+)$	< 3.9	$\times 10^{-6}$	CL=90%
Γ ₃₆₇	$a_0(980)^0K^+ \times B(a_0(980)^0 \rightarrow \eta\pi^0)$	< 2.5	$\times 10^{-6}$	CL=90%
Γ ₃₆₈	$K^*(892)^0\pi^+$	(1.01 ± 0.08)	$\times 10^{-5}$	
Γ ₃₆₉	$K^*(892)^+\pi^0$	(6.8 ± 0.9)	$\times 10^{-6}$	

Γ ₃₇₀	$K^+\pi^-\pi^+$	(5.10 ± 0.29)	$\times 10^{-5}$	
Γ ₃₇₁	$K^+\pi^-\pi^+$ nonresonant	(1.63 ± 0.21)	$\times 10^{-5}$	
Γ ₃₇₂	$\omega(782)K^+$	(6 ± 9)	$\times 10^{-6}$	
Γ ₃₇₃	$K^+f_0(980) \times B(f_0(980) \rightarrow \pi^+\pi^-)$	(9.4 ± 1.0)	$\times 10^{-6}$	
Γ ₃₇₄	$f_2(1270)^0K^+$	(1.07 ± 0.27)	$\times 10^{-6}$	
Γ ₃₇₅	$f_0(1370)^0K^+ \times B(f_0(1370)^0 \rightarrow \pi^+\pi^-)$	< 1.07	$\times 10^{-5}$	CL=90%
Γ ₃₇₆	$\rho^0(1450)K^+ \times B(\rho^0(1450) \rightarrow \pi^+\pi^-)$	< 1.17	$\times 10^{-5}$	CL=90%
Γ ₃₇₇	$f_2'(1525)K^+ \times B(f_2'(1525) \rightarrow \pi^+\pi^-)$	< 3.4	$\times 10^{-6}$	CL=90%
Γ ₃₇₈	$K^+\rho^0$	(3.7 ± 0.5)	$\times 10^{-6}$	
Γ ₃₇₉	$K_0^*(1430)^0\pi^+$	(3.9 ± 0.6)	$\times 10^{-5}$	S=1.4
Γ ₃₈₀	$K_0^*(1430)^+\pi^0$	(1.19 ± 0.20)	$\times 10^{-5}$	
Γ ₃₈₁	$K_2^*(1430)^0\pi^+$	(5.6 ± 2.2)	$\times 10^{-6}$	
Γ ₃₈₂	$K^*(1410)^0\pi^+$	< 4.5	$\times 10^{-5}$	CL=90%
Γ ₃₈₃	$K^*(1680)^0\pi^+$	< 1.2	$\times 10^{-5}$	CL=90%
Γ ₃₈₄	$K^+\pi^0\pi^0$	(1.62 ± 0.19)	$\times 10^{-5}$	
Γ ₃₈₅	$f_0(980)K^+ \times B(f_0 \rightarrow \pi^0\pi^0)$	(2.8 ± 0.8)	$\times 10^{-6}$	
Γ ₃₈₆	$K^-\pi^+\pi^+$	< 4.6	$\times 10^{-8}$	CL=90%
Γ ₃₈₇	$K^-\pi^+\pi^+$ nonresonant	< 5.6	$\times 10^{-5}$	CL=90%
Γ ₃₈₈	$K_1(1270)^0\pi^+$	< 4.0	$\times 10^{-5}$	CL=90%
Γ ₃₈₉	$K_1(1400)^0\pi^+$	< 3.9	$\times 10^{-5}$	CL=90%
Γ ₃₉₀	$K^0\pi^+\pi^0$	< 6.6	$\times 10^{-5}$	CL=90%
Γ ₃₉₁	$K^0\rho^+$	(7.3 ± 1.0)	$\times 10^{-6}$	
Γ ₃₉₂	$K^*(892)^+\pi^+\pi^-$	(7.5 ± 1.0)	$\times 10^{-5}$	
Γ ₃₉₃	$K^*(892)^+\rho^0$	(4.6 ± 1.1)	$\times 10^{-6}$	
Γ ₃₉₄	$K^*(892)^+f_0(980)$	(4.2 ± 0.7)	$\times 10^{-6}$	
Γ ₃₉₅	$a_1^+K^0$	(3.5 ± 0.7)	$\times 10^{-5}$	
Γ ₃₉₆	$b_1^+K^0 \times B(b_1^+ \rightarrow \omega\pi^+)$	(9.6 ± 1.9)	$\times 10^{-6}$	
Γ ₃₉₇	$K^*(892)^0\rho^+$	(9.2 ± 1.5)	$\times 10^{-6}$	
Γ ₃₉₈	$K_1(1400)^+\rho^0$	< 7.8	$\times 10^{-4}$	CL=90%
Γ ₃₉₉	$K_2^*(1430)^+\rho^0$	< 1.5	$\times 10^{-3}$	CL=90%
Γ ₄₀₀	$b_1^0K^+ \times B(b_1^0 \rightarrow \omega\pi^0)$	(9.1 ± 2.0)	$\times 10^{-6}$	
Γ ₄₀₁	$b_1^+K^{*0} \times B(b_1^+ \rightarrow \omega\pi^+)$	< 5.9	$\times 10^{-6}$	CL=90%
Γ ₄₀₂	$b_1^0K^{*+} \times B(b_1^0 \rightarrow \omega\pi^0)$	< 6.7	$\times 10^{-6}$	CL=90%
Γ ₄₀₃	$\bar{K}^0K^+\pi^0$	(1.31 ± 0.17)	$\times 10^{-6}$	S=1.2
Γ ₄₀₄	$K^+K_0^*K_0^0$	< 2.4	$\times 10^{-5}$	CL=90%
Γ ₄₀₅	$K^+K_0^*K_0^0$	(1.05 ± 0.04)	$\times 10^{-5}$	
Γ ₄₀₆	$f_0(980)K^+, f_0 \rightarrow K_S^0K_S^0$	(1.47 ± 0.33)	$\times 10^{-5}$	
Γ ₄₀₇	$f_0(1710)K^+, f_0 \rightarrow K_S^0K_S^0$	(4.8 ± 4.0)	$\times 10^{-7}$	
Γ ₄₀₈	$K^+K_S^0K_S^0$ nonresonant	(2.0 ± 0.4)	$\times 10^{-5}$	
Γ ₄₀₉	$K_S^0K_S^0\pi^+$	< 5.1	$\times 10^{-7}$	CL=90%
Γ ₄₁₀	$K^+K^-\pi^+$	(5.2 ± 0.4)	$\times 10^{-6}$	
Γ ₄₁₁	$K^+K^-\pi^+$ nonresonant	(1.68 ± 0.26)	$\times 10^{-6}$	
Γ ₄₁₂	$K^+\bar{K}^*(892)^0$	(5.9 ± 0.8)	$\times 10^{-7}$	
Γ ₄₁₃	$K^+\bar{K}_0^*(1430)^0$	(3.8 ± 1.3)	$\times 10^{-7}$	
Γ ₄₁₄	$\pi^+(K^+K^-) s\text{-wave}$	(8.5 ± 0.9)	$\times 10^{-7}$	
Γ ₄₁₅	$K^+K^+\pi^-$	< 1.1	$\times 10^{-8}$	CL=90%
Γ ₄₁₆	$K^+K^+\pi^-$ nonresonant	< 8.79	$\times 10^{-5}$	CL=90%
Γ ₄₁₇	$f_2'(1525)K^+$	(1.8 ± 0.5)	$\times 10^{-6}$	S=1.1
Γ ₄₁₈	$K^+f_J(2220)$			
Γ ₄₁₉	$K^{*+}\pi^+K^-$	< 1.18	$\times 10^{-5}$	CL=90%
Γ ₄₂₀	$K^*(892)^+K^*(892)^0$	(9.1 ± 2.9)	$\times 10^{-7}$	
Γ ₄₂₁	$K^{*+}K^+\pi^-$	< 6.1	$\times 10^{-6}$	CL=90%
Γ ₄₂₂	$K^+K^-K^+$	(3.40 ± 0.14)	$\times 10^{-5}$	S=1.4
Γ ₄₂₃	$K^+\phi$	(8.8 ± 0.7)	$\times 10^{-6}$	S=1.1
Γ ₄₂₄	$f_0(980)K^+ \times B(f_0(980) \rightarrow K^+K^-)$	(9.4 ± 3.2)	$\times 10^{-6}$	
Γ ₄₂₅	$a_2(1320)K^+ \times B(a_2(1320) \rightarrow K^+K^-)$	< 1.1	$\times 10^{-6}$	CL=90%
Γ ₄₂₆	$X_0(1550)K^+ \times B(X_0(1550) \rightarrow K^+K^-)$	(4.3 ± 0.7)	$\times 10^{-6}$	
Γ ₄₂₇	$\phi(1680)K^+ \times B(\phi(1680) \rightarrow K^+K^-)$	< 8	$\times 10^{-7}$	CL=90%
Γ ₄₂₈	$f_0(1710)K^+ \times B(f_0(1710) \rightarrow K^+K^-)$	(1.1 ± 0.6)	$\times 10^{-6}$	
Γ ₄₂₉	$K^+K^-K^+$ nonresonant	(2.38 ± 0.28)	$\times 10^{-5}$	

Γ ₄₃₀	$K^*(892)^+ K^+ K^-$	(3.6 ± 0.5) × 10 ⁻⁵	
Γ ₄₃₁	$K^*(892)^+ \phi$	(10.0 ± 2.0) × 10 ⁻⁶	S=1.7
Γ ₄₃₂	$\phi(K\pi)^{*+}$	(8.3 ± 1.6) × 10 ⁻⁶	
Γ ₄₃₃	$\phi K_1(1270)^+$	(6.1 ± 1.9) × 10 ⁻⁶	
Γ ₄₃₄	$\phi K_1(1400)^+$	< 3.2 × 10 ⁻⁶	CL=90%
Γ ₄₃₅	$\phi K^*(1410)^+$	< 4.3 × 10 ⁻⁶	CL=90%
Γ ₄₃₆	$\phi K_0^*(1430)^+$	(7.0 ± 1.6) × 10 ⁻⁶	
Γ ₄₃₇	$\phi K_2^*(1430)^+$	(8.4 ± 2.1) × 10 ⁻⁶	
Γ ₄₃₈	$\phi K_2^*(1770)^+$	< 1.50 × 10 ⁻⁵	CL=90%
Γ ₄₃₉	$\phi K_2^*(1820)^+$	< 1.63 × 10 ⁻⁵	CL=90%
Γ ₄₄₀	$a_1^+ K^{*0}$	< 3.6 × 10 ⁻⁶	CL=90%
Γ ₄₄₁	$K^+ \phi \phi$	(5.0 ± 1.2) × 10 ⁻⁶	S=2.3
Γ ₄₄₂	$\eta' \eta' K^+$	< 2.5 × 10 ⁻⁵	CL=90%
Γ ₄₄₃	$\omega \phi K^+$	< 1.9 × 10 ⁻⁶	CL=90%
Γ ₄₄₄	$X(1812) K^+ \times B(X \rightarrow \omega \phi)$	< 3.2 × 10 ⁻⁷	CL=90%
Γ ₄₄₅	$K^*(892)^+ \gamma$	(3.92 ± 0.22) × 10 ⁻⁵	S=1.7
Γ ₄₄₆	$K_1(1270)^+ \gamma$	(4.4 ± 0.7) × 10 ⁻⁵	
Γ ₄₄₇	$\eta K^+ \gamma$	(7.9 ± 0.9) × 10 ⁻⁶	
Γ ₄₄₈	$\eta' K^+ \gamma$	(2.9 ± 1.0 / 0.9) × 10 ⁻⁶	
Γ ₄₄₉	$\phi K^+ \gamma$	(2.7 ± 0.4) × 10 ⁻⁶	S=1.2
Γ ₄₅₀	$K^+ \pi^- \pi^+ \gamma$	(2.58 ± 0.15) × 10 ⁻⁵	S=1.3
Γ ₄₅₁	$K^*(892)^0 \pi^+ \gamma$	(2.33 ± 0.12) × 10 ⁻⁵	
Γ ₄₅₂	$K^+ \rho^0 \gamma$	(8.2 ± 0.9) × 10 ⁻⁶	
Γ ₄₅₃	$(K^+ \pi^-)_{NR} \pi^+ \gamma$	(9.9 ± 1.7 / -2.0) × 10 ⁻⁶	
Γ ₄₅₄	$K^0 \pi^+ \pi^0 \gamma$	(4.6 ± 0.5) × 10 ⁻⁵	
Γ ₄₅₅	$K_1(1400)^+ \gamma$	(10 ± 5 / 4) × 10 ⁻⁶	
Γ ₄₅₆	$K^*(1410)^+ \gamma$	(2.7 ± 0.8 / 0.6) × 10 ⁻⁵	
Γ ₄₅₇	$K_0^*(1430)^0 \pi^+ \gamma$	(1.32 ± 0.26 / -0.32) × 10 ⁻⁶	
Γ ₄₅₈	$K_2^*(1430)^+ \gamma$	(1.4 ± 0.4) × 10 ⁻⁵	
Γ ₄₅₉	$K^*(1680)^+ \gamma$	(6.7 ± 1.7 / -1.4) × 10 ⁻⁵	
Γ ₄₆₀	$K_3^*(1780)^+ \gamma$	< 3.9 × 10 ⁻⁵	CL=90%
Γ ₄₆₁	$K_4^*(2045)^+ \gamma$	< 9.9 × 10 ⁻³	CL=90%

Light unflavored meson modes

Γ ₄₆₂	$\rho^+ \gamma$	(9.8 ± 2.5) × 10 ⁻⁷	
Γ ₄₆₃	$\pi^+ \pi^0$	(5.5 ± 0.4) × 10 ⁻⁶	S=1.2
Γ ₄₆₄	$\pi^+ \pi^+ \pi^-$	(1.52 ± 0.14) × 10 ⁻⁵	
Γ ₄₆₅	$\rho^0 \pi^+$	(8.3 ± 1.2) × 10 ⁻⁶	
Γ ₄₆₆	$\pi^+ f_0(980), f_0 \rightarrow \pi^+ \pi^-$	< 1.5 × 10 ⁻⁶	CL=90%
Γ ₄₆₇	$\pi^+ f_2(1270)$	(2.2 ± 0.7 / -0.4) × 10 ⁻⁶	
Γ ₄₆₈	$\rho(1450)^0 \pi^+, \rho^0 \rightarrow \pi^+ \pi^-$	(1.4 ± 0.6 / 0.9) × 10 ⁻⁶	
Γ ₄₆₉	$\rho(1450)^0 \pi^+, \rho^0 \rightarrow K^+ K^-$	(1.60 ± 0.14) × 10 ⁻⁶	
Γ ₄₇₀	$f_0(1370) \pi^+, f_0 \rightarrow \pi^+ \pi^-$	< 4.0 × 10 ⁻⁶	CL=90%
Γ ₄₇₁	$f_0(500) \pi^+, f_0 \rightarrow \pi^+ \pi^-$	< 4.1 × 10 ⁻⁶	CL=90%
Γ ₄₇₂	$\pi^+ \pi^- \pi^+$ nonresonant	(5.3 ± 1.5 / 1.1) × 10 ⁻⁶	
Γ ₄₇₃	$\pi^+ \pi^0 \pi^0$	< 8.9 × 10 ⁻⁴	CL=90%
Γ ₄₇₄	$\rho^+ \pi^0$	(1.09 ± 0.14) × 10 ⁻⁵	
Γ ₄₇₅	$\pi^+ \pi^- \pi^+ \pi^0$	< 4.0 × 10 ⁻³	CL=90%
Γ ₄₇₆	$\rho^+ \rho^0$	(2.40 ± 0.19) × 10 ⁻⁵	
Γ ₄₇₇	$\rho^+ f_0(980), f_0 \rightarrow \pi^+ \pi^-$	< 2.0 × 10 ⁻⁶	CL=90%
Γ ₄₇₈	$a_1(1260)^+ \pi^0$	(2.6 ± 0.7) × 10 ⁻⁵	
Γ ₄₇₉	$a_1(1260)^0 \pi^+$	(2.0 ± 0.6) × 10 ⁻⁵	
Γ ₄₈₀	$\omega \pi^+$	(6.9 ± 0.5) × 10 ⁻⁶	
Γ ₄₈₁	$\omega \rho^+$	(1.59 ± 0.21) × 10 ⁻⁵	
Γ ₄₈₂	$\eta \pi^+$	(4.02 ± 0.27) × 10 ⁻⁶	
Γ ₄₈₃	$\eta \rho^+$	(7.0 ± 2.9) × 10 ⁻⁶	S=2.8
Γ ₄₈₄	$\eta' \pi^+$	(2.7 ± 0.9) × 10 ⁻⁶	S=1.9
Γ ₄₈₅	$\eta' \rho^+$	(9.7 ± 2.2) × 10 ⁻⁶	
Γ ₄₈₆	$\phi \pi^+$	(3.2 ± 1.5) × 10 ⁻⁸	
Γ ₄₈₇	$\phi \rho^+$	< 3.0 × 10 ⁻⁶	CL=90%
Γ ₄₈₈	$a_0(980)^0 \pi^+, a_0^0 \rightarrow \eta \pi^0$	< 5.8 × 10 ⁻⁶	CL=90%
Γ ₄₈₉	$a_0(980)^+ \pi^0, a_0^+ \rightarrow \eta \pi^+$	< 1.4 × 10 ⁻⁶	CL=90%
Γ ₄₉₀	$\pi^+ \pi^+ \pi^+ \pi^-$	< 8.6 × 10 ⁻⁴	CL=90%
Γ ₄₉₁	$\rho^0 a_1(1260)^+$	< 6.2 × 10 ⁻⁴	CL=90%
Γ ₄₉₂	$\rho^0 a_2(1320)^+$	< 7.2 × 10 ⁻⁴	CL=90%
Γ ₄₉₃	$b_1^0 \pi^+, b_1^0 \rightarrow \omega \pi^0$	(6.7 ± 2.0) × 10 ⁻⁶	
Γ ₄₉₄	$b_1^+ \pi^0, b_1^+ \rightarrow \omega \pi^+$	< 3.3 × 10 ⁻⁶	CL=90%
Γ ₄₉₅	$\pi^+ \pi^+ \pi^+ \pi^- \pi^- \pi^0$	< 6.3 × 10 ⁻³	CL=90%

Γ ₄₉₆	$b_1^+ \rho^0, b_1^+ \rightarrow \omega \pi^+$	< 5.2 × 10 ⁻⁶	CL=90%
Γ ₄₉₇	$a_1(1260)^+ a_1(1260)^0$	< 1.3 %	CL=90%
Γ ₄₉₈	$b_1^0 \rho^+, b_1^0 \rightarrow \omega \pi^0$	< 3.3 × 10 ⁻⁶	CL=90%

Charged particle (h^\pm) modes

$h^\pm = K^\pm \text{ or } \pi^\pm$			
Γ ₄₉₉	$h^+ \pi^0$	(1.6 ± 0.7 / 0.6) × 10 ⁻⁵	
Γ ₅₀₀	ωh^+	(1.38 ± 0.27 / -0.24) × 10 ⁻⁵	
Γ ₅₀₁	$h^+ \chi^0(\text{Familon})$	< 4.9 × 10 ⁻⁵	CL=90%
Γ ₅₀₂	$K^+ \chi^0, \chi^0 \rightarrow \mu^+ \mu^-$	< 1 × 10 ⁻⁷	CL=95%

Baryon modes

Γ ₅₀₃	$p \bar{p} \pi^+$	(1.62 ± 0.20) × 10 ⁻⁶	
Γ ₅₀₄	$p \bar{p} \pi^+$ nonresonant	< 5.3 × 10 ⁻⁵	CL=90%
Γ ₅₀₅	$p \bar{p} \pi^+ \pi^+$	(5.9 ± 0.5) × 10 ⁻⁶	S=1.5
Γ ₅₀₆	$p \bar{p} K^+$	[g] < 9.1 × 10 ⁻⁸	CL=90%
Γ ₅₀₇	$\Theta(1710)^{++} \bar{p}, \Theta^{++} \rightarrow p K^+$	[g] < 9.1 × 10 ⁻⁸	CL=90%
Γ ₅₀₈	$f_J(2220) K^+, f_J \rightarrow p \bar{p}$	[g] < 4.1 × 10 ⁻⁷	CL=90%
Γ ₅₀₉	$\rho \bar{\Lambda}(1520)$	(3.1 ± 0.6) × 10 ⁻⁷	
Γ ₅₁₀	$p \bar{p} K^+$ nonresonant	< 8.9 × 10 ⁻⁵	CL=90%
Γ ₅₁₁	$p \bar{p} K^*(892)^+$	(3.6 ± 0.8 / 0.7) × 10 ⁻⁶	
Γ ₅₁₂	$f_J(2220) K^{*+}, f_J \rightarrow p \bar{p}$	< 7.7 × 10 ⁻⁷	CL=90%
Γ ₅₁₃	$\rho \bar{\Lambda}$	(2.4 ± 1.0 / 0.9) × 10 ⁻⁷	
Γ ₅₁₄	$\rho \bar{\Lambda} \gamma$	(2.4 ± 0.5 / -0.4) × 10 ⁻⁶	
Γ ₅₁₅	$\rho \bar{\Lambda} \pi^0$	(3.0 ± 0.7 / 0.6) × 10 ⁻⁶	
Γ ₅₁₆	$\rho \bar{\Sigma}(1385)^0$	< 4.7 × 10 ⁻⁷	CL=90%
Γ ₅₁₇	$\Delta^+ \bar{\Lambda}$	< 8.2 × 10 ⁻⁷	CL=90%
Γ ₅₁₈	$\rho \bar{\Sigma} \gamma$	< 4.6 × 10 ⁻⁶	CL=90%
Γ ₅₁₉	$\rho \bar{\Lambda} \pi^+ \pi^-$	(1.13 ± 0.13) × 10 ⁻⁵	
Γ ₅₂₀	$\rho \bar{\Lambda} \pi^+ \pi^-$ nonresonant	(5.9 ± 1.1) × 10 ⁻⁶	
Γ ₅₂₁	$\rho \bar{\Lambda} \rho^0, \rho^0 \rightarrow \pi^+ \pi^-$	(4.8 ± 0.9) × 10 ⁻⁶	
Γ ₅₂₂	$\rho \bar{\Lambda} f_2(1270), f_2 \rightarrow \pi^+ \pi^-$	(2.0 ± 0.8) × 10 ⁻⁶	
Γ ₅₂₃	$\rho \bar{\Lambda} K^+ K^-$	(4.1 ± 0.7) × 10 ⁻⁶	
Γ ₅₂₄	$\rho \bar{\Lambda} \phi$	(8.0 ± 2.2) × 10 ⁻⁷	
Γ ₅₂₅	$\bar{p} \bar{\Lambda} K^+ K^-$	(3.7 ± 0.6) × 10 ⁻⁶	
Γ ₅₂₆	$\bar{\Lambda} \bar{\Lambda} \pi^+$	< 9.4 × 10 ⁻⁷	CL=90%
Γ ₅₂₇	$\bar{\Lambda} \bar{\Lambda} K^+$	(3.4 ± 0.6) × 10 ⁻⁶	
Γ ₅₂₈	$\bar{\Lambda} \bar{\Lambda} K^{*+}$	(2.2 ± 1.2 / -0.9) × 10 ⁻⁶	
Γ ₅₂₉	$\Lambda(1520) \bar{\Lambda} K^+$	(2.2 ± 0.7) × 10 ⁻⁶	
Γ ₅₃₀	$\bar{\Lambda} \bar{\Lambda}(1520) K^+$	< 2.08 × 10 ⁻⁶	
Γ ₅₃₁	$\bar{\Delta}^0 \rho$	< 1.38 × 10 ⁻⁶	CL=90%
Γ ₅₃₂	$\bar{\Delta}^{++} \bar{p}$	< 1.4 × 10 ⁻⁷	CL=90%
Γ ₅₃₃	$D^+ p \bar{p}$	< 1.5 × 10 ⁻⁵	CL=90%
Γ ₅₃₄	$D^*(2010)^+ p \bar{p}$	< 1.5 × 10 ⁻⁵	CL=90%
Γ ₅₃₅	$\bar{D}^0 p \bar{p} \pi^+$	(3.72 ± 0.27) × 10 ⁻⁴	
Γ ₅₃₆	$\bar{D}^{*0} p \bar{p} \pi^+$	(3.73 ± 0.32) × 10 ⁻⁴	
Γ ₅₃₇	$D^- p \bar{p} \pi^+ \pi^-$	(1.66 ± 0.30) × 10 ⁻⁴	
Γ ₅₃₈	$D^{*-} p \bar{p} \pi^+ \pi^-$	(1.86 ± 0.25) × 10 ⁻⁴	
Γ ₅₃₉	$\rho \bar{\Lambda}^0 \bar{D}^0$	(1.43 ± 0.32) × 10 ⁻⁵	
Γ ₅₄₀	$\rho \bar{\Lambda}^0 \bar{D}^*(2007)^0$	< 5 × 10 ⁻⁵	CL=90%
Γ ₅₄₁	$\bar{\Lambda}_c^- p \pi^+$	(2.3 ± 0.4) × 10 ⁻⁴	S=2.2
Γ ₅₄₂	$\bar{\Lambda}_c^- \Delta(1232)^{++}$	< 1.9 × 10 ⁻⁵	CL=90%
Γ ₅₄₃	$\bar{\Lambda}_c^- \Delta_X(1600)^{++}$	(4.7 ± 1.0) × 10 ⁻⁵	
Γ ₅₄₄	$\bar{\Lambda}_c^- \Delta_X(2420)^{++}$	(3.7 ± 0.8) × 10 ⁻⁵	
Γ ₅₄₅	$(\bar{\Lambda}_c^- p)_s \pi^+$	[h] (3.1 ± 0.7) × 10 ⁻⁵	
Γ ₅₄₆	$\bar{\Sigma}_c(2520)^0 p$	< 3 × 10 ⁻⁶	CL=90%
Γ ₅₄₇	$\bar{\Sigma}_c(2800)^0 p$	(2.6 ± 0.9) × 10 ⁻⁵	
Γ ₅₄₈	$\bar{\Lambda}_c^- p \pi^+ \pi^0$	(1.8 ± 0.6) × 10 ⁻³	
Γ ₅₄₉	$\bar{\Lambda}_c^- p \pi^+ \pi^+ \pi^-$	(2.2 ± 0.7) × 10 ⁻³	
Γ ₅₅₀	$\bar{\Lambda}_c^- p \pi^+ \pi^+ \pi^- \pi^0$	< 1.34 %	CL=90%
Γ ₅₅₁	$\Lambda_c^+ \bar{\Lambda}_c^- K^+$	(4.9 ± 0.7) × 10 ⁻⁴	
Γ ₅₅₂	$\Xi_c(2930) \Lambda_c^+, \Xi_c \rightarrow K^+ \bar{\Lambda}_c^-$	(1.7 ± 0.5) × 10 ⁻⁴	
Γ ₅₅₃	$\bar{\Sigma}_c(2455)^0 p$	(2.9 ± 0.7) × 10 ⁻⁵	
Γ ₅₅₄	$\bar{\Sigma}_c(2455)^0 p \pi^0$	(3.5 ± 1.1) × 10 ⁻⁴	
Γ ₅₅₅	$\bar{\Sigma}_c(2455)^0 p \pi^- \pi^+$	(3.5 ± 1.1) × 10 ⁻⁴	
Γ ₅₅₆	$\bar{\Sigma}_c(2455)^- p \pi^+ \pi^+$	(2.37 ± 0.20) × 10 ⁻⁴	
Γ ₅₅₇	$\bar{\Lambda}_c(2593)^- / \bar{\Lambda}_c(2625)^- p \pi^+$	< 1.9 × 10 ⁻⁴	CL=90%
Γ ₅₅₈	$\Xi_c^0 \Lambda_c^+$	(9.5 ± 2.3) × 10 ⁻⁴	
Γ ₅₅₉	$\Xi_c^0 \Lambda_c^+, \Xi_c^0 \rightarrow \Xi^+ \pi^-$	(1.76 ± 0.29) × 10 ⁻⁵	

Meson Particle Listings

 B^\pm

Γ_{560}	$\Xi_c^0 \Lambda_c^+, \Xi_c^0 \rightarrow \Lambda K^+ \pi^-$	(1.14 ± 0.26) × 10 ⁻⁵
Γ_{561}	$\Xi_c^0 \Lambda_c^+, \Xi_c^0 \rightarrow p K^- K^- \pi^+$	(5.5 ± 1.9) × 10 ⁻⁶
Γ_{562}	$\Lambda_c^+ \Xi_c^0$	< 6.5 × 10 ⁻⁴ CL=90%
Γ_{563}	$\Lambda_c^+ \Xi_c^0 (2645)^0$	< 7.9 × 10 ⁻⁴ CL=90%
Γ_{564}	$\Lambda_c^+ \Xi_c^0 (2790)^0$	(1.1 ± 0.4) × 10 ⁻³

Lepton Family number (LF) or Lepton number (L) or Baryon number (B) violating modes, or/and $\Delta B = 1$ weak neutral current ($B1$) modes

Γ_{565}	$\pi^+ \ell^+ \ell^-$	$B1$	< 4.9	× 10 ⁻⁸	CL=90%
Γ_{566}	$\pi^+ e^+ e^-$	$B1$	< 8.0	× 10 ⁻⁸	CL=90%
Γ_{567}	$\pi^+ \mu^+ \mu^-$	$B1$	(1.75 ± 0.22)	× 10 ⁻⁸	
Γ_{568}	$\pi^+ \nu \bar{\nu}$	$B1$	< 1.4	× 10 ⁻⁵	CL=90%
Γ_{569}	$K^+ \ell^+ \ell^-$	$B1$	[a] (4.51 ± 0.23)	× 10 ⁻⁷	S=1.1
Γ_{570}	$K^+ e^+ e^-$	$B1$	(5.5 ± 0.7)	× 10 ⁻⁷	
Γ_{571}	$K^+ \mu^+ \mu^-$	$B1$	(4.41 ± 0.22)	× 10 ⁻⁷	S=1.2
Γ_{572}	$K^+ \mu^+ \mu^-$ nonresonant	$B1$	(4.37 ± 0.27)	× 10 ⁻⁷	
Γ_{573}	$K^+ \tau^+ \tau^-$	$B1$	< 2.25	× 10 ⁻³	CL=90%
Γ_{574}	$K^+ \nu \bar{\nu}$	$B1$	< 1.6	× 10 ⁻⁵	CL=90%
Γ_{575}	$\rho^+ \nu \bar{\nu}$	$B1$	< 3.0	× 10 ⁻⁵	CL=90%
Γ_{576}	$K^*(892)^+ \ell^+ \ell^-$	$B1$	[a] (1.01 ± 0.11)	× 10 ⁻⁶	S=1.1
Γ_{577}	$K^*(892)^+ e^+ e^-$	$B1$	(1.55 ± 0.40)	× 10 ⁻⁶	
Γ_{578}	$K^*(892)^+ \mu^+ \mu^-$	$B1$	(9.6 ± 1.0)	× 10 ⁻⁷	
Γ_{579}	$K^*(892)^+ \nu \bar{\nu}$	$B1$	< 4.0	× 10 ⁻⁵	CL=90%
Γ_{580}	$K^+ \pi^+ \pi^- \mu^+ \mu^-$	$B1$	(4.3 ± 0.4)	× 10 ⁻⁷	
Γ_{581}	$\phi K^+ \mu^+ \mu^-$	$B1$	(7.9 ± 2.1)	× 10 ⁻⁸	
Γ_{582}	$\bar{\Lambda} p \nu \bar{\nu}$		< 3.0	× 10 ⁻⁵	CL=90%
Γ_{583}	$\pi^+ e^+ \mu^-$	LF	< 6.4	× 10 ⁻³	CL=90%
Γ_{584}	$\pi^+ e^- \mu^+$	LF	< 6.4	× 10 ⁻³	CL=90%
Γ_{585}	$\pi^+ e^\pm \mu^\mp$	LF	< 1.7	× 10 ⁻⁷	CL=90%
Γ_{586}	$\pi^+ e^+ \tau^-$	LF	< 7.4	× 10 ⁻⁵	CL=90%
Γ_{587}	$\pi^+ e^- \tau^+$	LF	< 2.0	× 10 ⁻⁵	CL=90%
Γ_{588}	$\pi^+ e^\pm \tau^\mp$	LF	< 7.5	× 10 ⁻⁵	CL=90%
Γ_{589}	$\pi^+ \mu^+ \tau^-$	LF	< 6.2	× 10 ⁻⁵	CL=90%
Γ_{590}	$\pi^+ \mu^- \tau^+$	LF	< 4.5	× 10 ⁻⁵	CL=90%
Γ_{591}	$\pi^+ \mu^\pm \tau^\mp$	LF	< 7.2	× 10 ⁻⁵	CL=90%
Γ_{592}	$K^+ e^+ \mu^-$	LF	< 7.0	× 10 ⁻⁹	CL=90%
Γ_{593}	$K^+ e^- \mu^+$	LF	< 6.4	× 10 ⁻⁹	CL=90%
Γ_{594}	$K^+ e^\pm \mu^\mp$	LF	< 9.1	× 10 ⁻⁸	CL=90%
Γ_{595}	$K^+ e^+ \tau^-$	LF	< 4.3	× 10 ⁻⁵	CL=90%
Γ_{596}	$K^+ e^- \tau^+$	LF	< 1.5	× 10 ⁻⁵	CL=90%
Γ_{597}	$K^+ e^\pm \tau^\mp$	LF	< 3.0	× 10 ⁻⁵	CL=90%
Γ_{598}	$K^+ \mu^+ \tau^-$	LF	< 4.5	× 10 ⁻⁵	CL=90%
Γ_{599}	$K^+ \mu^- \tau^+$	LF	< 2.8	× 10 ⁻⁵	CL=90%
Γ_{600}	$K^+ \mu^\pm \tau^\mp$	LF	< 4.8	× 10 ⁻⁵	CL=90%
Γ_{601}	$K^*(892)^+ e^+ \mu^-$	LF	< 1.3	× 10 ⁻⁶	CL=90%
Γ_{602}	$K^*(892)^+ e^- \mu^+$	LF	< 9.9	× 10 ⁻⁷	CL=90%
Γ_{603}	$K^*(892)^+ e^\pm \mu^\mp$	LF	< 1.4	× 10 ⁻⁶	CL=90%
Γ_{604}	$\pi^- e^+ e^+$	L	< 2.3	× 10 ⁻⁸	CL=90%
Γ_{605}	$\pi^- \mu^+ \mu^+$	L	< 4.0	× 10 ⁻⁹	CL=95%
Γ_{606}	$\pi^- e^+ \mu^+$	L	< 1.5	× 10 ⁻⁷	CL=90%
Γ_{607}	$\rho^- e^+ e^+$	L	< 1.7	× 10 ⁻⁷	CL=90%
Γ_{608}	$\rho^- \mu^+ \mu^+$	L	< 4.2	× 10 ⁻⁷	CL=90%
Γ_{609}	$\rho^- e^+ \mu^+$	L	< 4.7	× 10 ⁻⁷	CL=90%
Γ_{610}	$K^- e^+ e^+$	L	< 3.0	× 10 ⁻⁸	CL=90%
Γ_{611}	$K^- \mu^+ \mu^+$	L	< 4.1	× 10 ⁻⁸	CL=90%
Γ_{612}	$K^- e^+ \mu^+$	L	< 1.6	× 10 ⁻⁷	CL=90%
Γ_{613}	$K^*(892)^- e^+ e^+$	L	< 4.0	× 10 ⁻⁷	CL=90%
Γ_{614}	$K^*(892)^- \mu^+ \mu^+$	L	< 5.9	× 10 ⁻⁷	CL=90%
Γ_{615}	$K^*(892)^- e^+ \mu^+$	L	< 3.0	× 10 ⁻⁷	CL=90%
Γ_{616}	$D^- e^+ e^+$	L	< 2.6	× 10 ⁻⁶	CL=90%
Γ_{617}	$D^- e^+ \mu^+$	L	< 1.8	× 10 ⁻⁶	CL=90%
Γ_{618}	$D^- \mu^+ \mu^+$	L	< 6.9	× 10 ⁻⁷	CL=95%
Γ_{619}	$D^* \mu^+ \mu^+$	L	< 2.4	× 10 ⁻⁶	CL=95%
Γ_{620}	$D_s^- \mu^+ \mu^+$	L	< 5.8	× 10 ⁻⁷	CL=95%
Γ_{621}	$\bar{D}^0 \pi^- \mu^+ \mu^+$	L	< 1.5	× 10 ⁻⁶	CL=95%
Γ_{622}	$\Lambda^0 \mu^+$	L, B	< 6	× 10 ⁻⁸	CL=90%
Γ_{623}	$\Lambda^0 e^+$	L, B	< 3.2	× 10 ⁻⁸	CL=90%
Γ_{624}	$\bar{\Lambda}^0 \mu^+$	L, B	< 6	× 10 ⁻⁸	CL=90%
Γ_{625}	$\bar{\Lambda}^0 e^+$	L, B	< 8	× 10 ⁻⁸	CL=90%

[a] An ℓ indicates an e or a μ mode, not a sum over these modes.

[b] An $CP(\pm 1)$ indicates the $CP=+1$ and $CP=-1$ eigenstates of the D^0 - \bar{D}^0 system.

[c] D denotes D^0 or \bar{D}^0 .

[d] D_{CP+}^0 decays into $D^0 \pi^0$ with the D^0 reconstructed in CP -even eigenstates $K^+ K^-$ and $\pi^+ \pi^-$.

[e] \bar{D}^{**} represents an excited state with mass $2.2 < M < 2.8$ GeV/ c^2 .

[f] $\chi_{c1}(3872)^+$ is a hypothetical charged partner of the $\chi_{c1}(3872)$.

[g] $\Theta(1710)^{++}$ is a possible narrow pentaquark state and $G(2220)$ is a possible glueball resonance.

[h] $(\bar{\Lambda}_c^- p)_s$ denotes a low-mass enhancement near 3.35 GeV/ c^2 .

CONSTRAINED FIT INFORMATION

An overall fit to 3 branching ratios uses 6 measurements and one constraint to determine 3 parameters. The overall fit has a $\chi^2 = 3.7$ for 4 degrees of freedom.

The following *off-diagonal* array elements are the correlation coefficients $\langle \delta x_i \delta x_j \rangle / (\delta x_i \delta x_j)$, in percent, from the fit to the branching fractions, $x_i \equiv \Gamma_i / \Gamma_{\text{total}}$. The fit constrains the x_i whose labels appear in this array to sum to one.

x_{403}	10
	x_{342}

CONSTRAINED FIT INFORMATION

An overall fit to 18 branching ratios uses 58 measurements and one constraint to determine 12 parameters. The overall fit has a $\chi^2 = 55.9$ for 47 degrees of freedom.

The following *off-diagonal* array elements are the correlation coefficients $\langle \delta x_i \delta x_j \rangle / (\delta x_i \delta x_j)$, in percent, from the fit to the branching fractions, $x_i \equiv \Gamma_i / \Gamma_{\text{total}}$. The fit constrains the x_i whose labels appear in this array to sum to one.

x_7	33									
x_{49}	0	0								
x_{105}	0	0	7							
x_{146}	0	0	1	13						
x_{275}	0	0	0	0	0					
x_{280}	0	0	0	0	0	0				
x_{299}	0	0	0	0	0	92	0			
x_{311}	0	0	0	0	0	56	0	52		
x_{571}	0	0	0	0	0	13	0	12	7	
x_{578}	0	0	0	0	0	0	5	0	0	
	x_6	x_7	x_{49}	x_{105}	x_{146}	x_{275}	x_{280}	x_{299}	x_{311}	x_{571}

 B^+ BRANCHING RATIOS

$\Gamma(\ell^+ \nu_\ell X) / \Gamma_{\text{total}}$ Γ_1 / Γ

"OUR EVALUATION" is an average using rescaled values of the data listed below. The average and rescaling were performed by the Heavy Flavor Averaging Group (HFLAV) and are described at <https://hflav.web.cern.ch/>. The averaging/rescaling procedure takes into account correlations between the measurements.

VALUE (units 10 ⁻²)	DOCUMENT ID	TECN	COMMENT
---------------------------------	-------------	------	---------

10.99 ± 0.28 OUR EVALUATION

10.76 ± 0.32 OUR AVERAGE

Error includes scale factor of 1.1.

11.17 ± 0.25 ± 0.28 ¹ URQUIJO 07 BELL $e^+ e^- \rightarrow T(4S)$

10.28 ± 0.26 ± 0.39 ² AUBERT,B 06Y BABR $e^+ e^- \rightarrow T(4S)$

10.25 ± 0.57 ± 0.65 ³ ARTUSO 97 CLE2 $e^+ e^- \rightarrow T(4S)$

••• We do not use the following data for averages, fits, limits, etc. •••

11.15 ± 0.26 ± 0.41 ⁴ OKABE 05 BELL Repl. by URQUIJO 07

10.1 ± 1.8 ± 1.5 ATHANAS 94 CLE2 Sup. by ARTUSO 97

¹ URQUIJO 07 report a measurement of $(10.34 \pm 0.23 \pm 0.25)\%$ for the partial branching fraction of $B^+ \rightarrow e^+ \nu_e X_c$ decay with electron energy above 0.6 GeV. We converted the result to $B^+ \rightarrow e^+ \nu_e X$ branching fraction.

² The measurements are obtained for charged and neutral B mesons partial rates of semileptonic decay to electrons with momentum above 0.6 GeV/ c in the B rest frame. The best precision on the ratio is achieved for a momentum threshold of 1.0 GeV: $B(B^+ \rightarrow e^+ \nu_e X) / B(B^0 \rightarrow e^+ \nu_e X) = 1.074 \pm 0.041 \pm 0.026$.

³ ARTUSO 97 uses partial reconstruction of $B \rightarrow D^* \ell \nu_\ell$ and inclusive semileptonic branching ratio from BARISH 96B $(0.1049 \pm 0.0017 \pm 0.0043)$.

⁴ The measurements are obtained for charged and neutral B mesons partial rates of semileptonic decay to electrons with momentum above 0.6 GeV/ c in the B rest frame, and their ratio of $B(B^+ \rightarrow e^+ \nu_e X) / B(B^0 \rightarrow e^+ \nu_e X) = 1.08 \pm 0.05 \pm 0.02$.

$\Gamma(e^+ \nu_e X_c) / \Gamma_{\text{total}}$ Γ_2 / Γ

VALUE (units 10 ⁻²)	DOCUMENT ID	TECN	COMMENT
---------------------------------	-------------	------	---------

10.79 ± 0.25 ± 0.27

¹ URQUIJO 07 BELL $e^+ e^- \rightarrow T(4S)$

¹ Measure the independent B^+ and B^0 partial branching fractions with electron threshold energies of 0.4 GeV.

$\Gamma(\overline{D}^0 \ell^+ \nu_\ell)/\Gamma_{\text{total}}$ Γ_4/Γ
 "OUR EVALUATION" is an average using rescaled values of the data listed below. The average and rescaling were performed by the Heavy Flavor Averaging Group (HFLAV) and are described at <https://hflav.web.cern.ch/>. The averaging/rescaling procedure takes into account correlations between the measurements. $\ell = e$ or μ , not sum over e and μ modes.

VALUE (%) DOCUMENT ID TECN COMMENT
2.35 ± 0.03 ± 0.09 OUR EVALUATION
2.29 ± 0.08 OUR AVERAGE

2.29 ± 0.08 ± 0.09	¹ AUBERT	10	BABR	$e^+e^- \rightarrow \Upsilon(4S)$
2.34 ± 0.03 ± 0.13	AUBERT	09A	BABR	$e^+e^- \rightarrow \Upsilon(4S)$
2.21 ± 0.13 ± 0.19	² BARTELT	99	CLE2	$e^+e^- \rightarrow \Upsilon(4S)$
1.6 ± 0.6 ± 0.3	³ FULTON	91	CLEO	$e^+e^- \rightarrow \Upsilon(4S)$

- • • We do not use the following data for averages, fits, limits, etc. • • •
- 2.33 ± 0.09 ± 0.09 ¹ AUBERT 08Q BABR Repl. by AUBERT 09A
- 1.94 ± 0.15 ± 0.34 ⁴ ATHANAS 97 CLE2 Repl. by BARTELT 99

$\Gamma(\overline{D}^0 \ell^+ \nu_\ell)/\Gamma(\ell^+ \nu_\ell X)$ Γ_4/Γ_1

VALUE DOCUMENT ID TECN COMMENT
0.255 ± 0.009 ± 0.009 ¹ AUBERT 10 BABR $e^+e^- \rightarrow \Upsilon(4S)$

- ¹ Uses a fully reconstructed B meson on the recoil side.

$\Gamma(\overline{D}^0 \ell^+ \nu_\ell)/\Gamma(D \ell^+ \nu_\ell X)$ Γ_4/Γ_3

VALUE DOCUMENT ID TECN COMMENT
0.230 ± 0.020 OUR AVERAGE

0.25 ± 0.06	¹ AAIJ	19AC	LHCB	pp at 7 and 8 TeV
0.227 ± 0.014 ± 0.016	² AUBERT	07AN	BABR	$e^+e^- \rightarrow \Upsilon(4S)$

- ¹ The relative branching fractions of $B^- \rightarrow D^0, D^{*0}, D^{*0}$ in the $B^- \rightarrow D^0 X \mu^- \overline{\nu}$ channel are determined by fitting the distribution of the missing mass in $\overline{B}_s^{*0} \rightarrow B^- K^+$ decays.
- ² Uses a fully reconstructed B meson on the recoil side.

$\Gamma(\overline{D}^0 \tau^+ \nu_\tau)/\Gamma_{\text{total}}$ Γ_5/Γ

VALUE (units 10^{-2}) DOCUMENT ID TECN COMMENT
0.77 ± 0.22 ± 0.12 ¹ BOZEK 10 BELL $e^+e^- \rightarrow \Upsilon(4S)$

- • • We do not use the following data for averages, fits, limits, etc. • • •
- 0.67 ± 0.37 ± 0.13 ² AUBERT 08N BABR Repl. by AUBERT 09s
- ¹ Assumes equal production of B^+ and B^0 at the $\Upsilon(4S)$.
- ² Uses a fully reconstructed B meson as a tag on the recoil side.

$\Gamma(\overline{D}^0 \tau^+ \nu_\tau)/\Gamma(\overline{D}^0 \ell^+ \nu_\ell)$ Γ_5/Γ_4

VALUE DOCUMENT ID TECN COMMENT
0.429 ± 0.082 ± 0.052 ^{1,2} LEES 12D BABR $e^+e^- \rightarrow \Upsilon(4S)$

- • • We do not use the following data for averages, fits, limits, etc. • • •
- 0.314 ± 0.170 ± 0.049 ¹ AUBERT 09s BABR Repl. by LEES 12D
- ¹ Uses a fully reconstructed B meson as a tag on the recoil side.
- ² Uses $\tau^+ \rightarrow e^+ \nu_e \overline{\nu}_\tau$ and $\tau^+ \rightarrow \mu^+ \nu_\mu \overline{\nu}_\tau$ and e^+ or μ^+ as ℓ^+ .

$\Gamma(\overline{D}^*(2007)^0 \ell^+ \nu_\ell)/\Gamma_{\text{total}}$ Γ_6/Γ

"OUR EVALUATION" is an average using rescaled values of the data listed below. The average and rescaling were performed by the Heavy Flavor Averaging Group (HFLAV) and are described at <https://hflav.web.cern.ch/>. The averaging/rescaling procedure takes into account correlations between the measurements. $\ell = e$ or μ , not sum over e and μ modes.

VALUE (%) EVTS DOCUMENT ID TECN COMMENT
5.66 ± 0.07 ± 0.21 OUR EVALUATION

5.60 ± 0.26 OUR FIT Error includes scale factor of 1.5.
5.58 ± 0.26 OUR AVERAGE Error includes scale factor of 1.5. See the ideogram below.

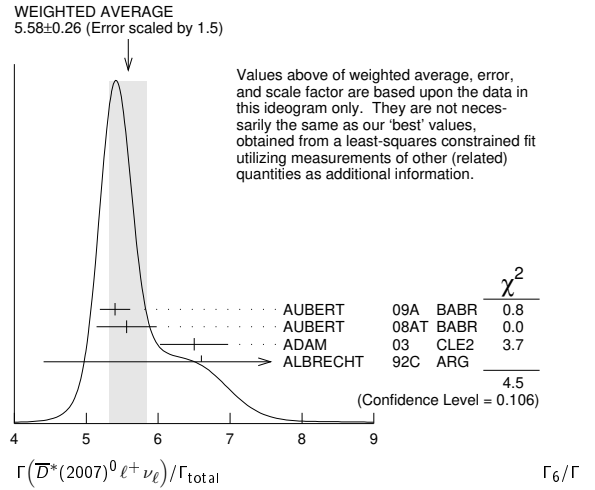
5.40 ± 0.02 ± 0.21	AUBERT	09A	BABR	$e^+e^- \rightarrow \Upsilon(4S)$
5.56 ± 0.08 ± 0.41	¹ AUBERT	08AT	BABR	$e^+e^- \rightarrow \Upsilon(4S)$
6.50 ± 0.20 ± 0.43	² ADAM	03	CLE2	$e^+e^- \rightarrow \Upsilon(4S)$
6.6 ± 1.6 ± 1.5	³ ALBRECHT	92C	ARG	$e^+e^- \rightarrow \Upsilon(4S)$

- • • We do not use the following data for averages, fits, limits, etc. • • •
- 5.83 ± 0.15 ± 0.30 ⁴ AUBERT 08Q BABR Repl. by AUBERT 09A
- 6.50 ± 0.20 ± 0.43 ⁵ BRIERE 02 CLE2 $e^+e^- \rightarrow \Upsilon(4S)$
- 5.13 ± 0.54 ± 0.64 ⁶ BARISH 95 CLE2 Repl. by ADAM 03
- seen 398 ⁷ SANGHERA 93 CLE2 $e^+e^- \rightarrow \Upsilon(4S)$
- 4.1 ± 0.8 ± 0.8 ⁸ FULTON 91 CLEO $e^+e^- \rightarrow \Upsilon(4S)$
- 7.0 ± 1.8 ± 1.4 ⁹ ANTREASYAN 90B CBAL $e^+e^- \rightarrow \Upsilon(4S)$
- ¹ Measured using the dependence of $B^- \rightarrow D^{*0} e^- \overline{\nu}_e$ decay differential rate and the form factor description by CAPRINI 98.
- ² Simultaneous measurements of both $B^0 \rightarrow D^*(2010)^- \ell \nu$ and $B^+ \rightarrow \overline{D}^*(2007)^0 \ell \nu$.
- ³ ALBRECHT 92C reports $0.058 \pm 0.014 \pm 0.013$. We rescale using the method described in STONE 94 but with the updated PDG 94 $B(D^0 \rightarrow K^- \pi^+)$. Assumes equal production of $B^0 \overline{B}^0$ and $B^+ B^-$ at the $\Upsilon(4S)$.
- ⁴ Uses a fully reconstructed B meson as a tag on the recoil side.
- ⁵ The results are based on the same analysis and data sample reported in ADAM 03.
- ⁶ BARISH 95 use $B(D^0 \rightarrow K^- \pi^+) = (3.91 \pm 0.08 \pm 0.17)\%$ and $B(D^{*0} \rightarrow D^0 \pi^0) = (63.6 \pm 2.3 \pm 3.3)\%$.

⁷ Combining $\overline{D}^{*0} \ell^+ \nu_\ell$ and $\overline{D}^{*-} \ell^+ \nu_\ell$ SANGHERA 93 test $V-A$ structure and fit the decay angular distributions to obtain $A_{FB} = 3/4 * (\Gamma^- - \Gamma^+)/\Gamma = 0.14 \pm 0.06 \pm 0.03$. Assuming a value of V_{cb} , they measure $V, A_1,$ and A_2 , the three form factors for the $D^* \ell \nu_\ell$ decay, where results are slightly dependent on model assumptions.

⁸ Assumes equal production of $B^0 \overline{B}^0$ and $B^+ B^-$ at the $\Upsilon(4S)$. Uncorrected for D and D^* branching ratio assumptions.

⁹ ANTREASYAN 90B is average over B and $\overline{D}^*(2010)$ charge states.



$\Gamma(\overline{D}^*(2007)^0 \ell^+ \nu_\ell)/\Gamma(D \ell^+ \nu_\ell X)$ Γ_6/Γ_3

VALUE DOCUMENT ID TECN COMMENT
0.582 ± 0.018 ± 0.030 ¹ AUBERT 07AN BABR $e^+e^- \rightarrow \Upsilon(4S)$

- ¹ Uses a fully reconstructed B meson on the recoil side.

$\Gamma(\overline{D}^*(2007)^0 \tau^+ \nu_\tau)/\Gamma_{\text{total}}$ Γ_7/Γ

VALUE (units 10^{-2}) DOCUMENT ID TECN COMMENT
1.88 ± 0.20 OUR FIT

2.12 ± 0.28 ± 0.29 ¹ BOZEK 10 BELL $e^+e^- \rightarrow \Upsilon(4S)$

- • • We do not use the following data for averages, fits, limits, etc. • • •
- 2.25 ± 0.48 ± 0.28 ² AUBERT 08N BABR Repl. by AUBERT 09s
- ¹ Assumes equal production of B^+ and B^0 at the $\Upsilon(4S)$.
- ² Uses a fully reconstructed B meson as a tag on the recoil side.

$\Gamma(\overline{D}^*(2007)^0 \tau^+ \nu_\tau)/\Gamma(\overline{D}^*(2007)^0 \ell^+ \nu_\ell)$ Γ_7/Γ_6

VALUE DOCUMENT ID TECN COMMENT
0.335 ± 0.034 OUR FIT

0.322 ± 0.032 ± 0.022 ^{1,2} LEES 12D BABR $e^+e^- \rightarrow \Upsilon(4S)$

- • • We do not use the following data for averages, fits, limits, etc. • • •
- 0.346 ± 0.073 ± 0.034 ¹ AUBERT 09s BABR Repl. by LEES 12D
- ¹ Uses a fully reconstructed B meson as a tag on the recoil side.
- ² Uses $\tau^+ \rightarrow e^+ \nu_e \overline{\nu}_\tau$ and $\tau^+ \rightarrow \mu^+ \nu_\mu \overline{\nu}_\tau$ and e^+ or μ^+ as ℓ^+ .

$\Gamma(D^- \pi^+ \ell^+ \nu_\ell)/\Gamma_{\text{total}}$ Γ_8/Γ

VALUE (units 10^{-3}) DOCUMENT ID TECN COMMENT
4.4 ± 0.4 OUR AVERAGE

4.55 ± 0.27 ± 0.39 VOSSEN 18 BELL $e^+e^- \rightarrow \Upsilon(4S)$

4.2 ± 0.6 ± 0.3 ¹ AUBERT 08Q BABR $e^+e^- \rightarrow \Upsilon(4S)$

4.4 ± 0.6 ± 0.2 ^{1,2} LIVENTSEV 08 BELL Repl. by VOSSEN 18

5.8 ± 1.0 ± 0.2 ³ LIVENTSEV 05 BELL Repl. by LIVENTSEV 08

- ¹ Uses a fully reconstructed B meson as a tag on the recoil side.
- ² LIVENTSEV 08 reports $(4.0 \pm 0.4 \pm 0.6) \times 10^{-3}$ from a measurement of $[\Gamma(B^+ \rightarrow D^- \pi^+ \ell^+ \nu_\ell)/\Gamma_{\text{total}}] / [B(B^+ \rightarrow \overline{D}^0 \ell^+ \nu_\ell)]$ assuming $B(B^+ \rightarrow \overline{D}^0 \ell^+ \nu_\ell) = (2.15 \pm 0.22) \times 10^{-2}$, which we rescale to our best value $B(B^+ \rightarrow \overline{D}^0 \ell^+ \nu_\ell) = (2.35 \pm 0.09) \times 10^{-2}$. Our first error is their experiment's error and our second error is the systematic error from using our best value.
- ³ LIVENTSEV 05 reports $[\Gamma(B^+ \rightarrow D^- \pi^+ \ell^+ \nu_\ell)/\Gamma_{\text{total}}] / [B(B^0 \rightarrow D^- \ell^+ \nu_\ell)] = 0.25 \pm 0.03 \pm 0.03$ which we multiply by our best value $B(B^0 \rightarrow D^- \ell^+ \nu_\ell) = (2.31 \pm 0.10) \times 10^{-2}$. Our first error is their experiment's error and our second error is the systematic error from using our best value.

$\Gamma(\overline{D}_s^*(2420)^0 \ell^+ \nu_\ell, \overline{D}_s^{*0} \rightarrow D^- \pi^+)/\Gamma_{\text{total}}$ Γ_9/Γ

VALUE (units 10^{-3}) DOCUMENT ID TECN COMMENT
2.5 ± 0.5 OUR AVERAGE

2.6 ± 0.5 ± 0.4 ¹ AUBERT 08BL BABR $e^+e^- \rightarrow \Upsilon(4S)$

2.4 ± 0.4 ± 0.6 ¹ LIVENTSEV 08 BELL $e^+e^- \rightarrow \Upsilon(4S)$

- ¹ Uses a fully reconstructed B meson as a tag on the recoil side.

Meson Particle Listings

 B^\pm $\Gamma(\overline{D}_2^*(2460)^0 \ell^+ \nu_\ell, \overline{D}_2^{*0} \rightarrow D^- \pi^+) / \Gamma_{\text{total}}$ Γ_{10} / Γ

VALUE (units 10^{-3})	DOCUMENT ID	TECN	COMMENT
1.53 ± 0.16 OUR AVERAGE			
1.42 ± 0.15 ± 0.15	¹ AUBERT	09Y	BABR $e^+ e^- \rightarrow \Upsilon(4S)$
1.5 ± 0.2 ± 0.2	² AUBERT	08BL	BABR $e^+ e^- \rightarrow \Upsilon(4S)$
2.2 ± 0.3 ± 0.4	² LIVENTSEV	08	BELL $e^+ e^- \rightarrow \Upsilon(4S)$

- ¹ Uses a simultaneous fit of all B semileptonic decays without full reconstruction of events. AUBERT 09Y reports $B(B^+ \rightarrow \overline{D}_2^*(2460)^0 \ell^+ \nu_\ell) \cdot B(\overline{D}_2^*(2460)^0 \rightarrow D^{(*)-} \pi^+) = (2.29 \pm 0.23 \pm 0.21) \times 10^{-3}$ and the authors have provided us the individual measurement.
- ² Uses a fully reconstructed B meson as a tag on the recoil side.

 $\Gamma(D^{(*)-} n \pi \ell^+ \nu_\ell (n \geq 1)) / \Gamma(D \ell^+ \nu_\ell X)$ Γ_{11} / Γ_3

VALUE	DOCUMENT ID	TECN	COMMENT
0.193 ± 0.022 OUR AVERAGE			
0.21 ± 0.07	^{1,2} AAIJ	19AC	LHCB pp at 7 and 8 TeV
0.191 ± 0.013 ± 0.019	³ AUBERT	07AN	BABR $e^+ e^- \rightarrow \Upsilon(4S)$

- ¹ The relative branching fractions of $B^- \rightarrow D^0, D^{*0}, D^{*0}$ in the $B^- \rightarrow D^0 X \mu^- \overline{\nu}$ channel are determined by fitting the distribution of the missing mass in $\overline{B}_s^0 \rightarrow B^- K^+$ decays.
- ² In this measurement of $f_{D^{*0}} = B(B^- \rightarrow (D^{*0} \rightarrow D^0 X) \mu^- \overline{\nu}) / B(B^- \rightarrow D^0 X \mu^- \overline{\nu})$, D^{*0} refers collectively to L = 1 states $D_{01}^*(2400), D_1(2420), D_1(2430)$, and $D_2^*(2460)$, as well as other resonances such as radially excited D mesons, and to nonresonant contributions with additional pions.
- ³ Uses a fully reconstructed B meson on the recoil side.

 $\Gamma(D^{*-} \pi^+ \ell^+ \nu_\ell) / \Gamma_{\text{total}}$ Γ_{12} / Γ

VALUE (units 10^{-3})	DOCUMENT ID	TECN	COMMENT
6.0 ± 0.4 OUR AVERAGE			
6.03 ± 0.43 ± 0.38		VOSSEN	18 BELL $e^+ e^- \rightarrow \Upsilon(4S)$
5.9 ± 0.5 ± 0.4	¹ AUBERT	08Q	BABR $e^+ e^- \rightarrow \Upsilon(4S)$

- • • We do not use the following data for averages, fits, limits, etc. • • •
- 7.0 ± 1.1 ± 0.3 ^{1,2} LIVENTSEV 08 BELL Repl. by VOSSEN 18
- 6.1 ± 1.4 ± 0.2 ^{3,4} LIVENTSEV 05 BELL Repl. by LIVENTSEV 08
- ¹ Uses a fully reconstructed B meson as a tag on the recoil side.
- ² LIVENTSEV 08 reports $(6.4 \pm 0.8 \pm 0.9) \times 10^{-3}$ from a measurement of $[\Gamma(B^+ \rightarrow D^{*-} \pi^+ \ell^+ \nu_\ell) / \Gamma_{\text{total}}] / [B(B^+ \rightarrow \overline{D}^0 \ell^+ \nu_\ell)]$ assuming $B(B^+ \rightarrow \overline{D}^0 \ell^+ \nu_\ell) = (2.15 \pm 0.22) \times 10^{-2}$, which we rescale to our best value $B(B^+ \rightarrow \overline{D}^0 \ell^+ \nu_\ell) = (2.35 \pm 0.09) \times 10^{-2}$. Our first error is their experiment's error and our second error is the systematic error from using our best value.
- ³ Excludes D^{*+} contribution to D modes.
- ⁴ LIVENTSEV 05 reports $[\Gamma(B^+ \rightarrow D^{*-} \pi^+ \ell^+ \nu_\ell) / \Gamma_{\text{total}}] / [B(B^0 \rightarrow D^*(2010)^- \ell^+ \nu_\ell)] = 0.12 \pm 0.02 \pm 0.02$ which we multiply by our best value $B(B^0 \rightarrow D^*(2010)^- \ell^+ \nu_\ell) = (5.05 \pm 0.14) \times 10^{-2}$. Our first error is their experiment's error and our second error is the systematic error from using our best value.

 $\Gamma(\overline{D}_1(2420)^0 \ell^+ \nu_\ell, \overline{D}_1^0 \rightarrow D^{*-} \pi^+) / \Gamma_{\text{total}}$ Γ_{13} / Γ

VALUE (units 10^{-3})	DOCUMENT ID	TECN	COMMENT
3.03 ± 0.20 OUR AVERAGE			
2.97 ± 0.17 ± 0.17	¹ AUBERT	09Y	BABR $e^+ e^- \rightarrow \Upsilon(4S)$
2.9 ± 0.3 ± 0.3	² AUBERT	08BL	BABR $e^+ e^- \rightarrow \Upsilon(4S)$
4.2 ± 0.7 ± 0.7	² LIVENTSEV	08	BELL $e^+ e^- \rightarrow \Upsilon(4S)$
3.73 ± 0.85 ± 0.57	³ ANASTASSOV	98	CLE2 $e^+ e^- \rightarrow \Upsilon(4S)$

- ¹ Uses a simultaneous measurement of all B semileptonic decays without full reconstruction of events.
- ² Uses a fully reconstructed B meson as a tag on the recoil side.
- ³ Assumes equal production of B^+ and B^0 at the $\Upsilon(4S)$.

 $\Gamma(\overline{D}_1^*(2430)^0 \ell^+ \nu_\ell, \overline{D}_1^{*0} \rightarrow D^{*-} \pi^+) / \Gamma_{\text{total}}$ Γ_{14} / Γ

VALUE (units 10^{-3})	CL%	DOCUMENT ID	TECN	COMMENT
2.7 ± 0.4 ± 0.5		¹ AUBERT	08BL	BABR $e^+ e^- \rightarrow \Upsilon(4S)$
<0.7	90	¹ LIVENTSEV	08	BELL $e^+ e^- \rightarrow \Upsilon(4S)$

- ¹ Uses a fully reconstructed B meson as a tag on the recoil side.

 $\Gamma(\overline{D}_2^*(2460)^0 \ell^+ \nu_\ell, \overline{D}_2^{*0} \rightarrow D^{*-} \pi^+) / \Gamma_{\text{total}}$ Γ_{15} / Γ

VALUE (units 10^{-3})	CL%	DOCUMENT ID	TECN	COMMENT
1.01 ± 0.24 OUR AVERAGE				Error includes scale factor of 2.0.
0.87 ± 0.11 ± 0.07		¹ AUBERT	09Y	BABR $e^+ e^- \rightarrow \Upsilon(4S)$
1.5 ± 0.2 ± 0.2		² AUBERT	08BL	BABR $e^+ e^- \rightarrow \Upsilon(4S)$
1.8 ± 0.6 ± 0.3		² LIVENTSEV	08	BELL $e^+ e^- \rightarrow \Upsilon(4S)$
<1.6	90	³ ANASTASSOV	98	CLE2 $e^+ e^- \rightarrow \Upsilon(4S)$

- ¹ Uses a simultaneous fit of all B semileptonic decays without full reconstruction of events. AUBERT 09Y reports $B(B^+ \rightarrow \overline{D}_2^*(2460)^0 \ell^+ \nu_\ell) \cdot B(\overline{D}_2^*(2460)^0 \rightarrow D^{(*)-} \pi^+) = (2.29 \pm 0.23 \pm 0.21) \times 10^{-3}$ and the authors have provided us the individual measurement.
- ² Uses a fully reconstructed B meson as a tag on the recoil side.
- ³ Assumes equal production of B^+ and B^0 at the $\Upsilon(4S)$.

 $\Gamma(\overline{D}^0 \pi^+ \pi^- \ell^+ \nu_\ell) / \Gamma(\overline{D}^0 \ell^+ \nu_\ell)$ Γ_{16} / Γ_4

VALUE (units 10^{-2})	DOCUMENT ID	TECN	COMMENT
7.1 ± 1.3 ± 0.8	¹ LEES	16	BABR $e^+ e^- \rightarrow \Upsilon(4S)$

- ¹ Measurement used electrons and muons as leptons.

 $\Gamma(\overline{D}^{*0} \pi^+ \pi^- \ell^+ \nu_\ell) / \Gamma(\overline{D}^{*0} \ell^+ \nu_\ell)$ Γ_{17} / Γ_6

VALUE (units 10^{-2})	DOCUMENT ID	TECN	COMMENT
1.4 ± 0.7 ± 0.4	¹ LEES	16	BABR $e^+ e^- \rightarrow \Upsilon(4S)$

- ¹ Measurement used electrons and muons as leptons.

 $\Gamma(D_s^{(*)-} K^+ \ell^+ \nu_\ell) / \Gamma_{\text{total}}$ Γ_{18} / Γ

VALUE (units 10^{-4})	DOCUMENT ID	TECN	COMMENT
6.1 ± 1.0 OUR AVERAGE			
5.9 ± 1.2 ± 1.5	¹ STYPULA	12	BELL $e^+ e^- \rightarrow \Upsilon(4S)$
6.13 ^{+1.04} _{-1.03} ± 0.67	¹ DEL-AMO-SA...11L	BABR	$e^+ e^- \rightarrow \Upsilon(4S)$

- ¹ Assumes equal production of B^+ and B^0 at the $\Upsilon(4S)$.

 $\Gamma(D_s^- K^+ \ell^+ \nu_\ell) / \Gamma_{\text{total}}$ Γ_{19} / Γ

VALUE (units 10^{-4})	DOCUMENT ID	TECN	COMMENT
3.0 ± 0.9^{+1.1}_{-0.8}	¹ STYPULA	12	BELL $e^+ e^- \rightarrow \Upsilon(4S)$

- ¹ Assumes equal production of B^+ and B^0 at the $\Upsilon(4S)$.

 $\Gamma(D_s^{*-} K^+ \ell^+ \nu_\ell) / \Gamma_{\text{total}}$ Γ_{20} / Γ

VALUE (units 10^{-4})	DOCUMENT ID	TECN	COMMENT
2.9 ± 1.6^{+1.1}_{-1.0}	^{1,2} STYPULA	12	BELL $e^+ e^- \rightarrow \Upsilon(4S)$

- ¹ Assumes equal production of B^+ and B^0 at the $\Upsilon(4S)$.
- ² STYPULA 12 provides also an upper limit of 0.56×10^{-3} at 90% CL for the same data. Also measures branching fraction of the combined modes of $D_s^- K^+ \ell^+ \nu_\ell$ and $D_s^{*-} K^+ \ell^+ \nu_\ell$ as $B(B^+ \rightarrow D_s^{*-} K^+ \ell^+ \nu_\ell) = (5.9 \pm 1.2 \pm 1.5) \times 10^{-4}$.

 $\Gamma(\pi^0 \ell^+ \nu_\ell) / \Gamma_{\text{total}}$ Γ_{21} / Γ

"OUR EVALUATION" is an average using rescaled values of the data listed below. The average and rescaling were performed by the Heavy Flavor Averaging Group (HFAG) and are described at <https://hfag.web.cern.ch/>. The averaging/rescaling procedure takes into account correlations between the measurements.

VALUE (units 10^{-4})	DOCUMENT ID	TECN	COMMENT
0.780 ± 0.027 OUR EVALUATION			
0.748 ± 0.029 OUR AVERAGE			
0.80 ± 0.08 ± 0.04	¹ SIBIDANOV	13	BELL $e^+ e^- \rightarrow \Upsilon(4S)$
0.77 ± 0.04 ± 0.03	² LEES	12AA	BABR $e^+ e^- \rightarrow \Upsilon(4S)$
0.705 ± 0.025 ± 0.035	³ DEL-AMO-SA...11c	BABR	$e^+ e^- \rightarrow \Upsilon(4S)$
0.82 ± 0.09 ± 0.05	³ AUBERT	08AV	BABR $e^+ e^- \rightarrow \Upsilon(4S)$
0.77 ± 0.14 ± 0.08	⁴ HOKUUE	07	BELL $e^+ e^- \rightarrow \Upsilon(4S)$
0.74 ± 0.05 ± 0.10	⁵ AUBERT,B	05o	BABR Repl. by DEL-AMO-SANCHEZ 11c

- ¹ The signal events are tagged by a second B meson reconstructed in the fully hadronic decays.
- ² Uses loose neutrino reconstruction technique. Assumes $B(Y(4S) \rightarrow B^+ B^-) = (51.6 \pm 0.6)\%$ and $B(Y(4S) \rightarrow B^0 \overline{B}^0) = (48.4 \pm 0.6)\%$.
- ³ Using the isospin symmetry relation, B^+ and B^0 branching fractions are combined.
- ⁴ The signal events are tagged by a second B meson reconstructed in the semileptonic mode $B \rightarrow D^{(*)} \ell \nu_\ell$.
- ⁵ B^+ and B^0 decays combined assuming isospin symmetry. Systematic errors include both experimental and form-factor uncertainties.

 $\Gamma(\pi^0 e^+ \nu_e) / \Gamma_{\text{total}}$ Γ_{22} / Γ

VALUE (units 10^{-4})	CL%	DOCUMENT ID	TECN	COMMENT
0.9 ± 0.2 ± 0.2		¹ ALEXANDER	96T	CLE2 $e^+ e^- \rightarrow \Upsilon(4S)$
<2.2	90	ANTREASNYAN	90B	CBAL $e^+ e^- \rightarrow \Upsilon(4S)$

- ¹ Derived based in the reported B^0 result by assuming isospin symmetry: $\Gamma(B^0 \rightarrow \pi^- \ell^+ \nu) = 2\Gamma(B^+ \rightarrow \pi^0 \ell^+ \nu)$.

 $\Gamma(\eta \ell^+ \nu_\ell) / \Gamma_{\text{total}}$ Γ_{23} / Γ

VALUE (units 10^{-4})	CL%	DOCUMENT ID	TECN	COMMENT
0.39 ± 0.05 OUR AVERAGE				
0.42 ± 0.11 ± 0.03		¹ BELENO	17	BELL $e^+ e^- \rightarrow \Upsilon(4S)$
0.38 ± 0.05 ± 0.05		² LEES	12AA	BABR $e^+ e^- \rightarrow \Upsilon(4S)$
0.31 ± 0.06 ± 0.08		² AUBERT	09Q	BABR $e^+ e^- \rightarrow \Upsilon(4S)$
0.64 ± 0.20 ± 0.03		³ AUBERT	08AV	BABR $e^+ e^- \rightarrow \Upsilon(4S)$

- • • We do not use the following data for averages, fits, limits, etc. • • •
- 0.36 ± 0.05 ± 0.04 2 DEL-AMO-SA...11F BABR Repl. by LEES 12AA
- <1.01 90 4 ADAM 07 CLE2 e⁺e⁻ → T(4S)
- 0.84 ± 0.31 ± 0.18 5 ATHAR 03 CLE2 Repl. by ADAM 07

¹ Uses missing-mass technique by fully reconstructing the hadronic decay chain of the accompanying B .

² Uses loose neutrino reconstruction technique. Assumes $B(\Upsilon(4S) \rightarrow B^+B^-) = (51.6 \pm 0.6)\%$ and $B(\Upsilon(4S) \rightarrow B^0\bar{B}^0) = (48.4 \pm 0.6)\%$.

³ Assumes equal production of B^+ and B^0 at the $\Upsilon(4S)$.

⁴ The B^0 and B^+ results are combined assuming the isospin, B lifetimes, and relative charged/neutral B production at the $\Upsilon(4S)$.

⁵ ATHAR 03 reports systematic errors 0.16 ± 0.09 , which are experimental systematic and systematic due to model dependence. We combine these in quadrature.

$\Gamma(\eta^{\pm}\ell^{\pm}\nu_{\ell})/\Gamma_{\text{total}}$		Γ_{24}/Γ	
VALUE (units 10^{-4})	CL%	DOCUMENT ID	TECN COMMENT
0.23 ± 0.08 OUR AVERAGE			
0.24 ± 0.08 ± 0.03		1 LEES 12AA BABR e ⁺ e ⁻ → T(4S)	
0.04 ± 0.22 ^{+0.05} _{-0.02}		2 AUBERT 08AV BABR e ⁺ e ⁻ → T(4S)	
2.66 ± 0.80 ± 0.56		3 ADAM 07 CLE2 e ⁺ e ⁻ → T(4S)	

- • • We do not use the following data for averages, fits, limits, etc. • • •
- <0.72 90 4 BELENO 17 BELL e⁺e⁻ → T(4S)
- 0.24 ± 0.08 ± 0.03 1 DEL-AMO-SA...11F BABR Repl. by LEES 12AA

¹ Uses loose neutrino reconstruction technique. Assumes $B(\Upsilon(4S) \rightarrow B^+B^-) = (51.6 \pm 0.6)\%$ and $B(\Upsilon(4S) \rightarrow B^0\bar{B}^0) = (48.4 \pm 0.6)\%$.

² Assumes equal production of B^+ and B^0 at the $\Upsilon(4S)$.

³ The B^0 and B^+ results are combined assuming the isospin, B lifetimes, and relative charged/neutral B production at the $\Upsilon(4S)$. Corresponds to 90% CL interval $(1.20-4.46) \times 10^{-4}$.

⁴ Uses missing-mass technique by fully reconstructing the hadronic decay chain of the accompanying B .

$\Gamma(\omega\ell^{\pm}\nu_{\ell})/\Gamma_{\text{total}}$		Γ_{25}/Γ	
VALUE (units 10^{-4})	CL%	DOCUMENT ID	TECN COMMENT
1.19 ± 0.09 OUR AVERAGE			
1.21 ± 0.16 ± 0.01		1,2 LEES 13A BABR e ⁺ e ⁻ → T(4S)	
1.35 ± 0.21 ± 0.11		3 LEES 13T BABR e ⁺ e ⁻ → T(4S)	
1.07 ± 0.16 ± 0.07		4 SIBIDANOV 13 BELL e ⁺ e ⁻ → T(4S)	
1.19 ± 0.16 ± 0.09		2,5 LEES 12AA BABR e ⁺ e ⁻ → T(4S)	
1.3 ± 0.4 ± 0.4		6 SCHWA NDA 04 BELL e ⁺ e ⁻ → T(4S)	

- • • We do not use the following data for averages, fits, limits, etc. • • •
- 1.14 ± 0.16 ± 0.08 2 AUBERT 09Q BABR Repl. by LEES 13A
- <2.1 90 7 BEAN 93B CLE2 e⁺e⁻ → T(4S)

¹ LEES 13A reports $(1.21 \pm 0.14 \pm 0.08) \times 10^{-4}$ from a measurement of $[\Gamma(B^+ \rightarrow \omega\ell^+\nu_{\ell})/\Gamma_{\text{total}}] \times [B(\omega(782) \rightarrow \pi^+\pi^-\pi^0)]$ assuming $B(\omega(782) \rightarrow \pi^+\pi^-\pi^0) = (89.2 \pm 0.7) \times 10^{-2}$, which we rescale to our best value $B(\omega(782) \rightarrow \pi^+\pi^-\pi^0) = (89.3 \pm 0.6) \times 10^{-2}$. Our first error is their experiment's error and our second error is the systematic error from using our best value.

² Uses $B(\Upsilon(4S) \rightarrow B^+B^-) = (51.6 \pm 0.6)\%$ and $B(\Upsilon(4S) \rightarrow B^0\bar{B}^0) = (48.4 \pm 0.6)\%$.

³ Uses semileptonic tagging. Assumes $B(\omega \rightarrow \pi^+\pi^-\pi^0) = (89.2 \pm 0.7)\%$ and that the production ratio of B^+B^- to $B^0\bar{B}^0$ from $\Upsilon(4S)$ is 1.056 ± 0.028 . The partial branching fractions in three bins of q^2 are also reported.

⁴ The signal events are tagged by a second B meson reconstructed in the fully hadronic decays.

⁵ Uses loose neutrino reconstruction technique.

⁶ Assumes equal production of B^+ and B^0 at the $\Upsilon(4S)$.

⁷ BEAN 93B limit set using ISGW Model. Using isospin and the quark model to combine $\Gamma(\rho^0\ell^+\nu_{\ell})$ and $\Gamma(\rho^-\ell^+\nu_{\ell})$ with this result, they obtain a limit $<(1.6-2.7) \times 10^{-4}$ at 90% CL for $B^+ \rightarrow \omega\ell^+\nu_{\ell}$. The range corresponds to the ISGW, WSB, and KS models. An upper limit on $|V_{ub}/V_{cb}| < 0.8-0.13$ at 90% CL is derived as well.

$\Gamma(\omega\mu^+\nu_{\mu})/\Gamma_{\text{total}}$		Γ_{26}/Γ	
VALUE	CL%	DOCUMENT ID	TECN COMMENT
• • • We do not use the following data for averages, fits, limits, etc. • • •			
seen		1 ALBRECHT 91c ARG	

- • • We do not use the following data for averages, fits, limits, etc. • • •
- <3.5 90 2 YOOK 15 BELL e⁺e⁻ → T(4S)
- <8 90 1 AUBERT 10E BABR e⁺e⁻ → T(4S)
- <1.9 90 1 AUBERT 09V BABR e⁺e⁻ → T(4S)
- <5.2 90 1 AUBERT 08AD BABR e⁺e⁻ → T(4S)
- <15 90 ARTUSO 95 CLE2 e⁺e⁻ → T(4S)

¹ Assumes equal production of B^+ and B^0 at the $\Upsilon(4S)$.

² Based on phase-space model; if $V-A$ model is used, the 90% CL upper limit becomes $<1.2 \times 10^{-3}$.

$\Gamma(\rho^0\ell^+\nu_{\ell})/\Gamma_{\text{total}}$		Γ_{27}/Γ	
VALUE (units 10^{-4})	CL%	DOCUMENT ID	TECN COMMENT
1.58 ± 0.11 OUR EVALUATION			
1.42 ± 0.23 OUR AVERAGE			
1.83 ± 0.10 ± 0.10		1 SIBIDANOV 13 BELL e ⁺ e ⁻ → T(4S)	
0.94 ± 0.08 ± 0.14		2 DEL-AMO-SA...11c BABR e ⁺ e ⁻ → T(4S)	
1.33 ± 0.23 ± 0.18		3 HOKUUE 07 BELL e ⁺ e ⁻ → T(4S)	
1.34 ± 0.15 ^{+0.28} _{-0.32}		4 BEHRENS 00 CLE2 e ⁺ e ⁻ → T(4S)	

“OUR EVALUATION” is an average using rescaled values of the data listed below. The average and rescaling were performed by the Heavy Flavor Averaging Group (HFLAV) and are described at <https://hflav.web.cern.ch/>. The averaging/rescaling procedure takes into account correlations between the measurements and asymmetric lifetime errors.

¹ Includes scale factor of 2.4. See the ideogram below.

- • • We do not use the following data for averages, fits, limits, etc. • • •
- 1.16 ± 0.11 ± 0.30 2 AUBERT,B 05o BABR Repl. by DEL-AMO-SANCHEZ 11c
- 1.40 ± 0.21^{+0.32}_{-0.33} 4 BEHRENS 00 CLE2 e⁺e⁻ → T(4S)
- 1.2 ± 0.2^{+0.3}_{-0.4} 4 ALEXANDER 96T CLE2 e⁺e⁻ → T(4S)
- <2.1 90 5 BEAN 93B CLE2 e⁺e⁻ → T(4S)

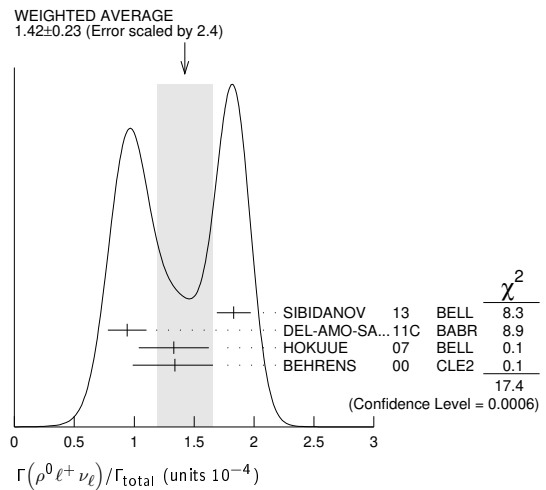
¹ The signal events are tagged by a second B meson reconstructed in the fully hadronic decays.

² B^+ and B^0 decays combined assuming isospin symmetry. Systematic errors include both experimental and form-factor uncertainties.

³ The signal events are tagged by a second B meson reconstructed in the semileptonic mode $B \rightarrow D^{(*)}\ell\nu_{\ell}$.

⁴ Derived based in the reported B^0 result by assuming isospin symmetry: $\Gamma(B^0 \rightarrow \rho^-\ell^+\nu) = 2\Gamma(B^+ \rightarrow \rho^0\ell^+\nu) \approx 2\Gamma(B^+ \rightarrow \omega\ell^+\nu)$.

⁵ BEAN 93B limit set using ISGW Model. Using isospin and the quark model to combine $\Gamma(\omega^0\ell^+\nu_{\ell})$ and $\Gamma(\rho^-\ell^+\nu_{\ell})$ with this result, they obtain a limit $<(1.6-2.7) \times 10^{-4}$ at 90% CL for $B^+ \rightarrow \rho^0\ell^+\nu_{\ell}$. The range corresponds to the ISGW, WSB, and KS models. An upper limit on $|V_{ub}/V_{cb}| < 0.8-0.13$ at 90% CL is derived as well.



$\Gamma(\rho^{\pm}\ell^{\pm}\nu_{\ell})/\Gamma_{\text{total}}$		Γ_{28}/Γ	
VALUE (units 10^{-6})	CL%	DOCUMENT ID	TECN COMMENT
5.8 ± 2.1 ± 0.9		1 TIEN 14 BELL e ⁺ e ⁻ → T(4S)	

¹ Assumes equal production of B^+ and B^0 at the $\Upsilon(4S)$.

$\Gamma(\rho^{\pm}\ell^{\pm}\nu_{\mu})/\Gamma_{\text{total}}$		Γ_{29}/Γ	
VALUE	CL%	DOCUMENT ID	TECN COMMENT
<8.5 × 10⁻⁶	90	1 TIEN 14 BELL e ⁺ e ⁻ → T(4S)	

¹ Assumes equal production of B^+ and B^0 at the $\Upsilon(4S)$.

$\Gamma(\rho^{\pm}\ell^{\pm}\nu_e)/\Gamma_{\text{total}}$		Γ_{30}/Γ	
VALUE (units 10^{-6})	CL%	DOCUMENT ID	TECN COMMENT
8.2^{+3.7}_{-3.2} ± 0.6		1 TIEN 14 BELL e ⁺ e ⁻ → T(4S)	

- • • We do not use the following data for averages, fits, limits, etc. • • •
- <5200 90 2 ADAM 03B CLE2 e⁺e⁻ → T(4S)

¹ Assumes equal production of B^+ and B^0 at the $\Upsilon(4S)$.

² Based on phase-space model; if $V-A$ model is used, the 90% CL upper limit becomes $<1.2 \times 10^{-3}$.

$\Gamma(e^{\pm}\nu_{\ell})/\Gamma_{\text{total}}$		Γ_{31}/Γ	
VALUE (units 10^{-6})	CL%	DOCUMENT ID	TECN COMMENT
<0.98	90	1 SATOYAMA 07 BELL e ⁺ e ⁻ → T(4S)	

- • • We do not use the following data for averages, fits, limits, etc. • • •
- <3.5 90 2 YOOK 15 BELL e⁺e⁻ → T(4S)
- <8 90 1 AUBERT 10E BABR e⁺e⁻ → T(4S)
- <1.9 90 1 AUBERT 09V BABR e⁺e⁻ → T(4S)
- <5.2 90 1 AUBERT 08AD BABR e⁺e⁻ → T(4S)
- <15 90 ARTUSO 95 CLE2 e⁺e⁻ → T(4S)

¹ Assumes equal production of B^+ and B^0 at the $\Upsilon(4S)$.

² Assumes $B(\Upsilon(4S) \rightarrow B^+B^-) = 0.513 \pm 0.006$.

Meson Particle Listings

 B^\pm $\Gamma(\mu^+\nu_\mu)/\Gamma_{\text{total}}$ Γ_{32}/Γ

VALUE (units 10^{-6})	CL%	DOCUMENT ID	TECN	COMMENT
0.29 to 1.07	90	¹ SIBIDANOV 18	BELL	$e^+e^- \rightarrow \Upsilon(4S)$
< 2.7	90	² YOOK 15	BELL	$e^+e^- \rightarrow \Upsilon(4S)$
< 11	90	³ AUBERT 10E	BABR	$e^+e^- \rightarrow \Upsilon(4S)$
< 1.0	90	³ AUBERT 09V	BABR	$e^+e^- \rightarrow \Upsilon(4S)$
< 5.6	90	³ AUBERT 08AD	BABR	$e^+e^- \rightarrow \Upsilon(4S)$
< 1.7	90	^{3,4} SATOYAMA 07	BELL	$e^+e^- \rightarrow \Upsilon(4S)$
< 6.6	90	AUBERT 04o	BABR	Repl. by AUBERT 09V
< 21	90	ARTUSO 95	CLE2	$e^+e^- \rightarrow \Upsilon(4S)$

¹ This is a 90% confidence interval in the frequentist approach. A 2.4 standard deviation signal above the background is found, with a measured branching fraction $(6.46 \pm 2.22 \pm 1.60) \times 10^{-7}$.

² Assumes $B(\Upsilon(4S) \rightarrow B^+B^-) = 0.513 \pm 0.006$.

³ Assumes equal production of B^+ and B^0 at the $\Upsilon(4S)$.

⁴ Superseded by SIBIDANOV 18.

 $\Gamma(\tau^+\nu_\tau)/\Gamma_{\text{total}}$ Γ_{33}/Γ

See the note on "Decay Constants of Charged Pseudoscalar Mesons" in the D_s^+ Listings.

VALUE (units 10^{-4})	CL%	DOCUMENT ID	TECN	COMMENT
1.09 ± 0.24 OUR AVERAGE		Error includes scale factor of 1.2.		
$1.25 \pm 0.28 \pm 0.27$		^{1,2} KRONENBIT... 15	BELL	$e^+e^- \rightarrow \Upsilon(4S)$
$0.72_{-0.25}^{+0.27} \pm 0.11$		³ HARA 13	BELL	$e^+e^- \rightarrow \Upsilon(4S)$
$1.83_{-0.49}^{+0.53} \pm 0.24$		^{2,4} LEES 13K	BABR	$e^+e^- \rightarrow \Upsilon(4S)$
$1.7 \pm 0.8 \pm 0.2$		^{2,5} AUBERT 10E	BABR	$e^+e^- \rightarrow \Upsilon(4S)$
$1.54_{-0.37}^{+0.38} \pm 0.29$		^{2,6} HARA 10	BELL	Repl. by KRONENBIT-TER 15
$1.8_{-0.8}^{+0.9} \pm 0.45$		^{2,7} AUBERT 08D	BABR	Repl. by LEES 13K
$0.9 \pm 0.6 \pm 0.1$		^{2,5} AUBERT 07AL	BABR	Repl. by AUBERT 10E
< 2.6	90	² AUBERT 06K	BABR	$e^+e^- \rightarrow \Upsilon(4S)$
$1.79_{-0.49}^{+0.56} \pm 0.46$		^{2,7} IKADO 06	BELL	Repl. by HARA 13
< 4.2	90	² AUBERT,B 05B	BABR	Repl. by AUBERT 06k
< 8.3	90	⁸ BARATE 01E	ALEP	$e^+e^- \rightarrow Z$
< 8.4	90	² BROWDER 01	CLE2	$e^+e^- \rightarrow \Upsilon(4S)$
< 5.7	90	⁹ ACCIARRI 97F	L3	$e^+e^- \rightarrow Z$
< 104	90	¹⁰ ALBRECHT 95D	ARG	$e^+e^- \rightarrow \Upsilon(4S)$
< 22	90	ARTUSO 95	CLE2	$e^+e^- \rightarrow \Upsilon(4S)$
< 18	90	¹¹ BUSKULIC 95	ALEP	$e^+e^- \rightarrow Z$

¹ Requires one reconstructed semileptonic B decay $B^- \rightarrow D^{(*)0} \ell^- \bar{\nu}_\ell$ in the recoil.

² Assumes equal production of B^+ and B^0 at the $\Upsilon(4S)$.

³ The authors combine their result with that from HARA 10 obtaining $B(B^- \rightarrow \tau^- \bar{\nu}_\tau) = (0.96 \pm 0.26) \times 10^{-4}$ and deriving $f_B |V_{ub}| = (7.4 \pm 0.8 \pm 0.5) \times 10^{-4}$ GeV.

⁴ Requires a fully reconstructed hadronic B -decay in the recoil. Reports that this result combined with AUBERT 10E value gives $B(B^- \rightarrow \tau^- \bar{\nu}_\tau) = (1.79 \pm 0.48) \times 10^{-4}$.

⁵ Requires one reconstructed semileptonic B decay $B^- \rightarrow D^0 \ell^- \bar{\nu}_\ell X$ in the recoil.

⁶ Requires one reconstructed semileptonic B decay $B^- \rightarrow D^{(*)0} \ell^- \bar{\nu}_\ell X$ in the recoil.

⁷ The analysis is based on a sample of events with one fully reconstructed tag B in a hadronic decay mode $B^- \rightarrow D^{(*)0} X^-$.

⁸ The energy-flow and b -tagging algorithms were used.

⁹ ACCIARRI 97F uses missing-energy technique and $f(b \rightarrow B^-) = (38.2 \pm 2.5)\%$.

¹⁰ ALBRECHT 95D uses full reconstruction of one B decay as tag.

¹¹ BUSKULIC 95 uses same missing-energy technique as in $\bar{b} \rightarrow \tau^+ \nu_\tau X$, but analysis is restricted to endpoint region of missing-energy distribution.

 $\Gamma(\ell^+\nu_\ell)/\Gamma_{\text{total}}$ Γ_{34}/Γ

VALUE	CL%	DOCUMENT ID	TECN	COMMENT
$< 3.0 \times 10^{-6}$	90	^{1,2} GELB 18	BELL	$e^+e^- \rightarrow \Upsilon(4S)$
$< 3.5 \times 10^{-6}$	90	^{2,3} HELLER 15	BELL	$e^+e^- \rightarrow \Upsilon(4S)$
$< 15.6 \times 10^{-6}$	90	² AUBERT 09AT	BABR	$e^+e^- \rightarrow \Upsilon(4S)$

¹ Supersedes HELLER 15.

² Assumes equal production of B^+ and B^0 at the $\Upsilon(4S)$.

³ Superseded by GELB 18.

 $\Gamma(e^+\nu_e)/\Gamma_{\text{total}}$ Γ_{35}/Γ

VALUE	CL%	DOCUMENT ID	TECN	COMMENT
$< 4.3 \times 10^{-6}$	90	^{1,2} GELB 18	BELL	$e^+e^- \rightarrow \Upsilon(4S)$
$< 6.1 \times 10^{-6}$	90	^{2,3} HELLER 15	BELL	$e^+e^- \rightarrow \Upsilon(4S)$
$< 17 \times 10^{-6}$	90	² AUBERT 09AT	BABR	$e^+e^- \rightarrow \Upsilon(4S)$
$< 200 \times 10^{-6}$	90	⁴ BROWDER 97	CLE2	$e^+e^- \rightarrow \Upsilon(4S)$

¹ Supersedes HELLER 15.

² Assumes equal production of B^+ and B^0 at the $\Upsilon(4S)$.

³ Superseded by GELB 18.

⁴ BROWDER 97 uses the hermiticity of the CLEOII detector to reconstruct the neutrino energy and momentum.

 $\Gamma(\mu^+\nu_\mu\gamma)/\Gamma_{\text{total}}$ Γ_{36}/Γ

VALUE	CL%	DOCUMENT ID	TECN	COMMENT
$< 3.4 \times 10^{-6}$	90	^{1,2} GELB 18	BELL	$e^+e^- \rightarrow \Upsilon(4S)$
$< 3.4 \times 10^{-6}$	90	^{2,3} HELLER 15	BELL	$e^+e^- \rightarrow \Upsilon(4S)$
$< 24 \times 10^{-6}$	90	^{2,4} AUBERT 09AT	BABR	$e^+e^- \rightarrow \Upsilon(4S)$
$< 52 \times 10^{-6}$	90	⁵ BROWDER 97	CLE2	$e^+e^- \rightarrow \Upsilon(4S)$

¹ Supersedes HELLER 15.

² Assumes equal production of B^+ and B^0 at the $\Upsilon(4S)$.

³ Superseded by GELB 18.

⁴ Note that the value given by AUBERT 09AT is 24×10^{-6} in the paper abstract, and 26×10^{-6} in the paper itself (Table I).

⁵ BROWDER 97 uses the hermiticity of the CLEOII detector to reconstruct the neutrino energy and momentum.

 $\Gamma(\mu^+\mu^-\mu^+\nu_\mu)/\Gamma_{\text{total}}$ Γ_{37}/Γ

VALUE	CL%	DOCUMENT ID	TECN	COMMENT
$< 1.6 \times 10^{-8}$	95	¹ AAIJ 19P	LHCB	pp at 7, 8, 13 TeV

¹ AAIJ 19P limit established for the kinematic region where the lower of the two $M(\mu^+\mu^-)$ is less than $980 \text{ MeV}/c^2$.

 $\Gamma(D^0X)/\Gamma_{\text{total}}$ Γ_{38}/Γ

VALUE	DOCUMENT ID	TECN	COMMENT
$0.086 \pm 0.006 \pm 0.004$	¹ AUBERT 07N	BABR	$e^+e^- \rightarrow \Upsilon(4S)$
$0.098 \pm 0.009 \pm 0.006$	¹ AUBERT,BE 04B	BABR	Repl. by AUBERT 07N

¹ Events are selected by completely reconstructing one B and searching for a reconstructed charmed particle in the rest of the event. The last error includes systematic and charm branching ratio uncertainties.

 $\Gamma(\bar{D}^0X)/\Gamma_{\text{total}}$ Γ_{39}/Γ

VALUE	DOCUMENT ID	TECN	COMMENT
$0.786 \pm 0.016_{-0.033}^{+0.034}$	¹ AUBERT 07N	BABR	$e^+e^- \rightarrow \Upsilon(4S)$
$0.793 \pm 0.025_{-0.044}^{+0.045}$	¹ AUBERT,BE 04B	BABR	Repl. by AUBERT 07N

¹ Events are selected by completely reconstructing one B and searching for a reconstructed charmed particle in the rest of the event. The last error includes systematic and charm branching ratio uncertainties.

 $\Gamma(D^0X)/[\Gamma(D^0X) + \Gamma(\bar{D}^0X)]$ $\Gamma_{38}/(\Gamma_{38} + \Gamma_{39})$

VALUE	DOCUMENT ID	TECN	COMMENT
$0.098 \pm 0.007 \pm 0.001$	AUBERT 07N	BABR	$e^+e^- \rightarrow \Upsilon(4S)$
$0.110 \pm 0.010 \pm 0.003$	AUBERT,BE 04B	BABR	Repl. by AUBERT 07N

¹ Events are selected by completely reconstructing one B and searching for a reconstructed charmed particle in the rest of the event. The last error includes systematic and charm branching ratio uncertainties.

 $\Gamma(D^+X)/\Gamma_{\text{total}}$ Γ_{40}/Γ

VALUE	DOCUMENT ID	TECN	COMMENT
$0.025 \pm 0.005 \pm 0.002$	¹ AUBERT 07N	BABR	$e^+e^- \rightarrow \Upsilon(4S)$
$0.038 \pm 0.009 \pm 0.005$	¹ AUBERT,BE 04B	BABR	Repl. by AUBERT 07N

¹ Events are selected by completely reconstructing one B and searching for a reconstructed charmed particle in the rest of the event. The last error includes systematic and charm branching ratio uncertainties.

 $\Gamma(D^-X)/\Gamma_{\text{total}}$ Γ_{41}/Γ

VALUE	DOCUMENT ID	TECN	COMMENT
$0.099 \pm 0.008 \pm 0.009$	¹ AUBERT 07N	BABR	$e^+e^- \rightarrow \Upsilon(4S)$
$0.098 \pm 0.012 \pm 0.014$	¹ AUBERT,BE 04B	BABR	Repl. by AUBERT 07N

¹ Events are selected by completely reconstructing one B and searching for a reconstructed charmed particle in the rest of the event. The last error includes systematic and charm branching ratio uncertainties.

 $\Gamma(D^+X)/[\Gamma(D^+X) + \Gamma(D^-X)]$ $\Gamma_{40}/(\Gamma_{40} + \Gamma_{41})$

VALUE	DOCUMENT ID	TECN	COMMENT
$0.204 \pm 0.035 \pm 0.001$	AUBERT 07N	BABR	$e^+e^- \rightarrow \Upsilon(4S)$
$0.278 \pm 0.052 \pm 0.009$	AUBERT,BE 04B	BABR	Repl. by AUBERT 07N

¹ Events are selected by completely reconstructing one B and searching for a reconstructed charmed particle in the rest of the event. The last error includes systematic and charm branching ratio uncertainties.

 $\Gamma(D_s^+X)/\Gamma_{\text{total}}$ Γ_{42}/Γ

VALUE	DOCUMENT ID	TECN	COMMENT
$0.079 \pm 0.006_{-0.011}^{+0.013}$	¹ AUBERT 07N	BABR	$e^+e^- \rightarrow \Upsilon(4S)$
$0.143 \pm 0.016_{-0.034}^{+0.051}$	¹ AUBERT,BE 04B	BABR	Repl. by AUBERT 07N

¹ Events are selected by completely reconstructing one B and searching for a reconstructed charmed particle in the rest of the event. The last error includes systematic and charm branching ratio uncertainties.

$\Gamma(D_s^{\pm} X)/\Gamma_{total}$					Γ_{43}/Γ
VALUE	CL%	DOCUMENT ID	TECN	COMMENT	

$0.011 \pm 0.004 + 0.002$ $-0.003 - 0.001$		1 AUBERT	07N	BABR $e^+e^- \rightarrow \Upsilon(4S)$	
<0.022	90	1 AUBERT, BE	04B	BABR Repl. by AUBERT 07N	

• • • We do not use the following data for averages, fits, limits, etc. • • •
 1 Events are selected by completely reconstructing one B and searching for a reconstructed charmed particle in the rest of the event. The last error includes systematic and charm branching ratio uncertainties.

$\Gamma(D_s^{\pm} X)/[\Gamma(D_s^{\pm} X) + \Gamma(D_s^{\mp} X)]$					$\Gamma_{42}/(\Gamma_{42} + \Gamma_{43})$
VALUE	CL%	DOCUMENT ID	TECN	COMMENT	

$0.884 \pm 0.038 \pm 0.002$		AUBERT	07N	BABR $e^+e^- \rightarrow \Upsilon(4S)$	
$0.966 \pm 0.039 \pm 0.012$		AUBERT, BE	04B	BABR Repl. by AUBERT 07N	

$\Gamma(D_s^{\pm} X)/[\Gamma(D_s^{\pm} X) + \Gamma(D_s^{\mp} X)]$					$\Gamma_{43}/(\Gamma_{42} + \Gamma_{43})$
VALUE	CL%	DOCUMENT ID	TECN	COMMENT	

<0.126	90	AUBERT, BE	04B	BABR $e^+e^- \rightarrow \Upsilon(4S)$	
--------	----	------------	-----	--	--

$\Gamma(A_c^{\pm} X)/\Gamma_{total}$					Γ_{44}/Γ
VALUE	CL%	DOCUMENT ID	TECN	COMMENT	

$0.021 \pm 0.005 + 0.008$ -0.004		1 AUBERT	07N	BABR $e^+e^- \rightarrow \Upsilon(4S)$	
$0.029 \pm 0.008 + 0.011$ -0.007		1 AUBERT, BE	04B	BABR Repl. by AUBERT 07N	

• • • We do not use the following data for averages, fits, limits, etc. • • •
 1 Events are selected by completely reconstructing one B and searching for a reconstructed charmed particle in the rest of the event. The last error includes systematic and charm branching ratio uncertainties.

$\Gamma(\bar{A}_c^{\pm} X)/\Gamma_{total}$					Γ_{45}/Γ
VALUE	CL%	DOCUMENT ID	TECN	COMMENT	

$0.028 \pm 0.005 + 0.010$ -0.007		1 AUBERT	07N	BABR $e^+e^- \rightarrow \Upsilon(4S)$	
$0.035 \pm 0.008 + 0.013$ -0.009		1 AUBERT, BE	04B	BABR Repl. by AUBERT 07N	

• • • We do not use the following data for averages, fits, limits, etc. • • •
 1 Events are selected by completely reconstructing one B and searching for a reconstructed charmed particle in the rest of the event. The last error includes systematic and charm branching ratio uncertainties.

$\Gamma(A_c^{\pm} X)/[\Gamma(A_c^{\pm} X) + \Gamma(\bar{A}_c^{\pm} X)]$					$\Gamma_{44}/(\Gamma_{44} + \Gamma_{45})$
VALUE	CL%	DOCUMENT ID	TECN	COMMENT	

$0.427 \pm 0.071 \pm 0.001$		AUBERT	07N	BABR $e^+e^- \rightarrow \Upsilon(4S)$	
$0.452 \pm 0.090 \pm 0.003$		AUBERT, BE	04B	BABR Repl. by AUBERT 07N	

$\Gamma(\bar{c} X)/\Gamma_{total}$					Γ_{46}/Γ
VALUE	CL%	DOCUMENT ID	TECN	COMMENT	

$0.968 \pm 0.019 + 0.041$ -0.039		1 AUBERT	07N	BABR $e^+e^- \rightarrow \Upsilon(4S)$	
$0.983 \pm 0.030 + 0.054$ -0.051		1 AUBERT, BE	04B	BABR Repl. by AUBERT 07N	

• • • We do not use the following data for averages, fits, limits, etc. • • •
 1 Events are selected by completely reconstructing one B and searching for a reconstructed charmed particle in the rest of the event. The last error includes systematic and charm branching ratio uncertainties.

$\Gamma(c X)/\Gamma_{total}$					Γ_{47}/Γ
VALUE	CL%	DOCUMENT ID	TECN	COMMENT	

$0.234 \pm 0.012 + 0.018$ -0.014		1 AUBERT	07N	BABR $e^+e^- \rightarrow \Upsilon(4S)$	
$0.330 \pm 0.022 + 0.055$ -0.037		1 AUBERT, BE	04B	BABR Repl. by AUBERT 07N	

• • • We do not use the following data for averages, fits, limits, etc. • • •
 1 Events are selected by completely reconstructing one B and searching for a reconstructed charmed particle in the rest of the event. The last error includes systematic and charm branching ratio uncertainties.

$\Gamma(c/\bar{c} X)/\Gamma_{total}$					Γ_{48}/Γ
VALUE	CL%	DOCUMENT ID	TECN	COMMENT	

$1.202 \pm 0.023 + 0.053$ -0.049		1 AUBERT	07N	BABR $e^+e^- \rightarrow \Upsilon(4S)$	
$1.313 \pm 0.037 + 0.088$ -0.075		1 AUBERT, BE	04B	BABR Repl. by AUBERT 07N	

• • • We do not use the following data for averages, fits, limits, etc. • • •
 1 Events are selected by completely reconstructing one B and searching for a reconstructed charmed particle in the rest of the event. The last error includes systematic and charm branching ratio uncertainties.

$\Gamma(D^0 \pi^+)/\Gamma_{total}$					Γ_{49}/Γ
VALUE (units 10^{-3})	EVTs	DOCUMENT ID	TECN	COMMENT	

4.68 ± 0.13 OUR FIT					
4.70 ± 0.13 OUR AVERAGE					
$4.34 \pm 0.10 \pm 0.23$		1 KATO	18	BELL $e^+e^- \rightarrow \Upsilon(4S)$	
$4.90 \pm 0.07 \pm 0.22$		2 AUBERT	07H	BABR $e^+e^- \rightarrow \Upsilon(4S)$	

$5.0 \pm 0.6 \pm 0.3$		3 ABULENCIA	06J	CDF $p\bar{p}$ at 1.96 TeV	
$4.49 \pm 0.21 \pm 0.23$		4 AUBERT, BE	06J	BABR $e^+e^- \rightarrow \Upsilon(4S)$	
$4.97 \pm 0.12 \pm 0.29$		2,5 AHMED	02B	CLE2 $e^+e^- \rightarrow \Upsilon(4S)$	
$5.0 \pm 0.7 \pm 0.6$	54	6 BORTOLETTO	92	CLEO $e^+e^- \rightarrow \Upsilon(4S)$	
$5.4 + 1.8 + 1.2$ $-1.5 - 0.9$	14	7 BEBEK	87	CLEO $e^+e^- \rightarrow \Upsilon(4S)$	
$4.67 \pm 0.26 \pm 0.04$		8 AUBERT, B	04P	BABR Repl. by AUBERT 07H	
$5.5 \pm 0.4 \pm 0.5$	304	9 ALAM	94	CLE2 Repl. by AHMED 02B	
$2.0 \pm 0.8 \pm 0.6$	12	6 ALBRECHT	90J	ARG $e^+e^- \rightarrow \Upsilon(4S)$	
$1.9 \pm 1.0 \pm 0.6$	7	10 ALBRECHT	88k	ARG $e^+e^- \rightarrow \Upsilon(4S)$	

• • • We do not use the following data for averages, fits, limits, etc. • • •
 1 Measures absolute branching fractions using a missing-mass technique.
 2 Assumes equal production of B^+ and B^0 at the $\Upsilon(4S)$.
 3 ABULENCIA 06J reports $[\Gamma(B^+ \rightarrow \bar{D}^0 \pi^+)/\Gamma_{total}] / [B(B^0 \rightarrow D^- \pi^+)] = 1.97 \pm 0.10 \pm 0.21$ which we multiply by our best value $B(B^0 \rightarrow D^- \pi^+) = (2.52 \pm 0.13) \times 10^{-3}$. Our first error is their experiment's error and our second error is the systematic error from using our best value.
 4 Uses a missing-mass method. Does not depend on D branching fractions or B^+/B^0 production rates.
 5 AHMED 02B reports an additional uncertainty on the branching ratios to account for 4.5% uncertainty on relative production of B^0 and B^+ , which is not included here.
 6 Assumes equal production of B^+ and B^0 at the $\Upsilon(4S)$ and uses the Mark III branching fractions for the D .
 7 BEBEK 87 value has been updated in BERKELMAN 91 to use same assumptions as noted for BORTOLETTO 92.
 8 AUBERT, B 04P reports $[\Gamma(B^+ \rightarrow \bar{D}^0 \pi^+)/\Gamma_{total}] \times [B(D^0 \rightarrow K^- \pi^+)] = (1.846 \pm 0.032 \pm 0.097) \times 10^{-4}$ which we divide by our best value $B(D^0 \rightarrow K^- \pi^+) = (3.950 \pm 0.031) \times 10^{-2}$. Our first error is their experiment's error and our second error is the systematic error from using our best value.
 9 ALAM 94 assume equal production of B^+ and B^0 at the $\Upsilon(4S)$ and use the CLEO II absolute $B(D^0 \rightarrow K^- \pi^+)$ and the PDG 1992 $B(D^0 \rightarrow K^- \pi^+ \pi^0)/B(D^0 \rightarrow K^- \pi^+)$ and $B(D^0 \rightarrow K^- 2\pi^+ \pi^-)/B(D^0 \rightarrow K^- \pi^+)$.
 10 ALBRECHT 88k assumes $B^0 \bar{B}^0, B^+ B^-$ ratio is 45:55. Superseded by ALBRECHT 90J.

$\Gamma(D^0 \rho^+)/\Gamma_{total}$					Γ_{52}/Γ
VALUE	EVTs	DOCUMENT ID	TECN	COMMENT	

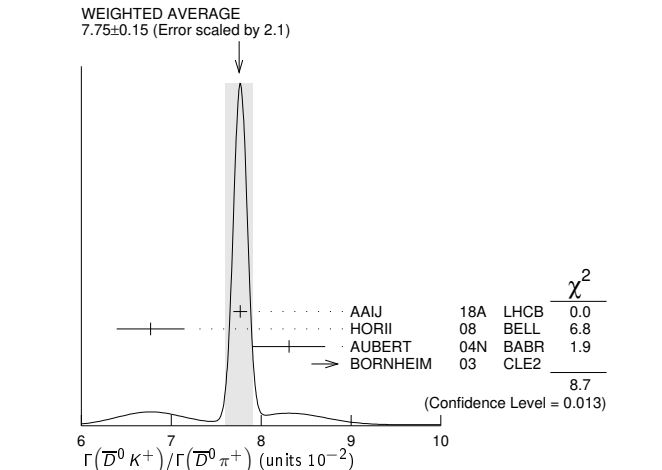
0.0134 ± 0.0018 OUR AVERAGE					
$0.0135 \pm 0.0012 \pm 0.0015$	212	1 ALAM	94	CLE2 $e^+e^- \rightarrow \Upsilon(4S)$	
$0.013 \pm 0.004 \pm 0.004$	19	2 ALBRECHT	90J	ARG $e^+e^- \rightarrow \Upsilon(4S)$	
$0.021 \pm 0.008 \pm 0.009$	10	3 ALBRECHT	88k	ARG $e^+e^- \rightarrow \Upsilon(4S)$	

• • • We do not use the following data for averages, fits, limits, etc. • • •
 1 ALAM 94 assume equal production of B^+ and B^0 at the $\Upsilon(4S)$ and use the CLEO II absolute $B(D^0 \rightarrow K^- \pi^+)$ and the PDG 1992 $B(D^0 \rightarrow K^- \pi^+ \pi^0)/B(D^0 \rightarrow K^- \pi^+)$ and $B(D^0 \rightarrow K^- 2\pi^+ \pi^-)/B(D^0 \rightarrow K^- \pi^+)$.
 2 Assumes equal production of B^+ and B^0 at the $\Upsilon(4S)$ and uses the Mark III branching fractions for the D .
 3 ALBRECHT 88k assumes $B^0 \bar{B}^0, B^+ B^-$ ratio is 45:55.

$\Gamma(D^0 K^+)/\Gamma(D^0 \pi^+)$					Γ_{53}/Γ_{49}
VALUE (units 10^{-2})	EVTs	DOCUMENT ID	TECN	COMMENT	

7.75 ± 0.15 OUR AVERAGE					
$7.768 \pm 0.038 \pm 0.066$		1 AAIJ	18A	LHCB $p\bar{p}$ at 7, 8, 13 TeV	
$6.77 \pm 0.23 \pm 0.30$		HORII	08	BELL $e^+e^- \rightarrow \Upsilon(4S)$	
$8.31 \pm 0.35 \pm 0.20$		AUBERT	04N	BABR $e^+e^- \rightarrow \Upsilon(4S)$	
$9.9 + 1.4 + 0.7$ $-1.2 - 0.6$		BORNHEIM	03	CLE2 $e^+e^- \rightarrow \Upsilon(4S)$	

• • • We do not use the following data for averages, fits, limits, etc. • • •
 1 AAIJ 16L LHCB $p\bar{p}$ at 7, 8 TeV
 2 AAIJ 16L LHCB $p\bar{p}$ at 7, 8 TeV
 2 AAIJ 13AE LHCB Repl. by AAIJ 16L
 AAIJ 12M LHCB Repl. by AAIJ 16L
 ABE 03D BELL Repl. by SWAIN 03
 SWAIN 03 BELL Repl. by HORII 08
 ABE 01I BELL Repl. by ABE 03D
 ATHANAS 98 CLE2 Repl. by BORNHEIM 03



1 Supersedes AAIJ 16L.

Meson Particle Listings

 B^\pm ² Uses $B^\pm \rightarrow [K^\pm \pi^\mp \pi^+ \pi^-]_D h^\pm$ mode. $\Gamma(D_{CP(+)} K^+)/\Gamma(D_{CP(+)} \pi^+)$ Γ_{54}/Γ_{50}

VALUE	DOCUMENT ID	TECN	COMMENT
0.088 ± 0.007 OUR AVERAGE			
0.088 ± 0.008 ± 0.002	^{1,2} ABE	06	BELL $e^+ e^- \rightarrow \Upsilon(4S)$
0.088 ± 0.016 ± 0.005	³ AUBERT	04N	BABR $e^+ e^- \rightarrow \Upsilon(4S)$
••• We do not use the following data for averages, fits, limits, etc. •••			
0.125 ± 0.036 ± 0.010	³ ABE	03D	BELL Repl. by SWAIN 03
0.093 ± 0.018 ± 0.008	³ SWAIN	03	BELL Repl. by ABE 06

¹ Reports a double ratio of $B(B^+ \rightarrow D_{CP(+)} K^+)/B(B^+ \rightarrow D_{CP(+)} \pi^+)$ and $B(B^+ \rightarrow \bar{D}^0 K^+)/B(B^+ \rightarrow \bar{D}^0 \pi^+)$, $1.13 \pm 0.16 \pm 0.08$. We multiply by our best value of $B(B^+ \rightarrow \bar{D}^0 K^+)/B(B^+ \rightarrow \bar{D}^0 \pi^+) = 0.083 \pm 0.006$. Our first error is their experiment's error and the second error is systematic error from using our best value.

² ABE 06 reports $[\Gamma(B^+ \rightarrow D_{CP(+)} K^+)/\Gamma(B^+ \rightarrow D_{CP(+)} \pi^+)] / [\Gamma(B^+ \rightarrow \bar{D}^0 K^+)/\Gamma(B^+ \rightarrow \bar{D}^0 \pi^+)] = 1.13 \pm 0.06 \pm 0.08$ which we multiply by our best value $\Gamma(B^+ \rightarrow \bar{D}^0 K^+)/\Gamma(B^+ \rightarrow \bar{D}^0 \pi^+) = 0.0775 \pm 0.0015$. Our first error is their experiment's error and our second error is the systematic error from using our best value.

³ $CP=+1$ eigenstate of $D^0 \bar{D}^0$ system is reconstructed via $K^+ K^-$ and $\pi^+ \pi^-$.

 $\Gamma(D_{CP(+)} K^+)/\Gamma(\bar{D}^0 K^+)$ Γ_{54}/Γ_{53}

VALUE	DOCUMENT ID	TECN	COMMENT
0.495 ± 0.007 OUR AVERAGE			
0.494 ± 0.008 ± 0.006	¹ AAIJ	18A	LHCB pp at 7, 8, 13 TeV
0.496 ± 0.014 ± 0.008	² AAIJ	18A	LHCB pp at 7, 8, 13 TeV
0.489 ± 0.010 ± 0.009	³ AAIJ	16L	LHCB pp at 7, 8 TeV
0.65 ± 0.12 ± 0.06	⁴ AALTONEN	10A	CDF $p\bar{p}$ at 1.96 TeV
0.590 ± 0.045 ± 0.025	⁵ DEL-AMO-SA..10G	BABR	$e^+ e^- \rightarrow \Upsilon(4S)$
••• We do not use the following data for averages, fits, limits, etc. •••			
0.504 ± 0.019 ± 0.006	⁶ AAIJ	12M	LHCB Repl. by AAIJ 16L
0.53 ± 0.05 ± 0.025	AUBERT	08AA	BABR Repl. by DEL-AMO-SANCHEZ 10G
0.45 ± 0.06 ± 0.02	AUBERT	06J	BABR Repl. by AUBERT 08AA

¹ Uses $D \rightarrow K^+ K^-$ decay mode and reports $R_{CP+} = 0.988 \pm 0.015 \pm 0.011$ which we have divided by 2.

² Uses $D \rightarrow \pi^+ \pi^-$ decay mode and reports $R_{CP+} = 0.992 \pm 0.027 \pm 0.015$ which we have divided by 2.

³ AAIJ 16L reports $R_{CP+} = 0.978 \pm 0.019 \pm 0.018$ which we have divided by 2.

⁴ Reports $R_{CP+} = 2 (B(B^- \rightarrow D_{CP(+)} K^-) + B(B^+ \rightarrow D_{CP(+)} K^+)) / (B(B^- \rightarrow D^0 K^-) + B(B^+ \rightarrow \bar{D}^0 K^+)) = 1.30 \pm 0.24 \pm 0.12$ that we have divided by 2.

⁵ Reports $R_{CP+} = 1.18 \pm 0.09 \pm 0.05$ that we have divided by 2.

⁶ AAIJ 12M reports $R_{CP+} = 1.007 \pm 0.038 \pm 0.012$ which we have divided by 2.

 $\Gamma(D_{CP(-)} K^+)/\Gamma(D_{CP(-)} \pi^+)$ Γ_{55}/Γ_{51}

VALUE	DOCUMENT ID	TECN	COMMENT
0.097 ± 0.016 ± 0.007			
0.097 ± 0.016 ± 0.007	¹ ABE	06	BELL $e^+ e^- \rightarrow \Upsilon(4S)$
••• We do not use the following data for averages, fits, limits, etc. •••			
0.119 ± 0.028 ± 0.006	² ABE	03D	BELL Repl. by SWAIN 03
0.108 ± 0.019 ± 0.007	² SWAIN	03	BELL Repl. by ABE 06

¹ Reports a double ratio of $B(B^+ \rightarrow D_{CP(-)} K^+)/B(B^+ \rightarrow D_{CP(-)} \pi^+)$ and $B(B^+ \rightarrow \bar{D}^0 K^+)/B(B^+ \rightarrow \bar{D}^0 \pi^+)$, $1.17 \pm 0.14 \pm 0.14$. We multiply by our best value of $B(B^+ \rightarrow \bar{D}^0 K^+)/B(B^+ \rightarrow \bar{D}^0 \pi^+) = 0.083 \pm 0.006$. Our first error is their experiment's error and the second error is systematic error from using our best value.

² $CP=-1$ eigenstate of $D^0 \bar{D}^0$ system is reconstructed via $K_S^0 \pi^0$, $K_S^0 \omega$, $K_S^0 \phi$, $K_S^0 \eta$, and $K_S^0 \eta'$.

 $\Gamma(D_{CP(-)} K^+)/\Gamma(\bar{D}^0 K^+)$ Γ_{55}/Γ_{53}

VALUE	DOCUMENT ID	TECN	COMMENT
0.54 ± 0.04 ± 0.02			
0.54 ± 0.04 ± 0.02	¹ DEL-AMO-SA..10G	BABR	$e^+ e^- \rightarrow \Upsilon(4S)$
••• We do not use the following data for averages, fits, limits, etc. •••			
0.515 ± 0.05 ± 0.025	AUBERT	08AA	BABR Repl. by DEL-AMO-SANCHEZ 10G
0.43 ± 0.05 ± 0.02	AUBERT	06J	BABR Repl. by AUBERT 08AA

¹ Reports $R_{CP+} = 1.07 \pm 0.08 \pm 0.04$ that we have divided by 2.

 $\Gamma(D^0 K^+)/\Gamma(\bar{D}^0 K^+)$ Γ_{56}/Γ_{53}

"OUR EVALUATION" is derived from $r_B(B^+ \rightarrow D^0 K^+)$ data block listed in "CP violation parameters" section.

VALUE (units 10^{-3})	DOCUMENT ID
9.86 ± 0.91 OUR EVALUATION	

 $\Gamma([K^- \pi^+]_D K^+)/\Gamma_{total}$ Γ_{57}/Γ

VALUE	CL%	DOCUMENT ID	TECN	COMMENT
< 2.8 × 10⁻⁷	90	HORII	08	BELL $e^+ e^- \rightarrow \Upsilon(4S)$
••• We do not use the following data for averages, fits, limits, etc. •••				
< 6.3 × 10 ⁻⁷	90	SAIGO	05	BELL $e^+ e^- \rightarrow \Upsilon(4S)$

 $\Gamma([K^- \pi^+]_D K^+)/\Gamma([K^+ \pi^-]_D K^+)$ Γ_{57}/Γ_{58}

VALUE (units 10^{-3})	CL%	DOCUMENT ID	TECN	COMMENT
18.3 ± 1.4 OUR AVERAGE				
18.8 ± 1.1 ± 1.0		AAIJ	16L	LHCB pp at 7, 8 TeV
22.0 ± 8.6 ± 2.6		¹ AALTONEN	11AJ	CDF $p\bar{p}$ at 1.96 TeV
16.3 ^{+4.4+0.7} _{-4.1-1.3}		HORII	11	BELL $e^+ e^- \rightarrow \Upsilon(4S)$
11 ± 6 ± 2		DEL-AMO-SA..10H	BABR	$e^+ e^- \rightarrow \Upsilon(4S)$
••• We do not use the following data for averages, fits, limits, etc. •••				
15.2 ± 2.0 ± 0.4		AAIJ	12M	LHCB Repl. by AAIJ 16L
7.8 ^{+6.2+2.0} _{-5.7-2.8}		HORII	08	BELL Repl. by HORII 11
< 29	90	² AUBERT	05G	BABR Repl. by DEL-AMO-SANCHEZ 10H
< 44	90	³ SAIGO	05	BELL $e^+ e^- \rightarrow \Upsilon(4S)$
< 26	90	⁴ AUBERT,B	04L	BABR Repl. by AUBERT 05G

¹ AALTONEN 11AJ also measures the ratio separately for B^+ ($R^+(K)$) and B^- ($R^-(K)$) and obtains: $R^+(K) = (42.6 \pm 13.7 \pm 2.8) \times 10^{-3}$, $R^-(K) = (3.8 \pm 10.3 \pm 2.7) \times 10^{-3}$.

² AUBERT 05G extract a constraint on the magnitude of the ratio of amplitudes $|A(B^+ \rightarrow D^0 K^+)/A(B^+ \rightarrow \bar{D}^0 K^+)| < 0.23$ at 90% CL (Bayesian). Similar measurements from $B^+ \rightarrow D^{*0} K^+$ are also reported.

³ SAIGO 05 extract a constraint on the magnitude of the ratio of amplitudes $|A(B^+ \rightarrow D^0 K^+)/A(B^+ \rightarrow \bar{D}^0 K^+)| < 0.27$ at 90% CL.

⁴ AUBERT,B 04L extract a constraint on the magnitude of the ratio of amplitudes $|A(B^+ \rightarrow D^0 K^+)/A(B^+ \rightarrow \bar{D}^0 K^+)| < 0.22$ at 90% CL.

 $\Gamma([K^- \pi^+ \pi^0]_D K^+)/\Gamma([K^+ \pi^- \pi^0]_D K^+)$ Γ_{59}/Γ_{60}

VALUE (units 10^{-3})	CL%	DOCUMENT ID	TECN	COMMENT
16 ± 4 OUR AVERAGE				
14.0 ± 4.7 ± 2.1		¹ AAIJ	15W	LHCB pp at 7, 8 TeV
19.8 ± 6.2 ± 2.4		NAYAK	13	BELL $e^+ e^- \rightarrow \Upsilon(4S)$
••• We do not use the following data for averages, fits, limits, etc. •••				
< 21	90	² LEES	11D	BABR $e^+ e^- \rightarrow \Upsilon(4S)$
< 39	95	³ AUBERT	07BN	BABR Repl. by LEES 11D

¹ Uses $D^0 \rightarrow K^- \pi^+ \pi^0$ for the favored mode, and $D^0 \rightarrow K^+ \pi^- \pi^0$ for the suppressed mode.

² Extracts a constraint on the magnitude of the ratio of amplitudes $|A(B^+ \rightarrow D^0 K^+)/A(B^+ \rightarrow \bar{D}^0 K^+)| < 0.13$ at 95% CL.

³ Extracts a constraint on the magnitude of the ratio of amplitudes $|A(B^+ \rightarrow D^0 K^+)/A(B^+ \rightarrow \bar{D}^0 K^+)| < 0.19$ at 95% CL.

 $\Gamma([K^- \pi^+ \pi^+ \pi^-]_D K^+)/\Gamma([K^+ \pi^- \pi^+ \pi^-]_D K^+)$ Γ_{61}/Γ_{62}

VALUE (units 10^{-2})	DOCUMENT ID	TECN	COMMENT
1.40 ± 0.15 ± 0.06			
1.40 ± 0.15 ± 0.06	AAIJ	16L	LHCB pp at 7, 8 TeV
••• We do not use the following data for averages, fits, limits, etc. •••			
1.24 ± 0.27	AAIJ	13AE	LHCB Repl. by AAIJ 16L

 $\Gamma([\pi^+ \pi^+ \pi^- \pi^-]_D K^+)/\Gamma([K^+ \pi^- \pi^+ \pi^-]_D K^+)$ Γ_{63}/Γ_{62}

VALUE	DOCUMENT ID	TECN	COMMENT
0.975 ± 0.037 ± 0.019			
0.975 ± 0.037 ± 0.019	AAIJ	16L	LHCB pp at 7, 8 TeV

 $\Gamma([K^- \pi^+]_D K^*(892)^+)/\Gamma([K^+ \pi^-]_D K^*(892)^+)$ Γ_{65}/Γ_{66}

VALUE	DOCUMENT ID	TECN	COMMENT
0.012 ± 0.004 OUR AVERAGE			
0.011 ± 0.004 ± 0.001	AAIJ	17B0	LHCB pp at 7, 8, 13 TeV
0.066 ± 0.031 ± 0.010	AUBERT	09AJ	BABR $e^+ e^- \rightarrow \Upsilon(4S)$
••• We do not use the following data for averages, fits, limits, etc. •••			
0.046 ± 0.031 ± 0.008	AUBERT,B	05V	BABR Repl. by AUBERT 09AJ

 $\Gamma([K^- \pi^+ \pi^- \pi^+]_D K^*(892)^+)/\Gamma([K^+ \pi^- \pi^+ \pi^-]_D K^*(892)^+)$ Γ_{67}/Γ_{68}

VALUE	DOCUMENT ID	TECN	COMMENT
0.011 ± 0.005 ± 0.003			
0.011 ± 0.005 ± 0.003	AAIJ	17B0	LHCB pp at 7, 8, 13 TeV

 $\Gamma([\pi^+ \pi^- \pi^+ \pi^-]_D K^*(892)^+)/\Gamma([K^+ \pi^- \pi^+ \pi^-]_D K^*(892)^+)$ Γ_{64}/Γ_{68}

VALUE	DOCUMENT ID	TECN	COMMENT
1.08 ± 0.13 ± 0.03			
1.08 ± 0.13 ± 0.03	AAIJ	17B0	LHCB pp at 7, 8, 13 TeV

 $\Gamma([K^- \pi^+]_D \pi^+)/\Gamma_{total}$ Γ_{69}/Γ

VALUE (units 10^{-7})	DOCUMENT ID	TECN	COMMENT
6.29^{+1.02+0.37}_{-0.98-0.48}			
6.29 ^{+1.02+0.37} _{-0.98-0.48}	HORII	08	BELL $e^+ e^- \rightarrow \Upsilon(4S)$
••• We do not use the following data for averages, fits, limits, etc. •••			
6.6 ^{+1.9} _{-1.7} ± 0.5	SAIGO	05	BELL Repl. by HORII 08

 $\Gamma([K^- \pi^+]_D \pi^+)/\Gamma([K^+ \pi^-]_D \pi^+)$ Γ_{69}/Γ_{70}

VALUE (units 10^{-3})	DOCUMENT ID	TECN	COMMENT
3.53 ± 0.14 OUR AVERAGE			
3.60 ± 0.12 ± 0.09	AAIJ	16L	LHCB pp at 7, 8 TeV
2.8 ± 0.7 ± 0.4	¹ AALTONEN	11AJ	CDF $p\bar{p}$ at 1.96 TeV
3.28 ^{+0.38+0.12} _{-0.36-0.18}	HORII	11	BELL $e^+ e^- \rightarrow \Upsilon(4S)$
3.3 ± 0.6 ± 0.4	DEL-AMO-SA..10H	BABR	$e^+ e^- \rightarrow \Upsilon(4S)$

• • • We do not use the following data for averages, fits, limits, etc. • • •

4.10 ± 0.25 ± 0.05	AAIJ	12M	LHCB	Repl. by AAIJ 16L
3.40 ^{+0.55+0.15} _{-0.53-0.22}	HORII	08	BELL	Repl. by HORII 11
3.5 ^{+1.0} _{-0.9} ± 0.2	SAIGO	05	BELL	Repl. by HORII 08

¹ AALTONEN 11AJ also measures the ratio separately for B⁺ (R⁺(π)) and B⁻ (R⁻(π)) and obtains: R⁺(π) = (2.4 ± 1.0 ± 0.4) × 10⁻³, R⁻(K) = (3.1 ± 1.1 ± 0.4) × 10⁻³.

Γ([K⁻π⁺π⁰]_Dπ⁺)/Γ([K⁺π⁻π⁰]_Dπ⁺) Γ₇₁/Γ₇₂

VALUE (units 10 ⁻³)	DOCUMENT ID	TECN	COMMENT
2.2 ± 0.4 OUR AVERAGE			
2.35 ± 0.49 ± 0.06	¹ AAIJ	15W	LHCB pp at 7, 8 TeV
1.89 ± 0.54 ^{+0.22} _{-0.25}	NAYAK	13	BELL e ⁺ e ⁻ → γ(4S)

¹ Uses D⁰ → K⁻π⁺π⁰ for the favored mode, and D⁰ → K⁺π⁻π⁰ for the suppressed mode.

Γ([K⁻π⁺π⁺π⁻]_Dπ⁺)/Γ([K⁺π⁻π⁺π⁻]_Dπ⁺) Γ₇₃/Γ₇₄

VALUE (units 10 ⁻³)	DOCUMENT ID	TECN	COMMENT
3.77 ± 0.18 ± 0.06	AAIJ	16L	LHCB pp at 7, 8 TeV
3.7 ± 0.4	AAIJ	13AE	LHCB Repl. by AAIJ 16L

• • • We do not use the following data for averages, fits, limits, etc. • • •

Γ([K⁻π⁺]_(Dπ)π⁺)/Γ([K⁺π⁻]_(Dπ)π⁺) Γ₇₅/Γ₇₆

VALUE (units 10 ⁻³)	DOCUMENT ID	TECN	COMMENT
3.2 ± 0.9 ± 0.8	DEL-AMO-SA..10H	BABR	e ⁺ e ⁻ → γ(4S)

Γ([K⁻π⁺]_(Dγ)π⁺)/Γ([K⁺π⁻]_(Dγ)π⁺) Γ₇₇/Γ₇₈

VALUE (units 10 ⁻³)	DOCUMENT ID	TECN	COMMENT
2.7 ± 1.4 ± 2.2	DEL-AMO-SA..10H	BABR	e ⁺ e ⁻ → γ(4S)

Γ([K⁻π⁺]_(Dπ)K⁺)/Γ([K⁺π⁻]_(Dπ)K⁺) Γ₇₉/Γ₈₀

VALUE (units 10 ⁻³)	DOCUMENT ID	TECN	COMMENT
1.8 ± 0.9 ± 0.4	DEL-AMO-SA..10H	BABR	e ⁺ e ⁻ → γ(4S)

Γ([K⁻π⁺]_(Dγ)K⁺)/Γ([K⁺π⁻]_(Dγ)K⁺) Γ₈₁/Γ₈₂

VALUE (units 10 ⁻³)	DOCUMENT ID	TECN	COMMENT
1.3 ± 1.4 ± 0.8	DEL-AMO-SA..10H	BABR	e ⁺ e ⁻ → γ(4S)

Γ([π⁺π⁻π⁰]_DK⁻)/Γ_{total} Γ₈₃/Γ

VALUE (units 10 ⁻⁶)	DOCUMENT ID	TECN	COMMENT
4.6 ± 0.8 ± 0.4	¹ AUBERT	07BJ	BABR e ⁺ e ⁻ → γ(4S)
5.5 ± 1.0 ± 0.7	¹ AUBERT,B	05T	BABR Repl. by AUBERT 07BJ

¹ Assumes equal production of B⁺ and B⁰ at the γ(4S).

Γ([K_S⁰K⁺π⁻]_DK⁺)/Γ([K_S⁰K⁺π⁻]_Dπ⁺) Γ₈₄/Γ₈₉

VALUE	DOCUMENT ID	TECN	COMMENT
0.092 ± 0.009 ± 0.004	¹ AAIJ	14V	LHCB pp at 7, 8 TeV

¹ The analysis uses all of D → K_S⁰Kπ Dalitz decays.

Γ([K_S⁰K⁻π⁺]_DK⁺)/Γ([K_S⁰K⁻π⁺]_Dπ⁺) Γ₈₅/Γ₈₇

VALUE	DOCUMENT ID	TECN	COMMENT
0.066 ± 0.009 ± 0.002	¹ AAIJ	14V	LHCB pp at 7, 8 TeV

¹ The analysis uses all of D → K_S⁰Kπ Dalitz decays.

Γ([K_S⁰K⁻π⁺]_DK⁺)/Γ([K_S⁰K⁺π⁻]_Dπ⁺) Γ₈₅/Γ₈₉

VALUE	DOCUMENT ID	TECN	COMMENT
0.084 ± 0.011 ± 0.003	¹ AAIJ	14V	LHCB pp at 7, 8 TeV

¹ The Analysis uses D → K*(892)K → K_S⁰Kπ decays.

Γ([K*(892)⁺K⁻]_DK⁺)/Γ([K*(892)⁻K⁺]_Dπ⁺) Γ₈₆/Γ₉₀

VALUE	DOCUMENT ID	TECN	COMMENT
0.056 ± 0.013 ± 0.002	¹ AAIJ	14V	LHCB pp at 7, 8 TeV

¹ The Analysis uses D → K*(892)K → K_S⁰Kπ decays.

Γ([K⁺K⁻π⁰]_DK⁺)/Γ([K⁺K⁻π⁰]_Dπ⁺) Γ₉₁/Γ₉₂

VALUE	DOCUMENT ID	TECN	COMMENT
0.95 ± 0.22 ± 0.05	¹ AAIJ	15W	LHCB pp at 7, 8 TeV

¹ Uses D → K⁺K⁻π⁰ mode.

Γ([π⁺π⁻π⁰]_DK⁺)/Γ([π⁺π⁻π⁰]_Dπ⁺) Γ₉₃/Γ₉₄

VALUE	DOCUMENT ID	TECN	COMMENT
0.98 ± 0.11 ± 0.05	¹ AAIJ	15W	LHCB pp at 7, 8 TeV

¹ Uses D → π⁺π⁻π⁰ mode.

Γ([K_S⁰K⁺π⁻]_Dπ⁺)/Γ([K_S⁰K⁺π⁻]_Dπ⁺) Γ₈₉/Γ₈₇

VALUE	DOCUMENT ID	TECN	COMMENT
1.528 ± 0.058 ± 0.025	¹ AAIJ	14V	LHCB pp at 7, 8 TeV

¹ The analysis uses all of D → K_S⁰Kπ Dalitz decays.

Γ([K*(892)⁻K⁺]_Dπ⁺)/Γ([K*(892)⁺K⁻]_Dπ⁺) Γ₉₀/Γ₈₈

VALUE	DOCUMENT ID	TECN	COMMENT
2.57 ± 0.13 ± 0.06	¹ AAIJ	14V	LHCB pp at 7, 8 TeV

¹ The Analysis uses D → K*(892)K → K_S⁰Kπ decays.

Γ(D⁰K*(892)⁺)/Γ_{total} Γ₉₅/Γ

VALUE (units 10 ⁻⁴)	DOCUMENT ID	TECN	COMMENT
5.3 ± 0.4 OUR AVERAGE			
5.29 ± 0.30 ± 0.34	¹ AUBERT	06Z	BABR e ⁺ e ⁻ → γ(4S)
6.1 ± 1.6 ± 1.7	¹ MAHAPATRA	02	CLE2 e ⁺ e ⁻ → γ(4S)
6.3 ± 0.7 ± 0.5	¹ AUBERT	04Q	BABR Repl. by AUBERT 06Z

¹ Assumes equal production of B⁺ and B⁰ at the γ(4S).

Γ(D_{CP(-)}}K*(892)⁺)/Γ(D⁰K*(892)⁺) Γ₉₆/Γ₉₅

VALUE	DOCUMENT ID	TECN	COMMENT
0.515 ± 0.135 ± 0.065	¹ AUBERT	09AJ	BABR e ⁺ e ⁻ → γ(4S)
0.325 ± 0.13 ± 0.04	² AUBERT,B	05U	BABR Repl. by AUBERT 09AJ

¹ The authors report R_{CP-} = 1.03 ± 0.27 ± 0.13 which is, assuming CP conservation, twice the value of the quoted above branching ratio,

² The authors report R_{CP-} = 0.65 ± 0.26 ± 0.08 which is, assuming CP conservation, twice the value of the quoted above branching ratio.

Γ(D_{CP(+)}}K*(892)⁺)/Γ(D⁰K*(892)⁺) Γ₉₇/Γ₉₅

VALUE	DOCUMENT ID	TECN	COMMENT
1.16 ± 0.08 OUR AVERAGE			
1.18 ± 0.08 ± 0.02	¹ AAIJ	18X	LHCB pp at 7, 8, 13 TeV
1.085 ± 0.175 ± 0.045	² AUBERT	09AJ	BABR e ⁺ e ⁻ → γ(4S)
1.18 ± 0.08 ± 0.01	³ AAIJ	17B0	LHCB Repl. by AAIJ 18X
0.98 ± 0.20 ± 0.055	⁴ AUBERT,B	05U	BABR Repl. by AUBERT 09AJ

¹ Measures the ratio separately for K⁺K⁻ and π⁺π⁻ final states, R_{KK} = 1.22 ± 0.09 ± 0.02 and R_{ππ} = 1.08 ± 0.14 ± 0.03, and combines the two results.

² The authors report R_{CP+} = 2.17 ± 0.35 ± 0.09 which is, assuming CP conservation, twice the value of the quoted above branching ratio,

³ Measures the ratio separately for K⁺K⁻ and π⁺π⁻ final states, R_{KK} = 1.22 ± 0.09 ± 0.01 and R_{ππ} = 1.08 ± 0.14 ± 0.03, and combines the two results.

⁴ The authors report R_{CP+} = 1.96 ± 0.40 ± 0.11 which is, assuming CP conservation, twice the value of the quoted above branching ratio.

Γ(D⁰K*(892)⁺)/Γ(D⁰K*(892)⁺) Γ₉₈/Γ₉₅

"OUR EVALUATION" is derived from Γ_B(B⁺ → D⁰K⁺) data block listed in "CP violation parameters" section.

Γ(D⁰K⁺π⁺π⁻)/Γ(D⁰π⁺π⁺π⁻) Γ₉₉/Γ₁₀₅

VALUE (units 10 ⁻³)	DOCUMENT ID	TECN	COMMENT
5.8 ± 3.0 OUR EVALUATION			
9.4 ± 1.3 ± 0.9	AAIJ	12T	LHCB pp at 7 TeV

Γ(D_{CP(+)}}K⁺π⁻π⁺)/Γ([K⁺π⁻]_DK⁺π⁻π⁺) Γ₁₀₂/Γ₁₀₀

VALUE	DOCUMENT ID	TECN	COMMENT
1.040 ± 0.064	AAIJ	15Bc	LHCB pp at 7, 8 TeV

Γ([K⁻π⁺]_DK⁺π⁻π⁺)/Γ([K⁺π⁻]_DK⁺π⁻π⁺) Γ₁₀₁/Γ₁₀₀

VALUE (units 10 ⁻⁴)	DOCUMENT ID	TECN	COMMENT
85⁺³⁶₋₃₃	AAIJ	15Bc	LHCB pp at 7, 8 TeV

Γ(D⁰K⁺K⁰)/Γ_{total} Γ₁₀₃/Γ

VALUE (units 10 ⁻⁴)	DOCUMENT ID	TECN	COMMENT
5.5 ± 1.4 ± 0.8	¹ DRUTSKOY	02	BELL e ⁺ e ⁻ → γ(4S)

¹ Assumes equal production of B⁺ and B⁰ at the γ(4S).

Γ(D⁰K⁺K⁰(892)⁰)/Γ_{total} Γ₁₀₄/Γ

VALUE (units 10 ⁻⁴)	DOCUMENT ID	TECN	COMMENT
7.5 ± 1.3 ± 1.1	¹ DRUTSKOY	02	BELL e ⁺ e ⁻ → γ(4S)

¹ Assumes equal production of B⁺ and B⁰ at the γ(4S).

Γ(D⁰π⁺π⁺π⁻)/Γ_{total} Γ₁₀₅/Γ

VALUE	DOCUMENT ID	TECN	COMMENT
0.0056 ± 0.0021 OUR FIT			Error includes scale factor of 3.6.
0.0115 ± 0.0029 ± 0.0021	¹ BORTOLETTO92	CLEO	e ⁺ e ⁻ → γ(4S)

¹ BORTOLETTO 92 assumes equal production of B⁺ and B⁰ at the γ(4S) and uses MarkIII branching fractions for the D.

Γ(D⁰π⁺π⁺π⁻)/Γ(D⁰π⁺) Γ₁₀₅/Γ₄₉

VALUE	DOCUMENT ID	TECN	COMMENT
1.2 ± 0.4 OUR FIT			Error includes scale factor of 3.7.
1.27 ± 0.06 ± 0.11	AAIJ	11E	LHCB pp at 7 TeV

Meson Particle Listings

B^\pm

$\Gamma([K^-\pi^+]_D\pi^+\pi^-)/\Gamma([K^-\pi^-]_D K^+\pi^-\pi^+)$				$\Gamma_{106}/\Gamma_{100}$
VALUE (units 10^{-4})	DOCUMENT ID	TECN	COMMENT	
42.7±5.6	AAIJ	15bc	LHCB pp at 7, 8 TeV	

$\Gamma(\bar{D}^0\pi^+\pi^+\pi^-\text{nonresonant})/\Gamma_{\text{total}}$				Γ_{107}/Γ
VALUE	DOCUMENT ID	TECN	COMMENT	
0.0051±0.0034±0.0023	¹ BORTOLETTO92	CLEO	$e^+e^- \rightarrow \Upsilon(4S)$	

¹BORTOLETTO 92 assumes equal production of B^+ and B^0 at the $\Upsilon(4S)$ and uses Mark III branching fractions for the D .

$\Gamma(\bar{D}^0\pi^+\rho^0)/\Gamma_{\text{total}}$				Γ_{108}/Γ
VALUE	DOCUMENT ID	TECN	COMMENT	
0.0042±0.0023±0.0020	¹ BORTOLETTO92	CLEO	$e^+e^- \rightarrow \Upsilon(4S)$	

¹BORTOLETTO 92 assumes equal production of B^+ and B^0 at the $\Upsilon(4S)$ and uses Mark III branching fractions for the D .

$\Gamma(\bar{D}^0 a_1(1260)^+)/\Gamma_{\text{total}}$				Γ_{109}/Γ
VALUE	DOCUMENT ID	TECN	COMMENT	
0.0045±0.0019±0.0031	¹ BORTOLETTO92	CLEO	$e^+e^- \rightarrow \Upsilon(4S)$	

¹BORTOLETTO 92 assumes equal production of B^+ and B^0 at the $\Upsilon(4S)$ and uses Mark III branching fractions for the D .

$\Gamma(\bar{D}^0\omega\pi^+)/\Gamma_{\text{total}}$				Γ_{110}/Γ
VALUE	DOCUMENT ID	TECN	COMMENT	
0.0041±0.0007±0.0006	¹ ALEXANDER 018	CLE2	$e^+e^- \rightarrow \Upsilon(4S)$	

¹Assumes equal production of B^+ and B^0 at the $\Upsilon(4S)$. The signal is consistent with all observed $\omega\pi^+$ having proceeded through the ρ^+ resonance at mass $1349 \pm 25_{-10}^{+15}$ MeV and width $547 \pm 86_{-45}^{+46}$ MeV.

$\Gamma(D^*(2010)^-\pi^+\pi^+)/\Gamma_{\text{total}}$				Γ_{111}/Γ	
VALUE (units 10^{-3})	CL%	EVTS	DOCUMENT ID	TECN	COMMENT
1.35±0.22 OUR AVERAGE					
1.25±0.08±0.22			¹ ABE	04D	BELL $e^+e^- \rightarrow \Upsilon(4S)$
1.9±0.7±0.3	14		² ALAM	94	CLE2 $e^+e^- \rightarrow \Upsilon(4S)$
2.6±1.4±0.7	11		³ ALBRECHT	90J	ARG $e^+e^- \rightarrow \Upsilon(4S)$
2.4 $^{+1.7}_{-1.6}$ $^{+1.0}_{-0.6}$	3		⁴ BEBEK	87	CLEO $e^+e^- \rightarrow \Upsilon(4S)$

<. . . We do not use the following data for averages, fits, limits, etc.					
<.4.	90		⁵ BORTOLETTO92	CLEO	$e^+e^- \rightarrow \Upsilon(4S)$
5. ±2. ±3.	7		⁶ ALBRECHT	87c	ARG $e^+e^- \rightarrow \Upsilon(4S)$

¹Assumes equal production of B^+ and B^0 at the $\Upsilon(4S)$.
²ALAM 94 assume equal production of B^+ and B^0 at the $\Upsilon(4S)$ and use the CLEO II $B(D^*(2010)^+ \rightarrow D^0\pi^+)$ and absolute $B(D^0 \rightarrow K^-\pi^+)$ and the PDG 1992 $B(D^0 \rightarrow K^-\pi^+\pi^0)/B(D^0 \rightarrow K^-\pi^+)$ and $B(D^0 \rightarrow K^-2\pi^+\pi^-)/B(D^0 \rightarrow K^-\pi^+)$.
³Assumes equal production of B^+ and B^0 at the $\Upsilon(4S)$ and uses the Mark III branching fractions for the D .
⁴BEBEK 87 value has been updated in BERKELMAN 91 to use same assumptions as noted for BORTOLETTO 92.
⁵BORTOLETTO 92 assumes equal production of B^+ and B^0 at the $\Upsilon(4S)$ and uses Mark III branching fractions for the D and $D^*(2010)$. The authors also find the product branching fraction into $D^{**}\pi$ followed by $D^{**} \rightarrow D^*(2010)\pi$ to be $0.0014^{+0.0008}_{-0.0006}$ where D^{**} represents all orbitally excited D mesons.
⁶ALBRECHT 87c use PDG 86 branching ratios for D and $D^*(2010)$ and assume $B(\Upsilon(4S) \rightarrow B^+B^-) = 55\%$ and $B(\Upsilon(4S) \rightarrow B^0\bar{B}^0) = 45\%$. Superseded by ALBRECHT 90J.

$\Gamma(D^*(2010)^-K^+\pi^+)/\Gamma_{\text{total}}$				Γ_{112}/Γ
VALUE (units 10^{-5})	DOCUMENT ID	TECN	COMMENT	
8.2±0.3±1.4	¹ AAIJ	17AR	LHCB pp at 7, 8 TeV	

¹The branching fraction of the normalization mode $B^+ \rightarrow D^{*-}\pi^+\pi^+$ is rescaled to the updated ratio of $\Upsilon(4S) \rightarrow B^+B^-$ to $\Upsilon(4S) \rightarrow B^0\bar{B}^0$ decay rates of 1.058 ± 0.024 .

$\Gamma(D^*(2010)^-K^+\pi^+)/\Gamma(D^*(2010)^-\pi^+\pi^+)$				$\Gamma_{112}/\Gamma_{111}$
VALUE (units 10^{-2})	DOCUMENT ID	TECN	COMMENT	
6.39±0.27±0.48	¹ AAIJ	17AR	LHCB pp at 7, 8 TeV	

¹Uses $D^{*-} \rightarrow \bar{D}^0\pi^-$ and $\bar{D}^0 \rightarrow K^+\pi^-$ decays.

$\Gamma(\bar{D}_1^-(2420)^0\pi^+, \bar{D}_1^0 \rightarrow D^*(2010)^-\pi^+)/\Gamma(\bar{D}^0\pi^+\pi^+\pi^-)$				$\Gamma_{113}/\Gamma_{105}$
VALUE (units 10^{-2})	DOCUMENT ID	TECN	COMMENT	
9.3±1.6±0.9	¹ AAIJ	11E	LHCB pp at 7 TeV	

¹AAIJ 11E reports $(9.3 \pm 1.6 \pm 0.9) \times 10^{-2}$ from a measurement of $[\Gamma(B^+ \rightarrow \bar{D}_1^-(2420)^0\pi^+, \bar{D}_1^0 \rightarrow D^*(2010)^-\pi^+)/\Gamma(B^+ \rightarrow \bar{D}^0\pi^+\pi^+\pi^-)] \times [B(D^*(2010)^+ \rightarrow D^0\pi^+)]$ assuming $B(D^*(2010)^+ \rightarrow D^0\pi^+) = (67.7 \pm 0.5) \times 10^{-2}$.

$\Gamma(D^-\pi^+\pi^+)/\Gamma_{\text{total}}$				Γ_{114}/Γ	
VALUE (units 10^{-3})	CL%	EVTS	DOCUMENT ID	TECN	COMMENT
1.07±0.05 OUR AVERAGE					
1.08±0.03±0.05			¹ AUBERT	09AB	BABR $e^+e^- \rightarrow \Upsilon(4S)$
1.02±0.04±0.15			¹ ABE	04D	BELL $e^+e^- \rightarrow \Upsilon(4S)$

. . . We do not use the following data for averages, fits, limits, etc.

<.1.4	90		² ALAM	94	CLE2 $e^+e^- \rightarrow \Upsilon(4S)$
<.7	90		³ BORTOLETTO92	CLEO	$e^+e^- \rightarrow \Upsilon(4S)$
2.5 $^{+4.1}_{-2.3}$ $^{+2.4}_{-0.8}$	1		⁴ BEBEK	87	CLEO $e^+e^- \rightarrow \Upsilon(4S)$

¹Assumes equal production of B^+ and B^0 at the $\Upsilon(4S)$.
²ALAM 94 assume equal production of B^+ and B^0 at the $\Upsilon(4S)$ and use the Mark III $B(D^+ \rightarrow K^-2\pi^+)$.
³BORTOLETTO 92 assumes equal production of B^+ and B^0 at the $\Upsilon(4S)$ and uses Mark III branching fractions for the D . The product branching fraction into $D_0^*(2340)\pi$ followed by $D_0^*(2340) \rightarrow D\pi$ is < 0.005 at 90%CL and into $D_2^*(2460)$ followed by $D_2^*(2460) \rightarrow D\pi$ is < 0.004 at 90%CL.
⁴BEBEK 87 assume the $\Upsilon(4S)$ decays 43% to $B^0\bar{B}^0$. $B(D^- \rightarrow K^+\pi^-\pi^-) = (9.1 \pm 1.3 \pm 0.4)\%$ is assumed.

$\Gamma(D^-K^+\pi^+)/\Gamma(D^-\pi^+\pi^+)$				$\Gamma_{115}/\Gamma_{114}$
VALUE (units 10^{-2})	DOCUMENT ID	TECN	COMMENT	
7.20±0.19±0.21	AAIJ	15v	LHCB pp at 7, 8 TeV	

$\Gamma(D_0^*(2300)^0K^+, D_0^* \rightarrow D^-\pi^+)/\Gamma_{\text{total}}$				Γ_{116}/Γ
VALUE (units 10^{-6})	DOCUMENT ID	TECN	COMMENT	
6.1±1.9±1.5	¹ AAIJ	15v	LHCB pp at 7, 8 TeV	

¹Performs the amplitude analysis by fitting the square-Dalitz-plot distribution.

$\Gamma(D_2^*(2460)^0K^+, D_2^* \rightarrow D^-\pi^+)/\Gamma_{\text{total}}$				Γ_{117}/Γ
VALUE (units 10^{-6})	DOCUMENT ID	TECN	COMMENT	
23.2±1.1±2.0	¹ AAIJ	15v	LHCB pp at 7, 8 TeV	

¹Performs the amplitude analysis by fitting the square-Dalitz-plot distribution.

$\Gamma(D_1^*(2760)^0K^+, D_1^* \rightarrow D^-\pi^+)/\Gamma_{\text{total}}$				Γ_{118}/Γ
VALUE (units 10^{-6})	DOCUMENT ID	TECN	COMMENT	
3.6±0.9±0.8	¹ AAIJ	15v	LHCB pp at 7, 8 TeV	

¹Performs the amplitude analysis by fitting the square-Dalitz-plot distribution.

$\Gamma(D^+K^0)/\Gamma_{\text{total}}$				Γ_{119}/Γ
VALUE (units 10^{-6})	CL%	DOCUMENT ID	TECN	COMMENT
<.2.9	90	¹ DEL-AMO-SA...10K	BABR	$e^+e^- \rightarrow \Upsilon(4S)$

. . . We do not use the following data for averages, fits, limits, etc.

<.5.0	90		¹ AUBERT,B	05E	BABR Repl. by DEL-AMO-SANCHEZ 10K
-------	----	--	-----------------------	-----	-----------------------------------

¹Assumes equal production of B^+ and B^0 at the $\Upsilon(4S)$.

$\Gamma(D^+K^+\pi^-)/\Gamma(D^-K^+\pi^+)$				$\Gamma_{120}/\Gamma_{115}$
VALUE (units 10^{-2})	DOCUMENT ID	TECN	COMMENT	
7.3±1.2±0.7	AAIJ	16M	LHCB pp at 7, 8 TeV	

$\Gamma(D_2^*(2460)^0K^+, D_2^* \rightarrow D^+\pi^-)/\Gamma_{\text{total}}$				Γ_{121}/Γ
VALUE	CL%	DOCUMENT ID	TECN	COMMENT
<.6.3 × 10 ⁻⁷	90	AAIJ	16R	LHCB pp at 7, 8 TeV

$\Gamma(D^+K^*0)/\Gamma_{\text{total}}$				Γ_{122}/Γ
VALUE	CL%	DOCUMENT ID	TECN	COMMENT
<.4.9 × 10 ⁻⁷	90	AAIJ	16M	LHCB pp at 7, 8 TeV

. . . We do not use the following data for averages, fits, limits, etc.

<.1.8 × 10 ⁻⁶	90	AAIJ	13R	LHCB Repl. by AAJ 16M
<.3.0 × 10 ⁻⁶	90	¹ DEL-AMO-SA...10K	BABR	$e^+e^- \rightarrow \Upsilon(4S)$

¹Assumes equal production of B^+ and B^0 at the $\Upsilon(4S)$.

$\Gamma(D^+\bar{K}^*0)/\Gamma_{\text{total}}$				Γ_{123}/Γ
VALUE (units 10^{-6})	CL%	DOCUMENT ID	TECN	COMMENT
<.1.4	90	AAIJ	13R	LHCB pp at 7 TeV

$\Gamma(\bar{D}^*(2007)^0\pi^+)/\Gamma_{\text{total}}$				Γ_{124}/Γ
VALUE (units 10^{-3})	EVTS	DOCUMENT ID	TECN	COMMENT
4.90 ±0.17 OUR AVERAGE				
4.664±0.029±0.268		AAIJ	18A	LHCB pp at 7, 8, 13 TeV
4.82±0.12±0.35		¹ KATO	18	BELL $e^+e^- \rightarrow \Upsilon(4S)$
5.52±0.17±0.42		² AUBERT	07H	BABR $e^+e^- \rightarrow \Upsilon(4S)$
5.3±0.4±0.1		^{3,4} AUBERT,BE	06J	BABR $e^+e^- \rightarrow \Upsilon(4S)$
4.34±0.47±0.18		⁵ BRANDENB...	98	CLE2 $e^+e^- \rightarrow \Upsilon(4S)$
5.2±0.7±0.7	71	⁶ ALAM	94	CLE2 $e^+e^- \rightarrow \Upsilon(4S)$
7.2±1.8±1.6		⁷ BORTOLETTO92	CLEO	$e^+e^- \rightarrow \Upsilon(4S)$
4.0±1.4±1.2	9	⁷ ALBRECHT	90J	ARG $e^+e^- \rightarrow \Upsilon(4S)$

. . . We do not use the following data for averages, fits, limits, etc.

2.7±4.4		⁸ BEBEK	87	CLEO $e^+e^- \rightarrow \Upsilon(4S)$
---------	--	--------------------	----	--

¹Measures absolute branching fractions using a missing-mass technique.
²Assumes equal production of B^+ and B^0 at the $\Upsilon(4S)$.
³AUBERT,BE 06J reports $[\Gamma(B^+ \rightarrow \bar{D}^*(2007)^0\pi^+)/\Gamma_{\text{total}}] / [B(B^+ \rightarrow \bar{D}^0\pi^+)] = 1.14 \pm 0.07 \pm 0.04$ which we multiply by our best value $B(B^+ \rightarrow \bar{D}^0\pi^+) = (4.68 \pm 0.13) \times 10^{-3}$. Our first error is their experiment's error and our second error is the systematic error from using our best value.

See key on page 999

Meson Particle Listings

 B^\pm

⁴ Uses a missing-mass method. Does not depend on D branching fractions or B^+/B^0 production rates.

⁵ BRANDENBURG 98 assume equal production of B^+ and B^0 at $\Upsilon(4S)$ and use the D^* reconstruction technique. The first error is their experiment's error and the second error is the systematic error from the PDG 96 value of $B(D^* \rightarrow D\pi)$.

⁶ ALAM 94 assume equal production of B^+ and B^0 at the $\Upsilon(4S)$ and use the CLEO II $B(D^*(2007)^0 \rightarrow D^0\pi^0)$ and absolute $B(D^0 \rightarrow K^-\pi^+)$ and the PDG 1992 $B(D^0 \rightarrow K^-\pi^+\pi^0)/B(D^0 \rightarrow K^-\pi^+)$ and $B(D^0 \rightarrow K^-2\pi^+\pi^-)/B(D^0 \rightarrow K^-\pi^+)$.

⁷ Assumes equal production of B^+ and B^0 at the $\Upsilon(4S)$ and uses Mark III branching fractions for the D and $D^*(2010)$.

⁸ This is a derived branching ratio, using the inclusive pion spectrum and other two-body B decays. BEBEK 87 assume the $\Upsilon(4S)$ decays 43% to $B^0\bar{B}^0$.

$\Gamma(\bar{D}^*(2007)^0 \omega \pi^+)/\Gamma_{\text{total}}$ Γ_{127}/Γ

VALUE	DOCUMENT ID	TECN	COMMENT
0.0045 ± 0.0010 ± 0.0007	¹ ALEXANDER 01B	CLE2	$e^+e^- \rightarrow \Upsilon(4S)$

¹ Assumes equal production of B^+ and B^0 at the $\Upsilon(4S)$. The signal is consistent with all observed $\omega\pi^+$ having proceeded through the ρ^+ resonance at mass $1349 \pm 25^{+10}_{-5}$ MeV and width $547 \pm 86^{+46}_{-45}$ MeV.

$\Gamma(\bar{D}^*(2007)^0 \rho^+)/\Gamma_{\text{total}}$ Γ_{128}/Γ

VALUE	DOCUMENT ID	TECN	COMMENT
0.0098 ± 0.0017 OUR AVERAGE			
0.0098 ± 0.0006 ± 0.0017	¹ CSORNA 03	CLE2	$e^+e^- \rightarrow \Upsilon(4S)$
0.010 ± 0.006 ± 0.004	² ALBRECHT 90J	ARG	$e^+e^- \rightarrow \Upsilon(4S)$

• • • We do not use the following data for averages, fits, limits, etc. • • •

0.0168 ± 0.0021 ± 0.0028 86 ³ALAM 94 CLE2 $e^+e^- \rightarrow \Upsilon(4S)$

¹ Assumes equal production of B^0 and B^+ at the $\Upsilon(4S)$ resonance. The second error combines the systematic and theoretical uncertainties in quadrature. CSORNA 03 includes data used in ALAM 94. A full angular fit to three complex helicity amplitudes is performed.

² Assumes equal production of B^+ and B^0 at the $\Upsilon(4S)$ and uses Mark III branching fractions for the D and $D^*(2010)$.

³ ALAM 94 assume equal production of B^+ and B^0 at the $\Upsilon(4S)$ and use the CLEO II $B(D^*(2007)^0 \rightarrow D^0\pi^0)$ and absolute $B(D^0 \rightarrow K^-\pi^+)$ and the PDG 1992 $B(D^0 \rightarrow K^-\pi^+\pi^0)/B(D^0 \rightarrow K^-\pi^+)$ and $B(D^0 \rightarrow K^-2\pi^+\pi^-)/B(D^0 \rightarrow K^-\pi^+)$. The nonresonant $\pi^+\pi^0$ contribution under the ρ^+ is negligible.

$\Gamma(\bar{D}^*(2007)^0 K^+)/\Gamma_{\text{total}}$ Γ_{129}/Γ

VALUE (units 10^{-4})	DOCUMENT ID	TECN	COMMENT
3.97 ± 0.31 ± 0.28 OUR AVERAGE			
3.98 ± 0.28 ± 0.13	¹ AUBERT 05N	BABR	$e^+e^- \rightarrow \Upsilon(4S)$
3.8 ± 1.0 ± 0.1	² ABE 01i	BELL	$e^+e^- \rightarrow \Upsilon(4S)$

¹ AUBERT 05N reports $[\Gamma(B^+ \rightarrow \bar{D}^*(2007)^0 K^+)/\Gamma_{\text{total}}] / [B(B^+ \rightarrow \bar{D}^*(2007)^0 \pi^+)] = 0.0813 \pm 0.0040 \pm 0.0042 \pm 0.0031$ which we multiply by our best value $B(B^+ \rightarrow \bar{D}^*(2007)^0 \pi^+) = (4.90 \pm 0.17) \times 10^{-3}$. Our first error is their experiment's error and our second error is the systematic error from using our best value.

² ABE 01i reports $[\Gamma(B^+ \rightarrow \bar{D}^*(2007)^0 K^+)/\Gamma_{\text{total}}] / [B(B^+ \rightarrow \bar{D}^*(2007)^0 \pi^+)] = 0.078 \pm 0.019 \pm 0.009$ which we multiply by our best value $B(B^+ \rightarrow \bar{D}^*(2007)^0 \pi^+) = (4.90 \pm 0.17) \times 10^{-3}$. Our first error is their experiment's error and our second error is the systematic error from using our best value.

$\Gamma(\bar{D}_{CP(1)}^{*0} K^+)/\Gamma_{\text{total}}$ Γ_{130}/Γ

VALUE (units 10^{-4})	DOCUMENT ID	TECN	COMMENT
2.60 ± 0.27 ± 0.20 ± 0.18	¹ AUBERT 08BF	BABR	$e^+e^- \rightarrow \Upsilon(4S)$

¹ AUBERT 08BF reports $[\Gamma(B^+ \rightarrow \bar{D}_{CP(1)}^{*0} K^+)/\Gamma_{\text{total}}] / [B(B^+ \rightarrow \bar{D}^*(2007)^0 K^+)] = 0.655 \pm 0.065 \pm 0.020$ which we multiply by our best value $B(B^+ \rightarrow \bar{D}^*(2007)^0 K^+) = (3.97 \pm 0.31 \pm 0.28) \times 10^{-4}$. Our first error is their experiment's error and our second error is the systematic error from using our best value.

$\Gamma(\bar{D}^*(2007)^0 K^+)/\Gamma(\bar{D}^*(2007)^0 \pi^+)$ $\Gamma_{129}/\Gamma_{124}$

VALUE (units 10^{-2})	DOCUMENT ID	TECN	COMMENT
7.930 ± 0.110 ± 0.560	AALJ	18A	LHCB pp at 7, 8, 13 TeV

$\Gamma(\bar{D}_{CP(1)}^{*0} K^+)/\Gamma(\bar{D}_{CP(1)}^{*0} \pi^+)$ $\Gamma_{130}/\Gamma_{125}$

VALUE	DOCUMENT ID	TECN	COMMENT
0.095 ± 0.017 OUR AVERAGE			
0.11 ± 0.02 ± 0.02	¹ ABE 06	BELL	$e^+e^- \rightarrow \Upsilon(4S)$
0.086 ± 0.021 ± 0.007	² AUBERT 05N	BABR	$e^+e^- \rightarrow \Upsilon(4S)$

¹ Reports a double ratio of $B(B^+ \rightarrow D_{CP(1)}^{*0} K^+)/B(B^+ \rightarrow D_{CP(1)}^{*0} \pi^+)$ and $B(B^+ \rightarrow \bar{D}^*(2007)^0 K^+)/B(B^+ \rightarrow \bar{D}^*(2007)^0 \pi^+)$. We multiply by our best value of $B(B^+ \rightarrow \bar{D}^*(2007)^0 K^+)/B(B^+ \rightarrow \bar{D}^*(2007)^0 \pi^+) = 0.080 \pm 0.011$. Our first error is their experiment's error and the second error is systematic error from using our best value.

² Uses $D^0 \rightarrow D^0\pi^0$ with D^0 reconstructed in the CP -even eigenstates K^+K^- and $\pi^+\pi^-$.

$\Gamma(\bar{D}_{CP(-1)}^{*0} K^+)/\Gamma_{\text{total}}$ Γ_{131}/Γ

VALUE (units 10^{-4})	DOCUMENT ID	TECN	COMMENT
2.19 ± 0.25 ± 0.17 ± 0.15	¹ AUBERT 08BF	BABR	$e^+e^- \rightarrow \Upsilon(4S)$

¹ AUBERT 08BF reports $[\Gamma(B^+ \rightarrow \bar{D}_{CP(-1)}^{*0} K^+)/\Gamma_{\text{total}}] / [B(B^+ \rightarrow \bar{D}^*(2007)^0 K^+)] = 0.55 \pm 0.06 \pm 0.02$ which we multiply by our best value $B(B^+ \rightarrow \bar{D}^*(2007)^0 K^+) = (3.97 \pm 0.31 \pm 0.28) \times 10^{-4}$. Our first error is their experiment's error and our second error is the systematic error from using our best value.

$\Gamma(\bar{D}_{CP(-1)}^{*0} K^+)/\Gamma(D_{CP(-1)}^{*0} \pi^+)$ $\Gamma_{131}/\Gamma_{126}$

VALUE	DOCUMENT ID	TECN	COMMENT
0.09 ± 0.03 ± 0.01	¹ ABE 06	BELL	$e^+e^- \rightarrow \Upsilon(4S)$

¹ Reports a double ratio of $B(B^+ \rightarrow (D_{CP(-1)}^{*0})^0 K^+)/B(B^+ \rightarrow (D_{CP(-1)}^{*0})^0 \pi^+)$ and $B(B^+ \rightarrow \bar{D}^*(2007)^0 K^+)/B(B^+ \rightarrow \bar{D}^*(2007)^0 \pi^+) = 1.15 \pm 0.31 \pm 0.12$. We multiply by our best value of $B(B^+ \rightarrow \bar{D}^*(2007)^0 K^+)/B(B^+ \rightarrow \bar{D}^*(2007)^0 \pi^+) = 0.080 \pm 0.011$. Our first error is their experiment's error and the second error is systematic error from using our best value.

$\Gamma(D^*(2007)^0 K^+)/\Gamma(\bar{D}^*(2007)^0 K^+)$ $\Gamma_{132}/\Gamma_{129}$

"OUR EVALUATION" is derived from $\Gamma(B^+ \rightarrow D^0 K^+)$ data block listed in "CP violation parameters" section.

VALUE (units 10^{-2})	DOCUMENT ID
1.96 ± 0.53 OUR EVALUATION	

$\Gamma(\bar{D}^*(2007)^0 K^*(892)^+)/\Gamma_{\text{total}}$ Γ_{133}/Γ

VALUE (units 10^{-4})	DOCUMENT ID	TECN	COMMENT
8.1 ± 1.4 OUR AVERAGE			
8.3 ± 1.1 ± 1.0	¹ AUBERT 04k	BABR	$e^+e^- \rightarrow \Upsilon(4S)$
7.2 ± 2.2 ± 2.6	² MAHAPATRA 02	CLE2	$e^+e^- \rightarrow \Upsilon(4S)$

¹ Assumes equal production of B^+ and B^0 at the $\Upsilon(4S)$.
² Assumes equal production of B^+ and B^0 at the $\Upsilon(4S)$ and an unpolarized final state.

$\Gamma(\bar{D}^*(2007)^0 K^+ \bar{K}^0)/\Gamma_{\text{total}}$ Γ_{134}/Γ

VALUE (units 10^{-4})	CL%	DOCUMENT ID	TECN	COMMENT
<10.6	90	¹ DRUTSKOY 02	BELL	$e^+e^- \rightarrow \Upsilon(4S)$

¹ Assumes equal production of B^+ and B^0 at the $\Upsilon(4S)$.

$\Gamma(\bar{D}^*(2007)^0 K^+ \bar{K}^*(892)^0)/\Gamma_{\text{total}}$ Γ_{135}/Γ

VALUE (units 10^{-4})	DOCUMENT ID	TECN	COMMENT
15.3 ± 3.1 ± 2.9	¹ DRUTSKOY 02	BELL	$e^+e^- \rightarrow \Upsilon(4S)$

¹ Assumes equal production of B^+ and B^0 at the $\Upsilon(4S)$.

$\Gamma(\bar{D}^*(2007)^0 \pi^+ \pi^+ \pi^-)/\Gamma_{\text{total}}$ Γ_{136}/Γ

VALUE (units 10^{-2})	EVTS	DOCUMENT ID	TECN	COMMENT
1.03 ± 0.12 OUR AVERAGE				
1.055 ± 0.047 ± 0.129		¹ MAJUMDER 04	BELL	$e^+e^- \rightarrow \Upsilon(4S)$
0.94 ± 0.20 ± 0.17	48	^{2,3} ALAM 94	CLE2	$e^+e^- \rightarrow \Upsilon(4S)$

¹ Assumes equal production of B^+ and B^0 at the $\Upsilon(4S)$.
² ALAM 94 assume equal production of B^+ and B^0 at the $\Upsilon(4S)$ and use the CLEO II $B(D^*(2007)^0 \rightarrow D^0\pi^0)$ and absolute $B(D^0 \rightarrow K^-\pi^+)$ and the PDG 1992 $B(D^0 \rightarrow K^-\pi^+\pi^0)/B(D^0 \rightarrow K^-\pi^+)$ and $B(D^0 \rightarrow K^-2\pi^+\pi^-)/B(D^0 \rightarrow K^-\pi^+)$.

³ The three pion mass is required to be between 1.0 and 1.6 GeV consistent with an a_1 meson. (If this channel is dominated by a_1^+ , the branching ratio for $\bar{D}^{*0} a_1^+$ is twice that for $\bar{D}^{*0} \pi^+ \pi^+ \pi^-$.)

$\Gamma(\bar{D}^*(2007)^0 a_1(1260)^+)/\Gamma_{\text{total}}$ Γ_{137}/Γ

VALUE	DOCUMENT ID	TECN	COMMENT
0.0188 ± 0.0040 ± 0.0034	^{1,2} ALAM 94	CLE2	$e^+e^- \rightarrow \Upsilon(4S)$

¹ ALAM 94 value is twice their $\Gamma(\bar{D}^*(2007)^0 \pi^+ \pi^+ \pi^-)/\Gamma_{\text{total}}$ value based on their observation that the three pions are dominantly in the $a_1(1260)$ mass range 1.0 to 1.6 GeV.

² ALAM 94 assume equal production of B^+ and B^0 at the $\Upsilon(4S)$ and use the CLEO II $B(D^*(2007)^0 \rightarrow D^0\pi^0)$ and absolute $B(D^0 \rightarrow K^-\pi^+)$ and the PDG 1992 $B(D^0 \rightarrow K^-\pi^+\pi^0)/B(D^0 \rightarrow K^-\pi^+)$ and $B(D^0 \rightarrow K^-2\pi^+\pi^-)/B(D^0 \rightarrow K^-\pi^+)$.

$\Gamma(\bar{D}^*(2007)^0 \pi^+ \pi^+ \pi^0)/\Gamma_{\text{total}}$ Γ_{138}/Γ

VALUE	DOCUMENT ID	TECN	COMMENT
0.0180 ± 0.0024 ± 0.0027	¹ ALEXANDER 01B	CLE2	$e^+e^- \rightarrow \Upsilon(4S)$

¹ Assumes equal production of B^+ and B^0 at the $\Upsilon(4S)$. The signal is consistent with all observed $\omega\pi^+$ having proceeded through the ρ^+ resonance at mass $1349 \pm 25^{+10}_{-5}$ MeV and width $547 \pm 86^{+46}_{-45}$ MeV.

$\Gamma(\bar{D}^{*0} 3\pi^+ 2\pi^-)/\Gamma_{\text{total}}$ Γ_{139}/Γ

VALUE (units 10^{-3})	DOCUMENT ID	TECN	COMMENT
5.67 ± 0.91 ± 0.85	¹ MAJUMDER 04	BELL	$e^+e^- \rightarrow \Upsilon(4S)$

¹ Assumes equal production of B^+ and B^0 at the $\Upsilon(4S)$.

Meson Particle Listings

 B^\pm $\Gamma(D^*(2010)^+\pi^0)/\Gamma_{\text{total}}$ Γ_{140}/Γ

VALUE	CL%	DOCUMENT ID	TECN	COMMENT
$<3.6 \times 10^{-6}$		¹ IWABUCHI 08	BELL	$e^+e^- \rightarrow \Upsilon(4S)$
$<1.7 \times 10^{-4}$	90	² BRANDENB... 98	CLE2	$e^+e^- \rightarrow \Upsilon(4S)$

- ¹ Assumes equal production of B^+ and B^0 at the $\Upsilon(4S)$.
² BRANDENBURG 98 assume equal production of B^+ and B^0 at $\Upsilon(4S)$ and use the D^* partial reconstruction technique. The first error is their experiment's error and the second error is the systematic error from the PDG 96 value of $B(D^* \rightarrow D\pi)$.

 $\Gamma(D^*(2010)^+K^0)/\Gamma_{\text{total}}$ Γ_{141}/Γ

VALUE	CL%	DOCUMENT ID	TECN	COMMENT
$<9.0 \times 10^{-6}$	90	¹ AUBERT,B 05E	BABR	$e^+e^- \rightarrow \Upsilon(4S)$
$<9.5 \times 10^{-5}$	90	¹ GRITSAN 01	CLE2	$e^+e^- \rightarrow \Upsilon(4S)$

- ¹ Assumes equal production of B^+ and B^0 at the $\Upsilon(4S)$.

 $\Gamma(D^*(2010)^-\pi^+\pi^+\pi^0)/\Gamma_{\text{total}}$ Γ_{142}/Γ

VALUE	EVTs	DOCUMENT ID	TECN	COMMENT
$0.0152 \pm 0.0071 \pm 0.0001$	26	¹ ALBRECHT 90j	ARG	$e^+e^- \rightarrow \Upsilon(4S)$
$0.043 \pm 0.013 \pm 0.026$	24	² ALBRECHT 87c	ARG	$e^+e^- \rightarrow \Upsilon(4S)$

- ¹ ALBRECHT 90j reports $0.018 \pm 0.007 \pm 0.005$ from a measurement of $[\Gamma(B^+ \rightarrow D^*(2010)^-\pi^+\pi^+\pi^0)/\Gamma_{\text{total}}] \times [B(D^*(2010)^+ \rightarrow D^0\pi^+)]$ assuming $B(D^*(2010)^+ \rightarrow D^0\pi^+) = 0.57 \pm 0.06$, which we rescale to our best value $B(D^*(2010)^+ \rightarrow D^0\pi^+) = (67.7 \pm 0.5) \times 10^{-2}$. Our first error is their experiment's error and our second error is the systematic error from using our best value. Assumes equal production of B^+ and B^0 at the $\Upsilon(4S)$ and uses MarkIII branching fractions for the D .
² ALBRECHT 87c use PDG 86 branching ratios for D and $D^*(2010)$ and assume $B(\Upsilon(4S) \rightarrow B^+B^-) = 55\%$ and $B(\Upsilon(4S) \rightarrow B^0\bar{B}^0) = 45\%$. Superseded by ALBRECHT 90j.

 $\Gamma(D^*(2010)^-\pi^+\pi^+\pi^-\pi^0)/\Gamma_{\text{total}}$ Γ_{143}/Γ

VALUE (units 10^{-3})	CL%	DOCUMENT ID	TECN	COMMENT
$2.56 \pm 0.26 \pm 0.33$		¹ MAJUMDER 04	BELL	$e^+e^- \rightarrow \Upsilon(4S)$
<10	90	² ALBRECHT 90j	ARG	$e^+e^- \rightarrow \Upsilon(4S)$

- ¹ Assumes equal production of B^+ and B^0 at the $\Upsilon(4S)$.
² Assumes equal production of B^+ and B^0 at the $\Upsilon(4S)$ and uses MarkIII branching fractions for the D and $D^*(2010)$.

 $\Gamma(\bar{D}^{*0}\pi^+)/\Gamma_{\text{total}}$ Γ_{144}/Γ

\bar{D}^{*0} represents an excited state with mass $2.2 < M < 2.8$ GeV/ c^2 .

VALUE (units 10^{-3})	DOCUMENT ID	TECN	COMMENT
$5.7 \pm 1.2 \pm 0.2$	^{1,2} AUBERT,BE 06j	BABR	$e^+e^- \rightarrow \Upsilon(4S)$

- ¹ AUBERT,BE 06j reports $[\Gamma(B^+ \rightarrow \bar{D}^{*0}\pi^+)/\Gamma_{\text{total}}] / [B(B^+ \rightarrow \bar{D}^0\pi^+)] = 1.22 \pm 0.13 \pm 0.23$ which we multiply by our best value $B(B^+ \rightarrow \bar{D}^0\pi^+) = (4.68 \pm 0.13) \times 10^{-3}$. Our first error is their experiment's error and our second error is the systematic error from using our best value.
² Uses a missing-mass method. Does not depend on D branching fractions or B^+/\bar{B}^0 production rates.

 $\Gamma(\bar{D}_1^*(2420)^0\pi^+)/\Gamma_{\text{total}}$ Γ_{145}/Γ

VALUE	EVTs	DOCUMENT ID	TECN	COMMENT
0.0015 ± 0.0006 OUR AVERAGE		Error includes scale factor of 1.3.		
$0.0011 \pm 0.0005 \pm 0.0002$	8	¹ ALAM 94	CLE2	$e^+e^- \rightarrow \Upsilon(4S)$
$0.0025 \pm 0.0007 \pm 0.0006$		² ALBRECHT 94D	ARG	$e^+e^- \rightarrow \Upsilon(4S)$

- ¹ ALAM 94 assume equal production of B^+ and B^0 at the $\Upsilon(4S)$ and use the CLEOII $B(D^*(2010)^+ \rightarrow D^0\pi^+)$ and absolute $B(D^0 \rightarrow K^-\pi^+)$ and the PDG 1992 $B(D^0 \rightarrow K^-\pi^+\pi^0)/B(D^0 \rightarrow K^-\pi^+)$ and assuming $B(D_1(2420)^0 \rightarrow D^*(2010)^+\pi^-) = 67\%$.
² ALBRECHT 94D assume equal production of B^+ and B^0 at the $\Upsilon(4S)$ and use the CLEOII $B(D^*(2010)^+ \rightarrow D^0\pi^+)$ assuming $B(D_1(2420)^0 \rightarrow D^*(2010)^+\pi^-) = 67\%$.

 $\Gamma(\bar{D}_1(2420)^0\pi^+ \times B(\bar{D}_1^0 \rightarrow \bar{D}^0\pi^+\pi^-))/\Gamma_{\text{total}}$ Γ_{146}/Γ

VALUE (units 10^{-4})	DOCUMENT ID	TECN	COMMENT
$2.5 \pm 1.6 \pm 1.4$ OUR FIT	Error includes scale factor of 3.9.		
$1.85 \pm 0.29 \pm 0.35 \pm 0.55$	¹ ABE 05A	BELL	$e^+e^- \rightarrow \Upsilon(4S)$

- ¹ Assumes equal production of B^+ and B^0 at the $\Upsilon(4S)$.

 $\Gamma(\bar{D}_1(2420)^0\pi^+ \times B(\bar{D}_1^0 \rightarrow \bar{D}^0\pi^+\pi^-))/\Gamma(\bar{D}^0\pi^+\pi^+\pi^-)$ $\Gamma_{146}/\Gamma_{105}$

VALUE (units 10^{-2})	DOCUMENT ID	TECN	COMMENT
$4.6 \pm 3.3 \pm 2.7$ OUR FIT	Error includes scale factor of 3.9.		
$10.3 \pm 1.5 \pm 0.9$	AAIJ 11E	LHCB	pp at 7 TeV

 $\Gamma(\bar{D}_1(2420)^0\pi^+ \times B(\bar{D}_1^0 \rightarrow \bar{D}^0\pi^+\pi^- (\text{nonresonant}))/\Gamma(\bar{D}^0\pi^+\pi^+\pi^-)$ $\Gamma_{147}/\Gamma_{105}$

VALUE (units 10^{-2})	DOCUMENT ID	TECN	COMMENT
$4.0 \pm 0.7 \pm 0.5$	¹ AAJ 11E	LHCB	pp at 7 TeV

- ¹ Excludes decays where $\bar{D}_1(2420)^0 \rightarrow D^*(2010)^-\pi^+$.

 $\Gamma(\bar{D}_2^*(2462)^0\pi^+ \times B(\bar{D}_2^0(2462)^0 \rightarrow D^-\pi^+))/\Gamma_{\text{total}}$ Γ_{148}/Γ

VALUE (units 10^{-4})	DOCUMENT ID	TECN	COMMENT
3.56 ± 0.24 OUR AVERAGE			
$3.62 \pm 0.06 \pm 0.30$	¹ AAJ 16AH	LHCB	pp at 7, 8 TeV
$3.5 \pm 0.2 \pm 0.4$	² AUBERT 09AB	BABR	$e^+e^- \rightarrow \Upsilon(4S)$
$3.4 \pm 0.3 \pm 0.72$	² ABE 04D	BELL	$e^+e^- \rightarrow \Upsilon(4S)$

- ¹ Measured using a Dalitz plot analysis of $B^- \rightarrow D^+\pi^-\pi^-$ decays.
² Assumes equal production of B^+ and B^0 at the $\Upsilon(4S)$.

 $\Gamma(\bar{D}_2^*(2462)^0\pi^+ \times B(\bar{D}_2^0(2462)^0 \rightarrow \bar{D}^0\pi^-\pi^+))/\Gamma(\bar{D}^0\pi^+\pi^+\pi^-)$ $\Gamma_{149}/\Gamma_{105}$

VALUE (units 10^{-4})	DOCUMENT ID	TECN	COMMENT
$4.0 \pm 1.0 \pm 0.4$	AAIJ 11E	LHCB	pp at 7 TeV

 $\Gamma(\bar{D}_2^*(2462)^0\pi^+ \times B(\bar{D}_2^0(2462)^0 \rightarrow \bar{D}^0\pi^-\pi^+ (\text{nonresonant}))/\Gamma(\bar{D}^0\pi^+\pi^+\pi^-)$ $\Gamma_{150}/\Gamma_{105}$

VALUE	CL%	DOCUMENT ID	TECN	COMMENT
$<3.0 \times 10^{-2}$	90	¹ AAJ 11E	LHCB	pp at 7 TeV

- ¹ Excludes decays where $\bar{D}_2^*(2462)^0 \rightarrow D^*(2010)^-\pi^+$.

 $\Gamma(\bar{D}_2^*(2462)^0\pi^+ \times B(\bar{D}_2^0(2462)^0 \rightarrow D^*(2010)^-\pi^+))/\Gamma(\bar{D}^0\pi^+\pi^+\pi^-)$ $\Gamma_{151}/\Gamma_{105}$

VALUE (units 10^{-2})	DOCUMENT ID	TECN	COMMENT
$3.9 \pm 1.2 \pm 0.4$	¹ AAJ 11E	LHCB	pp at 7 TeV

- ¹ Uses $B(D^*(2010)^+ \rightarrow D^0\pi^+) = (67.7 \pm 0.5)\%$.

 $\Gamma(\bar{D}_0^*(2400)^0\pi^+ \times B(\bar{D}_0^0(2400)^0 \rightarrow D^-\pi^+))/\Gamma_{\text{total}}$ Γ_{152}/Γ

VALUE (units 10^{-4})	DOCUMENT ID	TECN	COMMENT
6.4 ± 1.4 OUR AVERAGE			
$6.8 \pm 0.3 \pm 2.0$	¹ AUBERT 09AB	BABR	$e^+e^- \rightarrow \Upsilon(4S)$
$6.1 \pm 0.6 \pm 1.8$	¹ ABE 04D	BELL	$e^+e^- \rightarrow \Upsilon(4S)$

- ¹ Assumes equal production of B^+ and B^0 at the $\Upsilon(4S)$.

 $\Gamma(\bar{D}_1(2421)^0\pi^+ \times B(\bar{D}_1^0(2421)^0 \rightarrow D^-\pi^+))/\Gamma_{\text{total}}$ Γ_{153}/Γ

VALUE (units 10^{-4})	DOCUMENT ID	TECN	COMMENT
$6.8 \pm 0.7 \pm 1.3$	¹ ABE 04D	BELL	$e^+e^- \rightarrow \Upsilon(4S)$

- ¹ Assumes equal production of B^+ and B^0 at the $\Upsilon(4S)$.

 $\Gamma(\bar{D}_2^*(2462)^0\pi^+ \times B(\bar{D}_2^0(2462)^0 \rightarrow D^-\pi^+))/\Gamma_{\text{total}}$ Γ_{154}/Γ

VALUE (units 10^{-4})	DOCUMENT ID	TECN	COMMENT
$1.8 \pm 0.3 \pm 0.4$	¹ ABE 04D	BELL	$e^+e^- \rightarrow \Upsilon(4S)$

- ¹ Assumes equal production of B^+ and B^0 at the $\Upsilon(4S)$.

 $\Gamma(\bar{D}_1^*(2427)^0\pi^+ \times B(\bar{D}_1^0(2427)^0 \rightarrow D^-\pi^+))/\Gamma_{\text{total}}$ Γ_{155}/Γ

VALUE (units 10^{-4})	DOCUMENT ID	TECN	COMMENT
$5.0 \pm 0.4 \pm 1.1$	¹ ABE 04D	BELL	$e^+e^- \rightarrow \Upsilon(4S)$

- ¹ Assumes equal production of B^+ and B^0 at the $\Upsilon(4S)$.

 $\Gamma(\bar{D}_1(2420)^0\pi^+ \times B(\bar{D}_1^0 \rightarrow \bar{D}^0\pi^+\pi^-))/\Gamma_{\text{total}}$ Γ_{156}/Γ

VALUE (units 10^{-4})	CL%	DOCUMENT ID	TECN	COMMENT
<0.06	90	¹ ABE 05A	BELL	$e^+e^- \rightarrow \Upsilon(4S)$

- ¹ Assumes equal production of B^+ and B^0 at the $\Upsilon(4S)$.

 $\Gamma(\bar{D}_1^*(2420)^0\rho^+)/\Gamma_{\text{total}}$ Γ_{157}/Γ

VALUE	CL%	DOCUMENT ID	TECN	COMMENT
<0.0014	90	¹ ALAM 94	CLE2	$e^+e^- \rightarrow \Upsilon(4S)$

- ¹ ALAM 94 assume equal production of B^+ and B^0 at the $\Upsilon(4S)$ and use the CLEOII $B(D^*(2010)^+ \rightarrow D^0\pi^+)$ assuming $B(D_1(2420)^0 \rightarrow D^*(2010)^+\pi^-) = 67\%$.

 $\Gamma(\bar{D}_2^*(2460)^0\pi^+)/\Gamma_{\text{total}}$ Γ_{158}/Γ

VALUE	CL%	DOCUMENT ID	TECN	COMMENT
<0.0013	90	¹ ALAM 94	CLE2	$e^+e^- \rightarrow \Upsilon(4S)$
<0.0028	90	² ALAM 94	CLE2	$e^+e^- \rightarrow \Upsilon(4S)$
<0.0023	90	³ ALBRECHT 94D	ARG	$e^+e^- \rightarrow \Upsilon(4S)$

- ¹ ALAM 94 assume equal production of B^+ and B^0 at the $\Upsilon(4S)$ and use the MarkIII $B(D^+ \rightarrow K^-2\pi^+)$ and $B(D_2^*(2460)^0 \rightarrow D^+\pi^-) = 30\%$.
² ALAM 94 assume equal production of B^+ and B^0 at the $\Upsilon(4S)$ and use the MarkIII $B(D^+ \rightarrow K^-2\pi^+)$, the CLEOII $B(D^*(2010)^+ \rightarrow D^0\pi^+)$ and $B(D_2^*(2460)^0 \rightarrow D^*(2010)^+\pi^-) = 20\%$.
³ ALBRECHT 94D assume equal production of B^+ and B^0 at the $\Upsilon(4S)$ and use the CLEOII $B(D^*(2010)^+ \rightarrow D^0\pi^+)$ and $B(D_2^*(2460)^0 \rightarrow D^*(2010)^+\pi^-) = 30\%$.

See key on page 999

Meson Particle Listings

B^\pm

$\Gamma(\overline{D}_2^*(2460)^0 \pi^+ \times B(\overline{D}_2^{*0} \rightarrow \overline{D}^{*0} \pi^+ \pi^-))/\Gamma_{\text{total}}$					Γ_{159}/Γ
VALUE (units 10^{-4})	CL%	DOCUMENT ID	TECN	COMMENT	
<0.22	90	1 ABE	05A	BELL $e^+e^- \rightarrow \Upsilon(4S)$	

¹ Assumes equal production of B^+ and B^0 at the $\Upsilon(4S)$.

$\Gamma(\overline{D}_2^*(2460)^0 \rho^+)/\Gamma_{\text{total}}$					Γ_{163}/Γ
VALUE	CL%	DOCUMENT ID	TECN	COMMENT	
<0.0047	90	1 ALAM	94	CLE2 $e^+e^- \rightarrow \Upsilon(4S)$	
<0.005	90	2 ALAM	94	CLE2 $e^+e^- \rightarrow \Upsilon(4S)$	

¹ ALAM 94 assume equal production of B^+ and B^0 at the $\Upsilon(4S)$ and use the MarkIII $B(D^+ \rightarrow K^- 2\pi^+)$ and $B(D_2^*(2460)^0 \rightarrow D^+ \pi^-) = 30\%$.

² ALAM 94 assume equal production of B^+ and B^0 at the $\Upsilon(4S)$ and use the MarkIII $B(D^+ \rightarrow K^- 2\pi^+)$, the CLEO II $B(D^*(2010)^+ \rightarrow D^0 \pi^+)$ and $B(D_2^*(2460)^0 \rightarrow D^*(2010)^+ \pi^-) = 20\%$.

$\Gamma(\overline{D}_1^*(2680)^0 \pi^+, \overline{D}_1^*(2680)^0 \rightarrow D^- \pi^+)/\Gamma_{\text{total}}$					Γ_{160}/Γ
VALUE (units 10^{-4})		DOCUMENT ID	TECN	COMMENT	
$0.84 \pm 0.06 \pm 0.20$		1 AAIJ	16AH	LHCB pp at 7, 8 TeV	

¹ Measured using a Dalitz plot analysis of $B^+ \rightarrow D^- \pi^+ \pi^+$ decays.

$\Gamma(\overline{D}_3^*(2760)^0 \pi^+, \overline{D}_3^*(2760)^0 \pi^+ \rightarrow D^- \pi^+)/\Gamma_{\text{total}}$					Γ_{161}/Γ
VALUE (units 10^{-5})		DOCUMENT ID	TECN	COMMENT	
$1.0 \pm 0.1 \pm 0.2$		1 AAIJ	16AH	LHCB pp at 7, 8 TeV	

¹ Measured using a Dalitz plot analysis of $B^+ \rightarrow D^- \pi^+ \pi^+$ decays.

$\Gamma(\overline{D}_2^*(3000)^0 \pi^+, \overline{D}_2^*(3000)^0 \pi^+ \rightarrow D^- \pi^+)/\Gamma_{\text{total}}$					Γ_{162}/Γ
VALUE (units 10^{-6})		DOCUMENT ID	TECN	COMMENT	
$2 \pm 1 \pm 1$		1 AAIJ	16AH	LHCB pp at 7, 8 TeV	

¹ Measured using a Dalitz plot analysis of $B^+ \rightarrow D^- \pi^+ \pi^+$ decays.

$\Gamma(D^0 D_s^+)/\Gamma_{\text{total}}$					Γ_{164}/Γ
VALUE (units 10^{-3})		DOCUMENT ID	TECN	COMMENT	
9.0 ± 0.9 OUR AVERAGE					
$8.6 \pm 0.2 \pm 1.1$		1 AAIJ	13AP	LHCB pp at 7 TeV	
$9.5 \pm 2.0 \pm 0.8$		2 AUBERT	06N	BABR $e^+e^- \rightarrow \Upsilon(4S)$	
$9.8 \pm 2.6 \pm 0.9$		3 GIBAUT	96	CLE2 $e^+e^- \rightarrow \Upsilon(4S)$	
$14 \pm 8 \pm 1$		4 ALBRECHT	92G	ARG $e^+e^- \rightarrow \Upsilon(4S)$	
$13 \pm 6 \pm 1$		5 BORTOLETTO	90	CLEO $e^+e^- \rightarrow \Upsilon(4S)$	

¹ Uses $B(B^0 \rightarrow D^- D_s^+) = (7.2 \pm 0.8) \times 10^{-3}$.

² AUBERT 06N reports $(0.92 \pm 0.14 \pm 0.18) \times 10^{-2}$ from a measurement of $[\Gamma(B^+ \rightarrow \overline{D}^0 D_s^+)/\Gamma_{\text{total}}] \times [B(D_s^+ \rightarrow \phi \pi^+)]$ assuming $B(D_s^+ \rightarrow \phi \pi^+) = 0.0462 \pm 0.0062$, which we rescale to our best value $B(D_s^+ \rightarrow \phi \pi^+) = (4.5 \pm 0.4) \times 10^{-2}$. Our first error is their experiment's error and our second error is the systematic error from using our best value.

³ GIBAUT 96 reports $0.0126 \pm 0.0022 \pm 0.0025$ from a measurement of $[\Gamma(B^+ \rightarrow \overline{D}^0 D_s^+)/\Gamma_{\text{total}}] \times [B(D_s^+ \rightarrow \phi \pi^+)]$ assuming $B(D_s^+ \rightarrow \phi \pi^+) = 0.035$, which we rescale to our best value $B(D_s^+ \rightarrow \phi \pi^+) = (4.5 \pm 0.4) \times 10^{-2}$. Our first error is their experiment's error and our second error is the systematic error from using our best value.

⁴ ALBRECHT 92G reports $0.024 \pm 0.012 \pm 0.004$ from a measurement of $[\Gamma(B^+ \rightarrow \overline{D}^0 D_s^+)/\Gamma_{\text{total}}] \times [B(D_s^+ \rightarrow \phi \pi^+)]$ assuming $B(D_s^+ \rightarrow \phi \pi^+) = 0.027$, which we rescale to our best value $B(D_s^+ \rightarrow \phi \pi^+) = (4.5 \pm 0.4) \times 10^{-2}$. Our first error is their experiment's error and our second error is the systematic error from using our best value. Assumes PDG 1990 D^0 branching ratios, e.g., $B(D^0 \rightarrow K^- \pi^+) = 3.71 \pm 0.25\%$.

⁵ BORTOLETTO 90 reports 0.029 ± 0.013 from a measurement of $[\Gamma(B^+ \rightarrow \overline{D}^0 D_s^+)/\Gamma_{\text{total}}] \times [B(D_s^+ \rightarrow \phi \pi^+)]$ assuming $B(D_s^+ \rightarrow \phi \pi^+) = 0.02$, which we rescale to our best value $B(D_s^+ \rightarrow \phi \pi^+) = (4.5 \pm 0.4) \times 10^{-2}$. Our first error is their experiment's error and our second error is the systematic error from using our best value.

$\Gamma(D_{s0}^*(2317)^+ \overline{D}^0, D_{s0}^*(2317)^+ \rightarrow D_s^+ \pi^0)/\Gamma_{\text{total}}$					Γ_{165}/Γ
VALUE (units 10^{-3})		DOCUMENT ID	TECN	COMMENT	
$0.80 \pm 0.16 \pm 0.13$ OUR AVERAGE					
$0.80 \pm 0.17 \pm 0.16 \pm 0.02$		1,2 CHOI	15A	BELL $e^+e^- \rightarrow \Upsilon(4S)$	
$0.80 \pm 0.35 \pm 0.21 \pm 0.07$		2,3 AUBERT,B	04S	BABR $e^+e^- \rightarrow \Upsilon(4S)$	

• • • We do not use the following data for averages, fits, limits, etc. • • •

$0.65 \pm 0.26 \pm 0.06$ ^{2,4} KROKOVNY 03B BELL Repl. by CHOI 15A

¹ CHOI 15A reports $(8.0 \pm 1.3 \pm 1.1 \pm 0.4) \times 10^{-4}$ from a measurement of $[\Gamma(B^+ \rightarrow D_{s0}^*(2317)^+ \overline{D}^0, D_{s0}^*(2317)^+ \rightarrow D_s^+ \pi^0)/\Gamma_{\text{total}}] \times [B(D_s^+ \rightarrow K^+ K^- \pi^+)]$ assuming $B(D_s^+ \rightarrow K^+ K^- \pi^+) = (5.39 \pm 0.21) \times 10^{-2}$, which we rescale to our best value $B(D_s^+ \rightarrow K^+ K^- \pi^+) = (5.39 \pm 0.15) \times 10^{-2}$. Our first error is their experiment's error and our second error is the systematic error from using our best value.

² Assumes equal production of B^+ and B^0 at the $\Upsilon(4S)$.

³ AUBERT,B 04S reports $(1.0 \pm 0.3 \pm 0.2) \times 10^{-3}$ from a measurement of $[\Gamma(B^+ \rightarrow D_{s0}^*(2317)^+ \overline{D}^0, D_{s0}^*(2317)^+ \rightarrow D_s^+ \pi^0)/\Gamma_{\text{total}}] \times [B(D_s^+ \rightarrow \phi \pi^+)]$ assuming $B(D_s^+ \rightarrow \phi \pi^+) = 0.036 \pm 0.009$, which we rescale to our best value $B(D_s^+ \rightarrow \phi \pi^+) = (4.5 \pm 0.4) \times 10^{-2}$. Our first error is their experiment's error and our second error is the systematic error from using our best value.

$0.4) \times 10^{-2}$. Our first error is their experiment's error and our second error is the systematic error from using our best value.

⁴ KROKOVNY 03B reports $(0.81 \pm 0.30 \pm 0.24) \times 10^{-3}$ from a measurement of $[\Gamma(B^+ \rightarrow D_{s0}^*(2317)^+ \overline{D}^0, D_{s0}^*(2317)^+ \rightarrow D_s^+ \pi^0)/\Gamma_{\text{total}}] \times [B(D_s^+ \rightarrow \phi \pi^+)]$ assuming $B(D_s^+ \rightarrow \phi \pi^+) = 0.036 \pm 0.009$, which we rescale to our best value $B(D_s^+ \rightarrow \phi \pi^+) = (4.5 \pm 0.4) \times 10^{-2}$. Our first error is their experiment's error and our second error is the systematic error from using our best value.

$\Gamma(D_{s0}(2317)^+ \overline{D}^0 \times B(D_{s0}(2317)^+ \rightarrow D_s^+ \gamma))/\Gamma_{\text{total}}$					Γ_{166}/Γ
VALUE (units 10^{-3})	CL%	DOCUMENT ID	TECN	COMMENT	
<0.76	90	1 KROKOVNY	03B	BELL $e^+e^- \rightarrow \Upsilon(4S)$	

¹ Assumes equal production of B^+ and B^0 at the $\Upsilon(4S)$.

$\Gamma(D_{s0}(2317)^+ \overline{D}^*(2007)^0 \times B(D_{s0}(2317)^+ \rightarrow D_s^+ \pi^0))/\Gamma_{\text{total}}$					Γ_{167}/Γ
VALUE (units 10^{-3})		DOCUMENT ID	TECN	COMMENT	
$0.9 \pm 0.6 \pm 0.4 \pm 0.3$		1 AUBERT,B	04S	BABR $e^+e^- \rightarrow \Upsilon(4S)$	

¹ Assumes equal production of B^+ and B^0 at the $\Upsilon(4S)$.

$\Gamma(D_{sJ}(2457)^+ \overline{D}^0)/\Gamma_{\text{total}}$					Γ_{168}/Γ
VALUE (units 10^{-3})		DOCUMENT ID	TECN	COMMENT	
$3.1 \pm 1.0 \pm 0.9$ OUR AVERAGE					
$4.3 \pm 1.6 \pm 1.3$		1 AUBERT	06N	BABR $e^+e^- \rightarrow \Upsilon(4S)$	
$4.6 \pm 1.8 \pm 1.0$		2,3 AUBERT,B	04S	BABR $e^+e^- \rightarrow \Upsilon(4S)$	
$2.1 \pm 1.1 \pm 0.9 \pm 0.5$		2,4 KROKOVNY	03B	BELL $e^+e^- \rightarrow \Upsilon(4S)$	

¹ Uses a missing-mass method in the events that one of the B mesons is fully reconstructed.

² Assumes equal production of B^+ and B^0 at the $\Upsilon(4S)$.

³ AUBERT,B 04S reports $[\Gamma(B^+ \rightarrow D_{sJ}(2457)^+ \overline{D}^0)/\Gamma_{\text{total}}] \times [B(D_{s1}(2460)^+ \rightarrow D_s^+ \pi^0)] = (2.2 \pm 0.8 \pm 0.3) \times 10^{-3}$ which we divide by our best value $B(D_{s1}(2460)^+ \rightarrow D_s^+ \pi^0) = (48 \pm 11) \times 10^{-2}$. Our first error is their experiment's error and our second error is the systematic error from using our best value.

⁴ KROKOVNY 03B reports $[\Gamma(B^+ \rightarrow D_{sJ}(2457)^+ \overline{D}^0)/\Gamma_{\text{total}}] \times [B(D_{s1}(2460)^+ \rightarrow D_s^+ \pi^0)] = (1.0 \pm 0.5 \pm 0.1) \times 10^{-3}$ which we divide by our best value $B(D_{s1}(2460)^+ \rightarrow D_s^+ \pi^0) = (48 \pm 11) \times 10^{-2}$. Our first error is their experiment's error and our second error is the systematic error from using our best value.

$\Gamma(D_{sJ}(2457)^+ \overline{D}^0 \times B(D_{sJ}(2457)^+ \rightarrow D_s^+ \gamma))/\Gamma_{\text{total}}$					Γ_{169}/Γ
VALUE (units 10^{-3})		DOCUMENT ID	TECN	COMMENT	
$0.46 \pm 0.13 \pm 0.11$ OUR AVERAGE					
$0.48 \pm 0.19 \pm 0.13 \pm 0.04$		1,2 AUBERT,B	04S	BABR $e^+e^- \rightarrow \Upsilon(4S)$	
$0.45 \pm 0.15 \pm 0.04$		1,3 KROKOVNY	03B	BELL $e^+e^- \rightarrow \Upsilon(4S)$	

¹ Assumes equal production of B^+ and B^0 at the $\Upsilon(4S)$.

² AUBERT,B 04S reports $(0.6 \pm 0.2 \pm 0.2) \times 10^{-3}$ from a measurement of $[\Gamma(B^+ \rightarrow D_{sJ}(2457)^+ \overline{D}^0 \times B(D_{sJ}(2457)^+ \rightarrow D_s^+ \gamma))/\Gamma_{\text{total}}] \times [B(D_s^+ \rightarrow \phi \pi^+)]$ assuming $B(D_s^+ \rightarrow \phi \pi^+) = 0.036 \pm 0.009$, which we rescale to our best value $B(D_s^+ \rightarrow \phi \pi^+) = (4.5 \pm 0.4) \times 10^{-2}$. Our first error is their experiment's error and our second error is the systematic error from using our best value.

³ KROKOVNY 03B reports $(0.56 \pm 0.16 \pm 0.17) \times 10^{-3}$ from a measurement of $[\Gamma(B^+ \rightarrow D_{sJ}(2457)^+ \overline{D}^0 \times B(D_{sJ}(2457)^+ \rightarrow D_s^+ \gamma))/\Gamma_{\text{total}}] \times [B(D_s^+ \rightarrow \phi \pi^+)]$ assuming $B(D_s^+ \rightarrow \phi \pi^+) = 0.036 \pm 0.009$, which we rescale to our best value $B(D_s^+ \rightarrow \phi \pi^+) = (4.5 \pm 0.4) \times 10^{-2}$. Our first error is their experiment's error and our second error is the systematic error from using our best value.

$\Gamma(D_{sJ}(2457)^+ \overline{D}^0 \times B(D_{sJ}(2457)^+ \rightarrow D_s^+ \pi^+ \pi^-))/\Gamma_{\text{total}}$					Γ_{170}/Γ
VALUE (units 10^{-3})	CL%	DOCUMENT ID	TECN	COMMENT	
<0.22	90	1 KROKOVNY	03B	BELL $e^+e^- \rightarrow \Upsilon(4S)$	

¹ Assumes equal production of B^+ and B^0 at the $\Upsilon(4S)$.

$\Gamma(D_{sJ}(2457)^+ \overline{D}^0 \times B(D_{sJ}(2457)^+ \rightarrow D_s^+ \pi^0))/\Gamma_{\text{total}}$					Γ_{171}/Γ
VALUE (units 10^{-3})	CL%	DOCUMENT ID	TECN	COMMENT	
<0.27	90	1 KROKOVNY	03B	BELL $e^+e^- \rightarrow \Upsilon(4S)$	

¹ Assumes equal production of B^+ and B^0 at the $\Upsilon(4S)$.

$\Gamma(D_{sJ}(2457)^+ \overline{D}^0 \times B(D_{sJ}(2457)^+ \rightarrow D_s^+ \gamma))/\Gamma_{\text{total}}$					Γ_{172}/Γ
VALUE (units 10^{-3})	CL%	DOCUMENT ID	TECN	COMMENT	
<0.98	90	1 KROKOVNY	03B	BELL $e^+e^- \rightarrow \Upsilon(4S)$	

¹ Assumes equal production of B^+ and B^0 at the $\Upsilon(4S)$.

Meson Particle Listings

B^\pm

$\Gamma(D_{sJ}(2457)^+ \bar{D}^*(2007)^0)/\Gamma_{\text{total}}$		Γ_{173}/Γ	
VALUE (units 10^{-3})	DOCUMENT ID	TECN	COMMENT
12.0 ± 3.0 OUR AVERAGE			
11.2 ± 2.6 ± 2.0	¹ AUBERT	06N	BABR $e^+e^- \rightarrow \Upsilon(4S)$
16 $^{+8}_{-6} \pm 4$	^{2,3} AUBERT,B	04s	BABR $e^+e^- \rightarrow \Upsilon(4S)$

¹ Uses a missing-mass method in the events that one of the B mesons is fully reconstructed.
² AUBERT,B 04s reports $[\Gamma(B^+ \rightarrow D_{sJ}(2457)^+ \bar{D}^*(2007)^0)/\Gamma_{\text{total}}] \times [B(D_{s1}(2460)^+ \rightarrow D_s^{*+} \pi^0)] = (7.6 \pm 1.7^{+3.2}_{-2.4}) \times 10^{-3}$ which we divide by our best value $B(D_{s1}(2460)^+ \rightarrow D_s^{*+} \pi^0) = (48 \pm 11) \times 10^{-2}$. Our first error is their experiment's error and our second error is the systematic error from using our best value.
³ Assumes equal production of B^+ and B^0 at the $\Upsilon(4S)$.

$\Gamma(D_{sJ}(2457)^+ \bar{D}^*(2007)^0 \times B(D_{sJ}(2457)^+ \rightarrow D_s^{*+} \gamma))/\Gamma_{\text{total}}$		Γ_{174}/Γ	
VALUE (units 10^{-3})	DOCUMENT ID	TECN	COMMENT
1.4 ± 0.4 $^{+0.6}_{-0.4}$	¹ AUBERT,B	04s	BABR $e^+e^- \rightarrow \Upsilon(4S)$

¹ Assumes equal production of B^+ and B^0 at the $\Upsilon(4S)$.

$\Gamma(\bar{D}^0 D_{s1}(2536)^+ \times B(D_{s1}(2536)^+ \rightarrow D^*(2007)^0 K^+))/\Gamma_{\text{total}}$		Γ_{176}/Γ	
VALUE (units 10^{-4})	CL%	DOCUMENT ID	TECN COMMENT
2.16 ± 0.52 ± 0.45		¹ AUBERT	08B BABR $e^+e^- \rightarrow \Upsilon(4S)$
• • • We do not use the following data for averages, fits, limits, etc. • • •			
< 2	90	AUBERT	03x BABR Repl. by AUBERT 08B

¹ Assumes equal production of B^+ and B^0 at the $\Upsilon(4S)$.

$\Gamma(\bar{D}^0 D_{s1}(2536)^+ \times B(D_{s1}(2536)^+ \rightarrow D^*(2007)^0 K^+ + D^*(2010)^+ K^0))/\Gamma_{\text{total}}$		Γ_{175}/Γ	
VALUE (units 10^{-4})	DOCUMENT ID	TECN	COMMENT
3.97 ± 0.85 ± 0.56	^{1,2} AUSHEV	11	BELL $e^+e^- \rightarrow \Upsilon(4S)$

¹ Uses $\Gamma(D^*(2007)^0 \rightarrow D^0 \pi^0) / \Gamma(D^*(2007)^0 \rightarrow D^0 \gamma) = 1.74 \pm 0.13$ and $\Gamma(D_{s1}(2536)^+ \rightarrow D^*(2007)^0 K^+) / \Gamma(D_{s1}(2536)^+ \rightarrow D^*(2010)^+ K^0) = 1.36 \pm 0.2$.
² Assumes equal production of B^+ and B^0 at the $\Upsilon(4S)$.

$\Gamma(\bar{D}^*(2007)^0 D_{s1}(2536)^+ \times B(D_{s1}(2536)^+ \rightarrow D^*(2007)^0 K^+))/\Gamma_{\text{total}}$		Γ_{177}/Γ	
VALUE (units 10^{-4})	CL%	DOCUMENT ID	TECN COMMENT
5.46 ± 1.17 ± 1.04		¹ AUBERT	08B BABR $e^+e^- \rightarrow \Upsilon(4S)$
• • • We do not use the following data for averages, fits, limits, etc. • • •			
< 7	90	AUBERT	03x BABR Repl. by AUBERT 08B

¹ Assumes equal production of B^+ and B^0 at the $\Upsilon(4S)$.

$\Gamma(\bar{D}^0 D_{s1}(2536)^+ \times B(D_{s1}(2536)^+ \rightarrow D^{*+} K^0))/\Gamma_{\text{total}}$		Γ_{178}/Γ	
VALUE (units 10^{-4})	DOCUMENT ID	TECN	COMMENT
2.30 ± 0.98 ± 0.43	¹ AUBERT	08B	BABR $e^+e^- \rightarrow \Upsilon(4S)$

¹ Assumes equal production of B^+ and B^0 at the $\Upsilon(4S)$.

$\Gamma(\bar{D}^0 D_{sJ}(2700)^+ \times B(D_{sJ}(2700)^+ \rightarrow D^0 K^+))/\Gamma_{\text{total}}$		Γ_{179}/Γ	
VALUE (units 10^{-4})	DOCUMENT ID	TECN	COMMENT
5.6 ± 1.8 OUR AVERAGE	Error includes scale factor of 1.7.		
5.02 ± 0.71 ± 0.93	¹ LEES	15c	BABR $e^+e^- \rightarrow \Upsilon(4S)$
11.3 ± 2.2 $^{+1.4}_{-2.8}$	¹ BRODZICKA	08	BELL $e^+e^- \rightarrow \Upsilon(4S)$

¹ Assumes equal production of B^+ and B^0 at the $\Upsilon(4S)$.

$\Gamma(\bar{D}^{*0} D_{s1}(2536)^+, D_{s1}^+ \rightarrow D^{*+} K^0)/\Gamma_{\text{total}}$		Γ_{180}/Γ	
VALUE (units 10^{-4})	DOCUMENT ID	TECN	COMMENT
3.92 ± 2.46 ± 0.83	¹ AUBERT	08B	BABR $e^+e^- \rightarrow \Upsilon(4S)$

¹ Assumes equal production of B^+ and B^0 at the $\Upsilon(4S)$.

$\Gamma(\bar{D}^0 D_{sJ}(2573)^+, D_{sJ}^+ \rightarrow D^0 K^+)/\Gamma_{\text{total}}$		Γ_{181}/Γ	
VALUE (units 10^{-4})	DOCUMENT ID	TECN	COMMENT
0.08 ± 0.14 ± 0.05	¹ LEES	15c	BABR $e^+e^- \rightarrow \Upsilon(4S)$

¹ Assumes equal production of B^+ and B^0 at the $\Upsilon(4S)$.

$\Gamma(\bar{D}^{*0} D_{sJ}(2573), D_{sJ}^+ \rightarrow D^0 K^+)/\Gamma_{\text{total}}$		Γ_{182}/Γ	
VALUE (units 10^{-4})	CL%	DOCUMENT ID	TECN COMMENT
< 2	90	AUBERT	03x BABR $e^+e^- \rightarrow \Upsilon(4S)$

$\Gamma(\bar{D}^*(2007)^0 D_{sJ}(2573), D_{sJ}^+ \rightarrow D^0 K^+)/\Gamma_{\text{total}}$		Γ_{183}/Γ	
VALUE (units 10^{-4})	CL%	DOCUMENT ID	TECN COMMENT
< 5	90	AUBERT	03x BABR $e^+e^- \rightarrow \Upsilon(4S)$

$\Gamma(\bar{D}^0 D_s^{*+})/\Gamma_{\text{total}}$		Γ_{184}/Γ	
VALUE	DOCUMENT ID	TECN	COMMENT
0.0076 ± 0.0016 OUR AVERAGE			
0.0079 ± 0.0017 ± 0.0007	¹ AUBERT	06N	BABR $e^+e^- \rightarrow \Upsilon(4S)$
0.0068 ± 0.0025 ± 0.0006	² GIBAUT	96	CLE2 $e^+e^- \rightarrow \Upsilon(4S)$
0.010 ± 0.007 ± 0.001	³ ALBRECHT	92G	ARG $e^+e^- \rightarrow \Upsilon(4S)$

¹ AUBERT 06N reports $(0.77 \pm 0.15 \pm 0.13) \times 10^{-2}$ from a measurement of $[\Gamma(B^+ \rightarrow \bar{D}^0 D_s^{*+})/\Gamma_{\text{total}}] \times [B(D_s^+ \rightarrow \phi \pi^+)]$ assuming $B(D_s^+ \rightarrow \phi \pi^+) = 0.0462 \pm 0.0062$, which we rescale to our best value $B(D_s^+ \rightarrow \phi \pi^+) = (4.5 \pm 0.4) \times 10^{-2}$. Our first error is their experiment's error and our second error is the systematic error from using our best value.
² GIBAUT 96 reports $0.0087 \pm 0.0027 \pm 0.0017$ from a measurement of $[\Gamma(B^+ \rightarrow \bar{D}^0 D_s^{*+})/\Gamma_{\text{total}}] \times [B(D_s^+ \rightarrow \phi \pi^+)]$ assuming $B(D_s^+ \rightarrow \phi \pi^+) = 0.035$, which we rescale to our best value $B(D_s^+ \rightarrow \phi \pi^+) = (4.5 \pm 0.4) \times 10^{-2}$. Our first error is their experiment's error and our second error is the systematic error from using our best value.
³ ALBRECHT 92G reports $0.016 \pm 0.012 \pm 0.003$ from a measurement of $[\Gamma(B^+ \rightarrow \bar{D}^0 D_s^{*+})/\Gamma_{\text{total}}] \times [B(D_s^+ \rightarrow \phi \pi^+)]$ assuming $B(D_s^+ \rightarrow \phi \pi^+) = 0.027$, which we rescale to our best value $B(D_s^+ \rightarrow \phi \pi^+) = (4.5 \pm 0.4) \times 10^{-2}$. Our first error is their experiment's error and our second error is the systematic error from using our best value. Assumes PDG 1990 D^0 branching ratios, e.g., $B(D^0 \rightarrow K^- \pi^+) = 3.71 \pm 0.25\%$.

$\Gamma(\bar{D}^*(2007)^0 D_s^+)/\Gamma_{\text{total}}$		Γ_{185}/Γ	
VALUE	DOCUMENT ID	TECN	COMMENT
0.0082 ± 0.0017 OUR AVERAGE			
0.0078 ± 0.0018 ± 0.0007	¹ AUBERT	06N	BABR $e^+e^- \rightarrow \Upsilon(4S)$
0.011 ± 0.004 ± 0.001	² GIBAUT	96	CLE2 $e^+e^- \rightarrow \Upsilon(4S)$
0.008 ± 0.006 ± 0.001	³ ALBRECHT	92G	ARG $e^+e^- \rightarrow \Upsilon(4S)$

¹ AUBERT 06N reports $(0.76 \pm 0.15 \pm 0.13) \times 10^{-2}$ from a measurement of $[\Gamma(B^+ \rightarrow \bar{D}^*(2007)^0 D_s^+)/\Gamma_{\text{total}}] \times [B(D_s^+ \rightarrow \phi \pi^+)]$ assuming $B(D_s^+ \rightarrow \phi \pi^+) = 0.0462 \pm 0.0062$, which we rescale to our best value $B(D_s^+ \rightarrow \phi \pi^+) = (4.5 \pm 0.4) \times 10^{-2}$. Our first error is their experiment's error and our second error is the systematic error from using our best value.
² GIBAUT 96 reports $0.0140 \pm 0.0043 \pm 0.0035$ from a measurement of $[\Gamma(B^+ \rightarrow \bar{D}^*(2007)^0 D_s^+)/\Gamma_{\text{total}}] \times [B(D_s^+ \rightarrow \phi \pi^+)]$ assuming $B(D_s^+ \rightarrow \phi \pi^+) = 0.035$, which we rescale to our best value $B(D_s^+ \rightarrow \phi \pi^+) = (4.5 \pm 0.4) \times 10^{-2}$. Our first error is their experiment's error and our second error is the systematic error from using our best value.
³ ALBRECHT 92G reports $0.013 \pm 0.009 \pm 0.002$ from a measurement of $[\Gamma(B^+ \rightarrow \bar{D}^*(2007)^0 D_s^+)/\Gamma_{\text{total}}] \times [B(D_s^+ \rightarrow \phi \pi^+)]$ assuming $B(D_s^+ \rightarrow \phi \pi^+) = 0.027$, which we rescale to our best value $B(D_s^+ \rightarrow \phi \pi^+) = (4.5 \pm 0.4) \times 10^{-2}$. Our first error is their experiment's error and our second error is the systematic error from using our best value. Assumes PDG 1990 D^0 and $D^*(2007)^0$ branching ratios, e.g., $B(D^0 \rightarrow K^- \pi^+) = 3.71 \pm 0.25\%$ and $B(D^*(2007)^0 \rightarrow D^0 \pi^0) = 55 \pm 6\%$.

$\Gamma(\bar{D}^*(2007)^0 D_s^{*+})/\Gamma_{\text{total}}$		Γ_{186}/Γ	
VALUE	DOCUMENT ID	TECN	COMMENT
0.0171 ± 0.0024 OUR AVERAGE			
0.0167 ± 0.0019 ± 0.0015	¹ AUBERT	06N	BABR $e^+e^- \rightarrow \Upsilon(4S)$
0.024 ± 0.009 ± 0.002	² GIBAUT	96	CLE2 $e^+e^- \rightarrow \Upsilon(4S)$
0.019 ± 0.010 ± 0.002	³ ALBRECHT	92G	ARG $e^+e^- \rightarrow \Upsilon(4S)$

¹ AUBERT 06N reports $(1.62 \pm 0.22 \pm 0.18) \times 10^{-2}$ from a measurement of $[\Gamma(B^+ \rightarrow \bar{D}^*(2007)^0 D_s^{*+})/\Gamma_{\text{total}}] \times [B(D_s^+ \rightarrow \phi \pi^+)]$ assuming $B(D_s^+ \rightarrow \phi \pi^+) = 0.0462 \pm 0.0062$, which we rescale to our best value $B(D_s^+ \rightarrow \phi \pi^+) = (4.5 \pm 0.4) \times 10^{-2}$. Our first error is their experiment's error and our second error is the systematic error from using our best value.
² GIBAUT 96 reports $0.0310 \pm 0.0088 \pm 0.0065$ from a measurement of $[\Gamma(B^+ \rightarrow \bar{D}^*(2007)^0 D_s^{*+})/\Gamma_{\text{total}}] \times [B(D_s^+ \rightarrow \phi \pi^+)]$ assuming $B(D_s^+ \rightarrow \phi \pi^+) = 0.035$, which we rescale to our best value $B(D_s^+ \rightarrow \phi \pi^+) = (4.5 \pm 0.4) \times 10^{-2}$. Our first error is their experiment's error and our second error is the systematic error from using our best value.
³ ALBRECHT 92G reports $0.031 \pm 0.016 \pm 0.005$ from a measurement of $[\Gamma(B^+ \rightarrow \bar{D}^*(2007)^0 D_s^{*+})/\Gamma_{\text{total}}] \times [B(D_s^+ \rightarrow \phi \pi^+)]$ assuming $B(D_s^+ \rightarrow \phi \pi^+) = 0.027$, which we rescale to our best value $B(D_s^+ \rightarrow \phi \pi^+) = (4.5 \pm 0.4) \times 10^{-2}$. Our first error is their experiment's error and our second error is the systematic error from using our best value. Assumes PDG 1990 D^0 and $D^*(2007)^0$ branching ratios, e.g., $B(D^0 \rightarrow K^- \pi^+) = 3.71 \pm 0.25\%$ and $B(D^*(2007)^0 \rightarrow D^0 \pi^0) = 55 \pm 6\%$.

$\Gamma(D_s^{*+} \bar{D}^{*0})/\Gamma_{\text{total}}$		Γ_{187}/Γ	
VALUE	DOCUMENT ID	TECN	COMMENT
(2.73 ± 0.93 ± 0.68) × 10⁻²	¹ AHMED	00B	CLE2 $e^+e^- \rightarrow \Upsilon(4S)$

¹ AHMED 00B reports their experiment's uncertainties $(\pm 0.78 \pm 0.48 \pm 0.68)\%$, where the first error is statistical, the second is systematic, and the third is the uncertainty in the $D_s \rightarrow \phi \pi$ branching fraction. We combine the first two in quadrature.

$\Gamma(\bar{D}^*(2007)^0 D^*(2010)^+)/\Gamma_{\text{total}}$		Γ_{188}/Γ	
VALUE (units 10^{-4})	CL%	DOCUMENT ID	TECN COMMENT
8.1 ± 1.2 ± 1.2		¹ AUBERT,B	06A BABR $e^+e^- \rightarrow \Upsilon(4S)$
• • • We do not use the following data for averages, fits, limits, etc. • • •			
< 110	90	BARATE	98Q ALEP $e^+e^- \rightarrow Z$

¹ Assumes equal production of B^+ and B^0 at the $\Upsilon(4S)$.

See key on page 999

Meson Particle Listings

B^\pm

$\Gamma(\bar{D}^0 D^*(2010)^+) + \Gamma(\bar{D}^*(2007)^0 D^+)/\Gamma_{total}$ Γ_{189}/Γ

VALUE (units 10^{-4})	CL%	DOCUMENT ID	TECN	COMMENT
<130	90	BARATE	98Q	ALEP $e^+e^- \rightarrow Z$

$\Gamma(\bar{D}^0 D^*(2010)^+)/\Gamma_{total}$ Γ_{190}/Γ

VALUE (units 10^{-4})	DOCUMENT ID	TECN	COMMENT
3.9 ± 0.5 OUR AVERAGE			
3.6 ± 0.5 ± 0.4	¹ AUBERT,B	06A	BABR $e^+e^- \rightarrow \Upsilon(4S)$
4.57 ± 0.71 ± 0.56	¹ MAJUMDER	05	BELL $e^+e^- \rightarrow \Upsilon(4S)$

¹ Assumes equal production of B^+ and B^0 at the $\Upsilon(4S)$.

$\Gamma(\bar{D}^0 D^+)/\Gamma_{total}$ Γ_{191}/Γ

VALUE (units 10^{-4})	CL%	DOCUMENT ID	TECN	COMMENT
3.8 ± 0.4 OUR AVERAGE				
3.85 ± 0.31 ± 0.38		¹ ADACHI	08	BELL $e^+e^- \rightarrow \Upsilon(4S)$
3.8 ± 0.6 ± 0.5		¹ AUBERT,B	06A	BABR $e^+e^- \rightarrow \Upsilon(4S)$
••• We do not use the following data for averages, fits, limits, etc. •••				
4.83 ± 0.78 ± 0.58		¹ MAJUMDER	05	BELL Repl. by ADACHI 08
<67	90	BARATE	98Q	ALEP $e^+e^- \rightarrow Z$

¹ Assumes equal production of B^+ and B^0 at the $\Upsilon(4S)$.

$\Gamma(\bar{D}^0 D^+ K^0)/\Gamma_{total}$ Γ_{192}/Γ

VALUE (units 10^{-3})	CL%	DOCUMENT ID	TECN	COMMENT
1.55 ± 0.17 ± 0.13		¹ DEL-AMO-SA..11B	BABR	$e^+e^- \rightarrow \Upsilon(4S)$
••• We do not use the following data for averages, fits, limits, etc. •••				
<2.8	90	¹ AUBERT	03X	BABR Repl. by DEL-AMO-SANCHEZ 11B

¹ Assumes equal production of B^+ and B^0 at the $\Upsilon(4S)$.

$\Gamma(D^+ \bar{D}^*(2007)^0)/\Gamma_{total}$ Γ_{193}/Γ

VALUE (units 10^{-4})	DOCUMENT ID	TECN	COMMENT
6.3 ± 1.4 ± 1.0	¹ AUBERT,B	06A	BABR $e^+e^- \rightarrow \Upsilon(4S)$

¹ Assumes equal production of B^+ and B^0 at the $\Upsilon(4S)$.

$\Gamma(\bar{D}^*(2007)^0 D^+ K^0)/\Gamma_{total}$ Γ_{194}/Γ

VALUE (units 10^{-3})	CL%	DOCUMENT ID	TECN	COMMENT
2.06 ± 0.38 ± 0.30		¹ DEL-AMO-SA..11B	BABR	$e^+e^- \rightarrow \Upsilon(4S)$
••• We do not use the following data for averages, fits, limits, etc. •••				
<6.1	90	¹ AUBERT	03X	BABR Repl. by DEL-AMO-SANCHEZ 11B

¹ Assumes equal production of B^+ and B^0 at the $\Upsilon(4S)$.

$\Gamma(\bar{D}^0 D^*(2010)^+ K^0)/\Gamma_{total}$ Γ_{195}/Γ

VALUE (units 10^{-3})	DOCUMENT ID	TECN	COMMENT
3.81 ± 0.31 ± 0.23	¹ DEL-AMO-SA..11B	BABR	$e^+e^- \rightarrow \Upsilon(4S)$
••• We do not use the following data for averages, fits, limits, etc. •••			
5.2 $^{+1.0}_{-0.9}$ ± 0.7	¹ AUBERT	03X	BABR Repl. by DEL-AMO-SANCHEZ 11B

¹ Assumes equal production of B^+ and B^0 at the $\Upsilon(4S)$.

$\Gamma(\bar{D}^*(2007)^0 D^*(2010)^+ K^0)/\Gamma_{total}$ Γ_{196}/Γ

VALUE (units 10^{-3})	DOCUMENT ID	TECN	COMMENT
9.17 ± 0.83 ± 0.90	¹ DEL-AMO-SA..11B	BABR	$e^+e^- \rightarrow \Upsilon(4S)$
••• We do not use the following data for averages, fits, limits, etc. •••			
7.8 $^{+2.3}_{-2.1}$ ± 1.4	¹ AUBERT	03X	BABR Repl. by DEL-AMO-SANCHEZ 11B

¹ Assumes equal production of B^+ and B^0 at the $\Upsilon(4S)$.

$\Gamma(\bar{D}^0 D^0 K^+)/\Gamma_{total}$ Γ_{197}/Γ

VALUE (units 10^{-3})	DOCUMENT ID	TECN	COMMENT
1.45 ± 0.33 OUR AVERAGE			Error includes scale factor of 2.6.
1.31 ± 0.07 ± 0.12	¹ DEL-AMO-SA..11B	BABR	$e^+e^- \rightarrow \Upsilon(4S)$
2.22 ± 0.22 $^{+0.26}_{-0.24}$	¹ BRODZICKA	08	BELL $e^+e^- \rightarrow \Upsilon(4S)$
••• We do not use the following data for averages, fits, limits, etc. •••			
1.17 ± 0.21 ± 0.15	¹ CHISTOV	04	BELL Repl. by BRODZICKA 08
1.9 ± 0.3 ± 0.3	¹ AUBERT	03X	BABR Repl. by DEL-AMO-SANCHEZ 11B

¹ Assumes equal production of B^+ and B^0 at the $\Upsilon(4S)$.

$\Gamma(\bar{D}^*(2007)^0 D^0 K^+)/\Gamma_{total}$ Γ_{198}/Γ

VALUE (units 10^{-3})	DOCUMENT ID	TECN	COMMENT	
2.26 ± 0.16 ± 0.17	¹ DEL-AMO-SA..11B	BABR	$e^+e^- \rightarrow \Upsilon(4S)$	
••• We do not use the following data for averages, fits, limits, etc. •••				
<3.8	90	¹ AUBERT	03X	BABR Repl. by DEL-AMO-SANCHEZ 11B

¹ Assumes equal production of B^+ and B^0 at the $\Upsilon(4S)$.

$\Gamma(\bar{D}^0 D^*(2007)^0 K^+)/\Gamma_{total}$ Γ_{199}/Γ

VALUE (units 10^{-3})	DOCUMENT ID	TECN	COMMENT
6.32 ± 0.19 ± 0.45	¹ DEL-AMO-SA..11B	BABR	$e^+e^- \rightarrow \Upsilon(4S)$
••• We do not use the following data for averages, fits, limits, etc. •••			
4.7 ± 0.7 ± 0.7	¹ AUBERT	03X	BABR Repl. by DEL-AMO-SANCHEZ 11B

¹ Assumes equal production of B^+ and B^0 at the $\Upsilon(4S)$.

$\Gamma(\bar{D}^*(2007)^0 D^*(2007)^0 K^+)/\Gamma_{total}$ Γ_{200}/Γ

VALUE (units 10^{-3})	DOCUMENT ID	TECN	COMMENT
11.23 ± 0.36 ± 1.26	¹ DEL-AMO-SA..11B	BABR	$e^+e^- \rightarrow \Upsilon(4S)$
••• We do not use the following data for averages, fits, limits, etc. •••			
5.3 $^{+1.1}_{-1.0}$ ± 1.2	¹ AUBERT	03X	BABR Repl. by DEL-AMO-SANCHEZ 11B

¹ Assumes equal production of B^+ and B^0 at the $\Upsilon(4S)$.

$\Gamma(D^- D^+ K^+)/\Gamma_{total}$ Γ_{201}/Γ

VALUE (units 10^{-3})	CL%	DOCUMENT ID	TECN	COMMENT
0.22 ± 0.05 ± 0.05		¹ DEL-AMO-SA..11B	BABR	$e^+e^- \rightarrow \Upsilon(4S)$
••• We do not use the following data for averages, fits, limits, etc. •••				
<0.90	90	¹ CHISTOV	04	BELL $e^+e^- \rightarrow \Upsilon(4S)$
<0.4	90	¹ AUBERT	03X	BABR Repl. by DEL-AMO-SANCHEZ 11B

¹ Assumes equal production of B^+ and B^0 at the $\Upsilon(4S)$.

$\Gamma(D^- D^*(2010)^+ K^+)/\Gamma_{total}$ Γ_{202}/Γ

VALUE (units 10^{-3})	CL%	DOCUMENT ID	TECN	COMMENT
0.63 ± 0.09 ± 0.06		¹ DEL-AMO-SA..11B	BABR	$e^+e^- \rightarrow \Upsilon(4S)$
••• We do not use the following data for averages, fits, limits, etc. •••				
<0.7	90	¹ AUBERT	03X	BABR Repl. by DEL-AMO-SANCHEZ 11B

¹ Assumes equal production of B^+ and B^0 at the $\Upsilon(4S)$.

$\Gamma(D^*(2010)^- D^+ K^+)/\Gamma_{total}$ Γ_{203}/Γ

VALUE (units 10^{-3})	DOCUMENT ID	TECN	COMMENT
0.60 ± 0.10 ± 0.08	¹ DEL-AMO-SA..11B	BABR	$e^+e^- \rightarrow \Upsilon(4S)$
••• We do not use the following data for averages, fits, limits, etc. •••			
1.5 ± 0.3 ± 0.2	¹ AUBERT	03X	BABR Repl. by DEL-AMO-SANCHEZ 11B

¹ Assumes equal production of B^+ and B^0 at the $\Upsilon(4S)$.

$\Gamma(D^*(2010)^- D^*(2010)^+ K^+)/\Gamma_{total}$ Γ_{204}/Γ

VALUE (units 10^{-3})	CL%	DOCUMENT ID	TECN	COMMENT
1.32 ± 0.13 ± 0.12		¹ DEL-AMO-SA..11B	BABR	$e^+e^- \rightarrow \Upsilon(4S)$
••• We do not use the following data for averages, fits, limits, etc. •••				
<1.8	90	¹ AUBERT	03X	BABR Repl. by DEL-AMO-SANCHEZ 11B

¹ Assumes equal production of B^+ and B^0 at the $\Upsilon(4S)$.

$\Gamma((\bar{D}^+ \bar{D}^*)(D^+ D^*) K)/\Gamma_{total}$ Γ_{205}/Γ

VALUE (units 10^{-2})	DOCUMENT ID	TECN	COMMENT
4.05 ± 0.11 ± 0.28	¹ DEL-AMO-SA..11B	BABR	$e^+e^- \rightarrow \Upsilon(4S)$
••• We do not use the following data for averages, fits, limits, etc. •••			
3.5 ± 0.3 ± 0.5	¹ AUBERT	03X	BABR Repl. by DEL-AMO-SANCHEZ 11B

¹ Assumes equal production of B^+ and B^0 at the $\Upsilon(4S)$.

$\Gamma(D_s^+ \pi^0)/\Gamma_{total}$ Γ_{206}/Γ

VALUE (units 10^{-5})	CL%	DOCUMENT ID	TECN	COMMENT
1.6 $^{+0.6}_{-0.5}$ ± 0.1		¹ AUBERT	07M	BABR $e^+e^- \rightarrow \Upsilon(4S)$
••• We do not use the following data for averages, fits, limits, etc. •••				
<16	90	² ALEXANDER	93B	CLE2 $e^+e^- \rightarrow \Upsilon(4S)$

¹ AUBERT 07M reports $[\Gamma(B^+ \rightarrow D_s^+ \pi^0)/\Gamma_{total}] \times [B(D_s^+ \rightarrow \phi\pi^+)] = (7.0 \pm 2.4 + 0.6) \times 10^{-7}$ which we divide by our best value $B(D_s^+ \rightarrow \phi\pi^+) = (4.5 \pm 0.4) \times 10^{-2}$. Our first error is their experiment's error and our second error is the systematic error from using our best value.

² ALEXANDER 93B reports $< 2.0 \times 10^{-4}$ from a measurement of $[\Gamma(B^+ \rightarrow D_s^+ \pi^0)/\Gamma_{total}] \times [B(D_s^+ \rightarrow \phi\pi^+)]$ assuming $B(D_s^+ \rightarrow \phi\pi^+) = 0.037$, which we rescale to our best value $B(D_s^+ \rightarrow \phi\pi^+) = 4.5 \times 10^{-2}$.

$[\Gamma(D_s^+ \pi^0) + \Gamma(D_s^{*+} \pi^0)]/\Gamma_{total}$ $(\Gamma_{206} + \Gamma_{207})/\Gamma$

VALUE	CL%	DOCUMENT ID	TECN	COMMENT
<5 × 10⁻⁴	90	¹ ALBRECHT	93E	ARG $e^+e^- \rightarrow \Upsilon(4S)$

¹ ALBRECHT 93E reports $< 0.9 \times 10^{-3}$ from a measurement of $[\Gamma(B^+ \rightarrow D_s^+ \pi^0) + \Gamma(B^+ \rightarrow D_s^{*+} \pi^0)]/\Gamma_{total} \times [B(D_s^+ \rightarrow \phi\pi^+)]$ assuming $B(D_s^+ \rightarrow \phi\pi^+) = 0.027$, which we rescale to our best value $B(D_s^+ \rightarrow \phi\pi^+) = 4.5 \times 10^{-2}$.

Meson Particle Listings

 B^\pm

$\Gamma(D_s^{*+}\pi^0)/\Gamma_{\text{total}}$					Γ_{207}/Γ
VALUE	CL%	DOCUMENT ID	TECN	COMMENT	
$<2.6 \times 10^{-4}$	90	¹ ALEXANDER 93B	CLE2	$e^+e^- \rightarrow \Upsilon(4S)$	
¹ ALEXANDER 93B reports $< 3.2 \times 10^{-4}$ from a measurement of $[\Gamma(B^+ \rightarrow D_s^{*+}\pi^0)/\Gamma_{\text{total}}] \times [B(D_s^+ \rightarrow \phi\pi^+)]$ assuming $B(D_s^+ \rightarrow \phi\pi^+) = 0.037$, which we rescale to our best value $B(D_s^+ \rightarrow \phi\pi^+) = 4.5 \times 10^{-2}$.					

$\Gamma(D_s^{*+}\eta)/\Gamma_{\text{total}}$					Γ_{208}/Γ
VALUE	CL%	DOCUMENT ID	TECN	COMMENT	
$<4 \times 10^{-4}$	90	¹ ALEXANDER 93B	CLE2	$e^+e^- \rightarrow \Upsilon(4S)$	
¹ ALEXANDER 93B reports $< 4.6 \times 10^{-4}$ from a measurement of $[\Gamma(B^+ \rightarrow D_s^{*+}\eta)/\Gamma_{\text{total}}] \times [B(D_s^+ \rightarrow \phi\pi^+)]$ assuming $B(D_s^+ \rightarrow \phi\pi^+) = 0.037$, which we rescale to our best value $B(D_s^+ \rightarrow \phi\pi^+) = 4.5 \times 10^{-2}$.					

$\Gamma(D_s^{*+}\eta)/\Gamma_{\text{total}}$					Γ_{209}/Γ
VALUE	CL%	DOCUMENT ID	TECN	COMMENT	
$<6 \times 10^{-4}$	90	¹ ALEXANDER 93B	CLE2	$e^+e^- \rightarrow \Upsilon(4S)$	
¹ ALEXANDER 93B reports $< 7.5 \times 10^{-4}$ from a measurement of $[\Gamma(B^+ \rightarrow D_s^{*+}\eta)/\Gamma_{\text{total}}] \times [B(D_s^+ \rightarrow \phi\pi^+)]$ assuming $B(D_s^+ \rightarrow \phi\pi^+) = 0.037$, which we rescale to our best value $B(D_s^+ \rightarrow \phi\pi^+) = 4.5 \times 10^{-2}$.					

$\Gamma(D_s^{*+}\rho^0)/\Gamma_{\text{total}}$					Γ_{210}/Γ
VALUE	CL%	DOCUMENT ID	TECN	COMMENT	
$<3.0 \times 10^{-4}$	90	¹ ALEXANDER 93B	CLE2	$e^+e^- \rightarrow \Upsilon(4S)$	
¹ ALEXANDER 93B reports $< 3.7 \times 10^{-4}$ from a measurement of $[\Gamma(B^+ \rightarrow D_s^{*+}\rho^0)/\Gamma_{\text{total}}] \times [B(D_s^+ \rightarrow \phi\pi^+)]$ assuming $B(D_s^+ \rightarrow \phi\pi^+) = 0.037$, which we rescale to our best value $B(D_s^+ \rightarrow \phi\pi^+) = 4.5 \times 10^{-2}$.					

$[\Gamma(D_s^{*+}\rho^0) + \Gamma(D_s^{*+}\bar{K}^*(892)^0)]/\Gamma_{\text{total}}$					$(\Gamma_{210} + \Gamma_{221})/\Gamma$
VALUE	CL%	DOCUMENT ID	TECN	COMMENT	
$<2.0 \times 10^{-3}$	90	¹ ALBRECHT 93E	ARG	$e^+e^- \rightarrow \Upsilon(4S)$	
¹ ALBRECHT 93E reports $< 3.4 \times 10^{-3}$ from a measurement of $[\Gamma(B^+ \rightarrow D_s^{*+}\rho^0) + \Gamma(B^+ \rightarrow D_s^{*+}\bar{K}^*(892)^0)]/\Gamma_{\text{total}} \times [B(D_s^+ \rightarrow \phi\pi^+)]$ assuming $B(D_s^+ \rightarrow \phi\pi^+) = 0.027$, which we rescale to our best value $B(D_s^+ \rightarrow \phi\pi^+) = 4.5 \times 10^{-2}$.					

$\Gamma(D_s^{*+}\rho^0)/\Gamma_{\text{total}}$					Γ_{211}/Γ
VALUE	CL%	DOCUMENT ID	TECN	COMMENT	
$<4 \times 10^{-4}$	90	¹ ALEXANDER 93B	CLE2	$e^+e^- \rightarrow \Upsilon(4S)$	
¹ ALEXANDER 93B reports $< 4.8 \times 10^{-4}$ from a measurement of $[\Gamma(B^+ \rightarrow D_s^{*+}\rho^0)/\Gamma_{\text{total}}] \times [B(D_s^+ \rightarrow \phi\pi^+)]$ assuming $B(D_s^+ \rightarrow \phi\pi^+) = 0.037$, which we rescale to our best value $B(D_s^+ \rightarrow \phi\pi^+) = 4.5 \times 10^{-2}$.					

$[\Gamma(D_s^{*+}\rho^0) + \Gamma(D_s^{*+}\bar{K}^*(892)^0)]/\Gamma_{\text{total}}$					$(\Gamma_{211} + \Gamma_{223})/\Gamma$
VALUE	CL%	DOCUMENT ID	TECN	COMMENT	
$<1.2 \times 10^{-3}$	90	¹ ALBRECHT 93E	ARG	$e^+e^- \rightarrow \Upsilon(4S)$	
¹ ALBRECHT 93E reports $< 2.0 \times 10^{-3}$ from a measurement of $[\Gamma(B^+ \rightarrow D_s^{*+}\rho^0) + \Gamma(B^+ \rightarrow D_s^{*+}\bar{K}^*(892)^0)]/\Gamma_{\text{total}} \times [B(D_s^+ \rightarrow \phi\pi^+)]$ assuming $B(D_s^+ \rightarrow \phi\pi^+) = 0.027$, which we rescale to our best value $B(D_s^+ \rightarrow \phi\pi^+) = 4.5 \times 10^{-2}$.					

$\Gamma(D_s^{*+}\omega)/\Gamma_{\text{total}}$					Γ_{212}/Γ
VALUE	CL%	DOCUMENT ID	TECN	COMMENT	
$<4 \times 10^{-4}$	90	¹ ALEXANDER 93B	CLE2	$e^+e^- \rightarrow \Upsilon(4S)$	
••• We do not use the following data for averages, fits, limits, etc. •••					
$<2.0 \times 10^{-3}$	90	² ALBRECHT 93E	ARG	$e^+e^- \rightarrow \Upsilon(4S)$	
¹ ALEXANDER 93B reports $< 4.8 \times 10^{-4}$ from a measurement of $[\Gamma(B^+ \rightarrow D_s^{*+}\omega)/\Gamma_{\text{total}}] \times [B(D_s^+ \rightarrow \phi\pi^+)]$ assuming $B(D_s^+ \rightarrow \phi\pi^+) = 0.037$, which we rescale to our best value $B(D_s^+ \rightarrow \phi\pi^+) = 4.5 \times 10^{-2}$.					
² ALBRECHT 93E reports $< 3.4 \times 10^{-3}$ from a measurement of $[\Gamma(B^+ \rightarrow D_s^{*+}\omega)/\Gamma_{\text{total}}] \times [B(D_s^+ \rightarrow \phi\pi^+)]$ assuming $B(D_s^+ \rightarrow \phi\pi^+) = 0.027$, which we rescale to our best value $B(D_s^+ \rightarrow \phi\pi^+) = 4.5 \times 10^{-2}$.					

$\Gamma(D_s^{*+}\omega)/\Gamma_{\text{total}}$					Γ_{213}/Γ
VALUE	CL%	DOCUMENT ID	TECN	COMMENT	
$<6 \times 10^{-4}$	90	¹ ALEXANDER 93B	CLE2	$e^+e^- \rightarrow \Upsilon(4S)$	
••• We do not use the following data for averages, fits, limits, etc. •••					
$<1.1 \times 10^{-3}$	90	² ALBRECHT 93E	ARG	$e^+e^- \rightarrow \Upsilon(4S)$	
¹ ALEXANDER 93B reports $< 6.8 \times 10^{-4}$ from a measurement of $[\Gamma(B^+ \rightarrow D_s^{*+}\omega)/\Gamma_{\text{total}}] \times [B(D_s^+ \rightarrow \phi\pi^+)]$ assuming $B(D_s^+ \rightarrow \phi\pi^+) = 0.037$, which we rescale to our best value $B(D_s^+ \rightarrow \phi\pi^+) = 4.5 \times 10^{-2}$.					
² ALBRECHT 93E reports $< 1.9 \times 10^{-3}$ from a measurement of $[\Gamma(B^+ \rightarrow D_s^{*+}\omega)/\Gamma_{\text{total}}] \times [B(D_s^+ \rightarrow \phi\pi^+)]$ assuming $B(D_s^+ \rightarrow \phi\pi^+) = 0.027$, which we rescale to our best value $B(D_s^+ \rightarrow \phi\pi^+) = 4.5 \times 10^{-2}$.					

$\Gamma(D_s^{*+}a_1(1260)^0)/\Gamma_{\text{total}}$					Γ_{214}/Γ
VALUE	CL%	DOCUMENT ID	TECN	COMMENT	
$<1.8 \times 10^{-3}$	90	¹ ALBRECHT 93E	ARG	$e^+e^- \rightarrow \Upsilon(4S)$	
¹ ALBRECHT 93E reports $< 3.0 \times 10^{-3}$ from a measurement of $[\Gamma(B^+ \rightarrow D_s^{*+}a_1(1260)^0)/\Gamma_{\text{total}}] \times [B(D_s^+ \rightarrow \phi\pi^+)]$ assuming $B(D_s^+ \rightarrow \phi\pi^+) = 0.027$, which we rescale to our best value $B(D_s^+ \rightarrow \phi\pi^+) = 4.5 \times 10^{-2}$.					

$\Gamma(D_s^{*+}a_1(1260)^0)/\Gamma_{\text{total}}$					Γ_{215}/Γ
VALUE	CL%	DOCUMENT ID	TECN	COMMENT	
$<1.3 \times 10^{-3}$	90	¹ ALBRECHT 93E	ARG	$e^+e^- \rightarrow \Upsilon(4S)$	
¹ ALBRECHT 93E reports $< 2.2 \times 10^{-3}$ from a measurement of $[\Gamma(B^+ \rightarrow D_s^{*+}a_1(1260)^0)/\Gamma_{\text{total}}] \times [B(D_s^+ \rightarrow \phi\pi^+)]$ assuming $B(D_s^+ \rightarrow \phi\pi^+) = 0.027$, which we rescale to our best value $B(D_s^+ \rightarrow \phi\pi^+) = 4.5 \times 10^{-2}$.					

$\Gamma(D_s^+K^+K^-)/\Gamma(\bar{D}^0D_s^+)$					$\Gamma_{216}/\Gamma_{164}$
VALUE (units 10^{-4})		DOCUMENT ID	TECN	COMMENT	
$8.0 \pm 0.9 \pm 0.1$		¹ AAIJ 18B	LHCB	pp at 7, 8, 13 TeV	
¹ AAIJ 18B reports $[\Gamma(B^+ \rightarrow D_s^+K^+K^-)/\Gamma(B^+ \rightarrow \bar{D}^0D_s^+)] / [B(D^0 \rightarrow K^+K^-)] = 0.197 \pm 0.015 \pm 0.017$ which we multiply by our best value $B(D^0 \rightarrow K^+K^-) = (4.08 \pm 0.06) \times 10^{-3}$. Our first error is their experiment's error and our second error is the systematic error from using our best value.					

$\Gamma(D_s^+\phi)/\Gamma_{\text{total}}$					Γ_{217}/Γ
VALUE (units 10^{-6})	CL%	DOCUMENT ID	TECN	COMMENT	
< 0.42	90	¹ AAIJ 18B	LHCB	pp at 7, 8, 13 TeV	
••• We do not use the following data for averages, fits, limits, etc. •••					
$1.7^{+1.1}_{-0.7} \pm 0.2$		² AAIJ 13R	LHCB	Repl. by AAJ 18B	
< 1.9	90	³ AUBERT 06F	BABR	$e^+e^- \rightarrow \Upsilon(4S)$	
< 1000	90	⁴ ALBRECHT 93E	ARG	$e^+e^- \rightarrow \Upsilon(4S)$	
< 260	90	⁵ ALEXANDER 93B	CLE2	$e^+e^- \rightarrow \Upsilon(4S)$	

- ¹AAIJ 18B uses $B^+ \rightarrow D_s^+\bar{D}^0$ decays for normalization.
- ²AAIJ 13R reports $(1.87^{+1.25}_{-0.73} \pm 0.19 \pm 0.32) \times 10^{-6}$ from a measurement of $[\Gamma(B^+ \rightarrow D_s^+\phi)/\Gamma_{\text{total}}] / [B(B^+ \rightarrow \bar{D}^0D_s^+)]$ assuming $B(B^+ \rightarrow \bar{D}^0D_s^+) = (10.0 \pm 1.7) \times 10^{-3}$, which we rescale to our best value $B(B^+ \rightarrow \bar{D}^0D_s^+) = (9.0 \pm 0.9) \times 10^{-3}$. Our first error is their experiment's error and our second error is the systematic error from using our best value.
- ³Assumes equal production of B^+ and B^0 at the $\Upsilon(4S)$.
- ⁴ALBRECHT 93E reports $< 1.7 \times 10^{-3}$ from a measurement of $[\Gamma(B^+ \rightarrow D_s^+\phi)/\Gamma_{\text{total}}] \times [B(D_s^+ \rightarrow \phi\pi^+)]$ assuming $B(D_s^+ \rightarrow \phi\pi^+) = 0.027$, which we rescale to our best value $B(D_s^+ \rightarrow \phi\pi^+) = 4.5 \times 10^{-2}$.
- ⁵ALEXANDER 93B reports $< 3.1 \times 10^{-4}$ from a measurement of $[\Gamma(B^+ \rightarrow D_s^+\phi)/\Gamma_{\text{total}}] \times [B(D_s^+ \rightarrow \phi\pi^+)]$ assuming $B(D_s^+ \rightarrow \phi\pi^+) = 0.037$, which we rescale to our best value $B(D_s^+ \rightarrow \phi\pi^+) = 4.5 \times 10^{-2}$.

$\Gamma(D_s^{*+}\phi)/\Gamma_{\text{total}}$					Γ_{218}/Γ
VALUE	CL%	DOCUMENT ID	TECN	COMMENT	
$<1.2 \times 10^{-5}$	90	¹ AUBERT 06F	BABR	$e^+e^- \rightarrow \Upsilon(4S)$	
••• We do not use the following data for averages, fits, limits, etc. •••					
$<1.3 \times 10^{-3}$	90	² ALBRECHT 93E	ARG	$e^+e^- \rightarrow \Upsilon(4S)$	
$<3.5 \times 10^{-4}$	90	³ ALEXANDER 93B	CLE2	$e^+e^- \rightarrow \Upsilon(4S)$	

- ¹Assumes equal production of B^+ and B^0 at the $\Upsilon(4S)$.
- ²ALBRECHT 93E reports $< 2.1 \times 10^{-3}$ from a measurement of $[\Gamma(B^+ \rightarrow D_s^{*+}\phi)/\Gamma_{\text{total}}] \times [B(D_s^+ \rightarrow \phi\pi^+)]$ assuming $B(D_s^+ \rightarrow \phi\pi^+) = 0.027$, which we rescale to our best value $B(D_s^+ \rightarrow \phi\pi^+) = 4.5 \times 10^{-2}$.
- ³ALEXANDER 93B reports $< 4.2 \times 10^{-4}$ from a measurement of $[\Gamma(B^+ \rightarrow D_s^{*+}\phi)/\Gamma_{\text{total}}] \times [B(D_s^+ \rightarrow \phi\pi^+)]$ assuming $B(D_s^+ \rightarrow \phi\pi^+) = 0.037$, which we rescale to our best value $B(D_s^+ \rightarrow \phi\pi^+) = 4.5 \times 10^{-2}$.

$\Gamma(D_s^{*+}\bar{K}^0)/\Gamma_{\text{total}}$					Γ_{219}/Γ
VALUE	CL%	DOCUMENT ID	TECN	COMMENT	
$<8 \times 10^{-4}$	90	¹ ALEXANDER 93B	CLE2	$e^+e^- \rightarrow \Upsilon(4S)$	
••• We do not use the following data for averages, fits, limits, etc. •••					
$<1.5 \times 10^{-3}$	90	² ALBRECHT 93E	ARG	$e^+e^- \rightarrow \Upsilon(4S)$	
¹ ALEXANDER 93B reports $< 10.3 \times 10^{-4}$ from a measurement of $[\Gamma(B^+ \rightarrow D_s^{*+}\bar{K}^0)/\Gamma_{\text{total}}] \times [B(D_s^+ \rightarrow \phi\pi^+)]$ assuming $B(D_s^+ \rightarrow \phi\pi^+) = 0.037$, which we rescale to our best value $B(D_s^+ \rightarrow \phi\pi^+) = 4.5 \times 10^{-2}$.					
² ALBRECHT 93E reports $< 2.5 \times 10^{-3}$ from a measurement of $[\Gamma(B^+ \rightarrow D_s^{*+}\bar{K}^0)/\Gamma_{\text{total}}] \times [B(D_s^+ \rightarrow \phi\pi^+)]$ assuming $B(D_s^+ \rightarrow \phi\pi^+) = 0.027$, which we rescale to our best value $B(D_s^+ \rightarrow \phi\pi^+) = 4.5 \times 10^{-2}$.					

$\Gamma(D_s^{*+} \bar{K}^0)/\Gamma_{total}$ Γ_{220}/Γ

VALUE	CL%	DOCUMENT ID	TECN	COMMENT
$<9 \times 10^{-4}$	90	¹ ALEXANDER 93B	CLE2	$e^+e^- \rightarrow \Upsilon(4S)$
••• We do not use the following data for averages, fits, limits, etc. ••• $<1.9 \times 10^{-3}$ 90 ² ALBRECHT 93E ARG $e^+e^- \rightarrow \Upsilon(4S)$ ¹ ALEXANDER 93B reports $<10.9 \times 10^{-4}$ from a measurement of $[\Gamma(B^+ \rightarrow D_s^{*+} \bar{K}^0)/\Gamma_{total}] \times [B(D_s^+ \rightarrow \phi\pi^+)]$ assuming $B(D_s^+ \rightarrow \phi\pi^+) = 0.037$, which we rescale to our best value $B(D_s^+ \rightarrow \phi\pi^+) = 4.5 \times 10^{-2}$. ² ALBRECHT 93E reports $<3.1 \times 10^{-3}$ from a measurement of $[\Gamma(B^+ \rightarrow D_s^{*+} \bar{K}^0)/\Gamma_{total}] \times [B(D_s^+ \rightarrow \phi\pi^+)]$ assuming $B(D_s^+ \rightarrow \phi\pi^+) = 0.027$, which we rescale to our best value $B(D_s^+ \rightarrow \phi\pi^+) = 4.5 \times 10^{-2}$.				

$\Gamma(D_s^+ \bar{K}^*(892)^0)/\Gamma_{total}$ Γ_{221}/Γ

VALUE	CL%	DOCUMENT ID	TECN	COMMENT
$<4.4 \times 10^{-6}$	90	AAIJ	13R	LHCb pp at 7 TeV
••• We do not use the following data for averages, fits, limits, etc. ••• $<4 \times 10^{-4}$ 90 ¹ ALEXANDER 93B CLE2 $e^+e^- \rightarrow \Upsilon(4S)$ ¹ ALEXANDER 93B reports $<4.4 \times 10^{-4}$ from a measurement of $[\Gamma(B^+ \rightarrow D_s^+ \bar{K}^*(892)^0)/\Gamma_{total}] \times [B(D_s^+ \rightarrow \phi\pi^+)]$ assuming $B(D_s^+ \rightarrow \phi\pi^+) = 0.037$, which we rescale to our best value $B(D_s^+ \rightarrow \phi\pi^+) = 4.5 \times 10^{-2}$.				

$\Gamma(D_s^+ K^*0)/\Gamma_{total}$ Γ_{222}/Γ

VALUE (units 10^{-6})	CL%	DOCUMENT ID	TECN	COMMENT
<3.5	90	AAIJ	13R	LHCb pp at 7 TeV

$\Gamma(D_s^{*+} \bar{K}^*(892)^0)/\Gamma_{total}$ Γ_{223}/Γ

VALUE	CL%	DOCUMENT ID	TECN	COMMENT
$<3.5 \times 10^{-4}$	90	¹ ALEXANDER 93B	CLE2	$e^+e^- \rightarrow \Upsilon(4S)$
••• We do not use the following data for averages, fits, limits, etc. ••• ¹ ALEXANDER 93B reports $<4.3 \times 10^{-4}$ from a measurement of $[\Gamma(B^+ \rightarrow D_s^{*+} \bar{K}^*(892)^0)/\Gamma_{total}] \times [B(D_s^+ \rightarrow \phi\pi^+)]$ assuming $B(D_s^+ \rightarrow \phi\pi^+) = 0.037$, which we rescale to our best value $B(D_s^+ \rightarrow \phi\pi^+) = 4.5 \times 10^{-2}$.				

$\Gamma(D_s^- \pi^+ K^+)/\Gamma_{total}$ Γ_{224}/Γ

VALUE (units 10^{-4})	CL%	DOCUMENT ID	TECN	COMMENT
1.80 ± 0.22 OUR AVERAGE				
$1.71^{+0.09}_{-0.07} \pm 0.25$		¹ WIECHCZYN...09	BELL	$e^+e^- \rightarrow \Upsilon(4S)$
$2.02 \pm 0.13 \pm 0.38$		¹ AUBERT 08G	BABR	$e^+e^- \rightarrow \Upsilon(4S)$
••• We do not use the following data for averages, fits, limits, etc. ••• <7 90 ² ALBRECHT 93E ARG $e^+e^- \rightarrow \Upsilon(4S)$ ¹ Assumes equal production of B^+ and B^0 at the $\Upsilon(4S)$. ² ALBRECHT 93E reports $<1.1 \times 10^{-3}$ from a measurement of $[\Gamma(B^+ \rightarrow D_s^- \pi^+ K^+)/\Gamma_{total}] \times [B(D_s^+ \rightarrow \phi\pi^+)]$ assuming $B(D_s^+ \rightarrow \phi\pi^+) = 0.027$, which we rescale to our best value $B(D_s^+ \rightarrow \phi\pi^+) = 4.5 \times 10^{-2}$.				

$\Gamma(D_s^- \pi^+ K^+)/\Gamma_{total}$ Γ_{225}/Γ

VALUE (units 10^{-4})	CL%	DOCUMENT ID	TECN	COMMENT
1.45 ± 0.24 OUR AVERAGE				
$1.31^{+0.13}_{-0.12} \pm 0.28$		¹ WIECHCZYN...09	BELL	$e^+e^- \rightarrow \Upsilon(4S)$
$1.67 \pm 0.16 \pm 0.35$		¹ AUBERT 08G	BABR	$e^+e^- \rightarrow \Upsilon(4S)$
••• We do not use the following data for averages, fits, limits, etc. ••• <10 90 ² ALBRECHT 93E ARG $e^+e^- \rightarrow \Upsilon(4S)$ ¹ Assumes equal production of B^+ and B^0 at the $\Upsilon(4S)$. ² ALBRECHT 93E reports $<1.6 \times 10^{-3}$ from a measurement of $[\Gamma(B^+ \rightarrow D_s^{*-} \pi^+ K^+)/\Gamma_{total}] \times [B(D_s^+ \rightarrow \phi\pi^+)]$ assuming $B(D_s^+ \rightarrow \phi\pi^+) = 0.027$, which we rescale to our best value $B(D_s^+ \rightarrow \phi\pi^+) = 4.5 \times 10^{-2}$.				

$\Gamma(D_s^- \pi^+ K^*(892)^+)/\Gamma_{total}$ Γ_{226}/Γ

VALUE	CL%	DOCUMENT ID	TECN	COMMENT
$<5 \times 10^{-3}$	90	¹ ALBRECHT 93E	ARG	$e^+e^- \rightarrow \Upsilon(4S)$
¹ ALBRECHT 93E reports $<8.6 \times 10^{-3}$ from a measurement of $[\Gamma(B^+ \rightarrow D_s^- \pi^+ K^*(892)^+)/\Gamma_{total}] \times [B(D_s^+ \rightarrow \phi\pi^+)]$ assuming $B(D_s^+ \rightarrow \phi\pi^+) = 0.027$, which we rescale to our best value $B(D_s^+ \rightarrow \phi\pi^+) = 4.5 \times 10^{-2}$.				

$\Gamma(D_s^{*-} \pi^+ K^*(892)^+)/\Gamma_{total}$ Γ_{227}/Γ

VALUE	CL%	DOCUMENT ID	TECN	COMMENT
$<7 \times 10^{-3}$	90	¹ ALBRECHT 93E	ARG	$e^+e^- \rightarrow \Upsilon(4S)$
¹ ALBRECHT 93E reports $<1.1 \times 10^{-2}$ from a measurement of $[\Gamma(B^+ \rightarrow D_s^{*-} \pi^+ K^*(892)^+)/\Gamma_{total}] \times [B(D_s^+ \rightarrow \phi\pi^+)]$ assuming $B(D_s^+ \rightarrow \phi\pi^+) = 0.027$, which we rescale to our best value $B(D_s^+ \rightarrow \phi\pi^+) = 4.5 \times 10^{-2}$.				

$\Gamma(D_s^- K^+ K^+)/\Gamma_{total}$ Γ_{228}/Γ

VALUE (units 10^{-5})	DOCUMENT ID	TECN	COMMENT
0.97 ± 0.21 OUR AVERAGE			
$0.93 \pm 0.22 \pm 0.10$	¹ WIECHCZYN...15	BELL	$e^+e^- \rightarrow \Upsilon(4S)$
$1.1 \pm 0.4 \pm 0.2$	¹ AUBERT 08G	BABR	$e^+e^- \rightarrow \Upsilon(4S)$
¹ Assumes equal production of B^+ and B^0 at the $\Upsilon(4S)$.			

$\Gamma(D_s^- K^+ K^+)/\Gamma(D_s^- \pi^+ K^+)$ $\Gamma_{228}/\Gamma_{224}$

VALUE	DOCUMENT ID	TECN	COMMENT
$0.054 \pm 0.013 \pm 0.006$	WIECHCZYN...15	BELL	$e^+e^- \rightarrow \Upsilon(4S)$

$\Gamma(D_s^{*-} K^+ K^+)/\Gamma_{total}$ Γ_{229}/Γ

VALUE (units 10^{-4})	CL%	DOCUMENT ID	TECN	COMMENT
<0.15	90	¹ AUBERT 08G	BABR	$e^+e^- \rightarrow \Upsilon(4S)$
¹ Assumes equal production of B^+ and B^0 at the $\Upsilon(4S)$.				

$\Gamma(\eta_c K^+)/\Gamma_{total}$ Γ_{230}/Γ

VALUE (units 10^{-3})	DOCUMENT ID	TECN	COMMENT
1.06 ± 0.09 OUR AVERAGE	Error includes scale factor of 1.2.		
$0.74^{+0.09}_{-0.08} \pm 0.25$	¹ CHILIKIN 19	BELL	$e^+e^- \rightarrow \Upsilon(4S)$
$1.20 \pm 0.08 \pm 0.07$	² KATO 18	BELL	$e^+e^- \rightarrow \Upsilon(4S)$
0.87 ± 0.15	^{2,3} AUBERT 06E	BABR	$e^+e^- \rightarrow \Upsilon(4S)$
$1.24^{+0.25}_{-0.19} \pm 0.12$	⁴ AUBERT,B 05L	BABR	$e^+e^- \rightarrow \Upsilon(4S)$
$1.25 \pm 0.14^{+0.39}_{-0.40}$	⁵ FANG 03	BELL	$e^+e^- \rightarrow \Upsilon(4S)$
$0.69^{+0.26}_{-0.21} \pm 0.22$	⁶ EDWARDS 01	CLE2	$e^+e^- \rightarrow \Upsilon(4S)$
••• We do not use the following data for averages, fits, limits, etc. ••• $1.01 \pm 0.12 \pm 0.05$ ^{3,7} AUBERT,B 04B BABR $e^+e^- \rightarrow \Upsilon(4S)$			

¹ CHILIKIN 19 reports $[\Gamma(B^+ \rightarrow \eta_c K^+)/\Gamma_{total}] \times [B(\eta_c(1S) \rightarrow \pi^+\pi^-\rho\bar{p})] = (39.4^{+4.1+2.2}_{-3.9-1.8}) \times 10^{-7}$ which we divide by our best value $B(\eta_c(1S) \rightarrow \pi^+\pi^-\rho\bar{p}) = (5.3 \pm 1.8) \times 10^{-3}$. Our first error is their experiment's error and our second error is the systematic error from using our best value.
² Measures absolute branching fractions using a missing-mass technique.
³ The ratio of $B(B^\pm \rightarrow K^\pm \eta_c) B(\eta_c \rightarrow K\bar{K}\pi) = (7.4 \pm 0.5 \pm 0.7) \times 10^{-5}$ reported in AUBERT,B 04B and $B(B^\pm \rightarrow K^\pm \eta_c) = (8.7 \pm 1.5) \times 10^{-3}$ reported in AUBERT 06E contribute to the determination of $B(\eta_c \rightarrow K\bar{K}\pi)$, which is used by others for normalization.
⁴ AUBERT,B 05L reports $[\Gamma(B^+ \rightarrow \eta_c K^+)/\Gamma_{total}] \times [B(\eta_c(1S) \rightarrow \rho\bar{p})] = (1.8^{+0.3}_{-0.2}) \times 10^{-6}$ which we divide by our best value $B(\eta_c(1S) \rightarrow \rho\bar{p}) = (1.45 \pm 0.14) \times 10^{-3}$. Our first error is their experiment's error and our second error is the systematic error from using our best value.
⁵ Assumes equal production of B^+ and B^0 at the $\Upsilon(4S)$.
⁶ EDWARDS 01 assumes equal production of B^0 and B^+ at the $\Upsilon(4S)$. The correlated uncertainties (28.3)% from $B(J/\psi(1S) \rightarrow \gamma\eta_c)$ in those modes have been accounted for.
⁷ AUBERT,B 04B reports $[\Gamma(B^+ \rightarrow \eta_c K^+)/\Gamma_{total}] \times [B(\eta_c(1S) \rightarrow K\bar{K}\pi)] = (0.074 \pm 0.005 \pm 0.007) \times 10^{-3}$ which we divide by our best value $B(\eta_c(1S) \rightarrow K\bar{K}\pi) = (7.3 \pm 0.4) \times 10^{-2}$. Our first error is their experiment's error and our second error is the systematic error from using our best value.

$\Gamma(B^+ \rightarrow \eta_c K^+)/\Gamma_{total} \times \Gamma(\eta_c(1S) \rightarrow \gamma\gamma)/\Gamma_{total}$ $\Gamma_{230}/\Gamma \times \Gamma_{49}^{\eta_c(1S)}/\Gamma_{\eta_c(1S)}$

VALUE (units 10^{-6})	DOCUMENT ID	TECN	COMMENT
$0.22^{+0.09+0.04}_{-0.07-0.02}$	¹ WICHT 08	BELL	$e^+e^- \rightarrow \Upsilon(4S)$
¹ Assumes equal production of B^+ and B^0 at the $\Upsilon(4S)$.			

$\Gamma(\eta_c K^+, \eta_c \rightarrow K_S^0 K^\mp \pi^\pm)/\Gamma_{total}$ Γ_{231}/Γ

VALUE (units 10^{-6})	DOCUMENT ID	TECN	COMMENT
$26.7 \pm 1.4^{+5.7}_{-5.5}$	^{1,2} VINOKUROVA 11	BELL	$e^+e^- \rightarrow \Upsilon(4S)$
¹ Assumes equal production of B^0 and B^+ from Upsilon(4S) decays. ² VINOKUROVA 11 reports $(26.7 \pm 1.4^{+2.9}_{-2.9} \pm 4.9) \times 10^{-6}$, where the first uncertainty is statistical, the second is due to systematics, and the third comes from interference of $\eta_c(1S) \rightarrow K_S^0 K^\pm \pi^\mp$ with nonresonant $K_S^0 K^\pm \pi^\mp$. We combined both systematic uncertainties to single values.			

$\Gamma(\eta_c K^*(892)^+)/\Gamma_{total}$ Γ_{232}/Γ

VALUE (units 10^{-3})	DOCUMENT ID	TECN	COMMENT
$1.1^{+0.5}_{-0.4} \pm 0.1$	^{1,2} AUBERT 07AV	BABR	$e^+e^- \rightarrow \Upsilon(4S)$
¹ AUBERT 07AV reports $[\Gamma(B^+ \rightarrow \eta_c K^*(892)^+)/\Gamma_{total}] \times [B(\eta_c(1S) \rightarrow \rho\bar{p})] = (1.57^{+0.56+0.45}_{-0.46-0.36}) \times 10^{-6}$ which we divide by our best value $B(\eta_c(1S) \rightarrow \rho\bar{p}) = (1.45 \pm 0.14) \times 10^{-3}$. Our first error is their experiment's error and our second error is the systematic error from using our best value. ² Assumes equal production of B^+ and B^0 at the $\Upsilon(4S)$.			

$\Gamma(\eta_c K^+ \pi^+ \pi^-)/\Gamma_{total}$ Γ_{233}/Γ

VALUE	CL%	DOCUMENT ID	TECN	COMMENT
$<3.9 \times 10^{-4}$	90	VINOKUROVA 15	BELL	$e^+e^- \rightarrow \Upsilon(4S)$

Meson Particle Listings

B^\pm

$\Gamma(\eta_c K^+ \omega(782))/\Gamma_{\text{total}}$				Γ_{234}/Γ
VALUE	CL%	DOCUMENT ID	TECN	COMMENT
$<3.3 \times 10^{-4}$	90	VINOKUROVA 15	BELL	$e^+e^- \rightarrow \Upsilon(4S)$

$\Gamma(\eta_c K^+ \eta)/\Gamma_{\text{total}}$				Γ_{235}/Γ
VALUE	CL%	DOCUMENT ID	TECN	COMMENT
$<2.2 \times 10^{-4}$	90	VINOKUROVA 15	BELL	$e^+e^- \rightarrow \Upsilon(4S)$

$\Gamma(\eta_c K^+ \pi^0)/\Gamma_{\text{total}}$				Γ_{236}/Γ
VALUE	CL%	DOCUMENT ID	TECN	COMMENT
$<6.2 \times 10^{-5}$	90	VINOKUROVA 15	BELL	$e^+e^- \rightarrow \Upsilon(4S)$

$\Gamma(\eta_c(2S)K^+)/\Gamma_{\text{total}}$				Γ_{237}/Γ
VALUE (units 10^{-4})	CL%	DOCUMENT ID	TECN	COMMENT
4.4 ± 1.0 OUR AVERAGE				
4.8 ± 1.1 ± 0.3		1 KATO 18	BELL	$e^+e^- \rightarrow \Upsilon(4S)$
3.4 ± 1.8 ± 0.3		1 AUBERT 06E	BABR	$e^+e^- \rightarrow \Upsilon(4S)$

1 Measures absolute branching fractions using a missing-mass technique.

$\Gamma(\eta_c(2S)K^+, \eta_c \rightarrow \rho\bar{p})/\Gamma_{\text{total}}$				Γ_{238}/Γ
VALUE (units 10^{-8})	CL%	DOCUMENT ID	TECN	COMMENT
3.47 ± 0.72 ± 0.26		1 AAIJ 17AD	LHCB	pp at 7 and 8 TeV

• • • We do not use the following data for averages, fits, limits, etc. • • •
 <10.6 95 2 AAIJ 13s LHCB Repl. by AAIJ 17AD

1 Measured relative to $B^+ \rightarrow J/\psi K^+$ decay with charmonia reconstructed in $p\bar{p}$ final state and using $B(B^+ \rightarrow J/\psi K^+) \times B(J/\psi \rightarrow \rho\bar{p}) = (2.17 \pm 0.08) \times 10^{-6}$. The last uncertainty includes the uncertainty of $B(B^+ \rightarrow J/\psi K^+) \times B(J/\psi \rightarrow \rho\bar{p})$.

2 Measured relative to $B^+ \rightarrow J/\psi K^+$ decay with charmonia reconstructed in $p\bar{p}$ final state and using $B(B^+ \rightarrow J/\psi K^+) = (1.013 \pm 0.034) \times 10^{-3}$ and $B(J/\psi \rightarrow \rho\bar{p}) = (2.17 \pm 0.07) \times 10^{-3}$.

$\Gamma(\eta_c(2S)K^+, \eta_c \rightarrow \rho\bar{p}\pi^+\pi^-)/\Gamma_{\text{total}}$				Γ_{240}/Γ
VALUE (units 10^{-7})	CL%	DOCUMENT ID	TECN	COMMENT
11.2 ± 1.8 ± 0.5 -1.6 - 0.7		CHILIKIN 19	BELL	$e^+e^- \rightarrow \Upsilon(4S)$

$\Gamma(B^+ \rightarrow h_c(1P)K^+)/\Gamma_{\text{total}} \times \Gamma(h_c(1P) \rightarrow \gamma\eta_c(1S))/\Gamma_{\text{total}}$				$\Gamma_{340}/\Gamma \times \Gamma_{12}^{h_c(1P)}/\Gamma_{h_c(1P)}$
VALUE (units 10^{-4})	CL%	DOCUMENT ID	TECN	COMMENT
<0.48	90	1 AUBERT 08AB	BABR	$e^+e^- \rightarrow \Upsilon(4S)$

1 Uses the production ratio of $(B^+B^-)/(B^0\bar{B}^0) = 1.026 \pm 0.032$ at $\Upsilon(4S)$.

$\Gamma(B^+ \rightarrow \eta_c(2S)K^+)/\Gamma_{\text{total}} \times \Gamma(\eta_c(2S) \rightarrow \gamma\gamma)/\Gamma_{\text{total}}$				$\Gamma_{237}/\Gamma \times \Gamma_{16}^{\eta_c(2S)}/\Gamma_{\eta_c(2S)}$
VALUE (units 10^{-6})	CL%	DOCUMENT ID	TECN	COMMENT
<0.18	90	1 WICHT 08	BELL	$e^+e^- \rightarrow \Upsilon(4S)$

1 Assumes equal production of B^+ and B^0 at the $\Upsilon(4S)$.

$\Gamma(\eta_c(2S)K^+, \eta_c \rightarrow K_S^0 K^\mp \pi^\pm)/\Gamma_{\text{total}}$				Γ_{239}/Γ
VALUE (units 10^{-6})	CL%	DOCUMENT ID	TECN	COMMENT
3.4 ± 2.2 ± 0.5 -1.5 - 0.4		1,2 VINOKUROVA 11	BELL	$e^+e^- \rightarrow \Upsilon(4S)$

1 Assumes equal production of B^0 and B^+ from Upsilon(4S) decays.
 2 The first uncertainty includes both statistical and interference effects while the second is due to systematics.

$\Gamma(J/\psi(1S)K^+)/\Gamma_{\text{total}}$				Γ_{275}/Γ
VALUE (units 10^{-4})	CL%	DOCUMENT ID	TECN	COMMENT
10.06 ± 0.27 OUR FIT				
9.97 ± 0.30 OUR AVERAGE				

9.4 ± 0.7 ± 0.8		1 CHILIKIN 19	BELL	$e^+e^- \rightarrow \Upsilon(4S)$
8.9 ± 0.6 ± 0.5		2 KATO 18	BELL	$e^+e^- \rightarrow \Upsilon(4S)$
8.1 ± 1.3 ± 0.7		2 AUBERT 06E	BABR	$e^+e^- \rightarrow \Upsilon(4S)$
10.61 ± 0.15 ± 0.48		3 AUBERT 05J	BABR	$e^+e^- \rightarrow \Upsilon(4S)$
10.4 ± 1.1 ± 0.1		4 AUBERT,B 05L	BABR	$e^+e^- \rightarrow \Upsilon(4S)$
10.1 ± 0.2 ± 0.7		3 ABE 03B	BELL	$e^+e^- \rightarrow \Upsilon(4S)$
10.2 ± 0.8 ± 0.7		3 JESSOP 97	CLE2	$e^+e^- \rightarrow \Upsilon(4S)$
9.24 ± 3.04 ± 0.05		5 BORTOLETTO92	CLEO	$e^+e^- \rightarrow \Upsilon(4S)$
8.09 ± 3.50 ± 0.04	6	6 ALBRECHT 90J	ARG	$e^+e^- \rightarrow \Upsilon(4S)$

• • • We do not use the following data for averages, fits, limits, etc. • • •
 10.1 ± 0.3 ± 0.5 3 AUBERT 02 BABR Repl. by AUBERT 05J
 11.0 ± 1.5 ± 0.9 59 3 ALAM 94 CLE2 Repl. by JESSOP 97
 22 ± 10 ± 2 BUSKULIC 92G ALEP $e^+e^- \rightarrow Z$
 7 ± 4 3 7 ALBRECHT 87D ARG $e^+e^- \rightarrow \Upsilon(4S)$
 10 ± 7 ± 2 3 8 BEBEK 87 CLEO $e^+e^- \rightarrow \Upsilon(4S)$
 9 ± 5 3 9 ALAM 86 CLEO $e^+e^- \rightarrow \Upsilon(4S)$

1 CHILIKIN 19 reports $[\Gamma(B^+ \rightarrow J/\psi(1S)K^+)/\Gamma_{\text{total}}] \times [B(J/\psi(1S) \rightarrow \rho\bar{p}\pi^+\pi^-)] = (56.4^{+3.3+2.7}_{-3.2-2.5}) \times 10^{-7}$ which we divide by our best value $B(J/\psi(1S) \rightarrow \rho\bar{p}\pi^+\pi^-) = (6.0 \pm 0.5) \times 10^{-3}$. Our first error is their experiment's error and our second error is the systematic error from using our best value.

2 Measures absolute branching fractions using a missing-mass technique.
 3 Assumes equal production of B^+ and B^0 at the $\Upsilon(4S)$.
 4 AUBERT,B 05L reports $[\Gamma(B^+ \rightarrow J/\psi(1S)K^+)/\Gamma_{\text{total}}] \times [B(J/\psi(1S) \rightarrow \rho\bar{p})] = (2.2 \pm 0.2 \pm 0.1) \times 10^{-6}$ which we divide by our best value $B(J/\psi(1S) \rightarrow \rho\bar{p}) = (2.121 \pm 0.029) \times 10^{-3}$. Our first error is their experiment's error and our second error is the systematic error from using our best value.
 5 BORTOLETTO 92 reports $(8 \pm 2 \pm 2) \times 10^{-4}$ from a measurement of $[\Gamma(B^+ \rightarrow J/\psi(1S)K^+)/\Gamma_{\text{total}}] \times [B(J/\psi(1S) \rightarrow e^+e^-)]$ assuming $B(J/\psi(1S) \rightarrow e^+e^-) = 0.069 \pm 0.009$, which we rescale to our best value $B(J/\psi(1S) \rightarrow e^+e^-) = (5.971 \pm 0.032) \times 10^{-2}$. Our first error is their experiment's error and our second error is the systematic error from using our best value. Assumes equal production of B^+ and B^0 at the $\Upsilon(4S)$.
 6 ALBRECHT 90J reports $(7 \pm 3 \pm 1) \times 10^{-4}$ from a measurement of $[\Gamma(B^+ \rightarrow J/\psi(1S)K^+)/\Gamma_{\text{total}}] \times [B(J/\psi(1S) \rightarrow e^+e^-)]$ assuming $B(J/\psi(1S) \rightarrow e^+e^-) = 0.069 \pm 0.009$, which we rescale to our best value $B(J/\psi(1S) \rightarrow e^+e^-) = (5.971 \pm 0.032) \times 10^{-2}$. Our first error is their experiment's error and our second error is the systematic error from using our best value. Assumes equal production of B^+ and B^0 at the $\Upsilon(4S)$.
 7 ALBRECHT 87D assume $B^+B^-/B^0\bar{B}^0$ ratio is 55/45. Superseded by ALBRECHT 90J.
 8 BEBEK 87 value has been updated in BERKELMAN 91 to use same assumptions as noted for BORTOLETTO 92.
 9 ALAM 86 assumes B^\pm/B^0 ratio is 60/40.

$\Gamma(\eta_c K^+)/\Gamma(J/\psi(1S)K^+)$				$\Gamma_{230}/\Gamma_{275}$
VALUE	CL%	DOCUMENT ID	TECN	COMMENT
0.87 ± 0.10 OUR AVERAGE				

0.84 ± 0.06 ± 0.08 1 AAIJ 13s LHCB pp at 7 TeV
 1.33 ± 0.10 ± 0.43 2 AUBERT,B 04B BABR $e^+e^- \rightarrow \Upsilon(4S)$

1 AAIJ 13s reports $[\Gamma(B^+ \rightarrow \eta_c K^+)/\Gamma(B^+ \rightarrow J/\psi(1S)K^+)] \times [B(\eta_c(1S) \rightarrow \rho\bar{p})] / [B(J/\psi(1S) \rightarrow \rho\bar{p})] = 0.578 \pm 0.035 \pm 0.026$ which we multiply or divide by our best values $B(\eta_c(1S) \rightarrow \rho\bar{p}) = (1.45 \pm 0.14) \times 10^{-3}$, $B(J/\psi(1S) \rightarrow \rho\bar{p}) = (2.121 \pm 0.029) \times 10^{-3}$. Our first error is their experiment's error and our second error is the systematic error from using our best values.
 2 Uses BABAR measurement of $B(B^+ \rightarrow J/\psi K^+) = (10.1 \pm 0.3 \pm 0.5) \times 10^{-4}$.

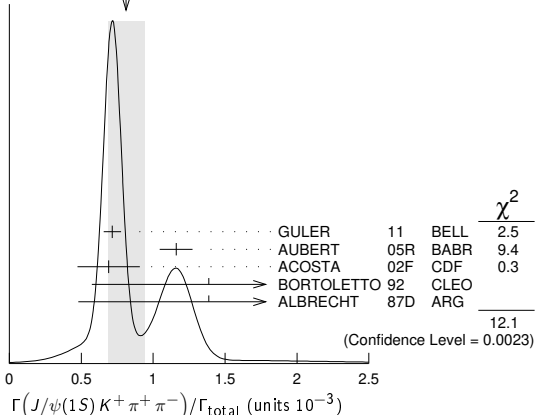
$\Gamma(B^+ \rightarrow J/\psi(1S)K^+)/\Gamma_{\text{total}} \times \Gamma(J/\psi(1S) \rightarrow \gamma\gamma)/\Gamma_{\text{total}}$				$\Gamma_{275}/\Gamma \times \Gamma_{303}^{J/\psi(1S)}/\Gamma_{J/\psi(1S)}$
VALUE (units 10^{-6})	CL%	DOCUMENT ID	TECN	COMMENT
<0.16	90	1 WICHT 08	BELL	$e^+e^- \rightarrow \Upsilon(4S)$

1 Assumes equal production of B^+ and B^0 at the $\Upsilon(4S)$.

$\Gamma(J/\psi(1S)K^+\pi^+\pi^-)/\Gamma_{\text{total}}$				Γ_{277}/Γ
VALUE (units 10^{-3})	CL%	DOCUMENT ID	TECN	COMMENT
0.81 ± 0.13 OUR AVERAGE				

Error includes scale factor of 2.5. See the ideogram below.
 0.716 ± 0.010 ± 0.060 1 GULER 11 BELL $e^+e^- \rightarrow \Upsilon(4S)$
 1.16 ± 0.07 ± 0.09 1 AUBERT 05R BABR $e^+e^- \rightarrow \Upsilon(4S)$
 0.69 ± 0.18 ± 0.12 2 ACOSTA 02F CDF $p\bar{p}$ 1.8 TeV
 1.39 ± 0.81 ± 0.01 3 BORTOLETTO92 CLEO $e^+e^- \rightarrow \Upsilon(4S)$
 1.39 ± 0.91 ± 0.01 6 4 ALBRECHT 87D ARG $e^+e^- \rightarrow \Upsilon(4S)$
 • • • We do not use the following data for averages, fits, limits, etc. • • •
 <1.8 90 5 ALBRECHT 90J ARG $e^+e^- \rightarrow \Upsilon(4S)$

WEIGHTED AVERAGE
 0.81 ± 0.13 (Error scaled by 2.5)



1 Assumes equal production of B^+ and B^0 at the $\Upsilon(4S)$.
 2 ACOSTA 02F uses as reference of $B(B \rightarrow J/\psi(1S)K^+) = (10.1 \pm 0.6) \times 10^{-4}$. The second error includes the systematic error and the uncertainties of the branching ratio.
 3 BORTOLETTO 92 reports $(1.2 \pm 0.6 \pm 0.4) \times 10^{-3}$ from a measurement of $[\Gamma(B^+ \rightarrow J/\psi(1S)K^+\pi^+\pi^-)/\Gamma_{\text{total}}] \times [B(J/\psi(1S) \rightarrow e^+e^-)]$ assuming $B(J/\psi(1S) \rightarrow e^+e^-) = 0.069 \pm 0.009$, which we rescale to our best value

$B(J/\psi(1S) \rightarrow e^+e^-) = (5.971 \pm 0.032) \times 10^{-2}$. Our first error is their experiment's error and our second error is the systematic error from using our best value. Assumes equal production of B^+ and B^0 at the $\Upsilon(4S)$.

⁴ALBRECHT 87D reports $(1.2 \pm 0.8) \times 10^{-3}$ from a measurement of $[\Gamma(B^+ \rightarrow J/\psi(1S) K^+ \pi^+ \pi^-)/\Gamma_{\text{total}}] \times [B(J/\psi(1S) \rightarrow e^+e^-)]$ assuming $B(J/\psi(1S) \rightarrow e^+e^-) = 0.069 \pm 0.009$, which we rescale to our best value $B(J/\psi(1S) \rightarrow e^+e^-) = (5.971 \pm 0.032) \times 10^{-2}$. Our first error is their experiment's error and our second error is the systematic error from using our best value. They actually report 0.0011 ± 0.0007 assuming $B^+ B^-/B^0 \bar{B}^0$ ratio is 55/45. We rescale to 50/50. Analysis explicitly removes $B^+ \rightarrow \psi(2S) K^+$.

⁵ALBRECHT 90J reports $< 1.6 \times 10^{-3}$ from a measurement of $[\Gamma(B^+ \rightarrow J/\psi(1S) K^+ \pi^+ \pi^-)/\Gamma_{\text{total}}] \times [B(J/\psi(1S) \rightarrow e^+e^-)]$ assuming $B(J/\psi(1S) \rightarrow e^+e^-) = 0.069$, which we rescale to our best value $B(J/\psi(1S) \rightarrow e^+e^-) = 5.971 \times 10^{-2}$. Assumes equal production of B^+ and B^0 at the $\Upsilon(4S)$.

$\Gamma(J/\psi(1S) K^+ K^- K^+)/\Gamma_{\text{total}}$		Γ_{278}/Γ	
VALUE (units 10^{-6})	DOCUMENT ID	TECN	COMMENT
$33.7 \pm 2.5 \pm 1.4$	LEES	15	BABR $e^+e^- \rightarrow \Upsilon(4S)$

$\Gamma(h_c(1P) K^+, h_c \rightarrow J/\psi \pi^+ \pi^-)/\Gamma_{\text{total}}$		Γ_{241}/Γ	
VALUE	CL%	DOCUMENT ID	TECN COMMENT
$< 3.4 \times 10^{-6}$	90	¹ AUBERT 05R	BABR $e^+e^- \rightarrow \Upsilon(4S)$
¹ Assumes equal production of B^+ and B^0 at the $\Upsilon(4S)$.			

$\Gamma(X(3730)^0 K^+, X^0 \rightarrow \eta_c \eta)/\Gamma_{\text{total}}$		Γ_{242}/Γ	
VALUE	CL%	DOCUMENT ID	TECN COMMENT
$< 4.6 \times 10^{-5}$	90	VINOKUROVA 15	BELL $e^+e^- \rightarrow \Upsilon(4S)$

$\Gamma(X(3730)^0 K^+, X^0 \rightarrow \eta_c \pi^0)/\Gamma_{\text{total}}$		Γ_{243}/Γ	
VALUE	CL%	DOCUMENT ID	TECN COMMENT
$< 5.7 \times 10^{-6}$	90	VINOKUROVA 15	BELL $e^+e^- \rightarrow \Upsilon(4S)$

$\Gamma(\chi_{c1}(3872) K^+)/\Gamma_{\text{total}}$		Γ_{244}/Γ	
VALUE	CL%	DOCUMENT ID	TECN COMMENT
$< 2.6 \times 10^{-4}$	90	¹ KATO 18	BELL $e^+e^- \rightarrow \Upsilon(4S)$
••• We do not use the following data for averages, fits, limits, etc. •••			
$< 3.2 \times 10^{-4}$	90	¹ AUBERT 06E	BABR $e^+e^- \rightarrow \Upsilon(4S)$
¹ Measures absolute branching fractions using a missing-mass technique.			

$\Gamma(B^+ \rightarrow \chi_{c1}(3872) K^+)/\Gamma_{\text{total}} \times \Gamma(\chi_{c1}(3872) \rightarrow \gamma \gamma)/\Gamma_{\text{total}}$		$\Gamma_{244}/\Gamma \times \Gamma_{\chi_{c1}(3872)}/\Gamma_{\chi_{c1}(3872)}$	
VALUE (units 10^{-6})	CL%	DOCUMENT ID	TECN COMMENT
< 0.24	90	¹ WICHT 08	BELL $e^+e^- \rightarrow \Upsilon(4S)$
¹ Assumes equal production of B^+ and B^0 at the $\Upsilon(4S)$.			

$\Gamma(\chi_{c1}(3872) K^+, \chi_{c1} \rightarrow J/\psi \pi^+ \pi^-)/\Gamma_{\text{total}}$		Γ_{246}/Γ	
VALUE (units 10^{-6})	DOCUMENT ID	TECN	COMMENT
8.6 ± 0.8 OUR AVERAGE	Error includes scale factor of 1.1.		
$8.63 \pm 0.82 \pm 0.52$	¹ CHOI 11	BELL	$e^+e^- \rightarrow \Upsilon(4S)$
$8.4 \pm 1.5 \pm 0.7$	¹ AUBERT 08Y	BABR	$e^+e^- \rightarrow \Upsilon(4S)$
••• We do not use the following data for averages, fits, limits, etc. •••			
$10.1 \pm 2.5 \pm 1.0$	¹ AUBERT 06	BABR	Repl. by AUBERT 08Y
12.8 ± 4.1	¹ AUBERT 05R	BABR	Repl. by AUBERT 06
$12.4 \pm 2.8 \pm 0.4$	² CHOI 03	BELL	Repl. by CHOI 11
¹ Assumes equal production of B^+ and B^0 at the $\Upsilon(4S)$.			
² CHOI 03 reports $[\Gamma(B^+ \rightarrow \chi_{c1}(3872) K^+, \chi_{c1} \rightarrow J/\psi \pi^+ \pi^-)/\Gamma_{\text{total}}] / [B(B^+ \rightarrow \psi(2S) K^+)] = 0.0200 \pm 0.0038 \pm 0.0023$ which we multiply by our best value $B(B^+ \rightarrow \psi(2S) K^+) = (6.19 \pm 0.22) \times 10^{-4}$. Our first error is their experiment's error and our second error is the systematic error from using our best value.			

$\Gamma(\chi_{c1}(3872) K^+, \chi_{c1} \rightarrow J/\psi \gamma)/\Gamma_{\text{total}}$		Γ_{247}/Γ	
VALUE (units 10^{-6})	DOCUMENT ID	TECN	COMMENT
2.1 ± 0.4 OUR AVERAGE	Error includes scale factor of 1.1.		
$1.78^{+0.48}_{-0.44} \pm 0.12$	¹ BHARDWAJ 11	BELL	$e^+e^- \rightarrow \Upsilon(4S)$
$2.8 \pm 0.8 \pm 0.1$	² AUBERT 09B	BABR	$e^+e^- \rightarrow \Upsilon(4S)$
••• We do not use the following data for averages, fits, limits, etc. •••			
$3.3 \pm 1.0 \pm 0.3$	¹ AUBERT, BE 06M	BABR	Repl. by AUBERT 09B
¹ Assumes equal production of B^+ and B^0 at the $\Upsilon(4S)$.			
² Uses $B(\Upsilon(4S) \rightarrow B^+ B^-) = (51.6 \pm 0.6)\%$ and $B(\Upsilon(4S) \rightarrow B^0 \bar{B}^0) = (48.4 \pm 0.6)\%$.			

$\Gamma(\chi_{c1}(3872) K^*(892)^+, \chi_{c1} \rightarrow J/\psi \gamma)/\Gamma_{\text{total}}$		Γ_{265}/Γ	
VALUE (units 10^{-6})	CL%	DOCUMENT ID	TECN COMMENT
< 4.8	90	¹ AUBERT 09B	BABR $e^+e^- \rightarrow \Upsilon(4S)$
¹ Uses $B(\Upsilon(4S) \rightarrow B^+ B^-) = (51.6 \pm 0.6)\%$ and $B(\Upsilon(4S) \rightarrow B^0 \bar{B}^0) = (48.4 \pm 0.6)\%$.			

$\Gamma(\chi_{c1}(3872) K^+, \chi_{c1} \rightarrow \psi(2S) \gamma)/\Gamma_{\text{total}}$		Γ_{248}/Γ	
VALUE (units 10^{-6})	DOCUMENT ID	TECN	COMMENT
4 ± 4 OUR AVERAGE	Error includes scale factor of 2.5.		
$0.83^{+1.98}_{-1.83} \pm 0.44$	^{1,2} BHARDWAJ 11	BELL	$e^+e^- \rightarrow \Upsilon(4S)$
$9.5 \pm 2.7 \pm 0.6$	³ AUBERT 09B	BABR	$e^+e^- \rightarrow \Upsilon(4S)$
¹ BHARDWAJ 11 measurement is equivalent to a limit of $< 3.45 \times 10^{-6}$ at 90% CL.			
² Assumes equal production of B^+ and B^0 at the $\Upsilon(4S)$.			
³ Uses $B(\Upsilon(4S) \rightarrow B^+ B^-) = (51.6 \pm 0.6)\%$ and $B(\Upsilon(4S) \rightarrow B^0 \bar{B}^0) = (48.4 \pm 0.6)\%$.			

$\Gamma(\chi_{c1}(3872) K^*(892)^+, \chi_{c1} \rightarrow \psi(2S) \gamma)/\Gamma_{\text{total}}$		Γ_{266}/Γ	
VALUE (units 10^{-6})	CL%	DOCUMENT ID	TECN COMMENT
< 28	90	¹ AUBERT 09B	BABR $e^+e^- \rightarrow \Upsilon(4S)$
¹ Uses $B(\Upsilon(4S) \rightarrow B^+ B^-) = (51.6 \pm 0.6)\%$ and $B(\Upsilon(4S) \rightarrow B^0 \bar{B}^0) = (48.4 \pm 0.6)\%$.			

$\Gamma(\chi_{c1}(3872) K^+, \chi_{c1} \rightarrow D^0 \bar{D}^0)/\Gamma_{\text{total}}$		Γ_{250}/Γ	
VALUE	CL%	DOCUMENT ID	TECN COMMENT
$< 6.0 \times 10^{-5}$	90	¹ CHISTOV 04	BELL $e^+e^- \rightarrow \Upsilon(4S)$
¹ Assumes equal production of B^+ and B^0 at the $\Upsilon(4S)$.			

$\Gamma(\chi_{c1}(3872) K^+, \chi_{c1} \rightarrow D^+ D^-)/\Gamma_{\text{total}}$		Γ_{251}/Γ	
VALUE	CL%	DOCUMENT ID	TECN COMMENT
$< 4.0 \times 10^{-5}$	90	¹ CHISTOV 04	BELL $e^+e^- \rightarrow \Upsilon(4S)$
¹ Assumes equal production of B^+ and B^0 at the $\Upsilon(4S)$.			

$\Gamma(\chi_{c1}(3872) K^+, \chi_{c1} \rightarrow D^0 \bar{D}^0 \pi^0)/\Gamma_{\text{total}}$		Γ_{252}/Γ	
VALUE (units 10^{-4})	CL%	DOCUMENT ID	TECN COMMENT
$1.02 \pm 0.31^{+0.21}_{-0.29}$	90	¹ GOKHROO 06	BELL $e^+e^- \rightarrow \Upsilon(4S)$
••• We do not use the following data for averages, fits, limits, etc. •••			
< 0.6	90	² CHISTOV 04	BELL Repl. by GOKHROO 06
¹ Measure the near-threshold enhancements in the $(D^0 \bar{D}^0 \pi^0)$ system at a mass $3875.2 \pm 0.7^{+0.3}_{-1.6} \pm 0.8$ MeV/c ² .			
² Assumes equal production of B^+ and B^0 at the $\Upsilon(4S)$.			

$\Gamma(\chi_{c1}(3872) K^+, \chi_{c1} \rightarrow \bar{D}^{*0} D^0)/\Gamma_{\text{total}}$		Γ_{253}/Γ	
VALUE (units 10^{-4})	CL%	DOCUMENT ID	TECN COMMENT
0.85 ± 0.26 OUR AVERAGE	Error includes scale factor of 1.4.		
$0.77 \pm 0.16 \pm 0.10$	¹ AUSHEV 10	BELL	$e^+e^- \rightarrow \Upsilon(4S)$
$1.67 \pm 0.36 \pm 0.47$	¹ AUBERT 08B	BABR	$e^+e^- \rightarrow \Upsilon(4S)$
¹ Assumes equal production of B^+ and B^0 at the $\Upsilon(4S)$.			

$\Gamma(\chi_{c1}(3872)^0 K^+, \chi_{c1}^0 \rightarrow \eta_c \pi^+ \pi^-)/\Gamma_{\text{total}}$		Γ_{254}/Γ	
VALUE	CL%	DOCUMENT ID	TECN COMMENT
$< 3.0 \times 10^{-5}$	90	VINOKUROVA 15	BELL $e^+e^- \rightarrow \Upsilon(4S)$

$\Gamma(\chi_{c1}(3872)^0 K^+, \chi_{c1}^0 \rightarrow \eta_c \omega(782))/\Gamma_{\text{total}}$		Γ_{255}/Γ	
VALUE	CL%	DOCUMENT ID	TECN COMMENT
$< 6.9 \times 10^{-5}$	90	VINOKUROVA 15	BELL $e^+e^- \rightarrow \Upsilon(4S)$

$\Gamma(\chi_{c1}(3872) K^+, \chi_{c1} \rightarrow \chi_{c1}(1P) \pi^+ \pi^-)/\Gamma_{\text{total}}$		Γ_{256}/Γ	
VALUE	CL%	DOCUMENT ID	TECN COMMENT
$< 1.5 \times 10^{-6}$	90	¹ BHARDWAJ 16	BELL $e^+e^- \rightarrow \Upsilon(4S)$
¹ Assumes equal production of B^+ and B^0 at the $\Upsilon(4S)$.			

$\Gamma(\chi_{c1}(3872) K^+, \chi_{c1}(3872) \rightarrow \chi_{c1}(1P) \pi^0)/\Gamma_{\text{total}}$		Γ_{257}/Γ	
VALUE	CL%	DOCUMENT ID	TECN COMMENT
$< 8.1 \times 10^{-6}$	90	¹ BHARDWAJ 19	BELL $e^+e^- \rightarrow \Upsilon(4S)$
¹ Assumes equal production of B^+ and B^0 at the $\Upsilon(4S)$.			

$\Gamma(X(3915) K^+)/\Gamma_{\text{total}}$		Γ_{258}/Γ	
VALUE	CL%	DOCUMENT ID	TECN COMMENT
$< 2.8 \times 10^{-4}$	90	¹ KATO 18	BELL $e^+e^- \rightarrow \Upsilon(4S)$
¹ Measures absolute branching fractions using a missing-mass technique.			

$\Gamma(X(3915)^0 K^+, X^0 \rightarrow \eta_c \eta)/\Gamma_{\text{total}}$		Γ_{259}/Γ	
VALUE	CL%	DOCUMENT ID	TECN COMMENT
$< 4.7 \times 10^{-5}$	90	¹ VINOKUROVA 15	BELL $e^+e^- \rightarrow \Upsilon(4S)$
¹ Upper limit is corrected in the Erratum.			

$\Gamma(X(3915)^0 K^+, X^0 \rightarrow \eta_c \pi^0)/\Gamma_{\text{total}}$		Γ_{260}/Γ	
VALUE	CL%	DOCUMENT ID	TECN COMMENT
$< 1.7 \times 10^{-5}$	90	¹ VINOKUROVA 15	BELL $e^+e^- \rightarrow \Upsilon(4S)$
¹ Upper limit is corrected in the Erratum.			

$\Gamma(X(4014)^0 K^+, X^0 \rightarrow \eta_c \eta)/\Gamma_{\text{total}}$		Γ_{261}/Γ	
VALUE	CL%	DOCUMENT ID	TECN COMMENT
$< 3.9 \times 10^{-5}$	90	VINOKUROVA 15	BELL $e^+e^- \rightarrow \Upsilon(4S)$

Meson Particle Listings

 B^\pm

$\Gamma(X(4014)^0 K^+, X^0 \rightarrow \eta_c \pi^0)/\Gamma_{\text{total}}$					Γ_{262}/Γ
VALUE	CL%	DOCUMENT ID	TECN	COMMENT	
$<1.2 \times 10^{-5}$	90	VINOKUROVA 15	BELL	$e^+ e^- \rightarrow \Upsilon(4S)$	

$\Gamma(Z_c(3900)^0 K^+, Z_c^0 \rightarrow \eta_c \pi^+ \pi^-)/\Gamma_{\text{total}}$					Γ_{263}/Γ
VALUE	CL%	DOCUMENT ID	TECN	COMMENT	
$<4.7 \times 10^{-5}$	90	VINOKUROVA 15	BELL	$e^+ e^- \rightarrow \Upsilon(4S)$	

$\Gamma(X(4020)^0 K^+, X^0 \rightarrow \eta_c \pi^+ \pi^-)/\Gamma_{\text{total}}$					Γ_{264}/Γ
VALUE	CL%	DOCUMENT ID	TECN	COMMENT	
$<1.6 \times 10^{-5}$	90	VINOKUROVA 15	BELL	$e^+ e^- \rightarrow \Upsilon(4S)$	

$\Gamma(\chi_{c1}(3872) K^+, \chi_{c1} \rightarrow J/\psi(1S)\eta)/\Gamma_{\text{total}}$					Γ_{249}/Γ
VALUE	CL%	DOCUMENT ID	TECN	COMMENT	
$<7.7 \times 10^{-6}$	90	¹ AUBERT	04Y BABR	$e^+ e^- \rightarrow \Upsilon(4S)$	

¹ Assumes equal production of B^+ and B^0 at the $\Upsilon(4S)$.

$\Gamma(\chi_{c1}(3872)^+ K^0, \chi_{c1}^+ \rightarrow J/\psi(1S)\pi^+ \pi^0)/\Gamma_{\text{total}}$					Γ_{267}/Γ
VALUE (units 10^{-6})	CL%	DOCUMENT ID	TECN	COMMENT	
<6.1	90	^{1,2} CHOI	11 BELL	$e^+ e^- \rightarrow \Upsilon(4S)$	

• • • We do not use the following data for averages, fits, limits, etc. • • •

<22 90 ³AUBERT 05B BABR $e^+ e^- \rightarrow \Upsilon(4S)$

¹ Assumes $\pi^+ \pi^0$ originates from ρ^+ .

² Assumes equal production of B^+ and B^0 at the $\Upsilon(4S)$.

³ Assumes equal production of B^+ and B^0 at the $\Upsilon(4S)$. The isovector- X hypothesis is excluded with a likelihood test at 1×10^{-4} level.

$\Gamma(\chi_{c1}(3872) K^0 \pi^+, \chi_{c1} \rightarrow J/\psi(1S)\pi^+ \pi^-)/\Gamma_{\text{total}}$					Γ_{268}/Γ
VALUE (units 10^{-6})	CL%	DOCUMENT ID	TECN	COMMENT	
$10.6 \pm 3.0 \pm 0.9$		BALA 15	BELL	$e^+ e^- \rightarrow \Upsilon(4S)$	

$\Gamma(Z_c(4430)^+ K^0, Z_c^+ \rightarrow J/\psi \pi^+)/\Gamma_{\text{total}}$					Γ_{269}/Γ
VALUE (units 10^{-5})	CL%	DOCUMENT ID	TECN	COMMENT	
<1.5	95	¹ AUBERT	09AA BABR	$e^+ e^- \rightarrow \Upsilon(4S)$	

¹ Assumes equal production of B^+ and B^0 at the $\Upsilon(4S)$.

$\Gamma(Z_c(4430)^+ K^0, Z_c^+ \rightarrow \psi(2S)\pi^+)/\Gamma_{\text{total}}$					Γ_{270}/Γ
VALUE (units 10^{-5})	CL%	DOCUMENT ID	TECN	COMMENT	
<4.7	95	¹ AUBERT	09AA BABR	$e^+ e^- \rightarrow \Upsilon(4S)$	

¹ Assumes equal production of B^+ and B^0 at the $\Upsilon(4S)$.

$\Gamma(\psi(4260)^0 K^+, \psi^0 \rightarrow J/\psi \pi^+ \pi^-)/\Gamma_{\text{total}}$					Γ_{271}/Γ
VALUE (units 10^{-6})	CL%	DOCUMENT ID	TECN	COMMENT	
<15.6	95	^{1,2} GARG	19 BELL	$e^+ e^- \rightarrow \Upsilon(4S)$	

• • • We do not use the following data for averages, fits, limits, etc. • • •

<29 95 ²AUBERT 06 BABR $e^+ e^- \rightarrow \Upsilon(4S)$

¹ Corresponds to a 90% CL upper limit of $< 14 \times 10^{-6}$.

² Assumes equal production of B^+ and B^0 at the $\Upsilon(4S)$.

$\Gamma(X(3915) K^+, X \rightarrow J/\psi \gamma)/\Gamma_{\text{total}}$					Γ_{272}/Γ
VALUE (units 10^{-6})	CL%	DOCUMENT ID	TECN	COMMENT	
<14	90	¹ AUBERT, BE	06M BABR	$e^+ e^- \rightarrow \Upsilon(4S)$	

¹ Assumes equal production of B^+ and B^0 at the $\Upsilon(4S)$.

$\Gamma(X(3915) K^+, X \rightarrow \chi_{c1}(1P)\pi^0)/\Gamma_{\text{total}}$					Γ_{273}/Γ
VALUE	CL%	DOCUMENT ID	TECN	COMMENT	
$<3.8 \times 10^{-5}$	90	¹ BHARDWAJ	19 BELL	$e^+ e^- \rightarrow \Upsilon(4S)$	

¹ Assumes equal production of B^+ and B^0 at the $\Upsilon(4S)$.

$\Gamma(X(3930)^0 K^+, X^0 \rightarrow J/\psi \gamma)/\Gamma_{\text{total}}$					Γ_{274}/Γ
VALUE (units 10^{-6})	CL%	DOCUMENT ID	TECN	COMMENT	
<2.5	90	¹ AUBERT, BE	06M BABR	$e^+ e^- \rightarrow \Upsilon(4S)$	

¹ Assumes equal production of B^+ and B^0 at the $\Upsilon(4S)$.

$\Gamma(J/\psi(1S) K^0 \pi^+)/\Gamma_{\text{total}}$					Γ_{276}/Γ
VALUE (units 10^{-3})	CL%	DOCUMENT ID	TECN	COMMENT	
1.101 ± 0.021		¹ AUBERT	09AA BABR	$e^+ e^- \rightarrow \Upsilon(4S)$	

• • • We do not use the following data for averages, fits, limits, etc. • • •

¹ Does not report systematic uncertainties.

$\Gamma(J/\psi(1S) K^*(892)^+)/\Gamma_{\text{total}}$					Γ_{280}/Γ
VALUE (units 10^{-3})	CL%	DOCUMENT ID	TECN	COMMENT	
1.43 ± 0.08		OUR FIT			
1.43 ± 0.08		OUR AVERAGE			

For polarization information see the Listings at the end of the " B^0 Branching Ratios" section.

VALUE (units 10^{-3})	CL%	DOCUMENT ID	TECN	COMMENT	
1.78 ± 0.36					
-0.32 ± 0.02		^{1,2} AUBERT	07AV BABR	$e^+ e^- \rightarrow \Upsilon(4S)$	

VALUE (units 10^{-3})	CL%	DOCUMENT ID	TECN	COMMENT	
$1.454 \pm 0.047 \pm 0.097$		² AUBERT	05J BABR	$e^+ e^- \rightarrow \Upsilon(4S)$	
$1.28 \pm 0.07 \pm 0.14$		² ABE	02N BELL	$e^+ e^- \rightarrow \Upsilon(4S)$	
$1.41 \pm 0.23 \pm 0.24$		² JESSOP	97 CLE2	$e^+ e^- \rightarrow \Upsilon(4S)$	
$1.58 \pm 0.47 \pm 0.27$		³ ABE	96H CDF	$p\bar{p}$ at 1.8 TeV	

VALUE (units 10^{-3})	CL%	DOCUMENT ID	TECN	COMMENT	
$1.50 \pm 1.08 \pm 0.01$		⁴ BORTOLETTO	92 CLEO	$e^+ e^- \rightarrow \Upsilon(4S)$	
$1.85 \pm 1.30 \pm 0.01$		² ALBRECHT	90J ARG	$e^+ e^- \rightarrow \Upsilon(4S)$	

• • • We do not use the following data for averages, fits, limits, etc. • • •

¹ AUBERT 07AV reports $[\Gamma(B^+ \rightarrow J/\psi(1S) K^*(892)^+)/\Gamma_{\text{total}}] \times [\text{B}(J/\psi(1S) \rightarrow p\bar{p})] = (3.78 \pm 0.72 \pm 0.28 - 0.64 - 0.23) \times 10^{-6}$ which we divide by our best value $\text{B}(J/\psi(1S) \rightarrow p\bar{p}) = (2.121 \pm 0.029) \times 10^{-3}$. Our first error is their experiment's error and our second error is the systematic error from using our best value.

² Assumes equal production of B^+ and B^0 at the $\Upsilon(4S)$.

³ ABE 96H assumes that $\text{B}(B^+ \rightarrow J/\psi K^+) = (1.02 \pm 0.14) \times 10^{-3}$.

⁴ BORTOLETTO 92 reports $(1.3 \pm 0.9 \pm 0.3) \times 10^{-3}$ from a measurement of $[\Gamma(B^+ \rightarrow J/\psi(1S) K^*(892)^+)/\Gamma_{\text{total}}] \times [\text{B}(J/\psi(1S) \rightarrow e^+ e^-)]$ assuming $\text{B}(J/\psi(1S) \rightarrow e^+ e^-) = 0.069 \pm 0.009$, which we rescale to our best value $\text{B}(J/\psi(1S) \rightarrow e^+ e^-) = (5.971 \pm 0.032) \times 10^{-2}$. Our first error is their experiment's error and our second error is the systematic error from using our best value. Assumes equal production of B^+ and B^0 at the $\Upsilon(4S)$.

⁵ ALBRECHT 90J reports $(1.6 \pm 1.1 \pm 0.3) \times 10^{-3}$ from a measurement of $[\Gamma(B^+ \rightarrow J/\psi(1S) K^*(892)^+)/\Gamma_{\text{total}}] \times [\text{B}(J/\psi(1S) \rightarrow e^+ e^-)]$ assuming $\text{B}(J/\psi(1S) \rightarrow e^+ e^-) = 0.069 \pm 0.009$, which we rescale to our best value $\text{B}(J/\psi(1S) \rightarrow e^+ e^-) = (5.971 \pm 0.032) \times 10^{-2}$. Our first error is their experiment's error and our second error is the systematic error from using our best value. Assumes equal production of B^+ and B^0 at the $\Upsilon(4S)$.

$\Gamma(J/\psi(1S) K^*(892)^+)/\Gamma(J/\psi(1S) K^+)$					$\Gamma_{280}/\Gamma_{275}$
VALUE	CL%	DOCUMENT ID	TECN	COMMENT	
1.39 ± 0.09		OUR AVERAGE			

VALUE	CL%	DOCUMENT ID	TECN	COMMENT	
$1.37 \pm 0.05 \pm 0.08$		AUBERT	05J BABR	$e^+ e^- \rightarrow \Upsilon(4S)$	
$1.45 \pm 0.20 \pm 0.17$		¹ JESSOP	97 CLE2	$e^+ e^- \rightarrow \Upsilon(4S)$	
$1.92 \pm 0.60 \pm 0.17$		ABE	96Q CDF	$p\bar{p}$	

• • • We do not use the following data for averages, fits, limits, etc. • • •

$1.37 \pm 0.10 \pm 0.08$ ²AUBERT 02 BABR Repl. by AUBERT 05J

¹ JESSOP 97 assumes equal production of B^+ and B^0 at the $\Upsilon(4S)$. The measurement is actually measured as an average over kaon charged and neutral states.

² Assumes equal production of B^+ and B^0 at the $\Upsilon(4S)$.

$\Gamma(J/\psi(1S) K(1270)^+)/\Gamma_{\text{total}}$					Γ_{281}/Γ
VALUE (units 10^{-3})	CL%	DOCUMENT ID	TECN	COMMENT	
$1.80 \pm 0.34 \pm 0.39$		¹ ABE	01L BELL	$e^+ e^- \rightarrow \Upsilon(4S)$	

¹ Uses the PDG value of $\text{B}(B^+ \rightarrow J/\psi(1S) K^+) = (1.00 \pm 0.10) \times 10^{-3}$.

$\Gamma(J/\psi(1S) K(1400)^+)/\Gamma(J/\psi(1S) K(1270)^+)$					$\Gamma_{282}/\Gamma_{281}$
VALUE	CL%	DOCUMENT ID	TECN	COMMENT	
<0.30	90	ABE	01L BELL	$e^+ e^- \rightarrow \Upsilon(4S)$	

$\Gamma(J/\psi(1S) \eta K^+)/\Gamma_{\text{total}}$					Γ_{283}/Γ
VALUE (units 10^{-5})	CL%	DOCUMENT ID	TECN	COMMENT	
12.4 ± 1.4		OUR AVERAGE			
$12.7 \pm 1.1 \pm 1.1$		¹ IWASHITA	14 BELL	$e^+ e^- \rightarrow \Upsilon(4S)$	
$10.8 \pm 2.3 \pm 2.4$		¹ AUBERT	04Y BABR	$e^+ e^- \rightarrow \Upsilon(4S)$	

¹ Assumes equal production of B^+ and B^0 at the $\Upsilon(4S)$.

$\Gamma(\chi_{c1-odd}(3872) K^+, \chi_{c1-odd} \rightarrow J/\psi \eta)/\Gamma_{\text{total}}$					Γ_{284}/Γ
VALUE	CL%	DOCUMENT ID	TECN	COMMENT	
$<3.8 \times 10^{-6}$	90	IWASHITA	14 BELL	$e^+ e^- \rightarrow \Upsilon(4S)$	

$\Gamma(\psi(4160) K^+, \psi \rightarrow J/\psi \eta)/\Gamma_{\text{total}}$					Γ_{285}/Γ
VALUE	CL%	DOCUMENT ID	TECN	COMMENT	
$<7.4 \times 10^{-6}$	90	IWASHITA	14 BELL	$e^+ e^- \rightarrow \Upsilon(4S)$	

$\Gamma(J/\psi(1S) \eta' K^+)/\Gamma_{\text{total}}$					Γ_{286}/Γ
VALUE (units 10^{-5})	CL%	DOCUMENT ID	TECN	COMMENT	
<8.8	90	¹ XIE	07 BELL	$e^+ e^- \rightarrow \Upsilon(4S)$	

¹ Assumes equal production of B^+ and B^0 at the $\Upsilon(4S)$.

See key on page 999

Meson Particle Listings

B^\pm

$\Gamma(J/\psi(1S)\phi K^+)/\Gamma_{total}$ Γ_{287}/Γ

VALUE (units 10^{-5})	DOCUMENT ID	TECN	COMMENT
5.0 ± 0.4 OUR AVERAGE			
5.00 ± 0.37 ± 0.15	LEES 15	BABR	$e^+e^- \rightarrow \Upsilon(4S)$
4.4 ± 1.4 ± 0.5	¹ AUBERT 030	BABR	$e^+e^- \rightarrow \Upsilon(4S)$
8.8 $^{+3.5}_{-3.0}$ ± 1.3	² ANASTASSOV 00	CLE2	$e^+e^- \rightarrow \Upsilon(4S)$

¹ Assumes equal production of B^+ and B^0 at the $\Upsilon(4S)$.
² ANASTASSOV 00 finds 10 events on a background of 0.5 ± 0.2 . Assumes equal production of B^0 and B^+ at the $\Upsilon(4S)$, a uniform Dalitz plot distribution, isotropic $J/\psi(1S)$ and ϕ decays, and $B(B^+ \rightarrow J/\psi(1S)\phi K^+) = B(B^0 \rightarrow J/\psi(1S)\phi K^0)$.

$\Gamma(J/\psi(1S)K_1(1650), K_1 \rightarrow \phi K^+)/\Gamma(J/\psi(1S)\phi K^+)$ $\Gamma_{288}/\Gamma_{287}$

VALUE	DOCUMENT ID	TECN	COMMENT
0.12 ± 0.10 $^{+0.17}_{-0.06}$	¹ AAIJ 17	LHCB	pp at 7, 8 TeV

¹ Measured in amplitude analysis of $B^+ \rightarrow J/\psi(1S)\phi K^+$.

$\Gamma(J/\psi(1S)K^*(1680)^+, K^* \rightarrow \phi K^+)/\Gamma(J/\psi(1S)\phi K^+)$ $\Gamma_{289}/\Gamma_{287}$

VALUE (units 10^{-2})	DOCUMENT ID	TECN	COMMENT
6.7 ± 1.9 $^{+3.2}_{-3.9}$	¹ AAIJ 17	LHCB	pp at 7, 8 TeV

¹ Measured in amplitude analysis of $B^+ \rightarrow J/\psi(1S)\phi K^+$.

$\Gamma(J/\psi(1S)K_2^*(1980), K_2^* \rightarrow \phi K^+)/\Gamma(J/\psi(1S)\phi K^+)$ $\Gamma_{290}/\Gamma_{287}$

VALUE (units 10^{-2})	DOCUMENT ID	TECN	COMMENT
2.9 ± 0.8 $^{+1.7}_{-0.7}$	¹ AAIJ 17	LHCB	pp at 7, 8 TeV

¹ Measured in amplitude analysis of $B^+ \rightarrow J/\psi(1S)\phi K^+$.

$\Gamma(J/\psi(1S)K(1830)^+, K(1830)^+ \rightarrow \phi K^+)/\Gamma(J/\psi(1S)\phi K^+)$ $\Gamma_{291}/\Gamma_{287}$

VALUE (units 10^{-2})	DOCUMENT ID	TECN	COMMENT
2.6 ± 1.1 $^{+2.3}_{-1.8}$	¹ AAIJ 17	LHCB	pp at 7, 8 TeV

¹ Measured in amplitude analysis of $B^+ \rightarrow J/\psi(1S)\phi K^+$.

$\Gamma(\chi_{c1}(4140)K^+, \chi_{c1} \rightarrow J/\psi(1S)\phi)/\Gamma(J/\psi(1S)\phi K^+)$ $\Gamma_{292}/\Gamma_{287}$

VALUE	CL%	DOCUMENT ID	TECN	COMMENT
0.19 ± 0.08 OUR AVERAGE				
0.13 ± 0.032 $^{+4.8}_{-2.0}$		¹ AAIJ 17	LHCB	pp at 7, 8 TeV
0.19 ± 0.07 ± 0.04		² ABAZOV 14A	D0	$p\bar{p}$ at 1.96 TeV
••• We do not use the following data for averages, fits, limits, etc. •••				
<0.133	90	LEES 15	BABR	$e^+e^- \rightarrow \Upsilon(4S)$
<0.07	90	³ AAIJ 12AA	LHCB	pp at 7 TeV

¹ Measured in amplitude analysis of $B^+ \rightarrow J/\psi(1S)\phi K^+$.
² Reported a threshold enhancement in the $J/\psi\phi$ mass distribution consistent with the $\chi_{c1}(4140)$ state with a statistical significance of 3.1 standard deviations.
³ Branching fractions are normalized to 382 ± 22 events of $B^+ \rightarrow J/\psi\phi K^+$.

$\Gamma(\chi_{c1}(4274)K^+, \chi_{c1} \rightarrow J/\psi(1S)\phi)/\Gamma(J/\psi(1S)\phi K^+)$ $\Gamma_{293}/\Gamma_{287}$

VALUE (units 10^{-2})	CL%	DOCUMENT ID	TECN	COMMENT
7.1 ± 2.5 $^{+3.5}_{-2.4}$		¹ AAIJ 17	LHCB	pp at 7, 8 TeV
••• We do not use the following data for averages, fits, limits, etc. •••				
<18.1	90	LEES 15	BABR	$e^+e^- \rightarrow \Upsilon(4S)$
< 8	90	² AAIJ 12AA	LHCB	Repl. by AAIJ 17

¹ Measured in amplitude analysis of $B^+ \rightarrow J/\psi(1S)\phi K^+$.
² Branching fractions are normalized to 382 ± 22 events of $B^+ \rightarrow J/\psi\phi K^+$.

$\Gamma(\chi_{c0}(4500)K^+, \chi_{c0}^0 \rightarrow J/\psi(1S)\phi)/\Gamma(J/\psi(1S)\phi K^+)$ $\Gamma_{294}/\Gamma_{287}$

VALUE (units 10^{-2})	DOCUMENT ID	TECN	COMMENT
6.6 ± 2.4 $^{+3.5}_{-2.3}$	¹ AAIJ 17	LHCB	pp at 7, 8 TeV

¹ Measured in amplitude analysis of $B^+ \rightarrow J/\psi(1S)\phi K^+$.

$\Gamma(\chi_{c0}(4700)K^+, \chi_{c0} \rightarrow J/\psi(1S)\phi)/\Gamma(J/\psi(1S)\phi K^+)$ $\Gamma_{295}/\Gamma_{287}$

VALUE	DOCUMENT ID	TECN	COMMENT
0.12 ± 0.05 $^{+0.09}_{-0.05}$	¹ AAIJ 17	LHCB	pp at 7, 8 TeV

¹ Measured in amplitude analysis of $B^+ \rightarrow J/\psi(1S)\phi K^+$.

$\Gamma(J/\psi(1S)\omega K^+)/\Gamma_{total}$ Γ_{296}/Γ

VALUE (units 10^{-4})	DOCUMENT ID	TECN	COMMENT
3.2 ± 0.1 $^{+0.6}_{-0.3}$	¹ DEL-AMO-SA...10B	BABR	$e^+e^- \rightarrow \Upsilon(4S)$
••• We do not use the following data for averages, fits, limits, etc. •••			
3.5 ± 0.2 ± 0.4	¹ AUBERT 08w	BABR	Repl. by DEL-AMO-SANCHEZ 10B

¹ Assumes equal production of B^+ and B^0 at the $\Upsilon(4S)$.

$\Gamma(\chi_{c1}(3872)K^+, \chi_{c1} \rightarrow J/\psi\omega)/\Gamma_{total}$ Γ_{297}/Γ

VALUE (units 10^{-6})	DOCUMENT ID	TECN	COMMENT
6 ± 2 ± 1	¹ DEL-AMO-SA...10B	BABR	$e^+e^- \rightarrow \Upsilon(4S)$
¹ Assumes equal production of B^+ and B^0 at the $\Upsilon(4S)$.			

$\Gamma(\chi_{c1}(3872)K^+, \chi_{c1} \rightarrow p\bar{p})/\Gamma_{total}$ Γ_{245}/Γ

VALUE	CL%	DOCUMENT ID	TECN	COMMENT
<0.5 × 10⁻⁸	95	¹ AAIJ 17AD	LHCB	pp at 7 and 8 TeV
••• We do not use the following data for averages, fits, limits, etc. •••				
<1.7 × 10 ⁻⁸	95	² AAIJ 13s	LHCB	Repl. by AAIJ 17AD
¹ Measured relative to $B^+ \rightarrow J/\psi K^+$ decay with charmonia reconstructed in $p\bar{p}$ final state and using $B(B^+ \rightarrow J/\psi K^+) \times B(J/\psi \rightarrow p\bar{p}) = (2.17 \pm 0.08) \times 10^{-6}$.				
² Measured relative to $B^+ \rightarrow J/\psi K^+$ decay with charmonia reconstructed in $p\bar{p}$ final state and using $B(B^+ \rightarrow J/\psi K^+) = (1.013 \pm 0.034) \times 10^{-3}$ and $B(J/\psi \rightarrow p\bar{p}) = (2.17 \pm 0.07) \times 10^{-3}$.				

$\Gamma(X(3915)K^+, X \rightarrow J/\psi\omega)/\Gamma_{total}$ Γ_{298}/Γ

VALUE (units 10^{-5})	DOCUMENT ID	TECN	COMMENT
3.0 $^{+0.7+0.5}_{-0.6-0.3}$	¹ DEL-AMO-SA...10B	BABR	$e^+e^- \rightarrow \Upsilon(4S)$
••• We do not use the following data for averages, fits, limits, etc. •••			
4.9 $^{+1.0}_{-0.9}$ ± 0.5	¹ AUBERT 08w	BABR	Repl. by DEL-AMO-SANCHEZ 10B
¹ Assumes equal production of B^+ and B^0 at the $\Upsilon(4S)$.			

$\Gamma(X(3915)K^+, X \rightarrow p\bar{p})/\Gamma_{total}$ Γ_{279}/Γ

VALUE	CL%	DOCUMENT ID	TECN	COMMENT
<7.1 × 10⁻⁸	95	¹ AAIJ 13s	LHCB	pp at 7 TeV
¹ Measured relative to $B^+ \rightarrow J/\psi K^+$ decay with charmonia reconstructed in $p\bar{p}$ final state and using $B(B^+ \rightarrow J/\psi K^+) = (1.013 \pm 0.034) \times 10^{-3}$ and $B(J/\psi \rightarrow p\bar{p}) = (2.17 \pm 0.07) \times 10^{-3}$.				

$\Gamma(J/\psi(1S)\pi^+)/\Gamma_{total}$ Γ_{299}/Γ

VALUE	DOCUMENT ID	TECN	COMMENT
(3.87 ± 0.11) × 10⁻⁵ OUR FIT			
(3.8 ± 0.6 ± 0.3) × 10⁻⁵	¹ ABE 03B	BELL	$e^+e^- \rightarrow \Upsilon(4S)$
¹ Assumes equal production of B^+ and B^0 at the $\Upsilon(4S)$.			

$\Gamma(J/\psi(1S)\pi^+)/\Gamma(J/\psi(1S)K^+)$ $\Gamma_{299}/\Gamma_{275}$

VALUE (units 10^{-2})	EVTS	DOCUMENT ID	TECN	COMMENT
3.85 ± 0.04 OUR FIT				
3.85 ± 0.04 OUR AVERAGE				
3.83 ± 0.03 ± 0.03		AAIJ 17o	LHCB	pp at 7, 8 TeV
3.5 ± 0.3 ± 1.2		AABOUD 16L	ATLS	pp at 7, 8 TeV
4.86 ± 0.82 ± 0.15		ABULENCIA 09	CDF	$p\bar{p}$ at 1.96 TeV
5.37 ± 0.45 ± 0.11		AUBERT 04P	BABR	$e^+e^- \rightarrow \Upsilon(4S)$
5.0 $^{+1.9}_{-1.7}$ ± 0.1		ABE 96R	CDF	$p\bar{p}$ 1.8 TeV
5.2 ± 2.4		BISHAI 96	CLE2	$e^+e^- \rightarrow \Upsilon(4S)$
••• We do not use the following data for averages, fits, limits, etc. •••				
3.83 ± 0.11 ± 0.07		AAIJ 12AC	LHCB	Repl. by AAIJ 17o
3.91 ± 0.78 ± 0.19		AUBERT 02F	BABR	Repl. by AUBERT 04P
4.3 ± 2.3	5	¹ ALEXANDER 95	CLE2	Sup. by BISHAI 96
¹ Assumes equal production of B^+B^- and $B^0\bar{B}^0$ on $\Upsilon(4S)$.				

$\Gamma(J/\psi(1S)\pi^+\pi^+\pi^-\pi^-)/\Gamma(\psi(2S)K^+)$ $\Gamma_{300}/\Gamma_{311}$

VALUE (units 10^{-2})	DOCUMENT ID	TECN	COMMENT
1.88 ± 0.17 ± 0.09	¹ AAIJ 17K	LHCB	pp at 7 and 8 TeV
¹ Contains also the contribution from $B^+ \rightarrow \psi(2S)[\rightarrow J/\psi\pi^+\pi^-]\pi^+\pi^-\pi^-$ decays.			

$\Gamma(\psi(2S)\pi^+\pi^-\pi^-)/\Gamma(\psi(2S)K^+)$ $\Gamma_{301}/\Gamma_{311}$

VALUE (units 10^{-2})	DOCUMENT ID	TECN	COMMENT
3.04 ± 0.50 ± 0.26	AAIJ 17K	LHCB	pp at 7 and 8 TeV

$\Gamma(J/\psi(1S)\rho^+)/\Gamma_{total}$ Γ_{302}/Γ

VALUE (units 10^{-5})	CL%	DOCUMENT ID	TECN	COMMENT
4.1 ± 0.5 OUR AVERAGE				Error includes scale factor of 1.4.
3.81 $^{+0.25}_{-0.24}$ ± 0.35		AAIJ 19o	LHCB	pp at 7 and 8 TeV
5.0 ± 0.7 ± 0.3		¹ AUBERT 07AC	BABR	$e^+e^- \rightarrow \Upsilon(4S)$
••• We do not use the following data for averages, fits, limits, etc. •••				
<77	90	BISHAI 96	CLE2	$e^+e^- \rightarrow \Upsilon(4S)$
¹ Assumes equal production of B^+ and B^0 at the $\Upsilon(4S)$.				

$\Gamma(J/\psi(1S)\pi^+\pi^0 \text{ nonresonant})/\Gamma_{total}$ Γ_{303}/Γ

VALUE (units 10^{-5})	CL%	DOCUMENT ID	TECN	COMMENT
<0.73	90	¹ AUBERT 07AC	BABR	$e^+e^- \rightarrow \Upsilon(4S)$
¹ Assumes equal production of B^+ and B^0 at the $\Upsilon(4S)$.				

$\Gamma(J/\psi(1S)a_1(1260)^+)/\Gamma_{total}$ Γ_{304}/Γ

VALUE	CL%	DOCUMENT ID	TECN	COMMENT
<1.2 × 10⁻³	90	BISHAI 96	CLE2	$e^+e^- \rightarrow \Upsilon(4S)$

Meson Particle Listings

 B^\pm

$\Gamma(J/\psi(1S)\rho\bar{p}\pi^+)/\Gamma_{\text{total}}$					Γ_{305}/Γ
VALUE	CL%	DOCUMENT ID	TECN	COMMENT	
$<5.0 \times 10^{-7}$	90	¹ AAIJ	13z	LHCB pp at 7 TeV	
¹ Uses $B(B_S^0 \rightarrow J/\psi(1S)\pi^+\pi^-) = (1.98 \pm 0.20) \times 10^{-4}$.					

$\Gamma(J/\psi(1S)\rho\bar{\Lambda})/\Gamma_{\text{total}}$					Γ_{306}/Γ
VALUE (units 10^{-6})	CL%	DOCUMENT ID	TECN	COMMENT	
14.6 ± 1.2 OUR AVERAGE					
$15.1 \pm 0.8 \pm 1.0$		¹ SIRUNYAN	19CM	CMS pp at 8 TeV	
$11.7 \pm 2.8^{+1.8}_{-2.3}$		² XIE	05	BELL $e^+e^- \rightarrow \Upsilon(4S)$	
12^{+9}_{-6}		² AUBERT	03k	BABR $e^+e^- \rightarrow \Upsilon(4S)$	

• • • We do not use the following data for averages, fits, limits, etc. • • •

VALUE	CL%	DOCUMENT ID	TECN	COMMENT
<41	90	ZANG	04	BELL $e^+e^- \rightarrow \Upsilon(4S)$

¹ SIRUNYAN 19CM reports $B(B^+ \rightarrow J/\psi\bar{\Lambda}p)/B(B^+ \rightarrow J/\psi K^*(892)) = (1.054 \pm 0.057 \pm 0.035 \pm 0.011) \times 10^{-2}$ and rescaled with the best value of $B(B^+ \rightarrow J/\psi K^*(892)) = (1.43 \pm 0.08) \times 10^{-3}$, where the last uncertainty is the uncertainty from the branching fractions of $\bar{\Lambda}$ and $K^*(892)$ to reconstructed final states.

² Assumes equal production of B^+ and B^0 at the $\Upsilon(4S)$.

$\Gamma(J/\psi(1S)\bar{\Sigma}^0 p)/\Gamma_{\text{total}}$					Γ_{307}/Γ
VALUE	CL%	DOCUMENT ID	TECN	COMMENT	
$<1.1 \times 10^{-5}$	90	¹ XIE	05	BELL $e^+e^- \rightarrow \Upsilon(4S)$	
¹ Assumes equal production of B^+ and B^0 at the $\Upsilon(4S)$.					

$\Gamma(J/\psi(1S)D^+)/\Gamma_{\text{total}}$					Γ_{308}/Γ
VALUE (units 10^{-5})	CL%	DOCUMENT ID	TECN	COMMENT	
<12	90	¹ AUBERT	05u	BABR $e^+e^- \rightarrow \Upsilon(4S)$	
¹ Assumes equal production of B^+ and B^0 at the $\Upsilon(4S)$.					

$\Gamma(J/\psi(1S)\bar{D}^0\pi^+)/\Gamma_{\text{total}}$					Γ_{309}/Γ
VALUE (units 10^{-5})	CL%	DOCUMENT ID	TECN	COMMENT	
<2.5	90	¹ ZHANG	05b	BELL $e^+e^- \rightarrow \Upsilon(4S)$	
• • • We do not use the following data for averages, fits, limits, etc. • • •					
<5.2	90	¹ AUBERT	05r	BABR $e^+e^- \rightarrow \Upsilon(4S)$	
¹ Assumes equal production of B^+ and B^0 at the $\Upsilon(4S)$.					

$\Gamma(\psi(2S)\pi^+)/\Gamma_{\text{total}}$					Γ_{310}/Γ
VALUE (units 10^{-5})		DOCUMENT ID	TECN	COMMENT	
$2.44 \pm 0.22 \pm 0.20$		¹ BHARDWAJ	08	BELL $e^+e^- \rightarrow \Upsilon(4S)$	
¹ Assumes equal production of B^+ and B^0 at the $\Upsilon(4S)$.					

$\Gamma(\psi(2S)\pi^+)/\Gamma(\psi(2S)K^+)$					$\Gamma_{310}/\Gamma_{311}$
VALUE (units 10^{-2})		DOCUMENT ID	TECN	COMMENT	
3.97 ± 0.29 OUR AVERAGE					
$3.95 \pm 0.40 \pm 0.12$		AAIJ	12Ac	LHCB pp at 7 TeV	
$3.99 \pm 0.36 \pm 0.17$		BHARDWAJ	08	BELL $e^+e^- \rightarrow \Upsilon(4S)$	

$\Gamma(\psi(2S)K^+)/\Gamma_{\text{total}}$					Γ_{311}/Γ
VALUE (units 10^{-4})	EVTS	DOCUMENT ID	TECN	COMMENT	
6.19 ± 0.22 OUR FIT					
6.48 ± 0.34 OUR AVERAGE					
$6.4 \pm 1.0 \pm 0.4$		¹ KATO	18	BELL $e^+e^- \rightarrow \Upsilon(4S)$	
$6.65 \pm 0.17 \pm 0.55$		² GULER	11	BELL $e^+e^- \rightarrow \Upsilon(4S)$	
$4.9 \pm 1.6 \pm 0.4$		¹ AUBERT	06E	BABR $e^+e^- \rightarrow \Upsilon(4S)$	
$6.17 \pm 0.32 \pm 0.44$		² AUBERT	05j	BABR $e^+e^- \rightarrow \Upsilon(4S)$	
$7.8 \pm 0.7 \pm 0.9$		² RICHICHI	01	CLE2 $e^+e^- \rightarrow \Upsilon(4S)$	
$18 \pm 8 \pm 4$	5	² ALBRECHT	90j	ARG $e^+e^- \rightarrow \Upsilon(4S)$	
• • • We do not use the following data for averages, fits, limits, etc. • • •					
6.9 ± 0.6		² ABE	03b	BELL Repl. by GULER 11	
$6.4 \pm 0.5 \pm 0.8$		² AUBERT	02	BABR Repl. by AUBERT 05j	
$6.1 \pm 2.3 \pm 0.9$	7	² ALAM	94	CLE2 Repl. by RICHICHI 01	
<5 at 90% CL		² BORTOLETTO	92	CLEO $e^+e^- \rightarrow \Upsilon(4S)$	
22 ± 17	3	³ ALBRECHT	87d	ARG $e^+e^- \rightarrow \Upsilon(4S)$	
¹ Measures absolute branching fractions using a missing-mass technique.					
² Assumes equal production of B^+ and B^0 at the $\Upsilon(4S)$.					
³ ALBRECHT 87d assume $B^+B^-/B^0\bar{B}^0$ ratio is 55/45. Superseded by ALBRECHT 90j.					

$\Gamma(\psi(2S)K^+)/\Gamma(J/\psi(1S)K^+)$					$\Gamma_{311}/\Gamma_{275}$
VALUE		DOCUMENT ID	TECN	COMMENT	
0.616 ± 0.018 OUR FIT					
0.605 ± 0.021 OUR AVERAGE					
$0.58 \pm 0.11 \pm 0.02$		¹ AAIJ	13s	LHCB pp at 7 TeV	
$0.607 \pm 0.018 \pm 0.013$		^{2,3} AAIJ	12L	LHCB pp at 7 TeV	
$0.63 \pm 0.05 \pm 0.08$		ABAZOV	09Y	D0 $p\bar{p}$ at 1.96 TeV	
$0.558 \pm 0.082 \pm 0.056$		ABE	98o	CDF $p\bar{p}$ 1.8 TeV	
• • • We do not use the following data for averages, fits, limits, etc. • • •					
$0.64 \pm 0.06 \pm 0.07$		⁴ AUBERT	02	BABR $e^+e^- \rightarrow \Upsilon(4S)$	
¹ AAIJ 13s reports $[\Gamma(B^+ \rightarrow \psi(2S)K^+)/\Gamma(B^+ \rightarrow J/\psi(1S)K^+)] \times [B(\psi(2S) \rightarrow p\bar{p})] / [B(J/\psi(1S) \rightarrow p\bar{p})] = 0.080 \pm 0.012 \pm 0.009$ which we multiply or divide by our best values $B(\psi(2S) \rightarrow p\bar{p}) = (2.94 \pm 0.08) \times 10^{-4}$, $B(J/\psi(1S) \rightarrow p\bar{p}) =$					

$(2.121 \pm 0.029) \times 10^{-3}$. Our first error is their experiment's error and our second error is the systematic error from using our best values.

² AAIJ 12L reports $0.594 \pm 0.006 \pm 0.016 \pm 0.015$ from a measurement of $[\Gamma(B^+ \rightarrow \psi(2S)K^+)/\Gamma(B^+ \rightarrow J/\psi(1S)K^+)] \times [B(J/\psi(1S) \rightarrow e^+e^-)] / [B(\psi(2S) \rightarrow e^+e^-)]$ assuming $B(J/\psi(1S) \rightarrow e^+e^-) = (5.94 \pm 0.06) \times 10^{-2}$, $B(\psi(2S) \rightarrow e^+e^-) = (7.72 \pm 0.17) \times 10^{-3}$, which we rescale to our best values $B(J/\psi(1S) \rightarrow e^+e^-) = (5.971 \pm 0.032) \times 10^{-2}$, $B(\psi(2S) \rightarrow e^+e^-) = (7.93 \pm 0.17) \times 10^{-3}$. Our first error is their experiment's error and our second error is the systematic error from using our best values.

³ Assumes $B(J/\psi \rightarrow \mu^+\mu^-) / B(\psi(2S) \rightarrow \mu^+\mu^-) = B(J/\psi \rightarrow e^+e^-) / B(\psi(2S) \rightarrow e^+e^-) = 7.69 \pm 0.19$.

⁴ Assumes equal production of B^+ and B^0 at the $\Upsilon(4S)$.

$\Gamma(\psi(2S)K^*(892^+)/\Gamma_{\text{total}}$					Γ_{312}/Γ
VALUE (units 10^{-4})	CL%	DOCUMENT ID	TECN	COMMENT	
6.7 ± 1.4 OUR AVERAGE					
$5.92 \pm 0.85 \pm 0.89$		¹ AUBERT	05j	BABR $e^+e^- \rightarrow \Upsilon(4S)$	
$9.2 \pm 1.9 \pm 1.2$		¹ RICHICHI	01	CLE2 $e^+e^- \rightarrow \Upsilon(4S)$	
• • • We do not use the following data for averages, fits, limits, etc. • • •					
<30	90	¹ ALAM	94	CLE2 Repl. by RICHICHI 01	
<35	90	¹ BORTOLETTO	092	CLEO $e^+e^- \rightarrow \Upsilon(4S)$	
<49	90	¹ ALBRECHT	90j	ARG $e^+e^- \rightarrow \Upsilon(4S)$	
¹ Assumes equal production of B^+ and B^0 at the $\Upsilon(4S)$.					

$\Gamma(\psi(2S)K^*(892^+)/\Gamma(\psi(2S)K^+)$					$\Gamma_{312}/\Gamma_{311}$
VALUE		DOCUMENT ID	TECN	COMMENT	
$0.96 \pm 0.15 \pm 0.09$		AUBERT	05j	BABR $e^+e^- \rightarrow \Upsilon(4S)$	

$\Gamma(\psi(2S)K^0\pi^+)/\Gamma_{\text{total}}$					Γ_{313}/Γ
VALUE (units 10^{-3})		DOCUMENT ID	TECN	COMMENT	
0.588 ± 0.034		¹ AUBERT	09AA	BABR $e^+e^- \rightarrow \Upsilon(4S)$	
• • • We do not use the following data for averages, fits, limits, etc. • • •					
¹ Does not report systematic uncertainties.					

$\Gamma(\psi(2S)K^+\pi^+\pi^-)/\Gamma_{\text{total}}$					Γ_{314}/Γ
VALUE (units 10^{-4})	EVTS	DOCUMENT ID	TECN	COMMENT	
4.3 ± 0.5 OUR AVERAGE					
$4.31 \pm 0.20 \pm 0.50$		¹ GULER	11	BELL $e^+e^- \rightarrow \Upsilon(4S)$	
$19 \pm 11 \pm 4$	3	¹ ALBRECHT	90j	ARG $e^+e^- \rightarrow \Upsilon(4S)$	
¹ Assumes equal production of B^+ and B^0 at the $\Upsilon(4S)$.					

$\Gamma(\psi(2S)\phi(1020)K^+)/\Gamma_{\text{total}}$					Γ_{315}/Γ
VALUE (units 10^{-6})		DOCUMENT ID	TECN	COMMENT	
$4.0 \pm 0.4 \pm 0.6$		^{1,2} KHACHATRY..17c	CMS	pp at 8 TeV	
¹ Measured using $B^+ \rightarrow \psi(2S)K^+$ as a normalization channel. The second error represents total systematic uncertainties including those from branching fractions which were taken from PDG 16 as $B(\phi \rightarrow K^+K^-) = 0.489 \pm 0.005$ and $B(B^+ \rightarrow \psi(2S)K^+) = (6.26 \pm 0.24) \times 10^{-4}$.					
² An upper limit on the fraction of the non- ϕ component in $B^+ \rightarrow \psi(2S)K^+K^-K^+$ decays is set as 0.26 at the 95% confidence level.					

$\Gamma(\psi(3770)K^+)/\Gamma_{\text{total}}$					Γ_{316}/Γ
VALUE (units 10^{-3})	CL%	DOCUMENT ID	TECN	COMMENT	
0.49 ± 0.13 OUR AVERAGE					
$3.5 \pm 2.5 \pm 0.3$		¹ AUBERT	06E	BABR $e^+e^- \rightarrow \Upsilon(4S)$	
$0.48 \pm 0.11 \pm 0.07$		² CHISTOV	04	BELL $e^+e^- \rightarrow \Upsilon(4S)$	
• • • We do not use the following data for averages, fits, limits, etc. • • •					
<0.23	90	¹ KATO	18	BELL $e^+e^- \rightarrow \Upsilon(4S)$	
¹ Measures absolute branching fractions using a missing-mass technique.					
² Assumes equal production of B^+ and B^0 at the $\Upsilon(4S)$.					

$\Gamma(\psi(3770)K^+, \psi \rightarrow D^0\bar{D}^0)/\Gamma_{\text{total}}$					Γ_{317}/Γ
VALUE (units 10^{-4})		DOCUMENT ID	TECN	COMMENT	
1.5 ± 0.5 OUR AVERAGE					
$1.18 \pm 0.41 \pm 0.15$		¹ LEES	15c	BABR $e^+e^- \rightarrow \Upsilon(4S)$	
$2.2 \pm 0.5 \pm 0.3$		¹ BRODZICKA	08	BELL $e^+e^- \rightarrow \Upsilon(4S)$	
• • • We do not use the following data for averages, fits, limits, etc. • • •					
$1.41 \pm 0.30 \pm 0.22$		¹ AUBERT	08b	BABR Repl. by LEES 15c	
$3.4 \pm 0.8 \pm 0.5$		¹ CHISTOV	04	BELL Repl. by BRODZICKA 08	
¹ Assumes equal production of B^+ and B^0 at the $\Upsilon(4S)$.					

$\Gamma(\psi(3770)K^+, \psi \rightarrow D^+D^-)/\Gamma_{\text{total}}$					Γ_{318}/Γ
VALUE (units 10^{-4})		DOCUMENT ID	TECN	COMMENT	
0.94 ± 0.35 OUR AVERAGE					
$0.84 \pm 0.32 \pm 0.21$		¹ AUBERT	08b	BABR $e^+e^- \rightarrow \Upsilon(4S)$	
$1.4 \pm 0.8 \pm 0.2$		¹ CHISTOV	04	BELL $e^+e^- \rightarrow \Upsilon(4S)$	
¹ Assumes equal production of B^+ and B^0 at the $\Upsilon(4S)$.					

$\Gamma(\psi(3770)K^+, \psi \rightarrow p\bar{p})/\Gamma_{\text{total}}$					Γ_{319}/Γ
VALUE	CL%	DOCUMENT ID	TECN	COMMENT	
$<2 \times 10^{-7}$	95	¹ AAIJ	17Ad	LHCB pp at 7 and 8 TeV	
¹ Measured relative to $B^+ \rightarrow J/\psi K^+$ decay with charmonia reconstructed in $p\bar{p}$ final state and using $B(B^+ \rightarrow J/\psi K^+) \times B(J/\psi \rightarrow p\bar{p}) = (2.17 \pm 0.08) \times 10^{-6}$.					

See key on page 999

Meson Particle Listings

B^\pm

$\Gamma(\psi(4040) K^+)/\Gamma_{\text{total}}$ Γ_{320}/Γ

VALUE	CL%	DOCUMENT ID	TECN	COMMENT
$<1.3 \times 10^{-4}$	90	AAIJ	13bc LHCB	pp at 7, 8 TeV
••• We do not use the following data for averages, fits, limits, etc. •••				
$<3.0 \times 10^{-3}$	90	¹ IWASHITA	14 BELL	$e^+e^- \rightarrow \Upsilon(4S)$
¹ IWASHITA 14 reports $[\Gamma(B^+ \rightarrow \psi(4040) K^+)/\Gamma_{\text{total}}] \times [B(\psi(4040) \rightarrow J/\psi\eta)] < 15.5 \times 10^{-6}$ which we divide by our best value $B(\psi(4040) \rightarrow J/\psi\eta) = 5.2 \times 10^{-3}$.				

$\Gamma(\psi(4160) K^+)/\Gamma_{\text{total}}$ Γ_{321}/Γ

VALUE (units 10^{-4})	DOCUMENT ID	TECN	COMMENT
$5.1^{+1.3+2.5}_{-1.2-2.4}$	¹ AAIJ	13bc LHCB	pp at 7, 8 TeV
¹ AAIJ 13bc reports $[\Gamma(B^+ \rightarrow \psi(4160) K^+)/\Gamma_{\text{total}}] \times B(\psi(4160) \rightarrow \mu^+\mu^-) = (3.5^{+0.9}_{-0.8}) \times 10^{-9}$ which we divide by our best value $B(\psi(4160) \rightarrow e^+e^-) = (6.9 \pm 3.3) \times 10^{-6}$ assuming lepton universality. Our first error is their experiment's error and our second error is the systematic error from using our best value.			

$\Gamma(\psi(4160) K^+, \psi \rightarrow \bar{D}^0 D^0)/\Gamma_{\text{total}}$ Γ_{322}/Γ

VALUE (units 10^{-4})	DOCUMENT ID	TECN	COMMENT
$0.84 \pm 0.41 \pm 0.33$	¹ LEES	15c BABR	$e^+e^- \rightarrow \Upsilon(4S)$
¹ Assumes equal production of B^+ and B^0 at the $\Upsilon(4S)$.			

$\Gamma(\chi_{c0} \pi^+, \chi_{c0} \rightarrow \pi^+ \pi^-)/\Gamma_{\text{total}}$ Γ_{323}/Γ

VALUE (units 10^{-6})	CL%	DOCUMENT ID	TECN	COMMENT
<0.1	90	¹ AUBERT	09L BABR	$e^+e^- \rightarrow \Upsilon(4S)$
••• We do not use the following data for averages, fits, limits, etc. •••				
<0.3	90	¹ AUBERT,B	05G BABR	Repl. by AUBERT 09L
¹ Assumes equal production of B^+ and B^0 at the $\Upsilon(4S)$.				

$\Gamma(\chi_{c0} K^+)/\Gamma_{\text{total}}$ Γ_{324}/Γ

VALUE (units 10^{-4})	CL%	DOCUMENT ID	TECN	COMMENT
$1.50^{+0.15}_{-0.13}$ OUR AVERAGE				
$1.8^{+0.6}_{-0.5} \pm 0.6$		¹ CHILIKIN	19 BELL	$e^+e^- \rightarrow \Upsilon(4S)$
$1.84 \pm 0.25 \pm 0.14$		^{2,3} LEES	12o BABR	$e^+e^- \rightarrow \Upsilon(4S)$
$1.68 \pm 0.32 \pm 0.16$		^{2,4} LEES	12o BABR	$e^+e^- \rightarrow \Upsilon(4S)$
$1.8 \pm 0.8 \pm 0.1$		⁵ LEES	11i BABR	$e^+e^- \rightarrow \Upsilon(4S)$
$1.23^{+0.28}_{-0.25} \pm 0.05$		^{2,6} AUBERT	08Ai BABR	$e^+e^- \rightarrow \Upsilon(4S)$
$4.3 \pm 2.0 \pm 0.2$		⁷ AUBERT, BE	06M BABR	$e^+e^- \rightarrow \Upsilon(4S)$
$1.12 \pm 0.12^{+0.30}_{-0.20}$		² GARMASH	06 BELL	$e^+e^- \rightarrow \Upsilon(4S)$
••• We do not use the following data for averages, fits, limits, etc. •••				
<3.3	90	⁸ KATO	18 BELL	$e^+e^- \rightarrow \Upsilon(4S)$
<2.7	95	⁹ AAIJ	13s LHCB	pp at 7 TeV
<5	90	^{2,10} WICHT	08 BELL	$e^+e^- \rightarrow \Upsilon(4S)$
<1.8	90	⁸ AUBERT	06E BABR	$e^+e^- \rightarrow \Upsilon(4S)$
$1.84 \pm 0.32 \pm 0.31$		^{2,11} AUBERT	06o BABR	Repl. by LEES 12o
<8.9	90	² AUBERT	05k BABR	$e^+e^- \rightarrow \Upsilon(4S)$
$1.39 \pm 0.49 \pm 0.11$		¹² AUBERT,B	05N BABR	Repl. by AUBERT 08Ai
$1.96 \pm 0.35^{+2.00}_{-0.42}$		² GARMASH	05 BELL	Repl. by GARMASH 06
2.7 ± 0.7		¹³ AUBERT	04T BABR	Repl. by AUBERT,B 04P
$3.0 \pm 0.8 \pm 0.3$		¹⁴ AUBERT,B	04P BABR	Repl. by AUBERT,B 05N
$6.0^{+2.1}_{-1.8} \pm 1.1$		¹⁵ ABE	02B BELL	Repl. by GARMASH 05
<4.8	90	¹⁶ EDWARDS	01 CLE2	$e^+e^- \rightarrow \Upsilon(4S)$

- ¹ CHILIKIN 19 reports $[\Gamma(B^+ \rightarrow \chi_{c0} K^+)/\Gamma_{\text{total}}] \times [B(\chi_{c0}(1P) \rightarrow p\bar{p}\pi^+\pi^-)] = (3.7^{+1.2+0.2}_{-1.0-0.3}) \times 10^{-7}$ which we divide by our best value $B(\chi_{c0}(1P) \rightarrow p\bar{p}\pi^+\pi^-) = (2.1 \pm 0.7) \times 10^{-3}$. Our first error is their experiment's error and our second error is the systematic error from using our best value.
- ² Assumes equal production of B^+ and B^0 at the $\Upsilon(4S)$.
- ³ Measured in the $B^+ \rightarrow K^+ K^- K^+$ decay.
- ⁴ Measured in the $B^+ \rightarrow K^+ K_S^0 K_S^0$ decay.
- ⁵ LEES 11i reports $[\Gamma(B^+ \rightarrow \chi_{c0} K^+)/\Gamma_{\text{total}}] \times [B(\chi_{c0}(1P) \rightarrow \pi\pi)] = (1.53 \pm 0.66 \pm 0.27) \times 10^{-6}$ which we divide by our best value $B(\chi_{c0}(1P) \rightarrow \pi\pi) = (8.51 \pm 0.33) \times 10^{-3}$. Our first error is their experiment's error and our second error is the systematic error from using our best value.
- ⁶ AUBERT 08Ai reports $(0.70 \pm 0.10^{+0.13}_{-0.10}) \times 10^{-6}$ for $B(B^+ \rightarrow \chi_{c0} K^+) \times B(\chi_{c0} \rightarrow \pi^+\pi^-)$. We compute $B(B^+ \rightarrow \chi_{c0} K^+)$ using the PDG value $B(\chi_{c0} \rightarrow \pi\pi) = (8.51 \pm 0.33) \times 10^{-3}$ and 2/3 for the $\pi^+\pi^-$ fraction. Our first error is their experiment's error and the second error is systematic error from using our best value.
- ⁷ AUBERT, BE 06M reports $[\Gamma(B^+ \rightarrow \chi_{c0} K^+)/\Gamma_{\text{total}}] \times [B(\chi_{c0}(1P) \rightarrow \gamma J/\psi(1S))] = (6.1 \pm 2.6 \pm 1.1) \times 10^{-6}$ which we divide by our best value $B(\chi_{c0}(1P) \rightarrow \gamma J/\psi(1S)) = (1.40 \pm 0.05) \times 10^{-2}$. Our first error is their experiment's error and our second error is the systematic error from using our best value. The significance of the observed signal is 2.4 σ .
- ⁸ Measures absolute branching fractions using a missing-mass technique.
- ⁹ AAIJ 13s reports $[\Gamma(B^+ \rightarrow \chi_{c0} K^+)/\Gamma_{\text{total}}] \times [B(\chi_{c0}(1P) \rightarrow p\bar{p})] < 6 \times 10^{-8}$ which we divide by our best value $B(\chi_{c0}(1P) \rightarrow p\bar{p}) = 2.21 \times 10^{-4}$.
- ¹⁰ WICHT 08 reports $[\Gamma(B^+ \rightarrow \chi_{c0} K^+)/\Gamma_{\text{total}}] \times [B(\chi_{c0}(1P) \rightarrow \gamma\gamma)] < 0.11 \times 10^{-6}$ which we divide by our best value $B(\chi_{c0}(1P) \rightarrow \gamma\gamma) = 2.04 \times 10^{-4}$.

- ¹¹ Measured in the $B^+ \rightarrow K^+ K^- K^+$ decay.
- ¹² AUBERT,B 05N reports $(0.66 \pm 0.22 \pm 0.08) \times 10^{-6}$ for $B(B^+ \rightarrow \chi_{c0}^0 K^+) \times B(\chi_{c0}^0 \rightarrow \pi^+\pi^-)$. We compute $B(B^+ \rightarrow \chi_{c0}^0 K^+)$ using the PDG value $B(\chi_{c0}^0 \rightarrow \pi^+\pi^-) = (7.1 \pm 0.6) \times 10^{-3}$ and 2/3 for the $\pi^+\pi^-$ fraction.
- ¹³ The measurement performed using decay channels $\chi_{c0} \rightarrow \pi^+\pi^-$ and $\chi_{c0} \rightarrow K^+K^-$. The ratio of the branching ratios for these channels is found to be consistent with world average.
- ¹⁴ AUBERT 04P reports $B(B^+ \rightarrow \chi_{c0} K^+) \times B(\chi_{c0} \rightarrow \pi^+\pi^-) = (1.5 \pm 0.4 \pm 0.1) \times 10^{-6}$ and used PDG value of $B(\chi_{c0} \rightarrow \pi\pi) = (7.4 \pm 0.8) \times 10^{-3}$ and Clebsh-Gordan coefficient to compute $B(B^+ \rightarrow \chi_{c0} K^+)$.
- ¹⁵ ABE 02b measures the ratio of $B(B^+ \rightarrow \chi_{c0} K^+)/B(B^+ \rightarrow J/\psi(1S) K^+) = 0.60 \pm 0.21 - 0.18 \pm 0.05 \pm 0.08$, where the third error is due to the uncertainty in the $B(\chi_{c0} \rightarrow \pi^+\pi^-)$, and uses $B(B^+ \rightarrow J/\psi(1S) K^+) = (10.0 \pm 1.0) \times 10^{-4}$ to obtain the result.
- ¹⁶ EDWARDS 01 assumes equal production of B^0 and B^+ at the $\Upsilon(4S)$. The correlated uncertainties (28.3)% from $B(J/\psi(1S) \rightarrow \gamma\eta_c)$ in those modes have been accounted for.

$\Gamma(\chi_{c0} K^*(892^+)/\Gamma_{\text{total}}$ Γ_{325}/Γ

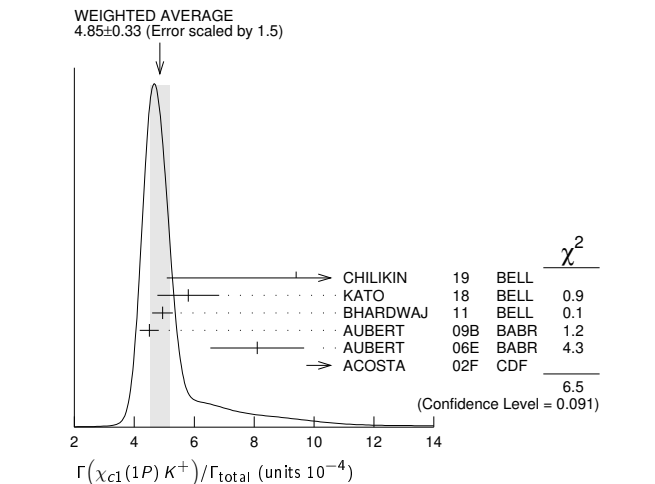
VALUE (units 10^{-4})	CL%	DOCUMENT ID	TECN	COMMENT
<2.1	90	¹ AUBERT	08BD BABR	$e^+e^- \rightarrow \Upsilon(4S)$
••• We do not use the following data for averages, fits, limits, etc. •••				
<28.6	90	¹ AUBERT	05k BABR	Repl. by AUBERT 08BD
¹ Assumes equal production of B^+ and B^0 at the $\Upsilon(4S)$.				

$\Gamma(\chi_{c1}(1P) \pi^+)/\Gamma_{\text{total}}$ Γ_{326}/Γ

VALUE (units 10^{-5})	DOCUMENT ID	TECN	COMMENT
$2.2 \pm 0.4 \pm 0.3$	¹ KUMAR	06 BELL	$e^+e^- \rightarrow \Upsilon(4S)$
¹ Assumes equal production of B^+ and B^0 at the $\Upsilon(4S)$.			

$\Gamma(\chi_{c1}(1P) K^+)/\Gamma_{\text{total}}$ Γ_{327}/Γ

VALUE (units 10^{-4})	EVTS	DOCUMENT ID	TECN	COMMENT
4.85 ± 0.33 OUR AVERAGE				Error includes scale factor of 1.5. See the ideogram below.
$9^{+3}_{-2} \pm 4$		¹ CHILIKIN	19 BELL	$e^+e^- \rightarrow \Upsilon(4S)$
$5.8 \pm 0.9 \pm 0.5$		² KATO	18 BELL	$e^+e^- \rightarrow \Upsilon(4S)$
$4.94 \pm 0.11 \pm 0.33$		³ BHARDWAJ	11 BELL	$e^+e^- \rightarrow \Upsilon(4S)$
$4.5 \pm 0.1 \pm 0.3$		⁴ AUBERT	09B BABR	$e^+e^- \rightarrow \Upsilon(4S)$
$8.1 \pm 1.4 \pm 0.7$		² AUBERT	06E BABR	$e^+e^- \rightarrow \Upsilon(4S)$
$15.5 \pm 5.4 \pm 2.0$		⁵ ACOSTA	02F CDF	$p\bar{p}$ 1.8 TeV
••• We do not use the following data for averages, fits, limits, etc. •••				
$5.1 \pm 0.4 \pm 0.1$		⁶ AUBERT, BE	06M BABR	Repl. by AUBERT 09B
$4.49 \pm 0.19 \pm 0.53$		³ SONI	06 BELL	Repl. by BHARDWAJ 11
$5.79 \pm 0.26 \pm 0.65$		³ AUBERT	05J BABR	Repl. by AUBERT, BE 06M
$6.0 \pm 0.9 \pm 0.2$		⁷ AUBERT	02 BABR	Repl. by AUBERT 05J
$9.7 \pm 4.0 \pm 0.9$		³ ALAM	94 CLE2	$e^+e^- \rightarrow \Upsilon(4S)$
$19 \pm 13 \pm 6$		⁸ ALBRECHT	92E ARG	$e^+e^- \rightarrow \Upsilon(4S)$



- ¹ CHILIKIN 19 reports $[\Gamma(B^+ \rightarrow \chi_{c1}(1P) K^+)/\Gamma_{\text{total}}] \times [B(\chi_{c1}(1P) \rightarrow p\bar{p}\pi^+\pi^-)] = (4.7^{+1.3+0.4}_{-1.2-0.2}) \times 10^{-7}$ which we divide by our best value $B(\chi_{c1}(1P) \rightarrow p\bar{p}\pi^+\pi^-) = (5.0 \pm 1.9) \times 10^{-4}$. Our first error is their experiment's error and our second error is the systematic error from using our best value.
- ² Measures absolute branching fractions using a missing-mass technique.
- ³ Assumes equal production of B^+ and B^0 at the $\Upsilon(4S)$.
- ⁴ Uses $\chi_{c1,2} \rightarrow J/\psi\gamma$. Assumes $B(\Upsilon(4S) \rightarrow B^+ B^-) = (51.6 \pm 0.6)\%$ and $B(\Upsilon(4S) \rightarrow B^0 \bar{B}^0) = (48.4 \pm 0.6)\%$.
- ⁵ ACOSTA 02F uses as reference of $B(B \rightarrow J/\psi(1S) K^+) = (10.1 \pm 0.6) \times 10^{-4}$. The second error includes the systematic error and the uncertainties of the branching ratio.

Meson Particle Listings

B^\pm

⁶ AUBERT, BE 06M reports $[\Gamma(B^+ \rightarrow \chi_{c1}(1P)K^+)/\Gamma_{\text{total}}] \times [B(\chi_{c1}(1P) \rightarrow \gamma J/\psi(1S))] = (1.76 \pm 0.07 \pm 0.12) \times 10^{-4}$ which we divide by our best value $B(\chi_{c1}(1P) \rightarrow \gamma J/\psi(1S)) = (34.3 \pm 1.0) \times 10^{-2}$. Our first error is their experiment's error and our second error is the systematic error from using our best value.

⁷ AUBERT 02 reports $(7.5 \pm 0.9 \pm 0.8) \times 10^{-4}$ from a measurement of $[\Gamma(B^+ \rightarrow \chi_{c1}(1P)K^+)/\Gamma_{\text{total}}] \times [B(\chi_{c1}(1P) \rightarrow \gamma J/\psi(1S))]$ assuming $B(\chi_{c1}(1P) \rightarrow \gamma J/\psi(1S)) = 0.273 \pm 0.016$, which we rescale to our best value $B(\chi_{c1}(1P) \rightarrow \gamma J/\psi(1S)) = (34.3 \pm 1.0) \times 10^{-2}$. Our first error is their experiment's error and our second error is the systematic error from using our best value. Assumes equal production of B^+ and B^0 at the $\Upsilon(4S)$.

⁸ ALBRECHT 92E assumes no $\chi_{c2}(1P)$ production and $B(\Upsilon(4S) \rightarrow B^+B^-) = 50\%$.

$\Gamma(\chi_{c1}(1P)K^+)/\Gamma(J/\psi(1S)K^+)$		$\Gamma_{327}/\Gamma_{275}$	
VALUE	DOCUMENT ID	TECN	COMMENT
0.60 ± 0.07 ± 0.02	¹ AUBERT	02	BABR $e^+e^- \rightarrow \Upsilon(4S)$

¹ AUBERT 02 reports $0.75 \pm 0.08 \pm 0.05$ from a measurement of $[\Gamma(B^+ \rightarrow \chi_{c1}(1P)K^+)/\Gamma(B^+ \rightarrow J/\psi(1S)K^+)] \times [B(\chi_{c1}(1P) \rightarrow \gamma J/\psi(1S))]$ assuming $B(\chi_{c1}(1P) \rightarrow \gamma J/\psi(1S)) = 0.273 \pm 0.016$, which we rescale to our best value $B(\chi_{c1}(1P) \rightarrow \gamma J/\psi(1S)) = (34.3 \pm 1.0) \times 10^{-2}$. Our first error is their experiment's error and our second error is the systematic error from using our best value. Assumes equal production of B^+ and B^0 at the $\Upsilon(4S)$.

$\Gamma(\chi_{c1}(1P)\pi^+)/\Gamma(\chi_{c1}(1P)K^+)$		$\Gamma_{326}/\Gamma_{327}$	
VALUE	DOCUMENT ID	TECN	COMMENT
0.043 ± 0.008 ± 0.003	¹ KUMAR	06	BELL $e^+e^- \rightarrow \Upsilon(4S)$

¹ Assumes equal production of B^+ and B^0 at the $\Upsilon(4S)$.

$\Gamma(\chi_{c1}(1P)K^*(892)^+)/\Gamma_{\text{total}}$		Γ_{328}/Γ	
VALUE (units 10^{-4})	CL%	DOCUMENT ID	TECN
3.0 ± 0.6 OUR AVERAGE		Error includes scale factor of 1.1.	
2.6 ± 0.5 ± 0.4		¹ AUBERT	09B BABR $e^+e^- \rightarrow \Upsilon(4S)$
4.05 ± 0.59 ± 0.95		² SONI	06 BELL $e^+e^- \rightarrow \Upsilon(4S)$

• • • We do not use the following data for averages, fits, limits, etc. • • •

2.94 ± 0.95 ± 0.98		² AUBERT	05J BABR Repl. by AUBERT 09B
< 21	90	² ALAM	94 CLE2 $e^+e^- \rightarrow \Upsilon(4S)$

¹ Uses $\chi_{c1,2} \rightarrow J/\psi\gamma$. Assumes $B(\Upsilon(4S) \rightarrow B^+B^-) = (51.6 \pm 0.6)\%$ and $B(\Upsilon(4S) \rightarrow B^0\bar{B}^0) = (48.4 \pm 0.6)\%$.

² Assumes equal production of B^+ and B^0 at the $\Upsilon(4S)$.

$\Gamma(\chi_{c1}(1P)K^*(892)^+)/\Gamma(\chi_{c1}(1P)K^+)$		$\Gamma_{328}/\Gamma_{327}$	
VALUE	DOCUMENT ID	TECN	COMMENT
0.51 ± 0.17 ± 0.16	AUBERT	05J	BABR $e^+e^- \rightarrow \Upsilon(4S)$

$\Gamma(\chi_{c1}(1P)K^0\pi^+)/\Gamma_{\text{total}}$		Γ_{329}/Γ	
VALUE (units 10^{-4})	CL%	DOCUMENT ID	TECN
5.75 ± 0.26 ± 0.32		¹ BHARDWAJ	16 BELL $e^+e^- \rightarrow \Upsilon(4S)$

¹ Assumes equal production of B^+ and B^0 at the $\Upsilon(4S)$.

$\Gamma(\chi_{c1}(1P)K^0\pi^+)/\Gamma(J/\psi(1S)K^0\pi^+)$		$\Gamma_{329}/\Gamma_{276}$	
VALUE	DOCUMENT ID	TECN	COMMENT
0.503 ± 0.030 ± 0.014	¹ LEES	12B	BABR $e^+e^- \rightarrow \Upsilon(4S)$

¹ LEES 12B reports $0.501 \pm 0.024 \pm 0.028$ from a measurement of $[\Gamma(B^+ \rightarrow \chi_{c1}(1P)K^0\pi^+)/\Gamma(B^+ \rightarrow J/\psi(1S)K^0\pi^+)] \times [B(\chi_{c1}(1P) \rightarrow \gamma J/\psi(1S))]$ assuming $B(\chi_{c1}(1P) \rightarrow \gamma J/\psi(1S)) = (34.4 \pm 1.5) \times 10^{-2}$, which we rescale to our best value $B(\chi_{c1}(1P) \rightarrow \gamma J/\psi(1S)) = (34.3 \pm 1.0) \times 10^{-2}$. Our first error is their experiment's error and our second error is the systematic error from using our best value.

$\Gamma(\chi_{c1}(1P)K^+\pi^0)/\Gamma_{\text{total}}$		Γ_{330}/Γ	
VALUE (units 10^{-4})	CL%	DOCUMENT ID	TECN
3.29 ± 0.29 ± 0.19		¹ BHARDWAJ	16 BELL $e^+e^- \rightarrow \Upsilon(4S)$

¹ Assumes equal production of B^+ and B^0 at the $\Upsilon(4S)$.

$\Gamma(\chi_{c1}(1P)K^+\pi^-\pi^-)/\Gamma_{\text{total}}$		Γ_{331}/Γ	
VALUE (units 10^{-4})	CL%	DOCUMENT ID	TECN
3.74 ± 0.18 ± 0.24		¹ BHARDWAJ	16 BELL $e^+e^- \rightarrow \Upsilon(4S)$

¹ Assumes equal production of B^+ and B^0 at the $\Upsilon(4S)$.

$\Gamma(\chi_{c1}(2P)K^+, \chi_{c1}(2P) \rightarrow \pi^+\pi^-\chi_{c1}(1P))/\Gamma_{\text{total}}$		Γ_{332}/Γ	
VALUE	CL%	DOCUMENT ID	TECN
< 1.1 × 10⁻⁵	90	^{1,2} BHARDWAJ	16 BELL $e^+e^- \rightarrow \Upsilon(4S)$

¹ BHARDWAJ 16 analysis fixes mass and width of the $\chi_{c1}(2P)$ state to 3920 MeV and 20 MeV.

² Assumes equal production of B^+ and B^0 at the $\Upsilon(4S)$.

$\Gamma(\chi_{c2}K^+)/\Gamma_{\text{total}}$		Γ_{333}/Γ	
VALUE (units 10^{-5})	CL%	DOCUMENT ID	TECN
1.11 + 0.36 - 0.34 ± 0.09		¹ BHARDWAJ	11 BELL $e^+e^- \rightarrow \Upsilon(4S)$

• • • We do not use the following data for averages, fits, limits, etc. • • •

< 1.8	90	² AUBERT	09B BABR $e^+e^- \rightarrow \Upsilon(4S)$
< 2.0	90	³ AUBERT	06E BABR $e^+e^- \rightarrow \Upsilon(4S)$
< 2.9	90	¹ SONI	06 BELL Repl. by BHARDWAJ 11
< 3.0	90	¹ AUBERT	05K BABR Repl. by AUBERT 06E

¹ Assumes equal production of B^+ and B^0 at the $\Upsilon(4S)$.

² Uses $\chi_{c1,2} \rightarrow J/\psi\gamma$. Assumes $B(\Upsilon(4S) \rightarrow B^+B^-) = (51.6 \pm 0.6)\%$ and $B(\Upsilon(4S) \rightarrow B^0\bar{B}^0) = (48.4 \pm 0.6)\%$.

³ Perform measurements of absolute branching fractions using a missing mass technique.

$\Gamma(\chi_{c2}K^+, \chi_{c2} \rightarrow p\bar{p}\pi^+\pi^-)/\Gamma_{\text{total}}$		Γ_{334}/Γ	
VALUE	DOCUMENT ID	TECN	COMMENT
< 1.9 × 10⁻⁷	CHILIKIN	19	BELL $e^+e^- \rightarrow \Upsilon(4S)$

$\Gamma(B^+ \rightarrow \chi_{c2}K^+)/\Gamma_{\text{total}} \times \Gamma(\chi_{c2}(1P) \rightarrow \gamma\gamma)/\Gamma_{\text{total}}$		$\Gamma_{333}/\Gamma \times \Gamma_{93}^{\chi_{c2}(1P)}/\Gamma_{\chi_{c2}(1P)}$	
VALUE (units 10^{-6})	CL%	DOCUMENT ID	TECN
< 0.09	90	¹ WICHT	08 BELL $e^+e^- \rightarrow \Upsilon(4S)$

¹ Assumes equal production of B^+ and B^0 at the $\Upsilon(4S)$.

$\Gamma(\chi_{c2}K^*(892)^+)/\Gamma_{\text{total}}$		Γ_{335}/Γ	
VALUE	CL%	DOCUMENT ID	TECN
< 12 × 10⁻⁵	90	¹ AUBERT	09B BABR $e^+e^- \rightarrow \Upsilon(4S)$

• • • We do not use the following data for averages, fits, limits, etc. • • •

< 12.7 × 10 ⁻⁵	90	² SONI	06 BELL $e^+e^- \rightarrow \Upsilon(4S)$
< 1.2 × 10 ⁻⁵	90	² AUBERT	05K BABR Repl. by AUBERT 09B

¹ Uses $\chi_{c1,2} \rightarrow J/\psi\gamma$. Assumes $B(\Upsilon(4S) \rightarrow B^+B^-) = (51.6 \pm 0.6)\%$ and $B(\Upsilon(4S) \rightarrow B^0\bar{B}^0) = (48.4 \pm 0.6)\%$.

² Assumes equal production of B^+ and B^0 at the $\Upsilon(4S)$.

$\Gamma(\chi_{c2}K^0\pi^+)/\Gamma_{\text{total}}$		Γ_{336}/Γ	
VALUE (units 10^{-4})	CL%	DOCUMENT ID	TECN
1.16 ± 0.22 ± 0.12		¹ BHARDWAJ	16 BELL $e^+e^- \rightarrow \Upsilon(4S)$

¹ Assumes equal production of B^+ and B^0 at the $\Upsilon(4S)$.

$\Gamma(\chi_{c2}K^+\pi^0)/\Gamma_{\text{total}}$		Γ_{337}/Γ	
VALUE	CL%	DOCUMENT ID	TECN
< 0.62 × 10⁻⁴	90	¹ BHARDWAJ	16 BELL $e^+e^- \rightarrow \Upsilon(4S)$

¹ Assumes equal production of B^+ and B^0 at the $\Upsilon(4S)$.

$\Gamma(\chi_{c2}K^+\pi^-\pi^-)/\Gamma_{\text{total}}$		Γ_{338}/Γ	
VALUE (units 10^{-4})	CL%	DOCUMENT ID	TECN
1.34 ± 0.17 ± 0.09		¹ BHARDWAJ	16 BELL $e^+e^- \rightarrow \Upsilon(4S)$

¹ Assumes equal production of B^+ and B^0 at the $\Upsilon(4S)$.

$\Gamma(\chi_{c2}(3930)\pi^+, \chi_{c2} \rightarrow \pi^+\pi^-)/\Gamma_{\text{total}}$		Γ_{339}/Γ	
VALUE (units 10^{-6})	CL%	DOCUMENT ID	TECN
< 0.1	90	¹ AUBERT	09L BABR $e^+e^- \rightarrow \Upsilon(4S)$

¹ Assumes equal production of B^+ and B^0 at the $\Upsilon(4S)$.

$\Gamma(h_c(1P)K^+)/\Gamma_{\text{total}}$		Γ_{340}/Γ	
VALUE (units 10^{-5})	CL%	DOCUMENT ID	TECN
3.7 + 1.0 + 0.8 - 0.9 - 0.8		CHILIKIN	19 BELL $e^+e^- \rightarrow \Upsilon(4S)$

• • • We do not use the following data for averages, fits, limits, etc. • • •

< 3.8	90	¹ FANG	06 BELL $e^+e^- \rightarrow \Upsilon(4S)$
-------	----	-------------------	---

¹ Assumes equal production of B^+ and B^0 at the $\Upsilon(4S)$ and $B(h_c \rightarrow \eta_c\gamma) = 50\%$.

$\Gamma(h_c(1P)K^+, h_c \rightarrow p\bar{p})/\Gamma_{\text{total}}$		Γ_{341}/Γ	
VALUE	CL%	DOCUMENT ID	TECN
< 6.4 × 10⁻⁸	95	¹ AAIJ	13s LHCB $p\bar{p}$ at 7 TeV

¹ Measured relative to $B^+ \rightarrow J/\psi K^+$ decay with charmonia reconstructed in $p\bar{p}$ final state and using $B(B^+ \rightarrow J/\psi K^+) = (1.013 \pm 0.034) \times 10^{-3}$ and $B(J/\psi \rightarrow p\bar{p}) = (2.17 \pm 0.07) \times 10^{-3}$.

$\Gamma(K^0\pi^+)/\Gamma_{\text{total}}$		Γ_{342}/Γ	
VALUE (units 10^{-6})	CL%	DOCUMENT ID	TECN
23.7 ± 0.8 OUR FIT			
23.8 ± 0.7 OUR AVERAGE			

23.97 ± 0.53 ± 0.71		¹ DUH	13 BELL $e^+e^- \rightarrow \Upsilon(4S)$
23.9 ± 1.1 ± 1.0		¹ AUBERT, BE	06c BABR $e^+e^- \rightarrow \Upsilon(4S)$
18.8 + 3.7 + 2.1 - 3.3 - 1.8		¹ BORNHEIM	03 CLE2 $e^+e^- \rightarrow \Upsilon(4S)$

• • • We do not use the following data for averages, fits, limits, etc. • • •

Table with columns: VALUE (units 10^-6), CL%, DOCUMENT ID, TECN, COMMENT. Rows include LIN 07 BELL, AUBERT, BE 05E BABR, AUBERT 04M BABR, CHAO 04 BELL, CASEY 02 BELL, ABE 01H BELL, AUBERT 01E BABR, CRONIN-HEN..00 CLE2, GODANG 98 CLE2, ASNER 96 CLE2, ALBRECHT 91B ARG, AVERY 89B CLEO, AVERY 87 CLEO.

1 Assumes equal production of B+ and B0 at the T(4S).
2 AVERY 89B reports < 9 x 10^-5 assuming the T(4S) decays 43% to B0 B0. We rescale to 50%.

Gamma(K+ pi0) / Gamma total 343 / Gamma

Table with columns: VALUE (units 10^-6), CL%, DOCUMENT ID, TECN, COMMENT. Rows include DUH 13 BELL, AUBERT 07bc BABR, BORNHEIM 03 CLE2.

• • • We do not use the following data for averages, fits, limits, etc. • • •

Table with columns: VALUE (units 10^-6), CL%, DOCUMENT ID, TECN, COMMENT. Rows include LIN 07A BELL, AUBERT 05L BABR, CHAO 04 BELL, AUBERT 03L BABR, CASEY 02 BELL, ABE 01H BELL, AUBERT 01E BABR, CRONIN-HEN..00 CLE2, GODANG 98 CLE2, ASNER 96 CLE2.

1 Assumes equal production of B+ and B0 at the T(4S).

Gamma(K+ pi0) / Gamma(K0 pi+) 343 / Gamma 342

Table with columns: VALUE, DOCUMENT ID, TECN, COMMENT. Row: LIN 07A BELL.

• • • We do not use the following data for averages, fits, limits, etc. • • •

Table with columns: VALUE, DOCUMENT ID, TECN, COMMENT. Row: ABE 01H BELL.

Gamma(eta' K+) / Gamma total 344 / Gamma

Table with columns: VALUE (units 10^-6), DOCUMENT ID, TECN, COMMENT. Rows include AUBERT 09Av BABR, WICHT 08 BELL, SCHUEMANN 06 BELL, RICHICHI 00 CLE2.

• • • We do not use the following data for averages, fits, limits, etc. • • •

Table with columns: VALUE (units 10^-6), DOCUMENT ID, TECN, COMMENT. Rows include AUBERT 07AE BABR, AUBERT 05M BABR, AUBERT 03W BABR, ABE 01M BELL, AUBERT 01G BABR, BEHRENS 98 CLE2.

1 Assumes equal production of B+ and B0 at the T(4S).
2 WICHT 08 reports [Gamma(B+ -> eta' K+) / Gamma total] x [B(eta'(958) -> gamma gamma)] = (1.40 +0.16 +0.15 -0.12) x 10^-6 which we divide by our best value B(eta'(958) -> gamma gamma) = (2.307 +/- 0.33) x 10^-2. Our first error is their experiment's error and our second error is the systematic error from using our best value.

Gamma(eta' K*(892)+) / Gamma total 345 / Gamma

Table with columns: VALUE (units 10^-6), CL%, DOCUMENT ID, TECN, COMMENT. Row: DEL-AMO-SA..10A BABR.

• • • We do not use the following data for averages, fits, limits, etc. • • •

Table with columns: VALUE (units 10^-6), CL%, DOCUMENT ID, TECN, COMMENT. Rows include AUBERT 07E BABR, SCHUEMANN 07 BELL, AUBERT, B 04D BABR, RICHICHI 00 CLE2, BEHRENS 98 CLE2.

Gamma(eta' K2(1430)+) / Gamma total 346 / Gamma

Table with columns: VALUE (units 10^-6), DOCUMENT ID, TECN, COMMENT. Row: DEL-AMO-SA..10A BABR.

1 Assumes equal production of B+ and B0 at the T(4S).

Gamma(eta' K2(1430)+) / Gamma total 347 / Gamma

Table with columns: VALUE (units 10^-6), DOCUMENT ID, TECN, COMMENT. Row: DEL-AMO-SA..10A BABR.

1 Assumes equal production of B+ and B0 at the T(4S).

Gamma(K+) / Gamma total 348 / Gamma

Table with columns: VALUE (units 10^-6), CL%, DOCUMENT ID, TECN, COMMENT. Rows include HOI 12 BELL, AUBERT 09Av BABR, RICHICHI 00 CLE2.

• • • We do not use the following data for averages, fits, limits, etc. • • •

Table with columns: VALUE (units 10^-6), CL%, DOCUMENT ID, TECN, COMMENT. Rows include WICHT 08 BELL, AUBERT 07AE BABR, CHANG 07B BELL, AUBERT, B 05K BABR, CHANG 05A BELL, AUBERT 04H BABR, BEHRENS 98 CLE2.

1 Assumes equal production of B+ and B0 at the T(4S).
2 WICHT 08 reports [Gamma(B+ -> eta K+) / Gamma total] x [B(eta -> 2 gamma)] = (0.87 +0.16 +0.10 -0.15 -0.07) x 10^-6 which we divide by our best value B(eta -> 2 gamma) = (39.41 +/- 0.20) x 10^-2. Our first error is their experiment's error and our second error is the systematic error from using our best value.

Gamma(eta K*(892)+) / Gamma total 349 / Gamma

Table with columns: VALUE (units 10^-6), CL%, DOCUMENT ID, TECN, COMMENT. Rows include WANG 07B BELL, AUBERT, B 06H BABR, RICHICHI 00 CLE2.

• • • We do not use the following data for averages, fits, limits, etc. • • •

Table with columns: VALUE (units 10^-6), CL%, DOCUMENT ID, TECN, COMMENT. Rows include AUBERT, B 04D BABR, BEHRENS 98 CLE2.

1 Assumes equal production of B+ and B0 at the T(4S).

Gamma(eta K0(1430)+) / Gamma total 350 / Gamma

Table with columns: VALUE (units 10^-6), DOCUMENT ID, TECN, COMMENT. Row: AUBERT, B 06H BABR.

1 Assumes equal production of B+ and B0 at the T(4S).

Gamma(eta K2(1430)+) / Gamma total 351 / Gamma

Table with columns: VALUE (units 10^-6), DOCUMENT ID, TECN, COMMENT. Row: AUBERT, B 06H BABR.

1 Assumes equal production of B+ and B0 at the T(4S).

Gamma(eta(1295) K+ x B(eta(1295) -> eta pi pi)) / Gamma total 352 / Gamma

Table with columns: VALUE (units 10^-6), DOCUMENT ID, TECN, COMMENT. Row: AUBERT 08x BABR.

1 Assumes equal production of B+ and B0 at the T(4S).

Gamma(eta(1405) K+ x B(eta(1405) -> eta pi pi)) / Gamma total 353 / Gamma

Table with columns: VALUE (units 10^-6), CL%, DOCUMENT ID, TECN, COMMENT. Row: AUBERT 08x BABR.

1 Assumes equal production of B+ and B0 at the T(4S).

Gamma(eta(1405) K+ x B(eta(1405) -> K* K)) / Gamma total 354 / Gamma

Table with columns: VALUE (units 10^-6), CL%, DOCUMENT ID, TECN, COMMENT. Row: AUBERT 08x BABR.

1 Assumes equal production of B+ and B0 at the T(4S).

Meson Particle Listings

 B^\pm $\Gamma(\eta(1475) K^+ \times B(\eta(1475) \rightarrow K^* K))/\Gamma_{\text{total}}$ Γ_{355}/Γ

VALUE (units 10^{-6})	CL%	DOCUMENT ID	TECN	COMMENT
$13.8^{+1.8+1.0}_{-1.7-0.6}$		1 AUBERT	08x BABR	$e^+ e^- \rightarrow \Upsilon(4S)$

¹ Assumes equal production of B^+ and B^0 at the $\Upsilon(4S)$.

 $\Gamma(f_1(1285) K^+)/\Gamma_{\text{total}}$ Γ_{356}/Γ

VALUE (units 10^{-6})	CL%	DOCUMENT ID	TECN	COMMENT
<2.0	90	1 AUBERT	08x BABR	$e^+ e^- \rightarrow \Upsilon(4S)$

¹ Assumes equal production of B^+ and B^0 at the $\Upsilon(4S)$.

 $\Gamma(f_1(1420) K^+ \times B(f_1(1420) \rightarrow \eta \pi \pi))/\Gamma_{\text{total}}$ Γ_{357}/Γ

VALUE (units 10^{-6})	CL%	DOCUMENT ID	TECN	COMMENT
<2.9	90	1 AUBERT	08x BABR	$e^+ e^- \rightarrow \Upsilon(4S)$

¹ Assumes equal production of B^+ and B^0 at the $\Upsilon(4S)$.

 $\Gamma(f_1(1420) K^+ \times B(f_1(1420) \rightarrow K^* K))/\Gamma_{\text{total}}$ Γ_{358}/Γ

VALUE (units 10^{-6})	CL%	DOCUMENT ID	TECN	COMMENT
<4.1	90	1 AUBERT	08x BABR	$e^+ e^- \rightarrow \Upsilon(4S)$

¹ Assumes equal production of B^+ and B^0 at the $\Upsilon(4S)$.

 $\Gamma(\phi(1680) K^+ \times B(\phi(1680) \rightarrow K^* K))/\Gamma_{\text{total}}$ Γ_{359}/Γ

VALUE (units 10^{-6})	CL%	DOCUMENT ID	TECN	COMMENT
<3.4	90	1 AUBERT	08x BABR	$e^+ e^- \rightarrow \Upsilon(4S)$

¹ Assumes equal production of B^+ and B^0 at the $\Upsilon(4S)$.

 $\Gamma(f_0(1500) K^+)/\Gamma_{\text{total}}$ Γ_{360}/Γ

VALUE (units 10^{-6})	CL%	DOCUMENT ID	TECN	COMMENT
3.7 ± 2.2 OUR AVERAGE				
$17 \pm 4 \pm 12$		1 LEES	12o BABR	$e^+ e^- \rightarrow \Upsilon(4S)$
$20 \pm 10 \pm 27$		2 LEES	12o BABR	$e^+ e^- \rightarrow \Upsilon(4S)$
$3.2^{+2.3}_{-2.3} \pm 0.2$		3,4 AUBERT	08A1 BABR	$e^+ e^- \rightarrow \Upsilon(4S)$

• • • We do not use the following data for averages, fits, limits, etc. • • •

<19	90	4,5 AUBERT,B	05N BABR	Repl. by AUBERT 08A1
-------	----	--------------	----------	----------------------

¹ Measured in the $B^+ \rightarrow K^+ K^- K^+$ decay.

² Measured in the $B^+ \rightarrow K^+ K_S^0 K_S^0$ decay.

³ AUBERT 08A1 reports $B(B^+ \rightarrow f_0(1500) K^+) \cdot B(f_0(1500) \rightarrow \pi^+ \pi^-) = (0.73 \pm 0.21_{-0.48}^{+0.47}) \times 10^{-6}$. We divide this result by our best value of $B(f_0(1500) \rightarrow \pi \pi) = (34.5 \pm 2.2) \times 10^{-2}$ multiplied by 2/3 to account for the $\pi^+ \pi^-$ fraction. Our first quoted uncertainty is the combined experiment's uncertainty and our second is the systematic uncertainty from using our best value.

⁴ Assumes equal production of B^+ and B^0 at the $\Upsilon(4S)$.

⁵ AUBERT,B 05N reports $B(B^+ \rightarrow f_0(1500) K^+) \cdot B(f_0(1500) \rightarrow \pi^+ \pi^-) < 4.4 \times 10^{-6}$. We divide this result by our best value of $B(f_0(1500) \rightarrow \pi \pi) = (34.5 \pm 2.2) \times 10^{-2}$ multiplied by 2/3 to account for the $\pi^+ \pi^-$ fraction. Our first quoted uncertainty is the combined experiment's uncertainty and our second is the systematic uncertainty from using our best value.

 $\Gamma(\omega K^+)/\Gamma_{\text{total}}$ Γ_{361}/Γ

VALUE (units 10^{-6})	CL%	DOCUMENT ID	TECN	COMMENT
6.5 ± 0.4 OUR AVERAGE				
$6.8 \pm 0.4 \pm 0.4$		1 CHOBANOVA	14 BELL	$e^+ e^- \rightarrow \Upsilon(4S)$
$6.3 \pm 0.5 \pm 0.3$		1 AUBERT	07AE BABR	$e^+ e^- \rightarrow \Upsilon(4S)$
$3.2^{+2.4}_{-1.9} \pm 0.8$		1 JESSOP	00 CLE2	$e^+ e^- \rightarrow \Upsilon(4S)$

• • • We do not use the following data for averages, fits, limits, etc. • • •

$6.1 \pm 0.6 \pm 0.4$		1 AUBERT,B	06E BABR	AUBERT 07AE
$8.1 \pm 0.6 \pm 0.6$		1 JEN	06 BELL	Repl. by CHOBANOVA 14
$4.8 \pm 0.8 \pm 0.4$		1 AUBERT	04H BABR	Repl. by AUBERT,B 06E
$6.5^{+1.3}_{-1.2} \pm 0.6$		1 WANG	04A BELL	Repl. by JEN 06
$9.2^{+2.6}_{-2.3} \pm 1.0$		1 LU	02 BELL	Repl. by WANG 04A
<4	90	1 AUBERT	01G BABR	$e^+ e^- \rightarrow \Upsilon(4S)$
$1.5^{+7}_{-6} \pm 2$		1 BERGFELD	98 CLE2	Repl. by JESSOP 00

¹ Assumes equal production of B^+ and B^0 at the $\Upsilon(4S)$.

 $\Gamma(\omega K^*(892)^+)/\Gamma_{\text{total}}$ Γ_{362}/Γ

VALUE (units 10^{-6})	CL%	DOCUMENT ID	TECN	COMMENT
<7.4	90	1 AUBERT	09H BABR	$e^+ e^- \rightarrow \Upsilon(4S)$

• • • We do not use the following data for averages, fits, limits, etc. • • •

<3.4	90	1 AUBERT,B	06T BABR	Repl. by AUBERT 09H
<7.4	90	1 AUBERT	05o BABR	Repl. by AUBERT,B 06T
<87	90	1 BERGFELD	98 CLE2	

¹ Assumes equal production of B^+ and B^0 at the $\Upsilon(4S)$.

 $\Gamma(\omega(K\pi)_0^{*+})/\Gamma_{\text{total}}$ Γ_{363}/Γ

($K\pi)_0^{*+}$ is the total S-wave composed of $K_0^0(1430)$ and nonresonant that are described using LASS shape.

VALUE (units 10^{-6})	CL%	DOCUMENT ID	TECN	COMMENT
$27.5 \pm 3.0 \pm 2.6$		1 AUBERT	09H BABR	$e^+ e^- \rightarrow \Upsilon(4S)$

¹ Assumes equal production of B^+ and B^0 at the $\Upsilon(4S)$.

 $\Gamma(\omega K_0^*(1430)^+)/\Gamma_{\text{total}}$ Γ_{364}/Γ

VALUE (units 10^{-6})	CL%	DOCUMENT ID	TECN	COMMENT
$24.0 \pm 2.6 \pm 4.4$		1 AUBERT	09H BABR	$e^+ e^- \rightarrow \Upsilon(4S)$

¹ Assumes equal production of B^+ and B^0 at the $\Upsilon(4S)$.

 $\Gamma(\omega K_2^*(1430)^+)/\Gamma_{\text{total}}$ Γ_{365}/Γ

VALUE (units 10^{-6})	CL%	DOCUMENT ID	TECN	COMMENT
$21.5 \pm 3.6 \pm 2.4$		1 AUBERT	09H BABR	$e^+ e^- \rightarrow \Upsilon(4S)$

¹ Assumes equal production of B^+ and B^0 at the $\Upsilon(4S)$.

 $\Gamma(a_0(980)^0 K^+ \times B(a_0(980)^0 \rightarrow \eta \pi^0))/\Gamma_{\text{total}}$ Γ_{367}/Γ

VALUE (units 10^{-6})	CL%	DOCUMENT ID	TECN	COMMENT
<2.5	90	1 AUBERT,BE	04 BABR	$e^+ e^- \rightarrow \Upsilon(4S)$

¹ Assumes equal production of charged and neutral B mesons from $\Upsilon(4S)$ decays.

 $\Gamma(a_0(980)^+ K^0 \times B(a_0(980)^+ \rightarrow \eta \pi^+))/\Gamma_{\text{total}}$ Γ_{366}/Γ

VALUE (units 10^{-6})	CL%	DOCUMENT ID	TECN	COMMENT
<3.9	90	1 AUBERT,BE	04 BABR	$e^+ e^- \rightarrow \Upsilon(4S)$

¹ Assumes equal production of charged and neutral B mesons from $\Upsilon(4S)$ decays.

 $\Gamma(K^*(892)^0 \pi^+)/\Gamma_{\text{total}}$ Γ_{368}/Γ

VALUE (units 10^{-6})	CL%	DOCUMENT ID	TECN	COMMENT
10.1 ± 0.8 OUR AVERAGE				
$10.1 \pm 1.7 \pm 1.0$		1 LEES	17G BABR	$e^+ e^- \rightarrow \Upsilon(4S)$
$10.8 \pm 0.6^{+1.2}_{-1.4}$		2 AUBERT	08A1 BABR	$e^+ e^- \rightarrow \Upsilon(4S)$
$9.67 \pm 0.64^{+0.81}_{-0.89}$		2 GARMASH	06 BELL	$e^+ e^- \rightarrow \Upsilon(4S)$

• • • We do not use the following data for averages, fits, limits, etc. • • •

$13.5 \pm 1.2^{+0.8}_{-0.9}$		2 AUBERT,B	05N BABR	Repl. by AUBERT 08A1
$9.8 \pm 0.9^{+1.1}_{-1.2}$		2 GARMASH	05 BELL	Repl. by GARMASH 06
$15.5 \pm 1.8^{+1.5}_{-4.0}$		2,3 AUBERT,B	04P BABR	Repl. by AUBERT,B 05N
$19.4^{+4.2+4.1}_{-3.9-7.1}$		4 GARMASH	02 BELL	Repl. by GARMASH 05
<119	90	5 ABE	00C SLD	$e^+ e^- \rightarrow Z$
<16	90	2 JESSOP	00 CLE2	$e^+ e^- \rightarrow \Upsilon(4S)$
<390	90	6 ADAM	96D DLPH	$e^+ e^- \rightarrow Z$
<41	90	ASNER	96 CLE2	Repl. by JESSOP 00
<480	90	6 ABREU	95N DLPH	Sup. by ADAM 96D
<170	90	ALBRECHT	91B ARG	$e^+ e^- \rightarrow \Upsilon(4S)$
<150	90	7 AVERY	89B CLEO	$e^+ e^- \rightarrow \Upsilon(4S)$
<260	90	AVERY	87 CLEO	$e^+ e^- \rightarrow \Upsilon(4S)$

¹ Obtains the result from a Dalitz analysis of $B^+ \rightarrow K_S^0 \pi^+ \pi^0$ decays. The first error is statistical, the second combines all the systematic uncertainties reported in the paper, including signal modelling.

² Assumes equal production of B^+ and B^0 at the $\Upsilon(4S)$.

³ AUBERT 04P also report a branching ratio for $B^+ \rightarrow$ "higher K^* resonances" π^+ , $K^* \rightarrow K^+ \pi^-$, $(25.1 \pm 2.0^{+11.0}_{-5.7}) \times 10^{-6}$.

⁴ Uses a reference decay mode $B^+ \rightarrow \bar{D}^0 \pi^+$ and $\bar{D}^0 \rightarrow K^+ \pi^-$ with $B(B^+ \rightarrow \bar{D}^0 \pi^+) \cdot B(\bar{D}^0 \rightarrow K^+ \pi^-) = (20.3 \pm 2.0) \times 10^{-5}$.

⁵ ABE 00c assumes $B(Z \rightarrow b\bar{b}) = (21.7 \pm 0.1)\%$ and the B fractions $f_{B^0} = f_{B^+} = (39.7^{+1.8}_{-2.2})\%$ and $f_{B_S} = (10.5^{+1.8}_{-2.2})\%$.

⁶ Assumes a B^0, B^- production fraction of 0.39 and a B_S production fraction of 0.12.

⁷ AVERY 89B reports $< 1.3 \times 10^{-4}$ assuming the $\Upsilon(4S)$ decays 43% to $B^0 \bar{B}^0$. We rescale to 50%.

 $\Gamma(K^*(892)^+ \pi^0)/\Gamma_{\text{total}}$ Γ_{369}/Γ

VALUE (units 10^{-6})	CL%	DOCUMENT ID	TECN	COMMENT
6.8 ± 0.9 OUR AVERAGE				
$6.4 \pm 0.9^{+0.4}_{-0.5}$		1 LEES	17G BABR	$e^+ e^- \rightarrow \Upsilon(4S)$
$8.2 \pm 1.5 \pm 1.1$		2 LEES	11i BABR	$e^+ e^- \rightarrow \Upsilon(4S)$

• • • We do not use the following data for averages, fits, limits, etc. • • •

$6.9 \pm 2.0 \pm 1.3$		2 AUBERT	05x BABR	Repl. by LEES 11i
<31	90	2 JESSOP	00 CLE2	$e^+ e^- \rightarrow \Upsilon(4S)$
<99	90	ASNER	96 CLE2	Repl. by JESSOP 00

¹ Obtains the result from a Dalitz analysis of $B^+ \rightarrow K_S^0 \pi^+ \pi^0$ decays. The first error is statistical, the second combines all the systematic uncertainties reported in the paper, including signal modelling.

² Assumes equal production of B^+ and B^0 at the $\Upsilon(4S)$.

$\Gamma(K^+\pi^-\pi^+)/\Gamma_{total}$ **Γ_{370}/Γ**

VALUE (units 10 ⁻⁶)	DOCUMENT ID	TECN	COMMENT
51.0 ± 2.9 OUR AVERAGE			
54.4 ± 1.1 ± 4.6	¹ AUBERT	08AI	BABR e ⁺ e ⁻ → $\Upsilon(4S)$
48.8 ± 1.1 ± 3.6	¹ GARMASH	06	BELL e ⁺ e ⁻ → $\Upsilon(4S)$
• • • We do not use the following data for averages, fits, limits, etc. • • •			
64.1 ± 2.4 ± 4.0	¹ AUBERT,B	05N	BABR Repl. by AUBERT 08AI
46.6 ± 2.1 ± 4.3	¹ GARMASH	05	BELL Repl. by GARMASH 06
53.6 ± 3.1 ± 5.1	¹ GARMASH	04	BELL Repl. by GARMASH 05
59.1 ± 3.8 ± 3.2	² AUBERT	03M	BABR Repl. by AUBERT,B 05N
55.6 ± 5.8 ± 7.7	³ GARMASH	02	BELL Repl. by GARMASH 04

- Assumes equal production of B⁺ and B⁰ at the $\Upsilon(4S)$.
- Assumes equal production of B⁰ and B⁺ at the $\Upsilon(4S)$; charm and charmonium contributions are subtracted, otherwise no assumptions about intermediate resonances.
- Uses a reference decay mode B⁺ → $\bar{D}^0\pi^+$ and $\bar{D}^0 \rightarrow K^+\pi^-$ with B(B⁺ → $\bar{D}^0\pi^+$)·B($\bar{D}^0 \rightarrow K^+\pi^-$) = (20.3 ± 2.0) × 10⁻⁵.

$\Gamma(K^+\pi^-\pi^+ \text{ nonresonant})/\Gamma_{total}$ **Γ_{371}/Γ**

VALUE (units 10 ⁻⁶)	CL%	DOCUMENT ID	TECN	COMMENT
16.3 ± 2.1 OUR AVERAGE				
9.3 ± 1.0 ± 1.7		^{1,2} AUBERT	08AI	BABR e ⁺ e ⁻ → $\Upsilon(4S)$
16.9 ± 1.3 ± 1.7		¹ GARMASH	06	BELL e ⁺ e ⁻ → $\Upsilon(4S)$
• • • We do not use the following data for averages, fits, limits, etc. • • •				
2.9 ± 0.6 ± 0.5		¹ AUBERT,B	05N	BABR Repl. by AUBERT 08AI
17.3 ± 1.7 ± 17.2		¹ GARMASH	05	BELL Repl. by GARMASH 06
< 17	90	¹ AUBERT,B	04P	BABR Repl. by AUBERT,B 05N
< 330	90	³ ADAM	96D	DLPH e ⁺ e ⁻ → Z
< 28	90	BERGFELD	96B	CLE2 e ⁺ e ⁻ → $\Upsilon(4S)$
< 400	90	³ ABREU	95N	DLPH Sup. by ADAM 96D
< 330	90	ALBRECHT	91E	ARG e ⁺ e ⁻ → $\Upsilon(4S)$
< 190	90	⁴ AVERY	89B	CLEO e ⁺ e ⁻ → $\Upsilon(4S)$

- Assumes equal production of B⁺ and B⁰ at the $\Upsilon(4S)$.
- Calculate the total nonresonant contribution by combining the S-wave composed of K₀^{*}(1430) and nonresonant that are described using LASS shape.
- Assumes a B⁰, B⁻ production fraction of 0.39 and a B_s production fraction of 0.12.
- AVERY 89B reports < 1.7 × 10⁻⁴ assuming the $\Upsilon(4S)$ decays 43% to B⁰ \bar{B}^0 . We rescale to 50%.

$\Gamma(\omega(782)K^+)/\Gamma_{total}$ **Γ_{372}/Γ**

VALUE (units 10 ⁻⁶)	DOCUMENT ID	TECN	COMMENT	
5.9 ± 0.8 OUR AVERAGE				
10.3 ± 0.5 ± 2.0	^{1,2} AUBERT	08AI	BABR e ⁺ e ⁻ → $\Upsilon(4S)$	
8.78 ± 0.82 ± 0.85	¹ GARMASH	06	BELL e ⁺ e ⁻ → $\Upsilon(4S)$	
• • • We do not use the following data for averages, fits, limits, etc. • • •				
9.47 ± 0.97 ± 0.62	¹ AUBERT,B	05N	BABR Repl. by AUBERT 08AI	
7.55 ± 1.24 ± 1.63	¹ GARMASH	05	BELL Repl. by GARMASH 06	
9.2 ± 1.2 ± 2.1	² AUBERT,B	04P	BABR Repl. by AUBERT,B 05N	
9.6 ± 2.5 ± 3.7	³ GARMASH	02	BELL Repl. by GARMASH 05	
< 80	90	⁴ AVERY	89B	CLEO e ⁺ e ⁻ → $\Upsilon(4S)$

- Assumes equal production of B⁺ and B⁰ at the $\Upsilon(4S)$.
- AUBERT 08AI reports [$\Gamma(B^+ \rightarrow \omega(782)K^+)/\Gamma_{total}$] × [B($\omega(782) \rightarrow \pi^+\pi^-$)] = (0.09 ± 0.13 ± 0.036) × 10⁻⁶ which we divide by our best value B($\omega(782) \rightarrow \pi^+\pi^-$) = (1.53 ± 0.06) × 10⁻². Our first error is their experiment's error and our second error is the systematic error from using our best value.

$\Gamma(K^+f_0(980) \times B(f_0(980) \rightarrow \pi^+\pi^-))/\Gamma_{total}$ **Γ_{373}/Γ**

VALUE (units 10 ⁻⁶)	CL%	DOCUMENT ID	TECN	COMMENT
9.4 ± 1.0 OUR AVERAGE				
10.3 ± 0.5 ± 2.0		¹ AUBERT	08AI	BABR e ⁺ e ⁻ → $\Upsilon(4S)$
8.78 ± 0.82 ± 0.85		¹ GARMASH	06	BELL e ⁺ e ⁻ → $\Upsilon(4S)$
• • • We do not use the following data for averages, fits, limits, etc. • • •				
9.47 ± 0.97 ± 0.62		¹ AUBERT,B	05N	BABR Repl. by AUBERT 08AI
7.55 ± 1.24 ± 1.63		¹ GARMASH	05	BELL Repl. by GARMASH 06
9.2 ± 1.2 ± 2.1		² AUBERT,B	04P	BABR Repl. by AUBERT,B 05N
9.6 ± 2.5 ± 3.7		³ GARMASH	02	BELL Repl. by GARMASH 05
< 80	90	⁴ AVERY	89B	CLEO e ⁺ e ⁻ → $\Upsilon(4S)$

- Assumes equal production of B⁺ and B⁰ at the $\Upsilon(4S)$.
- AUBERT,B 04P also reports B(B⁺ → "higher f₀ resonances" π^+ , f(980)⁰ → $\pi^+\pi^-$) = (3.2 ± 1.2 ± 6.0, -2.9) × 10⁻⁶.
- Uses a reference decay mode B⁺ → $\bar{D}^0\pi^+$ and $\bar{D}^0 \rightarrow K^+\pi^-$ with B(B⁺ → $\bar{D}^0\pi^+$)·B($\bar{D}^0 \rightarrow K^+\pi^-$) = (20.3 ± 2.0) × 10⁻⁵. Only charged pions from the f₀(980) are used.
- AVERY 89B reports < 7 × 10⁻⁵ assuming the $\Upsilon(4S)$ decays 43% to B⁰ \bar{B}^0 . We rescale to 50%.

$\Gamma(f_2(1270)^0 K^+)/\Gamma_{total}$ **Γ_{374}/Γ**

VALUE (units 10 ⁻⁶)	CL%	DOCUMENT ID	TECN	COMMENT
1.07 ± 0.27 OUR AVERAGE				
0.89 ± 0.38 ± 0.01		^{1,2} AUBERT	08AI	BABR e ⁺ e ⁻ → $\Upsilon(4S)$
-0.33 - 0.03		¹ GARMASH	06	BELL e ⁺ e ⁻ → $\Upsilon(4S)$
1.33 ± 0.30 ± 0.23		¹ GARMASH	06	BELL e ⁺ e ⁻ → $\Upsilon(4S)$
• • • We do not use the following data for averages, fits, limits, etc. • • •				
< 16	90	³ AUBERT,B	05N	BABR Repl. by AUBERT 08AI
< 2.3	90	⁴ GARMASH	05	BELL Repl. by GARMASH 06

- Assumes equal production of B⁺ and B⁰ at the $\Upsilon(4S)$.
- AUBERT 08AI reports (0.50 ± 0.15 ± 0.15) × 10⁻⁶ for B(B⁺ → f₂(1270) K⁺) × B(f₂ → $\pi^+\pi^-$). We compute B(B⁺ → f₂(1270) K⁺) using the PDG value B(f₂(1270) → $\pi\pi$) = (84.2 ± 2.9, -0.3) × 10⁻² and 2/3 for the $\pi^+\pi^-$ fraction. Our first error is their experiment's error and the second error is systematic error from using our best value.
- AUBERT,B 05N reports 8.9 × 10⁻⁶ at 90% CL for B(B⁺ → f₂(1270) K⁺) × B(f₂(1270) → $\pi^+\pi^-$). We rescaled it using the PDG value B(f₂(1270) → $\pi\pi$) = 84.7% and 2/3 for the $\pi^+\pi^-$ fraction.
- GARMASH 05 reports 1.3 × 10⁻⁶ at 90% CL for B(B⁺ → f₂(1270) K⁺) × B(f₂(1270) → $\pi^+\pi^-$). We rescaled it using the PDG value B(f₂(1270) → $\pi\pi$) = 84.7% and 2/3 for the $\pi^+\pi^-$ fraction.

$\Gamma(f_0(1370)^0 K^+ \times B(f_0(1370)^0 \rightarrow \pi^+\pi^-))/\Gamma_{total}$ **Γ_{375}/Γ**

VALUE	CL%	DOCUMENT ID	TECN	COMMENT
< 10.7 × 10⁻⁶				
	90	¹ AUBERT,B	05N	BABR e ⁺ e ⁻ → $\Upsilon(4S)$
• • • We do not use the following data for averages, fits, limits, etc. • • •				
Assumes equal production of B ⁺ and B ⁰ at the $\Upsilon(4S)$.				

$\Gamma(\rho^0(1450) K^+ \times B(\rho^0(1450) \rightarrow \pi^+\pi^-))/\Gamma_{total}$ **Γ_{376}/Γ**

VALUE	CL%	DOCUMENT ID	TECN	COMMENT
< 11.7 × 10⁻⁶				
	90	¹ AUBERT,B	05N	BABR e ⁺ e ⁻ → $\Upsilon(4S)$
Assumes equal production of B ⁺ and B ⁰ at the $\Upsilon(4S)$.				

$\Gamma(f_2'(1525) K^+ \times B(f_2'(1525) \rightarrow \pi^+\pi^-))/\Gamma_{total}$ **Γ_{377}/Γ**

VALUE	CL%	DOCUMENT ID	TECN	COMMENT
< 3.4 × 10⁻⁶				
	90	¹ AUBERT,B	05N	BABR e ⁺ e ⁻ → $\Upsilon(4S)$
Assumes equal production of B ⁺ and B ⁰ at the $\Upsilon(4S)$.				

$\Gamma(K^+\rho^0)/\Gamma_{total}$ **Γ_{378}/Γ**

VALUE (units 10 ⁻⁶)	CL%	DOCUMENT ID	TECN	COMMENT
3.7 ± 0.5 OUR AVERAGE				
3.56 ± 0.45 ± 0.57		¹ AUBERT	08AI	BABR e ⁺ e ⁻ → $\Upsilon(4S)$
-0.46		¹ GARMASH	06	BELL e ⁺ e ⁻ → $\Upsilon(4S)$
3.89 ± 0.47 ± 0.43		¹ GARMASH	06	BELL e ⁺ e ⁻ → $\Upsilon(4S)$
-0.41		¹ AUBERT,B	05N	BABR Repl. by AUBERT 08AI
5.07 ± 0.75 ± 0.55		¹ AUBERT,B	05N	BABR Repl. by AUBERT 08AI
-0.88		¹ GARMASH	05	BELL Repl. by GARMASH 06
4.78 ± 0.75 ± 1.01		¹ GARMASH	05	BELL Repl. by GARMASH 06
-0.97		² AUBERT,B	04P	BABR Repl. by AUBERT,B 05N
< 6.2	90	³ GARMASH	02	BELL e ⁺ e ⁻ → $\Upsilon(4S)$
< 12	90	⁴ ABE	00C	SLD e ⁺ e ⁻ → Z
< 86	90	¹ ABE	00C	SLD e ⁺ e ⁻ → Z
< 17	90	¹ JESSOP	00	CLE2 e ⁺ e ⁻ → $\Upsilon(4S)$
< 120	90	⁵ ADAM	96D	DLPH e ⁺ e ⁻ → Z
< 19	90	⁶ ASNER	96	CLE2 Repl. by JESSOP 00
< 190	90	⁵ ABREU	95N	DLPH Sup. by ADAM 96D
< 180	90	⁶ ALBRECHT	91B	ARG e ⁺ e ⁻ → $\Upsilon(4S)$
< 80	90	⁶ AVERY	89B	CLEO e ⁺ e ⁻ → $\Upsilon(4S)$
< 260	90	⁶ AVERY	87	CLEO e ⁺ e ⁻ → $\Upsilon(4S)$

- Assumes equal production of B⁺ and B⁰ at the $\Upsilon(4S)$.
- AUBERT 04P reports a central value of (3.9 ± 1.2 ± 1.3) × 10⁻⁶ for this branching ratio.
- Uses a reference decay mode B⁺ → $\bar{D}^0\pi^+$ and $\bar{D}^0 \rightarrow K^+\pi^-$ with B(B⁺ → $\bar{D}^0\pi^+$)·B($\bar{D}^0 \rightarrow K^+\pi^-$) = (20.3 ± 2.0) × 10⁻⁵.
- ABE 00C assumes B(Z → b \bar{b}) = (21.7 ± 0.1)% and the B fractions f_{B⁰} = f_{B⁺} = (39.7 ± 1.8, -2.2)% and f_{B_s} = (10.5 ± 1.8, -2.2)%.
- Assumes production fractions f_{B⁰} = f_{B⁺} = 0.39 and f_{B_s} = 0.12.
- AVERY 89B reports < 7 × 10⁻⁵ assuming the $\Upsilon(4S)$ decays 43% to B⁰ \bar{B}^0 . We rescale to 50%.

$\Gamma(K_0^*(1430)^0 \pi^+)/\Gamma_{total}$ **Γ_{379}/Γ**

VALUE (units 10 ⁻⁶)	DOCUMENT ID	TECN	COMMENT
39 ± 5 OUR AVERAGE Error includes scale factor of 1.4. See the ideogram below.			
34.6 ± 3.3 ± 4.6	¹ LEES	17G	BABR e ⁺ e ⁻ → $\Upsilon(4S)$
32.0 ± 1.2 ± 10.8	² AUBERT	08AI	BABR e ⁺ e ⁻ → $\Upsilon(4S)$
6.0	² GARMASH	06	BELL e ⁺ e ⁻ → $\Upsilon(4S)$
51.6 ± 1.7 ± 7.0	² GARMASH	06	BELL e ⁺ e ⁻ → $\Upsilon(4S)$

Meson Particle Listings

 B^\pm

• • • We do not use the following data for averages, fits, limits, etc. • • •

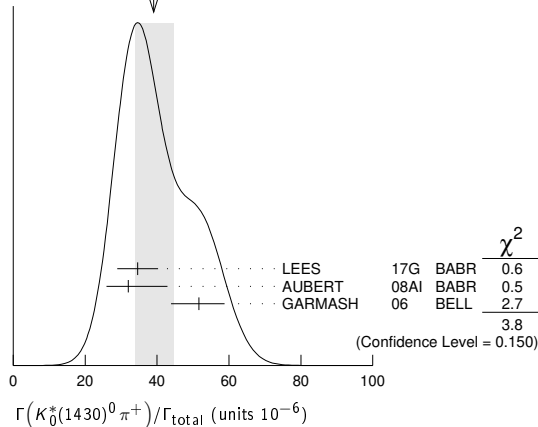
$44.4 \pm 2.2 \pm 5.3$	^{2,3} AUBERT,B	05N	BABR	Repl. by AUBERT 08AI
$45.0 \pm 2.9^{+15.0}_{-10.7}$	² GARMASH	05	BELL	Repl. by GARMASH 06

¹ Obtains the result from a Dalitz analysis of $B^+ \rightarrow K_S^0 \pi^+ \pi^0$ decays. The first error is statistical, the second combines all the systematic uncertainties reported in the paper, including signal modelling.

² Assumes equal production of B^+ and B^0 at the $\Upsilon(4S)$.

³ See erratum: AUBERT,BE 06A.

WEIGHTED AVERAGE
39+6-5 (Error scaled by 1.4)



$\Gamma(K_S^*(1430)^0 \pi^+) / \Gamma_{\text{total}}$ Γ381/Γ

VALUE (units 10^{-6})	CL%	DOCUMENT ID	TECN	COMMENT
$5.6^{+2.2}_{-1.5} \pm 0.1$		^{1,2} AUBERT	08AI	BABR $e^+ e^- \rightarrow \Upsilon(4S)$

• • • We do not use the following data for averages, fits, limits, etc. • • •

< 23	90	³ AUBERT,B	05N	BABR Repl. by AUBERT 08AI
< 6.9	90	⁴ GARMASH	05	BELL $e^+ e^- \rightarrow \Upsilon(4S)$
< 680	90	ALBRECHT	91B	ARG $e^+ e^- \rightarrow \Upsilon(4S)$

¹ Assumes equal production of B^+ and B^0 at the $\Upsilon(4S)$.

² AUBERT 08AI reports $(1.85 \pm 0.41^{+0.61}_{-0.29}) \times 10^{-6}$ for $B(B^+ \rightarrow K_S^*(1430)^0 \pi^+) \times B(K_S^*(1430)^0 \rightarrow K^+ \pi^-)$. We compute $B(B^+ \rightarrow K_S^*(1430)^0 \pi^+)$ using the PDG value $B(K_S^*(1430)^0 \rightarrow K\pi) = (49.9 \pm 1.2) \times 10^{-2}$ and 2/3 for the $K^+ \pi^-$ fraction. Our first error is their experiment's and the second error is systematic error from using our best value.

³ AUBERT,B 05N reports 7.7×10^{-6} at 90% CL for $B(B^+ \rightarrow K_S^*(1430)^0 \pi^+) \times B(K_S^*(1430)^0 \rightarrow K^+ \pi^-)$. We rescaled it using the PDG value $B(K_S^*(1430)^0 \rightarrow K\pi) = 49.9\%$ and 2/3 for the $K^+ \pi^-$ fraction.

⁴ GARMASH 05 reports 2.3×10^{-6} at 90% CL for $B(B^+ \rightarrow K_S^*(1430)^0 \pi^+) \times B(K_S^*(1430)^0 \rightarrow K^+ \pi^-)$. We rescaled it using the PDG value $B(K_S^*(1430)^0 \rightarrow K\pi) = 49.9\%$ and 2/3 for the $K^+ \pi^-$ mode.

$\Gamma(K_S^*(1430)^+ \pi^+) / \Gamma_{\text{total}}$ Γ380/Γ

VALUE (units 10^{-6})	DOCUMENT ID	TECN	COMMENT
$11.9 \pm 1.7^{+1.0}_{-1.6}$	¹ LEES	17G	BABR $e^+ e^- \rightarrow \Upsilon(4S)$

¹ Obtains the result from a Dalitz analysis of $B^+ \rightarrow K_S^0 \pi^+ \pi^0$ decays. The first error is statistical, the second combines all the systematic uncertainties reported in the paper, including signal modelling.

$\Gamma(K^*(1410)^0 \pi^+) / \Gamma_{\text{total}}$ Γ382/Γ

VALUE (units 10^{-6})	CL%	DOCUMENT ID	TECN	COMMENT
< 45	90	¹ GARMASH	05	BELL $e^+ e^- \rightarrow \Upsilon(4S)$

¹ GARMASH 05 reports 2.0×10^{-6} at 90% CL for $B(B^+ \rightarrow K^*(1410)^0 \pi^+) \times B(K^*(1410)^0 \rightarrow K^+ \pi^-)$. We rescaled it using the PDG value $B(K^*(1410)^0 \rightarrow K\pi) = 6.6\%$ and 2/3 for the $K^+ \pi^-$ mode.

$\Gamma(K^*(1680)^0 \pi^+) / \Gamma_{\text{total}}$ Γ383/Γ

VALUE (units 10^{-6})	CL%	DOCUMENT ID	TECN	COMMENT
< 12	90	¹ GARMASH	05	BELL $e^+ e^- \rightarrow \Upsilon(4S)$

• • • We do not use the following data for averages, fits, limits, etc. • • •

< 15	90	² AUBERT,B	05N	BABR $e^+ e^- \rightarrow \Upsilon(4S)$
--------	----	-----------------------	-----	---

¹ GARMASH 05 reports 3.1×10^{-6} at 90% CL for $B(B^+ \rightarrow K^*(1680)^0 \pi^+) \times B(K^*(1680)^0 \rightarrow K^+ \pi^-)$. We rescaled it using the PDG value $B(K^*(1680)^0 \rightarrow K\pi) = 38.7\%$ and 2/3 for the $K^+ \pi^-$ mode.

² AUBERT,B 05N reports 3.8×10^{-6} at 90% CL for $B(B^+ \rightarrow K^*(1680)^0 \pi^+) \times B(K^*(1680)^0 \rightarrow K^+ \pi^-)$. We rescaled it using the PDG value $B(K^*(1680)^0 \rightarrow K\pi) = 38.7\%$ and 2/3 for the $K^+ \pi^-$ fraction.

$\Gamma(K^+ \pi^0 \pi^0) / \Gamma_{\text{total}}$ Γ384/Γ

VALUE (units 10^{-6})	DOCUMENT ID	TECN	COMMENT
$16.2 \pm 1.2 \pm 1.5$	¹ LEES	11I	BABR $e^+ e^- \rightarrow \Upsilon(4S)$

¹ Assumes equal production of B^+ and B^0 at the $\Upsilon(4S)$.

$\Gamma(\rho(980) K^+ \times B(\rho_0 \rightarrow \pi^0 \pi^0)) / \Gamma_{\text{total}}$ Γ385/Γ

VALUE (units 10^{-6})	DOCUMENT ID	TECN	COMMENT
$2.8 \pm 0.6 \pm 0.5$	¹ LEES	11I	BABR $e^+ e^- \rightarrow \Upsilon(4S)$

¹ Assumes equal production of B^+ and B^0 at the $\Upsilon(4S)$.

$\Gamma(K^- \pi^+ \pi^+) / \Gamma_{\text{total}}$ Γ386/Γ

VALUE	CL%	DOCUMENT ID	TECN	COMMENT
$< 4.6 \times 10^{-8}$	90	AAIJ	17E	LHCB pp at 7, 8 TeV

• • • We do not use the following data for averages, fits, limits, etc. • • •

$< 9.5 \times 10^{-7}$	90	¹ AUBERT	08BE	BABR $e^+ e^- \rightarrow \Upsilon(4S)$
$< 4.5 \times 10^{-6}$	90	¹ GARMASH	04	BELL $e^+ e^- \rightarrow \Upsilon(4S)$
$< 1.8 \times 10^{-6}$	90	² AUBERT	03M	BABR Repl. by AUBERT 08BE
$< 7.0 \times 10^{-6}$	90	³ GARMASH	02	BELL $e^+ e^- \rightarrow \Upsilon(4S)$

¹ Assumes equal production of B^+ and B^0 at the $\Upsilon(4S)$.

² Assumes equal production of B^0 and B^+ at the $\Upsilon(4S)$; charm and charmonium contributions are subtracted, otherwise no assumptions about intermediate resonances.

³ Uses a reference decay mode $B^+ \rightarrow \bar{D}^0 \pi^+$ and $\bar{D}^0 \rightarrow K^+ \pi^-$ with $B(B^+ \rightarrow \bar{D}^0 \pi^+) \cdot B(\bar{D}^0 \rightarrow K^+ \pi^-) = (20.3 \pm 2.0) \times 10^{-5}$.

$\Gamma(K^- \pi^+ \pi^+ \text{nonresonant}) / \Gamma_{\text{total}}$ Γ387/Γ

VALUE (units 10^{-6})	CL%	DOCUMENT ID	TECN	COMMENT
< 56	90	BERGFELD	96B	CLE2 $e^+ e^- \rightarrow \Upsilon(4S)$

$\Gamma(K_1(1270)^0 \pi^+) / \Gamma_{\text{total}}$ Γ388/Γ

VALUE	CL%	DOCUMENT ID	TECN	COMMENT
$< 4.0 \times 10^{-5}$	90	¹ AUBERT	10D	BABR $e^+ e^- \rightarrow \Upsilon(4S)$

¹ Assumes equal production of B^+ and B^0 at the $\Upsilon(4S)$.

$\Gamma(K_1(1400)^0 \pi^+) / \Gamma_{\text{total}}$ Γ389/Γ

VALUE	CL%	DOCUMENT ID	TECN	COMMENT
$< 3.9 \times 10^{-5}$	90	¹ AUBERT	10D	BABR $e^+ e^- \rightarrow \Upsilon(4S)$

• • • We do not use the following data for averages, fits, limits, etc. • • •

$< 2.6 \times 10^{-3}$	90	ALBRECHT	91B	ARG $e^+ e^- \rightarrow \Upsilon(4S)$
------------------------	----	----------	-----	--

¹ Assumes equal production of B^+ and B^0 at the $\Upsilon(4S)$.

$\Gamma(K^0 \pi^+ \pi^0) / \Gamma_{\text{total}}$ Γ390/Γ

VALUE (units 10^{-6})	CL%	DOCUMENT ID	TECN	COMMENT
$31.8 \pm 1.8^{+6.3}_{-2.1}$		¹ LEES	17G	BABR $e^+ e^- \rightarrow \Upsilon(4S)$
< 66	90	² ECKHART	02	CLE2 $e^+ e^- \rightarrow \Upsilon(4S)$

¹ Obtains the result from a Dalitz analysis of $B^+ \rightarrow K_S^0 \pi^+ \pi^0$ decays. The first error is statistical, the second combines all the systematic uncertainties reported in the paper, including signal modelling.

² Assumes equal production of B^+ and B^0 at the $\Upsilon(4S)$.

$\Gamma(K^0 \rho^+) / \Gamma_{\text{total}}$ Γ391/Γ

VALUE (units 10^{-6})	CL%	DOCUMENT ID	TECN	COMMENT
$7.3 \pm 1.0^{+1.0}_{-1.2}$ OUR AVERAGE				

$6.5 \pm 1.1^{+0.8}_{-1.9}$	¹ LEES	17G	BABR $e^+ e^- \rightarrow \Upsilon(4S)$
-----------------------------	-------------------	-----	---

$8.0 \pm 1.4^{+0.6}_{-1.3}$	AUBERT	07Z	BABR $e^+ e^- \rightarrow \Upsilon(4S)$
-----------------------------	--------	-----	---

• • • We do not use the following data for averages, fits, limits, etc. • • •

< 48	90	ASNER	96	CLE2 $e^+ e^- \rightarrow \Upsilon(4S)$
--------	----	-------	----	---

¹ Obtains the result from a Dalitz analysis of $B^+ \rightarrow K_S^0 \pi^+ \pi^0$ decays. The first error is statistical, the second combines all the systematic uncertainties reported in the paper, including signal modelling.

$\Gamma(K^*(892)^+ \pi^+ \pi^-) / \Gamma_{\text{total}}$ Γ392/Γ

VALUE (units 10^{-6})	CL%	DOCUMENT ID	TECN	COMMENT
$75.3 \pm 6.0 \pm 8.1$		¹ AUBERT,B	06U	BABR $e^+ e^- \rightarrow \Upsilon(4S)$

• • • We do not use the following data for averages, fits, limits, etc. • • •

< 1100	90	ALBRECHT	91E	ARG $e^+ e^- \rightarrow \Upsilon(4S)$
----------	----	----------	-----	--

¹ Assumes equal production of B^+ and B^0 at the $\Upsilon(4S)$.

$\Gamma(K^*(892)^+ \rho^0) / \Gamma_{\text{total}}$ Γ393/Γ

VALUE (units 10^{-6})	CL%	DOCUMENT ID	TECN	COMMENT
$4.6 \pm 1.0 \pm 0.4$		¹ DEL-AMO-SA...11D	BABR	$e^+ e^- \rightarrow \Upsilon(4S)$

• • • We do not use the following data for averages, fits, limits, etc. • • •

< 6.1	90	¹ AUBERT,B	06G	BABR Repl. by DEL-AMO-SANCHEZ 11D
---------	----	-----------------------	-----	-----------------------------------

$10.6 \pm 3.0^{+2.4}_{-2.6}$	¹ AUBERT	03V	BABR	Repl. by AUBERT,B 06G
------------------------------	---------------------	-----	------	-----------------------

< 74	90	² GODANG	02	CLE2 $e^+ e^- \rightarrow \Upsilon(4S)$
--------	----	---------------------	----	---

< 900	90	ALBRECHT	91B	ARG $e^+ e^- \rightarrow \Upsilon(4S)$
---------	----	----------	-----	--

¹ Assumes equal production of B^+ and B^0 at the $\Upsilon(4S)$.

² Assumes a helicity 00 configuration. For a helicity 11 configuration, the limit decreases to 4.9×10^{-5} .

$\Gamma(K^*(892)^+ f_0(980))/\Gamma_{total}$ Γ_{394}/Γ

VALUE (units 10^{-6})	DOCUMENT ID	TECN	COMMENT
4.2 ± 0.6 ± 0.3	¹ DEL-AMO-SA..11D	BABR	$e^+e^- \rightarrow \Upsilon(4S)$
• • • We do not use the following data for averages, fits, limits, etc. • • •			
5.2 ± 1.2 ± 0.5	¹ AUBERT,B 06G	BABR	Repl. by DEL-A MO-SANCHEZ 11D
¹ Assumes equal production of B^+ and B^0 at the $\Upsilon(4S)$.			

$\Gamma(a_1^+ K^0)/\Gamma_{total}$ Γ_{395}/Γ

VALUE (units 10^{-6})	DOCUMENT ID	TECN	COMMENT
34.9 ± 5.0 ± 4.4	^{1,2} AUBERT 08F	BABR	$e^+e^- \rightarrow \Upsilon(4S)$
¹ Assumes equal production of B^+ and B^0 at the $\Upsilon(4S)$.			
² Assumes a_1^\pm decays only to 3π and $B(a_1^\pm \rightarrow \pi^\pm \pi^\mp \pi^\pm) = 0.5$.			

$\Gamma(b_1^+ K^0 \times B(b_1^+ \rightarrow \omega \pi^+))/\Gamma_{total}$ Γ_{396}/Γ

VALUE (units 10^{-6})	DOCUMENT ID	TECN	COMMENT
9.6 ± 1.7 ± 0.9	¹ AUBERT 08AG	BABR	$e^+e^- \rightarrow \Upsilon(4S)$
¹ Assumes equal production of B^+ and B^0 at the $\Upsilon(4S)$.			

$\Gamma(K^*(892)^0 \rho^+)/\Gamma_{total}$ Γ_{397}/Γ

VALUE (units 10^{-6})	DOCUMENT ID	TECN	COMMENT
9.2 ± 1.5 OUR AVERAGE			
9.6 ± 1.7 ± 1.5	¹ AUBERT,B 06G	BABR	$e^+e^- \rightarrow \Upsilon(4S)$
8.9 ± 1.7 ± 1.2	¹ ZHANG 05D	BELL	$e^+e^- \rightarrow \Upsilon(4S)$
¹ Assumes equal production of B^+ and B^0 at the $\Upsilon(4S)$.			

$\Gamma(K_1^+(1400)^+ \rho^+)/\Gamma_{total}$ Γ_{398}/Γ

VALUE	CL%	DOCUMENT ID	TECN	COMMENT
< 7.8 × 10⁻⁴	90	ALBRECHT 91B	ARG	$e^+e^- \rightarrow \Upsilon(4S)$

$\Gamma(K_2^+(1430)^+ \rho^+)/\Gamma_{total}$ Γ_{399}/Γ

VALUE	CL%	DOCUMENT ID	TECN	COMMENT
< 1.5 × 10⁻³	90	ALBRECHT 91B	ARG	$e^+e^- \rightarrow \Upsilon(4S)$

$\Gamma(b_1^0 K^+ \times B(b_1^0 \rightarrow \omega \pi^0))/\Gamma_{total}$ Γ_{400}/Γ

VALUE (units 10^{-6})	DOCUMENT ID	TECN	COMMENT
9.1 ± 1.7 ± 1.0	¹ AUBERT 07Bi	BABR	$e^+e^- \rightarrow \Upsilon(4S)$
¹ Assumes equal production of B^+ and B^0 at the $\Upsilon(4S)$.			

$\Gamma(b_1^+ K^{*0} \times B(b_1^+ \rightarrow \omega \pi^+))/\Gamma_{total}$ Γ_{401}/Γ

VALUE	CL%	DOCUMENT ID	TECN	COMMENT
< 5.9 × 10⁻⁶	90	¹ AUBERT 09AF	BABR	$e^+e^- \rightarrow \Upsilon(4S)$
¹ Assumes equal production of B^+ and B^0 at the $\Upsilon(4S)$.				

$\Gamma(b_1^0 K^{*+} \times B(b_1^0 \rightarrow \omega \pi^0))/\Gamma_{total}$ Γ_{402}/Γ

VALUE	CL%	DOCUMENT ID	TECN	COMMENT
< 6.7 × 10⁻⁶	90	¹ AUBERT 09AF	BABR	$e^+e^- \rightarrow \Upsilon(4S)$
¹ Assumes equal production of B^+ and B^0 at the $\Upsilon(4S)$.				

$\Gamma(K^+ \bar{K}^0)/\Gamma_{total}$ Γ_{403}/Γ

VALUE (units 10^{-6})	CL%	DOCUMENT ID	TECN	COMMENT
1.31 ± 0.17 OUR FIT		Error includes scale factor of 1.2.		
1.19 ± 0.18 OUR AVERAGE				
1.11 ± 0.19 ± 0.05		¹ DUH 13	BELL	$e^+e^- \rightarrow \Upsilon(4S)$
1.61 ± 0.44 ± 0.09		¹ AUBERT,BE 06c	BABR	$e^+e^- \rightarrow \Upsilon(4S)$
• • • We do not use the following data for averages, fits, limits, etc. • • •				
1.22 ± 0.32 ± 0.13		¹ LIN 07	BELL	Repl. by DUH 13
-0.28 - 0.16		¹ ABE 05G	BELL	Repl. by LIN 07
1.0 ± 0.4 ± 0.1		¹ AUBERT,BE 05E	BABR	Repl. by AUBERT,BE 06c
1.5 ± 0.5 ± 0.1		¹ AUBERT 04M	BABR	Repl. by AUBERT,BE 05E
< 2.5	90	¹ CHAO 04	BELL	$e^+e^- \rightarrow \Upsilon(4S)$
< 3.3	90	¹ BORNHEIM 03	CLE2	$e^+e^- \rightarrow \Upsilon(4S)$
< 3.3	90	¹ CASEY 02	BELL	Repl. by CHAO 04
< 2.0	90	¹ ABE 01H	BELL	$e^+e^- \rightarrow \Upsilon(4S)$
< 5.0	90	¹ AUBERT 01E	BABR	$e^+e^- \rightarrow \Upsilon(4S)$
< 2.4	90	¹ CRONIN-HEN..00	CLE2	$e^+e^- \rightarrow \Upsilon(4S)$
< 5.1	90	GODANG 98	CLE2	Repl. by CRONIN-HENNESSY 00
< 21	90			
¹ Assumes equal production of B^+ and B^0 at the $\Upsilon(4S)$.				

$\Gamma(K^+ \bar{K}^0)/\Gamma(K^0 \pi^+)$ $\Gamma_{403}/\Gamma_{342}$

VALUE	DOCUMENT ID	TECN	COMMENT
0.055 ± 0.007 OUR FIT	Error includes scale factor of 1.2.		
0.064 ± 0.009 ± 0.004	AAIJ 13Bs	LHCB	pp at 7 TeV

$\Gamma(\bar{K}^0 K^+ \pi^0)/\Gamma_{total}$ Γ_{404}/Γ

VALUE	CL%	DOCUMENT ID	TECN	COMMENT
< 24 × 10⁻⁶	90	¹ ECKHART 02	CLE2	$e^+e^- \rightarrow \Upsilon(4S)$
¹ Assumes equal production of B^+ and B^0 at the $\Upsilon(4S)$.				

$\Gamma(K^+ K_S^0 K_S^0)/\Gamma_{total}$ Γ_{405}/Γ

VALUE (units 10^{-6})	DOCUMENT ID	TECN	COMMENT
10.5 ± 0.4 OUR AVERAGE			
10.42 ± 0.43 ± 0.22	¹ KALIYAR 19	BELL	$e^+e^- \rightarrow \Upsilon(4S)$
10.6 ± 0.5 ± 0.3	^{1,2} LEES 12o	BABR	$e^+e^- \rightarrow \Upsilon(4S)$
• • • We do not use the following data for averages, fits, limits, etc. • • •			
10.7 ± 1.2 ± 1.0	¹ AUBERT,B 04V	BABR	Repl. by LEES 12o
13.4 ± 1.9 ± 1.5	¹ GARMASH 04	BELL	Repl. by KALIYAR 19
¹ Assumes equal production of B^+ and B^0 at the $\Upsilon(4S)$.			
² All intermediate charmonium and charm resonances are removed, except of χ_{c0} .			

$\Gamma(f_0(980) K^+, f_0 \rightarrow K_S^0 K_S^0)/\Gamma_{total}$ Γ_{406}/Γ

VALUE (units 10^{-6})	DOCUMENT ID	TECN	COMMENT
14.7 ± 2.8 ± 1.8	¹ LEES 12o	BABR	$e^+e^- \rightarrow \Upsilon(4S)$
¹ Assumes equal production of B^+ and B^0 at the $\Upsilon(4S)$.			

$\Gamma(f_0(1710) K^+, f_0 \rightarrow K_S^0 K_S^0)/\Gamma_{total}$ Γ_{407}/Γ

VALUE (units 10^{-6})	DOCUMENT ID	TECN	COMMENT
0.48 ± 0.40 ± 0.11	¹ LEES 12o	BABR	$e^+e^- \rightarrow \Upsilon(4S)$
¹ Assumes equal production of B^+ and B^0 at the $\Upsilon(4S)$.			

$\Gamma(K^+ K_S^0 K_S^0 \text{ nonresonant})/\Gamma_{total}$ Γ_{408}/Γ

VALUE (units 10^{-6})	DOCUMENT ID	TECN	COMMENT
19.8 ± 3.7 ± 2.5	¹ LEES 12o	BABR	$e^+e^- \rightarrow \Upsilon(4S)$
¹ Assumes equal production of B^+ and B^0 at the $\Upsilon(4S)$.			

$\Gamma(K_S^0 K_S^0 \pi^+)/\Gamma_{total}$ Γ_{409}/Γ

VALUE	CL%	DOCUMENT ID	TECN	COMMENT
< 5.1 × 10⁻⁷	90	¹ AUBERT 09i	BABR	$e^+e^- \rightarrow \Upsilon(4S)$
• • • We do not use the following data for averages, fits, limits, etc. • • •				
< 8.7 × 10 ⁻⁷		¹ KALIYAR 19	BELL	$e^+e^- \rightarrow \Upsilon(4S)$
< 3.2 × 10 ⁻⁶	90	¹ GARMASH 04	BELL	$e^+e^- \rightarrow \Upsilon(4S)$
¹ Assumes equal production of B^+ and B^0 at the $\Upsilon(4S)$.				

$\Gamma(K^+ K^- \pi^+)/\Gamma_{total}$ Γ_{410}/Γ

VALUE (units 10^{-6})	CL%	DOCUMENT ID	TECN	COMMENT
5.2 ± 0.4 OUR AVERAGE				
5.38 ± 0.40 ± 0.35		^{1,2} HSU 17	BELL	$e^+e^- \rightarrow \Upsilon(4S)$
5.0 ± 0.5 ± 0.5		² AUBERT 07bB	BABR	$e^+e^- \rightarrow \Upsilon(4S)$
• • • We do not use the following data for averages, fits, limits, etc. • • •				
< 13	90	² GARMASH 04	BELL	$e^+e^- \rightarrow \Upsilon(4S)$
< 6.3	90	^{2,3} AUBERT 03M	BABR	Repl. by AUBERT 07bB
< 12	90	⁴ GARMASH 02	BELL	$e^+e^- \rightarrow \Upsilon(4S)$
¹ HSU 17 provides also measurement as a function of $K^+ K^-$ invariant mass.				
² Assumes equal production of B^+ and B^0 at the $\Upsilon(4S)$.				
³ Charm and charmonium contributions are subtracted, otherwise no assumptions about intermediate resonances.				
⁴ Uses a reference decay mode $B^+ \rightarrow \bar{D}^0 \pi^+$ and $\bar{D}^0 \rightarrow K^+ \pi^-$ with $B(B^+ \rightarrow \bar{D}^0 \pi^+) \cdot B(\bar{D}^0 \rightarrow K^+ \pi^-) = (20.3 \pm 2.0) \times 10^{-5}$.				

$\Gamma(K^+ K^- \pi^+ \text{ nonresonant})/\Gamma_{total}$ Γ_{411}/Γ

VALUE (units 10^{-6})	CL%	DOCUMENT ID	TECN	COMMENT
1.68 ± 0.23 ± 0.13		¹ AAIJ 19AL	LHCB	pp at 7, 8 TeV
• • • We do not use the following data for averages, fits, limits, etc. • • •				
< 75	90	BERGFELD 96B	CLE2	$e^+e^- \rightarrow \Upsilon(4S)$
¹ AAIJ 19AL reports $0.323 \pm 0.015 \pm 0.041$ fit fraction for $B^+ \rightarrow K^+ K^- \pi^+$ nonresonant from the amplitude analysis of $B^\pm \rightarrow \pi^\pm K^+ K^-$ decays. We use the PDG 19 value $B(B^+ \rightarrow K^+ K^- \pi^+) = (5.2 \pm 0.4) \times 10^{-6}$ to obtain $B(B^+ \rightarrow K^+ K^- \pi^+ \text{ nonresonant})$. Our first error is the experiment's error and the second error is systematic error from using our best value.				

$\Gamma(K^+ \bar{K}^*(892)^0)/\Gamma_{total}$ Γ_{412}/Γ

VALUE (units 10^{-7})	CL%	DOCUMENT ID	TECN	COMMENT
5.9 ± 0.6 ± 0.5		¹ AAIJ 19AL	LHCB	pp at 7, 8 TeV
• • • We do not use the following data for averages, fits, limits, etc. • • •				
< 11	90	² AUBERT 07AR	BABR	$e^+e^- \rightarrow \Upsilon(4S)$
< 1290	90	ABBIENDI 00B	OPAL	$e^+e^- \rightarrow Z$
< 1380	90	³ ABE 00c	SLD	$e^+e^- \rightarrow Z$
< 53	90	² JESSOP 00	CLE2	$e^+e^- \rightarrow \Upsilon(4S)$
¹ AAIJ 19AL reports $(7.5 \pm 0.6 \pm 0.5) \times 10^{-2}$ fit fraction for $B^+ \rightarrow K^+ \bar{K}^*(892)^0$ from the amplitude analysis of $B^\pm \rightarrow \pi^\pm K^+ K^-$ decays. We use the PDG 19 value $B(B^+ \rightarrow K^+ K^- \pi^+) = (5.2 \pm 0.4) \times 10^{-6}$ to obtain $B(B^+ \rightarrow K^+ \bar{K}^*(892)^0, \bar{K}^*(892)^0 \rightarrow K^+ \pi^-)$. We compute $B(B^+ \rightarrow K^+ \bar{K}^*(892)^0)$ using 2/3 of $B(\bar{K}^*(892)^0 \rightarrow (K\pi)^0) = (99.754 \pm 0.021)\%$ for the $K^+ \pi^-$ fraction. Our first error is the experiment's error and the second error is systematic error from using our best value.				
² Assumes equal production of B^+ and B^0 at the $\Upsilon(4S)$.				
³ ABE 00c assumes $B(Z \rightarrow b\bar{b}) = (21.7 \pm 0.1)\%$ and the B fractions $f_{B^0} = f_{B^+} = (39.7 \pm 1.8)\%$ and $f_{B_s} = (10.5 \pm 1.8)\%$.				

Meson Particle Listings

B^\pm

$\Gamma(K^+ \bar{K}_0^*(1430)^0)/\Gamma_{\text{total}}$ Γ_{413}/Γ

VALUE (units 10^{-6})	CL%	DOCUMENT ID	TECN	COMMENT
--------------------------	-----	-------------	------	---------

0.38 ± 0.12 ± 0.05 ¹AAIJ 19AL LHCB pp at 7, 8 TeV

• • • We do not use the following data for averages, fits, limits, etc. • • •
 <2.2 90 ²AUBERT 07AR BABR $e^+e^- \rightarrow \Upsilon(4S)$

¹AAIJ 19AL reports $(4.5 \pm 0.7 \pm 1.2) \times 10^{-2}$ for fit fraction for $B^+ \rightarrow K^+ \bar{K}_0^*(1430)^0$ from the amplitude analysis of $B^\pm \rightarrow \pi^\pm K^+ K^-$ decays. We use the PDG 19 value $B(B^+ \rightarrow K^+ K^- \pi^+) = (5.2 \pm 0.4) \times 10^{-6}$ to obtain $B(B^+ \rightarrow K^+ \bar{K}_0^*(1430)^0, \bar{K}_0^*(1430)^0 \rightarrow K^+ \pi^-)$. We compute $B(B^+ \rightarrow K^+ \bar{K}_0^*(1430)^0)$ using 2/3 of PDG 19 value $B(K_0^*(1430)^0 \rightarrow K\pi) = (93 \pm 10)\%$ for the $K^+ \pi^-$ fraction. Our first error is the experiment's error and the second error is systematic error from using our best value. ²Assumes equal production of B^+ and B^0 at the $\Upsilon(4S)$.

$\Gamma(\rho(1450)^0 \pi^+, \rho^0 \rightarrow K^+ K^-)/\Gamma_{\text{total}}$ Γ_{469}/Γ

VALUE (units 10^{-6})	CL%	DOCUMENT ID	TECN	COMMENT
--------------------------	-----	-------------	------	---------

1.60 ± 0.08 ± 0.12 ¹AAIJ 19AL LHCB pp at 7, 8 TeV

¹AAIJ 19AL reports $0.307 \pm 0.012 \pm 0.009$ fit fraction for $B^+ \rightarrow \rho(1450)\pi^+$ from the amplitude analysis of $B^\pm \rightarrow \pi^\pm K^+ K^-$ decays. We use the PDG 19 value $B(B^+ \rightarrow K^+ K^- \pi^+) = (5.2 \pm 0.4) \times 10^{-6}$ to obtain $B(B^+ \rightarrow \rho(1450)\pi^+, \rho(1450) \rightarrow K^+ K^-)$. Our first error is the experiment's error and the second error is systematic error from using our best value.

$\Gamma(\pi^+(K^+ K^-)_{S\text{-wave}})/\Gamma_{\text{total}}$ Γ_{414}/Γ

VALUE (units 10^{-7})	CL%	DOCUMENT ID	TECN	COMMENT
--------------------------	-----	-------------	------	---------

8.53 ± 0.67 ± 0.66 ¹AAIJ 19AL LHCB pp at 7, 8 TeV

¹AAIJ 19AL reports $0.164 \pm 0.008 \pm 0.011$ fit fraction for $B^+ \rightarrow \pi^+(K^+ K^-)_{S\text{-wave}}$ in the region of $0.95 < m(K^+ K^-) < 1.42 \text{ GeV}/c^2$ from the amplitude analysis of $B^\pm \rightarrow \pi^\pm K^+ K^-$ decays. We use the PDG 19 value $B(B^+ \rightarrow K^+ K^- \pi^+) = (5.2 \pm 0.4) \times 10^{-6}$ to obtain $B(B^+ \rightarrow \pi^+(K^+ K^-)_{S\text{-wave}})$. Our first error is the experiment's error and the second error is systematic error from using our best value.

$\Gamma(K^+ K^+ \pi^-)/\Gamma_{\text{total}}$ Γ_{415}/Γ

VALUE	CL%	DOCUMENT ID	TECN	COMMENT
-------	-----	-------------	------	---------

<1.1 × 10⁻⁸ 90 AAJ 17E LHCB pp at 7, 8 TeV

• • • We do not use the following data for averages, fits, limits, etc. • • •

<1.6 × 10⁻⁷ 90 ¹AUBERT 08BE BABR $e^+e^- \rightarrow \Upsilon(4S)$

<2.4 × 10⁻⁶ 90 ¹GARMASH 04 BELL $e^+e^- \rightarrow \Upsilon(4S)$

<1.3 × 10⁻⁶ 90 ²AUBERT 03M BABR Repl. by AUBERT 08BE

<3.2 × 10⁻⁶ 90 ³GARMASH 02 BELL $e^+e^- \rightarrow \Upsilon(4S)$

¹Assumes equal production of B^+ and B^0 at the $\Upsilon(4S)$.
²Assumes equal production of B^0 and B^+ at the $\Upsilon(4S)$; charm and charmonium contributions are subtracted, otherwise no assumptions about intermediate resonances.
³Uses a reference decay mode $B^+ \rightarrow \bar{D}^0 \pi^+$ and $\bar{D}^0 \rightarrow K^+ \pi^-$ with $B(B^+ \rightarrow \bar{D}^0 \pi^+) \cdot B(\bar{D}^0 \rightarrow K^+ \pi^-) = (20.3 \pm 2.0) \times 10^{-5}$.

$\Gamma(K^+ K^+ \pi^- \text{nonresonant})/\Gamma_{\text{total}}$ Γ_{416}/Γ

VALUE (units 10^{-6})	CL%	DOCUMENT ID	TECN	COMMENT
--------------------------	-----	-------------	------	---------

<87.9 90 ABBIENDI 00B OPAL $e^+e^- \rightarrow Z$

$\Gamma(f_2'(1525) K^+)/\Gamma_{\text{total}}$ Γ_{417}/Γ

VALUE (units 10^{-6})	CL%	DOCUMENT ID	TECN	COMMENT
--------------------------	-----	-------------	------	---------

1.8 ± 0.5 OUR AVERAGE Error includes scale factor of 1.1.

1.56 ± 0.36 ± 0.30 ^{1,2}LEES 12o BABR $e^+e^- \rightarrow \Upsilon(4S)$

2.8 ± 0.9 ^{+0.5}_{-0.4} ^{1,3}LEES 12o BABR $e^+e^- \rightarrow \Upsilon(4S)$

• • • We do not use the following data for averages, fits, limits, etc. • • •

<8 90 ^{1,4}GARMASH 05 BELL $e^+e^- \rightarrow \Upsilon(4S)$

¹Assumes equal production of B^+ and B^0 at the $\Upsilon(4S)$.
²Measured in the $B^+ \rightarrow K^+ K^- K^+$ decay.
³Measured in the $B^+ \rightarrow K^+ K_S^0 K_S^0$ decay.
⁴GARMASH 05 reports $B(B^+ \rightarrow f_2'(1525) K^+) \cdot B(f_2'(1525) \rightarrow K^+ K^-) < 4.9 \times 10^{-6}$ at 90% CL. We divide this result by our best value of $B(f_2'(1525) \rightarrow K\bar{K}) = 87.6 \times 10^{-2}$ multiplied by 2/3 to account for the $K^+ K^-$ fraction.

$\Gamma(K^+ f_J(2220))/\Gamma_{\text{total}}$ Γ_{418}/Γ

VALUE (units 10^{-6})	CL%	DOCUMENT ID	TECN	COMMENT
--------------------------	-----	-------------	------	---------

not seen ¹HUANG 03 BELL $e^+e^- \rightarrow \Upsilon(4S)$

¹No evidence is found for such decay and set a limit on $B(B^+ \rightarrow f_J(2220)) \times B(f_J(2220) \rightarrow \phi\phi) < 1.2 \times 10^{-6}$ at 90%CL where the $f_J(2220)$ is a possible glueball state.

$\Gamma(K^* \pi^+ K^-)/\Gamma_{\text{total}}$ Γ_{419}/Γ

VALUE (units 10^{-6})	CL%	DOCUMENT ID	TECN	COMMENT
--------------------------	-----	-------------	------	---------

<11.8 90 ¹AUBERT,B 06u BABR $e^+e^- \rightarrow \Upsilon(4S)$

¹Assumes equal production of B^+ and B^0 at the $\Upsilon(4S)$.

$\Gamma(K^*(892) + K^*(892)^0)/\Gamma_{\text{total}}$ Γ_{420}/Γ

VALUE (units 10^{-6})	CL%	DOCUMENT ID	TECN	COMMENT
--------------------------	-----	-------------	------	---------

0.91 ± 0.29 OUR AVERAGE

0.77 ^{+0.35}_{-0.30} ± 0.12 ¹GOH 15 BELL $e^+e^- \rightarrow \Upsilon(4S)$

1.2 ± 0.5 ± 0.1 ²AUBERT 09F BABR $e^+e^- \rightarrow \Upsilon(4S)$

• • • We do not use the following data for averages, fits, limits, etc. • • •

<71 90 ³GODANG 02 CLE2 $e^+e^- \rightarrow \Upsilon(4S)$

¹Signal significance is 2.7 standard deviations. This measurement corresponds to an upper limit of $< 1.31 \times 10^{-6}$ at 90% CL.
²Signal significance is 3.7 standard deviations.
³Assumes a helicity 00 configuration. For a helicity 11 configuration, the limit decreases to 4.8×10^{-5} .

$\Gamma(K^* K^+ \pi^-)/\Gamma_{\text{total}}$ Γ_{421}/Γ

VALUE (units 10^{-6})	CL%	DOCUMENT ID	TECN	COMMENT
--------------------------	-----	-------------	------	---------

<6.1 90 ¹AUBERT,B 06u BABR $e^+e^- \rightarrow \Upsilon(4S)$

¹Assumes equal production of B^+ and B^0 at the $\Upsilon(4S)$.

$\Gamma(K^+ K^- K^+)/\Gamma_{\text{total}}$ Γ_{422}/Γ

VALUE (units 10^{-6})	CL%	DOCUMENT ID	TECN	COMMENT
--------------------------	-----	-------------	------	---------

34.0 ± 1.4 OUR AVERAGE Error includes scale factor of 1.4.

34.6 ± 0.6 ± 0.9 ^{1,2}LEES 12o BABR $e^+e^- \rightarrow \Upsilon(4S)$

30.6 ± 1.2 ± 2.3 ¹GARMASH 05 BELL $e^+e^- \rightarrow \Upsilon(4S)$

• • • We do not use the following data for averages, fits, limits, etc. • • •

35.2 ± 0.9 ± 1.6 ¹AUBERT 06o BABR Repl. by LEES 12o

32.8 ± 1.8 ± 2.8 ¹GARMASH 04 BELL Repl. by GARMASH 05

29.6 ± 2.1 ± 1.6 ³AUBERT 03M BABR Repl. by AUBERT 06o

35.3 ± 3.7 ± 4.5 ⁴GARMASH 02 BELL Repl. by GARMASH 04

<200 90 ⁵ADAM 96d DLPH $e^+e^- \rightarrow Z$

<320 90 ⁵ABREU 95N DLPH Sup. by ADAM 96d

<350 90 ALBRECHT 91E ARG $e^+e^- \rightarrow \Upsilon(4S)$

¹Assumes equal production of B^+ and B^0 at the $\Upsilon(4S)$.
²All intermediate charmonium and charm resonances are removed, except of χ_{c0} .
³Assumes equal production of B^0 and B^+ at the $\Upsilon(4S)$; charm and charmonium contributions are subtracted, otherwise no assumptions about intermediate resonances.
⁴Uses a reference decay mode $B^+ \rightarrow \bar{D}^0 \pi^+$ and $\bar{D}^0 \rightarrow K^+ \pi^-$ with $B(B^+ \rightarrow \bar{D}^0 \pi^+) \cdot B(\bar{D}^0 \rightarrow K^+ \pi^-) = (20.3 \pm 2.0) \times 10^{-5}$.
⁵Assumes B^0 and B^- production fractions of 0.39, and B_S production fraction of 0.12.

$\Gamma(K^+ \phi)/\Gamma_{\text{total}}$ Γ_{423}/Γ

VALUE (units 10^{-6})	CL%	DOCUMENT ID	TECN	COMMENT
--------------------------	-----	-------------	------	---------

8.8 ^{+0.7}_{-0.6} OUR AVERAGE Error includes scale factor of 1.1.

9.2 ± 0.4 ^{+0.7}_{-0.5} ¹LEES 12o BABR $e^+e^- \rightarrow \Upsilon(4S)$

7.6 ± 1.3 ± 0.6 ²ACOSTA 05J CDF $p\bar{p}$ at 1.96 TeV

9.60 ± 0.92 ^{+1.05}_{-0.85} ¹GARMASH 05 BELL $e^+e^- \rightarrow \Upsilon(4S)$

5.5 ^{+2.1}_{-1.8} ± 0.6 ¹BRIERE 01 CLE2 $e^+e^- \rightarrow \Upsilon(4S)$

• • • We do not use the following data for averages, fits, limits, etc. • • •

8.4 ± 0.7 ± 0.7 ¹AUBERT 06o BABR Repl. by LEES 12o

10.0 ^{+0.9}_{-0.8} ± 0.5 ¹AUBERT 04A BABR Repl. by AUBERT 06o

9.4 ± 1.1 ± 0.7 ¹CHEN 03B BELL Repl. by GARMASH 05

14.6 ^{+3.0}_{-2.8} ± 2.0 ³GARMASH 02 BELL Repl. by CHEN 03B

7.7 ^{+1.6}_{-1.4} ± 0.8 ¹AUBERT 01d BABR $e^+e^- \rightarrow \Upsilon(4S)$

<144 90 ⁴ABE 00c SLD $e^+e^- \rightarrow Z$

< 5 90 ¹BERGFELD 98 CLE2

<280 90 ⁵ADAM 96d DLPH $e^+e^- \rightarrow Z$

< 12 90 ASNER 96 CLE2 $e^+e^- \rightarrow \Upsilon(4S)$

<440 90 ⁶ABREU 95N DLPH Sup. by ADAM 96d

<180 90 ALBRECHT 91B ARG $e^+e^- \rightarrow \Upsilon(4S)$

< 90 90 ⁷AVERY 89B CLEO $e^+e^- \rightarrow \Upsilon(4S)$

<210 90 AVERY 87 CLEO $e^+e^- \rightarrow \Upsilon(4S)$

¹Assumes equal production of B^+ and B^0 at the $\Upsilon(4S)$.
²Uses $B(B^+ \rightarrow J/\psi K^+) = (1.00 \pm 0.04) \times 10^{-3}$ and $B(J/\psi \rightarrow \mu^+ \mu^-) = 0.0588 \pm 0.0010$.
³Uses a reference decay mode $B^+ \rightarrow \bar{D}^0 \pi^+$ and $\bar{D}^0 \rightarrow K^+ \pi^-$ with $B(B^+ \rightarrow \bar{D}^0 \pi^+) \cdot B(\bar{D}^0 \rightarrow K^+ \pi^-) = (20.3 \pm 2.0) \times 10^{-5}$.
⁴ABE 00c assumes $B(Z \rightarrow b\bar{b}) = (21.7 \pm 0.1)\%$ and the B fractions $f_{B^0} = f_{B^+} = (39.7 \pm 1.8)\%$ and $f_{B_S} = (10.5 \pm 1.8)\%$.
⁵ADAM 96d assumes $f_{B^0} = f_{B^-} = 0.39$ and $f_{B_S} = 0.12$.
⁶Assumes a B^0, B^- production fraction of 0.39 and a B_S production fraction of 0.12.
⁷AVERY 89B reports $< 8 \times 10^{-5}$ assuming the $\Upsilon(4S)$ decays 43% to $B^0 \bar{B}^0$. We rescale to 50%.

See key on page 999

Meson Particle Listings

B^\pm

$\Gamma(\phi_0(980) K^+ \times B(\phi_0(980) \rightarrow K^+ K^-) / \Gamma_{total}$ Γ_{424} / Γ

VALUE (units 10^{-6})	CL%	DOCUMENT ID	TECN	COMMENT
9.4 ± 1.6 ± 2.8		¹ LEES	120	BABR $e^+ e^- \rightarrow \Upsilon(4S)$
• • • We do not use the following data for averages, fits, limits, etc. • • •				
6.5 ± 2.5 ± 1.6		¹ AUBERT	060	BABR $e^+ e^- \rightarrow \Upsilon(4S)$
<2.9	90	¹ GARMASH	05	BELL $e^+ e^- \rightarrow \Upsilon(4S)$
¹ Assumes equal production of B^+ and B^0 at the $\Upsilon(4S)$.				

$\Gamma(a_2(1320) K^+ \times B(a_2(1320) \rightarrow K^+ K^-) / \Gamma_{total}$ Γ_{425} / Γ

VALUE	CL%	DOCUMENT ID	TECN	COMMENT
<1.1 × 10⁻⁶	90	¹ GARMASH	05	BELL $e^+ e^- \rightarrow \Upsilon(4S)$
¹ Assumes equal production of B^+ and B^0 at the $\Upsilon(4S)$.				

$\Gamma(X_0(1550) K^+ \times B(X_0(1550) \rightarrow K^+ K^-) / \Gamma_{total}$ Γ_{426} / Γ

$X_0(1550)$ is a possible spin zero state near 1.55 GeV/c² invariant mass of $K^+ K^-$.

VALUE (units 10^{-6})	DOCUMENT ID	TECN	COMMENT
4.3 ± 0.6 ± 0.3	¹ AUBERT	060	BABR $e^+ e^- \rightarrow \Upsilon(4S)$
¹ Assumes equal production of B^+ and B^0 at the $\Upsilon(4S)$.			

$\Gamma(\phi(1680) K^+ \times B(\phi(1680) \rightarrow K^+ K^-) / \Gamma_{total}$ Γ_{427} / Γ

VALUE	CL%	DOCUMENT ID	TECN	COMMENT
<0.8 × 10⁻⁶	90	¹ GARMASH	05	BELL $e^+ e^- \rightarrow \Upsilon(4S)$
¹ Assumes equal production of B^+ and B^0 at the $\Upsilon(4S)$.				

$\Gamma(\phi_0(1710) K^+ \times B(\phi_0(1710) \rightarrow K^+ K^-) / \Gamma_{total}$ Γ_{428} / Γ

VALUE (units 10^{-6})	DOCUMENT ID	TECN	COMMENT
1.12 ± 0.25 ± 0.50	¹ LEES	120	BABR $e^+ e^- \rightarrow \Upsilon(4S)$
• • • We do not use the following data for averages, fits, limits, etc. • • •			
1.7 ± 1.0 ± 0.3	¹ AUBERT	060	BABR Repl. by LEES 120
¹ Assumes equal production of B^+ and B^0 at the $\Upsilon(4S)$.			

$\Gamma(K^+ K^- K^+ \text{ nonresonant}) / \Gamma_{total}$ Γ_{429} / Γ

VALUE (units 10^{-6})	CL%	DOCUMENT ID	TECN	COMMENT
23.8 ± 2.8 OUR AVERAGE				
22.8 ± 2.7 ± 7.6		¹ LEES	120	BABR $e^+ e^- \rightarrow \Upsilon(4S)$
24.0 ± 1.5 ± 2.6		¹ GARMASH	05	BELL $e^+ e^- \rightarrow \Upsilon(4S)$
• • • We do not use the following data for averages, fits, limits, etc. • • •				
50.0 ± 6.0 ± 4.0		¹ AUBERT	060	BABR Repl. by LEES 120
<38	90	BERGFELD	96B	CLE2 $e^+ e^- \rightarrow \Upsilon(4S)$
¹ Assumes equal production of B^+ and B^0 at the $\Upsilon(4S)$.				

$\Gamma(K^*(892) K^+ K^-) / \Gamma_{total}$ Γ_{430} / Γ

VALUE (units 10^{-6})	CL%	DOCUMENT ID	TECN	COMMENT
36.2 ± 3.3 ± 3.6				
• • • We do not use the following data for averages, fits, limits, etc. • • •				
<1600	90	ALBRECHT	91E	ARG $e^+ e^- \rightarrow \Upsilon(4S)$
¹ Assumes equal production of B^+ and B^0 at the $\Upsilon(4S)$.				

$\Gamma(K^*(892) \phi) / \Gamma_{total}$ Γ_{431} / Γ

VALUE (units 10^{-6})	CL%	DOCUMENT ID	TECN	COMMENT
10.0 ± 2.0 OUR AVERAGE Error includes scale factor of 1.7.				
11.2 ± 1.0 ± 0.9		¹ AUBERT	07BA	BABR $e^+ e^- \rightarrow \Upsilon(4S)$
6.7 ± 2.1 ± 0.7		¹ CHEN	03B	BELL $e^+ e^- \rightarrow \Upsilon(4S)$
• • • We do not use the following data for averages, fits, limits, etc. • • •				
12.7 ± 2.2		¹ AUBERT	03V	BABR Repl. by AUBERT 07BA
9.7 ± 4.2		¹ AUBERT	01D	BABR Repl. by AUBERT 03V
< 22.5	90	¹ BRIERE	01	CLE2 $e^+ e^- \rightarrow \Upsilon(4S)$
< 41	90	¹ BERGFELD	98	CLE2
< 70	90	ASNER	96	CLE2 $e^+ e^- \rightarrow \Upsilon(4S)$
<1300	90	ALBRECHT	91B	ARG $e^+ e^- \rightarrow \Upsilon(4S)$
¹ Assumes equal production of B^+ and B^0 at the $\Upsilon(4S)$.				

$\Gamma(\phi(K\pi)_0^{*+}) / \Gamma_{total}$ Γ_{432} / Γ

$(K\pi)_0^{*+}$ is the total S-wave composed of $K_0^*(1430)$ and nonresonant that are described using LA SS shape.

VALUE (units 10^{-6})	DOCUMENT ID	TECN	COMMENT
8.3 ± 1.4 ± 0.8	¹ AUBERT	08B1	BABR $e^+ e^- \rightarrow \Upsilon(4S)$
¹ Assumes equal production of B^+ and B^0 at the $\Upsilon(4S)$.			

$\Gamma(\phi K_1(1270)^+) / \Gamma_{total}$ Γ_{433} / Γ

VALUE (units 10^{-6})	DOCUMENT ID	TECN	COMMENT
6.1 ± 1.6 ± 1.1	¹ AUBERT	08B1	BABR $e^+ e^- \rightarrow \Upsilon(4S)$
¹ Assumes equal production of B^+ and B^0 at the $\Upsilon(4S)$.			

$\Gamma(\phi K_1(1400)^+) / \Gamma_{total}$ Γ_{434} / Γ

VALUE (units 10^{-6})	CL%	DOCUMENT ID	TECN	COMMENT
< 3.2	90	¹ AUBERT	08B1	BABR $e^+ e^- \rightarrow \Upsilon(4S)$
• • • We do not use the following data for averages, fits, limits, etc. • • •				
<1100	90	ALBRECHT	91B	ARG $e^+ e^- \rightarrow \Upsilon(4S)$
¹ Assumes equal production of B^+ and B^0 at the $\Upsilon(4S)$.				

$\Gamma(\phi K^*(1410)^+) / \Gamma_{total}$ Γ_{435} / Γ

VALUE (units 10^{-6})	CL%	DOCUMENT ID	TECN	COMMENT
<4.3	90	¹ AUBERT	08B1	BABR $e^+ e^- \rightarrow \Upsilon(4S)$
¹ Assumes equal production of B^+ and B^0 at the $\Upsilon(4S)$.				

$\Gamma(\phi K_0^*(1430)^+) / \Gamma_{total}$ Γ_{436} / Γ

VALUE (units 10^{-6})	DOCUMENT ID	TECN	COMMENT
7.0 ± 1.3 ± 0.9	¹ AUBERT	08B1	BABR $e^+ e^- \rightarrow \Upsilon(4S)$
¹ Assumes equal production of B^+ and B^0 at the $\Upsilon(4S)$.			

$\Gamma(\phi K_2^*(1430)^+) / \Gamma_{total}$ Γ_{437} / Γ

VALUE (units 10^{-6})	CL%	DOCUMENT ID	TECN	COMMENT
8.4 ± 1.8 ± 1.0		¹ AUBERT	08B1	BABR $e^+ e^- \rightarrow \Upsilon(4S)$
• • • We do not use the following data for averages, fits, limits, etc. • • •				
<3400	90	ALBRECHT	91B	ARG $e^+ e^- \rightarrow \Upsilon(4S)$
¹ Assumes equal production of B^+ and B^0 at the $\Upsilon(4S)$.				

$\Gamma(\phi K_2^*(1770)^+) / \Gamma_{total}$ Γ_{438} / Γ

VALUE (units 10^{-6})	CL%	DOCUMENT ID	TECN	COMMENT
<15.0	90	¹ AUBERT	08B1	BABR $e^+ e^- \rightarrow \Upsilon(4S)$
¹ Assumes equal production of B^+ and B^0 at the $\Upsilon(4S)$.				

$\Gamma(\phi K_2^*(1820)^+) / \Gamma_{total}$ Γ_{439} / Γ

VALUE (units 10^{-6})	CL%	DOCUMENT ID	TECN	COMMENT
<16.3	90	¹ AUBERT	08B1	BABR $e^+ e^- \rightarrow \Upsilon(4S)$
¹ Assumes equal production of B^+ and B^0 at the $\Upsilon(4S)$.				

$\Gamma(a_1^{*+} K^0) / \Gamma_{total}$ Γ_{440} / Γ

VALUE (units 10^{-6})	CL%	DOCUMENT ID	TECN	COMMENT
<3.6	90	^{1,2} DEL-AMO-SA...101	BABR	$e^+ e^- \rightarrow \Upsilon(4S)$
¹ Assumes $B(a_1^{\pm} \rightarrow \pi^{\pm} \pi^{\mp} \pi^{\pm}) = 0.5$				
² Assumes equal production of B^+ and B^0 at the $\Upsilon(4S)$.				

$\Gamma(K^+ \phi) / \Gamma_{total}$ Γ_{441} / Γ

VALUE (units 10^{-6})	DOCUMENT ID	TECN	COMMENT
5.0 ± 1.2 OUR AVERAGE Error includes scale factor of 2.3.			
5.6 ± 0.5 ± 0.3	¹ LEES	11A	BABR $e^+ e^- \rightarrow \Upsilon(4S)$
2.6 ± 1.1	¹ HUANG	03	BELL $e^+ e^- \rightarrow \Upsilon(4S)$
0.9 ± 0.3	• • • We do not use the following data for averages, fits, limits, etc. • • •		
7.5 ± 1.0 ± 0.7	¹ AUBERT, BE	06H	BABR Repl. by LEES 11A
¹ Assumes equal production of B^0 and B^+ at the $\Upsilon(4S)$ and for a ϕ invariant mass below 2.85 GeV/c ² .			

$\Gamma(\eta' \eta' K^+) / \Gamma_{total}$ Γ_{442} / Γ

VALUE (units 10^{-6})	CL%	DOCUMENT ID	TECN	COMMENT
<25	90	¹ AUBERT, B	06P	BABR $e^+ e^- \rightarrow \Upsilon(4S)$
¹ Assumes equal production of B^+ and B^0 at the $\Upsilon(4S)$.				

$\Gamma(\omega \phi K^+) / \Gamma_{total}$ Γ_{443} / Γ

VALUE (units 10^{-6})	CL%	DOCUMENT ID	TECN	COMMENT
<1.9	90	¹ LIU	09	BELL $e^+ e^- \rightarrow \Upsilon(4S)$
¹ Assumes equal production of B^+ and B^0 at the $\Upsilon(4S)$.				

$\Gamma(X(1812) K^+ \times B(X \rightarrow \omega \phi) / \Gamma_{total}$ Γ_{444} / Γ

VALUE (units 10^{-6})	CL%	DOCUMENT ID	TECN	COMMENT
<0.32	90	¹ LIU	09	BELL $e^+ e^- \rightarrow \Upsilon(4S)$
¹ Assumes equal production of B^+ and B^0 at the $\Upsilon(4S)$.				

$\Gamma(K^*(892) \gamma) / \Gamma_{total}$ Γ_{445} / Γ

VALUE (units 10^{-5})	CL%	DOCUMENT ID	TECN	COMMENT
3.92 ± 0.22 OUR AVERAGE Error includes scale factor of 1.7.				
3.76 ± 0.10 ± 0.12		¹ HORIGUCHI	17	BELL $e^+ e^- \rightarrow \Upsilon(4S)$
4.22 ± 0.14 ± 0.16		² AUBERT	09a0	BABR $e^+ e^- \rightarrow \Upsilon(4S)$
3.76 ± 0.89		³ COAN	00	CLE2 $e^+ e^- \rightarrow \Upsilon(4S)$
-0.83 ± 0.28				

Meson Particle Listings

B^\pm

- • • We do not use the following data for averages, fits, limits, etc. • • •

3.87 ± 0.28 ± 0.26	4	AUBERT,BE	04A	BABR	Repl. by AUBERT 09A0
4.25 ± 0.31 ± 0.24	3	NAKAO	04	BELL	Repl. by HORIGUCHI 17
3.83 ± 0.62 ± 0.22	3	AUBERT	02c	BABR	Repl. by AUBERT,BE 04A
5.7 ± 3.1 ± 1.1	5	AMMAR	93	CLE2	Repl. by COAN 00

< 55	90	6	ALBRECHT	89G	ARG	$e^+e^- \rightarrow \Upsilon(4S)$
< 55	90	6	AVERY	89B	CLEO	$e^+e^- \rightarrow \Upsilon(4S)$
< 180	90		AVERY	87	CLEO	$e^+e^- \rightarrow \Upsilon(4S)$

 - 1 Uses $B(\Upsilon(4S) \rightarrow B^+B^-) = (51.4 \pm 0.6)\%$ and $B(\Upsilon(4S) \rightarrow B^0\bar{B}^0) = (48.6 \pm 0.6)\%$.
 - 2 Uses $B(\Upsilon(4S) \rightarrow B^+B^-) = (51.6 \pm 0.6)\%$ and $B(\Upsilon(4S) \rightarrow B^0\bar{B}^0) = (48.4 \pm 0.6)\%$.
 - 3 Assumes equal production of B^+ and B^0 at the $\Upsilon(4S)$.
 - 4 Uses the production ratio of charged and neutral B from $\Upsilon(4S)$ decays $R^{+0} = 1.006 \pm 0.048$.
 - 5 AMMAR 93 observed 4.1 ± 2.3 events above background.
 - 6 Assumes the $\Upsilon(4S)$ decays 43% to $B^0\bar{B}^0$.

$\Gamma(K_1(1270)^+\gamma)/\Gamma_{total}$ Γ_{446}/Γ

VALUE (units 10^{-5})	CL%	DOCUMENT ID	TECN	COMMENT	
4.4 $\pm_{-0.6}^{+0.7}$ OUR AVERAGE					
4.41 $\pm_{-0.44}^{+0.63} \pm 0.58$	1,2	DEL-AMO-SA...16	BABR	$e^+e^- \rightarrow \Upsilon(4S)$	
4.3 $\pm 0.9 \pm 0.9$	3	YANG	05	BELL	$e^+e^- \rightarrow \Upsilon(4S)$

- • • We do not use the following data for averages, fits, limits, etc. • • •

< 9.9	90	3	NISHIDA	02	BELL	Repl. by YANG 05
< 730	90	4	ALBRECHT	89G	ARG	$e^+e^- \rightarrow \Upsilon(4S)$

 - 1 Requires $M_{K\pi\pi} < 1.8 \text{ GeV}/c^2$.
 - 2 Uses $B(\Upsilon(4S) \rightarrow B^+B^-) = 0.513 \pm 0.006$.
 - 3 Assumes equal production of B^+ and B^0 at the $\Upsilon(4S)$.
 - 4 ALBRECHT 89G reports < 0.0066 assuming the $\Upsilon(4S)$ decays 45% to $B^0\bar{B}^0$. We rescale to 50%.

$\Gamma(\eta K^+\gamma)/\Gamma_{total}$ Γ_{447}/Γ

VALUE (units 10^{-6})	DOCUMENT ID	TECN	COMMENT
7.9 ± 0.9 OUR AVERAGE			
7.7 ± 1.0 ± 0.4	1,2	AUBERT	09 BABR $e^+e^- \rightarrow \Upsilon(4S)$
8.4 ± 1.5 $\pm_{-0.9}^{+1.2}$	2,3	NISHIDA	05 BELL $e^+e^- \rightarrow \Upsilon(4S)$

- • • We do not use the following data for averages, fits, limits, etc. • • •

10.0 ± 1.3 ± 0.5	1,2	AUBERT,B	06M	BABR	Repl. by AUBERT 09
------------------	-----	----------	-----	------	--------------------

 - 1 $m_{\eta K} < 3.25 \text{ GeV}/c^2$.
 - 2 Assumes equal production of B^+ and B^0 at the $\Upsilon(4S)$.
 - 3 $m_{\eta K} < 2.4 \text{ GeV}/c^2$.

$\Gamma(\eta' K^+\gamma)/\Gamma_{total}$ Γ_{448}/Γ

VALUE (units 10^{-6})	DOCUMENT ID	TECN	COMMENT
2.9 $\pm_{-0.9}^{+1.0}$ OUR AVERAGE			
3.6 ± 1.2 ± 0.4	1,2	WEDD	10 BELL $e^+e^- \rightarrow \Upsilon(4S)$
1.9 $\pm_{-1.2}^{+1.5} \pm 0.1$	1,3	AUBERT,B	06M BABR $e^+e^- \rightarrow \Upsilon(4S)$

- 1 Assumes equal production of B^+ and B^0 at the $\Upsilon(4S)$.
- 2 $m_{\eta' K} < 3.4 \text{ GeV}/c^2$.
- 3 Set the upper limit of 4.2×10^{-6} at 90% CL with $m_{\eta' K} < 3.25 \text{ GeV}/c^2$.

$\Gamma(\phi K^+\gamma)/\Gamma_{total}$ Γ_{449}/Γ

VALUE (units 10^{-6})	DOCUMENT ID	TECN	COMMENT
2.7 ± 0.4 OUR AVERAGE	Error includes scale factor of 1.2.		
2.48 ± 0.30 ± 0.24	1	SAHOO	11A BELL $e^+e^- \rightarrow \Upsilon(4S)$
3.5 ± 0.6 ± 0.4	1	AUBERT	07Q BABR $e^+e^- \rightarrow \Upsilon(4S)$

- • • We do not use the following data for averages, fits, limits, etc. • • •

3.4 ± 0.9 ± 0.4	1	DRUTSKOY	04 BELL	Repl. by SAHOO 11A
-----------------	---	----------	---------	--------------------

 - 1 Assumes equal production of B^+ and B^0 at $\Upsilon(4S)$.

$\Gamma(K^+\pi^-\pi^+\gamma)/\Gamma_{total}$ Γ_{450}/Γ

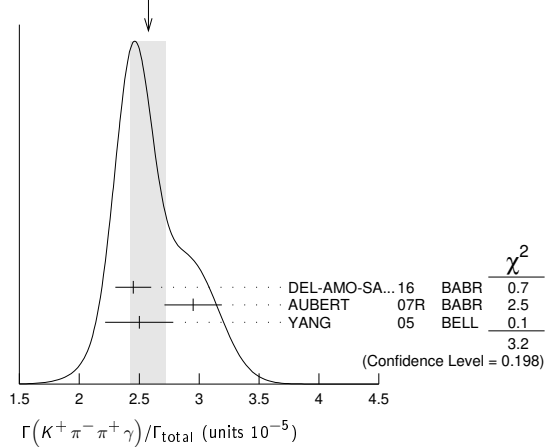
VALUE (units 10^{-5})	DOCUMENT ID	TECN	COMMENT
2.58 ± 0.15 OUR AVERAGE	Error includes scale factor of 1.3. See the ideogram below.		
2.45 ± 0.09 ± 0.12	1,2	DEL-AMO-SA...16	BABR $e^+e^- \rightarrow \Upsilon(4S)$
2.95 ± 0.13 ± 0.20	1,3	AUBERT	07R BABR $e^+e^- \rightarrow \Upsilon(4S)$
2.50 ± 0.18 ± 0.22	3,4	YANG	05 BELL $e^+e^- \rightarrow \Upsilon(4S)$

- • • We do not use the following data for averages, fits, limits, etc. • • •

2.4 ± 0.5 $\pm_{-0.2}^{+0.4}$	3,5	NISHIDA	02 BELL	Repl. by YANG 05
-------------------------------	-----	---------	---------	------------------

 - 1 $M_{K\pi\pi} < 1.8 \text{ GeV}/c^2$.
 - 2 Uses $B(\Upsilon(4S) \rightarrow B^+B^-) = 0.513 \pm 0.006$.
 - 3 Assumes equal production of B^+ and B^0 at the $\Upsilon(4S)$.
 - 4 $M_{K\pi\pi} < 2.0 \text{ GeV}/c^2$.
 - 5 $M_{K\pi\pi} < 2.4 \text{ GeV}/c^2$.

WEIGHTED AVERAGE
2.58 ± 0.15 (Error scaled by 1.3)



$\Gamma(K^*(892)^0\pi^+\gamma)/\Gamma_{total}$ Γ_{451}/Γ

VALUE (units 10^{-5})	DOCUMENT ID	TECN	COMMENT
2.33 ± 0.12 OUR AVERAGE			
2.34 ± 0.09 $\pm_{-0.07}^{+0.08}$	1,2	DEL-AMO-SA...16	BABR $e^+e^- \rightarrow \Upsilon(4S)$
2.0 $\pm_{-0.6}^{+0.7} \pm 0.2$	3,4	NISHIDA	02 BELL $e^+e^- \rightarrow \Upsilon(4S)$

- 1 Requires $M_{K\pi\pi} < 1.8 \text{ GeV}/c^2$.
- 2 Uses $B(\Upsilon(4S) \rightarrow B^+B^-) = 0.513 \pm 0.006$.
- 3 Assumes equal production of B^+ and B^0 at the $\Upsilon(4S)$.
- 4 $M_{K\pi\pi} < 2.4 \text{ GeV}/c^2$.

$\Gamma(K^+\rho^0\gamma)/\Gamma_{total}$ Γ_{452}/Γ

VALUE (units 10^{-6})	DOCUMENT ID	TECN	COMMENT
8.2 ± 0.4 ± 0.8	1,2	DEL-AMO-SA...16	BABR $e^+e^- \rightarrow \Upsilon(4S)$

- • • We do not use the following data for averages, fits, limits, etc. • • •

< 20	90	3,4	NISHIDA	02 BELL	$e^+e^- \rightarrow \Upsilon(4S)$
------	----	-----	---------	---------	-----------------------------------

 - 1 Requires $M_{K\pi\pi} < 1.8 \text{ GeV}/c^2$.
 - 2 Uses $B(\Upsilon(4S) \rightarrow B^+B^-) = 0.513 \pm 0.006$.
 - 3 Assumes equal production of B^+ and B^0 at the $\Upsilon(4S)$.
 - 4 $M_{K\pi\pi} < 2.4 \text{ GeV}/c^2$.

$\Gamma((K^+\pi^-)NR\pi^+\gamma)/\Gamma_{total}$ Γ_{453}/Γ

VALUE (units 10^{-6})	CL%	DOCUMENT ID	TECN	COMMENT
9.9 ± 0.7 $\pm_{-1.9}^{+1.5}$		1,2	DEL-AMO-SA...16	BABR $e^+e^- \rightarrow \Upsilon(4S)$

- • • We do not use the following data for averages, fits, limits, etc. • • •

< 9.2	90	3,4	NISHIDA	02 BELL	$e^+e^- \rightarrow \Upsilon(4S)$
-------	----	-----	---------	---------	-----------------------------------

 - 1 Requires $M_{K\pi\pi} < 1.8 \text{ GeV}/c^2$.
 - 2 Uses $B(\Upsilon(4S) \rightarrow B^+B^-) = 0.513 \pm 0.006$.
 - 3 Assumes equal production of B^+ and B^0 at the $\Upsilon(4S)$.
 - 4 $M_{K\pi\pi} < 2.4 \text{ GeV}/c^2$.

$\Gamma(K^0\pi^+\pi^0\gamma)/\Gamma_{total}$ Γ_{454}/Γ

VALUE (units 10^{-5})	DOCUMENT ID	TECN	COMMENT
4.56 ± 0.42 ± 0.31	1,2	AUBERT	07R BABR $e^+e^- \rightarrow \Upsilon(4S)$

- 1 $M_{K\pi\pi} < 1.8 \text{ GeV}/c^2$.
- 2 Assumes equal production of B^+ and B^0 at the $\Upsilon(4S)$.

$\Gamma(K_1(1400)^+\gamma)/\Gamma_{total}$ Γ_{455}/Γ

VALUE (units 10^{-6})	DOCUMENT ID	TECN	COMMENT
9.7 $\pm_{-2.9}^{+4.6} \pm_{-2.4}^{+2.9}$	1,2	DEL-AMO-SA...16	BABR $e^+e^- \rightarrow \Upsilon(4S)$

- • • We do not use the following data for averages, fits, limits, etc. • • •

< 15	90	3	YANG	05 BELL	$e^+e^- \rightarrow \Upsilon(4S)$
< 50	90	3	NISHIDA	02 BELL	Repl. by YANG 05
< 2200	90	4	ALBRECHT	89G	ARG $e^+e^- \rightarrow \Upsilon(4S)$

 - 1 Requires $M_{K\pi\pi} < 1.8 \text{ GeV}/c^2$.
 - 2 Uses $B(\Upsilon(4S) \rightarrow B^+B^-) = 0.513 \pm 0.006$.
 - 3 Assumes equal production of B^+ and B^0 at the $\Upsilon(4S)$.
 - 4 ALBRECHT 89G reports < 0.0020 assuming the $\Upsilon(4S)$ decays 45% to $B^0\bar{B}^0$. We rescale to 50%.

$\Gamma(K^*(1410)^+\gamma)/\Gamma_{total}$ Γ_{456}/Γ

VALUE (units 10^{-5})	DOCUMENT ID	TECN	COMMENT
2.71 $\pm_{-0.48}^{+0.54} \pm 0.59$	1,2	DEL-AMO-SA...16	BABR $e^+e^- \rightarrow \Upsilon(4S)$

- 1 Requires $M_{K\pi\pi} < 1.8 \text{ GeV}/c^2$.
- 2 Uses $B(\Upsilon(4S) \rightarrow B^+B^-) = 0.513 \pm 0.006$.

See key on page 999

Meson Particle Listings

B^{\pm}

$\Gamma(K_S^*(1430)^0 \pi^+ \gamma) / \Gamma_{total}$ Γ_{457} / Γ

VALUE (units 10^{-6})	DOCUMENT ID	TECN	COMMENT
1.32 ± 0.09 + 0.24 -0.10 - 0.30	1,2 DEL-AMO-SA...16	BABR	$e^+ e^- \rightarrow \Upsilon(4S)$

1 Requires $M_{K\pi\pi} < 1.8 \text{ GeV}/c^2$.
2 Uses $B(\Upsilon(4S) \rightarrow B^+ B^-) = 0.513 \pm 0.006$.

$\Gamma(K_S^*(1430)^+ \gamma) / \Gamma_{total}$ Γ_{458} / Γ

VALUE (units 10^{-5})	CL%	DOCUMENT ID	TECN	COMMENT
1.4 ± 0.4 OUR AVERAGE				
0.87 ± 0.70 + 0.87 -0.53 - 1.04		1,2 DEL-AMO-SA...16	BABR	$e^+ e^- \rightarrow \Upsilon(4S)$
1.45 ± 0.40 ± 0.15		3 AUBERT,B 04U	BABR	$e^+ e^- \rightarrow \Upsilon(4S)$

• • • We do not use the following data for averages, fits, limits, etc. • • •

<140	90	4 ALBRECHT 89G	ARG	$e^+ e^- \rightarrow \Upsilon(4S)$
------	----	----------------	-----	------------------------------------

1 Requires $M_{K\pi\pi} < 1.8 \text{ GeV}/c^2$.
2 Uses $B(\Upsilon(4S) \rightarrow B^+ B^-) = 0.513 \pm 0.006$.
3 Assumes equal production of B^+ and B^0 at the $\Upsilon(4S)$.
4 ALBRECHT 89G reports < 0.0013 assuming the $\Upsilon(4S)$ decays 45% to $B^0 \bar{B}^0$. We rescale to 50%.

$\Gamma(K^*(1680)^+ \gamma) / \Gamma_{total}$ Γ_{459} / Γ

VALUE (units 10^{-5})	CL%	DOCUMENT ID	TECN	COMMENT
6.67 ± 0.93 + 1.44 -0.76 - 1.14		1,2 DEL-AMO-SA...16	BABR	$e^+ e^- \rightarrow \Upsilon(4S)$

• • • We do not use the following data for averages, fits, limits, etc. • • •

<190	90	3 ALBRECHT 89G	ARG	$e^+ e^- \rightarrow \Upsilon(4S)$
------	----	----------------	-----	------------------------------------

1 Requires $M_{K\pi\pi} < 1.8 \text{ GeV}/c^2$.
2 Uses $B(\Upsilon(4S) \rightarrow B^+ B^-) = 0.513 \pm 0.006$.
3 ALBRECHT 89G reports < 0.0017 assuming the $\Upsilon(4S)$ decays 45% to $B^0 \bar{B}^0$. We rescale to 50%.

$\Gamma(K_S^*(1780)^+ \gamma) / \Gamma_{total}$ Γ_{460} / Γ

VALUE (units 10^{-6})	CL%	DOCUMENT ID	TECN	COMMENT
< 39	90	1,2 NISHIDA 05	BELL	$e^+ e^- \rightarrow \Upsilon(4S)$

• • • We do not use the following data for averages, fits, limits, etc. • • •

<5500	90	3 ALBRECHT 89G	ARG	$e^+ e^- \rightarrow \Upsilon(4S)$
-------	----	----------------	-----	------------------------------------

1 Assumes equal production of B^+ and B^0 at the $\Upsilon(4S)$.
2 Uses $B(K_S^*(1780) \rightarrow \eta K) = 0.11 \pm 0.05$.
3 ALBRECHT 89G reports < 0.005 assuming the $\Upsilon(4S)$ decays 45% to $B^0 \bar{B}^0$. We rescale to 50%.

$\Gamma(K_S^*(2045)^+ \gamma) / \Gamma_{total}$ Γ_{461} / Γ

VALUE	CL%	DOCUMENT ID	TECN	COMMENT
< 0.0099	90	1 ALBRECHT 89G	ARG	$e^+ e^- \rightarrow \Upsilon(4S)$

1 ALBRECHT 89G reports < 0.0090 assuming the $\Upsilon(4S)$ decays 45% to $B^0 \bar{B}^0$. We rescale to 50%.

$\Gamma(\rho^+ \gamma) / \Gamma_{total}$ Γ_{462} / Γ

VALUE (units 10^{-6})	CL%	DOCUMENT ID	TECN	COMMENT
0.98 ± 0.25 OUR AVERAGE				
1.20 ± 0.42 ± 0.20 -0.37 - 0.20		1 AUBERT 08BH	BABR	$e^+ e^- \rightarrow \Upsilon(4S)$
0.87 ± 0.29 + 0.09 -0.27 - 0.11		1 TANIGUCHI 08	BELL	$e^+ e^- \rightarrow \Upsilon(4S)$

• • • We do not use the following data for averages, fits, limits, etc. • • •

1.10 ± 0.37 ± 0.09 -0.33 - 0.09		1 AUBERT 07L	BABR	Repl. by AUBERT 08BH
0.55 ± 0.42 + 0.09 -0.36 - 0.08		1 MOHAPATRA 06	BELL	Repl. by TANIGUCHI 08
0.9 ± 0.6 ± 0.1 -0.5 - 0.1	90	1 AUBERT 05	BABR	Repl. by AUBERT 07L
< 2.2	90	1 MOHAPATRA 05	BELL	$e^+ e^- \rightarrow \Upsilon(4S)$
< 2.1	90	1 AUBERT 04c	BABR	$e^+ e^- \rightarrow \Upsilon(4S)$
<13	90	1,2 COAN 00	CLE2	$e^+ e^- \rightarrow \Upsilon(4S)$

1 Assumes equal production of B^+ and B^0 at $\Upsilon(4S)$.
2 No evidence for a nonresonant $K\pi\gamma$ contamination was seen; the central value assumes no contamination.

$\Gamma(\pi^+ \pi^0) / \Gamma_{total}$ Γ_{463} / Γ

VALUE (units 10^{-6})	CL%	DOCUMENT ID	TECN	COMMENT
5.5 ± 0.4 OUR AVERAGE				Error includes scale factor of 1.2.
5.86 ± 0.26 ± 0.38		1 DUH 13	BELL	$e^+ e^- \rightarrow \Upsilon(4S)$
5.02 ± 0.46 ± 0.29		1 AUBERT 07Bc	BABR	$e^+ e^- \rightarrow \Upsilon(4S)$
4.6 ± 1.8 + 0.6 -1.6 - 0.7		1 BORNHEIM 03	CLE2	$e^+ e^- \rightarrow \Upsilon(4S)$

• • • We do not use the following data for averages, fits, limits, etc. • • •

6.5 ± 0.4 ± 0.4		1 LIN 07A	BELL	Repl. by DUH 13
5.8 ± 0.6 ± 0.4		1 AUBERT 05L	BABR	Repl. by AUBERT 07Bc
5.0 ± 1.2 ± 0.5		1 CHAO 04	BELL	Repl. by LIN 07A
5.5 ± 1.0 ± 0.6 -1.9 - 0.6		1 AUBERT 03L	BABR	Repl. by AUBERT 05L
7.4 ± 2.3 ± 0.9 -2.2 - 0.9		1 CASEY 02	BELL	Repl. by CHAO 04
< 13.4	90	1 ABE 01H	BELL	$e^+ e^- \rightarrow \Upsilon(4S)$

< 9.6	90	1 AUBERT 01E	BABR	$e^+ e^- \rightarrow \Upsilon(4S)$
< 12.7	90	1 CRONIN-HEN.00	CLE2	$e^+ e^- \rightarrow \Upsilon(4S)$
< 20	90	GODANG 98	CLE2	Repl. by CRONIN-HENNESSY 00
< 17	90	ASNER 96	CLE2	Repl. by GODANG 98
< 240	90	1 ALBRECHT 90B	ARG	$e^+ e^- \rightarrow \Upsilon(4S)$
<2300	90	2 BEBEK 87	CLEO	$e^+ e^- \rightarrow \Upsilon(4S)$

1 Assumes equal production of B^+ and B^0 at the $\Upsilon(4S)$.
2 BEBEK 87 assume the $\Upsilon(4S)$ decays 43% to $B^0 \bar{B}^0$.

$\Gamma(\pi^+ \pi^0) / \Gamma(K^0 \pi^+)$ $\Gamma_{463} / \Gamma_{342}$

VALUE	DOCUMENT ID	TECN	COMMENT
0.285 ± 0.02 ± 0.02	LIN 07A	BELL	$e^+ e^- \rightarrow \Upsilon(4S)$

$\Gamma(\pi^+ \pi^+ \pi^-) / \Gamma_{total}$ Γ_{464} / Γ

VALUE (units 10^{-6})	CL%	DOCUMENT ID	TECN	COMMENT
15.2 ± 0.6 ± 1.3 -1.2		1 AUBERT 09L	BABR	$e^+ e^- \rightarrow \Upsilon(4S)$

• • • We do not use the following data for averages, fits, limits, etc. • • •

16.2 ± 1.2 ± 0.9		1 AUBERT,B 05G	BABR	Repl. by AUBERT 09L
10.9 ± 3.3 ± 1.6		1 AUBERT 03M	BABR	Repl. by AUBERT 05G
<130	90	2 ADAM 96D	DLPH	$e^+ e^- \rightarrow Z$
<220	90	3 ABREU 95N	DLPH	Sup. by ADAM 96D
<450	90	4 ALBRECHT 90B	ARG	$e^+ e^- \rightarrow \Upsilon(4S)$
<190	90	5 BORTOLETTO89	CLEO	$e^+ e^- \rightarrow \Upsilon(4S)$

1 Assumes equal production of B^0 and B^+ at the $\Upsilon(4S)$; charm and charmonium contributions are subtracted, otherwise no assumptions about intermediate resonances.
2 ADAM 96D assumes $f_{B^0} = f_{B^-} = 0.39$ and $f_{B_s} = 0.12$.
3 Assumes a B^0, B^- production fraction of 0.39 and a B_s production fraction of 0.12.
4 ALBRECHT 90B limit assumes equal production of $B^0 \bar{B}^0$ and $B^+ B^-$ at $\Upsilon(4S)$.
5 BORTOLETTO 89 reports $< 1.7 \times 10^{-4}$ assuming the $\Upsilon(4S)$ decays 43% to $B^0 \bar{B}^0$. We rescale to 50%.

$\Gamma(\rho^0 \pi^+) / \Gamma_{total}$ Γ_{465} / Γ

VALUE (units 10^{-6})	CL%	DOCUMENT ID	TECN	COMMENT
8.3 ± 1.2 OUR AVERAGE				
8.1 ± 0.7 + 1.3 -1.6		1 AUBERT 09L	BABR	$e^+ e^- \rightarrow \Upsilon(4S)$
8.0 ± 2.3 ± 0.7 -2.0		1 GORDON 02	BELL	$e^+ e^- \rightarrow \Upsilon(4S)$
10.4 ± 3.3 ± 2.1 -3.4		1 JESSOP 00	CLE2	$e^+ e^- \rightarrow \Upsilon(4S)$

• • • We do not use the following data for averages, fits, limits, etc. • • •

8.8 ± 1.0 ± 0.6 -0.9		1 AUBERT,B 05G	BABR	Repl. by AUBERT 09L
9.5 ± 1.1 ± 0.9		1 AUBERT 04Z	BABR	Repl. by AUBERT 05G
< 83	90	2 ABE 00c	SLD	$e^+ e^- \rightarrow Z$
<160	90	3 ADAM 96D	DLPH	$e^+ e^- \rightarrow Z$
< 43	90	ASNER 96	CLE2	Repl. by JESSOP 00
<260	90	4 ABREU 95N	DLPH	Sup. by ADAM 96D
<150	90	1 ALBRECHT 90B	ARG	$e^+ e^- \rightarrow \Upsilon(4S)$
<170	90	5 BORTOLETTO89	CLEO	$e^+ e^- \rightarrow \Upsilon(4S)$
<230	90	5 BEBEK 87	CLEO	$e^+ e^- \rightarrow \Upsilon(4S)$
<600	90	GILES 84	CLEO	Repl. by BEBEK 87

1 Assumes equal production of B^+ and B^0 at the $\Upsilon(4S)$.
2 ABE 00c assumes $B(Z \rightarrow b\bar{b}) = (21.7 \pm 0.1)\%$ and the B fractions $f_{B^0} = f_{B^+} = (39.7 \pm 1.8)\%$ and $f_{B_s} = (10.5 \pm 1.8)\%$.
3 ADAM 96D assumes $f_{B^0} = f_{B^-} = 0.39$ and $f_{B_s} = 0.12$.
4 Assumes a B^0, B^- production fraction of 0.39 and a B_s production fraction of 0.12.
5 Papers assume the $\Upsilon(4S)$ decays 43% to $B^0 \bar{B}^0$. We rescale to 50%.

$[\Gamma(K^*(892)^0 \pi^+) + \Gamma(\rho^0 \pi^+)] / \Gamma_{total}$ $(\Gamma_{368} + \Gamma_{465}) / \Gamma$

VALUE (units 10^{-6})	DOCUMENT ID	TECN	COMMENT
170 ± 120 ± 20	1 ADAM 96D	DLPH	$e^+ e^- \rightarrow Z$

1 ADAM 96D assumes $f_{B^0} = f_{B^-} = 0.39$ and $f_{B_s} = 0.12$.

$\Gamma(\pi^+ f_0(980), f_0 \rightarrow \pi^+ \pi^-) / \Gamma_{total}$ Γ_{466} / Γ

VALUE (units 10^{-6})	CL%	DOCUMENT ID	TECN	COMMENT
< 1.5	90	1 AUBERT 09L	BABR	$e^+ e^- \rightarrow \Upsilon(4S)$

• • • We do not use the following data for averages, fits, limits, etc. • • •

< 3.0	90	1 AUBERT,B 05G	BABR	Repl. by AUBERT 09L
<140	90	2 BORTOLETTO89	CLEO	$e^+ e^- \rightarrow \Upsilon(4S)$

1 Assumes equal production of B^+ and B^0 at the $\Upsilon(4S)$.
2 BORTOLETTO 89 reports $< 1.2 \times 10^{-4}$ assuming the $\Upsilon(4S)$ decays 43% to $B^0 \bar{B}^0$. We rescale to 50%.

Meson Particle Listings

 B^\pm

$\Gamma(\pi^+ f_2(1270))/\Gamma_{\text{total}}$ Γ_{467}/Γ

VALUE (units 10^{-6})	CL%	DOCUMENT ID	TECN	COMMENT
--------------------------	-----	-------------	------	---------

2.2 \pm 0.7 \pm 0.4 OUR AVERAGE

17.0 \pm 2.4 \pm 2.1 ¹AAIJ 19AL LHCb $p\bar{p}$ at 7, 8 TeV
 1.60 \pm 0.67 \pm 0.02 ^{2,3}AUBERT 09L BABR $e^+e^- \rightarrow \Upsilon(4S)$

• • • We do not use the following data for averages, fits, limits, etc. • • •

4.10 \pm 1.28 \pm 0.04 ^{3,4}AUBERT,B 05G BABR Repl. by AUBERT 09L
 <240 90 ⁵BORTOLETTO89 CLEO $e^+e^- \rightarrow \Upsilon(4S)$

¹AAIJ 19AL reports $0.075 \pm 0.008 \pm 0.007$ fit fraction for $B^+ \rightarrow f_2(1270)\pi^+$ from the amplitude analysis of $B^\pm \rightarrow \pi^\pm K^+ K^-$ decays. We use the PDG 19 value $B(B^+ \rightarrow K^+ K^- \pi^+) = (5.2 \pm 0.4) \times 10^{-6}$ to obtain $B(B^+ \rightarrow f_2(1270)\pi^+, f_2(1270) \rightarrow K^+ K^-)$. We compute $B(B^+ \rightarrow f_2(1270)\pi^+)$ using 1/2 of PDG 19 value of $B(f_2(1270) \rightarrow K^+ K^-) = (4.6^{+0.5}_{-0.4})\%$ for $K^+ K^-$ fraction. Our first error is the experiment's error and the second error is systematic error from using our best value.

²AUBERT 09L reports $[\Gamma(B^+ \rightarrow \pi^+ f_2(1270))/\Gamma_{\text{total}}] \times [B(f_2(1270) \rightarrow \pi^+ \pi^-)] = (0.9 \pm 0.2 \pm 0.1^{+0.3}_{-0.1}) \times 10^{-6}$ which we divide by our best value $B(f_2(1270) \rightarrow \pi^+ \pi^-) = (56.2^{+1.9}_{-0.6}) \times 10^{-2}$. Our first error is their experiment's error and our second error is the systematic error from using our best value.

³Assumes equal production of B^+ and B^0 at the $\Upsilon(4S)$.

⁴AUBERT,B 05G reports $[\Gamma(B^+ \rightarrow \pi^+ f_2(1270))/\Gamma_{\text{total}}] \times [B(f_2(1270) \rightarrow \pi^+ \pi^-)] = (2.3 \pm 0.6 \pm 0.4) \times 10^{-6}$ which we divide by our best value $B(f_2(1270) \rightarrow \pi^+ \pi^-) = (56.2^{+1.9}_{-0.6}) \times 10^{-2}$. Our first error is their experiment's error and our second error is the systematic error from using our best value.

⁵BORTOLETTO 89 reports $< 2.1 \times 10^{-4}$ assuming the $\Upsilon(4S)$ decays 43% to $B^0 \bar{B}^0$. We rescale to 50%.

$\Gamma(\rho(1450)^0 \pi^+, \rho^0 \rightarrow \pi^+ \pi^-)/\Gamma_{\text{total}}$ Γ_{468}/Γ

VALUE (units 10^{-6})	CL%	DOCUMENT ID	TECN	COMMENT
--------------------------	-----	-------------	------	---------

1.4 \pm 0.4 \pm 0.5 \pm 0.8

• • • We do not use the following data for averages, fits, limits, etc. • • •

<2.3 90 ¹AUBERT,B 05G BABR Repl. by AUBERT 09L

¹Assumes equal production of B^+ and B^0 at the $\Upsilon(4S)$.

$\Gamma(f_0(1370)\pi^+, f_0 \rightarrow \pi^+ \pi^-)/\Gamma_{\text{total}}$ Γ_{470}/Γ

VALUE (units 10^{-6})	CL%	DOCUMENT ID	TECN	COMMENT
--------------------------	-----	-------------	------	---------

<4.0 90 ¹AUBERT 09L BABR $e^+e^- \rightarrow \Upsilon(4S)$

• • • We do not use the following data for averages, fits, limits, etc. • • •

<3.0 90 ¹AUBERT,B 05G BABR Repl. by AUBERT 09L

¹Assumes equal production of B^+ and B^0 at the $\Upsilon(4S)$.

$\Gamma(f_0(500)\pi^+, f_0 \rightarrow \pi^+ \pi^-)/\Gamma_{\text{total}}$ Γ_{471}/Γ

VALUE (units 10^{-6})	CL%	DOCUMENT ID	TECN	COMMENT
--------------------------	-----	-------------	------	---------

<4.1 90 ¹AUBERT,B 05G BABR $e^+e^- \rightarrow \Upsilon(4S)$

¹Assumes equal production of B^+ and B^0 at the $\Upsilon(4S)$.

$\Gamma(\pi^+ \pi^- \pi^+ \text{nonresonant})/\Gamma_{\text{total}}$ Γ_{472}/Γ

VALUE (units 10^{-6})	CL%	DOCUMENT ID	TECN	COMMENT
--------------------------	-----	-------------	------	---------

5.3 \pm 0.7 \pm 1.3 \pm 0.8

• • • We do not use the following data for averages, fits, limits, etc. • • •

< 4.6 90 ¹AUBERT,B 05G BABR Repl. by AUBERT 09L

<41 90 BERGFELD 96B CLE2 $e^+e^- \rightarrow \Upsilon(4S)$

¹Assumes equal production of B^+ and B^0 at the $\Upsilon(4S)$.

$\Gamma(\pi^+ \pi^0 \pi^0)/\Gamma_{\text{total}}$ Γ_{473}/Γ

VALUE	CL%	DOCUMENT ID	TECN	COMMENT
-------	-----	-------------	------	---------

<8.9 \times 10⁻⁴ 90 ¹ALBRECHT 90B ARG $e^+e^- \rightarrow \Upsilon(4S)$

¹ALBRECHT 90B limit assumes equal production of $B^0 \bar{B}^0$ and $B^+ B^-$ at $\Upsilon(4S)$.

$\Gamma(\rho^+ \pi^0)/\Gamma_{\text{total}}$ Γ_{474}/Γ

VALUE (units 10^{-6})	CL%	DOCUMENT ID	TECN	COMMENT
--------------------------	-----	-------------	------	---------

10.9 \pm 1.4 OUR AVERAGE

10.2 \pm 1.4 \pm 0.9 ¹AUBERT 07X BABR $e^+e^- \rightarrow \Upsilon(4S)$

13.2 \pm 2.3 \pm 1.4 ¹ZHANG 05A BELL $e^+e^- \rightarrow \Upsilon(4S)$

• • • We do not use the following data for averages, fits, limits, etc. • • •

10.9 \pm 1.9 \pm 1.9 ¹AUBERT 04Z BABR Repl. by AUBERT 07X

< 43 90 ^{1,2}JESSOP 00 CLE2 $e^+e^- \rightarrow \Upsilon(4S)$

< 77 90 ASNER 96 CLE2 Repl. by JESSOP 00

<550 90 ¹ALBRECHT 90B ARG $e^+e^- \rightarrow \Upsilon(4S)$

¹Assumes equal production of B^+ and B^0 at the $\Upsilon(4S)$.

²Assumes no nonresonant contributions of $B^+ \rightarrow \pi^+ \pi^0 \pi^0$.

$\Gamma(\pi^+ \pi^- \pi^+ \pi^0)/\Gamma_{\text{total}}$ Γ_{475}/Γ

VALUE	CL%	DOCUMENT ID	TECN	COMMENT
-------	-----	-------------	------	---------

<4.0 \times 10⁻³ 90 ¹ALBRECHT 90B ARG $e^+e^- \rightarrow \Upsilon(4S)$

¹ALBRECHT 90B limit assumes equal production of $B^0 \bar{B}^0$ and $B^+ B^-$ at $\Upsilon(4S)$.

$\Gamma(\rho^+ \rho^0)/\Gamma_{\text{total}}$ Γ_{476}/Γ

VALUE (units 10^{-6})	CL%	DOCUMENT ID	TECN	COMMENT
--------------------------	-----	-------------	------	---------

24.0 \pm 1.9 OUR AVERAGE

23.7 \pm 1.4 \pm 1.4 ¹AUBERT 09G BABR $e^+e^- \rightarrow \Upsilon(4S)$

31.7 \pm 7.1 \pm 3.8 ^{1,2}ZHANG 03B BELL $e^+e^- \rightarrow \Upsilon(4S)$

• • • We do not use the following data for averages, fits, limits, etc. • • •

16.8 \pm 2.2 \pm 2.3 ¹AUBERT,BE 06G BABR Repl. by AUBERT 09G

22.5 \pm 5.7 \pm 5.8 ¹AUBERT 03V BABR Repl. by AUBERT,BE 06G

< 1000 90 ¹ALBRECHT 90B ARG $e^+e^- \rightarrow \Upsilon(4S)$

¹Assumes equal production of B^+ and B^0 at the $\Upsilon(4S)$.

²The systematic error includes the error associated with the helicity-mix uncertainty.

$\Gamma(\rho^+ f_0(980), f_0 \rightarrow \pi^+ \pi^-)/\Gamma_{\text{total}}$ Γ_{477}/Γ

VALUE (units 10^{-6})	CL%	DOCUMENT ID	TECN	COMMENT
--------------------------	-----	-------------	------	---------

<2.0 90 ¹AUBERT 09G BABR $e^+e^- \rightarrow \Upsilon(4S)$

• • • We do not use the following data for averages, fits, limits, etc. • • •

<1.9 90 ¹AUBERT,BE 06G BABR Repl. by AUBERT 09G

¹Assumes equal production of B^+ and B^0 at the $\Upsilon(4S)$.

$\Gamma(a_1(1260)^+ \pi^0)/\Gamma_{\text{total}}$ Γ_{478}/Γ

VALUE (units 10^{-6})	CL%	DOCUMENT ID	TECN	COMMENT
--------------------------	-----	-------------	------	---------

26.4 \pm 5.4 \pm 4.1 ^{1,2}AUBERT 07BL BABR $e^+e^- \rightarrow \Upsilon(4S)$

• • • We do not use the following data for averages, fits, limits, etc. • • •

<1700 90 ¹ALBRECHT 90B ARG $e^+e^- \rightarrow \Upsilon(4S)$

¹Assumes equal production of B^+ and B^0 at the $\Upsilon(4S)$.

²Assumes a_1^+ decays only to 3π and $B(a_1^+ \rightarrow \pi^\pm \pi^\mp \pi^+) = 0.5$.

$\Gamma(a_1(1260)^0 \pi^+)/\Gamma_{\text{total}}$ Γ_{479}/Γ

VALUE (units 10^{-6})	CL%	DOCUMENT ID	TECN	COMMENT
--------------------------	-----	-------------	------	---------

20.4 \pm 4.7 \pm 3.4 ^{1,2}AUBERT 07BL BABR $e^+e^- \rightarrow \Upsilon(4S)$

• • • We do not use the following data for averages, fits, limits, etc. • • •

<900 90 ¹ALBRECHT 90B ARG $e^+e^- \rightarrow \Upsilon(4S)$

¹Assumes equal production of B^+ and B^0 at the $\Upsilon(4S)$.

²Assumes a_1^0 decays only to 3π and $B(a_1^0 \rightarrow \pi^\pm \pi^\mp \pi^0) = 1.0$.

$\Gamma(\omega \pi^+)/\Gamma_{\text{total}}$ Γ_{480}/Γ

VALUE (units 10^{-6})	CL%	DOCUMENT ID	TECN	COMMENT
--------------------------	-----	-------------	------	---------

6.9 \pm 0.5 OUR AVERAGE

6.7 \pm 0.5 \pm 0.4 ¹AUBERT 07AE BABR $e^+e^- \rightarrow \Upsilon(4S)$

6.9 \pm 0.6 \pm 0.5 ¹JEN 06 BELL $e^+e^- \rightarrow \Upsilon(4S)$

11.3 \pm 3.3 \pm 1.4 ¹JESSOP 00 CLE2 $e^+e^- \rightarrow \Upsilon(4S)$

• • • We do not use the following data for averages, fits, limits, etc. • • •

6.1 \pm 0.7 \pm 0.4 ¹AUBERT,B 06E BABR Repl. by AUBERT 07AE

5.5 \pm 0.9 \pm 0.5 ¹AUBERT 04H BABR Repl. by AUBERT,B 06E

5.7 \pm 1.4 \pm 0.6 ¹WANG 04A BELL Repl. by JEN 06

4.2 \pm 2.0 \pm 0.5 ¹LU 02 BELL Repl. by WANG 04A

6.6 \pm 2.1 \pm 0.7 ¹AUBERT 01G BABR Repl. by AUBERT 04H

< 23 90 ¹BERGFELD 98 CLE2 Repl. by JESSOP 00

<400 90 ¹ALBRECHT 90B ARG $e^+e^- \rightarrow \Upsilon(4S)$

¹Assumes equal production of B^+ and B^0 at the $\Upsilon(4S)$.

$\Gamma(\omega \rho^+)/\Gamma_{\text{total}}$ Γ_{481}/Γ

VALUE (units 10^{-6})	CL%	DOCUMENT ID	TECN	COMMENT
--------------------------	-----	-------------	------	---------

15.9 \pm 1.6 \pm 1.4 ¹AUBERT 09H BABR $e^+e^- \rightarrow \Upsilon(4S)$

• • • We do not use the following data for averages, fits, limits, etc. • • •

10.6 \pm 2.1 \pm 1.6 ¹AUBERT,B 06T BABR Repl. by AUBERT 09H

12.6 \pm 3.7 \pm 1.6 ¹AUBERT 05O BABR Repl. by AUBERT,B 06T

<61 90 ¹BERGFELD 98 CLE2

¹Assumes equal production of B^+ and B^0 at the $\Upsilon(4S)$.

$\Gamma(\eta \pi^+)/\Gamma_{\text{total}}$ Γ_{482}/Γ

VALUE (units 10^{-6})	CL%	DOCUMENT ID	TECN	COMMENT
--------------------------	-----	-------------	------	---------

4.02 \pm 0.27 OUR AVERAGE

4.07 \pm 0.26 \pm 0.21 ¹HOI 12 BELL $e^+e^- \rightarrow \Upsilon(4S)$

4.00 \pm 0.40 \pm 0.24 ¹AUBERT 09AV BABR $e^+e^- \rightarrow \Upsilon(4S)$

1.2 \pm 2.8 \pm 1.2 ¹RICHICHI 00 CLE2 $e^+e^- \rightarrow \Upsilon(4S)$

• • • We do not use the following data for averages, fits, limits, etc. • • •

5.0 \pm 0.5 \pm 0.3 ¹AUBERT 07AE BABR Repl. by AUBERT 09AV

4.2 \pm 0.4 \pm 0.2 ¹CHANG 07B BELL Repl. by HOI 12

5.1 \pm 0.6 \pm 0.3 ¹AUBERT,B 05K BABR Repl. by AUBERT 07AE

4.8 \pm 0.7 \pm 0.3 ¹CHANG 05A BELL Repl. by CHANG 07B

5.3 \pm 1.0 \pm 0.3 ¹AUBERT 04H BABR Repl. by AUBERT,B 05K

< 15 90 BEHRENS 98 CLE2 Repl. by RICHICHI 00

<700 90 ¹ALBRECHT 90B ARG $e^+e^- \rightarrow \Upsilon(4S)$

¹Assumes equal production of B^+ and B^0 at the $\Upsilon(4S)$.

See key on page 999

Meson Particle Listings

B^{\pm}

$\Gamma(\eta\rho^+)/\Gamma_{total}$ Γ_{483}/Γ

VALUE (units 10^{-6})	CL%	DOCUMENT ID	TECN	COMMENT
7.0 ± 2.9 OUR AVERAGE		Error includes scale factor of 2.8.		
9.9 ± 1.2 ± 0.8		¹ AUBERT	08AH BABR	$e^+e^- \rightarrow \mathcal{T}(4S)$
4.1 $^{+1.4}_{-1.3}$ ± 0.4		¹ WANG	07B BELL	$e^+e^- \rightarrow \mathcal{T}(4S)$
• • • We do not use the following data for averages, fits, limits, etc. • • •				
8.4 ± 1.9 ± 1.1		¹ AUBERT,B	05K BABR	Repl. by AUBERT 08AH
<14	90	¹ AUBERT,B	04D BABR	Repl. by AUBERT,B 05K
<15	90	¹ RICHICHI	00 CLE2	$e^+e^- \rightarrow \mathcal{T}(4S)$
<32	90	¹ BEHRENS	98 CLE2	Repl. by RICHICHI 00
¹ Assumes equal production of B^+ and B^0 at the $\mathcal{T}(4S)$.				

$\Gamma(\eta'\pi^+)/\Gamma_{total}$ Γ_{484}/Γ

VALUE (units 10^{-6})	CL%	DOCUMENT ID	TECN	COMMENT
2.7 ± 0.9 OUR AVERAGE		Error includes scale factor of 1.9.		
3.5 ± 0.6 ± 0.2		¹ AUBERT	09AV BABR	$e^+e^- \rightarrow \mathcal{T}(4S)$
1.76 $^{+0.67+0.15}_{-0.62-0.14}$		¹ SCHUEMANN	06 BELL	$e^+e^- \rightarrow \mathcal{T}(4S)$
• • • We do not use the following data for averages, fits, limits, etc. • • •				
3.9 ± 0.7 ± 0.3		¹ AUBERT	07AE BABR	Repl. by AUBERT 09AV
4.0 ± 0.8 ± 0.4		¹ AUBERT,B	05K BABR	Repl. by AUBERT 07AE
< 4.5	90	¹ AUBERT	04H BABR	Repl. by AUBERT,B 05K
< 7.0	90	¹ ABE	01M BELL	$e^+e^- \rightarrow \mathcal{T}(4S)$
<12	90	¹ AUBERT	01G BABR	$e^+e^- \rightarrow \mathcal{T}(4S)$
<12	90	¹ RICHICHI	00 CLE2	$e^+e^- \rightarrow \mathcal{T}(4S)$
<31	90	¹ BEHRENS	98 CLE2	Repl. by RICHICHI 00
¹ Assumes equal production of B^+ and B^0 at the $\mathcal{T}(4S)$.				

$\Gamma(\eta'\rho^+)/\Gamma_{total}$ Γ_{485}/Γ

VALUE (units 10^{-6})	CL%	DOCUMENT ID	TECN	COMMENT
9.7 $^{+1.9}_{-1.8}$ ± 1.1		¹ DEL-AMO-SA..10A	BABR	$e^+e^- \rightarrow \mathcal{T}(4S)$
• • • We do not use the following data for averages, fits, limits, etc. • • •				
8.7 $^{+3.1+2.3}_{-2.8-1.3}$		¹ AUBERT	07E BABR	Repl. by DEL-AMO-SANCHEZ 10A
< 5.8	90	¹ SCHUEMANN	07 BELL	$e^+e^- \rightarrow \mathcal{T}(4S)$
<22	90	¹ AUBERT,B	04D BABR	Repl. by AUBERT 07E
<33	90	¹ RICHICHI	00 CLE2	$e^+e^- \rightarrow \mathcal{T}(4S)$
<47	90	¹ BEHRENS	98 CLE2	Repl. by RICHICHI 00
¹ Assumes equal production of B^+ and B^0 at the $\mathcal{T}(4S)$.				

$\Gamma(\phi\pi^+)/\Gamma_{total}$ Γ_{486}/Γ

VALUE (units 10^{-8})	CL%	DOCUMENT ID	TECN	COMMENT
3.2 ± 1.5 ± 0.3		¹ AAIJ	19AL LHCB	pp at 7, 8 TeV
• • • We do not use the following data for averages, fits, limits, etc. • • •				
< 15	90	² AAIJ	14A LHCB	Repl. by AAIJ 19AL
< 33	90	³ KIM	12A BELL	$e^+e^- \rightarrow \mathcal{T}(4S)$
< 24	90	³ AUBERT,B	06C BABR	$e^+e^- \rightarrow \mathcal{T}(4S)$
< 41	90	³ AUBERT	04A BABR	Repl. by AUBERT,B 06C
< 140	90	³ AUBERT	01D BABR	$e^+e^- \rightarrow \mathcal{T}(4S)$
<15300	90	⁴ ABE	00C SLD	$e^+e^- \rightarrow Z$
< 500	90	³ BERGFELD	98 CLE2	
¹ AAIJ 19AL reports $(0.3 \pm 0.1 \pm 0.1) \times 10^{-2}$ fit fraction for $B^+ \rightarrow \phi(1020)\pi^+$ from the amplitude analysis of $B^{\pm} \rightarrow \pi^{\pm}K^+K^-$ decays. We use the PDG 19 value $B(B^+ \rightarrow K^+K^-\pi^+) = (5.2 \pm 0.4) \times 10^{-6}$ to obtain $B(B^+ \rightarrow \phi(1020)\pi^+, \phi(1020) \rightarrow K^+K^-) = (49.2 \pm 0.5)\%$. Our first error is the experiment's error and the second error is systematic error from using our best value.				
² Measures $B(B^+ \rightarrow \phi\pi^+)/B(B^+ \rightarrow \phi K^+) < 0.018$ at 90% C.L. and assumes $B(B^+ \rightarrow \phi K^+) = (8.8^{+0.7}_{-0.6}) \times 10^{-6}$.				
³ Assumes equal production of B^+ and B^0 at the $\mathcal{T}(4S)$.				
⁴ ABE 00c assumes $B(Z \rightarrow b\bar{b}) = (21.7 \pm 0.1)\%$ and the B fractions $f_{B^0} = f_{B^+} = (39.7^{+1.8}_{-2.2})\%$ and $f_{B_s} = (10.5^{+1.8}_{-2.2})\%$.				

$\Gamma(\phi\rho^+)/\Gamma_{total}$ Γ_{487}/Γ

VALUE (units 10^{-6})	CL%	DOCUMENT ID	TECN	COMMENT
< 3.0	90	¹ AUBERT	08BK BABR	$e^+e^- \rightarrow \mathcal{T}(4S)$
• • • We do not use the following data for averages, fits, limits, etc. • • •				
<16		¹ BERGFELD	98 CLE2	
¹ Assumes equal production of B^+ and B^0 at the $\mathcal{T}(4S)$.				

$\Gamma(a_0(980)^0\pi^+, a_0^0 \rightarrow \eta\pi^0)/\Gamma_{total}$ Γ_{488}/Γ

VALUE (units 10^{-6})	CL%	DOCUMENT ID	TECN	COMMENT
< 5.8	90	¹ AUBERT,BE	04 BABR	$e^+e^- \rightarrow \mathcal{T}(4S)$
¹ Assumes equal production of charged and neutral B mesons from $\mathcal{T}(4S)$ decays.				

$\Gamma(a_0(980)^+\pi^0, a_0^+ \rightarrow \eta\pi^+)/\Gamma_{total}$ Γ_{489}/Γ

VALUE (units 10^{-6})	CL%	DOCUMENT ID	TECN	COMMENT
< 1.4	90	¹ AUBERT	08A BABR	$e^+e^- \rightarrow \mathcal{T}(4S)$
¹ Assumes equal production of B^+ and B^0 at the $\mathcal{T}(4S)$.				

$\Gamma(\pi^+\pi^+\pi^-\pi^-\pi^0)/\Gamma_{total}$ Γ_{490}/Γ

VALUE	CL%	DOCUMENT ID	TECN	COMMENT
< 8.6 × 10⁻⁴	90	¹ ALBRECHT	90B ARG	$e^+e^- \rightarrow \mathcal{T}(4S)$
¹ ALBRECHT 90B limit assumes equal production of $B^0\bar{B}^0$ and B^+B^- at $\mathcal{T}(4S)$.				

$\Gamma(\rho^0 a_1(1260)^+)/\Gamma_{total}$ Γ_{491}/Γ

VALUE	CL%	DOCUMENT ID	TECN	COMMENT
< 6.2 × 10⁻⁴	90	¹ BORTOLETTO89	CLEO	$e^+e^- \rightarrow \mathcal{T}(4S)$
• • • We do not use the following data for averages, fits, limits, etc. • • •				
< 6.0 × 10 ⁻⁴	90	² ALBRECHT	90B ARG	$e^+e^- \rightarrow \mathcal{T}(4S)$
< 3.2 × 10 ⁻³	90	¹ BEBEK	87 CLEO	$e^+e^- \rightarrow \mathcal{T}(4S)$
¹ BORTOLETTO 89 reports $< 5.4 \times 10^{-4}$ assuming the $\mathcal{T}(4S)$ decays 43% to $B^0\bar{B}^0$. We rescale to 50%.				
² ALBRECHT 90B limit assumes equal production of $B^0\bar{B}^0$ and B^+B^- at $\mathcal{T}(4S)$.				

$\Gamma(\rho^0 a_2(1320)^+)/\Gamma_{total}$ Γ_{492}/Γ

VALUE	CL%	DOCUMENT ID	TECN	COMMENT
< 7.2 × 10⁻⁴	90	¹ BORTOLETTO89	CLEO	$e^+e^- \rightarrow \mathcal{T}(4S)$
• • • We do not use the following data for averages, fits, limits, etc. • • •				
< 2.6 × 10 ⁻³	90	² BEBEK	87 CLEO	$e^+e^- \rightarrow \mathcal{T}(4S)$
¹ BORTOLETTO 89 reports $< 6.3 \times 10^{-4}$ assuming the $\mathcal{T}(4S)$ decays 43% to $B^0\bar{B}^0$. We rescale to 50%.				
² BEBEK 87 reports $< 2.3 \times 10^{-3}$ assuming the $\mathcal{T}(4S)$ decays 43% to $B^0\bar{B}^0$. We rescale to 50%.				

$\Gamma(b_1^0\pi^+, b_1^0 \rightarrow \omega\pi^0)/\Gamma_{total}$ Γ_{493}/Γ

VALUE (units 10^{-6})	CL%	DOCUMENT ID	TECN	COMMENT
6.7 ± 1.7 ± 1.0		¹ AUBERT	07Bi BABR	$e^+e^- \rightarrow \mathcal{T}(4S)$
¹ Assumes equal production of B^+ and B^0 at the $\mathcal{T}(4S)$.				

$\Gamma(b_1^+\pi^0, b_1^+ \rightarrow \omega\pi^+)/\Gamma_{total}$ Γ_{494}/Γ

VALUE (units 10^{-6})	CL%	DOCUMENT ID	TECN	COMMENT
< 3.3	90	¹ AUBERT	08AG BABR	$e^+e^- \rightarrow \mathcal{T}(4S)$
¹ Assumes equal production of B^+ and B^0 at the $\mathcal{T}(4S)$.				

$\Gamma(\pi^+\pi^+\pi^-\pi^-\pi^0)/\Gamma_{total}$ Γ_{495}/Γ

VALUE	CL%	DOCUMENT ID	TECN	COMMENT
< 6.3 × 10⁻³	90	¹ ALBRECHT	90B ARG	$e^+e^- \rightarrow \mathcal{T}(4S)$
¹ ALBRECHT 90B limit assumes equal production of $B^0\bar{B}^0$ and B^+B^- at $\mathcal{T}(4S)$.				

$\Gamma(b_1^+\rho^0, b_1^+ \rightarrow \omega\pi^+)/\Gamma_{total}$ Γ_{496}/Γ

VALUE	CL%	DOCUMENT ID	TECN	COMMENT
< 5.2 × 10⁻⁶	90	¹ AUBERT	09AF BABR	$e^+e^- \rightarrow \mathcal{T}(4S)$
¹ Assumes equal production of B^+ and B^0 at the $\mathcal{T}(4S)$.				

$\Gamma(b_1^0\rho^+, b_1^0 \rightarrow \omega\pi^0)/\Gamma_{total}$ Γ_{498}/Γ

VALUE	CL%	DOCUMENT ID	TECN	COMMENT
< 3.3 × 10⁻⁶	90	¹ AUBERT	09AF BABR	$e^+e^- \rightarrow \mathcal{T}(4S)$
¹ Assumes equal production of B^+ and B^0 at the $\mathcal{T}(4S)$.				

$\Gamma(a_1(1260)^0 a_1(1260)^0)/\Gamma_{total}$ Γ_{497}/Γ

VALUE	CL%	DOCUMENT ID	TECN	COMMENT
< 1.3 × 10⁻²	90	¹ ALBRECHT	90B ARG	$e^+e^- \rightarrow \mathcal{T}(4S)$
¹ ALBRECHT 90B limit assumes equal production of $B^0\bar{B}^0$ and B^+B^- at $\mathcal{T}(4S)$.				

$\Gamma(h^+\pi^0)/\Gamma_{total}$ Γ_{499}/Γ

VALUE (units 10^{-6})	CL%	DOCUMENT ID	TECN	COMMENT
16 $^{+6}_{-5}$ ± 3.6		GODANG	98 CLE2	$e^+e^- \rightarrow \mathcal{T}(4S)$

$\Gamma(\omega h^+)/\Gamma_{total}$ Γ_{500}/Γ

VALUE (units 10^{-6})	CL%	DOCUMENT ID	TECN	COMMENT
13.8 $^{+2.7}_{-2.4}$ OUR AVERAGE				
13.4 $^{+3.3}_{-2.9}$ ± 1.1		¹ LU	02 BELL	$e^+e^- \rightarrow \mathcal{T}(4S)$
14.3 $^{+3.6}_{-3.2}$ ± 2.0		¹ JESSOP	00 CLE2	$e^+e^- \rightarrow \mathcal{T}(4S)$
• • • We do not use the following data for averages, fits, limits, etc. • • •				
25 $^{+8}_{-7}$ ± 3		¹ BERGFELD	98 CLE2	Repl. by JESSOP 00
¹ Assumes equal production of B^+ and B^0 at the $\mathcal{T}(4S)$.				

$\Gamma(h^+X^0(\text{Familon}))/\Gamma_{total}$ Γ_{501}/Γ

VALUE (units 10^{-6})	CL%	DOCUMENT ID	TECN	COMMENT
< 49	90	¹ AMMAR	01B CLE2	$e^+e^- \rightarrow \mathcal{T}(4S)$
¹ AMMAR 01B searched for the two-body decay of the B meson to a massless neutral feebly-interacting particle X^0 such as the familon, the Nambu-Goldstone boson associated with a spontaneously broken global family symmetry.				

Meson Particle Listings

 B^\pm $\Gamma(K^+ X^0, X^0 \rightarrow \mu^+ \mu^-)/\Gamma_{\text{total}}$ Γ_{502}/Γ

X^0 stands here for a long-lived scalar particle.

VALUE	CL%	DOCUMENT ID	TECN	COMMENT
$<1 \times 10^{-7}$	95	¹ AAIJ	17AQ LHCb	pp at 7, 8 TeV

¹ AAIJ 17AQ searched for a long-lived scalar particle $X^0 \rightarrow \mu^+ \mu^-$ in the mass range 250–4700 MeV and lifetime range 0.1–1000 ps. The limit is between 10^{-7} and 2×10^{-10} in these ranges except in vetoed mass regions around $K_S^0, J/\psi, \psi(2S)$, and $\psi(3770)$.

 $\Gamma(p\bar{p}\pi^+)/\Gamma_{\text{total}}$ Γ_{503}/Γ

VALUE (units 10^{-6})	CL%	DOCUMENT ID	TECN	COMMENT
1.62 ± 0.20 OUR AVERAGE				
1.60 ± 0.22	± 0.12	^{1,2,3} WEI	08 BELL	$e^+ e^- \rightarrow \Upsilon(4S)$
1.69 ± 0.29	± 0.26	¹ AUBERT	07AV BABR	$e^+ e^- \rightarrow \Upsilon(4S)$
• • • We do not use the following data for averages, fits, limits, etc. • • •				
1.07 ± 0.11	± 0.11	⁴ AAIJ	14AF LHCb	pp at 7, 8 TeV
3.06 ± 0.73	± 0.37	^{1,3} WANG	04 BELL	Repl. by WEI 08
< 3.7	90	^{1,2} ABE	02K BELL	Repl. by WANG 04
< 500	90	⁵ ABREU	95N DLPH	Repl. by ADAM 96D
< 160	90	⁶ BEBEK	89 CLEO	$e^+ e^- \rightarrow \Upsilon(4S)$
570 ± 150	± 210	⁷ ALBRECHT	88F ARG	$e^+ e^- \rightarrow \Upsilon(4S)$

¹ Assumes equal production of B^+ and B^0 at the $\Upsilon(4S)$.
² Explicitly vetoes resonant production of $p\bar{p}$ from Charmonium states.
³ Also provides results with $m_{p\bar{p}} < 2.85 \text{ GeV}/c^2$ and angular asymmetry of $p\bar{p}$ system.
⁴ Requires $m_{p\bar{p}} < 2.85 \text{ GeV}/c^2$.
⁵ Assumes a B^0, B^- production fraction of 0.39 and a B_S production fraction of 0.12.
⁶ BEBEK 89 reports $< 1.4 \times 10^{-4}$ assuming the $\Upsilon(4S)$ decays 43% to $B^0 \bar{B}^0$. We rescale to 50%.
⁷ ALBRECHT 88F reports $(5.2 \pm 1.4 \pm 1.9) \times 10^{-4}$ assuming the $\Upsilon(4S)$ decays 45% to $B^0 \bar{B}^0$. We rescale to 50%.

 $\Gamma(p\bar{p}\pi^+ \text{nonresonant})/\Gamma_{\text{total}}$ Γ_{504}/Γ

VALUE (units 10^{-6})	CL%	DOCUMENT ID	TECN	COMMENT
< 53	90	BERGFELD	96B CLE2	$e^+ e^- \rightarrow \Upsilon(4S)$

 $\Gamma(p\bar{p}\pi^+ \pi^+ \pi^-)/\Gamma_{\text{total}}$ Γ_{505}/Γ

VALUE	CL%	DOCUMENT ID	TECN	COMMENT
$< 5.2 \times 10^{-4}$	90	¹ ALBRECHT	88F ARG	$e^+ e^- \rightarrow \Upsilon(4S)$

¹ ALBRECHT 88F reports $< 4.7 \times 10^{-4}$ assuming the $\Upsilon(4S)$ decays 45% to $B^0 \bar{B}^0$. We rescale to 50%.

 $\Gamma(p\bar{p}K^+)/\Gamma_{\text{total}}$ Γ_{506}/Γ

VALUE (units 10^{-6})	CL%	DOCUMENT ID	TECN	COMMENT
5.9 ± 0.5 OUR AVERAGE				Error includes scale factor of 1.5.
5.54 ± 0.27	± 0.36	^{1,2,3} WEI	08 BELL	$e^+ e^- \rightarrow \Upsilon(4S)$
6.7 ± 0.5	± 0.4	^{1,3} AUBERT,B	05L BABR	$e^+ e^- \rightarrow \Upsilon(4S)$
• • • We do not use the following data for averages, fits, limits, etc. • • •				
4.59 ± 0.38	± 0.50	^{1,2,3} WANG	05A BELL	Repl. by WEI 08
5.66 ± 0.67	± 0.62	^{1,2,3} WANG	04 BELL	Repl. by WANG 05A
4.3 ± 1.1	± 0.9	^{1,2} ABE	02K BELL	Repl. by WANG 04

¹ Assumes equal production of B^+ and B^0 at the $\Upsilon(4S)$.
² Explicitly vetoes resonant production of $p\bar{p}$ from Charmonium states.
³ Provides also results with $m_{p\bar{p}} < 2.85 \text{ GeV}/c^2$ and angular asymmetry of $p\bar{p}$ system.

 $\Gamma(p\bar{p}K^+)/\Gamma(J/\psi(1S)K^+)$ $\Gamma_{506}/\Gamma_{275}$

VALUE	DOCUMENT ID	TECN	COMMENT
$0.0104 \pm 0.0005 \pm 0.0001$	^{1,2} AAIJ	13S LHCb	pp at 7 TeV

¹ AAIJ 13S reports $[\Gamma(B^+ \rightarrow p\bar{p}K^+)/\Gamma(B^+ \rightarrow J/\psi(1S)K^+)] / [B(J/\psi(1S) \rightarrow p\bar{p})] = 4.91 \pm 0.19 \pm 0.14$ which we multiply by our best value $B(J/\psi(1S) \rightarrow p\bar{p}) = (2.121 \pm 0.029) \times 10^{-3}$. Our first error is their experiment's error and our second error is the systematic error from using our best value.
² Measurement includes contribution where $p\bar{p}$ is produced in charmonia decays.

 $\Gamma(\Theta(1710)^{++\bar{p}}, \Theta^{++} \rightarrow pK^+)/\Gamma_{\text{total}}$ Γ_{507}/Γ

VALUE (units 10^{-6})	CL%	DOCUMENT ID	TECN	COMMENT
< 0.091	90	¹ WANG	05A BELL	$e^+ e^- \rightarrow \Upsilon(4S)$

• • • We do not use the following data for averages, fits, limits, etc. • • •

< 0.1	90	^{1,2} AUBERT,B	05L BABR	$e^+ e^- \rightarrow \Upsilon(4S)$
---------	----	-------------------------	----------	------------------------------------

¹ Assumes equal production of B^+ and B^0 at the $\Upsilon(4S)$.
² Provides upper limits depending on the pentaquark masses between 1.43 to 2.0 GeV/c^2 .

 $\Gamma(f_J(2220)K^+, f_J \rightarrow p\bar{p})/\Gamma_{\text{total}}$ Γ_{508}/Γ

VALUE (units 10^{-6})	CL%	DOCUMENT ID	TECN	COMMENT
< 0.41	90	¹ WANG	05A BELL	$e^+ e^- \rightarrow \Upsilon(4S)$

¹ Assumes equal production of B^+ and B^0 at the $\Upsilon(4S)$.

 $\Gamma(p\bar{\Lambda}(1520))/\Gamma_{\text{total}}$ Γ_{509}/Γ

VALUE (units 10^{-7})	CL%	DOCUMENT ID	TECN	COMMENT
$3.15 \pm 0.48 \pm 0.27$		¹ AAIJ	14AF LHCb	pp at 7, 8 TeV

• • • We do not use the following data for averages, fits, limits, etc. • • •

3.9 ± 1.0	± 0.3	¹ AAIJ	13AU LHCb	Repl. by AAIJ 14AF
< 15	90	² AUBERT,B	05L BABR	$e^+ e^- \rightarrow \Upsilon(4S)$

¹ Uses $B(B^+ \rightarrow J/\psi K^+) = (1.016 \pm 0.033) \times 10^{-3}$, $B(J/\psi \rightarrow p\bar{p}) = (2.17 \pm 0.07) \times 10^{-3}$ and $B(\Lambda(1520) \rightarrow K^- p) = 0.234 \pm 0.016$.
² Assumes equal production of B^+ and B^0 at the $\Upsilon(4S)$.

 $\Gamma(p\bar{p}K^+ \text{nonresonant})/\Gamma_{\text{total}}$ Γ_{510}/Γ

VALUE (units 10^{-6})	CL%	DOCUMENT ID	TECN	COMMENT
< 89	90	BERGFELD	96B CLE2	$e^+ e^- \rightarrow \Upsilon(4S)$

 $\Gamma(p\bar{p}K^*(892)^+)/\Gamma_{\text{total}}$ Γ_{511}/Γ

VALUE (units 10^{-6})	CL%	DOCUMENT ID	TECN	COMMENT
3.6 ± 0.8 OUR AVERAGE				
3.38 ± 0.73	± 0.39	^{1,2} CHEN	08c BELL	$e^+ e^- \rightarrow \Upsilon(4S)$
5.3 ± 1.5	± 1.3	² AUBERT	07AV BABR	$e^+ e^- \rightarrow \Upsilon(4S)$

• • • We do not use the following data for averages, fits, limits, etc. • • •

10.3 ± 3.6	± 1.3	^{2,3} WANG	04 BELL	Repl. by CHEN 08c
----------------	-----------	---------------------	---------	-------------------

¹ Explicitly vetoes resonant production of $p\bar{p}$ from charmonium states.
² Assumes equal production of B^+ and B^0 at the $\Upsilon(4S)$.
³ Explicitly vetoes resonant production of $p\bar{p}$ from charmonium states. The branching fraction for $M_{p\bar{p}} < 2.85 \text{ GeV}/c^2$ is also reported.

 $\Gamma(f_J(2220)K^{*+}, f_J \rightarrow p\bar{p})/\Gamma_{\text{total}}$ Γ_{512}/Γ

VALUE (units 10^{-6})	CL%	DOCUMENT ID	TECN	COMMENT
< 0.77	90	¹ AUBERT	07AV BABR	$e^+ e^- \rightarrow \Upsilon(4S)$

¹ Assumes equal production of B^+ and B^0 at the $\Upsilon(4S)$.

 $\Gamma(p\bar{\Lambda})/\Gamma_{\text{total}}$ Γ_{513}/Γ

VALUE (units 10^{-6})	CL%	DOCUMENT ID	TECN	COMMENT
0.24 ± 0.10 OUR AVERAGE				
0.24 ± 0.10	± 0.03	¹ AAIJ	17R LHCb	pp at 7, 8 TeV

• • • We do not use the following data for averages, fits, limits, etc. • • •

< 0.32	90	² TSAI	07 BELL	$e^+ e^- \rightarrow \Upsilon(4S)$
< 0.49	90	² CHANG	05 BELL	Repl. by TSAI 07
< 1.5	90	² BORNHEIM	03 CLE2	$e^+ e^- \rightarrow \Upsilon(4S)$
< 2.2	90	² ABE	020 BELL	$e^+ e^- \rightarrow \Upsilon(4S)$
< 2.6	90	² COAN	99 CLE2	$e^+ e^- \rightarrow \Upsilon(4S)$
< 60	90	³ AVERY	89B CLEO	$e^+ e^- \rightarrow \Upsilon(4S)$
< 93	90	⁴ ALBRECHT	88F ARG	$e^+ e^- \rightarrow \Upsilon(4S)$

¹ Statistical significance of the signal is 4.1 standard deviations where the normalisation is based on $B(B^+ \rightarrow K_S^0 \pi^+) = (11.895 \pm 0.375) \times 10^{-6}$.
² Assumes equal production of B^+ and B^0 at the $\Upsilon(4S)$.
³ AVERY 89B reports $< 5 \times 10^{-5}$ assuming the $\Upsilon(4S)$ decays 43% to $B^0 \bar{B}^0$. We rescale to 50%.
⁴ ALBRECHT 88F reports $< 8.5 \times 10^{-5}$ assuming the $\Upsilon(4S)$ decays 45% to $B^0 \bar{B}^0$. We rescale to 50%.

 $\Gamma(p\bar{\Lambda}\gamma)/\Gamma_{\text{total}}$ Γ_{514}/Γ

VALUE (units 10^{-6})	CL%	DOCUMENT ID	TECN	COMMENT
2.45 ± 0.44 OUR AVERAGE				
2.45 ± 0.44	± 0.22	¹ WANG	07c BELL	$e^+ e^- \rightarrow \Upsilon(4S)$

• • • We do not use the following data for averages, fits, limits, etc. • • •

2.16 ± 0.58	± 0.20	¹ LEE	05 BELL	Repl. by WANG 07c
< 3.9	90	² EDWARDS	03 CLE2	$e^+ e^- \rightarrow \Upsilon(4S)$

¹ Assumes equal production of B^+ and B^0 at the $\Upsilon(4S)$.
² Corresponds to $E_\gamma > 1.5 \text{ GeV}$. The limit changes to 3.3×10^{-6} for $E_\gamma > 2.0 \text{ GeV}$.

 $\Gamma(p\bar{\Lambda}\pi^0)/\Gamma_{\text{total}}$ Γ_{515}/Γ

VALUE (units 10^{-6})	CL%	DOCUMENT ID	TECN	COMMENT
3.00 ± 0.61 OUR AVERAGE				
3.00 ± 0.61	± 0.33	¹ WANG	07c BELL	$e^+ e^- \rightarrow \Upsilon(4S)$

¹ Assumes equal production of B^+ and B^0 at the $\Upsilon(4S)$.

 $\Gamma(p\bar{\Sigma}^-(1385)^0)/\Gamma_{\text{total}}$ Γ_{516}/Γ

VALUE (units 10^{-6})	CL%	DOCUMENT ID	TECN	COMMENT
< 0.47	90	¹ WANG	07c BELL	$e^+ e^- \rightarrow \Upsilon(4S)$

¹ Assumes equal production of B^+ and B^0 at the $\Upsilon(4S)$.

 $\Gamma(\Delta^+ \bar{\Lambda})/\Gamma_{\text{total}}$ Γ_{517}/Γ

VALUE (units 10^{-6})	CL%	DOCUMENT ID	TECN	COMMENT
< 0.82	90	¹ WANG	07c BELL	$e^+ e^- \rightarrow \Upsilon(4S)$

¹ Assumes equal production of B^+ and B^0 at the $\Upsilon(4S)$.

$\Gamma(\rho\bar{\Sigma}\gamma)/\Gamma_{\text{total}}$ Γ_{518}/Γ

VALUE (units 10^{-6})	CL%	DOCUMENT ID	TECN	COMMENT
<4.6	90	¹ LEE	05 BELL	$e^+e^- \rightarrow \Upsilon(4S)$
••• We do not use the following data for averages, fits, limits, etc. •••				
<7.9	90	² EDWARDS	03 CLE2	$e^+e^- \rightarrow \Upsilon(4S)$
¹ Assumes equal production of B^+ and B^0 at the $\Upsilon(4S)$.				
² Corresponds to $E_\gamma > 1.5$ GeV. The limit changes to 6.4×10^{-6} for $E_\gamma > 2.0$ GeV.				

 $\Gamma(\rho\bar{\Lambda}\pi^+\pi^-)/\Gamma_{\text{total}}$ Γ_{519}/Γ

VALUE (units 10^{-6})	CL%	DOCUMENT ID	TECN	COMMENT
$11.28^{+0.91}_{-0.72} \pm 1.03$		¹ CHEN	09c BELL	$e^+e^- \rightarrow \Upsilon(4S)$
••• We do not use the following data for averages, fits, limits, etc. •••				
<200	90	² ALBRECHT	88F ARG	$e^+e^- \rightarrow \Upsilon(4S)$
¹ Assumes equal production of B^+ and B^0 at the $\Upsilon(4S)$.				
² ALBRECHT 88F reports $< 1.8 \times 10^{-4}$ assuming the $\Upsilon(4S)$ decays 45% to $B^0\bar{B}^0$. We rescale to 50%.				

 $\Gamma(\rho\bar{\Lambda}\pi^+\pi^- \text{ nonresonant})/\Gamma_{\text{total}}$ Γ_{520}/Γ

VALUE (units 10^{-6})	CL%	DOCUMENT ID	TECN	COMMENT
$5.92^{+0.88}_{-0.84} \pm 0.69$		¹ CHEN	09c BELL	$e^+e^- \rightarrow \Upsilon(4S)$
¹ Assumes equal production of B^+ and B^0 at the $\Upsilon(4S)$.				

 $\Gamma(\rho\bar{\Lambda}\rho^0, \rho^0 \rightarrow \pi^+\pi^-)/\Gamma_{\text{total}}$ Γ_{521}/Γ

VALUE (units 10^{-6})	CL%	DOCUMENT ID	TECN	COMMENT
$4.78^{+0.67}_{-0.64} \pm 0.60$		¹ CHEN	09c BELL	$e^+e^- \rightarrow \Upsilon(4S)$
¹ Assumes equal production of B^+ and B^0 at the $\Upsilon(4S)$.				

 $\Gamma(\rho\bar{\Lambda}f_2(1270), f_2 \rightarrow \pi^+\pi^-)/\Gamma_{\text{total}}$ Γ_{522}/Γ

VALUE (units 10^{-6})	CL%	DOCUMENT ID	TECN	COMMENT
$2.03^{+0.77}_{-0.72} \pm 0.27$		¹ CHEN	09c BELL	$e^+e^- \rightarrow \Upsilon(4S)$
¹ Assumes equal production of B^+ and B^0 at the $\Upsilon(4S)$.				

 $\Gamma(\rho\bar{\Lambda}K^+K^-)/\Gamma_{\text{total}}$ Γ_{523}/Γ

VALUE (units 10^{-6})	CL%	DOCUMENT ID	TECN	COMMENT
$4.10^{+0.45}_{-0.43} \pm 0.50$		¹ LU	19 BELL	$e^+e^- \rightarrow \Upsilon(4S)$
¹ Assumes equal production of B^+ and B^0 at the $\Upsilon(4S)$.				

 $\Gamma(\rho\bar{\Lambda}\phi)/\Gamma_{\text{total}}$ Γ_{524}/Γ

VALUE (units 10^{-6})	CL%	DOCUMENT ID	TECN	COMMENT
$0.795 \pm 0.209 \pm 0.077$		¹ LU	19 BELL	$e^+e^- \rightarrow \Upsilon(4S)$
¹ Assumes equal production of B^+ and B^0 at the $\Upsilon(4S)$.				

 $\Gamma(\bar{P}\Lambda K^+K^-)/\Gamma_{\text{total}}$ Γ_{525}/Γ

VALUE (units 10^{-6})	CL%	DOCUMENT ID	TECN	COMMENT
$3.70^{+0.39}_{-0.37} \pm 0.44$		¹ LU	19 BELL	$e^+e^- \rightarrow \Upsilon(4S)$
¹ Assumes equal production of B^+ and B^0 at the $\Upsilon(4S)$.				

 $\Gamma(\bar{\Lambda}\bar{\Lambda}\pi^+)/\Gamma_{\text{total}}$ Γ_{526}/Γ

VALUE (units 10^{-6})	CL%	DOCUMENT ID	TECN	COMMENT
<0.94	90	^{1,2} CHANG	09 BELL	Repl. by CHANG 09
••• We do not use the following data for averages, fits, limits, etc. •••				
<2.8	90	² LEE	04 BELL	$e^+e^- \rightarrow \Upsilon(4S)$
¹ For $m_{\bar{\Lambda}\bar{\Lambda}} < 2.85$ GeV/ c^2 .				
² Assumes equal production of B^+ and B^0 at the $\Upsilon(4S)$.				

 $\Gamma(\bar{\Lambda}\bar{\Lambda}K^+)/\Gamma_{\text{total}}$ Γ_{527}/Γ

VALUE (units 10^{-6})	CL%	DOCUMENT ID	TECN	COMMENT
$3.38^{+0.41}_{-0.36} \pm 0.41$		^{1,2} CHANG	09 BELL	$e^+e^- \rightarrow \Upsilon(4S)$
••• We do not use the following data for averages, fits, limits, etc. •••				
$2.91^{+0.9}_{-0.70} \pm 0.38$		² LEE	04 BELL	Repl. by CHANG 09
¹ Excluding charmonium events in $2.85 < m_{\bar{\Lambda}\bar{\Lambda}} < 3.128$ GeV/ c^2 and $3.315 < m_{\bar{\Lambda}\bar{\Lambda}} < 3.735$ GeV/ c^2 . Measurements in various $m_{\bar{\Lambda}\bar{\Lambda}}$ bins are also reported.				
² Assumes equal production of B^+ and B^0 at the $\Upsilon(4S)$.				

 $\Gamma(\bar{\Lambda}\bar{\Lambda}K^{*+})/\Gamma_{\text{total}}$ Γ_{528}/Γ

VALUE (units 10^{-6})	CL%	DOCUMENT ID	TECN	COMMENT
$2.19^{+1.13}_{-0.88} \pm 0.33$		^{1,2} CHANG	09 BELL	$e^+e^- \rightarrow \Upsilon(4S)$
¹ For $m_{\bar{\Lambda}\bar{\Lambda}} < 2.85$ GeV/ c^2 .				
² Assumes equal production of B^+ and B^0 at the $\Upsilon(4S)$.				

 $\Gamma(\bar{\Lambda}(1520)\bar{\Lambda}K^+)/\Gamma_{\text{total}}$ Γ_{529}/Γ

VALUE (units 10^{-6})	CL%	DOCUMENT ID	TECN	COMMENT
$2.23 \pm 0.63 \pm 0.25$		¹ LU	19 BELL	$e^+e^- \rightarrow \Upsilon(4S)$
¹ Assumes equal production of B^+ and B^0 at the $\Upsilon(4S)$.				

 $\Gamma(\bar{\Lambda}\bar{\Lambda}(1520)K^+)/\Gamma_{\text{total}}$ Γ_{530}/Γ

VALUE (units 10^{-6})	CL%	DOCUMENT ID	TECN	COMMENT
$<2.08 \times 10^{-6}$		¹ LU	19 BELL	$e^+e^- \rightarrow \Upsilon(4S)$
¹ Assumes equal production of B^+ and B^0 at the $\Upsilon(4S)$.				

 $\Gamma(\bar{D}^0\rho)/\Gamma_{\text{total}}$ Γ_{531}/Γ

VALUE (units 10^{-6})	CL%	DOCUMENT ID	TECN	COMMENT
< 1.38	90	¹ WEI	08 BELL	$e^+e^- \rightarrow \Upsilon(4S)$
••• We do not use the following data for averages, fits, limits, etc. •••				
<380	90	² BORTOLETTO	89 CLEO	$e^+e^- \rightarrow \Upsilon(4S)$
¹ Assumes equal production of B^+ and B^0 at the $\Upsilon(4S)$.				
² BORTOLETTO 89 reports $< 3.3 \times 10^{-4}$ assuming the $\Upsilon(4S)$ decays 43% to $B^0\bar{B}^0$. We rescale to 50%.				

 $\Gamma(\bar{D}^{*+}\bar{p})/\Gamma_{\text{total}}$ Γ_{532}/Γ

VALUE (units 10^{-6})	CL%	DOCUMENT ID	TECN	COMMENT
< 0.14	90	¹ WEI	08 BELL	$e^+e^- \rightarrow \Upsilon(4S)$
••• We do not use the following data for averages, fits, limits, etc. •••				
<150	90	² BORTOLETTO	89 CLEO	$e^+e^- \rightarrow \Upsilon(4S)$
¹ Assumes equal production of B^+ and B^0 at the $\Upsilon(4S)$.				
² BORTOLETTO 89 reports $< 1.3 \times 10^{-4}$ assuming the $\Upsilon(4S)$ decays 43% to $B^0\bar{B}^0$. We rescale to 50%.				

 $\Gamma(\bar{D}^+\rho\bar{p})/\Gamma_{\text{total}}$ Γ_{533}/Γ

VALUE (units 10^{-6})	CL%	DOCUMENT ID	TECN	COMMENT
$<1.5 \times 10^{-5}$	90	¹ ABE	02w BELL	$e^+e^- \rightarrow \Upsilon(4S)$
¹ Assumes equal production of B^+ and B^0 at the $\Upsilon(4S)$.				

 $\Gamma(\bar{D}^*(2010)^+\rho\bar{p})/\Gamma_{\text{total}}$ Γ_{534}/Γ

VALUE (units 10^{-6})	CL%	DOCUMENT ID	TECN	COMMENT
$<1.5 \times 10^{-5}$	90	¹ ABE	02w BELL	$e^+e^- \rightarrow \Upsilon(4S)$
¹ Assumes equal production of B^+ and B^0 at the $\Upsilon(4S)$.				

 $\Gamma(\bar{D}^0\rho\bar{p}\pi^+)/\Gamma_{\text{total}}$ Γ_{535}/Γ

VALUE (units 10^{-4})	CL%	DOCUMENT ID	TECN	COMMENT
$3.72 \pm 0.11 \pm 0.25$		^{1,2} DEL-AMO-SA...	12 BABR	$e^+e^- \rightarrow \Upsilon(4S)$
¹ Uses the values of D and D^* branching fractions from PDG 08.				
² Assumes equal production of B^+ and B^0 at the $\Upsilon(4S)$.				

 $\Gamma(\bar{D}^{*0}\rho\bar{p}\pi^+)/\Gamma_{\text{total}}$ Γ_{536}/Γ

VALUE (units 10^{-4})	CL%	DOCUMENT ID	TECN	COMMENT
$3.73 \pm 0.17 \pm 0.27$		^{1,2} DEL-AMO-SA...	12 BABR	$e^+e^- \rightarrow \Upsilon(4S)$
¹ Uses the values of D and D^* branching fractions from PDG 08.				
² Assumes equal production of B^+ and B^0 at the $\Upsilon(4S)$.				

 $\Gamma(\bar{D}^-\rho\bar{p}\pi^+\pi^-)/\Gamma_{\text{total}}$ Γ_{537}/Γ

VALUE (units 10^{-4})	CL%	DOCUMENT ID	TECN	COMMENT
$1.66 \pm 0.13 \pm 0.27$		^{1,2} DEL-AMO-SA...	12 BABR	$e^+e^- \rightarrow \Upsilon(4S)$
¹ Uses the values of D and D^* branching fractions from PDG 08.				
² Assumes equal production of B^+ and B^0 at the $\Upsilon(4S)$.				

 $\Gamma(\bar{D}^{*0}\rho\bar{p}\pi^+\pi^-)/\Gamma_{\text{total}}$ Γ_{538}/Γ

VALUE (units 10^{-4})	CL%	DOCUMENT ID	TECN	COMMENT
$1.86 \pm 0.16 \pm 0.19$		^{1,2} DEL-AMO-SA...	12 BABR	$e^+e^- \rightarrow \Upsilon(4S)$
¹ Uses the values of D and D^* branching fractions from PDG 08.				
² Assumes equal production of B^+ and B^0 at the $\Upsilon(4S)$.				

 $\Gamma(\rho\bar{\Lambda}^0\bar{D}^0)/\Gamma_{\text{total}}$ Γ_{539}/Γ

VALUE (units 10^{-5})	CL%	DOCUMENT ID	TECN	COMMENT
$1.43^{+0.28}_{-0.25} \pm 0.18$		^{1,2} CHEN	11F BELL	$e^+e^- \rightarrow \Upsilon(4S)$
¹ Uses $B(\Lambda \rightarrow p\pi^-) = 63.9 \pm 0.5\%$, $B(D^0 \rightarrow K^-\pi^+) = 3.89 \pm 0.05\%$, and $B(D^0 \rightarrow K^-\pi^+\pi^0) = 13.9 \pm 0.5\%$.				
² Assumes equal production of B^0 and B^+ from Upsilon(4S) decays.				

 $\Gamma(\rho\bar{\Lambda}^0\bar{D}^*(2007)^0)/\Gamma_{\text{total}}$ Γ_{540}/Γ

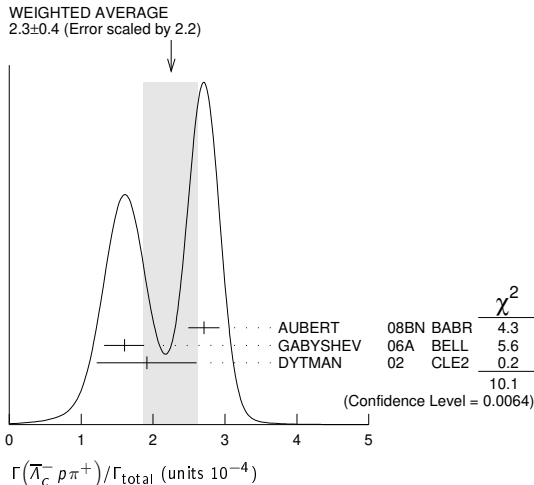
VALUE (units 10^{-5})	CL%	DOCUMENT ID	TECN	COMMENT
<5	90	^{1,2,3} CHEN	11F BELL	$e^+e^- \rightarrow \Upsilon(4S)$
¹ CHEN 11F reports $< 4.8 \times 10^{-5}$ from a measurement of $[\Gamma(B^+ \rightarrow \rho\bar{\Lambda}^0\bar{D}^*(2007)^0)/\Gamma_{\text{total}}] / [B(D^*(2007)^0 \rightarrow D^0\pi^0)]$ assuming $B(D^*(2007)^0 \rightarrow D^0\pi^0) = (61.9 \pm 2.9) \times 10^{-2}$, which we rescale to our best value $B(D^*(2007)^0 \rightarrow D^0\pi^0) = 64.7 \times 10^{-2}$.				
² Uses $B(\Lambda \rightarrow p\pi^-) = 63.9 \pm 0.5\%$ and $B(D^0 \rightarrow K^-\pi^+) = 3.89 \pm 0.05\%$.				
³ Assumes equal production of B^0 and B^+ from Upsilon(4S) decays.				

Meson Particle Listings

B^\pm

$\Gamma(\bar{A}_c^- \rho \pi^+)/\Gamma_{\text{total}}$	DOCUMENT ID	TECN	COMMENT	Γ_{541}/Γ
2.3 ± 0.4 OUR AVERAGE	Error includes scale factor of 2.2. See the ideogram below.			
$2.71 \pm 0.16 \pm 0.14$	1,2 AUBERT	08BN BABR	$e^+ e^- \rightarrow \Upsilon(4S)$	
$1.60 \pm 0.20 \pm 0.08$	1,3 GABYSHEV	06A BELL	$e^+ e^- \rightarrow \Upsilon(4S)$	
$1.9 \pm 0.5 \pm 0.1$	1,4 DYTMAN	02 CLE2	$e^+ e^- \rightarrow \Upsilon(4S)$	
$1.5 \pm 0.4 \pm 0.1$	1,5 GABYSHEV	02 BELL	Repl. by GABYSHEV 06A	
$6.2 \pm_{-2.0}^{+2.3} \pm 1.6$	1,6 FU	97 CLE2	Repl. by DYTMAN 02	

- 1 Assumes equal production of B^+ and B^0 at the $\Upsilon(4S)$.
- 2 AUBERT 08BN reports $(3.4 \pm 0.1 \pm 0.9) \times 10^{-4}$ from a measurement of $[\Gamma(B^+ \rightarrow \bar{A}_c^- \rho \pi^+)/\Gamma_{\text{total}}] \times [B(\Lambda_c^+ \rightarrow p K^- \pi^+)]$ assuming $B(\Lambda_c^+ \rightarrow p K^- \pi^+) = (5.0 \pm 1.3) \times 10^{-2}$, which we rescale to our best value $B(\Lambda_c^+ \rightarrow p K^- \pi^+) = (6.28 \pm 0.32) \times 10^{-2}$. Our first error is their experiment's error and our second error is the systematic error from using our best value.
- 3 GABYSHEV 06A reports $(2.01 \pm 0.15 \pm 0.20) \times 10^{-4}$ from a measurement of $[\Gamma(B^+ \rightarrow \bar{A}_c^- \rho \pi^+)/\Gamma_{\text{total}}] \times [B(\Lambda_c^+ \rightarrow p K^- \pi^+)]$ assuming $B(\Lambda_c^+ \rightarrow p K^- \pi^+) = 0.05$, which we rescale to our best value $B(\Lambda_c^+ \rightarrow p K^- \pi^+) = (6.28 \pm 0.32) \times 10^{-2}$. Our first error is their experiment's error and our second error is the systematic error from using our best value.
- 4 DYTMAN 02 reports $(2.4 \pm_{-0.62}^{+0.63}) \times 10^{-4}$ from a measurement of $[\Gamma(B^+ \rightarrow \bar{A}_c^- \rho \pi^+)/\Gamma_{\text{total}}] \times [B(\Lambda_c^+ \rightarrow p K^- \pi^+)]$ assuming $B(\Lambda_c^+ \rightarrow p K^- \pi^+) = 0.05$, which we rescale to our best value $B(\Lambda_c^+ \rightarrow p K^- \pi^+) = (6.28 \pm 0.32) \times 10^{-2}$. Our first error is their experiment's error and our second error is the systematic error from using our best value.
- 5 GABYSHEV 02 reports $(1.87 \pm_{-0.49}^{+0.51}) \times 10^{-4}$ from a measurement of $[\Gamma(B^+ \rightarrow \bar{A}_c^- \rho \pi^+)/\Gamma_{\text{total}}] \times [B(\Lambda_c^+ \rightarrow p K^- \pi^+)]$ assuming $B(\Lambda_c^+ \rightarrow p K^- \pi^+) = 0.05$, which we rescale to our best value $B(\Lambda_c^+ \rightarrow p K^- \pi^+) = (6.28 \pm 0.32) \times 10^{-2}$. Our first error is their experiment's error and our second error is the systematic error from using our best value.
- 6 FU 97 uses PDG 96 values of Λ_c branching fraction.



$\Gamma(\bar{A}_c^- \Delta(1232)^+)/\Gamma_{\text{total}}$	DOCUMENT ID	TECN	COMMENT	Γ_{542}/Γ
<1.9	90	GABYSHEV 06A	BELL $e^+ e^- \rightarrow \Upsilon(4S)$	

$\Gamma(\bar{A}_c^- \Delta_X(1600)^+)/\Gamma_{\text{total}}$	DOCUMENT ID	TECN	COMMENT	Γ_{543}/Γ
$4.7 \pm 0.9 \pm 0.2$	1 GABYSHEV	06A BELL	$e^+ e^- \rightarrow \Upsilon(4S)$	

1 GABYSHEV 06A reports $(5.9 \pm 1.0 \pm 0.6) \times 10^{-5}$ from a measurement of $[\Gamma(B^+ \rightarrow \bar{A}_c^- \Delta_X(1600)^+)/\Gamma_{\text{total}}] \times [B(\Lambda_c^+ \rightarrow p K^- \pi^+)]$ assuming $B(\Lambda_c^+ \rightarrow p K^- \pi^+) = 0.05$, which we rescale to our best value $B(\Lambda_c^+ \rightarrow p K^- \pi^+) = (6.28 \pm 0.32) \times 10^{-2}$. Our first error is their experiment's error and our second error is the systematic error from using our best value.

$\Gamma(\bar{A}_c^- \Delta_X(2420)^+)/\Gamma_{\text{total}}$	DOCUMENT ID	TECN	COMMENT	Γ_{544}/Γ
$3.7 \pm_{-0.8}^{+0.9} \pm 0.2$	1 GABYSHEV	06A BELL	$e^+ e^- \rightarrow \Upsilon(4S)$	

1 GABYSHEV 06A reports $(4.7 \pm_{-0.9}^{+1.0} \pm 0.4) \times 10^{-5}$ from a measurement of $[\Gamma(B^+ \rightarrow \bar{A}_c^- \Delta_X(2420)^+)/\Gamma_{\text{total}}] \times [B(\Lambda_c^+ \rightarrow p K^- \pi^+)]$ assuming $B(\Lambda_c^+ \rightarrow p K^- \pi^+) = 0.05$, which we rescale to our best value $B(\Lambda_c^+ \rightarrow p K^- \pi^+) = (6.28 \pm 0.32) \times 10^{-2}$. Our first error is their experiment's error and our second error is the systematic error from using our best value.

$\Gamma(\bar{A}_c^- \rho_s \pi^+)/\Gamma_{\text{total}}$	DOCUMENT ID	TECN	COMMENT	Γ_{545}/Γ
$3.1 \pm_{-0.6}^{+0.7} \pm 0.2$	1 GABYSHEV	06A BELL	$e^+ e^- \rightarrow \Upsilon(4S)$	

$(\bar{A}_c^- \rho)_s$ denotes a low-mass enhancement near 3.35 GeV/c².
 1 GABYSHEV 06A reports $(3.9 \pm_{-0.7}^{+0.8} \pm 0.4) \times 10^{-5}$ from a measurement of $[\Gamma(B^+ \rightarrow \bar{A}_c^- \rho_s \pi^+)/\Gamma_{\text{total}}] \times [B(\Lambda_c^+ \rightarrow p K^- \pi^+)]$ assuming $B(\Lambda_c^+ \rightarrow p K^- \pi^+) = 0.05$, which we rescale to our best value $B(\Lambda_c^+ \rightarrow p K^- \pi^+) = (6.28 \pm 0.32) \times 10^{-2}$. Our first error is their experiment's error and our second error is the systematic error from using our best value.

$\Gamma(\Sigma_c(2520)^0 \rho)/\Gamma_{\text{total}}$	CL%	DOCUMENT ID	TECN	COMMENT	Γ_{546}/Γ
<0.3	90	1,2 AUBERT	08BN BABR	$e^+ e^- \rightarrow \Upsilon(4S)$	
<2.7	90	1,2 GABYSHEV	06A BELL	$e^+ e^- \rightarrow \Upsilon(4S)$	
<4.6	90	1,2 GABYSHEV	02 BELL	Repl. by GABYSHEV 06A	

- 1 Assumes equal production of B^+ and B^0 at the $\Upsilon(4S)$.
- 2 Uses the value for $\Lambda_c \rightarrow p K^- \pi^+$ branching ratio $(5.0 \pm 1.3)\%$.

$\Gamma(\Sigma_c(2520)^0 \rho)/\Gamma(\bar{A}_c^- \rho \pi^+)$	DOCUMENT ID	TECN	COMMENT	$\Gamma_{546}/\Gamma_{541}$
<9	90	AUBERT	08BN BABR	$e^+ e^- \rightarrow \Upsilon(4S)$

$\Gamma(\Sigma_c(2800)^0 \rho)/\Gamma_{\text{total}}$	DOCUMENT ID	TECN	COMMENT	Γ_{547}/Γ
$2.6 \pm 0.7 \pm 0.4$	1 AUBERT	08BN BABR	$e^+ e^- \rightarrow \Upsilon(4S)$	

1 AUBERT 08BN reports $[\Gamma(B^+ \rightarrow \Sigma_c(2800)^0 \rho)/\Gamma_{\text{total}}] / [B(B^+ \rightarrow \bar{A}_c^- \rho \pi^+)] = 0.117 \pm 0.023 \pm 0.024$ which we multiply by our best value $B(B^+ \rightarrow \bar{A}_c^- \rho \pi^+) = (2.3 \pm 0.4) \times 10^{-4}$. Our first error is their experiment's error and our second error is the systematic error from using our best value.

$\Gamma(\bar{A}_c^- \rho \pi^+ \pi^0)/\Gamma_{\text{total}}$	DOCUMENT ID	TECN	COMMENT	Γ_{548}/Γ
$1.81 \pm 0.29 \pm_{-0.50}^{+0.52}$	1,2 DYTMAN	02 CLE2	$e^+ e^- \rightarrow \Upsilon(4S)$	

- 1 Assumes equal production of B^+ and B^0 at the $\Upsilon(4S)$.
- 2 DYTMAN 02 measurement uses $B(\Lambda_c^- \rightarrow \bar{p} K^+ \pi^-) = 5.0 \pm 1.3\%$. The second error includes the systematic and the uncertainty of the branching ratio.
- 3 FU 97 uses PDG 96 values of Λ_c branching ratio.

$\Gamma(\bar{A}_c^- \rho \pi^+ \pi^+ \pi^-)/\Gamma_{\text{total}}$	DOCUMENT ID	TECN	COMMENT	Γ_{549}/Γ
$2.25 \pm 0.25 \pm_{-0.61}^{+0.63}$	1,2 DYTMAN	02 CLE2	$e^+ e^- \rightarrow \Upsilon(4S)$	

- 1 Assumes equal production of B^+ and B^0 at the $\Upsilon(4S)$.
- 2 DYTMAN 02 measurement uses $B(\Lambda_c^- \rightarrow \bar{p} K^+ \pi^-) = 5.0 \pm 1.3\%$. The second error includes the systematic and the uncertainty of the branching ratio.
- 3 FU 97 uses PDG 96 values of Λ_c branching ratio.

$\Gamma(\bar{A}_c^- \rho \pi^+ \pi^+ \pi^- \pi^0)/\Gamma_{\text{total}}$	DOCUMENT ID	TECN	COMMENT	Γ_{550}/Γ
$<1.34 \times 10^{-2}$	1 FU	97 CLE2	$e^+ e^- \rightarrow \Upsilon(4S)$	

1 FU 97 uses PDG 96 values of Λ_c branching ratio.

$\Gamma(\Lambda_c^+ \Lambda_c^- K^+)/\Gamma_{\text{total}}$	DOCUMENT ID	TECN	COMMENT	Γ_{551}/Γ
4.9 ± 0.7 OUR AVERAGE				
$4.80 \pm 0.43 \pm 0.60$	LI	18A BELL	$e^+ e^- \rightarrow \Upsilon(4S)$	
$9.1 \pm 4.5 \pm 0.5$	1,2 AUBERT	08H BABR	$e^+ e^- \rightarrow \Upsilon(4S)$	

- 1 AUBERT 08H reports $(1.14 \pm 0.15 \pm 0.62) \times 10^{-3}$ from a measurement of $[\Gamma(B^+ \rightarrow \Lambda_c^+ \Lambda_c^- K^+)/\Gamma_{\text{total}}] \times [B(\Lambda_c^+ \rightarrow p K^- \pi^+)]$ assuming $B(\Lambda_c^+ \rightarrow p K^- \pi^+) = (5.0 \pm 1.3) \times 10^{-2}$, which we rescale to our best value $B(\Lambda_c^+ \rightarrow p K^- \pi^+) = (6.28 \pm 0.32) \times 10^{-2}$. Our first error is their experiment's error and our second error is the systematic error from using our best value.
- 2 Assumes equal production of B^+ and B^0 at the $\Upsilon(4S)$.
- 3 GABYSHEV 06 reports $(7.9 \pm_{-0.9}^{+1.0} \pm 3.6) \times 10^{-4}$ from a measurement of $[\Gamma(B^+ \rightarrow \Lambda_c^+ \Lambda_c^- K^+)/\Gamma_{\text{total}}] \times [B(\Lambda_c^+ \rightarrow p K^- \pi^+)]$ assuming $B(\Lambda_c^+ \rightarrow p K^- \pi^+) = (5.0 \pm 1.3) \times 10^{-2}$, which we rescale to our best value $B(\Lambda_c^+ \rightarrow p K^- \pi^+) = (6.28 \pm 0.32) \times 10^{-2}$. Our first error is their experiment's error and our second error is the systematic error from using our best value.

$\Gamma(\Xi_c(2930)\Lambda_c^+ \Xi_c \rightarrow K^+\Lambda_c^-)/\Gamma_{\text{total}}$		Γ_{552}/Γ	
VALUE (units 10^{-4})	DOCUMENT ID	TECN	COMMENT
1.73 ± 0.45 ± 0.21	¹ LI	18A	BELL $e^+e^- \rightarrow \Upsilon(4S)$

¹ The $\Xi_c(2930)$ is found in its decay to $K^-\Lambda_c^+$ in $B^- \rightarrow K^-\Lambda_c^+\Lambda_c^+$ with a significance more than 5 sigma.

$\Gamma(\Sigma_c(2455)^0 p)/\Gamma_{\text{total}}$		Γ_{553}/Γ	
VALUE (units 10^{-5})	CL%	DOCUMENT ID	TECN COMMENT
2.9 ± 0.6 ± 0.2 0.1		^{1,2} GABYSHEV	06A BELL $e^+e^- \rightarrow \Upsilon(4S)$

• • • We do not use the following data for averages, fits, limits, etc. • • •

<8	90	^{1,3} DYTMAN	02 CLE2 $e^+e^- \rightarrow \Upsilon(4S)$
<9.3	90	^{1,4} GABYSHEV	02 BELL Repl. by GABYSHEV 06A

- Assumes equal production of B^+ and B^0 at the $\Upsilon(4S)$.
- GABYSHEV 06A reports $(3.7 \pm 0.7 \pm 0.4) \times 10^{-5}$ from a measurement of $[\Gamma(B^+ \rightarrow \Sigma_c(2455)^0 p)/\Gamma_{\text{total}}] \times [B(\Lambda_c^+ \rightarrow pK^-\pi^+)]$ assuming $B(\Lambda_c^+ \rightarrow pK^-\pi^+) = 0.05$, which we rescale to our best value $B(\Lambda_c^+ \rightarrow pK^-\pi^+) = (6.28 \pm 0.32) \times 10^{-2}$. Our first error is their experiment's error and our second error is the systematic error from using our best value.
- DYTMAN 02 measurement uses $B(\Lambda_c^- \rightarrow \bar{p}K^+\pi^-) = 5.0 \pm 1.3\%$. The second error includes the systematic and the uncertainty of the branching ratio.
- Uses the value for $\Lambda_c \rightarrow pK^-\pi^+$ branching ratio $(5.0 \pm 1.3)\%$.

$\Gamma(\Sigma_c(2455)^0 p)/\Gamma(\Lambda_c^- p\pi^+)$		$\Gamma_{553}/\Gamma_{541}$	
VALUE	DOCUMENT ID	TECN	COMMENT
0.123 ± 0.012 ± 0.008	¹ AUBERT	08BN	BABR $e^+e^- \rightarrow \Upsilon(4S)$

¹ Assumes equal production of B^+ and B^0 at the $\Upsilon(4S)$.

$\Gamma(\Sigma_c(2455)^0 p\pi^0)/\Gamma_{\text{total}}$		Γ_{554}/Γ	
VALUE (units 10^{-4})	DOCUMENT ID	TECN	COMMENT
3.5 ± 1.1 ± 0.2	^{1,2} DYTMAN	02	CLE2 $e^+e^- \rightarrow \Upsilon(4S)$

- DYTMAN 02 reports $(4.4 \pm 1.4) \times 10^{-4}$ from a measurement of $[\Gamma(B^+ \rightarrow \Sigma_c(2455)^0 p\pi^0)/\Gamma_{\text{total}}] \times [B(\Lambda_c^+ \rightarrow pK^-\pi^+)]$ assuming $B(\Lambda_c^+ \rightarrow pK^-\pi^+) = 0.05$, which we rescale to our best value $B(\Lambda_c^+ \rightarrow pK^-\pi^+) = (6.28 \pm 0.32) \times 10^{-2}$. Our first error is their experiment's error and our second error is the systematic error from using our best value.
- Assumes equal production of B^+ and B^0 at the $\Upsilon(4S)$.

$\Gamma(\Sigma_c(2455)^0 p\pi^-\pi^+)/\Gamma_{\text{total}}$		Γ_{555}/Γ	
VALUE (units 10^{-4})	DOCUMENT ID	TECN	COMMENT
3.5 ± 1.0 ± 0.2	^{1,2} DYTMAN	02	CLE2 $e^+e^- \rightarrow \Upsilon(4S)$

- DYTMAN 02 reports $(4.4 \pm 1.3) \times 10^{-4}$ from a measurement of $[\Gamma(B^+ \rightarrow \Sigma_c(2455)^0 p\pi^-\pi^+)/\Gamma_{\text{total}}] \times [B(\Lambda_c^+ \rightarrow pK^-\pi^+)]$ assuming $B(\Lambda_c^+ \rightarrow pK^-\pi^+) = 0.05$, which we rescale to our best value $B(\Lambda_c^+ \rightarrow pK^-\pi^+) = (6.28 \pm 0.32) \times 10^{-2}$. Our first error is their experiment's error and our second error is the systematic error from using our best value.
- Assumes equal production of B^+ and B^0 at the $\Upsilon(4S)$.

$\Gamma(\Sigma_c(2455)^-- p\pi^+\pi^+)/\Gamma_{\text{total}}$		Γ_{556}/Γ	
VALUE (units 10^{-4})	DOCUMENT ID	TECN	COMMENT
2.37 ± 0.20 OUR AVERAGE			

2.37 ± 0.16 ± 0.13 -0.12	^{1,2} LEES	12Z	BABR $e^+e^- \rightarrow \Upsilon(4S)$
2.2 ± 0.8 ± 0.1	^{1,3} DYTMAN	02	CLE2 $e^+e^- \rightarrow \Upsilon(4S)$

- Assumes equal production of B^+ and B^0 at the $\Upsilon(4S)$.
- LEES 12Z reports $(2.98 \pm 0.16 \pm 0.15 \pm 0.77) \times 10^{-4}$ from a measurement of $[\Gamma(B^+ \rightarrow \Sigma_c(2455)^-- p\pi^+\pi^+)/\Gamma_{\text{total}}] \times [B(\Lambda_c^+ \rightarrow pK^-\pi^+)]$ assuming $B(\Lambda_c^+ \rightarrow pK^-\pi^+) = (5.0 \pm 1.3) \times 10^{-2}$, which we rescale to our best value $B(\Lambda_c^+ \rightarrow pK^-\pi^+) = (6.28 \pm 0.32) \times 10^{-2}$. Our first error is their experiment's error and our second error is the systematic error from using our best value.
- DYTMAN 02 reports $(2.8 \pm 0.9 \pm 0.5 \pm 0.7) \times 10^{-4}$ from a measurement of $[\Gamma(B^+ \rightarrow \Sigma_c(2455)^-- p\pi^+\pi^+)/\Gamma_{\text{total}}] \times [B(\Lambda_c^+ \rightarrow pK^-\pi^+)]$ assuming $B(\Lambda_c^+ \rightarrow pK^-\pi^+) = (5.0 \pm 1.3) \times 10^{-2}$, which we rescale to our best value $B(\Lambda_c^+ \rightarrow pK^-\pi^+) = (6.28 \pm 0.32) \times 10^{-2}$. Our first error is their experiment's error and our second error is the systematic error from using our best value.

$\Gamma(\Lambda_c(2593)^-/\Lambda_c(2625)^- p\pi^+)/\Gamma_{\text{total}}$		Γ_{557}/Γ	
VALUE	CL%	DOCUMENT ID	TECN COMMENT
<1.9 × 10⁻⁴	90	^{1,2} DYTMAN	02 CLE2 $e^+e^- \rightarrow \Upsilon(4S)$

- Assumes equal production of B^+ and B^0 at the $\Upsilon(4S)$.
- DYTMAN 02 measurement uses $B(\Lambda_c^- \rightarrow \bar{p}K^+\pi^-) = 5.0 \pm 1.3\%$. The second error includes the systematic and the uncertainty of the branching ratio.

$\Gamma(\Xi_c^0\Lambda_c^+)/\Gamma_{\text{total}}$		Γ_{558}/Γ	
VALUE (units 10^{-4})	DOCUMENT ID	TECN	COMMENT
9.51 ± 2.10 ± 0.88	¹ LI	19A	BELL $e^+e^- \rightarrow \Upsilon(4S)$

¹ First measured the absolute branching fraction using a missing-mass technique.

$\Gamma(\Xi_c^0\Lambda_c^+, \Xi_c^0 \rightarrow \Xi^+\pi^-)/\Gamma_{\text{total}}$		Γ_{559}/Γ	
VALUE (units 10^{-5})	DOCUMENT ID	TECN	COMMENT
1.76 ± 0.29 OUR AVERAGE			

1.71 ± 0.28 ± 0.15	¹ LI	19A	BELL $e^+e^- \rightarrow \Upsilon(4S)$
2.0 ± 0.7 ± 0.1	^{2,3} AUBERT	08H	BABR $e^+e^- \rightarrow \Upsilon(4S)$
4.5 ^{+1.8} _{-1.5} ± 0.2	^{3,4} CHISTOV	06A	BELL Repl. by LI 19A

- • • We do not use the following data for averages, fits, limits, etc. • • •
- Using a hadronic B -tagging method based on a full reconstruction.
 - AUBERT 08H reports $(2.51 \pm 0.89 \pm 0.61) \times 10^{-5}$ from a measurement of $[\Gamma(B^+ \rightarrow \Xi_c^0\Lambda_c^+, \Xi_c^0 \rightarrow \Xi^+\pi^-)/\Gamma_{\text{total}}] \times [B(\Lambda_c^+ \rightarrow pK^-\pi^+)]$ assuming $B(\Lambda_c^+ \rightarrow pK^-\pi^+) = (5.0 \pm 1.3) \times 10^{-2}$, which we rescale to our best value $B(\Lambda_c^+ \rightarrow pK^-\pi^+) = (6.28 \pm 0.32) \times 10^{-2}$. Our first error is their experiment's error and our second error is the systematic error from using our best value.
 - Assumes equal production of B^+ and B^0 at the $\Upsilon(4S)$.
 - CHISTOV 06A reports $(5.6 ^{+1.9}_{-1.5} ± 1.9) \times 10^{-5}$ from a measurement of $[\Gamma(B^+ \rightarrow \Xi_c^0\Lambda_c^+, \Xi_c^0 \rightarrow \Xi^+\pi^-)/\Gamma_{\text{total}}] \times [B(\Lambda_c^+ \rightarrow pK^-\pi^+)]$ assuming $B(\Lambda_c^+ \rightarrow pK^-\pi^+) = (5.0 \pm 1.3) \times 10^{-2}$, which we rescale to our best value $B(\Lambda_c^+ \rightarrow pK^-\pi^+) = (6.28 \pm 0.32) \times 10^{-2}$. Our first error is their experiment's error and our second error is the systematic error from using our best value.

$\Gamma(\Xi_c^0\Lambda_c^+, \Xi_c^0 \rightarrow \Lambda K^+\pi^-)/\Gamma_{\text{total}}$		Γ_{560}/Γ	
VALUE (units 10^{-5})	DOCUMENT ID	TECN	COMMENT
1.14 ± 0.26 OUR AVERAGE			

1.11 ± 0.26 ± 0.10	¹ LI	19A	BELL $e^+e^- \rightarrow \Upsilon(4S)$
1.4 ± 0.8 ± 0.1	^{2,3} AUBERT	08H	BABR $e^+e^- \rightarrow \Upsilon(4S)$
3.2 ^{+1.1} _{-0.9} ± 0.2	^{3,4} CHISTOV	06A	BELL Repl. by LI 19A

- • • We do not use the following data for averages, fits, limits, etc. • • •
- Using a hadronic B -tagging method based on a full reconstruction.
 - AUBERT 08H reports $(1.70 \pm 0.93 \pm 0.53) \times 10^{-5}$ from a measurement of $[\Gamma(B^+ \rightarrow \Xi_c^0\Lambda_c^+, \Xi_c^0 \rightarrow \Lambda K^+\pi^-)/\Gamma_{\text{total}}] \times [B(\Lambda_c^+ \rightarrow pK^-\pi^+)]$ assuming $B(\Lambda_c^+ \rightarrow pK^-\pi^+) = (5.0 \pm 1.3) \times 10^{-2}$, which we rescale to our best value $B(\Lambda_c^+ \rightarrow pK^-\pi^+) = (6.28 \pm 0.32) \times 10^{-2}$. Our first error is their experiment's error and our second error is the systematic error from using our best value.
 - Assumes equal production of B^+ and B^0 at the $\Upsilon(4S)$.
 - CHISTOV 06A reports $(4.0 ^{+1.1}_{-0.9} ± 1.3) \times 10^{-5}$ from a measurement of $[\Gamma(B^+ \rightarrow \Xi_c^0\Lambda_c^+, \Xi_c^0 \rightarrow \Lambda K^+\pi^-)/\Gamma_{\text{total}}] \times [B(\Lambda_c^+ \rightarrow pK^-\pi^+)]$ assuming $B(\Lambda_c^+ \rightarrow pK^-\pi^+) = (5.0 \pm 1.3) \times 10^{-2}$, which we rescale to our best value $B(\Lambda_c^+ \rightarrow pK^-\pi^+) = (6.28 \pm 0.32) \times 10^{-2}$. Our first error is their experiment's error and our second error is the systematic error from using our best value.

$\Gamma(\Xi_c^0\Lambda_c^+, \Xi_c^0 \rightarrow pK^-K^-\pi^+)/\Gamma_{\text{total}}$		Γ_{561}/Γ	
VALUE (units 10^{-6})	DOCUMENT ID	TECN	COMMENT
5.47 ± 1.78 ± 0.57	¹ LI	19A	BELL $e^+e^- \rightarrow \Upsilon(4S)$

¹ Using a hadronic B -tagging method based on a full reconstruction.

$\Gamma(\Lambda_c^+\Xi_c^0)/\Gamma_{\text{total}}$		Γ_{562}/Γ	
VALUE	CL%	DOCUMENT ID	TECN COMMENT
<6.5 × 10⁻⁴	90	¹ LI	19G BELL $e^+e^- \rightarrow \Upsilon(4S)$

¹ Uses fully reconstructed B^+ meson on tag side and recoil against Λ_c^+ on signal side.

$\Gamma(\Lambda_c^+\Xi_c(2645)^0)/\Gamma_{\text{total}}$		Γ_{563}/Γ	
VALUE	CL%	DOCUMENT ID	TECN COMMENT
<7.9 × 10⁻⁴	90	¹ LI	19G BELL $e^+e^- \rightarrow \Upsilon(4S)$

¹ Uses fully reconstructed B^+ meson on tag side and recoil against Λ_c^+ on signal side.

$\Gamma(\Lambda_c^+\Xi_c(2790)^0)/\Gamma_{\text{total}}$		Γ_{564}/Γ	
VALUE (units 10^{-3})	DOCUMENT ID	TECN	COMMENT
1.1 ± 0.4 ± 0.2	¹ LI	19G	BELL $e^+e^- \rightarrow \Upsilon(4S)$

¹ Uses fully reconstructed B^+ meson on tag side and recoil against Λ_c^+ on signal side.

$\Gamma(\pi^+\ell^+\ell^-)/\Gamma_{\text{total}}$		Γ_{565}/Γ	
VALUE	CL%	DOCUMENT ID	TECN COMMENT
<4.9 × 10⁻⁸	90	¹ WEI	08A BELL $e^+e^- \rightarrow \Upsilon(4S)$

- • • We do not use the following data for averages, fits, limits, etc. • • •
- | | | | |
|-------------------------|----|---------------------|---|
| <6.6 × 10 ⁻⁸ | 90 | ¹ LEES | 13M BABR $e^+e^- \rightarrow \Upsilon(4S)$ |
| <1.2 × 10 ⁻⁷ | 90 | ¹ AUBERT | 07AG BABR $e^+e^- \rightarrow \Upsilon(4S)$ |
- ¹ Assumes equal production of B^+ and B^0 at the $\Upsilon(4S)$.

$\Gamma(\pi^+e^+e^-)/\Gamma_{\text{total}}$		Γ_{566}/Γ	
VALUE	CL%	DOCUMENT ID	TECN COMMENT
< 8.0 × 10⁻⁸	90	¹ WEI	08A BELL $e^+e^- \rightarrow \Upsilon(4S)$

- • • We do not use the following data for averages, fits, limits, etc. • • •
- | | | | |
|--------------------------|----|---------------------|---|
| <12.5 × 10 ⁻⁸ | 90 | ¹ LEES | 13M BABR $e^+e^- \rightarrow \Upsilon(4S)$ |
| <18 × 10 ⁻⁸ | 90 | ¹ AUBERT | 07AG BABR $e^+e^- \rightarrow \Upsilon(4S)$ |
| < 3.9 × 10 ⁻³ | 90 | ² WEIR | 90B MRK2 e^+e^- 29 GeV |
- ¹ Assumes equal production of B^+ and B^0 at the $\Upsilon(4S)$.
- ² WEIR 90B assumes B^+ production cross section from LUND.

Meson Particle Listings

 B^\pm

$\Gamma(\pi^+\mu^+\mu^-)/\Gamma_{\text{total}}$ Γ_{567}/Γ
 Test for $\Delta B=1$ weak neutral current. Allowed by higher-order electroweak interactions.

VALUE (units 10^{-8})	CL%	DOCUMENT ID	TECN	COMMENT
$1.75 \pm 0.22 \pm 0.05$		¹ AAIJ	15AR LHCb	pp at 7, 8 TeV
< 5.5	90	² LEES	13M BABR	$e^+e^- \rightarrow \Upsilon(4S)$
$2.3 \pm 0.6 \pm 0.1$		AAIJ	12AY LHCb	Repl. by AAIJ 15AR
< 6.9	90	² WEI	08A BELL	$e^+e^- \rightarrow \Upsilon(4S)$
< 28	90	² AUBERT	07AG BABR	$e^+e^- \rightarrow \Upsilon(4S)$

¹ AAIJ 15AR reports $(1.83 \pm 0.24 \pm 0.05) \times 10^{-8}$ from a measurement of $[\Gamma(B^+ \rightarrow \pi^+\mu^+\mu^-)/\Gamma_{\text{total}}] / [B(B^+ \rightarrow J/\psi(1S)K^+) / [B(J/\psi(1S) \rightarrow \mu^+\mu^-)]]$ assuming $B(B^+ \rightarrow J/\psi(1S)K^+) = (1.05 \pm 0.05) \times 10^{-3}$, $B(J/\psi(1S) \rightarrow \mu^+\mu^-) = (5.961 \pm 0.033) \times 10^{-2}$, which we rescale to our best values $B(B^+ \rightarrow J/\psi(1S)K^+) = (1.006 \pm 0.027) \times 10^{-3}$, $B(J/\psi(1S) \rightarrow \mu^+\mu^-) = (5.961 \pm 0.033) \times 10^{-2}$. Our first error is their experiment's error and our second error is the systematic error from using our best values.

² Assumes equal production of B^+ and B^0 at the $\Upsilon(4S)$.

$\Gamma(\pi^+\mu^+\mu^-)/\Gamma(K^+\mu^+\mu^-)$ $\Gamma_{567}/\Gamma_{571}$

VALUE	DOCUMENT ID	TECN	COMMENT
$0.053 \pm 0.014 \pm 0.001$	AAIJ	12AY LHCb	Repl. by AAIJ 15AR

$\Gamma(\pi^+\nu\bar{\nu})/\Gamma_{\text{total}}$ Γ_{568}/Γ
 Test for $\Delta B=1$ weak neutral current. Allowed by higher-order electroweak interactions.

VALUE	CL%	DOCUMENT ID	TECN	COMMENT
$< 1.4 \times 10^{-5}$	90	¹ GRYGIER	17 BELL	$e^+e^- \rightarrow \Upsilon(4S)$
$< 9.8 \times 10^{-5}$	90	¹ LUTZ	13 BELL	$e^+e^- \rightarrow \Upsilon(4S)$
$< 1.7 \times 10^{-4}$	90	¹ CHEN	07D BELL	$e^+e^- \rightarrow \Upsilon(4S)$
$< 1.0 \times 10^{-4}$	90	¹ AUBERT	05H BABR	$e^+e^- \rightarrow \Upsilon(4S)$

¹ Assumes equal production of B^+ and B^0 at the $\Upsilon(4S)$.

$\Gamma(K^+e^+e^-)/\Gamma_{\text{total}}$ Γ_{569}/Γ
 Test for $\Delta B=1$ weak neutral current. Allowed by higher-order electroweak interactions.

VALUE (units 10^{-7})	DOCUMENT ID	TECN	COMMENT
4.51 ± 0.23 OUR AVERAGE			Error includes scale factor of 1.1.
$4.36 \pm 0.15 \pm 0.18$	¹ AAIJ	13H LHCb	pp at 7 TeV
$4.8 \pm 0.9 \pm 0.2$	² AUBERT	09T BABR	$e^+e^- \rightarrow \Upsilon(4S)$
$5.3 \pm 0.6 \pm 0.3$	² WEI	09A BELL	$e^+e^- \rightarrow \Upsilon(4S)$

••• We do not use the following data for averages, fits, limits, etc. **•••**

$3.8 \pm 0.9 \pm 0.2$	² AUBERT,B	06J BABR	Repl. by AUBERT 09T
$5.3 \pm 1.1 \pm 0.3$	² ISHIKAWA	03 BELL	Repl. by WEI 09A

¹ Uses $B(B^+ \rightarrow J/\psi K^+ \rightarrow \mu^+\mu^-K^+) = (6.01 \pm 0.21) \times 10^{-5}$.

² Assumes equal production of B^+ and B^0 at the $\Upsilon(4S)$.

$\Gamma(K^+e^+e^-)/\Gamma_{\text{total}}$ Γ_{570}/Γ
 Test for $\Delta B=1$ weak neutral current. Allowed by higher-order electroweak interactions.

VALUE (units 10^{-7})	CL%	DOCUMENT ID	TECN	COMMENT
5.5 ± 0.7 OUR AVERAGE				
$5.1 \pm 1.2 \pm 0.2$		¹ AUBERT	09T BABR	$e^+e^- \rightarrow \Upsilon(4S)$
$5.7 \pm 0.9 \pm 0.3$		¹ WEI	09A BELL	$e^+e^- \rightarrow \Upsilon(4S)$

••• We do not use the following data for averages, fits, limits, etc. **•••**

$4.2 \pm 1.2 \pm 0.2$		¹ AUBERT,B	06J BABR	Repl. by AUBERT 09T
$10.5 \pm 2.5 \pm 0.7$		¹ AUBERT	03U BABR	Repl. by AUBERT,B 06J
$6.3 \pm 1.9 \pm 0.3$		² ISHIKAWA	03 BELL	Repl. by WEI 09A

< 14 90 ¹ ABE 02 BELL $e^+e^- \rightarrow \Upsilon(4S)$

< 9 90 ¹ AUBERT 02L BABR $e^+e^- \rightarrow \Upsilon(4S)$

< 24 90 ³ ANDERSON 01B CLE2 $e^+e^- \rightarrow \Upsilon(4S)$

< 990 90 ⁴ ALBRECHT 91E ARG $e^+e^- \rightarrow \Upsilon(4S)$

< 68000 90 ⁵ WEIR 90B MRK2 $e^+e^- 29$ GeV

< 600 90 ⁶ AVERY 89B CLEO $e^+e^- \rightarrow \Upsilon(4S)$

< 2500 90 ⁷ AVERY 87 CLEO $e^+e^- \rightarrow \Upsilon(4S)$

¹ Assumes equal production of B^+ and B^0 at the $\Upsilon(4S)$.

² Assumes equal production of B^0 and B^+ at $\Upsilon(4S)$. The second error is a total of systematic uncertainties including model dependence.

³ The result is for di-lepton masses above 0.5 GeV.

⁴ ALBRECHT 91E reports $< 9.0 \times 10^{-5}$ assuming the $\Upsilon(4S)$ decays 45% to $B^0\bar{B}^0$. We rescale to 50%.

⁵ WEIR 90B assumes B^+ production cross section from LUND.

⁶ AVERY 89B reports $< 5 \times 10^{-5}$ assuming the $\Upsilon(4S)$ decays 43% to $B^0\bar{B}^0$. We rescale to 50%.

⁷ AVERY 87 reports $< 2.1 \times 10^{-4}$ assuming the $\Upsilon(4S)$ decays 40% to $B^0\bar{B}^0$. We rescale to 50%.

$\Gamma(K^+\mu^+\mu^-)/\Gamma_{\text{total}}$ Γ_{571}/Γ
 Test for $\Delta B=1$ weak neutral current. Allowed by higher-order electroweak interactions.

VALUE (units 10^{-7})	CL%	DOCUMENT ID	TECN	COMMENT
4.41 ± 0.22 OUR FIT				Error includes scale factor of 1.2.
4.36 ± 0.27 OUR AVERAGE				Error includes scale factor of 1.3.
$4.29 \pm 0.07 \pm 0.21$		¹ AAIJ	14M LHCb	pp at 7, 8 TeV
$4.1 \pm 1.6 \pm 0.2$		² AUBERT	09T BABR	$e^+e^- \rightarrow \Upsilon(4S)$
$5.3 \pm 0.8 \pm 0.3$		² WEI	09A BELL	$e^+e^- \rightarrow \Upsilon(4S)$

••• We do not use the following data for averages, fits, limits, etc. **•••**

$4.36 \pm 0.15 \pm 0.18$		³ AAIJ	13H LHCb	Repl. by AAIJ 14M
$3.1 \pm 1.5 \pm 0.3$		² AUBERT,B	06J BABR	Repl. by AUBERT 09T
$0.7 \pm 1.9 \pm 0.2$		² AUBERT	03U BABR	Repl. by AUBERT,B 06J
$4.5 \pm 1.4 \pm 0.3$		⁴ ISHIKAWA	03 BELL	Repl. by WEI 09A
$9.8 \pm 4.6 \pm 1.6$		² ABE	02 BELL	Repl. by ISHIKAWA 03
< 12	90	² AUBERT	02L BABR	$e^+e^- \rightarrow \Upsilon(4S)$
< 36.8	90	⁵ ANDERSON	01B CLE2	$e^+e^- \rightarrow \Upsilon(4S)$
< 52	90	⁶ AFFOLDER	99B CDF	$p\bar{p}$ at 1.8 TeV
< 100	90	⁷ ABE	96L CDF	Repl. by AFFOLDER 99B
< 2400	90	⁸ ALBRECHT	91E ARG	$e^+e^- \rightarrow \Upsilon(4S)$
< 64000	90	⁹ WEIR	90B MRK2	$e^+e^- 29$ GeV
< 1700	90	¹⁰ AVERY	89B CLEO	$e^+e^- \rightarrow \Upsilon(4S)$
< 3800	90	¹¹ AVERY	87 CLEO	$e^+e^- \rightarrow \Upsilon(4S)$

¹ Uses $B(B^+ \rightarrow J/\psi(1S)K^+) = (0.998 \pm 0.014 \pm 0.040) \times 10^{-3}$ for normalization.

² Assumes equal production of B^+ and B^0 at the $\Upsilon(4S)$.

³ Uses $B(B^+ \rightarrow J/\psi K^+ \rightarrow \mu^+\mu^-K^+) = (6.01 \pm 0.21) \times 10^{-5}$.

⁴ Assumes equal production of B^0 and B^+ at $\Upsilon(4S)$. The second error is a total of systematic uncertainties including model dependence.

⁵ The result is for di-lepton masses above 0.5 GeV.

⁶ AFFOLDER 99B measured relative to $B^+ \rightarrow J/\psi(1S)K^+$.

⁷ ABE 96L measured relative to $B^+ \rightarrow J/\psi(1S)K^+$ using PDG 94 branching ratios.

⁸ ALBRECHT 91E reports $< 2.2 \times 10^{-4}$ assuming the $\Upsilon(4S)$ decays 45% to $B^0\bar{B}^0$. We rescale to 50%.

⁹ WEIR 90B assumes B^+ production cross section from LUND.

¹⁰ AVERY 89B reports $< 1.5 \times 10^{-4}$ assuming the $\Upsilon(4S)$ decays 43% to $B^0\bar{B}^0$. We rescale to 50%.

¹¹ AVERY 87 reports $< 3.2 \times 10^{-4}$ assuming the $\Upsilon(4S)$ decays 40% to $B^0\bar{B}^0$. We rescale to 50%.

$\Gamma(K^+\mu^+\mu^- \text{ nonresonant})/\Gamma_{\text{total}}$ Γ_{572}/Γ

VALUE (units 10^{-7})	DOCUMENT ID	TECN	COMMENT
$4.37 \pm 0.15 \pm 0.23$	¹ AAIJ	17Y LHCb	pp at 7, 8 TeV

¹ Measured in amplitude analysis using model including short-distance $K^+\mu^+\mu^-$ and $\rho(770)$, $\omega(782)$, $\phi(1020)$, J/ψ , $\psi(2S)$, $\psi(3770)$, $\psi(4040)$, $\psi(4160)$, and $\psi(4415)$ contributions.

$\Gamma(K^+\tau^+\tau^-)/\Gamma_{\text{total}}$ Γ_{573}/Γ

VALUE	CL%	DOCUMENT ID	TECN	COMMENT
$< 2.25 \times 10^{-3}$	90	^{1,2} LEES	17 BABR	$e^+e^- \rightarrow \Upsilon(4S)$

¹ Uses only leptonic decays of τ and the quoted limit combines the final states $K^+e^+e^-$, $K^+\mu^+\mu^-$, and $K^+e^\pm\mu^\mp$.

² If observed events are interpreted as a signal the branching fraction measurement becomes $(1.31 \pm 0.66 \pm 0.35) \times 10^{-3}$.

$\Gamma(K^+\mu^+\mu^-)/\Gamma(J/\psi(1S)K^+)$ $\Gamma_{571}/\Gamma_{275}$

VALUE (units 10^{-3})	DOCUMENT ID	TECN	COMMENT
0.439 ± 0.024 OUR FIT			Error includes scale factor of 1.1.
$0.46 \pm 0.04 \pm 0.02$	AALTONEN	11A CDF	$p\bar{p}$ at 1.96 TeV

••• We do not use the following data for averages, fits, limits, etc. **•••**

$0.38 \pm 0.05 \pm 0.02$ AALTONEN 11L CDF Repl. by AALTONEN 11A

$0.59 \pm 0.15 \pm 0.03$ AALTONEN 09B CDF Repl. by AALTONEN 11L

$\Gamma(K^+\nu\bar{\nu})/\Gamma_{\text{total}}$ Γ_{574}/Γ
 Test for $\Delta B=1$ weak neutral current. Allowed by higher-order electroweak interactions.

VALUE	CL%	DOCUMENT ID	TECN	COMMENT
$< 1.6 \times 10^{-5}$	90	^{1,2} LEES	13I BABR	$e^+e^- \rightarrow \Upsilon(4S)$

••• We do not use the following data for averages, fits, limits, etc. **•••**

$< 1.9 \times 10^{-5}$ 90 ^{1,3} GRYGIER 17 BELL $e^+e^- \rightarrow \Upsilon(4S)$

$< 5.5 \times 10^{-5}$ 90 ¹ LUTZ 13 BELL $e^+e^- \rightarrow \Upsilon(4S)$

$< 1.3 \times 10^{-5}$ 90 ¹ DEL-AMO-SAL0Q BABR Repl. by LEES 13I

$< 1.4 \times 10^{-5}$ 90 ¹ CHEN 07D BELL $e^+e^- \rightarrow \Upsilon(4S)$

$< 5.2 \times 10^{-5}$ 90 ¹ AUBERT 05H BABR $e^+e^- \rightarrow \Upsilon(4S)$

$< 2.4 \times 10^{-4}$ 90 ¹ BROWDER 01 CLE2 $e^+e^- \rightarrow \Upsilon(4S)$

¹ Assumes equal production of B^+ and B^0 at the $\Upsilon(4S)$.

² Also reported a limit $< 3.7 \times 10^{-5}$ at 90% CL obtained using a fully reconstructed hadronic B -tag events.

³ The result was reported in arXiv:1702.03224, but missing from the publication by mistake.

$\Gamma(\rho^+ \nu \bar{\nu})/\Gamma_{\text{total}}$ Γ_{575}/Γ
 Test for $\Delta B = 1$ weak neutral current. Allowed by higher-order electroweak interaction.

VALUE (units 10^{-7})	CL%	DOCUMENT ID	TECN	COMMENT
$<3.0 \times 10^{-5}$	90	¹ GRYGIER 17	BELL	$e^+e^- \rightarrow \Upsilon(4S)$
• • • We do not use the following data for averages, fits, limits, etc. • • •				
$<2.13 \times 10^{-4}$	90	¹ LUTZ 13	BELL	$e^+e^- \rightarrow \Upsilon(4S)$
$<1.5 \times 10^{-4}$	90	¹ CHEN 07D	BELL	Repl. by LUTZ 13

$\Gamma(K^*(892)^+ \ell^+ \ell^-)/\Gamma_{\text{total}}$ Γ_{576}/Γ
 Test for $\Delta B = 1$ weak neutral current. Allowed by higher-order electroweak interactions.

VALUE (units 10^{-7})	CL%	DOCUMENT ID	TECN	COMMENT
10.1 ± 1.1 OUR AVERAGE		Error includes scale factor of 1.1.		
$9.24 \pm 0.93 \pm 0.67$		AAIJ 14M	LHCB	pp at 7, 8 TeV
$14.0 \pm 4.0 \pm 3.7$		¹ AUBERT 09T	BABR	$e^+e^- \rightarrow \Upsilon(4S)$
$12.4 \pm 2.3 \pm 2.1$		¹ WEI 09A	BELL	$e^+e^- \rightarrow \Upsilon(4S)$
• • • We do not use the following data for averages, fits, limits, etc. • • •				
11.6 ± 1.9		² AAIJ 12AH	LHCB	Repl. by AAIJ 14M
$7.3 \pm 5.0 \pm 4.2$		¹ AUBERT,B 06J	BABR	Repl. by AUBERT 09T
<22	90	¹ ISHIKAWA 03	BELL	$e^+e^- \rightarrow \Upsilon(4S)$

¹ Assumes equal production of B^+ and B^0 at the $\Upsilon(4S)$.
² Measured in $B^+ \rightarrow K^*(892)^+ \mu^+ \mu^-$ decays.

$\Gamma(K^*(892)^+ e^+ e^-)/\Gamma_{\text{total}}$ Γ_{577}/Γ
 Test for $\Delta B = 1$ weak neutral current. Allowed by higher-order electroweak interactions.

VALUE (units 10^{-7})	CL%	DOCUMENT ID	TECN	COMMENT
15.5 ± 4.0 ± 3.1 OUR AVERAGE				
$13.8 \pm 4.7 \pm 4.2$		¹ AUBERT 09T	BABR	$e^+e^- \rightarrow \Upsilon(4S)$
$17.3 \pm 5.0 \pm 4.2$		¹ WEI 09A	BELL	$e^+e^- \rightarrow \Upsilon(4S)$
• • • We do not use the following data for averages, fits, limits, etc. • • •				
$7.5 \pm 7.6 \pm 6.5$		¹ AUBERT,B 06J	BABR	Repl. by AUBERT 09T
$2.0 \pm 13.4 \pm 8.7$		¹ AUBERT 03U	BABR	$e^+e^- \rightarrow \Upsilon(4S)$
< 46	90	² ISHIKAWA 03	BELL	$e^+e^- \rightarrow \Upsilon(4S)$
< 89	90	¹ ABE 02	BELL	Repl. by ISHIKAWA 03
< 95	90	¹ AUBERT 02L	BABR	$e^+e^- \rightarrow \Upsilon(4S)$
< 690	90	³ ALBRECHT 91E	ARG	$e^+e^- \rightarrow \Upsilon(4S)$

¹ Assumes equal production of B^+ and B^0 at the $\Upsilon(4S)$.
² Assumes equal production of B^0 and B^+ at $\Upsilon(4S)$. The second error is a total of systematic uncertainties including model dependence.
³ ALBRECHT 91E reports $< 6.3 \times 10^{-4}$ assuming the $\Upsilon(4S)$ decays 45% to $B^0 \bar{B}^0$. We rescale to 50%.

$\Gamma(K^*(892)^+ \mu^+ \mu^-)/\Gamma_{\text{total}}$ Γ_{578}/Γ
 Test for $\Delta B = 1$ weak neutral current. Allowed by higher-order electroweak interactions.

VALUE (units 10^{-7})	CL%	DOCUMENT ID	TECN	COMMENT
9.6 ± 1.0 OUR FIT				
9.6 ± 1.1 OUR AVERAGE				
$9.24 \pm 0.93 \pm 0.67$		¹ AAIJ 14M	LHCB	pp at 7, 8 TeV
$14.6 \pm 7.9 \pm 7.5$		² AUBERT 09T	BABR	$e^+e^- \rightarrow \Upsilon(4S)$
$11.1 \pm 3.2 \pm 2.7$		² WEI 09A	BELL	$e^+e^- \rightarrow \Upsilon(4S)$
• • • We do not use the following data for averages, fits, limits, etc. • • •				
11.6 ± 1.9		AAIJ 12AH	LHCB	Repl. by AAIJ 14M
$9.7 \pm 9.4 \pm 6.9$		² AUBERT,B 06J	BABR	Repl. by AUBERT 09T
$30.7 \pm 25.8 \pm 17.8$		² AUBERT 03U	BABR	$e^+e^- \rightarrow \Upsilon(4S)$
$6.5 \pm 6.9 \pm 5.3$		³ ISHIKAWA 03	BELL	Repl. by WEI 09A
< 39	90	² ABE 02	BELL	Repl. by ISHIKAWA 03
< 170	90	² AUBERT 02L	BABR	$e^+e^- \rightarrow \Upsilon(4S)$

¹ Uses $B(B^+ \rightarrow J/\psi(1S) K^*(892)^+) = (1.431 \pm 0.027 \pm 0.090) \times 10^{-3}$ for normalization.
² Assumes equal production of B^+ and B^0 at the $\Upsilon(4S)$.
³ Assumes equal production of B^0 and B^+ at $\Upsilon(4S)$. The second error is a total of systematic uncertainties including model dependence. The 90% C.L. upper limit is 2.2×10^{-6} .

$\Gamma(K^*(892)^+ \mu^+ \mu^-)/\Gamma(J/\psi(1S) K^*(892)^+)$ $\Gamma_{578}/\Gamma_{280}$

VALUE (units 10^{-3})	DOCUMENT ID	TECN	COMMENT
0.67 ± 0.08 OUR FIT			
0.67 ± 0.22 ± 0.04	AALTONEN 11AI	CDF	pp at 1.96 TeV

$\Gamma(K^*(892)^+ \nu \bar{\nu})/\Gamma_{\text{total}}$ Γ_{579}/Γ
 Test for $\Delta B = 1$ weak neutral current. Allowed by higher-order electroweak interaction.

VALUE	CL%	DOCUMENT ID	TECN	COMMENT
$<4.0 \times 10^{-5}$	90	¹ LUTZ 13	BELL	$e^+e^- \rightarrow \Upsilon(4S)$
• • • We do not use the following data for averages, fits, limits, etc. • • •				
$<6.1 \times 10^{-5}$	90	¹ GRYGIER 17	BELL	$e^+e^- \rightarrow \Upsilon(4S)$
$<6.4 \times 10^{-5}$	90	^{1,2} LEES 13I	BABR	$e^+e^- \rightarrow \Upsilon(4S)$
$<8 \times 10^{-5}$	90	AUBERT 08Bc	BABR	Repl. by LEES 13I
$<1.4 \times 10^{-4}$	90	¹ CHEN 07D	BELL	$e^+e^- \rightarrow \Upsilon(4S)$

¹ Assumes equal production of B^+ and B^0 at the $\Upsilon(4S)$.
² Also reported a limit $< 11.6 \times 10^{-5}$ at 90% CL obtained using a fully reconstructed hadronic B -tag events.

$\Gamma(K^+ \pi^+ \pi^- \mu^+ \mu^-)/\Gamma(\psi(2S) K^+)$ $\Gamma_{580}/\Gamma_{311}$

VALUE (units 10^{-4})	DOCUMENT ID	TECN	COMMENT
6.95 ± 0.46 ± 0.43	AAIJ 14AZ	LHCB	pp at 7, 8 TeV

$\Gamma(\phi K^+ \mu^+ \mu^-)/\Gamma(J/\psi(1S) \phi K^+)$ $\Gamma_{581}/\Gamma_{287}$

VALUE (units 10^{-3})	DOCUMENT ID	TECN	COMMENT
1.50 ± 0.36 ± 0.19 ± 0.32 ± 0.07	AAIJ 14AZ	LHCB	pp at 7, 8 TeV

$\Gamma(\bar{A} \rho \nu \bar{\nu})/\Gamma_{\text{total}}$ Γ_{582}/Γ

VALUE	CL%	DOCUMENT ID	TECN	COMMENT
$<3.0 \times 10^{-5}$	90	¹ LEES 19C	BABR	$e^+e^- \rightarrow \Upsilon(4S)$

¹ Signal candidates are identified by first fully reconstructing B^+ in one of many possible exclusive decays to hadronic final states.

$\Gamma(\pi^+ e^+ \mu^-)/\Gamma_{\text{total}}$ Γ_{583}/Γ
 Test of lepton family number conservation.

VALUE	CL%	DOCUMENT ID	TECN	COMMENT
<0.0064	90	¹ WEIR 90B	MRK2	e^+e^- 29 GeV

¹ WEIR 90B assumes B^+ production cross section from LUND.

$\Gamma(\pi^+ e^- \mu^+)/\Gamma_{\text{total}}$ Γ_{584}/Γ
 Test of lepton family number conservation.

VALUE	CL%	DOCUMENT ID	TECN	COMMENT
<0.0064	90	¹ WEIR 90B	MRK2	e^+e^- 29 GeV

¹ WEIR 90B assumes B^+ production cross section from LUND.

$\Gamma(\pi^+ e^\pm \mu^\mp)/\Gamma_{\text{total}}$ Γ_{585}/Γ

VALUE	CL%	DOCUMENT ID	TECN	COMMENT
$<1.7 \times 10^{-7}$	90	¹ AUBERT 07AG	BABR	$e^+e^- \rightarrow \Upsilon(4S)$

¹ Assumes equal production of B^+ and B^0 at the $\Upsilon(4S)$.

$\Gamma(\pi^+ e^+ \tau^-)/\Gamma_{\text{total}}$ Γ_{586}/Γ
 Test of lepton family number conservation.

VALUE (units 10^{-6})	CL%	DOCUMENT ID	TECN	COMMENT
<74	90	¹ LEES 12P	BABR	$e^+e^- \rightarrow \Upsilon(4S)$

¹ Uses a fully reconstructed hadronic B decay as a tag on the recoil side.

$\Gamma(\pi^+ e^- \tau^+)/\Gamma_{\text{total}}$ Γ_{587}/Γ
 Test of lepton family number conservation.

VALUE (units 10^{-6})	CL%	DOCUMENT ID	TECN	COMMENT
<20	90	¹ LEES 12P	BABR	$e^+e^- \rightarrow \Upsilon(4S)$

¹ Uses a fully reconstructed hadronic B decay as a tag on the recoil side.

$\Gamma(\pi^+ e^\pm \tau^\mp)/\Gamma_{\text{total}}$ Γ_{588}/Γ
 Test of lepton family number conservation.

VALUE (units 10^{-6})	CL%	DOCUMENT ID	TECN	COMMENT
<75	90	^{1,2} LEES 12P	BABR	$e^+e^- \rightarrow \Upsilon(4S)$

¹ Assumes $B(B^+ \rightarrow h^+ \ell^+ \tau^-) = B(B^+ \rightarrow h^+ \ell^- \tau^+)$.
² Uses a fully reconstructed hadronic B decay as a tag on the recoil side.

$\Gamma(\pi^+ \mu^\pm \tau^\mp)/\Gamma_{\text{total}}$ Γ_{589}/Γ
 Test of lepton family number conservation.

VALUE (units 10^{-6})	CL%	DOCUMENT ID	TECN	COMMENT
<62	90	¹ LEES 12P	BABR	$e^+e^- \rightarrow \Upsilon(4S)$

¹ Uses a fully reconstructed hadronic B decay as a tag on the recoil side.

$\Gamma(\pi^+ \mu^- \tau^+)/\Gamma_{\text{total}}$ Γ_{590}/Γ
 Test of lepton family number conservation.

VALUE (units 10^{-6})	CL%	DOCUMENT ID	TECN	COMMENT
<45	90	¹ LEES 12P	BABR	$e^+e^- \rightarrow \Upsilon(4S)$

¹ Uses a fully reconstructed hadronic B decay as a tag on the recoil side.

$\Gamma(\pi^+ \mu^\pm \tau^\mp)/\Gamma_{\text{total}}$ Γ_{591}/Γ
 Test of lepton family number conservation.

VALUE (units 10^{-6})	CL%	DOCUMENT ID	TECN	COMMENT
<72	90	^{1,2} LEES 12P	BABR	$e^+e^- \rightarrow \Upsilon(4S)$

¹ Assumes $B(B^+ \rightarrow h^+ \ell^+ \tau^-) = B(B^+ \rightarrow h^+ \ell^- \tau^+)$.
² Uses a fully reconstructed hadronic B decay as a tag on the recoil side.

Meson Particle Listings

 B^\pm $\Gamma(K^+ e^+ \mu^-)/\Gamma_{\text{total}}$ Γ_{592}/Γ

Test of lepton family number conservation.

VALUE	CL%	DOCUMENT ID	TECN	COMMENT
$<7.0 \times 10^{-9}$	90	AAIJ	19AMLHCB	pp at 7, 8 TeV
••• We do not use the following data for averages, fits, limits, etc. •••				
$<0.91 \times 10^{-7}$	90	¹ AUBERT,B	06J BABR	$e^+e^- \rightarrow \Upsilon(4S)$
$<8 \times 10^{-7}$	90	¹ AUBERT	02L BABR	Repl. by AUBERT,B 06J
$<6.4 \times 10^{-3}$	90	² WEIR	90B MRK2	e^+e^- 29 GeV

¹ Assumes equal production of B^+ and B^0 at the $\Upsilon(4S)$.
² WEIR 90B assumes B^+ production cross section from LUND.

 $\Gamma(K^+ e^- \mu^+)/\Gamma_{\text{total}}$ Γ_{593}/Γ

Test of lepton family number conservation.

VALUE	CL%	DOCUMENT ID	TECN	COMMENT
$<6.4 \times 10^{-9}$	90	AAIJ	19AMLHCB	pp at 7, 8 TeV
••• We do not use the following data for averages, fits, limits, etc. •••				
$<1.3 \times 10^{-7}$	90	¹ AUBERT,B	06J BABR	$e^+e^- \rightarrow \Upsilon(4S)$
$<6.4 \times 10^{-3}$	90	² WEIR	90B MRK2	e^+e^- 29 GeV

¹ Assumes equal production of B^+ and B^0 at the $\Upsilon(4S)$.
² WEIR 90B assumes B^+ production cross section from LUND.

 $\Gamma(K^+ e^\pm \mu^\mp)/\Gamma_{\text{total}}$ Γ_{594}/Γ

Test of lepton family number conservation.

VALUE (units 10^{-7})	CL%	DOCUMENT ID	TECN	COMMENT
<0.91	90	¹ AUBERT,B	06J BABR	$e^+e^- \rightarrow \Upsilon(4S)$

¹ Assumes equal production of B^+ and B^0 at the $\Upsilon(4S)$.

 $\Gamma(K^+ e^+ \tau^-)/\Gamma_{\text{total}}$ Γ_{595}/Γ

Test of lepton family number conservation.

VALUE (units 10^{-6})	CL%	DOCUMENT ID	TECN	COMMENT
<43	90	¹ LEES	12P BABR	$e^+e^- \rightarrow \Upsilon(4S)$

¹ Uses a fully reconstructed hadronic B decay as a tag on the recoil side.

 $\Gamma(K^+ e^- \tau^+)/\Gamma_{\text{total}}$ Γ_{596}/Γ

Test of lepton family number conservation.

VALUE (units 10^{-6})	CL%	DOCUMENT ID	TECN	COMMENT
<15	90	¹ LEES	12P BABR	$e^+e^- \rightarrow \Upsilon(4S)$

¹ Uses a fully reconstructed hadronic B decay as a tag on the recoil side.

 $\Gamma(K^+ e^\pm \tau^\mp)/\Gamma_{\text{total}}$ Γ_{597}/Γ

Test of lepton family number conservation.

VALUE (units 10^{-6})	CL%	DOCUMENT ID	TECN	COMMENT
<30	90	^{1,2} LEES	12P BABR	$e^+e^- \rightarrow \Upsilon(4S)$

¹ Assumes $B(B^+ \rightarrow h^+ \ell^+ \tau^-) = B(B^+ \rightarrow h^+ \ell^- \tau^+)$.
² Uses a fully reconstructed hadronic B decay as a tag on the recoil side.

 $\Gamma(K^+ \mu^+ \tau^-)/\Gamma_{\text{total}}$ Γ_{598}/Γ

Test of lepton family number conservation.

VALUE (units 10^{-6})	CL%	DOCUMENT ID	TECN	COMMENT
<45	90	¹ LEES	12P BABR	$e^+e^- \rightarrow \Upsilon(4S)$

¹ Uses a fully reconstructed hadronic B decay as a tag on the recoil side.

 $\Gamma(K^+ \mu^- \tau^+)/\Gamma_{\text{total}}$ Γ_{599}/Γ

Test of lepton family number conservation.

VALUE (units 10^{-6})	CL%	DOCUMENT ID	TECN	COMMENT
<28	90	¹ LEES	12P BABR	$e^+e^- \rightarrow \Upsilon(4S)$

¹ Uses a fully reconstructed hadronic B decay as a tag on the recoil side.

 $\Gamma(K^+ \mu^\pm \tau^\mp)/\Gamma_{\text{total}}$ Γ_{600}/Γ

Test of lepton family number conservation.

VALUE (units 10^{-6})	CL%	DOCUMENT ID	TECN	COMMENT
<48	90	^{1,2} LEES	12P BABR	$e^+e^- \rightarrow \Upsilon(4S)$
••• We do not use the following data for averages, fits, limits, etc. •••				
<77	90	¹ AUBERT	07AZ BABR	Repl. by LEES 12P

¹ Uses a fully reconstructed hadronic B decay as a tag on the recoil side.
² Assumes $B(B^+ \rightarrow h^+ \ell^+ \tau^-) = B(B^+ \rightarrow h^+ \ell^- \tau^+)$.

 $\Gamma(K^*(892)^+ e^+ \mu^-)/\Gamma_{\text{total}}$ Γ_{601}/Γ

Test of lepton family number conservation.

VALUE (units 10^{-7})	CL%	DOCUMENT ID	TECN	COMMENT
<13	90	¹ AUBERT,B	06J BABR	$e^+e^- \rightarrow \Upsilon(4S)$

¹ Assumes equal production of B^+ and B^0 at the $\Upsilon(4S)$.

 $\Gamma(K^*(892)^+ e^- \mu^+)/\Gamma_{\text{total}}$ Γ_{602}/Γ

Test of lepton family number conservation.

VALUE (units 10^{-7})	CL%	DOCUMENT ID	TECN	COMMENT
<9.9	90	¹ AUBERT,B	06J BABR	$e^+e^- \rightarrow \Upsilon(4S)$

¹ Assumes equal production of B^+ and B^0 at the $\Upsilon(4S)$.

 $\Gamma(K^*(892)^+ e^\pm \mu^\mp)/\Gamma_{\text{total}}$ Γ_{603}/Γ

Test of lepton family number conservation.

VALUE	CL%	DOCUMENT ID	TECN	COMMENT
$<1.4 \times 10^{-6}$	90	¹ AUBERT,B	06J BABR	$e^+e^- \rightarrow \Upsilon(4S)$
••• We do not use the following data for averages, fits, limits, etc. •••				
$<7.9 \times 10^{-6}$	90	¹ AUBERT	02L BABR	Repl. by AUBERT,B 06J

¹ Assumes equal production of B^+ and B^0 at the $\Upsilon(4S)$.

 $\Gamma(\pi^- e^- e^+)/\Gamma_{\text{total}}$ Γ_{604}/Γ

Test of total lepton number conservation.

VALUE	CL%	DOCUMENT ID	TECN	COMMENT
$<2.3 \times 10^{-8}$	90	¹ LEES	12J BABR	$e^+e^- \rightarrow \Upsilon(4S)$
••• We do not use the following data for averages, fits, limits, etc. •••				
$<1.6 \times 10^{-6}$	90	¹ EDWARDS	02B CLE2	$e^+e^- \rightarrow \Upsilon(4S)$
<0.0039	90	² WEIR	90B MRK2	e^+e^- 29 GeV

¹ Assumes equal production of B^+ and B^0 at the $\Upsilon(4S)$.
² WEIR 90B assumes B^+ production cross section from LUND.

 $\Gamma(\pi^- \mu^+ \mu^+)/\Gamma_{\text{total}}$ Γ_{605}/Γ

Test of total lepton number conservation.

VALUE	CL%	DOCUMENT ID	TECN	COMMENT
$<4.0 \times 10^{-9}$	95	¹ AAIJ	14AC LHCB	pp at 7, 8 TeV
••• We do not use the following data for averages, fits, limits, etc. •••				
$<1.3 \times 10^{-8}$	95	² AAIJ	12AD LHCB	Repl. by AAIJ 14AC
$<4.4 \times 10^{-8}$	90	AAIJ	12C LHCB	pp at 7 TeV
$<10.7 \times 10^{-8}$	90	³ LEES	12J BABR	$e^+e^- \rightarrow \Upsilon(4S)$
$<1.4 \times 10^{-6}$	90	³ EDWARDS	02B CLE2	$e^+e^- \rightarrow \Upsilon(4S)$
$<9.1 \times 10^{-3}$	90	⁴ WEIR	90B MRK2	e^+e^- 29 GeV

¹ Uses $B^+ \rightarrow J/\psi K^+$, $J/\psi \rightarrow \mu^+ \mu^-$ mode for normalization. Obtains neutrino-mass-dependent upper limits in the range $0.4\text{--}4.0 \times 10^{-9}$. This limit is applicable for Majorana neutrino lifetime < 1 ps.
² Uses $B^+ \rightarrow J/\psi K^+$, $J/\psi \rightarrow \mu^+ \mu^-$ mode for normalization. Obtains neutrino-mass-dependent upper limits in the range $0.4\text{--}1.0 \times 10^{-8}$.
³ Assumes equal production of B^+ and B^0 at the $\Upsilon(4S)$.
⁴ WEIR 90B assumes B^+ production cross section from LUND.

 $\Gamma(\pi^- e^+ \mu^+)/\Gamma_{\text{total}}$ Γ_{606}/Γ

Test of total lepton number conservation.

VALUE	CL%	DOCUMENT ID	TECN	COMMENT
$<1.5 \times 10^{-7}$	90	¹ LEES	14A BABR	$e^+e^- \rightarrow \Upsilon(4S)$
••• We do not use the following data for averages, fits, limits, etc. •••				
$<1.3 \times 10^{-6}$	90	¹ EDWARDS	02B CLE2	$e^+e^- \rightarrow \Upsilon(4S)$
<0.0064	90	² WEIR	90B MRK2	e^+e^- 29 GeV

¹ Assumes equal production of B^+ and B^0 at the $\Upsilon(4S)$.
² WEIR 90B assumes B^+ production cross section from LUND.

 $\Gamma(\rho^- e^- e^+)/\Gamma_{\text{total}}$ Γ_{607}/Γ

Test of total lepton number conservation.

VALUE (units 10^{-6})	CL%	DOCUMENT ID	TECN	COMMENT
<0.17	90	¹ LEES	14A BABR	$e^+e^- \rightarrow \Upsilon(4S)$
••• We do not use the following data for averages, fits, limits, etc. •••				
<2.6	90	¹ EDWARDS	02B CLE2	$e^+e^- \rightarrow \Upsilon(4S)$

¹ Assumes equal production of B^+ and B^0 at the $\Upsilon(4S)$.

 $\Gamma(\rho^- \mu^+ \mu^+)/\Gamma_{\text{total}}$ Γ_{608}/Γ

Test of total lepton number conservation.

VALUE (units 10^{-6})	CL%	DOCUMENT ID	TECN	COMMENT
<0.42	90	LEES	14A BABR	$e^+e^- \rightarrow \Upsilon(4S)$
••• We do not use the following data for averages, fits, limits, etc. •••				
<5.0	90	¹ EDWARDS	02B CLE2	$e^+e^- \rightarrow \Upsilon(4S)$

¹ Assumes equal production of B^+ and B^0 at the $\Upsilon(4S)$.

 $\Gamma(\rho^- e^- \mu^+)/\Gamma_{\text{total}}$ Γ_{609}/Γ

Test of total lepton number conservation.

VALUE (units 10^{-6})	CL%	DOCUMENT ID	TECN	COMMENT
<0.47	90	¹ LEES	14A BABR	$e^+e^- \rightarrow \Upsilon(4S)$
••• We do not use the following data for averages, fits, limits, etc. •••				
<3.3	90	¹ EDWARDS	02B CLE2	$e^+e^- \rightarrow \Upsilon(4S)$

¹ Assumes equal production of B^+ and B^0 at the $\Upsilon(4S)$.

 $\Gamma(K^- e^+ e^+)/\Gamma_{\text{total}}$ Γ_{610}/Γ

Test of total lepton number conservation.

VALUE	CL%	DOCUMENT ID	TECN	COMMENT
$<3.0 \times 10^{-8}$	90	¹ LEES	12J BABR	$e^+e^- \rightarrow \Upsilon(4S)$
••• We do not use the following data for averages, fits, limits, etc. •••				
$<1.0 \times 10^{-6}$	90	¹ EDWARDS	02B CLE2	$e^+e^- \rightarrow \Upsilon(4S)$
<0.0039	90	² WEIR	90B MRK2	e^+e^- 29 GeV

¹ Assumes equal production of B^+ and B^0 at the $\Upsilon(4S)$.
² WEIR 90B assumes B^+ production cross section from LUND.

$\Gamma(K^- \mu^+ \mu^+)/\Gamma_{\text{total}}$ Γ_{611}/Γ
 Test of total lepton number conservation.

VALUE	CL%	DOCUMENT ID	TECN	COMMENT
$<4.1 \times 10^{-8}$	90	AAIJ	12c	LHCB pp at 7 TeV
$<6.7 \times 10^{-8}$	90	1 LEES	12j	BABR $e^+e^- \rightarrow \Upsilon(4S)$
$<1.8 \times 10^{-6}$	90	1 EDWARDS	02b	CLE2 $e^+e^- \rightarrow \Upsilon(4S)$
$<9.1 \times 10^{-3}$	90	2 WEIR	90b	MRK2 e^+e^- 29 GeV

••• We do not use the following data for averages, fits, limits, etc. •••

¹ Assumes equal production of B^+ and B^0 at the $\Upsilon(4S)$.
² WEIR 90b assumes B^+ production cross section from LUND.

$\Gamma(K^- e^+ \mu^+)/\Gamma_{\text{total}}$ Γ_{612}/Γ
 Test of total lepton number conservation.

VALUE	CL%	DOCUMENT ID	TECN	COMMENT
$<1.6 \times 10^{-7}$	90	1 LEES	14a	BABR $e^+e^- \rightarrow \Upsilon(4S)$
$<2.0 \times 10^{-6}$	90	1 EDWARDS	02b	CLE2 $e^+e^- \rightarrow \Upsilon(4S)$
<0.0064	90	2 WEIR	90b	MRK2 e^+e^- 29 GeV

••• We do not use the following data for averages, fits, limits, etc. •••

¹ Assumes equal production of B^+ and B^0 at the $\Upsilon(4S)$.
² WEIR 90b assumes B^+ production cross section from LUND.

$\Gamma(K^*(892)^- e^+ e^+)/\Gamma_{\text{total}}$ Γ_{613}/Γ
 Test of total lepton number conservation.

VALUE (units 10^{-6})	CL%	DOCUMENT ID	TECN	COMMENT
<0.40	90	1 LEES	14a	BABR $e^+e^- \rightarrow \Upsilon(4S)$
<2.8	90	1 EDWARDS	02b	CLE2 $e^+e^- \rightarrow \Upsilon(4S)$

••• We do not use the following data for averages, fits, limits, etc. •••

¹ Assumes equal production of B^+ and B^0 at the $\Upsilon(4S)$.

$\Gamma(K^*(892)^- \mu^+ \mu^+)/\Gamma_{\text{total}}$ Γ_{614}/Γ
 Test of total lepton number conservation.

VALUE (units 10^{-6})	CL%	DOCUMENT ID	TECN	COMMENT
<0.59	90	1 LEES	14a	BABR $e^+e^- \rightarrow \Upsilon(4S)$
<8.3	90	1 EDWARDS	02b	CLE2 $e^+e^- \rightarrow \Upsilon(4S)$

••• We do not use the following data for averages, fits, limits, etc. •••

¹ Assumes equal production of B^+ and B^0 at the $\Upsilon(4S)$.

$\Gamma(K^*(892)^- e^+ \mu^+)/\Gamma_{\text{total}}$ Γ_{615}/Γ
 Test of total lepton number conservation.

VALUE (units 10^{-6})	CL%	DOCUMENT ID	TECN	COMMENT
<0.30	90	1 LEES	14a	BABR $e^+e^- \rightarrow \Upsilon(4S)$
<4.4	90	1 EDWARDS	02b	CLE2 $e^+e^- \rightarrow \Upsilon(4S)$

••• We do not use the following data for averages, fits, limits, etc. •••

¹ Assumes equal production of B^+ and B^0 at the $\Upsilon(4S)$.

$\Gamma(D^- e^+ e^+)/\Gamma_{\text{total}}$ Γ_{616}/Γ

VALUE	CL%	DOCUMENT ID	TECN	COMMENT
$<2.6 \times 10^{-6}$	90	1 LEES	14a	BABR $e^+e^- \rightarrow \Upsilon(4S)$
$<2.6 \times 10^{-6}$	90	1,2 SEON	11	BELL $e^+e^- \rightarrow \Upsilon(4S)$

¹ Assumes equal production of B^0 and B^+ from Upsilon(4S) decays.
² Uses $D^- \rightarrow K^+ \pi^- \pi^-$ mode and 3-body phase-space hypothesis for the signal decays.

$\Gamma(D^- e^+ \mu^+)/\Gamma_{\text{total}}$ Γ_{617}/Γ

VALUE	CL%	DOCUMENT ID	TECN	COMMENT
$<1.8 \times 10^{-6}$	90	1,2 SEON	11	BELL $e^+e^- \rightarrow \Upsilon(4S)$
$<2.1 \times 10^{-6}$	90	1 LEES	14a	BABR $e^+e^- \rightarrow \Upsilon(4S)$

••• We do not use the following data for averages, fits, limits, etc. •••

¹ Assumes equal production of B^0 and B^+ from Upsilon(4S) decays.
² Uses $D^- \rightarrow K^+ \pi^- \pi^-$ mode and 3-body phase-space hypothesis for the signal decays.

$\Gamma(D^- \mu^+ \mu^+)/\Gamma_{\text{total}}$ Γ_{618}/Γ

VALUE	CL%	DOCUMENT ID	TECN	COMMENT
$<6.9 \times 10^{-7}$	95	1 AAIJ	12AD	LHCB pp at 7 TeV
$<17 \times 10^{-7}$	90	2 LEES	14a	BABR $e^+e^- \rightarrow \Upsilon(4S)$
$<1.1 \times 10^{-6}$	90	2,3 SEON	11	BELL $e^+e^- \rightarrow \Upsilon(4S)$

••• We do not use the following data for averages, fits, limits, etc. •••

¹ Uses $B^+ \rightarrow \psi(2S) K^+$, $\psi(2S) \rightarrow J/\psi \pi^+ \pi^-$ mode for normalization.
² Assumes equal production of B^0 and B^+ from Upsilon(4S) decays.
³ Uses $D^- \rightarrow K^+ \pi^- \pi^-$ mode and 3-body phase-space hypothesis for the signal decays.

$\Gamma(D^{*-} \mu^+ \mu^+)/\Gamma_{\text{total}}$ Γ_{619}/Γ

VALUE	CL%	DOCUMENT ID	TECN	COMMENT
$<2.4 \times 10^{-6}$	95	1 AAIJ	12AD	LHCB pp at 7 TeV

¹ Uses $B^+ \rightarrow \psi(2S) K^+$, $\psi(2S) \rightarrow J/\psi \pi^+ \pi^-$ mode for normalization.

$\Gamma(D_s^- \mu^+ \mu^+)/\Gamma_{\text{total}}$ Γ_{620}/Γ

VALUE	CL%	DOCUMENT ID	TECN	COMMENT
$<5.8 \times 10^{-7}$	95	1 AAIJ	12AD	LHCB pp at 7 TeV

¹ Uses $B^+ \rightarrow \psi(2S) K^+$, $\psi(2S) \rightarrow J/\psi \pi^+ \pi^-$ mode for normalization. Obtains neutrino-mass-dependent upper limits in the range $1.5-8.0 \times 10^{-7}$.

$\Gamma(\bar{D}^0 \pi^- \mu^+ \mu^+)/\Gamma_{\text{total}}$ Γ_{621}/Γ

VALUE	CL%	DOCUMENT ID	TECN	COMMENT
$<1.5 \times 10^{-6}$	95	1 AAIJ	12AD	LHCB pp at 7 TeV

¹ Uses $B^+ \rightarrow \psi(2S) K^+$, $\psi(2S) \rightarrow J/\psi \pi^+ \pi^-$ mode for normalization. Obtains neutrino-mass-dependent upper limits in the range $0.3-1.5 \times 10^{-6}$.

$\Gamma(\Lambda^0 \mu^+)/\Gamma_{\text{total}}$ Γ_{622}/Γ

VALUE	CL%	DOCUMENT ID	TECN	COMMENT
$<6 \times 10^{-8}$	90	1,2 DEL-AMO-SA...	11k	BABR $e^+e^- \rightarrow \Upsilon(4S)$

¹ DEL-AMO-SANCHEZ 11k reports $<6.1 \times 10^{-8}$ from a measurement of $[\Gamma(B^+ \rightarrow \Lambda^0 \mu^+)/\Gamma_{\text{total}}] \times [B(\Lambda \rightarrow p \pi^-)]$ assuming $B(\Lambda \rightarrow p \pi^-) = (63.9 \pm 0.5) \times 10^{-2}$.
² Uses $B(\Upsilon(4S) \rightarrow B^0 \bar{B}^0) = (51.6 \pm 0.6)\%$ and $B(\Upsilon(4S) \rightarrow B^+ B^-) = (48.4 \pm 0.6)\%$.

$\Gamma(\Lambda^0 e^+)/\Gamma_{\text{total}}$ Γ_{623}/Γ

VALUE	CL%	DOCUMENT ID	TECN	COMMENT
$<3.2 \times 10^{-8}$	90	1,2 DEL-AMO-SA...	11k	BABR $e^+e^- \rightarrow \Upsilon(4S)$

¹ DEL-AMO-SANCHEZ 11k reports $<3.2 \times 10^{-8}$ from a measurement of $[\Gamma(B^+ \rightarrow \Lambda^0 e^+)/\Gamma_{\text{total}}] \times [B(\Lambda \rightarrow p \pi^-)]$ assuming $B(\Lambda \rightarrow p \pi^-) = (63.9 \pm 0.5) \times 10^{-2}$.
² Uses $B(\Upsilon(4S) \rightarrow B^0 \bar{B}^0) = (51.6 \pm 0.6)\%$ and $B(\Upsilon(4S) \rightarrow B^+ B^-) = (48.4 \pm 0.6)\%$.

$\Gamma(\bar{\Lambda}^0 \mu^+)/\Gamma_{\text{total}}$ Γ_{624}/Γ

VALUE	CL%	DOCUMENT ID	TECN	COMMENT
$<6 \times 10^{-8}$	90	1,2 DEL-AMO-SA...	11k	BABR $e^+e^- \rightarrow \Upsilon(4S)$

¹ DEL-AMO-SANCHEZ 11k reports $<6.2 \times 10^{-8}$ from a measurement of $[\Gamma(B^+ \rightarrow \bar{\Lambda}^0 \mu^+)/\Gamma_{\text{total}}] \times [B(\Lambda \rightarrow p \pi^-)]$ assuming $B(\Lambda \rightarrow p \pi^-) = (63.9 \pm 0.5) \times 10^{-2}$.
² Uses $B(\Upsilon(4S) \rightarrow B^0 \bar{B}^0) = (51.6 \pm 0.6)\%$ and $B(\Upsilon(4S) \rightarrow B^+ B^-) = (48.4 \pm 0.6)\%$.

$\Gamma(\bar{\Lambda}^0 e^+)/\Gamma_{\text{total}}$ Γ_{625}/Γ

VALUE	CL%	DOCUMENT ID	TECN	COMMENT
$<8 \times 10^{-8}$	90	1,2 DEL-AMO-SA...	11k	BABR $e^+e^- \rightarrow \Upsilon(4S)$

¹ DEL-AMO-SANCHEZ 11k reports $<8.1 \times 10^{-8}$ from a measurement of $[\Gamma(B^+ \rightarrow \bar{\Lambda}^0 e^+)/\Gamma_{\text{total}}] \times [B(\Lambda \rightarrow p \pi^-)]$ assuming $B(\Lambda \rightarrow p \pi^-) = (63.9 \pm 0.5) \times 10^{-2}$.
² Uses $B(\Upsilon(4S) \rightarrow B^0 \bar{B}^0) = (51.6 \pm 0.6)\%$ and $B(\Upsilon(4S) \rightarrow B^+ B^-) = (48.4 \pm 0.6)\%$.

POLARIZATION IN B^+ DECAY

In decays involving two vector mesons, one can distinguish among the states in which meson polarizations are both longitudinal (L) or both are transverse and parallel (\parallel) or perpendicular (\perp) to each other with the parameters Γ_L/Γ , $\Gamma_{\parallel}/\Gamma$, and the relative phases ϕ_{\parallel} and ϕ_{\perp} . See the definitions in the note on "Polarization in B Decays" review in the B^0 Particle Listings.

Γ_L/Γ in $B^+ \rightarrow \bar{D}^{*0} \rho^+$

VALUE	DOCUMENT ID	TECN	COMMENT
$0.892 \pm 0.018 \pm 0.016$	CSORNA	03	CLE2 $e^+e^- \rightarrow \Upsilon(4S)$

Γ_L/Γ in $B^+ \rightarrow \bar{D}^{*0} K^{*+}$

VALUE	DOCUMENT ID	TECN	COMMENT
$0.86 \pm 0.06 \pm 0.03$	AUBERT	04k	BABR $e^+e^- \rightarrow \Upsilon(4S)$

Γ_L/Γ in $B^+ \rightarrow J/\psi K^{*+}$

VALUE	DOCUMENT ID	TECN	COMMENT
$0.604 \pm 0.015 \pm 0.018$	ITOH	05	BELL $e^+e^- \rightarrow \Upsilon(4S)$

Γ_{\perp}/Γ in $B^+ \rightarrow J/\psi K^{*+}$

VALUE	DOCUMENT ID	TECN	COMMENT
$0.180 \pm 0.014 \pm 0.010$	ITOH	05	BELL $e^+e^- \rightarrow \Upsilon(4S)$

Γ_L/Γ in $B^+ \rightarrow \omega K^{*+}$

VALUE	DOCUMENT ID	TECN	COMMENT
$0.41 \pm 0.18 \pm 0.05$	AUBERT	09h	BABR $e^+e^- \rightarrow \Upsilon(4S)$

Γ_L/Γ in $B^+ \rightarrow \omega K_2^*(1430)^+$

VALUE	DOCUMENT ID	TECN	COMMENT
$0.56 \pm 0.10 \pm 0.04$	AUBERT	09h	BABR $e^+e^- \rightarrow \Upsilon(4S)$

Γ_L/Γ in $B^+ \rightarrow K^{*+} \bar{K}^{*0}$

VALUE	DOCUMENT ID	TECN	COMMENT
$0.82^{+0.15}_{-0.21}$ OUR AVERAGE			
$1.06 \pm 0.30 \pm 0.14$	1 GOH	15	BELL $e^+e^- \rightarrow \Upsilon(4S)$
$0.75^{+0.16}_{-0.26} \pm 0.03$	2,3 AUBERT	09f	BABR $e^+e^- \rightarrow \Upsilon(4S)$

¹ Signal significance 2.7 standard deviations.
² Signal significance 3.7 standard deviations.
³ Assumes equal production of B^+ and B^0 at the $\Upsilon(4S)$.

Γ_L/Γ in $B^+ \rightarrow \phi K^*(892)^+$

VALUE	DOCUMENT ID	TECN	COMMENT
0.50 ± 0.05 OUR AVERAGE			
$0.49 \pm 0.05 \pm 0.03$	AUBERT	07BA	BABR $e^+e^- \rightarrow \Upsilon(4S)$
$0.52 \pm 0.08 \pm 0.03$	CHEN	05A	BELL $e^+e^- \rightarrow \Upsilon(4S)$
$0.46 \pm 0.12 \pm 0.03$	AUBERT	03v	BABR Repl. by AUBERT 07BA

••• We do not use the following data for averages, fits, limits, etc. •••

Meson Particle Listings

B^\pm

Γ_\perp/Γ in $B^+ \rightarrow \phi K^{*+}$

VALUE	DOCUMENT ID	TECN	COMMENT
0.20 ± 0.05 OUR AVERAGE			
0.21 ± 0.05 ± 0.02	AUBERT	07BA	BABR $e^+ e^- \rightarrow \Upsilon(4S)$
0.19 ± 0.08 ± 0.02	CHEN	05A	BELL $e^+ e^- \rightarrow \Upsilon(4S)$

ϕ_\parallel in $B^+ \rightarrow \phi K^{*+}$

VALUE (°)	DOCUMENT ID	TECN	COMMENT
2.34 ± 0.18 OUR AVERAGE			
2.47 ± 0.20 ± 0.07	AUBERT	07BA	BABR $e^+ e^- \rightarrow \Upsilon(4S)$
2.10 ± 0.28 ± 0.04	CHEN	05A	BELL $e^+ e^- \rightarrow \Upsilon(4S)$

ϕ_\perp in $B^+ \rightarrow \phi K^{*+}$

VALUE (°)	DOCUMENT ID	TECN	COMMENT
2.58 ± 0.17 OUR AVERAGE			
2.69 ± 0.20 ± 0.03	AUBERT	07BA	BABR $e^+ e^- \rightarrow \Upsilon(4S)$
2.31 ± 0.30 ± 0.07	CHEN	05A	BELL $e^+ e^- \rightarrow \Upsilon(4S)$

$\delta_0(B^+ \rightarrow \phi K^{*+})$

VALUE (rad)	DOCUMENT ID	TECN	COMMENT
3.07 ± 0.18 ± 0.06			
	AUBERT	07BA	BABR $e^+ e^- \rightarrow \Upsilon(4S)$

$A_{CP}^0(B^+ \rightarrow \phi K^{*+})$

VALUE	DOCUMENT ID	TECN	COMMENT
0.17 ± 0.11 ± 0.02			
	AUBERT	07BA	BABR $e^+ e^- \rightarrow \Upsilon(4S)$

$A_{CP}^\perp(B^+ \rightarrow \phi K^{*+})$

VALUE	DOCUMENT ID	TECN	COMMENT
0.22 ± 0.24 ± 0.08			
	AUBERT	07BA	BABR $e^+ e^- \rightarrow \Upsilon(4S)$

$\Delta\phi_\parallel(B^+ \rightarrow \phi K^{*+})$

VALUE (rad)	DOCUMENT ID	TECN	COMMENT
0.07 ± 0.20 ± 0.05			
	AUBERT	07BA	BABR $e^+ e^- \rightarrow \Upsilon(4S)$

$\Delta\phi_\perp(B^+ \rightarrow \phi K^{*+})$

VALUE (rad)	DOCUMENT ID	TECN	COMMENT
0.19 ± 0.20 ± 0.07			
	AUBERT	07BA	BABR $e^+ e^- \rightarrow \Upsilon(4S)$

$\Delta\delta_0(B^+ \rightarrow \phi K^{*+})$

VALUE (rad)	DOCUMENT ID	TECN	COMMENT
0.20 ± 0.18 ± 0.03			
	AUBERT	07BA	BABR $e^+ e^- \rightarrow \Upsilon(4S)$

Γ_L/Γ in $B^+ \rightarrow \phi K_1(1270)^+$

VALUE	DOCUMENT ID	TECN	COMMENT
0.46^{+0.12+0.06}_{-0.13-0.07}			
	AUBERT	08B1	BABR $e^+ e^- \rightarrow \Upsilon(4S)$

Γ_L/Γ in $B^+ \rightarrow \phi K_2^*(1430)^+$

VALUE	DOCUMENT ID	TECN	COMMENT
0.80^{+0.09}_{-0.10} ± 0.03			
	AUBERT	08B1	BABR $e^+ e^- \rightarrow \Upsilon(4S)$

$\delta_0(B^+ \rightarrow \phi K_2^*(1430)^+)$

VALUE (rad)	DOCUMENT ID	TECN	COMMENT
3.59 ± 0.19 ± 0.12			
	AUBERT	08B1	BABR $e^+ e^- \rightarrow \Upsilon(4S)$

$\Delta\delta_0(B^+ \rightarrow \phi K_2^*(1430)^+)$

VALUE (rad)	DOCUMENT ID	TECN	COMMENT
-0.05 ± 0.19 ± 0.06			
	AUBERT	08B1	BABR $e^+ e^- \rightarrow \Upsilon(4S)$

Γ_L/Γ in $B^+ \rightarrow \rho^0 K^*(892)^+$

VALUE	DOCUMENT ID	TECN	COMMENT
0.78 ± 0.12 ± 0.03			
	DEL-AMO-SA...11d	BABR	$e^+ e^- \rightarrow \Upsilon(4S)$
• • • We do not use the following data for averages, fits, limits, etc. • • •			
0.96 ^{+0.04} _{-0.15} ± 0.04	AUBERT	03v	BABR Repl. by DEL-A-MO-SANCHEZ 11d

$\Gamma_L/\Gamma(B^+ \rightarrow K^*(892)^0 \rho^+)$

VALUE	DOCUMENT ID	TECN	COMMENT
0.48 ± 0.08 OUR AVERAGE			
0.52 ± 0.10 ± 0.04	AUBERT,B	06G	BABR $e^+ e^- \rightarrow \Upsilon(4S)$
0.43 ± 0.11 ^{+0.05} _{-0.02}	ZHANG	05D	BELL $e^+ e^- \rightarrow \Upsilon(4S)$

Γ_L/Γ in $B^+ \rightarrow \rho^+ \rho^0$

VALUE	DOCUMENT ID	TECN	COMMENT
0.950 ± 0.016 OUR AVERAGE			
0.950 ± 0.015 ± 0.006	AUBERT	09G	BABR $e^+ e^- \rightarrow \Upsilon(4S)$
0.948 ± 0.106 ± 0.021	ZHANG	03B	BELL $e^+ e^- \rightarrow \Upsilon(4S)$
• • • We do not use the following data for averages, fits, limits, etc. • • •			
0.905 ± 0.042 ^{+0.023} _{-0.027}	AUBERT,BE	06G	BABR Repl. by AUBERT 09G
0.97 ^{+0.03} _{-0.07} ± 0.04	AUBERT	03v	BABR Repl. by AUBERT,BE 06G

Γ_L/Γ in $B^+ \rightarrow \omega \rho^+$

VALUE	DOCUMENT ID	TECN	COMMENT
0.90 ± 0.05 ± 0.03			
	AUBERT	09H	BABR $e^+ e^- \rightarrow \Upsilon(4S)$
• • • We do not use the following data for averages, fits, limits, etc. • • •			
0.82 ± 0.11 ± 0.02	AUBERT,B	06T	BABR Repl. by AUBERT 09H
0.88 ^{+0.12} _{-0.15} ± 0.03	AUBERT	05o	BABR Repl. by AUBERT,B 06T

Γ_L/Γ in $B^+ \rightarrow \rho \bar{p} K^*(892)^+$

VALUE	DOCUMENT ID	TECN	COMMENT
0.32 ± 0.17 ± 0.09			
	CHEN	08c	BELL $e^+ e^- \rightarrow \Upsilon(4S)$

CP VIOLATION

A_{CP} is defined as

$$\frac{B(B^- \rightarrow \bar{f}) - B(B^+ \rightarrow f)}{B(B^- \rightarrow \bar{f}) + B(B^+ \rightarrow f)}$$

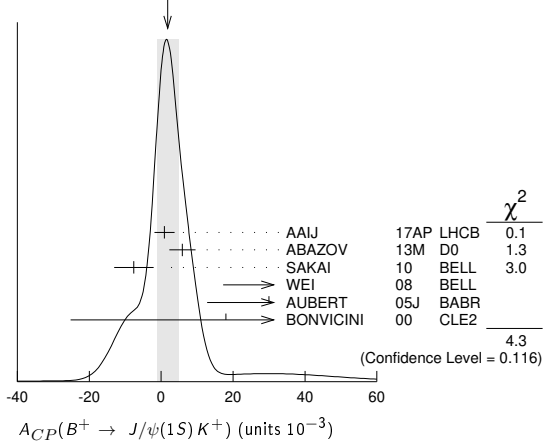
the CP-violation charge asymmetry of exclusive B^- and B^+ decay.

$A_{CP}(B^+ \rightarrow J/\psi(1S)K^+)$

VALUE (units 10^{-3})	DOCUMENT ID	TECN	COMMENT
1.8 ± 3.0 OUR AVERAGE			Error includes scale factor of 1.5. See the ideogram below.
0.9 ± 2.7 ± 0.7	AAIJ	17AP	LHCB pp at 7, 8 TeV
5.9 ± 3.6 ± 0.7	ABAZOV	13M	D0 $p\bar{p}$ at 1.96 TeV
-7.6 ± 5.0 ± 2.2	SAKAI	10	BELL $e^+ e^- \rightarrow \Upsilon(4S)$
90 ± 70 ± 20	¹ WEI	08	BELL $e^+ e^- \rightarrow \Upsilon(4S)$
30 ± 14 ± 10	² AUBERT	05J	BABR $e^+ e^- \rightarrow \Upsilon(4S)$
18 ± 43 ± 4	³ BONVICINI	00	CLE2 $e^+ e^- \rightarrow \Upsilon(4S)$
• • • We do not use the following data for averages, fits, limits, etc. • • •			
7.5 ± 6.1 ± 3.0	⁴ ABAZOV	08o	D0 Repl. by ABAZOV 13M
30 ± 15 ± 6	AUBERT	04P	BABR Repl. by AUBERT 05J
-26 ± 22 ± 17	ABE	03B	BELL Repl. by SAKAI 10
3 ± 30 ± 4	AUBERT	02F	BABR Repl. by AUBERT 04P

- Uses $B^+ \rightarrow J/\psi K^+$, where $J/\psi \rightarrow p\bar{p}$.
- The result reported corresponds to $-A_{CP}$.
- A +0.3% correction is applied due to a slightly higher reconstruction efficiency for the positive kaons.
- Uses $J/\psi \rightarrow \mu^+ \mu^-$ decay.

WEIGHTED AVERAGE
1.8 ± 3.0 (Error scaled by 1.5)



$A_{CP}(B^+ \rightarrow J/\psi(1S)\pi^+)$

VALUE (units 10^{-2})	DOCUMENT ID	TECN	COMMENT
1.8 ± 1.2 OUR AVERAGE			Error includes scale factor of 1.3.
1.91 ± 0.89 ± 0.16	¹ AAIJ	17o	LHCB pp at 7, 8 TeV
-4.2 ± 4.4 ± 0.9	ABAZOV	13M	D0 $p\bar{p}$ at 1.96 TeV
12.3 ± 8.5 ± 0.4	AUBERT	04P	BABR $e^+ e^- \rightarrow \Upsilon(4S)$
-2.3 ± 16.4 ± 1.5	ABE	03B	BELL $e^+ e^- \rightarrow \Upsilon(4S)$
• • • We do not use the following data for averages, fits, limits, etc. • • •			
0.5 ± 2.7 ± 1.1	² AAIJ	12Ac	LHCB Repl. by AAIJ 17o
-9 ± 8 ± 3	³ ABAZOV	08o	D0 Repl. by ABAZOV 13M
1 ± 22 ± 1	AUBERT	02F	BABR Repl. by AUBERT 04P
¹ Obtained by using LHCb measurement of $A_{CP}(B^+ \rightarrow J/\psi K^+) = (0.09 \pm 0.27 \pm 0.07) \times 10^{-2}$ of AAIJ 17AP. ² Uses $A_{CP}(B^+ \rightarrow J/\psi K^+) = 0.001 \pm 0.007$ to extract production asymmetry. ³ Uses $J/\psi \rightarrow \mu^+ \mu^-$ decay.			

$A_{CP}(B^+ \rightarrow J/\psi \rho^+)$

VALUE	DOCUMENT ID	TECN	COMMENT
-0.05 ± 0.05 OUR AVERAGE			
-0.045 ^{+0.056} _{-0.057} ± 0.008	AAIJ	19o	LHCB pp at 7 and 8 TeV
-0.11 ± 0.12 ± 0.08	AUBERT	07Ac	BABR $e^+ e^- \rightarrow \Upsilon(4S)$

A_{CP}(B⁺ → J/ψK*(892)⁺)

VALUE	DOCUMENT ID	TECN	COMMENT
-0.048 ± 0.029 ± 0.016	¹ AUBERT	05J	BABR e ⁺ e ⁻ → T(4S)

¹ The result reported corresponds to -A_{CP}.

A_{CP}(B⁺ → η_cK⁺)

VALUE	DOCUMENT ID	TECN	COMMENT
0.01 ± 0.07 OUR AVERAGE	Error includes scale factor of 2.2.		
0.040 ± 0.034 ± 0.004	¹ AAIJ	14AF	LHCB pp at 7, 8 TeV
-0.16 ± 0.08 ± 0.02	¹ WEI	08	BELL e ⁺ e ⁻ → T(4S)
• • • We do not use the following data for averages, fits, limits, etc. • • •			
0.046 ± 0.057 ± 0.007	¹ AAIJ	13AU	LHCB Repl. by AAIJ 14AF

¹ Uses B⁺ → η_cK⁺, where η_c → p \bar{p} .

A_{CP}(B⁺ → ψ(2S)π⁺)

VALUE	DOCUMENT ID	TECN	COMMENT
0.03 ± 0.06 OUR AVERAGE			
0.048 ± 0.090 ± 0.011	¹ AAIJ	12AC	LHCB pp at 7 TeV
0.022 ± 0.085 ± 0.016	BHARDWAJ	08	BELL e ⁺ e ⁻ → T(4S)

¹ Uses A_{CP}(B⁺ → J/ψK⁺) = 0.001 ± 0.007 to extract production asymmetry.

A_{CP}(B⁺ → ψ(2S)K⁺)

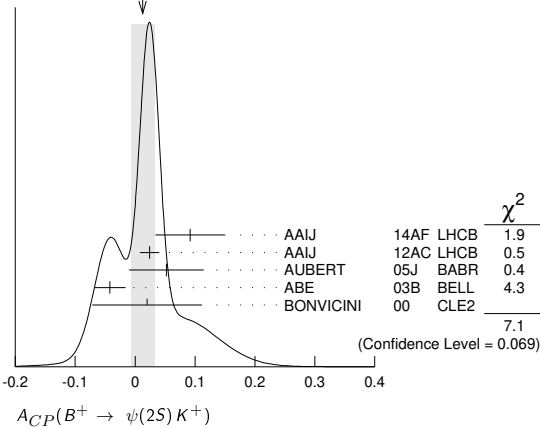
VALUE	DOCUMENT ID	TECN	COMMENT
0.012 ± 0.020 OUR AVERAGE	Error includes scale factor of 1.5. See the ideogram below.		
0.092 ± 0.058 ± 0.004	¹ AAIJ	14AF	LHCB pp at 7, 8 TeV
0.024 ± 0.014 ± 0.008	² AAIJ	12AC	LHCB pp at 7 TeV
0.052 ± 0.059 ± 0.020	AUBERT	05J	BABR e ⁺ e ⁻ → T(4S)
-0.042 ± 0.020 ± 0.017	ABE	03B	BELL e ⁺ e ⁻ → T(4S)
0.02 ± 0.091 ± 0.01	³ BONVICINI	00	CLE2 e ⁺ e ⁻ → T(4S)

• • • We do not use the following data for averages, fits, limits, etc. • • •

-0.002 ± 0.123 ± 0.012 ^{1,2} AAIJ 13AU LHCB Repl. by AAIJ 14AF

¹ Uses ψ(2S) → p \bar{p} decays.
² Uses A_{CP}(B⁺ → J/ψK⁺) = 0.001 ± 0.007 to extract production asymmetry.
³ A + 0.3% correction is applied due to a slightly higher reconstruction efficiency for the positive kaons.

WEIGHTED AVERAGE
0.012 ± 0.020 (Error scaled by 1.5)



A_{CP}(B⁺ → ψ(2S)K*(892)⁺)

VALUE	DOCUMENT ID	TECN	COMMENT
0.077 ± 0.207 ± 0.051	¹ AUBERT	05J	BABR e ⁺ e ⁻ → T(4S)

¹ The result reported corresponds to -A_{CP}.

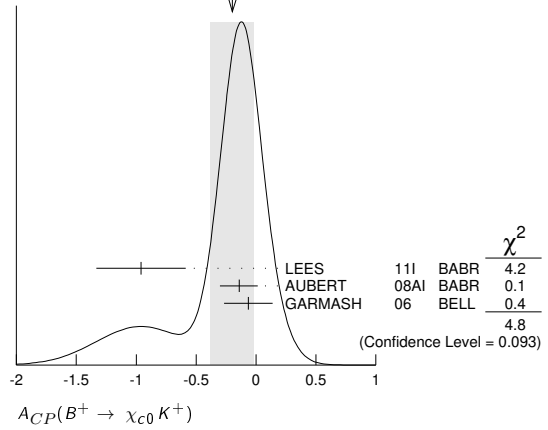
A_{CP}(B⁺ → χ₀₁(1P)π⁺)

VALUE	DOCUMENT ID	TECN	COMMENT
0.07 ± 0.18 ± 0.02	KUMAR	06	BELL e ⁺ e ⁻ → T(4S)

A_{CP}(B⁺ → χ₀₀K⁺)

VALUE	DOCUMENT ID	TECN	COMMENT
-0.20 ± 0.18 OUR AVERAGE	Error includes scale factor of 1.5. See the ideogram below.		
-0.96 ± 0.37 ± 0.04	LEES	11I	BABR e ⁺ e ⁻ → T(4S)
-0.14 ± 0.15 ^{+0.03} / _{-0.06}	AUBERT	08AI	BABR e ⁺ e ⁻ → T(4S)
-0.065 ± 0.20 ^{+0.035} / _{-0.024}	GARMASH	06	BELL e ⁺ e ⁻ → T(4S)

WEIGHTED AVERAGE
-0.20 ± 0.18 (Error scaled by 1.5)



A_{CP}(B⁺ → χ₀₁K⁺)

VALUE	DOCUMENT ID	TECN	COMMENT
-0.009 ± 0.033 OUR AVERAGE			
-0.01 ± 0.03 ± 0.02	KUMAR	06	BELL e ⁺ e ⁻ → T(4S)
-0.003 ± 0.076 ± 0.017	¹ AUBERT	05J	BABR e ⁺ e ⁻ → T(4S)

¹ The result reported corresponds to -A_{CP}.

A_{CP}(B⁺ → χ₀₁K*(892)⁺)

VALUE	DOCUMENT ID	TECN	COMMENT
0.471 ± 0.378 ± 0.268	¹ AUBERT	05J	BABR e ⁺ e ⁻ → T(4S)

¹ The result reported corresponds to -A_{CP}.

A_{CP}(B⁺ → D⁰ℓ⁺ν_ℓ)

VALUE (units 10 ⁻²)	DOCUMENT ID	TECN	COMMENT
-0.14 ± 0.14 ± 0.14	¹ ABZOV	17A	D0 p \bar{p} at 1.96 TeV

¹ Uses D⁰ → K⁻π⁺ decays and f(B⁺) = 0.56 ± 0.01 from 10.4 fb⁻¹ of Run II data.

A_{CP}(B⁺ → D⁰π⁺)

VALUE	DOCUMENT ID	TECN	COMMENT
-0.007 ± 0.007 OUR AVERAGE			
-0.006 ± 0.005 ± 0.010	¹ AAIJ	13AE	LHCB pp at 7 TeV
-0.008 ± 0.008	ABE	06	BELL e ⁺ e ⁻ → T(4S)

¹ Uses B[±] → [K[±]π[∓]π[±]π⁻]_Dh[±] mode.

A_{CP}(B⁺ → D_{CP(+1)}π⁺)

VALUE	DOCUMENT ID	TECN	COMMENT
-0.0080 ± 0.0026 OUR AVERAGE			
-0.008 ± 0.003 ± 0.002	¹ AAIJ	18A	LHCB pp at 7, 8, 13 TeV
-0.008 ± 0.006 ± 0.002	² AAIJ	18A	LHCB pp at 7, 8, 13 TeV
-0.0098 ± 0.0043 ± 0.0021	AAIJ	16L	LHCB pp at 7, 8 TeV
0.035 ± 0.024	ABE	06	BELL e ⁺ e ⁻ → T(4S)

¹ Uses D → K⁺K⁻ decay mode.
² Uses D → π⁺π⁻ decay mode.

A_{CP}(B⁺ → D_{CP(-1)}π⁺)

VALUE	DOCUMENT ID	TECN	COMMENT
0.017 ± 0.026	ABE	06	BELL e ⁺ e ⁻ → T(4S)

A_{CP}([K[∓]π[±]π[±]π⁻]_Dπ⁺)

VALUE	DOCUMENT ID	TECN	COMMENT
0.023 ± 0.048 ± 0.005	AAIJ	16L	LHCB pp at 7, 8 TeV
0.13 ± 0.10	AAIJ	13AE	LHCB Repl. by AAIJ 16L

• • • We do not use the following data for averages, fits, limits, etc. • • •

A_{CP}(B⁺ → [π⁺π⁺π⁻π⁻]_DK⁺)

VALUE	DOCUMENT ID	TECN	COMMENT
0.100 ± 0.034 ± 0.018	AAIJ	16L	LHCB pp at 7, 8 TeV

A_{CP}(B⁺ → [π⁺π⁻π⁺π⁻]_DK*(892)⁺)

VALUE	DOCUMENT ID	TECN	COMMENT
0.02 ± 0.11 ± 0.01	AAIJ	17Bo	LHCB pp at 7, 8, 13 TeV

A_{CP}(B⁺ → D⁰K⁺)

VALUE	DOCUMENT ID	TECN	COMMENT
-0.017 ± 0.005 OUR AVERAGE			
-0.019 ± 0.005 ± 0.002	¹ AAIJ	18A	LHCB pp at 7, 8, 13 TeV
-0.0194 ± 0.0072 ± 0.0060	AAIJ	16L	LHCB pp at 7, 8 TeV
0.010 ± 0.026 ± 0.005	² AAIJ	15W	LHCB pp at 7, 8 TeV
0.066 ± 0.036	ABE	06	BELL e ⁺ e ⁻ → T(4S)

Meson Particle Listings

 B^\pm

• • • We do not use the following data for averages, fits, limits, etc. • • •

$0.000 \pm 0.012 \pm 0.002$	³ AAIJ	16L LHCb	pp at 7, 8 TeV
$-0.029 \pm 0.020 \pm 0.018$	³ AAIJ	13AE LHCb	Repl. by AAIJ 16L
$0.003 \pm 0.080 \pm 0.037$	⁴ ABE	03D BELL	Repl. by SWAIN 03
$0.04 \pm 0.06 \pm 0.03$	⁵ SWAIN	03 BELL	Repl. by ABE 06

¹ Supersedes AAIJ 16L.

² Uses $D^0 \rightarrow K^- \pi^+ \pi^0$ for the favored mode, and $D^0 \rightarrow K^+ \pi^- \pi^0$ for the suppressed mode.

³ Uses $B^\pm \rightarrow [K^\pm \pi^\mp \pi^\pm \pi^\mp]_D h^\pm$ mode.

⁴ Corresponds to 90% confidence range $-0.15 < A_{CP} < 0.16$.

⁵ Corresponds to 90% confidence range $-0.07 < A_{CP} < 0.15$.

 $A_{CP}([K^\mp \pi^\pm \pi^\pm \pi^\mp]_D K^+)$

VALUE	DOCUMENT ID	TECN	COMMENT
$-0.313 \pm 0.102 \pm 0.038$	AAIJ	16L LHCb	pp at 7, 8 TeV

• • • We do not use the following data for averages, fits, limits, etc. • • •

-0.42 ± 0.22	AAIJ	13AE LHCb	Repl. by AAIJ 16L
------------------	------	-----------	-------------------

 $A_{CP}(B^+ \rightarrow [\pi^+ \pi^+ \pi^- \pi^-]_D \pi^+)$

VALUE (units 10^{-3})	DOCUMENT ID	TECN	COMMENT
$-4.1 \pm 7.9 \pm 2.4$	AAIJ	16L LHCb	pp at 7, 8 TeV

 $A_{CP}(B^+ \rightarrow [K^- \pi^+]_D K^+)$

VALUE	DOCUMENT ID	TECN	COMMENT
-0.58 ± 0.21 OUR AVERAGE			

$-0.82 \pm 0.44 \pm 0.09$	AALTONEN	11AJ CDF	$p\bar{p}$ at 1.96 TeV
---------------------------	----------	----------	------------------------

$-0.39 \pm 0.26 \pm 0.04$ -0.28 ± 0.03	HORII	11 BELL	$e^+ e^- \rightarrow \Upsilon(4S)$
---	-------	---------	------------------------------------

$-0.86 \pm 0.47 \pm 0.12$ -0.16	DEL-AMO-SA...10H	BABR	$e^+ e^- \rightarrow \Upsilon(4S)$
--------------------------------------	------------------	------	------------------------------------

• • • We do not use the following data for averages, fits, limits, etc. • • •

$-0.1 \pm 0.8 \pm 0.4$ -1.0	HORII	08 BELL	Repl. by HORII 11
----------------------------------	-------	---------	-------------------

$+0.88 \pm 0.77 \pm 0.06$ -0.62	SAIGO	05 BELL	Repl. by HORII 08
--------------------------------------	-------	---------	-------------------

 $A_{CP}(B^+ \rightarrow [K^- \pi^+ \pi^0]_D K^+)$

VALUE	DOCUMENT ID	TECN	COMMENT
0.07 ± 0.30 OUR AVERAGE			Error includes scale factor of 1.5.

$-0.20 \pm 0.27 \pm 0.04$	¹ AAIJ	15W LHCb	pp at 7, 8 TeV
---------------------------	-------------------	----------	------------------

$0.41 \pm 0.30 \pm 0.05$	NAYAK	13 BELL	$e^+ e^- \rightarrow \Upsilon(4S)$
--------------------------	-------	---------	------------------------------------

¹ Uses $D^0 \rightarrow K^- \pi^+ \pi^0$ for the favored mode, and $D^0 \rightarrow K^+ \pi^- \pi^0$ for the suppressed mode.

 $A_{CP}(B^+ \rightarrow [K^+ K^- \pi^0]_D K^+)$

VALUE	DOCUMENT ID	TECN	COMMENT
$0.30 \pm 0.20 \pm 0.02$	¹ AAIJ	15W LHCb	pp at 7, 8 TeV

¹ Uses $D \rightarrow K^+ K^- \pi^0$ mode.

 $A_{CP}(B^+ \rightarrow [\pi^+ \pi^- \pi^0]_D K^+)$

VALUE	DOCUMENT ID	TECN	COMMENT
$0.054 \pm 0.091 \pm 0.011$	¹ AAIJ	15W LHCb	pp at 7, 8 TeV

¹ Uses $D \rightarrow \pi^+ \pi^- \pi^0$ mode.

 $A_{CP}(B^+ \rightarrow \bar{D}^0 K^*(892)^+)$

VALUE	DOCUMENT ID	TECN	COMMENT
-0.007 ± 0.019 OUR AVERAGE			

$-0.004 \pm 0.023 \pm 0.008$	¹ AAIJ	17B0 LHCb	pp at 7, 8, 13 TeV
------------------------------	-------------------	-----------	----------------------

$-0.013 \pm 0.031 \pm 0.009$	² AAIJ	17B0 LHCb	pp at 7, 8, 13 TeV
------------------------------	-------------------	-----------	----------------------

¹ Uses $B^\pm \rightarrow [K^\pm \pi^\mp]_D K^*(892)^\pm$ decay mode.

² Uses $B^\pm \rightarrow [K^\pm \pi^\mp \pi^\pm \pi^\mp]_D K^*(892)^\pm$ decay mode.

 $A_{CP}(B^+ \rightarrow [K^- \pi^+]_D K^*(892)^+)$

VALUE	DOCUMENT ID	TECN	COMMENT
-0.75 ± 0.16 OUR AVERAGE			

$-0.81 \pm 0.17 \pm 0.04$	AAIJ	17B0 LHCb	pp at 7, 8, 13 TeV
---------------------------	------	-----------	----------------------

$-0.34 \pm 0.43 \pm 0.16$	AUBERT	09AJ BABR	$e^+ e^- \rightarrow \Upsilon(4S)$
---------------------------	--------	-----------	------------------------------------

• • • We do not use the following data for averages, fits, limits, etc. • • •

$-0.22 \pm 0.61 \pm 0.17$	AUBERT,B	05V BABR	Repl. by AUBERT 09AJ
---------------------------	----------	----------	----------------------

 $A_{CP}(B^+ \rightarrow [K^- \pi^+ \pi^- \pi^+]_D K^*(892)^+)$

VALUE	DOCUMENT ID	TECN	COMMENT
$-0.45 \pm 0.21 \pm 0.14$	AAIJ	17B0 LHCb	pp at 7, 8, 13 TeV

 $A_{CP}(B^+ \rightarrow [K^- \pi^+]_D \pi^+)$

VALUE	DOCUMENT ID	TECN	COMMENT
0.00 ± 0.09 OUR AVERAGE			

$0.13 \pm 0.25 \pm 0.02$	AALTONEN	11AJ CDF	$p\bar{p}$ at 1.96 TeV
--------------------------	----------	----------	------------------------

$-0.04 \pm 0.11 \pm 0.02$ -0.01	HORII	11 BELL	$e^+ e^- \rightarrow \Upsilon(4S)$
--------------------------------------	-------	---------	------------------------------------

$0.03 \pm 0.17 \pm 0.04$	DEL-AMO-SA...10H	BABR	$e^+ e^- \rightarrow \Upsilon(4S)$
--------------------------	------------------	------	------------------------------------

• • • We do not use the following data for averages, fits, limits, etc. • • •

$-0.02 \pm 0.15 \pm 0.04$ -0.16	HORII	08 BELL	Repl. by HORII 11
--------------------------------------	-------	---------	-------------------

$+0.30 \pm 0.29 \pm 0.06$ -0.25	SAIGO	05 BELL	Repl. by HORII 08
--------------------------------------	-------	---------	-------------------

 $A_{CP}(B^+ \rightarrow [K^- \pi^+ \pi^0]_D \pi^+)$

VALUE	DOCUMENT ID	TECN	COMMENT
0.35 ± 0.16 OUR AVERAGE			

$0.438 \pm 0.190 \pm 0.011$	¹ AAIJ	15W LHCb	pp at 7, 8 TeV
-----------------------------	-------------------	----------	------------------

$0.16 \pm 0.27 \pm 0.03$ -0.04	NAYAK	13 BELL	$e^+ e^- \rightarrow \Upsilon(4S)$
-------------------------------------	-------	---------	------------------------------------

¹ Uses $D^0 \rightarrow K^- \pi^+ \pi^0$ for the favored mode, and $D^0 \rightarrow K^+ \pi^- \pi^0$ for the suppressed mode.

 $A_{CP}(B^+ \rightarrow [K^+ K^- \pi^0]_D \pi^+)$

VALUE	DOCUMENT ID	TECN	COMMENT
$-0.030 \pm 0.040 \pm 0.005$	¹ AAIJ	15W LHCb	pp at 7, 8 TeV

¹ Uses $D \rightarrow K^+ K^-$ mode.

 $A_{CP}(B^+ \rightarrow [\pi^+ \pi^- \pi^0]_D \pi^+)$

VALUE	DOCUMENT ID	TECN	COMMENT
$-0.016 \pm 0.020 \pm 0.004$	¹ AAIJ	15W LHCb	pp at 7, 8 TeV

¹ Uses $D \rightarrow \pi^+ \pi^-$ mode.

 $A_{CP}(B^+ \rightarrow [K^- \pi^+]_{(D\pi)} \pi^+)$

VALUE	DOCUMENT ID	TECN	COMMENT
$-0.09 \pm 0.27 \pm 0.05$	DEL-AMO-SA...10H	BABR	$e^+ e^- \rightarrow \Upsilon(4S)$

 $A_{CP}(B^+ \rightarrow [K^- \pi^+]_{(D\gamma)} \pi^+)$

VALUE	DOCUMENT ID	TECN	COMMENT
$-0.65 \pm 0.55 \pm 0.22$	DEL-AMO-SA...10H	BABR	$e^+ e^- \rightarrow \Upsilon(4S)$

 $A_{CP}(B^+ \rightarrow [K^- \pi^+]_{(D\pi)} K^+)$

VALUE	DOCUMENT ID	TECN	COMMENT
$0.77 \pm 0.35 \pm 0.12$	DEL-AMO-SA...10H	BABR	$e^+ e^- \rightarrow \Upsilon(4S)$

$-0.86 \pm 0.47 \pm 0.12$ -0.16	DEL-AMO-SA...10H	BABR	$e^+ e^- \rightarrow \Upsilon(4S)$
--------------------------------------	------------------	------	------------------------------------

 $A_{CP}(B^+ \rightarrow [K^- \pi^+]_{(D\gamma)} K^+)$

VALUE	DOCUMENT ID	TECN	COMMENT
$0.36 \pm 0.94 \pm 0.25$ -0.41	DEL-AMO-SA...10H	BABR	$e^+ e^- \rightarrow \Upsilon(4S)$

$-0.1 \pm 0.8 \pm 0.4$ -1.0	HORII	08 BELL	Repl. by HORII 11
----------------------------------	-------	---------	-------------------

 $A_{CP}(B^+ \rightarrow [\pi^+ \pi^- \pi^0]_D K^+)$

VALUE	DOCUMENT ID	TECN	COMMENT
$-0.02 \pm 0.15 \pm 0.03$	¹ AUBERT	07BJ BABR	$e^+ e^- \rightarrow \Upsilon(4S)$

• • • We do not use the following data for averages, fits, limits, etc. • • •

$-0.02 \pm 0.16 \pm 0.03$	AUBERT,B	05T BABR	Repl. by AUBERT 07BJ
---------------------------	----------	----------	----------------------

¹ Uses a Dalitz plot analysis of $D^0 \rightarrow \pi^+ \pi^- \pi^0$. Also reports the one-sigma regions: $0.06 < r_B < 0.78$, $-30^\circ < \gamma < 76^\circ$, and $-27^\circ < \delta < 78^\circ$.

 $A_{CP}(B^+ \rightarrow [K_S^0 K^+ \pi^-]_D K^+)$

VALUE	DOCUMENT ID	TECN	COMMENT
$0.040 \pm 0.091 \pm 0.018$	¹ AAIJ	14V LHCb	pp at 7, 8 TeV

¹ The analysis uses all of $D \rightarrow K_S^0 K \pi$ Dalitz decays.

 $A_{CP}(B^+ \rightarrow [K_S^0 K^- \pi^+]_D K^+)$

VALUE	DOCUMENT ID	TECN	COMMENT
$0.233 \pm 0.129 \pm 0.024$	¹ AAIJ	14V LHCb	pp at 7, 8 TeV

¹ The analysis uses all of $D \rightarrow K_S^0 K \pi$ Dalitz decays.

 $A_{CP}(B^+ \rightarrow [K_S^0 K^- \pi^+]_D \pi^+)$

VALUE	DOCUMENT ID	TECN	COMMENT
$-0.052 \pm 0.029 \pm 0.017$	¹ AAIJ	14V LHCb	pp at 7, 8 TeV

¹ The analysis uses all of $D \rightarrow K_S^0 K \pi$ Dalitz decays.

 $A_{CP}(B^+ \rightarrow [K_S^0 K^+ \pi^-]_D \pi^+)$

VALUE	DOCUMENT ID	TECN	COMMENT
$-0.025 \pm 0.024 \pm 0.010$	¹ AAIJ	14V LHCb	pp at 7, 8 TeV

¹ The analysis uses all of $D \rightarrow K_S^0 K \pi$ Dalitz decays.

 $A_{CP}(B^+ \rightarrow [K^*(892)^- K^+]_D K^+)$

VALUE	DOCUMENT ID	TECN	COMMENT
$0.026 \pm 0.109 \pm 0.029$	¹ AAIJ	14V LHCb	pp at 7, 8 TeV

¹ The Analysis uses $D \rightarrow K^*(892) K \rightarrow K_S^0 K \pi$ decays.

 $A_{CP}(B^+ \rightarrow [K^*(892)^+ K^-]_D K^+)$

VALUE	DOCUMENT ID	TECN	COMMENT
$0.336 \pm 0.208 \pm 0.026$	¹ AAIJ	14V LHCb	pp at 7, 8 TeV

¹ The Analysis uses $D \rightarrow K^*(892) K \rightarrow K_S^0 K \pi$ decays.

 $A_{CP}(B^+ \rightarrow [K^*(892)^+ K^-]_D \pi^+)$

VALUE	DOCUMENT ID	TECN	COMMENT
$-0.054 \pm 0.043 \pm 0.017$	¹ AAIJ	14V LHCb	pp at 7, 8 TeV

¹ The Analysis uses $D \rightarrow K^*(892) K \rightarrow K_S^0 K \pi$ decays.

 $A_{CP}(B^+ \rightarrow [K^*(892)^- K^+]_D \pi^+)$

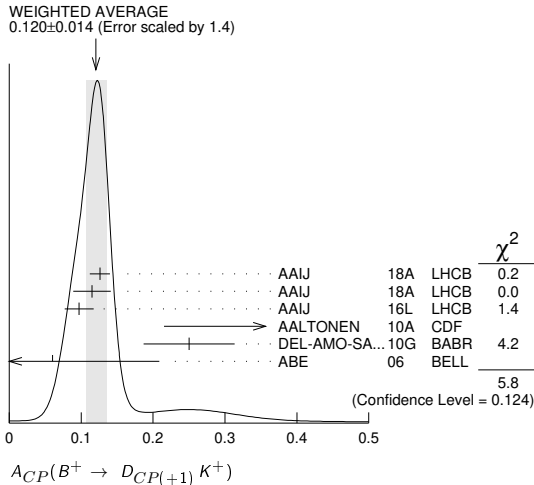
VALUE	DOCUMENT ID	TECN	COMMENT
$-0.012 \pm 0.028 \pm 0.010$	¹ AAIJ	14V LHCb	pp at 7, 8 TeV

¹ The Analysis uses $D \rightarrow K^*(892) K \rightarrow K_S^0 K \pi$ decays.

A_{CP}(B[±] → D_{CP(+1)}K[±])

VALUE	DOCUMENT ID	TECN	COMMENT
0.120±0.014 OUR AVERAGE	Error includes scale factor of 1.4. See the ideogram below.		
0.126±0.014±0.002	¹ AAIJ	18A LHCb	pp at 7, 8, 13 TeV
0.115±0.025±0.007	² AAIJ	18A LHCb	pp at 7, 8, 13 TeV
0.097±0.018±0.009	AAIJ	16L LHCb	pp at 7, 8 TeV
0.39 ±0.17 ±0.04	AALTONEN	10A CDF	p \bar{p} at 1.96 TeV
0.25 ±0.06 ±0.02	³ DEL-AMO-SA...	10G BABR	e ⁺ e ⁻ → $\Upsilon(4S)$
0.06 ±0.14 ±0.05	ABE	06 BELL	e ⁺ e ⁻ → $\Upsilon(4S)$
••• We do not use the following data for averages, fits, limits, etc. •••			
0.145±0.032±0.010	⁴ AAIJ	12M LHCb	Repl. by AAIJ 16L
0.27 ±0.09 ±0.04	AUBERT	08AA BABR	Repl. by DEL-AMO-SANCHEZ 10G
0.35 ±0.13 ±0.04	AUBERT	06J BABR	Repl. by AUBERT 08AA
0.07 ±0.17 ±0.06	AUBERT	04N BABR	Repl. by AUBERT 06J
0.29 ±0.26 ±0.05	⁵ ABE	03D BELL	Repl. by SWAIN 03
0.06 ±0.19 ±0.04	⁶ SWAIN	03 BELL	Repl. by ABE 06

- ¹ Uses D → K⁺K⁻ decay mode.
- ² Uses D → $\pi^+\pi^-$ decay mode.
- ³ Reports the first evidence for direct CP violation in B → DK decays with 3.6 standard deviations.
- ⁴ AAIJ 12M reports an evidence of direct CP violation in B[±] → DK[±] decays with a total significance of 5.8 σ .
- ⁵ Corresponds to 90% confidence range -0.14 < A_{CP} < 0.73.
- ⁶ Corresponds to 90% confidence range -0.26 < A_{CP} < 0.38.



A_{ADS}(B[±] → DK[±])

$$A_{ADS}(B^+ \rightarrow DK^+) = \frac{(R_K^- - R_K^+)}{(R_K^- + R_K^+)}$$

where

$$R_K^- = \Gamma(B^- \rightarrow [K^-\pi^-]_D K^-) / \Gamma(B^- \rightarrow [K^-\pi^+]_D K^-)$$

$$R_K^+ = \Gamma(B^+ \rightarrow [K^-\pi^+]_D K^+) / \Gamma(B^+ \rightarrow [K^+\pi^-]_D K^+)$$

VALUE	DOCUMENT ID	TECN	COMMENT
-0.403±0.056±0.011	AAIJ	16L LHCb	pp at 7, 8 TeV
••• We do not use the following data for averages, fits, limits, etc. •••			
-0.52 ±0.15 ±0.02	AAIJ	12M LHCb	Repl. by AAIJ 16L

A_{ADS}(B[±] → D π^+)

$$A_{ADS}(B^+ \rightarrow D\pi^+) = \frac{(R_\pi^- - R_\pi^+)}{(R_\pi^- + R_\pi^+)}$$

where

$$R_\pi^- = \Gamma(B^- \rightarrow [K^+\pi^-]_D \pi^-) / \Gamma(B^- \rightarrow [K^-\pi^+]_D \pi^-)$$

$$R_\pi^+ = \Gamma(B^+ \rightarrow [K^-\pi^+]_D \pi^+) / \Gamma(B^+ \rightarrow [K^+\pi^-]_D \pi^+)$$

VALUE	DOCUMENT ID	TECN	COMMENT
0.100±0.031±0.009	AAIJ	16L LHCb	pp at 7, 8 TeV
••• We do not use the following data for averages, fits, limits, etc. •••			
0.143±0.062±0.011	AAIJ	12M LHCb	Repl. by AAIJ 16L

A_{ADS}(B[±] → [K⁻ π^+]_DK[±] $\pi^-\pi^+$)

VALUE	DOCUMENT ID	TECN	COMMENT
-0.33^{+0.36}_{-0.34}	AAIJ	15bc LHCb	pp at 7, 8 TeV

A_{ADS}(B[±] → [K⁻ π^+]_D $\pi^+\pi^-\pi^+$)

VALUE	DOCUMENT ID	TECN	COMMENT
-0.013±0.087	AAIJ	15bc LHCb	pp at 7, 8 TeV

A_{CP}(B[±] → D_{CP(-1)}K[±])

VALUE	DOCUMENT ID	TECN	COMMENT
-0.10±0.07 OUR AVERAGE	Error includes scale factor of 1.4. See the ideogram below.		
-0.09±0.07±0.02	DEL-AMO-SA...	10G BABR	e ⁺ e ⁻ → $\Upsilon(4S)$
-0.12±0.14±0.05	ABE	06 BELL	e ⁺ e ⁻ → $\Upsilon(4S)$
••• We do not use the following data for averages, fits, limits, etc. •••			
-0.09±0.09±0.02	AUBERT	08AA BABR	Repl. by DEL-AMO-SANCHEZ 10G
-0.06±0.13±0.04	AUBERT	06J BABR	Repl. by AUBERT 08AA
-0.22±0.24±0.04	¹ ABE	03D BELL	Repl. by SWAIN 03
-0.19±0.17±0.05	² SWAIN	03 BELL	Repl. by ABE 06
¹ Corresponds to 90% confidence range -0.62 < A _{CP} < 0.18.			
² Corresponds to 90% confidence range -0.47 < A _{CP} < 0.11.			

A_{CP}(B[±] → [K⁺K⁻]_DK[±] $\pi^-\pi^+$)

VALUE	DOCUMENT ID	TECN	COMMENT
-0.045±0.064±0.011	AAIJ	15bc LHCb	pp at 7, 8 TeV

A_{CP}(B[±] → [$\pi^+\pi^-$]_DK[±] $\pi^-\pi^+$)

VALUE	DOCUMENT ID	TECN	COMMENT
-0.054±0.101±0.011	AAIJ	15bc LHCb	pp at 7, 8 TeV

A_{CP}(B[±] → [K⁻ π^+]_DK[±] $\pi^-\pi^+$)

VALUE	DOCUMENT ID	TECN	COMMENT
0.013±0.019±0.013	AAIJ	15bc LHCb	pp at 7, 8 TeV

A_{CP}(B[±] → [K⁺K⁻]_D $\pi^+\pi^-\pi^+$)

VALUE	DOCUMENT ID	TECN	COMMENT
-0.019±0.011±0.010	AAIJ	15bc LHCb	pp at 7, 8 TeV

A_{CP}(B[±] → [$\pi^+\pi^-$]_D $\pi^+\pi^-\pi^+$)

VALUE	DOCUMENT ID	TECN	COMMENT
-0.013±0.016±0.010	AAIJ	15bc LHCb	pp at 7, 8 TeV

A_{CP}(B[±] → [K⁻ π^+]_D $\pi^+\pi^-\pi^+$)

VALUE	DOCUMENT ID	TECN	COMMENT
-0.002±0.003±0.011	AAIJ	15bc LHCb	pp at 7, 8 TeV

A_{CP}(B[±] → D^{0*} π^+)

VALUE	DOCUMENT ID	TECN	COMMENT
0.0010±0.0028 OUR AVERAGE	Error includes scale factor of 1.2.		
0.000 ±0.006 ±0.001	¹ AAIJ	18A LHCb	pp at 7, 8, 13 TeV
0.002 ±0.003 ±0.001	² AAIJ	18A LHCb	pp at 7, 8, 13 TeV
-0.014 ±0.015	ABE	06 BELL	e ⁺ e ⁻ → $\Upsilon(4S)$
¹ Uses D ^{0*} → D ⁰ γ decay mode.			
² Uses D ^{0*} → D ⁰ π^0 decay mode.			

A_{CP}(B[±] → (D^{0*}_{CP(+1)})⁰ π^+)

VALUE	DOCUMENT ID	TECN	COMMENT
0.016±0.010 OUR AVERAGE	Error includes scale factor of 1.2.		
-0.003±0.017±0.002	¹ AAIJ	18A LHCb	pp at 7, 8, 13 TeV
0.025±0.010±0.003	² AAIJ	18A LHCb	pp at 7, 8, 13 TeV
-0.021±0.045	ABE	06 BELL	e ⁺ e ⁻ → $\Upsilon(4S)$
¹ Uses D ^{0*} → D ⁰ γ decay mode.			
² Uses D ^{0*} → D ⁰ π^0 decay mode.			

A_{CP}(B[±] → (D^{0*}_{CP(-1)})⁰ π^+)

VALUE	DOCUMENT ID	TECN	COMMENT
-0.090±0.051	ABE	06 BELL	e ⁺ e ⁻ → $\Upsilon(4S)$

A_{CP}(B[±] → D^{0*}K[±])

VALUE	DOCUMENT ID	TECN	COMMENT
-0.001±0.011 OUR AVERAGE	Error includes scale factor of 1.1.		
0.001±0.021±0.007	¹ AAIJ	18A LHCb	pp at 7, 8, 13 TeV
0.006±0.012±0.004	² AAIJ	18A LHCb	pp at 7, 8, 13 TeV
-0.06 ±0.04 ±0.01	AUBERT	08BF BABR	e ⁺ e ⁻ → $\Upsilon(4S)$
-0.089±0.086	ABE	06 BELL	e ⁺ e ⁻ → $\Upsilon(4S)$
¹ Uses D ^{0*} → D ⁰ γ decay mode.			
² Uses D ^{0*} → D ⁰ π^0 decay mode.			

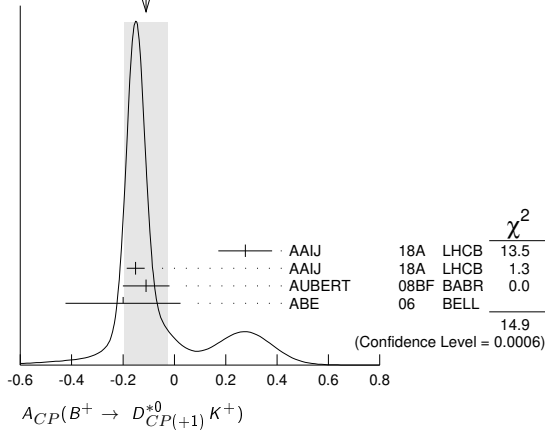
A_{CP}(B[±] → D^{0*}_{CP(+1)}K[±])

VALUE	DOCUMENT ID	TECN	COMMENT
-0.11 ±0.08 OUR AVERAGE	Error includes scale factor of 2.7. See the ideogram below.		
0.276±0.094±0.047	¹ AAIJ	18A LHCb	pp at 7, 8, 13 TeV
-0.151±0.033±0.011	² AAIJ	18A LHCb	pp at 7, 8, 13 TeV
-0.11 ±0.09 ±0.01	AUBERT	08BF BABR	e ⁺ e ⁻ → $\Upsilon(4S)$
-0.20 ±0.22 ±0.04	ABE	06 BELL	e ⁺ e ⁻ → $\Upsilon(4S)$
••• We do not use the following data for averages, fits, limits, etc. •••			
-0.10 ±0.23 ^{+0.03} _{-0.04}	AUBERT	05N BABR	Repl. by AUBERT 08BF
¹ Uses D ^{0*} → D ⁰ γ decay mode.			
² Uses D ^{0*} → D ⁰ π^0 decay mode.			

Meson Particle Listings

B^\pm

WEIGHTED AVERAGE
 -0.11 ± 0.08 (Error scaled by 2.7)



$A_{CP}(B^+ \rightarrow D_{CP(-)}^* K^+)$

VALUE	DOCUMENT ID	TECN	COMMENT
0.07 ± 0.10 OUR AVERAGE			
$+0.06 \pm 0.10 \pm 0.02$	AUBERT	08BF BABR	$e^+e^- \rightarrow \Upsilon(4S)$
$+0.13 \pm 0.30 \pm 0.08$	ABE	06 BELL	$e^+e^- \rightarrow \Upsilon(4S)$

$A_{CP}(B^+ \rightarrow D_{CP(+)} K^*(892)^+)$

VALUE	DOCUMENT ID	TECN	COMMENT
0.08 ± 0.06 OUR AVERAGE			
$0.08 \pm 0.06 \pm 0.01$	¹ AAIJ	17B0 LHCb	pp at 7, 8, 13 TeV
$0.09 \pm 0.13 \pm 0.06$	AUBERT	09AJ BABR	$e^+e^- \rightarrow \Upsilon(4S)$
$-0.08 \pm 0.19 \pm 0.08$	AUBERT,B	05U BABR	Repl. by AUBERT 09AJ

• • • We do not use the following data for averages, fits, limits, etc. • • •

¹ Measures the asymmetry separately for K^+K^- and $\pi^+\pi^-$ final states, $A(KK) = 0.06 \pm 0.07 \pm 0.01$ and $A(\pi\pi) = 0.15 \pm 0.13 \pm 0.01$, and combines the two results. The value of $A(\pi\pi)$ was updated in AAJ 18x.

$A_{CP}(B^+ \rightarrow D_{CP(-)} K^*(892)^+)$

VALUE	DOCUMENT ID	TECN	COMMENT
$-0.23 \pm 0.21 \pm 0.07$	AUBERT	09AJ BABR	$e^+e^- \rightarrow \Upsilon(4S)$
$-0.26 \pm 0.40 \pm 0.12$	AUBERT,B	05U BABR	Repl. by AUBERT 09AJ

$A_{CP}(B^+ \rightarrow D_s^+ \phi)$

VALUE	DOCUMENT ID	TECN	COMMENT
$-0.01 \pm 0.41 \pm 0.03$	AAIJ	13R LHCb	pp at 7 TeV

$A_{CP}(B^+ \rightarrow D_s^+ \bar{D}^0)$

VALUE (%)	DOCUMENT ID	TECN	COMMENT
$-0.4 \pm 0.5 \pm 0.5$	AAIJ	18W LHCb	pp at 7, 8 TeV

$A_{CP}(B^+ \rightarrow D^{*+} \bar{D}^{*0})$

VALUE	DOCUMENT ID	TECN	COMMENT
$-0.15 \pm 0.11 \pm 0.02$	AUBERT,B	06A BABR	$e^+e^- \rightarrow \Upsilon(4S)$

$A_{CP}(B^+ \rightarrow D^{*+} \bar{D}^0)$

VALUE	DOCUMENT ID	TECN	COMMENT
$-0.06 \pm 0.13 \pm 0.02$	AUBERT,B	06A BABR	$e^+e^- \rightarrow \Upsilon(4S)$

$A_{CP}(B^+ \rightarrow D^+ \bar{D}^{*0})$

VALUE	DOCUMENT ID	TECN	COMMENT
$0.13 \pm 0.18 \pm 0.04$	AUBERT,B	06A BABR	$e^+e^- \rightarrow \Upsilon(4S)$

$A_{CP}(B^+ \rightarrow D^+ \bar{D}^0)$

VALUE	DOCUMENT ID	TECN	COMMENT
0.016 ± 0.025 OUR AVERAGE			
$0.023 \pm 0.027 \pm 0.004$	AAIJ	18W LHCb	pp at 7, 8 TeV
$0.00 \pm 0.08 \pm 0.02$	ADACHI	08 BELL	$e^+e^- \rightarrow \Upsilon(4S)$
$-0.13 \pm 0.14 \pm 0.02$	AUBERT,B	06A BABR	$e^+e^- \rightarrow \Upsilon(4S)$

$A_{CP}(B^+ \rightarrow K_S^0 \pi^+)$

VALUE	DOCUMENT ID	TECN	COMMENT
-0.017 ± 0.016 OUR AVERAGE			
$-0.022 \pm 0.025 \pm 0.010$	AAIJ	13Bs LHCb	pp at 7 TeV
$-0.011 \pm 0.021 \pm 0.006$	DUH	13 BELL	$e^+e^- \rightarrow \Upsilon(4S)$
$-0.029 \pm 0.039 \pm 0.010$	¹ AUBERT, BE	06c BABR	$e^+e^- \rightarrow \Upsilon(4S)$
0.18 ± 0.24	² CHEN	00 CLE2	$e^+e^- \rightarrow \Upsilon(4S)$

- • • We do not use the following data for averages, fits, limits, etc. • • •
 - $0.03 \pm 0.03 \pm 0.01$ LIN 07 BELL Repl. by DUH 13
 - $-0.09 \pm 0.05 \pm 0.01$ ³AUBERT, BE 05E BABR Repl. by AUBERT, BE 06c
 - $0.05 \pm 0.05 \pm 0.01$ ⁴CHAO 05A BELL Repl. by LIN 07
 - $-0.05 \pm 0.08 \pm 0.01$ ⁵AUBERT 04M BABR Repl. by AUBERT, BE 05E
 - $0.07 \pm 0.09 \pm 0.01$ ⁶UNNO 03 BELL Repl. by CHAO 05A
 - -0.08 ± 0.03 ⁷CASEY 02 BELL Repl. by UNNO 03
 - $0.46 \pm 0.15 \pm 0.02$ ⁸ABE 01K BELL Repl. by CASEY 02
 - $0.098 \pm 0.430 \pm 0.020$ ⁹AUBERT 01E BABR Repl. by AUBERT 04M
 - -0.343 ± 0.063
 - $-0.21 \pm 0.18 \pm 0.03$
- ¹ Corresponds to 90% confidence range $-0.092 < A_{CP} < 0.036$.
² Corresponds to 90% confidence range $-0.22 < A_{CP} < 0.56$.
³ Corresponds to 90% confidence range $-0.16 < A_{CP} < -0.02$.
⁴ Corresponds to 90% confidence range $-0.04 < A_{CP} < 0.13$.
⁵ Corresponds to 90% confidence range $-0.18 < A_{CP} < 0.08$.
⁶ Corresponds to 90% confidence range $-0.10 < A_{CP} < +0.22$.
⁷ Corresponds to 90% confidence range $+0.19 < A_{CP} < +0.72$.
⁸ Corresponds to 90% confidence range $-0.53 < A_{CP} < 0.82$.
⁹ Corresponds to 90% confidence range $-0.51 < A_{CP} < 0.09$.

$A_{CP}(B^+ \rightarrow K^+ \pi^0)$

VALUE	DOCUMENT ID	TECN	COMMENT
0.037 ± 0.021 OUR AVERAGE			
$0.043 \pm 0.024 \pm 0.002$	DUH	13 BELL	$e^+e^- \rightarrow \Upsilon(4S)$
$0.030 \pm 0.039 \pm 0.010$	AUBERT	07Bc BABR	$e^+e^- \rightarrow \Upsilon(4S)$
-0.29 ± 0.23	¹ CHEN	00 CLE2	$e^+e^- \rightarrow \Upsilon(4S)$

- • • We do not use the following data for averages, fits, limits, etc. • • •
 - $0.07 \pm 0.03 \pm 0.01$ LIN 08 BELL Repl. by DUH 13
 - $0.06 \pm 0.06 \pm 0.01$ ²AUBERT 05L BABR Repl. by AUBERT 07Bc
 - $0.06 \pm 0.06 \pm 0.02$ ²CHAO 05A BELL Repl. by CHAO 04B
 - $0.04 \pm 0.05 \pm 0.02$ ³CHAO 04B BELL Repl. by LIN 08
 - $-0.09 \pm 0.09 \pm 0.01$ ⁴AUBERT 03L BABR Repl. by AUBERT 05L
 - $-0.02 \pm 0.19 \pm 0.02$ ⁵CASEY 02 BELL Repl. by CHAO 04B
 - $-0.059 \pm 0.222 \pm 0.055$ ⁶ABE 01K BELL Repl. by CASEY 02
 - -0.196 ± 0.017
 - $0.00 \pm 0.18 \pm 0.04$ ⁷AUBERT 01E BABR Repl. by AUBERT 03L
- ¹ Corresponds to 90% confidence range $-0.67 < A_{CP} < 0.09$.
² Corresponds to a 90% CL interval of $-0.06 < A_{CP} < 0.18$.
³ Corresponds to 90% CL interval of $-0.05 < A_{CP} < 0.13$.
⁴ Corresponds to 90% confidence range $-0.24 < A_{CP} < 0.06$.
⁵ Corresponds to 90% confidence range $-0.35 < A_{CP} < +0.30$.
⁶ Corresponds to 90% confidence range $-0.40 < A_{CP} < 0.36$.
⁷ Corresponds to 90% confidence range $-0.30 < A_{CP} < +0.30$.

$A_{CP}(B^+ \rightarrow \eta' K^+)$

VALUE	DOCUMENT ID	TECN	COMMENT
0.004 ± 0.011 OUR AVERAGE			
$-0.002 \pm 0.012 \pm 0.006$	¹ AAIJ	15o LHCb	pp at 7, 8 TeV
$0.008 \pm 0.017 \pm 0.009$	AUBERT	09AV BABR	$e^+e^- \rightarrow \Upsilon(4S)$
$0.028 \pm 0.028 \pm 0.021$	SCHUEMANN	06 BELL	$e^+e^- \rightarrow \Upsilon(4S)$
0.03 ± 0.12	² CHEN	00 CLE2	$e^+e^- \rightarrow \Upsilon(4S)$

- • • We do not use the following data for averages, fits, limits, etc. • • •
 - $0.010 \pm 0.022 \pm 0.006$ AUBERT 07AE BABR Repl. by AUBERT 09AV
 - $0.033 \pm 0.028 \pm 0.005$ ³AUBERT 05M BABR Repl. by AUBERT 07AE
 - $0.037 \pm 0.045 \pm 0.011$ ⁴AUBERT 03W BABR Repl. by AUBERT 05M
 - $-0.11 \pm 0.11 \pm 0.02$ ⁵AUBERT 02E BABR Repl. by AUBERT 05M
 - $-0.015 \pm 0.070 \pm 0.009$ ⁶CHEN 02B BELL Repl. by SCHUEMANN 06
 - $0.06 \pm 0.15 \pm 0.01$ ⁷ABE 01M BELL Repl. by CHEN 02B
- ¹ Obtained using $A_{CP}(B^\pm \rightarrow J/\psi K^\pm) = (0.3 \pm 0.6) \times 10^{-2}$.
² Corresponds to 90% confidence range $-0.17 < A_{CP} < 0.23$.
³ Corresponds to 90% confidence range $-0.012 < A_{CP} < 0.078$.
⁴ Corresponds to 90% confidence range $-0.04 < A_{CP} < 0.11$.
⁵ Corresponds to 90% confidence range $-0.28 < A_{CP} < 0.07$.
⁶ Corresponds to 90% confidence range $-0.13 < A_{CP} < 0.10$.
⁷ Corresponds to 90% confidence range $-0.20 < A_{CP} < 0.32$.

$A_{CP}(B^+ \rightarrow \eta' K^*(892)^+)$

VALUE	DOCUMENT ID	TECN	COMMENT
$-0.26 \pm 0.27 \pm 0.02$	DEL-AMO-SA..10A	BABR	$e^+e^- \rightarrow \Upsilon(4S)$

- • • We do not use the following data for averages, fits, limits, etc. • • •
 - $-0.30 \pm 0.33 \pm 0.02$ ¹AUBERT 07E BABR Repl. by DEL-AMO-SANCHEZ 10A
- ¹ Reports A_{CP} with the opposite sign convention.

$A_{CP}(B^+ \rightarrow \eta' K_0^*(1430)^+)$

VALUE	DOCUMENT ID	TECN	COMMENT
$0.06 \pm 0.20 \pm 0.02$	DEL-AMO-SA..10A	BABR	$e^+e^- \rightarrow \Upsilon(4S)$

$A_{CP}(B^+ \rightarrow \eta' K_2^*(1430)^+)$

VALUE	DOCUMENT ID	TECN	COMMENT
$0.15 \pm 0.13 \pm 0.02$	DEL-AMO-SA..10A	BABR	$e^+e^- \rightarrow \Upsilon(4S)$

See key on page 999

Meson Particle Listings

 B^\pm $A_{CP}(B^+ \rightarrow \eta K^+)$

VALUE	DOCUMENT ID	TECN	COMMENT
-0.37 ± 0.08 OUR AVERAGE			
$-0.38 \pm 0.11 \pm 0.01$	HOI 12	BELL	$e^+ e^- \rightarrow \Upsilon(4S)$
$-0.36 \pm 0.11 \pm 0.03$	AUBERT 09AV	BABR	$e^+ e^- \rightarrow \Upsilon(4S)$
• • • We do not use the following data for averages, fits, limits, etc. • • •			
$-0.22 \pm 0.11 \pm 0.01$	AUBERT 07AE	BABR	Repl. by AUBERT 09AV
$-0.39 \pm 0.16 \pm 0.03$	CHANG 07B	BELL	Repl. by HOI 12
$-0.20 \pm 0.15 \pm 0.01$	AUBERT,B 05K	BABR	Repl. by AUBERT 07AE
$-0.49 \pm 0.31 \pm 0.07$	CHANG 05A	BELL	Repl. by CHANG 07B
$-0.52 \pm 0.24 \pm 0.01$	AUBERT 04H	BABR	Repl. by AUBERT,B 05K

 $A_{CP}(B^+ \rightarrow \eta K^*(892)^+)$

VALUE	DOCUMENT ID	TECN	COMMENT
0.02 ± 0.06 OUR AVERAGE			
$0.03 \pm 0.10 \pm 0.01$	WANG 07B	BELL	$e^+ e^- \rightarrow \Upsilon(4S)$
$0.01 \pm 0.08 \pm 0.02$	AUBERT,B 06H	BABR	$e^+ e^- \rightarrow \Upsilon(4S)$
• • • We do not use the following data for averages, fits, limits, etc. • • •			
$0.13 \pm 0.14 \pm 0.02$	AUBERT,B 04D	BABR	Repl. by AUBERT,B 06H

 $A_{CP}(B^+ \rightarrow \eta K_0^*(1430)^+)$

VALUE	DOCUMENT ID	TECN	COMMENT
$0.05 \pm 0.13 \pm 0.02$	AUBERT,B 06H	BABR	$e^+ e^- \rightarrow \Upsilon(4S)$

 $A_{CP}(B^+ \rightarrow \eta K_2^*(1430)^+)$

VALUE	DOCUMENT ID	TECN	COMMENT
$-0.45 \pm 0.30 \pm 0.02$	AUBERT,B 06H	BABR	$e^+ e^- \rightarrow \Upsilon(4S)$

 $A_{CP}(B^+ \rightarrow \omega K^+)$

VALUE	DOCUMENT ID	TECN	COMMENT
-0.02 ± 0.04 OUR AVERAGE			
$-0.03 \pm 0.04 \pm 0.01$	CHOBANOVA 14	BELL	$e^+ e^- \rightarrow \Upsilon(4S)$
$-0.01 \pm 0.07 \pm 0.01$	AUBERT 07AE	BABR	$e^+ e^- \rightarrow \Upsilon(4S)$
• • • We do not use the following data for averages, fits, limits, etc. • • •			
$0.05 \pm 0.09 \pm 0.01$	AUBERT,B 06E	BABR	Repl. by AUBERT 07AE
$0.05 \pm 0.08 \pm 0.01$	JEN 06	BELL	Repl. by CHOBANOVA 14
$-0.09 \pm 0.17 \pm 0.01$	AUBERT 04H	BABR	Repl. by AUBERT,B 06E
$0.06 \pm 0.21 \pm 0.01$	¹ WANG 04A	BELL	Repl. by JEN 06
$-0.21 \pm 0.28 \pm 0.03$	² LU 02	BELL	Repl. by WANG 04A

¹ Corresponds to 90% CL interval $0.15 < A_{CP} < 0.90$ ² Corresponds to 90% confidence range $-0.70 < A_{CP} < +0.38$. $A_{CP}(B^+ \rightarrow \omega K^{*+})$

VALUE	DOCUMENT ID	TECN	COMMENT
$+0.29 \pm 0.35 \pm 0.02$	AUBERT 09H	BABR	$e^+ e^- \rightarrow \Upsilon(4S)$

 $A_{CP}(B^+ \rightarrow \omega(K\pi)_0^{*+})$

VALUE	DOCUMENT ID	TECN	COMMENT
$-0.10 \pm 0.09 \pm 0.02$	AUBERT 09H	BABR	$e^+ e^- \rightarrow \Upsilon(4S)$

 $A_{CP}(B^+ \rightarrow \omega K_2^*(1430)^+)$

VALUE	DOCUMENT ID	TECN	COMMENT
$+0.14 \pm 0.15 \pm 0.02$	AUBERT 09H	BABR	$e^+ e^- \rightarrow \Upsilon(4S)$

 $A_{CP}(B^+ \rightarrow K^{*0} \pi^+)$

VALUE	DOCUMENT ID	TECN	COMMENT
-0.04 ± 0.09 OUR AVERAGE			Error includes scale factor of 2.1.
$-0.12 \pm 0.21 \pm 0.08$	¹ LEES 17G	BABR	$e^+ e^- \rightarrow \Upsilon(4S)$
$0.032 \pm 0.052 \pm 0.016$	AUBERT 08AI	BABR	$e^+ e^- \rightarrow \Upsilon(4S)$
$-0.149 \pm 0.064 \pm 0.022$	GARMASH 06	BELL	$e^+ e^- \rightarrow \Upsilon(4S)$
• • • We do not use the following data for averages, fits, limits, etc. • • •			
$0.068 \pm 0.078 \pm 0.070$	AUBERT,B 05N	BABR	Repl. by AUBERT 08AI

¹ Obtains the result from a Dalitz analysis of $B^+ \rightarrow K_S^0 \pi^+ \pi^0$ decays. The first error is statistical, the second combines all the systematic uncertainties reported in the paper, including signal modelling. $A_{CP}(B^+ \rightarrow K^*(892)^+ \pi^0)$

VALUE	DOCUMENT ID	TECN	COMMENT
-0.39 ± 0.21 OUR AVERAGE			Error includes scale factor of 1.6.
$-0.52 \pm 0.14 \pm 0.06$	¹ LEES 17G	BABR	$e^+ e^- \rightarrow \Upsilon(4S)$
$-0.06 \pm 0.24 \pm 0.04$	LEES 11I	BABR	$e^+ e^- \rightarrow \Upsilon(4S)$
• • • We do not use the following data for averages, fits, limits, etc. • • •			
$0.04 \pm 0.29 \pm 0.05$	AUBERT 05X	BABR	Repl. by LEES 11I

¹ Obtains the result from a Dalitz analysis of $B^+ \rightarrow K_S^0 \pi^+ \pi^0$ decays. The first error is statistical, the second combines all the systematic uncertainties reported in the paper, including signal modelling. $A_{CP}(B^+ \rightarrow K^+ \pi^- \pi^+)$

VALUE	DOCUMENT ID	TECN	COMMENT
0.027 ± 0.008 OUR AVERAGE			
$0.025 \pm 0.004 \pm 0.008$	¹ AAIJ 14B0	LHCB	pp at 7, 8 TeV
$0.028 \pm 0.020 \pm 0.023$	AUBERT 08AI	BABR	$e^+ e^- \rightarrow \Upsilon(4S)$
$0.049 \pm 0.026 \pm 0.020$	GARMASH 06	BELL	$e^+ e^- \rightarrow \Upsilon(4S)$
• • • We do not use the following data for averages, fits, limits, etc. • • •			
$0.032 \pm 0.008 \pm 0.008$	AAIJ 13AZ	LHCB	Repl. by AAIJ 14B0
$-0.013 \pm 0.037 \pm 0.011$	AUBERT,B 05N	BABR	Repl. by AUBERT 08AI
$0.01 \pm 0.07 \pm 0.03$	AUBERT 03M	BABR	Repl. by AUBERT,B 05N
¹ AAIJ 14B0 reports also CP asymmetries in restricted regions of phase space.			

 $A_{CP}(B^+ \rightarrow K^+ K^- K^+ \text{nonresonant})$

VALUE	DOCUMENT ID	TECN	COMMENT
$0.060 \pm 0.044 \pm 0.019$	LEES 12O	BABR	$e^+ e^- \rightarrow \Upsilon(4S)$

 $A_{CP}(B^+ \rightarrow f(980)^0 K^+)$

VALUE	DOCUMENT ID	TECN	COMMENT
$-0.08 \pm 0.08 \pm 0.04$	¹ LEES 12O	BABR	$e^+ e^- \rightarrow \Upsilon(4S)$
¹ Measured in the $B^+ \rightarrow K^+ K^- K^+$ decay.			

 $A_{CP}(B^+ \rightarrow f_2(1270) K^+)$

VALUE	DOCUMENT ID	TECN	COMMENT
-0.68 ± 0.19 OUR AVERAGE			
$-0.85 \pm 0.22 \pm 0.26$	AUBERT 08AI	BABR	$e^+ e^- \rightarrow \Upsilon(4S)$
$-0.59 \pm 0.22 \pm 0.036$	GARMASH 06	BELL	$e^+ e^- \rightarrow \Upsilon(4S)$

 $A_{CP}(B^+ \rightarrow f_0(1500) K^+)$

VALUE	DOCUMENT ID	TECN	COMMENT
$0.28 \pm 0.26 \pm 0.15$	AUBERT 08AI	BABR	$e^+ e^- \rightarrow \Upsilon(4S)$

 $A_{CP}(B^+ \rightarrow f_2'(1525)^0 K^+)$

VALUE	DOCUMENT ID	TECN	COMMENT
-0.08 ± 0.05 OUR AVERAGE			
$0.18 \pm 0.18 \pm 0.04$	¹ LEES 11I	BABR	$e^+ e^- \rightarrow \Upsilon(4S)$
$-0.106 \pm 0.050 \pm 0.036$	AUBERT 08AI	BABR	$e^+ e^- \rightarrow \Upsilon(4S)$
$-0.077 \pm 0.065 \pm 0.046$	GARMASH 06	BELL	$e^+ e^- \rightarrow \Upsilon(4S)$
• • • We do not use the following data for averages, fits, limits, etc. • • •			
$-0.14 \pm 0.10 \pm 0.04$	² LEES 12O	BABR	$e^+ e^- \rightarrow \Upsilon(4S)$
$-0.31 \pm 0.25 \pm 0.08$	³ AUBERT 06O	BABR	Repl. by LEES 12O
$0.088 \pm 0.095 \pm 0.097$	AUBERT,B 05N	BABR	Repl. by AUBERT 08AI

¹ Measured in $B^+ \rightarrow f_0 K^+$ with $f_0 \rightarrow \pi^0 \pi^0$ decay.² Measured in the $B^+ \rightarrow K^+ K^- K^+$ decay assuming $A_{CP}(B^+ \rightarrow f_2'(1525)^0 K^+) = A_{CP}(B^+ \rightarrow f_0(1500)^0 K^+) = A_{CP}(B^+ \rightarrow f_0(1710)^0 K^+)$ ³ Measured in the $B^+ \rightarrow K^+ K^- K^+$ decay. $A_{CP}(B^+ \rightarrow \rho^0 K^+)$

VALUE	DOCUMENT ID	TECN	COMMENT
0.37 ± 0.10 OUR AVERAGE			
$0.44 \pm 0.10 \pm 0.06$	AUBERT 08AI	BABR	$e^+ e^- \rightarrow \Upsilon(4S)$
$0.30 \pm 0.11 \pm 0.11$	GARMASH 06	BELL	$e^+ e^- \rightarrow \Upsilon(4S)$
• • • We do not use the following data for averages, fits, limits, etc. • • •			
$0.32 \pm 0.13 \pm 0.10$	AUBERT,B 05N	BABR	Repl. by AUBERT 08AI

 $A_{CP}(B^+ \rightarrow K^0 \pi^+ \pi^0)$

VALUE	DOCUMENT ID	TECN	COMMENT
$0.07 \pm 0.05 \pm 0.04$	¹ LEES 17G	BABR	$e^+ e^- \rightarrow \Upsilon(4S)$
¹ Obtains the result from a Dalitz analysis of $B^+ \rightarrow K_S^0 \pi^+ \pi^0$ decays. The first error is statistical, the second combines all the systematic uncertainties reported in the paper, including signal modelling.			

 $A_{CP}(B^+ \rightarrow K_0^*(1430)^0 \pi^+)$

VALUE	DOCUMENT ID	TECN	COMMENT
0.061 ± 0.032 OUR AVERAGE			
$0.14 \pm 0.10 \pm 0.14$	¹ LEES 17G	BABR	$e^+ e^- \rightarrow \Upsilon(4S)$
$0.032 \pm 0.035 \pm 0.034$	AUBERT 08AI	BABR	$e^+ e^- \rightarrow \Upsilon(4S)$
$0.076 \pm 0.038 \pm 0.028$	GARMASH 06	BELL	$e^+ e^- \rightarrow \Upsilon(4S)$
• • • We do not use the following data for averages, fits, limits, etc. • • •			
$-0.064 \pm 0.032 \pm 0.023$	AUBERT,B 05N	BABR	Repl. by AUBERT 08AI
¹ Obtains the result from a Dalitz analysis of $B^+ \rightarrow K_S^0 \pi^+ \pi^0$ decays. The first error is statistical, the second combines all the systematic uncertainties reported in the paper, including signal modelling.			

$A_{CP}(B^+ \rightarrow \phi K^*(892)^+)$

VALUE	DOCUMENT ID	TECN	COMMENT
-0.01 ± 0.08 OUR AVERAGE			
0.00 ± 0.09 ± 0.04	AUBERT	07BA BABR	$e^+ e^- \rightarrow \Upsilon(4S)$
-0.02 ± 0.14 ± 0.03	1 CHEN	05A BELL	$e^+ e^- \rightarrow \Upsilon(4S)$
••• We do not use the following data for averages, fits, limits, etc. •••			
0.16 ± 0.17 ± 0.03	AUBERT	03v BABR	Repl. by AUBERT 07Ba
-0.13 ± 0.29 ^{+0.08} / _{-0.11}	2 CHEN	03B BELL	Repl. by CHEN 05A
-0.43 ± 0.36 ^{+0.06} / _{-0.30}	3 AUBERT	02E BABR	Repl. by AUBERT 03v
1 Corresponds to 90% confidence range $-0.25 < A_{CP} < 0.22$.			
2 Corresponds to 90% confidence range $-0.64 < A_{CP} < 0.36$.			
3 Corresponds to 90% confidence range $-0.88 < A_{CP} < 0.18$.			

$A_{CP}(B^+ \rightarrow \phi(K\pi)_0^{*+})$

VALUE	DOCUMENT ID	TECN	COMMENT
0.04 ± 0.15 ± 0.04			
	AUBERT	08B1 BABR	$e^+ e^- \rightarrow \Upsilon(4S)$

$A_{CP}(B^+ \rightarrow \phi K_1(1270)^+)$

VALUE	DOCUMENT ID	TECN	COMMENT
0.15 ± 0.19 ± 0.05			
	AUBERT	08B1 BABR	$e^+ e^- \rightarrow \Upsilon(4S)$

$A_{CP}(B^+ \rightarrow \phi K_2^*(1430)^+)$

VALUE	DOCUMENT ID	TECN	COMMENT
-0.23 ± 0.19 ± 0.06			
	AUBERT	08B1 BABR	$e^+ e^- \rightarrow \Upsilon(4S)$

$A_{CP}(B^+ \rightarrow K^+ \phi\phi)$

VALUE	DOCUMENT ID	TECN	COMMENT
-0.10 ± 0.08 ± 0.02			
	1 LEES	11A BABR	$e^+ e^- \rightarrow \Upsilon(4S)$
1 $m_{\phi\phi} < 2.85 \text{ GeV}/c^2$.			

$A_{CP}(B^+ \rightarrow K^+[\phi\phi]_{\eta_c})$

VALUE	DOCUMENT ID	TECN	COMMENT
0.09 ± 0.10 ± 0.02			
	1 LEES	11A BABR	$e^+ e^- \rightarrow \Upsilon(4S)$
1 $m_{\phi\phi}$ is consistent with η_c mass $[2.94, 3.02] \text{ GeV}/c^2$.			

$A_{CP}(B^+ \rightarrow K^*(892)^+ \gamma)$

VALUE	DOCUMENT ID	TECN	COMMENT
0.014 ± 0.018 OUR AVERAGE			
0.011 ± 0.023 ± 0.003	1 HORIGUCHI	17 BELL	$e^+ e^- \rightarrow \Upsilon(4S)$
0.018 ± 0.028 ± 0.007	AUBERT	09A0 BABR	$e^+ e^- \rightarrow \Upsilon(4S)$
1 Uses $B(\Upsilon(4S) \rightarrow B^+ B^-) = (51.4 \pm 0.6)\%$ and $B(\Upsilon(4S) \rightarrow B^0 \bar{B}^0) = (48.6 \pm 0.6)\%$.			

$A_{CP}(B^+ \rightarrow X_s \gamma)$

VALUE	DOCUMENT ID	TECN	COMMENT
0.0275 ± 0.0184 ± 0.0032			
	1 WATA NUKI	19 BELL	$e^+ e^- \rightarrow \Upsilon(4S)$
1 Using a sum-of-exclusive technique with $m_{X_s} < 2.8 \text{ GeV}/c^2$.			

$A_{CP}(B^+ \rightarrow \eta K^+ \gamma)$

VALUE	DOCUMENT ID	TECN	COMMENT
-0.12 ± 0.07 OUR AVERAGE			
-0.09 ± 0.10 ± 0.01	1 AUBERT	09 BABR	$e^+ e^- \rightarrow \Upsilon(4S)$
-0.16 ± 0.09 ± 0.06	2 NISHIDA	05 BELL	$e^+ e^- \rightarrow \Upsilon(4S)$
••• We do not use the following data for averages, fits, limits, etc. •••			
-0.09 ± 0.12 ± 0.01	1 AUBERT,B	06M BABR	Repl. by AUBERT 09
1 $m_{\eta K} < 3.25 \text{ GeV}/c^2$.			
2 $m_{\eta K} < 2.4 \text{ GeV}/c^2$.			

$A_{CP}(B^+ \rightarrow \phi K^+ \gamma)$

VALUE	DOCUMENT ID	TECN	COMMENT
-0.13 ± 0.11 OUR AVERAGE Error includes scale factor of 1.1.			
-0.03 ± 0.11 ± 0.08	SAHO0	11A BELL	$e^+ e^- \rightarrow \Upsilon(4S)$
-0.26 ± 0.14 ± 0.05	AUBERT	07Q BABR	$e^+ e^- \rightarrow \Upsilon(4S)$

$A_{CP}(B^+ \rightarrow \rho^+ \gamma)$

VALUE	DOCUMENT ID	TECN	COMMENT
-0.11 ± 0.32 ± 0.09			
	TANIGUCHI	08 BELL	$e^+ e^- \rightarrow \Upsilon(4S)$

$A_{CP}(B^+ \rightarrow \pi^+ \pi^0)$

VALUE	DOCUMENT ID	TECN	COMMENT
0.03 ± 0.04 OUR AVERAGE			
0.025 ± 0.043 ± 0.007	DUH	13 BELL	$e^+ e^- \rightarrow \Upsilon(4S)$
0.03 ± 0.08 ± 0.01	AUBERT	07Bc BABR	$e^+ e^- \rightarrow \Upsilon(4S)$
••• We do not use the following data for averages, fits, limits, etc. •••			
0.07 ± 0.06 ± 0.01	LIN	08 BELL	Repl. by DUH 13
-0.01 ± 0.10 ± 0.02	1 AUBERT	05L BABR	Repl. by AUBERT 07Bc
-0.00 ± 0.10 ± 0.02	2 CHAO	05A BELL	Repl. by CHAO 04B
-0.02 ± 0.10 ± 0.01	3 CHAO	04B BELL	Repl. by LIN 08
-0.03 ± 0.18 ^{+0.02} / _{-0.17}	4 AUBERT	03L BABR	Repl. by AUBERT 05L
0.30 ± 0.30 ± 0.06 ^{+0.06} / _{-0.04}	5 CASEY	02 BELL	Repl. by CHAO 04B

1 Corresponds to a 90% CL interval of $-0.19 < A_{CP} < 0.21$.
 2 Corresponds to a 90% CL interval of $-0.17 < A_{CP} < 0.16$.
 3 This corresponds to 90% CL interval of $-0.18 < A_{CP} < 0.14$.
 4 Corresponds to 90% confidence range $-0.32 < A_{CP} < 0.27$.
 5 Corresponds to 90% confidence range $-0.23 < A_{CP} < +0.86$.

$A_{CP}(B^+ \rightarrow \pi^+ \pi^- \pi^+)$

VALUE	DOCUMENT ID	TECN	COMMENT
0.057 ± 0.013 OUR AVERAGE			
0.058 ± 0.008 ± 0.011	1 AAIJ	14B0 LHCB	pp at 7, 8 TeV
0.032 ± 0.044 ^{+0.040} / _{-0.037}	AUBERT	09L BABR	$e^+ e^- \rightarrow \Upsilon(4S)$
••• We do not use the following data for averages, fits, limits, etc. •••			
0.117 ± 0.021 ± 0.011	2 AAIJ	14 LHCB	Repl. by AAIJ 14B0
-0.007 ± 0.077 ± 0.025	AUBERT,B	05G BABR	Repl. by AUBERT 09L
-0.39 ± 0.33 ± 0.12	AUBERT	03M BABR	Repl. by AUBERT 05G
1 AAIJ 14B0 reports also CP asymmetries in restricted regions of phase space.			
2 AAIJ 14 reports $A_{CP}(B^+ \rightarrow \pi^+ \pi^- \pi^+) = 0.584 \pm 0.082 \pm 0.027 \pm 0.007$ in the Dalitz plot region of $m_{\pi^+ \pi^-}^2 > 15 \text{ GeV}^2/c^4$ or $m_{\pi^+ \pi^-}^2 < 0.4 \text{ GeV}^2/c^4$. The third uncertainty is due to the CP asymmetry of the $B^\pm \rightarrow J/\psi K^\pm$ reference mode uncertainty.			

$A_{CP}(B^+ \rightarrow \rho^0 \pi^+)$

VALUE	DOCUMENT ID	TECN	COMMENT
0.009 ± 0.019 OUR AVERAGE			
0.007 ± 0.011 ± 0.016	1 AAIJ	20A LHCB	pp at 7, 8 TeV
0.18 ± 0.07 ^{+0.05} / _{-0.15}	AUBERT	09L BABR	$e^+ e^- \rightarrow \Upsilon(4S)$
••• We do not use the following data for averages, fits, limits, etc. •••			
-0.074 ± 0.120 ^{+0.035} / _{-0.055}	AUBERT,B	05G BABR	Repl. by AUBERT 09L
-0.19 ± 0.11 ± 0.02	AUBERT	04Z BABR	Repl. by AUBERT,B 05G
1 This result is obtained with an amplitude analysis of $B^+ \rightarrow \pi^+ \pi^+ \pi^-$ decays, using the isobar model within the mass range $1.0 < m(\pi^+ \pi^-) < 1.5 \text{ GeV}$ to describe the $\pi^+ \pi^-$ S-wave contribution.			

$A_{CP}(B^+ \rightarrow f_2(1270) \pi^+)$

VALUE	DOCUMENT ID	TECN	COMMENT
0.40 ± 0.06 OUR AVERAGE			
0.468 ± 0.061 ± 0.046	1 AAIJ	20A LHCB	pp at 7, 8 TeV
0.267 ± 0.102 ± 0.048	2 AAIJ	19AL LHCB	pp at 7, 8 TeV
0.41 ± 0.25 ^{+0.18} / _{-0.15}	AUBERT	09L BABR	$e^+ e^- \rightarrow \Upsilon(4S)$
••• We do not use the following data for averages, fits, limits, etc. •••			
-0.004 ± 0.247 ^{+0.028} / _{-0.032}	AUBERT,B	05G BABR	Repl. by AUBERT 09L

1 This result is obtained with an amplitude analysis of $B^+ \rightarrow \pi^+ \pi^+ \pi^-$ decays, using the isobar model within the mass range $1.0 < m(\pi^+ \pi^-) < 1.5 \text{ GeV}$ to describe the $\pi^+ \pi^-$ S-wave contribution.
 2 Uses amplitude analysis of $B^\pm \rightarrow \pi^\pm K^+ K^-$ decays.

$A_{CP}(B^+ \rightarrow \rho^0(1450) \pi^+)$

VALUE	DOCUMENT ID	TECN	COMMENT
-0.11 ± 0.05 OUR AVERAGE			
-0.129 ± 0.033 ± 0.359	1 AAIJ	20A LHCB	pp at 7, 8 TeV
-0.109 ± 0.044 ± 0.024	2 AAIJ	19AL LHCB	pp at 7, 8 TeV
-0.06 ± 0.28 ^{+0.23} / _{-0.40}	AUBERT	09L BABR	$e^+ e^- \rightarrow \Upsilon(4S)$
1 This result is obtained with an amplitude analysis of $B^+ \rightarrow \pi^+ \pi^+ \pi^-$ decays, using the isobar model within the mass range $1.0 < m(\pi^+ \pi^-) < 1.5 \text{ GeV}$ to describe the $\pi^+ \pi^-$ S-wave contribution.			
2 Uses amplitude analysis of $B^\pm \rightarrow \pi^\pm K^+ K^-$ decays.			

$A_{CP}(B^+ \rightarrow \rho_3(1690) \pi^+)$

VALUE	DOCUMENT ID	TECN	COMMENT
-0.801 ± 0.114 ± 0.253			
	1 AAIJ	20A LHCB	pp at 7, 8 TeV
1 This result is obtained with an amplitude analysis of $B^+ \rightarrow \pi^+ \pi^+ \pi^-$ decays, using the isobar model within the mass range $1.0 < m(\pi^+ \pi^-) < 1.5 \text{ GeV}$ to describe the $\pi^+ \pi^-$ S-wave contribution.			

$A_{CP}(B^+ \rightarrow f_0(1370) \pi^+)$

VALUE	DOCUMENT ID	TECN	COMMENT
0.72 ± 0.15 ± 0.16			
	AUBERT	09L BABR	$e^+ e^- \rightarrow \Upsilon(4S)$

$A_{CP}(B^+ \rightarrow \pi^+ \pi^- \pi^+ \text{ nonresonant})$

VALUE	DOCUMENT ID	TECN	COMMENT
-0.14 ± 0.14 ± 0.18 ^{+0.18} / _{-0.08}			
	AUBERT	09L BABR	$e^+ e^- \rightarrow \Upsilon(4S)$

$A_{CP}(B^+ \rightarrow \rho^+ \pi^0)$

VALUE	DOCUMENT ID	TECN	COMMENT
0.02 ± 0.11 OUR AVERAGE			
-0.01 ± 0.13 ± 0.02	AUBERT	07X BABR	$e^+ e^- \rightarrow \Upsilon(4S)$
0.06 ± 0.17 ^{+0.04} / _{-0.05}	ZHANG	05A BELL	$e^+ e^- \rightarrow \Upsilon(4S)$
••• We do not use the following data for averages, fits, limits, etc. •••			
0.24 ± 0.16 ± 0.06	AUBERT	04Z BABR	Repl. by AUBERT 07X

$A_{CP}(B^+ \rightarrow \rho^+ \rho^0)$

VALUE	DOCUMENT ID	TECN	COMMENT
-0.05 ± 0.05 OUR AVERAGE			
-0.054 ± 0.055 ± 0.010	AUBERT	09G BABR	$e^+ e^- \rightarrow \Upsilon(4S)$
0.00 ± 0.22 ± 0.03	ZHANG	03B BELL	$e^+ e^- \rightarrow \Upsilon(4S)$
••• We do not use the following data for averages, fits, limits, etc. •••			
-0.12 ± 0.13 ± 0.10	AUBERT,BE	06G BABR	Repl. by AUBERT 09G
-0.19 ± 0.23 ± 0.03	AUBERT	03v BABR	Repl. by AUBERT,BE 06G

Meson Particle Listings

 B^\pm $A_{CP}(B^+ \rightarrow \omega\pi^+)$

VALUE	DOCUMENT ID	TECN	COMMENT
-0.04 ± 0.05 OUR AVERAGE			
$-0.048 \pm 0.065 \pm 0.038$	¹ AAIJ	20A	LHCB pp at 7, 8 TeV
$-0.02 \pm 0.08 \pm 0.01$	AUBERT	07AE	BABR $e^+e^- \rightarrow \Upsilon(4S)$
$-0.02 \pm 0.09 \pm 0.01$	JEN	06	BELL $e^+e^- \rightarrow \Upsilon(4S)$
-0.34 ± 0.25	² CHEN	00	CLE2 $e^+e^- \rightarrow \Upsilon(4S)$
• • • We do not use the following data for averages, fits, limits, etc. • • •			
$-0.01 \pm 0.10 \pm 0.01$	AUBERT,B	06E	BABR Repl. by AUBERT 07AE
$0.03 \pm 0.16 \pm 0.01$	AUBERT	04H	BABR Repl. by AUBERT,B 06E
$0.50 \pm 0.23 \pm 0.02$	³ WANG	04A	BELL Repl. by JEN 06
$-0.01 \pm 0.29 \pm 0.03$	⁴ AUBERT	02E	BABR Repl. by AUBERT 04H

¹This result is obtained with an amplitude analysis of $B^+ \rightarrow \pi^+\pi^+\pi^-$ decays, using the isobar model within the mass range $1.0 < m(\pi^+\pi^-) < 1.5$ GeV to describe the $\pi^+\pi^-$ S-wave contribution.

²Corresponds to 90% confidence range $-0.75 < A_{CP} < 0.07$.

³Corresponds to 90% CL interval $-0.25 < A_{CP} < 0.41$

⁴Corresponds to 90% confidence range $-0.50 < A_{CP} < 0.46$.

 $A_{CP}(B^+ \rightarrow \omega\rho^+)$

VALUE	DOCUMENT ID	TECN	COMMENT
$-0.20 \pm 0.09 \pm 0.02$	AUBERT	09H	BABR $e^+e^- \rightarrow \Upsilon(4S)$
• • • We do not use the following data for averages, fits, limits, etc. • • •			
$0.04 \pm 0.18 \pm 0.02$	AUBERT,B	06T	BABR Repl. by AUBERT 09H
$0.05 \pm 0.26 \pm 0.02$	AUBERT	05o	BABR Repl. by AUBERT,B 06T

 $A_{CP}(B^+ \rightarrow \eta\pi^+)$

VALUE	DOCUMENT ID	TECN	COMMENT
-0.14 ± 0.07 OUR AVERAGE			Error includes scale factor of 1.4.
$-0.19 \pm 0.06 \pm 0.01$	HOI	12	BELL $e^+e^- \rightarrow \Upsilon(4S)$
$-0.03 \pm 0.09 \pm 0.03$	AUBERT	09AV	BABR $e^+e^- \rightarrow \Upsilon(4S)$
• • • We do not use the following data for averages, fits, limits, etc. • • •			
$-0.08 \pm 0.10 \pm 0.01$	AUBERT	07AE	BABR Repl. by AUBERT 09AV
$-0.23 \pm 0.09 \pm 0.02$	CHANG	07B	BELL Repl. by HOI 12
$-0.13 \pm 0.12 \pm 0.01$	AUBERT,B	05K	BABR Repl. by AUBERT 07AE
$0.07 \pm 0.15 \pm 0.03$	CHANG	05A	BELL Repl. by CHANG 07B
$-0.44 \pm 0.18 \pm 0.01$	AUBERT	04H	BABR Repl. by AUBERT,B 05K

 $A_{CP}(B^+ \rightarrow \eta\rho^+)$

VALUE	DOCUMENT ID	TECN	COMMENT
0.11 ± 0.11 OUR AVERAGE			
$0.13 \pm 0.11 \pm 0.02$	AUBERT	08AH	BABR $e^+e^- \rightarrow \Upsilon(4S)$
$-0.04 \pm 0.34 \pm 0.01$	WANG	07B	BELL $e^+e^- \rightarrow \Upsilon(4S)$
• • • We do not use the following data for averages, fits, limits, etc. • • •			
$0.02 \pm 0.18 \pm 0.02$	AUBERT,B	05K	BABR Repl. by AUBERT 08AH

 $A_{CP}(B^+ \rightarrow \eta'\pi^+)$

VALUE	DOCUMENT ID	TECN	COMMENT
0.06 ± 0.16 OUR AVERAGE			
$0.03 \pm 0.17 \pm 0.02$	AUBERT	09AV	BABR $e^+e^- \rightarrow \Upsilon(4S)$
$0.20 \pm 0.37 \pm 0.04$	SCHUEMANN	06	BELL $e^+e^- \rightarrow \Upsilon(4S)$
• • • We do not use the following data for averages, fits, limits, etc. • • •			
$0.21 \pm 0.17 \pm 0.01$	AUBERT	07AE	BABR Repl. by AUBERT 09AV
$0.14 \pm 0.16 \pm 0.01$	AUBERT,B	05K	BABR Repl. by AUBERT 07AE

 $A_{CP}(B^+ \rightarrow \eta'\rho^+)$

VALUE	DOCUMENT ID	TECN	COMMENT
$0.26 \pm 0.17 \pm 0.02$	DEL-AMO-SA...10A	BABR	$e^+e^- \rightarrow \Upsilon(4S)$
• • • We do not use the following data for averages, fits, limits, etc. • • •			
$0.04 \pm 0.28 \pm 0.02$	¹ AUBERT	07E	BABR Repl. by DEL-AMO-SANCHEZ 10A

¹Reports A_{CP} with the opposite sign convention.

 $A_{CP}(B^+ \rightarrow b_1^0\pi^+)$

VALUE	DOCUMENT ID	TECN	COMMENT
$+0.05 \pm 0.16 \pm 0.02$	AUBERT	07Bi	BABR $e^+e^- \rightarrow \Upsilon(4S)$

 $A_{CP}(B^+ \rightarrow \rho\bar{\rho}\pi^+)$

VALUE	DOCUMENT ID	TECN	COMMENT
0.00 ± 0.04 OUR AVERAGE			
$-0.02 \pm 0.05 \pm 0.02$	¹ WEI	08	BELL $e^+e^- \rightarrow \Upsilon(4S)$
$+0.04 \pm 0.07 \pm 0.04$	AUBERT	07AV	BABR $e^+e^- \rightarrow \Upsilon(4S)$
• • • We do not use the following data for averages, fits, limits, etc. • • •			
$-0.16 \pm 0.22 \pm 0.01$	WANG	04	BELL Repl. by WEI 08

¹Requires $m_{p\bar{p}} < 2.85$ GeV/c².

 $A_{CP}(B^+ \rightarrow \rho\bar{p}K^+)$

VALUE	DOCUMENT ID	TECN	COMMENT
0.00 ± 0.04 OUR AVERAGE			Error includes scale factor of 2.2.
$0.021 \pm 0.020 \pm 0.004$	¹ AAIJ	14AF	LHCB pp at 7, 8 TeV
$-0.17 \pm 0.10 \pm 0.02$	¹ WEI	08	BELL $e^+e^- \rightarrow \Upsilon(4S)$
$-0.16 \pm 0.07 \pm 0.04$	¹ AUBERT,B	05L	BABR $e^+e^- \rightarrow \Upsilon(4S)$
• • • We do not use the following data for averages, fits, limits, etc. • • •			
$-0.047 \pm 0.036 \pm 0.007$	¹ AAIJ	13AU	LHCB Repl. by AAIJ 14AF
$-0.05 \pm 0.11 \pm 0.01$	WANG	04	BELL Repl. by WEI 08
¹ Requires $m_{p\bar{p}} < 2.85$ GeV/c ² .			

 $A_{CP}(B^+ \rightarrow \rho\bar{p}K^*(892)^+)$

VALUE	DOCUMENT ID	TECN	COMMENT
0.21 ± 0.16 OUR AVERAGE			Error includes scale factor of 1.4.
$-0.01 \pm 0.19 \pm 0.02$	CHEN	08c	BELL $e^+e^- \rightarrow \Upsilon(4S)$
$+0.32 \pm 0.13 \pm 0.05$	AUBERT	07AV	BABR $e^+e^- \rightarrow \Upsilon(4S)$

 $A_{CP}(B^+ \rightarrow \rho\bar{\Lambda}\gamma)$

VALUE	DOCUMENT ID	TECN	COMMENT
$+0.17 \pm 0.16 \pm 0.05$	WANG	07c	BELL $e^+e^- \rightarrow \Upsilon(4S)$

 $A_{CP}(B^+ \rightarrow \rho\bar{\Lambda}\pi^0)$

VALUE	DOCUMENT ID	TECN	COMMENT
$+0.01 \pm 0.17 \pm 0.04$	WANG	07c	BELL $e^+e^- \rightarrow \Upsilon(4S)$

 $A_{CP}(B^+ \rightarrow K^+\ell^+\ell^-)$

VALUE	DOCUMENT ID	TECN	COMMENT
-0.02 ± 0.08 OUR AVERAGE			
$-0.03 \pm 0.14 \pm 0.01$	¹ LEES	12s	BABR $e^+e^- \rightarrow \Upsilon(4S)$
$-0.18 \pm 0.18 \pm 0.01$	AUBERT	09T	BABR $e^+e^- \rightarrow \Upsilon(4S)$
$+0.04 \pm 0.10 \pm 0.02$	WEI	09A	BELL $e^+e^- \rightarrow \Upsilon(4S)$
• • • We do not use the following data for averages, fits, limits, etc. • • •			
$-0.07 \pm 0.22 \pm 0.02$	AUBERT,B	06j	BABR Repl. by AUBERT 09T
¹ Measured in the union of $0.10 < q^2 < 8.12$ GeV ² /c ⁴ and $q^2 > 10.11$ GeV ² /c ⁴ . LEES 12s reports also individual measurements $A_{CP}(B^+ \rightarrow K^+\ell^+\ell^-) = 0.02 \pm 0.18 \pm 0.01$ for $0.10 < q^2 < 8.12$ GeV ² /c ⁴ and $A_{CP}(B^+ \rightarrow K^+\ell^+\ell^-) = -0.06 \pm 0.22 \pm 0.01$ for $q^2 > 10.11$ GeV ² /c ⁴ .			

 $A_{CP}(B^+ \rightarrow K^+e^+e^-)$

VALUE	DOCUMENT ID	TECN	COMMENT
$+0.14 \pm 0.14 \pm 0.03$	WEI	09A	BELL $e^+e^- \rightarrow \Upsilon(4S)$

 $A_{CP}(B^+ \rightarrow K^+\mu^+\mu^-)$

VALUE	DOCUMENT ID	TECN	COMMENT
0.011 ± 0.017 OUR AVERAGE			
$0.012 \pm 0.017 \pm 0.001$	AAIJ	14AN	LHCB pp at 7, 8 TeV
$-0.05 \pm 0.13 \pm 0.03$	WEI	09A	BELL $e^+e^- \rightarrow \Upsilon(4S)$
• • • We do not use the following data for averages, fits, limits, etc. • • •			
$0.000 \pm 0.033 \pm 0.009$	AAIJ	13BN	LHCB Repl. by AAIJ 14AN

 $A_{CP}(B^+ \rightarrow \pi^+\mu^+\mu^-)$

VALUE	DOCUMENT ID	TECN	COMMENT
$-0.11 \pm 0.12 \pm 0.01$	AAIJ	15AR	LHCB pp at 7, 8 TeV

 $A_{CP}(B^+ \rightarrow K^*+\ell^+\ell^-)$

VALUE	DOCUMENT ID	TECN	COMMENT
-0.09 ± 0.14 OUR AVERAGE			
$0.01 \pm 0.26 \pm 0.02$	AUBERT	09T	BABR $e^+e^- \rightarrow \Upsilon(4S)$
$-0.13 \pm 0.17 \pm 0.01$	WEI	09A	BELL $e^+e^- \rightarrow \Upsilon(4S)$
• • • We do not use the following data for averages, fits, limits, etc. • • •			
$0.03 \pm 0.23 \pm 0.03$	AUBERT,B	06j	BABR Repl. by AUBERT 09T

 $A_{CP}(B^+ \rightarrow K^*e^+e^-)$

VALUE	DOCUMENT ID	TECN	COMMENT
$-0.14 \pm 0.23 \pm 0.02$	WEI	09A	BELL $e^+e^- \rightarrow \Upsilon(4S)$

 $A_{CP}(B^+ \rightarrow K^*\mu^+\mu^-)$

VALUE	DOCUMENT ID	TECN	COMMENT
$-0.12 \pm 0.24 \pm 0.02$	WEI	09A	BELL $e^+e^- \rightarrow \Upsilon(4S)$

CP VIOLATION PARAMETERS IN $B^+ \rightarrow DK^+$ AND SIMILAR DECAYS

The parameters r_{B^+} and δ_{B^+} are the magnitude ratio and strong phase difference between the amplitudes of $A(B^+ \rightarrow \bar{D}^{(*)0}K^{(*)+})$ and $A(B^+ \rightarrow D^{(*)0}K^{(*)-})$. The measured observables are defined as $x_\pm = r_{B^+} \cos(\delta_{B^+} \pm \gamma)$ and $y_\pm = r_{B^+} \sin(\delta_{B^+} \pm \gamma)$, and can be used to measure the CKM angle γ .

"OUR EVALUATION" is provided by the Heavy Flavor Averaging Group (HFLAV). It is derived from combinations of their results on $B^+ \rightarrow DK^+$ and related processes.

7 For angle γ(φ3) of the CKM unitarity triangle, see the review on “CP Violation” in the Reviews section.

“OUR EVALUATION” is provided by the Heavy Flavor Averaging Group (HFLAV).

Table with 5 columns: VALUE (°), CL%, DOCUMENT ID, TECN, COMMENT. Row 1: 71.1+4.6 / -5.3 OUR EVALUATION. Rows 2-26: Data points for various experiments like RESMI, AAIJ, LHCb, Belle, etc.

- 1 Uses binned analysis of D → K_S^0 π^+ π^- π^0 from B± → DK± modes over the phase space.
2 Uses binned Dalitz plot analysis of D → K_S^0 π^+ π^- and K_S^0 K^+ K^- from B± → DK± modes.
3 Measured in B_S^0 → D_S^∓ K± decays, constraining -2β_S by the measurement of φ_S = 0.030 ± 0.033 from HFLAV.
... 26 POLUEKTOV 04 BELL Repl. by POLUEKTOV 06

- 15 Reports combination of published measurements using GGSZ, GLW, and ADS methods.
16 Reports combined statistical and systematic uncertainties.
17 Uses binned Dalitz plot of D^0 → K_S^0 π^+ π^- decays from B^+ → D^0 K^+.
... 26 Uses a Dalitz plot analysis of the 3-body D → K_S^0 π^+ π^- decays coming from B± → DK± and B± → D*K± followed by D* → Dπ^0.

r_B(B^+ → D^0 K^+) r_B and δ_B are the amplitude ratio and relative strong phase between the amplitudes of A(B^+ → D^0 K^+) and A(B^+ → D^0 K^+).

“OUR EVALUATION” is provided by the Heavy Flavor Averaging Group (HFLAV).

Table with 5 columns: VALUE, CL%, DOCUMENT ID, TECN, COMMENT. Row 1: 0.0993±0.0046 OUR EVALUATION. Rows 2-16: Data points for various experiments like RESMI, AAIJ, LHCb, Belle, etc.

- 1 Uses binned analysis of D → K_S^0 π^+ π^- π^0 from B± → DK± modes over the phase space.
2 Uses binned Dalitz plot analysis of D → K_S^0 π^+ π^- and K_S^0 K^+ K^- from B± → DK± modes.
3 Uses binned Dalitz plot analysis of B^+ → DK^+ decays, with D → K_S^0 π^+ π^- and D → K_S^0 K^+ K^-.
... 16 AUBERT,B 05Y BABR Repl. by AUBERT 08AL

Meson Particle Listings

 B^\pm

⁹We combined the systematics in quadrature. The authors report separately the contribution to the systematic uncertainty due to the uncertainty on the bin-averaged strong phase difference between D^0 and \bar{D}^0 amplitudes.

- ¹⁰Uses decays of neutral D to $K^-\pi^+\pi^0$.
- ¹¹Uses Dalitz plot analysis of $\bar{D}^0 \rightarrow K_S^0\pi^+\pi^-$, $K_S^0K^+K^-$ decays from $B^+ \rightarrow D^{(*)}K^{(*)+}$ modes. The corresponding two standard deviation interval is $0.037 < r_B < 0.155$.
- ¹²Uses the Cabibbo suppressed decay of $B^+ \rightarrow \bar{D}^0K^+$ followed by $\bar{D}^0 \rightarrow K^-\pi^+$.
- ¹³Uses Dalitz plot analysis of $\bar{D}^0 \rightarrow K_S^0\pi^+\pi^-$ decays from $B^+ \rightarrow D^0K^+$ modes. The corresponding two standard deviation interval is $0.084 < r_B < 0.239$.
- ¹⁴Uses Dalitz plot analysis of $\bar{D}^0 \rightarrow K_S^0\pi^+\pi^-$ and $\bar{D}^0 \rightarrow K_S^0K^+K^-$ decays coming from $B^\pm \rightarrow D^{(*)}K^{(*)\pm}$ modes.
- ¹⁵Uses a Dalitz plot analysis of the $\bar{D}^0 \rightarrow K_S^0\pi^+\pi^-$ decays; Combines the DK^+ , D^*K^+ and DK^{*+} modes.
- ¹⁶Uses a Dalitz analysis of neutral D decays to $K_S^0\pi^+\pi^-$ in the processes $B^\pm \rightarrow D^{(*)}K^\pm$, $D^* \rightarrow D\pi^0$, $D\gamma$.

 $\delta_B(B^+ \rightarrow D^0K^+)$

"OUR EVALUATION" is provided by the Heavy Flavor Averaging Group (HFLAV).

VALUE (°)	DOCUMENT ID	TECN	COMMENT
-----------	-------------	------	---------

129.6^{+5.0}_{-6.0} OUR EVALUATION

• • • We do not use the following data for averages, fits, limits, etc. • • •			
83.4 ^{+18.3} _{-16.6} ± 5.1	¹ RESMI	19 BELL	$e^+e^- \rightarrow \Upsilon(4S)$
101 ± 11	² AAIJ	18AD LHCb	pp at 13 TeV
134 ⁺¹⁴ ₋₁₅	³ AAIJ	14BA LHCb	pp at 7, 8 TeV
115 ⁺⁴¹ ₋₅₁	⁴ AAIJ	14BE LHCb	Repl. by AAIJ 14BA
105 ⁺¹⁶ ₋₁₇	⁵ LEES	13B BABR	$e^+e^- \rightarrow \Upsilon(4S)$
137 ⁺³⁵ ₋₄₆	^{6,7} AAIJ	12AQ LHCb	pp at 7 TeV
129.9 ± 15.0 ± 6.0	^{7,8} AIHARA	12 BELL	$e^+e^- \rightarrow \Upsilon(4S)$
119 ⁺¹⁹ ₋₂₀ ± 4	⁹ DEL-AMO-SA..10F	BABR	Repl. by LEES 13B
136.7 ^{+13.0} _{-15.8} ± 23.2	¹⁰ POLUEKTOV	10 BELL	$e^+e^- \rightarrow \Upsilon(4S)$
109 ⁺²⁷ ₋₃₀ ± 8	¹¹ AUBERT	08AL BABR	Repl. by DEL-AMO-SANCHEZ 10F
145.7 ^{+19.0} _{-19.7} ± 23.1	¹² POLUEKTOV	06 BELL	Repl. by POLUEKTOV 10
104 ± 45 ⁺²³ ₋₃₂	¹³ AUBERT,B	05Y BABR	Repl. by AUBERT 08AL

¹Uses binned analysis of $D \rightarrow K_S^0\pi^+\pi^-$ from $B^\pm \rightarrow DK^\pm$ modes over the phase space. Strong phase measurements from RESMI 18 analysis of CLEO-c data of the D decay over the phase space binning are used as input.

²Uses binned Dalitz plot analysis of $D \rightarrow K_S^0\pi^+\pi^-$ and $K_S^0K^+K^-$ from $B^\pm \rightarrow DK^\pm$ modes. Strong phase measurements from CLEO-c of the D decay over the Dalitz plot are used as input.

³Uses binned Dalitz plot analysis of $B^+ \rightarrow DK^+$ decays, with $D \rightarrow K_S^0\pi^+\pi^-$ and $D \rightarrow K_S^0K^+K^-$. Strong phase measurements from CLEO-c (LIBBY 10) of the D decay over the Dalitz plot are used as input.

⁴AAIJ 14BE uses model-dependent analysis of $D \rightarrow K_S^0\pi^+\pi^-$ amplitudes. The model is the same as in DEL-AMO-SANCHEZ 10F.

⁵Reports combination of published measurements using GGSZ, GLW, and ADS methods. Reports combined statistical and systematic uncertainties.

⁷Uses binned Dalitz plot of $\bar{D}^0 \rightarrow K_S^0\pi^+\pi^-$ decays from $B^+ \rightarrow \bar{D}^0K^+$. Measurement of strong phases in $\bar{D}^0 \rightarrow K_S^0\pi^+\pi^-$ Dalitz plot from LIBBY 10 is used as input.

⁸We combined the systematics in quadrature. The authors report separately the contribution to the systematic uncertainty due to the uncertainty on the bin-averaged strong phase difference between D^0 and \bar{D}^0 amplitudes.

⁹Uses Dalitz plot analysis of $\bar{D}^0 \rightarrow K_S^0\pi^+\pi^-$, $K_S^0K^+K^-$ decays from $B^+ \rightarrow D^{(*)}K^{(*)+}$ modes. The corresponding two standard deviation interval is $75^\circ < \delta_B < 157^\circ$.

¹⁰Uses Dalitz plot analysis of $\bar{D}^0 \rightarrow K_S^0\pi^+\pi^-$ decays from $B^+ \rightarrow \bar{D}^0K^+$ modes. The corresponding two standard deviation interval is $102.2^\circ < \delta_B < 162.3^\circ$.

¹¹Uses Dalitz plot analysis of $\bar{D}^0 \rightarrow K_S^0\pi^+\pi^-$ and $\bar{D}^0 \rightarrow K_S^0K^+K^-$ decays coming from $B^\pm \rightarrow D^{(*)}K^{(*)\pm}$ modes.

¹²Uses a Dalitz plot analysis of the $\bar{D}^0 \rightarrow K_S^0\pi^+\pi^-$ decays; Combines the DK^+ , D^*K^+ and DK^{*+} modes.

¹³Uses a Dalitz analysis of neutral D decays to $K_S^0\pi^+\pi^-$ in the processes $B^\pm \rightarrow D^{(*)}K^\pm$, $D^* \rightarrow D\pi^0$, $D\gamma$.

 $r_B(B^+ \rightarrow D^0K^{*+})$

r_B and δ_B are the amplitude ratio and relative strong phase between the amplitudes of $A_{CP}(B^+ \rightarrow D^0K^{*+})$ and $A_{CP}(B^+ \rightarrow \bar{D}^0K^{*+})$.

"OUR EVALUATION" is provided by the Heavy Flavor Averaging Group (HFLAV).

VALUE	DOCUMENT ID	TECN	COMMENT
-------	-------------	------	---------

0.076 ± 0.020 OUR EVALUATION

• • • We do not use the following data for averages, fits, limits, etc. • • •			
0.143 ^{+0.048} _{-0.049}	¹ LEES	13B BABR	$e^+e^- \rightarrow \Upsilon(4S)$
0.166 ^{+0.073} _{-0.069}	² DEL-AMO-SA..10F	BABR	Repl. by LEES 13B
0.31 ± 0.07	³ AUBERT	09AJ BABR	Repl. by LEES 13B
0.181 ^{+0.088} _{-0.108} ± 0.042	⁴ AUBERT	08AL BABR	Repl. by AUBERT 09AJ
0.564 ^{+0.216} _{-0.155} ± 0.093	⁵ POLUEKTOV	06 BELL	$e^+e^- \rightarrow \Upsilon(4S)$

¹Reports combination of published measurements using GGSZ, GLW, and ADS methods.

²DEL-AMO-SANCHEZ 10F reports $r_B \cdot k = 0.149^{+0.066}_{-0.062}$ for $k = 0.9$.

³Obtained by combining the GLW and ADS methods. The 2-sigma range corresponds to [0.17, 0.43].

⁴Uses Dalitz plot analysis of $\bar{D}^0 \rightarrow K_S^0\pi^+\pi^-$ and $\bar{D}^0 \rightarrow K_S^0K^+K^-$ decays coming from $B^\pm \rightarrow D^{(*)}K^{(*)\pm}$ modes.

⁵Uses a Dalitz plot analysis of the $\bar{D}^0 \rightarrow K_S^0\pi^+\pi^-$ decays; Combines the DK^+ , D^*K^+ and DK^{*+} modes.

 $\delta_B(B^+ \rightarrow D^0K^{*+})$

"OUR EVALUATION" is provided by the Heavy Flavor Averaging Group (HFLAV).

VALUE (°)	DOCUMENT ID	TECN	COMMENT
-----------	-------------	------	---------

98⁺¹⁸₋₃₇ OUR EVALUATION

• • • We do not use the following data for averages, fits, limits, etc. • • •			
101 ± 43	¹ LEES	13B BABR	$e^+e^- \rightarrow \Upsilon(4S)$
111 ± 32	DEL-AMO-SA..10F	BABR	Repl. by LEES 13B
104 ⁺³⁹ ₋₃₇ ± 18	² AUBERT	08AL BABR	Repl. by LEES 13B
242.6 ^{+20.2} _{-23.2} ± 49.4	³ POLUEKTOV	06 BELL	$e^+e^- \rightarrow \Upsilon(4S)$
¹ Reports combination of published measurements using GGSZ, GLW, and ADS methods.			
² Uses Dalitz plot analysis of $\bar{D}^0 \rightarrow K_S^0\pi^+\pi^-$ and $\bar{D}^0 \rightarrow K_S^0K^+K^-$ decays coming from $B^\pm \rightarrow D^{(*)}K^{(*)\pm}$ modes.			
³ Uses a Dalitz plot analysis of the $\bar{D}^0 \rightarrow K_S^0\pi^+\pi^-$ decays; Combines the DK^+ , D^*K^+ and DK^{*+} modes.			

 $r_B(B^+ \rightarrow D^{*0}K^+)$

r_B and δ_B are the amplitude ratio and relative strong phase between the amplitudes of $A(B^+ \rightarrow D^{*0}K^+)$ and $A(B^+ \rightarrow \bar{D}^{*0}K^+)$.

"OUR EVALUATION" is provided by the Heavy Flavor Averaging Group (HFLAV).

VALUE	DOCUMENT ID	TECN	COMMENT
-------	-------------	------	---------

0.140 ± 0.019 OUR EVALUATION

• • • We do not use the following data for averages, fits, limits, etc. • • •			
0.106 ^{+0.019} _{-0.036}	¹ LEES	13B BABR	$e^+e^- \rightarrow \Upsilon(4S)$
0.133 ^{+0.042} _{-0.039} ± 0.013	² DEL-AMO-SA..10F	BABR	Repl. by LEES 13B
0.096 ^{+0.035} _{-0.051}	³ DEL-AMO-SA..10H	BABR	Repl. by LEES 13B
0.196 ^{+0.072+0.064} _{-0.069-0.017}	⁴ POLUEKTOV	10 BELL	$e^+e^- \rightarrow \Upsilon(4S)$
0.135 ± 0.050 ± 0.012	⁵ AUBERT	08AL BABR	Repl. by DEL-AMO-SANCHEZ 10F
0.175 ^{+0.108} _{-0.099} ± 0.050	⁶ POLUEKTOV	06 BELL	Repl. by POLUEKTOV 10
0.17 ± 0.10 ± 0.04	⁷ AUBERT,B	05Y BABR	Repl. by AUBERT 08AL

¹Reports combination of published measurements using GGSZ, GLW, and ADS methods.

²Uses Dalitz plot analysis of $\bar{D}^0 \rightarrow K_S^0\pi^+\pi^-$, $K_S^0K^+K^-$ decays from $B^+ \rightarrow D^{(*)}K^{(*)+}$ modes. The corresponding two standard deviation interval is $0.049 < r_B < 0.215$.

³Uses the Cabibbo suppressed decay of $B^+ \rightarrow \bar{D}^{*0}K^+$ followed by $\bar{D}^{*0} \rightarrow \bar{D}\pi^0$ or $\bar{D}\gamma$, and $\bar{D} \rightarrow K^-\pi^+$.

⁴Uses Dalitz plot analysis of $\bar{D}^0 \rightarrow K_S^0\pi^+\pi^-$ decays from $B^+ \rightarrow D^{*0}K^+$ modes. The corresponding two standard deviation interval is $0.061 < r_B < 0.271$.

⁵Uses Dalitz plot analysis of $\bar{D}^0 \rightarrow K_S^0\pi^+\pi^-$ and $\bar{D}^0 \rightarrow K_S^0K^+K^-$ decays coming from $B^\pm \rightarrow D^{(*)}K^{(*)\pm}$ modes.

⁶Uses a Dalitz plot analysis of the $\bar{D}^0 \rightarrow K_S^0\pi^+\pi^-$ decays; Combines the DK^+ , D^*K^+ and DK^{*+} modes.

⁷Uses a Dalitz analysis of neutral D decays to $K_S^0\pi^+\pi^-$ in the processes $B^\pm \rightarrow D^{(*)}K^\pm$, $D^* \rightarrow D\pi^0$, $D\gamma$.

 $\delta_B(B^+ \rightarrow D^{*0}K^+)$

"OUR EVALUATION" is provided by the Heavy Flavor Averaging Group (HFLAV).

VALUE (°)	DOCUMENT ID	TECN	COMMENT
-----------	-------------	------	---------

319.2^{+7.7}_{-8.7} OUR EVALUATION

• • • We do not use the following data for averages, fits, limits, etc. • • •			
294 ⁺²¹ ₋₃₁	¹ LEES	13B BABR	$e^+e^- \rightarrow \Upsilon(4S)$
278 ± 21 ± 6	² DEL-AMO-SA..10F	BABR	Repl. by LEES 13B
341.9 ^{+18.0} _{-19.6} ± 23.1	³ POLUEKTOV	10 BELL	$e^+e^- \rightarrow \Upsilon(4S)$
297 ⁺²⁷ ₋₂₉ ± 6.4	⁴ AUBERT	08AL BABR	Repl. by DEL-AMO-SANCHEZ 10F
302.0 ^{+33.8} _{-35.1} ± 23.7	⁵ POLUEKTOV	06 BELL	Repl. by POLUEKTOV 10
296 ± 41 ⁺²⁰ ₋₁₉	⁶ AUBERT,B	05Y BABR	Repl. by AUBERT 08AL

¹Reports combination of published measurements using GGSZ, GLW, and ADS methods. We added 360° to the value of $(-66^{+21}_{-31})^\circ$ quoted by LEES 13B.

²Uses Dalitz plot analysis of $\bar{D}^0 \rightarrow K_S^0\pi^+\pi^-$, $K_S^0K^+K^-$ decays from $B^+ \rightarrow D^{(*)}K^{(*)+}$ modes. The corresponding two standard deviation interval is $236^\circ < \delta_B^* < 322^\circ$.

³ Uses Dalitz plot analysis of $\bar{D}^0 \rightarrow K_S^0 \pi^+ \pi^-$ decays from $B^+ \rightarrow D^* K^+$ modes. The corresponding two standard deviation interval is $296.5^\circ < \delta_B^* < 382.7^\circ$.

⁴ Uses Dalitz plot analysis of $\bar{D}^0 \rightarrow K_S^0 \pi^+ \pi^-$ and $\bar{D}^0 \rightarrow K_S^0 K^+ K^-$ decays coming from $B^\pm \rightarrow D^{(*)} K^{(*)\pm}$ modes.

⁵ Uses a Dalitz plot analysis of the $\bar{D}^0 \rightarrow K_S^0 \pi^+ \pi^-$ decays; Combines the $D K^+$, $D^* K^+$ and $D K^{*+}$ modes.

⁶ Uses a Dalitz analysis of neutral D decays to $K_S^0 \pi^+ \pi^-$ in the processes $B^\pm \rightarrow D^{(*)} K^\pm, D^* \rightarrow D \pi^0, D \gamma$.

PARTIAL BRANCHING FRACTIONS

B(B+ → K*+ ℓ+ ℓ-) (q² < 2.0 GeV²/c⁴)

VALUE (units 10 ⁻⁷)	DOCUMENT ID	TECN	COMMENT
1.4 ± 0.5 OUR AVERAGE			
1.37 ^{+0.60} _{-0.58}	AAIJ	12AH LHCb	pp at 7 TeV
1.30 ± 0.98 ± 0.14	AALTONEN	11AI CDF	p̄p̄ at 1.96 TeV

B(B+ → K*+ ℓ+ ℓ-) (2.0 < q² < 4.3 GeV²/c⁴)

VALUE (units 10 ⁻⁷)	DOCUMENT ID	TECN	COMMENT
1.1 ± 0.5 OUR AVERAGE			
1.24 ^{+0.60} _{-0.55}	AAIJ	12AH LHCb	pp at 7 TeV
0.71 ± 1.00 ± 0.15	AALTONEN	11AI CDF	p̄p̄ at 1.96 TeV

B(B+ → K*+ ℓ+ ℓ-) (4.3 < q² < 8.68 GeV²/c⁴)

VALUE (units 10 ⁻⁷)	DOCUMENT ID	TECN	COMMENT
2.4^{+0.8}_{-0.7} OUR AVERAGE			
2.50 ^{+0.88} _{-0.74}	AAIJ	12AH LHCb	pp at 7 TeV
1.71 ± 1.58 ± 0.49	AALTONEN	11AI CDF	p̄p̄ at 1.96 TeV

B(B+ → K*+ ℓ+ ℓ-) (10.09 < q² < 12.86 GeV²/c⁴)

VALUE (units 10 ⁻⁷)	DOCUMENT ID	TECN	COMMENT
2.1 ± 0.6 OUR AVERAGE			
2.13 ^{+0.72} _{-0.66}	AAIJ	12AH LHCb	pp at 7 TeV
1.97 ± 0.99 ± 0.22	AALTONEN	11AI CDF	p̄p̄ at 1.96 TeV

B(B+ → K*+ ℓ+ ℓ-) (14.18 < q² < 16.0 GeV²/c⁴)

VALUE (units 10 ⁻⁷)	DOCUMENT ID	TECN	COMMENT
0.86^{+0.40}_{-0.32} OUR AVERAGE			
1.00 ^{+0.47} _{-0.38}	AAIJ	12AH LHCb	pp at 7 TeV
0.52 ± 0.61 ± 0.09	AALTONEN	11AI CDF	p̄p̄ at 1.96 TeV

B(B+ → K*+ ℓ+ ℓ-) (15.0 < q² < 19.0 GeV²/c⁴)

VALUE (units 10 ⁻⁷)	DOCUMENT ID	TECN	COMMENT
1.50^{+0.32}_{-0.25} ± 0.11	¹ AAIJ	14M LHCb	pp at 7, 8 TeV
¹ Uses B(B+ → J/ψ(1S) K*(892)+) = (1.431 ± 0.027 ± 0.090) × 10 ⁻³ for normalization and μ+ μ- as a lepton pair.			

B(B+ → K*+ ℓ+ ℓ-) (q² > 16.0 GeV²/c⁴)

VALUE (units 10 ⁻⁷)	DOCUMENT ID	TECN	COMMENT
1.3 ± 0.4 OUR AVERAGE			
1.25 ± 0.46	AAIJ	12AH LHCb	pp at 7 TeV
1.57 ± 0.96 ± 0.17	AALTONEN	11AI CDF	p̄p̄ at 1.96 TeV

B(B+ → K*+ ℓ+ ℓ-) (1.0 < q² < 6.0 GeV²/c⁴)

VALUE (units 10 ⁻⁷)	DOCUMENT ID	TECN	COMMENT
1.8 ± 0.4 OUR AVERAGE			
1.79 ^{+0.41} _{-0.37} ± 0.13	¹ AAIJ	14M LHCb	pp at 7, 8 TeV
2.57 ± 1.61 ± 0.40	AALTONEN	11AI CDF	p̄p̄ at 1.96 TeV
• • • We do not use the following data for averages, fits, limits, etc. • • •			
2.90 ^{+0.90} _{-0.85}	AAIJ	12AH LHCb	Repl. by AAIJ 14M

¹ Uses B(B+ → J/ψ(1S) K*(892)+) = (1.431 ± 0.027 ± 0.090) × 10⁻³ for normalization and μ+ μ- as a lepton pair. Measured in 1.1 < q² < 6.0 GeV²/c⁴.

B(B+ → K*+ ℓ+ ℓ-) (0.0 < q² < 4.3 GeV²/c⁴)

VALUE (units 10 ⁻⁷)	DOCUMENT ID	TECN	COMMENT
2.01 ± 1.39 ± 0.27	AALTONEN	11AI CDF	p̄p̄ at 1.96 TeV

B(B+ → K+ ℓ+ ℓ-) (q² < 2.0 GeV²/c⁴)

VALUE (units 10 ⁻⁷)	DOCUMENT ID	TECN	COMMENT
0.51 ± 0.08 OUR AVERAGE			Error includes scale factor of 1.5.
0.556 ± 0.053 ± 0.027	¹ AAIJ	13H LHCb	pp at 7 TeV
0.36 ± 0.11 ± 0.03	AALTONEN	11AI CDF	p̄p̄ at 1.96 TeV

¹ Measured in 0.05 < q² < 2.0 GeV²/c⁴ range.

B(B+ → K+ ℓ+ ℓ-) (2.0 < q² < 4.3 GeV²/c⁴)

VALUE (units 10 ⁻⁷)	DOCUMENT ID	TECN	COMMENT
0.60 ± 0.07 OUR AVERAGE			Error includes scale factor of 1.3.
0.573 ± 0.053 ± 0.023	AAIJ	13H LHCb	pp at 7 TeV
0.80 ± 0.15 ± 0.05	AALTONEN	11AI CDF	p̄p̄ at 1.96 TeV

B(B+ → K+ ℓ+ ℓ-) (4.3 < q² < 8.68 GeV²/c⁴)

VALUE (units 10 ⁻⁷)	DOCUMENT ID	TECN	COMMENT
1.03 ± 0.07 OUR AVERAGE			
1.003 ± 0.070 ± 0.039	AAIJ	13H LHCb	pp at 7 TeV
1.18 ± 0.19 ± 0.09	AALTONEN	11AI CDF	p̄p̄ at 1.96 TeV

B(B+ → K+ ℓ+ ℓ-) (10.09 < q² < 12.86 GeV²/c⁴)

VALUE (units 10 ⁻⁷)	DOCUMENT ID	TECN	COMMENT
0.58 ± 0.05 OUR AVERAGE			
0.565 ± 0.050 ± 0.022	AAIJ	13H LHCb	pp at 7 TeV
0.68 ± 0.12 ± 0.05	AALTONEN	11AI CDF	p̄p̄ at 1.96 TeV

B(B+ → K+ ℓ+ ℓ-) (14.18 < q² < 16.0 GeV²/c⁴)

VALUE (units 10 ⁻⁷)	DOCUMENT ID	TECN	COMMENT
0.40 ± 0.05 OUR AVERAGE			Error includes scale factor of 1.4.
0.377 ± 0.036 ± 0.015	AAIJ	13H LHCb	pp at 7 TeV
0.53 ± 0.10 ± 0.03	AALTONEN	11AI CDF	p̄p̄ at 1.96 TeV

B(B+ → K+ ℓ+ ℓ-) (16.0 < q² < 18.0 GeV²/c⁴)

VALUE (units 10 ⁻⁷)	DOCUMENT ID	TECN	COMMENT
0.354 ± 0.036 ± 0.018	AAIJ	13H LHCb	pp at 7 TeV

B(B+ → K+ ℓ+ ℓ-) (18.0 < q² < 22.0 GeV²/c⁴)

VALUE (units 10 ⁻⁷)	DOCUMENT ID	TECN	COMMENT
0.312 ± 0.040 ± 0.016	AAIJ	13H LHCb	pp at 7 TeV
F_H is a fractional contribution of (pseudo) scalar and tensor amplitudes to the decay width in the massless muon approximation.			

B(B+ → K+ ℓ+ ℓ-) (15.0 < q² < 22.0 GeV²/c⁴)

VALUE (units 10 ⁻⁷)	DOCUMENT ID	TECN	COMMENT
0.85 ± 0.03 ± 0.04	¹ AAIJ	14M LHCb	pp at 7, 8 TeV
¹ Uses B(B+ → J/ψ(1S) K+) = (0.998 ± 0.014 ± 0.040) × 10 ⁻³ for normalization and μ+ μ- as a lepton pair.			

B(B+ → K+ ℓ+ ℓ-) (16.0 < q² < 18.0 GeV²/c⁴)

VALUE (units 10 ⁻⁷)	DOCUMENT ID	TECN	COMMENT
0.48 ± 0.11 ± 0.03	AALTONEN	11AI CDF	p̄p̄ at 1.96 TeV

B(B+ → K+ ℓ+ ℓ-) (1.0 < q² < 6.0 GeV²/c⁴)

VALUE (units 10 ⁻⁷)	DOCUMENT ID	TECN	COMMENT
1.21 ± 0.06 OUR AVERAGE			
1.40 ^{+0.98} _{-0.34} ± 0.69	¹ AAIJ	19S LHCb	pp at 7, 8, 13 TeV
1.19 ± 0.034 ± 0.059	² AAIJ	14M LHCb	pp at 7, 8 TeV
1.41 ± 0.20 ± 0.10	AALTONEN	11AI CDF	p̄p̄ at 1.96 TeV
• • • We do not use the following data for averages, fits, limits, etc. • • •			
1.56 ^{+0.19} _{-0.15} ± 0.06	³ AAIJ	14AR LHCb	pp at 7, 8 TeV
1.205 ± 0.085 ± 0.070	AAIJ	13H LHCb	Repl. by AAIJ 14M

¹ Measured by taking the ratio of the branching fraction from $B^+ \rightarrow K^+ e^+ e^-$ and $B^+ \rightarrow J/\psi(e^+ e^-) K^+$ decays and multiplying it by the measured value of $B^+ \rightarrow J/\psi K^+$ and $J/\psi \rightarrow e^+ e^-$ as in PDG 18. The branching fraction of $B^+ \rightarrow K^+ e^+ e^-$ is determined in the region $1.1 < q^2 < 6 \text{ GeV}^2/c^4$.

² Uses $B(B^+ \rightarrow J/\psi(1S) K^+) = (0.998 \pm 0.014 \pm 0.040) \times 10^{-3}$ for normalization and $\mu^+ \mu^-$ for leptons. Measured for $1.1 < q^2 < 6.0 \text{ GeV}^2/c^4$.

³ Measured by taking the ratio of the branching fraction from $B^+ \rightarrow K^+ e^+ e^-$ and $B^+ \rightarrow J/\psi(e^+ e^-) K^+$ decays and multiplying it by the measured value of $B^+ \rightarrow J/\psi K^+$ and $J/\psi \rightarrow e^+ e^-$ as in PDG 12. The branching fraction of $B^+ \rightarrow K^+ e^+ e^-$ is determined in the region $1 < q^2 < 6 \text{ GeV}^2/c^4$.

B(B+ → K+ μ+ μ-) / B(B+ → K+ e+ e-) (1.0 < q² < 6.0 GeV²/c⁴)

VALUE	DOCUMENT ID	TECN	COMMENT
0.846^{+0.060}_{-0.054} ± 0.016	¹ AAIJ	19S LHCb	pp at 7, 8, 13 TeV
• • • We do not use the following data for averages, fits, limits, etc. • • •			
0.745 ^{+0.090} _{-0.074} ± 0.036	² AAIJ	14AR LHCb	pp at 7, 8 TeV

¹ The ratio is determined using the relative branching fractions of the decays $B^+ \rightarrow K^+ \ell^+ \ell^-$ and $B^+ \rightarrow J/\psi(\ell^+ \ell^-) K^+$, with $\ell = e, \mu$. Measured for the region $1.1 < q^2 < 6.0 \text{ GeV}^2/c^4$.

² The ratio is determined using the relative branching fractions of the decays $B^+ \rightarrow K^+ \ell^+ \ell^-$ and $B^+ \rightarrow J/\psi(\ell^+ \ell^-) K^+$, with $\ell = e, \mu$.

B(B+ → K+ ℓ+ ℓ-) (0.0 < q² < 4.3 GeV²/c⁴)

VALUE (units 10 ⁻⁷)	DOCUMENT ID	TECN	COMMENT
1.13 ± 0.19 ± 0.08	AALTONEN	11AI CDF	p̄p̄ at 1.96 TeV

Meson Particle Listings

 B^\pm

ABE	06	PR D73 051106	K. Abe et al.	(BELLE Collab.)	NAKAO	04	PR D69 112001	M. Nakao et al.	(BELLE Collab.)
ABUENCIA	06J	PRL 96 191801	A. Abulencia et al.	(CDF Collab.)	POLUEKTOV	04	PR D70 072003	A. Poluektov et al.	(BELLE Collab.)
ACOSTA	06	PRL 96 202001	D. Acosta et al.	(CDF Collab.)	SCHWANDA	04	PRL 93 131803	C. Schwanda et al.	(BELLE Collab.)
AUBERT	06	PR D73 011101	B. Aubert et al.	(BABAR Collab.)	WANG	04	PRL 92 131801	M.Z. Wang et al.	(BELLE Collab.)
AUBERT	06E	PRL 96 052002	B. Aubert et al.	(BABAR Collab.)	WANG	04A	PR D70 012001	C.H. Wang et al.	(BELLE Collab.)
AUBERT	06F	PR D73 011103	B. Aubert et al.	(BABAR Collab.)	ZANG	04	PR D69 017101	S.L. Zang et al.	(BELLE Collab.)
AUBERT	06J	PR D73 051105	B. Aubert et al.	(BABAR Collab.)	ABE	03B	PR D67 032003	K. Abe et al.	(BELLE Collab.)
AUBERT	06K	PR D73 057101	B. Aubert et al.	(BABAR Collab.)	ABE	03D	PRL 90 131803	K. Abe et al.	(BELLE Collab.)
AUBERT	06N	PR D74 031103	B. Aubert et al.	(BABAR Collab.)	ADAM	03	PR D67 032001	N.E. Adam et al.	(CLEO Collab.)
AUBERT	06O	PR D74 032003	B. Aubert et al.	(BABAR Collab.)	ADAM	03B	PR D68 012004	N.E. Adam et al.	(CLEO Collab.)
AUBERT	06Z	PR D73 111104	B. Aubert et al.	(BABAR Collab.)	ATHAR	03	PR D68 072003	S.B. Athar et al.	(CLEO Collab.)
AUBERT,B	06A	PR D73 112004	B. Aubert et al.	(BABAR Collab.)	AUBERT	03K	PRL 90 231801	B. Aubert et al.	(BABAR Collab.)
AUBERT,B	06C	PR D74 011102	B. Aubert et al.	(BABAR Collab.)	AUBERT	03L	PRL 91 021801	B. Aubert et al.	(BABAR Collab.)
AUBERT,B	06E	PR D74 011106	B. Aubert et al.	(BABAR Collab.)	AUBERT	03M	PRL 91 051801	B. Aubert et al.	(BABAR Collab.)
AUBERT,B	06G	PRL 97 201801	B. Aubert et al.	(BABAR Collab.)	AUBERT	03O	PRL 91 071801	B. Aubert et al.	(BABAR Collab.)
AUBERT,B	06H	PRL 97 201802	B. Aubert et al.	(BABAR Collab.)	AUBERT	03U	PRL 91 221802	B. Aubert et al.	(BABAR Collab.)
AUBERT,B	06J	PR D73 092001	B. Aubert et al.	(BABAR Collab.)	AUBERT	03V	PRL 91 171802	B. Aubert et al.	(BABAR Collab.)
AUBERT,B	06M	PR D74 031102	B. Aubert et al.	(BABAR Collab.)	AUBERT	03W	PRL 91 161801	B. Aubert et al.	(BABAR Collab.)
AUBERT,B	06P	PR D74 031102	B. Aubert et al.	(BABAR Collab.)	AUBERT	03X	PR D68 092001	B. Aubert et al.	(BABAR Collab.)
AUBERT,B	06T	PR D74 051102	B. Aubert et al.	(BABAR Collab.)	BORNHEIM	03	PR D68 052002	A. Bornheim et al.	(CLEO Collab.)
AUBERT,B	06U	PR D74 051104	B. Aubert et al.	(BABAR Collab.)	CHEN	03B	PRL 91 201801	K.-F. Chen et al.	(BELLE Collab.)
AUBERT,B	06Y	PR D74 091105	B. Aubert et al.	(BABAR Collab.)	CHOI	03	PRL 91 262001	S.-K. Choi et al.	(BELLE Collab.)
AUBERT,BE	06A	PR D74 099903 (errat.)	B. Aubert et al.	(BABAR Collab.)	CSORNA	03	PR D67 112002	S.E. Csorna et al.	(CLEO Collab.)
AUBERT,BE	06C	PRL 97 171805	B. Aubert et al.	(BABAR Collab.)	EDWARDS	03	PR D68 011102	K.W. Edwards et al.	(CLEO Collab.)
AUBERT,BE	06G	PRL 97 261801	B. Aubert et al.	(BABAR Collab.)	FANG	03	PRL 90 071801	F. Fang et al.	(BELLE Collab.)
AUBERT,BE	06H	PRL 97 261803	B. Aubert et al.	(BABAR Collab.)	HUANG	03	PRL 91 241802	H.-C. Huang et al.	(BELLE Collab.)
AUBERT,BE	06J	PR D74 111102	B. Aubert et al.	(BABAR Collab.)	ISHIKAWA	03	PRL 91 261601	A. Ishikawa et al.	(BELLE Collab.)
AUBERT,BE	06M	PR D74 071101	B. Aubert et al.	(BABAR Collab.)	KROKOVNY	03B	PRL 91 262002	P. Krokovny et al.	(BELLE Collab.)
CHISTOV	06A	PR D74 111105	R. Chistov et al.	(BELLE Collab.)	SWAIN	03	PR D68 051101	S.K. Swain et al.	(BELLE Collab.)
FANG	06	PR D74 012007	F. Fang et al.	(BELLE Collab.)	URNO	03	PR D68 011103	Y. Urno et al.	(CLEO Collab.)
GABYSHEV	06	PRL 97 202003	N. Gabyshev et al.	(BELLE Collab.)	ZHANG	03B	PRL 91 221801	J. Zhang et al.	(BELLE Collab.)
GABYSHEV	06A	PRL 97 242001	N. Gabyshev et al.	(BELLE Collab.)	ABE	02	PRL 88 021801	K. Abe et al.	(BELLE Collab.)
GARMASH	06	PRL 96 251803	A. Garmash et al.	(BELLE Collab.)	ABE	02B	PRL 88 031802	K. Abe et al.	(BELLE Collab.)
GOKHROO	06	PRL 97 162002	G. Gokhroo et al.	(BELLE Collab.)	ABE	02H	PRL 88 171801	K. Abe et al.	(BELLE Collab.)
IKADO	06	PRL 97 251802	K. Ikado et al.	(BELLE Collab.)	ABE	02K	PRL 88 181803	K. Abe et al.	(BELLE Collab.)
JEN	06	PR D74 111101	C.-M. Jen et al.	(BELLE Collab.)	ABE	02N	PL B538 11	K. Abe et al.	(BELLE Collab.)
KUMAR	06	PR D74 051103	R. Kumar et al.	(BELLE Collab.)	ABE	02O	PR D65 091103	K. Abe et al.	(BELLE Collab.)
MOHAPATRA	06	PRL 96 221601	D. Mohapatra et al.	(BELLE Collab.)	ABE	02W	PRL 89 151802	K. Abe et al.	(BELLE Collab.)
POLUEKTOV	06	PR D73 112009	A. Poluektov et al.	(BELLE Collab.)	ACOSTA	02F	PR D65 092009	D. Acosta et al.	(CDF Collab.)
SCHUEMANN	06	PRL 97 061802	J. Schuemann et al.	(BELLE Collab.)	ACOSTA	02C	PR D66 052005	D. Acosta et al.	(CDF Collab.)
SONI	06	PL B634 155	N. Soni et al.	(BELLE Collab.)	AHMED	02B	PR D66 031101	S. Ahmed et al.	(CLEO Collab.)
ABE	05A	PRL 94 221805	K. Abe et al.	(BELLE Collab.)	AUBERT	02	PR D65 032001	B. Aubert et al.	(BABAR Collab.)
ABE	05B	PR D71 072003	K. Abe et al.	(BELLE Collab.)	AUBERT	02C	PRL 88 101805	B. Aubert et al.	(BABAR Collab.)
Also		PR D71 079903 (errat.)	K. Abe et al.	(BELLE Collab.)	AUBERT	02E	PR D65 051101	B. Aubert et al.	(BABAR Collab.)
ABE	05G	PRL 95 231802	K. Abe et al.	(BELLE Collab.)	AUBERT	02F	PR D65 091101	B. Aubert et al.	(BABAR Collab.)
ACOSTA	05J	PRL 95 031801	D. Acosta et al.	(CDF Collab.)	AUBERT	02L	PRL 88 241801	B. Aubert et al.	(BABAR Collab.)
AUBERT	05	PRL 94 011801	B. Aubert et al.	(BABAR Collab.)	BRIERE	02	PRL 89 081803	R. Briere et al.	(CLEO Collab.)
AUBERT	05B	PR D71 031501	B. Aubert et al.	(BABAR Collab.)	CASEY	02	PR D66 092002	B.C.K. Casey et al.	(BELLE Collab.)
AUBERT	05G	PR D72 032004	B. Aubert et al.	(BABAR Collab.)	CHEN	02B	PL B546 196	K.-F. Chen et al.	(BELLE Collab.)
AUBERT	05H	PRL 94 101801	B. Aubert et al.	(BABAR Collab.)	DRUTSKOY	02	PL B542 171	A. Drutskoy et al.	(BELLE Collab.)
AUBERT	05J	PRL 94 141801	B. Aubert et al.	(BABAR Collab.)	DYTMAN	02	PR D66 091101	S.A. Dytman et al.	(CLEO Collab.)
AUBERT	05K	PRL 94 171801	B. Aubert et al.	(BABAR Collab.)	ECKHART	02	PRL 89 251801	E. Eckhart et al.	(CLEO Collab.)
AUBERT	05L	PR D74 041801	B. Aubert et al.	(BABAR Collab.)	EDWARDS	02B	PR D65 031102	R.W. Edwards et al.	(CLEO Collab.)
AUBERT	05M	PRL 94 191802	B. Aubert et al.	(BABAR Collab.)	GABYSHEV	02	PR D66 011102	N. Gabyshev et al.	(BELLE Collab.)
AUBERT	05N	PR D71 031102	B. Aubert et al.	(BABAR Collab.)	GARMASH	02	PR D65 092005	A. Garmash et al.	(BELLE Collab.)
AUBERT	05O	PR D71 031103	B. Aubert et al.	(BABAR Collab.)	GODANG	02	PRL 88 021802	R. Godang et al.	(CLEO Collab.)
AUBERT	05R	PR D71 071103	B. Aubert et al.	(BABAR Collab.)	GORDON	02	PL B542 183	A. Gordon et al.	(BELLE Collab.)
AUBERT	05U	PR D71 091103	B. Aubert et al.	(BABAR Collab.)	LU	02	PRL 89 191801	R.-S. Lu et al.	(BELLE Collab.)
AUBERT	05X	PR D71 111101	B. Aubert et al.	(BABAR Collab.)	MAHAPATRA	02	PRL 88 101803	R. Mahapatra et al.	(CLEO Collab.)
AUBERT,B	05B	PRL 95 041804	B. Aubert et al.	(BABAR Collab.)	NISHIDA	02	PRL 89 231801	S. Nishida et al.	(BELLE Collab.)
AUBERT,B	05E	PR D72 011102	B. Aubert et al.	(BABAR Collab.)	ABE	01H	PRL 87 101801	K. Abe et al.	(BELLE Collab.)
AUBERT,B	05G	PR D72 052002	B. Aubert et al.	(BABAR Collab.)	ABE	01I	PRL 87 111801	K. Abe et al.	(BELLE Collab.)
AUBERT,B	05K	PRL 95 131803	B. Aubert et al.	(BABAR Collab.)	ABE	01K	PR D64 071101	K. Abe et al.	(BELLE Collab.)
AUBERT,B	05L	PR D72 051101	B. Aubert et al.	(BABAR Collab.)	ABE	01L	PRL 87 161801	K. Abe et al.	(BELLE Collab.)
AUBERT,B	05N	PR D72 072003	B. Aubert et al.	(BABAR Collab.)	ABE	01M	PL B517 309	K. Abe et al.	(BELLE Collab.)
Also		PR D74 099903 (errat.)	B. Aubert et al.	(BABAR Collab.)	ALEXANDER	01B	PR D64 092001	J.P. Alexander et al.	(CLEO Collab.)
AUBERT,B	05O	PR D72 051102	B. Aubert et al.	(BABAR Collab.)	AMMAR	01B	PRL 87 271801	R. Ammar et al.	(CLEO Collab.)
AUBERT,B	05T	PR D72 071102	B. Aubert et al.	(BABAR Collab.)	ANDERSON	01B	PRL 87 181803	S. Anderson et al.	(CLEO Collab.)
AUBERT,B	05U	PR D72 071103	B. Aubert et al.	(BABAR Collab.)	AUBERT	01D	PRL 87 151801	B. Aubert et al.	(BABAR Collab.)
AUBERT,B	05V	PR D72 071104	B. Aubert et al.	(BABAR Collab.)	AUBERT	01E	PRL 87 151802	B. Aubert et al.	(BABAR Collab.)
AUBERT,B	05Y	PRL 95 121802	B. Aubert et al.	(BABAR Collab.)	AUBERT	01F	PRL 87 201803	B. Aubert et al.	(BABAR Collab.)
AUBERT,BE	05E	PRL 95 221801	B. Aubert et al.	(BABAR Collab.)	AUBERT	01G	PRL 87 221802	B. Aubert et al.	(BABAR Collab.)
CHANG	05	PR D71 072007	M.-C. Chang et al.	(BELLE Collab.)	BARATE	01E	EPJ C19 213	R. Barate et al.	(ALEPH CERN)
CHANG	05A	PR D71 091106	P. Chang et al.	(BELLE Collab.)	BRIERE	01	PRL 86 3718	R.A. Briere et al.	(CLEO Collab.)
CHAO	05A	PR D71 091104	Y. Chao et al.	(BELLE Collab.)	BROWDER	01	PRL 85 2950	T.E. Browder et al.	(CLEO Collab.)
CHEN	05A	PRL 94 221804	K.-F. Chen et al.	(BELLE Collab.)	EDWARDS	01	PRL 86 30	K.W. Edwards et al.	(CLEO Collab.)
GARMASH	05	PR D71 092003	A. Garmash et al.	(BELLE Collab.)	GRITSAN	01	PR D64 077501	A. Gritsan et al.	(CLEO Collab.)
ITHO	05	PRL 95 091601	R. Itho et al.	(BELLE Collab.)	RICHICHI	01	PR D63 031103	S.J. Richichi et al.	(CLEO Collab.)
LEE	05	PRL 95 061802	Y.-J. Lee et al.	(BELLE Collab.)	ABBIENDI	00C	PL B476 233	G. Abbiendi et al.	(OPAL Collab.)
LIVENTSEV	05	PR D72 051109	D. Liventsev et al.	(BELLE Collab.)	ABE	00B	PR D62 071101	K. Abe et al.	(SLD Collab.)
MAJUMDER	05	PRL 95 041803	G. Majumder et al.	(BELLE Collab.)	AHMED	00B	PR D62 112003	S. Ahmed et al.	(CLEO Collab.)
MOHAPATRA	05	PR D72 011101	D. Mohapatra et al.	(BELLE Collab.)	ANASTASSOV	00	PRL 84 1393	A. Anastassov et al.	(CLEO Collab.)
NISHIDA	05	PL B610 23	S. Nishida et al.	(BELLE Collab.)	BARATE	00R	PL B492 275	R. Barate et al.	(ALEPH CERN)
OKABE	05	PL B614 27	T. Okabe et al.	(BELLE Collab.)	BEHRENS	00	PR D61 052001	B.H. Behrens et al.	(CLEO Collab.)
SAIGO	05	PRL 94 091601	M. Saigo et al.	(BELLE Collab.)	BONVICINI	00	PRL 84 5940	G. Bonvicini et al.	(CLEO Collab.)
WANG	05A	PL B617 141	M.-Z. Wang et al.	(BELLE Collab.)	CHEN	00	PRL 85 925	S. Chen et al.	(CLEO Collab.)
XIE	05	PR D72 051105	Q.L. Xie et al.	(BELLE Collab.)	COAN	00	PRL 84 5283	T.E. Coan et al.	(CLEO Collab.)
YANG	05	PRL 94 111802	H. Yang et al.	(BELLE Collab.)	CRONIN-HENNESSY	00	PR D61 111101	D. Cronin-Hennessy et al.	(CLEO Collab.)
ZHANG	05A	PRL 94 031801	J. Zhang et al.	(BELLE Collab.)	CSORNA	00	PR D61 111101	S.E. Csorna et al.	(CLEO Collab.)
ZHANG	05B	PR D71 091107	L.M. Zhang et al.	(BELLE Collab.)	JESSOP	00	PRL 85 2881	C.P. Jessop et al.	(CLEO Collab.)
ZHANG	05D	PRL 95 141801	J. Zhang et al.	(BELLE Collab.)	RICHICHI	00	PRL 85 520	S.J. Richichi et al.	(CLEO Collab.)
ABDALLAH	04E	EPJ C33 307	J. Abdallah et al.	(DELPHI Collab.)	ABBIENDI	99J	EPJ C12 609	G. Abbiendi et al.	(OPAL Collab.)
ABE	04D	PR D69 112002	K. Abe et al.	(BELLE Collab.)	AFFOLDER	99B	PRL 83 3378	T. Affolder et al.	(CDF Collab.)
AUBERT	04A	PR D69 011102	B. Aubert et al.	(BABAR Collab.)	BARTELT	99	PRL 82 3746	J. Bartelt et al.	(CLEO Collab.)
AUBERT	04C	PRL 92 111801	B. Aubert et al.	(BABAR Collab.)	COAN	99	PR D59 111101	T.E. Coan et al.	(CLEO Collab.)
AUBERT	04H	PRL 92 061801	B. Aubert et al.	(BABAR Collab.)	ABE	98B	PR D57 5382	F. Abe et al.	(CDF Collab.)
AUBERT	04K	PRL 92 141801	B. Aubert et al.	(BABAR Collab.)	ABE	98O	PR D58 072001	F. Abe et al.	(CDF Collab.)
AUBERT	04M	PRL 92 201802	B. Aubert et al.	(BABAR Collab.)	ABE	98Q	PR D58 092002	F. Abe et al.	(CDF Collab.)
AUBERT	04N	PRL 92 202002	B. Aubert et al.	(BABAR Collab.)	ACCARIARI	98S	PL B438 417	M. Acciarri et al.	(L3 Collab.)
AUBERT	04O	PRL 92 221803	B. Aubert et al.	(BABAR Collab.)	ANASTASSOV	98	PRL 80 4127	A. Anastassov et al.	(CLEO Collab.)
AUBERT	04P	PRL 92 241802	B. Aubert et al.	(BABAR Collab.)	ATHANAS	98	PRL 80 5493	M. Athanas et al.	(CLEO Collab.)
AUBERT	04Q	PR D69 051101	B. Aubert et al.	(BABAR Collab.)	BARATE	98Q	EPJ C4 387	R. Barate et al.	(ALEPH CERN)
AUBERT	04T	PR D69 071103	B. Aubert et al.	(BABAR Collab.)	BEHRENS	98	PRL 80 3710	B.H. Behrens et al.	(CLEO Collab.)
AUBERT	04Y	PRL 93 041801	B. Aubert et al.	(BABAR Collab.)	BERGFELD	98	PRL 81 272	T. Bergfeld et al.	(CLEO Collab.)
AUBERT	04Z	PRL 93 051802	B. Aubert et al.	(BABAR Collab.)	BRANDENB...	98	PRL 80 2762	G. Brandenb...	(CLEO Collab.)
AUBERT,B	04B	PR D70 011101	B. Aubert et al.	(BABAR Collab.)	CAPRINI	98	NP B530 153	I. Caprini, L. Leflouch, M. Neubert	(BCIP CERN)
AUBERT,B	04D	PR D70 032006	B. Aubert et al.	(BABAR Collab.)	GODANG	98	PRL 80 3456	R. Godang et al.	(CLEO Collab.)
AUBERT,B	04L	PRL 93 131804	B. Aubert et al.	(BABAR Collab.)	ABE	97J	PRL 79 590	K. Abe et al.	(SLD Collab.)
AUBERT,B	04P	PR D70 092001	B. Aubert et al.	(BABAR Collab.)	ACCARIARI	97F	PL B396 327	M. Acciarri et al.	(L3 Collab.)
AUBERT,B	04S	PRL 93 181801	B. Aubert et al.	(BABAR Collab.)	ARTUSO	97	PL B399 321	M. Artuso et al.	(CLEO Collab.)
AUBERT,B	04U	PR D70 091105	B. Aubert et al.	(BABAR Collab.)	ATHANAS	97	PRL 79 2208	M. Athanas et al.	(CLEO Collab.)
AUBERT,B	04V	PRL 93 181805	B. Aubert et al.	(BABAR Collab.)	BROWDER	97	PR D56 11	T. Browder et al.	(CLEO Collab.)
AUBERT,BE	04	PR D70 111102	B. Aubert et al.	(BABAR Collab.)	FU	97	PRL 79 3125	X. Fu et al.	(CLEO Collab.)
AUBERT,BE	04A	PR D70 112006	B. Aubert et al.	(BABAR Collab.)	JESSOP	97	PRL 79 4533	C.P. Jessop et al.	(CLEO Collab.)
AUBERT,BE	04B	PR D70 091106	B. Aubert et al.	(BABAR Collab.)	ABE	96B	PR D		

ASNER	96	PR D53 1039	D.M. Asner et al.	(CLEO Collab.)
BARISH	96B	PRL 76 1570	B.C. Barish et al.	(CLEO Collab.)
BERGFELD	96B	PRL 77 4503	T. Bergfeld et al.	(CLEO Collab.)
BISHAI	96	PL B369 186	M. Bishai et al.	(CLEO Collab.)
BUSKULIC	96J	ZPHY C71 31	D. Buskulic et al.	(ALEPH Collab.)
GIBAUT	96	PR D53 4734	D. Gibaut et al.	(CLEO Collab.)
PDG	96	PL D54 1	R. M. Barnett et al.	(PDG Collab.)
ABREU	95N	PL B357 255	P. Abreu et al.	(DELPHI Collab.)
ABREU	95Q	ZPHY C68 13	P. Abreu et al.	(DELPHI Collab.)
ADAM	95	ZPHY C68 363	W. Adam et al.	(DELPHI Collab.)
AKERS	95T	ZPHY C67 379	R. Akers et al.	(OPAL Collab.)
ALBRECHT	95D	PL B353 554	H. Albrecht et al.	(ARGUS Collab.)
ALEXANDER	95	PL B341 435	J. Alexander et al.	(CLEO Collab.)
Also		PL B347 469 (erratum)	J. Alexander et al.	(CLEO Collab.)
ARTUSO	95	PRL 75 785	M. Artuso et al.	(CLEO Collab.)
BARISH	95	PR D51 1014	B.C. Barish et al.	(CLEO Collab.)
BUSKULIC	95	PL B343 444	D. Buskulic et al.	(ALEPH Collab.)
ABE	94D	PRL 72 3456	F. ABE et al.	(CDF Collab.)
ALAM	94	PR D50 43	M.S. Alam et al.	(CLEO Collab.)
ALBRECHT	94D	PL B335 526	H. Albrecht et al.	(ARGUS Collab.)
ATHANAS	94	PRL 73 3503	M. Athanas et al.	(CLEO Collab.)
Also		PRL 74 3090 (erratum)	M. Athanas et al.	(CLEO Collab.)
PDG	94	PR D50 1173	L. Montanet et al.	(CERN, LBL, BOST+)
STONE	94	HEPSY 93-11	S. Stone	(Scientific, Singapore)
Published in B Decays, 2nd Edition, World Scientific, Singapore				
ABREU	93D	ZPHY C57 181	P. Abreu et al.	(DELPHI Collab.)
ABREU	93G	PL B312 253	P. Abreu et al.	(DELPHI Collab.)
ACTION	93C	PL B307 247	P.D. Acton et al.	(OPAL Collab.)
ALBRECHT	93E	ZPHY C60 11	H. Albrecht et al.	(ARGUS Collab.)
ALEXANDER	93B	PL B319 365	J. Alexander et al.	(CLEO Collab.)
AMMAR	93	PRL 71 674	R. Ammar et al.	(CLEO Collab.)
BEAN	93B	PRL 70 2681	A. Bean et al.	(CLEO Collab.)
BUSKULIC	93D	PL B307 194	D. Buskulic et al.	(ALEPH Collab.)
Also		PL B325 537 (erratum)	D. Buskulic et al.	(ALEPH Collab.)
SANGHERA	93	PR D47 791	S. Sanghera et al.	(CLEO Collab.)
ALBRECHT	92C	PL B275 195	H. Albrecht et al.	(ARGUS Collab.)
ALBRECHT	92E	PL B277 209	H. Albrecht et al.	(ARGUS Collab.)
ALBRECHT	92G	ZPHY C54 1	H. Albrecht et al.	(ARGUS Collab.)
BORTOLETTO	92	PR D45 21	D. Bortoletto et al.	(CLEO Collab.)
BUSKULIC	92G	PL B295 396	D. Buskulic et al.	(ALEPH Collab.)
ALBRECHT	91B	PL B254 288	H. Albrecht et al.	(ARGUS Collab.)
ALBRECHT	91C	PL B255 297	H. Albrecht et al.	(ARGUS Collab.)
ALBRECHT	91E	PL B262 148	H. Albrecht et al.	(ARGUS Collab.)
BERKELMAN	91	ARNPS 41 1	K. Berkelman, S. Stone	(CORN, SYRA)
"Decays of B Mesons"				
FULTON	91	PR D43 651	R. Fulton et al.	(CLEO Collab.)
ALBRECHT	90B	PL B241 278	H. Albrecht et al.	(ARGUS Collab.)
ALBRECHT	90J	ZPHY C48 543	H. Albrecht et al.	(ARGUS Collab.)
ANTREASAYAN	90B	ZPHY C48 553	D. Antreasyan et al.	(Crystal Ball Collab.)
BORTOLETTO	90	PRL 64 2117	D. Bortoletto et al.	(CLEO Collab.)
Also		PR D45 21	D. Bortoletto et al.	(CLEO Collab.)
WEIR	90B	PR D41 1384	A.J. Weir et al.	(Mark II Collab.)
ALBRECHT	89G	PL B229 304	H. Albrecht et al.	(ARGUS Collab.)
AVERY	89B	PL B223 470	P. Avery et al.	(CLEO Collab.)
BEBEK	89	PRL 62 8	C. Bebek et al.	(CLEO Collab.)
BORTOLETTO	89	PRL 62 2436	D. Bortoletto et al.	(CLEO Collab.)
ALBRECHT	88F	PL B209 119	H. Albrecht et al.	(ARGUS Collab.)
ALBRECHT	88K	PL B215 424	H. Albrecht et al.	(ARGUS Collab.)
ALBRECHT	87C	PL B185 218	H. Albrecht et al.	(ARGUS Collab.)
ALBRECHT	87D	PL B199 451	H. Albrecht et al.	(ARGUS Collab.)
AVERY	87	PL B183 429	P. Avery et al.	(CLEO Collab.)
BEBEK	87	PR D36 1289	C. Bebek et al.	(CLEO Collab.)
ALAM	86	PR D34 3379	M.S. Alam et al.	(CLEO Collab.)
PDG	86	PL 170B 1	M. Aguilar-Benitez et al.	(CERN, CIT+)
GILES	84	PR D30 2279	R. Giles et al.	(CLEO Collab.)

5 CSORNA 00 uses fully reconstructed 135 $B^0 \rightarrow J/\psi(\ell) K_S^0$ events and invariant masses without beam constraint.
 6 ALBRECHT 90J assumes 10580 for $\Upsilon(4S)$ mass. Supersedes ALBRECHT 87c and ALBRECHT 87D.
 7 Found using fully reconstructed decays with J/ψ . ALBRECHT 87D assume $m_{\Upsilon(4S)} = 10577$ MeV.

$m_{B^0} - m_{B^+}$

VALUE (MeV)	DOCUMENT ID	TECN	COMMENT
0.31 ± 0.05 OUR FIT			
0.32 ± 0.05 OUR AVERAGE			
0.20 ± 0.17 ± 0.11	1 AAIJ	12E LHCb	$p\bar{p}$ at 7 TeV
0.33 ± 0.05 ± 0.03	2 AUBERT	08AF BABR	$e^+e^- \rightarrow \Upsilon(4S)$
0.53 ± 0.67 ± 0.14	3 ACOSTA	06 CDF	$p\bar{p}$ at 1.96 TeV
0.41 ± 0.25 ± 0.19	ALAM	94 CLE2	$e^+e^- \rightarrow \Upsilon(4S)$
-0.4 ± 0.6 ± 0.5	BORTOLETTO92	CLEO	$e^+e^- \rightarrow \Upsilon(4S)$
-0.9 ± 1.2 ± 0.5	ALBRECHT	90J ARG	$e^+e^- \rightarrow \Upsilon(4S)$
2.0 ± 1.1 ± 0.3	4 BEBEK	87 CLEO	$e^+e^- \rightarrow \Upsilon(4S)$

1 Uses exclusively reconstructed final states containing a $J/\psi \rightarrow \mu^+\mu^-$ decay.
 2 Uses the B -momentum distributions in the e^+e^- rest frame.
 3 Uses exclusively reconstructed final states containing a $J/\psi \rightarrow \mu^+\mu^-$ decays.
 4 BEBEK 87 actually measure the difference between half of E_{cm} and the B^\pm or B^0 mass, so the $m_{B^0} - m_{B^\pm}$ is more accurate. Assume $m_{\Upsilon(4S)} = 10580$ MeV.

$m_{B_H^0} - m_{B_L^0}$

See the $B^0-\bar{B}^0$ MIXING PARAMETERS section near the end of these B^0 Listings.

B^0 MEAN LIFE

See $B^\pm/B^0/B_s^0/b$ -baryon ADMIXTURE section for data on B -hadron mean life averaged over species of bottom particles.

"OUR EVALUATION" is an average using rescaled values of the data listed below. The average and rescaling were performed by the Heavy Flavor Averaging Group (HFLAV) and are described at <https://hflav.web.cern.ch/>. The averaging/rescaling procedure takes into account correlations between the measurements and asymmetric lifetime errors.

VALUE (10^{-12} s)	EVTS	DOCUMENT ID	TECN	COMMENT
1.519 ± 0.004 OUR EVALUATION				
1.515 ± 0.005 ± 0.006	1	SIRUNYAN	18BY CMS	$p\bar{p}$ at 8 TeV
1.534 ± 0.019 ± 0.021	2	ABAZOV	15A D0	$p\bar{p}$ at 1.96 TeV
1.499 ± 0.013 ± 0.005	3	AAIJ	14E LHCb	$p\bar{p}$ at 7 TeV
1.524 ± 0.006 ± 0.004	4	AAIJ	14E LHCb	$p\bar{p}$ at 7 TeV
1.524 ± 0.011 ± 0.004	5	AAIJ	14R LHCb	$p\bar{p}$ at 7 TeV
1.509 ± 0.012 ± 0.018	6	AAD	13U ATLAS	$p\bar{p}$ at 7 TeV
1.508 ± 0.025 ± 0.043	7	ABAZOV	12U D0	$p\bar{p}$ at 1.96 TeV
1.507 ± 0.010 ± 0.008	8	AALTONEN	11 CDF	$p\bar{p}$ at 1.96 TeV
1.414 ± 0.018 ± 0.034	9	ABAZOV	09E D0	$p\bar{p}$ at 1.96 TeV
1.504 ± 0.013 +0.018 -0.013	10	AUBERT	06G BABR	$e^+e^- \rightarrow \Upsilon(4S)$
1.534 ± 0.008 ± 0.010	11	ABE	05B BELL	$e^+e^- \rightarrow \Upsilon(4S)$
1.531 ± 0.021 ± 0.031	12	ABDALLAH	04E DLPH	$e^+e^- \rightarrow Z$
1.523 +0.024 -0.023 ± 0.022	13	AUBERT	03C BABR	$e^+e^- \rightarrow \Upsilon(4S)$
1.533 ± 0.034 ± 0.038	14	AUBERT	03H BABR	$e^+e^- \rightarrow \Upsilon(4S)$
1.497 ± 0.073 ± 0.032	15	ACOSTA	02C CDF	$p\bar{p}$ at 1.8 TeV
1.529 ± 0.012 ± 0.029	16	AUBERT	02H BABR	$e^+e^- \rightarrow \Upsilon(4S)$
1.546 ± 0.032 ± 0.022	17	AUBERT	01F BABR	$e^+e^- \rightarrow \Upsilon(4S)$
1.541 ± 0.028 ± 0.023	18	ABBIENDI,G	00B OPAL	$e^+e^- \rightarrow Z$
1.518 ± 0.053 ± 0.034	19	BARATE	00R ALEP	$e^+e^- \rightarrow Z$
1.523 ± 0.057 ± 0.053	20	ABBIENDI	99J OPAL	$e^+e^- \rightarrow Z$
1.474 ± 0.039 +0.052 -0.051	21	ABE	98Q CDF	$p\bar{p}$ at 1.8 TeV
1.52 ± 0.06 ± 0.04	22	ACCIAARRI	98S L3	$e^+e^- \rightarrow Z$
1.64 ± 0.08 ± 0.08	23	ABE	97J SLD	$e^+e^- \rightarrow Z$
1.532 ± 0.041 ± 0.040	24	ABREU	97F DLPH	$e^+e^- \rightarrow Z$
1.25 +0.15 -0.13 ± 0.05	25	BUSKULIC	96J ALEP	$e^+e^- \rightarrow Z$
1.49 +0.17 +0.08 -0.15 -0.06 ± 0.05	26	BUSKULIC	96J ALEP	$e^+e^- \rightarrow Z$
1.61 +0.14 -0.13 ± 0.08	27,21	ABREU	95Q DLPH	$e^+e^- \rightarrow Z$
1.63 ± 0.14 ± 0.13	28	ADAM	95S DLPH	$e^+e^- \rightarrow Z$
1.53 ± 0.12 ± 0.08	29,23	AKERS	95T OPAL	$e^+e^- \rightarrow Z$
••• We do not use the following data for averages, fits, limits, etc. •••				
1.501 +0.078 -0.074 ± 0.050	30	ABAZOV	07s D0	Repl. by ABAZOV 12u
1.524 ± 0.030 ± 0.016	31	ABULENCIA	07A CDF	Repl. by AALTONEN 11
1.473 +0.052 -0.055 ± 0.023	32	ABAZOV	05B D0	Repl. by ABAZOV 05w
1.40 +0.11 -0.10 ± 0.03	33	ABAZOV	05c D0	Repl. by ABAZOV 07s
1.530 ± 0.043 ± 0.023	34	ABAZOV	05W D0	Repl. by ABAZOV 09E
1.54 ± 0.05 ± 0.02	35	ACOSTA	05 CDF	Repl. by AALTONEN 11
1.554 ± 0.030 ± 0.019	36	ABE	02H BELL	Repl. by ABE 05b
1.58 ± 0.09 ± 0.02	37	ABE	98B CDF	Repl. by ACOSTA 02c

B^0

$I(J^P) = \frac{1}{2}(0^-)$

Quantum numbers not measured. Values shown are quark-model predictions.

See also the B^\pm/B^0 ADMIXTURE and $B^\pm/B^0/B_s^0/b$ -baryon ADMIXTURE sections.

See the Note "Production and Decay of b -flavored Hadrons" at the beginning of the B^\pm Particle Listings and the Note " $B^0-\bar{B}^0$ Mixing" near the end of the B^0 Particle Listings.

B^0 MASS

The fit uses m_{B^+} , ($m_{B^0} - m_{B^+}$), and m_{B^0} to determine m_{B^+} , m_{B^0} , and the mass difference.

VALUE (MeV)	EVTS	DOCUMENT ID	TECN	COMMENT
5279.65 ± 0.12 OUR FIT				
5279.63 ± 0.20 OUR AVERAGE				
5279.74 ± 0.30 ± 0.10	1	AAIJ	19U LHCb	$p\bar{p}$ at 7, 8, 13 TeV
5279.6 ± 0.2 ± 1.0	2	AAD	13U ATLAS	$p\bar{p}$ at 7 TeV
5279.58 ± 0.15 ± 0.28	3	AAIJ	12E LHCb	$p\bar{p}$ at 7 TeV
5279.63 ± 0.53 ± 0.33	4	ACOSTA	06 CDF	$p\bar{p}$ at 1.96 TeV
5279.1 ± 0.7 ± 0.3	135	5 CSORNA	00 CLE2	$e^+e^- \rightarrow \Upsilon(4S)$
5281.3 ± 2.2 ± 1.4	51	ABE	96B CDF	$p\bar{p}$ at 1.8 TeV
••• We do not use the following data for averages, fits, limits, etc. •••				
5279.2 ± 0.54 ± 2.0	340	ALAM	94 CLE2	$e^+e^- \rightarrow \Upsilon(4S)$
5278.0 ± 0.4 ± 2.0		BORTOLETTO92	CLEO	$e^+e^- \rightarrow \Upsilon(4S)$
5279.6 ± 0.7 ± 2.0	40	6 ALBRECHT	90J ARG	$e^+e^- \rightarrow \Upsilon(4S)$
5278.2 ± 1.0 ± 3.0	40	ALBRECHT	87c ARG	$e^+e^- \rightarrow \Upsilon(4S)$
5279.5 ± 1.6 ± 3.0	7	7 ALBRECHT	87D ARG	$e^+e^- \rightarrow \Upsilon(4S)$
5280.6 ± 0.8 ± 2.0		BEBEK	87 CLEO	$e^+e^- \rightarrow \Upsilon(4S)$

1 Uses $B^0 \rightarrow J/\psi p\bar{p}$ decays.
 2 Measured with $B_d^0 \rightarrow J/\psi(\mu^+\mu^-) K_S^0(\pi^+\pi^-)$ decays.
 3 Uses $B^0 \rightarrow J/\psi K^0$ fully reconstructed decays.
 4 Uses exclusively reconstructed final states containing a $J/\psi \rightarrow \mu^+\mu^-$ decays.

Meson Particle Listings

 B^0

1.54 ± 0.08 ± 0.06	17	ABE	96c	CDF	Repl. by ABE 98Q	
1.55 ± 0.06 ± 0.03	25	BUSKULIC	96J	ALEP	$e^+e^- \rightarrow Z$	
1.61 ± 0.07 ± 0.04	17	BUSKULIC	96J	ALEP	Repl. by BARATE 00R	
1.62 ± 0.12	26	ADAM	95	DLPH	$e^+e^- \rightarrow Z$	
1.57 ± 0.18 ± 0.08	121	14	ABE	94D	CDF	Repl. by ABE 98B
1.17 $^{+0.29}_{-0.23}$ ± 0.16	96	17	ABREU	93D	DLPH	Sup. by ABREU 95Q
1.55 ± 0.25 ± 0.18	76	22	ABREU	93G	DLPH	Sup. by ADAM 95
1.51 $^{+0.24}_{-0.23}$ ± 0.12 $^{+0.07}_{-0.14}$	78	17	ACTON	93c	OPAL	Sup. by AKERS 95T
1.52 $^{+0.20}_{-0.18}$ ± 0.07 $^{+0.07}_{-0.13}$	77	17	BUSKULIC	93D	ALEP	Sup. by BUSKULIC 96J
1.20 $^{+0.52}_{-0.36}$ ± 0.16 $^{+0.16}_{-0.14}$	15	27	WAGNER	90	MRK2	$E_{\text{cm}}^{\text{ee}} = 29$ GeV
0.82 $^{+0.57}_{-0.37}$ ± 0.27	28	AVERRILL	89	HRS	$E_{\text{cm}}^{\text{ee}} = 29$ GeV	

- Measured using $B^0 \rightarrow J/\psi K^*(892)^0$ and $B^0 \rightarrow J/\psi K_S^0$ decays.
- Measured using $B^0 \rightarrow D^-\mu^+\nu_X$ decays.
- Measured mean life using $B^0 \rightarrow J/\psi K_S^0$ decays.
- Measured using $B^0 \rightarrow J/\psi K^*0$ decays.
- Measured using $B^0 \rightarrow K^+\pi^-$ decays.
- Measured with $B_d^0 \rightarrow J/\psi(\mu^+\mu^-)K_S^0(\pi^+\pi^-)$ decays.
- Measured mean life using fully reconstructed decays ($J/\psi K^*$).
- Measured mean life using $B^0 \rightarrow J/\psi K^*0$ decays.
- Measured using a simultaneous fit of the B^0 lifetime and $\bar{B}^0 B^0$ oscillation frequency Δm_d in the partially reconstructed $B^0 \rightarrow D^{*-}\ell\nu$ decays.
- Measurement performed using a combined fit of CP -violation, mixing and lifetimes.
- Measurement performed using an inclusive reconstruction and B flavor identification technique.
- AUBERT 03c uses a sample of approximately 14,000 exclusively reconstructed $B^0 \rightarrow D^*(2010)^-\ell\nu$ and simultaneously measures the lifetime and oscillation frequency.
- Measurement performed with decays $B^0 \rightarrow D^{*-}\pi^+$ and $B^0 \rightarrow D^{*-}\rho^+$ using a partial reconstruction technique.
- Measured mean life using fully reconstructed decays.
- Data analyzed using partially reconstructed $\bar{B}^0 \rightarrow D^{*+}\ell^-\bar{\nu}$ decays.
- Events are selected in which one B meson is fully reconstructed while the second B meson is reconstructed inclusively.
- Data analyzed using $D/D^* \ell X$ event vertices.
- Data analyzed using charge of secondary vertex.
- Data analyzed using inclusive $D/D^* \ell X$.
- Measured mean life using partially reconstructed $D^{*-}\pi^+ X$ vertices.
- ABREU 95Q assumes $B(B^0 \rightarrow D^{*-}\ell^+\nu_\ell) = 3.2 \pm 1.7\%$.
- Data analyzed using vertex-charge technique to tag B charge.
- AKERS 95T assumes $B(B^0 \rightarrow D_s^{*+}D^0(*)^0) = 5.0 \pm 0.9\%$ to find B^+ / B^0 yield.
- Measured using the time-dependent angular analysis of $B_d^0 \rightarrow J/\psi K^*0$ decays.
- Combined result of $D/D^* \ell X$ analysis, fully reconstructed B analysis, and partially reconstructed $D^{*-}\pi^+ X$ analysis.
- Combined ABREU 95Q and ADAM 95 result.
- WAGNER 90 tagged B^0 mesons by their decays into $D^{*-}e^+\nu$ and $D^{*-}\mu^+\nu$ where the D^{*-} is tagged by its decay into $\pi^-\bar{D}^0$.
- AVERRILL 89 is an estimate of the B^0 mean lifetime assuming that $B^0 \rightarrow D^{*+} + X$ always.

 $\tau_{B^0} / \tau_{\bar{B}^0}$

VALUE	DOCUMENT ID	TECN	COMMENT
1.000 ± 0.008 ± 0.009	1 AAIJ	14E	LHCB pp at 7 TeV

- Measured using $B^0 \rightarrow J/\psi K^*0$ decays.

MEAN LIFE RATIO τ_{B^+} / τ_{B^0} τ_{B^+} / τ_{B^0} (direct measurements)

"OUR EVALUATION" is an average using rescaled values of the data listed below. The average and rescaling were performed by the Heavy Flavor Averaging Group (HFLAV) and are described at <https://hflav.web.cern.ch/>. The averaging/rescaling procedure takes into account correlations between the measurements and asymmetric lifetime errors.

VALUE	EVTS	DOCUMENT ID	TECN	COMMENT
1.076 ± 0.004 OUR EVALUATION				
1.074 ± 0.005 ± 0.003	1	AAIJ	14E	LHCB pp at 7 TeV
1.088 ± 0.009 ± 0.004	2	AALTONEN	11	CDF $p\bar{p}$ at 1.96 TeV
1.080 ± 0.016 ± 0.014	3	ABAZOV	05D	D0 $p\bar{p}$ at 1.96 TeV
1.066 ± 0.008 ± 0.008	4	ABE	05B	BELL $e^+e^- \rightarrow \Upsilon(4S)$
1.060 ± 0.021 ± 0.024	5	ABDALLAH	04E	DLPH $e^+e^- \rightarrow Z$
1.093 ± 0.066 ± 0.028	6	ACOSTA	02c	CDF $p\bar{p}$ at 1.8 TeV
1.082 ± 0.026 ± 0.012	7	AUBERT	01F	BABR $e^+e^- \rightarrow \Upsilon(4S)$
1.085 ± 0.059 ± 0.018	3	BARATE	00R	ALEP $e^+e^- \rightarrow Z$
1.079 ± 0.064 ± 0.041	8	ABBIENDI	99J	OPAL $e^+e^- \rightarrow Z$
1.110 ± 0.056 $^{+0.033}_{-0.030}$	3	ABE	98Q	CDF $p\bar{p}$ at 1.8 TeV
1.09 ± 0.07 ± 0.03	8	ACCIARRI	98S	L3 $e^+e^- \rightarrow Z$
1.01 ± 0.07 ± 0.06	8	ABE	97J	SLD $e^+e^- \rightarrow Z$
1.27 $^{+0.23}_{-0.19}$ ± 0.03 $^{+0.03}_{-0.02}$	6	BUSKULIC	96J	ALEP $e^+e^- \rightarrow Z$
1.00 $^{+0.17}_{-0.15}$ ± 0.10	3,9	ABREU	95Q	DLPH $e^+e^- \rightarrow Z$
1.06 $^{+0.13}_{-0.11}$ ± 0.10	10	ADAM	95	DLPH $e^+e^- \rightarrow Z$
0.99 ± 0.14 $^{+0.05}_{-0.04}$	3,11	AKERS	95T	OPAL $e^+e^- \rightarrow Z$

• • • We do not use the following data for averages, fits, limits, etc. • • •

1.091 ± 0.023 ± 0.014	7	ABE	02H	BELL	Repl. by ABE 05B	
1.06 ± 0.07 ± 0.02	6	ABE	98B	CDF	Repl. by ACOSTA 02c	
1.01 ± 0.11 ± 0.02	3	ABE	96C	CDF	Repl. by ABE 98Q	
1.03 ± 0.08 ± 0.02	12	BUSKULIC	96J	ALEP	$e^+e^- \rightarrow Z$	
0.98 ± 0.08 ± 0.03	3	BUSKULIC	96J	ALEP	Repl. by BARATE 00R	
1.02 ± 0.16 ± 0.05	269	6	ABE	94D	CDF	Repl. by ABE 98B
1.11 $^{+0.51}_{-0.39}$ ± 0.11	188	3	ABREU	93D	DLPH	Sup. by ABREU 95Q
1.01 $^{+0.29}_{-0.22}$ ± 0.12	253	10	ABREU	93G	DLPH	Sup. by ADAM 95
1.0 $^{+0.33}_{-0.25}$ ± 0.08	130		ACTON	93c	OPAL	Sup. by AKERS 95T
0.96 $^{+0.19}_{-0.15}$ $^{+0.18}_{-0.12}$	154	3	BUSKULIC	93D	ALEP	Sup. by BUSKULIC 96J

- Measured using $B \rightarrow J/\psi K^*$ decays.
- Measured mean life using fully reconstructed decays ($J/\psi K^*$).
- Data analyzed using $D/D^* \mu X$ vertices.
- Measurement performed using a combined fit of CP -violation, mixing and lifetimes.
- Measurement performed using an inclusive reconstruction and B flavor identification technique.
- Measured using fully reconstructed decays.
- Events are selected in which one B meson is fully reconstructed while the second B meson is reconstructed inclusively.
- Data analyzed using charge of secondary vertex.
- ABREU 95Q assumes $B(B^0 \rightarrow D^{*-}\ell^+\nu_\ell) = 3.2 \pm 1.7\%$.
- Data analyzed using vertex-charge technique to tag B charge.
- AKERS 95T assumes $B(B^0 \rightarrow D_s^{*+}D^0(*)^0) = 5.0 \pm 0.9\%$ to find B^+ / B^0 yield.
- Combined result of $D/D^* \ell X$ analysis and fully reconstructed B analysis.

 τ_{B^+} / τ_{B^0} (inferred from branching fractions)

These measurements are inferred from the branching fractions for semileptonic decay or other spectator-dominated decays by assuming that the rates for such decays are equal for B^0 and B^+ . We do not use measurements which assume equal production of B^0 and B^+ because of the large uncertainty in the production ratio.

"OUR EVALUATION" has been obtained by the Heavy Flavor Averaging Group (HFLAV) by taking into account correlations between measurements.

VALUE	CL%	EVTS	DOCUMENT ID	TECN	COMMENT		
1.076 ± 0.034 OUR EVALUATION							
1.07 ± 0.04 OUR AVERAGE							
1.07 ± 0.04 ± 0.03			URQUIJO	07	BELL $e^+e^- \rightarrow \Upsilon(4S)$		
1.067 ± 0.041 ± 0.033			AUBERT,B	06Y	BABR $e^+e^- \rightarrow \Upsilon(4S)$		
• • • We do not use the following data for averages, fits, limits, etc. • • •							
0.95 $^{+0.117}_{-0.080}$ ± 0.091			1	ARTUSO	97	CLE2 $e^+e^- \rightarrow \Upsilon(4S)$	
1.15 ± 0.17 ± 0.06			2	JESSOP	97	CLE2 $e^+e^- \rightarrow \Upsilon(4S)$	
0.93 ± 0.18 ± 0.12			3	ATHANAS	94	CLE2	Sup. by ARTUSO 97
0.91 ± 0.27 ± 0.21			4	ALBRECHT	92c	ARG	$e^+e^- \rightarrow \Upsilon(4S)$
1.0 ± 0.4		29	4,5	ALBRECHT	92G	ARG	$e^+e^- \rightarrow \Upsilon(4S)$
0.89 ± 0.19 ± 0.13			4	FULTON	91	CLEO	$e^+e^- \rightarrow \Upsilon(4S)$
1.00 ± 0.23 ± 0.14			4	ALBRECHT	89L	ARG	$e^+e^- \rightarrow \Upsilon(4S)$
0.49 to 2.3		90	6	BEAN	87B	CLEO	$e^+e^- \rightarrow \Upsilon(4S)$

- ARTUSO 97 uses partial reconstruction of $B \rightarrow D^* \ell \nu_\ell$ and independent of B^0 and B^+ production fraction.
- Assumes equal production of B^+ and B^0 at the $\Upsilon(4S)$.
- ATHANAS 94 uses events tagged by fully reconstructed B^- decays and partially or fully reconstructed B^0 decays.
- Assumes equal production of B^0 and B^+ .
- ALBRECHT 92G data analyzed using $B \rightarrow D_s \bar{D}, D_s \bar{D}^*, D_s^* \bar{D}, D_s^* \bar{D}^*$ events.
- BEAN 87B assume the fraction of $B^0 \bar{B}^0$ events at the $\Upsilon(4S)$ is 0.41.

 $\Delta\Gamma_{B_d^0} / \Gamma_{B_d^0}$

$\Gamma_{B_d^0}$ and $\Delta\Gamma_{B_d^0}$ are the decay rate average and difference between two B_d^0 CP eigenstates (light – heavy). The λ_{CP} characterizes B^0 and \bar{B}^0 decays to states of charmonium plus K_L^0 , see the review on "CP Violation" in the reviews section.

"OUR EVALUATION" has been obtained by the Heavy Flavor Averaging Group (HFLAV) by taking into account correlations between measurements.

VALUE (units 10^{-2})	CL%	DOCUMENT ID	TECN	COMMENT	
0.1 ± 1.0 OUR EVALUATION					
0.1 ± 1.0 OUR AVERAGE					
3.4 ± 2.3 ± 2.4		1	SIRUNYAN	18BY	CMS pp at 8 TeV
– 0.1 ± 1.1 ± 0.9		2	AABOUD	16G	ATLS pp at 7, 8 TeV
– 4.4 ± 2.5 ± 1.1		3	AAIJ	14E	LHCB pp at 7 TeV
1.7 ± 1.8 ± 1.1		4	HIGUCHI	12	BELL $e^+e^- \rightarrow \Upsilon(4S)$
0.8 ± 3.7 ± 1.8		5	AUBERT,B	04C	BABR $e^+e^- \rightarrow \Upsilon(4S)$
0 ± 0.9		6	ABDALLAH	03B	DLPH $e^+e^- \rightarrow Z$

• • • We do not use the following data for averages, fits, limits, etc. • • •
 0.50 ± 1.38 ABAZOV 14 D0 $p\bar{p}$ at 1.96 TeV
 < 80 95 7 BEHRENS 00B CLE2 $e^+e^- \rightarrow \Upsilon(4S)$
¹ Measured using $B^0 \rightarrow J/\psi K^*(892)^0$ and $B^0 \rightarrow J/\psi K_S^0$ decays, and assuming $\beta = 21.9 \pm 0.7$ degrees.
² Measured from the ratio of decay time distributions of $B^0 \rightarrow J/\psi K_S^0$ and $B^0 \rightarrow J/\psi K^{*0}$ decays.
³ Measured using the effective lifetimes of $B^0 \rightarrow J/\psi K_S^0$ and $B^0 \rightarrow J/\psi K^{*0}$ decays.
⁴ Reports $-\Delta\Gamma_d/\Gamma_d$ using $B^0 \rightarrow J/\psi K_S^0, J/\psi K_L^0, D^-\pi^+, D^{*-}\pi^+, D^{*-}\rho^+$, and $D^{*-}\ell^+\nu$ decays.
⁵ Corresponds to 90% confidence range [-0.084, 0.068].
⁶ Used the measured $\tau_{B^0} = 1.55 \pm 0.03$ ps. Corresponds to an upper limit of < 0.18 at 95% C.L.
⁷ BEHRENS 00B uses high-momentum lepton tags and partially reconstructed $\bar{B}^0 \rightarrow D^{*+}\pi^-, \rho^-$ decays to determine the flavor of the B meson. Assumes $\Delta_{md} = 0.478 \pm 0.018$ ps⁻¹ and $\tau_{B^0} = 1.548 \pm 0.032$ ps.

B^0 DECAY MODES

\bar{B}^0 modes are charge conjugates of the modes below. Reactions indicate the weak decay vertex and do not include mixing. Modes which do not identify the charge state of the B are listed in the B^\pm/B^0 ADMIXTURE section.

The branching fractions listed below assume 50% $B^0\bar{B}^0$ and 50% B^+B^- production at the $\Upsilon(4S)$. We have attempted to bring older measurements up to date by rescaling their assumed $\Upsilon(4S)$ production ratio to 50:50 and their assumed D, D_s, D^* , and ψ branching ratios to current values whenever this would affect our averages and best limits significantly.

Indentation is used to indicate a subchannel of a previous reaction. All resonant subchannels have been corrected for resonance branching fractions to the final state so the sum of the subchannel branching fractions can exceed that of the final state.

For inclusive branching fractions, e.g., $B \rightarrow D^\pm X$, the values usually are multiplicities, not branching fractions. They can be greater than one.

Mode	Fraction (Γ_i/Γ)	Scale factor/ Confidence level
Γ_1 $\ell^+ \nu_\ell X$	[a] (10.33 ± 0.28) %	
Γ_2 $e^+ \nu_e X_c$	(10.1 ± 0.4) %	
Γ_3 $D \ell^+ \nu_\ell X$	(9.4 ± 0.9) %	
Γ_4 $D^- \ell^+ \nu_\ell$	[a] (2.31 ± 0.10) %	
Γ_5 $D^- \tau^+ \nu_\tau$	(1.08 ± 0.23) %	
Γ_6 $D^*(2010)^- \ell^+ \nu_\ell$	[a] (5.05 ± 0.14) %	
Γ_7 $D^*(2010)^- \tau^+ \nu_\tau$	(1.57 ± 0.09) %	S=1.1
Γ_8 $\bar{D}^0 \pi^- \ell^+ \nu_\ell$	(4.1 ± 0.5) × 10 ⁻³	
Γ_9 $D_0^*(2300)^- \ell^+ \nu_\ell, D_0^{*-} \rightarrow \bar{D}^0 \pi^-$	(3.0 ± 1.2) × 10 ⁻³	S=1.8
Γ_{10} $D_2^*(2460)^- \ell^+ \nu_\ell, D_2^{*-} \rightarrow \bar{D}^0 \pi^-$	(1.21 ± 0.33) × 10 ⁻³	S=1.8
Γ_{11} $\bar{D}^{(*)0} n \pi \ell^+ \nu_\ell (n \geq 1)$	(2.3 ± 0.5) %	
Γ_{12} $\bar{D}^{*0} \pi^- \ell^+ \nu_\ell$	(5.8 ± 0.8) × 10 ⁻³	S=1.4
Γ_{13} $D_1(2420)^- \ell^+ \nu_\ell, D_1^- \rightarrow \bar{D}^{*0} \pi^-$	(2.80 ± 0.28) × 10 ⁻³	
Γ_{14} $D_1'(2430)^- \ell^+ \nu_\ell, D_1'^- \rightarrow \bar{D}^{*0} \pi^-$	(3.1 ± 0.9) × 10 ⁻³	
Γ_{15} $D_2^*(2460)^- \ell^+ \nu_\ell, D_2^{*-} \rightarrow \bar{D}^{*0} \pi^-$	(6.8 ± 1.2) × 10 ⁻⁴	
Γ_{16} $D^- \pi^+ \pi^- \ell^+ \nu_\ell$	(1.3 ± 0.5) × 10 ⁻³	
Γ_{17} $D^{*-} \pi^+ \pi^- \ell^+ \nu_\ell$	(1.4 ± 0.5) × 10 ⁻³	
Γ_{18} $\rho^- \ell^+ \nu_\ell$	[a] (2.94 ± 0.21) × 10 ⁻⁴	
Γ_{19} $\pi^- \ell^+ \nu_\ell$	[a] (1.50 ± 0.06) × 10 ⁻⁴	
Γ_{20} $\pi^- \mu^+ \nu_\mu$		
Γ_{21} $\pi^- \tau^+ \nu_\tau$	< 2.5 × 10 ⁻⁴	CL=90%
Inclusive modes		
Γ_{22} $K^\pm X$	(78 ± 8) %	
Γ_{23} $D^0 X$	(8.1 ± 1.5) %	
Γ_{24} $\bar{D}^0 X$	(47.4 ± 2.8) %	
Γ_{25} $D^+ X$	< 3.9 %	CL=90%
Γ_{26} $D^- X$	(36.9 ± 3.3) %	
Γ_{27} $D_s^+ X$	(10.3 ± 2.1 / 1.8) %	
Γ_{28} $D_s^- X$	< 2.6 %	CL=90%
Γ_{29} $\Lambda_c^+ X$	< 3.1 %	CL=90%
Γ_{30} $\bar{\Lambda}_c^- X$	(5.0 ± 2.1 / 1.5) %	
Γ_{31} $\bar{c} X$	(95 ± 5) %	
Γ_{32} $c X$	(24.6 ± 3.1) %	
Γ_{33} $\bar{c}/c X$	(119 ± 6) %	

D, D^* , or D_s modes

Γ_{34} $D^- \pi^+$	(2.52 ± 0.13) × 10 ⁻³	S=1.1
Γ_{35} $D^- \rho^+$	(7.6 ± 1.2) × 10 ⁻³	
Γ_{36} $D^- K^0 \pi^+$	(4.9 ± 0.9) × 10 ⁻⁴	
Γ_{37} $D^- K^*(892)^+$	(4.5 ± 0.7) × 10 ⁻⁴	
Γ_{38} $D^- \omega \pi^+$	(2.8 ± 0.6) × 10 ⁻³	
Γ_{39} $D^- K^+$	(1.86 ± 0.20) × 10 ⁻⁴	
Γ_{40} $D^- K^+ \pi^+ \pi^-$	(3.5 ± 0.8) × 10 ⁻⁴	
Γ_{41} $D^- K^+ \bar{K}^0$	< 3.1 × 10 ⁻⁴	CL=90%
Γ_{42} $D^- K^+ \bar{K}^*(892)^0$	(8.8 ± 1.9) × 10 ⁻⁴	
Γ_{43} $\bar{D}^0 \pi^+ \pi^-$	(8.8 ± 0.5) × 10 ⁻⁴	
Γ_{44} $D^*(2010)^- \pi^+$	(2.74 ± 0.13) × 10 ⁻³	
Γ_{45} $\bar{D}^0 K^+ K^-$	(5.9 ± 0.5) × 10 ⁻⁵	
Γ_{46} $D^- \pi^+ \pi^+ \pi^-$	(6.0 ± 0.7) × 10 ⁻³	S=1.1
Γ_{47} $(D^- \pi^+ \pi^+ \pi^-)$ nonresonant	(3.9 ± 1.9) × 10 ⁻³	
Γ_{48} $D^- \pi^+ \rho^0$	(1.1 ± 1.0) × 10 ⁻³	
Γ_{49} $D^- a_1(1260)^+$	(6.0 ± 3.3) × 10 ⁻³	
Γ_{50} $D^*(2010)^- \pi^+ \pi^0$	(1.5 ± 0.5) %	
Γ_{51} $D^*(2010)^- \rho^+$	(6.8 ± 0.9) × 10 ⁻³	
Γ_{52} $D^*(2010)^- K^+$	(2.12 ± 0.15) × 10 ⁻⁴	
Γ_{53} $D^*(2010)^- K^0 \pi^+$	(3.0 ± 0.8) × 10 ⁻⁴	
Γ_{54} $D^*(2010)^- K^*(892)^+$	(3.3 ± 0.6) × 10 ⁻⁴	
Γ_{55} $D^*(2010)^- K^+ \bar{K}^0$	< 4.7 × 10 ⁻⁴	CL=90%
Γ_{56} $D^*(2010)^- K^+ \bar{K}^*(892)^0$	(1.29 ± 0.33) × 10 ⁻³	
Γ_{57} $D^*(2010)^- \pi^+ \pi^+ \pi^-$	(7.21 ± 0.29) × 10 ⁻³	
Γ_{58} $(D^*(2010)^- \pi^+ \pi^+ \pi^-)$ non-resonant	(0.0 ± 2.5) × 10 ⁻³	
Γ_{59} $D^*(2010)^- \pi^+ \rho^0$	(5.7 ± 3.2) × 10 ⁻³	
Γ_{60} $D^*(2010)^- a_1(1260)^+$	(1.30 ± 0.27) %	
Γ_{61} $\bar{D}_1(2420)^0 \pi^- \pi^+, \bar{D}_1^0 \rightarrow D^{*-} \pi^+$	(1.47 ± 0.35) × 10 ⁻⁴	
Γ_{62} $D^*(2010)^- K^+ \pi^- \pi^+$	(4.7 ± 0.4) × 10 ⁻⁴	
Γ_{63} $D^*(2010)^- \pi^+ \pi^+ \pi^- \pi^0$	(1.76 ± 0.27) %	
Γ_{64} $D^{*-} 3\pi^+ 2\pi^-$	(4.7 ± 0.9) × 10 ⁻³	
Γ_{65} $D^*(2010)^- \omega \pi^+$	(2.46 ± 0.18) × 10 ⁻³	S=1.2
Γ_{66} $\bar{D}_1(2430)^0 \omega, \bar{D}_1^0 \rightarrow D^{*-} \pi^+$	(2.7 ± 0.8 / 0.4) × 10 ⁻⁴	
Γ_{67} $D^{*-} \rho(1450)^+, \rho^+ \rightarrow \omega \pi^+$	(1.07 ± 0.40 / 0.34) × 10 ⁻³	
Γ_{68} $\bar{D}_1(2420)^0 \omega, \bar{D}_1^0 \rightarrow D^{*-} \pi^+$	(7.0 ± 2.2) × 10 ⁻⁵	
Γ_{69} $\bar{D}_2^*(2460)^0 \omega, \bar{D}_2^0 \rightarrow D^{*-} \pi^+$	(4.0 ± 1.4) × 10 ⁻⁵	
Γ_{70} $D^{*-} b_1(1235)^+, b_1^+ \rightarrow \omega \pi^+$	< 7 × 10 ⁻⁵	CL=90%
Γ_{71} $\bar{D}^{*-} \pi^+$	[b] (1.9 ± 0.9) × 10 ⁻³	
Γ_{72} $D_1(2420)^- \pi^+, D_1^- \rightarrow \bar{D}^{*0} \pi^-$	(9.9 ± 2.0 / 2.5) × 10 ⁻⁵	
Γ_{73} $D_1(2420)^- \pi^+, D_1^- \rightarrow \bar{D}^{*0} \pi^-$	< 3.3 × 10 ⁻⁵	CL=90%
Γ_{74} $\bar{D}_2^*(2460)^- \pi^+, (D_2^*)^- \rightarrow \bar{D}^{*0} \pi^-$	(2.38 ± 0.16) × 10 ⁻⁴	
Γ_{75} $\bar{D}_0^*(2400)^- \pi^+, (D_0^*)^- \rightarrow \bar{D}^{*0} \pi^-$	(7.6 ± 0.8) × 10 ⁻⁵	
Γ_{76} $D_2^*(2460)^- \pi^+, (D_2^*)^- \rightarrow \bar{D}^{*0} \pi^-$	< 2.4 × 10 ⁻⁵	CL=90%
Γ_{77} $\bar{D}_s^*(2460)^- \rho^+$	< 4.9 × 10 ⁻³	CL=90%
Γ_{78} $D^0 \bar{D}^0$	(1.4 ± 0.7) × 10 ⁻⁵	
Γ_{79} $D^{*0} \bar{D}^0$	< 2.9 × 10 ⁻⁴	CL=90%
Γ_{80} $D^- D^+$	(2.11 ± 0.18) × 10 ⁻⁴	
Γ_{81} $D^\pm D^{*\mp}$ (CP -averaged)	(6.1 ± 0.6) × 10 ⁻⁴	
Γ_{82} $D^- D_s^+$	(7.2 ± 0.8) × 10 ⁻³	
Γ_{83} $D^*(2010)^- D_s^+$	(8.0 ± 1.1) × 10 ⁻³	
Γ_{84} $D^- D_s^{*+}$	(7.4 ± 1.6) × 10 ⁻³	
Γ_{85} $D^*(2010)^- D_s^{*+}$	(1.77 ± 0.14) %	
Γ_{86} $D_{s0}(2317)^- K^+, D_{s0}^- \rightarrow D_s^- \pi^0$	(4.2 ± 1.4) × 10 ⁻⁵	
Γ_{87} $D_{s0}(2317)^- \pi^+, D_{s0}^- \rightarrow D_s^- \pi^0$	< 2.5 × 10 ⁻⁵	CL=90%
Γ_{88} $D_{s,J}(2457)^- K^+, D_{s,J}^- \rightarrow D_s^- \pi^0$	< 9.4 × 10 ⁻⁶	CL=90%
Γ_{89} $D_{s,J}(2457)^- \pi^+, D_{s,J}^- \rightarrow D_s^- \pi^0$	< 4.0 × 10 ⁻⁶	CL=90%
Γ_{90} $D_s^- D_s^+$	< 3.6 × 10 ⁻⁵	CL=90%
Γ_{91} $D_s^{*-} D_s^+$	< 1.3 × 10 ⁻⁴	CL=90%
Γ_{92} $D_s^{*0} D_s^{*+}$	< 2.4 × 10 ⁻⁴	CL=90%
Γ_{93} $D_{s0}^+(2317)^+ D^-, D_{s0}^{*+} \rightarrow D_s^+ \pi^0$	(1.06 ± 0.16) × 10 ⁻³	S=1.1

Meson Particle Listings

B^0

Γ ₉₄	$D_{s0}(2317)+D^-, D_{s0}^+ \rightarrow D_s^{*+}\gamma$	< 9.5	$\times 10^{-4}$	CL=90%	Γ ₁₄₇	$[\pi^+ K^- \pi^+ \pi^-]_D K^{*0}$		
Γ ₉₅	$D_{s0}(2317)+D^*(2010)^-, D_{s0}^+ \rightarrow D_s^+ \pi^0$	(1.5 ± 0.6)	$\times 10^{-3}$		Γ ₁₄₈	$[K^+ \pi^- \pi^+ \pi^-]_D K^{*0}$		
Γ ₉₆	$D_{sJ}(2457)+D^-$	(3.5 ± 1.1)	$\times 10^{-3}$		Γ ₁₄₉	$\bar{D}^0 \pi^0$	(2.63 ± 0.14)	$\times 10^{-4}$
Γ ₉₇	$D_{sJ}(2457)+D^-, D_{sJ}^+ \rightarrow D_s^+ \gamma$	(6.5 ± 1.7)	$\times 10^{-4}$		Γ ₁₅₀	$\bar{D}^0 \rho^0$	(3.21 ± 0.21)	$\times 10^{-4}$
Γ ₉₈	$D_{sJ}(2457)+D^-, D_{sJ}^+ \rightarrow D_s^{*+}\gamma$	(6.5 ± 1.4)	$\times 10^{-4}$		Γ ₁₅₁	$\bar{D}^0 f_2$	(1.56 ± 0.21)	$\times 10^{-4}$
Γ ₉₉	$D_{sJ}(2457)+D^-, D_{sJ}^+ \rightarrow D_s^+ \pi^+ \pi^-$	< 6.0	$\times 10^{-4}$	CL=90%	Γ ₁₅₂	$\bar{D}^0 \eta$	(2.36 ± 0.32)	$\times 10^{-4}$
Γ ₁₀₀	$D_{sJ}(2457)+D^-, D_{sJ}^+ \rightarrow D_s^+ \pi^0$	< 2.0	$\times 10^{-4}$	CL=90%	Γ ₁₅₃	$\bar{D}^0 \eta'$	(1.38 ± 0.16)	$\times 10^{-4}$
Γ ₁₀₁	$D^*(2010)^- D_{sJ}(2457)^+$	(9.3 ± 2.2)	$\times 10^{-3}$		Γ ₁₅₄	$\bar{D}^0 \omega$	(2.54 ± 0.16)	$\times 10^{-4}$
Γ ₁₀₂	$D_{sJ}(2457)+D^*(2010), D_{sJ}^+ \rightarrow D_s^+ \gamma$	(2.3 ± 0.9)	$\times 10^{-3}$		Γ ₁₅₅	$D^0 \phi$	< 2.3	$\times 10^{-6}$
Γ ₁₀₃	$D^- D_{s1}(2536)^+, D_{s1}^+ \rightarrow D^{*0} K^+ + D^{*+} K^0$	(2.8 ± 0.7)	$\times 10^{-4}$		Γ ₁₅₆	$D^0 K^+ \pi^-$	(5.3 ± 3.2)	$\times 10^{-6}$
Γ ₁₀₄	$D^- D_{s1}(2536)^+, D_{s1}^+ \rightarrow D^{*0} K^+$	(1.7 ± 0.6)	$\times 10^{-4}$		Γ ₁₅₇	$D^0 K^*(892)^0$	(2.2 ± 0.9)	$\times 10^{-6}$
Γ ₁₀₅	$D^- D_{s1}(2536)^+, D_{s1}^+ \rightarrow D^{*+} K^0$	(2.6 ± 1.1)	$\times 10^{-4}$		Γ ₁₅₈	$\bar{D}^{*0} \gamma$	< 2.5	$\times 10^{-5}$
Γ ₁₀₆	$D^*(2010)^- D_{s1}(2536)^+, D_{s1}^+ \rightarrow D^{*0} K^+ + D^{*+} K^0$	(5.0 ± 1.4)	$\times 10^{-4}$		Γ ₁₅₉	$\bar{D}^*(2007)^0 \pi^0$	(2.2 ± 0.6)	$\times 10^{-4}$
Γ ₁₀₇	$D^*(2010)^- D_{s1}(2536)^+, D_{s1}^+ \rightarrow D^{*0} K^+$	(3.3 ± 1.1)	$\times 10^{-4}$		Γ ₁₆₀	$\bar{D}^*(2007)^0 \rho^0$	< 5.1	$\times 10^{-4}$
Γ ₁₀₈	$D^{*-} D_{s1}(2536)^+, D_{s1}^+ \rightarrow D^{*+} K^0$	(5.0 ± 1.7)	$\times 10^{-4}$		Γ ₁₆₁	$\bar{D}^*(2007)^0 \eta$	(2.3 ± 0.6)	$\times 10^{-4}$
Γ ₁₀₉	$D^- D_{sJ}(2573)^+, D_{sJ}^+ \rightarrow D^0 K^+$	(3.4 ± 1.8)	$\times 10^{-5}$		Γ ₁₆₂	$\bar{D}^*(2007)^0 \eta'$	(1.40 ± 0.22)	$\times 10^{-4}$
Γ ₁₁₀	$D^*(2010)^- D_{sJ}(2573)^+, D_{sJ}^+ \rightarrow D^0 K^+$	< 2	$\times 10^{-4}$	CL=90%	Γ ₁₆₃	$\bar{D}^*(2007)^0 \pi^+ \pi^-$	(6.2 ± 2.2)	$\times 10^{-4}$
Γ ₁₁₁	$D^- D_{sJ}(2700)^+, D_{sJ}^+ \rightarrow D^0 K^+$	(7.1 ± 1.2)	$\times 10^{-4}$		Γ ₁₆₄	$\bar{D}^*(2007)^0 K^0$	(3.6 ± 1.2)	$\times 10^{-5}$
Γ ₁₁₂	$D^+ \pi^-$	(7.4 ± 1.3)	$\times 10^{-7}$		Γ ₁₆₅	$\bar{D}^*(2007)^0 K^*(892)^0$	< 6.9	$\times 10^{-5}$
Γ ₁₁₃	$D_s^+ \pi^-$	(2.16 ± 0.26)	$\times 10^{-5}$		Γ ₁₆₆	$D^*(2007)^0 K^*(892)^0$	< 4.0	$\times 10^{-5}$
Γ ₁₁₄	$D_s^{*+} \pi^-$	(2.1 ± 0.4)	$\times 10^{-5}$	S=1.4	Γ ₁₆₇	$D^*(2007)^0 \pi^+ \pi^+ \pi^- \pi^-$	(2.7 ± 0.5)	$\times 10^{-3}$
Γ ₁₁₅	$D_s^+ \rho^-$	< 2.4	$\times 10^{-5}$	CL=90%	Γ ₁₆₈	$D^*(2010)^+ D^*(2010)^-$	(8.0 ± 0.6)	$\times 10^{-4}$
Γ ₁₁₆	$D_s^{*+} \rho^-$	(4.1 ± 1.3)	$\times 10^{-5}$		Γ ₁₆₉	$\bar{D}^*(2007)^0 \omega$	(3.6 ± 1.1)	$\times 10^{-4}$
Γ ₁₁₇	$D_s^+ a_0^-$	< 1.9	$\times 10^{-5}$	CL=90%	Γ ₁₇₀	$D^*(2010)^+ D^-$	(6.1 ± 1.5)	$\times 10^{-4}$
Γ ₁₁₈	$D_s^{*+} a_0^-$	< 3.6	$\times 10^{-5}$	CL=90%	Γ ₁₇₁	$D^*(2007)^0 \bar{D}^*(2007)^0$	< 9	$\times 10^{-5}$
Γ ₁₁₉	$D_s^+ a_1(1260)^-$	< 2.1	$\times 10^{-3}$	CL=90%	Γ ₁₇₂	$D^- D^0 K^+$	(1.07 ± 0.11)	$\times 10^{-3}$
Γ ₁₂₀	$D_s^+ a_1(1260)^-$	< 1.7	$\times 10^{-3}$	CL=90%	Γ ₁₇₃	$D^- D^*(2007)^0 K^+$	(3.5 ± 0.4)	$\times 10^{-3}$
Γ ₁₂₁	$D_s^+ a_2^-$	< 1.9	$\times 10^{-4}$	CL=90%	Γ ₁₇₄	$D^*(2010)^- D^0 K^+$	(2.47 ± 0.21)	$\times 10^{-3}$
Γ ₁₂₂	$D_s^+ a_2^-$	< 2.0	$\times 10^{-4}$	CL=90%	Γ ₁₇₅	$D^*(2010)^- D^*(2007)^0 K^+$	(1.06 ± 0.09)	%
Γ ₁₂₃	$D_s^- K^+$	(2.7 ± 0.5)	$\times 10^{-5}$	S=2.7	Γ ₁₇₆	$D^- D^+ K^0$	(7.5 ± 1.7)	$\times 10^{-4}$
Γ ₁₂₄	$D_s^{*-} K^+$	(2.19 ± 0.30)	$\times 10^{-5}$		Γ ₁₇₇	$D^*(2010)^- D^+ K^0 + D^- D^*(2010)^+ K^0$	(6.4 ± 0.5)	$\times 10^{-3}$
Γ ₁₂₅	$D_s^- K^*(892)^+$	(3.5 ± 1.0)	$\times 10^{-5}$		Γ ₁₇₈	$D^*(2010)^- D^*(2010)^+ K^0$	(8.1 ± 0.7)	$\times 10^{-3}$
Γ ₁₂₆	$D_s^{*-} K^*(892)^+$	(3.2 ± 1.3)	$\times 10^{-5}$		Γ ₁₇₉	$D^{*-} D_{s1}(2536)^+, D_{s1}^+ \rightarrow D^{*+} K^0$	(8.0 ± 2.4)	$\times 10^{-4}$
Γ ₁₂₇	$D_s^- \pi^+ K^0$	(9.7 ± 1.4)	$\times 10^{-5}$		Γ ₁₈₀	$\bar{D}^0 D^0 K^0$	(2.7 ± 1.1)	$\times 10^{-4}$
Γ ₁₂₈	$D_s^{*-} \pi^+ K^0$	< 1.10	$\times 10^{-4}$	CL=90%	Γ ₁₈₁	$\bar{D}^0 D^*(2007)^0 K^0 + \bar{D}^*(2007)^0 D^0 K^0$	(1.1 ± 0.5)	$\times 10^{-3}$
Γ ₁₂₉	$D_s^- K^+ \pi^+ \pi^-$	(1.7 ± 0.5)	$\times 10^{-4}$		Γ ₁₈₂	$\bar{D}^*(2007)^0 D^*(2007)^0 K^0$	(2.4 ± 0.9)	$\times 10^{-3}$
Γ ₁₃₀	$D_s^- \pi^+ K^*(892)^0$	< 3.0	$\times 10^{-3}$	CL=90%	Γ ₁₈₃	$(\bar{D} + \bar{D}^*)(D + D^*)K$	(3.68 ± 0.26)	%
Γ ₁₃₁	$D_s^{*-} \pi^+ K^*(892)^0$	< 1.6	$\times 10^{-3}$	CL=90%	Charmonium modes			
Γ ₁₃₂	$\bar{D}^0 K^0$	(5.2 ± 0.7)	$\times 10^{-5}$		Γ ₁₈₄	$\eta_c K^0$	(8.0 ± 1.1)	$\times 10^{-4}$
Γ ₁₃₃	$\bar{D}^0 K^+ \pi^-$	(8.8 ± 1.7)	$\times 10^{-5}$		Γ ₁₈₅	$\eta_c(1S) K^+ \pi^-$	(6.0 ± 0.7)	$\times 10^{-4}$
Γ ₁₃₄	$\bar{D}^0 K^*(892)^0$	(4.5 ± 0.6)	$\times 10^{-5}$		Γ ₁₈₆	$\eta_c(1S) K^+ \pi^-$ (NR)	(6.2 ± 1.3)	$\times 10^{-5}$
Γ ₁₃₅	$\bar{D}^0 K^*(1410)^0$	< 6.7	$\times 10^{-5}$	CL=90%	Γ ₁₈₇	$X(4100)^- K^+, X^- \rightarrow \eta_c \pi^-$	(2.0 ± 1.0)	$\times 10^{-5}$
Γ ₁₃₆	$\bar{D}^0 K_0^*(1430)^0$	(7 ± 7)	$\times 10^{-6}$		Γ ₁₈₈	$\eta_c(1S) K^*(1410)^0$	(1.9 ± 1.5)	$\times 10^{-4}$
Γ ₁₃₇	$\bar{D}^0 K_2^*(1430)^0$	(2.1 ± 0.9)	$\times 10^{-5}$		Γ ₁₈₉	$\eta_c(1S) K_0^*(1430)^0$	(1.6 ± 0.4)	$\times 10^{-4}$
Γ ₁₃₈	$D_0^*(2300)^- K^+, D_0^{*-} \rightarrow \bar{D}^0 \pi^-$	(1.9 ± 0.9)	$\times 10^{-5}$		Γ ₁₉₀	$\eta_c(1S) K_2^*(1430)^0$	(4.9 ± 2.2)	$\times 10^{-5}$
Γ ₁₃₉	$D_2^*(2460)^- K^+, D_2^{*-} \rightarrow \bar{D}^0 \pi^-$	(2.03 ± 0.35)	$\times 10^{-5}$		Γ ₁₉₁	$\eta_c(1S) K^*(1680)^0$	(3 ± 4)	$\times 10^{-5}$
Γ ₁₄₀	$D_3^*(2760)^- K^+, D_3^{*-} \rightarrow \bar{D}^0 \pi^-$	< 1.0	$\times 10^{-6}$	CL=90%	Γ ₁₉₂	$\eta_c(1S) K_0^*(1950)^0$	(4.4 ± 2.9)	$\times 10^{-5}$
Γ ₁₄₁	$\bar{D}^0 K^+ \pi^-$ nonresonant	< 3.7	$\times 10^{-5}$	CL=90%	Γ ₁₉₃	$\eta_c K^*(892)^0$	(5.2 ± 0.7)	$\times 10^{-4}$
Γ ₁₄₂	$[K^+ K^-]_D K^*(892)^0$	(4.2 ± 0.7)	$\times 10^{-5}$		Γ ₁₉₄	$\eta_c(2S) K_S^0, \eta_c \rightarrow p \bar{p} \pi^+ \pi^-$	(4.2 ± 1.4)	$\times 10^{-7}$
Γ ₁₄₃	$[\pi^+ \pi^-]_D K^*(892)^0$	(6.0 ± 1.1)	$\times 10^{-5}$		Γ ₁₉₅	$\eta_c(2S) K^*0$	< 3.9	$\times 10^{-4}$
Γ ₁₄₄	$[\pi^+ K^-]_D K^*(892)^0$				Γ ₁₉₆	$h_c(1P) K_S^0$	< 1.4	$\times 10^{-5}$
Γ ₁₄₅	$[K^+ \pi^-]_D K^*(892)^0$				Γ ₁₉₇	$h_c(1P) K^*0$	< 4	$\times 10^{-4}$
Γ ₁₄₆	$[\pi^+ \pi^- \pi^+ \pi^-]_D K^*0$	(4.6 ± 0.9)	$\times 10^{-5}$		Γ ₁₉₈	$J/\psi(1S) K^0$	(8.68 ± 0.30)	$\times 10^{-4}$
					Γ ₁₉₉	$J/\psi(1S) K^+ \pi^-$	(1.15 ± 0.05)	$\times 10^{-3}$
					Γ ₂₀₀	$J/\psi(1S) K^*(892)^0$	(1.27 ± 0.05)	$\times 10^{-3}$
					Γ ₂₀₁	$J/\psi(1S) \eta K_S^0$	(5.4 ± 0.9)	$\times 10^{-5}$
					Γ ₂₀₂	$J/\psi(1S) \eta' K_S^0$	< 2.5	$\times 10^{-5}$
					Γ ₂₀₃	$J/\psi(1S) \phi K^0$	(4.9 ± 1.0)	$\times 10^{-5}$
					Γ ₂₀₄	$J/\psi(1S) \omega K^0$	(2.3 ± 0.4)	$\times 10^{-4}$
					Γ ₂₀₅	$\chi_{c1}(3872) K^0, \chi_{c1} \rightarrow J/\psi \omega$	(6.0 ± 3.2)	$\times 10^{-6}$
					Γ ₂₀₆	$X(3915), X \rightarrow J/\psi \omega$	(2.1 ± 0.9)	$\times 10^{-5}$
					Γ ₂₀₇	$J/\psi(1S) K(1270)^0$	(1.3 ± 0.5)	$\times 10^{-3}$
					Γ ₂₀₈	$J/\psi(1S) \pi^0$	(1.66 ± 0.10)	$\times 10^{-5}$
					Γ ₂₀₉	$J/\psi(1S) \eta$	(1.08 ± 0.23)	$\times 10^{-5}$
					Γ ₂₁₀	$J/\psi(1S) \pi^+ \pi^-$	(3.94 ± 0.17)	$\times 10^{-5}$
					Γ ₂₁₁	$J/\psi(1S) \pi^+ \pi^-$ nonresonant	< 1.2	$\times 10^{-5}$
					Γ ₂₁₂	$J/\psi(1S) f_0(500), f_0 \rightarrow \pi \pi$	(8.8 ± 1.2)	$\times 10^{-6}$
					Γ ₂₁₃	$J/\psi(1S) f_2$	(3.3 ± 0.5)	$\times 10^{-6}$

Γ ₂₁₄	$J/\psi(1S)\rho^0$	$(2.55^{+0.18}_{-0.16}) \times 10^{-5}$		Γ ₂₇₁	$\chi_{c2}\pi^+\pi^-K^0$	< 1.70	$\times 10^{-4}$	CL=90%	
Γ ₂₁₅	$J/\psi(1S)f_0(980), f_0 \rightarrow \pi^+\pi^-$	< 1.1	$\times 10^{-6}$	CL=90%	Γ ₂₇₂	$\chi_{c2}\pi^-\pi^0K^+$	< 7.4	$\times 10^{-5}$	CL=90%
Γ ₂₁₆	$J/\psi(1S)\rho(1450)^0, \rho^0 \rightarrow \pi\pi$	$(2.9^{+1.6}_{-0.7}) \times 10^{-6}$		Γ ₂₇₃	$\psi(4660)K^0, \psi \rightarrow \Lambda_c^+\Lambda_c^-$	< 2.3	$\times 10^{-4}$	CL=90%	
Γ ₂₁₇	$J/\psi\rho(1700)^0, \rho^0 \rightarrow \pi^+\pi^-$	$(2.0 \pm 1.3) \times 10^{-6}$		Γ ₂₇₄	$\psi(4260)^0K^0, \psi^0 \rightarrow J/\psi\pi^+\pi^-$	< 1.7	$\times 10^{-5}$	CL=90%	
Γ ₂₁₈	$J/\psi(1S)\omega$	$(1.8^{+0.7}_{-0.5}) \times 10^{-5}$		K or K* modes					
Γ ₂₁₉	$J/\psi(1S)K^+K^-$	$(2.50 \pm 0.35) \times 10^{-6}$		Γ ₂₇₅	$K^+\pi^-$	$(1.96 \pm 0.05) \times 10^{-5}$			
Γ ₂₂₀	$J/\psi(1S)a_0(980), a_0 \rightarrow K^+K^-$	$(4.7 \pm 3.4) \times 10^{-7}$		Γ ₂₇₆	$K^0\pi^0$	$(9.9 \pm 0.5) \times 10^{-6}$			
Γ ₂₂₁	$J/\psi(1S)\phi$	< 1.9	$\times 10^{-7}$	CL=90%	Γ ₂₇₇	$\eta'K^0$	$(6.6 \pm 0.4) \times 10^{-5}$	S=1.4	
Γ ₂₂₂	$J/\psi(1S)\eta'(958)$	$(7.6 \pm 2.4) \times 10^{-6}$		Γ ₂₇₈	$\eta'K^*(892)^0$	$(2.8 \pm 0.6) \times 10^{-6}$			
Γ ₂₂₃	$J/\psi(1S)K^0\pi^+\pi^-$	$(4.3 \pm 0.4) \times 10^{-4}$		Γ ₂₇₉	$\eta'K^*(1430)^0$	$(6.3 \pm 1.6) \times 10^{-6}$			
Γ ₂₂₄	$J/\psi(1S)K^0K^-\pi^+ + c.c.$	< 2.1	$\times 10^{-5}$	CL=90%	Γ ₂₈₀	$\eta'K^*(1430)^0$	$(1.37 \pm 0.32) \times 10^{-5}$		
Γ ₂₂₅	$J/\psi(1S)K^0K^+K^-$	$(2.5 \pm 0.7) \times 10^{-5}$	S=1.8	Γ ₂₈₁	ηK^0	$(1.23^{+0.27}_{-0.24}) \times 10^{-6}$			
Γ ₂₂₆	$J/\psi(1S)K^0K^\pm\pi^\mp$			Γ ₂₈₂	$\eta K^*(892)^0$	$(1.59 \pm 0.10) \times 10^{-5}$			
Γ ₂₂₇	$J/\psi(1S)K^0\rho^0$	$(5.4 \pm 3.0) \times 10^{-4}$		Γ ₂₈₃	$\eta K^*(1430)^0$	$(1.10 \pm 0.22) \times 10^{-5}$			
Γ ₂₂₈	$J/\psi(1S)K^*(892)^+\pi^-$	$(8 \pm 4) \times 10^{-4}$		Γ ₂₈₄	$\eta K^*(1430)^0$	$(9.6 \pm 2.1) \times 10^{-6}$			
Γ ₂₂₉	$J/\psi(1S)\pi^+\pi^-\pi^+\pi^-$	$(1.42 \pm 0.12) \times 10^{-5}$		Γ ₂₈₅	ωK^0	$(4.8 \pm 0.4) \times 10^{-6}$			
Γ ₂₃₀	$J/\psi(1S)f_1(1285)$	$(8.4 \pm 2.1) \times 10^{-6}$		Γ ₂₈₆	$a_0(980)^0K^0, a_0^0 \rightarrow \eta\pi^0$	< 7.8	$\times 10^{-6}$	CL=90%	
Γ ₂₃₁	$J/\psi(1S)K^*(892)^0\pi^+\pi^-$	$(6.6 \pm 2.2) \times 10^{-4}$		Γ ₂₈₇	$b_1^0K^0, b_1^0 \rightarrow \omega\pi^0$	< 7.8	$\times 10^{-6}$	CL=90%	
Γ ₂₃₂	$\chi_{c1}(3872)^-K^+$	< 5	$\times 10^{-4}$	CL=90%	Γ ₂₈₈	$a_0(980)^\pm K^\mp, a_0^\pm \rightarrow \eta\pi^\pm$	< 1.9	$\times 10^{-6}$	CL=90%
Γ ₂₃₃	$\chi_{c1}(3872)^-K^+, \chi_{c1}(3872)^- \rightarrow J/\psi(1S)\pi^-\pi^0$	[c] < 4.2	$\times 10^{-6}$	CL=90%	Γ ₂₈₉	$b_1^-K^+, b_1^- \rightarrow \omega\pi^-$	$(7.4 \pm 1.4) \times 10^{-6}$		
Γ ₂₃₄	$\chi_{c1}(3872)K^0, \chi_{c1} \rightarrow J/\psi\pi^+\pi^-$	$(4.3 \pm 1.3) \times 10^{-6}$		Γ ₂₉₀	$b_1^0K^{*0}, b_1^0 \rightarrow \omega\pi^0$	< 8.0	$\times 10^{-6}$	CL=90%	
Γ ₂₃₅	$\chi_{c1}(3872)K^0, \chi_{c1} \rightarrow J/\psi\gamma$	< 2.4	$\times 10^{-6}$	CL=90%	Γ ₂₉₁	$b_1^-K^{*+}, b_1^- \rightarrow \omega\pi^-$	< 5.0	$\times 10^{-6}$	CL=90%
Γ ₂₃₆	$\chi_{c1}(3872)K^*(892)^0, \chi_{c1} \rightarrow J/\psi\gamma$	< 2.8	$\times 10^{-6}$	CL=90%	Γ ₂₉₂	$a_0(1450)^\pm K^\mp, a_0^\pm \rightarrow \eta\pi^\pm$	< 3.1	$\times 10^{-6}$	CL=90%
Γ ₂₃₇	$\chi_{c1}(3872)K^0, \chi_{c1} \rightarrow \psi(2S)\gamma$	< 6.62	$\times 10^{-6}$	CL=90%	Γ ₂₉₃	$K_S^0X^0$ (Familon)	< 5.3	$\times 10^{-5}$	CL=90%
Γ ₂₃₈	$\chi_{c1}(3872)K^*(892)^0, \chi_{c1} \rightarrow \psi(2S)\gamma$	< 4.4	$\times 10^{-6}$	CL=90%	Γ ₂₉₄	$\omega K^*(892)^0$	$(2.0 \pm 0.5) \times 10^{-6}$		
Γ ₂₃₉	$\chi_{c1}(3872)K^0, \chi_{c1} \rightarrow D^0\bar{D}^0\pi^0$	$(1.7 \pm 0.8) \times 10^{-4}$		Γ ₂₉₅	$\omega(K\pi)_0^0$	$(1.84 \pm 0.25) \times 10^{-5}$			
Γ ₂₄₀	$\chi_{c1}(3872)K^0, \chi_{c1} \rightarrow \bar{D}^*D^0$	$(1.2 \pm 0.4) \times 10^{-4}$		Γ ₂₉₆	$\omega K^*(1430)^0$	$(1.60 \pm 0.34) \times 10^{-5}$			
Γ ₂₄₁	$\chi_{c1}(3872)K^+\pi^-, \chi_{c1} \rightarrow J/\psi\pi^+\pi^-$	$(7.9 \pm 1.4) \times 10^{-6}$		Γ ₂₉₇	$\omega K^*(1430)^0$	$(1.01 \pm 0.23) \times 10^{-5}$			
Γ ₂₄₂	$\chi_{c1}(3872)K^*(892)^0, \chi_{c1} \rightarrow J/\psi\pi^+\pi^-$	$(4.0 \pm 1.5) \times 10^{-6}$		Γ ₂₉₈	$\omega K^+\pi^-$ nonresonant	$(5.1 \pm 1.0) \times 10^{-6}$			
Γ ₂₄₃	$\chi_{c1}(3872)\gamma, \chi_{c1} \rightarrow J/\psi\pi^+\pi^-$	< 5.1	$\times 10^{-7}$	CL=90%	Γ ₂₉₉	$K^+\pi^-\pi^0$	$(3.78 \pm 0.32) \times 10^{-5}$		
Γ ₂₄₄	$Z_c(4430)^\pm K^\mp, Z_c^\pm \rightarrow \psi(2S)\pi^\pm$	$(6.0^{+3.0}_{-2.4}) \times 10^{-5}$		Γ ₃₀₀	$K^+\rho^-$	$(7.0 \pm 0.9) \times 10^{-6}$			
Γ ₂₄₅	$Z_c(4430)^\pm K^\mp, Z_c^\pm \rightarrow J/\psi\pi^\pm$	$(5.4^{+4.0}_{-1.2}) \times 10^{-6}$		Γ ₃₀₁	$K^+\rho(1450)^-$	$(2.4 \pm 1.2) \times 10^{-6}$			
Γ ₂₄₆	$Z_c(3900)^\pm K^\mp, Z_c^\pm \rightarrow J/\psi\pi^\pm$	< 9	$\times 10^{-7}$		Γ ₃₀₂	$K^+\rho(1700)^-$	$(6 \pm 7) \times 10^{-7}$		
Γ ₂₄₇	$Z_c(4200)^\pm K^\mp, X^\pm \rightarrow J/\psi\pi^\pm$	$(2.2^{+1.3}_{-0.8}) \times 10^{-5}$		Γ ₃₀₃	$(K^+\pi^-\pi^0)$ nonresonant	$(2.8 \pm 0.6) \times 10^{-6}$			
Γ ₂₄₈	$J/\psi(1S)p\bar{p}$	$(4.5 \pm 0.6) \times 10^{-7}$		Γ ₃₀₄	$(K\pi)_0^{*+}\pi^-, (K\pi)_0^{*+} \rightarrow K^+\pi^0$	$(3.4 \pm 0.5) \times 10^{-5}$			
Γ ₂₄₉	$J/\psi(1S)\gamma$	< 1.5	$\times 10^{-6}$	CL=90%	Γ ₃₀₅	$(K\pi)_0^{*0}\pi^0, (K\pi)_0^{*0} \rightarrow K^+\pi^-$	$(8.6 \pm 1.7) \times 10^{-6}$		
Γ ₂₅₀	$J/\psi(1S)\bar{D}^0$	< 1.3	$\times 10^{-5}$	CL=90%	Γ ₃₀₆	$K_S^*(1430)^0\pi^0$	< 4.0	$\times 10^{-6}$	CL=90%
Γ ₂₅₁	$\psi(2S)\pi^0$	$(1.17 \pm 0.19) \times 10^{-5}$		Γ ₃₀₇	$K^*(1680)^0\pi^0$	< 7.5	$\times 10^{-6}$	CL=90%	
Γ ₂₅₂	$\psi(2S)K^0$	$(5.8 \pm 0.5) \times 10^{-4}$		Γ ₃₀₈	$K_x^{*0}\pi^0$	[d] $(6.1 \pm 1.6) \times 10^{-6}$			
Γ ₂₅₃	$\psi(3770)K^0, \psi \rightarrow \bar{D}^0D^0$	< 1.23	$\times 10^{-4}$	CL=90%	Γ ₃₀₉	$K^0\pi^+\pi^-$	$(4.97 \pm 0.18) \times 10^{-5}$		
Γ ₂₅₄	$\psi(3770)K^0, \psi \rightarrow D^-D^+$	< 1.88	$\times 10^{-4}$	CL=90%	Γ ₃₁₀	$K^0\pi^+\pi^-$ nonresonant	$(1.39^{+0.26}_{-0.18}) \times 10^{-5}$	S=1.6	
Γ ₂₅₅	$\psi(2S)\pi^+\pi^-$	$(2.21 \pm 0.35) \times 10^{-5}$		Γ ₃₁₁	$K^0\rho^0$	$(3.4 \pm 1.1) \times 10^{-6}$		S=2.3	
Γ ₂₅₆	$\psi(2S)K^+\pi^-$	$(5.8 \pm 0.4) \times 10^{-4}$		Γ ₃₁₂	$K^*(892)^+\pi^-$	$(7.5 \pm 0.4) \times 10^{-6}$			
Γ ₂₅₇	$\psi(2S)K^*(892)^0$	$(5.9 \pm 0.4) \times 10^{-4}$		Γ ₃₁₃	$K^*(1430)^+\pi^-$	$(3.3 \pm 0.7) \times 10^{-5}$		S=2.0	
Γ ₂₅₈	$\chi_{c0}K^0$	$(1.11^{+0.24}_{-0.21}) \times 10^{-6}$		Γ ₃₁₄	$K_x^{*+}\pi^-$	[d] $(5.1 \pm 1.6) \times 10^{-6}$			
Γ ₂₅₉	$\chi_{c0}K^*(892)^0$	$(1.7 \pm 0.4) \times 10^{-4}$		Γ ₃₁₅	$K^*(1410)^+\pi^-, K^{*+} \rightarrow K^0\pi^+$	< 3.8	$\times 10^{-6}$	CL=90%	
Γ ₂₆₀	$\chi_{c1}\pi^0$	$(1.12 \pm 0.28) \times 10^{-5}$		Γ ₃₁₆	$(K\pi)_0^{*+}\pi^-, (K\pi)_0^{*+} \rightarrow K^0\pi^+$	$(1.62 \pm 0.13) \times 10^{-5}$			
Γ ₂₆₁	$\chi_{c1}K^0$	$(3.95 \pm 0.27) \times 10^{-4}$		Γ ₃₁₇	$f_0(980)K^0, f_0 \rightarrow \pi^+\pi^-$	$(8.1 \pm 0.8) \times 10^{-6}$		S=1.3	
Γ ₂₆₂	$\chi_{c1}\pi^-K^+$	$(4.97 \pm 0.30) \times 10^{-4}$		Γ ₃₁₈	$K^0f_0(500)$	$(1.6^{+2.5}_{-1.6}) \times 10^{-7}$			
Γ ₂₆₃	$\chi_{c1}K^*(892)^0$	$(2.38 \pm 0.19) \times 10^{-4}$	S=1.2	Γ ₃₁₉	$K^0f_0(1500)$	$(1.3 \pm 0.8) \times 10^{-6}$			
Γ ₂₆₄	$X(4051)^-K^+, X^- \rightarrow \chi_{c1}\pi^-$	$(3.0^{+4.0}_{-1.8}) \times 10^{-5}$		Γ ₃₂₀	$f_2(1270)K^0$	$(2.7^{+1.3}_{-1.2}) \times 10^{-6}$			
Γ ₂₆₅	$X(4248)^-K^+, X^- \rightarrow \chi_{c1}\pi^-$	$(4.0^{+20.0}_{-1.0}) \times 10^{-5}$		Γ ₃₂₁	$f_x(1300)K^0, f_x \rightarrow \pi^+\pi^-$	$(1.8 \pm 0.7) \times 10^{-6}$			
Γ ₂₆₆	$\chi_{c1}\pi^+\pi^-K^0$	$(3.2 \pm 0.5) \times 10^{-4}$		Γ ₃₂₂	$K^*(892)^0\pi^0$	$(3.3 \pm 0.6) \times 10^{-6}$			
Γ ₂₆₇	$\chi_{c1}\pi^-\pi^0K^+$	$(3.5 \pm 0.6) \times 10^{-4}$		Γ ₃₂₃	$K_S^*(1430)^+\pi^-$	$(3.65 \pm 0.34) \times 10^{-6}$			
Γ ₂₆₈	$\chi_{c2}K^0$	< 1.5	$\times 10^{-5}$	CL=90%	Γ ₃₂₄	$K^*(1680)^+\pi^-$	$(1.41 \pm 0.10) \times 10^{-5}$		
Γ ₂₆₉	$\chi_{c2}K^*(892)^0$	$(4.9 \pm 1.2) \times 10^{-5}$	S=1.1	Γ ₃₂₅	$K^+\pi^-\pi^+\pi^-$	[e] < 2.3	$\times 10^{-4}$	CL=90%	
Γ ₂₇₀	$\chi_{c2}\pi^-K^+$	$(7.2 \pm 1.0) \times 10^{-5}$		Γ ₃₂₆	$\rho^0K^+\pi^-$	$(2.8 \pm 0.7) \times 10^{-6}$			
				Γ ₃₂₇	$f_0(980)K^+\pi^-, f_0 \rightarrow \pi\pi$	$(1.4^{+0.5}_{-0.6}) \times 10^{-6}$			
				Γ ₃₂₈	$K^+\pi^-\pi^+\pi^-$ nonresonant	< 2.1	$\times 10^{-6}$	CL=90%	
				Γ ₃₂₉	$K^*(892)^0\pi^+\pi^-$	$(5.5 \pm 0.5) \times 10^{-5}$			
				Γ ₃₃₀	$K^*(892)^0\rho^0$	$(3.9 \pm 1.3) \times 10^{-6}$		S=1.9	
				Γ ₃₃₁	$K^*(892)^0f_0(980), f_0 \rightarrow \pi\pi$	$(3.9^{+2.1}_{-1.8}) \times 10^{-6}$		S=3.9	
				Γ ₃₃₂	$K_1(1270)^+\pi^-$	< 3.0	$\times 10^{-5}$	CL=90%	
				Γ ₃₃₃	$K_1(1400)^+\pi^-$	< 2.7	$\times 10^{-5}$	CL=90%	
				Γ ₃₃₄	$a_1(1260)^-K^+$	[e] $(1.6 \pm 0.4) \times 10^{-5}$			

Γ_{470}	$p\bar{p}\bar{p}$	< 2.0	$\times 10^{-7}$	CL=90%
Γ_{471}	$p\bar{\Lambda}\pi^-$	(3.14 ± 0.29)	$\times 10^{-6}$	
Γ_{472}	$p\bar{\Lambda}\pi^-\gamma$	< 6.5	$\times 10^{-7}$	CL=90%
Γ_{473}	$p\bar{\Sigma}^-(1385)^-$	< 2.6	$\times 10^{-7}$	CL=90%
Γ_{474}	$\Delta(1232)^+\bar{p} + \Delta(1232)^-\rho$	< 1.6	$\times 10^{-6}$	
Γ_{475}	$\Delta^0\bar{\Lambda}$	< 9.3	$\times 10^{-7}$	CL=90%
Γ_{476}	$p\bar{\Lambda}K^-$	< 8.2	$\times 10^{-7}$	CL=90%
Γ_{477}	$p\bar{\Lambda}D^-$	(2.5 ± 0.4)	$\times 10^{-5}$	
Γ_{478}	$p\bar{\Lambda}D^{*-}$	(3.4 ± 0.8)	$\times 10^{-5}$	
Γ_{479}	$p\bar{\Sigma}^0\pi^-$	< 3.8	$\times 10^{-6}$	CL=90%
Γ_{480}	$\bar{\Lambda}\Lambda$	< 3.2	$\times 10^{-7}$	CL=90%
Γ_{481}	$\bar{\Lambda}\Lambda K^0$	(4.8 ± 1.0 / 0.9)	$\times 10^{-6}$	
Γ_{482}	$\bar{\Lambda}\Lambda K^{*0}$	(2.5 ± 0.9 / 0.8)	$\times 10^{-6}$	
Γ_{483}	$\bar{\Lambda}\Lambda D^0$	(1.00 ± 0.30 / 0.26)	$\times 10^{-5}$	
Γ_{484}	$D^0\Sigma^0\bar{\Lambda} + c.c.$	< 3.1	$\times 10^{-5}$	CL=90%
Γ_{485}	$\Delta^0\bar{\Delta}^0$	< 1.5	$\times 10^{-3}$	CL=90%
Γ_{486}	$\Delta^{++}\bar{\Delta}^{--}$	< 1.1	$\times 10^{-4}$	CL=90%
Γ_{487}	$\bar{D}^0 p\bar{p}$	(1.04 ± 0.07)	$\times 10^{-4}$	
Γ_{488}	$D_c^-\bar{\Lambda}p$	(2.8 ± 0.9)	$\times 10^{-5}$	
Γ_{489}	$\bar{D}^*(2007)^0 p\bar{p}$	(9.9 ± 1.1)	$\times 10^{-5}$	
Γ_{490}	$D^*(2010)^-\rho\bar{p}$	(1.4 ± 0.4)	$\times 10^{-3}$	
Γ_{491}	$D^-\rho\bar{p}\pi^+$	(3.32 ± 0.31)	$\times 10^{-4}$	
Γ_{492}	$D^*(2010)^-\rho\bar{p}\pi^+$	(4.7 ± 0.5)	$\times 10^{-4}$	S=1.2
Γ_{493}	$\bar{D}^0 p\bar{p}\pi^+\pi^-$	(3.0 ± 0.5)	$\times 10^{-4}$	
Γ_{494}	$\bar{D}^{*0} p\bar{p}\pi^+\pi^-$	(1.9 ± 0.5)	$\times 10^{-4}$	
Γ_{495}	$\Theta_c\bar{p}\pi^+, \Theta_c \rightarrow D^-p$	< 9	$\times 10^{-6}$	CL=90%
Γ_{496}	$\Theta_c\bar{p}\pi^+, \Theta_c \rightarrow D^{*-}p$	< 1.4	$\times 10^{-5}$	CL=90%
Γ_{497}	$\bar{\Sigma}_c^-\Delta^{++}$	< 8	$\times 10^{-4}$	CL=90%
Γ_{498}	$\bar{\Lambda}_c^-p\pi^+\pi^-$	(1.02 ± 0.14)	$\times 10^{-3}$	S=1.3
Γ_{499}	$\bar{\Lambda}_c^-p$	(1.54 ± 0.18)	$\times 10^{-5}$	
Γ_{500}	$\bar{\Lambda}_c^-p\pi^0$	(1.55 ± 0.19)	$\times 10^{-4}$	
Γ_{501}	$\bar{\Sigma}_c(2455)^-p$	< 2.4	$\times 10^{-5}$	
Γ_{502}	$\bar{\Lambda}_c^-p\pi^+\pi^-\pi^0$	< 5.07	$\times 10^{-3}$	CL=90%
Γ_{503}	$\bar{\Lambda}_c^-p\pi^+\pi^-\pi^+\pi^-$	< 2.74	$\times 10^{-3}$	CL=90%
Γ_{504}	$\bar{\Lambda}_c^-p\pi^+\pi^-$ (nonresonant)	(5.5 ± 1.0)	$\times 10^{-4}$	S=1.3
Γ_{505}	$\bar{\Sigma}_c(2520)^{--}p\pi^+$	(1.02 ± 0.18)	$\times 10^{-4}$	
Γ_{506}	$\bar{\Sigma}_c(2520)^0 p\pi^-$	< 3.1	$\times 10^{-5}$	CL=90%
Γ_{507}	$\bar{\Sigma}_c(2455)^0 p\pi^-$	(1.08 ± 0.16)	$\times 10^{-4}$	
Γ_{508}	$\bar{\Sigma}_c(2455)^0 N^0, N^0 \rightarrow p\pi^-$	(6.4 ± 1.7)	$\times 10^{-5}$	
Γ_{509}	$\bar{\Sigma}_c(2455)^{--}p\pi^+$	(1.83 ± 0.24)	$\times 10^{-4}$	
Γ_{510}	$\bar{\Lambda}_c^-pK^+\pi^-$	(3.4 ± 0.7)	$\times 10^{-5}$	
Γ_{511}	$\bar{\Sigma}_c(2455)^{--}pK^+, \bar{\Sigma}_c^{--} \rightarrow \bar{\Lambda}_c^-\pi^-$	(8.8 ± 2.5)	$\times 10^{-6}$	
Γ_{512}	$\bar{\Lambda}_c^-pK^*(892)^0$	< 2.42	$\times 10^{-5}$	CL=90%
Γ_{513}	$\bar{\Lambda}_c^-pK^+K^-$	(2.0 ± 0.4)	$\times 10^{-5}$	
Γ_{514}	$\bar{\Lambda}_c^-p\phi$	< 1.0	$\times 10^{-5}$	CL=90%
Γ_{515}	$\bar{\Lambda}_c^-p\bar{p}p$	< 2.8	$\times 10^{-6}$	
Γ_{516}	$\bar{\Lambda}_c^-\Lambda K^+$	(4.8 ± 1.1)	$\times 10^{-5}$	
Γ_{517}	$\bar{\Lambda}_c^-\Lambda_c^+$	< 1.6	$\times 10^{-5}$	CL=95%
Γ_{518}	$\bar{\Lambda}_c^-(2593)^- / \bar{\Lambda}_c^-(2625)^-p$	< 1.1	$\times 10^{-4}$	CL=90%
Γ_{519}	$\Xi_c^-\Lambda_c^+$	(1.2 ± 0.8)	$\times 10^{-3}$	
Γ_{520}	$\Xi_c^-\Lambda_c^+, \Xi_c^- \rightarrow \Xi^+\pi^-\pi^-$	(2.4 ± 1.1)	$\times 10^{-5}$	S=1.8
Γ_{521}	$\Xi_c^-\Lambda_c^+, \Xi_c^- \rightarrow \bar{p}K^+\pi^-$	(5.3 ± 1.7)	$\times 10^{-6}$	
Γ_{522}	$\Lambda_c^+\Lambda_c^-K^0$	(4.0 ± 0.9)	$\times 10^{-4}$	
Γ_{523}	$\Xi_c^-(2930)^-\Lambda_c^+, \Xi_c^- \rightarrow \Lambda_c^-K^0$	(2.4 ± 0.6)	$\times 10^{-4}$	

Lepton Family number (LF) or Lepton number (L) or Baryon number (B) violating modes, or/and $\Delta B = 1$ weak neutral current (BI) modes

Γ_{524}	$\gamma\gamma$	B1	< 3.2	$\times 10^{-7}$	CL=90%
Γ_{525}	e^+e^-	B1	< 8.3	$\times 10^{-8}$	CL=90%
Γ_{526}	$e^+e^-\gamma$	B1	< 1.2	$\times 10^{-7}$	CL=90%
Γ_{527}	$\mu^+\mu^-$	B1	(1.1 ± 1.4 / 1.3)	$\times 10^{-10}$	S=1.6
Γ_{528}	$\mu^+\mu^-\gamma$	B1	< 1.6	$\times 10^{-7}$	CL=90%
Γ_{529}	$\mu^+\mu^-\mu^+\mu^-$	B1	< 6.9	$\times 10^{-10}$	CL=95%
Γ_{530}	$SP, S \rightarrow \mu^+\mu^-, P \rightarrow \mu^+\mu^-$	B1 [j]	< 6.0	$\times 10^{-10}$	CL=95%

Γ_{531}	$\tau^+\tau^-$	B1	< 2.1	$\times 10^{-3}$	CL=95%
Γ_{532}	$\pi^0\ell^+\ell^-$	B1	< 5.3	$\times 10^{-8}$	CL=90%
Γ_{533}	$\pi^0e^+e^-$	B1	< 8.4	$\times 10^{-8}$	CL=90%
Γ_{534}	$\pi^0\mu^+\mu^-$	B1	< 6.9	$\times 10^{-8}$	CL=90%
Γ_{535}	$\eta\ell^+\ell^-$	B1	< 6.4	$\times 10^{-8}$	CL=90%
Γ_{536}	ηe^+e^-	B1	< 1.08	$\times 10^{-7}$	CL=90%
Γ_{537}	$\eta\mu^+\mu^-$	B1	< 1.12	$\times 10^{-7}$	CL=90%
Γ_{538}	$\pi^0\nu\bar{\nu}$	B1	< 9	$\times 10^{-6}$	CL=90%
Γ_{539}	$K^0\ell^+\ell^-$	B1 [a]	(3.1 ± 0.8 / 0.7)	$\times 10^{-7}$	
Γ_{540}	$K^0e^+e^-$	B1	(1.6 ± 1.0 / 0.8)	$\times 10^{-7}$	
Γ_{541}	$K^0\mu^+\mu^-$	B1	(3.39 ± 0.34)	$\times 10^{-7}$	
Γ_{542}	$K^0\nu\bar{\nu}$	B1	< 2.6	$\times 10^{-5}$	CL=90%
Γ_{543}	$\rho^0\nu\bar{\nu}$	B1	< 4.0	$\times 10^{-5}$	CL=90%
Γ_{544}	$K^*(892)^0\ell^+\ell^-$	B1 [a]	(9.9 ± 1.2 / 1.1)	$\times 10^{-7}$	
Γ_{545}	$K^*(892)^0e^+e^-$	B1	(1.03 ± 0.19 / 0.17)	$\times 10^{-6}$	
Γ_{546}	$K^*(892)^0\mu^+\mu^-$	B1	(9.4 ± 0.5)	$\times 10^{-7}$	
Γ_{547}	$K^*(892)^0\chi, \chi \rightarrow \mu^+\mu^-$				
Γ_{548}	$\pi^+\pi^-\mu^+\mu^-$	B1	(2.1 ± 0.5)	$\times 10^{-8}$	
Γ_{549}	$K^*(892)^0\nu\bar{\nu}$	B1	< 1.8	$\times 10^{-5}$	CL=90%
Γ_{550}	invisible	B1	< 2.4	$\times 10^{-5}$	CL=90%
Γ_{551}	$\nu\bar{\nu}\gamma$	B1	< 1.7	$\times 10^{-5}$	CL=90%
Γ_{552}	$\phi\nu\bar{\nu}$	B1	< 1.27	$\times 10^{-4}$	CL=90%
Γ_{553}	$e^\pm\mu^\mp$	LF [h]	< 1.0	$\times 10^{-9}$	CL=90%
Γ_{554}	$\pi^0e^\pm\mu^\mp$	LF	< 1.4	$\times 10^{-7}$	CL=90%
Γ_{555}	$K^0e^\pm\mu^\mp$	LF	< 2.7	$\times 10^{-7}$	CL=90%
Γ_{556}	$K^*(892)^0e^+\mu^-$	LF	< 1.6	$\times 10^{-7}$	CL=90%
Γ_{557}	$K^*(892)^0e^-\mu^+$	LF	< 1.2	$\times 10^{-7}$	CL=90%
Γ_{558}	$K^*(892)^0e^\pm\mu^\mp$	LF	< 1.8	$\times 10^{-7}$	CL=90%
Γ_{559}	$e^\pm\tau^\mp$	LF [h]	< 2.8	$\times 10^{-5}$	CL=90%
Γ_{560}	$\mu^\pm\tau^\mp$	LF [h]	< 1.4	$\times 10^{-5}$	CL=95%
Γ_{561}	$\Lambda_c^+\mu^-$	L,B	< 1.4	$\times 10^{-6}$	CL=90%
Γ_{562}	$\Lambda_c^+e^-$	L,B	< 4	$\times 10^{-6}$	CL=90%

[a] An ℓ indicates an e or a μ mode, not a sum over these modes.

[b] \bar{D}^{*0} represents an excited state with mass $2.2 < M < 2.8$ GeV/ c^2 .

[c] $\chi_{c1}(3872)^+$ is a hypothetical charged partner of the $\chi_{c1}(3872)$.

[d] Stands for the possible candidates of $K^*(1410)$, $K_0^*(1430)$ and $K_2^*(1430)$.

[e] B^0 and B_s^0 contributions not separated. Limit is on weighted average of the two decay rates.

[f] This decay refers to the coherent sum of resonant and nonresonant $J^P = 0^+ K\pi$ components with $1.60 < m_{K\pi} < 2.15$ GeV/ c^2 .

[g] $X(214)$ is a hypothetical particle of mass 214 MeV/ c^2 reported by the HyperCP experiment, Physical Review Letters **94** 021801 (2005)

[h] The value is for the sum of the charge states or particle/antiparticle states indicated.

[i] $\Theta(1540)^+$ denotes a possible narrow pentaquark state.

[j] Here S and P are the hypothetical scalar and pseudoscalar particles with masses of 2.5 GeV/ c^2 and 214.3 MeV/ c^2 , respectively.

CONSTRAINED FIT INFORMATION

An overall fit to 34 branching ratios uses 89 measurements and one constraint to determine 22 parameters. The overall fit has a $\chi^2 = 64.3$ for 68 degrees of freedom.

The following *off-diagonal* array elements are the correlation coefficients $\langle \delta x_i \delta x_j \rangle / (\delta x_i \delta x_j)$, in percent, from the fit to the branching fractions, $x_i \equiv \Gamma_i / \Gamma_{\text{total}}$. The fit constrains the x_i whose labels appear in this array to sum to one.

See key on page 999

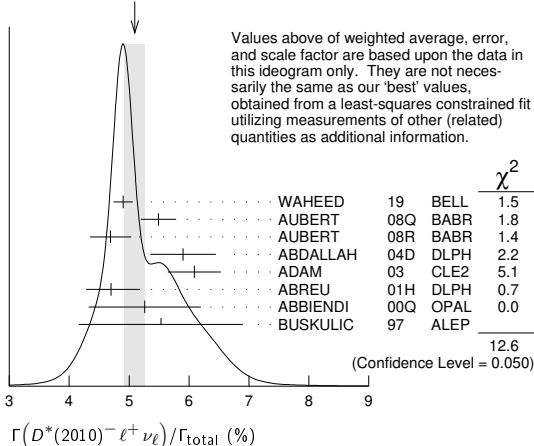
Meson Particle Listings

B⁰

4.5 ± 0.3 ± 0.4		16	ALBRECHT	94	ARG	e ⁺ e ⁻ → $\Upsilon(4S)$
4.7 ± 0.5 ± 0.5	235	17	ALBRECHT	93	ARG	e ⁺ e ⁻ → $\Upsilon(4S)$
seen	398	18	SANGHERA	93	CLE2	e ⁺ e ⁻ → $\Upsilon(4S)$
7.0 ± 1.8 ± 1.4		19	ANTREASIAN	90B	CBAL	e ⁺ e ⁻ → $\Upsilon(4S)$
		20	ALBRECHT	89c	ARG	e ⁺ e ⁻ → $\Upsilon(4S)$
6.0 ± 1.0 ± 1.4		21	ALBRECHT	89j	ARG	e ⁺ e ⁻ → $\Upsilon(4S)$
4.0 ± 0.4 ± 0.6		22	BORTOLETTO	89B	CLEO	e ⁺ e ⁻ → $\Upsilon(4S)$
7.0 ± 1.2 ± 1.9	47	23	ALBRECHT	87j	ARG	e ⁺ e ⁻ → $\Upsilon(4S)$

- ¹ Uses fully reconstructed $D^{*-}\ell^+\nu$ events ($\ell = e$ or μ).
- ² Uses a fully reconstructed B meson as a tag on the recoil side.
- ³ Measured using fully reconstructed D^* sample and a simultaneous fit to the Capriuni-Lellouch-Neubert form factor parameters: $\rho^2 = 1.191 \pm 0.048 \pm 0.028$, $R_1(1) = 1.429 \pm 0.061 \pm 0.044$, and $R_2(1) = 0.827 \pm 0.038 \pm 0.022$.
- ⁴ Measured using fully reconstructed D^* sample.
- ⁵ Uses the combined fit of both $B^0 \rightarrow D^*(2010)^-\ell\nu$ and $B^+ \rightarrow \overline{D}(2077)^0\ell\nu$ samples.
- ⁶ ABREU 01H measured using about 5000 partial reconstructed D^* sample.
- ⁷ ABBIENDI 00Q assumes the fraction $B(b \rightarrow B^0) = (39.7_{-2.2}^{+1.8})\%$. This result is an average of two methods using exclusive and partial D^* reconstruction.
- ⁸ BUSKULIC 97 assumes fraction (B^+) = fraction (B^0) = $(37.8 \pm 2.2)\%$ and PDG 96 values for B lifetime and D^* and D branching fractions.
- ⁹ Combines with previous partial reconstructed D^* measurement.
- ¹⁰ Assumes equal production of B^+ and B^0 at the $\Upsilon(4S)$.
- ¹¹ The results are based on the same analysis and data sample reported in ADAM 03.
- ¹² ACKERSTAFF 97G assumes fraction (B^+) = fraction (B^0) = $(37.8 \pm 2.2)\%$ and PDG 96 values for B lifetime and branching ratio of D^* and D decays.
- ¹³ ABREU 96P result is the average of two methods using exclusive and partial D^* reconstruction.
- ¹⁴ BARISH 95 use $B(D^0 \rightarrow K^-\pi^+) = (3.91 \pm 0.08 \pm 0.17)\%$ and $B(D^{*+} \rightarrow D^0\pi^+) = (68.1 \pm 1.0 \pm 1.3)\%$.
- ¹⁵ BUSKULIC 95N assumes fraction (B^+) = fraction (B^0) = $38.2 \pm 1.3 \pm 2.2\%$ and $\tau_{B^0} = 1.58 \pm 0.06$ ps. $\Gamma(D^{*-}\ell^+\nu_\ell)/\text{total} = [5.18 - 0.13(\text{fraction}(B^0) - 38.2) - 1.5(\tau_{B^0} - 1.58)]\%$.
- ¹⁶ ALBRECHT 94 assumes $B(D^{*+} \rightarrow D^0\pi^+) = 68.1 \pm 1.0 \pm 1.3\%$. Uses partial reconstruction of D^{*+} and is independent of D^0 branching ratios.
- ¹⁷ ALBRECHT 93 reports $0.052 \pm 0.005 \pm 0.006$. We rescale using the method described in STONE 94 but with the updated PDG 94 $B(D^0 \rightarrow K^-\pi^+)$. We have taken their average e and μ value. They also obtain $\alpha = 2\Gamma^0/(\Gamma^- + \Gamma^+) - 1 = 1.1 \pm 0.4 \pm 0.2$, $A_{AF} = 3/4 * (\Gamma^- - \Gamma^+)/\Gamma = 0.2 \pm 0.08 \pm 0.06$ and a value of $|V_{cb}| = 0.036 - 0.045$ depending on model assumptions.
- ¹⁸ Combining $\overline{D}^{*0}\ell^+\nu_\ell$ and $\overline{D}^{*-}\ell^+\nu_\ell$ SANGHERA 93 test $V-A$ structure and fit the decay angular distributions to obtain $A_{FB} = 3/4 * (\Gamma^- - \Gamma^+)/\Gamma = 0.14 \pm 0.06 \pm 0.03$. Assuming a value of V_{cb} , they measure V , A_1 , and A_2 , the three form factors for the $D^*\ell\nu_\ell$ decay, where results are slightly dependent on model assumptions.
- ¹⁹ ANTREASIAN 90B is average over B and $\overline{D}^*(2010)$ charge states.
- ²⁰ The measurement of ALBRECHT 89c suggests a D^* polarization γ_L/γ_T of 0.85 ± 0.45 , or $\alpha = 0.7 \pm 0.9$.
- ²¹ ALBRECHT 89j is ALBRECHT 87j value rescaled using $B(D^*(2010)^- \rightarrow D^0\pi^-) = 0.57 \pm 0.04 \pm 0.04$. Superseded by ALBRECHT 93.
- ²² We have taken average of the the BORTOLETTO 89B values for electrons and muons, $0.046 \pm 0.005 \pm 0.007$. We rescale using the method described in STONE 94 but with the updated PDG 94 $B(D^0 \rightarrow K^-\pi^+)$. The measurement suggests a D^* polarization parameter value $\alpha = 0.65 \pm 0.66 \pm 0.25$.
- ²³ ALBRECHT 87j assume μ -e universality, the $B(\Upsilon(4S) \rightarrow B^0\overline{B}^0) = 0.45$, the $B(D^0 \rightarrow K^-\pi^+) = (0.042 \pm 0.004 \pm 0.004)$, and the $B(D^*(2010)^- \rightarrow D^0\pi^-) = 0.49 \pm 0.08$. Superseded by ALBRECHT 89j.

WEIGHTED AVERAGE
5.09±0.17 (Error scaled by 1.4)



Values above of weighted average, error, and scale factor are based upon the data in this ideogram only. They are not necessarily the same as our 'best' values, obtained from a least-squares constrained fit utilizing measurements of other (related) quantities as additional information.

$\Gamma(D^*(2010)^-\ell^+\nu_\ell)/\Gamma(D\ell^+\nu_\ell X)$				Γ_6/Γ_3
VALUE	DOCUMENT ID	TECN	COMMENT	
0.537 ± 0.031 ± 0.036	¹ AUBERT	07AN	BABR	e ⁺ e ⁻ → $\Upsilon(4S)$

¹ Uses a fully reconstructed B meson on the recoil side.

$\Gamma(D^*(2010)^-\tau^+\nu_\tau)/\Gamma_{\text{total}}$				Γ_7/Γ
---	--	--	--	-------------------

VALUE (units 10^{-2})	DOCUMENT ID	TECN	COMMENT	
1.57 ± 0.09 OUR FIT	Error includes scale factor of 1.1.			
1.48 ± 0.18 OUR AVERAGE	Error includes scale factor of 1.1.			
1.42 ± 0.094 ± 0.140	¹ AAIJ	18D	LHCB	pp at 7, 8 TeV
2.02 ^{+0.40} _{-0.37} ± 0.37	² MATYJA	07	BELL	e ⁺ e ⁻ → $\Upsilon(4S)$
• • •	We do not use the following data for averages, fits, limits, etc. • • •			
1.11 ± 0.51 ± 0.06	³ AUBERT	08N	BABR	Repl. by AUBERT 09s
¹ Normalizes to $B(B^0 \rightarrow D^*(2010)^-\pi^+\pi^-) = (7.214 \pm 0.28) \times 10^{-3}$.				
² Observed in the recoil of the accompanying B meson.				
³ Uses a fully reconstructed B meson as a tag on the recoil side.				

$\Gamma(D^*(2010)^-\tau^+\nu_\tau)/\Gamma(D^*(2010)^-\ell^+\nu_\ell)$				Γ_7/Γ_6
---	--	--	--	---------------------

VALUE	DOCUMENT ID	TECN	COMMENT	
0.309 ± 0.016 OUR FIT				
0.315 ± 0.018 OUR AVERAGE				
0.291 ± 0.019 ± 0.029	¹ AAIJ	18D	LHCB	pp at 7, 8 TeV
0.302 ± 0.030 ± 0.011	² SATO	16B	BELL	e ⁺ e ⁻ → $\Upsilon(4S)$
0.336 ± 0.027 ± 0.030	³ AAIJ	15Q	LHCB	pp at 7, 8 TeV
0.355 ± 0.039 ± 0.021	^{4,5} LEES	12D	BABR	e ⁺ e ⁻ → $\Upsilon(4S)$
• • •	We do not use the following data for averages, fits, limits, etc. • • •			
0.207 ± 0.095 ± 0.008	⁴ AUBERT	09s	BABR	Repl. by LEES 12d
¹ Uses $\tau^+ \rightarrow \pi^+\pi^-\pi^+\overline{\nu}_\tau$ and $\tau^+ \rightarrow \pi^+\pi^-\pi^+\pi^0\overline{\nu}_\tau$, and μ^+ as ℓ^+ .				
² Uses semileptonic B decay events for tagging and $\tau^+ \rightarrow \ell^+\nu_\ell\overline{\nu}_\tau$ mode.				
³ Uses $\tau^+ \rightarrow \mu^+\nu_\mu\overline{\nu}_\tau$ and μ^+ as ℓ^+ .				
⁴ Uses a fully reconstructed B meson as a tag on the recoil side.				
⁵ Uses $\tau^+ \rightarrow e^+\nu_e\overline{\nu}_\tau$ and $\tau^+ \rightarrow \mu^+\nu_\mu\overline{\nu}_\tau$ and e^+ or μ^+ as ℓ^+ .				

$\Gamma(D^*(2010)^-\tau^+\nu_\tau)/\Gamma(D^*(2010)^-\pi^+\pi^-\pi^-)$				Γ_7/Γ_{57}
--	--	--	--	------------------------

VALUE	DOCUMENT ID	TECN	COMMENT	
1.97 ± 0.13 ± 0.18	¹ AAIJ	18D	LHCB	pp at 7, 8 TeV
¹ Uses $\tau^+ \rightarrow \pi^+\pi^-\pi^+\overline{\nu}_\tau$ and $\tau^+ \rightarrow \pi^+\pi^-\pi^+\pi^0\overline{\nu}_\tau$ modes.				

$\Gamma(\overline{D}^0\pi^-\ell^+\nu_\ell)/\Gamma_{\text{total}}$				Γ_8/Γ
---	--	--	--	-------------------

VALUE (units 10^{-3})	DOCUMENT ID	TECN	COMMENT	
4.1 ± 0.5 OUR AVERAGE				
4.05 ± 0.36 ± 0.41	VOSSEN	18	BELL	e ⁺ e ⁻ → $\Upsilon(4S)$
4.3 ± 0.8 ± 0.3	¹ AUBERT	08Q	BABR	e ⁺ e ⁻ → $\Upsilon(4S)$
• • •	We do not use the following data for averages, fits, limits, etc. • • •			
4.6 ± 0.9 ± 0.2	^{1,2} LIVENTSEV	08	BELL	Repl. by VOSSEN 18
3.5 ± 1.0 ± 0.1	³ LIVENTSEV	05	BELL	Repl. by LIVENTSEV 08
¹ Uses a fully reconstructed B meson as a tag on the recoil side.				
² LIVENTSEV 08 reports $(4.2 \pm 0.7 \pm 0.6) \times 10^{-3}$ from a measurement of $[\Gamma(B^0 \rightarrow \overline{D}^0\pi^-\ell^+\nu_\ell)/\Gamma_{\text{total}}] / [B(B^0 \rightarrow D^-\ell^+\nu_\ell)]$ assuming $B(B^0 \rightarrow D^-\ell^+\nu_\ell) = (2.12 \pm 0.20) \times 10^{-2}$, which we rescale to our best value $B(B^0 \rightarrow D^-\ell^+\nu_\ell) = (2.31 \pm 0.10) \times 10^{-2}$. Our first error is their experiment's error and our second error is the systematic error from using our best value.				
³ LIVENTSEV 05 reports $[\Gamma(B^0 \rightarrow \overline{D}^0\pi^-\ell^+\nu_\ell)/\Gamma_{\text{total}}] / [B(B^+ \rightarrow \overline{D}^0\ell^+\nu_\ell)] = 0.15 \pm 0.03 \pm 0.03$ which we multiply by our best value $B(B^+ \rightarrow \overline{D}^0\ell^+\nu_\ell) = (2.35 \pm 0.09) \times 10^{-2}$. Our first error is their experiment's error and our second error is the systematic error from using our best value.				

$\Gamma(D_2^*(2300)^-\ell^+\nu_\ell, D_2^{*-} \rightarrow \overline{D}^0\pi^-)/\Gamma_{\text{total}}$				Γ_9/Γ
---	--	--	--	-------------------

VALUE (units 10^{-3})	DOCUMENT ID	TECN	COMMENT	
3.0 ± 1.2 OUR AVERAGE	Error includes scale factor of 1.8.			
4.4 ± 0.8 ± 0.6	¹ AUBERT	08BL	BABR	e ⁺ e ⁻ → $\Upsilon(4S)$
2.0 ± 0.7 ± 0.5	¹ LIVENTSEV	08	BELL	e ⁺ e ⁻ → $\Upsilon(4S)$
¹ Uses a fully reconstructed B meson as a tag on the recoil side.				

$\Gamma(D_2^*(2460)^-\ell^+\nu_\ell, D_2^{*-} \rightarrow \overline{D}^0\pi^-)/\Gamma_{\text{total}}$				Γ_{10}/Γ
---	--	--	--	----------------------

VALUE (units 10^{-3})	DOCUMENT ID	TECN	COMMENT	
1.21 ± 0.33 OUR AVERAGE	Error includes scale factor of 1.8.			
1.10 ± 0.17 ± 0.08	¹ AUBERT	09Y	BABR	e ⁺ e ⁻ → $\Upsilon(4S)$
2.2 ± 0.4 ± 0.4	² LIVENTSEV	08	BELL	e ⁺ e ⁻ → $\Upsilon(4S)$
¹ Uses a simultaneous fit of all B semileptonic decays without full reconstruction of events. AUBERT 09Y reports $B(B^0 \rightarrow \overline{D}_2^*(2460)^-\ell^+\nu_\ell) \cdot B(\overline{D}_2^*(2460)^- \rightarrow \overline{D}^{(*)0}\pi^-) = (1.77 \pm 0.26 \pm 0.11) \times 10^{-3}$ and the authors have provided us the individual measurement.				
² Uses a fully reconstructed B meson as a tag on the recoil side.				

$\Gamma(\overline{D}^{*+}n\pi\ell^+\nu_\ell (n \geq 1))/\Gamma(D\ell^+\nu_\ell X)$				Γ_{11}/Γ_3
--	--	--	--	------------------------

VALUE	DOCUMENT ID	TECN	COMMENT	
0.248 ± 0.032 ± 0.030	¹ AUBERT	07AN	BABR	e ⁺ e ⁻ → $\Upsilon(4S)$
¹ Uses a fully reconstructed B meson on the recoil side.				

Meson Particle Listings

B^0

$\Gamma(\overline{D}^{*0} \pi^- \ell^+ \nu_\ell) / \Gamma_{\text{total}}$ Γ_{12} / Γ

VALUE (units 10^{-3})	DOCUMENT ID	TECN	COMMENT
5.8 ± 0.8 OUR AVERAGE	Error includes scale factor of 1.4.		
6.46 ± 0.53 ± 0.52	VOSSEN 18	BELL	$e^+ e^- \rightarrow \Upsilon(4S)$
4.8 ± 0.8 ± 0.4	¹ AUBERT 08Q	BABR	$e^+ e^- \rightarrow \Upsilon(4S)$
6.1 ± 2.4 ± 0.3	^{1,2} LIVENTSEV 08	BELL	Repl. by VOSSEN 18
5.7 ± 1.3 ± 0.2	^{3,4} LIVENTSEV 05	BELL	Repl. by LIVENTSEV 08

• • • We do not use the following data for averages, fits, limits, etc. • • •

¹ Uses a fully reconstructed B meson as a tag on the recoil side.
² LIVENTSEV 08 reports $(5.6 \pm 2.1 \pm 0.8) \times 10^{-3}$ from a measurement of $[\Gamma(B^0 \rightarrow \overline{D}^{*0} \pi^- \ell^+ \nu_\ell) / \Gamma_{\text{total}}] / [B(B^0 \rightarrow D^- \ell^+ \nu_\ell)]$ assuming $B(B^0 \rightarrow D^- \ell^+ \nu_\ell) = (2.12 \pm 0.20) \times 10^{-2}$, which we rescale to our best value $B(B^0 \rightarrow D^- \ell^+ \nu_\ell) = (2.31 \pm 0.10) \times 10^{-2}$. Our first error is their experiment's error and our second error is the systematic error from using our best value.
³ Excludes D^{*+} contribution to $D \pi$ modes.
⁴ LIVENTSEV 05 reports $[\Gamma(B^0 \rightarrow \overline{D}^{*0} \pi^- \ell^+ \nu_\ell) / \Gamma_{\text{total}}] / [B(B^+ \rightarrow \overline{D}^{*0} \ell^+ \nu_\ell)] = 0.10 \pm 0.02 \pm 0.01$ which we multiply by our best value $B(B^+ \rightarrow \overline{D}^{*0} \ell^+ \nu_\ell) = (5.66 \pm 0.22) \times 10^{-2}$. Our first error is their experiment's error and our second error is the systematic error from using our best value.

$\Gamma(D_1(2420)^- \ell^+ \nu_\ell, D_1^- \rightarrow \overline{D}^{*0} \pi^-) / \Gamma_{\text{total}}$ Γ_{13} / Γ

VALUE (units 10^{-3})	DOCUMENT ID	TECN	COMMENT
2.80 ± 0.28 OUR AVERAGE			
2.78 ± 0.24 ± 0.25	¹ AUBERT 09Y	BABR	$e^+ e^- \rightarrow \Upsilon(4S)$
2.7 ± 0.4 ± 0.3	² AUBERT 08BL	BABR	$e^+ e^- \rightarrow \Upsilon(4S)$
5.4 ± 1.9 ± 0.9	² LIVENTSEV 08	BELL	$e^+ e^- \rightarrow \Upsilon(4S)$

• • • We do not use the following data for averages, fits, limits, etc. • • •

¹ Uses a simultaneous measurement of all B semileptonic decays without full reconstruction of events.
² Uses a fully reconstructed B meson as a tag on the recoil side.

$\Gamma(D_1'(2430)^- \ell^+ \nu_\ell, D_1'^- \rightarrow \overline{D}^{*0} \pi^-) / \Gamma_{\text{total}}$ Γ_{14} / Γ

VALUE (units 10^{-3})	CL%	DOCUMENT ID	TECN	COMMENT
3.1 ± 0.7 ± 0.5		¹ AUBERT 08BL	BABR	$e^+ e^- \rightarrow \Upsilon(4S)$
<5.0	90	¹ LIVENTSEV 08	BELL	$e^+ e^- \rightarrow \Upsilon(4S)$

• • • We do not use the following data for averages, fits, limits, etc. • • •

¹ Uses a fully reconstructed B meson as a tag on the recoil side.

$\Gamma(D_2^*(2460)^- \ell^+ \nu_\ell, D_2^{*-} \rightarrow \overline{D}^{*0} \pi^-) / \Gamma_{\text{total}}$ Γ_{15} / Γ

VALUE (units 10^{-3})	CL%	DOCUMENT ID	TECN	COMMENT
0.68 ± 0.12 OUR AVERAGE				
0.67 ± 0.12 ± 0.05		¹ AUBERT 09Y	BABR	$e^+ e^- \rightarrow \Upsilon(4S)$
0.7 ± 0.2 ± 0.2		² AUBERT 08BL	BABR	$e^+ e^- \rightarrow \Upsilon(4S)$
<3.0	90	² LIVENTSEV 08	BELL	$e^+ e^- \rightarrow \Upsilon(4S)$

• • • We do not use the following data for averages, fits, limits, etc. • • •

¹ Uses a simultaneous fit of all B semileptonic decays without full reconstruction of events. AUBERT 09Y reports $B(B^0 \rightarrow \overline{D}_2^*(2460)^- \ell^+ \nu_\ell) \cdot B(\overline{D}_2^*(2460)^- \rightarrow \overline{D}^{*0} \pi^-) = (1.77 \pm 0.26 \pm 0.11) \times 10^{-3}$ and the authors have provided us the individual measurement.
² Uses a fully reconstructed B meson as a tag on the recoil side.

$\Gamma(D^- \pi^+ \pi^- \ell^+ \nu_\ell) / \Gamma(D^- \ell^+ \nu_\ell)$ Γ_{16} / Γ_4

VALUE (units 10^{-2})	DOCUMENT ID	TECN	COMMENT
5.8 ± 1.8 ± 1.2			
	¹ LEES 16	BABR	$e^+ e^- \rightarrow \Upsilon(4S)$

¹ Measurement used electrons and muons as leptons.

$\Gamma(D^{*-} \pi^+ \pi^- \ell^+ \nu_\ell) / \Gamma(D^{*0}(2010)^- \ell^+ \nu_\ell)$ Γ_{17} / Γ_6

VALUE (units 10^{-2})	DOCUMENT ID	TECN	COMMENT
2.8 ± 0.8 ± 0.6			
	¹ LEES 16	BABR	$e^+ e^- \rightarrow \Upsilon(4S)$

¹ Measurement used electrons and muons as leptons.

$\Gamma(\rho^- \ell^+ \nu_\ell) / \Gamma_{\text{total}}$ Γ_{18} / Γ

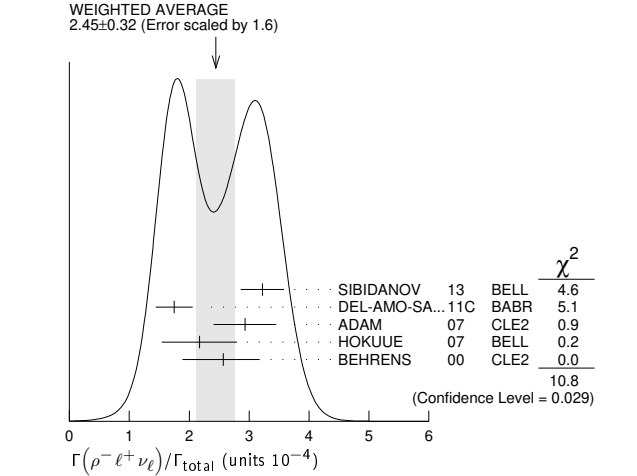
$\ell = e$ or μ , not sum over e and μ modes.
 "OUR EVALUATION" has been obtained by the Heavy Flavor Averaging Group (HFLAV) by including both B^0 and B^+ decays. The average assumes equality of the semileptonic decay width for these isospin conjugate states.

VALUE (units 10^{-4})	CL%	DOCUMENT ID	TECN	COMMENT
2.94 ± 0.11 ± 0.18 OUR EVALUATION				
2.45 ± 0.32 OUR AVERAGE	Error includes scale factor of 1.6. See the ideogram below.			
3.22 ± 0.27 ± 0.24		¹ SIBIDANOV 13	BELL	$e^+ e^- \rightarrow \Upsilon(4S)$
1.75 ± 0.15 ± 0.27		² DEL-AMO-SA...11c	BABR	$e^+ e^- \rightarrow \Upsilon(4S)$
2.93 ± 0.37 ± 0.37		³ ADAM 07	CLE2	$e^+ e^- \rightarrow \Upsilon(4S)$
2.17 ± 0.54 ± 0.32		⁴ HOKUUE 07	BELL	$e^+ e^- \rightarrow \Upsilon(4S)$
2.57 ± 0.29 ^{+0.53} / _{-0.62}		⁵ BEHRENS 00	CLE2	$e^+ e^- \rightarrow \Upsilon(4S)$

• • • We do not use the following data for averages, fits, limits, etc. • • •

2.14 ± 0.21 ± 0.56	² AUBERT,B	05o	BABR	Repl. by DEL-AMO-SANCHEZ 11c
2.17 ± 0.34 ^{+0.62} / _{-0.68}	⁶ ATHAR	03	CLE2	Repl. by ADAM 07
3.29 ± 0.42 ± 0.72	⁷ AUBERT	03E	BABR	Repl. by AUBERT,B 05o
2.69 ± 0.41 ^{+0.61} / _{-0.64}	⁸ BEHRENS	00	CLE2	$e^+ e^- \rightarrow \Upsilon(4S)$
2.5 ± 0.4 ^{+0.7} / _{-0.9}	⁹ ALEXANDER	96T	CLE2	Repl. by BEHRENS 00
<4.1	90	¹⁰ BEAN	93B	CLE2 $e^+ e^- \rightarrow \Upsilon(4S)$

¹ The signal events are tagged by a second B meson reconstructed in the fully hadronic decays.
² B^+ and B^0 decays combined assuming isospin symmetry. Systematic errors include both experimental and form-factor uncertainties.
³ The B^0 and B^+ results are combined assuming the isospin, B lifetimes, and relative charged/neutral B production at the $\Upsilon(4S)$.
⁴ The signal events are tagged by a second B meson reconstructed in the semileptonic mode $B \rightarrow D^{(*)} \ell \nu_\ell$.
⁵ Averaging with ALEXANDER 96T results including experimental and theoretical correlations considered, BEHRENS 00 reports systematic errors $+0.33 \pm 0.41$, where the second error is theoretical model dependence. We combine these in quadrature.
⁶ ATHAR 03 reports systematic errors $+0.47 \pm 0.41 \pm 0.01$, which are experimental systematic, systematic due to residual form-factor uncertainties in the signal, and systematic due to residual form-factor uncertainties in the cross-feed modes, respectively. We combine these in quadrature.
⁷ Uses isospin constraints and extrapolation to all electron energies according to five different form-factor calculations. The second error combines the systematic and theoretical uncertainties in quadrature.
⁸ BEHRENS 00 reports $+0.35 \pm 0.50$, where the second error is the theoretical model dependence. We combine these in quadrature. B^+ and B^0 decays combined using isospin symmetry: $\Gamma(B^0 \rightarrow \rho^- \ell^+ \nu) = 2\Gamma(B^+ \rightarrow \rho^0 \ell^+ \nu) \approx 2\Gamma(B^+ \rightarrow \omega \ell^+ \nu)$. No evidence for $\omega \ell \nu$ is reported.
⁹ ALEXANDER 96T reports $+0.5 \pm 0.5$ where the second error is the theoretical model dependence. We combine these in quadrature. B^+ and B^0 decays combined using isospin symmetry: $\Gamma(B^0 \rightarrow \rho^- \ell^+ \nu) = 2\Gamma(B^+ \rightarrow \rho^0 \ell^+ \nu) \approx 2\Gamma(B^+ \rightarrow \omega \ell^+ \nu)$. No evidence for $\omega \ell \nu$ is reported.
¹⁰ BEAN 93B limit set using ISGW Model. Using isospin and the quark model to combine $\Gamma(\rho^0 \ell^+ \nu_\ell)$ and $\Gamma(\omega \ell^+ \nu_\ell)$ with this result, they obtain a limit $<(1.6-2.7) \times 10^{-4}$ at 90% CL for $B^+ \rightarrow (\omega \text{ or } \rho^0) \ell^+ \nu_\ell$. The range corresponds to the ISGW, WSB, and KS models. An upper limit on $|V_{ub}/V_{cb}| < 0.08-0.13$ at 90% CL is derived as well.



$\Gamma(\pi^- \ell^+ \nu_\ell) / \Gamma_{\text{total}}$ Γ_{19} / Γ

"OUR EVALUATION" is provided by the Heavy Flavor Averaging Group (HFLAV) and the procedure is described at <https://hflav.web.cern.ch/>.

VALUE (units 10^{-4})	DOCUMENT ID	TECN	COMMENT
1.50 ± 0.06 OUR EVALUATION			
1.46 ± 0.04 OUR AVERAGE			
1.49 ± 0.09 ± 0.07	¹ SIBIDANOV 13	BELL	$e^+ e^- \rightarrow \Upsilon(4S)$
1.47 ± 0.05 ± 0.06	^{2,3} LEES 12AA	BABR	$e^+ e^- \rightarrow \Upsilon(4S)$
1.41 ± 0.05 ± 0.07	⁴ DEL-AMO-SA...11c	BABR	$e^+ e^- \rightarrow \Upsilon(4S)$
1.49 ± 0.04 ± 0.07	² HA 11	BELL	$e^+ e^- \rightarrow \Upsilon(4S)$
1.54 ± 0.17 ± 0.09	⁴ AUBERT 08AV	BABR	$e^+ e^- \rightarrow \Upsilon(4S)$
1.37 ± 0.15 ± 0.11	^{5,6} ADAM 07	CLE2	$e^+ e^- \rightarrow \Upsilon(4S)$
1.38 ± 0.19 ± 0.14	⁷ HOKUUE 07	BELL	$e^+ e^- \rightarrow \Upsilon(4S)$

• • • We do not use the following data for averages, fits, limits, etc. • • •

1.42±0.05±0.08	² DEL-AMO-SA..11F	BABR	Repl. by LEES 12AA
1.46±0.07±0.08	⁸ AUBERT	07J	BABR Repl. by DEL-AMO-SANCHEZ 11F
1.33±0.17±0.11	⁹ AUBERT,B	06K	BABR Repl. by AUBERT 08AV
1.38±0.10±0.18	¹⁰ AUBERT,B	05O	BABR Repl. by DEL-AMO-SANCHEZ 11C
1.33±0.18±0.13	¹¹ ATHAR	03	CLE2 Repl. by ADAM 07
1.8 ± 0.4 ± 0.4	¹² ALEXANDER	96T	CLE2 Repl. by ATHAR 03

- The signal events are tagged by a second B meson reconstructed in the fully hadronic decays.
- Uses loose neutrino reconstruction technique. Assumes $B(\Upsilon(4S) \rightarrow B^+ B^-) = (51.6 \pm 0.6)\%$ and $B(\Upsilon(4S) \rightarrow B^0 \bar{B}^0) = (48.4 \pm 0.6)\%$.
- Reports also a branching fraction value $B(B^0 \rightarrow \pi^- \ell^+ \nu) = (1.45 \pm 0.04 \pm 0.06) \times 10^{-4}$ from the decays of B^+ and B^0 that are combined using the isospin symmetry relation.
- Using the isospin symmetry relation, B^+ and B^0 branching fractions are combined.
- The B^0 and B^+ results are combined assuming the isospin, B lifetimes, and relative charged/neutral B production at the $\Upsilon(4S)$.
- Also report the rate for $q^2 > 16 \text{ GeV}^2$ of $(0.41 \pm 0.08 \pm 0.04) \times 10^{-4}$ from which they obtain $|V_{ub}| = 3.6 \pm 0.4 \pm 0.2^{+0.6}_{-0.4}$ (last error is from theory).
- The signal events are tagged by a second B meson reconstructed in the semileptonic mode $B \rightarrow D^{(*)} \ell \nu_\ell$.
- The analysis uses events in which the signal B decays are reconstructed with an innovative loose neutrino reconstruction technique.
- The signals are tagged by a second B meson reconstructed in a semileptonic or hadronic decay. The B^0 and B^+ results are combined assuming the isospin symmetry.
- B^+ and B^0 decays combined assuming isospin symmetry. Systematic errors include both experimental and form-factor uncertainties.
- ATHAR 03 reports systematic errors $0.11 \pm 0.01 \pm 0.07$, which are experimental systematic, systematic due to residual form-factor uncertainties in the signal, and systematic due to residual form-factor uncertainties in the cross-feed modes, respectively. We combine these in quadrature.
- ALEXANDER 96T gives systematic errors $\pm 0.3 \pm 0.2$ where the second error reflects the estimated model dependence. We combine these in quadrature. Assumes isospin symmetry: $\Gamma(B^0 \rightarrow \pi^- \ell^+ \nu) = 2 \times \Gamma(B^+ \rightarrow \pi^0 \ell^+ \nu)$.

$\Gamma(\pi^- \mu^+ \nu_\mu) / \Gamma_{\text{total}}$ Γ_{20} / Γ

VALUE	DOCUMENT ID	TECN	COMMENT
• • • We do not use the following data for averages, fits, limits, etc. • • •			
seen	¹ ALBRECHT	91c	ARG

- In ALBRECHT 91c, one event is fully reconstructed providing evidence for the $b \rightarrow u$ transition.

$\Gamma(\pi^- \tau^+ \nu_\tau) / \Gamma_{\text{total}}$ Γ_{21} / Γ

VALUE	CL%	DOCUMENT ID	TECN	COMMENT
$< 2.5 \times 10^{-4}$	90	¹ HAMER	16	BELL $e^+ e^- \rightarrow \Upsilon(4S)$

- Assumes equal production of B^+ and B^0 at the $\Upsilon(4S)$.

$\Gamma(K^\pm X) / \Gamma_{\text{total}}$ Γ_{22} / Γ

VALUE	DOCUMENT ID	TECN	COMMENT
0.78±0.08	¹ ALBRECHT	96D	ARG $e^+ e^- \rightarrow \Upsilon(4S)$

- Average multiplicity.

$\Gamma(D^0 X) / \Gamma_{\text{total}}$ Γ_{23} / Γ

VALUE	DOCUMENT ID	TECN	COMMENT
0.081±0.014±0.005	¹ AUBERT	07N	BABR $e^+ e^- \rightarrow \Upsilon(4S)$

- • • We do not use the following data for averages, fits, limits, etc. • • •
- | | | | |
|-------------------|------------------------|-----|--------------------------|
| 0.063±0.019±0.005 | ¹ AUBERT,BE | 04B | BABR Repl. by AUBERT 07N |
|-------------------|------------------------|-----|--------------------------|
- Events are selected by completely reconstructing one B and searching for a reconstructed charmed particle in the rest of the event. The last error includes systematic and charm branching ratio uncertainties.

$\Gamma(\bar{D}^0 X) / \Gamma_{\text{total}}$ Γ_{24} / Γ

VALUE	DOCUMENT ID	TECN	COMMENT
0.474±0.020^{+0.020}_{-0.019}	¹ AUBERT	07N	BABR $e^+ e^- \rightarrow \Upsilon(4S)$

- • • We do not use the following data for averages, fits, limits, etc. • • •
- | | | | |
|-------------------|------------------------|-----|--------------------------|
| 0.511±0.031±0.028 | ¹ AUBERT,BE | 04B | BABR Repl. by AUBERT 07N |
|-------------------|------------------------|-----|--------------------------|
- Events are selected by completely reconstructing one B and searching for a reconstructed charmed particle in the rest of the event. The last error includes systematic and charm branching ratio uncertainties.

$\Gamma(D^0 X) / [\Gamma(D^0 X) + \Gamma(\bar{D}^0 X)]$ $\Gamma_{23} / (\Gamma_{23} + \Gamma_{24})$

VALUE	DOCUMENT ID	TECN	COMMENT
0.146±0.022±0.006	AUBERT	07N	BABR $e^+ e^- \rightarrow \Upsilon(4S)$

• • • We do not use the following data for averages, fits, limits, etc. • • •

0.110±0.031±0.008	AUBERT,BE	04B	BABR Repl. by AUBERT 07N
-------------------	-----------	-----	--------------------------

$\Gamma(D^+ X) / \Gamma_{\text{total}}$ Γ_{25} / Γ

VALUE	CL%	DOCUMENT ID	TECN	COMMENT
< 0.039	90	¹ AUBERT	07N	BABR $e^+ e^- \rightarrow \Upsilon(4S)$

• • • We do not use the following data for averages, fits, limits, etc. • • •

< 0.051	90	¹ AUBERT,BE	04B	BABR Repl. by AUBERT 07N
---------	----	------------------------	-----	--------------------------

- Events are selected by completely reconstructing one B and searching for a reconstructed charmed particle in the rest of the event. The last error includes systematic and charm branching ratio uncertainties.

$\Gamma(D^- X) / \Gamma_{\text{total}}$ Γ_{26} / Γ

VALUE	DOCUMENT ID	TECN	COMMENT
0.369±0.016^{+0.030}_{-0.027}	¹ AUBERT	07N	BABR $e^+ e^- \rightarrow \Upsilon(4S)$

- • • We do not use the following data for averages, fits, limits, etc. • • •
- | | | | |
|---|------------------------|-----|--------------------------|
| 0.397±0.030 ^{+0.040} _{-0.038} | ¹ AUBERT,BE | 04B | BABR Repl. by AUBERT 07N |
|---|------------------------|-----|--------------------------|
- Events are selected by completely reconstructing one B and searching for a reconstructed charmed particle in the rest of the event. The last error includes systematic and charm branching ratio uncertainties.

$\Gamma(D^+ X) / [\Gamma(D^+ X) + \Gamma(D^- X)]$ $\Gamma_{25} / (\Gamma_{25} + \Gamma_{26})$

VALUE	DOCUMENT ID	TECN	COMMENT
0.058±0.028±0.006	AUBERT	07N	BABR $e^+ e^- \rightarrow \Upsilon(4S)$

• • • We do not use the following data for averages, fits, limits, etc. • • •

0.055±0.040±0.006	AUBERT,BE	04B	BABR Repl. by AUBERT 07N
-------------------	-----------	-----	--------------------------

$\Gamma(D_s^+ X) / \Gamma_{\text{total}}$ Γ_{27} / Γ

VALUE	DOCUMENT ID	TECN	COMMENT
0.103±0.012^{+0.017}_{-0.014}	¹ AUBERT	07N	BABR $e^+ e^- \rightarrow \Upsilon(4S)$

• • • We do not use the following data for averages, fits, limits, etc. • • •

0.109±0.021 ^{+0.039} _{-0.024}	¹ AUBERT,BE	04B	BABR Repl. by AUBERT 07N
---	------------------------	-----	--------------------------

- Events are selected by completely reconstructing one B and searching for a reconstructed charmed particle in the rest of the event. The last error includes systematic and charm branching ratio uncertainties.

$\Gamma(D_s^- X) / \Gamma_{\text{total}}$ Γ_{28} / Γ

VALUE	CL%	DOCUMENT ID	TECN	COMMENT
< 0.026	90	¹ AUBERT	07N	BABR $e^+ e^- \rightarrow \Upsilon(4S)$

• • • We do not use the following data for averages, fits, limits, etc. • • •

< 0.087	90	¹ AUBERT,BE	04B	BABR Repl. by AUBERT 07N
---------	----	------------------------	-----	--------------------------

- Events are selected by completely reconstructing one B and searching for a reconstructed charmed particle in the rest of the event. The last error includes systematic and charm branching ratio uncertainties.

$\Gamma(D_s^+ X) / [\Gamma(D_s^+ X) + \Gamma(D_s^- X)]$ $\Gamma_{27} / (\Gamma_{27} + \Gamma_{28})$

VALUE	DOCUMENT ID	TECN	COMMENT
0.879±0.066±0.005	AUBERT	07N	BABR $e^+ e^- \rightarrow \Upsilon(4S)$

• • • We do not use the following data for averages, fits, limits, etc. • • •

0.733±0.092±0.010	AUBERT,BE	04B	BABR Repl. by AUBERT 07N
-------------------	-----------	-----	--------------------------

$\Gamma(A_c^+ X) / \Gamma_{\text{total}}$ Γ_{29} / Γ

VALUE	CL%	DOCUMENT ID	TECN	COMMENT
< 0.031	90	¹ AUBERT	07N	BABR $e^+ e^- \rightarrow \Upsilon(4S)$

• • • We do not use the following data for averages, fits, limits, etc. • • •

< 0.038	90	¹ AUBERT,BE	04B	BABR Repl. by AUBERT 07N
---------	----	------------------------	-----	--------------------------

- Events are selected by completely reconstructing one B and searching for a reconstructed charmed particle in the rest of the event. The last error includes systematic and charm branching ratio uncertainties.

$\Gamma(\bar{A}_c^- X) / \Gamma_{\text{total}}$ Γ_{30} / Γ

VALUE	DOCUMENT ID	TECN	COMMENT
0.05 ± 0.010^{+0.019}_{-0.011}	¹ AUBERT	07N	BABR $e^+ e^- \rightarrow \Upsilon(4S)$

• • • We do not use the following data for averages, fits, limits, etc. • • •

0.049±0.017 ^{+0.018} _{-0.011}	¹ AUBERT,BE	04B	BABR Repl. by AUBERT 07N
---	------------------------	-----	--------------------------

- Events are selected by completely reconstructing one B and searching for a reconstructed charmed particle in the rest of the event. The last error includes systematic and charm branching ratio uncertainties.

$\Gamma(A_c^+ X) / [\Gamma(A_c^+ X) + \Gamma(\bar{A}_c^- X)]$ $\Gamma_{29} / (\Gamma_{29} + \Gamma_{30})$

VALUE	DOCUMENT ID	TECN	COMMENT
0.243±0.119^{+0.021}_{-0.121}±0.003	AUBERT	07N	BABR $e^+ e^- \rightarrow \Upsilon(4S)$

• • • We do not use the following data for averages, fits, limits, etc. • • •

0.286±0.142±0.007	AUBERT,BE	04B	BABR Repl. by AUBERT 07N
-------------------	-----------	-----	--------------------------

$\Gamma(\bar{X}) / \Gamma_{\text{total}}$ Γ_{31} / Γ

VALUE	DOCUMENT ID	TECN	COMMENT
0.947±0.030^{+0.045}_{-0.040}	¹ AUBERT	07N	BABR $e^+ e^- \rightarrow \Upsilon(4S)$

• • • We do not use the following data for averages, fits, limits, etc. • • •

1.039±0.051 ^{+0.063} _{-0.058}	¹ AUBERT,BE	04B	BABR Repl. by AUBERT 07N
---	------------------------	-----	--------------------------

- Events are selected by completely reconstructing one B and searching for a reconstructed charmed particle in the rest of the event. The last error includes systematic and charm branching ratio uncertainties.

Meson Particle Listings

 B^0

$\Gamma(cX)/\Gamma_{\text{total}}$ Γ_{32}/Γ
 VALUE DOCUMENT ID TECN COMMENT

$0.246 \pm 0.024^{+0.021}_{-0.017}$ ¹AUBERT 07N BABR $e^+e^- \rightarrow \Upsilon(4S)$

• • • We do not use the following data for averages, fits, limits, etc. • • •

$0.237 \pm 0.036^{+0.041}_{-0.027}$ ¹AUBERT,BE 04B BABR Repl. by AUBERT 07N

¹ Events are selected by completely reconstructing one B and searching for a reconstructed charmed particle in the rest of the event. The last error includes systematic and charm branching ratio uncertainties.

$\Gamma(\bar{c}/cX)/\Gamma_{\text{total}}$ Γ_{33}/Γ
 VALUE DOCUMENT ID TECN COMMENT

$1.193 \pm 0.030^{+0.053}_{-0.049}$ ¹AUBERT 07N BABR $e^+e^- \rightarrow \Upsilon(4S)$

• • • We do not use the following data for averages, fits, limits, etc. • • •

$1.276 \pm 0.062^{+0.088}_{-0.074}$ ¹AUBERT,BE 04B BABR Repl. by AUBERT 07N

¹ Events are selected by completely reconstructing one B and searching for a reconstructed charmed particle in the rest of the event. The last error includes systematic and charm branching ratio uncertainties.

$\Gamma(D^-\pi^+)/\Gamma_{\text{total}}$ Γ_{34}/Γ
 VALUE (units 10^{-3}) EVTS DOCUMENT ID TECN COMMENT

2.52 ± 0.13 OUR FIT Error includes scale factor of 1.1.

2.68 ± 0.13 OUR AVERAGE

$2.55 \pm 0.05 \pm 0.16$ ¹AUBERT 07H BABR $e^+e^- \rightarrow \Upsilon(4S)$

$3.03 \pm 0.23 \pm 0.23$ ²AUBERT,BE 06J BABR $e^+e^- \rightarrow \Upsilon(4S)$

$2.68 \pm 0.12 \pm 0.24$ ^{1,3}AHMED 02B CLE2 $e^+e^- \rightarrow \Upsilon(4S)$

$2.7 \pm 0.6 \pm 0.5$ ⁴BORTOLETTO92 CLEO $e^+e^- \rightarrow \Upsilon(4S)$

$4.8 \pm 1.1 \pm 1.1$ ²² ⁵ALBRECHT 90J ARG $e^+e^- \rightarrow \Upsilon(4S)$

$5.1^{+2.8}_{-2.5}^{+1.3}_{-1.2}$ ⁴ ⁶BEBEK 87 CLEO $e^+e^- \rightarrow \Upsilon(4S)$

• • • We do not use the following data for averages, fits, limits, etc. • • •

$2.73 \pm 0.19 \pm 0.05$ ^{1,7}AUBERT,B 04O BABR Repl. by AUBERT 07H

$2.83 \pm 0.42 \pm 0.05$ ⁸¹ ⁸ALAM 94 CLE2 Repl. by AHMED 02B

$3.1 \pm 1.3 \pm 1.0$ ⁷ ⁵ALBRECHT 88K ARG $e^+e^- \rightarrow \Upsilon(4S)$

¹ Assumes equal production of B^+ and B^0 at the $\Upsilon(4S)$.

² Uses a missing-mass method. Does not depend on D branching fractions or B^{\pm}/B^0 production rates.

³ AHMED 02B reports an additional uncertainty on the branching ratios to account for 4.5% uncertainty on relative production of B^0 and B^+ , which is not included here.

⁴ BORTOLETTO 92 assumes equal production of B^+ and B^0 at the $\Upsilon(4S)$ and uses Mark III branching fractions for the D .

⁵ ALBRECHT 88K assumes $B^0\bar{B}^0:B^+B^-$ production ratio is 45:55. Superseded by ALBRECHT 90J which assumes 50:50.

⁶ BEBEK 87 value has been updated in BERKELMAN 91 to use same assumptions as noted for BORTOLETTO 92.

⁷ AUBERT,B 04O reports $[\Gamma(B^0 \rightarrow D^-\pi^+)/\Gamma_{\text{total}}] \times [B(D^+ \rightarrow K_S^0\pi^+)] = (42.7 \pm 2.1 \pm 2.2) \times 10^{-6}$ which we divide by our best value $B(D^+ \rightarrow K_S^0\pi^+) = (1.562 \pm 0.031) \times 10^{-2}$. Our first error is their experiment's error and our second error is the systematic error from using our best value.

⁸ ALAM 94 reports $[\Gamma(B^0 \rightarrow D^-\pi^+)/\Gamma_{\text{total}}] \times [B(D^+ \rightarrow K^-2\pi^+)] = (0.265 \pm 0.032 \pm 0.023) \times 10^{-3}$ which we divide by our best value $B(D^+ \rightarrow K^-2\pi^+) = (9.38 \pm 0.16) \times 10^{-2}$. Our first error is their experiment's error and our second error is the systematic error from using our best value. Assumes equal production of B^+ and B^0 at the $\Upsilon(4S)$.

$\Gamma(D^-\ell^+\nu_\ell)/\Gamma(D^-\pi^+)$ Γ_4/Γ_{34}
 VALUE DOCUMENT ID TECN COMMENT

$9.9 \pm 1.0 \pm 0.9$ AALTONEN 09E CDF $p\bar{p}$ at 1.96 TeV

$\Gamma(D^-\rho^+)/\Gamma_{\text{total}}$ Γ_{35}/Γ
 VALUE EVTS DOCUMENT ID TECN COMMENT

0.0076 ± 0.0012 OUR AVERAGE

$0.0075 \pm 0.0013 \pm 0.0001$ ⁷⁹ ¹ALAM 94 CLE2 $e^+e^- \rightarrow \Upsilon(4S)$

$0.009 \pm 0.005 \pm 0.003$ ⁹ ²ALBRECHT 90J ARG $e^+e^- \rightarrow \Upsilon(4S)$

• • • We do not use the following data for averages, fits, limits, etc. • • •

$0.022 \pm 0.012 \pm 0.009$ ⁶ ²ALBRECHT 88K ARG $e^+e^- \rightarrow \Upsilon(4S)$

¹ ALAM 94 reports $[\Gamma(B^0 \rightarrow D^-\rho^+)/\Gamma_{\text{total}}] \times [B(D^+ \rightarrow K^-2\pi^+)] = 0.000704 \pm 0.000096 \pm 0.000070$ which we divide by our best value $B(D^+ \rightarrow K^-2\pi^+) = (9.38 \pm 0.16) \times 10^{-2}$. Our first error is their experiment's error and our second error is the systematic error from using our best value. Assumes equal production of B^+ and B^0 at the $\Upsilon(4S)$.

² ALBRECHT 88K assumes $B^0\bar{B}^0:B^+B^-$ production ratio is 45:55. Superseded by ALBRECHT 90J which assumes 50:50.

$\Gamma(D^-K^0\pi^+)/\Gamma_{\text{total}}$ Γ_{36}/Γ
 VALUE (units 10^{-4}) DOCUMENT ID TECN COMMENT

$4.9 \pm 0.7 \pm 0.5$ ¹AUBERT,BE 05B BABR $e^+e^- \rightarrow \Upsilon(4S)$

¹ Assumes equal production of B^+ and B^0 at the $\Upsilon(4S)$.

$\Gamma(D^-K^*(892)^+)/\Gamma_{\text{total}}$ Γ_{37}/Γ
 VALUE (units 10^{-4}) DOCUMENT ID TECN COMMENT

4.5 ± 0.7 OUR AVERAGE

$4.6 \pm 0.6 \pm 0.5$ ¹AUBERT,BE 05B BABR $e^+e^- \rightarrow \Upsilon(4S)$

$3.7 \pm 1.5 \pm 1.0$ ¹MAHAPATRA 02 CLE2 $e^+e^- \rightarrow \Upsilon(4S)$

¹ Assumes equal production of B^+ and B^0 at the $\Upsilon(4S)$.

$\Gamma(D^-\omega\pi^+)/\Gamma_{\text{total}}$ Γ_{38}/Γ
 VALUE DOCUMENT ID TECN COMMENT

$0.0028 \pm 0.0005 \pm 0.0004$ ¹ALEXANDER 01B CLE2 $e^+e^- \rightarrow \Upsilon(4S)$

¹ Assumes equal production of B^+ and B^0 at the $\Upsilon(4S)$. The signal is consistent with all observed $\omega\pi^+$ having proceeded through the ρ^+ resonance at mass $1349 \pm 25^{+10}_{-5}$ MeV and width $547 \pm 86^{+46}_{-45}$ MeV.

$\Gamma(D^-K^+)/\Gamma_{\text{total}}$ Γ_{39}/Γ
 VALUE (units 10^{-4}) DOCUMENT ID TECN COMMENT

1.86 ± 0.20 OUR AVERAGE

$1.89 \pm 0.19 \pm 0.10$ ¹AAIJ 11F LHCB pp at 7 TeV

$1.7 \pm 0.4 \pm 0.1$ ²ABE 01I BELL $e^+e^- \rightarrow \Upsilon(4S)$

¹ AAIJ 11F reports $(2.01 \pm 0.18 \pm 0.14) \times 10^{-4}$ from a measurement of $[\Gamma(B^0 \rightarrow D^-K^+)/\Gamma_{\text{total}}] / [B(B^0 \rightarrow D^-\pi^+)]$ assuming $B(B^0 \rightarrow D^-\pi^+) = (2.68 \pm 0.13) \times 10^{-3}$, which we rescale to our best value $B(B^0 \rightarrow D^-\pi^+) = (2.52 \pm 0.13) \times 10^{-3}$. Our first error is their experiment's error and our second error is the systematic error from using our best value.

² ABE 01I reports $[\Gamma(B^0 \rightarrow D^-K^+)/\Gamma_{\text{total}}] / [B(B^0 \rightarrow D^-\pi^+)] = (6.8 \pm 1.5 \pm 0.7) \times 10^{-2}$ which we multiply by our best value $B(B^0 \rightarrow D^-\pi^+) = (2.52 \pm 0.13) \times 10^{-3}$. Our first error is their experiment's error and our second error is the systematic error from using our best value.

$\Gamma(D^-K^+)/\Gamma(D^-\pi^+)$ Γ_{39}/Γ_{34}
 VALUE (units 10^{-2}) DOCUMENT ID TECN COMMENT

$8.22 \pm 0.11 \pm 0.25$ AAIJ 13P LHCB pp at 7 TeV

$\Gamma(D^-K^+\pi^+\pi^-)/\Gamma(D^-\pi^+\pi^+\pi^-)$ Γ_{40}/Γ_{46}
 VALUE (units 10^{-2}) DOCUMENT ID TECN COMMENT

$5.9 \pm 1.1 \pm 0.5$ AAIJ 12T LHCB pp at 7 TeV

$\Gamma(D^-K^+\bar{K}^0)/\Gamma_{\text{total}}$ Γ_{41}/Γ
 VALUE (units 10^{-4}) CL% DOCUMENT ID TECN COMMENT

< 3.1 ⁹⁰ ¹DRUTSKOY 02 BELL $e^+e^- \rightarrow \Upsilon(4S)$

¹ Assumes equal production of B^+ and B^0 at the $\Upsilon(4S)$.

$\Gamma(D^-K^+\bar{K}^*(892)^0)/\Gamma_{\text{total}}$ Γ_{42}/Γ
 VALUE (units 10^{-4}) DOCUMENT ID TECN COMMENT

$8.8 \pm 1.1 \pm 1.5$ ¹DRUTSKOY 02 BELL $e^+e^- \rightarrow \Upsilon(4S)$

¹ Assumes equal production of B^+ and B^0 at the $\Upsilon(4S)$.

$\Gamma(\bar{D}^0\pi^+\pi^-)/\Gamma_{\text{total}}$ Γ_{43}/Γ
 VALUE (units 10^{-4}) CL% EVTS DOCUMENT ID TECN COMMENT

8.8 ± 0.5 OUR AVERAGE

$8.95 \pm 0.15 \pm 0.52$ ¹AAIJ 15Y LHCB pp at 7, 8 TeV

$8.4 \pm 0.4 \pm 0.8$ ²KUZMIN 07 BELL $e^+e^- \rightarrow \Upsilon(4S)$

• • • We do not use the following data for averages, fits, limits, etc. • • •

$8.0 \pm 0.6 \pm 1.5$ ^{2,3}SATPATHY 03 BELL Repl. by KUZMIN 07

< 16 ⁹⁰ ²ALAM 94 CLE2 $e^+e^- \rightarrow \Upsilon(4S)$

< 70 ⁹⁰ ⁴BORTOLETTO92 CLEO $e^+e^- \rightarrow \Upsilon(4S)$

< 340 ⁹⁰ ⁵BEBEK 87 CLEO $e^+e^- \rightarrow \Upsilon(4S)$

700 ± 500 ⁵ ⁶BEHRENDTS 83 CLEO $e^+e^- \rightarrow \Upsilon(4S)$

¹ The second uncertainty combines in quadrature all systematic uncertainties quoted in the paper. AAIJ 15Y reports $B(B^0 \rightarrow \bar{D}^0\pi^+\pi^-) = (8.46 \pm 0.14 \pm 0.49) \times 10^{-4}$ in the kinematic region $m(\bar{D}^0\pi^+) > 2.1$ GeV which we corrected to the full phase-space dividing by 0.945 from Belle.

² Assumes equal production of B^+ and B^0 at the $\Upsilon(4S)$.

³ No assumption about the intermediate mechanism is made in the analysis.

⁴ BORTOLETTO 92 assumes equal production of B^+ and B^0 at the $\Upsilon(4S)$ and uses Mark III branching fractions for the D . The product branching fraction into $D_1^*(2340)\pi$ followed by $D_1^*(2340) \rightarrow D^0\pi$ is < 0.0001 at 90% CL and into $D_2^*(2460)\pi$ followed by $D_2^*(2460) \rightarrow D^0\pi$ is < 0.0004 at 90% CL.

⁵ BEBEK 87 assume the $\Upsilon(4S)$ decays 43% to $B^0\bar{B}^0$. We rescale to 50%. $B(D^0 \rightarrow K^-\pi^+) = (4.2 \pm 0.4 \pm 0.4)\%$ and $B(D^0 \rightarrow K^-\pi^+\pi^+\pi^-) = (9.1 \pm 0.8 \pm 0.8)\%$ were used.

⁶ Corrected by us using assumptions: $B(D^0 \rightarrow K^-\pi^+) = (0.042 \pm 0.006)$ and $B(\Upsilon(4S) \rightarrow B^0\bar{B}^0) = 50\%$. The product branching ratio is $B(B^0 \rightarrow \bar{D}^0\pi^+\pi^-)B(\bar{D}^0 \rightarrow K^+\pi^-) = (0.39 \pm 0.26) \times 10^{-2}$.

See key on page 999

Meson Particle Listings

B^0

$\Gamma(D^*(2010)^-\pi^+)/\Gamma_{total}$			Γ_{44}/Γ		
VALUE (units 10^{-3})	EVTS	DOCUMENT ID	TECN	COMMENT	
2.74 ± 0.13 OUR AVERAGE					
2.79 ± 0.08 ± 0.17		1 AUBERT	07H	BABR	$e^+e^- \rightarrow \Upsilon(4S)$
2.50 ± 0.34 ± 0.13		2,3 AUBERT, BE	06J	BABR	$e^+e^- \rightarrow \Upsilon(4S)$
2.81 ± 0.24 ± 0.05		4 BRANDENB...	98	CLE2	$e^+e^- \rightarrow \Upsilon(4S)$
2.6 ± 0.3 ± 0.4	82	5 ALAM	94	CLE2	$e^+e^- \rightarrow \Upsilon(4S)$
3.37 ± 0.96 ± 0.02		6 BOROLETTO92	CLEO	$e^+e^- \rightarrow \Upsilon(4S)$	
2.36 ± 0.88 ± 0.02	12	7 ALBRECHT	90J	ARG	$e^+e^- \rightarrow \Upsilon(4S)$
2.36 ^{+1.50} _{-1.10} ± 0.02	5	8 BEBEK	87	CLEO	$e^+e^- \rightarrow \Upsilon(4S)$

• • • We do not use the following data for averages, fits, limits, etc. • • •

10 ± 4 ± 1	8	9 AKERS	94J	OPAL	$e^+e^- \rightarrow Z$
2.7 ± 1.4 ± 1.0	5	10 ALBRECHT	87c	ARG	$e^+e^- \rightarrow \Upsilon(4S)$
3.5 ± 2 ± 2		11 ALBRECHT	86F	ARG	$e^+e^- \rightarrow \Upsilon(4S)$
17 ± 5 ± 5	41	12 GILES	84	CLEO	$e^+e^- \rightarrow \Upsilon(4S)$

1 Assumes equal production of B^+ and B^0 at the $\Upsilon(4S)$.
 2 AUBERT, BE 06J reports $[\Gamma(B^0 \rightarrow D^*(2010)^-\pi^+)/\Gamma_{total}] / [B(B^0 \rightarrow D^-\pi^+)] = 0.99 \pm 0.11 \pm 0.08$ which we multiply by our best value $B(B^0 \rightarrow D^-\pi^+) = (2.52 \pm 0.13) \times 10^{-3}$. Our first error is their experiment's error and our second error is the systematic error from using our best value.
 3 Uses a missing-mass method. Does not depend on D branching fractions or $B^+\pi^0$ production rates.
 4 BRANDENBURG 98 assume equal production of B^+ and B^0 at $\Upsilon(4S)$ and use the D^* reconstruction technique. The first error is their experiment's error and the second error is the systematic error from the PDG 96 value of $B(D^* \rightarrow D\pi)$.
 5 ALAM 94 assume equal production of B^+ and B^0 at the $\Upsilon(4S)$ and use the CLEO II $B(D^*(2010)^+ \rightarrow D^0\pi^+)$ and absolute $B(D^0 \rightarrow K^-\pi^+)$ and the PDG 1992 $B(D^0 \rightarrow K^-\pi^+\pi^0)/B(D^0 \rightarrow K^-\pi^+)$ and $B(D^0 \rightarrow K^-2\pi^+\pi^-)/B(D^0 \rightarrow K^-\pi^+)$.
 6 BOROLETTO 92 reports $(4.0 \pm 1.0 \pm 0.7) \times 10^{-3}$ from a measurement of $[\Gamma(B^0 \rightarrow D^*(2010)^-\pi^+)/\Gamma_{total}] \times [B(D^*(2010)^+ \rightarrow D^0\pi^+)]$ assuming $B(D^*(2010)^+ \rightarrow D^0\pi^+) = 0.57 \pm 0.06$, which we rescale to our best value $B(D^*(2010)^+ \rightarrow D^0\pi^+) = (67.7 \pm 0.5) \times 10^{-2}$. Our first error is their experiment's error and our second error is the systematic error from using our best value. Assumes equal production of B^+ and B^0 at the $\Upsilon(4S)$ and uses Mark III branching fractions for the D .
 7 ALBRECHT 90J reports $(2.8 \pm 0.9 \pm 0.6) \times 10^{-3}$ from a measurement of $[\Gamma(B^0 \rightarrow D^*(2010)^-\pi^+)/\Gamma_{total}] \times [B(D^*(2010)^+ \rightarrow D^0\pi^+)]$ assuming $B(D^*(2010)^+ \rightarrow D^0\pi^+) = 0.57 \pm 0.06$, which we rescale to our best value $B(D^*(2010)^+ \rightarrow D^0\pi^+) = (67.7 \pm 0.5) \times 10^{-2}$. Our first error is their experiment's error and our second error is the systematic error from using our best value. Assumes equal production of B^+ and B^0 at the $\Upsilon(4S)$ and uses Mark III branching fractions for the D .
 8 BEBEK 87 reports $(2.8^{+1.5+1.0}_{-1.2-0.6}) \times 10^{-3}$ from a measurement of $[\Gamma(B^0 \rightarrow D^*(2010)^-\pi^+)/\Gamma_{total}] \times [B(D^*(2010)^+ \rightarrow D^0\pi^+)]$ assuming $B(D^*(2010)^+ \rightarrow D^0\pi^+) = 0.57 \pm 0.06$, which we rescale to our best value $B(D^*(2010)^+ \rightarrow D^0\pi^+) = (67.7 \pm 0.5) \times 10^{-2}$. Our first error is their experiment's error and our second error is the systematic error from using our best value. Updated in BERKELMAN 91 to use same assumptions as noted for BOROLETTO 92 and ALBRECHT 90J.
 9 Assumes $B(Z \rightarrow b\bar{b}) = 0.217$ and 38% B_d production fraction.
 10 ALBRECHT 87c use PDG 86 branching ratios for D and $D^*(2010)$ and assume $B(\Upsilon(4S) \rightarrow B^+B^-) = 55\%$ and $B(\Upsilon(4S) \rightarrow B^0\bar{B}^0) = 45\%$. Superseded by ALBRECHT 90J.
 11 ALBRECHT 86F uses pseudomass that is independent of D^0 and D^+ branching ratios.
 12 Assumes $B(D^*(2010)^+ \rightarrow D^0\pi^+) = 0.60^{+0.08}_{-0.15}$. Assumes $B(\Upsilon(4S) \rightarrow B^0\bar{B}^0) = 0.40 \pm 0.02$. Does not depend on D branching ratios.

$\Gamma(D^*(2010)^-\ell^+\nu_\ell)/\Gamma(D^*(2010)^-\pi^+)$			Γ_6/Γ_{44}		
VALUE	DOCUMENT ID	TECN	COMMENT		
16.5 ± 2.3 ± 1.1					
	AALTONEN	09E	CDF	$p\bar{p}$ at 1.96 TeV	

$\Gamma(D^0 K^+ K^-)/\Gamma(D^0 \pi^+ \pi^-)$			Γ_{45}/Γ_{43}		
VALUE	DOCUMENT ID	TECN	COMMENT		
0.067 ± 0.005 OUR AVERAGE					
0.069 ± 0.004 ± 0.003	AAIJ	18AZ	LHCB	$p\bar{p}$ at 7, 8 TeV	
0.056 ± 0.011 ± 0.007	AAIJ	12AMLHCB		$p\bar{p}$ at 7 TeV	

$\Gamma(D^-\pi^+\pi^+\pi^-)/\Gamma_{total}$			Γ_{46}/Γ		
VALUE	DOCUMENT ID	TECN	COMMENT		
0.0060 ± 0.0007 OUR FIT Error includes scale factor of 1.1.					
0.0080 ± 0.0021 ± 0.0014					
	1 BOROLETTO92	CLEO	$e^+e^- \rightarrow \Upsilon(4S)$		

1 BOROLETTO 92 assumes equal production of B^+ and B^0 at the $\Upsilon(4S)$ and uses Mark III branching fractions for the D .

$\Gamma(D^-\pi^+\pi^+\pi^-)/\Gamma(D^-\pi^+)$			Γ_{46}/Γ_{34}		
VALUE	DOCUMENT ID	TECN	COMMENT		
2.39 ± 0.23 OUR FIT					
2.38 ± 0.11 ± 0.21					
	AAIJ	11E	LHCB	$p\bar{p}$ at 7 TeV	

$\Gamma((D^-\pi^+\pi^+\pi^-)_{nonresonant})/\Gamma_{total}$			Γ_{47}/Γ		
VALUE	DOCUMENT ID	TECN	COMMENT		
0.0039 ± 0.0014 ± 0.0013					
	1 BOROLETTO92	CLEO	$e^+e^- \rightarrow \Upsilon(4S)$		

1 BOROLETTO 92 assumes equal production of B^+ and B^0 at the $\Upsilon(4S)$ and uses Mark III branching fractions for the D .

$\Gamma(D^-\pi^+\rho^0)/\Gamma_{total}$			Γ_{48}/Γ		
VALUE	DOCUMENT ID	TECN	COMMENT		
0.0011 ± 0.0009 ± 0.0004					
	1 BOROLETTO92	CLEO	$e^+e^- \rightarrow \Upsilon(4S)$		

1 BOROLETTO 92 assumes equal production of B^+ and B^0 at the $\Upsilon(4S)$ and uses Mark III branching fractions for the D .

$\Gamma(D^-\pi_1(1260)^+)/\Gamma_{total}$			Γ_{49}/Γ		
VALUE	DOCUMENT ID	TECN	COMMENT		
0.0060 ± 0.0022 ± 0.0024					
	1 BOROLETTO92	CLEO	$e^+e^- \rightarrow \Upsilon(4S)$		

1 BOROLETTO 92 assumes equal production of B^+ and B^0 at the $\Upsilon(4S)$ and uses Mark III branching fractions for the D .

$\Gamma(D^*(2010)^-\pi^+\pi^0)/\Gamma_{total}$			Γ_{50}/Γ		
VALUE	EVTS	DOCUMENT ID	TECN	COMMENT	
0.0152 ± 0.0052 ± 0.0001					
• • • We do not use the following data for averages, fits, limits, etc. • • •					
0.015 ± 0.008 ± 0.008	8	2 ALBRECHT	87c	ARG	$e^+e^- \rightarrow \Upsilon(4S)$

1 ALBRECHT 90J reports $0.018 \pm 0.004 \pm 0.005$ from a measurement of $[\Gamma(B^0 \rightarrow D^*(2010)^-\pi^+\pi^0)/\Gamma_{total}] \times [B(D^*(2010)^+ \rightarrow D^0\pi^+)]$ assuming $B(D^*(2010)^+ \rightarrow D^0\pi^+) = 0.57 \pm 0.06$, which we rescale to our best value $B(D^*(2010)^+ \rightarrow D^0\pi^+) = (67.7 \pm 0.5) \times 10^{-2}$. Our first error is their experiment's error and our second error is the systematic error from using our best value. Assumes equal production of B^+ and B^0 at the $\Upsilon(4S)$ and uses Mark III branching fractions for the D .
 2 ALBRECHT 87c use PDG 86 branching ratios for D and $D^*(2010)$ and assume $B(\Upsilon(4S) \rightarrow B^+B^-) = 55\%$ and $B(\Upsilon(4S) \rightarrow B^0\bar{B}^0) = 45\%$. Superseded by ALBRECHT 90J.

$\Gamma(D^*(2010)^-\rho^+)/\Gamma_{total}$			Γ_{51}/Γ		
VALUE (units 10^{-3})	EVTS	DOCUMENT ID	TECN	COMMENT	
6.8 ± 0.9 OUR AVERAGE					
6.8 ± 0.3 ± 0.9		1,2 CSORNA	03	CLE2	$e^+e^- \rightarrow \Upsilon(4S)$
16.0 ± 11.3 ± 0.1		3 BOROLETTO92	CLEO	$e^+e^- \rightarrow \Upsilon(4S)$	
5.89 ± 3.52 ± 0.04	19	4 ALBRECHT	90J	ARG	$e^+e^- \rightarrow \Upsilon(4S)$
• • • We do not use the following data for averages, fits, limits, etc. • • •					
7.4 ± 1.0 ± 1.4	76	2,5 MATVIENKO	15	BELL	$e^+e^- \rightarrow \Upsilon(4S)$
		6,7 ALAM	94	CLE2	$e^+e^- \rightarrow \Upsilon(4S)$
81 ± 29 ⁺⁵⁹ ₋₂₄	19	8 CHEN	85	CLEO	$e^+e^- \rightarrow \Upsilon(4S)$

1 The second error combines the systematic and theoretical uncertainties in quadrature. CSORNA 03 includes data used in ALAM 94. A full angular fit to three complex helicity amplitudes is performed.
 2 Assumes equal production of B^0 and B^+ at the $\Upsilon(4S)$ resonance.
 3 BOROLETTO 92 reports $0.019 \pm 0.008 \pm 0.011$ from a measurement of $[\Gamma(B^0 \rightarrow D^*(2010)^-\rho^+)/\Gamma_{total}] \times [B(D^*(2010)^+ \rightarrow D^0\pi^+)]$ assuming $B(D^*(2010)^+ \rightarrow D^0\pi^+) = 0.57 \pm 0.06$, which we rescale to our best value $B(D^*(2010)^+ \rightarrow D^0\pi^+) = (67.7 \pm 0.5) \times 10^{-2}$. Our first error is their experiment's error and our second error is the systematic error from using our best value. Assumes equal production of B^+ and B^0 at the $\Upsilon(4S)$ and uses Mark III branching fractions for the D .
 4 ALBRECHT 90J reports $0.007 \pm 0.003 \pm 0.003$ from a measurement of $[\Gamma(B^0 \rightarrow D^*(2010)^-\rho^+)/\Gamma_{total}] \times [B(D^*(2010)^+ \rightarrow D^0\pi^+)]$ assuming $B(D^*(2010)^+ \rightarrow D^0\pi^+) = 0.57 \pm 0.06$, which we rescale to our best value $B(D^*(2010)^+ \rightarrow D^0\pi^+) = (67.7 \pm 0.5) \times 10^{-2}$. Our first error is their experiment's error and our second error is the systematic error from using our best value. Assumes equal production of B^+ and B^0 at the $\Upsilon(4S)$ and uses Mark III branching fractions for the D .
 5 MATVIENKO 15 reports $B(B^0 \rightarrow D^*(2010)^-\rho^+, \rho^+ \rightarrow \omega\pi^+) = (1.48 \pm 0.27^{+0.15+0.21}_{-0.09-0.56}) \times 10^{-3}$. The last uncertainty is a model one.
 6 ALAM 94 assume equal production of B^+ and B^0 at the $\Upsilon(4S)$ and use the CLEO II $B(D^*(2010)^+ \rightarrow D^0\pi^+)$ and absolute $B(D^0 \rightarrow K^-\pi^+)$ and the PDG 1992 $B(D^0 \rightarrow K^-\pi^+\pi^0)/B(D^0 \rightarrow K^-\pi^+)$ and $B(D^0 \rightarrow K^-2\pi^+\pi^-)/B(D^0 \rightarrow K^-\pi^+)$.
 7 This decay is nearly completely longitudinally polarized, $\Gamma_L/\Gamma = (93 \pm 5 \pm 5)\%$, as expected from the factorization hypothesis (ROSNER 90). The nonresonant $\pi^+\pi^0$ contribution under the ρ^+ is less than 9% at 90% CL.
 8 Uses $B(D^* \rightarrow D^0\pi^+) = 0.6 \pm 0.15$ and $B(\Upsilon(4S) \rightarrow B^0\bar{B}^0) = 0.4$. Does not depend on D branching ratios.

$\Gamma(D^*(2010)^-K^+)/\Gamma_{total}$			Γ_{52}/Γ		
VALUE (units 10^{-4})	DOCUMENT ID	TECN	COMMENT		
2.12 ± 0.15 OUR AVERAGE					
2.13 ± 0.12 ± 0.10		1 AUBERT	06A	BABR	$e^+e^- \rightarrow \Upsilon(4S)$
2.0 ± 0.4 ± 0.1		2 ABE	01I	BELL	$e^+e^- \rightarrow \Upsilon(4S)$

1 AUBERT 06A reports $[\Gamma(B^0 \rightarrow D^*(2010)^-K^+)/\Gamma_{total}] / [B(B^0 \rightarrow D^*(2010)^-\pi^+)] = 0.0776 \pm 0.0034 \pm 0.0029$ which we multiply by our best value $B(B^0 \rightarrow D^*(2010)^-\pi^+) = (2.74 \pm 0.13) \times 10^{-3}$. Our first error is their experiment's error and our second error is the systematic error from using our best value.
 2 ABE 01I reports $[\Gamma(B^0 \rightarrow D^*(2010)^-K^+)/\Gamma_{total}] / [B(B^0 \rightarrow D^*(2010)^-\pi^+)] = 0.074 \pm 0.015 \pm 0.006$ which we multiply by our best value $B(B^0 \rightarrow D^*(2010)^-\pi^+) = (2.74 \pm 0.13) \times 10^{-3}$. Our first error is their experiment's error and our second error is the systematic error from using our best value.

$\Gamma(D^*(2010)^-K^+)/\Gamma(D^*(2010)^-\pi^+)$			Γ_{52}/Γ_{44}		
VALUE	DOCUMENT ID	TECN	COMMENT		
(7.76 ± 0.34 ± 0.26) × 10⁻²					
	AAIJ	13AO	LHCB	$p\bar{p}$ at 7 TeV	

Meson Particle Listings

 B^0 $\Gamma(D^*(2010)^- K^0 \pi^+)/\Gamma_{\text{total}}$ Γ_{53}/Γ

VALUE (units 10^{-4})	DOCUMENT ID	TECN	COMMENT
3.0 ± 0.7 ± 0.3	1 AUBERT, BE	05B	BABR $e^+e^- \rightarrow \Upsilon(4S)$

¹ Assumes equal production of B^+ and B^0 at the $\Upsilon(4S)$.

 $\Gamma(D^*(2010)^- K^*(892)^+)/\Gamma_{\text{total}}$ Γ_{54}/Γ

VALUE (units 10^{-4})	DOCUMENT ID	TECN	COMMENT
3.3 ± 0.6 OUR AVERAGE			
3.2 ± 0.6 ± 0.3	1 AUBERT, BE	05B	BABR $e^+e^- \rightarrow \Upsilon(4S)$
3.8 ± 1.3 ± 0.8	2 MAHAPATRA	02	CLE2 $e^+e^- \rightarrow \Upsilon(4S)$

¹ Assumes equal production of B^+ and B^0 at the $\Upsilon(4S)$.

² Assumes equal production of B^+ and B^0 at the $\Upsilon(4S)$ and an unpolarized final state.

 $\Gamma(D^*(2010)^- K^+ \bar{K}^0)/\Gamma_{\text{total}}$ Γ_{55}/Γ

VALUE (units 10^{-4})	CL%	DOCUMENT ID	TECN	COMMENT
<4.7	90	1 DRUTSKOY	02	BELL $e^+e^- \rightarrow \Upsilon(4S)$

¹ Assumes equal production of B^+ and B^0 at the $\Upsilon(4S)$.

 $\Gamma(D^*(2010)^- K^+ \bar{K}^*(892)^0)/\Gamma_{\text{total}}$ Γ_{56}/Γ

VALUE (units 10^{-4})	DOCUMENT ID	TECN	COMMENT
12.9 ± 2.2 ± 2.5	1 DRUTSKOY	02	BELL $e^+e^- \rightarrow \Upsilon(4S)$

¹ Assumes equal production of B^+ and B^0 at the $\Upsilon(4S)$.

 $\Gamma(D^*(2010)^- \pi^+ \pi^+ \pi^-)/\Gamma_{\text{total}}$ Γ_{57}/Γ

VALUE (units 10^{-3})	CL%	DOCUMENT ID	TECN	COMMENT
7.21 ± 0.29 OUR AVERAGE				
7.26 ± 0.11 ± 0.31		1 LEES	16H	BABR $e^+e^- \rightarrow \Upsilon(4S)$
6.81 ± 0.23 ± 0.72		2 MAJUMDER	04	BELL $e^+e^- \rightarrow \Upsilon(4S)$
6.3 ± 1.0 ± 1.1		3,4 ALAM	94	CLE2 $e^+e^- \rightarrow \Upsilon(4S)$
13.4 ± 3.6 ± 0.1		5 BORTOLETTO	92	CLEO $e^+e^- \rightarrow \Upsilon(4S)$
10.1 ± 4.1 ± 0.1		6 ALBRECHT	90J	ARG $e^+e^- \rightarrow \Upsilon(4S)$
• • • We do not use the following data for averages, fits, limits, etc. • • •				
33 ± 9 ± 16		7 ALBRECHT	87c	ARG $e^+e^- \rightarrow \Upsilon(4S)$
<42	90	8 BEBEK	87	CLEO $e^+e^- \rightarrow \Upsilon(4S)$

¹ Assumes $B(\Upsilon(4S)) \rightarrow B^0 \bar{B}^0 = 0.486 \pm 0.006$.

² Assumes equal production of B^+ and B^0 at the $\Upsilon(4S)$.

³ ALAM 94 assume equal production of B^+ and B^0 at the $\Upsilon(4S)$ and use the CLEO II $B(D^*(2010)^+ \rightarrow D^0 \pi^+)$ and absolute $B(D^0 \rightarrow K^- \pi^+)$ and the PDG 1992 $B(D^0 \rightarrow K^- \pi^+ \pi^0)/B(D^0 \rightarrow K^- \pi^+)$ and $B(D^0 \rightarrow K^- 2\pi^+ \pi^-)/B(D^0 \rightarrow K^- \pi^+)$.

⁴ The three pion mass is required to be between 1.0 and 1.6 GeV consistent with an a_1 meson. (If this channel is dominated by a_1^+ , the branching ratio for $\bar{D}^{*-} a_1^+$ is twice that for $\bar{D}^{*-} \pi^+ \pi^+ \pi^-$.)

⁵ BORTOLETTO 92 reports $0.0159 \pm 0.0028 \pm 0.0037$ from a measurement of $[\Gamma(B^0 \rightarrow D^*(2010)^- \pi^+ \pi^+ \pi^-)/\Gamma_{\text{total}}] \times [B(D^*(2010)^+ \rightarrow D^0 \pi^+)]$ assuming $B(D^*(2010)^+ \rightarrow D^0 \pi^+) = 0.57 \pm 0.06$, which we rescale to our best value $B(D^*(2010)^+ \rightarrow D^0 \pi^+) = (67.7 \pm 0.5) \times 10^{-2}$. Our first error is their experiment's error and our second error is the systematic error from using our best value. Assumes equal production of B^+ and B^0 at the $\Upsilon(4S)$ and uses Mark III branching fractions for the D .

⁶ ALBRECHT 90J reports $0.012 \pm 0.003 \pm 0.004$ from a measurement of $[\Gamma(B^0 \rightarrow D^*(2010)^- \pi^+ \pi^+ \pi^-)/\Gamma_{\text{total}}] \times [B(D^*(2010)^+ \rightarrow D^0 \pi^+)]$ assuming $B(D^*(2010)^+ \rightarrow D^0 \pi^+) = 0.57 \pm 0.06$, which we rescale to our best value $B(D^*(2010)^+ \rightarrow D^0 \pi^+) = (67.7 \pm 0.5) \times 10^{-2}$. Our first error is their experiment's error and our second error is the systematic error from using our best value. Assumes equal production of B^+ and B^0 at the $\Upsilon(4S)$ and uses Mark III branching fractions for the D .

⁷ ALBRECHT 87c use PDG 86 branching ratios for D and $D^*(2010)$ and assume $B(\Upsilon(4S)) \rightarrow B^+ B^- = 55\%$ and $B(\Upsilon(4S)) \rightarrow B^0 \bar{B}^0 = 45\%$. Superseded by ALBRECHT 90J.

⁸ BEBEK 87 value has been updated in BERKELMAN 91 to use same assumptions as noted for BORTOLETTO 92.

 $\Gamma((D^*(2010)^- \pi^+ \pi^+ \pi^-) \text{ nonresonant})/\Gamma_{\text{total}}$ Γ_{58}/Γ

VALUE	DOCUMENT ID	TECN	COMMENT
0.0000 ± 0.0019 ± 0.0016	1 BORTOLETTO	92	CLEO $e^+e^- \rightarrow \Upsilon(4S)$

¹ BORTOLETTO 92 assumes equal production of B^+ and B^0 at the $\Upsilon(4S)$ and uses Mark III branching fractions for the D and $D^*(2010)$.

 $\Gamma(D^*(2010)^- \pi^+ \rho^0)/\Gamma_{\text{total}}$ Γ_{59}/Γ

VALUE	DOCUMENT ID	TECN	COMMENT
0.00573 ± 0.00317 ± 0.00004	1 BORTOLETTO	92	CLEO $e^+e^- \rightarrow \Upsilon(4S)$

¹ BORTOLETTO 92 reports $0.0068 \pm 0.0032 \pm 0.0021$ from a measurement of $[\Gamma(B^0 \rightarrow D^*(2010)^- \pi^+ \rho^0)/\Gamma_{\text{total}}] \times [B(D^*(2010)^+ \rightarrow D^0 \pi^+)]$ assuming $B(D^*(2010)^+ \rightarrow D^0 \pi^+) = 0.57 \pm 0.06$, which we rescale to our best value $B(D^*(2010)^+ \rightarrow D^0 \pi^+) = (67.7 \pm 0.5) \times 10^{-2}$. Our first error is their experiment's error and our second error is the systematic error from using our best value. Assumes equal production of B^+ and B^0 at the $\Upsilon(4S)$ and uses Mark III branching fractions for the D .

 $\Gamma(D^*(2010)^- a_1(1260)^+)/\Gamma_{\text{total}}$ Γ_{60}/Γ

VALUE	DOCUMENT ID	TECN	COMMENT
0.0130 ± 0.0027 OUR AVERAGE			
0.0126 ± 0.0020 ± 0.0022	1,2 ALAM	94	CLE2 $e^+e^- \rightarrow \Upsilon(4S)$
0.0152 ± 0.0070 ± 0.0001	3 BORTOLETTO	92	CLEO $e^+e^- \rightarrow \Upsilon(4S)$

¹ ALAM 94 value is twice their $\Gamma(D^*(2010)^- \pi^+ \pi^+ \pi^-)/\Gamma_{\text{total}}$ value based on their observation that the three pions are dominantly in the $a_1(1260)$ mass range 1.0 to 1.6 GeV.

² ALAM 94 assume equal production of B^+ and B^0 at the $\Upsilon(4S)$ and use the CLEO II $B(D^*(2010)^+ \rightarrow D^0 \pi^+)$ and absolute $B(D^0 \rightarrow K^- \pi^+)$ and the PDG 1992 $B(D^0 \rightarrow K^- \pi^+ \pi^0)/B(D^0 \rightarrow K^- \pi^+)$ and $B(D^0 \rightarrow K^- 2\pi^+ \pi^-)/B(D^0 \rightarrow K^- \pi^+)$.

³ BORTOLETTO 92 reports $0.018 \pm 0.006 \pm 0.006$ from a measurement of $[\Gamma(B^0 \rightarrow D^*(2010)^- a_1(1260)^+)/\Gamma_{\text{total}}] \times [B(D^*(2010)^+ \rightarrow D^0 \pi^+)]$ assuming $B(D^*(2010)^+ \rightarrow D^0 \pi^+) = 0.57 \pm 0.06$, which we rescale to our best value $B(D^*(2010)^+ \rightarrow D^0 \pi^+) = (67.7 \pm 0.5) \times 10^{-2}$. Our first error is their experiment's error and our second error is the systematic error from using our best value. Assumes equal production of B^+ and B^0 at the $\Upsilon(4S)$ and uses Mark III branching fractions for the D .

 $\Gamma(\bar{D}_1^0(2420)^0 \pi^- \pi^+, \bar{D}_1^0 \rightarrow D^{*-} \pi^+)/\Gamma(D^*(2010)^- \pi^+ \pi^+ \pi^-)$ Γ_{61}/Γ_{57}

VALUE	DOCUMENT ID	TECN	COMMENT
(2.04 ± 0.42 ± 0.22) × 10⁻²	AAIJ	13a0	LHCb pp at 7 TeV

 $\Gamma(D^*(2010)^- K^+ \pi^- \pi^+)/\Gamma(D^*(2010)^- \pi^+ \pi^+ \pi^-)$ Γ_{62}/Γ_{57}

VALUE	DOCUMENT ID	TECN	COMMENT
(6.47 ± 0.37 ± 0.35) × 10⁻²	AAIJ	13a0	LHCb pp at 7 TeV

 $\Gamma(D^*(2010)^- \pi^+ \pi^+ \pi^- \pi^0)/\Gamma_{\text{total}}$ Γ_{63}/Γ

VALUE	EVTs	DOCUMENT ID	TECN	COMMENT
0.0176 ± 0.0027 OUR AVERAGE				
0.0172 ± 0.0014 ± 0.0024		1 ALEXANDER	01B	CLE2 $e^+e^- \rightarrow \Upsilon(4S)$
0.0345 ± 0.0181 ± 0.0003	28	2 ALBRECHT	90J	ARG $e^+e^- \rightarrow \Upsilon(4S)$

¹ Assumes equal production of B^+ and B^0 at the $\Upsilon(4S)$. The signal is consistent with all observed $\omega \pi^+$ having proceeded through the ρ^+ resonance at mass $1349 \pm 25^{+10}_{-5}$ MeV and width $547 \pm 86^{+46}_{-45}$ MeV.

² ALBRECHT 90J reports $0.041 \pm 0.015 \pm 0.016$ from a measurement of $[\Gamma(B^0 \rightarrow D^*(2010)^- \pi^+ \pi^+ \pi^- \pi^0)/\Gamma_{\text{total}}] \times [B(D^*(2010)^+ \rightarrow D^0 \pi^+)]$ assuming $B(D^*(2010)^+ \rightarrow D^0 \pi^+) = 0.57 \pm 0.06$, which we rescale to our best value $B(D^*(2010)^+ \rightarrow D^0 \pi^+) = (67.7 \pm 0.5) \times 10^{-2}$. Our first error is their experiment's error and our second error is the systematic error from using our best value. Assumes equal production of B^+ and B^0 at the $\Upsilon(4S)$ and uses Mark III branching fractions for the D .

 $\Gamma(D^{*-} 3\pi^+ 2\pi^-)/\Gamma_{\text{total}}$ Γ_{64}/Γ

VALUE (units 10^{-3})	DOCUMENT ID	TECN	COMMENT
4.72 ± 0.59 ± 0.71	1 MAJUMDER	04	BELL $e^+e^- \rightarrow \Upsilon(4S)$

¹ Assumes equal production of B^+ and B^0 at the $\Upsilon(4S)$.

 $\Gamma(D^*(2010)^- \omega \pi^+)/\Gamma_{\text{total}}$ Γ_{65}/Γ

VALUE (units 10^{-3})	DOCUMENT ID	TECN	COMMENT
2.46 ± 0.18 OUR AVERAGE			Error includes scale factor of 1.2.
2.31 ± 0.11 ± 0.14	1 MATVIENKO	15	BELL $e^+e^- \rightarrow \Upsilon(4S)$
2.88 ± 0.21 ± 0.31	1 AUBERT	06L	BABR $e^+e^- \rightarrow \Upsilon(4S)$
2.9 ± 0.3 ± 0.4	1,2 ALEXANDER	01B	CLE2 $e^+e^- \rightarrow \Upsilon(4S)$

¹ Assumes equal production of B^+ and B^0 at the $\Upsilon(4S)$.

² The signal is consistent with all observed $\omega \pi^+$ having proceeded through the ρ^+ resonance at mass $1349 \pm 25^{+10}_{-5}$ MeV and width $547 \pm 86^{+46}_{-45}$ MeV.

 $\Gamma(\bar{D}_1^0(2430)^0 \omega, \bar{D}_1^0 \rightarrow D^{*-} \pi^+)/\Gamma_{\text{total}}$ Γ_{66}/Γ

VALUE (units 10^{-4})	DOCUMENT ID	TECN	COMMENT
2.7 ± 0.8 OUR AVERAGE			
2.5 ± 0.4 ± 0.8	1,2 MATVIENKO	15	BELL $e^+e^- \rightarrow \Upsilon(4S)$
4.1 ± 1.2 ± 1.1	3 AUBERT	06L	BABR $e^+e^- \rightarrow \Upsilon(4S)$

¹ Assumes equal production of B^+ and B^0 .

² The measurement is obtained by amplitude analysis of $B^0 \rightarrow D^{*-} \omega \pi^+$. The second uncertainty combines in quadrature experimental systematic and model uncertainties.

³ Obtained by fitting the events with $\cos \theta_{D^*} < 0.5$ and scaling up the result by a factor of 4/3. No interference effects between $B^0 \rightarrow D_1^0 \omega$ and $D^* \omega \pi^+$ are assumed.

 $\Gamma(D^{*-} \rho(1450)^+, \rho^+ \rightarrow \omega \pi^+)/\Gamma_{\text{total}}$ Γ_{67}/Γ

VALUE (units 10^{-3})	DOCUMENT ID	TECN	COMMENT
1.07 ± 0.15 ± 0.40	1,2 MATVIENKO	15	BELL $e^+e^- \rightarrow \Upsilon(4S)$
-0.31 - 0.13			

¹ Obtained by amplitude analysis of $\bar{B}^0 \rightarrow D^{*-} \omega \pi^+$. The second uncertainty combines in quadrature experimental systematic and model uncertainties.

² Assumes equal production of B^0 and B^+ at $\Upsilon(4S)$.

$\Gamma(\bar{D}_1^0(2420)^0 \omega, \bar{D}_1^0 \rightarrow D^{*-} \pi^+) / \Gamma_{\text{total}}$	Γ_{68} / Γ		
VALUE (units 10^{-4})	DOCUMENT ID	TECN	COMMENT
$0.7 \pm 0.2 \pm 0.1$	1,2	MATVIENKO 15	BELL $e^+ e^- \rightarrow \Upsilon(4S)$

¹ Obtained by amplitude analysis of $\bar{B}^0 \rightarrow D^{*-} \omega \pi^+$. The second uncertainty combines in quadrature experimental systematic and model uncertainties.
² Assumes equal production of B^0 and B^+ at $\Upsilon(4S)$.

$\Gamma(\bar{D}_2^*(2460)^0 \omega, \bar{D}_2^* \rightarrow D^{*-} \pi^+) / \Gamma_{\text{total}}$	Γ_{69} / Γ		
VALUE (units 10^{-4})	DOCUMENT ID	TECN	COMMENT
$0.4 \pm 0.1 \pm 0.1$	1,2	MATVIENKO 15	BELL $e^+ e^- \rightarrow \Upsilon(4S)$

¹ Obtained by amplitude analysis of $\bar{B}^0 \rightarrow D^{*-} \omega \pi^+$. The second uncertainty combines in quadrature experimental systematic and model uncertainties.
² Assumes equal production of B^0 and B^+ at $\Upsilon(4S)$.

$\Gamma(D^{*-} b_1(1235)^+, b_1^+ \rightarrow \omega \pi^+) / \Gamma_{\text{total}}$	Γ_{70} / Γ			
VALUE	CL%	DOCUMENT ID	TECN	COMMENT
$< 0.7 \times 10^{-4}$	90	1	MATVIENKO 15	BELL $e^+ e^- \rightarrow \Upsilon(4S)$

¹ Assumes equal production of B^0 and B^+ at $\Upsilon(4S)$.

$\Gamma(\bar{D}^{*-} \pi^+) / \Gamma_{\text{total}}$	Γ_{71} / Γ		
VALUE (units 10^{-3})	DOCUMENT ID	TECN	COMMENT
$1.9 \pm 0.9 \pm 0.1$	1,2	AUBERT,BE 06J	BABR $e^+ e^- \rightarrow \Upsilon(4S)$

D^{*-} represents an excited state with mass $2.2 < M < 2.8$ GeV/ c^2 .
¹ AUBERT,BE 06J reports $[\Gamma(\bar{B}^0 \rightarrow \bar{D}^{*-} \pi^+) / \Gamma_{\text{total}}] / [\Gamma(\bar{B}^0 \rightarrow D^- \pi^+)] = 0.77 \pm 0.22 \pm 0.29$ which we multiply by our best value $B(B^0 \rightarrow D^- \pi^+) = (2.52 \pm 0.13) \times 10^{-3}$. Our first error is their experiment's error and our second error is the systematic error from using our best value.
² Uses a missing-mass method. Does not depend on D branching fractions or B^+ / B^0 production rates.

$\Gamma(D_1^-(2420) \pi^+, D_1^- \rightarrow D^- \pi^+ \pi^-) / \Gamma_{\text{total}}$	Γ_{72} / Γ		
VALUE (units 10^{-4})	DOCUMENT ID	TECN	COMMENT
$0.99 \pm_{-0.25}^{+0.29}$ OUR FIT			

$0.89 \pm 0.15 \pm_{-0.32}^{+0.17}$	1	ABE 05A	BELL $e^+ e^- \rightarrow \Upsilon(4S)$
---	---	---------	---

¹ Assumes equal production of B^+ and B^0 at the $\Upsilon(4S)$.

$\Gamma(D_1^-(2420) \pi^+, D_1^- \rightarrow D^- \pi^+ \pi^-) / \Gamma(D^- \pi^+ \pi^-)$	$\Gamma_{72} / \Gamma_{46}$		
VALUE (units 10^{-2})	DOCUMENT ID	TECN	COMMENT
$1.65 \pm_{-0.40}^{+0.35}$ OUR FIT			

$2.1 \pm 0.5 \pm_{-0.5}^{+0.3}$	AAIJ	11E	LHCb pp at 7 TeV
---	------	-----	--------------------

$\Gamma(D_1^-(2420) \pi^+, D_1^- \rightarrow D^{*-} \pi^+ \pi^-) / \Gamma_{\text{total}}$	Γ_{73} / Γ			
VALUE (units 10^{-4})	CL%	DOCUMENT ID	TECN	COMMENT
< 0.33	90	1	ABE 05A	BELL $e^+ e^- \rightarrow \Upsilon(4S)$

¹ Assumes equal production of B^+ and B^0 at the $\Upsilon(4S)$.

$\Gamma(D^*(2010) \pi^+ \pi^+ \pi^-) / \Gamma(D^*(2010) \pi^+)$	$\Gamma_{57} / \Gamma_{44}$		
VALUE	DOCUMENT ID	TECN	COMMENT
$2.64 \pm 0.04 \pm 0.13$	AAIJ	13A0	LHCb pp at 7 TeV

$\Gamma(\bar{D}_2^*(2460) \pi^+, (D_2^*)^- \rightarrow D^0 \pi^-) / \Gamma_{\text{total}}$	Γ_{74} / Γ			
VALUE (units 10^{-4})	CL%	DOCUMENT ID	TECN	COMMENT
2.38 ± 0.16 OUR AVERAGE				

$2.44 \pm 0.07 \pm 0.16$	1	AAIJ	15Y	LHCb pp at 7, 8 TeV
$2.15 \pm 0.17 \pm 0.31$	2,3	KUZMIN 07	BELL	$e^+ e^- \rightarrow \Upsilon(4S)$

• • • We do not use the following data for averages, fits, limits, etc. **• • •**
 < 14.7 90 2 ALAM 94 CLE2 $e^+ e^- \rightarrow \Upsilon(4S)$

¹ Result obtained using the isobar formalism. The second uncertainty combines in quadrature all systematic uncertainties quoted in the paper.
² Assumes equal production of B^+ and B^0 at the $\Upsilon(4S)$.
³ Our second uncertainty combines systematics and model errors quoted in the paper.

$\Gamma(\bar{D}_0^*(2400) \pi^+, (D_0^*)^- \rightarrow D^0 \pi^-) / \Gamma_{\text{total}}$	Γ_{75} / Γ		
VALUE (units 10^{-4})	DOCUMENT ID	TECN	COMMENT
0.76 ± 0.08 OUR AVERAGE			

$0.77 \pm 0.05 \pm 0.06$	1	AAIJ	15Y	LHCb pp at 7, 8 TeV
$0.60 \pm 0.13 \pm 0.27$	2,3	KUZMIN 07	BELL	$e^+ e^- \rightarrow \Upsilon(4S)$

¹ Result obtained using the isobar formalism. The second uncertainty combines in quadrature all systematic uncertainties quoted in the paper.
² Assumes equal production of B^+ and B^0 at the $\Upsilon(4S)$.
³ Our second uncertainty combines systematics and model errors quoted in the paper.

$\Gamma(D_2^*(2460) \pi^+, (D_2^*)^- \rightarrow D^{*-} \pi^+ \pi^-) / \Gamma_{\text{total}}$	Γ_{76} / Γ			
VALUE (units 10^{-4})	CL%	DOCUMENT ID	TECN	COMMENT
< 0.24	90	1	ABE 05A	BELL $e^+ e^- \rightarrow \Upsilon(4S)$

¹ Assumes equal production of B^+ and B^0 at the $\Upsilon(4S)$.

$\Gamma(\bar{D}_2^*(2460) \rho^+) / \Gamma_{\text{total}}$	Γ_{77} / Γ			
VALUE	CL%	DOCUMENT ID	TECN	COMMENT
< 0.0049	90	1	ALAM 94	CLE2 $e^+ e^- \rightarrow \Upsilon(4S)$

¹ ALAM 94 assumes equal production of B^+ and B^0 at the $\Upsilon(4S)$ and use the CLEO II absolute $B(D^0 \rightarrow K^- \pi^+)$ and $B(D_2^*(2460)^+ \rightarrow D^0 \pi^+) = 30\%$.

$\Gamma(D^0 \bar{D}^0) / \Gamma_{\text{total}}$	Γ_{78} / Γ			
VALUE (units 10^{-4})	CL%	DOCUMENT ID	TECN	COMMENT
$0.14 \pm 0.06 \pm 0.03$		1	AAIJ	13AP LHCb pp at 7 TeV

• • • We do not use the following data for averages, fits, limits, etc. **• • •**
 < 0.43 90 2 ADACHI 08 BELL $e^+ e^- \rightarrow \Upsilon(4S)$
 < 0.6 90 2 AUBERT,B 06A BABR $e^+ e^- \rightarrow \Upsilon(4S)$

¹ Uses $B(B^0 \rightarrow D^- D^+) = (2.11 \pm 0.31) \times 10^{-4}$ and $B(B^+ \rightarrow \bar{D}^0 D_s^+) = (10.1 \pm 1.7) \times 10^{-3}$.
² Assumes equal production of B^+ and B^0 at the $\Upsilon(4S)$.

$\Gamma(D^{*0} \bar{D}^0) / \Gamma_{\text{total}}$	Γ_{79} / Γ			
VALUE (units 10^{-4})	CL%	DOCUMENT ID	TECN	COMMENT
< 2.9	90	1	AUBERT,B 06A	BABR $e^+ e^- \rightarrow \Upsilon(4S)$

¹ Assumes equal production of B^+ and B^0 at the $\Upsilon(4S)$.

$\Gamma(D^- D^+) / \Gamma_{\text{total}}$	Γ_{80} / Γ			
VALUE (units 10^{-4})	CL%	DOCUMENT ID	TECN	COMMENT
2.11 ± 0.18 OUR AVERAGE				

$2.12 \pm 0.16 \pm 0.18$	1	ROHRKEN 12	BELL	$e^+ e^- \rightarrow \Upsilon(4S)$
$1.97 \pm 0.20 \pm 0.20$	1	FRATINA 07	BELL	$e^+ e^- \rightarrow \Upsilon(4S)$
$2.8 \pm 0.4 \pm 0.5$	1	AUBERT,B 06A	BABR	$e^+ e^- \rightarrow \Upsilon(4S)$

• • • We do not use the following data for averages, fits, limits, etc. **• • •**
 $1.91 \pm 0.51 \pm 0.30$ 1 MAJUMDER 05 BELL Repl. by FRATINA 07
 < 9.4 90 1 LIPELES 00 CLE2 $e^+ e^- \rightarrow \Upsilon(4S)$
 < 59 90 BARATE 98Q ALEP $e^+ e^- \rightarrow Z$
 < 12 90 ASNER 97 CLE2 $e^+ e^- \rightarrow \Upsilon(4S)$

¹ Assumes equal production of B^+ and B^0 at the $\Upsilon(4S)$.

$\Gamma(D^\pm D^{*\mp} (CP\text{-averaged})) / \Gamma_{\text{total}}$	Γ_{81} / Γ		
VALUE (units 10^{-4})	DOCUMENT ID	TECN	COMMENT
$6.14 \pm 0.29 \pm 0.50$	1	ROHRKEN 12	BELL $e^+ e^- \rightarrow \Upsilon(4S)$

¹ Assumes equal production of B^+ and B^0 at the $\Upsilon(4S)$.

$\Gamma(D^- D_s^+) / \Gamma_{\text{total}}$	Γ_{82} / Γ			
VALUE	EVT%	DOCUMENT ID	TECN	COMMENT
0.0072 ± 0.0008 OUR AVERAGE				

$0.0073 \pm 0.0004 \pm 0.0007$	1	ZUPANC 07	BELL	$e^+ e^- \rightarrow \Upsilon(4S)$
$0.0066 \pm 0.0014 \pm 0.0006$	2	AUBERT 06N	BABR	$e^+ e^- \rightarrow \Upsilon(4S)$
$0.0068 \pm 0.0024 \pm 0.0006$	3	GIBAUT 96	CLE2	$e^+ e^- \rightarrow \Upsilon(4S)$
$0.010 \pm 0.009 \pm 0.001$	4	ALBRECHT 92G	ARG	$e^+ e^- \rightarrow \Upsilon(4S)$
$0.0053 \pm 0.0030 \pm 0.0005$	5	BORTOLETTO92	CLEO	$e^+ e^- \rightarrow \Upsilon(4S)$

• • • We do not use the following data for averages, fits, limits, etc. **• • •**
 0.012 ± 0.007 3 6 BORTOLETTO90 CLEO $e^+ e^- \rightarrow \Upsilon(4S)$

¹ ZUPANC 07 reports $(7.5 \pm 0.2 \pm 1.1) \times 10^{-3}$ from a measurement of $[\Gamma(B^0 \rightarrow D^- D_s^+) / \Gamma_{\text{total}}] \times [B(D_s^+ \rightarrow \phi \pi^+)]$ assuming $B(D_s^+ \rightarrow \phi \pi^+) = (4.4 \pm 0.6) \times 10^{-2}$, which we rescale to our best value $B(D_s^+ \rightarrow \phi \pi^+) = (4.5 \pm 0.4) \times 10^{-2}$. Our first error is their experiment's error and our second error is the systematic error from using our best value.

² AUBERT 06N reports $(0.64 \pm 0.13 \pm 0.10) \times 10^{-2}$ from a measurement of $[\Gamma(B^0 \rightarrow D^- D_s^+) / \Gamma_{\text{total}}] \times [B(D_s^+ \rightarrow \phi \pi^+)]$ assuming $B(D_s^+ \rightarrow \phi \pi^+) = 0.0462 \pm 0.0062$, which we rescale to our best value $B(D_s^+ \rightarrow \phi \pi^+) = (4.5 \pm 0.4) \times 10^{-2}$. Our first error is their experiment's error and our second error is the systematic error from using our best value.

³ GIBAUT 96 reports $0.0087 \pm 0.0024 \pm 0.0020$ from a measurement of $[\Gamma(B^0 \rightarrow D^- D_s^+) / \Gamma_{\text{total}}] \times [B(D_s^+ \rightarrow \phi \pi^+)]$ assuming $B(D_s^+ \rightarrow \phi \pi^+) = 0.035$, which we rescale to our best value $B(D_s^+ \rightarrow \phi \pi^+) = (4.5 \pm 0.4) \times 10^{-2}$. Our first error is their experiment's error and our second error is the systematic error from using our best value.

⁴ ALBRECHT 92G reports $0.017 \pm 0.013 \pm 0.006$ from a measurement of $[\Gamma(B^0 \rightarrow D^- D_s^+) / \Gamma_{\text{total}}] \times [B(D_s^+ \rightarrow \phi \pi^+)]$ assuming $B(D_s^+ \rightarrow \phi \pi^+) = 0.027$, which we rescale to our best value $B(D_s^+ \rightarrow \phi \pi^+) = (4.5 \pm 0.4) \times 10^{-2}$. Our first error is their experiment's error and our second error is the systematic error from using our best value. Assumes PDG 1990 D^+ branching ratios, e.g., $B(D^+ \rightarrow K^- 2\pi^+) = 7.7 \pm 1.0\%$.

⁵ BORTOLETTO 92 reports $0.0080 \pm 0.0045 \pm 0.0030$ from a measurement of $[\Gamma(B^0 \rightarrow D^- D_s^+) / \Gamma_{\text{total}}] \times [B(D_s^+ \rightarrow \phi \pi^+)]$ assuming $B(D_s^+ \rightarrow \phi \pi^+) = 0.030 \pm 0.011$, which we rescale to our best value $B(D_s^+ \rightarrow \phi \pi^+) = (4.5 \pm 0.4) \times 10^{-2}$. Our first error is their experiment's error and our second error is the systematic error from using our best value. Assumes equal production of B^+ and B^0 at the $\Upsilon(4S)$ and uses Mark III branching fractions for the D .

⁶ BORTOLETTO 90 assume $B(D_s \rightarrow \phi \pi^+) = 2\%$. Superseded by BORTOLETTO 92.

Meson Particle Listings

B^0

$\Gamma(D^*(2010)^- D_s^+)/\Gamma_{total}$ Γ_{83}/Γ

VALUE	EVTS	DOCUMENT ID	TECN	COMMENT
0.0080 ± 0.0011 OUR AVERAGE				
0.0073 ± 0.0013 ± 0.0007		1 AUBERT 06N	BABR	$e^+e^- \rightarrow \Upsilon(4S)$
0.0083 ± 0.0015 ± 0.0007		2 AUBERT 03i	BABR	$e^+e^- \rightarrow \Upsilon(4S)$
0.0088 ± 0.0017 ± 0.0008		3 AHMED 00b	CLE2	$e^+e^- \rightarrow \Upsilon(4S)$
0.008 ± 0.006 ± 0.001		4 ALBRECHT 92G	ARG	$e^+e^- \rightarrow \Upsilon(4S)$
0.011 ± 0.006 ± 0.001		5 BORTOLETTO92	CLEO	$e^+e^- \rightarrow \Upsilon(4S)$
• • • We do not use the following data for averages, fits, limits, etc. • • •				
0.0072 ± 0.0022 ± 0.0006		6 GIBAUT 96	CLE2	Repl. by AHMED 00b
0.024 ± 0.014	3	7 BORTOLETTO90	CLEO	$e^+e^- \rightarrow \Upsilon(4S)$

- AUBERT 06N reports $(0.71 \pm 0.13 \pm 0.09) \times 10^{-2}$ from a measurement of $[\Gamma(B^0 \rightarrow D^*(2010)^- D_s^+)/\Gamma_{total}] \times [B(D_s^+ \rightarrow \phi\pi^+)]$ assuming $B(D_s^+ \rightarrow \phi\pi^+) = 0.0462 \pm 0.0062$, which we rescale to our best value $B(D_s^+ \rightarrow \phi\pi^+) = (4.5 \pm 0.4) \times 10^{-2}$. Our first error is their experiment's error and our second error is the systematic error from using our best value.
- AUBERT 03i reports 0.0103 ± 0.0014 ± 0.0013 from a measurement of $[\Gamma(B^0 \rightarrow D^*(2010)^- D_s^+)/\Gamma_{total}] \times [B(D_s^+ \rightarrow \phi\pi^+)]$ assuming $B(D_s^+ \rightarrow \phi\pi^+) = 0.036$, which we rescale to our best value $B(D_s^+ \rightarrow \phi\pi^+) = (4.5 \pm 0.4) \times 10^{-2}$. Our first error is their experiment's error and our second error is the systematic error from using our best value.
- AHMED 00b reports $0.0110 \pm 0.0018 \pm 0.0011$ from a measurement of $[\Gamma(B^0 \rightarrow D^*(2010)^- D_s^+)/\Gamma_{total}] \times [B(D_s^+ \rightarrow \phi\pi^+)]$ assuming $B(D_s^+ \rightarrow \phi\pi^+) = 0.036$, which we rescale to our best value $B(D_s^+ \rightarrow \phi\pi^+) = (4.5 \pm 0.4) \times 10^{-2}$. Our first error is their experiment's error and our second error is the systematic error from using our best value.
- ALBRECHT 92G reports $0.014 \pm 0.010 \pm 0.003$ from a measurement of $[\Gamma(B^0 \rightarrow D^*(2010)^- D_s^+)/\Gamma_{total}] \times [B(D_s^+ \rightarrow \phi\pi^+)]$ assuming $B(D_s^+ \rightarrow \phi\pi^+) = 0.027$, which we rescale to our best value $B(D_s^+ \rightarrow \phi\pi^+) = (4.5 \pm 0.4) \times 10^{-2}$. Our first error is their experiment's error and our second error is the systematic error from using our best value. Assumes PDG 1990 D^+ and $D^*(2010)^+$ branching ratios, e.g., $B(D^0 \rightarrow K^-\pi^+) = 3.71 \pm 0.25\%$, $B(D^+ \rightarrow K^-2\pi^+) = 7.1 \pm 1.0\%$, and $B(D^*(2010)^+ \rightarrow D^0\pi^+) = 55 \pm 4\%$.
- BORTOLETTO 92 reports $0.016 \pm 0.009 \pm 0.006$ from a measurement of $[\Gamma(B^0 \rightarrow D^*(2010)^- D_s^+)/\Gamma_{total}] \times [B(D_s^+ \rightarrow \phi\pi^+)]$ assuming $B(D_s^+ \rightarrow \phi\pi^+) = 0.030 \pm 0.011$, which we rescale to our best value $B(D_s^+ \rightarrow \phi\pi^+) = (4.5 \pm 0.4) \times 10^{-2}$. Our first error is their experiment's error and our second error is the systematic error from using our best value. Assumes equal production of B^+ and B^0 at the $\Upsilon(4S)$ and uses Mark III branching fractions for the D and $D^*(2010)$.
- GIBAUT 96 reports $0.0093 \pm 0.0023 \pm 0.0016$ from a measurement of $[\Gamma(B^0 \rightarrow D^*(2010)^- D_s^+)/\Gamma_{total}] \times [B(D_s^+ \rightarrow \phi\pi^+)]$ assuming $B(D_s^+ \rightarrow \phi\pi^+) = 0.035$, which we rescale to our best value $B(D_s^+ \rightarrow \phi\pi^+) = (4.5 \pm 0.4) \times 10^{-2}$. Our first error is their experiment's error and our second error is the systematic error from using our best value.
- BORTOLETTO 90 assume $B(D_s \rightarrow \phi\pi^+) = 2\%$. Superseded by BORTOLETTO 92.

$\Gamma(D^- D_s^+)/\Gamma_{total}$ Γ_{84}/Γ

VALUE	DOCUMENT ID	TECN	COMMENT
0.0074 ± 0.0016 OUR AVERAGE			
0.0071 ± 0.0016 ± 0.0006	1 AUBERT 06N	BABR	$e^+e^- \rightarrow \Upsilon(4S)$
0.0078 ± 0.0032 ± 0.0007	2 GIBAUT 96	CLE2	$e^+e^- \rightarrow \Upsilon(4S)$
0.016 ± 0.012 ± 0.001	3 ALBRECHT 92G	ARG	$e^+e^- \rightarrow \Upsilon(4S)$

- AUBERT 06n reports $(0.69 \pm 0.16 \pm 0.09) \times 10^{-2}$ from a measurement of $[\Gamma(B^0 \rightarrow D^- D_s^+)/\Gamma_{total}] \times [B(D_s^+ \rightarrow \phi\pi^+)]$ assuming $B(D_s^+ \rightarrow \phi\pi^+) = 0.0462 \pm 0.0062$, which we rescale to our best value $B(D_s^+ \rightarrow \phi\pi^+) = (4.5 \pm 0.4) \times 10^{-2}$. Our first error is their experiment's error and our second error is the systematic error from using our best value.
- GIBAUT 96 reports $0.0100 \pm 0.0035 \pm 0.0022$ from a measurement of $[\Gamma(B^0 \rightarrow D^- D_s^+)/\Gamma_{total}] \times [B(D_s^+ \rightarrow \phi\pi^+)]$ assuming $B(D_s^+ \rightarrow \phi\pi^+) = 0.035$, which we rescale to our best value $B(D_s^+ \rightarrow \phi\pi^+) = (4.5 \pm 0.4) \times 10^{-2}$. Our first error is their experiment's error and our second error is the systematic error from using our best value.
- ALBRECHT 92G reports $0.027 \pm 0.017 \pm 0.009$ from a measurement of $[\Gamma(B^0 \rightarrow D^- D_s^+)/\Gamma_{total}] \times [B(D_s^+ \rightarrow \phi\pi^+)]$ assuming $B(D_s^+ \rightarrow \phi\pi^+) = 0.027$, which we rescale to our best value $B(D_s^+ \rightarrow \phi\pi^+) = (4.5 \pm 0.4) \times 10^{-2}$. Our first error is their experiment's error and our second error is the systematic error from using our best value. Assumes PDG 1990 D^+ branching ratios, e.g., $B(D^+ \rightarrow K^-2\pi^+) = 7.7 \pm 1.0\%$.

$\Gamma(D^*(2010)^- D_s^{*+})/\Gamma_{total}$ Γ_{85}/Γ

VALUE	DOCUMENT ID	TECN	COMMENT
0.0177 ± 0.0014 OUR AVERAGE			
0.0173 ± 0.0018 ± 0.0015	1 AUBERT 06N	BABR	$e^+e^- \rightarrow \Upsilon(4S)$
0.0188 ± 0.0009 ± 0.0017	2 AUBERT 05v	BABR	$e^+e^- \rightarrow \Upsilon(4S)$
0.0158 ± 0.0027 ± 0.0014	3 AUBERT 03i	BABR	$e^+e^- \rightarrow \Upsilon(4S)$
0.015 ± 0.004 ± 0.001	4 AHMED 00b	CLE2	$e^+e^- \rightarrow \Upsilon(4S)$
0.016 ± 0.009 ± 0.001	5 ALBRECHT 92G	ARG	$e^+e^- \rightarrow \Upsilon(4S)$
• • • We do not use the following data for averages, fits, limits, etc. • • •			
0.016 ± 0.005 ± 0.001	6 GIBAUT 96	CLE2	Repl. by AHMED 00b

- AUBERT 06N reports $(1.68 \pm 0.21 \pm 0.19) \times 10^{-2}$ from a measurement of $[\Gamma(B^0 \rightarrow D^*(2010)^- D_s^{*+})/\Gamma_{total}] \times [B(D_s^{*+} \rightarrow \phi\pi^+)]$ assuming $B(D_s^{*+} \rightarrow \phi\pi^+) = 0.0462 \pm$

- 0.0062, which we rescale to our best value $B(D_s^{*+} \rightarrow \phi\pi^+) = (4.5 \pm 0.4) \times 10^{-2}$. Our first error is their experiment's error and our second error is the systematic error from using our best value.
- A partial reconstruction technique is used and the result is independent of the particle decay rate of D_s^+ meson. It also provides a model-independent determination of $B(D_s^+ \rightarrow \phi\pi^+) = (4.81 \pm 0.52 \pm 0.38)\%$.
- AUBERT 03i reports $0.0197 \pm 0.0015 \pm 0.0030$ from a measurement of $[\Gamma(B^0 \rightarrow D^*(2010)^- D_s^{*+})/\Gamma_{total}] \times [B(D_s^+ \rightarrow \phi\pi^+)]$ assuming $B(D_s^+ \rightarrow \phi\pi^+) = 0.036$, which we rescale to our best value $B(D_s^+ \rightarrow \phi\pi^+) = (4.5 \pm 0.4) \times 10^{-2}$. Our first error is their experiment's error and our second error is the systematic error from using our best value.
- AHMED 00b reports $0.0182 \pm 0.0037 \pm 0.0025$ from a measurement of $[\Gamma(B^0 \rightarrow D^*(2010)^- D_s^{*+})/\Gamma_{total}] \times [B(D_s^+ \rightarrow \phi\pi^+)]$ assuming $B(D_s^+ \rightarrow \phi\pi^+) = 0.036$, which we rescale to our best value $B(D_s^+ \rightarrow \phi\pi^+) = (4.5 \pm 0.4) \times 10^{-2}$. Our first error is their experiment's error and our second error is the systematic error from using our best value.
- ALBRECHT 92G reports $0.026 \pm 0.014 \pm 0.006$ from a measurement of $[\Gamma(B^0 \rightarrow D^*(2010)^- D_s^{*+})/\Gamma_{total}] \times [B(D_s^+ \rightarrow \phi\pi^+)]$ assuming $B(D_s^+ \rightarrow \phi\pi^+) = 0.027$, which we rescale to our best value $B(D_s^+ \rightarrow \phi\pi^+) = (4.5 \pm 0.4) \times 10^{-2}$. Our first error is their experiment's error and our second error is the systematic error from using our best value. Assumes PDG 1990 D^+ and $D^*(2010)^+$ branching ratios, e.g., $B(D^0 \rightarrow K^-\pi^+) = 3.71 \pm 0.25\%$, $B(D^+ \rightarrow K^-2\pi^+) = 7.1 \pm 1.0\%$, and $B(D^*(2010)^+ \rightarrow D^0\pi^+) = 55 \pm 4\%$.
- GIBAUT 96 reports $0.0203 \pm 0.0050 \pm 0.0036$ from a measurement of $[\Gamma(B^0 \rightarrow D^*(2010)^- D_s^{*+})/\Gamma_{total}] \times [B(D_s^+ \rightarrow \phi\pi^+)]$ assuming $B(D_s^+ \rightarrow \phi\pi^+) = 0.035$, which we rescale to our best value $B(D_s^+ \rightarrow \phi\pi^+) = (4.5 \pm 0.4) \times 10^{-2}$. Our first error is their experiment's error and our second error is the systematic error from using our best value.

$[\Gamma(D^*(2010)^- D_s^+) + \Gamma(D^*(2010)^- D_s^{*+})]/\Gamma_{total}$ $(\Gamma_{83} + \Gamma_{85})/\Gamma$

VALUE (units 10^{-2})	EVTS	DOCUMENT ID	TECN	COMMENT
2.5 ± 0.4 OUR AVERAGE				
2.40 ± 0.35 ± 0.22		1 AUBERT 03i	BABR	$e^+e^- \rightarrow \Upsilon(4S)$
3.3 ± 0.9 ± 0.3	22	2 BORTOLETTO90	CLEO	$e^+e^- \rightarrow \Upsilon(4S)$

- AUBERT 03i reports $(3.00 \pm 0.19 \pm 0.39) \times 10^{-2}$ from a measurement of $[\Gamma(B^0 \rightarrow D^*(2010)^- D_s^+) + \Gamma(B^0 \rightarrow D^*(2010)^- D_s^{*+})]/\Gamma_{total}] \times [B(D_s^+ \rightarrow \phi\pi^+)]$ assuming $B(D_s^+ \rightarrow \phi\pi^+) = 0.036$, which we rescale to our best value $B(D_s^+ \rightarrow \phi\pi^+) = (4.5 \pm 0.4) \times 10^{-2}$. Our first error is their experiment's error and our second error is the systematic error from using our best value.
- BORTOLETTO 90 reports $(7.5 \pm 2.0) \times 10^{-2}$ from a measurement of $[\Gamma(B^0 \rightarrow D^*(2010)^- D_s^+) + \Gamma(B^0 \rightarrow D^*(2010)^- D_s^{*+})]/\Gamma_{total}] \times [B(D_s^+ \rightarrow \phi\pi^+)]$ assuming $B(D_s^+ \rightarrow \phi\pi^+) = 0.02$, which we rescale to our best value $B(D_s^+ \rightarrow \phi\pi^+) = (4.5 \pm 0.4) \times 10^{-2}$. Our first error is their experiment's error and our second error is the systematic error from using our best value.

$\Gamma(D_{s0}(2317)^- K^+, D_{s0}^- \rightarrow D_s^- \pi^0)/\Gamma_{total}$ Γ_{86}/Γ

VALUE (units 10^{-5})	DOCUMENT ID	TECN	COMMENT
4.2 ± 1.4 ± 0.4			
	1 DRUTSKOY 05	BELL	$e^+e^- \rightarrow \Upsilon(4S)$

- DRUTSKOY 05 reports $(5.3^{+1.5}_{-1.3} \pm 1.6) \times 10^{-5}$ from a measurement of $[\Gamma(B^0 \rightarrow D_{s0}(2317)^- K^+, D_{s0}^- \rightarrow D_s^- \pi^0)/\Gamma_{total}] \times [B(D_s^+ \rightarrow \phi\pi^+)]$ assuming $B(D_s^+ \rightarrow \phi\pi^+) = 0.036 \pm 0.009$, which we rescale to our best value $B(D_s^+ \rightarrow \phi\pi^+) = (4.5 \pm 0.4) \times 10^{-2}$. Our first error is their experiment's error and our second error is the systematic error from using our best value.

$\Gamma(D_{s0}(2317)^- \pi^+, D_{s0}^- \rightarrow D_s^- \pi^0)/\Gamma_{total}$ Γ_{87}/Γ

VALUE (units 10^{-5})	CL%	DOCUMENT ID	TECN	COMMENT
< 2.5	90	1 DRUTSKOY 05	BELL	$e^+e^- \rightarrow \Upsilon(4S)$

- Assumes equal production of B^+ and B^0 at the $\Upsilon(4S)$.

$\Gamma(D_{sJ}(2457)^- K^+, D_{sJ}^- \rightarrow D_s^- \pi^0)/\Gamma_{total}$ Γ_{88}/Γ

VALUE (units 10^{-5})	CL%	DOCUMENT ID	TECN	COMMENT
< 0.94	90	1 DRUTSKOY 05	BELL	$e^+e^- \rightarrow \Upsilon(4S)$

- Assumes equal production of B^+ and B^0 at the $\Upsilon(4S)$.

$\Gamma(D_{sJ}(2457)^- \pi^+, D_{sJ}^- \rightarrow D_s^- \pi^0)/\Gamma_{total}$ Γ_{89}/Γ

VALUE (units 10^{-5})	CL%	DOCUMENT ID	TECN	COMMENT
< 0.40	90	1 DRUTSKOY 05	BELL	$e^+e^- \rightarrow \Upsilon(4S)$

- Assumes equal production of B^+ and B^0 at the $\Upsilon(4S)$.

$\Gamma(D_s^- D_s^+)/\Gamma_{total}$ Γ_{90}/Γ

VALUE	CL%	DOCUMENT ID	TECN	COMMENT
< 3.6 × 10⁻⁵	90	1 ZUPANC 07	BELL	$e^+e^- \rightarrow \Upsilon(4S)$

- • • We do not use the following data for averages, fits, limits, etc. • • •

< 10 × 10 ⁻⁵	90	1 AUBERT,BE	05F	BABR $e^+e^- \rightarrow \Upsilon(4S)$
-------------------------	----	-------------	-----	--

- Assumes equal production of B^+ and B^0 at the $\Upsilon(4S)$.

See key on page 999

Meson Particle Listings

B^0

$\Gamma(D_s^{*-} D_s^+)/\Gamma_{total}$					Γ_{91}/Γ
VALUE	CL%	DOCUMENT ID	TECN	COMMENT	
$<1.3 \times 10^{-4}$	90	1 AUBERT,BE	05F	BABR $e^+e^- \rightarrow \Upsilon(4S)$	

¹ Assumes equal production of B^+ and B^0 at the $\Upsilon(4S)$.

$\Gamma(D_s^{*+} D_s^+)/\Gamma_{total}$					Γ_{92}/Γ
VALUE	CL%	DOCUMENT ID	TECN	COMMENT	
$<2.4 \times 10^{-4}$	90	1 AUBERT,BE	05F	BABR $e^+e^- \rightarrow \Upsilon(4S)$	

¹ Assumes equal production of B^+ and B^0 at the $\Upsilon(4S)$.

$\Gamma(D_{s0}^*(2317)^+ D^- , D_{s0}^{*+} \rightarrow D_s^+ \pi^0)/\Gamma_{total}$					Γ_{93}/Γ
VALUE (units 10^{-3})	CL%	DOCUMENT ID	TECN	COMMENT	
1.06 ± 0.16 OUR AVERAGE				Error includes scale factor of 1.1.	
$0.99^{+0.16}_{-0.15} \pm 0.03$		1,2 CHOI	15A	BELL $e^+e^- \rightarrow \Upsilon(4S)$	

1,4 $^{+0.5}_{-0.4} \pm 0.1$ 2,3 AUBERT,B 04s BABR $e^+e^- \rightarrow \Upsilon(4S)$

• • • We do not use the following data for averages, fits, limits, etc. • • •

0.69 $^{+0.29}_{-0.24} \pm 0.06$ 2,4 KROKOVNY 03B BELL Repl. by CHOI 15A

¹ CHOI 15A reports $(10.2^{+1.3}_{-1.2} \pm 1.0 \pm 0.4) \times 10^{-4}$ from a measurement of $[\Gamma(B^0 \rightarrow D_s^*(2317)^+ D^- , D_{s0}^{*+} \rightarrow D_s^+ \pi^0)/\Gamma_{total}] \times [B(D_s^+ \rightarrow K^+ K^- \pi^+)] \times [B(D^+ \rightarrow K^- 2\pi^+)]$ assuming $B(D_s^+ \rightarrow K^+ K^- \pi^+) = (5.39 \pm 0.21) \times 10^{-2}$, $B(D^+ \rightarrow K^- 2\pi^+) = (9.13 \pm 0.19) \times 10^{-2}$, which we rescale to our best values $B(D_s^+ \rightarrow K^+ K^- \pi^+) = (5.39 \pm 0.15) \times 10^{-2}$, $B(D^+ \rightarrow K^- 2\pi^+) = (9.38 \pm 0.16) \times 10^{-2}$. Our first error is their experiment's error and our second error is the systematic error from using our best values.

² Assumes equal production of B^+ and B^0 at the $\Upsilon(4S)$.

³ AUBERT,B 04s reports $(1.8 \pm 0.4^{+0.7}_{-0.5}) \times 10^{-3}$ from a measurement of $[\Gamma(B^0 \rightarrow D_s^*(2317)^+ D^- , D_{s0}^{*+} \rightarrow D_s^+ \pi^0)/\Gamma_{total}] \times [B(D_s^+ \rightarrow \phi \pi^+)]$ assuming $B(D_s^+ \rightarrow \phi \pi^+) = 0.036 \pm 0.009$, which we rescale to our best value $B(D_s^+ \rightarrow \phi \pi^+) = (4.5 \pm 0.4) \times 10^{-2}$. Our first error is their experiment's error and our second error is the systematic error from using our best value.

⁴ KROKOVNY 03B reports $(0.86^{+0.33}_{-0.26} \pm 0.26) \times 10^{-3}$ from a measurement of $[\Gamma(B^0 \rightarrow D_s^*(2317)^+ D^- , D_{s0}^{*+} \rightarrow D_s^+ \pi^0)/\Gamma_{total}] \times [B(D_s^+ \rightarrow \phi \pi^+)]$ assuming $B(D_s^+ \rightarrow \phi \pi^+) = 0.036 \pm 0.009$, which we rescale to our best value $B(D_s^+ \rightarrow \phi \pi^+) = (4.5 \pm 0.4) \times 10^{-2}$. Our first error is their experiment's error and our second error is the systematic error from using our best value.

$\Gamma(D_{s0}(2317)^+ D^- , D_{s0}^{*+} \rightarrow D_s^{*+} \gamma)/\Gamma_{total}$					Γ_{94}/Γ
VALUE (units 10^{-3})	CL%	DOCUMENT ID	TECN	COMMENT	
<0.95	90	1 KROKOVNY 03B	BELL	$e^+e^- \rightarrow \Upsilon(4S)$	

¹ Assumes equal production of B^+ and B^0 at the $\Upsilon(4S)$.

$\Gamma(D_{s0}(2317)^+ D^*(2010)^- , D_{s0}^{*+} \rightarrow D_s^+ \pi^0)/\Gamma_{total}$					Γ_{95}/Γ
VALUE (units 10^{-3})	CL%	DOCUMENT ID	TECN	COMMENT	
$1.5 \pm 0.4^{+0.5}_{-0.4}$		1 AUBERT,B	04s	BABR $e^+e^- \rightarrow \Upsilon(4S)$	

¹ Assumes equal production of B^+ and B^0 at the $\Upsilon(4S)$.

$\Gamma(D_{sJ}(2457)^+ D^-)/\Gamma_{total}$					Γ_{96}/Γ
VALUE (units 10^{-3})	CL%	DOCUMENT ID	TECN	COMMENT	
3.5 ± 1.1 OUR AVERAGE					
$2.6 \pm 1.5 \pm 0.7$		1 AUBERT	06N	BABR $e^+e^- \rightarrow \Upsilon(4S)$	
$4.8^{+2.2}_{-1.6} \pm 1.1$		2,3 AUBERT,B	04s	BABR $e^+e^- \rightarrow \Upsilon(4S)$	
$3.9^{+1.5}_{-1.3} \pm 0.9$		2,4 KROKOVNY	03B	BELL $e^+e^- \rightarrow \Upsilon(4S)$	

¹ Uses a missing-mass method in the events that one of the B mesons is fully reconstructed.

² Assumes equal production of B^+ and B^0 at the $\Upsilon(4S)$.

³ AUBERT,B 04s reports $[\Gamma(B^0 \rightarrow D_{sJ}(2457)^+ D^-)/\Gamma_{total}] \times [B(D_{s1}(2460)^+ \rightarrow D_s^{*+} \pi^0)] = (2.3^{+1.0}_{-0.7} \pm 0.3) \times 10^{-3}$ which we divide by our best value $B(D_{s1}(2460)^+ \rightarrow D_s^{*+} \pi^0) = (48 \pm 11) \times 10^{-2}$. Our first error is their experiment's error and our second error is the systematic error from using our best value.

⁴ KROKOVNY 03B reports $[\Gamma(B^0 \rightarrow D_{sJ}(2457)^+ D^-)/\Gamma_{total}] \times [B(D_{s1}(2460)^+ \rightarrow D_s^{*+} \pi^0)] = (1.9^{+0.7}_{-0.6} \pm 0.2) \times 10^{-3}$ which we divide by our best value $B(D_{s1}(2460)^+ \rightarrow D_s^{*+} \pi^0) = (48 \pm 11) \times 10^{-2}$. Our first error is their experiment's error and our second error is the systematic error from using our best value.

$\Gamma(D_{sJ}(2457)^+ D^- , D_{sJ}^{*+} \rightarrow D_s^+ \gamma)/\Gamma_{total}$					Γ_{97}/Γ
VALUE (units 10^{-3})	CL%	DOCUMENT ID	TECN	COMMENT	
$0.65^{+0.17}_{-0.14}$ OUR AVERAGE					
$0.64^{+0.24}_{-0.16} \pm 0.06$		1,2 AUBERT,B	04s	BABR $e^+e^- \rightarrow \Upsilon(4S)$	
$0.66^{+0.21}_{-0.19} \pm 0.06$		1,3 KROKOVNY	03B	BELL $e^+e^- \rightarrow \Upsilon(4S)$	

¹ Assumes equal production of B^+ and B^0 at the $\Upsilon(4S)$.

² AUBERT,B 04s reports $(0.8 \pm 0.2^{+0.3}_{-0.2}) \times 10^{-3}$ from a measurement of $[\Gamma(B^0 \rightarrow D_{sJ}(2457)^+ D^- , D_{sJ}^{*+} \rightarrow D_s^+ \gamma)/\Gamma_{total}] \times [B(D_s^+ \rightarrow \phi \pi^+)]$ assuming $B(D_s^+ \rightarrow \phi \pi^+) = 0.036 \pm 0.009$, which we rescale to our best value $B(D_s^+ \rightarrow \phi \pi^+) = (4.5 \pm 0.4) \times 10^{-2}$. Our first error is their experiment's error and our second error is the systematic error from using our best value.

$\phi \pi^+) = 0.036 \pm 0.009$, which we rescale to our best value $B(D_s^+ \rightarrow \phi \pi^+) = (4.5 \pm 0.4) \times 10^{-2}$. Our first error is their experiment's error and our second error is the systematic error from using our best value.

³ KROKOVNY 03B reports $(0.82^{+0.22}_{-0.19} \pm 0.25) \times 10^{-3}$ from a measurement of $[\Gamma(B^0 \rightarrow D_{sJ}(2457)^+ D^- , D_{sJ}^{*+} \rightarrow D_s^+ \gamma)/\Gamma_{total}] \times [B(D_s^+ \rightarrow \phi \pi^+)]$ assuming $B(D_s^+ \rightarrow \phi \pi^+) = 0.036 \pm 0.009$, which we rescale to our best value $B(D_s^+ \rightarrow \phi \pi^+) = (4.5 \pm 0.4) \times 10^{-2}$. Our first error is their experiment's error and our second error is the systematic error from using our best value.

$\Gamma(D_{sJ}(2457)^+ D^- , D_{sJ}^{*+} \rightarrow D_s^{*+} \gamma)/\Gamma_{total}$					Γ_{98}/Γ
VALUE (units 10^{-3})	CL%	DOCUMENT ID	TECN	COMMENT	
<0.60	90	1 KROKOVNY 03B	BELL	$e^+e^- \rightarrow \Upsilon(4S)$	

¹ Assumes equal production of B^+ and B^0 at the $\Upsilon(4S)$.

$\Gamma(D_{sJ}(2457)^+ D^- , D_{sJ}^{*+} \rightarrow D_s^+ \pi^+ \pi^-)/\Gamma_{total}$					Γ_{99}/Γ
VALUE (units 10^{-3})	CL%	DOCUMENT ID	TECN	COMMENT	
<0.20	90	1 KROKOVNY 03B	BELL	$e^+e^- \rightarrow \Upsilon(4S)$	

¹ Assumes equal production of B^+ and B^0 at the $\Upsilon(4S)$.

$\Gamma(D_{sJ}(2457)^+ D^- , D_{sJ}^{*+} \rightarrow D_s^+ \pi^0)/\Gamma_{total}$					Γ_{100}/Γ
VALUE (units 10^{-3})	CL%	DOCUMENT ID	TECN	COMMENT	
<0.36	90	1 KROKOVNY 03B	BELL	$e^+e^- \rightarrow \Upsilon(4S)$	

¹ Assumes equal production of B^+ and B^0 at the $\Upsilon(4S)$.

$\Gamma(D^*(2010)^- D_{sJ}(2457)^+)/\Gamma_{total}$					Γ_{101}/Γ
VALUE (units 10^{-3})	CL%	DOCUMENT ID	TECN	COMMENT	
9.3 ± 2.2 OUR AVERAGE					
$8.8 \pm 2.0 \pm 1.4$		1 AUBERT	06N	BABR $e^+e^- \rightarrow \Upsilon(4S)$	
$11^{+5}_{-4} \pm 3$		2,3 AUBERT,B	04s	BABR $e^+e^- \rightarrow \Upsilon(4S)$	

¹ Uses a missing-mass method in the events that one of the B mesons is fully reconstructed.

² AUBERT,B 04s reports $[\Gamma(B^0 \rightarrow D^*(2010)^- D_{sJ}(2457)^+)/\Gamma_{total}] \times [B(D_{s1}(2460)^+ \rightarrow D_s^{*+} \pi^0)] = (5.5 \pm 1.2^{+2.2}_{-1.6}) \times 10^{-3}$ which we divide by our best value $B(D_{s1}(2460)^+ \rightarrow D_s^{*+} \pi^0) = (48 \pm 11) \times 10^{-2}$. Our first error is their experiment's error and our second error is the systematic error from using our best value.

³ Assumes equal production of B^+ and B^0 at the $\Upsilon(4S)$.

$\Gamma(D_{sJ}(2457)^+ D^*(2010)^- , D_{sJ}^{*+} \rightarrow D_s^+ \gamma)/\Gamma_{total}$					Γ_{102}/Γ
VALUE (units 10^{-3})	CL%	DOCUMENT ID	TECN	COMMENT	
$2.3 \pm 0.3^{+0.9}_{-0.6}$		1 AUBERT,B	04s	BABR $e^+e^- \rightarrow \Upsilon(4S)$	

¹ Assumes equal production of B^+ and B^0 at the $\Upsilon(4S)$.

$[\Gamma(D^- D_{s1}(2536)^+ , D_{s1}^{*+} \rightarrow D^{*0} K^+) + \Gamma(D^{*+} K^0)]/\Gamma_{total}$					$\Gamma_{103}/\Gamma = (\Gamma_{104} + \Gamma_{105})/\Gamma$
VALUE (units 10^{-4})	CL%	DOCUMENT ID	TECN	COMMENT	
$2.75 \pm 0.62 \pm 0.36$		1,2 AUSHEV	11	BELL $e^+e^- \rightarrow \Upsilon(4S)$	

¹ Uses $\Gamma(D^*(2007)^0 \rightarrow D^0 \pi^0) / \Gamma(D^*(2007)^0 \rightarrow D^0 \gamma) = 1.74 \pm 0.13$ and $\Gamma(D_{s1}(2536)^+ \rightarrow D^*(2007)^0 K^+) / \Gamma(D_{s1}(2536)^+ \rightarrow D^*(2010)^+ K^0) = 1.36 \pm 0.2$.

² Assumes equal production of B^+ and B^0 at the $\Upsilon(4S)$.

$\Gamma(D^- D_{s1}(2536)^+ , D_{s1}^{*+} \rightarrow D^{*0} K^+)/\Gamma_{total}$					Γ_{104}/Γ
VALUE (units 10^{-4})	CL%	DOCUMENT ID	TECN	COMMENT	
$1.71 \pm 0.48 \pm 0.32$		1 AUBERT	08B	BABR $e^+e^- \rightarrow \Upsilon(4S)$	

• • • We do not use the following data for averages, fits, limits, etc. • • •

<5 90 AUBERT 03X BABR Repl. by AUBERT 08B

¹ Assumes equal production of B^+ and B^0 at the $\Upsilon(4S)$.

$\Gamma(D^- D_{s1}(2536)^+ , D_{s1}^{*+} \rightarrow D^{*+} K^0)/\Gamma_{total}$					Γ_{105}/Γ
VALUE (units 10^{-4})	CL%	DOCUMENT ID	TECN	COMMENT	
$2.61 \pm 1.03 \pm 0.31$		1 AUBERT	08B	BABR $e^+e^- \rightarrow \Upsilon(4S)$	

¹ Assumes equal production of B^+ and B^0 at the $\Upsilon(4S)$.

$[\Gamma(D^*(2010)^- D_{s1}(2536)^+ , D_{s1}^{*+} \rightarrow D^{*0} K^+) + \Gamma(D^{*+} K^0)]/\Gamma_{total}$					$\Gamma_{106}/\Gamma = (\Gamma_{107} + \Gamma_{108})/\Gamma$
VALUE (units 10^{-4})	CL%	DOCUMENT ID	TECN	COMMENT	
$5.01 \pm 1.21 \pm 0.70$		1,2 AUSHEV	11	BELL $e^+e^- \rightarrow \Upsilon(4S)$	

¹ Uses $\Gamma(D^*(2007)^0 \rightarrow D^0 \pi^0) / \Gamma(D^*(2007)^0 \rightarrow D^0 \gamma) = 1.74 \pm 0.13$ and $\Gamma(D_{s1}(2536)^+ \rightarrow D^*(2007)^0 K^+) / \Gamma(D_{s1}(2536)^+ \rightarrow D^*(2010)^+ K^0) = 1.36 \pm 0.2$.

² Assumes equal production of B^+ and B^0 at the $\Upsilon(4S)$.

$\Gamma(D^*(2010)^- D_{s1}(2536)^+ , D_{s1}^{*+} \rightarrow D^{*0} K^+)/\Gamma_{total}$					Γ_{107}/Γ
VALUE (units 10^{-4})	CL%	DOCUMENT ID	TECN	COMMENT	
$3.32 \pm 0.88 \pm 0.66$		1 AUBERT	08B	BABR $e^+e^- \rightarrow \Upsilon(4S)$	

• • • We do not use the following data for averages, fits, limits, etc. • • •

<7 90 AUBERT 03X BABR Repl. by AUBERT 08B

¹ Assumes equal production of B^+ and B^0 at the $\Upsilon(4S)$.

Meson Particle Listings

 B^0 $\Gamma(D^{*-} D_{s1}(2536)^+, D_{s1}^+ \rightarrow D^{*+} K^0)/\Gamma_{\text{total}}$ Γ_{108}/Γ

VALUE (units 10^{-4})	CL%	DOCUMENT ID	TECN	COMMENT
5.00 ± 1.51 ± 0.67		1 AUBERT 08B	BABR	$e^+ e^- \rightarrow \Upsilon(4S)$

¹ Assumes equal production of B^+ and B^0 at the $\Upsilon(4S)$.

 $\Gamma(D^- D_{sJ}(2573)^+, D_{sJ}^+ \rightarrow D^0 K^+)/\Gamma_{\text{total}}$ Γ_{109}/Γ

VALUE (units 10^{-5})	CL%	DOCUMENT ID	TECN	COMMENT
3.4 ± 1.7 ± 0.5		1 LEES 15c	BABR	$e^+ e^- \rightarrow \Upsilon(4S)$

• • • We do not use the following data for averages, fits, limits, etc. • • •

<10	90	AUBERT 03X	BABR	$e^+ e^- \rightarrow \Upsilon(4S)$
-----	----	------------	------	------------------------------------

¹ Assumes equal production of B^+ and B^0 at the $\Upsilon(4S)$.

 $\Gamma(D^{*+}(2010)^- D_{sJ}(2573)^+, D_{sJ}^+ \rightarrow D^0 K^+)/\Gamma_{\text{total}}$ Γ_{110}/Γ

VALUE (units 10^{-4})	CL%	DOCUMENT ID	TECN	COMMENT
<2	90	AUBERT 03X	BABR	$e^+ e^- \rightarrow \Upsilon(4S)$

 $\Gamma(D^- D_{sJ}(2700)^+, D_{sJ}^+ \rightarrow D^0 K^+)/\Gamma_{\text{total}}$ Γ_{111}/Γ

VALUE (units 10^{-4})	CL%	DOCUMENT ID	TECN	COMMENT
7.14 ± 0.96 ± 0.69		1 LEES 15c	BABR	$e^+ e^- \rightarrow \Upsilon(4S)$

¹ Assumes equal production of B^+ and B^0 at the $\Upsilon(4S)$.

 $\Gamma(D^+ \pi^-)/\Gamma_{\text{total}}$ Γ_{112}/Γ

VALUE (units 10^{-7})	CL%	DOCUMENT ID	TECN	COMMENT
7.4 ± 1.2 ± 0.4		1,2 DAS 10	BELL	$e^+ e^- \rightarrow \Upsilon(4S)$

¹ DAS 10 reports $[\Gamma(B^0 \rightarrow D^+ \pi^-)/\Gamma_{\text{total}}] / [B(B^0 \rightarrow D^+ \pi^-)] = (2.92 \pm 0.38 \pm 0.31) \times 10^{-4}$ which we multiply by our best value $B(B^0 \rightarrow D^+ \pi^-) = (2.52 \pm 0.13) \times 10^{-3}$. Our first error is their experiment's error and our second error is the systematic error from using our best value.

² Derived using $\tan(\theta_C) f_D/f_{D_s} \sqrt{B(B^0 \rightarrow D_s^+ \pi^-)/B(B^0 \rightarrow D^+ \pi^-)}$ by assuming the flavor SU(3) symmetry, where θ_C is the Cabibbo angle, f_D (f_{D_s}) is the D (D_s) meson decay constant.

 $\Gamma(D_s^+ \pi^-)/\Gamma_{\text{total}}$ Γ_{113}/Γ

VALUE (units 10^{-6})	CL%	DOCUMENT ID	TECN	COMMENT
21.6 ± 2.6 OUR AVERAGE				

19.9 ± 2.6 ± 1.8		1 DAS 10	BELL	$e^+ e^- \rightarrow \Upsilon(4S)$
25 ± 4 ± 2		1 AUBERT 08AJ	BABR	$e^+ e^- \rightarrow \Upsilon(4S)$

• • • We do not use the following data for averages, fits, limits, etc. • • •

14.0 ± 3.5 ± 1.3		2 AUBERT 07K	BABR	Repl. by AUBERT 08AJ
25 ± 9 ± 2		3 AUBERT 03D	BABR	Repl. by AUBERT 07K
19 ± 9 ± 2		4 KROKOVNY 02	BELL	Repl. by DAS 10

< 220	90	5 ALEXANDER 93B	CLE2	$e^+ e^- \rightarrow \Upsilon(4S)$
< 1300	90	6 BORTOLETTO90	CLEO	$e^+ e^- \rightarrow \Upsilon(4S)$

¹ Assumes equal production of B^+ and B^0 at the $\Upsilon(4S)$.

² AUBERT 07K reports $[\Gamma(B^0 \rightarrow D_s^+ \pi^-)/\Gamma_{\text{total}}] \times [B(D_s^+ \rightarrow \phi \pi^+)] = (0.63 \pm 0.15 \pm 0.05) \times 10^{-6}$ which we divide by our best value $B(D_s^+ \rightarrow \phi \pi^+) = (4.5 \pm 0.4) \times 10^{-2}$. Our first error is their experiment's error and our second error is the systematic error from using our best value.

³ AUBERT 03D reports $[\Gamma(B^0 \rightarrow D_s^+ \pi^-)/\Gamma_{\text{total}}] \times [B(D_s^+ \rightarrow \phi \pi^+)] = (1.13 \pm 0.33 \pm 0.21) \times 10^{-6}$ which we divide by our best value $B(D_s^+ \rightarrow \phi \pi^+) = (4.5 \pm 0.4) \times 10^{-2}$. Our first error is their experiment's error and our second error is the systematic error from using our best value.

⁴ KROKOVNY 02 reports $[\Gamma(B^0 \rightarrow D_s^+ \pi^-)/\Gamma_{\text{total}}] \times [B(D_s^+ \rightarrow \phi \pi^+)] = (0.86^{+0.37}_{-0.30} \pm 0.11) \times 10^{-6}$ which we divide by our best value $B(D_s^+ \rightarrow \phi \pi^+) = (4.5 \pm 0.4) \times 10^{-2}$. Our first error is their experiment's error and our second error is the systematic error from using our best value.

⁵ ALEXANDER 93B reports $< 270 \times 10^{-6}$ from a measurement of $[\Gamma(B^0 \rightarrow D_s^+ \pi^-)/\Gamma_{\text{total}}] \times [B(D_s^+ \rightarrow \phi \pi^+)]$ assuming $B(D_s^+ \rightarrow \phi \pi^+) = 0.037$, which we rescale to our best value $B(D_s^+ \rightarrow \phi \pi^+) = 4.5 \times 10^{-2}$.

⁶ BORTOLETTO 90 assume $B(D_s \rightarrow \phi \pi^+) = 2\%$.

 $[\Gamma(D_s^+ \pi^-) + \Gamma(D_s^- K^+)]/\Gamma_{\text{total}}$ $(\Gamma_{113} + \Gamma_{123})/\Gamma$

VALUE	CL%	DOCUMENT ID	TECN	COMMENT
< 1.0 × 10⁻³	90	1 ALBRECHT 93E	ARG	$e^+ e^- \rightarrow \Upsilon(4S)$

¹ ALBRECHT 93E reports $< 1.7 \times 10^{-3}$ from a measurement of $[\Gamma(B^0 \rightarrow D_s^+ \pi^-) + \Gamma(B^0 \rightarrow D_s^- K^+)]/\Gamma_{\text{total}} \times [B(D_s^+ \rightarrow \phi \pi^+)]$ assuming $B(D_s^+ \rightarrow \phi \pi^+) = 0.027$, which we rescale to our best value $B(D_s^+ \rightarrow \phi \pi^+) = 4.5 \times 10^{-2}$.

 $\Gamma(D_s^{*+} \pi^-)/\Gamma_{\text{total}}$ Γ_{114}/Γ

VALUE (units 10^{-5})	CL%	DOCUMENT ID	TECN	COMMENT
2.1 ± 0.4 OUR AVERAGE				Error includes scale factor of 1.4.

1.75 ± 0.34 ± 0.20		1 JOSHI 10	BELL	$e^+ e^- \rightarrow \Upsilon(4S)$
2.6 ± 0.5 ± 0.2		1 AUBERT 08AJ	BABR	$e^+ e^- \rightarrow \Upsilon(4S)$

• • • We do not use the following data for averages, fits, limits, etc. • • •

2.9 ± 0.7 ± 0.3		2 AUBERT 07K	BABR	Repl. by AUBERT 08AJ
< 4.1	90	AUBERT 03D	BABR	Repl. by AUBERT 07K
< 40	90	3 ALEXANDER 93B	CLE2	$e^+ e^- \rightarrow \Upsilon(4S)$

¹ Assumes equal production of B^+ and B^0 at the $\Upsilon(4S)$.

² AUBERT 07K reports $[\Gamma(B^0 \rightarrow D_s^{*+} \pi^-)/\Gamma_{\text{total}}] \times [B(D_s^+ \rightarrow \phi \pi^+)] = (1.32 \pm 0.27 \pm 0.15) \times 10^{-6}$ which we divide by our best value $B(D_s^+ \rightarrow \phi \pi^+) = (4.5 \pm 0.4) \times 10^{-2}$. Our first error is their experiment's error and our second error is the systematic error from using our best value.

³ ALEXANDER 93B reports $< 44 \times 10^{-5}$ from a measurement of $[\Gamma(B^0 \rightarrow D_s^{*+} \pi^-)/\Gamma_{\text{total}}] \times [B(D_s^+ \rightarrow \phi \pi^+)]$ assuming $B(D_s^+ \rightarrow \phi \pi^+) = 0.037$, which we rescale to our best value $B(D_s^+ \rightarrow \phi \pi^+) = 4.5 \times 10^{-2}$.

 $[\Gamma(D_s^{*+} \pi^-) + \Gamma(D_s^{*-} K^+)]/\Gamma_{\text{total}}$ $(\Gamma_{114} + \Gamma_{124})/\Gamma$

VALUE	CL%	DOCUMENT ID	TECN	COMMENT
< 7 × 10⁻⁴	90	1 ALBRECHT 93E	ARG	$e^+ e^- \rightarrow \Upsilon(4S)$

¹ ALBRECHT 93E reports $< 1.2 \times 10^{-3}$ from a measurement of $[\Gamma(B^0 \rightarrow D_s^{*+} \pi^-) + \Gamma(B^0 \rightarrow D_s^{*-} K^+)]/\Gamma_{\text{total}} \times [B(D_s^+ \rightarrow \phi \pi^+)]$ assuming $B(D_s^+ \rightarrow \phi \pi^+) = 0.027$, which we rescale to our best value $B(D_s^+ \rightarrow \phi \pi^+) = 4.5 \times 10^{-2}$.

 $\Gamma(D_s^+ \rho^-)/\Gamma_{\text{total}}$ Γ_{115}/Γ

VALUE (units 10^{-5})	CL%	DOCUMENT ID	TECN	COMMENT
< 2.4	90	1 AUBERT 08AJ	BABR	$e^+ e^- \rightarrow \Upsilon(4S)$

• • • We do not use the following data for averages, fits, limits, etc. • • •

< 130	90	2 ALBRECHT 93E	ARG	$e^+ e^- \rightarrow \Upsilon(4S)$
< 50	90	3 ALEXANDER 93B	CLE2	$e^+ e^- \rightarrow \Upsilon(4S)$

¹ Assumes equal production of B^+ and B^0 at the $\Upsilon(4S)$.

² ALBRECHT 93E reports $< 2.2 \times 10^{-3}$ from a measurement of $[\Gamma(B^0 \rightarrow D_s^+ \rho^-)/\Gamma_{\text{total}}] \times [B(D_s^+ \rightarrow \phi \pi^+)]$ assuming $B(D_s^+ \rightarrow \phi \pi^+) = 0.027$, which we rescale to our best value $B(D_s^+ \rightarrow \phi \pi^+) = 4.5 \times 10^{-2}$.

³ ALEXANDER 93B reports $< 6.6 \times 10^{-4}$ from a measurement of $[\Gamma(B^0 \rightarrow D_s^+ \rho^-)/\Gamma_{\text{total}}] \times [B(D_s^+ \rightarrow \phi \pi^+)]$ assuming $B(D_s^+ \rightarrow \phi \pi^+) = 0.037$, which we rescale to our best value $B(D_s^+ \rightarrow \phi \pi^+) = 4.5 \times 10^{-2}$.

 $\Gamma(D_s^{*+} \rho^-)/\Gamma_{\text{total}}$ Γ_{116}/Γ

VALUE (units 10^{-5})	CL%	DOCUMENT ID	TECN	COMMENT
4.1 ± 1.3 ± 0.4		1 AUBERT 08AJ	BABR	$e^+ e^- \rightarrow \Upsilon(4S)$

• • • We do not use the following data for averages, fits, limits, etc. • • •

< 150	90	2 ALBRECHT 93E	ARG	$e^+ e^- \rightarrow \Upsilon(4S)$
< 60	90	3 ALEXANDER 93B	CLE2	$e^+ e^- \rightarrow \Upsilon(4S)$

¹ Assumes equal production of B^+ and B^0 at the $\Upsilon(4S)$.

² ALBRECHT 93E reports $< 2.5 \times 10^{-3}$ from a measurement of $[\Gamma(B^0 \rightarrow D_s^{*+} \rho^-)/\Gamma_{\text{total}}] \times [B(D_s^+ \rightarrow \phi \pi^+)]$ assuming $B(D_s^+ \rightarrow \phi \pi^+) = 0.027$, which we rescale to our best value $B(D_s^+ \rightarrow \phi \pi^+) = 4.5 \times 10^{-2}$.

³ ALEXANDER 93B reports $< 7.4 \times 10^{-4}$ from a measurement of $[\Gamma(B^0 \rightarrow D_s^{*+} \rho^-)/\Gamma_{\text{total}}] \times [B(D_s^+ \rightarrow \phi \pi^+)]$ assuming $B(D_s^+ \rightarrow \phi \pi^+) = 0.037$, which we rescale to our best value $B(D_s^+ \rightarrow \phi \pi^+) = 4.5 \times 10^{-2}$.

 $\Gamma(D_s^+ a_0^-)/\Gamma_{\text{total}}$ Γ_{117}/Γ

VALUE (units 10^{-5})	CL%	DOCUMENT ID	TECN	COMMENT
< 1.9	90	1 AUBERT 06X	BABR	$e^+ e^- \rightarrow \Upsilon(4S)$

¹ Assumes equal production of B^+ and B^0 at the $\Upsilon(4S)$.

 $\Gamma(D_s^{*+} a_0^-)/\Gamma_{\text{total}}$ Γ_{118}/Γ

VALUE (units 10^{-5})	CL%	DOCUMENT ID	TECN	COMMENT
< 3.6	90	1 AUBERT 06X	BABR	$e^+ e^- \rightarrow \Upsilon(4S)$

¹ Assumes equal production of B^+ and B^0 at the $\Upsilon(4S)$.

 $\Gamma(D_s^+ a_1(1260)^-)/\Gamma_{\text{total}}$ Γ_{119}/Γ

VALUE	CL%	DOCUMENT ID	TECN	COMMENT
< 2.1 × 10⁻³	90	1 ALBRECHT 93E	ARG	$e^+ e^- \rightarrow \Upsilon(4S)$

¹ ALBRECHT 93E reports $< 3.5 \times 10^{-3}$ from a measurement of $[\Gamma(B^0 \rightarrow D_s^+ a_1(1260)^-)/\Gamma_{\text{total}}] \times [B(D_s^+ \rightarrow \phi \pi^+)]$ assuming $B(D_s^+ \rightarrow \phi \pi^+) = 0.027$, which we rescale to our best value $B(D_s^+ \rightarrow \phi \pi^+) = 4.5 \times 10^{-2}$.

 $\Gamma(D_s^{*+} a_1(1260)^-)/\Gamma_{\text{total}}$ Γ_{120}/Γ

VALUE	CL%	DOCUMENT ID	TECN	COMMENT
< 1.7 × 10⁻³	90	1 ALBRECHT 93E	ARG	$e^+ e^- \rightarrow \Upsilon(4S)$

¹ ALBRECHT 93E reports $< 2.9 \times 10^{-3}$ from a measurement of $[\Gamma(B^0 \rightarrow D_s^{*+} a_1(1260)^-)/\Gamma_{\text{total}}] \times [B(D_s^+ \rightarrow \phi \pi^+)]$ assuming $B(D_s^+ \rightarrow \phi \pi^+) = 0.027$, which we rescale to our best value $B(D_s^+ \rightarrow \phi \pi^+) = 4.5 \times 10^{-2}$.

$\Gamma(D_s^{*+} a_2^-)/\Gamma_{total}$					Γ_{121}/Γ
VALUE (units 10^{-5})	CL%	DOCUMENT ID	TECN	COMMENT	
<19	90	1 AUBERT	06x BABR	$e^+e^- \rightarrow \Upsilon(4S)$	
1 Assumes equal production of B^+ and B^0 at the $\Upsilon(4S)$.					

$\Gamma(D_s^{*+} a_2^-)/\Gamma_{total}$					Γ_{122}/Γ
VALUE (units 10^{-5})	CL%	DOCUMENT ID	TECN	COMMENT	
<20	90	1 AUBERT	06x BABR	$e^+e^- \rightarrow \Upsilon(4S)$	
1 Assumes equal production of B^+ and B^0 at the $\Upsilon(4S)$.					

$\Gamma(D_s^- K^+)/\Gamma_{total}$					Γ_{123}/Γ
VALUE (units 10^{-6})	CL%	DOCUMENT ID	TECN	COMMENT	
27 ± 5 OUR FIT		Error includes scale factor of 2.7.			
22 ± 5 OUR AVERAGE		Error includes scale factor of 1.8.			
19.1 ± 2.4 ± 1.7		1 DAS	10 BELL	$e^+e^- \rightarrow \Upsilon(4S)$	
29 ± 4 ± 2		1 AUBERT	08AJ BABR	$e^+e^- \rightarrow \Upsilon(4S)$	
• • • We do not use the following data for averages, fits, limits, etc. • • •					
27 ± 5 ± 2		2 AUBERT	07k BABR	Repl. by AUBERT 08AJ	
26 ± 10 ± 2		3 AUBERT	03D BABR	Repl. by AUBERT 07k	
36 +11 -10 ± 3		4 KROKOVNY	02 BELL	Repl. by DAS 10	
< 190	90	5 ALEXANDER	93B CLE2	$e^+e^- \rightarrow \Upsilon(4S)$	
<1300	90	6 BORTOLETTO	090 CLEO	$e^+e^- \rightarrow \Upsilon(4S)$	

1 Assumes equal production of B^+ and B^0 at the $\Upsilon(4S)$.
 2 AUBERT 07k reports $[\Gamma(B^0 \rightarrow D_s^- K^+)/\Gamma_{total}] \times [B(D_s^+ \rightarrow \phi\pi^+)] = (1.21 \pm 0.17 \pm 0.11) \times 10^{-6}$ which we divide by our best value $B(D_s^+ \rightarrow \phi\pi^+) = (4.5 \pm 0.4) \times 10^{-2}$. Our first error is their experiment's error and our second error is the systematic error from using our best value.
 3 AUBERT 03D reports $[\Gamma(B^0 \rightarrow D_s^- K^+)/\Gamma_{total}] \times [B(D_s^+ \rightarrow \phi\pi^+)] = (1.16 \pm 0.36 \pm 0.24) \times 10^{-6}$ which we divide by our best value $B(D_s^+ \rightarrow \phi\pi^+) = (4.5 \pm 0.4) \times 10^{-2}$. Our first error is their experiment's error and our second error is the systematic error from using our best value.
 4 KROKOVNY 02 reports $[\Gamma(B^0 \rightarrow D_s^- K^+)/\Gamma_{total}] \times [B(D_s^+ \rightarrow \phi\pi^+)] = (1.61 \pm 0.45 \pm 0.38 \pm 0.21) \times 10^{-6}$ which we divide by our best value $B(D_s^+ \rightarrow \phi\pi^+) = (4.5 \pm 0.4) \times 10^{-2}$. Our first error is their experiment's error and our second error is the systematic error from using our best value.
 5 ALEXANDER 93B reports $< 230 \times 10^{-6}$ from a measurement of $[\Gamma(B^0 \rightarrow D_s^- K^+)/\Gamma_{total}] \times [B(D_s^+ \rightarrow \phi\pi^+)]$ assuming $B(D_s^+ \rightarrow \phi\pi^+) = 0.037$, which we rescale to our best value $B(D_s^+ \rightarrow \phi\pi^+) = 4.5 \times 10^{-2}$.
 6 BORTOLETTO 90 assume $B(D_s \rightarrow \phi\pi^+) = 2\%$.

$\Gamma(D_s^{*-} K^+)/\Gamma_{total}$					Γ_{124}/Γ
VALUE (units 10^{-5})	CL%	DOCUMENT ID	TECN	COMMENT	
2.19 ± 0.30 OUR AVERAGE					
2.02 ± 0.33 ± 0.22		1 JOSHI	10 BELL	$e^+e^- \rightarrow \Upsilon(4S)$	
2.4 ± 0.4 ± 0.2		1 AUBERT	08AJ BABR	$e^+e^- \rightarrow \Upsilon(4S)$	
• • • We do not use the following data for averages, fits, limits, etc. • • •					
2.2 ± 0.6 ± 0.2		2 AUBERT	07k BABR	Repl. by AUBERT 08AJ	
< 2.5	90	AUBERT	03D BABR	Repl. by AUBERT 07k	
<14	90	3 ALEXANDER	93B CLE2	$e^+e^- \rightarrow \Upsilon(4S)$	

1 Assumes equal production of B^+ and B^0 at the $\Upsilon(4S)$.
 2 AUBERT 07k reports $[\Gamma(B^0 \rightarrow D_s^{*-} K^+)/\Gamma_{total}] \times [B(D_s^+ \rightarrow \phi\pi^+)] = (0.97 \pm 0.24 \pm 0.12) \times 10^{-6}$ which we divide by our best value $B(D_s^+ \rightarrow \phi\pi^+) = (4.5 \pm 0.4) \times 10^{-2}$. Our first error is their experiment's error and our second error is the systematic error from using our best value.
 3 ALEXANDER 93B reports $< 17 \times 10^{-5}$ from a measurement of $[\Gamma(B^0 \rightarrow D_s^{*-} K^+)/\Gamma_{total}] \times [B(D_s^+ \rightarrow \phi\pi^+)]$ assuming $B(D_s^+ \rightarrow \phi\pi^+) = 0.037$, which we rescale to our best value $B(D_s^+ \rightarrow \phi\pi^+) = 4.5 \times 10^{-2}$.

$\Gamma(D_s^- K^+)/\Gamma(D^- \pi^+)$					Γ_{123}/Γ_{34}
VALUE (units 10^{-2})	CL%	DOCUMENT ID	TECN	COMMENT	
1.09 ± 0.19 OUR FIT		Error includes scale factor of 2.6.			
1.29 ± 0.05 ± 0.08		AAIJ	15Ac LHCb	pp at 7, 8 TeV	

$\Gamma(D_s^- K^*(892)^+)/\Gamma_{total}$					Γ_{125}/Γ
VALUE (units 10^{-5})	CL%	DOCUMENT ID	TECN	COMMENT	
3.5 ± 1.0 ± 0.9 ± 0.4		1 AUBERT	08AJ BABR	$e^+e^- \rightarrow \Upsilon(4S)$	
• • • We do not use the following data for averages, fits, limits, etc. • • •					
<280	90	2 ALBRECHT	93E ARG	$e^+e^- \rightarrow \Upsilon(4S)$	
< 80	90	3 ALEXANDER	93B CLE2	$e^+e^- \rightarrow \Upsilon(4S)$	

1 Assumes equal production of B^+ and B^0 at the $\Upsilon(4S)$.
 2 ALBRECHT 93E reports $< 4.6 \times 10^{-3}$ from a measurement of $[\Gamma(B^0 \rightarrow D_s^- K^*(892)^+)/\Gamma_{total}] \times [B(D_s^+ \rightarrow \phi\pi^+)]$ assuming $B(D_s^+ \rightarrow \phi\pi^+) = 0.027$, which we rescale to our best value $B(D_s^+ \rightarrow \phi\pi^+) = 4.5 \times 10^{-2}$.
 3 ALEXANDER 93B reports $< 9.7 \times 10^{-4}$ from a measurement of $[\Gamma(B^0 \rightarrow D_s^- K^*(892)^+)/\Gamma_{total}] \times [B(D_s^+ \rightarrow \phi\pi^+)]$ assuming $B(D_s^+ \rightarrow \phi\pi^+) = 0.037$, which we rescale to our best value $B(D_s^+ \rightarrow \phi\pi^+) = 4.5 \times 10^{-2}$.

$\Gamma(D_s^{*-} K^*(892)^+)/\Gamma_{total}$					Γ_{126}/Γ
VALUE (units 10^{-5})	CL%	DOCUMENT ID	TECN	COMMENT	
3.2 ± 1.4 ± 0.4		1 AUBERT	08AJ BABR	$e^+e^- \rightarrow \Upsilon(4S)$	
• • • We do not use the following data for averages, fits, limits, etc. • • •					
<350	90	2 ALBRECHT	93E ARG	$e^+e^- \rightarrow \Upsilon(4S)$	
< 90	90	3 ALEXANDER	93B CLE2	$e^+e^- \rightarrow \Upsilon(4S)$	

1 Assumes equal production of B^+ and B^0 at the $\Upsilon(4S)$.
 2 ALBRECHT 93E reports $< 5.8 \times 10^{-3}$ from a measurement of $[\Gamma(B^0 \rightarrow D_s^{*-} K^*(892)^+)/\Gamma_{total}] \times [B(D_s^+ \rightarrow \phi\pi^+)]$ assuming $B(D_s^+ \rightarrow \phi\pi^+) = 0.027$, which we rescale to our best value $B(D_s^+ \rightarrow \phi\pi^+) = 4.5 \times 10^{-2}$.
 3 ALEXANDER 93B reports $< 11.0 \times 10^{-4}$ from a measurement of $[\Gamma(B^0 \rightarrow D_s^{*-} K^*(892)^+)/\Gamma_{total}] \times [B(D_s^+ \rightarrow \phi\pi^+)]$ assuming $B(D_s^+ \rightarrow \phi\pi^+) = 0.037$, which we rescale to our best value $B(D_s^+ \rightarrow \phi\pi^+) = 4.5 \times 10^{-2}$.

$\Gamma(D_s^- \pi^+ K^0)/\Gamma_{total}$					Γ_{127}/Γ
VALUE (units 10^{-4})	CL%	DOCUMENT ID	TECN	COMMENT	
0.97 ± 0.14 OUR AVERAGE					
0.94 ± 0.12 ± 0.10		1 WIECHCZYN...	15 BELL	$e^+e^- \rightarrow \Upsilon(4S)$	
1.10 ± 0.26 ± 0.20		1 AUBERT	08G BABR	$e^+e^- \rightarrow \Upsilon(4S)$	
• • • We do not use the following data for averages, fits, limits, etc. • • •					
<40	90	2 ALBRECHT	93E ARG	$e^+e^- \rightarrow \Upsilon(4S)$	

1 Assumes equal production of B^+ and B^0 at the $\Upsilon(4S)$.
 2 ALBRECHT 93E reports $< 7.3 \times 10^{-3}$ from a measurement of $[\Gamma(B^0 \rightarrow D_s^- \pi^+ K^0)/\Gamma_{total}] \times [B(D_s^+ \rightarrow \phi\pi^+)]$ assuming $B(D_s^+ \rightarrow \phi\pi^+) = 0.027$, which we rescale to our best value $B(D_s^+ \rightarrow \phi\pi^+) = 4.5 \times 10^{-2}$.

$\Gamma(D_s^{*-} \pi^+ K^0)/\Gamma_{total}$					Γ_{128}/Γ
VALUE (units 10^{-4})	CL%	DOCUMENT ID	TECN	COMMENT	
< 1.10	90	1 AUBERT	08G BABR	$e^+e^- \rightarrow \Upsilon(4S)$	
• • • We do not use the following data for averages, fits, limits, etc. • • •					
<25	90	2 ALBRECHT	93E ARG	$e^+e^- \rightarrow \Upsilon(4S)$	

1 Assumes equal production of B^+ and B^0 at the $\Upsilon(4S)$.
 2 ALBRECHT 93E reports $< 4.2 \times 10^{-3}$ from a measurement of $[\Gamma(B^0 \rightarrow D_s^{*-} \pi^+ K^0)/\Gamma_{total}] \times [B(D_s^+ \rightarrow \phi\pi^+)]$ assuming $B(D_s^+ \rightarrow \phi\pi^+) = 0.027$, which we rescale to our best value $B(D_s^+ \rightarrow \phi\pi^+) = 4.5 \times 10^{-2}$.

$\Gamma(D_s^- K^+ \pi^+ \pi^-)/\Gamma_{total}$					Γ_{129}/Γ
VALUE (units 10^{-4})	CL%	DOCUMENT ID	TECN	COMMENT	
1.73 ± 0.32 ± 0.35		1 AAIJ	12Ax LHCb	pp at 7 TeV	

1 AAIJ 12Ax reports $[\Gamma(B^0 \rightarrow D_s^- K^+ \pi^+ \pi^-)/\Gamma_{total}] / [B(B_s^0 \rightarrow D_s^- K^+ \pi^+ \pi^-)] = 0.54 \pm 0.07 \pm 0.07$ which we multiply by our best value $B(B_s^0 \rightarrow D_s^- K^+ \pi^+ \pi^-) = (3.2 \pm 0.6) \times 10^{-4}$. Our first error is their experiment's error and our second error is the systematic error from using our best value.

$\Gamma(D_s^- \pi^+ K^*(892)^0)/\Gamma_{total}$					Γ_{130}/Γ
VALUE	CL%	DOCUMENT ID	TECN	COMMENT	
<3.0 × 10⁻³		1 ALBRECHT	93E ARG	$e^+e^- \rightarrow \Upsilon(4S)$	
1 ALBRECHT 93E reports $< 5.0 \times 10^{-3}$ from a measurement of $[\Gamma(B^0 \rightarrow D_s^- \pi^+ K^*(892)^0)/\Gamma_{total}] \times [B(D_s^+ \rightarrow \phi\pi^+)]$ assuming $B(D_s^+ \rightarrow \phi\pi^+) = 0.027$, which we rescale to our best value $B(D_s^+ \rightarrow \phi\pi^+) = 4.5 \times 10^{-2}$.					

$\Gamma(D_s^{*-} \pi^+ K^*(892)^0)/\Gamma_{total}$					Γ_{131}/Γ
VALUE	CL%	DOCUMENT ID	TECN	COMMENT	
<1.6 × 10⁻³		1 ALBRECHT	93E ARG	$e^+e^- \rightarrow \Upsilon(4S)$	
1 ALBRECHT 93E reports $< 2.7 \times 10^{-3}$ from a measurement of $[\Gamma(B^0 \rightarrow D_s^{*-} \pi^+ K^*(892)^0)/\Gamma_{total}] \times [B(D_s^+ \rightarrow \phi\pi^+)]$ assuming $B(D_s^+ \rightarrow \phi\pi^+) = 0.027$, which we rescale to our best value $B(D_s^+ \rightarrow \phi\pi^+) = 4.5 \times 10^{-2}$.					

$\Gamma(D^0 K^0)/\Gamma_{total}$					Γ_{132}/Γ
VALUE (units 10^{-5})	CL%	DOCUMENT ID	TECN	COMMENT	
5.2 ± 0.7 OUR AVERAGE					
5.3 ± 0.7 ± 0.3		1 AUBERT,B	06L BABR	$e^+e^- \rightarrow \Upsilon(4S)$	
5.0 ± 1.3 ± 0.6		1 KROKOVNY	03 BELL	$e^+e^- \rightarrow \Upsilon(4S)$	
1 Assumes equal production of B^+ and B^0 at the $\Upsilon(4S)$.					

$\Gamma(D^0 K^+ \pi^-)/\Gamma_{total}$					Γ_{133}/Γ
VALUE (units 10^{-6})	CL%	DOCUMENT ID	TECN	COMMENT	
88 ± 15 ± 9		1 AUBERT	06A BABR	$e^+e^- \rightarrow \Upsilon(4S)$	
1 Assumes equal production of B^+ and B^0 at the $\Upsilon(4S)$.					

$\Gamma(D^0 K^+ \pi^-)/\Gamma(D^0 \pi^+ \pi^-)$					Γ_{133}/Γ_{43}
VALUE	CL%	DOCUMENT ID	TECN	COMMENT	
0.106 ± 0.007 ± 0.008		AAIJ	13Aq LHCb	pp at 7 TeV	

Meson Particle Listings

B^0

$\Gamma(\bar{D}^0 K^*(892)^0)/\Gamma_{\text{total}}$ Γ_{134}/Γ

VALUE (units 10^{-5})	DOCUMENT ID	TECN	COMMENT
4.5 ± 0.6 OUR AVERAGE			
5.4 ± 0.3 ± 1.1	1,2 AAIJ	15X	LHCB pp at 7, 8 TeV
4.0 ± 0.7 ± 0.3	3 AUBERT,B	06L	BABR $e^+e^- \rightarrow \Upsilon(4S)$
4.8 ± 1.1 ± 0.5	3 KROKOVNY	03	BELL $e^+e^- \rightarrow \Upsilon(4S)$

• • • We do not use the following data for averages, fits, limits, etc. • • •

5.7 ± 0.9 ± 0.6 ³AUBERT 06A BABR Repl. by AUBERT,B 06L

¹ AAIJ 15x reports $(5.13 \pm 0.20 \pm 0.15 \pm 0.24 \pm 0.60) \times 10^{-5}$ from a measurement of $[\Gamma(B^0 \rightarrow \bar{D}^0 K^*(892)^0)/\Gamma_{\text{total}}] \times [B(B^0 \rightarrow \bar{D}^0 K^+ \pi^-)]$ assuming $B(B^0 \rightarrow \bar{D}^0 K^+ \pi^-) = (9.2 \pm 0.6 \pm 0.7 \pm 0.6) \times 10^{-5}$, which we rescale to our best value $B(B^0 \rightarrow \bar{D}^0 K^+ \pi^-) = (8.8 \pm 1.7) \times 10^{-5}$. Our first error is their experiment's error and our second error is the systematic error from using our best value.

² Measured via amplitude analysis of $B^0 \rightarrow \bar{D}^0 K^+ \pi^-$, which excludes contribution from decay via $D^*(2010)^-$ resonance.

³ Assumes equal production of B^+ and B^0 at the $\Upsilon(4S)$.

$\Gamma(\bar{D}^0 K^*(1430)^0)/\Gamma_{\text{total}}$ Γ_{135}/Γ

VALUE	CL%	DOCUMENT ID	TECN	COMMENT
<6.7 × 10⁻⁵	90	1 AAIJ	15X	LHCB pp at 7, 8 TeV

¹ Measured via amplitude analysis of $B^0 \rightarrow \bar{D}^0 K^+ \pi^-$, which excludes contribution from decay via $D^*(2010)^-$ resonance.

$\Gamma(\bar{D}^0 K_0^*(1430)^0)/\Gamma_{\text{total}}$ Γ_{136}/Γ

VALUE (units 10^{-5})	DOCUMENT ID	TECN	COMMENT
0.7 ± 0.7 ± 0.1	1,2 AAIJ	15X	LHCB pp at 7, 8 TeV

¹ AAIJ 15x reports $(0.71 \pm 0.27 \pm 0.33 \pm 0.47 \pm 0.08) \times 10^{-5}$ from a measurement of $[\Gamma(B^0 \rightarrow \bar{D}^0 K_0^*(1430)^0)/\Gamma_{\text{total}}] \times [B(B^0 \rightarrow \bar{D}^0 K^+ \pi^-)]$ assuming $B(B^0 \rightarrow \bar{D}^0 K^+ \pi^-) = (9.2 \pm 0.6 \pm 0.7 \pm 0.6) \times 10^{-5}$, which we rescale to our best value $B(B^0 \rightarrow \bar{D}^0 K^+ \pi^-) = (8.8 \pm 1.7) \times 10^{-5}$. Our first error is their experiment's error and our second error is the systematic error from using our best value.

² Measured via amplitude analysis of $B^0 \rightarrow \bar{D}^0 K^+ \pi^-$, which excludes contribution from decay via $D^*(2010)^-$ resonance.

$\Gamma(\bar{D}^0 K_2^*(1430)^0)/\Gamma_{\text{total}}$ Γ_{137}/Γ

VALUE (units 10^{-5})	DOCUMENT ID	TECN	COMMENT
2.1 ± 0.8 ± 0.4	1,2 AAIJ	15X	LHCB pp at 7, 8 TeV

¹ AAIJ 15x reports $(2.04 \pm 0.45 \pm 0.30 \pm 0.54 \pm 0.25) \times 10^{-5}$ from a measurement of $[\Gamma(B^0 \rightarrow \bar{D}^0 K_2^*(1430)^0)/\Gamma_{\text{total}}] \times [B(B^0 \rightarrow \bar{D}^0 K^+ \pi^-)]$ assuming $B(B^0 \rightarrow \bar{D}^0 K^+ \pi^-) = (9.2 \pm 0.6 \pm 0.7 \pm 0.6) \times 10^{-5}$, which we rescale to our best value $B(B^0 \rightarrow \bar{D}^0 K^+ \pi^-) = (8.8 \pm 1.7) \times 10^{-5}$. Our first error is their experiment's error and our second error is the systematic error from using our best value.

² Measured via amplitude analysis of $B^0 \rightarrow \bar{D}^0 K^+ \pi^-$, which excludes contribution from decay via $D^*(2010)^-$ resonance.

$\Gamma(D_0^*(2300)^- K^+, D_0^{*-} \rightarrow \bar{D}^0 \pi^-)/\Gamma_{\text{total}}$ Γ_{138}/Γ

VALUE (units 10^{-5})	DOCUMENT ID	TECN	COMMENT
1.9 ± 0.8 ± 0.4	1,2 AAIJ	15X	LHCB pp at 7, 8 TeV

¹ AAIJ 15x reports $(1.77 \pm 0.26 \pm 0.19 \pm 0.67 \pm 0.20) \times 10^{-5}$ from a measurement of $[\Gamma(B^0 \rightarrow D_0^*(2300)^- K^+, D_0^{*-} \rightarrow \bar{D}^0 \pi^-)/\Gamma_{\text{total}}] \times [B(B^0 \rightarrow \bar{D}^0 K^+ \pi^-)]$ assuming $B(B^0 \rightarrow \bar{D}^0 K^+ \pi^-) = (9.2 \pm 0.6 \pm 0.7 \pm 0.6) \times 10^{-5}$, which we rescale to our best value $B(B^0 \rightarrow \bar{D}^0 K^+ \pi^-) = (8.8 \pm 1.7) \times 10^{-5}$. Our first error is their experiment's error and our second error is the systematic error from using our best value.

² Measured via amplitude analysis of $B^0 \rightarrow \bar{D}^0 K^+ \pi^-$, which excludes contribution from decay via $D^*(2010)^-$ resonance.

$\Gamma(D_2^*(2460)^- K^+, D_2^{*-} \rightarrow \bar{D}^0 \pi^-)/\Gamma_{\text{total}}$ Γ_{139}/Γ

VALUE (units 10^{-6})	DOCUMENT ID	TECN	COMMENT
20.3 ± 3.5 OUR AVERAGE			
22 ± 2 ± 4	1,2 AAIJ	15X	LHCB pp at 7, 8 TeV
18.3 ± 4.0 ± 3.1	3 AUBERT	06A	BABR $e^+e^- \rightarrow \Upsilon(4S)$

¹ AAIJ 15x reports $(2.12 \pm 0.10 \pm 0.11 \pm 0.11 \pm 0.25) \times 10^{-5}$ from a measurement of $[\Gamma(B^0 \rightarrow D_2^*(2460)^- K^+, D_2^{*-} \rightarrow \bar{D}^0 \pi^-)/\Gamma_{\text{total}}] \times [B(B^0 \rightarrow \bar{D}^0 K^+ \pi^-)]$ assuming $B(B^0 \rightarrow \bar{D}^0 K^+ \pi^-) = (9.2 \pm 0.6 \pm 0.7 \pm 0.6) \times 10^{-5}$, which we rescale to our best value $B(B^0 \rightarrow \bar{D}^0 K^+ \pi^-) = (8.8 \pm 1.7) \times 10^{-5}$. Our first error is their experiment's error and our second error is the systematic error from using our best value.

² Measured via amplitude analysis of $B^0 \rightarrow \bar{D}^0 K^+ \pi^-$, which excludes contribution from decay via $D^*(2010)^-$ resonance.

³ Assumes equal production of B^+ and B^0 at the $\Upsilon(4S)$.

$\Gamma(D_3^*(2760)^- K^+, D_3^{*-} \rightarrow \bar{D}^0 \pi^-)/\Gamma_{\text{total}}$ Γ_{140}/Γ

VALUE	CL%	DOCUMENT ID	TECN	COMMENT
<0.10 × 10⁻⁵	90	1 AAIJ	15X	LHCB pp at 7, 8 TeV

¹ Measured via amplitude analysis of $B^0 \rightarrow \bar{D}^0 K^+ \pi^-$, which excludes contribution from decay via $D^*(2010)^-$ resonance.

$\Gamma(\bar{D}^0 K^+ \pi^- \text{ nonresonant})/\Gamma_{\text{total}}$ Γ_{141}/Γ

VALUE (units 10^{-6})	CL%	DOCUMENT ID	TECN	COMMENT
<37	90	1 AUBERT	06A	BABR $e^+e^- \rightarrow \Upsilon(4S)$

¹ Assumes equal production of B^+ and B^0 at the $\Upsilon(4S)$.

$\Gamma([\bar{K}^+ K^-]_D K^*(892)^0)/\Gamma(\bar{D}^0 K^*(892)^0)$ $\Gamma_{142}/\Gamma_{134}$

VALUE	DOCUMENT ID	TECN	COMMENT
0.92 ± 0.10 ± 0.02	AAIJ	19N	LHCB pp at 7, 8, 13 TeV
• • • We do not use the following data for averages, fits, limits, etc. • • •			
1.05 ^{+0.17} _{-0.15} ± 0.04	AAIJ	14BN	LHCB Repl. by AAIJ 16s
1.36 ^{+0.37} _{-0.32} ± 0.07	AAIJ	13L	LHCB Repl. by AAIJ 14BN

$\Gamma([\pi^+ \pi^-]_D K^*(892)^0)/\Gamma(\bar{D}^0 K^*(892)^0)$ $\Gamma_{143}/\Gamma_{134}$

VALUE	DOCUMENT ID	TECN	COMMENT
1.32 ± 0.19 ± 0.03	AAIJ	19N	LHCB pp at 7, 8, 13 TeV
• • • We do not use the following data for averages, fits, limits, etc. • • •			
1.21 ^{+0.28} _{-0.25} ± 0.05	AAIJ	14BN	LHCB Repl. by AAIJ 16s

$\Gamma([\pi^+ K^-]_D K^*(892)^0)/\Gamma([\bar{K}^+ \pi^-]_D K^*(892)^0)$ $\Gamma_{144}/\Gamma_{145}$

VALUE	DOCUMENT ID	TECN	COMMENT
0.080 ± 0.015 ± 0.002	AAIJ	19N	LHCB pp at 7, 8, 13 TeV

$\Gamma([\pi^+ \pi^- \pi^+ \pi^-]_D K^*(892)^0)/\Gamma(\bar{D}^0 K^*(892)^0)$ $\Gamma_{146}/\Gamma_{134}$

VALUE	DOCUMENT ID	TECN	COMMENT
1.01 ± 0.16 ± 0.04	AAIJ	19N	LHCB pp at 7, 8, 13 TeV

$\Gamma([\pi^+ K^- \pi^+ \pi^-]_D K^*(892)^0)/\Gamma([\bar{K}^+ \pi^- \pi^+ \pi^-]_D K^*(892)^0)$ $\Gamma_{147}/\Gamma_{148}$

VALUE	DOCUMENT ID	TECN	COMMENT
0.073 ± 0.018 ± 0.002	AAIJ	19N	LHCB pp at 7, 8, 13 TeV

$\Gamma(\bar{D}^0 \pi^0)/\Gamma_{\text{total}}$ Γ_{149}/Γ

VALUE (units 10^{-4})	CL%	DOCUMENT ID	TECN	COMMENT
2.63 ± 0.14 OUR AVERAGE				
2.69 ± 0.09 ± 0.13		1 LEES	11M	BABR $e^+e^- \rightarrow \Upsilon(4S)$
2.25 ± 0.14 ± 0.35		1 BLYTH	06	BELL $e^+e^- \rightarrow \Upsilon(4S)$
2.74 ^{+0.36} _{-0.32} ± 0.55		1 COAN	02	CLE2 $e^+e^- \rightarrow \Upsilon(4S)$
• • • We do not use the following data for averages, fits, limits, etc. • • •				
2.9 ± 0.2 ± 0.3		1 AUBERT	04B	BABR Repl. by LEES 11M
3.1 ± 0.4 ± 0.5		1 ABE	02J	BELL Repl. by BLYTH 06
<1.2	90	2 NEMATI	98	CLE2 Repl. by COAN 02
<4.8	90	3 ALAM	94	CLE2 Repl. by NEMATI 98

¹ Assumes equal production of B^+ and B^0 at the $\Upsilon(4S)$.

² NEMATI 98 assumes equal production of B^+ and B^0 at the $\Upsilon(4S)$ and use the PDG 96 values for $D^0, D^{*0}, \eta, \eta',$ and ω branching fractions.

³ ALAM 94 assume equal production of B^+ and B^0 at the $\Upsilon(4S)$ and use the CLEO II absolute $B(D^0 \rightarrow K^- \pi^+)$ and the PDG 1992 $B(D^0 \rightarrow K^- \pi^+ \pi^0)/B(D^0 \rightarrow K^- \pi^+)$ and $B(D^0 \rightarrow K^- 2\pi^+ \pi^-)/B(D^0 \rightarrow K^- \pi^+)$.

$\Gamma(\bar{D}^0 \rho^0)/\Gamma_{\text{total}}$ Γ_{150}/Γ

VALUE (units 10^{-4})	CL%	DOCUMENT ID	TECN	COMMENT
3.21 ± 0.21 OUR AVERAGE				
3.21 ± 0.10 ± 0.21		1 AAIJ	15Y	LHCB pp at 7, 8 TeV
3.19 ± 0.20 ± 0.45		2,3 KUZMIN	07	BELL $e^+e^- \rightarrow \Upsilon(4S)$
• • • We do not use the following data for averages, fits, limits, etc. • • •				
2.9 ± 1.0 ± 0.4		2 SATPATHY	03	BELL Repl. by KUZMIN 07
< 3.9	90	4 NEMATI	98	CLE2 $e^+e^- \rightarrow \Upsilon(4S)$
< 5.5	90	5 ALAM	94	CLE2 Repl. by NEMATI 98
< 6.0	90	6 BORTOLETTO92	CLEO	$e^+e^- \rightarrow \Upsilon(4S)$
<27.0	90	7 ALBRECHT	88k	ARG $e^+e^- \rightarrow \Upsilon(4S)$

¹ Measured using isobar formalism in the decay chain $B^0 \rightarrow \bar{D}^0 \rho(770), \rho \rightarrow \pi^+ \pi^-$ assuming $B(\rho(770) \rightarrow \pi^+ \pi^-) = 1$. The second uncertainty combines in quadrature all systematic uncertainties quoted in the paper.

² Assumes equal production of B^+ and B^0 at the $\Upsilon(4S)$.

³ Our second uncertainty combines systematics and model errors quoted in the paper.

⁴ NEMATI 98 assumes equal production of B^+ and B^0 at the $\Upsilon(4S)$ and use the PDG 96 values for $D^0, D^{*0}, \eta, \eta',$ and ω branching fractions.

⁵ ALAM 94 assume equal production of B^+ and B^0 at the $\Upsilon(4S)$ and use the CLEO II absolute $B(D^0 \rightarrow K^- \pi^+)$ and the PDG 1992 $B(D^0 \rightarrow K^- \pi^+ \pi^0)/B(D^0 \rightarrow K^- \pi^+)$ and $B(D^0 \rightarrow K^- 2\pi^+ \pi^-)/B(D^0 \rightarrow K^- \pi^+)$.

⁶ BORTOLETTO 92 assumes equal production of B^+ and B^0 at the $\Upsilon(4S)$ and uses Mark III branching fractions for the D .

⁷ ALBRECHT 88k reports < 0.003 assuming $B^0 \bar{B}^0, B^+ B^-$ production ratio is 45:55. We rescale to 50%.

$\Gamma(\bar{D}^0 f_2)/\Gamma_{\text{total}}$ Γ_{151}/Γ

VALUE (units 10^{-4})	DOCUMENT ID	TECN	COMMENT
1.56 ± 0.21 OUR AVERAGE			
1.68 ± 0.11 ± 0.21	1 AAIJ	15Y	LHCB pp at 7, 8 TeV
1.20 ± 0.18 ± 0.38	2,3 KUZMIN	07	BELL $e^+e^- \rightarrow \Upsilon(4S)$

¹ Result obtained using the isobar formalism. The second uncertainty combines in quadrature all systematic uncertainties quoted in the paper. Measured in the decay chain $B^0 \rightarrow \bar{D}^0 f_2(1270), f_2 \rightarrow \pi^+ \pi^-$.

² Assumes equal production of B^+ and B^0 at the $\Upsilon(4S)$.

³ Our second uncertainty combines systematics and model errors quoted in the paper.

$\Gamma(\bar{D}^0 \eta)/\Gamma_{\text{total}}$ Γ_{152}/Γ

VALUE (units 10 ⁻⁴)	CL%	DOCUMENT ID	TECN	COMMENT
2.36 ± 0.32 OUR AVERAGE		Error includes scale factor of 2.5.		
2.53 ± 0.09 ± 0.11		1 LEES	11M BABR	e ⁺ e ⁻ → T(4S)
1.77 ± 0.16 ± 0.21		1 BLYTH	06 BELL	e ⁺ e ⁻ → T(4S)
• • • We do not use the following data for averages, fits, limits, etc. • • •				
2.5 ± 0.2 ± 0.3		1 AUBERT	04B BABR	Repl. by LEES 11M
1.4 ^{+0.5} _{-0.4} ± 0.3		1 ABE	02J BELL	Repl. by BLYTH 06
<1.3	90	2 NEMAT1	98 CLE2	e ⁺ e ⁻ → T(4S)
<6.8	90	3 ALAM	94 CLE2	Repl. by NEMAT1 98

1 Assumes equal production of B⁺ and B⁰ at the T(4S).
 2 NEMAT1 98 assumes equal production of B⁺ and B⁰ at the T(4S) and use the PDG 96 values for D⁰, D^{*0}, η, η', and ω branching fractions.
 3 ALAM 94 assume equal production of B⁺ and B⁰ at the T(4S) and use the CLEO II absolute B(D⁰ → K⁻π⁺) and the PDG 1992 B(D⁰ → K⁻π⁺π⁰)/B(D⁰ → K⁻π⁺) and B(D⁰ → K⁻2π⁺π⁻)/B(D⁰ → K⁻π⁺).

$\Gamma(\bar{D}^0 \eta')/\Gamma_{\text{total}}$ Γ_{153}/Γ

VALUE (units 10 ⁻⁴)	CL%	DOCUMENT ID	TECN	COMMENT
1.38 ± 0.16 OUR AVERAGE		Error includes scale factor of 1.3.		
1.48 ± 0.13 ± 0.07		1 LEES	11M BABR	e ⁺ e ⁻ → T(4S)
1.14 ± 0.20 ^{+0.10} _{-0.13}		1 SCHUMANN	05 BELL	e ⁺ e ⁻ → T(4S)
• • • We do not use the following data for averages, fits, limits, etc. • • •				
1.7 ± 0.4 ± 0.2		1 AUBERT	04B BABR	Repl. by LEES 11M
<9.4	90	2 NEMAT1	98 CLE2	e ⁺ e ⁻ → T(4S)
<8.6	90	3 ALAM	94 CLE2	Repl. by NEMAT1 98

1 Assumes equal production of B⁺ and B⁰ at the T(4S).
 2 NEMAT1 98 assumes equal production of B⁺ and B⁰ at the T(4S) and use the PDG 96 values for D⁰, D^{*0}, η, η', and ω branching fractions.
 3 ALAM 94 assume equal production of B⁺ and B⁰ at the T(4S) and use the CLEO II absolute B(D⁰ → K⁻π⁺) and the PDG 1992 B(D⁰ → K⁻π⁺π⁰)/B(D⁰ → K⁻π⁺) and B(D⁰ → K⁻2π⁺π⁻)/B(D⁰ → K⁻π⁺).

$\Gamma(\bar{D}^0 \eta')/\Gamma(\bar{D}^0 \eta)$ $\Gamma_{153}/\Gamma_{152}$

VALUE	DOCUMENT ID	TECN	COMMENT
0.54 ± 0.07 ± 0.01	LEES	11M BABR	e ⁺ e ⁻ → T(4S)
• • • We do not use the following data for averages, fits, limits, etc. • • •			
0.7 ± 0.2 ± 0.1	AUBERT	04B BABR	Repl. by LEES 11M

$\Gamma(\bar{D}^0 \omega)/\Gamma_{\text{total}}$ Γ_{154}/Γ

VALUE (units 10 ⁻⁴)	CL%	DOCUMENT ID	TECN	COMMENT
2.54 ± 0.16 OUR AVERAGE				
2.75 ± 0.72 ± 0.35		1 AAIJ	15Y LHCB	pp at 7, 8 TeV
2.57 ± 0.11 ± 0.14		2 LEES	11M BABR	e ⁺ e ⁻ → T(4S)
2.37 ± 0.23 ± 0.28		2 BLYTH	06 BELL	e ⁺ e ⁻ → T(4S)
• • • We do not use the following data for averages, fits, limits, etc. • • •				
3.0 ± 0.3 ± 0.4		2 AUBERT	04B BABR	Repl. by LEES 11M
1.8 ± 0.5 ^{+0.4} _{-0.3}		2 ABE	02J BELL	Repl. by BLYTH 06
<5.1	90	3 NEMAT1	98 CLE2	e ⁺ e ⁻ → T(4S)
<6.3	90	4 ALAM	94 CLE2	Repl. by NEMAT1 98

1 Result obtained using the isobar model. The second uncertainty combines in quadrature all systematic uncertainties quoted in the paper.
 2 Assumes equal production of B⁺ and B⁰ at the T(4S).
 3 NEMAT1 98 assumes equal production of B⁺ and B⁰ at the T(4S) and use the PDG 96 values for D⁰, D^{*0}, η, η', and ω branching fractions.
 4 ALAM 94 assume equal production of B⁺ and B⁰ at the T(4S) and use the CLEO II absolute B(D⁰ → K⁻π⁺) and the PDG 1992 B(D⁰ → K⁻π⁺π⁰)/B(D⁰ → K⁻π⁺) and B(D⁰ → K⁻2π⁺π⁻)/B(D⁰ → K⁻π⁺).

$\Gamma(D^0 \phi)/\Gamma_{\text{total}}$ Γ_{155}/Γ

VALUE	CL%	DOCUMENT ID	TECN	COMMENT
< 2.3 × 10⁻⁶	95	AAIJ	18AY LHCB	pp at 7 and 8 TeV
• • • We do not use the following data for averages, fits, limits, etc. • • •				
<11.6 × 10 ⁻⁶	90	1 AUBERT	07A0 BABR	e ⁺ e ⁻ → T(4S)
1 Assumes equal production of B ⁺ and B ⁰ at the T(4S).				

$\Gamma(D^0 K^+ \pi^-)/\Gamma_{\text{total}}$ Γ_{156}/Γ

VALUE (units 10 ⁻⁶)	CL%	DOCUMENT ID	TECN	COMMENT
• • • We do not use the following data for averages, fits, limits, etc. • • •				
<19	90	1 AUBERT	06A BABR	Repl. by AUBERT 09AE
1 Assumes equal production of B ⁺ and B ⁰ at the T(4S).				

$\Gamma(D^0 K^+ \pi^-)/\Gamma(\bar{D}^0 K^+ \pi^-)$ $\Gamma_{156}/\Gamma_{133}$

VALUE	DOCUMENT ID	TECN	COMMENT
0.060 ± 0.034 OUR AVERAGE			
0.045 ^{+0.056} _{-0.050} ± 0.028	1,2 NEGISHI	12 BELL	e ⁺ e ⁻ → T(4S)
0.068 ± 0.042	3 AUBERT	09AE BABR	e ⁺ e ⁻ → T(4S)

1 Assumes equal production of B⁰ and B⁺ at T(4S).
 2 Uses D⁰ → K⁻π⁺ mode. Restricts K⁺π⁻ mass within ±50 MeV of the nominal K⁺π⁻ mass. Corresponds to the upper limit, < 0.16 at 95% CL.
 3 Reports a signal at the level of 2.5 standard deviations after combining results from D⁰ → K⁺π⁻, K⁺π⁻π⁰, and K⁺π⁻π⁺π⁻.

$\Gamma(D^0 K^*(892)^0)/\Gamma_{\text{total}}$ Γ_{157}/Γ

VALUE (units 10 ⁻⁵)	CL%	DOCUMENT ID	TECN	COMMENT
• • • We do not use the following data for averages, fits, limits, etc. • • •				
<1.1	90	1 AUBERT,B	06L BABR	e ⁺ e ⁻ → T(4S)
<1.8	90	1 KROKOVNY	03 BELL	e ⁺ e ⁻ → T(4S)
1 Assumes equal production of B ⁺ and B ⁰ at the T(4S).				

$\Gamma(D^0 K^*(892)^0)/\Gamma(\bar{D}^0 K^*(892)^0)$ $\Gamma_{157}/\Gamma_{134}$

"OUR EVALUATION" is derived from r_{B⁰}(B⁰ → D K^{*0}) data block listed in "CP violation parameters" section.

VALUE (units 10 ⁻²)	DOCUMENT ID
4.84^{+1.80}_{-2.07} OUR EVALUATION	

$\Gamma(\bar{D}^{*0} \gamma)/\Gamma_{\text{total}}$ Γ_{158}/Γ

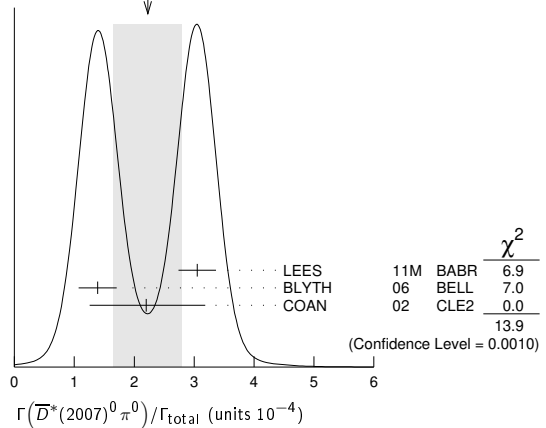
VALUE	CL%	DOCUMENT ID	TECN	COMMENT
<2.5 × 10⁻⁵	90	1 AUBERT,B	05Q BABR	e ⁺ e ⁻ → T(4S)
• • • We do not use the following data for averages, fits, limits, etc. • • •				
<5.0 × 10 ⁻⁵	90	1 ARTUSO	00 CLE2	e ⁺ e ⁻ → T(4S)
1 Assumes equal production of B ⁺ and B ⁰ at the T(4S).				

$\Gamma(\bar{D}^*(2007)^0 \pi^0)/\Gamma_{\text{total}}$ Γ_{159}/Γ

VALUE (units 10 ⁻⁴)	CL%	DOCUMENT ID	TECN	COMMENT
2.2 ± 0.6 OUR AVERAGE		Error includes scale factor of 2.6. See the ideogram below.		
3.05 ± 0.14 ± 0.28		1 LEES	11M BABR	e ⁺ e ⁻ → T(4S)
1.39 ± 0.18 ± 0.26		1 BLYTH	06 BELL	e ⁺ e ⁻ → T(4S)
2.20 ^{+0.59} _{-0.52} ± 0.79		1 COAN	02 CLE2	e ⁺ e ⁻ → T(4S)
• • • We do not use the following data for averages, fits, limits, etc. • • •				
2.9 ± 0.4 ± 0.5		1 AUBERT	04B BABR	Repl. by LEES 11M
2.7 ± 0.8 ^{+0.5} _{-0.7} ± 0.6		1 ABE	02J BELL	Repl. by BLYTH 06
<4.4	90	2 NEMAT1	98 CLE2	Repl. by COAN 02
<9.7	90	3 ALAM	94 CLE2	Repl. by NEMAT1 98

1 Assumes equal production of B⁺ and B⁰ at the T(4S).
 2 NEMAT1 98 assumes equal production of B⁺ and B⁰ at the T(4S) and use the PDG 96 values for D⁰, D^{*0}, η, η', and ω branching fractions.
 3 ALAM 94 assume equal production of B⁺ and B⁰ at the T(4S) and use the CLEO II B(D^{*}(2007)⁰ → D⁰π⁰) and absolute B(D⁰ → K⁻π⁺) and the PDG 1992 B(D⁰ → K⁻π⁺π⁰)/B(D⁰ → K⁻π⁺) and B(D⁰ → K⁻2π⁺π⁻)/B(D⁰ → K⁻π⁺).

WEIGHTED AVERAGE
2.2±0.6 (Error scaled by 2.6)



$\Gamma(D^0 \pi^0)/\Gamma(\bar{D}^*(2007)^0 \pi^0)$ $\Gamma_{149}/\Gamma_{159}$

VALUE	DOCUMENT ID	TECN	COMMENT
0.90 ± 0.08 OUR AVERAGE			
0.88 ± 0.05 ± 0.06	LEES	11M BABR	e ⁺ e ⁻ → T(4S)
1.62 ± 0.23 ± 0.35	BLYTH	06 BELL	e ⁺ e ⁻ → T(4S)
• • • We do not use the following data for averages, fits, limits, etc. • • •			
1.0 ± 0.1 ± 0.2	AUBERT	04B BABR	Repl. by LEES 11M

$\Gamma(\bar{D}^*(2007)^0 \rho^0)/\Gamma_{\text{total}}$ Γ_{160}/Γ

VALUE	CL%	DOCUMENT ID	TECN	COMMENT
<5.1 × 10⁻⁴	90	1 SATPATHY	03 BELL	e ⁺ e ⁻ → T(4S)
• • • We do not use the following data for averages, fits, limits, etc. • • •				
<0.00056	90	2 NEMAT1	98 CLE2	e ⁺ e ⁻ → T(4S)
<0.00117	90	3 ALAM	94 CLE2	Repl. by NEMAT1 98

1 Assumes equal production of B⁺ and B⁰ at the T(4S).
 2 NEMAT1 98 assumes equal production of B⁺ and B⁰ at the T(4S) and use the PDG 96 values for D⁰, D^{*0}, η, η', and ω branching fractions.
 3 ALAM 94 assume equal production of B⁺ and B⁰ at the T(4S) and use the CLEO II B(D^{*}(2007)⁰ → D⁰π⁰) and absolute B(D⁰ → K⁻π⁺) and the PDG 1992 B(D⁰ → K⁻π⁺π⁰)/B(D⁰ → K⁻π⁺) and B(D⁰ → K⁻2π⁺π⁻)/B(D⁰ → K⁻π⁺).

Meson Particle Listings

 B^0 $\Gamma(\bar{D}^*(2007)^0 \eta)/\Gamma_{\text{total}}$ Γ_{161}/Γ

VALUE (units 10^{-4})	CL%	DOCUMENT ID	TECN	COMMENT
2.3 ± 0.6 OUR AVERAGE				Error includes scale factor of 2.8.
2.69 ± 0.14 ± 0.23		¹ LEES	11M	BABR $e^+e^- \rightarrow \Upsilon(4S)$
1.40 ± 0.28 ± 0.26		¹ BLYTH	06	BELL $e^+e^- \rightarrow \Upsilon(4S)$
• • • We do not use the following data for averages, fits, limits, etc. • • •				
2.6 ± 0.4 ± 0.4		¹ AUBERT	04B	BABR Repl. by LEES 11M
<4.6	90	¹ ABE	02J	BELL $e^+e^- \rightarrow \Upsilon(4S)$
<2.6	90	² NEMAT1	98	CLE2 $e^+e^- \rightarrow \Upsilon(4S)$
<6.9	90	³ ALAM	94	CLE2 Repl. by NEMAT1 98

- ¹ Assumes equal production of B^+ and B^0 at the $\Upsilon(4S)$.
² NEMAT1 98 assumes equal production of B^+ and B^0 at the $\Upsilon(4S)$ and use the PDG 96 values for D^0 , D^{*0} , η , η' , and ω branching fractions.
³ ALAM 94 assume equal production of B^+ and B^0 at the $\Upsilon(4S)$ and use the CLEOII $B(D^*(2007)^0 \rightarrow D^0 \pi^0)$ and absolute $B(D^0 \rightarrow K^- \pi^+)$ and the PDG 1992 $B(D^0 \rightarrow K^- \pi^+ \pi^0)/B(D^0 \rightarrow K^- \pi^+)$ and $B(D^0 \rightarrow K^- 2\pi^+ \pi^-)/B(D^0 \rightarrow K^- \pi^+)$.

 $\Gamma(\bar{D}^0 \eta)/\Gamma(\bar{D}^*(2007)^0 \eta)$ $\Gamma_{152}/\Gamma_{161}$

VALUE	DOCUMENT ID	TECN	COMMENT
0.99 ± 0.10 OUR AVERAGE			
0.97 ± 0.07 ± 0.07	LEES	11M	BABR $e^+e^- \rightarrow \Upsilon(4S)$
1.27 ± 0.29 ± 0.25	BLYTH	06	BELL $e^+e^- \rightarrow \Upsilon(4S)$
• • • We do not use the following data for averages, fits, limits, etc. • • •			
0.9 ± 0.2 ± 0.1	AUBERT	04B	BABR Repl. by LEES 11M

 $\Gamma(\bar{D}^*(2007)^0 \eta')/\Gamma(\bar{D}^*(2007)^0 \eta)$ $\Gamma_{162}/\Gamma_{161}$

VALUE	DOCUMENT ID	TECN	COMMENT
0.61 ± 0.14 ± 0.02	LEES	11M	BABR $e^+e^- \rightarrow \Upsilon(4S)$
• • • We do not use the following data for averages, fits, limits, etc. • • •			
0.5 ± 0.3 ± 0.1	AUBERT	04B	BABR Repl. by LEES 11M

 $\Gamma(\bar{D}^*(2007)^0 \eta')/\Gamma_{\text{total}}$ Γ_{162}/Γ

VALUE (units 10^{-4})	CL%	DOCUMENT ID	TECN	COMMENT
1.40 ± 0.22 OUR AVERAGE				
1.48 ± 0.22 ± 0.13		¹ LEES	11M	BABR $e^+e^- \rightarrow \Upsilon(4S)$
1.21 ± 0.34 ± 0.22		¹ SCHUMANN	05	BELL $e^+e^- \rightarrow \Upsilon(4S)$
• • • We do not use the following data for averages, fits, limits, etc. • • •				
1.3 ± 0.7 ± 0.2		^{1,2} AUBERT	04B	BABR Repl. by LEES 11M
<14	90	BRANDENB...	98	CLE2 $e^+e^- \rightarrow \Upsilon(4S)$
<19	90	³ NEMAT1	98	CLE2 $e^+e^- \rightarrow \Upsilon(4S)$
<27	90	⁴ ALAM	94	CLE2 Repl. by NEMAT1 98

- ¹ Assumes equal production of B^+ and B^0 at the $\Upsilon(4S)$.
² Reports an upper limit $< 2.6 \times 10^{-4}$ at 90% CL.
³ NEMAT1 98 assumes equal production of B^+ and B^0 at the $\Upsilon(4S)$ and use the PDG 96 values for D^0 , D^{*0} , η , η' , and ω branching fractions.
⁴ ALAM 94 assume equal production of B^+ and B^0 at the $\Upsilon(4S)$ and use the CLEOII $B(D^*(2007)^0 \rightarrow D^0 \pi^0)$ and absolute $B(D^0 \rightarrow K^- \pi^+)$ and the PDG 1992 $B(D^0 \rightarrow K^- \pi^+ \pi^0)/B(D^0 \rightarrow K^- \pi^+)$ and $B(D^0 \rightarrow K^- 2\pi^+ \pi^-)/B(D^0 \rightarrow K^- \pi^+)$.

 $\Gamma(\bar{D}^0 \eta')/\Gamma(\bar{D}^*(2007)^0 \eta')$ $\Gamma_{153}/\Gamma_{162}$

VALUE	DOCUMENT ID	TECN	COMMENT
0.96 ± 0.18 ± 0.06	LEES	11M	BABR $e^+e^- \rightarrow \Upsilon(4S)$
• • • We do not use the following data for averages, fits, limits, etc. • • •			
1.3 ± 0.8 ± 0.2	AUBERT	04B	BABR Repl. by LEES 11M

 $\Gamma(\bar{D}^*(2007)^0 \pi^+ \pi^-)/\Gamma_{\text{total}}$ Γ_{163}/Γ

VALUE	DOCUMENT ID	TECN	COMMENT
(6.2 ± 1.2 ± 1.8) × 10⁻⁴	^{1,2} SATPATHY	03	BELL $e^+e^- \rightarrow \Upsilon(4S)$

- ¹ Assumes equal production of B^+ and B^0 at the $\Upsilon(4S)$.
² No assumption about the intermediate mechanism is made in the analysis.

 $\Gamma(\bar{D}^*(2007)^0 K^0)/\Gamma_{\text{total}}$ Γ_{164}/Γ

VALUE (units 10^{-5})	CL%	DOCUMENT ID	TECN	COMMENT
3.6 ± 1.2 ± 0.3		¹ AUBERT,B	06L	BABR $e^+e^- \rightarrow \Upsilon(4S)$
• • • We do not use the following data for averages, fits, limits, etc. • • •				
<6.6	90	¹ KROKOVNY	03	BELL $e^+e^- \rightarrow \Upsilon(4S)$

- ¹ Assumes equal production of B^+ and B^0 at the $\Upsilon(4S)$.

 $\Gamma(\bar{D}^*(2007)^0 K^*(892)^0)/\Gamma_{\text{total}}$ Γ_{165}/Γ

VALUE	CL%	DOCUMENT ID	TECN	COMMENT
<6.9 × 10⁻⁵	90	¹ KROKOVNY	03	BELL $e^+e^- \rightarrow \Upsilon(4S)$

- ¹ Assumes equal production of B^+ and B^0 at the $\Upsilon(4S)$.

 $\Gamma(D^*(2007)^0 K^*(892)^0)/\Gamma_{\text{total}}$ Γ_{166}/Γ

VALUE	CL%	DOCUMENT ID	TECN	COMMENT
<4.0 × 10⁻⁵	90	¹ KROKOVNY	03	BELL $e^+e^- \rightarrow \Upsilon(4S)$

- ¹ Assumes equal production of B^+ and B^0 at the $\Upsilon(4S)$.

 $\Gamma(D^*(2007)^0 \pi^+ \pi^+ \pi^- \pi^-)/\Gamma_{\text{total}}$ Γ_{167}/Γ

VALUE (units 10^{-3})	DOCUMENT ID	TECN	COMMENT
2.7 ± 0.5 OUR AVERAGE			
2.60 ± 0.47 ± 0.37	¹ MAJUMDER	04	BELL $e^+e^- \rightarrow \Upsilon(4S)$
3.0 ± 0.7 ± 0.6	¹ EDWARDS	02	CLE2 $e^+e^- \rightarrow \Upsilon(4S)$

- ¹ Assumes equal production of B^+ and B^0 at the $\Upsilon(4S)$.

 $\Gamma(D^*(2007)^0 \pi^+ \pi^+ \pi^- \pi^-)/\Gamma(D^*(2010)^- \pi^+ \pi^+ \pi^- \pi^0)$ Γ_{167}/Γ_{63}

VALUE	DOCUMENT ID	TECN	COMMENT
0.17 ± 0.04 ± 0.02	¹ EDWARDS	02	CLE2 $e^+e^- \rightarrow \Upsilon(4S)$

- ¹ Assumes equal production of B^+ and B^0 at the $\Upsilon(4S)$.

 $\Gamma(D^*(2010)^+ D^*(2010)^-)/\Gamma_{\text{total}}$ Γ_{168}/Γ

VALUE (units 10^{-4})	CL%	DOCUMENT ID	TECN	COMMENT
8.0 ± 0.6 OUR AVERAGE				
7.82 ± 0.38 ± 0.63		¹ KRONENBIT...	12	BELL $e^+e^- \rightarrow \Upsilon(4S)$
8.1 ± 0.6 ± 1.0		¹ AUBERT,B	06A	BABR $e^+e^- \rightarrow \Upsilon(4S)$
9.9 ^{+4.2} _{-3.3} ± 1.2		¹ LIPELES	00	CLE2 $e^+e^- \rightarrow \Upsilon(4S)$
• • • We do not use the following data for averages, fits, limits, etc. • • •				
8.1 ± 0.8 ± 1.1		¹ MIYAKE	05	BELL Repl. by KRONENBIT-TER 12
8.3 ± 1.6 ± 1.2		^{1,2} AUBERT	02M	BABR Repl. by AUBERT,B 06B
6.2 ^{+4.0} _{-2.9} ± 1.0		³ ARTUSO	99	CLE2 Repl. by LIPELES 00
<61	90	⁴ BARATE	98Q	ALEP $e^+e^- \rightarrow Z$
<22	90	⁵ ASNER	97	CLE2 Repl. by ARTUSO 99

- ¹ Assumes equal production of B^+ and B^0 at the $\Upsilon(4S)$.
² AUBERT 02M also assumes the measured CP-odd fraction of the final states is $0.22 \pm 0.18 \pm 0.03$.
³ ARTUSO 99 uses $B(\Upsilon(4S) \rightarrow B^0 \bar{D}^0) = (48 \pm 4)\%$.
⁴ BARATE 98Q (ALEPH) observes 2 events with an expected background of 0.10 ± 0.03 which corresponds to a branching ratio of $(2.3 ^{+1.9} _{-1.2} ± 0.4) \times 10^{-3}$.
⁵ ASNER 97 at CLEO observes 1 event with an expected background of 0.022 ± 0.011 . This corresponds to a branching ratio of $(5.3 ^{+7.1} _{-3.7} ± 1.0) \times 10^{-4}$.

 $\Gamma(\bar{D}^*(2007)^0 \omega)/\Gamma_{\text{total}}$ Γ_{169}/Γ

VALUE (units 10^{-4})	CL%	DOCUMENT ID	TECN	COMMENT
3.6 ± 1.1 OUR AVERAGE				Error includes scale factor of 3.1.
4.55 ± 0.24 ± 0.39		¹ LEES	11M	BABR $e^+e^- \rightarrow \Upsilon(4S)$
2.29 ± 0.39 ± 0.40		¹ BLYTH	06	BELL $e^+e^- \rightarrow \Upsilon(4S)$
• • • We do not use the following data for averages, fits, limits, etc. • • •				
4.2 ± 0.7 ± 0.9	90	¹ AUBERT	04B	BABR Repl. by LEES 11M
< 7.9	90	¹ ABE	02J	BELL $e^+e^- \rightarrow \Upsilon(4S)$
< 7.4	90	² NEMAT1	98	CLE2 $e^+e^- \rightarrow \Upsilon(4S)$
<21	90	³ ALAM	94	CLE2 Repl. by NEMAT1 98

- ¹ Assumes equal production of B^+ and B^0 at the $\Upsilon(4S)$.
² NEMAT1 98 assumes equal production of B^+ and B^0 at the $\Upsilon(4S)$ and use the PDG 96 values for D^0 , D^{*0} , η , η' , and ω branching fractions.
³ ALAM 94 assume equal production of B^+ and B^0 at the $\Upsilon(4S)$ and use the CLEOII $B(D^*(2007)^0 \rightarrow D^0 \pi^0)$ and absolute $B(D^0 \rightarrow K^- \pi^+)$ and the PDG 1992 $B(D^0 \rightarrow K^- \pi^+ \pi^0)/B(D^0 \rightarrow K^- \pi^+)$ and $B(D^0 \rightarrow K^- 2\pi^+ \pi^-)/B(D^0 \rightarrow K^- \pi^+)$.

 $\Gamma(\bar{D}^0 \omega)/\Gamma(\bar{D}^*(2007)^0 \omega)$ $\Gamma_{154}/\Gamma_{169}$

VALUE	DOCUMENT ID	TECN	COMMENT
0.58 ± 0.06 OUR AVERAGE			
0.56 ± 0.04 ± 0.04	LEES	11M	BABR $e^+e^- \rightarrow \Upsilon(4S)$
1.04 ± 0.20 ± 0.17	BLYTH	06	BELL $e^+e^- \rightarrow \Upsilon(4S)$
• • • We do not use the following data for averages, fits, limits, etc. • • •			
0.7 ± 0.1 ± 0.1	AUBERT	04B	BABR Repl. by LEES 11M

 $\Gamma(D^*(2010)^+ D^-)/\Gamma_{\text{total}}$ Γ_{170}/Γ

VALUE (units 10^{-4})	CL%	DOCUMENT ID	TECN	COMMENT
6.1 ± 1.5 OUR AVERAGE				Error includes scale factor of 1.6.
5.7 ± 0.7 ± 0.7		¹ AUBERT,B	06A	BABR $e^+e^- \rightarrow \Upsilon(4S)$
11.7 ± 2.6 ^{+2.2} _{-2.5}		^{1,2} ABE	02Q	BELL $e^+e^- \rightarrow \Upsilon(4S)$
• • • We do not use the following data for averages, fits, limits, etc. • • •				
8.8 ± 1.0 ± 1.3		¹ AUBERT	03J	BABR Repl. by AUBERT,B 06B
14.8 ± 3.8 ^{+2.8} _{-3.1}		^{1,3} ABE	02Q	BELL $e^+e^- \rightarrow \Upsilon(4S)$
< 6.3	90	¹ LIPELES	00	CLE2 $e^+e^- \rightarrow \Upsilon(4S)$
<56	90	BARATE	98Q	ALEP $e^+e^- \rightarrow Z$
<18	90	ASNER	97	CLE2 $e^+e^- \rightarrow \Upsilon(4S)$

- ¹ Assumes equal production of B^+ and B^0 at the $\Upsilon(4S)$.
² The measurement is performed using fully reconstructed D^* and D^+ decays.
³ The measurement is performed using a partial reconstruction technique for the D^* and fully reconstructed D^+ decays as a cross check.

 $\Gamma(D^*(2007)^0 \bar{D}^*(2007)^0)/\Gamma_{\text{total}}$ Γ_{171}/Γ

VALUE (units 10^{-4})	CL%	DOCUMENT ID	TECN	COMMENT
< 0.9	90	¹ AUBERT,B	06A	BABR $e^+e^- \rightarrow \Upsilon(4S)$
• • • We do not use the following data for averages, fits, limits, etc. • • •				
<270	90	BARATE	98Q	ALEP $e^+e^- \rightarrow Z$

- ¹ Assumes equal production of B^+ and B^0 at the $\Upsilon(4S)$.

See key on page 999

Meson Particle Listings

B^0

$\Gamma(D^- D^0 K^+)/\Gamma_{total}$ Γ_{172}/Γ

VALUE (units 10^{-3})	DOCUMENT ID	TECN	COMMENT
1.07 ± 0.07 ± 0.09	¹ DEL-AMO-SA..11B	BABR	$e^+ e^- \rightarrow \Upsilon(4S)$
• • • We do not use the following data for averages, fits, limits, etc. • • •			
1.7 ± 0.3 ± 0.3	¹ AUBERT	03x BABR	Repl. by DEL-AMO-SANCHEZ 11B

¹ Assumes equal production of B^+ and B^0 at the $\Upsilon(4S)$.

$\Gamma(D^- D^*(2007)^0 K^+)/\Gamma_{total}$ Γ_{173}/Γ

VALUE (units 10^{-3})	DOCUMENT ID	TECN	COMMENT
3.46 ± 0.18 ± 0.37	¹ DEL-AMO-SA..11B	BABR	$e^+ e^- \rightarrow \Upsilon(4S)$
• • • We do not use the following data for averages, fits, limits, etc. • • •			
4.6 ± 0.7 ± 0.7	¹ AUBERT	03x BABR	Repl. by DEL-AMO-SANCHEZ 11B

¹ Assumes equal production of B^+ and B^0 at the $\Upsilon(4S)$.

$\Gamma(D^*(2010)^- D^0 K^+)/\Gamma_{total}$ Γ_{174}/Γ

VALUE (units 10^{-3})	DOCUMENT ID	TECN	COMMENT
2.47 ± 0.10 ± 0.18	¹ DEL-AMO-SA..11B	BABR	$e^+ e^- \rightarrow \Upsilon(4S)$
• • • We do not use the following data for averages, fits, limits, etc. • • •			
3.1 $^{+0.4}_{-0.3}$ ± 0.4	¹ AUBERT	03x BABR	Repl. by DEL-AMO-SANCHEZ 11B

¹ Assumes equal production of B^+ and B^0 at the $\Upsilon(4S)$.

$\Gamma(D^*(2010)^- D^*(2007)^0 K^+)/\Gamma_{total}$ Γ_{175}/Γ

VALUE (units 10^{-3})	DOCUMENT ID	TECN	COMMENT
10.6 ± 0.33 ± 0.86	¹ DEL-AMO-SA..11B	BABR	$e^+ e^- \rightarrow \Upsilon(4S)$
• • • We do not use the following data for averages, fits, limits, etc. • • •			
11.8 ± 1.0 ± 1.7	¹ AUBERT	03x BABR	Repl. by DEL-AMO-SANCHEZ 11B

¹ Assumes equal production of B^+ and B^0 at the $\Upsilon(4S)$.

$\Gamma(D^- D^+ K^0)/\Gamma_{total}$ Γ_{176}/Γ

VALUE (units 10^{-3})	CL%	DOCUMENT ID	TECN	COMMENT
0.75 ± 0.12 ± 0.12		¹ DEL-AMO-SA..11B	BABR	$e^+ e^- \rightarrow \Upsilon(4S)$
• • • We do not use the following data for averages, fits, limits, etc. • • •				
<1.7	90	¹ AUBERT	03x BABR	Repl. by DEL-AMO-SANCHEZ 11B

¹ Assumes equal production of B^+ and B^0 at the $\Upsilon(4S)$.

$[\Gamma(D^*(2010)^- D^+ K^0) + \Gamma(D^- D^*(2010)^+ K^0)]/\Gamma_{total}$ Γ_{177}/Γ

VALUE (units 10^{-3})	DOCUMENT ID	TECN	COMMENT
6.41 ± 0.36 ± 0.39	¹ DEL-AMO-SA..11B	BABR	$e^+ e^- \rightarrow \Upsilon(4S)$
• • • We do not use the following data for averages, fits, limits, etc. • • •			
6.5 ± 1.2 ± 1.0	¹ AUBERT	03x BABR	Repl. by DEL-AMO-SANCHEZ 11B

¹ Assumes equal production of B^+ and B^0 at the $\Upsilon(4S)$.

$\Gamma(D^*(2010)^- D^*(2010)^+ K^0)/\Gamma_{total}$ Γ_{178}/Γ

VALUE (units 10^{-3})	DOCUMENT ID	TECN	COMMENT
8.1 ± 0.7 OUR AVERAGE			
8.26 ± 0.43 ± 0.67	¹ DEL-AMO-SA..11B	BABR	$e^+ e^- \rightarrow \Upsilon(4S)$
6.8 ± 0.8 ± 1.4	^{1,2} DALSENO	07 BELL	$e^+ e^- \rightarrow \Upsilon(4S)$
8.8 ± 0.8 ± 1.4	^{1,2} AUBERT,B	06Q BABR	$e^+ e^- \rightarrow \Upsilon(4S)$
• • • We do not use the following data for averages, fits, limits, etc. • • •			
8.8 $^{+1.5}_{-1.4}$ ± 1.3	¹ AUBERT	03x BABR	Repl. by AUBERT,B 06Q

¹ Assumes equal production of B^+ and B^0 at the $\Upsilon(4S)$.

² The result is rescaled by a factor of 2 to convert from K_S^0 to K^0 .

$\Gamma(D^{*-} D_{s1}(2536)^+, D_{s1}^+ \rightarrow D^{*+} K^0)/\Gamma_{total}$ Γ_{179}/Γ

VALUE (units 10^{-4})	DOCUMENT ID	TECN	COMMENT
8.0 ± 2.4 OUR AVERAGE			
7.6 $^{+4.8}_{-4.2}$ ± 1.4	^{1,2} DALSENO	07 BELL	$e^+ e^- \rightarrow \Upsilon(4S)$
8.2 ± 2.6 ± 1.2	^{1,2} AUBERT,B	06Q BABR	$e^+ e^- \rightarrow \Upsilon(4S)$

¹ Assumes equal production of B^+ and B^0 at the $\Upsilon(4S)$.

² The result is rescaled by a factor of 2 to convert from K_S^0 to K^0 .

$\Gamma(D^0 D^0 K^0)/\Gamma_{total}$ Γ_{180}/Γ

VALUE (units 10^{-3})	CL%	DOCUMENT ID	TECN	COMMENT
0.27 ± 0.10 ± 0.05		¹ DEL-AMO-SA..11B	BABR	$e^+ e^- \rightarrow \Upsilon(4S)$
• • • We do not use the following data for averages, fits, limits, etc. • • •				
<1.4	90	¹ AUBERT	03x BABR	Repl. by DEL-AMO-SANCHEZ 11B

¹ Assumes equal production of B^+ and B^0 at the $\Upsilon(4S)$.

$[\Gamma(\bar{D}^0 D^*(2007)^0 K^0) + \Gamma(\bar{D}^*(2007)^0 D^0 K^0)]/\Gamma_{total}$ Γ_{181}/Γ

VALUE (units 10^{-3})	CL%	DOCUMENT ID	TECN	COMMENT
1.08 ± 0.32 ± 0.36		¹ DEL-AMO-SA..11B	BABR	$e^+ e^- \rightarrow \Upsilon(4S)$
• • • We do not use the following data for averages, fits, limits, etc. • • •				
<3.7	90	¹ AUBERT	03x BABR	Repl. by DEL-AMO-SANCHEZ 11B

¹ Assumes equal production of B^+ and B^0 at the $\Upsilon(4S)$.

$\Gamma(\bar{D}^*(2007)^0 D^*(2007)^0 K^0)/\Gamma_{total}$ Γ_{182}/Γ

VALUE (units 10^{-3})	CL%	DOCUMENT ID	TECN	COMMENT
2.40 ± 0.55 ± 0.67		¹ DEL-AMO-SA..11B	BABR	$e^+ e^- \rightarrow \Upsilon(4S)$
• • • We do not use the following data for averages, fits, limits, etc. • • •				
<6.6	90	¹ AUBERT	03x BABR	Repl. by DEL-AMO-SANCHEZ 11B

¹ Assumes equal production of B^+ and B^0 at the $\Upsilon(4S)$.

$\Gamma((\bar{D}^+ \bar{D}^*)(D^+ D^*) K)/\Gamma_{total}$ Γ_{183}/Γ

VALUE (units 10^{-2})	DOCUMENT ID	TECN	COMMENT
3.68 ± 0.10 ± 0.24	¹ DEL-AMO-SA..11B	BABR	$e^+ e^- \rightarrow \Upsilon(4S)$
• • • We do not use the following data for averages, fits, limits, etc. • • •			
4.3 ± 0.3 ± 0.6	¹ AUBERT	03x BABR	Repl. by DEL-AMO-SANCHEZ 11B

¹ Assumes equal production of B^+ and B^0 at the $\Upsilon(4S)$.

$\Gamma(\eta_c K^0)/\Gamma_{total}$ Γ_{184}/Γ

VALUE (units 10^{-3})	DOCUMENT ID	TECN	COMMENT
0.80 ± 0.11 OUR AVERAGE			
0.71 $^{+0.12}_{-0.10}$ ± 0.24	¹ CHILIKIN	19 BELL	$e^+ e^- \rightarrow \Upsilon(4S)$
0.57 $^{+0.20}_{-0.18}$ ± 0.05	^{2,3} AUBERT	07AV BABR	$e^+ e^- \rightarrow \Upsilon(4S)$
0.89 ± 0.15 ± 0.05	^{2,4} AUBERT,B	04B BABR	$e^+ e^- \rightarrow \Upsilon(4S)$
1.23 ± 0.23 $^{+0.40}_{-0.41}$	² FANG	03 BELL	$e^+ e^- \rightarrow \Upsilon(4S)$
1.09 $^{+0.55}_{-0.42}$ ± 0.33	⁵ EDWARDS	01 CLE2	$e^+ e^- \rightarrow \Upsilon(4S)$

¹ CHILIKIN 19 reports $[\Gamma(B^0 \rightarrow \eta_c K^0)/\Gamma_{total}] \times [B(\eta_c(1S) \rightarrow \pi^+ \pi^- p\bar{p})] = (38.0^{+6.4+1.3}_{-2.9-4.7}) \times 10^{-7}$ which we divide by our best value $B(\eta_c(1S) \rightarrow \pi^+ \pi^- p\bar{p}) = (5.3 \pm 1.8) \times 10^{-3}$. Our first error is their experiment's error and our second error is the systematic error from using our best value.

² Assumes equal production of B^+ and B^0 at the $\Upsilon(4S)$.

³ AUBERT 07AV reports $[\Gamma(B^0 \rightarrow \eta_c K^0)/\Gamma_{total}] \times [B(\eta_c(1S) \rightarrow p\bar{p})] = (0.83^{+0.28}_{-0.26} \pm 0.05) \times 10^{-6}$ which we divide by our best value $B(\eta_c(1S) \rightarrow p\bar{p}) = (1.45 \pm 0.14) \times 10^{-3}$. Our first error is their experiment's error and our second error is the systematic error from using our best value.

⁴ AUBERT,B 04B reports $[\Gamma(B^0 \rightarrow \eta_c K^0)/\Gamma_{total}] \times [B(\eta_c(1S) \rightarrow K\bar{K}\pi)] = (0.0648 \pm 0.0085 \pm 0.0071) \times 10^{-3}$ which we divide by our best value $B(\eta_c(1S) \rightarrow K\bar{K}\pi) = (7.3 \pm 0.4) \times 10^{-2}$. Our first error is their experiment's error and our second error is the systematic error from using our best value.

⁵ EDWARDS 01 assumes equal production of B^0 and B^+ at the $\Upsilon(4S)$. The correlated uncertainties (28.3)% from $B(J/\psi(1S) \rightarrow \gamma\eta_c)$ in those modes have been accounted for.

$\Gamma(\eta_c K^0)/\Gamma(J/\psi(1S) K^0)$ $\Gamma_{184}/\Gamma_{198}$

VALUE	DOCUMENT ID	TECN	COMMENT
1.39 ± 0.20 ± 0.45	¹ AUBERT,B	04B BABR	$e^+ e^- \rightarrow \Upsilon(4S)$

¹ Uses BABAR measurement of $B(B^0 \rightarrow J/\psi K^0) = (8.5 \pm 0.5 \pm 0.6) \times 10^{-4}$.

$\Gamma(\eta_c(1S) K^+ \pi^-)/\Gamma(J/\psi(1S) K^+ \pi^-)$ $\Gamma_{185}/\Gamma_{199}$

VALUE	DOCUMENT ID	TECN	COMMENT
0.52 ± 0.02 ± 0.05	¹ AAIJ	18AN LHCB	pp at 7, 8, 13 TeV

¹ AAIJ 18AN reports $[\Gamma(B^0 \rightarrow \eta_c(1S) K^+ \pi^-)/\Gamma(B^0 \rightarrow J/\psi(1S) K^+ \pi^-)] \times [B(\eta_c(1S) \rightarrow p\bar{p})] / [B(J/\psi(1S) \rightarrow p\bar{p})] = 0.357 \pm 0.015 \pm 0.008$ which we multiply or divide by our best values $B(\eta_c(1S) \rightarrow p\bar{p}) = (1.45 \pm 0.14) \times 10^{-3}$, $B(J/\psi(1S) \rightarrow p\bar{p}) = (2.121 \pm 0.029) \times 10^{-3}$. Our first error is their experiment's error and our second error is the systematic error from using our best values.

$\Gamma(\eta_c(1S) K^*(1410)^0)/\Gamma(\eta_c(1S) K^+ \pi^-)$ $\Gamma_{188}/\Gamma_{185}$

VALUE (units 10^{-2})	DOCUMENT ID	TECN	COMMENT
32 ± 24 ± 6	¹ AAIJ	18AN LHCB	pp at 7, 8, 13 TeV

¹ AAIJ 18AN reports $[\Gamma(B^0 \rightarrow \eta_c(1S) K^*(1410)^0)/\Gamma(B^0 \rightarrow \eta_c(1S) K^+ \pi^-)] \times [B(K^*(1410) \rightarrow K\pi)] = 0.021 \pm 0.011 \pm 0.011$ which we divide by our best value $B(K^*(1410) \rightarrow K\pi) = (6.6 \pm 1.3) \times 10^{-2}$. Our first error is their experiment's error and our second error is the systematic error from using our best value.

$\Gamma(\eta_c(1S) K^+ \pi^- (NR))/\Gamma(\eta_c(1S) K^+ \pi^-)$ $\Gamma_{186}/\Gamma_{185}$

VALUE (units 10^{-2})	DOCUMENT ID	TECN	COMMENT
10.3 ± 1.4 $^{+1.0}_{-1.2}$	AAIJ	18AN LHCB	pp at 7, 8, 13 TeV

Meson Particle Listings

 B^0 $\Gamma(\eta_c(1S)K_0^*(1430)^0)/\Gamma(\eta_c(1S)K^+\pi^-)$ $\Gamma_{189}/\Gamma_{185}$

VALUE (units 10^{-2})	DOCUMENT ID	TECN	COMMENT
$27 \pm 5 \pm 3$	¹ AAIJ	18AN LHCB	pp at 7, 8, 13 TeV

¹AAIJ 18AN reports $[\Gamma(B^0 \rightarrow \eta_c(1S)K_0^*(1430)^0)/\Gamma(B^0 \rightarrow \eta_c(1S)K^+\pi^-)] \times [B(K_0^*(1430) \rightarrow K\pi)] = 0.253 \pm 0.035_{-0.028}^{+0.035}$ which we divide by our best value $B(K_0^*(1430) \rightarrow K\pi) = (93 \pm 10) \times 10^{-2}$. Our first error is their experiment's error and our second error is the systematic error from using our best value.

 $\Gamma(\eta_c(1S)K_2^*(1430)^0)/\Gamma(\eta_c(1S)K^+\pi^-)$ $\Gamma_{190}/\Gamma_{185}$

VALUE (units 10^{-2})	DOCUMENT ID	TECN	COMMENT
$8.2 \pm 3.6_{-4.4} \pm 0.2$	¹ AAIJ	18AN LHCB	pp at 7, 8, 13 TeV

¹AAIJ 18AN reports $[\Gamma(B^0 \rightarrow \eta_c(1S)K_2^*(1430)^0)/\Gamma(B^0 \rightarrow \eta_c(1S)K^+\pi^-)] \times [B(K_2^*(1430) \rightarrow K\pi)] = 0.041 \pm 0.015_{-0.016}^{+0.010}$ which we divide by our best value $B(K_2^*(1430) \rightarrow K\pi) = (49.9 \pm 2.5) \times 10^{-2}$. Our first error is their experiment's error and our second error is the systematic error from using our best value.

 $\Gamma(\eta_c(1S)K^*(1680)^0)/\Gamma(\eta_c(1S)K^+\pi^-)$ $\Gamma_{191}/\Gamma_{185}$

VALUE (units 10^{-2})	DOCUMENT ID	TECN	COMMENT
$5.7 \pm 6.5_{-6.8} \pm 0.4$	¹ AAIJ	18AN LHCB	pp at 7, 8, 13 TeV

¹AAIJ 18AN reports $[\Gamma(B^0 \rightarrow \eta_c(1S)K^*(1680)^0)/\Gamma(B^0 \rightarrow \eta_c(1S)K^+\pi^-)] \times [B(K^*(1680) \rightarrow K\pi)] = 0.022 \pm 0.020_{-0.017}^{+0.015}$ which we divide by our best value $B(K^*(1680) \rightarrow K\pi) = (38.7 \pm 2.5) \times 10^{-2}$. Our first error is their experiment's error and our second error is the systematic error from using our best value.

 $\Gamma(\eta_c(1S)K_0^*(1950)^0)/\Gamma(\eta_c(1S)K^+\pi^-)$ $\Gamma_{192}/\Gamma_{185}$

VALUE (units 10^{-2})	DOCUMENT ID	TECN	COMMENT
$7 \pm 4 \pm 2$	¹ AAIJ	18AN LHCB	pp at 7, 8, 13 TeV

¹AAIJ 18AN reports $[\Gamma(B^0 \rightarrow \eta_c(1S)K_0^*(1950)^0)/\Gamma(B^0 \rightarrow \eta_c(1S)K^+\pi^-)] \times [B(K_0^*(1950) \rightarrow K^-\pi^+)] = 0.038 \pm 0.018_{-0.025}^{+0.014}$ which we divide by our best value $B(K_0^*(1950) \rightarrow K^-\pi^+) = (52 \pm 14) \times 10^{-2}$. Our first error is their experiment's error and our second error is the systematic error from using our best value.

 $\Gamma(X(4100)^-K^+, X^- \rightarrow \eta_c\pi^-)/\Gamma(\eta_c(1S)K^+\pi^-)$ $\Gamma_{187}/\Gamma_{185}$

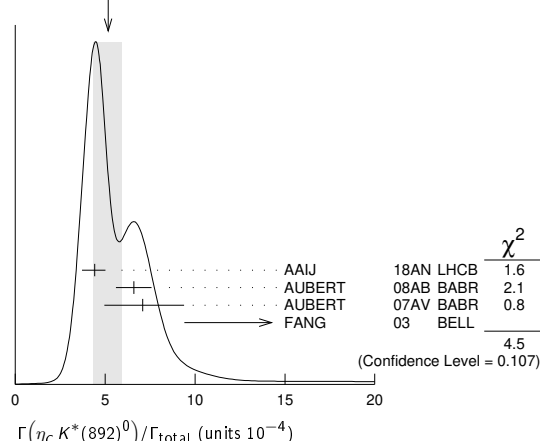
VALUE (units 10^{-2})	DOCUMENT ID	TECN	COMMENT
$3.3 \pm 1.1 \pm 1.2_{-1.1}$	AAIJ	18AN LHCB	pp at 7, 8, 13 TeV

 $\Gamma(\eta_c K^*(892)^0)/\Gamma_{total}$ Γ_{193}/Γ

VALUE (units 10^{-4})	DOCUMENT ID	TECN	COMMENT
$5.2 \pm 0.7_{-0.8}$ OUR AVERAGE	Error includes scale factor of 1.5. See the ideogram below.		

$4.42 \pm 0.24_{-0.66}^{+0.54}$	¹ AAIJ	18AN LHCB	pp at 7, 8, 13 TeV
$6.6 \pm 0.8 \pm 0.5$	^{2,3} AUBERT	08AB BABR	$e^+e^- \rightarrow \Upsilon(4S)$
$7.1 \pm 2.2_{-2.0} \pm 0.7$	^{4,5} AUBERT	07AV BABR	$e^+e^- \rightarrow \Upsilon(4S)$
$16.2 \pm 3.2 \pm 5.5_{-6.0}$	⁵ FANG	03 BELL	$e^+e^- \rightarrow \Upsilon(4S)$

WEIGHTED AVERAGE
 $5.2 \pm 0.7 - 0.8$ (Error scaled by 1.5)



¹AAIJ 18AN reports $B(B^0 \rightarrow \eta_c K^*(892)^0, K^*(892)^0 \rightarrow K^+\pi^-) = (2.95 \pm 0.16_{-0.44}^{+0.36}) \times 10^{-4}$ using the fitted fraction of $0.514 \pm 0.019_{-0.048}^{+0.017}$ from Dalitz decay of $B(B^0 \rightarrow \eta_c K^+\pi^-) = (5.73 \pm 0.24 \pm 0.67) \times 10^{-4}$ and corrected for $B(K^*(892)^0 \rightarrow K^+\pi^-) = 2/3$.

²AUBERT 08AB reports $[\Gamma(B^0 \rightarrow \eta_c K^*(892)^0)/\Gamma_{total}] / [B(B^+ \rightarrow \eta_c K^+)] = 0.62 \pm 0.06 \pm 0.05$ which we multiply by our best value $B(B^+ \rightarrow \eta_c K^+) = (1.06 \pm 0.09) \times 10^{-3}$. Our first error is their experiment's error and our second error is the systematic error from using our best value.

³Uses the production ratio of $(B^+ B^-)/(B^0 \bar{B}^0) = 1.026 \pm 0.032$ at $\Upsilon(4S)$.

⁴AUBERT 07AV reports $[\Gamma(B^0 \rightarrow \eta_c K^*(892)^0)/\Gamma_{total}] \times [B(\eta_c(1S) \rightarrow p\bar{p})] = (1.03 \pm 0.27_{-0.24} \pm 0.17) \times 10^{-6}$ which we divide by our best value $B(\eta_c(1S) \rightarrow p\bar{p}) = (1.45 \pm 0.14) \times 10^{-3}$. Our first error is their experiment's error and our second error is the systematic error from using our best value.

⁵Assumes equal production of B^+ and B^0 at the $\Upsilon(4S)$.

 $\Gamma(\eta_c(2S)K_S^0, \eta_c \rightarrow p\bar{p}\pi^+\pi^-)/\Gamma_{total}$ Γ_{194}/Γ

VALUE (units 10^{-7})	DOCUMENT ID	TECN	COMMENT
$4.2 \pm 1.4 \pm 0.3_{-1.2} \pm 0.3$	CHILIKIN	19 BELL	$e^+e^- \rightarrow \Upsilon(4S)$

 $\Gamma(\eta_c(2S)K^{*0})/\Gamma_{total}$ Γ_{195}/Γ

VALUE (units 10^{-4})	CL%	DOCUMENT ID	TECN	COMMENT
<3.9	90	¹ AUBERT	08AB BABR	$e^+e^- \rightarrow \Upsilon(4S)$

¹Uses the production ratio of $(B^+ B^-)/(B^0 \bar{B}^0) = 1.026 \pm 0.032$ at $\Upsilon(4S)$.

 $\Gamma(h_c(1P)K_S^0)/\Gamma_{total}$ Γ_{196}/Γ

VALUE	DOCUMENT ID	TECN	COMMENT
$<1.4 \times 10^{-5}$	CHILIKIN	19 BELL	$e^+e^- \rightarrow \Upsilon(4S)$

 $\Gamma(B^0 \rightarrow h_c(1P)K^{*0})/\Gamma_{total} \times \Gamma(h_c(1P) \rightarrow \gamma\eta_c(1S))/\Gamma_{total}$ $\Gamma_{197}/\Gamma \times \Gamma_{12}^{h_c(1P)}/\Gamma_{h_c(1P)}$

VALUE (units 10^{-4})	CL%	DOCUMENT ID	TECN	COMMENT
<2.2	90	¹ AUBERT	08AB BABR	$e^+e^- \rightarrow \Upsilon(4S)$

¹Uses the production ratio of $(B^+ B^-)/(B^0 \bar{B}^0) = 1.026 \pm 0.032$ at $\Upsilon(4S)$.

 $\Gamma(\eta_c K^*(892)^0)/\Gamma(\eta_c K^0)$ $\Gamma_{193}/\Gamma_{184}$

VALUE	DOCUMENT ID	TECN	COMMENT
$1.33 \pm 0.36 \pm 0.24_{-0.33}$	FANG	03 BELL	$e^+e^- \rightarrow \Upsilon(4S)$

 $\Gamma(J/\psi(1S)K^0)/\Gamma_{total}$ Γ_{198}/Γ

VALUE (units 10^{-4})	CL%	EVTS	DOCUMENT ID	TECN	COMMENT
8.68 ± 0.30 OUR FIT					
8.67 ± 0.30 OUR AVERAGE					

$8.1 \pm 0.9 \pm 0.6$	¹ CHILIKIN	19 BELL	$e^+e^- \rightarrow \Upsilon(4S)$
$8.8 \pm 1.4_{-1.3} \pm 0.1$	^{2,3} AUBERT	07AV BABR	$e^+e^- \rightarrow \Upsilon(4S)$
$8.69 \pm 0.22 \pm 0.30$	³ AUBERT	05J BABR	$e^+e^- \rightarrow \Upsilon(4S)$
$7.9 \pm 0.4 \pm 0.9$	³ ABE	03B BELL	$e^+e^- \rightarrow \Upsilon(4S)$
$9.5 \pm 0.8 \pm 0.6$	³ AVERY	00 CLE2	$e^+e^- \rightarrow \Upsilon(4S)$
$11.5 \pm 2.3 \pm 1.7$	⁴ ABE	96H CDF	$p\bar{p}$ at 1.8 TeV
$6.93 \pm 4.07 \pm 0.04$	⁵ BORTOLETTO	92 CLEO	$e^+e^- \rightarrow \Upsilon(4S)$
$9.24 \pm 7.21 \pm 0.05$	² ALBRECHT	90J ARG	$e^+e^- \rightarrow \Upsilon(4S)$

••• We do not use the following data for averages, fits, limits, etc. •••

$8.3 \pm 0.4 \pm 0.5$	³ AUBERT	02 BABR	Repl. by AUBERT 05J
$8.5 \pm 1.4_{-1.2} \pm 0.6$	³ JESSOP	97 CLE2	Repl. by AVERY 00
$7.5 \pm 2.4 \pm 0.8$	⁵ ALAM	94 CLE2	Sup. by JESSOP 97
<50	90	ALAM	86 CLEO $e^+e^- \rightarrow \Upsilon(4S)$

¹CHILIKIN 19 reports $[\Gamma(B^0 \rightarrow J/\psi(1S)K^0)/\Gamma_{total}] \times [B(J/\psi(1S) \rightarrow p\bar{p}\pi^+\pi^-)] = (48.6 \pm 4.6 \pm 2.4_{-4.4} \pm 2.6) \times 10^{-7}$ which we divide by our best value $B(J/\psi(1S) \rightarrow p\bar{p}\pi^+\pi^-) = (6.0 \pm 0.5) \times 10^{-3}$. Our first error is their experiment's error and our second error is the systematic error from using our best value.

²AUBERT 07AV reports $[\Gamma(B^0 \rightarrow J/\psi(1S)K^0)/\Gamma_{total}] \times [B(J/\psi(1S) \rightarrow p\bar{p})] = (1.87 \pm 0.28_{-0.26} \pm 0.07) \times 10^{-6}$ which we divide by our best value $B(J/\psi(1S) \rightarrow p\bar{p}) = (2.121 \pm 0.029) \times 10^{-3}$. Our first error is their experiment's error and our second error is the systematic error from using our best value.

³Assumes equal production of B^+ and B^0 at the $\Upsilon(4S)$.

⁴ABE 96H assumes that $B(B^+ \rightarrow J/\psi K^+) = (1.02 \pm 0.14) \times 10^{-3}$.

⁵BORTOLETTO 92 reports $(6 \pm 3 \pm 2) \times 10^{-4}$ from a measurement of $[\Gamma(B^0 \rightarrow J/\psi(1S)K^0)/\Gamma_{total}] \times [B(J/\psi(1S) \rightarrow e^+e^-)]$ assuming $B(J/\psi(1S) \rightarrow e^+e^-) = 0.069 \pm 0.009$, which we rescale to our best value $B(J/\psi(1S) \rightarrow e^+e^-) = (5.971 \pm 0.032) \times 10^{-2}$. Our first error is their experiment's error and our second error is the systematic error from using our best value. Assumes equal production of B^+ and B^0 at the $\Upsilon(4S)$.

⁶ALBRECHT 90J reports $(8 \pm 6 \pm 2) \times 10^{-4}$ from a measurement of $[\Gamma(B^0 \rightarrow J/\psi(1S)K^0)/\Gamma_{total}] \times [B(J/\psi(1S) \rightarrow e^+e^-)]$ assuming $B(J/\psi(1S) \rightarrow e^+e^-) = 0.069 \pm 0.009$, which we rescale to our best value $B(J/\psi(1S) \rightarrow e^+e^-) = (5.971 \pm 0.032) \times 10^{-2}$. Our first error is their experiment's error and our second error is the systematic error from using our best value. Assumes equal production of B^+ and B^0 at the $\Upsilon(4S)$.

Γ(J/ψ(1S)K⁺π⁻)/Γ_{total} Γ₁₉₉/Γ

Table with columns: VALUE (units 10^-3), CL%, DOCUMENT ID, TECN, COMMENT. Includes OUR AVERAGE and data from CHILIKIN, BORTOLETTO92, AUBERT, ALBRECHT, GILES.

BORTOLETTO 92 reports (1.0 ± 0.4 ± 0.3) × 10^-3 from a measurement of [Γ(B^0 → J/ψ(1S)K^+π^-)/Γ_{total}] × [B(J/ψ(1S) → e^+e^-)] assuming B(J/ψ(1S) → e^+e^-) = 0.069 ± 0.009...

Does not report systematic uncertainties. ALBRECHT 87D assume B^+B^-/B^0B^0 ratio is 55/45. Kπ system is specifically selected as nonresonant.

Γ(J/ψ(1S)K*(892)^0)/Γ_{total} Γ₂₀₀/Γ

Table with columns: VALUE (units 10^-3), EVTS, DOCUMENT ID, TECN, COMMENT. Includes OUR AVERAGE and data from CHILIKIN, AUBERT, ABE, JESSOP, BORTOLETTO92, ALBRECHT, BEBEK.

We do not use the following data for averages, fits, limits, etc.

Table with columns: VALUE (units 10^-3), EVTS, DOCUMENT ID, TECN, COMMENT. Includes data from AUBERT, ABE, ALAM, ALBRECHT, ALBAJAR, ALBRECHT, ALAM.

AUBERT 07AV reports [Γ(B^0 → J/ψ(1S)K*(892)^0)/Γ_{total}] × [B(J/ψ(1S) → pπ)] = (2.82^+0.30+0.36_-0.28-0.35) × 10^-6 which we divide by our best value B(J/ψ(1S) → pπ) = (2.121 ± 0.029) × 10^-3...

Assumes equal production of B^+ and B^0 at the T(4S).

ABE 98O reports [B(B^0 → J/ψ(1S)K*(892)^0)]/[B(B^+ → J/ψ(1S)K^+)] = 1.76 ± 0.14 ± 0.15. We multiply by our best value B(B^+ → J/ψ(1S)K^+) = (9.9 ± 1.0) × 10^-4. Our first error is their experiment's error and our second error is the systematic error from using our best value.

Assumes equal production of B^+ and B^0 at the T(4S).

BORTOLETTO 92 reports (1.1 ± 0.5 ± 0.3) × 10^-3 from a measurement of [Γ(B^0 → J/ψ(1S)K*(892)^0)/Γ_{total}] × [B(J/ψ(1S) → e^+e^-)] assuming B(J/ψ(1S) → e^+e^-) = 0.069 ± 0.009, which we rescale to our best value B(J/ψ(1S) → e^+e^-) = (5.971 ± 0.032) × 10^-2. Our first error is their experiment's error and our second error is the systematic error from using our best value. Assumes equal production of B^+ and B^0 at the T(4S).

ALBRECHT 90J reports (1.1 ± 0.5 ± 0.2) × 10^-3 from a measurement of [Γ(B^0 → J/ψ(1S)K*(892)^0)/Γ_{total}] × [B(J/ψ(1S) → e^+e^-)] assuming B(J/ψ(1S) → e^+e^-) = 0.069 ± 0.009, which we rescale to our best value B(J/ψ(1S) → e^+e^-) = (5.971 ± 0.032) × 10^-2. Our first error is their experiment's error and our second error is the systematic error from using our best value. Assumes equal production of B^+ and B^0 at the T(4S).

BEBEK 87 reports (3.5 ± 1.6 ± 0.3) × 10^-3 from a measurement of [Γ(B^0 → J/ψ(1S)K*(892)^0)/Γ_{total}] × [B(J/ψ(1S) → e^+e^-)] assuming B(J/ψ(1S) → e^+e^-) = 0.069 ± 0.009, which we rescale to our best value B(J/ψ(1S) → e^+e^-) = (5.971 ± 0.032) × 10^-2. Our first error is their experiment's error and our second error is the systematic error from using our best value. Updated in BORTOLETTO 92 to use the same assumptions.

ABE 96H assumes that B(B^+ → J/ψK^+) = (1.02 ± 0.14) × 10^-3.

The neutral and charged B events together are predominantly longitudinally polarized. Γ_L/Γ = 0.080 ± 0.08 ± 0.05. This can be compared with a prediction using HQET, 0.73 (KRAMER 92). This polarization indicates that the B → ψK* decay is dominated by the CP = -1 CP eigenstate. Assumes equal production of B^+ and B^0 at the T(4S).

ALBRECHT 94G measures the polarization in the vector-vector decay to be predominantly longitudinal, Γ_T/Γ = 0.03 ± 0.16 ± 0.15 making the neutral decay a CP eigenstate when the K*0 decays through K_S^0π^0.

ALBAJAR 91E assumes B₀⁰ production fraction of 36%.

ALBRECHT 87D assume B^+B^-/B^0B^0 ratio is 55/45. Superseded by ALBRECHT 90J.

ALAM 86 assumes B±/B^0 ratio is 60/40. The observation of the decay B^+ → J/ψK*(892)^+ (HAAS 85) has been retracted in this paper.

Γ(J/ψ(1S)K*(892)^0)/Γ(J/ψ(1S)K^0) Γ₂₀₀/Γ₁₉₈

Table with columns: VALUE, DOCUMENT ID, TECN, COMMENT. Includes OUR AVERAGE and data from AUBERT, ABE.

We do not use the following data for averages, fits, limits, etc.

Γ(J/ψ(1S)ηK_S^0)/Γ_{total} Γ₂₀₁/Γ

Table with columns: VALUE (units 10^-5), DOCUMENT ID, TECN, COMMENT. Includes OUR AVERAGE and data from IWASHITA, AUBERT.

Γ(J/ψ(1S)η'K_S^0)/Γ_{total} Γ₂₀₂/Γ

Table with columns: VALUE (units 10^-5), CL%, DOCUMENT ID, TECN, COMMENT. Includes data from XIE.

Γ(J/ψ(1S)ωK^0)/Γ_{total} Γ₂₀₄/Γ

Table with columns: VALUE (units 10^-4), DOCUMENT ID, TECN, COMMENT. Includes OUR AVERAGE and data from DEL-AMO-SA., AUBERT.

We do not use the following data for averages, fits, limits, etc.

Γ(χ_{c1}(3872)K^0, χ_{c1} → J/ψω)/Γ_{total} Γ₂₀₅/Γ

Table with columns: VALUE (units 10^-6), DOCUMENT ID, TECN, COMMENT. Includes data from DEL-AMO-SA.

Γ(X(3915), X → J/ψω)/Γ_{total} Γ₂₀₆/Γ

Table with columns: VALUE (units 10^-5), DOCUMENT ID, TECN, COMMENT. Includes OUR AVERAGE and data from DEL-AMO-SA., AUBERT.

Γ(J/ψ(1S)φK^0)/Γ_{total} Γ₂₀₃/Γ

Table with columns: VALUE (units 10^-5), DOCUMENT ID, TECN, COMMENT. Includes OUR AVERAGE and data from LEES, AUBERT, ANASTASSOV.

Assumes equal production of B^+ and B^0 at the T(4S).

ANASTASSOV 00 finds 10 events on a background of 0.5 ± 0.2. Assumes equal production of B^0 and B^+ at the T(4S), a uniform Dalitz plot distribution, isotropic J/ψ(1S) and φ decays, and B(B^+ → J/ψ(1S)φK^+) = B(B^0 → J/ψ(1S)φK^0).

Γ(J/ψ(1S)K(1270)^0)/Γ_{total} Γ₂₀₇/Γ

Table with columns: VALUE (units 10^-3), DOCUMENT ID, TECN, COMMENT. Includes data from ABE.

Assumes equal production of B^+ and B^0 at the T(4S) and uses the PDG value of B(B^+ → J/ψ(1S)K^+) = (1.00 ± 0.10) × 10^-3.

Γ(J/ψ(1S)π^0)/Γ_{total} Γ₂₀₈/Γ

Table with columns: VALUE (units 10^-5), CL%, DOCUMENT ID, TECN, COMMENT. Includes OUR AVERAGE and data from PAL, AUBERT, AVERY.

We do not use the following data for averages, fits, limits, etc.

Table with columns: VALUE, DOCUMENT ID, TECN, COMMENT. Includes data from AUBERT, ABE, AUBERT, ACCIARRI, BISHAI, ALEXANDER.

Assumes equal production of B^+ and B^0 at the T(4S).

ACCIARRI 97c assumes B₀⁰ production fraction (39.5 ± 4.0)% and B_S (12.0 ± 3.0)%.

See key on page 999

Meson Particle Listings

B⁰

Table with 4 columns: VALUE, DOCUMENT ID, TECN, COMMENT. Row 1: Γ(ψ(2S) K*(892)0)/Γ(ψ(2S) K0) Γ257/Γ252. Row 2: 1.02±0.10 OUR FIT. Row 3: 1.00±0.14±0.09 AUBERT 05J BABR e+e- -> T(4S)

Table with 4 columns: VALUE (units 10^-6), CL%, DOCUMENT ID, TECN, COMMENT. Row 1: Γ(χc0 K0)/Γtotal Γ258/Γ. Row 2: 1.11 ± 0.20 / 0.16 ± 0.14. Row 3: 1 AAIJ 18F LHCB pp at 7, 8 TeV

• • • We do not use the following data for averages, fits, limits, etc. • • •

Table with 4 columns: VALUE, CL%, DOCUMENT ID, TECN, COMMENT. Rows 1-6: 145 +103 / -85 ± 8 2,3 LEES 12l BABR e+e- -> T(4S); 148 ± 30 ± 13 2,4 LEES 12o BABR e+e- -> T(4S); 142 +55 / -44 ± 22 2,5 AUBERT 09AU BABR e+e- -> T(4S); < 113 90 5 GARMASH 07 BELL e+e- -> T(4S); < 1240 90 2 AUBERT 05K BABR e+e- -> T(4S); < 500 90 6 EDWARDS 01 CLE2 e+e- -> T(4S)

1 Uses Dalitz plot analysis of the B0 -> KS0 pi+ pi- final state decays. For the branching fraction of the reference mode, the PDG 18 average B(B0 -> KS0 pi+ pi-) = (4.96 ± 0.20) x 10^-5 is used.

2 Assumes equal production of B+ and B0 at the T(4S).

3 LEES 12l reports [Γ(B0 -> χc0 K0)/Γtotal] x [B(χc0(1P) -> KS0 KS0)] = (0.46 +/- 0.25 +/- 0.21) x 10^-6 which we divide by our best value B(χc0(1P) -> KS0 KS0) = (3.16 ± 0.17) x 10^-3. Our first error is their experiment's error and our second error is the systematic error from using our best value.

4 Measured in the B0 -> KS0 K+ K- decay.

5 Uses Dalitz plot analysis of the B0 -> K0 pi+ pi- final state decays.

6 EDWARDS 01 assumes equal production of B0 and B+ at the T(4S). The correlated uncertainties (28.3)% from B(J/ψ(1S) -> η ηc) in those modes have been accounted for.

Table with 4 columns: VALUE (units 10^-4), CL%, DOCUMENT ID, TECN, COMMENT. Row 1: Γ(χc0 K*(892)0)/Γtotal Γ259/Γ. Row 2: 1.7 ± 0.3 ± 0.2. Row 3: 1 AUBERT 08BD BABR e+e- -> T(4S). Row 4: < 7.7 90 1 AUBERT 05K BABR Repl. by AUBERT 08BD. Row 5: 1 Assumes equal production of B+ and B0 at the T(4S).

Table with 4 columns: VALUE (units 10^-5), DOCUMENT ID, TECN, COMMENT. Row 1: Γ(χc1 π0)/Γtotal Γ260/Γ. Row 2: 1.12 ± 0.25 ± 0.12. Row 3: 1 KUMAR 08 BELL e+e- -> T(4S). Row 4: 1 Assumes equal production of B+ and B0 at the T(4S).

Table with 4 columns: VALUE (units 10^-4), CL%, DOCUMENT ID, TECN, COMMENT. Row 1: Γ(χc1 K0)/Γtotal Γ261/Γ. Row 2: 3.95 ± 0.27 OUR AVERAGE. Row 3: 15 +5 / -4 ± 6 1 CHILIKIN 19 BELL e+e- -> T(4S); 3.78 +0.17 / -0.16 ± 0.33 2 BHARDWAJ 11 BELL e+e- -> T(4S); 4.2 ± 0.3 ± 0.3 3 AUBERT 09B BABR e+e- -> T(4S); 3.1 +1.5 / -1.1 ± 0.1 4 AVERY 00 CLE2 e+e- -> T(4S); 3.51 ± 0.33 ± 0.45 2 SONI 06 BELL Repl. by BHARDWAJ 11; 4.53 ± 0.41 ± 0.51 2 AUBERT 05J BABR Repl. by AUBERT 09B; 4.3 ± 1.4 ± 0.1 5 AUBERT 02 BABR Repl. by AUBERT 05J; < 27 90 2 ALAM 94 CLE2 e+e- -> T(4S)

1 CHILIKIN 19 reports [Γ(B0 -> χc1 K0)/Γtotal] x [B(χc1(1P) -> p p-bar π+ π-)] = (7.4 +/- 2.4 +/- 0.6 +/- 0.4) x 10^-7 which we divide by our best value B(χc1(1P) -> p p-bar π+ π-) = (5.0 ± 1.9) x 10^-4. Our first error is their experiment's error and our second error is the systematic error from using our best value.

2 Assumes equal production of B+ and B0 at the T(4S).

3 Uses χc1,2 -> J/ψ γ. Assumes B(T(4S) -> B+ B-) = (51.6 ± 0.6)% and B(T(4S) -> B0 B-bar) = (48.4 ± 0.6)%.

4 AVERY 00 reports (3.9 +/- 1.9 +/- 0.4) x 10^-4 from a measurement of [Γ(B0 -> χc1 K0)/Γtotal] x [B(χc1(1P) -> γ J/ψ(1S))] assuming B(χc1(1P) -> γ J/ψ(1S)) = 0.273 ± 0.016, which we rescale to our best value B(χc1(1P) -> γ J/ψ(1S)) = (34.3 ± 1.0) x 10^-2. Our first error is their experiment's error and our second error is the systematic error from using our best value. Assumes equal production of B+ and B0 at the T(4S).

5 AUBERT 02 reports (5.4 ± 1.4 ± 1.1) x 10^-4 from a measurement of [Γ(B0 -> χc1 K0)/Γtotal] x [B(χc1(1P) -> γ J/ψ(1S))] assuming B(χc1(1P) -> γ J/ψ(1S)) = 0.273 ± 0.016, which we rescale to our best value B(χc1(1P) -> γ J/ψ(1S)) = (34.3 ± 1.0) x 10^-2. Our first error is their experiment's error and our second error is the systematic error from using our best value. Assumes equal production of B+ and B0 at the T(4S).

Table with 4 columns: VALUE, DOCUMENT ID, TECN, COMMENT. Row 1: Γ(χc1 K0)/Γ(J/ψ(1S) K0) Γ261/Γ198. Row 2: 0.53 ± 0.16 ± 0.01. Row 3: 1 AUBERT 02 BABR e+e- -> T(4S)

1 AUBERT 02 reports 0.66 ± 0.11 ± 0.17 from a measurement of [Γ(B0 -> χc1 K0)/Γ(B0 -> J/ψ(1S) K0)] x [B(χc1(1P) -> γ J/ψ(1S))] assuming B(χc1(1P) -> γ J/ψ(1S)) = 0.273 ± 0.016, which we rescale to our best value B(χc1(1P) -> γ J/ψ(1S)) = (34.3 ± 1.0) x 10^-2. Our first error is their experiment's error and our second error is the systematic error from using our best value. Assumes equal production of B+ and B0 at the T(4S).

Table with 4 columns: VALUE (units 10^-4), DOCUMENT ID, TECN, COMMENT. Row 1: Γ(χc1 π- K+)/Γtotal Γ262/Γ. Row 2: 4.97 ± 0.12 ± 0.28. Row 3: 1 BHARDWAJ 16 BELL e+e- -> T(4S)

• • • We do not use the following data for averages, fits, limits, etc. • • •

3.83 ± 0.10 ± 0.39 1 MIZUK 08 BELL Repl. by BHARDWAJ 16

1 Assumes equal production of B+ and B0 at the T(4S).

Table with 4 columns: VALUE, DOCUMENT ID, TECN, COMMENT. Row 1: Γ(χc1 π- K+)/Γ(J/ψ(1S) K+ π-) Γ262/Γ199. Row 2: 0.476 ± 0.021 ± 0.013. Row 3: 1 LEES 12B BABR

1 LEES 12B reports 0.474 ± 0.013 ± 0.026 from a measurement of [Γ(B0 -> χc1 π- K+)/Γ(B0 -> J/ψ(1S) K+ π-)] x [B(χc1(1P) -> γ J/ψ(1S))] assuming B(χc1(1P) -> γ J/ψ(1S)) = (34.4 ± 1.5) x 10^-2, which we rescale to our best value B(χc1(1P) -> γ J/ψ(1S)) = (34.3 ± 1.0) x 10^-2. Our first error is their experiment's error and our second error is the systematic error from using our best value.

Table with 4 columns: VALUE (units 10^-4), CL%, DOCUMENT ID, TECN, COMMENT. Row 1: Γ(χc1 K*(892)0)/Γtotal Γ263/Γ. Row 2: 2.38 ± 0.19 OUR FIT Error includes scale factor of 1.2.

2.22 +0.40 / -0.31 OUR AVERAGE Error includes scale factor of 1.6.

2.5 ± 0.2 ± 0.2 1 AUBERT 09B BABR e+e- -> T(4S)

1.73 +0.15 +0.34 / -0.12 -0.22 2 MIZUK 08 BELL e+e- -> T(4S)

• • • We do not use the following data for averages, fits, limits, etc. • • •

3.14 ± 0.34 ± 0.72 2 SONI 06 BELL Repl. by MIZUK 08

3.27 ± 0.42 ± 0.64 2 AUBERT 05J BABR Repl. by AUBERT 09B

3.8 ± 1.3 ± 0.1 3 AUBERT 02 BABR Repl. by AUBERT 05J

< 21 90 4 ALAM 94 CLE2 e+e- -> T(4S)

1 Uses χc1,2 -> J/ψ γ. Assumes B(T(4S) -> B+ B-) = (51.6 ± 0.6)% and B(T(4S) -> B0 B-bar) = (48.4 ± 0.6)%.

2 Assumes equal production of B+ and B0 at the T(4S).

3 AUBERT 02 reports (4.8 ± 1.4 ± 0.9) x 10^-4 from a measurement of [Γ(B0 -> χc1 K*(892)0)/Γtotal] x [B(χc1(1P) -> γ J/ψ(1S))] assuming B(χc1(1P) -> γ J/ψ(1S)) = 0.273 ± 0.016, which we rescale to our best value B(χc1(1P) -> γ J/ψ(1S)) = (34.3 ± 1.0) x 10^-2. Our first error is their experiment's error and our second error is the systematic error from using our best value. Assumes equal production of B+ and B0 at the T(4S).

4 BORTOLETTO 92 assumes equal production of B+ and B0 at the T(4S).

Table with 4 columns: VALUE (units 10^-2), DOCUMENT ID, TECN, COMMENT. Row 1: Γ(χc1 K*(892)0)/Γ(J/ψ(1S) K*(892)0) Γ263/Γ200. Row 2: 18.8 ± 1.5 OUR FIT Error includes scale factor of 1.1.

19.8 ± 1.1 ± 1.5 1 AAIJ 13AC LHCB pp at 7 TeV

1 Uses B(χc1 -> J/ψ γ) = (34.4 ± 1.5)%.

Table with 4 columns: VALUE, DOCUMENT ID, TECN, COMMENT. Row 1: Γ(χc1 K*(892)0)/Γ(χc1 K0) Γ263/Γ261. Row 2: 0.72 ± 0.11 ± 0.12. Row 3: AUBERT 05J BABR e+e- -> T(4S)

• • • We do not use the following data for averages, fits, limits, etc. • • •

0.89 ± 0.34 ± 0.17 1 AUBERT 02 BABR Repl. by AUBERT 05J

1 Assumes equal production of B+ and B0 at the T(4S).

Table with 4 columns: VALUE (units 10^-5), CL%, DOCUMENT ID, TECN, COMMENT. Row 1: Γ(X(4051)- K+, X- -> χc1 π-)/Γtotal Γ264/Γ. Row 2: 3.0 +1.5 +3.7 / -0.8 -1.6. Row 3: 1 MIZUK 08 BELL e+e- -> T(4S)

• • • We do not use the following data for averages, fits, limits, etc. • • •

< 1.8 90 1,2 LEES 12B BABR

1 Assumes equal production of B+ and B0 at the T(4S).

2 Uses χc1 -> J/ψ γ mode. Uses χc1 -> J/ψ γ mode. Finds a good description of the data without this B0 -> X(4051)+ K- decay mode in a fit.

Table with 4 columns: VALUE (units 10^-5), CL%, DOCUMENT ID, TECN, COMMENT. Row 1: Γ(X(4248)- K+, X- -> χc1 π-)/Γtotal Γ265/Γ. Row 2: 4.0 +2.3 +19.7 / -0.9 -0.5. Row 3: 1 MIZUK 08 BELL e+e- -> T(4S)

• • • We do not use the following data for averages, fits, limits, etc. • • •

< 4.0 90 1,2 LEES 12B BABR

1 Assumes equal production of B+ and B0 at the T(4S).

2 Uses χc1 -> J/ψ γ mode. Finds a good description of the data without this B0 -> X(4248)+ K- decay mode in a fit.

Downloaded from https://academic.oup.com/ptep/article/2020/8/083C01/5891211 by guest on 20 August 2020

See key on page 999

Meson Particle Listings B⁰

Table with 4 columns: VALUE (units 10^-6), DOCUMENT ID, TECN, COMMENT. Section: Γ(η' K^0)/Γtotal Γ277/Γ. Includes OUR AVERAGE 66 ± 4 and various data points from AUBERT, SCHUEMANN, RICHIHI, etc.

Table with 4 columns: VALUE (units 10^-6), CL%, DOCUMENT ID, TECN, COMMENT. Section: Γ(η' K*(892)^0)/Γtotal Γ278/Γ. Includes OUR AVERAGE 2.8 ± 0.6 and various data points from SATO, DEL-AMO-SA..10A, AUBERT, etc.

Table with 4 columns: VALUE (units 10^-6), DOCUMENT ID, TECN, COMMENT. Section: Γ(η' K*(1430)^0)/Γtotal Γ279/Γ. Includes OUR AVERAGE 6.3 ± 1.3 ± 0.9 and data points from DEL-AMO-SA..10A.

Table with 4 columns: VALUE (units 10^-6), DOCUMENT ID, TECN, COMMENT. Section: Γ(η' K*(1430)^0)/Γtotal Γ280/Γ. Includes OUR AVERAGE 13.7 ± 3.0 ± 2.9 ± 1.2 and data points from DEL-AMO-SA..10A.

Table with 4 columns: VALUE (units 10^-6), CL%, DOCUMENT ID, TECN, COMMENT. Section: Γ(η K^0)/Γtotal Γ281/Γ. Includes OUR AVERAGE 1.23 ± 0.27 ± 0.24 and various data points from HOI, AUBERT, etc.

Table with 4 columns: VALUE (units 10^-6), CL%, DOCUMENT ID, TECN, COMMENT. Section: Γ(η K*(892)^0)/Γtotal Γ282/Γ. Includes OUR AVERAGE 15.9 ± 1.0 and various data points from WANG, AUBERT, RICHIHI, etc.

Table with 4 columns: VALUE (units 10^-6), DOCUMENT ID, TECN, COMMENT. Section: Γ(η K*(1430)^0)/Γtotal Γ283/Γ. Includes OUR AVERAGE 11.0 ± 1.6 ± 1.5 and data points from AUBERT, WANG.

Table with 4 columns: VALUE (units 10^-6), DOCUMENT ID, TECN, COMMENT. Section: Γ(η K*(1430)^0)/Γtotal Γ284/Γ. Includes OUR AVERAGE 9.6 ± 1.8 ± 1.1 and data points from AUBERT.

Table with 4 columns: VALUE (units 10^-6), CL%, DOCUMENT ID, TECN, COMMENT. Section: Γ(ω K^0)/Γtotal Γ285/Γ. Includes OUR AVERAGE 4.8 ± 0.4 and various data points from CHOBANOVA, AUBERT, JESSOP, etc.

Table with 4 columns: VALUE (units 10^-6), CL%, DOCUMENT ID, TECN, COMMENT. Section: Γ(a_0(980)^0 K^0, a_0^0 → ηπ^0)/Γtotal Γ286/Γ. Includes OUR AVERAGE <7.8 and data points from AUBERT, BE.

Table with 4 columns: VALUE (units 10^-6), CL%, DOCUMENT ID, TECN, COMMENT. Section: Γ(b_1^0 K^0, b_1^0 → ωπ^0)/Γtotal Γ287/Γ. Includes OUR AVERAGE <7.8 and data points from AUBERT.

Table with 4 columns: VALUE (units 10^-6), CL%, DOCUMENT ID, TECN, COMMENT. Section: Γ(a_0(980)^± K^±, a_0^± → ηπ^±)/Γtotal Γ288/Γ. Includes OUR AVERAGE <1.9 and data points from AUBERT.

Table with 4 columns: VALUE (units 10^-6), DOCUMENT ID, TECN, COMMENT. Section: Γ(b_1^- K^+, b_1^- → ωπ^-)/Γtotal Γ289/Γ. Includes OUR AVERAGE 7.4 ± 1.0 ± 1.0 and data points from AUBERT.

Table with 4 columns: VALUE (units 10^-6), CL%, DOCUMENT ID, TECN, COMMENT. Section: Γ(b_1^0 K^*0, b_1^0 → ωπ^0)/Γtotal Γ290/Γ. Includes OUR AVERAGE <8.0 x 10^-6 and data points from AUBERT.

Table with 4 columns: VALUE (units 10^-6), CL%, DOCUMENT ID, TECN, COMMENT. Section: Γ(b_1^- K^*+, b_1^- → ωπ^-)/Γtotal Γ291/Γ. Includes OUR AVERAGE <5.0 x 10^-6 and data points from AUBERT.

Table with 4 columns: VALUE (units 10^-6), CL%, DOCUMENT ID, TECN, COMMENT. Section: Γ(a_0(1450)^± K^±, a_0^± → ηπ^±)/Γtotal Γ292/Γ. Includes OUR AVERAGE <3.1 and data points from AUBERT.

Table with 4 columns: VALUE (units 10^-6), CL%, DOCUMENT ID, TECN, COMMENT. Section: Γ(K_S^0 X^0 (Familon))/Γtotal Γ293/Γ. Includes OUR AVERAGE <53 and data points from AMMAR.

Table with 4 columns: VALUE (units 10^-6), CL%, DOCUMENT ID, TECN, COMMENT. Section: Γ(ω K*(892)^0)/Γtotal Γ294/Γ. Includes OUR AVERAGE 2.0 ± 0.5 and various data points from AUBERT, GOLDENZWE..08, etc.

Table with 4 columns: VALUE (units 10^-6), DOCUMENT ID, TECN, COMMENT. Section: Γ(ω(Kπ)^0)/Γtotal Γ295/Γ. Includes OUR AVERAGE 18.4 ± 1.8 ± 1.7 and data points from AUBERT.

Downloaded from https://academic.oup.com/ptep/article/2020/8/083C01/5891211 by guest on 20 August 2020

Meson Particle Listings

B^0

$\Gamma(\omega K_0^*(1430)^0)/\Gamma_{total}$ Γ_{296}/Γ

VALUE (units 10^{-6})	DOCUMENT ID	TECN	COMMENT
16.0 ± 1.6 ± 3.0	1 AUBERT	09H BABR	$e^+e^- \rightarrow \Upsilon(4S)$

¹ Assumes equal production of B^+ and B^0 at the $\Upsilon(4S)$.

$\Gamma(\omega K_2^*(1430)^0)/\Gamma_{total}$ Γ_{297}/Γ

VALUE (units 10^{-6})	DOCUMENT ID	TECN	COMMENT
10.1 ± 2.0 ± 1.1	1 AUBERT	09H BABR	$e^+e^- \rightarrow \Upsilon(4S)$

¹ Assumes equal production of B^+ and B^0 at the $\Upsilon(4S)$.

$\Gamma(\omega K^+\pi^-\text{ nonresonant})/\Gamma_{total}$ Γ_{298}/Γ

VALUE (units 10^{-6})	DOCUMENT ID	TECN	COMMENT
5.1 ± 0.7 ± 0.7	1,2 GOLDENZWE..08	BELL	$e^+e^- \rightarrow \Upsilon(4S)$

¹ Assumes equal production of B^+ and B^0 at the $\Upsilon(4S)$.
² For the $K\pi$ mass range 0.755–1.250 GeV/ c^2 , excluding $K^*(892)$.

$\Gamma(K^+\pi^-\pi^0)/\Gamma_{total}$ Γ_{299}/Γ

VALUE (units 10^{-6})	CL%	DOCUMENT ID	TECN	COMMENT
37.8 ± 3.2 OUR AVERAGE				
38.5 ± 1.0 ± 3.9		1,2 LEES	11 BABR	$e^+e^- \rightarrow \Upsilon(4S)$
36.6 ^{+4.2} _{-4.3} ± 3.0		1 CHANG	04 BELL	$e^+e^- \rightarrow \Upsilon(4S)$

$\Gamma(K^+\rho^-)/\Gamma_{total}$ Γ_{300}/Γ

VALUE (units 10^{-6})	CL%	DOCUMENT ID	TECN	COMMENT
7.0 ± 0.9 OUR AVERAGE				
6.6 ± 0.5 ± 0.8		1,2 LEES	11 BABR	$e^+e^- \rightarrow \Upsilon(4S)$
15.1 ^{+3.4} _{-3.3} ± 2.4		1 CHANG	04 BELL	$e^+e^- \rightarrow \Upsilon(4S)$

$\Gamma(K^+\rho(1450)^-)/\Gamma_{total}$ Γ_{301}/Γ

VALUE (units 10^{-6})	CL%	DOCUMENT ID	TECN	COMMENT
2.4 ± 1.0 ± 0.6		1,2 LEES	11 BABR	$e^+e^- \rightarrow \Upsilon(4S)$
<2.1	90	1 AUBERT	08AQ BABR	Repl. by LEES 11

$\Gamma(K^+\rho(1700)^-)/\Gamma_{total}$ Γ_{302}/Γ

VALUE (units 10^{-6})	CL%	DOCUMENT ID	TECN	COMMENT
0.6 ± 0.6 ± 0.4		1,2 LEES	11 BABR	$e^+e^- \rightarrow \Upsilon(4S)$
<1.1	90	1 AUBERT	08AQ BABR	Repl. by LEES 11

$\Gamma((K^+\pi^-\pi^0)\text{ nonresonant})/\Gamma_{total}$ Γ_{303}/Γ

VALUE (units 10^{-6})	CL%	DOCUMENT ID	TECN	COMMENT
2.8 ± 0.5 ± 0.4		1,2 LEES	11 BABR	$e^+e^- \rightarrow \Upsilon(4S)$
4.4 ± 0.9 ± 0.5		1 AUBERT	08AQ BABR	Repl. by LEES 11
<9.4	90	1 CHANG	04 BELL	$e^+e^- \rightarrow \Upsilon(4S)$

$\Gamma((K\pi)_0^{*+}\pi^-, (K\pi)_0^{*+} \rightarrow K^+\pi^0)/\Gamma_{total}$ Γ_{304}/Γ

($K\pi)_0^{*+}$ is the total S-wave composed of $K_0^*(1430)$ and nonresonant that are described using LASS shape.

VALUE (units 10^{-6})	DOCUMENT ID	TECN	COMMENT
34.2 ± 2.4 ± 4.1	1,2 LEES	11 BABR	$e^+e^- \rightarrow \Upsilon(4S)$
9.4 ^{+1.1} _{-1.3} ± 2.3	1 AUBERT	08AQ BABR	Repl. by LEES 11

$\Gamma((K\pi)_0^{*0}\pi^0, (K\pi)_0^{*0} \rightarrow K^+\pi^-)/\Gamma_{total}$ Γ_{305}/Γ

($K\pi)_0^{*0}$ is the total S-wave composed of $K_0^*(1430)$ and nonresonant that are described using LASS shape.

VALUE (units 10^{-6})	DOCUMENT ID	TECN	COMMENT
8.6 ± 1.1 ± 1.3	1,2 LEES	11 BABR	$e^+e^- \rightarrow \Upsilon(4S)$
8.7 ^{+1.1} _{-0.9} ± 2.8	1 AUBERT	08AQ BABR	Repl. by LEES 11

$\Gamma(K^*(1680)^0\pi^0)/\Gamma_{total}$ Γ_{306}/Γ

VALUE (units 10^{-6})	CL%	DOCUMENT ID	TECN	COMMENT
<4.0	90	1 AUBERT	08AQ BABR	$e^+e^- \rightarrow \Upsilon(4S)$

$\Gamma(K^*(1680)^0\pi^0)/\Gamma_{total}$ Γ_{307}/Γ

VALUE (units 10^{-6})	CL%	DOCUMENT ID	TECN	COMMENT
<7.5	90	1 AUBERT	08AQ BABR	$e^+e^- \rightarrow \Upsilon(4S)$

$\Gamma(K_x^{*0}\pi^0)/\Gamma_{total}$ Γ_{308}/Γ

K_x^{*0} stands for the possible candidates of $K^*(1410)$, $K_0^*(1430)$ and $K_2^*(1430)$.

VALUE (units 10^{-6})	DOCUMENT ID	TECN	COMMENT
6.1 ± 1.6 ± 0.5 -1.5 - 0.6	1 CHANG	04 BELL	$e^+e^- \rightarrow \Upsilon(4S)$

$\Gamma(K^0\pi^+\pi^-)/\Gamma_{total}$ Γ_{309}/Γ

VALUE (units 10^{-6})	CL%	DOCUMENT ID	TECN	COMMENT
49.7 ± 1.8 OUR FIT 49.6 ± 2.0 OUR AVERAGE				
50.2 ± 1.5 ± 1.8		1 AUBERT	09AU BABR	$e^+e^- \rightarrow \Upsilon(4S)$
47.5 ± 2.4 ± 3.7		2 GARMASH	07 BELL	$e^+e^- \rightarrow \Upsilon(4S)$
50 ± 10 ₉ ± 7		1 ECKHART	02 CLE2	$e^+e^- \rightarrow \Upsilon(4S)$

$\Gamma(K^0\pi^+\pi^- \text{ nonresonant})/\Gamma_{total}$ Γ_{310}/Γ

VALUE (units 10^{-6})	DOCUMENT ID	TECN	COMMENT
13.9 ± 2.6 OUR AVERAGE			Error includes scale factor of 1.6. See the ideogram below.
12.1 ± 0.6 ± 2.9	1 AAIJ	18F LHCb	pp at 7, 8 TeV
11.1 ^{+2.5} _{-1.0} ± 0.9	2 AUBERT	09AU BABR	$e^+e^- \rightarrow \Upsilon(4S)$
19.9 ± 2.5 ± 1.7	3 GARMASH	07 BELL	$e^+e^- \rightarrow \Upsilon(4S)$

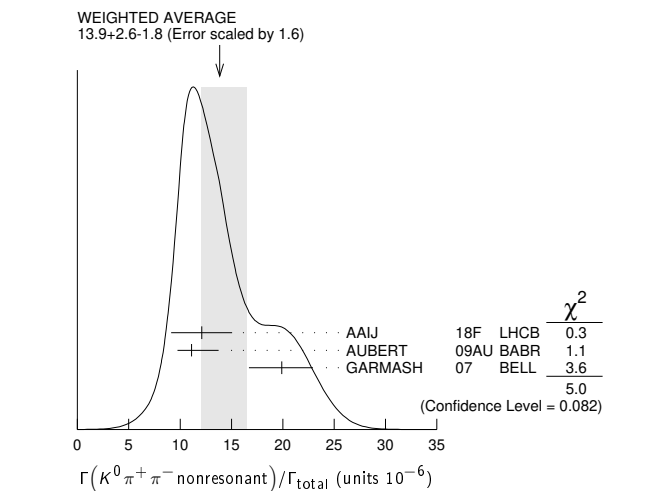
$\Gamma(K^0\pi^+\pi^- \text{ nonresonant})/\Gamma_{total}$ Γ_{311}/Γ

VALUE (units 10^{-6})	DOCUMENT ID	TECN	COMMENT
43.0 ± 2.3 ± 2.3	1 AUBERT	06i BABR	Repl. by AUBERT 09AU
43.7 ± 3.8 ± 3.4	1 AUBERT,B	04o BABR	Repl. by AUBERT 06i
45.4 ± 5.2 ± 5.9	1 GARMASH	04 BELL	Repl. by GARMASH 07
<440	90	ALBRECHT	91E ARG $e^+e^- \rightarrow \Upsilon(4S)$

$\Gamma(K^0\pi^+\pi^- \text{ nonresonant})/\Gamma_{total}$ Γ_{312}/Γ

VALUE (units 10^{-6})	DOCUMENT ID	TECN	COMMENT
50.2 ± 1.5 ± 1.8	1 AUBERT	09AU BABR	$e^+e^- \rightarrow \Upsilon(4S)$
47.5 ± 2.4 ± 3.7	2 GARMASH	07 BELL	$e^+e^- \rightarrow \Upsilon(4S)$
50 ± 10 ₉ ± 7	1 ECKHART	02 CLE2	$e^+e^- \rightarrow \Upsilon(4S)$

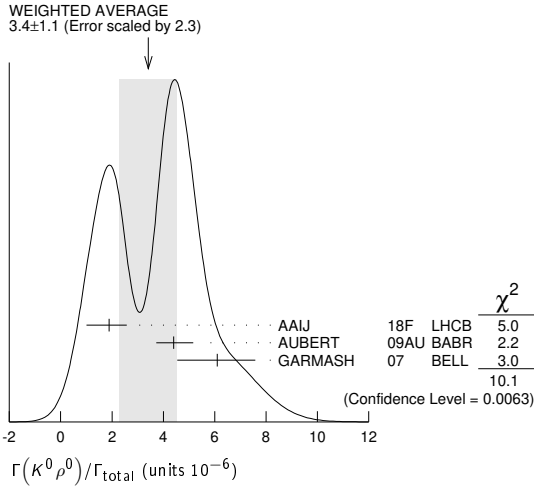
¹ Assumes equal production of B^+ and B^0 at the $\Upsilon(4S)$.
² Uses Dalitz plot analysis of the $B^0 \rightarrow K^0\pi^+\pi^-$ final state decays.
³ Uses Dalitz plot analysis of the $B^0 \rightarrow K^0\pi^+\pi^-$ final state decays.



$\Gamma(K^0 \rho^0)/\Gamma_{total}$ Γ_{311}/Γ

VALUE (units 10 ⁻⁶)	CL%	DOCUMENT ID	TECN	COMMENT
3.4 ± 1.1 OUR AVERAGE		Error includes scale factor of 2.3. See the ideogram below.		
1.89 ^{+0.55} _{-0.79} ± 0.40		1 AAIJ	18F LHCb	pp at 7, 8 TeV
4.4 ^{+0.7} _{-0.6} ± 0.3		2 AUBERT	09AU BABR	e ⁺ e ⁻ → $\Upsilon(4S)$
6.1 ± 1.0 ^{+1.1} _{-1.2}		3 GARMASH	07 BELL	e ⁺ e ⁻ → $\Upsilon(4S)$
• • • We do not use the following data for averages, fits, limits, etc. • • •				
4.9 ± 0.8 ± 0.9		2 AUBERT	07F BABR	Repl. by AUBERT 09AU
< 39	90	ASNER	96 CLEO	e ⁺ e ⁻ → $\Upsilon(4S)$
< 320	90	ALBRECHT	91B ARG	e ⁺ e ⁻ → $\Upsilon(4S)$
< 500	90	4 AVERY	89B CLEO	e ⁺ e ⁻ → $\Upsilon(4S)$

- 1 Uses Dalitz plot analysis of the B⁰ → K_S⁰π⁺π⁻ final state decays. For the branching fraction of the reference mode, the PDG 18 average B(B⁰ → K_S⁰π⁺π⁻) = (4.96 ± 0.20) × 10⁻⁵ is used.
- 2 Assumes equal production of B⁺ and B⁰ at the $\Upsilon(4S)$.
- 3 Uses Dalitz plot analysis of the B⁰ → K⁰π⁺π⁻ final state decays.
- 4 AVERY 89B reports < 5.8 × 10⁻⁴ assuming the $\Upsilon(4S)$ decays 43% to B⁰ \bar{B}^0 . We rescale to 50%.



$\Gamma(K^*(892)^+ \pi^-)/\Gamma_{total}$ Γ_{312}/Γ

VALUE (units 10 ⁻⁶)	CL%	DOCUMENT ID	TECN	COMMENT
7.5 ± 0.4 OUR AVERAGE				
7.02 ± 0.30 ± 0.45		1 AAIJ	18F LHCb	pp at 7, 8 TeV
8.0 ± 1.1 ± 0.8		2,3 LEES	11 BABR	e ⁺ e ⁻ → $\Upsilon(4S)$
8.3 ^{+0.9} _{-0.8} ± 0.8		3,4 AUBERT	09AU BABR	e ⁺ e ⁻ → $\Upsilon(4S)$
8.4 ± 1.1 ^{+1.0} _{-0.9}		4 GARMASH	07 BELL	e ⁺ e ⁻ → $\Upsilon(4S)$
16 ⁺⁶ ₋₅ ± 2		3 ECKHART	02 CLE2	e ⁺ e ⁻ → $\Upsilon(4S)$
• • • We do not use the following data for averages, fits, limits, etc. • • •				
12.6 ^{+2.7} _{-1.6} ± 0.9		2,3 AUBERT	08AQ BABR	Repl. by LEES 11
11.0 ± 1.5 ± 0.71		3 AUBERT	06i BABR	Repl. by AUBERT 09AU
12.9 ± 2.4 ± 1.4		3 AUBERT,B	04o BABR	Repl. by AUBERT 06i
14.8 ^{+4.6} _{-4.4} ± 2.8		3 CHANG	04 BELL	Repl. by GARMASH 07
< 72	90	ASNER	96 CLE2	e ⁺ e ⁻ → $\Upsilon(4S)$
< 620	90	ALBRECHT	91B ARG	e ⁺ e ⁻ → $\Upsilon(4S)$
< 380	90	5 AVERY	89B CLEO	e ⁺ e ⁻ → $\Upsilon(4S)$
< 560	90	6 AVERY	87 CLEO	e ⁺ e ⁻ → $\Upsilon(4S)$

- 1 Uses Dalitz plot analysis of the B⁰ → K_S⁰π⁺π⁻ final state decays. For the branching fraction of the reference mode, the PDG 18 average B(B⁰ → K_S⁰π⁺π⁻) = (4.96 ± 0.20) × 10⁻⁵ is used.
- 2 Uses Dalitz plot analysis of B⁰ → K⁺π⁻π⁰ decays.
- 3 Assumes equal production of B⁺ and B⁰ at the $\Upsilon(4S)$.
- 4 Uses Dalitz plot analysis of the B⁰ → K⁰π⁺π⁻ final state decays.
- 5 AVERY 89B reports < 4.4 × 10⁻⁴ assuming the $\Upsilon(4S)$ decays 43% to B⁰ \bar{B}^0 . We rescale to 50%.
- 6 AVERY 87 reports < 7 × 10⁻⁴ assuming the $\Upsilon(4S)$ decays 40% to B⁰ \bar{B}^0 . We rescale to 50%.

$\Gamma(K_S^0(1430)^+ \pi^-)/\Gamma_{total}$ Γ_{313}/Γ

VALUE (units 10 ⁻⁶)	DOCUMENT ID	TECN	COMMENT
33 ± 7 OUR AVERAGE	Error includes scale factor of 2.0.		
29.9 ^{+2.3} _{-1.7} ± 3.6	1,2 AUBERT	09AU BABR	e ⁺ e ⁻ → $\Upsilon(4S)$
49.7 ± 3.8 ^{+6.8} _{-8.2}	2 GARMASH	07 BELL	e ⁺ e ⁻ → $\Upsilon(4S)$

- 1 Assumes equal production of B⁺ and B⁰ at the $\Upsilon(4S)$.
- 2 Uses Dalitz plot analysis of the B⁰ → K⁰π⁺π⁻ final state decays.

$\Gamma((K\pi)_0^{*+} \pi^-, (K\pi)_0^{*+} \rightarrow K^0 \pi^+)/\Gamma_{total}$ Γ_{316}/Γ

VALUE (units 10 ⁻⁶)	DOCUMENT ID	TECN	COMMENT
16.2 ± 0.69 ± 1.15	1 AAIJ	18F LHCb	pp at 7, 8 TeV

- 1 Uses Dalitz plot analysis of the B⁰ → K_S⁰π⁺π⁻ final state decays. (Kπ)₀^{*+} is the S-wave component of K⁰π⁺. For the branching fraction of the reference mode, the PDG 18 average B(B⁰ → K_S⁰π⁺π⁻) = (4.96 ± 0.20) × 10⁻⁵ is used.

$\Gamma(K_x^{*+} \pi^-)/\Gamma_{total}$ Γ_{314}/Γ

K_x^{*+} stands for the possible candidates of K*(1410), K_S⁰(1430) and K₂^{*}(1430).

VALUE (units 10 ⁻⁶)	DOCUMENT ID	TECN	COMMENT
5.1 ± 1.5 ± 0.6 _{-0.7}	1 CHANG	04 BELL	e ⁺ e ⁻ → $\Upsilon(4S)$

- 1 Assumes equal production of B⁺ and B⁰ at the $\Upsilon(4S)$.

$\Gamma(K^*(1410)^+ \pi^-, K^{*+} \rightarrow K^0 \pi^+)/\Gamma_{total}$ Γ_{315}/Γ

VALUE (units 10 ⁻⁶)	CL%	DOCUMENT ID	TECN	COMMENT
< 3.8	90	1 GARMASH	07 BELL	e ⁺ e ⁻ → $\Upsilon(4S)$

- 1 Uses Dalitz plot analysis of the B⁰ → K⁰π⁺π⁻ final state decays.

$\Gamma(K^0 f_0(500))/\Gamma_{total}$ Γ_{318}/Γ

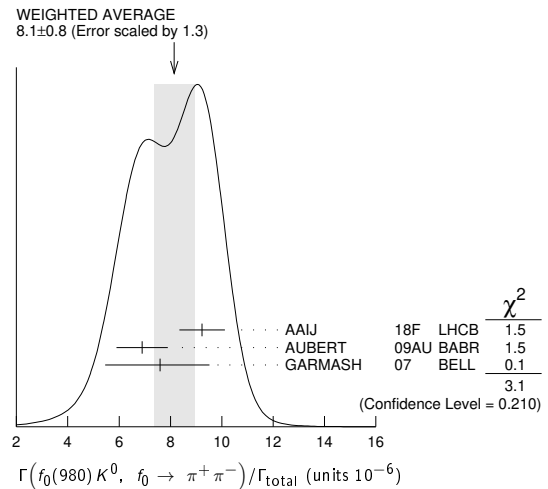
VALUE (units 10 ⁻⁶)	DOCUMENT ID	TECN	COMMENT
0.16 ± 0.20 ± 0.15	1 AAIJ	18F LHCb	pp at 7, 8 TeV

- 1 Uses Dalitz plot analysis of the B⁰ → K_S⁰π⁺π⁻ final state decays. For the branching fraction of the reference mode, the PDG 18 average B(B⁰ → K_S⁰π⁺π⁻) = (4.96 ± 0.20) × 10⁻⁵ is used.

$\Gamma(f_0(980) K^0, f_0 \rightarrow \pi^+ \pi^-)/\Gamma_{total}$ Γ_{317}/Γ

VALUE (units 10 ⁻⁶)	CL%	DOCUMENT ID	TECN	COMMENT
8.1 ± 0.8 OUR AVERAGE	Error includes scale factor of 1.3. See the ideogram below.			
9.23 ± 0.40 ± 0.79		1 AAIJ	18F LHCb	pp at 7, 8 TeV
6.9 ± 0.8 ± 0.6		2 AUBERT	09AU BABR	e ⁺ e ⁻ → $\Upsilon(4S)$
7.6 ± 1.7 ^{+0.9} _{-1.3}		3 GARMASH	07 BELL	e ⁺ e ⁻ → $\Upsilon(4S)$

- 1 Uses Dalitz plot analysis of the B⁰ → K_S⁰π⁺π⁻ final state decays. For the branching fraction of the reference mode, the PDG 18 average B(B⁰ → K_S⁰π⁺π⁻) = (4.96 ± 0.20) × 10⁻⁵ is used.
- 2 Assumes equal production of B⁺ and B⁰ at the $\Upsilon(4S)$.
- 3 Uses Dalitz plot analysis of the B⁰ → K⁰π⁺π⁻ final state decays.
- 4 AVERY 89B reports < 4.2 × 10⁻⁴ assuming the $\Upsilon(4S)$ decays 43% to B⁰ \bar{B}^0 . We rescale to 50%.



Meson Particle Listings

 B^0

$\Gamma(f_2(1270)K^0)/\Gamma_{\text{total}}$ Γ_{320}/Γ
 VALUE (units 10^{-6}) CL% DOCUMENT ID TECN COMMENT

$2.7^{+1.0}_{-0.8} \pm 0.9$ 1 AUBERT 09AU BABR $e^+e^- \rightarrow \Upsilon(4S)$
 ••• We do not use the following data for averages, fits, limits, etc. •••
 <2.5 90 2 GARMASH 07 BELL $e^+e^- \rightarrow \Upsilon(4S)$

¹ Assumes equal production of B^+ and B^0 at the $\Upsilon(4S)$.
² GARMASH 07 reports $B(B^0 \rightarrow f_2(1270)K^0) \times B(f_2(1270) \rightarrow \pi^+\pi^-) < 1.4 \times 10^{-6}$ using Dalitz plot analysis. We compute $B(B^0 \rightarrow f_2(1270)K^0)$ using the PDG value $B(f_2(1270) \rightarrow \pi\pi) = 84.2 \times 10^{-2}$ and 2/3 for the $\pi^+\pi^-$ fraction.

$\Gamma(f_x(1300)K^0, f_x \rightarrow \pi^+\pi^-)/\Gamma_{\text{total}}$ Γ_{321}/Γ
 VALUE (units 10^{-6}) CL% DOCUMENT ID TECN COMMENT

$1.81^{+0.55}_{-0.45} \pm 0.48$ 1 AUBERT 09AU BABR $e^+e^- \rightarrow \Upsilon(4S)$
¹ Assumes equal production of B^+ and B^0 at the $\Upsilon(4S)$.

$\Gamma(K^0 f_0(1500))/\Gamma_{\text{total}}$ Γ_{319}/Γ
 VALUE (units 10^{-6}) CL% DOCUMENT ID TECN COMMENT

$1.29 \pm 0.27 \pm 0.70$ 1 AAIJ 18F LHCb pp at 7, 8 TeV
¹ Uses Dalitz plot analysis of the $B^0 \rightarrow K_S^0 \pi^+ \pi^-$ final state decays. For the branching fraction of the reference mode, the PDG 18 average $B(B^0 \rightarrow K_S^0 \pi^+ \pi^-) = (4.96 \pm 0.20) \times 10^{-5}$ is used.

$\Gamma(K^*(892)^0 \pi^0)/\Gamma_{\text{total}}$ Γ_{322}/Γ
 VALUE (units 10^{-6}) CL% DOCUMENT ID TECN COMMENT

$3.3 \pm 0.5 \pm 0.4$ 1,2 LEES 11 BABR $e^+e^- \rightarrow \Upsilon(4S)$
 ••• We do not use the following data for averages, fits, limits, etc. •••
 $3.6 \pm 0.7 \pm 0.4$ 1,2 AUBERT 08AQ BABR Repl. by LEES 11
 < 3.5 90 2 CHANG 04 BELL $e^+e^- \rightarrow \Upsilon(4S)$
 < 3.6 90 JESSOP 00 CLE2 $e^+e^- \rightarrow \Upsilon(4S)$
 < 28 90 ASNER 96 CLE2 Repl. by JESSOP 00

¹ Uses Dalitz plot analysis of $B^0 \rightarrow K^+ \pi^- \pi^0$ decays.
² Assumes equal production of B^+ and B^0 at the $\Upsilon(4S)$.

$\Gamma(K_2^*(1430)^+ \pi^-)/\Gamma_{\text{total}}$ Γ_{323}/Γ
 VALUE (units 10^{-6}) CL% DOCUMENT ID TECN COMMENT

$3.65^{+0.15}_{-0.12} \pm 0.31$ 1 AAIJ 18F LHCb pp at 7, 8 TeV
 ••• We do not use the following data for averages, fits, limits, etc. •••
 < 16.2 90 2,3 AUBERT 08AQ BABR $e^+e^- \rightarrow \Upsilon(4S)$
 < 6 90 4 GARMASH 07 BELL $e^+e^- \rightarrow \Upsilon(4S)$
 < 18 90 3 GARMASH 04 BELL Repl. by GARMASH 07
 < 2600 90 ALBRECHT 91B ARG $e^+e^- \rightarrow \Upsilon(4S)$

¹ Uses Dalitz plot analysis of the $B^0 \rightarrow K_S^0 \pi^+ \pi^-$ final state decays. We compute $B(B^0 \rightarrow K_2^*(1430)^+ \pi^-)$ using the PDG 18 value $B(K_2^*(1430) \rightarrow K\pi) = 49.9 \times 10^{-2}$ and 2/3 for the $K^0 \pi^+$ fraction. For the branching fraction of the reference mode, the PDG 18 average $B(B^0 \rightarrow K_S^0 \pi^+ \pi^-) = (4.96 \pm 0.20) \times 10^{-5}$ is used.

² Uses Dalitz plot analysis of $B^0 \rightarrow K^+ \pi^- \pi^0$ decays.
³ Assumes equal production of B^+ and B^0 at the $\Upsilon(4S)$.
⁴ GARMASH 07 reports $B(B^0 \rightarrow K_2^*(1430)^+ \pi^-) \times B(K_2^* \rightarrow K^0 \pi^+) < 2.1 \times 10^{-6}$ using Dalitz plot analysis. We compute $B(B^0 \rightarrow K_2^*(1430)^+ \pi^-)$ using the PDG value $B(K_2^*(1430) \rightarrow K\pi) = 49.9 \times 10^{-2}$ and 2/3 for the $K^0 \pi^+$ fraction.

$\Gamma(K^*(1680)^+ \pi^-)/\Gamma_{\text{total}}$ Γ_{324}/Γ
 VALUE (units 10^{-6}) CL% DOCUMENT ID TECN COMMENT

$14.1 \pm 0.58 \pm 0.84$ 1 AAIJ 18F LHCb pp at 7, 8 TeV
 ••• We do not use the following data for averages, fits, limits, etc. •••
 < 25 90 2,3 AUBERT 08AQ BABR $e^+e^- \rightarrow \Upsilon(4S)$
 < 10 90 4 GARMASH 07 BELL $e^+e^- \rightarrow \Upsilon(4S)$

¹ Uses Dalitz plot analysis of the $B^0 \rightarrow K_S^0 \pi^+ \pi^-$ final state decays. We compute $B(B^0 \rightarrow K_2^*(1430)^+ \pi^-)$ using the PDG 18 value $B(K_2^*(1430) \rightarrow K\pi) = (49.9 \pm 1.2) \times 10^{-2}$ and 2/3 for the $K^0 \pi^+$ fraction. For the branching fraction of the reference mode, the PDG 18 average $B(B^0 \rightarrow K_S^0 \pi^+ \pi^-) = (4.96 \pm 0.20) \times 10^{-5}$ is used.

² Uses Dalitz plot analysis of $B^0 \rightarrow K^+ \pi^- \pi^0$ decays.
³ Assumes equal production of B^+ and B^0 at the $\Upsilon(4S)$.
⁴ GARMASH 07 reports $B(B^0 \rightarrow K^*(1680)^+ \pi^-) \times B(K^* \rightarrow K^0 \pi^+) < 2.6 \times 10^{-6}$ using Dalitz plot analysis. We compute $B(B^0 \rightarrow K^*(1680)^+ \pi^-)$ using the PDG value $B(K^*(1680) \rightarrow K\pi) = 38.7 \times 10^{-2}$ and 2/3 for the $K^0 \pi^+$ fraction.

$\Gamma(K^+ \pi^- \pi^+ \pi^-)/\Gamma_{\text{total}}$ Γ_{325}/Γ
 VALUE CL% DOCUMENT ID TECN COMMENT

$< 2.3 \times 10^{-4}$ 90 1 ADAM 96D DLPH $e^+e^- \rightarrow Z$
 ••• We do not use the following data for averages, fits, limits, etc. •••
 $< 2.1 \times 10^{-4}$ 90 2 ABREU 95N DLPH Sup. by ADAM 96D

¹ ADAM 96D assumes $f_{B^0} = f_{B^-} = 0.39$ and $f_{B_S} = 0.12$. Contributions from B^0 and B_S decays cannot be separated. Limits are given for the weighted average of the decay rates for the two neutral B mesons.
² Assumes a B^0 , B^- production fraction of 0.39 and a B_S production fraction of 0.12. Contributions from B^0 and B_S decays cannot be separated. Limits are given for the weighted average of the decay rates for the two neutral B mesons.

$\Gamma(\rho^0 K^+ \pi^-)/\Gamma_{\text{total}}$ Γ_{326}/Γ
 VALUE (units 10^{-6}) CL% DOCUMENT ID TECN COMMENT

$2.8 \pm 0.5 \pm 0.5$ 1,2 KYEONG 09 BELL $e^+e^- \rightarrow \Upsilon(4S)$
¹ Assumes equal production of B^+ and B^0 at the $\Upsilon(4S)$.
² Required $0.75 < m_{K^+ \pi^-} < 1.20$ GeV/ c^2 .

$\Gamma(f_0(980)K^+ \pi^-, f_0 \rightarrow \pi\pi)/\Gamma_{\text{total}}$ Γ_{327}/Γ
 VALUE (units 10^{-6}) CL% DOCUMENT ID TECN COMMENT

$1.4 \pm 0.4^{+0.3}_{-0.4}$ 1,2 KYEONG 09 BELL $e^+e^- \rightarrow \Upsilon(4S)$
¹ Assumes equal production of B^+ and B^0 at the $\Upsilon(4S)$.
² Required $0.75 < m_{K^+ K^-} < 1.2$ GeV/ c^2 .

$\Gamma(K^+ \pi^- \pi^+ \pi^- \text{ nonresonant})/\Gamma_{\text{total}}$ Γ_{328}/Γ
 VALUE CL% DOCUMENT ID TECN COMMENT

$< 2.1 \times 10^{-6}$ 90 1,2 KYEONG 09 BELL $e^+e^- \rightarrow \Upsilon(4S)$
¹ Assumes equal production of B^+ and B^0 at the $\Upsilon(4S)$.
² Required $0.55 < m_{\pi^+ \pi^-} < 1.42$ and $0.75 < m_{K^+ \pi^-} < 1.20$ GeV/ c^2 .

$\Gamma(K^*(892)^0 \pi^+ \pi^-)/\Gamma_{\text{total}}$ Γ_{329}/Γ
 VALUE (units 10^{-6}) CL% DOCUMENT ID TECN COMMENT

$54.5 \pm 2.9 \pm 4.3$ 1 AUBERT 07As BABR $e^+e^- \rightarrow \Upsilon(4S)$
 ••• We do not use the following data for averages, fits, limits, etc. •••
 $4.5^{+1.1+0.9}_{-1.0-1.6}$ 1,2 KYEONG 09 BELL $e^+e^- \rightarrow \Upsilon(4S)$
 < 1400 90 ALBRECHT 91E ARG $e^+e^- \rightarrow \Upsilon(4S)$
¹ Assumes equal production of B^+ and B^0 at the $\Upsilon(4S)$.
² Required $0.55 < m_{\pi^+ \pi^-} < 1.42$ GeV/ c^2 .

$\Gamma(K^*(892)^0 \rho^0)/\Gamma_{\text{total}}$ Γ_{330}/Γ
 VALUE (units 10^{-6}) CL% DOCUMENT ID TECN COMMENT

3.9 ± 1.3 OUR AVERAGE Error includes scale factor of 1.9.
 $5.1 \pm 0.6^{+0.6}_{-0.8}$ 1 LEES 12k BABR $e^+e^- \rightarrow \Upsilon(4S)$
 $2.1^{+0.8+0.9}_{-0.7-0.5}$ 1 KYEONG 09 BELL $e^+e^- \rightarrow \Upsilon(4S)$
 ••• We do not use the following data for averages, fits, limits, etc. •••
 $5.6 \pm 0.9 \pm 1.3$ 1 AUBERT,B 06G BABR Repl. by LEES 12k
 < 34 90 2 GODANG 02 CLE2 $e^+e^- \rightarrow \Upsilon(4S)$
 < 286 90 3 ABE 00c SLD $e^+e^- \rightarrow Z$
 < 460 90 ALBRECHT 91B ARG $e^+e^- \rightarrow \Upsilon(4S)$
 < 580 90 4 AVERY 89B CLEO $e^+e^- \rightarrow \Upsilon(4S)$
 < 960 90 5 AVERY 87 CLEO $e^+e^- \rightarrow \Upsilon(4S)$

¹ Assumes equal production of B^+ and B^0 at the $\Upsilon(4S)$.
² Assumes a helicity 00 configuration. For a helicity 11 configuration, the limit decreases to 2.4×10^{-5} .
³ ABE 00c assumes $B(Z \rightarrow b\bar{b}) = (21.7 \pm 0.1)\%$ and the B fractions $f_{B^0} = f_{B^+} = (39.7^{+1.8}_{-2.2})\%$ and $f_{B_S} = (10.5^{+1.8}_{-2.2})\%$.
⁴ AVERY 89B reports $< 6.7 \times 10^{-4}$ assuming the $\Upsilon(4S)$ decays 43% to $B^0 \bar{B}^0$. We rescale to 50%.
⁵ AVERY 87 reports $< 1.2 \times 10^{-3}$ assuming the $\Upsilon(4S)$ decays 40% to $B^0 \bar{B}^0$. We rescale to 50%.

$\Gamma(K^*(892)^0 f_0(980), f_0 \rightarrow \pi\pi)/\Gamma_{\text{total}}$ Γ_{331}/Γ
 VALUE (units 10^{-6}) CL% DOCUMENT ID TECN COMMENT

$3.9^{+2.1}_{-1.8}$ OUR AVERAGE Error includes scale factor of 3.9.
 $5.7 \pm 0.6 \pm 0.4$ 1 LEES 12k BABR $e^+e^- \rightarrow \Upsilon(4S)$
 $1.4^{+0.6+0.6}_{-0.5-0.4}$ 1,2 KYEONG 09 BELL $e^+e^- \rightarrow \Upsilon(4S)$
 ••• We do not use the following data for averages, fits, limits, etc. •••
 < 4.3 90 1 AUBERT,B 06G BABR $e^+e^- \rightarrow \Upsilon(4S)$
 < 170 90 3 AVERY 89B CLEO $e^+e^- \rightarrow \Upsilon(4S)$

¹ Assumes equal production of B^+ and B^0 at the $\Upsilon(4S)$.
² The upper limit is 2.2×10^{-6} at 90% CL.
³ AVERY 89B reports $< 2.0 \times 10^{-4}$ assuming the $\Upsilon(4S)$ decays 43% to $B^0 \bar{B}^0$. We rescale to 50%.

$\Gamma(K_1(1270)^+ \pi^-)/\Gamma_{\text{total}}$ Γ_{332}/Γ
 VALUE CL% DOCUMENT ID TECN COMMENT

$< 3.0 \times 10^{-5}$ 90 1 AUBERT 10D BABR $e^+e^- \rightarrow \Upsilon(4S)$
¹ Assumes equal production of B^+ and B^0 at the $\Upsilon(4S)$.

$\Gamma(K_1(1400)^+ \pi^-)/\Gamma_{\text{total}}$ Γ_{333}/Γ
 VALUE CL% DOCUMENT ID TECN COMMENT

$< 2.7 \times 10^{-5}$ 90 1 AUBERT 10D BABR $e^+e^- \rightarrow \Upsilon(4S)$
 ••• We do not use the following data for averages, fits, limits, etc. •••
 $< 1.1 \times 10^{-3}$ 90 ALBRECHT 91B ARG $e^+e^- \rightarrow \Upsilon(4S)$
¹ Assumes equal production of B^+ and B^0 at the $\Upsilon(4S)$.

See key on page 999

Meson Particle Listings

B^0

$\Gamma(a_1(1260)^- K^+)/\Gamma_{total}$ Γ_{334}/Γ

VALUE (units 10^{-6})	CL%	DOCUMENT ID	TECN	COMMENT
16.3 ± 2.9 ± 2.3		1,2 AUBERT	08F BABR	$e^+e^- \rightarrow \Upsilon(4S)$
<230	90	3 ADAM	96D DLPH	$e^+e^- \rightarrow Z$
<390	90	4 ABREU	95N DLPH	Sup. by ADAM 96D

- • • We do not use the following data for averages, fits, limits, etc. • • •
- ¹ Assumes equal production of B^+ and B^0 at the $\Upsilon(4S)$.
- ² Assumes a_1^\pm decays only to 3π and $B(a_1^\pm \rightarrow \pi^\pm \pi^\mp \pi^\pm) = 0.5$.
- ³ ADAM 96D assumes $f_{B^0} = f_{B^-} = 0.39$ and $f_{B_s} = 0.12$. Contributions from B^0 and B_s decays cannot be separated. Limits are given for the weighted average of the decay rates for the two neutral B mesons.
- ⁴ Assumes a B^0, B^- production fraction of 0.39 and a B_s production fraction of 0.12. Contributions from B^0 and B_s^0 decays cannot be separated. Limits are given for the weighted average of the decay rates for the two neutral B mesons.

$\Gamma(K^*(892)^+ \rho^-)/\Gamma_{total}$ Γ_{335}/Γ

VALUE (units 10^{-6})	CL%	DOCUMENT ID	TECN	COMMENT
10.3 ± 2.3 ± 1.3		1 LEES	12K BABR	$e^+e^- \rightarrow \Upsilon(4S)$
<12.0	90	1 AUBERT,B	06G BABR	Repl. by LEES 12K

- • • We do not use the following data for averages, fits, limits, etc. • • •
- ¹ Assumes equal production of B^+ and B^0 at the $\Upsilon(4S)$.

$\Gamma(K_S^0(1430)^+ \rho^-)/\Gamma_{total}$ Γ_{336}/Γ

VALUE (units 10^{-6})	CL%	DOCUMENT ID	TECN	COMMENT
28 ± 10 ± 6		1 LEES	12K BABR	$e^+e^- \rightarrow \Upsilon(4S)$

- ¹ Assumes equal production of B^+ and B^0 at the $\Upsilon(4S)$.

$\Gamma(K_1(1400)^0 \rho^0)/\Gamma_{total}$ Γ_{337}/Γ

VALUE	CL%	DOCUMENT ID	TECN	COMMENT
< 3.0 × 10⁻³	90	ALBRECHT	91B ARG	$e^+e^- \rightarrow \Upsilon(4S)$

$\Gamma(K_S^0(1430)^0 \rho^0)/\Gamma_{total}$ Γ_{338}/Γ

VALUE (units 10^{-6})	CL%	DOCUMENT ID	TECN	COMMENT
27 ± 4 ± 4		1 LEES	12K BABR	$e^+e^- \rightarrow \Upsilon(4S)$

$\Gamma(K_S^0(1430)^0 f_0(980), f_0 \rightarrow \pi\pi)/\Gamma_{total}$ Γ_{339}/Γ

VALUE (units 10^{-6})	CL%	DOCUMENT ID	TECN	COMMENT
2.7 ± 0.7 ± 0.6		1 LEES	12K BABR	$e^+e^- \rightarrow \Upsilon(4S)$

$\Gamma(K_S^0(1430)^0 f_0(980), f_0 \rightarrow \pi\pi)/\Gamma_{total}$ Γ_{340}/Γ

VALUE (units 10^{-6})	CL%	DOCUMENT ID	TECN	COMMENT
8.6 ± 1.7 ± 1.0		1 LEES	12K BABR	$e^+e^- \rightarrow \Upsilon(4S)$

$\Gamma(K^+ K^-)/\Gamma_{total}$ Γ_{341}/Γ

VALUE (units 10^{-8})	CL%	DOCUMENT ID	TECN	COMMENT
7.80 ± 1.27 ± 0.84		1 AAIJ	17G LHCB	pp at 7 and 8 TeV

- • • We do not use the following data for averages, fits, limits, etc. • • •
- 10 ± 8 ± 4
- 12 ± 8 ± 1
- 23 ± 10 ± 10
- < 70
- < 50
- < 41
- < 180
- < 37
- < 70
- < 80
- < 60
- < 90
- < 270
- < 250
- < 6600
- < 190
- < 430
- < 4600
- < 400
- < 1800
- < 12000
- < 700

- ¹ Supersedes results of AAIJ 12AR.
- ² DUH 13 reports also for the same data $B(B^0 \rightarrow K^+ K^-) < 0.20 \times 10^{-6}$ at 90% CL.
- ³ Assumes equal production of B^+ and B^0 at the $\Upsilon(4S)$.
- ⁴ AAIJ 12AR reports $[\Gamma(B^0 \rightarrow K^+ K^-)/\Gamma_{total}] / [B(B_s^0 \rightarrow K^+ K^-)] / [\Gamma(\bar{B} \rightarrow B^0)] / \Gamma(\bar{B} \rightarrow B^0) = 0.018^{+0.008}_{-0.007} \pm 0.009$ which we multiply by our best values $B(B_s^0 \rightarrow$

$K^+ K^-) = (2.66 \pm 0.22) \times 10^{-5}$, $\Gamma(\bar{B} \rightarrow B^0)/\Gamma(\bar{B} \rightarrow B^0) = 0.246 \pm 0.023$. Our first error is their experiment's error and our second error is the systematic error from using our best values.

- ⁵ Reported a central value of $(0.23 \pm 0.10 \pm 0.10) \times 10^{-6}$ using $B(B^0 \rightarrow K^+ \pi^-) = (19.4 \pm 0.6) \times 10^{-6}$.
- ⁶ Obtains this result from $B(K^+ K^-)/B(K^+ \pi^-) = 0.020 \pm 0.008 \pm 0.006$, assuming $B(B^0 \rightarrow K^+ \pi^-) = (19.4 \pm 0.6) \times 10^{-6}$.
- ⁷ ABULENCIA,A 06D obtains this from $\Gamma(K^+ K^-)/\Gamma(K^+ \pi^-) < 0.10$ at 90% CL, assuming $B(B^0 \rightarrow K^+ \pi^-) = (18.9 \pm 0.7) \times 10^{-6}$.
- ⁸ ABE 00c assumes $B(Z \rightarrow b\bar{b}) = (21.7 \pm 0.1)\%$ and the B fractions $f_{B^0} = f_{B^+} = (39.7^{+1.8}_{-2.2})\%$ and $f_{B_s} = (10.5^{+1.8}_{-2.2})\%$.
- ⁹ ADAM 96D assumes $f_{B^0} = f_{B^-} = 0.39$ and $f_{B_s} = 0.12$. Contributions from B^0 and B_s decays cannot be separated. Limits are given for the weighted average of the decay rates for the two neutral B mesons.
- ¹⁰ BUSKULIC 96v assumes PDG 96 production fractions for B^0, B^+, B_s, b baryons.
- ¹¹ Assumes a B^0, B^- production fraction of 0.39 and a B_s production fraction of 0.12. Contributions from B^0 and B_s^0 decays cannot be separated. Limits are given for the weighted average of the decay rates for the two neutral B mesons.

$\Gamma(K^0 \bar{K}^0)/\Gamma_{total}$ Γ_{342}/Γ

VALUE (units 10^{-6})	CL%	DOCUMENT ID	TECN	COMMENT
1.21 ± 0.16 OUR AVERAGE				
1.26 ± 0.19 ± 0.05		1 DUH	13 BELL	$e^+e^- \rightarrow \Upsilon(4S)$
1.08 ± 0.28 ± 0.11		1 AUBERT,BE	06c BABR	$e^+e^- \rightarrow \Upsilon(4S)$
0.87 ± 0.25 ± 0.09		1 LIN	07 BELL	Repl. by DUH 13
0.8 ± 0.3 ± 0.9		1 ABE	05G BELL	Repl. by LIN 07
1.19 ± 0.40 ± 0.13		1 AUBERT,BE	05E BABR	Repl. by AUBERT,BE 06c
< 1.8	90	1 AUBERT	04M BABR	$e^+e^- \rightarrow \Upsilon(4S)$
< 1.5	90	1 CHAO	04 BELL	Repl. by ABE 05G
< 3.3	90	1 BORNHEIM	03 CLE2	$e^+e^- \rightarrow \Upsilon(4S)$
< 4.1	90	1 CASEY	02 BELL	$e^+e^- \rightarrow \Upsilon(4S)$
< 17	90	1 GODANG	98 CLE2	$e^+e^- \rightarrow \Upsilon(4S)$

- ¹ Assumes equal production of B^+ and B^0 at the $\Upsilon(4S)$.

$\Gamma(K^0 K^- \pi^+)/\Gamma_{total}$ Γ_{343}/Γ

VALUE (units 10^{-6})	CL%	DOCUMENT ID	TECN	COMMENT
6.7 ± 0.5 OUR FIT				
7.0 ± 0.6 OUR AVERAGE				
7.2 ± 0.7 ± 0.3		1 LAI	19 BELL	$e^+e^- \rightarrow \Upsilon(4S)$
6.4 ± 1.0 ± 0.6		1 DEL-AMO-SA...	10E BABR	$e^+e^- \rightarrow \Upsilon(4S)$
< 18	90	1 GARMASH	04 BELL	$e^+e^- \rightarrow \Upsilon(4S)$
< 21	90	1 ECKHART	02 CLE2	$e^+e^- \rightarrow \Upsilon(4S)$

- • • We do not use the following data for averages, fits, limits, etc. • • •
- ¹ Assumes equal production of B^+ and B^0 at the $\Upsilon(4S)$.

$\Gamma(K^*(892)^\pm K^\mp)/\Gamma_{total}$ Γ_{344}/Γ

VALUE	CL%	DOCUMENT ID	TECN	COMMENT
< 0.4 × 10⁻⁶		90	AAIJ	14BMLHCB pp at 7 TeV

$\Gamma(K^0 K^- \pi^+)/\Gamma(K^0 \pi^+ \pi^-)$ $\Gamma_{343}/\Gamma_{309}$

VALUE	CL%	DOCUMENT ID	TECN	COMMENT
0.134 ± 0.011 OUR FIT				
0.123 ± 0.009 ± 0.015				
0.128 ± 0.017 ± 0.009		AAIJ	17BP LHCB	pp at 7, 8 TeV
		AAIJ	13BP LHCB	Repl. by AAIJ 17BP

$[\Gamma(K^* K^0) + \Gamma(K^* \bar{K}^0)]/\Gamma_{total}$ Γ_{345}/Γ

VALUE (units 10^{-6})	CL%	DOCUMENT ID	TECN	COMMENT
< 0.96	90	1 AAIJ	16 LHCB	pp at 7 TeV
< 1.9	90	2 AUBERT,BE	06N BABR	$e^+e^- \rightarrow \Upsilon(4S)$

- • • We do not use the following data for averages, fits, limits, etc. • • •
- ¹ Assumes $B(B^0 \rightarrow K^0 \pi^+ \pi^-) = (4.96 \pm 0.20) \times 10^{-5}$.
- ² Assumes equal production of B^+ and B^0 at the $\Upsilon(4S)$.

$\Gamma(K^+ K^- \pi^0)/\Gamma_{total}$ Γ_{346}/Γ

VALUE (units 10^{-6})	CL%	DOCUMENT ID	TECN	COMMENT
2.17 ± 0.60 ± 0.24		1 GAUR	13 BELL	$e^+e^- \rightarrow \Upsilon(4S)$
< 19	90	1 ECKHART	02 CLE2	$e^+e^- \rightarrow \Upsilon(4S)$

- ¹ Assumes equal production of B^+ and B^0 at the $\Upsilon(4S)$.

$\Gamma(K_S^0 K_S^0 \pi^0)/\Gamma_{total}$ Γ_{347}/Γ

VALUE	CL%	DOCUMENT ID	TECN	COMMENT
< 0.9 × 10⁻⁶	90	1 AUBERT	09AD BABR	$e^+e^- \rightarrow \Upsilon(4S)$

- ¹ Assumes equal production of B^+ and B^0 at the $\Upsilon(4S)$.

$\Gamma(K_S^0 K_S^0 \eta)/\Gamma_{total}$ Γ_{348}/Γ

VALUE	CL%	DOCUMENT ID	TECN	COMMENT
< 1.0 × 10⁻⁶	90	1 AUBERT	09AD BABR	$e^+e^- \rightarrow \Upsilon(4S)$

- ¹ Assumes equal production of B^+ and B^0 at the $\Upsilon(4S)$.

Meson Particle Listings

 B^0

$\Gamma(K_S^0 K_S^0 \eta)/\Gamma_{\text{total}}$				Γ_{349}/Γ
VALUE	CL%	DOCUMENT ID	TECN	COMMENT
$<2.0 \times 10^{-6}$	90	¹ AUBERT	09AD BABR	$e^+e^- \rightarrow \Upsilon(4S)$

¹ Assumes equal production of B^+ and B^0 at the $\Upsilon(4S)$.

$\Gamma(K^0 K^+ K^-)/\Gamma_{\text{total}}$				Γ_{350}/Γ
VALUE (units 10^{-6})	CL%	DOCUMENT ID	TECN	COMMENT
26.8 ± 1.1 OUR FIT				
26.6 ± 1.2 OUR AVERAGE				
26.5 ± 0.9 ± 0.8		^{1,2} LEES	12o BABR	$e^+e^- \rightarrow \Upsilon(4S)$
28.3 ± 3.3 ± 4.0		¹ GARMASH	04 BELL	$e^+e^- \rightarrow \Upsilon(4S)$
• • • We do not use the following data for averages, fits, limits, etc. • • •				
23.8 ± 2.0 ± 1.6		¹ AUBERT,B	04v BABR	Repl. by LEES 12o
<1300	90	ALBRECHT	91E ARG	$e^+e^- \rightarrow \Upsilon(4S)$

¹ Assumes equal production of B^+ and B^0 at the $\Upsilon(4S)$.² All intermediate charmonium and charm resonances are removed, except of χ_{c0} .

$\Gamma(K^0 K^+ K^-)/\Gamma(K^0 \pi^+ \pi^-)$				$\Gamma_{350}/\Gamma_{309}$
VALUE	CL%	DOCUMENT ID	TECN	COMMENT
0.539 ± 0.025 OUR FIT				
0.549 ± 0.018 ± 0.033		AAIJ	17BP LHCB	pp at 7, 8 TeV
• • • We do not use the following data for averages, fits, limits, etc. • • •				
0.385 ± 0.031 ± 0.023		AAIJ	13BP LHCB	Repl. by AAIJ 17BP

$\Gamma(K^0 \phi)/\Gamma_{\text{total}}$				Γ_{351}/Γ
VALUE (units 10^{-6})	CL%	DOCUMENT ID	TECN	COMMENT
7.3 ± 0.7 OUR AVERAGE				
7.1 ± 0.6 ± 0.4		¹ LEES	12o BABR	$e^+e^- \rightarrow \Upsilon(4S)$
9.0 ± 2.2 ± 0.7		¹ CHEN	03B BELL	$e^+e^- \rightarrow \Upsilon(4S)$
• • • We do not use the following data for averages, fits, limits, etc. • • •				
8.4 ± 1.5 ± 0.5		¹ AUBERT	04A BABR	Repl. by LEES 12o
8.1 ± 3.1 ± 0.8		¹ AUBERT	01D BABR	$e^+e^- \rightarrow \Upsilon(4S)$
< 12.3	90	¹ BRIERE	01 CLE2	$e^+e^- \rightarrow \Upsilon(4S)$
< 31	90	¹ BERGFELD	98 CLE2	
< 88	90	ASNER	96 CLE2	$e^+e^- \rightarrow \Upsilon(4S)$
< 720	90	ALBRECHT	91B ARG	$e^+e^- \rightarrow \Upsilon(4S)$
< 420	90	² AVERY	89B CLEO	$e^+e^- \rightarrow \Upsilon(4S)$
<1000	90	³ AVERY	87 CLEO	$e^+e^- \rightarrow \Upsilon(4S)$

¹ Assumes equal production of B^+ and B^0 at the $\Upsilon(4S)$.² AVERY 89B reports $< 4.9 \times 10^{-4}$ assuming the $\Upsilon(4S)$ decays 43% to $B^0 \bar{B}^0$. We rescale to 50%.³ AVERY 87 reports $< 1.3 \times 10^{-3}$ assuming the $\Upsilon(4S)$ decays 40% to $B^0 \bar{B}^0$. We rescale to 50%.

$\Gamma(f_0(980) K^0, f_0 \rightarrow K^+ K^-)/\Gamma_{\text{total}}$				Γ_{352}/Γ
VALUE (units 10^{-6})	CL%	DOCUMENT ID	TECN	COMMENT
7.0 ± 2.6 ± 1.8 ± 2.4		¹ LEES	12o BABR	$e^+e^- \rightarrow \Upsilon(4S)$

¹ Assumes equal production of B^+ and B^0 at the $\Upsilon(4S)$.

$\Gamma(f_0(1500) K^0)/\Gamma_{\text{total}}$				Γ_{353}/Γ
VALUE (units 10^{-6})	CL%	DOCUMENT ID	TECN	COMMENT
13.3 ± 5.8 ± 3.2		¹ LEES	12o BABR	$e^+e^- \rightarrow \Upsilon(4S)$

¹ Assumes equal production of B^+ and B^0 at the $\Upsilon(4S)$.

$\Gamma(f_2'(1525)^0 K^0)/\Gamma_{\text{total}}$				Γ_{354}/Γ
VALUE (units 10^{-6})	CL%	DOCUMENT ID	TECN	COMMENT
0.29 ± 0.27 ± 0.36		¹ LEES	12o BABR	$e^+e^- \rightarrow \Upsilon(4S)$

¹ Assumes equal production of B^+ and B^0 at the $\Upsilon(4S)$.

$\Gamma(f_0(1710) K^0, f_0 \rightarrow K^+ K^-)/\Gamma_{\text{total}}$				Γ_{355}/Γ
VALUE (units 10^{-6})	CL%	DOCUMENT ID	TECN	COMMENT
4.4 ± 0.7 ± 0.5		¹ LEES	12o BABR	$e^+e^- \rightarrow \Upsilon(4S)$

¹ Assumes equal production of B^+ and B^0 at the $\Upsilon(4S)$.

$\Gamma(K^0 K^+ K^- \text{ nonresonant})/\Gamma_{\text{total}}$				Γ_{356}/Γ
VALUE (units 10^{-6})	CL%	DOCUMENT ID	TECN	COMMENT
33 ± 5 ± 9		¹ LEES	12o BABR	$e^+e^- \rightarrow \Upsilon(4S)$

¹ Assumes equal production of B^+ and B^0 at the $\Upsilon(4S)$.

$\Gamma(K_S^0 K_S^0 K_S^0)/\Gamma_{\text{total}}$				Γ_{357}/Γ
VALUE (units 10^{-6})	CL%	DOCUMENT ID	TECN	COMMENT
6.0 ± 0.5 OUR AVERAGE				Error includes scale factor of 1.1.
6.19 ± 0.48 ± 0.19		¹ LEES	12i BABR	$e^+e^- \rightarrow \Upsilon(4S)$
4.2 ± 1.6 ± 0.8		¹ GARMASH	04 BELL	$e^+e^- \rightarrow \Upsilon(4S)$

¹ Assumes equal production of B^+ and B^0 at the $\Upsilon(4S)$.² Assumes equal production of B^+ and B^0 at the $\Upsilon(4S)$.³ Assumes equal production of B^+ and B^0 at the $\Upsilon(4S)$.⁴ Assumes equal production of B^+ and B^0 at the $\Upsilon(4S)$.⁵ Assumes equal production of B^+ and B^0 at the $\Upsilon(4S)$.⁶ Assumes equal production of B^+ and B^0 at the $\Upsilon(4S)$.⁷ Assumes equal production of B^+ and B^0 at the $\Upsilon(4S)$.

$\Gamma(f_0(980) K^0, f_0 \rightarrow K_S^0 K_S^0)/\Gamma_{\text{total}}$				Γ_{358}/Γ
VALUE (units 10^{-6})	CL%	DOCUMENT ID	TECN	COMMENT
2.7 ± 1.3 ± 1.3		^{1,2} LEES	12i BABR	$e^+e^- \rightarrow \Upsilon(4S)$

¹ Assumes equal production of B^+ and B^0 at the $\Upsilon(4S)$.² Uses Dalitz plot analysis of the $B^0 \rightarrow K_S^0 K_S^0 K_S^0$ decay.

$\Gamma(f_0(1710) K^0, f_0 \rightarrow K_S^0 K_S^0)/\Gamma_{\text{total}}$				Γ_{359}/Γ
VALUE (units 10^{-6})	CL%	DOCUMENT ID	TECN	COMMENT
0.50 ± 0.46 ± 0.11		^{1,2} LEES	12i BABR	$e^+e^- \rightarrow \Upsilon(4S)$

¹ Assumes equal production of B^+ and B^0 at the $\Upsilon(4S)$.² Uses Dalitz plot analysis of the $B^0 \rightarrow K_S^0 K_S^0 K_S^0$ decay.

$\Gamma(f_2(2010) K^0, f_2 \rightarrow K_S^0 K_S^0)/\Gamma_{\text{total}}$				Γ_{360}/Γ
VALUE (units 10^{-6})	CL%	DOCUMENT ID	TECN	COMMENT
0.54 ± 0.21 ± 0.52		^{1,2} LEES	12i BABR	$e^+e^- \rightarrow \Upsilon(4S)$

¹ Assumes equal production of B^+ and B^0 at the $\Upsilon(4S)$.² Uses Dalitz plot analysis of the $B^0 \rightarrow K_S^0 K_S^0 K_S^0$ decay.

$\Gamma(K_S^0 K_S^0 K_S^0 \text{ nonresonant})/\Gamma_{\text{total}}$				Γ_{361}/Γ
VALUE (units 10^{-6})	CL%	DOCUMENT ID	TECN	COMMENT
13.3 ± 2.3 ± 2.2		^{1,2} LEES	12i BABR	$e^+e^- \rightarrow \Upsilon(4S)$

¹ Assumes equal production of B^+ and B^0 at the $\Upsilon(4S)$.² Uses Dalitz plot analysis of the $B^0 \rightarrow K_S^0 K_S^0 K_S^0$ decay.

$\Gamma(K_S^0 K_S^0 K_L^0)/\Gamma_{\text{total}}$				Γ_{362}/Γ
VALUE (units 10^{-6})	CL%	DOCUMENT ID	TECN	COMMENT
<16	90	¹ AUBERT,B	06R BABR	$e^+e^- \rightarrow \Upsilon(4S)$

¹ Assumes equal production of B^+ and B^0 at the $\Upsilon(4S)$.

$\Gamma(K^*(892)^0 K^+ K^-)/\Gamma_{\text{total}}$				Γ_{363}/Γ
VALUE (units 10^{-6})	CL%	DOCUMENT ID	TECN	COMMENT
27.5 ± 1.3 ± 2.2		¹ AUBERT	07As BABR	$e^+e^- \rightarrow \Upsilon(4S)$
• • • We do not use the following data for averages, fits, limits, etc. • • •				
<610	90	ALBRECHT	91E ARG	$e^+e^- \rightarrow \Upsilon(4S)$

¹ Assumes equal production of B^+ and B^0 at the $\Upsilon(4S)$.

$\Gamma(K^*(892)^0 \phi)/\Gamma_{\text{total}}$				Γ_{364}/Γ
VALUE (units 10^{-6})	CL%	DOCUMENT ID	TECN	COMMENT
10.0 ± 0.5 OUR FIT				
10.0 ± 0.5 OUR AVERAGE				
10.4 ± 0.5 ± 0.6		¹ PRIM	13 BELL	$e^+e^- \rightarrow \Upsilon(4S)$
9.7 ± 0.5 ± 0.5		¹ AUBERT	08Bg BABR	$e^+e^- \rightarrow \Upsilon(4S)$
11.5 ± 4.5 ± 1.8		¹ BRIERE	01 CLE2	$e^+e^- \rightarrow \Upsilon(4S)$
-3.7 - 1.7				

¹ Assumes equal production of B^+ and B^0 at the $\Upsilon(4S)$.

9.2 ± 0.7 ± 0.6		¹ AUBERT	07D BABR	Repl. by AUBERT 08Bg
10.2 ± 0.9 ± 0.5		¹ AUBERT,B	04W BABR	Repl. by AUBERT 07D
11.2 ± 1.3 ± 0.8		¹ AUBERT	03v BABR	Repl. by AUBERT,B 04w
10.0 ± 1.6 ± 0.7		¹ CHEN	03B BELL	Repl. by PRIM 13
-1.5 - 0.8				
8.7 ± 2.5 ± 1.1		¹ AUBERT	01D BABR	Repl. by AUBERT 03v
<384	90	² ABE	00c SLD	$e^+e^- \rightarrow Z$
< 21	90	¹ BERGFELD	98 CLE2	
< 43	90	ASNER	96 CLE2	$e^+e^- \rightarrow \Upsilon(4S)$
<320	90	ALBRECHT	91B ARG	$e^+e^- \rightarrow \Upsilon(4S)$
<380	90	³ AVERY	89B CLEO	$e^+e^- \rightarrow \Upsilon(4S)$
<380	90	⁴ AVERY	87 CLEO	$e^+e^- \rightarrow \Upsilon(4S)$

¹ Assumes equal production of B^+ and B^0 at the $\Upsilon(4S)$.² ABE 00c assumes $B(Z \rightarrow b\bar{b}) = (21.7 \pm 0.1)\%$ and the B fractions $f_{B^0} = f_{B^+} = (39.7 \pm 2.2)\%$ and $f_{B_s} = (10.5 \pm 1.8)\%$.³ AVERY 89B reports $< 4.4 \times 10^{-4}$ assuming the $\Upsilon(4S)$ decays 43% to $B^0 \bar{B}^0$. We rescale to 50%.⁴ AVERY 87 reports $< 4.7 \times 10^{-4}$ assuming the $\Upsilon(4S)$ decays 40% to $B^0 \bar{B}^0$. We rescale to 50%.

$\Gamma(K^+ K^- \pi^+ \pi^- \text{ nonresonant})/\Gamma_{\text{total}}$				Γ_{365}/Γ
VALUE (units 10^{-6})	CL%	DOCUMENT ID	TECN	COMMENT
<71.7	90	^{1,2} CHIANG	10 BELL	$e^+e^- \rightarrow \Upsilon(4S)$

¹ Measured in the range $0.7 < m_{K\pi} < 1.7$ and corrected using PS assumption for the full $K\pi$ mass range.² Assumes equal production of B^+ and B^0 at the $\Upsilon(4S)$.

See key on page 999

Meson Particle Listings

B^0

$\Gamma(K^*(892)^0 K^- \pi^+)/\Gamma_{total}$ Γ_{366}/Γ

VALUE (units 10^{-6})	CL%	DOCUMENT ID	TECN	COMMENT
4.5 ± 1.3 OUR AVERAGE				
2.11 ^{+5.63+4.85} _{-5.26-4.75}		1,2 CHIANG	10	BELL $e^+e^- \rightarrow \Upsilon(4S)$
4.6 ± 1.1 ± 0.8		2 AUBERT	07As	BABR $e^+e^- \rightarrow \Upsilon(4S)$

¹ Measured in the range $0.7 < m_{K\pi} < 1.7$ and corrected using PS assumption for the full $K\pi$ mass range. The quoted result is equivalent to the upper limit of $< 13.9 \times 10^{-6}$ at 90% CL.
² Assumes equal production of B^+ and B^0 at the $\Upsilon(4S)$.

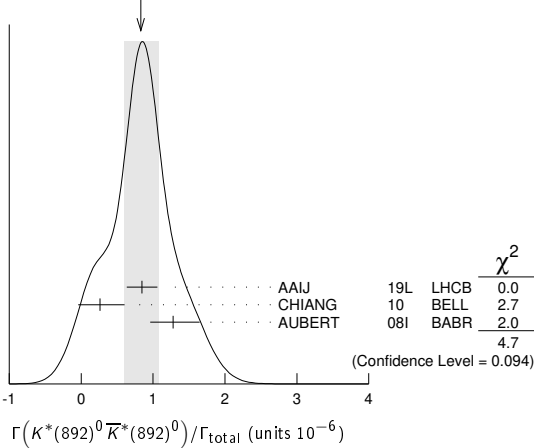
$\Gamma(K^*(892)^0 \bar{K}^*(892)^0)/\Gamma_{total}$ Γ_{367}/Γ

VALUE (units 10^{-6})	CL%	DOCUMENT ID	TECN	COMMENT
0.83 ± 0.24 OUR AVERAGE				Error includes scale factor of 1.5. See the ideogram below.
0.85 ± 0.07 ± 0.20		1 AAIJ	19L	LHCB pp at 7 and 8 TeV
0.26 ^{+0.33+0.10} _{-0.29-0.08}		2,3 CHIANG	10	BELL $e^+e^- \rightarrow \Upsilon(4S)$
1.28 ^{+0.35} _{-0.30} ± 0.11		3 AUBERT	08i	BABR $e^+e^- \rightarrow \Upsilon(4S)$

• • • We do not use the following data for averages, fits, limits, etc. • • •
 < 22 90 4 GODANG 02 CLE2 $e^+e^- \rightarrow \Upsilon(4S)$
 < 469 90 5 ABE 00c SLD $e^+e^- \rightarrow Z$

¹ AAIJ 19L reports $[\Gamma(B^0 \rightarrow K^*(892)^0 \bar{K}^*(892)^0)/\Gamma_{total}] / [B(B_S^0 \rightarrow \bar{K}^*(892)^0 K^*(892)^0)] = 0.0758 \pm 0.0057 \pm 0.0030$ which we multiply by our best value $B(B_S^0 \rightarrow \bar{K}^*(892)^0 K^*(892)^0) = (1.11 \pm 0.27) \times 10^{-5}$. Our first error is their experiment's error and our second error is the systematic error from using our best value.
² Measured in the range $0.7 < m_{K\pi} < 1.7$ and corrected using PS assumption for the full $K\pi$ mass range. The quoted result is equivalent to the upper limit of $< 0.8 \times 10^{-6}$ at 90% CL.
³ Assumes equal production of B^+ and B^0 at the $\Upsilon(4S)$.
⁴ Assumes a helicity 00 configuration. For a helicity 11 configuration, the limit decreases to 1.9×10^{-5} .
⁵ ABE 00c assumes $B(Z \rightarrow b\bar{b}) = (21.7 \pm 0.1)\%$ and the B fractions $f_{B^0} = f_{B^+} = (39.7 \pm 2.2)\%$ and $f_{B_s} = (10.5 \pm 1.8)\%$.

WEIGHTED AVERAGE
0.83±0.24 (Error scaled by 1.5)



$\Gamma(K^+ K^+ \pi^- \pi^- \text{nonresonant})/\Gamma_{total}$ Γ_{368}/Γ

VALUE (units 10^{-6})	CL%	DOCUMENT ID	TECN	COMMENT
< 6.0	90	1 CHIANG	10	BELL $e^+e^- \rightarrow \Upsilon(4S)$

¹ Assumes equal production of B^+ and B^0 at the $\Upsilon(4S)$.

$\Gamma(K^*(892)^0 K^+ \pi^-)/\Gamma_{total}$ Γ_{369}/Γ

VALUE (units 10^{-6})	CL%	DOCUMENT ID	TECN	COMMENT
< 2.2	90	1 AUBERT	07As	BABR $e^+e^- \rightarrow \Upsilon(4S)$
• • • We do not use the following data for averages, fits, limits, etc. • • •				
< 7.6	90	1 CHIANG	10	BELL $e^+e^- \rightarrow \Upsilon(4S)$

¹ Assumes equal production of B^+ and B^0 at the $\Upsilon(4S)$.

$\Gamma(K^*(892)^0 K^*(892)^0)/\Gamma_{total}$ Γ_{370}/Γ

VALUE (units 10^{-6})	CL%	DOCUMENT ID	TECN	COMMENT
< 0.2	90	1 CHIANG	10	BELL $e^+e^- \rightarrow \Upsilon(4S)$
• • • We do not use the following data for averages, fits, limits, etc. • • •				
< 0.41	90	1 AUBERT	08i	BABR $e^+e^- \rightarrow \Upsilon(4S)$
< 37	90	2 GODANG	02	CLE2 $e^+e^- \rightarrow \Upsilon(4S)$

¹ Assumes equal production of B^+ and B^0 at the $\Upsilon(4S)$.
² Assumes a helicity 00 configuration. For a helicity 11 configuration, the limit decreases to 2.9×10^{-5} .

$\Gamma(K^*(892)^+ K^*(892)^-)/\Gamma_{total}$ Γ_{371}/Γ

VALUE (units 10^{-6})	CL%	DOCUMENT ID	TECN	COMMENT
< 2.0	90	1 AUBERT	08AP	BABR $e^+e^- \rightarrow \Upsilon(4S)$
• • • We do not use the following data for averages, fits, limits, etc. • • •				
< 141	90	2 GODANG	02	CLE2 $e^+e^- \rightarrow \Upsilon(4S)$

¹ Assumes equal production of B^+ and B^0 at the $\Upsilon(4S)$.
² Assumes a helicity 00 configuration. For a helicity 11 configuration, the limit decreases to 8.9×10^{-5} .

$\Gamma(K_1(1400)^0 \phi)/\Gamma_{total}$ Γ_{372}/Γ

VALUE (units 10^{-6})	CL%	DOCUMENT ID	TECN	COMMENT
< 5.0 × 10⁻³	90	ALBRECHT	91B	ARG $e^+e^- \rightarrow \Upsilon(4S)$

$\Gamma(\phi(K\pi)_0^0)/\Gamma_{total}$ Γ_{373}/Γ

This decay refers to the coherent sum of resonant and nonresonant $J^P = 0^+ K\pi$ components with $1.13 < m_{K\pi} < 1.53 \text{ GeV}/c^2$.

VALUE (units 10^{-6})	CL%	DOCUMENT ID	TECN	COMMENT
4.3 ± 0.4 OUR AVERAGE				
4.3 ± 0.4 ± 0.4		1 PRIM	13	BELL $e^+e^- \rightarrow \Upsilon(4S)$
4.3 ± 0.6 ± 0.4		1 AUBERT	08BG	BABR $e^+e^- \rightarrow \Upsilon(4S)$
• • • We do not use the following data for averages, fits, limits, etc. • • •				
5.0 ± 0.8 ± 0.3		1 AUBERT	07D	BABR Repl. by AUBERT 08Bg

¹ Assumes equal production of B^+ and B^0 at the $\Upsilon(4S)$.

$\Gamma(\phi(K\pi)_0^0(1.60 < m_{K\pi} < 2.15))/\Gamma_{total}$ Γ_{374}/Γ

This decay refers to the coherent sum of resonant and nonresonant $J^P = 0^+ K\pi$ components with $1.60 < m_{K\pi} < 2.15 \text{ GeV}/c^2$.

VALUE (units 10^{-6})	CL%	DOCUMENT ID	TECN	COMMENT
< 1.7	90	1 AUBERT	07A0	BABR $e^+e^- \rightarrow \Upsilon(4S)$

¹ Assumes equal production of B^+ and B^0 at the $\Upsilon(4S)$.

$\Gamma(K_0^*(1430)^0 K^- \pi^+)/\Gamma_{total}$ Γ_{375}/Γ

VALUE (units 10^{-6})	CL%	DOCUMENT ID	TECN	COMMENT
< 31.8	90	1,2 CHIANG	10	BELL $e^+e^- \rightarrow \Upsilon(4S)$

¹ Measured in the range $0.7 < m_{K\pi} < 1.7$ and corrected using PS assumption for the full $K\pi$ mass range.
² Assumes equal production of B^+ and B^0 at the $\Upsilon(4S)$.

$\Gamma(K_0^*(1430)^0 \bar{K}^*(892)^0)/\Gamma_{total}$ Γ_{376}/Γ

VALUE (units 10^{-6})	CL%	DOCUMENT ID	TECN	COMMENT
< 3.3	90	1,2 CHIANG	10	BELL $e^+e^- \rightarrow \Upsilon(4S)$

¹ Measured in the range $0.7 < m_{K\pi} < 1.7$ and corrected using PS assumption for the full $K\pi$ mass range.
² Assumes equal production of B^+ and B^0 at the $\Upsilon(4S)$.

$\Gamma(K_0^*(1430)^0 \bar{K}_0^*(1430)^0)/\Gamma_{total}$ Γ_{377}/Γ

VALUE (units 10^{-6})	CL%	DOCUMENT ID	TECN	COMMENT
< 8.4	90	1,2 CHIANG	10	BELL $e^+e^- \rightarrow \Upsilon(4S)$

¹ Measured in the range $0.7 < m_{K\pi} < 1.7$ and corrected using PS assumption for the full $K\pi$ mass range.
² Assumes equal production of B^+ and B^0 at the $\Upsilon(4S)$.

$\Gamma(K_0^*(1430)^0 \phi)/\Gamma_{total}$ Γ_{378}/Γ

VALUE (units 10^{-6})	CL%	DOCUMENT ID	TECN	COMMENT
3.9 ± 0.5 ± 0.6		1 AUBERT	08BG	BABR $e^+e^- \rightarrow \Upsilon(4S)$
• • • We do not use the following data for averages, fits, limits, etc. • • •				
4.6 ± 0.7 ± 0.6		1 AUBERT	07D	BABR Repl. by AUBERT 08Bg
seen		2 AUBERT,B	04W	BABR Repl. by AUBERT 07D

¹ Assumes equal production of B^+ and B^0 at the $\Upsilon(4S)$.
² Observed 181 ± 17 events with statistical significance greater than 10σ .

$\Gamma(K_0^*(1430)^0 K^*(892)^0)/\Gamma_{total}$ Γ_{379}/Γ

VALUE (units 10^{-6})	CL%	DOCUMENT ID	TECN	COMMENT
< 1.7	90	1 CHIANG	10	BELL $e^+e^- \rightarrow \Upsilon(4S)$

¹ Assumes equal production of B^+ and B^0 at the $\Upsilon(4S)$.

$\Gamma(K_0^*(1430)^0 K_0^*(1430)^0)/\Gamma_{total}$ Γ_{380}/Γ

VALUE (units 10^{-6})	CL%	DOCUMENT ID	TECN	COMMENT
< 4.7	90	1 CHIANG	10	BELL $e^+e^- \rightarrow \Upsilon(4S)$

¹ Assumes equal production of B^+ and B^0 at the $\Upsilon(4S)$.

$\Gamma(K^*(1680)^0 \phi)/\Gamma_{total}$ Γ_{381}/Γ

VALUE (units 10^{-6})	CL%	DOCUMENT ID	TECN	COMMENT
< 3.5	90	1 AUBERT	07A0	BABR $e^+e^- \rightarrow \Upsilon(4S)$

¹ Assumes equal production of B^+ and B^0 at the $\Upsilon(4S)$.

$\Gamma(K^*(1780)^0 \phi)/\Gamma_{total}$ Γ_{382}/Γ

VALUE (units 10^{-6})	CL%	DOCUMENT ID	TECN	COMMENT
< 2.7	90	1 AUBERT	07A0	BABR $e^+e^- \rightarrow \Upsilon(4S)$

¹ Assumes equal production of B^+ and B^0 at the $\Upsilon(4S)$.

Meson Particle Listings

 B^0 $\Gamma(K^*(2045)^0 \phi) / \Gamma_{\text{total}}$ Γ_{383} / Γ

VALUE (units 10^{-6})	CL%	DOCUMENT ID	TECN	COMMENT
<15.3	90	¹ AUBERT	07A0 BABR	$e^+ e^- \rightarrow \Upsilon(4S)$

¹ Assumes equal production of B^+ and B^0 at the $\Upsilon(4S)$.

 $\Gamma(K_2^*(1430)^0 \rho^0) / \Gamma_{\text{total}}$ Γ_{384} / Γ

VALUE (units 10^{-6})	CL%	DOCUMENT ID	TECN	COMMENT
<1.1 $\times 10^3$	90	ALBRECHT	91B ARG	$e^+ e^- \rightarrow \Upsilon(4S)$

 $\Gamma(K_2^*(1430)^0 \phi) / \Gamma_{\text{total}}$ Γ_{385} / Γ

VALUE (units 10^{-6})	CL%	DOCUMENT ID	TECN	COMMENT
6.8 ± 0.9 OUR AVERAGE		Error includes scale factor of 1.2.		
$5.5^{+0.9}_{-0.7} \pm 1.0$		¹ PRIM	13 BELL	$e^+ e^- \rightarrow \Upsilon(4S)$
$7.5 \pm 0.9 \pm 0.5$		¹ AUBERT	08B0 BABR	$e^+ e^- \rightarrow \Upsilon(4S)$
• • • We do not use the following data for averages, fits, limits, etc. • • •				
$7.8 \pm 1.1 \pm 0.6$		¹ AUBERT	07D BABR	Repl. by AUBERT 08B0
		² AUBERT,B	04W BABR	Repl. by AUBERT 07D
<1400	90	ALBRECHT	91B ARG	$e^+ e^- \rightarrow \Upsilon(4S)$

¹ Assumes equal production of B^+ and B^0 at the $\Upsilon(4S)$.
² The angular distribution of $B \rightarrow \phi K^*(1430)$ provides evidence with statistical significance of 3.2σ .

 $\Gamma(K^0 \phi \phi) / \Gamma_{\text{total}}$ Γ_{386} / Γ

VALUE (units 10^{-6})	CL%	DOCUMENT ID	TECN	COMMENT
$4.5 \pm 0.8 \pm 0.3$		¹ LEES	11A BABR	$e^+ e^- \rightarrow \Upsilon(4S)$

• • • We do not use the following data for averages, fits, limits, etc. **• • •**

VALUE (units 10^{-6})	CL%	DOCUMENT ID	TECN	COMMENT
$4.1^{+1.7}_{-1.4} \pm 0.4$		¹ AUBERT,BE	06H BABR	Repl. by LEES 11A

¹ Assumes equal production of B^0 and B^+ at the $\Upsilon(4S)$ and for a $\phi\phi$ invariant mass below $2.85 \text{ GeV}/c^2$.

 $\Gamma(\eta' \eta' K^0) / \Gamma_{\text{total}}$ Γ_{387} / Γ

VALUE (units 10^{-6})	CL%	DOCUMENT ID	TECN	COMMENT
<31	90	¹ AUBERT,B	06P BABR	$e^+ e^- \rightarrow \Upsilon(4S)$

¹ Assumes equal production of B^+ and B^0 at the $\Upsilon(4S)$.

 $\Gamma(\eta K^0 \gamma) / \Gamma_{\text{total}}$ Γ_{388} / Γ

VALUE (units 10^{-6})	CL%	DOCUMENT ID	TECN	COMMENT
7.6 ± 1.8 OUR AVERAGE				
$7.1^{+2.1}_{-2.0} \pm 0.4$		^{1,2} AUBERT	09 BABR	$e^+ e^- \rightarrow \Upsilon(4S)$
$8.7^{+3.1+1.9}_{-2.7-1.6}$		^{2,3} NISHIDA	05 BELL	$e^+ e^- \rightarrow \Upsilon(4S)$
• • • We do not use the following data for averages, fits, limits, etc. • • •				
$11.3^{+2.8}_{-1.6} \pm 0.6$		^{1,2} AUBERT,B	06M BABR	Repl. by AUBERT 09

¹ $m_{\eta K} < 3.25 \text{ GeV}/c^2$.
² Assumes equal production of B^+ and B^0 at the $\Upsilon(4S)$.
³ $m_{\eta K} < 2.4 \text{ GeV}/c^2$.

 $\Gamma(\eta' K^0 \gamma) / \Gamma_{\text{total}}$ Γ_{389} / Γ

VALUE (units 10^{-6})	CL%	DOCUMENT ID	TECN	COMMENT
<6.4	90	^{1,2} WEDD	10 BELL	$e^+ e^- \rightarrow \Upsilon(4S)$
• • • We do not use the following data for averages, fits, limits, etc. • • •				
<6.6	90	^{1,3} AUBERT,B	06M BABR	$e^+ e^- \rightarrow \Upsilon(4S)$

¹ Assumes equal production of B^+ and B^0 at the $\Upsilon(4S)$.
² $m_{\eta' K} < 3.4 \text{ GeV}/c^2$.
³ $m_{\eta' K} < 3.25 \text{ GeV}/c^2$.

 $\Gamma(K^0 \phi \gamma) / \Gamma_{\text{total}}$ Γ_{390} / Γ

VALUE (units 10^{-6})	CL%	DOCUMENT ID	TECN	COMMENT
$2.74 \pm 0.60 \pm 0.32$		¹ SAHOO	11A BELL	$e^+ e^- \rightarrow \Upsilon(4S)$
• • • We do not use the following data for averages, fits, limits, etc. • • •				
<2.7	90	¹ AUBERT	07Q BABR	$e^+ e^- \rightarrow \Upsilon(4S)$
<8.3	90	¹ DRUTSKOY	04 BELL	$e^+ e^- \rightarrow \Upsilon(4S)$

¹ Assumes equal production of B^+ and B^0 at $\Upsilon(4S)$.

 $\Gamma(K^+ \pi^- \gamma) / \Gamma_{\text{total}}$ Γ_{391} / Γ

VALUE (units 10^{-6})	CL%	DOCUMENT ID	TECN	COMMENT
$(4.6^{+1.3+0.5}_{-1.2-0.7}) \times 10^{-6}$		^{1,2} NISHIDA	02 BELL	$e^+ e^- \rightarrow \Upsilon(4S)$

¹ Assumes equal production of B^+ and B^0 at the $\Upsilon(4S)$.
² $1.25 \text{ GeV}/c^2 < M_{K\pi} < 1.6 \text{ GeV}/c^2$

 $\Gamma(K^*(892)^0 \gamma) / \Gamma_{\text{total}}$ Γ_{392} / Γ

VALUE (units 10^{-6})	CL%	DOCUMENT ID	TECN	COMMENT
41.8 ± 2.5 OUR AVERAGE		Error includes scale factor of 2.1.		
$39.6 \pm 0.7 \pm 1.4$		¹ HORIGUCHI	17 BELL	$e^+ e^- \rightarrow \Upsilon(4S)$
$44.7 \pm 1.0 \pm 1.6$		² AUBERT	09A0 BABR	$e^+ e^- \rightarrow \Upsilon(4S)$
$45.5^{+7.2}_{-6.8} \pm 3.4$		³ COAN	00 CLE2	$e^+ e^- \rightarrow \Upsilon(4S)$
• • • We do not use the following data for averages, fits, limits, etc. • • •				
$39.2 \pm 2.0 \pm 2.4$		⁴ AUBERT,BE	04A BABR	Repl. by AUBERT 09A0
$40.1 \pm 2.1 \pm 1.7$		⁵ NAKAO	04 BELL	Repl. by HORIGUCHI 17
<110	90	ACOSTA	02G CDF	$p\bar{p}$ at 1.8 TeV
$42.3 \pm 4.0 \pm 2.2$		⁵ AUBERT	02C BABR	Repl. by AUBERT,BE 04A
<210	90	⁶ ADAM	96D DLPH	$e^+ e^- \rightarrow Z$
$40 \pm 17 \pm 8$		⁷ AMMAR	93 CLE2	Repl. by COAN 00
<420	90	ALBRECHT	89G ARG	$e^+ e^- \rightarrow \Upsilon(4S)$
<240	90	⁸ AVERY	89B CLEO	$e^+ e^- \rightarrow \Upsilon(4S)$
<2100	90	AVERY	87 CLEO	$e^+ e^- \rightarrow \Upsilon(4S)$

¹ Uses $B(\Upsilon(4S) \rightarrow B^+ B^-) = (51.4 \pm 0.6)\%$ and $B(\Upsilon(4S) \rightarrow B^0 \bar{B}^0) = (48.6 \pm 0.6)\%$.
² Uses $B(\Upsilon(4S) \rightarrow B^+ B^-) = (51.6 \pm 0.6)\%$ and $B(\Upsilon(4S) \rightarrow B^0 \bar{B}^0) = (48.4 \pm 0.6)\%$.
³ Assumes equal production of B^+ and B^0 at the $\Upsilon(4S)$. No evidence for a nonresonant $K\pi\gamma$ contamination was seen; the central value assumes no contamination.
⁴ Uses the production ratio of charged and neutral B from $\Upsilon(4S)$ decays $R^{+0} = 1.006 \pm 0.048$.
⁵ Assumes equal production of B^+ and B^0 at the $\Upsilon(4S)$.
⁶ ADAM 96d assumes $f_{B^0} = f_{B^-} = 0.39$ and $f_{B_s} = 0.12$.
⁷ AMMAR 93 observed 6.6 ± 2.8 events above background.
⁸ AVERY 89b reports $< 2.8 \times 10^{-4}$ assuming the $\Upsilon(4S)$ decays 43% to $B^0 \bar{B}^0$. We rescale to 50%.

 $\Gamma(K^*(1410)\gamma) / \Gamma_{\text{total}}$ Γ_{393} / Γ

VALUE (units 10^{-4})	CL%	DOCUMENT ID	TECN	COMMENT
<1.3 $\times 10^{-4}$	90	¹ NISHIDA	02 BELL	$e^+ e^- \rightarrow \Upsilon(4S)$

¹ Assumes equal production of B^+ and B^0 at the $\Upsilon(4S)$.

 $\Gamma(K^+ \pi^- \gamma \text{ nonresonant}) / \Gamma_{\text{total}}$ Γ_{394} / Γ

VALUE (units 10^{-6})	CL%	DOCUMENT ID	TECN	COMMENT
<2.6 $\times 10^{-6}$	90	^{1,2} NISHIDA	02 BELL	$e^+ e^- \rightarrow \Upsilon(4S)$

¹ Assumes equal production of B^+ and B^0 at the $\Upsilon(4S)$.
² $1.25 \text{ GeV}/c^2 < M_{K\pi} < 1.6 \text{ GeV}/c^2$

 $\Gamma(K^*(892)^0 X(214), X \rightarrow \mu^+ \mu^-) / \Gamma_{\text{total}}$ Γ_{395} / Γ

$X(214)$ is a hypothetical particle of mass $214 \text{ MeV}/c^2$ reported by the HyperCP experiment (PARK 05)

VALUE (units 10^{-8})	CL%	DOCUMENT ID	TECN	COMMENT
<2.26	90	^{1,2} HYUN	10 BELL	$e^+ e^- \rightarrow \Upsilon(4S)$

¹ Assumes equal production of B^+ and B^0 at the $\Upsilon(4S)$.
² Based on scalar nature of X particle. With a vector X assumption, the upper limit is 2.27×10^{-8} .

 $\Gamma(K^0 \pi^+ \pi^- \gamma) / \Gamma_{\text{total}}$ Γ_{396} / Γ

VALUE (units 10^{-5})	CL%	DOCUMENT ID	TECN	COMMENT
1.99 ± 0.18 OUR AVERAGE				
$2.05 \pm 0.20^{+0.26}_{-0.22}$		^{1,2} DEL-AMO-SA..16	BABR	$e^+ e^- \rightarrow \Upsilon(4S)$
$1.85 \pm 0.21 \pm 0.12$		^{1,3} AUBERT	07R BABR	$e^+ e^- \rightarrow \Upsilon(4S)$
$2.40 \pm 0.4 \pm 0.3$		^{3,4} YANG	05 BELL	$e^+ e^- \rightarrow \Upsilon(4S)$

¹ $M_{K\pi\pi} < 1.8 \text{ GeV}/c^2$.
² Uses $B(\Upsilon(4S) \rightarrow B^+ B^-) = 0.513 \pm 0.006$.
³ Assumes equal production of B^+ and B^0 at the $\Upsilon(4S)$.
⁴ $M_{K\pi\pi} < 2.0 \text{ GeV}/c^2$.

 $\Gamma(K^+ \pi^- \pi^0 \gamma) / \Gamma_{\text{total}}$ Γ_{397} / Γ

VALUE (units 10^{-5})	CL%	DOCUMENT ID	TECN	COMMENT
$4.07 \pm 0.22 \pm 0.31$		^{1,2} AUBERT	07R BABR	$e^+ e^- \rightarrow \Upsilon(4S)$

¹ $M_{K\pi\pi} < 1.8 \text{ GeV}/c^2$.
² Assumes equal production of B^+ and B^0 at the $\Upsilon(4S)$.

 $\Gamma(K_1(1270)^0 \gamma) / \Gamma_{\text{total}}$ Γ_{398} / Γ

VALUE (units 10^{-5})	CL%	DOCUMENT ID	TECN	COMMENT
< 5.8	90	¹ YANG	05 BELL	$e^+ e^- \rightarrow \Upsilon(4S)$
• • • We do not use the following data for averages, fits, limits, etc. • • •				
<700	90	² ALBRECHT	89G ARG	$e^+ e^- \rightarrow \Upsilon(4S)$

¹ Assumes equal production of B^+ and B^0 at the $\Upsilon(4S)$.
² ALBRECHT 89g reports < 0.0078 assuming the $\Upsilon(4S)$ decays 45% to $B^0 \bar{B}^0$. We rescale to 50%.

 $\Gamma(K_1(1400)^0 \gamma) / \Gamma_{\text{total}}$ Γ_{399} / Γ

VALUE (units 10^{-5})	CL%	DOCUMENT ID	TECN	COMMENT
< 1.2	90	¹ YANG	05 BELL	$e^+ e^- \rightarrow \Upsilon(4S)$
• • • We do not use the following data for averages, fits, limits, etc. • • •				
<430	90	² ALBRECHT	89G ARG	$e^+ e^- \rightarrow \Upsilon(4S)$

¹ Assumes equal production of B^+ and B^0 at the $\Upsilon(4S)$.
² ALBRECHT 89g reports < 0.0048 assuming the $\Upsilon(4S)$ decays 45% to $B^0 \bar{B}^0$. We rescale to 50%.

$\Gamma(K_S^0(1430)^0 \gamma) / \Gamma_{\text{total}}$		Γ_{400} / Γ		
VALUE (units 10 ⁻⁵)	CL%	DOCUMENT ID	TECN	COMMENT
1.24 ± 0.24 OUR AVERAGE				
1.22 ± 0.25 ± 0.10		¹ AUBERT,B	04U BABR	e ⁺ e ⁻ → T(4S)
1.3 ± 0.5 ± 0.1		¹ NISHIDA	02 BELL	e ⁺ e ⁻ → T(4S)
• • • We do not use the following data for averages, fits, limits, etc. • • •				
<40	90	² ALBRECHT	89G ARG	e ⁺ e ⁻ → T(4S)
¹ Assumes equal production of B ⁺ and B ⁰ at the T(4S).				
² ALBRECHT 89G reports < 4.4 × 10 ⁻⁴ assuming the T(4S) decays 45% to B ⁰ \bar{B}^0 . We rescale to 50%.				

$\Gamma(K^*(1680)^0 \gamma) / \Gamma_{\text{total}}$		Γ_{401} / Γ		
VALUE	CL%	DOCUMENT ID	TECN	COMMENT
<0.0020				
	90	¹ ALBRECHT	89G ARG	e ⁺ e ⁻ → T(4S)
¹ ALBRECHT 89G reports < 0.0022 assuming the T(4S) decays 45% to B ⁰ \bar{B}^0 . We rescale to 50%.				

$\Gamma(K_S^0(1780)^0 \gamma) / \Gamma_{\text{total}}$		Γ_{402} / Γ		
VALUE (units 10 ⁻⁶)	CL%	DOCUMENT ID	TECN	COMMENT
< 83				
	90	^{1,2} NISHIDA	05 BELL	e ⁺ e ⁻ → T(4S)
• • • We do not use the following data for averages, fits, limits, etc. • • •				
<10000	90	³ ALBRECHT	89G ARG	e ⁺ e ⁻ → T(4S)
¹ Assumes equal production of B ⁺ and B ⁰ at the T(4S).				
² Uses B(K _S ⁰ (1780) → ηK) = 0.11 ^{+0.05} _{-0.04} .				
³ ALBRECHT 89G reports < 0.011 assuming the T(4S) decays 45% to B ⁰ \bar{B}^0 . We rescale to 50%.				

$\Gamma(K_S^0(2045)^0 \gamma) / \Gamma_{\text{total}}$		Γ_{403} / Γ		
VALUE	CL%	DOCUMENT ID	TECN	COMMENT
<0.0043				
	90	¹ ALBRECHT	89G ARG	e ⁺ e ⁻ → T(4S)
¹ ALBRECHT 89G reports < 0.0048 assuming the T(4S) decays 45% to B ⁰ \bar{B}^0 . We rescale to 50%.				

$\Gamma(\rho^0 \gamma) / \Gamma_{\text{total}}$		Γ_{404} / Γ		
VALUE (units 10 ⁻⁶)	CL%	DOCUMENT ID	TECN	COMMENT
0.86 ± 0.15 OUR AVERAGE				
0.97 ^{+0.24} _{-0.22} ± 0.06		¹ AUBERT	08BH BABR	e ⁺ e ⁻ → T(4S)
0.78 ^{+0.17+0.09} _{-0.16-0.10}		¹ TANIGUCHI	08 BELL	e ⁺ e ⁻ → T(4S)
• • • We do not use the following data for averages, fits, limits, etc. • • •				
0.79 ^{+0.22} _{-0.20} ± 0.06		¹ AUBERT	07L BABR	Repl. by AUBERT 08BH
1.25 ^{+0.37+0.07} _{-0.33-0.06}		¹ MOHAPATRA	06 BELL	Repl. by TANIGUCHI 08
0.0 ± 0.2 ± 0.1	90	¹ AUBERT	05 BABR	Repl. by AUBERT 07L
< 0.8	90	¹ MOHAPATRA	05 BELL	e ⁺ e ⁻ → T(4S)
< 1.2	90	¹ AUBERT	04C BABR	e ⁺ e ⁻ → T(4S)
<17	90	¹ COAN	00 CLE2	e ⁺ e ⁻ → T(4S)
¹ Assumes equal production of B ⁺ and B ⁰ at the T(4S).				

$\Gamma(\rho^0 X(214), X \rightarrow \mu^+ \mu^-) / \Gamma_{\text{total}}$		Γ_{405} / Γ		
VALUE (units 10 ⁻⁸)	CL%	DOCUMENT ID	TECN	COMMENT
<1.73				
	90	^{1,2} HYUN	10 BELL	e ⁺ e ⁻ → T(4S)
¹ Assumes equal production of B ⁺ and B ⁰ at the T(4S).				
² The result is the same for a scalar or vector X particle.				

$\Gamma(\rho^0 \gamma) / \Gamma(K^*(892)^0 \gamma)$		$\Gamma_{404} / \Gamma_{392}$		
VALUE (units 10 ⁻²)	CL%	DOCUMENT ID	TECN	COMMENT
2.06^{+0.45+0.14}_{-0.43-0.16}				
		TANIGUCHI	08 BELL	e ⁺ e ⁻ → T(4S)

$\Gamma(\omega \gamma) / \Gamma_{\text{total}}$		Γ_{406} / Γ		
VALUE (units 10 ⁻⁶)	CL%	DOCUMENT ID	TECN	COMMENT
0.44^{+0.18}_{-0.16} OUR AVERAGE				
0.50 ^{+0.27} _{-0.23} ± 0.09		¹ AUBERT	08BH BABR	e ⁺ e ⁻ → T(4S)
0.40 ^{+0.19} _{-0.17} ± 0.13		¹ TANIGUCHI	08 BELL	e ⁺ e ⁻ → T(4S)
• • • We do not use the following data for averages, fits, limits, etc. • • •				
0.40 ^{+0.24} _{-0.20} ± 0.05		¹ AUBERT	07L BABR	Repl. by AUBERT 08BH
0.56 ^{+0.34+0.05} _{-0.27-0.10}		¹ MOHAPATRA	06 BELL	Repl. by TANIGUCHI 08
<1.0	90	¹ AUBERT	05 BABR	Repl. by AUBERT 07L
<0.8	90	¹ MOHAPATRA	05 BELL	Repl. by MOHAPATRA 06
<1.0	90	¹ AUBERT	04C BABR	e ⁺ e ⁻ → T(4S)
<9.2	90	¹ COAN	00 CLE2	e ⁺ e ⁻ → T(4S)
¹ Assumes equal production of B ⁺ and B ⁰ at the T(4S).				

$\Gamma(\phi \gamma) / \Gamma_{\text{total}}$		Γ_{407} / Γ		
VALUE	CL%	DOCUMENT ID	TECN	COMMENT
<1.0 × 10⁻⁷				
	90	¹ KING	16 BELL	e ⁺ e ⁻ → T(4S)
• • • We do not use the following data for averages, fits, limits, etc. • • •				
<8.5 × 10 ⁻⁷	90	¹ AUBERT,BE	05C BABR	e ⁺ e ⁻ → T(4S)
<3.3 × 10 ⁻⁶	90	¹ COAN	00 CLE2	e ⁺ e ⁻ → T(4S)
¹ Assumes equal production of B ⁺ and B ⁰ at the T(4S).				

$\Gamma(\pi^+ \pi^-) / \Gamma_{\text{total}}$		Γ_{408} / Γ		
VALUE (units 10 ⁻⁶)	CL%	DOCUMENT ID	TECN	COMMENT
5.12 ± 0.19 OUR FIT				
5.13 ± 0.24 OUR AVERAGE				
5.04 ± 0.21 ± 0.18		¹ DUH	13 BELL	e ⁺ e ⁻ → T(4S)
5.5 ± 0.4 ± 0.3		¹ AUBERT	07B BABR	e ⁺ e ⁻ → T(4S)
4.5 ^{+1.4+0.5} _{-1.2-0.4}		¹ BORNHEIM	03 CLE2	e ⁺ e ⁻ → T(4S)
• • • We do not use the following data for averages, fits, limits, etc. • • •				
5.1 ± 0.2 ± 0.2		¹ LIN	07A BELL	Repl. by DUH 13
4.4 ± 0.6 ± 0.3		¹ CHAO	04 BELL	Repl. by LIN 07A
4.7 ± 0.6 ± 0.2		¹ AUBERT	02Q BABR	Repl. by AUBERT 07B
5.4 ± 1.2 ± 0.5		¹ CASEY	02 BELL	Repl. by CHAO 04
5.6 ^{+2.3+0.4} _{-2.0-0.5}		¹ ABE	01H BELL	Repl. by CASEY 02
4.1 ± 1.0 ± 0.7		¹ AUBERT	01E BABR	Repl. by AUBERT 02Q
< 6.1	90	² ABE	00C SLD	e ⁺ e ⁻ → Z
4.3 ^{+1.6} _{-1.4} ± 0.5		¹ CRONIN-HEN..	00 CLE2	Repl. by BORNHEIM 03
< 15	90	GODANG	98 CLE2	Repl. by CRONIN-HENNESSY 00
< 45	90	³ ADAM	96D DLPH	e ⁺ e ⁻ → Z
< 20	90	ASNER	96 CLE2	Repl. by GODANG 98
< 41	90	⁴ BUSKULIC	96V ALEP	e ⁺ e ⁻ → Z
< 55	90	⁵ ABREU	95N DLPH	Sup. by ADAM 96D
< 47	90	⁶ AKERS	94L OPAL	e ⁺ e ⁻ → Z
< 29	90	¹ BATTLE	93 CLE2	e ⁺ e ⁻ → T(4S)
<130	90	¹ ALBRECHT	90B ARG	e ⁺ e ⁻ → T(4S)
< 77	90	⁷ BORTOLETTO	89 CLEO	e ⁺ e ⁻ → T(4S)
<260	90	⁷ BEBEK	87 CLEO	e ⁺ e ⁻ → T(4S)
<500	90	GILES	84 CLEO	e ⁺ e ⁻ → T(4S)
¹ Assumes equal production of B ⁺ and B ⁰ at the T(4S).				
² ABE 00C assumes B(Z → b \bar{b}) = (21.7 ± 0.1)% and the B fractions f _{B⁰} = f _{B⁺} = (39.7 ^{+1.8} _{-2.2})% and f _{B_s} = (10.5 ^{+1.8} _{-2.2})%.				
³ ADAM 96D assumes f _{B⁰} = f _{B⁻} = 0.39 and f _{B_s} = 0.12.				
⁴ BUSKULIC 96V assumes PDG 96 production fractions for B ⁰ , B ⁺ , B _s , b baryons.				
⁵ Assumes a B ⁰ , B ⁻ production fraction of 0.39 and a B _s production fraction of 0.12.				
⁶ Assumes B(Z → b \bar{b}) = 0.217 and B _d ⁰ (B _d ⁰) fraction 39.5% (12%).				
⁷ Paper assumes the T(4S) decays 43% to B ⁰ \bar{B}^0 . We rescale to 50%.				

$\Gamma(\pi^+ \pi^-) / \Gamma(K^+ \pi^-)$		$\Gamma_{408} / \Gamma_{275}$		
VALUE	CL%	DOCUMENT ID	TECN	COMMENT
0.261 ± 0.010 OUR FIT				
0.261 ± 0.015 OUR AVERAGE				
0.262 ± 0.009 ± 0.017		AALJ	12AR LHCB	pp at 7 TeV
0.259 ± 0.017 ± 0.016		AALTONEN	11N CDF	p \bar{p} at 1.96 TeV
• • • We do not use the following data for averages, fits, limits, etc. • • •				
0.21 ± 0.05 ± 0.03		ABULENCIA,A	06D CDF	Repl. by AALTONEN 11N

$\Gamma(\pi^0 \pi^0) / \Gamma_{\text{total}}$		Γ_{409} / Γ		
VALUE (units 10 ⁻⁶)	CL%	DOCUMENT ID	TECN	COMMENT
1.59 ± 0.26 OUR AVERAGE				
1.31 ± 0.19 ± 0.19		¹ JULIUS	17 BELL	e ⁺ e ⁻ → T(4S)
1.83 ± 0.21 ± 0.13		¹ LEES	13D BABR	e ⁺ e ⁻ → T(4S)
• • • We do not use the following data for averages, fits, limits, etc. • • •				
1.47 ± 0.25 ± 0.12		¹ AUBERT	07Bc BABR	Repl. by LEES 13D
1.17 ± 0.32 ± 0.10		¹ AUBERT	05L BABR	Repl. by AUBERT 07Bc
2.3 ^{+0.4+0.2} _{-0.5-0.3}		¹ CHAO	05 BELL	Repl. by JULIUS 17
< 3.6	90	¹ AUBERT	03L BABR	e ⁺ e ⁻ → T(4S)
2.1 ± 0.6 ± 0.3		¹ AUBERT	03s BABR	Repl. by AUBERT 05L
< 4.4	90	¹ BORNHEIM	03 CLE2	e ⁺ e ⁻ → T(4S)
1.7 ± 0.6 ± 0.2		¹ LEE	03 BELL	Repl. by CHAO 05
< 5.7	90	¹ ASNER	02 CLE2	e ⁺ e ⁻ → T(4S)
< 6.4	90	¹ CASEY	02 BELL	e ⁺ e ⁻ → T(4S)
< 9.3	90	GODANG	98 CLE2	Repl. by ASNER 02
< 9.1	90	ASNER	96 CLE2	Repl. by GODANG 98
<60	90	² ACCIARRI	95H L3	e ⁺ e ⁻ → Z
¹ Assumes equal production of B ⁺ and B ⁰ at the T(4S).				
² ACCIARRI 95H assumes f _{B⁰} = 39.5 ± 4.0 and f _{B_s} = 12.0 ± 3.0%.				

Meson Particle Listings

 B^0

$\Gamma(\eta\pi^0)/\Gamma_{\text{total}}$ Γ_{410}/Γ

VALUE (units 10^{-6})	CL%	DOCUMENT ID	TECN	COMMENT
$0.41^{+0.17+0.05}_{-0.15-0.07}$		1,2 PAL	15 BELL	$e^+e^- \rightarrow \Upsilon(4S)$

• • • We do not use the following data for averages, fits, limits, etc. • • •

< 1.5	90	² AUBERT	08AH BABR	$e^+e^- \rightarrow \Upsilon(4S)$
< 1.3	90	² AUBERT	06W BABR	Repl. by AUBERT 08AH
< 2.5	90	² CHANG	05A BELL	Repl. by PAL 15
< 2.5	90	² AUBERT,B	04D BABR	Repl. by AUBERT 06W
< 2.9	90	² RICHICHI	00 CLE2	$e^+e^- \rightarrow \Upsilon(4S)$
< 8	90	BEHRENS	98 CLE2	Repl. by RICHICHI 00
< 250	90	³ ACCIARRI	95H L3	$e^+e^- \rightarrow Z$
< 1800	90	² ALBRECHT	90B ARG	$e^+e^- \rightarrow \Upsilon(4S)$

¹ PAL 15 signal significance is 3.0 standard deviations. The measurement corresponds to 90% CL upper limit of $< 6.5 \times 10^{-7}$.

² Assumes equal production of B^+ and B^0 at the $\Upsilon(4S)$.

³ ACCIARRI 95H assumes $f_{B^0} = 39.5 \pm 4.0$ and $f_{B_s} = 12.0 \pm 3.0\%$.

$\Gamma(\eta)/\Gamma_{\text{total}}$ Γ_{411}/Γ

VALUE (units 10^{-6})	CL%	DOCUMENT ID	TECN	COMMENT
< 1.0	90	¹ AUBERT	09AV BABR	$e^+e^- \rightarrow \Upsilon(4S)$

• • • We do not use the following data for averages, fits, limits, etc. • • •

< 1.8	90	¹ AUBERT,B	06V BABR	Repl. by AUBERT 09AV
< 2.0	90	¹ CHANG	05A BELL	$e^+e^- \rightarrow \Upsilon(4S)$
< 2.8	90	¹ AUBERT,B	04X BABR	$e^+e^- \rightarrow \Upsilon(4S)$
< 18	90	BEHRENS	98 CLE2	$e^+e^- \rightarrow \Upsilon(4S)$
< 410	90	² ACCIARRI	95H L3	$e^+e^- \rightarrow Z$

¹ Assumes equal production of B^+ and B^0 at the $\Upsilon(4S)$.

² ACCIARRI 95H assumes $f_{B^0} = 39.5 \pm 4.0$ and $f_{B_s} = 12.0 \pm 3.0\%$.

$\Gamma(\eta'\pi^0)/\Gamma_{\text{total}}$ Γ_{412}/Γ

VALUE (units 10^{-6})	CL%	DOCUMENT ID	TECN	COMMENT
1.2 ± 0.6 OUR AVERAGE		Error includes scale factor of 1.7.		
$0.9 \pm 0.4 \pm 0.1$		¹ AUBERT	08AH BABR	$e^+e^- \rightarrow \Upsilon(4S)$
$2.8 \pm 1.0 \pm 0.3$		¹ SCHUEMANN	06 BELL	$e^+e^- \rightarrow \Upsilon(4S)$

• • • We do not use the following data for averages, fits, limits, etc. • • •

$0.8^{+0.8}_{-0.6} \pm 0.1$		¹ AUBERT	06W BABR	Repl. by AUBERT 08AH
$1.0^{+1.4}_{-1.0} \pm 0.8$	90	¹ AUBERT,B	04D BABR	Repl. by AUBERT 06W
< 5.7	90	¹ RICHICHI	00 CLE2	$e^+e^- \rightarrow \Upsilon(4S)$
< 11	90	BEHRENS	98 CLE2	Repl. by RICHICHI 00

¹ Assumes equal production of B^+ and B^0 at the $\Upsilon(4S)$.

$\Gamma(\eta'\eta)/\Gamma_{\text{total}}$ Γ_{413}/Γ

VALUE (units 10^{-6})	CL%	DOCUMENT ID	TECN	COMMENT
< 1.7	90	¹ AUBERT	09AV BABR	$e^+e^- \rightarrow \Upsilon(4S)$

• • • We do not use the following data for averages, fits, limits, etc. • • •

< 6.5	90	¹ SCHUEMANN	07 BELL	$e^+e^- \rightarrow \Upsilon(4S)$
< 2.4	90	¹ AUBERT,B	06V BABR	Repl. by AUBERT 09AV
< 10	90	¹ AUBERT,B	04X BABR	Repl. by AUBERT,B 06V
< 47	90	BEHRENS	98 CLE2	$e^+e^- \rightarrow \Upsilon(4S)$

¹ Assumes equal production of B^+ and B^0 at the $\Upsilon(4S)$.

$\Gamma(\eta'\eta)/\Gamma_{\text{total}}$ Γ_{414}/Γ

VALUE (units 10^{-6})	CL%	DOCUMENT ID	TECN	COMMENT
< 1.2	90	¹ AUBERT	08AH BABR	$e^+e^- \rightarrow \Upsilon(4S)$

• • • We do not use the following data for averages, fits, limits, etc. • • •

< 4.5	90	¹ SCHUEMANN	07 BELL	$e^+e^- \rightarrow \Upsilon(4S)$
< 1.7	90	¹ AUBERT	06W BABR	Repl. by AUBERT 08AH
< 4.6	90	¹ AUBERT,B	04X BABR	$e^+e^- \rightarrow \Upsilon(4S)$
< 27	90	BEHRENS	98 CLE2	$e^+e^- \rightarrow \Upsilon(4S)$

¹ Assumes equal production of B^+ and B^0 at the $\Upsilon(4S)$.

$\Gamma(\eta'\rho^0)/\Gamma_{\text{total}}$ Γ_{415}/Γ

VALUE (units 10^{-6})	CL%	DOCUMENT ID	TECN	COMMENT
< 1.3	90	¹ SCHUEMANN	07 BELL	$e^+e^- \rightarrow \Upsilon(4S)$

• • • We do not use the following data for averages, fits, limits, etc. • • •

< 2.8	90	¹ DEL-AMO-SA..10A	BABR	$e^+e^- \rightarrow \Upsilon(4S)$
< 3.7	90	AUBERT	07E BABR	Repl. by DEL-AMO-SANCHEZ 10A
< 4.3	90	¹ AUBERT,B	04D BABR	Repl. by AUBERT 07E
< 12	90	¹ RICHICHI	00 CLE2	$e^+e^- \rightarrow \Upsilon(4S)$
< 23	90	BEHRENS	98 CLE2	Repl. by RICHICHI 00

¹ Assumes equal production of B^+ and B^0 at the $\Upsilon(4S)$.

$\Gamma(\eta'f_0(980), f_0 \rightarrow \pi^+\pi^-)/\Gamma_{\text{total}}$ Γ_{416}/Γ

VALUE (units 10^{-6})	CL%	DOCUMENT ID	TECN	COMMENT
< 0.9	90	¹ DEL-AMO-SA..10A	BABR	$e^+e^- \rightarrow \Upsilon(4S)$

• • • We do not use the following data for averages, fits, limits, etc. • • •

< 1.5	90	AUBERT	07E BABR	Repl. by DEL-AMO-SANCHEZ 10A
-------	----	--------	----------	------------------------------

¹ Assumes equal production of B^+ and B^0 at the $\Upsilon(4S)$.

$\Gamma(\eta\rho^0)/\Gamma_{\text{total}}$ Γ_{417}/Γ

VALUE (units 10^{-6})	CL%	DOCUMENT ID	TECN	COMMENT
< 1.5	90	¹ AUBERT	07Y BABR	$e^+e^- \rightarrow \Upsilon(4S)$

• • • We do not use the following data for averages, fits, limits, etc. • • •

< 1.9	90	¹ WANG	07B BELL	$e^+e^- \rightarrow \Upsilon(4S)$
< 1.5	90	¹ AUBERT,B	04D BABR	Repl. by AUBERT 07Y
< 10	90	¹ RICHICHI	00 CLE2	$e^+e^- \rightarrow \Upsilon(4S)$
< 13	90	BEHRENS	98 CLE2	Repl. by RICHICHI 00

¹ Assumes equal production of B^+ and B^0 at the $\Upsilon(4S)$.

$\Gamma(\eta f_0(980), f_0 \rightarrow \pi^+\pi^-)/\Gamma_{\text{total}}$ Γ_{418}/Γ

VALUE (units 10^{-6})	CL%	DOCUMENT ID	TECN	COMMENT
< 0.4	90	¹ AUBERT	07Y BABR	$e^+e^- \rightarrow \Upsilon(4S)$

¹ Assumes equal production of B^+ and B^0 at the $\Upsilon(4S)$.

$\Gamma(\omega\eta)/\Gamma_{\text{total}}$ Γ_{419}/Γ

VALUE (units 10^{-6})	CL%	DOCUMENT ID	TECN	COMMENT
$0.94^{+0.35}_{-0.30} \pm 0.09$		¹ AUBERT	09AV BABR	$e^+e^- \rightarrow \Upsilon(4S)$

• • • We do not use the following data for averages, fits, limits, etc. • • •

< 1.9	90	¹ AUBERT,B	05K BABR	Repl. by AUBERT 09AV
$4.0^{+1.3}_{-1.2} \pm 0.4$		¹ AUBERT,B	04X BABR	Repl. by AUBERT,B 05K
< 12	90	¹ BERGFELD	98 CLE2	

¹ Assumes equal production of B^+ and B^0 at the $\Upsilon(4S)$.

$\Gamma(\omega\eta')/\Gamma_{\text{total}}$ Γ_{420}/Γ

VALUE (units 10^{-6})	CL%	DOCUMENT ID	TECN	COMMENT
$1.01^{+0.46}_{-0.38} \pm 0.09$		¹ AUBERT	09AV BABR	$e^+e^- \rightarrow \Upsilon(4S)$

• • • We do not use the following data for averages, fits, limits, etc. • • •

< 2.2	90	¹ SCHUEMANN	07 BELL	$e^+e^- \rightarrow \Upsilon(4S)$
< 2.8	90	¹ AUBERT,B	04X BABR	$e^+e^- \rightarrow \Upsilon(4S)$
< 60	90	¹ BERGFELD	98 CLE2	

¹ Assumes equal production of B^+ and B^0 at the $\Upsilon(4S)$.

$\Gamma(\omega\rho^0)/\Gamma_{\text{total}}$ Γ_{421}/Γ

VALUE (units 10^{-6})	CL%	DOCUMENT ID	TECN	COMMENT
< 1.6	90	¹ AUBERT	09H BABR	$e^+e^- \rightarrow \Upsilon(4S)$

• • • We do not use the following data for averages, fits, limits, etc. • • •

< 1.5	90	¹ AUBERT,B	06T BABR	Repl. by AUBERT 09H
< 3.3	90	¹ AUBERT	05o BABR	Repl. by AUBERT,B 06T
< 11	90	¹ BERGFELD	98 CLE2	

¹ Assumes equal production of B^+ and B^0 at the $\Upsilon(4S)$.

$\Gamma(\omega f_0(980), f_0 \rightarrow \pi^+\pi^-)/\Gamma_{\text{total}}$ Γ_{422}/Γ

VALUE (units 10^{-6})	CL%	DOCUMENT ID	TECN	COMMENT
< 1.5	90	¹ AUBERT	09H BABR	$e^+e^- \rightarrow \Upsilon(4S)$

• • • We do not use the following data for averages, fits, limits, etc. • • •

< 1.5	90	¹ AUBERT,B	06T BABR	Repl. by AUBERT 09H
-------	----	-----------------------	----------	---------------------

¹ Assumes equal production of B^+ and B^0 at the $\Upsilon(4S)$.

$\Gamma(\omega\omega)/\Gamma_{\text{total}}$ Γ_{423}/Γ

VALUE (units 10^{-6})	CL%	DOCUMENT ID	TECN	COMMENT
$1.2 \pm 0.3^{+0.3}_{-0.2}$		¹ LEES	14 BABR	$e^+e^- \rightarrow \Upsilon(4S)$

• • • We do not use the following data for averages, fits, limits, etc. • • •

< 4.0	90	¹ AUBERT,B	06T BABR	Repl. by LEES 14
< 19	90	¹ BERGFELD	98 CLE2	

¹ Assumes equal production of B^+ and B^0 at the $\Upsilon(4S)$.

$\Gamma(\phi\pi^0)/\Gamma_{\text{total}}$ Γ_{424}/Γ

VALUE (units 10^{-6})	CL%	DOCUMENT ID	TECN	COMMENT
< 0.15	90	¹ KIM	12A BELL	$e^+e^- \rightarrow \Upsilon(4S)$

• • • We do not use the following data for averages, fits, limits, etc. • • •

< 0.28	90	¹ AUBERT,B	06c BABR	$e^+e^- \rightarrow \Upsilon(4S)$
< 1.0	90	¹ AUBERT,B	04D BABR	Repl. by AUBERT,B 06c
< 5	90	¹ BERGFELD	98 CLE2	

¹ Assumes equal production of B^+ and B^0 at the $\Upsilon(4S)$.

$\Gamma(\phi\eta)/\Gamma_{\text{total}}$ Γ_{425}/Γ

VALUE (units 10^{-6})	CL%	DOCUMENT ID	TECN	COMMENT
< 0.5	90	¹ AUBERT	09AV BABR	$e^+e^- \rightarrow \Upsilon(4S)$

• • • We do not use the following data for averages, fits, limits, etc. • • •

< 0.6	90	¹ AUBERT,B	06V BABR	Repl. by AUBERT 09AV
< 1.0	90	¹ AUBERT,B	04X BABR	Repl. by AUBERT,B 06V
< 9	90	¹ BERGFELD	98 CLE2	

¹ Assumes equal production of B^+ and B^0 at the $\Upsilon(4S)$.

$\Gamma(\phi\eta)/\Gamma_{total}$ Γ_{426}/Γ

VALUE (units 10 ⁻⁶)	CL%	DOCUMENT ID	TECN	COMMENT
< 0.5	90	¹ SCHUEMANN 07	BELL	e ⁺ e ⁻ → $\Upsilon(4S)$
••• We do not use the following data for averages, fits, limits, etc. •••				
< 1.1	90	¹ AUBERT 09AV	BABR	e ⁺ e ⁻ → $\Upsilon(4S)$
< 1.0	90	¹ AUBERT,B 06V	BABR	Repl. by AUBERT 09AV
< 4.5	90	¹ AUBERT,B 04X	BABR	Repl. by AUBERT,B 06V
<31	90	¹ BERGFELD 98	CLE2	
¹ Assumes equal production of B ⁺ and B ⁰ at the $\Upsilon(4S)$.				

$\Gamma(\phi\pi^+\pi^-)/\Gamma_{total}$ Γ_{427}/Γ

VALUE (units 10 ⁻⁷)	DOCUMENT ID	TECN	COMMENT
1.82 ± 0.25 ± 0.43	¹ AAIJ 17A	LHCB	pp at 7, 8 TeV
¹ Signal evidence is 4.5 standard deviations.			

$\Gamma(\phi\rho^0)/\Gamma_{total}$ Γ_{428}/Γ

VALUE (units 10 ⁻⁶)	CL%	DOCUMENT ID	TECN	COMMENT
< 0.33	90	¹ AUBERT 08BK	BABR	e ⁺ e ⁻ → $\Upsilon(4S)$
••• We do not use the following data for averages, fits, limits, etc. •••				
<156	90	² ABE 00c	SLD	e ⁺ e ⁻ → Z
< 13	90	¹ BERGFELD 98	CLE2	
¹ Assumes equal production of B ⁺ and B ⁰ at the $\Upsilon(4S)$.				
² ABE 00c assumes B(Z → b \bar{b})=(21.7 ± 0.1)% and the B fractions f _{B⁰} =f _{B⁺} =(39.7 ^{+1.8} _{-2.2})% and f _{B_s} =(10.5 ^{+1.8} _{-2.2})%.				

$\Gamma(\phi f_0(980), f_0 \rightarrow \pi^+\pi^-)/\Gamma_{total}$ Γ_{429}/Γ

VALUE (units 10 ⁻⁶)	CL%	DOCUMENT ID	TECN	COMMENT
<0.38	90	¹ AUBERT 08BK	BABR	e ⁺ e ⁻ → $\Upsilon(4S)$
¹ Assumes equal production of B ⁺ and B ⁰ at the $\Upsilon(4S)$.				

$\Gamma(\phi\omega)/\Gamma_{total}$ Γ_{430}/Γ

VALUE (units 10 ⁻⁶)	CL%	DOCUMENT ID	TECN	COMMENT
< 0.7	90	¹ LEES 14	BABR	e ⁺ e ⁻ → $\Upsilon(4S)$
••• We do not use the following data for averages, fits, limits, etc. •••				
< 1.2	90	¹ AUBERT,B 06T	BABR	Repl. by LEES 14
<21	90	¹ BERGFELD 98	CLE2	
¹ Assumes equal production of B ⁺ and B ⁰ at the $\Upsilon(4S)$.				

$\Gamma(\phi\phi)/\Gamma_{total}$ Γ_{431}/Γ

VALUE	CL%	DOCUMENT ID	TECN	COMMENT
<2.7 × 10 ⁻⁸	90	AAIJ 19AP	LHCB	pp at 7, 8 and 13 TeV
••• We do not use the following data for averages, fits, limits, etc. •••				
<2.8 × 10 ⁻⁸	90	AAIJ 15AS	LHCB	Repl. by AAIJ 19AP
<2 × 10 ⁻⁷	90	¹ AUBERT 08BK	BABR	e ⁺ e ⁻ → $\Upsilon(4S)$
<1.5 × 10 ⁻⁶	90	¹ AUBERT,B 04X	BABR	Repl. by AUBERT 08BK
<3.21 × 10 ⁻⁴	90	² ABE 00c	SLD	e ⁺ e ⁻ → Z
<1.2 × 10 ⁻⁵	90	¹ BERGFELD 98	CLE2	
<3.9 × 10 ⁻⁵	90	ASNER 96	CLE2	e ⁺ e ⁻ → $\Upsilon(4S)$
¹ Assumes equal production of B ⁺ and B ⁰ at the $\Upsilon(4S)$.				
² ABE 00c assumes B(Z → b \bar{b})=(21.7 ± 0.1)% and the B fractions f _{B⁰} =f _{B⁺} =(39.7 ^{+1.8} _{-2.2})% and f _{B_s} =(10.5 ^{+1.8} _{-2.2})%.				

$\Gamma(a_0(980)\pm\pi^\mp, a_0^\pm \rightarrow \eta\pi^\pm)/\Gamma_{total}$ Γ_{432}/Γ

VALUE (units 10 ⁻⁶)	CL%	DOCUMENT ID	TECN	COMMENT
<3.1	90	¹ AUBERT 07Y	BABR	e ⁺ e ⁻ → $\Upsilon(4S)$
••• We do not use the following data for averages, fits, limits, etc. •••				
<5.1	90	¹ AUBERT,BE 04	BABR	Repl. by AUBERT 07Y
¹ Assumes equal production of B ⁺ and B ⁰ at the $\Upsilon(4S)$.				

$\Gamma(a_0(1450)\pm\pi^\mp, a_0^\pm \rightarrow \eta\pi^\pm)/\Gamma_{total}$ Γ_{433}/Γ

VALUE (units 10 ⁻⁶)	CL%	DOCUMENT ID	TECN	COMMENT
<2.3	90	¹ AUBERT 07Y	BABR	e ⁺ e ⁻ → $\Upsilon(4S)$
¹ Assumes equal production of B ⁺ and B ⁰ at the $\Upsilon(4S)$.				

$\Gamma(\pi^+\pi^-\pi^0)/\Gamma_{total}$ Γ_{434}/Γ

VALUE	CL%	DOCUMENT ID	TECN	COMMENT
<7.2 × 10 ⁻⁴	90	¹ ALBRECHT 90B	ARG	e ⁺ e ⁻ → $\Upsilon(4S)$
¹ ALBRECHT 90B limit assumes equal production of B ⁰ \bar{B}^0 and B ⁺ B ⁻ at $\Upsilon(4S)$.				

$\Gamma(\rho^0\pi^0)/\Gamma_{total}$ Γ_{435}/Γ

VALUE (units 10 ⁻⁶)	CL%	DOCUMENT ID	TECN	COMMENT
2.0 ± 0.5 OUR AVERAGE				
3.0 ± 0.5 ± 0.7		^{1,2} KUSAKA 08	BELL	e ⁺ e ⁻ → $\Upsilon(4S)$
1.4 ± 0.6 ± 0.3		¹ AUBERT 04Z	BABR	e ⁺ e ⁻ → $\Upsilon(4S)$
1.6 ^{+2.0} _{-1.4} ± 0.8		¹ JESSOP 00	CLEO	e ⁺ e ⁻ → $\Upsilon(4S)$

••• We do not use the following data for averages, fits, limits, etc. •••

3.12 ^{+0.88+0.60} _{-0.82-0.76}		¹ DRAGIC 06	BELL	Repl. by KUSAKA 08
5.1 ± 1.6 ± 0.9		DRAGIC 04	BELL	Repl. by DRAGIC 06
< 5.3	90	¹ GORDON 02	BELL	Repl. by DRAGIC 04
< 24	90	ASNER 96	CLEO	Repl. by JESSOP 00
<400	90	¹ ALBRECHT 90B	ARG	e ⁺ e ⁻ → $\Upsilon(4S)$
¹ Assumes equal production of B ⁺ and B ⁰ at the $\Upsilon(4S)$.				
² This is the first measurement that excludes contributions from $\rho(1450)$ and $\rho(1570)$ resonances.				

$\Gamma(\rho^\mp\pi^\pm)/\Gamma_{total}$ Γ_{436}/Γ

VALUE (units 10 ⁻⁶)	CL%	DOCUMENT ID	TECN	COMMENT
23.0 ± 2.3 OUR AVERAGE				
22.6 ± 1.1 ± 4.4		^{1,2} KUSAKA 08	BELL	e ⁺ e ⁻ → $\Upsilon(4S)$
22.6 ± 1.8 ± 2.2		¹ AUBERT 03T	BABR	e ⁺ e ⁻ → $\Upsilon(4S)$
27.6 ^{+8.4} _{-7.4} ± 4.2		¹ JESSOP 00	CLE2	e ⁺ e ⁻ → $\Upsilon(4S)$
••• We do not use the following data for averages, fits, limits, etc. •••				

20.8 ^{+6.0+2.8} _{-6.3-3.1}		¹ GORDON 02	BELL	Repl. by KUSAKA 08
< 88	90	ASNER 96	CLE2	Repl. by JESSOP 00
< 520	90	¹ ALBRECHT 90B	ARG	e ⁺ e ⁻ → $\Upsilon(4S)$
<5200	90	³ BEBEK 87	CLEO	e ⁺ e ⁻ → $\Upsilon(4S)$
¹ Assumes equal production of B ⁺ and B ⁰ at the $\Upsilon(4S)$.				
² This is the first measurement that excludes contributions from $\rho(1450)$ and $\rho(1570)$ resonances.				
³ BEBEK 87 reports < 6.1 × 10 ⁻³ assuming the $\Upsilon(4S)$ decays 43% to B ⁰ \bar{B}^0 . We rescale to 50%.				

$\Gamma(\pi^+\pi^-\pi^+\pi^-)/\Gamma_{total}$ Γ_{437}/Γ

VALUE	CL%	DOCUMENT ID	TECN	COMMENT
<11.2 × 10 ⁻⁶	90	¹ VANHOEFER 14	BELL	e ⁺ e ⁻ → $\Upsilon(4S)$
••• We do not use the following data for averages, fits, limits, etc. •••				
<23.1 × 10 ⁻⁶	90	¹ AUBERT 08BB	BABR	e ⁺ e ⁻ → $\Upsilon(4S)$
<19.3 × 10 ⁻⁶	90	¹ CHIANG 08	BELL	Repl. by VANHOEFER 14
< 2.3 × 10 ⁻⁴	90	² ADAM 96D	DLPH	e ⁺ e ⁻ → Z
< 2.8 × 10 ⁻⁴	90	³ ABREU 95N	DLPH	Sup. by ADAM 96D
< 6.7 × 10 ⁻⁴	90	¹ ALBRECHT 90B	ARG	e ⁺ e ⁻ → $\Upsilon(4S)$
¹ Assumes equal production of B ⁺ and B ⁰ at the $\Upsilon(4S)$.				
² ADAM 96D assumes f _{B⁰} = f _{B⁻} = 0.39 and f _{B_s} = 0.12.				
³ Assumes a B ⁰ , B ⁻ production fraction of 0.39 and a B _s production fraction of 0.12.				

$\Gamma(\rho^0\pi^+\pi^-)/\Gamma_{total}$ Γ_{438}/Γ

VALUE (units 10 ⁻⁶)	CL%	DOCUMENT ID	TECN	COMMENT
< 8.8	90	¹ AUBERT 08BB	BABR	e ⁺ e ⁻ → $\Upsilon(4S)$
••• We do not use the following data for averages, fits, limits, etc. •••				
<12.0	90	¹ VANHOEFER 14	BELL	e ⁺ e ⁻ → $\Upsilon(4S)$
<12.0	90	¹ CHIANG 08	BELL	Repl. by VANHOEFER 14
¹ Assumes equal production of B ⁺ and B ⁰ at the $\Upsilon(4S)$.				

$\Gamma(\rho^0\rho^0)/\Gamma_{total}$ Γ_{439}/Γ

VALUE (units 10 ⁻⁶)	CL%	DOCUMENT ID	TECN	COMMENT
0.96 ± 0.15 OUR FIT				
0.97 ± 0.24 OUR AVERAGE				
1.02 ± 0.30 ± 0.15		^{1,2} VANHOEFER 14	BELL	e ⁺ e ⁻ → $\Upsilon(4S)$
0.92 ± 0.32 ± 0.14		² AUBERT 08BB	BABR	e ⁺ e ⁻ → $\Upsilon(4S)$
••• We do not use the following data for averages, fits, limits, etc. •••				
0.4 ± 0.4 ^{+0.2} _{-0.3}		² CHIANG 08	BELL	Repl. by VANHOEFER 14
1.07 ± 0.33 ± 0.19		² AUBERT 07G	BABR	Repl. by AUBERT 08BB
< 1.1	90	² AUBERT 05I	BABR	Repl. by AUBERT 07G
< 2.1	90	² AUBERT 03V	BABR	Repl. by AUBERT 05I
< 18	90	³ GODANG 02	CLE2	e ⁺ e ⁻ → $\Upsilon(4S)$
<136	90	⁴ ABE 00c	SLD	e ⁺ e ⁻ → Z
<280	90	² ALBRECHT 90B	ARG	e ⁺ e ⁻ → $\Upsilon(4S)$
<290	90	⁵ BORTOLETTO 089	CLEO	e ⁺ e ⁻ → $\Upsilon(4S)$
<430	90	⁵ BEBEK 87	CLEO	e ⁺ e ⁻ → $\Upsilon(4S)$

¹ Signal significance 3.4 standard deviations.
² Assumes equal production of B⁺ and B⁰ at the $\Upsilon(4S)$.
³ Assumes a helicity 00 configuration. For a helicity 11 configuration, the limit decreases to 1.4 × 10⁻⁵.
⁴ ABE 00c assumes B(Z → b \bar{b})=(21.7 ± 0.1)% and the B fractions f_{B⁰}=f_{B⁺}=(39.7^{+1.8}_{-2.2})% and f_{B_s}=(10.5^{+1.8}_{-2.2})%.
⁵ Paper assumes the $\Upsilon(4S)$ decays 43% to B⁰ \bar{B}^0 . We rescale to 50%.

$\Gamma(\rho^0\rho^0)/\Gamma(K^*(892)^0\phi)$ $\Gamma_{439}/\Gamma_{364}$

VALUE (units 10 ⁻²)	DOCUMENT ID	TECN	COMMENT
9.5 ± 1.5 OUR FIT			
9.4 ± 1.7 ± 0.9	AAIJ 15T	LHCB	pp at 7, 8 TeV

Meson Particle Listings

 B^0 $\Gamma(\rho(980)\pi^+\pi^-, f_0 \rightarrow \pi^+\pi^-)/\Gamma_{\text{total}}$ Γ_{440}/Γ

VALUE	CL%	DOCUMENT ID	TECN	COMMENT
$<3.0 \times 10^{-6}$	90	¹ VANHOEFER 14	BELL	$e^+e^- \rightarrow \Upsilon(4S)$
••• We do not use the following data for averages, fits, limits, etc. •••				
$<3.8 \times 10^{-6}$	90	¹ CHIANG 08	BELL	$e^+e^- \rightarrow \Upsilon(4S)$
¹ Assumes equal production of B^+ and B^0 at the $\Upsilon(4S)$.				

 $\Gamma(\rho^0 f_0(980), f_0 \rightarrow \pi^+\pi^-)/\Gamma_{\text{total}}$ Γ_{441}/Γ

VALUE (units 10^{-7})	CL%	DOCUMENT ID	TECN	COMMENT
$7.8 \pm 2.2 \pm 1.1$		^{1,2} VANHOEFER 14	BELL	$e^+e^- \rightarrow \Upsilon(4S)$
••• We do not use the following data for averages, fits, limits, etc. •••				
<8.1	90	A A I J 15 ^T	LHCB	pp at 7, 8 TeV
<4.0	90	² AUBERT 08 ^{BB}	BABR	$e^+e^- \rightarrow \Upsilon(4S)$
<3	90	² CHIANG 08	BELL	Repl. by VANHOEFER 14
<5.3	90	² AUBERT 07 ^G	BABR	Repl. by AUBERT 08 ^{BB}
¹ Signal significance of 3.1 standard deviations.				
² Assumes equal production of B^+ and B^0 at the $\Upsilon(4S)$.				

 $\Gamma(f_0(980) f_0(980), f_0 \rightarrow \pi^+\pi^-, f_0 \rightarrow \pi^+\pi^-)/\Gamma_{\text{total}}$ Γ_{442}/Γ

VALUE (units 10^{-6})	CL%	DOCUMENT ID	TECN	COMMENT
<0.19	90	¹ AUBERT 08 ^{BB}	BABR	$e^+e^- \rightarrow \Upsilon(4S)$
••• We do not use the following data for averages, fits, limits, etc. •••				
<0.2	90	¹ VANHOEFER 14	BELL	$e^+e^- \rightarrow \Upsilon(4S)$
<0.1	90	¹ CHIANG 08	BELL	Repl. by VANHOEFER 14
<0.16	90	¹ AUBERT 07 ^G	BABR	Repl. by AUBERT 08 ^{BB}
¹ Assumes equal production of B^+ and B^0 at the $\Upsilon(4S)$.				

 $\Gamma(f_0(980) f_0(980), f_0 \rightarrow \pi^+\pi^-, f_0 \rightarrow K^+K^-)/\Gamma_{\text{total}}$ Γ_{443}/Γ

VALUE (units 10^{-6})	CL%	DOCUMENT ID	TECN	COMMENT
<0.23	90	¹ AUBERT 08 ^{BB}	BABR	$e^+e^- \rightarrow \Upsilon(4S)$
¹ Assumes equal production of B^+ and B^0 at the $\Upsilon(4S)$.				

 $\Gamma(a_1(1260)\pi^+\pi^-)/\Gamma_{\text{total}}$ Γ_{444}/Γ

VALUE (units 10^{-6})	CL%	DOCUMENT ID	TECN	COMMENT
26 ± 5	OUR AVERAGE	Error includes scale factor of 1.9.		
$22.2 \pm 2.0 \pm 2.8$		^{1,2} DALSENO 12	BELL	$e^+e^- \rightarrow \Upsilon(4S)$
$33.2 \pm 3.8 \pm 3.0$		^{2,3} AUBERT 06 ^V	BABR	$e^+e^- \rightarrow \Upsilon(4S)$
••• We do not use the following data for averages, fits, limits, etc. •••				
<630	90	² ALBRECHT 90 ^B	ARG	$e^+e^- \rightarrow \Upsilon(4S)$
<490	90	⁴ BORTOLETTO ⁰⁸⁹	CLEO	$e^+e^- \rightarrow \Upsilon(4S)$
<1000	90	⁴ BEBEK 87	CLEO	$e^+e^- \rightarrow \Upsilon(4S)$
¹ DALSENO 12 reports $B(B^0 \rightarrow a_1^\pm \pi^\mp) B(a_1^\pm \rightarrow \pi^\pm \pi^+ \pi^-) = (11.1 \pm 1.0 \pm 1.4) \times 10^{-6}$ which we rescaled assuming $a_1(1260)$ decays only to 3π and $B(a_1^\pm \rightarrow \pi^\pm \pi^+ \pi^-) = 0.5$.				
² Assumes equal production of B^+ and B^0 at the $\Upsilon(4S)$.				
³ Assumes $a_1(1260)$ decays only to 3π and $B(a_1^\pm \rightarrow \pi^\pm \pi^+ \pi^-) = 0.5$.				
⁴ Paper assumes the $\Upsilon(4S)$ decays 43% to $B^0 \bar{B}^0$. We rescale to 50%.				

 $\Gamma(a_2(1320)\pi^+\pi^-)/\Gamma_{\text{total}}$ Γ_{445}/Γ

VALUE	CL%	DOCUMENT ID	TECN	COMMENT
$<6.3 \times 10^{-6}$	90	¹ DALSENO 12	BELL	$e^+e^- \rightarrow \Upsilon(4S)$
••• We do not use the following data for averages, fits, limits, etc. •••				
$<3.0 \times 10^{-4}$	90	² BORTOLETTO ⁰⁸⁹	CLEO	$e^+e^- \rightarrow \Upsilon(4S)$
$<1.4 \times 10^{-3}$	90	² BEBEK 87	CLEO	$e^+e^- \rightarrow \Upsilon(4S)$
¹ DALSENO 12 reports $B(B^0 \rightarrow a_2^\pm \pi^\mp) B(a_2^\pm \rightarrow \pi^\pm \pi^+ \pi^-) < 2.2 \times 10^{-6}$ which we rescaled using $B(a_2^\pm \rightarrow \pi^\pm \pi^+ \pi^-) = 1/2 B(a_2^\pm \rightarrow 3\pi) = 0.35 \pm 0.013$.				
² Paper assumes the $\Upsilon(4S)$ decays 43% to $B^0 \bar{B}^0$. We rescale to 50%.				

 $\Gamma(\pi^+\pi^-\pi^0\pi^0)/\Gamma_{\text{total}}$ Γ_{446}/Γ

VALUE	CL%	DOCUMENT ID	TECN	COMMENT
$<3.1 \times 10^{-3}$	90	¹ ALBRECHT 90 ^B	ARG	$e^+e^- \rightarrow \Upsilon(4S)$
¹ ALBRECHT 90 ^B limit assumes equal production of $B^0 \bar{B}^0$ and $B^+ B^-$ at $\Upsilon(4S)$.				

 $\Gamma(\rho^+\rho^-)/\Gamma_{\text{total}}$ Γ_{447}/Γ

VALUE (units 10^{-6})	CL%	DOCUMENT ID	TECN	COMMENT
27.7 ± 1.9	OUR AVERAGE			
$28.3 \pm 1.5 \pm 1.5$		¹ VANHOEFER 16	BELL	$e^+e^- \rightarrow \Upsilon(4S)$
$25.5 \pm 2.1 \pm 3.6$		¹ AUBERT 07 ^{BF}	BABR	$e^+e^- \rightarrow \Upsilon(4S)$
••• We do not use the following data for averages, fits, limits, etc. •••				
$22.8 \pm 3.8 \pm 2.3$		¹ SOMOV 06	BELL	Repl. by VANHOEFER 16
$25 \pm 7 \pm 5$		¹ AUBERT 04 ^G	BABR	Repl. by AUBERT, B 04 ^R
$30 \pm 4 \pm 5$		^{1,2} AUBERT, B 04 ^R	BABR	Repl. by AUBERT 07 ^{BF}
<2200	90	¹ ALBRECHT 90 ^B	ARG	$e^+e^- \rightarrow \Upsilon(4S)$
¹ Assumes equal production of B^+ and B^0 at the $\Upsilon(4S)$.				
² The quoted result is obtained after combining with AUBERT 04 ^G result by AUBERT 04 ^R alone gives $(33 \pm 4 \pm 5) \times 10^{-6}$.				

 $\Gamma(a_1(1260)^0\pi^0)/\Gamma_{\text{total}}$ Γ_{448}/Γ

VALUE	CL%	DOCUMENT ID	TECN	COMMENT
$<1.1 \times 10^{-3}$	90	¹ ALBRECHT 90 ^B	ARG	$e^+e^- \rightarrow \Upsilon(4S)$
¹ ALBRECHT 90 ^B limit assumes equal production of $B^0 \bar{B}^0$ and $B^+ B^-$ at $\Upsilon(4S)$.				

 $\Gamma(\omega\pi^0)/\Gamma_{\text{total}}$ Γ_{449}/Γ

VALUE (units 10^{-6})	CL%	DOCUMENT ID	TECN	COMMENT
<0.5	90	¹ AUBERT 08 ^{AH}	BABR	$e^+e^- \rightarrow \Upsilon(4S)$
••• We do not use the following data for averages, fits, limits, etc. •••				
<2.0	90	¹ JEN 06	BELL	$e^+e^- \rightarrow \Upsilon(4S)$
<1.2	90	¹ AUBERT, B 04 ^D	BABR	Repl. by AUBERT 08 ^{AH}
<1.9	90	¹ WANG 04 ^A	BELL	$e^+e^- \rightarrow \Upsilon(4S)$
<3	90	¹ AUBERT 01 ^G	BABR	$e^+e^- \rightarrow \Upsilon(4S)$
<5.5	90	¹ JESSOP 00	CLE2	$e^+e^- \rightarrow \Upsilon(4S)$
<14	90	¹ BERGFELD 98	CLE2	Repl. by JESSOP 00
<460	90	² ALBRECHT 90 ^B	ARG	$e^+e^- \rightarrow \Upsilon(4S)$
¹ Assumes equal production of B^+ and B^0 at the $\Upsilon(4S)$.				
² ALBRECHT 90 ^B limit assumes equal production of $B^0 \bar{B}^0$ and $B^+ B^-$ at $\Upsilon(4S)$.				

 $\Gamma(\pi^+\pi^+\pi^-\pi^0)/\Gamma_{\text{total}}$ Γ_{450}/Γ

VALUE	CL%	DOCUMENT ID	TECN	COMMENT
$<9.0 \times 10^{-3}$	90	¹ ALBRECHT 90 ^B	ARG	$e^+e^- \rightarrow \Upsilon(4S)$
¹ ALBRECHT 90 ^B limit assumes equal production of $B^0 \bar{B}^0$ and $B^+ B^-$ at $\Upsilon(4S)$.				

 $\Gamma(a_1(1260)^+\rho^-)/\Gamma_{\text{total}}$ Γ_{451}/Γ

VALUE (units 10^{-6})	CL%	DOCUMENT ID	TECN	COMMENT
<61	90	^{1,2} AUBERT, B 06 ^O	BABR	$e^+e^- \rightarrow \Upsilon(4S)$
••• We do not use the following data for averages, fits, limits, etc. •••				
<3400	90	¹ ALBRECHT 90 ^B	ARG	$e^+e^- \rightarrow \Upsilon(4S)$
¹ Assumes equal production of B^+ and B^0 at the $\Upsilon(4S)$.				
² Assumes $a_1(1260)$ decays only to 3π and $B(a_1^\pm \rightarrow \pi^\pm \pi^+ \pi^-) = 0.5$.				

 $\Gamma(a_1(1260)^0\rho^0)/\Gamma_{\text{total}}$ Γ_{452}/Γ

VALUE	CL%	DOCUMENT ID	TECN	COMMENT
$<2.4 \times 10^{-3}$	90	¹ ALBRECHT 90 ^B	ARG	$e^+e^- \rightarrow \Upsilon(4S)$
¹ ALBRECHT 90 ^B limit assumes equal production of $B^0 \bar{B}^0$ and $B^+ B^-$ at $\Upsilon(4S)$.				

 $\Gamma(b_1^-\pi^\pm, b_1^{\mp} \rightarrow \omega\pi^\mp)/\Gamma_{\text{total}}$ Γ_{453}/Γ

VALUE (units 10^{-6})	CL%	DOCUMENT ID	TECN	COMMENT
$10.9 \pm 1.2 \pm 0.9$		¹ AUBERT 07 ^{BI}	BABR	$e^+e^- \rightarrow \Upsilon(4S)$
¹ Assumes equal production of B^+ and B^0 at the $\Upsilon(4S)$.				

 $\Gamma(b_1^0\rho^0, b_1^0 \rightarrow \omega\pi^0)/\Gamma_{\text{total}}$ Γ_{454}/Γ

VALUE (units 10^{-6})	CL%	DOCUMENT ID	TECN	COMMENT
<1.9	90	¹ AUBERT 08 ^{AG}	BABR	$e^+e^- \rightarrow \Upsilon(4S)$
¹ Assumes equal production of B^+ and B^0 at the $\Upsilon(4S)$.				

 $\Gamma(b_1^-\rho^+, b_1^- \rightarrow \omega\pi^-)/\Gamma_{\text{total}}$ Γ_{455}/Γ

VALUE	CL%	DOCUMENT ID	TECN	COMMENT
$<1.4 \times 10^{-6}$	90	¹ AUBERT 09 ^{AF}	BABR	$e^+e^- \rightarrow \Upsilon(4S)$
¹ Assumes equal production of B^+ and B^0 at the $\Upsilon(4S)$.				

 $\Gamma(b_1^0\rho^0, b_1^0 \rightarrow \omega\pi^0)/\Gamma_{\text{total}}$ Γ_{456}/Γ

VALUE	CL%	DOCUMENT ID	TECN	COMMENT
$<3.4 \times 10^{-6}$	90	¹ AUBERT 09 ^{AF}	BABR	$e^+e^- \rightarrow \Upsilon(4S)$
¹ Assumes equal production of B^+ and B^0 at the $\Upsilon(4S)$.				

 $\Gamma(\pi^+\pi^+\pi^-\pi^-\pi^0)/\Gamma_{\text{total}}$ Γ_{457}/Γ

VALUE	CL%	DOCUMENT ID	TECN	COMMENT
$<3.0 \times 10^{-3}$	90	¹ ALBRECHT 90 ^B	ARG	$e^+e^- \rightarrow \Upsilon(4S)$
¹ ALBRECHT 90 ^B limit assumes equal production of $B^0 \bar{B}^0$ and $B^+ B^-$ at $\Upsilon(4S)$.				

 $\Gamma(a_1(1260)^+ a_1(1260)^-, a_1^+ \rightarrow 2\pi^+\pi^-, a_1^- \rightarrow 2\pi^-\pi^+)/\Gamma_{\text{total}}$ Γ_{458}/Γ

VALUE (units 10^{-6})	CL%	DOCUMENT ID	TECN	COMMENT
$11.8 \pm 2.6 \pm 1.6$		¹ AUBERT 09 ^{AL}	BABR	$e^+e^- \rightarrow \Upsilon(4S)$
••• We do not use the following data for averages, fits, limits, etc. •••				
<6000	90	¹ ALBRECHT 90 ^B	ARG	$e^+e^- \rightarrow \Upsilon(4S)$
<2800	90	² BORTOLETTO ⁰⁸⁹	CLEO	$e^+e^- \rightarrow \Upsilon(4S)$
¹ Assumes equal production of $B^0 \bar{B}^0$ and $B^+ B^-$ at $\Upsilon(4S)$.				
² BORTOLETTO 89 reports $< 3.2 \times 10^{-3}$ assuming the $\Upsilon(4S)$ decays 43% to $B^0 \bar{B}^0$. We rescale to 50%.				

 $\Gamma(\pi^+\pi^+\pi^-\pi^-\pi^0)/\Gamma_{\text{total}}$ Γ_{459}/Γ

VALUE	CL%	DOCUMENT ID	TECN	COMMENT
$<1.1 \times 10^{-2}$	90	¹ ALBRECHT 90 ^B	ARG	$e^+e^- \rightarrow \Upsilon(4S)$
¹ ALBRECHT 90 ^B limit assumes equal production of $B^0 \bar{B}^0$ and $B^+ B^-$ at $\Upsilon(4S)$.				

$\Gamma(p\bar{p})/\Gamma_{\text{total}}$		Γ_{460}/Γ		
VALUE (units 10^{-8})	CL%	DOCUMENT ID	TECN	COMMENT
1.25 ± 0.27 ± 0.18		¹ AAIJ	17B LHCb	pp at 7 and 8 TeV
1.47 ^{+0.62+0.35} _{-0.51-0.14}		² AAIJ	13Bq LHCb	Repl. by AAIJ 17Bj
< 11	90	³ TSAI	07 BELL	$e^+e^- \rightarrow \Upsilon(4S)$
< 41	90	³ CHANG	05 BELL	$e^+e^- \rightarrow \Upsilon(4S)$
< 27	90	³ AUBERT	04U BABR	$e^+e^- \rightarrow \Upsilon(4S)$
< 140	90	³ BORNHEIM	03 CLE2	$e^+e^- \rightarrow \Upsilon(4S)$
< 120	90	³ ABE	02o BELL	$e^+e^- \rightarrow \Upsilon(4S)$
< 700	90	³ COAN	99 CLE2	$e^+e^- \rightarrow \Upsilon(4S)$
< 1800	90	⁴ BUSKULIC	96V ALEP	$e^+e^- \rightarrow Z$
< 35000	90	⁵ ABREU	95N DLPH	Sup. by ADAM 96D
< 3400	90	⁶ BORTOLETTO	089 CLEO	$e^+e^- \rightarrow \Upsilon(4S)$
< 12000	90	⁷ ALBRECHT	88F ARG	$e^+e^- \rightarrow \Upsilon(4S)$
< 17000	90	⁶ BEBEK	87 CLEO	$e^+e^- \rightarrow \Upsilon(4S)$

¹ Uses normalization mode $B(B^0 \rightarrow K^+\pi^-) = (19.6 \pm 0.5) \times 10^{-6}$.
² Uses normalization mode $B(B^0 \rightarrow K^+\pi^-) = (19.55 \pm 0.54) \times 10^{-6}$.
³ Assumes equal production of B^+ and B^0 at the $\Upsilon(4S)$.
⁴ BUSKULIC 96V assumes PDG 96 production fractions for B^0, B^+, B_s, b baryons.
⁵ Assumes a B^0, B^- production fraction of 0.39 and a B_s production fraction of 0.12.
⁶ Paper assumes the $\Upsilon(4S)$ decays 43% to $B^0\bar{B}^0$. We rescale to 50%.
⁷ ALBRECHT 88F reports $< 1.3 \times 10^{-4}$ assuming the $\Upsilon(4S)$ decays 45% to $B^0\bar{B}^0$. We rescale to 50%.

$\Gamma(p\bar{p}\pi^+\pi^-)/\Gamma_{\text{total}}$		Γ_{461}/Γ		
VALUE (units 10^{-6})	CL%	DOCUMENT ID	TECN	COMMENT
2.87 ± 0.15 ± 0.11		^{1,2} AAIJ	17Bd LHCb	pp at 7, 8 TeV
< 950	90	³ ABREU	95N DLPH	Sup. by ADAM 96D
< 250	90	⁴ BEBEK	89 CLEO	$e^+e^- \rightarrow \Upsilon(4S)$
540 ± 180 ± 200		⁵ ALBRECHT	88F ARG	$e^+e^- \rightarrow \Upsilon(4S)$

¹ AAIJ 17Bd reports $[\Gamma(B^0 \rightarrow p\bar{p}\pi^+\pi^-)/\Gamma_{\text{total}}] / [B(B^0 \rightarrow J/\psi(1S)K^*(892)^0)] / [B(J/\psi(1S) \rightarrow p\bar{p})] / [B(K^*(892) \rightarrow (K\pi)^\pm)] = 1.07 \pm 0.04 \pm 0.04$ which we multiply by our best values $B(B^0 \rightarrow J/\psi(1S)K^*(892)^0) = (1.27 \pm 0.05) \times 10^{-3}$, $B(J/\psi(1S) \rightarrow p\bar{p}) = (2.121 \pm 0.029) \times 10^{-3}$, $B(K^*(892) \rightarrow (K\pi)^\pm) = (99.901 \pm 0.009) \times 10^{-2}$. Our first error is their experiment's error and our second error is the systematic error from using our best values.
² The branching ratio is given for $m_{p\bar{p}} < 2.85$ GeV.
³ Assumes a B^0, B^- production fraction of 0.39 and a B_s production fraction of 0.12.
⁴ BEBEK 89 reports $< 2.9 \times 10^{-4}$ assuming the $\Upsilon(4S)$ decays 43% to $B^0\bar{B}^0$. We rescale to 50%.
⁵ ALBRECHT 88F reports $6.0 \pm 2.0 \pm 2.2$ assuming the $\Upsilon(4S)$ decays 45% to $B^0\bar{B}^0$. We rescale to 50%.

$\Gamma(p\bar{p}\pi^+\pi^-)/\Gamma(p\bar{p}K^+\pi^-)$		$\Gamma_{461}/\Gamma_{462}$		
VALUE		DOCUMENT ID	TECN	COMMENT
0.46 ± 0.02 ± 0.02		¹ AAIJ	17Bd LHCb	pp at 7, 8 TeV

¹ The ratio is given for $m_{p\bar{p}} < 2.85$ GeV.

$\Gamma(p\bar{p}K^0)/\Gamma_{\text{total}}$		Γ_{463}/Γ		
VALUE (units 10^{-6})	CL%	DOCUMENT ID	TECN	COMMENT
2.66 ± 0.32 OUR AVERAGE				
2.51 ^{+0.35} _{-0.29} ± 0.21		^{1,2} CHEN	08c BELL	$e^+e^- \rightarrow \Upsilon(4S)$
3.0 ± 0.5 ± 0.3		² AUBERT	07AV BABR	$e^+e^- \rightarrow \Upsilon(4S)$
2.40 ^{+0.64} _{-0.44} ± 0.28		^{2,3,4} WANG	05A BELL	Repl. by CHEN 08c
1.88 ^{+0.77} _{-0.60} ± 0.23		^{2,3,5} WANG	04 BELL	Repl. by WANG 05A
< 7.2	90	^{2,3} ABE	02k BELL	Repl. by WANG 04

¹ Explicitly vetoes resonant production of $p\bar{p}$ from charmonium states.
² Assumes equal production of B^+ and B^0 at the $\Upsilon(4S)$.
³ Explicitly vetoes resonant production of $p\bar{p}$ from charmonium states and pK^0 production from Λ_c .
⁴ Provides also results with $M_{p\bar{p}} < 2.85$ GeV/ c^2 and angular asymmetry of $p\bar{p}$ system.
⁵ The branching fraction for $M_{p\bar{p}} < 2.85$ is also reported.

$\Gamma(\Theta(1540)^+\bar{p}, \Theta^+ \rightarrow pK_S^0)/\Gamma_{\text{total}}$		Γ_{464}/Γ		
VALUE (units 10^{-6})	CL%	DOCUMENT ID	TECN	COMMENT
< 0.05		¹ AUBERT	07AV BABR	$e^+e^- \rightarrow \Upsilon(4S)$
< 0.23	90	¹ WANG	05A BELL	$e^+e^- \rightarrow \Upsilon(4S)$

¹ Assumes equal production of B^+ and B^0 at the $\Upsilon(4S)$.

$\Gamma(f_J(2220)K^0, f_J \rightarrow p\bar{p})/\Gamma_{\text{total}}$		Γ_{465}/Γ		
VALUE (units 10^{-6})	CL%	DOCUMENT ID	TECN	COMMENT
< 0.45		¹ AUBERT	07AV BABR	$e^+e^- \rightarrow \Upsilon(4S)$

¹ Assumes equal production of B^+ and B^0 at the $\Upsilon(4S)$.

$\Gamma(p\bar{p}K^+\pi^-)/\Gamma_{\text{total}}$		Γ_{462}/Γ		
VALUE (units 10^{-8})		DOCUMENT ID	TECN	COMMENT
6.3 ± 0.5 ± 0.2		^{1,2} AAIJ	17Bd LHCb	pp at 7, 8 TeV

¹ AAIJ 17Bd reports $[\Gamma(B^0 \rightarrow p\bar{p}K^+\pi^-)/\Gamma_{\text{total}}] / [B(B^0 \rightarrow J/\psi(1S)K^*(892)^0)] / [B(J/\psi(1S) \rightarrow p\bar{p})] / [B(K^*(892) \rightarrow (K\pi)^\pm)] = 2.34 \pm 0.12 \pm 0.12$ which we multiply by our best values $B(B^0 \rightarrow J/\psi(1S)K^*(892)^0) = (1.27 \pm 0.05) \times 10^{-3}$, $B(J/\psi(1S) \rightarrow p\bar{p}) = (2.121 \pm 0.029) \times 10^{-3}$, $B(K^*(892) \rightarrow (K\pi)^\pm) = (99.901 \pm 0.009) \times 10^{-2}$. Our first error is their experiment's error and our second error is the systematic error from using our best values.
² The branching ratio is given for $m_{p\bar{p}} < 2.85$ GeV.

$\Gamma(p\bar{p}K^*(892)^0)/\Gamma_{\text{total}}$		Γ_{466}/Γ		
VALUE (units 10^{-6})	CL%	DOCUMENT ID	TECN	COMMENT
1.24 ± 0.28 ± 0.25 OUR AVERAGE				
1.18 ^{+0.29} _{-0.25} ± 0.11		^{1,2} CHEN	08c BELL	$e^+e^- \rightarrow \Upsilon(4S)$
1.47 ± 0.45 ± 0.40		² AUBERT	07AV BABR	$e^+e^- \rightarrow \Upsilon(4S)$
< 7.6	90	² WANG	04 BELL	$e^+e^- \rightarrow \Upsilon(4S)$

¹ Explicitly vetoes resonant production of $p\bar{p}$ from charmonium states.
² Assumes equal production of B^+ and B^0 at the $\Upsilon(4S)$.

$\Gamma(p\bar{p}\pi^0)/\Gamma_{\text{total}}$		Γ_{469}/Γ		
VALUE (units 10^{-7})		DOCUMENT ID	TECN	COMMENT
5.0 ± 1.8 ± 0.6		PAL	19 BELL	$e^+e^- \rightarrow \Upsilon(4S)$

$\Gamma(f_J(2220)K_S^0, f_J \rightarrow p\bar{p})/\Gamma_{\text{total}}$		Γ_{467}/Γ		
VALUE (units 10^{-6})	CL%	DOCUMENT ID	TECN	COMMENT
< 0.15		¹ AUBERT	07AV BABR	$e^+e^- \rightarrow \Upsilon(4S)$

¹ Assumes equal production of B^+ and B^0 at the $\Upsilon(4S)$.

$\Gamma(p\bar{p}K^+K^-)/\Gamma_{\text{total}}$		Γ_{468}/Γ		
VALUE (units 10^{-8})		DOCUMENT ID	TECN	COMMENT
12.1 ± 3.1 ± 0.5		^{1,2} AAIJ	17Bd LHCb	pp at 7, 8 TeV

¹ AAIJ 17Bd reports $[\Gamma(B^0 \rightarrow p\bar{p}K^+K^-)/\Gamma_{\text{total}}] / [B(B^0 \rightarrow J/\psi(1S)K^*(892)^0)] / [B(J/\psi(1S) \rightarrow p\bar{p})] / [B(K^*(892) \rightarrow (K\pi)^\pm)] = 0.045 \pm 0.011 \pm 0.004$ which we multiply by our best values $B(B^0 \rightarrow J/\psi(1S)K^*(892)^0) = (1.27 \pm 0.05) \times 10^{-3}$, $B(J/\psi(1S) \rightarrow p\bar{p}) = (2.121 \pm 0.029) \times 10^{-3}$, $B(K^*(892) \rightarrow (K\pi)^\pm) = (99.901 \pm 0.009) \times 10^{-2}$. Our first error is their experiment's error and our second error is the systematic error from using our best values.
² The branching ratio is given for $m_{p\bar{p}} < 2.85$ GeV.

$\Gamma(p\bar{p}K^+K^-)/\Gamma(p\bar{p}K^+\pi^-)$		$\Gamma_{468}/\Gamma_{462}$		
VALUE (%)		DOCUMENT ID	TECN	COMMENT
1.9 ± 0.5 ± 0.2		¹ AAIJ	17Bd LHCb	pp at 7, 8 TeV

¹ The ratio is given for $m_{p\bar{p}} < 2.85$ GeV.

$\Gamma(p\bar{p}p\bar{p})/\Gamma_{\text{total}}$		Γ_{470}/Γ		
VALUE	CL%	DOCUMENT ID	TECN	COMMENT
< 2.0 × 10⁻⁷		¹ LEES	18c BABR	$e^+e^- \rightarrow \Upsilon(4S)$

¹ Assumes equal production of B^+ and B^0 at the $\Upsilon(4S)$.

$\Gamma(p\bar{p}\pi^-)/\Gamma_{\text{total}}$		Γ_{471}/Γ		
VALUE (units 10^{-6})	CL%	DOCUMENT ID	TECN	COMMENT
3.14 ± 0.29 OUR AVERAGE				
3.07 ± 0.31 ± 0.23		¹ AUBERT	09Ac BABR	$e^+e^- \rightarrow \Upsilon(4S)$
3.23 ^{+0.33} _{-0.29} ± 0.29		¹ WANG	07c BELL	$e^+e^- \rightarrow \Upsilon(4S)$
2.62 ^{+0.44} _{-0.40} ± 0.31		^{1,2} WANG	05A BELL	Repl. by WANG 07c
3.97 ^{+1.00} _{-0.80} ± 0.56		¹ WANG	03 BELL	Repl. by WANG 05A
< 13	90	¹ COAN	99 CLE2	$e^+e^- \rightarrow \Upsilon(4S)$
< 180	90	³ ALBRECHT	88F ARG	$e^+e^- \rightarrow \Upsilon(4S)$

¹ Assumes equal production of B^+ and B^0 at the $\Upsilon(4S)$.
² Provides also results with $M_{p\bar{p}} < 2.85$ GeV/ c^2 and angular asymmetry of $p\bar{p}$ system.
³ ALBRECHT 88F reports $< 2.0 \times 10^{-4}$ assuming the $\Upsilon(4S)$ decays 45% to $B^0\bar{B}^0$. We rescale to 50%.

$\Gamma(p\bar{p}\pi^-\gamma)/\Gamma_{\text{total}}$		Γ_{472}/Γ		
VALUE	CL%	DOCUMENT ID	TECN	COMMENT
< 6.5 × 10⁻⁷		¹ LAI	14 BELL	$e^+e^- \rightarrow \Upsilon(4S)$

¹ Assumes equal production of B^+ and B^0 at the $\Upsilon(4S)$.

$\Gamma(p\bar{p}\Sigma^-(1385)^-)/\Gamma_{\text{total}}$		Γ_{473}/Γ		
VALUE (units 10^{-6})	CL%	DOCUMENT ID	TECN	COMMENT
< 0.26		¹ WANG	07c BELL	$e^+e^- \rightarrow \Upsilon(4S)$

¹ Assumes equal production of B^+ and B^0 at the $\Upsilon(4S)$.

Meson Particle Listings

 B^0

$\Gamma(\Delta(1232)^+ \bar{p}) + \Gamma(\Delta(1232)^- p) / \Gamma_{\text{total}}$				Γ_{474} / Γ
VALUE	DOCUMENT ID	TECN	COMMENT	
$<1.6 \times 10^{-6}$	PAL	19	BELL $e^+ e^- \rightarrow \Upsilon(4S)$	

$\Gamma(\Delta^0 \bar{\Lambda}) / \Gamma_{\text{total}}$				Γ_{475} / Γ
VALUE (units 10^{-6})	CL%	DOCUMENT ID	TECN	COMMENT
<0.93	90	1 WANG	07c	BELL $e^+ e^- \rightarrow \Upsilon(4S)$
¹ Assumes equal production of B^+ and B^0 at the $\Upsilon(4S)$.				

$\Gamma(p \bar{\Lambda} K^-) / \Gamma_{\text{total}}$				Γ_{476} / Γ
VALUE (units 10^{-6})	CL%	DOCUMENT ID	TECN	COMMENT
<0.82	90	1 WANG	03	BELL $e^+ e^- \rightarrow \Upsilon(4S)$
¹ Assumes equal production of B^+ and B^0 at the $\Upsilon(4S)$.				

$\Gamma(p \bar{\Lambda} D^-) / \Gamma_{\text{total}}$				Γ_{477} / Γ
VALUE (units 10^{-6})	CL%	DOCUMENT ID	TECN	COMMENT
$25.1 \pm 2.6 \pm 3.5$		1 CHANG	15	BELL $e^+ e^- \rightarrow \Upsilon(4S)$
¹ Assumes equal production of B^+ and B^0 at the $\Upsilon(4S)$.				

$\Gamma(p \bar{\Lambda} D^{*-}) / \Gamma_{\text{total}}$				Γ_{478} / Γ
VALUE (units 10^{-6})	CL%	DOCUMENT ID	TECN	COMMENT
$33.6 \pm 6.3 \pm 4.4$		1 CHANG	15	BELL $e^+ e^- \rightarrow \Upsilon(4S)$
¹ Assumes equal production of B^+ and B^0 at the $\Upsilon(4S)$.				

$\Gamma(p \Sigma^0 \pi^-) / \Gamma_{\text{total}}$				Γ_{479} / Γ
VALUE	CL%	DOCUMENT ID	TECN	COMMENT
$<3.8 \times 10^{-6}$	90	1 WANG	03	BELL $e^+ e^- \rightarrow \Upsilon(4S)$
¹ Assumes equal production of B^+ and B^0 at the $\Upsilon(4S)$.				

$\Gamma(\bar{\Lambda}) / \Gamma_{\text{total}}$				Γ_{480} / Γ
VALUE (units 10^{-6})	CL%	DOCUMENT ID	TECN	COMMENT
<0.32	90	1 TSAI	07	BELL $e^+ e^- \rightarrow \Upsilon(4S)$
• • • We do not use the following data for averages, fits, limits, etc. • • •				
<0.69	90	1 CHANG	05	BELL Repl. by TSAI 07
<1.2	90	1 BORNHEIM	03	CLE2 $e^+ e^- \rightarrow \Upsilon(4S)$
<1.0	90	1 ABE	02o	BELL Repl. by CHANG 05
<3.9	90	1 COAN	99	CLE2 $e^+ e^- \rightarrow \Upsilon(4S)$
¹ Assumes equal production of B^+ and B^0 at the $\Upsilon(4S)$.				

$\Gamma(\bar{\Lambda} \Lambda K^0) / \Gamma_{\text{total}}$				Γ_{481} / Γ
VALUE (units 10^{-6})	CL%	DOCUMENT ID	TECN	COMMENT
$4.76 \pm 0.84 \pm 0.61$		1,2 CHANG	09	BELL $e^+ e^- \rightarrow \Upsilon(4S)$
¹ Excluding charmonium events in $2.85 < m_{\Lambda \bar{\Lambda}} < 3.128 \text{ GeV}/c^2$ and $3.315 < m_{\Lambda \bar{\Lambda}} < 3.735 \text{ GeV}/c^2$. Measurements in various $m_{\Lambda \bar{\Lambda}}$ bins are also reported.				
² Assumes equal production of B^+ and B^0 at the $\Upsilon(4S)$.				

$\Gamma(\bar{\Lambda} \Lambda K^{*0}) / \Gamma_{\text{total}}$				Γ_{482} / Γ
VALUE (units 10^{-6})	CL%	DOCUMENT ID	TECN	COMMENT
$2.46 \pm 0.87 \pm 0.72 \pm 0.34$		1,2 CHANG	09	BELL $e^+ e^- \rightarrow \Upsilon(4S)$
¹ Excluding charmonium events in $2.85 < m_{\Lambda \bar{\Lambda}} < 3.128 \text{ GeV}/c^2$ and $3.315 < m_{\Lambda \bar{\Lambda}} < 3.735 \text{ GeV}/c^2$. Measurements in various $m_{\Lambda \bar{\Lambda}}$ bins are also reported.				
² Assumes equal production of B^+ and B^0 at the $\Upsilon(4S)$.				

$\Gamma(\bar{\Lambda} \Lambda D^0) / \Gamma_{\text{total}}$				Γ_{483} / Γ
VALUE (units 10^{-5})	CL%	DOCUMENT ID	TECN	COMMENT
$1.00 \pm 0.30 \pm 0.26$ OUR AVERAGE				
$0.90 \pm 0.29 \pm 0.19$		1,2 LEES	14b	BABR $e^+ e^- \rightarrow \Upsilon(4S)$
$1.05 \pm 0.57 \pm 0.14$		2 CHANG	09	BELL $e^+ e^- \rightarrow \Upsilon(4S)$
¹ Evidence for 3.4 st. dev. signal significance.				
² Assumes equal production of B^+ and B^0 at the $\Upsilon(4S)$.				

$\Gamma(D^0 \Sigma^0 \bar{\Lambda} + \text{c.c.}) / \Gamma_{\text{total}}$				Γ_{484} / Γ
VALUE	CL%	DOCUMENT ID	TECN	COMMENT
$<3.1 \times 10^{-5}$	90	1,2 LEES	14b	BABR $e^+ e^- \rightarrow \Upsilon(4S)$
¹ Here $\Sigma^0 \rightarrow \Lambda \gamma$.				
² Assumes equal production of B^+ and B^0 at the $\Upsilon(4S)$.				

$\Gamma(\Delta^0 \bar{D}^0) / \Gamma_{\text{total}}$				Γ_{485} / Γ
VALUE	CL%	DOCUMENT ID	TECN	COMMENT
<0.0015	90	1 BORTOLETTO89	CLEO	$e^+ e^- \rightarrow \Upsilon(4S)$
¹ BORTOLETTO 89 reports < 0.0018 assuming $\Upsilon(4S)$ decays 43% to $B^0 \bar{B}^0$. We rescale to 50%.				

$\Gamma(D^{*+} \bar{D}^{*-}) / \Gamma_{\text{total}}$				Γ_{486} / Γ
VALUE	CL%	DOCUMENT ID	TECN	COMMENT
$<1.1 \times 10^{-4}$	90	1 BORTOLETTO89	CLEO	$e^+ e^- \rightarrow \Upsilon(4S)$
¹ BORTOLETTO 89 reports $< 1.3 \times 10^{-4}$ assuming $\Upsilon(4S)$ decays 43% to $B^0 \bar{B}^0$. We rescale to 50%.				

$\Gamma(D^0 p \bar{p}) / \Gamma_{\text{total}}$				Γ_{487} / Γ
VALUE (units 10^{-4})	CL%	DOCUMENT ID	TECN	COMMENT
1.04 ± 0.07 OUR AVERAGE				
$1.02 \pm 0.04 \pm 0.06$		1,2 DEL-AMO-SA...12	BABR	$e^+ e^- \rightarrow \Upsilon(4S)$
$1.18 \pm 0.15 \pm 0.16$		2 ABE	02w	BELL $e^+ e^- \rightarrow \Upsilon(4S)$
• • • We do not use the following data for averages, fits, limits, etc. • • •				
$1.13 \pm 0.06 \pm 0.08$		2 AUBERT,B	06s	BABR Repl. by DEL-AMO-SANCHEZ 12
¹ Uses the values of D and D^* branching fractions from PDG 08.				
² Assumes equal production of B^+ and B^0 at the $\Upsilon(4S)$.				

$\Gamma(D_s^- \bar{\Lambda} p) / \Gamma_{\text{total}}$				Γ_{488} / Γ
VALUE (units 10^{-5})	CL%	DOCUMENT ID	TECN	COMMENT
$2.8 \pm 0.8 \pm 0.3$		1,2 MEDVEDEVA	07	BELL $e^+ e^- \rightarrow \Upsilon(4S)$
¹ Assumes equal production of B^+ and B^0 at the $\Upsilon(4S)$.				
² MEDVEDEVA 07 reports $(2.9 \pm 0.7 \pm 0.5 \pm 0.4) \times 10^{-5}$ from a measurement of $[\Gamma(B^0 \rightarrow D_s^- \bar{\Lambda} p) / \Gamma_{\text{total}}] \times [B(D_s^+ \rightarrow \phi \pi^+)]$ assuming $B(D_s^+ \rightarrow \phi \pi^+) = (4.4 \pm 0.6) \times 10^{-2}$, which we rescale to our best value $B(D_s^+ \rightarrow \phi \pi^+) = (4.5 \pm 0.4) \times 10^{-2}$. Our first error is their experiment's error and our second error is the systematic error from using our best value.				

$\Gamma(D^{*+} (2007)^0 p \bar{p}) / \Gamma_{\text{total}}$				Γ_{489} / Γ
VALUE (units 10^{-4})	CL%	DOCUMENT ID	TECN	COMMENT
0.99 ± 0.11 OUR AVERAGE				
$0.97 \pm 0.07 \pm 0.09$		1,2 DEL-AMO-SA...12	BABR	$e^+ e^- \rightarrow \Upsilon(4S)$
$1.20 \pm 0.33 \pm 0.21$		2 ABE	02w	BELL $e^+ e^- \rightarrow \Upsilon(4S)$
• • • We do not use the following data for averages, fits, limits, etc. • • •				
$1.01 \pm 0.10 \pm 0.09$		2 AUBERT,B	06s	BABR Repl. by DEL-AMO-SANCHEZ 12
¹ Uses the values of D and D^* branching fractions from PDG 08.				
² Assumes equal production of B^+ and B^0 at the $\Upsilon(4S)$.				

$\Gamma(D^{*+} (2010)^- p \bar{n}) / \Gamma_{\text{total}}$				Γ_{490} / Γ
VALUE (units 10^{-4})	CL%	DOCUMENT ID	TECN	COMMENT
$14.5 \pm 3.4 \pm 2.7$		1 ANDERSON	01	CLE2 $e^+ e^- \rightarrow \Upsilon(4S)$
¹ Assumes equal production of B^+ and B^0 at the $\Upsilon(4S)$.				

$\Gamma(D^- p \bar{p} \pi^+) / \Gamma_{\text{total}}$				Γ_{491} / Γ
VALUE (units 10^{-4})	CL%	DOCUMENT ID	TECN	COMMENT
$3.32 \pm 0.10 \pm 0.29$		1,2 DEL-AMO-SA...12	BABR	$e^+ e^- \rightarrow \Upsilon(4S)$
• • • We do not use the following data for averages, fits, limits, etc. • • •				
$3.38 \pm 0.14 \pm 0.29$		2 AUBERT,B	06s	BABR Repl. by DEL-AMO-SANCHEZ 12
¹ Uses the values of D and D^* branching fractions from PDG 08.				
² Assumes equal production of B^+ and B^0 at the $\Upsilon(4S)$.				

$\Gamma(D^{*+} (2010)^- p \bar{p} \pi^+) / \Gamma_{\text{total}}$				Γ_{492} / Γ
VALUE (units 10^{-4})	CL%	DOCUMENT ID	TECN	COMMENT
4.7 ± 0.5 OUR AVERAGE				
$4.55 \pm 0.16 \pm 0.39$		1,2 DEL-AMO-SA...12	BABR	$e^+ e^- \rightarrow \Upsilon(4S)$
$6.5 \pm 1.3 \pm 1.0$		2 ANDERSON	01	CLE2 $e^+ e^- \rightarrow \Upsilon(4S)$
• • • We do not use the following data for averages, fits, limits, etc. • • •				
$4.81 \pm 0.22 \pm 0.44$		2 AUBERT,B	06s	BABR Repl. by DEL-AMO-SANCHEZ 12
¹ Uses the values of D and D^* branching fractions from PDG 08.				
² Assumes equal production of B^+ and B^0 at the $\Upsilon(4S)$.				

$\Gamma(D^0 p \bar{p} \pi^+ \pi^-) / \Gamma_{\text{total}}$				Γ_{493} / Γ
VALUE (units 10^{-4})	CL%	DOCUMENT ID	TECN	COMMENT
$2.99 \pm 0.21 \pm 0.45$		1,2 DEL-AMO-SA...12	BABR	$e^+ e^- \rightarrow \Upsilon(4S)$
¹ Uses the values of D and D^* branching fractions from PDG 08.				
² Assumes equal production of B^+ and B^0 at the $\Upsilon(4S)$.				

$\Gamma(D^{*0} p \bar{p} \pi^+ \pi^-) / \Gamma_{\text{total}}$				Γ_{494} / Γ
VALUE (units 10^{-4})	CL%	DOCUMENT ID	TECN	COMMENT
$1.91 \pm 0.36 \pm 0.29$		1,2 DEL-AMO-SA...12	BABR	$e^+ e^- \rightarrow \Upsilon(4S)$
¹ Uses the values of D and D^* branching fractions from PDG 08.				
² Assumes equal production of B^+ and B^0 at the $\Upsilon(4S)$.				

$\Gamma(\Theta_c^- \bar{p} \pi^+, \Theta_c^- \rightarrow D^- p) / \Gamma_{\text{total}}$				Γ_{495} / Γ
VALUE (units 10^{-6})	CL%	DOCUMENT ID	TECN	COMMENT
<9	90	1 AUBERT,B	06s	BABR $e^+ e^- \rightarrow \Upsilon(4S)$
¹ Assumes equal production of B^+ and B^0 at the $\Upsilon(4S)$.				

See key on page 999

Meson Particle Listings

B^0

$\Gamma(\Theta_c \bar{p} \pi^+, \Theta_c \rightarrow D^{*-} p) / \Gamma_{total}$ Γ_{496} / Γ

VALUE (units 10^{-6})	CL%	DOCUMENT ID	TECN	COMMENT
<14	90	¹ AUBERT,B	06s BABR	$e^+ e^- \rightarrow \Upsilon(4S)$

¹ Assumes equal production of B^+ and B^0 at the $\Upsilon(4S)$.

$\Gamma(\Sigma_c^{--} \Delta^{++}) / \Gamma_{total}$ Γ_{497} / Γ

VALUE	CL%	DOCUMENT ID	TECN	COMMENT
<8 × 10 ⁻⁴	90	¹ PROCARIO	94 CLE2	$e^+ e^- \rightarrow \Upsilon(4S)$

¹ PROCARIO 94 reports < 0.0012 from a measurement of $[\Gamma(B^0 \rightarrow \Sigma_c^{--} \Delta^{++}) / \Gamma_{total}] \times [B(\Lambda_c^+ \rightarrow p K^- \pi^+)]$ assuming $B(\Lambda_c^+ \rightarrow p K^- \pi^+) = 0.043$, which we rescale to our best value $B(\Lambda_c^+ \rightarrow p K^- \pi^+) = 6.28 \times 10^{-2}$.

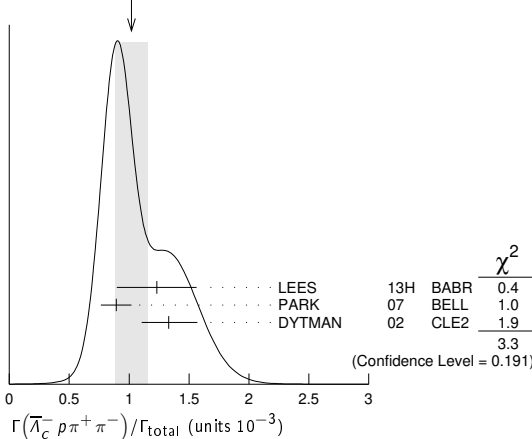
$\Gamma(\bar{\Lambda}_c^- p \pi^+ \pi^-) / \Gamma_{total}$ Γ_{498} / Γ

VALUE (units 10^{-3})	DOCUMENT ID	TECN	COMMENT
1.02 ± 0.14 OUR AVERAGE	Error includes scale factor of 1.3. See the ideogram below.		

1.23 ± 0.05 ± 0.33	^{1,2} LEES	13H BABR	$e^+ e^- \rightarrow \Upsilon(4S)$
0.89 ± 0.11 ± 0.05 -0.04	^{1,3} PARK	07 BELL	$e^+ e^- \rightarrow \Upsilon(4S)$
1.33 ± 0.22 ± 0.07 -0.20	⁴ DYTMAN	02 CLE2	$e^+ e^- \rightarrow \Upsilon(4S)$
0.88 ± 0.16 ± 0.05 -0.04	⁵ GABYSHEV	02 BELL	Repl. by PARK 07
1.33 ± 0.46 ± 0.37 -0.42	⁶ FU	97 CLE2	Repl. by DYTMAN 02

- ¹ Assumes equal production of B^+ and B^0 at the $\Upsilon(4S)$.
- ² Uses $\Lambda_c^+ \rightarrow p K^- \pi^+$ mode. The second error includes the uncertainty of the branching fraction of the Λ_c decay, $B(\Lambda_c^+ \rightarrow p K^- \pi^+) = (5.0 \pm 1.3)\%$.
- ³ PARK 07 reports $(11.2 \pm 0.5 \pm 3.2) \times 10^{-4}$ from a measurement of $[\Gamma(B^0 \rightarrow \bar{\Lambda}_c^- p \pi^+ \pi^-) / \Gamma_{total}] \times [B(\Lambda_c^+ \rightarrow p K^- \pi^+)]$ assuming $B(\Lambda_c^+ \rightarrow p K^- \pi^+) = (5.0 \pm 1.3) \times 10^{-2}$, which we rescale to our best value $B(\Lambda_c^+ \rightarrow p K^- \pi^+) = (6.28 \pm 0.32) \times 10^{-2}$. Our first error is their experiment's error and our second error is the systematic error from using our best value.
- ⁴ DYTMAN 02 reports $(1.67^{+0.27}_{-0.25}) \times 10^{-3}$ from a measurement of $[\Gamma(B^0 \rightarrow \bar{\Lambda}_c^- p \pi^+ \pi^-) / \Gamma_{total}] \times [B(\Lambda_c^+ \rightarrow p K^- \pi^+)]$ assuming $B(\Lambda_c^+ \rightarrow p K^- \pi^+) = 0.05$, which we rescale to our best value $B(\Lambda_c^+ \rightarrow p K^- \pi^+) = (6.28 \pm 0.32) \times 10^{-2}$. Our first error is their experiment's error and our second error is the systematic error from using our best value.
- ⁵ GABYSHEV 02 reports $(1.1 \pm 0.2) \times 10^{-3}$ from a measurement of $[\Gamma(B^0 \rightarrow \bar{\Lambda}_c^- p \pi^+ \pi^-) / \Gamma_{total}] \times [B(\Lambda_c^+ \rightarrow p K^- \pi^+)]$ assuming $B(\Lambda_c^+ \rightarrow p K^- \pi^+) = 0.05$, which we rescale to our best value $B(\Lambda_c^+ \rightarrow p K^- \pi^+) = (6.28 \pm 0.32) \times 10^{-2}$. Our first error is their experiment's error and our second error is the systematic error from using our best value.
- ⁶ FU 97 uses PDG 96 values of Λ_c branching fraction.

WEIGHTED AVERAGE
1.02 ± 0.14 (Error scaled by 1.3)



$\Gamma(\bar{\Lambda}_c^- p) / \Gamma_{total}$ Γ_{499} / Γ

VALUE (units 10^{-5})	CL%	DOCUMENT ID	TECN	COMMENT
1.54 ± 0.18 OUR AVERAGE	Error includes scale factor of 1.3.			

1.51 ± 0.16 ± 0.08	^{1,2} AUBERT	08BN BABR	$e^+ e^- \rightarrow \Upsilon(4S)$
2.19 ± 0.56 ± 0.65 -0.49	^{1,3} GABYSHEV	03 BELL	$e^+ e^- \rightarrow \Upsilon(4S)$
2.10 ± 0.67 ± 0.77 -0.55 - 0.46	^{1,4} AUBERT	07AV BABR	Repl. by AUBERT 08BN
< 9	90	^{1,5} DYTMAN	02 CLE2 $e^+ e^- \rightarrow \Upsilon(4S)$
< 3.1	90	^{1,4} GABYSHEV	02 BELL $e^+ e^- \rightarrow \Upsilon(4S)$
< 21	90	⁶ FU	97 CLE2 $e^+ e^- \rightarrow \Upsilon(4S)$

¹ Assumes equal production of B^+ and B^0 at the $\Upsilon(4S)$.

² AUBERT 08BN reports $(1.89 \pm 0.21 \pm 0.49) \times 10^{-5}$ from a measurement of $[\Gamma(B^0 \rightarrow \bar{\Lambda}_c^- p) / \Gamma_{total}] \times [B(\Lambda_c^+ \rightarrow p K^- \pi^+)]$ assuming $B(\Lambda_c^+ \rightarrow p K^- \pi^+) = (5.0 \pm 1.3) \times 10^{-2}$, which we rescale to our best value $B(\Lambda_c^+ \rightarrow p K^- \pi^+) = (6.28 \pm 0.32) \times 10^{-2}$. Our first error is their experiment's error and our second error is the systematic error from using our best value.

- ³ The second error for GABYSHEV 03 includes the systematic and the error of $\Lambda_c \rightarrow \bar{p} K^+ \pi^-$ decay branching fraction.
- ⁴ Uses the value for $\Lambda_c \rightarrow p K^- \pi^+$ branching ratio $(5.0 \pm 1.3)\%$.
- ⁵ DYTMAN 02 measurement uses $B(\Lambda_c^- \rightarrow \bar{p} K^+ \pi^-) = 5.0 \pm 1.3\%$. The second error includes the systematic and the uncertainty of the branching ratio.
- ⁶ FU 97 uses PDG 96 values of Λ_c branching ratio.

$\Gamma(\bar{\Lambda}_c^- p \pi^0) / \Gamma_{total}$ Γ_{500} / Γ

VALUE (units 10^{-4})	CL%	DOCUMENT ID	TECN	COMMENT
1.55 ± 0.17 ± 0.08	Error includes scale factor of 1.3. See the ideogram below.			

- • • We do not use the following data for averages, fits, limits, etc. • • •
- <5.9
- ¹ AUBERT 10H reports $(1.94 \pm 0.17 \pm 0.52) \times 10^{-4}$ from a measurement of $[\Gamma(B^0 \rightarrow \bar{\Lambda}_c^- p \pi^0) / \Gamma_{total}] \times [B(\Lambda_c^+ \rightarrow p K^- \pi^+)]$ assuming $B(\Lambda_c^+ \rightarrow p K^- \pi^+) = (5.0 \pm 1.3) \times 10^{-2}$, which we rescale to our best value $B(\Lambda_c^+ \rightarrow p K^- \pi^+) = (6.28 \pm 0.32) \times 10^{-2}$. Our first error is their experiment's error and our second error is the systematic error from using our best value.
- ² Assumes equal production of B^+ and B^0 at the $\Upsilon(4S)$.
- ³ FU 97 uses PDG 96 values of Λ_c branching ratio.

$\Gamma(\bar{\Lambda}_c^- p K^+ K^-) / \Gamma_{total}$ Γ_{513} / Γ

VALUE (units 10^{-5})	CL%	DOCUMENT ID	TECN	COMMENT
2.0 ± 0.4 ± 0.1	Error includes scale factor of 1.3. See the ideogram below.			

- ¹ LEES 15B reports $[\Gamma(B^0 \rightarrow \bar{\Lambda}_c^- p K^+ K^-) / \Gamma_{total}] \times [B(\Lambda_c^+ \rightarrow p K^- \pi^+)] = (12.5 \pm 2.0 \pm 1.0) \times 10^{-7}$ which we divide by our best value $B(\Lambda_c^+ \rightarrow p K^- \pi^+) = (6.28 \pm 0.32) \times 10^{-2}$. Our first error is their experiment's error and our second error is the systematic error from using our best value.
- ² Assumes equal production of B^+ and B^0 at the $\Upsilon(4S)$.

$\Gamma(\bar{\Lambda}_c^- p \phi) / \Gamma_{total}$ Γ_{514} / Γ

VALUE	CL%	DOCUMENT ID	TECN	COMMENT
<1.0 × 10 ⁻⁵	90	^{1,2} LEES	15B BABR	$e^+ e^- \rightarrow \Upsilon(4S)$

- ¹ LEES 15B reports < 1.2 × 10⁻⁵ from a measurement of $[\Gamma(B^0 \rightarrow \bar{\Lambda}_c^- p \phi) / \Gamma_{total}] \times [B(\Lambda_c^+ \rightarrow p K^- \pi^+)]$ assuming $B(\Lambda_c^+ \rightarrow p K^- \pi^+) = (5.0 \pm 1.3) \times 10^{-2}$, which we rescale to our best value $B(\Lambda_c^+ \rightarrow p K^- \pi^+) = 6.28 \times 10^{-2}$.
- ² Assumes equal production of B^+ and B^0 at the $\Upsilon(4S)$.

$\Gamma(\Sigma_c(2455)^- p) / \Gamma_{total}$ Γ_{501} / Γ

VALUE (units 10^{-6})	CL%	DOCUMENT ID	TECN	COMMENT
<24	Error includes scale factor of 1.3. See the ideogram below.			

- ¹ AUBERT 10H reports $[\Gamma(B^0 \rightarrow \Sigma_c(2455)^- p) / \Gamma_{total}] \times [B(\Lambda_c^+ \rightarrow p K^- \pi^+)] < 1.5 \times 10^{-6}$ which we divide by our best value $B(\Lambda_c^+ \rightarrow p K^- \pi^+) = 6.28 \times 10^{-2}$.
- ² Assumes equal production of B^+ and B^0 at the $\Upsilon(4S)$.

$\Gamma(\bar{\Lambda}_c^- p \pi^+ \pi^- \pi^0) / \Gamma_{total}$ Γ_{502} / Γ

VALUE	CL%	DOCUMENT ID	TECN	COMMENT
<5.07 × 10 ⁻³	90	¹ FU	97 CLE2	$e^+ e^- \rightarrow \Upsilon(4S)$

¹ FU 97 uses PDG 96 values of Λ_c branching ratio.

$\Gamma(\bar{\Lambda}_c^- p \pi^+ \pi^- \pi^+ \pi^-) / \Gamma_{total}$ Γ_{503} / Γ

VALUE	CL%	DOCUMENT ID	TECN	COMMENT
<2.74 × 10 ⁻³	90	¹ FU	97 CLE2	$e^+ e^- \rightarrow \Upsilon(4S)$

¹ FU 97 uses PDG 96 values of Λ_c branching ratio.

$\Gamma(\bar{\Lambda}_c^- p \pi^+ \pi^- (\text{nonresonant})) / \Gamma_{total}$ Γ_{504} / Γ

VALUE (units 10^{-4})	CL%	DOCUMENT ID	TECN	COMMENT
5.5 ± 1.0 OUR AVERAGE	Error includes scale factor of 1.3.			

- 7.9 ± 0.4 ± 2.0
- 5.1 ± 0.8 ± 0.3
- ¹ Assumes equal production of B^+ and B^0 at the $\Upsilon(4S)$.
- ² Uses $\Lambda_c^+ \rightarrow p K^- \pi^+$ mode. The second error includes the uncertainty of the branching fraction of the Λ_c decay, $B(\Lambda_c^+ \rightarrow p K^- \pi^+) = (5.0 \pm 1.3)\%$.
- ³ PARK 07 reports $(6.4 \pm 0.4 \pm 1.9) \times 10^{-4}$ from a measurement of $[\Gamma(B^0 \rightarrow \bar{\Lambda}_c^- p \pi^+ \pi^- (\text{nonresonant})) / \Gamma_{total}] \times [B(\Lambda_c^+ \rightarrow p K^- \pi^+)]$ assuming $B(\Lambda_c^+ \rightarrow p K^- \pi^+) = (5.0 \pm 1.3) \times 10^{-2}$, which we rescale to our best value $B(\Lambda_c^+ \rightarrow p K^- \pi^+) = (6.28 \pm 0.32) \times 10^{-2}$. Our first error is their experiment's error and our second error is the systematic error from using our best value.

Meson Particle Listings

B^0

$\Gamma(\overline{S}_C(2520)^{--} p\pi^+)/\Gamma_{\text{total}}$ Γ_{505}/Γ

VALUE (units 10^{-4})	DOCUMENT ID	TECN	COMMENT
1.02 ± 0.18 OUR AVERAGE			
1.15 ± 0.10 ± 0.30	1,2 LEES	13H BABR	$e^+e^- \rightarrow \mathcal{T}(4S)$
0.96 ± 0.21 ± 0.05	1,3 PARK	07 BELL	$e^+e^- \rightarrow \mathcal{T}(4S)$

- • • We do not use the following data for averages, fits, limits, etc. • • •
- 1,3 ± 0.5 ± 0.1 ⁴GABYSHEV 02 BELL Repl. by PARK 07
- ¹Assumes equal production of B^+ and B^0 at the $\mathcal{T}(4S)$.
- ²Uses $\Lambda_C^+ \rightarrow pK^-\pi^+$ mode. The second error includes the uncertainty of the branching fraction of the Λ_C decay, $B(\Lambda_C^+ \rightarrow pK^-\pi^+) = (5.0 \pm 1.3)\%$.
- ³PARK 07 reports $(1.2 \pm 0.1 \pm 0.4) \times 10^{-4}$ from a measurement of $[\Gamma(B^0 \rightarrow \overline{S}_C(2520)^{--} p\pi^+)/\Gamma_{\text{total}}] \times [B(\Lambda_C^+ \rightarrow pK^-\pi^+)]$ assuming $B(\Lambda_C^+ \rightarrow pK^-\pi^+) = (5.0 \pm 1.3) \times 10^{-2}$, which we rescale to our best value $B(\Lambda_C^+ \rightarrow pK^-\pi^+) = (6.28 \pm 0.32) \times 10^{-2}$. Our first error is their experiment's error and our second error is the systematic error from using our best value.
- ⁴GABYSHEV 02 reports $(1.63_{-0.58}^{+0.64}) \times 10^{-4}$ from a measurement of $[\Gamma(B^0 \rightarrow \overline{S}_C(2520)^{--} p\pi^+)/\Gamma_{\text{total}}] \times [B(\Lambda_C^+ \rightarrow pK^-\pi^+)]$ assuming $B(\Lambda_C^+ \rightarrow pK^-\pi^+) = 0.05$, which we rescale to our best value $B(\Lambda_C^+ \rightarrow pK^-\pi^+) = (6.28 \pm 0.32) \times 10^{-2}$. Our first error is their experiment's error and our second error is the systematic error from using our best value.

$\Gamma(\overline{S}_C(2520)^0 p\rho\pi^-)/\Gamma_{\text{total}}$ Γ_{506}/Γ

VALUE	CL%	DOCUMENT ID	TECN	COMMENT
<0.31 × 10⁻⁴	90	1,2 LEES	13H BABR	$e^+e^- \rightarrow \mathcal{T}(4S)$
<0.38 × 10 ⁻⁴	90	1 PARK	07 BELL	$e^+e^- \rightarrow \mathcal{T}(4S)$
<1.21 × 10 ⁻⁴	90	1,2 GABYSHEV	02 BELL	Repl. by PARK 07

- • • We do not use the following data for averages, fits, limits, etc. • • •
- ¹Assumes equal production of B^+ and B^0 at the $\mathcal{T}(4S)$.
- ²Uses the value for $\Lambda_C \rightarrow pK^-\pi^+$ branching ratio $(5.0 \pm 1.3)\%$.

$\Gamma(\overline{S}_C(2455)^0 N^0, N^0 \rightarrow p\rho\pi^-)/\Gamma_{\text{total}}$ Γ_{508}/Γ

N^0 is the $N(1440) P_{11}$ or $N(1535) S_{11}$ or an admixture of the two baryonic states.

VALUE (units 10^{-4})	DOCUMENT ID	TECN	COMMENT
0.64 ± 0.16 ± 0.03	1,2 KIM	08 BELL	$e^+e^- \rightarrow \mathcal{T}(4S)$

- ¹Assumes equal production of B^+ and B^0 at the $\mathcal{T}(4S)$.
- ²KIM 08 reports $(0.80 \pm 0.15 \pm 0.25) \times 10^{-4}$ from a measurement of $[\Gamma(B^0 \rightarrow \overline{S}_C(2455)^0 N^0, N^0 \rightarrow p\rho\pi^-)/\Gamma_{\text{total}}] \times [B(\Lambda_C^+ \rightarrow pK^-\pi^+)]$ assuming $B(\Lambda_C^+ \rightarrow pK^-\pi^+) = (5.0 \pm 1.3) \times 10^{-2}$, which we rescale to our best value $B(\Lambda_C^+ \rightarrow pK^-\pi^+) = (6.28 \pm 0.32) \times 10^{-2}$. Our first error is their experiment's error and our second error is the systematic error from using our best value.

$\Gamma(\overline{S}_C(2455)^0 p\rho\pi^-)/\Gamma_{\text{total}}$ Γ_{507}/Γ

VALUE (units 10^{-4})	CL%	DOCUMENT ID	TECN	COMMENT
1.08 ± 0.16 OUR AVERAGE				
0.91 ± 0.07 ± 0.24		1,2 LEES	13H BABR	$e^+e^- \rightarrow \mathcal{T}(4S)$
1.12 ± 0.21 ± 0.06		1,3 PARK	07 BELL	$e^+e^- \rightarrow \mathcal{T}(4S)$
1.8 ± 0.6 ± 0.1		4 DYTMAN	02 CLE2	$e^+e^- \rightarrow \mathcal{T}(4S)$

- • • We do not use the following data for averages, fits, limits, etc. • • •

- 0.38 ± $\frac{0.37}{0.33}$ ± 0.02 90 ⁵GABYSHEV 02 BELL Repl. by PARK 07
- ¹Assumes equal production of B^+ and B^0 at the $\mathcal{T}(4S)$.
- ²Uses $\Lambda_C^+ \rightarrow pK^-\pi^+$ mode. The second error includes the uncertainty of the branching fraction of the Λ_C decay, $B(\Lambda_C^+ \rightarrow pK^-\pi^+) = (5.0 \pm 1.3)\%$.
- ³PARK 07 reports $(1.4 \pm 0.2 \pm 0.4) \times 10^{-4}$ from a measurement of $[\Gamma(B^0 \rightarrow \overline{S}_C(2455)^0 p\rho\pi^-)/\Gamma_{\text{total}}] \times [B(\Lambda_C^+ \rightarrow pK^-\pi^+)]$ assuming $B(\Lambda_C^+ \rightarrow pK^-\pi^+) = (5.0 \pm 1.3) \times 10^{-2}$, which we rescale to our best value $B(\Lambda_C^+ \rightarrow pK^-\pi^+) = (6.28 \pm 0.32) \times 10^{-2}$. Our first error is their experiment's error and our second error is the systematic error from using our best value.
- ⁴DYTMAN 02 reports $(2.2 \pm 0.7) \times 10^{-4}$ from a measurement of $[\Gamma(B^0 \rightarrow \overline{S}_C(2455)^0 p\rho\pi^-)/\Gamma_{\text{total}}] \times [B(\Lambda_C^+ \rightarrow pK^-\pi^+)]$ assuming $B(\Lambda_C^+ \rightarrow pK^-\pi^+) = 0.05$, which we rescale to our best value $B(\Lambda_C^+ \rightarrow pK^-\pi^+) = (6.28 \pm 0.32) \times 10^{-2}$. Our first error is their experiment's error and our second error is the systematic error from using our best value.
- ⁵GABYSHEV 02 reports $(0.48_{-0.41}^{+0.46}) \times 10^{-4}$ from a measurement of $[\Gamma(B^0 \rightarrow \overline{S}_C(2455)^0 p\rho\pi^-)/\Gamma_{\text{total}}] \times [B(\Lambda_C^+ \rightarrow pK^-\pi^+)]$ assuming $B(\Lambda_C^+ \rightarrow pK^-\pi^+) = 0.05$, which we rescale to our best value $B(\Lambda_C^+ \rightarrow pK^-\pi^+) = (6.28 \pm 0.32) \times 10^{-2}$. Our first error is their experiment's error and our second error is the systematic error from using our best value.

$\Gamma(\overline{S}_C(2455)^{--} p\pi^+)/\Gamma_{\text{total}}$ Γ_{509}/Γ

VALUE (units 10^{-4})	DOCUMENT ID	TECN	COMMENT
1.83 ± 0.24 OUR AVERAGE			
2.13 ± 0.10 ± 0.56	1,2 LEES	13H BABR	$e^+e^- \rightarrow \mathcal{T}(4S)$
1.67 ± $\frac{0.25}{0.08}$ ± 0.09	1,3 PARK	07 BELL	$e^+e^- \rightarrow \mathcal{T}(4S)$
2.9 ± $\frac{0.9}{0.1}$ ± 0.2	4 DYTMAN	02 CLE2	$e^+e^- \rightarrow \mathcal{T}(4S)$

- • • We do not use the following data for averages, fits, limits, etc. • • •

1.9 $\frac{+0.6}{-0.5}$ ± 0.1 ⁵GABYSHEV 02 BELL Repl. by PARK 07

- ¹Assumes equal production of B^+ and B^0 at the $\mathcal{T}(4S)$.
- ²Uses $\Lambda_C^+ \rightarrow pK^-\pi^+$ mode. The second error includes the uncertainty of the branching fraction of the Λ_C decay, $B(\Lambda_C^+ \rightarrow pK^-\pi^+) = (5.0 \pm 1.3)\%$.
- ³PARK 07 reports $(2.1 \pm 0.2 \pm 0.6) \times 10^{-4}$ from a measurement of $[\Gamma(B^0 \rightarrow \overline{S}_C(2455)^{--} p\pi^+)/\Gamma_{\text{total}}] \times [B(\Lambda_C^+ \rightarrow pK^-\pi^+)]$ assuming $B(\Lambda_C^+ \rightarrow pK^-\pi^+) = (5.0 \pm 1.3) \times 10^{-2}$, which we rescale to our best value $B(\Lambda_C^+ \rightarrow pK^-\pi^+) = (6.28 \pm 0.32) \times 10^{-2}$. Our first error is their experiment's error and our second error is the systematic error from using our best value.
- ⁴DYTMAN 02 reports $(3.7 \pm 1.1) \times 10^{-4}$ from a measurement of $[\Gamma(B^0 \rightarrow \overline{S}_C(2455)^{--} p\pi^+)/\Gamma_{\text{total}}] \times [B(\Lambda_C^+ \rightarrow pK^-\pi^+)]$ assuming $B(\Lambda_C^+ \rightarrow pK^-\pi^+) = 0.05$, which we rescale to our best value $B(\Lambda_C^+ \rightarrow pK^-\pi^+) = (6.28 \pm 0.32) \times 10^{-2}$. Our first error is their experiment's error and our second error is the systematic error from using our best value.
- ⁵GABYSHEV 02 reports $(2.38_{-0.69}^{+0.75}) \times 10^{-4}$ from a measurement of $[\Gamma(B^0 \rightarrow \overline{S}_C(2455)^{--} p\pi^+)/\Gamma_{\text{total}}] \times [B(\Lambda_C^+ \rightarrow pK^-\pi^+)]$ assuming $B(\Lambda_C^+ \rightarrow pK^-\pi^+) = 0.05$, which we rescale to our best value $B(\Lambda_C^+ \rightarrow pK^-\pi^+) = (6.28 \pm 0.32) \times 10^{-2}$. Our first error is their experiment's error and our second error is the systematic error from using our best value.

$\Gamma(\Lambda_C^- pK^+\pi^-)/\Gamma_{\text{total}}$ Γ_{510}/Γ

VALUE (units 10^{-5})	DOCUMENT ID	TECN	COMMENT
3.4 ± 0.7 ± 0.2	1,2 AUBERT	09AG BABR	$e^+e^- \rightarrow \mathcal{T}(4S)$

- ¹AUBERT 09AG reports $(4.33 \pm 0.82 \pm 0.33 \pm 1.13) \times 10^{-5}$ from a measurement of $[\Gamma(B^0 \rightarrow \Lambda_C^- pK^+\pi^-)/\Gamma_{\text{total}}] \times [B(\Lambda_C^+ \rightarrow pK^-\pi^+)]$ assuming $B(\Lambda_C^+ \rightarrow pK^-\pi^+) = (5.0 \pm 1.3) \times 10^{-2}$, which we rescale to our best value $B(\Lambda_C^+ \rightarrow pK^-\pi^+) = (6.28 \pm 0.32) \times 10^{-2}$. Our first error is their experiment's error and our second error is the systematic error from using our best value.
- ²Assumes equal production of B^+ and B^0 at the $\mathcal{T}(4S)$.

$\Gamma(\overline{S}_C(2455)^{--} pK^+, \overline{S}_C^- \rightarrow \overline{\Lambda}_C^- \pi^-)/\Gamma_{\text{total}}$ Γ_{511}/Γ

VALUE (units 10^{-5})	DOCUMENT ID	TECN	COMMENT
0.88 ± 0.25 ± $\frac{0.05}{0.04}$	1,2 AUBERT	09AG BABR	$e^+e^- \rightarrow \mathcal{T}(4S)$

- ¹AUBERT 09AG reports $(1.11 \pm 0.30 \pm 0.09 \pm 0.29) \times 10^{-5}$ from a measurement of $[\Gamma(B^0 \rightarrow \overline{S}_C(2455)^{--} pK^+, \overline{S}_C^- \rightarrow \overline{\Lambda}_C^- \pi^-)/\Gamma_{\text{total}}] \times [B(\Lambda_C^+ \rightarrow pK^-\pi^+)]$ assuming $B(\Lambda_C^+ \rightarrow pK^-\pi^+) = (5.0 \pm 1.3) \times 10^{-2}$, which we rescale to our best value $B(\Lambda_C^+ \rightarrow pK^-\pi^+) = (6.28 \pm 0.32) \times 10^{-2}$. Our first error is their experiment's error and our second error is the systematic error from using our best value.
- ²Assumes equal production of B^+ and B^0 at the $\mathcal{T}(4S)$.

$\Gamma(\Lambda_C^- pK^*(892)^0)/\Gamma_{\text{total}}$ Γ_{512}/Γ

VALUE (units 10^{-5})	CL%	DOCUMENT ID	TECN	COMMENT
<2.42	90	1 AUBERT	09AG BABR	$e^+e^- \rightarrow \mathcal{T}(4S)$

- ¹Assumes equal production of B^+ and B^0 at the $\mathcal{T}(4S)$.

$\Gamma(\Lambda_C^- p\overline{p}p)/\Gamma_{\text{total}}$ Γ_{515}/Γ

VALUE (units 10^{-5})	DOCUMENT ID	TECN	COMMENT
<2.8	1 LEES	14c BABR	$e^+e^- \rightarrow \mathcal{T}(4S)$

- ¹Assumes equal production of B^+ and B^0 at the $\mathcal{T}(4S)$ and $B(\Lambda_C^+ \rightarrow pK^-\pi^+) = 0.050 \pm 0.013$.

$\Gamma(\overline{\Lambda}_C^- \Lambda K^+)/\Gamma_{\text{total}}$ Γ_{516}/Γ

VALUE (units 10^{-5})	DOCUMENT ID	TECN	COMMENT
4.8 ± 1.1 ± $\frac{0.2}{0.3}$	1,2 LEES	11F BABR	$e^+e^- \rightarrow \mathcal{T}(4S)$

- ¹Assumes equal production of B^0 and B^+ from Upsilon(4S) decays.
- ²LEES 11F reports $(3.8 \pm 0.8 \pm 0.2 \pm 1.0) \times 10^{-5}$ from a measurement of $[\Gamma(B^0 \rightarrow \overline{\Lambda}_C^- \Lambda K^+)/\Gamma_{\text{total}}] / [B(\Lambda_C^+ \rightarrow pK^-\pi^+)] / [B(\Lambda \rightarrow p\pi^-)]$ assuming $B(\Lambda_C^+ \rightarrow pK^-\pi^+) = (5.0 \pm 1.3) \times 10^{-2}$, $B(\Lambda \rightarrow p\pi^-) = (63.9 \pm 0.5) \times 10^{-2}$, which we rescale to our best values $B(\Lambda_C^+ \rightarrow pK^-\pi^+) = (6.28 \pm 0.32) \times 10^{-2}$, $B(\Lambda \rightarrow p\pi^-) = (63.9 \pm 0.5) \times 10^{-2}$. Our first error is their experiment's error and our second error is the systematic error from using our best values. The reported uncertainties are statistical, systematic, and $\overline{\Lambda}_C^-$ branching fraction uncertainty.

$\Gamma(\overline{\Lambda}_C^- \Lambda_C^+)/\Gamma_{\text{total}}$ Γ_{517}/Γ

VALUE (units 10^{-5})	CL%	DOCUMENT ID	TECN	COMMENT
<1.6	95	1 AAIJ	14AA LHCB	pp at 7 TeV

- • • We do not use the following data for averages, fits, limits, etc. • • •

- <6.2 90 ²UCHIDA 08 BELL $e^+e^- \rightarrow \mathcal{T}(4S)$
- ¹Uses $B(\overline{B}^0 \rightarrow D^+ D_s^-) = (7.2 \pm 0.8) \times 10^{-3}$.
- ²Assumes equal production of B^+ and B^0 at the $\mathcal{T}(4S)$.

See key on page 999

Meson Particle Listings

B^0

$\Gamma(\bar{A}_c(2593)^- / \bar{A}_c(2625^- p) / \Gamma_{total}$					Γ_{518} / Γ
VALUE	CL%	DOCUMENT ID	TECN	COMMENT	
$< 1.1 \times 10^{-4}$	90	1,2 DYTMAN	02	CLE2 $e^+e^- \rightarrow \Upsilon(4S)$	

- ¹ Assumes equal production of B^+ and B^0 at the $\Upsilon(4S)$.
- ² DYTMAN 02 measurement uses $B(\Lambda_c^- \rightarrow \bar{p}K^+\pi^-) = 5.0 \pm 1.3\%$. The second error includes the systematic and the uncertainty of the branching ratio.

$\Gamma(\Xi_c^+ \Lambda_c^+) / \Gamma_{total}$					Γ_{519} / Γ
VALUE (units 10^{-3})	DOCUMENT ID	TECN	COMMENT		
$1.2 \pm 0.7 \pm 0.3$	1,2 LI	19c	BELL $e^+e^- \rightarrow \Upsilon(4S)$		

- ¹ Uses fully reconstructed B^0 on tag side with recoil against Λ_c^+ .
- ² LI 19c reports $(1.16 \pm 0.74 \pm 0.33) \times 10^{-3}$ from a measurement of $[\Gamma(B^0 \rightarrow \Xi_c^+ \Lambda_c^+) / \Gamma_{total}] \times [B(\Lambda_c^+ \rightarrow pK^-\pi^+)]$ assuming $B(\Lambda_c^+ \rightarrow pK^-\pi^+) = (6.28 \pm 0.32) \times 10^{-2}$.

$\Gamma(\Xi_c^+ \Lambda_c^+, \Xi_c^- \rightarrow \Xi^+ \pi^- \pi^-) / \Gamma_{total}$					Γ_{520} / Γ
VALUE (units 10^{-5})	DOCUMENT ID	TECN	COMMENT		
2.4 ± 1.1 OUR AVERAGE	Error includes scale factor of 1.8.				
$3.3 \pm 0.7 \pm 0.3$	1 LI	19c	BELL $e^+e^- \rightarrow \Upsilon(4S)$		
$1.2 \pm 0.9 \pm 0.1$	2,3 AUBERT	08H	BABR $e^+e^- \rightarrow \Upsilon(4S)$		

- • •** We do not use the following data for averages, fits, limits, etc. **• • •**
- $7.4^{+3.3}_{-2.7} \pm 0.4$ 3,4 CHISTOV 06A BELL Repl. by LI 19c

¹ LI 19c reports $(3.32 \pm 0.74 \pm 0.33) \times 10^{-5}$ from a measurement of $[\Gamma(B^0 \rightarrow \Xi_c^+ \Lambda_c^+, \Xi_c^- \rightarrow \Xi^+ \pi^- \pi^-) / \Gamma_{total}] \times [B(\Lambda_c^+ \rightarrow pK^-\pi^+)]$ assuming $B(\Lambda_c^+ \rightarrow pK^-\pi^+) = (6.28 \pm 0.32) \times 10^{-2}$.

² AUBERT 08H reports $(1.5 \pm 1.07 \pm 0.44) \times 10^{-5}$ from a measurement of $[\Gamma(B^0 \rightarrow \Xi_c^+ \Lambda_c^+, \Xi_c^- \rightarrow \Xi^+ \pi^- \pi^-) / \Gamma_{total}] \times [B(\Lambda_c^+ \rightarrow pK^-\pi^+)]$ assuming $B(\Lambda_c^+ \rightarrow pK^-\pi^+) = (5.0 \pm 1.3) \times 10^{-2}$, which we rescale to our best value $B(\Lambda_c^+ \rightarrow pK^-\pi^+) = (6.28 \pm 0.32) \times 10^{-2}$. Our first error is their experiment's error and our second error is the systematic error from using our best value.

³ Assumes equal production of B^+ and B^0 at the $\Upsilon(4S)$.

⁴ CHISTOV 06A reports $(9.3^{+3.7}_{-2.8} \pm 3.1) \times 10^{-5}$ from a measurement of $[\Gamma(B^0 \rightarrow \Xi_c^+ \Lambda_c^+, \Xi_c^- \rightarrow \Xi^+ \pi^- \pi^-) / \Gamma_{total}] \times [B(\Lambda_c^+ \rightarrow pK^-\pi^+)]$ assuming $B(\Lambda_c^+ \rightarrow pK^-\pi^+) = (5.0 \pm 1.3) \times 10^{-2}$, which we rescale to our best value $B(\Lambda_c^+ \rightarrow pK^-\pi^+) = (6.28 \pm 0.32) \times 10^{-2}$. Our first error is their experiment's error and our second error is the systematic error from using our best value.

$\Gamma(\Xi_c^+ \Lambda_c^+, \Xi_c^- \rightarrow \bar{p}K^+\pi^-) / \Gamma_{total}$					Γ_{521} / Γ
VALUE (units 10^{-6})	DOCUMENT ID	TECN	COMMENT		
$5.3 \pm 1.5 \pm 0.7$	1 LI	19c	BELL $e^+e^- \rightarrow \Upsilon(4S)$		

¹ LI 19c reports $(5.27 \pm 1.51 \pm 0.69) \times 10^{-6}$ from a measurement of $[\Gamma(B^0 \rightarrow \Xi_c^+ \Lambda_c^+, \Xi_c^- \rightarrow \bar{p}K^+\pi^-) / \Gamma_{total}] \times [B(\Lambda_c^+ \rightarrow pK^-\pi^+)]$ assuming $B(\Lambda_c^+ \rightarrow pK^-\pi^+) = (6.28 \pm 0.32) \times 10^{-2}$.

$\Gamma(\Lambda_c^+ \Lambda_c^- K^0) / \Gamma_{total}$					Γ_{522} / Γ
VALUE (units 10^{-4})	DOCUMENT ID	TECN	COMMENT		
4.0 ± 0.9 OUR AVERAGE					
$3.99 \pm 0.76 \pm 0.51$	1 LI	18D	BELL $e^+e^- \rightarrow \Upsilon(4S)$		
$3.8 \pm 3.1 \pm 2.1$	2,3 AUBERT	08H	BABR $e^+e^- \rightarrow \Upsilon(4S)$		

- • •** We do not use the following data for averages, fits, limits, etc. **• • •**
- $7.9^{+2.9}_{-2.3} \pm 4.3$ 2,3 GABYSHEV 06 BELL Repl. by LI 18D

¹ Assumes $B(\Upsilon(4S) \rightarrow B^0 \bar{B}^0) = 48.6 \pm 0.6\%$ and $B(\Lambda_c^+ \rightarrow pK^-\pi^+) = 6.23 \pm 0.33\%$.

² Assumes $B(\Lambda_c^+ \rightarrow pK^-\pi^+) = 5.0 \pm 1.3\%$.

³ Assumes equal production of B^+ and B^0 at the $\Upsilon(4S)$.

$\Gamma(\Xi_c(2930)^- \Lambda_c^+, \Xi_c^- \rightarrow \Lambda_c^- K^0) / \Gamma_{total}$					Γ_{523} / Γ
VALUE (units 10^{-4})	DOCUMENT ID	TECN	COMMENT		
$2.37 \pm 0.51 \pm 0.31$	1 LI	18D	BELL $e^+e^- \rightarrow \Upsilon(4S)$		

¹ Assumes $B(\Upsilon(4S) \rightarrow B^0 \bar{B}^0) = 48.6 \pm 0.6\%$ and $B(\Lambda_c^+ \rightarrow pK^-\pi^+) = 6.23 \pm 0.33\%$.

$\Gamma(\gamma\gamma) / \Gamma_{total}$					Γ_{524} / Γ
Test for $\Delta B=1$ weak neutral current. Allowed by higher-order electroweak interactions.					
VALUE	CL%	DOCUMENT ID	TECN	COMMENT	
$< 3.2 \times 10^{-7}$	90	1 DEL-AMO-SA...11A	BABR	$e^+e^- \rightarrow \Upsilon(4S)$	

- • •** We do not use the following data for averages, fits, limits, etc. **• • •**
- $< 6.2 \times 10^{-7}$ 90 1 VILLA 06 BELL $e^+e^- \rightarrow \Upsilon(4S)$
- $< 1.7 \times 10^{-6}$ 90 1 AUBERT 01 BABR $e^+e^- \rightarrow \Upsilon(4S)$
- $< 3.9 \times 10^{-5}$ 90 2 ACCIARRI 95I L3 $e^+e^- \rightarrow Z$

¹ Assumes equal production of B^+ and B^0 at the $\Upsilon(4S)$.

² ACCIARRI 95I assumes $f_{B^0} = 39.5 \pm 4.0$ and $f_{B_s} = 12.0 \pm 3.0\%$.

$\Gamma(e^+e^-) / \Gamma_{total}$					Γ_{525} / Γ
Test for $\Delta B=1$ weak neutral current. Allowed by higher-order electroweak interactions.					
VALUE	CL%	DOCUMENT ID	TECN	COMMENT	
$< 8.3 \times 10^{-8}$	90	AALTONEN	09P	CDF $p\bar{p}$ at 1.96 TeV	

- • •** We do not use the following data for averages, fits, limits, etc. **• • •**
- $< 11.3 \times 10^{-8}$ 90 1 AUBERT 08P BABR $e^+e^- \rightarrow \Upsilon(4S)$
- $< 6.1 \times 10^{-8}$ 90 1 AUBERT 05W BABR Repl. by AUBERT 08P
- $< 1.9 \times 10^{-7}$ 90 1 CHANG 03 BELL $e^+e^- \rightarrow \Upsilon(4S)$
- $< 8.3 \times 10^{-7}$ 90 1 BERGFELD 00B CLE2 $e^+e^- \rightarrow \Upsilon(4S)$
- $< 1.4 \times 10^{-5}$ 90 2 ACCIARRI 97B L3 $e^+e^- \rightarrow Z$
- $< 5.9 \times 10^{-6}$ 90 AMMAR 94 CLE2 Repl. by BERGFELD 00B
- $< 2.6 \times 10^{-5}$ 90 3 AVERY 89B CLEO $e^+e^- \rightarrow \Upsilon(4S)$
- $< 7.6 \times 10^{-5}$ 90 4 ALBRECHT 87D ARG $e^+e^- \rightarrow \Upsilon(4S)$
- $< 6.4 \times 10^{-5}$ 90 5 AVERY 87 CLEO $e^+e^- \rightarrow \Upsilon(4S)$
- $< 3 \times 10^{-4}$ 90 GILES 84 CLEO Repl. by AVERY 87

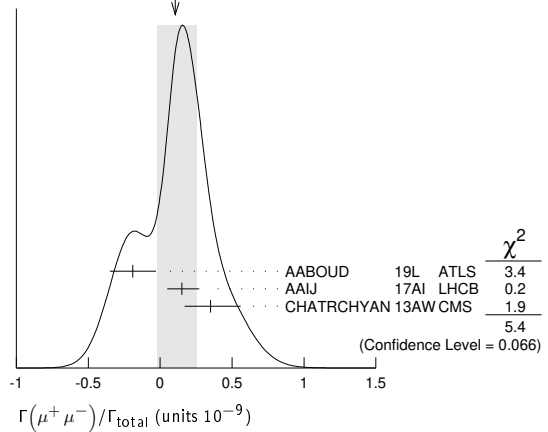
- ¹ Assumes equal production of B^+ and B^0 at the $\Upsilon(4S)$.
- ² ACCIARRI 97B assume PDG 96 production fractions for B^+, B^0, B_s , and Λ_b .
- ³ AVERY 89B reports $< 3 \times 10^{-5}$ assuming the $\Upsilon(4S)$ decays 43% to $B^0 \bar{B}^0$. We rescale to 50%.
- ⁴ ALBRECHT 87D reports $< 8.5 \times 10^{-5}$ assuming the $\Upsilon(4S)$ decays 45% to $B^0 \bar{B}^0$. We rescale to 50%.
- ⁵ AVERY 87 reports $< 8 \times 10^{-5}$ assuming the $\Upsilon(4S)$ decays 40% to $B^0 \bar{B}^0$. We rescale to 50%.

$\Gamma(e^+e^-\gamma) / \Gamma_{total}$					Γ_{526} / Γ
Test for $\Delta B=1$ weak neutral current. Allowed by higher-order electroweak interactions.					
VALUE	CL%	DOCUMENT ID	TECN	COMMENT	
$< 1.2 \times 10^{-7}$	90	AUBERT	08c	BABR $e^+e^- \rightarrow \Upsilon(4S)$	

$\Gamma(\mu^+\mu^-) / \Gamma_{total}$					Γ_{527} / Γ
Test for $\Delta B=1$ weak neutral current. Allowed by higher-order electroweak interactions.					
VALUE (units 10^{-3})	CL%	DOCUMENT ID	TECN	COMMENT	
$0.11^{+0.14}_{-0.13}$ OUR AVERAGE	Error includes scale factor of 1.6. See the ideogram below.				

- -0.19 ± 0.16 1,2 AABOUD 19L ATLS $p\bar{p}$ at 7, 8, 13 TeV
- $0.15^{+0.12+0.02}_{-0.10-0.01}$ 3 AAIJ 17AI LHCB $p\bar{p}$ at 7, 8, 13 TeV
- $0.35^{+0.21}_{-0.18}$ 4 CHATRCHYAN13AW CMS $p\bar{p}$ at 7, 8 TeV
- • •** We do not use the following data for averages, fits, limits, etc. **• • •**
- -0.25 ± 0.20 5 AABOUD 16L ATLS $p\bar{p}$ at 7, 8 TeV, Repl. by AABOUD 16L
- $0.39^{+0.16}_{-0.14}$ 6 KHACHATRY...15BE LHC $p\bar{p}$ at 7, 8 TeV
- < 0.80 90 7 AAIJ 13B LHCB Repl. by AAIJ 13BA
- < 0.63 90 8 AAIJ 13BA LHCB Repl. by KHACHA-TRYAN 15BE
- < 3.8 90 9 AALTONEN 13F CDF $p\bar{p}$ at 1.96 TeV
- < 2.6 90 7 AAIJ 12A LHCB Repl. by AAIJ 12W
- < 0.81 90 10 AAIJ 12W LHCB Repl. by AAIJ 13B
- < 1.4 90 10 CHATRCHYAN12A CMS $p\bar{p}$ at 7 TeV
- < 12 90 11 AAIJ 11B LHCB Repl. by AAIJ 12A
- < 5.0 90 10 AALTONEN 11AG CDF $p\bar{p}$ at 1.96 TeV
- < 3.7 90 10 CHATRCHYAN11T CMS Repl. by CHATRCHYAN 12A

WEIGHTED AVERAGE
0.11+0.14-0.13 (Error scaled by 1.6)



- ¹ Corresponds to a 95% CL upper limit of $< 2.1 \times 10^{-10}$.
- ² Uses normalization mode $B(B^+ \rightarrow J/\psi K^+) = (1.010 \pm 0.029) \times 10^{-3}$ and B production ratio $f(b \rightarrow B_s^0) / (b \rightarrow B^0) = 0.256 \pm 0.013$.
- ³ Corresponds to a 95% CL upper limit of $< 3.4 \times 10^{-10}$.
- ⁴ Reports also a limit of $< 9.2 \times 10^{-10}$ at 90% CL. and uses $B(B^+ \rightarrow J/\psi K^+ \rightarrow \mu^+ \mu^- K^+) = (6.0 \pm 0.2) \times 10^{-5}$ for normalization.

Meson Particle Listings

B^0

- ⁵ This value is obtained from a profile-likelihood fit, see Fig. 9. It corresponds to an upper limit of $< 0.42 \times 10^{-9}$ at 95% C.L.
- ⁶ Derived from the combined fit to CMS and LHCb data. Uncertainty includes both statistical and systematic component. Also reports $B(B^0 \rightarrow \mu^+ \mu^-)/B(B_s \rightarrow \mu^+ \mu^-) = 0.14^{+0.08}_{-0.06}$.
- ⁷ Uses $B(B^+ \rightarrow J/\psi K^+ \rightarrow \mu^+ \mu^- K^+) = (6.01 \pm 0.21) \times 10^{-5}$ and $B(B^0 \rightarrow K^+ \pi^-) = (1.94 \pm 0.06) \times 10^{-5}$ for normalization.
- ⁸ Reports also a limit of $< 7.4 \times 10^{-10}$ at 95% CL. Uses normalization modes $B^+ \rightarrow J/\psi K^+ \rightarrow \mu^+ \mu^- K^+$ and $B^0 \rightarrow K^+ \pi^-$.
- ⁹ Uses normalization mode $B(B^+ \rightarrow J/\psi K^+) = (10.22 \pm 0.35) \times 10^{-4}$.
- ¹⁰ Uses $B(B^+ \rightarrow J/\psi K^+ \rightarrow \mu^+ \mu^- K^+) = (6.01 \pm 0.21) \times 10^{-5}$.
- ¹¹ Uses B production ratio $f(\bar{b} \rightarrow B^+)/f(\bar{b} \rightarrow B_s^0) = 3.71 \pm 0.47$ and three normalization modes.

$\Gamma(\mu^+ \mu^- \gamma)/\Gamma_{total}$ Γ_{528}/Γ
 Test for $\Delta B=1$ weak neutral current. Allowed by higher-order electroweak interactions.

VALUE	CL%	DOCUMENT ID	TECN	COMMENT
$< 1.6 \times 10^{-7}$	90	AUBERT	08c	BABR $e^+ e^- \rightarrow \Upsilon(4S)$

$\Gamma(\tau^+ \tau^-)/\Gamma_{total}$ Γ_{531}/Γ
 Test for $\Delta B=1$ weak neutral current. Allowed by higher-order electroweak interactions.

VALUE	CL%	DOCUMENT ID	TECN	COMMENT
$< 2.1 \times 10^{-3}$	95	1 AAIJ	17AJ	LHCB pp at 7, 8 TeV
••• We do not use the following data for averages, fits, limits, etc. •••				
$< 4.1 \times 10^{-3}$	90	2 AUBERT	06s	BABR $e^+ e^- \rightarrow \Upsilon(4S)$
1 Assuming no contribution from $B_s^0 \rightarrow \tau^+ \tau^-$.				
2 Assumes equal production of B^+ and B^0 at the $\Upsilon(4S)$.				

$\Gamma(\mu^+ \mu^- \mu^+ \mu^-)/\Gamma_{total}$ Γ_{529}/Γ

VALUE	CL%	DOCUMENT ID	TECN	COMMENT
$< 6.9 \times 10^{-10}$	95	AAIJ	17N	LHCB pp at 7, 8 TeV
••• We do not use the following data for averages, fits, limits, etc. •••				
$< 5.3 \times 10^{-9}$	90	1 AAIJ	13AW	LHCB Repl. by AAIJ 17N
1 Also reports a limit of $< 6.6 \times 10^{-9}$ at 95% CL.				

$\Gamma(S, P, S \rightarrow \mu^+ \mu^-, P \rightarrow \mu^+ \mu^-)/\Gamma_{total}$ Γ_{530}/Γ
 Here S and P are the hypothetical scalar and pseudoscalar particles with masses of 2.5 GeV/c² and 214.3 MeV/c², respectively.

VALUE	CL%	DOCUMENT ID	TECN	COMMENT
$< 6.0 \times 10^{-10}$	95	AAIJ	17N	LHCB pp at 7, 8 TeV
••• We do not use the following data for averages, fits, limits, etc. •••				
$< 5.1 \times 10^{-9}$	90	1 AAIJ	13AW	LHCB Repl. by AAIJ 17N
1 Also reports a limit of $< 6.3 \times 10^{-9}$ at 95% CL.				

$\Gamma(\pi^0 \ell^+ \ell^-)/\Gamma_{total}$ Γ_{532}/Γ

VALUE	CL%	DOCUMENT ID	TECN	COMMENT
$< 5.3 \times 10^{-8}$	90	1 LEES	13M	BABR $e^+ e^- \rightarrow \Upsilon(4S)$
••• We do not use the following data for averages, fits, limits, etc. •••				
$< 1.5 \times 10^{-7}$	90	1 WEI	08A	BELL $e^+ e^- \rightarrow \Upsilon(4S)$
$< 1.2 \times 10^{-7}$	90	1 AUBERT	07AG	BABR Repl. by LEES 13M
1 Assumes equal production of B^+ and B^0 at the $\Upsilon(4S)$.				

$\Gamma(\pi^0 \nu \bar{\nu})/\Gamma_{total}$ Γ_{538}/Γ
 Test for $\Delta B = 1$ weak neutral current. Allowed by higher-order electroweak interaction.

VALUE	CL%	DOCUMENT ID	TECN	COMMENT
$< 0.9 \times 10^{-5}$	90	1 GRYGIER	17	BELL $e^+ e^- \rightarrow \Upsilon(4S)$
••• We do not use the following data for averages, fits, limits, etc. •••				
$< 6.9 \times 10^{-5}$	90	1 LUTZ	13	BELL $e^+ e^- \rightarrow \Upsilon(4S)$
$< 2.2 \times 10^{-4}$	90	1 CHEN	07D	BELL Repl. by LUTZ 13
1 Assumes equal production of B^+ and B^0 at the $\Upsilon(4S)$.				

$\Gamma(\pi^0 e^+ e^-)/\Gamma_{total}$ Γ_{533}/Γ

VALUE	CL%	DOCUMENT ID	TECN	COMMENT
$< 8.4 \times 10^{-8}$	90	1 LEES	13M	BABR $e^+ e^- \rightarrow \Upsilon(4S)$
••• We do not use the following data for averages, fits, limits, etc. •••				
$< 2.3 \times 10^{-7}$	90	1 WEI	08A	BELL $e^+ e^- \rightarrow \Upsilon(4S)$
$< 1.4 \times 10^{-7}$	90	1 AUBERT	07AG	BABR Repl. by LEES 13M
1 Assumes equal production of B^+ and B^0 at the $\Upsilon(4S)$.				

$\Gamma(\pi^0 \mu^+ \mu^-)/\Gamma_{total}$ Γ_{534}/Γ

VALUE	CL%	DOCUMENT ID	TECN	COMMENT
$< 6.9 \times 10^{-8}$	90	1 LEES	13M	BABR $e^+ e^- \rightarrow \Upsilon(4S)$
••• We do not use the following data for averages, fits, limits, etc. •••				
$< 1.8 \times 10^{-7}$	90	1 WEI	08A	BELL $e^+ e^- \rightarrow \Upsilon(4S)$
$< 5.1 \times 10^{-7}$	90	1 AUBERT	07AG	BABR $e^+ e^- \rightarrow \Upsilon(4S)$
1 Assumes equal production of B^+ and B^0 at the $\Upsilon(4S)$.				

$\Gamma(\eta \ell^+ \ell^-)/\Gamma_{total}$ Γ_{535}/Γ

VALUE	CL%	DOCUMENT ID	TECN	COMMENT
$< 6.4 \times 10^{-8}$	90	1 LEES	13M	BABR $e^+ e^- \rightarrow \Upsilon(4S)$
1 Assumes equal production of B^+ and B^0 at the $\Upsilon(4S)$.				

$\Gamma(\eta e^+ e^-)/\Gamma_{total}$ Γ_{536}/Γ

VALUE	CL%	DOCUMENT ID	TECN	COMMENT
$< 10.8 \times 10^{-8}$	90	1 LEES	13M	BABR $e^+ e^- \rightarrow \Upsilon(4S)$
1 Assumes equal production of B^+ and B^0 at the $\Upsilon(4S)$.				

$\Gamma(\eta \mu^+ \mu^-)/\Gamma_{total}$ Γ_{537}/Γ

VALUE	CL%	DOCUMENT ID	TECN	COMMENT
$< 11.2 \times 10^{-8}$	90	1 LEES	13M	BABR $e^+ e^- \rightarrow \Upsilon(4S)$
1 Assumes equal production of B^+ and B^0 at the $\Upsilon(4S)$.				

$\Gamma(K^0 \ell^+ \ell^-)/\Gamma_{total}$ Γ_{539}/Γ

VALUE (units 10^{-7})	CL%	DOCUMENT ID	TECN	COMMENT
3.1 \pm 0.8 OUR AVERAGE				
$2.1^{+1.5}_{-1.3} \pm 0.2$		1 AUBERT	09T	BABR $e^+ e^- \rightarrow \Upsilon(4S)$
$3.4^{+0.9}_{-0.8} \pm 0.2$		1 WEI	09A	BELL $e^+ e^- \rightarrow \Upsilon(4S)$
••• We do not use the following data for averages, fits, limits, etc. •••				
$2.9^{+1.6}_{-1.3} \pm 0.3$		1 AUBERT,B	06J	BABR Repl. by AUBERT 09T
< 6.8	90	1 ISHIKAWA	03	BELL $e^+ e^- \rightarrow \Upsilon(4S)$
1 Assumes equal production of B^0 and B^+ at $\Upsilon(4S)$.				

$\Gamma(K^0 e^+ e^-)/\Gamma_{total}$ Γ_{540}/Γ
 Test for $\Delta B=1$ weak neutral current. Allowed by higher-order electroweak interactions.

VALUE (units 10^{-7})	CL%	DOCUMENT ID	TECN	COMMENT
1.6 \pm 1.0 OUR AVERAGE				
$0.8^{+1.5}_{-1.2} \pm 0.1$		1 AUBERT	09T	BABR $e^+ e^- \rightarrow \Upsilon(4S)$
$2.0^{+1.4}_{-1.0} \pm 0.1$		1 WEI	09A	BELL $e^+ e^- \rightarrow \Upsilon(4S)$
••• We do not use the following data for averages, fits, limits, etc. •••				
$1.3^{+1.6}_{-1.1} \pm 0.2$		1 AUBERT,B	06J	BABR Repl. by AUBERT 09T
$- 2.1^{+2.3}_{-1.6} \pm 0.8$		1 AUBERT	03U	BABR $e^+ e^- \rightarrow \Upsilon(4S)$
< 5.4	90	2 ISHIKAWA	03	BELL $e^+ e^- \rightarrow \Upsilon(4S)$
< 27	90	1 ABE	02	BELL Repl. by ISHIKAWA 03
< 38	90	1 AUBERT	02L	BABR $e^+ e^- \rightarrow \Upsilon(4S)$
< 84.5	90	3 ANDERSON	01B	CLE2 $e^+ e^- \rightarrow \Upsilon(4S)$
< 3000	90	1 ALBRECHT	91E	ARG $e^+ e^- \rightarrow \Upsilon(4S)$
< 5200	90	4 AVERY	87	CLEO $e^+ e^- \rightarrow \Upsilon(4S)$
1 Assumes equal production of B^+ and B^0 at the $\Upsilon(4S)$.				
2 Assumes equal production of B^0 and B^+ at $\Upsilon(4S)$.				
3 The result is for di-lepton masses above 0.5 GeV.				
4 AVERY 87 reports $< 6.5 \times 10^{-4}$ assuming the $\Upsilon(4S)$ decays 40% to $B^0 \bar{B}^0$. We rescale to 50%.				

$\Gamma(K^0 \nu \bar{\nu})/\Gamma_{total}$ Γ_{542}/Γ
 Test for $\Delta B = 1$ weak neutral current. Allowed by higher-order electroweak interaction.

VALUE	CL%	DOCUMENT ID	TECN	COMMENT
$< 2.6 \times 10^{-5}$	90	1 GRYGIER	17	BELL $e^+ e^- \rightarrow \Upsilon(4S)$
••• We do not use the following data for averages, fits, limits, etc. •••				
$< 4.9 \times 10^{-5}$	90	1,2 LEES	13I	BABR $e^+ e^- \rightarrow \Upsilon(4S)$
$< 19.4 \times 10^{-5}$	90	1 LUTZ	13	BELL $e^+ e^- \rightarrow \Upsilon(4S)$
$< 5.6 \times 10^{-5}$	90	1 DEL-AMO-SA...	10Q	BABR Repl. by LEES 13I
$< 1.6 \times 10^{-4}$	90	1 CHEN	07D	BELL $e^+ e^- \rightarrow \Upsilon(4S)$
1 Assumes equal production of B^+ and B^0 at the $\Upsilon(4S)$.				
2 Also reported a limit $< 8.1 \times 10^{-5}$ at 90% CL obtained using a fully reconstructed hadronic B -tag evnets.				

$\Gamma(\rho^0 \nu \bar{\nu})/\Gamma_{total}$ Γ_{543}/Γ
 Test for $\Delta B = 1$ weak neutral current. Allowed by higher-order electroweak interaction.

VALUE	CL%	DOCUMENT ID	TECN	COMMENT
$< 4.0 \times 10^{-5}$	90	1 GRYGIER	17	BELL $e^+ e^- \rightarrow \Upsilon(4S)$
••• We do not use the following data for averages, fits, limits, etc. •••				
$< 2.08 \times 10^{-4}$	90	1 LUTZ	13	BELL $e^+ e^- \rightarrow \Upsilon(4S)$
$< 4.4 \times 10^{-4}$	90	1 CHEN	07D	BELL Repl. by LUTZ 13
1 Assumes equal production of B^+ and B^0 at the $\Upsilon(4S)$.				

$\Gamma(K^0 \mu^+ \mu^-)/\Gamma_{total}$ Γ_{541}/Γ
 Test for $\Delta B=1$ weak neutral current. Allowed by higher-order electroweak interactions.

VALUE (units 10^{-7})	CL%	DOCUMENT ID	TECN	COMMENT
3.39 \pm 0.34 OUR FIT				
3.4 \pm 0.4 OUR AVERAGE				
$3.27 \pm 0.34 \pm 0.17$		1 AAIJ	14M	LHCB pp at 7, 8 TeV
$4.9^{+2.9}_{-2.5} \pm 0.3$		2 AUBERT	09T	BABR $e^+ e^- \rightarrow \Upsilon(4S)$
$4.4^{+1.3}_{-1.1} \pm 0.3$		2 WEI	09A	BELL $e^+ e^- \rightarrow \Upsilon(4S)$

• • • We do not use the following data for averages, fits, limits, etc. • • •

Table with columns: Value, Document ID, TECN, COMMENT. Rows include AAIJ, AUBERT, B, ISHIKAWA, ABE, AUBERT, ANDERSON, ALBRECHT, AVERY.

- 1 Uses B(B^0 -> J/psi(1S) K^0) = (0.928 +/- 0.013 +/- 0.037) x 10^-3 for normalization.
2 Assumes equal production of B+ and B0 at the T(4S).
3 Assumes equal production of B0 and B+ at T(4S). The second error is a total of systematic uncertainties including model dependence.
4 The result is for di-lepton masses above 0.5 GeV.
5 AVERY 87 reports < 4.5 x 10^-4 assuming the T(4S) decays 40% to B0 B0-bar. We rescale to 50%.

Gamma(K^0 mu+ mu-)/Gamma(J/psi(1S) K^0) Gamma541/Gamma198. Value: 0.39 +/- 0.04 OUR FIT. Comment: AALTONEN 11A1 CDF pp at 1.96 TeV.

Gamma(K*(892)^0 l+ l-)/Gamma_total Gamma544/Gamma. Test for Delta B=1 weak neutral current. Value: 9.9 +/- 1.2 OUR AVERAGE.

Table with columns: Value, Document ID, TECN, COMMENT. Rows include AUBERT, WEI.

• • • We do not use the following data for averages, fits, limits, etc. • • •

Table with columns: Value, Document ID, TECN, COMMENT. Rows include AUBERT, B, ISHIKAWA.

- 1 Assumes equal production of B0 and B+ at T(4S).

Gamma(K*(892)^0 e+ e-)/Gamma_total Gamma545/Gamma. Test for Delta B=1 weak neutral current. Value: 10.3 +/- 1.9 OUR AVERAGE.

Table with columns: Value, Document ID, TECN, COMMENT. Rows include AUBERT, WEI.

• • • We do not use the following data for averages, fits, limits, etc. • • •

Table with columns: Value, Document ID, TECN, COMMENT. Rows include AUBERT, B, ISHIKAWA, ABE, AUBERT, ALBRECHT.

- 1 Assumes equal production of B+ and B0 at the T(4S).
2 Assumes equal production of B0 and B+ at T(4S).

Gamma(K*(892)^0 mu+ mu-)/Gamma_total Gamma546/Gamma. Test for Delta B=1 weak neutral current. Value: 9.4 +/- 0.6 OUR AVERAGE.

Table with columns: Value, Document ID, TECN, COMMENT. Rows include AAIJ, AUBERT, WEI.

• • • We do not use the following data for averages, fits, limits, etc. • • •

Table with columns: Value, Document ID, TECN, COMMENT. Rows include AAIJ, AUBERT, B, ISHIKAWA, ABE, AUBERT, AFFOLDER.

- 1 Uses B(B^0 -> J/psi K*(892)^0) = (1.19 +/- 0.01 +/- 0.08) x 10^-3. The second error is the total systematic uncertainty.
2 Assumes equal production of B+ and B0 at the T(4S).
3 Assumes equal production of B0 and B+ at T(4S). The second error is a total of systematic uncertainties including model dependence.
4 AFFOLDER 99B measured relative to B0 -> J/psi(1S) K*(892)^0.

Gamma(K*(892)^0 mu+ mu-)/Gamma(J/psi(1S) K*(892)^0) Gamma546/Gamma200

Table with columns: Value, Document ID, TECN, COMMENT. Rows include AALTONEN 11A1 CDF pp at 1.96 TeV, AALTONEN 11L CDF Repl. by AALTONEN 11A1, AALTONEN 09B CDF Repl. by AALTONEN 11L.

Gamma(K*(892)^0 chi -> mu+ mu-)/Gamma_total Gamma547/Gamma

Table with columns: Value, Document ID, TECN, COMMENT. Row: 1 AAIJ 15Az LHCb pp at 7, 8 TeV.

- 1 The limit is obtained as a function of di-muon mass. A normalizing mode branching fraction value of B(B^0 -> K*0 mu+ mu-) = (1.6 +/- 0.3) x 10^-7 is used.

Gamma(pi+ pi- mu+ mu-)/Gamma_total Gamma548/Gamma

Table with columns: Value, Document ID, TECN, COMMENT. Row: 1 AAIJ 15s LHCb pp at 7, 8 TeV.

- 1 AAIJ 15s reports (2.11 +/- 0.51 +/- 0.15 +/- 0.16) x 10^-8 from a measurement of [Gamma(B^0 -> pi+ pi- mu+ mu-)/Gamma_total] / [B(B^0 -> J/psi(1S) K*(892)^0)] assuming B(B^0 -> J/psi(1S) K*(892)^0) = (1.3 +/- 0.1) x 10^-3, which we rescale to our best value B(B^0 -> J/psi(1S) K*(892)^0) = (1.27 +/- 0.05) x 10^-3. Our first error is their experiment's error and our second error is the systematic error from using our best value.

Gamma(K*(892)^0 nu nu)/Gamma_total Gamma549/Gamma

Table with columns: Value, Document ID, TECN, COMMENT. Row: 1 GRYGIER 17 BELL e+ e- -> T(4S).

• • • We do not use the following data for averages, fits, limits, etc. • • •

Table with columns: Value, Document ID, TECN, COMMENT. Rows include LEES, LUTZ, AUBERT, CHEN, ADAM.

- 1 Assumes equal production of B+ and B0 at the T(4S).
2 Also reported a limit < 9.3 x 10^-5 at 90% CL obtained using a fully reconstructed hadronic B-tag evnets.
3 ADAM 96D assumes f_B0 = f_B- = 0.39 and f_Bs = 0.12.

Gamma(invisible)/Gamma_total Gamma550/Gamma

Table with columns: Value, Document ID, TECN, COMMENT. Row: 1 LEES 12T BABR e+ e- -> T(4S).

• • • We do not use the following data for averages, fits, limits, etc. • • •

Table with columns: Value, Document ID, TECN, COMMENT. Rows include HSU, AUBERT, B.

- 1 Uses the fully reconstructed B0 -> D(*)- l+ nu_l events as a tag.
2 Identified by fully reconstructing a hadronic decay of the accompanying B meson and requiring no other particles in the event.

Gamma(nu nu gamma)/Gamma_total Gamma551/Gamma

Table with columns: Value, Document ID, TECN, COMMENT. Row: 1 LEES 12T BABR e+ e- -> T(4S).

• • • We do not use the following data for averages, fits, limits, etc. • • •

Table with columns: Value, Document ID, TECN, COMMENT. Row: 1 AUBERT, B 04J BABR Repl. by LEES 12T.

Gamma(phi nu nu)/Gamma_total Gamma552/Gamma

Table with columns: Value, Document ID, TECN, COMMENT. Row: 1 LUTZ 13 BELL e+ e- -> T(4S).

• • • We do not use the following data for averages, fits, limits, etc. • • •

Table with columns: Value, Document ID, TECN, COMMENT. Row: 1 CHEN 07D BELL Repl. by LUTZ 13.

- 1 Assumes equal production of B+ and B0 at the T(4S).

Gamma(e+ e-)/Gamma_total Gamma553/Gamma

Table with columns: Value, Document ID, TECN, COMMENT. Row: 1 AAIJ 18T LHCb pp at 7, 8 TeV.

• • • We do not use the following data for averages, fits, limits, etc. • • •

Table with columns: Value, Document ID, TECN, COMMENT. Rows include AAIJ, AALTONEN, AUBERT, ABE, CHANG, BERGFELD, ABE, ACCIARRI, AMMAR, AVERY, ALBRECHT.

Meson Particle Listings

 B^0

VALUE	CL%	DOCUMENT ID	TECN	COMMENT
$< 7.7 \times 10^{-5}$	90	7 AVERY	87	CLEO $e^+e^- \rightarrow \Upsilon(4S)$
$< 3 \times 10^{-4}$	90	GILES	84	CLEO Repl. by AVERY 87

¹ AAIJ 18T uses normalization modes $B(B^0 \rightarrow K^+\pi^-) = (19.6 \pm 0.5) \times 10^{-6}$ and $B(B^+ \rightarrow J/\psi K^+) = (1.026 \pm 0.031) \times 10^{-3}$.
² Uses normalization mode $B(B^0 \rightarrow K^+\pi^-) = (19.4 \pm 0.6) \times 10^{-6}$.
³ Assumes equal production of B^+ and B^0 at the $\Upsilon(4S)$.
⁴ ACCIARRI 97B assume PDG 96 production fractions for B^+ , B^0 , B_s , and Λ_b .
⁵ Paper assumes the $\Upsilon(4S)$ decays 43% to $B^0\bar{B}^0$. We rescale to 50%.
⁶ ALBRECHT 87D reports $< 5 \times 10^{-5}$ assuming the $\Upsilon(4S)$ decays 45% to $B^0\bar{B}^0$. We rescale to 50%.
⁷ AVERY 87 reports $< 9 \times 10^{-5}$ assuming the $\Upsilon(4S)$ decays 40% to $B^0\bar{B}^0$. We rescale to 50%.

$\Gamma(\pi^0 e^\pm \mu^\mp)/\Gamma_{\text{total}}$	CL%	DOCUMENT ID	TECN	COMMENT
$< 1.4 \times 10^{-7}$	90	1 AUBERT	07AG	BABR $e^+e^- \rightarrow \Upsilon(4S)$

¹ Assumes equal production of B^+ and B^0 at the $\Upsilon(4S)$.

$\Gamma(K^0 e^\pm \mu^\mp)/\Gamma_{\text{total}}$	CL%	DOCUMENT ID	TECN	COMMENT
Test of lepton family number conservation.				
VALUE (units 10^{-7})	CL%	DOCUMENT ID	TECN	COMMENT
< 2.7	90	1 AUBERT,B	06J	BABR $e^+e^- \rightarrow \Upsilon(4S)$

••• We do not use the following data for averages, fits, limits, etc. •••
 < 40 90 1 AUBERT 02L BABR Repl. by AUBERT,B 06J
¹ Assumes equal production of B^+ and B^0 at the $\Upsilon(4S)$.

$\Gamma(K^*(892)^0 e^+ \mu^-)/\Gamma_{\text{total}}$	CL%	DOCUMENT ID	TECN	COMMENT
VALUE (units 10^{-7})	CL%	DOCUMENT ID	TECN	COMMENT
< 1.6	90	1 SANDILYA	18	BELL $e^+e^- \rightarrow \Upsilon(4S)$

••• We do not use the following data for averages, fits, limits, etc. •••
 < 5.3 90 2 AUBERT,B 06J BABR $e^+e^- \rightarrow \Upsilon(4S)$
¹ Uses $B(\Upsilon(4S) \rightarrow B^0\bar{B}^0) = 0.486 \pm 0.006$.
² Assumes equal production of B^0 and B^+ at $\Upsilon(4S)$.

$\Gamma(K^*(892)^0 e^- \mu^+)/\Gamma_{\text{total}}$	CL%	DOCUMENT ID	TECN	COMMENT
VALUE (units 10^{-7})	CL%	DOCUMENT ID	TECN	COMMENT
< 1.2	90	1 SANDILYA	18	BELL $e^+e^- \rightarrow \Upsilon(4S)$

••• We do not use the following data for averages, fits, limits, etc. •••
 < 3.4 90 2 AUBERT,B 06J BABR $e^+e^- \rightarrow \Upsilon(4S)$
¹ Uses $B(\Upsilon(4S) \rightarrow B^0\bar{B}^0) = 0.486 \pm 0.006$.
² Assumes equal production of B^0 and B^+ at $\Upsilon(4S)$.

$\Gamma(K^*(892)^0 e^\pm \mu^\mp)/\Gamma_{\text{total}}$	CL%	DOCUMENT ID	TECN	COMMENT
Test of lepton family number conservation.				
VALUE (units 10^{-7})	CL%	DOCUMENT ID	TECN	COMMENT
< 1.8	90	1 SANDILYA	18	BELL $e^+e^- \rightarrow \Upsilon(4S)$

••• We do not use the following data for averages, fits, limits, etc. •••
 < 5.8 90 2 AUBERT,B 06J BABR $e^+e^- \rightarrow \Upsilon(4S)$
 < 34 90 2 AUBERT 02L BABR Repl. by AUBERT,B 06J
¹ Uses $B(\Upsilon(4S) \rightarrow B^0\bar{B}^0) = 0.486 \pm 0.006$.
² Assumes equal production of B^+ and B^0 at the $\Upsilon(4S)$.

$\Gamma(e^\pm \tau^\mp)/\Gamma_{\text{total}}$	CL%	DOCUMENT ID	TECN	COMMENT
Test of lepton family number conservation. Allowed by higher-order electroweak interactions.				
VALUE	CL%	DOCUMENT ID	TECN	COMMENT
$< 2.8 \times 10^{-5}$	90	1 AUBERT	08AD	BABR $e^+e^- \rightarrow \Upsilon(4S)$

••• We do not use the following data for averages, fits, limits, etc. •••
 $< 1.1 \times 10^{-4}$ 90 BORNHEIM 04 CLE2 $e^+e^- \rightarrow \Upsilon(4S)$
 $< 5.3 \times 10^{-4}$ 90 AMMAR 94 CLE2 Repl. by BORNHEIM 04
¹ Assumes equal production of B^+ and B^0 at the $\Upsilon(4S)$.

$\Gamma(\mu^\pm \tau^\mp)/\Gamma_{\text{total}}$	CL%	DOCUMENT ID	TECN	COMMENT
Test of lepton family number conservation. Allowed by higher-order electroweak interactions.				
VALUE	CL%	DOCUMENT ID	TECN	COMMENT
$< 1.4 \times 10^{-5}$	95	1 AAIJ	19AK	LHCB pp at 7, 8 TeV

••• We do not use the following data for averages, fits, limits, etc. •••
 $< 2.2 \times 10^{-5}$ 90 2 AUBERT 08AD BABR $e^+e^- \rightarrow \Upsilon(4S)$
 $< 3.8 \times 10^{-5}$ 90 BORNHEIM 04 CLE2 $e^+e^- \rightarrow \Upsilon(4S)$
 $< 8.3 \times 10^{-4}$ 90 AMMAR 94 CLE2 Repl. by BORNHEIM 04
¹ Assuming no contribution from $B_s^0 \rightarrow \mu^\pm \tau^\mp$.
² Assumes equal production of B^+ and B^0 at the $\Upsilon(4S)$.

$\Gamma(\Lambda_c^+ \mu^-)/\Gamma_{\text{total}}$	CL%	DOCUMENT ID	TECN	COMMENT
VALUE	CL%	DOCUMENT ID	TECN	COMMENT
$< 1.4 \times 10^{-6}$	90	1,2 DEL-AMO-SA..11k	BABR	$e^+e^- \rightarrow \Upsilon(4S)$

¹ DEL-AMO-SANCHEZ 11k reports $< 180 \times 10^{-8}$ from a measurement of $[\Gamma(B^0 \rightarrow \Lambda_c^+ \mu^-)/\Gamma_{\text{total}}] \times [B(\Lambda_c^+ \rightarrow p K^- \pi^+)]$ assuming $B(\Lambda_c^+ \rightarrow p K^- \pi^+) = (5.0 \pm 1.3) \times 10^{-2}$, which we rescale to our best value $B(\Lambda_c^+ \rightarrow p K^- \pi^+) = 6.28 \times 10^{-2}$.
² Uses $B(\Upsilon(4S) \rightarrow B^0\bar{B}^0) = (51.6 \pm 0.6)\%$ and $B(\Upsilon(4S) \rightarrow B^+ B^-) = (48.4 \pm 0.6)\%$.

$\Gamma(\Lambda_c^+ e^-)/\Gamma_{\text{total}}$	CL%	DOCUMENT ID	TECN	COMMENT
VALUE	CL%	DOCUMENT ID	TECN	COMMENT
$< 4 \times 10^{-6}$	90	1,2 DEL-AMO-SA..11k	BABR	$e^+e^- \rightarrow \Upsilon(4S)$

¹ DEL-AMO-SANCHEZ 11k reports $< 520 \times 10^{-8}$ from a measurement of $[\Gamma(B^0 \rightarrow \Lambda_c^+ e^-)/\Gamma_{\text{total}}] \times [B(\Lambda_c^+ \rightarrow p K^- \pi^+)]$ assuming $B(\Lambda_c^+ \rightarrow p K^- \pi^+) = (5.0 \pm 1.3) \times 10^{-2}$, which we rescale to our best value $B(\Lambda_c^+ \rightarrow p K^- \pi^+) = 6.28 \times 10^{-2}$.
² Uses $B(\Upsilon(4S) \rightarrow B^0\bar{B}^0) = (51.6 \pm 0.6)\%$ and $B(\Upsilon(4S) \rightarrow B^+ B^-) = (48.4 \pm 0.6)\%$.

 B_s^0 CROSS-PARTICLE BRANCHING RATIOS

$\Gamma([K^+ K^-]_D K^*(892)^0)/\Gamma_{\text{total}} \times B(B_s^0 \rightarrow [K^+ K^-]_D K^*(892)^0)$	CL%	DOCUMENT ID	TECN	COMMENT
VALUE	CL% <td>DOCUMENT ID</td> <td>TECN</td> <td>COMMENT</td>	DOCUMENT ID	TECN	COMMENT
$0.10 \pm 0.02 \pm 0.01$		AAIJ	14BN	LHCB pp at 7, 8 TeV

$\Gamma([\pi^+ \pi^-]_D K^*(892)^0)/\Gamma_{\text{total}} \times B(B_s^0 \rightarrow [\pi^+ \pi^-]_D K^*(892)^0)$	CL%	DOCUMENT ID	TECN	COMMENT
VALUE	CL% <td>DOCUMENT ID</td> <td>TECN</td> <td>COMMENT</td>	DOCUMENT ID	TECN	COMMENT
$0.15 \pm 0.04 \pm 0.01$		AAIJ	14BN	LHCB pp at 7, 8 TeV

See the related review(s):
[Polarization in B Decays](#)

POLARIZATION IN B^0 DECAY

In decays involving two vector mesons, one can distinguish among the states in which meson polarizations are both longitudinal (L) or both are transverse and parallel (\parallel) or perpendicular (\perp) to each other with the parameters Γ_L/Γ , Γ_\perp/Γ , and the relative phases ϕ_\parallel and ϕ_\perp . See the definitions in the note on "Polarization in B Decays" review in the B^0 Particle Listings.

 Γ_L/Γ in $B^0 \rightarrow J/\psi(1S) K^*(892)^0$

VALUE	EVTS	DOCUMENT ID	TECN	COMMENT
0.571 ± 0.007 OUR AVERAGE				
0.572 ± 0.006 ± 0.014		1 AAIJ	13AT	LHCB pp at 7 TeV
0.587 ± 0.011 ± 0.013		2 ABAZOV	09E	D0 $p\bar{p}$ at 1.96 TeV
0.556 ± 0.009 ± 0.010		3 AUBERT	07AD	BABR $e^+e^- \rightarrow \Upsilon(4S)$
0.562 ± 0.026 ± 0.018		ACOSTA	05	CDF $p\bar{p}$ at 1.96 TeV
0.574 ± 0.012 ± 0.009		ITOH	05	BELL $e^+e^- \rightarrow \Upsilon(4S)$
0.59 ± 0.06 ± 0.01		4 AFFOLDER	00N	CDF $p\bar{p}$ at 1.8 TeV
0.52 ± 0.07 ± 0.04		5 JESSOP	97	CLE2 $e^+e^- \rightarrow \Upsilon(4S)$
0.65 ± 0.10 ± 0.04	65	ABE	95Z	CDF $p\bar{p}$ at 1.8 TeV
0.97 ± 0.16 ± 0.15	13	6 ALBRECHT	94G	ARG $e^+e^- \rightarrow \Upsilon(4S)$

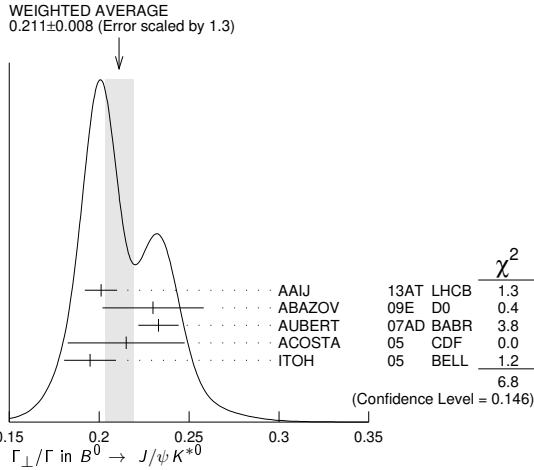
••• We do not use the following data for averages, fits, limits, etc. •••
 0.566 ± 0.012 ± 0.005 3 AUBERT 05P BABR Repl. by AUBERT 07AD
 0.62 ± 0.02 ± 0.03 7 ABE 02N BELL Repl. by ITOH 05
 0.597 ± 0.028 ± 0.024 8 AUBERT 01H BABR Repl. by AUBERT 07AD
 0.80 ± 0.08 ± 0.05 42 6 ALAM 94 CLE2 Sup. by JESSOP 97

¹ AAIJ 13AT obtains $\Gamma_\parallel/\Gamma = 0.227 \pm 0.004 \pm 0.011$. The relation $1 = (\Gamma_L + \Gamma_\perp + \Gamma_\parallel)/\Gamma$ is used to obtain Γ_L/Γ .
² Measured the angular and lifetime parameters for the time-dependent angular untagged decays $B_d^0 \rightarrow J/\psi K^{*0}$ and $B_s^0 \rightarrow J/\psi \phi$.
³ Obtained by combining the B^0 and B^+ modes.
⁴ AFFOLDER 00N measurements are based on 190 B^0 candidates obtained from a data sample of 89 pb⁻¹. The P -wave fraction is found to be $0.13_{-0.09}^{+0.12} \pm 0.06$.
⁵ JESSOP 97 is the average over a mixture of B^0 and B^+ decays. The P -wave fraction is found to be $0.16 \pm 0.08 \pm 0.04$.
⁶ Averaged over an admixture of B^0 and B^+ decays.
⁷ Averaged over an admixture of B^0 and B^+ decays and the P wave fraction is $(19 \pm 2 \pm 3)\%$.
⁸ Averaged over an admixture of B^0 and B^- decays and the P wave fraction is $(16.0 \pm 3.2 \pm 1.4) \times 10^{-2}$.

 Γ_\perp/Γ in $B^0 \rightarrow J/\psi K^{*0}$

VALUE	DOCUMENT ID	TECN	COMMENT
0.211 ± 0.008 OUR AVERAGE			
0.201 ± 0.004 ± 0.008	AAIJ	13AT	LHCB pp at 7 TeV
0.230 ± 0.013 ± 0.025	1 ABAZOV	09E	D0 $p\bar{p}$ at 1.96 TeV
0.233 ± 0.010 ± 0.005	2 AUBERT	07AD	BABR $e^+e^- \rightarrow \Upsilon(4S)$
0.215 ± 0.032 ± 0.006	ACOSTA	05	CDF $p\bar{p}$ at 1.96 TeV
0.195 ± 0.012 ± 0.008	ITOH	05	BELL $e^+e^- \rightarrow \Upsilon(4S)$

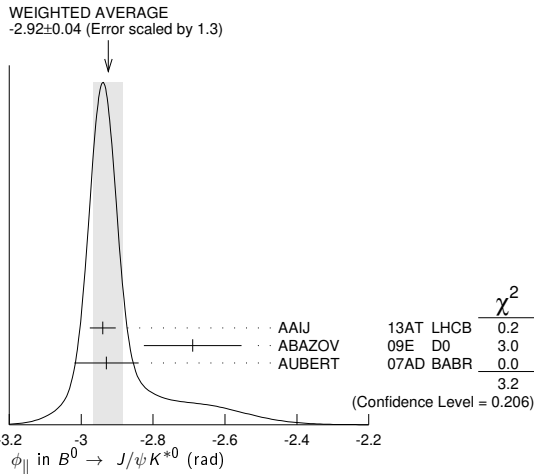
¹ Measured the angular and lifetime parameters for the time-dependent angular untagged decays $B_d^0 \rightarrow J/\psi K^{*0}$ and $B_s^0 \rightarrow J/\psi \phi$.
² Obtained by combining the B^0 and B^+ modes.



φ_{||} in B⁰ → J/ψK*⁰

VALUE (rad)	DOCUMENT ID	TECN	COMMENT
-2.92 ± 0.04 OUR AVERAGE	Error includes scale factor of 1.3. See the ideogram below.		
-2.94 ± 0.02 ± 0.03	AAIJ	13AT LHCb	pp at 7 TeV
-2.69 ± 0.08 ± 0.11	¹ ABAZOV	09E D0	p \bar{p} at 1.96 TeV
-2.93 ± 0.08 ± 0.04	² AUBERT	07AD BABR	e ⁺ e ⁻ → T(4S)

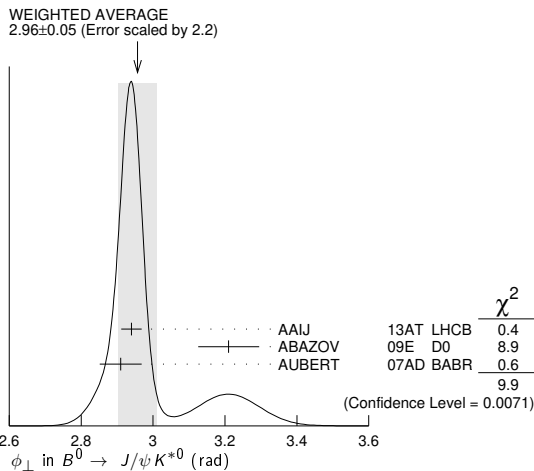
¹ Obtained φ_{||} as δ₂ - δ₁, assuming they are uncorrelated.
² Obtained by combining the B⁰ and B⁺ modes.



φ_⊥ in B⁰ → J/ψK*⁰

VALUE (rad)	DOCUMENT ID	TECN	COMMENT
2.96 ± 0.05 OUR AVERAGE	Error includes scale factor of 2.2. See the ideogram below.		
2.94 ± 0.02 ± 0.02	AAIJ	13AT LHCb	pp at 7 TeV
3.21 ± 0.06 ± 0.06	ABAZOV	09E D0	p \bar{p} at 1.96 TeV
2.91 ± 0.05 ± 0.03	¹ AUBERT	07AD BABR	e ⁺ e ⁻ → T(4S)

¹ Obtained by combining the B⁰ and B⁺ modes.



Γ_⊥/Γ in B⁰ → ψ(2S)K*(892)⁰

VALUE	DOCUMENT ID	TECN	COMMENT
0.463^{+0.028}_{-0.040} OUR AVERAGE			
0.455 ^{+0.031+0.014} _{-0.029-0.049}	CHILIKIN	13 BELL	e ⁺ e ⁻ → T(4S)
0.48 ± 0.05 ± 0.02	¹ AUBERT	07AD BABR	e ⁺ e ⁻ → T(4S)
0.45 ± 0.11 ± 0.04	² RICHICHI	01 CLE2	e ⁺ e ⁻ → T(4S)
••• We do not use the following data for averages, fits, limits, etc. •••			
0.448 ^{+0.040+0.040} _{-0.027-0.053}	MIZUK	09 BELL	e ⁺ e ⁻ → T(4S)

¹ Obtained by combining the B⁰ and B⁺ modes.
² Averages between charged and neutral B mesons.

Γ_⊥/Γ in B⁰ → ψ(2S)K*⁰

VALUE	DOCUMENT ID	TECN	COMMENT
0.30 ± 0.06 ± 0.02	¹ AUBERT	07AD BABR	e ⁺ e ⁻ → T(4S)

¹ Obtained by combining the B⁰ and B⁺ modes.

φ_{||} in B⁰ → ψ(2S)K*⁰

VALUE (rad)	DOCUMENT ID	TECN	COMMENT
-2.8 ± 0.4 ± 0.1	¹ AUBERT	07AD BABR	e ⁺ e ⁻ → T(4S)

¹ Obtained by combining the B⁰ and B⁺ modes.

φ_⊥ in B⁰ → ψ(2S)K*⁰

VALUE (rad)	DOCUMENT ID	TECN	COMMENT
2.8 ± 0.3 ± 0.1	¹ AUBERT	07AD BABR	e ⁺ e ⁻ → T(4S)

¹ Obtained by combining the B⁰ and B⁺ modes.

Γ_L/Γ in B⁰ → χ_{c1}K*(892)⁰

VALUE	DOCUMENT ID	TECN	COMMENT
0.83^{+0.06}_{-0.08} OUR AVERAGE	Error includes scale factor of 1.3.		
0.947 ^{+0.038+0.046} _{-0.048-0.099}	MIZUK	08 BELL	e ⁺ e ⁻ → T(4S)
0.77 ± 0.07 ± 0.04	¹ AUBERT	07AD BABR	e ⁺ e ⁻ → T(4S)

¹ Obtained by combining the B⁰ and B⁺ modes.

Γ_L/Γ in B⁰ → χ_{c1}K*(892)⁰

VALUE	DOCUMENT ID	TECN	COMMENT
0.03 ± 0.04 ± 0.02	¹ AUBERT	07AD BABR	e ⁺ e ⁻ → T(4S)

¹ Obtained by combining the B⁰ and B⁺ modes.

φ_{||} in B⁰ → χ_{c1}K*(892)⁰

VALUE (rad)	DOCUMENT ID	TECN	COMMENT
0.0 ± 0.3 ± 0.1	¹ AUBERT	07AD BABR	e ⁺ e ⁻ → T(4S)

¹ Obtained by combining the B⁰ and B⁺ modes.

Γ_L/Γ in B⁰ → D_s⁺D*⁻

VALUE	DOCUMENT ID	TECN	COMMENT
0.52 ± 0.05 OUR AVERAGE			
0.519 ± 0.050 ± 0.028	¹ AUBERT	03i BABR	e ⁺ e ⁻ → T(4S)
0.506 ± 0.139 ± 0.036	AHMED	00b CLE2	e ⁺ e ⁻ → T(4S)

¹ Measurement performed using partial reconstruction of D*⁻ decay.

Γ_L/Γ in B⁰ → D*⁻ρ⁺

VALUE	EVTS	DOCUMENT ID	TECN	COMMENT
0.885 ± 0.016 ± 0.012				
••• We do not use the following data for averages, fits, limits, etc. •••				
0.93 ± 0.05 ± 0.05	76	ALAM	94 CLE2	e ⁺ e ⁻ → T(4S)

Γ_L/Γ in B⁰ → D_s⁺ρ⁻

VALUE	DOCUMENT ID	TECN	COMMENT
0.84^{+0.25}_{-0.28} ± 0.13	¹ AUBERT	08AJ BABR	e ⁺ e ⁻ → T(4S)

¹ Assumes equal production of B⁺ and B⁰ at the T(4S).

Γ_L/Γ in B⁰ → D_s⁺K*⁻

VALUE	DOCUMENT ID	TECN	COMMENT
0.92^{+0.37}_{-0.31} ± 0.07	¹ AUBERT	08AJ BABR	e ⁺ e ⁻ → T(4S)

¹ Assumes equal production of B⁺ and B⁰ at the T(4S).

Γ_L/Γ in B⁰ → D*⁺D*⁻

VALUE	DOCUMENT ID	TECN	COMMENT
0.624 ± 0.029 ± 0.011			
••• We do not use the following data for averages, fits, limits, etc. •••			
0.57 ± 0.08 ± 0.02	MIYAKE	05 BELL	Repl. by KRONENBITTER 12

Meson Particle Listings

B^0

Γ_{\perp}/Γ in $B^0 \rightarrow D^{*+}D^{*-}$

VALUE	DOCUMENT ID	TECN	COMMENT
0.147 ± 0.019 OUR AVERAGE			
0.138 ± 0.024 ± 0.006	KRONENBIT...12	BELL	$e^+e^- \rightarrow \Upsilon(4S)$
0.158 ± 0.028 ± 0.006	AUBERT 09c	BABR	$e^+e^- \rightarrow \Upsilon(4S)$
• • • We do not use the following data for averages, fits, limits, etc. • • •			
0.125 ± 0.043 ± 0.023	VERVINK 09	BELL	Repl. by KRONENBITTER 12
0.143 ± 0.034 ± 0.008	AUBERT 07b0	BABR	Repl. by AUBERT 09c
0.125 ± 0.044 ± 0.007	AUBERT,BE 05A	BABR	Repl. by AUBERT 07b0
0.19 ± 0.08 ± 0.01	MIYAKE 05	BELL	Repl. by VERVINK 09
0.063 ± 0.055 ± 0.009	AUBERT 03q	BABR	Repl. by AUBERT,BE 05A

Γ_{\perp}/Γ in $B^0 \rightarrow \bar{D}^{*0}\omega$

VALUE	DOCUMENT ID	TECN	COMMENT
0.665 ± 0.047 ± 0.015	LEES 11m	BABR	$e^+e^- \rightarrow \Upsilon(4S)$

Γ_{\perp}/Γ in $B^0 \rightarrow \bar{D}_1(2430)^0\omega$

VALUE (%)	DOCUMENT ID	TECN	COMMENT
63.0 ± 9.1^{+5.5}_{-6.0}	1,2 MATVIENKO 15	BELL	$e^+e^- \rightarrow \Upsilon(4S)$

- ¹ Obtained by amplitude analysis of $\bar{B}^0 \rightarrow D^{*-}\omega\pi^+$. The second uncertainty combines in quadrature experimental systematic and model uncertainties.
- ² Assumes equal production of B^0 and B^+ at $\Upsilon(4S)$.

Γ_{\perp}/Γ in $B^0 \rightarrow \bar{D}_1(2420)^0\omega$

VALUE (%)	DOCUMENT ID	TECN	COMMENT
67.1 ± 11.7^{+2.3}_{-5.0}	1,2 MATVIENKO 15	BELL	$e^+e^- \rightarrow \Upsilon(4S)$

- ¹ Obtained by amplitude analysis of $\bar{B}^0 \rightarrow D^{*-}\omega\pi^+$. The second uncertainty combines in quadrature experimental systematic and model uncertainties.
- ² Assumes equal production of B^0 and B^+ at $\Upsilon(4S)$.

Γ_{\perp}/Γ in $B^0 \rightarrow \bar{D}_2^*(2460)^0\omega$

VALUE (%)	DOCUMENT ID	TECN	COMMENT
76.0^{+18.3+3.5}_{-8.5-2.8}	1,2 MATVIENKO 15	BELL	$e^+e^- \rightarrow \Upsilon(4S)$

- ¹ Obtained by amplitude analysis of $\bar{B}^0 \rightarrow D^{*-}\omega\pi^+$. The second uncertainty combines in quadrature experimental systematic and model uncertainties.
- ² Assumes equal production of B^0 and B^+ at $\Upsilon(4S)$.

Γ_{\perp}/Γ in $B^0 \rightarrow D^{*-}\omega\pi^+$

VALUE	DOCUMENT ID	TECN	COMMENT
0.654 ± 0.042 ± 0.016	¹ AUBERT 06L	BABR	$e^+e^- \rightarrow \Upsilon(4S)$

- ¹ Invariant mass of the $[\omega\pi]$ system is restricted in the region 1.1 and 1.9 GeV.

Γ_{\perp}/Γ in $B^0 \rightarrow \omega K^{*0}$

VALUE	DOCUMENT ID	TECN	COMMENT
0.69 ± 0.11 OUR AVERAGE			
0.68 ± 0.17 ± 0.16	AAIJ 19j	LHCB	pp at 7, 8 TeV
0.72 ± 0.14 ± 0.02	AUBERT 09H	BABR	$e^+e^- \rightarrow \Upsilon(4S)$
0.56 ± 0.29 ^{+0.18} _{-0.08}	GOLDENZWE..08	BELL	$e^+e^- \rightarrow \Upsilon(4S)$

Γ_{\perp}/Γ in $B^0 \rightarrow \omega K^*(892)^0$

VALUE	DOCUMENT ID	TECN	COMMENT
0.10 ± 0.09 ± 0.09	AAIJ 19j	LHCB	pp at 7, 8 TeV

A_{CP}^0 in $B^0 \rightarrow \omega K^*(892)^0$

VALUE	DOCUMENT ID	TECN	COMMENT
-0.13 ± 0.27 ± 0.13	AAIJ 19j	LHCB	pp at 7, 8 TeV

A_{CP}^{\perp} in $B^0 \rightarrow \omega K^*(892)^0$

VALUE	DOCUMENT ID	TECN	COMMENT
0.3 ± 0.8 ± 0.4	AAIJ 19j	LHCB	pp at 7, 8 TeV

A_{CP}^{\parallel} in $B^0 \rightarrow \omega K^*(892)^0$

VALUE	DOCUMENT ID	TECN	COMMENT
0.26 ± 0.55 ± 0.22	AAIJ 19j	LHCB	pp at 7, 8 TeV

ϕ_0 in $B^0 \rightarrow \omega K^*(892)^0$

VALUE	DOCUMENT ID	TECN	COMMENT
-0.86 ± 0.29 ± 0.71	AAIJ 19j	LHCB	pp at 7, 8 TeV

ϕ_{\perp} in $B^0 \rightarrow \omega K^*(892)^0$

VALUE	DOCUMENT ID	TECN	COMMENT
1.6 ± 0.4 ± 0.6	AAIJ 19j	LHCB	pp at 7, 8 TeV

ϕ_{\parallel} in $B^0 \rightarrow \omega K^*(892)^0$

VALUE	DOCUMENT ID	TECN	COMMENT
-1.83 ± 0.29 ± 0.32	AAIJ 19j	LHCB	pp at 7, 8 TeV

Γ_{\perp}/Γ in $B^0 \rightarrow \omega K_2^*(1430)^0$

VALUE	DOCUMENT ID	TECN	COMMENT
0.45 ± 0.12 ± 0.02	AUBERT 09H	BABR	$e^+e^- \rightarrow \Upsilon(4S)$

Γ_{\perp}/Γ in $B^0 \rightarrow K^{*0}\bar{K}^{*0}$

VALUE	DOCUMENT ID	TECN	COMMENT
0.74 ± 0.05 OUR AVERAGE			
0.724 ± 0.051 ± 0.016	¹ AAIJ 19L	LHCB	pp at 7 and 8 TeV
0.80 ^{+0.10} _{-0.12} ± 0.06	AUBERT 08i	BABR	$e^+e^- \rightarrow \Upsilon(4S)$

- ¹ Untagged and time-integrated analysis within 150 MeV of the K^{*0} mass.

Γ_{\perp}/Γ in $B^0 \rightarrow \phi K^*(892)^0$

VALUE	DOCUMENT ID	TECN	COMMENT
0.497 ± 0.017 OUR AVERAGE			
0.497 ± 0.019 ± 0.015	AAIJ 14AM	LHCB	pp at 7 TeV
0.499 ± 0.030 ± 0.018	PRIM 13	BELL	$e^+e^- \rightarrow \Upsilon(4S)$
0.494 ± 0.034 ± 0.013	AUBERT 08BG	BABR	$e^+e^- \rightarrow \Upsilon(4S)$
• • • We do not use the following data for averages, fits, limits, etc. • • •			
0.506 ± 0.040 ± 0.015	AUBERT 07D	BABR	Repl. by AUBERT 08BG
0.45 ± 0.05 ± 0.02	CHEN 05A	BELL	Repl. by PRIM 13
0.52 ± 0.05 ± 0.02	¹ AUBERT,B 04W	BABR	Repl. by AUBERT 07D
0.65 ± 0.07 ± 0.02	AUBERT 03V	BABR	Repl. by AUBERT,B 04W
0.41 ± 0.10 ± 0.04	CHEN 03B	BELL	Repl. by CHEN 05A

- ¹ AUBERT,B 04W also measures the fraction of parity-odd transverse contribution $f_{\perp} = 0.22 \pm 0.05 \pm 0.02$ and the phases of the parity-even and parity-odd transverse amplitudes relative to the longitudinal amplitude.

Γ_{\perp}/Γ in $B^0 \rightarrow \phi K^*(892)^0$

VALUE	DOCUMENT ID	TECN	COMMENT
0.224 ± 0.015 OUR AVERAGE			
0.221 ± 0.016 ± 0.013	AAIJ 14AM	LHCB	pp at 7 TeV
0.238 ± 0.026 ± 0.008	PRIM 13	BELL	$e^+e^- \rightarrow \Upsilon(4S)$
0.212 ± 0.032 ± 0.013	AUBERT 08BG	BABR	$e^+e^- \rightarrow \Upsilon(4S)$
• • • We do not use the following data for averages, fits, limits, etc. • • •			
0.227 ± 0.038 ± 0.013	AUBERT 07D	BABR	Repl. by AUBERT 08BG
0.31 ^{+0.06} _{-0.05} ± 0.02	¹ CHEN 05A	BELL	Repl. by PRIM 13
0.22 ± 0.05 ± 0.02	AUBERT,B 04W	BABR	Repl. by AUBERT 07D

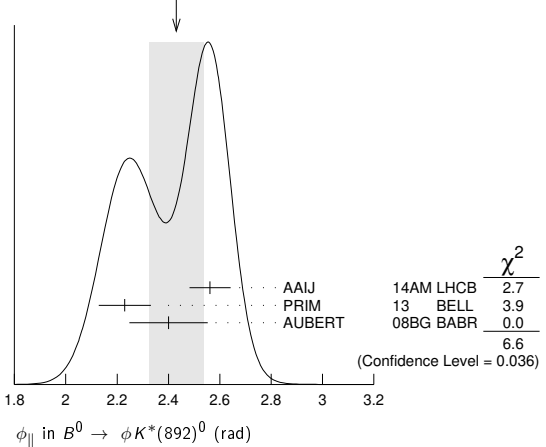
- ¹ This quantity was recalculated by the BELLE authors from numbers in the original paper.

ϕ_{\parallel} in $B^0 \rightarrow \phi K^*(892)^0$

VALUE (rad)	DOCUMENT ID	TECN	COMMENT
2.43 ± 0.11 OUR AVERAGE			Error includes scale factor of 1.8. See the ideogram below.
2.562 ± 0.069 ± 0.040	AAIJ 14AM	LHCB	pp at 7 TeV
2.23 ± 0.10 ± 0.02	PRIM 13	BELL	$e^+e^- \rightarrow \Upsilon(4S)$
2.40 ± 0.13 ± 0.08	AUBERT 08BG	BABR	$e^+e^- \rightarrow \Upsilon(4S)$
• • • We do not use the following data for averages, fits, limits, etc. • • •			
2.31 ± 0.14 ± 0.08	AUBERT 07D	BABR	Repl. by AUBERT 08BG
2.40 ^{+0.28} _{-0.24} ± 0.07	¹ CHEN 05A	BELL	Repl. by PRIM 13
2.34 ^{+0.23} _{-0.20} ± 0.05	AUBERT,B 04W	BABR	Repl. by AUBERT 07D

- ¹ This quantity was recalculated by the BELLE authors from numbers in the original paper.

WEIGHTED AVERAGE
2.43 ± 0.11 (Error scaled by 1.8)

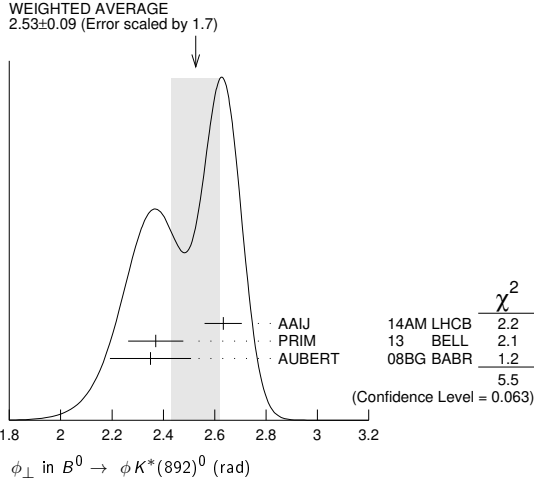


ϕ_{\perp} in $B^0 \rightarrow \phi K^*(892)^0$

VALUE (rad)	DOCUMENT ID	TECN	COMMENT
2.53 ± 0.09 OUR AVERAGE			Error includes scale factor of 1.7. See the ideogram below.
2.633 ± 0.062 ± 0.037	AAIJ 14AM	LHCB	pp at 7 TeV
2.37 ± 0.10 ± 0.04	PRIM 13	BELL	$e^+e^- \rightarrow \Upsilon(4S)$
2.35 ± 0.13 ± 0.09	AUBERT 08BG	BABR	$e^+e^- \rightarrow \Upsilon(4S)$

• • • We do not use the following data for averages, fits, limits, etc. • • •
 2.24 ± 0.15 ± 0.09 AUBERT 07D BABR Repl. by AUBERT 08Bg
 2.51 ± 0.25 ± 0.06 1 CHEN 05A BELL Repl. by PRIM 13
 2.47 ± 0.25 ± 0.05 AUBERT,B 04W BABR Repl. by AUBERT 07D

1 This quantity was recalculated by the BELLE authors from numbers in the original paper.



δ₀(B⁰ → φK*(892)⁰)
 VALUE (rad)
2.88±0.10 OUR AVERAGE
 2.91±0.10±0.08 PRIM 13 BELL e⁺e⁻ → γ(4S)
 2.82±0.15±0.09 AUBERT 08Bg BABR e⁺e⁻ → γ(4S)
 • • • We do not use the following data for averages, fits, limits, etc. • • •
 2.78±0.17±0.09 AUBERT 07D BABR Repl. by AUBERT 08Bg

A⁰_{CP} in B⁰ → φK*(892)⁰
 VALUE
-0.007±0.030 OUR AVERAGE
 -0.003±0.038±0.005 AAIJ 14AM LHCb pp at 7 TeV
 -0.030±0.061±0.007 PRIM 13 BELL e⁺e⁻ → γ(4S)
 0.01±0.07±0.02 AUBERT 08Bg BABR e⁺e⁻ → γ(4S)
 • • • We do not use the following data for averages, fits, limits, etc. • • •
 -0.03±0.08±0.02 AUBERT 07D BABR Repl. by AUBERT 08Bg
 0.13±0.12±0.04 1 CHEN 05A BELL Repl. by PRIM 13
 -0.06±0.10±0.01 AUBERT,B 04W BABR Repl. by AUBERT 07D
 1 This quantity was recalculated by the BELLE authors from numbers in the original paper.

A[⊥]_{CP} in B⁰ → φK*(892)⁰
 VALUE
-0.02 ± 0.06 OUR AVERAGE
 0.047±0.074±0.009 AAIJ 14AM LHCb pp at 7 TeV
 -0.14±0.11±0.01 PRIM 13 BELL e⁺e⁻ → γ(4S)
 -0.04±0.15±0.06 AUBERT 08Bg BABR e⁺e⁻ → γ(4S)
 • • • We do not use the following data for averages, fits, limits, etc. • • •
 -0.03±0.16±0.05 AUBERT 07D BABR Repl. by AUBERT 08Bg
 -0.20±0.18±0.04 1 CHEN 05A BELL Repl. by PRIM 13
 -0.10±0.24±0.05 AUBERT,B 04W BABR Repl. by AUBERT 07D
 1 This quantity was recalculated by the BELLE authors from numbers in the original paper.

Δφ_{||} in B⁰ → φK*(892)⁰
 VALUE (rad)
0.05 ± 0.05 OUR AVERAGE
 0.045±0.069±0.015 AAIJ 14AM LHCb pp at 7 TeV
 -0.02±0.10±0.01 PRIM 13 BELL e⁺e⁻ → γ(4S)
 0.22±0.12±0.08 AUBERT 08Bg BABR e⁺e⁻ → γ(4S)
 • • • We do not use the following data for averages, fits, limits, etc. • • •
 0.24±0.14±0.08 AUBERT 07D BABR Repl. by AUBERT 08Bg
 -0.32±0.27±0.07 1 CHEN 05A BELL Repl. by PRIM 13
 0.27 ± 0.20 ± 0.05 AUBERT,B 04W BABR Repl. by AUBERT 07D
 1 This quantity was recalculated by the BELLE authors from numbers in the original paper.

Δφ_⊥ in B⁰ → φK*(892)⁰
 VALUE (rad)
0.08 ± 0.05 OUR AVERAGE
 0.062±0.062±0.005 AAIJ 14AM LHCb pp at 7 TeV
 0.05±0.10±0.02 PRIM 13 BELL e⁺e⁻ → γ(4S)
 0.21±0.13±0.08 AUBERT 08Bg BABR e⁺e⁻ → γ(4S)
 • • • We do not use the following data for averages, fits, limits, etc. • • •
 0.19±0.15±0.08 AUBERT 07D BABR Repl. by AUBERT 08Bg
 -0.30±0.25±0.06 1 CHEN 05A BELL Repl. by PRIM 13
 0.36±0.25±0.05 AUBERT,B 04W BABR Repl. by AUBERT 07D
 1 This quantity was recalculated by the BELLE authors from numbers in the original paper.

Δδ₀(B⁰ → φK*(892)⁰)
 VALUE (rad)
0.13±0.09 OUR AVERAGE
 0.08±0.10±0.01 PRIM 13 BELL e⁺e⁻ → γ(4S)
 0.27±0.14±0.08 AUBERT 08Bg BABR e⁺e⁻ → γ(4S)
 • • • We do not use the following data for averages, fits, limits, etc. • • •
 0.21±0.17±0.08 AUBERT 07D BABR Repl. by AUBERT 08Bg

Δφ₀₀(B⁰ → φK₀^{*}(1430)⁰)
 VALUE (rad)
0.28±0.42±0.04
 AUBERT 08Bg BABR e⁺e⁻ → γ(4S)

Γ_L/Γ in B⁰ → φK₂^{*}(1430)⁰
 VALUE
0.913+0.028-0.050 OUR AVERAGE
 0.918+0.029-0.060±0.012 PRIM 13 BELL e⁺e⁻ → γ(4S)
 0.901+0.046-0.058±0.037 AUBERT 08Bg BABR e⁺e⁻ → γ(4S)
 • • • We do not use the following data for averages, fits, limits, etc. • • •
 0.853+0.061-0.069±0.036 AUBERT 07D BABR Repl. by AUBERT 08Bg

Γ_L/Γ in B⁰ → φK₂^{*}(1430)⁰
 VALUE
0.027+0.031-0.025 OUR AVERAGE Error includes scale factor of 1.1.
 0.056+0.050-0.035±0.009 PRIM 13 BELL e⁺e⁻ → γ(4S)
 0.002+0.018-0.002±0.031 AUBERT 08Bg BABR e⁺e⁻ → γ(4S)
 • • • We do not use the following data for averages, fits, limits, etc. • • •
 0.045+0.049-0.040±0.013 AUBERT 07D BABR Repl. by AUBERT 08Bg

φ_{||} in B⁰ → φK₂^{*}(1430)⁰
 VALUE (rad)
4.0 ± 0.4 OUR AVERAGE
 3.76±2.88±1.32 PRIM 13 BELL e⁺e⁻ → γ(4S)
 3.96±0.38±0.06 AUBERT 08Bg BABR e⁺e⁻ → γ(4S)
 • • • We do not use the following data for averages, fits, limits, etc. • • •
 2.90±0.39±0.06 AUBERT 07D BABR Repl. by AUBERT 08Bg

φ_⊥ in B⁰ → φK₂^{*}(1430)⁰
 VALUE (rad)
4.45+0.43-0.38±0.13
 PRIM 13 BELL e⁺e⁻ → γ(4S)
 • • • We do not use the following data for averages, fits, limits, etc. • • •
 5.72+0.55-0.87±0.11 AUBERT 07D BABR Repl. by AUBERT 08Bg

δ₀(B⁰ → φK₂^{*}(1430)⁰)
 VALUE (rad)
3.46±0.14 OUR AVERAGE
 3.53±0.11±0.19 PRIM 13 BELL e⁺e⁻ → γ(4S)
 3.41±0.13±0.13 AUBERT 08Bg BABR e⁺e⁻ → γ(4S)
 • • • We do not use the following data for averages, fits, limits, etc. • • •
 3.54+0.12-0.14±0.06 AUBERT 07D BABR Repl. by AUBERT 08Bg

A⁰_{CP} in B⁰ → φK₂^{*}(1430)⁰
 VALUE
-0.03 ± 0.04 OUR AVERAGE
 -0.016+0.066-0.051±0.008 PRIM 13 BELL e⁺e⁻ → γ(4S)
 -0.05 ± 0.06 ± 0.01 AUBERT 08Bg BABR e⁺e⁻ → γ(4S)

A[⊥]_{CP} in B⁰ → φK₂^{*}(1430)⁰
 VALUE
-0.01 ± 0.85-0.67±0.09
 PRIM 13 BELL e⁺e⁻ → γ(4S)

Δφ_{||}(B⁰ → φK₂^{*}(1430)⁰)
 VALUE (rad)
-0.9 ± 0.4 OUR AVERAGE
 -0.02±1.08±1.01 PRIM 13 BELL e⁺e⁻ → γ(4S)
 -1.00±0.38±0.09 AUBERT 08Bg BABR e⁺e⁻ → γ(4S)

Δφ_⊥(B⁰ → φK₂^{*}(1430)⁰)
 VALUE
-0.19±0.42±0.11
 PRIM 13 BELL e⁺e⁻ → γ(4S)

Δδ₀ in B⁰ → φK₂^{*}(1430)⁰
 VALUE (rad)
0.08±0.09 OUR AVERAGE
 0.06±0.11±0.02 PRIM 13 BELL e⁺e⁻ → γ(4S)
 0.11±0.13±0.06 AUBERT 08Bg BABR e⁺e⁻ → γ(4S)

Meson Particle Listings

 B^0 Γ_L/Γ in $B^0 \rightarrow K^*(892)^0 \rho^0$

VALUE	DOCUMENT ID	TECN	COMMENT
0.173 ± 0.026 OUR AVERAGE			
0.164 ± 0.015 ± 0.022	AAIJ	19j	LHCB pp at 7, 8 TeV
0.40 ± 0.08 ± 0.11	LEES	12k	BABR $e^+e^- \rightarrow \Upsilon(4S)$
• • • We do not use the following data for averages, fits, limits, etc. • • •			
0.57 ± 0.09 ± 0.08	AUBERT,B	06g	BABR Repl. by LEES 12k

 Γ_\perp/Γ in $B^0 \rightarrow K^*(892)^0 \rho^0$

VALUE	DOCUMENT ID	TECN	COMMENT
0.401 ± 0.016 ± 0.037	AAIJ	19j	LHCB pp at 7, 8 TeV

 A_{CP}^0 in $B^0 \rightarrow K^*(892)^0 \rho^0$

VALUE	DOCUMENT ID	TECN	COMMENT
-0.62 ± 0.09 ± 0.09	AAIJ	19j	LHCB pp at 7, 8 TeV

 A_{CP}^\perp in $B^0 \rightarrow K^*(892)^0 \rho^0$

VALUE	DOCUMENT ID	TECN	COMMENT
0.050 ± 0.039 ± 0.015	AAIJ	19j	LHCB pp at 7, 8 TeV

 A_{CP}^\parallel in $B^0 \rightarrow K^*(892)^0 \rho^0$

VALUE	DOCUMENT ID	TECN	COMMENT
0.188 ± 0.037 ± 0.022	AAIJ	19j	LHCB pp at 7, 8 TeV

 ϕ_0 in $B^0 \rightarrow K^*(892)^0 \rho^0$

VALUE	DOCUMENT ID	TECN	COMMENT
1.57 ± 0.08 ± 0.18	AAIJ	19j	LHCB pp at 7, 8 TeV

 ϕ_\perp in $B^0 \rightarrow K^*(892)^0 \rho^0$

VALUE	DOCUMENT ID	TECN	COMMENT
-2.365 ± 0.032 ± 0.054	AAIJ	19j	LHCB pp at 7, 8 TeV

 ϕ_\parallel in $B^0 \rightarrow K^*(892)^0 \rho^0$

VALUE	DOCUMENT ID	TECN	COMMENT
0.795 ± 0.030 ± 0.068	AAIJ	19j	LHCB pp at 7, 8 TeV

 Γ_L/Γ in $B^0 \rightarrow K^{*+} \rho^-$

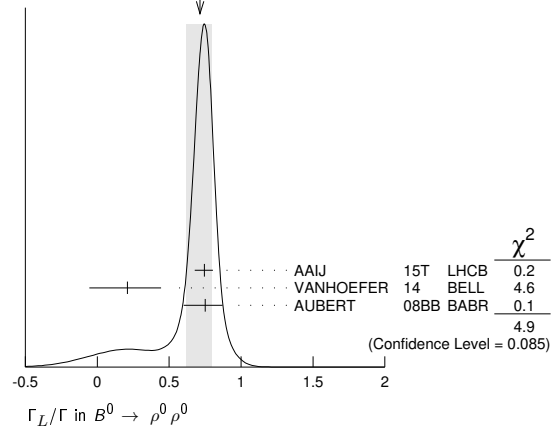
VALUE	DOCUMENT ID	TECN	COMMENT
0.38 ± 0.13 ± 0.03	LEES	12k	BABR $e^+e^- \rightarrow \Upsilon(4S)$

 Γ_L/Γ in $B^0 \rightarrow \rho^+ \rho^-$

VALUE	DOCUMENT ID	TECN	COMMENT
0.990^{+0.021}_{-0.019} OUR AVERAGE			
0.988 ± 0.012 ± 0.023	VANHOEFER	16	BELL $e^+e^- \rightarrow \Upsilon(4S)$
0.992 ± 0.024 ^{+0.026} _{-0.013}	AUBERT	07BF	BABR $e^+e^- \rightarrow \Upsilon(4S)$
• • • We do not use the following data for averages, fits, limits, etc. • • •			
0.941 ^{+0.034} _{-0.040} ± 0.030	SOMOV	06	BELL Repl. by VANHOEFER 16
0.978 ± 0.014 ^{+0.021} _{-0.029}	AUBERT,B	05c	BABR Repl. by AUBERT 07BF
0.98 ^{+0.02} _{-0.08} ± 0.03	AUBERT	04G	BABR Repl. by AUBERT,B 04R
0.99 ± 0.03 ^{+0.04} _{-0.03}	AUBERT,B	04R	BABR Repl. by AUBERT,B 05c

 Γ_L/Γ in $B^0 \rightarrow \rho^0 \rho^0$

VALUE	DOCUMENT ID	TECN	COMMENT
0.71^{+0.08}_{-0.09} OUR AVERAGE			
0.745 ^{+0.048} _{-0.058} ± 0.034	AAIJ	15T	LHCB pp at 7, 8 TeV
0.21 ^{+0.18} _{-0.22} ± 0.15	VANHOEFER	14	BELL $e^+e^- \rightarrow \Upsilon(4S)$
0.75 ^{+0.11} _{-0.14} ± 0.05	AUBERT	08BB	BABR $e^+e^- \rightarrow \Upsilon(4S)$
• • • We do not use the following data for averages, fits, limits, etc. • • •			
0.87 ± 0.13 ± 0.04	AUBERT	07G	BABR Repl. by AUBERT 08BB

WEIGHTED AVERAGE
0.71±0.08±0.09 (Error scaled by 1.6) Γ_L/Γ in $B^0 \rightarrow a_1(1260)^+ a_1(1260)^-$

VALUE	DOCUMENT ID	TECN	COMMENT
0.31 ± 0.22 ± 0.10	AUBERT	09AL	BABR $e^+e^- \rightarrow \Upsilon(4S)$

 Γ_L/Γ in $B^0 \rightarrow \rho^+ \rho^- K^*(892)^0$

VALUE	DOCUMENT ID	TECN	COMMENT
1.01 ± 0.13 ± 0.03	CHEN	08c	BELL $e^+e^- \rightarrow \Upsilon(4S)$

 Γ_L/Γ in $B^0 \rightarrow \Lambda \bar{\Lambda} K^*(892)^0$

VALUE	DOCUMENT ID	TECN	COMMENT
0.60 ± 0.22 ± 0.08	CHANG	09	BELL $e^+e^- \rightarrow \Upsilon(4S)$

 Γ_L/Γ in $B^0 \rightarrow K^*(892)^0 \mu^+ \mu^-$ ($0.04 < q^2 < 6.0 \text{ GeV}^2/c^4$)

VALUE	DOCUMENT ID	TECN	COMMENT
0.50 ± 0.06 ± 0.04	¹ AABOUD	18BY	ATLS pp at 8 TeV

¹A set of angular parameters obtained for this decay is also presented. Γ_L/Γ in $B^0 \rightarrow K^*(892)^0 e^+ e^-$ ($0.002 < q^2 < 1.120 \text{ GeV}^2/c^4$)

VALUE	DOCUMENT ID	TECN	COMMENT
0.16 ± 0.06 ± 0.03	AAIJ	15z	LHCB pp at 7, 8 TeV

 $A_T^{(2)}$ in $B^0 \rightarrow K^*(892)^0 e^+ e^-$ ($0.002 < q^2 < 1.120 \text{ GeV}^2/c^4$)

VALUE	DOCUMENT ID	TECN	COMMENT
-0.23 ± 0.23 ± 0.05	AAIJ	15z	LHCB pp at 7, 8 TeV

 $A_T^{\perp m}$ in $B^0 \rightarrow K^*(892)^0 e^+ e^-$ ($0.002 < q^2 < 1.120 \text{ GeV}^2/c^4$)

VALUE	DOCUMENT ID	TECN	COMMENT
0.14 ± 0.22 ± 0.05	AAIJ	15z	LHCB pp at 7, 8 TeV

 A_T^{Re} in $B^0 \rightarrow K^*(892)^0 e^+ e^-$ ($0.002 < q^2 < 1.120 \text{ GeV}^2/c^4$)

VALUE	DOCUMENT ID	TECN	COMMENT
0.10 ± 0.18 ± 0.05	AAIJ	15z	LHCB pp at 7, 8 TeV

Related to A_{FB}^e, F_L by $A_T^{Re} = (4/3) A_{FB}^e / (1 - F_L)$.

See the related review(s):

 $B^0 - \bar{B}^0$ Mixing $B^0 - \bar{B}^0$ MIXING PARAMETERSFor a discussion of $B^0 - \bar{B}^0$ mixing see the note on " $B^0 - \bar{B}^0$ Mixing" in the B^0 Particle Listings above. χ_d is a measure of the time-integrated $B^0 - \bar{B}^0$ mixing probability that a produced $B^0(\bar{B}^0)$ decays as a $\bar{B}^0(B^0)$. Mixing violates $\Delta B \neq 2$ rule.

$$\chi_d = \frac{x_d^2}{2(1+x_d^2)}$$

$$\chi_d = \frac{\Delta m_{B^0}}{\Gamma_{B^0}} = (m_{B_H^0} - m_{B_L^0}) \tau_{B^0}$$

where H, L stand for heavy and light states of two B^0 CP eigenstates and $\tau_{B^0} = \frac{1}{0.5(\Gamma_{B_H^0} + \Gamma_{B_L^0})}$.

See key on page 999

Meson Particle Listings

B^0

χ_d This $B^0\text{-}\bar{B}^0$ mixing parameter is the probability (integrated over time) that a produced B^0 (or \bar{B}^0) decays as a \bar{B}^0 (or B^0), e.g. for inclusive lepton decays

$$\chi_d = \Gamma(B^0 \rightarrow \ell^- X \text{ (via } \bar{B}^0)) / \Gamma(B^0 \rightarrow \ell^\pm X)$$

$$= \Gamma(\bar{B}^0 \rightarrow \ell^+ X \text{ (via } B^0)) / \Gamma(\bar{B}^0 \rightarrow \ell^\pm X)$$
 Where experiments have measured the parameter $r = \chi / (1 - \chi)$, we have converted to χ . Mixing violates the $\Delta B \neq 2$ rule.

Note that the measurement of χ at energies higher than the $\Upsilon(4S)$ have not separated χ_d from χ_s where the subscripts indicate $B^0(\bar{B}d)$ or $B_s^0(\bar{B}s)$. They are listed in the $B^\pm/B^0/B_s^0/b$ -baryon ADMIXTURE section.

The experiments at $\Upsilon(4S)$ make an assumption about the $B^0\bar{B}^0$ fraction and about the ratio of the B^\pm and B^0 semileptonic branching ratios (usually that it equals one).

“OUR EVALUATION” is an average using rescaled values of the data listed below. The average and rescaling were performed by the Heavy Flavor Averaging Group (HFLAV) and are described at <https://hflav.web.cern.ch/>. The averaging/rescaling procedure takes into account correlations between the measurements, includes χ_d calculated from Δm_{B^0} and τ_{B^0} .

VALUE	CL%	DOCUMENT ID	TECN	COMMENT
0.1858 ± 0.0011 OUR EVALUATION				
0.182 ± 0.015 OUR AVERAGE				
0.198 ± 0.013 ± 0.014		1 BEHRENS 00B	CLE2	$e^+e^- \rightarrow \Upsilon(4S)$
0.16 ± 0.04 ± 0.04		2 ALBRECHT 94	ARG	$e^+e^- \rightarrow \Upsilon(4S)$
0.149 ± 0.023 ± 0.022		3 BARTELT 93	CLE2	$e^+e^- \rightarrow \Upsilon(4S)$
0.171 ± 0.048		4 ALBRECHT 92L	ARG	$e^+e^- \rightarrow \Upsilon(4S)$
• • • We do not use the following data for averages, fits, limits, etc. • • •				
0.20 ± 0.13 ± 0.12		5 ALBRECHT 96D	ARG	$e^+e^- \rightarrow \Upsilon(4S)$
0.19 ± 0.07 ± 0.09		6 ALBRECHT 96D	ARG	$e^+e^- \rightarrow \Upsilon(4S)$
0.24 ± 0.12		7 ELSEN 90	JADE	e^+e^- 35–44 GeV
0.158 $^{+0.052}_{-0.059}$		ARTUSO 89	CLEO	$e^+e^- \rightarrow \Upsilon(4S)$
0.17 ± 0.05		8 ALBRECHT 87I	ARG	$e^+e^- \rightarrow \Upsilon(4S)$
<0.19	90	9 BEAN 87B	CLEO	$e^+e^- \rightarrow \Upsilon(4S)$
<0.27	90	10 AVERY 84	CLEO	$e^+e^- \rightarrow \Upsilon(4S)$

- BEHRENS 00B uses high-momentum lepton tags and partially reconstructed $\bar{B}^0 \rightarrow D^{*+}\pi^-, \rho^-$ decays to determine the flavor of the B meson.
- ALBRECHT 94 reports $r=0.194 \pm 0.062 \pm 0.054$. We convert to χ for comparison. Uses tagged events (lepton + pion from D^*).
- BARTELT 93 analysis performed using tagged events (lepton+pion from D^*). Using dilepton events they obtain $0.157 \pm 0.016 \pm^{+0.033}_{-0.028}$.
- ALBRECHT 92L is a combined measurement employing several lepton-based techniques. It uses all previous ARGUS data in addition to new data and therefore supersedes ALBRECHT 87I. A value of $r = 20.6 \pm 7.0\%$ is directly measured. The value can be used to measure $x = \Delta M/\Gamma = 0.72 \pm 0.15$ for the B_d meson. Assumes $f_{+,-}/f_0 = 1.0 \pm 0.05$ and uses $\tau_{B^\pm}/\tau_{B^0} = (0.95 \pm 0.14) (f_{+,-}/f_0)$.
- Uses $D^{*+}K^\pm$ correlations.
- Uses $(D^{*+}\ell^-)K^\pm$ correlations.
- These experiments see a combination of B_s and B_d mesons.
- ALBRECHT 87I is inclusive measurement with like-sign dileptons, with tagged B decays plus leptons, and one fully reconstructed event. Measures $r=0.21 \pm 0.08$. We convert to χ for comparison. Superseded by ALBRECHT 92L.
- BEAN 87B measured $r < 0.24$; we converted to χ .
- Same-sign dilepton events. Limit assumes semileptonic BR for B^+ and B^0 equal. If B^0/B^\pm ratio < 0.58 , no limit exists. The limit was corrected in BEAN 87B from $r < 0.30$ to $r < 0.37$. We converted this limit to χ .

$$\Delta m_{B^0} = m_{B_H^0} - m_{B_L^0}$$

Δm_{B^0} is a measure of 2π times the $B^0\text{-}\bar{B}^0$ oscillation frequency in time-dependent mixing experiments.

The second “OUR EVALUATION” is an average using rescaled values of the data listed below. The average and rescaling were performed by the Heavy Flavor Averaging Group (HFLAV) and are described at <https://hflav.web.cern.ch/>. The averaging/rescaling procedure takes into account correlations between the measurements.

The first “OUR EVALUATION”, also provided by the HFLAV, includes Δm_d calculated from χ_d measured at $\Upsilon(4S)$.

VALUE (10^{12} h s^{-1})	DOCUMENT ID	TECN	COMMENT
0.5065 ± 0.0019 OUR EVALUATION			
0.5065 ± 0.0019 OUR EVALUATION First			
0.5050 ± 0.0021 ± 0.0010	1 AAIJ 16AV	LHCB	pp at 7, 8 TeV
0.503 ± 0.011 ± 0.013	2 AAIJ 13CF	LHCB	pp at 7 TeV
0.5156 ± 0.0051 ± 0.0033	3 AAIJ 13F	LHCB	pp at 7 TeV
0.499 ± 0.032 ± 0.003	4 AAIJ 12I	LHCB	pp at 7 TeV
0.506 ± 0.020 ± 0.016	5 ABZOV 06W	D0	$p\bar{p}$ at 1.96 TeV
0.511 ± 0.007 $^{+0.007}_{-0.006}$	6 AUBERT 06G	BABR	$e^+e^- \rightarrow \Upsilon(4S)$
0.511 ± 0.005 ± 0.006	7 ABE 05B	BELL	$e^+e^- \rightarrow \Upsilon(4S)$
0.531 ± 0.025 ± 0.007	8 ABDALLAH 03B	DLPH	$e^+e^- \rightarrow Z$
0.492 ± 0.018 ± 0.013	9 AUBERT 03C	BABR	$e^+e^- \rightarrow \Upsilon(4S)$
0.503 ± 0.008 ± 0.010	10 HASTINGS 03	BELL	$e^+e^- \rightarrow \Upsilon(4S)$
0.509 ± 0.017 ± 0.020	11 ZHENG 03	BELL	$e^+e^- \rightarrow \Upsilon(4S)$
0.516 ± 0.016 ± 0.010	12 AUBERT 02I	BABR	$e^+e^- \rightarrow \Upsilon(4S)$
0.493 ± 0.012 ± 0.009	13 AUBERT 02J	BABR	$e^+e^- \rightarrow \Upsilon(4S)$
0.497 ± 0.024 ± 0.025	14 ABBIENDI,G 00B	OPAL	$e^+e^- \rightarrow Z$

0.503 ± 0.064 ± 0.071	15 ABE 99K	CDF	$p\bar{p}$ at 1.8 TeV
0.500 ± 0.052 ± 0.043	16 ABE 99Q	CDF	$p\bar{p}$ at 1.8 TeV
0.516 ± 0.099 $^{+0.029}_{-0.035}$	17 AFFOLDER 99C	CDF	$p\bar{p}$ at 1.8 TeV
0.471 $^{+0.078}_{-0.068}$ $^{+0.033}_{-0.034}$	18 ABE 98C	CDF	$p\bar{p}$ at 1.8 TeV
0.458 ± 0.046 ± 0.032	19 ACCIARRI 98D	L3	$e^+e^- \rightarrow Z$
0.437 ± 0.043 ± 0.044	20 ACCIARRI 98D	L3	$e^+e^- \rightarrow Z$
0.472 ± 0.049 ± 0.053	21 ACCIARRI 98D	L3	$e^+e^- \rightarrow Z$
0.523 ± 0.072 ± 0.043	22 ABREU 97N	DLPH	$e^+e^- \rightarrow Z$
0.493 ± 0.042 ± 0.027	20 ABREU 97N	DLPH	$e^+e^- \rightarrow Z$
0.499 ± 0.053 ± 0.015	23 ABREU 97N	DLPH	$e^+e^- \rightarrow Z$
0.480 ± 0.040 ± 0.051	19 ABREU 97N	DLPH	$e^+e^- \rightarrow Z$
0.444 ± 0.029 $^{+0.020}_{-0.017}$	20 ACKERSTAFF 97U	OPAL	$e^+e^- \rightarrow Z$
0.430 ± 0.043 $^{+0.028}_{-0.030}$	19 ACKERSTAFF 97V	OPAL	$e^+e^- \rightarrow Z$
0.482 ± 0.044 ± 0.024	24 BUSKULIC 97D	ALEP	$e^+e^- \rightarrow Z$
0.404 ± 0.045 ± 0.027	20 BUSKULIC 97D	ALEP	$e^+e^- \rightarrow Z$
0.452 ± 0.039 ± 0.044	19 BUSKULIC 97D	ALEP	$e^+e^- \rightarrow Z$
0.539 ± 0.060 ± 0.024	25 ALEXANDER 96V	OPAL	$e^+e^- \rightarrow Z$
0.567 ± 0.089 $^{+0.029}_{-0.023}$	26 ALEXANDER 96V	OPAL	$e^+e^- \rightarrow Z$

• • • We do not use the following data for averages, fits, limits, etc. • • •				
0.516 ± 0.016 ± 0.010	27 AUBERT 02N	BABR	$e^+e^- \rightarrow \Upsilon(4S)$	
0.494 ± 0.012 ± 0.015	28 HARA 02	BELL	Repl. by ABE 05B	
0.528 ± 0.017 ± 0.011	29 TOMURA 02	BELL	Repl. by ABE 05B	
0.463 ± 0.008 ± 0.016	13 ABE 01D	BELL	Repl. by HASTINGS 03	
0.444 ± 0.028 ± 0.028	30 ACCIARRI 98D	L3	$e^+e^- \rightarrow Z$	
0.497 ± 0.035	31 ABREU 97N	DLPH	$e^+e^- \rightarrow Z$	
0.467 ± 0.022 $^{+0.017}_{-0.015}$	32 ACKERSTAFF 97V	OPAL	$e^+e^- \rightarrow Z$	
0.446 ± 0.032	33 BUSKULIC 97D	ALEP	$e^+e^- \rightarrow Z$	
0.531 $^{+0.050}_{-0.046}$ ± 0.078	34 ABREU 96Q	DLPH	Sup. by ABREU 97N	
0.496 $^{+0.055}_{-0.051}$ ± 0.043	19 ACCIARRI 96E	L3	Repl. by ACCIARRI 98D	
0.548 ± 0.050 $^{+0.023}_{-0.019}$	35 ALEXANDER 96V	OPAL	$e^+e^- \rightarrow Z$	
0.496 ± 0.046	36 AKERS 95J	OPAL	Repl. by ACKERSTAFF 97V	
0.462 $^{+0.040}_{-0.053}$ $^{+0.052}_{-0.035}$	19 AKERS 95J	OPAL	Repl. by ACKERSTAFF 97V	
0.50 ± 0.12 ± 0.06	22 ABREU 94M	DLPH	Sup. by ABREU 97N	
0.508 ± 0.075 ± 0.025	25 AKERS 94C	OPAL	Repl. by ALEXANDER 96V	
0.57 ± 0.11 ± 0.02	26 AKERS 94H	OPAL	Repl. by ALEXANDER 96V	
0.50 $^{+0.07}_{-0.06}$ $^{+0.11}_{-0.10}$	19 BUSKULIC 94B	ALEP	Sup. by BUSKULIC 97D	
0.52 $^{+0.10}_{-0.11}$ $^{+0.04}_{-0.03}$	26 BUSKULIC 93K	ALEP	Sup. by BUSKULIC 97D	

- Uses semileptonic decays of $B^0 \rightarrow D^- \mu^+ \nu_\mu X$ and $B^0 \rightarrow D^{(*)-} \mu^+ \nu_\mu X$, where the D mesons are reconstructed in $D^- \rightarrow K^+ \pi^- \pi^-$ and $D^{(*)-} \rightarrow \bar{D}^0 \pi^-$ with $\bar{D}^0 \rightarrow K^+ \pi^-$.
- Uses semileptonic decays of $B^0 \rightarrow D^- \mu^+ \nu_\mu X$ where the D^- mesons are reconstructed in $D^- \rightarrow K^+ K^- \pi^-$.
- Measured using $B^0 \rightarrow D^- \pi^+$ and $B^0 \rightarrow J/\psi K^*(892)^0$ decays.
- Measured using $B^0 \rightarrow D^- \pi^+$.
- Uses opposite-side flavor-tagging with $B \rightarrow D^{(*)} \mu \nu_\mu X$ events.
- Measured using a simultaneous fit of the B^0 lifetime and $\bar{B}^0 B^0$ oscillation frequency Δm_d in the partially reconstructed $B^0 \rightarrow D^{*-} \ell \nu$ decays.
- Measurement performed using a combined fit of CP -violation, mixing and lifetimes.
- Events with a high transverse momentum lepton were removed and an inclusively reconstructed vertex was required.
- AUBERT 03C uses a sample of approximately 14,000 exclusively reconstructed $B^0 \rightarrow D^*(2010)^- \ell \nu$ and simultaneously measures the lifetime and oscillation frequency.
- HASTINGS 03 measurement based on the time evolution of dilepton events. It also reports $f_+/f_0 = 1.01 \pm 0.03 \pm 0.09$ and CPT violation parameters in $B^0\text{-}\bar{B}^0$ mixing.
- ZHENG 03 data analyzed using partially reconstructed $\bar{B}^0 \rightarrow D^{*-} \pi^+$ decay and a flavor tag based on the charge of the lepton from the accompanying B decay.
- Uses a tagged sample of fully-reconstructed neutral B decays at $\Upsilon(4S)$.
- Measured based on the time evolution of dilepton events in $\Upsilon(4S)$ decays.
- Data analyzed using partially reconstructed $\bar{B}^0 \rightarrow D^{*+} \ell^- \bar{\nu}$ decay and a combination of flavor tags from the rest of the event.
- Uses di-muon events.
- Uses jet-charge and lepton-flavor tagging.
- Uses $\ell^- D^{*+} - \ell$ events.
- Uses $\pi^- B$ in the same side.
- Uses $\ell\text{-}\ell$.
- Uses $\ell\text{-}Q_{\text{hem}}$.
- Uses $\ell\text{-}\ell$ with impact parameters.
- Uses $D^{*+}\text{-}Q_{\text{hem}}$.
- Uses $\pi_s^\pm \ell\text{-}Q_{\text{hem}}$.
- Uses $D^{*+}\text{-}\ell/Q_{\text{hem}}$.
- Uses $D^{*+}\text{-}\ell\text{-}Q_{\text{hem}}$.
- Uses $D^{*+}\text{-}\ell$.
- AUBERT 02N result based on the same analysis and data sample reported in AUBERT 02I.
- Uses a tagged sample of B^0 decays reconstructed in the mode $B^0 \rightarrow D^* \ell \nu$.
- Uses a tagged sample of fully-reconstructed hadronic B^0 decays at $\Upsilon(4S)$.
- ACCIARRI 98D combines results from $\ell\text{-}\ell$, $\ell\text{-}Q_{\text{hem}}$, and $\ell\text{-}\ell$ with impact parameters.

Meson Particle Listings

B^0

- ³¹ ABREU 97N combines results from $D^{*\pm} - Q_{\text{hem}}$, $\ell - Q_{\text{hem}}$, $\pi_S^{\pm} \ell - Q_{\text{hem}}$, and $\ell - \ell$.
- ³² ACKERSTAFF 97V combines results from $\ell - \ell$, $\ell - Q_{\text{hem}}$, $D^{*\pm} - \ell$, and $D^{*\pm} - Q_{\text{hem}}$.
- ³³ BUSKULIC 97D combines results from $D^{*\pm} - \ell / Q_{\text{hem}}$, $\ell - Q_{\text{hem}}$, and $\ell - \ell$.
- ³⁴ ABREU 96Q analysis performed using lepton, kaon, and jet-charge tags.
- ³⁵ ALEXANDER 96V combines results from $D^{*\pm} - \ell$ and $D^{*\pm} \ell - Q_{\text{hem}}$.
- ³⁶ AKERS 95J combines results from charge measurement, $D^{*\pm} \ell - Q_{\text{hem}}$ and $\ell - \ell$.

$\chi_d = \Delta m_{B^0} / \Gamma_{B^0}$

The second "OUR EVALUATION" is an average using rescaled values of the data listed below. The average and rescaling were performed by the Heavy Flavor Averaging Group (HFLAV) and are described at <https://hflav.web.cern.ch/>. The averaging/rescaling procedure takes into account correlations between the measurements.

The first "OUR EVALUATION", also provided by the HFLAV, includes χ_d measured at $\Upsilon(4S)$.

VALUE	DOCUMENT ID
0.769 ± 0.004 OUR EVALUATION	First
0.769 ± 0.004 OUR EVALUATION	Second

Re($\lambda_{CP} / |\lambda_{CP}|$) Re(z)

The λ_{CP} characterizes B^0 and \bar{B}^0 decays to states of charmonium plus K_S^0 . Parameter z is used to describe CPT violation in mixing, see the review on "CPT Violation" in the reviews section.

VALUE	DOCUMENT ID	TECN	COMMENT
0.047 ± 0.022 ± 0.003	1 LEES	16E	BABR $e^+ e^- \rightarrow \Upsilon(4S)$

- • • We do not use the following data for averages, fits, limits, etc. • • •
- 0.014 ± 0.035 ± 0.034 ² AUBERT,B 04C BABR Repl. by LEES 16E
- ¹ The first uncertainty is the uncertainty from Re(z) and the second uncertainty is from Re($\lambda/|\lambda|$).
- ² Corresponds to 90% confidence range [-0.072, 0.101].

$\Delta\Gamma$ Re(z)

VALUE	DOCUMENT ID	TECN	COMMENT
-0.0071 ± 0.0039 ± 0.0020	AUBERT	06T	BABR $e^+ e^- \rightarrow \Upsilon(4S)$

Re(z)

VALUE (units 10 ⁻²)	DOCUMENT ID	TECN	COMMENT
-4 ± 4 OUR AVERAGE	Error includes scale factor of 1.4.		
-6.5 ± 2.8 ± 1.4	1 LEES	16E	BABR $e^+ e^- \rightarrow \Upsilon(4S)$
1.9 ± 3.7 ± 3.3	2 HIGUCHI	12	BELL $e^+ e^- \rightarrow \Upsilon(4S)$
• • • We do not use the following data for averages, fits, limits, etc. • • •			
0 ± 12 ± 1	3 HASTINGS	03	BELL Repl. by HIGUCHI 12
¹ Measurement uses decays $B^0/\bar{B}^0 \rightarrow c\bar{c}K_S^0/K_L^0$.			
² Measured using $B^0 \rightarrow J/\psi K_S^0, J/\psi K_L^0, D^-\pi^+, D^{*-}\pi^+, D^{*-}\rho^+$, and $D^{*-}\ell^+\nu$ decays.			
³ Measured using inclusive dilepton events from B^0 decay.			

Im(z)

VALUE (units 10 ⁻²)	DOCUMENT ID	TECN	COMMENT
-0.8 ± 0.4 OUR AVERAGE			
1.0 ± 3.0 ± 1.3	1 LEES	16E	BABR $e^+ e^- \rightarrow \Upsilon(4S)$
-0.57 ± 0.33 ± 0.33	2 HIGUCHI	12	BELL $e^+ e^- \rightarrow \Upsilon(4S)$
-1.39 ± 0.73 ± 0.32	3 AUBERT	06T	BABR $e^+ e^- \rightarrow \Upsilon(4S)$
• • • We do not use the following data for averages, fits, limits, etc. • • •			
3.8 ± 2.9 ± 2.5	4 AUBERT,B	04C	BABR Repl. by AUBERT 06T
-3 ± 1 ± 3	5 HASTINGS	03	BELL Repl. by HIGUCHI 12
¹ Measurement uses decays $B^0/\bar{B}^0 \rightarrow c\bar{c}K_S^0/K_L^0$.			
² Measured using $B^0 \rightarrow J/\psi K_S^0, J/\psi K_L^0, D^-\pi^+, D^{*-}\pi^+, D^{*-}\rho^+$, and $D^{*-}\ell^+\nu$ decays.			
³ Measurement uses $B^0/\bar{B}^0 \rightarrow \ell^+ X/\ell^- X$ decays. Assuming $\Delta\Gamma = 0$, the result becomes $\text{Im}(z) = (-0.37 \pm 0.54) \times 10^{-2}$.			
⁴ Corresponds to 90% confidence range [-0.028, 0.104].			
⁵ Measured using inclusive dilepton events from B^0 decay.			

CP VIOLATION PARAMETERS

Re(ϵ_{B^0})/(1+ $|\epsilon_{B^0}|^2$)

CP impurity in B_d^0 system. It is obtained from either $a_{\ell\ell}$, the charge asymmetry in like-sign dilepton events or a_{CP} , the time-dependent asymmetry of inclusive B^0 and \bar{B}^0 decays.

"OUR EVALUATION" is an average obtained by the Heavy Flavor Averaging Group (HFLAV) and described at <https://hflav.web.cern.ch/>. It is the result of a fit to B_d and B_s CP asymmetries, which includes the B_d measurements listed below and the B_s measurements listed in the B_s section, taking into account correlations between those measurements.

VALUE (units 10 ⁻³)	DOCUMENT ID	TECN	COMMENT
-0.5 ± 0.4 OUR EVALUATION			
-0.1 ± 0.4 OUR AVERAGE			
-0.05 ± 0.48 ± 0.75	1 AAIJ	15F	LHCB pp at 7, 8 TeV
-0.975 ± 0.875 ± 0.475	2 LEES	15A	BABR $e^+ e^- \rightarrow \Upsilon(4S)$
1.55 ± 1.05	3 ABAZOV	14	D0 $p\bar{p}$ at 1.96 TeV
0.15 ± 0.42 ± 0.94 ± 0.81	4 LEES	13N	BABR $e^+ e^- \rightarrow \Upsilon(4S)$
-1.7 ± 1.1 ± 0.4	5 ABAZOV	12AC	D0 $p\bar{p}$ at 1.96 TeV
0.4 ± 1.3 ± 0.9	6 AUBERT	06T	BABR $e^+ e^- \rightarrow \Upsilon(4S)$
-0.3 ± 2.0 ± 2.1	7 NAKANO	06	BELL $e^+ e^- \rightarrow \Upsilon(4S)$
3.5 ± 10.3 ± 1.5	8 JAFFE	01	CLE2 $e^+ e^- \rightarrow \Upsilon(4S)$

- • • We do not use the following data for averages, fits, limits, etc. • • •

-0.3 ± 1.3	9 ABAZOV	11U	D0 Repl. by ABAZOV 14
-2.3 ± 1.1 ± 0.8	10 ABAZOV	06S	D0 Repl. by ABAZOV 11U
-14.7 ± 6.7 ± 5.7	11 AUBERT,B	04C	BABR Repl. by AUBERT 06T
1.2 ± 2.9 ± 3.6	2 AUBERT	02K	BABR Repl. by LEES 15A
-3.2 ± 6.5	12 BARATE	01D	ALEP $e^+ e^- \rightarrow Z$
4 ± 18 ± 3	13 BEHRENS	00B	CLE2 Repl. by JAFFE 01
1.2 ± 13.8 ± 3.2	14 ABBIENDI	99J	OPAL $e^+ e^- \rightarrow Z$
2 ± 7 ± 3	15 ACKERSTAFF	97U	OPAL $e^+ e^- \rightarrow Z$
< 45	16 BARTELT	93	CLE2 $e^+ e^- \rightarrow \Upsilon(4S)$

- ¹ AAIJ 15F uses semileptonic B^0 decays in the inclusive final states $D^-\mu^+$ and $D^{*-}\mu^+$, where the D^- meson decays into the $K^+\pi^-\pi^-$ final state, and the D^{*-} meson into the $\bar{D}^0(\rightarrow K^+\pi^-\pi^-)$ final state. Reports $A_{SL}^d = (-0.02 \pm 0.19 \pm 0.30)\%$, which equals to $4\text{Re}(\epsilon_{B^0})/(1+|\epsilon_{B^0}|^2)$.
- ² Uses the charge asymmetry in like-sign dilepton events. LEES 15A reports $A_{SL}^d = (-3.9 \pm 3.5 \pm 1.9) \times 10^{-3}$.
- ³ ABAZOV 14 uses the dimuon charge asymmetry with different impact parameters from which it reports $A_{SL}^d = (-0.62 \pm 0.42) \times 10^{-2}$.
- ⁴ Uses $B^0 \rightarrow D^{*-} X \ell^+ \nu_\ell$ and a kaon-tagged sample which yields measurement of $A_{SL}^d = (0.06 \pm 0.17_{-0.32}^{+0.38})\%$, corresponding to $\Delta_{CP} = 1-|q/p| = (0.29 \pm 0.84_{-1.88}^{+1.61}) \times 10^{-3}$.
- ⁵ ABAZOV 12AC uses $B^0 \rightarrow D^-\mu^+ X$ and $B^0 \rightarrow D^*(2010)^-\mu^+ X$ decays without initial state flavor tagging which yields measurement of $A_{SL}^d = (6.8 \pm 4.5 \pm 1.4) \times 10^{-3}$.
- ⁶ AUBERT 06T reports $|q/p|-1 = (-0.8 \pm 2.7 \pm 1.9) \times 10^{-3}$. We convert to $1-|q/p|/2$.
- ⁷ Uses the charge asymmetry in like-sign dilepton events and reports $|q/p| = 1.0005 \pm 0.0040 \pm 0.0043$.
- ⁸ JAFFE 01 finds $a_{\ell\ell} = 0.013 \pm 0.050 \pm 0.005$ and combines with the previous BEHRENS 00B independent measurement.
- ⁹ ABAZOV 11U uses the dimuon charge asymmetry with different impact parameters from which it reports $A_{SL}^d = (-1.2 \pm 5.2) \times 10^{-3}$.
- ¹⁰ Uses the dimuon charge asymmetry.
- ¹¹ AUBERT 04C reports $|q/p| = 1.029 \pm 0.013 \pm 0.011$ and we converted it to $(1-|q/p|)/2$.
- ¹² BARATE 01D measured by investigating time-dependent asymmetries in semileptonic and fully inclusive B_d^0 decays.
- ¹³ BEHRENS 00B uses high-momentum lepton tags and partially reconstructed $\bar{B}^0 \rightarrow D^{*+}\pi^-, \rho^-$ decays to determine the flavor of the B meson.
- ¹⁴ Data analyzed using the time-dependent asymmetry of inclusive B^0 decay. The production flavor of B^0 mesons is determined using both the jet charge and the charge of secondary vertex in the opposite hemisphere.
- ¹⁵ ACKERSTAFF 97U assumes CPT and is based on measuring the charge asymmetry in a sample of B^0 decays defined by lepton and Q_{hem} tags. If CPT is not invoked, $\text{Re}(\epsilon_B) = -0.006 \pm 0.010 \pm 0.006$ is found. The indirect CPT violation parameter is determined to $\text{Im}(\delta B) = -0.020 \pm 0.016 \pm 0.006$.
- ¹⁶ BARTELT 93 finds $a_{\ell\ell} = 0.031 \pm 0.096 \pm 0.032$ which corresponds to $|a_{\ell\ell}| < 0.18$, which yields the above $|\text{Re}(\epsilon_{B^0})/(1+|\epsilon_{B^0}|^2)|$.

$A_{T/CP}$

$A_{T/CP}$ is defined as

$$\frac{P(\bar{B}^0 \rightarrow B^0) - P(B^0 \rightarrow \bar{B}^0)}{P(\bar{B}^0 \rightarrow B^0) + P(B^0 \rightarrow \bar{B}^0)}$$

the CPT invariant asymmetry between the oscillation probabilities $P(\bar{B}^0 \rightarrow B^0)$ and $P(B^0 \rightarrow \bar{B}^0)$.

VALUE	DOCUMENT ID	TECN	COMMENT
0.005 ± 0.012 ± 0.014	1 AUBERT	02K	BABR $e^+ e^- \rightarrow \Upsilon(4S)$

- ¹ AUBERT 02K uses the charge asymmetry in like-sign dilepton events.

$A_{CP}(B^0 \rightarrow D^{*}(2010)^+ D^-)$

A_{CP} is defined as

$$\frac{B(\bar{B}^0 \rightarrow \bar{D}^+ B^0) - B(B^0 \rightarrow D^+ \bar{B}^0)}{B(\bar{B}^0 \rightarrow \bar{D}^+ B^0) + B(B^0 \rightarrow D^+ \bar{B}^0)}$$

the CP-violation charge asymmetry of exclusive B^0 and \bar{B}^0 decay.

VALUE	DOCUMENT ID	TECN	COMMENT
0.037 ± 0.034 OUR AVERAGE			
0.06 ± 0.05 ± 0.02	ROHRKEN	12	BELL $e^+ e^- \rightarrow \Upsilon(4S)$
0.008 ± 0.048 ± 0.013	AUBERT	09C	BABR $e^+ e^- \rightarrow \Upsilon(4S)$
0.07 ± 0.08 ± 0.04	1 AUSHEV	04	BELL $e^+ e^- \rightarrow \Upsilon(4S)$

- • • We do not use the following data for averages, fits, limits, etc. • • •

-0.12 ± 0.06 ± 0.02	AUBERT	07A1	BABR Repl. by AUBERT 09C
-0.03 ± 0.10 ± 0.02	AUBERT,B	06A	BABR Repl. by AUBERT 07A1
-0.03 ± 0.11 ± 0.05	AUBERT	03J	BABR Repl. by AUBERT,B 06B

- ¹ Combines results from fully and partially reconstructed $B^0 \rightarrow D^{*\pm} D^\mp$ decays.

$A_{CP}(B^0 \rightarrow [K^+ K^-]_D K^*(892)^0)$

VALUE	DOCUMENT ID	TECN	COMMENT
-0.05 ± 0.10 ± 0.01	AAIJ	19N	LHCB pp at 7, 8, 13 TeV

- • • We do not use the following data for averages, fits, limits, etc. • • •

-0.20 ± 0.15 ± 0.02	AAIJ	14BN	LHCB Repl. by AAIJ 16S
-0.45 ± 0.23 ± 0.02	AAIJ	13L	LHCB Repl. by AAIJ 14BN

See key on page 999

Meson Particle Listings
B⁰

$A_{CP}(B^0 \rightarrow [K^+ \pi^-]_D K^*(892)^0)$

VALUE	DOCUMENT ID	TECN	COMMENT
$0.047 \pm 0.027 \pm 0.010$	AAIJ	19N	LHCB <i>pp</i> at 7, 8, 13 TeV
• • • We do not use the following data for averages, fits, limits, etc. • • •			
$-0.03 \pm 0.04 \pm 0.02$	AAIJ	14BN	LHCB Repl. by AAIJ 19N
$-0.08 \pm 0.08 \pm 0.01$	AAIJ	13L	LHCB Repl. by AAIJ 14BN

$A_{CP}(B^0 \rightarrow [K^+ \pi^- \pi^+ \pi^-]_D K^*(892)^0)$

VALUE	DOCUMENT ID	TECN	COMMENT
$0.037 \pm 0.032 \pm 0.010$	AAIJ	19N	LHCB <i>pp</i> at 7, 8, 13 TeV

$A_{CP}(B^0 \rightarrow [K^- \pi^+]_D K^*(892)^0)$

VALUE	DOCUMENT ID	TECN	COMMENT
$0.19 \pm 0.19 \pm 0.01$	AAIJ	19N	LHCB <i>pp</i> at 7, 8, 13 TeV

$A_{CP}(B^0 \rightarrow [K^- \pi^+ \pi^+ \pi^-]_D K^*(892)^0)$

VALUE	DOCUMENT ID	TECN	COMMENT
$-0.01 \pm 0.24 \pm 0.01$	AAIJ	19N	LHCB <i>pp</i> at 7, 8, 13 TeV

$R_D^+ = \Gamma(B^0 \rightarrow [\pi^+ K^-]_D K^{*0}) / \Gamma(B^0 \rightarrow [\pi^- K^+]_D K^{*0})$

VALUE	DOCUMENT ID	TECN	COMMENT
$0.064 \pm 0.021 \pm 0.002$	AAIJ	19N	LHCB <i>pp</i> at 7, 8, 13 TeV
• • • We do not use the following data for averages, fits, limits, etc. • • •			
$0.06 \pm 0.03 \pm 0.01$	AAIJ	14BN	LHCB Repl. by AAIJ 19N

$R_D^- = \Gamma(\bar{B}^0 \rightarrow [\pi^- K^+]_D K^{*0}) / \Gamma(\bar{B}^0 \rightarrow [\pi^+ K^-]_D K^{*0})$

VALUE	DOCUMENT ID	TECN	COMMENT
$0.095 \pm 0.021 \pm 0.003$	AAIJ	19N	LHCB <i>pp</i> at 7, 8, 13 TeV
• • • We do not use the following data for averages, fits, limits, etc. • • •			
$0.06 \pm 0.03 \pm 0.01$	AAIJ	14BN	LHCB Repl. by AAIJ 19N

$A_{CP}(B^0 \rightarrow [\pi^+ \pi^-]_D K^*(892)^0)$

VALUE	DOCUMENT ID	TECN	COMMENT
$-0.18 \pm 0.14 \pm 0.01$	AAIJ	19N	LHCB <i>pp</i> at 7, 8, 13 TeV
• • • We do not use the following data for averages, fits, limits, etc. • • •			
$-0.09 \pm 0.22 \pm 0.02$	AAIJ	14BN	LHCB Repl. by AAIJ 16s

$A_{CP}(B^0 \rightarrow [\pi^+ \pi^- \pi^+ \pi^-]_D K^*(892)^0)$

VALUE	DOCUMENT ID	TECN	COMMENT
$-0.03 \pm 0.15 \pm 0.01$	AAIJ	19N	LHCB <i>pp</i> at 7, 8, 13 TeV

$R_D^+ = \Gamma(B^0 \rightarrow [\pi^+ K^- \pi^+ \pi^-]_D K^{*0}) / \Gamma(B^0 \rightarrow [\pi^- K^+ \pi^+ \pi^-]_D K^{*0})$

VALUE	DOCUMENT ID	TECN	COMMENT
$0.074 \pm 0.026 \pm 0.002$	AAIJ	19N	LHCB <i>pp</i> at 7, 8, 13 TeV

$R_D^- = \Gamma(\bar{B}^0 \rightarrow [\pi^- K^+ \pi^+ \pi^-]_D K^{*0}) / \Gamma(\bar{B}^0 \rightarrow [\pi^+ K^- \pi^+ \pi^-]_D K^{*0})$

VALUE	DOCUMENT ID	TECN	COMMENT
$0.072 \pm 0.025 \pm 0.003$	AAIJ	19N	LHCB <i>pp</i> at 7, 8, 13 TeV

$A_{CP}(B^0 \rightarrow K^+ \pi^-)$

VALUE	DOCUMENT ID	TECN	COMMENT
-0.083 ± 0.004 OUR AVERAGE			
$-0.084 \pm 0.004 \pm 0.003$	AAIJ	18o	LHCB <i>pp</i> at 7, 8 TeV
$-0.083 \pm 0.013 \pm 0.004$	AALTONEN	14P	CDF $p\bar{p}$ at 1.96 TeV
$-0.080 \pm 0.007 \pm 0.003$	AAIJ	13Ax	LHCB <i>pp</i> at 7 TeV
$-0.069 \pm 0.014 \pm 0.007$	DUH	13	BELL $e^+e^- \rightarrow T(4S)$
$-0.107 \pm 0.016 \pm 0.006$	LEES	13d	BABR $e^+e^- \rightarrow T(4S)$
-0.04 ± 0.16	¹ CHEN	00	CLE2 $e^+e^- \rightarrow T(4S)$
• • • We do not use the following data for averages, fits, limits, etc. • • •			
$-0.088 \pm 0.011 \pm 0.008$	AAIJ	12v	LHCB Repl. by AAIJ 13Ax
$-0.086 \pm 0.023 \pm 0.009$	AALTONEN	11n	CDF Repl. by AALTONEN 14P
$-0.094 \pm 0.018 \pm 0.008$	LIN	08	BELL Repl. by DUH 13
$-0.107 \pm 0.018 \pm 0.007$	AUBERT	07Af	BABR Repl. by LEES 13d
$-0.013 \pm 0.078 \pm 0.012$	ABULENCIA,A	06d	CDF Repl. by AALTONEN 11n
$-0.088 \pm 0.035 \pm 0.013$	² CHAO	05a	BELL Repl. by CHAO 04B
$-0.133 \pm 0.030 \pm 0.009$	³ AUBERT,B	04k	BABR Repl. by AUBERT 07Af
$-0.101 \pm 0.025 \pm 0.005$	⁴ CHAO	04b	BELL Repl. by LIN 08
$-0.07 \pm 0.08 \pm 0.02$	¹ AUBERT	02d	BABR Repl. by AUBERT 02q
$-0.102 \pm 0.050 \pm 0.016$	⁶ AUBERT	02q	BABR Repl. by AUBERT,B 04k
$-0.06 \pm 0.09 \pm 0.01$	⁷ CASEY	02	BELL Repl. by CHAO 04B
$0.044 \pm 0.186 \pm 0.018$	⁸ ABE	01k	BELL Repl. by CASEY 02
$-0.19 \pm 0.10 \pm 0.03$	⁹ AUBERT	01e	BABR Repl. by AUBERT 02q

¹ Corresponds to 90% confidence range $-0.30 < A_{CP} < 0.22$.
² Corresponds to a 90% CL interval of $-0.15 < A_{CP} < -0.03$.
³ Based on a total signal yield of $N(K^-\pi^+) + N(K^+\pi^-) = 1606 \pm 51$ events.
⁴ CHAO 04b reports significance of 3.9 standard deviation for deviation of A_{CP} from zero.
⁵ Corresponds to 90% confidence range $-0.21 < A_{CP} < 0.07$.
⁶ Corresponds to 90% confidence range $-0.188 < A_{CP} < -0.016$.
⁷ Corresponds to 90% confidence range $-0.21 < A_{CP} < +0.09$.
⁸ Corresponds to 90% confidence range $-0.25 < A_{CP} < 0.37$.
⁹ Corresponds to 90% confidence range $-0.35 < A_{CP} < -0.03$.

$A_{CP}(B^0 \rightarrow \eta' K^*(892)^0)$

VALUE	DOCUMENT ID	TECN	COMMENT
-0.07 ± 0.18 OUR AVERAGE			
$-0.22 \pm 0.29 \pm 0.07$	SATO	14	BELL $e^+e^- \rightarrow T(4S)$
$0.02 \pm 0.23 \pm 0.02$	DEL-AMO-SA...	10A	BABR $e^+e^- \rightarrow T(4S)$
• • • We do not use the following data for averages, fits, limits, etc. • • •			
$0.08 \pm 0.25 \pm 0.02$	¹ AUBERT	07E	BABR Repl. by DEL-AMO-SANCHEZ 10A

¹ Reports A_{CP} with the opposite sign convention.

$A_{CP}(B^0 \rightarrow \eta' K_0^*(1430)^0)$

VALUE	DOCUMENT ID	TECN	COMMENT
$-0.19 \pm 0.17 \pm 0.02$	DEL-AMO-SA...	10A	BABR $e^+e^- \rightarrow T(4S)$

$A_{CP}(B^0 \rightarrow \eta' K_2^*(1430)^0)$

VALUE	DOCUMENT ID	TECN	COMMENT
$0.14 \pm 0.18 \pm 0.02$	DEL-AMO-SA...	10A	BABR $e^+e^- \rightarrow T(4S)$

$A_{CP}(B^0 \rightarrow \eta K^*(892)^0)$

VALUE	DOCUMENT ID	TECN	COMMENT
0.19 ± 0.05 OUR AVERAGE			
$0.17 \pm 0.08 \pm 0.01$	WANG	07B	BELL $e^+e^- \rightarrow T(4S)$
$0.21 \pm 0.06 \pm 0.02$	AUBERT,B	06H	BABR $e^+e^- \rightarrow T(4S)$
• • • We do not use the following data for averages, fits, limits, etc. • • •			
$0.02 \pm 0.11 \pm 0.02$	AUBERT,B	04d	BABR Repl. by AUBERT,B 06H

$A_{CP}(B^0 \rightarrow \eta K_0^*(1430)^0)$

VALUE	DOCUMENT ID	TECN	COMMENT
$0.06 \pm 0.13 \pm 0.02$	AUBERT,B	06H	BABR $e^+e^- \rightarrow T(4S)$

$A_{CP}(B^0 \rightarrow \eta K_2^*(1430)^0)$

VALUE	DOCUMENT ID	TECN	COMMENT
$-0.07 \pm 0.19 \pm 0.02$	AUBERT,B	06H	BABR $e^+e^- \rightarrow T(4S)$

$A_{CP}(B^0 \rightarrow b_1 K^+)$

VALUE	DOCUMENT ID	TECN	COMMENT
$-0.07 \pm 0.12 \pm 0.02$	AUBERT	07Bi	BABR $e^+e^- \rightarrow T(4S)$

$A_{CP}(B^0 \rightarrow \omega K^{*0})$

VALUE	DOCUMENT ID	TECN	COMMENT
$0.45 \pm 0.25 \pm 0.02$	AUBERT	09H	BABR $e^+e^- \rightarrow T(4S)$

$A_{CP}(B^0 \rightarrow \omega(K\pi)_0^{*0})$

VALUE	DOCUMENT ID	TECN	COMMENT
$-0.07 \pm 0.09 \pm 0.02$	AUBERT	09H	BABR $e^+e^- \rightarrow T(4S)$

$A_{CP}(B^0 \rightarrow \omega K_2^*(1430)^0)$

VALUE	DOCUMENT ID	TECN	COMMENT
$-0.37 \pm 0.17 \pm 0.02$	AUBERT	09H	BABR $e^+e^- \rightarrow T(4S)$

$A_{CP}(B^0 \rightarrow K^+ \pi^- \pi^0)$

VALUE (units 10^{-2})	DOCUMENT ID	TECN	COMMENT
0 ± 6 OUR AVERAGE			
$-3.0^{+4.5}_{-5.1} \pm 5.5$	¹ AUBERT	08AQ	BABR $e^+e^- \rightarrow T(4S)$
$7 \pm 11 \pm 1$	² CHANG	04	BELL $e^+e^- \rightarrow T(4S)$

¹ Uses Dalitz plot analysis of $B^0 \rightarrow K^+ \pi^- \pi^0$ decays.
² Corresponds to 90% confidence range $-0.12 < A_{CP} < 0.26$.

$A_{CP}(B^0 \rightarrow \rho^- K^+)$

VALUE	DOCUMENT ID	TECN	COMMENT
0.20 ± 0.11 OUR AVERAGE			
$0.20 \pm 0.09 \pm 0.08$	¹ LEES	11	BABR $e^+e^- \rightarrow T(4S)$
$0.22^{+0.22+0.06}_{-0.23-0.02}$	² CHANG	04	BELL $e^+e^- \rightarrow T(4S)$
• • • We do not use the following data for averages, fits, limits, etc. • • •			
$0.11^{+0.14}_{-0.15} \pm 0.07$	¹ AUBERT	08AQ	BABR Repl. by LEES 11
$-0.28 \pm 0.17 \pm 0.08$	³ AUBERT	03T	BABR Repl. by AUBERT 08AQ

¹ Uses Dalitz plot analysis of $B^0 \rightarrow K^+ \pi^- \pi^0$ decays.
² Corresponds to 90% confidence range $-0.18 < A_{CP} < 0.64$.
³ The result reported corresponds to $-A_{CP}$.

$A_{CP}(B^0 \rightarrow \rho(1450)^- K^+)$

VALUE	DOCUMENT ID	TECN	COMMENT
$-0.10 \pm 0.32 \pm 0.09$	¹ LEES	11	BABR $e^+e^- \rightarrow T(4S)$

¹ Uses Dalitz plot analysis of $B^0 \rightarrow K^+ \pi^- \pi^0$ decays.

$A_{CP}(B^0 \rightarrow \rho(1700)^- K^+)$

VALUE	DOCUMENT ID	TECN	COMMENT
$-0.36 \pm 0.57 \pm 0.23$	¹ LEES	11	BABR $e^+e^- \rightarrow T(4S)$

¹ Uses Dalitz plot analysis of $B^0 \rightarrow K^+ \pi^- \pi^0$ decays.

Downloaded from https://academic.oup.com/ptep/article/2020/8/083C01/5891211 by guest on 20 August 2020

Meson Particle Listings

 B^0 $A_{CP}(B^0 \rightarrow K^+ \pi^- \pi^0 \text{ nonresonant})$

VALUE	DOCUMENT ID	TECN	COMMENT
$0.10 \pm 0.16 \pm 0.08$	¹ LEES	11	BABR $e^+ e^- \rightarrow \Upsilon(4S)$

••• We do not use the following data for averages, fits, limits, etc. •••

$0.23^{+0.19+0.11}_{-0.27-0.10}$	¹ AUBERT	08AQ	BABR Repl. by LEES 11
----------------------------------	---------------------	------	-----------------------

¹ Uses Dalitz plot analysis of $B^0 \rightarrow K^+ \pi^- \pi^0$ decays. The quoted value is only for the flat part of the non-resonant component.

 $A_{CP}(B^0 \rightarrow K^0 \pi^+ \pi^-)$

VALUE	DOCUMENT ID	TECN	COMMENT
$-0.01 \pm 0.05 \pm 0.01$	¹ AUBERT	09AU	BABR $e^+ e^- \rightarrow \Upsilon(4S)$

¹ Uses Dalitz plot analysis of $B^0 \rightarrow K^0 \pi^+ \pi^-$ decays and the first of two equivalent solutions is used.

 $A_{CP}(B^0 \rightarrow K^*(892)^+ \pi^-)$

VALUE	DOCUMENT ID	TECN	COMMENT
-0.27 ± 0.04 OUR AVERAGE			

$-0.308 \pm 0.060 \pm 0.016$	¹ AAIJ	18F	LHCB pp at 7, 8 TeV
$-0.29 \pm 0.11 \pm 0.02$	² LEES	11	BABR $e^+ e^- \rightarrow \Upsilon(4S)$
$-0.21 \pm 0.10 \pm 0.02$	^{3,4} AUBERT	09AU	BABR $e^+ e^- \rightarrow \Upsilon(4S)$
$-0.21 \pm 0.11 \pm 0.07$	⁵ DALSENO	09	BELL $e^+ e^- \rightarrow \Upsilon(4S)$
$0.26^{+0.33+0.10}_{-0.34-0.08}$	⁶ EISENSTEIN	03	CLE2 $e^+ e^- \rightarrow \Upsilon(4S)$

••• We do not use the following data for averages, fits, limits, etc. •••

$-0.19^{+0.20}_{-0.15} \pm 0.04$	² AUBERT	08AQ	BABR Repl. by LEES 11
$-0.11 \pm 0.14 \pm 0.05$	³ AUBERT	06i	BABR Repl. by AUBERT 09AU
$0.23 \pm 0.18^{+0.09}_{-0.06}$	AUBERT,B	04o	BABR Repl. by AUBERT 06i

¹ Uses Dalitz plot analysis of the $B^0 \rightarrow K_S^0 \pi^+ \pi^-$ final state decays.
² Uses Dalitz plot analysis of $B^0 \rightarrow K^+ \pi^- \pi^0$ decays.
³ Uses Dalitz plot analysis of $B^0 \rightarrow K^0 \pi^+ \pi^-$ decays.
⁴ The first of two equivalent solutions is used.
⁵ Uses Dalitz plot analysis of $B^0 \rightarrow K^0 \pi^+ \pi^-$ decays and the first of two consistent solutions that may be preferred.
⁶ Corresponds to 90% confidence range $-0.31 < A_{CP} < 0.78$.

 $A_{CP}(B^0 \rightarrow (K\pi)_0^{*+} \pi^-)$

VALUE	DOCUMENT ID	TECN	COMMENT
0.02 ± 0.04 OUR AVERAGE			

$-0.032 \pm 0.047 \pm 0.031$	¹ AAIJ	18F	LHCB pp at 7, 8 TeV
$0.07 \pm 0.14 \pm 0.01$	² LEES	11	BABR $e^+ e^- \rightarrow \Upsilon(4S)$
$0.09 \pm 0.07 \pm 0.03$	³ AUBERT	09AU	BABR $e^+ e^- \rightarrow \Upsilon(4S)$

••• We do not use the following data for averages, fits, limits, etc. •••

$0.17^{+0.11}_{-0.16} \pm 0.22$	² AUBERT	08AQ	BABR Repl. by LEES 11
---------------------------------	---------------------	------	-----------------------

¹ Uses Dalitz plot analysis of the $B^0 \rightarrow K_S^0 \pi^+ \pi^-$ final states decays.
² Uses Dalitz plot analysis of $B^0 \rightarrow K^+ \pi^- \pi^0$ decays.
³ Uses Dalitz plot analysis of $B^0 \rightarrow K^0 \pi^+ \pi^-$ decays and the first of two equivalent solutions is used.

 $A_{CP}(B^0 \rightarrow K_2^*(1430)^+ \pi^-)$

VALUE	DOCUMENT ID	TECN	COMMENT
$-0.29 \pm 0.22 \pm 0.09$	¹ AAIJ	18F	LHCB pp at 7, 8 TeV

¹ Uses Dalitz plot analysis of the $B^0 \rightarrow K_S^0 \pi^+ \pi^-$ final state decays.

 $A_{CP}(B^0 \rightarrow K^*(1680)^+ \pi^-)$

VALUE	DOCUMENT ID	TECN	COMMENT
$-0.07 \pm 0.13 \pm 0.04$	¹ AAIJ	18F	LHCB pp at 7, 8 TeV

¹ Uses Dalitz plot analysis of the $B^0 \rightarrow K_S^0 \pi^+ \pi^-$ final state decays.

 $A_{CP}(B^0 \rightarrow f_0(980) K_S^0)$

VALUE	DOCUMENT ID	TECN	COMMENT
$0.28 \pm 0.27 \pm 0.15$	¹ AAIJ	18F	LHCB pp at 7, 8 TeV

¹ Uses Dalitz plot analysis of the $B^0 \rightarrow K_S^0 \pi^+ \pi^-$ final state decays.

 $A_{CP}(B^0 \rightarrow (K\pi)_0^{*0} \pi^0)$

VALUE	DOCUMENT ID	TECN	COMMENT
$-0.15 \pm 0.10 \pm 0.04$	¹ LEES	11	BABR $e^+ e^- \rightarrow \Upsilon(4S)$

••• We do not use the following data for averages, fits, limits, etc. •••

$-0.22 \pm 0.12^{+0.30}_{-0.29}$	¹ AUBERT	08AQ	BABR Repl. by LEES 11
----------------------------------	---------------------	------	-----------------------

¹ Uses Dalitz plot analysis of $B^0 \rightarrow K^+ \pi^- \pi^0$ decays.

 $A_{CP}(B^0 \rightarrow K^{*0} \pi^0)$

VALUE	DOCUMENT ID	TECN	COMMENT
$-0.15 \pm 0.12 \pm 0.04$	¹ LEES	11	BABR $e^+ e^- \rightarrow \Upsilon(4S)$

••• We do not use the following data for averages, fits, limits, etc. •••

$-0.09^{+0.21}_{-0.24} \pm 0.09$	¹ AUBERT	08AQ	BABR Repl. by LEES 11
----------------------------------	---------------------	------	-----------------------

¹ Uses Dalitz plot analysis of $B^0 \rightarrow K^+ \pi^- \pi^0$ decays.

 $A_{CP}(B^0 \rightarrow K^*(892)^0 \pi^+ \pi^-)$

VALUE	DOCUMENT ID	TECN	COMMENT
$0.07 \pm 0.04 \pm 0.03$	AUBERT	07As	BABR $e^+ e^- \rightarrow \Upsilon(4S)$

 $A_{CP}(B^0 \rightarrow K^*(892)^0 \rho^0)$

VALUE	DOCUMENT ID	TECN	COMMENT
$-0.06 \pm 0.09 \pm 0.02$	LEES	12k	BABR $e^+ e^- \rightarrow \Upsilon(4S)$

••• We do not use the following data for averages, fits, limits, etc. •••

$0.09 \pm 0.19 \pm 0.02$	AUBERT,B	06G	BABR Repl. by LEES 12K
--------------------------	----------	-----	------------------------

 $A_{CP}(B^0 \rightarrow K^{*0} f_0(980))$

VALUE	DOCUMENT ID	TECN	COMMENT
$0.07 \pm 0.10 \pm 0.02$	LEES	12k	BABR $e^+ e^- \rightarrow \Upsilon(4S)$

••• We do not use the following data for averages, fits, limits, etc. •••

$-0.17 \pm 0.28 \pm 0.02$	AUBERT,B	06G	BABR Repl. by LEES 12K
---------------------------	----------	-----	------------------------

 $A_{CP}(B^0 \rightarrow K^{*+} \rho^-)$

VALUE	DOCUMENT ID	TECN	COMMENT
$0.21 \pm 0.15 \pm 0.02$	LEES	12k	BABR $e^+ e^- \rightarrow \Upsilon(4S)$

 $A_{CP}(B^0 \rightarrow K^*(892)^0 K^+ K^-)$

VALUE	DOCUMENT ID	TECN	COMMENT
$0.01 \pm 0.05 \pm 0.02$	AUBERT	07As	BABR $e^+ e^- \rightarrow \Upsilon(4S)$

 $A_{CP}(B^0 \rightarrow a_1^- K^+)$

VALUE	DOCUMENT ID	TECN	COMMENT
$-0.16 \pm 0.12 \pm 0.01$	AUBERT	08F	BABR $e^+ e^- \rightarrow \Upsilon(4S)$

 $A_{CP}(B^0 \rightarrow K^0 K^0)$

VALUE	DOCUMENT ID	TECN	COMMENT
$-0.58^{+0.73}_{-0.66} \pm 0.04$	LIN	07	BELL $e^+ e^- \rightarrow \Upsilon(4S)$

 $A_{CP}(B^0 \rightarrow K^*(892)^0 \phi)$

VALUE	DOCUMENT ID	TECN	COMMENT
0.00 ± 0.04 OUR AVERAGE			

$-0.007 \pm 0.048 \pm 0.021$	PRIM	13	BELL $e^+ e^- \rightarrow \Upsilon(4S)$
$0.01 \pm 0.06 \pm 0.03$	AUBERT	08BG	BABR $e^+ e^- \rightarrow \Upsilon(4S)$

••• We do not use the following data for averages, fits, limits, etc. •••

$-0.03 \pm 0.07 \pm 0.03$	AUBERT	07D	BABR Repl. by AUBERT 08BG
$0.02 \pm 0.09 \pm 0.02$	¹ CHEN	05A	BELL Repl. by PRIM 13
$-0.01 \pm 0.09 \pm 0.02$	AUBERT,B	04W	BABR Repl. by AUBERT 07D
$0.04 \pm 0.12 \pm 0.02$	AUBERT	03V	BABR Repl. by AUBERT 04W
$0.07 \pm 0.15^{+0.05}_{-0.03}$	² CHEN	03B	BELL Repl. by CHEN 05A
$0.00 \pm 0.27 \pm 0.03$	³ AUBERT	02E	BABR Repl. by AUBERT 03V

¹ Corresponds to 90% confidence range $-0.14 < A_{CP} < 0.17$.

² Corresponds to 90% confidence range $-0.18 < A_{CP} < 0.33$.

³ Corresponds to 90% confidence range $-0.44 < A_{CP} < 0.44$.

 $A_{CP}(B^0 \rightarrow K^*(892)^0 K^- \pi^+)$

VALUE	DOCUMENT ID	TECN	COMMENT
$0.22 \pm 0.33 \pm 0.20$	AUBERT	07As	BABR $e^+ e^- \rightarrow \Upsilon(4S)$

 $A_{CP}(B^0 \rightarrow \phi(K\pi)_0^{*0})$

VALUE	DOCUMENT ID	TECN	COMMENT
0.12 ± 0.08 OUR AVERAGE			

$0.093 \pm 0.094 \pm 0.017$	PRIM	13	BELL $e^+ e^- \rightarrow \Upsilon(4S)$
$0.20 \pm 0.14 \pm 0.06$	AUBERT	08BG	BABR $e^+ e^- \rightarrow \Upsilon(4S)$

••• We do not use the following data for averages, fits, limits, etc. •••

$0.17 \pm 0.15 \pm 0.03$	AUBERT	07D	BABR Repl. by AUBERT 08BG
--------------------------	--------	-----	---------------------------

 $A_{CP}(B^0 \rightarrow \phi K_2^*(1430)^0)$

VALUE	DOCUMENT ID	TECN	COMMENT
-0.11 ± 0.10 OUR AVERAGE			

$-0.155^{+0.152}_{-0.133} \pm 0.033$	PRIM	13	BELL $e^+ e^- \rightarrow \Upsilon(4S)$
$-0.08 \pm 0.12 \pm 0.05$	AUBERT	08BG	BABR $e^+ e^- \rightarrow \Upsilon(4S)$

••• We do not use the following data for averages, fits, limits, etc. •••

$-0.12 \pm 0.14 \pm 0.04$	AUBERT	07D	BABR Repl. by AUBERT 08BG
---------------------------	--------	-----	---------------------------

 $A_{CP}(B^0 \rightarrow K^*(892)^0 \gamma)$

VALUE	DOCUMENT ID	TECN	COMMENT
-0.006 ± 0.011 OUR AVERAGE			

$-0.013 \pm 0.017 \pm 0.004$	¹ HORIGUCHI	17	BELL $e^+ e^- \rightarrow \Upsilon(4S)$
$0.008 \pm 0.017 \pm 0.009$	AAIJ	13	LHCB pp at 7 TeV
$-0.016 \pm 0.022 \pm 0.007$	AUBERT	09Ao	BABR $e^+ e^- \rightarrow \Upsilon(4S)$

¹ Uses $B(\Upsilon(4S) \rightarrow B^+ B^-) = (51.4 \pm 0.6)\%$ and $B(\Upsilon(4S) \rightarrow B^0 \bar{B}^0) = (48.6 \pm 0.6)\%$.

 $A_{CP}(B^0 \rightarrow K_2^*(1430)^0 \gamma)$

VALUE	DOCUMENT ID	TECN	COMMENT
$-0.08 \pm 0.15 \pm 0.01$	AUBERT,B	04U	BABR $e^+ e^- \rightarrow \Upsilon(4S)$

See key on page 999

Meson Particle Listings

B^0

$A_{CP}(B^0 \rightarrow X_s \gamma)$

VALUE	DOCUMENT ID	TECN	COMMENT
$-0.0094 \pm 0.0174 \pm 0.0047$	¹ WATA NUKI	19 BELL	$e^+ e^- \rightarrow \Upsilon(4S)$

¹ Using a sum-of-exclusive technique with $m_{X_s} < 2.8 \text{ GeV}/c^2$.

$A_{CP}(B^0 \rightarrow \rho^+ \pi^-)$

VALUE	DOCUMENT ID	TECN	COMMENT
0.13 ± 0.06 OUR AVERAGE	Error includes scale factor of 1.1.		
$0.09 \pm 0.05 \pm 0.04$	¹ LEES	13J BABR	$e^+ e^- \rightarrow \Upsilon(4S)$
$0.21 \pm 0.08 \pm 0.04$	¹ KUSAKA	07 BELL	$e^+ e^- \rightarrow \Upsilon(4S)$
• • • We do not use the following data for averages, fits, limits, etc. • • •			
$0.03 \pm 0.07 \pm 0.04$	AUBERT	07AA BABR	Repl. by LEES 13J
$-0.02 \pm 0.16 \pm 0.05$	WANG	05 BELL	Repl. by KUSAKA 07
$-0.18 \pm 0.08 \pm 0.03$	AUBERT	03T BABR	Repl. by AUBERT 07AA
¹ Uses time-dependent Dalitz plot analysis of $B^0 \rightarrow \pi^+ \pi^- \pi^0$ decays.			

$A_{CP}(B^0 \rightarrow \rho^- \pi^+)$

VALUE	DOCUMENT ID	TECN	COMMENT
-0.08 ± 0.08 OUR AVERAGE	Error includes scale factor of 1.1.		
$-0.12 \pm 0.08 \pm 0.04$	¹ LEES	13J BABR	$e^+ e^- \rightarrow \Upsilon(4S)$
$0.08 \pm 0.16 \pm 0.11$	¹ KUSAKA	07 BELL	$e^+ e^- \rightarrow \Upsilon(4S)$
• • • We do not use the following data for averages, fits, limits, etc. • • •			
$-0.37 \pm 0.16 \pm 0.09$	AUBERT	07AA BABR	Repl. by LEES 13J
$-0.53 \pm 0.29 \pm 0.09$	WANG	05 BELL	Repl. by KUSAKA 07
¹ Uses time-dependent Dalitz plot analysis of $B^0 \rightarrow \pi^+ \pi^- \pi^0$ decays.			

$A_{CP}(B^0 \rightarrow a_1(1260)^\pm \pi^\mp)$

VALUE	DOCUMENT ID	TECN	COMMENT
-0.07 ± 0.06 OUR AVERAGE	Error includes scale factor of 1.1.		
$-0.06 \pm 0.05 \pm 0.07$	DALSENO	12 BELL	$e^+ e^- \rightarrow \Upsilon(4S)$
$-0.07 \pm 0.07 \pm 0.02$	AUBERT	07o BABR	$e^+ e^- \rightarrow \Upsilon(4S)$

$A_{CP}(B^0 \rightarrow b_1^- \pi^+)$

VALUE	DOCUMENT ID	TECN	COMMENT
$-0.05 \pm 0.10 \pm 0.02$	AUBERT	07Bi BABR	$e^+ e^- \rightarrow \Upsilon(4S)$

$A_{CP}(B^0 \rightarrow p\bar{p}K^*(892)^0)$

VALUE	DOCUMENT ID	TECN	COMMENT
0.05 ± 0.12 OUR AVERAGE	Error includes scale factor of 1.1.		
$-0.08 \pm 0.20 \pm 0.02$	CHEN	08c BELL	$e^+ e^- \rightarrow \Upsilon(4S)$
$0.11 \pm 0.13 \pm 0.06$	AUBERT	07AV BABR	$e^+ e^- \rightarrow \Upsilon(4S)$

$A_{CP}(B^0 \rightarrow \rho^0 \pi^+ \pi^-)$

VALUE	DOCUMENT ID	TECN	COMMENT
0.04 ± 0.07 OUR AVERAGE	Error includes scale factor of 1.1.		
$0.10 \pm 0.10 \pm 0.02$	AUBERT	09Ac BABR	$e^+ e^- \rightarrow \Upsilon(4S)$
$-0.02 \pm 0.10 \pm 0.03$	WANG	07c BELL	$e^+ e^- \rightarrow \Upsilon(4S)$

$A_{CP}(B^0 \rightarrow K^{*0} \ell^+ \ell^-)$

VALUE	DOCUMENT ID	TECN	COMMENT
-0.05 ± 0.10 OUR AVERAGE	Error includes scale factor of 1.1.		
$0.02 \pm 0.20 \pm 0.02$	AUBERT	09T BABR	$e^+ e^- \rightarrow \Upsilon(4S)$
$-0.08 \pm 0.12 \pm 0.02$	WEI	09A BELL	$e^+ e^- \rightarrow \Upsilon(4S)$

$A_{CP}(B^0 \rightarrow K^{*0} e^+ e^-)$

VALUE	DOCUMENT ID	TECN	COMMENT
$-0.21 \pm 0.19 \pm 0.02$	WEI	09A BELL	$e^+ e^- \rightarrow \Upsilon(4S)$

$A_{CP}(B^0 \rightarrow K^{*0} \mu^+ \mu^-)$

VALUE	DOCUMENT ID	TECN	COMMENT
-0.034 ± 0.024 OUR AVERAGE	Error includes scale factor of 1.1.		
$-0.035 \pm 0.024 \pm 0.003$	AAIJ	14AN LHCB	pp at 7, 8 TeV
$0.00 \pm 0.15 \pm 0.03$	WEI	09A BELL	$e^+ e^- \rightarrow \Upsilon(4S)$
• • • We do not use the following data for averages, fits, limits, etc. • • •			
$-0.072 \pm 0.040 \pm 0.005$	AAIJ	13E LHCB	Repl. by AAIJ 14AN

$C_{D^*(2010)^- D^+}(B^0 \rightarrow D^*(2010)^- D^+)$

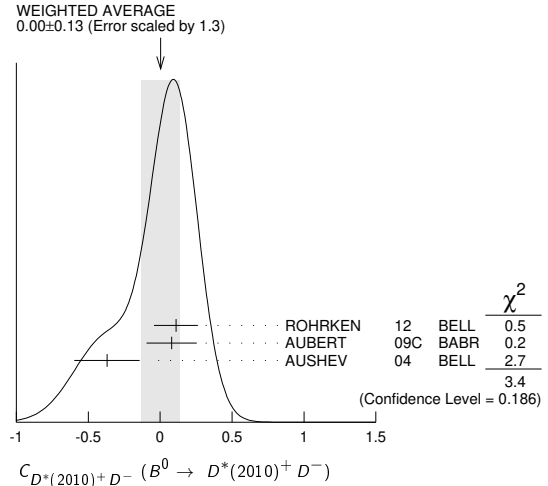
VALUE	DOCUMENT ID	TECN	COMMENT
-0.01 ± 0.11 OUR AVERAGE	Error includes scale factor of 1.6. See the ideogram below.		
$-0.13 \pm 0.16 \pm 0.05$	¹ ROHRKEN	12 BELL	$e^+ e^- \rightarrow \Upsilon(4S)$
$0.00 \pm 0.17 \pm 0.03$	AUBERT	09c BABR	$e^+ e^- \rightarrow \Upsilon(4S)$
$0.23 \pm 0.25 \pm 0.06$	² AUSHEV	04 BELL	$e^+ e^- \rightarrow \Upsilon(4S)$
• • • We do not use the following data for averages, fits, limits, etc. • • •			
$0.23 \pm 0.15 \pm 0.04$	AUBERT	07Ai BABR	Repl. by AUBERT 09c
$0.17 \pm 0.24 \pm 0.04$	AUBERT,B	05z BABR	Repl. by AUBERT 07Ai
$-0.22 \pm 0.37 \pm 0.10$	AUBERT	03j BABR	Repl. by AUBERT,B 05z
¹ ROHRKEN 12 reports the measurements of $C = -0.01 \pm 0.11 \pm 0.04$ and $\Delta C = 0.12 \pm 0.11 \pm 0.03$ such that $C_{D^*(2010)^- D^+} = C - \Delta C$.			
² Combines results from fully and partially reconstructed $B^0 \rightarrow D^{*\pm} D^\mp$ decays.			

$S_{D^*(2010)^- D^+}(B^0 \rightarrow D^*(2010)^- D^+)$

VALUE	DOCUMENT ID	TECN	COMMENT
-0.72 ± 0.15 OUR AVERAGE	Error includes scale factor of 1.3. See the ideogram below.		
$-0.65 \pm 0.22 \pm 0.07$	¹ ROHRKEN	12 BELL	$e^+ e^- \rightarrow \Upsilon(4S)$
$-0.73 \pm 0.23 \pm 0.050$	AUBERT	09c BABR	$e^+ e^- \rightarrow \Upsilon(4S)$
$-0.96 \pm 0.43 \pm 0.12$	² AUSHEV	04 BELL	$e^+ e^- \rightarrow \Upsilon(4S)$
• • • We do not use the following data for averages, fits, limits, etc. • • •			
$-0.44 \pm 0.22 \pm 0.06$	AUBERT	07Ai BABR	Repl. by AUBERT 09c
$-0.29 \pm 0.33 \pm 0.07$	AUBERT,B	05z BABR	Repl. by AUBERT 07Ai
$-0.24 \pm 0.69 \pm 0.12$	AUBERT	03j BABR	Repl. by AUBERT,B 05z
¹ ROHRKEN 12 reports the measurements of $S = -0.78 \pm 0.15 \pm 0.05$ and $\Delta S = -0.13 \pm 0.15 \pm 0.04$ such that $S_{D^*(2010)^- D^+} = S - \Delta S$.			
² Combines results from fully and partially reconstructed $B^0 \rightarrow D^{*\pm} D^\mp$ decays.			

$C_{D^*(2010)^+ D^-}(B^0 \rightarrow D^*(2010)^+ D^-)$

VALUE	DOCUMENT ID	TECN	COMMENT
0.00 ± 0.13 OUR AVERAGE	Error includes scale factor of 1.3. See the ideogram below.		
$0.11 \pm 0.14 \pm 0.06$	¹ ROHRKEN	12 BELL	$e^+ e^- \rightarrow \Upsilon(4S)$
$0.08 \pm 0.17 \pm 0.04$	AUBERT	09c BABR	$e^+ e^- \rightarrow \Upsilon(4S)$
$-0.37 \pm 0.22 \pm 0.06$	² AUSHEV	04 BELL	$e^+ e^- \rightarrow \Upsilon(4S)$
• • • We do not use the following data for averages, fits, limits, etc. • • •			
$0.18 \pm 0.15 \pm 0.04$	AUBERT	07Ai BABR	Repl. by AUBERT 09c
$0.09 \pm 0.25 \pm 0.06$	AUBERT,B	05z BABR	Repl. by AUBERT 07Ai
$-0.47 \pm 0.40 \pm 0.12$	AUBERT	03j BABR	Repl. by AUBERT,B 05z
¹ ROHRKEN 12 reports the measurements of $C = -0.01 \pm 0.11 \pm 0.04$ and $\Delta C = 0.12 \pm 0.11 \pm 0.03$ such that $C_{D^*(2010)^+ D^-} = C + \Delta C$.			
² Combines results from fully and partially reconstructed $B^0 \rightarrow D^{*\pm} D^\mp$ decays.			



$S_{D^*(2010)^+ D^-}(B^0 \rightarrow D^*(2010)^+ D^-)$

VALUE	DOCUMENT ID	TECN	COMMENT
-0.73 ± 0.14 OUR AVERAGE	Error includes scale factor of 1.6. See the ideogram below.		
$-0.90 \pm 0.21 \pm 0.07$	¹ ROHRKEN	12 BELL	$e^+ e^- \rightarrow \Upsilon(4S)$
$-0.62 \pm 0.21 \pm 0.03$	AUBERT	09c BABR	$e^+ e^- \rightarrow \Upsilon(4S)$
$-0.55 \pm 0.39 \pm 0.12$	² AUSHEV	04 BELL	$e^+ e^- \rightarrow \Upsilon(4S)$
• • • We do not use the following data for averages, fits, limits, etc. • • •			
$-0.79 \pm 0.21 \pm 0.06$	AUBERT	07Ai BABR	Repl. by AUBERT 09c
$-0.54 \pm 0.35 \pm 0.07$	AUBERT,B	05z BABR	Repl. by AUBERT 07Ai
$-0.82 \pm 0.75 \pm 0.14$	AUBERT	03j BABR	Repl. by AUBERT,B 05z
¹ ROHRKEN 12 reports the measurements of $S = -0.78 \pm 0.15 \pm 0.05$ and $\Delta S = -0.13 \pm 0.15 \pm 0.04$ such that $S_{D^*(2010)^+ D^-} = S + \Delta S$.			
² Combines results from fully and partially reconstructed $B^0 \rightarrow D^{*\pm} D^\mp$ decays.			

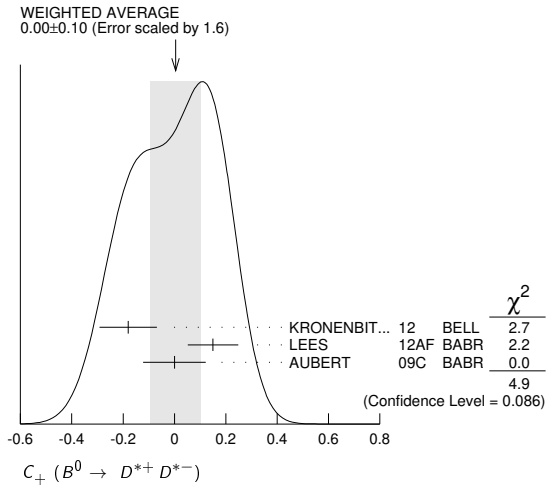
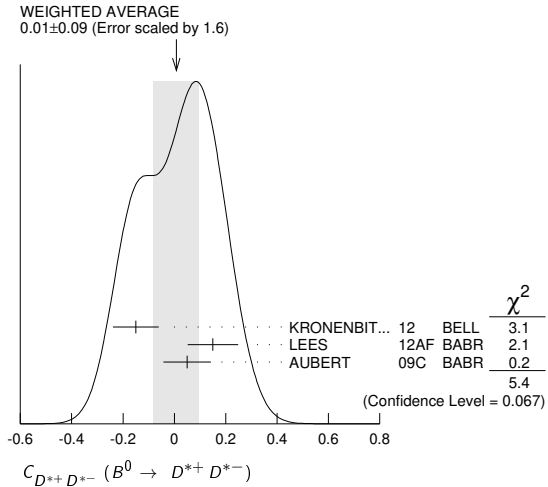
$C_{D^{*+} D^{*-}}(B^0 \rightarrow D^{*+} D^{*-})$

VALUE	DOCUMENT ID	TECN	COMMENT
0.01 ± 0.09 OUR AVERAGE	Error includes scale factor of 1.6. See the ideogram below.		
$-0.15 \pm 0.08 \pm 0.04$	^{1,2} KRONENBITTER	12 BELL	$e^+ e^- \rightarrow \Upsilon(4S)$
$+0.15 \pm 0.09 \pm 0.04$	³ LEES	12AF BABR	$e^+ e^- \rightarrow \Upsilon(4S)$
$0.05 \pm 0.09 \pm 0.02$	AUBERT	09c BABR	$e^+ e^- \rightarrow \Upsilon(4S)$
• • • We do not use the following data for averages, fits, limits, etc. • • •			
$-0.15 \pm 0.13 \pm 0.04$	² VERVINK	09 BELL	Repl. by KRONENBITTER 12
$-0.02 \pm 0.11 \pm 0.02$	¹ AUBERT	07Bo BABR	Repl. by AUBERT 09c
$0.26 \pm 0.26 \pm 0.06$	² MIYAKE	05 BELL	Repl. by VERVINK 09
$0.28 \pm 0.23 \pm 0.02$	⁴ AUBERT	03Q BABR	Repl. by AUBERT 07Bo
¹ Assumes both CP -even and CP -odd states having the CP asymmetry.			
² Belle Collab. quotes $A_{D^{*+} D^{*-}}$ which is equal to $-C_{D^{*+} D^{*-}}$.			
³ Measured partially reconstructed candidates when one D^0 meson is not explicitly reconstructed. Analysis does not separate CP -even and CP -odd component.			

Meson Particle Listings

B^0

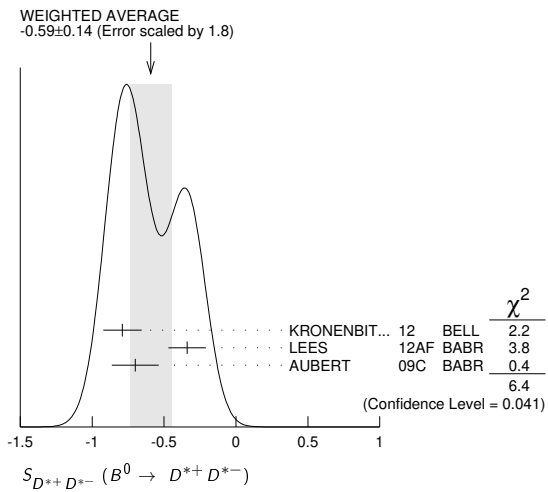
⁴AUBERT 03q reports $|\lambda|=0.75 \pm 0.19 \pm 0.02$ and $\text{Im}(\lambda)=0.05 \pm 0.29 \pm 0.10$. We convert them to S and C parameters taking into account correlations.



$S_{D^{*+}D^{*-}} (B^0 \to D^{*+}D^{*-})$

VALUE	DOCUMENT ID	TECN	COMMENT
-0.59 ± 0.14 OUR AVERAGE	Error includes scale factor of 1.8. See the ideogram below.		
-0.79 ± 0.13 ± 0.03	¹ KRONENBIT...12	BELL	$e^+e^- \to \Upsilon(4S)$
-0.34 ± 0.12 ± 0.05	² LEES	12AF BABR	$e^+e^- \to \Upsilon(4S)$
-0.70 ± 0.16 ± 0.03	¹ AUBERT	09c BABR	$e^+e^- \to \Upsilon(4S)$
••• We do not use the following data for averages, fits, limits, etc. •••			
-0.96 ± 0.25 ± 0.13	VERVINK	09 BELL	Repl. by KRONENBITTER 12
-0.66 ± 0.19 ± 0.04	¹ AUBERT	07B0 BABR	Repl. by AUBERT 09c
-0.75 ± 0.56 ± 0.12	MIYAKE	05 BELL	Repl. by VERVINK 09
0.06 ± 0.37 ± 0.13	³ AUBERT	03q BABR	Repl. by AUBERT 07B0

¹Assumes both CP -even and CP -odd states having the CP asymmetry.
²Measured partially reconstructed candidates when one D^0 meson is not explicitly reconstructed. Analysis does not separate CP -even and CP -odd component.
³AUBERT 03q reports $|\lambda|=0.75 \pm 0.19 \pm 0.02$ and $\text{Im}(\lambda)=0.05 \pm 0.29 \pm 0.10$. We convert them to S and C parameters taking into account correlations.



$C_{+} (B^0 \to D^{*+}D^{*-})$

See the note in the $C_{\pi\pi}$ datablock, but for CP even final state.

VALUE	DOCUMENT ID	TECN	COMMENT
0.00 ± 0.10 OUR AVERAGE	Error includes scale factor of 1.6. See the ideogram below.		
-0.18 ± 0.10 ± 0.05	¹ KRONENBIT...12	BELL	$e^+e^- \to \Upsilon(4S)$
+0.15 ± 0.09 ± 0.04	² LEES	12AF BABR	$e^+e^- \to \Upsilon(4S)$
0.00 ± 0.12 ± 0.02	AUBERT	09c BABR	$e^+e^- \to \Upsilon(4S)$
••• We do not use the following data for averages, fits, limits, etc. •••			
-0.05 ± 0.14 ± 0.02	AUBERT	07B0 BABR	Repl. by AUBERT 09c
0.06 ± 0.17 ± 0.03	³ AUBERT, BE	05A BABR	Repl. by AUBERT 07B0
¹ Belle Collab. quotes $A_{D^{*+}D^{*-}}$ which is equal to $-C_{D^{*+}D^{*-}}$.			
² Measured partially reconstructed candidates when one D^0 meson is not explicitly reconstructed. Extracted under assumption of equal C_{+} and C_{-} .			
³ AUBERT, BE 05A reports a CP -odd fraction $R_{\perp} = 0.125 \pm 0.044 \pm 0.007$.			

$S_{+} (B^0 \to D^{*+}D^{*-})$

See the note in the $S_{\pi\pi}$ datablock, but for CP even final state.

VALUE	DOCUMENT ID	TECN	COMMENT
-0.73 ± 0.09 OUR AVERAGE	Error includes scale factor of 1.6. See the ideogram below.		
-0.81 ± 0.13 ± 0.03	KRONENBIT...12	BELL	$e^+e^- \to \Upsilon(4S)$
-0.49 ± 0.18 ± 0.08	¹ LEES	12AF BABR	$e^+e^- \to \Upsilon(4S)$
-0.76 ± 0.16 ± 0.04	AUBERT	09c BABR	$e^+e^- \to \Upsilon(4S)$
••• We do not use the following data for averages, fits, limits, etc. •••			
-0.72 ± 0.19 ± 0.05	AUBERT	07B0 BABR	Repl. by AUBERT 09c
-0.75 ± 0.25 ± 0.03	² AUBERT, BE	05A BABR	Repl. by AUBERT 07B0
¹ Measured partially reconstructed candidates when one D^0 meson is not explicitly reconstructed. Analysis does not separate CP -even and CP -odd component. Value is obtained from $S = -0.34 \pm 0.12 \pm 0.05$ using $S = S_{+}(1 - 2R_{\perp})$ with $R_{\perp} = 0.158 \pm 0.029$.			
² AUBERT, BE 05A reports a CP -odd fraction $R_{\perp} = 0.125 \pm 0.044 \pm 0.007$.			

$C_{-} (B^0 \to D^{*+}D^{*-})$

See the note in the $C_{\pi\pi}$ datablock, but for CP odd final state.

VALUE	DOCUMENT ID	TECN	COMMENT
0.19 ± 0.31 OUR AVERAGE	Error includes scale factor of 1.6. See the ideogram below.		
0.05 ± 0.39 ± 0.08	¹ KRONENBIT...12	BELL	$e^+e^- \to \Upsilon(4S)$
0.41 ± 0.49 ± 0.08	AUBERT	09c BABR	$e^+e^- \to \Upsilon(4S)$
••• We do not use the following data for averages, fits, limits, etc. •••			
0.23 ± 0.67 ± 0.10	AUBERT	07B0 BABR	Repl. by AUBERT 09c
-0.20 ± 0.96 ± 0.11	² AUBERT, BE	05A BABR	Repl. by AUBERT 07B0
¹ Belle Collab. quotes $A_{D^{*+}D^{*-}}$ which is equal to $-C_{D^{*+}D^{*-}}$.			
² AUBERT, BE 05A reports a CP -odd fraction $R_{\perp} = 0.125 \pm 0.044 \pm 0.007$.			

$S_{-} (B^0 \to D^{*+}D^{*-})$

See the note in the $S_{\pi\pi}$ datablock, but for CP odd final state.

VALUE	DOCUMENT ID	TECN	COMMENT
0.1 ± 1.6 OUR AVERAGE	Error includes scale factor of 3.5.		
1.52 ± 0.62 ± 0.12	KRONENBIT...12	BELL	$e^+e^- \to \Upsilon(4S)$
-1.80 ± 0.70 ± 0.16	AUBERT	09c BABR	$e^+e^- \to \Upsilon(4S)$
••• We do not use the following data for averages, fits, limits, etc. •••			
-1.83 ± 1.04 ± 0.23	AUBERT	07B0 BABR	Repl. by AUBERT 09c
-1.75 ± 1.78 ± 0.22	¹ AUBERT, BE	05A BABR	Repl. by AUBERT 07B0
¹ AUBERT, BE 05A reports a CP -odd fraction $R_{\perp} = 0.125 \pm 0.044 \pm 0.007$.			

$C (B^0 \to D^{*}(2010)^+ D^{*}(2010)^- K_S^0)$

VALUE	DOCUMENT ID	TECN	COMMENT
0.01 ± 0.28 ± 0.09	¹ DALSENO	07 BELL	$e^+e^- \to \Upsilon(4S)$
¹ Reports value of A which is equal to $-C$.			

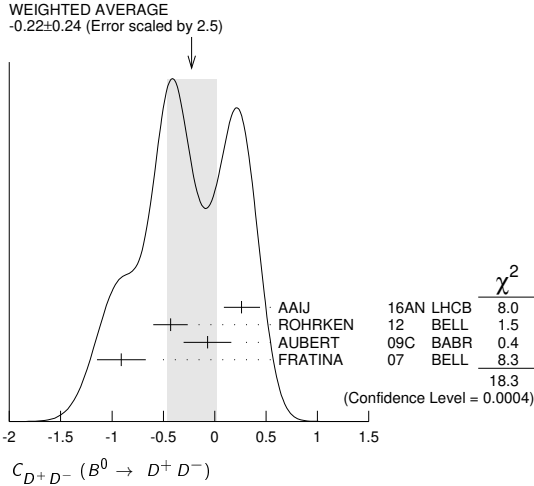
$S (B^0 \to D^{*}(2010)^+ D^{*}(2010)^- K_S^0)$

VALUE	DOCUMENT ID	TECN	COMMENT
0.06 ± 0.45 ± 0.06	¹ DALSENO	07 BELL	$e^+e^- \to \Upsilon(4S)$
¹ This value includes an unknown CP dilution factor D due to possible contributions from intermediate resonances and different partial waves.			

$C_{D^+D^-} (B^0 \to D^+D^-)$

VALUE	DOCUMENT ID	TECN	COMMENT
-0.22 ± 0.24 OUR AVERAGE	Error includes scale factor of 2.5. See the ideogram below.		
0.26 ± 0.18 ± 0.02	AAIJ	16AN LHCB	pp at 7, 8 TeV
-0.43 ± 0.16 ± 0.05	ROHRKEN	12 BELL	$e^+e^- \to \Upsilon(4S)$
-0.07 ± 0.23 ± 0.03	AUBERT	09c BABR	$e^+e^- \to \Upsilon(4S)$
-0.91 ± 0.23 ± 0.06	¹ FRATINA	07 BELL	$e^+e^- \to \Upsilon(4S)$

• • • We do not use the following data for averages, fits, limits, etc. • • •
 $0.11 \pm 0.22 \pm 0.07$ AUBERT 07AI BABR Repl. by AUBERT 09c
 $0.11 \pm 0.35 \pm 0.06$ AUBERT,B 05Z BABR Repl. by AUBERT 07AI
¹The paper reports A , which is equal to $-C$.



$S_{D^+D^-} (B^0 \rightarrow D^+ D^-)$

VALUE	DOCUMENT ID	TECN	COMMENT
$-0.76^{+0.15}_{-0.13}$ OUR AVERAGE	Error includes scale factor of 1.2.		
$-0.54^{+0.17}_{-0.16} \pm 0.05$	AAIJ	16AN	LHCB pp at 7, 8 TeV
$-1.06^{+0.21}_{-0.14} \pm 0.08$	ROHRKEN	12	BELL $e^+e^- \rightarrow \Upsilon(4S)$
$-0.63 \pm 0.36 \pm 0.05$	AUBERT	09C	BABR $e^+e^- \rightarrow \Upsilon(4S)$
$-1.13 \pm 0.37 \pm 0.09$	FRATINA	07	BELL $e^+e^- \rightarrow \Upsilon(4S)$
• • • We do not use the following data for averages, fits, limits, etc. • • •			
$-0.54 \pm 0.34 \pm 0.06$	AUBERT	07AI	BABR Repl. by AUBERT 09c
$-0.29 \pm 0.63 \pm 0.06$	AUBERT,B	05Z	BABR Repl. by AUBERT 07AI

$C_{J/\psi(1S)\pi^0} (B^0 \rightarrow J/\psi(1S)\pi^0)$

VALUE	DOCUMENT ID	TECN	COMMENT
0.03 ± 0.17 OUR AVERAGE	Error includes scale factor of 1.5.		
$0.15 \pm 0.14^{+0.04}_{-0.03}$	¹ PAL	18	BELL $e^+e^- \rightarrow \Upsilon(4S)$
$-0.20 \pm 0.19 \pm 0.03$	AUBERT	08AU	BABR $e^+e^- \rightarrow \Upsilon(4S)$
• • • We do not use the following data for averages, fits, limits, etc. • • •			
$-0.08 \pm 0.16 \pm 0.05$	¹ LEE	08A	BELL Repl. by PAL 18
$-0.21 \pm 0.26 \pm 0.06$	AUBERT,B	06B	BABR Repl. by AUBERT 08AU
$0.01 \pm 0.29 \pm 0.03$	¹ KATAOKA	04	BELL Repl. by LEE 08A
$0.38 \pm 0.41 \pm 0.09$	AUBERT	03N	BABR Repl. by AUBERT,B 06B
¹ BELLE Collab. quotes $A_{J/\psi\pi^0}$ which is equal to $-C_{J/\psi\pi^0}$.			

$S_{J/\psi(1S)\pi^0} (B^0 \rightarrow J/\psi(1S)\pi^0)$

VALUE	DOCUMENT ID	TECN	COMMENT
-0.88 ± 0.32 OUR AVERAGE	Error includes scale factor of 2.2.		
$-0.59 \pm 0.19 \pm 0.03$	PAL	18	BELL $e^+e^- \rightarrow \Upsilon(4S)$
$-1.23 \pm 0.21 \pm 0.04$	AUBERT	08AU	BABR $e^+e^- \rightarrow \Upsilon(4S)$
• • • We do not use the following data for averages, fits, limits, etc. • • •			
$-0.65 \pm 0.21 \pm 0.05$	LEE	08A	BELL Repl. by PAL 18
$-0.68 \pm 0.30 \pm 0.04$	AUBERT,B	06B	BABR Repl. by AUBERT 08AU
$-0.72 \pm 0.42 \pm 0.09$	KATAOKA	04	BELL Repl. by LEE 08A
$0.05 \pm 0.49 \pm 0.16$	AUBERT	03N	BABR Repl. by AUBERT,B 06B

$C(B^0 \rightarrow J/\psi(1S)\rho^0)$

VALUE	DOCUMENT ID	TECN	COMMENT
$-0.063 \pm 0.056^{+0.019}_{-0.014}$	¹ AAIJ	15J	LHCB pp at 7, 8 TeV

¹Time-dependent CP violation is measured in the $B^0 \rightarrow J/\psi\rho^0$ and was used to limit the size of penguin amplitude contributions to ϕ_S in $B^0_S \rightarrow J/\psi\phi$ decays to be between $[-1.05^\circ, 1.18^\circ]$ at 95% confidence level.

$S(B^0 \rightarrow J/\psi(1S)\rho^0)$

VALUE	DOCUMENT ID	TECN	COMMENT
$-0.66^{+0.13+0.09}_{-0.12-0.03}$	¹ AAIJ	15J	LHCB pp at 7, 8 TeV

¹Time-dependent CP violation is measured in the $B^0 \rightarrow J/\psi\rho^0$ and was used to limit the size of penguin amplitude contributions to ϕ_S in $B^0_S \rightarrow J/\psi\phi$ decays to be between $[-1.05^\circ, 1.18^\circ]$ at 95% confidence level.

$C_{D_{CP}^{(*)}h^0} (B^0 \rightarrow D_{CP}^{(*)}h^0)$

VALUE	DOCUMENT ID	TECN	COMMENT
$-0.02 \pm 0.07 \pm 0.03$	¹ ABDESSALAM 15		$e^+e^- \rightarrow \Upsilon(4S)$
• • • We do not use the following data for averages, fits, limits, etc. • • •			
$-0.23 \pm 0.16 \pm 0.04$	AUBERT	07AJ	BABR Repl. by ABDESSALAM 15

¹BABAR and BELLE combined analysis uses CP -eigenstate decay modes $D^0 \rightarrow K^+K^-$, $K_S^0\pi^0$, $K_S^0\omega$, and $h^0 = \pi^0, \eta, \omega$.

$S_{D_{CP}^{(*)}h^0} (B^0 \rightarrow D_{CP}^{(*)}h^0)$

VALUE	DOCUMENT ID	TECN	COMMENT
$-0.66 \pm 0.10 \pm 0.06$	¹ ABDESSALAM 15		$e^+e^- \rightarrow \Upsilon(4S)$
• • • We do not use the following data for averages, fits, limits, etc. • • •			
$-0.56 \pm 0.23 \pm 0.05$	AUBERT	07AJ	BABR Repl. by ABDESSALAM 15

¹BABAR and BELLE combined analysis uses CP -eigenstate decay modes $D^0 \rightarrow K^+K^-$, $K_S^0\pi^0$, $K_S^0\omega$, and $h^0 = \pi^0, \eta, \omega$.

$C_{K^0\pi^0} (B^0 \rightarrow K^0\pi^0)$

VALUE	DOCUMENT ID	TECN	COMMENT
0.00 ± 0.13 OUR AVERAGE	Error includes scale factor of 1.4.		
$-0.14 \pm 0.13 \pm 0.06$	¹ FUJIKAWA	10A	BELL $e^+e^- \rightarrow \Upsilon(4S)$
$0.13 \pm 0.13 \pm 0.03$	AUBERT	09I	BABR $e^+e^- \rightarrow \Upsilon(4S)$

• • • We do not use the following data for averages, fits, limits, etc. • • •

$0.24 \pm 0.15 \pm 0.03$	AUBERT	08E	BABR Repl. by AUBERT 09I
$0.05 \pm 0.14 \pm 0.05$	¹ CHAO	07	BELL Repl. by FUJIKAWA 10A
$0.06 \pm 0.18 \pm 0.03$	AUBERT	05Y	BABR Repl. by AUBERT 08E
$-0.16 \pm 0.29 \pm 0.05$	^{1,2} CHAO	05A	BELL Repl. by CHEN 05B
$0.11 \pm 0.20 \pm 0.09$	¹ CHEN	05B	BELL Repl. by CHAO 07
$-0.03 \pm 0.36 \pm 0.11$	¹ AUBERT	04M	BABR Repl. by AUBERT,B 04M
$0.40^{+0.27}_{-0.28} \pm 0.09$	³ AUBERT,B	04M	BABR Repl. by AUBERT 05Y

¹Reports A which is equal to $-C$.
²Corresponds to a 90% CL interval of $-0.33 < A_{CP} < 0.64$.
³Based on a total signal yield of 122 \pm 16 events.

$S_{K^0\pi^0} (B^0 \rightarrow K^0\pi^0)$

VALUE	DOCUMENT ID	TECN	COMMENT
0.58 ± 0.17 OUR AVERAGE			
$0.67 \pm 0.31 \pm 0.08$	FUJIKAWA	10A	BELL $e^+e^- \rightarrow \Upsilon(4S)$
$0.55 \pm 0.20 \pm 0.03$	AUBERT	09I	BABR $e^+e^- \rightarrow \Upsilon(4S)$

• • • We do not use the following data for averages, fits, limits, etc. • • •

$0.40 \pm 0.23 \pm 0.03$	AUBERT	08E	BABR Repl. by AUBERT 09I
$0.33 \pm 0.35 \pm 0.08$	CHAO	07	BELL Repl. by FUJIKAWA 10A
$0.35^{+0.30}_{-0.33} \pm 0.04$	AUBERT	05Y	BABR Repl. by AUBERT 08E
$0.32 \pm 0.61 \pm 0.13$	CHEN	05B	BELL Repl. by CHAO 07
$0.48^{+0.37}_{-0.48} \pm 0.06$	¹ AUBERT,B	04M	BABR Repl. by AUBERT 05Y

¹Based on a total signal yield of 122 \pm 16 events.

$C_{\eta(958)K_S^0} (B^0 \rightarrow \eta(958)K_S^0)$

See updated measurements in $C_{\eta'K^0}$

VALUE	DOCUMENT ID	TECN	COMMENT
-0.04 ± 0.20 OUR AVERAGE	Error includes scale factor of 2.5.		
$-0.21 \pm 0.10 \pm 0.02$	AUBERT	05M	BABR $e^+e^- \rightarrow \Upsilon(4S)$
$0.19 \pm 0.11 \pm 0.05$	¹ CHEN	05B	BELL $e^+e^- \rightarrow \Upsilon(4S)$

• • • We do not use the following data for averages, fits, limits, etc. • • •

$-0.26 \pm 0.22 \pm 0.03$	¹ ABE	03C	BELL Repl. by ABE 03H
$0.01 \pm 0.16 \pm 0.04$	¹ ABE	03H	BELL Repl. by CHEN 05B
$0.10 \pm 0.22 \pm 0.04$	AUBERT	03W	BABR Repl. by AUBERT 05M
$-0.13 \pm 0.32^{+0.06}_{-0.09}$	¹ CHEN	02B	BELL Repl. by ABE 03C

¹BELLE Collab. quotes $A_{\eta(958)K_S^0}$ which is equal to $-C_{\eta(958)K_S^0}$.

$S_{\eta(958)K_S^0} (B^0 \rightarrow \eta(958)K_S^0)$

See updated measurements in $S_{\eta'K^0}$

VALUE	DOCUMENT ID	TECN	COMMENT
0.43 ± 0.17 OUR AVERAGE	Error includes scale factor of 1.5.		
$0.30 \pm 0.14 \pm 0.02$	AUBERT	05M	BABR $e^+e^- \rightarrow \Upsilon(4S)$
$0.65 \pm 0.18 \pm 0.04$	CHEN	05B	BELL $e^+e^- \rightarrow \Upsilon(4S)$

• • • We do not use the following data for averages, fits, limits, etc. • • •

$0.71 \pm 0.37^{+0.05}_{-0.06}$	ABE	03C	BELL Repl. by ABE 03H
$0.43 \pm 0.27 \pm 0.05$	ABE	03H	BELL Repl. by CHEN 05B
$0.02 \pm 0.34 \pm 0.03$	AUBERT	03W	BABR Repl. by AUBERT 05M
$0.28 \pm 0.55^{+0.07}_{-0.08}$	CHEN	02B	BELL Repl. by ABE 03C

Meson Particle Listings

B^0

$C_{\eta} K^0 (B^0 \rightarrow \eta K^0)$

VALUE	DOCUMENT ID	TECN	COMMENT
-0.06 ± 0.04 OUR AVERAGE			
$-0.03 \pm 0.05 \pm 0.04$	¹ SANTELJ 14	BELL	$e^+ e^- \rightarrow \Upsilon(4S)$
$-0.08 \pm 0.06 \pm 0.02$	AUBERT 09i	BABR	$e^+ e^- \rightarrow \Upsilon(4S)$
• • • We do not use the following data for averages, fits, limits, etc. • • •			
$-0.16 \pm 0.07 \pm 0.03$	² AUBERT 07A	BABR	Repl. by AUBERT 09i
$0.01 \pm 0.07 \pm 0.05$	^{1,2} CHEN 07	BELL	Repl. by SANTELJ 14

¹ The paper reports A , which is equal to $-C$.
² The mixing-induced CP violation is reported with a significance of more than 5 standard deviations in this $b \rightarrow s$ penguin dominated mode.

$S_{\eta} K^0 (B^0 \rightarrow \eta K^0)$

VALUE	DOCUMENT ID	TECN	COMMENT
0.63 ± 0.06 OUR AVERAGE			
$0.68 \pm 0.07 \pm 0.03$	SANTELJ 14	BELL	$e^+ e^- \rightarrow \Upsilon(4S)$
$0.57 \pm 0.08 \pm 0.02$	AUBERT 09i	BABR	$e^+ e^- \rightarrow \Upsilon(4S)$
• • • We do not use the following data for averages, fits, limits, etc. • • •			
$0.58 \pm 0.10 \pm 0.03$	¹ AUBERT 07A	BABR	Repl. by AUBERT 09i
$0.64 \pm 0.10 \pm 0.04$	¹ CHEN 07A	BELL	Repl. by SANTELJ 14

¹ The mixing-induced CP violation is reported with a significance of more than 5 standard deviations in this $b \rightarrow s$ penguin dominated mode.

$C_{\omega} K_S^0 (B^0 \rightarrow \omega K_S^0)$

VALUE	DOCUMENT ID	TECN	COMMENT
0.0 ± 0.4 OUR AVERAGE			Error includes scale factor of 3.0.
$0.36 \pm 0.19 \pm 0.05$	¹ CHOBANOVA 14	BELL	$e^+ e^- \rightarrow \Upsilon(4S)$
$-0.52 \pm 0.22 \pm 0.03$	AUBERT 09i	BABR	$e^+ e^- \rightarrow \Upsilon(4S)$
• • • We do not use the following data for averages, fits, limits, etc. • • •			
$0.09 \pm 0.29 \pm 0.06$	¹ CHAO 07	BELL	Repl. by CHOBANOVA 14
$-0.55 \pm 0.28 \pm 0.03$	AUBERT,B 06E	BABR	Repl. by AUBERT 09i
$-0.27 \pm 0.48 \pm 0.15$	¹ CHEN 05B	BELL	Repl. by CHAO 07

¹ Belle Collab. quotes $A_{\omega K_S^0}$ which is equal to $-C_{\omega K_S^0}$.

$S_{\omega} K_S^0 (B^0 \rightarrow \omega K_S^0)$

VALUE	DOCUMENT ID	TECN	COMMENT
0.70 ± 0.21 OUR AVERAGE			
$0.91 \pm 0.32 \pm 0.05$	CHOBANOVA 14	BELL	$e^+ e^- \rightarrow \Upsilon(4S)$
$0.55 \pm 0.26 \pm 0.02$	AUBERT 09i	BABR	$e^+ e^- \rightarrow \Upsilon(4S)$
• • • We do not use the following data for averages, fits, limits, etc. • • •			
$0.11 \pm 0.46 \pm 0.07$	CHAO 07	BELL	Repl. by CHOBANOVA 14
$0.51 \pm 0.35 \pm 0.02$	AUBERT,B 06E	BABR	Repl. by AUBERT 09i
$0.76 \pm 0.65 \pm 0.13$	CHEN 05B	BELL	Repl. by CHAO 07

$C(B^0 \rightarrow K_S^0 \pi^0 \pi^0)$

VALUE	DOCUMENT ID	TECN	COMMENT
-0.21 ± 0.20 OUR AVERAGE			
$-0.28 \pm 0.21 \pm 0.04$	¹ YUSA 19	BELL	$e^+ e^- \rightarrow \Upsilon(4S)$
$0.23 \pm 0.52 \pm 0.13$	AUBERT 07AQ	BABR	$e^+ e^- \rightarrow \Upsilon(4S)$
¹ Reports value of A which is equal to $-C$.			

$S(B^0 \rightarrow K_S^0 \pi^0 \pi^0)$

VALUE	DOCUMENT ID	TECN	COMMENT
0.89 ± 0.27 OUR AVERAGE			
$0.92 \pm 0.27 \pm 0.11$	YUSA 19	BELL	$e^+ e^- \rightarrow \Upsilon(4S)$
$0.72 \pm 0.71 \pm 0.08$	AUBERT 07AQ	BABR	$e^+ e^- \rightarrow \Upsilon(4S)$

$C_{\rho} K_S^0 (B^0 \rightarrow \rho^0 K_S^0)$

VALUE	DOCUMENT ID	TECN	COMMENT
-0.04 ± 0.20 OUR AVERAGE			
$-0.05 \pm 0.26 \pm 0.10$	¹ AUBERT 09AU	BABR	$e^+ e^- \rightarrow \Upsilon(4S)$
$-0.03 \pm 0.24 \pm 0.15$	^{2,3} DALSENO 09	BELL	$e^+ e^- \rightarrow \Upsilon(4S)$
• • • We do not use the following data for averages, fits, limits, etc. • • •			
$0.64 \pm 0.41 \pm 0.20$	AUBERT 07F	BABR	Repl. by AUBERT 09AU

¹ Uses Dalitz plot analysis of $B^0 \rightarrow K^0 \pi^+ \pi^-$ decays and the first of two equivalent solutions is used.
² Quotes $A_{\rho^0(K_S^0)}$ which is equal to $-C_{\rho^0(K_S^0)}$.
³ Uses Dalitz plot analysis of $B^0 \rightarrow K^0 \pi^+ \pi^-$ decays and the first of two consistent solutions that may be preferred.

$S_{\rho} K_S^0 (B^0 \rightarrow \rho^0 K_S^0)$

VALUE	DOCUMENT ID	TECN	COMMENT
0.50 ± 0.17 OUR AVERAGE			
$0.35 \pm 0.26 \pm 0.07$	¹ AUBERT 09AU	BABR	$e^+ e^- \rightarrow \Upsilon(4S)$
$0.64 \pm 0.19 \pm 0.13$	² DALSENO 09	BELL	$e^+ e^- \rightarrow \Upsilon(4S)$
• • • We do not use the following data for averages, fits, limits, etc. • • •			
$0.20 \pm 0.52 \pm 0.24$	AUBERT 07F	BABR	Repl. by AUBERT 09AU

¹ Uses Dalitz plot analysis of $B^0 \rightarrow K^0 \pi^+ \pi^-$ decays and the first of two equivalent solutions is used.
² Uses Dalitz plot analysis of $B^0 \rightarrow K^0 \pi^+ \pi^-$ decays and the first of two consistent solutions that may be preferred.

$C_{f_0(980)} K_S^0 (B^0 \rightarrow f_0(980) K_S^0)$

VALUE	DOCUMENT ID	TECN	COMMENT
0.29 ± 0.20 OUR AVERAGE			
$0.28 \pm 0.24 \pm 0.09$	¹ LEES 12o	BABR	$e^+ e^- \rightarrow \Upsilon(4S)$
$0.30 \pm 0.29 \pm 0.14$	^{2,3} NAKAHAMA 10	BELL	$e^+ e^- \rightarrow \Upsilon(4S)$
• • • We do not use the following data for averages, fits, limits, etc. • • •			
$0.08 \pm 0.19 \pm 0.05$	⁴ AUBERT 09AU	BABR	Repl. by LEES 12o
$0.06 \pm 0.17 \pm 0.11$	^{2,5} DALSENO 09	BELL	Repl. by NAKAHAMA 10
$-0.41 \pm 0.23 \pm 0.07$	² AUBERT 07AX	BABR	Repl. by AUBERT 09AU
$0.15 \pm 0.15 \pm 0.07$	² CHAO 07	BELL	Repl. by DALSENO 09
$0.39 \pm 0.27 \pm 0.09$	² CHEN 05B	BELL	Repl. by CHAO 07

¹ Uses Dalitz plot analysis of the $B^0 \rightarrow K_S^0 K^+ K^-$ decay.
² Quotes $A_{f_0(980) K_S^0}$ which is equal to $-C_{f_0(980) K_S^0}$.
³ Uses Dalitz plot analysis of $B^0 \rightarrow K_S^0 K^+ K^-$ decays and the first of four consistent solutions that may be preferred.
⁴ Uses Dalitz plot analysis of $B^0 \rightarrow K^0 \pi^+ \pi^-$ decays and the first of two equivalent solutions is used.
⁵ Uses Dalitz plot analysis of $B^0 \rightarrow K^0 \pi^+ \pi^-$ decays and the first of two consistent solutions that may be preferred.

$S_{f_0(980)} K_S^0 (B^0 \rightarrow f_0(980) K_S^0)$

VALUE	DOCUMENT ID	TECN	COMMENT
-0.50 ± 0.16 OUR AVERAGE			
$-0.55 \pm 0.18 \pm 0.12$	¹ LEES 12o	BABR	$e^+ e^- \rightarrow \Upsilon(4S)$
$-0.43 \pm 0.22 \pm 0.14$	² DALSENO 09	BELL	$e^+ e^- \rightarrow \Upsilon(4S)$
• • • We do not use the following data for averages, fits, limits, etc. • • •			
$-0.96 \pm 0.21 \pm 0.04$	³ AUBERT 09AU	BABR	Repl. by LEES 12o
$-0.25 \pm 0.26 \pm 0.10$	⁴ AUBERT 07AX	BABR	Repl. by AUBERT 09AU
$0.18 \pm 0.23 \pm 0.11$	CHAO 07	BELL	Repl. by DALSENO 09
$0.47 \pm 0.41 \pm 0.08$	CHEN 05B	BELL	Repl. by CHAO 07

¹ Uses Dalitz plot analysis of the $B^0 \rightarrow K_S^0 K^+ K^-$ decay.
² Uses Dalitz plot analysis of $B^0 \rightarrow K^0 \pi^+ \pi^-$ decays and the first of two consistent solutions that may be preferred.
³ Uses Dalitz plot analysis of $B^0 \rightarrow K^0 \pi^+ \pi^-$ decays and the first of two equivalent solutions is used.
⁴ Reports β_{eff} . We quote S obtained from epaps: E-PRLTAO-99-076741.

$S_{f_2(1270)} K_S^0 (B^0 \rightarrow f_2(1270) K_S^0)$

VALUE	DOCUMENT ID	TECN	COMMENT
$-0.48 \pm 0.52 \pm 0.12$	¹ AUBERT 09AU	BABR	$e^+ e^- \rightarrow \Upsilon(4S)$
¹ Uses Dalitz plot analysis of $B^0 \rightarrow K^0 \pi^+ \pi^-$ decays and the first of two equivalent solutions is used.			

$C_{f_2(1270)} K_S^0 (B^0 \rightarrow f_2(1270) K_S^0)$

VALUE	DOCUMENT ID	TECN	COMMENT
0.28 ± 0.35 OUR AVERAGE			
$0.28 \pm 0.35 \pm 0.11$	¹ AUBERT 09AU	BABR	$e^+ e^- \rightarrow \Upsilon(4S)$
¹ Uses Dalitz plot analysis of $B^0 \rightarrow K^0 \pi^+ \pi^-$ decays and the first of two equivalent solutions is used.			

$S_{f_x(1300)} K_S^0 (B^0 \rightarrow f_x(1300) K_S^0)$

VALUE	DOCUMENT ID	TECN	COMMENT
$-0.20 \pm 0.52 \pm 0.10$	¹ AUBERT 09AU	BABR	$e^+ e^- \rightarrow \Upsilon(4S)$
¹ Uses Dalitz plot analysis of $B^0 \rightarrow K^0 \pi^+ \pi^-$ decays and the first of two equivalent solutions is used.			

$C_{f_x(1300)} K_S^0 (B^0 \rightarrow f_x(1300) K_S^0)$

VALUE	DOCUMENT ID	TECN	COMMENT
0.13 ± 0.33 OUR AVERAGE			
$0.13 \pm 0.33 \pm 0.10$	¹ AUBERT 09AU	BABR	$e^+ e^- \rightarrow \Upsilon(4S)$
¹ Uses Dalitz plot analysis of $B^0 \rightarrow K^0 \pi^+ \pi^-$ decays and the first of two equivalent solutions is used.			

$S_{K^0 \pi^+ \pi^-} (B^0 \rightarrow K^0 \pi^+ \pi^- \text{ nonresonant})$

VALUE	DOCUMENT ID	TECN	COMMENT
$-0.01 \pm 0.31 \pm 0.10$	¹ AUBERT 09AU	BABR	$e^+ e^- \rightarrow \Upsilon(4S)$
¹ Uses Dalitz plot analysis of $B^0 \rightarrow K^0 \pi^+ \pi^-$ decays and the first of two equivalent solutions is used.			

$C_{K^0\pi^+\pi^-} (B^0 \rightarrow K^0\pi^+\pi^- \text{ nonresonant})$

VALUE	DOCUMENT ID	TECN	COMMENT
0.01 ± 0.25 ± 0.08	¹ AUBERT	09AU	BABR $e^+e^- \rightarrow \Upsilon(4S)$

¹ Uses Dalitz plot analysis of $B^0 \rightarrow K^0\pi^+\pi^-$ decays and the first of two equivalent solutions is used.

$C_{K_S^0 K_S^0} (B^0 \rightarrow K_S^0 K_S^0)$

VALUE	DOCUMENT ID	TECN	COMMENT
0.0 ± 0.4 OUR AVERAGE	Error includes scale factor of 1.4.		
0.38 ± 0.38 ± 0.05	¹ NAKAHAMA	08	BELL $e^+e^- \rightarrow \Upsilon(4S)$
-0.40 ± 0.41 ± 0.06	AUBERT, BE	06C	BABR $e^+e^- \rightarrow \Upsilon(4S)$

¹ Reports $A_{K_S^0 K_S^0}$ which equals to $-C_{K_S^0 K_S^0}$.

$S_{K_S^0 K_S^0} (B^0 \rightarrow K_S^0 K_S^0)$

VALUE	DOCUMENT ID	TECN	COMMENT
-0.8 ± 0.5 OUR AVERAGE			
-0.38 ^{+0.69} _{-0.77} ± 0.09	NAKAHAMA	08	BELL $e^+e^- \rightarrow \Upsilon(4S)$
-1.28 ^{+0.80} _{-0.73} ± 0.11 ± 0.16	AUBERT, BE	06C	BABR $e^+e^- \rightarrow \Upsilon(4S)$

$C_{K^+K^-K_S^0} (B^0 \rightarrow K^+K^-K_S^0 \text{ nonresonant})$

VALUE	DOCUMENT ID	TECN	COMMENT
0.06 ± 0.08 OUR AVERAGE			
0.02 ± 0.09 ± 0.03	^{1,2} LEES	12o	BABR $e^+e^- \rightarrow \Upsilon(4S)$
0.14 ± 0.11 ± 0.09	^{3,4} NAKAHAMA	10	BELL $e^+e^- \rightarrow \Upsilon(4S)$

• • • We do not use the following data for averages, fits, limits, etc. • • •

0.054 ± 0.102 ± 0.060	^{3,5} AUBERT	07AX	BABR Repl. by LEES 12o
0.09 ± 0.10 ± 0.05	^{3,5} CHAO	07	BELL Repl. by NAKAHAMA 10
0.10 ± 0.14 ± 0.04	⁵ AUBERT	05T	BABR Repl. by AUBERT 07AX
0.09 ± 0.12 ± 0.07	³ CHEN	05B	BELL Repl. by CHAO 07
-0.10 ± 0.19 ± 0.10	⁵ AUBERT, B	04V	BABR Repl. by AUBERT 05T
0.40 ± 0.33 ^{+0.28} _{-0.10}	³ ABE	03C	BELL Repl. by ABE 03H
0.17 ± 0.16 ± 0.04	^{3,5} ABE	03H	BELL Repl. by CHEN 05B

¹ Uses Dalitz plot analysis of the $B^0 \rightarrow K_S^0 K^+ K^-$ decay.
² This measurement is performed on all the isobar components, excluding ϕK_S^0 and $f_0(980) K_S^0$.
³ Quotes $A_{K^+K^-K_S^0}$ which is equal to $-C_{K^+K^-K_S^0}$.
⁴ Uses Dalitz plot analysis of $B^0 \rightarrow K_S^0 K^+ K^-$ decays and the first of four consistent solutions that may be preferred.
⁵ Excludes the events from $B^0 \rightarrow \phi K_S^0$ decay. The results are derived from a combined sample of $K^+ K^- K_S^0$ and $K^+ K^- K_L^0$ decays.

$S_{K^+K^-K_S^0} (B^0 \rightarrow K^+K^-K_S^0 \text{ nonresonant})$

VALUE	DOCUMENT ID	TECN	COMMENT
-0.66 ± 0.11 OUR AVERAGE			
-0.65 ± 0.12 ± 0.03	^{1,2} LEES	12o	BABR $e^+e^- \rightarrow \Upsilon(4S)$
-0.68 ± 0.15 ^{+0.21} _{-0.13}	³ CHAO	07	BELL $e^+e^- \rightarrow \Upsilon(4S)$

• • • We do not use the following data for averages, fits, limits, etc. • • •

-0.764 ± 0.111 ^{+0.071} _{-0.040}	^{3,4} AUBERT	07AX	BABR Repl. by LEES 12o
-0.42 ± 0.17 ± 0.03	^{3,5} AUBERT	05T	BABR Repl. by AUBERT 07AX
-0.49 ± 0.18 ± 0.04	CHEN	05B	BELL Repl. by CHAO 07
-0.56 ± 0.25 ± 0.04	^{3,6} AUBERT, B	04V	BABR Repl. by AUBERT 05T
-0.49 ± 0.43 ± 0.11	ABE	03C	BELL Repl. by ABE 03H
-0.51 ± 0.26 ± 0.05	^{3,7} ABE	03H	BELL Repl. by CHEN 05B

¹ Uses Dalitz plot analysis of the $B^0 \rightarrow K_S^0 K^+ K^-$ decay.
² This measurement is performed on all the isobar components, excluding ϕK_S^0 and $f_0(980) K_S^0$. Note that the nonresonant component is not a CP eigenstate.
³ Excludes events from $B^0 \rightarrow \phi K_S^0$ decay. The results are derived from a combined sample of $K^+ K^- K_S^0$ and $K^+ K^- K_L^0$ decays.
⁴ Reports β_{eff} . We quote S obtained from epaps: E-PRLTAAO-99-076741.
⁵ The measured CP-even final states fraction is $0.89 \pm 0.08 \pm 0.06$.
⁶ The measured CP-even final states fraction is $0.98 \pm 0.15 \pm 0.04$.
⁷ The measured CP-even final states fraction is $1.03 \pm 0.15 \pm 0.05$.

$C_{K^+K^-K_S^0} (B^0 \rightarrow K^+K^-K_S^0 \text{ inclusive})$

VALUE	DOCUMENT ID	TECN	COMMENT
0.015 ± 0.077 ± 0.053	^{1,2} AUBERT	07AX	BABR $e^+e^- \rightarrow \Upsilon(4S)$

¹ Measured using full Dalitz plot fit including ϕ component.
² The results are derived from a combined sample of $K^+ K^- K_S^0$ and $K^+ K^- K_L^0$ decays.

$S_{K^+K^-K_S^0} (B^0 \rightarrow K^+K^-K_S^0 \text{ inclusive})$

VALUE	DOCUMENT ID	TECN	COMMENT
-0.647 ± 0.116 ± 0.040	¹ AUBERT	07AX	BABR $e^+e^- \rightarrow \Upsilon(4S)$

¹ Measured using full Dalitz plot fit including ϕ component.

$C_{\phi K_S^0} (B^0 \rightarrow \phi K_S^0)$

VALUE	DOCUMENT ID	TECN	COMMENT
0.01 ± 0.14 OUR AVERAGE			
0.05 ± 0.18 ± 0.05	¹ LEES	12o	BABR $e^+e^- \rightarrow \Upsilon(4S)$
-0.04 ± 0.20 ± 0.10	^{2,3} NAKAHAMA	10	BELL $e^+e^- \rightarrow \Upsilon(4S)$

• • • We do not use the following data for averages, fits, limits, etc. • • •

0.08 ± 0.18 ± 0.04	^{2,4} AUBERT	07AX	BABR Repl. by LEES 12o
-0.07 ± 0.15 ± 0.05	^{2,4} CHEN	07	BELL Repl. by NAKAHAMA 10
0.00 ± 0.23 ± 0.05	⁴ AUBERT	05T	BABR Repl. by AUBERT 07AX
-0.08 ± 0.22 ± 0.09	^{2,4} CHEN	05B	BELL Repl. by CHEN 07
0.01 ± 0.33 ± 0.10	⁴ AUBERT, B	04G	BABR Repl. by AUBERT 05T
0.56 ± 0.41 ± 0.16	² ABE	03C	BELL Repl. by ABE 03H
0.15 ± 0.29 ± 0.07	² ABE	03H	BELL Repl. by CHEN 05B

¹ Uses Dalitz plot analysis of the $B^0 \rightarrow K_S^0 K^+ K^-$ decay.
² Quotes $A_{\phi K_S^0}$ which is equal to $-C_{\phi K_S^0}$.
³ Uses Dalitz plot analysis of $B^0 \rightarrow K_S^0 K^+ K^-$ decays and the first of four consistent solutions that may be preferred.
⁴ Result combines B-meson final states ϕK_S^0 and ϕK_L^0 by assuming $S_{\phi K_S^0} = -S_{\phi K_L^0}$.

$S_{\phi K_S^0} (B^0 \rightarrow \phi K_S^0)$

VALUE	DOCUMENT ID	TECN	COMMENT
0.59 ± 0.14 OUR AVERAGE			
0.66 ± 0.17 ± 0.07	¹ LEES	12o	BABR $e^+e^- \rightarrow \Upsilon(4S)$
0.50 ± 0.21 ± 0.06	² CHEN	07	BELL $e^+e^- \rightarrow \Upsilon(4S)$

• • • We do not use the following data for averages, fits, limits, etc. • • •

0.21 ± 0.26 ± 0.11	^{2,3} AUBERT	07AX	BABR Repl. by LEES 12o
0.50 ± 0.25 ^{+0.07} _{-0.04}	² AUBERT	05T	BABR Repl. by AUBERT 07AX
0.08 ± 0.33 ± 0.09	² CHEN	05B	BELL Repl. by CHEN 07
0.47 ± 0.34 ^{+0.08} _{-0.06}	² AUBERT, B	04G	BABR Repl. by AUBERT 05T
-0.73 ± 0.64 ± 0.22	ABE	03C	BELL Repl. by ABE 03H
-0.96 ± 0.50 ^{+0.09} _{-0.11}	ABE	03H	BELL Repl. by CHEN 05B

¹ Uses Dalitz plot analysis of the $B^0 \rightarrow K_S^0 K^+ K^-$ decay.
² Result combines B-meson final states ϕK_S^0 and ϕK_L^0 by assuming $S_{\phi K_S^0} = -S_{\phi K_L^0}$.
³ Reports β_{eff} . We quote S obtained from epaps: E-PRLTAAO-99-076741.

$C_{K_S^0 K_S^0 K_S^0} (B^0 \rightarrow K_S^0 K_S^0 K_S^0)$

VALUE	DOCUMENT ID	TECN	COMMENT
-0.23 ± 0.14 OUR AVERAGE			
-0.17 ± 0.18 ± 0.04	LEES	12i	BABR $e^+e^- \rightarrow \Upsilon(4S)$
-0.31 ± 0.20 ± 0.07	¹ CHEN	07	BELL $e^+e^- \rightarrow \Upsilon(4S)$

• • • We do not use the following data for averages, fits, limits, etc. • • •

0.02 ± 0.21 ± 0.05	AUBERT	07AT	BABR Repl. by LEES 12i
-0.34 ± 0.28 ^{+0.25} _{-0.25} ± 0.05	AUBERT, B	05	BABR Repl. by AUBERT 07AT
-0.54 ± 0.34 ± 0.09	¹ SUMISAWA	05	BELL Repl. by CHEN 07

¹ Belle Collab. quotes $A_{K_S^0 K_S^0 K_S^0}$ which is equal to $-C_{K_S^0 K_S^0 K_S^0}$.

$S_{K_S^0 K_S^0 K_S^0} (B^0 \rightarrow K_S^0 K_S^0 K_S^0)$

VALUE	DOCUMENT ID	TECN	COMMENT
-0.5 ± 0.6 OUR AVERAGE	Error includes scale factor of 3.0.		
-0.94 ± 0.24 ^{+0.21} _{-0.21} ± 0.06	LEES	12i	BABR $e^+e^- \rightarrow \Upsilon(4S)$
0.30 ± 0.32 ± 0.08	CHEN	07	BELL $e^+e^- \rightarrow \Upsilon(4S)$

• • • We do not use the following data for averages, fits, limits, etc. • • •

-0.71 ± 0.24 ± 0.04	AUBERT	07AT	BABR Repl. by LEES 12i
-0.71 ± 0.38 ^{+0.32} _{-0.32} ± 0.04	AUBERT, B	05	BABR Repl. by AUBERT 07AT
1.26 ± 0.68 ± 0.20	SUMISAWA	05	BELL Repl. by CHEN 07.

$C_{K_S^0 \pi^0 \gamma} (B^0 \rightarrow K_S^0 \pi^0 \gamma)$

VALUE	DOCUMENT ID	TECN	COMMENT
0.36 ± 0.33 ± 0.04	¹ AUBERT	08BA	BABR $e^+e^- \rightarrow \Upsilon(4S)$

• • • We do not use the following data for averages, fits, limits, etc. • • •

0.20 ± 0.20 ± 0.06	^{2,3} USHIRODA	06	BELL $e^+e^- \rightarrow \Upsilon(4S)$
-1.0 ± 0.5 ± 0.2	¹ AUBERT, B	05P	BABR Repl. by AUBERT 08BA
-0.03 ± 0.34 ± 0.11	³ USHIRODA	05	BELL Repl. by USHIRODA 06

¹ Requires $1.1 < M_{K_S^0 \pi^0} < 1.8 \text{ GeV}/c^2$.
² Requires $M_{K_S^0 \pi^0} < 1.8 \text{ GeV}/c^2$.
³ Reports $A_{K_S^0 \pi^0 \gamma}$, which is $-C_{K_S^0 \pi^0 \gamma}$.

Meson Particle Listings

 B^0 $S_{K_S^0 \pi^0 \gamma} (B^0 \rightarrow K_S^0 \pi^0 \gamma)$

VALUE	DOCUMENT ID	TECN	COMMENT
$-0.78 \pm 0.59 \pm 0.09$	1 AUBERT	08BA BABR	$e^+ e^- \rightarrow \Upsilon(4S)$
• • • We do not use the following data for averages, fits, limits, etc. • • •			
$-0.10 \pm 0.31 \pm 0.07$	2 USHIRODA	06 BELL	$e^+ e^- \rightarrow \Upsilon(4S)$
$0.9 \pm 1.0 \pm 0.2$	1 AUBERT,B	05P BABR	Repl. by AUBERT 08BA
$-0.58 \pm 0.46 \pm 0.11$	USHIRODA	05 BELL	Repl. by USHIRODA 06
1 Requires $1.1 < M_{K_S^0 \pi^0} < 1.8 \text{ GeV}/c^2$.			
2 Requires $M_{K_S^0 \pi^0} < 1.8 \text{ GeV}/c^2$.			

 $C_{K_S^0 \pi^+ \pi^- \gamma} (B^0 \rightarrow K_S^0 \pi^+ \pi^- \gamma)$

VALUE	DOCUMENT ID	TECN	COMMENT
$-0.39 \pm 0.20 \pm 0.03$	1 DEL-AMO-SA...16	BABR	$e^+ e^- \rightarrow \Upsilon(4S)$
1 Requires $M_{K \pi \pi} < 1.8 \text{ GeV}/c^2$, $0.6 \text{ GeV}/c^2 < m_{\pi^+ \pi^-} < 0.9 \text{ GeV}/c^2$, $m_{K \pi} < 0.845 \text{ GeV}/c^2$ or $m_{K \pi} > 0.945 \text{ GeV}/c^2$.			

 $S_{K_S^0 \pi^+ \pi^- \gamma} (B^0 \rightarrow K_S^0 \pi^+ \pi^- \gamma)$

VALUE	DOCUMENT ID	TECN	COMMENT
$0.14 \pm 0.25 \pm 0.03$	1 DEL-AMO-SA...16	BABR	$e^+ e^- \rightarrow \Upsilon(4S)$
1 Requires $M_{K \pi \pi} < 1.8 \text{ GeV}/c^2$, $0.6 \text{ GeV}/c^2 < m_{\pi^+ \pi^-} < 0.9 \text{ GeV}/c^2$, $m_{K \pi} < 0.845 \text{ GeV}/c^2$ or $m_{K \pi} > 0.945 \text{ GeV}/c^2$.			

 $C_{K^*(892)^0 \gamma} (B^0 \rightarrow K^*(892)^0 \gamma)$

VALUE	DOCUMENT ID	TECN	COMMENT
-0.04 ± 0.16 OUR AVERAGE	Error includes scale factor of 1.2.		
$-0.14 \pm 0.16 \pm 0.03$	1 AUBERT	08BA BABR	$e^+ e^- \rightarrow \Upsilon(4S)$
$0.20 \pm 0.24 \pm 0.05$	1,2 USHIRODA	06 BELL	$e^+ e^- \rightarrow \Upsilon(4S)$
• • • We do not use the following data for averages, fits, limits, etc. • • •			
$-0.40 \pm 0.23 \pm 0.03$	AUBERT,B	05P BABR	Repl. by AUBERT 08BA
$-0.57 \pm 0.32 \pm 0.09$	3 AUBERT,B	04Z BABR	Repl. by AUBERT,B 05P
1 Requires $0.8 < M_{K_S^0 \pi^0} < 1.0 \text{ GeV}/c^2$.			
2 Reports value of A which is equal to $-C$.			
3 Based on a total signal of 105 ± 14 events with $K^*(892)^0 \rightarrow K_S^0 \pi^0$ only.			

 $S_{K^*(892)^0 \gamma} (B^0 \rightarrow K^*(892)^0 \gamma)$

VALUE	DOCUMENT ID	TECN	COMMENT
-0.15 ± 0.22 OUR AVERAGE	Error includes scale factor of 1.4.		
$-0.03 \pm 0.29 \pm 0.03$	1 AUBERT	08BA BABR	$e^+ e^- \rightarrow \Upsilon(4S)$
$-0.32 \pm 0.36 \pm 0.05$	1 USHIRODA	06 BELL	$e^+ e^- \rightarrow \Upsilon(4S)$
• • • We do not use the following data for averages, fits, limits, etc. • • •			
$-0.21 \pm 0.40 \pm 0.05$	AUBERT,B	05P BABR	Repl. by AUBERT 08BA
$-0.79 \pm 0.63 \pm 0.10$	2 USHIRODA	05 BELL	Repl. by USHIRODA 06
$0.25 \pm 0.63 \pm 0.14$	3 AUBERT,B	04Z BABR	Repl. by AUBERT,B 05P
1 Requires $0.8 < M_{K_S^0 \pi^0} < 1.0 \text{ GeV}/c^2$.			
2 Assumes $C(B^0 \rightarrow K^*(892)^0 \gamma) = 0$.			
3 Based on a total signal of 105 ± 14 events with $K^*(892)^0 \rightarrow K_S^0 \pi^0$ only.			

 $C_{\eta K^0 \gamma} (B^0 \rightarrow \eta K^0 \gamma)$

VALUE	DOCUMENT ID	TECN	COMMENT
0.1 ± 0.4 OUR AVERAGE	Error includes scale factor of 1.4.		
$0.48 \pm 0.41 \pm 0.07$	1,2 NAKANO	18 BELL	$e^+ e^- \rightarrow \Upsilon(4S)$
$-0.32 \pm 0.40 \pm 0.07$	3 AUBERT	09 BABR	$e^+ e^- \rightarrow \Upsilon(4S)$
1 Assuming $m_{\eta K_S^0} < 2.1 \text{ GeV}$.			
2 Reversed the sign for C=A.			
3 Assuming $m_{\eta K} < 3.25 \text{ GeV}$.			

 $S_{\eta K^0 \gamma} (B^0 \rightarrow \eta K^0 \gamma)$

VALUE	DOCUMENT ID	TECN	COMMENT
-0.5 ± 0.5 OUR AVERAGE	Error includes scale factor of 1.2.		
$-1.32 \pm 0.77 \pm 0.36$	1 NAKANO	18 BELL	$e^+ e^- \rightarrow \Upsilon(4S)$
$-0.18 \pm 0.49 \pm 0.12$	2 AUBERT	09 BABR	$e^+ e^- \rightarrow \Upsilon(4S)$
1 Assuming $m_{\eta K_S^0} < 2.1 \text{ GeV}$.			
2 Assuming $m_{\eta K} < 3.25 \text{ GeV}$.			

 $C_{K^0 \phi \gamma} (B^0 \rightarrow K^0 \phi \gamma)$

VALUE	DOCUMENT ID	TECN	COMMENT
$-0.35 \pm 0.58 \pm 0.10$	1 SAHOO	11A BELL	$e^+ e^- \rightarrow \Upsilon(4S)$
1 Reports value of A, which is equal to $-C$.			

 $S_{K^0 \phi \gamma} (B^0 \rightarrow K^0 \phi \gamma)$

VALUE	DOCUMENT ID	TECN	COMMENT
$0.74 \pm 0.72 \pm 0.10$	SAHOO	11A BELL	$e^+ e^- \rightarrow \Upsilon(4S)$
-1.05 -0.24			

 $C(B^0 \rightarrow K_S^0 \rho^0 \gamma)$

VALUE	DOCUMENT ID	TECN	COMMENT
$-0.05 \pm 0.18 \pm 0.06$	1,2 LI	08F BELL	$e^+ e^- \rightarrow \Upsilon(4S)$
1 Requires $M_{K_S^0 \pi^+ \pi^-} < 1.8 \text{ GeV}/c^2$ and $0.6 < m_{\pi^+ \pi^-} < 0.9 \text{ GeV}/c^2$.			
2 Reports value of A_{eff} which is equal to $-C$, and includes the non-resonant $\pi^+ \pi^-$ contribution in the ρ^0 region.			

 $S(B^0 \rightarrow K_S^0 \rho^0 \gamma)$

VALUE	DOCUMENT ID	TECN	COMMENT
-0.04 ± 0.23 OUR AVERAGE			
$-0.18 \pm 0.32 \pm 0.06$	1 DEL-AMO-SA...16	BABR	$e^+ e^- \rightarrow \Upsilon(4S)$
$0.11 \pm 0.33 \pm 0.05$	2 LI	08F BELL	$e^+ e^- \rightarrow \Upsilon(4S)$
1 Requires $M_{K \pi \pi} < 1.8 \text{ GeV}/c^2$, $0.6 \text{ GeV}/c^2 < m_{\pi^+ \pi^-} < 0.9 \text{ GeV}/c^2$, $m_{K \pi} < 0.845 \text{ GeV}/c^2$ or $m_{K \pi} > 0.945 \text{ GeV}/c^2$.			
2 Requires $M_{K \pi \pi} < 1.8 \text{ GeV}/c^2$.			

 $C(B^0 \rightarrow \rho^0 \gamma)$

VALUE	DOCUMENT ID	TECN	COMMENT
$0.44 \pm 0.49 \pm 0.14$	1 USHIRODA	08 BELL	$e^+ e^- \rightarrow \Upsilon(4S)$
1 Reports value of A which is equal to $-C$.			

 $S(B^0 \rightarrow \rho^0 \gamma)$

VALUE	DOCUMENT ID	TECN	COMMENT
$-0.83 \pm 0.65 \pm 0.18$	USHIRODA	08 BELL	$e^+ e^- \rightarrow \Upsilon(4S)$

 $C_{\pi \pi} (B^0 \rightarrow \pi^+ \pi^-)$

$C_{\pi \pi}$ is defined as $(1 - |\lambda|^2)/(1 + |\lambda|^2)$, where the quantity $\lambda = q/p \bar{A}_f/A_f$ is a phase convention independent observable quantity for the final state f . For details, see the review on "CP Violation" in the Reviews section.

VALUE	DOCUMENT ID	TECN	COMMENT
-0.32 ± 0.04 OUR AVERAGE			
$-0.34 \pm 0.06 \pm 0.01$	AAIJ	18o LHCB	pp at 7, 8 TeV
$-0.38 \pm 0.15 \pm 0.02$	AAIJ	13Bo LHCB	pp at 7 TeV
$-0.33 \pm 0.06 \pm 0.03$	1 DALSENO	13 BELL	$e^+ e^- \rightarrow \Upsilon(4S)$
$-0.25 \pm 0.08 \pm 0.02$	LEES	13D BABR	$e^+ e^- \rightarrow \Upsilon(4S)$
• • • We do not use the following data for averages, fits, limits, etc. • • •			
$-0.21 \pm 0.09 \pm 0.02$	AUBERT	07AF BABR	Repl. by LEES 13D
$-0.55 \pm 0.08 \pm 0.05$	1 ISHINO	07 BELL	Repl. by DALSENO 13
$-0.56 \pm 0.12 \pm 0.06$	1 ABE	05D BELL	Repl. by ISHINO 07
$-0.09 \pm 0.15 \pm 0.04$	AUBERT,BE	05 BABR	Repl. by AUBERT 07AF
$-0.58 \pm 0.15 \pm 0.07$	1 ABE	04E BELL	Repl. by ABE 05D
$-0.77 \pm 0.27 \pm 0.08$	1 ABE	03G BELL	Repl. by ABE 04E
$-0.94 \pm 0.31 \pm 0.25 \pm 0.09$	1 ABE	02M BELL	Repl. by ABE 03G
$-0.25 \pm 0.45 \pm 0.47 \pm 0.14$	2 AUBERT	02D BABR	Repl. by AUBERT 02Q
$-0.30 \pm 0.25 \pm 0.04$	3 AUBERT	02Q BABR	Repl. by AUBERT,BE 05
1 Paper reports $A_{\pi \pi}$ which equals to $-C_{\pi \pi}$.			
2 Corresponds to 90% confidence range $-1.0 < C_{\pi \pi} < 0.47$.			
3 Corresponds to 90% confidence range $-0.72 < C_{\pi \pi} < 0.12$.			

 $S_{\pi \pi} (B^0 \rightarrow \pi^+ \pi^-)$

$S_{\pi \pi} = 2\text{Im}(\lambda)/(1 + |\lambda|^2)$, see the note in the $C_{\pi \pi}$ datablock above.

VALUE	DOCUMENT ID	TECN	COMMENT
-0.65 ± 0.04 OUR AVERAGE			
$-0.63 \pm 0.05 \pm 0.01$	AAIJ	18o LHCB	pp at 7, 8 TeV
$-0.71 \pm 0.13 \pm 0.02$	AAIJ	13Bo LHCB	pp at 7 TeV
$-0.64 \pm 0.08 \pm 0.03$	1 DALSENO	13 BELL	$e^+ e^- \rightarrow \Upsilon(4S)$
$-0.68 \pm 0.10 \pm 0.03$	LEES	13D BABR	$e^+ e^- \rightarrow \Upsilon(4S)$
• • • We do not use the following data for averages, fits, limits, etc. • • •			
$-0.60 \pm 0.11 \pm 0.03$	AUBERT	07AF BABR	Repl. by LEES 13D
$-0.61 \pm 0.10 \pm 0.04$	1 ISHINO	07 BELL	Repl. by DALSENO 13
$-0.67 \pm 0.16 \pm 0.06$	2 ABE	05D BELL	Repl. by ISHINO 07
$-0.30 \pm 0.17 \pm 0.03$	AUBERT,BE	05 BABR	Repl. by AUBERT 07AF
$-1.00 \pm 0.21 \pm 0.07$	3 ABE	04E BELL	Repl. by ABE 05D
$-1.23 \pm 0.41 \pm 0.08 \pm 0.27 \pm 0.13$	ABE	03G BELL	Repl. by ABE 04E
$-1.21 \pm 0.38 \pm 0.16 \pm 0.27 \pm 0.13$	ABE	02M BELL	Repl. by ABE 03G
$0.03 \pm 0.52 \pm 0.56 \pm 0.11$	4 AUBERT	02D BABR	Repl. by AUBERT 02Q
$0.02 \pm 0.34 \pm 0.05$	5 AUBERT	02Q BABR	Repl. by AUBERT,BE 05
1 An isospin analysis using other BELLE measurements, disfavors the region of $23.8^\circ < \phi_2 < 66.8^\circ$ at 68% CL.			
2 Rule out the CP-conserving case, $C_{\pi \pi} = S_{\pi \pi} = 0$, at the 5.4 sigma level.			
3 Rule out the CP-conserving case, $C_{\pi \pi} = S_{\pi \pi} = 0$, at the 5.2 sigma level.			
4 Corresponds to 90% confidence range $-0.89 < S_{\pi \pi} < 0.85$.			
5 Corresponds to 90% confidence range $-0.54 < S_{\pi \pi} < 0.58$.			

C_{π⁰π⁰} (B⁰ → π⁰π⁰)

VALUE	DOCUMENT ID	TECN	COMMENT
-0.33 ± 0.22 OUR AVERAGE			
-0.14 ± 0.36 ± 0.10	1 JULIUS 17	BELL	e ⁺ e ⁻ → 7(4S)
-0.43 ± 0.26 ± 0.05	LEES 13D	BABR	e ⁺ e ⁻ → 7(4S)
• • • We do not use the following data for averages, fits, limits, etc. • • •			
-0.49 ± 0.35 ± 0.05	AUBERT 07Bc	BABR	Repl. by LEES 13D
-0.12 ± 0.56 ± 0.06	2 AUBERT 05L	BABR	Repl. by AUBERT 07Bc
-0.44 ^{+0.52} _{-0.53} ± 0.17	1 CHAO 05	BELL	Repl. by JULIUS 17

¹ BELLE Collab. quotes A_{π⁰π⁰} which is equal to -C_{π⁰π⁰}.
² Corresponds to a 90% CL interval of -0.88 < A_{CP} < 0.64.

C_{ρ⁺π⁻} (B⁰ → ρ⁺π⁻)

VALUE	DOCUMENT ID	TECN	COMMENT
-0.03 ± 0.07 OUR AVERAGE	Error includes scale factor of 1.2.		
0.016 ± 0.059 ± 0.036	1 LEES 13J	BABR	e ⁺ e ⁻ → 7(4S)
-0.13 ± 0.09 ± 0.05	1 KUSAKA 07	BELL	e ⁺ e ⁻ → 7(4S)
• • • We do not use the following data for averages, fits, limits, etc. • • •			
0.15 ± 0.09 ± 0.05	AUBERT 07AA	BABR	Repl. by LEES 13J
0.25 ± 0.17 ^{+0.02} _{-0.06}	WANG 05	BELL	Repl. by KUSAKA 07
0.36 ± 0.18 ± 0.04	AUBERT 03T	BABR	Repl. by AUBERT 07AA

¹ Uses time-dependent Dalitz plot analysis of B⁰ → π⁺π⁻π⁰ decays.

S_{ρ⁺π⁻} (B⁰ → ρ⁺π⁻)

VALUE	DOCUMENT ID	TECN	COMMENT
0.05 ± 0.07 OUR AVERAGE			
0.053 ± 0.081 ± 0.034	1 LEES 13J	BABR	e ⁺ e ⁻ → 7(4S)
0.06 ± 0.13 ± 0.05	1 KUSAKA 07	BELL	e ⁺ e ⁻ → 7(4S)
• • • We do not use the following data for averages, fits, limits, etc. • • •			
-0.03 ± 0.11 ± 0.04	AUBERT 07AA	BABR	Repl. by LEES 13J
-0.28 ± 0.23 ^{+0.10} _{-0.08}	WANG 05	BELL	Repl. by KUSAKA 07
0.19 ± 0.24 ± 0.03	AUBERT 03T	BABR	Repl. by AUBERT 07AA

¹ Uses time-dependent Dalitz plot analysis of B⁰ → π⁺π⁻π⁰ decays.

ΔC_{ρ⁺π⁻} (B⁰ → ρ⁺π⁻)

ΔC_{ρ⁺π⁻} describes the asymmetry between the rates Γ(B⁰ → ρ⁺π⁻) + Γ(B⁰ → ρ⁻π⁺) and Γ(B⁰ → ρ⁻π⁺) + Γ(B⁰ → ρ⁺π⁻).

VALUE	DOCUMENT ID	TECN	COMMENT
0.27 ± 0.06 OUR AVERAGE			
0.234 ± 0.061 ± 0.048	1 LEES 13J	BABR	e ⁺ e ⁻ → 7(4S)
0.36 ± 0.10 ± 0.05	1 KUSAKA 07	BELL	e ⁺ e ⁻ → 7(4S)
• • • We do not use the following data for averages, fits, limits, etc. • • •			
0.39 ± 0.09 ± 0.09	AUBERT 07AA	BABR	Repl. by LEES 13J
0.38 ± 0.18 ^{+0.02} _{-0.04}	WANG 05	BELL	Repl. by KUSAKA 07
0.28 ^{+0.18} _{-0.19} ± 0.04	AUBERT 03T	BABR	Repl. by AUBERT 07AA

¹ Uses time-dependent Dalitz plot analysis of B⁰ → π⁺π⁻π⁰ decays.

ΔS_{ρ⁺π⁻} (B⁰ → ρ⁺π⁻)

ΔS_{ρ⁺π⁻} is related to the strong phase difference between the amplitudes contributing to B⁰ → ρ⁺π⁻.

VALUE	DOCUMENT ID	TECN	COMMENT
0.01 ± 0.08 OUR AVERAGE			
0.054 ± 0.082 ± 0.039	1 LEES 13J	BABR	e ⁺ e ⁻ → 7(4S)
-0.08 ± 0.13 ± 0.05	1 KUSAKA 07	BELL	e ⁺ e ⁻ → 7(4S)
• • • We do not use the following data for averages, fits, limits, etc. • • •			
-0.01 ± 0.14 ± 0.06	AUBERT 07AA	BABR	Repl. by LEES 13J
-0.30 ± 0.24 ± 0.09	WANG 05	BELL	Repl. by KUSAKA 07
0.15 ± 0.25 ± 0.03	AUBERT 03T	BABR	Repl. by AUBERT 07AA

¹ Uses time-dependent Dalitz plot analysis of B⁰ → π⁺π⁻π⁰ decays.

C_{ρ⁰π⁰} (B⁰ → ρ⁰π⁰)

VALUE	DOCUMENT ID	TECN	COMMENT
0.27 ± 0.24 OUR AVERAGE			
0.19 ± 0.23 ± 0.15	1 LEES 13J	BABR	e ⁺ e ⁻ → 7(4S)
0.49 ± 0.36 ± 0.28	1,2 KUSAKA 07	BELL	e ⁺ e ⁻ → 7(4S)
• • • We do not use the following data for averages, fits, limits, etc. • • •			
-0.10 ± 0.40 ± 0.53	AUBERT 07AA	BABR	Repl. by LEES 13J
0.53 ^{+0.67} _{-0.84} ± 0.10	2 DRAGIC 06	BELL	Repl. by KUSAKA 07

¹ Uses time-dependent Dalitz plot analysis of B⁰ → π⁺π⁻π⁰ decays.
² Quotes A_{ρ⁰π⁰} which is equal to -C_{ρ⁰π⁰}.

S_{ρ⁰π⁰} (B⁰ → ρ⁰π⁰)

VALUE	DOCUMENT ID	TECN	COMMENT
-0.23 ± 0.34 OUR AVERAGE			
-0.37 ± 0.34 ± 0.20	1 LEES 13J	BABR	e ⁺ e ⁻ → 7(4S)
0.17 ± 0.57 ± 0.35	1 KUSAKA 07	BELL	e ⁺ e ⁻ → 7(4S)
• • • We do not use the following data for averages, fits, limits, etc. • • •			
0.04 ± 0.44 ± 0.18	AUBERT 07AA	BABR	Repl. by LEES 13J

¹ Uses time-dependent Dalitz plot analysis of B⁰ → π⁺π⁻π⁰ decays.

C_{a₁(1260)⁺π⁻} (B⁰ → a₁(1260)⁺π⁻)

VALUE	DOCUMENT ID	TECN	COMMENT
-0.05 ± 0.11 OUR AVERAGE			
-0.01 ± 0.11 ± 0.09	DALSENO 12	BELL	e ⁺ e ⁻ → 7(4S)
-0.10 ± 0.15 ± 0.09	AUBERT 07o	BABR	e ⁺ e ⁻ → 7(4S)

S_{a₁(1260)⁺π⁻} (B⁰ → a₁(1260)⁺π⁻)

VALUE	DOCUMENT ID	TECN	COMMENT
-0.2 ± 0.4 OUR AVERAGE	Error includes scale factor of 3.2.		
-0.51 ± 0.14 ± 0.08	DALSENO 12	BELL	e ⁺ e ⁻ → 7(4S)
0.37 ± 0.21 ± 0.07	AUBERT 07o	BABR	e ⁺ e ⁻ → 7(4S)

ΔC_{a₁(1260)⁺π⁻} (B⁰ → a₁(1260)⁺π⁻)

ΔC_{a₁(1260)⁺π⁻} describes the asymmetry between the rates Γ(B⁰ → a₁⁺π⁻) + Γ(B⁰ → a₁⁻π⁺) and Γ(B⁰ → a₁⁻π⁺) + Γ(B⁰ → a₁⁺π⁻).

VALUE	DOCUMENT ID	TECN	COMMENT
0.43 ± 0.14 OUR AVERAGE	Error includes scale factor of 1.3.		
0.54 ± 0.11 ± 0.07	DALSENO 12	BELL	e ⁺ e ⁻ → 7(4S)
0.26 ± 0.15 ± 0.07	AUBERT 07o	BABR	e ⁺ e ⁻ → 7(4S)

ΔS_{a₁(1260)⁺π⁻} (B⁰ → a₁(1260)⁺π⁻)

ΔS_{a₁(1260)⁺π⁻} is related to the strong phase difference between the amplitudes contributing to B⁰ → a₁π decays.

VALUE	DOCUMENT ID	TECN	COMMENT
-0.11 ± 0.12 OUR AVERAGE			
-0.09 ± 0.14 ± 0.06	DALSENO 12	BELL	e ⁺ e ⁻ → 7(4S)
-0.14 ± 0.21 ± 0.06	AUBERT 07o	BABR	e ⁺ e ⁻ → 7(4S)

C (B⁰ → b₁⁻K⁺)

VALUE	DOCUMENT ID	TECN	COMMENT
-0.22 ± 0.23 ± 0.05	AUBERT 07Bi	BABR	e ⁺ e ⁻ → 7(4S)

ΔC (B⁰ → b₁⁻π⁺)

VALUE	DOCUMENT ID	TECN	COMMENT
-1.04 ± 0.23 ± 0.08	AUBERT 07Bi	BABR	e ⁺ e ⁻ → 7(4S)

C_{ρ⁰ρ⁰} (B⁰ → ρ⁰ρ⁰)

VALUE	DOCUMENT ID	TECN	COMMENT
0.2 ± 0.8 ± 0.3	AUBERT 08Bb	BABR	e ⁺ e ⁻ → 7(4S)

S_{ρ⁰ρ⁰} (B⁰ → ρ⁰ρ⁰)

VALUE	DOCUMENT ID	TECN	COMMENT
0.3 ± 0.7 ± 0.2	AUBERT 08Bb	BABR	e ⁺ e ⁻ → 7(4S)

C_{ρ⁺ρ⁻} (B⁰ → ρ⁺ρ⁻)

VALUE	DOCUMENT ID	TECN	COMMENT
0.00 ± 0.09 OUR AVERAGE			
0.00 ± 0.10 ± 0.06	1 VANHOEFER 16	BELL	e ⁺ e ⁻ → 7(4S)
0.01 ± 0.15 ± 0.06	AUBERT 07Bf	BABR	e ⁺ e ⁻ → 7(4S)
• • • We do not use the following data for averages, fits, limits, etc. • • •			
-0.16 ± 0.21 ± 0.08	1 SOMOV 07	BELL	Repl. by VANHOEFER 16
-0.00 ± 0.30 ± 0.09	1 SOMOV 06	BELL	Repl. by SOMOV 07
-0.03 ± 0.18 ± 0.09	AUBERT,B 05c	BABR	Repl. by AUBERT 07Bf
-0.17 ± 0.27 ± 0.14	AUBERT,B 04R	BABR	Repl. by AUBERT,B 05c

¹ BELLE Collab. quotes A_{CP} which is equal to -C.

S_{ρ⁺ρ⁻} (B⁰ → ρ⁺ρ⁻)

VALUE	DOCUMENT ID	TECN	COMMENT
-0.14 ± 0.13 OUR AVERAGE			
-0.13 ± 0.15 ± 0.05	VANHOEFER 16	BELL	e ⁺ e ⁻ → 7(4S)
-0.17 ± 0.20 ^{+0.05} _{-0.06}	AUBERT 07Bf	BABR	e ⁺ e ⁻ → 7(4S)
• • • We do not use the following data for averages, fits, limits, etc. • • •			
0.19 ± 0.30 ± 0.08	SOMOV 07	BELL	Repl. by VANHOEFER 16
0.08 ± 0.41 ± 0.09	SOMOV 06	BELL	Repl. by SOMOV 07
-0.33 ± 0.24 ^{+0.08} _{-0.14}	AUBERT,B 05c	BABR	Repl. by AUBERT 07Bf
-0.42 ± 0.42 ± 0.14	AUBERT,B 04R	BABR	Repl. by AUBERT,B 05c

|λ| (B⁰ → J/ψ K*(892)⁰)

VALUE	CL%	DOCUMENT ID	TECN	COMMENT
<0.25	95	1 AUBERT,B 04H	BABR	e ⁺ e ⁻ → 7(4S)

¹ Uses the measured cosine coefficients C and C̄ and assumes |q/p| = 1.

cos 2β (B⁰ → J/ψ K*(892)⁰)

β (φ₁) is one of the angles of CKM unitarity triangle, see the review on "CP" Violation in the Reviews section.

VALUE	DOCUMENT ID	TECN	COMMENT
1.7^{+0.7}_{-0.9} OUR AVERAGE	Error includes scale factor of 1.6.		
2.72 ^{+0.50} _{-0.79} ± 0.27	1 AUBERT 05P	BABR	e ⁺ e ⁻ → 7(4S)
0.87 ± 0.74 ± 0.12	2 ITOH 05	BELL	e ⁺ e ⁻ → 7(4S)

¹ The measurement is obtained when sin 2β is fixed to 0.726 and the sign of cos 2β is positive with 86% confidence level.
² The measurement is obtained with sin 2β fixed to 0.731.

Meson Particle Listings

B^0

$\cos 2\beta (B^0 \rightarrow [K_S^0 \pi^+ \pi^-]_{D^{(*)}} h^0)$

VALUE	DOCUMENT ID	TECN	COMMENT
0.91 ± 0.22 ± 0.11	¹ ADACHI 18		$e^+ e^- \rightarrow \Upsilon(4S)$
1.06 ± 0.33 ^{+0.21} _{-0.15}	² VOROBYEV 16	BELL	$e^+ e^- \rightarrow \Upsilon(4S)$
0.42 ± 0.49 ± 0.16	³ AUBERT 07BH	BABR	$e^+ e^- \rightarrow \Upsilon(4S)$
1.87 ^{+0.40+0.22} _{-0.53-0.32}	⁴ KROKOVNY 06	BELL	Repl. by VOROBYEV 16

- ¹ Analyzes joint data sample of Belle and BaBar using Dalitz plot analysis of $D \rightarrow K_S^0 \pi^+ \pi^-$; the second error combines experimental systematic uncertainty and the Dalitz plot model uncertainty.
- ² A model-independent measurement uses the binned Dalitz plot technique.
- ³ AUBERT 07BH evaluates the likelihoods for the positive and negative solutions assuming $\sin(2\beta_{eff}) = 0.678$. It quotes $L_+ / (L_+ + L_-) = 0.86$ corresponding to a likelihood ratio of $L_+ / L_- = 6.14$ in favor of the positive solution.
- ⁴ KROKOVNY 06 evaluates the likelihoods for the positive and negative solutions assuming $\sin(2\beta_{eff}) = 0.689$. It quotes $L_+ / (L_+ + L_-) = 0.983$ corresponding to a likelihood ratio of $L_+ / L_- = 57.8$ in favor of the positive solution.

$(S_+ + S_-)/2 (B^0 \rightarrow D^{*-} \pi^+)$

$$S_{\pm} = -\frac{2Im(\lambda_{\pm})}{1+|\lambda_{\pm}|^2} \text{ where } \lambda_+ \text{ and } \lambda_- \text{ are defined in the } C_{\pi\pi} \text{ datablock above for } B^0 \rightarrow D^{*-} \pi^+ \text{ and } \bar{B}^0 \rightarrow D^{*+} \pi^-.$$

VALUE	DOCUMENT ID	TECN	COMMENT
-0.039 ± 0.011 OUR AVERAGE			
-0.046 ± 0.013 ± 0.015	¹ BAHINIPATI 11	BELL	$e^+ e^- \rightarrow \Upsilon(4S)$
-0.040 ± 0.023 ± 0.010	² AUBERT 06Y	BABR	$e^+ e^- \rightarrow \Upsilon(4S)$
-0.034 ± 0.014 ± 0.009	¹ AUBERT 05Z	BABR	$e^+ e^- \rightarrow \Upsilon(4S)$
-0.039 ± 0.020 ± 0.013	³ RONGA 06	BELL	Repl. by BAHINIPATI 11
-0.030 ± 0.028 ± 0.018	¹ GERSHON 05	BELL	Repl. by RONGA 06
-0.068 ± 0.038 ± 0.020	² AUBERT 04V	BABR	Repl. by AUBERT 06Y
-0.063 ± 0.024 ± 0.014	¹ AUBERT 04W	BABR	Repl. by AUBERT 05Z
0.060 ± 0.040 ± 0.019	² SARANGI 04	BELL	Repl. by RONGA 06

- ¹ Uses partially reconstructed $B^0 \rightarrow D^{*+} \pi^-$ decays.
- ² Uses fully reconstructed $B^0 \rightarrow D^{*+} \pi^-$ decays.
- ³ Combines the results from fully reconstructed and partially reconstructed $D^{*+} \pi^-$ events by taking weighted averages. Assumes that systematic errors from physics parameters and fit biases in the two measurements are 100% correlated.

$(S_- - S_+)/2 (B^0 \rightarrow D^{*-} \pi^+)$

VALUE	DOCUMENT ID	TECN	COMMENT
-0.009 ± 0.015 OUR AVERAGE			
-0.015 ± 0.013 ± 0.015	¹ BAHINIPATI 11	BELL	$e^+ e^- \rightarrow \Upsilon(4S)$
-0.049 ± 0.042 ± 0.015	² AUBERT 06Y	BABR	$e^+ e^- \rightarrow \Upsilon(4S)$
-0.019 ± 0.022 ± 0.013	¹ AUBERT 05Z	BABR	$e^+ e^- \rightarrow \Upsilon(4S)$
-0.011 ± 0.020 ± 0.013	³ RONGA 06	BELL	Repl. by BAHINIPATI 11
-0.005 ± 0.028 ± 0.018	¹ GERSHON 05	BELL	Repl. by RONGA 06
0.031 ± 0.070 ± 0.033	² AUBERT 04V	BABR	Repl. by AUBERT 06Y
-0.004 ± 0.037 ± 0.014	¹ AUBERT 04W	BABR	Repl. by AUBERT 05Z
0.049 ± 0.040 ± 0.019	² SARANGI 04	BELL	Repl. by RONGA 06

- ¹ Uses partially reconstructed $B^0 \rightarrow D^{*+} \pi^-$ decays.
- ² Uses fully reconstructed $B^0 \rightarrow D^{*+} \pi^-$ decays.
- ³ Combines the results from fully reconstructed and partially reconstructed $D^{*+} \pi^-$ events by taking weighted averages. Assumes that systematic errors from physics parameters and fit biases in the two measurements are 100% correlated.

$(S_+ + S_-)/2 (B^0 \rightarrow D^- \pi^+)$

VALUE	DOCUMENT ID	TECN	COMMENT
-0.046 ± 0.023 OUR AVERAGE			
-0.010 ± 0.023 ± 0.07	¹ AUBERT 06Y	BABR	$e^+ e^- \rightarrow \Upsilon(4S)$
-0.050 ± 0.021 ± 0.012	² RONGA 06	BELL	$e^+ e^- \rightarrow \Upsilon(4S)$
-0.022 ± 0.038 ± 0.020	¹ AUBERT 04V	BABR	Repl. by AUBERT 06Y
-0.062 ± 0.037 ± 0.018	¹ SARANGI 04	BELL	Repl. by RONGA 06

- ¹ Uses fully reconstructed $B^0 \rightarrow D^{\pm} \pi^{\mp}$ decays.
- ² Combines the results from fully reconstructed and partially reconstructed $D\pi$ events by taking weighted averages. Assumes that systematic errors from physics parameters and fit biases in the two measurements are 100% correlated.

$(S_- - S_+)/2 (B^0 \rightarrow D^- \pi^+)$

VALUE	DOCUMENT ID	TECN	COMMENT
-0.022 ± 0.021 OUR AVERAGE			
-0.033 ± 0.042 ± 0.012	¹ AUBERT 06Y	BABR	$e^+ e^- \rightarrow \Upsilon(4S)$
-0.019 ± 0.021 ± 0.012	² RONGA 06	BELL	$e^+ e^- \rightarrow \Upsilon(4S)$
0.025 ± 0.068 ± 0.033	¹ AUBERT 04V	BABR	Repl. by AUBERT 06Y
-0.025 ± 0.037 ± 0.018	¹ SARANGI 04	BELL	Repl. by RONGA 06

- ¹ Uses fully reconstructed $B^0 \rightarrow D^{\pm} \pi^{\mp}$ decays.
- ² Combines the results from fully reconstructed and partially reconstructed $D\pi$ events by taking weighted averages. Assumes that systematic errors from physics parameters and fit biases in the two measurements are 100% correlated.

$S_+ (B^0 \rightarrow D^- \pi^+)$

VALUE	DOCUMENT ID	TECN	COMMENT
0.058 ± 0.020 ± 0.011	¹ AAIJ 18Z	LHCB	pp at 7, 8 TeV

- ¹ Measured in the simultaneous analysis of $B^0 \rightarrow D^{\mp} \pi^{\pm}$ decays. AAIJ 18Z reports a statistical (systematic) correlation of 0.6 (-0.41) with the measured value of $S_-(B^0 \rightarrow D^+ \pi^-)$.

$S_- (B^0 \rightarrow D^+ \pi^-)$

VALUE	DOCUMENT ID	TECN	COMMENT
0.038 ± 0.020 ± 0.007	¹ AAIJ 18Z	LHCB	pp at 7, 8 TeV

- ¹ Measured in the simultaneous analysis of $B^0 \rightarrow D^{\mp} \pi^{\pm}$ decays. AAIJ 18Z reports a statistical (systematic) correlation of 0.6 (-0.41) with the measured value of $S_+(B^0 \rightarrow D^- \pi^+)$.

$(S_+ + S_-)/2 (B^0 \rightarrow D^- \rho^+)$

VALUE	DOCUMENT ID	TECN	COMMENT
-0.024 ± 0.031 ± 0.009	¹ AUBERT 06Y	BABR	$e^+ e^- \rightarrow \Upsilon(4S)$

- ¹ Uses fully reconstructed $B^0 \rightarrow D^- \rho^+$ decays.

$(S_- - S_+)/2 (B^0 \rightarrow D^- \rho^+)$

VALUE	DOCUMENT ID	TECN	COMMENT
-0.098 ± 0.055 ± 0.018	¹ AUBERT 06Y	BABR	$e^+ e^- \rightarrow \Upsilon(4S)$

- ¹ Uses fully reconstructed $B^0 \rightarrow D^- \rho^+$ decays.

$C_{\eta_c K_S^0} (B^0 \rightarrow \eta_c K_S^0)$

VALUE	DOCUMENT ID	TECN	COMMENT
0.080 ± 0.124 ± 0.029	AUBERT 09K	BABR	$e^+ e^- \rightarrow \Upsilon(4S)$

$S_{\eta_c K_S^0} (B^0 \rightarrow \eta_c K_S^0)$

VALUE	DOCUMENT ID	TECN	COMMENT
0.925 ± 0.160 ± 0.057	AUBERT 09K	BABR	$e^+ e^- \rightarrow \Upsilon(4S)$

$C_{c\bar{c}K^{(*)0}} (B^0 \rightarrow c\bar{c}K^{(*)0})$

"OUR EVALUATION" is an average using rescaled values of the data listed below. The average and rescaling were performed by the Heavy Flavor Averaging Group (HFLAV) and are described at <https://hflav.web.cern.ch/>. The averaging/rescaling procedure takes into account correlations between the measurements.

VALUE (units 10^{-2})	DOCUMENT ID	TECN	COMMENT
0.5 ± 1.7 OUR EVALUATION			
0.0 ± 1.4 OUR AVERAGE			
-1.7 ± 2.9	^{1,2} AAIJ	17BN LHCB	pp at 7, 8 TeV
-0.6 ± 1.6 ± 1.2	³ ADACHI 12A	BELL	$e^+ e^- \rightarrow \Upsilon(4S)$
-29 ⁺⁵³ ₋₄₄ ± 6	⁴ AUBERT 09AU	BABR	$e^+ e^- \rightarrow \Upsilon(4S)$
2.4 ± 2.0 ± 1.6	⁵ AUBERT 09K	BABR	$e^+ e^- \rightarrow \Upsilon(4S)$
-4 ± 7 ± 5	⁶ SAHOO 08	BELL	Repl. by ADACHI 12A
4.9 ± 2.3 ± 1.8	⁵ AUBERT 07AY	BABR	Repl. by AUBERT 09K
-1.8 ± 2.1 ± 1.4	⁷ CHEN 07	BELL	Repl. by ADACHI 12A
-0.7 ± 4.1 ± 3.3	⁸ ABE 05B	BELL	Repl. by CHEN 07
5.1 ± 3.2 ± 1.4	⁹ AUBERT 05F	BABR	Repl. by AUBERT 07AY
5.1 ± 5.1 ± 2.6	¹⁰ ABE 02Z	BELL	Repl. by ABE 05B
5.3 ± 5.4 ± 3.2	¹¹ AUBERT 02P	BABR	Repl. by AUBERT 05F

- ¹ Measurement based on $B^0 \rightarrow J/\psi K_S^0, B^0 \rightarrow \psi(2S) K_S^0$ with $J/\psi \rightarrow \mu^+ \mu^-, J/\psi \rightarrow e^+ e^-$ and $\psi(2S) \rightarrow \mu^+ \mu^-$.
- ² AAIJ 17BN provides the correlation coefficient $\rho=0.42$ between the uncertainties of $S_{B^0 \rightarrow c\bar{c}K^{(*)0}}$ and $C_{c\bar{c}K^{(*)0}}$ ($B^0 \rightarrow c\bar{c}K^{(*)0}$) measurements.
- ³ Measurement based on $B^0 \rightarrow J/\psi K_S^0, B^0 \rightarrow \psi(2S) K_S^0, B^0 \rightarrow J/\psi K_L^0$, and $B^0 \rightarrow \chi_{c1}(1P) K_S^0$ decays.
- ⁴ Uses Dalitz plot analysis of $B^0 \rightarrow K^0 \pi^+ \pi^-$ decays and the first of two equivalent solutions is used.
- ⁵ Measurement based on $B^0 \rightarrow c\bar{c}K^{(*)0}$ decays.
- ⁶ Reports value of A of $B^0 \rightarrow \psi(2S) K^0$ which is equal to $-C$.
- ⁷ Reports value of A of $B^0 \rightarrow J/\psi K^0$ which is equal to $-C$.
- ⁸ Measurement based on $15.2 \times 10^6 B\bar{B}$ pairs.
- ⁹ Measurement based on $227 \times 10^6 B\bar{B}$ pairs.
- ¹⁰ Measured with both $\eta_f = \pm 1$ samples.
- ¹¹ Measured with the high purity of $\eta_f = -1$ samples.

$\sin(2\beta)$

For a discussion of CP violation, see the review on "CP Violation" in the Reviews section. $\sin(2\beta)$ is a measure of the CP -violating amplitude in the $B^0_d \rightarrow J/\psi(1S) K_S^0$.

"OUR EVALUATION" is an average using rescaled values of the data listed below. The average and rescaling were performed by the Heavy Flavor Averaging Group (HFLAV) and are described at <https://hflav.web.cern.ch/>. The averaging/rescaling procedure takes into account correlations between the measurements.

VALUE	DOCUMENT ID	TECN	COMMENT
0.695 ± 0.019 OUR EVALUATION			
0.698 ± 0.027 OUR AVERAGE			Error includes scale factor of 1.6. See the ideogram below.
0.760 ± 0.034	^{1,2} AAIJ	17BN LHCB	pp at 7, 8 TeV
0.667 ± 0.023 ± 0.012	³ ADACHI 12A	BELL	$e^+ e^- \rightarrow \Upsilon(4S)$
0.57 ± 0.58 ± 0.06	⁴ SATO 12	BELL	$e^+ e^- \rightarrow \Upsilon(5S)$
0.69 ± 0.52 ± 0.08	⁵ AUBERT 09AU	BABR	$e^+ e^- \rightarrow \Upsilon(4S)$

See key on page 999

Meson Particle Listings

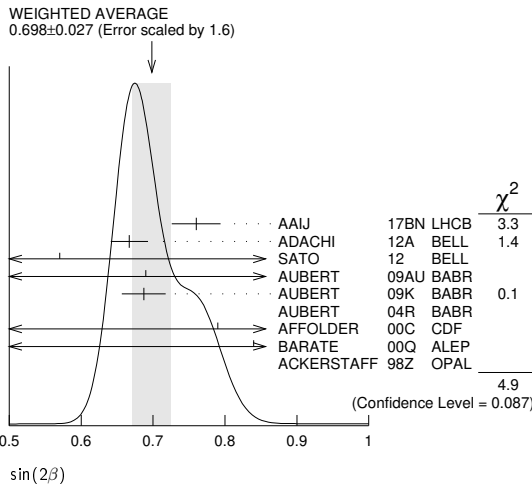
B^0

$0.687 \pm 0.028 \pm 0.012$	6	AUBERT	09K	BABR	$e^+e^- \rightarrow \Upsilon(4S)$
$1.56 \pm 0.42 \pm 0.21$	7	AUBERT	04R	BABR	$e^+e^- \rightarrow \Upsilon(4S)$
$0.79 \begin{smallmatrix} +0.41 \\ -0.44 \end{smallmatrix}$	8	AFFOLDER	00C	CDF	$p\bar{p}$ at 1.8 TeV
$0.84 \begin{smallmatrix} +0.82 \\ -1.04 \end{smallmatrix} \pm 0.16$	9	BARATE	00Q	ALEP	$e^+e^- \rightarrow Z$
$3.2 \begin{smallmatrix} +1.8 \\ -2.0 \end{smallmatrix} \pm 0.5$	10	ACKERSTAFF	98Z	OPAL	$e^+e^- \rightarrow Z$

• • • We do not use the following data for averages, fits, limits, etc. • • •

$0.72 \pm 0.09 \pm 0.03$	11	SAHOO	08	BELL	Repl. by ADACHI 12A
$0.714 \pm 0.032 \pm 0.018$	6	AUBERT	07AY	BABR	Repl. by AUBERT 09K
$0.642 \pm 0.031 \pm 0.017$		CHEN	07	BELL	Repl. by ADACHI 12A
$0.728 \pm 0.056 \pm 0.023$	12	ABE	05B	BELL	Repl. by CHEN 07
$0.722 \pm 0.040 \pm 0.023$	13	AUBERT	05F	BABR	Repl. by AUBERT 07AY
$0.99 \pm 0.14 \pm 0.06$	14	ABE	02U	BELL	$e^+e^- \rightarrow \Upsilon(4S)$
$0.719 \pm 0.074 \pm 0.035$	15	ABE	02Z	BELL	Repl. by ABE 05B
$0.59 \pm 0.14 \pm 0.05$	16	AUBERT	02N	BABR	$e^+e^- \rightarrow \Upsilon(4S)$
$0.741 \pm 0.067 \pm 0.034$	17	AUBERT	02P	BABR	Repl. by AUBERT 05F
$0.58 \begin{smallmatrix} +0.32 \\ -0.34 \end{smallmatrix} \pm 0.09$		ABASHIAN	01	BELL	Repl. by ABE 01G
$0.99 \pm 0.14 \pm 0.06$	18	ABE	01G	BELL	Repl. by ABE 02Z
$0.34 \pm 0.20 \pm 0.05$		AUBERT	01	BABR	Repl. by AUBERT 01B
$0.59 \pm 0.14 \pm 0.05$	18	AUBERT	01B	BABR	Repl. by AUBERT 02P
$1.8 \pm 1.1 \pm 0.3$	19	ABE	98U	CDF	Repl. by AFFOLDER 00C

- Measurement based on $B^0 \rightarrow J/\psi K_S^0, B^0 \rightarrow \psi(2S) K_S^0$ with $J/\psi \rightarrow \mu^+ \mu^-, J/\psi \rightarrow e^+ e^-$ and $\psi(2S) \rightarrow \mu^+ \mu^-$.
- AAIJ 17BN provides the correlation coefficient $\rho = 0.42$ between the uncertainties of $\sin(2\beta)$ and $\cos(2\beta)$ measurements.
- Measurement based on $B^0 \rightarrow J/\psi K_S^0, B^0 \rightarrow \psi(2S) K_S^0, B^0 \rightarrow J/\psi K_L^0$, and $B^0 \rightarrow \chi_{c1}(1P) K_S^0$ decays.
- SATO 12 uses 121 fb^{-1} data collected on $\Upsilon(5S)$ resonance. Uses the " $B - \pi$ tagging" where $B\pi^+$ and $B\pi^-$ tagged $J/\psi K_S^0$ events are compared.
- Uses Dalitz plot analysis of $B^0 \rightarrow K^0 \pi^+ \pi^-$ decays and the first of two equivalent solutions.
- Measurement based on $B^0 \rightarrow c\bar{c} K^0$ decays.
- Measurement in which the J/ψ decays to hadrons or to muons that do not satisfy the standard identification criteria.
- AFFOLDER 00C uses about 400 $B^0 \rightarrow J/\psi(1S) K_S^0$ events. The production flavor of B^0 was determined using three tagging algorithms: a same-side tag, a jet-charge tag, and a soft-lepton tag.
- BARATE 00Q uses 23 candidates for $B^0 \rightarrow J/\psi(1S) K_S^0$ decays. A combination of jet-charge, vertex-charge, and same-side tagging techniques were used to determine the B^0 production flavor.
- ACKERSTAFF 98Z uses 24 candidates for $B_d^0 \rightarrow J/\psi(1S) K_S^0$ decay. A combination of jet-charge and vertex-charge techniques were used to tag the B_d^0 production flavor.
- Based on $B^0 \rightarrow \psi(2S) K_S^0$ decays.
- Measurement based on $152 \times 10^6 B\bar{B}$ pairs.
- Measurement based on $227 \times 10^6 B\bar{B}$ pairs.
- ABE 02U result is based on the same analysis and data sample reported in ABE 01G.
- ABE 02Z result is based on $85 \times 10^6 B\bar{B}$ pairs.
- AUBERT 02N result based on the same analysis and data sample reported in AUBERT 01B.
- AUBERT 02P result is based on $88 \times 10^6 B\bar{B}$ pairs.
- First observation of CP violation in B^0 meson system.
- ABE 98U uses $198 \pm 17 B_d^0 \rightarrow J/\psi(1S) K^0$ events. The production flavor of B^0 was determined using the same side tagging technique.



$C_{J/\psi(nS) K^0} (B^0 \rightarrow J/\psi(nS) K^0)$

"OUR EVALUATION" is an average using rescaled values of the data listed below. The average and rescaling were performed by the Heavy Flavor Averaging Group (HFLAV) and are described at <https://hflav.web.cern.ch/>. The averaging/rescaling procedure takes into account correlations between the measurements.

VALUE (units 10^{-2})	DOCUMENT ID	TECN	COMMENT
0.5 ± 2.0 OUR EVALUATION			
-0.5 ± 1.6 OUR AVERAGE			
-1.7 ± 2.9	1,2	AAIJ	17BN LHCb $p\bar{p}$ at 7, 8 TeV
$1.5 \pm 2.1 \begin{smallmatrix} +2.3 \\ -4.5 \end{smallmatrix}$	3,4	ADACHI	12A BELL $e^+e^- \rightarrow \Upsilon(4S)$
$-10.4 \pm 5.5 \begin{smallmatrix} +2.7 \\ -4.7 \end{smallmatrix}$	4,5	ADACHI	12A BELL $e^+e^- \rightarrow \Upsilon(4S)$
$-1.9 \pm 2.6 \begin{smallmatrix} +4.1 \\ -1.7 \end{smallmatrix}$	4,6	ADACHI	12A BELL $e^+e^- \rightarrow \Upsilon(4S)$
$8.9 \pm 7.6 \pm 2.0$	5	AUBERT	09K BABR $e^+e^- \rightarrow \Upsilon(4S)$
$1.6 \pm 2.3 \pm 1.8$		AUBERT	09K BABR $e^+e^- \rightarrow \Upsilon(4S)$

• • • We do not use the following data for averages, fits, limits, etc. • • •

-1.4 ± 3.0	7	AAIJ	17BN LHCb $p\bar{p}$ at 7, 8 TeV
$-5 \pm 10 \pm 1$	8	AAIJ	17BN LHCb $p\bar{p}$ at 7, 8 TeV
$-3.8 \pm 3.2 \pm 0.5$	9	AAIJ	15N LHCb Repl. by AAIJ 17BN
$3 \pm 9 \pm 1$	10	AAIJ	13K LHCb Repl. by AAIJ 15N
$-4 \pm 7 \pm 5$	4,5	SAHOO	08 BELL Repl. by ADACHI 12A
$-1.8 \pm 2.1 \pm 1.4$	4	CHEN	07 BELL Repl. by ADACHI 12A

- Measurement based on $B^0 \rightarrow J/\psi K_S^0, B^0 \rightarrow \psi(2S) K_S^0$ with $J/\psi \rightarrow \mu^+ \mu^-, J/\psi \rightarrow e^+ e^-$ and $\psi(2S) \rightarrow \mu^+ \mu^-$.
- AAIJ 17BN provides the correlation coefficient $\rho = 0.42$ between the uncertainties of $S_{J/\psi(nS) K^0} (B^0 \rightarrow J/\psi(nS) K^0)$ and $C_{J/\psi(nS) K^0} (B^0 \rightarrow J/\psi(nS) K^0)$ measurements.
- Uses $B^0 \rightarrow J/\psi K_S^0$ decays.
- The paper reports A, which is equal to $-C$.
- Uses $B^0 \rightarrow \psi(2S) K_S^0$ decays.
- Uses $B^0 \rightarrow J/\psi K_L^0$ decays.
- Measurement based on $B^0 \rightarrow J/\psi K_S^0$ with $J/\psi \rightarrow \mu^+ \mu^-$ and $J/\psi \rightarrow e^+ e^-$.
- Measurement based on $B^0 \rightarrow \psi(2S) K_S^0$ with $\psi(2S) \rightarrow \mu^+ \mu^-$.
- AAIJ 15N uses 41,560 flavor-tagged $B_d \rightarrow J/\psi K_S^0$ events from 3 fb^{-1} of integrated luminosity. Provides the correlation coefficient $\rho = 0.483$ between the statistical uncertainties of and measurements.
- AAIJ 13K uses 8200 flavor-tagged $B_d \rightarrow J/\psi K_S^0$ events from 1 fb^{-1} of integrated luminosity. Provides the correlation coefficient $\rho = 0.42$ between the statistical uncertainties of $S_{J/\psi(nS) K^0} (B^0 \rightarrow J/\psi(nS) K^0)$ and $C_{J/\psi(nS) K^0} (B^0 \rightarrow J/\psi(nS) K^0)$ measurements.

$S_{J/\psi(nS) K^0} (B^0 \rightarrow J/\psi(nS) K^0)$

"OUR EVALUATION" is an average using rescaled values of the data listed below. The average and rescaling were performed by the Heavy Flavor Averaging Group (HFLAV) and are described at <https://hflav.web.cern.ch/>. The averaging/rescaling procedure takes into account correlations between the measurements.

VALUE	DOCUMENT ID	TECN	COMMENT
0.701 ± 0.017 OUR EVALUATION			
0.698 ± 0.024 OUR AVERAGE			Error includes scale factor of 1.4. See the ideogram below.
0.760 ± 0.034	1,2	AAIJ	17BN LHCb $p\bar{p}$ at 7, 8 TeV
$0.670 \pm 0.029 \pm 0.013$	3	ADACHI	12A BELL $e^+e^- \rightarrow \Upsilon(4S)$
$0.738 \pm 0.079 \pm 0.036$	4	ADACHI	12A BELL $e^+e^- \rightarrow \Upsilon(4S)$
$0.642 \pm 0.047 \pm 0.021$	5	ADACHI	12A BELL $e^+e^- \rightarrow \Upsilon(4S)$
$0.57 \pm 0.58 \pm 0.06$	6	SATO	12 BELL $e^+e^- \rightarrow \Upsilon(5S)$
$0.897 \pm 0.100 \pm 0.036$	4	AUBERT	09K BABR $e^+e^- \rightarrow \Upsilon(4S)$
$0.666 \pm 0.031 \pm 0.013$		AUBERT	09K BABR $e^+e^- \rightarrow \Upsilon(4S)$
$0.79 \begin{smallmatrix} +0.41 \\ -0.44 \end{smallmatrix}$	7	AFFOLDER	00C CDF $p\bar{p}$ at 1.8 TeV
$0.84 \begin{smallmatrix} +0.82 \\ -1.04 \end{smallmatrix} \pm 0.16$	8	BARATE	00Q ALEP $e^+e^- \rightarrow Z$
$3.2 \begin{smallmatrix} +1.8 \\ -2.0 \end{smallmatrix} \pm 0.5$	9	ACKERSTAFF	98Z OPAL $e^+e^- \rightarrow Z$

• • • We do not use the following data for averages, fits, limits, etc. • • •

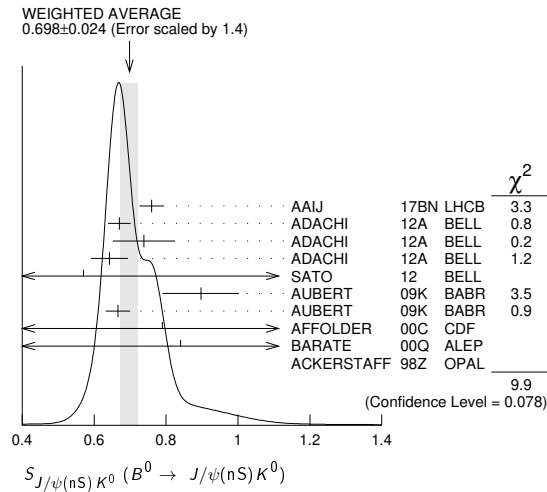
0.75 ± 0.04	10	AAIJ	17BN LHCb $p\bar{p}$ at 7, 8 TeV
$0.84 \pm 0.10 \pm 0.01$	11	AAIJ	17BN LHCb $p\bar{p}$ at 7, 8 TeV
$0.731 \pm 0.035 \pm 0.020$	12	AAIJ	15N LHCb Repl. by AAIJ 17BN
$0.73 \pm 0.07 \pm 0.04$	13	AAIJ	13K LHCb Repl. by AAIJ 15N
$0.650 \pm 0.029 \pm 0.018$	14	SAHOO	08 BELL Repl. by ADACHI 12A
$0.72 \pm 0.09 \pm 0.03$	4	SAHOO	08 BELL Repl. by ADACHI 12A
$0.642 \pm 0.031 \pm 0.017$		CHEN	07 BELL Repl. by ADACHI 12A

- Measurement based on $B^0 \rightarrow J/\psi K_S^0, B^0 \rightarrow \psi(2S) K_S^0$ with $J/\psi \rightarrow \mu^+ \mu^-, J/\psi \rightarrow e^+ e^-$ and $\psi(2S) \rightarrow \mu^+ \mu^-$.
- AAIJ 17BN provides the correlation coefficient $\rho = 0.42$ between the uncertainties of $S_{J/\psi(nS) K^0} (B^0 \rightarrow J/\psi(nS) K^0)$ and $C_{J/\psi(nS) K^0} (B^0 \rightarrow J/\psi(nS) K^0)$ measurements.
- Uses $B^0 \rightarrow J/\psi K_S^0$ decays.
- Based on $B^0 \rightarrow \psi(2S) K_S^0$ decays.
- Uses $B^0 \rightarrow J/\psi K_L^0$ decays.
- SATO 12 uses 121 fb^{-1} data collected at $\Upsilon(5S)$ resonance. Uses the " $B - \pi$ tagging" where $B\pi^+$ and $B\pi^-$ tagged $J/\psi K_S^0$ events are compared.
- AFFOLDER 00C uses about 400 $B^0 \rightarrow J/\psi(1S) K_S^0$ events. The production flavor of B^0 was determined using three tagging algorithms: a same-side tag, a jet-charge tag, and a soft-lepton tag.

Meson Particle Listings

B^0

- ⁸ BARATE 00q uses 23 candidates for $B^0 \rightarrow J/\psi(1S)K_S^0$ decays. A combination of jet-charge, vertex-charge, and same-side tagging techniques were used to determine the B^0 production flavor.
- ⁹ ACKERSTAFF 98z uses 24 candidates for $B^0 \rightarrow J/\psi(1S)K_S^0$ decay. A combination of jet-charge and vertex-charge techniques were used to tag the B^0 production flavor.
- ¹⁰ Measurement based on $B^0 \rightarrow J/\psi K_S^0$ with $J/\psi \rightarrow \mu^+ \mu^-$ and $J/\psi \rightarrow e^+ e^-$.
- ¹¹ Measurement based on $B^0 \rightarrow \psi(2S)K_S^0$ with $\psi(2S) \rightarrow \mu^+ \mu^-$.
- ¹² AAIJ 15N uses 41,560 flavor-tagged $B_d \rightarrow J/\psi K_S^0$ events from 3 fb⁻¹ of integrated luminosity. Provides the correlation coefficient $\rho = 0.483$ between the statistical uncertainties of and measurements.
- ¹³ AAIJ 13K uses 8200 flavor-tagged $B_d \rightarrow J/\psi K_S^0$ events from 1 fb⁻¹ of integrated luminosity. Provides the correlation coefficient $\rho = 0.42$ between the statistical uncertainties of $S_{J/\psi(nS)K^0}$ ($B^0 \rightarrow J/\psi(nS)K^0$) and $C_{J/\psi(nS)K^0}$ ($B^0 \rightarrow J/\psi(nS)K^0$) measurements.
- ¹⁴ Combined result of CHEN 07 and SAHOO 08.



$C_{J/\psi K^0} (B^0 \rightarrow J/\psi K^0)$

VALUE	DOCUMENT ID	TECN	COMMENT
$0.025 \pm 0.083 \pm 0.054$	¹ AUBERT	09K	BABR $e^+ e^- \rightarrow \Upsilon(4S)$

¹ Based on $B^0 \rightarrow J/\psi K^0, K^0 \rightarrow K_S^0 \pi^0$.

$S_{J/\psi K^0} (B^0 \rightarrow J/\psi K^0)$

VALUE	DOCUMENT ID	TECN	COMMENT
$0.601 \pm 0.239 \pm 0.087$	^{1,2} AUBERT	09K	BABR $e^+ e^- \rightarrow \Upsilon(4S)$

¹ Based on $B^0 \rightarrow J/\psi K^0, K^0 \rightarrow K_S^0 \pi^0$.

² This $S_{J/\psi K^0}$ value has been corrected for the dilution of the $\sin(\Delta M \Delta t)$ coefficient of the CP asymmetry by a factor of $1-R_{\perp}$, which arises from the mixture of CP-even and CP-odd B decay amplitudes.

$C_{\chi_{c0} K_S^0} (B^0 \rightarrow \chi_{c0} K_S^0)$

VALUE	DOCUMENT ID	TECN	COMMENT
$-0.29 \pm 0.53 \pm 0.06$	¹ AUBERT	09AU	BABR $e^+ e^- \rightarrow \Upsilon(4S)$

¹ Uses Dalitz plot analysis of $B^0 \rightarrow K^0 \pi^+ \pi^-$ decays and the first of two equivalent solutions is used.

$S_{\chi_{c0} K_S^0} (B^0 \rightarrow \chi_{c0} K_S^0)$

VALUE	DOCUMENT ID	TECN	COMMENT
$-0.69 \pm 0.52 \pm 0.08$	¹ AUBERT	09AU	BABR $e^+ e^- \rightarrow \Upsilon(4S)$

¹ Uses Dalitz plot analysis of $B^0 \rightarrow K^0 \pi^+ \pi^-$ decays and the first of two equivalent solutions is used.

$C_{\chi_{c1} K_S^0} (B^0 \rightarrow \chi_{c1} K_S^0)$

VALUE	DOCUMENT ID	TECN	COMMENT
0.06 ± 0.07 OUR AVERAGE			
$0.017 \pm 0.083 \pm 0.026$	ADACHI	12A	BELL $e^+ e^- \rightarrow \Upsilon(4S)$
$0.129 \pm 0.109 \pm 0.025$	AUBERT	09K	BABR $e^+ e^- \rightarrow \Upsilon(4S)$

$S_{\chi_{c1} K_S^0} (B^0 \rightarrow \chi_{c1} K_S^0)$

VALUE	DOCUMENT ID	TECN	COMMENT
0.63 ± 0.10 OUR AVERAGE			
$0.640 \pm 0.117 \pm 0.040$	ADACHI	12A	BELL $e^+ e^- \rightarrow \Upsilon(4S)$
$0.614 \pm 0.160 \pm 0.040$	AUBERT	09K	BABR $e^+ e^- \rightarrow \Upsilon(4S)$

$\sin(2\beta_{\text{eff}}) (B^0 \rightarrow \phi K^0)$

VALUE	DOCUMENT ID	TECN	COMMENT
$0.22 \pm 0.27 \pm 0.12$	AUBERT	07AX	BABR $e^+ e^- \rightarrow \Upsilon(4S)$

• • • We do not use the following data for averages, fits, limits, etc. • • •

$0.50 \pm 0.25 \pm 0.07$	¹ AUBERT	05T	BABR Repl. by AUBERT 07AX
--------------------------	---------------------	-----	---------------------------

¹ Obtained by constraining $C = 0$.

$\sin(2\beta_{\text{eff}}) (B^0 \rightarrow \phi K_0^*(1430)^0)$

VALUE	DOCUMENT ID	TECN	COMMENT
0.97 ± 0.03	¹ AUBERT	08BG	BABR $e^+ e^- \rightarrow \Upsilon(4S)$

¹ Measured using the CP-violation phase difference $\Delta\phi_{00}$ between the B and \bar{B} decay amplitude.

$\sin(2\beta_{\text{eff}}) (B^0 \rightarrow K^+ K^- K_S^0)$

VALUE	DOCUMENT ID	TECN	COMMENT
$0.77 \pm 0.11 \pm 0.07$	AUBERT	07AX	BABR $e^+ e^- \rightarrow \Upsilon(4S)$

• • • We do not use the following data for averages, fits, limits, etc. • • •

$0.55 \pm 0.22 \pm 0.12$	¹ AUBERT	05T	BABR Repl. by AUBERT 07AX
--------------------------	---------------------	-----	---------------------------

¹ Obtained by constraining $C = 0$.

$\sin(2\beta_{\text{eff}}) (B^0 \rightarrow [K_S^0 \pi^+ \pi^-]_{D^{(*)}} h^0)$

VALUE	DOCUMENT ID	TECN	COMMENT
$0.80 \pm 0.14 \pm 0.07$	¹ ADACHI	18	$e^+ e^- \rightarrow \Upsilon(4S)$

• • • We do not use the following data for averages, fits, limits, etc. • • •

$0.43 \pm 0.27 \pm 0.08$	² VOROBYEV	16	BELL $e^+ e^- \rightarrow \Upsilon(4S)$
$0.29 \pm 0.34 \pm 0.06$	AUBERT	07BH	BABR $e^+ e^- \rightarrow \Upsilon(4S)$
$0.78 \pm 0.44 \pm 0.22$	KROKOVNY	06	BELL Repl. by VOROBYEV 16

¹ Analyzes joint data sample of Belle and BaBar using Dalitz plot analysis of $D \rightarrow K_S^0 \pi^+ \pi^-$; the second error combines experimental systematic uncertainty and the Dalitz plot model uncertainty.

² A model-independent measurement uses the binned Dalitz plot technique.

$\beta_{\text{eff}} (B^0 \rightarrow [K_S^0 \pi^+ \pi^-]_{D^{(*)}} h^0)$

VALUE (°)	DOCUMENT ID	TECN	COMMENT
$22.5 \pm 4.4 \pm 1.3$	¹ ADACHI	18	$e^+ e^- \rightarrow \Upsilon(4S)$

• • • We do not use the following data for averages, fits, limits, etc. • • •

$11.7 \pm 7.8 \pm 2.1$	² VOROBYEV	16	BELL $e^+ e^- \rightarrow \Upsilon(4S)$
------------------------	-----------------------	----	---

¹ Analyzes joint data sample of Belle and BaBar using Dalitz plot analysis of $D \rightarrow K_S^0 \pi^+ \pi^-$; the second error combines experimental systematic uncertainty and the Dalitz plot model uncertainty.

² A model-independent measurement uses the binned Dalitz plot technique.

$2\beta_{\text{eff}} (B^0 \rightarrow J/\psi \rho^0)$

VALUE (°)	DOCUMENT ID	TECN	COMMENT
$41.7 \pm 9.6 \pm 2.8$	AAIJ	15J	LHCB pp at 7, 8 TeV

$|\lambda| (B^0 \rightarrow [K_S^0 \pi^+ \pi^-]_{D^{(*)}} h^0)$

VALUE	DOCUMENT ID	TECN	COMMENT
$1.01 \pm 0.08 \pm 0.02$	AUBERT	07BH	BABR $e^+ e^- \rightarrow \Upsilon(4S)$

$|\sin(2\beta + \gamma)|$

β (ϕ_1) and γ (ϕ_3) are angles of CKM unitarity triangle, see the review on "CP Violation" in the Reviews section.

VALUE	CL%	DOCUMENT ID	TECN	COMMENT
>0.40	90	¹ AUBERT	06Y	BABR $e^+ e^- \rightarrow \Upsilon(4S)$

• • • We do not use the following data for averages, fits, limits, etc. • • •

>0.77	68	² AAIJ	18Z	LHCB pp at 7, 8 TeV
>0.13	95	³ RONGA	06	BELL $e^+ e^- \rightarrow \Upsilon(4S)$
>0.07	95	³ RONGA	06	BELL $e^+ e^- \rightarrow \Upsilon(4S)$
>0.35	90	⁴ AUBERT	05Z	BABR $e^+ e^- \rightarrow \Upsilon(4S)$
>0.69	68	⁵ AUBERT	04V	BABR $e^+ e^- \rightarrow \Upsilon(4S)$
>0.58	95	⁶ AUBERT	04W	BABR Repl. by AUBERT 05Z

- ¹ Uses fully reconstructed $B^0 \rightarrow D^{(*)} \pi^{\pm} \pi^{\mp}$ and $D^{\pm} \rho^{\mp}$ decays and some theoretical assumptions.
- ² Uses a time dependent CP violation measurement in $B^0 \rightarrow D^{\mp} \pi^{\pm}$ decays with external input and some theoretical assumptions.
- ³ Combines the results from fully reconstructed and partially reconstructed $D^{(*)} \pi$ events by taking weighted averages. Assumes that systematic errors from physics parameters and fit biases in the two measurements are 100% correlated.
- ⁴ Uses partially reconstructed $B^0 \rightarrow D^{* \pm} \pi^{\mp}$ decays and some theoretical assumptions.
- ⁵ Uses fully reconstructed $B^0 \rightarrow D^{(*)} \pi^{\pm} \pi^{\mp}$ decays and some theoretical assumptions, such as the SU(3) symmetry relation.
- ⁶ Combining this measurement with the results from AUBERT 04v for fully reconstructed $B^0 \rightarrow D^{(*)} \pi^{\pm} \pi^{\mp}$ and some theoretical assumptions, such as the SU(3) symmetry relation.

$2\beta + \gamma$

VALUE (°)	DOCUMENT ID	TECN	COMMENT
$83 \pm 53 \pm 20$	¹ AUBERT	08AC	BABR $e^+ e^- \rightarrow \Upsilon(4S)$

¹ Used a time-dependent Dalitz-plot analysis of $B^0 \rightarrow D^{\mp} K^0 \pi^{\pm}$ assuming the ratio of the $b \rightarrow u$ and $b \rightarrow c$ decay amplitudes to be 0.3.

α
For angle $\alpha(\phi_2)$ of the CKM unitarity triangle, see the review on “CP violation” in the reviews section.
“OUR EVALUATION” is provided by the Heavy Flavor Averaging Group (HFLAV).

VALUE (°)	DOCUMENT ID	TECN	COMMENT
84.9^{+5.1}_{-4.5} OUR EVALUATION			
93.7±10.6	¹ VANHOEFER 16	BELL	$e^+e^- \rightarrow \Upsilon(4S)$
84.9±13.5	¹ VANHOEFER 14	BELL	Repl. by VANHOEFER 16
79 ± 7 ± 11	² AUBERT 10d	BABR	$e^+e^- \rightarrow \Upsilon(4S)$
92.4 ^{+6.0} _{-6.5}	¹ AUBERT 09g	BABR	$e^+e^- \rightarrow \Upsilon(4S)$
78.6± 7.3	³ AUBERT 07o	BABR	$e^+e^- \rightarrow \Upsilon(4S)$
88 ± 17	⁴ SOMOV 06	BELL	Repl. by VANHOEFER 14
100 ± 13	⁵ AUBERT,B 05c	BABR	Repl. by AUBERT 09g
102 ⁺¹⁶ ₋₁₂ ± 14	⁶ AUBERT,B 04r	BABR	Repl. by AUBERT,B 05c

- • • We do not use the following data for averages, fits, limits, etc. • • •
- ¹ Based on an isospin analysis of the $B \rightarrow \rho\rho$ system.
- ² Obtained using the time dependent analysis of $B^0 \rightarrow a_1(1260)\pi^\pm\pi^\mp$ and branching fraction measurements of $B \rightarrow a_1(1260)K$ and $B \rightarrow K_1\pi$. Uses SU(3) flavor relations.
- ³ The angle α_{eff} is obtained using the measured CP parameters of $B^0 \rightarrow a_1(1260)\pi^\pm\pi^\mp$ and choosing one of the four solutions that is compatible with the result of SM-based fits.
- ⁴ Obtained using isospin relation and selecting a solution closest to the CKM best fit average; the 90% CL allowed interval is $59^\circ < \phi_2 (\equiv \alpha) < 115^\circ$.
- ⁵ Obtained using isospin relation and selecting a solution closest to the CKM best fit average; 90% CL allowed interval is $79^\circ < \alpha < 123^\circ$.
- ⁶ Obtained from the measured CP parameters of the longitudinal polarization by selecting the solution closest to the CKM best fit central value of $\alpha = 95^\circ - 98^\circ$.

CP VIOLATION PARAMETERS IN $B^0 \rightarrow D^0 K^{*0}$ DECAY

The parameters r_{B^0} and δ_{B^0} are the magnitude ratio and strong phase difference between the amplitudes of $A(B^0 \rightarrow D^0 K^{*0})$ and $A(B^0 \rightarrow \bar{D}^0 K^{*0})$. The measured observables and are defined as $x_\pm = r_{B^0} \cos(\delta_{B^0} \pm \gamma)$ and $y_\pm = r_{B^0} \sin(\delta_{B^0} \pm \gamma)$ where γ is the CKM angle γ .

“OUR EVALUATION” is provided by the Heavy Flavor Averaging Group (HFLAV). The CKM angle γ is listed in the B⁺ section for “CP VIOLATION PARAMETERS IN $B^+ \rightarrow D K^+$ AND SIMILAR DECAYS.”

$x_+(B^0 \rightarrow DK^{*0})$

VALUE	DOCUMENT ID	TECN	COMMENT
0.04±0.17 OUR AVERAGE			
0.04±0.16±0.11	¹ AAIJ 16s	LHCB	pp at 7, 8 TeV
0.05±0.35±0.02	AAIJ 16z	LHCB	pp at 7, 8 TeV
• • • We do not use the following data for averages, fits, limits, etc. • • •			
0.05±0.24±0.04	² AAIJ 16AA	LHCB	Repl. by AAIJ 16z
¹ Uses Dalitz plot of $B^0 \rightarrow DK^+\pi^-$ with $D \rightarrow K^+K^-, \pi^+\pi^-,$ or $K^+\pi^-$.			
² Uses Dalitz plot analysis of $D \rightarrow K_S^0\pi^+\pi^-$ decays coming from $B^0 \rightarrow DK^*(892)^0$ modes.			

$x_-(B^0 \rightarrow DK^{*0})$

VALUE	DOCUMENT ID	TECN	COMMENT
-0.16±0.14 OUR AVERAGE			
-0.02±0.13±0.14	¹ AAIJ 16s	LHCB	pp at 7, 8 TeV
-0.15±0.20±0.04	AAIJ 16z	LHCB	pp at 7, 8 TeV
• • • We do not use the following data for averages, fits, limits, etc. • • •			
-0.15±0.14±0.03	² AAIJ 16AA	LHCB	Repl. by AAIJ 16z
¹ Uses Dalitz plot of $B^0 \rightarrow DK^+\pi^-$ with $D \rightarrow K^+K^-, \pi^+\pi^-,$ or $K^+\pi^-$.			
² Uses Dalitz plot analysis of $D \rightarrow K_S^0\pi^+\pi^-$ decays coming from $B^0 \rightarrow DK^*(892)^0$ modes.			

$y_+(B^0 \rightarrow DK^{*0})$

VALUE	DOCUMENT ID	TECN	COMMENT
-0.68±0.22 OUR AVERAGE			
-0.47±0.28±0.22	¹ AAIJ 16s	LHCB	pp at 7, 8 TeV
-0.81±0.28±0.06	AAIJ 16z	LHCB	pp at 7, 8 TeV
• • • We do not use the following data for averages, fits, limits, etc. • • •			
-0.65 ^{+0.24} _{-0.23} ± 0.08	² AAIJ 16AA	LHCB	Repl. by AAIJ 16z
¹ Uses Dalitz plot of $B^0 \rightarrow DK^+\pi^-$ with $D \rightarrow K^+K^-, \pi^+\pi^-,$ or $K^+\pi^-$.			
² Uses Dalitz plot analysis of $D \rightarrow K_S^0\pi^+\pi^-$ decays coming from $B^0 \rightarrow DK^*(892)^0$ modes.			

$y_-(B^0 \rightarrow DK^{*0})$

VALUE	DOCUMENT ID	TECN	COMMENT
0.20±0.25 OUR AVERAGE	Error includes scale factor of 1.2.		
-0.35±0.26±0.41	¹ AAIJ 16s	LHCB	pp at 7, 8 TeV
0.31±0.21±0.05	AAIJ 16z	LHCB	pp at 7, 8 TeV
• • • We do not use the following data for averages, fits, limits, etc. • • •			
0.25±0.15±0.06	² AAIJ 16AA	LHCB	Repl. by AAIJ 16z
¹ Uses Dalitz plot of $B^0 \rightarrow DK^+\pi^-$ with $D \rightarrow K^+K^-, \pi^+\pi^-,$ or $K^+\pi^-$.			
² Uses Dalitz plot analysis of $D \rightarrow K_S^0\pi^+\pi^-$ decays coming from $B^0 \rightarrow DK^*(892)^0$ modes.			

$r_{B^0}(B^0 \rightarrow DK^{*0})$

“OUR EVALUATION” is provided by the Heavy Flavor Averaging Group (HFLAV).

VALUE	DOCUMENT ID	TECN	COMMENT
0.220^{+0.041}_{-0.047} OUR EVALUATION			
• • • We do not use the following data for averages, fits, limits, etc. • • •			
0.39 ± 0.13	¹ AAIJ 16AA	LHCB	Repl. by AAIJ 16z
0.56 ± 0.17	² AAIJ 16z	LHCB	pp at 7, 8 TeV

- ¹ Uses Dalitz plot analysis of $D \rightarrow K_S^0\pi^+\pi^-$ decays coming from $B^0 \rightarrow DK^*(892)^0$ modes.
- ² Measurement is performed with $K^+\pi^-$ masses within 50 MeV of the K^{*0} mass and an absolute value of the cosine of the K^{*0} helicity angle greater than 0.4. Angle γ is required to satisfy $0 < \gamma < 180$ degrees.

$\delta_{B^0}(B^0 \rightarrow DK^{*0})$

“OUR EVALUATION” is provided by the Heavy Flavor Averaging Group (HFLAV).

VALUE (°)	DOCUMENT ID	TECN	COMMENT
194⁺³⁰₋₂₂ OUR EVALUATION			
• • • We do not use the following data for averages, fits, limits, etc. • • •			
197 ⁺²⁴ ₋₂₀	¹ AAIJ 16AA	LHCB	Repl. by AAIJ 16z
204 ⁺²¹ ₋₂₀	² AAIJ 16z	LHCB	pp at 7, 8 TeV

- ¹ Uses Dalitz plot analysis of $D \rightarrow K_S^0\pi^+\pi^-$ decays coming from $B^0 \rightarrow DK^*(892)^0$ modes.
- ² Measurement is performed with $K^+\pi^-$ masses within 50 MeV of the K^{*0} mass and an absolute value of the cosine of the K^{*0} helicity angle greater than 0.4. Angle γ is required to satisfy $0 < \gamma < 180$ degrees.

T and CPT VIOLATION PARAMETERS

Measured values of the T -, CP -, and CPT -asymmetry parameters, defined as the differences in $S_{\alpha,\beta}^\pm$ and $C_{\alpha,\beta}^\pm$ between symmetry-transformed transitions. The indices $\alpha = \ell^+, \ell^-$ and $\beta = K_S^0, K_L^0$ stand for reconstructed the flavor final state and the CP final states from $\Upsilon(4S)$ decay. The sign \pm indicates whether the decay to the flavor final state α occurs before or after the decay to the CP final state.

Alternatively, violations of CPT symmetry and Lorentz invariance are searched for by studying interference effects in B^0 mixing. Results are expressed in terms of the standard model extension parameter Δ_a , which describes the difference between the couplings of the valence quarks within B^0 meson with the Lorentz-violating fields.

$\Delta S_T^+(S_{\ell^-,K_S^0}^- - S_{\ell^+,K_S^0}^+)$

VALUE	DOCUMENT ID	TECN	COMMENT
-1.37±0.14±0.06	LEES 12w	BABR	$e^+e^- \rightarrow \Upsilon(4S)$

$\Delta S_T^-(S_{\ell^-,K_S^0}^+ - S_{\ell^+,K_S^0}^-)$

VALUE	DOCUMENT ID	TECN	COMMENT
1.17±0.18±0.11	LEES 12w	BABR	$e^+e^- \rightarrow \Upsilon(4S)$

$\Delta C_T^+(C_{\ell^-,K_S^0}^- - C_{\ell^+,K_S^0}^+)$

VALUE	DOCUMENT ID	TECN	COMMENT
0.10±0.14±0.08	LEES 12w	BABR	$e^+e^- \rightarrow \Upsilon(4S)$

$\Delta C_T^-(C_{\ell^-,K_S^0}^+ - C_{\ell^+,K_S^0}^-)$

VALUE	DOCUMENT ID	TECN	COMMENT
0.04±0.14±0.08	LEES 12w	BABR	$e^+e^- \rightarrow \Upsilon(4S)$

$\Delta S_{CP}^+(S_{\ell^-,K_S^0}^+ - S_{\ell^+,K_S^0}^-)$

VALUE	DOCUMENT ID	TECN	COMMENT
-1.30±0.11±0.07	LEES 12w	BABR	$e^+e^- \rightarrow \Upsilon(4S)$

$\Delta S_{CP}^-(S_{\ell^-,K_S^0}^- - S_{\ell^+,K_S^0}^+)$

VALUE	DOCUMENT ID	TECN	COMMENT
1.33±0.12±0.06	LEES 12w	BABR	$e^+e^- \rightarrow \Upsilon(4S)$

$\Delta C_{CP}^+(C_{\ell^-,K_S^0}^+ - C_{\ell^+,K_S^0}^-)$

VALUE	DOCUMENT ID	TECN	COMMENT
0.07±0.09±0.03	LEES 12w	BABR	$e^+e^- \rightarrow \Upsilon(4S)$

$\Delta C_{CP}^-(C_{\ell^-,K_S^0}^- - C_{\ell^+,K_S^0}^+)$

VALUE	DOCUMENT ID	TECN	COMMENT
0.08±0.10±0.04	LEES 12w	BABR	$e^+e^- \rightarrow \Upsilon(4S)$

$\Delta S_{CPT}^+(S_{\ell^+,K_S^0}^- - S_{\ell^-,K_S^0}^+)$

VALUE	DOCUMENT ID	TECN	COMMENT
0.16±0.21±0.09	LEES 12w	BABR	$e^+e^- \rightarrow \Upsilon(4S)$

Meson Particle Listings

B^0

$\Delta S_{CPT} (S^+_{\ell^+, K^0_S} - S^-_{\ell^+, K^0_S})$

VALUE	DOCUMENT ID	TECN	COMMENT
$-0.03 \pm 0.13 \pm 0.06$	LEES	12W	BABR $e^+ e^- \rightarrow \Upsilon(4S)$

$\Delta C^+_{CPT} (C^-_{\ell^+, K^0_S} - C^+_{\ell^+, K^0_S})$

VALUE	DOCUMENT ID	TECN	COMMENT
$0.14 \pm 0.15 \pm 0.07$	LEES	12W	BABR $e^+ e^- \rightarrow \Upsilon(4S)$

$\Delta C^-_{CPT} (C^+_{\ell^+, K^0_S} - C^-_{\ell^+, K^0_S})$

VALUE	DOCUMENT ID	TECN	COMMENT
$0.03 \pm 0.12 \pm 0.08$	LEES	12W	BABR $e^+ e^- \rightarrow \Upsilon(4S)$

$\Delta a_{||}$ CPT parameter in B^0 mixing

VALUE (10^{-15} GeV)	DOCUMENT ID	TECN	COMMENT
$-0.10 \pm 0.82 \pm 0.54$	¹ AAIJ	16E	LHCB pp at 7, 8 TeV

¹ Uses $B^0 \rightarrow J/\psi K^0_S$ decays.

Δa_{\perp} CPT parameter in B^0 mixing

VALUE (10^{-13} GeV)	DOCUMENT ID	TECN	COMMENT
$-0.20 \pm 0.22 \pm 0.04$	¹ AAIJ	16E	LHCB pp at 7, 8 TeV

¹ Uses $B^0 \rightarrow J/\psi K^0_S$ decays.

Δa_{χ} CPT parameter in B^0 mixing

VALUE (10^{-15} GeV)	DOCUMENT ID	TECN	COMMENT
$+1.97 \pm 1.30 \pm 0.29$	¹ AAIJ	16E	LHCB pp at 7, 8 TeV

¹ Uses $B^0 \rightarrow J/\psi K^0_S$ decays.

Δa_{γ} CPT parameter in B^0 mixing

VALUE (10^{-15} GeV)	DOCUMENT ID	TECN	COMMENT
$+0.44 \pm 1.26 \pm 0.29$	¹ AAIJ	16E	LHCB pp at 7, 8 TeV

¹ Uses $B^0 \rightarrow J/\psi K^0_S$ decays.

$B^0 \rightarrow D^{*-} \ell^+ \nu_{\ell}$ FORM FACTORS

R_1 (form factor ratio $\sim V/A_1$)

VALUE	DOCUMENT ID	TECN	COMMENT
1.239 ± 0.029 OUR AVERAGE			
$1.229 \pm 0.028 \pm 0.009$	¹ WAHEED	19	BELL $e^+ e^- \rightarrow \Upsilon(4S)$
$1.56 \pm 0.07 \pm 0.15$	AUBERT	09A	BABR $e^+ e^- \rightarrow \Upsilon(4S)$
$1.18 \pm 0.30 \pm 0.12$	DUBOSCQ	96	CLE2 $e^+ e^- \rightarrow \Upsilon(4S)$

• • • We do not use the following data for averages, fits, limits, etc. • • •

$1.401 \pm 0.034 \pm 0.018$	¹ DUNGEL	10	BELL Repl. by WAHEED 19
$1.429 \pm 0.061 \pm 0.044$	AUBERT	08R	BABR Repl. by AUBERT 09A
$1.396 \pm 0.060 \pm 0.044$	AUBERT,B	06Z	BABR Repl. by AUBERT 08R

¹ Uses fully reconstructed $D^{*-} \ell^+ \nu$ events ($\ell = e$ or μ).

R_2 (form factor ratio $\sim A_2/A_1$)

VALUE	DOCUMENT ID	TECN	COMMENT
0.84 ± 0.04 OUR AVERAGE			Error includes scale factor of 1.8.
$0.852 \pm 0.021 \pm 0.006$	¹ WAHEED	19	BELL $e^+ e^- \rightarrow \Upsilon(4S)$
$0.66 \pm 0.05 \pm 0.09$	AUBERT	09A	BABR $e^+ e^- \rightarrow \Upsilon(4S)$
$0.71 \pm 0.22 \pm 0.07$	DUBOSCQ	96	CLE2 $e^+ e^- \rightarrow \Upsilon(4S)$

• • • We do not use the following data for averages, fits, limits, etc. • • •

$0.864 \pm 0.024 \pm 0.008$	¹ DUNGEL	10	BELL Repl. by WAHEED 19
$0.827 \pm 0.038 \pm 0.022$	AUBERT	08R	BABR Repl. by AUBERT 09A
$0.885 \pm 0.040 \pm 0.026$	AUBERT,B	06Z	BABR Repl. by AUBERT 08R

¹ Uses fully reconstructed $D^{*-} \ell^+ \nu$ events ($\ell = e$ or μ).

$\rho^2_{A_1}$ (form factor slope)

VALUE	DOCUMENT ID	TECN	COMMENT
1.12 ± 0.04 OUR AVERAGE			Error includes scale factor of 1.5.
$1.106 \pm 0.031 \pm 0.007$	¹ WAHEED	19	BELL $e^+ e^- \rightarrow \Upsilon(4S)$
$1.22 \pm 0.02 \pm 0.07$	AUBERT	09A	BABR $e^+ e^- \rightarrow \Upsilon(4S)$
$0.91 \pm 0.15 \pm 0.06$	DUBOSCQ	96	CLE2 $e^+ e^- \rightarrow \Upsilon(4S)$

• • • We do not use the following data for averages, fits, limits, etc. • • •

$1.214 \pm 0.034 \pm 0.009$	¹ DUNGEL	10	BELL Repl. by WAHEED 19
$1.191 \pm 0.048 \pm 0.028$	AUBERT	08R	BABR Repl. by AUBERT 09A
$1.145 \pm 0.059 \pm 0.046$	AUBERT,B	06Z	BABR Repl. by AUBERT 08R

¹ Uses fully reconstructed $D^{*-} \ell^+ \nu$ events ($\ell = e$ or μ).

PARTIAL BRANCHING FRACTIONS IN $B^0 \rightarrow K^{(*)0} \ell^+ \ell^-$

$B(B^0 \rightarrow K^{*0} e^+ e^-) (0.0009 < q^2 < 1.0 \text{ GeV}^2/c^4)$

VALUE (units 10^{-7})	DOCUMENT ID	TECN	COMMENT
$3.1^{+0.9+0.2}_{-0.8-0.3} \pm 0.2$	¹ AAIJ	13U	LHCB pp at 7 TeV

¹ The last uncertainty is due to uncertainties of $B(B^0 \rightarrow J/\psi K^{*0})$ and $B(J/\psi \rightarrow e^+ e^-)$ branching fraction measurements.

$B(B^0 \rightarrow K^{*0} \ell^+ \ell^-) (0.1 < q^2 < 2.0 \text{ GeV}^2/c^4)$

VALUE (units 10^{-7})	DOCUMENT ID	TECN	COMMENT
$1.24^{+0.23}_{-0.27}$ OUR AVERAGE			Error includes scale factor of 1.6.
$1.14 \pm 0.11^{+0.11}_{-0.15}$	AAIJ	13Y	LHCB pp at 7 TeV, $K^{*0} \mu^+ \mu^-$
$1.80 \pm 0.36 \pm 0.11$	AALTONEN	11AI	CDF $p\bar{p}$ at 1.96 TeV

• • • We do not use the following data for averages, fits, limits, etc. • • •

$0.48^{+0.14}_{-0.12} \pm 0.04$	¹ CHATRCHYAN	13BL	CMS pp at 7 TeV
$1.16 \pm 0.23 \pm 0.11$	AAIJ	12U	LHCB Repl. by AAIJ 13Y

¹ CHATRCHYAN 13BL uses, for this bin, $1.0 < q^2 < 2.0 \text{ GeV}^2/c^4$.

$B(B^0 \rightarrow K^{*0} \ell^+ \ell^-) (2.0 < q^2 < 4.3 \text{ GeV}^2/c^4)$

VALUE (units 10^{-7})	DOCUMENT ID	TECN	COMMENT
0.76 ± 0.07 OUR AVERAGE			
$0.759 \pm 0.115 \pm 0.046$	KHACHATRY..	16D	CMS pp at 8 TeV
$0.69 \pm 0.07 \pm 0.09$	AAIJ	13Y	LHCB pp at 7 TeV, $K^{*0} \mu^+ \mu^-$
$0.87 \pm 0.16 \pm 0.07$	CHATRCHYAN	13BL	CMS pp at 7 TeV
$0.84 \pm 0.28 \pm 0.06$	AALTONEN	11AI	CDF $p\bar{p}$ at 1.96 TeV

• • • We do not use the following data for averages, fits, limits, etc. • • •

$0.78 \pm 0.21 \pm 0.05$	AAIJ	12U	LHCB Repl. by AAIJ 13Y
--------------------------	------	-----	------------------------

$B(B^0 \rightarrow K^{*0} \ell^+ \ell^-) (4.3 < q^2 < 8.68 \text{ GeV}^2/c^4)$

VALUE (units 10^{-7})	DOCUMENT ID	TECN	COMMENT
1.87 ± 0.21 OUR AVERAGE			
$2.15 \pm 0.18^{+0.22}_{-0.28}$	AAIJ	13Y	LHCB pp at 7 TeV, $K^{*0} \mu^+ \mu^-$
$1.62 \pm 0.31 \pm 0.18$	CHATRCHYAN	13BL	CMS pp at 7 TeV
$1.73 \pm 0.43 \pm 0.15$	AALTONEN	11AI	CDF $p\bar{p}$ at 1.96 TeV

• • • We do not use the following data for averages, fits, limits, etc. • • •

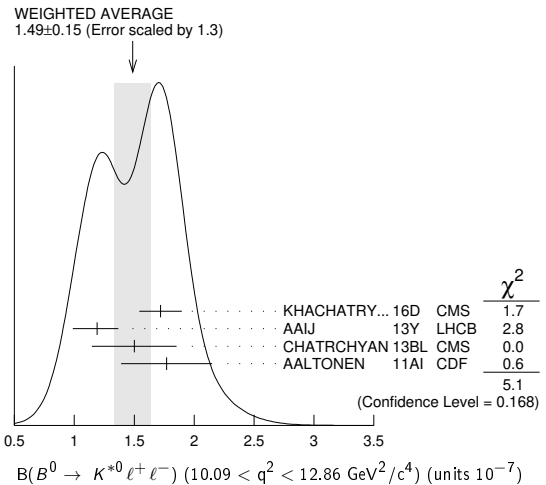
$3.02 \pm 0.35 \pm 0.22$	AAIJ	12U	LHCB Repl. by AAIJ 13Y
--------------------------	------	-----	------------------------

$B(B^0 \rightarrow K^{*0} \ell^+ \ell^-) (10.09 < q^2 < 12.86 \text{ GeV}^2/c^4)$

VALUE (units 10^{-7})	DOCUMENT ID	TECN	COMMENT
1.49 ± 0.15 OUR AVERAGE			Error includes scale factor of 1.3. See the ideogram below.
$1.72 \pm 0.11 \pm 0.14$	KHACHATRY..	16D	CMS pp at 8 TeV
$1.19 \pm 0.11^{+0.14}_{-0.17}$	AAIJ	13Y	LHCB pp at 7 TeV, $K^{*0} \mu^+ \mu^-$
$1.50 \pm 0.25 \pm 0.25$	CHATRCHYAN	13BL	CMS pp at 7 TeV
$1.77 \pm 0.36 \pm 0.12$	AALTONEN	11AI	CDF $p\bar{p}$ at 1.96 TeV

• • • We do not use the following data for averages, fits, limits, etc. • • •

$1.52 \pm 0.25 \pm 0.19$	AAIJ	12U	LHCB Repl. by AAIJ 13Y
--------------------------	------	-----	------------------------



$B(B^0 \rightarrow K^{*0} \ell^+ \ell^-) (14.18 < q^2 < 16.0 \text{ GeV}^2/c^4)$

VALUE (units 10^{-7})	DOCUMENT ID	TECN	COMMENT
1.09 ± 0.10 OUR AVERAGE			Error includes scale factor of 1.1.
$1.22 \pm 0.11 \pm 0.09$	KHACHATRY..	16D	CMS pp at 8 TeV
$1.02 \pm 0.11^{+0.11}_{-0.15}$	AAIJ	13Y	LHCB pp at 7 TeV, $K^{*0} \mu^+ \mu^-$
$0.84^{+0.16}_{-0.15} \pm 0.09$	CHATRCHYAN	13BL	CMS pp at 7 TeV
$1.34 \pm 0.26 \pm 0.08$	AALTONEN	11AI	CDF $p\bar{p}$ at 1.96 TeV

• • • We do not use the following data for averages, fits, limits, etc. • • •

$1.15 \pm 0.20 \pm 0.09$	AAIJ	12U	LHCB Repl. by AAIJ 13Y
--------------------------	------	-----	------------------------

See key on page 999

Meson Particle Listings

 B^0 $B(B^0 \rightarrow K^{*0} \ell^+ \ell^-) (16.0 < q^2 < 19.0 \text{ GeV}^2/c^4)$

VALUE (units 10^{-7})	DOCUMENT ID	TECN	COMMENT
1.27 ± 0.09 OUR AVERAGE			
1.26 ± 0.09 ± 0.09	KHACHATRY...16D	CMS	pp at 8 TeV
1.23 ± 0.12 ^{+0.15} _{-0.18}	AAIJ	13Y LHCb	pp at 7 TeV, $K^{*0} \mu^+ \mu^-$
1.56 ± 0.18 ± 0.15	CHATRCHYAN13BL	CMS	pp at 7 TeV
0.97 ± 0.26 ± 0.07	AALTONEN	11AI CDF	$p\bar{p}$ at 1.96 TeV
• • • We do not use the following data for averages, fits, limits, etc. • • •			
1.50 ± 0.24 ± 0.15	AAIJ	12U LHCb	Repl. by AAIJ 13Y

 $B(B^0 \rightarrow K^*(892)^0 \ell^+ \ell^-) (15.0 < q^2 < 19.0 \text{ GeV}^2/c^4)$

VALUE (units 10^{-7})	DOCUMENT ID	TECN	COMMENT
1.744^{+0.072}_{-0.076} ± 0.123	AAIJ	17Q LHCb	pp at 7, 8 TeV
• • • We do not use the following data for averages, fits, limits, etc. • • •			
1.95 ^{+0.08} _{-0.09} ± 0.13	AAIJ	16Ao LHCb	Repl. by AAIJ 17Q

 $B(B^0 \rightarrow K^{*0} \ell^+ \ell^-) (1.0 < q^2 < 6.0 \text{ GeV}^2/c^4)$

VALUE (units 10^{-7})	DOCUMENT ID	TECN	COMMENT
1.73 ± 0.11 OUR AVERAGE			
1.68 ± 0.083 ± 0.12	¹ AAIJ	17Q LHCb	pp at 7, 8 TeV
1.90 ± 0.20	KHACHATRY...16D	CMS	pp at 7, 8 TeV
1.42 ± 0.41 ± 0.12	AALTONEN	11AI CDF	$p\bar{p}$ at 1.96 TeV
• • • We do not use the following data for averages, fits, limits, etc. • • •			
1.92 ^{+0.10} _{-0.09} ± 0.14	AAIJ	16Ao LHCb	Repl. by AAIJ 17Q
1.70 ± 0.15 ^{+0.20} _{-0.25}	AAIJ	13Y LHCb	Repl. by AAIJ 16Ao
2.20 ± 0.30 ± 0.20	CHATRCHYAN13BL	CMS	Repl. by KHACHATRYAN 16D
2.10 ± 0.30 ± 0.15	AAIJ	12U LHCb	Repl. by AAIJ 13Y
¹ AAIJ 17Q result is determined for the range $1.1 < q^2 < 6.0 \text{ GeV}^2/c^2$.			

 $B(B^0 \rightarrow K^{*0} \ell^+ \ell^-) (0.0 < q^2 < 4.3 \text{ GeV}^2/c^4)$

VALUE (units 10^{-7})	DOCUMENT ID	TECN	COMMENT
2.60 ± 0.45 ± 0.17	AALTONEN	11AI CDF	$p\bar{p}$ at 1.96 TeV

 $B(B^0 \rightarrow K^{*0} \mu^+ \mu^-)/B(B^0 \rightarrow K^{*0} e^+ e^-) (0.045 < q^2 < 1.1 \text{ GeV}^2/c^4)$

VALUE	DOCUMENT ID	TECN	COMMENT
0.66^{+0.11}_{-0.07} ± 0.03	AAIJ	17W LHCb	pp at 7, 8 TeV

 $B(B^0 \rightarrow K^{*0} \mu^+ \mu^-)/B(B^0 \rightarrow K^{*0} e^+ e^-) (1.1 < q^2 < 6.0 \text{ GeV}^2/c^4)$

VALUE	DOCUMENT ID	TECN	COMMENT
0.69^{+0.11}_{-0.07} ± 0.05	AAIJ	17W LHCb	pp at 7, 8 TeV

 $B(B^0 \rightarrow K^0 \ell^+ \ell^-) (q^2 < 2.0 \text{ GeV}^2/c^4)$

VALUE (units 10^{-7})	DOCUMENT ID	TECN	COMMENT
0.24^{+0.22}_{-0.20} OUR AVERAGE			
0.21 ^{+0.27} _{-0.23}	AAIJ	12AH LHCb	pp at 7 TeV
0.31 ± 0.37 ± 0.02	AALTONEN	11AI CDF	$p\bar{p}$ at 1.96 TeV

 $B(B^0 \rightarrow K^0 \ell^+ \ell^-) (2.0 < q^2 < 4.3 \text{ GeV}^2/c^4)$

VALUE (units 10^{-7})	DOCUMENT ID	TECN	COMMENT
0.24^{+0.35}_{-0.30} OUR AVERAGE			Error includes scale factor of 1.6.
0.07 ^{+0.25} _{-0.21}	AAIJ	12AH LHCb	pp at 7 TeV
0.93 ± 0.49 ± 0.07	AALTONEN	11AI CDF	$p\bar{p}$ at 1.96 TeV

 $B(B^0 \rightarrow K^0 \ell^+ \ell^-) (4.3 < q^2 < 8.68 \text{ GeV}^2/c^4)$

VALUE (units 10^{-7})	DOCUMENT ID	TECN	COMMENT
1.08 ± 0.27 OUR AVERAGE			
1.23 ± 0.31	AAIJ	12AH LHCb	pp at 7 TeV
0.66 ± 0.51 ± 0.05	AALTONEN	11AI CDF	$p\bar{p}$ at 1.96 TeV

 $B(B^0 \rightarrow K^0 \ell^+ \ell^-) (10.09 < q^2 < 12.86 \text{ GeV}^2/c^4)$

VALUE (units 10^{-7})	DOCUMENT ID	TECN	COMMENT
0.27 ± 0.27 OUR AVERAGE			Error includes scale factor of 1.8.
0.50 ^{+0.22} _{-0.19}	AAIJ	12AH LHCb	pp at 7 TeV
-0.03 ± 0.22 ± 0.01	AALTONEN	11AI CDF	$p\bar{p}$ at 1.96 TeV

 $B(B^0 \rightarrow K^0 \ell^+ \ell^-) (14.18 < q^2 < 16.0 \text{ GeV}^2/c^4)$

VALUE (units 10^{-7})	DOCUMENT ID	TECN	COMMENT
0.29^{+0.21}_{-0.15} OUR AVERAGE			Error includes scale factor of 1.8.
0.20 ^{+0.13} _{-0.09}	AAIJ	12AH LHCb	pp at 7 TeV
0.73 ± 0.26 ± 0.06	AALTONEN	11AI CDF	$p\bar{p}$ at 1.96 TeV

 $B(B^0 \rightarrow K^0 \ell^+ \ell^-) (q^2 > 16.0 \text{ GeV}^2/c^4)$

VALUE (units 10^{-7})	DOCUMENT ID	TECN	COMMENT
0.31^{+0.16}_{-0.12} OUR AVERAGE			
0.35 ^{+0.21} _{-0.14}	AAIJ	12AH LHCb	pp at 7 TeV
0.21 ± 0.18 ± 0.16	AALTONEN	11AI CDF	$p\bar{p}$ at 1.96 TeV

 $B(B^0 \rightarrow K^0 \ell^+ \ell^-) (1.0 < q^2 < 6.0 \text{ GeV}^2/c^4)$

VALUE (units 10^{-7})	DOCUMENT ID	TECN	COMMENT
0.92 ± 0.16 OUR AVERAGE			
0.916 ^{+0.172} _{-0.157} ± 0.004	¹ AAIJ	14M LHCb	pp at 7, 8 TeV
0.98 ± 0.61 ± 0.08	AALTONEN	11AI CDF	$p\bar{p}$ at 1.96 TeV
• • • We do not use the following data for averages, fits, limits, etc. • • •			
0.65 ^{+0.45} _{-0.35}	AAIJ	12AH LHCb	Repl. by AAIJ 14M
¹ Uses $B(B^0 \rightarrow J/\psi(1S) K^0) = (0.928 \pm 0.013 \pm 0.037) \times 10^{-3}$ for normalisation and $\mu^+ \mu^-$ as a lepton pair. Measured in $1.1 < q^2 < 6.0 \text{ GeV}^2/c^4$.			

 $B(B^0 \rightarrow K^0 \ell^+ \ell^-) (0.0 < q^2 < 4.3 \text{ GeV}^2/c^4)$

VALUE (units 10^{-7})	DOCUMENT ID	TECN	COMMENT
1.27 ± 0.62 ± 0.10	AALTONEN	11AI CDF	$p\bar{p}$ at 1.96 TeV

 $B(B^0 \rightarrow K^0 \ell^+ \ell^-) (15.0 < q^2 < 22.0 \text{ GeV}^2/c^4)$

VALUE (units 10^{-7})	DOCUMENT ID	TECN	COMMENT
0.67^{+0.11}_{-0.11} ± 0.04	¹ AAIJ	14M LHCb	pp at 7, 8 TeV
¹ Uses $B(B^0 \rightarrow J/\psi(1S) K^0) = (0.928 \pm 0.013 \pm 0.037) \times 10^{-3}$ for normalisation and $\mu^+ \mu^-$ as a lepton pair.			

 $B(B^0 \rightarrow K_{0,2}^*(1430)^0 \mu^+ \mu^-) (1.10 < q^2 < 6.00 \text{ GeV}^2/c^4)$

VALUE (units 10^{-8})	DOCUMENT ID	TECN	COMMENT
4.02 ± 0.44 ± 0.31	^{1,2} AAIJ	16AP LHCb	pp at 7, 8 TeV
¹ Measured the differential branching fraction and angular moments of the decay $B^0 \rightarrow K^+ \pi^- \mu^+ \mu^-$ in the $K^+ \pi^-$ invariant mass range $1330 < m(K^+ \pi^-) < 1530 \text{ MeV}/c^2$.			
² The reported value is converted from the measured $d\mathcal{B}/dq^2 = (0.82 \pm 0.09 \pm 0.063) \times 10^{-8} (\text{GeV}^2/c^4)^{-1}$ by multiplying by the $\Delta q^2 = 4.9 \text{ GeV}^2/c^4$ range.			

 $F_H(B^0 \rightarrow K^0 \mu^+ \mu^-) (1.1 < q^2 < 6.0 \text{ GeV}^2/c^4)$

F_H is a fractional contribution of (pseudo) scalar and tensor amplitudes to the decay width in the massless muon approximation.

VALUE	DOCUMENT ID	TECN	COMMENT
0.78 ± 0.46 ± 0.09	¹ AAIJ	14o LHCb	pp at 7, 8 TeV
¹ AAIJ 14o reports 68% C.L. interval, which we encode as midpoint with uncertainty as half of the width of interval.			

 $F_H(B^0 \rightarrow K^0 \mu^+ \mu^-) (15.0 < q^2 < 22.0 \text{ GeV}^2/c^4)$

VALUE	DOCUMENT ID	TECN	COMMENT
0.34 ± 0.25 ± 0.03	¹ AAIJ	14o LHCb	pp at 7, 8 TeV
¹ AAIJ 14o reports 68% C.L. interval, which we encode as midpoint with uncertainty as half of the width of interval.			

PRODUCTION ASYMMETRIES

 $A_P(B^0)$

$$A_P(B^0) = [\sigma(\bar{B}^0) - \sigma(B^0)] / [\sigma(\bar{B}^0) + \sigma(B^0)]$$

VALUE (units 10^{-2})	DOCUMENT ID	TECN	COMMENT
-0.3 ± 0.6 OUR AVERAGE			Error includes scale factor of 1.7. See the ideogram below.
0.44 ± 0.88 ± 0.11	¹ AAIJ	17BF LHCb	pp at 7 TeV
-1.40 ± 0.55 ± 0.10	¹ AAIJ	17BF LHCb	pp at 8 TeV
0.25 ± 0.48 ± 0.05	² AABOUD	16G ATLS	pp at 7, 8 TeV
• • • We do not use the following data for averages, fits, limits, etc. • • •			
-0.35 ± 0.76 ± 0.28	³ AAIJ	14BP LHCb	Repl. by AAIJ 17BF, pp at 7 TeV

¹ AAIJ 17BF uses $B^0 \rightarrow J/\psi K^{*0}$ decays with B^0 transverse momenta p_T and rapidities y in the region of $0 < p_T < 30 \text{ GeV}/c$ and $2.1 < y < 4.5$.

² Based on time-dependent analysis of $B^0 \rightarrow J/\psi K^{*0}$ decay in kinematic range $p_T > 10 \text{ GeV}/c$ and $|\eta| < 2.5$.

³ Based on time-dependent analysis of $B^0 \rightarrow J/\psi K^{*0}$ and $B^0 \rightarrow D^- \pi^+$ in kinematic range $4 < p_T < 30 \text{ GeV}/c$ and $2.5 < \eta < 4.5$.

See key on page 999

Meson Particle Listings

B⁰

Table of meson particle listings including particle names (e.g., KRONENBIT, LEES), codes (e.g., 12, 12AA), and references (e.g., PR D86 071103). Includes a section for 'Also' with 'EPAPS Document No. E-PR/LTAO-102-060910' and a corresponding 'EPAPS Supplement'.

Meson Particle Listings

B⁰

Table with columns for particle name, quantum numbers, and author references. Includes particles like AUBERT.B, BABAR Collab., and various experimental collaborations. Includes a large black redaction box on the left side.

Downloaded from https://academic.oup.com/ptep/article/2020/8/083C01/5891211 by guest on 20 August 2020

Meson Particle Listings

 B^\pm/B^0 ADMIXTURE

Γ_{11}	$\bar{D}_1(2420)\ell^+\nu_\ell$ anything	(3.8 ± 1.3) × 10 ⁻³	S=2.4	Γ_{72}	$K_4^*(2045)\gamma$	< 1.0	× 10 ⁻³	CL=90%
Γ_{12}	$D\pi\ell^+\nu_\ell$ anything + $D^*\pi\ell^+\nu_\ell$ anything	(2.6 ± 0.5) %	S=1.5	Γ_{73}	$K\eta'(958)$	(8.3 ± 1.1) × 10 ⁻⁵		
Γ_{13}	$D\pi\ell^+\nu_\ell$ anything	(1.5 ± 0.6) %		Γ_{74}	$K^*(892)\eta'(958)$	(4.1 ± 1.1) × 10 ⁻⁶		
Γ_{14}	$D^*\pi\ell^+\nu_\ell$ anything	(1.9 ± 0.4) %		Γ_{75}	$K\eta$	< 5.2	× 10 ⁻⁶	CL=90%
Γ_{15}	$\bar{D}_2^*(2460)\ell^+\nu_\ell$ anything	(4.4 ± 1.6) × 10 ⁻³		Γ_{76}	$K^*(892)\eta$	(1.8 ± 0.5) × 10 ⁻⁵		
Γ_{16}	$D^*\pi^+\ell^+\nu_\ell$ anything	(1.00 ± 0.34) %		Γ_{77}	$K\phi\phi$	(2.3 ± 0.9) × 10 ⁻⁶		
Γ_{17}	$\bar{D}\pi^+\pi^-\ell^+\nu_\ell$	(1.62 ± 0.32) × 10 ⁻³		Γ_{78}	$\bar{b} \rightarrow \bar{s}\gamma$	(3.49 ± 0.19) × 10 ⁻⁴		
Γ_{18}	$\bar{D}^*\pi^+\pi^-\ell^+\nu_\ell$	(9.4 ± 3.2) × 10 ⁻⁴		Γ_{79}	$\bar{b} \rightarrow \bar{d}\gamma$	(9.2 ± 3.0) × 10 ⁻⁶		
Γ_{19}	$D_s^-\ell^+\nu_\ell$ anything	[b] < 7	× 10 ⁻³ CL=90%	Γ_{80}	$\bar{b} \rightarrow \bar{s}$ gluon	< 6.8	%	CL=90%
Γ_{20}	$D_s^-\ell^+\nu_\ell K^+$ anything	[b] < 5	× 10 ⁻³ CL=90%	Γ_{81}	η anything	(2.6 ± 0.5) × 10 ⁻⁴		
Γ_{21}	$D_s^-\ell^+\nu_\ell K^0$ anything	[b] < 7	× 10 ⁻³ CL=90%	Γ_{82}	η' anything	(4.2 ± 0.9) × 10 ⁻⁴		
Γ_{22}	$X_c\ell^+\nu_\ell$	(10.65 ± 0.16) %		Γ_{83}	K^+ gluon (charmless)	< 1.87	× 10 ⁻⁴	CL=90%
Γ_{23}	$X_u\ell^+\nu_\ell$	(2.13 ± 0.30) × 10 ⁻³		Γ_{84}	K^0 gluon (charmless)	(1.9 ± 0.7) × 10 ⁻⁴		
Γ_{24}	$K^+\ell^+\nu_\ell$ anything	[b] (6.3 ± 0.6) %		Light unflavored meson modes				
Γ_{25}	$K^-\ell^+\nu_\ell$ anything	[b] (10 ± 4) × 10 ⁻³		Γ_{85}	$\rho\gamma$	(1.39 ± 0.25) × 10 ⁻⁶		S=1.2
Γ_{26}	$K^0/\bar{K}^0\ell^+\nu_\ell$ anything	[b] (4.6 ± 0.5) %		Γ_{86}	$\rho/\omega\gamma$	(1.30 ± 0.23) × 10 ⁻⁶		S=1.2
Γ_{27}	$\bar{D}^*\tau^+\nu_\tau$	(9.9 ± 1.2) × 10 ⁻³		Γ_{87}	π^\pm anything	[f,i] (358 ± 7) %		
Γ_{28}	$D^*\tau^+\nu_\tau$	(1.50 ± 0.08) %		Γ_{88}	π^0 anything	(235 ± 11) %		
D, D*, or D_s modes				Γ_{89}	η anything	(17.6 ± 1.6) %		
Γ_{29}	D^\pm anything	(23.1 ± 1.2) %		Γ_{90}	ρ^0 anything	(21 ± 5) %		
Γ_{30}	D^0/\bar{D}^0 anything	(61.5 ± 2.9) %	S=1.3	Γ_{91}	ω anything	< 81	%	CL=90%
Γ_{31}	$D^*(2010)^\pm$ anything	(22.5 ± 1.5) %		Γ_{92}	ϕ anything	(3.43 ± 0.12) %		
Γ_{32}	$D^*(2007)^0$ anything	(26.0 ± 2.7) %		Γ_{93}	$\phi K^*(892)$	< 2.2	× 10 ⁻⁵	CL=90%
Γ_{33}	D_s^\pm anything	[f] (8.3 ± 0.8) %		Γ_{94}	$\bar{b} \rightarrow \bar{d}$ gluon			
Γ_{34}	D_s^\pm anything	(6.3 ± 1.0) %		Γ_{95}	π^+ gluon (charmless)	(3.7 ± 0.8) × 10 ⁻⁴		
Γ_{35}	$D_s^*\bar{D}^*(*)$	(3.4 ± 0.6) %		Baryon modes				
Γ_{36}	$\bar{D}D_{s0}(2317)$	seen		Γ_{96}	$\Lambda_c^+/\bar{\Lambda}_c^-$ anything	(3.6 ± 0.4) %		
Γ_{37}	$\bar{D}D_{sJ}(2457)$	seen		Γ_{97}	Λ_c^+ anything	< 1.3	%	CL=90%
Γ_{38}	$D^*(*)\bar{D}^*(*)K^0 + D^*(*)\bar{D}^*(*)K^\pm$ [f,g]	(7.1 ± 2.7) %		Γ_{98}	$\bar{\Lambda}_c^-$ anything	< 7	%	CL=90%
Γ_{39}	$b \rightarrow c\bar{c}s$	(22 ± 4) %		Γ_{99}	$\bar{\Lambda}_c^- \ell^+$ anything	< 9	× 10 ⁻⁴	CL=90%
Γ_{40}	$D_s^*(*)\bar{D}^*(*)$	[f,g] (3.9 ± 0.4) %		Γ_{100}	$\bar{\Lambda}_c^- e^+$ anything	< 1.8	× 10 ⁻³	CL=90%
Γ_{41}	$D^*(2010)^\pm$	[f] < 5.9	× 10 ⁻³ CL=90%	Γ_{101}	$\bar{\Lambda}_c^- \mu^+$ anything	< 1.4	× 10 ⁻³	CL=90%
Γ_{42}	$D D^*(2010)^\pm + D^* D^\pm$	[f] < 5.5	× 10 ⁻³ CL=90%	Γ_{102}	$\bar{\Lambda}_c^- p$ anything	(2.04 ± 0.33) %		
Γ_{43}	$D D^\pm$	[f] < 3.1	× 10 ⁻³ CL=90%	Γ_{103}	$\bar{\Lambda}_c^- p e^+\nu_e$	< 8	× 10 ⁻⁴	CL=90%
Γ_{44}	$D_s^*(*)\bar{D}^*(*)X(n\pi^\pm)$	[f,g] (9 ± 5) %		Γ_{104}	$\bar{\Sigma}_c^{--}$ anything	(3.3 ± 1.7) × 10 ⁻³		
Γ_{45}	$D^*(2010)\gamma$	< 1.1	× 10 ⁻³ CL=90%	Γ_{105}	$\bar{\Sigma}_c^-$ anything	< 8	× 10 ⁻³	CL=90%
Γ_{46}	$D_s^+\pi^-, D_s^{*+}\pi^-, D_s^+\rho^-, D_s^{*+}\rho^-, D_s^+\pi^0, D_s^{*+}\pi^0, D_s^+\eta, D_s^{*+}\eta, D_s^+\rho^0, D_s^{*+}\rho^0, D_s^+\omega, D_s^{*+}\omega$	[f] < 4	× 10 ⁻⁴ CL=90%	Γ_{106}	$\bar{\Sigma}_c^0$ anything	(3.7 ± 1.7) × 10 ⁻³		
Γ_{47}	$D_{s1}(2536)^+$ anything	< 9.5	× 10 ⁻³ CL=90%	Γ_{107}	$\bar{\Sigma}_c^0 N(N=p \text{ or } n)$	< 1.2	× 10 ⁻³	CL=90%
Charmonium modes				Γ_{108}	Ξ_c^0 anything, $\Xi_c^0 \rightarrow \Xi^- \pi^+$	(1.93 ± 0.30) × 10 ⁻⁴		S=1.1
Γ_{48}	$J/\psi(1S)$ anything	(1.094 ± 0.032) %	S=1.1	Γ_{109}	$\Xi_c^\pm, \Xi_c^\pm \rightarrow \Xi^- \pi^+ \pi^+$	(4.5 ± 1.3) × 10 ⁻⁴		
Γ_{49}	$J/\psi(1S)$ (direct) anything	(7.8 ± 0.4) × 10 ⁻³	S=1.1	Γ_{110}	$\rho/\bar{\rho}$ anything	[f] (8.0 ± 0.4) %		
Γ_{50}	$\psi(2S)$ anything	(3.07 ± 0.21) × 10 ⁻³		Γ_{111}	$\rho/\bar{\rho}$ (direct) anything	[f] (5.5 ± 0.5) %		
Γ_{51}	$\chi_{c1}(1P)$ anything	(3.55 ± 0.27) × 10 ⁻³	S=1.3	Γ_{112}	$\bar{\rho}e^+\nu_e$ anything	< 5.9	× 10 ⁻⁴	CL=90%
Γ_{52}	$\chi_{c1}(1P)$ (direct) anything	(3.08 ± 0.19) × 10 ⁻³		Γ_{113}	$\Lambda/\bar{\Lambda}$ anything	[f] (4.0 ± 0.5) %		
Γ_{53}	$\chi_{c2}(1P)$ anything	(10.0 ± 1.7) × 10 ⁻⁴	S=1.6	Γ_{114}	Λ anything	seen		
Γ_{54}	$\chi_{c2}(1P)$ (direct) anything	(7.5 ± 1.1) × 10 ⁻⁴		Γ_{115}	$\bar{\Lambda}$ anything	seen		
Γ_{55}	$\eta_c(1S)$ anything	< 9	× 10 ⁻³ CL=90%	Γ_{116}	Ξ^-/Ξ^+ anything	[f] (2.7 ± 0.6) × 10 ⁻³		
Γ_{56}	$K\chi_{c1}(3872), \chi_{c1} \rightarrow D^0\bar{D}^0\pi^0$	(1.2 ± 0.4) × 10 ⁻⁴		Γ_{117}	baryons anything	(6.8 ± 0.6) %		
Γ_{57}	$K\chi_{c1}(3872), \chi_{c1} \rightarrow D^{*0}D^0$	(8.0 ± 2.2) × 10 ⁻⁵		Γ_{118}	$p\bar{p}$ anything	(2.47 ± 0.23) %		
Γ_{58}	$KX(3940), X \rightarrow D^{*0}D^0$	< 6.7	× 10 ⁻⁵ CL=90%	Γ_{119}	$\Lambda\bar{\Lambda}/\bar{\Lambda}p$ anything	[f] (2.5 ± 0.4) %		
Γ_{59}	$KX(3915), X \rightarrow \omega J/\psi$	[h] (7.1 ± 3.4) × 10 ⁻⁵		Γ_{120}	$\Lambda\bar{\Lambda}$ anything	< 5	× 10 ⁻³	CL=90%
K or K* modes				Lepton Family number (LF) violating modes or $\Delta B = 1$ weak neutral current (B1) modes				
Γ_{60}	K^\pm anything	[f] (78.9 ± 2.5) %		Γ_{121}	se^+e^-	B1 (6.7 ± 1.7) × 10 ⁻⁶		S=2.0
Γ_{61}	K^+ anything	(66 ± 5) %		Γ_{122}	$s\mu^+\mu^-$	B1 (4.3 ± 1.0) × 10 ⁻⁶		
Γ_{62}	K^- anything	(13 ± 4) %		Γ_{123}	$s\ell^+\ell^-$	B1 [b] (5.8 ± 1.3) × 10 ⁻⁶		S=1.8
Γ_{63}	K^0/\bar{K}^0 anything	[f] (64 ± 4) %		Γ_{124}	$\pi\ell^+\ell^-$	B1 < 5.9	× 10 ⁻⁸	CL=90%
Γ_{64}	$K^*(892)^\pm$ anything	(18 ± 6) %		Γ_{125}	πe^+e^-	B1 < 1.10	× 10 ⁻⁷	CL=90%
Γ_{65}	$K^*(892)^0/\bar{K}^*(892)^0$ anything	[f] (14.6 ± 2.6) %		Γ_{126}	$\pi\mu^+\mu^-$	B1 < 5.0	× 10 ⁻⁸	CL=90%
Γ_{66}	$K^*(892)\gamma$	(4.2 ± 0.6) × 10 ⁻⁵		Γ_{127}	Ke^+e^-	B1 (4.4 ± 0.6) × 10 ⁻⁷		
Γ_{67}	$\eta K\gamma$	(8.5 ± 1.8) × 10 ⁻⁶		Γ_{128}	$K^*(892)e^+e^-$	B1 (1.19 ± 0.20) × 10 ⁻⁶		S=1.2
Γ_{68}	$K_1(1400)\gamma$	< 1.27	× 10 ⁻⁴ CL=90%	Γ_{129}	$K\mu^+\mu^-$	B1 (4.4 ± 0.4) × 10 ⁻⁷		
Γ_{69}	$K_2^0(1430)\gamma$	(1.7 ± 0.6) × 10 ⁻⁵		Γ_{130}	$K^*(892)\mu^+\mu^-$	B1 (1.06 ± 0.09) × 10 ⁻⁶		
Γ_{70}	$K_2(1770)\gamma$	< 1.2	× 10 ⁻³ CL=90%	Γ_{131}	$K\ell^+\ell^-$	B1 (4.8 ± 0.4) × 10 ⁻⁷		
Γ_{71}	$K_3^0(1780)\gamma$	< 3.7	× 10 ⁻⁵ CL=90%	Γ_{132}	$K^*(892)\ell^+\ell^-$	B1 (1.05 ± 0.10) × 10 ⁻⁶		
				Γ_{133}	$K\nu\bar{\nu}$	B1 < 1.6	× 10 ⁻⁵	CL=90%
				Γ_{134}	$K^*\nu\bar{\nu}$	B1 < 2.7	× 10 ⁻⁵	CL=90%
				Γ_{135}	$\pi\nu\bar{\nu}$	B1 < 8	× 10 ⁻⁶	CL=90%
				Γ_{136}	$\rho\nu\bar{\nu}$	B1 < 2.8	× 10 ⁻⁵	CL=90%
				Γ_{137}	$se^\pm\mu^\mp$	LF [f] < 2.2	× 10 ⁻⁵	CL=90%

Γ_{138}	$\pi e^\pm \mu^\mp$	LF	<	9.2	$\times 10^{-8}$	CL=90%
Γ_{139}	$\rho e^\pm \mu^\mp$	LF	<	3.2	$\times 10^{-6}$	CL=90%
Γ_{140}	$K e^\pm \mu^\mp$	LF	<	3.8	$\times 10^{-8}$	CL=90%
Γ_{141}	$K^*(892) e^\pm \mu^\mp$	LF	<	5.1	$\times 10^{-7}$	CL=90%

- [a] These values are model dependent.
- [b] An ℓ indicates an e or a μ mode, not a sum over these modes.
- [c] Here "anything" means at least one particle observed.
- [d] This is a $B(B^0 \rightarrow D^{*-} \ell^+ \nu_\ell)$ value.
- [e] D^{**} stands for the sum of the $D(1^1P_1)$, $D(1^3P_0)$, $D(1^3P_1)$, $D(1^3P_2)$, $D(2^1S_0)$, and $D(2^1S_1)$ resonances.
- [f] The value is for the sum of the charge states or particle/antiparticle states indicated.
- [g] $D^{(*)} \bar{D}^{(*)}$ stands for the sum of $D^* \bar{D}^*$, $D^* \bar{D}$, $D \bar{D}^*$, and $D \bar{D}$.
- [h] $X(3915)$ denotes a near-threshold enhancement in the $\omega J/\psi$ mass spectrum.
- [i] Inclusive branching fractions have a multiplicity definition and can be greater than 100%.

B^\pm/B^0 ADMIXTURE BRANCHING RATIOS

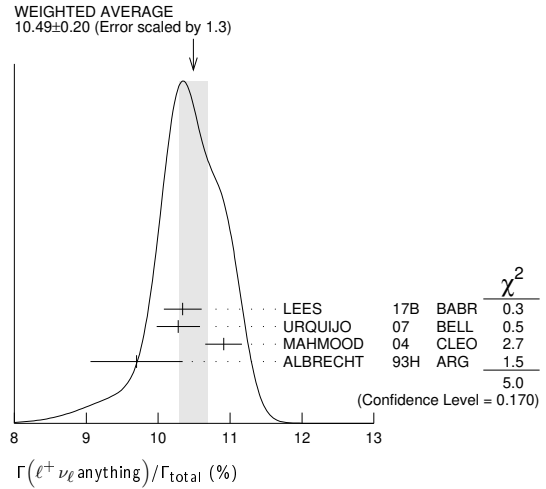
$\Gamma(\ell^+ \nu_\ell \text{ anything})/\Gamma_{\text{total}}$ Γ_3/Γ
 These branching fraction values are model dependent.

"OUR EVALUATION" assumes lepton universality and is an average using rescaled values of the data listed below. The average and rescaling were performed by the Heavy Flavor Averaging Group (HFLAV) and are described at <https://hflav.web.cern.ch/>. The averaging/rescaling procedure takes into account correlations between the measurements.

VALUE (%)	DOCUMENT ID	TECN	COMMENT
10.86 ± 0.16 OUR EVALUATION			
10.49 ± 0.20 OUR AVERAGE	Error includes scale factor of 1.3. See the ideogram below.		
10.34 ± 0.04 ± 0.26	1 LEES	17B	BABR $e^+ e^- \rightarrow \Upsilon(4S)$
10.28 ± 0.18 ± 0.24	2 URQUIJO	07	BELL $e^+ e^- \rightarrow \Upsilon(4S)$
10.91 ± 0.09 ± 0.24	3 MAHMOOD	04	CLEO $e^+ e^- \rightarrow \Upsilon(4S)$
9.7 ± 0.5 ± 0.4	4 ALBRECHT	93H	ARG $e^+ e^- \rightarrow \Upsilon(4S)$
• • • We do not use the following data for averages, fits, limits, etc. • • •			
9.96 ± 0.19 ± 0.32	5 AUBERT,B	06Y	BABR Repl. by LEES 17B
10.85 ± 0.21 ± 0.36	6 OKABE	05	BELL Repl. by URQUIJO 07
10.83 ± 0.16 ± 0.06	7 AUBERT	04X	BABR Repl. by AUBERT,B 06Y
10.36 ± 0.06 ± 0.23	8 AUBERT,B	04A	BABR $e^+ e^- \rightarrow \Upsilon(4S)$
10.87 ± 0.18 ± 0.30	9 AUBERT	03	BABR Repl. by AUBERT 04X
10.90 ± 0.12 ± 0.49	10 ABE	02Y	BELL Repl. by OKABE 05
10.49 ± 0.17 ± 0.43	11 BARISH	96B	CLE2 Repl. by MAHMOOD 04
10.80 ± 0.20 ± 0.56	12 HENDERSON	92	CLEO $e^+ e^- \rightarrow \Upsilon(4S)$
10.0 ± 0.4 ± 0.3	13 YANAGISAWA	91	CSB2 $e^+ e^- \rightarrow \Upsilon(4S)$
10.3 ± 0.6 ± 0.2	14 ALBRECHT	90H	ARG Direct e at $\Upsilon(4S)$
10.0 ± 0.6 ± 0.2	15 ALBRECHT	90H	ARG Direct μ at $\Upsilon(4S)$
11.7 ± 0.4 ± 1.0	16 WACHS	89	CBAL Direct e at $\Upsilon(4S)$
12.0 ± 0.7 ± 0.5	CHEN	84	CLEO Direct e at $\Upsilon(4S)$
10.8 ± 0.6 ± 1.0	CHEN	84	CLEO Direct μ at $\Upsilon(4S)$
11.2 ± 0.9 ± 1.0	LEVMAN	84	CUSB Direct e at $\Upsilon(4S)$
13.2 ± 0.8 ± 1.4	17 KLOPFEN...	83B	CUSB Direct e at $\Upsilon(4S)$

- 1 LEES 17B measurement is obtained from semileptonic decays to electrons. The result is averaged over B^\pm and B^0 mesons, assuming lepton universality.
- 2 URQUIJO 07 report a measurement of $(10.07 \pm 0.18 \pm 0.21)\%$ for the partial branching fraction of $B \rightarrow e \nu_e X_c$ decay with electron energy above 0.6 GeV. We converted the result to $B \rightarrow e \nu_e X$ branching fraction.
- 3 Uses charge and angular correlations in $\Upsilon(4S)$ events with a high-momentum lepton and an additional electron.
- 4 ALBRECHT 93H analysis performed using tagged semileptonic decays of the B . This technique is almost model independent for the lepton branching ratio.
- 5 The measurements are obtained for charged and neutral B mesons partial rates of semileptonic decay to electrons with momentum above 0.6 GeV/c in the B rest frame. The best precision on the ratio is achieved for a momentum threshold of 1.0 GeV: $B(B^+ \rightarrow e^+ \nu_e X) / B(B^0 \rightarrow e^+ \nu_e X) = 1.074 \pm 0.041 \pm 0.026$.
- 6 The measurements are obtained for charged and neutral B mesons partial rates of semileptonic decay to electrons with momentum above 0.6 GeV/c in the B rest frame, and their ratio of $B(B^+ \rightarrow e^+ \nu_e X)/B(B^0 \rightarrow e^+ \nu_e X) = 1.08 \pm 0.05 \pm 0.02$.
- 7 The semileptonic branching ratio, $|V_{cb}|$ and other heavy-quark parameters are determined from a simultaneous fit to moments of the hadronic-mass and lepton-energy distribution.
- 8 Uses the high-momentum lepton tag method and requires the electron energy above 0.6 GeV.
- 9 Uses the high-momentum lepton tag method. They also report $|V_{cb}| = 0.0423 \pm 0.0007(\text{exp}) \pm 0.0020(\text{theo.})$.
- 10 Uses the high-momentum lepton tag method. ABE 02Y also reports $|V_{cb}| = 0.0408 \pm 0.0010(\text{exp}) \pm 0.0025(\text{theo.})$. The second error is due to uncertainties of theoretical inputs.
- 11 BARISH 96B analysis performed using tagged semileptonic decays of the B . This technique is almost model independent for the lepton branching ratio.
- 12 HENDERSON 92 measurement employs e and μ . The systematic error contains 0.004 in quadrature from model dependence. The authors average a variation of the Isgur, Scora,

- Grinstein, and Wise model with that of the Altarelli-Cabibbo-Corbò-Maiani-Martinelli model for semileptonic decays to correct the acceptance.
- 13 YA NAGISAWA 91 also measures an average semileptonic branching ratio at the $\Upsilon(5S)$ of 9.6–10.5% depending on assumptions about the relative production of different B meson species.
- 14 ALBRECHT 90H uses the model of ALTARELLI 82 to correct over all lepton momenta. 0.099 ± 0.006 is obtained using ISGUR 89b.
- 15 ALBRECHT 90H uses the model of ALTARELLI 82 to correct over all lepton momenta. 0.097 ± 0.006 is obtained using ISGUR 89b.
- 16 Using data above $p(e) = 2.4$ GeV, WACHS 89 determine $\sigma(B \rightarrow e \nu \mu p)/\sigma(B \rightarrow e \nu \text{charm}) < 0.065$ at 90% CL.
- 17 Ratio $\sigma(b \rightarrow e \nu \mu p)/\sigma(b \rightarrow e \nu \text{charm}) < 0.055$ at CL = 90%.



$\Gamma(D^- \ell^+ \nu_\ell \text{ anything})/\Gamma(\ell^+ \nu_\ell \text{ anything})$ Γ_4/Γ_3
 $\ell = e \text{ or } \mu$.

VALUE	DOCUMENT ID	TECN	COMMENT
0.26 ± 0.07 ± 0.04	1 FULTON	91	CLEO $e^+ e^- \rightarrow \Upsilon(4S)$
1 FULTON 91 uses $B(D^+ \rightarrow K^- \pi^+ \pi^+) = (9.1 \pm 1.3 \pm 0.4)\%$ as measured by MARK III.			

$\Gamma(\bar{D}^0 \ell^+ \nu_\ell \text{ anything})/\Gamma(\ell^+ \nu_\ell \text{ anything})$ Γ_5/Γ_3
 $\ell = e \text{ or } \mu$.

VALUE	DOCUMENT ID	TECN	COMMENT
0.67 ± 0.09 ± 0.10	1 FULTON	91	CLEO $e^+ e^- \rightarrow \Upsilon(4S)$
1 FULTON 91 uses $B(D^0 \rightarrow K^- \pi^+) = (4.2 \pm 0.4 \pm 0.4)\%$ as measured by MARK III.			

$\Gamma(\bar{D} \ell^+ \nu_\ell)/\Gamma(\ell^+ \nu_\ell \text{ anything})$ Γ_6/Γ_3

VALUE	DOCUMENT ID	TECN	COMMENT
0.223 ± 0.006 ± 0.009	1 AUBERT	10	BABR $e^+ e^- \rightarrow \Upsilon(4S)$
1 Uses a fully reconstructed B meson as a tag on the recoil side.			

$\Gamma(D^{*-} \ell^+ \nu_\ell \text{ anything})/\Gamma_{\text{total}}$ Γ_7/Γ

VALUE (units 10^{-2})	DOCUMENT ID	TECN	COMMENT
0.67 ± 0.08 ± 0.10	ABDALLAH	04D	DLPH $e^+ e^- \rightarrow Z^0$
• • • We do not use the following data for averages, fits, limits, etc. • • •			
0.6 ± 0.3 ± 0.1	1 BARISH	95	CLE2 $e^+ e^- \rightarrow \Upsilon(4S)$

1 BARISH 95 use $B(D^0 \rightarrow K^- \pi^+) = (3.91 \pm 0.08 \pm 0.17)\%$ and $B(D^{*+} \rightarrow D^0 \pi^+) = (68.1 \pm 1.0 \pm 1.3)\%$.

$\Gamma(D^{*0} \ell^+ \nu_\ell \text{ anything})/\Gamma_{\text{total}}$ Γ_8/Γ

VALUE (units 10^{-2})	DOCUMENT ID	TECN	COMMENT
• • • We do not use the following data for averages, fits, limits, etc. • • •			
0.6 ± 0.6 ± 0.1	1 BARISH	95	CLE2 $e^+ e^- \rightarrow \Upsilon(4S)$

1 BARISH 95 use $B(D^0 \rightarrow K^- \pi^+) = (3.91 \pm 0.08 \pm 0.17)\%$, $B(D^{*+} \rightarrow D^0 \pi^+) = (68.1 \pm 1.0 \pm 1.3)\%$, $B(D^{*0} \rightarrow D^0 \pi^0) = (63.6 \pm 2.3 \pm 3.3)\%$.

$\Gamma(D^{**} \ell^+ \nu_\ell)/\Gamma_{\text{total}}$ Γ_{10}/Γ
 D^{**} stands for the sum of the $D(1^1P_1)$, $D(1^3P_0)$, $D(1^3P_1)$, $D(1^3P_2)$, $D(2^1S_0)$, and $D(2^1S_1)$ resonances. $\ell = e \text{ or } \mu$, not sum over e and μ modes.

VALUE	CL%	EVTS	DOCUMENT ID	TECN	COMMENT
0.027 ± 0.005 ± 0.005		63	1 ALBRECHT	93	ARG $e^+ e^- \rightarrow \Upsilon(4S)$
• • • We do not use the following data for averages, fits, limits, etc. • • •					
< 0.028		95	2 BARISH	95	CLE2 $e^+ e^- \rightarrow \Upsilon(4S)$

- 1 ALBRECHT 93 assumes the GISW model to correct for unseen modes. Using the BHK model, the result becomes $0.023 \pm 0.006 \pm 0.004$. Assumes $B(D^{*+} \rightarrow D^0 \pi^+) = 68.1\%$, $B(D^0 \rightarrow K^- \pi^+) = 3.65\%$, $B(D^0 \rightarrow K^- \pi^+ \pi^+) = 7.5\%$. We have taken their average e and μ value.
- 2 BARISH 95 use $B(D^0 \rightarrow K^- \pi^+) = (3.91 \pm 0.08 \pm 0.17)\%$, assume all nonresonant channels are zero, and use GISW model for relative abundances of D^{**} states.

Meson Particle Listings

 B^\pm/B^0 ADMIXTURE $\Gamma(\bar{D}_1(2420)\ell^+\nu_\ell\text{anything})/\Gamma_{\text{total}}$ Γ_{11}/Γ

VALUE	DOCUMENT ID	TECN	COMMENT
0.0038 ± 0.0013 OUR AVERAGE	Error includes scale factor of 2.4.		
0.0033 ± 0.0006	¹ ABAZOV 05o D0		$p\bar{p}$ at 1.96 TeV
0.0074 ± 0.0016	² BUSKULIC 97b ALEP		$e^+e^- \rightarrow Z$
• • • We do not use the following data for averages, fits, limits, etc. • • •			
seen	³ BUSKULIC 95b ALEP		Repl. by BUSKULIC 97b

- ¹ Assumes $B(D_1 \rightarrow D^*\pi) = 1$, $B(D_1 \rightarrow D^*\pi^\pm) = 2/3$, and $B(b \rightarrow B) = 0.397$.
² BUSKULIC 97b assumes $B(D_1(2420) \rightarrow D^*\pi) = 1$, $B(D_1(2420) \rightarrow D^*\pi^\pm) = 2/3$, and $B(b \rightarrow B) = 0.378 \pm 0.022$.
³ BUSKULIC 95b reports $f_B \times B(B \rightarrow \bar{D}_1(2420)^0\ell^+\nu_\ell\text{anything}) \times B(\bar{D}_1(2420)^0 \rightarrow \bar{D}^*(2010)^-\pi^+) = (2.04 \pm 0.58 \pm 0.34)10^{-3}$, where f_B is the production fraction for a single B charge state.

 $\Gamma(D\pi\ell^+\nu_\ell\text{anything}) + \Gamma(D^*\pi\ell^+\nu_\ell\text{anything})/\Gamma_{\text{total}}$ Γ_{12}/Γ

VALUE	DOCUMENT ID	TECN	COMMENT
0.026 ± 0.005 OUR AVERAGE	Error includes scale factor of 1.5.		
0.0340 ± 0.0052 ± 0.0032	¹ ABREU 00r DLPH		$e^+e^- \rightarrow Z$
0.0226 ± 0.0029 ± 0.0033	² BUSKULIC 97b ALEP		$e^+e^- \rightarrow Z$

- ¹ Assumes no contribution from B_s and b baryons. Further assumes contributions from single pion ($D\pi$ and $D^*\pi$) states only, allowing isospin conservation to relate the relative π^0 and π^\pm rates.
² BUSKULIC 97b assumes $B(b \rightarrow B) = 0.378 \pm 0.022$ and uses isospin invariance by assuming that all observed $D^0\pi^+$, $D^{*0}\pi^+$, $D^+\pi^-$, and $D^{*+}\pi^-$ are from D^{**} states. A correction has been applied to account for the production of B_s^0 and L_b^0 .

 $\Gamma(D\pi\ell^+\nu_\ell\text{anything})/\Gamma_{\text{total}}$ Γ_{13}/Γ

VALUE	DOCUMENT ID	TECN	COMMENT
0.0154 ± 0.0061	ABREU 00r DLPH		$e^+e^- \rightarrow Z$

 $\Gamma(D^*\pi\ell^+\nu_\ell\text{anything})/\Gamma_{\text{total}}$ Γ_{14}/Γ

VALUE	DOCUMENT ID	TECN	COMMENT
0.0186 ± 0.0038	ABREU 00r DLPH		$e^+e^- \rightarrow Z$

 $\Gamma(\bar{D}_2^*(2460)\ell^+\nu_\ell\text{anything})/\Gamma_{\text{total}}$ Γ_{15}/Γ

VALUE	CL%	DOCUMENT ID	TECN	COMMENT
0.0044 ± 0.0016		¹ ABAZOV 05o D0		$p\bar{p}$ at 1.96 TeV
• • • We do not use the following data for averages, fits, limits, etc. • • •				
<0.0065	95	² BUSKULIC 97b ALEP		$e^+e^- \rightarrow Z$
not seen		³ BUSKULIC 95b ALEP		$e^+e^- \rightarrow Z$

- ¹ Assumes $B(D_2^* \rightarrow D^*\pi^\pm) = 0.30 \pm 0.06$ and $B(b \rightarrow B) = 0.397$.
² A revised number based on BUSKULIC 97b which assumes $B(D_2^*(2460) \rightarrow D^*\pi^\pm) = 0.20$ and $B(b \rightarrow B) = 0.378 \pm 0.022$.
³ BUSKULIC 95b reports $f_B \times B(B \rightarrow \bar{D}_2^*(2460)^0\ell^+\nu_\ell\text{anything}) \times B(\bar{D}_2^*(2460)^0 \rightarrow \bar{D}^*(2010)^-\pi^+) \leq 0.81 \times 10^{-3}$ at CL=95%, where f_B is the production fraction for a single B charge state.

 $\Gamma(B \rightarrow \bar{D}_2^*(2460)\ell^+\nu_\ell\text{anything}) \times B(D_2^*(2460) \rightarrow D^*\pi^+)$ $\Gamma(B \rightarrow \bar{D}_1(2420)\ell^+\nu_\ell\text{anything}) \times B(\bar{D}_1(2420) \rightarrow D^*\pi^+)$

VALUE	DOCUMENT ID	TECN	COMMENT
0.39 ± 0.09 ± 0.12	ABAZOV 05o D0		$p\bar{p}$ at 1.96 TeV

 $\Gamma(D^*\pi^-\ell^+\nu_\ell\text{anything})/\Gamma_{\text{total}}$ Γ_{16}/Γ

VALUE (units 10^{-3})	DOCUMENT ID	TECN	COMMENT
10.0 ± 2.7 ± 2.1	¹ BUSKULIC 95b ALEP		$e^+e^- \rightarrow Z$
¹ BUSKULIC 95b reports $f_B \times B(B \rightarrow \bar{D}^*(2010)^-\pi^+\ell^+\nu_\ell\text{anything}) = (3.7 \pm 1.0 \pm 0.7)10^{-3}$. Above value assumes $f_B = 0.37 \pm 0.03$.			

 $\Gamma(\bar{D}\pi^+\pi^-\ell^+\nu_\ell)/\Gamma(\bar{D}\ell^+\nu_\ell)$ Γ_{17}/Γ_6

VALUE (units 10^{-2})	DOCUMENT ID	TECN	COMMENT
6.7 ± 1.0 ± 0.8	¹ LEES 16 BABR		$e^+e^- \rightarrow \Upsilon(4S)$

- ¹ Measurement used electrons and muons as leptons.

 $\Gamma(\bar{D}^*\pi^+\pi^-\ell^+\nu_\ell)/\Gamma(D^*\ell^+\nu_\ell)$ Γ_{18}/Γ_9

VALUE (units 10^{-2})	DOCUMENT ID	TECN	COMMENT
1.9 ± 0.5 ± 0.4	¹ LEES 16 BABR		$e^+e^- \rightarrow \Upsilon(4S)$

- ¹ Measurement used electrons and muons as leptons.

 $\Gamma(D_s^-\ell^+\nu_\ell\text{anything})/\Gamma_{\text{total}}$ Γ_{19}/Γ

VALUE	CL%	DOCUMENT ID	TECN	COMMENT
<7 × 10⁻³	90	¹ ALBRECHT 93E ARG		$e^+e^- \rightarrow \Upsilon(4S)$

- ¹ ALBRECHT 93E reports < 0.012 from a measurement of $[\Gamma(B \rightarrow D_s^-\ell^+\nu_\ell\text{anything})/\Gamma_{\text{total}}] \times [B(D_s^+ \rightarrow \phi\pi^+)]$ assuming $B(D_s^+ \rightarrow \phi\pi^+) = 0.027$, which we rescale to our best value $B(D_s^+ \rightarrow \phi\pi^+) = 4.5 \times 10^{-2}$.

 $\Gamma(D_s^-\ell^+\nu_\ell K^+\text{anything})/\Gamma_{\text{total}}$ Γ_{20}/Γ

VALUE	CL%	DOCUMENT ID	TECN	COMMENT
<5 × 10⁻³	90	¹ ALBRECHT 93E ARG		$e^+e^- \rightarrow \Upsilon(4S)$
¹ ALBRECHT reports < 0.008 from a measurement of $[\Gamma(B \rightarrow D_s^-\ell^+\nu_\ell K^+\text{anything})/\Gamma_{\text{total}}] \times [B(D_s^+ \rightarrow \phi\pi^+)]$ assuming $B(D_s^+ \rightarrow \phi\pi^+) = 0.027$, which we rescale to our best value $B(D_s^+ \rightarrow \phi\pi^+) = 4.5 \times 10^{-2}$.				

 $\Gamma(D_s^-\ell^+\nu_\ell K^0\text{anything})/\Gamma_{\text{total}}$ Γ_{21}/Γ

VALUE	CL%	DOCUMENT ID	TECN	COMMENT
<7 × 10⁻³	90	¹ ALBRECHT 93E ARG		$e^+e^- \rightarrow \Upsilon(4S)$
¹ ALBRECHT reports < 0.012 from a measurement of $[\Gamma(B \rightarrow D_s^-\ell^+\nu_\ell K^0\text{anything})/\Gamma_{\text{total}}] \times [B(D_s^+ \rightarrow \phi\pi^+)]$ assuming $B(D_s^+ \rightarrow \phi\pi^+) = 0.027$, which we rescale to our best value $B(D_s^+ \rightarrow \phi\pi^+) = 4.5 \times 10^{-2}$.				

 $\Gamma(X_c\ell^+\nu_\ell)/\Gamma_{\text{total}}$ Γ_{22}/Γ

"OUR EVALUATION" is an average using rescaled values of the data listed below. The average and rescaling were performed by the Heavy Flavor Averaging Group (HFLAV) and are described at <https://hflav.web.cern.ch/>. The averaging/rescaling procedure takes into account correlations between the measurements.

VALUE (%)	DOCUMENT ID	TECN	COMMENT
10.65 ± 0.16 OUR EVALUATION			
10.29 ± 0.19 OUR AVERAGE			
10.18 ± 0.03 ± 0.24	¹ LEES 17b BABR		$e^+e^- \rightarrow \Upsilon(4S)$
10.44 ± 0.19 ± 0.22	² URQUIJO 07 BELL		$e^+e^- \rightarrow \Upsilon(4S)$
• • • We do not use the following data for averages, fits, limits, etc. • • •			
10.64 ± 0.17 ± 0.06	³ AUBERT 10a BABR		Repl. by LEES 17b
10.61 ± 0.16 ± 0.06	⁴ AUBERT 04x BABR		Repl. by AUBERT 10a

- ¹ The measurement is obtained from semileptonic decays to electrons $B \rightarrow X_c e \nu$, and using a theoretical model (GAMBINO 07, GAMBINO 11) to predict the contribution from $B \rightarrow X_c \mu \nu$. The result is averaged over B^\pm and B^0 mesons, assuming lepton universality.
² Measured the independent B^+ and B^0 partial branching fractions with electron energy above 0.4 GeV.
³ Obtained from a combined fit to the moments of observed spectra in inclusive $B \rightarrow X_c \ell^+ \nu_\ell$ decay.
⁴ The semileptonic branching ratio, $|V_{cb}|$ and other heavy-quark parameters are determined from a simultaneous fit to moments of the hadronic-mass and lepton-energy distribution.

 $\Gamma(X_u\ell^+\nu_\ell)/\Gamma_{\text{total}}$ Γ_{23}/Γ

"OUR EVALUATION" is an average using rescaled values of the data listed below. The average and rescaling were performed by the Heavy Flavor Averaging Group (HFLAV) and are described at <https://hflav.web.cern.ch/>. The averaging/rescaling procedure takes into account correlations between the measurements.

VALUE (units 10^{-3})	DOCUMENT ID	TECN	COMMENT
2.13 ± 0.30 OUR EVALUATION			
1.665 ± 0.087 +0.103 -0.094	¹ LEES 17b BABR		$e^+e^- \rightarrow \Upsilon(4S)$
2.01 ± 0.15 ± 0.25	² LEES 12r BABR		$e^+e^- \rightarrow \Upsilon(4S)$
2.53 ± 0.24 ± 0.24	³ AUBERT,B 05x BABR		$e^+e^- \rightarrow \Upsilon(4S)$
2.80 ± 0.52 ± 0.41	⁴ LIMOSANI 05 BELL		$e^+e^- \rightarrow \Upsilon(4S)$
1.77 ± 0.29 ± 0.38	⁵ BORNHEIM 02 CLE2		$e^+e^- \rightarrow \Upsilon(4S)$
• • • We do not use the following data for averages, fits, limits, etc. • • •			
1.963 ± 0.173 ± 0.159	⁶ URQUIJO 10 BELL		$e^+e^- \rightarrow \Upsilon(4S)$
1.18 ± 0.09 ± 0.07	⁷ AUBERT 08as BABR		Repl. by LEES 12r
2.27 ± 0.26 +0.37 -0.33	⁸ AUBERT 06h BABR		Repl. by LEES 17b
2.24 ± 0.27 ± 0.47	^{9,10} AUBERT 04i BABR		Repl. by AUBERT,B 05x

- ¹ Obtained from the partial rate $\Delta B = (1.554 \pm 0.082 +0.095 -0.086) \times 10^{-3}$ for the electron momentum interval of 0.8–2.7 GeV/c based on GGOU method ($X_c \ell \nu$, m_c constraint fit of SF parameters).
² Measures several partial branching fractions in different phase space regions. The most precise result on the full branching fraction is obtained in the region for lepton momentum in B rest frame $p_\ell^* > 1$ GeV/c, where the measured partial branching fraction is $\Delta B = (1.80 \pm 0.13 \pm 0.15) \times 10^{-3}$. The acceptance in that region is reported in a private communication by the Authors to be 0.894. The corresponding $|V_{ub}|$ from the BLPN method is $(4.28 \pm 0.15 \pm 0.19) \times 10^{-3}$, where the last uncertainty comes from theoretical prediction.
³ Determined from the partial rate $\Delta B = (4.41 \pm 0.42 \pm 0.42) \times 10^{-4}$ measured for electron energy > 2 GeV and hadronic mass squared < 3.5 GeV², and calculated acceptance 0.174 in that region. The V_{ub} is measured as $(4.41 \pm 0.30 +0.65 -0.47 \pm 0.28) \times 10^{-3}$.
⁴ Uses electrons in the momentum interval 1.9–2.6 GeV/c in the center-of-mass frame. The V_{ub} is found to be $(5.08 \pm 0.47 +0.49 -0.48) \times 10^{-3}$.
⁵ BORNHEIM 02 uses the observed yield of leptons from semileptonic B decays in the end-point momentum interval 2.2–2.6 GeV/c with recent CLEO-2 data on $B \rightarrow X_s \gamma$. The V_{ub} is found to be $(4.08 \pm 0.34 \pm 0.53) \times 10^{-3}$.
⁶ Uses a multivariate analysis method and requires lepton momentum in the B rest frame, $p_\ell^{*B} > 1.0$ GeV/c.
⁷ Measures several partial branching fractions in different phase space regions. The most precise result is obtained in the region for hadronic mass $M_X < 1.55$ GeV/c², and is $\Delta B = (1.18 \pm 0.09 \pm 0.07) \times 10^{-3}$. The corresponding $|V_{ub}|$ from the BLPN method

See key on page 999

Meson Particle Listings
 B^\pm/B^0 ADMIXTURE

is $(4.27 \pm 0.16 \pm 0.13 \pm 0.30) \times 10^{-3}$, where the last uncertainty comes from the theoretical prediction of the partial rate in the given phase-space region.

⁸ Obtained from the partial rate $\Delta B = (0.572 \pm 0.041 \pm 0.065) \times 10^{-3}$ for the electron momentum interval of 2.0–2.6 GeV/c based on BLNP method.

⁹ Used BaBar measurement of Semileptonic branching fraction $B(B \rightarrow X \ell \nu_\ell) = (10.87 \pm 0.18 \pm 0.30)\%$ to convert the ratio of rates to branching fraction.

¹⁰ The third error includes the systematics and theoretical errors summed in quadrature.

$\Gamma(X_u \ell^+ \nu_\ell)/\Gamma(\ell^+ \nu_\ell \text{ anything})$ Γ_{23}/Γ_3
 ℓ denotes e or μ , not the sum. These experiments measure this ratio in very limited momentum intervals.

VALUE (units 10^{-2})	CL%	EVTS	DOCUMENT ID	TECN	COMMENT
2.06 ± 0.25 ± 0.42			¹ AUBERT 04i	BABR	$e^+e^- \rightarrow \Upsilon(4S)$
			² ALBRECHT 94c	ARG	$e^+e^- \rightarrow \Upsilon(4S)$
		107	³ BARTELT 93b	CLE2	$e^+e^- \rightarrow \Upsilon(4S)$
		77	⁴ ALBRECHT 91c	ARG	$e^+e^- \rightarrow \Upsilon(4S)$
		41	⁵ ALBRECHT 90	ARG	$e^+e^- \rightarrow \Upsilon(4S)$
		76	⁶ FULTON 90	CLEO	$e^+e^- \rightarrow \Upsilon(4S)$
			⁷ BEHREND 87	CLEO	$e^+e^- \rightarrow \Upsilon(4S)$
<4.0	90		CHEN 90	CLEO	Direct e at $\Upsilon(4S)$
<4.0	90		KLOPFEN... 83b	CUSB	Direct e at $\Upsilon(4S)$

¹ The third error includes the systematics and theoretical errors summed in quadrature.

² ALBRECHT 94c find $\Gamma(b \rightarrow c)/\Gamma(b \rightarrow \text{all}) = 0.99 \pm 0.02 \pm 0.04$.

³ BARTELT 93b (CLEO II) measures an excess of $107 \pm 15 \pm 11$ leptons in the lepton momentum interval 2.3–2.6 GeV/c which is attributed to $b \rightarrow u \ell \nu_\ell$. This corresponds to a model-dependent partial branching ratio Δ_{ub} between $(1.15 \pm 0.16 \pm 0.15) \times 10^{-4}$, as evaluated using the KS model (KOERNER 88), and $(1.54 \pm 0.22 \pm 0.20) \times 10^{-4}$ using the ACCMM model (ARTUSO 93). The corresponding values of $|V_{ub}/V_{cb}|$ are 0.056 ± 0.006 and 0.076 ± 0.008 , respectively.

⁴ ALBRECHT 91c result supersedes ALBRECHT 90. Two events are fully reconstructed providing evidence for the $b \rightarrow u$ transition. Using the model of ALTARELLI 82, they obtain $|V_{ub}/V_{cb}| = 0.11 \pm 0.012$ from 77 leptons in the 2.3–2.6 GeV momentum range.

⁵ ALBRECHT 90 observes 41 ± 10 excess e and μ (lepton) events in the momentum interval $p = 2.3$ –2.6 GeV signaling the presence of the $b \rightarrow u$ transition. The events correspond to a model-dependent measurement of $|V_{ub}/V_{cb}| = 0.10 \pm 0.01$.

⁶ FULTON 90 observe 76 ± 20 excess e and μ (lepton) events in the momentum interval $p = 2.4$ –2.6 GeV signaling the presence of the $b \rightarrow u$ transition. The average branching ratio, $(1.8 \pm 0.4 \pm 0.3) \times 10^{-4}$, corresponds to a model-dependent measurement of approximately $|V_{ub}/V_{cb}| = 0.1$ using $B(b \rightarrow c \ell \nu) = 10.2 \pm 0.2 \pm 0.7\%$.

⁷ The quoted possible limits range from 0.018 to 0.04 for the ratio, depending on which model or momentum range is chosen. We select the most conservative limit they have calculated. This corresponds to a limit on $|V_{ub}/V_{cb}| < 0.20$. While the endpoint technique employed is more robust than their previous results in CHEN 84, these results do not provide a numerical improvement in the limit.

$\Gamma(K^+ \ell^+ \nu_\ell \text{ anything})/\Gamma(\ell^+ \nu_\ell \text{ anything})$ Γ_{24}/Γ_3
 ℓ denotes e or μ , not the sum.

VALUE	DOCUMENT ID	TECN	COMMENT
0.58 ± 0.05 OUR AVERAGE			
0.594 ± 0.021 ± 0.056	ALBRECHT 94c	ARG	$e^+e^- \rightarrow \Upsilon(4S)$
0.54 ± 0.07 ± 0.06	¹ ALAM 87b	CLEO	$e^+e^- \rightarrow \Upsilon(4S)$

¹ ALAM 87b measurement relies on lepton-kaon correlations.

$\Gamma(K^- \ell^+ \nu_\ell \text{ anything})/\Gamma(\ell^+ \nu_\ell \text{ anything})$ Γ_{25}/Γ_3
 ℓ denotes e or μ , not the sum.

VALUE	DOCUMENT ID	TECN	COMMENT
0.092 ± 0.035 OUR AVERAGE			
0.086 ± 0.011 ± 0.044	ALBRECHT 94c	ARG	$e^+e^- \rightarrow \Upsilon(4S)$
0.10 ± 0.05 ± 0.02	¹ ALAM 87b	CLEO	$e^+e^- \rightarrow \Upsilon(4S)$

¹ ALAM 87b measurement relies on lepton-kaon correlations.

$\Gamma(K^0/\bar{K}^0 \ell^+ \nu_\ell \text{ anything})/\Gamma(\ell^+ \nu_\ell \text{ anything})$ Γ_{26}/Γ_3
 ℓ denotes e or μ , not the sum. Sum over K^0 and \bar{K}^0 states.

VALUE	DOCUMENT ID	TECN	COMMENT
0.42 ± 0.05 OUR AVERAGE			
0.452 ± 0.038 ± 0.056	¹ ALBRECHT 94c	ARG	$e^+e^- \rightarrow \Upsilon(4S)$
0.39 ± 0.06 ± 0.04	² ALAM 87b	CLEO	$e^+e^- \rightarrow \Upsilon(4S)$

¹ ALBRECHT 94c assume a K^0/\bar{K}^0 multiplicity twice that of K_S^0 .

² ALAM 87b measurement relies on lepton-kaon correlations.

$\Gamma(\bar{D}^+ \tau^+ \nu_\tau)/\Gamma(\bar{D}^+ \ell^+ \nu_\ell)$ Γ_{27}/Γ_6

“OUR EVALUATION” is an average using rescaled values of the data listed below. The average and rescaling were performed by the Heavy Flavor Averaging Group (HFLAV) and are described at <https://hflav.web.cern.ch/>. The averaging/rescaling procedure takes into account correlations between the measurements.

VALUE (units 10^{-2})	DOCUMENT ID	TECN	COMMENT
40.7 ± 4.6 OUR EVALUATION			
41.1 ± 5.0 OUR AVERAGE			
37.5 ± 6.4 ± 2.6	^{1,2} HUSCHLE 15	BELL	$e^+e^- \rightarrow \Upsilon(4S)$
44.0 ± 5.8 ± 4.2	^{1,2} LEES 12d	BABR	$e^+e^- \rightarrow \Upsilon(4S)$
			••• We do not use the following data for averages, fits, limits, etc. •••
4.16 ± 11.7 ± 5.2	¹ AUBERT 08N	BABR	Repl. by LEES 12d

¹ Uses a fully reconstructed B meson as a tag on the recoil side.

² Uses $\tau^+ \rightarrow e^+ \nu_e \bar{\nu}_\tau$ and $\tau^+ \rightarrow \mu^+ \nu_\mu \bar{\nu}_\tau$ and e^+ or μ^+ as ℓ^+ . Obtained from simultaneous fit to B^+ and B^0 assuming isospin symmetry.

$\Gamma(D^+ \tau^+ \nu_\tau)/\Gamma(D^+ \ell^+ \nu_\ell)$

Γ_{28}/Γ_9

“OUR EVALUATION” is an average using rescaled values of the data listed below. The average and rescaling were performed by the Heavy Flavor Averaging Group (HFLAV) and are described at <https://hflav.web.cern.ch/>. The averaging/rescaling procedure takes into account correlations between the measurements.

VALUE (units 10^{-2})	DOCUMENT ID	TECN	COMMENT
30.4 ± 1.5 OUR EVALUATION			
30.7 ± 2.1 OUR AVERAGE			
27.0 ± 3.5 ± 2.8	¹ HIROSE 17	BELL	$e^+e^- \rightarrow \Upsilon(4S)$
29.3 ± 3.8 ± 1.5	² HUSCHLE 15	BELL	$e^+e^- \rightarrow \Upsilon(4S)$
33.2 ± 2.4 ± 1.8	² LEES 12d	BABR	$e^+e^- \rightarrow \Upsilon(4S)$
			••• We do not use the following data for averages, fits, limits, etc. •••
29.7 ± 5.6 ± 1.8	³ AUBERT 08N	BABR	Repl. by LEES 12d

¹ Uses a fully reconstructed B meson as a tag on the recoil side.

² Uses $\tau^+ \rightarrow e^+ \nu_e \bar{\nu}_\tau$ and $\tau^+ \rightarrow \mu^+ \nu_\mu \bar{\nu}_\tau$ and e^+ or μ^+ as ℓ^+ . Obtained from simultaneous fit to B^+ and B^0 assuming isospin symmetry. Uses a fully reconstructed B meson as a tag on the recoil side.

³ Uses a fully reconstructed B meson as a tag on the recoil side. The results are normalized to the B^+ decay rate.

$\langle n_c \rangle$

VALUE	DOCUMENT ID	TECN	COMMENT
1.10 ± 0.05	¹ GIBBONS 97b	CLE2	$e^+e^- \rightarrow \Upsilon(4S)$
			••• We do not use the following data for averages, fits, limits, etc. •••
0.98 ± 0.16 ± 0.12	² ALAM 87b	CLEO	$e^+e^- \rightarrow \Upsilon(4S)$

¹ GIBBONS 97b from charm counting using $B(D_s^+ \rightarrow \phi \pi) = 0.036 \pm 0.009$ and $B(\Lambda_c^+ \rightarrow p K^- \pi^+) = 0.044 \pm 0.006$.

² From the difference between K^- and K^+ widths. ALAM 87b measurement relies on lepton-kaon correlations. It does not consider the possibility of $B\bar{B}$ mixing. We have thus removed it from the average.

$\Gamma(D^\pm \text{ anything})/\Gamma_{\text{total}}$ Γ_{29}/Γ

VALUE	EVTS	DOCUMENT ID	TECN	COMMENT
0.231 ± 0.012 OUR AVERAGE				
0.230 ± 0.012 ± 0.004		¹ GIBBONS 97b	CLE2	$e^+e^- \rightarrow \Upsilon(4S)$
0.241 ± 0.037 ± 0.004		² BORTOLETTO92	CLEO	$e^+e^- \rightarrow \Upsilon(4S)$
0.223 ± 0.051 ± 0.004		³ ALBRECHT 91h	ARG	$e^+e^- \rightarrow \Upsilon(4S)$

••• We do not use the following data for averages, fits, limits, etc. •••

⁴ BORTOLETTO87 20k ⁴ BORTOLETTO87 CLEO Sup. by BORTOLETTO 92

¹ GIBBONS 97b reports $[\Gamma(B \rightarrow D^\pm \text{ anything})/\Gamma_{\text{total}}] \times [B(D^+ \rightarrow K^- 2\pi^+)] = 0.0216 \pm 0.0008 \pm 0.00082$ which we divide by our best value $B(D^+ \rightarrow K^- 2\pi^+) = (9.38 \pm 0.16) \times 10^{-2}$. Our first error is their experiment's error and our second error is the systematic error from using our best value.

² BORTOLETTO 92 reports $[\Gamma(B \rightarrow D^\pm \text{ anything})/\Gamma_{\text{total}}] \times [B(D^+ \rightarrow K^- 2\pi^+)] = 0.0226 \pm 0.0030 \pm 0.0018$ which we divide by our best value $B(D^+ \rightarrow K^- 2\pi^+) = (9.38 \pm 0.16) \times 10^{-2}$. Our first error is their experiment's error and our second error is the systematic error from using our best value.

³ ALBRECHT 91h reports $[\Gamma(B \rightarrow D^\pm \text{ anything})/\Gamma_{\text{total}}] \times [B(D^+ \rightarrow K^- 2\pi^+)] = 0.0209 \pm 0.0027 \pm 0.0040$ which we divide by our best value $B(D^+ \rightarrow K^- 2\pi^+) = (9.38 \pm 0.16) \times 10^{-2}$. Our first error is their experiment's error and our second error is the systematic error from using our best value.

⁴ BORTOLETTO 87 reports $[\Gamma(B \rightarrow D^\pm \text{ anything})/\Gamma_{\text{total}}] \times [B(D^+ \rightarrow K^- 2\pi^+)] = 0.019 \pm 0.004 \pm 0.002$ which we divide by our best value $B(D^+ \rightarrow K^- 2\pi^+) = (9.38 \pm 0.16) \times 10^{-2}$. Our first error is their experiment's error and our second error is the systematic error from using our best value.

$\Gamma(D^0/\bar{D}^0 \text{ anything})/\Gamma_{\text{total}}$ Γ_{30}/Γ

VALUE	EVTS	DOCUMENT ID	TECN	COMMENT
0.615 ± 0.029 OUR AVERAGE				
0.635 ± 0.024 ± 0.005		¹ GIBBONS 97b	CLE2	$e^+e^- \rightarrow \Upsilon(4S)$
0.590 ± 0.047 ± 0.005		² BORTOLETTO92	CLEO	$e^+e^- \rightarrow \Upsilon(4S)$
0.491 ± 0.074 ± 0.004		³ ALBRECHT 91h	ARG	$e^+e^- \rightarrow \Upsilon(4S)$

••• We do not use the following data for averages, fits, limits, etc. •••

0.532 ± 0.065 ± 0.004 21k ⁴ BORTOLETTO87 CLEO $e^+e^- \rightarrow \Upsilon(4S)$

0.608 ± 0.183 ± 0.005 ⁵ GREEN 83 CLEO Repl. by BORTOLETTO 87

¹ GIBBONS 97b reports $[\Gamma(B \rightarrow D^0/\bar{D}^0 \text{ anything})/\Gamma_{\text{total}}] \times [B(D^0 \rightarrow K^- \pi^+)] = 0.0251 \pm 0.0006 \pm 0.00075$ which we divide by our best value $B(D^0 \rightarrow K^- \pi^+) = (3.950 \pm 0.031) \times 10^{-2}$. Our first error is their experiment's error and our second error is the systematic error from using our best value.

² BORTOLETTO 92 reports $[\Gamma(B \rightarrow D^0/\bar{D}^0 \text{ anything})/\Gamma_{\text{total}}] \times [B(D^0 \rightarrow K^- \pi^+)] = 0.0233 \pm 0.0012 \pm 0.0014$ which we divide by our best value $B(D^0 \rightarrow K^- \pi^+) = (3.950 \pm 0.031) \times 10^{-2}$. Our first error is their experiment's error and our second error is the systematic error from using our best value.

³ ALBRECHT 91h reports $[\Gamma(B \rightarrow D^0/\bar{D}^0 \text{ anything})/\Gamma_{\text{total}}] \times [B(D^0 \rightarrow K^- \pi^+)] = 0.0194 \pm 0.0015 \pm 0.0025$ which we divide by our best value $B(D^0 \rightarrow K^- \pi^+) = (3.950 \pm 0.031) \times 10^{-2}$. Our first error is their experiment's error and our second error is the systematic error from using our best value.

⁴ BORTOLETTO 87 reports $[\Gamma(B \rightarrow D^0/\bar{D}^0 \text{ anything})/\Gamma_{\text{total}}] \times [B(D^0 \rightarrow K^- \pi^+)] = 0.0210 \pm 0.0015 \pm 0.0021$ which we divide by our best value $B(D^0 \rightarrow K^- \pi^+) = (3.950 \pm 0.031) \times 10^{-2}$. Our first error is their experiment's error and our second error is the systematic error from using our best value.

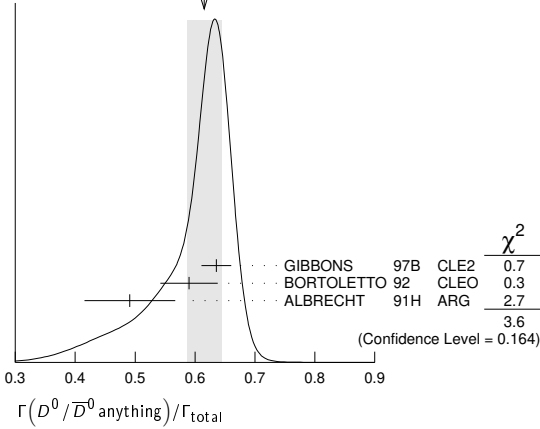
⁵ GREEN 83 reports $[\Gamma(B \rightarrow D^0/\bar{D}^0 \text{ anything})/\Gamma_{\text{total}}] \times [B(D^0 \rightarrow K^- \pi^+)] = 0.024 \pm 0.006 \pm 0.004$ which we divide by our best value $B(D^0 \rightarrow K^- \pi^+) = (3.950 \pm 0.031) \times$

Meson Particle Listings

B^\pm/B^0 ADMIXTURE

10^{-2} . Our first error is their experiment's error and our second error is the systematic error from using our best value.

WEIGHTED AVERAGE
0.615±0.029 (Error scaled by 1.3)



$\Gamma(D^- \ell^+ \nu_\ell \text{ anything})/\Gamma(D^0 \ell^+ \nu_\ell \text{ anything})$ Γ_4/Γ_5

VALUE	DOCUMENT ID	TECN	COMMENT
0.359±0.006±0.009	¹ AAIJ	19AD LHCb	$p\bar{p}$ at 13 TeV

¹ AAIJ 19AD uses $D^0 \rightarrow K^- \pi^+$ and $D^+ \rightarrow K^- \pi^+ \pi^+$ modes.

$\Gamma(D^*(2010)^\pm \text{ anything})/\Gamma_{\text{total}}$ Γ_{31}/Γ

VALUE	EVTS	DOCUMENT ID	TECN	COMMENT
0.225±0.015 OUR AVERAGE				
0.247±0.019±0.01		¹ GIBBONS 97B CLE2	$e^+e^- \rightarrow \Upsilon(4S)$	
0.205±0.019±0.007		² ALBRECHT 96D ARG	$e^+e^- \rightarrow \Upsilon(4S)$	
0.230±0.028±0.009		³ BORTOLETTO92 CLEO	$e^+e^- \rightarrow \Upsilon(4S)$	
• • • We do not use the following data for averages, fits, limits, etc. • • •				
0.283±0.053±0.002		⁴ ALBRECHT 91H ARG	Sup. by ALBRECHT 96D	
0.22 ± 0.04 $^{+0.07}_{-0.04}$	5200	⁵ BORTOLETTO87 CLEO	$e^+e^- \rightarrow \Upsilon(4S)$	
0.27 ± 0.06 $^{+0.08}_{-0.06}$	510	⁶ CSORNA 85 CLEO	Repl. by BORTOLETTO 87	

¹ GIBBONS 97B reports $B(B \rightarrow D^*(2010)^+ \text{ anything}) = 0.239 \pm 0.015 \pm 0.014 \pm 0.009$ using CLEO measured D and D^* branching fractions. We rescale to our PDG 96 values of D and D^* branching ratios. Our first error is their experiment's error and our second error is the systematic error from using our best value.

² ALBRECHT 96D reports $B(B \rightarrow D^*(2010)^+ \text{ anything}) = 0.196 \pm 0.019$ using CLEO measured $B(D^*(2010)^+ \rightarrow D^0 \pi^+) = 0.681 \pm 0.01 \pm 0.013$, $B(D^0 \rightarrow K^- \pi^+) = 0.0401 \pm 0.0014$, $B(D^0 \rightarrow K^- \pi^+ \pi^+) = 0.081 \pm 0.005$. We rescale to our PDG 96 values of D and D^* branching ratios. Our first error is their experiment's error and our second error is the systematic error from using our best value.

³ BORTOLETTO 92 reports $B(B \rightarrow D^*(2010)^+ \text{ anything}) = 0.25 \pm 0.03 \pm 0.04$ using MARK II $B(D^*(2010)^+ \rightarrow D^0 \pi^+) = 0.57 \pm 0.06$ and $B(D^0 \rightarrow K^- \pi^+) = 0.042 \pm 0.008$. We rescale to our PDG 96 values of D and D^* branching ratios. Our first error is their experiment's error and our second error is the systematic error from using our best value.

⁴ ALBRECHT 91H reports $0.348 \pm 0.060 \pm 0.035$ from a measurement of $[\Gamma(B \rightarrow D^*(2010)^\pm \text{ anything})/\Gamma_{\text{total}}] \times [B(D^*(2010)^+ \rightarrow D^0 \pi^+)]$ assuming $B(D^*(2010)^+ \rightarrow D^0 \pi^+) = 0.55 \pm 0.04$, which we rescale to our best value $B(D^*(2010)^+ \rightarrow D^0 \pi^+) = (67.7 \pm 0.5) \times 10^{-2}$. Our first error is their experiment's error and our second error is the systematic error from using our best value. Uses the PDG 90 $B(D^0 \rightarrow K^- \pi^+) = 0.0371 \pm 0.0025$.

⁵ BORTOLETTO 87 uses old MARK III (BALTRUSAITIS 86E) branching ratios $B(D^0 \rightarrow K^- \pi^+) = 0.056 \pm 0.004 \pm 0.003$ and also assumes $B(D^*(2010)^+ \rightarrow D^0 \pi^+) = 0.60^{+0.08}_{-0.15}$. The product branching ratio for $B(B \rightarrow D^*(2010)^+) B(D^*(2010)^+ \rightarrow D^0 \pi^+)$ is $0.13 \pm 0.02 \pm 0.012$. Superseded by BORTOLETTO 92.

⁶ $V-A$ momentum spectrum used to extrapolate below $p = 1$ GeV. We correct the value assuming $B(D^0 \rightarrow K^- \pi^+) = 0.042 \pm 0.006$ and $B(D^+ \rightarrow D^0 \pi^+) = 0.6^{+0.08}_{-0.15}$. The product branching fraction is $B(B \rightarrow D^*(2010)^+) B(D^*(2010)^+ \rightarrow D^0 \pi^+) = (68 \pm 15 \pm 9) \times 10^{-4}$.

$\Gamma(D^*(2007)^0 \text{ anything})/\Gamma_{\text{total}}$ Γ_{32}/Γ

VALUE	DOCUMENT ID	TECN	COMMENT
0.260±0.023±0.015	¹ GIBBONS 97B CLE2	$e^+e^- \rightarrow \Upsilon(4S)$	

¹ GIBBONS 97B reports $B(B \rightarrow D^*(2007)^0 \text{ anything}) = 0.247 \pm 0.012 \pm 0.018 \pm 0.018$ using CLEO measured D and D^* branching fractions. We rescale to our PDG 96 values of D and D^* branching ratios. Our first error is their experiment's error and our second error is the systematic error from using our best value.

$\Gamma(D_s^\pm \text{ anything})/\Gamma_{\text{total}}$ Γ_{33}/Γ

VALUE	EVTS	DOCUMENT ID	TECN	COMMENT
0.083±0.008 OUR AVERAGE				
0.089±0.010±0.008		¹ ARTUSO 05B CLE2	$e^+e^- \rightarrow \Upsilon(5S)$	
0.087±0.005±0.008		² AUBERT 02G BABR	$e^+e^- \rightarrow \Upsilon(4S)$	
0.065±0.011±0.006		³ ALBRECHT 92G ARG	$e^+e^- \rightarrow \Upsilon(4S)$	
0.068±0.010±0.006	257	⁴ BORTOLETTO90 CLEO	$e^+e^- \rightarrow \Upsilon(4S)$	
0.085±0.022±0.008		⁵ HAAS 86 CLEO	$e^+e^- \rightarrow \Upsilon(4S)$	
• • • We do not use the following data for averages, fits, limits, etc. • • •				
0.094±0.007±0.008		⁶ GIBAUT 96 CLE2	Repl. by ARTUSO 05B	
0.094±0.024±0.008		⁷ ALBRECHT 87H ARG	$e^+e^- \rightarrow \Upsilon(4S)$	

¹ ARTUSO 05B reports $0.0905 \pm 0.0025 \pm 0.0140$ from a measurement of $[\Gamma(B \rightarrow D_s^\pm \text{ anything})/\Gamma_{\text{total}}] \times [B(D_s^\pm \rightarrow \phi \pi^\pm)]$ assuming $B(D_s^\pm \rightarrow \phi \pi^\pm) = (4.4 \pm 0.5) \times 10^{-2}$, which we rescale to our best value $B(D_s^\pm \rightarrow \phi \pi^\pm) = (4.5 \pm 0.4) \times 10^{-2}$. Our first error is their experiment's error and our second error is the systematic error from using our best value.

² AUBERT 02G reports $[\Gamma(B \rightarrow D_s^\pm \text{ anything})/\Gamma_{\text{total}}] \times [B(D_s^\pm \rightarrow \phi \pi^\pm)] = 0.00393 \pm 0.00007 \pm 0.00021$ which we divide by our best value $B(D_s^\pm \rightarrow \phi \pi^\pm) = (4.5 \pm 0.4) \times 10^{-2}$. Our first error is their experiment's error and our second error is the systematic error from using our best value.

³ ALBRECHT 92G reports $[\Gamma(B \rightarrow D_s^\pm \text{ anything})/\Gamma_{\text{total}}] \times [B(D_s^\pm \rightarrow \phi \pi^\pm)] = 0.00292 \pm 0.00039 \pm 0.00031$ which we divide by our best value $B(D_s^\pm \rightarrow \phi \pi^\pm) = (4.5 \pm 0.4) \times 10^{-2}$. Our first error is their experiment's error and our second error is the systematic error from using our best value.

⁴ BORTOLETTO 90 reports $[\Gamma(B \rightarrow D_s^\pm \text{ anything})/\Gamma_{\text{total}}] \times [B(D_s^\pm \rightarrow \phi \pi^\pm)] = 0.00306 \pm 0.00047$ which we divide by our best value $B(D_s^\pm \rightarrow \phi \pi^\pm) = (4.5 \pm 0.4) \times 10^{-2}$. Our first error is their experiment's error and our second error is the systematic error from using our best value.

⁵ HAAS 86 reports $[\Gamma(B \rightarrow D_s^\pm \text{ anything})/\Gamma_{\text{total}}] \times [B(D_s^\pm \rightarrow \phi \pi^\pm)] = 0.0038 \pm 0.0010$ which we divide by our best value $B(D_s^\pm \rightarrow \phi \pi^\pm) = (4.5 \pm 0.4) \times 10^{-2}$. Our first error is their experiment's error and our second error is the systematic error from using our best value. 64 ± 22% decays are 2-body.

⁶ GIBAUT 96 reports $0.1211 \pm 0.0039 \pm 0.0088$ from a measurement of $[\Gamma(B \rightarrow D_s^\pm \text{ anything})/\Gamma_{\text{total}}] \times [B(D_s^\pm \rightarrow \phi \pi^\pm)]$ assuming $B(D_s^\pm \rightarrow \phi \pi^\pm) = 0.035$, which we rescale to our best value $B(D_s^\pm \rightarrow \phi \pi^\pm) = (4.5 \pm 0.4) \times 10^{-2}$. Our first error is their experiment's error and our second error is the systematic error from using our best value.

⁷ ALBRECHT 87H reports $[\Gamma(B \rightarrow D_s^\pm \text{ anything})/\Gamma_{\text{total}}] \times [B(D_s^\pm \rightarrow \phi \pi^\pm)] = 0.0042 \pm 0.0009 \pm 0.0006$ which we divide by our best value $B(D_s^\pm \rightarrow \phi \pi^\pm) = (4.5 \pm 0.4) \times 10^{-2}$. Our first error is their experiment's error and our second error is the systematic error from using our best value. 46 ± 16% of $B \rightarrow D_s X$ decays are 2-body. Superseded by ALBRECHT 92G.

$\Gamma(D_s^{*\pm} \text{ anything})/\Gamma_{\text{total}}$ Γ_{34}/Γ

VALUE	DOCUMENT ID	TECN	COMMENT
0.063±0.009±0.006	¹ AUBERT 02G BABR	$e^+e^- \rightarrow \Upsilon(4S)$	

¹ AUBERT 02G reports $[\Gamma(B \rightarrow D_s^{*\pm} \text{ anything})/\Gamma_{\text{total}}] \times [B(D_s^{*\pm} \rightarrow \phi \pi^\pm)] = 0.00284 \pm 0.00029 \pm 0.00025$ which we divide by our best value $B(D_s^{*\pm} \rightarrow \phi \pi^\pm) = (4.5 \pm 0.4) \times 10^{-2}$. Our first error is their experiment's error and our second error is the systematic error from using our best value.

$\Gamma(D_s^\pm \bar{D}^{(*)})/\Gamma(D_s^\pm \text{ anything})$ Γ_{35}/Γ_{34}

VALUE	DOCUMENT ID	TECN	COMMENT
0.533±0.037±0.037	AUBERT	02G BABR	$e^+e^- \rightarrow \Upsilon(4S)$

$\Gamma(\bar{D}_{S0}(2317))/\Gamma_{\text{total}}$ Γ_{36}/Γ

VALUE	DOCUMENT ID	TECN	COMMENT
seen	¹ KROKOVNY 03B BELL	$e^+e^- \rightarrow \Upsilon(4S)$	

¹ The product branching ratio for $B(B \rightarrow \bar{D}_{S0}(2317)^+) \times B(D_{S0}(2317)^+ \rightarrow D_s \pi^0)$ is measured to be $(8.5^{+2.1}_{-1.9} \pm 2.6) \times 10^{-4}$.

$\Gamma(\bar{D}_{S0}(2457))/\Gamma_{\text{total}}$ Γ_{37}/Γ

VALUE	DOCUMENT ID	TECN	COMMENT
seen	¹ KROKOVNY 03B BELL	$e^+e^- \rightarrow \Upsilon(4S)$	

¹ The product branching ratio for $B(B \rightarrow \bar{D}_{S0}(2457)^+) \times B(D_{S0}(2457)^+ \rightarrow D_s^{*+} \pi^0, D_s^+ \gamma)$ are measured to be $(17.8^{+4.5}_{-3.9} \pm 5.3) \times 10^{-4}$ and $(6.7^{+1.3}_{-1.2} \pm 2.0) \times 10^{-4}$, respectively.

$[\Gamma(D^{(*)} \bar{D}^{(*)} K^0) + \Gamma(D^{(*)} \bar{D}^{(*)} K^\pm)]/\Gamma_{\text{total}}$ Γ_{38}/Γ

VALUE	DOCUMENT ID	TECN	COMMENT
0.071±0.025±0.010 $^{+0.015}_{-0.009}$	¹ BARATE 98Q ALEP	$e^+e^- \rightarrow Z$	

¹ The systematic error includes the uncertainties due to the charm branching ratios.

$\Gamma(b \rightarrow c \bar{c} s)/\Gamma_{\text{total}}$ Γ_{39}/Γ

VALUE	DOCUMENT ID	TECN	COMMENT
0.219±0.037	¹ COAN 98 CLE2	$e^+e^- \rightarrow \Upsilon(4S)$	

¹ COAN 98 uses $D-\ell$ correlation.

See key on page 999

Meson Particle Listings

B^\pm/B^0 ADMIXTURE

$\Gamma(D_s^{(*)}\bar{D}^{(*)})/\Gamma(D_s^\pm \text{ anything})$ Γ_{40}/Γ_{33}

VALUE	DOCUMENT ID	TECN	COMMENT
0.469 ± 0.017 OUR AVERAGE			
0.464 ± 0.013 ± 0.015	AUBERT 02G	BABR	$e^+e^- \rightarrow \Upsilon(4S)$
0.56 ^{+0.21 +0.09} _{-0.15 -0.08}	¹ BARATE 98Q	ALEP	$e^+e^- \rightarrow Z$
0.457 ± 0.019 ± 0.037	GIBAUT 96	CLE2	$e^+e^- \rightarrow \Upsilon(4S)$
0.58 ± 0.07 ± 0.09	ALBRECHT 92G	ARG	$e^+e^- \rightarrow \Upsilon(4S)$
0.56 ± 0.10	BORTOLETTO90	CLEO	$e^+e^- \rightarrow \Upsilon(4S)$

¹BARATE 98Q measures $B(B \rightarrow D_s^{(*)}\bar{D}^{(*)}) = 0.056^{+0.021+0.009+0.019}_{-0.015-0.008-0.011}$, where the third error results from the uncertainty on the different D branching ratios and is dominated by the uncertainty on $B(D_s^+ \rightarrow \phi\pi^+)$. We divide $B(B \rightarrow D_s^{(*)}\bar{D}^{(*)})$ by our best value of $B(B \rightarrow D_s \text{ anything}) = 0.1 \pm 0.025$.

$\Gamma(D^*D^*(2010)^\pm)/\Gamma_{\text{total}}$ Γ_{41}/Γ

VALUE	CL%	DOCUMENT ID	TECN	COMMENT
<5.9 × 10⁻³	90	BARATE 98Q	ALEP	$e^+e^- \rightarrow Z$

$[\Gamma(D^*D^*(2010)^\pm) + \Gamma(D^*D^\pm)]/\Gamma_{\text{total}}$ Γ_{42}/Γ

VALUE	CL%	DOCUMENT ID	TECN	COMMENT
<5.5 × 10⁻³	90	BARATE 98Q	ALEP	$e^+e^- \rightarrow Z$

$\Gamma(D D^\pm)/\Gamma_{\text{total}}$ Γ_{43}/Γ

VALUE	CL%	DOCUMENT ID	TECN	COMMENT
<3.1 × 10⁻³	90	BARATE 98Q	ALEP	$e^+e^- \rightarrow Z$

$\Gamma(D_s^{(*)}\pm\bar{D}^{(*)}X(n\pi^\pm))/\Gamma_{\text{total}}$ Γ_{44}/Γ

VALUE	DOCUMENT ID	TECN	COMMENT
0.094^{+0.040+0.034}_{-0.031-0.024}	¹ BARATE 98Q	ALEP	$e^+e^- \rightarrow Z$

¹The systematic error includes the uncertainties due to the charm branching ratios.

$\Gamma(D^*(2010)\gamma)/\Gamma_{\text{total}}$ Γ_{45}/Γ

VALUE	CL%	DOCUMENT ID	TECN	COMMENT
<1.1 × 10⁻³	90	¹ LESIAK 92	CBAL	$e^+e^- \rightarrow \Upsilon(4S)$

¹LESIAK 92 set a limit on the inclusive process $B(b \rightarrow s\gamma) < 2.8 \times 10^{-3}$ at 90% CL for the range of masses of 892–2045 MeV, independent of assumptions about s-quark hadronization.

$\Gamma(D_s^+\pi^-, D_s^{*+}\pi^-, D_s^+\rho^-, D_s^{*+}\rho^-, D_s^+\pi^0, D_s^{*+}\pi^0, D_s^+\eta, D_s^{*+}\eta, D_s^+\rho^0, D_s^+\rho^0, D_s^+\omega, D_s^{*+}\omega)/\Gamma_{\text{total}}$ Γ_{46}/Γ

VALUE	CL%	DOCUMENT ID	TECN	COMMENT
<4 × 10⁻⁴	90	¹ ALEXANDER 93B	CLE2	$e^+e^- \rightarrow \Upsilon(4S)$

¹ALEXANDER 93B reports $< 4.8 \times 10^{-4}$ from a measurement of $[\Gamma(B \rightarrow D_s^+\pi^-, D_s^{*+}\pi^-, D_s^+\rho^-, D_s^{*+}\rho^-, D_s^+\pi^0, D_s^{*+}\pi^0, D_s^+\eta, D_s^{*+}\eta, D_s^+\rho^0, D_s^{*+}\rho^0, D_s^+\omega, D_s^{*+}\omega)/\Gamma_{\text{total}}] \times [B(D_s^+ \rightarrow \phi\pi^+)]$ assuming $B(D_s^+ \rightarrow \phi\pi^+) = 0.037$, which we rescale to our best value $B(D_s^+ \rightarrow \phi\pi^+) = 4.5 \times 10^{-2}$. This branching ratio limit provides a model-dependent upper limit $|V_{ub}|/|V_{cb}| < 0.16$ at CL=90%.

$\Gamma(D_{s1}(2536)^+ \text{ anything})/\Gamma_{\text{total}}$ Γ_{47}/Γ

VALUE	CL%	DOCUMENT ID	TECN	COMMENT
<0.0095	90	¹ BISHAI 98	CLE2	$e^+e^- \rightarrow \Upsilon(4S)$

¹Assuming factorization, the decay constant $f_{D_{s1}^+}$ is at least a factor of 2.5 times smaller than $f_{D_s^+}$.

$\Gamma(J/\psi(1S) \text{ anything})/\Gamma_{\text{total}}$ Γ_{48}/Γ

VALUE (units 10 ⁻²)	EVTs	DOCUMENT ID	TECN	COMMENT
1.094 ± 0.032 OUR AVERAGE				Error includes scale factor of 1.1.
1.057 ± 0.012 ± 0.040		¹ AUBERT 03F	BABR	$e^+e^- \rightarrow \Upsilon(4S)$
1.121 ± 0.013 ± 0.042		ANDERSON 02	CLE2	$e^+e^- \rightarrow \Upsilon(4S)$
1.29 ± 0.45 ± 0.01	27	² MASCHMANN 90	CBAL	$e^+e^- \rightarrow \Upsilon(4S)$
1.24 ± 0.27 ± 0.01	120	³ ALBRECHT 87D	ARG	$e^+e^- \rightarrow \Upsilon(4S)$
1.35 ± 0.24 ± 0.01	52	⁴ ALAM 86	CLEO	$e^+e^- \rightarrow \Upsilon(4S)$
••• We do not use the following data for averages, fits, limits, etc. •••				
1.12 ± 0.06 ± 0.01	1489	⁵ BALEST 95B	CLE2	$e^+e^- \rightarrow \Upsilon(4S)$
1.4 ^{+0.6} _{-0.5}	7	⁶ ALBRECHT 85H	ARG	$e^+e^- \rightarrow \Upsilon(4S)$
1.1 ± 0.21 ± 0.23	46	⁷ HAAS 85	CLEO	Repl. by ALAM 86

¹AUBERT 03F also reports the momentum distribution and helicity of $J/\psi \rightarrow \ell^+\ell^-$ in the $\Upsilon(4S)$ center-of-mass frame.
²MASCHMANN 90 reports $(1.12 \pm 0.33 \pm 0.25) \times 10^{-2}$ from a measurement of $[\Gamma(B \rightarrow J/\psi(1S) \text{ anything})/\Gamma_{\text{total}}] \times [B(J/\psi(1S) \rightarrow e^+e^-)]$ assuming $B(J/\psi(1S) \rightarrow e^+e^-) = 0.069 \pm 0.009$, which we rescale to our best value $B(J/\psi(1S) \rightarrow e^+e^-) = (5.971 \pm 0.032) \times 10^{-2}$. Our first error is their experiment's error and our second error is the systematic error from using our best value.
³ALBRECHT 87D reports $(1.07 \pm 0.16 \pm 0.22) \times 10^{-2}$ from a measurement of $[\Gamma(B \rightarrow J/\psi(1S) \text{ anything})/\Gamma_{\text{total}}] \times [B(J/\psi(1S) \rightarrow e^+e^-)]$ assuming $B(J/\psi(1S) \rightarrow e^+e^-) = 0.069 \pm 0.009$, which we rescale to our best value $B(J/\psi(1S) \rightarrow e^+e^-) = (5.971 \pm$

$0.032) \times 10^{-2}$. Our first error is their experiment's error and our second error is the systematic error from using our best value. ALBRECHT 87D find the branching ratio for J/ψ not from $\psi(2S)$ to be 0.0081 ± 0.0023 .

⁴ALAM 86 reports $(1.09 \pm 0.16 \pm 0.21) \times 10^{-2}$ from a measurement of $[\Gamma(B \rightarrow J/\psi(1S) \text{ anything})/\Gamma_{\text{total}}] \times [B(J/\psi(1S) \rightarrow \mu^+\mu^-)]$ assuming $B(J/\psi(1S) \rightarrow \mu^+\mu^-) = 0.074 \pm 0.012$, which we rescale to our best value $B(J/\psi(1S) \rightarrow \mu^+\mu^-) = (5.961 \pm 0.033) \times 10^{-2}$. Our first error is their experiment's error and our second error is the systematic error from using our best value.

⁵BALEST 95B reports $(1.12 \pm 0.04 \pm 0.06) \times 10^{-2}$ from a measurement of $[\Gamma(B \rightarrow J/\psi(1S) \text{ anything})/\Gamma_{\text{total}}] \times [B(J/\psi(1S) \rightarrow e^+e^-)]$ assuming $B(J/\psi(1S) \rightarrow e^+e^-) = 0.0599 \pm 0.0025$, which we rescale to our best value $B(J/\psi(1S) \rightarrow e^+e^-) = (5.971 \pm 0.032) \times 10^{-2}$. Our first error is their experiment's error and our second error is the systematic error from using our best value. They measure $J/\psi(1S) \rightarrow e^+e^-$ and $\mu^+\mu^-$ and use PDG 1994 values for the branching fractions. The rescaling is the same for either mode so we use e^+e^- .

⁶Statistical and systematic errors were added in quadrature. ALBRECHT 85H also report a CL = 90% limit of 0.007 for $B \rightarrow J/\psi(1S) + X$ where $m_X < 1$ GeV.

⁷Dimuon and dielectron events used.

$\Gamma(J/\psi(1S) \text{ (direct) anything})/\Gamma_{\text{total}}$ Γ_{49}/Γ

VALUE	DOCUMENT ID	TECN	COMMENT
0.0078 ± 0.0004 OUR AVERAGE			Error includes scale factor of 1.1.
0.00740 ± 0.00023 ± 0.00043	¹ AUBERT 03F	BABR	$e^+e^- \rightarrow \Upsilon(4S)$
0.00813 ± 0.00017 ± 0.00037	² ANDERSON 02	CLE2	$e^+e^- \rightarrow \Upsilon(4S)$
••• We do not use the following data for averages, fits, limits, etc. •••			
0.0080 ± 0.0008	³ BALEST 95B	CLE2	$e^+e^- \rightarrow \Upsilon(4S)$

¹AUBERT 03F also reports the helicity of $J/\psi \rightarrow \ell^+\ell^-$ produced directly in B decay.

²Also reports the measurement of $J/\psi \rightarrow \ell^+\ell^-$ polarization produced directly from B decay.

³BALEST 95B assume PDG 1994 values for sub mode branching ratios. $J/\psi(1S)$ mesons are reconstructed in $J/\psi(1S) \rightarrow e^+e^-$ and $J/\psi(1S) \rightarrow \mu^+\mu^-$. The $B \rightarrow J/\psi(1S)X$ branching ratio contains $J/\psi(1S)$ mesons directly from B decays and also from feeddown through $\psi(2S) \rightarrow J/\psi(1S)$, $\chi_{c1}(1P) \rightarrow J/\psi(1S)$, or $\chi_{c2}(1P) \rightarrow J/\psi(1S)$. Using the measured inclusive rates, BALEST 95B corrects for the feeddown and finds the $B \rightarrow J/\psi(1S)$ (direct) X branching ratio.

$\Gamma(\psi(2S) \text{ anything})/\Gamma_{\text{total}}$ Γ_{50}/Γ

VALUE	EVTs	DOCUMENT ID	TECN	COMMENT
0.00307 ± 0.00021 OUR AVERAGE				Error includes scale factor of 1.1.
0.00297 ± 0.00020 ± 0.00020		AUBERT 03F	BABR	$e^+e^- \rightarrow \Upsilon(4S)$
0.00316 ± 0.00014 ± 0.00028		¹ ANDERSON 02	CLE2	$e^+e^- \rightarrow \Upsilon(4S)$
0.0046 ± 0.0017 ± 0.0011	8	ALBRECHT 87D	ARG	$e^+e^- \rightarrow \Upsilon(4S)$
••• We do not use the following data for averages, fits, limits, etc. •••				
0.0034 ± 0.0004 ± 0.0003	240	² BALEST 95B	CLE2	$e^+e^- \rightarrow \Upsilon(4S)$

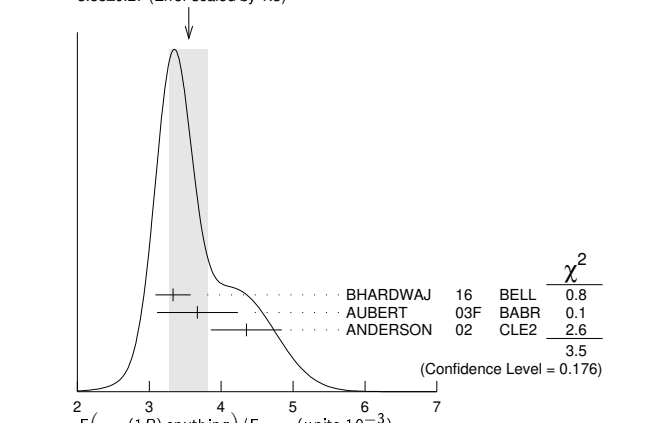
¹Also reports the measurement of $\psi(2S) \rightarrow \ell^+\ell^-$ polarization produced directly from B decay.

²BALEST 95B assume PDG 1994 values for sub mode branching ratios. They find $B(B \rightarrow \psi(2S)X, \psi(2S) \rightarrow \ell^+\ell^-) = 0.30 \pm 0.05 \pm 0.04$ and $B(B \rightarrow \psi(2S)X, \psi(2S) \rightarrow J/\psi(1S)\pi^+\pi^-) = 0.37 \pm 0.05 \pm 0.05$. Weighted average is quoted for $B(B \rightarrow \psi(2S)X)$.

$\Gamma(\chi_{c1}(1P) \text{ anything})/\Gamma_{\text{total}}$ Γ_{51}/Γ

VALUE (units 10 ⁻³)	EVTs	DOCUMENT ID	TECN	COMMENT
3.55 ± 0.27 OUR AVERAGE				Error includes scale factor of 1.3. See the ideogram below.
3.33 ± 0.05 ± 0.24		¹ BHARDWAJ 16	BELL	$e^+e^- \rightarrow \Upsilon(4S)$
3.67 ± 0.35 ± 0.44		AUBERT 03F	BABR	$e^+e^- \rightarrow \Upsilon(4S)$
4.35 ± 0.29 ± 0.40		ANDERSON 02	CLE2	$e^+e^- \rightarrow \Upsilon(4S)$
••• We do not use the following data for averages, fits, limits, etc. •••				
3.63 ± 0.22 ± 0.34		² ABE 02L	BELL	Repl. by BHARDWAJ 16
3.30 ± 0.35 ± 0.09		³ CHEN 01	CLE2	$e^+e^- \rightarrow \Upsilon(4S)$
4.0 ± 0.6 ± 0.4	112	⁴ BALEST 95B	CLE2	Repl. by CHEN 01
10.5 ± 3.5 ± 2.5		⁵ ALBRECHT 92E	ARG	$e^+e^- \rightarrow \Upsilon(4S)$

WEIGHTED AVERAGE
 3.55 ± 0.27 (Error scaled by 1.3)



¹Assumes equal production of B^+ and B^0 at the $\Upsilon(4S)$.

Downloaded from https://academic.oup.com/ptep/article/2020/8/083C01/5891211 by guest on 20 August 2020

Meson Particle Listings

 B^\pm/B^0 ADMIXTURE

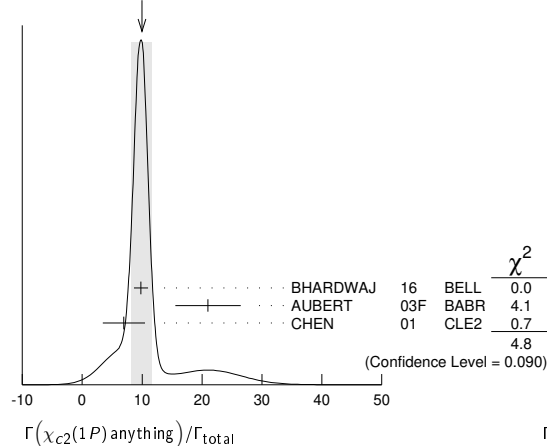
- ²ABE 02L uses PDG 01 values for $B(J/\psi(1S) \rightarrow \ell^+ \ell^-)$ and $B(\chi_{c1,c2} \rightarrow J/\psi(1S)\gamma)$.
- ³CHEN 01 reports $0.00414 \pm 0.00031 \pm 0.00040$ from a measurement of $[\Gamma(B \rightarrow \chi_{c1}(1P) \text{ anything})/\Gamma_{\text{total}}] \times [B(\chi_{c1}(1P) \rightarrow \gamma J/\psi(1S))]$ assuming $B(\chi_{c1}(1P) \rightarrow \gamma J/\psi(1S)) = 0.273 \pm 0.016$, which we rescale to our best value $B(\chi_{c1}(1P) \rightarrow \gamma J/\psi(1S)) = (34.3 \pm 1.0) \times 10^{-2}$. Our first error is their experiment's error and our second error is the systematic error from using our best value. Assumes equal production of B^+ and B^0 at the $T(4S)$.
- ⁴BALEST 95B assume $B(\chi_{c1}(1P) \rightarrow J/\psi(1S)\gamma) = (27.3 \pm 1.6) \times 10^{-2}$, the PDG 1994 value. Fit to ψ -photon invariant mass distribution allows for a $\chi_{c1}(1P)$ and a $\chi_{c2}(1P)$ component.
- ⁵ALBRECHT 92E assumes no $\chi_{c2}(1P)$ production.

$\Gamma(\chi_{c1}(1P) \text{ (direct) anything})/\Gamma_{\text{total}}$				Γ_{52}/Γ
VALUE (units 10^{-3})	DOCUMENT ID	TECN	COMMENT	
3.08 ± 0.19 OUR AVERAGE				
$3.03 \pm 0.05 \pm 0.24$	¹ BHARDWAJ 16	BELL	$e^+ e^- \rightarrow T(4S)$	
$3.41 \pm 0.35 \pm 0.42$	AUBERT 03F	BABR	$e^+ e^- \rightarrow T(4S)$	
$3.1 \pm 0.4 \pm 0.1$	² CHEN 01	CLE2	$e^+ e^- \rightarrow T(4S)$	
• • • We do not use the following data for averages, fits, limits, etc. • • •				
$3.32 \pm 0.22 \pm 0.34$	³ ABE 02L	BELL	Repl. by BHARDWAJ 16	
3.7 ± 0.7	⁴ BALEST 95B	CLE2	Repl. by CHEN 01	

- ¹Assumes equal production of B^+ and B^0 at the $T(4S)$.
- ²CHEN 01 reports $0.00383 \pm 0.00031 \pm 0.00040$ from a measurement of $[\Gamma(B \rightarrow \chi_{c1}(1P) \text{ (direct) anything})/\Gamma_{\text{total}}] \times [B(\chi_{c1}(1P) \rightarrow \gamma J/\psi(1S))]$ assuming $B(\chi_{c1}(1P) \rightarrow \gamma J/\psi(1S)) = 0.273 \pm 0.016$, which we rescale to our best value $B(\chi_{c1}(1P) \rightarrow \gamma J/\psi(1S)) = (34.3 \pm 1.0) \times 10^{-2}$. Our first error is their experiment's error and our second error is the systematic error from using our best value. Assumes equal production of B^+ and B^0 at the $T(4S)$.
- ³ABE 02L uses PDG 01 values for $B(J/\psi(1S) \rightarrow \ell^+ \ell^-)$ and $B(\chi_{c1,c2} \rightarrow J/\psi(1S)\gamma)$.
- ⁴BALEST 95B assume PDG 1994 values. $J/\psi(1S)$ mesons are reconstructed in the $e^+ e^-$ and $\mu^+ \mu^-$ modes. The $B \rightarrow \chi_{c1}(1P)X$ branching ratio contains $\chi_{c1}(1P)$ mesons directly from B decays and also from feeddown through $\psi(2S) \rightarrow \chi_{c1}(1P)\gamma$. Using the measured inclusive rates, BALEST 95B corrects for the feeddown and finds the $B \rightarrow \chi_{c1}(1P) \text{ (direct) } X$ branching ratio.

$\Gamma(\chi_{c2}(1P) \text{ anything})/\Gamma_{\text{total}}$				Γ_{53}/Γ
VALUE (units 10^{-4})	CL%	DOCUMENT ID	TECN	COMMENT
10.0 ± 1.7 OUR AVERAGE				Error includes scale factor of 1.6. See the ideogram below.
$9.8 \pm 0.6 \pm 1.0$		¹ BHARDWAJ 16	BELL	$e^+ e^- \rightarrow T(4S)$
$21.0 \pm 4.5 \pm 3.1$		AUBERT 03F	BABR	$e^+ e^- \rightarrow T(4S)$
$7.0 \pm 3.5 \pm 0.2$		² CHEN 01	CLE2	$e^+ e^- \rightarrow T(4S)$
• • • We do not use the following data for averages, fits, limits, etc. • • •				
$18.0^{+2.3}_{-2.8} \pm 2.6$		³ ABE 02L	BELL	Repl. by BHARDWAJ 16
<38	90	⁴ BALEST 95B	CLE2	Repl. by CHEN 01

- ¹Assumes equal production of B^+ and B^0 at the $T(4S)$.
- ²CHEN 01 reports $(9.8 \pm 4.8 \pm 1.5) \times 10^{-4}$ from a measurement of $[\Gamma(B \rightarrow \chi_{c2}(1P) \text{ anything})/\Gamma_{\text{total}}] \times [B(\chi_{c2}(1P) \rightarrow \gamma J/\psi(1S))]$ assuming $B(\chi_{c2}(1P) \rightarrow \gamma J/\psi(1S)) = 0.135 \pm 0.011$, which we rescale to our best value $B(\chi_{c2}(1P) \rightarrow \gamma J/\psi(1S)) = (19.0 \pm 0.5) \times 10^{-2}$. Our first error is their experiment's error and our second error is the systematic error from using our best value. Assumes equal production of B^+ and B^0 at the $T(4S)$.
- ³ABE 02L uses PDG 01 values for $B(J/\psi(1S) \rightarrow \ell^+ \ell^-)$ and $B(\chi_{c1,c2} \rightarrow J/\psi(1S)\gamma)$.
- ⁴BALEST 95B assume $B(\chi_{c2}(1P) \rightarrow J/\psi(1S)\gamma) = (13.5 \pm 1.1) \times 10^{-2}$, the PDG 1994 value. $J/\psi(1S)$ mesons are reconstructed in the $e^+ e^-$ and $\mu^+ \mu^-$ modes, and PDG 1994 branching fractions are used. If interpreted as signal, the 35 ± 13 events correspond to $B(B \rightarrow \chi_{c2}(1P)X) = (0.25 \pm 0.10 \pm 0.03) \times 10^{-2}$.

WEIGHTED AVERAGE
10.0 ± 1.7 (Error scaled by 1.6)

$\Gamma(\chi_{c2}(1P) \text{ (direct) anything})/\Gamma_{\text{total}}$				Γ_{54}/Γ
VALUE (units 10^{-3})	DOCUMENT ID	TECN	COMMENT	
0.75 ± 0.11 OUR AVERAGE				
$0.70 \pm 0.06 \pm 0.10$	¹ BHARDWAJ 16	BELL	$e^+ e^- \rightarrow T(4S)$	
$1.90 \pm 0.45 \pm 0.29$	AUBERT 03F	BABR	$e^+ e^- \rightarrow T(4S)$	
• • • We do not use the following data for averages, fits, limits, etc. • • •				
$1.53^{+0.23}_{-0.28} \pm 0.27$	² ABE 02L	BELL	Repl. by BHARDWAJ 16	
¹ Assumes equal production of B^+ and B^0 at the $T(4S)$.				
² ABE 02L uses PDG 01 values for $B(J/\psi(1S) \rightarrow \ell^+ \ell^-)$ and $B(\chi_{c1,c2} \rightarrow J/\psi(1S)\gamma)$.				

$\Gamma(\eta_c(1S) \text{ anything})/\Gamma_{\text{total}}$				Γ_{55}/Γ
VALUE	CL%	DOCUMENT ID	TECN	COMMENT
<0.009		¹ BALEST 95B	CLE2	$e^+ e^- \rightarrow T(4S)$
¹ BALEST 95B assume PDG 1994 values for sub mode branching ratios. $J/\psi(1S)$ mesons are reconstructed in $J/\psi(1S) \rightarrow e^+ e^-$ and $J/\psi(1S) \rightarrow \mu^+ \mu^-$. Search region $2960 < m_{\eta_c(1S)} < 3010$ MeV/ c^2 .				

$\Gamma(K\chi_{c1}(3872), \chi_{c1} \rightarrow D^0 \bar{D}^0 \pi^0)/\Gamma_{\text{total}}$				Γ_{56}/Γ
VALUE (units 10^{-4})	DOCUMENT ID	TECN	COMMENT	
1.22 ± 0.31 ± 0.23	¹ GOKHROO 06	BELL	$e^+ e^- \rightarrow T(4S)$	
¹ Measure the near-threshold enhancements in the $(D^0 \bar{D}^0 \pi^0)$ system at a mass $3875.2 \pm 0.7^{+0.3}_{-1.6} \pm 0.8$ MeV/ c^2 .				

$\Gamma(K\chi_{c1}(3872), \chi_{c1} \rightarrow D^{*0} D^0)/\Gamma_{\text{total}}$				Γ_{57}/Γ
VALUE (units 10^{-4})	DOCUMENT ID	TECN	COMMENT	
0.80 ± 0.20 ± 0.10	AUSHEV 10	BELL	$e^+ e^- \rightarrow T(4S)$	

$\Gamma(KX(3940), X \rightarrow D^{*0} D^0)/\Gamma_{\text{total}}$				Γ_{58}/Γ
VALUE (units 10^{-4})	CL%	DOCUMENT ID	TECN	COMMENT
<0.67	90	AUSHEV 10	BELL	$e^+ e^- \rightarrow T(4S)$

$\Gamma(KX(3915), X \rightarrow \omega J/\psi)/\Gamma_{\text{total}}$				Γ_{59}/Γ
VALUE (units 10^{-5})	DOCUMENT ID	TECN	COMMENT	
7.1 ± 1.3 ± 3.1	¹ CHOI 05	BELL	$e^+ e^- \rightarrow T(4S)$	
¹ CHOI 05 reports the observation of a near-threshold enhancement in the $\omega J/\psi$ mass spectrum in exclusive $B \rightarrow K\omega J/\psi$. The new state, denoted as $X(3915)$, is measured to have a mass of $3943 \pm 11 \pm 13$ GeV/ c^2 and a width $\Gamma = 87 \pm 22 \pm 26$ MeV.				

$\Gamma(K^\pm \text{ anything})/\Gamma_{\text{total}}$				Γ_{60}/Γ
VALUE	DOCUMENT ID	TECN	COMMENT	
0.789 ± 0.025 OUR AVERAGE				
$0.82 \pm 0.01 \pm 0.05$	ALBRECHT 94c	ARG	$e^+ e^- \rightarrow T(4S)$	
$0.775 \pm 0.015 \pm 0.025$	¹ ALBRECHT 93i	ARG	$e^+ e^- \rightarrow T(4S)$	
$0.85 \pm 0.07 \pm 0.09$	ALAM 87b	CLEO	$e^+ e^- \rightarrow T(4S)$	
• • • We do not use the following data for averages, fits, limits, etc. • • •				
seen	² BRODY 82	CLEO	$e^+ e^- \rightarrow T(4S)$	
seen	³ GIANNINI 82	CUSB	$e^+ e^- \rightarrow T(4S)$	

- ¹ALBRECHT 93i value is not independent of the sum of $B \rightarrow K^+ \text{ anything}$ and $B \rightarrow K^- \text{ anything}$ ALBRECHT 94c values.
- ²Assuming $T(4S) \rightarrow B\bar{B}$, a total of $3.38 \pm 0.34 \pm 0.68$ kaons per $T(4S)$ decay is found (the second error is systematic). In the context of the standard B -decay model, this leads to a value for $(b\text{-quark} \rightarrow c\text{-quark})/(b\text{-quark} \rightarrow \text{all})$ of $1.09 \pm 0.33 \pm 0.13$.
- ³GIANNINI 82 at CESR-CUSB observed 1.58 ± 0.35 K^0 per hadronic event much higher than 0.82 ± 0.10 below threshold. Consistent with predominant $b \rightarrow cX$ decay.

$\Gamma(K^+ \text{ anything})/\Gamma_{\text{total}}$				Γ_{61}/Γ
VALUE	DOCUMENT ID	TECN	COMMENT	
0.66 ± 0.05	¹ ALBRECHT 94c	ARG	$e^+ e^- \rightarrow T(4S)$	
• • • We do not use the following data for averages, fits, limits, etc. • • •				
$0.620 \pm 0.013 \pm 0.038$	² ALBRECHT 94c	ARG	$e^+ e^- \rightarrow T(4S)$	
$0.66 \pm 0.05 \pm 0.07$	² ALAM 87b	CLEO	$e^+ e^- \rightarrow T(4S)$	
¹ Measurement relies on lepton-kaon correlations. It is for the weak decay vertex and does not include mixing of the neutral B meson. Mixing effects were corrected for by assuming a mixing parameter r of $(18.1 \pm 4.3)\%$.				
² Measurement relies on lepton-kaon correlations. It includes production through mixing of the neutral B meson.				

$\Gamma(K^- \text{ anything})/\Gamma_{\text{total}}$				Γ_{62}/Γ
VALUE	DOCUMENT ID	TECN	COMMENT	
0.13 ± 0.04	¹ ALBRECHT 94c	ARG	$e^+ e^- \rightarrow T(4S)$	
• • • We do not use the following data for averages, fits, limits, etc. • • •				
$0.165 \pm 0.011 \pm 0.036$	² ALBRECHT 94c	ARG	$e^+ e^- \rightarrow T(4S)$	
$0.19 \pm 0.05 \pm 0.02$	² ALAM 87b	CLEO	$e^+ e^- \rightarrow T(4S)$	
¹ Measurement relies on lepton-kaon correlations. It is for the weak decay vertex and does not include mixing of the neutral B meson. Mixing effects were corrected for by assuming a mixing parameter r of $(18.1 \pm 4.3)\%$.				
² Measurement relies on lepton-kaon correlations. It includes production through mixing of the neutral B meson.				

See key on page 999

Meson Particle Listings

B^\pm/B^0 ADMIXTURE

$\Gamma(K^0/\bar{K}^0 \text{ anything})/\Gamma_{\text{total}}$ Γ_{63}/Γ

VALUE	DOCUMENT ID	TECN	COMMENT
0.64 ± 0.04 OUR AVERAGE			
0.642 ± 0.010 ± 0.042	¹ ALBRECHT 94C	ARG	$e^+e^- \rightarrow \Upsilon(4S)$
0.63 ± 0.06 ± 0.06	ALAM	87B CLEO	$e^+e^- \rightarrow \Upsilon(4S)$

¹ ALBRECHT 94C assume a K^0/\bar{K}^0 multiplicity twice that of K_S^0 .

$\Gamma(K^*(892)^\pm \text{ anything})/\Gamma_{\text{total}}$ Γ_{64}/Γ

VALUE	DOCUMENT ID	TECN	COMMENT
0.182 ± 0.054 ± 0.024	ALBRECHT 94J	ARG	$e^+e^- \rightarrow \Upsilon(4S)$

$\Gamma(K^*(892)^0/\bar{K}^*(892)^0 \text{ anything})/\Gamma_{\text{total}}$ Γ_{65}/Γ

VALUE	DOCUMENT ID	TECN	COMMENT
0.146 ± 0.016 ± 0.020	ALBRECHT 94J	ARG	$e^+e^- \rightarrow \Upsilon(4S)$

$\Gamma(K^*(892)\gamma)/\Gamma_{\text{total}}$ Γ_{66}/Γ

VALUE (units 10^{-5})	CL%	DOCUMENT ID	TECN	COMMENT
4.24 ± 0.54 ± 0.32		¹ COAN 00	CLE2	$e^+e^- \rightarrow \Upsilon(4S)$
< 15.0	90	² LESIAK 92	CBAL	$e^+e^- \rightarrow \Upsilon(4S)$
< 24	90	ALBRECHT 88H	ARG	$e^+e^- \rightarrow \Upsilon(4S)$

• • • We do not use the following data for averages, fits, limits, etc. • • •

¹ An average of $B(B^+ \rightarrow K^*(892)^+\gamma)$ and $B(B^0 \rightarrow K^*(892)^0\gamma)$ measurements reported in COAN 00 by assuming full correlated systematic errors.

² LESIAK 92 set a limit on the inclusive process $B(b \rightarrow s\gamma) < 2.8 \times 10^{-3}$ at 90% CL for the range of masses of 892–2045 MeV, independent of assumptions about s-quark hadronization.

$\Gamma(\eta K\gamma)/\Gamma_{\text{total}}$ Γ_{67}/Γ

VALUE (units 10^{-6})	DOCUMENT ID	TECN	COMMENT
8.5 ± 1.3^{+1.2}_{-0.9}	¹ NISHIDA 05	BELL	$e^+e^- \rightarrow \Upsilon(4S)$

¹ $m_{\eta K} < 2.4 \text{ GeV}/c^2$

$\Gamma(K_1(1400)\gamma)/\Gamma_{\text{total}}$ Γ_{68}/Γ

VALUE	CL%	DOCUMENT ID	TECN	COMMENT
< 12.7 × 10⁻⁵	90	¹ COAN 00	CLE2	$e^+e^- \rightarrow \Upsilon(4S)$
< 1.6 × 10 ⁻³	90	² LESIAK 92	CBAL	$e^+e^- \rightarrow \Upsilon(4S)$
< 4.1 × 10 ⁻⁴	90	ALBRECHT 88H	ARG	$e^+e^- \rightarrow \Upsilon(4S)$

• • • We do not use the following data for averages, fits, limits, etc. • • •

¹ Assumes equal production of B^+ and B^0 at the $\Upsilon(4S)$.

² LESIAK 92 set a limit on the inclusive process $B(b \rightarrow s\gamma) < 2.8 \times 10^{-3}$ at 90% CL for the range of masses of 892–2045 MeV, independent of assumptions about s-quark hadronization.

$\Gamma(K_2^*(1430)\gamma)/\Gamma_{\text{total}}$ Γ_{69}/Γ

VALUE (units 10^{-5})	CL%	DOCUMENT ID	TECN	COMMENT
1.66 ± 0.59 ± 0.13		¹ COAN 00	CLE2	$e^+e^- \rightarrow \Upsilon(4S)$
< 83	90	ALBRECHT 88H	ARG	$e^+e^- \rightarrow \Upsilon(4S)$

• • • We do not use the following data for averages, fits, limits, etc. • • •

¹ COAN 00 obtains a fitted signal yield of $15.9^{+5.7}_{-5.2}$ events. A search for contamination by $K^*(1410)$ yielded a rate consistent with 0; the central value assumes no contamination.

$\Gamma(K_2(1770)\gamma)/\Gamma_{\text{total}}$ Γ_{70}/Γ

VALUE	CL%	DOCUMENT ID	TECN	COMMENT
< 1.2 × 10⁻³	90	¹ LESIAK 92	CBAL	$e^+e^- \rightarrow \Upsilon(4S)$

¹ LESIAK 92 set a limit on the inclusive process $B(b \rightarrow s\gamma) < 2.8 \times 10^{-3}$ at 90% CL for the range of masses of 892–2045 MeV, independent of assumptions about s-quark hadronization.

$\Gamma(K_3^*(1780)\gamma)/\Gamma_{\text{total}}$ Γ_{71}/Γ

VALUE	CL%	DOCUMENT ID	TECN	COMMENT
< 3.7 × 10⁻⁵	90	¹ NISHIDA 05	BELL	$e^+e^- \rightarrow \Upsilon(4S)$

• • • We do not use the following data for averages, fits, limits, etc. • • •

< 3.0 × 10⁻³ ⁹⁰ ALBRECHT 88H ARG $e^+e^- \rightarrow \Upsilon(4S)$

¹ Uses $B(K_3^*(1780) \rightarrow \eta K) = 0.11^{+0.05}_{-0.04}$.

$\Gamma(K_3^*(2045)\gamma)/\Gamma_{\text{total}}$ Γ_{72}/Γ

VALUE	CL%	DOCUMENT ID	TECN	COMMENT
< 1.0 × 10⁻³	90	¹ LESIAK 92	CBAL	$e^+e^- \rightarrow \Upsilon(4S)$

¹ LESIAK 92 set a limit on the inclusive process $B(b \rightarrow s\gamma) < 2.8 \times 10^{-3}$ at 90% CL for the range of masses of 892–2045 MeV, independent of assumptions about s-quark hadronization.

$\Gamma(K\eta(958))/\Gamma_{\text{total}}$ Γ_{73}/Γ

VALUE	DOCUMENT ID	TECN	COMMENT
(8.3^{+0.9}_{-0.8} ± 0.7) × 10⁻⁵	¹ RICHICHI 00	CLE2	$e^+e^- \rightarrow \Upsilon(4S)$

¹ Assumes equal production of B^+ and B^0 at the $\Upsilon(4S)$.

$\Gamma(K^*(892)\eta'(958))/\Gamma_{\text{total}}$ Γ_{74}/Γ

VALUE (units 10^{-6})	CL%	DOCUMENT ID	TECN	COMMENT
4.1^{+1.0}_{-0.9} ± 0.5		¹ AUBERT 07E	BABR	$e^+e^- \rightarrow \Upsilon(4S)$

• • • We do not use the following data for averages, fits, limits, etc. • • •

< 22 ⁹⁰ ¹ RICHICHI 00 CLE2 $e^+e^- \rightarrow \Upsilon(4S)$

¹ Assumes equal production of B^+ and B^0 at the $\Upsilon(4S)$.

$\Gamma(K\eta)/\Gamma_{\text{total}}$ Γ_{75}/Γ

VALUE	CL%	DOCUMENT ID	TECN	COMMENT
< 5.2 × 10⁻⁶	90	¹ RICHICHI 00	CLE2	$e^+e^- \rightarrow \Upsilon(4S)$

¹ Assumes equal production of B^+ and B^0 at the $\Upsilon(4S)$.

$\Gamma(K^*(892)\eta)/\Gamma_{\text{total}}$ Γ_{76}/Γ

VALUE	DOCUMENT ID	TECN	COMMENT
(1.80 ± 0.49 ± 0.18) × 10⁻⁵	¹ RICHICHI 00	CLE2	$e^+e^- \rightarrow \Upsilon(4S)$

¹ Assumes equal production of B^+ and B^0 at the $\Upsilon(4S)$.

$\Gamma(K\phi\phi)/\Gamma_{\text{total}}$ Γ_{77}/Γ

VALUE (units 10^{-6})	DOCUMENT ID	TECN	COMMENT
2.3^{+0.9}_{-0.8} ± 0.3	¹ HUANG 03	BELL	$e^+e^- \rightarrow \Upsilon(4S)$

¹ Assumes equal production of charged and neutral B meson pairs and isospin symmetry.

$\Gamma(\bar{b} \rightarrow \bar{s}\gamma)/\Gamma_{\text{total}}$ Γ_{78}/Γ

VALUE (units 10^{-4})	DOCUMENT ID	TECN	COMMENT
3.49 ± 0.19 OUR AVERAGE			

3.75 ± 0.18 ± 0.35	^{1,2} SAITO 15	BELL	$e^+e^- \rightarrow \Upsilon(4S)$
3.52 ± 0.20 ± 0.51	^{1,3} LEES 12u	BABR	$e^+e^- \rightarrow \Upsilon(4S)$
3.32 ± 0.16 ± 0.31	^{1,4} LEES 12v	BABR	$e^+e^- \rightarrow \Upsilon(4S)$
3.47 ± 0.15 ± 0.40	^{1,5} LIMOSANI 09	BELL	$e^+e^- \rightarrow \Upsilon(4S)$
3.90 ± 0.91 ± 0.64	^{1,6} AUBERT 08o	BABR	$e^+e^- \rightarrow \Upsilon(4S)$
3.29 ± 0.44 ± 0.29	^{1,7} CHEN 01c	CLE2	$e^+e^- \rightarrow \Upsilon(4S)$

• • • We do not use the following data for averages, fits, limits, etc. • • •

⁸ DEL-AMO-SA...10M BABR $e^+e^- \rightarrow \Upsilon(4S)$

⁹ AUBERT 09u BABR Repl. by DEL-AMO-SANCHEZ 10M

^{1,10} AUBERT, BE 06b BABR Repl. by LEES 12v

^{3.49 ± 0.20 ± 0.59} ^{1,11} AUBERT, B 05r BABR Repl. by LEES 12u

^{3.50 ± 0.32 ± 0.31} ^{1,12} KOPPENBURG 04 BELL Repl. by LIMOSANI 09

^{3.36 ± 0.53 ± 0.65} ¹³ ABE 01f BELL Repl. by SAITO 15

^{2.32 ± 0.57 ± 0.35} ALAM 95 CLE2 Repl. by CHEN 01c

¹ We extrapolate the measured value to $E_\gamma > 1.6 \text{ GeV}$ using the method of BUCHMUELLER 06 (average of three theoretical models).

² SAITO 15 measured $(3.51 \pm 0.17 \pm 0.33) \times 10^{-4}$ using a sum-of-exclusive approach in which 38 of the hadronic final states with $m_{X_S} < 2.8 \text{ GeV}/c^2$ are reconstructed. The cut of minimum photon energy is $E_\gamma > 1.9 \text{ GeV}$.

³ Reports $(3.29 \pm 0.19 \pm 0.48) \times 10^{-4}$ for $E_\gamma > 1.9 \text{ GeV}$.

⁴ Reports $(3.21 \pm 0.15 \pm 0.29 \pm 0.08) \times 10^{-4}$ for $1.8 < E_\gamma < 2.8 \text{ GeV}$, where the last systematic uncertainty is for model dependency. Results with other cutoffs are also reported.

⁵ The measurement reported is $(3.45 \pm 0.15 \pm 0.40) \times 10^{-4}$ for $E_\gamma > 1.7 \text{ GeV}$.

⁶ Uses a fully reconstructed B meson as a tag on the recoil side. The measurement reported is $(3.66 \pm 0.85 \pm 0.60) \times 10^{-4}$ for $E_\gamma > 1.9 \text{ GeV}$.

⁷ The measurement reported is $(3.21 \pm 0.43^{+0.32}_{-0.29}) \times 10^{-4}$ for $E_\gamma > 2.0 \text{ GeV}$.

⁸ Measured using sums of seven exclusive final states $B \rightarrow X_{d(s)}\gamma$ where $X_{d(s)}$ is a nonstrange (strange) charmless hadronic system in mass range 0.5–2.0 GeV/c^2 .

⁹ Measured using sums of seven exclusive final states $B \rightarrow X_{d(s)}\gamma$ where $X_{d(s)}$ is a nonstrange (strange) charmless hadronic system in mass range 0.6–1.8 GeV/c^2 .

¹⁰ The measurement reported is $(3.67 \pm 0.29 \pm 0.45) \times 10^{-4}$ for $E_\gamma > 1.9 \text{ GeV}$.

¹¹ The measurement reported is $(3.27 \pm 0.18^{+0.55}_{-0.42}) \times 10^{-4}$ for $E_\gamma > 1.9 \text{ GeV}$.

¹² The measurement reported is $(3.55 \pm 0.32 \pm 0.32) \times 10^{-4}$ for $E_\gamma > 1.8 \text{ GeV}$.

¹³ ABE 01f reports their systematic errors $(\pm 0.42^{+0.50}_{-0.54}) \times 10^{-4}$, where the second error is due to the theoretical uncertainty. We combine them in quadrature.

$\Gamma(\bar{b} \rightarrow \bar{d}\gamma)/\Gamma_{\text{total}}$ Γ_{79}/Γ

VALUE (units 10^{-6})	DOCUMENT ID	TECN	COMMENT
9.2 ± 2.0 ± 2.3	¹ DEL-AMO-SA...10M	BABR	$e^+e^- \rightarrow \Upsilon(4S)$

• • • We do not use the following data for averages, fits, limits, etc. • • •

14 ± 5 ± 4 ² AUBERT 09u BABR Repl. by DEL-AMO-SANCHEZ 10M

¹ Measured using sums of seven exclusive final states $B \rightarrow X_{d(s)}\gamma$ where $X_{d(s)}$ is a nonstrange (strange) charmless hadronic system in mass range 0.5–2.0 GeV/c^2 .

² Measured using sums of seven exclusive final states $B \rightarrow X_{d(s)}\gamma$ where $X_{d(s)}$ is a nonstrange (strange) charmless hadronic system in mass range 0.6–1.8 GeV/c^2 .

Meson Particle Listings

 B^\pm/B^0 ADMIXTURE $\Gamma(\bar{b} \rightarrow \bar{s}\gamma)/\Gamma(\bar{b} \rightarrow \bar{s}\gamma)$ Γ_{79}/Γ_{78}

VALUE	DOCUMENT ID	TECN	COMMENT
0.040 ± 0.009 ± 0.010	1 DEL-AMO-SA..10M	BABR	$e^+e^- \rightarrow \Upsilon(4S)$
0.033 ± 0.013 ± 0.009	2 AUBERT	09u	Repl. by DEL-AMO-SANCHEZ 10M

- 1 Measured using sums of seven exclusive final states $B \rightarrow X_{d(s)}\gamma$ where $X_{d(s)}$ is a nonstrange (strange) charmless hadronic system in mass range 0.5–2.0 GeV/c².
 2 Measured using sums of seven exclusive final states $B \rightarrow X_{d(s)}\gamma$ where $X_{d(s)}$ is a nonstrange (strange) charmless hadronic system in mass range 0.6–1.8 GeV/c².

 $\Gamma(\bar{b} \rightarrow \bar{s}\text{gluon})/\Gamma_{\text{total}}$ Γ_{80}/Γ

VALUE	CL%	EVTS	DOCUMENT ID	TECN	COMMENT
<0.068	90		1 COAN	98	CLE2 $e^+e^- \rightarrow \Upsilon(4S)$
<0.08	2		2 ALBRECHT	95D	ARG $e^+e^- \rightarrow \Upsilon(4S)$

- 1 COAN 98 uses D - ℓ correlation.
 2 ALBRECHT 95D use full reconstruction of one B decay as tag. Two candidate events for charmless B decay can be interpreted as either $b \rightarrow \text{sgluon}$ or $b \rightarrow u$ transition. If interpreted as $b \rightarrow \text{sgluon}$ they find a branching ratio of ~ 0.026 or the upper limit quoted above. Result is highly model dependent.

 $\Gamma(\eta \text{ anything})/\Gamma_{\text{total}}$ Γ_{81}/Γ

VALUE (units 10^{-4})	CL%	DOCUMENT ID	TECN	COMMENT
2.61 ± 0.30^{+0.44}_{-0.74}		1 NISHIMURA	10	BELL $e^+e^- \rightarrow \Upsilon(4S)$
1.69 ± 0.29 ^{+0.36} _{-0.62}		2 NISHIMURA	10	BELL $e^+e^- \rightarrow \Upsilon(4S)$
<4.4	90	3 BROWDER	98	CLE2 $e^+e^- \rightarrow \Upsilon(4S)$

- 1 Uses $B \rightarrow \eta X_S$ with $0.4 < m_{X_S} < 2.6$ GeV/c².
 2 Uses $B \rightarrow \eta X_S$ with $1.8 < m_{X_S} < 2.6$ GeV/c².
 3 BROWDER 98 search for high momentum $B \rightarrow \eta X_S$ between 2.1 and 2.7 GeV/c.

 $\Gamma(\eta' \text{ anything})/\Gamma_{\text{total}}$ Γ_{82}/Γ

VALUE (units 10^{-4})	DOCUMENT ID	TECN	COMMENT
4.2 ± 0.9 OUR AVERAGE			
3.9 ± 0.8 ± 0.9	1 AUBERT,B	04F	BABR $e^+e^- \rightarrow \Upsilon(4S)$
4.6 ± 1.1 ± 0.6	2 BONVICINI	03	CLE2 $e^+e^- \rightarrow \Upsilon(4S)$
6.2 ± 1.6 ^{+1.3} _{-2.0}	3 BROWDER	98	CLE2 $e^+e^- \rightarrow \Upsilon(4S)$

- 1 AUBERT,B 04F reports branching ratio $B \rightarrow \eta' X_S$ for high momentum η' between 2.0 and 2.7 GeV/c in the $\Upsilon(4S)$ center-of-mass frame. X_S represents a recoil system consisting of a kaon and zero to four pions.
 2 BONVICINI 03 observed a signal of 61.2 ± 13.9 events in $B \rightarrow \eta' X_{nc}$ production for high momentum η' between 2.0 and 2.7 GeV/c in the $\Upsilon(4S)$ center-of-mass frame. The X_{nc} denotes "charmless" hadronic states recoiling against η' . The second error combines systematic and background subtraction uncertainties in quadrature.
 3 BROWDER 98 observed a signal of 39.0 ± 11.6 events in high momentum $B \rightarrow \eta' X_S$ production between 2.0 and 2.7 GeV/c. The branching fraction is based on the interpretation of $b \rightarrow \text{sg}$, where the last error includes additional uncertainties due to the color-suppressed $b \rightarrow \text{backgrounds}$.

 $\Gamma(K^+ \text{ gluon (charmless)})/\Gamma_{\text{total}}$ Γ_{83}/Γ

VALUE (units 10^{-4})	CL%	DOCUMENT ID	TECN	COMMENT
<1.87	90	1 DEL-AMO-SA..11	BABR	$e^+e^- \rightarrow \Upsilon(4S)$

- 1 $B \rightarrow K^+ X$ with $m_X < 1.69$ GeV/c².

 $\Gamma(K^0 \text{ gluon (charmless)})/\Gamma_{\text{total}}$ Γ_{84}/Γ

VALUE (units 10^{-4})	DOCUMENT ID	TECN	COMMENT
1.95^{+0.51}_{-0.45} ± 0.50	1 DEL-AMO-SA..11	BABR	$e^+e^- \rightarrow \Upsilon(4S)$

- 1 $B \rightarrow K^0 X$ with $m_X < 1.69$ GeV/c².

 $\Gamma(\rho\gamma)/\Gamma_{\text{total}}$ Γ_{85}/Γ

VALUE (units 10^{-6})	CL%	DOCUMENT ID	TECN	COMMENT
1.39 ± 0.25 OUR AVERAGE				Error includes scale factor of 1.2.
1.73 ^{+0.34} _{-0.32} ± 0.17		1,2 AUBERT	08BH	BABR $e^+e^- \rightarrow \Upsilon(4S)$
1.21 ^{+0.24} _{-0.22} ± 0.12		1,2 TANIGUCHI	08	BELL $e^+e^- \rightarrow \Upsilon(4S)$
1.36 ^{+0.29} _{-0.27} ± 0.10		1,3 AUBERT	07L	BABR Repl. by AUBERT 08BH
< 1.9	90	1,3 AUBERT	04c	BABR Repl. by AUBERT 07L
< 14	90	1,4 COAN	00	CLE2 $e^+e^- \rightarrow \Upsilon(4S)$

- 1 Assumes equal production of B^+ and B^0 at the $\Upsilon(4S)$.
 2 Assumes $\Gamma(B \rightarrow \rho\gamma) = \Gamma(B^+ \rightarrow \rho^+\gamma) = 2\Gamma(B^0 \rightarrow \rho^0\gamma)$ and uses lifetime ratio of $\tau_{B^+}/\tau_{B^0} = 1.071 \pm 0.009$.
 3 Assumes $\Gamma(B \rightarrow \rho\gamma) = \Gamma(B^+ \rightarrow \rho^+\gamma) = 2\Gamma(B^0 \rightarrow \rho^0\gamma)$ and uses lifetime ratio of $\tau_{B^+}/\tau_{B^0} = 1.083 \pm 0.017$.
 4 COAN 00 reports $B(B \rightarrow \rho\gamma)/B(B \rightarrow K^*(892)\gamma) < 0.32$ at 90%CL and scaled by the central value of $B(B \rightarrow K^*(892)\gamma) = (4.24 \pm 0.54 \pm 0.32) \times 10^{-5}$.

 $\Gamma(\rho\gamma)/\Gamma(K^*(892)\gamma)$ Γ_{85}/Γ_{66}

VALUE (units 10^{-2})	DOCUMENT ID	TECN	COMMENT
3.02 ± 0.60 ± 0.26 -0.55 - 0.28	TANIGUCHI	08	BELL $e^+e^- \rightarrow \Upsilon(4S)$

 $\Gamma(\rho/\omega\gamma)/\Gamma_{\text{total}}$ Γ_{86}/Γ

VALUE (units 10^{-6})	CL%	DOCUMENT ID	TECN	COMMENT
1.30 ± 0.23 OUR AVERAGE				Error includes scale factor of 1.2.
1.63 ^{+0.30} _{-0.28} ± 0.16		1,2,3 AUBERT	08BH	BABR $e^+e^- \rightarrow \Upsilon(4S)$
1.14 ± 0.20 ^{+0.10} _{-0.12}		1,3 TANIGUCHI	08	BELL $e^+e^- \rightarrow \Upsilon(4S)$
1.25 ^{+0.25} _{-0.24} ± 0.09		4 AUBERT	07L	BABR Repl. by AUBERT 08BH
1.32 ^{+0.34} _{-0.31} ± 0.10		4 MOHAPATRA	06	BELL Repl. by TANIGUCHI 08
0.6 ± 0.3 ± 0.1		4 AUBERT	05	BABR Repl. by AUBERT 07L
< 1.4	90	4 MOHAPATRA	05	BELL $e^+e^- \rightarrow \Upsilon(4S)$

- 1 Assumes $\Gamma(B \rightarrow \rho\gamma) = \Gamma(B^+ \rightarrow \rho^+\gamma) = 2\Gamma(B^0 \rightarrow \rho^0\gamma)$ and uses lifetime ratio of $\tau_{B^+}/\tau_{B^0} = 1.071 \pm 0.009$.
 2 Also reports $|V_{td}/V_{ts}| = 0.233^{+0.025}_{-0.024} - 0.021$.
 3 Assumes equal production of B^+ and B^0 at the $\Upsilon(4S)$.
 4 Assumes $\Gamma(B \rightarrow \rho\gamma) = \Gamma(B^+ \rightarrow \rho^+\gamma) = 2\Gamma(B^0 \rightarrow \rho^0\gamma)$ and uses lifetime ratio of $\tau_{B^+}/\tau_{B^0} = 1.083 \pm 0.017$.

 $\Gamma(\rho/\omega\gamma)/\Gamma(K^*(892)\gamma)$ Γ_{86}/Γ_{66}

VALUE (units 10^{-2})	CL%	DOCUMENT ID	TECN	COMMENT
2.84 ± 0.50^{+0.27}_{-0.29}		1 TANIGUCHI	08	BELL $e^+e^- \rightarrow \Upsilon(4S)$
< 3.5	90	MOHAPATRA	05	BELL Repl. by TANIGUCHI 08

- 1 Also reports $|V_{td}/V_{ts}| = 0.195^{+0.020}_{-0.019} ± 0.015$.

 $\Gamma(\pi^\pm \text{ anything})/\Gamma_{\text{total}}$ Γ_{87}/Γ

VALUE	DOCUMENT ID	TECN	COMMENT
3.985 ± 0.025 ± 0.070	1 ALBRECHT	93i	ARG $e^+e^- \rightarrow \Upsilon(4S)$

- 1 ALBRECHT 93 excludes π^\pm from K_S^0 and Λ decays. If included, they find $4.105 \pm 0.025 \pm 0.080$.

 $\Gamma(\pi^0 \text{ anything})/\Gamma_{\text{total}}$ Γ_{88}/Γ

VALUE	DOCUMENT ID	TECN	COMMENT
2.35 ± 0.02 ± 0.11	1 ABE	01J	BELL $e^+e^- \rightarrow \Upsilon(4S)$

- 1 From fully inclusive π^0 yield with no corrections from decays of K_S^0 or other particles.

 $\Gamma(\eta \text{ anything})/\Gamma_{\text{total}}$ Γ_{89}/Γ

VALUE	DOCUMENT ID	TECN	COMMENT
0.176 ± 0.011 ± 0.012	KUBOTA	96	CLE2 $e^+e^- \rightarrow \Upsilon(4S)$

 $\Gamma(\rho^0 \text{ anything})/\Gamma_{\text{total}}$ Γ_{90}/Γ

VALUE	DOCUMENT ID	TECN	COMMENT
0.208 ± 0.042 ± 0.032	ALBRECHT	94J	ARG $e^+e^- \rightarrow \Upsilon(4S)$

 $\Gamma(\omega \text{ anything})/\Gamma_{\text{total}}$ Γ_{91}/Γ

VALUE	CL%	DOCUMENT ID	TECN	COMMENT
<0.81	90	ALBRECHT	94J	ARG $e^+e^- \rightarrow \Upsilon(4S)$

 $\Gamma(\phi \text{ anything})/\Gamma_{\text{total}}$ Γ_{92}/Γ

VALUE	DOCUMENT ID	TECN	COMMENT
0.0343 ± 0.0012 OUR AVERAGE			
0.0353 ± 0.0005 ± 0.0030	HUANG	07	CLEO $e^+e^- \rightarrow \Upsilon(4S)$
0.0341 ± 0.0006 ± 0.0012	AUBERT	04s	BABR $e^+e^- \rightarrow \Upsilon(4S)$
0.0390 ± 0.0030 ± 0.0035	ALBRECHT	94J	ARG $e^+e^- \rightarrow \Upsilon(4S)$
0.023 ± 0.006 ± 0.005	BORTOLETTO	086	CLEO $e^+e^- \rightarrow \Upsilon(4S)$

 $\Gamma(\phi K^*(892))/\Gamma_{\text{total}}$ Γ_{93}/Γ

VALUE	CL%	DOCUMENT ID	TECN	COMMENT
<2.2 × 10⁻⁵	90	1 BERGFELD	98	CLE2

- 1 Assumes equal production of B^+ and B^0 at the $\Upsilon(4S)$.

 $\Gamma(\pi^+ \text{ gluon (charmless)})/\Gamma_{\text{total}}$ Γ_{95}/Γ

VALUE (units 10^{-4})	DOCUMENT ID	TECN	COMMENT
3.72^{+0.59}_{-0.47} ± 0.59	1 DEL-AMO-SA..11	BABR	$e^+e^- \rightarrow \Upsilon(4S)$

- 1 $B \rightarrow \pi^+ X$ with $m_X < 1.71$ GeV/c².

$\Gamma(\Lambda_c^+ / \bar{\Lambda}_c^- \text{ anything}) / \Gamma_{\text{total}}$ Γ_{96} / Γ

VALUE (%)	CL%	DOCUMENT ID	TECN	COMMENT
$3.59 \pm 0.32 \pm 0.19$ -0.18		1 AUBERT 07c	BABR	$e^+e^- \rightarrow \Upsilon(4S)$
6.4 ± 0.8 ± 0.8		2 CRAWFORD 92	CLEO	$e^+e^- \rightarrow \Upsilon(4S)$
14 ± 9		3 ALBRECHT 88E	ARG	$e^+e^- \rightarrow \Upsilon(4S)$
<11.2	90	4 ALAM 87	CLEO	$e^+e^- \rightarrow \Upsilon(4S)$

• • • We do not use the following data for averages, fits, limits, etc. • • •

¹ AUBERT 07c reports $0.045 \pm 0.003 \pm 0.012$ from a measurement of $[\Gamma(B \rightarrow \Lambda_c^+ / \bar{\Lambda}_c^- \text{ anything}) / \Gamma_{\text{total}}] \times [B(\Lambda_c^+ \rightarrow pK^- \pi^+)]$ assuming $B(\Lambda_c^+ \rightarrow pK^- \pi^+) = (5.0 \pm 1.3) \times 10^{-2}$, which we rescale to our best value $B(\Lambda_c^+ \rightarrow pK^- \pi^+) = (6.28 \pm 0.32) \times 10^{-2}$. Our first error is their experiment's error and our second error is the systematic error from using our best value.

² CRAWFORD 92 result derived from lepton baryon correlations. Assumes all charmed baryons in B^0 and B^\pm decay are Λ_c .

³ ALBRECHT 88E measured $B(B \rightarrow \Lambda_c^+ X) \cdot B(\Lambda_c^+ \rightarrow pK^- \pi^+) = (0.30 \pm 0.12 \pm 0.06)\%$ and used $B(\Lambda_c^+ \rightarrow pK^- \pi^+) = (2.2 \pm 1.0)\%$ from ABRAMS 80 to obtain above number.

⁴ Assuming all baryons result from charmed baryons, ALAM 86 conclude the branching fraction is $7.4 \pm 2.9\%$. The limit given above is model independent.

$\Gamma(\Lambda_c^+ \text{ anything}) / \Gamma(\bar{\Lambda}_c^- \text{ anything})$ $\Gamma_{97} / \Gamma_{98}$

VALUE	DOCUMENT ID	TECN	COMMENT
$0.19 \pm 0.13 \pm 0.04$	1 AMMAR 97	CLE2	$e^+e^- \rightarrow \Upsilon(4S)$

¹ AMMAR 97 uses a high-momentum lepton tag ($P_\ell > 1.4 \text{ GeV}/c^2$).

$\Gamma(\bar{\Lambda}_c^- \mu^+ \text{ anything}) / \Gamma(\bar{\Lambda}_c^- \text{ anything})$ $\Gamma_{101} / \Gamma_{98}$

VALUE (units 10^{-2})	DOCUMENT ID	TECN	COMMENT
$-2.0 \pm 2.0 \pm 1.9$	LEES 12	BABR	$e^+e^- \rightarrow \Upsilon(4S)$

$\Gamma(\bar{\Lambda}_c^- \ell^+ \text{ anything}) / \Gamma(\Lambda_c^+ / \bar{\Lambda}_c^- \text{ anything})$ $\Gamma_{99} / \Gamma_{96}$

VALUE	CL%	DOCUMENT ID	TECN	COMMENT
$<2.5 \times 10^{-2}$	90	1 LEES 12	BABR	$e^+e^- \rightarrow \Upsilon(4S)$

¹ LEES 12 quotes also the measurement $\Gamma(B \rightarrow \bar{\Lambda}_c^- \ell^+ \text{ anything}) / \Gamma(B \rightarrow \Lambda_c^+ / \bar{\Lambda}_c^- \text{ anything}) = (1.2 \pm 0.7 \pm 0.4) \times 10^{-2}$.

$\Gamma(\bar{\Lambda}_c^- e^+ \text{ anything}) / \Gamma(\Lambda_c^+ / \bar{\Lambda}_c^- \text{ anything})$ $\Gamma_{100} / \Gamma_{96}$

VALUE	CL%	DOCUMENT ID	TECN	COMMENT
<0.05	90	1 BONVICINI 98	CLE2	$e^+e^- \rightarrow \Upsilon(4S)$

¹ BONVICINI 98 uses the electron with momentum above 0.6 GeV/c.

$\Gamma(\bar{\Lambda}_c^- e^+ \text{ anything}) / \Gamma(\bar{\Lambda}_c^- \text{ anything})$ $\Gamma_{100} / \Gamma_{98}$

VALUE (units 10^{-2})	DOCUMENT ID	TECN	COMMENT
$2.5 \pm 1.1 \pm 0.6$	1 LEES 12	BABR	$e^+e^- \rightarrow \Upsilon(4S)$

¹ Uses the full reconstruction of the recoiling B in a hadronic decay as a tag.

$\Gamma(\bar{\Lambda}_c^- \ell^+ \text{ anything}) / \Gamma(\bar{\Lambda}_c^- \text{ anything})$ $\Gamma_{99} / \Gamma_{98}$

VALUE	CL%	DOCUMENT ID	TECN	COMMENT
$<3.5 \times 10^{-2}$	90	1 LEES 12	BABR	$e^+e^- \rightarrow \Upsilon(4S)$

¹ LEES 12 quotes also the measurement $\Gamma(B \rightarrow \bar{\Lambda}_c^- \ell^+ \text{ anything}) / \Gamma(B \rightarrow \bar{\Lambda}_c^- \text{ anything}) = (1.7 \pm 1.0 \pm 0.6) \times 10^{-2}$.

$\Gamma(\bar{\Lambda}_c^- p \text{ anything}) / \Gamma(\Lambda_c^+ / \bar{\Lambda}_c^- \text{ anything})$ $\Gamma_{102} / \Gamma_{96}$

VALUE	DOCUMENT ID	TECN	COMMENT
$0.57 \pm 0.05 \pm 0.05$	BONVICINI 98	CLE2	$e^+e^- \rightarrow \Upsilon(4S)$

$\Gamma(\bar{\Lambda}_c^- p e^+ \nu_e) / \Gamma(\bar{\Lambda}_c^- p \text{ anything})$ $\Gamma_{103} / \Gamma_{102}$

VALUE	CL%	DOCUMENT ID	TECN	COMMENT
<0.04	90	1 BONVICINI 98	CLE2	$e^+e^- \rightarrow \Upsilon(4S)$

¹ BONVICINI 98 uses the electron with momentum above 0.6 GeV/c.

$\Gamma(\Sigma_c^{--} \text{ anything}) / \Gamma_{\text{total}}$ Γ_{104} / Γ

VALUE	EVTS	DOCUMENT ID	TECN	COMMENT
$0.0033 \pm 0.0017 \pm 0.0002$	77	1 PROCARIO 94	CLE2	$e^+e^- \rightarrow \Upsilon(4S)$

¹ PROCARIO 94 reports $[\Gamma(B \rightarrow \Sigma_c^{--} \text{ anything}) / \Gamma_{\text{total}}] \times [B(\Lambda_c^+ \rightarrow pK^- \pi^+)] = 0.00021 \pm 0.00008 \pm 0.00007$ which we divide by our best value $B(\Lambda_c^+ \rightarrow pK^- \pi^+) = (6.28 \pm 0.32) \times 10^{-2}$. Our first error is their experiment's error and our second error is the systematic error from using our best value.

$\Gamma(\Sigma_c^- \text{ anything}) / \Gamma_{\text{total}}$ Γ_{105} / Γ

VALUE	CL%	DOCUMENT ID	TECN	COMMENT
$<8 \times 10^{-3}$	90	1 PROCARIO 94	CLE2	$e^+e^- \rightarrow \Upsilon(4S)$

¹ PROCARIO 94 reports $[\Gamma(B \rightarrow \Sigma_c^- \text{ anything}) / \Gamma_{\text{total}}] \times [B(\Lambda_c^+ \rightarrow pK^- \pi^+)] < 0.00048$ which we divide by our best value $B(\Lambda_c^+ \rightarrow pK^- \pi^+) = 6.28 \times 10^{-2}$.

$\Gamma(\Sigma_c^0 \text{ anything}) / \Gamma_{\text{total}}$ Γ_{106} / Γ

VALUE	EVTS	DOCUMENT ID	TECN	COMMENT
$0.0037 \pm 0.0017 \pm 0.0002$	76	1 PROCARIO 94	CLE2	$e^+e^- \rightarrow \Upsilon(4S)$

¹ PROCARIO 94 reports $[\Gamma(B \rightarrow \Sigma_c^0 \text{ anything}) / \Gamma_{\text{total}}] \times [B(\Lambda_c^+ \rightarrow pK^- \pi^+)] = 0.00023 \pm 0.00008 \pm 0.00007$ which we divide by our best value $B(\Lambda_c^+ \rightarrow pK^- \pi^+) = (6.28 \pm 0.32) \times 10^{-2}$. Our first error is their experiment's error and our second error is the systematic error from using our best value.

$\Gamma(\Sigma_c^0 N(N = p \text{ or } n)) / \Gamma_{\text{total}}$ Γ_{107} / Γ

VALUE	CL%	DOCUMENT ID	TECN	COMMENT
$<1.2 \times 10^{-3}$	90	1 PROCARIO 94	CLE2	$e^+e^- \rightarrow \Upsilon(4S)$

¹ PROCARIO 94 reports < 0.0017 from a measurement of $[\Gamma(B \rightarrow \Sigma_c^0 N(N = p \text{ or } n)) / \Gamma_{\text{total}}] \times [B(\Lambda_c^+ \rightarrow pK^- \pi^+)]$ assuming $B(\Lambda_c^+ \rightarrow pK^- \pi^+) = 0.043$, which we rescale to our best value $B(\Lambda_c^+ \rightarrow pK^- \pi^+) = 6.28 \times 10^{-2}$.

$\Gamma(\Xi_c^0 \text{ anything}, \Xi_c^0 \rightarrow \Xi^- \pi^+) / \Gamma_{\text{total}}$ Γ_{108} / Γ

VALUE (units 10^{-3})	DOCUMENT ID	TECN	COMMENT
0.193 ± 0.030 OUR AVERAGE	Error includes scale factor of 1.1.		
$0.211 \pm 0.019 \pm 0.025$	1 AUBERT B 05M	BABR	$e^+e^- \rightarrow \Upsilon(4S)$
$0.144 \pm 0.048 \pm 0.021$	2 BARISH 97	CLE2	$e^+e^- \rightarrow \Upsilon(4S)$

¹ The yield is obtained by requiring the momentum $P < 2.15 \text{ GeV}/c$.

² BARISH 97 find $79 \pm 27 \Xi_c^0$ events.

$\Gamma(\Xi_c^+ \Xi_c^+ \rightarrow \Xi^- \pi^+ \pi^+) / \Gamma_{\text{total}}$ Γ_{109} / Γ

VALUE (units 10^{-3})	DOCUMENT ID	TECN	COMMENT
$0.453 \pm 0.096 \pm 0.085$ -0.065	1 BARISH 97	CLE2	$e^+e^- \rightarrow \Upsilon(4S)$

¹ BARISH 97 find $125 \pm 28 \Xi_c^+$ events.

$\Gamma(p/\bar{p} \text{ anything}) / \Gamma_{\text{total}}$ Γ_{110} / Γ

Includes p and \bar{p} from Λ and $\bar{\Lambda}$ decay.

VALUE	EVTS	DOCUMENT ID	TECN	COMMENT
0.080 ± 0.004 OUR AVERAGE				
$0.080 \pm 0.005 \pm 0.005$		ALBRECHT 93i	ARG	$e^+e^- \rightarrow \Upsilon(4S)$
$0.080 \pm 0.005 \pm 0.003$		CRAWFORD 92	CLEO	$e^+e^- \rightarrow \Upsilon(4S)$
$0.082 \pm 0.005 \pm 0.013$ -0.010	2163	1 ALBRECHT 89k	ARG	$e^+e^- \rightarrow \Upsilon(4S)$

• • • We do not use the following data for averages, fits, limits, etc. • • •

>0.021

² ALAM 83b reported their result as $> 0.036 \pm 0.006 \pm 0.009$. Data are consistent with equal yields of p and \bar{p} . Using assumed yields below cut, $B(B \rightarrow p + X) = 0.03$ not including protons from Λ decays.

$\Gamma(p/\bar{p} \text{ (direct) anything}) / \Gamma_{\text{total}}$ Γ_{111} / Γ

VALUE	EVTS	DOCUMENT ID	TECN	COMMENT
0.055 ± 0.005 OUR AVERAGE				
$0.055 \pm 0.005 \pm 0.0035$		ALBRECHT 93i	ARG	$e^+e^- \rightarrow \Upsilon(4S)$
$0.056 \pm 0.006 \pm 0.005$		CRAWFORD 92	CLEO	$e^+e^- \rightarrow \Upsilon(4S)$
0.055 ± 0.016	1220	1 ALBRECHT 89k	ARG	$e^+e^- \rightarrow \Upsilon(4S)$

¹ ALBRECHT 89k subtract contribution of Λ decay from the inclusive proton yield.

$\Gamma(\bar{p} e^+ \nu_e \text{ anything}) / \Gamma_{\text{total}}$ Γ_{112} / Γ

VALUE	CL%	DOCUMENT ID	TECN	COMMENT
$< 5.9 \times 10^{-4}$	90	1 ADAM 03B	CLE2	$e^+e^- \rightarrow \Upsilon(4S)$

• • • We do not use the following data for averages, fits, limits, etc. • • •

$<16 \times 10^{-4}$

90 ALBRECHT 90H ARG $e^+e^- \rightarrow \Upsilon(4S)$

¹ Based on $V-A$ model.

$\Gamma(\Lambda/\bar{\Lambda} \text{ anything}) / \Gamma_{\text{total}}$ Γ_{113} / Γ

VALUE	EVTS	DOCUMENT ID	TECN	COMMENT
0.040 ± 0.005 OUR AVERAGE				
$0.038 \pm 0.004 \pm 0.006$	2998	CRAWFORD 92	CLEO	$e^+e^- \rightarrow \Upsilon(4S)$
$0.042 \pm 0.005 \pm 0.006$	943	ALBRECHT 89k	ARG	$e^+e^- \rightarrow \Upsilon(4S)$

• • • We do not use the following data for averages, fits, limits, etc. • • •

$0.022 \pm 0.003 \pm 0.0022$

>0.011

¹ ACKERSTAFF 97N OPAL $e^+e^- \rightarrow Z$

² ALAM 83B CLEO $e^+e^- \rightarrow \Upsilon(4S)$

¹ ACKERSTAFF 97N assumes $B(b \rightarrow B) = 0.868 \pm 0.041$, i.e., an admixture of B^0, B^\pm , and B_s .

² ALAM 83b reported their result as $> 0.022 \pm 0.007 \pm 0.004$. Values are for $(B(\Lambda X) + B(\bar{\Lambda} X))/2$. Data are consistent with equal yields of p and \bar{p} . Using assumed yields below cut, $B(B \rightarrow \Lambda X) = 0.03$.

$\Gamma(\Lambda \text{ anything}) / \Gamma(\bar{\Lambda} \text{ anything})$ $\Gamma_{114} / \Gamma_{115}$

VALUE	DOCUMENT ID	TECN	COMMENT
$0.43 \pm 0.09 \pm 0.07$	1 AMMAR 97	CLE2	$e^+e^- \rightarrow \Upsilon(4S)$

¹ AMMAR 97 uses a high-momentum lepton tag ($P_\ell > 1.4 \text{ GeV}/c^2$).

$\Gamma(\Xi^- / \Xi^+ \text{ anything}) / \Gamma_{\text{total}}$ Γ_{116} / Γ

VALUE	EVTS	DOCUMENT ID	TECN	COMMENT
0.0027 ± 0.0006 OUR AVERAGE				
$0.0027 \pm 0.0005 \pm 0.0004$	147	CRAWFORD 92	CLEO	$e^+e^- \rightarrow \Upsilon(4S)$
0.0028 ± 0.0014	54	ALBRECHT 89k	ARG	$e^+e^- \rightarrow \Upsilon(4S)$

Meson Particle Listings

B^\pm/B^0 ADMIXTURE

$\Gamma(\text{baryons anything})/\Gamma_{\text{total}}$ Γ_{117}/Γ

VALUE	DOCUMENT ID	TECN	COMMENT
0.068 ± 0.005 ± 0.003	¹ ALBRECHT 92a	ARG	$e^+e^- \rightarrow \Upsilon(4S)$

• • • We do not use the following data for averages, fits, limits, etc. • • •
 0.076 ± 0.014 ² ALBRECHT 89k ARG $e^+e^- \rightarrow \Upsilon(4S)$

¹ ALBRECHT 92a result is from simultaneous analysis of p and Λ yields, $p\bar{p}$ and $\Lambda\bar{\Lambda}$ correlations, and various lepton-baryon and lepton-baryon-antibaryon correlations. Supersedes ALBRECHT 89k.

² ALBRECHT 89k obtain this result by adding their their measurements (5.5 ± 1.6)% for direct protons and (4.2 ± 0.5 ± 0.6)% for inclusive Λ production. They then assume (5.5 ± 1.6)% for neutron production and add it in also. Since each B decay has two baryons, they divide by 2 to obtain (7.6 ± 1.4)%.

$\Gamma(p\bar{p} \text{ anything})/\Gamma_{\text{total}}$ Γ_{118}/Γ

Includes p and \bar{p} from Λ and $\bar{\Lambda}$ decay.

VALUE	EVTS	DOCUMENT ID	TECN	COMMENT
0.0247 ± 0.0023 OUR AVERAGE				
0.024 ± 0.001 ± 0.004		CRAWFORD 92	CLEO	$e^+e^- \rightarrow \Upsilon(4S)$
0.025 ± 0.002 ± 0.002	918	ALBRECHT 89k	ARG	$e^+e^- \rightarrow \Upsilon(4S)$

$\Gamma(p\bar{p} \text{ anything})/\Gamma(p/\bar{p} \text{ anything})$ $\Gamma_{118}/\Gamma_{110}$

Includes p and \bar{p} from Λ and $\bar{\Lambda}$ decay.

VALUE	DOCUMENT ID	TECN	COMMENT
0.30 ± 0.02 ± 0.05	¹ CRAWFORD 92	CLEO	$e^+e^- \rightarrow \Upsilon(4S)$

¹ CRAWFORD 92 value is not independent of their $\Gamma(p\bar{p} \text{ anything})/\Gamma_{\text{total}}$ value.

$\Gamma(\Lambda\bar{\Lambda} \text{ anything})/\Gamma_{\text{total}}$ Γ_{119}/Γ

Includes p and \bar{p} from Λ and $\bar{\Lambda}$ decay.

VALUE	EVTS	DOCUMENT ID	TECN	COMMENT
0.025 ± 0.004 OUR AVERAGE				
0.029 ± 0.005 ± 0.005		CRAWFORD 92	CLEO	$e^+e^- \rightarrow \Upsilon(4S)$
0.023 ± 0.004 ± 0.003	165	ALBRECHT 89k	ARG	$e^+e^- \rightarrow \Upsilon(4S)$

$\Gamma(\Lambda\bar{\Lambda} \text{ anything})/\Gamma(\Lambda/\bar{\Lambda} \text{ anything})$ $\Gamma_{119}/\Gamma_{113}$

Includes p and \bar{p} from Λ and $\bar{\Lambda}$ decay.

VALUE	DOCUMENT ID	TECN	COMMENT
0.76 ± 0.11 ± 0.08	¹ CRAWFORD 92	CLEO	$e^+e^- \rightarrow \Upsilon(4S)$

¹ CRAWFORD 92 value is not independent of their $[\Gamma(\Lambda\bar{\Lambda} \text{ anything}) + \Gamma(\Lambda/\bar{\Lambda} \text{ anything})]/\Gamma_{\text{total}}$ value.

$\Gamma(\Lambda\bar{\Lambda} \text{ anything})/\Gamma_{\text{total}}$ Γ_{120}/Γ

Includes p and \bar{p} from Λ and $\bar{\Lambda}$ decay.

VALUE	CL%	EVTS	DOCUMENT ID	TECN	COMMENT
<0.005	90		CRAWFORD 92	CLEO	$e^+e^- \rightarrow \Upsilon(4S)$
<0.0088	90	12	ALBRECHT 89k	ARG	$e^+e^- \rightarrow \Upsilon(4S)$

$\Gamma(\Lambda\bar{\Lambda} \text{ anything})/\Gamma(\Lambda/\bar{\Lambda} \text{ anything})$ $\Gamma_{120}/\Gamma_{113}$

Includes p and \bar{p} from Λ and $\bar{\Lambda}$ decay.

VALUE	CL%	DOCUMENT ID	TECN	COMMENT
<0.13	90	¹ CRAWFORD 92	CLEO	$e^+e^- \rightarrow \Upsilon(4S)$

¹ CRAWFORD 92 value is not independent of their $\Gamma(\Lambda\bar{\Lambda} \text{ anything})/\Gamma_{\text{total}}$ value.

$\Gamma(s e^+ e^-)/\Gamma_{\text{total}}$ Γ_{121}/Γ

Test for $\Delta B = 1$ weak neutral current. Allowed by higher-order electroweak interactions.

VALUE (units 10^{-6})	CL%	DOCUMENT ID	TECN	COMMENT
6.7 ± 1.7 OUR AVERAGE				Error includes scale factor of 2.0.
7.69 ^{+0.82} _{-0.77} ± 0.71 ^{+0.63} _{-0.60}		¹ LEES 14d	BABR	$e^+e^- \rightarrow \Upsilon(4S)$
4.04 ± 1.30 ^{+0.87} _{-0.83}		² IWASAKI 05	BELL	$e^+e^- \rightarrow \Upsilon(4S)$

• • • We do not use the following data for averages, fits, limits, etc. • • •
 6.0 ± 1.7 ± 1.3 ² AUBERT,B 04i BABR Repl. by LEES 14d
 5.0 ± 2.3^{+1.3}_{-1.1} ² KANEKO 03 BELL Repl. by IWASAKI 05

< 57 90 GLENN 98 CLEO $e^+e^- \rightarrow \Upsilon(4S)$
 <50000 90 BEBEK 81 CLEO $e^+e^- \rightarrow \Upsilon(4S)$

¹ Measured from sum of exclusive modes through K^+ , $K^+\pi^0$, $K^+\pi^-$, $K^+\pi^-\pi^0$, $K^+\pi^-\pi^+$, K_S^0 , $K_S^0\pi^0$, $K_S^0\pi^+$, $K_S^0\pi^+\pi^0$, and $K_S^0\pi^+\pi^-$ corrected for unobserved modes.

² Requires $M_{e^+e^-} > 0.2 \text{ GeV}/c^2$.

$\Gamma(s\mu^+\mu^-)/\Gamma_{\text{total}}$ Γ_{122}/Γ

Test for $\Delta B = 1$ weak neutral current. Allowed by higher-order electroweak interactions.

VALUE (units 10^{-6})	CL%	DOCUMENT ID	TECN	COMMENT
4.3 ± 1.0 OUR AVERAGE				
4.41 ^{+1.31} _{-1.17} ± 0.63 ^{+0.63} _{-0.50}		¹ LEES 14d	BABR	$e^+e^- \rightarrow \Upsilon(4S)$
4.13 ± 1.05 ^{+0.85} _{-0.81}		² IWASAKI 05	BELL	$e^+e^- \rightarrow \Upsilon(4S)$

• • • We do not use the following data for averages, fits, limits, etc. • • •
 5.0 ± 2.8 ± 1.2 AUBERT,B 04i BABR Repl. by LEES 14d
 7.9 ± 2.1^{+2.1}_{-1.5} KANEKO 03 BELL Repl. by IWASAKI 05

< 58 90 GLENN 98 CLEO $e^+e^- \rightarrow \Upsilon(4S)$
 <17000 90 CHADWICK 81 CLEO $e^+e^- \rightarrow \Upsilon(4S)$

¹ Measured from sum of exclusive modes through K^+ , $K^+\pi^0$, $K^+\pi^-$, $K^+\pi^-\pi^0$, $K^+\pi^-\pi^+$, K_S^0 , $K_S^0\pi^0$, $K_S^0\pi^+$, $K_S^0\pi^+\pi^0$, and $K_S^0\pi^+\pi^-$ corrected for unobserved modes.

² Requires $M_{e^+e^-} > 0.2 \text{ GeV}/c^2$.

$[\Gamma(s e^+ e^-) + \Gamma(s\mu^+\mu^-)]/\Gamma_{\text{total}}$ $(\Gamma_{121} + \Gamma_{122})/\Gamma$

Test for $\Delta B = 1$ weak neutral current. Allowed by higher-order electroweak interactions.

VALUE	CL%	DOCUMENT ID	TECN	COMMENT
<4.2 × 10⁻⁵	90	GLENN 98	CLEO	$e^+e^- \rightarrow \Upsilon(4S)$

• • • We do not use the following data for averages, fits, limits, etc. • • •
 <0.0024 90 ¹ BEAN 87 CLEO Repl. by GLENN 98
 <0.0062 90 ² AVERY 98 CLEO Repl. by BEAN 87

¹ BEAN 87 reports $[(\mu^+\mu^-) + (e^+e^-)]/2$ and we converted it.

² Determine ratio of B^+ to B^0 semileptonic decays to be in the range 0.25–2.9.

$\Gamma(s\ell^+\ell^-)/\Gamma_{\text{total}}$ Γ_{123}/Γ

Test for $\Delta B = 1$ weak neutral current.

VALUE (units 10^{-6})	CL%	DOCUMENT ID	TECN	COMMENT
5.8 ± 1.3 OUR AVERAGE				Error includes scale factor of 1.8.
6.73 ^{+0.70} _{-0.64} ± 0.60 ^{+0.60} _{-0.56}		¹ LEES 14d	BABR	$e^+e^- \rightarrow \Upsilon(4S)$
4.11 ± 0.83 ^{+0.85} _{-0.81}		² IWASAKI 05	BELL	$e^+e^- \rightarrow \Upsilon(4S)$

• • • We do not use the following data for averages, fits, limits, etc. • • •
 5.6 ± 1.5 ± 1.3 ³ AUBERT,B 04i BABR Repl. by LEES 14d
 6.1 ± 1.4^{+1.4}_{-1.1} ³ KANEKO 03 BELL Repl. by IWASAKI 05

¹ Measured from sum of exclusive modes through K^+ , $K^+\pi^0$, $K^+\pi^-$, $K^+\pi^-\pi^0$, $K^+\pi^-\pi^+$, K_S^0 , $K_S^0\pi^0$, $K_S^0\pi^+$, $K_S^0\pi^+\pi^0$, and $K_S^0\pi^+\pi^-$ corrected for unobserved modes.

² Requires $M_{e^+e^-} > 0.2 \text{ GeV}/c^2$.

³ Requires $M_{e^+e^-} > 0.2 \text{ GeV}/c^2$.

$\Gamma(\pi\ell^+\ell^-)/\Gamma_{\text{total}}$ Γ_{124}/Γ

Includes p and \bar{p} from Λ and $\bar{\Lambda}$ decay.

VALUE	CL%	DOCUMENT ID	TECN	COMMENT
<5.9 × 10⁻⁸	90	¹ LEES 13m	BABR	$e^+e^- \rightarrow \Upsilon(4S)$

• • • We do not use the following data for averages, fits, limits, etc. • • •
 <6.2 × 10⁻⁸ 90 ¹ WEI 08a BELL $e^+e^- \rightarrow \Upsilon(4S)$
 <9.1 × 10⁻⁸ 90 ¹ AUBERT 07aG BABR $e^+e^- \rightarrow \Upsilon(4S)$

¹ Assumes equal production of B^+ and B^0 at the $\Upsilon(4S)$.

$\Gamma(\pi e^+ e^-)/\Gamma_{\text{total}}$ Γ_{125}/Γ

Includes p and \bar{p} from Λ and $\bar{\Lambda}$ decay.

VALUE	CL%	DOCUMENT ID	TECN	COMMENT
<11.0 × 10⁻⁸	90	¹ LEES 13m	BABR	$e^+e^- \rightarrow \Upsilon(4S)$

¹ Assumes equal production of B^+ and B^0 at the $\Upsilon(4S)$.

$\Gamma(\pi\mu^+\mu^-)/\Gamma_{\text{total}}$ Γ_{126}/Γ

Includes p and \bar{p} from Λ and $\bar{\Lambda}$ decay.

VALUE	CL%	DOCUMENT ID	TECN	COMMENT
<5.0 × 10⁻⁸	90	¹ LEES 13m	BABR	$e^+e^- \rightarrow \Upsilon(4S)$

¹ Assumes equal production of B^+ and B^0 at the $\Upsilon(4S)$.

$\Gamma(K e^+ e^-)/\Gamma_{\text{total}}$ Γ_{127}/Γ

Test for $\Delta B = 1$ weak neutral current. Allowed by higher-order electroweak interactions.

VALUE (units 10^{-7})	CL%	DOCUMENT ID	TECN	COMMENT
4.4 ± 0.6 OUR AVERAGE				
3.9 ^{+0.9} _{-0.8} ± 0.2		¹ AUBERT 09t	BABR	$e^+e^- \rightarrow \Upsilon(4S)$
4.8 ^{+0.8} _{-0.7} ± 0.3		¹ WEI 09a	BELL	$e^+e^- \rightarrow \Upsilon(4S)$

• • • We do not use the following data for averages, fits, limits, etc. • • •
 3.3^{+0.9}_{-0.8} ± 0.2 ¹ AUBERT,B 06j BABR Repl. by AUBERT 09t
 7.4^{+1.8}_{-1.6} ± 0.5 ¹ AUBERT 03u BABR Repl. by AUBERT,B 06j

4.8^{+1.5}_{-1.3} ± 0.3 ^{1,2} ISHIKAWA 03 BELL Repl. by WEI 09a
 <13 90 ABE 02 BELL Repl. by ISHIKAWA 03

¹ Assumes equal production of B^+ and B^0 at the $\Upsilon(4S)$.

² The second error is a total of systematic uncertainties including model dependence.

Meson Particle Listings

B^\pm/B^0 ADMIXTURE

$\Gamma(K^*(892)e^+e^-)/\Gamma_{\text{total}}$ Γ_{128}/Γ

Test for $\Delta B = 1$ weak neutral current. Allowed by higher-order electroweak interactions.

VALUE (units 10^{-7})	CL%	DOCUMENT ID	TECN	COMMENT
11.9 ± 2.0 OUR AVERAGE		Error includes scale factor of 1.2.		
$9.9^{+2.3}_{-2.1} \pm 0.6$		1 AUBERT	09T BABR	$e^+e^- \rightarrow \Upsilon(4S)$
$13.9^{+2.3}_{-2.0} \pm 1.2$		1 WEI	09A BELL	$e^+e^- \rightarrow \Upsilon(4S)$
• • • We do not use the following data for averages, fits, limits, etc. • • •				
$9.7^{+3.0}_{-2.7} \pm 1.4$		1 AUBERT,B	06J BABR	Repl. by AUBERT 09T
$9.8^{+5.0}_{-4.2} \pm 1.1$		1 AUBERT	03U BABR	Repl. by AUBERT,B 06J
$14.9^{+5.2+1.2}_{-4.6-1.3}$		2 ISHIKAWA	03 BELL	Repl. by WEI 09A
<56	90	ABE	02 BELL	Repl. by ISHIKAWA 03

¹ Assumes equal production of B^+ and B^0 at the $\Upsilon(4S)$.
² Assumes equal production of B^0 and B^+ at $\Upsilon(4S)$. The second error is a total of systematic uncertainties including model dependence.

$\Gamma(K\mu^+\mu^-)/\Gamma_{\text{total}}$ Γ_{129}/Γ

Test for $\Delta B = 1$ weak neutral current. Allowed by higher-order electroweak interactions.

VALUE (units 10^{-7})	DOCUMENT ID	TECN	COMMENT
4.4 ± 0.4 OUR AVERAGE			
$4.2 \pm 0.4 \pm 0.2$	AALTONEN	11A1 CDF	$p\bar{p}$ at 1.96 TeV
$4.1^{+1.3}_{-1.2} \pm 0.2$	1 AUBERT	09T BABR	$e^+e^- \rightarrow \Upsilon(4S)$
$5.0 \pm 0.6 \pm 0.3$	1 WEI	09A BELL	$e^+e^- \rightarrow \Upsilon(4S)$
• • • We do not use the following data for averages, fits, limits, etc. • • •			
$3.5^{+1.3}_{-1.1} \pm 0.3$	1 AUBERT,B	06J BABR	Repl. by AUBERT 09T
$4.5^{+2.3}_{-1.9} \pm 0.4$	1 AUBERT	03U BABR	Repl. by AUBERT,B 06J
$4.8^{+1.2}_{-1.1} \pm 0.4$	1,2 ISHIKAWA	03 BELL	Repl. by WEI 09A
$9.9^{+4.0+1.3}_{-3.2-1.0}$	ABE	02 BELL	Repl. by ISHIKAWA 03

¹ Assumes equal production of B^+ and B^0 at the $\Upsilon(4S)$.
² The second error is a total of systematic uncertainties including model dependence.

$\Gamma(K\mu^+\mu^-)/\Gamma(Ke^+e^-)$ $\Gamma_{129}/\Gamma_{127}$

VALUE	DOCUMENT ID	TECN	COMMENT
1.01 ± 0.15 OUR AVERAGE			
$1.00^{+0.31}_{-0.25} \pm 0.07$	1 LEES	12s BABR	$e^+e^- \rightarrow \Upsilon(4S)$
$0.96^{+0.44}_{-0.34} \pm 0.05$	AUBERT	09T BABR	$e^+e^- \rightarrow \Upsilon(4S)$
$1.03 \pm 0.19 \pm 0.06$	WEI	09A BELL	$e^+e^- \rightarrow \Upsilon(4S)$
• • • We do not use the following data for averages, fits, limits, etc. • • •			
$1.06 \pm 0.48 \pm 0.08$	AUBERT,B	06J BABR	Repl. by AUBERT 09T
¹ Measured in the union of $0.10 < q^2 < 8.12 \text{ GeV}^2/c^4$ and $q^2 > 10.11 \text{ GeV}^2/c^4$. LEES 12s reports also individual measurements $\Gamma(B \rightarrow K\mu^+\mu^-)/\Gamma(B \rightarrow Ke^+e^-) = 0.74^{+0.40}_{-0.31} \pm 0.06$ for $0.10 < q^2 < 8.12 \text{ GeV}^2/c^4$ and $\Gamma(B \rightarrow K\mu^+\mu^-)/\Gamma(B \rightarrow Ke^+e^-) = 1.43^{+0.65}_{-0.44} \pm 0.12$ for $q^2 > 10.11 \text{ GeV}^2/c^4$.			

$\Gamma(K^*(892)\mu^+\mu^-)/\Gamma_{\text{total}}$ Γ_{130}/Γ

Test for $\Delta B = 1$ weak neutral current. Allowed by higher-order electroweak interactions.

VALUE (units 10^{-7})	CL%	DOCUMENT ID	TECN	COMMENT
10.6 ± 0.9 OUR AVERAGE				
$10.1 \pm 1.0 \pm 0.5$		AALTONEN	11A1 CDF	$p\bar{p}$ at 1.96 TeV
$13.5^{+3.5}_{-3.3} \pm 1.0$		1 AUBERT	09T BABR	$e^+e^- \rightarrow \Upsilon(4S)$
$11.0^{+1.6}_{-1.4} \pm 0.8$		1 WEI	09A BELL	$e^+e^- \rightarrow \Upsilon(4S)$
• • • We do not use the following data for averages, fits, limits, etc. • • •				
$8.8^{+3.5}_{-3.0} \pm 1.2$		1 AUBERT,B	06J BABR	Repl. by AUBERT 09T
$12.7^{+7.6}_{-6.1} \pm 1.6$		1 AUBERT	03U BABR	Repl. by AUBERT,B 06J
$11.7^{+3.6}_{-3.1} \pm 1.0$		2 ISHIKAWA	03 BELL	Repl. by WEI 09A
<31	90	ABE	02 BELL	Repl. by ISHIKAWA 03

¹ Assumes equal production of B^+ and B^0 at the $\Upsilon(4S)$.
² Assumes equal production of B^0 and B^+ at $\Upsilon(4S)$. The second error is a total of systematic uncertainties including model dependence.

$\Gamma(K^*(892)\mu^+\mu^-)/\Gamma(K^*(892)e^+e^-)$ $\Gamma_{130}/\Gamma_{128}$

VALUE	DOCUMENT ID	TECN	COMMENT
0.98 ± 0.15 OUR AVERAGE			
$1.13^{+0.34}_{-0.26} \pm 0.10$	1 LEES	12s BABR	$e^+e^- \rightarrow \Upsilon(4S)$
$1.37^{+0.53}_{-0.40} \pm 0.09$	AUBERT	09T BABR	$e^+e^- \rightarrow \Upsilon(4S)$
$0.83 \pm 0.17 \pm 0.08$	WEI	09A BELL	$e^+e^- \rightarrow \Upsilon(4S)$

• • • We do not use the following data for averages, fits, limits, etc. • • •
 $0.91 \pm 0.45 \pm 0.06$ AUBERT,B 06J BABR Repl. by AUBERT 09T

¹ Measured in the union of $0.10 < q^2 < 8.12 \text{ GeV}^2/c^4$ and $q^2 > 10.11 \text{ GeV}^2/c^4$. LEES 12s reports also individual measurements $\Gamma(B \rightarrow K^*(892)\mu^+\mu^-)/\Gamma(B \rightarrow K^*(892)e^+e^-) = 1.06^{+0.48}_{-0.33} \pm 0.08$ for $0.10 < q^2 < 8.12 \text{ GeV}^2/c^4$ and $\Gamma(B \rightarrow K^*(892)\mu^+\mu^-)/\Gamma(B \rightarrow K^*(892)e^+e^-) = 1.18^{+0.55}_{-0.37} \pm 0.11$ for $q^2 > 10.11 \text{ GeV}^2/c^4$.

$\Gamma(K\ell^+\ell^-)/\Gamma_{\text{total}}$ Γ_{131}/Γ

Test for $\Delta B = 1$ weak neutral current. Allowed by higher-order electroweak interactions.

VALUE (units 10^{-7})	CL%	DOCUMENT ID	TECN	COMMENT
4.8 ± 0.4 OUR AVERAGE				
$4.7 \pm 0.6 \pm 0.2$		LEES	12s BABR	$e^+e^- \rightarrow \Upsilon(4S)$
$4.8^{+0.5}_{-0.4} \pm 0.3$		WEI	09A BELL	$e^+e^- \rightarrow \Upsilon(4S)$
• • • We do not use the following data for averages, fits, limits, etc. • • •				
$3.9 \pm 0.7 \pm 0.2$		1 AUBERT	09T BABR	Repl. by LEES 12s
$3.4 \pm 0.7 \pm 0.2$		1 AUBERT,B	06J BABR	Repl. by AUBERT 09T
$6.5^{+1.4}_{-1.3} \pm 0.4$		2 AUBERT	03U BABR	Repl. by AUBERT,B 06J
$4.8^{+1.0}_{-0.9} \pm 0.3$		3 ISHIKAWA	03 BELL	Repl. by WEI 09A
$7.5^{+2.5}_{-2.1} \pm 0.6$		4 ABE	02 BELL	Repl. by ISHIKAWA 03
< 5.1	90	1 AUBERT	02L BABR	$e^+e^- \rightarrow \Upsilon(4S)$
<17	90	5 ANDERSON	01B CLE2	$e^+e^- \rightarrow \Upsilon(4S)$

¹ Assumes equal production of B^+ and B^0 at the $\Upsilon(4S)$.
² Assumes all four $B \rightarrow K\ell^+\ell^-$ modes having equal partial widths in the fit.
³ Assumes equal production rate for charge and neutral B meson pairs, isospin invariance, lepton universality for $B \rightarrow K\ell^+\ell^-$, and $B(B \rightarrow K^*(892)\mu^+\mu^-) = 1.33$. The second error is total systematic uncertainties including model dependence.
⁴ Assumes lepton universality.
⁵ The result is for di-lepton masses above 0.5 GeV.

$\Gamma(K^*(892)\ell^+\ell^-)/\Gamma_{\text{total}}$ Γ_{132}/Γ

Test for $\Delta B = 1$ weak neutral current. Allowed by higher-order electroweak interactions.

VALUE (units 10^{-7})	CL%	DOCUMENT ID	TECN	COMMENT
10.5 ± 1.0 OUR AVERAGE				
$10.2^{+1.4}_{-1.3} \pm 0.5$		LEES	12s BABR	$e^+e^- \rightarrow \Upsilon(4S)$
$10.7^{+1.1}_{-1.0} \pm 0.9$		WEI	09A BELL	$e^+e^- \rightarrow \Upsilon(4S)$
• • • We do not use the following data for averages, fits, limits, etc. • • •				
$11.1^{+1.9}_{-1.8} \pm 0.7$		1 AUBERT	09T BABR	Repl. by LEES 12s
$7.8^{+1.9}_{-1.7} \pm 1.1$		1 AUBERT,B	06J BABR	Repl. by AUBERT 09T
$8.8^{+3.3}_{-2.9} \pm 1.0$		2 AUBERT	03U BABR	Repl. by AUBERT,B 06J
$11.5^{+2.6}_{-2.4} \pm 0.8$		3 ISHIKAWA	03 BELL	Repl. by WEI 09A
<31	90	1,4 AUBERT	02L BABR	Repl. by AUBERT 03U
<33	90	5 ANDERSON	01B CLE2	$e^+e^- \rightarrow \Upsilon(4S)$

¹ Assumes equal production of B^+ and B^0 at the $\Upsilon(4S)$.
² Assumes the partial width ratio of electron and muon modes to be $\Gamma(B \rightarrow K^*(892)e^+e^-)/\Gamma(B \rightarrow K^*(892)\mu^+\mu^-) = 1.33$.
³ Assumes equal production rate for charge and neutral B meson pairs, isospin invariance, lepton universality for $B \rightarrow K\ell^+\ell^-$, and $B(B \rightarrow K^*(892)\mu^+\mu^-) = 1.33$. The second error is total systematic uncertainties including model dependence.
⁴ For averaging $K^*(892)\mu^+\mu^-$ and $K^*(892)e^+e^-$ modes, AUBERT 02L assumed $B(B \rightarrow K^*(892)e^+e^-)/B(B \rightarrow K^*(892)\mu^+\mu^-) = 1.2$.
⁵ The result is for di-lepton masses above 0.5 GeV.

$\Gamma(K\nu\bar{\nu})/\Gamma_{\text{total}}$ Γ_{133}/Γ

Test for $\Delta B = 1$ weak neutral current.

VALUE	CL%	DOCUMENT ID	TECN	COMMENT
$<1.6 \times 10^{-5}$		1 GRYGIER	17 BELL	$e^+e^- \rightarrow \Upsilon(4S)$
< 1.7×10^{-5}	90	1,2 LEES	13i BABR	$e^+e^- \rightarrow \Upsilon(4S)$
< 1.4×10^{-5}	90	1 DEL-AMO-SA...	10q BABR	Repl. by LEES 13i

¹ Assumes equal production of B^+ and B^0 at the $\Upsilon(4S)$.
² Also reported a limit $< 3.2 \times 10^{-5}$ at 90% CL obtained using a fully reconstructed hadronic B -tag events.

$\Gamma(K^*\nu\bar{\nu})/\Gamma_{\text{total}}$ Γ_{134}/Γ

Test for $\Delta B = 1$ weak neutral current.

VALUE	CL%	DOCUMENT ID	TECN	COMMENT
$<2.7 \times 10^{-5}$		1 GRYGIER	17 BELL	$e^+e^- \rightarrow \Upsilon(4S)$
• • • We do not use the following data for averages, fits, limits, etc. • • •				
< 7.6×10^{-5}	90	1,2 LEES	13i BABR	$e^+e^- \rightarrow \Upsilon(4S)$
< 8×10^{-5}	90	AUBERT	08bc BABR	Repl. by LEES 13i

¹ Assumes equal production of B^+ and B^0 at the $\Upsilon(4S)$.
² Also reported a limit $< 7.9 \times 10^{-5}$ at 90% CL obtained using a fully reconstructed hadronic B -tag events.

Meson Particle Listings

 B^\pm/B^0 ADMIXTURE

$\Gamma(\pi\nu\bar{\nu})/\Gamma_{\text{total}}$ Γ_{135}/Γ

VALUE	CL%	DOCUMENT ID	TECN	COMMENT
$<0.8 \times 10^{-5}$	90	¹ GRYGIER 17	BELL	$e^+e^- \rightarrow \Upsilon(4S)$

¹ Assumes equal production of B^+ and B^0 at the $\Upsilon(4S)$.

$\Gamma(\rho\nu\bar{\nu})/\Gamma_{\text{total}}$ Γ_{136}/Γ

VALUE	CL%	DOCUMENT ID	TECN	COMMENT
$<2.8 \times 10^{-5}$	90	¹ GRYGIER 17	BELL	$e^+e^- \rightarrow \Upsilon(4S)$

¹ Assumes equal production of B^+ and B^0 at the $\Upsilon(4S)$.

$\Gamma(s e^\pm \mu^\mp)/\Gamma_{\text{total}}$ Γ_{137}/Γ

Test of lepton family number conservation. Allowed by higher-order electroweak interactions.

VALUE	CL%	DOCUMENT ID	TECN	COMMENT
$<2.2 \times 10^{-5}$	90	GLENN 98	CLEO	$e^+e^- \rightarrow \Upsilon(4S)$

$\Gamma(\pi e^\pm \mu^\mp)/\Gamma_{\text{total}}$ Γ_{138}/Γ

Test of lepton family number conservation.

VALUE	CL%	DOCUMENT ID	TECN	COMMENT
$<9.2 \times 10^{-8}$	90	¹ AUBERT 07AG	BABR	$e^+e^- \rightarrow \Upsilon(4S)$
••• We do not use the following data for averages, fits, limits, etc. •••				
$<1.6 \times 10^{-6}$	90	¹ EDWARDS 02B	CLE2	$e^+e^- \rightarrow \Upsilon(4S)$

¹ Assumes equal production of B^+ and B^0 at the $\Upsilon(4S)$.

$\Gamma(\rho e^\pm \mu^\mp)/\Gamma_{\text{total}}$ Γ_{139}/Γ

Test of lepton family number conservation.

VALUE	CL%	DOCUMENT ID	TECN	COMMENT
$<3.2 \times 10^{-6}$	90	¹ EDWARDS 02B	CLE2	$e^+e^- \rightarrow \Upsilon(4S)$

¹ Assumes equal production of B^+ and B^0 at the $\Upsilon(4S)$.

$\Gamma(K e^\pm \mu^\mp)/\Gamma_{\text{total}}$ Γ_{140}/Γ

Test of lepton family number conservation.

VALUE (units 10^{-7})	CL%	DOCUMENT ID	TECN	COMMENT
<0.38	90	¹ AUBERT,B 06J	BABR	$e^+e^- \rightarrow \Upsilon(4S)$
••• We do not use the following data for averages, fits, limits, etc. •••				
<16	90	¹ EDWARDS 02B	CLE2	$e^+e^- \rightarrow \Upsilon(4S)$

¹ Assumes equal production of B^+ and B^0 at the $\Upsilon(4S)$.

$\Gamma(K^*(892) e^\pm \mu^\mp)/\Gamma_{\text{total}}$ Γ_{141}/Γ

Test of lepton family number conservation.

VALUE (units 10^{-7})	CL%	DOCUMENT ID	TECN	COMMENT
<5.1	90	¹ AUBERT,B 06J	BABR	$e^+e^- \rightarrow \Upsilon(4S)$
••• We do not use the following data for averages, fits, limits, etc. •••				
<62	90	¹ EDWARDS 02B	CLE2	$e^+e^- \rightarrow \Upsilon(4S)$

¹ Assumes equal production of B^+ and B^0 at the $\Upsilon(4S)$.

CP VIOLATION

A_{CP} is defined as

$$\frac{B(\bar{B} \rightarrow \bar{f}) - B(B \rightarrow f)}{B(\bar{B} \rightarrow \bar{f}) + B(B \rightarrow f)},$$

the CP-violation charge asymmetry of inclusive B^\pm and B^0 decay.

$A_{CP}(B \rightarrow K^*(892)\gamma)$

VALUE	DOCUMENT ID	TECN	COMMENT
-0.003 ± 0.011 OUR AVERAGE			
$-0.004 \pm 0.014 \pm 0.003$	¹ HORIGUCHI 17	BELL	$e^+e^- \rightarrow \Upsilon(4S)$
$-0.003 \pm 0.017 \pm 0.007$	² AUBERT 09A0	BABR	$e^+e^- \rightarrow \Upsilon(4S)$
$0.08 \pm 0.13 \pm 0.03$	³ COAN 00	CLE2	$e^+e^- \rightarrow \Upsilon(4S)$
••• We do not use the following data for averages, fits, limits, etc. •••			
$-0.013 \pm 0.036 \pm 0.010$	⁴ AUBERT,BE 04A	BABR	Repl. by AUBERT 09A0
$-0.015 \pm 0.044 \pm 0.012$	³ NAKAO 04	BELL	Repl. by HORIGUCHI 17
$-0.044 \pm 0.076 \pm 0.012$	⁵ AUBERT 02c	BABR	Repl. by AUBERT,BE 04A

¹ Uses $B(\Upsilon(4S) \rightarrow B^+B^-) = (51.4 \pm 0.6)\%$ and $B(\Upsilon(4S) \rightarrow B^0\bar{B}^0) = (48.6 \pm 0.6)\%$.

² Corresponds to a 90% CL interval $-0.033 < A_{CP} < 0.028$.

³ Assumes equal production of B^+ and B^0 at the $\Upsilon(4S)$.

⁴ Corresponds to a 90% CL allowed region, $-0.074 < A_{CP} < 0.049$.

⁵ A 90% CL range is $-0.170 < A_{CP} < 0.082$.

$A_{CP}(B \rightarrow s\gamma)$

VALUE	DOCUMENT ID	TECN	COMMENT
0.015 ± 0.011 OUR AVERAGE			
$0.0144 \pm 0.0128 \pm 0.0011$	¹ WATANUKI 19	BELL	$e^+e^- \rightarrow \Upsilon(4S)$
$0.017 \pm 0.019 \pm 0.010$	² LEES 14k	BABR	$e^+e^- \rightarrow \Upsilon(4S)$
••• We do not use the following data for averages, fits, limits, etc. •••			
$-0.011 \pm 0.030 \pm 0.014$	³ AUBERT 08Bj	BABR	Repl. by LEES 14k
$0.025 \pm 0.050 \pm 0.015$	⁴ AUBERT,B 04E	BABR	Repl. by AUBERT 08Bj
$0.002 \pm 0.050 \pm 0.030$	⁵ NISHIDA 04	BELL	Repl. by WATANUKI 19

¹ Using a sum-of-exclusive technique with $m_{X_S} < 2.8 \text{ GeV}/c^2$.

² Measured with 16 exclusively reconstructed $B \rightarrow X_S\gamma$ decays with $0.6 < m_{X_S} < 2.0 \text{ GeV}/c^2$ (ten charged and six neutral self-tagging B modes).

³ Uses a sum of exclusively reconstructed $B \rightarrow X_S$ decay modes, with X_S mass between 0.6 and $2.8 \text{ GeV}/c^2$.

⁴ Corresponds to $-0.06 < A_{CP} < 0.11$ at 90% CL.

⁵ This measurement is performed inclusively for recoil mass X_S less than 2.1 GeV , which corresponds to $-0.093 < A_{CP} < 0.096$ at 90% CL.

$A_{CP}(B \rightarrow (s+d)\gamma)$

VALUE	DOCUMENT ID	TECN	COMMENT
0.010 ± 0.031 OUR AVERAGE			
$0.022 \pm 0.039 \pm 0.009$	¹ PESANTEZ 15	BELL	$e^+e^- \rightarrow \Upsilon(4S)$
$0.057 \pm 0.060 \pm 0.018$	LEES 12v	BABR	$e^+e^- \rightarrow \Upsilon(4S)$
$-0.10 \pm 0.18 \pm 0.05$	² AUBERT 08o	BABR	$e^+e^- \rightarrow \Upsilon(4S)$
$-0.110 \pm 0.115 \pm 0.017$	AUBERT,BE 06b	BABR	$e^+e^- \rightarrow \Upsilon(4S)$
$-0.079 \pm 0.108 \pm 0.022$	³ COAN 01	CLE2	$e^+e^- \rightarrow \Upsilon(4S)$

¹ Assumes equal production of B^+ and B^0 at the $\Upsilon(4S)$. Uses an opposite side lepton tag. Requires center-of-mass frame $E_\gamma > 2.1 \text{ GeV}$.

² Uses a fully reconstructed B meson as a tag on the recoil side. Requires $E_\gamma > 2.2 \text{ GeV}$.

³ Corresponds to $-0.27 < A_{CP} < 0.10$ at 90% CL.

$A_{CP}(B \rightarrow X_S \ell^+ \ell^-)$

VALUE	DOCUMENT ID	TECN	COMMENT
$0.04 \pm 0.11 \pm 0.01$	¹ LEES 14D	BABR	$e^+e^- \rightarrow \Upsilon(4S)$
••• We do not use the following data for averages, fits, limits, etc. •••			
$-0.22 \pm 0.26 \pm 0.02$	² AUBERT,B 04i	BABR	Repl. by LEES 14D
$0.04 \pm 0.11 \pm 0.01$			
$0.04 \pm 0.11 \pm 0.01$			

¹ Measured from sum of exclusive modes through K^+ , $K^+\pi^0$, $K^+\pi^-$, $K^+\pi^-\pi^0$, $K^+\pi^-\pi^+$, $K_S^0\pi^+$, and $K_S^0\pi^-\pi^0$.

² The final state flavor is determined by the kaon and pion charges where modes with $X_S = K_S^0$, $K_S^0\pi^0$ or $K_S^0\pi^+\pi^-$ are not used.

$A_{CP}(B \rightarrow X_S \ell^+ \ell^-) (1.0 < q^2 < 6.0 \text{ GeV}^2/c^4)$

VALUE	DOCUMENT ID	TECN	COMMENT
$-0.06 \pm 0.22 \pm 0.01$	¹ LEES 14D	BABR	$e^+e^- \rightarrow \Upsilon(4S)$

¹ Measured from sum of exclusive modes through K^+ , $K^+\pi^0$, $K^+\pi^-$, $K^+\pi^-\pi^0$, $K^+\pi^-\pi^+$, $K_S^0\pi^+$, and $K_S^0\pi^-\pi^0$.

$A_{CP}(B \rightarrow X_S \ell^+ \ell^-) (10.1 < q^2 < 12.9 \text{ or } q^2 > 14.2 \text{ GeV}^2/c^4)$

VALUE	DOCUMENT ID	TECN	COMMENT
$0.19 \pm 0.18 \pm 0.01$	¹ LEES 14D	BABR	$e^+e^- \rightarrow \Upsilon(4S)$

¹ Measured from sum of exclusive modes through K^+ , $K^+\pi^0$, $K^+\pi^-$, $K^+\pi^-\pi^0$, $K^+\pi^-\pi^+$, $K_S^0\pi^+$, and $K_S^0\pi^-\pi^0$.

VALUE	DOCUMENT ID	TECN	COMMENT
$-0.18 \pm 0.15 \pm 0.01$	WEI 09A	BELL	$e^+e^- \rightarrow \Upsilon(4S)$

VALUE	DOCUMENT ID	TECN	COMMENT
$-0.03 \pm 0.13 \pm 0.02$	WEI 09A	BELL	$e^+e^- \rightarrow \Upsilon(4S)$

VALUE	DOCUMENT ID	TECN	COMMENT
-0.04 ± 0.07 OUR AVERAGE			
$0.03 \pm 0.13 \pm 0.01$	¹ LEES 12s	BABR	$e^+e^- \rightarrow \Upsilon(4S)$
$+0.01 \pm 0.16 \pm 0.01$	AUBERT 09t	BABR	$e^+e^- \rightarrow \Upsilon(4S)$
$-0.10 \pm 0.10 \pm 0.01$	WEI 09A	BELL	$e^+e^- \rightarrow \Upsilon(4S)$

¹ Measured in the union of $0.10 < q^2 < 8.12 \text{ GeV}^2/c^4$ and $q^2 > 10.11 \text{ GeV}^2/c^4$.

LEES 12s reports also individual measurements $A_{CP}(B \rightarrow K^*\ell^+\ell^-) = -0.13 \pm 0.18 \pm 0.01$ for $0.10 < q^2 < 8.12 \text{ GeV}^2/c^4$ and $A_{CP}(B \rightarrow K^*\ell^+\ell^-) = 0.16 \pm 0.18 \pm 0.01$ for $q^2 > 10.11 \text{ GeV}^2/c^4$.

$A_{CP}(B \rightarrow \eta \text{ anything})$

VALUE	DOCUMENT ID	TECN	COMMENT
$-0.13 \pm 0.04 \pm 0.02$	¹ NISHIMURA 10	BELL	$e^+e^- \rightarrow \Upsilon(4S)$

¹ Uses $B \rightarrow \eta X_S$ with $0.4 < m_{X_S} < 2.6 \text{ GeV}/c^2$.

$\Delta A_{CP}(X_S\gamma) = A_{CP}(B^\pm \rightarrow X_S\gamma) - A_{CP}(B^0 \rightarrow X_S\gamma)$

This is the isospin difference of the CP asymmetries.

VALUE	DOCUMENT ID	TECN	COMMENT
0.041 ± 0.023 OUR AVERAGE			
$0.0369 \pm 0.0265 \pm 0.0076$	¹ WATANUKI 19	BELL	$e^+e^- \rightarrow \Upsilon(4S)$
$0.050 \pm 0.039 \pm 0.015$	² LEES 14k	BABR	$e^+e^- \rightarrow \Upsilon(4S)$

¹ Using a sum-of-exclusive technique with $m_{X_S} < 2.8 \text{ GeV}/c^2$.

² Measured with 16 exclusively reconstructed $B \rightarrow X_S\gamma$ decays with $0.6 < m_{X_S} < 2.0 \text{ GeV}/c^2$ (ten charged and six neutral self-tagging B modes).

$\bar{A}_{CP}(B \rightarrow X_S\gamma) = (A_{CP}(B^+ \rightarrow X_S\gamma) + A_{CP}(B^0 \rightarrow X_S\gamma))/2$

VALUE	DOCUMENT ID	TECN	COMMENT
$0.0091 \pm 0.0121 \pm 0.0013$	¹ WATANUKI 19	BELL	$e^+e^- \rightarrow \Upsilon(4S)$

¹ Using a sum-of-exclusive technique with $m_{X_S} < 2.8 \text{ GeV}/c^2$.

$\Delta A_{CP}(B \rightarrow K^*\gamma) = A_{CP}(B^+ \rightarrow K^{*+}\gamma) - A_{CP}(B^0 \rightarrow K^{*0}\gamma)$

This is the isospin difference of the CP asymmetries.

VALUE	DOCUMENT ID	TECN	COMMENT
$0.024 \pm 0.028 \pm 0.005$	¹ HORIGUCHI 17	BELL	$e^+e^- \rightarrow \Upsilon(4S)$

¹ Uses $B(\Upsilon(4S) \rightarrow B^+B^-) = (51.4 \pm 0.6)\%$ and $B(\Upsilon(4S) \rightarrow B^0\bar{B}^0) = (48.6 \pm 0.6)\%$.

See key on page 999

Meson Particle Listings

B^\pm/B^0 ADMIXTURE

$\overline{A}_{CP}(B \rightarrow K^*\gamma) = (A_{CP}(B^+ \rightarrow K^{*+}\gamma) + A_{CP}(B^0 \rightarrow K^{*0}\gamma))/2$

This is the average CP asymmetry.

VALUE	DOCUMENT ID	TECN	COMMENT
$-0.001 \pm 0.014 \pm 0.003$	¹ Horiguchi 17	BELL	$e^+e^- \rightarrow \Upsilon(4S)$

¹ Uses $B(\Upsilon(4S) \rightarrow B^+B^-) = (51.4 \pm 0.6)\%$ and $B(\Upsilon(4S) \rightarrow B^0\overline{B}^0) = (48.6 \pm 0.6)\%$.

POLARIZATION IN B DECAY

In decays involving two vector mesons, one can distinguish among the states in which meson polarizations are both longitudinal (L) or both are transverse and parallel (||) or perpendicular (⊥) to each other with the parameters Γ_L/Γ , $\Gamma_{\parallel}/\Gamma$, and the relative phases ϕ_{\parallel} and ϕ_{\perp} . See the definitions in the note on "Polarization in B Decays" review in the B^0 Particle Listings.

$F_L(B \rightarrow K^*\ell^+\ell^-) (q^2 > 0.1 \text{ GeV}^2/c^4)$

VALUE	DOCUMENT ID	TECN	COMMENT
$0.63^{+0.18}_{-0.19} \pm 0.05$	¹ Aubert, B	06J	BABR $e^+e^- \rightarrow \Upsilon(4S)$

¹ Results with different q^2 cuts are also reported.

$F_L(B \rightarrow K^*\ell^+\ell^-) (m_{\ell\ell} < 2.5 \text{ GeV}/c^2)$

VALUE	DOCUMENT ID	TECN	COMMENT
$0.35 \pm 0.16 \pm 0.04$	Aubert	09N	BABR $e^+e^- \rightarrow \Upsilon(4S)$

$F_L(B \rightarrow K^*\ell^+\ell^-) (m_{\ell\ell} > 3.2 \text{ GeV}/c^2)$

VALUE	DOCUMENT ID	TECN	COMMENT
$0.71^{+0.20}_{-0.22} \pm 0.04$	Aubert	09N	BABR $e^+e^- \rightarrow \Upsilon(4S)$

$F_L(B \rightarrow K^*\ell^+\ell^-) (0.10 < q^2 < 0.98 \text{ GeV}^2/c^4)$

VALUE	DOCUMENT ID	TECN	COMMENT
$0.263^{+0.045}_{-0.044} \pm 0.017$	AAIJ	16B	LHCB pp at 7, 8 TeV

$F_L(B \rightarrow K^*\ell^+\ell^-) (1.1 < q^2 < 2.5 \text{ GeV}^2/c^4)$

VALUE	DOCUMENT ID	TECN	COMMENT
$0.660^{+0.083}_{-0.077} \pm 0.022$	AAIJ	16B	LHCB pp at 7, 8 TeV

$F_L(B \rightarrow K^*\ell^+\ell^-) (0.1 < q^2 < 2.0 \text{ GeV}^2/c^4)$

VALUE	DOCUMENT ID	TECN	COMMENT
$0.34^{+0.08}_{-0.07} \pm 0.019$	OUR AVERAGE		

$0.37^{+0.10}_{-0.09} \pm 0.04$	AAIJ	13Y	LHCB pp at 7 TeV, $K^{*0}\mu^+\mu^-$
$0.30 \pm 0.16 \pm 0.02$	AALTONEN	12I	CDF $p\overline{p}$ at 1.96 TeV
$0.29^{+0.21}_{-0.18} \pm 0.02$	WEI	09A	BELL $e^+e^- \rightarrow \Upsilon(4S)$

• • • We do not use the following data for averages, fits, limits, etc. • • •

$0.60^{+0.00}_{-0.28} \pm 0.19$	¹ Chatrchyan 13BL	CMS	pp at 7 TeV
$0.00^{+0.13}_{-0.06} \pm 0.02$	AAIJ	12U	LHCB Repl. by AAIJ 13Y
$0.53^{+0.32}_{-0.34} \pm 0.07$	AALTONEN	11L	CDF Repl. by AALTONEN 12I

¹ Chatrchyan 13BL uses, for this bin, $1.0 < q^2 < 2.0 \text{ GeV}^2/c^4$.

$F_L(B \rightarrow K^*\ell^+\ell^-) (2.0 < q^2 < 4.3 \text{ GeV}^2/c^4)$

VALUE	DOCUMENT ID	TECN	COMMENT
0.77 ± 0.05	OUR AVERAGE		

$0.876^{+0.109}_{-0.097} \pm 0.017$	¹ AAIJ	16B	LHCB pp at 7, 8 TeV
$0.80 \pm 0.08 \pm 0.06$	Khachatryan...16D	CMS	pp at 8 TeV
$0.74^{+0.10}_{-0.09} \pm 0.02$	AAIJ	13Y	LHCB pp at 7 TeV, $K^{*0}\mu^+\mu^-$
$0.65 \pm 0.17 \pm 0.03$	Chatrchyan 13BL	CMS	pp at 7 TeV
$0.37^{+0.25}_{-0.24} \pm 0.10$	AALTONEN	12I	CDF $p\overline{p}$ at 1.96 TeV
$0.71 \pm 0.24 \pm 0.05$	WEI	09A	BELL $e^+e^- \rightarrow \Upsilon(4S)$
$0.77 \pm 0.15 \pm 0.03$	AAIJ	12U	LHCB Repl. by AAIJ 13Y
$0.40^{+0.32}_{-0.33} \pm 0.08$	AALTONEN	11L	CDF Repl. by AALTONEN 12I

¹ Measured in $2.5 < q^2 < 4.0 \text{ GeV}^2/c^4$.

$F_L(B \rightarrow K^*\ell^+\ell^-) (4.0 < q^2 < 6.0 \text{ GeV}^2/c^4)$

VALUE	DOCUMENT ID	TECN	COMMENT
$0.611^{+0.052}_{-0.053} \pm 0.017$	AAIJ	16B	LHCB pp at 7, 8 TeV

$F_L(B \rightarrow K^*\ell^+\ell^-) (6.0 < q^2 < 8.0 \text{ GeV}^2/c^4)$

VALUE	DOCUMENT ID	TECN	COMMENT
$0.579 \pm 0.046 \pm 0.015$	AAIJ	16B	LHCB pp at 7, 8 TeV

$F_L(B \rightarrow K^*\ell^+\ell^-) (4.3 < q^2 < 8.6 \text{ GeV}^2/c^4)$

VALUE	DOCUMENT ID	TECN	COMMENT
0.64 ± 0.06	OUR AVERAGE		

$0.57 \pm 0.07 \pm 0.03$	AAIJ	13Y	LHCB pp at 7 TeV, $K^{*0}\mu^+\mu^-$
$0.81^{+0.13}_{-0.12} \pm 0.05$	Chatrchyan 13BL	CMS	pp at 7 TeV
$0.68^{+0.15}_{-0.17} \pm 0.09$	AALTONEN	12I	CDF $p\overline{p}$ at 1.96 TeV
$0.64^{+0.23}_{-0.24} \pm 0.07$	WEI	09A	BELL $e^+e^- \rightarrow \Upsilon(4S)$

• • • We do not use the following data for averages, fits, limits, etc. • • •

$0.60^{+0.06}_{-0.07} \pm 0.01$	AAIJ	12U	LHCB Repl. by AAIJ 13Y
$0.82^{+0.19}_{-0.23} \pm 0.07$	AALTONEN	11L	CDF Repl. by AALTONEN 12I

$F_L(B \rightarrow K^*\ell^+\ell^-) (10.09 < q^2 < 12.86 \text{ GeV}^2/c^4)$

VALUE	DOCUMENT ID	TECN	COMMENT
0.448 ± 0.033	OUR AVERAGE		

$0.493^{+0.049}_{-0.047} \pm 0.013$	¹ AAIJ	16B	LHCB pp at 7, 8 TeV
$0.39 \pm 0.05 \pm 0.04$	Khachatryan...16D	CMS	pp at 8 TeV
$0.48^{+0.08}_{-0.09} \pm 0.03$	AAIJ	13Y	LHCB pp at 7 TeV, $K^{*0}\mu^+\mu^-$
$0.45^{+0.10}_{-0.11} \pm 0.04$	Chatrchyan 13BL	CMS	pp at 7 TeV
$0.47 \pm 0.14 \pm 0.03$	AALTONEN	12I	CDF $p\overline{p}$ at 1.96 TeV
$0.17^{+0.17}_{-0.15} \pm 0.03$	WEI	09A	BELL $e^+e^- \rightarrow \Upsilon(4S)$

• • • We do not use the following data for averages, fits, limits, etc. • • •

$0.41 \pm 0.11 \pm 0.03$	AAIJ	12U	LHCB Repl. by AAIJ 13Y
$0.31^{+0.19}_{-0.18} \pm 0.02$	AALTONEN	11L	CDF Repl. by AALTONEN 12I

¹ Measured in $11.0 < q^2 < 12.5 \text{ GeV}^2/c^4$.

$F_L(B \rightarrow K^*\ell^+\ell^-) (15.0 < q^2 < 17.0 \text{ GeV}^2/c^4)$

VALUE	DOCUMENT ID	TECN	COMMENT
$0.349 \pm 0.039 \pm 0.009$	AAIJ	16B	LHCB pp at 7, 8 TeV

$F_L(B \rightarrow K^*\ell^+\ell^-) (17.0 < q^2 < 19.0 \text{ GeV}^2/c^4)$

VALUE	DOCUMENT ID	TECN	COMMENT
$0.354^{+0.049}_{-0.048} \pm 0.025$	AAIJ	16B	LHCB pp at 7, 8 TeV

$F_L(B \rightarrow K^*\ell^+\ell^-) (14.18 < q^2 < 16.0 \text{ GeV}^2/c^4)$

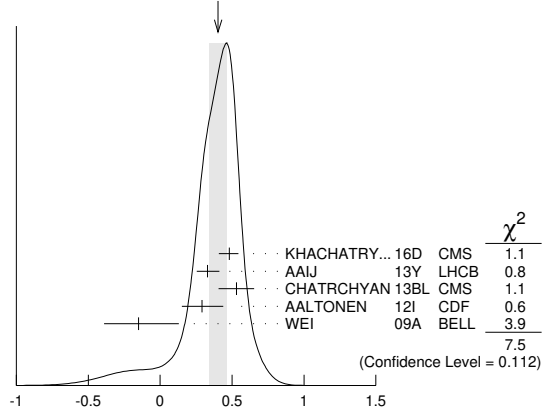
VALUE	DOCUMENT ID	TECN	COMMENT
0.40 ± 0.06	OUR AVERAGE		

$0.48^{+0.05}_{-0.06} \pm 0.04$	Khachatryan...16D	CMS	pp at 8 TeV
$0.33^{+0.08+0.02}_{-0.07-0.03}$	AAIJ	13Y	LHCB pp at 7 TeV, $K^{*0}\mu^+\mu^-$
$0.53 \pm 0.12 \pm 0.03$	Chatrchyan 13BL	CMS	pp at 7 TeV
$0.29^{+0.14}_{-0.13} \pm 0.05$	AALTONEN	12I	CDF $p\overline{p}$ at 1.96 TeV
$-0.15^{+0.27}_{-0.23} \pm 0.07$	WEI	09A	BELL $e^+e^- \rightarrow \Upsilon(4S)$

• • • We do not use the following data for averages, fits, limits, etc. • • •

$0.37 \pm 0.09 \pm 0.05$	AAIJ	12U	LHCB Repl. by AAIJ 13Y
$0.55^{+0.17}_{-0.18} \pm 0.02$	AALTONEN	11L	CDF Repl. by AALTONEN 12I

WEIGHTED AVERAGE
0.40±0.06 (Error scaled by 1.4)



$F_L(B \rightarrow K^*\ell^+\ell^-) (14.18 < q^2 < 16.0 \text{ GeV}^2/c^4)$

Meson Particle Listings

B^\pm/B^0 ADMIXTURE

$F_L(B \rightarrow K^* \ell^+ \ell^-)$ ($16.0 < q^2 < 19.0 \text{ GeV}^2/c^4$)

VALUE	DOCUMENT ID	TECN	COMMENT
0.353 ± 0.024 OUR AVERAGE			
0.344 ^{+0.028} _{-0.030} ± 0.008	¹ AAIJ 16B	LHCB	pp at 7, 8 TeV
0.38 ^{+0.05} _{-0.06} ± 0.04	KHACHATRY...16D	CMS	pp at 8 TeV
0.38 ^{+0.09} _{-0.07} ± 0.03	AAIJ 13Y	LHCB	pp at 7 TeV, $K^{*0} \mu^+ \mu^-$
0.44 ± 0.07 ± 0.03	CHATRCHYAN13BL	CMS	pp at 7 TeV
0.20 ^{+0.19} _{-0.17} ± 0.05	AALTONEN 12i	CDF	$p\bar{p}$ at 1.96 TeV
0.12 ^{+0.15} _{-0.13} ± 0.02	WEI 09A	BELL	$e^+ e^- \rightarrow \Upsilon(4S)$
0.26 ^{+0.10} _{-0.08} ± 0.03	AAIJ 12u	LHCB	Repl. by AAIJ 13Y
0.09 ^{+0.18} _{-0.14} ± 0.03	AALTONEN 11L	CDF	Repl. by AALTONEN 12i

¹ Measured in $15.0 < q^2 < 19.0 \text{ GeV}^2/c^4$.

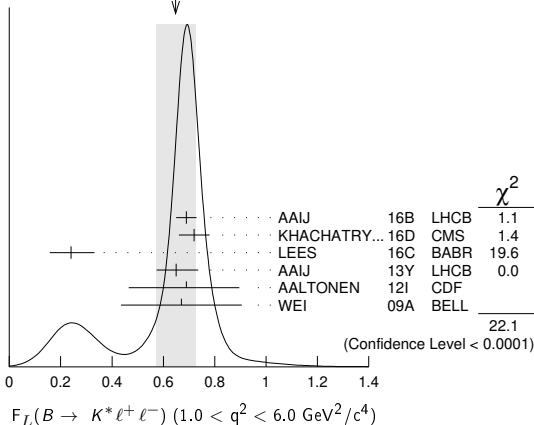
$F_L(B \rightarrow K^* \ell^+ \ell^-)$ ($1.0 < q^2 < 6.0 \text{ GeV}^2/c^4$)

VALUE	DOCUMENT ID	TECN	COMMENT
0.65 ± 0.08 OUR AVERAGE			Error includes scale factor of 2.7. See the ideogram below.
0.690 ^{+0.035} _{-0.036} ± 0.017	¹ AAIJ 16B	LHCB	pp at 7, 8 TeV
0.72 ± 0.06	KHACHATRY...16D	CMS	pp at 7, 8 TeV
0.24 ^{+0.09} _{-0.08} ± 0.02	² LEES 16C	BABR	$e^+ e^- \rightarrow \Upsilon(4S)$
0.65 ^{+0.08} _{-0.07} ± 0.03	AAIJ 13Y	LHCB	pp at 7 TeV, $K^{*0} \mu^+ \mu^-$
0.69 ^{+0.19} _{-0.21} ± 0.08	AALTONEN 12i	CDF	$p\bar{p}$ at 1.96 TeV
0.67 ± 0.23 ± 0.05	WEI 09A	BELL	$e^+ e^- \rightarrow \Upsilon(4S)$
0.68 ± 0.10 ± 0.02	CHATRCHYAN13BL	CMS	Repl. by KHACHATRYAN 16D
0.55 ± 0.10 ± 0.03	AAIJ 12u	LHCB	Repl. by AAIJ 13Y
0.50 ^{+0.27} _{-0.30} ± 0.03	AALTONEN 11L	CDF	Repl. by AALTONEN 12i

¹ Measured in $1.1 < q^2 < 6.0 \text{ GeV}^2/c^4$.

² Measured by combining B^0 and B^+ with e and μ as leptons. Results are also provided separately for B^0 and B^+ .

WEIGHTED AVERAGE
0.65±0.08 (Error scaled by 2.7)



$F_L(B \rightarrow K^* \ell^+ \ell^-)$ ($0.0 < q^2 < 4.3 \text{ GeV}^2/c^4$)

VALUE	DOCUMENT ID	TECN	COMMENT
0.33^{+0.14}_{-0.13} ± 0.03	AALTONEN 12i	CDF	$p\bar{p}$ at 1.96 TeV
0.47 ^{+0.23} _{-0.24} ± 0.03	AALTONEN 11L	CDF	Repl. by AALTONEN 12i

$P_\tau(B \rightarrow D^* \tau^+ \nu_\tau)$

Measures difference in decay widths with positive and negative τ^+ helicities normalized to the sum of those decay widths.

VALUE	DOCUMENT ID	TECN	COMMENT
-0.38 ± 0.51^{+0.21}_{-0.16}	¹ HIROSE 17	BELL	$e^+ e^- \rightarrow \Upsilon(4S)$

¹ Uses a fully reconstructed B meson as a tag on the recoil side.

PARTIAL BRANCHING FRACTIONS IN $B \rightarrow K^{(*)} \ell^+ \ell^-$

$B(B \rightarrow K^* \ell^+ \ell^-)$ ($q^2 < 2.0 \text{ GeV}^2/c^4$)

VALUE (units 10^{-7})	DOCUMENT ID	TECN	COMMENT
1.68 ± 0.23 OUR AVERAGE			
1.89 ^{+0.52} _{-0.46} ± 0.06	¹ LEES 12s	BABR	$e^+ e^- \rightarrow \Upsilon(4S)$
1.73 ± 0.33 ± 0.10	AALTONEN 11A	CDF	$p\bar{p}$ at 1.96 TeV
1.46 ^{+0.40} _{-0.35} ± 0.11	WEI 09A	BELL	$e^+ e^- \rightarrow \Upsilon(4S)$
0.98 ± 0.40 ± 0.09	AALTONEN 11L	CDF	Repl. by AALTONEN 11A

¹ The value reported here from LEES 12s refers to $0.1 < q^2 < 2.0 \text{ GeV}^2/c^2$.

$B(B \rightarrow K^* \ell^+ \ell^-)$ ($2.0 < q^2 < 4.3 \text{ GeV}^2/c^4$)

VALUE (units 10^{-7})	DOCUMENT ID	TECN	COMMENT
0.87 ± 0.17 OUR AVERAGE			
0.95 ^{+0.35} _{-0.30} ± 0.04	LEES 12s	BABR	$e^+ e^- \rightarrow \Upsilon(4S)$
0.82 ± 0.26 ± 0.06	AALTONEN 11A	CDF	$p\bar{p}$ at 1.96 TeV
0.86 ^{+0.31} _{-0.27} ± 0.07	WEI 09A	BELL	$e^+ e^- \rightarrow \Upsilon(4S)$
1.00 ± 0.38 ± 0.09	AALTONEN 11L	CDF	Repl. by AALTONEN 11A

$B(B \rightarrow K^* \ell^+ \ell^-)$ ($4.3 < q^2 < 8.68 \text{ GeV}^2/c^4$)

VALUE (units 10^{-7})	DOCUMENT ID	TECN	COMMENT
1.67 ± 0.29 OUR AVERAGE			
1.82 ^{+0.56} _{-0.52} ± 0.09	¹ LEES 12s	BABR	$e^+ e^- \rightarrow \Upsilon(4S)$
1.72 ± 0.41 ± 0.14	AALTONEN 11A	CDF	$p\bar{p}$ at 1.96 TeV
1.37 ^{+0.47} _{-0.42} ± 0.39	WEI 09A	BELL	$e^+ e^- \rightarrow \Upsilon(4S)$
1.69 ± 0.57 ± 0.15	AALTONEN 11L	CDF	Repl. by AALTONEN 11A

¹ The value reported here from LEES 12s refers to $4.3 < q^2 < 8.12 \text{ GeV}^2/c^2$.

$B(B \rightarrow K^* \ell^+ \ell^-)$ ($10.09 < q^2 < 12.86 \text{ GeV}^2/c^4$)

VALUE (units 10^{-7})	DOCUMENT ID	TECN	COMMENT
1.93 ± 0.25 OUR AVERAGE			
1.86 ^{+0.52} _{-0.48} ± 0.10	¹ LEES 12s	BABR	$e^+ e^- \rightarrow \Upsilon(4S)$
1.77 ± 0.34 ± 0.11	AALTONEN 11A	CDF	$p\bar{p}$ at 1.96 TeV
2.24 ^{+0.44} _{-0.40} ± 0.19	WEI 09A	BELL	$e^+ e^- \rightarrow \Upsilon(4S)$
1.97 ± 0.47 ± 0.17	AALTONEN 11L	CDF	Repl. by AALTONEN 11A

¹ The value reported here from LEES 12s refers to $10.11 < q^2 < 12.89 \text{ GeV}^2/c^2$.

$B(B \rightarrow K^* \ell^+ \ell^-)$ ($14.18 < q^2 < 16.0 \text{ GeV}^2/c^4$)

VALUE (units 10^{-7})	DOCUMENT ID	TECN	COMMENT
1.21 ± 0.17 OUR AVERAGE			
1.46 ^{+0.41} _{-0.36} ± 0.06	¹ LEES 12s	BABR	$e^+ e^- \rightarrow \Upsilon(4S)$
1.21 ± 0.24 ± 0.07	AALTONEN 11A	CDF	$p\bar{p}$ at 1.96 TeV
1.05 ^{+0.29} _{-0.26} ± 0.08	WEI 09A	BELL	$e^+ e^- \rightarrow \Upsilon(4S)$
1.51 ± 0.36 ± 0.13	AALTONEN 11L	CDF	Repl. by AALTONEN 11A

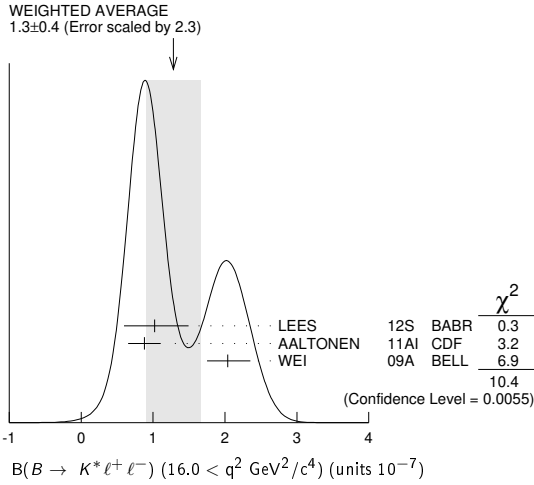
¹ The value reported here from LEES 12s refers to $14.21 < q^2 < 16.0 \text{ GeV}^2/c^2$.

$B(B \rightarrow K^* \ell^+ \ell^-)$ ($16.0 < q^2 \text{ GeV}^2/c^4$)

VALUE (units 10^{-7})	DOCUMENT ID	TECN	COMMENT
1.3 ± 0.4 OUR AVERAGE			Error includes scale factor of 2.3. See the ideogram below.
1.02 ^{+0.47} _{-0.42} ± 0.06	LEES 12s	BABR	$e^+ e^- \rightarrow \Upsilon(4S)$
0.88 ± 0.22 ± 0.05	AALTONEN 11A	CDF	$p\bar{p}$ at 1.96 TeV
2.04 ^{+0.27} _{-0.24} ± 0.16	WEI 09A	BELL	$e^+ e^- \rightarrow \Upsilon(4S)$
1.35 ± 0.37 ± 0.12	AALTONEN 11L	CDF	Repl. by AALTONEN 11A

Meson Particle Listings

B^\pm/B^0 ADMIXTURE



$B(B \rightarrow K^* \ell^+ \ell^-)$ ($1.0 < q^2 < 6.0 \text{ GeV}^2/c^4$)

VALUE (units 10^{-7})	DOCUMENT ID	TECN	COMMENT
1.64±0.26 OUR AVERAGE	Error includes scale factor of 1.4. See the ideogram below.		
$2.05^{+0.53}_{-0.48} \pm 0.07$	LEES	12s BABR	$e^+e^- \rightarrow \Upsilon(4S)$
$1.48 \pm 0.39 \pm 0.12$	AALTONEN	11A1 CDF	$p\bar{p}$ at 1.96 TeV
$1.49^{+0.45}_{-0.40} \pm 0.12$	WEI	09A BELL	$e^+e^- \rightarrow \Upsilon(4S)$
••• We do not use the following data for averages, fits, limits, etc. •••			
$1.60 \pm 0.54 \pm 0.14$	AALTONEN	11L CDF	Repl. by AALTONEN 11A1

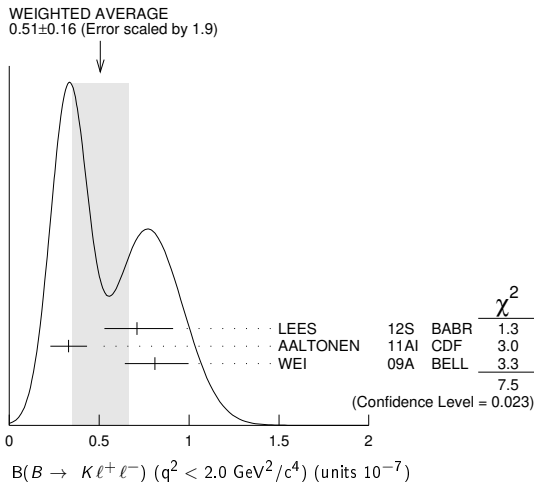
$B(B \rightarrow K^* \ell^+ \ell^-)$ ($0.0 < q^2 < 4.3 \text{ GeV}^2/c^4$)

VALUE (units 10^{-7})	DOCUMENT ID	TECN	COMMENT
2.53±0.43±0.15	AALTONEN	11A1 CDF	$p\bar{p}$ at 1.96 TeV
••• We do not use the following data for averages, fits, limits, etc. •••			
$1.98 \pm 0.55 \pm 0.18$	AALTONEN	11L CDF	Repl. by AALTONEN 11A1

$B(B \rightarrow K \ell^+ \ell^-)$ ($q^2 < 2.0 \text{ GeV}^2/c^4$)

VALUE (units 10^{-7})	DOCUMENT ID	TECN	COMMENT
0.51±0.16 OUR AVERAGE	Error includes scale factor of 1.9. See the ideogram below.		
$0.71^{+0.20}_{-0.18} \pm 0.02$	¹ LEES	12s BABR	$e^+e^- \rightarrow \Upsilon(4S)$
$0.33 \pm 0.10 \pm 0.02$	AALTONEN	11A1 CDF	$p\bar{p}$ at 1.96 TeV
$0.81^{+0.18}_{-0.16} \pm 0.05$	WEI	09A BELL	$e^+e^- \rightarrow \Upsilon(4S)$
••• We do not use the following data for averages, fits, limits, etc. •••			
$0.38 \pm 0.16 \pm 0.03$	AALTONEN	11L CDF	Repl. by AALTONEN 11A1

¹ The value reported here from LEES 12s refers to $0.1 < q^2 < 2.0 \text{ GeV}^2/c^2$.



$B(B \rightarrow K \ell^+ \ell^-)$ ($2.0 < q^2 < 4.3 \text{ GeV}^2/c^4$)

VALUE (units 10^{-7})	DOCUMENT ID	TECN	COMMENT
0.57±0.10±0.09 OUR AVERAGE	Error includes scale factor of 1.2.		
$0.49^{+0.15}_{-0.13} \pm 0.01$	LEES	12s BABR	$e^+e^- \rightarrow \Upsilon(4S)$
$0.77 \pm 0.14 \pm 0.05$	AALTONEN	11A1 CDF	$p\bar{p}$ at 1.96 TeV
$0.46^{+0.14}_{-0.12} \pm 0.03$	WEI	09A BELL	$e^+e^- \rightarrow \Upsilon(4S)$
••• We do not use the following data for averages, fits, limits, etc. •••			
$0.58 \pm 0.19 \pm 0.04$	AALTONEN	11L CDF	Repl. by AALTONEN 11A1

$B(B \rightarrow K \ell^+ \ell^-)$ ($4.3 < q^2 < 8.68 \text{ GeV}^2/c^4$)

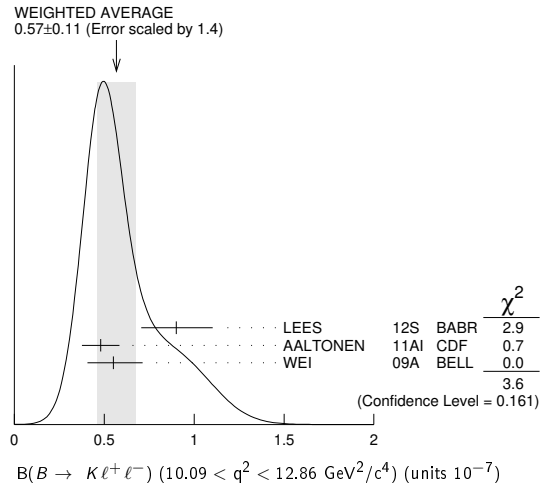
VALUE (units 10^{-7})	DOCUMENT ID	TECN	COMMENT
1.00±0.11 OUR AVERAGE	Error includes scale factor of 1.4. See the ideogram below.		
$0.94^{+0.20}_{-0.19} \pm 0.02$	¹ LEES	12s BABR	$e^+e^- \rightarrow \Upsilon(4S)$
$1.05 \pm 0.17 \pm 0.07$	AALTONEN	11A1 CDF	$p\bar{p}$ at 1.96 TeV
$1.00^{+0.19}_{-0.18} \pm 0.06$	WEI	09A BELL	$e^+e^- \rightarrow \Upsilon(4S)$
••• We do not use the following data for averages, fits, limits, etc. •••			
$0.93 \pm 0.25 \pm 0.06$	AALTONEN	11L CDF	Repl. by AALTONEN 11A1

¹ The value reported here from LEES 12s refers to $4.3 < q^2 < 8.12 \text{ GeV}^2/c^2$.

$B(B \rightarrow K \ell^+ \ell^-)$ ($10.09 < q^2 < 12.86 \text{ GeV}^2/c^4$)

VALUE (units 10^{-7})	DOCUMENT ID	TECN	COMMENT
0.57±0.11 OUR AVERAGE	Error includes scale factor of 1.4. See the ideogram below.		
$0.90^{+0.20}_{-0.19} \pm 0.04$	¹ LEES	12s BABR	$e^+e^- \rightarrow \Upsilon(4S)$
$0.48 \pm 0.10 \pm 0.03$	AALTONEN	11A1 CDF	$p\bar{p}$ at 1.96 TeV
$0.55^{+0.16}_{-0.14} \pm 0.03$	WEI	09A BELL	$e^+e^- \rightarrow \Upsilon(4S)$
••• We do not use the following data for averages, fits, limits, etc. •••			
$0.72 \pm 0.17 \pm 0.05$	AALTONEN	11L CDF	Repl. by AALTONEN 11A1

¹ The value reported here from LEES 12s refers to $10.11 < q^2 < 12.89 \text{ GeV}^2/c^2$.



$B(B \rightarrow K \ell^+ \ell^-)$ ($14.18 < q^2 < 16.0 \text{ GeV}^2/c^4$)

VALUE (units 10^{-7})	DOCUMENT ID	TECN	COMMENT
0.49±0.07 OUR AVERAGE	Error includes scale factor of 2.1. See the ideogram below.		
$0.49^{+0.15}_{-0.14} \pm 0.02$	¹ LEES	12s BABR	$e^+e^- \rightarrow \Upsilon(4S)$
$0.52 \pm 0.09 \pm 0.03$	AALTONEN	11A1 CDF	$p\bar{p}$ at 1.96 TeV
$0.38^{+0.19}_{-0.12} \pm 0.02$	WEI	09A BELL	$e^+e^- \rightarrow \Upsilon(4S)$
••• We do not use the following data for averages, fits, limits, etc. •••			
$0.38 \pm 0.12 \pm 0.03$	AALTONEN	11L CDF	Repl. by AALTONEN 11A1

¹ The value reported here from LEES 12s refers to $14.21 < q^2 < 16.0 \text{ GeV}^2/c^2$.

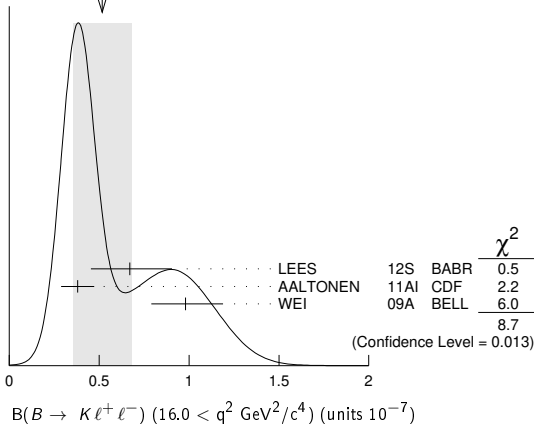
$B(B \rightarrow K \ell^+ \ell^-)$ ($16.0 < q^2 < 16.0 \text{ GeV}^2/c^4$)

VALUE (units 10^{-7})	DOCUMENT ID	TECN	COMMENT
0.52±0.16 OUR AVERAGE	Error includes scale factor of 2.1. See the ideogram below.		
$0.67^{+0.23}_{-0.21} \pm 0.05$	LEES	12s BABR	$e^+e^- \rightarrow \Upsilon(4S)$
$0.38 \pm 0.09 \pm 0.02$	AALTONEN	11A1 CDF	$p\bar{p}$ at 1.96 TeV
$0.98^{+0.20}_{-0.18} \pm 0.06$	WEI	09A BELL	$e^+e^- \rightarrow \Upsilon(4S)$
••• We do not use the following data for averages, fits, limits, etc. •••			
$0.35 \pm 0.13 \pm 0.02$	AALTONEN	11L CDF	Repl. by AALTONEN 11A1

Meson Particle Listings

B^\pm/B^0 ADMIXTURE

WEIGHTED AVERAGE
0.52±0.16 (Error scaled by 2.1)



$B(B \rightarrow K \ell^+ \ell^-)$ ($1.0 < q^2 < 6.0 \text{ GeV}^2/c^4$)

VALUE (units 10^{-7})	DOCUMENT ID	TECN	COMMENT
1.33 ± 0.13 OUR AVERAGE			
1.36 ^{+0.27} _{-0.24} ± 0.03	LEES	12s BABR	$e^+e^- \rightarrow \Upsilon(4S)$
1.29 ± 0.18 ± 0.08	AALTONEN	11AI CDF	$p\bar{p}$ at 1.96 TeV
1.36 ^{+0.23} _{-0.21} ± 0.08	WEI	09A BELL	$e^+e^- \rightarrow \Upsilon(4S)$
• • • We do not use the following data for averages, fits, limits, etc. • • •			
1.01 ± 0.26 ± 0.07	AALTONEN	11L CDF	Repl. by AALTONEN 11AI

$B(B \rightarrow K \ell^+ \ell^-)$ ($0.0 < q^2 < 4.3 \text{ GeV}^2/c^4$)

VALUE (units 10^{-7})	DOCUMENT ID	TECN	COMMENT
1.07 ± 0.17 ± 0.07	AALTONEN	11AI CDF	$p\bar{p}$ at 1.96 TeV
• • • We do not use the following data for averages, fits, limits, etc. • • •			
0.96 ± 0.25 ± 0.06	AALTONEN	11L CDF	Repl. by AALTONEN 11AI

$B(B \rightarrow X_s \ell^+ \ell^-)$ ($1.0 < q^2 < 6.0 \text{ GeV}^2/c^4$)

VALUE (units 10^{-6})	DOCUMENT ID	TECN	COMMENT
1.60^{+0.41}_{-0.39} ± 0.25 ± 0.22	¹ LEES	14D BABR	$e^+e^- \rightarrow \Upsilon(4S)$
¹ Measured from sum of exclusive modes through K^+ , $K^+\pi^0$, $K^+\pi^-$, $K^+\pi^-\pi^0$, $K^+\pi^-\pi^+$, K_S^0 , $K_S^0\pi^0$, $K_S^0\pi^+$, $K_S^0\pi^+\pi^0$, and $K_S^0\pi^+\pi^-$ corrected for unobserved modes.			

$B(B \rightarrow X_s e^+ e^-)$ ($1.0 < q^2 < 6.0 \text{ GeV}^2/c^4$)

VALUE (units 10^{-6})	DOCUMENT ID	TECN	COMMENT
1.93^{+0.47}_{-0.45} ± 0.28 ± 0.24	¹ LEES	14D BABR	$e^+e^- \rightarrow \Upsilon(4S)$
¹ Measured from sum of exclusive modes through K^+ , $K^+\pi^0$, $K^+\pi^-$, $K^+\pi^-\pi^0$, $K^+\pi^-\pi^+$, K_S^0 , $K_S^0\pi^0$, $K_S^0\pi^+$, $K_S^0\pi^+\pi^0$, and $K_S^0\pi^+\pi^-$ corrected for unobserved modes.			

$B(B \rightarrow X_s \mu^+ \mu^-)$ ($1.0 < q^2 < 6.0 \text{ GeV}^2/c^4$)

VALUE (units 10^{-6})	DOCUMENT ID	TECN	COMMENT
0.66^{+0.82}_{-0.76} ± 0.31 ± 0.25	¹ LEES	14D BABR	$e^+e^- \rightarrow \Upsilon(4S)$
¹ Measured from sum of exclusive modes through K^+ , $K^+\pi^0$, $K^+\pi^-$, $K^+\pi^-\pi^0$, $K^+\pi^-\pi^+$, K_S^0 , $K_S^0\pi^0$, $K_S^0\pi^+$, $K_S^0\pi^+\pi^0$, and $K_S^0\pi^+\pi^-$ corrected for unobserved modes.			

$B(B \rightarrow X_s \ell^+ \ell^-)$ ($14.2 < q^2 < 17.0 \text{ GeV}^2/c^4$)

VALUE (units 10^{-6})	DOCUMENT ID	TECN	COMMENT
0.57^{+0.16}_{-0.15} ± 0.03 ± 0.02	¹ LEES	14D BABR	$e^+e^- \rightarrow \Upsilon(4S)$
¹ Measured from sum of exclusive modes through K^+ , $K^+\pi^0$, $K^+\pi^-$, $K^+\pi^-\pi^0$, $K^+\pi^-\pi^+$, K_S^0 , $K_S^0\pi^0$, $K_S^0\pi^+$, $K_S^0\pi^+\pi^0$, and $K_S^0\pi^+\pi^-$ corrected for unobserved modes.			

$B(B \rightarrow X_s e^+ e^-)$ ($14.2 < q^2 < 17.0 \text{ GeV}^2/c^4$)

VALUE (units 10^{-6})	DOCUMENT ID	TECN	COMMENT
0.56^{+0.19}_{-0.18} ± 0.03 ± 0.03	¹ LEES	14D BABR	$e^+e^- \rightarrow \Upsilon(4S)$
¹ Measured from sum of exclusive modes through K^+ , $K^+\pi^0$, $K^+\pi^-$, $K^+\pi^-\pi^0$, $K^+\pi^-\pi^+$, K_S^0 , $K_S^0\pi^0$, $K_S^0\pi^+$, $K_S^0\pi^+\pi^0$, and $K_S^0\pi^+\pi^-$ corrected for unobserved modes.			

$B(B \rightarrow X_s \mu^+ \mu^-)$ ($14.2 < q^2 < 17.0 \text{ GeV}^2/c^4$)

VALUE (units 10^{-6})	DOCUMENT ID	TECN	COMMENT
0.60^{+0.31}_{-0.29} ± 0.05 ± 0.04	¹ LEES	14D BABR	$e^+e^- \rightarrow \Upsilon(4S)$
¹ Measured from sum of exclusive modes through K^+ , $K^+\pi^0$, $K^+\pi^-$, $K^+\pi^-\pi^0$, $K^+\pi^-\pi^+$, K_S^0 , $K_S^0\pi^0$, $K_S^0\pi^+$, $K_S^0\pi^+\pi^0$, and $K_S^0\pi^+\pi^-$ corrected for unobserved modes.			

LEPTON (HADRON) FORWARD-BACKWARD ASYMMETRY IN $B \rightarrow K^{(*)} \ell^+ \ell^-$ ($B \rightarrow K/\pi h^+ h^-$) DECAY

The forward-backward angular asymmetry of the lepton pair in $B \rightarrow K^{(*)} \ell^+ \ell^-$ ($B \rightarrow K/\pi h^+ h^-$) decay is defined as

$$A_{FB}(s) = \frac{N(\cos\theta > 0) - N(\cos\theta < 0)}{N(\cos\theta > 0) + N(\cos\theta < 0)}$$

where $s = q^2/m_B^2$, and θ is the angle of the ℓ^- (h^-) with respect to the flight direction of the B meson, measured in the dilepton (dihadron) rest frame. In addition, the fraction of longitudinal polarization F_L of the K^* and F_S , the relative contribution from scalar and pseudoscalar penguin amplitudes in $B \rightarrow K \ell^+ \ell^-$, can be measured from the angular distribution of its decay products.

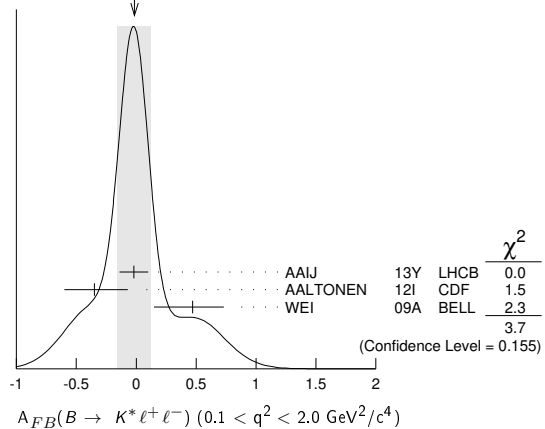
$A_{FB}(B \rightarrow K^* \ell^+ \ell^-)$ ($q^2 > 0.1 \text{ GeV}^2/c^4$)

VALUE	CL%	DOCUMENT ID	TECN	COMMENT
0.50 ± 0.15 ± 0.02		¹ ISHIKAWA	06 BELL	$e^+e^- \rightarrow \Upsilon(4S)$
• • • We do not use the following data for averages, fits, limits, etc. • • •				
> 0.55	95	² AUBERT,B	06J BABR	$e^+e^- \rightarrow \Upsilon(4S)$
¹ Using an unbinned max. likelihood fits to the M_{bc} distribution in five q^2 bins for $\cos\theta > 0$ and $\cos\theta < 0$.				
² Results with different q^2 cuts are also reported.				

$A_{FB}(B \rightarrow K^* \ell^+ \ell^-)$ ($0.1 < q^2 < 2.0 \text{ GeV}^2/c^4$)

VALUE	DOCUMENT ID	TECN	COMMENT
-0.01 ± 0.14 OUR AVERAGE	Error includes scale factor of 1.4. See the ideogram below.		
-0.02 ± 0.12 ± 0.01	AAIJ	13Y LHCb	$p\bar{p}$ at 7 TeV, $K^*0 \mu^+ \mu^-$
-0.35 ^{+0.26} _{-0.23} ± 0.10	AALTONEN	12I CDF	$p\bar{p}$ at 1.96 TeV
0.47 ^{+0.26} _{-0.32} ± 0.03	WEI	09A BELL	$e^+e^- \rightarrow \Upsilon(4S)$
• • • We do not use the following data for averages, fits, limits, etc. • • •			
-0.29 ^{+0.37} _{-0.00} ± 0.18	¹ CHATRCHYAN	13BL CMS	$p\bar{p}$ at 7 TeV
-0.15 ± 0.20 ± 0.06	AAIJ	12U LHCb	Repl. by AAIJ 13Y
0.13 ^{+1.65} _{-0.75} ± 0.25	AALTONEN	11L CDF	Repl. by AALTONEN 12I
¹ CHATRCHYAN 13BL uses, for this bin, $1.0 < q^2 < 2.0 \text{ GeV}^2/c^4$.			

WEIGHTED AVERAGE
-0.01±0.14 (Error scaled by 1.4)



$A_{FB}(B \rightarrow K^* \ell^+ \ell^-)$ ($m_{\ell\ell} < 2.5 \text{ GeV}/c^2$)

VALUE	DOCUMENT ID	TECN	COMMENT
0.24^{+0.18}_{-0.23} ± 0.05	AUBERT	09N BABR	$e^+e^- \rightarrow \Upsilon(4S)$

$A_{FB}(B \rightarrow K^* \ell^+ \ell^-)$ ($m_{\ell\ell} > 3.2 \text{ GeV}/c^2$)

VALUE	DOCUMENT ID	TECN	COMMENT
0.76^{+0.52}_{-0.32} ± 0.07	AUBERT	09N BABR	$e^+e^- \rightarrow \Upsilon(4S)$

$A_{FB}(B \rightarrow K^* \ell^+ \ell^-)$ ($0.10 < q^2 < 0.98 \text{ GeV}^2/c^4$)

VALUE	DOCUMENT ID	TECN	COMMENT
-0.003^{+0.058}_{-0.057} ± 0.009	AAIJ	16B LHCb	$p\bar{p}$ at 7, 8 TeV

Meson Particle Listings

B^\pm/B^0 ADMIXTURE

$A_{FB}(B \rightarrow K^* \ell^+ \ell^-)$ ($1.1 < q^2 < 2.5 \text{ GeV}^2/c^4$)

VALUE	DOCUMENT ID	TECN	COMMENT
$-0.191 \pm_{-0.080}^{+0.068} \pm 0.012$	AAIJ	16b LHCb	pp at 7, 8 TeV

$A_{FB}(B \rightarrow K^* \ell^+ \ell^-)$ ($2.0 < q^2 < 4.3 \text{ GeV}^2/c^4$)

VALUE	DOCUMENT ID	TECN	COMMENT
-0.14 ± 0.05 OUR AVERAGE			
$-0.118 \pm_{-0.090}^{+0.082} \pm 0.007$	¹ AAIJ	16b LHCb	pp at 7, 8 TeV
$-0.12 \pm_{-0.17}^{+0.15} \pm 0.05$	KHACHATRY...16D	CMS	pp at 8 TeV
$-0.20 \pm 0.08 \pm 0.01$	AAIJ	13Y LHCb	pp at 7 TeV, $K^{*0} \mu^+ \mu^-$
$-0.07 \pm 0.20 \pm 0.02$	CHATRCHYAN13BL	CMS	pp at 7 TeV
$0.29 \pm_{-0.35}^{+0.32} \pm 0.15$	AALTONEN	12i CDF	$p\bar{p}$ at 1.96 TeV
$0.11 \pm_{-0.36}^{+0.31} \pm 0.07$	WEI	09A BELL	$e^+e^- \rightarrow \Upsilon(4S)$
$0.05 \pm_{-0.20}^{+0.16} \pm 0.04$	AAIJ	12u LHCb	Repl. by AAIJ 13Y
$0.19 \pm_{-0.41}^{+0.40} \pm 0.14$	AALTONEN	11L CDF	Repl. by AALTONEN 12i

¹ Measured in $2.5 < q^2 < 4.0 \text{ GeV}^2/c^4$.

$A_{FB}(B \rightarrow K^* \ell^+ \ell^-)$ ($0.0 < q^2 < 4.3 \text{ GeV}^2/c^4$)

VALUE	DOCUMENT ID	TECN	COMMENT
$-0.08 \pm_{-0.20}^{+0.21} \pm 0.05$	AALTONEN	12i CDF	$p\bar{p}$ at 1.96 TeV
$0.21 \pm_{-0.33}^{+0.31} \pm 0.05$	AALTONEN	11L CDF	Repl. by AALTONEN 12i

$A_{FB}(B \rightarrow K^* \ell^+ \ell^-)$ ($4.0 < q^2 < 6.0 \text{ GeV}^2/c^4$)

VALUE	DOCUMENT ID	TECN	COMMENT
$0.025 \pm_{-0.052}^{+0.051} \pm 0.004$	AAIJ	16b LHCb	pp at 7, 8 TeV

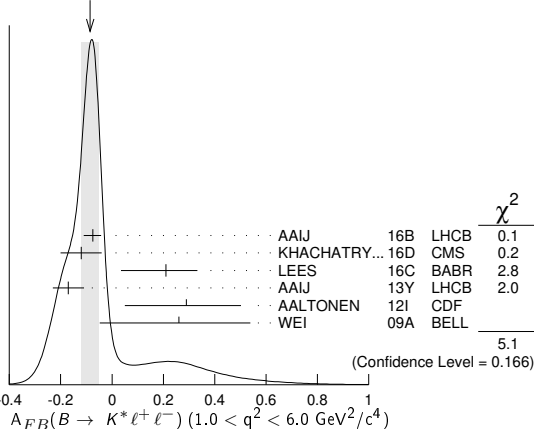
$A_{FB}(B \rightarrow K^* \ell^+ \ell^-)$ ($6.0 < q^2 < 8.0 \text{ GeV}^2/c^4$)

VALUE	DOCUMENT ID	TECN	COMMENT
$0.152 \pm_{-0.040}^{+0.041} \pm 0.008$	AAIJ	16b LHCb	pp at 7, 8 TeV

$A_{FB}(B \rightarrow K^* \ell^+ \ell^-)$ ($1.0 < q^2 < 6.0 \text{ GeV}^2/c^4$)

VALUE	DOCUMENT ID	TECN	COMMENT
-0.085 ± 0.035 OUR AVERAGE			Error includes scale factor of 1.3. See the ideogram below.
$-0.075 \pm_{-0.034}^{+0.032} \pm 0.007$	¹ AAIJ	16b LHCb	pp at 7, 8 TeV
-0.12 ± 0.08	KHACHATRY...16D	CMS	pp at 7, 8 TeV
$0.21 \pm_{-0.15}^{+0.10} \pm_{-0.09}^{+0.07}$	² LEES	16c BABR	$e^+e^- \rightarrow \Upsilon(4S)$
$-0.17 \pm 0.06 \pm 0.01$	AAIJ	13Y LHCb	pp at 7 TeV, $K^{*0} \mu^+ \mu^-$
$0.29 \pm_{-0.23}^{+0.20} \pm 0.07$	AALTONEN	12i CDF	$p\bar{p}$ at 1.96 TeV
$0.26 \pm_{-0.30}^{+0.27} \pm 0.07$	WEI	09A BELL	$e^+e^- \rightarrow \Upsilon(4S)$
0.55 ± 0.43	³ SATO	16 BELL	$e^+e^- \rightarrow \Upsilon(4S)$
$-0.07 \pm 0.12 \pm 0.01$	CHATRCHYAN13BL	CMS	Repl. by KHACHATRYAN 16D
$-0.06 \pm_{-0.14}^{+0.13} \pm 0.07$	AAIJ	12u LHCb	Repl. by AAIJ 13Y
$0.43 \pm_{-0.37}^{+0.36} \pm 0.06$	AALTONEN	11L CDF	Repl. by AALTONEN 12i

WEIGHTED AVERAGE
 -0.085 ± 0.035 (Error scaled by 1.3)



¹ Measured in $1.1 < q^2 < 6.0 \text{ GeV}^2/c^4$.

² Measured by combining B^0 and B^+ with e and μ as leptons. Results are also provided separately for B^0 and B^+ .

³ Uses $K^* \rightarrow K^- \pi^+$, $K^- \pi^0$, $K_S^0 \pi^-$ in the range $M(K\pi) < 1.1 \text{ GeV}/c^2$. Uncertainty is statistical only.

$A_{FB}(B \rightarrow K^* \ell^+ \ell^-)$ ($4.3 < q^2 < 8.6 \text{ GeV}^2/c^4$)

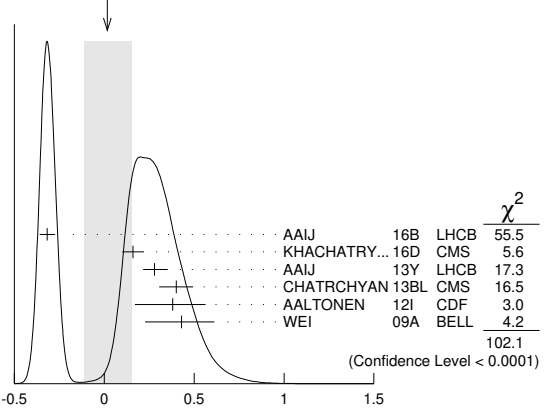
VALUE	DOCUMENT ID	TECN	COMMENT
$0.13 \pm_{-0.05}^{+0.06}$ OUR AVERAGE			Error includes scale factor of 1.1.
$0.16 \pm_{-0.05}^{+0.06} \pm 0.01$	AAIJ	13Y LHCb	pp at 7 TeV, $K^{*0} \mu^+ \mu^-$
$-0.01 \pm 0.11 \pm 0.03$	CHATRCHYAN13BL	CMS	pp at 7 TeV
$0.01 \pm 0.20 \pm 0.09$	AALTONEN	12i CDF	$p\bar{p}$ at 1.96 TeV
$0.45 \pm_{-0.21}^{+0.15} \pm 0.15$	WEI	09A BELL	$e^+e^- \rightarrow \Upsilon(4S)$
$0.27 \pm_{-0.08}^{+0.06} \pm 0.02$	AAIJ	12u LHCb	Repl. by AAIJ 13Y
$-0.06 \pm_{-0.28}^{+0.30} \pm 0.05$	AALTONEN	11L CDF	Repl. by AALTONEN 12i

$A_{FB}(B \rightarrow K^* \ell^+ \ell^-)$ ($10.09 < q^2 < 12.86 \text{ GeV}^2/c^4$)

VALUE	DOCUMENT ID	TECN	COMMENT
0.02 ± 0.13 OUR AVERAGE			Error includes scale factor of 4.5. See the ideogram below.
$-0.318 \pm_{-0.040}^{+0.044} \pm 0.009$	¹ AAIJ	16B LHCb	pp at 7, 8 TeV
$0.16 \pm 0.06 \pm 0.01$	KHACHATRY...16D	CMS	pp at 8 TeV
$0.28 \pm_{-0.06}^{+0.07} \pm 0.02$	AAIJ	13Y LHCb	pp at 7 TeV, $K^{*0} \mu^+ \mu^-$
$0.40 \pm 0.08 \pm 0.05$	CHATRCHYAN13BL	CMS	pp at 7 TeV
$0.38 \pm_{-0.19}^{+0.16} \pm 0.09$	AALTONEN	12i CDF	$p\bar{p}$ at 1.96 TeV
$0.43 \pm_{-0.20}^{+0.18} \pm 0.03$	WEI	09A BELL	$e^+e^- \rightarrow \Upsilon(4S)$
$0.27 \pm_{-0.13}^{+0.11} \pm 0.02$	AAIJ	12u LHCb	Repl. by AAIJ 13Y
$0.66 \pm_{-0.20}^{+0.23} \pm 0.07$	AALTONEN	11L CDF	Repl. by AALTONEN 12i

¹ Measured in $11.0 < q^2 < 12.5 \text{ GeV}^2/c^4$.

WEIGHTED AVERAGE
 0.02 ± 0.13 (Error scaled by 4.5)

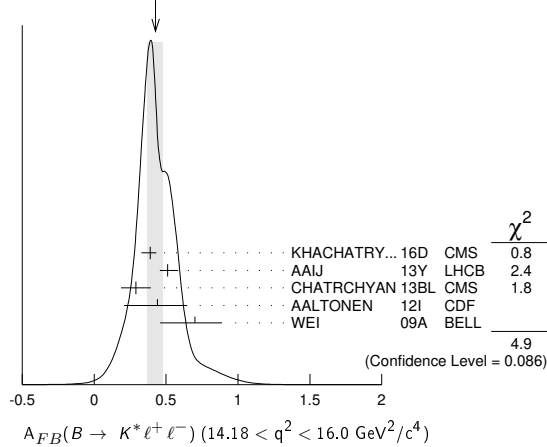


$A_{FB}(B \rightarrow K^* \ell^+ \ell^-)$ ($14.18 < q^2 < 16.0 \text{ GeV}^2/c^4$)

VALUE	DOCUMENT ID	TECN	COMMENT
$0.43 \pm_{-0.06}^{+0.05}$ OUR AVERAGE			Error includes scale factor of 1.6. See the ideogram below.
$0.39 \pm_{-0.06}^{+0.04} \pm 0.01$	KHACHATRY...16D	CMS	pp at 8 TeV
$0.51 \pm_{-0.05}^{+0.07} \pm 0.02$	AAIJ	13Y LHCb	pp at 7 TeV, $K^{*0} \mu^+ \mu^-$
$0.29 \pm 0.09 \pm 0.05$	CHATRCHYAN13BL	CMS	pp at 7 TeV
$0.44 \pm_{-0.21}^{+0.18} \pm 0.10$	AALTONEN	12i CDF	$p\bar{p}$ at 1.96 TeV
$0.70 \pm_{-0.22}^{+0.16} \pm 0.10$	WEI	09A BELL	$e^+e^- \rightarrow \Upsilon(4S)$
$0.47 \pm_{-0.08}^{+0.06} \pm 0.03$	AAIJ	12u LHCb	Repl. by AAIJ 13Y
$0.42 \pm 0.16 \pm 0.09$	AALTONEN	11L CDF	Repl. by AALTONEN 12i

¹ We do not use the following data for averages, fits, limits, etc.

Meson Particle Listings

 B^\pm/B^0 ADMIXTUREWEIGHTED AVERAGE
0.43±0.05-0.06 (Error scaled by 1.6) $A_{FB}(B \rightarrow K^* \ell^+ \ell^-)$ (15.0 < q^2 < 17.0 GeV^2/c^4)

VALUE	DOCUMENT ID	TECN	COMMENT
$0.411^{+0.41}_{-0.037} \pm 0.008$	AAIJ	16B	LHCB pp at 7, 8 TeV

 $A_{FB}(B \rightarrow K^* \ell^+ \ell^-)$ (17.0 < q^2 < 19.0 GeV^2/c^4)

VALUE	DOCUMENT ID	TECN	COMMENT
$0.305^{+0.049}_{-0.048} \pm 0.013$	AAIJ	16B	LHCB pp at 7, 8 TeV

 $A_{FB}(B \rightarrow K^* \ell^+ \ell^-)$ (16.0 < q^2 < 19.0 GeV^2/c^4)

VALUE	DOCUMENT ID	TECN	COMMENT
0.367 ± 0.024 OUR AVERAGE	Error includes scale factor of 1.1.		
$0.355 \pm 0.027 \pm 0.009$	¹ AAIJ	16B	LHCB pp at 7, 8 TeV
$0.35 \pm 0.07 \pm 0.01$	KHACHATRY...	16D	CMS pp at 8 TeV
$0.30 \pm 0.08^{+0.01}_{-0.02}$	AAIJ	13Y	LHCB pp at 7 TeV, $K^*0 \mu^+ \mu^-$
$0.41 \pm 0.05 \pm 0.03$	CHATRCHYAN	13BL	CMS pp at 7 TeV
$0.65^{+0.17}_{-0.18} \pm 0.16$	AALTONEN	12I	CDF $p\bar{p}$ at 1.96 TeV
$0.66^{+0.11}_{-0.16} \pm 0.04$	WEI	09A	BELL $e^+ e^- \rightarrow \Upsilon(4S)$
••• We do not use the following data for averages, fits, limits, etc. •••			
$0.16^{+0.11}_{-0.13} \pm 0.06$	AAIJ	12U	LHCB Repl. by AAIJ 13Y
$0.70^{+0.16}_{-0.25} \pm 0.10$	AALTONEN	11L	CDF Repl. by AALTONEN 12I

¹ Measured in $15.0 < q^2 < 19.0 \text{ GeV}^2/c^4$. $A_{FB}(B \rightarrow K \ell^+ \ell^-)$ ($q^2 > 0.1 \text{ GeV}^2/c^4$)

VALUE	DOCUMENT ID	TECN	COMMENT
0.11 ± 0.12 OUR AVERAGE			
$0.15^{+0.21}_{-0.23} \pm 0.08$	¹ AUBERT,B	06J	BABR $e^+ e^- \rightarrow \Upsilon(4S)$
$0.10 \pm 0.14 \pm 0.01$	² ISHIKAWA	06	BELL $e^+ e^- \rightarrow \Upsilon(4S)$

¹ Results with different q^2 cuts are also reported.² Using an unbinned max. likelihood fits to the M_{bc} distribution in five q^2 bins for $\cos \theta > 0$ and $\cos \theta < 0$. $A_{FB}(B \rightarrow K \ell^+ \ell^-)$ ($q^2 < 2.0 \text{ GeV}^2/c^4$)

VALUE	DOCUMENT ID	TECN	COMMENT
$0.00^{+0.06}_{-0.05}$ OUR AVERAGE			
$0.00^{+0.06+0.03}_{-0.05-0.01}$	AAIJ	13H	LHCB pp at 7 TeV
$0.13^{+0.42}_{-0.43} \pm 0.07$	AALTONEN	12I	CDF $p\bar{p}$ at 1.96 TeV
$0.06^{+0.32}_{-0.35} \pm 0.02$	WEI	09A	BELL $e^+ e^- \rightarrow \Upsilon(4S)$
••• We do not use the following data for averages, fits, limits, etc. •••			
$-0.15^{+0.46}_{-0.39} \pm 0.08$	AALTONEN	11L	CDF Repl. by AALTONEN 12I

 $A_{FB}(B \rightarrow K \ell^+ \ell^-)$ (2.0 < q^2 < 4.3 GeV^2/c^4)

VALUE	DOCUMENT ID	TECN	COMMENT
$0.09^{+0.10}_{-0.07}$ OUR AVERAGE	Error includes scale factor of 1.4.		
$0.07^{+0.08+0.02}_{-0.05-0.01}$	AAIJ	13H	LHCB pp at 7 TeV
$0.32^{+0.15}_{-0.16} \pm 0.05$	AALTONEN	12I	CDF $p\bar{p}$ at 1.96 TeV
$-0.43^{+0.38}_{-0.40} \pm 0.09$	WEI	09A	BELL $e^+ e^- \rightarrow \Upsilon(4S)$
••• We do not use the following data for averages, fits, limits, etc. •••			
$0.72^{+0.40}_{-0.35} \pm 0.07$	AALTONEN	11L	CDF Repl. by AALTONEN 12I

 $A_{FB}(B \rightarrow K \ell^+ \ell^-)$ (0.0 < q^2 < 4.3 GeV^2/c^4)

VALUE	DOCUMENT ID	TECN	COMMENT
$0.31 \pm 0.16 \pm 0.04$	AALTONEN	12I	CDF $p\bar{p}$ at 1.96 TeV
••• We do not use the following data for averages, fits, limits, etc. •••			
$0.36^{+0.24}_{-0.26} \pm 0.06$	AALTONEN	11L	CDF Repl. by AALTONEN 12I

 $A_{FB}(B \rightarrow K \ell^+ \ell^-)$ (1.0 < q^2 < 6.0 GeV^2/c^4)

VALUE	DOCUMENT ID	TECN	COMMENT
$0.034^{+0.040}_{-0.029}$ OUR AVERAGE			
$0.02^{+0.05+0.02}_{-0.03-0.01}$	AAIJ	13H	LHCB pp at 7 TeV
$0.13 \pm 0.09 \pm 0.02$	AALTONEN	12I	CDF $p\bar{p}$ at 1.96 TeV
$-0.04^{+0.13}_{-0.16} \pm 0.05$	WEI	09A	BELL $e^+ e^- \rightarrow \Upsilon(4S)$
••• We do not use the following data for averages, fits, limits, etc. •••			
0.00 ± 0.13	¹ SATO	16	BELL $e^+ e^- \rightarrow \Upsilon(4S)$
$0.08^{+0.27}_{-0.22} \pm 0.07$	AALTONEN	11L	CDF Repl. by AALTONEN 12I

¹ Statistical uncertainty only. $A_{FB}(B \rightarrow K \ell^+ \ell^-)$ (4.3 < q^2 < 8.6 GeV^2/c^4)

VALUE	DOCUMENT ID	TECN	COMMENT
$-0.04^{+0.04}_{-0.05}$ OUR AVERAGE			
$-0.02^{+0.03}_{-0.05} \pm 0.03$	AAIJ	13H	LHCB pp at 7 TeV
$0.01^{+0.13}_{-0.10} \pm 0.01$	AALTONEN	12I	CDF $p\bar{p}$ at 1.96 TeV
$-0.20^{+0.12}_{-0.14} \pm 0.03$	WEI	09A	BELL $e^+ e^- \rightarrow \Upsilon(4S)$
••• We do not use the following data for averages, fits, limits, etc. •••			
$-0.20^{+0.17}_{-0.28} \pm 0.03$	AALTONEN	11L	CDF Repl. by AALTONEN 12I

 $A_{FB}(B \rightarrow K \ell^+ \ell^-)$ (10.09 < q^2 < 12.86 GeV^2/c^4)

VALUE	DOCUMENT ID	TECN	COMMENT
-0.05 ± 0.06 OUR AVERAGE			
$-0.03 \pm 0.07 \pm 0.01$	AAIJ	13H	LHCB pp at 7 TeV
$-0.03^{+0.11}_{-0.10} \pm 0.04$	AALTONEN	12I	CDF $p\bar{p}$ at 1.96 TeV
$-0.21^{+0.17}_{-0.15} \pm 0.06$	WEI	09A	BELL $e^+ e^- \rightarrow \Upsilon(4S)$
••• We do not use the following data for averages, fits, limits, etc. •••			
$-0.10^{+0.17}_{-0.15} \pm 0.07$	AALTONEN	11L	CDF Repl. by AALTONEN 12I

 $A_{FB}(B \rightarrow K \ell^+ \ell^-)$ (14.18 < q^2 < 16.0 GeV^2/c^4)

VALUE	DOCUMENT ID	TECN	COMMENT
$-0.02^{+0.07}_{-0.05}$ OUR AVERAGE			
$-0.01^{+0.12}_{-0.06} \pm 0.01$	AAIJ	13H	LHCB pp at 7 TeV
$-0.05^{+0.09}_{-0.11} \pm 0.03$	AALTONEN	12I	CDF $p\bar{p}$ at 1.96 TeV
$0.04^{+0.32}_{-0.26} \pm 0.05$	WEI	09A	BELL $e^+ e^- \rightarrow \Upsilon(4S)$
••• We do not use the following data for averages, fits, limits, etc. •••			
$0.03^{+0.49}_{-0.16} \pm 0.04$	AALTONEN	11L	CDF Repl. by AALTONEN 12I

 $A_{FB}(B \rightarrow K \ell^+ \ell^-)$ (16.0 < q^2 < 18.0 GeV^2/c^4)

VALUE	DOCUMENT ID	TECN	COMMENT
$-0.09^{+0.07+0.02}_{-0.09-0.01}$	AAIJ	13H	LHCB pp at 7 TeV

 $A_{FB}(B \rightarrow K \ell^+ \ell^-)$ (18.0 < q^2 < 22.0 GeV^2/c^4)

VALUE	DOCUMENT ID	TECN	COMMENT
$0.02 \pm 0.11 \pm 0.01$	AAIJ	13H	LHCB pp at 7 TeV

 $A_{FB}(B \rightarrow K \ell^+ \ell^-)$ ($q^2 > 16.0 \text{ GeV}^2/c^4$)

VALUE	DOCUMENT ID	TECN	COMMENT
$0.04^{+0.09}_{-0.07}$ OUR AVERAGE			
$0.09^{+0.17}_{-0.13} \pm 0.03$	AALTONEN	12I	CDF $p\bar{p}$ at 1.96 TeV
$0.02^{+0.11}_{-0.08} \pm 0.02$	WEI	09A	BELL $e^+ e^- \rightarrow \Upsilon(4S)$
••• We do not use the following data for averages, fits, limits, etc. •••			
$0.07^{+0.30}_{-0.23} \pm 0.02$	AALTONEN	11L	CDF Repl. by AALTONEN 12I

 $A_{FB}(B \rightarrow X_s \ell^+ \ell^-)$ (1.0 < q^2 < 6.0 GeV^2/c^4)

VALUE	DOCUMENT ID	TECN	COMMENT
0.74 ± 0.54	¹ SATO	16	BELL $e^+ e^- \rightarrow \Upsilon(4S)$
••• We do not use the following data for averages, fits, limits, etc. •••			
¹ Uses the sum of 10 exclusive X_s modes in the range $M(X_s) > 1.1 \text{ GeV}/c^2$. Uncertainty is statistical only.			

See key on page 999

Meson Particle Listings

B^\pm/B^0 ADMIXTURE

$F_S(B \rightarrow K\ell^+\ell^-)$ ($q^2 > 0.1 \text{ GeV}^2/c^4$)

VALUE	DOCUMENT ID	TECN	COMMENT
$0.81^{+0.58}_{-0.61} \pm 0.46$	¹ AUBERT,B	06J	BABR $e^+e^- \rightarrow \Upsilon(4S)$

¹ Results with different q^2 cuts are also reported.

$A_{FB}(B \rightarrow K\rho\bar{\rho})$ ($m_{\rho\bar{\rho}} < 2.85 \text{ GeV}/c^2$)

VALUE	DOCUMENT ID	TECN	COMMENT
$0.495 \pm 0.012 \pm 0.007$	¹ AAIJ	14AF	LHCB pp at 7, 8 TeV

¹ Measured in $B^+ \rightarrow K^+\rho\bar{\rho}$ decays.

$A_{FB}(B \rightarrow \pi\rho\bar{\rho})$ ($m_{\rho\bar{\rho}} < 2.85 \text{ GeV}/c^2$)

VALUE	DOCUMENT ID	TECN	COMMENT
$-0.409 \pm 0.033 \pm 0.006$	¹ AAIJ	14AF	LHCB pp at 7, 8 TeV

¹ Measured in $B^+ \rightarrow \pi^+\rho\bar{\rho}$ decays.

ISOSPIN ASYMMETRY

Δ_{0-} is defined as

$$\frac{\Gamma(\bar{B}^0 \rightarrow f_{\pi}) - \Gamma(B^- \rightarrow f_{\pi})}{\Gamma(\bar{B}^0 \rightarrow f_{\pi}) + \Gamma(B^- \rightarrow f_{\pi})},$$

the isospin asymmetry of inclusive neutral and charged B decay.

$\Delta_{0-}(B \rightarrow X_S\gamma)$

VALUE	DOCUMENT ID	TECN	COMMENT
-0.005 ± 0.020 OUR AVERAGE			
$-0.0048 \pm 0.0149 \pm 0.0150$	¹ WATANUKI	19	BELL $e^+e^- \rightarrow \Upsilon(4S)$
$-0.006 \pm 0.058 \pm 0.026$	AUBERT,B	05R	BABR $e^+e^- \rightarrow \Upsilon(4S)$

¹ Using a sum-of-exclusive technique with $m_{X_S} < 2.8 \text{ GeV}/c^2$.

$\Delta_{0-}(B \rightarrow X_S+d\gamma)$

VALUE	DOCUMENT ID	TECN	COMMENT
$-0.06 \pm 0.15 \pm 0.07$	¹ AUBERT	08o	BABR $e^+e^- \rightarrow \Upsilon(4S)$

¹ Uses a fully reconstructed B meson as a tag on the recoil side. The result is for $E_\gamma > 2.2 \text{ GeV}$.

$\Delta_{0+}(B \rightarrow K^*(892)\gamma)$

Δ_{0+} describes the isospin asymmetry between $\Gamma(B^0 \rightarrow K^*(892)^0\gamma)$ and $\Gamma(B^+ \rightarrow K^*(892)^+\gamma)$.

VALUE	DOCUMENT ID	TECN	COMMENT
0.063 ± 0.017 OUR AVERAGE			
$0.062 \pm 0.015 \pm 0.013$	¹ HORIGUCHI	17	BELL $e^+e^- \rightarrow \Upsilon(4S)$
$0.066 \pm 0.021 \pm 0.022$	² AUBERT	09A0	BABR $e^+e^- \rightarrow \Upsilon(4S)$
$0.050 \pm 0.045 \pm 0.037$	³ AUBERT,BE	04A	BABR Repl. by AUBERT 09A0
$0.012 \pm 0.044 \pm 0.026$	NAKAO	04	BELL Repl. by HORIGUCHI 17

••• We do not use the following data for averages, fits, limits, etc. •••

¹ Uses $B(\Upsilon(4S) \rightarrow B^+B^-) = (51.4 \pm 0.6)\%$ and $B(\Upsilon(4S) \rightarrow B^0\bar{B}^0) = (48.6 \pm 0.6)\%$.
² Uses the production ratio of charged and neutral B from $\Upsilon(4S)$ decays and the lifetime ratio $\tau_{B^+}/\tau_{B^0} = 1.071 \pm 0.009$. The 90% CL interval is $0.017 < \Delta_{0+} < 0.116$.
³ Uses the production ratio of charged and neutral B from $\Upsilon(4S)$ decays $R^{+0} = 1.006 \pm 0.048$ and the lifetime ratio of $\tau_{B^+} / \tau_{B^0} = 1.083 \pm 0.017$. The 90% CL interval is $-0.046 < \Delta_{0+} < 0.146$.

$\Delta_{\rho\gamma} = \Gamma(B^+ \rightarrow \rho^+\gamma) / (2 \cdot \Gamma(B^0 \rightarrow \rho^0\gamma)) - 1$

VALUE	DOCUMENT ID	TECN	COMMENT
-0.46 ± 0.17 OUR AVERAGE			
$-0.43^{+0.25}_{-0.22} \pm 0.10$	AUBERT	08BH	BABR $e^+e^- \rightarrow \Upsilon(4S)$
$-0.48^{+0.21+0.08}_{-0.19-0.09}$	TANIGUCHI	08	BELL $e^+e^- \rightarrow \Upsilon(4S)$

$\Delta_{0-}(B \rightarrow K\ell^+\ell^-)$

VALUE	DOCUMENT ID	TECN	COMMENT
-0.13 ± 0.06 OUR AVERAGE			Error includes scale factor of 1.1.
$-0.10^{+0.08}_{-0.09} \pm 0.02$	¹ AAIJ	14M	LHCB pp at 7, 8 TeV
$-0.09^{+0.08}_{-0.08} \pm 0.02$	² AAIJ	14M	LHCB pp at 7, 8 TeV
$-0.58^{+0.29}_{-0.37} \pm 0.02$	³ LEES	12s	BABR $e^+e^- \rightarrow \Upsilon(4S)$
$-0.31^{+0.17}_{-0.14} \pm 0.08$	⁴ WEI	09A	BELL $e^+e^- \rightarrow \Upsilon(4S)$
$-0.35^{+0.23}_{-0.27}$	⁵ AAIJ	12AH	LHCB Repl. by AAIJ 14M
$-1.43^{+0.56}_{-0.85} \pm 0.05$	^{6,7} AUBERT	09T	BABR Repl. by LEES 12s

••• We do not use the following data for averages, fits, limits, etc. •••

¹ For $1.1 < q^2 < 6.0 \text{ GeV}^2/c^4$ using $\mu^+\mu^-$ as a lepton pair and assuming isospin symmetry for the $B \rightarrow J/\psi(1S)K$. Measurements in other q^2 bins are also reported.
² For $15.0 < q^2 < 19.0 \text{ GeV}^2/c^4$ using $\mu^+\mu^-$ as a lepton pair and assuming isospin symmetry for the $B \rightarrow J/\psi(1S)K$. Measurements in other q^2 bins are also reported.
³ For $0.10 < q^2 < 8.12 \text{ GeV}^2/c^4$. Measurements in other q^2 bins are also reported.
⁴ For $q^2 < 8.68 \text{ GeV}^2/c^4$.
⁵ For $1 < q^2 < 6 \text{ GeV}^2/c^4$.
⁶ For $0.1 < m_{\ell^+\ell^-}^2 < 7.02 \text{ GeV}^2/c^4$.
⁷ Assumes equal production of B^+ and B^0 at the $\Upsilon(4S)$.

$\Delta_{0-}(B(B \rightarrow K^*\ell^+\ell^-))$

VALUE	DOCUMENT ID	TECN	COMMENT
$-0.03^{+0.08}_{-0.07}$ OUR AVERAGE			Error includes scale factor of 1.2.
$0.00^{+0.12}_{-0.10} \pm 0.02$	¹ AAIJ	14M	LHCB pp at 7, 8 TeV
$0.06^{+0.10}_{-0.09} \pm 0.02$	² AAIJ	14M	LHCB pp at 7, 8 TeV
$-0.25^{+0.20}_{-0.17} \pm 0.03$	³ LEES	12s	BABR $e^+e^- \rightarrow \Upsilon(4S)$
$-0.29 \pm 0.16 \pm 0.09$	⁴ WEI	09A	BELL $e^+e^- \rightarrow \Upsilon(4S)$
-0.15 ± 0.16	⁵ AAIJ	12AH	LHCB Repl. by AAIJ 14M
$-0.56^{+0.17}_{-0.15} \pm 0.03$	^{6,7} AUBERT	09T	BABR Repl. by LEES 12s

••• We do not use the following data for averages, fits, limits, etc. •••

¹ For $1.1 < q^2 < 6.0 \text{ GeV}^2/c^4$ using $\mu^+\mu^-$ as a lepton pair and assuming isospin symmetry for the $B(B \rightarrow J/\psi(1S)K^*(892))$. Measurements in other q^2 bins are also reported.
² For $15.0 < q^2 < 22.0 \text{ GeV}^2/c^4$ using $\mu^+\mu^-$ as a lepton pair and assuming isospin symmetry for the $B(B \rightarrow J/\psi(1S)K^*(892))$. Measurements in other q^2 bins are also reported.
³ For $0.10 < q^2 < 8.12 \text{ GeV}^2/c^4$. Measurements in other q^2 bins are also reported.
⁴ For $q^2 < 8.68 \text{ GeV}^2/c^4$.
⁵ For $1 < q^2 < 6 \text{ GeV}^2/c^4$.
⁶ For $0.1 < m_{\ell^+\ell^-}^2 < 7.02 \text{ GeV}^2/c^4$.
⁷ Assumes equal production of B^+ and B^0 at the $\Upsilon(4S)$.

$\Delta_{0-}(B(B \rightarrow K^*(*)\ell^+\ell^-))$

VALUE	DOCUMENT ID	TECN	COMMENT
-0.45 ± 0.17 OUR AVERAGE			Error includes scale factor of 1.7.
$-0.64^{+0.15}_{-0.14} \pm 0.03$	^{1,2} AUBERT	09T	BABR $e^+e^- \rightarrow \Upsilon(4S)$
$-0.30^{+0.12}_{-0.11} \pm 0.08$	³ WEI	09A	BELL $e^+e^- \rightarrow \Upsilon(4S)$

¹ For $0.1 < m_{\ell^+\ell^-}^2 < 7.02 \text{ GeV}^2/c^4$.
² Assumes equal production of B^+ and B^0 at the $\Upsilon(4S)$.
³ For $q^2 < 8.68 \text{ GeV}^2/c^2$.

$B \rightarrow X_c \ell \nu$ HADRONIC MASS MOMENTS

$\langle M_X^2 - \bar{M}_D^2 \rangle$ (First Moments)

VALUE (GeV ²)	DOCUMENT ID	TECN	COMMENT
0.36 ± 0.08 OUR AVERAGE			Error includes scale factor of 1.8.
$0.467 \pm 0.038 \pm 0.068$	¹ ACOSTA	05F	CDF $p\bar{p}$ at 1.96 TeV
$0.293 \pm 0.012 \pm 0.058$	² CSORNA	04	CLE2 $e^+e^- \rightarrow \Upsilon(4S)$
$0.251 \pm 0.023 \pm 0.062$	³ CRONIN-HEN..01B	CLE2	$e^+e^- \rightarrow \Upsilon(4S)$

••• We do not use the following data for averages, fits, limits, etc. •••

¹ Moments are measured with a minimum lepton momentum of 0.7 GeV/c in the B rest frame;
² Uses minimum lepton energy of 1.5 GeV and also reports moments with $E_\ell > 1.0 \text{ GeV}$.
³ The leptons are required to have $P_\ell > 1.5 \text{ GeV}/c$.

$\langle M_X^2 \rangle$ (First Moments)

VALUE (GeV ²)	DOCUMENT ID	TECN	COMMENT
4.156 ± 0.029 OUR AVERAGE			
$4.144 \pm 0.028 \pm 0.022$	¹ SCHWANDA	07	BELL $e^+e^- \rightarrow \Upsilon(4S)$
$4.18 \pm 0.04 \pm 0.03$	¹ AUBERT,B	04	BABR $e^+e^- \rightarrow \Upsilon(4S)$

¹ The leptons are required to have $E_\ell > 1.5 \text{ GeV}/c$.

$\langle (M_X^2 - \bar{M}_X^2)^2 \rangle$ (Second Moments)

VALUE (GeV ⁴)	DOCUMENT ID	TECN	COMMENT
0.55 ± 0.08 OUR AVERAGE			
$0.515 \pm 0.061 \pm 0.064$	¹ SCHWANDA	07	BELL $e^+e^- \rightarrow \Upsilon(4S)$
$0.629 \pm 0.031 \pm 0.143$	² CSORNA	04	CLE2 $e^+e^- \rightarrow \Upsilon(4S)$
$1.05 \pm 0.26 \pm 0.13$	³ ACOSTA	05F	CDF $p\bar{p}$ at 1.96 TeV
$0.576 \pm 0.048 \pm 0.168$	¹ CRONIN-HEN..01B	CLE2	$e^+e^- \rightarrow \Upsilon(4S)$

••• We do not use the following data for averages, fits, limits, etc. •••

¹ The leptons are required to have $E_\ell > 1.5 \text{ GeV}/c$.
² Uses minimum lepton energy of 1.5 GeV and also reports moments with $E_\ell > 1.0 \text{ GeV}$.
³ Moments are measured with a minimum lepton momentum of 0.7 GeV/c in the B rest frame;

$\langle (M_X^2 - \bar{M}_D^2)^2 \rangle$ (Second Moments)

VALUE (GeV ⁴)	DOCUMENT ID	TECN	COMMENT
$0.639 \pm 0.056 \pm 0.178$	¹ CRONIN-HEN..01B	CLE2	$e^+e^- \rightarrow \Upsilon(4S)$

¹ The leptons are required to have $E_\ell > 1.5 \text{ GeV}/c$.

$B \rightarrow X_c \ell \nu$ LEPTON MOMENTUM MOMENTS

R_0 ($\Gamma_{E_\ell > 1.7 \text{ GeV}} / \Gamma_{E_\ell > 1.5 \text{ GeV}}$)

VALUE	DOCUMENT ID	TECN	COMMENT
$0.6187 \pm 0.0014 \pm 0.0016$	¹ MAHMOOD	03	CLE2 $e^+e^- \rightarrow \Upsilon(4S)$

¹ The leptons are required to have $E_\ell > 1.5 \text{ GeV}$ in the B rest frame.

Meson Particle Listings

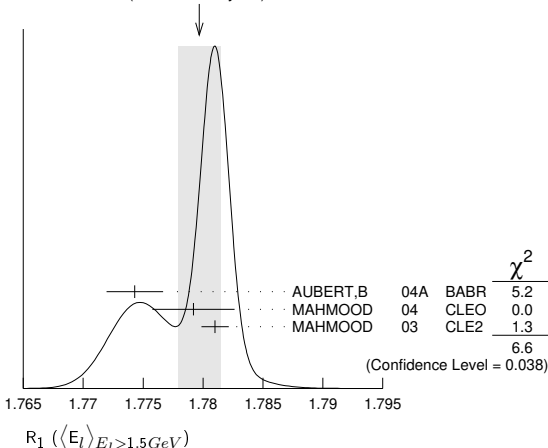
B±/B⁰ ADMIXTURE

R₁ (⟨Eᵢ⟩Eᵢ>1.5GeV)

Table with columns: VALUE, DOCUMENT ID, TECN, COMMENT. Contains experimental data for R1 and a weighted average of 1.7797 ± 0.0018.

- 1 The leptons are required to have E_l > 1.5 GeV in the B rest frame. The result with E_l > 0.6 GeV is also given.
2 Uses E_e > 1.5 GeV and also reports moments with other minimum minimum E_e conditions, as low as E_e > 0.6 GeV.
3 The leptons are required to have E_l > 1.5 GeV in the B rest frame.

WEIGHTED AVERAGE
1.7797 ± 0.0018 (Error scaled by 1.8)



R₂ (⟨Eᵢ² - Eᵢ⟩Eᵢ>1.5GeV)

Table with columns: VALUE (10⁻³ GeV²), DOCUMENT ID, TECN, COMMENT. Contains experimental data for R2 and a weighted average of 30.3 ± 0.9 ± 0.5.

- 1 The leptons are required to have E_l > 1.5 GeV in the B rest frame. The result with E_l > 0.6 GeV is also given.
2 Uses E_e > 1.5 GeV and also reports moments with other minimum minimum E_e conditions, as low as E_e > 0.6 GeV.

R₃ (⟨Eᵢ³ - Eᵢ²⟩Eᵢ>1.5GeV)

Table with columns: VALUE (10⁻³ GeV³), DOCUMENT ID, TECN, COMMENT. Contains experimental data for R3 and a weighted average of 2.12 ± 0.47 ± 0.20.

- 1 The leptons are required to have E_l > 1.5 GeV in the B rest frame. The result with E_l > 0.6 GeV is also given.

B → Xₛγ PHOTON ENERGY MOMENTS

⟨Eᵞ⟩

Table with columns: VALUE (GeV), DOCUMENT ID, TECN, COMMENT. Contains experimental data for photon energy moments and a weighted average of 2.314 ± 0.011.

- 1 LEES 12U uses E_γ > 1.897 GeV to calculate the moments; the moments are used to calculate the HQET parameters...
2 Results for different E_γ threshold values are also measured.
3 The result is for E_γ > 1.9 GeV.
4 Uses a fully reconstructed B meson as a tag on the recoil side.

⟨Eᵞ²⟩ - ⟨Eᵞ⟩²

Table with columns: VALUE (10⁻² GeV²), DOCUMENT ID, TECN, COMMENT. Contains experimental data for photon energy variance and a weighted average of 3.03 ± 0.25.

- • • We do not use the following data for averages, fits, limits, etc. • • •
3.28 ± 0.40 ± 0.43
3 AUBERT,BE 06B BABR Repl. by LEES 12v

- 1 LEES 12U uses E_γ > 1.897 GeV to calculate the moments; the moments are used to calculate the HQET parameters...
2 Results for different E_γ threshold values are also measured.
3 The result is for E_γ > 1.9 GeV.
4 Uses a fully reconstructed B meson as a tag on the recoil side.

B±/B⁰ ADMIXTURE REFERENCES

List of references for B±/B⁰ admixture, including works by Aaij, Watanuki, Grygier, Hirose, etc.

See key on page 999

Meson Particle Listings

B±/B0 ADMIXTURE, B±/B0/Bs0/b-baryon ADMIXTURE

Table listing meson and baryon decays with columns for particle name, experiment code, reference, and collaboration.

Table listing meson and baryon decays with columns for particle name, experiment code, reference, and collaboration.

B±/B0/Bs0/b-baryon ADMIXTURE

B±/B0/Bs0/b-baryon ADMIXTURE MEAN LIFE

Each measurement of the B mean life is an average over an admixture of various bottom mesons and baryons which decay weakly.

“OUR EVALUATION” is an average using rescaled values of the data listed below. The average and rescaling were performed by the Heavy Flavor Averaging Group (HFLAV) and are described at https://hflav.web.cern.ch/.

Table with columns: VALUE (10^-12 s), EVTS, DOCUMENT ID, TECN, COMMENT. Includes 'OUR EVALUATION' and various decay channels like ABDELLAH, ABE, ACCIARRI, etc.

- 1 Measurement performed using an inclusive reconstruction and B flavor identification technique.
2 Measured using inclusive J/psi(1S) -> mu+ mu- vertex.
3 ACCIARRI 98 uses inclusively reconstructed secondary vertex and lepton impact parameter.
...
17 ACTON 92 is combined result of muon and electron impact parameter analyses.

Downloaded from https://academic.oup.com/ptep/article/2020/8/083C01/5891211 by guest on 20 August 2020

Meson Particle Listings

$B^\pm/B^0/B_s^0/b$ -baryon ADMIXTURE

- ¹⁸BUSKULIC 92F uses the lepton impact parameter distribution for data from the 1991 run.
¹⁹BUSKULIC 92c use $J/\psi(1S)$ tags to measure the average b lifetime. This is comparable to other methods only if the $J/\psi(1S)$ branching fractions of the different b -flavored hadrons are in the same ratio.
²⁰Using $Z \rightarrow e^+X$ or μ^+X , ADEVA 91H determined the average lifetime for an admixture of B hadrons from the impact parameter distribution of the lepton.
²¹Using $Z \rightarrow J/\psi(1S)X$, $J/\psi(1S) \rightarrow \ell^+\ell^-$, ALEXANDER 91G determined the average lifetime for an admixture of B hadrons from the decay point of the $J/\psi(1S)$.
²²Using $Z \rightarrow eX$ or μX , DECAMP 91c determines the average lifetime for an admixture of B hadrons from the signed impact parameter distribution of the lepton.
²³HAGEMANN 90 uses electrons and muons in an impact parameter analysis.
²⁴LYONS 90 combine the results of the B lifetime measurements of ONG 89, BRAUN-SCHWEIG 89B, KLEM 88, and ASH 87, and JADE data by private communication. They use statistical techniques which include variation of the error with the mean life, and possible correlations between the systematic errors. This result is not independent of the measured results used in our average.
²⁵We have combined an overall scale error of 15% in quadrature with the systematic error of ± 0.7 to obtain ± 2.1 systematic error.
²⁶Statistical and systematic errors were combined by BROM 87.

$$\text{cor}(B_s^0, B^\pm=B^0) = -0.633$$

$$\text{cor}(b\text{-baryon}, B^\pm=B^0) = -0.813.$$

The notation for production fractions varies in the literature (f_b, d_{B^0} , $f(b \rightarrow \bar{B}^0)$, $\text{Br}(b \rightarrow \bar{B}^0)$). We use our own branching fraction notation here, $\text{B}(\bar{b} \rightarrow B^0)$.

Note these production fractions are b -hadronization fractions, not the conventional branching fractions of b -quark to a B -hadron, which may have considerable dependence on the initial and final state kinematic and production environment.

Γ_1	B^+	(40.8 ± 0.7) %
Γ_2	B^0	(40.8 ± 0.7) %
Γ_3	B_s^0	(10.0 ± 0.8) %
Γ_4	B_c^+	
Γ_5	b -baryon	(8.4 ± 1.1) %

CHARGED b -HADRON ADMIXTURE MEAN LIFE

VALUE (10^{-12} s)	DOCUMENT ID	TECN	COMMENT
1.72 ± 0.08 ± 0.06	¹ ADAM	95	DLPH $e^+e^- \rightarrow Z$

¹ADAM 95 data analyzed using vertex-charge technique to tag b -hadron charge.

NEUTRAL b -HADRON ADMIXTURE MEAN LIFE

VALUE (10^{-12} s)	DOCUMENT ID	TECN	COMMENT
1.58 ± 0.11 ± 0.09	¹ ADAM	95	DLPH $e^+e^- \rightarrow Z$

¹ADAM 95 data analyzed using vertex-charge technique to tag b -hadron charge.

MEAN LIFE RATIO $\tau_{\text{charged } b\text{-hadron}}/\tau_{\text{neutral } b\text{-hadron}}$

VALUE	DOCUMENT ID	TECN	COMMENT
1.09 $^{+0.11}_{-0.10}$ ± 0.08	¹ ADAM	95	DLPH $e^+e^- \rightarrow Z$

¹ADAM 95 data analyzed using vertex-charge technique to tag b -hadron charge.

$$\left| \frac{\Delta\tau_b}{\tau_{b,\bar{b}}} \right|$$

$\tau_{b,\bar{b}}$ and $|\Delta\tau_b|$ are the mean life average and difference between b and \bar{b} hadrons.

VALUE	DOCUMENT ID	TECN	COMMENT
-0.001 ± 0.012 ± 0.008	¹ ABBIENDI	99j	OPAL $e^+e^- \rightarrow Z$

¹Data analyzed using both the jet charge and the charge of secondary vertex in the opposite hemisphere.

\bar{b} PRODUCTION FRACTIONS AND DECAY MODES

The branching fraction measurements are for an admixture of B mesons and baryons at energies above the $T(4S)$. Only the highest energy results (LHC, LEP, Tevatron, $S\bar{p}\bar{S}$) are used in the branching fraction averages. In the following, we assume that the production fractions are the same at the LHC, LEP, and at the Tevatron.

For inclusive branching fractions, e.g., $B \rightarrow D^\pm$ anything, the values usually are multiplicities, not branching fractions. They can be greater than one.

The modes below are listed for a \bar{b} initial state. b modes are their charge conjugates. Reactions indicate the weak decay vertex and do not include mixing.

Mode	Fraction (Γ_j/Γ)	Scale factor/ Confidence level
------	--------------------------------	-----------------------------------

PRODUCTION FRACTIONS

The production fractions for weakly decaying b -hadrons at high energy have been calculated from the best values of mean lives, mixing parameters, and branching fractions in this edition by the Heavy Flavor Averaging Group (HFLAV) as described in the note " $B^0\text{-}\bar{B}^0$ Mixing" in the B^0 Particle Listings. We no longer provide world averages of the b -hadron production fractions, where results from LEP, Tevatron and LHC are averaged together; indeed the available data (from CDF and LHCb) shows that the fractions depend on the kinematics (in particular the p_T) of the produced b hadron. Hence we would like to list the fractions in Z decays instead, which are well-defined physics observables. The production fractions in $p\bar{p}$ collisions at the Tevatron are also listed at the end of the section. Values assume

$$\text{B}(\bar{b} \rightarrow B^+) = \text{B}(\bar{b} \rightarrow B^0)$$

$$\text{B}(\bar{b} \rightarrow B^+) + \text{B}(\bar{b} \rightarrow B^0) + \text{B}(\bar{b} \rightarrow B_s^0) + \text{B}(b \rightarrow b\text{-baryon}) = 100\%.$$

The correlation coefficients between production fractions are also reported:

$$\text{cor}(B_s^0, b\text{-baryon}) = 0.064$$

DECAY MODES

Semileptonic and leptonic modes

Γ_6	ν anything	(23.1 ± 1.5) %	
Γ_7	$\ell^+ \nu_\ell$ anything	[a] (10.69 ± 0.22) %	
Γ_8	$e^+ \nu_e$ anything	(10.86 ± 0.35) %	
Γ_9	$\mu^+ \nu_\mu$ anything	(10.95 $^{+0.29}_{-0.25}$) %	
Γ_{10}	$D^- \ell^+ \nu_\ell$ anything	[a] (2.2 ± 0.4) %	S=1.9
Γ_{11}	$D^- \pi^+ \ell^+ \nu_\ell$ anything	(4.9 ± 1.9) × 10^{-3}	
Γ_{12}	$D^- \pi^- \ell^+ \nu_\ell$ anything	(2.6 ± 1.6) × 10^{-3}	
Γ_{13}	$\bar{D}^0 \ell^+ \nu_\ell$ anything	[a] (6.79 ± 0.34) %	
Γ_{14}	$\bar{D}^0 \pi^- \ell^+ \nu_\ell$ anything	(1.07 ± 0.27) %	
Γ_{15}	$\bar{D}^0 \pi^+ \ell^+ \nu_\ell$ anything	(2.3 ± 1.6) × 10^{-3}	
Γ_{16}	$D^{*-} \ell^+ \nu_\ell$ anything	[a] (2.75 ± 0.19) %	
Γ_{17}	$D^{*-} \pi^- \ell^+ \nu_\ell$ anything	(6 ± 7) × 10^{-4}	
Γ_{18}	$D^{*-} \pi^+ \ell^+ \nu_\ell$ anything	(4.8 ± 1.0) × 10^{-3}	
Γ_{19}	$\bar{D}_j^0 \ell^+ \nu_\ell$ anything × $\text{B}(\bar{D}_j^0 \rightarrow D^{*+} \pi^-)$	[a,b] (2.6 ± 0.9) × 10^{-3}	
Γ_{20}	$D_j^- \ell^+ \nu_\ell$ anything × $\text{B}(D_j^- \rightarrow D^0 \pi^-)$	[a,b] (7.0 ± 2.3) × 10^{-3}	
Γ_{21}	$\bar{D}_2^*(2460)^0 \ell^+ \nu_\ell$ anything × $\text{B}(\bar{D}_2^*(2460)^0 \rightarrow$ $D^{*-} \pi^+)$	< 1.4 × 10^{-3}	CL=90%
Γ_{22}	$D_2^*(2460)^- \ell^+ \nu_\ell$ anything × $\text{B}(D_2^*(2460)^- \rightarrow$ $D^0 \pi^-)$	(4.2 $^{+1.5}_{-1.8}$) × 10^{-3}	
Γ_{23}	$\bar{D}_2^*(2460)^0 \ell^+ \nu_\ell$ anything × $\text{B}(\bar{D}_2^*(2460)^0 \rightarrow$ $D^- \pi^+)$	(1.6 ± 0.8) × 10^{-3}	
Γ_{24}	charmless $\ell \bar{\nu}_\ell$	[a] (1.7 ± 0.5) × 10^{-3}	
Γ_{25}	$\tau^+ \nu_\tau$ anything	(2.41 ± 0.23) %	
Γ_{26}	$D^{*-} \tau \nu_\tau$ anything	(9 ± 4) × 10^{-3}	
Γ_{27}	$\bar{c} \rightarrow \ell^- \bar{\nu}_\ell$ anything	[a] (8.02 ± 0.19) %	
Γ_{28}	$c \rightarrow \ell^+ \nu$ anything	(1.6 $^{+0.4}_{-0.5}$) %	

Charmed meson and baryon modes

Γ_{29}	\bar{D}^0 anything	(58.7 ± 2.8) %	
Γ_{30}	$D^0 D_s^\pm$ anything	[c] (9.1 $^{+4.0}_{-2.8}$) %	
Γ_{31}	$D^\mp D_s^\pm$ anything	[c] (4.0 $^{+2.3}_{-1.8}$) %	
Γ_{32}	$\bar{D}^0 D^0$ anything	[c] (5.1 $^{+2.0}_{-1.8}$) %	
Γ_{33}	$D^0 D^\pm$ anything	[c] (2.7 $^{+1.8}_{-1.6}$) %	
Γ_{34}	$D^\pm D^\mp$ anything	[c] < 9 × 10^{-3}	CL=90%
Γ_{35}	D^0 anything		
Γ_{36}	D^+ anything		
Γ_{37}	D^- anything	(22.7 ± 1.6) %	
Γ_{38}	$D^*(2010)^+$ anything	(17.3 ± 2.0) %	
Γ_{39}	$D_1(2420)^0$ anything	(5.0 ± 1.5) %	
Γ_{40}	$D^*(2010)^\mp D_s^\pm$ anything	[c] (3.3 $^{+1.6}_{-1.3}$) %	
Γ_{41}	$D^0 D^*(2010)^\pm$ anything	[c] (3.0 $^{+1.1}_{-0.9}$) %	
Γ_{42}	$D^*(2010)^\pm D^\mp$ anything	[c] (2.5 $^{+1.2}_{-1.0}$) %	
Γ_{43}	$D^*(2010)^\pm D^*(2010)^\mp$ anything	[c] (1.2 ± 0.4) %	
Γ_{44}	$\bar{D} D$ anything	(10 $^{+11}_{-10}$) %	

See key on page 999

Meson Particle Listings

$B^\pm/B^0/B_s^0/b$ -baryon ADMIXTURE

Γ_{45}	$D_2^*(2460)^0$ anything	(4.7 ± 2.7) %	
Γ_{46}	D_s^- anything	(14.7 ± 2.1) %	
Γ_{47}	D_s^+ anything	(10.1 ± 3.1) %	
Γ_{48}	Λ_c^+ anything	(7.7 ± 1.1) %	
Γ_{49}	\bar{c}/c anything	[d] (116.2 ± 3.2) %	
Charmonium modes			
Γ_{50}	$J/\psi(1S)$ anything	(1.16 ± 0.10) %	
Γ_{51}	$\psi(2S)$ anything	(2.86 ± 0.28) × 10 ⁻³	
Γ_{52}	$\chi_{c0}(1P)$ anything	(1.5 ± 0.6) %	
Γ_{53}	$\chi_{c1}(1P)$ anything	(1.4 ± 0.4) %	
Γ_{54}	$\chi_{c2}(1P)$ anything	(6.2 ± 2.9) × 10 ⁻³	
Γ_{55}	$\chi_c(2P)$ anything, $\chi_c \rightarrow \phi\phi$	< 2.8 × 10 ⁻⁷	CL=95%
Γ_{56}	$\eta_c(1S)$ anything	(4.5 ± 1.9) %	
Γ_{57}	$\eta_c(2S)$ anything, $\eta_c \rightarrow \phi\phi$	(3.2 ± 1.7) × 10 ⁻⁶	
Γ_{58}	$\chi_{c1}(3872)$ anything, $\chi_{c1} \rightarrow \phi\phi$	< 4.5 × 10 ⁻⁷	CL=95%
Γ_{59}	$X(3915)$ anything, $X \rightarrow \phi\phi$	< 3.1 × 10 ⁻⁷	CL=95%
K or K* modes			
Γ_{60}	$\bar{S}\gamma$	(3.1 ± 1.1) × 10 ⁻⁴	
Γ_{61}	$\bar{S}\bar{\nu}$	< 6.4 × 10 ⁻⁴	CL=90%
Γ_{62}	K^\pm anything	(74 ± 6) %	
Γ_{63}	K_S^0 anything	(29.0 ± 2.9) %	
Pion modes			
Γ_{64}	π^\pm anything	(397 ± 21) %	
Γ_{65}	π^0 anything	[d] (278 ± 60) %	
Γ_{66}	ϕ anything	(2.82 ± 0.23) %	
Baryon modes			
Γ_{67}	p/\bar{p} anything	(13.1 ± 1.1) %	
Γ_{68}	$\Lambda/\bar{\Lambda}$ anything	(5.9 ± 0.6) %	
Γ_{69}	b -baryon anything	(10.2 ± 2.8) %	
Γ_{70}	$\bar{\Lambda}_b^0$ anything		
Γ_{71}	$\bar{\Xi}_b^+$ anything		
Other modes			
Γ_{72}	charged anything	[d] (497 ± 7) %	
Γ_{73}	hadron ⁺ hadron ⁻	(1.7 + 1.0 - 0.7) × 10 ⁻⁵	
Γ_{74}	charmless	(7 ± 21) × 10 ⁻³	
$\Delta B = 1$ weak neutral current (BI) modes			
Γ_{75}	e^+e^- anything		
Γ_{76}	$\mu^+\mu^-$ anything	BI < 3.2 × 10 ⁻⁴	CL=90%
Γ_{77}	$\nu\bar{\nu}$ anything		

- [a] An ℓ indicates an e or a μ mode, not a sum over these modes.
 [b] D_j represents an unresolved mixture of pseudoscalar and tensor D^{**} (P -wave) states.
 [c] The value is for the sum of the charge states or particle/antiparticle states indicated.
 [d] Inclusive branching fractions have a multiplicity definition and can be greater than 100%.

$B^\pm/B^0/B_s^0/b$ -baryon ADMIXTURE BRANCHING RATIOS

$\Gamma(B^+)/\Gamma_{\text{total}}$		Γ_1/Γ	
"OUR EVALUATION" is an average from Z decay obtained by the Heavy Flavor Averaging Group (HFLAV) as described at https://hflav.web.cern.ch/ .			
VALUE	DOCUMENT ID	TECN	COMMENT
0.408 ± 0.007 OUR EVALUATION			
0.4099 ± 0.0082 ± 0.0111	¹ ABDALLAH	03k DLPH	$e^+e^- \rightarrow Z$
¹ The analysis is based on a neural network, to estimate the charge of the weakly-decaying b -hadron by distinguishing its decay products from particles produced at the primary vertex.			
$\Gamma(B^+)/\Gamma(B^0)$		Γ_1/Γ_2	
VALUE	DOCUMENT ID	TECN	COMMENT
1.054 ± 0.018 +0.052 -0.074	AALTONEN	08N CDF	$p\bar{p}$ at 1.96 TeV

$$\frac{\Gamma(B_s^0)}{[\Gamma(B^+) + \Gamma(B^0)]} \quad \Gamma_3/(\Gamma_1 + \Gamma_2)$$

"OUR EVALUATION" is an average from Z decay obtained by the Heavy Flavor Averaging Group (HFLAV) as described at <https://hflav.web.cern.ch/>.

VALUE	DOCUMENT ID	TECN	COMMENT
0.1230 ± 0.0115 OUR EVALUATION			
• • • We do not use the following data for averages, fits, limits, etc. • • •			
0.122 ± 0.006	¹ AAIJ	19AD LHCb	$p\bar{p}$ at 13 TeV
0.134 ± 0.004 +0.011 -0.010	² AAIJ	12J LHCb	$p\bar{p}$ at 7 TeV
0.1265 ± 0.0085 ± 0.0131	³ AAIJ	11F LHCb	$p\bar{p}$ at 7 TeV
0.128 +0.011 -0.010 ± 0.011	⁴ AALTONEN	08N CDF	$p\bar{p}$ at 1.96 TeV
0.213 ± 0.068	⁵ AFFOLDER	00E CDF	$p\bar{p}$ at 1.8 TeV
0.21 ± 0.036 +0.038 -0.030	⁶ ABE	99P CDF	$p\bar{p}$ at 1.8 TeV
¹ AAIJ 19AD measured the average value using b -hadron semileptonic decays and assuming isospin symmetry for b -hadron p_T of 4 and 25 GeV and η of 2 and 5.			
² AAIJ 12J measured this value using b -hadron semileptonic decays and assuming isospin symmetry.			
³ AAIJ 11F measured $f_s/f_d = 0.253 ± 0.017 ± 0.017 ± 0.020$, where the errors are statistical, systematic, and theoretical. We divide their value by 2. Our second error combines systematic and theoretical uncertainties.			
⁴ AALTONEN 08N reports $[\Gamma(\bar{b} \rightarrow B_s^0)/[\Gamma(\bar{b} \rightarrow B^+) + \Gamma(\bar{b} \rightarrow B^0)]] \times [B(D_s^+ \rightarrow \phi\pi^+)] = (5.76 ± 0.18 +0.45 -0.42) \times 10^{-3}$ which we divide by our best value $B(D_s^+ \rightarrow \phi\pi^+) = (4.5 ± 0.4) \times 10^{-2}$. Our first error is their experiment's error and our second error is the systematic error from using our best value.			
⁵ AFFOLDER 00E uses several electron-charm final states in $b \rightarrow ce^-X$.			
⁶ ABE 99P uses the numbers of $K^*(892)^0$, $K^*(892)^+$, and $\phi(1020)$ events produced in association with the double semileptonic decays $b \rightarrow c\mu^-X$ with $c \rightarrow s\mu^+X$.			

$$\frac{\Gamma(B_s^0)}{\Gamma(B^0)} \quad \Gamma_3/\Gamma_2$$

"OUR EVALUATION" has been provided by the Heavy Flavor Averaging Group (HFLAV, <https://hflav.web.cern.ch/>).

VALUE	DOCUMENT ID	TECN	COMMENT
0.246 ± 0.023 OUR EVALUATION			
0.239 ± 0.016 OUR AVERAGE			
0.240 ± 0.004 ± 0.020	¹ AAD	15CMATLS	$p\bar{p}$ at 7 TeV
0.238 ± 0.004 ± 0.015 ± 0.021	² AAIJ	13P LHCb	$p\bar{p}$ at 7 TeV
¹ The measurement is derived from the observed $B_s^0 \rightarrow J/\psi\phi$ and $B_d^0 \rightarrow J/\psi K^{*0}$ yields and a recent theory prediction of $B(B_s^0 \rightarrow J/\psi\phi)/B(B_d^0 \rightarrow J/\psi K^{*0})$. The second uncertainty combines in quadrature systematic and theoretical uncertainties.			
² AAIJ 13P studies also separately the $p_T(B)$ and $\eta(B)$ dependency of $\Gamma(\bar{b} \rightarrow B_s^0)/\Gamma(\bar{b} \rightarrow B^0)$, finding $f_s/f_d(p_T) = (0.256 ± 0.020) + (-2.0 ± 0.6) 10^{-3} / \text{GeV}/c (p_T - \langle p_T \rangle)$ and $f_s/f_d(\eta) = (0.256 ± 0.020) + (0.005 ± 0.006) (\eta - \langle \eta \rangle)$, where $\langle p_T \rangle = 10.4 \text{ GeV}/c$ and $\langle \eta \rangle = 3.28$.			

$$\frac{\Gamma(B_c^+)}{[\Gamma(B^+) + \Gamma(B^0)]} \quad \Gamma_4/(\Gamma_1 + \Gamma_2)$$

VALUE (units 10 ⁻³)	DOCUMENT ID	TECN	COMMENT
3.7 ± 0.6 OUR AVERAGE			
3.63 ± 0.08 ± 0.87	¹ AAIJ	19A LHCb	$p\bar{p}$ at 7 TeV
3.78 ± 0.04 ± 0.90	¹ AAIJ	19A LHCb	$p\bar{p}$ at 13 TeV
¹ Measured using B_c^+ semileptonic decays.			

$$\frac{\Gamma(b\text{-baryon})}{[\Gamma(B^+) + \Gamma(B^0)]} \quad \Gamma_5/(\Gamma_1 + \Gamma_2)$$

"OUR EVALUATION" is an average from Z decay obtained by the Heavy Flavor Averaging Group (HFLAV) as described at <https://hflav.web.cern.ch/>.

VALUE	DOCUMENT ID	TECN	COMMENT
0.103 ± 0.015 OUR EVALUATION			
• • • We do not use the following data for averages, fits, limits, etc. • • •			
0.259 ± 0.018	¹ AAIJ	19AD LHCb	$p\bar{p}$ at 13 TeV
0.305 ± 0.010 ± 0.081	² AAIJ	12J LHCb	$p\bar{p}$ at 7 TeV
0.31 ± 0.11 +0.12 -0.08	³ AALTONEN	09E CDF	$p\bar{p}$ at 1.8 TeV
0.22 +0.08 -0.07 ± 0.01	⁴ AALTONEN	08N CDF	$p\bar{p}$ at 1.96 TeV
0.118 ± 0.042	^{3,5} AFFOLDER	00E CDF	$p\bar{p}$ at 1.8 TeV
¹ AAIJ 19AD measured the average value for Λ_b^0 using semileptonic decays and assuming isospin symmetry for b -hadron p_T of 4 and 25 GeV and η of 2 and 5.			
² AAIJ 12J measured the ratio to be $(0.404 ± 0.017 ± 0.027 ± 0.105) \times [1 - (0.031 ± 0.004 ± 0.003) \times p_T]$ using b -hadron semileptonic decays where the p_T is the momentum of charmed hadron-muon pair in GeV/c. We quote their weighted average value where the second error combines systematic and the error on $B(\Lambda_c^+ \rightarrow pK^-\pi^+)$.			
³ AALTONEN 09E errata to the measurement reported in AFFOLDER 00E using the p_T spectra from fully reconstructed B^0 and Λ_b decays.			
⁴ AALTONEN 08N reports $[\Gamma(\bar{b} \rightarrow b\text{-baryon})/[\Gamma(\bar{b} \rightarrow B^+) + \Gamma(\bar{b} \rightarrow B^0)]] \times [B(\Lambda_c^+ \rightarrow pK^-\pi^+)] = (14.1 ± 0.6 +5.3 -4.4) \times 10^{-3}$ which we divide by our best value $B(\Lambda_c^+ \rightarrow pK^-\pi^+) = (6.28 ± 0.32) \times 10^{-2}$. Our first error is their experiment's error and our second error is the systematic error from using our best value.			
⁵ AFFOLDER 00E uses several electron-charm final states in $b \rightarrow ce^-X$.			

Meson Particle Listings

 $B^\pm/B^0/B_s^0/b$ -baryon ADMIXTURE

$\Gamma(\nu \text{ anything})/\Gamma_{\text{total}}$ Γ_6/Γ
 VALUE DOCUMENT ID TECN COMMENT

0.2308 ± 0.0077 ± 0.0124 1,2 ACCIARRI 96c L3 $e^+e^- \rightarrow Z$

¹ ACCIARRI 96c assumes relative b semileptonic decay rates $e:\mu:\tau$ of 1:1:0.25. Based on missing-energy spectrum.

² Assumes Standard Model value for R_B .

$\Gamma(\ell^+ \nu_\ell \text{ anything})/\Gamma_{\text{total}}$ Γ_7/Γ

"OUR EVALUATION" is an average of the data listed below, excluding all asymmetry measurements, performed by the LEP Electroweak Working Group as described in the "Note on the Z boson" in the Z Particle Listings.

VALUE DOCUMENT ID TECN COMMENT

0.1069 ± 0.0022 OUR EVALUATION
0.1064 ± 0.0016 OUR AVERAGE

0.1070 ± 0.0010 ± 0.0035 1 HEISTER 02G ALEP $e^+e^- \rightarrow Z$

0.1070 ± 0.0008 ± 0.0037 2 ABREU 01L DLPH $e^+e^- \rightarrow Z$
 - 0.0049

0.1083 ± 0.0010 ± 0.0028 3 ABBIENZI 00E OPAL $e^+e^- \rightarrow Z$
 - 0.0024

0.1016 ± 0.0013 ± 0.0030 4 ACCIARRI 00 L3 $e^+e^- \rightarrow Z$

0.1085 ± 0.0012 ± 0.0047 5,6 ACCIARRI 96c L3 $e^+e^- \rightarrow Z$

• • • We do not use the following data for averages, fits, limits, etc. • • •

0.1106 ± 0.0039 ± 0.0022 7 ABREU 95D DLPH $e^+e^- \rightarrow Z$

0.114 ± 0.003 ± 0.004 8 BUSKULIC 94G ALEP $e^+e^- \rightarrow Z$

0.100 ± 0.007 ± 0.007 9 ABREU 93c DLPH $e^+e^- \rightarrow Z$

0.105 ± 0.006 ± 0.005 10 AKERS 93B OPAL Repl. by ABBI-
 ENDI 00E

¹ Uses the combination of lepton transverse momentum spectrum and the correlation between the charge of the lepton and opposite jet charge. The first error is statistical and the second error is the total systematic error including the modeling.

² The experimental systematic and model uncertainties are combined in quadrature.

³ ABBIENZI 00E result is determined by comparing the distribution of several kinematic variables of leptonic events in a lifetime tagged $Z \rightarrow b\bar{b}$ sample using artificial neural network techniques. The first error is statistical; the second error is the total systematic error.

⁴ ACCIARRI 00 result obtained from a combined fit of $R_D = \Gamma(Z \rightarrow b\bar{b})/\Gamma(Z \rightarrow \text{hadrons})$ and $B(b \rightarrow \ell\nu X)$, using double-tagging method.

⁵ ACCIARRI 96c result obtained by a fit to the single lepton spectrum.

⁶ Assumes Standard Model value for R_B .

⁷ ABREU 95D give systematic errors ±0.0019 (model) and 0.0012 (R_c). We combine these in quadrature.

⁸ BUSKULIC 94G uses e and μ events. This value is from a global fit to the lepton p and p_T (relative to jet) spectra which also determines the b and c production fractions, the fragmentation functions, and the forward-backward asymmetries. This branching ratio depends primarily on the ratio of dileptons to single leptons at high p_T , but the lower p_T portion of the lepton spectrum is included in the global fit to reduce the model dependence. The model dependence is ±0.0026 and is included in the systematic error.

⁹ ABREU 93c event count includes $e\bar{e}$ events. Combining $e\bar{e}$, $\mu\mu$, and $e\mu$ events, they obtain $0.100 \pm 0.007 \pm 0.007$.

¹⁰ AKERS 93B analysis performed using single and dilepton events.

$\Gamma(e^+ \nu_e \text{ anything})/\Gamma_{\text{total}}$ Γ_8/Γ

VALUE EVTS DOCUMENT ID TECN COMMENT

0.1086 ± 0.0035 OUR AVERAGE

0.1078 ± 0.0008 ± 0.0050 1 ABBIENZI 00E OPAL $e^+e^- \rightarrow Z$
 - 0.0046

0.1089 ± 0.0020 ± 0.0051 2,3 ACCIARRI 96c L3 $e^+e^- \rightarrow Z$

0.107 ± 0.015 ± 0.007 260 4 ABREU 93c DLPH $e^+e^- \rightarrow Z$

0.138 ± 0.032 ± 0.008 5 ADEVA 91c L3 $e^+e^- \rightarrow Z$

• • • We do not use the following data for averages, fits, limits, etc. • • •

0.086 ± 0.027 ± 0.008 6 ABE 93E VNS $E_{\text{cm}}^{ee} = 58 \text{ GeV}$

0.109 ± 0.014 ± 0.0055 2719 7 AKERS 93B OPAL Repl. by ABBI-
 ENDI 00E

0.111 ± 0.028 ± 0.026 BEHREND 90D CELL $E_{\text{cm}}^{ee} = 43 \text{ GeV}$

0.150 ± 0.011 ± 0.022 BEHREND 90D CELL $E_{\text{cm}}^{ee} = 35 \text{ GeV}$

0.112 ± 0.009 ± 0.011 ONG 88 MRK2 $E_{\text{cm}}^{ee} = 29 \text{ GeV}$

0.149 ± 0.022 ± 0.019 PAL 86 DLCO $E_{\text{cm}}^{ee} = 29 \text{ GeV}$

0.110 ± 0.018 ± 0.010 AIHARA 85 TPC $E_{\text{cm}}^{ee} = 29 \text{ GeV}$

0.111 ± 0.034 ± 0.040 ALTHOFF 84J TASS $E_{\text{cm}}^{ee} = 34.6 \text{ GeV}$

0.146 ± 0.028 KOOP 84 DLCO Repl. by PAL 86

0.116 ± 0.021 ± 0.017 NELSON 83 MRK2 $E_{\text{cm}}^{ee} = 29 \text{ GeV}$

¹ ABBIENZI 00E result is determined by comparing the distribution of several kinematic variables of leptonic events in a lifetime tagged $Z \rightarrow b\bar{b}$ sample using artificial neural network techniques. The first error is statistical; the second error is the total systematic error.

² ACCIARRI 96c result obtained by a fit to the single lepton spectrum.

³ Assumes Standard Model value for R_B .

⁴ ABREU 93c event count includes $e\bar{e}$ events. Combining $e\bar{e}$, $\mu\mu$, and $e\mu$ events, they obtain $0.100 \pm 0.007 \pm 0.007$.

⁵ ADEVA 91c measure the average $B(b \rightarrow eX)$ branching ratio using single and double tagged b enhanced Z events. Combining e and μ results, they obtain $0.113 \pm 0.010 \pm 0.006$. Constraining the initial number of b quarks by the Standard Model prediction ($378 \pm 3 \text{ MeV}$) for the decay of the Z into $b\bar{b}$, the electron result gives $0.112 \pm 0.004 \pm 0.008$. They obtain $0.119 \pm 0.003 \pm 0.006$ when e and μ results are combined. Used to measure the $b\bar{b}$ width itself, this electron result gives $370 \pm 12 \pm 24 \text{ MeV}$ and combined with the muon result gives $385 \pm 7 \pm 22 \text{ MeV}$.

⁶ ABE 93E experiment also measures forward-backward asymmetries and fragmentation functions for b and c .

⁷ AKERS 93B analysis performed using single and dilepton events.

$\Gamma(\mu^+ \nu_\mu \text{ anything})/\Gamma_{\text{total}}$ Γ_9/Γ
 VALUE EVTS DOCUMENT ID TECN COMMENT

0.1095 ± 0.0029 OUR AVERAGE
 - 0.0025

0.1096 ± 0.0008 ± 0.0034 1 ABBIENZI 00E OPAL $e^+e^- \rightarrow Z$
 - 0.0027

0.1082 ± 0.0015 ± 0.0059 2,3 ACCIARRI 96c L3 $e^+e^- \rightarrow Z$

0.110 ± 0.012 ± 0.007 656 4 ABREU 93c DLPH $e^+e^- \rightarrow Z$

0.113 ± 0.012 ± 0.006 5 ADEVA 91c L3 $e^+e^- \rightarrow Z$

• • • We do not use the following data for averages, fits, limits, etc. • • •

0.122 ± 0.006 ± 0.007 3 UENO 96 AMY e^+e^- at 57.9 GeV

0.101 ± 0.010 ± 0.0055 4248 6 AKERS 93B OPAL Repl. by ABBI-
 ENDI 00E

0.104 ± 0.023 ± 0.016 BEHREND 90D CELL $E_{\text{cm}}^{ee} = 43 \text{ GeV}$

0.148 ± 0.010 ± 0.016 BEHREND 90D CELL $E_{\text{cm}}^{ee} = 35 \text{ GeV}$

0.118 ± 0.012 ± 0.010 ONG 88 MRK2 $E_{\text{cm}}^{ee} = 29 \text{ GeV}$

0.117 ± 0.016 ± 0.015 BARTEL 87 JADE $E_{\text{cm}}^{ee} = 34.6 \text{ GeV}$

0.114 ± 0.018 ± 0.025 BARTEL 85J JADE Repl. by BARTEL 87

0.117 ± 0.028 ± 0.010 ALTHOFF 84G TASS $E_{\text{cm}}^{ee} = 34.5 \text{ GeV}$

0.105 ± 0.015 ± 0.013 ADEVA 83B MRKJ $E_{\text{cm}}^{ee} = 33-38.5 \text{ GeV}$

0.155 ± 0.054 ± 0.029 FERNANDEZ 83D MAC $E_{\text{cm}}^{ee} = 29 \text{ GeV}$

¹ ABBIENZI 00E result is determined by comparing the distribution of several kinematic variables of leptonic events in a lifetime tagged $Z \rightarrow b\bar{b}$ sample using artificial neural network techniques. The first error is statistical; the second error is the total systematic error.

² ACCIARRI 96c result obtained by a fit to the single lepton spectrum.

³ Assumes Standard Model value for R_B .

⁴ ABREU 93c event count includes $\mu\mu$ events. Combining $e\bar{e}$, $\mu\mu$, and $e\mu$ events, they obtain $0.100 \pm 0.007 \pm 0.007$.

⁵ ADEVA 91c measure the average $B(b \rightarrow eX)$ branching ratio using single and double tagged b enhanced Z events. Combining e and μ results, they obtain $0.113 \pm 0.010 \pm 0.006$. Constraining the initial number of b quarks by the Standard Model prediction ($378 \pm 3 \text{ MeV}$) for the decay of the Z into $b\bar{b}$, the muon result gives $0.123 \pm 0.003 \pm 0.006$. They obtain $0.119 \pm 0.003 \pm 0.006$ when e and μ results are combined. Used to measure the $b\bar{b}$ width itself, this muon result gives $394 \pm 9 \pm 22 \text{ MeV}$ and combined with the electron result gives $385 \pm 7 \pm 22 \text{ MeV}$.

⁶ AKERS 93B analysis performed using single and dilepton events.

$\Gamma(D^- \ell^+ \nu_\ell \text{ anything})/\Gamma_{\text{total}}$ Γ_{10}/Γ

VALUE DOCUMENT ID TECN COMMENT

0.022 ± 0.004 OUR AVERAGE Error includes scale factor of 1.9.

0.0272 ± 0.0028 ± 0.0018 1 ABREU 00R DLPH $e^+e^- \rightarrow Z$

0.0194 ± 0.0025 ± 0.0003 2 AKERS 95Q OPAL $e^+e^- \rightarrow Z$

¹ ABREU 00R reports their experiment's uncertainties ±0.0019 ± 0.0016 ± 0.0018, where the first error is statistical, the second is systematic, and the third is the uncertainty due to the D branching fraction. We combine first two in quadrature.

² AKERS 95Q reports $[\Gamma(\bar{D}^- \rightarrow D^- \ell^+ \nu_\ell \text{ anything})/\Gamma_{\text{total}}] \times [B(D^+ \rightarrow K^- 2\pi^+)] = (1.82 \pm 0.20 \pm 0.12) \times 10^{-3}$ which we divide by our best value $B(D^+ \rightarrow K^- 2\pi^+) = (9.38 \pm 0.16) \times 10^{-2}$. Our first error is their experiment's error and our second error is the systematic error from using our best value.

$\Gamma(D^- \pi^+ \ell^+ \nu_\ell \text{ anything})/\Gamma_{\text{total}}$ Γ_{11}/Γ

VALUE DOCUMENT ID TECN COMMENT

0.0049 ± 0.0018 ± 0.0007 ABREU 00R DLPH $e^+e^- \rightarrow Z$

$\Gamma(D^- \pi^- \ell^+ \nu_\ell \text{ anything})/\Gamma_{\text{total}}$ Γ_{12}/Γ

VALUE DOCUMENT ID TECN COMMENT

0.0026 ± 0.0015 ± 0.0004 ABREU 00R DLPH $e^+e^- \rightarrow Z$

$\Gamma(D^0 \ell^+ \nu_\ell \text{ anything})/\Gamma_{\text{total}}$ Γ_{13}/Γ

VALUE DOCUMENT ID TECN COMMENT

0.0679 ± 0.0034 OUR AVERAGE

0.0704 ± 0.0040 ± 0.0017 1 ABREU 00R DLPH $e^+e^- \rightarrow Z$

0.0638 ± 0.0056 ± 0.0005 2 AKERS 95Q OPAL $e^+e^- \rightarrow Z$

¹ ABREU 00R reports their experiment's uncertainties ±0.0034 ± 0.0036 ± 0.0017, where the first error is statistical, the second is systematic, and the third is the uncertainty due to the D branching fraction. We combine first two in quadrature.

² AKERS 95Q reports $[\Gamma(\bar{D}^0 \rightarrow D^0 \ell^+ \nu_\ell \text{ anything})/\Gamma_{\text{total}}] \times [B(D^0 \rightarrow K^- \pi^+)] = (2.52 \pm 0.14 \pm 0.17) \times 10^{-3}$ which we divide by our best value $B(D^0 \rightarrow K^- \pi^+) = (3.950 \pm 0.031) \times 10^{-2}$. Our first error is their experiment's error and our second error is the systematic error from using our best value.

$\Gamma(D^0 \pi^- \ell^+ \nu_\ell \text{ anything})/\Gamma_{\text{total}}$ Γ_{14}/Γ

VALUE DOCUMENT ID TECN COMMENT

0.0107 ± 0.0025 ± 0.0011 ABREU 00R DLPH $e^+e^- \rightarrow Z$

$\Gamma(D^0 \pi^+ \ell^+ \nu_\ell \text{ anything})/\Gamma_{\text{total}}$ Γ_{15}/Γ

VALUE DOCUMENT ID TECN COMMENT

0.0023 ± 0.0015 ± 0.0004 ABREU 00R DLPH $e^+e^- \rightarrow Z$

Meson Particle Listings

 $B^\pm/B^0/B_s^0/b$ -baryon ADMIXTURE

$\Gamma(D^\pm D^\mp \text{ anything})/\Gamma_{\text{total}}$		Γ_{34}/Γ		
VALUE	CL%	DOCUMENT ID	TECN	COMMENT
<0.009	90	BARATE	98Q	ALEP $e^+e^- \rightarrow Z$

$[\Gamma(D^0 \text{ anything}) + \Gamma(D^+ \text{ anything})]/\Gamma_{\text{total}}$		$(\Gamma_{35} + \Gamma_{36})/\Gamma$		
VALUE	CL%	DOCUMENT ID	TECN	COMMENT
$0.093 \pm 0.017 \pm 0.014$		1 ABDALLAH	03E	DLPH $e^+e^- \rightarrow Z$

¹ The second error is the total of systematic uncertainties including the branching fractions used in the measurement.

$\Gamma(D^- \text{ anything})/\Gamma_{\text{total}}$		Γ_{37}/Γ		
VALUE	CL%	DOCUMENT ID	TECN	COMMENT
$0.227 \pm 0.016 \pm 0.004$		1 BUSKULIC	96Y	ALEP $e^+e^- \rightarrow Z$

¹ BUSKULIC 96Y reports $0.234 \pm 0.013 \pm 0.010$ from a measurement of $[\Gamma(\bar{D}^- \rightarrow D^- \text{ anything})/\Gamma_{\text{total}}] \times [B(D^+ \rightarrow K^- 2\pi^+)]$ assuming $B(D^+ \rightarrow K^- 2\pi^+) = 0.091$, which we rescale to our best value $B(D^+ \rightarrow K^- 2\pi^+) = (9.38 \pm 0.16) \times 10^{-2}$. Our first error is their experiment's error and our second error is the systematic error from using our best value.

$\Gamma(D^*(2010)^+ \text{ anything})/\Gamma_{\text{total}}$		Γ_{38}/Γ		
VALUE	CL%	DOCUMENT ID	TECN	COMMENT
$0.173 \pm 0.016 \pm 0.012$		1 ACKERSTAFF	98E	OPAL $e^+e^- \rightarrow Z$

¹ Uses lepton tags to select $Z \rightarrow b\bar{b}$ events.

$\Gamma(D_1(2420)^0 \text{ anything})/\Gamma_{\text{total}}$		Γ_{39}/Γ		
VALUE	CL%	DOCUMENT ID	TECN	COMMENT
$0.050 \pm 0.014 \pm 0.006$		1 ACKERSTAFF	97W	OPAL $e^+e^- \rightarrow Z$

¹ ACKERSTAFF 97W assumes $B(D_1^0(2460) \rightarrow D^+ \pi^-) = 0.21 \pm 0.04$ and $\Gamma_{b\bar{b}}/\Gamma_{\text{hadrons}} = 0.216$ at Z decay.

$\Gamma(D^*(2010)^0 D_s^\pm \text{ anything})/\Gamma_{\text{total}}$		Γ_{40}/Γ		
VALUE	CL%	DOCUMENT ID	TECN	COMMENT
$0.033 + 0.010 + 0.012$ $-0.009 - 0.009$		1 BARATE	98Q	ALEP $e^+e^- \rightarrow Z$

¹ The systematic error includes the uncertainties due to the charm branching ratios.

$\Gamma(D^0 D^*(2010)^\pm \text{ anything})/\Gamma_{\text{total}}$		Γ_{41}/Γ		
VALUE	CL%	DOCUMENT ID	TECN	COMMENT
$0.030 + 0.009 + 0.007$ $-0.008 - 0.005$		1 BARATE	98Q	ALEP $e^+e^- \rightarrow Z$

¹ The systematic error includes the uncertainties due to the charm branching ratios.

$\Gamma(D^*(2010)^\pm D^\mp \text{ anything})/\Gamma_{\text{total}}$		Γ_{42}/Γ		
VALUE	CL%	DOCUMENT ID	TECN	COMMENT
$0.025 + 0.010 + 0.006$ $-0.009 - 0.005$		1 BARATE	98Q	ALEP $e^+e^- \rightarrow Z$

¹ The systematic error includes the uncertainties due to the charm branching ratios.

$\Gamma(D^*(2010)^\pm D^*(2010)^\mp \text{ anything})/\Gamma_{\text{total}}$		Γ_{43}/Γ		
VALUE	CL%	DOCUMENT ID	TECN	COMMENT
$0.012 + 0.004$ -0.003 ± 0.002		1 BARATE	98Q	ALEP $e^+e^- \rightarrow Z$

¹ The systematic error includes the uncertainties due to the charm branching ratios.

$\Gamma(\bar{D} D \text{ anything})/\Gamma_{\text{total}}$		Γ_{44}/Γ		
VALUE	CL%	DOCUMENT ID	TECN	COMMENT
$0.10 \pm 0.032 + 0.107$ -0.095		1 ABBIENDI	04I	OPAL $e^+e^- \rightarrow Z$

¹ Measurement performed using an inclusive identification of B mesons and the D candidates.

$\Gamma(D_s^*(2460)^0 \text{ anything})/\Gamma_{\text{total}}$		Γ_{45}/Γ		
VALUE	CL%	DOCUMENT ID	TECN	COMMENT
$0.047 \pm 0.024 \pm 0.013$		1 ACKERSTAFF	97W	OPAL $e^+e^- \rightarrow Z$

¹ ACKERSTAFF 97W assumes $B(D_s^*(2460) \rightarrow D^+ \pi^-) = 0.21 \pm 0.04$ and $\Gamma_{b\bar{b}}/\Gamma_{\text{hadrons}} = 0.216$ at Z decay.

$\Gamma(D_s^- \text{ anything})/\Gamma_{\text{total}}$		Γ_{46}/Γ		
VALUE	CL%	DOCUMENT ID	TECN	COMMENT
$0.147 \pm 0.017 \pm 0.013$		1 BUSKULIC	96Y	ALEP $e^+e^- \rightarrow Z$

¹ BUSKULIC 96Y reports $0.183 \pm 0.019 \pm 0.009$ from a measurement of $[\Gamma(\bar{D}^- \rightarrow D_s^- \text{ anything})/\Gamma_{\text{total}}] \times [B(D_s^+ \rightarrow \phi \pi^+)]$ assuming $B(D_s^+ \rightarrow \phi \pi^+) = 0.036$, which we rescale to our best value $B(D_s^+ \rightarrow \phi \pi^+) = (4.5 \pm 0.4) \times 10^{-2}$. Our first error is their experiment's error and our second error is the systematic error from using our best value.

$\Gamma(D_s^+ \text{ anything})/\Gamma_{\text{total}}$		Γ_{47}/Γ		
VALUE	CL%	DOCUMENT ID	TECN	COMMENT
$0.101 \pm 0.010 \pm 0.029$		1 ABDALLAH	03E	DLPH $e^+e^- \rightarrow Z$

¹ The second error is the total of systematic uncertainties including the branching fractions used in the measurement.

$\Gamma(b \rightarrow \Lambda_c^+ \text{ anything})/\Gamma_{\text{total}}$		Γ_{48}/Γ		
VALUE	CL%	DOCUMENT ID	TECN	COMMENT
$0.077 \pm 0.011 \pm 0.004$		1 BUSKULIC	96Y	ALEP $e^+e^- \rightarrow Z$

¹ BUSKULIC 96Y reports $0.110 \pm 0.014 \pm 0.006$ from a measurement of $[\Gamma(b \rightarrow \Lambda_c^+ \text{ anything})/\Gamma_{\text{total}}] \times [B(\Lambda_c^+ \rightarrow p K^- \pi^+)]$ assuming $B(\Lambda_c^+ \rightarrow p K^- \pi^+) = 0.044$, which we rescale to our best value $B(\Lambda_c^+ \rightarrow p K^- \pi^+) = (6.28 \pm 0.32) \times 10^{-2}$. Our first error is their experiment's error and our second error is the systematic error from using our best value.

$\Gamma(\tau/c \text{ anything})/\Gamma_{\text{total}}$		Γ_{49}/Γ		
VALUE	CL%	DOCUMENT ID	TECN	COMMENT
1.162 ± 0.032		OUR AVERAGE		

VALUE	CL%	DOCUMENT ID	TECN	COMMENT
1.12 ± 0.11 -0.10		1 ABBIENDI	04I	OPAL $e^+e^- \rightarrow Z$
$1.166 \pm 0.031 \pm 0.080$		2 ABREU	00	DLPH $e^+e^- \rightarrow Z$
1.147 ± 0.041		3 ABREU	98D	DLPH $e^+e^- \rightarrow Z$
$1.230 \pm 0.036 \pm 0.065$		4 BUSKULIC	96Y	ALEP $e^+e^- \rightarrow Z$

¹ Measurement performed using an inclusive identification of B mesons and the D candidates.

² Evaluated via summation of exclusive and inclusive channels.

³ ABREU 98D results are extracted from a fit to the b -tagging probability distribution based on the impact parameter.

⁴ BUSKULIC 96Y assumes PDG 96 production fractions for B^0, B^+, B_s, b baryons, and PDG 96 branching ratios for charm decays. This is sum of their inclusive $\bar{D}^0, D^-, \bar{D}_s, \Lambda_c$ branching ratios, corrected to include inclusive Ξ_c and charmonium.

$\Gamma(J/\psi(1S) \text{ anything})/\Gamma_{\text{total}}$		Γ_{50}/Γ			
VALUE (units 10^{-2})	CL%	EVTS	DOCUMENT ID	TECN	COMMENT
1.16 ± 0.10		OUR AVERAGE			

VALUE	CL%	DOCUMENT ID	TECN	COMMENT
$1.12 \pm 0.12 \pm 0.10$		1 ABREU	94P	DLPH $e^+e^- \rightarrow Z$
$1.16 \pm 0.16 \pm 0.14$		2 ADRIANI	93J	L3 $e^+e^- \rightarrow Z$
$1.21 \pm 0.13 \pm 0.08$	121	BUSKULIC	92G	ALEP $e^+e^- \rightarrow Z$

• • • We do not use the following data for averages, fits, limits, etc. • • •

VALUE	CL%	DOCUMENT ID	TECN	COMMENT
$1.3 \pm 0.2 \pm 0.2$		3 ADRIANI	92	L3 $e^+e^- \rightarrow Z$
<4.9	90	MATTEUZZI	83	MRK2 $E_{\text{cm}}^{\text{res}} = 29$ GeV

¹ ABREU 94P is an inclusive measurement from b decays at the Z . Uses $J/\psi(1S) \rightarrow e^+e^-$ and $\mu^+\mu^-$ channels. Assumes $\Gamma(Z \rightarrow b\bar{b})/\Gamma_{\text{hadron}} = 0.22$.

² ADRIANI 93J is an inclusive measurement from b decays at the Z . Uses $J/\psi(1S) \rightarrow \mu^+\mu^-$ and $J/\psi(1S) \rightarrow e^+e^-$ channels.

³ ADRIANI 92 measurement is an inclusive result for $B(Z \rightarrow J/\psi(1S) X) = (4.1 \pm 0.7 \pm 0.3) \times 10^{-3}$ which is used to extract the b -hadron contribution to $J/\psi(1S)$ production.

$\Gamma(\psi(2S) \text{ anything})/\Gamma_{\text{total}}$		Γ_{51}/Γ		
VALUE	CL%	DOCUMENT ID	TECN	COMMENT
$0.0048 \pm 0.0022 \pm 0.0010$		1 ABREU	94P	DLPH $e^+e^- \rightarrow Z$

¹ ABREU 94P is an inclusive measurement from b decays at the Z . Uses $\psi(2S) \rightarrow J/\psi(1S) \pi^+ \pi^-, J/\psi(1S) \rightarrow \mu^+ \mu^-$ channels. Assumes $\Gamma(Z \rightarrow b\bar{b})/\Gamma_{\text{hadron}} = 0.22$.

$\Gamma(\psi(2S) \text{ anything})/\Gamma(J/\psi(1S) \text{ anything})$		Γ_{51}/Γ_{50}		
VALUE	CL%	DOCUMENT ID	TECN	COMMENT
0.245 ± 0.013		OUR AVERAGE		

VALUE	CL%	DOCUMENT ID	TECN	COMMENT
$0.240 \pm 0.015 \pm 0.005$		1,2 AAIJ	12BD	LHCb pp at 7 TeV
$0.257 \pm 0.015 \pm 0.019$		3,4	CHATRCHYAN	12AK CMS pp at 7 TeV

¹ AAIJ 12BD reports $0.235 \pm 0.005 \pm 0.015$ from a measurement of $[\Gamma(\bar{D}^- \rightarrow \psi(2S) \text{ anything})/\Gamma(\bar{D}^- \rightarrow J/\psi(1S) \text{ anything})] \times [B(J/\psi(1S) \rightarrow \mu^+ \mu^-)] / [B(\psi(2S) \rightarrow e^+ e^-)]$ assuming $B(J/\psi(1S) \rightarrow \mu^+ \mu^-) = (5.93 \pm 0.06) \times 10^{-2}, B(\psi(2S) \rightarrow e^+ e^-) = (7.72 \pm 0.17) \times 10^{-3}$, which we rescale to our best values $B(J/\psi(1S) \rightarrow \mu^+ \mu^-) = (5.961 \pm 0.033) \times 10^{-2}, B(\psi(2S) \rightarrow e^+ e^-) = (7.93 \pm 0.17) \times 10^{-3}$. Our first error is their experiment's error and our second error is the systematic error from using our best values.

² Assumes lepton universality imposing $B(\psi(2S) \rightarrow \mu^+ \mu^-) = B(\psi(2S) \rightarrow e^+ e^-)$.

³ CHATRCHYAN 12AK really reports $\Gamma_{51}/\Gamma = (3.08 \pm 0.12 \pm 0.13 \pm 0.42) \times 10^{-3}$ assuming PDG 10 value of $\Gamma_{50}/\Gamma = (1.16 \pm 0.10) \times 10^{-2}$ which we present as a ratio of $\Gamma_{51}/\Gamma_{50} = (26.5 \pm 1.0 \pm 1.1 \pm 2.8) \times 10^{-2}$.

⁴ CHATRCHYAN 12AK reports $(26.5 \pm 1.0 \pm 1.1 \pm 2.8) \times 10^{-2}$ from a measurement of $[\Gamma(\bar{D}^- \rightarrow \psi(2S) \text{ anything})/\Gamma(\bar{D}^- \rightarrow J/\psi(1S) \text{ anything})] \times [B(\psi(2S) \rightarrow \mu^+ \mu^-)] / [B(J/\psi(1S) \rightarrow \mu^+ \mu^-)]$ assuming $B(\psi(2S) \rightarrow \mu^+ \mu^-) = (7.7 \pm 0.8) \times 10^{-3}, B(J/\psi(1S) \rightarrow \mu^+ \mu^-) = (5.93 \pm 0.06) \times 10^{-2}$, which we rescale to our best values $B(\psi(2S) \rightarrow \mu^+ \mu^-) = (8.0 \pm 0.6) \times 10^{-3}, B(J/\psi(1S) \rightarrow \mu^+ \mu^-) = (5.961 \pm 0.033) \times 10^{-2}$. Our first error is their experiment's error and our second error is the systematic error from using our best values.

$\Gamma(\chi_{c0}(1P) \text{ anything})/\Gamma(\eta_c(1S) \text{ anything})$		Γ_{52}/Γ_{56}		
VALUE	CL%	DOCUMENT ID	TECN	COMMENT
$0.33 \pm 0.06 \pm 0.05$		1 AAIJ	17Bb	LHCb pp at 7, 8 TeV

¹ AAIJ 17Bb reports $[\Gamma(\bar{D}^- \rightarrow \chi_{c0}(1P) \text{ anything})/\Gamma(\bar{D}^- \rightarrow \eta_c(1S) \text{ anything})] / [B(\eta_c(1S) \rightarrow \phi \phi)] \times [B(\chi_{c0}(1P) \rightarrow \phi \phi)] = 0.147 \pm 0.023 \pm 0.011$ which we multiply or divide by our best values $B(\eta_c(1S) \rightarrow \phi \phi) = (1.77 \pm 0.19) \times 10^{-3}, B(\chi_{c0}(1P) \rightarrow \phi \phi) = (8.0 \pm 0.7) \times 10^{-4}$. Our first error is their experiment's error and our second error is the systematic error from using our best values.

Meson Particle Listings

 $B^\pm/B^0/B_s^0/b$ -baryon ADMIXTURE $\Gamma(\text{charmless})/\Gamma_{\text{total}}$

VALUE	DOCUMENT ID	TECN	COMMENT	Γ_{74}/Γ
0.007 ± 0.021	1 ABREU	98D	DLPH $e^+e^- \rightarrow Z$	

¹ ABREU 98D results are extracted from a fit to the b -tagging probability distribution based on the impact parameter. The expected hidden charm contribution of 0.026 ± 0.004 has been subtracted.

 $\Gamma(\mu^+\mu^- \text{ anything})/\Gamma_{\text{total}}$

VALUE	CL%	DOCUMENT ID	TECN	COMMENT	Γ_{76}/Γ
<3.2 × 10⁻⁴	90	ABBOTT	98B	D0 $p\bar{p}$ 1.8 TeV	

• • • We do not use the following data for averages, fits, limits, etc. • • •

<5.0 × 10 ⁻⁵	90	1 ALBAJAR	91c	UA1 $E_{\text{cm}}^e = 630$ GeV	
<0.02	95	ALTHOFF	84G	TASS $E_{\text{cm}}^e = 34.5$ GeV	
<0.007	95	ADEVA	83	MRKJ $E_{\text{cm}}^e = 30\text{--}38$ GeV	
<0.007	95	BARTEL	83B	JADE $E_{\text{cm}}^e = 33\text{--}37$ GeV	

¹ Both ABBOTT 98B and GLENN 98 claim that the efficiency quoted in ALBAJAR 91c was overestimated by a large factor.

 $[\Gamma(e^+e^- \text{ anything}) + \Gamma(\mu^+\mu^- \text{ anything})]/\Gamma_{\text{total}}$

Test for $\Delta B = 1$ weak neutral current.

VALUE	CL%	DOCUMENT ID	TECN	COMMENT	$(\Gamma_{75} + \Gamma_{76})/\Gamma$
<0.008	90	MATTEUZZI	83	MRK2 $E_{\text{cm}}^e = 29$ GeV	

 $\Gamma(\nu \bar{\nu} \text{ anything})/\Gamma_{\text{total}}$

VALUE	DOCUMENT ID	TECN	COMMENT	Γ_{77}/Γ
<3.9 × 10 ⁻⁴	1 GROSSMAN	96	RVUE $e^+e^- \rightarrow Z$	

• • • We do not use the following data for averages, fits, limits, etc. • • •
¹ GROSSMAN 96 limit is derived from the ALEPH BUSKULIC 95 limit $B(B^+ \rightarrow \tau^+ \nu_\tau) < 1.8 \times 10^{-3}$ at CL=90% using conservative simplifying assumptions.

 χ_b AT HIGH ENERGY

For a discussion of $B\text{--}\bar{B}$ mixing, see the note on “ $B^0\text{--}\bar{B}^0$ Mixing” in the B^0 Particle Listings.

χ_b is the average $B\text{--}\bar{B}$ mixing parameter at high-energy $\chi_b = f_d' \chi_d + f_s' \chi_s$ where f_d' and f_s' are the fractions of B^0 and B_s^0 hadrons in an unbiased sample of semileptonic b -hadron decays.

“OUR EVALUATION” is an average using rescaled values of the data listed below. The average and rescaling were performed by the Heavy Flavor Averaging Group (HFLAV) and are described at <https://hflav.web.cern.ch/>. The averaging/rescaling procedure takes into account correlations between the measurements.

VALUE	EVTS	DOCUMENT ID	TECN	COMMENT
0.1284 ± 0.0069 OUR EVALUATION				
0.129 ± 0.004 OUR AVERAGE				
0.132 ± 0.001 ± 0.024		1 ABAZOV	06s	D0 $p\bar{p}$ at 1.96 TeV
0.152 ± 0.007 ± 0.011		2 ACOSTA	04A	CDF $p\bar{p}$ at 1.8 TeV
0.1312 ± 0.0049 ± 0.0042		3 ABBIENDI	03P	OPAL $e^+e^- \rightarrow Z$
0.127 ± 0.013 ± 0.006		4 ABREU	01L	DLPH $e^+e^- \rightarrow Z$
0.1192 ± 0.0068 ± 0.0051		5 ACCIARRI	99D	L3 $e^+e^- \rightarrow Z$
0.121 ± 0.016 ± 0.006		6 ABREU	94J	DLPH $e^+e^- \rightarrow Z$
0.114 ± 0.014 ± 0.008		7 BUSKULIC	94G	ALEP $e^+e^- \rightarrow Z$
0.129 ± 0.022		8 BUSKULIC	92B	ALEP $e^+e^- \rightarrow Z$
0.176 ± 0.031 ± 0.032	1112	9 ABE	91G	CDF $p\bar{p}$ 1.8 TeV
0.148 ± 0.029 ± 0.017		10 ALBAJAR	91D	UA1 $p\bar{p}$ 630 GeV
• • • We do not use the following data for averages, fits, limits, etc. • • •				
0.131 ± 0.020 ± 0.016		11 ABE	97I	CDF Repl. by ACOSTA 04A
0.1107 ± 0.0062 ± 0.0055		12 ALEXANDER	96	OPAL Rep. by ABBIENDI 03P
0.136 ± 0.037 ± 0.040		13 UENO	96	AMY e^+e^- at 57.9 GeV
0.144 ± 0.014 ± 0.017		14 ABREU	94F	DLPH Sup. by ABREU 94J
0.131 ± 0.014		15 ABREU	94J	DLPH $e^+e^- \rightarrow Z$
0.123 ± 0.012 ± 0.008		ACCIARRI	94D	L3 Repl. by ACCIARRI 99D
0.157 ± 0.020 ± 0.032		16 ALBAJAR	94	UA1 $\sqrt{s} = 630$ GeV
0.121 ± 0.044 ± 0.017	1665	17 ABREU	93C	DLPH Sup. by ABREU 94J
0.143 ± 0.022 ± 0.007		18 AKERS	93B	OPAL Sup. by ALEXANDER 96
0.145 ± 0.041 ± 0.018		19 ACTON	92C	OPAL $e^+e^- \rightarrow Z$
0.121 ± 0.017 ± 0.006		20 ADEVA	92C	L3 Sup. by ACCIARRI 94D
0.132 ± 0.22 ± 0.015	823	21 DECAMP	91	ALEP $e^+e^- \rightarrow Z$
0.178 ± 0.049 ± 0.020		22 ADEVA	90P	L3 $e^+e^- \rightarrow Z$
0.17 ± 0.15 ± 0.08		23,24 WEIR	90	MRK2 e^+e^- 29 GeV
0.21 ± 0.29 ± 0.15		23 BAND	88	MAC $E_{\text{cm}}^e = 29$ GeV
>0.02 at 90% CL		23 BAND	88	MAC $E_{\text{cm}}^e = 29$ GeV
0.121 ± 0.047		23,25 ALBAJAR	87C	UA1 Repl. by ALBAJAR 91D
<0.12 at 90% CL		23,26 SCHAAD	85	MRK2 $E_{\text{cm}}^e = 29$ GeV

¹ Uses the dimuon charge asymmetry. Averaged over the mix of b -flavored hadrons.

² Measurement performed using events containing a dimuon or an e/μ pair.

³ The average B mixing parameter is determined simultaneously with b and c forward-backward asymmetries in the fit.

⁴ The experimental systematic and model uncertainties are combined in quadrature.

⁵ ACCIARRI 99D uses maximum-likelihood fits to extract χ_b as well as the A_{FB}^b in $Z \rightarrow b\bar{b}$ events containing prompt leptons.

⁶ This ABREU 94J result is from 5182 $\ell\ell$ and 279 $\ell\ell$ events. The systematic error includes 0.004 for model dependence.

⁷ BUSKULIC 94G data analyzed using ee , $e\mu$, and $\mu\mu$ events.

⁸ BUSKULIC 92B uses a jet charge technique combined with electrons and muons.

⁹ ABE 91G measurement of χ is done with $e\mu$ and ee events.

¹⁰ ALBAJAR 91D measurement of χ is done with dimuons.

¹¹ Uses di-muon events.

¹² ALEXANDER 96 uses a maximum likelihood fit to simultaneously extract χ as well as the forward-backward asymmetries in $e^+e^- \rightarrow Z \rightarrow b\bar{b}$ and $c\bar{c}$.

¹³ UENO 96 extracted χ from the energy dependence of the forward-backward asymmetry.

¹⁴ ABREU 94F uses the average electric charge sum of the jets recoiling against a b -quark jet tagged by a high p_T muon. The result is for $\bar{\chi} = f_d \chi_d + 0.9 f_s \chi_s$.

¹⁵ This ABREU 94J result combines $\ell\ell$, $\ell\ell$, and jet-charge ℓ (ABREU 94F) analyses. It is for $\bar{\chi} = f_d \chi_d + 0.96 f_s \chi_s$.

¹⁶ ALBAJAR 94 uses dimuon events. Not independent of ALBAJAR 91D.

¹⁷ ABREU 93C data analyzed using ee , $e\mu$, and $\mu\mu$ events.

¹⁸ AKERS 93B analysis performed using dilepton events.

¹⁹ ACTON 92C uses electrons and muons. Superseded by AKERS 93B.

²⁰ ADEVA 92C uses electrons and muons.

²¹ DECAMP 91 done with opposite and like-sign dileptons. Superseded by BUSKULIC 92B.

²² ADEVA 90P measurement uses ee , $\mu\mu$, and $e\mu$ events from 118k events at the Z. Superseded by ADEVA 92C.

²³ These experiments are not in the average because the combination of B_s and B_d mesons which they see could differ from those at higher energy.

²⁴ The WEIR 90 measurement supersedes the limit obtained in SCHAAD 85. The 90% CL are 0.06 and 0.38.

²⁵ ALBAJAR 87C measured $\chi = (\bar{B}^0 \rightarrow B^0 \rightarrow \mu^+ X)$ divided by the average production weighted semileptonic branching fraction for B hadrons at 546 and 630 GeV.

²⁶ Limit is average probability for hadron containing B quark to produce a positive lepton.

CP VIOLATION PARAMETERS in semileptonic b -hadron decays. $\text{Re}(\epsilon_b) / (1 + |\epsilon_b|^2)$

CP impurity in semileptonic b -hadron decays.

VALUE (units 10 ⁻³)	DOCUMENT ID	TECN	COMMENT
• • • We do not use the following data for averages, fits, limits, etc. • • •			
-6.2 ± 5.2 ± 4.7	1 AABOUD	17E	ATLS $p\bar{p}$ at 8 TeV
-1.24 ± 0.38 ± 0.18	2 ABAZOV	14	D0 $p\bar{p}$ at 1.96 TeV
-1.97 ± 0.43 ± 0.23	3 ABAZOV	11U	D0 Repl. by ABAZOV 14
-2.39 ± 0.63 ± 0.37	4 ABAZOV	10H	D0 Repl. by ABAZOV 11U

¹ AABOUD 17E reports a measurement of charge asymmetry of $A_{SL}^b = (-25 \pm 21 \pm 19) \times 10^{-3}$ in lepton + jets $t\bar{t}$ events in which a b -hadron decays semileptonically to a soft muon.

² ABAZOV 14 reports a measurement of like-sign dimuon charge asymmetry of $A_{SL}^b = (-4.96 \pm 1.53 \pm 0.72) \times 10^{-3}$ in semileptonic b -hadron decays.

³ ABAZOV 11U reports a measurement of like-sign dimuon charge asymmetry of $A_{SL}^b = (-7.87 \pm 1.72 \pm 0.93) \times 10^{-3}$ in semileptonic b -hadron decays.

⁴ ABAZOV 10H reports a measurement of like-sign dimuon charge asymmetry of $A_{SL}^b = (-9.57 \pm 2.51 \pm 1.46) \times 10^{-3}$ in semileptonic b -hadron decays. Using the measured production ratio of B_d^0 and B_s^0 , and the asymmetry of $B_d^0, A_{SL}^d = (-4.7 \pm 4.6) \times 10^{-3}$ measured from B -factories, they obtain the asymmetry for B_s^0 as $A_{SL}^s = (-14.6 \pm 7.5) \times 10^{-3}$.

B-HADRON PRODUCTION FRACTIONS IN $p\bar{p}$ COLLISIONS AT Tevatron

The production fractions for b -hadrons in $p\bar{p}$ collisions at the Tevatron have been calculated from the best values of mean lifetimes, mixing parameters, and branching fractions in this edition by the Heavy Flavor Averaging Group (HFLAV) (see <https://hflav.web.cern.ch/>).

The values reported below assume:

$$f(\bar{b} \rightarrow B^+) = f(\bar{b} \rightarrow B^0) \\ f(\bar{b} \rightarrow B^+) + f(\bar{b} \rightarrow B^0) + f(\bar{b} \rightarrow B_s^0) + f(b \rightarrow b\text{-baryon}) = 1$$

The values are:

$$f(\bar{b} \rightarrow B^+) = f(\bar{b} \rightarrow B^0) = 0.344 \pm 0.021$$

$$f(\bar{b} \rightarrow B_s^0) = 0.115 \pm 0.013$$

$$f(b \rightarrow b\text{-baryon}) = 0.198 \pm 0.046$$

$$f(\bar{b} \rightarrow B_s^0) / f(\bar{b} \rightarrow B^0) = 0.334 \pm 0.041$$

and their correlation coefficients are:

$$\text{cor}(B_s^0, b\text{-baryon}) = -0.429$$

$$\text{cor}(B_s^0, B^+ = B^0) = +0.159$$

$$\text{cor}(b\text{-baryon}, B^+ = B^0) = -0.960$$

as obtained with the Tevatron average of time-integrated mixing parameter

$$\bar{\chi} = 0.147 \pm 0.011.$$

See key on page 999

Meson Particle Listings

B±/B0/Bs0/b-baryon ADMIXTURE, Vcb and Vub CKM Matrix Elements

PRODUCTION ASYMMETRIES

AbC

AbC = [N(Dy > 0) - N(Dy < 0)] / [N(Dy > 0) + N(Dy < 0)] with Dy = |yb| - |yb| where yb/B is rapidity of b or B quarks.

Table with columns: VALUE (units 10^-2), DOCUMENT ID, TECN, COMMENT. Contains data for various experiments like AAIJ, LHCb, etc.

B±/B0/Bs0/b-baryon ADMIXTURE REFERENCES

Large table listing references for B±/B0/Bs0/b-baryon admixture, including columns for author, document ID, and comment.

Table listing references for Vcb and Vub CKM matrix elements, including columns for author, document ID, and comment.

Vcb and Vub CKM Matrix Elements

OMITTED FROM SUMMARY TABLE

See the related review(s): Semileptonic B Hadron Decays, Determination of Vcb and Vub

Vcb MEASUREMENTS

For the discussion of Vcb measurements, which is not repeated here, see the review on "Determination of |Vcb| and |Vub|." The CKM matrix element |Vcb| can be determined by studying the rate of the semileptonic decay B -> D(*) l nu as a function of the recoil kinematics of D(*) mesons.

"OUR EVALUATION" is an average using rescaled values of the data listed below. The average and rescaling were performed by the Heavy Flavor Averaging Group (HFLAV) and are described at https://hflav.web.cern.ch/.

|Vcb| x F(1) (from B0 -> D*- l+ nu)

Table listing Vcb measurements with columns: VALUE, DOCUMENT ID, TECN, COMMENT. Includes entries like 0.03561 +/- 0.00043 OUR EVALUATION and 0.0355 +/- 0.0008 OUR AVERAGE.

Downloaded from https://academic.oup.com/ptep/article/2020/8/083C01/5891211 by guest on 20 August 2020

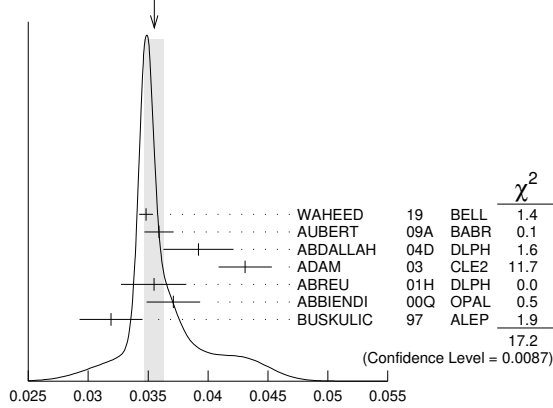
Meson Particle Listings

V_{cb} and V_{ub} CKM Matrix Elements, B^*

0.0431 ± 0.0013 ± 0.0018	14 BRIERE	02 CLE2	$e^+e^- \rightarrow \Upsilon(4S)$
0.0328 ± 0.0019 ± 0.0022	ACKERSTAFF	97G OPAL	Repl. by ABBIENDI 00Q
0.0350 ± 0.0019 ± 0.0023	15 ABREU	96P DLPH	Repl. by ABREU 01H
0.0351 ± 0.0019 ± 0.0020	16 BARISH	95 CLE2	Repl. by ADAM 03
0.0314 ± 0.0023 ± 0.0025	BUSKULIC	95N ALEP	Repl. by BUSKULIC 97

- Uses fully reconstructed $D^{*+} \ell^+ \nu$ events ($\ell = e$ or μ) and $\eta_{EW} = 1.0066$.
- Obtained from a global fit to $B \rightarrow D^{(*)} \ell \nu \ell$ events, with reconstructed $D^0 \ell$ and $D^+ \ell$ final states and $\rho^2 = 1.22 \pm 0.02 \pm 0.07$.
- Measurement using fully reconstructed D^* sample with a $\rho^2 = 1.32 \pm 0.15 \pm 0.33$.
- Average of the $B^0 \rightarrow D^{*}(2010)^- \ell^+ \nu$ and $B^+ \rightarrow \bar{D}^{*}(2007)^+ \ell^+ \nu$ modes with $\rho^2 = 1.61 \pm 0.09 \pm 0.21$ and $f_{+,-} = 0.521 \pm 0.012$.
- ABREU 01H measured using about 5000 partial reconstructed D^* sample with a $\rho^2 = 1.34 \pm 0.14^{+0.24}_{-0.22}$.
- ABBIENDI 00Q: measured using both inclusively and exclusively reconstructed $D^{*\pm}$ samples with a $\rho^2 = 1.21 \pm 0.12 \pm 0.20$. The statistical and systematic correlations between $|V_{cb}| \times F(1)$ and ρ^2 are 0.90 and 0.54 respectively.
- BUSKULIC 97: measured using exclusively reconstructed $D^{*\pm}$ with a $a^2 = 0.31 \pm 0.17 \pm 0.08$. The statistical correlation is 0.92.
- Uses fully reconstructed $D^{*+} \ell^+ \nu$ events ($\ell = e$ or μ).
- Measured using the dependence of $B^- \rightarrow D^{*0} e^- \bar{\nu}_e$ decay differential rate and the form factor description by CAPRINI 98 with $\rho^2 = 1.16 \pm 0.06 \pm 0.08$.
- Measured using fully reconstructed D^* sample and a simultaneous fit to the Caprini-Lellouch-Neubert form factor parameters: $\rho^2 = 1.191 \pm 0.048 \pm 0.028$, $R_1(1) = 1.429 \pm 0.061 \pm 0.044$, and $R_2(1) = 0.827 \pm 0.038 \pm 0.022$.
- Measurement using fully reconstructed D^* sample with a $\rho^2 = 1.29 \pm 0.03 \pm 0.27$.
- Combines with previous partial reconstructed D^* measurement with a $\rho^2 = 1.39 \pm 0.10 \pm 0.33$.
- Measured using exclusive $B^0 \rightarrow D^{*}(892)^- e^+ \nu$ decays with $\rho^2 = 1.35 \pm 0.17 \pm 0.19$ and a correlation of 0.91.
- BRIERE 02 result is based on the same analysis and data sample reported in ADAM 03.
- ABREU 96P: measured using both inclusively and exclusively reconstructed $D^{*\pm}$ samples.
- BARISH 95: measured using both exclusive reconstructed $B^0 \rightarrow D^{*-} \ell^+ \nu$ and $B^+ \rightarrow D^{*0} \ell^+ \nu$ samples. They report their experiment's uncertainties $\pm 0.0019 \pm 0.0018 \pm 0.0008$, where the first error is statistical, the second is systematic, and the third is the uncertainty in the lifetimes. We combine the last two in quadrature.

WEIGHTED AVERAGE
0.0355 ± 0.0008 (Error scaled by 1.7)



$|V_{cb}| \times G(1)$ (from $B \rightarrow D^* \ell^+ \nu$)

VALUE	DOCUMENT ID	TECN	COMMENT
0.04157 ± 0.00100 OUR EVALUATION	with $\rho^2 = 1.128 \pm 0.033$ and a correlation of 0.751. The fitted χ^2 is 4.7 for 8 degrees of freedom.		
0.0422 ± 0.0010 OUR AVERAGE			
0.04229 ± 0.00137	1 GLATTAUER	16 BELL	$e^+e^- \rightarrow \Upsilon(4S)$
0.0423 ± 0.0019 ± 0.0014	2 AUBERT	10 BABR	$e^+e^- \rightarrow \Upsilon(4S)$
0.0431 ± 0.0008 ± 0.0023	3 AUBERT	09A BABR	$e^+e^- \rightarrow \Upsilon(4S)$
0.0416 ± 0.0047 ± 0.0037	4 BARTELT	99 CLE2	$e^+e^- \rightarrow \Upsilon(4S)$
0.0278 ± 0.0068 ± 0.0065	5 BUSKULIC	97 ALEP	$e^+e^- \rightarrow Z$
••• We do not use the following data for averages, fits, limits, etc. •••			
0.0411 ± 0.0044 ± 0.0052	6 ABE	02E BELL	Repl. by GLATTAUER 16
0.0337 ± 0.0044 ± 0.0072 ± 0.0049	7 ATHANAS	97 CLE2	Repl. by BARTELT 99

- Obtained from a fit to the combined partially reconstructed $B \rightarrow \bar{D} \ell \nu \ell$ sample while tagged by the other fully reconstructed B meson in the event. Also reports fitted $\rho^2 = 1.09 \pm 0.05$.
- Obtained from a fit to the combined $B \rightarrow \bar{D} \ell^+ \nu \ell$ sample in which a hadronic decay of the second B meson is fully reconstructed and $\rho^2 = 1.20 \pm 0.09 \pm 0.04$.
- Obtained from a global fit to $B \rightarrow D^{(*)} \ell \nu \ell$ events, with reconstructed $D^0 \ell$ and $D^+ \ell$ final states and $\rho^2 = 1.20 \pm 0.04 \pm 0.07$.
- BARTELT 99: measured using both exclusive reconstructed $B^0 \rightarrow D^- \ell^+ \nu$ and $B^+ \rightarrow D^0 \ell^+ \nu$ samples.
- BUSKULIC 97: measured using exclusively reconstructed D^\pm with a $a^2 = -0.05 \pm 0.53 \pm 0.38$. The statistical correlation is 0.99.

- Using the missing energy and momentum to extract kinematic information about the undetected neutrino in the $B^0 \rightarrow D^- \ell^+ \nu$ decay.
- ATHANAS 97: measured using both exclusive reconstructed $B^0 \rightarrow D^- \ell^+ \nu$ and $B^+ \rightarrow D^0 \ell^+ \nu$ samples with a $\rho^2 = 0.59 \pm 0.22 \pm 0.12^{+0.59}_{-0}$. They report their experiment's uncertainties $\pm 0.0044 \pm 0.0048^{+0.0053}_{-0.0012}$, where the first error is statistical, the second is systematic, and the third is the uncertainty due to the form factor model variations. We combine the last two in quadrature.

V_{ub} MEASUREMENTS

For the discussion of V_{ub} measurements, which is not repeated here, see the review on "Determination of $|V_{cb}|$ and $|V_{ub}|$."

The CKM matrix element $|V_{ub}|$ can be determined by studying the rate of the charmless semileptonic decay $b \rightarrow u \ell \nu$. The relevant branching ratio measurements based on exclusive and inclusive decays can be found in the B Listings, and are not repeated here.

V_{cb} and V_{ub} CKM Matrix Elements REFERENCES

WAHEED	19	PR D100 052007	E. Waheed <i>et al.</i>	(BELLE Collab.)
GLATTAUER	16	PR D93 032006	R. Glattauer <i>et al.</i>	(BELLE Collab.)
AUBERT	10	PRL 104 011802	B. Aubert <i>et al.</i>	(BABAR Collab.)
DUNDEL	10	PR D82 112007	W. Dungenl <i>et al.</i>	(BELLE Collab.)
AUBERT	09A	PR D79 012002	B. Aubert <i>et al.</i>	(BABAR Collab.)
AUBERT	08AT	PRL 100 231803	B. Aubert <i>et al.</i>	(BABAR Collab.)
AUBERT	08R	PR D77 032002	B. Aubert <i>et al.</i>	(BABAR Collab.)
AUBERT	05E	PR D71 051502	B. Aubert <i>et al.</i>	(BABAR Collab.)
ABDALLAH	04D	EPJ C33 213	J. Abdallah <i>et al.</i>	(DELPHI Collab.)
ADAM	03	PR D67 032001	N.E. Adam <i>et al.</i>	(CLEO Collab.)
ABE	02E	PL B526 258	K. Abe <i>et al.</i>	(BELLE Collab.)
ABE	02F	PL B526 247	K. Abe <i>et al.</i>	(BELLE Collab.)
BRIERE	02	PRL 89 081803	R. Briere <i>et al.</i>	(CLEO Collab.)
ABREU	01H	PL B510 55	P. Abreu <i>et al.</i>	(DELPHI Collab.)
ABBIENDI	00Q	PL B482 15	G. Abbiendi <i>et al.</i>	(OPAL Collab.)
BARTELT	99	PRL 82 3746	J. Bartelt <i>et al.</i>	(CLEO Collab.)
CAPRINI	98	NP B530 153	I. Caprini, L. Lellouch, M. Neubert	(BCIP, CERN)
ACKERSTAFF	97G	PL B395 128	K. Ackerstaff <i>et al.</i>	(OPAL Collab.)
ATHANAS	97	PRL 79 2208	M. Athanas <i>et al.</i>	(CLEO Collab.)
BUSKULIC	97	PL B395 373	D. Buskulic <i>et al.</i>	(ALEPH Collab.)
ABREU	96P	ZPHY C71 539	P. Abreu <i>et al.</i>	(DELPHI Collab.)
BARISH	95	PR D51 1014	B.C. Barish <i>et al.</i>	(CLEO Collab.)
BUSKULIC	95N	PL B359 236	D. Buskulic <i>et al.</i>	(ALEPH Collab.)

B^*

$$I(J^P) = \frac{1}{2}(1^-)$$

I, J, P need confirmation.

Quantum numbers shown are quark-model predictions.

B^* MASS

From mass difference below and the average of our B masses ($m_{B^\pm} + m_{B^0}$)/2.

VALUE (MeV)	DOCUMENT ID
5324.70 ± 0.21 OUR FIT	

$m_{B^*} - m_B$

VALUE (MeV)	EVTS	DOCUMENT ID	TECN	COMMENT
45.21 ± 0.21 OUR FIT				
45.42 ± 0.26 OUR AVERAGE				Includes data from the datablock that follows this one.
46.2 ± 0.3 ± 0.8		1 ACKERSTAFF 97M	OPAL	$e^+e^- \rightarrow Z$
45.3 ± 0.35 ± 0.87	4227	1 BUSKULIC 96D	ALEP	$E_{cm}^{ee} = 88-94$ GeV
45.5 ± 0.3 ± 0.8		1 ABREU 95R	DLPH	$E_{cm}^{ee} = 88-94$ GeV
46.3 ± 1.9	1378	1 ACCIARRI 95B	L3	$E_{cm}^{ee} = 88-94$ GeV
46.4 ± 0.3 ± 0.8		2 AKERIB 91	CLE2	$e^+e^- \rightarrow \gamma X$
45.6 ± 0.8		2 WU 91	CSB2	$e^+e^- \rightarrow \gamma X, \gamma \ell X$
45.4 ± 1.0		3 LEE-FRANZINI 90	CSB2	$e^+e^- \rightarrow \Upsilon(5S)$
52 ± 2 ± 4	1400	4 HAN 85	CUSB	$e^+e^- \rightarrow \gamma e X$

- u, d, s flavor averaged.
- These papers report E_γ in the B^* center of mass. The $m_{B^*} - m_B$ is 0.2 MeV higher. $E_{cm} = 10.61-10.7$ GeV. Admixture of B^0 and B^+ mesons, but not B_s .
- LEE-FRANZINI 90 value is for an admixture of B^0 and B^+ . They measure $46.7 \pm 0.4 \pm 0.2$ MeV for an admixture of B^0, B^+ , and B_s , and use the shape of the photon line to separate the above value.
- HAN 85 is for $E_{cm} = 10.6-11.2$ GeV, giving an admixture of B^0, B^+ , and B_s .

$m_{B^{*+}} - m_{B^+}$

VALUE (MeV)	DOCUMENT ID	TECN	COMMENT
The data in this block is included in the average printed for a previous datablock.			

VALUE (MeV)	CL%	DOCUMENT ID	TECN	COMMENT
45.37 ± 0.21 OUR FIT				
45.01 ± 0.30 ± 0.23		5 AAIJ 130	LHCb	pp at 7 TeV

- Obtained the mass difference between $B^{*+} K^-$ and $B^+ K^-$ from $B_{s2}^*(5840)^0$ decay.

$|(m_{B^{*+}} - m_{B^+}) - (m_{B^0} - m_{B^+})|$

VALUE (MeV)	CL%	DOCUMENT ID	TECN	COMMENT
<6	95	ABREU 95R	DLPH	$E_{cm}^{ee} = 88-94$ GeV

See key on page 999

Meson Particle Listings

$B^*, B_1(5721)^+, B_1(5721)^0, B_J^*(5732)$

B^* DECAY MODES

Mode	Fraction (Γ_i/Γ)
$\Gamma_1 B \gamma$	seen

B^* REFERENCES

AAIJ	13O	PRL 110 151803	R. Aaij <i>et al.</i>	(LHCb Collab.)
ACKERSTAFF	97M	ZPHY C74 413	K. Ackerstaff <i>et al.</i>	(OPAL Collab.)
BUSKULIC	96D	ZPHY C69 393	D. Buskulic <i>et al.</i>	(ALEPH Collab.)
ABREU	95R	ZPHY C68 353	P. Abreu <i>et al.</i>	(DELPHI Collab.)
ACCIARRI	95B	PL B345 589	M. Acciari <i>et al.</i>	(L3 Collab.)
AKERIB	91	PRL 67 1692	D.S. Akerib <i>et al.</i>	(CLEO Collab.)
WU	91	PL B273 177	Q.W. Wu <i>et al.</i>	(CUSB II Collab.)
LEE-FRANZINI	90	PRL 65 2947	J. Lee-Franzini <i>et al.</i>	(CUSB II Collab.)
HAN	85	PRL 55 36	K. Han <i>et al.</i>	(COLU, LSU, MPIM, STON)

$B_1(5721)^+$

$I(J^P) = \frac{1}{2}(1^+)$
 I, J, P need confirmation.

Quantum numbers shown are quark-model predictions.

$B_1(5721)^+$ MASS

OUR FIT uses m_{B^*0} and $m_{B^+} - m_{B^*0}$ to determine $m_{B_1(5721)^+}$.

VALUE (MeV)	DOCUMENT ID
5725.9 ± 2.5 ± 2.7 OUR FIT	

$m_{B^+} - m_{B^*0}$

VALUE (MeV)	EVTS	DOCUMENT ID	TECN	COMMENT
401.2 ± 2.4 ± 2.7 OUR FIT				
401.2 ± 2.4 ± 2.7 OUR AVERAGE				
400.5 ± 1.8 ± 3.1	8K	¹ AAIJ	15AB LHCB	$p\bar{p}$ at 7, 8 TeV
402 ± 3 ± 1		² AALTONEN	14i CDF	$p\bar{p}$ at 1.96 TeV

¹AAIJ 15AB reports $[m_{B^+} - m_{B^*0}] - (m_{B^*0} - m_{B^0}) - m_{\pi^+} = 260.9 \pm 1.8 \pm 3.1$ MeV which we adjust by the π^+ mass and assume $(m_{B^*0} - m_{B^0}) = (m_{B^{*+}} - m_{B^+}) = 45.01 \pm 0.30 \pm 0.23$ MeV. The masses inside the square brackets were measured for each candidate event.
²AALTONEN 14i reports $m_{B_1(5721)^+} - m_{B^*0} - m_{\pi^+} = 262 \pm 3^{+1}_{-3}$ MeV which we adjusted by the π^+ mass.

$B_1(5721)^+$ WIDTH

VALUE (MeV)	EVTS	DOCUMENT ID	TECN	COMMENT
31 ± 6 OUR AVERAGE				Error includes scale factor of 1.1.
29.1 ± 3.6 ± 4.3	8K	AAIJ	15AB LHCB	$p\bar{p}$ at 7, 8 TeV
49 ± 12 ± 13		AALTONEN	14i CDF	$p\bar{p}$ at 1.96 TeV

$B_1(5721)^+$ DECAY MODES

Mode	Fraction (Γ_i/Γ)
$\Gamma_1 B^*0 \pi^+$	seen

$B_1(5721)^+$ BRANCHING RATIOS

$\Gamma(B^*0 \pi^+)/\Gamma_{total}$	EVTS	DOCUMENT ID	TECN	COMMENT	Γ_1/Γ
seen	8K	AAIJ	15AB LHCB	$p\bar{p}$ at 7, 8 TeV	
seen		AALTONEN	14i CDF	$p\bar{p}$ at 1.96 TeV	

$B_1(5721)^+$ REFERENCES

AAIJ	15AB	JHEP 1504 024	R. Aaij <i>et al.</i>	(LHCb Collab.)
AALTONEN	14i	PR D90 012013	T. Aaltonen <i>et al.</i>	(CDF Collab.)

$B_1(5721)^0$

$I(J^P) = \frac{1}{2}(1^+)$
 I, J, P need confirmation.

Quantum numbers shown are quark-model predictions.

$B_1(5721)^0$ MASS

OUR FIT uses mass differences measurements listed below to determine the mass $m_{B_1(5721)^0}$.

VALUE (MeV)	DOCUMENT ID
5726.1 ± 1.3 OUR FIT	Error includes scale factor of 1.2.

$m_{B_1^0} - m_{B^+}$

VALUE (MeV)	DOCUMENT ID	TECN	COMMENT
446.7 ± 1.3 OUR FIT	Error includes scale factor of 1.2.		
441.5 ± 2.4 ± 1.3	¹ ABAZOV	07T D0	$p\bar{p}$ at 1.96 TeV
• • • We do not use the following data for averages, fits, limits, etc. • • •			
446.2 ± 1.9 ± 1.0	¹ AALTONEN	09D CDF	Repl. by AALTONEN 14i
-2.1 ± 1.2			
¹ Observed in $B_1^0 \rightarrow B^* + \pi^-$.			

$m_{B_1^0} - m_{B^{*+}}$

VALUE (MeV)	EVTS	DOCUMENT ID	TECN	COMMENT
401.4 ± 1.2 OUR FIT				Error includes scale factor of 1.2.
402.8 ± 1.1 OUR AVERAGE				
403.4 ± 0.7 ± 1.5	35K	¹ AAIJ	15AB LHCB	$p\bar{p}$ at 7, 8 TeV
402.3 ± 0.9 ± 1.1		² AALTONEN	14i CDF	$p\bar{p}$ at 1.96 TeV
-1.2				
¹ AAIJ 15AB reports $[m_{B_1^0} - m_{B^+}] - (m_{B^{*+}} - m_{B^+}) - m_{\pi^-} = 263.9 \pm 0.7 \pm 1.4$ MeV which we adjust by the π^- mass and $(m_{B^{*+}} - m_{B^+}) = 45.01 \pm 0.30 \pm 0.23$ MeV. The masses inside the square brackets were measured for each candidate event. ² AALTONEN 14i reports $m_{B_1(5721)^0} - m_{B^{*+}} - m_{\pi^-} = 262.7 \pm 0.9^{+1.1}_{-1.2}$ MeV which we adjusted by the π^- mass.				

$B_1(5721)^0$ WIDTH

VALUE (MeV)	EVTS	DOCUMENT ID	TECN	COMMENT
27.5 ± 3.4 OUR AVERAGE				Error includes scale factor of 1.1.
30.1 ± 1.5 ± 3.5	35k	AAIJ	15AB LHCB	$p\bar{p}$ at 7, 8 TeV
23 ± 3 ± 4		AALTONEN	14i CDF	$p\bar{p}$ at 1.96 TeV

$B_1(5721)^0$ DECAY MODES

Mode	Fraction (Γ_i/Γ)
$\Gamma_1 B^{*+} \pi^-$	seen

$B_1(5721)^0$ BRANCHING RATIOS

$\Gamma(B^{*+} \pi^-)/\Gamma_{total}$	EVTS	DOCUMENT ID	TECN	COMMENT	Γ_1/Γ
seen	35K	AAIJ	15AB LHCB	$p\bar{p}$ at 7, 8 TeV	
seen		AALTONEN	09D CDF	$p\bar{p}$ at 1.96 TeV	
seen		¹ ABAZOV	07T D0	$p\bar{p}$ at 1.96 TeV	
¹ Observed in $B_1^0 \rightarrow B^* + \pi^-$ with $B^* \rightarrow B^+ \gamma$ and $B^+ \rightarrow J/\psi \pi^+$.					

$B_1(5721)^0$ REFERENCES

AAIJ	15AB	JHEP 1504 024	R. Aaij <i>et al.</i>	(LHCb Collab.)
AALTONEN	14i	PR D90 012013	T. Aaltonen <i>et al.</i>	(CDF Collab.)
AALTONEN	09D	PRL 102 102003	T. Aaltonen <i>et al.</i>	(CDF Collab.)
ABAZOV	07T	PRL 99 172001	V.M. Abazov <i>et al.</i>	(D0 Collab.)

$B_J^*(5732)$

$I(J^P) = ?(?^?)$
 I, J, P need confirmation.

OMITTED FROM SUMMARY TABLE
 also known as B^{**}

Quantum numbers shown are quark-model predictions. Signal can be interpreted as stemming from several narrow and broad resonances.

$B_J^*(5732)$ MASS

VALUE (MeV)	EVTS	DOCUMENT ID	TECN	COMMENT
5698 ± 8 OUR AVERAGE				Error includes scale factor of 1.2.
5710 ± 20		¹ AFFOLDER	01F CDF	$p\bar{p}$ at 1.8 TeV
5695 ± 17		² BARATE	98L ALEP	$e^+ e^- \rightarrow Z$
-19				
5704 ± 4 ± 10	1944	³ BUSKULIC	96D ALEP	$E_{cm}^{e^+e^-} = 88-94$ GeV
5732 ± 5 ± 20	2157	ABREU	95B DLPH	$E_{cm}^{e^+e^-} = 88-94$ GeV
5681 ± 11	1738	AKERS	95E OPAL	$E_{cm}^{e^+e^-} = 88-94$ GeV

Meson Particle Listings

$B_J^*(5732), B_2^*(5747)^+, B_2^*(5747)^0$

- • • We do not use the following data for averages, fits, limits, etc. • • •
- 5713 ± 2 ⁴ ACCIARRI 99N L3 $e^+e^- \rightarrow Z$
- ¹ AFFOLDER 01F uses the reconstructed B meson through semileptonic decay channels. The fraction of light B mesons that are produced at $L=1$ B^{**} states is measured to be $0.28 \pm 0.06 \pm 0.03$.
- ² BARATE 98L uses fully reconstructed B mesons to search for B^{**} production in the $B\pi^\pm$ system. In the framework of heavy quark symmetry (HQs), they also measured the mass of B_2^* to be 5739^{+8+6}_{-11-4} MeV/ c^2 and the relative production rate of $B(b \rightarrow B_2^* \rightarrow B^*(*)\pi)/B(b \rightarrow B_{u,d}) = (31 \pm 9^{+6}_{-5})\%$.
- ³ Using $m_{B\pi} - m_B = 424 \pm 4 \pm 10$ MeV.
- ⁴ ACCIARRI 99N uses inclusive reconstructed B mesons to search for B^{**} production in the $B^*(*)\pi^\pm$ system. In the framework of HQET, they measured the mass of B_1^* and B_2^* to be $5670 \pm 10 \pm 13$ MeV and $5768 \pm 5 \pm 6$ with the $B(b \rightarrow B^{**}) = (32 \pm 3 \pm 6) \times 10^{-2}$. They also reported the evidence for the existence of an excited B -meson state or mixture of states in the region 5.9–6.0 GeV.

$B_J^*(5732)$ WIDTH

VALUE (MeV)	EVTS	DOCUMENT ID	TECN	COMMENT
128 ± 16 OUR AVERAGE				
145 ± 28	2157	ABREU	95B DLPH	$E_{cm}^{ec} = 88-94$ GeV
116 ± 24	1738	AKERS	95E OPAL	$E_{cm}^{ec} = 88-94$ GeV

$B_J^*(5732)$ DECAY MODES

Mode	Fraction (Γ_i/Γ)
Γ_1 $B^*\pi + B\pi$	seen
Γ_2 $B^*\pi(X)$	[a] (85 ± 29) %

[a] X refers to decay modes with or without additional accompanying decay particles.

$B_J^*(5732)$ BRANCHING RATIOS

X refers to decay modes with or without additional accompanying decay particles.

$\Gamma(B^*\pi(X))/\Gamma_{total}$	DOCUMENT ID	TECN	COMMENT	Γ_2/Γ
0.85 \pm 0.26 \pm 0.12	ABBIENDI	02E OPAL	$e^+e^- \rightarrow Z$	

$B_J^*(5732)$ REFERENCES

ABBIENDI 02E EPJ C23 437	G. Abbiendi et al.	(OPAL Collab.)
AFFOLDER 01F PR D64 072002	T. Affolder et al.	(CDF Collab.)
ACCIARRI 99N PL B465 323	M. Acciarrri et al.	(L3 Collab.)
BARATE 98L PL B425 215	R. Barate et al.	(ALEPH Collab.)
BUSKULIC 96D ZPHY C69 393	D. Buskulic et al.	(ALEPH Collab.)
ABREU 95B PL B345 590	P. Abreu et al.	(DELPHI Collab.)
AKERS 95E ZPHY C66 19	R. Akers et al.	(OPAL Collab.)

$B_2^*(5747)^+$

 $I(J^P) = \frac{1}{2}(2^+)$
 I, J, P need confirmation.
 Quantum numbers shown are quark-model predictions.

$B_2^*(5747)^+$ MASS

OUR FIT uses m_{B_0} and $m_{B_2^{*+}} - m_{B_0}$ to determine $m_{B_2^*(5747)^+}$.

VALUE (MeV)	DOCUMENT ID
5737.2 ± 0.7 OUR FIT	

$m_{B_2^{*+}} - m_{B_0}$

VALUE (MeV)	EVTS	DOCUMENT ID	TECN	COMMENT
457.5 ± 0.7 OUR FIT				
457.5 ± 0.7 OUR AVERAGE				
457.62 ± 0.72 ± 0.40	4K	¹ AAIJ	15AB LHCB	$p\bar{p}$ at 7, 8 TeV
457.3 ± 1.3 \pm 0.3 \pm 0.9		² AALTONEN	14i CDF	$p\bar{p}$ at 1.96 TeV

- ¹ AAIJ 15AB reports $[m_{B_2^{*+}} - m_{B_0}] - m_{\pi^+} = 318.1 \pm 0.7 \pm 0.4$ MeV which we adjust by the π^+ mass. The masses inside the square brackets were measured for each candidate event.
- ² AALTONEN 14i reports $m_{B_2^*(5747)^+} - m_{B_0} - m_{\pi^+} = 317.7 \pm 1.2^{+0.3}_{-0.9}$ MeV which we adjusted by the π^+ mass.

$B_2^*(5747)^+$ WIDTH

VALUE (MeV)	EVTS	DOCUMENT ID	TECN	COMMENT
20 ± 5 OUR AVERAGE				Error includes scale factor of 2.2.
23.6 ± 2.0 ± 2.1	4K	AAIJ	15AB LHCB	$p\bar{p}$ at 7, 8 TeV
11 \pm 4 \pm 3 \pm 4		AALTONEN	14i CDF	$p\bar{p}$ at 1.96 TeV

$B_2^*(5747)^+$ DECAY MODES

Mode	Fraction (Γ_i/Γ)
Γ_1 $B^0\pi^+$	seen
Γ_2 $B^{*0}\pi^+$	seen

$B_2^*(5747)^+$ BRANCHING RATIOS

$\Gamma(B^0\pi^+)/\Gamma_{total}$	DOCUMENT ID	TECN	COMMENT	Γ_1/Γ
seen	4K	AAIJ	15AB LHCB	$p\bar{p}$ at 7, 8 TeV
seen		AALTONEN	14i CDF	$p\bar{p}$ at 1.96 TeV

$\Gamma(B^{*0}\pi^+)/\Gamma_{total}$	DOCUMENT ID	TECN	COMMENT	Γ_2/Γ
seen	4k	AAIJ	15AB LHCB	$p\bar{p}$ at 7, 8 TeV

$\Gamma(B^{*0}\pi^+)/\Gamma(B^0\pi^+)$	DOCUMENT ID	TECN	COMMENT	Γ_2/Γ_1
1.0 ± 0.5 ± 0.8	4k	AAIJ	15AB LHCB	$p\bar{p}$ at 7, 8 TeV

$B_2^*(5747)^+$ REFERENCES

AAIJ 15AB JHEP 1504 024	R. Aaij et al.	(LHCb Collab.)
AALTONEN 14i PR D90 012013	T. Aaltonen et al.	(CDF Collab.)

$B_2^*(5747)^0$

$I(J^P) = \frac{1}{2}(2^+)$
 I, J, P need confirmation.

Quantum numbers shown are quark-model predictions.

$B_2^*(5747)^0$ MASS

OUR FIT uses $m_{B^{*+}}, m_{B_1^0} - m_{B^{*+}}$, and $m_{B_2^0} - m_{B_1^0}$ to determine $m_{B_2^*(5747)^0}$. The -0.659 correlation between statistical uncertainties of $m_{B_1^0} - m_{B^{*+}}$ and $m_{B_2^0} - m_{B_1^0}$ measurements reported by AB AZOV 07r is taken into account.

VALUE (MeV)	DOCUMENT ID
5739.5 ± 0.7 OUR FIT	Error includes scale factor of 1.4.

$m_{B_2^0} - m_{B_1^0}$

VALUE (MeV)	DOCUMENT ID	TECN	COMMENT
13.4 ± 1.4 OUR FIT	Error includes scale factor of 1.3.		
45.9 ± 0.8 OUR AVERAGE	¹ AB AZOV 07r D0		$p\bar{p}$ at 1.96 TeV
14.9 \pm 2.2 \pm 1.2 \pm 2.5 \pm 1.4	¹ AALTONEN 09D CDF		Repl. by AALTONEN 14i

- • • We do not use the following data for averages, fits, limits, etc. • • •
- ¹ Observed in $B_2^0 \rightarrow B^{*+}\pi^-$ and $B_2^0 \rightarrow B^+\pi^-$.

$m_{B_2^0} - m_{B^+}$

VALUE (MeV)	EVTS	DOCUMENT ID	TECN	COMMENT
460.2 ± 0.6 OUR FIT				Error includes scale factor of 1.4.
459.9 ± 0.8 OUR AVERAGE				Error includes scale factor of 1.8.
460.18 ± 0.37 ± 0.33	17K	¹ AAIJ	15AB LHCB	$p\bar{p}$ at 7, 8 TeV
457.5 ± 1.2 \pm 0.8 \pm 0.9		² AALTONEN	14i CDF	$p\bar{p}$ at 1.96 TeV

- ¹ AAIJ 15AB reports $[m_{B_2^0} - m_{B^+}] - m_{\pi^-} = 320.6 \pm 0.4 \pm 0.3$ MeV which we adjust by the π^- mass. The masses inside the square brackets were measured for each candidate event.
- ² AALTONEN 14i reports $m_{B_2^*(5747)^0} - m_{B^+} - m_{\pi^-} = 317.9 \pm 1.2^{+0.8}_{-0.9}$ MeV which we adjusted by the π^- mass.

$B_2^*(5747)^0$ WIDTH

VALUE (MeV)	EVTS	DOCUMENT ID	TECN	COMMENT
24.2 ± 1.7 OUR AVERAGE				
24.5 ± 1.0 ± 1.5	17K	AAIJ	15AB LHCB	$p\bar{p}$ at 7, 8 TeV
22 \pm 3 \pm 4		AALTONEN	14i CDF	$p\bar{p}$ at 1.96 TeV
• • • We do not use the following data for averages, fits, limits, etc. • • •				
22.7 \pm 3.8 \pm 3.2 \pm 3.2 \pm 10.2		AALTONEN	09D CDF	Repl. by AALTONEN 14i

$B_2^*(5747)^0$ DECAY MODES

Mode	Fraction (Γ_i/Γ)
Γ_1 $B^+\pi^-$	seen
Γ_2 $B^{*+}\pi^-$	seen

See key on page 999

Meson Particle Listings

$B_2^*(5747)^0, B_J(5840)^+, B_J(5840)^0$

$B_2^*(5747)^0$ BRANCHING RATIOS

$\Gamma(B^+\pi^-)/\Gamma_{total}$					Γ_1/Γ
VALUE	EVTS	DOCUMENT ID	TECN	COMMENT	
seen	17K	AAIJ	15AB LHCB	pp at 7, 8 TeV	
seen		AALTONEN	09D CDF	$p\bar{p}$ at 1.96 TeV	
seen		ABAZOV	07T D0	$p\bar{p}$ at 1.96 TeV	

$\Gamma(B^{*+}\pi^-)/\Gamma_{total}$					Γ_2/Γ
VALUE	EVTS	DOCUMENT ID	TECN	COMMENT	
seen	17K	AAIJ	15AB LHCB	pp at 7, 8 TeV	
seen		AALTONEN	09D CDF	$p\bar{p}$ at 1.96 TeV	
seen		ABAZOV	07T D0	$p\bar{p}$ at 1.96 TeV	

$\Gamma(B^{*+}\pi^-)/\Gamma(B^+\pi^-)$					Γ_2/Γ_1
VALUE	EVTS	DOCUMENT ID	TECN	COMMENT	
0.82 ± 0.28 OUR AVERAGE					
0.71 ± 0.14 ± 0.30	17K	AAIJ	15AB LHCB	pp at 7, 8 TeV	
1.10 ± 0.42 ± 0.31		¹ ABAZOV	07T D0	$p\bar{p}$ at 1.96 TeV	

¹ Converted from measured ratio of $R = B(B_2^{*0} \rightarrow B^{*+}\pi^-) / B(B_2^{*0} \rightarrow B^{(*)+}\pi^-) = 0.475 \pm 0.095 \pm 0.069$.

$B_2^*(5747)^0$ REFERENCES

AAIJ	15AB JHEP 1504 024	R. Aaij et al.	(LHCb Collab.)
AALTONEN	14I PR D90 012013	T. Aaltonen et al.	(CDF Collab.)
AALTONEN	09D PRL 102 102003	T. Aaltonen et al.	(CDF Collab.)
ABAZOV	07T PRL 99 172001	V.M. Abazov et al.	(D0 Collab.)

$B_J(5840)^+$

$I(J^P) = \frac{1}{2}(?^?)$
I, J, P need confirmation.

OMITTED FROM SUMMARY TABLE
Quantum numbers shown are quark-model predictions.

$B_J(5840)^+$ MASS

OUR FIT uses m_{B^0} and $m_{B_J(5840)^+} - m_{B^0}$ to determine $m_{B_J(5840)^+}$.

VALUE (MeV)	DOCUMENT ID
5851 ± 19 OUR FIT	

$m_{B_J(5840)^+} - m_{B^0}$

VALUE (MeV)	EVTS	DOCUMENT ID	TECN	COMMENT
571 ± 19 OUR FIT				
571 ± 13 ± 14	7k	¹ AAIJ	15AB LHCB	pp at 7, 8 TeV
• • • We do not use the following data for averages, fits, limits, etc. • • •				
595 ± 26 ± 14	7k	² AAIJ	15AB LHCB	pp at 7, 8 TeV

¹ AAIJ 15AB reports $[m_{B_J^+} - m_{B^0}] - m_{\pi^+} = 431 \pm 13 \pm 14$ MeV which we adjust by the π^+ mass. The masses inside the square brackets were measured for each candidate event. The result assumes $P = (-1)^J$ and uses two relativistic Breit-Wigner functions in the fit for mass difference.

² AAIJ 15AB reports $[m_{B_J^+} - m_{B^0}] - m_{\pi^+} = 455 \pm 26 \pm 14$ MeV which we adjust by the π^+ mass. The masses inside the square brackets were measured for each candidate event. The result assumes $P = (-1)^J$ and uses three relativistic Breit-Wigner functions in the fit for mass difference.

$m_{B_J(5840)^+} - m_{B^0}$

VALUE (MeV)	EVTS	DOCUMENT ID	TECN	COMMENT
• • • We do not use the following data for averages, fits, limits, etc. • • •				
565 ± 15 ± 14	7k	¹ AAIJ	15AB LHCB	pp at 7, 8 TeV

¹ AAIJ 15AB reports $[m_{B_J^+} - m_{B^0}] - (m_{B^{*+}} - m_{B^+}) - m_{\pi^+} = 425 \pm 15 \pm 14$ MeV which we adjust by the π^+ mass. The masses inside the square brackets were measured for each candidate event. The result assumes $P = (-1)^J, (m_{B^{*0}} - m_{B^0}) = (m_{B^{*+}} - m_{B^+}) = 45.01 \pm 0.30 \pm 0.23$ MeV, and uses three relativistic Breit-Wigner functions in the fit for mass difference.

$B_J(5840)^+$ WIDTH

VALUE (MeV)	EVTS	DOCUMENT ID	TECN	COMMENT
224 ± 24 ± 80	7k	¹ AAIJ	15AB LHCB	pp at 7, 8 TeV
• • • We do not use the following data for averages, fits, limits, etc. • • •				
215 ± 27 ± 80	7k	² AAIJ	15AB LHCB	pp at 7, 8 TeV
229 ± 27 ± 80	7k	³ AAIJ	15AB LHCB	pp at 7, 8 TeV

¹ Assuming $P = (-1)^J$ and using two relativistic Breit-Wigner functions in the fit for mass difference.
² Assuming $P = (-1)^J$ and using three relativistic Breit-Wigner functions in the fit for mass difference.
³ Assuming $P = (-1)^J$ and using three relativistic Breit-Wigner functions in the fit for mass difference.

$B_J(5840)^+$ DECAY MODES

Mode	Fraction (Γ_i/Γ)
Γ_1 $B^{*0}\pi^+$	seen
Γ_2 $B^0\pi^+$	possibly seen

$B_J(5840)^+$ BRANCHING RATIOS

$\Gamma(B^{*0}\pi^+)/\Gamma_{total}$					Γ_1/Γ
VALUE	EVTS	DOCUMENT ID	TECN	COMMENT	
seen	7k	AAIJ	15AB LHCB	pp at 7, 8 TeV	

$\Gamma(B^0\pi^+)/\Gamma_{total}$					Γ_2/Γ
VALUE	EVTS	DOCUMENT ID	TECN	COMMENT	
possibly seen	7k	¹ AAIJ	15AB LHCB	pp at 7, 8 TeV	

¹ A $B\pi$ decay is forbidden from a $P = -(-1)^J$ parent, whereas $B^*\pi$ is allowed.

$B_J(5840)^+$ REFERENCES

AAIJ	15AB JHEP 1504 024	R. Aaij et al.	(LHCb Collab.)
------	--------------------	----------------	----------------

$B_J(5840)^0$

$I(J^P) = \frac{1}{2}(?^?)$
I, J, P need confirmation.

OMITTED FROM SUMMARY TABLE
Quantum numbers shown are quark-model predictions.

$B_J(5840)^0$ MASS

OUR FIT uses m_{B^+} and $m_{B_J(5840)^0} - m_{B^+}$ to determine $m_{B_J(5840)^0}$.

VALUE (MeV)	DOCUMENT ID
5863 ± 9 OUR FIT	

$m_{B_J(5840)^0} - m_{B^+}$

VALUE (MeV)	EVTS	DOCUMENT ID	TECN	COMMENT
584 ± 9 OUR FIT				
584 ± 5 ± 7	12k	¹ AAIJ	15AB LHCB	pp at 7, 8 TeV
• • • We do not use the following data for averages, fits, limits, etc. • • •				
610 ± 22 ± 7	12k	² AAIJ	15AB LHCB	pp at 7, 8 TeV

¹ AAIJ 15AB reports $[m_{B_J^0} - m_{B^+}] - m_{\pi^-} = 444 \pm 5 \pm 7$ MeV which we adjust by

the π^- mass. The masses inside the square brackets were measured for each candidate event. The result assumes $P = (-1)^J$ and uses two relativistic Breit-Wigner functions in the fit for mass difference.

² AAIJ 15AB reports $[m_{B_J^0} - m_{B^+}] - m_{\pi^-} = 471 \pm 22 \pm 7$ MeV which we adjust by

the π^- mass. The masses inside the square brackets were measured for each candidate event. The result assumes $P = (-1)^J$ and uses three relativistic Breit-Wigner functions in the fit for mass difference.

$m_{B_J(5840)^0} - m_{B^{*+}}$

VALUE (MeV)	EVTS	DOCUMENT ID	TECN	COMMENT
• • • We do not use the following data for averages, fits, limits, etc. • • •				
584 ± 5 ± 7	12k	¹ AAIJ	15AB LHCB	pp at 7, 8 TeV

¹ AAIJ 15AB reports $[m_{B_J^0} - m_{B^+}] - (m_{B^{*+}} - m_{B^+}) - m_{\pi^-} = 444 \pm 5 \pm 7$ MeV which we adjust by the π^- mass. The masses inside the square brackets were measured for each candidate event. The result assumes $P = -(-1)^J, (m_{B^{*0}} - m_{B^0}) = 45.01 \pm 0.30 \pm 0.23$ MeV, and uses three relativistic Breit-Wigner functions in the fit for mass difference.

$B_J(5840)^0$ WIDTH

VALUE (MeV)	EVTS	DOCUMENT ID	TECN	COMMENT
127 ± 17 ± 34	12k	¹ AAIJ	15AB LHCB	pp at 7, 8 TeV
• • • We do not use the following data for averages, fits, limits, etc. • • •				
107 ± 20 ± 34	12k	² AAIJ	15AB LHCB	pp at 7, 8 TeV
119 ± 17 ± 34	12k	³ AAIJ	15AB LHCB	pp at 7, 8 TeV

¹ Assuming $P = (-1)^J$ and using two relativistic Breit-Wigner functions in the fit for mass difference.

² Assuming $P = (-1)^J$ and using three relativistic Breit-Wigner functions in the fit for mass difference.

³ Assuming $P = -(-1)^J$ and using three relativistic Breit-Wigner functions in the fit for mass difference.

$B_J(5840)^0$ DECAY MODES

Mode	Fraction (Γ_i/Γ)
Γ_1 $B^{*+}\pi^-$	seen
Γ_2 $B^+\pi^-$	possibly seen

Meson Particle Listings

 $B_J(5840)^0, B_J(5970)^+, B_J(5970)^0$ $B_J(5840)^0$ BRANCHING RATIOS

$\Gamma(B^{*+}\pi^-)/\Gamma_{\text{total}}$					Γ_1/Γ
VALUE	EVTS	DOCUMENT ID	TECN	COMMENT	
seen	12k	AAIJ	15AB LHCb	$p\bar{p}$ at 7, 8 TeV	

$\Gamma(B^+\pi^-)/\Gamma_{\text{total}}$					Γ_2/Γ
VALUE	EVTS	DOCUMENT ID	TECN	COMMENT	
possibly seen		¹ AAIJ	15AB LHCb	$p\bar{p}$ at 7, 8 TeV	

¹A $B\pi$ decay is forbidden from a $P = -(-1)^J$ parent, whereas $B^*\pi$ is allowed.

 $B_J(5840)^0$ REFERENCES

AAIJ 15AB JHEP 1504 024 R. Aaij *et al.* (LHCb Collab.)

$B_J(5970)^+$	$I(J^P) = \frac{1}{2}(??)$
	I, J, P need confirmation.
Quantum numbers shown are quark-model predictions.	

 $B_J(5970)^+$ MASS

OUR FIT uses m_{B^0} and $m_{B_J(5970)^+} - m_{B^0}$ to determine $m_{B_J(5970)^+}$.

VALUE (MeV)	DOCUMENT ID
5964 ± 5 OUR FIT	

 $m_{B_J(5970)^+} - m_{B^0}$

VALUE (MeV)	EVTS	DOCUMENT ID	TECN	COMMENT
685 ± 5 OUR FIT				
685 ± 5 OUR AVERAGE				
685.3 ± 4.1 ± 2.5	2K	¹ AAIJ	15AB LHCb	$p\bar{p}$ at 7, 8 TeV
681 ± 5 ± 12	1.4k	² AALTONEN	14i CDF	$p\bar{p}$ at 1.96 TeV

• • • We do not use the following data for averages, fits, limits, etc. • • •

686.8 ± 4.5 ± 2.5 2K ³AAIJ 15AB LHCb $p\bar{p}$ at 7, 8 TeV

¹AAIJ 15AB reports $[m_{B_J^+} - m_{B^0}] - m_{\pi^+} = 545.8 \pm 4.1 \pm 2.5$ MeV which we adjust by

the π^+ mass. The masses inside the square brackets were measured for each candidate event. The result assumes $P = (-1)^J$ and uses two relativistic Breit-Wigner functions in the fit for mass difference.

²AALTONEN 14i reports $m_{B_J(5970)^+} - m_{B^0} - m_{\pi^+} = 541 \pm 5 \pm 12$ MeV which we adjust by the π^+ mass.

³AAIJ 15AB reports $[m_{B_J^+} - m_{B^0}] - m_{\pi^+} = 547 \pm 5 \pm 3$ MeV which we adjust by

the π^+ mass. The masses inside the square brackets were measured for each candidate event. The result assumes $P = (-1)^J$ and uses three relativistic Breit-Wigner functions in the fit for mass difference.

 $m_{B_J(5970)^+} - m_{B^{*0}}$

VALUE (MeV)	EVTS	DOCUMENT ID	TECN	COMMENT
• • • We do not use the following data for averages, fits, limits, etc. • • •				
686.0 ± 4.0 ± 2.5	2k	¹ AAIJ	15AB LHCb	$p\bar{p}$ at 7, 8 TeV

¹AAIJ 15AB reports $[m_{B_J^+} - m_{B^0}] - (m_{B^{*+}} - m_{B^+}) - m_{\pi^+} = 547 \pm 4 \pm 3$ MeV which

we adjust by the π^+ mass. The masses inside the square brackets were measured for each candidate event. The result assumes $P = -(-1)^J$, $(m_{B^{*0}} - m_{B^0}) = (m_{B^{*+}} - m_{B^+}) = 45.01 \pm 0.30 \pm 0.23$ MeV, and uses three relativistic Breit-Wigner functions in the fit for mass difference.

 $B_J(5970)^+$ WIDTH

VALUE (MeV)	EVTS	DOCUMENT ID	TECN	COMMENT
62 ± 20 OUR AVERAGE				
63 ± 15 ± 17	2K	¹ AAIJ	15AB LHCb	$p\bar{p}$ at 7, 8 TeV
60 ± 30 ± 40	1.4k	AALTONEN	14i CDF	$p\bar{p}$ at 1.96 TeV

• • • We do not use the following data for averages, fits, limits, etc. • • •

61 ± 14 ± 17 2K ²AAIJ 15AB LHCb $p\bar{p}$ at 7, 8 TeV

61 ± 15 ± 17 2K ³AAIJ 15AB LHCb $p\bar{p}$ at 7, 8 TeV

¹Assuming $P = (-1)^J$ and using two relativistic Breit-Wigner functions in the fit for mass difference.

²Assuming $P = (-1)^J$ and using three relativistic Breit-Wigner functions in the fit for mass difference.

³Assuming $P = -(-1)^J$ and using three relativistic Breit-Wigner functions in the fit for mass difference.

 $B_J(5970)^+$ DECAY MODES

Mode	Fraction (Γ_i/Γ)
Γ_1 $B^0\pi^+$	possibly seen
Γ_2 $B^{*0}\pi^+$	seen

 $B_J(5970)^+$ BRANCHING RATIOS

$\Gamma(B^0\pi^+)/\Gamma_{\text{total}}$					Γ_1/Γ
VALUE	EVTS	DOCUMENT ID	TECN	COMMENT	
possibly seen	2K	¹ AAIJ	15AB LHCb	$p\bar{p}$ at 7, 8 TeV	
possibly seen	1.4k	AALTONEN	14i CDF	$p\bar{p}$ at 1.96 TeV	

¹A $B\pi$ decay is forbidden from a $P = -(-1)^J$ parent, whereas $B^*\pi$ is allowed.

$\Gamma(B^{*0}\pi^+)/\Gamma_{\text{total}}$					Γ_2/Γ
VALUE	EVTS	DOCUMENT ID	TECN	COMMENT	
seen	2k	AAIJ	15AB LHCb	$p\bar{p}$ at 7, 8 TeV	
seen	1.4k	AALTONEN	14i CDF	$p\bar{p}$ at 1.96 TeV	

 $B_J(5970)^+$ REFERENCES

AAIJ 15AB JHEP 1504 024 R. Aaij *et al.* (LHCb Collab.)
AALTONEN 14i PR D90 012013 T. Aaltonen *et al.* (CDF Collab.)

$B_J(5970)^0$	$I(J^P) = \frac{1}{2}(??)$
	I, J, P need confirmation.
Quantum numbers shown are quark-model predictions.	

 $B_J(5970)^0$ MASS

OUR FIT uses m_{B^+} and $m_{B_J(5970)^0} - m_{B^+}$ to determine $m_{B_J(5970)^0}$.

VALUE (MeV)	DOCUMENT ID
5971 ± 5 OUR FIT	

 $m_{B_J(5970)^0} - m_{B^+}$

VALUE (MeV)	EVTS	DOCUMENT ID	TECN	COMMENT
691 ± 5 OUR FIT				
691 ± 5 OUR AVERAGE				
689.9 ± 2.9 ± 5.1	10K	¹ AAIJ	15AB LHCb	$p\bar{p}$ at 7, 8 TeV
698 ± 5 ± 12	2.6k	² AALTONEN	14i CDF	$p\bar{p}$ at 1.96 TeV

• • • We do not use the following data for averages, fits, limits, etc. • • •

714.3 ± 6.4 ± 5.1 10K ³AAIJ 15AB LHCb $p\bar{p}$ at 7, 8 TeV

¹AAIJ 15AB reports $[m_{B_J^0} - m_{B^+}] - m_{\pi^-} = 550.4 \pm 2.9 \pm 5.1$ MeV which we adjust by

the π^- mass. The masses inside the square brackets were measured for each candidate event. The result assumes $P = (-1)^J$ and uses two relativistic Breit-Wigner functions in the fit for mass difference.

²AALTONEN 14i reports $m_{B_J(5970)^0} - m_{B^+} - m_{\pi^-} = 558 \pm 5 \pm 12$ MeV which we adjust by the π^- mass.

³AAIJ 15AB reports $[m_{B_J^0} - m_{B^+}] - m_{\pi^-} = 575 \pm 6 \pm 5$ MeV which we adjust by

the π^- mass. The masses inside the square brackets were measured for each candidate event. The result assumes $P = (-1)^J$ and uses three relativistic Breit-Wigner functions in the fit for mass difference.

 $m_{B_J(5970)^0} - m_{B^{*+}}$

VALUE (MeV)	EVTS	DOCUMENT ID	TECN	COMMENT
• • • We do not use the following data for averages, fits, limits, etc. • • •				
691.6 ± 3.7 ± 5.1	10k	¹ AAIJ	15AB LHCb	$p\bar{p}$ at 7, 8 TeV

¹AAIJ 15AB reports $[m_{B_J^0} - m_{B^+}] - (m_{B^{*+}} - m_{B^+}) - m_{\pi^-} = 552 \pm 4 \pm 5$ MeV

which we adjust by the π^- mass. The masses inside the square brackets were measured for each candidate event. The result assumes $P = -(-1)^J$, $(m_{B^{*+}} - m_{B^+}) = 45.01 \pm 0.30 \pm 0.23$ MeV, and uses three relativistic Breit-Wigner functions in the fit for mass difference.

 $B_J(5970)^0$ WIDTH

VALUE (MeV)	EVTS	DOCUMENT ID	TECN	COMMENT
81 ± 12 OUR AVERAGE				
82 ± 8 ± 9	10K	¹ AAIJ	15AB LHCb	$p\bar{p}$ at 7, 8 TeV
70 ± 30 ± 30	2.6k	AALTONEN	14i CDF	$p\bar{p}$ at 1.96 TeV

• • • We do not use the following data for averages, fits, limits, etc. • • •

56 ± 7 ± 9 10K ²AAIJ 15AB LHCb $p\bar{p}$ at 7, 8 TeV

82 ± 10 ± 9 10K ³AAIJ 15AB LHCb $p\bar{p}$ at 7, 8 TeV

¹Assuming $P = (-1)^J$ and using two relativistic Breit-Wigner functions in the fit for mass difference.

²Assuming $P = (-1)^J$ and using three relativistic Breit-Wigner functions in the fit for mass difference.

³Assuming $P = -(-1)^J$ and using three relativistic Breit-Wigner functions in the fit for mass difference.

 $B_J(5970)^0$ DECAY MODES

Mode	Fraction (Γ_i/Γ)
Γ_1 $B^+\pi^-$	possibly seen
Γ_2 $B^{*+}\pi^-$	seen

See key on page 999

Meson Particle Listings

 $B_J(5970)^0$ $B_J(5970)^0$ BRANCHING RATIOS $B_J(5970)^0$ REFERENCES

$\Gamma(B^+\pi^-)/\Gamma_{\text{total}}$					Γ_1/Γ
VALUE	EVTs	DOCUMENT ID	TECN	COMMENT	
possibly seen	10K	¹ AAIJ	15AB LHCb	pp at 7, 8 TeV	
possibly seen	2.6k	AALTONEN	14i CDF	$p\bar{p}$ at 1.96 TeV	

¹ A $B\pi$ decay is forbidden from a $P = -(-1)^J$ parent, whereas $B^*\pi$ is allowed.

$\Gamma(B^*\pi^-)/\Gamma_{\text{total}}$					Γ_2/Γ
VALUE	EVTs	DOCUMENT ID	TECN	COMMENT	
seen	10K	AAIJ	15AB LHCb	pp at 7, 8 TeV	
seen	2.6k	AALTONEN	14i CDF	$p\bar{p}$ at 1.96 TeV	

AAIJ	15AB	JHEP 1504 024	R. Aaij et al.	(LHCb Collab.)
AALTONEN	14i	PR D90 012013	T. Aaltonen et al.	(CDF Collab.)

Meson Particle Listings

B_s^0

BOTTOM, STRANGE MESONS

$(B = \pm 1, S = \mp 1)$

$B_s^0 = s\bar{b}, \bar{B}_s^0 = \bar{s}b$, similarly for B_s^{*s}

B_s^0

$$I(J^P) = 0(0^-)$$

I, J, P need confirmation. Quantum numbers shown are quark-model predictions.

B_s^0 MASS

VALUE (MeV)	EVTS	DOCUMENT ID	TECN	COMMENT
5366.88 ± 0.14 OUR FIT				
5366.84 ± 0.15 OUR AVERAGE				
5366.85 ± 0.19 ± 0.13		1 AAIJ	19U	LHCB pp at 7, 8, 13 TeV
5366.83 ± 0.25 ± 0.27		2 AAIJ	18AC	LHCB pp at 7, 8, 13 TeV
5367.08 ± 0.38 ± 0.15	128	3 AAIJ	16U	LHCB pp at 7, 8 TeV
5366.90 ± 0.28 ± 0.23		4 AAIJ	12E	LHCB pp at 7 TeV
5364.4 ± 1.3 ± 0.7		LOUVOT	09	BELL $e^+e^- \rightarrow \Upsilon(5S)$
5366.01 ± 0.73 ± 0.33		5 ACOSTA	06	CDF $p\bar{p}$ at 1.96 TeV
5369.9 ± 2.3 ± 1.3	32	6 ABE	96B	CDF $p\bar{p}$ at 1.8 TeV
5374 ± 16 ± 2	3	ABREU	94D	DLPH $e^+e^- \rightarrow Z$
5359 ± 19 ± 7	1	6 AKERS	94J	OPAL $e^+e^- \rightarrow Z$
5368.6 ± 5.6 ± 1.5	2	BUSKULIC	93G	ALEP $e^+e^- \rightarrow Z$
• • • We do not use the following data for averages, fits, limits, etc. • • •				
5370 ± 1 ± 3		DRUTSKOY	07A	BELL Repl. by LOUVOT 09
5370 ± 40	6	7 AKERS	94J	OPAL $e^+e^- \rightarrow Z$
5383.3 ± 4.5 ± 5.0	14	ABE	93F	CDF Repl. by ABE 96B

- 1 Uses $B_s^0 \rightarrow J/\psi p\bar{p}$ decays.
- 2 Uses $B_s \rightarrow \chi_{c1} K^+ K^-$ mode.
- 3 Uses $J/\psi \rightarrow \mu^+ \mu^-, \phi \rightarrow K^+ K^-$ decays, and observes 128 ± 13 events of $B_s^0 \rightarrow J/\psi \phi$.
- 4 Uses $B_s^0 \rightarrow J/\psi \phi$ fully reconstructed decays.
- 5 Uses exclusively reconstructed final states containing a $J/\psi \rightarrow \mu^+ \mu^-$ decays.
- 6 From the decay $B_s \rightarrow J/\psi(1S) \phi$.
- 7 From the decay $B_s \rightarrow D_s^- \pi^+$.

$m_{B_s^0} - m_B$

m_B is the average of our B masses $(m_{B^\pm} + m_{B^0})/2$.

VALUE (MeV)	CL%	DOCUMENT ID	TECN	COMMENT
87.38 ± 0.16 OUR FIT				
87.42 ± 0.24 OUR AVERAGE				
87.60 ± 0.44 ± 0.09		1 AAIJ	15U	LHCB pp at 7, 8 TeV
87.42 ± 0.30 ± 0.09		2 AAIJ	12E	LHCB pp at 7 TeV
86.64 ± 0.80 ± 0.08		3 ACOSTA	06	CDF $p\bar{p}$ at 1.96 TeV
• • • We use the following data for averages but not for fits. • • •				
89.7 ± 2.7 ± 1.2		ABE	96B	CDF $p\bar{p}$ at 1.8 TeV
• • • We do not use the following data for averages, fits, limits, etc. • • •				
80 to 130	68	LEE-FRANZINI	90	CSB2 $e^+e^- \rightarrow \Upsilon(5S)$

- 1 The reported result is $m_{B_s^0} - m_{B^0} = 87.45 \pm 0.44 \pm 0.09$ MeV. We convert it to the mass difference with respect to the average of $(m_{B^\pm} + m_{B^0})/2$. Uses the mode $B_s^0 \rightarrow \psi(2S) K^- \pi^+$.
- 2 The reported result is $m_{B_s^0} - m_{B^+} = 87.52 \pm 0.30 \pm 0.12$ MeV. We convert it to the mass difference with respect to the average of $(m_{B^\pm} + m_{B^0})/2$.
- 3 The reported result is $m_{B_s^0} - m_{B^0} = 86.38 \pm 0.90 \pm 0.06$ MeV. We convert it to the mass difference with respect to the average of $(m_{B^\pm} + m_{B^0})/2$.

$m_{B_s^0 H} - m_{B_s^0 L}$

See the $B_s^0 \bar{B}_s^0$ MIXING section near the end of these B_s^0 Listings.

B_s^0 MEAN LIFE

"OUR EVALUATION" is provided by the Heavy Flavor Averaging Group (HFLAV, <https://hflav.web.cern.ch/>). It is derived from the average of $\Gamma_{B_s^0}$.

VALUE (10^{-12} s)	EVTS	DOCUMENT ID	TECN	COMMENT
1.515 ± 0.004 OUR EVALUATION				
• • • We do not use the following data for averages, fits, limits, etc. • • •				
1.518 ± 0.041 ± 0.027		1 AALTONEN	11AP	CDF $p\bar{p}$ at 1.96 TeV

1.398 ± 0.044 ± 0.028 -0.025		2 ABAZOV	06V	D0 $p\bar{p}$ at 1.96 TeV
1.42 ± 0.14 ± 0.03 -0.13		3 ABREU	00Y	DLPH $e^+e^- \rightarrow Z$
1.53 ± 0.16 ± 0.07 -0.15		4 ABREU,P	00G	DLPH $e^+e^- \rightarrow Z$
1.36 ± 0.09 ± 0.06 -0.05		5 ABE	99D	CDF $p\bar{p}$ at 1.8 TeV
1.72 ± 0.20 ± 0.18 -0.19 -0.17		6 ACKERSTAFF	98F	OPAL $e^+e^- \rightarrow Z$
1.50 ± 0.16 ± 0.04 -0.15		5 ACKERSTAFF	98G	OPAL $e^+e^- \rightarrow Z$
1.47 ± 0.14 ± 0.08		4 BARATE	98C	ALEP $e^+e^- \rightarrow Z$
1.51 ± 0.11		7 BARATE	98C	ALEP $e^+e^- \rightarrow Z$
1.56 ± 0.29 ± 0.08 -0.26 -0.07		5 ABREU	96F	DLPH Repl. by ABREU 00Y
1.65 ± 0.34 ± 0.12 -0.31		4 ABREU	96F	DLPH Repl. by ABREU 00Y
1.76 ± 0.20 ± 0.15 -0.10		8 ABREU	96F	DLPH Repl. by ABREU 00Y
1.60 ± 0.26 ± 0.13 -0.15		9 ABREU	96F	DLPH Repl. by ABREU,P 00G
1.67 ± 0.14		10 ABREU	96F	DLPH $e^+e^- \rightarrow Z$
1.61 ± 0.30 ± 0.18 -0.29 -0.16	90	4 BUSKULIC	96E	ALEP Repl. by BARATE 98C
1.54 ± 0.14 ± 0.04 -0.13		5 BUSKULIC	96M	ALEP $e^+e^- \rightarrow Z$
1.42 ± 0.27 ± 0.11 -0.23	76	5 ABE	95R	CDF Repl. by ABE 99D
1.74 ± 1.08 ± 0.07 -0.69	8	11 ABE	95R	CDF Sup. by ABE 96N
1.54 ± 0.25 ± 0.06 -0.21	79	5 AKERS	95G	OPAL Repl. by ACKERSTAFF 98G
1.59 ± 0.17 ± 0.03 -0.15	134	5 BUSKULIC	95O	ALEP Sup. by BUSKULIC 96M
0.96 ± 0.37	41	12 ABREU	94E	DLPH Sup. by ABREU 96F
1.92 ± 0.45 ± 0.04 -0.35	31	5 BUSKULIC	94C	ALEP Sup. by BUSKULIC 95O
1.13 ± 0.35 ± 0.09 -0.26	22	5 ACTON	93H	OPAL Sup. by AKERS 95G

- 1 AALTONEN 11AP combines the fully reconstructed $B_s^0 \rightarrow D_s^- \pi^+$ decays and partially reconstructed $B_s^0 \rightarrow D_s^- X$ decays.
- 2 Measured using $D_s \mu^+$ vertices.
- 3 Uses $D_s^- \ell^+$, and $\phi \ell^+$ vertices.
- 4 Measured using D_s hadron vertices.
- 5 Measured using $D_s^- \ell^+$ vertices.
- 6 ACKERSTAFF 98F use fully reconstructed $D_s^- \rightarrow \phi \pi^-$ and $D_s^- \rightarrow K^*0 K^-$ in the inclusive B_s^0 decay.
- 7 Combined results from $D_s^- \ell^+$ and D_s hadron.
- 8 Measured using $\phi \ell$ vertices.
- 9 Measured using inclusive D_s vertices.
- 10 Combined result for the four ABREU 96F methods.
- 11 Exclusive reconstruction of $B_s \rightarrow \psi \phi$.
- 12 ABREU 94E uses the flight-distance distribution of D_s vertices, ϕ -lepton vertices, and $D_s \mu$ vertices.

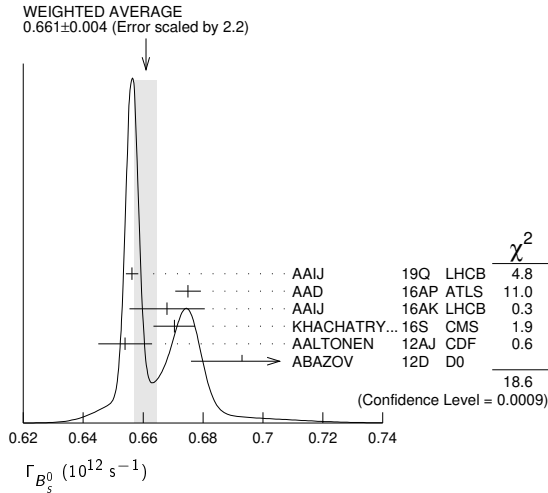
$\Gamma_{B_s^0}$

"OUR EVALUATION" is an average performed by the Heavy Flavor Averaging Group (HFLAV, <https://hflav.web.cern.ch/>) as described in our "Review on $B-\bar{B}$ Mixing" in the B^0 section of these Listings. It includes the measurements of Γ_{B^0} and $\Delta \Gamma_{B^0}$ listed in this section, as well as constraints from effective lifetimes with pure CP modes and flavor-specific modes.

VALUE (10^{12} s $^{-1}$)	DOCUMENT ID	TECN	COMMENT
0.6600 ± 0.0016 OUR EVALUATION			
0.661 ± 0.004 OUR AVERAGE			Error includes scale factor of 2.2. See the ideogram below.
0.6563 ± 0.0021	1 AAIJ	19Q	LHCB pp at 7, 8, 13 TeV
0.675 ± 0.003 ± 0.003	2 AAD	16AP	ATLS pp at 7, 8 TeV
0.668 ± 0.011 ± 0.006	3 AAIJ	16AK	LHCB pp at 7, 8 TeV
0.6704 ± 0.0043 ± 0.0055	2 KHACHATRY...	16S	CMS pp at 8 TeV
0.654 ± 0.008 ± 0.004	2 AALTONEN	12AJ	CDF $p\bar{p}$ at 1.96 TeV
0.693 ± 0.018 -0.017	2 ABAZOV	12D	D0 $p\bar{p}$ at 1.96 TeV
• • • We do not use the following data for averages, fits, limits, etc. • • •			
0.650 ± 0.006 ± 0.004	1 AAIJ	17V	LHCB Repl. by AAIJ 19Q
0.6603 ± 0.0027 ± 0.0015	4 AAIJ	15I	LHCB Repl. by AAIJ 19Q
0.677 ± 0.007 ± 0.004	2 AAD	14U	ATLS Repl. by AAD 16AP
0.661 ± 0.004 ± 0.006	5 AAIJ	13AR	LHCB Repl. by AAIJ 15I
0.677 ± 0.007 ± 0.004	2 AAD	12CV	ATLS Repl. by AAD 14U
0.657 ± 0.009 ± 0.008	2 AAIJ	12D	LHCB Repl. by AAIJ 13AR
0.654 ± 0.011 ± 0.005	2.6 AALTONEN	12D	CDF Repl. by AALTONEN 12AJ
0.672 ± 0.027 ± 0.013	2 ABAZOV	09E	D0 Repl. by ABAZOV 08AM
0.658 ± 0.017 ± 0.009	2.7 AALTONEN	08J	CDF Repl. by AALTONEN 12D
0.658 ± 0.022 ± 0.004	2 ABAZOV	08AM	D0 Repl. by ABAZOV 12D
0.658 ± 0.035 ± 0.0130 -0.004	2.7 ABAZOV	07	D0 Repl. by ABAZOV 09E
0.714 ± 0.007 ± 0.010 -0.008	2.7 ACOSTA	05	CDF Repl. by AALTONEN 08J

- 1 Measured using time-dependent angular analysis of $B_S^0 \rightarrow J/\psi K^+ K^-$ in the region $m(KK) > 1.05$ GeV.
- 2 Measured using a time-dependent angular analysis of $B_S^0 \rightarrow J/\psi \phi$ decays.
- 3 Measured using a time-dependent angular analysis of $B_S^0 \rightarrow \psi(2S) \phi$ decays.
- 4 Measured using a time-dependent angular analysis of $B_S^0 \rightarrow J/\psi K^+ K^-$ decays.
- 5 Measured using a combined time-dependent angular analysis of $B_S^0 \rightarrow J/\psi K^+ K^-$ and $B_S^0 \rightarrow J/\psi \pi^+ \pi^-$ decays.
- 6 Assuming CPV phase $\phi_S = -0.04$.
- 7 Assuming CPV phase $\phi_S = 0$.

- 7 Uses the time-dependent angular analysis of $B_S^0 \rightarrow J/\psi \phi$ decays and assuming CP-violating angle $\beta_S(B^0 \rightarrow J/\psi \phi) = 0.02$.
- 8 Measured the angular and lifetime parameters for the time-dependent angular untagged decays $B_d^0 \rightarrow J/\psi K^{*0}$ and $B_S^0 \rightarrow J/\psi \phi$.
- 9 Measured using the time-dependent angular analysis of $B_S^0 \rightarrow J/\psi \phi$ decays and assuming CP-violating phase $\phi_S = 0$.
- 10 Obtains 90% CL interval $-0.06 < \Delta\Gamma_S < 0.30$.
- 11 ABAZOV 07 reports $0.17 \pm 0.09 \pm 0.02$ with CP-violating phase ϕ_S as a free parameter.
- 12 Combines D^0 measurements of time-dependent angular distributions in $B_S^0 \rightarrow J/\psi \phi$ and charge asymmetry in semileptonic decays. There is a 4-fold ambiguity in the solution.



$\Delta\Gamma_{B_S^0}/\Gamma_{B_S^0}$

$\Gamma_{B_S^0}$ and $\Delta\Gamma_{B_S^0}$ are the decay rate average and difference between two B_S^0 CP eigenstates (light – heavy).

"OUR EVALUATION" is provided by the Heavy Flavor Averaging Group (HFLAV, <https://hflav.web.cern.ch/>). It is derived from the averages of $\Gamma_{B_S^0}$ and $\Delta\Gamma_{B_S^0}$ (and their correlation).

VALUE	CL%	DOCUMENT ID	TECN	COMMENT
0.129 ± 0.006 OUR EVALUATION				
• • • We do not use the following data for averages, fits, limits, etc. • • •				
$0.090 \pm 0.009 \pm 0.023$		1 ESEN 13 BELL	BELL	$e^+ e^- \rightarrow \Upsilon(5S)$
		2 AAIJ 12D LHCb	LHCb	$p\bar{p}$ at 7 TeV
		3 AALTONEN 12D CDF	CDF	$p\bar{p}$ at 1.96 TeV
		4 ABAZOV 12D D0	D0	$p\bar{p}$ at 1.96 TeV
$0.147^{+0.036+0.042}_{-0.030-0.041}$		1 ESEN 10 BELL	BELL	$e^+ e^- \rightarrow \Upsilon(5S)$
$0.072 \pm 0.021 \pm 0.022$		5 ABAZOV 09I D0	D0	$p\bar{p}$ at 1.96 TeV
> 0.012	95	5 AALTONEN 08F CDF	CDF	$p\bar{p}$ at 1.96 TeV
$0.116^{+0.09}_{-0.10} \pm 0.010$		6 AALTONEN 08J CDF	CDF	Repl. by AALTONEN 12D
$0.079^{+0.038+0.031}_{-0.035-0.030}$		5 ABAZOV 07Y D0	D0	Repl. by ABAZOV 09I
$0.24^{+0.28+0.03}_{-0.38-0.04}$		6,7 ABAZOV 05W D0	D0	Repl. by ABAZOV 08AM
$0.65^{+0.25}_{-0.33} \pm 0.01$		6 ACOSTA 05 CDF	CDF	Repl. by AALTONEN 08J
< 0.46	95	8 ABREU 00Y DLPH	DLPH	$e^+ e^- \rightarrow Z$
< 0.69	95	9 ABREU,P 00G DLPH	DLPH	$e^+ e^- \rightarrow Z$
$0.25^{+0.21}_{-0.14}$		10 BARATE 00K ALEP	ALEP	$e^+ e^- \rightarrow Z$
< 0.83	95	11 ABE 99D CDF	CDF	$p\bar{p}$ at 1.8 TeV
< 0.67	95	12 ACCIARRI 98s L3	L3	$e^+ e^- \rightarrow Z$

$\Delta\Gamma_{B_S^0}$

"OUR EVALUATION" is an average performed by the Heavy Flavor Averaging Group (HFLAV, <https://hflav.web.cern.ch/>) as described in our "Review on $B-\bar{B}$ Mixing" in the B^0 section of these Listings. It includes the measurements of $\Gamma_{B_S^0}$ and $\Delta\Gamma_{B_S^0}$ listed in this section, as well as constraints from effective lifetimes with pure CP modes and flavor-specific modes.

VALUE ($10^{12} s^{-1}$)	DOCUMENT ID	TECN	COMMENT
0.085 ± 0.004 OUR EVALUATION			
0.081 ± 0.006 OUR AVERAGE			
$0.077 \pm 0.008 \pm 0.003$	1 AAIJ 19Q LHCb	LHCb	$p\bar{p}$ at 13 TeV
$0.066 \pm 0.018 \pm 0.010$	2 AAIJ 17V LHCb	LHCb	$p\bar{p}$ at 7, 8 TeV
$0.085 \pm 0.011 \pm 0.007$	3 AAD 16AP ATLS	ATLS	$p\bar{p}$ at 7, 8 TeV
$0.066^{+0.041}_{-0.044} \pm 0.007$	4 AAIJ 16AK LHCb	LHCb	$p\bar{p}$ at 7, 8 TeV
$0.095 \pm 0.013 \pm 0.007$	3 KHACHATRY... 16S CMS	CMS	$p\bar{p}$ at 8 TeV
$0.068 \pm 0.026 \pm 0.009$	3 AALTONEN 12AJ CDF	CDF	$p\bar{p}$ at 1.96 TeV
$0.163^{+0.065}_{-0.064}$	3,5 ABAZOV 12D D0	D0	$p\bar{p}$ at 1.96 TeV
• • • We do not use the following data for averages, fits, limits, etc. • • •			
$0.0805 \pm 0.0091 \pm 0.0032$	1 AAIJ 15I LHCb	LHCb	Repl. by AAIJ 19Q
$0.053 \pm 0.021 \pm 0.010$	3 AAD 14U ATLS	ATLS	Repl. by AAD 16AP
$0.106 \pm 0.011 \pm 0.007$	6 AAIJ 13AR LHCb	LHCb	Repl. by AAIJ 15I
$0.053 \pm 0.021 \pm 0.010$	3 AAD 12CV ATLS	ATLS	Repl. by AAD 14U
$0.123 \pm 0.029 \pm 0.011$	3 AAIJ 12D LHCb	LHCb	Repl. by AAIJ 13AR
$0.075 \pm 0.035 \pm 0.006$	7 AALTONEN 12D CDF	CDF	Repl. by AALTONEN 12AJ
$0.085^{+0.072}_{-0.078} \pm 0.001$	8 ABAZOV 09E D0	D0	Repl. by ABAZOV 08AM
$0.076^{+0.059}_{-0.063} \pm 0.006$	9 AALTONEN 08J CDF	CDF	Repl. by AALTONEN 12D
$0.19 \pm 0.07^{+0.02}_{-0.01}$	3,10 ABAZOV 08AMD0	D0	Repl. by ABAZOV 12D
$0.12^{+0.08}_{-0.10} \pm 0.02$	9,11 ABAZOV 07 D0	D0	Repl. by ABAZOV 07N
0.13 ± 0.09	12 ABAZOV 07N D0	D0	Repl. by ABAZOV 09E
$0.47^{+0.19}_{-0.24} \pm 0.01$	9 ACOSTA 05 CDF	CDF	Repl. by AALTONEN 08J

- 1 Measured using time-dependent angular analysis of $B_S^0 \rightarrow J/\psi K^+ K^-$ decays.
- 2 Measured using time-dependent angular analysis of $B_S^0 \rightarrow J/\psi K^+ K^-$ in the region $m(KK) > 1.05$ GeV.
- 3 Measured using the time-dependent angular analysis of $B_S^0 \rightarrow J/\psi \phi$ decays.
- 4 Measured using time-dependent angular analysis of $B_S^0 \rightarrow \psi(2S) \phi$ decays.
- 5 The error includes both statistical and systematic uncertainties.
- 6 AAIJ 13AR result comes from a combined fit to $B_S^0 \rightarrow J/\psi K^+ K^-$ and $B_S^0 \rightarrow J/\psi \pi^+ \pi^-$ data sets. Also reports $\Delta\Gamma_S = 0.100 \pm 0.016 \pm 0.003 \text{ ps}^{-1}$ from a fit to $B_S^0 \rightarrow J/\psi K^+ K^-$ decays.

- 1 Assumes CP violation is negligible.
- 2 Measured using the time-dependent angular analysis of $B_S^0 \rightarrow J/\psi \phi$ decays.
- 3 Uses the time-dependent angular analysis of $B_S^0 \rightarrow J/\psi \phi$ decays and assuming CP-violating angle $\beta_S(B^0 \rightarrow J/\psi \phi) = 0.02$.
- 4 Measured using fully reconstructed $B_S \rightarrow J/\psi \phi$ decays.
- 5 Assumes $2 \text{B}(B_S^0 \rightarrow D_S^{(*)} D_S^{(*)}) \simeq \Delta\Gamma_S^{CP} / \Gamma_S$.
- 6 Measured using the time-dependent angular analysis of $B_S^0 \rightarrow J/\psi \phi$ decays.
- 7 Uses $|A_0|^2 - |A_{||}|^2 = 0.355 \pm 0.066$ from ACOSTA 05.
- 8 Uses $D_S^- \ell^+$, and $\phi \ell^+$ vertices.
- 9 Measured using D_S hadron vertices.
- 10 Uses $\phi \phi$ correlations from $B_S^0 \rightarrow D_S^{(*)+} D_S^{(*)-}$.
- 11 ABE 99D assumes $\tau_{B_S^0} = 1.55 \pm 0.05 \text{ ps}$.
- 12 ACCIARRI 98s assumes $\tau_{B_S^0} = 1.49 \pm 0.06 \text{ ps}$ and PDG 98 values of b production fraction.

B_{SH}^0 MEAN LIFE

B_{SH}^0 is the heavy mass state of two B_S^0 CP eigenstates.

"OUR EVALUATION" is provided by the Heavy Flavor Averaging Group (HFLAV, <https://hflav.web.cern.ch/>). It is derived from the averages of $\Gamma_{B_S^0}$ and $\Delta\Gamma_{B_S^0}$ (and their correlation).

VALUE ($10^{-12} s$)	DOCUMENT ID	TECN	COMMENT
1.620 ± 0.007 OUR EVALUATION			
• • • We do not use the following data for averages, fits, limits, etc. • • •			
$1.677 \pm 0.034 \pm 0.011$	1 SIRU NYAN 18BY CMS	CMS	$p\bar{p}$ at 8 TeV
$2.04 \pm 0.44 \pm 0.05$	2 AAIJ 17AI LHCb	LHCb	$p\bar{p}$ at 7, 8, 13 TeV
$1.70 \pm 0.14 \pm 0.05$	3 ABAZOV 16C D0	D0	$p\bar{p}$ at 1.96 TeV
$1.75 \pm 0.12 \pm 0.07$	4 AAIJ 13AB LHCb	LHCb	$p\bar{p}$ at 7 TeV
$1.652 \pm 0.024 \pm 0.024$	5 AAIJ 13AR LHCb	LHCb	$p\bar{p}$ at 7 TeV
$1.700 \pm 0.040 \pm 0.026$	6 AAIJ 12AN LHCb	LHCb	$p\bar{p}$ at 7 TeV
	7 AALTONEN 12D CDF	CDF	$p\bar{p}$ at 1.96 TeV
$1.70^{+0.12}_{-0.11} \pm 0.03$	6 AALTONEN 11AB CDF	CDF	$p\bar{p}$ at 1.96 TeV
$1.613^{+0.123}_{-0.113}$	8,9 AALTONEN 08J CDF	CDF	Repl. by AALTONEN 12D
$1.58^{+0.39+0.01}_{-0.42-0.02}$	9 ABAZOV 05W D0	D0	Repl. by ABAZOV 08AM
$2.07^{+0.58}_{-0.46} \pm 0.03$	9 ACOSTA 05 CDF	CDF	Repl. by AALTONEN 08J

Meson Particle Listings

 B_S^0

- Measured using $B_S^0 \rightarrow J/\psi \pi^+ \pi^-$ decays with $0.9240 < m(\pi\pi) < 1.0204$ GeV, which is dominated by the $f_0(980)$ resonance, making it a CP -odd state.
- Measured using $B_S \rightarrow \mu^+ \mu^-$ decays which, in the Standard Model, correspond to B_{SH}^0 decays. Assumes $-2 \operatorname{Re}(\lambda)/(1 + |\lambda|^2) = 1$.
- Measured using $J/\psi \pi^+ \pi^-$ mode with $0.880 < m(\pi\pi) < 1.080$ GeV/ c^2 , which is mostly $J/\psi f(0)(980)$ mode, a pure CP -odd final state.
- Measured using a pure CP -odd final state $J/\psi K_S^0$ with the assumption that contributions from penguin diagrams are small.
- Measured using $B_S \rightarrow J/\psi \pi^+ \pi^-$ decays which, in the limit of $\phi_S = 0$ and $|\lambda| = 1$, correspond to B_{SH}^0 decays.
- Measured using a pure CP -odd final state $J/\psi f_0(980)$.
- Uses the time-dependent angular analysis of $B_S^0 \rightarrow J/\psi \phi$ decays assuming CP -violating angle $\beta_S(B^0 \rightarrow J/\psi \phi) = 0.02$.
- Obtained from $\Delta\Gamma_S$ and Γ_S fit with a correlation of 0.6.
- Measured using the time-dependent angular analysis of $B_S^0 \rightarrow J/\psi \phi$ decays.

 B_{sL}^0 MEAN LIFE

B_{sL}^0 is the light mass state of two B_S^0 CP eigenstates.

"OUR EVALUATION" is provided by the Heavy Flavor Averaging Group (HFLAV, <https://hflav.web.cern.ch/>). It is derived from the averages of $\Gamma_{B_S^0}$ and $\Delta\Gamma_{B_S^0}$ (and their correlation).

VALUE (10^{-12} s)	DOCUMENT ID	TECN	COMMENT
-----------------------	-------------	------	---------

1.423 ± 0.005 OUR EVALUATION

VALUE (10^{-12} s)	DOCUMENT ID	TECN	COMMENT
1.40 ± 0.02	1 SIRUNYAN	18BY CMS	pp at 8 TeV
1.479 ± 0.034 ± 0.011	2 AAIJ	16AL LHCb	pp at 7, 8 TeV
1.379 ± 0.026 ± 0.017	3 AAIJ	14F LHCb	pp at 7, 8 TeV
1.407 ± 0.016 ± 0.007	4 AAIJ	14R LHCb	pp at 7 TeV
1.440 ± 0.096 ± 0.009	4 AAIJ	12 LHCb	Repl. by AAIJ 14R
1.455 ± 0.046 ± 0.006	4 AAIJ	12R LHCb	Repl. by AAIJ 14R
	5 AALTONEN	12D CDF	$p\bar{p}$ at 1.96 TeV
1.437 ^{+0.054} _{-0.047}	6,7 AALTONEN	08J CDF	Repl. by AALTONEN 12D
1.24 ^{+0.14} _{-0.11} ^{+0.01} _{-0.02}	7 ABAZOV	05W D0	Repl. by ABAZOV 08AM
1.05 ^{+0.16} _{-0.13} ± 0.02	7 ACOSTA	05 CDF	Repl. by AALTONEN 08J
1.27 ± 0.33 ± 0.08	8 BARATE	00K ALEP	$e^+e^- \rightarrow Z$

- Measured using results in SIRUNYAN 18BY for the heavy B_S^0 lifetime obtained from $B_S^0 \rightarrow J/\psi \pi^+ \pi^-$ decays and the average effective $B_S^0 \rightarrow J/\psi \phi$ lifetime, and magnitude squared of the CP -odd amplitude $|A_{\perp}|^2 = 0.250 \pm 0.006$. The uncertainty includes all statistical and systematic contributions.
- Measured using $B_S^0 \rightarrow J/\psi \eta$ decays.
- Measured using $B_S^0 \rightarrow D_S^- D_S^+$. The effective lifetime is translated into a decay width of $\Gamma_L = 0.725 \pm 0.014 \pm 0.009$ ps $^{-1}$.
- Measured using $B_S^0 \rightarrow K^+ K^-$ decays. There may still be CPV in the decay.
- Uses the time-dependent angular analysis of $B_S^0 \rightarrow J/\psi \phi$ decays and assuming CP -violating angle $\beta_S(B^0 \rightarrow J/\psi \phi) = 0.02$.
- Obtained from $\Delta\Gamma_S$ and Γ_S fit with a correlation of 0.6.
- Measured using the time-dependent angular analysis of $B_S^0 \rightarrow J/\psi \phi$ decays.
- Uses ϕ correlations from $B_S^0 \rightarrow D_S^{(*)+} D_S^{(*)-}$.

 B_S^0 MEAN LIFE (Flavor specific)

VALUE (10^{-12} s)	DOCUMENT ID	TECN	COMMENT
-----------------------	-------------	------	---------

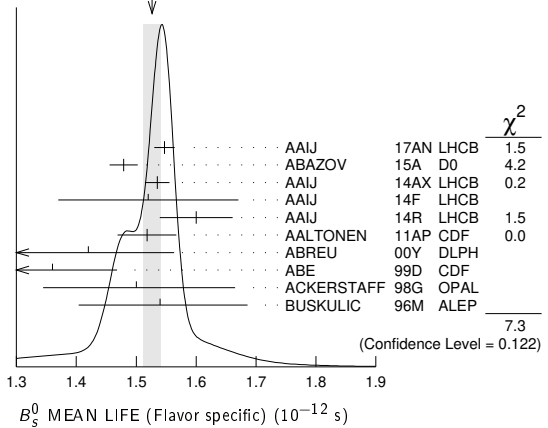
1.527 ± 0.011 OUR EVALUATION

VALUE (10^{-12} s)	DOCUMENT ID	TECN	COMMENT
1.526 ± 0.015 OUR AVERAGE	Error includes scale factor of 1.3. See the ideogram below.		
1.547 ± 0.013 ± 0.011	1 AAIJ	17AN LHCb	pp at 7, 8 TeV
1.479 ± 0.010 ± 0.021	2 ABAZOV	15A D0	$p\bar{p}$ at 1.96 TeV
1.535 ± 0.015 ± 0.014	3 AAIJ	14AX LHCb	pp at 7 TeV
1.52 ± 0.15 ± 0.01	4 AAIJ	14F LHCb	pp at 7, 8 TeV
1.60 ± 0.06 ± 0.01	5 AAIJ	14R LHCb	pp at 7 TeV
1.518 ± 0.041 ± 0.027	6 AALTONEN	11AP CDF	$p\bar{p}$ at 1.96 TeV
1.42 ^{+0.14} _{-0.13} ± 0.03	7 ABREU	00Y DLPH	$e^+e^- \rightarrow Z$
1.36 ± 0.09 ^{+0.06} _{-0.05}	8 ABE	99D CDF	$p\bar{p}$ at 1.8 TeV
1.50 ^{+0.16} _{-0.15} ± 0.04	8 ACKERSTAFF	98G OPAL	$e^+e^- \rightarrow Z$
1.54 ^{+0.14} _{-0.13} ± 0.04	8 BUSKULIC	96M ALEP	$e^+e^- \rightarrow Z$
1.398 ± 0.044 ^{+0.028} _{-0.025}	9 ABAZOV	06V D0	Repl. by ABAZOV 15A

- AAIJ 17AN value was measured using $B_S^0 \rightarrow D_S^{(*)-} \mu^+ \nu_\mu$ decays relative to $B^0 \rightarrow D^{(*)-} \mu^+ \nu_\mu$ decays.
- Measured using $B_S^0 \rightarrow D_S^- \mu^+ \nu_\mu X$ decays.
- Measured using the $B_S^0 \rightarrow D_S^- \pi^+$ decays.
- Measured using $B_S^0 \rightarrow D^+ D_S^-$.

- Measured using $B_S^0 \rightarrow \pi^+ K^-$ decays.
- AALTONEN 11AP combines the fully reconstructed $B_S^0 \rightarrow D_S^- \pi^+$ decays and partially reconstructed $B_S^0 \rightarrow D_S X$ decays.
- Uses $D_S^- \ell^+$, and $\phi \ell^+$ vertices.
- Measured using $D_S^- \ell^+$ vertices.
- Measured using $D_S^- \mu^+$ vertices.

WEIGHTED AVERAGE
1.526 ± 0.015 (Error scaled by 1.3)

 B_S^0 MEAN LIFE ($B_S \rightarrow J/\psi \phi$)

VALUE (10^{-12} s)	DOCUMENT ID	TECN	COMMENT
-----------------------	-------------	------	---------

1.480 ± 0.007 OUR EVALUATION

VALUE (10^{-12} s)	DOCUMENT ID	TECN	COMMENT
1.480 ± 0.007 ± 0.005	1 SIRUNYAN	18BY CMS	pp at 8 TeV
1.480 ± 0.011 ± 0.005	1 AAIJ	14E LHCb	pp at 7 TeV
1.444 ^{+0.098} _{-0.090} ± 0.020	1 ABAZOV	05B D0	$p\bar{p}$ at 1.96 TeV
1.34 ^{+0.23} _{-0.19} ± 0.05	2 ABE	98B CDF	$p\bar{p}$ at 1.8 TeV
1.39 ^{+0.13} _{-0.16} ^{+0.01} _{-0.02}	2 ABAZOV	05W D0	$p\bar{p}$ at 1.96 TeV
1.34 ^{+0.23} _{-0.19} ± 0.05	3 ABE	96N CDF	Repl. by ABE 98B

- Measured using fully reconstructed $B_S \rightarrow J/\psi \phi$ decays.
- Measured using the time-dependent angular analysis of $B_S^0 \rightarrow J/\psi \phi$ decays.
- ABE 96N uses 58 ± 12 exclusive $B_S \rightarrow J/\psi \phi$ events.

 $\tau_{B_S^0}/\tau_{B^0}$ MEAN LIFE RATIO

$\tau_{B_S^0}/\tau_{B^0}$ (direct measurements)

VALUE	DOCUMENT ID	TECN	COMMENT
-------	-------------	------	---------

0.980 ± 0.006 ± 0.003

- SIRUNYAN 18BY CMS pp at 8 TeV
- Measured using $B_S^0 \rightarrow J/\psi \phi(1020)$ and $B^0 \rightarrow J/\psi K^*(892)^0$ decays.

 $\Gamma_{B_S^0} - \Gamma_{B^0}$

VALUE (10^{12} s $^{-1}$)	DOCUMENT ID	TECN	COMMENT
-------------------------------	-------------	------	---------

-0.0041 ± 0.0024 ± 0.0015

- AAIJ 19Q LHCb pp at 13 TeV
- Measured using time-dependent angular analysis of $B_S^0 \rightarrow J/\psi K^+ K^-$ decays.

 $\Gamma_{B_{SH}^0} - \Gamma_{B^0}$

VALUE (10^{12} s $^{-1}$)	DOCUMENT ID	TECN	COMMENT
-------------------------------	-------------	------	---------

-0.05 ± 0.004 ± 0.004

- AAIJ 19AF LHCb pp at 7, 8, 13 TeV
- Measured in $B_S^0 \rightarrow J/\psi \pi^+ \pi^-$ decays.

 B_S^0 DECAY MODES

These branching fractions all scale with $B(\bar{B} \rightarrow B_S^0)$.

The branching fraction $B(B_S^0 \rightarrow D_S^- \ell^+ \nu_\ell \text{ anything})$ is not a pure measurement since the measured product branching fraction $B(\bar{B} \rightarrow B_S^0) \times B(B_S^0 \rightarrow D_S^- \ell^+ \nu_\ell \text{ anything})$ was used to determine $B(\bar{B} \rightarrow B_S^0)$, as described in the note on " B^0 - \bar{B}^0 Mixing"

For inclusive branching fractions, e.g., $B \rightarrow D^\pm \text{ anything}$, the values usually are multiplicities, not branching fractions. They can be greater than one.

Mode	Fraction (Γ_i/Γ)	Scale factor/ Confidence level			
$\Gamma_1 D_s^-$ anything	(93 ± 25) %		$\Gamma_{60} J/\psi(1S) f_2(1270), f_2 \rightarrow$	$(1.1 \pm 0.4) \times 10^{-6}$	
$\Gamma_2 \ell \nu_\ell X$	(9.6 ± 0.8) %		$\Gamma_{61} J/\psi(1S) f_2(1270)_0, f_2 \rightarrow$	$(7.5 \pm 1.8) \times 10^{-7}$	
$\Gamma_3 e^+ \nu X^-$	(9.1 ± 0.8) %		$\Gamma_{62} J/\psi(1S) f_2(1270)_\parallel, f_2 \rightarrow$	$(1.09 \pm 0.34) \times 10^{-6}$	
$\Gamma_4 \mu^+ \nu X^-$	(10.2 ± 1.0) %		$\Gamma_{63} J/\psi(1S) f_2(1270)_\perp, f_2 \rightarrow$	$(1.3 \pm 0.8) \times 10^{-6}$	
$\Gamma_5 D_s^- \ell^+ \nu_\ell$ anything	[a] (8.1 ± 1.3) %		$\Gamma_{64} J/\psi(1S) f_0(1370), f_0 \rightarrow$	$(4.5 \pm_{-4.0}^{+0.7}) \times 10^{-5}$	
$\Gamma_6 D_s^{*-} \ell^+ \nu_\ell$ anything	(5.4 ± 1.1) %		$\Gamma_{65} J/\psi(1S) f_0(1500), f_0 \rightarrow$	$(2.11 \pm_{-0.29}^{+0.40}) \times 10^{-5}$	
$\Gamma_7 D_{s1}(2536)^- \mu^+ \nu_\mu, D_{s1}^- \rightarrow$ $D^{*-} K_S^0$	(2.7 ± 0.7) × 10 ⁻³		$\Gamma_{66} J/\psi(1S) f_2'(1525)_0, f_2' \rightarrow$	$(1.07 \pm 0.24) \times 10^{-6}$	
$\Gamma_8 D_{s1}(2536)^- X \mu^+ \nu, D_{s1}^- \rightarrow$ $\bar{D}^0 K^+$	(4.4 ± 1.3) × 10 ⁻³		$\Gamma_{67} J/\psi(1S) f_2'(1525)_\parallel, f_2' \rightarrow$	$(1.3 \pm_{-0.9}^{+2.7}) \times 10^{-7}$	
$\Gamma_9 D_{s2}(2573)^- X \mu^+ \nu, D_{s2}^- \rightarrow$ $\bar{D}^0 K^+$	(2.7 ± 1.0) × 10 ⁻³		$\Gamma_{68} J/\psi(1S) f_2'(1525)_\perp, f_2' \rightarrow$	$(5 \pm 4) \times 10^{-7}$	
$\Gamma_{10} D_s^- \pi^+$	(3.00 ± 0.23) × 10 ⁻³		$\Gamma_{69} J/\psi(1S) f_0(1790), f_0 \rightarrow$	$(5.0 \pm_{-1.1}^{+11.0}) \times 10^{-6}$	
$\Gamma_{11} D_s^- \rho^+$	(6.9 ± 1.4) × 10 ⁻³		$\Gamma_{70} J/\psi(1S) \pi^+ \pi^-$ (nonresonant)	$(1.8 \pm_{-0.4}^{+1.1}) \times 10^{-5}$	
$\Gamma_{12} D_s^- \pi^+ \pi^+ \pi^-$	(6.1 ± 1.0) × 10 ⁻³		$\Gamma_{71} J/\psi(1S) \bar{K}^0 \pi^+ \pi^-$	$< 4.4 \times 10^{-5}$	CL=90%
$\Gamma_{13} D_{s1}(2536)^- \pi^+, D_{s1}^- \rightarrow$ $D_s^- \pi^+ \pi^-$	(2.5 ± 0.8) × 10 ⁻⁵		$\Gamma_{72} J/\psi(1S) K^+ K^-$	$(7.9 \pm 0.7) \times 10^{-4}$	
$\Gamma_{14} D_s^{\mp} K^\pm$	(2.27 ± 0.19) × 10 ⁻⁴		$\Gamma_{73} J/\psi(1S) K^0 K^- \pi^+ + c.c.$	$(9.2 \pm 1.3) \times 10^{-4}$	
$\Gamma_{15} D_s^- K^+ \pi^+ \pi^-$	(3.2 ± 0.6) × 10 ⁻⁴		$\Gamma_{74} J/\psi(1S) \bar{K}^0 K^+ K^-$	$< 1.2 \times 10^{-5}$	CL=90%
$\Gamma_{16} D_s^+ D_s^-$	(4.4 ± 0.5) × 10 ⁻³		$\Gamma_{75} J/\psi(1S) f_2'(1525)$	$(2.6 \pm 0.6) \times 10^{-4}$	
$\Gamma_{17} D_s^- D^+$	(2.8 ± 0.5) × 10 ⁻⁴		$\Gamma_{76} J/\psi(1S) \rho \bar{\rho}$	$(3.6 \pm 0.4) \times 10^{-6}$	
$\Gamma_{18} D^+ D^-$	(2.2 ± 0.6) × 10 ⁻⁴		$\Gamma_{77} J/\psi(1S) \gamma$	$< 7.3 \times 10^{-6}$	CL=90%
$\Gamma_{19} D^0 \bar{D}^0$	(1.9 ± 0.5) × 10 ⁻⁴		$\Gamma_{78} J/\psi(1S) \pi^+ \pi^- \pi^+ \pi^-$	$(7.8 \pm 1.0) \times 10^{-5}$	
$\Gamma_{20} D_s^{*-} \pi^+$	(2.0 ± 0.5) × 10 ⁻³		$\Gamma_{79} J/\psi(1S) f_1(1285)$	$(7.2 \pm 1.4) \times 10^{-5}$	
$\Gamma_{21} D_s^{\mp} K^\pm$	(1.33 ± 0.35) × 10 ⁻⁴		$\Gamma_{80} \psi(2S) \eta$	$(3.3 \pm 0.9) \times 10^{-4}$	
$\Gamma_{22} D_s^{\mp} \rho^+$	(9.6 ± 2.1) × 10 ⁻³		$\Gamma_{81} \psi(2S) \eta'$	$(1.29 \pm 0.35) \times 10^{-4}$	
$\Gamma_{23} D_s^{*+} D_s^- + D_s^{*-} D_s^+$	(1.39 ± 0.17) %		$\Gamma_{82} \psi(2S) \pi^+ \pi^-$	$(7.1 \pm 1.3) \times 10^{-5}$	
$\Gamma_{24} D_s^{*+} D_s^{*-}$	(1.44 ± 0.21) %	S=1.1	$\Gamma_{83} \psi(2S) \phi$	$(5.4 \pm 0.6) \times 10^{-4}$	
$\Gamma_{25} D_s^{(*)+} D_s^{(*)-}$	(4.5 ± 1.4) %		$\Gamma_{84} \psi(2S) K^- \pi^+$	$(3.1 \pm 0.4) \times 10^{-5}$	
$\Gamma_{26} \bar{D}^{*0} \bar{K}^0$	(2.8 ± 1.1) × 10 ⁻⁴		$\Gamma_{85} \psi(2S) \bar{K}^*(892)^0$	$(3.3 \pm 0.5) \times 10^{-5}$	
$\Gamma_{27} \bar{D}^0 \bar{K}^0$	(4.3 ± 0.9) × 10 ⁻⁴		$\Gamma_{86} \chi_{c1} \phi$	$(2.04 \pm 0.30) \times 10^{-4}$	
$\Gamma_{28} \bar{D}^0 K^- \pi^+$	(1.04 ± 0.13) × 10 ⁻³		$\Gamma_{87} \chi_{c1} K^+ K^-$		
$\Gamma_{29} \bar{D}^0 \bar{K}^*(892)^0$	(4.4 ± 0.6) × 10 ⁻⁴		$\Gamma_{88} \chi_{c2} K^+ K^-$		
$\Gamma_{30} \bar{D}^0 \bar{K}^*(1410)$	(3.9 ± 3.5) × 10 ⁻⁴		$\Gamma_{89} \pi^+ \pi^-$	$(7.0 \pm 1.0) \times 10^{-7}$	
$\Gamma_{31} \bar{D}^0 \bar{K}_0^*(1430)$	(3.0 ± 0.7) × 10 ⁻⁴		$\Gamma_{90} \pi^0 \pi^0$	$< 2.1 \times 10^{-4}$	CL=90%
$\Gamma_{32} \bar{D}^0 \bar{K}_2^*(1430)$	(1.1 ± 0.4) × 10 ⁻⁴		$\Gamma_{91} \eta \pi^0$	$< 1.0 \times 10^{-3}$	CL=90%
$\Gamma_{33} \bar{D}^0 \bar{K}^*(1680)$	$< 7.8 \times 10^{-5}$	CL=90%	$\Gamma_{92} \eta \eta$	$< 1.5 \times 10^{-3}$	CL=90%
$\Gamma_{34} \bar{D}^0 \bar{K}_0^*(1950)$	$< 1.1 \times 10^{-4}$	CL=90%	$\Gamma_{93} \rho^0 \rho^0$	$< 3.20 \times 10^{-4}$	CL=90%
$\Gamma_{35} \bar{D}^0 \bar{K}_2^*(1780)$	$< 2.6 \times 10^{-5}$	CL=90%	$\Gamma_{94} \eta' \eta'$	$(3.3 \pm 0.7) \times 10^{-5}$	
$\Gamma_{36} \bar{D}^0 \bar{K}_4^*(2045)$	$< 3.1 \times 10^{-5}$	CL=90%	$\Gamma_{95} \eta' \phi$	$< 8.2 \times 10^{-7}$	CL=90%
$\Gamma_{37} \bar{D}^0 K^- \pi^+$ (non-resonant)	(2.1 ± 0.8) × 10 ⁻⁴		$\Gamma_{96} \phi f_0(980), f_0(980) \rightarrow \pi^+ \pi^-$	$(1.12 \pm 0.21) \times 10^{-6}$	
$\Gamma_{38} D_{s2}^*(2573)^- \pi^+, D_{s2}^* \rightarrow$ $\bar{D}^0 K^-$	(2.6 ± 0.4) × 10 ⁻⁴		$\Gamma_{97} \phi f_2(1270), f_2(1270) \rightarrow$ $\pi^+ \pi^-$	$(6.1 \pm_{-1.5}^{+1.8}) \times 10^{-7}$	
$\Gamma_{39} D_{s1}^*(2700)^- \pi^+, D_{s1}^* \rightarrow$ $\bar{D}^0 K^-$	(1.6 ± 0.8) × 10 ⁻⁵		$\Gamma_{98} \phi \rho^0$	$(2.7 \pm 0.8) \times 10^{-7}$	
$\Gamma_{40} D_{s1}^*(2860)^- \pi^+, D_{s1}^* \rightarrow$ $\bar{D}^0 K^-$	(5 ± 4) × 10 ⁻⁵		$\Gamma_{99} \phi \pi^+ \pi^-$	$(3.5 \pm 0.5) \times 10^{-6}$	
$\Gamma_{41} D_{s3}^*(2860)^- \pi^+, D_{s3}^* \rightarrow$ $\bar{D}^0 K^-$	(2.2 ± 0.6) × 10 ⁻⁵		$\Gamma_{100} \phi \phi$	$(1.87 \pm 0.15) \times 10^{-5}$	
$\Gamma_{42} \bar{D}^0 K^+ K^-$	(5.5 ± 0.8) × 10 ⁻⁵		$\Gamma_{101} \phi \phi \phi$	$(2.2 \pm 0.7) \times 10^{-6}$	
$\Gamma_{43} \bar{D}^0 f_0(980)$	$< 3.1 \times 10^{-6}$	CL=90%	$\Gamma_{102} \pi^+ K^-$	$(5.8 \pm 0.7) \times 10^{-6}$	
$\Gamma_{44} \bar{D}^0 \phi$	(3.0 ± 0.5) × 10 ⁻⁵		$\Gamma_{103} K^+ K^-$	$(2.66 \pm 0.22) \times 10^{-5}$	
$\Gamma_{45} \bar{D}^{*0} \phi$	(3.7 ± 0.6) × 10 ⁻⁵		$\Gamma_{104} K^0 \bar{K}^0$	$(2.0 \pm 0.6) \times 10^{-5}$	
$\Gamma_{46} D^{*\mp} \pi^\pm$	$< 6.1 \times 10^{-6}$	CL=90%	$\Gamma_{105} K^0 \pi^+ \pi^-$	$(9.5 \pm 2.1) \times 10^{-6}$	
$\Gamma_{47} \eta_c \phi$	(5.0 ± 0.9) × 10 ⁻⁴		$\Gamma_{106} K^0 K^\pm \pi^\mp$	$(8.4 \pm 0.9) \times 10^{-5}$	
$\Gamma_{48} \eta_c \pi^+ \pi^-$	(1.8 ± 0.7) × 10 ⁻⁴		$\Gamma_{107} K^*(892)^- \pi^+$	$(2.9 \pm 1.1) \times 10^{-6}$	
$\Gamma_{49} J/\psi(1S) \phi$	(1.08 ± 0.08) × 10 ⁻³		$\Gamma_{108} K^*(892)^\pm K^\mp$	$(1.9 \pm 0.5) \times 10^{-5}$	
$\Gamma_{50} J/\psi(1S) \phi \phi$	$(1.24 \pm_{-0.19}^{+0.17}) \times 10^{-5}$		$\Gamma_{109} K_0^*(1430)^\pm K^\mp$	$(3.1 \pm 2.5) \times 10^{-5}$	
$\Gamma_{51} J/\psi(1S) \pi^0$	$< 1.2 \times 10^{-3}$	CL=90%	$\Gamma_{110} K_2^*(1430)^\pm K^\mp$	$(1.0 \pm 1.7) \times 10^{-5}$	
$\Gamma_{52} J/\psi(1S) \eta$	(4.0 ± 0.7) × 10 ⁻⁴	S=1.4	$\Gamma_{111} K^*(892)^0 \bar{K}^0 + c.c.$	$(2.0 \pm 0.6) \times 10^{-5}$	
$\Gamma_{53} J/\psi(1S) K_S^0$	(1.88 ± 0.15) × 10 ⁻⁵		$\Gamma_{112} K_0^*(1430) \bar{K}^0 + c.c.$	$(3.3 \pm 1.0) \times 10^{-5}$	
$\Gamma_{54} J/\psi(1S) \bar{K}^*(892)^0$	(4.1 ± 0.4) × 10 ⁻⁵		$\Gamma_{113} K_2^*(1430)^0 \bar{K}^0 + c.c.$	$(1.7 \pm 2.2) \times 10^{-5}$	
$\Gamma_{55} J/\psi(1S) \eta'$	(3.3 ± 0.4) × 10 ⁻⁴		$\Gamma_{114} K_0^0 \bar{K}^*(892)^0 + c.c.$	$(1.6 \pm 0.4) \times 10^{-5}$	
$\Gamma_{56} J/\psi(1S) \pi^+ \pi^-$	(2.09 ± 0.23) × 10 ⁻⁴	S=1.3	$\Gamma_{115} K^0 K^+ K^-$	$(1.3 \pm 0.6) \times 10^{-6}$	
$\Gamma_{57} J/\psi(1S) f_0(500), f_0 \rightarrow$ $\pi^+ \pi^-$	$< 4 \times 10^{-6}$	CL=90%	$\Gamma_{116} \bar{K}^*(892)^0 \rho^0$	$< 7.67 \times 10^{-4}$	CL=90%
$\Gamma_{58} J/\psi(1S) \rho, \rho \rightarrow \pi^+ \pi^-$	$< 4 \times 10^{-6}$	CL=90%	$\Gamma_{117} \bar{K}^*(892)^0 K^*(892)^0$	$(1.11 \pm 0.27) \times 10^{-5}$	
$\Gamma_{59} J/\psi(1S) f_0(980), f_0 \rightarrow$ $\pi^+ \pi^-$	(1.28 ± 0.18) × 10 ⁻⁴	S=1.7	$\Gamma_{118} K^*(892)^0 \bar{K}_2^*(1430)^0$		
			$\Gamma_{119} K_2^*(1430)^0 \bar{K}^*(892)^0$		
			$\Gamma_{120} K_2^*(1430)^0 \bar{K}_2^*(1430)^0$		
			$\Gamma_{121} \phi K^*(892)^0$	$(1.14 \pm 0.30) \times 10^{-6}$	
			$\Gamma_{122} \rho \bar{\rho}$	$< 1.5 \times 10^{-8}$	CL=90%

Meson Particle Listings

B_s^0

Γ_{123}	$p\bar{p}K^+K^-$		$(4.5 \pm 0.5) \times 10^{-6}$	
Γ_{124}	$p\bar{p}K^+\pi^-$		$(1.39 \pm 0.26) \times 10^{-6}$	
Γ_{125}	$p\bar{p}\pi^+\pi^-$		$(4.3 \pm 2.0) \times 10^{-7}$	
Γ_{126}	$p\bar{p}K^- + c.c.$		$(5.5 \pm 1.0) \times 10^{-6}$	
Γ_{127}	$\Lambda_c^- \Lambda\pi^+$		$(3.6 \pm 1.6) \times 10^{-4}$	
Γ_{128}	$\Lambda_c^- \Lambda_c^+$		$< 8.0 \times 10^{-5}$	CL=95%

Lepton Family number (LF) violating modes or $\Delta B = 1$ weak neutral current (B1) modes

Γ_{129}	$\gamma\gamma$	B1	$< 3.1 \times 10^{-6}$	CL=90%
Γ_{130}	$\phi\gamma$	B1	$(3.4 \pm 0.4) \times 10^{-5}$	
Γ_{131}	$\mu^+\mu^-$	B1	$(3.0 \pm 0.4) \times 10^{-9}$	
Γ_{132}	e^+e^-	B1	$< 2.8 \times 10^{-7}$	CL=90%
Γ_{133}	$\tau^+\tau^-$	B1	$< 6.8 \times 10^{-3}$	CL=95%
Γ_{134}	$\mu^+\mu^-\mu^+\mu^-$	B1	$< 2.5 \times 10^{-9}$	CL=95%
Γ_{135}	$SP, S \rightarrow \mu^+\mu^-, P \rightarrow \mu^+\mu^-$	B1	$[b] < 2.2 \times 10^{-9}$	CL=95%
Γ_{136}	$\phi(1020)\mu^+\mu^-$	B1	$(8.2 \pm 1.2) \times 10^{-7}$	
Γ_{137}	$K^*(892)^0\mu^+\mu^-$		$(2.9 \pm 1.1) \times 10^{-8}$	
Γ_{138}	$\pi^+\pi^-\mu^+\mu^-$	B1	$(8.4 \pm 1.7) \times 10^{-8}$	
Γ_{139}	$\phi\nu\bar{\nu}$	B1	$< 5.4 \times 10^{-3}$	CL=90%
Γ_{140}	$e^\pm\mu^\mp$	LF	$[c] < 5.4 \times 10^{-9}$	CL=90%
Γ_{141}	$\mu^\pm\tau^\mp$		$< 4.2 \times 10^{-5}$	CL=95%

- [a] Not a pure measurement. See note at head of B_s^0 Decay Modes.
- [b] Here S and P are the hypothetical scalar and pseudoscalar particles with masses of 2.5 GeV/c² and 214.3 MeV/c², respectively.
- [c] The value is for the sum of the charge states or particle/antiparticle states indicated.

CONSTRAINED FIT INFORMATION

An overall fit to 12 branching ratios uses 20 measurements and one constraint to determine 8 parameters. The overall fit has a $\chi^2 = 26.7$ for 13 degrees of freedom.

The following *off-diagonal* array elements are the correlation coefficients $\langle \delta x_i \delta x_j \rangle / (\delta x_i \delta x_j)$, in percent, from the fit to the branching fractions, $x_i \equiv \Gamma_i / \Gamma_{total}$. The fit constrains the x_i whose labels appear in this array to sum to one.

x_{12}	28					
x_{14}	92	26				
x_{49}	0	0	0			
x_{56}	0	0	0	72		
x_{59}	0	0	0	57	67	
x_{100}	0	0	0	29	21	17
	x_{10}	x_{12}	x_{14}	x_{49}	x_{56}	x_{59}

B_s^0 BRANCHING RATIOS

$\Gamma(D_s^- \text{ anything}) / \Gamma_{total}$ Γ_1 / Γ

VALUE	EVTS	DOCUMENT ID	TECN	COMMENT
0.93 ± 0.25 OUR AVERAGE				
0.91 ± 0.18 ± 0.41		¹ DRUTSKOY 07	BELL	$e^+e^- \rightarrow \Upsilon(4S)$
0.81 ± 0.24 ± 0.22	90	² BUSKULIC 96E	ALEP	$e^+e^- \rightarrow Z$
1.56 ± 0.58 ± 0.44	147	³ ACTON 92N	OPAL	$e^+e^- \rightarrow Z$

- The extraction of this result takes into account the correlation between the measurements of $B(\Upsilon(5S) \rightarrow D_s X)$ and $B(\Upsilon(5S) \rightarrow D^0 X)$.
- BUSKULIC 96E separate $c\bar{c}$ and $b\bar{b}$ sources of D_s^+ mesons using a lifetime tag, subtract generic $\bar{b} \rightarrow W^+ \rightarrow D_s^+$ events, and obtain $B(\bar{b} \rightarrow B_s^0) \times B(B_s^0 \rightarrow D_s^- \text{ anything}) = 0.088 \pm 0.020 \pm 0.020$ assuming $B(D_s \rightarrow \phi\pi) = (3.5 \pm 0.4) \times 10^{-2}$ and PDG 1994 values for the relative partial widths to other D_s channels. We evaluate using our current values $B(\bar{b} \rightarrow B_s^0) = 0.107 \pm 0.014$ and $B(D_s \rightarrow \phi\pi) = 0.036 \pm 0.009$. Our first error is their experiment's and our second error is that due to $B(\bar{b} \rightarrow B_s^0)$ and $B(D_s \rightarrow \phi\pi)$.
- ACTON 92N assume that excess of $147 \pm 48 D_s^0$ events over that expected from $B^0, B^+,$ and $c\bar{c}$ is all from B_s^0 decay. The product branching fraction is measured to be $B(\bar{b} \rightarrow B_s^0)B(B_s^0 \rightarrow D_s^- \text{ anything}) \times B(D_s^- \rightarrow \phi\pi^-) = (5.9 \pm 1.9 \pm 1.1) \times 10^{-3}$. We evaluate using our current values $B(\bar{b} \rightarrow B_s^0) = 0.107 \pm 0.014$ and $B(D_s \rightarrow \phi\pi) = 0.036 \pm 0.009$. Our first error is their experiment's and our second error is that due to $B(\bar{b} \rightarrow B_s^0)$ and $B(D_s \rightarrow \phi\pi)$.

$\Gamma(\ell\nu_e X) / \Gamma_{total}$ Γ_2 / Γ

VALUE (units 10^{-2})	DOCUMENT ID	TECN	COMMENT
9.6 ± 0.8 OUR AVERAGE			
9.6 ± 0.4 ± 0.7	¹ OSWALD 13	BELL	$e^+e^- \rightarrow \Upsilon(5S)$
9.5 ^{+2.5+1.1} _{-2.0-1.9}	² LEES 12A	BABR	e^+e^-

- The measurement corresponds to the average of the electron and muon branching fractions.
- The measurement corresponds to a branching fraction where the lepton originates from bottom decay and is the average between the electron and muon branching fractions. LEES 12A uses the correlation of the production of ϕ mesons in association with a lepton in e^+e^- data taken at center-of-mass energies between 10.54 and 11.2 GeV.

$\Gamma(e^+ \nu X^-) / \Gamma_{total}$ Γ_3 / Γ

VALUE (units 10^{-2})	DOCUMENT ID	TECN	COMMENT
9.1 ± 0.5 ± 0.6			
	OSWALD 13	BELL	$e^+e^- \rightarrow \Upsilon(5S)$

$\Gamma(\mu^+ \nu X^-) / \Gamma_{total}$ Γ_4 / Γ

VALUE (units 10^{-2})	DOCUMENT ID	TECN	COMMENT
10.2 ± 0.6 ± 0.8			
	OSWALD 13	BELL	$e^+e^- \rightarrow \Upsilon(5S)$

$\Gamma(D_s^- \ell^+ \nu_\ell \text{ anything}) / \Gamma_{total}$ Γ_5 / Γ

The values and averages in this section serve only to show what values result if one assumes our $B(\bar{b} \rightarrow B_s^0)$. They cannot be thought of as measurements since the underlying product branching fractions were also used to determine $B(\bar{b} \rightarrow B_s^0)$ as described in the note on "Production and Decay of b-Flavored Hadrons."

VALUE (units 10^{-2})	EVTS	DOCUMENT ID	TECN	COMMENT
8.1 ± 1.3 OUR AVERAGE				
8.2 ± 0.2 ± 1.5		¹ OSWALD 15	BELL	$e^+e^- \rightarrow \Upsilon(5S)$
7.6 ± 1.2 ± 2.1	134	² BUSKULIC 95O	ALEP	$e^+e^- \rightarrow Z$
10.7 ± 4.3 ± 2.9		³ ABREU 92M	DLPH	$e^+e^- \rightarrow Z$
10.3 ± 3.6 ± 2.8	18	⁴ ACTON 92N	OPAL	$e^+e^- \rightarrow Z$
13 ± 4 ± 4	27	⁵ BUSKULIC 92E	ALEP	$e^+e^- \rightarrow Z$

- We do not use the following data for averages, fits, limits, etc. •••
- Obtains $B_s \rightarrow D_s X e \nu$, and $D_s X \mu \nu$ separately, then combines them by assuming systematic uncertainties are fully correlated, except for the one on lepton identification. The third uncertainty adds in quadrature systematic uncertainties from external sources (number of B_s events, and $D_s^{(*)}$ branching fractions). OSWALD 15 also measures the cross-section $\sigma(e^+e^- \rightarrow B_s^{(*)} \bar{B}_s^{(*)}) = 53.8 \pm 1.4 \pm 5.3$ pb at $\sqrt{s} = 10.86$ GeV.
 - BUSKULIC 95O use $D_s \ell$ correlations. The measured product branching ratio is $B(\bar{b} \rightarrow B_s) \times B(B_s \rightarrow D_s^- \ell^+ \nu_\ell \text{ anything}) = (0.82 \pm 0.09_{-0.13}^{+0.13})\%$ assuming $B(D_s \rightarrow \phi\pi) = (3.5 \pm 0.4) \times 10^{-2}$ and PDG 1994 values for the relative partial widths to the six other D_s channels used in this analysis. Combined with results from $\Upsilon(4S)$ experiments this can be used to extract $B(\bar{b} \rightarrow B_s) = (11.0 \pm 1.2_{-2.6}^{+2.5})\%$. We evaluate using our current values $B(\bar{b} \rightarrow B_s^0) = 0.107 \pm 0.014$ and $B(D_s \rightarrow \phi\pi) = 0.036 \pm 0.009$. Our first error is their experiment's and our second error is that due to $B(\bar{b} \rightarrow B_s^0)$ and $B(D_s \rightarrow \phi\pi)$.
 - ABREU 92M measured muons only and obtained product branching ratio $B(Z \rightarrow b\bar{b}) \times B(\bar{b} \rightarrow B_s) \times B(B_s \rightarrow D_s \mu^+ \nu_\mu \text{ anything}) \times B(D_s \rightarrow \phi\pi) = (18 \pm 8) \times 10^{-5}$. We evaluate using our current values $B(\bar{b} \rightarrow B_s^0) = 0.107 \pm 0.014$ and $B(D_s \rightarrow \phi\pi) = 0.036 \pm 0.009$. Our first error is their experiment's and our second error is that due to $B(\bar{b} \rightarrow B_s^0)$ and $B(D_s \rightarrow \phi\pi)$. We use $B(Z \rightarrow b\bar{b}) = 2B(Z \rightarrow b\bar{b}) = 2 \times (0.2212 \pm 0.0019)$.
 - ACTON 92N is measured using $D_s \rightarrow \phi\pi^+$ and $K^*(892)^0 K^+$ events. The product branching fraction measured is measured to be $B(\bar{b} \rightarrow B_s^0)B(B_s^0 \rightarrow D_s^- \ell^+ \nu_\ell \text{ anything}) \times B(D_s^- \rightarrow \phi\pi^-) = (3.9 \pm 1.1 \pm 0.8) \times 10^{-4}$. We evaluate using our current values $B(\bar{b} \rightarrow B_s^0) = 0.107 \pm 0.014$ and $B(D_s \rightarrow \phi\pi) = 0.036 \pm 0.009$. Our first error is their experiment's and our second error is that due to $B(\bar{b} \rightarrow B_s^0)$ and $B(D_s \rightarrow \phi\pi)$.
 - BUSKULIC 92E is measured using $D_s \rightarrow \phi\pi^+$ and $K^*(892)^0 K^+$ events. They use $2.7 \pm 0.7\%$ for the $\phi\pi^+$ branching fraction. The average product branching fraction is measured to be $B(\bar{b} \rightarrow B_s^0)B(B_s^0 \rightarrow D_s^- \ell^+ \nu_\ell \text{ anything}) = 0.020 \pm 0.0055_{-0.006}^{+0.005}$. We evaluate using our current values $B(\bar{b} \rightarrow B_s^0) = 0.107 \pm 0.014$ and $B(D_s \rightarrow \phi\pi) = 0.036 \pm 0.009$. Our first error is their experiment's and our second error is that due to $B(\bar{b} \rightarrow B_s^0)$ and $B(D_s \rightarrow \phi\pi)$. Superseded by BUSKULIC 95O.

$\Gamma(D_s^- \ell^+ \nu_\ell \text{ anything}) / \Gamma_{total}$ Γ_6 / Γ

VALUE (units 10^{-2})	DOCUMENT ID	TECN	COMMENT
5.4 ± 0.4 ± 1.0			
	¹ OSWALD 15	BELL	$e^+e^- \rightarrow \Upsilon(5S)$

- Obtains $B_s \rightarrow D_s^* X e \nu$, and $D_s^* X \mu \nu$ separately, then combines them by assuming systematic uncertainties are fully correlated, except for the one on lepton identification. The third uncertainty adds in quadrature systematic uncertainties from external sources (number of B_s events, and $D_s^{(*)}$ branching fractions). OSWALD 15 also measures the cross-section $\sigma(e^+e^- \rightarrow B_s^{(*)} \bar{B}_s^{(*)}) = 53.8 \pm 1.4 \pm 5.3$ pb at $\sqrt{s} = 10.86$ GeV.

$\Gamma(D_{s1}(2536)^- \mu^+ \nu_\mu, D_{s1}^- \rightarrow D^{*-} K_S^0)/\Gamma_{total}$	Γ_7/Γ		
VALUE (units 10 ⁻³)	DOCUMENT ID	TECN	COMMENT
2.7 ± 0.7 ± 0.2	¹ ABAZOV	09G	D0 $p\bar{p}$ at 1.96 TeV

¹ ABAZOV 09G reports $[\Gamma(B_s^0 \rightarrow D_{s1}(2536)^- \mu^+ \nu_\mu, D_{s1}^- \rightarrow D^{*-} K_S^0)/\Gamma_{total}] \times [B(\bar{b} \rightarrow B_s^0)] = (2.66 \pm 0.52 \pm 0.45) \times 10^{-4}$ which we divide by our best value $B(\bar{b} \rightarrow B_s^0) = (10.0 \pm 0.8) \times 10^{-2}$. Our first error is their experiment's error and our second error is the systematic error from using our best value.

$\Gamma(D_{s1}(2536)^- X \mu^+ \nu, D_{s1}^- \rightarrow \bar{D}^0 K^+)/\Gamma(D_s^- \ell^+ \nu_\ell \text{ anything})$	Γ_8/Γ_5		
VALUE (units 10 ⁻²)	DOCUMENT ID	TECN	COMMENT
5.4 ± 1.2 ± 0.5	AAIJ	11A	LHCB pp at 7 TeV

$\Gamma(D_{s2}(2573)^- X \mu^+ \nu, D_{s2}^- \rightarrow \bar{D}^0 K^+)/\Gamma(D_s^- \ell^+ \nu_\ell \text{ anything})$	Γ_9/Γ_5		
VALUE (units 10 ⁻²)	DOCUMENT ID	TECN	COMMENT
3.3 ± 1.0 ± 0.4	AAIJ	11A	LHCB pp at 7 TeV

$\Gamma(D_{s1}(2536)^- X \mu^+ \nu, D_{s1}^- \rightarrow \bar{D}^0 K^+)/\Gamma(D_{s2}(2573)^- X \mu^+ \nu, D_{s2}^- \rightarrow \bar{D}^0 K^+)$	Γ_8/Γ_9		
VALUE	DOCUMENT ID	TECN	COMMENT
0.61 ± 0.14 ± 0.05	¹ AAIJ	11A	LHCB pp at 7 TeV
¹ Not independent of other AAIJ 11A measurements.			

$\Gamma(D_s^- \pi^+)/\Gamma_{total}$	Γ_{10}/Γ			
VALUE (units 10 ⁻³)	EVTS	DOCUMENT ID	TECN	COMMENT
3.00 ± 0.23 OUR FIT				
2.99 ± 0.24 OUR AVERAGE				
2.95 ± 0.05 +0.25 / -0.28	¹ AAIJ	12AG	LHCB	pp at 7 TeV
3.6 ± 0.5 ± 0.5	² LOUVOT	09	BELL	$e^+ e^- \rightarrow \Upsilon(5S)$
2.8 ± 0.6 ± 0.1	³ ABULENCIA	07c	CDF	$p\bar{p}$ at 1.96 TeV
• • • We do not use the following data for averages, fits, limits, etc. • • •				
6.8 ± 2.2 ± 1.6		DRUTSKOY	07A	BELL Repl. by LOUVOT 09
3.3 ± 1.1 ± 0.2		⁴ ABULENCIA	06j	CDF Repl. by ABULENCIA 07c
<130 seen	⁶ AKERS	94j	OPAL	$e^+ e^- \rightarrow Z$
	¹ BUSKULIC	93g	ALEP	$e^+ e^- \rightarrow Z$

¹ AAIJ 12AG reports $(2.95 \pm 0.05 \pm 0.17 +0.18 / -0.22) \times 10^{-3}$ where the last uncertainty comes from the semileptonic f_S/f_d measurement. We combined the systematics in quadrature.

² LOUVOT 09 reports $(3.67_{-0.33}^{+0.35} -0.645) \times 10^{-3}$ from a measurement of $[\Gamma(B_s^0 \rightarrow D_s^- \pi^+)/\Gamma_{total}] \times [B(\Upsilon(10860) \rightarrow B_s^{(*)} \bar{B}_s^{(*)})]$ assuming $B(\Upsilon(10860) \rightarrow B_s^{(*)} \bar{B}_s^{(*)}) = (19.5 \pm 2.6) \times 10^{-2}$, which we rescale to our best value $B(\Upsilon(10860) \rightarrow B_s^{(*)} \bar{B}_s^{(*)}) = (20.1 \pm 3.1) \times 10^{-2}$. Our first error is their experiment's error and our second error is the systematic error from using our best value.

³ ABULENCIA 07c reports $[\Gamma(B_s^0 \rightarrow D_s^- \pi^+)/\Gamma_{total}] / [B(B^0 \rightarrow D^- \pi^+)] = 1.13 \pm 0.08 \pm 0.23$ which we multiply by our best value $B(B^0 \rightarrow D^- \pi^+) = (2.52 \pm 0.13) \times 10^{-3}$. Our first error is their experiment's error and our second error is the systematic error from using our best value.

⁴ ABULENCIA 06j reports $[\Gamma(B_s^0 \rightarrow D_s^- \pi^+)/\Gamma_{total}] / [B(B^0 \rightarrow D^- \pi^+)] = 1.32 \pm 0.18 \pm 0.38$ which we multiply by our best value $B(B^0 \rightarrow D^- \pi^+) = (2.52 \pm 0.13) \times 10^{-3}$. Our first error is their experiment's error and our second error is the systematic error from using our best value.

⁵ AKERS 94j sees ≤ 6 events and measures the limit on the product branching fraction $f(\bar{b} \rightarrow B_s^0) \cdot B(B_s^0 \rightarrow D_s^- \pi^+) < 1.3\%$ at CL = 90%. We divide by our current value $B(\bar{b} \rightarrow B_s^0) = 0.105$.

$\Gamma(D_s^- \rho^+)/\Gamma(D_s^- \pi^+)$	Γ_{11}/Γ_{10}		
VALUE	DOCUMENT ID	TECN	COMMENT
2.3 ± 0.4 ± 0.2	LOUVOT	10	BELL $e^+ e^- \rightarrow \Upsilon(5S)$

$\Gamma(D_s^- \pi^+ \pi^+ \pi^-)/\Gamma_{total}$	Γ_{12}/Γ		
VALUE (units 10 ⁻³)	DOCUMENT ID	TECN	COMMENT
6.1 ± 1.0 OUR FIT			
6.3 ± 1.5 ± 0.7	¹ ABULENCIA	07c	CDF $p\bar{p}$ at 1.96 TeV

¹ ABULENCIA 07c reports $[\Gamma(B_s^0 \rightarrow D_s^- \pi^+ \pi^+ \pi^-)/\Gamma_{total}] / [B(B^0 \rightarrow D^- \pi^+ \pi^+ \pi^-)] = 1.05 \pm 0.10 \pm 0.22$ which we multiply by our best value $B(B^0 \rightarrow D^- \pi^+ \pi^+ \pi^-) = (6.0 \pm 0.7) \times 10^{-3}$. Our first error is their experiment's error and our second error is the systematic error from using our best value.

$\Gamma(D_s^- \pi^+ \pi^+ \pi^-)/\Gamma(D_s^- \pi^+)$	Γ_{12}/Γ_{10}		
VALUE	DOCUMENT ID	TECN	COMMENT
2.05 ± 0.34 OUR FIT			
2.01 ± 0.37 ± 0.20	AAIJ	11E	LHCB pp at 7 TeV

$\Gamma(D_{s1}(2536)^- \pi^+, D_{s1}^- \rightarrow D_s^- \pi^+ \pi^-)/\Gamma(D_s^- \pi^+ \pi^+ \pi^-)$	Γ_{13}/Γ_{12}		
VALUE (units 10 ⁻³)	DOCUMENT ID	TECN	COMMENT
4.0 ± 1.0 ± 0.4	AAIJ	12AX	LHCB pp at 7 TeV

$\Gamma(D_s^- K^+)/\Gamma_{total}$	Γ_{14}/Γ		
VALUE (units 10 ⁻⁴)	DOCUMENT ID	TECN	COMMENT
2.27 ± 0.19 OUR FIT			
2.3 +1.2 -1.0 +0.4 -0.3	¹ LOUVOT	09	BELL $e^+ e^- \rightarrow \Upsilon(5S)$

¹ LOUVOT 09 reports $(2.4_{-1.0}^{+1.2} \pm 0.42) \times 10^{-4}$ from a measurement of $[\Gamma(B_s^0 \rightarrow D_s^- K^+)/\Gamma_{total}] \times [B(\Upsilon(10860) \rightarrow B_s^{(*)} \bar{B}_s^{(*)})]$ assuming $B(\Upsilon(10860) \rightarrow B_s^{(*)} \bar{B}_s^{(*)}) = (19.5 \pm 2.6) \times 10^{-2}$, which we rescale to our best value $B(\Upsilon(10860) \rightarrow B_s^{(*)} \bar{B}_s^{(*)}) = (20.1 \pm 3.1) \times 10^{-2}$. Our first error is their experiment's error and our second error is the systematic error from using our best value.

$\Gamma(D_s^- K^+)/\Gamma(D_s^- \pi^+)$	Γ_{14}/Γ_{10}		
VALUE (units 10 ⁻²)	DOCUMENT ID	TECN	COMMENT
7.55 ± 0.24 OUR FIT			
7.55 ± 0.24 OUR AVERAGE			
7.52 ± 0.15 ± 0.19	AAIJ	15AC	LHCB pp at 7, 8 TeV
9.7 ± 1.8 ± 0.9	AALTONEN	09AQ	CDF $p\bar{p}$ at 1.96 TeV
• • • We do not use the following data for averages, fits, limits, etc. • • •			
6.46 ± 0.43 ± 0.25	AAIJ	12AG	LHCB Repl. by AAIJ 15AC

$\Gamma(D_s^- K^+ \pi^+ \pi^-)/\Gamma(D_s^- \pi^+ \pi^+ \pi^-)$	Γ_{15}/Γ_{12}		
VALUE (units 10 ⁻²)	DOCUMENT ID	TECN	COMMENT
5.2 ± 0.5 ± 0.3	AAIJ	12AX	LHCB pp at 7 TeV

$\Gamma(D_s^+ D_s^-)/\Gamma_{total}$	Γ_{16}/Γ			
VALUE (units 10 ⁻³)	CL%	DOCUMENT ID	TECN	COMMENT
4.4 ± 0.5 OUR AVERAGE				
4.0 ± 0.2 ± 0.5		¹ AAIJ	13AP	LHCB pp at 7 TeV
5.8 +1.1 / -0.9 ± 1.3		² ESEN	13	BELL $e^+ e^- \rightarrow \Upsilon(5S)$
5.4 ± 0.8 ± 0.8		³ AALTONEN	12c	CDF $p\bar{p}$ at 1.96 TeV
• • • We do not use the following data for averages, fits, limits, etc. • • •				
10.3 +3.9+2.6 / -3.2-2.5		⁴ ESEN	10	BELL Repl. by ESEN 13
10.4 +3.5+1.1 / -3.2-2.5		⁵ AALTONEN	08F	CDF Repl. by AALTONEN 12c
<67	90	DRUTSKOY	07A	BELL Repl. by ESEN 10

¹ Uses $B(B^0 \rightarrow D^- D_s^+) = (7.2 \pm 0.8) \times 10^{-3}$.

² Uses $\Upsilon(5S) \rightarrow B_s^* \bar{B}_s^*$ decays assuming $B(\Upsilon(5S) \rightarrow B_s^* \bar{B}_s^*) = (17.1 \pm 3.0)\%$ and $\Gamma(\Upsilon(5S) \rightarrow B_s^* \bar{B}_s^*) / \Gamma(\Upsilon(5S) \rightarrow B_s^{(*)} \bar{B}_s^{(*)}) = (87.0 \pm 1.7)\%$.

³ AALTONEN 12c reports $(f_S/f_d) (B(B_s^0 \rightarrow D_s^+ D_s^-) / B(B^0 \rightarrow D^- D_s^+)) = 0.183 \pm 0.021 \pm 0.017$. We multiply this result by our best value of $B(B^0 \rightarrow D^- D_s^+) = (7.2 \pm 0.8) \times 10^{-3}$ and divide by our best value of f_S/f_d , where $1/2 f_S/f_d = 0.1230 \pm 0.0115$. Our first quoted uncertainty is the combined experiment's uncertainty and our second is the systematic uncertainty from using our best values.

⁴ Uses $\Upsilon(10860) \rightarrow B_s^* \bar{B}_s^*$ assuming $B(\Upsilon(10860) \rightarrow B_s^{(*)} \bar{B}_s^{(*)}) = (19.3 \pm 2.9)\%$ and $\Gamma(\Upsilon(10860) \rightarrow B_s^* \bar{B}_s^*) / \Gamma(\Upsilon(10860) \rightarrow B_s^{(*)} \bar{B}_s^{(*)}) = (90.1_{-4.0}^{+3.8})\%$.

⁵ AALTONEN 08F reports $[\Gamma(B_s^0 \rightarrow D_s^+ D_s^-)/\Gamma_{total}] / [B(B^0 \rightarrow D^- D_s^+)] = 1.44_{-0.44}^{+0.48}$ which we multiply by our best value $B(B^0 \rightarrow D^- D_s^+) = (7.2 \pm 0.8) \times 10^{-3}$. Our first error is their experiment's error and our second error is the systematic error from using our best value.

$\Gamma(D_s^- D^+)/\Gamma_{total}$	Γ_{17}/Γ		
VALUE (units 10 ⁻⁴)	DOCUMENT ID	TECN	COMMENT
2.8 ± 0.4 ± 0.3	¹ AAIJ	14AA	LHCB pp at 7 TeV
• • • We do not use the following data for averages, fits, limits, etc. • • •			
3.6 ± 0.6 ± 0.5	² AAIJ	13AP	LHCB Repl. by AAIJ 14AA

¹ AAIJ 14AA reports $[\Gamma(B_s^0 \rightarrow D_s^- D^+)/\Gamma_{total}] / [B(B^0 \rightarrow D^- D_s^+)] = 0.038 \pm 0.004 \pm 0.003$ which we multiply by our best value $B(B^0 \rightarrow D^- D_s^+) = (7.2 \pm 0.8) \times 10^{-3}$. Our first error is their experiment's error and our second error is the systematic error from using our best value.

² Uses $B(B^0 \rightarrow D^- D_s^+) = (7.2 \pm 0.8) \times 10^{-3}$.

$\Gamma(D^+ D^-)/\Gamma_{total}$	Γ_{18}/Γ		
VALUE (units 10 ⁻⁴)	DOCUMENT ID	TECN	COMMENT
2.2 ± 0.4 ± 0.4	¹ AAIJ	13AP	LHCB pp at 7 TeV

¹ Uses $B(B^0 \rightarrow D^- D^+) = (2.11 \pm 0.31) \times 10^{-4}$ and $B(B^+ \rightarrow \bar{D}^0 D_s^+) = (10.1 \pm 1.7) \times 10^{-3}$.

$\Gamma(D^0 \bar{D}^0)/\Gamma_{total}$	Γ_{19}/Γ		
VALUE (units 10 ⁻⁴)	DOCUMENT ID	TECN	COMMENT
1.9 ± 0.3 ± 0.4	¹ AAIJ	13AP	LHCB pp at 7 TeV

¹ Uses $B(B^0 \rightarrow D^- D^+) = (2.11 \pm 0.31) \times 10^{-4}$ and $B(B^+ \rightarrow \bar{D}^0 D_s^+) = (10.1 \pm 1.7) \times 10^{-3}$.

$\Gamma(D_s^{*-} \pi^+)/\Gamma(D_s^- \pi^+)$	Γ_{20}/Γ_{10}		
VALUE	DOCUMENT ID	TECN	COMMENT
0.65 +0.15 / -0.13 ± 0.07	LOUVOT	10	BELL $e^+ e^- \rightarrow \Upsilon(5S)$

Meson Particle Listings

B_s^0

$\Gamma(D_s^{*\mp} K^\pm)/\Gamma(D_s^{*-} \pi^+)$		Γ_{21}/Γ_{20}	
VALUE	DOCUMENT ID	TECN	COMMENT
$0.068 \pm 0.005 \pm 0.003$ <small>-0.002</small>	AAIJ	15AD	LHCB pp at 7, 8 TeV

$\Gamma(D_s^{*-} \rho^+)/\Gamma(D_s^- \pi^+)$		Γ_{22}/Γ_{10}	
VALUE	DOCUMENT ID	TECN	COMMENT
$3.2 \pm 0.6 \pm 0.3$	LOUVOT	10	BELL $e^+ e^- \rightarrow \Upsilon(5S)$

$\Gamma(D_s^{*-} \rho^+)/\Gamma(D_s^- \rho^+)$		Γ_{22}/Γ_{11}	
VALUE	DOCUMENT ID	TECN	COMMENT
$1.4 \pm 0.3 \pm 0.1$	LOUVOT	10	BELL $e^+ e^- \rightarrow \Upsilon(5S)$
••• We do not use the following data for averages, fits, limits, etc. ••• 1 Not independent of other LOUVOT 10 measurements.			

$[\Gamma(D_s^{*+} D_s^-) + \Gamma(D_s^{*-} D_s^+)]/\Gamma_{total}$		Γ_{23}/Γ	
VALUE (units 10^{-3})	CL%	DOCUMENT ID	TECN COMMENT
13.9 ± 1.7 OUR AVERAGE			
13.6 ± 1.0 ± 1.4		1 AAIJ	16P LHCB pp at 7 TeV
17.6 ± 2.3 ± 4.0		2 ESEN	13 BELL $e^+ e^- \rightarrow \Upsilon(5S)$
12.5 ± 1.7 ± 1.8		3 AALTONEN	12c CDF $p\bar{p}$ at 1.96 TeV
••• We do not use the following data for averages, fits, limits, etc. •••			
27.5 ± 8.3 ± 6.9		4 ESEN	10 BELL Repl. by ESEN 13
<121	90	DRUTSKOY	07A BELL Repl. by ESEN 10

1 AAIJ 16P reports $[\Gamma(B_s^0 \rightarrow D_s^{*+} D_s^-) + \Gamma(D_s^{*-} D_s^+)]/\Gamma_{total} / [B(B^0 \rightarrow D^- D_s^+)] = 1.88 \pm 0.08 \pm 0.12$ which we multiply by our best value $B(B^0 \rightarrow D^- D_s^+) = (7.2 \pm 0.8) \times 10^{-3}$. Our first error is their experiment's error and our second error is the systematic error from using our best value.

2 Use $\Upsilon(5S) \rightarrow B_s^* \bar{B}_s^*$ decays assuming $B(\Upsilon(5S) \rightarrow B_s^* \bar{B}_s^*) = (17.1 \pm 3.0)\%$ and $\Gamma(\Upsilon(5S) \rightarrow B_s^* \bar{B}_s^*) / \Gamma(\Upsilon(5S) \rightarrow B_s^{(*)} \bar{B}_s^{(*)}) = (87.0 \pm 1.7)\%$.

3 AALTONEN 12c reports $(f_s/f_d) (B(B_s^0 \rightarrow D_s^{*+} D_s^- + D_s^{*-} D_s^+) / B(B^0 \rightarrow D^- D_s^+)) = 0.424 \pm 0.046 \pm 0.035$. We multiply this result by our best value of $B(B^0 \rightarrow D^- D_s^+) = (7.2 \pm 0.8) \times 10^{-3}$ and divide by our best value of f_s/f_d , where $1/2 f_s/f_d = 0.1230 \pm 0.0115$. Our first quoted uncertainty is the combined experiment's uncertainty and our second is the systematic uncertainty from using our best values.

4 Uses $\Upsilon(10860) \rightarrow B_s^* \bar{B}_s^*$ assuming $B(\Upsilon(10860) \rightarrow B_s^{(*)} \bar{B}_s^{(*)}) = (19.3 \pm 2.9)\%$ and $\Gamma(\Upsilon(10860) \rightarrow B_s^* \bar{B}_s^*) / \Gamma(\Upsilon(10860) \rightarrow B_s^{(*)} \bar{B}_s^{(*)}) = (90.1 \pm 3.8)_{-4.0}^{\%}$.

$\Gamma(D_s^{*+} D_s^{*-})/\Gamma_{total}$		Γ_{24}/Γ	
VALUE (units 10^{-3})	CL%	DOCUMENT ID	TECN COMMENT
14.4 ± 2.1 OUR AVERAGE			
12.7 ± 1.3 ± 1.4		1 AAIJ	16P LHCB pp at 7 TeV
19.8 ± 3.3 ± 5.2 <small>-3.1 -5.0</small>		2 ESEN	13 BELL $e^+ e^- \rightarrow \Upsilon(5S)$
19.2 ± 2.9 ± 2.7		3 AALTONEN	12c CDF $p\bar{p}$ at 1.96 TeV
••• We do not use the following data for averages, fits, limits, etc. •••			
30.8 ± 12.2 ± 8.5 <small>-10.4 -8.6</small>		4 ESEN	10 BELL Repl. by ESEN 13
<257	90	DRUTSKOY	07A BELL Repl. by ESEN 10

1 AAIJ 16P reports $[\Gamma(B_s^0 \rightarrow D_s^{*+} D_s^{*-})/\Gamma_{total}] / [B(B^0 \rightarrow D^- D_s^+)] = 1.76 \pm 0.11 \pm 0.14$ which we multiply by our best value $B(B^0 \rightarrow D^- D_s^+) = (7.2 \pm 0.8) \times 10^{-3}$. Our first error is their experiment's error and our second error is the systematic error from using our best value.

2 Use $\Upsilon(5S) \rightarrow B_s^* \bar{B}_s^*$ decays assuming $B(\Upsilon(5S) \rightarrow B_s^* \bar{B}_s^*) = (17.1 \pm 3.0)\%$ and $\Gamma(\Upsilon(5S) \rightarrow B_s^* \bar{B}_s^*) / \Gamma(\Upsilon(5S) \rightarrow B_s^{(*)} \bar{B}_s^{(*)}) = (87.0 \pm 1.7)\%$.

3 AALTONEN 12c reports $(f_s/f_d) (B(B_s^0 \rightarrow D_s^{*+} D_s^{*-}) / B(B^0 \rightarrow D^- D_s^+)) = 0.654 \pm 0.072 \pm 0.065$. We multiply this result by our best value of $B(B^0 \rightarrow D^- D_s^+) = (7.2 \pm 0.8) \times 10^{-3}$ and divide by our best value of f_s/f_d , where $1/2 f_s/f_d = 0.1230 \pm 0.0115$. Our first quoted uncertainty is the combined experiment's uncertainty and our second is the systematic uncertainty from using our best values.

4 Uses $\Upsilon(10860) \rightarrow B_s^* \bar{B}_s^*$ assuming $B(\Upsilon(10860) \rightarrow B_s^{(*)} \bar{B}_s^{(*)}) = (19.3 \pm 2.9)\%$ and $\Gamma(\Upsilon(10860) \rightarrow B_s^* \bar{B}_s^*) / \Gamma(\Upsilon(10860) \rightarrow B_s^{(*)} \bar{B}_s^{(*)}) = (90.1 \pm 3.8)_{-4.0}^{\%}$.

$\Gamma(D_s^{*+} D_s^{*-})/\Gamma_{total}$		Γ_{25}/Γ	
VALUE (%)	CL%	DOCUMENT ID	TECN COMMENT
4.5 ± 1.4 OUR EVALUATION			
3.4 ± 0.4 OUR AVERAGE			
3.07 ± 0.22 ± 0.33		1 AAIJ	16P LHCB pp at 7 TeV
4.32 ± 0.42 ± 1.04 <small>-0.39 -1.03</small>		2 ESEN	13 BELL $e^+ e^- \rightarrow \Upsilon(5S)$
3.7 ± 0.4 ± 0.5		3 AALTONEN	12c CDF $p\bar{p}$ at 1.96 TeV
3.5 ± 1.0 ± 1.1		4 ABAZOV	09I D0 $p\bar{p}$ at 1.96 TeV
14 ± 6 ± 3		5,6 BARATE	00K ALEP $e^+ e^- \rightarrow Z$

"OUR EVALUATION" is an average using rescaled values of the data listed below. The average and rescaling were performed by the Heavy Flavor Averaging Group (HFLAV, <https://hflav.web.cern.ch/>) and are described at <https://hflav.web.cern.ch/>. The averaging/rescaling procedure takes into account correlations between the measurements.

••• We do not use the following data for averages, fits, limits, etc. •••

6.85 ± 1.53 ± 1.79
-1.30 -1.80 7,8 ESEN 10 BELL Repl. by ESEN 13

3.9 ± 1.9 ± 1.6
-1.7 -1.5 4 ABAZOV 07Y D0 Repl. by ABAZOV 09I

<0.218 90 BARATE 98Q ALEP $e^+ e^- \rightarrow Z$

1 AAIJ 16P reports $[\Gamma(B_s^0 \rightarrow D_s^{*+} D_s^{*-})/\Gamma_{total}] / [B(B^0 \rightarrow D^- D_s^+)] = 4.24 \pm 0.14 \pm 0.27$ which we multiply by our best value $B(B^0 \rightarrow D^- D_s^+) = (7.2 \pm 0.8) \times 10^{-3}$. Our first error is their experiment's error and our second error is the systematic error from using our best value.

2 Use $\Upsilon(5S) \rightarrow B_s^* \bar{B}_s^*$ decays assuming $B(\Upsilon(5S) \rightarrow B_s^* \bar{B}_s^*) = (17.1 \pm 3.0)\%$ and $\Gamma(\Upsilon(5S) \rightarrow B_s^* \bar{B}_s^*) / \Gamma(\Upsilon(5S) \rightarrow B_s^{(*)} \bar{B}_s^{(*)}) = (87.0 \pm 1.7)\%$.

3 AALTONEN 12c reports $(f_s/f_d) (B(B_s^0 \rightarrow D_s^{*+} D_s^{*-}) / B(B^0 \rightarrow D^- D_s^+)) = 1.261 \pm 0.095 \pm 0.112$. We multiply this result by our best value of $B(B^0 \rightarrow D^- D_s^+) = (7.2 \pm 0.8) \times 10^{-3}$ and divide by our best value of f_s/f_d , where $1/2 f_s/f_d = 0.1230 \pm 0.0115$. Our first quoted uncertainty is the combined experiment's uncertainty and our second is the systematic uncertainty from using our best values.

4 Uses the final states where $D_s^+ \rightarrow \phi \pi^+$ and $D_s^- \rightarrow \phi \mu^- \bar{\nu}_\mu$.

5 Reports $B(B_s^0 \text{ (short)} \rightarrow D_s^{*+} D_s^{*-}) = (0.23 \pm 0.10 \pm 0.05) \cdot [0.17/B(D_s \rightarrow \phi \chi)]^2$ assuming $B(B_s^0 \rightarrow B_s^0 \text{ (short)}) = 50\%$. We use our best value of $B(D_s \rightarrow \phi \chi) = 15.7 \pm 1.0\%$ to obtain the quoted result.

6 Uses $\phi\phi$ correlations from $B_s^0 \text{ (short)} \rightarrow D_s^{*+} D_s^{*-}$.

7 Sum of exclusive $B_s \rightarrow D_s^+ D_s^-$, $B_s \rightarrow D_s^+ D_s^-$ and $B_s \rightarrow D_s^+ D_s^-$.

8 Uses $\Upsilon(10860) \rightarrow B_s^* \bar{B}_s^*$ assuming $B(\Upsilon(10860) \rightarrow B_s^{(*)} \bar{B}_s^{(*)}) = (19.3 \pm 2.9)\%$ and $\Gamma(\Upsilon(10860) \rightarrow B_s^* \bar{B}_s^*) / \Gamma(\Upsilon(10860) \rightarrow B_s^{(*)} \bar{B}_s^{(*)}) = (90.1 \pm 3.8)_{-4.0}^{\%}$.

$\Gamma(\bar{D}^0 \bar{K}^0)/\Gamma_{total}$		Γ_{26}/Γ	
VALUE (units 10^{-4})	DOCUMENT ID	TECN	COMMENT
2.8 ± 1.0 ± 0.5			
	1 AAIJ	16c	LHCB pp at 7, 8 TeV
1 Measured and normalized to the $B_s^0 \rightarrow \bar{D}^0 \bar{K}_S^0$ decay with $f_s/f_d = 0.259 \pm 0.015$. Signal significance is 4.4 standard deviations.			

$\Gamma(\bar{D}^0 \bar{K}^0)/\Gamma_{total}$		Γ_{27}/Γ	
VALUE (units 10^{-4})	DOCUMENT ID	TECN	COMMENT
4.3 ± 0.5 ± 0.7			
	1 AAIJ	16c	LHCB pp at 7, 8 TeV
1 Measured and normalized to the $B^0 \rightarrow \bar{D}^0 \bar{K}_S^0$ decay with $f_s/f_d = 0.259 \pm 0.015$.			

$\Gamma(\bar{D}^0 K^- \pi^+)/\Gamma_{total}$		Γ_{28}/Γ	
VALUE (units 10^{-4})	DOCUMENT ID	TECN	COMMENT
10.4 ± 1.1 ± 0.5			
	1 AAIJ	13AQ	LHCB pp at 7 TeV
1 AAIJ 13AQ reports $[\Gamma(B_s^0 \rightarrow \bar{D}^0 K^- \pi^+)/\Gamma_{total}] / [B(B^0 \rightarrow \bar{D}^0 \pi^+ \pi^-)] = 1.18 \pm 0.05 \pm 0.12$ which we multiply by our best value $B(B^0 \rightarrow \bar{D}^0 \pi^+ \pi^-) = (8.8 \pm 0.5) \times 10^{-4}$. Our first error is their experiment's error and our second error is the systematic error from using our best value.			

$\Gamma(\bar{D}^0 \bar{K}^*(892)^0)/\Gamma_{total}$		Γ_{29}/Γ	
VALUE (units 10^{-4})	DOCUMENT ID	TECN	COMMENT
4.4 ± 0.6 OUR AVERAGE			
4.29 ± 0.09 ± 0.65	1 AAIJ	14BH	LHCB pp at 7, 8 TeV
4.7 ± 1.2 ± 0.3	2 AAIJ	11D	LHCB pp at 7 TeV
••• We do not use the following data for averages, fits, limits, etc. •••			
3.5 ± 0.4 ± 0.4	3 AAIJ	13BX	LHCB Repl. by AAIJ 14BH

1 Uses Dalitz plot analysis of $B^0 \rightarrow \bar{D}^0 K^- \pi^+$ decays.

2 AAIJ 11D reports $[\Gamma(B_s^0 \rightarrow \bar{D}^0 \bar{K}^*(892)^0)/\Gamma_{total}] / [B(B^0 \rightarrow \bar{D}^0 \rho^0)] = 1.48 \pm 0.34 \pm 0.19$ which we multiply by our best value $B(B^0 \rightarrow \bar{D}^0 \rho^0) = (3.21 \pm 0.21) \times 10^{-4}$. Our first error is their experiment's error and our second error is the systematic error from using our best value.

3 AAIJ 13BX reports $[\Gamma(B_s^0 \rightarrow \bar{D}^0 \bar{K}^*(892)^0)/\Gamma_{total}] / [B(B^0 \rightarrow \bar{D}^0 K^*(892)^0)] = 7.8 \pm 0.7 \pm 0.3 \pm 0.6$ which we multiply by our best value $B(B^0 \rightarrow \bar{D}^0 K^*(892)^0) = (4.5 \pm 0.6) \times 10^{-6}$. Our first error is their experiment's error and our second error is the systematic error from using our best value.

$\Gamma(\bar{D}^0 \bar{K}^*(1410))/\Gamma_{total}$		Γ_{30}/Γ	
VALUE (units 10^{-5})	DOCUMENT ID	TECN	COMMENT
38.6 ± 11.4 ± 33.3			
	1 AAIJ	14BH	LHCB pp at 7, 8 TeV
1 Uses Dalitz plot analysis of $B_s^0 \rightarrow \bar{D}^0 K^- \pi^+$ decays.			

$\Gamma(\bar{D}^0 \bar{K}_0^*(1430))/\Gamma_{total}$		Γ_{31}/Γ	
VALUE (units 10^{-5})	DOCUMENT ID	TECN	COMMENT
30.0 ± 2.4 ± 6.8			
	1 AAIJ	14BH	LHCB pp at 7, 8 TeV
1 Uses Dalitz plot analysis of $B_s^0 \rightarrow \bar{D}^0 K^- \pi^+$ decays. Corresponds to the resonant $K_0^*(1430)$ part of LASS parametrization.			

$\Gamma(\bar{D}^0 \bar{K}_2^*(1430))/\Gamma_{total}$		Γ_{32}/Γ	
VALUE (units 10^{-5})	DOCUMENT ID	TECN	COMMENT
11.1 ± 1.8 ± 3.8			
	1 AAIJ	14BH	LHCB pp at 7, 8 TeV
1 Uses Dalitz plot analysis of $B_s^0 \rightarrow \bar{D}^0 K^- \pi^+$ decays.			

$\Gamma(\overline{D}^0 \overline{K}^*(1680))/\Gamma_{\text{total}}$					Γ_{33}/Γ
VALUE (units 10^{-5})	CL%	DOCUMENT ID	TECN	COMMENT	
<7.8	90	¹ AAIJ	14BH LHCb	pp at 7, 8 TeV	

¹ Uses Dalitz plot analysis of $B_s^0 \rightarrow \overline{D}^0 K^- \pi^+$ decays.

$\Gamma(\overline{D}^0 \overline{K}_0^*(1950))/\Gamma_{\text{total}}$					Γ_{34}/Γ
VALUE (units 10^{-5})	CL%	DOCUMENT ID	TECN	COMMENT	
<11	90	¹ AAIJ	14BH LHCb	pp at 7, 8 TeV	

¹ Uses Dalitz plot analysis of $B_s^0 \rightarrow \overline{D}^0 K^- \pi^+$ decays.

$\Gamma(\overline{D}^0 \overline{K}_3^*(1780))/\Gamma_{\text{total}}$					Γ_{35}/Γ
VALUE (units 10^{-5})	CL%	DOCUMENT ID	TECN	COMMENT	
<2.6	90	¹ AAIJ	14BH LHCb	pp at 7, 8 TeV	

¹ Uses Dalitz plot analysis of $B_s^0 \rightarrow \overline{D}^0 K^- \pi^+$ decays.

$\Gamma(\overline{D}^0 \overline{K}_4^*(2045))/\Gamma_{\text{total}}$					Γ_{36}/Γ
VALUE (units 10^{-5})	CL%	DOCUMENT ID	TECN	COMMENT	
<3.1	90	¹ AAIJ	14BH LHCb	pp at 7, 8 TeV	

¹ Uses Dalitz plot analysis of $B_s^0 \rightarrow \overline{D}^0 K^- \pi^+$ decays.

$\Gamma(\overline{D}^0 K^- \pi^+ (\text{non-resonant}))/\Gamma_{\text{total}}$					Γ_{37}/Γ
VALUE (units 10^{-5})	CL%	DOCUMENT ID	TECN	COMMENT	
$20.6 \pm 3.8 \pm 7.3$		¹ AAIJ	14BH LHCb	pp at 7, 8 TeV	

¹ Uses Dalitz plot analysis of $B_s^0 \rightarrow \overline{D}^0 K^- \pi^+$ decays. Corresponds to the non-resonant part of the LASS parametrization.

$\Gamma(D_{s2}^*(2573)^- \pi^+, D_{s2}^* \rightarrow \overline{D}^0 K^-)/\Gamma_{\text{total}}$					Γ_{38}/Γ
VALUE (units 10^{-5})	CL%	DOCUMENT ID	TECN	COMMENT	
$25.7 \pm 0.7 \pm 4.0$		¹ AAIJ	14BH LHCb	pp at 7, 8 TeV	

¹ Uses Dalitz plot analysis of $B_s^0 \rightarrow \overline{D}^0 K^- \pi^+$ decays.

$\Gamma(D_{s1}^*(2700)^- \pi^+, D_{s1}^* \rightarrow \overline{D}^0 K^-)/\Gamma_{\text{total}}$					Γ_{39}/Γ
VALUE (units 10^{-5})	CL%	DOCUMENT ID	TECN	COMMENT	
$1.6 \pm 0.4 \pm 0.7$		¹ AAIJ	14BH LHCb	pp at 7, 8 TeV	

¹ Uses Dalitz plot analysis of $B_s^0 \rightarrow \overline{D}^0 K^- \pi^+$ decays.

$\Gamma(D_{s1}^*(2860)^- \pi^+, D_{s1}^* \rightarrow \overline{D}^0 K^-)/\Gamma_{\text{total}}$					Γ_{40}/Γ
VALUE (units 10^{-5})	CL%	DOCUMENT ID	TECN	COMMENT	
$5.0 \pm 1.2 \pm 3.4$		¹ AAIJ	14BH LHCb	pp at 7, 8 TeV	

¹ Uses Dalitz plot analysis of $B_s^0 \rightarrow \overline{D}^0 K^- \pi^+$ decays.

$\Gamma(D_{s3}^*(2860)^- \pi^+, D_{s3}^* \rightarrow \overline{D}^0 K^-)/\Gamma_{\text{total}}$					Γ_{41}/Γ
VALUE (units 10^{-5})	CL%	DOCUMENT ID	TECN	COMMENT	
$2.2 \pm 0.1 \pm 0.6$		¹ AAIJ	14BH LHCb	pp at 7, 8 TeV	

¹ Uses Dalitz plot analysis of $B_s^0 \rightarrow \overline{D}^0 K^- \pi^+$ decays.

$\Gamma(\overline{D}^0 K^+ K^-)/\Gamma_{\text{total}}$					Γ_{42}/Γ
VALUE (units 10^{-5})	CL%	DOCUMENT ID	TECN	COMMENT	
$5.5 \pm 0.7 \pm 0.5$		¹ AAIJ	18AZ LHCb	pp at 7, 8 TeV	

• • • We do not use the following data for averages, fits, limits, etc. • • •
 $5.3 \pm 2.0 \pm 0.5$ ^{2,3} AAIJ 12AMLHCb Repl. by AAIJ 18AZ

¹ AAIJ 18AZ reports $[\Gamma(B_s^0 \rightarrow \overline{D}^0 K^+ K^-)/\Gamma_{\text{total}}] / [B(B^0 \rightarrow \overline{D}^0 K^+ K^-)] = 0.930 \pm 0.089 \pm 0.069$ which we multiply by our best value $B(B^0 \rightarrow \overline{D}^0 K^+ K^-) = (5.9 \pm 0.5) \times 10^{-5}$. Our first error is their experiment's error and our second error is the systematic error from using our best value.

² AAIJ 12AM reports $[\Gamma(B_s^0 \rightarrow \overline{D}^0 K^+ K^-)/\Gamma_{\text{total}}] / [B(B^0 \rightarrow \overline{D}^0 K^+ K^-)] = 0.90 \pm 0.27 \pm 0.20$ which we multiply by our best value $B(B^0 \rightarrow \overline{D}^0 K^+ K^-) = (5.9 \pm 0.5) \times 10^{-5}$. Our first error is their experiment's error and our second error is the systematic error from using our best value.

³ Uses $B(b \rightarrow B_s^0)/B(b \rightarrow B^0) = 0.267_{-0.020}^{+0.023}$ measured by the same authors.

$\Gamma(\overline{D}^0 f_0(980))/\Gamma_{\text{total}}$					Γ_{43}/Γ
VALUE	CL%	DOCUMENT ID	TECN	COMMENT	
< 3.1×10^{-6}	90	AAIJ	15AG LHCb	pp at 7, 8 TeV	

$\Gamma(\overline{D}^0 \phi)/\Gamma(\overline{D}^0 \overline{K}^*(892)^0)$					Γ_{44}/Γ_{29}
VALUE	CL%	DOCUMENT ID	TECN	COMMENT	
$0.069 \pm 0.013 \pm 0.007$		AAIJ	13BX LHCb	Repl. by AAIJ 18AY	

$\Gamma(\overline{D}^0 \phi)/\Gamma_{\text{total}}$					Γ_{44}/Γ
VALUE (units 10^{-5})	CL%	DOCUMENT ID	TECN	COMMENT	
$3.0 \pm 0.4 \pm 0.2$		¹ AAIJ	18AY LHCb	pp at 7 and 8 TeV	

¹ AAIJ 18AY reports $[\Gamma(B_s^0 \rightarrow \overline{D}^0 \phi)/\Gamma_{\text{total}}] / [B(B^0 \rightarrow \overline{D}^0 \pi^+ \pi^-)] = (3.4 \pm 0.4 \pm 0.3) \times 10^{-2}$ which we multiply by our best value $B(B^0 \rightarrow \overline{D}^0 \pi^+ \pi^-) = (8.8 \pm 0.5) \times 10^{-4}$. Our first error is their experiment's error and our second error is the systematic error from using our best value.

$\Gamma(\overline{D}^{*0} \phi)/\Gamma_{\text{total}}$					Γ_{45}/Γ
VALUE (units 10^{-5})	CL%	DOCUMENT ID	TECN	COMMENT	
$3.7 \pm 0.6 \pm 0.2$		¹ AAIJ	18AY LHCb	pp at 7 and 8 TeV	

¹ AAIJ 18AY reports $[\Gamma(B_s^0 \rightarrow \overline{D}^{*0} \phi)/\Gamma_{\text{total}}] / [B(B^0 \rightarrow \overline{D}^0 \pi^+ \pi^-)] = (4.2 \pm 0.5 \pm 0.4) \times 10^{-2}$ which we multiply by our best value $B(B^0 \rightarrow \overline{D}^0 \pi^+ \pi^-) = (8.8 \pm 0.5) \times 10^{-4}$. Our first error is their experiment's error and our second error is the systematic error from using our best value.

$\Gamma(D^{*+} \pi^-)/\Gamma_{\text{total}}$					Γ_{46}/Γ
VALUE	CL%	DOCUMENT ID	TECN	COMMENT	
< 6.1×10^{-6}	90	¹ AAIJ	13AL LHCb	pp at 7 TeV	

¹ Uses $f_s/f_d = 0.256 \pm 0.020$ and $B(B^0 \rightarrow D^{*+} \pi^-) = (2.76 \pm 0.13) \times 10^{-3}$.

$\Gamma(\eta_c \phi)/\Gamma_{\text{total}}$					Γ_{47}/Γ
VALUE (units 10^{-4})	CL%	DOCUMENT ID	TECN	COMMENT	
$5.01 \pm 0.53 \pm 0.68$		¹ AAIJ	17U LHCb	pp at 7, 8 TeV	

¹ The last uncertainty includes the limited knowledge of the external branching fractions where the η_c is reconstructed in the $p\overline{p}, K^+ K^- \pi^+ \pi^-, \pi^+ \pi^- \pi^+ \pi^-$, and $K^+ K^- K^+ K^-$ decays and $\phi(1020) \rightarrow K^+ K^-$.

$\Gamma(\eta_c \pi^+ \pi^-)/\Gamma_{\text{total}}$					Γ_{48}/Γ
VALUE (units 10^{-4})	CL%	DOCUMENT ID	TECN	COMMENT	
$1.76 \pm 0.59 \pm 0.31$		¹ AAIJ	17U LHCb	pp at 7, 8 TeV	

¹ The last uncertainty includes the limited knowledge of the external branching fractions where the η_c is reconstructed in the $p\overline{p}, K^+ K^- \pi^+ \pi^-, \pi^+ \pi^- \pi^+ \pi^-$, and $K^+ K^- K^+ K^-$ decays. The significance of the signal, including systematic uncertainties, is 4.6 standard deviations.

$\Gamma(J/\psi(1S) \phi)/\Gamma_{\text{total}}$					Γ_{49}/Γ
VALUE (units 10^{-3})	CL%	DOCUMENT ID	TECN	COMMENT	
1.08 ± 0.08		OUR FIT			
1.10 ± 0.09		OUR AVERAGE			

¹ AAIJ 13AN LHCb pp at 7 TeV
² THORNE 13 BELL $e^+ e^- \rightarrow \Upsilon(5S)$
³ ABE 96Q CDF $p\overline{p}$

• • • We do not use the following data for averages, fits, limits, etc. • • •
 <6 ¹ AKERS 94J OPAL $e^+ e^- \rightarrow Z$
 seen 14 ⁵ ABE 93F CDF $p\overline{p}$ at 1.8 TeV
 seen 1 ⁶ ACTON 92N OPAL Sup. by AKERS 94J

¹ Uses $f_s/f_d = 0.256 \pm 0.020$ and $B(B^+ \rightarrow J/\psi K^+) = (10.18 \pm 0.42) \times 10^{-4}$.

² Uses $f_s = (17.2 \pm 3.0)\%$ as the fraction of $\Upsilon(5S)$ decaying to $B_s^{(*)} \overline{B}_s^{(*)}$.

³ ABE 96Q reports $[\Gamma(B_s^0 \rightarrow J/\psi(1S) \phi)/\Gamma_{\text{total}}] \times [\Gamma(\overline{B} \rightarrow B_s^0)/\Gamma(\overline{B} \rightarrow B^+) + \Gamma(\overline{B} \rightarrow B^0)] = (0.185 \pm 0.055 \pm 0.020) \times 10^{-3}$ which we divide by our best value $\Gamma(\overline{B} \rightarrow B_s^0)/[\Gamma(\overline{B} \rightarrow B^+) + \Gamma(\overline{B} \rightarrow B^0)] = 0.1230 \pm 0.0115$. Our first error is their experiment's error and our second error is the systematic error from using our best value.

⁴ AKERS 94J sees one event and measures the limit on the product branching fraction $f(\overline{B} \rightarrow B_s^0) \cdot B(B_s^0 \rightarrow J/\psi(1S) \phi) < 7 \times 10^{-4}$ at CL = 90%. We divide by $B(\overline{B} \rightarrow B_s^0) = 0.112$.

⁵ ABE 93F measured using $J/\psi(1S) \rightarrow \mu^+ \mu^-$ and $\phi \rightarrow K^+ K^-$.

⁶ In ACTON 92N a limit on the product branching fraction is measured to be $f(\overline{B} \rightarrow B_s^0) \cdot B(B_s^0 \rightarrow J/\psi(1S) \phi) \leq 0.22 \times 10^{-2}$.

$\Gamma(J/\psi(1S) \phi \phi)/\Gamma(J/\psi(1S) \phi)$					Γ_{50}/Γ_{49}
VALUE (units 10^{-2})	CL%	DOCUMENT ID	TECN	COMMENT	
$1.15 \pm 0.12 \pm 0.05$	90	¹ AAIJ	16U LHCb	pp at 7, 8 TeV	

¹ Uses $J/\psi \rightarrow \mu^+ \mu^-$, $\phi \rightarrow K^+ K^-$ decays, and observes 128 ± 13 events of $B_s^0 \rightarrow J/\psi \phi \phi$.

$\Gamma(J/\psi(1S) \pi^0)/\Gamma_{\text{total}}$					Γ_{51}/Γ
VALUE	CL%	DOCUMENT ID	TECN	COMMENT	
< 1.2×10^{-3}	90	¹ ACCIARRI	97c L3		

¹ ACCIARRI 97c assumes B^0 production fraction $(39.5 \pm 4.0\%)$ and B_s $(12.0 \pm 3.0\%)$.

$\Gamma(J/\psi(1S) \eta)/\Gamma_{\text{total}}$					Γ_{52}/Γ
VALUE (units 10^{-4})	CL%	DOCUMENT ID	TECN	COMMENT	
4.0 ± 0.7		OUR AVERAGE		Error includes scale factor of 1.4.	
$3.6_{-0.6}^{+0.5+0.3}$		¹ AAIJ	13A LHCb	pp at 7 TeV	

¹ AAIJ 13A reports $[\Gamma(B_s^0 \rightarrow J/\psi(1S) \eta)/\Gamma_{\text{total}}] / [B(B^0 \rightarrow J/\psi(1S) \rho^0)] = (2.55_{-0.16}^{+0.18-1.5-1.0}) \times 10^{-5}$. Our first error is their experiment's error and our second error is the systematic error from using our best value.

• • • We do not use the following data for averages, fits, limits, etc. • • •
 <38 ² LI 12 BELL $e^+ e^- \rightarrow \Upsilon(4S)$
³ ACCIARRI 97c L3

¹ AAIJ 13A reports $[\Gamma(B_s^0 \rightarrow J/\psi(1S) \eta)/\Gamma_{\text{total}}] / [B(B^0 \rightarrow J/\psi(1S) \rho^0)] = 14.0 \pm 1.2_{-1.5-1.0}^{+1.1+1.1}$ which we multiply by our best value $B(B^0 \rightarrow J/\psi(1S) \rho^0) = (2.55_{-0.16}^{+0.18-1.5-1.0}) \times 10^{-5}$. Our first error is their experiment's error and our second error is the systematic error from using our best value.

² Observed for the first time with significances over 10σ . The second error are total systematic uncertainties including the error on $N(B_s^{(*)} \overline{B}_s^{(*)})$.

³ ACCIARRI 97c assumes B^0 production fraction $(39.5 \pm 4.0\%)$ and B_s $(12.0 \pm 3.0\%)$.

Meson Particle Listings

 B_S^0

$\Gamma(J/\psi(1S)K_S^0)/\Gamma_{total}$	Γ_{53}/Γ		
VALUE (units 10^{-5})	DOCUMENT ID	TECN	COMMENT
1.88±0.15 OUR AVERAGE			
1.87±0.14±0.06	1 AAIJ	15AL LHCB	$p\bar{p}$ at 7, 8 TeV
1.9 ±0.4 ±0.2	2 AALTONEN	11A CDF	$p\bar{p}$ at 1.96 TeV
• • • We do not use the following data for averages, fits, limits, etc. • • •			
1.98±0.16±0.20	3 AAIJ	13AB LHCB	Repl. by AAIJ 15AL
1.98±0.25±0.20	4 AAIJ	12O LHCB	Repl. by AAIJ 13AB

- ¹ AAIJ 15AL reports $[\Gamma(B_S^0 \rightarrow J/\psi(1S)K_S^0)/\Gamma_{total}] / [B(B^0 \rightarrow J/\psi(1S)K_S^0)] = (4.31 \pm 0.17 \pm 0.12 \pm 0.25) \times 10^{-2}$ which we multiply by our best value $B(B^0 \rightarrow J/\psi(1S)K_S^0) = (4.34 \pm 0.15) \times 10^{-4}$. Our first error is their experiment's error and our second error is the systematic error from using our best value.
- ² AALTONEN 11A reports $[\Gamma(B_S^0 \rightarrow J/\psi(1S)K_S^0)/\Gamma_{total}] \times [B(\bar{B}^0 \rightarrow B_S^0)] / [B(\bar{B}^0 \rightarrow B^0)] / [B(B^0 \rightarrow J/\psi(1S)K_S^0)] = (1.09 \pm 0.19 \pm 0.11) \times 10^{-2}$ which we multiply or divide by our best values $B(\bar{B}^0 \rightarrow B_S^0) = (10.0 \pm 0.8) \times 10^{-2}$, $B(\bar{B}^0 \rightarrow B^0) = (40.8 \pm 0.7) \times 10^{-2}$, $B(B^0 \rightarrow J/\psi(1S)K_S^0) = 1/2 \times B(B^0 \rightarrow J/\psi(1S)K^0) = 1/2 \times (8.68 \pm 0.30) \times 10^{-4}$. Our first error is their experiment's error and our second error is the systematic error from using our best values.
- ³ AAIJ 13AB reports $(1.97 \pm 0.14 \pm 0.07 \pm 0.15 \pm 0.08) \times 10^{-5}$ from a measurement of $[\Gamma(B_S^0 \rightarrow J/\psi(1S)K_S^0)/\Gamma_{total}] / [B(B^0 \rightarrow J/\psi(1S)K^0)] \times [\Gamma(\bar{B}^0 \rightarrow B_S^0)/\Gamma(\bar{B}^0 \rightarrow B^0)]$ assuming $B(B^0 \rightarrow J/\psi(1S)K^0) = (8.98 \pm 0.35) \times 10^{-4}$, $\Gamma(\bar{B}^0 \rightarrow B_S^0)/\Gamma(\bar{B}^0 \rightarrow B^0) = 0.256 \pm 0.020$, which we rescale to our best values $B(B^0 \rightarrow J/\psi(1S)K^0) = (8.68 \pm 0.30) \times 10^{-4}$, $\Gamma(\bar{B}^0 \rightarrow B_S^0)/\Gamma(\bar{B}^0 \rightarrow B^0) = 0.246 \pm 0.023$. Our first error is their experiment's error and our second error is the systematic error from using our best values.
- ⁴ AAIJ 12O reports $(1.83 \pm 0.21 \pm 0.10 \pm 0.14 \pm 0.07) \times 10^{-5}$ from a measurement of $[\Gamma(B_S^0 \rightarrow J/\psi(1S)K_S^0)/\Gamma_{total}] / [B(B^0 \rightarrow J/\psi(1S)K^0)] \times [\Gamma(\bar{B}^0 \rightarrow B_S^0)/\Gamma(\bar{B}^0 \rightarrow B^0)]$ assuming $B(B^0 \rightarrow J/\psi(1S)K^0) = (8.71 \pm 0.32) \times 10^{-4}$, $\Gamma(\bar{B}^0 \rightarrow B_S^0)/\Gamma(\bar{B}^0 \rightarrow B^0) = 0.267^{+0.021}_{-0.02}$, which we rescale to our best values $B(B^0 \rightarrow J/\psi(1S)K^0) = (8.68 \pm 0.30) \times 10^{-4}$, $\Gamma(\bar{B}^0 \rightarrow B_S^0)/\Gamma(\bar{B}^0 \rightarrow B^0) = 0.246 \pm 0.023$. Our first error is their experiment's error and our second error is the systematic error from using our best values.

$\Gamma(J/\psi(1S)\bar{K}^*(892)^0)/\Gamma_{total}$	Γ_{54}/Γ		
VALUE (units 10^{-5})	DOCUMENT ID	TECN	COMMENT
4.14±0.18±0.35	1 AAIJ	15AV LHCB	$p\bar{p}$ at 7, 8 TeV
• • • We do not use the following data for averages, fits, limits, etc. • • •			
4.4 $^{+0.5}_{-0.4}$ ±0.8	2 AAIJ	12AP LHCB	Repl. by AAIJ 15AV
9 ±4 ±1	3 AALTONEN	11A CDF	$p\bar{p}$ at 1.96 TeV

- ¹ AAIJ 15AV result combines two measurements with different normalizing modes of $B^0 \rightarrow J/\psi K^*(892)^0$ and $B_S^0 \rightarrow J/\psi\phi$.
- ² AAIJ 12AP reports $B(B_S^0 \rightarrow J/\psi(1S)\bar{K}^*(892)^0)/B(B^0 \rightarrow J/\psi(1S)K^*(892)^0) = (3.43^{+0.34}_{-0.36} \pm 0.50) \times 10^{-2}$ and $B(B^0 \rightarrow J/\psi(1S)K^*(892)^0) = (1.29 \pm 0.05 \pm 0.13) \times 10^{-3}$ after correcting for the contribution from $K\pi$ S-wave beneath the K^* peak.
- ³ AALTONEN 11A reports $[\Gamma(B_S^0 \rightarrow J/\psi(1S)\bar{K}^*(892)^0)/\Gamma_{total}] \times [B(\bar{B}^0 \rightarrow B_S^0)] / [B(\bar{B}^0 \rightarrow B^0)] / [B(B^0 \rightarrow J/\psi(1S)K^*(892)^0)] = 0.0168 \pm 0.0024 \pm 0.0068$ which we multiply or divide by our best values $B(\bar{B}^0 \rightarrow B_S^0) = (10.0 \pm 0.8) \times 10^{-2}$, $B(\bar{B}^0 \rightarrow B^0) = (40.8 \pm 0.7) \times 10^{-2}$, $B(B^0 \rightarrow J/\psi(1S)K^*(892)^0) = (1.27 \pm 0.05) \times 10^{-3}$. Our first error is their experiment's error and our second error is the systematic error from using our best values.

$\Gamma(J/\psi(1S)\eta)/\Gamma_{total}$	Γ_{55}/Γ		
VALUE (units 10^{-4})	DOCUMENT ID	TECN	COMMENT
3.3 ±0.4 OUR AVERAGE			
3.2 $^{+0.4}_{-0.5}$ ±0.2	1 AAIJ	13A LHCB	$p\bar{p}$ at 7 TeV
3.71±0.61±0.85 -0.60	2 LI	12 BELL	$e^+e^- \rightarrow \Upsilon(4S)$

- ¹ AAIJ 13A reports $[\Gamma(B_S^0 \rightarrow J/\psi(1S)\eta)/\Gamma_{total}] / [B(B^0 \rightarrow J/\psi(1S)\rho^0)] = 12.7 \pm 1.1^{+0.5+1.0}_{-1.3-0.9}$ which we multiply by our best value $B(B^0 \rightarrow J/\psi(1S)\rho^0) = (2.55^{+0.18}_{-0.16}) \times 10^{-5}$. Our first error is their experiment's error and our second error is the systematic error from using our best value.
- ² Observed for the first time with significances over 10σ . The second error are total systematic uncertainties including the error on $N(B_S^{(*)}\bar{B}_S^{(*)})$.

$\Gamma(J/\psi(1S)\eta')/\Gamma(J/\psi(1S)\eta)$	Γ_{55}/Γ_{52}		
VALUE	DOCUMENT ID	TECN	COMMENT
0.87 ±0.06 OUR AVERAGE			
0.902±0.072±0.045	1 AAIJ	15D LHCB	$p\bar{p}$ at 7, 8 TeV
0.90 ±0.09 $^{+0.06}_{-0.02}$	2 AAIJ	13A LHCB	$p\bar{p}$ at 7 TeV
0.73 ±0.14 ±0.02	2 LI	12 BELL	$e^+e^- \rightarrow \Upsilon(4S)$

- ¹ Uses $J/\psi \rightarrow \mu^+\mu^-$, $\eta' \rightarrow \rho^0\gamma$, and $\eta' \rightarrow \eta\pi^+\pi^-$ decays.
- ² Strongly correlated with measurements of $\Gamma(J/\psi(1S)\eta)/\Gamma$ and $\Gamma(J/\psi(1S)\eta')/\Gamma$ reported in the same reference.

$\Gamma(J/\psi(1S)\pi^+\pi^-)/\Gamma(J/\psi(1S)\phi)$	Γ_{56}/Γ_{49}		
VALUE (units 10^{-2})	DOCUMENT ID	TECN	COMMENT
19.4±1.5 OUR FIT			Error includes scale factor of 2.2.
19.9±0.7±0.2	1 AAIJ	12A0 LHCB	$p\bar{p}$ at 7 TeV

- ¹ AAIJ 12A0 reports $(19.79 \pm 0.47 \pm 0.52) \times 10^{-2}$ from a measurement of $[\Gamma(B_S^0 \rightarrow J/\psi(1S)\pi^+\pi^-)/\Gamma(B_S^0 \rightarrow J/\psi(1S)\phi)] / [B(\phi(1020) \rightarrow K^+K^-)]$ assuming $B(\phi(1020) \rightarrow K^+K^-) = (48.9 \pm 0.5) \times 10^{-2}$, which we rescale to our best value $B(\phi(1020) \rightarrow K^+K^-) = (49.2 \pm 0.5) \times 10^{-2}$. Our first error is their experiment's error and our second error is the systematic error from using our best value.

$\Gamma(J/\psi(1S)f_0(980), f_0 \rightarrow \pi^+\pi^-)/\Gamma_{total}$	Γ_{59}/Γ		
VALUE (units 10^{-4})	DOCUMENT ID	TECN	COMMENT
1.28±0.18 OUR FIT			Error includes scale factor of 1.7.
1.16 $^{+0.31}_{-0.19}$ ±0.25	1 LI	11 BELL	$e^+e^- \rightarrow \Upsilon(5S)$

- ¹ The second error includes both the detector systematic and the uncertainty in the number of produced $\Upsilon(5S) \rightarrow B_S^{(*)}\bar{B}_S^{(*)}$ pairs.

$\Gamma(J/\psi(1S)f_0(500), f_0 \rightarrow \pi^+\pi^-)/\Gamma(J/\psi(1S)f_0(980), f_0 \rightarrow \pi^+\pi^-)$	Γ_{57}/Γ_{59}		
VALUE	CL%	DOCUMENT ID	TECN COMMENT
<0.034	90	1 AAIJ	14BR LHCB $p\bar{p}$ at 7, 8 TeV

- ¹ Reported first of two solutions using the full Dalitz analysis.

$\Gamma(J/\psi(1S)\rho, \rho \rightarrow \pi^+\pi^-)/\Gamma(J/\psi(1S)\pi^+\pi^-)$	Γ_{58}/Γ_{56}		
VALUE	CL%	DOCUMENT ID	TECN COMMENT
<0.017	90	1 AAIJ	14BR LHCB $p\bar{p}$ at 7, 8 TeV

- ¹ Reported first of two solutions using the full Dalitz analysis.

$\Gamma(J/\psi(1S)f_0(980), f_0 \rightarrow \pi^+\pi^-)/\Gamma(J/\psi(1S)\pi^+\pi^-)$	Γ_{59}/Γ_{56}		
VALUE	DOCUMENT ID	TECN	COMMENT
0.61 $^{+0.06}_{-0.07}$ OUR FIT			Error includes scale factor of 2.1.
0.703±0.015 $^{+0.004}_{-0.051}$	1 AAIJ	14BR LHCB	$p\bar{p}$ at 7, 8 TeV

- ¹ Reported first of two solutions using the full Dalitz analysis.

$\Gamma(J/\psi(1S)f_2(1270)_0, f_2 \rightarrow \pi^+\pi^-)/\Gamma(J/\psi(1S)\pi^+\pi^-)$	Γ_{61}/Γ_{56}		
VALUE (%)	DOCUMENT ID	TECN	COMMENT
0.36±0.07±0.03	1 AAIJ	14BR LHCB	$p\bar{p}$ at 7, 8 TeV

- ¹ Reported first of two solutions using the full Dalitz analysis.

$\Gamma(J/\psi(1S)f_2(1270)_\parallel, f_2 \rightarrow \pi^+\pi^-)/\Gamma(J/\psi(1S)\pi^+\pi^-)$	Γ_{62}/Γ_{56}		
VALUE (%)	DOCUMENT ID	TECN	COMMENT
0.52±0.15 $^{+0.05}_{-0.02}$	1 AAIJ	14BR LHCB	$p\bar{p}$ at 7, 8 TeV

- ¹ Reported first of two solutions using the full Dalitz analysis.

$\Gamma(J/\psi(1S)f_2(1270)_\perp, f_2 \rightarrow \pi^+\pi^-)/\Gamma(J/\psi(1S)\pi^+\pi^-)$	Γ_{63}/Γ_{56}		
VALUE (%)	DOCUMENT ID	TECN	COMMENT
0.63±0.34 $^{+0.16}_{-0.08}$	1 AAIJ	14BR LHCB	$p\bar{p}$ at 7, 8 TeV

- ¹ Reported first of two solutions using the full Dalitz analysis.

$\Gamma(J/\psi(1S)f_0(1500), f_0 \rightarrow \pi^+\pi^-)/\Gamma(J/\psi(1S)\pi^+\pi^-)$	Γ_{65}/Γ_{56}		
VALUE	DOCUMENT ID	TECN	COMMENT
0.101±0.008 $^{+0.011}_{-0.003}$	1 AAIJ	14BR LHCB	$p\bar{p}$ at 7, 8 TeV

- ¹ Reported first of two solutions using the full Dalitz analysis.

$\Gamma(J/\psi(1S)f_2'(1525)_0, f_2' \rightarrow \pi^+\pi^-)/\Gamma(J/\psi(1S)\pi^+\pi^-)$	Γ_{66}/Γ_{56}		
VALUE (%)	DOCUMENT ID	TECN	COMMENT
0.51±0.09 $^{+0.05}_{-0.04}$	1 AAIJ	14BR LHCB	$p\bar{p}$ at 7, 8 TeV

- ¹ Reported first of two solutions using the full Dalitz analysis.

$\Gamma(J/\psi(1S)f_2'(1525)_\parallel, f_2' \rightarrow \pi^+\pi^-)/\Gamma(J/\psi(1S)\pi^+\pi^-)$	Γ_{67}/Γ_{56}		
VALUE (%)	DOCUMENT ID	TECN	COMMENT
0.06 $^{+0.13}_{-0.04}$ ±0.01	1 AAIJ	14BR LHCB	$p\bar{p}$ at 7, 8 TeV

- ¹ Reported first of two solutions using the full Dalitz analysis.

$\Gamma(J/\psi(1S)f_2'(1525)_\perp, f_2' \rightarrow \pi^+\pi^-)/\Gamma(J/\psi(1S)\pi^+\pi^-)$	Γ_{68}/Γ_{56}		
VALUE (%)	DOCUMENT ID	TECN	COMMENT
0.26±0.18 $^{+0.06}_{-0.04}$	1 AAIJ	14BR LHCB	$p\bar{p}$ at 7, 8 TeV

- ¹ Reported first of two solutions using the full Dalitz analysis.

$\Gamma(J/\psi(1S)f_0(1790), f_0 \rightarrow \pi^+\pi^-)/\Gamma(J/\psi(1S)\pi^+\pi^-)$	Γ_{69}/Γ_{56}		
VALUE	DOCUMENT ID	TECN	COMMENT
0.024±0.004 $^{+0.050}_{-0.002}$	1 AAIJ	14BR LHCB	$p\bar{p}$ at 7, 8 TeV

- ¹ Reported first of two solutions using the full Dalitz analysis.

$\Gamma(J/\psi(1S) f_0(980), f_0 \rightarrow \pi^+ \pi^-) / \Gamma(J/\psi(1S) \phi)$ $\Gamma_{59} / \Gamma_{49}$

VALUE	DOCUMENT ID	TECN	COMMENT
-------	-------------	------	---------

0.119^{+0.013}_{-0.014} OUR FIT Error includes scale factor of 2.4.

0.111^{+0.020}_{-0.018} OUR AVERAGE Error includes scale factor of 2.5. See the ideogram below.

0.069 ± 0.012 ± 0.001	1 KHACHATRYAN	16Q CMS	pp at 7 TeV
0.140 ± 0.026 _{-0.013} ± 0.002	2,3 AAIJ	12A0 LHCB	pp at 7 TeV
0.135 ± 0.036 ± 0.001	4 ABAZOV	12C D0	p \bar{p} at 1.96 TeV
0.126 ± 0.012 ± 0.001	5 AALTONEN	11AB CDF	p \bar{p} at 1.96 TeV

• • • We do not use the following data for averages, fits, limits, etc. • • •

0.124 ± 0.026_{-0.023} ± 0.001 $\Gamma_{59} / \Gamma_{49}$

1 KHACHATRYAN 16Q reports $[\Gamma(B_s^0 \rightarrow J/\psi(1S) f_0(980), f_0 \rightarrow \pi^+ \pi^-) / \Gamma(B_s^0 \rightarrow J/\psi(1S) \phi)] / [B(\phi(1020) \rightarrow K^+ K^-)] = 0.140 \pm 0.008 \pm 0.023$ which we multiply by our best value $B(\phi(1020) \rightarrow K^+ K^-) = (49.2 \pm 0.5) \times 10^{-2}$. Our first error is their experiment's error and our second error is the systematic error from using our best value.

2 AAIJ 12A0 reports $(13.9 \pm 0.6 + 2.5) \times 10^{-2}$ from a measurement of $[\Gamma(B_s^0 \rightarrow J/\psi(1S) f_0(980), f_0 \rightarrow \pi^+ \pi^-) / \Gamma(B_s^0 \rightarrow J/\psi(1S) \phi)] / [B(\phi(1020) \rightarrow K^+ K^-)]$ assuming $B(\phi(1020) \rightarrow K^+ K^-) = (48.9 \pm 0.5) \times 10^{-2}$, which we rescale to our best value $B(\phi(1020) \rightarrow K^+ K^-) = (49.2 \pm 0.5) \times 10^{-2}$. Our first error is their experiment's error and our second error is the systematic error from using our best value.

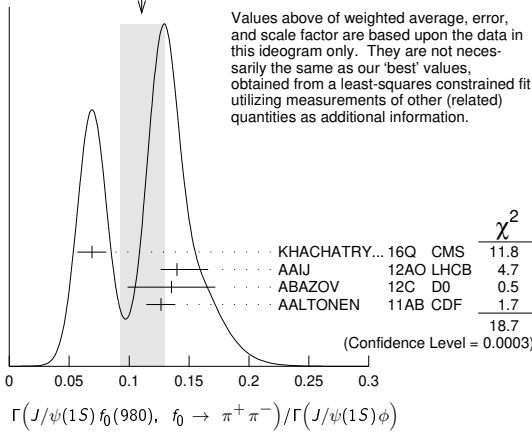
3 Measured in Dalitz plot like analysis of $B_s \rightarrow J/\psi \pi^+ \pi^-$ decays.

4 ABAZOV 12C reports $[\Gamma(B_s^0 \rightarrow J/\psi(1S) f_0(980), f_0 \rightarrow \pi^+ \pi^-) / \Gamma(B_s^0 \rightarrow J/\psi(1S) \phi)] / [B(\phi(1020) \rightarrow K^+ K^-)] = 0.275 \pm 0.041 \pm 0.061$ which we multiply by our best value $B(\phi(1020) \rightarrow K^+ K^-) = (49.2 \pm 0.5) \times 10^{-2}$. Our first error is their experiment's error and our second error is the systematic error from using our best value.

5 AALTONEN 11AB reports $[\Gamma(B_s^0 \rightarrow J/\psi(1S) f_0(980), f_0 \rightarrow \pi^+ \pi^-) / \Gamma(B_s^0 \rightarrow J/\psi(1S) \phi)] / [B(\phi(1020) \rightarrow K^+ K^-)] = 0.257 \pm 0.020 \pm 0.014$ which we multiply by our best value $B(\phi(1020) \rightarrow K^+ K^-) = (49.2 \pm 0.5) \times 10^{-2}$. Our first error is their experiment's error and our second error is the systematic error from using our best value.

6 AAIJ 11 reports $[\Gamma(B_s^0 \rightarrow J/\psi(1S) f_0(980), f_0 \rightarrow \pi^+ \pi^-) / \Gamma(B_s^0 \rightarrow J/\psi(1S) \phi)] / [B(\phi(1020) \rightarrow K^+ K^-)] = 0.252 \pm 0.046 + 0.027 - 0.032 - 0.033$ which we multiply by our best value $B(\phi(1020) \rightarrow K^+ K^-) = (49.2 \pm 0.5) \times 10^{-2}$. Our first error is their experiment's error and our second error is the systematic error from using our best value.

WEIGHTED AVERAGE
0.111±0.020-0.018 (Error scaled by 2.5)



Values above of weighted average, error, and scale factor are based upon the data in this ideogram only. They are not necessarily the same as our 'best' values, obtained from a least-squares constrained fit utilizing measurements of other (related) quantities as additional information.

$\Gamma(J/\psi(1S) f_0(1370), f_0 \rightarrow \pi^+ \pi^-) / \Gamma_{total}$ Γ_{64} / Γ

VALUE (units 10^{-4})	DOCUMENT ID	TECN	COMMENT
--------------------------	-------------	------	---------

• • • We do not use the following data for averages, fits, limits, etc. • • •

0.34^{+0.11+0.085}_{-0.14-0.054} Γ_{64} / Γ

1 The second error includes both the detector systematic and the uncertainty in the number of produced $Y(5S) \rightarrow B_s^{(*)} \bar{B}_s^{(*)}$ pairs.

$\Gamma(J/\psi(1S) f_0(1370), f_0 \rightarrow \pi^+ \pi^-) / \Gamma(J/\psi(1S) \phi)$ $\Gamma_{64} / \Gamma_{49}$

VALUE (units 10^{-2})	DOCUMENT ID	TECN	COMMENT
--------------------------	-------------	------	---------

4.22^{+0.55}_{-3.76} ± 0.05 $\Gamma_{64} / \Gamma_{49}$

1 AAIJ 12A0 reports $(4.19 \pm 0.53 + 0.12 - 3.7) \times 10^{-2}$ from a measurement of $[\Gamma(B_s^0 \rightarrow J/\psi(1S) f_0(1370), f_0 \rightarrow \pi^+ \pi^-) / \Gamma(B_s^0 \rightarrow J/\psi(1S) \phi)] / [B(\phi(1020) \rightarrow K^+ K^-)]$ assuming $B(\phi(1020) \rightarrow K^+ K^-) = (48.9 \pm 0.5) \times 10^{-2}$, which we rescale to our best value $B(\phi(1020) \rightarrow K^+ K^-) = (49.2 \pm 0.5) \times 10^{-2}$. Our first error is their experiment's error and our second error is the systematic error from using our best value.

2 Measured in Dalitz plot like analysis of $B_s \rightarrow J/\psi \pi^+ \pi^-$ decays.

$\Gamma(J/\psi(1S) f_2(1270), f_2 \rightarrow \pi^+ \pi^-) / \Gamma(J/\psi(1S) \phi)$ $\Gamma_{60} / \Gamma_{49}$

VALUE (units 10^{-4})	DOCUMENT ID	TECN	COMMENT
--------------------------	-------------	------	---------

9.9 ± 3.4_{-3.6} ± 0.1 $\Gamma_{60} / \Gamma_{49}$

1,2 AAIJ 12A0 reports $(0.098 \pm 0.033 + 0.006 - 0.015) \times 10^{-2}$ from a measurement of $[\Gamma(B_s^0 \rightarrow J/\psi(1S) f_2(1270), f_2 \rightarrow \pi^+ \pi^-) / \Gamma(B_s^0 \rightarrow J/\psi(1S) \phi)] / [B(\phi(1020) \rightarrow K^+ K^-)]$ assuming $B(\phi(1020) \rightarrow K^+ K^-) = (48.9 \pm 0.5) \times 10^{-2}$, which we rescale to our best value $B(\phi(1020) \rightarrow K^+ K^-) = (49.2 \pm 0.5) \times 10^{-2}$. Our first error is their experiment's error and our second error is the systematic error from using our best value.

2 Measured in Dalitz plot like analysis of $B_s \rightarrow J/\psi \pi^+ \pi^-$ decays for the f_2 helicity state $\lambda = 0$.

$\Gamma(J/\psi(1S) \pi^+ \pi^- (\text{nonresonant})) / \Gamma(J/\psi(1S) \phi)$ $\Gamma_{70} / \Gamma_{49}$

VALUE (units 10^{-2})	DOCUMENT ID	TECN	COMMENT
--------------------------	-------------	------	---------

1.67^{+1.02}_{-0.32} ± 0.02 $\Gamma_{70} / \Gamma_{49}$

1 AAIJ 12A0 reports $(1.66 \pm 0.31 + 0.96 - 0.08) \times 10^{-2}$ from a measurement of $[\Gamma(B_s^0 \rightarrow J/\psi(1S) \pi^+ \pi^- (\text{nonresonant})) / \Gamma(B_s^0 \rightarrow J/\psi(1S) \phi)] / [B(\phi(1020) \rightarrow K^+ K^-)]$ assuming $B(\phi(1020) \rightarrow K^+ K^-) = (48.9 \pm 0.5) \times 10^{-2}$, which we rescale to our best value $B(\phi(1020) \rightarrow K^+ K^-) = (49.2 \pm 0.5) \times 10^{-2}$. Our first error is their experiment's error and our second error is the systematic error from using our best value.

2 Measured in Dalitz plot like analysis of $B_s \rightarrow J/\psi \pi^+ \pi^-$ decays.

$\Gamma(J/\psi(1S) \bar{K}^0 \pi^+ \pi^-) / \Gamma_{total}$ Γ_{71} / Γ

VALUE	CL%	DOCUMENT ID	TECN	COMMENT
-------	-----	-------------	------	---------

<4.4 × 10⁻⁵ Γ_{71} / Γ

1 Measured with $B(B_s^0 \rightarrow J/\psi K_S^0 \pi^+ \pi^-) / B(B^0 \rightarrow J/\psi K_S^0 \pi^+ \pi^-)$ using PDG 12 values for the involved branching fractions.

$\Gamma(J/\psi(1S) K^+ K^-) / \Gamma_{total}$ Γ_{72} / Γ

VALUE (units 10^{-4})	DOCUMENT ID	TECN	COMMENT
--------------------------	-------------	------	---------

7.9 ± 0.7 OUR AVERAGE Γ_{72} / Γ

7.70 ± 0.08 ± 0.72 Γ_{72} / Γ

10.1 ± 0.9 ± 2.1 Γ_{72} / Γ

1 Uses $f_s / f_d = 0.256 \pm 0.020$ and $B(B^+ \rightarrow J/\psi K^+) = (10.18 \pm 0.42) \times 10^{-4}$.

2 Uses $f_s = (17.2 \pm 3.0)\%$ as the fraction of $\Upsilon(5S)$ decaying to $B_s^{(*)} \bar{B}_s^{(*)}$.

$\Gamma(J/\psi(1S) K^0 K^- \pi^+ + \text{c.c.}) / \Gamma_{total}$ Γ_{73} / Γ

VALUE (units 10^{-4})	DOCUMENT ID	TECN	COMMENT
--------------------------	-------------	------	---------

9.2 ± 1.0 ± 0.9 Γ_{73} / Γ

1 AAIJ 14L reports $[\Gamma(B_s^0 \rightarrow J/\psi(1S) K^0 K^- \pi^+ + \text{c.c.}) / \Gamma_{total}] / [B(B^0 \rightarrow J/\psi(1S) K^0 \pi^+ \pi^-)] = 2.12 \pm 0.15 \pm 0.18$ which we multiply by our best value $B(B^0 \rightarrow J/\psi(1S) K^0 \pi^+ \pi^-) = (4.3 \pm 0.4) \times 10^{-4}$. Our first error is their experiment's error and our second error is the systematic error from using our best value. This is an observation of $B_s^0 \rightarrow J/\psi K_S^0 K^\pm \pi^\mp$ with more than 10 standard deviations.

$\Gamma(J/\psi(1S) \bar{K}^0 K^+ K^-) / \Gamma_{total}$ Γ_{74} / Γ

VALUE	CL%	DOCUMENT ID	TECN	COMMENT
-------	-----	-------------	------	---------

<12 × 10⁻⁶ Γ_{74} / Γ

1 Measured with $B(B_s^0 \rightarrow J/\psi K_S^0 K^+ K^-) / B(B^0 \rightarrow J/\psi K_S^0 \pi^+ \pi^-)$ using PDG 12 values for the involved branching fractions.

$\Gamma(J/\psi(1S) f_2'(1525)) / \Gamma(J/\psi(1S) \phi)$ $\Gamma_{75} / \Gamma_{49}$

VALUE (units 10^{-2})	DOCUMENT ID	TECN	COMMENT
--------------------------	-------------	------	---------

21 ± 4 OUR AVERAGE $\Gamma_{75} / \Gamma_{49}$

21.5 ± 4.9 ± 2.6 $\Gamma_{75} / \Gamma_{49}$

21 ± 7 ± 1 $\Gamma_{75} / \Gamma_{49}$

• • • We do not use the following data for averages, fits, limits, etc. • • •

27 ± 4 ± 1 $\Gamma_{75} / \Gamma_{49}$

1 Uses $B(f_2'(1525) \rightarrow K^+ K^-) = (44.4 \pm 1.1)\%$.

2 ABAZOV 12AF reports $[\Gamma(B_s^0 \rightarrow J/\psi(1S) f_2'(1525)) / \Gamma(B_s^0 \rightarrow J/\psi(1S) \phi)] \times B(f_2'(1525) \rightarrow K^+ K^-) / B(\phi(1020) \rightarrow K^+ K^-) = 0.19 \pm 0.05 \pm 0.04$ which we divide and multiply by our best values $B(f_2'(1525) \rightarrow K^+ K^-) = \frac{1}{2} (87.6 \pm 2.2) \times 10^{-2}$, $B(\phi(1020) \rightarrow K^+ K^-) = (49.2 \pm 0.5) \times 10^{-2}$. Our first error is their experiment's error and our second error is the systematic error from using our best values.

3 ABAZOV 12AF fits the invariant masses of the $K^+ K^-$ pair in the range $1.35 < M(K^+ K^-) < 2$ GeV.

4 AAIJ 12S reports $[(26.4 \pm 2.7 \pm 2.4) \times 10^{-2}]$ from a measurement of $[\Gamma(B_s^0 \rightarrow J/\psi(1S) f_2'(1525)) / \Gamma(B_s^0 \rightarrow J/\psi(1S) \phi)] \times B(f_2'(1525) \rightarrow K^+ K^-) / B(\phi(1020) \rightarrow K^+ K^-)$ assuming $B(f_2'(1525) \rightarrow K^+ K^-) = (44.4 \pm 1.1) \times 10^{-2}$, $B(\phi(1020) \rightarrow K^+ K^-) = (48.9 \pm 0.5) \times 10^{-2}$, which we rescale to our best values $B(f_2'(1525) \rightarrow K^+ K^-) = \frac{1}{2} (87.6 \pm 2.2) \times 10^{-2}$, $B(\phi(1020) \rightarrow K^+ K^-) = (49.2 \pm 0.5) \times 10^{-2}$. Our first error is their experiment's error and our second error is the systematic error from using our best values.

$\Gamma(J/\psi(1S) f_2'(1525)) / \Gamma_{total}$ Γ_{75} / Γ

VALUE (units 10^{-4})	DOCUMENT ID	TECN	COMMENT
--------------------------	-------------	------	---------

2.61 ± 0.20 ± 0.56_{-0.50} Γ_{75} / Γ

1 Uses $f_s / f_d = 0.256 \pm 0.020$ and $B(B^+ \rightarrow J/\psi K^+) = (10.18 \pm 0.42) \times 10^{-4}$.

Meson Particle Listings

 B_s^0 $\Gamma(\psi(2S)\eta)/\Gamma(J/\psi(1S)\eta)$ Γ_{80}/Γ_{52}

VALUE	DOCUMENT ID	TECN	COMMENT
0.83±0.14±0.12	¹ AAIJ	13AA LHCb	pp at 7 TeV

¹ Assuming lepton universality for dimuon decay modes of J/ψ and $\psi(2S)$ mesons, the ratio $B(J/\psi \rightarrow \mu^+\mu^-)/B(\psi(2S) \rightarrow \mu^+\mu^-) = B(J/\psi \rightarrow e^+e^-)/B(\psi(2S) \rightarrow e^+e^-) = 7.69 \pm 0.19$ was used.

 $\Gamma(\psi(2S)\eta')/\Gamma(J/\psi(1S)\eta')$ Γ_{81}/Γ_{55}

VALUE (units 10^{-2})	DOCUMENT ID	TECN	COMMENT
38.7±9.0±1.6	¹ AAIJ	15D LHCb	pp at 7, 8 TeV

¹ Uses $J/\psi \rightarrow \mu^+\mu^-$, $\eta' \rightarrow \rho^0\gamma$, and $\eta' \rightarrow \eta\pi^+\pi^-$ decays.

 $\Gamma(J/\psi(1S)\rho\bar{\rho})/\Gamma_{total}$ Γ_{76}/Γ

VALUE (units 10^{-6})	CL%	DOCUMENT ID	TECN	COMMENT
3.58±0.19±0.39		¹ AAIJ	19U LHCb	pp at 7, 8, 13 TeV

• • • We do not use the following data for averages, fits, limits, etc. • • •

<4.8	90	² AAIJ	13Z LHCb	Repl. by AAIJ 2019U
------	----	-------------------	----------	---------------------

¹ Measured relative to $B_s^0 \rightarrow J/\psi\phi$ assuming $B(B_s^0 \rightarrow J/\psi\phi) = (10.5 \pm 0.13 \pm 0.64) \times 10^{-4}$ and taking into account small K^+K^-S -wave contribution.
² Uses $B(B_s^0 \rightarrow J/\psi(1S)\pi^+\pi^-) = (1.98 \pm 0.20) \times 10^{-4}$.

 $\Gamma(J/\psi(1S)\gamma)/\Gamma_{total}$ Γ_{77}/Γ

VALUE	CL%	DOCUMENT ID	TECN	COMMENT
<7.3 × 10⁻⁶	90	¹ AAIJ	15BB LHCb	pp at 7, 8 TeV

¹ Branching fractions of normalization modes $B_s^0 \rightarrow J/\psi\gamma X$ taken from PDG 14. Uses $f_s/f_d = 0.259 \pm 0.015$.

 $\Gamma(J/\psi(1S)\pi^+\pi^-\pi^+\pi^-)/\Gamma(J/\psi(1S)\pi^+\pi^-)$ Γ_{78}/Γ_{56}

VALUE	DOCUMENT ID	TECN	COMMENT
0.371±0.015±0.022	¹ AAIJ	14Y LHCb	pp at 7, 8 TeV

¹ Excludes contributions from $\psi(2S)$ and $\chi_{c1}(3872)$ decaying to $J/\psi(1S)\pi^+\pi^-$.

 $\Gamma(J/\psi(1S)f_1(1285))/\Gamma_{total}$ Γ_{79}/Γ

VALUE (units 10^{-5})	DOCUMENT ID	TECN	COMMENT
7.2±1.3±0.4	¹ AAIJ	14Y LHCb	pp at 7, 8 TeV

¹ AAIJ 14Y reports $(7.14 \pm 0.90_{-0.91}^{+0.83} \pm 0.41) \times 10^{-5}$ from a measurement of $\Gamma(B_s^0 \rightarrow J/\psi(1S)f_1(1285))/\Gamma_{total} \times [B(f_1(1285) \rightarrow 2\pi^+2\pi^-)]$ assuming $B(f_1(1285) \rightarrow 2\pi^+2\pi^-) = 0.11 \pm 0.007_{-0.006}^{+0.007}$, which we rescale to our best value $B(f_1(1285) \rightarrow 2\pi^+2\pi^-) = (10.9 \pm 0.6) \times 10^{-2}$. Our first error is their experiment's error and our second error is the systematic error from using our best value.

 $\Gamma(\psi(2S)\phi)/\Gamma_{total}$ Γ_{83}/Γ

VALUE (units 10^{-4})	EVTS	DOCUMENT ID	TECN	COMMENT
• • • We do not use the following data for averages, fits, limits, etc. • • •				

seen ¹ BUSKULIC 93G ALEP $e^+e^- \rightarrow Z$

 $\Gamma(\psi(2S)\phi)/\Gamma(J/\psi(1S)\phi)$ Γ_{83}/Γ_{49}

VALUE	DOCUMENT ID	TECN	COMMENT
0.503±0.034 OUR AVERAGE			

0.500±0.034±0.011	^{1,2} AAIJ	12L LHCb	pp at 7 TeV
0.53 ± 0.10 ± 0.09	ABAZOV	09Y D0	$p\bar{p}$ at 1.96 TeV
0.52 ± 0.13 ± 0.07	ABULENCIA	06N CDF	$p\bar{p}$ at 1.96 TeV

¹ AAIJ 12L reports $0.489 \pm 0.026 \pm 0.021$ from a measurement of $\Gamma(B_s^0 \rightarrow \psi(2S)\phi)/\Gamma(B_s^0 \rightarrow J/\psi(1S)\phi) \times [B(J/\psi(1S) \rightarrow e^+e^-)] / [B(\psi(2S) \rightarrow e^+e^-)]$ assuming $B(J/\psi(1S) \rightarrow e^+e^-) = (5.94 \pm 0.06) \times 10^{-2}$, $B(\psi(2S) \rightarrow e^+e^-) = (7.72 \pm 0.17) \times 10^{-3}$, which we rescale to our best values $B(J/\psi(1S) \rightarrow e^+e^-) = (5.971 \pm 0.032) \times 10^{-2}$, $B(\psi(2S) \rightarrow e^+e^-) = (7.93 \pm 0.17) \times 10^{-3}$. Our first error is their experiment's error and our second error is the systematic error from using our best values.
² Assumes $B(J/\psi \rightarrow \mu^+\mu^-) / B(\psi(2S) \rightarrow \mu^+\mu^-) = B(J/\psi \rightarrow e^+e^-) / B(\psi(2S) \rightarrow e^+e^-) = 7.69 \pm 0.19$.

 $\Gamma(\psi(2S)K^-\pi^+)/\Gamma_{total}$ Γ_{84}/Γ

VALUE (units 10^{-5})	DOCUMENT ID	TECN	COMMENT
3.12±0.30±0.21	¹ AAIJ	15U LHCb	pp at 7, 8 TeV

¹ AAIJ 15U reports $[\Gamma(B_s^0 \rightarrow \psi(2S)K^-\pi^+)/\Gamma_{total}] / [B(B^0 \rightarrow \psi(2S)K^+\pi^-)] = (5.38 \pm 0.36 \pm 0.22 \pm 0.31) \times 10^{-2}$ which we multiply by our best value $B(B^0 \rightarrow \psi(2S)K^+\pi^-) = (5.8 \pm 0.4) \times 10^{-4}$. Our first error is their experiment's error and our second error is the systematic error from using our best value.

 $\Gamma(\psi(2S)K^*(892)^0)/\Gamma_{total}$ Γ_{85}/Γ

VALUE (units 10^{-5})	DOCUMENT ID	TECN	COMMENT
3.3±0.5±0.2	¹ AAIJ	15U LHCb	pp at 7, 8 TeV

¹ AAIJ 15U reports $[\Gamma(B_s^0 \rightarrow \psi(2S)K^*(892)^0)/\Gamma_{total}] / [B(B^0 \rightarrow \psi(2S)K^*(892)^0)] = (5.58 \pm 0.57 \pm 0.40 \pm 0.32) \times 10^{-2}$ which we multiply by our best value $B(B^0 \rightarrow \psi(2S)K^*(892)^0) = (5.9 \pm 0.4) \times 10^{-4}$. Our first error is their experiment's error and our second error is the systematic error from using our best value.

 $\Gamma(\chi_{c1}\phi)/\Gamma(J/\psi(1S)\phi)$ Γ_{86}/Γ_{49}

VALUE (units 10^{-2})	DOCUMENT ID	TECN	COMMENT
18.9±1.8±1.5	¹ AAIJ	13Ac LHCb	pp at 7 TeV

¹ Uses $B(\chi_{c1} \rightarrow J/\psi\gamma) = (34.4 \pm 1.5)\%$.

 $\Gamma(\chi_{c2}K^+K^-)/\Gamma(\chi_{c1}K^+K^-)$ Γ_{88}/Γ_{87}

VALUE (units 10^{-2})	DOCUMENT ID	TECN	COMMENT
17.1±3.1±1.0	¹ AAIJ	18Ac LHCb	pp at 7, 8, 13 TeV

¹ Measures the ratio for ± 15 MeV window around ϕ mass.

 $\Gamma(\psi(2S)\pi^+\pi^-)/\Gamma(J/\psi(1S)\pi^+\pi^-)$ Γ_{82}/Γ_{56}

VALUE	DOCUMENT ID	TECN	COMMENT
0.34±0.04±0.03	¹ AAIJ	13AA LHCb	pp at 7 TeV

¹ Assuming lepton universality for dimuon decay modes of J/ψ and $\psi(2S)$ mesons, the ratio $B(J/\psi \rightarrow \mu^+\mu^-)/B(\psi(2S) \rightarrow \mu^+\mu^-) = B(J/\psi \rightarrow e^+e^-)/B(\psi(2S) \rightarrow e^+e^-) = 7.69 \pm 0.19$ was used.

 $\Gamma(\pi^+\pi^-)/\Gamma_{total}$ Γ_{89}/Γ

VALUE (units 10^{-7})	CL%	DOCUMENT ID	TECN	COMMENT
7.0±1.0 OUR AVERAGE				

7.3±0.9±0.7		¹ AAIJ	17G LHCb	pp at 7 and 8 TeV
6.4±1.8±0.6		² AALTONEN	12L CDF	$p\bar{p}$ at 1.96 TeV

• • • We do not use the following data for averages, fits, limits, etc. • • •

10.4 ^{+2.4} _{-2.1} ±1.0		³ AAIJ	12AR LHCb	Repl. by AAIJ 17G
< 120	90	⁴ PENG	10 BELL	$e^+e^- \rightarrow \Upsilon(5S)$
< 12	90	⁵ AALTONEN	09C CDF	Repl. by AALTONEN 12L
< 17	90	⁶ ABULENCIA,A	06D CDF	Repl. by AALTONEN 09c
<2320	90	⁷ ABE	00C SLD	$e^+e^- \rightarrow Z$
<1700	90	⁸ BUSKULIC	96V ALEP	$e^+e^- \rightarrow Z$

¹ AAIJ 17G reports $[\Gamma(B_s^0 \rightarrow \pi^+\pi^-)/\Gamma_{total}] / [B(B^0 \rightarrow K^+\pi^-)] \times [\Gamma(\bar{B} \rightarrow B_s^0)/\Gamma(\bar{B} \rightarrow B^0)] = (9.15 \pm 0.71 \pm 0.83) \times 10^{-3}$ which we multiply or divide by our best values $B(B^0 \rightarrow K^+\pi^-) = (1.96 \pm 0.05) \times 10^{-5}$, $\Gamma(\bar{B} \rightarrow B_s^0)/\Gamma(\bar{B} \rightarrow B^0) = 0.246 \pm 0.023$. Our first error is their experiment's error and our second error is the systematic error from using our best values.

² AALTONEN 12L reports $[\Gamma(B_s^0 \rightarrow \pi^+\pi^-)/\Gamma_{total}] / [B(B^0 \rightarrow K^+\pi^-)] \times [\Gamma(\bar{B} \rightarrow B_s^0)/\Gamma(\bar{B} \rightarrow B^0)] = 0.008 \pm 0.002 \pm 0.001$ which we multiply or divide by our best values $B(B^0 \rightarrow K^+\pi^-) = (1.96 \pm 0.05) \times 10^{-5}$, $\Gamma(\bar{B} \rightarrow B_s^0)/\Gamma(\bar{B} \rightarrow B^0) = 0.246 \pm 0.023$. Our first error is their experiment's error and our second error is the systematic error from using our best values.

³ AAIJ 12AR reports $[\Gamma(B_s^0 \rightarrow \pi^+\pi^-)/\Gamma_{total}] / [B(B^0 \rightarrow \pi^+\pi^-)] \times [\Gamma(\bar{B} \rightarrow B_s^0)/\Gamma(\bar{B} \rightarrow B^0)] = 0.050_{-0.009}^{+0.011} \pm 0.004$ which we multiply or divide by our best values $B(B^0 \rightarrow \pi^+\pi^-) = (5.12 \pm 0.19) \times 10^{-6}$, $\Gamma(\bar{B} \rightarrow B_s^0)/\Gamma(\bar{B} \rightarrow B^0) = 0.246 \pm 0.023$. Our first error is their experiment's error and our second error is the systematic error from using our best values.

⁴ Uses $\Upsilon(10860) \rightarrow B_s^* \bar{B}_s^*$ and assumes $B(\Upsilon(10860) \rightarrow B_s^* \bar{B}_s^*) = (19.3 \pm 2.9)\%$ and $\Gamma(\Upsilon(10860) \rightarrow B_s^* \bar{B}_s^*) / \Gamma(\Upsilon(10860) \rightarrow B_s^* \bar{B}_s^*) = (90.1 \pm 3.8)_{-4.0}^{\pm 3.8}\%$.

⁵ Obtains this result from $(f_s/f_d) \cdot B(B_s \rightarrow \pi^+\pi^-)/B(B^0 \rightarrow K^+\pi^-) = 0.007 \pm 0.004 \pm 0.005$, assuming $f_s/f_d = 0.276 \pm 0.034$ and $B(B^0 \rightarrow K^+\pi^-) = (19.4 \pm 0.6) \times 10^{-6}$.

⁶ ABULENCIA,A 06D obtains this from $B(B_s \rightarrow \pi^+\pi^-) / B(B_s \rightarrow K^+K^-) < 0.05$ at 90% CL, assuming $B(B_s \rightarrow K^+K^-) = (33 \pm 6 \pm 7) \times 10^{-6}$.

⁷ ABE 00c assumes $B(Z \rightarrow b\bar{b}) = (21.7 \pm 0.1)\%$ and the B fractions $f_{B^0} = f_{B^+} = (39.7 \pm 1.8)_{-2.2}^{\pm 1.8}\%$ and $f_{B_s} = (10.5 \pm 1.8)_{-2.2}^{\pm 1.8}\%$.

⁸ BUSKULIC 96V assumes PDG 96 production fractions for B^0, B^+, B_s, b baryons.

 $\Gamma(\pi^0\pi^0)/\Gamma_{total}$ Γ_{90}/Γ

VALUE	CL%	DOCUMENT ID	TECN	COMMENT
<2.1 × 10⁻⁴	90	¹ ACCIARRI	95H L3	$e^+e^- \rightarrow Z$

¹ ACCIARRI 95H assumes $f_{B^0} = 39.5 \pm 4.0$ and $f_{B_s} = 12.0 \pm 3.0\%$.

 $\Gamma(\eta\pi^0)/\Gamma_{total}$ Γ_{91}/Γ

VALUE	CL%	DOCUMENT ID	TECN	COMMENT
<1.0 × 10⁻³	90	¹ ACCIARRI	95H L3	$e^+e^- \rightarrow Z$

¹ ACCIARRI 95H assumes $f_{B^0} = 39.5 \pm 4.0$ and $f_{B_s} = 12.0 \pm 3.0\%$.

 $\Gamma(\eta\eta)/\Gamma_{total}$ Γ_{92}/Γ

VALUE	CL%	DOCUMENT ID	TECN	COMMENT
<1.5 × 10⁻³	90	¹ ACCIARRI	95H L3	$e^+e^- \rightarrow Z$

¹ ACCIARRI 95H assumes $f_{B^0} = 39.5 \pm 4.0$ and $f_{B_s} = 12.0 \pm 3.0\%$.

 $\Gamma(\rho^0\rho^0)/\Gamma_{total}$ Γ_{93}/Γ

VALUE	CL%	DOCUMENT ID	TECN	COMMENT
<3.20 × 10⁻⁴	90	¹ ABE	00c SLD	$e^+e^- \rightarrow Z$

¹ ABE 00c assumes $B(Z \rightarrow b\bar{b}) = (21.7 \pm 0.1)\%$ and the B fractions $f_{B^0} = f_{B^+} = (39.7 \pm 1.8)_{-2.2}^{\pm 1.8}\%$ and $f_{B_s} = (10.5 \pm 1.8)_{-2.2}^{\pm 1.8}\%$.

Γ(η'η')/Γ_{total} Γ₉₄/Γ

Table with columns: VALUE (units 10^-5), CL%, DOCUMENT ID, TECN, COMMENT. Row 1: 3.3 ± 0.7 ± 0.1, 1 AAIJ, 150 LHCb, pp at 7, 8 TeV

1 AAIJ 150 reports [Γ(B_s⁰ → η'η')/Γ_{total}] / [B(B⁺ → η'K⁺)] = 0.47 ± 0.09 ± 0.04 which we multiply by our best value B(B⁺ → η'K⁺) = (7.04 ± 0.25) × 10⁻⁵. Our first error is their experiment's error and our second error is the systematic error from using our best value.

Γ(η'φ)/Γ_{total} Γ₉₅/Γ

Table with columns: VALUE, CL%, DOCUMENT ID, TECN, COMMENT. Row 1: <0.82 × 10^-6, 90, 1 AAIJ, 17B LHCb, pp at 7, 8 TeV

1 Corresponds to the 95% CL upper limit 1.01 × 10⁻⁶. Uses the normalization mode B⁺ → η'K⁺ with branching fraction (70.6 ± 2.5) × 10⁻⁶ and the ratio of hadronisation fractions f_s/f_d = 0.259 ± 0.015, which is assumed equal to f_s/f_u.

Γ(φπ⁺π⁻)/Γ_{total} Γ₉₉/Γ

Table with columns: VALUE (units 10^-6), CL%, DOCUMENT ID, TECN, COMMENT. Row 1: 3.48 ± 0.23 ± 0.39, 1 AAIJ, 17A LHCb, pp at 7, 8 TeV

1 Inclusive decays in mass range 400 < m(π⁺π⁻) < 1600 MeV/c².

Γ(φρ⁰)/Γ_{total} Γ₉₈/Γ

Table with columns: VALUE (units 10^-7), CL%, DOCUMENT ID, TECN, COMMENT. Row 1: 2.7 ± 0.7 ± 0.3, 1 AAIJ, 17A LHCb, pp at 7, 8 TeV

• • • We do not use the following data for averages, fits, limits, etc. • • • <6170 90 2 ABE 00c SLD e⁺e⁻ → Z
1 Signal evidence is 4 standard deviations.
2 ABE 00c assumes B(Z → b**bar**) = (21.7 ± 0.1)% and the B fractions f_{B⁰} = f_{B⁺} = (39.7^{+1.8}_{-2.2})% and f_{B_s} = (10.5^{+1.8}_{-2.2})%.

Γ(φf₀(980), f₀(980) → π⁺π⁻)/Γ_{total} Γ₉₆/Γ

Table with columns: VALUE (units 10^-6), CL%, DOCUMENT ID, TECN, COMMENT. Row 1: 1.12 ± 0.16 ± 0.14, 1 AAIJ, 17A LHCb, pp at 7, 8 TeV

1 Signal is observed with 8 standard deviations significance.

Γ(φf₂(1270), f₂(1270) → π⁺π⁻)/Γ_{total} Γ₉₇/Γ

Table with columns: VALUE (units 10^-6), CL%, DOCUMENT ID, TECN, COMMENT. Row 1: 0.61 ± 0.13 ± 0.13 ± 0.08, 1 AAIJ, 17A LHCb, pp at 7, 8 TeV

1 Signal is observed with 5 standard deviations significance.

Γ(φφ)/Γ_{total} Γ₁₀₀/Γ

Table with columns: VALUE (units 10^-6), CL%, DOCUMENT ID, TECN, COMMENT. Row 1: 18.7 ± 1.5 OUR FIT, 18.5 ± 1.4 ± 1.0, 1 AAIJ, 15AS LHCb, pp at 7, 8 TeV

• • • We do not use the following data for averages, fits, limits, etc. • • • 14 +6/-5 ± 6 2 ACOSTA 05J CDF Repl. by AALTONEN 11AN <1183 90 3 ABE 00c SLD e⁺e⁻ → Z
1 AAIJ 15AS reports [Γ(B_s⁰ → φφ)/Γ_{total}] / [B(B⁰ → K*(892)⁰φ)] = 1.84 ± 0.05 ± 0.13 which we multiply by our best value B(B⁰ → K*(892)⁰φ) = (1.00 ± 0.05) × 10⁻⁵. Our first error is their experiment's error and our second error is the systematic error from using our best value.
2 Uses B(B⁰ → J/ψφ) = (1.38 ± 0.49) × 10⁻³ and production cross-section ratio of σ(B_s)/σ(B⁰) = 0.26 ± 0.04.
3 ABE 00c assumes B(Z → b**bar**) = (21.7 ± 0.1)% and the B fractions f_{B⁰} = f_{B⁺} = (39.7^{+1.8}_{-2.2})% and f_{B_s} = (10.5^{+1.8}_{-2.2})%.

Γ(φφ)/Γ(J/ψ(1S)φ) Γ₁₀₀/Γ₄₉

Table with columns: VALUE (units 10^-2), DOCUMENT ID, TECN, COMMENT. Row 1: 1.73 ± 0.16 OUR FIT, 1.78 ± 0.14 ± 0.20, AALTONEN 11AN CDF, p**bar** at 1.96 TeV

Γ(φφφ)/Γ(φφ) Γ₁₀₁/Γ₁₀₀

Table with columns: VALUE, DOCUMENT ID, TECN, COMMENT. Row 1: 0.117 ± 0.030 ± 0.015, AAIJ, 17Bb LHCb, pp at 7, 8 TeV

Γ(π⁺K⁻)/Γ_{total} Γ₁₀₂/Γ

Table with columns: VALUE (units 10^-6), CL%, DOCUMENT ID, TECN, COMMENT. Row 1: 5.8 ± 0.7 OUR AVERAGE, 5.9 ± 0.7 ± 0.6, 5.7 ± 1.0 ± 0.5

• • • We do not use the following data for averages, fits, limits, etc. • • • < 26 90 3 PENG 10 BELL e⁺e⁻ → Υ(5S) < 5.6 90 4 ABULENCIA,A 06D CDF Repl. by AALTONEN 09c <261 90 5 ABE 00c SLD e⁺e⁻ → Z <210 90 6 BUSKULIC 96v ALEP e⁺e⁻ → Z <260 90 7 AKERS 94L OPAL e⁺e⁻ → Z
1 AAIJ 12AR reports [Γ(B_s⁰ → π⁺K⁻)/Γ_{total}] / [B(B⁰ → K⁺π⁻)] × [Γ(**bar** → B_s⁰)/Γ(**bar** → B⁰)] = 0.074 ± 0.006 ± 0.006 which we multiply or divide by our best values B(B⁰ → K⁺π⁻) = (1.96 ± 0.05) × 10⁻⁵, Γ(**bar** → B_s⁰)/Γ(**bar** → B⁰) = 0.246 ± 0.023.

Our first error is their experiment's error and our second error is the systematic error from using our best values.

2 AALTONEN 09c reports [Γ(B_s⁰ → π⁺K⁻)/Γ_{total}] / [B(B⁰ → K⁺π⁻)] × [B(**bar** → B_s⁰)] / [B(**bar** → B⁰)] = 0.071 ± 0.010 ± 0.007 which we multiply or divide by our best values B(B⁰ → K⁺π⁻) = (1.96 ± 0.05) × 10⁻⁵, B(**bar** → B_s⁰) = (10.0 ± 0.8) × 10⁻², B(**bar** → B⁰) = (40.8 ± 0.7) × 10⁻². Our first error is their experiment's error and our second error is the systematic error from using our best values.
3 Uses Υ(10860) → B_s^{*}B_s^{*} and assumes B(Υ(10860) → B_s^{*}B_s^{*}) = (19.3 ± 2.9)% and Γ(Υ(10860) → B_s^{*}B_s^{*}) / Γ(Υ(10860) → B_s^{*}B_s^{*}) = (90.1 ± 3.8)_{-4.0}%.
4 ABULENCIA,A 06D obtains this from (f_s/f_d) (B(B_s → π⁺K⁻) / B(B⁰ → K⁺π⁻)) < 0.08 at 90% CL, assuming f_s/f_d = 0.260 ± 0.039 and B(B⁰ → K⁺π⁻) = (18.9 ± 0.7) × 10⁻⁶.
5 ABE 00c assumes B(Z → b**bar**) = (21.7 ± 0.1)% and the B fractions f_{B⁰} = f_{B⁺} = (39.7^{+1.8}_{-2.2})% and f_{B_s} = (10.5^{+1.8}_{-2.2})%.
6 BUSKULIC 96v assumes PDG 96 production fractions for B⁰, B⁺, B_s, b baryons.
7 Assumes B(Z → b**bar**) = 0.217 and B_d⁰ (B_s⁰) fraction 39.5% (12%).

Γ(K⁺K⁻)/Γ_{total} Γ₁₀₃/Γ

Table with columns: VALUE (units 10^-6), CL%, DOCUMENT ID, TECN, COMMENT. Row 1: 26.6 ± 2.2 OUR AVERAGE, 25.2 ± 1.7 ± 2.4, 27.6 ± 2.3 ± 2.7

1 AAIJ 12AR LHCb pp at 7 TeV
2 AALTONEN 11N CDF p**bar** at 1.96 TeV
3 PENG 10 BELL e⁺e⁻ → Υ(5S)
• • • We do not use the following data for averages, fits, limits, etc. • • • <310 90 DRUTSKOY 07A BELL e⁺e⁻ → Υ(5S) 33 ± 6 ± 7 4 ABULENCIA,A 06D CDF Repl. by AALTONEN 11N <283 90 5 ABE 00c SLD e⁺e⁻ → Z < 59 90 6 BUSKULIC 96v ALEP e⁺e⁻ → Z <140 90 7 AKERS 94L OPAL e⁺e⁻ → Z

1 AAIJ 12AR reports [Γ(B_s⁰ → K⁺K⁻)/Γ_{total}] / [B(B⁰ → K⁺π⁻)] × [Γ(**bar** → B_s⁰)/Γ(**bar** → B⁰)] = 0.316 ± 0.009 ± 0.019 which we multiply or divide by our best values B(B⁰ → K⁺π⁻) = (1.96 ± 0.05) × 10⁻⁵, Γ(**bar** → B_s⁰)/Γ(**bar** → B⁰) = 0.246 ± 0.023. Our first error is their experiment's error and our second error is the systematic error from using our best values.
2 AALTONEN 11N reports (f_s/f_d) (B(B_s⁰ → K⁺K⁻) / B(B⁰ → K⁺π⁻)) = 0.347 ± 0.020 ± 0.021. We multiply this result by our best value of B(B⁰ → K⁺π⁻) = (1.96 ± 0.05) × 10⁻⁵ and divide by our best value of f_s/f_d, where 1/2 f_s/f_d = 0.1230 ± 0.0115. Our first quoted uncertainty is the combined experiment's uncertainty and our second is the systematic uncertainty from using our best values.
3 Uses Υ(10860) → B_s^{*}B_s^{*} and assumes B(Υ(10860) → B_s^{*}B_s^{*}) = (19.3 ± 2.9)% and Γ(Υ(10860) → B_s^{*}B_s^{*}) / Γ(Υ(10860) → B_s^{*}B_s^{*}) = (90.1 ± 3.8)_{-4.0}%.
4 ABULENCIA,A 06D obtains this from (f_s/f_d) (B(B_s → K⁺K⁻) / B(B⁰ → K⁺π⁻)) = 0.46 ± 0.08 ± 0.07, assuming f_s/f_d = 0.260 ± 0.039 and B(B⁰ → K⁺π⁻) = (18.9 ± 0.7) × 10⁻⁶.
5 ABE 00c assumes B(Z → b**bar**) = (21.7 ± 0.1)% and the B fractions f_{B⁰} = f_{B⁺} = (39.7^{+1.8}_{-2.2})% and f_{B_s} = (10.5^{+1.8}_{-2.2})%.
6 BUSKULIC 96v assumes PDG 96 production fractions for B⁰, B⁺, B_s, b baryons.
7 Assumes B(Z → b**bar**) = 0.217 and B_d⁰ (B_s⁰) fraction 39.5% (12%).

Γ(K⁰K⁰)/Γ_{total} Γ₁₀₄/Γ

Table with columns: VALUE (units 10^-5), CL%, DOCUMENT ID, TECN, COMMENT. Row 1: 1.96 ± 0.58 ± 0.51 ± 0.10 ± 0.20, 1 PAL, 16 BELL e⁺e⁻ → Υ(5S)

• • • We do not use the following data for averages, fits, limits, etc. • • • <6.6 90 2 PENG 10 BELL Repl. by PAL 16
1 Observed in B_s⁰ → K_S⁰K_S⁰ with significance of 5.1 σ. The last uncertainty is due to the uncertainty of the total number of B_S⁰B_S⁰ pairs.
2 Uses Υ(10860) → B_s^{*}B_s^{*} and assumes B(Υ(10860) → B_s^{*}B_s^{*}) = (19.3 ± 2.9)% and Γ(Υ(10860) → B_s^{*}B_s^{*}) / Γ(Υ(10860) → B_s^{*}B_s^{*}) = (90.1 ± 3.8)_{-4.0}%.

Γ(K⁰π⁺π⁻)/Γ_{total} Γ₁₀₅/Γ

Table with columns: VALUE (units 10^-6), DOCUMENT ID, TECN, COMMENT. Row 1: 9.5 ± 2.1 ± 0.3, 1,2 AAIJ, 17B LHCb, pp at 7, 8 TeV

• • • We do not use the following data for averages, fits, limits, etc. • • • 14 ± 4 ± 1 3 AAIJ 13BP LHCb Repl. by AAIJ 17BP
1 AAIJ 17BP reports [Γ(B_s⁰ → K⁰π⁺π⁻)/Γ_{total}] / [B(B⁰ → K⁰π⁺π⁻)] = 0.191 ± 0.027 ± 0.033 which we multiply by our best value B(B⁰ → K⁰π⁺π⁻) = (4.97 ± 0.18) × 10⁻⁵. Our first error is their experiment's error and our second error is the systematic error from using our best value.
2 Used f_s/f_d = 0.259 ± 0.015.
3 AAIJ 13BP reports [Γ(B_s⁰ → K⁰π⁺π⁻)/Γ_{total}] / [B(B⁰ → K⁰π⁺π⁻)] = 0.29 ± 0.06 ± 0.04 which we multiply by our best value B(B⁰ → K⁰π⁺π⁻) = (4.97 ± 0.18) × 10⁻⁵. Our first error is their experiment's error and our second error is the systematic error from using our best value.

Meson Particle Listings

 B_S^0 $\Gamma(K^*(892)^-\pi^+)/\Gamma_{\text{total}}$ Γ_{107}/Γ

VALUE (units 10^{-6})	DOCUMENT ID	TECN	COMMENT
$2.9 \pm 1.0 \pm 0.2$	1,2 AAIJ	14BMLHCB	pp at 7 TeV
1 AAIJ 14BML reports $[\Gamma(B_S^0 \rightarrow K^*(892)^-\pi^+)/\Gamma_{\text{total}}] / [B(B^0 \rightarrow K^*(892)^+\pi^-)] = 0.39 \pm 0.13 \pm 0.05$ which we multiply by our best value $B(B^0 \rightarrow K^*(892)^+\pi^-) = (7.5 \pm 0.4) \times 10^{-6}$. Our first error is their experiment's error and our second error is the systematic error from using our best value. 2 Uses $f_s/f_d = 0.259 \pm 0.015$.			

 $\Gamma(K^0 K^\pm \pi^\mp)/\Gamma_{\text{total}}$ Γ_{106}/Γ

VALUE (units 10^{-5})	DOCUMENT ID	TECN	COMMENT
$8.4 \pm 0.8 \pm 0.3$	1,2 AAIJ	17BP LHCb	pp at 7, 8 TeV
1 AAIJ 17BP reports $[\Gamma(B_S^0 \rightarrow K^0 K^\pm \pi^\mp)/\Gamma_{\text{total}}] / [B(B^0 \rightarrow K^0 \pi^+ \pi^-)] = 1.70 \pm 0.07 \pm 0.15$ which we multiply by our best value $B(B^0 \rightarrow K^0 \pi^+ \pi^-) = (4.97 \pm 0.18) \times 10^{-5}$. Our first error is their experiment's error and our second error is the systematic error from using our best value. 2 Used $f_s/f_d = 0.259 \pm 0.015$. 3 AAIJ 13BP reports $[\Gamma(B_S^0 \rightarrow K^0 K^\pm \pi^\mp)/\Gamma_{\text{total}}] / [B(B^0 \rightarrow K^0 \pi^+ \pi^-)] = 1.48 \pm 0.12 \pm 0.14$ which we multiply by our best value $B(B^0 \rightarrow K^0 \pi^+ \pi^-) = (4.97 \pm 0.18) \times 10^{-5}$. Our first error is their experiment's error and our second error is the systematic error from using our best value.			

 $\Gamma(K^*(892)^\pm K^\mp)/\Gamma_{\text{total}}$ Γ_{108}/Γ

VALUE (units 10^{-5})	DOCUMENT ID	TECN	COMMENT
$1.86 \pm 0.12 \pm 0.45$	1,2 AAIJ	19K LHCb	pp at 7, 8 TeV
1 AAIJ 19K reports $(18.6 \pm 1.2 \pm 0.8 \pm 4.0 \pm 2.0) \times 10^{-6}$ as the measured value. We have combined in quadrature all systematic uncertainties into a single one. 2 Measured in Dalitz plot analysis of $B_S^0 \rightarrow K_S^0 K^\pm \pi^\mp$ decays. 3 AAIJ 14BM reports $[\Gamma(B_S^0 \rightarrow K^*(892)^\pm K^\mp)/\Gamma_{\text{total}}] / [B(B^0 \rightarrow K^*(892)^+\pi^-)] = 1.49 \pm 0.22 \pm 0.18$ which we multiply by our best value $B(B^0 \rightarrow K^*(892)^+\pi^-) = (7.5 \pm 0.4) \times 10^{-6}$. Our first error is their experiment's error and our second error is the systematic error from using our best value. 4 Uses $f_s/f_d = 0.259 \pm 0.015$.			

 $\Gamma(K_S^0(1430)^\pm K^\mp)/\Gamma_{\text{total}}$ Γ_{109}/Γ

VALUE (units 10^{-5})	DOCUMENT ID	TECN	COMMENT
$3.13 \pm 0.23 \pm 2.53$	1,2 AAIJ	19K LHCb	pp at 7, 8 TeV
1 AAIJ 19K reports $(31.3 \pm 2.3 \pm 0.7 \pm 25.1 \pm 3.3) \times 10^{-6}$ as the measured value. We have combined in quadrature all systematic uncertainties into a single one. 2 Measured in Dalitz plot analysis of $B_S^0 \rightarrow K_S^0 K^\pm \pi^\mp$ decays.			

 $\Gamma(K_S^0(1430)^\pm K^\mp)/\Gamma_{\text{total}}$ Γ_{110}/Γ

VALUE (units 10^{-5})	DOCUMENT ID	TECN	COMMENT
$1.03 \pm 0.25 \pm 1.64$	1,2 AAIJ	19K LHCb	pp at 7, 8 TeV
1 AAIJ 19K reports $(10.3 \pm 2.5 \pm 1.1 \pm 16.3 \pm 1.1) \times 10^{-6}$ as the measured value. We have combined in quadrature all systematic uncertainties into a single one. 2 Measured in Dalitz plot analysis of $B_S^0 \rightarrow K_S^0 K^\pm \pi^\mp$ decays.			

 $\Gamma(K^*(892)^0 \bar{K}^0 + c.c.)/\Gamma_{\text{total}}$ Γ_{111}/Γ

VALUE (units 10^{-5})	DOCUMENT ID	TECN	COMMENT
$1.98 \pm 0.28 \pm 0.50$	1,2 AAIJ	19K LHCb	pp at 7, 8 TeV
1 AAIJ 19K reports $(19.8 \pm 2.8 \pm 1.2 \pm 4.4 \pm 2.1) \times 10^{-6}$ as the measured value. We have combined in quadrature all systematic uncertainties into a single one. 2 Measured in Dalitz plot analysis of $B_S^0 \rightarrow K_S^0 K^\pm \pi^\mp$ decays.			

 $\Gamma(K_S^0(1430) \bar{K}^0 + c.c.)/\Gamma_{\text{total}}$ Γ_{112}/Γ

VALUE (units 10^{-5})	DOCUMENT ID	TECN	COMMENT
$3.30 \pm 0.25 \pm 0.98$	1,2 AAIJ	19K LHCb	pp at 7, 8 TeV
1 AAIJ 19K reports $(33.0 \pm 2.5 \pm 0.9 \pm 9.1 \pm 3.5) \times 10^{-6}$ as the measured value. We have combined in quadrature all systematic uncertainties into a single one. 2 Measured in Dalitz plot analysis of $B_S^0 \rightarrow K_S^0 K^\pm \pi^\mp$ decays.			

 $\Gamma(K_S^0(1430) \bar{K}^0 + c.c.)/\Gamma_{\text{total}}$ Γ_{113}/Γ

VALUE (units 10^{-5})	DOCUMENT ID	TECN	COMMENT
$1.68 \pm 0.45 \pm 2.13$	1,2 AAIJ	19K LHCb	pp at 7, 8 TeV
1 AAIJ 19K reports $(16.8 \pm 4.5 \pm 1.7 \pm 21.2 \pm 1.8) \times 10^{-6}$ as the measured value. We have combined in quadrature all systematic uncertainties into a single one. 2 Measured in Dalitz plot analysis of $B_S^0 \rightarrow K_S^0 K^\pm \pi^\mp$ decays.			

 $\Gamma(K_S^0 \bar{K}^*(892)^0 + c.c.)/\Gamma_{\text{total}}$ Γ_{114}/Γ

VALUE (units 10^{-6})	DOCUMENT ID	TECN	COMMENT
$16.4 \pm 3.4 \pm 2.3$	1 AAIJ	16 LHCb	pp at 7 TeV
1 Measured relative to $B^0 \rightarrow K_S^0 \pi^+ \pi^-$ using the value of $B(B^0 \rightarrow K^0 \pi^+ \pi^-) = (4.96 \pm 0.2) \times 10^{-5}$.			

 $\Gamma(K^0 K^+ K^-)/\Gamma_{\text{total}}$ Γ_{115}/Γ

VALUE (units 10^{-7})	CL%	DOCUMENT ID	TECN	COMMENT
$12.9 \pm 6.5 \pm 0.5$		1,2,3 AAIJ	17BP LHCb	pp at 7, 8 TeV
$\bullet \bullet \bullet$ We do not use the following data for averages, fits, limits, etc. $\bullet \bullet \bullet$ <34 90 4 AAIJ 13BP LHCb Repl. by AAIJ 17BP 1 AAIJ 17BP reports $[\Gamma(B_S^0 \rightarrow K^0 K^+ K^-)/\Gamma_{\text{total}}] / [B(B^0 \rightarrow K^0 \pi^+ \pi^-)] = 0.026 \pm 0.011 \pm 0.007$ which we multiply by our best value $B(B^0 \rightarrow K^0 \pi^+ \pi^-) = (4.97 \pm 0.18) \times 10^{-5}$. Our first error is their experiment's error and our second error is the systematic error from using our best value. 2 AAIJ 17BP also set the limit range $4-25 \times 10^{-7}$ at 90% CL using the world average value $B(B^0 \rightarrow K^0 \pi^+ \pi^-) = (4.96 \pm 0.20) \times 10^{-5}$. 3 Used $f_s/f_d = 0.259 \pm 0.015$. 4 AAIJ 13BP reports $[\Gamma(B_S^0 \rightarrow K^0 K^+ K^-)/\Gamma_{\text{total}}] / [B(B^0 \rightarrow K^0 \pi^+ \pi^-)] < 0.068$ which we multiply by our best value $B(B^0 \rightarrow K^0 \pi^+ \pi^-) = 4.97 \times 10^{-5}$.				

 $\Gamma(\bar{K}^*(892)^0 \rho^0)/\Gamma_{\text{total}}$ Γ_{116}/Γ

VALUE	CL%	DOCUMENT ID	TECN	COMMENT
$<7.67 \times 10^{-4}$		90 1 ABE	00c SLD	$e^+e^- \rightarrow Z$
1 ABE 00c assumes $B(Z \rightarrow b\bar{b}) = (21.7 \pm 0.1)\%$ and the B fractions $f_{B^0} = f_{B^+} = (39.7 \pm 1.8)_{-2.2}^{\pm 1.8}\%$ and $f_{B_S} = (10.5 \pm 1.8)_{-2.2}^{\pm 1.8}\%$.				

 $\Gamma(\bar{K}^*(892)^0 K^*(892)^0)/\Gamma_{\text{total}}$ Γ_{117}/Γ

VALUE (units 10^{-5})	CL%	DOCUMENT ID	TECN	COMMENT
$1.11 \pm 0.26 \pm 0.06$		1 AAIJ	15AF LHCb	pp at 7 TeV
$\bullet \bullet \bullet$ We do not use the following data for averages, fits, limits, etc. $\bullet \bullet \bullet$ $2.81 \pm 0.46 \pm 0.56$ 2 AAIJ 12F LHCb Repl. by AAIJ 15AF <168.1 90 3 ABE 00c SLD $e^+e^- \rightarrow Z$ 1 AAIJ 15AF reports $[\Gamma(B_S^0 \rightarrow \bar{K}^*(892)^0 K^*(892)^0)/\Gamma_{\text{total}}] / [B(B^0 \rightarrow K^*(892)^0 \phi)] = 1.11 \pm 0.22 \pm 0.12 \pm 0.06$ which we multiply by our best value $B(B^0 \rightarrow K^*(892)^0 \phi) = (1.00 \pm 0.05) \times 10^{-5}$. Our first error is their experiment's error and our second error is the systematic error from using our best value. 2 Uses $B^0 \rightarrow J/\psi K^{*0}$ for normalization and assumes $B(B^0 \rightarrow J/\psi K^{*0}) B(J/\psi \rightarrow \mu^+ \mu^-) B(K^{*0} \rightarrow K^+ \pi^-) = (1.33 \pm 0.06) \times 10^{-3}$ and $f_s/f_d = 0.253 \pm 0.031$. The second quoted error is total uncertainty including the error of 0.34 on f_s/f_d . 3 ABE 00c assumes $B(Z \rightarrow b\bar{b}) = (21.7 \pm 0.1)\%$ and the B fractions $f_{B^0} = f_{B^+} = (39.7 \pm 1.8)_{-2.2}^{\pm 1.8}\%$ and $f_{B_S} = (10.5 \pm 1.8)_{-2.2}^{\pm 1.8}\%$.				

 $\Gamma(\phi K^*(892)^0)/\Gamma_{\text{total}}$ Γ_{121}/Γ

VALUE (units 10^{-6})	CL%	DOCUMENT ID	TECN	COMMENT
$1.14 \pm 0.29 \pm 0.06$		1 AAIJ	13BW LHCb	pp at 7 TeV
$\bullet \bullet \bullet$ We do not use the following data for averages, fits, limits, etc. $\bullet \bullet \bullet$ <1013 90 2 ABE 00c SLD $e^+e^- \rightarrow Z$ 1 AAIJ 13BW reports $[\Gamma(B_S^0 \rightarrow \phi K^*(892)^0)/\Gamma_{\text{total}}] / [B(B^0 \rightarrow K^*(892)^0 \phi)] = 0.113 \pm 0.024 \pm 0.016$ which we multiply by our best value $B(B^0 \rightarrow K^*(892)^0 \phi) = (1.00 \pm 0.05) \times 10^{-5}$. Our first error is their experiment's error and our second error is the systematic error from using our best value. 2 ABE 00c assumes $B(Z \rightarrow b\bar{b}) = (21.7 \pm 0.1)\%$ and the B fractions $f_{B^0} = f_{B^+} = (39.7 \pm 1.8)_{-2.2}^{\pm 1.8}\%$ and $f_{B_S} = (10.5 \pm 1.8)_{-2.2}^{\pm 1.8}\%$.				

 $\Gamma(\rho\bar{\rho})/\Gamma_{\text{total}}$ Γ_{122}/Γ

VALUE (units 10^{-8})	CL%	DOCUMENT ID	TECN	COMMENT
<1.5		90 1 AAIJ	17Bj LHCb	pp at 7 and 8 TeV
$\bullet \bullet \bullet$ We do not use the following data for averages, fits, limits, etc. $\bullet \bullet \bullet$ $2.84 \pm 2.03 \pm 0.85$ 2 AAIJ 13Bq LHCb Repl. by AAIJ 17Bj -1.68 ± 0.18 <5900 90 3 BUSKULIC 96v ALEP $e^+e^- \rightarrow Z$ 1 Uses normalization mode $B(B^0 \rightarrow K^+ \pi^-) = (19.6 \pm 0.5) \times 10^{-6}$ and B production ratio $f(\bar{b} \rightarrow B_S^0)/f(\bar{b} \rightarrow B_d^0) = 0.259 \pm 0.015$. 2 Uses normalization mode $B(B^0 \rightarrow K^+ \pi^-) = (19.55 \pm 0.54) \times 10^{-6}$ and B production ratio $f(\bar{b} \rightarrow B_S^0)/f(\bar{b} \rightarrow B_d^0) = 0.256 \pm 0.020$. 3 BUSKULIC 96v assumes PDG 96 production fractions for B^0, B^+, B_S, b baryons.				

 $\Gamma(\rho\bar{\rho} K^+ K^-)/\Gamma_{\text{total}}$ Γ_{123}/Γ

VALUE (units 10^{-6})	DOCUMENT ID	TECN	COMMENT
$4.5 \pm 0.4 \pm 0.2$	1,2 AAIJ	17BD LHCb	pp at 7, 8 TeV
1 AAIJ 17BD reports $[\Gamma(B_S^0 \rightarrow \rho\bar{\rho} K^+ K^-)/\Gamma_{\text{total}}] / [B(B^0 \rightarrow J/\psi(1S) K^*(892)^0)] / [B(J/\psi(1S) \rightarrow \rho\bar{\rho})] / [B(K^*(892) \rightarrow (K\pi)^\pm)] = 1.67 \pm 0.12 \pm 0.11$ which we multiply by our best values $B(B^0 \rightarrow J/\psi(1S) K^*(892)^0) = (1.27 \pm 0.05) \times 10^{-3}$, $B(J/\psi(1S) \rightarrow \rho\bar{\rho}) = (2.121 \pm 0.029) \times 10^{-3}$, $B(K^*(892) \rightarrow (K\pi)^\pm) = (99.901 \pm 0.009) \times 10^{-2}$. Our first error is their experiment's error and our second error is the systematic error from using our best values. Reported value assumes $f_s/f_d = 0.259 \pm 0.015$. 2 The branching ratio is given for $m_{\rho\bar{\rho}} < 2.85$ GeV.			

See key on page 999

Meson Particle Listings

B_s^0

$\Gamma(p\bar{p}K^+\pi^-)/\Gamma_{total}$ Γ_{124}/Γ

VALUE (units 10^{-7})	DOCUMENT ID	TECN	COMMENT
13.9 ± 2.5 ± 0.5	1,2 AAIJ	17Bd LHCB	pp at 7, 8 TeV

¹ AAIJ 17Bd reports $[\Gamma(B_s^0 \rightarrow p\bar{p}K^+\pi^-)/\Gamma_{total}] / [B(B^0 \rightarrow J/\psi(1S)K^*(892)^0)] / [B(J/\psi(1S) \rightarrow p\bar{p}) / [B(K^*(892) \rightarrow (K\pi)^\pm)]] = 0.52 \pm 0.08 \pm 0.05$ which we multiply by our best values $B(B^0 \rightarrow J/\psi(1S)K^*(892)^0) = (1.27 \pm 0.05) \times 10^{-3}$, $B(J/\psi(1S) \rightarrow p\bar{p}) = (2.121 \pm 0.029) \times 10^{-3}$, $B(K^*(892) \rightarrow (K\pi)^\pm) = (99.901 \pm 0.009) \times 10^{-2}$. Our first error is their experiment's error and our second error is the systematic error from using our best values. Reported value assumes $f_s/f_d = 0.259 \pm 0.015$.

² The branching ratio is given for $m_{p\bar{p}} < 2.85$ GeV.

$\Gamma(p\bar{p}K^+\pi^-)/\Gamma(p\bar{p}K^+K^-)$ $\Gamma_{124}/\Gamma_{123}$

VALUE	DOCUMENT ID	TECN	COMMENT
0.31 ± 0.05 ± 0.02	1,2 AAIJ	17Bd LHCB	pp at 7, 8 TeV

¹ Reports $B(B_s^0 \rightarrow p\bar{p}K^+\pi^-) / B(B^0 \rightarrow p\bar{p}K^+\pi^-) = 0.22 \pm 0.04 \pm 0.02 \pm 0.01$, where the third error is due to f_s/f_d .

² The ratio is given for $m_{p\bar{p}} < 2.85$ GeV and assuming $f_s/f_d = 0.259 \pm 0.015$.

$\Gamma(p\bar{p}\pi^+\pi^-)/\Gamma_{total}$ Γ_{125}/Γ

VALUE (units 10^{-7})	DOCUMENT ID	TECN	COMMENT
4.3 ± 2.0 ± 0.2	1,2 AAIJ	17Bd LHCB	pp at 7, 8 TeV

¹ AAIJ 17Bd reports $[\Gamma(B_s^0 \rightarrow p\bar{p}\pi^+\pi^-)/\Gamma_{total}] / [B(B^0 \rightarrow J/\psi(1S)K^*(892)^0)] / [B(J/\psi(1S) \rightarrow p\bar{p})] / [B(K^*(892) \rightarrow (K\pi)^\pm)] = 0.16 \pm 0.07 \pm 0.02$ which we multiply by our best values $B(B^0 \rightarrow J/\psi(1S)K^*(892)^0) = (1.27 \pm 0.05) \times 10^{-3}$, $B(J/\psi(1S) \rightarrow p\bar{p}) = (2.121 \pm 0.029) \times 10^{-3}$, $B(K^*(892) \rightarrow (K\pi)^\pm) = (99.901 \pm 0.009) \times 10^{-2}$. Our first error is their experiment's error and our second error is the systematic error from using our best values. Reported value assumes $f_s/f_d = 0.259 \pm 0.015$.

² The branching ratio is given for $m_{p\bar{p}} < 2.85$ GeV.

$\Gamma(p\bar{p}K^- + c.c.)/\Gamma_{total}$ Γ_{126}/Γ

VALUE (units 10^{-6})	DOCUMENT ID	TECN	COMMENT
5.5 ± 0.6 ± 0.8	1,2 AAIJ	17AL LHCB	pp at 7, 8 TeV

¹ AAIJ 17AL reports $(5.46 \pm 0.61 \pm 0.82) \times 10^{-6}$ from a measurement of $[\Gamma(B_s^0 \rightarrow p\bar{p}K^- + c.c.)/\Gamma_{total}] / [B(B^0 \rightarrow p\bar{p}\pi^-)]$ assuming $B(B^0 \rightarrow p\bar{p}\pi^-) = (3.14 \pm 0.29) \times 10^{-6}$.

² AAIJ 17AL value represents the sum of $B_s^0 \rightarrow p\bar{p}K^-$ and $B_s^0 \rightarrow p\bar{p}K^+$ and assumes the fraction $f_s/f_d = 0.259 \pm 0.015$.

$\Gamma(\Lambda_c^- \Lambda\pi^+)/\Gamma_{total}$ Γ_{127}/Γ

VALUE (units 10^{-4})	DOCUMENT ID	TECN	COMMENT
3.6 ± 1.1 ± 1.2	1 SOLOVIEVA	13 BELL	$e^+e^- \rightarrow \Upsilon(4S)$

¹ The second error is the total systematic uncertainty including the Λ_c absolute branching fractions and the normalization number of B_s events.

$\Gamma(\Lambda_c^- \Lambda_c^+)/\Gamma_{total}$ Γ_{128}/Γ

VALUE	CL%	DOCUMENT ID	TECN	COMMENT
< 8.0 × 10⁻⁵	95	1 AAIJ	14AA LHCB	pp at 7 TeV

¹ Uses $B(\bar{B}^0 \rightarrow D^+ D_s^-) = (7.2 \pm 0.8) \times 10^{-3}$.

$\Gamma(\gamma)/\Gamma_{total}$ Γ_{129}/Γ

Test for $\Delta B=1$ weak neutral current.

VALUE (units 10^{-6})	CL%	DOCUMENT ID	TECN	COMMENT
< 3.1	90	1 DUTTA	15 BELL	$e^+e^- \rightarrow \Upsilon(5S)$
• • •				We do not use the following data for averages, fits, limits, etc. • • •
< 8.7	90	2 WICHT	08A BELL	Repl. by DUTTA 15
< 5.3	90	DRUTSKOY	07A BELL	Repl. by WICHT 08A
< 148	90	3 ACCIARRI	95i L3	$e^+e^- \rightarrow Z$

¹ Assumes the fraction of $B_s^{(*)}\bar{B}_s^{(*)}$ in $b\bar{b}$ events is $f_s = (17.2 \pm 3.0)\%$.

² Assumes $\Upsilon(5S) \rightarrow B_s^* \bar{B}_s^* = (19.5 \pm 3.0)\%$.

³ ACCIARRI 95i assumes $f_{B^0} = 39.5 \pm 4.0$ and $f_{B_s} = (12.0 \pm 3.0)\%$.

$\Gamma(\phi\gamma)/\Gamma_{total}$ Γ_{130}/Γ

VALUE (units 10^{-6})	CL%	DOCUMENT ID	TECN	COMMENT
34 ± 4 OUR AVERAGE				
36 ± 5 ± 7		1 DUTTA	15 BELL	$e^+e^- \rightarrow \Upsilon(5S)$
33.8 ± 3.4 ± 2.0		2 AAIJ	13 LHCB	pp at 7 TeV

• • • We do not use the following data for averages, fits, limits, etc. **• • •**

39 ± 5		3 AAIJ	12AE LHCB	Repl. by AAIJ 13
57 +18 +12 / -15 -11		4 WICHT	08A BELL	Repl. by DUTTA 15
< 390	90	DRUTSKOY	07A BELL	$e^+e^- \rightarrow \Upsilon(5S)$
< 120	90	ACOSTA	02G CDF	$p\bar{p}$ at 1.8 TeV
< 700	90	5 ADAM	96D DLPH	$e^+e^- \rightarrow Z$

¹ Assumes the fraction of $B_s^{(*)}\bar{B}_s^{(*)}$ in $b\bar{b}$ events is $f_s = (17.2 \pm 3.0)\%$. The systematic uncertainty from f_s is 0.6×10^{-5} .

² AAIJ 13 reports $[\Gamma(B_s^0 \rightarrow \phi\gamma)/\Gamma_{total}] / [B(B^0 \rightarrow K^*(892)^0\gamma)] = 0.81 \pm 0.04 \pm 0.07$ which we multiply by our best value $B(B^0 \rightarrow K^*(892)^0\gamma) = (4.18 \pm 0.25) \times 10^{-5}$. Our first error is their experiment's error and our second error is the systematic error from using our best value.

³ Measures $B(B^0 \rightarrow K^{*0}\gamma)/B(B_s \rightarrow \phi\gamma) = 1.12 \pm 0.08(\text{stat}) + 0.06(\text{sys}) + 0.09(f_s/f_d)$ and uses current world-average value of $B(B^0 \rightarrow K^{*0}\gamma) = (4.33 \pm 0.15) \times 10^{-5}$.

⁴ Assumes $\Upsilon(5S) \rightarrow B_s^* \bar{B}_s^* = (19.5 \pm 3.0)\%$.

⁵ ADAM 96d assumes $f_{B^0} = f_{B^-} = 0.39$ and $f_{B_s} = 0.12$.

$\Gamma(\mu^+\mu^-)/\Gamma_{total}$ Γ_{131}/Γ

Test for $\Delta B = 1$ weak neutral current.

VALUE (units 10^{-3})	CL%	DOCUMENT ID	TECN	COMMENT
3.0 ± 0.4 OUR AVERAGE				

2.8 +0.8 / -0.7		1 AABOUD	19L ATLS	pp at 7, 8, 13 TeV
3.0 ± 0.6 +0.3 / -0.2		AAIJ	17Al LHCB	pp at 7, 8, 13 TeV
13 +9 / -7		2 AALTONEN	13F CDF	$p\bar{p}$ at 1.96 TeV
3.0 +1.0 / -0.9		3 CHATRCHYAN	13AW CMS	pp at 7, 8 TeV
• • •				We do not use the following data for averages, fits, limits, etc. • • •
0.9 +1.1 / -0.8		4 AABOUD	16L ATLS	pp at 7, 8 TeV, Repl. by AABOUD 19L
2.8 +0.7 / -0.6		5 KHACHATRYAN	15BE LHC	pp at 7, 8 TeV
3.2 +1.4 +0.5 / -1.2 -0.3		6 AAIJ	13B LHCB	Repl. by AAIJ 13BA
2.9 +1.1 +0.3 / -1.0 -0.1		7 AAIJ	13BA LHCB	Repl. by KHACHATRYAN 15BE
< 12	90	8 ABAZOV	13C D0	$p\bar{p}$ at 1.96 TeV
< 19	90	9 AAD	12AE ATLS	pp at 7 TeV
< 12	90	10 AAIJ	12A LHCB	Repl. by AAIJ 12W
< 3.8	90	11 AAIJ	12W LHCB	Repl. by AAIJ 13B
< 6.4	90	12 CHATRCHYAN	12A CMS	pp at 7 TeV
< 43	90	13 AAIJ	11B LHCB	Repl. by AAIJ 12A
< 35	90	14 AALTONEN	11AG CDF	$p\bar{p}$ at 1.96 TeV
< 16	90	15 CHATRCHYAN	11T CMS	Repl. by CHATRCHYAN 12A
< 42	90	16 ABAZOV	10S D0	$p\bar{p}$ at 1.96 TeV

¹ Uses normalization mode $B(B^+ \rightarrow J/\psi K^+) = (1.010 \pm 0.029) \times 10^{-3}$ and B production ratio $f(b \rightarrow B_s^0)/f(b \rightarrow B^0) = 0.256 \pm 0.013$.

² Uses normalization mode $B(B^+ \rightarrow J/\psi K^+) = (10.22 \pm 0.35) \times 10^{-4}$ and B production ratio $f(\bar{b} \rightarrow B_s^0)/f(\bar{b} \rightarrow B^0) = 0.28 \pm 0.04$.

³ Uses B production ratio $f(\bar{b} \rightarrow B_s^0)/f(\bar{b} \rightarrow B^0) = 0.256 \pm 0.020$ and $B(B^+ \rightarrow J/\psi K^+ \rightarrow \mu^+ \mu^- K^+) = (6.0 \pm 0.2) \times 10^{-5}$ for normalization.

⁴ This value corresponds to an upper limit of $< 3.0 \times 10^{-9}$ at 95% C.L. It uses $f_s/f_d = 0.24 \pm 0.02$.

⁵ Determined from the joint fit to CMS and LHCb data. Uncertainty includes both statistical and systematic component.

⁶ Uses B production ratio $f(\bar{b} \rightarrow B_s^0)/f(\bar{b} \rightarrow B^0) = 0.256 \pm 0.020$ and two normalization modes: $B(B^+ \rightarrow J/\psi K^+ \rightarrow \mu^+ \mu^- K^+) = (6.01 \pm 0.21) \times 10^{-5}$ and $B(B^0 \rightarrow K^+ \pi^-) = (1.94 \pm 0.06) \times 10^{-5}$.

⁷ Uses B production ratio $f(\bar{b} \rightarrow B_s^0)/f(\bar{b} \rightarrow B^0) = 0.259 \pm 0.015$ and normalization modes $B^+ \rightarrow J/\psi K^+ \rightarrow \mu^+ \mu^- K^+$ and $B^0 \rightarrow K^+ \pi^-$.

⁸ Uses normalization mode $B(B^+ \rightarrow J/\psi K^+ \rightarrow \mu^+ \mu^- K^+) = (6.01 \pm 0.21) \times 10^{-5}$ and B production ratio $f(\bar{b} \rightarrow B_s^0)/f(\bar{b} \rightarrow B^0) = 0.263 \pm 0.017$.

⁹ Uses B production ratio $f(\bar{b} \rightarrow B^+)/f(\bar{b} \rightarrow B_s^0) = 3.75 \pm 0.29$ and $B(B^+ \rightarrow J/\psi K^+ \rightarrow \mu^+ \mu^- K^+) = (6.0 \pm 0.2) \times 10^{-5}$.

¹⁰ Uses B production ratio $f(\bar{b} \rightarrow B_s^0)/f(\bar{b} \rightarrow B^0) = 0.267 \pm 0.021$ and three normalization modes $B(B^+ \rightarrow J/\psi K^+ \rightarrow \mu^+ \mu^- K^+) = (6.01 \pm 0.21) \times 10^{-5}$, $B(B^0 \rightarrow K^+ \pi^-) = (1.94 \pm 0.06) \times 10^{-5}$, and $B(B_s^0 \rightarrow J/\psi\phi \rightarrow \mu^+ \mu^- K^+ K^-) = (3.4 \pm 0.9) \times 10^{-5}$.

¹¹ Uses B production ratio $f(\bar{b} \rightarrow B_s^0)/f(\bar{b} \rightarrow B^0) = 0.267 \pm 0.021$ and three normalization modes of $B^+ \rightarrow J/\psi K^+$, $B^0 \rightarrow K^+ \pi^-$, and $B_s^0 \rightarrow J/\psi\phi$.

¹² Uses $f_s/f_d = 0.267 \pm 0.021$ and $B(B^+ \rightarrow J/\psi K^+ \rightarrow \mu^+ \mu^- K^+) = (6.0 \pm 0.2) \times 10^{-5}$.

¹³ Uses B production ratio $f(\bar{b} \rightarrow B^+)/f(\bar{b} \rightarrow B_s^0) = 3.71 \pm 0.47$ and three normalization modes.

¹⁴ Uses B production ratio $f(\bar{b} \rightarrow B^+)/f(\bar{b} \rightarrow B_s^0) = 3.55 \pm 0.47$ and $B(B^+ \rightarrow J/\psi K^+ \rightarrow \mu^+ \mu^- K^+) = (6.01 \pm 0.21) \times 10^{-5}$.

¹⁵ Uses B production ratio $f(\bar{b} \rightarrow B^+)/f(\bar{b} \rightarrow B_s^0) = 3.55 \pm 0.42$ and $B(B^+ \rightarrow J/\psi K^+ \rightarrow \mu^+ \mu^- K^+) = (6.0 \pm 0.2) \times 10^{-5}$.

¹⁶ Uses B production ratio $f(\bar{b} \rightarrow B^+)/f(\bar{b} \rightarrow B_s^0) = 3.86 \pm 0.59$, and the number of $B^+ \rightarrow J/\psi K^+$ decays.

$\Gamma(e^+e^-)/\Gamma_{total}$ Γ_{132}/Γ

Test for $\Delta B = 1$ weak neutral current.

VALUE	CL%	DOCUMENT ID	TECN	COMMENT
< 2.8 × 10⁻⁷				

• • • We do not use the following data for averages, fits, limits, etc. **• • •**

< 5.4 × 10 ⁻⁵	90	1 ACCIARRI	97B L3	$e^+e^- \rightarrow Z$
--------------------------	----	------------	--------	------------------------

¹ ACCIARRI 97B assume PDG 96 production fractions for B^+ , B^0 , B_s , and Λ_b .

$\Gamma(\tau^+\tau^-)/\Gamma_{total}$ Γ_{133}/Γ

VALUE	CL%	DOCUMENT ID	TECN	COMMENT
< 6.8 × 10⁻³	95	1 AAIJ	17Al LHCB	pp at 7, 8 TeV

¹ Assuming no contribution from $B^0 \rightarrow \tau^+\tau^-$.

Meson Particle Listings

 B_S^0 $\Gamma(\mu^+\mu^-\mu^+\mu^-)/\Gamma_{\text{total}}$ Γ_{134}/Γ

VALUE	CL%	DOCUMENT ID	TECN	COMMENT
$<2.5 \times 10^{-9}$	95	AAIJ	17N LHCB	pp at 7, 8 TeV
••• We do not use the following data for averages, fits, limits, etc. •••				
$<1.2 \times 10^{-8}$	90	1AAIJ	13AW LHCB	Repl. by AAIJ 17N
¹ Also reports a limit of $<1.6 \times 10^{-8}$ at 95% CL.				

 $\Gamma(SP, S \rightarrow \mu^+\mu^-, P \rightarrow \mu^+\mu^-)/\Gamma_{\text{total}}$ Γ_{135}/Γ

Here S and P are the hypothetical scalar and pseudoscalar particles with masses of 2.5 GeV/ c^2 and 214.3 MeV/ c^2 , respectively.

VALUE	CL%	DOCUMENT ID	TECN	COMMENT
$<2.2 \times 10^{-9}$	95	AAIJ	17N LHCB	pp at 7, 8 TeV
••• We do not use the following data for averages, fits, limits, etc. •••				
$<1.2 \times 10^{-8}$	90	1AAIJ	13AW LHCB	Repl. by AAIJ 17N
¹ Also reports a limit of $<1.6 \times 10^{-8}$ at 95% CL.				

 $\Gamma(\phi(1020)\mu^+\mu^-)/\Gamma_{\text{total}}$ Γ_{136}/Γ

Test for $\Delta B = 1$ weak neutral current.

VALUE (units 10^{-7})	CL%	DOCUMENT ID	TECN	COMMENT
<32	90	1ABAZOV	06G D0	$p\bar{p}$ at 1.96 TeV
$<4.7 \times 10^2$	90	ACOSTA	02D CDF	$p\bar{p}$ at 1.8 TeV
••• We do not use the following data for averages, fits, limits, etc. •••				
¹ Uses $B(B_S^0 \rightarrow J/\psi\phi) = 9.3 \times 10^{-4}$.				

 $\Gamma(\phi(1020)\mu^+\mu^-)/\Gamma(J/\psi(1S)\phi)$ Γ_{136}/Γ_{49}

VALUE (units 10^{-3})	CL%	DOCUMENT ID	TECN	COMMENT
0.76 ± 0.09	OUR AVERAGE	Error includes scale factor of 1.9.		
$0.741^{+0.042}_{-0.040} \pm 0.029$		AAIJ	15AQ LHCB	pp at 7, 8 TeV
$1.13 \pm 0.19 \pm 0.07$		AALTONEN	11AI CDF	$p\bar{p}$ at 1.96 TeV
••• We do not use the following data for averages, fits, limits, etc. •••				
$0.674^{+0.061}_{-0.056} \pm 0.016$		1AAIJ	13X LHCB	Repl. by AAIJ 15AQ
$1.11 \pm 0.25 \pm 0.09$		AALTONEN	11L CDF	Repl. by AALTONEN 11AI
<2.3	90	AALTONEN	09B CDF	Repl. by AALTONEN 11L
¹ Replaced by AAIJ 15AQ.				

 $\Gamma(\bar{K}^*(892)^0\mu^+\mu^-)/\Gamma_{\text{total}}$ Γ_{137}/Γ

VALUE (units 10^{-8})	CL%	DOCUMENT ID	TECN	COMMENT
$2.9 \pm 1.0 \pm 0.4$		1AAIJ	18AB LHCB	pp at 7, 8, 13 TeV
¹ Normalizes to $B(B^0 \rightarrow J/\psi K^{*0}) = 1.19 \pm 0.01 \pm 0.08\%$ and $B(J/\psi \rightarrow \mu^+\mu^-) = 5.96 \pm 0.03\%$, and uses $f_s/f_d = 0.259 \pm 0.015$.				

 $\Gamma(\pi^+\pi^-\mu^+\mu^-)/\Gamma_{\text{total}}$ Γ_{138}/Γ

VALUE (units 10^{-8})	CL%	DOCUMENT ID	TECN	COMMENT
$8.4 \pm 1.6 \pm 0.3$		1AAIJ	15S LHCB	pp at 7, 8 TeV
¹ AAIJ 15S reports $(8.6 \pm 1.5 \pm 0.7 \pm 0.7) \times 10^{-8}$ from a measurement of $[\Gamma(B_S^0 \rightarrow \pi^+\pi^-\mu^+\mu^-)/\Gamma_{\text{total}}] / [B(B^0 \rightarrow J/\psi(1S)K^*(892)^0)]$ assuming $B(B^0 \rightarrow J/\psi(1S)K^*(892)^0) = (1.3 \pm 0.1) \times 10^{-3}$, which we rescale to our best value $B(B^0 \rightarrow J/\psi(1S)K^*(892)^0) = (1.27 \pm 0.05) \times 10^{-3}$. Our first error is their experiment's error and our second error is the systematic error from using our best value.				

 $\Gamma(\phi\nu\bar{\nu})/\Gamma_{\text{total}}$ Γ_{139}/Γ

Test for $\Delta B = 1$ weak neutral current.

VALUE	CL%	DOCUMENT ID	TECN	COMMENT
$<5.4 \times 10^{-3}$	90	1ADAM	96D DLPH	$e^+e^- \rightarrow Z$
¹ ADAM 96D assumes $f_{B^0} = f_{B^-} = 0.39$ and $f_{B_S} = 0.12$.				

 $\Gamma(e^{\pm}\mu^{\mp})/\Gamma_{\text{total}}$ Γ_{140}/Γ

Test of lepton family number conservation.

VALUE	CL%	DOCUMENT ID	TECN	COMMENT
$<5.4 \times 10^{-9}$	90	1AAIJ	18T LHCB	pp at 7, 8 TeV
••• We do not use the following data for averages, fits, limits, etc. •••				
$<1.1 \times 10^{-8}$	90	2AAIJ	13BM LHCB	Repl. by AAIJ 18T
$<2.0 \times 10^{-7}$	90	AALTONEN	09P CDF	$p\bar{p}$ at 1.96 TeV
$<6.1 \times 10^{-6}$	90	ABE	98V CDF	Repl. by AALTONEN 09P
$<4.1 \times 10^{-5}$	90	3ACCIARRI	97B L3	$e^+e^- \rightarrow Z$

¹ AAIJ 18T uses normalization modes $B(B^0 \rightarrow K^+\pi^-) = (19.6 \pm 0.5) \times 10^{-6}$ and $B(B^+ \rightarrow J/\psi K^+) = (1.026 \pm 0.031) \times 10^{-3}$ with B production ratio $f(\bar{b} \rightarrow B_S^0)/f(\bar{b} \rightarrow B_d^0) = 0.259 \pm 0.015$. The upper limit increases to 6×10^{-9} with the assumption of B_L -dominated decay amplitude.

² Uses normalization mode $B(B^0 \rightarrow K^+\pi^-) = (19.4 \pm 0.6) \times 10^{-6}$ and B production ratio $f(\bar{b} \rightarrow B_S^0)/f(\bar{b} \rightarrow B_d^0) = 0.256 \pm 0.020$.

³ ACCIARRI 97B assume PDG 96 production fractions for B^+ , B^0 , B_S , and Λ_b .

 $\Gamma(\mu^{\pm}\tau^{\mp})/\Gamma_{\text{total}}$ Γ_{141}/Γ

VALUE	CL%	DOCUMENT ID	TECN	COMMENT
$<4.2 \times 10^{-5}$	95	1AAIJ	19AK LHCB	pp at 7, 8 TeV
¹ Assuming no contribution from $B^0 \rightarrow \mu^{\pm}\tau^{\mp}$.				

POLARIZATION IN B_S^0 DECAY

In decays involving two vector mesons, one can distinguish among the states in which meson polarizations are both longitudinal (L), or both are transverse and parallel (\parallel), or perpendicular (\perp) to each other with the parameters Γ_L/Γ , $\Gamma_{\parallel}/\Gamma$, and the relative phases ϕ_{\parallel} and ϕ_{\perp} . In decays involving two tensor mesons, the transverse polarization states are described by parameters $\Gamma_{\parallel 1}$, $\Gamma_{\parallel 2}$, $\Gamma_{\perp 1}$, $\Gamma_{\perp 2}$ and their relative phases $\phi_{\parallel 1}$, $\phi_{\parallel 2}$, $\phi_{\perp 1}$, $\phi_{\perp 2}$. See also the review on "Polarization in B Decays."

 Γ_L/Γ in $B_S^0 \rightarrow D_s^*\rho^+$

VALUE	DOCUMENT ID	TECN	COMMENT
$1.05^{+0.08+0.03}_{-0.10-0.04}$	LOUVOT	10 BELL	$e^+e^- \rightarrow T(5S)$

 Γ_L/Γ in $B_S^0 \rightarrow J/\psi(1S)\phi$

VALUE	DOCUMENT ID	TECN	COMMENT
0.5199 ± 0.0035	OUR AVERAGE	Error includes scale factor of 1.1.	
$0.5186 \pm 0.0029 \pm 0.0024$	AAIJ	19Q LHCB	pp at 13 TeV
$0.522 \pm 0.003 \pm 0.007$	1AAD	16AP ATLS	pp at 7, 8 TeV
$0.510 \pm 0.005 \pm 0.011$	KHACHATRY..16s	CMS	pp at 8 TeV
$0.524 \pm 0.013 \pm 0.015$	2AALTONEN	12D CDF	$p\bar{p}$ at 1.96 TeV
$0.558^{+0.017}_{-0.019}$	2,3ABAZOV	12D D0	$p\bar{p}$ at 1.96 TeV
$0.61 \pm 0.14 \pm 0.02$	4AFFOLDER	00N CDF	$p\bar{p}$ at 1.8 TeV
$0.56 \pm 0.21^{+0.02}_{-0.04}$	ABE	95Z CDF	$p\bar{p}$ at 1.8 TeV

••• We do not use the following data for averages, fits, limits, etc. •••

$0.5241 \pm 0.0034 \pm 0.0067$ AAIJ 15I LHCB Repl. by AAIJ 19Q

$0.529 \pm 0.006 \pm 0.012$ 1AAD 14U ATLS Repl. by AAD 16AP

$0.539 \pm 0.014 \pm 0.016$ 2AAD 12CV ATLS Repl. by AAD 14U

$0.555 \pm 0.027 \pm 0.006$ 5ABAZOV 09E D0 Repl. by ABAZOV 12D

$0.531 \pm 0.020 \pm 0.007$ 2AALTONEN 08J CDF Repl. by AALTONEN 12D

$0.62 \pm 0.06 \pm 0.01$ ACOSTA 05 CDF Repl. by AALTONEN 08J

¹ Measured using the flavor tagged, time-dependent angular analysis of $B_S^0 \rightarrow J/\psi\phi$ decays.

² Measured using the time-dependent angular analysis of $B_S^0 \rightarrow J/\psi\phi$ decays.

³ The error includes both statistical and systematic uncertainties.

⁴ AFFOLDER 00N measurements are based on 40 B_S^0 candidates obtained from a data sample of 89 pb $^{-1}$. The P -wave fraction is found to be $0.23 \pm 0.19 \pm 0.04$.

⁵ Measured the angular and lifetime parameters for the time-dependent angular untagged decays $B_d^0 \rightarrow J/\psi K^{*0}$ and $B_S^0 \rightarrow J/\psi\phi$.

 Γ_L/Γ in $B_S^0 \rightarrow D_s^* D_s^{*-}$

VALUE	DOCUMENT ID	TECN	COMMENT
$0.06^{+0.19}_{-0.17} \pm 0.03$	ESEN	13 BELL	$e^+e^- \rightarrow T(5S)$

 $\Gamma_{\parallel}/\Gamma$ in $B_S^0 \rightarrow J/\psi(1S)\phi$

VALUE	DOCUMENT ID	TECN	COMMENT
0.228 ± 0.007	OUR AVERAGE		
$0.227 \pm 0.004 \pm 0.006$	1AAD	16AP ATLS	pp at 7, 8 TeV
$0.231 \pm 0.014 \pm 0.015$	2AALTONEN	12D CDF	$p\bar{p}$ at 1.96 TeV
$0.231^{+0.024}_{-0.030}$	2,3ABAZOV	12D D0	$p\bar{p}$ at 1.96 TeV
••• We do not use the following data for averages, fits, limits, etc. •••			
$0.220 \pm 0.008 \pm 0.009$	1AAD	14U ATLS	Repl. by AAD 16AP
$0.224 \pm 0.010 \pm 0.009$	2AAD	12CV ATLS	Repl. by AAD 14U
$0.244 \pm 0.032 \pm 0.014$	4ABAZOV	09E D0	Repl. by ABAZOV 12D
$0.230 \pm 0.029 \pm 0.011$	2AALTONEN	08J CDF	Repl. by AALTONEN 12D
$0.260 \pm 0.084 \pm 0.013$	ACOSTA	05 CDF	Repl. by AALTONEN 08J

¹ Measured using a tagged, time-dependent angular analysis of $B_S^0 \rightarrow J/\psi\phi$ decays.

² Measured using the time-dependent angular analysis of $B_S^0 \rightarrow J/\psi\phi$ decays.

³ The error includes both statistical and systematic uncertainties.

⁴ Measured the angular and lifetime parameters for the time-dependent angular untagged decays $B_d^0 \rightarrow J/\psi K^{*0}$ and $B_S^0 \rightarrow J/\psi\phi$.

 Γ_{\perp}/Γ in $B_S^0 \rightarrow J/\psi(1S)\phi$

VALUE	DOCUMENT ID	TECN	COMMENT
0.245 ± 0.004	OUR AVERAGE		
$0.2456 \pm 0.0040 \pm 0.0019$	AAIJ	19Q LHCB	pp at 13 TeV
$0.243 \pm 0.008 \pm 0.012$	KHACHATRY..16s	CMS	pp at 8 TeV
••• We do not use the following data for averages, fits, limits, etc. •••			
$0.2504 \pm 0.0049 \pm 0.0036$	AAIJ	15I LHCB	Repl. by AAIJ 19Q

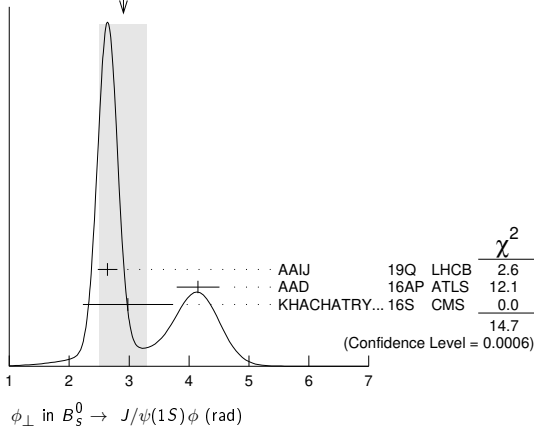
 ϕ_{\parallel} in $B_S^0 \rightarrow J/\psi(1S)\phi$

VALUE (rad)	DOCUMENT ID	TECN	COMMENT
3.10 ± 0.06	OUR AVERAGE		
$3.06^{+0.08}_{-0.07} \pm 0.04$	AAIJ	19Q LHCB	pp at 13 TeV
$3.15 \pm 0.10 \pm 0.05$	AAD	16AP ATLS	pp at 7, 8 TeV
$3.48^{+0.07}_{-0.09} \pm 0.68$	KHACHATRY..16s	CMS	pp at 8 TeV
3.15 ± 0.22	1ABAZOV	12D D0	$p\bar{p}$ at 1.96 TeV
••• We do not use the following data for averages, fits, limits, etc. •••			
$3.26^{+0.10+0.06}_{-0.17-0.07}$	AAIJ	15I LHCB	Repl. by AAIJ 19Q
$2.72^{+1.12}_{-0.27} \pm 0.26$	ABAZOV	09E D0	Repl. by ABAZOV 12D

¹ The error includes both statistical and systematic uncertainties.

ϕ_{\perp} in $B_s^0 \rightarrow J/\psi(1S)\phi$

VALUE (rad)	DOCUMENT ID	TECN	COMMENT
2.9 ± 0.4 OUR AVERAGE	Error includes scale factor of 2.7. See the ideogram below.		
$2.64 \pm 0.13 \pm 0.10$	AAIJ	19q	LHCB pp at 13 TeV
$4.15 \pm 0.32 \pm 0.16$	¹ AAD	16AP	ATLS pp at 7, 8 TeV
$2.98 \pm 0.36 \pm 0.66$	KHACHATRY...	16s	CMS pp at 8 TeV
• • • We do not use the following data for averages, fits, limits, etc. • • •			
$3.08^{+0.14}_{-0.15} \pm 0.06$	AAIJ	15i	LHCB Repl. by AAIJ 19q
$3.89 \pm 0.47 \pm 0.11$	¹ AAD	14u	ATLS Repl. by AAD 16AP
¹ Measured using a tagged, time-dependent angular analysis of $B_s^0 \rightarrow J/\psi\phi$ decays.			

WEIGHTED AVERAGE
 2.9 ± 0.4 (Error scaled by 2.7) Γ_{\perp}/Γ in $B_s^0 \rightarrow \psi(2S)\phi$

VALUE	DOCUMENT ID	TECN	COMMENT
$0.264^{+0.024}_{-0.023} \pm 0.002$	¹ AAIJ	16AK	LHCB pp at 7, 8 TeV
¹ Measured using time-dependent angular analysis of $B_s^0 \rightarrow \psi(2S)\phi$ decays.			

 ϕ_{\parallel} in $B_s^0 \rightarrow \psi(2S)\phi$

VALUE (rad)	DOCUMENT ID	TECN	COMMENT
$3.67^{+0.13}_{-0.18} \pm 0.03$	¹ AAIJ	16AK	LHCB pp at 7, 8 TeV
¹ Measured using time-dependent angular analysis of $B_s^0 \rightarrow \psi(2S)\phi$ decays.			

 ϕ_{\perp} in $B_s^0 \rightarrow \psi(2S)\phi$

VALUE (rad)	DOCUMENT ID	TECN	COMMENT
$3.29^{+0.43}_{-0.39} \pm 0.04$	¹ AAIJ	16AK	LHCB pp at 7, 8 TeV
¹ Measured using time-dependent angular analysis of $B_s^0 \rightarrow \psi(2S)\phi$ decays.			

 Γ_L/Γ for $B_s^0 \rightarrow J/\psi(1S)\bar{K}^*(892)^0$ Longitudinal polarization fraction, equals to f_L using notation of "Polarization in B decays" review.

VALUE	DOCUMENT ID	TECN	COMMENT
$0.497 \pm 0.025 \pm 0.025$	AAIJ	15AV	LHCB pp at 7, 8 TeV
• • • We do not use the following data for averages, fits, limits, etc. • • •			
$0.50 \pm 0.08 \pm 0.02$	¹ AAIJ	12AP	LHCB Repl. by AAIJ 15AV
¹ The non-resonant $K\pi$ background contributions are subtracted. Also reports an S-wave amplitude $ A_S ^2 = 0.07^{+0.15}_{-0.07}$.			

 $\Gamma_{\parallel}/\Gamma$ for $B_s^0 \rightarrow J/\psi(1S)\bar{K}^*(892)^0$ Parallel polarization fraction, equals to $1 - f_L - f_{\perp}$ using notation of "Polarization in B decays" review.

VALUE	DOCUMENT ID	TECN	COMMENT
$0.179 \pm 0.027 \pm 0.013$	AAIJ	15AV	LHCB pp at 7, 8 TeV
• • • We do not use the following data for averages, fits, limits, etc. • • •			
$0.19^{+0.10}_{-0.08} \pm 0.02$	¹ AAIJ	12AP	LHCB Repl. by AAIJ 15AV
¹ The non-resonant $K\pi$ background contributions are subtracted. Also reports an S-wave amplitude $ A_S ^2 = 0.07^{+0.15}_{-0.07}$.			

 $\Gamma_{\parallel}/\Gamma$ of $K^*(892)^0$ in $B_s^0 \rightarrow \psi(2S)\bar{K}^*(892)^0$

VALUE	DOCUMENT ID	TECN	COMMENT
$0.524 \pm 0.056 \pm 0.029$	AAIJ	15u	LHCB pp at 7, 8 TeV

 Γ_L/Γ in $B_s^0 \rightarrow \phi\phi$

VALUE	DOCUMENT ID	TECN	COMMENT
0.378 ± 0.013 OUR AVERAGE			
$0.381 \pm 0.007 \pm 0.012$	AAIJ	19AP	LHCB pp at 7, 8 and 13 TeV
$0.348 \pm 0.041 \pm 0.021$	AALTONEN	11AN	CDF $p\bar{p}$ at 1.96 TeV
• • • We do not use the following data for averages, fits, limits, etc. • • •			
$0.364 \pm 0.012 \pm 0.009$	AAIJ	14AE	LHCB Repl. by AAIJ 19AP
$0.365 \pm 0.022 \pm 0.012$	AAIJ	12P	LHCB Repl. by AAIJ 14AE

 Γ_{\perp}/Γ in $B_s^0 \rightarrow \phi\phi$

VALUE	DOCUMENT ID	TECN	COMMENT
0.292 ± 0.009 OUR AVERAGE			
$0.290 \pm 0.008 \pm 0.005$	¹ AAIJ	19AP	LHCB pp at 7, 8 and 13 TeV
$0.365 \pm 0.044 \pm 0.027$	AALTONEN	11AN	CDF $p\bar{p}$ at 1.96 TeV
• • • We do not use the following data for averages, fits, limits, etc. • • •			
$0.305 \pm 0.013 \pm 0.005$	AAIJ	14AE	LHCB Repl. by AAIJ 19AP
$0.291 \pm 0.024 \pm 0.010$	AAIJ	12P	LHCB Repl. by AAIJ 14AE
¹ Note: in the summary of AAIJ 19AP the systematic uncertainty is 0.007. We take the systematic uncertainty as given in Table 5 in the paper.			

 ϕ_{\parallel} in $B_s^0 \rightarrow \phi\phi$

VALUE (rad)	DOCUMENT ID	TECN	COMMENT
2.56 ± 0.06 OUR AVERAGE			
$2.559 \pm 0.045 \pm 0.033$	AAIJ	19AP	LHCB pp at 7, 8 and 13 TeV
$2.71^{+0.31}_{-0.36} \pm 0.22$	¹ AALTONEN	11AN	CDF $p\bar{p}$ at 1.96 TeV
• • • We do not use the following data for averages, fits, limits, etc. • • •			
$2.54 \pm 0.07 \pm 0.09$	² AAIJ	14AE	LHCB Repl. by AAIJ 19AP
$2.57 \pm 0.15 \pm 0.06$	³ AAIJ	12P	LHCB Repl. by AAIJ 14AE
¹ AALTONEN 11AN quotes $\cos\phi_{\parallel} = -0.91^{+0.15}_{-0.13} \pm 0.09$ which we convert to ϕ_{\parallel} taking the smaller solution.			
² AAIJ 14AE reports measurement of ϕ_{\perp} and $\phi_{\perp} - \phi_{\parallel}$, which we convert into ϕ_{\parallel} . Statistical uncertainty includes correlation between measured parameters, while systematic uncertainties are assumed uncorrelated.			
³ AAIJ 12P quotes $\cos\phi_{\parallel} = -0.844 \pm 0.068 \pm 0.029$ which we convert to ϕ_{\parallel} , taking the smaller solution.			

 ϕ_{\perp} in $B_s^0 \rightarrow \phi\phi$

VALUE (rad)	DOCUMENT ID	TECN	COMMENT
$2.818 \pm 0.178 \pm 0.073$	AAIJ	19AP	LHCB pp at 7, 8 and 13 TeV
• • • We do not use the following data for averages, fits, limits, etc. • • •			
$2.67 \pm 0.23 \pm 0.07$	AAIJ	14AE	LHCB Repl. by AAIJ 19AP

 Γ_L/Γ in $B_s^0 \rightarrow K^{*0}\bar{K}^{*0}$

VALUE	DOCUMENT ID	TECN	COMMENT
$0.240 \pm 0.031 \pm 0.025$	¹ AAIJ	19L	LHCB pp at 7 and 8 TeV
• • • We do not use the following data for averages, fits, limits, etc. • • •			
$0.208 \pm 0.032 \pm 0.046$	² AAIJ	18s	LHCB Repl. by AAIJ 19L
$0.201 \pm 0.057 \pm 0.040$	³ AAIJ	15AF	LHCB Repl. by AAIJ 18s
$0.31 \pm 0.12 \pm 0.04$	AAIJ	12F	LHCB Repl. by AAIJ 15AF
¹ Untagged and time-integrated analysis within 150 MeV of the K^{*0} mass.			
² Measured in angular analysis, which takes into account S-, P- and D-wave contributions.			
³ Measured in angular analysis, which takes into account S-wave contributions.			

 Γ_{\perp}/Γ in $B_s^0 \rightarrow K^{*0}\bar{K}^{*0}$

VALUE	DOCUMENT ID	TECN	COMMENT
$0.38 \pm 0.11 \pm 0.04$	AAIJ	12F	LHCB pp at 7 TeV

 $\Gamma_{\parallel}/\Gamma$ in $B_s^0 \rightarrow K^*(892)^0\bar{K}^*(892)^0$

VALUE	DOCUMENT ID	TECN	COMMENT
$0.297 \pm 0.029 \pm 0.042$	¹ AAIJ	18s	LHCB pp at 7, 8 TeV
• • • We do not use the following data for averages, fits, limits, etc. • • •			
$0.215 \pm 0.046 \pm 0.015$	AAIJ	15AF	LHCB Repl. by AAIJ 18s
¹ Measured in angular analysis, which takes into account S-, P- and D-wave contributions.			

 Φ_{\parallel} in $B_s^0 \rightarrow K^*(892)^0\bar{K}^*(892)^0$

VALUE	DOCUMENT ID	TECN	COMMENT
$2.40 \pm 0.11 \pm 0.33$	¹ AAIJ	18s	LHCB pp at 7, 8 TeV
• • • We do not use the following data for averages, fits, limits, etc. • • •			
$5.31 \pm 0.24 \pm 0.14$	AAIJ	15AF	LHCB Repl. by AAIJ 18s
¹ Measured in angular analysis, which takes into account S-, P- and D-wave contributions.			

 Φ_{\perp} in $B_s^0 \rightarrow K^*(892)^0\bar{K}^*(892)^0$

VALUE (rad)	DOCUMENT ID	TECN	COMMENT
$2.62 \pm 0.26 \pm 0.64$	¹ AAIJ	18s	LHCB pp at 7, 8 TeV
¹ Measured in angular analysis, which takes into account S-, P- and D-wave contributions.			

 Γ_L/Γ in $B_s^0 \rightarrow \phi\bar{K}^{*0}$

VALUE	DOCUMENT ID	TECN	COMMENT
$0.51 \pm 0.15 \pm 0.07$	AAIJ	13BW	LHCB pp at 7 TeV

Meson Particle Listings

B_s^0

$\Gamma_{\parallel} / \Gamma$ in $B_s^0 \rightarrow \phi \bar{K}^{*0}$

VALUE	DOCUMENT ID	TECN	COMMENT
$0.21 \pm 0.11 \pm 0.02$	AAIJ	13BW	LHCB pp at 7 TeV

ϕ_{\parallel} in $B_s^0 \rightarrow \phi \bar{K}^{*0}$

VALUE (rad)	DOCUMENT ID	TECN	COMMENT
$1.75 \pm 0.53 \pm 0.29$	¹ AAIJ	13BW	LHCB pp at 7 TeV

¹ Measures $\cos(\phi_{\parallel}) = -0.18 \pm 0.52 \pm 0.29$, which we convert to ϕ_{\parallel} by taking the smaller solution.

Γ_L / Γ in $B_s^0 \rightarrow \bar{D}^{*0} \phi$

VALUE	DOCUMENT ID	TECN	COMMENT
$0.73 \pm 0.15 \pm 0.04$	AAIJ	18AY	LHCB pp at 7 and 8 TeV

Γ_L / Γ in $B_s^0 \rightarrow K^*(892)^0 \bar{K}_2^*(1430)^0$

VALUE	DOCUMENT ID	TECN	COMMENT
$0.911 \pm 0.020 \pm 0.165$	¹ AAIJ	18s	LHCB pp at 7, 8 TeV

¹ Measured in angular analysis, which takes into account S -, P - and D -wave. contributions.

$\Gamma_{\parallel} / \Gamma$ in $B_s^0 \rightarrow K^*(892)^0 \bar{K}_2^*(1430)^0$

VALUE	DOCUMENT ID	TECN	COMMENT
$0.012 \pm 0.008 \pm 0.053$	¹ AAIJ	18s	LHCB pp at 7, 8 TeV

¹ Measured in angular analysis, which takes into account S -, P - and D -wave. contributions.

Γ_L / Γ in $B_s^0 \rightarrow K_2^*(1430)^0 \bar{K}^*(892)^0$

VALUE	DOCUMENT ID	TECN	COMMENT
$0.62 \pm 0.16 \pm 0.25$	¹ AAIJ	18s	LHCB pp at 7, 8 TeV

¹ Measured in angular analysis, which takes into account S -, P - and D -wave. contributions.

$\Gamma_{\parallel} / \Gamma$ in $B_s^0 \rightarrow K_2^*(1430)^0 \bar{K}^*(892)^0$

VALUE	DOCUMENT ID	TECN	COMMENT
$0.24 \pm 0.10 \pm 0.14$	¹ AAIJ	18s	LHCB pp at 7, 8 TeV

¹ Measured in angular analysis, which takes into account S -, P - and D -wave. contributions.

Γ_L / Γ in $B_s^0 \rightarrow K_2^*(1430)^0 \bar{K}_2^*(1430)^0$

VALUE	DOCUMENT ID	TECN	COMMENT
$0.25 \pm 0.14 \pm 0.18$	¹ AAIJ	18s	LHCB pp at 7, 8 TeV

¹ Measured in angular analysis, which takes into account S -, P - and D -wave. contributions.

$\Gamma_{\parallel 1} / \Gamma$ in $B_s^0 \rightarrow K_2^*(1430)^0 \bar{K}_2^*(1430)^0$

VALUE	DOCUMENT ID	TECN	COMMENT
$0.17 \pm 0.11 \pm 0.14$	¹ AAIJ	18s	LHCB pp at 7, 8 TeV

¹ Measured in angular analysis, which takes into account S -, P - and D -wave. contributions.

$\Gamma_{\parallel 1} / \Gamma$ in $B_s^0 \rightarrow K_2^*(1430)^0 \bar{K}_2^*(1430)^0$

VALUE	DOCUMENT ID	TECN	COMMENT
$0.30 \pm 0.18 \pm 0.21$	¹ AAIJ	18s	LHCB pp at 7, 8 TeV

¹ Measured in angular analysis, which takes into account S -, P - and D -wave. contributions.

$\Gamma_{\parallel 2} / \Gamma$ in $B_s^0 \rightarrow K_2^*(1430)^0 \bar{K}_2^*(1430)^0$

VALUE	DOCUMENT ID	TECN	COMMENT
$0.015 \pm 0.033 \pm 0.107$	¹ AAIJ	18s	LHCB pp at 7, 8 TeV

¹ Measured in angular analysis, which takes into account S -, P - and D -wave. contributions.

$F_L(B_s^0 \rightarrow \phi \mu^+ \mu^-)$ ($0.10 < q^2 < 2.00 \text{ GeV}^2/c^4$)

VALUE	DOCUMENT ID	TECN	COMMENT
$0.20^{+0.08}_{-0.09} \pm 0.02$	AAIJ	15AQ	LHCB pp at 7, 8 TeV

••• We do not use the following data for averages, fits, limits, etc. •••

$0.37^{+0.19}_{-0.17} \pm 0.07$	AAIJ	13X	LHCB Repl. by AAIJ 15AQ
---------------------------------	------	-----	-------------------------

$F_L(B_s^0 \rightarrow \phi \mu^+ \mu^-)$ ($2.00 < q^2 < 5.0 \text{ GeV}^2/c^4$)

VALUE	DOCUMENT ID	TECN	COMMENT
$0.68^{+0.16}_{-0.13} \pm 0.03$	AAIJ	15AQ	LHCB pp at 7, 8 TeV

••• We do not use the following data for averages, fits, limits, etc. •••

$0.53^{+0.25}_{-0.23} \pm 0.10$	¹ AAIJ	13X	LHCB Repl. by AAIJ 15AQ
---------------------------------	-------------------	-----	-------------------------

¹ Measured in $2.0 < q^2 < 4.3 \text{ GeV}^2/c^4$.

$F_L(B_s^0 \rightarrow \phi \mu^+ \mu^-)$ ($5.0 < q^2 < 8.0 \text{ GeV}^2/c^4$)

VALUE	DOCUMENT ID	TECN	COMMENT
$0.54^{+0.10}_{-0.09} \pm 0.02$	AAIJ	15AQ	LHCB pp at 7, 8 TeV

••• We do not use the following data for averages, fits, limits, etc. •••

$0.81^{+0.11}_{-0.13} \pm 0.05$	¹ AAIJ	13X	LHCB Repl. by AAIJ 15AQ
---------------------------------	-------------------	-----	-------------------------

¹ Measured in $4.3 < q^2 < 8.68 \text{ GeV}^2/c^4$.

$F_L(B_s^0 \rightarrow \phi \mu^+ \mu^-)$ ($11.0 < q^2 < 12.5 \text{ GeV}^2/c^4$)

VALUE	DOCUMENT ID	TECN	COMMENT
$0.29 \pm 0.11 \pm 0.04$	AAIJ	15AQ	LHCB pp at 7, 8 TeV

••• We do not use the following data for averages, fits, limits, etc. •••

$0.33^{+0.14}_{-0.12} \pm 0.06$	¹ AAIJ	13X	LHCB Repl. by AAIJ 15AQ
---------------------------------	-------------------	-----	-------------------------

¹ Measured in $10.09 < q^2 < 12.90 \text{ GeV}^2/c^4$.

$F_L(B_s^0 \rightarrow \phi \mu^+ \mu^-)$ ($15.0 < q^2 < 17.0 \text{ GeV}^2/c^4$)

VALUE	DOCUMENT ID	TECN	COMMENT
$0.23^{+0.09}_{-0.08} \pm 0.02$	AAIJ	15AQ	LHCB pp at 7, 8 TeV

••• We do not use the following data for averages, fits, limits, etc. •••

$0.34^{+0.18}_{-0.17} \pm 0.07$	¹ AAIJ	13X	LHCB Repl. by AAIJ 15AQ
---------------------------------	-------------------	-----	-------------------------

¹ Measured in $14.18 < q^2 < 16 \text{ GeV}^2/c^4$.

$F_L(B_s^0 \rightarrow \phi \mu^+ \mu^-)$ ($17.0 < q^2 < 19.0 \text{ GeV}^2/c^4$)

VALUE	DOCUMENT ID	TECN	COMMENT
$0.40^{+0.13}_{-0.15} \pm 0.02$	AAIJ	15AQ	LHCB pp at 7, 8 TeV

••• We do not use the following data for averages, fits, limits, etc. •••

$0.16^{+0.17}_{-0.10} \pm 0.07$	¹ AAIJ	13X	LHCB Repl. by AAIJ 15AQ
---------------------------------	-------------------	-----	-------------------------

¹ Measured in $16.0 < q^2 < 19.0 \text{ GeV}^2/c^4$.

$F_L(B_s^0 \rightarrow \phi \mu^+ \mu^-)$ ($1.00 < q^2 < 6.00 \text{ GeV}^2/c^4$)

VALUE	DOCUMENT ID	TECN	COMMENT
$0.63^{+0.09}_{-0.09} \pm 0.03$	AAIJ	15AQ	LHCB pp at 7, 8 TeV

••• We do not use the following data for averages, fits, limits, etc. •••

$0.56^{+0.17}_{-0.16} \pm 0.09$	AAIJ	13X	LHCB Repl. by AAIJ 15AQ
---------------------------------	------	-----	-------------------------

$B_s^0\text{-}\bar{B}_s^0$ MIXING

For a discussion of $B_s^0\text{-}\bar{B}_s^0$ mixing see the note on " $B^0\text{-}\bar{B}^0$ Mixing" in the B^0 Particle Listings above.

χ_s is a measure of the time-integrated $B_s^0\text{-}\bar{B}_s^0$ mixing probability that produced $B_s^0(\bar{B}_s^0)$ decays as a $\bar{B}_s^0(B_s^0)$. Mixing violates $\Delta B \neq 2$ rule.

$$\chi_s = \frac{x_s^2}{2(1+x_s^2)}$$

$$x_s = \frac{\Delta m_{B_s^0}}{\Gamma_{B_s^0}} = (m_{B_{sH}} - m_{B_{sL}}) \tau_{B_s^0}$$

where H, L stand for heavy and light states of two B_s^0 CP eigenstates and $\tau_{B_s^0} = \frac{1}{0.5(\Gamma_{B_{sH}} + \Gamma_{B_{sL}})}$.

$$\Delta m_{B_s^0} = m_{B_{sH}} - m_{B_{sL}}$$

$\Delta m_{B_s^0}$ is a measure of 2π times the $B_s^0\text{-}\bar{B}_s^0$ oscillation frequency in time-dependent mixing experiments.

"OUR EVALUATION" is provided by the Heavy Flavor Averaging Group (HFLAV, <https://hflav.web.cern.ch/>) by taking into account correlations between measurements.

VALUE (10^{12} s^{-1})	CL%	DOCUMENT ID	TECN	COMMENT
17.749 ± 0.020 OUR EVALUATION				
17.756 ± 0.021 OUR AVERAGE				
$17.703 \pm 0.059 \pm 0.018$		¹ AAIJ	19Q	LHCB pp at 13 TeV
$17.768 \pm 0.023 \pm 0.006$		² AAIJ	13BI	LHCB pp at 7 TeV
$17.93 \pm 0.22 \pm 0.15$		³ AAIJ	13CF	LHCB pp at 7 TeV
$17.63 \pm 0.11 \pm 0.02$		⁴ AAIJ	12I	LHCB pp at 7 TeV
$17.77 \pm 0.10 \pm 0.07$		⁵ ABULENCIA,A	06G	CDF $p\bar{p}$ at 1.96 TeV
••• We do not use the following data for averages, fits, limits, etc. •••				
$17.711^{+0.055}_{-0.057} \pm 0.011$		¹ AAIJ	15I	LHCB Repl. by AAIJ 19Q
17–21	90	⁶ ABAZOV	06B	D0 $p\bar{p}$ at 1.96 TeV
17.31	$^{+0.33}_{-0.18} \pm 0.07$	⁷ ABULENCIA	06Q	CDF Repl. by ABULENCIA,A 06G
> 8.0	95	⁸ ABDALLAH	04J	DLPH $e^+e^- \rightarrow Z^0$
> 4.9	95	⁹ ABDALLAH	04J	DLPH $e^+e^- \rightarrow Z^0$
> 8.5	95	¹⁰ ABDALLAH	04J	DLPH $e^+e^- \rightarrow Z^0$
> 5.0	95	¹¹ ABDALLAH	03B	DLPH $e^+e^- \rightarrow Z$
> 10.3	95	¹² ABE	03	SLD $e^+e^- \rightarrow Z$
> 10.9	95	¹³ HEISTER	03E	ALEP $e^+e^- \rightarrow Z$
> 5.3	95	¹⁴ ABE	02V	SLD $e^+e^- \rightarrow Z$
> 1.0	95	¹⁵ ABBIENDI	01D	OPAL $e^+e^- \rightarrow Z$
> 7.4	95	¹⁶ ABREU	00Y	DLPH Repl. by ABDALLAH 04J
> 4.0	95	¹⁷ ABREU,P	00G	DLPH $e^+e^- \rightarrow Z$

> 5.2	95	18	ABBIENDI	99S	OPAL	$e^+e^- \rightarrow Z$
< 96	95	19	ABE	99D	CDF	$p\bar{p}$ at 1.8 TeV
> 5.8	95	20	ABE	99J	CDF	$p\bar{p}$ at 1.8 TeV
> 9.6	95	21	BARATE	99J	ALEP	$e^+e^- \rightarrow Z$
> 7.9	95	22	BARATE	98C	ALEP	Repl. by BARATE 99J
> 3.1	95	23	ACKERSTAFF	97U	OPAL	Repl. by ABBIENDI 99S
> 2.2	95	24	ACKERSTAFF	97V	OPAL	Repl. by ABBIENDI 99S
> 6.5	95	25	ADAM	97	DLPH	Repl. by ABREU 00Y
> 6.6	95	26	BUSKULIC	96M	ALEP	Repl. by BARATE 98C
> 2.2	95	24	AKERS	95J	OPAL	Sup. by ACKERSTAFF 97V
> 5.7	95	27	BUSKULIC	95J	ALEP	$e^+e^- \rightarrow Z$
> 1.8	95	24	BUSKULIC	94B	ALEP	$e^+e^- \rightarrow Z$

- Measured using time-dependent angular analysis of $B_s^0 \rightarrow J/\psi K^+ K^-$ decays.
- Measured using $B_s^0 \rightarrow D_s^- \pi^+$ decays.
- Measured using $B_s^0 \rightarrow D_s^- \mu^+ \nu_\mu X$ decays.
- Measured using $B_s^0 \rightarrow D_s^- \pi^+$ and $D_s^- \pi^+ \pi^- \pi^+$ decays.
- Significance of oscillation signal is 5.4σ . Also reports $|V_{td} / V_{ts}| = 0.2060 \pm 0.0007^{+0.0008}_{-0.0060}$.
- A likelihood scan over the oscillation frequency, Δm_s , gives a most probable value of 19 ps^{-1} and a range of $17 < \Delta m_s < 21 \text{ (ps}^{-1})$ at 90% C.L. assuming Gaussian uncertainties. Also excludes $\Delta m_s < 14.8 \text{ ps}^{-1}$ at 95% C.L.
- Significance of oscillation signal is 0.2%. Also reported the value $|V_{td} / V_{ts}| = 0.208^{+0.001+0.008}_{-0.002-0.006}$.
- Uses leptons emitted with large momentum transverse to a jet and improved techniques for vertexing and flavor-tagging.
- Updates of D_s -lepton analysis.
- Combined results from all Delphi analyses.
- Events with a high transverse momentum lepton were removed and an inclusively reconstructed vertex was required.
- ABE 03 uses the novel "charge dipole" technique to reconstruct separate secondary and tertiary vertices originating from the $B \rightarrow D$ decay chain. The analysis excludes $\Delta m_s < 4.9 \text{ ps}^{-1}$ and $7.9 < \Delta m_s < 10.3 \text{ ps}^{-1}$.
- Three analyses based on complementary event selections: (1) fully-reconstructed hadronic decays; (2) semileptonic decays with D_s exclusively reconstructed; (3) inclusive semileptonic decays.
- ABE 02v uses exclusively reconstructed D_s^- mesons and excludes $\Delta m_s < 1.4 \text{ ps}^{-1}$ and $2.4 < \Delta m_s < 5.3 \text{ ps}^{-1}$ at 95% C.L.
- Uses fully or partially reconstructed $D_s \ell$ vertices and a mixing tag as a flavor tagging.
- Replaced by ABDALLAH 04A. Uses $D_s^- \ell^+$, and $\phi \ell^+$ vertices, and a multi-variable discriminant as a flavor tagging.
- Uses inclusive D_s vertices and fully reconstructed B_s decays and a multi-variable discriminant as a flavor tagging.
- Uses ℓ - Q_{hem} and ℓ - ℓ .
- ABE 99D assumes $\tau_{B_s^0} = 1.55 \pm 0.05 \text{ ps}$ and $\Delta\Gamma/\Delta m = (5.6 \pm 2.6) \times 10^{-3}$.
- ABE 99J uses ϕ ℓ - ℓ correlation.
- BARATE 99J uses combination of an inclusive lepton and D_s^- -based analyses.
- BARATE 98C combines results from $D_s h\ell/Q_{\text{hem}}$, $D_s hK$ in the same side, $D_s \ell\ell/Q_{\text{hem}}$ and $D_s \ell K$ in the same side.
- Uses ℓ - Q_{hem} .
- Uses ℓ - ℓ .
- ADAM 97 combines results from $D_s \ell$ - Q_{hem} , ℓ - Q_{hem} , and ℓ - ℓ .
- BUSKULIC 96M uses D_s lepton correlations and lepton, kaon, and jet charge tags.
- BUSKULIC 95J uses ℓ - Q_{hem} . They find $\Delta m_s > 5.6$ [> 6.1] for $r_s=10\%$ [12%]. We interpolate to our central value $r_s=10.5\%$.

$x_s = \Delta m_{B_s^0} / \Gamma_{B_s^0}$
 This is derived by the Heavy Flavor Averaging Group (HFLAV, <https://hflav.web.cern.ch/>) from the results on $\Delta m_{B_s^0}$ and "OUR EVALUATION" of the B_s^0 mean lifetime.

VALUE DOCUMENT ID
26.89 ± 0.07 OUR EVALUATION

X_s
 This is a $B_s^0 \bar{B}_s^0$ integrated mixing parameter derived from x_s above and OUR EVALUATION of $\Delta\Gamma_{B_s^0} / \Gamma_{B_s^0}$.

VALUE DOCUMENT ID
0.49931 ± 0.00004 OUR EVALUATION

CP VIOLATION PARAMETERS in B_s^0

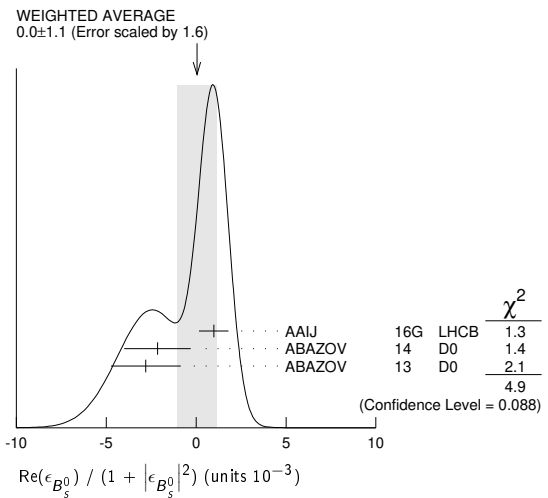
$\text{Re}(\epsilon_{B_s^0}) / (1 + |\epsilon_{B_s^0}|^2)$
 CP impurity in B_s^0 system.

"OUR EVALUATION" is an average obtained by the Heavy Flavor Averaging Group (HFLAV, <https://hflav.web.cern.ch/>) and described at <https://hflav.web.cern.ch/>. It is the result of a fit to B_d and B_s CP asymmetries, which includes the B_s measurements listed below and the B_d measurements listed in the B_d section, and takes into account correlations between those measurements.

VALUE (units 10^{-3})	DOCUMENT ID	TECN	COMMENT
-0.15 ± 0.70 OUR EVALUATION			Error includes scale factor of 1.6. See the ideogram below.
0.0 ± 1.1 OUR AVERAGE			
0.98 ± 0.65 ± 0.5	1	AAIJ	16G LHCb pp at 7, 8 TeV
-2.15 ± 1.85	2	ABAZOV	14 D0 $p\bar{p}$ at 1.96 TeV
-2.8 ± 1.9 ± 0.4	3	ABAZOV	13 D0 $p\bar{p}$ at 1.96 TeV

- We do not use the following data for averages, fits, limits, etc.

-0.15 ± 1.25 ± 0.90	4	AAIJ	14D LHCb	Repl. by AAJ 16G
-4.5 ± 2.7	5	ABAZOV	11U D0	Repl. by ABAZOV 14
-0.4 ± 2.3 ± 0.4	6	ABAZOV	10E D0	Repl. by ABAZOV 13
-3.6 ± 1.9	7	ABAZOV	10H D0	Repl. by ABAZOV 11U
6.1 ± 4.8 ± 0.9	8	ABAZOV	07A D0	Repl. by ABAZOV 10E
- AAIJ 16G reports a measurement of time-integrated flavor-specific asymmetry in $B_s^0 \rightarrow \mu^+ D_s^- X$ decays, $A_{SL}^s = (0.39 \pm 0.26 \pm 0.20)\%$, which is approximately equal to $4 \times \text{Re}(\epsilon_{B_s^0}) / (1 + |\epsilon_{B_s^0}|^2)$.
- ABAZOV 14 uses the dimuon charge asymmetry with different impact parameters from which it reports $A_{SL}^s = (-0.86 \pm 0.74) \times 10^{-2}$.
- ABAZOV 13 reports a measurement of time-integrated flavor-specific asymmetry in mixed semileptonic $B_s^0 \rightarrow \mu^+ D_s^- X$ decays $A_{SL}^s = (-1.12 \pm 0.74 \pm 0.17)\%$ which is approximately equal to $4 \times \text{Re}(\epsilon_{B_s^0}) / (1 + |\epsilon_{B_s^0}|^2)$.
- AAIJ 14D reports a measurement of time-integrated flavor-specific asymmetry in $B_s^0 \rightarrow \mu^+ D_s^- X$ decays, $A_{SL}^s = (-0.06 \pm 0.50 \pm 0.36)\%$, which is approximately equal to $4 \times \text{Re}(\epsilon_{B_s^0}) / (1 + |\epsilon_{B_s^0}|^2)$.
- ABAZOV 11U uses the dimuon charge asymmetry with different impact parameters from which it reports $A_{SL}^s = (-18.1 \pm 10.6) \times 10^{-3}$.
- ABAZOV 10E reports a measurement of flavor-specific asymmetry in $B_{(s)}^0 \rightarrow \mu^+ D_{(s)}^{*-} X$ decays with a decay-time analysis including initial-state flavor tagging, $A_{SL}^s = (-1.7 \pm 9.1^{+1.4}_{-1.5}) \times 10^{-3}$ which is approximately equal to $4 \times \text{Re}(\epsilon_{B_s^0}) / (1 + |\epsilon_{B_s^0}|^2)$.
- ABAZOV 10H reports a measurement of like-sign dimuon charge asymmetry of $A_{SL}^s = (-9.57 \pm 2.51 \pm 1.46) \times 10^{-3}$ in semileptonic b -hadron decays. Using the measured production ratio of B_d^0 and B_s^0 , and the asymmetry of B_d^0 , $A_{SL}^s = (-4.7 \pm 4.6) \times 10^{-3}$ measured from B -factories, they obtain the asymmetry for B_s^0 .
- The first direct measurement of the time integrated flavor untagged charge asymmetry in semileptonic B_s^0 decays is reported as $2 \times A_{SL}^s(\text{untagged}) = A_{SL}^s = (2.45 \pm 1.93 \pm 0.35) \times 10^{-2}$.



$C_{KK}(B_s^0 \rightarrow K^+ K^-)$
 VALUE DOCUMENT ID TECN COMMENT
0.14 ± 0.11 ± 0.03 AAJ 13B0 LHCb pp at 7 TeV

$S_{KK}(B_s^0 \rightarrow K^+ K^-)$
 VALUE DOCUMENT ID TECN COMMENT
0.30 ± 0.12 ± 0.04 AAJ 13B0 LHCb pp at 7 TeV

$r_B(B_s^0 \rightarrow D_s^\mp K^\pm)$
 r_B and ϕ_B are the amplitude ratio and relative strong phase between the amplitudes of $A(B_s^0 \rightarrow D_s^\mp K^\pm)$ and $A(B_s^0 \rightarrow D_s^\mp K^\mp)$.

VALUE DOCUMENT ID TECN COMMENT
0.37^{+0.10}_{-0.09} 1 AAJ 18U LHCb pp at 7, 8 TeV

- We do not use the following data for averages, fits, limits, etc.

0.53 ^{+0.17} _{-0.16}	2	AAIJ	14BF LHCb	Repl. by AAJ 18U
--	---	------	-----------	------------------

- Measured in $B_s^0 \rightarrow D_s^\mp K^\pm$ decays, constraining $-2\beta_s$ by the measurement of $\phi_s = -0.030 \pm 0.033$ from HFLAV.
- Measured in $B_s^0 \rightarrow D_s^\mp K^\pm$ decays, constraining $-2\beta_s$ by the measurement of $\phi_s = 0.01 \pm 0.07 \pm 0.0$ from AAJ 13AR. At 68% CL.

Meson Particle Listings

B_s^0

$\delta_B(B_s^0 \rightarrow D_s^\pm K^\mp)$

VALUE (°)	DOCUMENT ID	TECN	COMMENT
358⁺¹³₋₁₄	¹ AAIJ	18U LHCb	pp at 7, 8 TeV
• • • We do not use the following data for averages, fits, limits, etc. • • •			
3^{+19} -20	² AAIJ	148F LHCb	Repl. by AAIJ 18U

¹ Measured in $B_s^0 \rightarrow D_s^\mp K^\pm$ decays, constraining $-2\beta_S$ by the measurement of $\phi_S = 0.030 \pm 0.033$ from HFLAV. The value is modulo 180° .
² Measured in $B_s^0 \rightarrow D_s^\mp K^\pm$ decays, constraining $-2\beta_S$ by the measurement of $\phi_S = 0.01 \pm 0.07 \pm 0.0$ from AAIJ 13AR. The value is modulo 180° at 68% CL.

CP Violation phase β_S

$-2\beta_S$ is the weak phase difference between B_s^0 mixing amplitude and the $B_s^0 \rightarrow J/\psi\phi$ decay amplitude driven by the $b \rightarrow c\bar{c}s$ transition (such as $B_s \rightarrow J/\psi\phi, J/\psi K^+ K^-$, $J/\psi\pi^+\pi^-$, and $D_s^+ D_s^-$). The Standard Model value of β_S is $\arg(-\frac{V_{ts}V_{tb}}{V_{cs}V_{cb}})$ if penguin contributions are neglected.

“OUR EVALUATION” is an average using rescaled values of the data listed below. The average and rescaling were performed by the Heavy Flavor Averaging Group (HFLAV, <https://hflav.web.cern.ch/>) and are described at <https://hflav.web.cern.ch/>. The averaging/scaling procedure takes into account correlation between the measurements.

VALUE (10 ⁻² rad)	DOCUMENT ID	TECN	COMMENT
2.55 ± 1.15 OUR EVALUATION			
2.6 ± 1.4 OUR AVERAGE			
- 0.1 ± 2.2 ± 0.6	¹ AAIJ	19AF LHCb	pp at 7, 8, 13 TeV
4.15 ± 2.05 ± 0.30	² AAIJ	19Q LHCb	pp at 13 TeV
11.9 ± 10.7 ± 3.4	³ AAIJ	17V LHCb	pp at 7, 8 TeV
4.5 ± 3.9 ± 2.1	⁴ AAD	16AP ATLS	pp at 7, 8 TeV
-11.5 ⁺¹⁴ _{-14.5} ± 1	⁵ AAIJ	16AK LHCb	pp at 7, 8 TeV
3.75 ± 4.85 ± 1.55	⁶ KHACHATRYAN...16s	CMS	pp at 8 TeV
- 1 ± 9 ± 1	⁷ AAIJ	14AY LHCb	pp at 7, 8 TeV
	⁸ AALTONEN	12AJ CDF	$p\bar{p}$ at 1.96 TeV
28 ⁺¹⁸ ₋₁₉	⁹ ABZOV	12D D0	$p\bar{p}$ at 1.96 TeV
• • • We do not use the following data for averages, fits, limits, etc. • • •			
3.7 ± 5.8 ± 1.4	^{10,11} AAIJ	19AP LHCb	pp at 7, 8, 13 TeV
5.0 ± 6.5 ± 7.0	¹² AAIJ	18s LHCb	pp at 7, 8 TeV
2.9 ± 2.5 ± 0.3	¹³ AAIJ	15i LHCb	Repl. by AAIJ 19Q
6 ⁺⁸ ₋₇	^{14,15} AAIJ	15K LHCb	pp at 7, 8 TeV
- 6 ± 13 ± 3	¹⁶ AAD	14U ATLS	Repl. by AAD 16AP
8.5 ± 7.5 ± 1.5	¹⁷ AAIJ	14AE LHCb	Repl. by AAIJ 19AF
- 3.5 ± 3.4 ± 0.4	¹⁸ AAIJ	14s LHCb	Repl. by AAIJ 19AF
- 0.5 ± 3.5 ± 0.5	¹⁹ AAIJ	13AR LHCb	Repl. by AAIJ 15i
	²⁰ AAIJ	13AY LHCb	pp at 7 TeV
-11.0 ± 20.5 ± 5.0	²¹ AAD	12CV ATLS	Repl. by AAD 14U
22 ± 22 ± 1	²² AAIJ	12B LHCb	Repl. by AAIJ 12Q
- 8 ± 9 ± 3	²³ AAIJ	12D LHCb	Repl. by AAIJ 13AR
0.95 ^{+8.70+0.15} _{-8.65-0.20}	²⁴ AAIJ	12Q LHCb	Repl. by AAIJ 13AR
	²⁵ AALTONEN	12D CDF	Repl. by AALTONEN 12AJ
	²⁶ AALTONEN	08G CDF	Repl. by AALTONEN 12D
28 ⁺¹² ₋₁₅ ⁺⁴ ₋₁	^{9,27} ABZOV	08AMD0	Repl. by ABZOV 12D
39.5 ± 28.0 ^{+0.5} _{-7.0}	^{28,29} ABZOV	07 D0	Repl. by ABZOV 07N
35 ⁺²⁰ ₋₂₄	^{29,30} ABZOV	07N D0	Repl. by ABZOV 08AM

¹ AAIJ 19AF reports $\phi_S = -2\beta_S = 0.002 \pm 0.044 \pm 0.012$ rad. and $|\lambda| = 0.949 \pm 0.036 \pm 0.019$, when direct CP violation is allowed. Measured using a time-dependent fit to $B_s^0 \rightarrow J/\psi\pi^+\pi^-$ decays, which is sensitive to $\phi_S(s\bar{s}s)$, not $\phi_S(c\bar{c}s)$.
² AAIJ 19Q reports $\phi_S = -2\beta_S = -0.083 \pm 0.041 \pm 0.006$ rad. that was measured using a time-dependent angular analysis of $B_s^0 \rightarrow J/\psi K^+ K^-$ decays.
³ Measured using time-dependent angular analysis of $B_s^0 \rightarrow J/\psi K^+ K^-$ in the region $m(KK) > 1.05$ GeV.
⁴ AAD 16AP reports $\phi_S = -2\beta_S = -0.090 \pm 0.078 \pm 0.041$ rad. that was measured using a time-dependent angular analysis of $B_s^0 \rightarrow J/\psi\phi$ decays.
⁵ AAIJ 16AK reports $\phi_S = -2\beta_S = 0.23^{+0.29}_{-0.28} \pm 0.02$ rad. that was measured using a time-dependent angular analysis of $B_s^0 \rightarrow \psi(2S)\phi$ decays.
⁶ KHACHATRYAN 16s reports $\phi_S = -2\beta_S = -0.075 \pm 0.097 \pm 0.031$ rad. that was measured using a time-dependent angular analysis of $B_s^0 \rightarrow J/\psi\phi$ decays.
⁷ AAIJ 14AY reports $\phi_S = -2\beta_S = 0.02 \pm 0.17 \pm 0.02$ rad. in a time-dependent fit to $B_s^0 \rightarrow D_s^+ D_s^-$, while allowing CP violation in decay.
⁸ AALTONEN 12AJ reports $-\pi/2 < \beta_S < -1.51$ or $-0.06 < \beta_S < 0.30$, or $1.26 < \beta_S < \pi/2$ rad. at 68% CL. Measured using the time-dependent angular analysis of $B_s^0 \rightarrow J/\psi\phi$ decays.
⁹ ABZOV 12D reports $\phi_S = -2\beta_S = -0.55^{+0.38}_{-0.36}$ rad. that was measured using a time-dependent angular analysis of $B_s^0 \rightarrow J/\psi\phi$ decays. A single error includes both statistical and systematic uncertainties.
¹⁰ AAIJ 19AP reports $\phi_S^{S\bar{S}} = -0.073 \pm 0.115 \pm 0.027$ rad and $|\lambda| = 0.99 \pm 0.05 \pm 0.01$. Measured using a time-dependent fit to $B_s^0 \rightarrow \phi\phi$ decays, assuming independence of the helicity of the ϕ decay.

¹¹ AAIJ 19AP reports also polarisation-dependent results assuming that the longitudinal weak phase is CP -conserving and that there is no direct CP violation, giving $\phi_{S,\parallel} = 0.014 \pm 0.055 \pm 0.011$ rad and $\phi_{S,\perp} = 0.044 \pm 0.059 \pm 0.019$ rad.
¹² AAIJ 18s reports $\phi_S = -2\beta_S = -0.10 \pm 0.13 \pm 0.14$ rad measured in $B_s^0 \rightarrow (K^+\pi^-)(K^-\pi^+)$ in the region $0.75 < m(K^\pm\pi^\mp) < 1.6$ GeV. This is a $b \rightarrow d\bar{d}s$ transition with a decay amplitude phase different from that of $b \rightarrow c\bar{c}s$ transition.
¹³ AAIJ 15i reports $\phi_S = -2\beta_S = -0.058 \pm 0.049 \pm 0.006$ rad. that was measured using a time-dependent angular analysis of $B_s^0 \rightarrow J/\psi K^+ K^-$ decays. It also combines this result with that of AAIJ 14s and quotes $\phi_S = -2\beta_S = -0.010 \pm 0.039$ rad.
¹⁴ AAIJ 15K reports $-2\beta_S = -0.12^{+0.14}_{-0.16}$ rad. The value was obtained by measuring time-dependent CP asymmetry in $B_s^0 \rightarrow K^+ K^-$ and using a U-spin relation between $B_s^0 \rightarrow K^+ K^-$ and $B^0 \rightarrow \pi^+ \pi^-$.
¹⁵ Results are also presented using additional inputs on $B^0 \rightarrow \pi^0\pi^0$ and $B^+ \rightarrow \pi^+\pi^0$ decays from other experiments and isospin symmetry assumptions. The dependence of the results on the maximum allowed amount of U-spin breaking up to 50% is also included.
¹⁶ AAD 14U reports $\phi_S = -2\beta_S = 0.12 \pm 0.25 \pm 0.05$ rad. that was measured using a time-dependent angular analysis of $B_s^0 \rightarrow J/\psi\phi$ decays.
¹⁷ AAIJ 14AE value measured in $B_s^0 \rightarrow \phi\phi$ decays. This is a $b \rightarrow s\bar{s}s$ transition with a decay amplitude phase different from that of $b \rightarrow c\bar{c}s$ transition. Also reports $\phi_S = -0.17 \pm 0.15 \pm 0.03$ rad.
¹⁸ AAIJ 14s reports $\phi_S = -2\beta_S = 0.070 \pm 0.068 \pm 0.008$ rad. and $|\lambda| = 0.89 \pm 0.05 \pm 0.01$, when direct CP violation is allowed. Measured using a time-dependent fit to $B_s^0 \rightarrow J/\psi\pi^+\pi^-$ decays.
¹⁹ AAIJ 13AR reports $\phi_S = -2\beta_S = 0.01 \pm 0.07 \pm 0.01$ rad. obtained from combined fit to $B_s^0 \rightarrow J/\psi K^+ K^-$ and $B_s^0 \rightarrow J/\psi\pi^+\pi^-$ data sets. Also reports separate results of $\phi_S = 0.07 \pm 0.09 \pm 0.01$ rad. from $B_s^0 \rightarrow J/\psi K^+ K^-$ decays and $\phi_S = -0.14^{+0.17}_{-0.16} \pm 0.01$ rad. from $B_s^0 \rightarrow J/\psi\pi^+\pi^-$ decays.
²⁰ AAIJ 13AY uses $B_s^0 \rightarrow \phi\phi$ mode, and reports the 68% CL interval of $\phi_S = -2\beta_S$ as $[-2.46, -0.76]$ rad.
²¹ AAD 12CV reports $\phi_S = -2\beta_S = 0.22 \pm 0.41 \pm 0.10$ rad. that was measured using a time-dependent angular analysis of $B_s^0 \rightarrow J/\psi\phi$ decays.
²² Reports $\phi_S = -2\beta_S = -0.44 \pm 0.44 \pm 0.02$ rad. that was measured using a time-dependent fit to $B_s^0 \rightarrow J/\psi\eta(980)$ decays.
²³ Reports $\phi_S = -2\beta_S = 0.15 \pm 0.18 \pm 0.06$ rad. that was measured using a time-dependent angular analysis of $B_s^0 \rightarrow J/\psi\phi$ decays.
²⁴ Reports $\phi_S = -2\beta_S = -0.019^{+0.173+0.004}_{-0.174-0.003}$ rad. which was measured using a time-dependent fit to $B_s^0 \rightarrow J/\psi\pi^+\pi^-$ decays, with the $\pi^+\pi^-$ mass within 775–1550 MeV. Searches for, but finds no evidence, for direct CP violation in $B_s^0 \rightarrow J/\psi\pi\pi$ decays.
²⁵ Reports $0.02 < \phi_S < 0.52$ or $1.08 < \phi_S < 1.55$ rad. at 68% C.L. confidence regions in the two-dimensional space of ϕ_S and $\Delta\Gamma_{B_s^0}$ from $B_s^0 \rightarrow J/\psi\phi$ decays.
²⁶ Reports $0.32 < 2\beta_S < 2.82$ rad. at 68% C.L. and confidence regions in the two-dimensional space of $2\beta_S$ and $\Delta\Gamma$ from the first measurement of $B_s^0 \rightarrow J/\psi\phi$ decays using flavor tagging. The probability of a deviation from SM prediction as large as the level of observed data is 15%.
²⁷ Reports $\phi_S = -2\beta_S$ and obtains 90% CL interval $-0.03 < \beta_S < 0.60$ rad.
²⁸ The first direct measurement of the CP -violating mixing phase is reported from the time-dependent analysis of flavor untagged $B_s^0 \rightarrow J/\psi\phi$ decays.
²⁹ Reports ϕ_S which equals to $-2\beta_S$.
³⁰ Combines D0 collaboration measurements of time-dependent angular distributions in $B_s^0 \rightarrow J/\psi\phi$ and charge asymmetry in semileptonic decays. There is a 4-fold ambiguity in the solution.

$|\lambda| (B_s^0 \rightarrow J/\psi(1S)\phi)$

VALUE	DOCUMENT ID	TECN	COMMENT
1.012 ± 0.016 ± 0.006	AAIJ	19Q LHCb	pp at 13 TeV
• • • We do not use the following data for averages, fits, limits, etc. • • •			
0.964 ± 0.019 ± 0.007	AAIJ	15i LHCb	Repl. by AAIJ 19Q

$|\lambda|$

VALUE	DOCUMENT ID	TECN	COMMENT
0.999 ± 0.017 OUR AVERAGE			
0.99 ± 0.05 ± 0.01	¹ AAIJ	19AP LHCb	pp at 7, 8, 13 TeV
1.035 ± 0.034 ± 0.089	² AAIJ	18s LHCb	pp at 7, 8 TeV
0.994 ± 0.018 ± 0.006	³ AAIJ	17V LHCb	pp at 7, 8 TeV
1.045 ^{+0.069} _{-0.050} ± 0.007	⁴ AAIJ	16AK LHCb	pp at 7, 8 TeV
0.91 ^{+0.18} _{-0.15} ± 0.02	⁵ AAIJ	14AY LHCb	pp at 7, 8 TeV
• • • We do not use the following data for averages, fits, limits, etc. • • •			
0.949 ± 0.036 ± 0.019	⁶ AAIJ	19AF LHCb	pp at 7, 8, 13 TeV
1.04 ± 0.07 ± 0.03	⁷ AAIJ	14AE LHCb	Repl. by AAIJ 19AP

¹ Measured in $B_s^0 \rightarrow \phi\phi$ decays.
² Measured in $B_s^0 \rightarrow (K^+\pi^-)(K^-\pi^+)$ in the region $0.75 < m(K^\pm\pi^\mp) < 1.6$ GeV.
³ Measured using time-dependent angular analysis of $B_s^0 \rightarrow J/\psi K^+ K^-$ in the region $m(KK) > 1.05$ GeV.
⁴ Measured using time-dependent angular analysis of $B_s^0 \rightarrow \psi(2S)\phi$ decays.
⁵ Measured in $B_s^0 \rightarrow D_s^+ D_s^-$ decays.
⁶ Measured using time-dependent analysis of $B_s^0 \rightarrow J/\psi\pi^+\pi^-$ decays.
⁷ Measured in $B_s^0 \rightarrow \phi\phi$ decays.

A, CP violation parameter

$$A = -2 \operatorname{Re}(\lambda) / (1 + |\lambda|^2)$$

VALUE	DOCUMENT ID	TECN	COMMENT
-0.75 ± 0.12 OUR AVERAGE			
-0.79 ± 0.07 ± 0.10	¹ AAIJ	18o LHCb	pp at 7, 8 TeV
0.49 ^{+0.77} _{-0.65} ± 0.06	² AAIJ	15AL LHCb	pp at 7, 8 TeV
¹ Measured in $B_s^0 \rightarrow K^+ K^-$ decays.			
² Measured in $B_s^0 \rightarrow J/\psi K_S^0$ decays.			

C, CP violation parameter

$$C = (1 - |\lambda|^2) / (1 + |\lambda|^2)$$

VALUE	DOCUMENT ID	TECN	COMMENT
0.19 ± 0.06 OUR AVERAGE			
0.20 ± 0.06 ± 0.02	¹ AAIJ	18o LHCb	pp at 7, 8 TeV
-0.28 ± 0.41 ± 0.08	² AAIJ	15AL LHCb	pp at 7, 8 TeV
¹ Measured in $B_s^0 \rightarrow K^+ K^-$ decays.			
² Measured in $B_s^0 \rightarrow J/\psi K_S^0$ decays.			

S, CP violation parameter

$$S = -2 \operatorname{Im}(\lambda) / (1 + |\lambda|^2)$$

VALUE	DOCUMENT ID	TECN	COMMENT
0.17 ± 0.06 OUR AVERAGE			
0.18 ± 0.06 ± 0.02	¹ AAIJ	18o LHCb	pp at 7, 8 TeV
-0.08 ± 0.40 ± 0.08	² AAIJ	15AL LHCb	pp at 7, 8 TeV
¹ Measured in $B_s^0 \rightarrow K^+ K^-$ decays.			
² Measured in $B_s^0 \rightarrow J/\psi K_S^0$ decays.			

$A_{CP}^L(B_s \rightarrow J/\psi \bar{K}^*(892)^0)$

VALUE	DOCUMENT ID	TECN	COMMENT
-0.048 ± 0.057 ± 0.020	AAIJ	15AV LHCb	pp at 7, 8 TeV

$A_{CP}^{\parallel}(B_s \rightarrow J/\psi \bar{K}^*(892)^0)$

VALUE	DOCUMENT ID	TECN	COMMENT
0.171 ± 0.152 ± 0.028	AAIJ	15AV LHCb	pp at 7, 8 TeV

$A_{CP}^{\perp}(B_s \rightarrow J/\psi \bar{K}^*(892)^0)$

VALUE	DOCUMENT ID	TECN	COMMENT
-0.049 ± 0.096 ± 0.025	AAIJ	15AV LHCb	pp at 7, 8 TeV

$A_{CP}(B_s \rightarrow \pi^+ K^-)$

A_{CP} is defined as

$$\frac{B(\bar{B}_s^0 \rightarrow f) - B(B_s^0 \rightarrow \bar{f})}{B(\bar{B}_s^0 \rightarrow f) + B(B_s^0 \rightarrow \bar{f})},$$

the CP-violation asymmetry of exclusive B_s^0 and \bar{B}_s^0 decay.

VALUE	DOCUMENT ID	TECN	COMMENT
0.221 ± 0.015 OUR AVERAGE			
0.213 ± 0.015 ± 0.007	AAIJ	18o LHCb	pp at 7, 8 TeV
0.22 ± 0.07 ± 0.02	AALTONEN	14P CDF	p \bar{p} at 1.96 TeV
0.27 ± 0.04 ± 0.01	AAIJ	13AX LHCb	pp at 7 TeV
• • • We do not use the following data for averages, fits, limits, etc. • • •			
0.27 ± 0.08 ± 0.02	AAIJ	12V LHCb	Repl. by AAIJ 13AX
0.39 ± 0.15 ± 0.08	AALTONEN	11N CDF	Repl. by AALTONEN 14P

$A_{CP}(B_s^0 \rightarrow [K^+ K^-]_D \bar{K}^*(892)^0)$

VALUE	DOCUMENT ID	TECN	COMMENT
-0.04 ± 0.07 ± 0.02	AAIJ	14BN LHCb	pp at 7, 8 TeV
• • • We do not use the following data for averages, fits, limits, etc. • • •			
0.04 ± 0.16 ± 0.01	AAIJ	13L LHCb	Repl. by AAIJ 14BN

$A_{CP}(B_s^0 \rightarrow [\pi^+ K^-]_D K^*(892)^0)$

VALUE	DOCUMENT ID	TECN	COMMENT
-0.01 ± 0.03 ± 0.02	AAIJ	14BN LHCb	pp at 7, 8 TeV

$A_{CP}(B_s^0 \rightarrow [\pi^+ \pi^-]_D K^*(892)^0)$

VALUE	DOCUMENT ID	TECN	COMMENT
0.06 ± 0.13 ± 0.02	AAIJ	14BN LHCb	pp at 7, 8 TeV

$S(B_s^0 \rightarrow \phi\gamma)$

VALUE	DOCUMENT ID	TECN	COMMENT
0.43 ± 0.30 ± 0.11	¹ AAIJ	19AE LHCb	pp at 7, 8 TeV
¹ Measured in flavor tagged time dependent analysis.			

$C(B_s^0 \rightarrow \phi\gamma)$

VALUE	DOCUMENT ID	TECN	COMMENT
0.11 ± 0.29 ± 0.11	¹ AAIJ	19AE LHCb	pp at 7, 8 TeV
¹ Measured in flavor tagged time dependent analysis.			

$A^\Delta(B_s \rightarrow \phi\gamma)$

$A^\Delta(B_s \rightarrow \phi\gamma)$ is the multiplicative coefficient of the $\sinh(\Delta\Gamma/2)$ term in the $B_s \rightarrow \phi\gamma$ decay rate time dependence.

VALUE	DOCUMENT ID	TECN	COMMENT
-0.67 ± 0.37 ± 0.41 ± 0.17			
	¹ AAIJ	19AE LHCb	pp at 7, 8 TeV
• • • We do not use the following data for averages, fits, limits, etc. • • •			
-0.98 ± 0.46 ± 0.23	² AAIJ	17B LHCb	Repl. by AAIJ 19AE
-0.52 ± 0.20			
¹ Measured in flavor tagged time dependent analysis, using tagged and un-tagged events. This result updates AAIJ 17B with better selection efficiency and other analysis improvements.			
² Measured in time dependent analysis without initial flavor tagging.			

CPT VIOLATION PARAMETERS

In the B_s^0 mixing, propagating mass eigenstates can be written as

$$|B_{sL}\rangle \propto p \sqrt{1-\xi} |B_s^0\rangle + q \sqrt{1+\xi} |\bar{B}_s^0\rangle$$

$$|B_{sH}\rangle \propto p \sqrt{1+\xi} |B_s^0\rangle - q \sqrt{1-\xi} |\bar{B}_s^0\rangle$$

where parameter ξ controls CPT violation. If ξ is zero, then CPT is conserved. The parameter ξ can be written as

$$\xi = \frac{2(M_{11}-M_{22})-i(\Gamma_{11}-\Gamma_{22})}{-2\Delta m_s+i\Delta\Gamma_s} \approx \frac{-2\beta^\mu \Delta a_\mu}{2\Delta m_s-i\Delta\Gamma_s},$$

where M_{ii} , Γ_{ii} , Δm_s , and $\Delta\Gamma_s$ are parameters of Hamiltonian governing B_s oscillations, β^μ is the B_s^0 meson velocity and Δa_μ characterizes Lorentz-invariance violation.

Δa_\perp

VALUE (10^{-12} GeV)	CL%	DOCUMENT ID	TECN	COMMENT
-0.47 ± 0.39 ± 0.08		¹ AAIJ	16E LHCb	pp at 7, 8 TeV
< 1.2	95	² ABAZOV	15L D0	p \bar{p} at 1.96 TeV
¹ Uses $B_s^0 \rightarrow J/\psi K^+ K^-$ decays.				
² Measured in semileptonic $B_s^0 \rightarrow D_s^- \mu^+ X$ decays. Also extracts limit on time and longitudinal components ($-0.8 < \Delta a_T - 0.396 \Delta a_Z < 3.9$) 10^{-13} GeV.				

Δa_\parallel

VALUE (10^{-14} GeV)	DOCUMENT ID	TECN	COMMENT
-0.89 ± 1.41 ± 0.36	¹ AAIJ	16E LHCb	pp at 7, 8 TeV
¹ Uses $B_s^0 \rightarrow J/\psi K^+ K^-$ decays.			

Δa_χ

VALUE (10^{-14} GeV)	DOCUMENT ID	TECN	COMMENT
+1.01 ± 2.08 ± 0.71	¹ AAIJ	16E LHCb	pp at 7, 8 TeV
¹ Uses $B_s^0 \rightarrow J/\psi K^+ K^-$ decays.			

Δa_γ

VALUE (10^{-14} GeV)	DOCUMENT ID	TECN	COMMENT
-3.83 ± 2.09 ± 0.71	¹ AAIJ	16E LHCb	pp at 7, 8 TeV
¹ Uses $B_s^0 \rightarrow J/\psi K^+ K^-$ decays.			

Re(ξ)

VALUE	DOCUMENT ID	TECN	COMMENT
-0.022 ± 0.033 ± 0.003	¹ AAIJ	16E LHCb	pp at 7, 8 TeV
¹ Uses $B_s^0 \rightarrow J/\psi K^+ K^-$ decays.			

Im(ξ)

VALUE	DOCUMENT ID	TECN	COMMENT
0.004 ± 0.011 ± 0.002	¹ AAIJ	16E LHCb	pp at 7, 8 TeV
¹ Uses $B_s^0 \rightarrow J/\psi K^+ K^-$ decays.			

PARTIAL BRANCHING FRACTIONS IN $B_s \rightarrow \phi \ell^+ \ell^-$

$B(B_s \rightarrow \phi \ell^+ \ell^-) (0.1 < q^2 < 2.0 \text{ GeV}^2/c^4)$

VALUE (units 10^{-7})	DOCUMENT ID	TECN	COMMENT
1.14 ± 0.16 OUR AVERAGE			
1.11 ^{+0.14} _{-0.13} ± 0.09	¹ AAIJ	15AQ LHCb	pp at 7, 8 TeV
2.78 ± 0.95 ± 0.89	AALTONEN	11AI CDF	p \bar{p} at 1.96 TeV
• • • We do not use the following data for averages, fits, limits, etc. • • •			
0.897 ^{+0.207} _{-0.186} ± 0.097	¹ AAIJ	13X LHCb	Repl. by AAIJ 15AQ
¹ Measured in $B_s^0 \rightarrow \phi \mu^+ \mu^-$ decays.			

$B(B_s \rightarrow \phi \ell^+ \ell^-) (2.0 < q^2 < 5.0 \text{ GeV}^2/c^4)$

VALUE (units 10^{-7})	DOCUMENT ID	TECN	COMMENT
0.77 ± 0.12 ± 0.06			
	¹ AAIJ	15AQ LHCb	pp at 7, 8 TeV
• • • We do not use the following data for averages, fits, limits, etc. • • •			
0.529 ^{+0.182} _{-0.159} ± 0.057	^{1,2} AAIJ	13X LHCb	Repl. by AAIJ 15AQ
0.58 ± 0.55 ± 0.19	² AALTONEN	11AI CDF	p \bar{p} at 1.96 TeV
¹ Measured in $B_s^0 \rightarrow \phi \mu^+ \mu^-$ decays.			
² Measured in $2 < q^2 < 4.3 \text{ GeV}^2/c^4$.			

Meson Particle Listings

B_s^* , $X(5568)^\pm$, $B_{s1}(5830)^0$

$X(5568)^\pm$

$$I(J^P) = ?(??)$$

OMITTED FROM SUMMARY TABLE

Seen as a peak in the $B_s \pi^\pm$ mass spectrum with a significance of more than 3σ by ABAZOV 16E and ABAZOV 18A in inclusive $p\bar{p}$ collisions at 1.96 TeV. Not seen by AAIJ 16AI, AABOUD 18L, AALTONEN 18A, and SIRUNYAN 18J. Needs confirmation.

$X(5568)^\pm$ MASS

VALUE (MeV)	EVTS	DOCUMENT ID	TECN	COMMENT
$5566.9^{+3.2+0.6}_{-3.1-1.2}$	278	¹ ABAZOV	18A D0	$p\bar{p} \rightarrow B_s^0 \pi^\pm X$
$5567.8 \pm 2.9^{+0.9}_{-1.9}$	133	² ABAZOV	16E D0	$p\bar{p} \rightarrow B_s^0 \pi^\pm X$

- • • We do not use the following data for averages, fits, limits, etc. • • •
- ¹ From the combined analysis of $B_s^0 \rightarrow J/\psi \phi$ and $B_s^0 \rightarrow D_s^\pm \mu^\mp X$ decays.
- ² Assumes $X(5568)^\pm \rightarrow B_s \pi^\pm$ decay. If $X(5568)^\pm \rightarrow B_s^* \pi^\pm$ decay is assumed, the mass shifts upward by 49 MeV.

$X(5568)^\pm$ WIDTH

VALUE (MeV)	EVTS	DOCUMENT ID	TECN	COMMENT
$18.6^{+7.9+3.5}_{-6.1-3.8}$	278	¹ ABAZOV	18A D0	$p\bar{p} \rightarrow B_s \pi^\pm X$
$21.9 \pm 6.4^{+5.0}_{-2.5}$	133	ABAZOV	16E D0	$p\bar{p} \rightarrow B_s \pi^\pm X$

- • • We do not use the following data for averages, fits, limits, etc. • • •
- ¹ From the combined analysis of $B_s^0 \rightarrow J/\psi \phi$ and $B_s^0 \rightarrow D_s^\pm \mu^\mp X$ decays.

$X(5568)^\pm$ DECAY MODES

Mode	Fraction (Γ_i/Γ)
$\Gamma_1 B_s \pi^\pm$	seen

$\Gamma(B_s \pi^\pm)/\Gamma_{total}$

VALUE	EVTS	DOCUMENT ID	TECN	COMMENT	Γ_1/Γ
seen	145	¹ ABAZOV	18A D0	$p\bar{p} \rightarrow B_s^0 \pi^\pm X$	
seen	133	² ABAZOV	16E D0	$p\bar{p} \rightarrow B_s^0 \pi^\pm X$	
not seen		³ AABOUD	18L ATLS	$pp \rightarrow B_s^0 \pi^\pm X$	
not seen		⁴ AALTONEN	18A CDF	$p\bar{p} \rightarrow B_s^0 \pi^\pm X$	
not seen		⁵ SIRUNYAN	18J CMS	$pp \rightarrow B_s^0 \pi^\pm X$	
not seen		⁶ AAIJ	16AI LHCB	$pp \rightarrow B_s^0 \pi^\pm X$	

- • • We do not use the following data for averages, fits, limits, etc. • • •
- ¹ With B_s mesons reconstructed in decays to $D_s^\pm \mu^\mp X$.
- ² Seen in $p\bar{p}$ collisions at 1.96 TeV at a rate of $(8.6 \pm 1.9 \pm 1.4)\%$ relative to inclusive B_s production in the kinematic region $10 < p_T(B_s) < 30$ GeV/c, with B_s mesons reconstructed in decays to $J/\psi \phi$. An alternative possibility, $X(5568)^\pm \rightarrow B_s^* \pi^\pm$ with a missing γ , could not be ruled out.
- ³ Not seen in 24.4 fb^{-1} of pp collision data at $\sqrt{s} = 7$ and 8 TeV with B_s mesons reconstructed in decays to $J/\psi \phi$. An upper limit on the production rate times branching fraction for $X(5568)^\pm \rightarrow B_s \pi^\pm$ relative to inclusive B_s production is less than 1.5% at $p_T(B_s) > 10$ GeV/c and less than 1.6% at $p_T(B_s) > 15$ GeV/c at 95% CL.
- ⁴ Not seen in 9.6 fb^{-1} of $p\bar{p}$ collision data at $\sqrt{s} = 1.96$ TeV with B_s mesons reconstructed in decays to $J/\psi \phi$. An upper limit on the production rate times branching fraction for $X(5568)^\pm \rightarrow B_s \pi^\pm$ relative to inclusive B_s production is less than 6.7% at 95% CL.
- ⁵ Not seen in 19.7 fb^{-1} of pp collisions data at $\sqrt{s} = 8$ TeV with B_s mesons reconstructed in decays to $J/\psi \phi$. An upper limit on the production rate times branching fraction for $X(5568)^\pm \rightarrow B_s \pi^\pm$ relative to inclusive B_s production is less than 1.1% at $p_T(B_s) > 10$ GeV/c and less than 1.0% at $p_T(B_s) > 15$ GeV/c at 95% CL.
- ⁶ Not seen in 3 fb^{-1} of pp collision data at $\sqrt{s} = 7$ and 8 TeV in a scan over the $X(5568)$ mass and width, with B_s mesons reconstructed in decays to $D_s^\pm \pi^\mp$ or $J/\psi \phi$. An upper limit on the production rate times branching fraction for $X(5568)^\pm \rightarrow B_s \pi^\pm$ relative to inclusive B_s production is less than 2.1% at $p_T(B_s) > 10$ GeV/c at 90% CL.

$X(5568)^\pm$ REFERENCES

AABOUD	18L	PRL 120 202007	M. Aaboud et al.	(ATLAS Collab.)
AALTONEN	18A	PRL 120 202006	T. Aaltonen et al.	(CDF Collab.)
ABAZOV	18A	PR D97 092004	V.M. Abazov et al.	(D0 Collab.)
SIRUNYAN	18J	PRL 120 202005	A.M. Sirunyan et al.	(CMS Collab.)
AAIJ	16AI	PRL 117 152003	R. Aaij et al.	(LHCb Collab.)
ABAZOV	16E	PRL 117 022003	V.M. Abazov et al.	(D0 Collab.)

$B_{s1}(5830)^0$

$$I(J^P) = 0(1^+)$$

I, J, P need confirmation.

Quantum numbers shown are quark-model predictions.

$B_{s1}(5830)^0$ MASS

VALUE (MeV)	DOCUMENT ID	TECN	COMMENT
5828.70 ± 0.20 OUR FIT			
5828.65 ± 0.24 OUR AVERAGE			
$5828.78 \pm 0.09 \pm 0.29$	SIRUNYAN	18DF CMS	pp at 8 TeV
$5828.40 \pm 0.04 \pm 0.41$	¹ AAIJ	13o LHCB	pp at 7 TeV
5829.4 ± 0.7	² AALTONEN	08K CDF	Repl. by AALTONEN 14I

• • • We do not use the following data for averages, fits, limits, etc. • • •

- ¹ Uses $B_{s1}(5830)^0 \rightarrow B^{*+} K^-$ decay.
- ² Uses two-body decays into K^- and B^+ mesons reconstructed as $B^+ \rightarrow J/\psi K^+$, $J/\psi \rightarrow \mu^+ \mu^-$ or $B^+ \rightarrow \bar{D}^0 \pi^+$, $\bar{D}^0 \rightarrow K^+ \pi^-$.

$m_{B_{s1}^0} - m_{B^{*+}}$

VALUE (MeV)	DOCUMENT ID	TECN	COMMENT
504.00 ± 0.17 OUR FIT			
504.03 ± 0.12 ± 0.15			
$504.41 \pm 0.21 \pm 0.14$	¹ AALTONEN	14I CDF	$p\bar{p}$ at 1.96 TeV
$504.41 \pm 0.21 \pm 0.14$	² AALTONEN	08K CDF	Repl. by AALTONEN 14I

• • • We do not use the following data for averages, fits, limits, etc. • • •

- ¹ AALTONEN 14I reports $m_{B_{s1}(5830)^0} - m_{B^{*+}} - m_{K^-} = 10.35 \pm 0.12 \pm 0.15$ MeV which we adjusted by the K^- mass.
- ² Uses two-body decays into K^- and B^+ mesons reconstructed as $B^+ \rightarrow J/\psi K^+$, $J/\psi \rightarrow \mu^+ \mu^-$ or $B^+ \rightarrow \bar{D}^0 \pi^+$, $\bar{D}^0 \rightarrow K^+ \pi^-$.

$B_{s1}(5830)^0$ WIDTH

VALUE (MeV)	DOCUMENT ID	TECN	COMMENT
0.5 ± 0.3 ± 0.3	AALTONEN	14I CDF	$p\bar{p}$ at 1.96 TeV

$B_{s1}(5830)^0$ DECAY MODES

Mode	Fraction (Γ_i/Γ)
$\Gamma_1 B^{*+} K^-$	seen
$\Gamma_2 B^{*0} K_S^0$	

$B_{s1}(5830)^0$ BRANCHING RATIOS

$\Gamma(B^{*+} K^-)/\Gamma_{total}$	Γ_1/Γ
seen	
$\Gamma(B^{*0} K_S^0)/\Gamma(B^{*+} K^-)$	Γ_2/Γ_1
0.49 ± 0.12 ± 0.07	¹ SIRUNYAN
	18DF CMS
	pp at 8 TeV

¹ With the branching fractions $B(B^{*+} \rightarrow J/\psi K^+) = (1.026 \pm 0.031) \times 10^{-3}$ and $B(B^0 \rightarrow J/\psi K^{*0}) = (1.28 \pm 0.05) \times 10^{-3}$.

$B_{s1}(5830)^0$ REFERENCES

SIRUNYAN	18DF	EPJ C78 939	A.M. Sirunyan et al.	(CMS Collab.)
AALTONEN	14I	PR D90 012013	T. Aaltonen et al.	(CDF Collab.)
AAIJ	13O	PRL 110 151803	R. Aaij et al.	(LHCb Collab.)
AALTONEN	08K	PRL 100 082001	T. Aaltonen et al.	(CDF Collab.)

See key on page 999

Meson Particle Listings

$B_{s2}^*(5840)^0, B_{sJ}^*(5850)$

$B_{s2}^*(5840)^0$
 $I(J^P) = 0(2^+)$
I, J, P need confirmation.
 Quantum numbers shown are quark-model predictions.

$B_{s2}^*(5840)^0$ MASS

VALUE (MeV)	DOCUMENT ID	TECN	COMMENT
5839.86 ± 0.12 OUR FIT			
5839.92 ± 0.14 OUR AVERAGE			
5839.86 ± 0.09 ± 0.17	SIRUNYAN	18DF CMS	<i>pp</i> at 8 TeV
5839.99 ± 0.05 ± 0.20	AAIJ	13o LHCB	<i>pp</i> at 7 TeV
5839.6 ± 1.1 ± 0.7	¹ ABAZOV	08E D0	<i>p</i> \bar{p} at 1.96 TeV
• • • We do not use the following data for averages, fits, limits, etc. • • •			
5839.7 ± 0.7	² AALTONEN	08K CDF	Repl. by AALTONEN 14i
¹ Observed in $B_{s2}^{*0} \rightarrow B^+ K^-$. Measured production rate of B_{s2}^{*0} relative to B^+ to be $(1.15 \pm 0.23 \pm 0.13)\%$.			
² Uses two-body decays into K^- and B^+ mesons reconstructed as $B^+ \rightarrow J/\psi K^+$, $J/\psi \rightarrow \mu^+ \mu^-$ or $B^+ \rightarrow \bar{D}^0 \pi^+$, $\bar{D}^0 \rightarrow K^+ \pi^-$.			

$m_{B_{s2}^{*0}} - m_{B_{s1}^0}$

VALUE (MeV)	DOCUMENT ID	TECN	COMMENT
• • • We do not use the following data for averages, fits, limits, etc. • • •			
10.5 ± 0.6	¹ AALTONEN	08K CDF	Repl. by AALTONEN 14i
¹ Uses two-body decays into K^- and B^+ mesons reconstructed as $B^+ \rightarrow J/\psi K^+$, $J/\psi \rightarrow \mu^+ \mu^-$ or $B^+ \rightarrow \bar{D}^0 \pi^+$, $\bar{D}^0 \rightarrow K^+ \pi^-$.			

$m_{B_{s2}^{*0}} - m_{B^+}$

VALUE (MeV)	DOCUMENT ID	TECN	COMMENT
560.52 ± 0.14 OUR FIT			
560.41 ± 0.13 ± 0.14	¹ AALTONEN	14i CDF	<i>p</i> \bar{p} at 1.96 TeV
¹ AALTONEN 14i reports $m_{B_{s2}^*(5840)^0} - m_{B^+} - m_{K^-} = 66.73 \pm 0.13 \pm 0.14$ MeV which we adjusted by the K^- mass.			

$B_{s2}^*(5840)^0$ WIDTH

VALUE (MeV)	DOCUMENT ID	TECN	COMMENT
1.49 ± 0.27 OUR AVERAGE			
1.52 ± 0.34 ± 0.30	SIRUNYAN	18DF CMS	<i>pp</i> at 8 TeV
1.4 ± 0.4 ± 0.2	AALTONEN	14i CDF	<i>p</i> \bar{p} at 1.96 TeV
1.56 ± 0.13 ± 0.47	¹ AAIJ	13o LHCB	<i>pp</i> at 7 TeV
¹ Uses $B_{s2}^*(5840)^0 \rightarrow B^{*+} K^-$ decays.			

$B_{s2}^*(5840)^0$ DECAY MODES

Mode	Fraction (Γ_j/Γ)
Γ_1 $B^+ K^-$	DEFINED AS 1
Γ_2 $B^{*+} K^-$	0.093 ± 0.018
Γ_3 $B^0 K_S^0$	0.43 ± 0.11
Γ_4 $B^{*0} K_S^0$	0.04 ± 0.04

$B_{s2}^*(5840)^0$ BRANCHING RATIOS

$\Gamma(B^+ K^-)/\Gamma_{total}$	DOCUMENT ID	TECN	COMMENT	Γ_1/Γ
<u>VALUE</u>				
seen	AALTONEN	08K CDF	<i>p</i> \bar{p} at 1.96 TeV	
seen	¹ ABAZOV	08E D0	<i>p</i> \bar{p} at 1.96 TeV	
¹ Measured production rate of B_{s2}^{*0} relative to B^+ to be $(1.15 \pm 0.23 \pm 0.13)\%$.				
$\Gamma(B^{*+} K^-)/\Gamma(B^+ K^-)$				Γ_2/Γ_1
<u>VALUE</u>				
0.093 ± 0.013 ± 0.012	AAIJ	13o LHCB	<i>pp</i> at 7 TeV	
$\Gamma(B^{*0} K_S^0)/\Gamma(B^0 K_S^0)$				Γ_4/Γ_3
<u>VALUE</u>				
0.093 ± 0.086 ± 0.014	¹ SIRUNYAN	18DF CMS	<i>pp</i> at 8 TeV	
¹ With the branching fraction $B(B^0 \rightarrow J/\psi K^*0) = (1.28 \pm 0.05) \times 10^{-3}$.				
$\Gamma(B^0 K_S^0)/\Gamma(B^+ K^-)$				Γ_3/Γ_1
<u>VALUE</u>				
0.432 ± 0.077 ± 0.078	¹ SIRUNYAN	18DF CMS	<i>pp</i> at 8 TeV	
¹ With the branching fractions $B(B^+ \rightarrow J/\psi K^+) = (1.026 \pm 0.031) \times 10^{-3}$ and $B(B^0 \rightarrow J/\psi K^*0) = (1.28 \pm 0.05) \times 10^{-3}$.				
$\Gamma(B^{*+} K^-)/\Gamma(B^+ K^-)$				Γ_2/Γ_1
<u>VALUE</u>				
0.081 ± 0.021 ± 0.015	¹ SIRUNYAN	18DF CMS	<i>pp</i> at 8 TeV	
¹ With the branching fraction $B(B^+ \rightarrow J/\psi K^+) = (1.026 \pm 0.031) \times 10^{-3}$.				

$B_{s2}^*(5840)^0$ REFERENCES

SIRUNYAN	18DF EPJ C78 939	A.M. Sirunyan <i>et al.</i>	(CMS Collab.)
AALTONEN	14i PR D90 012013	T. Aaltonen <i>et al.</i>	(CDF Collab.)
AAIJ	13O PRL 110 151803	R. Aaij <i>et al.</i>	(LHCb Collab.)
AALTONEN	08K PRL 100 082001	T. Aaltonen <i>et al.</i>	(CDF Collab.)
ABAZOV	08E PRL 100 082002	V.M. Abazov <i>et al.</i>	(D0 Collab.)

$B_{sJ}^*(5850)$

$I(J^P) = ?(??)$
I, J, P need confirmation.

OMITTED FROM SUMMARY TABLE
 Signal can be interpreted as coming from $\bar{b}s$ states. Needs confirmation.

$B_{sJ}^*(5850)$ MASS

VALUE (MeV)	EVTS	DOCUMENT ID	TECN	COMMENT
5853 ± 15	141	AKERS	95E OPAL	$E_{cm}^{95} = 88-94$ GeV

$B_{sJ}^*(5850)$ WIDTH

VALUE (MeV)	EVTS	DOCUMENT ID	TECN	COMMENT
47 ± 22	141	AKERS	95E OPAL	$E_{cm}^{95} = 88-94$ GeV

$B_{sJ}^*(5850)$ REFERENCES

AKERS	95E ZPHY C66 19	R. Akers <i>et al.</i>	(OPAL Collab.)
-------	-----------------	------------------------	----------------

Meson Particle Listings

B_c^+

BOTTOM, CHARMED MESONS

($B = C = \pm 1$)

$B_c^+ = c\bar{b}, B_c^- = \bar{c}b$, similarly for B_c^{*} 's

B_c^+

$I(J^P) = 0(0^-)$
I, J, P need confirmation.

Quantum numbers shown are quark-model predictions.

B_c^+ MASS

VALUE (MeV)	DOCUMENT ID	TECN	COMMENT
6274.9 ± 0.8 OUR AVERAGE			
6274.28 ± 1.40 ± 0.32	¹ AAIJ	17L LHCB	pp at 7, 8 TeV
6274.0 ± 1.8 ± 0.4	² AAIJ	14AQ LHCB	pp at 7, 8 TeV
6276.28 ± 1.44 ± 0.36	³ AAIJ	13AS LHCB	pp at 7, 8 TeV
6273.7 ± 1.3 ± 1.6	⁴ AAIJ	12AV LHCB	pp at 7 TeV
6275.6 ± 2.9 ± 2.5	⁵ AALTONEN	08M CDF	$p\bar{p}$ at 1.96 TeV
6300 ± 14 ± 5	⁵ ABAZOV	08T D0	$p\bar{p}$ at 1.96 TeV
6400 ± 390 ± 130	⁶ ABE	98M CDF	$p\bar{p}$ at 1.8 TeV
6285.7 ± 5.3 ± 1.2	⁵ ABULENCIA	06C CDF	Repl. by AALTONEN 08M
6320 ± 60	⁷ ACKERSTAFF	98o OPAL	$e^+e^- \rightarrow Z$

- • • We do not use the following data for averages, fits, limits, etc. • • •
- ¹ Measured using $B_c^+ \rightarrow J/\psi D^0 K^+$ decays.
- ² Uses $B_c^+ \rightarrow J/\psi p \bar{p} \pi^+$ decays.
- ³ AAIJ 13AS uses the $B_c^+ \rightarrow J/\psi D_s^+$.
- ⁴ AAIJ 12AV uses the $B_c^+ \rightarrow J/\psi \pi^+$ mode and also measures the mass difference $M(B_c^+) - M(B^+) = 994.6 \pm 1.3 \pm 0.6$ MeV/ c^2 .
- ⁵ Measured using a fully reconstructed decay mode of $B_c \rightarrow J/\psi \pi$.
- ⁶ ABE 98M observed $20.4^{+6.2}_{-5.5}$ events in the $B_c^+ \rightarrow J/\psi(1S) \ell \nu_\ell$ with a significance of > 4.8 standard deviations. The mass value is estimated from $m(J/\psi(1S) \ell)$.
- ⁷ ACKERSTAFF 98o observed 2 candidate events in the $B_c^+ \rightarrow J/\psi(1S) \pi^+$ channel with an estimated background of 0.63 ± 0.20 events.

B_c^+ MEAN LIFE

"OUR EVALUATION" is an average using rescaled values of the data listed below. The average and rescaling were performed by the Heavy Flavor Averaging Group (HFLAV) and are described at <https://hfav.web.cern.ch/>. The averaging/rescaling procedure takes into account correlations between the measurements.

VALUE (10^{-12} s)	DOCUMENT ID	TECN	COMMENT
0.510 ± 0.009 OUR EVALUATION			
0.510 ± 0.009 OUR AVERAGE			
0.541 ± 0.026 ± 0.014	¹ SIRUNYAN	18BY CMS	pp at 8 TeV
0.5134 ± 0.0110 ± 0.0057	^{2,3} AAIJ	15G LHCB	pp at 7, 8 TeV
0.509 ± 0.008 ± 0.012	⁴ AAIJ	14G LHCB	pp at 8 TeV
0.452 ± 0.048 ± 0.027	³ AALTONEN	13 CDF	$p\bar{p}$ at 1.96 TeV
0.448 ± 0.038 ± 0.036 ± 0.032	⁵ ABAZOV	09H D0	$p\bar{p}$ at 1.96 TeV
0.463 ± 0.073 ± 0.065 ± 0.036	⁵ ABULENCIA	06o CDF	$p\bar{p}$ at 1.96 TeV
0.46 ± 0.18 ± 0.16 ± 0.03	⁵ ABE	98M CDF	$p\bar{p}$ 1.8 TeV

- ¹ The lifetime is measured using the decays $B_c^+ \rightarrow J/\psi \pi^+$ and $B^+ \rightarrow J/\psi K^+$.
- ² Also measures the width difference $\Delta\Gamma = \Gamma_{B_c^+} - \Gamma_{B^+} = 4.46 \pm 0.14 \pm 0.07$ $\text{mm}^{-1}c$.
- ³ Uses fully reconstructed $B_c^+ \rightarrow J/\psi \pi^+$ decays.
- ⁴ Measured using $B_c^+ \rightarrow J/\psi \mu^+ \nu_\mu X$ decays.
- ⁵ The lifetime is measured from the $J/\psi e$ decay vertices.

B_c^+ DECAY MODES × $B(\bar{b} \rightarrow B_c)$

B_c^- modes are charge conjugates of the modes below.

Mode	Fraction (Γ_i/Γ)	Confidence level
The following quantities are not pure branching ratios; rather the fraction $\Gamma_i/\Gamma \times B(\bar{b} \rightarrow B_c)$.		
Γ_1	$J/\psi(1S) \ell^+ \nu_\ell \text{ anything}$	$(8.1 \pm 1.2) \times 10^{-5}$
Γ_2	$J/\psi(1S) \mu^+ \nu_\mu$	
Γ_3	$J/\psi(1S) \tau^+ \nu_\tau$	
Γ_4	$J/\psi(1S) \pi^+$	seen
Γ_5	$J/\psi(1S) K^+$	seen
Γ_6	$J/\psi(1S) \pi^+ \pi^+ \pi^-$	seen
Γ_7	$J/\psi(1S) a_1(1260)$	< 1.2 × 10 ⁻³ 90%

Γ_8	$J/\psi(1S) K^+ K^- \pi^+$	seen
Γ_9	$J/\psi(1S) \pi^+ \pi^+ \pi^+ \pi^- \pi^-$	seen
Γ_{10}	$\psi(2S) \pi^+$	seen
Γ_{11}	$J/\psi(1S) D^0 K^+$	seen
Γ_{12}	$J/\psi(1S) D^*(2007)^0 K^+$	seen
Γ_{13}	$J/\psi(1S) D^*(2010)^+ K^{*0}$	seen
Γ_{14}	$J/\psi(1S) D^+ K^{*0}$	seen
Γ_{15}	$J/\psi(1S) D_s^+$	seen
Γ_{16}	$J/\psi(1S) D_s^{*+}$	seen
Γ_{17}	$J/\psi(1S) \rho \bar{p} \pi^+$	seen
Γ_{18}	$\chi_c^0 \pi^+$	$(2.4 \pm 0.9 \pm 0.8) \times 10^{-5}$
Γ_{19}	$p \bar{p} \pi^+$	not seen
Γ_{20}	$D^0 K^+$	$(3.8 \pm 1.2 \pm 1.1) \times 10^{-7}$
Γ_{21}	$D^0 \pi^+$	< 1.6 × 10 ⁻⁷ 95%
Γ_{22}	$D^{*0} \pi^+$	< 4 × 10 ⁻⁷ 95%
Γ_{23}	$D^{*0} K^+$	< 4 × 10 ⁻⁷ 95%
Γ_{24}	$D_s^+ \bar{D}^0$	< 1.4 × 10 ⁻⁷ 90%
Γ_{25}	$D_s^+ D^0$	< 6 × 10 ⁻⁸ 90%
Γ_{26}	$D^+ \bar{D}^0$	< 3.0 × 10 ⁻⁶ 90%
Γ_{27}	$D^+ D^0$	< 1.9 × 10 ⁻⁶ 90%
Γ_{28}	$D_s^{*+} \bar{D}^0$	
Γ_{29}	$D_s^{*+} \bar{D}^*(2007)^0$	
Γ_{30}	$D_s^{*+} D^0$	
Γ_{31}	$D_s^+ D^*(2007)^0$	
Γ_{32}	$D^*(2010)^+ \bar{D}^0$	< 6.2 × 10 ⁻³ 90%
Γ_{33}	$D^*(2010)^+ \bar{D}^0, D^{*+} \rightarrow D^+ \pi^0 / \gamma$	
Γ_{34}	$D^+ \bar{D}^*(2007)^0$	
Γ_{35}	$D^*(2010)^+ \bar{D}^0, D^{*+} \rightarrow D^+ \pi^0 / \gamma$	
Γ_{36}	$D^+ D^*(2007)^0$	
Γ_{37}	$D_s^{*+} \bar{D}^*(2007)^0$	< 1.7 × 10 ⁻⁶ 90%
Γ_{38}	$D_s^{*+} D^*(2007)^0$	< 3.1 × 10 ⁻⁶ 90%
Γ_{39}	$D^*(2010)^+ \bar{D}^*(2007)^0$	< 1.0 × 10 ⁻⁴ 90%
Γ_{40}	$D^*(2010)^+ D^*(2007)^0$	< 2.0 × 10 ⁻⁵ 90%
Γ_{41}	$D^+ K^{*0}$	< 0.20 × 10 ⁻⁶ 90%
Γ_{42}	$D^+ \bar{K}^{*0}$	< 0.16 × 10 ⁻⁶ 90%
Γ_{43}	$D_s^+ K^{*0}$	< 0.28 × 10 ⁻⁶ 90%
Γ_{44}	$D_s^+ \bar{K}^{*0}$	< 0.4 × 10 ⁻⁶ 90%
Γ_{45}	$D_s^+ \phi$	< 0.32 × 10 ⁻⁶ 90%
Γ_{46}	$K^+ K^0$	< 4.6 × 10 ⁻⁷ 90%
Γ_{47}	$B_s^0 \pi^+ / B(\bar{b} \rightarrow B_s)$	$(2.37 \pm 0.37 \pm 0.35) \times 10^{-3}$

B_c^+ BRANCHING RATIOS

VALUE (units 10 ⁻⁵)	CL%	DOCUMENT ID	TECN	COMMENT	$\Gamma_1/\Gamma \times B$
8.1 ± 1.2 OUR AVERAGE		Error includes scale factor of 1.3.			
8.7 ± 1.0 ± 0.3		^{1,2} AALTONEN	16A CDF	$p\bar{p}$ at 1.96 TeV	
5.2 ± 2.4 ± 2.1		³ ABE	98M CDF	$p\bar{p}$ 1.8 TeV	

- • • We do not use the following data for averages, fits, limits, etc. • • •
- <16 90 ⁴ACKERSTAFF 98o OPAL $e^+e^- \rightarrow Z$
- <19 90 ⁵ABREU 97E DLPH $e^+e^- \rightarrow Z$
- <12 90 ⁶BARATE 97H ALEP $e^+e^- \rightarrow Z$
- ¹ AALTONEN 16A reports $[\Gamma(B_c^+ \rightarrow J/\psi(1S) \ell^+ \nu_\ell \text{ anything})/\Gamma_{\text{total}} \times B(\bar{b} \rightarrow B_c)] / [B(\bar{b} \rightarrow B^+)] / [B(B^+ \rightarrow J/\psi(1S) K^+)] = 0.211 \pm 0.012 \pm 0.021$ which we multiply by our best values $B(\bar{b} \rightarrow B^+) = (40.8 \pm 0.7) \times 10^{-2}$, $B(B^+ \rightarrow J/\psi(1S) K^+) = (1.006 \pm 0.027) \times 10^{-3}$. Our first error is their experiment's error and our second error is the systematic error from using our best values.
- ² AALTONEN 16A also measures the cross-section $\sigma(B_c) \times B(B_c \rightarrow J/\psi \mu \nu_\mu) = 0.60 \pm 0.09$ nb and estimates the total cross-section $\sigma(B_c)$ to be in the range 25 ± 4 to 52 ± 8 nb for $p_T(B_c) > 6$ GeV/ c and $|y(B_c)| < 1$.
- ³ ABE 98M result is derived from the measurement of $[\sigma(B_c) \times B(B_c \rightarrow J/\psi(1S) \ell \nu_\ell)] / [\sigma(B^+) \times B(B^+ \rightarrow J/\psi(1S) K^+)] = 0.132 \pm 0.041 \pm 0.037$ (stat) ± 0.031 (sys) ± 0.032 (lifetime) by using PDG 98 values of $B(b \rightarrow B^+)$ and $B(B^+ \rightarrow J/\psi(1S) K^+)$.
- ⁴ ACKERSTAFF 98o reports $B(Z \rightarrow B_c X)/B(Z \rightarrow q q) \times B(B_c \rightarrow J/\psi(1S) \ell \nu_\ell) < 6.95 \times 10^{-5}$ at 90%CL. We rescale to our PDG 98 values of $B(Z \rightarrow b \bar{b})$.
- ⁵ ABREU 97E value listed is for an assumed $\tau_{B_c} = 0.4$ ps and improves to 1.6×10^{-4} for $\tau_{B_c} = 1.4$ ps.
- ⁶ BARATE 97H reports $B(Z \rightarrow B_c X)/B(Z \rightarrow q q) \times B(B_c \rightarrow J/\psi(1S) \ell \nu_\ell) < 5.2 \times 10^{-5}$ at 90%CL. We rescale to our PDG 96 values of $B(Z \rightarrow b \bar{b})$. A $B_c^+ \rightarrow J/\psi(1S) \mu^+ \nu_\mu$ candidate event is found, compared to all the known background sources 2×10^{-3} , which gives $m_{B_c} = 5.96 \pm 0.25$ GeV and $\tau_{B_c} = 1.77 \pm 0.17$ ps.

See key on page 999

Meson Particle Listings

B⁺_c

Table with 4 columns: VALUE, DOCUMENT ID, TECN, COMMENT. Row 1: 0.71 ± 0.17 ± 0.18, 1 AAIJ, 18c LHCB, pp at 7, 8 TeV. Includes a footnote about the ratio value.

Table with 4 columns: VALUE, CL%, DOCUMENT ID, TECN, COMMENT. Rows include measurements from AAIJ, CMS, CDF, LHCb, OPAL, DPH, ALEP, and ABE.

• • • We do not use the following data for averages, fits, limits, etc. • • •
1 AAIJ 15M reports a measurement of B(B_c⁺ → J/ψπ⁺) / B(B⁺ → J/ψK⁺) · f_c/f_u = (0.683 ± 0.018 ± 0.009)% at p_T(B) < 20 GeV and 2.0 < y(B) < 4.5.

Table with 4 columns: VALUE (units 10⁻²), DOCUMENT ID, TECN, COMMENT. Row 1: 4.69 ± 0.28 ± 0.46, 1 AAIJ, 14W LHCB, pp at 7 TeV. Includes a footnote about the measurement region.

Table with 4 columns: VALUE, EVTS, DOCUMENT ID, TECN, COMMENT. Row 1: 0.079 ± 0.007 ± 0.003, AAIJ, 16AF LHCB, pp at 7, 8 TeV. Includes a footnote about data usage.

Table with 4 columns: VALUE, CL%, DOCUMENT ID, TECN, COMMENT. Row 1: 0.069 ± 0.019 ± 0.005, 50 AAIJ, 13BY LHCB, Repl. by AAIJ 16AF. Includes a footnote about the independent value.

Table with 4 columns: VALUE, DOCUMENT ID, TECN, COMMENT. Row 1: 2.4 ± 0.4 OUR AVERAGE, KHACHATRY...15AA CMS, pp at 7 TeV. Row 2: 2.55 ± 0.80 ± 0.33^{+0.04}_{-0.01}, AAIJ, 12Y LHCB, pp at 7 TeV.

Table with 4 columns: VALUE, CL%, DOCUMENT ID, TECN, COMMENT. Row 1: <1.2 × 10⁻³, 90 ACKERSTAFF 980 OPAL, e⁺e⁻ → Z. Includes a footnote about the rescaled value.

Table with 4 columns: VALUE, DOCUMENT ID, TECN, COMMENT. Row 1: 2.41 ± 0.30 ± 0.33, AAIJ, 12Y LHCB, pp at 7 TeV. Includes a footnote about the signal yield.

Table with 4 columns: VALUE, DOCUMENT ID, TECN, COMMENT. Row 1: 0.53 ± 0.10 ± 0.05, 1 AAIJ, 13CA LHCB, pp at 7, 8 TeV. Includes a footnote about the signal yield.

Table with 4 columns: VALUE, DOCUMENT ID, TECN, COMMENT. Row 1: 1.74 ± 0.44 ± 0.24, 1 AAIJ, 14P LHCB, pp at 7, 8 TeV. Includes a footnote about the signal yield.

Table with 4 columns: VALUE, DOCUMENT ID, TECN, COMMENT. Row 1: 0.268 ± 0.032 ± 0.007 ± 0.006, 1 AAIJ, 15AY LHCB, pp at 7, 8 TeV. Includes a footnote about data usage.

Table with 4 columns: VALUE, DOCUMENT ID, TECN, COMMENT. Row 1: 0.432 ± 0.136 ± 0.028, AAIJ, 17L LHCB, pp at 7, 8 TeV.

Table with 4 columns: VALUE, DOCUMENT ID, TECN, COMMENT. Row 1: 5.1 ± 1.8 ± 0.4, AAIJ, 17L LHCB, pp at 7, 8 TeV.

Table with 4 columns: VALUE, DOCUMENT ID, TECN, COMMENT. Row 1: 2.10 ± 1.08 ± 0.34, AAIJ, 17L LHCB, pp at 7, 8 TeV.

Table with 4 columns: VALUE, DOCUMENT ID, TECN, COMMENT. Row 1: 0.63 ± 0.39 ± 0.08, AAIJ, 17L LHCB, pp at 7, 8 TeV.

Table with 4 columns: VALUE, DOCUMENT ID, TECN, COMMENT. Row 1: 3.1 ± 0.5 OUR AVERAGE, AAD, 16H ATLS, pp at 7, 8 TeV. Row 2: 3.8 ± 1.1 ± 0.4, AAIJ, 13As LHCB, pp at 7, 8 TeV.

Table with 4 columns: VALUE, DOCUMENT ID, TECN, COMMENT. Row 1: 10.4 ± 3.1 ± 1.6, AAD, 16H ATLS, pp at 7, 8 TeV.

Table with 4 columns: VALUE, DOCUMENT ID, TECN, COMMENT. Row 1: 2.5 ± 0.5 OUR AVERAGE, AAD, 16H ATLS, pp at 7, 8 TeV. Row 2: 2.8^{+1.2}_{-0.8} ± 0.3, AAIJ, 13As LHCB, pp at 7, 8 TeV.

Table with 4 columns: VALUE, DOCUMENT ID, TECN, COMMENT. Row 1: 0.143^{+0.041}_{-0.036}, AAIJ, 14AQ LHCB, pp at 7, 8 TeV.

Table with 4 columns: VALUE (units 10⁻⁶), DOCUMENT ID, TECN, COMMENT. Row 1: 24.0^{+8.6}_{-7.6} ± 0.4, 1,2 AAIJ, 16AT LHCB, pp at 7 and 8 TeV. Includes a footnote about the ratio value.

Table with 4 columns: VALUE, DOCUMENT ID, TECN, COMMENT. Row 1: not seen, 1 AAIJ, 16K LHCB, pp at 7, 8 TeV. Includes a footnote about the ratio measurement.

Table with 4 columns: VALUE (units 10⁻⁷), DOCUMENT ID, TECN, COMMENT. Row 1: 3.8 ± 1.2 ± 0.1, 1 AAIJ, 17AG LHCB, pp at 7, 8 TeV.

1 AAIJ 17AG reports [Γ(B_c⁺ → D⁰K⁺)/Γ_{total} × B(B_c⁺ → B_c⁺) / [B(B_c⁺ → B_c⁺)] = (9.3^{+2.8}_{-2.5} ± 0.6) × 10⁻⁷ which we multiply by our best value B(B_c⁺ → B_c⁺) = (40.8 ± 0.7) × 10⁻².

Table with 4 columns: VALUE, CL%, DOCUMENT ID, TECN, COMMENT. Row 1: <1.6 × 10⁻⁷, 95, 1 AAIJ, 17AG LHCB, pp at 7, 8 TeV. Includes a footnote about the ratio measurement.

Meson Particle Listings

 B_c^+

$\Gamma(D^{*0}\pi^+)/\Gamma_{\text{total}} \times B(\bar{b} \rightarrow B_c)$ $\Gamma_{22}/\Gamma \times B$

VALUE	CL%	DOCUMENT ID	TECN	COMMENT
$<4 \times 10^{-7}$	95	¹ AAIJ	17AG LHCB	pp at 7, 8 TeV

¹AAIJ 17AG reports $[\Gamma(B_c^+ \rightarrow D^{*0}\pi^+)/\Gamma_{\text{total}} \times B(\bar{b} \rightarrow B_c)] / [B(\bar{b} \rightarrow B^+)] < 1.1 \times 10^{-6}$ which we multiply by our best value $B(\bar{b} \rightarrow B^+) = 40.8 \times 10^{-2}$.

$\Gamma(D^{*0}K^+)/\Gamma_{\text{total}} \times B(\bar{b} \rightarrow B_c)$ $\Gamma_{23}/\Gamma \times B$

VALUE	CL%	DOCUMENT ID	TECN	COMMENT
$<4 \times 10^{-7}$	95	¹ AAIJ	17AG LHCB	pp at 7, 8 TeV

¹AAIJ 17AG reports $[\Gamma(B_c^+ \rightarrow D^{*0}K^+)/\Gamma_{\text{total}} \times B(\bar{b} \rightarrow B_c)] / [B(\bar{b} \rightarrow B^+)] < 1.1 \times 10^{-6}$ which we multiply by our best value $B(\bar{b} \rightarrow B^+) = 40.8 \times 10^{-2}$.

$\Gamma(D_s^+\bar{D}^0)/\Gamma_{\text{total}} \times B(\bar{b} \rightarrow B_c)$ $\Gamma_{24}/\Gamma \times B$

VALUE	CL%	DOCUMENT ID	TECN	COMMENT
$<1.4 \times 10^{-7}$	90	¹ AAIJ	18P LHCB	pp at 7, 8 TeV

¹AAIJ 18P reports $[\Gamma(B_c^+ \rightarrow D_s^+\bar{D}^0)/\Gamma_{\text{total}} \times B(\bar{b} \rightarrow B_c)] / [B(\bar{b} \rightarrow B^+)] / [B(B^+ \rightarrow \bar{D}^0 D^+)] < 0.9 \times 10^{-3}$ which we multiply by our best values $B(\bar{b} \rightarrow B^+) = 40.8 \times 10^{-2}$, $B(B^+ \rightarrow \bar{D}^0 D^+) = 3.8 \times 10^{-4}$.

$\Gamma(D_s^+ D^0)/\Gamma_{\text{total}} \times B(\bar{b} \rightarrow B_c)$ $\Gamma_{25}/\Gamma \times B$

VALUE	CL%	DOCUMENT ID	TECN	COMMENT
$<6 \times 10^{-8}$	90	¹ AAIJ	18P LHCB	pp at 7, 8 TeV

¹AAIJ 18P reports $[\Gamma(B_c^+ \rightarrow D_s^+ D^0)/\Gamma_{\text{total}} \times B(\bar{b} \rightarrow B_c)] / [B(\bar{b} \rightarrow B^+)] / [B(B^+ \rightarrow \bar{D}^0 D^+)] < 3.7 \times 10^{-4}$ which we multiply by our best values $B(\bar{b} \rightarrow B^+) = 40.8 \times 10^{-2}$, $B(B^+ \rightarrow \bar{D}^0 D^+) = 3.8 \times 10^{-4}$.

$\Gamma(D^+\bar{D}^0)/\Gamma_{\text{total}} \times B(\bar{b} \rightarrow B_c)$ $\Gamma_{26}/\Gamma \times B$

VALUE	CL%	DOCUMENT ID	TECN	COMMENT
$<3.0 \times 10^{-6}$	90	¹ AAIJ	18P LHCB	pp at 7, 8 TeV

¹AAIJ 18P reports $[\Gamma(B_c^+ \rightarrow D^+\bar{D}^0)/\Gamma_{\text{total}} \times B(\bar{b} \rightarrow B_c)] / [B(\bar{b} \rightarrow B^+)] / [B(B^+ \rightarrow \bar{D}^0 D^+)] < 1.9 \times 10^{-2}$ which we multiply by our best values $B(\bar{b} \rightarrow B^+) = 40.8 \times 10^{-2}$, $B(B^+ \rightarrow \bar{D}^0 D^+) = 3.8 \times 10^{-4}$.

$\Gamma(D^+ D^0)/\Gamma_{\text{total}} \times B(\bar{b} \rightarrow B_c)$ $\Gamma_{27}/\Gamma \times B$

VALUE	CL%	DOCUMENT ID	TECN	COMMENT
$<1.9 \times 10^{-6}$	90	¹ AAIJ	18P LHCB	pp at 7, 8 TeV

¹AAIJ 18P reports $[\Gamma(B_c^+ \rightarrow D^+ D^0)/\Gamma_{\text{total}} \times B(\bar{b} \rightarrow B_c)] / [B(\bar{b} \rightarrow B^+)] / [B(B^+ \rightarrow \bar{D}^0 D^+)] < 1.2 \times 10^{-2}$ which we multiply by our best values $B(\bar{b} \rightarrow B^+) = 40.8 \times 10^{-2}$, $B(B^+ \rightarrow \bar{D}^0 D^+) = 3.8 \times 10^{-4}$.

$[\Gamma(D_s^+\bar{D}^0) + \Gamma(D_s^+\bar{D}^*(2007)^0)]/\Gamma_{\text{total}} \times B(\bar{b} \rightarrow B_c)$ $(\Gamma_{28} + \Gamma_{29})/\Gamma \times B$

VALUE	CL%	DOCUMENT ID	TECN	COMMENT
$<4 \times 10^{-7}$	90	¹ AAIJ	18P LHCB	pp at 7, 8 TeV

¹AAIJ 18P reports $[\Gamma(B_c^+ \rightarrow D_s^+\bar{D}^0) + \Gamma(B_c^+ \rightarrow D_s^+\bar{D}^*(2007)^0)]/\Gamma_{\text{total}} \times B(\bar{b} \rightarrow B_c)] / [B(\bar{b} \rightarrow B^+)] / [B(B^+ \rightarrow \bar{D}^0 D^+)] < 2.8 \times 10^{-3}$ which we multiply by our best values $B(\bar{b} \rightarrow B^+) = 40.8 \times 10^{-2}$, $B(B^+ \rightarrow \bar{D}^0 D^+) = 3.8 \times 10^{-4}$.

$[\Gamma(D_s^+ D^0) + \Gamma(D_s^+ D^*(2007)^0)]/\Gamma_{\text{total}} \times B(\bar{b} \rightarrow B_c)$ $(\Gamma_{30} + \Gamma_{31})/\Gamma \times B$

VALUE	CL%	DOCUMENT ID	TECN	COMMENT
$<5 \times 10^{-7}$	90	¹ AAIJ	18P LHCB	pp at 7, 8 TeV

¹AAIJ 18P reports $[\Gamma(B_c^+ \rightarrow D_s^+ D^0) + \Gamma(B_c^+ \rightarrow D_s^+ D^*(2007)^0)]/\Gamma_{\text{total}} \times B(\bar{b} \rightarrow B_c)] / [B(\bar{b} \rightarrow B^+)] / [B(B^+ \rightarrow \bar{D}^0 D^+)] < 3.0 \times 10^{-3}$ which we multiply by our best values $B(\bar{b} \rightarrow B^+) = 40.8 \times 10^{-2}$, $B(B^+ \rightarrow \bar{D}^0 D^+) = 3.8 \times 10^{-4}$.

$\Gamma(D^*(2010)^+\bar{D}^0)/\Gamma_{\text{total}} \times B(\bar{b} \rightarrow B_c)$ $\Gamma_{32}/\Gamma \times B$

VALUE	CL%	DOCUMENT ID	TECN	COMMENT
$<6.2 \times 10^{-3}$	90	¹ BARATE	98Q ALEP	$e^+e^- \rightarrow Z$

¹BARATE 98Q reports $B(Z \rightarrow B_c X) \times B(B_c \rightarrow D^*(2010)^+\bar{D}^0) < 1.9 \times 10^{-3}$ at 90%CL. We rescale to our PDG 98 values of $B(Z \rightarrow b\bar{b})$.

$[\Gamma(D^*(2010)^+\bar{D}^0, D^{*+} \rightarrow D^+\pi^0/\gamma) + \Gamma(D^+\bar{D}^*(2007)^0)]/\Gamma_{\text{total}} \times B(\bar{b} \rightarrow B_c)$ $(\Gamma_{33} + \Gamma_{34})/\Gamma \times B$

VALUE	CL%	DOCUMENT ID	TECN	COMMENT
$<9 \times 10^{-6}$	90	¹ AAIJ	18P LHCB	pp at 7, 8 TeV

¹AAIJ 18P reports $[\Gamma(B_c^+ \rightarrow D^*(2010)^+\bar{D}^0, D^{*+} \rightarrow D^+\pi^0/\gamma) + \Gamma(B_c^+ \rightarrow D^+\bar{D}^*(2007)^0)]/\Gamma_{\text{total}} \times B(\bar{b} \rightarrow B_c)] / [B(\bar{b} \rightarrow B^+)] / [B(B^+ \rightarrow \bar{D}^0 D^+)] < 5.5 \times 10^{-2}$ which we multiply by our best values $B(\bar{b} \rightarrow B^+) = 40.8 \times 10^{-2}$, $B(B^+ \rightarrow \bar{D}^0 D^+) = 3.8 \times 10^{-4}$.

$[\Gamma(D^*(2010)^+ D^0, D^{*+} \rightarrow D^+\pi^0/\gamma) + \Gamma(D^+ D^*(2007)^0)]/\Gamma_{\text{total}} \times B(\bar{b} \rightarrow B_c)$ $(\Gamma_{35} + \Gamma_{36})/\Gamma \times B$

VALUE	CL%	DOCUMENT ID	TECN	COMMENT
$<3.4 \times 10^{-6}$	90	¹ AAIJ	18P LHCB	pp at 7, 8 TeV

¹AAIJ 18P reports $[\Gamma(B_c^+ \rightarrow D^*(2010)^+ D^0, D^{*+} \rightarrow D^+\pi^0/\gamma) + \Gamma(B_c^+ \rightarrow D^+ D^*(2007)^0)]/\Gamma_{\text{total}} \times B(\bar{b} \rightarrow B_c)] / [B(\bar{b} \rightarrow B^+)] / [B(B^+ \rightarrow \bar{D}^0 D^+)] < 2.2 \times 10^{-2}$ which we multiply by our best values $B(\bar{b} \rightarrow B^+) = 40.8 \times 10^{-2}$, $B(B^+ \rightarrow \bar{D}^0 D^+) = 3.8 \times 10^{-4}$.

$\Gamma(D_s^+\bar{D}^*(2007)^0)/\Gamma_{\text{total}} \times B(\bar{b} \rightarrow B_c)$ $\Gamma_{37}/\Gamma \times B$

VALUE	CL%	DOCUMENT ID	TECN	COMMENT
$<1.7 \times 10^{-6}$	90	¹ AAIJ	18P LHCB	pp at 7, 8 TeV

¹AAIJ 18P reports $[\Gamma(B_c^+ \rightarrow D_s^+\bar{D}^*(2007)^0)/\Gamma_{\text{total}} \times B(\bar{b} \rightarrow B_c)] / [B(\bar{b} \rightarrow B^+)] / [B(B^+ \rightarrow \bar{D}^0 D^+)] < 1.1 \times 10^{-2}$ which we multiply by our best values $B(\bar{b} \rightarrow B^+) = 40.8 \times 10^{-2}$, $B(B^+ \rightarrow \bar{D}^0 D^+) = 3.8 \times 10^{-4}$.

$\Gamma(D_s^+ D^*(2007)^0)/\Gamma_{\text{total}} \times B(\bar{b} \rightarrow B_c)$ $\Gamma_{38}/\Gamma \times B$

VALUE	CL%	DOCUMENT ID	TECN	COMMENT
$<3.1 \times 10^{-6}$	90	¹ AAIJ	18P LHCB	pp at 7, 8 TeV

¹AAIJ 18P reports $[\Gamma(B_c^+ \rightarrow D_s^+ D^*(2007)^0)/\Gamma_{\text{total}} \times B(\bar{b} \rightarrow B_c)] / [B(\bar{b} \rightarrow B^+)] / [B(B^+ \rightarrow \bar{D}^0 D^+)] < 2.0 \times 10^{-2}$ which we multiply by our best values $B(\bar{b} \rightarrow B^+) = 40.8 \times 10^{-2}$, $B(B^+ \rightarrow \bar{D}^0 D^+) = 3.8 \times 10^{-4}$.

$\Gamma(D^*(2010)^+\bar{D}^*(2007)^0)/\Gamma_{\text{total}} \times B(\bar{b} \rightarrow B_c)$ $\Gamma_{39}/\Gamma \times B$

VALUE	CL%	DOCUMENT ID	TECN	COMMENT
$<1.0 \times 10^{-4}$	90	¹ AAIJ	18P LHCB	pp at 7, 8 TeV

¹AAIJ 18P reports $[\Gamma(B_c^+ \rightarrow D^*(2010)^+\bar{D}^*(2007)^0)/\Gamma_{\text{total}} \times B(\bar{b} \rightarrow B_c)] / [B(\bar{b} \rightarrow B^+)] / [B(B^+ \rightarrow \bar{D}^0 D^+)] < 6.5 \times 10^{-1}$ which we multiply by our best values $B(\bar{b} \rightarrow B^+) = 40.8 \times 10^{-2}$, $B(B^+ \rightarrow \bar{D}^0 D^+) = 3.8 \times 10^{-4}$.

$\Gamma(D^*(2010)^+ D^*(2007)^0)/\Gamma_{\text{total}} \times B(\bar{b} \rightarrow B_c)$ $\Gamma_{40}/\Gamma \times B$

VALUE	CL%	DOCUMENT ID	TECN	COMMENT
$<2.0 \times 10^{-5}$	90	¹ AAIJ	18P LHCB	pp at 7, 8 TeV

¹AAIJ 18P reports $[\Gamma(B_c^+ \rightarrow D^*(2010)^+ D^*(2007)^0)/\Gamma_{\text{total}} \times B(\bar{b} \rightarrow B_c)] / [B(\bar{b} \rightarrow B^+)] / [B(B^+ \rightarrow \bar{D}^0 D^+)] < 1.3 \times 10^{-1}$ which we multiply by our best values $B(\bar{b} \rightarrow B^+) = 40.8 \times 10^{-2}$, $B(B^+ \rightarrow \bar{D}^0 D^+) = 3.8 \times 10^{-4}$.

$\Gamma(D^+ K^*)/\Gamma_{\text{total}} \times B(\bar{b} \rightarrow B_c)$ $\Gamma_{41}/\Gamma \times B$

VALUE	CL%	DOCUMENT ID	TECN	COMMENT
$<2.0 \times 10^{-7}$	90	¹ AAIJ	13R LHCB	pp at 7 TeV

¹AAIJ 13R reports $[\Gamma(B_c^+ \rightarrow D^+ K^*)/\Gamma_{\text{total}} \times B(\bar{b} \rightarrow B_c)] / [B(\bar{b} \rightarrow B^+)] < 0.5 \times 10^{-6}$ which we multiply by our best value $B(\bar{b} \rightarrow B^+) = 40.8 \times 10^{-2}$.

$\Gamma(D^+ \bar{K}^*)/\Gamma_{\text{total}} \times B(\bar{b} \rightarrow B_c)$ $\Gamma_{42}/\Gamma \times B$

VALUE	CL%	DOCUMENT ID	TECN	COMMENT
$<1.6 \times 10^{-7}$	90	¹ AAIJ	13R LHCB	pp at 7 TeV

¹AAIJ 13R reports $[\Gamma(B_c^+ \rightarrow D^+ \bar{K}^*)/\Gamma_{\text{total}} \times B(\bar{b} \rightarrow B_c)] / [B(\bar{b} \rightarrow B^+)] < 0.4 \times 10^{-6}$ which we multiply by our best value $B(\bar{b} \rightarrow B^+) = 40.8 \times 10^{-2}$.

$\Gamma(D_s^+ K^*)/\Gamma_{\text{total}} \times B(\bar{b} \rightarrow B_c)$ $\Gamma_{43}/\Gamma \times B$

VALUE	CL%	DOCUMENT ID	TECN	COMMENT
$<2.9 \times 10^{-7}$	90	¹ AAIJ	13R LHCB	pp at 7 TeV

¹AAIJ 13R reports $[\Gamma(B_c^+ \rightarrow D_s^+ K^*)/\Gamma_{\text{total}} \times B(\bar{b} \rightarrow B_c)] / [B(\bar{b} \rightarrow B^+)] < 0.7 \times 10^{-6}$ which we multiply by our best value $B(\bar{b} \rightarrow B^+) = 40.8 \times 10^{-2}$.

$\Gamma(D_s^+ \bar{K}^*)/\Gamma_{\text{total}} \times B(\bar{b} \rightarrow B_c)$ $\Gamma_{44}/\Gamma \times B$

VALUE	CL%	DOCUMENT ID	TECN	COMMENT
$<4 \times 10^{-7}$	90	¹ AAIJ	13R LHCB	pp at 7 TeV

¹AAIJ 13R reports $[\Gamma(B_c^+ \rightarrow D_s^+ \bar{K}^*)/\Gamma_{\text{total}} \times B(\bar{b} \rightarrow B_c)] / [B(\bar{b} \rightarrow B^+)] < 1.1 \times 10^{-6}$ which we multiply by our best value $B(\bar{b} \rightarrow B^+) = 40.8 \times 10^{-2}$.

$\Gamma(D_s^+ \phi)/\Gamma_{\text{total}} \times B(\bar{b} \rightarrow B_c)$ $\Gamma_{45}/\Gamma \times B$

VALUE	CL%	DOCUMENT ID	TECN	COMMENT
$<3.3 \times 10^{-7}$	90	¹ AAIJ	13R LHCB	pp at 7 TeV

¹AAIJ 13R reports $[\Gamma(B_c^+ \rightarrow D_s^+ \phi)/\Gamma_{\text{total}} \times B(\bar{b} \rightarrow B_c)] / [B(\bar{b} \rightarrow B^+)] < 0.8 \times 10^{-6}$ which we multiply by our best value $B(\bar{b} \rightarrow B^+) = 40.8 \times 10^{-2}$.

$\Gamma(K^+ K^0)/\Gamma_{\text{total}} \times B(\bar{b} \rightarrow B_c)$ $\Gamma_{46}/\Gamma \times B$

VALUE	CL%	DOCUMENT ID	TECN	COMMENT
$<4.6 \times 10^{-7}$	90	¹ AAIJ	13bs LHCB	pp at 7 TeV

¹Derived from $\Gamma(K^+ K^0)/\Gamma \times B(\bar{b} \rightarrow B_c) / (B(B^+ \rightarrow K^0 \pi^+) B(\bar{b} \rightarrow B^+)) < 5.8\%$ at 90% CL using normalization mode $B(B^+ \rightarrow K^0 \pi^+) = (23.97 \pm 0.53 \pm 0.71) \times 10^{-6}$ and assuming a B production ratio $f(\bar{b} \rightarrow B^+) = 0.33$.

$\Gamma(B_s^0 \pi^+)/\Gamma_{\text{total}} \times B(\bar{b} \rightarrow B_c)$ $\Gamma_{47}/\Gamma \times B$

VALUE (units 10^{-3})	CL%	DOCUMENT ID	TECN	COMMENT
$2.37 \pm 0.31 \pm 0.11 \pm 0.13$		¹ AAIJ	13bu LHCB	pp at 7, 8 TeV

¹The last uncertainty is due to the uncertainty of the B_c^+ lifetime measurement.

POLARIZATION IN B_c^+ DECAY

In decays involving two vector mesons, one can distinguish among the states in which meson polarizations are both longitudinal (L) or both are transverse and parallel (\parallel) or perpendicular (\perp) to each other with the parameters Γ_L/Γ , Γ_\perp/Γ , and the relative phases ϕ_\parallel and ϕ_\perp . See the definitions in the note on "Polarization in B Decays" review in the B^0 Particle Listings.

Γ_L/Γ in $B_c^+ \rightarrow J/\psi D_s^{*\pm}$

VALUE	DOCUMENT ID	TECN	COMMENT
0.54 ± 0.15 OUR AVERAGE			
0.62 ± 0.24	¹ AAD	16H ATLS	pp at 7, 8 TeV
0.48 ± 0.20	² AAIJ	13As LHCb	pp at 7, 8 TeV
¹ AAD 16H measures $1 - \Gamma_\perp/\Gamma = 0.38 \pm 0.24$.			
² AAIJ 13As measures $1 - \Gamma_\perp/\Gamma = 0.52 \pm 0.20$.			

$A_P(B_c^+)$

$$A_P(B_c^+) = [\sigma(B_c^-) - \sigma(B_c^+)] / [\sigma(B_c^-) + \sigma(B_c^+)]$$

VALUE (units 10^{-2})	DOCUMENT ID	TECN	COMMENT
-1.0 ± 1.0 OUR AVERAGE			
-2.5 ± 2.1 ± 0.5	¹ AAIJ	19Al LHCb	pp at 7 TeV
-0.5 ± 1.1 ± 0.4	¹ AAIJ	19Al LHCb	pp at 13 TeV
¹ Measured using B_c^+ semileptonic decays.			

B_c^+ REFERENCES

AAIJ	19Al	PR D100 112006	R. Aaij et al.	(LHCb Collab.)
AAIJ	18C	PRL 120 121801	R. Aaij et al.	(LHCb Collab.)
AAIJ	18P	NP B930 563	R. Aaij et al.	(CMS Collab.)
SIRUNYAN	18BY	EPJ C78 457	A.M. Sirunyan et al.	(CMS Collab.)
AAIJ	17AG	PRL 118 111803	R. Aaij et al.	(LHCb Collab.)
AAIJ	17L	PR D95 032005	R. Aaij et al.	(LHCb Collab.)
AAD	16H	EPJ C76 4	G. Aad et al.	(ATLAS Collab.)
AAIJ	16AF	JHEP 1609 153	R. Aaij et al.	(LHCb Collab.)
AAIJ	16AT	PR D94 091102	R. Aaij et al.	(LHCb Collab.)
AAIJ	16K	PL B759 313	R. Aaij et al.	(LHCb Collab.)
AALTONEN	16A	PR D93 052001	T. Aaltonen et al.	(CDF Collab.)
AAIJ	15AY	PR D92 072007	R. Aaij et al.	(LHCb Collab.)
AAIJ	15G	PL B742 29	R. Aaij et al.	(LHCb Collab.)
AAIJ	15M	PRL 114 132001	R. Aaij et al.	(LHCb Collab.)
KHACHATRYAN	15AA	JHEP 1501 063	V. Khachatryan et al.	(CMS Collab.)
AAIJ	14AQ	PRL 113 152003	R. Aaij et al.	(LHCb Collab.)
AAIJ	14G	EPJ C74 2839	R. Aaij et al.	(LHCb Collab.)
AAIJ	14P	JHEP 1405 148	R. Aaij et al.	(LHCb Collab.)
AAIJ	14W	PR D90 032009	R. Aaij et al.	(LHCb Collab.)
AAIJ	13AM	PR D87 071103	R. Aaij et al.	(LHCb Collab.)
AAIJ	13AS	PR D87 112012	R. Aaij et al.	(LHCb Collab.)
Also		PR D89 019301 (errat.)	R. Aaij et al.	(LHCb Collab.)
AAIJ	13BS	PL B726 646	R. Aaij et al.	(LHCb Collab.)
AAIJ	13BU	PRL 111 181801	R. Aaij et al.	(LHCb Collab.)
AAIJ	13BY	JHEP 1309 075	R. Aaij et al.	(LHCb Collab.)
AAIJ	13CA	JHEP 1311 094	R. Aaij et al.	(LHCb Collab.)
AAIJ	13R	JHEP 1302 043	R. Aaij et al.	(LHCb Collab.)
AALTONEN	13	PR D87 011101	T. Aaltonen et al.	(CDF Collab.)
AAIJ	12AV	PRL 109 232001	R. Aaij et al.	(LHCb Collab.)
AAIJ	12Y	PRL 108 251802	R. Aaij et al.	(LHCb Collab.)
ABAZOV	09H	PRL 102 092001	V.M. Abazov et al.	(DO Collab.)
AALTONEN	08M	PRL 100 182002	T. Aaltonen et al.	(CDF Collab.)
ABAZOV	08T	PRL 101 012001	V.M. Abazov et al.	(DO Collab.)
ABULENCIA	06C	PRL 96 082002	A. Abulencia et al.	(CDF Collab.)
ABULENCIA	06O	PRL 97 012002	A. Abulencia et al.	(CDF Collab.)
ABE	98M	PRL 81 2432	F. Abe et al.	(CDF Collab.)
Also		PR D58 112004	F. Abe et al.	(CDF Collab.)
ACKERSTAFF	98O	PL B420 157	K. Ackerstaff et al.	(OPAL Collab.)
BARATE	98Q	EPJ C4 387	R. Barate et al.	(ALEPH Collab.)
PDG	98	EPJ C3 1	C. Caso et al.	(PDG Collab.)
ABREU	97E	PL B398 207	P. Abreu et al.	(DELPHI Collab.)
BARATE	97H	PL B402 213	R. Barate et al.	(ALEPH Collab.)
ABE	96R	PRL 77 5176	F. Abe et al.	(CDF Collab.)
PDG	96	PR D54 1	R. M. Barnett et al.	(PDG Collab.)

$B_c(2S)^\pm$

$$I(J^P) = 0(0^-)$$

OMITTED FROM SUMMARY TABLE
Quantum numbers neither measured nor confirmed.

$B_c(2S)^\pm$ MASS

VALUE (MeV)	EVTS	DOCUMENT ID	TECN	COMMENT
6871.6 ± 1.1 OUR AVERAGE				
6872.1 ± 1.3 ± 0.8	24	^{1,2} AAIJ	19Y LHCb	pp at 7, 8, 13 TeV
6871.0 ± 1.4 ± 0.8	51	^{3,4} SIRUNYAN	19M CMS	pp at 13 TeV
• • • We do not use the following data for averages, fits, limits, etc. • • •				
not seen		⁵ AAIJ	18AL LHCb	pp at 8 TeV
6842 ± 4 ± 5	57	^{6,7} AAD	14AQ ATLS	pp at 7, 8 TeV

- ¹ AAIJ 19Y observed $B_c(2S)^+$ in the decay mode $B_c(2S)^+ \rightarrow B_c^+ \pi^+ \pi^-$ ($B_c^+ \rightarrow J/\psi \pi^+$) with 2.2 (3.2) global (local) standard deviations significance.
- ² AAIJ 19Y reports mass difference measurement of $M(B_c(2S)^+) - M(B_c^+) = 597.2 \pm 1.3 \pm 0.1$ MeV. We have adjusted this measurement with our best value of $M(B_c^+) = 6274.9 \pm 0.8$ MeV. The first uncertainty of the $M(B_c(2S)^+)$ value is a total of uncertainties reported by the experiment and the second one comes from our best value of $M(B_c^+)$.
- ³ SIRUNYAN 19M observed $B_c(2S)^+$ in the decay mode $B_c(2S)^+ \rightarrow B_c^+ \pi^+ \pi^-$ ($B_c^+ \rightarrow J/\psi \pi^+$) with 6.5 standard deviations significance.
- ⁴ SIRUNYAN 19M reports mass difference measurement of $M(B_c(2S)^+) - M(B_c^+) = 596.1 \pm 1.2 \pm 0.8$ MeV. We have adjusted this measurement with our best value of $M(B_c^+) = 6274.9 \pm 0.8$ MeV. The first uncertainty of the $M(B_c(2S)^+)$ value is a total of uncertainties reported by the experiment and the second one comes from our best value of $M(B_c^+)$.
- ⁵ AAIJ 18AL reports an upper limit on the ratio of production cross sections for $[\sigma(B_c(2S)^+)/\sigma(B_c^+)] \cdot B(B_c(2S)^+ \rightarrow B_c^+ \pi^+ \pi^-) < 0.04-0.09$ at 95% CL for the mass value reported by AAD 14AQ.
- ⁶ Observed in the decay mode $B_c(2S)^+ \rightarrow B_c^+ \pi^+ \pi^-$ ($B_c^+ \rightarrow J/\psi \pi^+$) with 5.2 standard deviations significance.
- ⁷ Might be the $B_c^*(2S)$.

$B_c(2S)^\pm$ DECAY MODES

Mode	Fraction (Γ_i/Γ)
$\Gamma_1 B_c^+ \pi^+ \pi^-$	seen

$B_c(2S)^\pm$ BRANCHING RATIOS

$\Gamma(B_c^+ \pi^+ \pi^-)/\Gamma_{total}$	Γ_1/Γ			
VALUE	EVTS	DOCUMENT ID	TECN	COMMENT
seen	57	¹ AAD	14AQ ATLS	pp at 7, 8 TeV
• • • We do not use the following data for averages, fits, limits, etc. • • •				
not seen		² AAIJ	18AL LHCb	pp at 8 TeV

- ¹ Observed with 5.2 standard deviations significance.
- ² AAIJ 18AL reports an upper limit on the ratio of production cross sections for $[\sigma(B_c(2S)^+)/\sigma(B_c^+)] \cdot B(B_c(2S)^+ \rightarrow B_c^+ \pi^+ \pi^-) < 0.04-0.09$ at 95% CL for the mass value reported by AAD 14AQ.

$B_c(2S)^\pm$ REFERENCES

AAIJ	19Y	PRL 122 232001	R. Aaij et al.	(LHCb Collab.)
SIRUNYAN	19M	PRL 122 132001	A.M. Sirunyan et al.	(CMS Collab.)
AAIJ	18AL	JHEP 1801 138	R. Aaij et al.	(LHCb Collab.)
AAD	14AQ	PRL 113 212004	G. Aad et al.	(ATLAS Collab.)

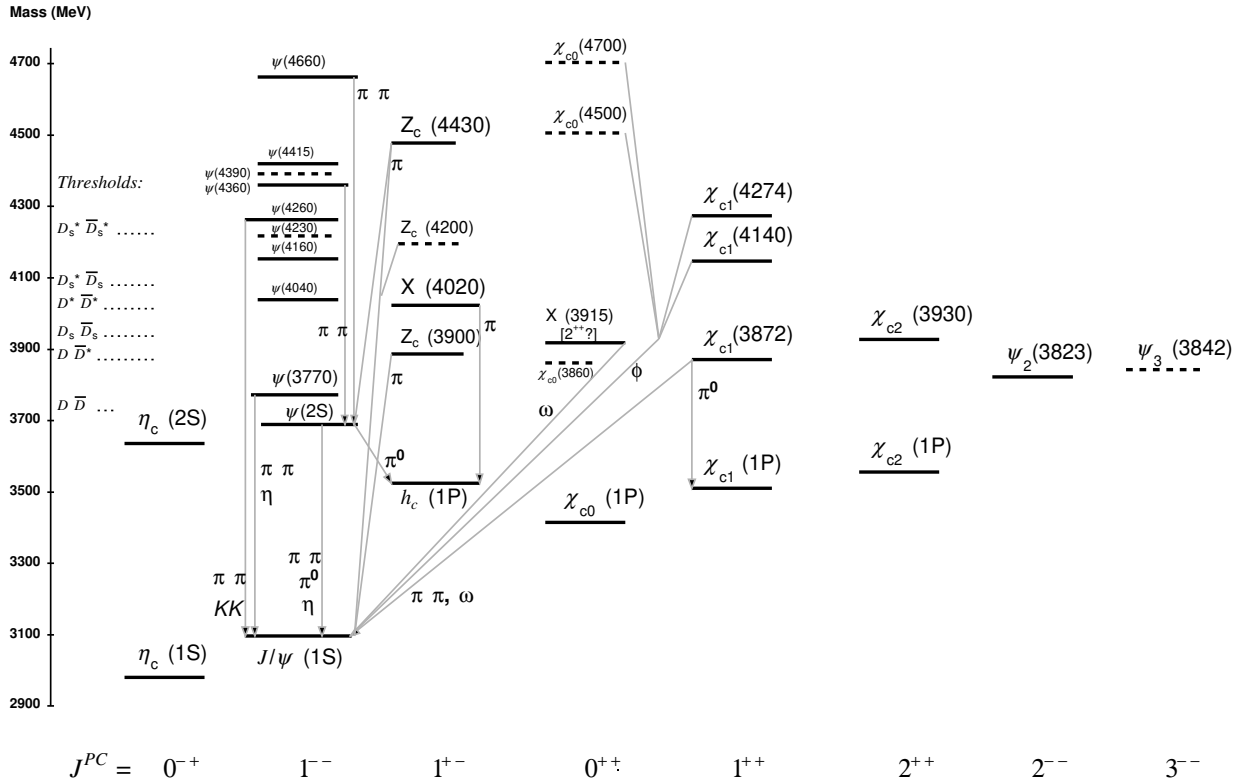
See the related review(s):

Spectroscopy of Mesons Containing Two Heavy Quarks

Meson Particle Listings

Charmonium, $\eta_c(1S)$

$c\bar{c}$ MESONS
(including possibly non- $q\bar{q}$ states)



The level scheme of meson states containing a minimal quark content of $c\bar{c}$. The name of a state is determined by its quantum numbers $I^G J^{PC}$ (see the review “Naming Scheme for Hadrons”). States with unestablished quantum numbers are called X and are drawn according to our best estimate of their likely J^{PC} . States included in the Summary Tables are shown with solid lines; selected states not in the Summary Tables, but with assigned quantum numbers, are shown with dotted lines. The arrows indicate the most dominant hadronic transitions. Single photon transitions, including $\psi(nS) \rightarrow \gamma\eta_c(mS)$, $\psi(nS) \rightarrow \gamma\chi_{cJ}(1P)$, and $\chi_{cJ}(1P) \rightarrow \gamma J/\psi$, are omitted for clarity. For orientation, the location of the thresholds related to a pair of ground state open charm mesons is indicated in the figure.

$\eta_c(1S)$ $I^G(J^{PC}) = 0^+(0^-+)$

VALUE (MeV)	EVTS	DOCUMENT ID	TECN	COMMENT
2983.9 ± 0.5	OUR AVERAGE	Error includes scale factor of 1.3. See the ideogram below.		
2985.9 ± 0.7 ± 2.1	1705	ABL IKIM	19AV BES3	$J/\psi \rightarrow \gamma\omega\omega$
2984.6 ± 0.7 ± 2.2	2673	XU	18 BELL	$e^+e^- \rightarrow \pi^+\pi^-\pi^0$
2986.7 ± 0.5 ± 0.9	11K	1 AAIJ	17AD LHCB	$pp \rightarrow B^+X \rightarrow p\bar{p}K^+X$
2982.8 ± 1.0 ± 0.5	6.4k	2 AAIJ	17BB LHCB	$pp \rightarrow b\bar{b}X \rightarrow 2(K^+K^-)X$
2982.2 ± 1.5 ± 0.1	2.0k	3 AAIJ	15BI LHCB	$pp \rightarrow \eta_c(1S)X$
2983.5 ± 1.4 ± 1.6	3.6	4 ANASHIN	14 KEDR	$J/\psi \rightarrow \gamma\eta_c$
2979.8 ± 0.8 ± 3.5	4.5k	5,6 LEES	14E BABR	$\gamma\gamma \rightarrow K^+K^-\pi^0$
2984.1 ± 1.1 ± 2.1	900	5,6,7 LEES	14E BABR	$\gamma\gamma \rightarrow K^+K^-\eta$
2984.3 ± 0.6 ± 0.6		8,9 ABLIKIM	12F BES3	$\psi(2S) \rightarrow \gamma\eta_c$
2984.49 ± 1.16 ± 0.52	832	5 ABLIKIM	12N BES3	$\psi(2S) \rightarrow \pi^0\gamma$ hadrons
2982.7 ± 1.8 ± 2.2	486	ZHANG	12A BELL	$e^+e^- \rightarrow \pi^+\pi^-\pi^0$
2984.5 ± 0.8 ± 3.1	11k	DEL-AMO-SA...11M	BABR	$\gamma\gamma \rightarrow K^+K^-\pi^+\pi^-\pi^0$
2985.4 ± 1.5 ± 2.0	920	9 VINOKUROVA	11 BELL	$B^\pm \rightarrow K^\pm(K_S^0 K^\pm\pi^\mp)$

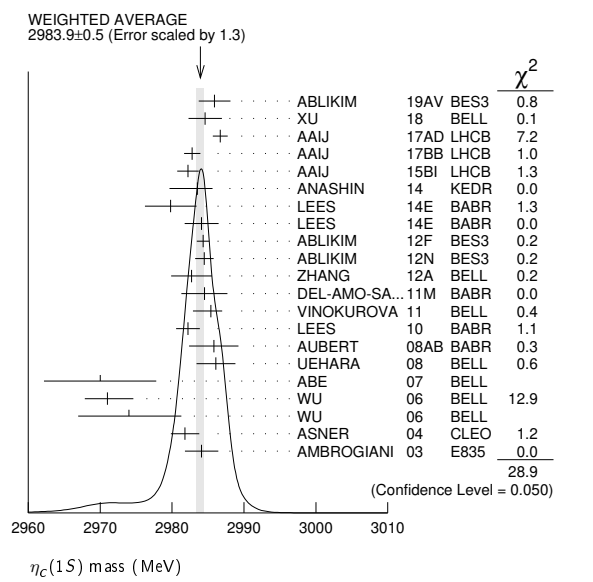
2982.2 ± 0.4 ± 1.6	14k	10 LEES	10 BABR	$10.6 e^+e^- \rightarrow e^+e^-K_S^0 K^\pm\pi^\mp$
2985.8 ± 1.5 ± 3.1	0.9k	AUBERT	08AB BABR	$B \rightarrow \eta_c(1S)K^*(*) \rightarrow K\bar{K}\pi K^*(*)$
2986.1 ± 1.0 ± 2.5	7.5k	UEHARA	08 BELL	$\gamma\gamma \rightarrow \eta_c \rightarrow$ hadrons
2970 ± 5 ± 6	5.01	11 ABE	07 BELL	$e^+e^- \rightarrow J/\psi(c\bar{c})$
2971 ± 3 ± 2	1.95	WU	06 BELL	$B^+ \rightarrow p\bar{p}K^+$
2974 ± 7 ± 2	20	WU	06 BELL	$B^+ \rightarrow \Lambda\bar{\Lambda}K^+$
2981.8 ± 1.3 ± 1.5	5.92	ASNER	04 CLEO	$\gamma\gamma \rightarrow \eta_c \rightarrow K_S^0 K^\pm\pi^\mp$
2984.1 ± 2.1 ± 1.0	190	12 AMBROGIANI	03 E835	$\bar{p}p \rightarrow \eta_c \rightarrow \gamma\gamma$
••• We do not use the following data for averages, fits, limits, etc. •••				
2982.5 ± 0.4 ± 1.4	12k	13 DEL-AMO-SA...11M	BABR	$\gamma\gamma \rightarrow K_S^0 K^\pm\pi^\mp$
2982.2 ± 0.6		14 MITCHELL	09 CLEO	$e^+e^- \rightarrow \gamma X$
2982 ± 5	270	15 AUBERT	06E BABR	$B^\pm \rightarrow K^\pm X_{c\bar{c}}$
2982.5 ± 1.1 ± 0.9	2.5k	16 AUBERT	04D BABR	$\gamma\gamma \rightarrow \eta_c(1S) \rightarrow K\bar{K}\pi$
2977.5 ± 1.0 ± 1.2		14,17 BAI	03 BES	$J/\psi \rightarrow \gamma\eta_c$
2979.6 ± 2.3 ± 1.6	180	18 FANG	03 BELL	$B \rightarrow \eta_c K$
2976.3 ± 2.3 ± 1.2		14,19 BAI	00F BES	$J/\psi, \psi(2S) \rightarrow \gamma\eta_c$
2976.6 ± 2.9 ± 1.3	140	14,20 BAI	00F BES	$J/\psi \rightarrow \gamma\eta_c$
2980.4 ± 2.3 ± 0.6		21 BRANDENB...	00B CLE2	$\gamma\gamma \rightarrow \eta_c \rightarrow K^\pm K_S^0\pi^\mp$
2975.8 ± 3.9 ± 1.2		20 BAI	99B BES	Sup. by BAI 00F
2999 ± 8	25	ABREU	98O DLPH	$e^+e^- \rightarrow e^+e^-$ hadrons

Table of experimental data for eta_c(1S) decays, including columns for mass, width, and decay mode. Includes entries for ARMSTRONG 95F E760, BISELLO 91 DM2, BAI 90B MRK3, BAGLIN 87B SPEC, BALTRUSAIT...86 MRK3, GAISSER 86 CBAL, HIMEL 80B MRK2, and PARTRIDGE 80B CBAL.

Continuation of experimental data for eta_c(1S) decays, including entries for AAIJ 17AD LHCb, ANASHIN 14 KEDR, LEES 14E BABR, ABLIKIM 12F BES3, ZHANG 12A BELL, DEL-AMO-SA...11M BABR, VINOKUROVA 11 BELL, and AUBERT 08AB BABR.

- 1 AAIJ 17AD report m_{J/\psi} - m_{\eta_c(1S)} = 110.2 \pm 0.5 \pm 0.9 MeV. We use the current value m_{J/\psi} = 3096.900 \pm 0.006 MeV to obtain the quoted mass.
2 From a fit of the \phi\phi invariant mass with the mass and width of \eta_c(1S) as free parameters.
3 AAIJ 15BI reports m_{J/\psi} - m_{\eta_c(1S)} = 114.7 \pm 1.5 \pm 0.1 MeV from a sample of \eta_c(1S) and J/\psi produced in b-hadron decays.
4 Taking into account an asymmetric photon lineshape.
5 With floating width.
6 Ignoring possible interference with the non-resonant 0^- amplitude.
7 Using both, \eta \to \gamma\gamma and \eta \to \pi^+\pi^-\pi^0 decays.
8 From a simultaneous fit to six decay modes of the \eta_c.
9 Accounts for interference with non-resonant continuum.
10 Taking into account interference with the non-resonant J^P = 0^- amplitude.
11 From a fit of the J/\psi recoil mass spectrum. Supersedes ABE,K 02 and ABE 04g.
12 Using mass of \psi(2S) = 3686.00 MeV.
13 Not independent from the measurements reported by LEES 10.
14 MITCHELL 09 observes a significant asymmetry in the lineshapes of \psi(2S) \to \gamma\eta_c and J/\psi \to \gamma\eta_c transitions.
15 From the fit of the kaon momentum spectrum. Systematic errors not evaluated.
16 Superseded by LEES 10.
17 From a simultaneous fit of five decay modes of the \eta_c.
18 Superseded by VINOKUROVA 11.
19 Weighted average of the \psi(2S) and J/\psi(1S) samples. Using an \eta_c width of 13.2 MeV.
20 Average of several decay modes. Using an \eta_c width of 13.2 MeV.
21 Superseded by ASNER 04.
22 Average of several decay modes.
23 \eta_c \to \phi\phi.
24 Mass adjusted by us to correspond to J/\psi(1S) mass = 3097 MeV.

- 31.4 \pm 3.5 \pm 2.0 6.4k 1 AAIJ 17BB LHCb pp \to b\bar{b}X \to 2(K^+K^-)X
27.2 \pm 3.1^{+5.4}_{-2.6} 2 ANASHIN 14 KEDR J/\psi \to \gamma\eta_c
25.2 \pm 2.6 \pm 2.4 4.5k 3,4 LEES 14E BABR \gamma\gamma \to K^+K^-\pi^0
34.8 \pm 3.1 \pm 4.0 900 3,4,5 LEES 14E BABR \gamma\gamma \to K^+K^-\eta
32.0 \pm 1.2 \pm 1.0 6,7 ABLIKIM 12F BES3 \psi(2S) \to \gamma\eta_c
36.4 \pm 3.2 \pm 1.7 832 3 ABLIKIM 12N BES3 \psi(2S) \to \pi^0\gamma hadrons
37.8 \pm 5.8_{-5.3} \pm 3.1 486 ZHANG 12A BELL e^+e^- \to e^+e^-\eta/\pi^+\pi^-
36.2 \pm 2.8 \pm 3.0 11k DEL-AMO-SA...11M BABR \gamma\gamma \to K^+K^-\pi^+\pi^-
35.1 \pm 3.1^{+1.0}_{-1.6} 920 7 VINOKUROVA 11 BELL B^\pm \to K^\pm(K_S^0 K^\pm\pi^\mp)
31.7 \pm 1.2 \pm 0.8 14k 8 LEES 10 BABR 10.6 e^+e^- \to e^+e^-K_S^0 K^\pm\pi^\mp
36.3 \pm 3.7_{-3.6} \pm 4.4 0.9k AUBERT 08AB BABR B \to \eta_c(1S) K^*(*) \to K\bar{K}\pi K^*(*)
28.1 \pm 3.2 \pm 2.2 7.5k UEHARA 08 BELL \gamma\gamma \to \eta_c \to hadrons
48 \pm 8_{-7} \pm 5 195 WU 06 BELL B^+ \to \rho\bar{p}K^+
40 \pm 19 \pm 5 20 WU 06 BELL B^+ \to \Lambda\bar{\Lambda}K^+
24.8 \pm 3.4 \pm 3.5 592 ASNER 04 CLEO \gamma\gamma \to \eta_c \to K_S^0 K^\pm\pi^\mp
20.4 \pm 7.7_{-6.7} \pm 2.0 190 AMBROGIANI 03 E835 \bar{p}p \to \eta_c \to \gamma\gamma
23.9 \pm 12.6_{-7.1} \pm 1.1 ARMSTRONG 95F E760 \bar{p}p \to \gamma\gamma
••• We do not use the following data for averages, fits, limits, etc. •••
32.1 \pm 1.1 \pm 1.3 12k 9 DEL-AMO-SA...11M BABR \gamma\gamma \to K_S^0 K^\pm\pi^\mp
34.3 \pm 2.3 \pm 0.9 2.5k 10 AUBERT 04D BABR \gamma\gamma \to \eta_c(1S) \to K\bar{K}\pi
17.0 \pm 3.7 \pm 7.4 11 BAI 03 BES J/\psi \to \gamma\eta_c
29 \pm 8 \pm 6 180 12 FANG 03 BELL B \to \eta_c K
11.0 \pm 8.1 \pm 4.1 13 BAI 00F BES J/\psi \to \gamma\eta_c and \psi(2S) \to \gamma\eta_c
27.0 \pm 5.8 \pm 1.4 14 BRANDENB... 00B CLE2 \gamma\gamma \to \eta_c \to K^\pm K_S^0 \pi^\mp
7.0 \pm 7.5_{-7.0} \pm 1.2 12 BAGLIN 87B SPEC \bar{p}p \to \gamma\gamma
10.1 \pm 33.0_{-8.2} \pm 1.5 23 15 BALTRUSAIT...86 MRK3 J/\psi \to \gamma\rho\bar{\rho}
11.5 \pm 4.5 GAISSER 86 CBAL J/\psi \to \gamma X, \psi(2S) \to \gamma X
< 40 90% CL 18 HIMEL 80B MRK2 e^+e^- \to e^+e^-
< 20 90% CL PARTRIDGE 80B CBAL e^+e^-



- 1 From a fit of the \phi\phi invariant mass with the mass and width of \eta_c(1S) as free parameters.
2 Taking into account an asymmetric photon lineshape.
3 With floating mass.
4 Ignoring possible interference with the non-resonant 0^- amplitude.
5 Using both, \eta \to \gamma\gamma and \eta \to \pi^+\pi^-\pi^0 decays.
6 From a simultaneous fit to six decay modes of the \eta_c.
7 Accounts for interference with non-resonant continuum.
8 Taking into account interference with the non-resonant J^P = 0^- amplitude.
9 Not independent from the measurements reported by LEES 10.
10 Superseded by LEES 10.
11 From a simultaneous fit of five decay modes of the \eta_c.
12 Superseded by VINOKUROVA 11.
13 From a fit to the 4-prong invariant mass in \psi(2S) \to \gamma\eta_c and J/\psi(1S) \to \gamma\eta_c decays.
14 Superseded by ASNER 04.
15 Positive and negative errors correspond to 90% confidence level.

$\eta_c(1S)$ DECAY MODES

Table listing decay modes of eta_c(1S). Columns: Mode, Fraction (\Gamma_i/\Gamma), Confidence level. Includes modes like \eta'(958)\pi\pi, \rho\rho, K^*(892)^0 K^-\pi^+ + c.c., K^*(892)^0 \bar{K}^*(892), K^*(892)^0 \bar{K}^*(892)^0 \pi^+\pi^-, \phi K^+ K^-, \phi\phi, \phi 2(\pi^+\pi^-), a_0(980)\pi, a_2(1320)\pi, K^*(892)\bar{K} + c.c., f_2(1270)\eta, \omega\omega, \omega\phi, f_2(1270)f_2(1270), f_2(1270)f_2'(1525), f_0(980)\eta, f_0(1500)\eta, f_0(2200)\eta.

$\eta_c(1S)$ WIDTH

Table summarizing the width of eta_c(1S). Columns: VALUE (MeV), EVTS, DOCUMENT ID, TECN, COMMENT. Includes 'OUR FIT' and 'OUR AVERAGE' values, and experimental data from ABLIKIM, XU, and AAIJ.

Meson Particle Listings

$\eta_c(1S)$

Γ_{20}	$a_0(980)\pi$	seen
Γ_{21}	$a_0(1320)\pi$	seen
Γ_{22}	$a_0(1450)\pi$	seen
Γ_{23}	$a_0(1950)\pi$	seen
Γ_{24}	$K_0^*(1430)\bar{K}$	seen
Γ_{25}	$K_0^*(1430)\bar{K}$	seen
Γ_{26}	$K_0^*(1950)\bar{K}$	seen

Γ_{31}	$K^+ K^- \pi^+ \pi^-$	0.220 ± 0.034
Γ_{35}	$2(K^+ K^-)$	0.047 ± 0.010
Γ_{38}	$2(\pi^+ \pi^-)$	0.31 ± 0.04
Γ_{41}	$\rho\bar{\rho}$	0.046 ± 0.005
Γ_{43}	$\Lambda\bar{\Lambda}$	0.034 ± 0.008
Γ_{49}	$\gamma\gamma$	0.00506 ± 0.00034

Decays into stable hadrons

Γ_{27}	$K\bar{K}\pi$	(7.3 ± 0.4) %	
Γ_{28}	$K\bar{K}\eta$	(1.36 ± 0.15) %	
Γ_{29}	$\eta\pi^+\pi^-$	(1.7 ± 0.5) %	
Γ_{30}	$\eta 2(\pi^+\pi^-)$	(4.4 ± 1.3) %	
Γ_{31}	$K^+ K^- \pi^+ \pi^-$	(6.9 ± 1.0) × 10 ⁻³	
Γ_{32}	$K^+ K^- \pi^+ \pi^- \pi^0$	(3.5 ± 0.6) %	
Γ_{33}	$K^0 K^- \pi^+ \pi^- \pi^+ + c.c.$	(5.6 ± 1.5) %	
Γ_{34}	$K^+ K^- 2(\pi^+\pi^-)$	(7.5 ± 2.4) × 10 ⁻³	
Γ_{35}	$2(K^+ K^-)$	(1.46 ± 0.30) × 10 ⁻³	
Γ_{36}	$\pi^+ \pi^- \pi^0$	< 5 × 10 ⁻⁴	90%
Γ_{37}	$\pi^+ \pi^- \pi^0 \pi^0$	(4.7 ± 1.0) %	
Γ_{38}	$2(\pi^+\pi^-)$	(9.7 ± 1.2) × 10 ⁻³	
Γ_{39}	$2(\pi^+\pi^-\pi^0)$	(16.1 ± 2.0) %	
Γ_{40}	$3(\pi^+\pi^-)$	(1.8 ± 0.4) %	
Γ_{41}	$\rho\bar{\rho}$	(1.45 ± 0.14) × 10 ⁻³	
Γ_{42}	$\rho\bar{\rho}\pi^0$	(3.6 ± 1.3) × 10 ⁻³	
Γ_{43}	$\Lambda\bar{\Lambda}$	(1.07 ± 0.24) × 10 ⁻³	
Γ_{44}	$K^+ \bar{p} \Lambda + c.c.$	(2.6 ± 0.4) × 10 ⁻³	
Γ_{45}	$\bar{\Lambda}(1520)\Lambda + c.c.$	(3.1 ± 1.4) × 10 ⁻³	
Γ_{46}	$\Sigma^+ \bar{\Sigma}^-$	(2.1 ± 0.6) × 10 ⁻³	
Γ_{47}	$\Xi^- \bar{\Xi}^+$	(9.0 ± 2.6) × 10 ⁻⁴	
Γ_{48}	$\pi^+ \pi^- \rho\bar{\rho}$	(5.3 ± 1.8) × 10 ⁻³	

Radiative decays

Γ_{49}	$\gamma\gamma$	(1.58 ± 0.11) × 10 ⁻⁴
---------------	----------------	----------------------------------

Charge conjugation (C), Parity (P), Lepton family number (LF) violating modes

Γ_{50}	$\pi^+ \pi^-$	P, CP < 1.1 × 10 ⁻⁴	90%
Γ_{51}	$\pi^0 \pi^0$	P, CP < 4 × 10 ⁻⁵	90%
Γ_{52}	$K^+ K^-$	P, CP < 6 × 10 ⁻⁴	90%
Γ_{53}	$K_S^0 K_S^0$	P, CP < 3.1 × 10 ⁻⁴	90%

CONSTRAINED FIT INFORMATION

An overall fit to the total width, 8 combinations of partial widths obtained from integrated cross section, and 19 branching ratios uses 93 measurements and one constraint to determine 13 parameters. The overall fit has a $\chi^2 = 121.6$ for 81 degrees of freedom.

The following off-diagonal array elements are the correlation coefficients $\langle \delta p_i \delta p_j \rangle / (\delta p_i \delta p_j)$, in percent, from the fit to parameters p_i , including the branching fractions, $x_i \equiv \Gamma_i / \Gamma_{total}$. The fit constrains the x_i whose labels appear in this array to sum to one.

x_7	15																					
x_{15}	3	5																				
x_{27}	17	33	6																			
x_{28}	7	15	3	45																		
x_{31}	9	17	3	19	9																	
x_{35}	7	12	2	20	9	8																
x_{38}	11	21	4	24	11	13	9															
x_{41}	10	19	3	25	11	11	9	14														
x_{43}	2	4	1	6	3	3	2	3	23													
x_{49}	-26	-49	-9	-56	-25	-30	-22	-37	-36	-8												
Γ	-1	-2	0	-3	-1	-2	-1	-2	6	1												
	x_4	x_7	x_{15}	x_{27}	x_{28}	x_{31}	x_{35}	x_{38}	x_{41}	x_{43}												
Γ	-29																					
	x_{49}																					

Mode	Rate (MeV)	
Γ_4	$K^*(892)\bar{K}^*(892)$	0.22 ± 0.04
Γ_7	$\phi\phi$	0.057 ± 0.006
Γ_{15}	$f_2(1270)f_2(1270)$	0.31 ± 0.08
Γ_{27}	$K\bar{K}\pi$	2.33 ± 0.13
Γ_{28}	$K\bar{K}\eta$	0.43 ± 0.05

$\eta_c(1S)$ PARTIAL WIDTHS

$\Gamma(\gamma\gamma)$	VALUE (keV)	EVTS	DOCUMENT ID	TECN	COMMENT	Γ_{49}
5.06 ± 0.34 OUR FIT						
• • • We do not use the following data for averages, fits, limits, etc. • • •						
	5.8 ± 1.1	486	¹ ZHANG	12A	BELL $e^+e^- \rightarrow e^+e^- \eta' \pi^+ \pi^-$	
	5.2 ± 1.2	273 ± 43	^{2,3} AUBERT	06E	BABR $B^\pm \rightarrow K^\pm X_c \bar{c}$	
	5.5 ± 1.2 ± 1.8	57 ± 33	⁴ KUO	05	BELL $\gamma\gamma \rightarrow \rho\bar{\rho}$	
	7.4 ± 0.4 ± 2.3		⁵ ASNER	04	CLEO $\gamma\gamma \rightarrow \eta_c \rightarrow K_S^0 K^\pm \pi^\mp$	
	13.9 ± 2.0 ± 3.0	41	⁶ ABDALLAH	03J	DLPH $\gamma\gamma \rightarrow \eta_c$	
	3.8 ± 1.1 + 1.9 - 1.0 - 1.0	190	⁷ AMBROGIANI	03	E835 $\bar{p}p \rightarrow \eta_c \rightarrow \gamma\gamma$	
	7.6 ± 0.8 ± 2.3		^{5,8} BRANDENB...	00B	CLE2 $\gamma\gamma \rightarrow \eta_c \rightarrow K^\pm K_S^0 \pi^\mp$	
	6.9 ± 1.7 ± 2.1	76	⁹ ACCIARRI	99T	L3 $e^+e^- \rightarrow e^+e^- \eta_c$	
	27 ± 16 ± 10	5	⁵ SHIRAI	98	AMY 58 e^+e^-	
	6.7 ± 2.4 ± 2.3		⁴ ARMSTRONG	95F	E760 $\bar{p}p \rightarrow \gamma\gamma$	
	11.3 ± 4.2		¹⁰ ALBRECHT	94H	ARG $e^+e^- \rightarrow e^+e^- \eta_c$	
	8.0 ± 2.3 ± 2.4	17	¹¹ ADRIANI	93N	L3 $e^+e^- \rightarrow e^+e^- \eta_c$	
	5.9 ± 2.1 ± 1.9		⁷ CHEN	90B	CLEO $e^+e^- \rightarrow e^+e^- \eta_c$	
	6.4 ± 5.0 - 3.4		¹² AIHARA	88D	TPC $e^+e^- \rightarrow e^+e^- X$	
	4.3 ± 3.4 ± 2.4		⁴ BAGLIN	87B	SPEC $\bar{p}p \rightarrow \gamma\gamma$	
	28 ± 15		^{5,13} BERGER	86	PLUT $\gamma\gamma \rightarrow K\bar{K}\pi$	

- Assuming there is no interference with the non-resonant background.
- Calculated by us using $\Gamma(\eta_c \rightarrow K\bar{K}\pi) \times \Gamma(\eta_c \rightarrow \gamma\gamma) / \Gamma = 0.44 \pm 0.05$ keV from PDG 06 and $B(\eta_c \rightarrow K\bar{K}\pi) = (8.5 \pm 1.8)\%$ from AUBERT 06E.
- Systematic errors not evaluated.
- Normalized to $B(\eta_c \rightarrow \rho\bar{\rho}) = (1.3 \pm 0.4) \times 10^{-3}$.
- Normalized to $B(\eta_c \rightarrow K^\pm K_S^0 \pi^\mp)$.
- Average of $K_S^0 K^\pm \pi^\mp$, $\pi^+ \pi^- K^+ K^-$, and $2(K^+ K^-)$ decay modes.
- Normalized to the sum of $B(\eta_c \rightarrow K^\pm K_S^0 \pi^\mp)$, $B(\eta_c \rightarrow K^+ K^- \pi^+ \pi^-)$, and $B(\eta_c \rightarrow 2\pi^+ 2\pi^-)$.
- Superseded by ASNER 04.
- Normalized to the sum of 9 branching ratios.
- Normalized to the sum of $B(\eta_c \rightarrow K^\pm K_S^0 \pi^\mp)$, $B(\eta_c \rightarrow \phi\phi)$, $B(\eta_c \rightarrow K^+ K^- \pi^+ \pi^-)$, and $B(\eta_c \rightarrow 2\pi^+ 2\pi^-)$.
- Superseded by ACCIARRI 99T.
- Normalized to the sum of $B(\eta_c \rightarrow K^\pm K_S^0 \pi^\mp)$, $B(\eta_c \rightarrow 2K^+ 2K^-)$, $B(\eta_c \rightarrow K^+ K^- \pi^+ \pi^-)$, and $B(\eta_c \rightarrow 2\pi^+ 2\pi^-)$.
- Re-evaluated by AIHARA 88D.

$\eta_c(1S)$ $\Gamma(i)\Gamma(\gamma\gamma)/\Gamma(\text{total})$

$\Gamma(\eta'(958)\pi\pi) \times \Gamma(\gamma\gamma)/\Gamma_{total}$	VALUE (eV)	EVTS	DOCUMENT ID	TECN	COMMENT	$\Gamma_1 \Gamma_{49}/\Gamma$
98.1 ± 3.9 ± 11.7						
	2673		XU	18	BELL $e^+e^- \rightarrow e^+e^- \eta' \pi^+ \pi^-$	
• • • We do not use the following data for averages, fits, limits, etc. • • •						
	75.8 ± 6.3 ± 8.4	486	¹ ZHANG	12A	BELL $e^+e^- \rightarrow e^+e^- \eta' \pi^+ \pi^-$	
¹ Superseded by XU 18.						

$\Gamma(\rho\rho) \times \Gamma(\gamma\gamma)/\Gamma_{total}$	VALUE (eV)	CL%	EVTS	DOCUMENT ID	TECN	COMMENT	$\Gamma_2 \Gamma_{49}/\Gamma$
• • • We do not use the following data for averages, fits, limits, etc. • • •							
	<39		90 < 1556	UEHARA	08	BELL $\gamma\gamma \rightarrow 2(\pi^+ \pi^-)$	

$\Gamma(K^*(892)\bar{K}^*(892)) \times \Gamma(\gamma\gamma)/\Gamma_{total}$	VALUE (eV)	EVTS	DOCUMENT ID	TECN	COMMENT	$\Gamma_4 \Gamma_{49}/\Gamma$
36 ± 6 OUR FIT						
	32.4 ± 4.2 ± 5.8	882 ± 115	UEHARA	08	BELL $\gamma\gamma \rightarrow \pi^+ \pi^- K^+ K^-$	

$\Gamma(\phi\phi) \times \Gamma(\gamma\gamma)/\Gamma_{total}$	VALUE (eV)	EVTS	DOCUMENT ID	TECN	COMMENT	$\Gamma_7 \Gamma_{49}/\Gamma$
9.0 ± 0.8 OUR FIT						
	7.75 ± 0.66 ± 0.62	386 ± 31	¹ LIU	12B	BELL $\gamma\gamma \rightarrow 2(K^+ K^-)$	
• • • We do not use the following data for averages, fits, limits, etc. • • •						
	6.8 ± 1.2 ± 1.3	132 ± 23	UEHARA	08	BELL $\gamma\gamma \rightarrow 2(K^+ K^-)$	
¹ Supersedes UEHARA 08. Using $B(\phi \rightarrow K^+ K^-) = (48.9 \pm 0.5)\%$.						

$\Gamma(\omega) \times \Gamma(\gamma\gamma)/\Gamma_{total}$		$\Gamma_{13}\Gamma_{49}/\Gamma$		
VALUE (eV)	EVTS	DOCUMENT ID	TECN	COMMENT
8.67 ± 2.86 ± 0.96	85 ± 29	¹ LIU	12B BELL	$\gamma\gamma \rightarrow 2(\pi^+ \pi^- \pi^0)$
¹ Using $B(\omega \rightarrow \pi^+ \pi^- \pi^0) = (89.2 \pm 0.7)\%$.				

$\Gamma(\omega\phi) \times \Gamma(\gamma\gamma)/\Gamma_{total}$		$\Gamma_{14}\Gamma_{49}/\Gamma$		
VALUE (eV)	CL%	DOCUMENT ID	TECN	COMMENT
••• We do not use the following data for averages, fits, limits, etc. •••				
<0.49	90	¹ LIU	12B BELL	$\gamma\gamma \rightarrow K^+ K^- \pi^+ \pi^- \pi^0$
¹ Using $B(\phi \rightarrow K^+ K^-) = (48.9 \pm 0.5)\%$ and $B(\omega \rightarrow \pi^+ \pi^- \pi^0) = (89.2 \pm 0.7)\%$.				

$\Gamma(f_2(1270) f_2'(1270)) \times \Gamma(\gamma\gamma)/\Gamma_{total}$		$\Gamma_{15}\Gamma_{49}/\Gamma$		
VALUE (eV)	EVTS	DOCUMENT ID	TECN	COMMENT
59 ± 13 OUR FIT				
69 ± 17 ± 12	3182 ± 766	UEHARA	08 BELL	$\gamma\gamma \rightarrow 2(\pi^+ \pi^-)$

$\Gamma(f_2(1270) f_2'(1525)) \times \Gamma(\gamma\gamma)/\Gamma_{total}$		$\Gamma_{16}\Gamma_{49}/\Gamma$		
VALUE (eV)	EVTS	DOCUMENT ID	TECN	COMMENT
49 ± 9 ± 13	1128 ± 206	UEHARA	08 BELL	$\gamma\gamma \rightarrow \pi^+ \pi^- K^+ K^-$

$\Gamma(K\bar{K}\pi) \times \Gamma(\gamma\gamma)/\Gamma_{total}$		$\Gamma_{27}\Gamma_{49}/\Gamma$		
VALUE (keV)	CL% EVTS	DOCUMENT ID	TECN	COMMENT
0.369 ± 0.020 OUR FIT				
0.407 ± 0.027 OUR AVERAGE Error includes scale factor of 1.2.				
0.374 ± 0.009 ± 0.031	14k	¹ LEES	10 BABR	$10.6 e^+ e^- \rightarrow e^+ e^- K_S^0 K_{S\pi}^{\pm\mp}$
0.407 ± 0.022 ± 0.028		^{2,3} ASNER	04 CLEO	$\gamma\gamma \rightarrow \eta_C \rightarrow K_S^0 K_{S\pi}^{\pm\mp}$
0.60 ± 0.12 ± 0.09	41	^{3,4} ABDALLAH	03J DLPH	$\gamma\gamma \rightarrow K_S^0 K_{S\pi}^{\pm\mp}$
1.47 ± 0.87 ± 0.27		³ SHIRAI	98 AMY	$\gamma\gamma \rightarrow \eta_C \rightarrow K_{S\pi}^{\pm\mp}$
0.84 ± 0.21		³ ALBRECHT	94H ARG	$\gamma\gamma \rightarrow K_{S\pi}^{\pm\mp}$
0.60 ± 0.23 ± 0.20		³ CHEN	90B CLEO	$\gamma\gamma \rightarrow \eta_C K_{S\pi}^{\pm\mp}$
1.06 ± 0.41 ± 0.27	11	³ BRAUNSCH...	89 TASS	$\gamma\gamma \rightarrow K\bar{K}\pi$
1.5 ± 0.60 ± 0.3 ± 0.45	7	³ BERGER	86 PLUT	$\gamma\gamma \rightarrow K\bar{K}\pi$

••• We do not use the following data for averages, fits, limits, etc. •••

0.386 ± 0.008 ± 0.021 12k ⁵ DEL-AMO-SA...11M BABR $\gamma\gamma \rightarrow K_S^0 K_{S\pi}^{\pm\mp}$

0.418 ± 0.044 ± 0.022 ^{3,6} BRANDENB... 00B CLE2 $\gamma\gamma \rightarrow \eta_C \rightarrow K_{S\pi}^{\pm\mp}$

<0.63 95 ³ BEHREND 89 CELL $\gamma\gamma \rightarrow K_S^0 K_{S\pi}^{\pm\mp}$

<4.4 95 ALTHOFF 85B TASS $\gamma\gamma \rightarrow K\bar{K}\pi$

¹ From the corrected and unfolded mass spectrum.

² Calculated by us from the value reported in ASNER 04 that assumes $B(\eta_C \rightarrow K\bar{K}\pi) = 5.5 \pm 1.7\%$.

³ We have multiplied $K_{S\pi}^{\pm\mp}$ measurement by 3 to obtain $K\bar{K}\pi$.

⁴ Calculated by us from the value reported in ABDALLAH 03J, which uses $B(\eta_C \rightarrow K_S^0 K_{S\pi}^{\pm\mp}) = (1.5 \pm 0.4)\%$.

⁵ Not independent from the measurements reported by LEES 10.

⁶ Superseded by ASNER 04.

$\Gamma(K^+ K^- \pi^+ \pi^-) \times \Gamma(\gamma\gamma)/\Gamma_{total}$		$\Gamma_{31}\Gamma_{49}/\Gamma$		
VALUE (eV)	EVTS	DOCUMENT ID	TECN	COMMENT
35 ± 5 OUR FIT				
27 ± 6 OUR AVERAGE				
25.7 ± 3.2 ± 4.9	2019 ± 248	UEHARA	08 BELL	$\gamma\gamma \rightarrow \pi^+ \pi^- K^+ K^-$
280 ± 100 ± 60	42	¹ ABDALLAH	03J DLPH	$\gamma\gamma \rightarrow \pi^+ \pi^- K^+ K^-$
170 ± 80 ± 20	13.9 ± 6.6	ALBRECHT	94H ARG	$\gamma\gamma \rightarrow \pi^+ \pi^- K^+ K^-$
¹ Calculated by us from the value reported in ABDALLAH 03J, which uses $B(\eta_C \rightarrow \pi^+ \pi^- K^+ K^-) = (2.0 \pm 0.7)\%$.				

$\Gamma(K^+ K^- \pi^+ \pi^- \pi^0) \times \Gamma(\gamma\gamma)/\Gamma_{total}$		$\Gamma_{32}\Gamma_{49}/\Gamma$		
VALUE (keV)	EVTS	DOCUMENT ID	TECN	COMMENT
••• We do not use the following data for averages, fits, limits, etc. •••				
0.190 ± 0.006 ± 0.028	11k	¹ DEL-AMO-SA...11M BABR		$\gamma\gamma \rightarrow K^+ K^- \pi^+ \pi^- \pi^0$
¹ Not independent from other measurements reported in DEL-AMO-SANCHEZ 11M.				

$\Gamma(2(K^+ K^-)) \times \Gamma(\gamma\gamma)/\Gamma_{total}$		$\Gamma_{35}\Gamma_{49}/\Gamma$		
VALUE (eV)	EVTS	DOCUMENT ID	TECN	COMMENT
7.4 ± 1.5 OUR FIT				
5.8 ± 1.9 OUR AVERAGE				
5.6 ± 1.1 ± 1.6	216 ± 42	UEHARA	08 BELL	$\gamma\gamma \rightarrow 2(K^+ K^-)$
350 ± 90 ± 60	46	¹ ABDALLAH	03J DLPH	$\gamma\gamma \rightarrow 2(K^+ K^-)$
231 ± 90 ± 23	9.1 ± 3.3	² ALBRECHT	94H ARG	$\gamma\gamma \rightarrow 2(K^+ K^-)$
¹ Calculated by us from the value reported in ABDALLAH 03J, which uses $B(\eta_C \rightarrow 2(K^+ K^-)) = (2.1 \pm 1.2)\%$.				
² Includes all topological modes except $\eta_C \rightarrow \phi\phi$.				

$\Gamma(2(\pi^+ \pi^-)) \times \Gamma(\gamma\gamma)/\Gamma_{total}$		$\Gamma_{38}\Gamma_{49}/\Gamma$		
VALUE (eV)	EVTS	DOCUMENT ID	TECN	COMMENT
49 ± 6 OUR FIT				
42 ± 6 OUR AVERAGE				
40.7 ± 3.7 ± 5.3	5381 ± 492	UEHARA	08 BELL	$\gamma\gamma \rightarrow 2(\pi^+ \pi^-)$
180 ± 70 ± 20	21.4 ± 8.6	ALBRECHT	94H ARG	$\gamma\gamma \rightarrow 2(\pi^+ \pi^-)$

$\Gamma(\rho\bar{\rho}) \times \Gamma(\gamma\gamma)/\Gamma_{total}$		$\Gamma_{41}\Gamma_{49}/\Gamma$		
VALUE (eV)	EVTS	DOCUMENT ID	TECN	COMMENT
7.4 ± 0.7 OUR FIT				
7.20 ± 1.53 ± 0.67 ± 0.75 157 ± 33 ¹ KUO 05 BELL $\gamma\gamma \rightarrow \rho\bar{\rho}$				

••• We do not use the following data for averages, fits, limits, etc. •••

4.6 ^{+1.3} _{-1.1} ± 0.4 190 ¹ AMBROGIANI 03 E835 $\bar{p}p \rightarrow \gamma\gamma$

8.1 ^{+2.9} _{-2.0} ¹ ARMSTRONG 95F E760 $\bar{p}p \rightarrow \gamma\gamma$

¹ Not independent from the $\Gamma_{\gamma\gamma}$ reported by the same experiment.

$\Gamma(K_S^0 K_S^0) \times \Gamma(\gamma\gamma)/\Gamma_{total}$		$\Gamma_{53}\Gamma_{49}/\Gamma$		
VALUE (eV)	CL%	DOCUMENT ID	TECN	COMMENT
<1.6 90 ¹ UEHARA 13 BELL $\gamma\gamma \rightarrow K_S^0 K_S^0$				
••• We do not use the following data for averages, fits, limits, etc. •••				
<0.29	90	² UEHARA	13 BELL	$\gamma\gamma \rightarrow K_S^0 K_S^0$
¹ Taking into account interference with the non-resonant continuum.				
² Neglecting interference with the non-resonant continuum.				

$\eta_c(1S)$ BRANCHING RATIOS

HADRONIC DECAYS

$\Gamma(\eta'(958) \pi\pi)/\Gamma_{total}$		Γ_1/Γ		
VALUE	EVTS	DOCUMENT ID	TECN	COMMENT
0.041 ± 0.017	14	¹ BALTRUSAIT...86	MRK3	$J/\psi \rightarrow \eta_C \gamma$
¹ The quoted branching ratios use $B(J/\psi(1S) \rightarrow \gamma\eta_c(1S)) = 0.0127 \pm 0.0036$.				

$\Gamma(\rho\rho)/\Gamma_{total}$		Γ_2/Γ		
VALUE (units 10^{-3})	CL% EVTS	DOCUMENT ID	TECN	COMMENT
18 ± 5 OUR AVERAGE				
12.6 ± 3.8 ± 5.1	72	¹ ABLIKIM	05L BES2	$J/\psi \rightarrow \pi^+ \pi^- \pi^+ \pi^-$
26.0 ± 2.4 ± 8.8	113	¹ BISELLO	91 DM2	$J/\psi \rightarrow \gamma\rho^0\rho^0$
23.6 ± 10.6 ± 8.2	32	¹ BISELLO	91 DM2	$J/\psi \rightarrow \gamma\rho^+ \rho^-$
••• We do not use the following data for averages, fits, limits, etc. •••				
<14	90	¹ BALTRUSAIT...86	MRK3	$J/\psi \rightarrow \eta_C \gamma$

¹ The quoted branching ratios use $B(J/\psi(1S) \rightarrow \gamma\eta_c(1S)) = 0.0127 \pm 0.0036$. Where relevant, the error in this branching ratio is treated as a common systematic in computing averages.

$\Gamma(K^*(892)^0 K^- \pi^+ + c.c.)/\Gamma_{total}$		Γ_3/Γ		
VALUE	EVTS	DOCUMENT ID	TECN	COMMENT
0.02 ± 0.007	63	^{1,2} BALTRUSAIT...86	MRK3	$J/\psi \rightarrow \eta_C \gamma$
¹ BALTRUSAIT'S 86 has an error according to Partridge.				
² The quoted branching ratios use $B(J/\psi(1S) \rightarrow \gamma\eta_c(1S)) = 0.0127 \pm 0.0036$.				

$\Gamma(K^*(892) \bar{K}^*(892))/\Gamma_{total}$		Γ_4/Γ		
VALUE (units 10^{-4})	EVTS	DOCUMENT ID	TECN	COMMENT
70 ± 13 OUR FIT				
91 ± 26 OUR AVERAGE				
108 ± 25 ± 44	60	¹ ABLIKIM	05L BES2	$J/\psi \rightarrow K^+ K^- \pi^+ \pi^- \gamma$
82 ± 28 ± 27	14	¹ BISELLO	91 DM2	$e^+ e^- \rightarrow \gamma K^+ K^- \pi^+ \pi^-$
90 ± 50	9	¹ BALTRUSAIT...86	MRK3	$J/\psi \rightarrow \eta_C \gamma$

¹ The quoted branching ratios use $B(J/\psi(1S) \rightarrow \gamma\eta_c(1S)) = 0.0127 \pm 0.0036$. Where relevant, the error in this branching ratio is treated as a common systematic in computing averages.

$\Gamma(K^*(892)^0 \bar{K}^*(892)^0 \pi^+ \pi^-)/\Gamma_{total}$		Γ_5/Γ		
VALUE (units 10^{-4})	EVTS	DOCUMENT ID	TECN	COMMENT
113 ± 47 ± 24 45 ¹ ABLIKIM 06A BES2 $J/\psi \rightarrow K^{*0} \bar{K}^{*0} \pi^+ \pi^- \gamma$				
[BLIKIM 06A reports $[\Gamma(\eta_c(1S) \rightarrow K^*(892)^0 \bar{K}^*(892)^0 \pi^+ \pi^-)/\Gamma_{total}] \times [B(J/\psi(1S) \rightarrow \gamma\eta_c(1S))] = (1.91 \pm 0.64 \pm 0.48) \times 10^{-4}$ which we divide by our best value $B(J/\psi(1S) \rightarrow \gamma\eta_c(1S)) = (1.7 \pm 0.4) \times 10^{-2}$. Our first error is their experiment's error and our second error is the systematic error from using our best value.				

$\Gamma(\phi K^+ K^-)/\Gamma_{total}$		Γ_6/Γ		
VALUE (units 10^{-3})	EVTS	DOCUMENT ID	TECN	COMMENT
2.9 ± 0.9 ± 1.1	14.1 ± 4.4 ± 3.7	¹ HUANG	03 BELL	$B^+ \rightarrow (\phi K^+ K^-) K^+$
¹ Using $B(B^+ \rightarrow \eta_C K^+) = (1.25 \pm 0.12 \pm 0.10) \times 10^{-3}$ from FANG 03 and $B(\eta_C \rightarrow K\bar{K}\pi) = (5.5 \pm 1.7) \times 10^{-2}$.				

Meson Particle Listings

 $\eta_c(1S)$ $\Gamma(\phi\phi)/\Gamma_{\text{total}}$ Γ_7/Γ

VALUE (units 10^{-4})	EVTS	DOCUMENT ID	TECN	COMMENT
17.7 ± 1.9 OUR FIT				
28 ± 4 OUR AVERAGE				
26 $\pm \frac{4}{8} \pm 5$	1.2k	¹ ABLIKIM	17P BES3	$J/\psi \rightarrow K^+ K^- K^+ K^- \gamma$
25.3 ± 5.1 ± 9.1	72	² ABLIKIM	05L BES2	$J/\psi \rightarrow K^+ K^- K^+ K^- \gamma$
26 ± 9	357	² BAI	04 BES	$J/\psi \rightarrow \gamma K^+ K^- K^+ K^-$
31 ± 7 ± 10	19	² BISELLO	91 DM2	$J/\psi \rightarrow \gamma K^+ K^- K^+ K^-$
30 $\pm \frac{18}{-12} \pm 10$	5	² BISELLO	91 DM2	$J/\psi \rightarrow \gamma K^+ K^- K_S^0 K_L^0$
74 ± 18 ± 24	80	² BAI	90B MRK3	$J/\psi \rightarrow \gamma K^+ K^- K^+ K^-$
67 ± 21 ± 24		² BAI	90B MRK3	$J/\psi \rightarrow \gamma K^+ K^- K_S^0 K_L^0$

• • • We do not use the following data for averages, fits, limits, etc. • • •

18 $\pm \frac{8}{6} \pm 7$	7	³ HUANG	03 BELL	$B^+ \rightarrow (\phi\phi) K^+$
----------------------------	---	--------------------	---------	----------------------------------

¹ ABLIKIM 17P reports $[\Gamma(\eta_c(1S) \rightarrow \phi\phi)/\Gamma_{\text{total}}] \times [B(J/\psi(1S) \rightarrow \gamma\eta_c(1S))] = (4.3 \pm 0.5 \pm 0.5) \times 10^{-5}$ which we divide by our best value $B(J/\psi(1S) \rightarrow \gamma\eta_c(1S)) = (1.7 \pm 0.4) \times 10^{-2}$. Our first error is their experiment's error and our second error is the systematic error from using our best value.

² The quoted branching ratios use $B(J/\psi(1S) \rightarrow \gamma\eta_c(1S)) = 0.0127 \pm 0.0036$. Where relevant, the error in this branching ratio is treated as a common systematic in computing averages.

³ Using $B(B^+ \rightarrow \eta_c K^+) = (1.25 \pm 0.12 \pm 0.10) \times 10^{-3}$ from FANG 03 and $B(\eta_c \rightarrow K\bar{K}\pi) = (5.5 \pm 1.7) \times 10^{-2}$.

 $\Gamma(\phi\phi)/\Gamma(K\bar{K}\pi)$ Γ_7/Γ_{27}

VALUE	EVTS	DOCUMENT ID	TECN	COMMENT
0.0243 ± 0.0025 OUR FIT				
0.044 $\pm \frac{0.012}{-0.010}$ OUR AVERAGE				
0.055 ± 0.014 ± 0.005		AUBERT,B	04B BABR	$B^\pm \rightarrow K^\pm \eta_c$
0.032 $\pm \frac{0.014}{-0.010} \pm 0.009$	7	¹ HUANG	03 BELL	$B^\pm \rightarrow K^\pm \phi$

¹ Using $B(B^+ \rightarrow \eta_c K^+) = (1.25 \pm 0.12 \pm 0.10) \times 10^{-3}$ from FANG 03 and $B(\eta_c \rightarrow K\bar{K}\pi) = (5.5 \pm 1.7) \times 10^{-2}$.

 $\Gamma(\phi\phi)/\Gamma(p\bar{p})$ Γ_7/Γ_{41}

VALUE	EVTS	DOCUMENT ID	TECN	COMMENT
1.79 ± 0.14 ± 0.32	6.4k	¹ AAIJ	17Bb LHCB	$pp \rightarrow b\bar{b} X \rightarrow 2(K^+ K^-) X$

¹ Using inputs from AAIJ 15As and AAIJ 15B1 and $\Gamma(b \rightarrow J/\psi(1S) \text{ anything})/\Gamma_{\text{total}} = (1.16 \pm 0.10)\%$ and $\Gamma(J/\psi(1S) \rightarrow p\bar{p})/\Gamma_{\text{total}} = (2.120 \pm 0.029) \times 10^{-3}$ from PDG 16.

 $\Gamma(\phi_2(\pi^+ \pi^-))/\Gamma_{\text{total}}$ Γ_8/Γ

VALUE (units 10^{-4})	CL%	DOCUMENT ID	TECN	COMMENT
<40	90	¹ ABLIKIM	06A BES2	$J/\psi \rightarrow \phi_2(\pi^+ \pi^-) \gamma$

¹ ABLIKIM 06A reports $[\Gamma(\eta_c(1S) \rightarrow \phi_2(\pi^+ \pi^-))/\Gamma_{\text{total}}] \times [B(J/\psi(1S) \rightarrow \gamma\eta_c(1S))] < 0.603 \times 10^{-4}$ which we divide by our best value $B(J/\psi(1S) \rightarrow \gamma\eta_c(1S)) = 1.7 \times 10^{-2}$.

 $\Gamma(a_0(980)\pi)/\Gamma_{\text{total}}$ Γ_9/Γ

VALUE	CL%	DOCUMENT ID	TECN	COMMENT
<0.02	90	^{1,2} BALTRUSAIT..86	MRK3	$J/\psi \rightarrow \eta_c \gamma$

¹ The quoted branching ratios use $B(J/\psi(1S) \rightarrow \gamma\eta_c(1S)) = 0.0127 \pm 0.0036$.

² We are assuming $B(a_0(980) \rightarrow \eta\pi) > 0.5$.

 $\Gamma(a_2(1320)\pi)/\Gamma_{\text{total}}$ Γ_{10}/Γ

VALUE	CL%	DOCUMENT ID	TECN	COMMENT
<0.02	90	¹ BALTRUSAIT..86	MRK3	$J/\psi \rightarrow \eta_c \gamma$

¹ The quoted branching ratios use $B(J/\psi(1S) \rightarrow \gamma\eta_c(1S)) = 0.0127 \pm 0.0036$.

 $\Gamma(K^*(892)\bar{K} + c.c.)/\Gamma_{\text{total}}$ Γ_{11}/Γ

VALUE	CL%	DOCUMENT ID	TECN	COMMENT
<0.0128	90	¹ BISELLO	91 DM2	$J/\psi \rightarrow \gamma K_S^0 K^\pm \pi^\mp$
<0.0132	90	¹ BISELLO	91 DM2	$J/\psi \rightarrow \gamma K^+ K^- \pi^0$

¹ The quoted branching ratios use $B(J/\psi(1S) \rightarrow \gamma\eta_c(1S)) = 0.0127 \pm 0.0036$.

 $\Gamma(f_2(1270)\eta)/\Gamma_{\text{total}}$ Γ_{12}/Γ

VALUE	CL%	DOCUMENT ID	TECN	COMMENT
<0.011	90	¹ BALTRUSAIT..86	MRK3	$J/\psi \rightarrow \eta_c \gamma$

¹ The quoted branching ratios use $B(J/\psi(1S) \rightarrow \gamma\eta_c(1S)) = 0.0127 \pm 0.0036$.

 $\Gamma(\omega\omega)/\Gamma_{\text{total}}$ Γ_{13}/Γ

VALUE (units 10^{-3})	CL%	EVTS	DOCUMENT ID	TECN	COMMENT
2.9 ± 0.5 ± 0.6		1705	¹ ABLIKIM	19AP BES3	$J/\psi \rightarrow \gamma\omega\omega$

• • • We do not use the following data for averages, fits, limits, etc. • • •

<6.3	90	² ABLIKIM	05L BES2	$J/\psi \rightarrow 2(\pi^+ \pi^- \pi^0) \gamma$
<6.3	90	² BISELLO	91 DM2	$J/\psi \rightarrow \gamma\omega\omega$
<3.1	90	² BALTRUSAIT..86	MRK3	$J/\psi \rightarrow \eta_c \gamma$

¹ ABLIKIM 19AP reports $[\Gamma(\eta_c(1S) \rightarrow \omega\omega)/\Gamma_{\text{total}}] \times [B(J/\psi(1S) \rightarrow \gamma\eta_c(1S))] = (4.90 \pm 0.17 \pm 0.77) \times 10^{-3}$ which we divide by our best value $B(J/\psi(1S) \rightarrow \gamma\eta_c(1S)) = (1.7 \pm 0.4) \times 10^{-2}$. Our first error is their experiment's error and our second error is the systematic error from using our best value.

² The quoted branching ratios use $B(J/\psi(1S) \rightarrow \gamma\eta_c(1S)) = 0.0127 \pm 0.0036$. Where relevant, the error in this branching ratio is treated as a common systematic in computing averages.

 $\Gamma(\omega\phi)/\Gamma_{\text{total}}$ Γ_{14}/Γ

VALUE	CL%	DOCUMENT ID	TECN	COMMENT
< 2.5 × 10⁻⁴	90	¹ ABLIKIM	17P BES3	$J/\psi \rightarrow \pi^+ \pi^- \pi^0 K^+ K^- \gamma$

• • • We do not use the following data for averages, fits, limits, etc. • • •

<17 × 10 ⁻⁴	90	² ABLIKIM	05L BES2	$J/\psi \rightarrow \pi^+ \pi^- \pi^0 K^+ K^- \gamma$
------------------------	----	----------------------	----------	---

¹ Using $B(J/\psi \rightarrow \gamma\eta_c) = 0.017 \pm 0.004$.

² The quoted branching ratios use $B(J/\psi(1S) \rightarrow \gamma\eta_c(1S)) = 0.0127 \pm 0.0036$.

 $\Gamma(f_2(1270)f_2(1270))/\Gamma_{\text{total}}$ Γ_{15}/Γ

VALUE (units 10^{-2})	EVTS	DOCUMENT ID	TECN	COMMENT
0.98 ± 0.25 OUR FIT				
0.77 $\pm \frac{0.25}{-0.30} \pm 0.17$	91.2 ± 19.8	¹ ABLIKIM	04M BES	$J/\psi \rightarrow \gamma 2\pi^+ 2\pi^-$

¹ ABLIKIM 04M reports $[\Gamma(\eta_c(1S) \rightarrow f_2(1270)f_2(1270))/\Gamma_{\text{total}}] \times [B(J/\psi(1S) \rightarrow \gamma\eta_c(1S))] = (1.3 \pm 0.3 \pm 0.3) \times 10^{-4}$ which we divide by our best value $B(J/\psi(1S) \rightarrow \gamma\eta_c(1S)) = (1.7 \pm 0.4) \times 10^{-2}$. Our first error is their experiment's error and our second error is the systematic error from using our best value.

 $\Gamma(f_0(980)\eta)/\Gamma_{\text{total}}$ Γ_{17}/Γ

VALUE	DOCUMENT ID	TECN	COMMENT
seen	LEES	14E BABR	Dalitz anal. of $\eta_c \rightarrow K^+ K^- \eta$

 $\Gamma(f_0(1500)\eta)/\Gamma_{\text{total}}$ Γ_{18}/Γ

VALUE	DOCUMENT ID	TECN	COMMENT
seen	LEES	14E BABR	Dalitz anal. of $\eta_c \rightarrow K^+ K^- \eta$

 $\Gamma(f_0(2200)\eta)/\Gamma_{\text{total}}$ Γ_{19}/Γ

VALUE	DOCUMENT ID	TECN	COMMENT
seen	LEES	14E BABR	Dalitz anal. of $\eta_c \rightarrow K^+ K^- \eta$

 $\Gamma(a_0(980)\pi)/\Gamma_{\text{total}}$ Γ_{20}/Γ

VALUE	DOCUMENT ID	TECN	COMMENT
seen	LEES	14E BABR	Dalitz anal. of $\eta_c \rightarrow K^+ K^- \pi^0$

 $\Gamma(a_0(1320)\pi)/\Gamma_{\text{total}}$ Γ_{21}/Γ

VALUE	DOCUMENT ID	TECN	COMMENT
seen	LEES	14E BABR	Dalitz anal. of $\eta_c \rightarrow K^+ K^- \pi^0$

 $\Gamma(a_0(1450)\pi)/\Gamma_{\text{total}}$ Γ_{22}/Γ

VALUE	DOCUMENT ID	TECN	COMMENT
seen	LEES	14E BABR	Dalitz anal. of $\eta_c \rightarrow K^+ K^- \pi^0$

 $\Gamma(a_0(1950)\pi)/\Gamma_{\text{total}}$ Γ_{23}/Γ

VALUE	EVTS	DOCUMENT ID	TECN	COMMENT
seen	12k	¹ LEES	16A BABR	$\gamma\gamma \rightarrow \eta_c(1S) \rightarrow K\bar{K}\pi$

¹ From a model-independent partial wave analysis.

 $\Gamma(K_0^*(1430)\bar{K})/\Gamma_{\text{total}}$ Γ_{24}/Γ

VALUE	EVTS	DOCUMENT ID	TECN	COMMENT
seen	12k	¹ LEES	16A BABR	$\gamma\gamma \rightarrow \eta_c(1S) \rightarrow K\bar{K}\pi$
seen		LEES	14E BABR	Dalitz anal. of $\eta_c \rightarrow K^+ K^- \eta/\pi^0$

¹ From a model-independent partial wave analysis.

 $\Gamma(K_2^*(1430)\bar{K})/\Gamma_{\text{total}}$ Γ_{25}/Γ

VALUE	DOCUMENT ID	TECN	COMMENT
seen	LEES	14E BABR	Dalitz anal. of $\eta_c \rightarrow K^+ K^- \pi^0$

 $\Gamma(K_0^*(1950)\bar{K})/\Gamma_{\text{total}}$ Γ_{26}/Γ

VALUE	EVTS	DOCUMENT ID	TECN	COMMENT
seen	12K	¹ LEES	16A BABR	$\gamma\gamma \rightarrow \eta_c(1S) \rightarrow K\bar{K}\pi$
seen		LEES	14E BABR	Dalitz anal. of $\eta_c \rightarrow K^+ K^- \eta/\pi^0$

¹ From a Dalitz plot analysis using an isobar model.

 $\Gamma(K\bar{K}\pi)/\Gamma_{\text{total}}$ Γ_{27}/Γ

VALUE (units 10^{-2})	EVTS	DOCUMENT ID	TECN	COMMENT
7.3 ± 0.4 OUR FIT				
6.9 ± 0.4 OUR AVERAGE				
6.9 ± 0.7 ± 0.6	146	¹ ABLIKIM	19AP BES3	$h_c \rightarrow \gamma\eta_c$
7.8 ± 0.6 ± 0.6	267	² ABLIKIM	19AP BES3	$h_c \rightarrow \gamma\eta_c$
6.3 ± 1.3 ± 0.6	55	^{3,4} ABLIKIM	12N BES3	$\psi(2S) \rightarrow \pi^0 \gamma K^+ K^- \pi^0$
7.9 ± 1.4 ± 0.7	107	^{5,6} ABLIKIM	12N BES3	$\psi(2S) \rightarrow \pi^0 \gamma K_S^0 K^\mp \pi^\pm$
8.5 ± 1.8		⁷ AUBERT	06E BABR	$B^\pm \rightarrow K^\pm X_{c\bar{c}}$
5.1 ± 2.1	0.6k	⁸ BAI	04 BES	$J/\psi \rightarrow \gamma K^\pm \pi^\mp K_S^0$
6.90 ± 1.42 ± 1.32	33	⁸ BISELLO	91 DM2	$J/\psi \rightarrow \gamma K^+ K^- \pi^0$
5.43 ± 0.94 ± 0.94	68	⁸ BISELLO	91 DM2	$J/\psi \rightarrow \gamma K^\pm \pi^\mp K_S^0$
4.8 ± 1.7	95	^{8,9} BALTRUSAIT..86	MRK3	$J/\psi \rightarrow \eta_c \gamma$
16.1 $\pm \frac{9.2}{-7.3}$		^{10,11} HIMEL	80B MRK2	$\psi(2S) \rightarrow \eta_c \gamma$

- • • We do not use the following data for averages, fits, limits, etc. • • •
- < 10.7 90% CL ^{8,12} PARTRIDGE 80B CBAL $J/\psi \rightarrow \eta_c \gamma$
- ¹ ABLIKIM 19AP quotes $B(\eta_c \rightarrow K^+ K^- \pi^0) = (1.15 \pm 0.12 \pm 0.10) \times 10^{-2}$ which we multiply by 6 to account for isospin symmetry.
- ² ABLIKIM 19AP quotes $B(\eta_c \rightarrow K_S^0 K^\pm \pi^\mp) = (2.60 \pm 0.21 \pm 0.20) \times 10^{-2}$ which we multiply by 3 to account for isospin symmetry.
- ³ ABLIKIM 12N quotes $B(\psi(2S) \rightarrow \pi^0 h_c) \cdot B(h_c \rightarrow \gamma \eta_c) \cdot B(\eta_c \rightarrow K^+ K^- \pi^0) = (4.54 \pm 0.76 \pm 0.48) \times 10^{-6}$ which we multiply by 6 to account for isospin symmetry.
- ⁴ ABLIKIM 12N reports $[\Gamma(\eta_c(1S) \rightarrow K \bar{K} \pi)/\Gamma_{\text{total}}] \times [\Gamma(h_c(1P) \rightarrow \gamma \eta_c(1S))/\Gamma_{\text{total}} \times \Gamma(\psi(2S) \rightarrow \pi^0 h_c(1P))/\Gamma_{\text{total}}] = (27.24 \pm 4.56 \pm 2.88) \times 10^{-6}$ which we divide by our best value $\Gamma(h_c(1P) \rightarrow \gamma \eta_c(1S))/\Gamma_{\text{total}} \times \Gamma(\psi(2S) \rightarrow \pi^0 h_c(1P))/\Gamma_{\text{total}} = (4.3 \pm 0.4) \times 10^{-4}$. Our first error is their experiment's error and our second error is the systematic error from using our best value.
- ⁵ ABLIKIM 12N quotes $B(\psi(2S) \rightarrow \pi^0 h_c) \cdot B(h_c \rightarrow \gamma \eta_c) \cdot B(\eta_c \rightarrow K_S^0 K^\pm \pi^\mp) = (11.35 \pm 1.25 \pm 1.50) \times 10^{-6}$ which we multiply by 3 to account for isospin symmetry.
- ⁶ ABLIKIM 12N reports $[\Gamma(\eta_c(1S) \rightarrow K \bar{K} \pi)/\Gamma_{\text{total}}] \times [\Gamma(h_c(1P) \rightarrow \gamma \eta_c(1S))/\Gamma_{\text{total}} \times \Gamma(\psi(2S) \rightarrow \pi^0 h_c(1P))/\Gamma_{\text{total}}] = (34.05 \pm 3.75 \pm 4.50) \times 10^{-6}$ which we divide by our best value $\Gamma(h_c(1P) \rightarrow \gamma \eta_c(1S))/\Gamma_{\text{total}} \times \Gamma(\psi(2S) \rightarrow \pi^0 h_c(1P))/\Gamma_{\text{total}} = (4.3 \pm 0.4) \times 10^{-4}$. Our first error is their experiment's error and our second error is the systematic error from using our best value.
- ⁷ Determined from the ratio of $B(B^\pm \rightarrow K^\pm \eta_c) B(\eta_c \rightarrow K \bar{K} \pi) = (7.4 \pm 0.5 \pm 0.7) \times 10^{-5}$ reported in AUBERT, B 04B and $B(B^\pm \rightarrow K^\pm \eta_c) = (8.7 \pm 1.5) \times 10^{-3}$ reported in AUBERT 06E.
- ⁸ The quoted branching ratios use $B(J/\psi(1S) \rightarrow \gamma \eta_c(1S)) = 0.0127 \pm 0.0036$. Where relevant, the error in this branching ratio is treated as a common systematic in computing averages.
- ⁹ Average from $K^+ K^- \pi^0$ and $K^\pm K_S^0 \pi^\mp$ decay channels.
- ¹⁰ $K^\pm K_S^0 \pi^\mp$ corrected to $K \bar{K} \pi$ by factor 3. KS, MR.
- ¹¹ Estimated using $B(\psi(2S) \rightarrow \gamma \eta_c(1S)) = 0.0028 \pm 0.0006$.
- ¹² $K^+ K^- \pi^0$ corrected to $K \bar{K} \pi$ by factor 6. KS, MR

$\Gamma(\phi K^+ K^-)/\Gamma(K \bar{K} \pi)$ Γ_6/Γ_{27}

VALUE	EVTS	DOCUMENT ID	TECN	COMMENT
0.052 ± 0.016 ± 0.014	7	¹ HUANG 03	BELL	$B^\pm \rightarrow K^\pm \phi$

¹ Using $B(B^+ \rightarrow \eta_c K^+) = (1.25 \pm 0.12_{-0.10}^{+0.10}) \times 10^{-3}$ from FANG 03 and $B(\eta_c \rightarrow K \bar{K} \pi) = (5.5 \pm 1.7) \times 10^{-2}$.

$\Gamma(K \bar{K} \eta)/\Gamma_{\text{total}}$ Γ_{28}/Γ

VALUE (units 10 ⁻²)	CL%	EVTS	DOCUMENT ID	TECN	COMMENT
1.36 ± 0.15 OUR FIT					
1.0 ± 0.5 ± 0.2		7	^{1,2} ABLIKIM 12N	BES3	$\psi(2S) \rightarrow \pi^0 \gamma \eta K^+ K^-$

- • • We do not use the following data for averages, fits, limits, etc. • • •
- < 3.1 90 ³ BALTRUSAIT...86 MRK3 $J/\psi \rightarrow \eta_c \gamma$
- ¹ ABLIKIM 12N quotes $B(\psi(2S) \rightarrow \pi^0 h_c) \cdot B(h_c \rightarrow \gamma \eta_c) \cdot B(\eta_c \rightarrow K^+ K^- \eta) = (2.11 \pm 1.01 \pm 0.32) \times 10^{-6}$ which we multiply by 2 to account for isospin symmetry.
- ² ABLIKIM 12N reports $[\Gamma(\eta_c(1S) \rightarrow K \bar{K} \eta)/\Gamma_{\text{total}}] \times [B(\psi(2S) \rightarrow \pi^0 h_c(1P))] \times [B(h_c(1P) \rightarrow \gamma \eta_c(1S))] = (4.22 \pm 2.02 \pm 0.64) \times 10^{-6}$ which we divide by our best values $B(\psi(2S) \rightarrow \pi^0 h_c(1P)) = (8.6 \pm 1.3) \times 10^{-4}$, $B(h_c(1P) \rightarrow \gamma \eta_c(1S)) = (51 \pm 6) \times 10^{-2}$. Our first error is their experiment's error and our second error is the systematic error from using our best values.
- ³ The quoted branching ratios use $B(J/\psi(1S) \rightarrow \gamma \eta_c(1S)) = 0.0127 \pm 0.0036$.

$\Gamma(K \bar{K} \eta)/\Gamma(K \bar{K} \pi)$ Γ_{28}/Γ_{27}

VALUE	EVTS	DOCUMENT ID	TECN	COMMENT
0.186 ± 0.018 OUR FIT				
0.190 ± 0.008 ± 0.017	5.4k	¹ LEES 14E	BABR	$\gamma \gamma \rightarrow K^+ K^- \eta/\pi^0$

¹ LEES 14E reports $B(\eta_c(1S) \rightarrow K^+ K^- \eta)/B(\eta_c(1S) \rightarrow K^+ K^- \pi^0) = 0.571 \pm 0.025 \pm 0.051$, which we divide by 3 to account for isospin symmetry. It uses both $\eta \rightarrow \gamma \gamma$ and $\eta \rightarrow \pi^+ \pi^- \pi^0$ decays.

$\Gamma(\eta \pi^+ \pi^-)/\Gamma_{\text{total}}$ Γ_{29}/Γ

VALUE (units 10 ⁻²)	EVTS	DOCUMENT ID	TECN	COMMENT
1.7 ± 0.4 ± 0.1	33	¹ ABLIKIM 12N	BES3	$\psi(2S) \rightarrow \pi^0 \gamma \eta \pi^+ \pi^-$

- • • We do not use the following data for averages, fits, limits, etc. • • •
- 5.4 ± 2.0 ² BALTRUSAIT...86 MRK3 $J/\psi \rightarrow \eta_c \gamma$
- 3.7 ± 1.3 ± 2.0 ² PARTRIDGE 80B CBAL $J/\psi \rightarrow \eta \pi^+ \pi^- \gamma$
- ¹ ABLIKIM 12N reports $[\Gamma(\eta_c(1S) \rightarrow \eta \pi^+ \pi^-)/\Gamma_{\text{total}}] \times [\Gamma(h_c(1P) \rightarrow \gamma \eta_c(1S))/\Gamma_{\text{total}} \times \Gamma(\psi(2S) \rightarrow \pi^0 h_c(1P))/\Gamma_{\text{total}}] = (7.22 \pm 1.47 \pm 1.11) \times 10^{-6}$ which we divide by our best value $\Gamma(h_c(1P) \rightarrow \gamma \eta_c(1S))/\Gamma_{\text{total}} \times \Gamma(\psi(2S) \rightarrow \pi^0 h_c(1P))/\Gamma_{\text{total}} = (4.3 \pm 0.4) \times 10^{-4}$. Our first error is their experiment's error and our second error is the systematic error from using our best value.
- ² The quoted branching ratios use $B(J/\psi(1S) \rightarrow \gamma \eta_c(1S)) = 0.0127 \pm 0.0036$. Where relevant, the error in this branching ratio is treated as a common systematic in computing averages.

$\Gamma(\eta(2\pi^+ \pi^-))/\Gamma_{\text{total}}$ Γ_{30}/Γ

VALUE (units 10 ⁻²)	EVTS	DOCUMENT ID	TECN	COMMENT
4.4 ± 1.2 ± 0.4	39	¹ ABLIKIM 12N	BES3	$\psi(2S) \rightarrow \pi^0 \gamma \eta(2\pi^+ \pi^-)$

¹ ABLIKIM 12N reports $[\Gamma(\eta_c(1S) \rightarrow \eta(2\pi^+ \pi^-))/\Gamma_{\text{total}}] \times [\Gamma(h_c(1P) \rightarrow \gamma \eta_c(1S))/\Gamma_{\text{total}} \times \Gamma(\psi(2S) \rightarrow \pi^0 h_c(1P))/\Gamma_{\text{total}}] = (19.17 \pm 3.77 \pm 3.72) \times 10^{-6}$ which we divide by our best value $\Gamma(h_c(1P) \rightarrow \gamma \eta_c(1S))/\Gamma_{\text{total}} \times \Gamma(\psi(2S) \rightarrow \pi^0 h_c(1P))/\Gamma_{\text{total}} = (4.3 \pm 0.4) \times 10^{-4}$. Our first error is their experiment's error and our second error is the systematic error from using our best value.

$\Gamma(K^+ K^- \pi^+ \pi^-)/\Gamma_{\text{total}}$ Γ_{31}/Γ

VALUE (units 10 ⁻³)	EVTS	DOCUMENT ID	TECN	COMMENT
6.9 ± 1.0 OUR FIT				
11.2 ± 1.9 OUR AVERAGE				
9.7 ± 2.2 ± 0.9	38	¹ ABLIKIM 12N	BES3	$\psi(2S) \rightarrow \pi^0 \gamma K^+ K^- \pi^+ \pi^-$
12 ± 4	0.4k	² BAI 04	BES	$J/\psi \rightarrow \gamma K^+ K^- \pi^+ \pi^-$
21 ± 7	110	² BALTRUSAIT...86	MRK3	$J/\psi \rightarrow \eta_c \gamma$
14 ± ⁺²² / ₉		³ HIMEL	.80B	MRK2 $\psi(2S) \rightarrow \eta_c \gamma$

- ¹ ABLIKIM 12N reports $[\Gamma(\eta_c(1S) \rightarrow K^+ K^- \pi^+ \pi^-)/\Gamma_{\text{total}}] \times [\Gamma(h_c(1P) \rightarrow \gamma \eta_c(1S))/\Gamma_{\text{total}} \times \Gamma(\psi(2S) \rightarrow \pi^0 h_c(1P))/\Gamma_{\text{total}}] = (4.16 \pm 0.76 \pm 0.59) \times 10^{-6}$ which we divide by our best value $\Gamma(h_c(1P) \rightarrow \gamma \eta_c(1S))/\Gamma_{\text{total}} \times \Gamma(\psi(2S) \rightarrow \pi^0 h_c(1P))/\Gamma_{\text{total}} = (4.3 \pm 0.4) \times 10^{-4}$. Our first error is their experiment's error and our second error is the systematic error from using our best value.
- ² The quoted branching ratios use $B(J/\psi(1S) \rightarrow \gamma \eta_c(1S)) = 0.0127 \pm 0.0036$. Where relevant, the error in this branching ratio is treated as a common systematic in computing averages.
- ³ Estimated using $B(\psi(2S) \rightarrow \gamma \eta_c(1S)) = 0.0028 \pm 0.0006$.

$\Gamma(K^+ K^- \pi^+ \pi^- \pi^0)/\Gamma(K \bar{K} \pi)$ Γ_{32}/Γ_{27}

VALUE	EVTS	DOCUMENT ID	TECN	COMMENT
0.477 ± 0.017 ± 0.070	11k	¹ DEL-AMO-SA...11M	BABR	$\gamma \gamma \rightarrow K^+ K^- \pi^+ \pi^- \pi^0$

¹ We have multiplied the value of $\Gamma(K^+ K^- \pi^+ \pi^- \pi^0)/\Gamma(K_S^0 K^\pm \pi^\mp)$ reported in DEL-AMO-SANCHEZ 11M by a factor 1/3 to obtain $\Gamma(K^+ K^- \pi^+ \pi^- \pi^0)/\Gamma(K \bar{K} \pi)$. Not independent from other measurements reported in DEL-AMO-SANCHEZ 11M.

$\Gamma(K^0 K^- \pi^+ \pi^- \pi^+ + c.c.)/\Gamma_{\text{total}}$ Γ_{33}/Γ

VALUE (units 10 ⁻²)	EVTS	DOCUMENT ID	TECN	COMMENT
5.6 ± 1.4 ± 0.5	43	^{1,2} ABLIKIM 12N	BES3	$\psi(2S) \rightarrow \pi^0 \gamma K_S^0 K^\mp \pi^\mp 2\pi^\pm$

- ¹ ABLIKIM 12N quotes $B(\psi(2S) \rightarrow \pi^0 h_c) \cdot B(h_c \rightarrow \gamma \eta_c) \cdot B(\eta_c \rightarrow K_S^0 K^- \pi^- 2\pi^+) = (12.01 \pm 2.22 \pm 2.04) \times 10^{-6}$ which we multiply by 2 to take c.c. into account.
- ² ABLIKIM 12N reports $[\Gamma(\eta_c(1S) \rightarrow K^0 K^- \pi^+ \pi^- \pi^+ + c.c.)/\Gamma_{\text{total}}] \times [\Gamma(h_c(1P) \rightarrow \gamma \eta_c(1S))/\Gamma_{\text{total}} \times \Gamma(\psi(2S) \rightarrow \pi^0 h_c(1P))/\Gamma_{\text{total}}] = (24.02 \pm 4.44 \pm 4.08) \times 10^{-6}$ which we divide by our best value $\Gamma(h_c(1P) \rightarrow \gamma \eta_c(1S))/\Gamma_{\text{total}} \times \Gamma(\psi(2S) \rightarrow \pi^0 h_c(1P))/\Gamma_{\text{total}} = (4.3 \pm 0.4) \times 10^{-4}$. Our first error is their experiment's error and our second error is the systematic error from using our best value.

$\Gamma(K^+ K^- 2(\pi^+ \pi^-))/\Gamma_{\text{total}}$ Γ_{34}/Γ

VALUE (units 10 ⁻³)	EVTS	DOCUMENT ID	TECN	COMMENT
7.5 ± 2.4 OUR AVERAGE				
8 ± 4 ± 1	10	¹ ABLIKIM 12N	BES3	$\psi(2S) \rightarrow \pi^0 \gamma K^+ K^- 2(\pi^+ \pi^-)$
7.2 ± 2.4 ± 1.5	100	² ABLIKIM 06A	BES2	$J/\psi \rightarrow K^+ K^- 2(\pi^+ \pi^-) \gamma$

- ¹ ABLIKIM 12N reports $[\Gamma(\eta_c(1S) \rightarrow K^+ K^- 2(\pi^+ \pi^-))/\Gamma_{\text{total}}] \times [\Gamma(h_c(1P) \rightarrow \gamma \eta_c(1S))/\Gamma_{\text{total}} \times \Gamma(\psi(2S) \rightarrow \pi^0 h_c(1P))/\Gamma_{\text{total}}] = (3.60 \pm 1.71 \pm 0.64) \times 10^{-6}$ which we divide by our best value $\Gamma(h_c(1P) \rightarrow \gamma \eta_c(1S))/\Gamma_{\text{total}} \times \Gamma(\psi(2S) \rightarrow \pi^0 h_c(1P))/\Gamma_{\text{total}} = (4.3 \pm 0.4) \times 10^{-4}$. Our first error is their experiment's error and our second error is the systematic error from using our best value.
- ² ABLIKIM 06A reports $[\Gamma(\eta_c(1S) \rightarrow K^+ K^- 2(\pi^+ \pi^-))/\Gamma_{\text{total}}] \times [B(J/\psi(1S) \rightarrow \gamma \eta_c(1S))] = (1.21 \pm 0.32 \pm 0.24) \times 10^{-4}$ which we divide by our best value $B(J/\psi(1S) \rightarrow \gamma \eta_c(1S)) = (1.7 \pm 0.4) \times 10^{-2}$. Our first error is their experiment's error and our second error is the systematic error from using our best value.

$\Gamma(2(K^+ K^-))/\Gamma_{\text{total}}$ Γ_{35}/Γ

VALUE (units 10 ⁻³)	EVTS	DOCUMENT ID	TECN	COMMENT
1.46 ± 0.30 OUR FIT				
2.2 ± 0.9 ± 0.2	7	¹ ABLIKIM 12N	BES3	$\psi(2S) \rightarrow \pi^0 \gamma 2(K^+ K^-)$

- • • We do not use the following data for averages, fits, limits, etc. • • •
- 1.4 ± ^{0.5}/_{0.4} ± 0.6 ² HUANG 03 BELL $B^+ \rightarrow 2(K^+ K^-) K^+$
- 21 ± 10 ± 6 ³ ALBRECHT 94H ARG $\gamma \gamma \rightarrow K^+ K^- K^+ K^-$
- ¹ ABLIKIM 12N reports $[\Gamma(\eta_c(1S) \rightarrow 2(K^+ K^-))/\Gamma_{\text{total}}] \times [\Gamma(h_c(1P) \rightarrow \gamma \eta_c(1S))/\Gamma_{\text{total}} \times \Gamma(\psi(2S) \rightarrow \pi^0 h_c(1P))/\Gamma_{\text{total}}] = (0.94 \pm 0.37 \pm 0.14) \times 10^{-6}$ which we divide by our best value $\Gamma(h_c(1P) \rightarrow \gamma \eta_c(1S))/\Gamma_{\text{total}} \times \Gamma(\psi(2S) \rightarrow \pi^0 h_c(1P))/\Gamma_{\text{total}} = (4.3 \pm 0.4) \times 10^{-4}$. Our first error is their experiment's error and our second error is the systematic error from using our best value.
- ² Using $B(B^+ \rightarrow \eta_c K^+) = (1.25 \pm 0.12_{-0.10}^{+0.10}) \times 10^{-3}$ from FANG 03 and $B(\eta_c \rightarrow K \bar{K} \pi) = (5.5 \pm 1.7) \times 10^{-2}$.
- ³ Normalized to the sum of $B(\eta_c \rightarrow K^\pm K_S^0 \pi^\mp)$, $B(\eta_c \rightarrow \phi \phi)$, $B(\eta_c \rightarrow K^+ K^- \pi^+ \pi^-)$, and $B(\eta_c \rightarrow 2\pi^+ 2\pi^-)$.

$\Gamma(2(K^+ K^-))/\Gamma(K \bar{K} \pi)$ Γ_{35}/Γ_{27}

VALUE	EVTS	DOCUMENT ID	TECN	COMMENT
0.020 ± 0.004 OUR FIT				
0.024 ± 0.007 OUR AVERAGE				
0.023 ± 0.007 ± 0.006		AUBERT, B 04B	BABR	$B^\pm \rightarrow K^\pm \eta_c$
0.026 ± 0.009 ± 0.007	15	¹ HUANG 03	BELL	$B^\pm \rightarrow K^\pm (2K^+ 2K^-)$

¹ Using $B(B^+ \rightarrow \eta_c K^+) = (1.25 \pm 0.12_{-0.10}^{+0.10}) \times 10^{-3}$ from FANG 03 and $B(\eta_c \rightarrow K \bar{K} \pi) = (5.5 \pm 1.7) \times 10^{-2}$.

Meson Particle Listings

 $\eta_c(1S)$

$\Gamma(\pi^+\pi^-\pi^0)/\Gamma_{\text{total}}$ Γ_{36}/Γ

VALUE	CL%	DOCUMENT ID	TECN	COMMENT
$<5 \times 10^{-4}$	90	1 ABLIKIM	17AJ BES3	$\psi(2S) \rightarrow \gamma\pi^+\pi^-\pi^0$

¹ ABLIKIM 17AJ reports $[\Gamma(\eta_c(1S) \rightarrow \pi^+\pi^-\pi^0)/\Gamma_{\text{total}}] \times [B(\psi(2S) \rightarrow \gamma\eta_c(1S))]$ $< 1.6 \times 10^{-6}$ which we divide by our best value $B(\psi(2S) \rightarrow \gamma\eta_c(1S)) = 3.4 \times 10^{-3}$.

$\Gamma(\pi^+\pi^-\pi^0\pi^0)/\Gamma_{\text{total}}$ Γ_{37}/Γ

VALUE (units 10^{-2})	EVTS	DOCUMENT ID	TECN	COMMENT
$4.7 \pm 0.9 \pm 0.4$	118	1 ABLIKIM	12N BES3	$\psi(2S) \rightarrow \pi^0\gamma\pi^+\pi^-\pi^0$

¹ ABLIKIM 12N reports $[\Gamma(\eta_c(1S) \rightarrow \pi^+\pi^-\pi^0\pi^0)/\Gamma_{\text{total}}] \times [\Gamma(h_c(1P) \rightarrow \gamma\eta_c(1S))/\Gamma_{\text{total}} \times \Gamma(\psi(2S) \rightarrow \pi^0 h_c(1P))/\Gamma_{\text{total}}] = (20.31 \pm 2.20 \pm 3.33) \times 10^{-6}$ which we divide by our best value $\Gamma(h_c(1P) \rightarrow \gamma\eta_c(1S))/\Gamma_{\text{total}} \times \Gamma(\psi(2S) \rightarrow \pi^0 h_c(1P))/\Gamma_{\text{total}} = (4.3 \pm 0.4) \times 10^{-4}$. Our first error is their experiment's error and our second error is the systematic error from using our best value.

$\Gamma(2(\pi^+\pi^-))/\Gamma_{\text{total}}$ Γ_{38}/Γ

VALUE (units 10^{-2})	EVTS	DOCUMENT ID	TECN	COMMENT
0.97 ± 0.12 OUR FIT				
1.35 ± 0.21 OUR AVERAGE				
$1.74 \pm 0.32 \pm 0.15$	100	1 ABLIKIM	12N BES3	$\psi(2S) \rightarrow \pi^0\gamma 2(\pi^+\pi^-)$
1.0 ± 0.5	542 ± 75	2 BAI	04 BES	$J/\psi \rightarrow \gamma 2(\pi^+\pi^-)$
$1.05 \pm 0.17 \pm 0.34$	137	2 BISELLO	91 DM2	$J/\psi \rightarrow \gamma 2\pi^+ 2\pi^-$
1.3 ± 0.6	25	2 BALTRUSAIT..86	MRK3	$J/\psi \rightarrow \eta_c\gamma$
2.0 ± 1.5		3 HIMEL	80B MRK2	$\psi(2S) \rightarrow \eta_c\gamma$

¹ ABLIKIM 12N reports $[\Gamma(\eta_c(1S) \rightarrow 2(\pi^+\pi^-))/\Gamma_{\text{total}}] \times [\Gamma(h_c(1P) \rightarrow \gamma\eta_c(1S))/\Gamma_{\text{total}} \times \Gamma(\psi(2S) \rightarrow \pi^0 h_c(1P))/\Gamma_{\text{total}}] = (7.51 \pm 0.85 \pm 1.11) \times 10^{-6}$ which we divide by our best value $\Gamma(h_c(1P) \rightarrow \gamma\eta_c(1S))/\Gamma_{\text{total}} \times \Gamma(\psi(2S) \rightarrow \pi^0 h_c(1P))/\Gamma_{\text{total}} = (4.3 \pm 0.4) \times 10^{-4}$. Our first error is their experiment's error and our second error is the systematic error from using our best value.

² The quoted branching ratios use $B(J/\psi(1S) \rightarrow \gamma\eta_c(1S)) = 0.0127 \pm 0.0036$. Where relevant, the error in this branching ratio is treated as a common systematic in computing averages.

³ Estimated using $B(\psi(2S) \rightarrow \gamma\eta_c(1S)) = 0.0028 \pm 0.0006$.

$\Gamma(2(\pi^+\pi^-\pi^0))/\Gamma_{\text{total}}$ Γ_{39}/Γ

VALUE (units 10^{-2})	EVTS	DOCUMENT ID	TECN	COMMENT
16.1 ± 2.0 OUR AVERAGE				
$15.3 \pm 1.8 \pm 1.8$	333	ABLIKIM	19AP BES3	$h_c \rightarrow \gamma\eta_c$
$17.4 \pm 2.9 \pm 1.5$	175	1 ABLIKIM	12N BES3	$\psi(2S) \rightarrow \pi^0\gamma 2(\pi^+\pi^-\pi^0)$

¹ ABLIKIM 12N reports $[\Gamma(\eta_c(1S) \rightarrow 2(\pi^+\pi^-\pi^0))/\Gamma_{\text{total}}] \times [\Gamma(h_c(1P) \rightarrow \gamma\eta_c(1S))/\Gamma_{\text{total}} \times \Gamma(\psi(2S) \rightarrow \pi^0 h_c(1P))/\Gamma_{\text{total}}] = (75.13 \pm 7.42 \pm 9.99) \times 10^{-6}$ which we divide by our best value $\Gamma(h_c(1P) \rightarrow \gamma\eta_c(1S))/\Gamma_{\text{total}} \times \Gamma(\psi(2S) \rightarrow \pi^0 h_c(1P))/\Gamma_{\text{total}} = (4.3 \pm 0.4) \times 10^{-4}$. Our first error is their experiment's error and our second error is the systematic error from using our best value.

$\Gamma(3(\pi^+\pi^-))/\Gamma_{\text{total}}$ Γ_{40}/Γ

VALUE (units 10^{-3})	EVTS	DOCUMENT ID	TECN	COMMENT
18 ± 4 OUR AVERAGE				
$20 \pm 5 \pm 2$	51	1 ABLIKIM	12N BES3	$\psi(2S) \rightarrow \pi^0\gamma 3(\pi^+\pi^-)$
$15.4 \pm 3.4 \pm 3.3$	479	2 ABLIKIM	06A BES2	$J/\psi \rightarrow 3(\pi^+\pi^-)\gamma$

¹ ABLIKIM 12N reports $[\Gamma(\eta_c(1S) \rightarrow 3(\pi^+\pi^-))/\Gamma_{\text{total}}] \times [\Gamma(h_c(1P) \rightarrow \gamma\eta_c(1S))/\Gamma_{\text{total}} \times \Gamma(\psi(2S) \rightarrow \pi^0 h_c(1P))/\Gamma_{\text{total}}] = (8.82 \pm 1.57 \pm 1.59) \times 10^{-6}$ which we divide by our best value $\Gamma(h_c(1P) \rightarrow \gamma\eta_c(1S))/\Gamma_{\text{total}} \times \Gamma(\psi(2S) \rightarrow \pi^0 h_c(1P))/\Gamma_{\text{total}} = (4.3 \pm 0.4) \times 10^{-4}$. Our first error is their experiment's error and our second error is the systematic error from using our best value.

² ABLIKIM 06A reports $[\Gamma(\eta_c(1S) \rightarrow 3(\pi^+\pi^-))/\Gamma_{\text{total}}] \times [B(J/\psi(1S) \rightarrow \gamma\eta_c(1S))] = (2.59 \pm 0.32 \pm 0.47) \times 10^{-4}$ which we divide by our best value $B(J/\psi(1S) \rightarrow \gamma\eta_c(1S)) = (1.7 \pm 0.4) \times 10^{-2}$. Our first error is their experiment's error and our second error is the systematic error from using our best value.

$\Gamma(\rho\bar{\rho})/\Gamma_{\text{total}}$ Γ_{41}/Γ

VALUE (units 10^{-4})	EVTS	DOCUMENT ID	TECN	COMMENT
14.5 ± 1.4 OUR FIT				
12.7 ± 2.0 OUR AVERAGE				
$12.0 \pm 2.6 \pm 1.5$	34	ABLIKIM	19APBES3	$h_c \rightarrow \gamma\eta_c$
$15 \pm 5 \pm 1$	15	1 ABLIKIM	12N BES3	$\psi(2S) \rightarrow \pi^0\gamma\rho\bar{\rho}$
15 ± 6	213 ± 33	2 BAI	04 BES	$J/\psi \rightarrow \gamma\rho\bar{\rho}$
$10 \pm 3 \pm 4$	18	2 BISELLO	91 DM2	$J/\psi \rightarrow \gamma\rho\bar{\rho}$
11 ± 6	23	2 BALTRUSAIT..86	MRK3	$J/\psi \rightarrow \eta_c\gamma$
29 ± 29		3 HIMEL	80B MRK2	$\psi(2S) \rightarrow \eta_c\gamma$

• • • We do not use the following data for averages, fits, limits, etc. • • •

$13.4 \pm 1.9 \pm 1.1$ 195 4 WU 06 BELL $B^+ \rightarrow \rho\bar{\rho}K^+$

¹ ABLIKIM 12N reports $[\Gamma(\eta_c(1S) \rightarrow \rho\bar{\rho})/\Gamma_{\text{total}}] \times [\Gamma(h_c(1P) \rightarrow \gamma\eta_c(1S))/\Gamma_{\text{total}} \times \Gamma(\psi(2S) \rightarrow \pi^0 h_c(1P))/\Gamma_{\text{total}}] = (0.65 \pm 0.19 \pm 0.10) \times 10^{-6}$ which we divide by our best value $\Gamma(h_c(1P) \rightarrow \gamma\eta_c(1S))/\Gamma_{\text{total}} \times \Gamma(\psi(2S) \rightarrow \pi^0 h_c(1P))/\Gamma_{\text{total}} = (4.3 \pm 0.4) \times 10^{-4}$. Our first error is their experiment's error and our second error is the systematic error from using our best value.

² The quoted branching ratios use $B(J/\psi(1S) \rightarrow \gamma\eta_c(1S)) = 0.0127 \pm 0.0036$. Where relevant, the error in this branching ratio is treated as a common systematic in computing averages.

³ Estimated using $B(\psi(2S) \rightarrow \gamma\eta_c(1S)) = 0.0028 \pm 0.0006$.

⁴ WU 06 reports $[\Gamma(\eta_c(1S) \rightarrow \rho\bar{\rho})/\Gamma_{\text{total}}] \times [B(B^+ \rightarrow \eta_c K^+)] = (1.42 \pm 0.11 \pm 0.16) \times 10^{-6}$ which we divide by our best value $B(B^+ \rightarrow \eta_c K^+) = (1.06 \pm 0.09) \times 10^{-3}$. Our first error is their experiment's error and our second error is the systematic error from using our best value.

$\Gamma(\rho\bar{\rho})/\Gamma(K\bar{K}\pi)$ Γ_{41}/Γ_{27}

VALUE	EVTS	DOCUMENT ID	TECN	COMMENT
0.0199 ± 0.0019 OUR FIT				
$0.021 \pm 0.002 \pm 0.004$	195	1 WU	06 BELL	$B^\pm \rightarrow K^\pm \rho\bar{\rho}$

¹ Using $B(B^+ \rightarrow \eta_c K^+) = (1.25 \pm 0.12 \pm 0.10) \times 10^{-3}$ from FANG 03 and $B(\eta_c \rightarrow K\bar{K}\pi) = (5.5 \pm 1.7) \times 10^{-2}$.

$\Gamma(\rho\bar{\rho})/\Gamma_{\text{total}} \times \Gamma(\phi\phi)/\Gamma_{\text{total}}$ $\Gamma_{41}/\Gamma \times \Gamma_7/\Gamma$

VALUE (units 10^{-5})	DOCUMENT ID	TECN	COMMENT
0.26 ± 0.04 OUR FIT			
4.0 ± 3.5	BAGLIN	89 SPEC	$\bar{p}p \rightarrow K^+ K^- K^+ K^-$

$\Gamma(\rho\bar{\rho}\pi^0)/\Gamma_{\text{total}}$ Γ_{42}/Γ

VALUE (units 10^{-2})	EVTS	DOCUMENT ID	TECN	COMMENT
0.36 ± 0.13 ± 0.03	14	1 ABLIKIM	12N BES3	$\psi(2S) \rightarrow \pi^0\gamma\rho\bar{\rho}\pi^0$

¹ ABLIKIM 12N reports $[\Gamma(\eta_c(1S) \rightarrow \rho\bar{\rho}\pi^0)/\Gamma_{\text{total}}] \times [\Gamma(h_c(1P) \rightarrow \gamma\eta_c(1S))/\Gamma_{\text{total}} \times \Gamma(\psi(2S) \rightarrow \pi^0 h_c(1P))/\Gamma_{\text{total}}] = (1.53 \pm 0.49 \pm 0.23) \times 10^{-6}$ which we divide by our best value $\Gamma(h_c(1P) \rightarrow \gamma\eta_c(1S))/\Gamma_{\text{total}} \times \Gamma(\psi(2S) \rightarrow \pi^0 h_c(1P))/\Gamma_{\text{total}} = (4.3 \pm 0.4) \times 10^{-4}$. Our first error is their experiment's error and our second error is the systematic error from using our best value.

$\Gamma(\Lambda\bar{\Lambda})/\Gamma_{\text{total}}$ Γ_{43}/Γ

VALUE (units 10^{-4})	CL%	EVTS	DOCUMENT ID	TECN	COMMENT
10.7 ± 2.4 OUR FIT					
11.8 ± 2.3 ± 2.5			1 ABLIKIM	12B BES3	

• • • We do not use the following data for averages, fits, limits, etc. • • •

$8.9 \pm 2.5 \pm 0.7$ 20 2 WU 06 BELL $B^+ \rightarrow \Lambda\bar{\Lambda}K^+$

<20 90 3 BISELLO 91 DM2 $e^+e^- \rightarrow \gamma\Lambda\bar{\Lambda}$

¹ ABLIKIM 12B reports $[\Gamma(\eta_c(1S) \rightarrow \Lambda\bar{\Lambda})/\Gamma_{\text{total}}] \times [B(J/\psi(1S) \rightarrow \gamma\eta_c(1S))] = (0.198 \pm 0.021 \pm 0.032) \times 10^{-4}$ which we divide by our best value $B(J/\psi(1S) \rightarrow \gamma\eta_c(1S)) = (1.7 \pm 0.4) \times 10^{-2}$. Our first error is their experiment's error and our second error is the systematic error from using our best value.

² WU 06 reports $[\Gamma(\eta_c(1S) \rightarrow \Lambda\bar{\Lambda})/\Gamma_{\text{total}}] \times [B(B^+ \rightarrow \eta_c K^+)] = (0.95 \pm 0.25 \pm 0.08) \times 10^{-6}$ which we divide by our best value $B(B^+ \rightarrow \eta_c K^+) = (1.06 \pm 0.09) \times 10^{-3}$. Our first error is their experiment's error and our second error is the systematic error from using our best value.

³ The quoted branching ratios use $B(J/\psi(1S) \rightarrow \gamma\eta_c(1S)) = 0.0127 \pm 0.0036$.

$\Gamma(\Lambda\bar{\Lambda})/\Gamma(\rho\bar{\rho})$ Γ_{43}/Γ_{41}

VALUE	DOCUMENT ID	TECN	COMMENT
0.73 ± 0.16 OUR FIT			
$0.67 \pm 0.19 \pm 0.12$	1 WU	06 BELL	$B^+ \rightarrow \rho\bar{\rho}K^+, \Lambda\bar{\Lambda}K^+$

¹ Not independent from other $\eta_c \rightarrow \Lambda\bar{\Lambda}, \rho\bar{\rho}$ branching ratios reported by WU 06.

$\Gamma(K^+\bar{p}\Lambda + c.c.)/\Gamma_{\text{total}}$ Γ_{44}/Γ

VALUE (units 10^{-3})	EVTS	DOCUMENT ID	TECN	COMMENT
2.56 ± 0.35 ± 0.21	157	1 LU	19 BELL	$B^+ \rightarrow \bar{p}\Lambda K^+ K^+$

¹ LU 19 reports $(2.83 \pm 0.36 \pm 0.35) \times 10^{-3}$ from a measurement of $[\Gamma(\eta_c(1S) \rightarrow K^+\bar{p}\Lambda + c.c.)/\Gamma_{\text{total}}] \times [B(B^+ \rightarrow \eta_c K^+)]$ assuming $B(B^+ \rightarrow \eta_c K^+) = (9.6 \pm 1.1) \times 10^{-4}$, which we rescale to our best value $B(B^+ \rightarrow \eta_c K^+) = (1.06 \pm 0.09) \times 10^{-3}$. Our first error is their experiment's error and our second error is the systematic error from using our best value.

$\Gamma(\bar{\Lambda}(1520)\Lambda + c.c.)/\Gamma_{\text{total}}$ Γ_{45}/Γ

VALUE (units 10^{-3})	EVTS	DOCUMENT ID	TECN	COMMENT
3.1 ± 1.4 ± 0.3	43	1 LU	19 BELL	$B^+ \rightarrow \bar{p}\Lambda K^+ K^+$

¹ LU 19 reports $(3.48 \pm 1.48 \pm 0.46) \times 10^{-3}$ from a measurement of $[\Gamma(\eta_c(1S) \rightarrow \bar{\Lambda}(1520)\Lambda + c.c.)/\Gamma_{\text{total}}] \times [B(B^+ \rightarrow \eta_c K^+)]$ assuming $B(B^+ \rightarrow \eta_c K^+) = (9.6 \pm 1.1) \times 10^{-4}$, which we rescale to our best value $B(B^+ \rightarrow \eta_c K^+) = (1.06 \pm 0.09) \times 10^{-3}$. Our first error is their experiment's error and our second error is the systematic error from using our best value.

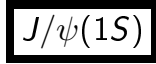
$\Gamma(\Sigma^+\Sigma^-)/\Gamma_{\text{total}}$ Γ_{46}/Γ

VALUE (units 10^{-3})	EVTS	DOCUMENT ID	TECN	COMMENT
2.1 ± 0.3 ± 0.5	112	1 ABLIKIM	13C BES3	$J/\psi \rightarrow \gamma\rho\bar{\rho}\pi^0\pi^0$

¹ ABLIKIM 13C reports $[\Gamma(\eta_c(1S) \rightarrow \Sigma^+\Sigma^-)/\Gamma_{\text{total}}] \times [B(J/\psi(1S) \rightarrow \gamma\eta_c(1S))] = (3.60 \pm 0.48 \pm 0.31) \times 10^{-5}$ which we divide by our best value $B(J/\psi(1S) \rightarrow \gamma\eta_c(1S)) = (1.7 \pm 0.4) \times 10^{-2}$. Our first error is their experiment's error and our second error is the systematic error from using our best value.

Meson Particle Listings

$J/\psi(1S)$



$$I^G(J^{PC}) = 0^-(1^{--})$$

$J/\psi(1S)$ MASS

VALUE (MeV)	EVTs	DOCUMENT ID	TECN	COMMENT
3096.900 ± 0.006 OUR AVERAGE				
3096.900 ± 0.002 ± 0.006		1 ANASHIN 15	KEDR	$e^+e^- \rightarrow$ hadrons
3096.89 ± 0.09	502	2 ARTAMONOV 00	OLYA	$e^+e^- \rightarrow$ hadrons
3096.91 ± 0.03 ± 0.01		3 ARMSTRONG 93B	E760	$\bar{p}p \rightarrow e^+e^-$
3096.95 ± 0.1 ± 0.3	193	BAGLIN 87	SPEC	$\bar{p}p \rightarrow e^+e^-X$
• • • We do not use the following data for averages, fits, limits, etc. • • •				
3096.66 ± 0.19 ± 0.02	6.1k	4 AAIJ 15B1	LHCB	$pp \rightarrow J/\psi X$
3096.917 ± 0.010 ± 0.007		AULCHENKO 03	KEDR	$e^+e^- \rightarrow$ hadrons
3097.5 ± 0.3		GRIBUSHIN 96	FMP5	$515 \pi^-Be \rightarrow 2\mu X$
3098.4 ± 2.0	38k	LEMOIGNE 82	GOLI	$185 \pi^-Be \rightarrow \gamma \mu^+ \mu^- A$
3096.93 ± 0.09	502	5 ZHOLENTZ 80	REDE	e^+e^-
3097.0 ± 1		6 BRANDELIK 79c	DASP	e^+e^-

1 Supersedes AULCHENKO 03.
 2 Reanalysis of ZHOLENTZ 80 using new electron mass (COHEN 87) and radiative corrections (KURAEV 85).
 3 Mass central value and systematic error recalculated by us according to Eq. (16) in ARMSTRONG 93B, using the value for the $\psi(2S)$ mass from AULCHENKO 03.
 4 From a sample of $\eta_c(1S)$ and J/ψ produced in b -hadron decays. Systematic uncertainties not estimated.
 5 Superseded by ARTAMONOV 00.
 6 From a simultaneous fit to e^+e^- , $\mu^+\mu^-$ and hadronic channels assuming $\Gamma(e^+e^-) = \Gamma(\mu^+\mu^-)$.

$J/\psi(1S)$ WIDTH

VALUE (keV)	EVTs	DOCUMENT ID	TECN	COMMENT
92.9 ± 2.8 OUR AVERAGE				Error includes scale factor of 1.1.
96.1 ± 3.2	13k	1 ADAMS 06A	CLEO	$e^+e^- \rightarrow \mu^+\mu^-\gamma$
84.4 ± 8.9		BAI 95B	BES	e^+e^-
91 ± 11 ± 6		2 ARMSTRONG 93B	E760	$\bar{p}p \rightarrow e^+e^-$
85.5 ± 6.1 ± 5.8		3 HSUEH 92	RVUE	See Υ mini-review
• • • We do not use the following data for averages, fits, limits, etc. • • •				
92.94 ± 1.83		4 ANASHIN 18A	KEDR	e^+e^-
94.1 ± 2.7		5 ANASHIN 10	KEDR	$3.097 e^+e^- \rightarrow e^+e^-$, $\mu^+\mu^-$
93.7 ± 3.5	7.8k	1 AUBERT 04	BABR	$e^+e^- \rightarrow \mu^+\mu^-\gamma$

1 Calculated by us from the reported values of $\Gamma(e^+e^-) \times B(\mu^+\mu^-)$ using $B(e^+e^-) = (5.94 \pm 0.06)\%$ and $B(\mu^+\mu^-) = (5.93 \pm 0.06)\%$.
 2 The initial-state radiation correction reevaluated by ANDREOTTI 07 in its Ref. [4].
 3 Using data from COFFMAN 92, BALDINI-CELIO 75, BOYARSKI 75, ESPOSITO 75B, BRANDELIK 79c.
 4 Using $\Gamma(e^+e^-)$ from ANASHIN 18A and $B(J/\psi(1S) \rightarrow e^+e^-) = (5.971 \pm 0.032)\%$ from PDG 16.
 5 Assuming $\Gamma(e^+e^-) = \Gamma(\mu^+\mu^-)$ and using $\Gamma(e^+e^-)/\Gamma_{\text{total}} = (5.94 \pm 0.06)\%$.

$J/\psi(1S)$ DECAY MODES

Mode	Fraction (Γ_i/Γ)	Scale factor/ Confidence level
Γ_1 hadrons	(87.7 ± 0.5) %	
Γ_2 virtual $\gamma \rightarrow$ hadrons	(13.50 ± 0.30) %	
Γ_3 ggg	(64.1 ± 1.0) %	
Γ_4 γgg	(8.8 ± 1.1) %	
Γ_5 e^+e^-	(5.971 ± 0.032) %	
Γ_6 $e^+e^-\gamma$	[a] (8.8 ± 1.4) × 10 ⁻³	
Γ_7 $\mu^+\mu^-$	(5.961 ± 0.033) %	

Decays involving hadronic resonances

Γ_8 $\rho\pi$	(1.69 ± 0.15) %	S=2.4
Γ_9 $\rho^0\pi^0$	(5.6 ± 0.7) × 10 ⁻³	
Γ_{10} $\rho(770)^\mp K^\pm K_S^0$	(1.9 ± 0.4) × 10 ⁻³	
Γ_{11} $\rho(1450)\pi$		
Γ_{12} $\rho(1450)\pi \rightarrow \pi^+\pi^-\pi^0$	(2.3 ± 0.7) × 10 ⁻³	
Γ_{13} $\rho(1450)^\pm \pi^\mp \rightarrow K_S^0 K^\pm \pi^\mp$	(3.5 ± 0.6) × 10 ⁻⁴	
Γ_{14} $\rho(1450)^0 \pi^0 \rightarrow K^+K^-\pi^0$	(2.7 ± 0.6) × 10 ⁻⁴	
Γ_{15} $\rho(1450)\eta'(958) \rightarrow \pi^+\pi^-\eta'(958)$	(3.3 ± 0.7) × 10 ⁻⁶	
Γ_{16} $\rho(1700)\pi$		
Γ_{17} $\rho(1700)\pi \rightarrow \pi^+\pi^-\pi^0$	(1.7 ± 1.1) × 10 ⁻⁴	
Γ_{18} $\rho(2150)\pi$		
Γ_{19} $\rho(2150)\pi \rightarrow \pi^+\pi^-\pi^0$	(8 ± 40) × 10 ⁻⁶	
Γ_{20} $\rho_3(1690)\pi \rightarrow \pi^+\pi^-\pi^0$		
Γ_{21} $a_2(1320)\rho$	(1.09 ± 0.22) %	
Γ_{22} $\omega\pi^+\pi^+\pi^-\pi^-$	(8.5 ± 3.4) × 10 ⁻³	

Γ_{23} $\omega\pi^+\pi^-\pi^0$	(4.0 ± 0.7) × 10 ⁻³	
Γ_{24} $\omega\pi^+\pi^-$	(7.2 ± 1.0) × 10 ⁻³	
Γ_{25} $\omega f_2(1270)$	(4.3 ± 0.6) × 10 ⁻³	
Γ_{26} $K^*(892)^0 \bar{K}^*(892)^0$	(2.3 ± 0.6) × 10 ⁻⁴	
Γ_{27} $K^*(892)^\pm K^*(892)^\mp$	(1.00 ± 0.22 ± 0.40) × 10 ⁻³	
Γ_{28} $K^*(892)^\pm K^*(700)^\mp$	(1.1 ± 1.0 ± 0.6) × 10 ⁻³	
Γ_{29} $K_S^0 \pi^- K^*(892)^+ + \text{c.c.}$	(2.0 ± 0.5) × 10 ⁻³	
Γ_{30} $K_S^0 \pi^- K^*(892)^+ + \text{c.c.} \rightarrow K_S^0 K_S^0 \pi^+ \pi^-$	(6.7 ± 2.2) × 10 ⁻⁴	
Γ_{31} $K_S^0 K^*(892)^0 \rightarrow \gamma K_S^0 K_S^0$	(6.3 ± 0.6 ± 0.5) × 10 ⁻⁶	
Γ_{32} $K_2^*(1430)^+ K^- + \text{c.c.} \rightarrow K^+ K^- \pi^0$	(2.69 ± 0.25 ± 0.19) × 10 ⁻⁴	
Γ_{33} $K_2^*(1980)^+ K^- + \text{c.c.} \rightarrow K^+ K^- \pi^0$	(1.10 ± 0.60 ± 0.14) × 10 ⁻⁵	
Γ_{34} $K_4^*(2045)^+ K^- + \text{c.c.} \rightarrow K^+ K^- \pi^0$	(6.2 ± 2.9 ± 1.6) × 10 ⁻⁶	
Γ_{35} $\eta K^*(892)^0 \bar{K}^*(892)^0$	(1.15 ± 0.26) × 10 ⁻³	
Γ_{36} $\eta' K^* K^\mp$	(1.48 ± 0.13) × 10 ⁻³	
Γ_{37} $\eta' K^* \bar{K}^0 + \text{c.c.}$	(1.66 ± 0.21) × 10 ⁻³	
Γ_{38} $\eta' h_1(1415) \rightarrow \eta' K^* \bar{K}^0 + \text{c.c.}$	(2.16 ± 0.31) × 10 ⁻⁴	
Γ_{39} $\eta' h_1(1415) \rightarrow \eta' K^* K^\mp$	(1.51 ± 0.23) × 10 ⁻⁴	
Γ_{40} $K^*(1410) \bar{K} + \text{c.c.}$		
Γ_{41} $K^*(1410) \bar{K} + \text{c.c.} \rightarrow K^\pm K^\mp \pi^0$	(7 ± 4) × 10 ⁻⁵	
Γ_{42} $K^*(1410) \bar{K} + \text{c.c.} \rightarrow K_S^0 K^\pm \pi^\mp$	(8 ± 6) × 10 ⁻⁵	
Γ_{43} $K_2^*(1430) \bar{K} + \text{c.c.}$		
Γ_{44} $K_2^*(1430) \bar{K} + \text{c.c.} \rightarrow K^\pm K^\mp \pi^0$	(1.0 ± 0.5) × 10 ⁻⁴	
Γ_{45} $K_2^*(1430) \bar{K} + \text{c.c.} \rightarrow K_S^0 K^\pm \pi^\mp$	(4.0 ± 1.0) × 10 ⁻⁴	
Γ_{46} $K^*(892)^0 \bar{K}_2^*(1430)^0 + \text{c.c.}$	(4.66 ± 0.31) × 10 ⁻³	
Γ_{47} $K^*(892)^+ K_2^*(1430)^- + \text{c.c.}$	(3.4 ± 2.9) × 10 ⁻³	
Γ_{48} $K^*(892)^+ K_2^*(1430)^- + \text{c.c.} \rightarrow K^*(892)^+ K_S^0 \pi^- + \text{c.c.}$	(4 ± 4) × 10 ⁻⁴	
Γ_{49} $K^*(892)^0 \bar{K}_2^*(1770)^0 + \text{c.c.} \rightarrow K^*(892)^0 K^- \pi^+ + \text{c.c.}$	(6.9 ± 0.9) × 10 ⁻⁴	
Γ_{50} $\omega K^*(892) \bar{K} + \text{c.c.}$	(6.1 ± 0.9) × 10 ⁻³	
Γ_{51} $\bar{K} K^*(892) + \text{c.c.}$		
Γ_{52} $\bar{K} K^*(892) + \text{c.c.} \rightarrow K_S^0 K^\pm \pi^\mp$	(5.0 ± 0.5) × 10 ⁻³	
Γ_{53} $K^+ K^*(892)^- + \text{c.c.}$	(6.0 ± 0.8 ± 1.0) × 10 ⁻³	S=2.9
Γ_{54} $K^+ K^*(892)^- + \text{c.c.} \rightarrow K^+ K^- \pi^0$	(2.69 ± 0.13 ± 0.20) × 10 ⁻³	
Γ_{55} $K^+ K^*(892)^- + \text{c.c.} \rightarrow K^0 K^\pm \pi^\mp + \text{c.c.}$	(3.0 ± 0.4) × 10 ⁻³	
Γ_{56} $K^0 \bar{K}^*(892)^0 + \text{c.c.}$	(4.2 ± 0.4) × 10 ⁻³	
Γ_{57} $K^0 \bar{K}^*(892)^0 + \text{c.c.} \rightarrow K^0 K^\pm \pi^\mp + \text{c.c.}$	(3.2 ± 0.4) × 10 ⁻³	
Γ_{58} $K_1(1400)^\pm K^\mp$	(3.8 ± 1.4) × 10 ⁻³	
Γ_{59} $\bar{K}^*(892)^0 K^+ \pi^- + \text{c.c.}$	(7.7 ± 1.6) × 10 ⁻³	
Γ_{60} $K^*(892)^\pm K^\mp \pi^0$	(4.1 ± 1.3) × 10 ⁻³	
Γ_{61} $K^*(892)^0 K_S^0 \pi^0$	(6 ± 4) × 10 ⁻⁴	
Γ_{62} $\omega\pi^0\pi^0$	(3.4 ± 0.8) × 10 ⁻³	
Γ_{63} $\omega\pi^0\eta$	(3.4 ± 1.7) × 10 ⁻⁴	
Γ_{64} $b_1(1235)^\pm \pi^\mp$	[b] (3.0 ± 0.5) × 10 ⁻³	
Γ_{65} $\omega K^\pm K_S^0 \pi^\mp$	[b] (3.4 ± 0.5) × 10 ⁻³	
Γ_{66} $b_1(1235)^0 \pi^0$	(2.3 ± 0.6) × 10 ⁻³	
Γ_{67} $\eta K^\pm K_S^0 \pi^\mp$	[b] (2.2 ± 0.4) × 10 ⁻³	
Γ_{68} $\phi K^*(892) \bar{K} + \text{c.c.}$	(2.18 ± 0.23) × 10 ⁻³	
Γ_{69} $\omega K \bar{K}$	(1.9 ± 0.4) × 10 ⁻³	
Γ_{70} $\omega f_0(1710) \rightarrow \omega K \bar{K}$	(4.8 ± 1.1) × 10 ⁻⁴	
Γ_{71} $\phi_2(\pi^+\pi^-)$	(1.60 ± 0.32) × 10 ⁻³	
Γ_{72} $\Delta(1232)^{++} \bar{p}\pi^-$	(1.6 ± 0.5) × 10 ⁻³	
Γ_{73} $\omega\eta$	(1.74 ± 0.20) × 10 ⁻³	S=1.6
Γ_{74} $\omega\eta' \pi^+ \pi^-$	(1.12 ± 0.13) × 10 ⁻³	
Γ_{75} $\phi K \bar{K}$	(1.77 ± 0.16) × 10 ⁻³	S=1.3
Γ_{76} $\phi K_S^0 K_S^0$	(5.9 ± 1.5) × 10 ⁻⁴	
Γ_{77} $\phi f_0(1710) \rightarrow \phi K \bar{K}$	(3.6 ± 0.6) × 10 ⁻⁴	
Γ_{78} $\phi K^+ K^-$	(8.3 ± 1.2) × 10 ⁻⁴	
Γ_{79} $\phi f_2(1270)$	(3.2 ± 0.6) × 10 ⁻⁴	

Γ_{80}	$\Delta(1232)^{++}\bar{\Delta}(1232)^{--}$	$(1.10 \pm 0.29) \times 10^{-3}$		Γ_{148}	$\pi^+\pi^-K_S^0K_L^0$	$(3.8 \pm 0.6) \times 10^{-3}$	
Γ_{81}	$\Sigma(1385)^-\bar{\Sigma}(1385)^+$ (or c.c.)	[b] $(1.16 \pm 0.05) \times 10^{-3}$		Γ_{149}	$\pi^+\pi^-K_S^0K_S^0$	$(1.68 \pm 0.19) \times 10^{-3}$	
Γ_{82}	$\Sigma(1385)^0\bar{\Sigma}(1385)^0$	$(1.07 \pm 0.08) \times 10^{-3}$		Γ_{150}	$\pi^\pm\pi^0K^\mp K_S^0$	$(5.7 \pm 0.5) \times 10^{-3}$	
Γ_{83}	$K^+K^-f_2'(1525)$	$(1.05 \pm 0.35) \times 10^{-3}$		Γ_{151}	$K^+K^-K_S^0K_S^0$	$(4.1 \pm 0.8) \times 10^{-4}$	
Γ_{84}	$\phi f_2'(1525)$	$(8 \pm 4) \times 10^{-4}$	S=2.7	Γ_{152}	$\pi^+\pi^-K^+K^-\eta$	$(4.7 \pm 0.7) \times 10^{-3}$	
Γ_{85}	$\phi\pi^+\pi^-$	$(9.4 \pm 1.5) \times 10^{-4}$	S=1.7	Γ_{153}	$\pi^0\pi^0K^+K^-$	$(2.12 \pm 0.23) \times 10^{-3}$	
Γ_{86}	$\phi\pi^0\pi^0$	$(5.0 \pm 1.0) \times 10^{-4}$		Γ_{154}	$\pi^0\pi^0K_S^0K_L^0$	$(1.9 \pm 0.4) \times 10^{-3}$	
Γ_{87}	$\phi K^\pm K_S^0\pi^\mp$	[b] $(7.2 \pm 0.8) \times 10^{-4}$		Γ_{155}	$K\bar{K}\pi$	$(6.1 \pm 1.0) \times 10^{-3}$	
Γ_{88}	$\omega f_1(1420)$	$(6.8 \pm 2.4) \times 10^{-4}$		Γ_{156}	$K^+K^-\pi^0$	$(2.88 \pm 0.12) \times 10^{-3}$	
Γ_{89}	$\phi\eta$	$(7.4 \pm 0.8) \times 10^{-4}$	S=1.5	Γ_{157}	$K_S^0K^\pm\pi^\mp$	$(5.6 \pm 0.5) \times 10^{-3}$	
Γ_{90}	$\Xi^0\Xi^0$	$(1.17 \pm 0.04) \times 10^{-3}$		Γ_{158}	$K_S^0K_L^0\pi^0$	$(2.06 \pm 0.27) \times 10^{-3}$	
Γ_{91}	$\Xi(1530)^-\bar{\Xi}^++$ + c.c.	$(3.18 \pm 0.08) \times 10^{-4}$		Γ_{159}	$K^*(892)^0\bar{K}^0$ + c.c. \rightarrow	$(1.21 \pm 0.18) \times 10^{-3}$	
Γ_{92}	$\rho K^-\bar{\Sigma}(1385)^0$	$(5.1 \pm 3.2) \times 10^{-4}$			$K_S^0K_L^0\pi^0$		
Γ_{93}	$\omega\pi^0$	$(4.5 \pm 0.5) \times 10^{-4}$	S=1.4	Γ_{160}	$K_2^*(1430)^0\bar{K}^0$ + c.c. \rightarrow	$(4.3 \pm 1.3) \times 10^{-4}$	
Γ_{94}	$\omega\pi^0 \rightarrow \pi^+\pi^-\pi^0$	$(1.7 \pm 0.8) \times 10^{-5}$			$K_S^0K_L^0\pi^0$		
Γ_{95}	$\phi\eta'(958)$	$(4.6 \pm 0.5) \times 10^{-4}$	S=2.2	Γ_{161}	$K_S^0K_L^0\eta$	$(1.44 \pm 0.34) \times 10^{-3}$	
Γ_{96}	$\phi f_0(980)$	$(3.2 \pm 0.9) \times 10^{-4}$	S=1.9	Γ_{162}	$2(\pi^+\pi^-)$	$(3.57 \pm 0.30) \times 10^{-3}$	
Γ_{97}	$\phi f_0(980) \rightarrow \phi\pi^+\pi^-$	$(2.59 \pm 0.34) \times 10^{-4}$		Γ_{163}	$3(\pi^+\pi^-)$	$(4.3 \pm 0.4) \times 10^{-3}$	
Γ_{98}	$\phi f_0(980) \rightarrow \phi\pi^0\pi^0$	$(1.8 \pm 0.5) \times 10^{-4}$		Γ_{164}	$2(\pi^+\pi^-\pi^0)$	$(1.61 \pm 0.21) \%$	
Γ_{99}	$\phi\eta\eta'$	$(2.32 \pm 0.17) \times 10^{-4}$		Γ_{165}	$2(\pi^+\pi^-\eta)$	$(2.26 \pm 0.28) \times 10^{-3}$	
Γ_{100}	$\phi\pi^0 f_0(980) \rightarrow \phi\pi^0\pi^+\pi^-$	$(4.5 \pm 1.0) \times 10^{-6}$		Γ_{166}	$3(\pi^+\pi^-\eta)$	$(7.2 \pm 1.5) \times 10^{-4}$	
Γ_{101}	$\phi\pi^0 f_0(980) \rightarrow \phi\pi^0\rho^0\pi^0$	$(1.7 \pm 0.6) \times 10^{-6}$		Γ_{167}	$\pi^+\pi^-\pi^0\pi^0\eta$	$(2.3 \pm 0.5) \times 10^{-3}$	
Γ_{102}	$\eta\phi f_0(980) \rightarrow \eta\phi\pi^+\pi^-$	$(3.2 \pm 1.0) \times 10^{-4}$		Γ_{168}	$\rho^\pm\pi^\mp\pi^0\eta$	$(1.9 \pm 0.8) \times 10^{-3}$	
Γ_{103}	$\phi a_0(980)^0 \rightarrow \phi\eta\pi^0$	$(4.4 \pm 1.4) \times 10^{-6}$		Γ_{169}	$\rho\bar{\rho}$	$(2.121 \pm 0.029) \times 10^{-3}$	
Γ_{104}	$\Xi(1530)^0\Xi^0$	$(3.2 \pm 1.4) \times 10^{-4}$		Γ_{170}	$\rho\bar{\rho}\pi^0$	$(1.19 \pm 0.08) \times 10^{-3}$	S=1.1
Γ_{105}	$\Sigma(1385)^-\bar{\Sigma}^+$ (or c.c.)	[b] $(3.1 \pm 0.5) \times 10^{-4}$		Γ_{171}	$\rho\bar{\rho}\pi^+\pi^-$	$(6.0 \pm 0.5) \times 10^{-3}$	S=1.3
Γ_{106}	$\phi f_1(1285)$	$(2.6 \pm 0.5) \times 10^{-4}$		Γ_{172}	$\rho\bar{\rho}\pi^+\pi^-\pi^0$	[c] $(2.3 \pm 0.9) \times 10^{-3}$	S=1.9
Γ_{107}	$\phi f_1(1285) \rightarrow \phi\pi^0 f_0(980) \rightarrow$ $\phi\pi^0\pi^+\pi^-$	$(9.4 \pm 2.8) \times 10^{-7}$		Γ_{173}	$\rho\bar{\rho}\eta$	$(2.00 \pm 0.12) \times 10^{-3}$	
Γ_{108}	$\phi f_1(1285) \rightarrow \phi\pi^0 f_0(980) \rightarrow$ $\phi\pi^0\pi^0\pi^0$	$(2.1 \pm 2.2) \times 10^{-7}$		Γ_{174}	$\rho\bar{\rho}\rho$	< 3.1 $\times 10^{-4}$	CL=90%
Γ_{109}	$\eta\pi^+\pi^-$	$(3.8 \pm 0.7) \times 10^{-4}$		Γ_{175}	$\rho\bar{\rho}\omega$	$(9.8 \pm 1.0) \times 10^{-4}$	S=1.3
Γ_{110}	$\eta\rho$	$(1.93 \pm 0.23) \times 10^{-4}$		Γ_{176}	$\rho\bar{\rho}\eta'(958)$	$(1.29 \pm 0.14) \times 10^{-4}$	S=2.0
Γ_{111}	$\omega\eta'(958)$	$(1.89 \pm 0.18) \times 10^{-4}$		Γ_{177}	$\rho\bar{\rho}a_0(980) \rightarrow \rho\bar{\rho}\pi^0\eta$	$(6.8 \pm 1.8) \times 10^{-5}$	
Γ_{112}	$\omega f_0(980)$	$(1.4 \pm 0.5) \times 10^{-4}$		Γ_{178}	$\rho\bar{\rho}\phi$	$(5.19 \pm 0.33) \times 10^{-5}$	
Γ_{113}	$\rho\eta'(958)$	$(8.1 \pm 0.8) \times 10^{-5}$	S=1.6	Γ_{179}	$n\bar{n}$	$(2.09 \pm 0.16) \times 10^{-3}$	
Γ_{114}	$a_2(1320)^\pm\pi^\mp$	[b] < 4.3 $\times 10^{-3}$	CL=90%	Γ_{180}	$n\bar{n}\pi^+\pi^-$	$(4 \pm 4) \times 10^{-3}$	
Γ_{115}	$K\bar{K}_2^*(1430)$ + c.c.	< 4.0 $\times 10^{-3}$	CL=90%	Γ_{181}	$\Sigma^+\bar{\Sigma}^-$	$(1.50 \pm 0.24) \times 10^{-3}$	
Γ_{116}	$K_1(1270)^\pm K^\mp$	< 3.0 $\times 10^{-3}$	CL=90%	Γ_{182}	$\Sigma^0\bar{\Sigma}^0$	$(1.172 \pm 0.032) \times 10^{-3}$	S=1.4
Γ_{117}	$K_1(1270)K_S^0 \rightarrow \gamma K_S^0K_S^0$	$(8.5 \pm 2.5) \times 10^{-7}$		Γ_{183}	$2(\pi^+\pi^-)K^+K^-$	$(3.1 \pm 1.3) \times 10^{-3}$	
Γ_{118}	$K_S^0\pi^-K_2^*(1430)^+ + c.c.$	$(3.6 \pm 1.8) \times 10^{-3}$		Γ_{184}	$\rho\bar{n}\pi^-$	$(2.12 \pm 0.09) \times 10^{-3}$	
Γ_{119}	$K_2^*(1430)^0\bar{K}_2^*(1430)^0$	< 2.9 $\times 10^{-3}$	CL=90%	Γ_{185}	$nN(1440)$	seen	
Γ_{120}	$\phi\pi^0$	3×10^{-6} or 1×10^{-7}		Γ_{186}	$nN(1520)$	seen	
Γ_{121}	$\phi\eta(1405) \rightarrow \phi\eta\pi^+\pi^-$	$(2.0 \pm 1.0) \times 10^{-5}$		Γ_{187}	$nN(1535)$	seen	
Γ_{122}	$\omega f_2'(1525)$	< 2.2 $\times 10^{-4}$	CL=90%	Γ_{188}	$\Xi^-\bar{\Xi}^+$	$(9.7 \pm 0.8) \times 10^{-4}$	S=1.4
Γ_{123}	$\omega X(1835) \rightarrow \omega\rho\bar{\rho}$	< 3.9 $\times 10^{-6}$	CL=95%	Γ_{189}	$\Lambda\bar{\Lambda}$	$(1.89 \pm 0.09) \times 10^{-3}$	S=2.8
Γ_{124}	$\omega X(1835), X \rightarrow \eta'\pi^+\pi^-$	< 6.2 $\times 10^{-5}$		Γ_{190}	$\Lambda\bar{\Sigma}^-\pi^+$ (or c.c.)	[b] $(8.3 \pm 0.7) \times 10^{-4}$	S=1.2
Γ_{125}	$\phi X(1835) \rightarrow \phi\rho\bar{\rho}$	< 2.1 $\times 10^{-7}$	CL=90%	Γ_{191}	$\rho K^-\bar{\Lambda} + c.c.$	$(8.7 \pm 1.1) \times 10^{-4}$	
Γ_{126}	$\phi X(1835) \rightarrow \phi\eta\pi^+\pi^-$	< 2.8 $\times 10^{-4}$	CL=90%	Γ_{192}	$2(K^+K^-)$	$(7.2 \pm 0.8) \times 10^{-4}$	
Γ_{127}	$\phi X(1870) \rightarrow \phi\eta\pi^+\pi^-$	< 6.13 $\times 10^{-5}$	CL=90%	Γ_{193}	$\rho K^-\bar{\Sigma}^0$	$(2.9 \pm 0.8) \times 10^{-4}$	
Γ_{128}	$\eta\phi(2170) \rightarrow \eta\phi f_0(980) \rightarrow$ $\eta\phi\pi^+\pi^-$	$(1.2 \pm 0.4) \times 10^{-4}$		Γ_{194}	K^+K^-	$(2.86 \pm 0.21) \times 10^{-4}$	
Γ_{129}	$\eta\phi(2170) \rightarrow$ $\eta K^*(892)^0\bar{K}^*(892)^0$	< 2.52 $\times 10^{-4}$	CL=90%	Γ_{195}	$K_S^0K_L^0$	$(1.95 \pm 0.11) \times 10^{-4}$	S=2.4
Γ_{130}	$\Sigma(1385)^0\bar{\Lambda} + c.c.$	< 8.2 $\times 10^{-6}$	CL=90%	Γ_{196}	$\Lambda\bar{\Lambda}\pi^+\pi^-$	$(4.3 \pm 1.0) \times 10^{-3}$	
Γ_{131}	$\Delta(1232)^+\bar{p}$	< 1 $\times 10^{-4}$	CL=90%	Γ_{197}	$\Lambda\bar{\Lambda}\eta$	$(1.62 \pm 0.17) \times 10^{-4}$	
Γ_{132}	$\Lambda(1520)\bar{\Lambda} + c.c. \rightarrow \gamma\Lambda\bar{\Lambda}$	< 4.1 $\times 10^{-6}$	CL=90%	Γ_{198}	$\Lambda\bar{\Lambda}\pi^0$	$(3.8 \pm 0.4) \times 10^{-5}$	
Γ_{133}	$\bar{\Lambda}(1520)\Lambda + c.c.$	< 1.80 $\times 10^{-3}$	CL=90%	Γ_{199}	$\bar{\Lambda}nK_S^0 + c.c.$	$(6.5 \pm 1.1) \times 10^{-4}$	
Γ_{134}	$\Theta(1540)\bar{\Theta}(1540) \rightarrow$ $K_S^0\rho K^-\bar{p} + c.c.$	< 1.1 $\times 10^{-5}$	CL=90%	Γ_{200}	$\pi^+\pi^-$	$(1.47 \pm 0.14) \times 10^{-4}$	
Γ_{135}	$\Theta(1540)K^-\bar{n} \rightarrow K_S^0\rho K^-\bar{n}$	< 2.1 $\times 10^{-5}$	CL=90%	Γ_{201}	$\Lambda\bar{\Sigma} + c.c.$	$(2.83 \pm 0.23) \times 10^{-5}$	
Γ_{136}	$\Theta(1540)K_S^0\bar{p} \rightarrow K_S^0\bar{p}K^+n$	< 1.6 $\times 10^{-5}$	CL=90%	Γ_{202}	$K_S^0K_S^0$	< 1.4 $\times 10^{-8}$	CL=95%
Γ_{137}	$\bar{\Theta}(1540)K^+n \rightarrow K_S^0\bar{p}K^+n$	< 5.6 $\times 10^{-5}$	CL=90%				
Γ_{138}	$\bar{\Theta}(1540)K_S^0p \rightarrow K_S^0\rho K^-\bar{n}$	< 1.1 $\times 10^{-5}$	CL=90%				
Decays into stable hadrons							
Γ_{139}	$2(\pi^+\pi^-)\pi^0$	$(3.73 \pm 0.32) \%$	S=1.4	Γ_{203}	3γ	$(1.16 \pm 0.22) \times 10^{-5}$	
Γ_{140}	$3(\pi^+\pi^-)\pi^0$	$(2.9 \pm 0.6) \%$		Γ_{204}	4γ	< 9 $\times 10^{-6}$	CL=90%
Γ_{141}	$\pi^+\pi^-\pi^0$	$(2.10 \pm 0.08) \%$	S=1.6	Γ_{205}	5γ	< 1.5 $\times 10^{-5}$	CL=90%
Γ_{142}	$\pi^+\pi^-\pi^0\pi^0\pi^0$	$(2.71 \pm 0.29) \%$		Γ_{206}	$\gamma\pi^0\pi^0$	$(1.15 \pm 0.05) \times 10^{-3}$	
Γ_{143}	$\rho^\pm\pi^\mp\pi^0\pi^0$	$(1.41 \pm 0.22) \%$		Γ_{207}	$\gamma\eta\pi^0$	$(2.14 \pm 0.31) \times 10^{-5}$	
Γ_{144}	$\rho^+\rho^-\pi^0$	$(6.0 \pm 1.1) \times 10^{-3}$		Γ_{208}	$\gamma a_0(980)^0 \rightarrow \gamma\eta\pi^0$	< 2.5 $\times 10^{-6}$	CL=95%
Γ_{145}	$\pi^+\pi^-\pi^0K^+K^-$	$(1.20 \pm 0.30) \%$		Γ_{209}	$\gamma a_2(1320)^0 \rightarrow \gamma\eta\pi^0$	< 6.6 $\times 10^{-6}$	CL=95%
Γ_{146}	$4(\pi^+\pi^-)\pi^0$	$(9.0 \pm 3.0) \times 10^{-3}$		Γ_{210}	$\gamma K_S^0K_S^0$	$(8.1 \pm 0.4) \times 10^{-4}$	
Γ_{147}	$\pi^+\pi^-K^+K^-$	$(6.84 \pm 0.32) \times 10^{-3}$		Γ_{211}	$\gamma\eta_c(1S)$	$(1.7 \pm 0.4) \%$	S=1.5
				Γ_{212}	$\gamma\eta_c(1S) \rightarrow 3\gamma$	$(3.8 \pm 1.3) \times 10^{-6}$	S=1.1
				Γ_{213}	$\gamma\pi^+\pi^-2\pi^0$	$(8.3 \pm 3.1) \times 10^{-3}$	
				Γ_{214}	$\gamma\eta\pi\pi$	$(6.1 \pm 1.0) \times 10^{-3}$	
				Γ_{215}	$\gamma\eta_2(1870) \rightarrow \gamma\eta\pi^+\pi^-$	$(6.2 \pm 2.4) \times 10^{-4}$	
				Γ_{216}	$\gamma\eta(1405/1475) \rightarrow \gamma K\bar{K}\pi$	[d] $(2.8 \pm 0.6) \times 10^{-3}$	S=1.6
				Γ_{217}	$\gamma\eta(1405/1475) \rightarrow \gamma\gamma\rho^0$	$(7.8 \pm 2.0) \times 10^{-5}$	S=1.8

Meson Particle Listings

$J/\psi(1S)$

Γ_{218}	$\gamma\eta(1405/1475) \rightarrow \gamma\eta\pi^+\pi^-$	$(3.0 \pm 0.5) \times 10^{-4}$	
Γ_{219}	$\gamma\eta(1405/1475) \rightarrow \gamma\eta\phi$	$< 8.2 \times 10^{-5}$	CL=95%
Γ_{220}	$\gamma\eta(1405) \rightarrow \gamma\gamma\gamma$	$< 2.63 \times 10^{-6}$	CL=90%
Γ_{221}	$\gamma\eta(1475) \rightarrow \gamma\gamma\gamma$	$< 1.86 \times 10^{-6}$	CL=90%
Γ_{222}	$\gamma\rho\rho$	$(4.5 \pm 0.8) \times 10^{-3}$	
Γ_{223}	$\gamma\rho\omega$	$< 5.4 \times 10^{-4}$	CL=90%
Γ_{224}	$\gamma\rho\phi$	$< 8.8 \times 10^{-5}$	CL=90%
Γ_{225}	$\gamma\eta'(958)$	$(5.25 \pm 0.07) \times 10^{-3}$	S=1.3
Γ_{226}	$\gamma 2\pi^+ 2\pi^-$	$(2.8 \pm 0.5) \times 10^{-3}$	S=1.9
Γ_{227}	$\gamma f_2(1270) f_2(1270)$	$(9.5 \pm 1.7) \times 10^{-4}$	
Γ_{228}	$\gamma f_2(1270) f_2(1270)$ (non resonant)	$(8.2 \pm 1.9) \times 10^{-4}$	
Γ_{229}	$\gamma K^+ K^- \pi^+ \pi^-$	$(2.1 \pm 0.6) \times 10^{-3}$	
Γ_{230}	$\gamma f_4(2050)$	$(2.7 \pm 0.7) \times 10^{-3}$	
Γ_{231}	$\gamma\omega\omega$	$(1.61 \pm 0.33) \times 10^{-3}$	
Γ_{232}	$\gamma\eta(1405/1475) \rightarrow \gamma\rho^0\rho^0$	$(1.7 \pm 0.4) \times 10^{-3}$	S=1.3
Γ_{233}	$\gamma f_2(1270)$	$(1.64 \pm 0.12) \times 10^{-3}$	S=1.3
Γ_{234}	$\gamma f_2(1270) \rightarrow \gamma K_S^0 K_S^0$	$(2.58 \pm 0.60) \times 10^{-5}$	
Γ_{235}	$\gamma f_0(1370) \rightarrow \gamma K\bar{K}$	$(4.2 \pm 1.5) \times 10^{-4}$	
Γ_{236}	$\gamma f_0(1370) \rightarrow \gamma K_S^0 K_S^0$	$(1.1 \pm 0.4) \times 10^{-5}$	
Γ_{237}	$\gamma f_0(1500) \rightarrow \gamma K_S^0 K_S^0$	$(1.59 \pm 0.24) \times 10^{-5}$	
Γ_{238}	$\gamma f_0(1710) \rightarrow \gamma K\bar{K}$	$(9.5 \pm 1.0) \times 10^{-4}$	S=1.5
Γ_{239}	$\gamma f_0(1710) \rightarrow \gamma\pi\pi$	$(3.8 \pm 0.5) \times 10^{-4}$	
Γ_{240}	$\gamma f_0(1710) \rightarrow \gamma\omega\omega$	$(3.1 \pm 1.0) \times 10^{-4}$	
Γ_{241}	$\gamma f_0(1710) \rightarrow \gamma\eta\eta$	$(2.4 \pm 0.7) \times 10^{-4}$	
Γ_{242}	$\gamma\eta$	$(1.108 \pm 0.027) \times 10^{-3}$	
Γ_{243}	$\gamma f_1(1420) \rightarrow \gamma K\bar{K}\pi$	$(7.9 \pm 1.3) \times 10^{-4}$	
Γ_{244}	$\gamma f_1(1285)$	$(6.1 \pm 0.8) \times 10^{-4}$	
Γ_{245}	$\gamma f_1(1510) \rightarrow \gamma\eta\pi^+\pi^-$	$(4.5 \pm 1.2) \times 10^{-4}$	
Γ_{246}	$\gamma f_2'(1525)$	$(5.7 \pm 0.8) \times 10^{-4}$	S=1.5
Γ_{247}	$\gamma f_2'(1525) \rightarrow \gamma K_S^0 K_S^0$	$(8.0 \pm 0.7) \times 10^{-5}$	
Γ_{248}	$\gamma f_2'(1525) \rightarrow \gamma\eta\eta$	$(3.4 \pm 1.4) \times 10^{-5}$	
Γ_{249}	$\gamma f_2(1640) \rightarrow \gamma\omega\omega$	$(2.8 \pm 1.8) \times 10^{-4}$	
Γ_{250}	$\gamma f_2(1910) \rightarrow \gamma\omega\omega$	$(2.0 \pm 1.4) \times 10^{-4}$	
Γ_{251}	$\gamma f_0(1750) \rightarrow \gamma K_S^0 K_S^0$	$(1.11 \pm 0.20) \times 10^{-5}$	
Γ_{252}	$\gamma f_0(1800) \rightarrow \gamma\omega\phi$	$(2.5 \pm 0.6) \times 10^{-4}$	
Γ_{253}	$\gamma f_2(1810) \rightarrow \gamma\eta\eta$	$(5.4 \pm 3.5) \times 10^{-5}$	
Γ_{254}	$\gamma f_2(1950) \rightarrow \gamma K^*(892)\bar{K}^*(892)$	$(7.0 \pm 2.2) \times 10^{-4}$	
Γ_{255}	$\gamma K^*(892)\bar{K}^*(892)$	$(4.0 \pm 1.3) \times 10^{-3}$	
Γ_{256}	$\gamma\phi\phi$	$(4.0 \pm 1.2) \times 10^{-4}$	S=2.1
Γ_{257}	$\gamma\rho\bar{\rho}$	$(3.8 \pm 1.0) \times 10^{-4}$	
Γ_{258}	$\gamma\eta(2225)$	$(3.14 \pm 0.50) \times 10^{-4}$	
Γ_{259}	$\gamma\eta(1760) \rightarrow \gamma\rho^0\rho^0$	$(1.3 \pm 0.9) \times 10^{-4}$	
Γ_{260}	$\gamma\eta(1760) \rightarrow \gamma\omega\omega$	$(1.98 \pm 0.33) \times 10^{-3}$	
Γ_{261}	$\gamma\eta(1760) \rightarrow \gamma\gamma\gamma$	$< 4.80 \times 10^{-6}$	CL=90%
Γ_{262}	$\gamma X(1835) \rightarrow \gamma\pi^+\pi^-\eta'$	$(2.77 \pm 0.34) \times 10^{-4}$	S=1.1
Γ_{263}	$\gamma X(1835) \rightarrow \gamma\rho\bar{\rho}$	$(7.7 \pm 1.5) \times 10^{-5}$	
Γ_{264}	$\gamma X(1835) \rightarrow \gamma K_S^0 K_S^0 \eta$	$(3.3 \pm 2.0) \times 10^{-5}$	
Γ_{265}	$\gamma X(1835) \rightarrow \gamma\gamma\phi(1020)$		
Γ_{266}	$\gamma X(1835) \rightarrow \gamma\gamma\gamma$	$< 3.56 \times 10^{-6}$	CL=90%
Γ_{267}	$\gamma X(1840) \rightarrow \gamma 3(\pi^+\pi^-)$	$(2.4 \pm 0.7) \times 10^{-5}$	
Γ_{268}	$\gamma(K\bar{K}\pi) [J^{PC} = 0^- +]$	$(7 \pm 4) \times 10^{-4}$	S=2.1
Γ_{269}	$\gamma\pi^0$	$(3.56 \pm 0.17) \times 10^{-5}$	
Γ_{270}	$\gamma\rho\bar{\rho}\pi^+\pi^-$	$< 7.9 \times 10^{-4}$	CL=90%
Γ_{271}	$\gamma A\bar{A}$	$< 1.3 \times 10^{-4}$	CL=90%
Γ_{272}	$\gamma f_0(2100) \rightarrow \gamma\eta\eta$	$(1.13 \pm 0.60) \times 10^{-4}$	
Γ_{273}	$\gamma f_0(2100) \rightarrow \gamma\pi\pi$	$(6.2 \pm 1.0) \times 10^{-4}$	
Γ_{274}	$\gamma f_0(2200)$		
Γ_{275}	$\gamma f_0(2200) \rightarrow \gamma K\bar{K}$	$(5.9 \pm 1.3) \times 10^{-4}$	
Γ_{276}	$\gamma f_0(2200) \rightarrow \gamma K_S^0 K_S^0$	$(2.72 \pm 0.19) \times 10^{-4}$	
Γ_{277}	$\gamma f_J(2220)$		
Γ_{278}	$\gamma f_J(2220) \rightarrow \gamma\pi\pi$	$< 3.9 \times 10^{-5}$	CL=90%
Γ_{279}	$\gamma f_J(2220) \rightarrow \gamma K\bar{K}$	$< 4.1 \times 10^{-5}$	CL=90%
Γ_{280}	$\gamma f_J(2220) \rightarrow \gamma\rho\bar{\rho}$	$(1.5 \pm 0.8) \times 10^{-5}$	
Γ_{281}	$\gamma f_0(2330) \rightarrow \gamma K_S^0 K_S^0$	$(4.9 \pm 0.7) \times 10^{-5}$	

Γ_{282}	$\gamma f_2(2340) \rightarrow \gamma\eta\eta$	$(5.6 \pm 2.4) \times 10^{-5}$	
Γ_{283}	$\gamma f_2(2340) \rightarrow \gamma K_S^0 K_S^0$	$(5.5 \pm 4.0) \times 10^{-5}$	
Γ_{284}	$\gamma f_0(1500) \rightarrow \gamma\pi\pi$	$(1.09 \pm 0.24) \times 10^{-4}$	
Γ_{285}	$\gamma f_0(1500) \rightarrow \gamma\eta\eta$	$(1.7 \pm 1.4) \times 10^{-5}$	
Γ_{286}	$\gamma A \rightarrow \gamma$ invisible	$[e] < 6.3$	$\times 10^{-6}$ CL=90%
Γ_{287}	$\gamma A^0 \rightarrow \gamma\mu^+\mu^-$	$[f] < 5$	$\times 10^{-6}$ CL=90%

Dalitz decays

Γ_{288}	$\pi^0 e^+ e^-$	$(7.6 \pm 1.4) \times 10^{-7}$	
Γ_{289}	$\eta e^+ e^-$	$(1.43 \pm 0.07) \times 10^{-5}$	
Γ_{290}	$\eta'(958) e^+ e^-$	$(6.59 \pm 0.18) \times 10^{-5}$	
Γ_{291}	$\eta U \rightarrow \eta e^+ e^-$	< 9.11	$\times 10^{-7}$ CL=90%
Γ_{292}	$\eta'(958) U \rightarrow \eta'(958) e^+ e^-$	< 2.0	$\times 10^{-7}$ CL=90%
Γ_{293}	$\phi e^+ e^-$	< 1.2	$\times 10^{-7}$ CL=90%

Weak decays

Γ_{294}	$D^- e^+ \nu_e + c.c.$	< 1.2	$\times 10^{-5}$ CL=90%
Γ_{295}	$\bar{D}^0 e^+ e^- + c.c.$	< 8.5	$\times 10^{-8}$ CL=90%
Γ_{296}	$D_s^- e^+ \nu_e + c.c.$	< 1.3	$\times 10^{-6}$ CL=90%
Γ_{297}	$D_s^- e^+ \nu_e + c.c.$	< 1.8	$\times 10^{-6}$ CL=90%
Γ_{298}	$D^- \pi^+ + c.c.$	< 7.5	$\times 10^{-5}$ CL=90%
Γ_{299}	$\bar{D}^0 \bar{K}^0 + c.c.$	< 1.7	$\times 10^{-4}$ CL=90%
Γ_{300}	$\bar{D}^0 \bar{K}^{*0} + c.c.$	< 2.5	$\times 10^{-6}$ CL=90%
Γ_{301}	$D_s^- \pi^+ + c.c.$	< 1.3	$\times 10^{-4}$ CL=90%
Γ_{302}	$D_s^- \rho^+ + c.c.$	< 1.3	$\times 10^{-5}$ CL=90%

Charge conjugation (C), Parity (P), Lepton Family number (LF) violating modes

Γ_{303}	$\gamma\gamma$	C	< 2.7	$\times 10^{-7}$ CL=90%
Γ_{304}	$\gamma\phi$	C	< 1.4	$\times 10^{-6}$ CL=90%
Γ_{305}	$e^\pm \mu^\mp$	LF	< 1.6	$\times 10^{-7}$ CL=90%
Γ_{306}	$e^\pm \tau^\mp$	LF	< 8.3	$\times 10^{-6}$ CL=90%
Γ_{307}	$\mu^\pm \tau^\mp$	LF	< 2.0	$\times 10^{-6}$ CL=90%
Γ_{308}	$A_C^\pm e^- + c.c.$		< 6.9	$\times 10^{-8}$ CL=90%

Other decays

Γ_{309}	invisible	< 7	$\times 10^{-4}$ CL=90%
----------------	-----------	-------	-------------------------

[a] For $E_\gamma > 100$ MeV.

[b] The value is for the sum of the charge states or particle/antiparticle states indicated.

[c] Includes $p\bar{p}\pi^+\pi^-\gamma$ and excludes $p\bar{p}\eta, p\bar{p}\omega, p\bar{p}\eta'$.

[d] See the "Note on the $\eta(1405)$ " in the $\eta(1405)$ Particle Listings.

[e] For a narrow state A with mass less than 960 MeV.

[f] For a narrow scalar or pseudoscalar A^0 with mass 0.21–3.0 GeV.

$J/\psi(1S)$ PARTIAL WIDTHS

$\Gamma(\text{hadrons})$		Γ_1		
VALUE (keV)	DOCUMENT ID	TECN	COMMENT	
●●● We do not use the following data for averages, fits, limits, etc. ●●●				
74.1 ± 8.1	BAI	95B	BES	e^+e^-
59 ± 24	BALDINI...	75	FRAG	e^+e^-
59 ± 14	BOYARSKI	75	MRK1	e^+e^-
50 ± 25	ESPOSITO	75B	FRAM	e^+e^-
$\Gamma(e^+e^-)$		Γ_5		
VALUE (keV)	EVTS	DOCUMENT ID	TECN	COMMENT
5.53 ± 0.10	OUR AVERAGE			
$5.550 \pm 0.056 \pm 0.089$		¹ ANASHIN	18A	KEDR e^+e^-
5.36 ± 0.29		² HSUEH	92	RVUE See \mathcal{T} mini-review
5.36 ± 0.28				
●●● We do not use the following data for averages, fits, limits, etc. ●●●				
$5.58 \pm 0.05 \pm 0.08$		³ ABLIKIM	16q	BES3 $3.773 e^+e^- \rightarrow \mu^+\mu^-\gamma$
5.71 ± 0.16	13k	⁴ ADAMS	06A	CLEO $e^+e^- \rightarrow \mu^+\mu^-\gamma$
5.57 ± 0.19	7.8k	⁴ AUBERT	04	BABR $e^+e^- \rightarrow \mu^+\mu^-\gamma$
5.14 ± 0.39		BAI	95B	BES e^+e^-
4.72 ± 0.35		ALEXANDER	89	RVUE See \mathcal{T} mini-review
4.4 ± 0.6		² BRANDELIK	79C	DASP e^+e^-
4.6 ± 0.8		⁵ BALDINI...	75	FRAG e^+e^-
4.8 ± 0.6		BOYARSKI	75	MRK1 e^+e^-
4.6 ± 1.0		ESPOSITO	75B	FRAM e^+e^-
¹ From the cross sections of $e^+e^- \rightarrow e^+e^-$ and $e^+e^- \rightarrow \text{hadrons}$ near the $J/\psi(1S)$ peak. ² From a simultaneous fit to e^+e^- , $\mu^+\mu^-$, and hadronic channels assuming $\Gamma(e^+e^-) = \Gamma(\mu^+\mu^-)$. ³ Using $B(J/\psi \rightarrow \mu^+\mu^-) = (5.973 \pm 0.007 \pm 0.037)\%$ from ABLIKIM 13R. ⁴ Calculated by us from the reported values of $\Gamma(e^+e^-) \times B(\mu^+\mu^-)$ using $B(\mu^+\mu^-) = (5.93 \pm 0.06)\%$. ⁵ Assuming equal partial widths for e^+e^- and $\mu^+\mu^-$.				

Γ(μ+μ-) Γ7

Table with columns: VALUE (keV), DOCUMENT ID, TECN, COMMENT. Includes data for BAI, BOYARSKI, ESPOSITO.

Γ(γγ) Γ303

Table with columns: VALUE (eV), CL%, DOCUMENT ID, TECN, COMMENT. Includes data for BRANDELIK.

J/ψ(1S) Γ(i)Γ(e+e-)/Γ(total)

This combination of a partial width with the partial width into e+e- and with the total width is obtained from the integrated cross section into channel i in the e+e- annihilation.

Γ(hadrons) × Γ(e+e-)/Γtotal Γ1Γ5/Γ

Table with columns: VALUE (keV), DOCUMENT ID, TECN, COMMENT. Includes data for ANASHIN, BALDINI, ESPOSITO.

1 From the cross sections of e+e- -> e+e- and e+e- -> hadrons near the J/ψ(1S) peak. 2 Data redundant with branching ratios or partial widths above.

Γ(e+e-) × Γ(e+e-)/Γtotal Γ5Γ5/Γ

Table with columns: VALUE (eV), DOCUMENT ID, TECN, COMMENT. Includes data for ANASHIN, BRANDELIK, BALDINI, ESPOSITO, FORD.

1 From the cross sections of e+e- -> e+e- and e+e- -> hadrons near the J/ψ(1S) peak. 2 Data redundant with branching ratios or partial widths above.

Γ(μ+μ-) × Γ(e+e-)/Γtotal Γ7Γ5/Γ

Table with columns: VALUE (eV), EVTS, DOCUMENT ID, TECN, COMMENT. Includes data for ABLIKIM, ANASHIN, ADAMS, AUBERT, DASP, ESPOSITO.

1 Data redundant with branching ratios or partial widths above.

Γ(ρ(770)±K±K0S) × Γ(e+e-)/Γtotal Γ10Γ5/Γ

Table with columns: VALUE (eV), EVTS, DOCUMENT ID, TECN, COMMENT. Includes data for LEES.

Γ(ωπ+π-π0) × Γ(e+e-)/Γtotal Γ23Γ5/Γ

Table with columns: VALUE (10^-2 keV), EVTS, DOCUMENT ID, TECN, COMMENT. Includes data for AUBERT.

Γ(ωπ+π-) × Γ(e+e-)/Γtotal Γ24Γ5/Γ

Table with columns: VALUE (eV), EVTS, DOCUMENT ID, TECN, COMMENT. Includes data for AUBERT.

1 AUBERT 07AU reports [Γ(J/ψ(1S) -> ωπ+π-) × Γ(J/ψ(1S) -> e+e-)/Γtotal] × [B(ω(782) -> π+π-π0)] = 47.8 ± 3.1 ± 3.2 eV which we divide by our best value B(ω(782) -> π+π-π0) = (89.3 ± 0.6) × 10^-2. Our first error is their experiment's error and our second error is the systematic error from using our best value.

Γ(ωπ0π0) × Γ(e+e-)/Γtotal Γ62Γ5/Γ

Table with columns: VALUE (eV), EVTS, DOCUMENT ID, TECN, COMMENT. Includes data for LEES.

1 LEES 18E reports [Γ(J/ψ(1S) -> ωπ0π0) × Γ(J/ψ(1S) -> e+e-)/Γtotal] × [B(ω(782) -> π+π-π0)] = 24.8 ± 1.8 ± 2.5 eV which we divide by our best value B(ω(782) -> π+π-π0) = (89.3 ± 0.6) × 10^-2. Our first error is their experiment's error and our second error is the systematic error from using our best value.

Γ(K*(892)0K*(892)0) × Γ(e+e-)/Γtotal Γ26Γ5/Γ

Table with columns: VALUE (eV), EVTS, DOCUMENT ID, TECN, COMMENT. Includes data for LEES.

••• We do not use the following data for averages, fits, limits, etc. ••• 1.28 ± 0.40 ± 0.11 25 ± 8 1,2 AUBERT 07AK BABR 10.6 e+e- -> π+π-K+K-γ 1 Dividing by (2/3)^2 to take twice into account that B(K*0 -> K+π-) = 2/3 B(K*0 -> Kπ). 2 Superseded by LEES 12F.

Γ(K*(892)±K*(892)∓) × Γ(e+e-)/Γtotal Γ27Γ5/Γ

Table with columns: VALUE (eV), EVTS, DOCUMENT ID, TECN, COMMENT. Includes data for LEES.

1 Dividing by (1/4)^2 to take twice into account B(K*(892) -> K0Sπ) = 1/4.

Γ(K0Sπ-K*(892)+ + c.c.) × Γ(e+e-)/Γtotal Γ29Γ5/Γ

Table with columns: VALUE (eV), EVTS, DOCUMENT ID, TECN, COMMENT. Includes data for LEES.

1 Dividing by 1/2 to take into account B(K*(892)± -> K±π∓) = 1/2. 2 Dividing by 1/4 to take into account B(K*(892) -> K0Sπ) = 1/4.

Γ(K0Sπ-K*(892)+ + c.c. -> K0SK0Sπ+π-) × Γ(e+e-)/Γtotal Γ30Γ5/Γ

Table with columns: VALUE (eV), EVTS, DOCUMENT ID, TECN, COMMENT. Includes data for LEES.

Γ(K*(892)0K2(1430)0 + c.c.) × Γ(e+e-)/Γtotal Γ46Γ5/Γ

Table with columns: VALUE (eV), EVTS, DOCUMENT ID, TECN, COMMENT. Includes data for LEES.

••• We do not use the following data for averages, fits, limits, etc. ••• 33 ± 4 ± 1 317 2,4 AUBERT 07AK BABR 10.6 e+e- -> π+π-K+K-γ 1 LEES 12F reports [Γ(J/ψ(1S) -> K*(892)0K2(1430)0 + c.c.) × Γ(J/ψ(1S) -> e+e-)/Γtotal] × [B(K2(1430) -> Kπ)] = 12.89 ± 0.54 ± 0.41 eV which we divide by our best value B(K2(1430) -> Kπ) = (49.9 ± 1.2) × 10^-2. Our first error is their experiment's error and our second error is the systematic error from using our best value. 2 Dividing by 2/3 to take into account that B(K*0 -> K+π-) = 2/3 B(K*0 -> Kπ). 3 The K2(1430) cannot be distinguished from the K0(1430). 4 Superseded by LEES 12F. AUBERT 07AK reports [Γ(J/ψ(1S) -> K*(892)0K2(1430)0 + c.c.) × Γ(J/ψ(1S) -> e+e-)/Γtotal] × [B(K2(1430) -> Kπ)] = 16.4 ± 1.1 ± 1.4 eV which we divide by our best value B(K2(1430) -> Kπ) = (49.9 ± 1.2) × 10^-2. Our first error is their experiment's error and our second error is the systematic error from using our best value.

Γ(K*(892)+K2(1430)- + c.c.) × Γ(e+e-)/Γtotal Γ47Γ5/Γ

Table with columns: VALUE (eV), EVTS, DOCUMENT ID, TECN, COMMENT. Includes data for LEES.

1 Dividing by (1/4)^2 to take into account B(K*(892) -> K0Sπ) = 1/4 and B(K*(1430) -> K0Sπ) = 1/4 B(K*(1430) -> Kπ). 2 LEES 14H reports [Γ(J/ψ(1S) -> K*(892)+K2(1430)- + c.c.) × Γ(J/ψ(1S) -> e+e-)/Γtotal] × [B(K2(1430) -> Kπ)] = 9.28 ± 8.0 ± 0.32 eV which we divide by our best value B(K2(1430) -> Kπ) = (49.9 ± 1.2) × 10^-2. Our first error is their experiment's error and our second error is the systematic error from using our best value.

Γ(K*(892)+K2(1430)- + c.c. -> K*(892)+K0Sπ- + c.c.) × Γ(e+e-)/Γtotal Γ48Γ5/Γ

Table with columns: VALUE (eV), EVTS, DOCUMENT ID, TECN, COMMENT. Includes data for LEES.

1 Dividing by 1/4 to take into account B(K*(892) -> K0Sπ) = 1/4.

Γ(K*(892)0K2(1770)0 + c.c. -> K*(892)0K-π+ + c.c.) × Γ(e+e-)/Γtotal Γ49Γ5/Γ

Table with columns: VALUE (eV), EVTS, DOCUMENT ID, TECN, COMMENT. Includes data for AUBERT.

1 Dividing by 2/3 to take into account that B(K*0 -> K+π-) = 2/3.

Γ(K+K*(892)- + c.c.) × Γ(e+e-)/Γtotal Γ53Γ5/Γ

Table with columns: VALUE (eV), DOCUMENT ID, TECN, COMMENT. Includes data for AUBERT.

Γ(K+K*(892)- + c.c. -> K+K-π0) × Γ(e+e-)/Γtotal Γ54Γ5/Γ

Table with columns: VALUE (eV), EVTS, DOCUMENT ID, TECN, COMMENT. Includes data for AUBERT.

Γ(K+K*(892)- + c.c. -> K+K-π0)/Γtotal Γ54/Γ

Table with columns: VALUE (units 10^-3), EVTS, DOCUMENT ID, TECN, COMMENT. Includes data for ABLIKIM.

Meson Particle Listings

 $J/\psi(1S)$

$\Gamma(K^+ K^*(892)^- + c.c. \rightarrow K^0 K^\pm \pi^\mp + c.c.) \times \Gamma(e^+ e^-)/\Gamma_{total}$					$\Gamma_{55}\Gamma_5/\Gamma$
VALUE (eV)	EVTS	DOCUMENT ID	TECN	COMMENT	
$16.76 \pm 1.70 \pm 1.00$	89	AUBERT	08s	BABR	$10.6 e^+ e^- \rightarrow K_S^0 K^\pm \pi^\mp \gamma$

$\Gamma(K^0 \bar{K}^*(892)^0 + c.c.) \times \Gamma(e^+ e^-)/\Gamma_{total}$					$\Gamma_{56}\Gamma_5/\Gamma$
VALUE (eV)	DOCUMENT ID	TECN	COMMENT		
$26.6 \pm 2.5 \pm 1.5$	AUBERT	08s	BABR	$10.6 e^+ e^- \rightarrow K^0 \bar{K}^*(892)^0 \gamma$	

$\Gamma(K^0 \bar{K}^*(892)^0 + c.c. \rightarrow K^0 K^\pm \pi^\mp + c.c.) \times \Gamma(e^+ e^-)/\Gamma_{total}$					$\Gamma_{57}\Gamma_5/\Gamma$
VALUE (eV)	EVTS	DOCUMENT ID	TECN	COMMENT	
$17.70 \pm 1.70 \pm 1.00$	94	AUBERT	08s	BABR	$10.6 e^+ e^- \rightarrow K_S^0 K^\pm \pi^\mp \gamma$

$\Gamma(K_S^0 K^*(892)^0 \rightarrow \gamma K_S^0 K_S^0)/\Gamma_{total}$					Γ_{31}/Γ
VALUE (units 10^{-6})	DOCUMENT ID	TECN	COMMENT		
$6.20 \pm 0.16 + 0.59 - 0.17 - 0.52$	ABLIKIM	18AA	BES3	$J/\psi \rightarrow \gamma K_S^0 K_S^0$	

$\Gamma(K^*(892)^0 K^+ \pi^- + c.c.) \times \Gamma(e^+ e^-)/\Gamma_{total}$					$\Gamma_{59}\Gamma_5/\Gamma$
VALUE (eV)	EVTS	DOCUMENT ID	TECN	COMMENT	
$42.6 \pm 4.8 \pm 7.2$	99	1 LEES	17D	BABR	$e^+ e^- \rightarrow K_S^0 K^\pm \pi^\mp \pi^0 \gamma$
1 Dividing by 1/6 to account for $B(K^*(892)^0 \rightarrow K_S^0 \pi^0) = 1/6$.					

$\Gamma(K^*(892)^\pm K^\mp \pi^0) \times \Gamma(e^+ e^-)/\Gamma_{total}$					$\Gamma_{60}\Gamma_5/\Gamma$
VALUE (eV)	EVTS	DOCUMENT ID	TECN	COMMENT	
$22.8 \pm 2.8 \pm 6.8$	80	1 LEES	17D	BABR	$e^+ e^- \rightarrow K_S^0 K^\pm \pi^\mp \pi^0 \gamma$
1 Dividing by 1/4 to account for $B(K^*(892)^\pm \rightarrow K_S^0 \pi^\pm) = 1/4$.					

$\Gamma(K_S^0(1430)^+ K^- + c.c. \rightarrow K^+ K^- \pi^0)/\Gamma_{total}$					Γ_{32}/Γ
VALUE (units 10^{-4})	EVTS	DOCUMENT ID	TECN	COMMENT	
$2.69 \pm 0.04 + 0.25 - 0.19$	183k	ABLIKIM	19AQ	BES	$J/\psi \rightarrow K^+ K^- \pi^0$

$\Gamma(K_S^0(1980)^+ K^- + c.c. \rightarrow K^+ K^- \pi^0)/\Gamma_{total}$					Γ_{33}/Γ
VALUE (units 10^{-5})	EVTS	DOCUMENT ID	TECN	COMMENT	
$1.1 \pm 0.1 + 0.6 - 0.1$	183k	ABLIKIM	19AQ	BES	$J/\psi \rightarrow K^+ K^- \pi^0$

$\Gamma(K_S^0(2045)^+ K^- + c.c. \rightarrow K^+ K^- \pi^0)/\Gamma_{total}$					Γ_{34}/Γ
VALUE (units 10^{-6})	EVTS	DOCUMENT ID	TECN	COMMENT	
$6.2 \pm 0.7 + 1.8 - 1.4$	183k	ABLIKIM	19AQ	BES	$J/\psi \rightarrow K^+ K^- \pi^0$

$\Gamma(K^*(892)^0 K_S^0 \pi^0) \times \Gamma(e^+ e^-)/\Gamma_{total}$					$\Gamma_{61}\Gamma_5/\Gamma$
VALUE (eV)	EVTS	DOCUMENT ID	TECN	COMMENT	
$3.60 \pm 0.75 \pm 2.25$	34	1 LEES	17D	BABR	$e^+ e^- \rightarrow K_S^0 K^\pm \pi^\mp \pi^0 \gamma$
1 Dividing by 2/3 to account for $B(K^*(892)^0 \rightarrow K^+ \pi^-) = 2/3$.					

$\Gamma(\eta K^\pm K_S^0 \pi^\mp) \times \Gamma(e^+ e^-)/\Gamma_{total}$					$\Gamma_{67}\Gamma_5/\Gamma$
VALUE (eV)	EVTS	DOCUMENT ID	TECN	COMMENT	
$7.3 \pm 1.4 \pm 0.4$	44	LEES	17D	BABR	$e^+ e^- \rightarrow K_S^0 K^\pm \pi^\mp \pi^0 \gamma$

$\Gamma(\omega K \bar{K}) \times \Gamma(e^+ e^-)/\Gamma_{total}$					$\Gamma_{69}\Gamma_5/\Gamma$
VALUE (eV)	EVTS	DOCUMENT ID	TECN	COMMENT	
$3.70 \pm 1.98 \pm 0.03$	24	1 AUBERT	07AU	BABR	$10.6 e^+ e^- \rightarrow \omega K^+ K^- \gamma$
1 AUBERT 07AU reports $[\Gamma(J/\psi(1S) \rightarrow \omega K \bar{K}) \times \Gamma(J/\psi(1S) \rightarrow e^+ e^-)/\Gamma_{total}] \times [B(\omega(782) \rightarrow \pi^+ \pi^- \pi^0)] = 3.3 \pm 1.3 \pm 1.2$ eV which we divide by our best value $B(\omega(782) \rightarrow \pi^+ \pi^- \pi^0) = (89.3 \pm 0.6) \times 10^{-2}$. Our first error is their experiment's error and our second error is the systematic error from using our best value.					

$\Gamma(\phi(2\pi^+ \pi^-)) \times \Gamma(e^+ e^-)/\Gamma_{total}$					$\Gamma_{71}\Gamma_5/\Gamma$
VALUE (10^{-2} keV)	EVTS	DOCUMENT ID	TECN	COMMENT	
$0.95 \pm 0.19 \pm 0.01$	35	1 AUBERT	06D	BABR	$10.6 e^+ e^- \rightarrow \phi(2\pi^+ \pi^-) \gamma$
1 AUBERT 06D reports $[\Gamma(J/\psi(1S) \rightarrow \phi(2\pi^+ \pi^-)) \times \Gamma(J/\psi(1S) \rightarrow e^+ e^-)/\Gamma_{total}] \times [B(\phi(1020) \rightarrow K^+ K^-)] = (0.47 \pm 0.09 \pm 0.03) \times 10^{-2}$ keV which we divide by our best value $B(\phi(1020) \rightarrow K^+ K^-) = (49.2 \pm 0.5) \times 10^{-2}$. Our first error is their experiment's error and our second error is the systematic error from using our best value.					

$\Gamma(\phi K_S^0 K_S^0) \times \Gamma(e^+ e^-)/\Gamma_{total}$					$\Gamma_{76}\Gamma_5/\Gamma$
VALUE (eV)	EVTS	DOCUMENT ID	TECN	COMMENT	
$3.25 \pm 0.84 \pm 0.03$	29	1 LEES	14H	BABR	$e^+ e^- \rightarrow K_S^0 K_S^0 K^+ K^- \gamma$
1 LEES 14H reports $[\Gamma(J/\psi(1S) \rightarrow \phi K_S^0 K_S^0) \times \Gamma(J/\psi(1S) \rightarrow e^+ e^-)/\Gamma_{total}] \times [B(\phi(1020) \rightarrow K^+ K^-)] = 1.6 \pm 0.4 \pm 0.1$ eV which we divide by our best value $B(\phi(1020) \rightarrow K^+ K^-) = (49.2 \pm 0.5) \times 10^{-2}$. Our first error is their experiment's error and our second error is the systematic error from using our best value.					

$\Gamma(\phi K^+ K^-) \times \Gamma(e^+ e^-)/\Gamma_{total}$					$\Gamma_{78}\Gamma_5/\Gamma$
VALUE (eV)	EVTS	DOCUMENT ID	TECN	COMMENT	
$4.59 \pm 0.62 \pm 0.05$	163	1 LEES	12F	BABR	$10.6 e^+ e^- \rightarrow K^+ K^- K^+ K^- \gamma$

1 LEES 12F reports $[\Gamma(J/\psi(1S) \rightarrow \phi K^+ K^-) \times \Gamma(J/\psi(1S) \rightarrow e^+ e^-)/\Gamma_{total}] \times [B(\phi(1020) \rightarrow K^+ K^-)] = 2.26 \pm 0.26 \pm 0.16$ eV which we divide by our best value $B(\phi(1020) \rightarrow K^+ K^-) = (49.2 \pm 0.5) \times 10^{-2}$. Our first error is their experiment's error and our second error is the systematic error from using our best value.

$\Gamma(\phi f_2(1270)) \times \Gamma(e^+ e^-)/\Gamma_{total}$					$\Gamma_{79}\Gamma_5/\Gamma$	
VALUE (eV)	EVTS	DOCUMENT ID	TECN	COMMENT		
$1.79 \pm 0.32 + 0.02 - 0.06$	61	1,2,3	LEES	12F	BABR	$10.6 e^+ e^- \rightarrow \pi^+ \pi^- K^+ K^- \gamma$

• • • We do not use the following data for averages, fits, limits, etc. • • •

$4.08 \pm 0.73 + 0.04 - 0.14$	44	2,4	AUBERT	07AK	BABR	$10.6 e^+ e^- \rightarrow \pi^+ \pi^- K^+ K^- \gamma$
-------------------------------	----	-----	--------	------	------	---

1 LEES 12F reports $[\Gamma(J/\psi(1S) \rightarrow \phi f_2(1270)) \times \Gamma(J/\psi(1S) \rightarrow e^+ e^-)/\Gamma_{total}] \times [B(f_2(1270) \rightarrow \pi\pi)] = 1.51 \pm 0.25 \pm 0.10$ eV which we divide by our best value $B(f_2(1270) \rightarrow \pi\pi) = (84.2 \pm 2.9) \times 10^{-2}$. Our first error is their experiment's error and our second error is the systematic error from using our best value.

2 Using $B(\phi \rightarrow K^+ K^-) = (48.9 \pm 0.5)\%$.

3 Using $\pi^+ \pi^-$ invariant mass between 1.1 and 1.5 GeV. May include other sources such as $f_0(1370)$.

4 Superseded by LEES 12F. AUBERT 07AK reports $[\Gamma(J/\psi(1S) \rightarrow \phi f_2(1270)) \times \Gamma(J/\psi(1S) \rightarrow e^+ e^-)/\Gamma_{total}] \times [B(f_2(1270) \rightarrow \pi\pi)] = 3.44 \pm 0.55 \pm 0.28$ eV which we divide by our best value $B(f_2(1270) \rightarrow \pi\pi) = (84.2 \pm 2.9) \times 10^{-2}$. Our first error is their experiment's error and our second error is the systematic error from using our best value.

$\Gamma(K^+ K^- f_2'(1525)) \times \Gamma(e^+ e^-)/\Gamma_{total}$					$\Gamma_{83}\Gamma_5/\Gamma$	
VALUE (eV)	EVTS	DOCUMENT ID	TECN	COMMENT		
$5.8 \pm 1.9 \pm 0.1$	16	1,2	LEES	14H	BABR	$e^+ e^- \rightarrow K_S^0 K_S^0 K^+ K^- \gamma$

1 Dividing by 1/4 to take into account $B(f_2'(1525) \rightarrow K_S^0 K_S^0) = 1/4$ $B(f_2'(1525) \rightarrow K \bar{K})$.

2 LEES 14H reports $[\Gamma(J/\psi(1S) \rightarrow K^+ K^- f_2'(1525)) \times \Gamma(J/\psi(1S) \rightarrow e^+ e^-)/\Gamma_{total}] \times [B(f_2'(1525) \rightarrow K \bar{K})] = 5.12 \pm 1.68 \pm 0.20$ eV which we divide by our best value $B(f_2'(1525) \rightarrow K \bar{K}) = (87.6 \pm 2.2) \times 10^{-2}$. Our first error is their experiment's error and our second error is the systematic error from using our best value.

$\Gamma(\phi f_2'(1525)) \times \Gamma(e^+ e^-)/\Gamma_{total}$					$\Gamma_{84}\Gamma_5/\Gamma$	
VALUE (eV)	EVTS	DOCUMENT ID	TECN	COMMENT		
$8.2 \pm 3.2 \pm 0.2$	11	1,2	LEES	14H	BABR	$e^+ e^- \rightarrow K_S^0 K_S^0 K^+ K^- \gamma$

1 Dividing by 1/4 to take into account $B(f_2'(1525) \rightarrow K_S^0 K_S^0) = 1/4$ $B(f_2'(1525) \rightarrow K \bar{K})$ and using $B(\phi \rightarrow K^+ K^-) = (48.9 \pm 0.5)\%$.

2 LEES 14H reports $[\Gamma(J/\psi(1S) \rightarrow \phi f_2'(1525)) \times \Gamma(J/\psi(1S) \rightarrow e^+ e^-)/\Gamma_{total}] \times [B(f_2'(1525) \rightarrow K \bar{K})] = 7.2 \pm 2.8 \pm 0.3$ eV which we divide by our best value $B(f_2'(1525) \rightarrow K \bar{K}) = (87.6 \pm 2.2) \times 10^{-2}$. Our first error is their experiment's error and our second error is the systematic error from using our best value.

$\Gamma(\phi \pi^+ \pi^-) \times \Gamma(e^+ e^-)/\Gamma_{total}$					$\Gamma_{85}\Gamma_5/\Gamma$
VALUE (eV)	EVTS	DOCUMENT ID	TECN	COMMENT	
4.47 ± 0.35 OUR AVERAGE					

$4.45 \pm 0.49 \pm 0.05$	181	1	LEES	12F	BABR	$10.6 e^+ e^- \rightarrow K^+ K^- \pi^+ \pi^- \gamma$
$4.50 \pm 0.48 \pm 0.05$	254 ± 23	2	SHEN	09	BELL	$10.6 e^+ e^- \rightarrow K^+ K^- \pi^+ \pi^- \gamma$

• • • We do not use the following data for averages, fits, limits, etc. • • •

$5.3 \pm 0.7 \pm 0.1$	103	3	AUBERT, BE	06D	BABR	$10.6 e^+ e^- \rightarrow K^+ K^- \pi^+ \pi^- \gamma$
-----------------------	-----	---	------------	-----	------	---

1 LEES 12F reports $[\Gamma(J/\psi(1S) \rightarrow \phi \pi^+ \pi^-) \times \Gamma(J/\psi(1S) \rightarrow e^+ e^-)/\Gamma_{total}] \times [B(\phi(1020) \rightarrow K^+ K^-)] = 2.19 \pm 0.23 \pm 0.07$ eV which we divide by our best value $B(\phi(1020) \rightarrow K^+ K^-) = (49.2 \pm 0.5) \times 10^{-2}$. Our first error is their experiment's error and our second error is the systematic error from using our best value.

2 SHEN 09 reports $4.50 \pm 0.41 \pm 0.26$ eV from a measurement of $[\Gamma(J/\psi(1S) \rightarrow \phi \pi^+ \pi^-) \times \Gamma(J/\psi(1S) \rightarrow e^+ e^-)/\Gamma_{total}] \times [B(\phi(1020) \rightarrow K^+ K^-)]$ assuming $B(\phi(1020) \rightarrow K^+ K^-) = (49.2 \pm 0.6) \times 10^{-2}$, which we rescale to our best value $B(\phi(1020) \rightarrow K^+ K^-) = (49.2 \pm 0.5) \times 10^{-2}$. Our first error is their experiment's error and our second error is the systematic error from using our best value.

3 Superseded by LEES 12F. AUBERT, BE 06D reports $[\Gamma(J/\psi(1S) \rightarrow \phi \pi^+ \pi^-) \times \Gamma(J/\psi(1S) \rightarrow e^+ e^-)/\Gamma_{total}] \times [B(\phi(1020) \rightarrow K^+ K^-)] = 2.61 \pm 0.30 \pm 0.18$ eV which we divide by our best value $B(\phi(1020) \rightarrow K^+ K^-) = (49.2 \pm 0.5) \times 10^{-2}$. Our first error is their experiment's error and our second error is the systematic error from using our best value.

$\Gamma(\phi \pi^0 \pi^0) \times \Gamma(e^+ e^-)/\Gamma_{total}$					$\Gamma_{86}\Gamma_5/\Gamma$	
VALUE (eV)	EVTS	DOCUMENT ID	TECN	COMMENT		
$2.76 \pm 0.57 \pm 0.03$	45	1	LEES	12F	BABR	$10.6 e^+ e^- \rightarrow K^+ K^- \pi^0 \pi^0 \gamma$

••• We do not use the following data for averages, fits, limits, etc. •••
 $3.13 \pm 0.88 \pm 0.03$ 23 ² AUBERT,BE 06D BABR $10.6 e^+ e^- \rightarrow K^+ K^- \pi^0 \pi^0 \gamma$

¹ LEES 12F reports $[\Gamma(J/\psi(1S) \rightarrow \phi \pi^0 \pi^0) \times \Gamma(J/\psi(1S) \rightarrow e^+ e^-) / \Gamma_{\text{total}}] \times [B(\phi(1020) \rightarrow K^+ K^-)] = 1.36 \pm 0.27 \pm 0.07$ eV which we divide by our best value $B(\phi(1020) \rightarrow K^+ K^-) = (49.2 \pm 0.5) \times 10^{-2}$. Our first error is their experiment's error and our second error is the systematic error from using our best value.

² Superseded by LEES 12F. AUBERT,BE 06D reports $[\Gamma(J/\psi(1S) \rightarrow \phi \pi^0 \pi^0) \times \Gamma(J/\psi(1S) \rightarrow e^+ e^-) / \Gamma_{\text{total}}] \times [B(\phi(1020) \rightarrow K^+ K^-)] = 1.54 \pm 0.40 \pm 0.16$ eV which we divide by our best value $B(\phi(1020) \rightarrow K^+ K^-) = (49.2 \pm 0.5) \times 10^{-2}$. Our first error is their experiment's error and our second error is the systematic error from using our best value.

$\Gamma(\phi\eta) \times \Gamma(e^+ e^-) / \Gamma_{\text{total}}$					$\Gamma_{89} \Gamma_5 / \Gamma$
VALUE (eV)	EVTS	DOCUMENT ID	TECN	COMMENT	
6.1 ± 2.7 ± 0.4	6	¹ AUBERT	07AU BABR	$10.6 e^+ e^- \rightarrow \phi \eta \gamma$	

¹ AUBERT 07AU quotes $\Gamma_{ee}^{J/\psi} \cdot B(J/\psi \rightarrow \phi \eta) \cdot B(\phi \rightarrow K^+ K^-) \cdot B(\eta \rightarrow 3\pi) = 0.84 \pm 0.37 \pm 0.05$ eV.

$\Gamma(\phi f_0(980) \rightarrow \phi \pi^+ \pi^-) \times \Gamma(e^+ e^-) / \Gamma_{\text{total}}$					$\Gamma_{97} \Gamma_5 / \Gamma$
VALUE (eV)	EVTS	DOCUMENT ID	TECN	COMMENT	
1.44 ± 0.19 OUR AVERAGE					

$1.40 \pm 0.25 \pm 0.02$ 57 ± 9 ¹ LEES 12F BABR $10.6 e^+ e^- \rightarrow \pi^+ \pi^- K^+ K^- \gamma$
 $1.48 \pm 0.27 \pm 0.09$ 60 ± 11 ² SHEN 09 BELL $10.6 e^+ e^- \rightarrow K^+ K^- \pi^+ \pi^- \gamma$

••• We do not use the following data for averages, fits, limits, etc. •••
 $1.02 \pm 0.24 \pm 0.01$ 20 ± 5 ³ AUBERT 07AK BABR $10.6 e^+ e^- \rightarrow \pi^+ \pi^- K^+ K^- \gamma$

¹ LEES 12F reports $[\Gamma(J/\psi(1S) \rightarrow \phi f_0(980) \rightarrow \phi \pi^+ \pi^-) \times \Gamma(J/\psi(1S) \rightarrow e^+ e^-) / \Gamma_{\text{total}}] \times [B(\phi(1020) \rightarrow K^+ K^-)] = 0.69 \pm 0.11 \pm 0.05$ eV which we divide by our best value $B(\phi(1020) \rightarrow K^+ K^-) = (49.2 \pm 0.5) \times 10^{-2}$. Our first error is their experiment's error and our second error is the systematic error from using our best value.

² Multiplied by 2/3 to take into account the $\phi \pi^+ \pi^-$ mode only. Using $B(\phi \rightarrow K^+ K^-) = (49.2 \pm 0.6)\%$.

³ Superseded by LEES 12F. AUBERT 07AK reports $[\Gamma(J/\psi(1S) \rightarrow \phi f_0(980) \rightarrow \phi \pi^+ \pi^-) \times \Gamma(J/\psi(1S) \rightarrow e^+ e^-) / \Gamma_{\text{total}}] \times [B(\phi(1020) \rightarrow K^+ K^-)] = 0.50 \pm 0.11 \pm 0.04$ eV which we divide by our best value $B(\phi(1020) \rightarrow K^+ K^-) = (49.2 \pm 0.5) \times 10^{-2}$. Our first error is their experiment's error and our second error is the systematic error from using our best value.

$\Gamma(\phi f_0(980) \rightarrow \phi \pi^0 \pi^0) \times \Gamma(e^+ e^-) / \Gamma_{\text{total}}$					$\Gamma_{98} \Gamma_5 / \Gamma$
VALUE (eV)	EVTS	DOCUMENT ID	TECN	COMMENT	
0.98 ± 0.26 ± 0.01	16 ± 4	¹ LEES 12F BABR	$10.6 e^+ e^- \rightarrow \pi^0 \pi^0 K^+ K^- \gamma$		

••• We do not use the following data for averages, fits, limits, etc. •••
 $0.95 \pm 0.40 \pm 0.01$ 7.0 ± 2.8 ² AUBERT 07AK BABR $10.6 e^+ e^- \rightarrow \pi^0 \pi^0 K^+ K^- \gamma$

¹ LEES 12F reports $[\Gamma(J/\psi(1S) \rightarrow \phi f_0(980) \rightarrow \phi \pi^0 \pi^0) \times \Gamma(J/\psi(1S) \rightarrow e^+ e^-) / \Gamma_{\text{total}}] \times [B(\phi(1020) \rightarrow K^+ K^-)] = 0.48 \pm 0.12 \pm 0.05$ eV which we divide by our best value $B(\phi(1020) \rightarrow K^+ K^-) = (49.2 \pm 0.5) \times 10^{-2}$. Our first error is their experiment's error and our second error is the systematic error from using our best value.

² Superseded by LEES 12F. AUBERT 07AK reports $[\Gamma(J/\psi(1S) \rightarrow \phi f_0(980) \rightarrow \phi \pi^0 \pi^0) \times \Gamma(J/\psi(1S) \rightarrow e^+ e^-) / \Gamma_{\text{total}}] \times [B(\phi(1020) \rightarrow K^+ K^-)] = 0.47 \pm 0.19 \pm 0.05$ eV which we divide by our best value $B(\phi(1020) \rightarrow K^+ K^-) = (49.2 \pm 0.5) \times 10^{-2}$. Our first error is their experiment's error and our second error is the systematic error from using our best value.

$\Gamma(\eta \pi^+ \pi^-) \times \Gamma(e^+ e^-) / \Gamma_{\text{total}}$					$\Gamma_{109} \Gamma_5 / \Gamma$
VALUE (eV)	EVTS	DOCUMENT ID	TECN	COMMENT	
2.3 ± 0.4 OUR AVERAGE					

$2.34 \pm 0.43 \pm 0.16$ 49 LEES 18 BABR $e^+ e^- \rightarrow \eta \pi^+ \pi^- \gamma$
 $2.23 \pm 0.97 \pm 0.03$ 9 ¹ AUBERT 07AU BABR $10.6 e^+ e^- \rightarrow \eta \pi^+ \pi^- \gamma$

¹ AUBERT 07AU reports $[\Gamma(J/\psi(1S) \rightarrow \eta \pi^+ \pi^-) \times \Gamma(J/\psi(1S) \rightarrow e^+ e^-) / \Gamma_{\text{total}}] \times [B(\eta \rightarrow \pi^+ \pi^- \pi^0)] = 0.51 \pm 0.22 \pm 0.03$ eV which we divide by our best value $B(\eta \rightarrow \pi^+ \pi^- \pi^0) = (22.92 \pm 0.28) \times 10^{-2}$. Our first error is their experiment's error and our second error is the systematic error from using our best value.

$\Gamma(K_S^0 \pi^- K_2^*(1430)^+ + \text{c.c.}) \times \Gamma(e^+ e^-) / \Gamma_{\text{total}}$					$\Gamma_{118} \Gamma_5 / \Gamma$
VALUE (eV)	EVTS	DOCUMENT ID	TECN	COMMENT	
20.1 ± 9.8 ± 0.5	35	^{1,2} LEES	14H BABR	$e^+ e^- \rightarrow \pi^+ \pi^- K_S^0 K_S^0 \gamma$	

¹ Dividing by 1/4 to take into account $B(K^*(1430) \rightarrow K_S^0 \pi) = 1/4 B(K^*(1430) \rightarrow K \pi)$.

² LEES 14H reports $[\Gamma(J/\psi(1S) \rightarrow K_S^0 \pi^- K_2^*(1430)^+ + \text{c.c.}) \times \Gamma(J/\psi(1S) \rightarrow e^+ e^-) / \Gamma_{\text{total}}] \times [B(K_2^*(1430) \rightarrow K \pi)] = 10.0 \pm 4.8 \pm 0.8$ eV which we divide by our best value $B(K_2^*(1430) \rightarrow K \pi) = (49.9 \pm 1.2) \times 10^{-2}$. Our first error is their experiment's error and our second error is the systematic error from using our best value.

$\Gamma(2(\pi^+ \pi^-) \pi^0) \times \Gamma(e^+ e^-) / \Gamma_{\text{total}}$					$\Gamma_{139} \Gamma_5 / \Gamma$
VALUE (eV)	EVTS	DOCUMENT ID	TECN	COMMENT	
303 ± 5 ± 18	4990	AUBERT	07AU BABR	$10.6 e^+ e^- \rightarrow 2(\pi^+ \pi^-) \pi^0 \gamma$	

$\Gamma(\pi^+ \pi^- \pi^0) \times \Gamma(e^+ e^-) / \Gamma_{\text{total}}$					$\Gamma_{141} \Gamma_5 / \Gamma$
VALUE (keV)	EVTS	DOCUMENT ID	TECN	COMMENT	
0.122 ± 0.005 ± 0.008		AUBERT,B	04N BABR	$10.6 e^+ e^- \rightarrow \pi^+ \pi^- \pi^0 \gamma$	

$\Gamma(\pi^+ \pi^- \pi^0 \pi^0) \times \Gamma(e^+ e^-) / \Gamma_{\text{total}}$					$\Gamma_{142} \Gamma_5 / \Gamma$
VALUE (eV)	EVTS	DOCUMENT ID	TECN	COMMENT	
150.0 ± 4.0 ± 15.0	2.3k	LEES	18E BABR	$10.6 e^+ e^- \rightarrow \pi^+ \pi^- \pi^0 \pi^0 \gamma$	

$\Gamma(\rho^\pm \pi^\mp \pi^0) \times \Gamma(e^+ e^-) / \Gamma_{\text{total}}$					$\Gamma_{143} \Gamma_5 / \Gamma$
VALUE (eV)	EVTS	DOCUMENT ID	TECN	COMMENT	
78.0 ± 9.0 ± 8.0	1.2k	LEES	18E BABR	$10.6 e^+ e^- \rightarrow \pi^+ \pi^- \pi^0 \gamma$	

$\Gamma(\rho^\pm \rho^- \pi^0) \times \Gamma(e^+ e^-) / \Gamma_{\text{total}}$					$\Gamma_{144} \Gamma_5 / \Gamma$
VALUE (eV)	EVTS	DOCUMENT ID	TECN	COMMENT	
33.0 ± 5.0 ± 3.3	529	LEES	18E BABR	$10.6 e^+ e^- \rightarrow \pi^+ \pi^- \pi^0 \gamma$	

$\Gamma(\pi^+ \pi^- \pi^0 K^+ K^-) \times \Gamma(e^+ e^-) / \Gamma_{\text{total}}$					$\Gamma_{145} \Gamma_5 / \Gamma$
VALUE (eV)	EVTS	DOCUMENT ID	TECN	COMMENT	
107.0 ± 4.3 ± 6.4	768	AUBERT	07AU BABR	$10.6 e^+ e^- \rightarrow K^+ K^- \pi^+ \pi^- \pi^0 \gamma$	

$\Gamma(\pi^+ \pi^- K^+ K^-) \times \Gamma(e^+ e^-) / \Gamma_{\text{total}}$					$\Gamma_{147} \Gamma_5 / \Gamma$
VALUE (eV)	EVTS	DOCUMENT ID	TECN	COMMENT	
37.94 ± 0.81 ± 1.10	3.1k	LEES	12F BABR	$10.6 e^+ e^- \rightarrow \pi^+ \pi^- K^+ K^- \gamma$	

••• We do not use the following data for averages, fits, limits, etc. •••
 $36.3 \pm 1.3 \pm 2.1$ 1.5k ¹ AUBERT 07AK BABR $10.6 e^+ e^- \rightarrow \pi^+ \pi^- K^+ K^- \gamma$
 $33.6 \pm 2.7 \pm 2.7$ 233 ² AUBERT 05D BABR $10.6 e^+ e^- \rightarrow K^+ K^- \pi^+ \pi^- \gamma$

¹ Superseded by LEES 12F.
² Superseded by AUBERT 07AK.

$\Gamma(\pi^+ \pi^- K_S^0 K_L^0) \times \Gamma(e^+ e^-) / \Gamma_{\text{total}}$					$\Gamma_{148} \Gamma_5 / \Gamma$
VALUE (eV)	EVTS	DOCUMENT ID	TECN	COMMENT	
20.8 ± 2.3 ± 2.1	248	LEES	14H BABR	$e^+ e^- \rightarrow \pi^+ \pi^- K_S^0 K_L^0 \gamma$	

$\Gamma(\pi^+ \pi^- K_S^0 K_S^0) \times \Gamma(e^+ e^-) / \Gamma_{\text{total}}$					$\Gamma_{149} \Gamma_5 / \Gamma$
VALUE (eV)	EVTS	DOCUMENT ID	TECN	COMMENT	
9.3 ± 0.9 ± 0.5	133	LEES	14H BABR	$e^+ e^- \rightarrow \pi^+ \pi^- K_S^0 K_S^0 \gamma$	

$\Gamma(\pi^\pm \pi^0 K^\mp K_S^0) \times \Gamma(e^+ e^-) / \Gamma_{\text{total}}$					$\Gamma_{150} \Gamma_5 / \Gamma$
VALUE (eV)	EVTS	DOCUMENT ID	TECN	COMMENT	
31.7 ± 1.9 ± 1.8	393	LEES	17D BABR	$e^+ e^- \rightarrow K_S^0 K^\pm \pi^\mp \pi^0 \gamma$	

$\Gamma(K^+ K^- K_S^0 K_S^0) \times \Gamma(e^+ e^-) / \Gamma_{\text{total}}$					$\Gamma_{151} \Gamma_5 / \Gamma$
VALUE (eV)	EVTS	DOCUMENT ID	TECN	COMMENT	
2.3 ± 0.4 ± 0.1	29	LEES	14H BABR	$e^+ e^- \rightarrow K_S^0 K_S^0 K^+ K^- \gamma$	

$\Gamma(\pi^+ \pi^- K^+ K^- \eta) \times \Gamma(e^+ e^-) / \Gamma_{\text{total}}$					$\Gamma_{152} \Gamma_5 / \Gamma$
VALUE (eV)	EVTS	DOCUMENT ID	TECN	COMMENT	
25.9 ± 3.9 ± 0.1	73	¹ AUBERT	07AU BABR	$10.6 e^+ e^- \rightarrow K^+ K^- \pi^+ \pi^- \eta \gamma$	

¹ AUBERT 07AU reports $[\Gamma(J/\psi(1S) \rightarrow \pi^+ \pi^- K^+ K^- \eta) \times \Gamma(J/\psi(1S) \rightarrow e^+ e^-) / \Gamma_{\text{total}}] \times [B(\eta \rightarrow 2\gamma)] = 10.2 \pm 1.3 \pm 0.8$ eV which we divide by our best value $B(\eta \rightarrow 2\gamma) = (39.41 \pm 0.20) \times 10^{-2}$. Our first error is their experiment's error and our second error is the systematic error from using our best value.

$\Gamma(\pi^0 \pi^0 K^+ K^-) \times \Gamma(e^+ e^-) / \Gamma_{\text{total}}$					$\Gamma_{153} \Gamma_5 / \Gamma$
VALUE (eV)	EVTS	DOCUMENT ID	TECN	COMMENT	
11.75 ± 0.81 ± 0.90	388	LEES	12F BABR	$10.6 e^+ e^- \rightarrow \pi^0 \pi^0 K^+ K^- \gamma$	

••• We do not use the following data for averages, fits, limits, etc. •••
 $13.6 \pm 1.1 \pm 1.3$ 203 ¹ AUBERT 07AK BABR $10.6 e^+ e^- \rightarrow \pi^0 \pi^0 K^+ K^- \gamma$

¹ Superseded by LEES 12F.

$\Gamma(\pi^0 \pi^0 K_S^0 K_L^0) \times \Gamma(e^+ e^-) / \Gamma_{\text{total}}$					$\Gamma_{154} \Gamma_5 / \Gamma$
VALUE (eV)	EVTS	DOCUMENT ID	TECN	COMMENT	
10.3 ± 2.3 ± 0.5	47	LEES	17A BABR	$e^+ e^- \rightarrow K_S^0 K_L^0 \pi^0 \pi^0 \gamma$	

$\Gamma(K_S^0 K_L^0 \pi^0) \times \Gamma(e^+ e^-) / \Gamma_{\text{total}}$					$\Gamma_{158} \Gamma_5 / \Gamma$
VALUE (eV)	EVTS	DOCUMENT ID	TECN	COMMENT	
11.4 ± 1.3 ± 0.6	182	LEES	17A BABR	$e^+ e^- \rightarrow K_S^0 K_L^0 \pi^0 \gamma$	

$\Gamma(K^*(892)^0 \bar{K}^0 + \text{c.c.} \rightarrow K_S^0 K_L^0 \pi^0) \times \Gamma(e^+ e^-) / \Gamma_{\text{total}}$					$\Gamma_{159} \Gamma_5 / \Gamma$
VALUE (eV)	EVTS	DOCUMENT ID	TECN	COMMENT	
6.7 ± 0.9 ± 0.4	106	LEES	17A BABR	$e^+ e^- \rightarrow K_S^0 K_L^0 \pi^0 \gamma$	

$\Gamma(K_2^*(1430)^0 \bar{K}^0 + \text{c.c.} \rightarrow K_S^0 K_L^0 \pi^0) \times \Gamma(e^+ e^-) / \Gamma_{\text{total}}$					$\Gamma_{160} \Gamma_5 / \Gamma$
VALUE (eV)	EVTS	DOCUMENT ID	TECN	COMMENT	
2.4 ± 0.7 ± 0.1	37	LEES	17A BABR	$e^+ e^- \rightarrow K_S^0 K_L^0 \pi^0 \gamma$	

$\Gamma(K_S^0 K_L^0 \eta) \times \Gamma(e^+ e^-) / \Gamma_{\text{total}}$					$\Gamma_{161} \Gamma_5 / \Gamma$
VALUE (eV)	EVTS	DOCUMENT ID	TECN	COMMENT	
8.0 ± 1.8 ± 0.4	45	LEES	17A BABR	$e^+ e^- \rightarrow K_S^0 K_L^0 \eta \gamma$	

$\Gamma(2(\pi^+ \pi^-)) \times \Gamma(e^+ e^-) / \Gamma_{\text{total}}$					$\Gamma_{162} \Gamma_5 / \Gamma$
VALUE (eV)	EVTS	DOCUMENT ID	TECN	COMMENT	
20.4 ± 0.9 ± 0.4		LEES	12E BABR	$10.6 e^+ e^- \rightarrow 2\pi^+ 2\pi^- \gamma$	

Meson Particle Listings

$J/\psi(1S)$

••• We do not use the following data for averages, fits, limits, etc. •••

19.5 ± 1.4 ± 1.3	270	¹ AUBERT	05D	BABR	10.6 e ⁺ e ⁻ → 2(π ⁺ π ⁻)γ
¹ Superseded by LEES 12E.					

$\Gamma(3(\pi^+\pi^-)) \times \Gamma(e^+e^-)/\Gamma_{total}$ $\Gamma_{163}\Gamma_5/\Gamma$

VALUE (10 ⁻² keV)	EVTS	DOCUMENT ID	TECN	COMMENT
2.37 ± 0.16 ± 0.14	496	AUBERT	06D	BABR 10.6 e ⁺ e ⁻ → 3(π ⁺ π ⁻)γ

$\Gamma(2(\pi^+\pi^-\pi^0)) \times \Gamma(e^+e^-)/\Gamma_{total}$ $\Gamma_{164}\Gamma_5/\Gamma$

VALUE (10 ⁻² keV)	EVTS	DOCUMENT ID	TECN	COMMENT
8.9 ± 0.5 ± 1.0	761	AUBERT	06D	BABR 10.6 e ⁺ e ⁻ → 2(π ⁺ π ⁻ π ⁰)γ

$\Gamma(2(\pi^+\pi^-)\eta) \times \Gamma(e^+e^-)/\Gamma_{total}$ $\Gamma_{165}\Gamma_5/\Gamma$

VALUE (eV)	EVTS	DOCUMENT ID	TECN	COMMENT
13.1 ± 2.4 ± 0.1	85	¹ AUBERT	07AU	BABR 10.6 e ⁺ e ⁻ → 2(π ⁺ π ⁻)ηγ

¹ AUBERT 07AU reports [Γ(J/ψ(1S) → 2(π⁺π⁻)η) × Γ(J/ψ(1S) → e⁺e⁻)/Γ_{total}] × [B(η → 2γ)] = 5.16 ± 0.85 ± 0.39 eV which we divide by our best value B(η → 2γ) = (39.41 ± 0.20) × 10⁻². Our first error is their experiment's error and our second error is the systematic error from using our best value.

$\Gamma(\pi^+\pi^-\pi^0\eta) \times \Gamma(e^+e^-)/\Gamma_{total}$ $\Gamma_{167}\Gamma_5/\Gamma$

VALUE (eV)	EVTS	DOCUMENT ID	TECN	COMMENT
12.8 ± 1.8 ± 2.0	203	LEES	18E	BABR 10.6 e ⁺ e ⁻ → π ⁺ π ⁻ π ⁰ ηγ

$\Gamma(\omega\pi^0\eta) \times \Gamma(e^+e^-)/\Gamma_{total}$ $\Gamma_{63}\Gamma_5/\Gamma$

VALUE (eV)	EVTS	DOCUMENT ID	TECN	COMMENT
1.90 ± 0.96 ± 0.01	27	¹ LEES	18E	BABR 10.6 e ⁺ e ⁻ → π ⁺ π ⁻ π ⁰ ηγ

¹ LEES 18E reports [Γ(J/ψ(1S) → ωπ⁰η) × Γ(J/ψ(1S) → e⁺e⁻)/Γ_{total}] × [B(ω(782) → π⁺π⁻π⁰)] = 1.7 ± 0.8 ± 0.3 eV which we divide by our best value B(ω(782) → π⁺π⁻π⁰) = (89.3 ± 0.6) × 10⁻². Our first error is their experiment's error and our second error is the systematic error from using our best value.

$\Gamma(\rho^+\pi^-\pi^0\eta) \times \Gamma(e^+e^-)/\Gamma_{total}$ $\Gamma_{168}\Gamma_5/\Gamma$

VALUE (eV)	EVTS	DOCUMENT ID	TECN	COMMENT
10.5 ± 4.1 ± 1.6	168	LEES	18E	BABR 10.6 e ⁺ e ⁻ → π ⁺ π ⁻ π ⁰ ηγ

$\Gamma(\rho\bar{\rho}) \times \Gamma(e^+e^-)/\Gamma_{total}$ $\Gamma_{169}\Gamma_5/\Gamma$

VALUE (eV)	EVTS	DOCUMENT ID	TECN	COMMENT
11.9 ± 0.6 OUR AVERAGE	Error includes scale factor of 1.8. See the ideogram below.			

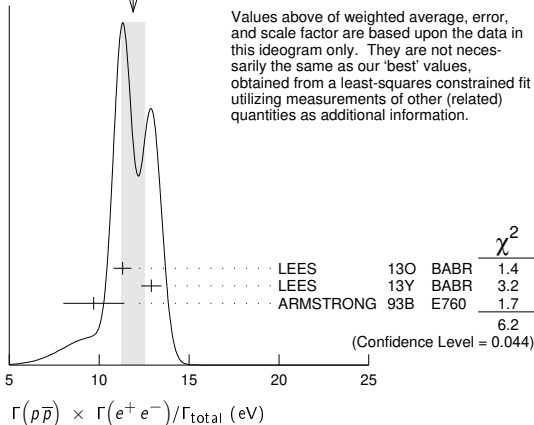
11.3 ± 0.4 ± 0.3	821	¹ LEES	13O	BABR e ⁺ e ⁻ → ρ ⁺ ρ ⁻ γ
12.9 ± 0.4 ± 0.4	918	² LEES	13Y	BABR e ⁺ e ⁻ → ρ ⁺ ρ ⁻ γ
9.7 ± 1.7		³ ARMSTRONG	93B	E760 $\bar{p}p$ → e ⁺ e ⁻

••• We do not use the following data for averages, fits, limits, etc. •••

12.0 ± 0.6 ± 0.5	438	⁴ AUBERT	06B	BABR e ⁺ e ⁻ → ρ ⁺ ρ ⁻ γ
------------------	-----	---------------------	-----	--

- ¹ISR photon reconstructed in the detector
- ²ISR photon undetected
- ³Using Γ_{total} = 85.5^{+6.1}_{-5.8} MeV.
- ⁴Superseded by LEES 13O

WEIGHTED AVERAGE
11.9 ± 0.6 (Error scaled by 1.8)



Values above of weighted average, error, and scale factor are based upon the data in this ideogram only. They are not necessarily the same as our 'best' values, obtained from a least-squares constrained fit utilizing measurements of other (related) quantities as additional information.

$\Gamma(\Sigma^0\bar{\Sigma}^0) \times \Gamma(e^+e^-)/\Gamma_{total}$ $\Gamma_{182}\Gamma_5/\Gamma$

VALUE (eV)	DOCUMENT ID	TECN	COMMENT
6.4 ± 1.2 ± 0.6	AUBERT	07Bd	BABR 10.6 e ⁺ e ⁻ → Σ ⁰ $\bar{\Sigma}$ ⁰ γ

$\Gamma(2(\pi^+\pi^-)K^+K^-) \times \Gamma(e^+e^-)/\Gamma_{total}$ $\Gamma_{183}\Gamma_5/\Gamma$

VALUE (10 ⁻² keV)	EVTS	DOCUMENT ID	TECN	COMMENT
2.75 ± 0.23 ± 0.17	205	AUBERT	06D	BABR 10.6 e ⁺ e ⁻ → K ⁺ K ⁻ 2(π ⁺ π ⁻)γ

$\Gamma(\Lambda\bar{\Lambda}) \times \Gamma(e^+e^-)/\Gamma_{total}$ $\Gamma_{189}\Gamma_5/\Gamma$

VALUE (eV)	DOCUMENT ID	TECN	COMMENT
10.7 ± 0.9 ± 0.7	AUBERT	07Bd	BABR 10.6 e ⁺ e ⁻ → Λ $\bar{\Lambda}$ γ

$\Gamma(2(K^+K^-)) \times \Gamma(e^+e^-)/\Gamma_{total}$ $\Gamma_{192}\Gamma_5/\Gamma$

VALUE (eV)	EVTS	DOCUMENT ID	TECN	COMMENT
4.00 ± 0.33 ± 0.29	287 ± 24	LEES	12F	BABR 10.6 e ⁺ e ⁻ → 2(K ⁺ K ⁻)γ

4.11 ± 0.39 ± 0.30	156 ± 15	¹ AUBERT	07AK	BABR 10.6 e ⁺ e ⁻ → 2(K ⁺ K ⁻)γ
4.0 ± 0.7 ± 0.6	38	² AUBERT	05D	BABR 10.6 e ⁺ e ⁻ → 2(K ⁺ K ⁻)γ

¹ Superseded by LEES 12F.
² Superseded by AUBERT 07AK.

$\Gamma(K^+K^-) \times \Gamma(e^+e^-)/\Gamma_{total}$ $\Gamma_{194}\Gamma_5/\Gamma$

VALUE (eV)	EVTS	DOCUMENT ID	TECN	COMMENT
1.78 ± 0.11 ± 0.05	462	¹ LEES	15J	BABR e ⁺ e ⁻ → K ⁺ K ⁻ γ
1.94 ± 0.11 ± 0.05	462	² LEES	15J	BABR e ⁺ e ⁻ → K ⁺ K ⁻ γ
1.42 ± 0.23 ± 0.08	51	³ LEES	13Q	BABR e ⁺ e ⁻ → K ⁺ K ⁻ γ

- We do not use the following data for averages, fits, limits, etc. •••
- ¹ sin φ > 0.
- ² sin φ < 0.
- ³ Interference with non-resonant K⁺K⁻ production not taken into account.

J/ψ(1S) BRANCHING RATIOS

For the first four branching ratios, see also the partial widths, and (partial widths) × Γ(e⁺e⁻)/Γ_{total} above.

$\Gamma(\text{hadrons})/\Gamma_{total}$ Γ_1/Γ

VALUE	DOCUMENT ID	TECN	COMMENT
0.877 ± 0.005 OUR AVERAGE			
0.878 ± 0.005	BAI	95B	BES e ⁺ e ⁻
0.86 ± 0.02	BOYARSKI	75	MRK1 e ⁺ e ⁻

$\Gamma(\text{virtual}\gamma \rightarrow \text{hadrons})/\Gamma_{total}$ Γ_2/Γ

VALUE	DOCUMENT ID	TECN	COMMENT	
0.135 ± 0.003	1,2	SETH	04	RVUE e ⁺ e ⁻
0.17 ± 0.02	¹	BOYARSKI	75	MRK1 e ⁺ e ⁻

- We do not use the following data for averages, fits, limits, etc. •••
- ¹Included in Γ(hadrons)/Γ_{total}.
- ²Using B(J/ψ → ℓ⁺ℓ⁻) = (5.90 ± 0.09)% from RPP-2002 and R = 2.28 ± 0.04 determined by a fit to data from BAI 00 and BAI 02c.

$\Gamma(g\bar{g})/\Gamma_{total}$ Γ_3/Γ

VALUE (units 10 ⁻²)	EVTS	DOCUMENT ID	TECN	COMMENT
64.1 ± 1.0	6 M	¹ BESSON	08	CLEO ψ(2S) → π ⁺ π ⁻ + hadrons

¹ Calculated using the value Γ(γγg)/Γ(gg) = 0.137 ± 0.001 ± 0.016 ± 0.004 from BESSON 08 and the PDG 08 values of B(ℓ⁺ℓ⁻), B(virtual γ → hadrons), and B(γη_c). The statistical error is negligible and the systematic error is partially correlated with that of Γ(γγg)/Γ_{total} measurement of BESSON 08.

$\Gamma(\gamma\bar{g})/\Gamma_{total}$ Γ_4/Γ

VALUE (units 10 ⁻²)	EVTS	DOCUMENT ID	TECN	COMMENT
8.79 ± 1.05	200 k	¹ BESSON	08	CLEO ψ(2S) → π ⁺ π ⁻ γ + hadrons

¹ Calculated using the value Γ(γγg)/Γ(gg) = 0.137 ± 0.001 ± 0.016 ± 0.004 from BESSON 08 and the value of Γ(gg)/Γ_{total}. The statistical error is negligible and the systematic error is partially correlated with that of Γ(gg)/Γ_{total} measurement of BESSON 08.

$\Gamma(\gamma\bar{g})/\Gamma(g\bar{g})$ Γ_4/Γ_3

VALUE (units 10 ⁻²)	EVTS	DOCUMENT ID	TECN	COMMENT
13.7 ± 0.1 ± 0.7	6 M	BESSON	08	CLEO ψ(2S) → π ⁺ π ⁻ J/ψ

$\Gamma(e^+e^-)/\Gamma_{total}$ Γ_5/Γ

VALUE (units 10 ⁻²)	EVTS	DOCUMENT ID	TECN	COMMENT
5.971 ± 0.032 OUR AVERAGE				
5.983 ± 0.007 ± 0.037	720k	ABLIKIM	13R	BES3 ψ(2S) → J/ψπ ⁺ π ⁻
5.945 ± 0.067 ± 0.042	15k	LI	05c	CLEO ψ(2S) → J/ψπ ⁺ π ⁻
5.90 ± 0.05 ± 0.10		BAI	98D	BES ψ(2S) → J/ψπ ⁺ π ⁻
6.09 ± 0.33		BAI	95B	BES e ⁺ e ⁻
5.92 ± 0.15 ± 0.20		COFFMAN	92	MRK3 ψ(2S) → J/ψπ ⁺ π ⁻
6.9 ± 0.9		BOYARSKI	75	MRK1 e ⁺ e ⁻

$\Gamma(e^+e^-\gamma)/\Gamma_{total}$ Γ_6/Γ

VALUE (units 10 ⁻³)	DOCUMENT ID	TECN	COMMENT
8.8 ± 1.3 ± 0.4	¹ ARMSTRONG	96	E760 $\bar{p}p$ → e ⁺ e ⁻ γ

¹ For E_γ > 100 MeV.

$\Gamma(\mu^+\mu^-)/\Gamma_{total}$					Γ_7/Γ
VALUE (units 10^{-2})	EVTS	DOCUMENT ID	TECN	COMMENT	
5.961 ± 0.033 OUR AVERAGE					
5.973 ± 0.007 ± 0.038	770k	ABLIKIM	13R	BES3 $\psi(2S) \rightarrow J/\psi \pi^+ \pi^-$	
5.960 ± 0.065 ± 0.050	17k	LI	05c	CLEO $\psi(2S) \rightarrow J/\psi \pi^+ \pi^-$	
5.84 ± 0.06 ± 0.10		BAI	98D	BES $\psi(2S) \rightarrow J/\psi \pi^+ \pi^-$	
6.08 ± 0.33		BAI	95B	BES $e^+ e^-$	
5.90 ± 0.15 ± 0.19		COFFMAN	92	MRK3 $\psi(2S) \rightarrow J/\psi \pi^+ \pi^-$	
6.9 ± 0.9		BOYARSKI	75	MRK1 $e^+ e^-$	

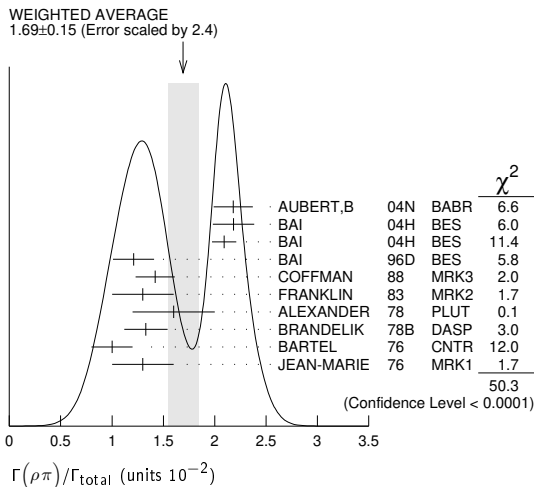
$\Gamma(e^+e^-)/\Gamma(\mu^+\mu^-)$					Γ_5/Γ_7
VALUE	DOCUMENT ID	TECN	COMMENT		
1.0016 ± 0.0031 OUR AVERAGE					
1.0022 ± 0.0044 ± 0.0048	¹ AULCHENKO	14	KEDR	3.097 $e^+ e^- \rightarrow e^+ e^- \mu^+ \mu^-$	
1.0017 ± 0.0017 ± 0.0033	² ABLIKIM	13R	BES3	$\psi(2S) \rightarrow J/\psi \pi^+ \pi^-$	
1.002 ± 0.021 ± 0.013	³ ANASHIN	10	KEDR	3.097 $e^+ e^- \rightarrow e^+ e^- \mu^+ \mu^-$	
0.997 ± 0.012 ± 0.006	LI	05c	CLEO	$\psi(2S) \rightarrow J/\psi \pi^+ \pi^-$	
• • • We do not use the following data for averages, fits, limits, etc. • • •					
1.011 ± 0.013 ± 0.016	BAI	98D	BES	$\psi(2S) \rightarrow J/\psi \pi^+ \pi^-$	
1.00 ± 0.07	BAI	95B	BES	$e^+ e^-$	
1.00 ± 0.05	BOYARSKI	75	MRK1	$e^+ e^-$	
0.91 ± 0.15	ESPOSITO	75B	FRAM	$e^+ e^-$	
0.93 ± 0.10	FORD	75	SPEC	$e^+ e^-$	

¹ From 235.3k $J/\psi \rightarrow e^+ e^-$ and 156.6k $J/\psi \rightarrow \mu^+ \mu^-$ observed events.
² Not independent of the corresponding measurements of $\Gamma(e^+e^-)/\Gamma_{total}$ and $\Gamma(\mu^+\mu^-)/\Gamma_{total}$.
³ Not independent of the corresponding measurements of $\Gamma(e^+e^-) \times \Gamma(e^+e^-)/\Gamma_{total}$ and $\Gamma(\mu^+\mu^-) \times \Gamma(e^+e^-)/\Gamma_{total}$.

HADRONIC DECAYS

$\Gamma(\rho\pi)/\Gamma_{total}$					Γ_8/Γ
VALUE (units 10^{-2})	EVTS	DOCUMENT ID	TECN	COMMENT	
1.69 ± 0.15 OUR AVERAGE					
2.18 ± 0.19		^{1,2} AUBERT,B	04N	BABR 10.6 $e^+ e^- \rightarrow \pi^+ \pi^- \pi^0 \gamma$	
2.184 ± 0.005 ± 0.201	220k	^{2,3} BAI	04H	BES $e^+ e^- \rightarrow J/\psi \rightarrow \pi^+ \pi^- \pi^0$	
2.091 ± 0.021 ± 0.116		^{2,4} BAI	04H	BES $\psi(2S) \rightarrow \pi^+ \pi^- J/\psi$	
1.21 ± 0.20		BAI	96D	BES $e^+ e^- \rightarrow \rho\pi$	
1.42 ± 0.01 ± 0.19		COFFMAN	88	MRK3 $e^+ e^-$	
1.3 ± 0.3	150	FRANKLIN	83	MRK2 $e^+ e^-$	
1.6 ± 0.4	183	ALEXANDER	78	PLUT $e^+ e^-$	
1.33 ± 0.21		BRANDELIK	78B	DASP $e^+ e^-$	
1.0 ± 0.2	543	BARTEL	76	CNTR $e^+ e^-$	
1.3 ± 0.3	153	JEAN-MARIE	76	MRK1 $e^+ e^-$	

¹ From the ratio of $\Gamma(e^+e^-) B(\pi^+ \pi^- \pi^0)$ and $\Gamma(e^+e^-) B(\mu^+ \mu^-)$ (AUBERT 04).
² Not independent of their $B(\pi^+ \pi^- \pi^0)$.
³ From $J/\psi \rightarrow \pi^+ \pi^- \pi^0$ events directly.
⁴ Obtained comparing the rates for $\pi^+ \pi^- \pi^0$ and $\mu^+ \mu^-$, using J/ψ events produced via $\psi(2S) \rightarrow \pi^+ \pi^- J/\psi$ and with $B(J/\psi \rightarrow \mu^+ \mu^-) = 5.88 \pm 0.10\%$.



$\Gamma(\rho\pi)/\Gamma(\pi^+\pi^-\pi^0)$					Γ_8/Γ_{141}
VALUE	EVTS	DOCUMENT ID	TECN	COMMENT	
1.142 ± 0.011 ± 0.026					
	20K	¹ LEES	17c	BABR $J/\psi \rightarrow \pi^+ \pi^- \pi^0$	
• • • We do not use the following data for averages, fits, limits, etc. • • •					
1.331 ± 0.033	20K	² LEES	17c	BABR $J/\psi \rightarrow \pi^+ \pi^- \pi^0$	

¹ From a Dalitz plot analysis in an isobar model.
² From a Dalitz plot analysis in a Veneziano model.

$\Gamma(\rho^0\pi^0)/\Gamma(\rho\pi)$					Γ_9/Γ_8
VALUE	DOCUMENT ID	TECN	COMMENT		
0.328 ± 0.005 ± 0.027					
	COFFMAN	88	MRK3	$e^+ e^-$	
• • • We do not use the following data for averages, fits, limits, etc. • • •					
0.35 ± 0.08	ALEXANDER	78	PLUT	$e^+ e^-$	
0.32 ± 0.08	BRANDELIK	78B	DASP	$e^+ e^-$	
0.39 ± 0.11	BARTEL	76	CNTR	$e^+ e^-$	
0.37 ± 0.09	JEAN-MARIE	76	MRK1	$e^+ e^-$	

$\Gamma(\rho(1450)\pi \rightarrow \pi^+\pi^-\pi^0)/\Gamma(\pi^+\pi^-\pi^0)$					Γ_{12}/Γ_{141}
VALUE (%)	EVTS	DOCUMENT ID	TECN	COMMENT	
10.9 ± 1.7 ± 2.7					
	20K	¹ LEES	17c	BABR $J/\psi \rightarrow \pi^+ \pi^- \pi^0$	
• • • We do not use the following data for averages, fits, limits, etc. • • •					
0.80 ± 0.27	20K	² LEES	17c	BABR $J/\psi \rightarrow \pi^+ \pi^- \pi^0$	

¹ From a Dalitz plot analysis in an isobar model.
² From a Dalitz plot analysis in a Veneziano model.

$\Gamma(\rho(1450)\pi \rightarrow K^0_S K^\pm \pi^\mp)/\Gamma(K^0_S K^\pm \pi^\mp)$					Γ_{13}/Γ_{157}
VALUE (%)	EVTS	DOCUMENT ID	TECN	COMMENT	
6.3 ± 0.8 ± 0.6					
	4K	¹ LEES	17c	BABR $J/\psi \rightarrow K^0_S K^\pm \pi^\mp$	

¹ From a Dalitz plot analysis in an isobar model.

$\Gamma(\rho(1450)\pi^0 \rightarrow K^+ K^- \pi^0)/\Gamma(K^+ K^- \pi^0)$					Γ_{14}/Γ_{156}
VALUE (%)	EVTS	DOCUMENT ID	TECN	COMMENT	
9.3 ± 2.0 ± 0.6					
	2K	¹ LEES	17c	BABR $J/\psi \rightarrow K^+ K^- \pi^0$	

¹ From a Dalitz plot analysis in an isobar model.

$\Gamma(\rho(1450)\eta(958) \rightarrow \pi^+\pi^-\eta(958))/\Gamma_{total}$					Γ_{15}/Γ
VALUE (units 10^{-6})	EVTS	DOCUMENT ID	TECN	COMMENT	
3.28 ± 0.55 ± 0.44					
	119	¹ ABLIKIM	17AK	BES3 $J/\psi \rightarrow \pi^+ \pi^- \eta'$	

¹ From a partial wave analysis of the decay $J/\psi \rightarrow \pi^+ \pi^- \eta'$.

$\Gamma(\rho(1700)\pi \rightarrow \pi^+\pi^-\pi^0)/\Gamma(\pi^+\pi^-\pi^0)$					Γ_{17}/Γ_{141}
VALUE (units 10^{-3})	EVTS	DOCUMENT ID	TECN	COMMENT	
8 ± 2 ± 5					
	20K	¹ LEES	17c	BABR $J/\psi \rightarrow \pi^+ \pi^- \pi^0$	
• • • We do not use the following data for averages, fits, limits, etc. • • •					
22 ± 6	20K	² LEES	17c	BABR $J/\psi \rightarrow \pi^+ \pi^- \pi^0$	

¹ From a Dalitz plot analysis in an isobar model.
² From a Dalitz plot analysis in a Veneziano model.

$\Gamma(\rho(2150)\pi \rightarrow \pi^+\pi^-\pi^0)/\Gamma(\pi^+\pi^-\pi^0)$					Γ_{19}/Γ_{141}
VALUE (units 10^{-4})	EVTS	DOCUMENT ID	TECN	COMMENT	
4 ± 1 ± 20					
	20K	¹ LEES	17c	BABR $J/\psi \rightarrow \pi^+ \pi^- \pi^0$	
• • • We do not use the following data for averages, fits, limits, etc. • • •					
600 ± 250	20K	² LEES	17c	BABR $J/\psi \rightarrow \pi^+ \pi^- \pi^0$	

¹ From a Dalitz plot analysis in an isobar model.
² From a Dalitz plot analysis in a Veneziano model.

$\Gamma(\rho_3(1690)\pi \rightarrow \pi^+\pi^-\pi^0)/\Gamma(\pi^+\pi^-\pi^0)$					Γ_{20}/Γ_{141}
VALUE (units 10^{-3})	EVTS	DOCUMENT ID	TECN	COMMENT	
4.0 ± 0.8					
	20K	¹ LEES	17c	BABR $J/\psi \rightarrow \pi^+ \pi^- \pi^0$	

¹ From a Dalitz plot analysis in a Veneziano model.

$\Gamma(\rho_2(1320)\rho)/\Gamma_{total}$					Γ_{21}/Γ
VALUE (units 10^{-3})	EVTS	DOCUMENT ID	TECN	COMMENT	
10.9 ± 2.2 OUR AVERAGE					
11.7 ± 0.7 ± 2.5	7584	AUGUSTIN	89	DM2 $J/\psi \rightarrow \rho^0 \rho^\pm \pi^\mp$	
8.4 ± 4.5	36	VANNUCCI	77	MRK1 $e^+ e^- \rightarrow 2(\pi^+ \pi^-) \pi^0$	

$\Gamma(\omega\pi^+\pi^-\pi^-\pi^0)/\Gamma_{total}$					Γ_{22}/Γ
VALUE (units 10^{-4})	EVTS	DOCUMENT ID	TECN	COMMENT	
85 ± 34					
	140	VANNUCCI	77	MRK1 $e^+ e^- \rightarrow 3(\pi^+ \pi^-) \pi^0$	

$\Gamma(\omega\pi^+\pi^-)/\Gamma_{total}$					Γ_{24}/Γ
VALUE (units 10^{-3})	EVTS	DOCUMENT ID	TECN	COMMENT	
7.2 ± 1.0 OUR AVERAGE					
7.0 ± 1.6	18058	AUGUSTIN	89	DM2 $J/\psi \rightarrow 2(\pi^+ \pi^-) \pi^0$	
7.8 ± 1.6	215	BURMESTER	77D	PLUT $e^+ e^-$	
6.8 ± 1.9	348	VANNUCCI	77	MRK1 $e^+ e^- \rightarrow 2(\pi^+ \pi^-) \pi^0$	

$\Gamma(\omega\eta'\pi^+\pi^-)/\Gamma_{total}$					Γ_{74}/Γ
VALUE (units 10^{-3})	EVTS	DOCUMENT ID	TECN	COMMENT	
1.12 ± 0.02 ± 0.13					
	14k	¹ ABLIKIM	19AC	BES3 $J/\psi \rightarrow \omega\eta'\pi^+\pi^-$	

¹ Using the decays $\omega \rightarrow \pi^+ \pi^- \pi^0$ and $\eta' \rightarrow \eta\pi^+\pi^-$.

Meson Particle Listings

$J/\psi(1S)$

$\Gamma(\omega f_2(1270))/\Gamma_{total}$ Γ_{25}/Γ

VALUE (units 10^{-3})	EVTS	DOCUMENT ID	TECN	COMMENT
4.3 ± 0.6 OUR AVERAGE				
4.3 ± 0.2 ± 0.6	5860	AUGUSTIN 89	DM2	e^+e^-
4.0 ± 1.6	70	BURMESTER 77D	PLUT	e^+e^-
• • • We do not use the following data for averages, fits, limits, etc. • • •				
1.9 ± 0.8	81	VANNUCCI 77	MRK1	$e^+e^- \rightarrow 2(\pi^+\pi^-)\pi^0$

$\Gamma(K^*(892)^0 \bar{K}^*(892)^0)/\Gamma_{total}$ Γ_{26}/Γ

VALUE (units 10^{-4})	CL%	DOCUMENT ID	TECN	COMMENT
• • • We do not use the following data for averages, fits, limits, etc. • • •				
<5	90	VANNUCCI 77	MRK1	$e^+e^- \rightarrow \pi^+\pi^-K^+K^-$

$\Gamma(K^*(892)^\pm K^*(892)^\mp)/\Gamma_{total}$ Γ_{27}/Γ

VALUE (units 10^{-3})	EVTS	DOCUMENT ID	TECN	COMMENT
1.00 ± 0.19 ± 0.11 ± 0.32	323	ABLIKIM 10E	BES2	$J/\psi \rightarrow K^\pm K_S^0 \pi^\mp \pi^0$

$\Gamma(K^*(892)^\pm K^*(700)^\mp)/\Gamma_{total}$ Γ_{28}/Γ

VALUE (units 10^{-3})	EVTS	DOCUMENT ID	TECN	COMMENT
1.09 ± 0.18 ± 0.94 ± 0.54	655	ABLIKIM 10E	BES2	$J/\psi \rightarrow K^\pm K_S^0 \pi^\mp \pi^0$

$\Gamma(\eta K^*(892)^0 \bar{K}^*(892)^0)/\Gamma_{total}$ Γ_{35}/Γ

VALUE (units 10^{-3})	EVTS	DOCUMENT ID	TECN	COMMENT
1.15 ± 0.13 ± 0.22	209	ABLIKIM 10C	BES2	$J/\psi \rightarrow \eta K^+\pi^-K^-\pi^+$

$\Gamma(K^*(1410)\bar{K} + c.c. \rightarrow K^\pm K^\mp \pi^0)/\Gamma(K^+K^-\pi^0)$ Γ_{41}/Γ_{156}

VALUE (%)	EVTS	DOCUMENT ID	TECN	COMMENT
2.3 ± 1.1 ± 0.7	2K	¹ LEES 17C	BABR	$J/\psi \rightarrow K^+K^-\pi^0$

¹ From a Dalitz plot analysis in an isobar model.

$\Gamma(K^*(1410)\bar{K} + c.c. \rightarrow K_S^0 K^\pm \pi^\mp)/\Gamma(K_S^0 K^\pm \pi^\mp)$ Γ_{42}/Γ_{157}

VALUE (%)	EVTS	DOCUMENT ID	TECN	COMMENT
1.5 ± 0.5 ± 0.9	4K	¹ LEES 17C	BABR	$J/\psi \rightarrow K_S^0 K^\pm \pi^\mp$

¹ From a Dalitz plot analysis in an isobar model.

$\Gamma(K_S^0(1430)\bar{K} + c.c. \rightarrow K^\pm K^\mp \pi^0)/\Gamma(K^+K^-\pi^0)$ Γ_{44}/Γ_{156}

VALUE (%)	EVTS	DOCUMENT ID	TECN	COMMENT
3.5 ± 1.3 ± 0.9	2K	¹ LEES 17C	BABR	$J/\psi \rightarrow K^+K^-\pi^0$

¹ From a Dalitz plot analysis in an isobar model.

$\Gamma(K_S^0(1430)\bar{K} + c.c. \rightarrow K_S^0 K^\pm \pi^\mp)/\Gamma(K_S^0 K^\pm \pi^\mp)$ Γ_{45}/Γ_{157}

VALUE (%)	EVTS	DOCUMENT ID	TECN	COMMENT
7.1 ± 1.3 ± 1.2	4K	¹ LEES 17C	BABR	$J/\psi \rightarrow K_S^0 K^\pm \pi^\mp$

¹ From a Dalitz plot analysis in an isobar model.

$\Gamma(K^*(892)^0 \bar{K}_S^0(1430)^0 + c.c.)/\Gamma_{total}$ Γ_{46}/Γ

VALUE (units 10^{-3})	EVTS	DOCUMENT ID	TECN	COMMENT
• • • We do not use the following data for averages, fits, limits, etc. • • •				
6.7 ± 2.6	40	VANNUCCI 77	MRK1	$e^+e^- \rightarrow \pi^+\pi^-K^+K^-$

$\Gamma(\omega K^*(892)\bar{K} + c.c.)/\Gamma_{total}$ Γ_{50}/Γ

VALUE (units 10^{-4})	EVTS	DOCUMENT ID	TECN	COMMENT
61 ± 9 OUR AVERAGE				
62.0 ± 6.8 ± 10.6	899 ± 98	ABLIKIM 08E	BES2	$J/\psi \rightarrow \omega K_S^0 K^\pm \pi^\mp$
65.3 ± 10.2 ± 13.5	176 ± 28	ABLIKIM 08E	BES2	$J/\psi \rightarrow \omega K^+K^-\pi^0$
53 ± 14 ± 14	530 ± 140	BECKER 87	MRK3	$e^+e^- \rightarrow \text{hadrons}$

$\Gamma(\bar{K}^*K^*(892) + c.c. \rightarrow K_S^0 K^\pm \pi^\mp)/\Gamma(K_S^0 K^\pm \pi^\mp)$ Γ_{52}/Γ_{157}

VALUE (%)	EVTS	DOCUMENT ID	TECN	COMMENT
90.5 ± 0.9 ± 3.8	4K	¹ LEES 17C	BABR	$J/\psi \rightarrow K_S^0 K^\pm \pi^\mp$

¹ From a Dalitz plot analysis in an isobar model.

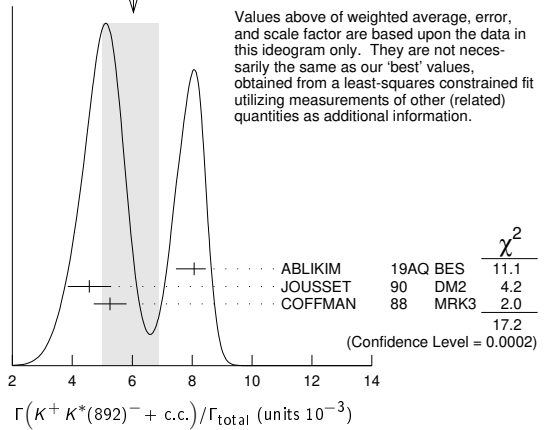
$\Gamma(K^+K^*(892)^- + c.c.)/\Gamma_{total}$ Γ_{53}/Γ

VALUE (units 10^{-3})	EVTS	DOCUMENT ID	TECN	COMMENT
6.0 ± 0.8 ± 1.0 OUR AVERAGE				Error includes scale factor of 2.9. See the ideogram below.
8.07 ± 0.04 ± 0.38 ± 0.61	183k	ABLIKIM 19AQ	BES	$J/\psi \rightarrow K^+K^-\pi^0$
4.57 ± 0.17 ± 0.70	2285	JOUSSET 90	DM2	$J/\psi \rightarrow \text{hadrons}$
5.26 ± 0.13 ± 0.53		COFFMAN 88	MRK3	$J/\psi \rightarrow K^\pm K_S^0 \pi^\mp, K^+K^-\pi^0$

• • • We do not use the following data for averages, fits, limits, etc. • • •

2.6 ± 0.6	24	FRANKLIN 83	MRK2	$J/\psi \rightarrow K^+K^-\pi^0$
3.2 ± 0.6	48	VANNUCCI 77	MRK1	$J/\psi \rightarrow K^\pm K_S^0 \pi^\mp$
4.1 ± 1.2	39	BRAUNSCH... 76	DASP	$J/\psi \rightarrow K^\pm X$

WEIGHTED AVERAGE
6.0±0.8-1.0 (Error scaled by 2.9)



$\Gamma(K^+K^*(892)^- + c.c. \rightarrow K^+K^-\pi^0)/\Gamma(K^+K^-\pi^0)$ Γ_{54}/Γ_{156}

VALUE (%)	EVTS	DOCUMENT ID	TECN	COMMENT
92.4 ± 1.5 ± 3.4	2K	¹ LEES 17C	BABR	$J/\psi \rightarrow K^+K^-\pi^0$

¹ From a Dalitz plot analysis in an isobar model.

$\Gamma(K^0 \bar{K}^*(892)^0 + c.c.)/\Gamma_{total}$ Γ_{56}/Γ

VALUE (units 10^{-3})	EVTS	DOCUMENT ID	TECN	COMMENT
4.2 ± 0.4 OUR AVERAGE				
3.96 ± 0.15 ± 0.60	1192	JOUSSET 90	DM2	$J/\psi \rightarrow \text{hadrons}$
4.33 ± 0.12 ± 0.45		COFFMAN 88	MRK3	$J/\psi \rightarrow K^\pm K_S^0 \pi^\mp$
• • • We do not use the following data for averages, fits, limits, etc. • • •				
2.7 ± 0.6	45	VANNUCCI 77	MRK1	$J/\psi \rightarrow K^\pm K_S^0 \pi^\mp$

$\Gamma(K_1(1400)^\pm K^\mp)/\Gamma_{total}$ Γ_{58}/Γ

VALUE (units 10^{-3})	DOCUMENT ID	TECN	COMMENT
3.8 ± 0.8 ± 1.2	¹ BAI 99C	BES	e^+e^-

¹ Assuming $B(K_1(1400) \rightarrow K^*\pi) = 0.94 \pm 0.06$

$\Gamma(\bar{K}^*(892)^0 K^+\pi^- + c.c.)/\Gamma_{total}$ Γ_{59}/Γ

VALUE	DOCUMENT ID	TECN	COMMENT
• • • We do not use the following data for averages, fits, limits, etc. • • •			
seen	¹ ABLIKIM 06C	BES2	$J/\psi \rightarrow \bar{K}^*(892)^0 K^+\pi^-$

¹ A $K_0^*(700)$ is observed by ABLIKIM 06C in the $K^+\pi^-$ mass spectrum of the $\bar{K}^*(892)^0 K^+\pi^-$ final state against the $\bar{K}^*(892)$. A corresponding branching fraction of the $J/\psi(1S)$ is not presented.

$\Gamma(\omega \pi^0 \pi^0)/\Gamma_{total}$ Γ_{62}/Γ

VALUE (units 10^{-3})	EVTS	DOCUMENT ID	TECN	COMMENT
3.4 ± 0.3 ± 0.7	509	AUGUSTIN 89	DM2	$J/\psi \rightarrow \pi^+\pi^-\pi^0$

$\Gamma(b_1(1235)^\pm \pi^\mp)/\Gamma_{total}$ Γ_{64}/Γ

VALUE (units 10^{-4})	EVTS	DOCUMENT ID	TECN	COMMENT
30 ± 5 OUR AVERAGE				
31 ± 6	4600	AUGUSTIN 89	DM2	$J/\psi \rightarrow 2(\pi^+\pi^-)\pi^0$
29 ± 7	87	BURMESTER 77D	PLUT	e^+e^-

$\Gamma(\omega K^\pm K_S^0 \pi^\mp)/\Gamma_{total}$ Γ_{65}/Γ

VALUE (units 10^{-4})	EVTS	DOCUMENT ID	TECN	COMMENT
34 ± 5 OUR AVERAGE				
37.7 ± 0.8 ± 5.8	1972 ± 41	ABLIKIM 08E	BES2	$e^+e^- \rightarrow J/\psi$
29.5 ± 1.4 ± 7.0	879 ± 41	BECKER 87	MRK3	$e^+e^- \rightarrow \text{hadrons}$

$\Gamma(b_1(1235)^0 \pi^0)/\Gamma_{total}$ Γ_{66}/Γ

VALUE (units 10^{-4})	EVTS	DOCUMENT ID	TECN	COMMENT
23 ± 3 ± 5	229	AUGUSTIN 89	DM2	e^+e^-

$\Gamma(\eta K^\pm K_S^0 \pi^\mp)/\Gamma_{total}$ Γ_{67}/Γ

VALUE (units 10^{-4})	EVTS	DOCUMENT ID	TECN	COMMENT
21.8 ± 2.2 ± 3.4	232 ± 23	ABLIKIM 08E	BES2	$e^+e^- \rightarrow J/\psi$

$\Gamma(\eta' K^* \bar{K}^0 + c.c.)/\Gamma_{total}$ Γ_{37}/Γ

VALUE (units 10^{-3})	DOCUMENT ID	TECN	COMMENT
1.66 ± 0.03 ± 0.21	¹ ABLIKIM 18AB	BES3	$J/\psi \rightarrow \eta' K^* \bar{K}$

¹ From $\eta' K_S^0 K^\pm \pi^\mp$.

$\Gamma(\eta' K^* \pm K^\mp)/\Gamma_{total}$ Γ_{36}/Γ

VALUE (units 10^{-3})	DOCUMENT ID	TECN	COMMENT
1.48 ± 0.13 OUR AVERAGE			
1.50 ± 0.02 ± 0.19	¹ ABLIKIM	18AB BES3	$J/\psi \rightarrow \eta' K^* \bar{K}$
1.47 ± 0.03 ± 0.17	² ABLIKIM	18AB BES3	$J/\psi \rightarrow \eta' K^* \bar{K}$
¹ From $\eta' K^+ K^- \pi^0$.			
² From $\eta' K_S^0 K^\pm \pi^\mp$.			

$\Gamma(\eta' h_1(1415) \rightarrow \eta' K^* \pm K^\mp)/\Gamma_{total}$ Γ_{39}/Γ

VALUE (units 10^{-4})	EVTS	DOCUMENT ID	TECN	COMMENT
1.51 ± 0.09 ± 0.21	1.0k	¹ ABLIKIM	18AB BES3	$J/\psi \rightarrow \eta' h_1 \rightarrow \eta' K^* \bar{K}$
¹ From $\eta' K^+ K^- \pi^0$.				

$\Gamma(\eta' h_1(1415) \rightarrow \eta' K^* \bar{K} + c.c.)/\Gamma_{total}$ Γ_{38}/Γ

VALUE (units 10^{-4})	EVTS	DOCUMENT ID	TECN	COMMENT
2.16 ± 0.12 ± 0.29	1.1k	¹ ABLIKIM	18AB BES3	$J/\psi \rightarrow \eta' h_1 \rightarrow \eta' K^* \bar{K}$
¹ From $\eta' K_S^0 K^\pm \pi^\mp$.				

$\Gamma(\phi K^*(892) \bar{K} + c.c.)/\Gamma_{total}$ Γ_{68}/Γ

VALUE (units 10^{-4})	EVTS	DOCUMENT ID	TECN	COMMENT
21.8 ± 2.3 OUR AVERAGE				
20.8 ± 2.7 ± 3.9	195 ± 25	ABLIKIM	08E BES2	$J/\psi \rightarrow \phi K_S^0 K^\pm \pi^\mp$
29.6 ± 3.7 ± 4.7	238 ± 30	ABLIKIM	08E BES2	$J/\psi \rightarrow \phi K^+ K^- \pi^0$
20.7 ± 2.4 ± 3.0		FALVARD	88 DM2	$J/\psi \rightarrow$ hadrons
20 ± 3 ± 3	155 ± 20	BECKER	87 MRK3	$e^+ e^- \rightarrow$ hadrons

$\Gamma(\omega K \bar{K})/\Gamma_{total}$ Γ_{69}/Γ

VALUE (units 10^{-4})	EVTS	DOCUMENT ID	TECN	COMMENT
19 ± 4 OUR AVERAGE				
19.8 ± 2.1 ± 3.9		¹ FALVARD	88 DM2	$J/\psi \rightarrow$ hadrons
16 ± 10	22	FELDMAN	77 MRK1	$e^+ e^-$
¹ Addition of $\omega K^+ K^-$ and $\omega K^0 \bar{K}^0$ branching ratios.				

$\Gamma(\omega f_0(1710) \rightarrow \omega K \bar{K})/\Gamma_{total}$ Γ_{70}/Γ

VALUE (units 10^{-4})	DOCUMENT ID	TECN	COMMENT
4.8 ± 1.1 ± 0.3	^{1,2} FALVARD	88 DM2	$J/\psi \rightarrow$ hadrons
¹ Includes unknown branching fraction $f_0(1710) \rightarrow K \bar{K}$.			
² Addition of $f_0(1710) \rightarrow K^+ K^-$ and $f_0(1710) \rightarrow K^0 \bar{K}^0$ branching ratios.			

$\Gamma(\phi 2(\pi^+ \pi^-))/\Gamma_{total}$ Γ_{71}/Γ

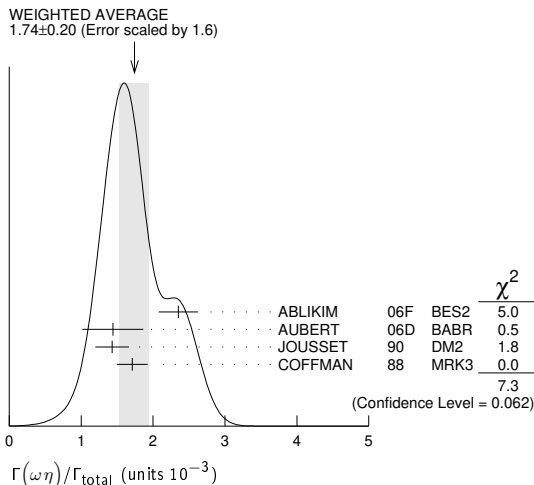
VALUE (units 10^{-4})	DOCUMENT ID	TECN	COMMENT
16.0 ± 1.0 ± 3.0	FALVARD	88 DM2	$J/\psi \rightarrow$ hadrons

$\Gamma(\Delta(1232)^{++} \bar{p} \pi^-)/\Gamma_{total}$ Γ_{72}/Γ

VALUE (units 10^{-3})	EVTS	DOCUMENT ID	TECN	COMMENT
1.58 ± 0.23 ± 0.40	332	EATON	84 MRK2	$e^+ e^-$

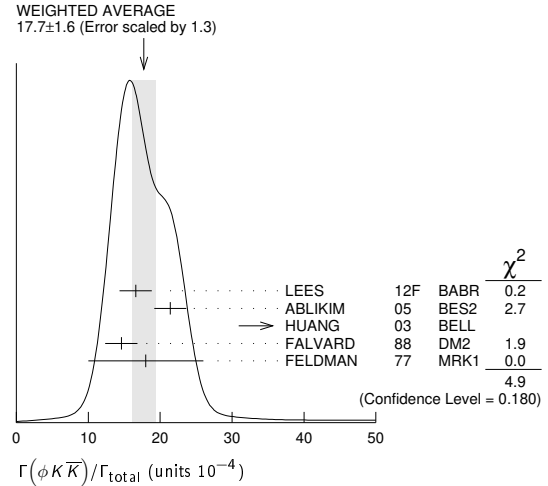
$\Gamma(\omega \eta)/\Gamma_{total}$ Γ_{73}/Γ

VALUE (units 10^{-3})	EVTS	DOCUMENT ID	TECN	COMMENT
1.74 ± 0.20 OUR AVERAGE				Error includes scale factor of 1.6. See the ideogram below.
2.352 ± 0.273	5k	¹ ABLIKIM	06F BES2	$J/\psi \rightarrow \omega \eta$
1.44 ± 0.40 ± 0.14	13	² AUBERT	06D BABR	10.6 $e^+ e^- \rightarrow \omega \eta \gamma$
1.43 ± 0.10 ± 0.21	378	JOUSSET	90 DM2	$J/\psi \rightarrow$ hadrons
1.71 ± 0.08 ± 0.20		COFFMAN	88 MRK3	$e^+ e^- \rightarrow 3\pi \eta$
¹ Using $B(\eta \rightarrow 2\gamma) = (39.43 \pm 0.26)\%$, $B(\eta \rightarrow \pi^+ \pi^- \pi^0) = 22.6 \pm 0.4\%$, $B(\eta \rightarrow \pi^+ \pi^- \gamma) = 4.68 \pm 0.11\%$, and $B(\omega \rightarrow \pi^+ \pi^- \pi^0) = (89.1 \pm 0.7)\%$.				
² Using $\Gamma(J/\psi \rightarrow e^+ e^-) = 5.52 \pm 0.14 \pm 0.04$ keV.				



$\Gamma(\phi K \bar{K})/\Gamma_{total}$ Γ_{75}/Γ

VALUE (units 10^{-4})	EVTS	DOCUMENT ID	TECN	COMMENT
17.7 ± 1.6 OUR AVERAGE				Error includes scale factor of 1.3. See the ideogram below.
16.6 ± 1.9 ± 1.2	163 ± 19	LEES	12F BABR	10.6 $e^+ e^- \rightarrow 2(K^+ K^-) \gamma$
21.4 ± 0.4 ± 2.2		ABLIKIM	05 BES2	$J/\psi \rightarrow \phi \pi^+ \pi^-$
48 $^{+20}_{-16}$ ± 6	9.0 $^{+3.7}_{-3.0}$	^{1,2} HUANG	03 BELL	$B^+ \rightarrow (\phi K^+ K^-) K^+$
14.6 ± 0.8 ± 2.1		³ FALVARD	88 DM2	$J/\psi \rightarrow$ hadrons
18 ± 8	14	FELDMAN	77 MRK1	$e^+ e^-$
¹ We have multiplied $K^+ K^-$ measurement by 2 to obtain $K \bar{K}$.				
² Using $B(B^+ \rightarrow J/\psi K^+) = (1.01 \pm 0.05) \times 10^{-3}$.				
³ Addition of $\phi K^+ K^-$ and $\phi K^0 \bar{K}^0$ branching ratios.				



$\Gamma(\phi f_0(1710) \rightarrow \phi K \bar{K})/\Gamma_{total}$ Γ_{77}/Γ

VALUE (units 10^{-4})	DOCUMENT ID	TECN	COMMENT
3.6 ± 0.2 ± 0.6	^{1,2} FALVARD	88 DM2	$J/\psi \rightarrow$ hadrons
¹ Including interference with $f_2'(1525)$.			
² Includes unknown branching fraction $f_0(1710) \rightarrow K \bar{K}$.			

$\Gamma(\phi f_2'(1270))/\Gamma_{total}$ Γ_{79}/Γ

VALUE (units 10^{-3})	CL%	DOCUMENT ID	TECN	COMMENT
• • • We do not use the following data for averages, fits, limits, etc. • • •				
< 0.45	90	FALVARD	88 DM2	$J/\psi \rightarrow$ hadrons
< 0.37	90	VANNUCCI	77 MRK1	$e^+ e^- \rightarrow \pi^+ \pi^- K^+ K^-$

$\Gamma(\Delta(1232)^{++} \bar{\Delta}(1232)^{--})/\Gamma_{total}$ Γ_{80}/Γ

VALUE (units 10^{-3})	EVTS	DOCUMENT ID	TECN	COMMENT
1.10 ± 0.09 ± 0.28	233	EATON	84 MRK2	$e^+ e^-$

$\Gamma(\Sigma(1385) - \bar{\Sigma}(1385)^+)/\Gamma_{total}$ Γ_{81}/Γ

VALUE (units 10^{-3})	EVTS	DOCUMENT ID	TECN	COMMENT
1.16 ± 0.05 OUR AVERAGE				
1.096 ± 0.012 ± 0.071	43k	ABLIKIM	16L BES3	$J/\psi \rightarrow \Sigma(1385) - \bar{\Sigma}(1385)^+$
1.258 ± 0.014 ± 0.078	53k	ABLIKIM	16L BES3	$J/\psi \rightarrow \Sigma(1385)^+ - \bar{\Sigma}(1385)^-$
1.23 ± 0.07 ± 0.30	0.8k	ABLIKIM	12P BES2	$J/\psi \rightarrow \Sigma(1385) - \bar{\Sigma}(1385)^+$
1.50 ± 0.08 ± 0.38	1k	ABLIKIM	12P BES2	$J/\psi \rightarrow \Sigma(1385)^+ - \bar{\Sigma}(1385)^-$
1.00 ± 0.04 ± 0.21	0.6k	HENRRARD	87 DM2	$e^+ e^- \rightarrow \Sigma^{*-}$
1.19 ± 0.04 ± 0.25	0.7k	HENRRARD	87 DM2	$e^+ e^- \rightarrow \Sigma^{*+}$
0.86 ± 0.18 ± 0.22	56	EATON	84 MRK2	$e^+ e^- \rightarrow \Sigma^{*-}$
1.03 ± 0.24 ± 0.25	68	EATON	84 MRK2	$e^+ e^- \rightarrow \Sigma^{*+}$

$\Gamma(\Sigma(1385)^0 \bar{\Sigma}(1385)^0)/\Gamma_{total}$ Γ_{82}/Γ

VALUE (units 10^{-3})	EVTS	DOCUMENT ID	TECN	COMMENT
1.071 ± 0.009 ± 0.082	103k	ABLIKIM	17E BES3	$e^+ e^- \rightarrow J/\psi \rightarrow$ hadrons

$\Gamma(\phi f_2'(1525))/\Gamma_{total}$ Γ_{84}/Γ

VALUE (units 10^{-4})	EVTS	DOCUMENT ID	TECN	COMMENT
8 ± 4 OUR AVERAGE				Error includes scale factor of 2.7.
12.3 ± 0.6 ± 2.0		^{1,2} FALVARD	88 DM2	$J/\psi \rightarrow$ hadrons
4.8 ± 1.8	46	¹ GIDAL	81 MRK2	$J/\psi \rightarrow K^+ K^- K^+ K^-$
¹ Re-evaluated using $B(f_2'(1525) \rightarrow K \bar{K}) = 0.713$.				
² Including interference with $f_0(1710)$.				

Meson Particle Listings

 $J/\psi(1S)$ $\Gamma(\phi\pi^+\pi^-)/\Gamma_{\text{total}}$ Γ_{85}/Γ

VALUE (units 10^{-3})	EVTS	DOCUMENT ID	TECN	COMMENT
0.94 ± 0.15	OUR AVERAGE	Error includes scale factor of 1.7.		
$1.09 \pm 0.02 \pm 0.13$		ABLIKIM	05 BES2	$J/\psi \rightarrow \phi\pi^+\pi^-$
$0.78 \pm 0.03 \pm 0.12$		FALVARD	88 DM2	$J/\psi \rightarrow$ hadrons
2.1 ± 0.9	23	FELDMAN	77 MRK1	e^+e^-

 $\Gamma(\phi K^\pm K_S^0 \pi^\mp)/\Gamma_{\text{total}}$ Γ_{87}/Γ

VALUE (units 10^{-4})	EVTS	DOCUMENT ID	TECN	COMMENT
7.2 ± 0.8	OUR AVERAGE			
$7.4 \pm 0.6 \pm 1.4$	227 \pm 19	ABLIKIM	08E BES2	$e^+e^- \rightarrow J/\psi$
$7.4 \pm 0.9 \pm 1.1$		FALVARD	88 DM2	$J/\psi \rightarrow$ hadrons
$7 \pm 0.6 \pm 1.0$	163 \pm 15	BECKER	87 MRK3	$e^+e^- \rightarrow$ hadrons

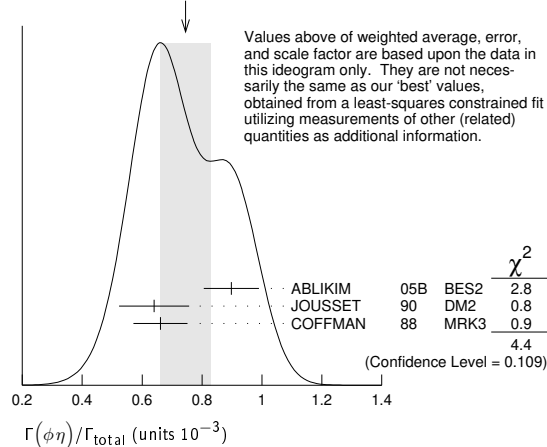
 $\Gamma(\omega f_1(1420))/\Gamma_{\text{total}}$ Γ_{88}/Γ

VALUE (units 10^{-4})	EVTS	DOCUMENT ID	TECN	COMMENT
6.8 ± 1.9	111 ± 31	OUR AVERAGE		
$6.8 \pm 1.6 \pm 1.7$	111 ± 26			
		BECKER	87 MRK3	$e^+e^- \rightarrow$ hadrons

 $\Gamma(\phi\eta)/\Gamma_{\text{total}}$ Γ_{89}/Γ

VALUE (units 10^{-3})	EVTS	DOCUMENT ID	TECN	COMMENT
0.74 ± 0.08	OUR AVERAGE	Error includes scale factor of 1.5. See the ideogram below.		
$0.898 \pm 0.024 \pm 0.089$		ABLIKIM	05B BES2	$e^+e^- \rightarrow J/\psi \rightarrow$ hadr
$0.64 \pm 0.04 \pm 0.11$	346	JOUSSET	90 DM2	$J/\psi \rightarrow$ hadrons
$0.661 \pm 0.045 \pm 0.078$		COFFMAN	88 MRK3	$e^+e^- \rightarrow K^+K^-\eta$

WEIGHTED AVERAGE
0.74 \pm 0.08 (Error scaled by 1.5)

 $\Gamma(\phi\eta\eta')/\Gamma_{\text{total}}$ Γ_{99}/Γ

VALUE (units 10^{-4})	EVTS	DOCUMENT ID	TECN	COMMENT
$2.32 \pm 0.06 \pm 0.16$	2.2k	OUR AVERAGE		
		1 ABLIKIM	19AN BES3	$e^+e^- \rightarrow J/\psi \rightarrow$ hadrons

¹ Including contributions from intermediate resonances. Evidence for an intermediate resonance at $M \approx 2$ GeV and $\Gamma \approx 150$ MeV decaying to $\phi\eta'$ with $J^P = 1^+$ or $J^P = 1^-$, and $B(J/\psi \rightarrow \eta X) \times B(X \rightarrow \phi\eta') \approx 10^{-4}$.

 $\Gamma(\Xi^0 \Xi^0)/\Gamma_{\text{total}}$ Γ_{90}/Γ

VALUE (units 10^{-3})	EVTS	DOCUMENT ID	TECN	COMMENT
1.17 ± 0.04	OUR AVERAGE			
$1.165 \pm 0.004 \pm 0.043$	135K			
		ABLIKIM	17E BES3	$e^+e^- \rightarrow J/\psi \rightarrow$ hadrons
$1.20 \pm 0.12 \pm 0.21$	206	ABLIKIM	08o BES2	$e^+e^- \rightarrow J/\psi$

 $\Gamma(\Xi(1530)^- \Xi^+ + c.c.)/\Gamma_{\text{total}}$ Γ_{91}/Γ

VALUE (units 10^{-3})	EVTS	DOCUMENT ID	TECN	COMMENT
0.318 ± 0.008	OUR AVERAGE			
$0.317 \pm 0.002 \pm 0.008$	70k			
		ABLIKIM	20 BES3	$e^+e^- \rightarrow J/\psi$
$0.59 \pm 0.09 \pm 0.12$	75	HENRARD	87 DM2	e^+e^-

 $\Gamma(pK^-\Sigma(1385)^0)/\Gamma_{\text{total}}$ Γ_{92}/Γ

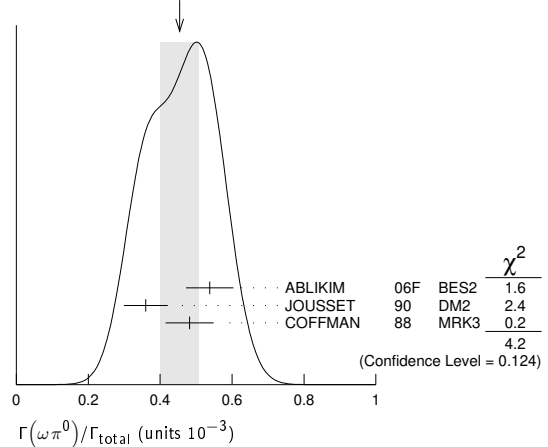
VALUE (units 10^{-3})	EVTS	DOCUMENT ID	TECN	COMMENT
$0.51 \pm 0.26 \pm 0.18$	89			
		EATON	84 MRK2	e^+e^-

 $\Gamma(\omega\pi^0)/\Gamma_{\text{total}}$ Γ_{93}/Γ

VALUE (units 10^{-3})	EVTS	DOCUMENT ID	TECN	COMMENT
0.45 ± 0.05	OUR AVERAGE	Error includes scale factor of 1.4. See the ideogram below.		
$0.538 \pm 0.012 \pm 0.065$	2090			
		1 ABLIKIM	06F BES2	$J/\psi \rightarrow \omega\pi^0$
$0.360 \pm 0.028 \pm 0.054$	222	JOUSSET	90 DM2	$J/\psi \rightarrow$ hadrons
$0.482 \pm 0.019 \pm 0.064$		COFFMAN	88 MRK3	$e^+e^- \rightarrow \pi^0\pi^+\pi^-\pi^0$

¹ Using $B(\omega \rightarrow \pi^+\pi^-\pi^0) = (89.1 \pm 0.7)\%$.

WEIGHTED AVERAGE
0.45 \pm 0.05 (Error scaled by 1.4)

 $\Gamma(\omega\pi^0 \rightarrow \pi^+\pi^-\pi^0)/\Gamma(\pi^+\pi^-\pi^0)$ Γ_{94}/Γ_{141}

VALUE (units 10^{-4})	EVTS	DOCUMENT ID	TECN	COMMENT
$8 \pm 3 \pm 2$	20K	OUR AVERAGE		
		1 LEES	17c BABR	$J/\psi \rightarrow \pi^+\pi^-\pi^0$

¹ From a Dalitz plot analysis in an isobar model and significance 4.9 σ .

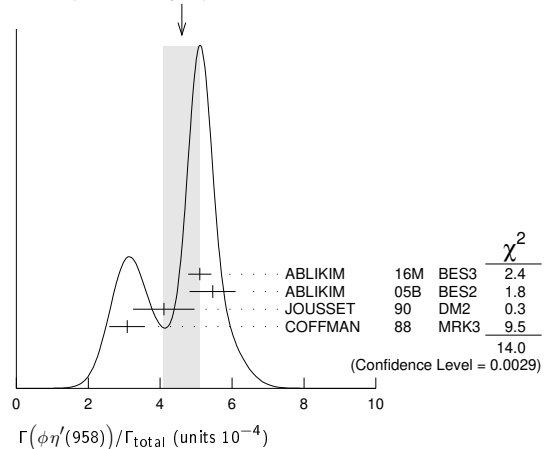
 $\Gamma(\phi\eta'(958))/\Gamma_{\text{total}}$ Γ_{95}/Γ

VALUE (units 10^{-4})	CL% EVTS	DOCUMENT ID	TECN	COMMENT
4.6 ± 0.5	OUR AVERAGE	Error includes scale factor of 2.2. See the ideogram below.		
$5.10 \pm 0.03 \pm 0.32$	31k	ABLIKIM	16M BES3	$e^+e^- \rightarrow J/\psi \rightarrow$ hadrons
$5.46 \pm 0.31 \pm 0.56$		ABLIKIM	05B BES2	$e^+e^- \rightarrow J/\psi \rightarrow$ hadrons
$4.1 \pm 0.3 \pm 0.8$	167	JOUSSET	90 DM2	$J/\psi \rightarrow$ hadrons
$3.08 \pm 0.34 \pm 0.36$		COFFMAN	88 MRK3	$e^+e^- \rightarrow K^+K^-\eta'$

••• We do not use the following data for averages, fits, limits, etc. •••

< 13 90 VANNUCCI 77 MRK1 e^+e^-

WEIGHTED AVERAGE
4.6 \pm 0.5 (Error scaled by 2.2)

 $\Gamma(\phi f_0(980))/\Gamma_{\text{total}}$ Γ_{96}/Γ

VALUE (units 10^{-4})	EVTS	DOCUMENT ID	TECN	COMMENT
3.2 ± 0.9	OUR AVERAGE	Error includes scale factor of 1.9.		
$4.6 \pm 0.4 \pm 0.8$		1 FALVARD	88 DM2	$J/\psi \rightarrow$ hadrons
2.6 ± 0.6	50	1 GIDAL	81 MRK2	$J/\psi \rightarrow K^+K^-K^+K^-$

¹ Assuming $B(f_0(980) \rightarrow \pi\pi) = 0.78$.

 $\Gamma(\phi\pi^0 f_0(980) \rightarrow \phi\pi^0\pi^+\pi^-)/\Gamma_{\text{total}}$ Γ_{100}/Γ

VALUE (units 10^{-6})	EVTS	DOCUMENT ID	TECN	COMMENT
$4.50 \pm 0.80 \pm 0.61$	355			
		ABLIKIM	15P BES3	$J/\psi \rightarrow K^+K^-3\pi$

 $\Gamma(\phi\pi^0 f_0(980) \rightarrow \phi\pi^0\rho^0\pi^0)/\Gamma_{\text{total}}$ Γ_{101}/Γ

VALUE (units 10^{-6})	EVTS	DOCUMENT ID	TECN	COMMENT
$1.67 \pm 0.50 \pm 0.24$	70			
		ABLIKIM	15P BES3	$J/\psi \rightarrow K^+K^-3\pi$

 $\Gamma(\eta\phi f_0(980) \rightarrow \eta\phi\pi^+\pi^-)/\Gamma_{\text{total}}$ Γ_{102}/Γ

VALUE (units 10^{-4})	EVTS	DOCUMENT ID	TECN	COMMENT
$3.23 \pm 0.75 \pm 0.73$	52			
		ABLIKIM	08F BES	$J/\psi \rightarrow \eta\phi f_0(980)$

$\Gamma(\phi a_0(980)^0 \rightarrow \phi \eta \pi^0)/\Gamma_{total}$ Γ_{103}/Γ

VALUE (units 10^{-6})	DOCUMENT ID	TECN	COMMENT
4.37 ± 1.35	¹ ABLIKIM 18D BES3		$J/\psi \rightarrow \phi \eta \pi^0$
• • • We do not use the following data for averages, fits, limits, etc. • • •			
5.0 ± 2.7 ± 2.5	² ABLIKIM 11D BES3		$J/\psi \rightarrow \phi \eta \pi^0$

¹ Assuming constructive interference between $a_0(980) - f_0(980)$ mixing and electromagnetic decay. Destructive interference gives a value of $(4.93 \pm 1.77) \times 10^{-6}$ for this branching fraction.
² Assuming $a_0(980) - f_0(980)$ mixing and isospin breaking via γ^* and $K^* K$ loops.

$\Gamma(\Xi(1530)^0 \Xi^0)/\Gamma_{total}$ Γ_{104}/Γ

VALUE (units 10^{-3})	EVTS	DOCUMENT ID	TECN	COMMENT
0.32 ± 0.12 ± 0.07	24 ± 9	HENRRARD 87	DM2	$e^+ e^-$

$\Gamma(\Sigma(1385)^- \Sigma^+ (or c.c.))/\Gamma_{total}$ Γ_{105}/Γ

VALUE (units 10^{-3})	EVTS	DOCUMENT ID	TECN	COMMENT
0.31 ± 0.05 OUR AVERAGE				
0.30 ± 0.03 ± 0.07	74 ± 8	HENRRARD 87	DM2	$e^+ e^- \rightarrow \Sigma^{*-}$
0.34 ± 0.04 ± 0.07	77 ± 9	HENRRARD 87	DM2	$e^+ e^- \rightarrow \Sigma^{*+}$
0.29 ± 0.11 ± 0.10	26	EATON 84	MRK2	$e^+ e^- \rightarrow \Sigma^{*-}$
0.31 ± 0.11 ± 0.11	28	EATON 84	MRK2	$e^+ e^- \rightarrow \Sigma^{*+}$

$\Gamma(\phi f_1(1285))/\Gamma_{total}$ Γ_{106}/Γ

VALUE (units 10^{-4})	EVTS	DOCUMENT ID	TECN	COMMENT
2.6 ± 0.5 OUR AVERAGE				
3.4 ± 1.8 ± 1.5	1.1k	¹ ABLIKIM 15H BES3		$e^+ e^- \rightarrow J/\psi \rightarrow \phi \eta \pi^+ \pi^-$
3.2 ± 0.6 ± 0.4		JOUSSET 90	DM2	$J/\psi \rightarrow \phi 2(\pi^+ \pi^-)$
2.1 ± 0.5 ± 0.4	25	² JOUSSET 90	DM2	$J/\psi \rightarrow \phi \eta \pi^+ \pi^-$
• • • We do not use the following data for averages, fits, limits, etc. • • •				
0.6 ± 0.2 ± 0.1	16	BECKER 87	MRK3	$J/\psi \rightarrow \phi K \bar{K} \pi$

¹ ABLIKIM 15H reports $[\Gamma(J/\psi(1S) \rightarrow \phi f_1(1285))/\Gamma_{total}] \times [B(f_1(1285) \rightarrow \eta \pi^+ \pi^-)] = (1.20 \pm 0.6 \pm 0.14) \times 10^{-4}$ which we divide by our best value $B(f_1(1285) \rightarrow \eta \pi^+ \pi^-) = (35 \pm 15) \times 10^{-2}$. Our first error is their experiment's error and our second error is the systematic error from using our best value.
² We attribute to the $f_1(1285)$ the signal observed in the $\pi^+ \pi^- \eta$ invariant mass distribution at 1297 MeV.

$\Gamma(\phi f_1(1285) \rightarrow \phi \pi^0 f_0(980) \rightarrow \phi \pi^0 \pi^+ \pi^-)/\Gamma_{total}$ Γ_{107}/Γ

VALUE (units 10^{-7})	EVTS	DOCUMENT ID	TECN	COMMENT
9.36 ± 2.31 ± 1.54	78	ABLIKIM 15P BES3		$J/\psi \rightarrow K^+ K^- 3\pi$

$\Gamma(\phi f_1(1285) \rightarrow \phi \pi^0 f_0(980) \rightarrow \phi \pi^0 \pi^0 \pi^0)/\Gamma_{total}$ Γ_{108}/Γ

VALUE (units 10^{-7})	EVTS	DOCUMENT ID	TECN	COMMENT
2.08 ± 1.63 ± 1.47	9	ABLIKIM 15P BES3		$J/\psi \rightarrow K^+ K^- 3\pi$

$\Gamma(\eta \pi^+ \pi^-)/\Gamma_{total}$ Γ_{109}/Γ

VALUE (units 10^{-4})	EVTS	DOCUMENT ID	TECN	COMMENT
3.78 ± 0.68	471	¹ ABLIKIM 19Q BES3		$e^+ e^- \rightarrow J/\psi \rightarrow \eta \pi^+ \pi^-$

¹ From an energy scan of $e^+ e^- \rightarrow J/\psi \rightarrow \eta \pi^+ \pi^-$ assuming PDG 16 values for $\Gamma(e^+ e^-)$, $\Gamma(\mu^+ \mu^-)$, and $\Gamma(total)$.

$\Gamma(\eta \rho)/\Gamma_{total}$ Γ_{110}/Γ

VALUE (units 10^{-3})	EVTS	DOCUMENT ID	TECN	COMMENT
0.193 ± 0.023 OUR AVERAGE				
0.194 ± 0.017 ± 0.029	299	JOUSSET 90	DM2	$J/\psi \rightarrow$ hadrons
0.193 ± 0.013 ± 0.029		COFFMAN 88	MRK3	$e^+ e^- \rightarrow \pi^+ \pi^- \eta$

$\Gamma(\omega \eta'(958))/\Gamma_{total}$ Γ_{111}/Γ

VALUE (units 10^{-4})	EVTS	DOCUMENT ID	TECN	COMMENT
1.89 ± 0.18 OUR AVERAGE				
2.08 ± 0.30 ± 0.14	137	¹ ABLIKIM 17AK BES3		$J/\psi \rightarrow \pi^+ \pi^- \eta'$
2.26 ± 0.43	218	² ABLIKIM 06F BES2		$J/\psi \rightarrow \omega \eta'$
1.8 ± 1.0 ± 0.3	6	JOUSSET 90	DM2	$J/\psi \rightarrow$ hadrons
1.66 ± 0.17 ± 0.19		COFFMAN 88	MRK3	$e^+ e^- \rightarrow 3\pi \eta'$

¹ From a partial wave analysis of the decay $J/\psi \rightarrow \pi^+ \pi^- \eta'$.
² Using $B(\eta' \rightarrow \pi^+ \pi^- \eta) = (44.3 \pm 1.5)\%$, $B(\eta' \rightarrow \pi^+ \pi^- \gamma) = 29.5 \pm 1.0\%$, $B(\eta \rightarrow 2\gamma) = 39.43 \pm 0.26\%$, and $B(\omega \rightarrow \pi^+ \pi^- \pi^0) = (89.1 \pm 0.7)\%$.

$\Gamma(\omega f_0(980))/\Gamma_{total}$ Γ_{112}/Γ

VALUE (units 10^{-4})	DOCUMENT ID	TECN	COMMENT
1.41 ± 0.27 ± 0.47	¹ AUGUSTIN 89	DM2	$J/\psi \rightarrow 2(\pi^+ \pi^-) \pi^0$

¹ Assuming $B(f_0(980) \rightarrow \pi \pi) = 0.78$.

$\Gamma(\rho \eta'(958))/\Gamma_{total}$ Γ_{113}/Γ

VALUE (units 10^{-5})	EVTS	DOCUMENT ID	TECN	COMMENT
8.1 ± 0.8 OUR AVERAGE Error includes scale factor of 1.6.				
7.90 ± 0.19 ± 0.49	3476	¹ ABLIKIM 17AK BES3		$J/\psi \rightarrow \pi^+ \pi^- \eta'$
8.3 ± 3.0 ± 1.2	19	JOUSSET 90	DM2	$J/\psi \rightarrow$ hadrons
11.4 ± 1.4 ± 1.6		COFFMAN 88	MRK3	$J/\psi \rightarrow \pi^+ \pi^- \eta'$

¹ From a partial wave analysis of the decay $J/\psi \rightarrow \pi^+ \pi^- \eta'$.

$\Gamma(a_2(1320)^\pm \pi^\mp)/\Gamma_{total}$ Γ_{114}/Γ

VALUE	CL%	DOCUMENT ID	TECN	COMMENT
< 43 × 10⁻⁴	90	BRAUNSCH... 76	DASP	$e^+ e^-$

$\Gamma(K \bar{K}_2^*(1430) + c.c.)/\Gamma_{total}$ Γ_{115}/Γ

VALUE	CL%	DOCUMENT ID	TECN	COMMENT
< 40 × 10⁻⁴	90	VANNUCCI 77	MRK1	$e^+ e^- \rightarrow K^0 \bar{K}_2^{*0}$
• • • We do not use the following data for averages, fits, limits, etc. • • •				
< 66 × 10 ⁻⁴	90	BRAUNSCH... 76	DASP	$e^+ e^- \rightarrow K^\pm \bar{K}_2^{*\mp}$

$\Gamma(K_1(1270)^\pm K^\mp)/\Gamma_{total}$ Γ_{116}/Γ

VALUE	CL%	DOCUMENT ID	TECN	COMMENT
< 3.0 × 10⁻³	90	¹ BAI 99c	BES	$e^+ e^-$
¹ Assuming $B(K_1(1270) \rightarrow K \rho) = 0.42 \pm 0.06$				

$\Gamma(K_1(1270) K_S^0 \rightarrow \gamma K_S^0 K_S^0)/\Gamma_{total}$ Γ_{117}/Γ

VALUE (units 10^{-7})	DOCUMENT ID	TECN	COMMENT
8.54 ± 1.07 + 2.35 - 1.20 - 2.13	ABLIKIM 18AA BES3		$J/\psi \rightarrow \gamma K_S^0 K_S^0$

$\Gamma(K_2^*(1430)^0 \bar{K}_2^*(1430)^0)/\Gamma_{total}$ Γ_{119}/Γ

VALUE	CL%	DOCUMENT ID	TECN	COMMENT
< 29 × 10⁻⁴	90	VANNUCCI 77	MRK1	$e^+ e^- \rightarrow \pi^+ \pi^- K^+ K^-$

$\Gamma(\phi \pi^0)/\Gamma_{total}$ Γ_{120}/Γ

The two different fit values of ABLIKIM 15K below have the same statistical significance of 6.4 σ and cannot be distinguished at this moment.

VALUE (units 10^{-6})	CL%	EVTS	DOCUMENT ID	TECN	COMMENT
2.94 ± 0.16 ± 0.16		0.8k	¹ ABLIKIM 15K	BES3	$e^+ e^- \rightarrow J/\psi \rightarrow K^+ K^- \gamma \gamma$
0.124 ± 0.033 ± 0.030		35 ± 9	² ABLIKIM 15K	BES3	$e^+ e^- \rightarrow J/\psi \rightarrow K^+ K^- \gamma \gamma$

• • • We do not use the following data for averages, fits, limits, etc. • • •
 < 6.4 90 ³ ABLIKIM 05B BES2 $e^+ e^- \rightarrow J/\psi \rightarrow \phi \gamma \gamma$
 < 6.8 90 COFFMAN 88 MRK3 $e^+ e^- \rightarrow K^+ K^- \pi^0$

¹ Corresponding to one of the two fit solutions with $\delta = (-95.9 \pm 1.5)^\circ$ for the phase angle between the resonant $J/\psi \rightarrow \phi \pi^0$ and non-phi $J/\psi \rightarrow K^+ K^- \pi^0$ contributions.
² Corresponding to one of the two fit solutions with $\delta = (-152.1 \pm 7.7)^\circ$ for the phase angle between the resonant $J/\psi \rightarrow \phi \pi^0$ and non-phi $J/\psi \rightarrow K^+ K^- \pi^0$ contributions.
³ Superseded by ABLIKIM 15K.

$\Gamma(\phi \eta(1405) \rightarrow \phi \eta \pi^+ \pi^-)/\Gamma_{total}$ Γ_{121}/Γ

VALUE (units 10^{-5})	CL%	EVTS	DOCUMENT ID	TECN	COMMENT
2.01 ± 0.58 ± 0.82	172	¹ ABLIKIM 15H	BES3		$e^+ e^- \rightarrow J/\psi \rightarrow \phi \eta \pi^+ \pi^-$

• • • We do not use the following data for averages, fits, limits, etc. • • •
 < 17 90 ² FALVARD 88 DM2 $J/\psi \rightarrow$ hadrons
¹ With 3.6 σ significance.
² Includes unknown branching fraction $\eta(1405) \rightarrow \eta \pi \pi$.

$\Gamma(\omega f_2'(1525))/\Gamma_{total}$ Γ_{122}/Γ

VALUE	CL%	DOCUMENT ID	TECN	COMMENT
< 2.2 × 10⁻⁴	90	¹ VANNUCCI 77	MRK1	$e^+ e^- \rightarrow \pi^+ \pi^- \pi^0 K^+ K^-$
• • • We do not use the following data for averages, fits, limits, etc. • • •				
< 2.8 × 10 ⁻⁴	90	¹ FALVARD 88	DM2	$J/\psi \rightarrow$ hadrons

¹ Re-evaluated assuming $B(f_2'(1525) \rightarrow K \bar{K}) = 0.713$.

$\Gamma(\omega X(1835) \rightarrow \omega \rho \bar{\rho})/\Gamma_{total}$ Γ_{123}/Γ

VALUE	CL%	DOCUMENT ID	TECN	COMMENT
< 3.9 × 10⁻⁶	95	ABLIKIM 13P	BES3	$J/\psi \rightarrow \gamma \pi^0 \rho \bar{\rho}$

$\Gamma(\omega X(1835), X \rightarrow \eta' \pi^+ \pi^-)/\Gamma_{total}$ Γ_{124}/Γ

VALUE	DOCUMENT ID	TECN	COMMENT
< 6.2 × 10⁻⁵	¹ ABLIKIM 19AC	BES3	$J/\psi \rightarrow \omega \eta' \pi^+ \pi^-$

¹ Using the decays $\omega \rightarrow \pi^+ \pi^- \pi^0$ and $\eta' \rightarrow \eta \pi^+ \pi^-$.

$\Gamma(\phi X(1835) \rightarrow \phi \rho \bar{\rho})/\Gamma_{total}$ Γ_{125}/Γ

VALUE	CL%	DOCUMENT ID	TECN	COMMENT
< 2.1 × 10⁻⁷	90	¹ ABLIKIM 16K	BES3	$J/\psi \rightarrow \rho \bar{\rho} K_S^0 K_L^0, \rho \bar{\rho} K^+ K^-$

¹ Upper limit applies to any $\rho \bar{\rho}$ mass enhancement near threshold.

$\Gamma(\phi X(1835) \rightarrow \phi \eta \pi^+ \pi^-)/\Gamma_{total}$ Γ_{126}/Γ

VALUE	CL%	DOCUMENT ID	TECN	COMMENT
< 2.8 × 10⁻⁴	90	ABLIKIM 15H	BES3	$e^+ e^- \rightarrow J/\psi \rightarrow \phi \eta \pi^+ \pi^-$

$\Gamma(\phi X(1870) \rightarrow \phi \eta \pi^+ \pi^-)/\Gamma_{total}$ Γ_{127}/Γ

VALUE	CL%	DOCUMENT ID	TECN	COMMENT
< 6.13 × 10⁻⁵	90	ABLIKIM 15H	BES3	$e^+ e^- \rightarrow J/\psi \rightarrow \phi \eta \pi^+ \pi^-$

Meson Particle Listings

$J/\psi(1S)$

$\Gamma(\eta\phi(2170) \rightarrow \eta\phi f_0(980) \rightarrow \eta\phi\pi^+\pi^-)/\Gamma_{total}$ Γ_{128}/Γ

VALUE (units 10^{-4})	EVTS	DOCUMENT ID	TECN	COMMENT
$1.20 \pm 0.14 \pm 0.37$	471	ABLIKIM	15H BES3	$e^+e^- \rightarrow J/\psi \rightarrow \phi\eta\pi^+\pi^-$

$\Gamma(\eta\phi(2170) \rightarrow \eta K^*(892)^0 \bar{K}^*(892)^0)/\Gamma_{total}$ Γ_{129}/Γ

VALUE	CL%	DOCUMENT ID	TECN	COMMENT
$<2.52 \times 10^{-4}$	90	ABLIKIM	10c BES2	$J/\psi \rightarrow \eta K^+\pi^- K^-\pi^+$

$\Gamma(\Sigma(1385)^0 \bar{\Lambda} + c.c.)/\Gamma_{total}$ Γ_{130}/Γ

VALUE	CL%	DOCUMENT ID	TECN	COMMENT
$<0.82 \times 10^{-5}$	90	ABLIKIM	13F BES3	$J/\psi \rightarrow \rho\bar{p}\pi^+\pi^-\gamma\gamma$
••• We do not use the following data for averages, fits, limits, etc. •••				
$<0.2 \times 10^{-3}$	90	HENRRARD	87 DM2	e^+e^-

$\Gamma(\Delta(1232)^+ \bar{p})/\Gamma_{total}$ Γ_{131}/Γ

VALUE	CL%	DOCUMENT ID	TECN	COMMENT
$<0.1 \times 10^{-3}$	90	HENRRARD	87 DM2	e^+e^-

$\Gamma(\Lambda(1520)\bar{\Lambda} + c.c. \rightarrow \gamma\Lambda\bar{\Lambda})/\Gamma_{total}$ Γ_{132}/Γ

VALUE	CL%	DOCUMENT ID	TECN	COMMENT
$<4.1 \times 10^{-6}$	90	ABLIKIM	12B BES3	$J/\psi \rightarrow \Lambda\bar{\Lambda}\gamma$

$\Gamma(\bar{\Lambda}(1520)\Lambda + c.c.)/\Gamma_{total}$ Γ_{133}/Γ

VALUE	CL%	DOCUMENT ID	TECN	COMMENT
$<1.80 \times 10^{-3}$	90	LU	19 BELL	$B^+ \rightarrow \bar{p}\Lambda K^+ K^+$

$\Gamma(\Theta(1540)\bar{\Theta}(1540) \rightarrow K_S^0 p K^-\bar{n} + c.c.)/\Gamma_{total}$ Γ_{134}/Γ

VALUE	CL%	DOCUMENT ID	TECN	COMMENT
$<1.1 \times 10^{-5}$	90	BAI	04G BES2	e^+e^-

$\Gamma(\Theta(1540)K^-\bar{n} \rightarrow K_S^0 p K^-\bar{n})/\Gamma_{total}$ Γ_{135}/Γ

VALUE	CL%	DOCUMENT ID	TECN	COMMENT
$<2.1 \times 10^{-5}$	90	BAI	04G BES2	e^+e^-

$\Gamma(\Theta(1540)K_S^0\bar{p} \rightarrow K_S^0\bar{p}K^+n)/\Gamma_{total}$ Γ_{136}/Γ

VALUE	CL%	DOCUMENT ID	TECN	COMMENT
$<1.6 \times 10^{-5}$	90	BAI	04G BES2	e^+e^-

$\Gamma(\bar{\Theta}(1540)K^+n \rightarrow K_S^0\bar{p}K^+n)/\Gamma_{total}$ Γ_{137}/Γ

VALUE	CL%	DOCUMENT ID	TECN	COMMENT
$<5.6 \times 10^{-5}$	90	BAI	04G BES2	e^+e^-

$\Gamma(\bar{\Theta}(1540)K_S^0p \rightarrow K_S^0pK^-\bar{n})/\Gamma_{total}$ Γ_{138}/Γ

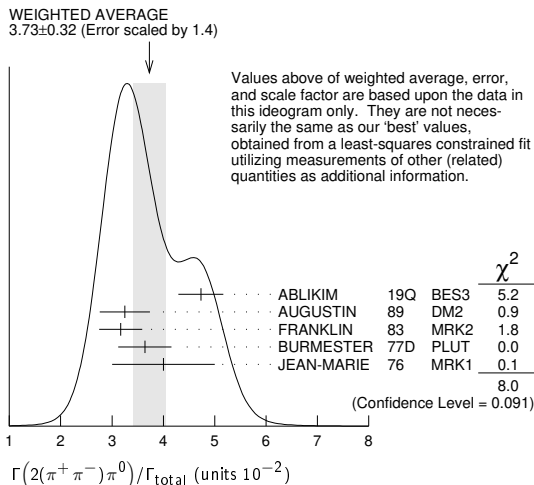
VALUE	CL%	DOCUMENT ID	TECN	COMMENT
$<1.1 \times 10^{-5}$	90	BAI	04G BES2	e^+e^-

STABLE HADRONS

$\Gamma(2(\pi^+\pi^-\pi^0))/\Gamma_{total}$ Γ_{139}/Γ

VALUE (units 10^{-2})	EVTS	DOCUMENT ID	TECN	COMMENT
3.73 ± 0.32 OUR AVERAGE		Error includes scale factor of 1.4. See the ideogram below.		
4.73 ± 0.44	228K	1 ABLIKIM	19Q BES3	$J/\psi \rightarrow 2(\pi^+\pi^-\pi^0)$
3.25 ± 0.49	46055	AUGUSTIN	89 DM2	$J/\psi \rightarrow 2(\pi^+\pi^-\pi^0)$
3.17 ± 0.42	147	FRANKLIN	83 MRK2	$e^+e^- \rightarrow$ hadrons
3.64 ± 0.52	1500	BURMESTER	77D PLUT	e^+e^-
4 ± 1	675	JEAN-MARIE	76 MRK1	e^+e^-

¹ From an energy scan of $e^+e^- \rightarrow J/\psi \rightarrow 2(\pi^+\pi^-\pi^0)$, assuming PDG 16 values for $\Gamma(e^+e^-)$, $\Gamma(\mu^+\mu^-)$, and $\Gamma(total)$, and for a phase difference between strong and electromagnetic amplitudes of $(84.9 \pm 3.6)^\circ$. An alternative solution is $(4.85 \pm 0.45)^\circ$ with a phase of $(-84.7 \pm 3.1)^\circ$.



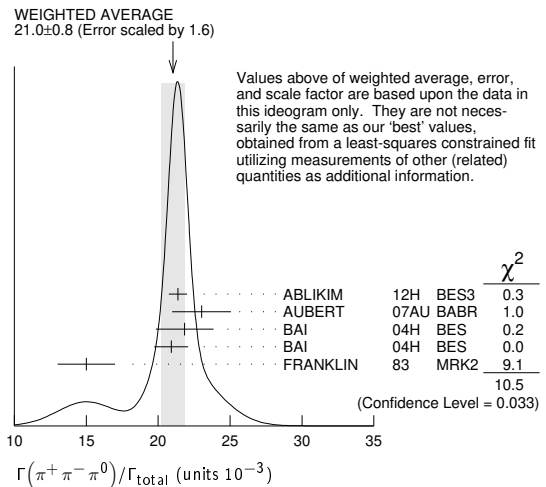
$\Gamma(3(\pi^+\pi^-\pi^0))/\Gamma_{total}$ Γ_{140}/Γ

VALUE	EVTS	DOCUMENT ID	TECN	COMMENT
0.029 ± 0.006 OUR AVERAGE				
0.028 ± 0.009	11	FRANKLIN	83 MRK2	$e^+e^- \rightarrow$ hadrons
0.029 ± 0.007	181	JEAN-MARIE	76 MRK1	e^+e^-

$\Gamma(\pi^+\pi^-\pi^0)/\Gamma_{total}$ Γ_{141}/Γ

VALUE (units 10^{-3})	EVTS	DOCUMENT ID	TECN	COMMENT
21.0 ± 0.8 OUR AVERAGE		Error includes scale factor of 1.6. See the ideogram below.		
21.37 ± 0.04 +0.64 -0.62	1.8M	1,2 ABLIKIM	12H BES3	$e^+e^- \rightarrow J/\psi$
23.0 ± 2.0 ± 0.4	256	3 AUBERT	07AU BABR	10.6 $e^+e^- \rightarrow J/\psi\pi^+\pi^-\gamma$
21.84 ± 0.05 ± 2.01	220k	1,4 BAI	04H BES	e^+e^-
20.91 ± 0.21 ± 1.16		4,5 BAI	04H BES	e^+e^-
15 ± 2	168	FRANKLIN	83 MRK2	e^+e^-

¹ From $J/\psi \rightarrow \pi^+\pi^-\pi^0$ events directly.
² The quoted systematic error includes a contribution of 1.23% (added in quadrature) from the uncertainty on the number of J/ψ events.
³ AUBERT 07AU reports $[\Gamma(J/\psi(1S) \rightarrow \pi^+\pi^-\pi^0)/\Gamma_{total}] \times [\Gamma(\psi(2S) \rightarrow J/\psi(1S)\pi^+\pi^-) \times \Gamma(\psi(2S) \rightarrow e^+e^-)]/\Gamma_{total} = (18.6 \pm 1.2 \pm 1.1) \times 10^{-3}$ keV which we divide by our best value $\Gamma(\psi(2S) \rightarrow J/\psi(1S)\pi^+\pi^-) \times \Gamma(\psi(2S) \rightarrow e^+e^-)/\Gamma_{total} = 0.808 \pm 0.013$ keV. Our first error is their experiment's error and our second error is the systematic error from using our best value.
⁴ Mostly $\rho\pi$, see also $\rho\pi$ subsection.
⁵ Obtained comparing the rates for $\pi^+\pi^-\pi^0$ and $\mu^+\mu^-$, using J/ψ events produced via $\psi(2S) \rightarrow \pi^+\pi^-J/\psi$ and with $B(J/\psi \rightarrow \mu^+\mu^-) = 5.88 \pm 0.10\%$.



$\Gamma(\pi^+\pi^-\pi^0 K^+K^-)/\Gamma_{total}$ Γ_{145}/Γ

VALUE (units 10^{-2})	EVTS	DOCUMENT ID	TECN	COMMENT
1.2 ± 0.3	309	VANNUCCI	77 MRK1	e^+e^-

$\Gamma(4(\pi^+\pi^-\pi^0))/\Gamma_{total}$ Γ_{146}/Γ

VALUE (units 10^{-4})	EVTS	DOCUMENT ID	TECN	COMMENT
90 ± 30	13	JEAN-MARIE	76 MRK1	e^+e^-

$\Gamma(\pi^+\pi^-K^+K^-)/\Gamma_{total}$ Γ_{147}/Γ

VALUE (units 10^{-3})	EVTS	DOCUMENT ID	TECN	COMMENT
7.2 ± 2.3	205	VANNUCCI	77 MRK1	e^+e^-

••• We do not use the following data for averages, fits, limits, etc. •••

$\Gamma(K\bar{K}\pi)/\Gamma_{total}$ Γ_{155}/Γ

VALUE (units 10^{-4})	EVTS	DOCUMENT ID	TECN	COMMENT
61 ± 10 OUR AVERAGE				
55.2 ± 12.0	25	FRANKLIN	83 MRK2	$e^+e^- \rightarrow K^+K^-\pi^0$
78.0 ± 21.0	126	VANNUCCI	77 MRK1	$e^+e^- \rightarrow K_S^0 K^\pm\pi^\mp$

$\Gamma(K^+K^-\pi^0)/\Gamma_{total}$ Γ_{156}/Γ

VALUE (units 10^{-3})	EVTS	DOCUMENT ID	TECN	COMMENT
$2.88 \pm 0.01 \pm 0.12$	183k	ABLIKIM	19AQ BES	$J/\psi \rightarrow K^+K^-\pi^0$

$\Gamma(K^+K^-\pi^0)/\Gamma(\pi^+\pi^-\pi^0)$ $\Gamma_{156}/\Gamma_{141}$

VALUE (%)	EVTS	DOCUMENT ID	TECN	COMMENT
$12.0 \pm 0.3 \pm 0.9$	23K	LEES	17c BABR	$J/\psi \rightarrow h^+h^-\pi^0$

$\Gamma(K_S^0 K^\pm\pi^\mp)/\Gamma(\pi^+\pi^-\pi^0)$ $\Gamma_{157}/\Gamma_{141}$

VALUE (%)	EVTS	DOCUMENT ID	TECN	COMMENT
$26.5 \pm 0.5 \pm 2.1$	24K	LEES	17c BABR	$J/\psi \rightarrow h^0 h^+ h^-$

See key on page 999

Meson Particle Listings

$J/\psi(1S)$

$\Gamma(2(\pi^+\pi^-))/\Gamma_{total}$ Γ_{162}/Γ

VALUE (units 10^{-3})	EVTS	DOCUMENT ID	TECN	COMMENT
3.57 ± 0.30 OUR AVERAGE				
3.53 ± 0.12 ± 0.29	1107	¹ ABLIKIM	05H BES2	$e^+e^- \rightarrow \psi(2S) \rightarrow J/\psi \pi^+\pi^-$, $J/\psi \rightarrow 2(\pi^+\pi^-)$
4.0 ± 1.0	76	JEAN-MARIE	76 MRK1	e^+e^-

¹ Computed using $B(J/\psi \rightarrow \mu^+\mu^-) = 0.0588 \pm 0.0010$.

$\Gamma(3(\pi^+\pi^-))/\Gamma_{total}$ Γ_{163}/Γ

VALUE (units 10^{-4})	EVTS	DOCUMENT ID	TECN	COMMENT
40 ± 20	32	JEAN-MARIE	76 MRK1	e^+e^-

• • • We do not use the following data for averages, fits, limits, etc. • • •

$\Gamma(2(\pi^+\pi^-\eta))/\Gamma_{total}$ Γ_{165}/Γ

VALUE (units 10^{-3})	EVTS	DOCUMENT ID	TECN	COMMENT
2.26 ± 0.08 ± 0.27	4.8k	ABLIKIM	05c BES2	$e^+e^- \rightarrow 2(\pi^+\pi^-\eta)$

$\Gamma(3(\pi^+\pi^-\eta))/\Gamma_{total}$ Γ_{166}/Γ

VALUE (units 10^{-4})	EVTS	DOCUMENT ID	TECN	COMMENT
7.24 ± 0.96 ± 1.11	616	ABLIKIM	05c BES2	$e^+e^- \rightarrow 3(\pi^+\pi^-\eta)$

$\Gamma(p\bar{p})/\Gamma_{total}$ Γ_{169}/Γ

VALUE (units 10^{-3})	EVTS	DOCUMENT ID	TECN	COMMENT
2.121 ± 0.029 OUR AVERAGE				
2.112 ± 0.004 ± 0.031	314k	ABLIKIM	12c BES3	e^+e^-
2.20 ± 0.16 ± 0.06	317	¹ WU	06 BELL	$B^+ \rightarrow p\bar{p}K^+$
2.26 ± 0.01 ± 0.14	63316	BAI	04E BES2	$e^+e^- \rightarrow J/\psi$
1.97 ± 0.22	99	BALDINI	98 FENI	e^+e^-
1.91 ± 0.04 ± 0.30		PALLIN	87 DM2	e^+e^-
2.16 ± 0.07 ± 0.15	1420	EATON	84 MRK2	e^+e^-
2.5 ± 0.4	133	BRANDELIK	79c DASP	e^+e^-
2.0 ± 0.5		BESCH	78 BONA	e^+e^-
2.2 ± 0.2	331	² PERUZZI	78 MRK1	e^+e^-
2.0 ± 0.3	48	ANTONELLI	93 SPEC	e^+e^-

• • • We do not use the following data for averages, fits, limits, etc. • • •

¹ WU 06 reports $[\Gamma(J/\psi(1S) \rightarrow p\bar{p})/\Gamma_{total}] \times [B(B^+ \rightarrow J/\psi(1S)K^+)] = (2.21 \pm 0.13 \pm 0.10) \times 10^{-6}$ which we divide by our best value $B(B^+ \rightarrow J/\psi(1S)K^+) = (1.006 \pm 0.027) \times 10^{-3}$. Our first error is their experiment's error and our second error is the systematic error from using our best value.

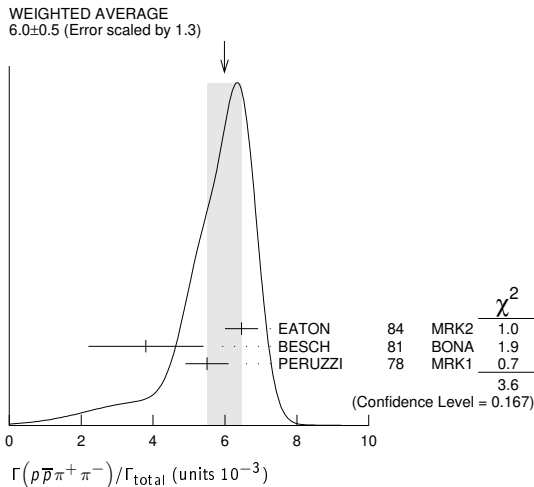
² Assuming angular distribution $(1 + \cos^2\theta)$.

$\Gamma(p\bar{p}\pi^0)/\Gamma_{total}$ Γ_{170}/Γ

VALUE (units 10^{-3})	EVTS	DOCUMENT ID	TECN	COMMENT
1.19 ± 0.08 OUR AVERAGE				Error includes scale factor of 1.1.
1.33 ± 0.02 ± 0.11	11k	ABLIKIM	09B BES2	e^+e^-
1.13 ± 0.09 ± 0.09	685	EATON	84 MRK2	e^+e^-
1.4 ± 0.4		BRANDELIK	79c DASP	e^+e^-
1.00 ± 0.15	109	PERUZZI	78 MRK1	e^+e^-

$\Gamma(p\bar{p}\pi^+\pi^-)/\Gamma_{total}$ Γ_{171}/Γ

VALUE (units 10^{-3})	EVTS	DOCUMENT ID	TECN	COMMENT
6.0 ± 0.5 OUR AVERAGE				Error includes scale factor of 1.3. See the ideogram below.
6.46 ± 0.17 ± 0.43	1435	EATON	84 MRK2	e^+e^-
3.8 ± 1.6	48	BESCH	81 BONA	e^+e^-
5.5 ± 0.6	533	PERUZZI	78 MRK1	e^+e^-



$\Gamma(p\bar{p}\pi^+\pi^-\pi^0)/\Gamma_{total}$ Γ_{172}/Γ

Including $p\bar{p}\pi^+\pi^-\pi^0$ and excluding ω, η, η'

VALUE (units 10^{-3})	EVTS	DOCUMENT ID	TECN	COMMENT
2.3 ± 0.9 OUR AVERAGE				Error includes scale factor of 1.9.
3.36 ± 0.65 ± 0.28	364	EATON	84 MRK2	e^+e^-
1.6 ± 0.6	39	PERUZZI	78 MRK1	e^+e^-

$\Gamma(p\bar{p}\eta)/\Gamma_{total}$ Γ_{173}/Γ

VALUE (units 10^{-3})	EVTS	DOCUMENT ID	TECN	COMMENT
2.00 ± 0.12 OUR AVERAGE				
1.91 ± 0.02 ± 0.17	13k	¹ ABLIKIM	09 BES2	e^+e^-
2.03 ± 0.13 ± 0.15	826	EATON	84 MRK2	e^+e^-
2.5 ± 1.2		BRANDELIK	79c DASP	e^+e^-
2.3 ± 0.4	197	PERUZZI	78 MRK1	e^+e^-

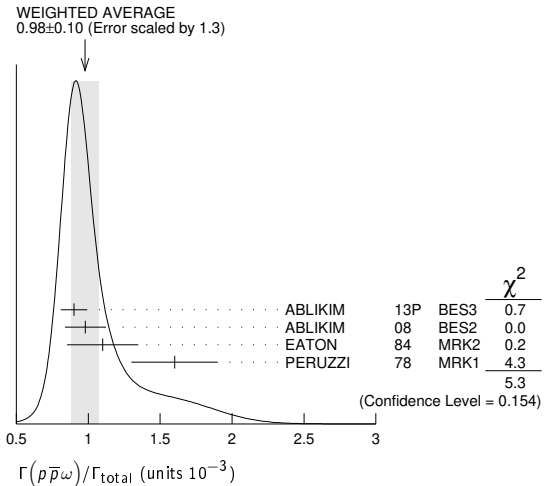
¹ From the combination of $p\bar{p}\eta \rightarrow p\bar{p}\gamma\gamma$ and $p\bar{p}\eta \rightarrow p\bar{p}\pi^+\pi^-\pi^0$ channels.

$\Gamma(p\bar{p}\rho)/\Gamma_{total}$ Γ_{174}/Γ

VALUE	CL%	DOCUMENT ID	TECN	COMMENT
< 0.31 × 10⁻³	90	EATON	84 MRK2	$e^+e^- \rightarrow \text{hadrons}\gamma$

$\Gamma(p\bar{p}\omega)/\Gamma_{total}$ Γ_{175}/Γ

VALUE (units 10^{-3})	EVTS	DOCUMENT ID	TECN	COMMENT
0.98 ± 0.10 OUR AVERAGE				Error includes scale factor of 1.3. See the ideogram below.
0.90 ± 0.02 ± 0.09	2670	ABLIKIM	13P BES3	e^+e^-
0.98 ± 0.03 ± 0.14	2449	ABLIKIM	08 BES2	e^+e^-
1.10 ± 0.17 ± 0.18	486	EATON	84 MRK2	e^+e^-
1.6 ± 0.3	77	PERUZZI	78 MRK1	e^+e^-



$\Gamma(p\bar{p}\eta'(958))/\Gamma_{total}$ Γ_{176}/Γ

VALUE (units 10^{-3})	EVTS	DOCUMENT ID	TECN	COMMENT
0.129 ± 0.014 OUR AVERAGE				Error includes scale factor of 2.0.
0.126 ± 0.002 ± 0.007	16K	¹ ABLIKIM	19N BES3	e^+e^-
0.200 ± 0.023 ± 0.028	265 ± 31	² ABLIKIM	09 BES2	e^+e^-
0.68 ± 0.23 ± 0.17	19	EATON	84 MRK2	e^+e^-
1.8 ± 0.6	19	PERUZZI	78 MRK1	e^+e^-

¹ From the combination of $p\bar{p}\eta' \rightarrow p\bar{p}\pi^+\pi^-\eta$ and $p\bar{p}\eta' \rightarrow p\bar{p}\pi^+\pi^-\gamma$ channels.

² From the combination of $p\bar{p}\eta' \rightarrow p\bar{p}\pi^+\pi^-\eta$ and $p\bar{p}\eta' \rightarrow p\bar{p}\gamma\rho^0$ channels.

$\Gamma(p\bar{p}a_0(980) \rightarrow p\bar{p}\pi^0\eta)/\Gamma_{total}$ Γ_{177}/Γ

VALUE (units 10^{-3})	DOCUMENT ID	TECN	COMMENT
6.8 ± 1.2 ± 1.3	ABLIKIM	14N BES3	$e^+e^- \rightarrow J/\psi$

$\Gamma(p\bar{p}\phi)/\Gamma_{total}$ Γ_{178}/Γ

VALUE (units 10^{-4})	EVTS	DOCUMENT ID	TECN	COMMENT
0.519 ± 0.033 OUR AVERAGE				
0.523 ± 0.006 ± 0.033	14K	ABLIKIM	16k BES3	$J/\psi \rightarrow p\bar{p}K_S^0 K_L^0$, $p\bar{p}K^+ K^-$
0.45 ± 0.13 ± 0.07		FALVARD	88 DM2	$J/\psi \rightarrow \text{hadrons}$

$\Gamma(n\bar{n})/\Gamma_{total}$ Γ_{179}/Γ

VALUE (units 10^{-3})	EVTS	DOCUMENT ID	TECN	COMMENT
2.09 ± 0.16 OUR AVERAGE				
2.07 ± 0.01 ± 0.17	36k	ABLIKIM	12c BES3	e^+e^-
2.31 ± 0.49	79	BALDINI	98 FENI	e^+e^-
1.8 ± 0.9		BESCH	78 BONA	e^+e^-
1.90 ± 0.55	40	ANTONELLI	93 SPEC	e^+e^-

• • • We do not use the following data for averages, fits, limits, etc. • • •

Meson Particle Listings

$J/\psi(1S)$

$\Gamma(n\bar{n}\pi^+\pi^-)/\Gamma_{total}$ Γ_{180}/Γ

VALUE (units 10^{-3})	EVTS	DOCUMENT ID	TECN	COMMENT
3.8 ± 3.6	5	BESCH	81	BONA e^+e^-

$\Gamma(\Sigma^+\bar{\Sigma}^-)/\Gamma_{total}$ Γ_{181}/Γ

VALUE (units 10^{-3})	EVTS	DOCUMENT ID	TECN	COMMENT
$1.50 \pm 0.10 \pm 0.22$	399	ABLIKIM	080	BES2 $e^+e^- \rightarrow J/\psi$

$\Gamma(\Sigma^0\bar{\Sigma}^0)/\Gamma_{total}$ Γ_{182}/Γ

VALUE (units 10^{-3})	EVTS	DOCUMENT ID	TECN	COMMENT
1.172 ± 0.032 OUR AVERAGE		Error includes scale factor of 1.4.		
$1.164 \pm 0.004 \pm 0.023$	111k	ABLIKIM	17L	BES3 $J/\psi \rightarrow \Sigma^0\bar{\Sigma}^0$
$1.33 \pm 0.04 \pm 0.11$	1.7k	ABLIKIM	06	BES2 $J/\psi \rightarrow \Sigma^0\bar{\Sigma}^0$
$1.06 \pm 0.04 \pm 0.23$	884	PALLIN	87	DM2 $e^+e^- \rightarrow \Sigma^0\bar{\Sigma}^0$
$1.58 \pm 0.16 \pm 0.25$	90	EATON	84	MRK2 $e^+e^- \rightarrow \Sigma^0\bar{\Sigma}^0$
1.3 ± 0.4	52	PERUZZI	78	MRK1 $e^+e^- \rightarrow \Sigma^0\bar{\Sigma}^0$
2.4 ± 2.6	3	BESCH	81	BONA $e^+e^- \rightarrow \Sigma^+\bar{\Sigma}^-$

• • • We do not use the following data for averages, fits, limits, etc. • • •

$\Gamma(2(\pi^+\pi^-)K^+K^-)/\Gamma_{total}$ Γ_{183}/Γ

VALUE (units 10^{-4})	EVTS	DOCUMENT ID	TECN	COMMENT
31 ± 13	30	VANNUCCI	77	MRK1 e^+e^-

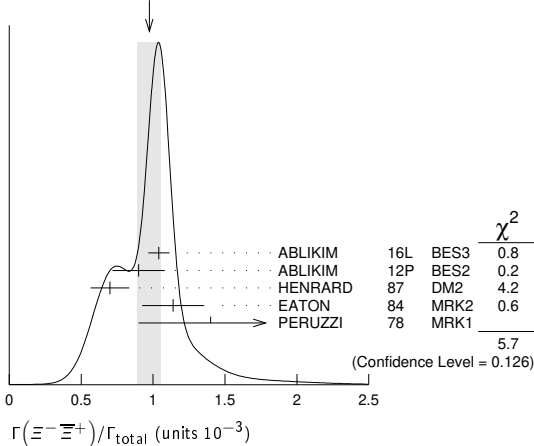
$\Gamma(\rho\bar{\rho}\pi^-)/\Gamma_{total}$ Γ_{184}/Γ

VALUE (units 10^{-3})	EVTS	DOCUMENT ID	TECN	COMMENT
2.12 ± 0.09 OUR AVERAGE				
$2.36 \pm 0.02 \pm 0.21$	59k	ABLIKIM	06k	BES2 $J/\psi \rightarrow \rho\pi^-\bar{\rho}$
$2.47 \pm 0.02 \pm 0.24$	55k	ABLIKIM	06k	BES2 $J/\psi \rightarrow \bar{\rho}\pi^+n$
$2.02 \pm 0.07 \pm 0.16$	1288	EATON	84	MRK2 $e^+e^- \rightarrow \rho\pi^-$
$1.93 \pm 0.07 \pm 0.16$	1191	EATON	84	MRK2 $e^+e^- \rightarrow \bar{\rho}\pi^+$
1.7 ± 0.7	32	BESCH	81	BONA $e^+e^- \rightarrow \rho\pi^-$
1.6 ± 1.2	5	BESCH	81	BONA $e^+e^- \rightarrow \bar{\rho}\pi^+$
2.16 ± 0.29	194	PERUZZI	78	MRK1 $e^+e^- \rightarrow \rho\pi^-$
2.04 ± 0.27	204	PERUZZI	78	MRK1 $e^+e^- \rightarrow \bar{\rho}\pi^+$

$\Gamma(\Xi^-\bar{\Xi}^+)/\Gamma_{total}$ Γ_{188}/Γ

VALUE (units 10^{-3})	EVTS	DOCUMENT ID	TECN	COMMENT
0.97 ± 0.08 OUR AVERAGE		Error includes scale factor of 1.4. See the ideogram below.		
$1.040 \pm 0.006 \pm 0.074$	43k	ABLIKIM	16L	BES3 $J/\psi \rightarrow \Xi^-\bar{\Xi}^+$
$0.90 \pm 0.03 \pm 0.18$	961	ABLIKIM	12P	BES2 $J/\psi \rightarrow \Xi^-\bar{\Xi}^+$
$0.70 \pm 0.06 \pm 0.12$	132	HENRRARD	87	DM2 $e^+e^- \rightarrow \Xi^-\bar{\Xi}^+$
$1.14 \pm 0.08 \pm 0.20$	194	EATON	84	MRK2 $e^+e^- \rightarrow \Xi^-\bar{\Xi}^+$
1.4 ± 0.5	51	PERUZZI	78	MRK1 $e^+e^- \rightarrow \Xi^-\bar{\Xi}^+$

WEIGHTED AVERAGE
 0.97 ± 0.08 (Error scaled by 1.4)



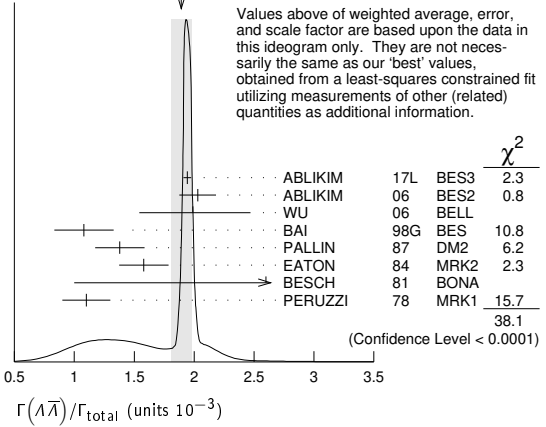
$\Gamma(\Lambda\bar{\Lambda})/\Gamma_{total}$ Γ_{189}/Γ

VALUE (units 10^{-3})	EVTS	DOCUMENT ID	TECN	COMMENT
1.89 ± 0.09 OUR AVERAGE		Error includes scale factor of 2.8. See the ideogram below.		
$1.943 \pm 0.003 \pm 0.033$	441k	ABLIKIM	17L	BES3 e^+e^-
$2.03 \pm 0.03 \pm 0.15$	8887	ABLIKIM	06	BES2 $J/\psi \rightarrow \Lambda\bar{\Lambda}$
$2.0 \pm 0.5 \pm 0.1$	46	¹ WU	06	BELL $B^+ \rightarrow \Lambda\bar{\Lambda}K^+$
$1.08 \pm 0.06 \pm 0.24$	631	BAI	98G	BES e^+e^-
$1.38 \pm 0.05 \pm 0.20$	1847	PALLIN	87	DM2 e^+e^-
$1.58 \pm 0.08 \pm 0.19$	365	EATON	84	MRK2 e^+e^-
2.6 ± 1.6	5	BESCH	81	BONA e^+e^-
1.1 ± 0.2	196	PERUZZI	78	MRK1 e^+e^-

¹WU 06 reports $[\Gamma(J/\psi(1S) \rightarrow \Lambda\bar{\Lambda})/\Gamma_{total}] \times [B(B^+ \rightarrow J/\psi(1S)K^+)] = (2.00 \pm 0.34 \pm 0.34) \times 10^{-6}$ which we divide by our best value $B(B^+ \rightarrow J/\psi(1S)K^+) = (1.006 \pm 0.027) \times 10^{-3}$. Our first error is their experiment's error and our second error is the systematic error from using our best value.

$= (1.006 \pm 0.027) \times 10^{-3}$. Our first error is their experiment's error and our second error is the systematic error from using our best value.

WEIGHTED AVERAGE
 1.89 ± 0.09 (Error scaled by 2.8)



$\Gamma(\Lambda\Sigma^-\pi^+ \text{ (or c.c.)})/\Gamma_{total}$ Γ_{190}/Γ

VALUE (units 10^{-3})	EVTS	DOCUMENT ID	TECN	COMMENT
0.83 ± 0.07 OUR AVERAGE		Error includes scale factor of 1.2.		
$0.770 \pm 0.051 \pm 0.083$	335	¹ ABLIKIM	07H	BES2 $e^+e^- \rightarrow \Lambda\Sigma^+\pi^-$
$0.747 \pm 0.056 \pm 0.076$	254	¹ ABLIKIM	07H	BES2 $e^+e^- \rightarrow \Lambda\Sigma^-\pi^+$
$0.90 \pm 0.06 \pm 0.16$	225 \pm 15	HENRRARD	87	DM2 $e^+e^- \rightarrow \Lambda\Sigma^+\pi^-$
$1.11 \pm 0.06 \pm 0.20$	342 \pm 18	HENRRARD	87	DM2 $e^+e^- \rightarrow \Lambda\Sigma^-\pi^+$
$1.53 \pm 0.17 \pm 0.38$	135	EATON	84	MRK2 $e^+e^- \rightarrow \Lambda\Sigma^+\pi^-$
$1.38 \pm 0.21 \pm 0.35$	118	EATON	84	MRK2 $e^+e^- \rightarrow \Lambda\Sigma^-\pi^+$

¹ Using $B(\Lambda \rightarrow \pi^-p) = 63.9\%$ and $B(\Sigma^+ \rightarrow \pi^0p) = 51.6\%$.

$\Gamma(\rho K^-\bar{\Lambda} + \text{c.c.})/\Gamma_{total}$ Γ_{191}/Γ

VALUE (units 10^{-3})	EVTS	DOCUMENT ID	TECN	COMMENT
0.87 ± 0.11 OUR AVERAGE				
$0.85 \pm 0.17 \pm 0.02$	45	¹ LU	19	BELL $B^+ \rightarrow \bar{\rho}\Lambda K^+ K^+$
$0.89 \pm 0.07 \pm 0.14$	307	EATON	84	MRK2 e^+e^-

¹LU 19 reports $(8.32 \pm 1.63 \pm 1.45) \times 10^{-4}$ from a measurement of $[\Gamma(J/\psi(1S) \rightarrow \rho K^-\bar{\Lambda} + \text{c.c.})/\Gamma_{total}] \times [B(B^+ \rightarrow J/\psi(1S)K^+)]$ assuming $B(B^+ \rightarrow J/\psi(1S)K^+) = (1.026 \pm 0.031) \times 10^{-3}$, which we rescale to our best value $B(B^+ \rightarrow J/\psi(1S)K^+) = (1.006 \pm 0.027) \times 10^{-3}$. Our first error is their experiment's error and our second error is the systematic error from using our best value.

$\Gamma(2(K^+K^-))/\Gamma_{total}$ Γ_{192}/Γ

VALUE (units 10^{-3})	EVTS	DOCUMENT ID	TECN	COMMENT
$1.4 \pm 0.5 \pm 0.2$	$11.0 \pm 4.3 \pm 3.5$	¹ HUANG	03	BELL $B^+ \rightarrow 2(K^+K^-)K^+$
0.7 ± 0.3		VANNUCCI	77	MRK1 e^+e^-

¹ Using $B(B^+ \rightarrow J/\psi K^+) = (1.01 \pm 0.05) \times 10^{-3}$.

$\Gamma(\rho K^-\Sigma^0)/\Gamma_{total}$ Γ_{193}/Γ

VALUE (units 10^{-3})	EVTS	DOCUMENT ID	TECN	COMMENT
$0.29 \pm 0.06 \pm 0.05$	90	EATON	84	MRK2 e^+e^-

$\Gamma(K^+K^-)/\Gamma_{total}$ Γ_{194}/Γ

VALUE (units 10^{-4})	EVTS	DOCUMENT ID	TECN	COMMENT
$2.86 \pm 0.09 \pm 0.19$	1k	¹ METREVELLI	12	$\psi(2S) \rightarrow \pi^+\pi^-K^+K^-$
$2.39 \pm 0.24 \pm 0.22$	107	² BALTRUSAIT...85D	MRK3	e^+e^-
2.2 ± 0.9	6	² BRANDELIK	79c	DASP e^+e^-

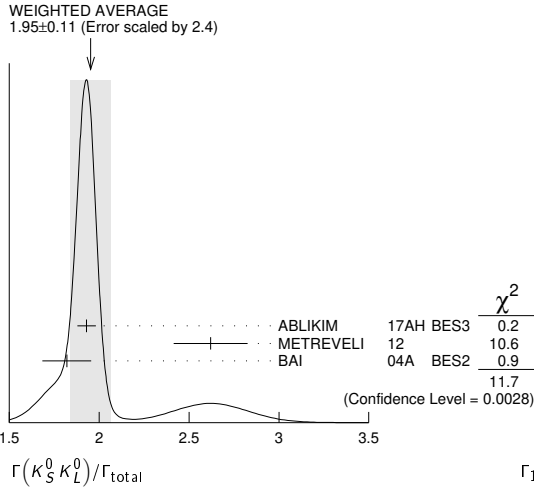
¹ Obtained by analyzing CLEO-c data but not authored by the CLEO Collaboration.
² Interference with non-resonant K^+K^- production not taken into account.

$\Gamma(K_S^0 K_L^0)/\Gamma_{total}$ Γ_{195}/Γ

VALUE (units 10^{-4})	EVTS	DOCUMENT ID	TECN	COMMENT
1.95 ± 0.11 OUR AVERAGE		Error includes scale factor of 2.4. See the ideogram below.		
$1.93 \pm 0.01 \pm 0.05$	110K	ABLIKIM	17AH	BES3 $J/\psi \rightarrow K_S^0 K_L^0 \rightarrow \pi^+\pi^-X$
$2.62 \pm 0.15 \pm 0.14$	0.3k	¹ METREVELLI	12	$\psi(2S) \rightarrow \pi^+\pi^-K_S^0 K_L^0$
$1.82 \pm 0.04 \pm 0.13$	2.1k	² BAI	04A	BES2 $J/\psi \rightarrow K_S^0 K_L^0 \rightarrow \pi^+\pi^-X$

• • • We do not use the following data for averages, fits, limits, etc. • • •

¹ Obtained by analyzing CLEO-c data but not authored by the CLEO Collaboration.
² Using $B(K_S^0 \rightarrow \pi^+\pi^-) = 0.6868 \pm 0.0027$.



RADIATIVE DECAYS

$\Gamma(K_S^0 K_L^0)/\Gamma_{total}$ Γ_{195}/Γ

$\Gamma(\Lambda\bar{\Lambda}\pi^+\pi^-)/\Gamma_{total}$ Γ_{196}/Γ
 VALUE (units 10⁻³) EVTS DOCUMENT ID TECN COMMENT
4.30 ± 0.13 ± 0.99 2.4k ABLIKIM 12P BES2 J/ψ

$\Gamma(\Lambda\bar{\Lambda}\eta)/\Gamma_{total}$ Γ_{197}/Γ
 VALUE (units 10⁻⁵) EVTS DOCUMENT ID TECN COMMENT
16.2 ± 1.7 OUR AVERAGE
 15.7 ± 0.80 ± 1.54 454 ¹ ABLIKIM 13F BES3 J/ψ → p p̄π⁺π⁻γγ
 26.2 ± 6.0 ± 4.4 44 ² ABLIKIM 07H BES2 e⁺e⁻ → ψ(2S)

¹ Using B(Λ → π⁻p) = 63.9% and B(η → γγ) = 39.31%.
² Using B(Λ → π⁻p) = 63.9% and B(η → γγ) = 39.4%.

$\Gamma(\Lambda\bar{\Lambda}\pi^0)/\Gamma_{total}$ Γ_{198}/Γ
 VALUE (units 10⁻⁵) CL% EVTS DOCUMENT ID TECN COMMENT
3.78 ± 0.27 ± 0.30 323 ¹ ABLIKIM 13F BES3 J/ψ → p p̄π⁺π⁻γγ
 ••• We do not use the following data for averages, fits, limits, etc. •••
 < 6.4 90 ² ABLIKIM 07H BES2 e⁺e⁻ → ψ(2S)
 23 ± 7 ± 8 11 BAI 98G BES e⁺e⁻
 22 ± 5 ± 5 19 HENRRARD 87 DM2 e⁺e⁻

¹ Using B(Λ → π⁻p) = 63.9% and B(π⁰ → γγ) = 98.8%.
² Using B(Λ → π⁻p) = 63.9%.

$\Gamma(\Lambda\bar{\Lambda}K_S^0 + c.c.)/\Gamma_{total}$ Γ_{199}/Γ
 VALUE (units 10⁻⁴) EVTS DOCUMENT ID TECN COMMENT
6.46 ± 0.20 ± 1.07 1058 ¹ ABLIKIM 08c BES2 e⁺e⁻ → J/ψ

¹ Using B(Λ → p̄π⁺) = 63.9% and B(K_S⁰ → π⁺π⁻) = 69.2%.

$\Gamma(\pi^+\pi^-)/\Gamma_{total}$ Γ_{200}/Γ
 VALUE (units 10⁻⁴) EVTS DOCUMENT ID TECN COMMENT
1.47 ± 0.14 OUR AVERAGE
 1.47 ± 0.13 ± 0.13 140 ¹ METREVELI 12 ψ(2S) → 2(π⁺π⁻)
 1.58 ± 0.20 ± 0.15 84 BALTRUSAIT...85D MRK3 e⁺e⁻
 1.0 ± 0.5 5 BRANDELIK 78B DASP e⁺e⁻
 1.6 ± 1.6 1 VANNUCCI 77 MRK1 e⁺e⁻

¹ Obtained by analyzing CLEO-c data but not authored by the CLEO Collaboration.

$\Gamma(\Lambda\bar{\Sigma} + c.c.)/\Gamma_{total}$ Γ_{201}/Γ
 VALUE (units 10⁻³) CL% EVTS DOCUMENT ID TECN COMMENT
2.83 ± 0.23 OUR AVERAGE
 2.74 ± 0.24 ± 0.22 234 ± 21 ¹ ABLIKIM 12B BES3 J/ψ → ΛΣ⁰
 2.92 ± 0.22 ± 0.24 308 ± 24 ² ABLIKIM 12B BES3 J/ψ → ΛΣ⁰

••• We do not use the following data for averages, fits, limits, etc. •••
 <18 ² HENRRARD 87 DM2 J/ψ → ΛΣ⁰
 <15 90 PERUZZI 78 MRK1 e⁺e⁻ → ΛX

¹ ABLIKIM 12B quotes B(J/ψ → ΛΣ⁰) which we multiply by 2.
² ABLIKIM 12B and HENRRARD 87 quote results for B(J/ψ → ΛΣ⁰) which we multiply by 2.

$\Gamma(K_S^0 K_S^0)/\Gamma_{total}$ Γ_{202}/Γ
 VALUE CL% EVTS DOCUMENT ID TECN COMMENT
<1.4 × 10⁻⁸ 95 ¹ ABLIKIM 17AH BES3 J/ψ → K_S⁰ K_S⁰ → π⁺π⁻π⁺π⁻

••• We do not use the following data for averages, fits, limits, etc. •••
 <1 × 10⁻⁶ 95 ¹ BAI 04D BES e⁺e⁻
 <5.2 × 10⁻⁶ 90 ¹ BALTRUSAIT...85c MRK3 e⁺e⁻

¹ Forbidden by CP.

$\Gamma(3\gamma)/\Gamma_{total}$ Γ_{203}/Γ
 VALUE (units 10⁻⁶) CL% EVTS DOCUMENT ID TECN COMMENT
11.6 ± 2.2 OUR AVERAGE
 11.3 ± 1.8 ± 2.0 113 ± 18 ABLIKIM 13i BES3 ψ(2S) → π⁺π⁻J/ψ
 12 ± 3 ± 2 24.2^{+7.2}_{-6.0} ADAMS 08 CLEO ψ(2S) → π⁺π⁻J/ψ

••• We do not use the following data for averages, fits, limits, etc. •••
 <55 90 PARTRIDGE 80 CBAL e⁺e⁻

$\Gamma(4\gamma)/\Gamma_{total}$ Γ_{204}/Γ
 VALUE CL% EVTS DOCUMENT ID TECN COMMENT
<9 × 10⁻⁶ 90 ADAMS 08 CLEO ψ(2S) → π⁺π⁻J/ψ

$\Gamma(5\gamma)/\Gamma_{total}$ Γ_{205}/Γ
 VALUE CL% EVTS DOCUMENT ID TECN COMMENT
<15 × 10⁻⁶ 90 ADAMS 08 CLEO ψ(2S) → π⁺π⁻J/ψ

$\Gamma(\gamma\pi^0\pi^0)/\Gamma_{total}$ Γ_{206}/Γ
 VALUE (units 10⁻³) DOCUMENT ID TECN COMMENT
1.15 ± 0.05 ¹ ABLIKIM 15AE BES3 J/ψ → γπ⁰π⁰

¹ The uncertainty is systematic as statistical is negligible.

$\Gamma(\gamma\eta\pi^0)/\Gamma_{total}$ Γ_{207}/Γ
 VALUE (units 10⁻⁶) EVTS DOCUMENT ID TECN COMMENT
21.4 ± 1.8 ± 2.5 596 ABLIKIM 16P BES3 J/ψ → 5γ

$\Gamma(\gamma a_0(980)^0 \rightarrow \gamma\eta\pi^0)/\Gamma_{total}$ Γ_{208}/Γ
 VALUE CL% EVTS DOCUMENT ID TECN COMMENT
<2.5 × 10⁻⁶ 95 ABLIKIM 16P BES3 J/ψ → 5γ

$\Gamma(\gamma a_2(1320)^0 \rightarrow \gamma\eta\pi^0)/\Gamma_{total}$ Γ_{209}/Γ
 VALUE CL% EVTS DOCUMENT ID TECN COMMENT
<6.6 × 10⁻⁶ 95 ABLIKIM 16P BES3 J/ψ → 5γ

$\Gamma(\gamma K_S^0 K_S^0)/\Gamma_{total}$ Γ_{210}/Γ
 VALUE (units 10⁻⁴) DOCUMENT ID TECN COMMENT
8.1 ± 0.4 ABLIKIM 18AA BES3 J/ψ → γK_S⁰ K_S⁰

$\Gamma(\gamma\eta_c(1S))/\Gamma_{total}$ Γ_{211}/Γ
 VALUE (units 10⁻²) EVTS DOCUMENT ID TECN COMMENT
1.7 ± 0.4 OUR AVERAGE Error includes scale factor of 1.5.
 2.00 ± 0.31 ± 0.02 ¹ MITCHELL 09 CLEO e⁺e⁻ → γX
 1.27 ± 0.36 GAISER 86 CBAL J/ψ → γX

••• We do not use the following data for averages, fits, limits, etc. •••
 seen ANASHIN 14 KEDR J/ψ → γη_c
 0.79 ± 0.20 273 ± 43 ² AUBERT 06E BABR B[±] → K[±]X_cπ̄
 seen 16 BALTRUSAIT...84 MRK3 J/ψ → 2φγ

¹ MITCHELL 09 reports (1.98 ± 0.09 ± 0.30) × 10⁻² from a measurement of [Γ(J/ψ(1S) → γη_c(1S))/Γ_{total}] × [B(ψ(2S) → J/ψ(1S)π⁺π⁻)] assuming B(ψ(2S) → J/ψ(1S)π⁺π⁻) = (35.04 ± 0.07 ± 0.77) × 10⁻², which we rescale to our best value B(ψ(2S) → J/ψ(1S)π⁺π⁻) = (34.68 ± 0.30) × 10⁻². Our first error is their experiment's error and our second error is the systematic error from using our best value.
² Calculated by the authors using an average of B(J/ψ → γη_c) × B(η_c → K[±]π) from BALTRUSAITIS 86, BISELLO 91, BAI 04 and B(η_c → K[±]π) = (8.5 ± 1.8)% from AUBERT 06E.

$\Gamma(\gamma\eta_c(1S) \rightarrow 3\gamma)/\Gamma_{total}$ Γ_{212}/Γ
 VALUE (units 10⁻⁶) EVTS DOCUMENT ID TECN COMMENT
3.8 ± 1.3 OUR AVERAGE Error includes scale factor of 1.1.
 4.5 ± 1.2 ± 0.6 33 ± 9 ABLIKIM 13i BES3 ψ(2S) → π⁺π⁻J/ψ
 1.2 ± 2.7_{-1.1} ± 0.3 1.2^{+2.8}_{-1.1} ADAMS 08 CLEO ψ(2S) → π⁺π⁻J/ψ

$\Gamma(\gamma\pi^+\pi^-2\pi^0)/\Gamma_{total}$ Γ_{213}/Γ
 VALUE (units 10⁻³) DOCUMENT ID TECN COMMENT
8.3 ± 0.2 ± 3.1 ¹ BALTRUSAIT...86B MRK3 J/ψ → 4πγ

¹ 4π mass less than 2.0 GeV.

$\Gamma(\gamma\eta\pi\pi)/\Gamma_{total}$ Γ_{214}/Γ
 VALUE (units 10⁻³) DOCUMENT ID TECN COMMENT
6.1 ± 1.0 OUR AVERAGE
 5.85 ± 0.3 ± 1.05 ¹ EDWARDS 83B CBAL J/ψ → ηπ⁺π⁻
 7.8 ± 1.2 ± 2.4 ¹ EDWARDS 83B CBAL J/ψ → η2π⁰

¹ Broad enhancement at 1700 MeV.

$\Gamma(\gamma\eta_2(1870) \rightarrow \gamma\eta\pi^+\pi^-)/\Gamma_{total}$ Γ_{215}/Γ
 VALUE (units 10⁻⁴) DOCUMENT ID TECN COMMENT
6.2 ± 2.2 ± 0.9 BAI 99 BES J/ψ → γηπ⁺π⁻

Meson Particle Listings

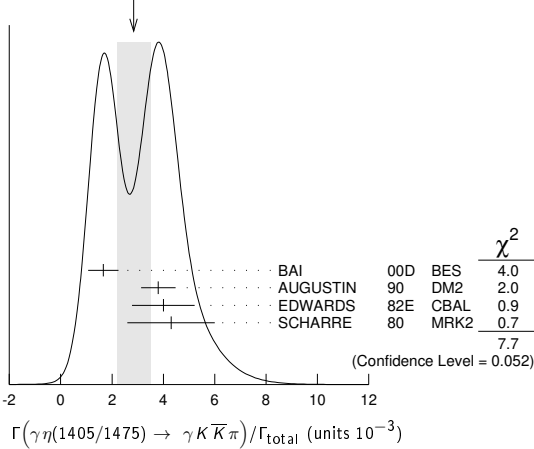
$J/\psi(1S)$

$\Gamma(\gamma\eta(1405/1475) \rightarrow \gamma K \bar{K} \pi) / \Gamma_{total}$ Γ_{216}/Γ

VALUE (units 10^{-3})	DOCUMENT ID	TECN	COMMENT
2.8 ± 0.6 OUR AVERAGE	Error includes scale factor of 1.6. See the ideogram below.		
1.66 ± 0.1 ± 0.58	1,2 BAI	00D BES	$J/\psi \rightarrow \gamma K^\pm K_S^0 \pi^\mp$
3.8 ± 0.3 ± 0.6	3 AUGUSTIN	90 DM2	$J/\psi \rightarrow \gamma K \bar{K} \pi$
4.0 ± 0.7 ± 1.0	3 EDWARDS	82E CBAL	$J/\psi \rightarrow K^+ K^- \pi^0 \gamma$
4.3 ± 1.7	3,4 SCHARRE	80 MRK2	$e^+ e^-$
• • • We do not use the following data for averages, fits, limits, etc. • • •			
1.78 ± 0.21 ± 0.33	3,5,6 AUGUSTIN	92 DM2	$J/\psi \rightarrow \gamma K \bar{K} \pi$
0.83 ± 0.13 ± 0.18	3,7,8 AUGUSTIN	92 DM2	$J/\psi \rightarrow \gamma K \bar{K} \pi$
0.66 ± 0.17 ± 0.24 -0.16 - 0.15	3,6,9 BAI	90C MRK3	$J/\psi \rightarrow \gamma K_S^0 K^\pm \pi^\mp$
1.03 ± 0.21 ± 0.26 -0.18 - 0.19	3,8,10 BAI	90C MRK3	$J/\psi \rightarrow \gamma K_S^0 K^\pm \pi^\mp$

- Interference with the $J/\psi(1S)$ radiative transition to the broad $K \bar{K} \pi$ pseudoscalar state around 1800 is $(0.15 \pm 0.01 \pm 0.05) \times 10^{-3}$.
- Interference with $J/\psi \rightarrow \gamma f_1(1420)$ is $(-0.03 \pm 0.01 \pm 0.01) \times 10^{-3}$.
- Includes unknown branching fraction $\eta(1405) \rightarrow K \bar{K} \pi$.
- Corrected for spin-zero hypothesis for $\eta(1405)$.
- From fit to the $a_0(980) \pi^0 \pi^+$ partial wave.
- $a_0(980) \pi$ mode.
- From fit to the $K^*(892) K^0 \pi^+$ partial wave.
- $K^* K$ mode.
- From $a_0(980) \pi$ final state.
- From $K^*(890) K$ final state.

WEIGHTED AVERAGE
2.8±0.6 (Error scaled by 1.6)



$\Gamma(\gamma\eta(1405/1475) \rightarrow \gamma\gamma\rho^0) / \Gamma_{total}$ Γ_{217}/Γ

VALUE (units 10^{-4})	DOCUMENT ID	TECN	COMMENT
0.78 ± 0.20 OUR AVERAGE	Error includes scale factor of 1.8.		
1.07 ± 0.17 ± 0.11	1 BAI	04J BES2	$J/\psi \rightarrow \gamma\gamma\pi^+\pi^-$
0.64 ± 0.12 ± 0.07	1 COFFMAN	90 MRK3	$J/\psi \rightarrow \gamma\gamma\pi^+\pi^-$

1 Includes unknown branching fraction $\eta(1405) \rightarrow \gamma\rho^0$.

$\Gamma(\gamma\eta(1405/1475) \rightarrow \gamma\eta\pi^+\pi^-) / \Gamma_{total}$ Γ_{218}/Γ

VALUE (units 10^{-4})	EVTS	DOCUMENT ID	TECN	COMMENT
3.0 ± 0.5 OUR AVERAGE				
2.6 ± 0.7 ± 0.4		BAI	99 BES	$J/\psi \rightarrow \gamma\eta\pi^+\pi^-$
3.38 ± 0.33 ± 0.64		1 BOLTON	92B MRK3	$J/\psi \rightarrow \gamma\eta\pi^+\pi^-$
• • • We do not use the following data for averages, fits, limits, etc. • • •				
7.0 ± 0.6 ± 1.1	261	2 AUGUSTIN	90 DM2	$J/\psi \rightarrow \gamma\eta\pi^+\pi^-$

1 Via $a_0(980) \pi$.
2 Includes unknown branching fraction to $\eta\pi^+\pi^-$.

$\Gamma(\gamma\eta(1405/1475) \rightarrow \gamma\gamma\phi) / \Gamma_{total}$ Γ_{219}/Γ

VALUE (units 10^{-6})	CL%	EVTS	DOCUMENT ID	TECN	COMMENT
<82	95		BAI	04J BES2	$J/\psi \rightarrow \gamma\gamma K^+ K^-$
• • • We do not use the following data for averages, fits, limits, etc. • • •					
7.03 ± 0.92 ± 0.91	1.3k	1	ABLIKIM	18I BES3	$J/\psi \rightarrow \gamma\gamma\phi(1020)$
10.36 ± 1.51 ± 1.54	1.9k	2	ABLIKIM	18I BES3	$J/\psi \rightarrow \gamma\gamma\phi(1020)$

1 Constructive interference between the $X(1835)$ and $\eta(1405)/\eta(1475)$ is assumed in a fit to the $\gamma\phi$ invariant mass.
2 Destructive interference between the $X(1835)$ and $\eta(1405)/\eta(1475)$ is assumed in a fit to the $\gamma\phi$ invariant mass.

$\Gamma(\gamma\eta(1405) \rightarrow \gamma\gamma\gamma) / \Gamma_{total}$ Γ_{220}/Γ

VALUE	CL%	DOCUMENT ID	TECN	COMMENT
<2.63 × 10⁻⁶	90	ABLIKIM	180 BES3	$\psi(2S) \rightarrow \pi^+\pi^-\gamma\gamma\gamma$

$\Gamma(\gamma\eta(1475) \rightarrow \gamma\gamma\gamma) / \Gamma_{total}$ Γ_{221}/Γ

VALUE	CL%	DOCUMENT ID	TECN	COMMENT
<1.86 × 10⁻⁶	90	ABLIKIM	180 BES3	$\psi(2S) \rightarrow \pi^+\pi^-\gamma\gamma\gamma$

$\Gamma(\gamma\rho\rho) / \Gamma_{total}$ Γ_{222}/Γ

VALUE (units 10^{-3})	CL%	DOCUMENT ID	TECN	COMMENT
4.5 ± 0.8 OUR AVERAGE				
4.7 ± 0.3 ± 0.9		1 BALTRUSAIT...86B	MRK3	$J/\psi \rightarrow 4\pi\gamma$
3.75 ± 1.05 ± 1.20		2 BURKE	82 MRK2	$J/\psi \rightarrow 4\pi\gamma$
• • • We do not use the following data for averages, fits, limits, etc. • • •				
<0.09	90	3 BISELLO	89B	$J/\psi \rightarrow 4\pi\gamma$

1 4π mass less than 2.0 GeV.
2 4π mass less than 2.0 GeV. We have multiplied $2\rho^0$ measurement by 3 to obtain 2ρ .
3 4π mass in the range 2.0–25 GeV.

$\Gamma(\gamma\rho\omega) / \Gamma_{total}$ Γ_{223}/Γ

VALUE	CL%	DOCUMENT ID	TECN	COMMENT
<5.4 × 10⁻⁴	90	ABLIKIM	08A BES2	$e^+e^- \rightarrow J/\psi$

$\Gamma(\gamma\rho\phi) / \Gamma_{total}$ Γ_{224}/Γ

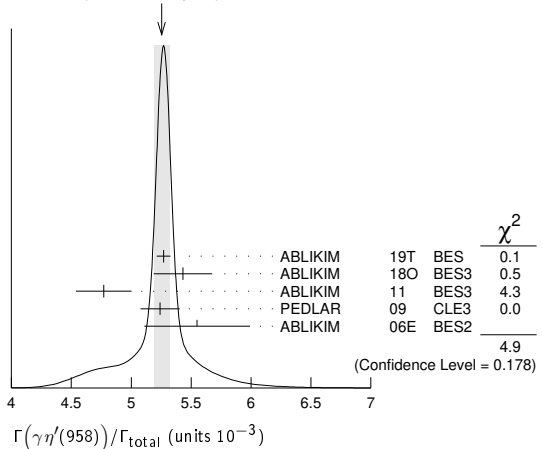
VALUE	CL%	DOCUMENT ID	TECN	COMMENT
<8.8 × 10⁻⁵	90	ABLIKIM	08A BES2	$e^+e^- \rightarrow J/\psi$

$\Gamma(\gamma\eta'(958)) / \Gamma_{total}$ Γ_{225}/Γ

VALUE (units 10^{-3})	EVTS	DOCUMENT ID	TECN	COMMENT
5.25 ± 0.07 OUR AVERAGE	Error includes scale factor of 1.3. See the ideogram below.			
5.27 ± 0.03 ± 0.05	36k	ABLIKIM	19T BES	$J/\psi \rightarrow \gamma\eta'$
5.43 ± 0.23 ± 0.09	5.0k	1 ABLIKIM	180 BES3	$\psi(2S) \rightarrow \pi^+\pi^-\gamma\gamma\gamma$
4.77 ± 0.22 ± 0.06		2 ABLIKIM	11 BES3	$J/\psi \rightarrow \eta'\gamma$
5.24 ± 0.12 ± 0.11		PEDLAR	09 CLE3	$J/\psi \rightarrow \eta'\gamma$
5.55 ± 0.44	35k	ABLIKIM	06E BES2	$J/\psi \rightarrow \eta'\gamma$
• • • We do not use the following data for averages, fits, limits, etc. • • •				
4.50 ± 0.14 ± 0.53		BOLTON	92B MRK3	$J/\psi \rightarrow \gamma\pi^+\pi^-\eta, \eta \rightarrow \gamma\gamma$
4.30 ± 0.31 ± 0.71		BOLTON	92B MRK3	$J/\psi \rightarrow \gamma\pi^+\pi^-\eta, \eta \rightarrow \pi^+\pi^-\pi^0$
4.04 ± 0.16 ± 0.85	622	AUGUSTIN	90 DM2	$J/\psi \rightarrow \gamma\eta\pi^+\pi^-$
4.39 ± 0.09 ± 0.66	2420	AUGUSTIN	90 DM2	$J/\psi \rightarrow \gamma\gamma\pi^+\pi^-$
4.1 ± 0.3 ± 0.6		BLOOM	83 CBAL	$e^+e^- \rightarrow 3\gamma + \text{hadrons}$
2.9 ± 1.1	6	BRANDELIK	79C DASP	$e^+e^- \rightarrow 3\gamma$
2.4 ± 0.7	57	BARTEL	76 CNTR	$e^+e^- \rightarrow 2\gamma\rho$

- 1 ABLIKIM 180 reports $[\Gamma(J/\psi(1S) \rightarrow \gamma\eta'(958)) / \Gamma_{total}] \times [B(\eta'(958) \rightarrow \gamma\gamma)] = (1.26 \pm 0.02 \pm 0.05) \times 10^{-4}$ from a measurement of $[\Gamma(J/\psi(1S) \rightarrow \gamma\eta'(958)) / \Gamma_{total}] \times [B(\eta'(958) \rightarrow \gamma\gamma)] \times [B(\psi(2S) \rightarrow J/\psi(1S)\pi^+\pi^-)]$ assuming $B(\psi(2S) \rightarrow J/\psi(1S)\pi^+\pi^-) = (34.49 \pm 0.30) \times 10^{-2}$, which we rescale to our best values $B(\eta'(958) \rightarrow \gamma\gamma) = (2.307 \pm 0.033) \times 10^{-2}$, $B(\psi(2S) \rightarrow J/\psi(1S)\pi^+\pi^-) = (34.68 \pm 0.30) \times 10^{-2}$. Our first error is their experiment's error and our second error is the systematic error from using our best values.
- 2 ABLIKIM 11 reports $(4.84 \pm 0.03 \pm 0.24) \times 10^{-3}$ from a measurement of $[\Gamma(J/\psi(1S) \rightarrow \gamma\eta'(958)) / \Gamma_{total}] / [B(\eta'(958) \rightarrow \pi^+\pi^-\eta)] / [B(\eta \rightarrow 2\gamma)]$ assuming $B(\eta'(958) \rightarrow \pi^+\pi^-\eta) = (43.2 \pm 0.7) \times 10^{-2}$, $B(\eta \rightarrow 2\gamma) = (39.31 \pm 0.20) \times 10^{-2}$, which we rescale to our best values $B(\eta'(958) \rightarrow \pi^+\pi^-\eta) = (42.5 \pm 0.5) \times 10^{-2}$, $B(\eta \rightarrow 2\gamma) = (39.41 \pm 0.20) \times 10^{-2}$. Our first error is their experiment's error and our second error is the systematic error from using our best values.

WEIGHTED AVERAGE
5.25±0.07 (Error scaled by 1.3)



See key on page 999

Meson Particle Listings

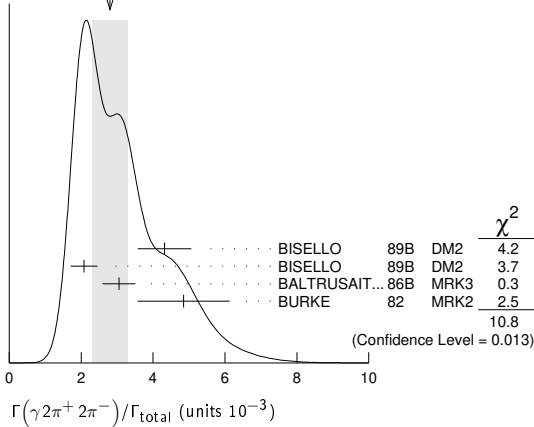
$J/\psi(1S)$

$\Gamma(\gamma 2\pi^+ 2\pi^-)/\Gamma_{total}$ Γ_{226}/Γ

VALUE (units 10^{-3})	DOCUMENT ID	TECN	COMMENT
2.8 ± 0.5 OUR AVERAGE	Error includes scale factor of 1.9. See the ideogram below.		
4.32 ± 0.14 ± 0.73	1 BISELLO	89B DM2	$J/\psi \rightarrow 4\pi\gamma$
2.08 ± 0.13 ± 0.35	2 BISELLO	89B DM2	$J/\psi \rightarrow 4\pi\gamma$
3.05 ± 0.08 ± 0.45	2 BALTRUSAIT...86B	MRK3	$J/\psi \rightarrow 4\pi\gamma$
4.85 ± 0.45 ± 1.20	3 BURKE	82 MRK2	e^+e^-

- ¹ 4π mass less than 3.0 GeV.
- ² 4π mass less than 2.0 GeV.
- ³ 4π mass less than 2.5 GeV.

WEIGHTED AVERAGE
2.8±0.5 (Error scaled by 1.9)



$\Gamma(\gamma f_2(1270) f_2(1270))/\Gamma_{total}$ Γ_{227}/Γ

VALUE (units 10^{-4})	EVTS	DOCUMENT ID	TECN	COMMENT
9.5 ± 0.7 ± 1.6	646 ± 45	ABLIKIM	04M BES	$J/\psi \rightarrow \gamma 2\pi^+ 2\pi^-$

$\Gamma(\gamma f_2(1270) f_2(1270) \text{ (non resonant)})/\Gamma_{total}$ Γ_{228}/Γ

VALUE (units 10^{-4})	DOCUMENT ID	TECN	COMMENT
8.2 ± 0.8 ± 1.7	1 ABLIKIM	04M BES	$J/\psi \rightarrow \gamma 2\pi^+ 2\pi^-$

¹ Subtracting contribution from intermediate $\eta_c(1S)$ decays.

$\Gamma(\gamma K^+ K^- \pi^+ \pi^-)/\Gamma_{total}$ Γ_{229}/Γ

VALUE (units 10^{-3})	EVTS	DOCUMENT ID	TECN	COMMENT
2.1 ± 0.1 ± 0.6	1516	BAI	00B BES	$J/\psi \rightarrow \gamma K^+ K^0 \pi^+ \pi^-$

$\Gamma(\gamma f_4(2050))/\Gamma_{total}$ Γ_{230}/Γ

VALUE (units 10^{-3})	DOCUMENT ID	TECN	COMMENT
2.7 ± 0.5 ± 0.5	1 BALTRUSAIT...87	MRK3	$J/\psi \rightarrow \gamma \pi^+ \pi^-$

¹ Assuming branching fraction $f_4(2050) \rightarrow \pi\pi/\text{total} = 0.167$.

$\Gamma(\gamma\omega)/\Gamma_{total}$ Γ_{231}/Γ

VALUE (units 10^{-3})	EVTS	DOCUMENT ID	TECN	COMMENT
1.61 ± 0.33 OUR AVERAGE				
6.0 ± 4.8 ± 1.8		ABLIKIM	08A BES2	$J/\psi \rightarrow \gamma\omega\pi^+\pi^-$
1.41 ± 0.2 ± 0.42	120 ± 17	BISELLO	87 SPEC	e^+e^- , hadrons γ
1.76 ± 0.09 ± 0.45		BALTRUSAIT...85c	MRK3	$e^+e^- \rightarrow \text{hadrons}\gamma$

$\Gamma(\gamma\eta(1405/1475) \rightarrow \gamma\rho^0\rho^0)/\Gamma_{total}$ Γ_{232}/Γ

VALUE (units 10^{-3})	DOCUMENT ID	TECN	COMMENT
1.7 ± 0.4 OUR AVERAGE	Error includes scale factor of 1.3.		
2.1 ± 0.4	BUGG	95 MRK3	$J/\psi \rightarrow \gamma\pi^+\pi^-\pi^+\pi^-$
1.36 ± 0.38	1,2 BISELLO	89B DM2	$J/\psi \rightarrow 4\pi\gamma$

- ¹ Estimated by us from various fits.
- ² Includes unknown branching fraction to $\rho^0\rho^0$.

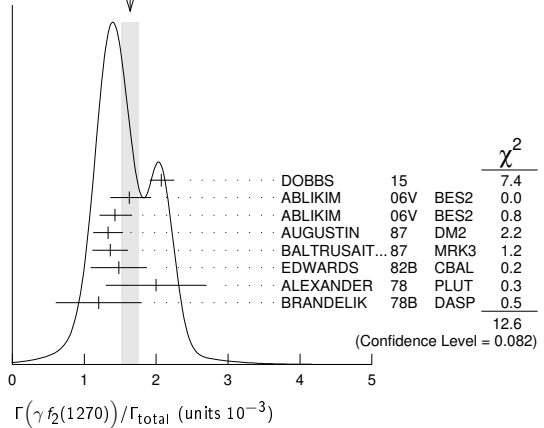
$\Gamma(\gamma f_2(1270))/\Gamma_{total}$ Γ_{233}/Γ

VALUE (units 10^{-3})	EVTS	DOCUMENT ID	TECN	COMMENT
1.64 ± 0.12 OUR AVERAGE				Error includes scale factor of 1.3. See the ideogram below.
2.07 ± 0.16 ± 0.02 ± 0.07	2.4k	1,2 DOBBS	15	$J/\psi \rightarrow \gamma\pi\pi$
1.63 ± 0.26 ± 0.02 ± 0.06		3 ABLIKIM	06v BES2	$e^+e^- \rightarrow J/\psi \rightarrow \gamma\pi^+\pi^-$
1.42 ± 0.21 ± 0.01 ± 0.05		4 ABLIKIM	06v BES2	$e^+e^- \rightarrow J/\psi \rightarrow \gamma\pi^0\pi^0$
1.33 ± 0.05 ± 0.20		5 AUGUSTIN	87 DM2	$J/\psi \rightarrow \gamma\pi^+\pi^-$
1.36 ± 0.09 ± 0.23		5 BALTRUSAIT...87	MRK3	$J/\psi \rightarrow \gamma\pi^+\pi^-$
1.48 ± 0.25 ± 0.30	178	EDWARDS	82B CBAL	$e^+e^- \rightarrow 2\pi^0\gamma$
2.0 ± 0.7	35	ALEXANDER	78 PLUT	e^+e^-
1.2 ± 0.6	30	6 BRANDELIK	78B DASP	$e^+e^- \rightarrow \pi^+\pi^-\gamma$

¹ Using CLEO-c data but not authored by the CLEO Collaboration.

- ² DOBBS 15 reports $[\Gamma(J/\psi(1S) \rightarrow \gamma f_2(1270))/\Gamma_{total}] \times [B(f_2(1270) \rightarrow \pi\pi)] = (1.744 \pm 0.052 \pm 0.122) \times 10^{-3}$ which we divide by our best value $B(f_2(1270) \rightarrow \pi\pi) = (84.2^{+2.9}_{-0.9}) \times 10^{-2}$. Our first error is their experiment's error and our second error is the systematic error from using our best value.
- ³ ABLIKIM 06v reports $[\Gamma(J/\psi(1S) \rightarrow \gamma f_2(1270))/\Gamma_{total}] \times [B(f_2(1270) \rightarrow \pi\pi)] = (1.371 \pm 0.010 \pm 0.222) \times 10^{-3}$ which we divide by our best value $B(f_2(1270) \rightarrow \pi\pi) = (84.2^{+2.9}_{-0.9}) \times 10^{-2}$. Our first error is their experiment's error and our second error is the systematic error from using our best value.
- ⁴ ABLIKIM 06v reports $[\Gamma(J/\psi(1S) \rightarrow \gamma f_2(1270))/\Gamma_{total}] \times [B(f_2(1270) \rightarrow \pi\pi)] = (1.200 \pm 0.027 \pm 0.174) \times 10^{-3}$ which we divide by our best value $B(f_2(1270) \rightarrow \pi\pi) = (84.2^{+2.9}_{-0.9}) \times 10^{-2}$. Our first error is their experiment's error and our second error is the systematic error from using our best value.
- ⁵ Estimated using $B(f_2(1270) \rightarrow \pi\pi) = 0.843 \pm 0.012$. The errors do not contain the uncertainty in the $f_2(1270)$ decay.
- ⁶ Restated by us to take account of spread of E1, M2, E3 transitions.

WEIGHTED AVERAGE
1.64±0.12 (Error scaled by 1.3)



$\Gamma(\gamma f_2(1270) \rightarrow \gamma K_S^0 K_S^0)/\Gamma_{total}$ Γ_{234}/Γ

VALUE (units 10^{-5})	DOCUMENT ID	TECN	COMMENT
2.58 ± 0.08 ± 0.59 ± 0.09 - 0.20	ABLIKIM	18AA BES3	$J/\psi \rightarrow \gamma K_S^0 K_S^0$

$\Gamma(\gamma f_0(1370) \rightarrow \gamma K\bar{K})/\Gamma_{total}$ Γ_{235}/Γ

VALUE (units 10^{-4})	EVTS	DOCUMENT ID	COMMENT
4.19 ± 0.73 ± 1.34	478	1 DOBBS	15 $J/\psi \rightarrow \gamma K\bar{K}$

¹ Using CLEO-c data but not authored by the CLEO Collaboration.

$\Gamma(\gamma f_0(1370) \rightarrow \gamma K_S^0 K_S^0)/\Gamma_{total}$ Γ_{236}/Γ

VALUE (units 10^{-5})	DOCUMENT ID	TECN	COMMENT
1.07 ± 0.08 ± 0.36 ± 0.07 - 0.34	ABLIKIM	18AA BES3	$J/\psi \rightarrow \gamma K_S^0 K_S^0$

$\Gamma(\gamma f_0(1500) \rightarrow \gamma K_S^0 K_S^0)/\Gamma_{total}$ Γ_{237}/Γ

VALUE (units 10^{-5})	DOCUMENT ID	TECN	COMMENT
1.59 ± 0.16 ± 0.18 ± 0.06	ABLIKIM	18AA BES3	$J/\psi \rightarrow \gamma K_S^0 K_S^0$

$\Gamma(\gamma f_0(1710) \rightarrow \gamma K\bar{K})/\Gamma_{total}$ Γ_{238}/Γ

VALUE (units 10^{-4})	CL%	EVTS	DOCUMENT ID	TECN	COMMENT
9.5 ± 1.0 ± 0.5 OUR AVERAGE					Error includes scale factor of 1.5. See the ideogram below.
8.00 ± 0.12 ± 1.24 ± 0.08 - 0.40			1 ABLIKIM	18AA BES3	$J/\psi \rightarrow \gamma K_S^0 K_S^0$
11.76 ± 0.54 ± 0.94	1.2k		2 DOBBS	15	$J/\psi \rightarrow \gamma K\bar{K}$
9.62 ± 0.29 ± 3.51 ± 1.86			3 BAI	03G BES	$J/\psi \rightarrow \gamma K\bar{K}$
5.0 ± 0.8 ± 1.8 ± 0.4			1,4 BAI	96C BES	$J/\psi \rightarrow \gamma K^+ K^-$
9.2 ± 1.4 ± 1.4			1 AUGUSTIN	88 DM2	$J/\psi \rightarrow \gamma K^+ K^-$
10.4 ± 1.2 ± 1.6			1 AUGUSTIN	88 DM2	$J/\psi \rightarrow \gamma K_S^0 K_S^0$
9.6 ± 1.2 ± 1.8			1 BALTRUSAIT...87	MRK3	$J/\psi \rightarrow \gamma K^+ K^-$

- • • We do not use the following data for averages, fits, limits, etc. • • •
- 1.6 ± 0.2 ± 0.6 ± 0.2
- 1.5 BAI 96C BES $J/\psi \rightarrow \gamma K^+ K^-$
- < 0.8 ± 0.4 ± 0.3
- 90
- 6 BISELLO 89B $J/\psi \rightarrow 4\pi\gamma$
- 7 BALTRUSAIT...87 MRK3 $J/\psi \rightarrow \gamma\pi^+\pi^-$
- 8 EDWARDS 82D CBAL $e^+e^- \rightarrow \eta\eta\gamma$

- ¹ Includes unknown branching fraction to K^+K^- or $K_S^0 K_S^0$. We have multiplied K^+K^- measurement by 2, and $K_S^0 K_S^0$ by 4 to obtain $K\bar{K}$ result.
- ² Using CLEO-c data but not authored by the CLEO Collaboration.

Meson Particle Listings

$J/\psi(1S)$

³Includes unknown branching ratio to K^+K^- or $K_S^0K_S^0$.

⁴Assuming $J^P = 2^+$ for $f_0(1710)$.

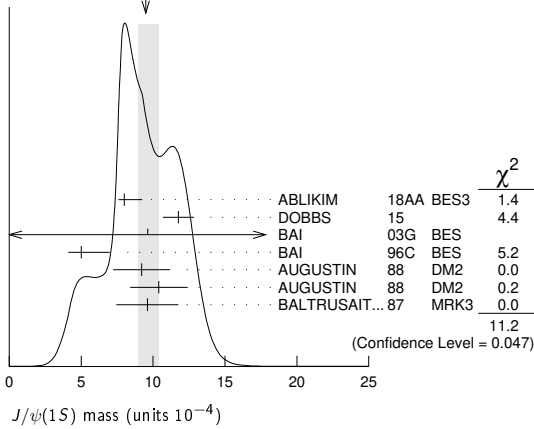
⁵Assuming $J^P = 0^+$ for $f_0(1710)$.

⁶Includes unknown branching fraction to $\rho^0\rho^0$.

⁷Includes unknown branching fraction to $\pi^+\pi^-$.

⁸Includes unknown branching fraction to $\eta\eta$.

WEIGHTED AVERAGE
9.5±1.0-0.5 (Error scaled by 1.5)



$\Gamma(\gamma f_0(1710) \rightarrow \gamma \pi \pi) / \Gamma_{total}$ Γ_{239} / Γ

VALUE (units 10^{-4})	EVTS	DOCUMENT ID	TECN	COMMENT
3.8 ± 0.5 OUR AVERAGE				
3.72 ± 0.30 ± 0.43	483	¹ DOBBS	15	$J/\psi \rightarrow \gamma \pi \pi$
3.96 ± 0.06 ± 1.12		² ABLIKIM	06V BES2	$e^+e^- \rightarrow J/\psi \rightarrow \gamma \pi^+\pi^-$
3.99 ± 0.15 ± 2.64		² ABLIKIM	06V BES2	$e^+e^- \rightarrow J/\psi \rightarrow \gamma \pi^0\pi^0$
• • • We do not use the following data for averages, fits, limits, etc. • • •				
2.5 ± 1.6 ± 0.8		BAI	98H BES	$J/\psi \rightarrow \gamma \pi^0\pi^0$

¹Using CLEO-c data but not authored by the CLEO Collaboration.
²Including unknown branching fraction to $\pi\pi$.

$\Gamma(\gamma f_0(1710) \rightarrow \gamma \omega \omega) / \Gamma_{total}$ Γ_{240} / Γ

VALUE (units 10^{-3})	EVTS	DOCUMENT ID	TECN	COMMENT
0.31 ± 0.06 ± 0.08	180	ABLIKIM	06H BES	$J/\psi \rightarrow \gamma \omega \omega$

$\Gamma(\gamma f_0(1710) \rightarrow \gamma \eta \eta) / \Gamma_{total}$ Γ_{241} / Γ

VALUE (units 10^{-4})	EVTS	DOCUMENT ID	TECN	COMMENT
2.35^{+0.13+1.24}_{-0.11-0.74}	5.5k	¹ ABLIKIM	13N BES3	$J/\psi \rightarrow \gamma \eta \eta$

¹From partial wave analysis including all possible combinations of 0^{++} , 2^{++} , and 4^{++} resonances.

$\Gamma(\gamma \eta) / \Gamma_{total}$ Γ_{242} / Γ

VALUE (units 10^{-3})	EVTS	DOCUMENT ID	TECN	COMMENT
1.108 ± 0.027 OUR AVERAGE				
1.12 ± 0.05 ± 0.01	18.6k	¹ ABLIKIM	180 BES3	$\psi(2S) \rightarrow \pi^+\pi^-\gamma\gamma\gamma$
1.101 ± 0.029 ± 0.022		PEDLAR	09 CLE3	$J/\psi \rightarrow \eta\gamma$
1.123 ± 0.089	11k	ABLIKIM	06E BES2	$J/\psi \rightarrow \eta\gamma$
• • • We do not use the following data for averages, fits, limits, etc. • • •				
0.88 ± 0.08 ± 0.11		BLOOM	83 CBAL	e^+e^-
0.82 ± 0.10		BRANDELIK	79C DASP	e^+e^-
1.3 ± 0.4	21	BARTEL	77 CNTR	e^+e^-

¹ABLIKIM 180 reports $[\Gamma(J/\psi(1S) \rightarrow \gamma \eta) / \Gamma_{total}] \times [B(\eta \rightarrow 2\gamma)] = (4.42 \pm 0.04 \pm 0.18) \times 10^{-4}$ from a measurement of $[\Gamma(J/\psi(1S) \rightarrow \gamma \eta) / \Gamma_{total}] \times [B(\eta \rightarrow 2\gamma)] \times [B(\psi(2S) \rightarrow J/\psi(1S)\pi^+\pi^-)]$ assuming $B(\psi(2S) \rightarrow J/\psi(1S)\pi^+\pi^-) = (34.49 \pm 0.30) \times 10^{-2}$, which we rescale to our best values $B(\eta \rightarrow 2\gamma) = (39.41 \pm 0.20) \times 10^{-2}$, $B(\psi(2S) \rightarrow J/\psi(1S)\pi^+\pi^-) = (34.68 \pm 0.30) \times 10^{-2}$. Our first error is their experiment's error and our second error is the systematic error from using our best values.

$\Gamma(\gamma f_1(1420) \rightarrow \gamma K \bar{K} \pi) / \Gamma_{total}$ Γ_{243} / Γ

VALUE (units 10^{-3})	DOCUMENT ID	TECN	COMMENT
0.79 ± 0.13 OUR AVERAGE			
0.68 ± 0.04 ± 0.24	BAI	00D BES	$J/\psi \rightarrow \gamma K^\pm K_S^0 \pi^\mp$
0.76 ± 0.15 ± 0.21	^{1,2} AUGUSTIN	92 DM2	$J/\psi \rightarrow \gamma K \bar{K} \pi$
0.87 ± 0.14 ^{+0.14} _{-0.11}	¹ BAI	90C MRK3	$J/\psi \rightarrow \gamma K_S^0 K^\pm \pi^\mp$

¹Included unknown branching fraction $f_1(1420) \rightarrow K \bar{K} \pi$.
²From fit to the $K^*(892)K1^{++}$ partial wave.

$\Gamma(\gamma f_1(1285)) / \Gamma_{total}$ Γ_{244} / Γ

VALUE (units 10^{-3})	DOCUMENT ID	TECN	COMMENT
0.61 ± 0.08 OUR AVERAGE			
0.69 ± 0.16 ± 0.20	¹ BAI	04J BES2	$J/\psi \rightarrow \gamma \gamma \rho^0$
0.61 ± 0.04 ± 0.21	² BAI	00D BES	$J/\psi \rightarrow \gamma K^\pm K_S^0 \pi^\mp$
0.45 ± 0.09 ± 0.17	³ BAI	99 BES	$J/\psi \rightarrow \gamma \eta \pi^+ \pi^-$
0.625 ± 0.063 ± 0.103	⁴ BOLTON	92 MRK3	$J/\psi \rightarrow \gamma f_1(1285)$
0.70 ± 0.08 ± 0.16	⁵ BOLTON	92B MRK3	$J/\psi \rightarrow \gamma \eta \pi^+ \pi^-$

¹Assuming $B(f_1(1285) \rightarrow \rho^0\gamma) = 0.055 \pm 0.013$.
²Assuming $\Gamma(f_1(1285) \rightarrow K \bar{K} \pi) / \Gamma_{total} = 0.090 \pm 0.004$.
³Assuming $\Gamma(f_1(1285) \rightarrow \eta \pi \pi) / \Gamma_{total} = 0.5 \pm 0.18$.
⁴Obtained summing the sequential decay channels
 $B(J/\psi \rightarrow \gamma f_1(1285), f_1(1285) \rightarrow \pi \pi \pi \pi) = (1.44 \pm 0.39 \pm 0.27) \times 10^{-4}$;
 $B(J/\psi \rightarrow \gamma f_1(1285), f_1(1285) \rightarrow a_0(980)\pi, a_0(980) \rightarrow \eta \pi) = (3.90 \pm 0.42 \pm 0.87) \times 10^{-4}$;
 $B(J/\psi \rightarrow \gamma f_1(1285), f_1(1285) \rightarrow a_0(980)\pi, a_0(980) \rightarrow K \bar{K}) = (0.66 \pm 0.26 \pm 0.29) \times 10^{-4}$;
 $B(J/\psi \rightarrow \gamma f_1(1285), f_1(1285) \rightarrow \gamma \rho^0) = (0.25 \pm 0.07 \pm 0.03) \times 10^{-4}$.
⁵Using $B(f_1(1285) \rightarrow a_0(980)\pi) = 0.37$, and including unknown branching ratio for $a_0(980) \rightarrow \eta \pi$.

$\Gamma(\gamma f_1(1510) \rightarrow \gamma \eta \pi^+ \pi^-) / \Gamma_{total}$ Γ_{245} / Γ

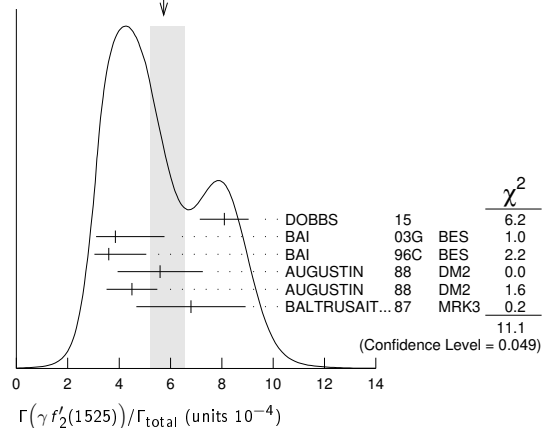
VALUE (units 10^{-4})	DOCUMENT ID	TECN	COMMENT
4.5 ± 1.0 ± 0.7	BAI	99 BES	$J/\psi \rightarrow \gamma \eta \pi^+ \pi^-$

$\Gamma(\gamma f_2'(1525)) / \Gamma_{total}$ Γ_{246} / Γ

VALUE (units 10^{-4})	CL%	EVTS	DOCUMENT ID	TECN	COMMENT	
5.7^{+0.8}_{-0.5} OUR AVERAGE					Error includes scale factor of 1.5. See the ideogram below.	
8.1 ± 0.9 ± 0.2		750	^{1,2} DOBBS	15	$J/\psi \rightarrow \gamma K \bar{K}$	
3.85 ± 0.17 ^{+1.91} _{-0.73}			³ BAI	03G BES	$J/\psi \rightarrow \gamma K \bar{K}$	
3.6 ± 0.4 ^{+1.4} _{-0.4}			³ BAI	96C BES	$J/\psi \rightarrow \gamma K^+ K^-$	
5.6 ± 1.4 ± 0.9			³ AUGUSTIN	88 DM2	$J/\psi \rightarrow \gamma K^+ K^-$	
4.5 ± 0.4 ± 0.9			³ AUGUSTIN	88 DM2	$J/\psi \rightarrow \gamma K_S^0 K_S^0$	
6.8 ± 1.6 ± 1.4			³ BALTRUSAIT...87	MRK3	$J/\psi \rightarrow \gamma K^+ K^-$	
• • • We do not use the following data for averages, fits, limits, etc. • • •						
<3.4		90	4	BRANDELIK	79C DASP	$e^+e^- \rightarrow \pi^+\pi^-\gamma$
<2.3		90	3	ALEXANDER	78 PLUT	$e^+e^- \rightarrow K^+ K^- \gamma$

¹Using CLEO-c data but not authored by the CLEO Collaboration.
²DOBBS 15 reports $[\Gamma(J/\psi(1S) \rightarrow \gamma f_2'(1525)) / \Gamma_{total}] \times [B(f_2'(1525) \rightarrow K \bar{K})] = (7.09 \pm 0.46 \pm 0.67) \times 10^{-4}$ which we divide by our best value $B(f_2'(1525) \rightarrow K \bar{K}) = (87.6 \pm 2.2) \times 10^{-2}$. Our first error is their experiment's error and our second error is the systematic error from using our best value.
³Using $B(f_2'(1525) \rightarrow K \bar{K}) = 0.888$.
⁴Assuming isotropic production and decay of the $f_2'(1525)$ and isospin.

WEIGHTED AVERAGE
5.7±0.8-0.5 (Error scaled by 1.5)



$\Gamma(\gamma f_2'(1525) \rightarrow \gamma K_S^0 K_S^0) / \Gamma_{total}$ Γ_{247} / Γ

VALUE (units 10^{-5})	DOCUMENT ID	TECN	COMMENT
7.99^{+0.03+0.69}_{-0.04-0.50}	ABLIKIM	18AA BES3	$J/\psi \rightarrow \gamma K_S^0 K_S^0$

$\Gamma(\gamma f_2'(1525) \rightarrow \gamma \eta \eta) / \Gamma_{total}$ Γ_{248} / Γ

VALUE (units 10^{-5})	EVTS	DOCUMENT ID	TECN	COMMENT
3.42^{+0.43+1.37}_{-0.51-1.30}	5.5k	¹ ABLIKIM	13N BES3	$J/\psi \rightarrow \gamma \eta \eta$

¹From partial wave analysis including all possible combinations of 0^{++} , 2^{++} , and 4^{++} resonances.

See key on page 999

Meson Particle Listings

$J/\psi(1S)$

$\Gamma(\gamma f_2(1640) \rightarrow \gamma\omega\phi)/\Gamma_{total}$					Γ_{249}/Γ
VALUE (units 10^{-3})	EVTS	DOCUMENT ID	TECN	COMMENT	
$0.28 \pm 0.05 \pm 0.17$	141	ABLIKIM	06H	BES	$J/\psi \rightarrow \gamma\omega\phi$

$\Gamma(\gamma f_2(1910) \rightarrow \gamma\omega\phi)/\Gamma_{total}$					Γ_{250}/Γ
VALUE (units 10^{-3})	EVTS	DOCUMENT ID	TECN	COMMENT	
$0.20 \pm 0.04 \pm 0.13$	151	ABLIKIM	06H	BES	$J/\psi \rightarrow \gamma\omega\phi$

$\Gamma(\gamma f_0(1750) \rightarrow \gamma K_S^0 K_S^0)/\Gamma_{total}$					Γ_{251}/Γ
VALUE (units 10^{-5})	EVTS	DOCUMENT ID	TECN	COMMENT	
$1.11 \pm 0.06 \pm 0.19$ -0.32		ABLIKIM	18AA	BES3	$J/\psi \rightarrow \gamma K_S^0 K_S^0$

$\Gamma(\gamma f_0(1800) \rightarrow \gamma\omega\phi)/\Gamma_{total}$					Γ_{252}/Γ
VALUE (units 10^{-4})	EVTS	DOCUMENT ID	TECN	COMMENT	
2.5 ± 0.6 OUR AVERAGE					
$2.00 \pm 0.08 \pm 1.38$ -1.64	1.3k	ABLIKIM	13J	BES3	$J/\psi \rightarrow \gamma\omega\phi$
$2.61 \pm 0.27 \pm 0.65$	95	ABLIKIM	06J	BES2	$J/\psi \rightarrow \gamma\omega\phi$

$\Gamma(\gamma f_2(1810) \rightarrow \gamma\eta\eta)/\Gamma_{total}$					Γ_{253}/Γ
VALUE (units 10^{-5})	EVTS	DOCUMENT ID	TECN	COMMENT	
$5.40 \pm 0.60 \pm 3.42$ $-0.67 - 2.35$	5.5k	¹ ABLIKIM	13N	BES3	$J/\psi \rightarrow \gamma\eta\eta$

¹ From partial wave analysis including all possible combinations of 0^{++} , 2^{++} , and 4^{++} resonances.

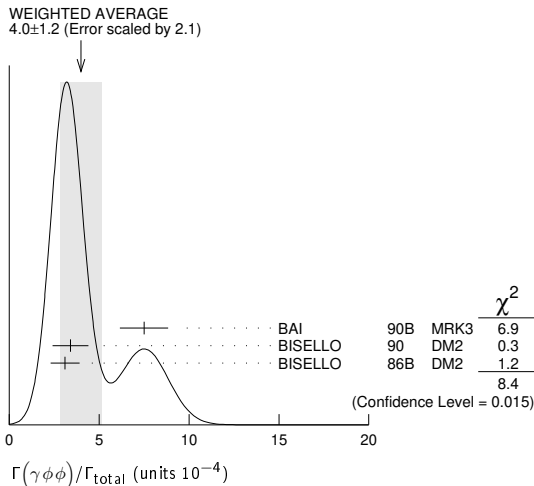
$\Gamma(\gamma f_2(1950) \rightarrow \gamma K^*(892) \bar{K}^*(892))/\Gamma_{total}$					Γ_{254}/Γ
VALUE (units 10^{-3})	EVTS	DOCUMENT ID	TECN	COMMENT	
$0.7 \pm 0.1 \pm 0.2$		BAI	00B	BES	$J/\psi \rightarrow \gamma K^+ K^0 \pi^+ \pi^-$

$\Gamma(\gamma K^*(892) \bar{K}^*(892))/\Gamma_{total}$					Γ_{255}/Γ
VALUE (units 10^{-3})	EVTS	DOCUMENT ID	TECN	COMMENT	
$4.0 \pm 0.3 \pm 1.3$	320	¹ BAI	00B	BES	$J/\psi \rightarrow \gamma K^+ K^0 \pi^+ \pi^-$

¹ Summed over all charges.

$\Gamma(\gamma\phi\phi)/\Gamma_{total}$					Γ_{256}/Γ
VALUE (units 10^{-4})	EVTS	DOCUMENT ID	TECN	COMMENT	
4.0 ± 1.2 OUR AVERAGE					Error includes scale factor of 2.1. See the ideogram below.
$7.5 \pm 0.6 \pm 1.2$	168	BAI	90B	MRK3	$J/\psi \rightarrow \gamma 4K$
$3.4 \pm 0.8 \pm 0.6$	33 ± 7	¹ BISELLO	90	DM2	$J/\psi \rightarrow \gamma K^+ K^- K_S^0 K_L^0$
$3.1 \pm 0.7 \pm 0.4$		¹ BISELLO	86B	DM2	$J/\psi \rightarrow \gamma K^+ K^- K^+ K^-$

¹ ϕ mass less than 2.9 GeV, η_C excluded.



$\Gamma(\gamma p\bar{p})/\Gamma_{total}$					Γ_{257}/Γ
VALUE (units 10^{-3})	CL%	EVTS	DOCUMENT ID	TECN	COMMENT
$0.38 \pm 0.07 \pm 0.07$		49	EATON	84	MRK2 e^+e^-
<0.11		90	PERUZZI	78	MRK1 e^+e^-

$\Gamma(\gamma\eta(2225))/\Gamma_{total}$					Γ_{258}/Γ
VALUE (units 10^{-4})	EVTS	DOCUMENT ID	TECN	COMMENT	
3.14 ± 0.50 OUR AVERAGE					
$2.40 \pm 0.10 \pm 2.47$ -0.18		^{1,2} ABLIKIM	16N	BES3	$J/\psi \rightarrow \gamma K^+ K^- K^+ K^-$
$4.4 \pm 0.4 \pm 0.8$	196	² ABLIKIM	08i	BES	$J/\psi \rightarrow \gamma K^+ K^- K_S^0 K_L^0$
$3.3 \pm 0.8 \pm 0.5$		² BAI	90b	MRK3	$J/\psi \rightarrow \gamma K^+ K^- K^+ K^-$

$2.7 \pm 0.6 \pm 0.6$		² BAI	90b	MRK3	$J/\psi \rightarrow \gamma K^+ K^- K_S^0 K_L^0$
2.4 ± 1.5 -1.0		^{3,4} BISELLO	89b	DM2	$J/\psi \rightarrow 4\pi\gamma$

¹ From a partial wave analysis of $J/\psi \rightarrow \gamma\phi\phi$ that also finds significant signals for $\eta(2100)$, 0^{-+} phase space, $f_0(2100)$, $f_2(2010)$, $f_2(2300)$, $f_2(2340)$, and a previously unseen 0^{-+} state $X(2500)$ ($M = 2470 \pm 15 \pm 101$ MeV, $\Gamma = 230 \pm 64 \pm 56$ MeV).

² Includes unknown branching fraction to $\phi\phi$.

³ Estimated by us from various fits.

⁴ Includes unknown branching fraction to $\rho^0\rho^0$.

$\Gamma(\gamma\eta(1760) \rightarrow \gamma\rho^0\rho^0)/\Gamma_{total}$					Γ_{259}/Γ
VALUE (units 10^{-3})	EVTS	DOCUMENT ID	TECN	COMMENT	
0.13 ± 0.09		^{1,2} BISELLO	89b	DM2	$J/\psi \rightarrow 4\pi\gamma$

¹ Estimated by us from various fits.

² Includes unknown branching fraction to $\rho^0\rho^0$.

$\Gamma(\gamma\eta(1760) \rightarrow \gamma\omega\omega)/\Gamma_{total}$					Γ_{260}/Γ
VALUE (units 10^{-3})	EVTS	DOCUMENT ID	TECN	COMMENT	
$1.98 \pm 0.08 \pm 0.32$	1045	ABLIKIM	06H	BES	$J/\psi \rightarrow \gamma\omega\omega$

$\Gamma(\gamma\eta(1760) \rightarrow \gamma\gamma\gamma)/\Gamma_{total}$					Γ_{261}/Γ
VALUE	CL%	DOCUMENT ID	TECN	COMMENT	
$<4.80 \times 10^{-6}$	90	ABLIKIM	18o	BES3	$\psi(2S) \rightarrow \pi^+ \pi^- \gamma\gamma\gamma$

$\Gamma(\gamma X(1835) \rightarrow \gamma\pi^+ \pi^- \eta')/\Gamma_{total}$					Γ_{262}/Γ
VALUE (units 10^{-4})	EVTS	DOCUMENT ID	TECN	COMMENT	
2.77 ± 0.34 -0.40 OUR AVERAGE					Error includes scale factor of 1.1.

$3.93 \pm 0.38 \pm 0.31$
 -0.84 ¹ABLIKIM 16j BES3 $J/\psi \rightarrow \gamma\pi^+ \pi^- \eta'$

$2.87 \pm 0.09 \pm 0.49$
 -0.52 ²ABLIKIM 11c BES3 $J/\psi \rightarrow \gamma\pi^+ \pi^- \eta'$

$2.2 \pm 0.4 \pm 0.4$ 264 ABLIKIM 05R BES2 $J/\psi \rightarrow \gamma\pi^+ \pi^- \eta'$

¹ From a fit of the measured $\pi^+ \pi^- \eta'$ lineshape that accounts for the abrupt distortion observed at the $p\bar{p}$ threshold with a Flatté formula in addition to known backgrounds and contributors, as well as an *ad hoc* Breit-Wigner ($M \approx 1919$ MeV; $\Gamma \approx 51$ MeV) that is required for a good fit. Another explanation for the distortion provided by ABLIKIM 16j is that a second resonance near 1870 MeV interferes with the $X(1835)$; fits to this possibility yield product branching fraction values compatible with that shown within the respective systematic uncertainties.

² From a fit of the $\pi^+ \pi^- \eta'$ mass distribution to a combination of $\gamma f_1(1510)$, $\gamma X(1835)$, and two unconfirmed states $\gamma X(2120)$, and $\gamma X(2370)$, for $M(p\bar{p}) < 2.8$ GeV, and accounting for backgrounds from non- η' events and $J/\psi \rightarrow \pi^0 \pi^+ \pi^- \eta'$.

$\Gamma(\gamma X(1835) \rightarrow \gamma p\bar{p})/\Gamma_{total}$					Γ_{263}/Γ
VALUE (units 10^{-4})	EVTS	DOCUMENT ID	TECN	COMMENT	
0.77 ± 0.15 -0.09 OUR AVERAGE					
$0.90 \pm 0.04 \pm 0.27$ $-0.11 - 0.55$		¹ ABLIKIM	12D	BES3	$J/\psi \rightarrow \gamma p\bar{p}$
$1.14 \pm 0.43 \pm 0.42$ $-0.30 - 0.26$	231	² ALEXANDER	10	CLEO	$J/\psi \rightarrow \gamma p\bar{p}$
$0.70 \pm 0.04 \pm 0.19$ -0.08		BAI	03F	BES2	$J/\psi \rightarrow \gamma p\bar{p}$

¹ From the fit including final state interaction effects in isospin 0 S-wave according to SIBIRTSSEV 05A.

² From a fit of the $p\bar{p}$ mass distribution to a combination of $\gamma X(1835)$, γR with $M(R) = 2100$ MeV and $\Gamma(R) = 160$ MeV, and $\gamma p\bar{p}$ phase space, for $M(p\bar{p}) < 2.85$ GeV.

$\Gamma(\gamma X(1835) \rightarrow \gamma K_S^0 K_S^0 \eta)/\Gamma_{total}$					Γ_{264}/Γ
VALUE (units 10^{-5})	EVTS	DOCUMENT ID	TECN	COMMENT	
$3.31 \pm 0.33 \pm 1.96$ $-0.30 - 1.29$		ABLIKIM	15T	BES3	$J/\psi \rightarrow \gamma K_S^0 K_S^0 \eta$

$\Gamma(\gamma X(1835) \rightarrow \gamma\gamma\phi(1020))/\Gamma_{total}$					Γ_{265}/Γ
VALUE (units 10^{-6})	EVTS	DOCUMENT ID	TECN	COMMENT	
$1.77 \pm 0.35 \pm 0.25$	305	¹ ABLIKIM	18i	BES3	$J/\psi \rightarrow \gamma\gamma\phi(1020)$
$8.09 \pm 1.99 \pm 1.36$	1.3k	² ABLIKIM	18i	BES3	$J/\psi \rightarrow \gamma\gamma\phi(1020)$

¹ Constructive interference between the $X(1835)$ and $\eta(1405)/\eta(1475)$ is assumed in a fit to the $\gamma\phi$ invariant mass.

² Destructive interference between the $X(1835)$ and $\eta(1405)/\eta(1475)$ is assumed in a fit to the $\gamma\phi$ invariant mass.

$\Gamma(\gamma X(1835) \rightarrow \gamma\gamma\gamma)/\Gamma_{total}$					Γ_{266}/Γ
VALUE	CL%	DOCUMENT ID	TECN	COMMENT	
$<3.56 \times 10^{-6}$	90	ABLIKIM	18o	BES3	$\psi(2S) \rightarrow \pi^+ \pi^- \gamma\gamma\gamma$

$\Gamma(\gamma X(1840) \rightarrow \gamma 3(\pi^+ \pi^-))/\Gamma_{total}$					Γ_{267}/Γ
VALUE (units 10^{-5})	EVTS	DOCUMENT ID	TECN	COMMENT	
$2.44 \pm 0.36 \pm 0.60$ -0.74	0.6k	ABLIKIM	13U	BES3	$J/\psi \rightarrow \gamma 3(\pi^+ \pi^-)$

Meson Particle Listings

 $J/\psi(1S)$ $\Gamma(\gamma(K\bar{K}\pi)[P^{PC}=0^{-+}])/ \Gamma_{\text{total}}$ Γ_{268}/Γ

VALUE (units 10^{-3})	DOCUMENT ID	TECN	COMMENT
0.7 ± 0.4 OUR AVERAGE	Error includes scale factor of 2.1.		
0.58 ± 0.03 ± 0.20	¹ BAI	00D	BES $J/\psi \rightarrow \gamma K^{\pm} K_S^0 \pi^{\mp}$
2.1 ± 0.1 ± 0.7	² BAI	00D	BES $J/\psi \rightarrow \gamma K^{\pm} K_S^0 \pi^{\mp}$

- ¹ For a broad structure around 1800 MeV.
² For a broad structure around 2040 MeV.

 $\Gamma(\gamma\pi^0)/ \Gamma_{\text{total}}$ Γ_{269}/Γ

VALUE (units 10^{-5})	EVTS	DOCUMENT ID	TECN	COMMENT
3.56 ± 0.17 OUR AVERAGE				
3.59 ± 0.20 ± 0.03	1.6k	¹ ABLIKIM	18o	BES3 $\psi(2S) \rightarrow \pi^+ \pi^- \gamma \gamma$
3.63 ± 0.36 ± 0.13		PEDLAR	09	CLE3 $J/\psi \rightarrow \pi^0 \gamma$
3.13 $^{+0.65}_{-0.47}$	586	ABLIKIM	06E	BES2 $J/\psi \rightarrow \pi^0 \gamma$

- • • We do not use the following data for averages, fits, limits, etc. • • •
 3.6 ± 1.1 ± 0.7 BLOOM 83 CBAL $e^+ e^-$
 7.3 ± 4.7 10 BRANDELIK 79c DASP $e^+ e^-$
¹ ABLIKIM 18o reports $[\Gamma(J/\psi(1S) \rightarrow \gamma\pi^0)/\Gamma_{\text{total}}] \times [B(\pi^0 \rightarrow 2\gamma)] = (3.57 \pm 0.12 \pm 0.16) \times 10^{-5}$ from a measurement of $[\Gamma(J/\psi(1S) \rightarrow \gamma\pi^0)/\Gamma_{\text{total}}] \times [B(\pi^0 \rightarrow 2\gamma)] \times [B(\psi(2S) \rightarrow J/\psi(1S)\pi^+\pi^-)]$ assuming $B(\psi(2S) \rightarrow J/\psi(1S)\pi^+\pi^-) = (34.49 \pm 0.30) \times 10^{-2}$, which we rescale to our best values $B(\pi^0 \rightarrow 2\gamma) = (98.823 \pm 0.034) \times 10^{-2}$, $B(\psi(2S) \rightarrow J/\psi(1S)\pi^+\pi^-) = (34.68 \pm 0.30) \times 10^{-2}$. Our first error is their experiment's error and our second error is the systematic error from using our best values.

 $\Gamma(\gamma\rho\bar{\rho}\pi^+\pi^-)/ \Gamma_{\text{total}}$ Γ_{270}/Γ

VALUE	CL%	DOCUMENT ID	TECN	COMMENT
< 0.79 × 10⁻³	90	EATON	84	MRK2 $e^+ e^-$

 $\Gamma(\gamma A\bar{A})/ \Gamma_{\text{total}}$ Γ_{271}/Γ

VALUE	CL%	DOCUMENT ID	TECN	COMMENT
< 0.13 × 10⁻³	90	HENRRARD	87	DM2 $e^+ e^-$
• • • We do not use the following data for averages, fits, limits, etc. • • •				
< 0.16 × 10 ⁻³	90	BAI	98G	BES $e^+ e^-$

 $\Gamma(\gamma f_0(2100) \rightarrow \gamma\eta\eta)/ \Gamma_{\text{total}}$ Γ_{272}/Γ

VALUE (units 10^{-4})	EVTS	DOCUMENT ID	TECN	COMMENT
1.13 $^{+0.09+0.64}_{-0.10-0.28}$	5.5k	¹ ABLIKIM	13N	BES3 $J/\psi \rightarrow \gamma\eta\eta$

- ¹ From partial wave analysis including all possible combinations of 0^{++} , 2^{++} , and 4^{++} resonances.

 $\Gamma(\gamma f_0(2100) \rightarrow \gamma\pi\pi)/ \Gamma_{\text{total}}$ Γ_{273}/Γ

VALUE (units 10^{-4})	EVTS	DOCUMENT ID	TECN	COMMENT
6.24 ± 0.48 ± 0.87	744	¹ DOBBS	15	$J/\psi \rightarrow \gamma\pi\pi$

- ¹ Using CLEO-c data but not authored by the CLEO Collaboration.

 $\Gamma(\gamma f_0(2200))/ \Gamma_{\text{total}}$ Γ_{274}/Γ

VALUE (units 10^{-4})	DOCUMENT ID	TECN	COMMENT
• • • We do not use the following data for averages, fits, limits, etc. • • •			
1.5	¹ AUGUSTIN	88	DM2 $J/\psi \rightarrow \gamma K_S^0 K_S^0$

- ¹ Includes unknown branching fraction to $K_S^0 K_S^0$.

 $\Gamma(\gamma f_0(2200) \rightarrow \gamma K\bar{K})/ \Gamma_{\text{total}}$ Γ_{275}/Γ

VALUE (units 10^{-4})	EVTS	DOCUMENT ID	TECN	COMMENT
5.86 ± 0.49 ± 1.20	490	¹ DOBBS	15	$J/\psi \rightarrow \gamma K\bar{K}$

- ¹ Using CLEO-c data but not authored by the CLEO Collaboration.

 $\Gamma(\gamma f_0(2200) \rightarrow \gamma K_S^0 K_S^0)/ \Gamma_{\text{total}}$ Γ_{276}/Γ

VALUE (units 10^{-4})	DOCUMENT ID	TECN	COMMENT
2.72 $^{+0.08+0.17}_{-0.06-0.47}$	ABLIKIM	18AA	BES3 $J/\psi \rightarrow \gamma K_S^0 K_S^0$

 $\Gamma(\gamma f_J(2220))/ \Gamma_{\text{total}}$ Γ_{277}/Γ

VALUE (units 10^{-5})	CL%	EVTS	DOCUMENT ID	TECN	COMMENT
• • • We do not use the following data for averages, fits, limits, etc. • • •					

>300		¹ BAI	96B	BES	$e^+ e^- \rightarrow \gamma \bar{p}p, K\bar{K}$
>250	99.9	² HASAN	96	SPEC	$\bar{p}p \rightarrow \pi^+ \pi^-$
< 2.3	95	³ AUGUSTIN	88	DM2	$J/\psi \rightarrow \gamma K^+ K^-$
< 1.6	95	³ AUGUSTIN	88	DM2	$J/\psi \rightarrow \gamma K_S^0 K_S^0$
12.4 $^{+6.4}_{-5.2}$ ± 2.8	23	³ BALTRUSAIT..86D	MRK3	$J/\psi \rightarrow \gamma K_S^0 K_S^0$	
8.4 $^{+3.4}_{-2.8}$ ± 1.6	93	³ BALTRUSAIT..86D	MRK3	$J/\psi \rightarrow \gamma K^+ K^-$	

- ¹ Using BARNES 93.
² Using BAI 96b.
³ Includes unknown branching fraction to $K^+ K^-$ or $K_S^0 K_S^0$.

 $\Gamma(\gamma f_J(2220) \rightarrow \gamma\pi\pi)/ \Gamma_{\text{total}}$ Γ_{278}/Γ

VALUE (units 10^{-5})	CL%	DOCUMENT ID	TECN	COMMENT
< 3.9	90	^{1,2} DOBBS	15	$J/\psi \rightarrow \gamma\pi\pi$
• • • We do not use the following data for averages, fits, limits, etc. • • •				
14 ± 8 ± 4		BAI	98H	BES $J/\psi \rightarrow \gamma\pi^0 \pi^0$
8.4 ± 2.6 ± 3.0		BAI	96B	BES $e^+ e^- \rightarrow J/\psi \rightarrow \gamma\pi^+ \pi^-$

- ¹ Using CLEO-c data but not authored by the CLEO Collaboration.
² For $\Gamma = 20/50$ MeV, the 90% CL upper limits for $\pi^+ \pi^-$ and $\pi^0 \pi^0$ are $2.6/5.2 \times 10^{-5}$ and $1.3/1.9 \times 10^{-5}$, respectively.

 $\Gamma(\gamma f_J(2220) \rightarrow \gamma K\bar{K})/ \Gamma_{\text{total}}$ Γ_{279}/Γ

VALUE (units 10^{-5})	CL%	DOCUMENT ID	TECN	COMMENT
< 4.1	90	^{1,2} DOBBS	15	$J/\psi \rightarrow \gamma K\bar{K}$
• • • We do not use the following data for averages, fits, limits, etc. • • •				
< 3.6		³ DEL-AMO-SA...10o	BABR	$e^+ e^- \rightarrow J/\psi \rightarrow \gamma K^+ K^-$
< 2.9		³ DEL-AMO-SA...10o	BABR	$e^+ e^- \rightarrow J/\psi \rightarrow \gamma K_S^0 K_S^0$
6.6 ± 2.9 ± 2.4		BAI	96B	BES $e^+ e^- \rightarrow J/\psi \rightarrow \gamma K^+ K^-$
10.8 ± 4.0 ± 3.2		BAI	96B	BES $e^+ e^- \rightarrow J/\psi \rightarrow \gamma K_S^0 K_S^0$

- ¹ Using CLEO-c data but not authored by the CLEO Collaboration.
² For $\Gamma = 20/50$ MeV, the 90% CL upper limits for $K^+ K^-$ and $K_S^0 K_S^0$ are $1.7/3.1 \times 10^{-5}$ and $1.2/2.0 \times 10^{-5}$, respectively.
³ For spin 2 and helicity 0; other combinations lead to more stringent upper limits.

 $\Gamma(\gamma f_J(2220) \rightarrow \gamma\rho\bar{\rho})/ \Gamma_{\text{total}}$ Γ_{280}/Γ

VALUE (units 10^{-5})	DOCUMENT ID	TECN	COMMENT
1.5 ± 0.6 ± 0.5	BAI	96B	BES $e^+ e^- \rightarrow J/\psi \rightarrow \gamma\rho\bar{\rho}$

 $\Gamma(\gamma f_0(2330) \rightarrow \gamma K_S^0 K_S^0)/ \Gamma_{\text{total}}$ Γ_{281}/Γ

VALUE (units 10^{-5})	DOCUMENT ID	TECN	COMMENT
4.95 ± 0.21 ± 0.66	ABLIKIM	18AA	BES3 $J/\psi \rightarrow \gamma K_S^0 K_S^0$

 $\Gamma(\gamma f_2(2340) \rightarrow \gamma\eta\eta)/ \Gamma_{\text{total}}$ Γ_{282}/Γ

VALUE (units 10^{-5})	EVTS	DOCUMENT ID	TECN	COMMENT
5.60 $^{+0.62+2.37}_{-0.65-2.07}$	5.5k	¹ ABLIKIM	13N	BES3 $J/\psi \rightarrow \gamma\eta\eta$

- ¹ From partial wave analysis including all possible combinations of 0^{++} , 2^{++} , and 4^{++} resonances.

 $\Gamma(\gamma f_2(2340) \rightarrow \gamma K_S^0 K_S^0)/ \Gamma_{\text{total}}$ Γ_{283}/Γ

VALUE (units 10^{-5})	DOCUMENT ID	TECN	COMMENT
5.54 $^{+0.34+3.82}_{-0.40-1.49}$	ABLIKIM	18AA	BES3 $J/\psi \rightarrow \gamma K_S^0 K_S^0$

 $\Gamma(\gamma f_0(1500) \rightarrow \gamma\pi\pi)/ \Gamma_{\text{total}}$ Γ_{284}/Γ

VALUE (units 10^{-4})	EVTS	DOCUMENT ID	TECN	COMMENT
1.09 ± 0.24 OUR AVERAGE				
1.21 ± 0.29 ± 0.24	174	¹ DOBBS	15	$J/\psi \rightarrow \gamma\pi\pi$
1.00 ± 0.03 ± 0.45		² ABLIKIM	06v	BES2 $e^+ e^- \rightarrow J/\psi \rightarrow \gamma\pi^+ \pi^-$
1.02 ± 0.09 ± 0.45		² ABLIKIM	06v	BES2 $e^+ e^- \rightarrow J/\psi \rightarrow \gamma\pi^0 \pi^0$
• • • We do not use the following data for averages, fits, limits, etc. • • •				
5.7 ± 0.8		^{3,4} BUGG	95	MRK3 $J/\psi \rightarrow \gamma\pi^+ \pi^- \pi^+ \pi^-$

- ¹ Using CLEO-c data but not authored by the CLEO Collaboration.
² Including unknown branching fraction to $\pi\pi$.
³ Including unknown branching ratio for $f_0(1500) \rightarrow \pi^+ \pi^- \pi^+ \pi^-$.
⁴ Assuming that $f_0(1500)$ decays only to two S-wave dipions.

 $\Gamma(\gamma f_0(1500) \rightarrow \gamma\eta\eta)/ \Gamma_{\text{total}}$ Γ_{285}/Γ

VALUE (units 10^{-5})	EVTS	DOCUMENT ID	TECN	COMMENT
1.65 $^{+0.26+0.51}_{-0.31-1.40}$	5.5k	¹ ABLIKIM	13N	BES3 $J/\psi \rightarrow \gamma\eta\eta$

- ¹ From partial wave analysis including all possible combinations of 0^{++} , 2^{++} , and 4^{++} resonances.

 $\Gamma(\gamma A \rightarrow \gamma \text{invisible})/ \Gamma_{\text{total}}$ (narrow state A with $m_A < 960$ MeV) Γ_{286}/Γ

VALUE	CL%	DOCUMENT ID	TECN	COMMENT
< 6.3 × 10⁻⁶	90	¹ INSLER	10	CLEO $e^+ e^- \rightarrow \pi^+ \pi^- J/\psi$

- ¹ The limit varies with mass m_A of a narrow state A and is 4.3×10^{-6} for $m_A = 0$ MeV, reaches its largest value of 6.3×10^{-6} at $m_A = 500$ MeV, and is 3.6×10^{-6} at $m_A = 960$ MeV.

 $\Gamma(\gamma A^0 \rightarrow \gamma\mu^+\mu^-)/ \Gamma_{\text{total}}$ (narrow state A⁰ with 0.2 GeV < m_{A^0} < 3 GeV) Γ_{287}/Γ

VALUE	CL%	DOCUMENT ID	TECN	COMMENT
< 0.5 × 10⁻⁵	90	¹ ABLIKIM	16E	BES3 $J/\psi \rightarrow \gamma\mu^+\mu^-$
• • • We do not use the following data for averages, fits, limits, etc. • • •				
< 2.1 × 10 ⁻⁵	90	² ABLIKIM	12	BES3 $J/\psi \rightarrow \gamma\mu^+\mu^-$

- ¹ For a narrow scalar or pseudoscalar, A^0 , with a mass in the range 0.212–3 GeV. The measured 90% CL limit as a function of m_{A^0} is in the range $(2.8\text{--}495.3) \times 10^{-8}$.
² For a narrow scalar or pseudoscalar, A^0 , with a mass in the range 0.21–3.00 GeV. The measured 90% CL limit as a function of m_{A^0} ranges from 4×10^{-7} to 2.1×10^{-5} .

DALITZ DECAYS

$\Gamma(\pi^0 e^+ e^-)/\Gamma_{\text{total}}$					Γ_{288}/Γ
VALUE (units 10^{-7})	EVTS	DOCUMENT ID	TECN	COMMENT	
$7.56 \pm 1.32 \pm 0.50$	39	ABLIKIM	14I	BES3	J/ψ → π ⁰ e ⁺ e ⁻

$\Gamma(\eta e^+ e^-)/\Gamma_{\text{total}}$					Γ_{289}/Γ
VALUE (units 10^{-5})	EVTS	DOCUMENT ID	TECN	COMMENT	
$1.43 \pm 0.04 \pm 0.06$	2.47k	1,2 ABLIKIM	19A	BES3	J/ψ → η e ⁺ e ⁻
• • • We do not use the following data for averages, fits, limits, etc. • • •					
$1.16 \pm 0.07 \pm 0.06$	320	1 ABLIKIM	14I	BES3	J/ψ → η e ⁺ e ⁻

¹ Using both η → γγ and η → π⁺ π⁻ π⁰ decays.
² Approximation of the transition form factor squared as an incoherent sum of the ρ-meson and one-pole non-resonant amplitudes gives the pole mass m(A) = 2.84 ± 0.11 ± 0.08 GeV. Supersedes ABLIKIM 14I.

$\Gamma(\eta'(958) e^+ e^-)/\Gamma_{\text{total}}$					Γ_{290}/Γ
VALUE (units 10^{-5})	EVTS	DOCUMENT ID	TECN	COMMENT	
$6.59 \pm 0.07 \pm 0.17$	8.9k	1 ABLIKIM	19H	BES3	J/ψ → η'(958) e ⁺ e ⁻
• • • We do not use the following data for averages, fits, limits, etc. • • •					
$5.81 \pm 0.16 \pm 0.31$	1.4k	1,2 ABLIKIM	14I	BES3	J/ψ → η'(958) e ⁺ e ⁻

¹ Using both η' → γπ⁺ π⁻ and η' → π⁺ π⁻ η decays.
² Superseded by ABLIKIM 19H.

$\Gamma(\eta U \rightarrow \eta e^+ e^-)/\Gamma_{\text{total}}$					Γ_{291}/Γ
VALUE	CL%	DOCUMENT ID	TECN	COMMENT	
$< 9.11 \times 10^{-7}$	90	1 ABLIKIM	19A	BES3	J/ψ → η e ⁺ e ⁻
¹ For a dark photon U with mass between 10 and 2400 MeV. Obtained 90% C.L. limits as a function of m _U range from 1.9 × 10 ⁻⁸ to 91.1 × 10 ⁻⁸ .					

$\Gamma(\eta'(958) U \rightarrow \eta'(958) e^+ e^-)/\Gamma_{\text{total}}$					Γ_{292}/Γ
VALUE	CL%	DOCUMENT ID	TECN	COMMENT	
$< 2.0 \times 10^{-7}$	90	1 ABLIKIM	19H	BES3	J/ψ → η'(958) e ⁺ e ⁻
¹ For a dark photon U with mass between 100 and 2100 MeV. Obtained 90% C.L. limits as a function of m _U range from 1.8 × 10 ⁻⁸ to 2.0 × 10 ⁻⁷ . The corresponding limits on the branching fraction J/ψ → η' U range from 5.7 × 10 ⁻⁸ to 7.4 × 10 ⁻⁷ .					

$\Gamma(\phi e^+ e^-)/\Gamma_{\text{total}}$					Γ_{293}/Γ
VALUE (units 10^{-7})	CL%	DOCUMENT ID	TECN	COMMENT	
< 1.2	90	1 ABLIKIM	19AB	BES3	J/ψ → φ e ⁺ e ⁻
¹ Using B(φ → K ⁺ K ⁻) = (48.9 ± 0.5)% and B(ψ(2S) → π ⁺ π ⁻ J/ψ) = (34.49 ± 0.30)%.					

WEAK DECAYS

$\Gamma(D^- e^+ \nu_e + \text{c.c.})/\Gamma_{\text{total}}$					Γ_{294}/Γ
VALUE	CL%	DOCUMENT ID	TECN	COMMENT	
$< 1.2 \times 10^{-5}$	90	ABLIKIM	06M	BES2	e ⁺ e ⁻ → J/ψ

$\Gamma(D^0 e^+ e^- + \text{c.c.})/\Gamma_{\text{total}}$					Γ_{295}/Γ
VALUE	CL%	DOCUMENT ID	TECN	COMMENT	
$< 8.5 \times 10^{-8}$	90	1 ABLIKIM	17AF	BES3	e ⁺ e ⁻ → J/ψ
• • • We do not use the following data for averages, fits, limits, etc. • • •					
$< 1.1 \times 10^{-5}$	90	ABLIKIM	06M	BES2	e ⁺ e ⁻ → J/ψ
¹ Using D ⁰ decays to K ⁻ π ⁺ , K ⁻ π ⁺ π ⁰ , and K ⁻ π ⁺ π ⁺ π ⁻ .					

$\Gamma(D_s^- e^+ \nu_e + \text{c.c.})/\Gamma_{\text{total}}$					Γ_{296}/Γ
VALUE	CL%	DOCUMENT ID	TECN	COMMENT	
$< 1.3 \times 10^{-6}$	90	ABLIKIM	14R	BES3	e ⁺ e ⁻ → J/ψ
• • • We do not use the following data for averages, fits, limits, etc. • • •					
$< 3.6 \times 10^{-5}$	90	1 ABLIKIM	06M	BES2	e ⁺ e ⁻ → J/ψ
¹ Using B(D _s ⁻ → φ π ⁻) = 4.4 ± 0.5 %.					

$\Gamma(D_s^- e^+ \nu_e + \text{c.c.})/\Gamma_{\text{total}}$					Γ_{297}/Γ
VALUE	CL%	DOCUMENT ID	TECN	COMMENT	
$< 1.8 \times 10^{-6}$	90	ABLIKIM	14R	BES3	e ⁺ e ⁻ → J/ψ

$\Gamma(D^- \pi^+ + \text{c.c.})/\Gamma_{\text{total}}$					Γ_{298}/Γ
VALUE	CL%	DOCUMENT ID	TECN	COMMENT	
$< 7.5 \times 10^{-5}$	90	ABLIKIM	08J	BES2	e ⁺ e ⁻ → J/ψ

$\Gamma(D^0 \bar{K}^0 + \text{c.c.})/\Gamma_{\text{total}}$					Γ_{299}/Γ
VALUE	CL%	DOCUMENT ID	TECN	COMMENT	
$< 1.7 \times 10^{-4}$	90	ABLIKIM	08J	BES2	e ⁺ e ⁻ → J/ψ

$\Gamma(D^0 \bar{K}^{*0} + \text{c.c.})/\Gamma_{\text{total}}$					Γ_{300}/Γ
VALUE	CL%	DOCUMENT ID	TECN	COMMENT	
$< 2.5 \times 10^{-6}$	90	ABLIKIM	14K	BES3	e ⁺ e ⁻ → J/ψ

$\Gamma(D_s^- \pi^+ + \text{c.c.})/\Gamma_{\text{total}}$				Γ_{301}/Γ	
VALUE	CL%	DOCUMENT ID	TECN	COMMENT	
$< 1.3 \times 10^{-4}$	90	ABLIKIM	08J	BES2	e ⁺ e ⁻ → J/ψ

$\Gamma(D_s^- \rho^+ + \text{c.c.})/\Gamma_{\text{total}}$				Γ_{302}/Γ	
VALUE	CL%	DOCUMENT ID	TECN	COMMENT	
$< 1.3 \times 10^{-5}$	90	ABLIKIM	14K	BES3	e ⁺ e ⁻ → J/ψ

CHARGE CONJUGATION (C), PARITY (P),
LEPTON FAMILY NUMBER (LF) VIOLATING MODES

$\Gamma(\gamma\gamma)/\Gamma_{\text{total}}$					Γ_{303}/Γ
VALUE	CL%	DOCUMENT ID	TECN	COMMENT	
$< 2.7 \times 10^{-7}$	90	ABLIKIM	14Q	BES3	ψ(2S) → π ⁺ π ⁻ J/ψ
• • • We do not use the following data for averages, fits, limits, etc. • • •					
$< 0.5 \times 10^{-5}$	90	ADAMS	08	CLEO	ψ(2S) → π ⁺ π ⁻ J/ψ
$< 1.6 \times 10^{-4}$	90	1 WICHT	08	BELL	B [±] → K [±] γγ
$< 2.2 \times 10^{-5}$	90	ABLIKIM	07J	BES2	ψ(2S) → J/ψ π ⁺ π ⁻
$< 50 \times 10^{-5}$	90	BARTEL	77	CNTR	e ⁺ e ⁻

¹ WICHT 08 reports [Γ(J/ψ(1S) → γγ)/Γ_{total}] × [B(B⁺ → J/ψ(1S) K⁺)] < 0.16 × 10⁻⁶ which we divide by our best value B(B⁺ → J/ψ(1S) K⁺) = 1.006 × 10⁻³.

$\Gamma(\gamma\phi)/\Gamma_{\text{total}}$					Γ_{304}/Γ
VALUE	CL%	DOCUMENT ID	TECN	COMMENT	
$< 1.4 \times 10^{-6}$	90	ABLIKIM	14Q	BES3	ψ(2S) → π ⁺ π ⁻ J/ψ

$\Gamma(e^\pm \mu^\mp)/\Gamma_{\text{total}}$					Γ_{305}/Γ
VALUE	CL%	DOCUMENT ID	TECN	COMMENT	
$< 1.6 \times 10^{-7}$	90	ABLIKIM	13L	BES3	e ⁺ e ⁻ → J/ψ
• • • We do not use the following data for averages, fits, limits, etc. • • •					
$< 1.1 \times 10^{-6}$	90	BAI	03D	BES	e ⁺ e ⁻ → J/ψ

$\Gamma(e^\pm \tau^\mp)/\Gamma_{\text{total}}$					Γ_{306}/Γ
VALUE	CL%	DOCUMENT ID	TECN	COMMENT	
$< 8.3 \times 10^{-6}$	90	ABLIKIM	04	BES	e ⁺ e ⁻ → J/ψ

$\Gamma(A_c^+ e^- + \text{c.c.})/\Gamma_{\text{total}}$					Γ_{308}/Γ
VALUE	CL%	DOCUMENT ID	TECN	COMMENT	
$< 6.9 \times 10^{-8}$	90	ABLIKIM	19AF	BES3	e ⁺ e ⁻ → J/ψ → p K ⁻ π ⁺ e ⁻ (+ c.c.)

$\Gamma(\mu^\pm \tau^\mp)/\Gamma_{\text{total}}$					Γ_{307}/Γ
VALUE	CL%	DOCUMENT ID	TECN	COMMENT	
$< 2.0 \times 10^{-6}$	90	ABLIKIM	04	BES	e ⁺ e ⁻ → J/ψ

OTHER DECAYS

$\Gamma(\text{invisible})/\Gamma(e^+ e^-)$					Γ_{309}/Γ_5
VALUE	CL%	DOCUMENT ID	TECN	COMMENT	
$< 6.6 \times 10^{-2}$	90	LEES	13I	BABR	B → K ^(*) J/ψ

$\Gamma(\text{invisible})/\Gamma(\mu^+ \mu^-)$					Γ_{309}/Γ_7
VALUE	CL%	DOCUMENT ID	TECN	COMMENT	
$< 1.2 \times 10^{-2}$	90	ABLIKIM	08G	BES2	ψ(2S) → π ⁺ π ⁻ J/ψ

J/ψ(1S) REFERENCES

ABLIKIM	20	PR D101 012004	M. Ablikim <i>et al.</i>	(BESIII Collab.)
ABLIKIM	19A	PR D99 012006	M. Ablikim <i>et al.</i>	(BESIII Collab.)
ABLIKIM	19AB	PR D99 052010	M. Ablikim <i>et al.</i>	(BESIII Collab.)
ABLIKIM	19AC	PR D99 071101	M. Ablikim <i>et al.</i>	(BESIII Collab.)
ABLIKIM	19AF	PR D99 072006	M. Ablikim <i>et al.</i>	(BESIII Collab.)
ABLIKIM	19AN	PR D99 112008	M. Ablikim <i>et al.</i>	(BESIII Collab.)
ABLIKIM	19AQ	PR D100 032004	M. Ablikim <i>et al.</i>	(BESIII Collab.)
ABLIKIM	19H	PR D99 012013	M. Ablikim <i>et al.</i>	(BESIII Collab.)
ABLIKIM	19N	PR D99 032006	M. Ablikim <i>et al.</i>	(BESIII Collab.)
ABLIKIM	19Q	PL B791 375	M. Ablikim <i>et al.</i>	(BESIII Collab.)
ABLIKIM	19T	PRL 122 142002	M. Ablikim <i>et al.</i>	(BESIII Collab.)
LU	19	PR D99 032003	P.-C. Lu <i>et al.</i>	(BELLE Collab.)
ABLIKIM	18AA	PR D98 072003	M. Ablikim <i>et al.</i>	(BESIII Collab.)
ABLIKIM	18AB	PR D98 072005	M. Ablikim <i>et al.</i>	(BESIII Collab.)
ABLIKIM	18D	PRL 121 022001	M. Ablikim <i>et al.</i>	(BESIII Collab.)
ABLIKIM	18I	PR D97 051101	M. Ablikim <i>et al.</i>	(BESIII Collab.)
ABLIKIM	18O	PR D97 072014	M. Ablikim <i>et al.</i>	(BESIII Collab.)
ANASHIN	18A	JHEP 1805 119	V.V. Anashin <i>et al.</i>	(KEDR Collab.)
LEES	18	PR D97 052007	J.P. Lees <i>et al.</i>	(BABAR Collab.)
LEES	18E	PR D98 112015	J.P. Lees <i>et al.</i>	(BABAR Collab.)
ABLIKIM	17AF	PR D96 111101	M. Ablikim <i>et al.</i>	(BESIII Collab.)
ABLIKIM	17AH	PR D96 112001	M. Ablikim <i>et al.</i>	(BESIII Collab.)
ABLIKIM	17AK	PR D96 112012	M. Ablikim <i>et al.</i>	(BESIII Collab.)
ABLIKIM	17E	PL B770 217	M. Ablikim <i>et al.</i>	(BESIII Collab.)
ABLIKIM	17L	PR D95 052003	M. Ablikim <i>et al.</i>	(BESIII Collab.)
LEES	17A	PR D95 052001	J.P. Lees <i>et al.</i>	(BABAR Collab.)
LEES	17C	PR D95 072007	J.P. Lees <i>et al.</i>	(BABAR Collab.)
LEES	17D	PR D95 092005	J.P. Lees <i>et al.</i>	(BABAR Collab.)
ABLIKIM	16E	PR D93 052005	M. Ablikim <i>et al.</i>	(BESIII Collab.)
ABLIKIM	16J	PRL 117 042002	M. Ablikim <i>et al.</i>	(BESIII Collab.)
ABLIKIM	16K	PR D93 052010	M. Ablikim <i>et al.</i>	(BESIII Collab.)
ABLIKIM	16L	PR D93 072003	M. Ablikim <i>et al.</i>	(BESIII Collab.)
ABLIKIM	16M	PR D93 072008	M. Ablikim <i>et al.</i>	(BESIII Collab.)
ABLIKIM	16N	PR D93 112011	M. Ablikim <i>et al.</i>	(BESIII Collab.)
ABLIKIM	16P	PR D94 072005	M. Ablikim <i>et al.</i>	(BESIII Collab.)
ABLIKIM	16Q	PL B761 98	M. Ablikim <i>et al.</i>	(BESIII Collab.)
PDG	16	CP C40 100001	C. Patrignani <i>et al.</i>	(PDG Collab.)

Meson Particle Listings

Branching Ratios of ψ 's and χ 's, $\chi_{c0}(1P)$

the required branching ratios. However, the values are frequently taken from the *Review of Particle Physics* (RPP), which in turn uses the branching ratio reported by the experiment in the following edition, giving rise either to correlations or to plain vicious circles, as discussed in more detail in earlier editions of this review [1,2].

The way to avoid these dependencies and correlations is to extract the branching ratios through a fit that uses the truly measured combinations of branching fractions and partial widths. This fit, in fact, should involve decays from the four concerned particles, $\psi(2S)$, χ_{c0} , χ_{c1} , and χ_{c2} , and occasionally some combinations of branching ratios of more than one of them. This is what is done since the 2002 edition [3].

The PDG policy is to quote the results of the collaborations in a manner as close as possible to what appears in their original publications. However, in order to avoid the problems mentioned above, we had in some cases to work out the values originally measured, using the number of events and detection efficiencies given by the collaborations, or rescaling back the published results. The information was sometimes spread over several articles, and some articles referred to papers still unpublished, which in turn contained the relevant numbers in footnotes.

Even though the experimental collaborations are entitled to extract whatever branching ratios they consider appropriate by using other published results, we would like to encourage them to also quote explicitly in their articles the actual quantities measured, so that they can be used directly in averages and fits of different experimental determinations.

To inform the reader how we computed some of the values used in this edition of RPP, we use footnotes to indicate the branching ratios actually given by the experiments and the quantities they use to derive them from the true combination of branching ratios actually measured.

None of the branching ratios of the $\chi_{c0,1,2}$ are measured independently of the $\psi(2S)$ radiative decays. We tried to identify those branching ratios which can be correlated in a non-trivial way, and although we cannot preclude the existence of other cases, we are confident that the most relevant correlations have already been removed. Nevertheless, correlations in the errors of different quantities measured by the same experiment have not been taken into account.

Fit information

This is an overall fit to 4 total widths, 1 partial width, 26 combinations of partial widths, 24 branching ratios, and 108 combinations of branching ratios. Of the latter 62 involve decays of more than one particle.

The overall fit uses 248 measurements to determine 49 parameters and has a χ^2 of 378.1 for 199 degrees of freedom.

The relatively high χ^2 of the fit, 1.9 per d.o.f., can be traced back to a few specific discrepancies in the data. No scaling factors to fit uncertainties have been applied.

In the listing we provide the inter-particle correlation coefficients $\langle \delta x_i \delta x_j \rangle / (\delta x_i \cdot \delta x_j)$, in percent, from the fit to the corresponding parameter x_i .

References

1. Y.F. Gu and X.H. Li, Phys. Lett. **B449**, 361 (1999).
2. C. Patrignani, Phys. Rev. **D64**, 034017 (2001).
3. Particle Data Group, K.Hagiwara *et al.*, Phys. Rev. **D68**, 010001 (2002).

$\chi_{c0}(1P)$

$$I^G(J^{PC}) = 0^+(0^{++})$$

$\chi_{c0}(1P)$ MASS

VALUE (MeV)	EVTs	DOCUMENT ID	TECN	COMMENT
3414.71 ± 0.30 OUR AVERAGE				
3413.0 ± 1.9 ± 0.6	933	1 AAIJ	17B8 LHCB	$\rho\rho \rightarrow b\bar{b}X \rightarrow 2(K+K^-)X$
3414.2 ± 0.5 ± 2.3	5.4k	UEHARA	08 BELL	$\gamma\gamma \rightarrow \chi_{c0} \rightarrow \text{hadrons}$
3406 ± 7 ± 6	230	2 ABE	07 BELL	$e^+e^- \rightarrow J/\psi(c\bar{c})$
3414.21 ± 0.39 ± 0.27		ABLIKIM	05G BES2	$\psi(2S) \rightarrow \gamma\chi_{c0}$
3414.7 ± 0.7 ± 0.6	± 0.2	3 ANDREOTTI	03 E835	$\bar{p}p \rightarrow \chi_{c0} \rightarrow \pi^0\pi^0$
3415.5 ± 0.4 ± 0.4	392	4 BAGNASCO	02 E835	$\bar{p}p \rightarrow \chi_{c0} \rightarrow J/\psi\gamma$
3417.4 ± 1.8 ± 1.9	± 0.2	3 AMBROGIANI	99B E835	$\bar{p}p \rightarrow e^+e^-\gamma$
3414.1 ± 0.6 ± 0.8		BAI	99B BES	$\psi(2S) \rightarrow \gamma X$
3417.8 ± 0.4 ± 4		3 GAISER	86 CBAL	$\psi(2S) \rightarrow \gamma X$
3416 ± 3 ± 4		5 TANENBAUM	78 MRK1	e^+e^-
••• We do not use the following data for averages, fits, limits, etc. •••				
3414.6 ± 1.1	266	UEHARA	13 BELL	$\gamma\gamma \rightarrow K_S^0 K_S^0$
3416.5 ± 3.0		EISENSTEIN	01 CLE2	$e^+e^- \rightarrow e^+e^-\chi_{c0}$
3422 ± 10		5 BARTEL	78B CNTR	$e^+e^- \rightarrow J/\psi 2\gamma$
3415 ± 9		5 BIDDICK	77 CNTR	$e^+e^- \rightarrow \gamma X$

¹ From a fit of the $\phi\phi$ invariant mass with the width of $\chi_{c0}(1P)$ fixed to the PDG 16 value.
² From a fit of the J/ψ recoil mass spectrum. Supersedes ABE,K 02 and ABE 04G.
³ Using mass of $\psi(2S) = 3686.0$ MeV.
⁴ Recalculated by ANDREOTTI 05A, using the value of $\psi(2S)$ mass from AULCHENKO 03.
⁵ Mass value shifted by us by amount appropriate for $\psi(2S)$ mass = 3686 MeV and $J/\psi(1S)$ mass = 3097 MeV.

$\chi_{c0}(1P)$ WIDTH

VALUE (MeV)	EVTs	DOCUMENT ID	TECN	COMMENT
10.8 ± 0.6 OUR FIT				
10.5 ± 0.8 OUR AVERAGE	Error includes scale factor of 1.1.			
10.6 ± 1.9 ± 2.6	5.4k	UEHARA	08 BELL	$\gamma\gamma \rightarrow \chi_{c0} \rightarrow \text{hadrons}$
12.6 ^{+1.5+0.9} _{-1.6-1.1}		ABLIKIM	05G BES2	$\psi(2S) \rightarrow \gamma\chi_{c0}$
8.6 ^{+1.7±0.1} _{-1.3}		ANDREOTTI	03 E835	$\bar{p}p \rightarrow \chi_{c0} \rightarrow \pi^0\pi^0$
9.7 ± 1.0	392	1 BAGNASCO	02 E835	$\bar{p}p \rightarrow \chi_{c0} \rightarrow J/\psi\gamma$
16.6 ^{+5.2±0.1} _{-3.7}		AMBROGIANI	99B E835	$\bar{p}p \rightarrow e^+e^-\gamma$
14.3 ± 2.0 ± 3.0		BAI	98I BES	$\psi(2S) \rightarrow \gamma\pi^+\pi^-$
13.5 ± 3.3 ± 4.2		GAISER	86 CBAL	$\psi(2S) \rightarrow \gamma X, \gamma\pi^0\pi^0$
••• We do not use the following data for averages, fits, limits, etc. •••				
13.2 ± 2.1	266	UEHARA	13 BELL	$\gamma\gamma \rightarrow K_S^0 K_S^0$

¹ Recalculated by ANDREOTTI 05A.

$\chi_{c0}(1P)$ DECAY MODES

Mode	Fraction (Γ_i/Γ)	Scale factor/ Confidence level
Hadronic decays		
Γ_1 $2(\pi^+\pi^-)$	(2.34 ± 0.18) %	
Γ_2 $\rho^0\pi^+\pi^-$	(9.1 ± 2.9) × 10 ⁻³	
Γ_3 $\rho^0\rho^0$		
Γ_4 $f_0(980)f_0(980)$	(6.6 ± 2.1) × 10 ⁻⁴	
Γ_5 $\pi^+\pi^-\pi^0\pi^0$	(3.3 ± 0.4) %	
Γ_6 $\rho^+\pi^-\pi^0 + \text{c.c.}$	(2.9 ± 0.4) %	
Γ_7 $4\pi^0$	(3.3 ± 0.4) × 10 ⁻³	
Γ_8 $\pi^+\pi^-K^+K^-$	(1.81 ± 0.14) %	
Γ_9 $K_0^*(1430)^0\bar{K}_0^*(1430)^0 \rightarrow \pi^+\pi^-K^+K^-$	(9.8 ^{+4.0} _{-2.8}) × 10 ⁻⁴	

Meson Particle Listings

$\chi_{c0}(1P)$

Γ_{10}	$K_0^*(1430)^0 \bar{K}_2^*(1430)^0 + c.c. \rightarrow \pi^+ \pi^- K^+ K^-$	$(8.0 \pm_{-2.4}^{+2.0}) \times 10^{-4}$	
Γ_{11}	$K_1(1270)^+ K^- + c.c. \rightarrow \pi^+ \pi^- K^+ K^-$	$(6.3 \pm 1.9) \times 10^{-3}$	
Γ_{12}	$K_1(1400)^+ K^- + c.c. \rightarrow \pi^+ \pi^- K^+ K^-$	$< 2.7 \times 10^{-3}$	CL=90%
Γ_{13}	$f_0(980) f_0(980)$	$(1.6 \pm_{-0.9}^{+1.0}) \times 10^{-4}$	
Γ_{14}	$f_0(980) f_0(2200)$	$(7.9 \pm_{-2.5}^{+2.0}) \times 10^{-4}$	
Γ_{15}	$f_0(1370) f_0(1370)$	$< 2.7 \times 10^{-4}$	CL=90%
Γ_{16}	$f_0(1370) f_0(1500)$	$< 1.7 \times 10^{-4}$	CL=90%
Γ_{17}	$f_0(1370) f_0(1710)$	$(6.7 \pm_{-2.3}^{+3.5}) \times 10^{-4}$	
Γ_{18}	$f_0(1500) f_0(1370)$	$< 1.3 \times 10^{-4}$	CL=90%
Γ_{19}	$f_0(1500) f_0(1500)$	$< 5 \times 10^{-5}$	CL=90%
Γ_{20}	$f_0(1500) f_0(1710)$	$< 7 \times 10^{-5}$	CL=90%
Γ_{21}	$K^+ K^- \pi^+ \pi^- \pi^0$	$(8.6 \pm 0.9) \times 10^{-3}$	
Γ_{22}	$K_S^0 K_S^0 \pi^+ \pi^-$	$(4.2 \pm 0.4) \times 10^{-3}$	
Γ_{23}	$K^+ K^- \pi^0 \pi^0$	$(5.6 \pm 0.9) \times 10^{-3}$	
Γ_{24}	$K^+ \pi^- \bar{K}^0 \pi^0 + c.c.$	$(2.49 \pm 0.33) \%$	
Γ_{25}	$\rho^+ K^- K^0 + c.c.$	$(1.21 \pm 0.21) \%$	
Γ_{26}	$K^*(892)^- K^+ \pi^0 \rightarrow K^+ \pi^- \bar{K}^0 \pi^0 + c.c.$	$(4.6 \pm 1.2) \times 10^{-3}$	
Γ_{27}	$K_S^0 K_S^0 \pi^+ \pi^-$	$(5.7 \pm 1.1) \times 10^{-3}$	
Γ_{28}	$K^+ K^- \eta \pi^0$	$(3.0 \pm 0.7) \times 10^{-3}$	
Γ_{29}	$3(\pi^+ \pi^-)$	$(1.20 \pm 0.18) \%$	
Γ_{30}	$K^+ \bar{K}^*(892)^0 \pi^- + c.c.$	$(7.5 \pm 1.6) \times 10^{-3}$	
Γ_{31}	$K^*(892)^0 \bar{K}^*(892)^0$	$(1.7 \pm 0.6) \times 10^{-3}$	
Γ_{32}	$\pi \pi$	$(8.51 \pm 0.33) \times 10^{-3}$	
Γ_{33}	$\pi^0 \eta$	$< 1.8 \times 10^{-4}$	
Γ_{34}	$\pi^0 \eta'$	$< 1.1 \times 10^{-3}$	
Γ_{35}	$\pi^0 \eta_c$	$< 1.6 \times 10^{-3}$	CL=90%
Γ_{36}	$\eta \eta$	$(3.01 \pm 0.19) \times 10^{-3}$	
Γ_{37}	$\eta \eta'$	$(9.1 \pm 1.1) \times 10^{-5}$	
Γ_{38}	$\eta' \eta'$	$(2.17 \pm 0.12) \times 10^{-3}$	
Γ_{39}	$\omega \omega$	$(9.7 \pm 1.1) \times 10^{-4}$	
Γ_{40}	$\omega \phi$	$(1.41 \pm 0.13) \times 10^{-4}$	
Γ_{41}	$\omega K^+ K^-$	$(1.94 \pm 0.21) \times 10^{-3}$	
Γ_{42}	$K^+ K^-$	$(6.05 \pm 0.31) \times 10^{-3}$	
Γ_{43}	$K_S^0 K_S^0$	$(3.16 \pm 0.17) \times 10^{-3}$	
Γ_{44}	$\pi^+ \pi^- \eta$	$< 2.0 \times 10^{-4}$	CL=90%
Γ_{45}	$\pi^+ \pi^- \eta'$	$< 4 \times 10^{-4}$	CL=90%
Γ_{46}	$\bar{K}^0 K^+ \pi^- + c.c.$	$< 9 \times 10^{-5}$	CL=90%
Γ_{47}	$K^+ K^- \pi^0$	$< 6 \times 10^{-5}$	CL=90%
Γ_{48}	$K^+ K^- \eta$	$< 2.3 \times 10^{-4}$	CL=90%
Γ_{49}	$K^+ K^- K_S^0 K_S^0$	$(1.4 \pm 0.5) \times 10^{-3}$	
Γ_{50}	$K_S^0 K_S^0 K_S^0 K_S^0$	$(5.8 \pm 0.5) \times 10^{-4}$	
Γ_{51}	$K^+ K^- K^+ K^-$	$(2.82 \pm 0.29) \times 10^{-3}$	
Γ_{52}	$K^+ K^- \phi$	$(9.7 \pm 2.5) \times 10^{-4}$	
Γ_{53}	$\bar{K}^0 K^+ \pi^- \phi + c.c.$	$(3.7 \pm 0.6) \times 10^{-3}$	
Γ_{54}	$K^+ K^- \pi^0 \phi$	$(1.90 \pm 0.35) \times 10^{-3}$	
Γ_{55}	$\phi \pi^+ \pi^- \pi^0$	$(1.18 \pm 0.15) \times 10^{-3}$	
Γ_{56}	$\phi \phi$	$(8.0 \pm 0.7) \times 10^{-4}$	
Γ_{57}	$\phi \phi \eta$	$(8.4 \pm 1.0) \times 10^{-4}$	
Γ_{58}	$\rho \bar{\rho}$	$(2.21 \pm 0.08) \times 10^{-4}$	
Γ_{59}	$\rho \bar{\rho} \pi^0$	$(7.0 \pm 0.7) \times 10^{-4}$	S=1.3
Γ_{60}	$\rho \bar{\rho} \eta$	$(3.5 \pm 0.4) \times 10^{-4}$	
Γ_{61}	$\rho \bar{\rho} \omega$	$(5.2 \pm 0.6) \times 10^{-4}$	
Γ_{62}	$\rho \bar{\rho} \phi$	$(6.0 \pm 1.4) \times 10^{-5}$	
Γ_{63}	$\rho \bar{\rho} \pi^+ \pi^-$	$(2.1 \pm 0.7) \times 10^{-3}$	S=1.4
Γ_{64}	$\rho \bar{\rho} \pi^0 \pi^0$	$(1.04 \pm 0.28) \times 10^{-3}$	
Γ_{65}	$\rho \bar{\rho} K^+ K^-$ (non-resonant)	$(1.22 \pm 0.26) \times 10^{-4}$	
Γ_{66}	$\rho \bar{\rho} K_S^0 K_S^0$	$< 8.8 \times 10^{-4}$	CL=90%
Γ_{67}	$\rho \bar{\rho} \pi^-$	$(1.27 \pm 0.11) \times 10^{-3}$	
Γ_{68}	$\rho \bar{\rho} \pi^+$	$(1.37 \pm 0.12) \times 10^{-3}$	
Γ_{69}	$\rho \bar{\rho} \pi^- \pi^0$	$(2.34 \pm 0.21) \times 10^{-3}$	
Γ_{70}	$\rho \bar{\rho} \pi^+ \pi^0$	$(2.21 \pm 0.18) \times 10^{-3}$	
Γ_{71}	$\Lambda \bar{\Lambda}$	$(3.27 \pm 0.24) \times 10^{-4}$	
Γ_{72}	$\Lambda \bar{\Lambda} \pi^+ \pi^-$	$(1.18 \pm 0.13) \times 10^{-3}$	
Γ_{73}	$\Lambda \bar{\Lambda} \pi^+ \pi^-$ (non-resonant)	$< 5 \times 10^{-4}$	CL=90%
Γ_{74}	$\Sigma(1385)^- \bar{\Lambda} \pi^- + c.c.$	$< 5 \times 10^{-4}$	CL=90%
Γ_{75}	$\Sigma(1385)^- \bar{\Lambda} \pi^+ + c.c.$	$< 5 \times 10^{-4}$	CL=90%
Γ_{76}	$K^+ \bar{p} \Lambda + c.c.$	$(1.25 \pm 0.12) \times 10^{-3}$	S=1.3
Γ_{77}	$K^*(892)^+ \bar{p} \Lambda + c.c.$	$(4.8 \pm 0.9) \times 10^{-4}$	
Γ_{78}	$K^+ \bar{p} \Lambda(1520) + c.c.$	$(2.9 \pm 0.7) \times 10^{-4}$	
Γ_{79}	$\Lambda(1520) \bar{\Lambda}(1520)$	$(3.1 \pm 1.2) \times 10^{-4}$	

Γ_{80}	$\Sigma^0 \bar{\Sigma}^0$	$(4.68 \pm 0.32) \times 10^{-4}$	
Γ_{81}	$\Sigma^+ \bar{p} K_S^0 + c.c.$	$(3.52 \pm 0.27) \times 10^{-4}$	
Γ_{82}	$\Sigma^+ \bar{\Sigma}^-$	$(4.6 \pm 0.8) \times 10^{-4}$	S=2.6
Γ_{83}	$\Sigma(1385)^+ \bar{\Sigma}(1385)^-$	$(1.6 \pm 0.6) \times 10^{-4}$	
Γ_{84}	$\Sigma(1385)^- \bar{\Sigma}(1385)^+$	$(2.3 \pm 0.7) \times 10^{-4}$	
Γ_{85}	$K^- \bar{\Lambda} \Xi^+ + c.c.$	$(1.94 \pm 0.35) \times 10^{-4}$	
Γ_{86}	$\Xi^0 \Xi^0$	$(3.1 \pm 0.8) \times 10^{-4}$	
Γ_{87}	$\Xi^- \Xi^+$	$(4.8 \pm 0.7) \times 10^{-4}$	
Γ_{88}	$\eta_c \pi^+ \pi^-$	$< 7 \times 10^{-4}$	CL=90%

Radiative decays

Γ_{89}	$\gamma J/\psi(1S)$	$(1.40 \pm 0.05) \%$	
Γ_{90}	$\gamma \rho^0$	$< 9 \times 10^{-6}$	CL=90%
Γ_{91}	$\gamma \omega$	$< 8 \times 10^{-6}$	CL=90%
Γ_{92}	$\gamma \phi$	$< 6 \times 10^{-6}$	CL=90%
Γ_{93}	$\gamma \gamma$	$(2.04 \pm 0.09) \times 10^{-4}$	
Γ_{94}	$e^+ e^- J/\psi(1S)$	$(1.33 \pm 0.29) \times 10^{-4}$	
Γ_{95}	$\mu^+ \mu^- J/\psi(1S)$	$< 1.9 \times 10^{-5}$	CL=90%

CONSTRAINED FIT INFORMATION

A multiparticle fit to $\chi_{c1}(1P)$, $\chi_{c0}(1P)$, $\chi_{c2}(1P)$, and $\psi(2S)$ with 4 total widths, a partial width, 25 combinations of partial widths obtained from integrated cross section, and 84 branching ratios uses 248 measurements to determine 49 parameters. The overall fit has a $\chi^2 = 378.1$ for 199 degrees of freedom.

The following *off-diagonal* array elements are the correlation coefficients $\langle \delta p_i \delta p_j \rangle / (\delta p_i \delta p_j)$, in percent, from the fit to parameters p_i , including the branching fractions, $x_i \equiv \Gamma_i / \Gamma_{\text{total}}$.

x_2	24									
x_8	9	2								
x_{30}	5	1	28							
x_{32}	8	2	10	3						
x_{36}	4	1	5	1	14					
x_{42}	8	2	8	3	18	11				
x_{43}	7	2	8	2	18	10	14			
x_{51}	5	1	5	2	9	5	7	7		
x_{56}	7	2	6	2	9	5	7	7	4	
x_{58}	3	1	4	1	3	-1	7	7	3	3
x_{71}	4	1	5	1	13	8	10	10	5	5
x_{89}	5	1	6	2	17	11	13	12	6	6
x_{93}	-8	-2	-2	-3	14	9	10	10	3	1
Γ	-26	-6	-19	-10	-15	-7	-14	-12	-10	-13
	x_1	x_2	x_8	x_{30}	x_{32}	x_{36}	x_{42}	x_{43}	x_{51}	x_{56}
x_{71}	5									
x_{89}	-19	9								
x_{93}	6	9	13							
Γ	-4	-7	-9	-38						
	x_{58}	x_{71}	x_{89}	x_{93}						

$\chi_{c0}(1P)$ PARTIAL WIDTHS

$$\chi_{c0}(1P) \Gamma(i) \Gamma(\gamma J/\psi(1S)) / \Gamma(\text{total})$$

$\Gamma(\rho \bar{\rho}) \times \Gamma(\gamma J/\psi(1S)) / \Gamma_{\text{total}}$	VALUE (eV)	EVTS	DOCUMENT ID	TECN	COMMENT
33.6 ± 2.3 OUR FIT					
• • • We do not use the following data for averages, fits, limits, etc. • • •					
26.6 ± 2.6 ± 1.4	392	1,2	BAGNASCO 02	E835	$\bar{p} p \rightarrow \chi_{c0} \rightarrow J/\psi \gamma$
48.7 ± 11.3 ± 2.4		1,2	AMBROGIANI 99B	E835	$\bar{p} p \rightarrow \gamma J/\psi$

¹ Calculated by us using $B(J/\psi(1S) \rightarrow e^+ e^-) = 0.0593 \pm 0.0010$.
² Values in $(\Gamma(\rho \bar{\rho}) \times \Gamma(\gamma J/\psi(1S)) / \Gamma_{\text{total}})$ and $(\Gamma(\rho \bar{\rho}) / \Gamma_{\text{total}} \times \Gamma(\gamma J/\psi(1S)) / \Gamma_{\text{total}})$ are not independent. The latter is used in the fit since it is less correlated to the total width.

$\chi_{c0}(1P) \Gamma(i) \Gamma(\gamma \gamma) / \Gamma(\text{total})$

$\Gamma(2(\pi^+ \pi^-)) \times \Gamma(\gamma \gamma) / \Gamma_{\text{total}}$	VALUE (eV)	EVTS	DOCUMENT ID	TECN	COMMENT
52 ± 4 OUR FIT					
49 ± 10 OUR AVERAGE					Error includes scale factor of 1.8.
44.7 ± 3.6 ± 4.9	3.6k		UEHARA 08	BELL	$\gamma \gamma \rightarrow \chi_{c0} \rightarrow 2(\pi^+ \pi^-)$
75 ± 13 ± 8			EISENSTEIN 01	CLE2	$e^+ e^- \rightarrow e^+ e^- \chi_{c0}$

$\Gamma(\rho^0 \rho^0) \times \Gamma(\gamma\gamma)/\Gamma_{total}$					$\Gamma_3 \Gamma_{93}/\Gamma$
VALUE (eV)	CL%	EVTS	DOCUMENT ID	TECN	COMMENT

• • • We do not use the following data for averages, fits, limits, etc. • • •
 <12 90 <252 UEHARA 08 BELL $\gamma\gamma \rightarrow \chi_{c0} \rightarrow 2(\pi^+ \pi^-)$

$\Gamma(\pi^+ \pi^- K^+ K^-) \times \Gamma(\gamma\gamma)/\Gamma_{total}$					$\Gamma_8 \Gamma_{93}/\Gamma$
VALUE (eV)	CL%	EVTS	DOCUMENT ID	TECN	COMMENT

40.0 ± 3.5 OUR FIT
38.8 ± 3.7 ± 4.7 1.7k UEHARA 08 BELL $\gamma\gamma \rightarrow \chi_{c0} \rightarrow K^+ K^- \pi^+ \pi^-$

$\Gamma(K^+ K^- \pi^+ \pi^- \pi^0) \times \Gamma(\gamma\gamma)/\Gamma_{total}$					$\Gamma_{21} \Gamma_{93}/\Gamma$
VALUE (eV)	CL%	EVTS	DOCUMENT ID	TECN	COMMENT

26 ± 4 ± 4 1094 DEL-AMO-SA...11M BABR $\gamma\gamma \rightarrow K^+ K^- \pi^+ \pi^- \pi^0$

$\Gamma(K^+ \bar{K}^*(892)^0 \pi^- + c.c.) \times \Gamma(\gamma\gamma)/\Gamma_{total}$					$\Gamma_{30} \Gamma_{93}/\Gamma$
VALUE (eV)	CL%	EVTS	DOCUMENT ID	TECN	COMMENT

16 ± 4 OUR FIT
16.7 ± 6.1 ± 3.0 495 ± 182 UEHARA 08 BELL $\gamma\gamma \rightarrow \chi_{c0} \rightarrow K^+ K^- \pi^+ \pi^-$

$\Gamma(K^*(892)^0 \bar{K}^*(892)^0) \times \Gamma(\gamma\gamma)/\Gamma_{total}$					$\Gamma_{31} \Gamma_{93}/\Gamma$
VALUE (eV)	CL%	EVTS	DOCUMENT ID	TECN	COMMENT

• • • We do not use the following data for averages, fits, limits, etc. • • •
 <6 90 <148 UEHARA 08 BELL $\gamma\gamma \rightarrow \chi_{c0} \rightarrow K^+ K^- \pi^+ \pi^-$

$\Gamma(\pi\pi) \times \Gamma(\gamma\gamma)/\Gamma_{total}$					$\Gamma_{32} \Gamma_{93}/\Gamma$
VALUE (eV)	CL%	EVTS	DOCUMENT ID	TECN	COMMENT

18.8 ± 1.3 OUR FIT
23 ± 5 OUR AVERAGE
 29.7^{+17.4}_{-12.0} ± 4.8 103⁺⁶⁰₋₄₂ 1 UEHARA 09 BELL 10.6 e⁺e⁻ → e⁺e⁻π⁰π⁰
 22.7 ± 3.2 ± 3.5 129 ± 18 2 NAKAZAWA 05 BELL 10.6 e⁺e⁻ → e⁺e⁻π⁺π⁻

¹ We multiplied the measurement by 3 to convert from π⁰π⁰ to ππ. Interference with the continuum included.
² We have multiplied π⁺π⁻ measurement by 3/2 to obtain ππ.

$\Gamma(\eta\eta) \times \Gamma(\gamma\gamma)/\Gamma_{total}$					$\Gamma_{36} \Gamma_{93}/\Gamma$
VALUE (eV)	CL%	EVTS	DOCUMENT ID	TECN	COMMENT

9.4 ± 2.3 ± 1.2 22 1 UEHARA 10A BELL 10.6 e⁺e⁻ → e⁺e⁻ηη
¹ Interference with the continuum not included.

$\Gamma(\omega\omega) \times \Gamma(\gamma\gamma)/\Gamma_{total}$					$\Gamma_{39} \Gamma_{93}/\Gamma$
VALUE (eV)	CL%	EVTS	DOCUMENT ID	TECN	COMMENT

• • • We do not use the following data for averages, fits, limits, etc. • • •
 <3.9 90 1 LIU 12B BELL $\gamma\gamma \rightarrow 2(\pi^+ \pi^- \pi^0)$
¹ Using B(ω → π⁺π⁻π⁰) = (89.2 ± 0.7)%.

$\Gamma(\omega\phi) \times \Gamma(\gamma\gamma)/\Gamma_{total}$					$\Gamma_{40} \Gamma_{93}/\Gamma$
VALUE (eV)	CL%	EVTS	DOCUMENT ID	TECN	COMMENT

• • • We do not use the following data for averages, fits, limits, etc. • • •
 <0.34 90 1 LIU 12B BELL $\gamma\gamma \rightarrow K^+ K^- \pi^+ \pi^- \pi^0$
¹ Using B(φ → K⁺K⁻) = (48.9 ± 0.5)% and B(ω → π⁺π⁻π⁰) = (89.2 ± 0.7)%.

$\Gamma(K^+ K^-) \times \Gamma(\gamma\gamma)/\Gamma_{total}$					$\Gamma_{42} \Gamma_{93}/\Gamma$
VALUE (eV)	CL%	EVTS	DOCUMENT ID	TECN	COMMENT

13.4 ± 1.0 OUR FIT
14.3 ± 1.6 ± 2.3 153 ± 17 NAKAZAWA 05 BELL 10.6 e⁺e⁻ → e⁺e⁻K⁺K⁻

$\Gamma(K_S^0 K_S^0) \times \Gamma(\gamma\gamma)/\Gamma_{total}$					$\Gamma_{43} \Gamma_{93}/\Gamma$
VALUE (eV)	CL%	EVTS	DOCUMENT ID	TECN	COMMENT

7.0 ± 0.5 OUR FIT
8.7 ± 1.7 ± 0.9 266 1 UEHARA 13 BELL $\gamma\gamma \rightarrow K_S^0 K_S^0$
 • • • We do not use the following data for averages, fits, limits, etc. • • •
 7.00 ± 0.65 ± 0.71 134 ± 12 CHEN 07B BELL e⁺e⁻ → e⁺e⁻χ_{c0}
¹ Supersedes CHEN 07B.

$\Gamma(K^+ K^- K^+ K^-) \times \Gamma(\gamma\gamma)/\Gamma_{total}$					$\Gamma_{51} \Gamma_{93}/\Gamma$
VALUE (eV)	CL%	EVTS	DOCUMENT ID	TECN	COMMENT

6.2 ± 0.7 OUR FIT
7.9 ± 1.3 ± 1.1 215 ± 36 UEHARA 08 BELL $\gamma\gamma \rightarrow \chi_{c0} \rightarrow 2(K^+ K^-)$

$\Gamma(\phi\phi) \times \Gamma(\gamma\gamma)/\Gamma_{total}$					$\Gamma_{56} \Gamma_{93}/\Gamma$
VALUE (eV)	CL%	EVTS	DOCUMENT ID	TECN	COMMENT

1.76 ± 0.18 OUR FIT
1.72 ± 0.33 ± 0.14 56 ± 11 1 LIU 12B BELL $\gamma\gamma \rightarrow 2(K^+ K^-)$
 • • • We do not use the following data for averages, fits, limits, etc. • • •
 2.3 ± 0.9 ± 0.4 23.6 ± 9.6 UEHARA 08 BELL $\gamma\gamma \rightarrow \chi_{c0} \rightarrow 2(K^+ K^-)$
¹ Supersedes UEHARA 08. Using B(φ → K⁺K⁻) = (48.9 ± 0.5)%.

$\chi_{c0}(1P)$ BRANCHING RATIOS

HADRONIC DECAYS

$\Gamma(2(\pi^+ \pi^-))/\Gamma_{total}$				Γ_1/Γ
VALUE	CL%	EVTS	DOCUMENT ID	COMMENT

0.0234 ± 0.0018 OUR FIT

$\Gamma(\rho^0 \pi^+ \pi^-)/\Gamma(2(\pi^+ \pi^-))$				Γ_2/Γ_1
VALUE	CL%	EVTS	DOCUMENT ID	COMMENT

0.39 ± 0.12 OUR FIT
0.39 ± 0.12 TANENBAUM 78 MRK1 $\psi(2S) \rightarrow \gamma\chi_{c0}$

$\Gamma(\rho^0 \pi^+ \pi^-)/\Gamma_{total}$				Γ_2/Γ
VALUE	CL%	EVTS	DOCUMENT ID	COMMENT

0.0091 ± 0.0029 OUR FIT

$\Gamma(f_0(980) f_0(980))/\Gamma_{total}$				Γ_4/Γ	
VALUE (units 10 ⁻⁴)	CL%	EVTS	DOCUMENT ID	TECN	COMMENT

6.6 ± 2.1 ± 0.1 36 ± 9 1 ABLIKIM 04G BES $\psi(2S) \rightarrow \gamma\pi^+ \pi^-$
¹ ABLIKIM 04G reports $[\Gamma(\chi_{c0}(1P) \rightarrow f_0(980) f_0(980))/\Gamma_{total}] \times [B(\psi(2S) \rightarrow \gamma\chi_{c0}(1P))]$ = (6.5 ± 1.6 ± 1.3) × 10⁻⁵ which we divide by our best value B(ψ(2S) → γχ_{c0}(1P)) = (9.79 ± 0.20) × 10⁻². Our first error is their experiment's error and our second error is the systematic error from using our best value.

$\Gamma(\pi^+ \pi^- \pi^0 \pi^0)/\Gamma_{total}$				Γ_5/Γ	
VALUE (%)	CL%	EVTS	DOCUMENT ID	TECN	COMMENT

3.3 ± 0.4 ± 0.1 1751.4 1 HE 08B CLEO e⁺e⁻ → γh⁺h⁻h⁰h⁰
¹ HE 08B reports 3.54 ± 0.10 ± 0.43 ± 0.18 % from a measurement of $[\Gamma(\chi_{c0}(1P) \rightarrow \pi^+ \pi^- \pi^0 \pi^0)/\Gamma_{total}] \times [B(\psi(2S) \rightarrow \gamma\chi_{c0}(1P))]$ assuming B(ψ(2S) → γχ_{c0}(1P)) = (9.22 ± 0.11 ± 0.46) × 10⁻², which we rescale to our best value B(ψ(2S) → γχ_{c0}(1P)) = (9.79 ± 0.20) × 10⁻². Our first error is their experiment's error and our second error is the systematic error from using our best value.
² Calculated by us. We have added the values from HE 08B for ρ⁺π⁻π⁰ and ρ⁻π⁺π⁰ decays assuming uncorrelated statistical and fully correlated systematic uncertainties.

$\Gamma(4\pi^0)/\Gamma_{total}$				Γ_7/Γ	
VALUE (units 10 ⁻³)	CL%	EVTS	DOCUMENT ID	TECN	COMMENT

3.3 ± 0.4 ± 0.1 3296 1 ABLIKIM 11A BES3 e⁺e⁻ → ψ(2S) → γχ_{c0}
¹ ABLIKIM 11A reports (3.34 ± 0.06 ± 0.44) × 10⁻³ from a measurement of $[\Gamma(\chi_{c0}(1P) \rightarrow 4\pi^0)/\Gamma_{total}] \times [B(\psi(2S) \rightarrow \gamma\chi_{c0}(1P))]$ assuming B(ψ(2S) → γχ_{c0}(1P)) = (9.62 ± 0.31) × 10⁻², which we rescale to our best value B(ψ(2S) → γχ_{c0}(1P)) = (9.79 ± 0.20) × 10⁻². Our first error is their experiment's error and our second error is the systematic error from using our best value.

$\Gamma(\pi^+ \pi^- K^+ K^-)/\Gamma_{total}$				Γ_8/Γ
VALUE (units 10 ⁻³)	CL%	EVTS	DOCUMENT ID	COMMENT

18.1 ± 1.4 OUR FIT

$\Gamma(K^+ \bar{K}^*(892)^0 \pi^- + c.c.)/\Gamma(\pi^+ \pi^- K^+ K^-)$				Γ_{30}/Γ_8	
VALUE	CL%	EVTS	DOCUMENT ID	TECN	COMMENT

0.41 ± 0.09 OUR FIT
0.41 ± 0.10 TANENBAUM 78 MRK1 $\psi(2S) \rightarrow \gamma\chi_{c0}$

$\Gamma(K_S^0(1430)^0 \bar{K}_S^0(1430)^0 \rightarrow \pi^+ \pi^- K^+ K^-)/\Gamma_{total}$				Γ_9/Γ	
VALUE (units 10 ⁻⁴)	CL%	EVTS	DOCUMENT ID	TECN	COMMENT

9.8 ± 3.6 ± 0.2 83 1 ABLIKIM 05q BES2 $\psi(2S) \rightarrow \gamma\pi^+ \pi^- K^+ K^-$
¹ ABLIKIM 05q reports (10.44 ± 2.37^{+3.05}_{-1.90}) × 10⁻⁴ from a measurement of $[\Gamma(\chi_{c0}(1P) \rightarrow K_S^0(1430)^0 \bar{K}_S^0(1430)^0)/\Gamma_{total}] \times [B(\psi(2S) \rightarrow \gamma\chi_{c0}(1P))]$ assuming B(ψ(2S) → γχ_{c0}(1P)) = (9.22 ± 0.11 ± 0.46) × 10⁻², which we rescale to our best value B(ψ(2S) → γχ_{c0}(1P)) = (9.79 ± 0.20) × 10⁻². Our first error is their experiment's error and our second error is the systematic error from using our best value.

$\Gamma(K_S^0(1430)^0 \bar{K}_S^0(1430)^0 + c.c. \rightarrow \pi^+ \pi^- K^+ K^-)/\Gamma_{total}$				Γ_{10}/Γ	
VALUE (units 10 ⁻⁴)	CL%	EVTS	DOCUMENT ID	TECN	COMMENT

8.0 ± 2.0 ± 0.2 62 1 ABLIKIM 05q BES2 $\psi(2S) \rightarrow \gamma\pi^+ \pi^- K^+ K^-$
¹ ABLIKIM 05q reports (8.49 ± 1.66^{+1.32}_{-1.99}) × 10⁻⁴ from a measurement of $[\Gamma(\chi_{c0}(1P) \rightarrow K_S^0(1430)^0 \bar{K}_S^0(1430)^0 + c.c. \rightarrow \pi^+ \pi^- K^+ K^-)/\Gamma_{total}] \times [B(\psi(2S) \rightarrow \gamma\chi_{c0}(1P))]$ assuming B(ψ(2S) → γχ_{c0}(1P)) = (9.22 ± 0.11 ± 0.46) × 10⁻², which we rescale to our best value B(ψ(2S) → γχ_{c0}(1P)) = (9.79 ± 0.20) × 10⁻². Our first error is their experiment's error and our second error is the systematic error from using our best value.

Meson Particle Listings

 $\chi_{c0}(1P)$ $\Gamma(K_1(1270)^+ K^- + c.c. \rightarrow \pi^+ \pi^- K^+ K^-) / \Gamma_{\text{total}}$ Γ_{11} / Γ

VALUE (units 10^{-3})	EVTS	DOCUMENT ID	TECN	COMMENT
$6.3 \pm 1.9 \pm 0.1$	68	¹ ABLIKIM	05q BES2	$\psi(2S) \rightarrow \gamma \pi^+ \pi^- K^+ K^-$
¹ ABLIKIM 05q reports $(6.66 \pm 1.31 \pm 1.60_{-1.51}) \times 10^{-3}$ from a measurement of $[\Gamma(\chi_{c0}(1P) \rightarrow K_1(1270)^+ K^- + c.c. \rightarrow \pi^+ \pi^- K^+ K^-) / \Gamma_{\text{total}}] \times [B(\psi(2S) \rightarrow \gamma \chi_{c0}(1P))]$ assuming $B(\psi(2S) \rightarrow \gamma \chi_{c0}(1P)) = (9.22 \pm 0.11 \pm 0.46) \times 10^{-2}$, which we rescale to our best value $B(\psi(2S) \rightarrow \gamma \chi_{c0}(1P)) = (9.79 \pm 0.20) \times 10^{-2}$. Our first error is their experiment's error and our second error is the systematic error from using our best value. The measurement assumes $B(K_1(1270) \rightarrow K \rho(770)) = 42 \pm 6\%$.				

 $\Gamma(K_1(1400)^+ K^- + c.c. \rightarrow \pi^+ \pi^- K^+ K^-) / \Gamma_{\text{total}}$ Γ_{12} / Γ

VALUE (units 10^{-3})	CL%	DOCUMENT ID	TECN	COMMENT
<2.7	90	¹ ABLIKIM	05q BES2	$\psi(2S) \rightarrow \gamma \pi^+ \pi^- K^+ K^-$
¹ ABLIKIM 05q reports $< 2.85 \times 10^{-3}$ from a measurement of $[\Gamma(\chi_{c0}(1P) \rightarrow K_1(1400)^+ K^- + c.c. \rightarrow \pi^+ \pi^- K^+ K^-) / \Gamma_{\text{total}}] \times [B(\psi(2S) \rightarrow \gamma \chi_{c0}(1P))]$ assuming $B(\psi(2S) \rightarrow \gamma \chi_{c0}(1P)) = (9.22 \pm 0.11 \pm 0.46) \times 10^{-2}$, which we rescale to our best value $B(\psi(2S) \rightarrow \gamma \chi_{c0}(1P)) = 9.79 \times 10^{-2}$. The measurement assumes $B(K_1(1400) \rightarrow K^*(892) \pi) = 94 \pm 6\%$.				

 $\Gamma(f_0(980) f_0(980)) / \Gamma_{\text{total}}$ Γ_{13} / Γ

VALUE (units 10^{-5})	EVTS	DOCUMENT ID	TECN	COMMENT
$16.2^{+10.4}_{-9.0} \pm 0.3$	28	¹ ABLIKIM	05q BES2	$\psi(2S) \rightarrow \gamma \pi^+ \pi^- K^+ K^-$
¹ ABLIKIM 05q reports $[\Gamma(\chi_{c0}(1P) \rightarrow f_0(980) f_0(980)) / \Gamma_{\text{total}}] \times [B(\psi(2S) \rightarrow \gamma \chi_{c0}(1P))]$ = $(1.59 \pm 0.50 \pm 0.89_{-0.72}) \times 10^{-5}$ which we divide by our best value $B(\psi(2S) \rightarrow \gamma \chi_{c0}(1P)) = (9.79 \pm 0.20) \times 10^{-2}$. Our first error is their experiment's error and our second error is the systematic error from using our best value. One of the $f_0(980)$ mesons is identified via decay to $\pi^+ \pi^-$ while the other via $K^+ K^-$ decay.				

 $\Gamma(f_0(980) f_0(2200)) / \Gamma_{\text{total}}$ Γ_{14} / Γ

VALUE (units 10^{-4})	EVTS	DOCUMENT ID	TECN	COMMENT
$7.9^{+2.0}_{-2.5} \pm 0.2$	77	¹ ABLIKIM	05q BES2	$\psi(2S) \rightarrow \gamma \pi^+ \pi^- K^+ K^-$
¹ ABLIKIM 05q reports $(8.42 \pm 1.42 \pm 1.65_{-2.29}) \times 10^{-4}$ from a measurement of $[\Gamma(\chi_{c0}(1P) \rightarrow f_0(980) f_0(2200)) / \Gamma_{\text{total}}] \times [B(\psi(2S) \rightarrow \gamma \chi_{c0}(1P))]$ assuming $B(\psi(2S) \rightarrow \gamma \chi_{c0}(1P)) = (9.22 \pm 0.11 \pm 0.46) \times 10^{-2}$, which we rescale to our best value $B(\psi(2S) \rightarrow \gamma \chi_{c0}(1P)) = (9.79 \pm 0.20) \times 10^{-2}$. Our first error is their experiment's error and our second error is the systematic error from using our best value. The f_0 mesons are identified via $f_0(980) \rightarrow \pi^+ \pi^-$ and $f_0(2200) \rightarrow K^+ K^-$ decays.				

 $\Gamma(f_0(1370) f_0(1370)) / \Gamma_{\text{total}}$ Γ_{15} / Γ

VALUE (units 10^{-4})	CL%	DOCUMENT ID	TECN	COMMENT
<2.7	90	¹ ABLIKIM	05q BES2	$\psi(2S) \rightarrow \gamma \pi^+ \pi^- K^+ K^-$
¹ ABLIKIM 05q reports $< 2.9 \times 10^{-4}$ from a measurement of $[\Gamma(\chi_{c0}(1P) \rightarrow f_0(1370) f_0(1370)) / \Gamma_{\text{total}}] \times [B(\psi(2S) \rightarrow \gamma \chi_{c0}(1P))]$ assuming $B(\psi(2S) \rightarrow \gamma \chi_{c0}(1P)) = (9.22 \pm 0.11 \pm 0.46) \times 10^{-2}$, which we rescale to our best value $B(\psi(2S) \rightarrow \gamma \chi_{c0}(1P)) = 9.79 \times 10^{-2}$. One of the $f_0(1370)$ mesons is identified via decay to $\pi^+ \pi^-$ while the other via $K^+ K^-$ decay. Both branching fractions for these f_0 decays are implicitly included in the quoted result.				

 $\Gamma(f_0(1370) f_0(1500)) / \Gamma_{\text{total}}$ Γ_{16} / Γ

VALUE (units 10^{-4})	CL%	DOCUMENT ID	TECN	COMMENT
<1.7	90	¹ ABLIKIM	05q BES2	$\psi(2S) \rightarrow \gamma \pi^+ \pi^- K^+ K^-$
¹ ABLIKIM 05q reports $< 1.8 \times 10^{-4}$ from a measurement of $[\Gamma(\chi_{c0}(1P) \rightarrow f_0(1370) f_0(1500)) / \Gamma_{\text{total}}] \times [B(\psi(2S) \rightarrow \gamma \chi_{c0}(1P))]$ assuming $B(\psi(2S) \rightarrow \gamma \chi_{c0}(1P)) = (9.22 \pm 0.11 \pm 0.46) \times 10^{-2}$, which we rescale to our best value $B(\psi(2S) \rightarrow \gamma \chi_{c0}(1P)) = 9.79 \times 10^{-2}$. The f_0 mesons are identified via $f_0(1370) \rightarrow \pi^+ \pi^-$ and $f_0(1500) \rightarrow K^+ K^-$ decays. Both branching fractions for these f_0 decays are implicitly included in the quoted result.				

 $\Gamma(f_0(1370) f_0(1710)) / \Gamma_{\text{total}}$ Γ_{17} / Γ

VALUE (units 10^{-4})	EVTS	DOCUMENT ID	TECN	COMMENT
$6.7^{+3.5}_{-2.3} \pm 0.1$	61	¹ ABLIKIM	05q BES2	$\psi(2S) \rightarrow \gamma \pi^+ \pi^- K^+ K^-$
¹ ABLIKIM 05q reports $(7.12 \pm 1.85 \pm 3.28_{-1.68}) \times 10^{-4}$ from a measurement of $[\Gamma(\chi_{c0}(1P) \rightarrow f_0(1370) f_0(1710)) / \Gamma_{\text{total}}] \times [B(\psi(2S) \rightarrow \gamma \chi_{c0}(1P))]$ assuming $B(\psi(2S) \rightarrow \gamma \chi_{c0}(1P)) = (9.22 \pm 0.11 \pm 0.46) \times 10^{-2}$, which we rescale to our best value $B(\psi(2S) \rightarrow \gamma \chi_{c0}(1P)) = (9.79 \pm 0.20) \times 10^{-2}$. Our first error is their experiment's error and our second error is the systematic error from using our best value. The f_0 mesons are identified via $f_0(1370) \rightarrow \pi^+ \pi^-$ and $f_0(1710) \rightarrow K^+ K^-$ decays. Both branching fractions for these f_0 decays are implicitly included in the quoted result.				

 $\Gamma(f_0(1500) f_0(1370)) / \Gamma_{\text{total}}$ Γ_{18} / Γ

VALUE (units 10^{-4})	CL%	DOCUMENT ID	TECN	COMMENT
<1.3	90	¹ ABLIKIM	05q BES2	$\psi(2S) \rightarrow \gamma \pi^+ \pi^- K^+ K^-$
¹ ABLIKIM 05q reports $< 1.4 \times 10^{-4}$ from a measurement of $[\Gamma(\chi_{c0}(1P) \rightarrow f_0(1500) f_0(1370)) / \Gamma_{\text{total}}] \times [B(\psi(2S) \rightarrow \gamma \chi_{c0}(1P))]$ assuming $B(\psi(2S) \rightarrow \gamma \chi_{c0}(1P)) = (9.22 \pm 0.11 \pm 0.46) \times 10^{-2}$, which we rescale to our best value $B(\psi(2S) \rightarrow \gamma \chi_{c0}(1P)) = 9.79 \times 10^{-2}$. The f_0 mesons are identified via $f_0(1500) \rightarrow \pi^+ \pi^-$ and $f_0(1370) \rightarrow K^+ K^-$ decays. Both branching fractions for these f_0 decays are implicitly included in the quoted result.				

 $\Gamma(f_0(1500) f_0(1500)) / \Gamma_{\text{total}}$ Γ_{19} / Γ

VALUE (units 10^{-4})	CL%	DOCUMENT ID	TECN	COMMENT
<0.5	90	¹ ABLIKIM	05q BES2	$\psi(2S) \rightarrow \gamma \pi^+ \pi^- K^+ K^-$
¹ ABLIKIM 05q reports $< 0.55 \times 10^{-4}$ from a measurement of $[\Gamma(\chi_{c0}(1P) \rightarrow f_0(1500) f_0(1500)) / \Gamma_{\text{total}}] \times [B(\psi(2S) \rightarrow \gamma \chi_{c0}(1P))]$ assuming $B(\psi(2S) \rightarrow \gamma \chi_{c0}(1P)) = (9.22 \pm 0.11 \pm 0.46) \times 10^{-2}$, which we rescale to our best value $B(\psi(2S) \rightarrow \gamma \chi_{c0}(1P)) = 9.79 \times 10^{-2}$. One of the $f_0(1500)$ is identified via decay to $\pi^+ \pi^-$ while the other via $K^+ K^-$ decay. Both branching fractions for these f_0 decays are implicitly included in the quoted result.				

 $\Gamma(f_0(1500) f_0(1710)) / \Gamma_{\text{total}}$ Γ_{20} / Γ

VALUE (units 10^{-4})	CL%	DOCUMENT ID	TECN	COMMENT
<0.7	90	¹ ABLIKIM	05q BES2	$\psi(2S) \rightarrow \gamma \pi^+ \pi^- K^+ K^-$
¹ ABLIKIM 05q reports $< 0.73 \times 10^{-4}$ from a measurement of $[\Gamma(\chi_{c0}(1P) \rightarrow f_0(1500) f_0(1710)) / \Gamma_{\text{total}}] \times [B(\psi(2S) \rightarrow \gamma \chi_{c0}(1P))]$ assuming $B(\psi(2S) \rightarrow \gamma \chi_{c0}(1P)) = (9.22 \pm 0.11 \pm 0.46) \times 10^{-2}$, which we rescale to our best value $B(\psi(2S) \rightarrow \gamma \chi_{c0}(1P)) = 9.79 \times 10^{-2}$. The f_0 mesons are identified via $f_0(1500) \rightarrow \pi^+ \pi^-$ and $f_0(1710) \rightarrow K^+ K^-$ decays. Both branching fractions for these f_0 decays are implicitly included in the quoted result.				

 $\Gamma(K^+ K^- \pi^+ \pi^-) / \Gamma_{\text{total}}$ Γ_{21} / Γ

VALUE (units 10^{-3})	EVTS	DOCUMENT ID	TECN	COMMENT
$8.61 \pm 0.13 \pm 0.94$	9.0k	¹ ABLIKIM	13B BES3	$e^+ e^- \rightarrow \psi(2S) \rightarrow \gamma \chi_{c0}$
¹ Using $1.06 \times 10^8 \psi(2S)$ mesons and $B(\psi(2S) \rightarrow \chi_{c0} \gamma) = (9.68 \pm 0.31)\%$.				

 $\Gamma(K_S^0 K^{\pm} \pi^{\mp} \pi^{\pm}) / \Gamma_{\text{total}}$ Γ_{22} / Γ

VALUE (units 10^{-3})	EVTS	DOCUMENT ID	TECN	COMMENT
$4.22 \pm 0.10 \pm 0.43$	2.7k	¹ ABLIKIM	13B BES3	$e^+ e^- \rightarrow \psi(2S) \rightarrow \gamma \chi_{c0}$
¹ Using $1.06 \times 10^8 \psi(2S)$ mesons and $B(\psi(2S) \rightarrow \chi_{c0} \gamma) = (9.68 \pm 0.31)\%$.				

 $\Gamma(K^+ K^- \pi^0 \pi^0) / \Gamma_{\text{total}}$ Γ_{23} / Γ

VALUE (%)	EVTS	DOCUMENT ID	TECN	COMMENT
$0.56 \pm 0.09 \pm 0.01$	213.5	¹ HE	08B CLEO	$e^+ e^- \rightarrow \gamma h^+ h^- h^0 h^0$
¹ HE 08B reports $0.59 \pm 0.05 \pm 0.08 \pm 0.03\%$ from a measurement of $[\Gamma(\chi_{c0}(1P) \rightarrow K^+ K^- \pi^0 \pi^0) / \Gamma_{\text{total}}] \times [B(\psi(2S) \rightarrow \gamma \chi_{c0}(1P))]$ assuming $B(\psi(2S) \rightarrow \gamma \chi_{c0}(1P)) = (9.22 \pm 0.11 \pm 0.46) \times 10^{-2}$, which we rescale to our best value $B(\psi(2S) \rightarrow \gamma \chi_{c0}(1P)) = (9.79 \pm 0.20) \times 10^{-2}$. Our first error is their experiment's error and our second error is the systematic error from using our best value.				

 $\Gamma(K^+ \pi^- \bar{K}^0 \pi^0 + c.c.) / \Gamma_{\text{total}}$ Γ_{24} / Γ

VALUE (%)	EVTS	DOCUMENT ID	TECN	COMMENT
$2.49 \pm 0.33 \pm 0.05$	401.7	¹ HE	08B CLEO	$e^+ e^- \rightarrow \gamma h^+ h^- h^0 h^0$
¹ HE 08B reports $2.64 \pm 0.15 \pm 0.31 \pm 0.14\%$ from a measurement of $[\Gamma(\chi_{c0}(1P) \rightarrow K^+ \pi^- \bar{K}^0 \pi^0 + c.c.) / \Gamma_{\text{total}}] \times [B(\psi(2S) \rightarrow \gamma \chi_{c0}(1P))]$ assuming $B(\psi(2S) \rightarrow \gamma \chi_{c0}(1P)) = (9.22 \pm 0.11 \pm 0.46) \times 10^{-2}$, which we rescale to our best value $B(\psi(2S) \rightarrow \gamma \chi_{c0}(1P)) = (9.79 \pm 0.20) \times 10^{-2}$. Our first error is their experiment's error and our second error is the systematic error from using our best value.				

 $\Gamma(\rho^+ K^- K^0 + c.c.) / \Gamma_{\text{total}}$ Γ_{25} / Γ

VALUE (%)	EVTS	DOCUMENT ID	TECN	COMMENT
$1.21 \pm 0.21 \pm 0.02$	179.7	¹ HE	08B CLEO	$e^+ e^- \rightarrow \gamma h^+ h^- h^0 h^0$
¹ HE 08B reports $1.28 \pm 0.16 \pm 0.15 \pm 0.07\%$ from a measurement of $[\Gamma(\chi_{c0}(1P) \rightarrow \rho^+ K^- K^0 + c.c.) / \Gamma_{\text{total}}] \times [B(\psi(2S) \rightarrow \gamma \chi_{c0}(1P))]$ assuming $B(\psi(2S) \rightarrow \gamma \chi_{c0}(1P)) = (9.22 \pm 0.11 \pm 0.46) \times 10^{-2}$, which we rescale to our best value $B(\psi(2S) \rightarrow \gamma \chi_{c0}(1P)) = (9.79 \pm 0.20) \times 10^{-2}$. Our first error is their experiment's error and our second error is the systematic error from using our best value.				

 $\Gamma(K^*(892) K^- \pi^0 \rightarrow K^+ \pi^- \bar{K}^0 \pi^0 + c.c.) / \Gamma_{\text{total}}$ Γ_{26} / Γ

VALUE (%)	EVTS	DOCUMENT ID	TECN	COMMENT
$0.46 \pm 0.12 \pm 0.01$	64.1	¹ HE	08B CLEO	$e^+ e^- \rightarrow \gamma h^+ h^- h^0 h^0$
¹ HE 08B reports $0.49 \pm 0.10 \pm 0.07 \pm 0.03\%$ from a measurement of $[\Gamma(\chi_{c0}(1P) \rightarrow K^*(892) K^- \pi^0 \rightarrow K^+ \pi^- \bar{K}^0 \pi^0 + c.c.) / \Gamma_{\text{total}}] \times [B(\psi(2S) \rightarrow \gamma \chi_{c0}(1P))]$ assuming $B(\psi(2S) \rightarrow \gamma \chi_{c0}(1P)) = (9.22 \pm 0.11 \pm 0.46) \times 10^{-2}$, which we rescale to our best value $B(\psi(2S) \rightarrow \gamma \chi_{c0}(1P)) = (9.79 \pm 0.20) \times 10^{-2}$. Our first error is their experiment's error and our second error is the systematic error from using our best value.				

 $\Gamma(K_S^0 K_S^0 \pi^+ \pi^-) / \Gamma_{\text{total}}$ Γ_{27} / Γ

VALUE (units 10^{-3})	EVTS	DOCUMENT ID	TECN	COMMENT
$5.7 \pm 1.0 \pm 0.1$	152 \pm 14	¹ ABLIKIM	05o BES2	$\psi(2S) \rightarrow \gamma \chi_{c0}$
¹ ABLIKIM 05o reports $[\Gamma(\chi_{c0}(1P) \rightarrow K_S^0 K_S^0 \pi^+ \pi^-) / \Gamma_{\text{total}}] \times [B(\psi(2S) \rightarrow \gamma \chi_{c0}(1P))]$ = $(0.558 \pm 0.051 \pm 0.089) \times 10^{-3}$ which we divide by our best value $B(\psi(2S) \rightarrow \gamma \chi_{c0}(1P)) = (9.79 \pm 0.20) \times 10^{-2}$. Our first error is their experiment's error and our second error is the systematic error from using our best value.				

$\Gamma(K^+ K^- \eta \pi^0)/\Gamma_{total}$		Γ_{28}/Γ	
VALUE (%)	EVTS	DOCUMENT ID	TECN COMMENT
0.30 ± 0.07 ± 0.01	56.4	¹ HE	08B CLEO $e^+e^- \rightarrow \gamma h^+ h^- h^0 h^0$

¹ HE 08B reports $0.32 \pm 0.05 \pm 0.05 \pm 0.02$ % from a measurement of $[\Gamma(\chi_{c0}(1P) \rightarrow K^+ K^- \eta \pi^0)/\Gamma_{total}] \times [B(\psi(2S) \rightarrow \gamma \chi_{c0}(1P))]$ assuming $B(\psi(2S) \rightarrow \gamma \chi_{c0}(1P)) = (9.22 \pm 0.11 \pm 0.46) \times 10^{-2}$, which we rescale to our best value $B(\psi(2S) \rightarrow \gamma \chi_{c0}(1P)) = (9.79 \pm 0.20) \times 10^{-2}$. Our first error is their experiment's error and our second error is the systematic error from using our best value.

$\Gamma(3(\pi^+ \pi^-))/\Gamma_{total}$		Γ_{29}/Γ	
VALUE (units 10^{-3})	DOCUMENT ID	TECN	COMMENT
12.0 ± 1.8 OUR EVALUATION	Treating systematic error as correlated.		
12.0 ± 1.7 OUR AVERAGE			
11.7 ± 1.0 ± 1.9	¹ BAI	99B BES	$\psi(2S) \rightarrow \gamma \chi_{c0}$
12.5 ± 2.9 ± 0.5	¹ TANENBAUM	78 MRK1	$\psi(2S) \rightarrow \gamma \chi_{c0}$

¹ Rescaled by us using $B(\psi(2S) \rightarrow \gamma \chi_{c0}) = (9.4 \pm 0.4)$ % and $B(\psi(2S) \rightarrow J/\psi(1S) \pi^+ \pi^-) = (32.6 \pm 0.5)$ %.

$\Gamma(K^+ \bar{K}^*(892)^0 \pi^- + c.c.)/\Gamma_{total}$		Γ_{30}/Γ	
VALUE	DOCUMENT ID	TECN	COMMENT
0.0075 ± 0.0016 OUR FIT			

$\Gamma(K^*(892)^0 \bar{K}^*(892)^0)/\Gamma_{total}$		Γ_{31}/Γ	
VALUE (units 10^{-3})	EVTS	DOCUMENT ID	TECN COMMENT
1.72 ± 0.60 ± 0.54 OUR AVERAGE	64	¹ ABLIKIM	05Q BES2 $\psi(2S) \rightarrow \gamma \pi^+ \pi^- K^+ K^-$

• • • We do not use the following data for averages, fits, limits, etc. • • •

1.56 ± 0.40 ± 0.03 30 ± 6 ^{2,3} ABLIKIM 04H BES Repl. by ABLIKIM 05Q

¹ ABLIKIM 05Q reports $[\Gamma(\chi_{c0}(1P) \rightarrow K^*(892)^0 \bar{K}^*(892)^0)/\Gamma_{total}] \times [B(\psi(2S) \rightarrow \gamma \chi_{c0}(1P))] = (0.168 \pm 0.035 \pm 0.047 \pm 0.040) \times 10^{-3}$ which we divide by our best value $B(\psi(2S) \rightarrow \gamma \chi_{c0}(1P)) = (9.79 \pm 0.20) \times 10^{-2}$. Our first error is their experiment's error and our second error is the systematic error from using our best value.

² Assumes $B(K^*(892)^0 \rightarrow K^- \pi^+) = 2/3$.

³ ABLIKIM 04H reports $[\Gamma(\chi_{c0}(1P) \rightarrow K^*(892)^0 \bar{K}^*(892)^0)/\Gamma_{total}] \times [B(\psi(2S) \rightarrow \gamma \chi_{c0}(1P))] = (1.53 \pm 0.29 \pm 0.26) \times 10^{-4}$ which we divide by our best value $B(\psi(2S) \rightarrow \gamma \chi_{c0}(1P)) = (9.79 \pm 0.20) \times 10^{-2}$. Our first error is their experiment's error and our second error is the systematic error from using our best value.

$\Gamma(\pi \pi)/\Gamma_{total}$		Γ_{32}/Γ	
VALUE (units 10^{-3})	DOCUMENT ID	TECN	COMMENT
8.51 ± 0.33 OUR FIT			

$\Gamma(\pi^0 \eta_c)/\Gamma_{total}$		Γ_{35}/Γ	
VALUE	CL%	DOCUMENT ID	TECN COMMENT
< 1.6 × 10⁻³		¹ ABLIKIM	15N BES3 $\psi(2S) e^+ e^- \rightarrow \gamma \pi^0 \eta_c$

¹ Using $B(\eta_c \rightarrow K_S^0 K^\pm \pi^\mp) \times B(K_S^0 \rightarrow \pi^+ \pi^-) \times B(\pi^0 \rightarrow \gamma \gamma) = (1.66 \pm 0.11) \times 10^{-2}$.

$\Gamma(\eta \eta)/\Gamma_{total}$		Γ_{36}/Γ	
VALUE (units 10^{-3})	DOCUMENT ID	TECN	COMMENT
3.01 ± 0.19 OUR FIT			

$\Gamma(\eta \eta)/\Gamma(\pi \pi)$		Γ_{36}/Γ_{32}	
VALUE	DOCUMENT ID	TECN	COMMENT
0.353 ± 0.025 OUR FIT			

• • • We do not use the following data for averages, fits, limits, etc. • • •

0.26 ± 0.09 ^{+0.03}/_{-0.02} ¹ ANDREOTTI 05c E835 $\bar{p}p \rightarrow 2$ mesons

0.24 ± 0.10 ± 0.08 ¹ BAI 03c BES $\psi(2S) \rightarrow 5\gamma$

¹ We have multiplied $\pi^0 \pi^0$ measurement by 3 to obtain $\pi \pi$.

$\Gamma(\eta \eta')/\Gamma_{total}$		Γ_{37}/Γ	
VALUE (units 10^{-5})	CL%	EVTS	DOCUMENT ID
9.1 ± 1.1 ± 0.2		85	¹ ABLIKIM 17A1 BES3 $\psi(2S) \rightarrow \gamma \eta' \eta$

• • • We do not use the following data for averages, fits, limits, etc. • • •

<24 90 35 ± 13 ² ASNER 09 CLEO $\psi(2S) \rightarrow \gamma \eta' \eta$

<50 90 ³ ADAMS 07 CLEO $\psi(2S) \rightarrow \gamma \chi_{c0}$

¹ ABLIKIM 17A1 reports $(8.92 \pm 0.84 \pm 0.65) \times 10^{-5}$ from a measurement of $[\Gamma(\chi_{c0}(1P) \rightarrow \eta \eta')/\Gamma_{total}] \times [B(\psi(2S) \rightarrow \gamma \chi_{c0}(1P))]$ assuming $B(\psi(2S) \rightarrow \gamma \chi_{c0}(1P)) = (9.99 \pm 0.27) \times 10^{-2}$, which we rescale to our best value $B(\psi(2S) \rightarrow \gamma \chi_{c0}(1P)) = (9.79 \pm 0.20) \times 10^{-2}$. Our first error is their experiment's error and our second error is the systematic error from using our best value.

² ASNER 09 reports $< 0.25 \times 10^{-3}$ from a measurement of $[\Gamma(\chi_{c0}(1P) \rightarrow \eta \eta')/\Gamma_{total}] \times [B(\psi(2S) \rightarrow \gamma \chi_{c0}(1P))]$ assuming $B(\psi(2S) \rightarrow \gamma \chi_{c0}(1P)) = (9.22 \pm 0.11 \pm 0.46) \times 10^{-2}$, which we rescale to our best value $B(\psi(2S) \rightarrow \gamma \chi_{c0}(1P)) = 9.79 \times 10^{-2}$.

³ Superseded by ASNER 09. ADAMS 07 reports $< 0.5 \times 10^{-3}$ from a measurement of $[\Gamma(\chi_{c0}(1P) \rightarrow \eta \eta')/\Gamma_{total}] \times [B(\psi(2S) \rightarrow \gamma \chi_{c0}(1P))]$ assuming $B(\psi(2S) \rightarrow \gamma \chi_{c0}(1P)) = (9.22 \pm 0.11 \pm 0.46) \times 10^{-2}$, which we rescale to our best value $B(\psi(2S) \rightarrow \gamma \chi_{c0}(1P)) = 9.79 \times 10^{-2}$.

$\Gamma(\eta' \eta')/\Gamma_{total}$		Γ_{38}/Γ	
VALUE (units 10^{-3})	EVTS	DOCUMENT ID	TECN COMMENT
2.17 ± 0.12 OUR AVERAGE			

2.23 ± 0.13 ± 0.05 2.5k ¹ ABLIKIM 17A1 BES3 $\psi(2S) \rightarrow \gamma \eta' \eta'$

2.00 ± 0.21 ± 0.04 0.4k ² ASNER 09 CLEO $\psi(2S) \rightarrow \gamma \eta' \eta'$

• • • We do not use the following data for averages, fits, limits, etc. • • •

1.60 ± 0.41 ± 0.03 23 ³ ADAMS 07 CLEO $\psi(2S) \rightarrow \gamma \chi_{c0}$

¹ ABLIKIM 17A1 reports $(2.19 \pm 0.03 \pm 0.14) \times 10^{-3}$ from a measurement of $[\Gamma(\chi_{c0}(1P) \rightarrow \eta' \eta')/\Gamma_{total}] \times [B(\psi(2S) \rightarrow \gamma \chi_{c0}(1P))]$ assuming $B(\psi(2S) \rightarrow \gamma \chi_{c0}(1P)) = (9.99 \pm 0.27) \times 10^{-2}$, which we rescale to our best value $B(\psi(2S) \rightarrow \gamma \chi_{c0}(1P)) = (9.79 \pm 0.20) \times 10^{-2}$. Our first error is their experiment's error and our second error is the systematic error from using our best value.

² ASNER 09 reports $(2.12 \pm 0.13 \pm 0.21) \times 10^{-3}$ from a measurement of $[\Gamma(\chi_{c0}(1P) \rightarrow \eta' \eta')/\Gamma_{total}] \times [B(\psi(2S) \rightarrow \gamma \chi_{c0}(1P))]$ assuming $B(\psi(2S) \rightarrow \gamma \chi_{c0}(1P)) = (9.22 \pm 0.11 \pm 0.46) \times 10^{-2}$, which we rescale to our best value $B(\psi(2S) \rightarrow \gamma \chi_{c0}(1P)) = (9.79 \pm 0.20) \times 10^{-2}$. Our first error is their experiment's error and our second error is the systematic error from using our best value.

³ Superseded by ASNER 09. ADAMS 07 reports $(1.7 \pm 0.4 \pm 0.2) \times 10^{-3}$ from a measurement of $[\Gamma(\chi_{c0}(1P) \rightarrow \eta' \eta')/\Gamma_{total}] \times [B(\psi(2S) \rightarrow \gamma \chi_{c0}(1P))]$ assuming $B(\psi(2S) \rightarrow \gamma \chi_{c0}(1P)) = 0.0922 \pm 0.0011 \pm 0.0046$, which we rescale to our best value $B(\psi(2S) \rightarrow \gamma \chi_{c0}(1P)) = (9.79 \pm 0.20) \times 10^{-2}$. Our first error is their experiment's error and our second error is the systematic error from using our best value.

$\Gamma(\omega \omega)/\Gamma_{total}$		Γ_{39}/Γ	
VALUE (units 10^{-3})	EVTS	DOCUMENT ID	TECN COMMENT
0.97 ± 0.11 OUR AVERAGE			

0.93 ± 0.11 ± 0.02 991 ¹ ABLIKIM 11K BES3 $\psi(2S) \rightarrow \gamma$ hadrons

2.16 ± 0.66 ± 0.04 38.1 ± 9.6 ² ABLIKIM 05N BES2 $\psi(2S) \rightarrow \gamma \chi_{c0} \rightarrow \gamma 6\pi$

¹ ABLIKIM 11K reports $(0.95 \pm 0.03 \pm 0.11) \times 10^{-3}$ from a measurement of $[\Gamma(\chi_{c0}(1P) \rightarrow \omega \omega)/\Gamma_{total}] \times [B(\psi(2S) \rightarrow \gamma \chi_{c0}(1P))]$ assuming $B(\psi(2S) \rightarrow \gamma \chi_{c0}(1P)) = (9.62 \pm 0.31) \times 10^{-2}$, which we rescale to our best value $B(\psi(2S) \rightarrow \gamma \chi_{c0}(1P)) = (9.79 \pm 0.20) \times 10^{-2}$. Our first error is their experiment's error and our second error is the systematic error from using our best value.

² ABLIKIM 05N reports $[\Gamma(\chi_{c0}(1P) \rightarrow \omega \omega)/\Gamma_{total}] \times [B(\psi(2S) \rightarrow \gamma \chi_{c0}(1P))] = (0.212 \pm 0.053 \pm 0.037) \times 10^{-3}$ which we divide by our best value $B(\psi(2S) \rightarrow \gamma \chi_{c0}(1P)) = (9.79 \pm 0.20) \times 10^{-2}$. Our first error is their experiment's error and our second error is the systematic error from using our best value.

$\Gamma(\omega \phi)/\Gamma_{total}$		Γ_{40}/Γ	
VALUE (units 10^{-4})	EVTS	DOCUMENT ID	TECN COMMENT
1.41 ± 0.13 ± 0.03	486	¹ ABLIKIM 19J	BES3 $\psi(2S) \rightarrow \gamma$ hadrons

• • • We do not use the following data for averages, fits, limits, etc. • • •

1.18 ± 0.22 ± 0.02 76 ^{2,3} ABLIKIM 11K BES3 $\psi(2S) \rightarrow \gamma$ hadrons

¹ ABLIKIM 19J reports $[\Gamma(\chi_{c0}(1P) \rightarrow \omega \phi)/\Gamma_{total}] \times [B(\psi(2S) \rightarrow \gamma \chi_{c0}(1P))] = (13.83 \pm 0.70 \pm 1.01) \times 10^{-6}$ which we divide by our best value $B(\psi(2S) \rightarrow \gamma \chi_{c0}(1P)) = (9.79 \pm 0.20) \times 10^{-2}$. Our first error is their experiment's error and our second error is the systematic error from using our best value.

² ABLIKIM 11K reports $(1.2 \pm 0.1 \pm 0.2) \times 10^{-4}$ from a measurement of $[\Gamma(\chi_{c0}(1P) \rightarrow \omega \phi)/\Gamma_{total}] \times [B(\psi(2S) \rightarrow \gamma \chi_{c0}(1P))]$ assuming $B(\psi(2S) \rightarrow \gamma \chi_{c0}(1P)) = (9.62 \pm 0.31) \times 10^{-2}$, which we rescale to our best value $B(\psi(2S) \rightarrow \gamma \chi_{c0}(1P)) = (9.79 \pm 0.20) \times 10^{-2}$. Our first error is their experiment's error and our second error is the systematic error from using our best value.

³ Superseded by ABLIKIM 19J.

$\Gamma(\omega K^+ K^-)/\Gamma_{total}$		Γ_{41}/Γ	
VALUE (units 10^{-3})	EVTS	DOCUMENT ID	TECN COMMENT
1.94 ± 0.06 ± 0.20	1.4k	¹ ABLIKIM 13B	BES3 $e^+e^- \rightarrow \psi(2S) \rightarrow \gamma \chi_{c0}$

¹ Using 1.06×10^8 $\psi(2S)$ mesons and $B(\psi(2S) \rightarrow \chi_{c0} \gamma) = (9.68 \pm 0.31)$ %.

$\Gamma(K^+ K^-)/\Gamma_{total}$		Γ_{42}/Γ	
VALUE (units 10^{-3})	DOCUMENT ID	TECN	COMMENT
6.05 ± 0.31 OUR FIT			

$\Gamma(K_S^0 K_S^0)/\Gamma_{total}$		Γ_{43}/Γ	
VALUE (units 10^{-3})	DOCUMENT ID	TECN	COMMENT
3.16 ± 0.17 OUR FIT			

$\Gamma(K_S^0 K_S^0)/\Gamma(\pi \pi)$		Γ_{43}/Γ_{32}	
VALUE	DOCUMENT ID	TECN	COMMENT
0.371 ± 0.023 OUR FIT			

• • • We do not use the following data for averages, fits, limits, etc. • • •

0.31 ± 0.05 ± 0.05 ^{1,2} CHEN 07B BELL $e^+e^- \rightarrow e^+e^- \chi_{c0}$

¹ Using $\Gamma(\pi \pi) \times \Gamma(\gamma \gamma)/\Gamma_{total}$ from the $\pi^+ \pi^-$ measurement of NAKAZAWA 05 rescaled by 3/2 to convert to $\pi \pi$.

² Not independent from other measurements.

$\Gamma(K_S^0 K_S^0)/\Gamma(K^+ K^-)$		Γ_{43}/Γ_{42}	
VALUE	DOCUMENT ID	TECN	COMMENT
0.52 ± 0.04 OUR FIT			

• • • We do not use the following data for averages, fits, limits, etc. • • •

0.49 ± 0.07 ± 0.08 ^{1,2} CHEN 07B BELL $e^+e^- \rightarrow e^+e^- \chi_{c0}$

¹ Using $\Gamma(K^+ K^-) \times \Gamma(\gamma \gamma)/\Gamma_{total}$ from NAKAZAWA 05.

² Not independent from other measurements.

Meson Particle Listings

 $\chi_{c0}(1P)$

$\Gamma(\pi^+\pi^-\eta)/\Gamma_{\text{total}}$ Γ_{44}/Γ

VALUE (units 10^{-3})	CL%	DOCUMENT ID	TECN	COMMENT
<0.20	90	¹ ATHAR	07 CLEO	$\psi(2S) \rightarrow \gamma h^+ h^- h^0$

• • • We do not use the following data for averages, fits, limits, etc. • • •

<1.0	90	² ABLIKIM	06R BES2	$\psi(2S) \rightarrow \gamma\chi_{c0}$
¹ ATHAR 07 reports $< 0.21 \times 10^{-3}$ from a measurement of $[\Gamma(\chi_{c0}(1P) \rightarrow \pi^+\pi^-\eta)/\Gamma_{\text{total}}] \times [B(\psi(2S) \rightarrow \gamma\chi_{c0}(1P))]$ assuming $B(\psi(2S) \rightarrow \gamma\chi_{c0}(1P)) = (9.22 \pm 0.11 \pm 0.46) \times 10^{-2}$, which we rescale to our best value $B(\psi(2S) \rightarrow \gamma\chi_{c0}(1P)) = 9.79 \times 10^{-2}$.				
² ABLIKIM 06R reports $< 1.1 \times 10^{-3}$ from a measurement of $[\Gamma(\chi_{c0}(1P) \rightarrow \pi^+\pi^-\eta)/\Gamma_{\text{total}}] \times [B(\psi(2S) \rightarrow \gamma\chi_{c0}(1P))]$ assuming $B(\psi(2S) \rightarrow \gamma\chi_{c0}(1P)) = (9.2 \pm 0.4) \times 10^{-2}$, which we rescale to our best value $B(\psi(2S) \rightarrow \gamma\chi_{c0}(1P)) = 9.79 \times 10^{-2}$.				

$\Gamma(\pi^+\pi^-\eta')/\Gamma_{\text{total}}$ Γ_{45}/Γ

VALUE (units 10^{-3})	CL%	DOCUMENT ID	TECN	COMMENT
<0.4	90	¹ ATHAR	07 CLEO	$\psi(2S) \rightarrow \gamma h^+ h^- h^0$

¹ ATHAR 07 reports $< 0.38 \times 10^{-3}$ from a measurement of $[\Gamma(\chi_{c0}(1P) \rightarrow \pi^+\pi^-\eta')/\Gamma_{\text{total}}] \times [B(\psi(2S) \rightarrow \gamma\chi_{c0}(1P))]$ assuming $B(\psi(2S) \rightarrow \gamma\chi_{c0}(1P)) = (9.22 \pm 0.11 \pm 0.46) \times 10^{-2}$, which we rescale to our best value $B(\psi(2S) \rightarrow \gamma\chi_{c0}(1P)) = 9.79 \times 10^{-2}$.

$\Gamma(\bar{K}^0 K^+ \pi^- + \text{c.c.})/\Gamma_{\text{total}}$ Γ_{46}/Γ

VALUE (units 10^{-3})	CL%	DOCUMENT ID	TECN	COMMENT
<0.09	90	¹ ATHAR	07 CLEO	$\psi(2S) \rightarrow \gamma h^+ h^- h^0$

• • • We do not use the following data for averages, fits, limits, etc. • • •

<0.7	90	^{2,3} ABLIKIM	06R BES2	$\psi(2S) \rightarrow \gamma\chi_{c0}$
<0.7	90	^{3,4} BAI	99B BES	$\psi(2S) \rightarrow \gamma\chi_{c0}$
¹ ATHAR 07 reports $< 0.10 \times 10^{-3}$ from a measurement of $[\Gamma(\chi_{c0}(1P) \rightarrow \bar{K}^0 K^+ \pi^- + \text{c.c.})/\Gamma_{\text{total}}] \times [B(\psi(2S) \rightarrow \gamma\chi_{c0}(1P))]$ assuming $B(\psi(2S) \rightarrow \gamma\chi_{c0}(1P)) = (9.22 \pm 0.11 \pm 0.46) \times 10^{-2}$, which we rescale to our best value $B(\psi(2S) \rightarrow \gamma\chi_{c0}(1P)) = 9.79 \times 10^{-2}$.				
² ABLIKIM 06R reports $< 0.70 \times 10^{-3}$ from a measurement of $[\Gamma(\chi_{c0}(1P) \rightarrow \bar{K}^0 K^+ \pi^- + \text{c.c.})/\Gamma_{\text{total}}] \times [B(\psi(2S) \rightarrow \gamma\chi_{c0}(1P))]$ assuming $B(\psi(2S) \rightarrow \gamma\chi_{c0}(1P)) = (9.2 \pm 0.4) \times 10^{-2}$, which we rescale to our best value $B(\psi(2S) \rightarrow \gamma\chi_{c0}(1P)) = 9.79 \times 10^{-2}$.				
³ We have multiplied the $K_S^0 K^+ \pi^-$ measurement by a factor of 2 to convert to $K^0 K^+ \pi^-$.				
⁴ Rescaled by us using $B(\psi(2S) \rightarrow \gamma\chi_{c0}) = (9.4 \pm 0.4)\%$ and $B(\psi(2S) \rightarrow J/\psi(1S) \pi^+ \pi^-) = (32.6 \pm 0.5)\%$.				

$\Gamma(K^+ K^- \pi^0)/\Gamma_{\text{total}}$ Γ_{47}/Γ

VALUE (units 10^{-3})	CL%	DOCUMENT ID	TECN	COMMENT
<0.06	90	¹ ATHAR	07 CLEO	$\psi(2S) \rightarrow \gamma h^+ h^- h^0$

¹ ATHAR 07 reports $< 0.06 \times 10^{-3}$ from a measurement of $[\Gamma(\chi_{c0}(1P) \rightarrow K^+ K^- \pi^0)/\Gamma_{\text{total}}] \times [B(\psi(2S) \rightarrow \gamma\chi_{c0}(1P))]$ assuming $B(\psi(2S) \rightarrow \gamma\chi_{c0}(1P)) = (9.22 \pm 0.11 \pm 0.46) \times 10^{-2}$, which we rescale to our best value $B(\psi(2S) \rightarrow \gamma\chi_{c0}(1P)) = 9.79 \times 10^{-2}$.

$\Gamma(K^+ K^- \eta)/\Gamma_{\text{total}}$ Γ_{48}/Γ

VALUE (units 10^{-3})	CL%	DOCUMENT ID	TECN	COMMENT
<0.23	90	¹ ATHAR	07 CLEO	$\psi(2S) \rightarrow \gamma h^+ h^- h^0$

¹ ATHAR 07 reports $< 0.24 \times 10^{-3}$ from a measurement of $[\Gamma(\chi_{c0}(1P) \rightarrow K^+ K^- \eta)/\Gamma_{\text{total}}] \times [B(\psi(2S) \rightarrow \gamma\chi_{c0}(1P))]$ assuming $B(\psi(2S) \rightarrow \gamma\chi_{c0}(1P)) = (9.22 \pm 0.11 \pm 0.46) \times 10^{-2}$, which we rescale to our best value $B(\psi(2S) \rightarrow \gamma\chi_{c0}(1P)) = 9.79 \times 10^{-2}$.

$\Gamma(K^+ K^- K_S^0 K_S^0)/\Gamma_{\text{total}}$ Γ_{49}/Γ

VALUE (units 10^{-3})	EVTS	DOCUMENT ID	TECN	COMMENT
$1.41 \pm 0.47 \pm 0.03$	16.8 ± 4.8	¹ ABLIKIM	05o BES2	$\psi(2S) \rightarrow \gamma\chi_{c0}$

¹ ABLIKIM 05o reports $[\Gamma(\chi_{c0}(1P) \rightarrow K^+ K^- K_S^0 K_S^0)/\Gamma_{\text{total}}] \times [B(\psi(2S) \rightarrow \gamma\chi_{c0}(1P))] = (0.138 \pm 0.039 \pm 0.025) \times 10^{-3}$ which we divide by our best value $B(\psi(2S) \rightarrow \gamma\chi_{c0}(1P)) = (9.79 \pm 0.20) \times 10^{-2}$. Our first error is their experiment's error and our second error is the systematic error from using our best value.

$\Gamma(K_S^0 K_S^0 K_S^0 K_S^0)/\Gamma_{\text{total}}$ Γ_{50}/Γ

VALUE (units 10^{-4})	EVTS	DOCUMENT ID	TECN	COMMENT
$5.8 \pm 0.5 \pm 0.1$	319	¹ ABLIKIM	19AA BES3	$\psi(2S) \rightarrow \gamma 4K_S^0$

¹ Using $B(K_S^0 \rightarrow \pi^+ \pi^-) = (69.20 \pm 0.05)\%$. ABLIKIM 19AA reports $[\Gamma(\chi_{c0}(1P) \rightarrow K_S^0 K_S^0 K_S^0 K_S^0)/\Gamma_{\text{total}}] \times [B(\psi(2S) \rightarrow \gamma\chi_{c0}(1P))] = (5.64 \pm 0.33 \pm 0.37) \times 10^{-5}$ which we divide by our best value $B(\psi(2S) \rightarrow \gamma\chi_{c0}(1P)) = (9.79 \pm 0.20) \times 10^{-2}$. Our first error is their experiment's error and our second error is the systematic error from using our best value..

$\Gamma(K^+ K^- K^+ K^-)/\Gamma_{\text{total}}$ Γ_{51}/Γ

VALUE (units 10^{-3})	DOCUMENT ID
2.82 ± 0.29 OUR FIT	

$\Gamma(K^+ K^- \phi)/\Gamma_{\text{total}}$ Γ_{52}/Γ

VALUE (units 10^{-3})	EVTS	DOCUMENT ID	TECN	COMMENT
$0.97 \pm 0.25 \pm 0.02$	38	¹ ABLIKIM	06T BES2	$\psi(2S) \rightarrow \gamma 2K^+ 2K^-$

¹ ABLIKIM 06T reports $(1.03 \pm 0.22 \pm 0.15) \times 10^{-3}$ from a measurement of $[\Gamma(\chi_{c0}(1P) \rightarrow K^+ K^- \phi)/\Gamma_{\text{total}}] \times [B(\psi(2S) \rightarrow \gamma\chi_{c0}(1P))]$ assuming $B(\psi(2S) \rightarrow \gamma\chi_{c0}(1P)) = (9.2 \pm 0.4) \times 10^{-2}$, which we rescale to our best value $B(\psi(2S) \rightarrow \gamma\chi_{c0}(1P)) = (9.79 \pm 0.20) \times 10^{-2}$. Our first error is their experiment's error and our second error is the systematic error from using our best value.

$\Gamma(\bar{K}^0 K^+ \pi^- \phi + \text{c.c.})/\Gamma_{\text{total}}$ Γ_{53}/Γ

VALUE (units 10^{-3})	DOCUMENT ID	TECN	COMMENT
$3.68 \pm 0.30 \pm 0.50$	ABLIKIM	15M BES3	$\psi(2S) \rightarrow \gamma\chi_{c0}$

$\Gamma(K^+ K^- \pi^0 \phi)/\Gamma_{\text{total}}$ Γ_{54}/Γ

VALUE (units 10^{-3})	DOCUMENT ID	TECN	COMMENT
$1.90 \pm 0.14 \pm 0.32$	ABLIKIM	15M BES3	$\psi(2S) \rightarrow \gamma\chi_{c0}$

$\Gamma(\phi \pi^+ \pi^- \pi^0)/\Gamma_{\text{total}}$ Γ_{55}/Γ

VALUE (units 10^{-3})	EVTS	DOCUMENT ID	TECN	COMMENT
$1.18 \pm 0.07 \pm 0.13$	538	¹ ABLIKIM	13B BES3	$e^+ e^- \rightarrow \psi(2S) \rightarrow \gamma\chi_{c0}$

¹ Using $1.06 \times 10^8 \psi(2S)$ mesons and $B(\psi(2S) \rightarrow \chi_{c0} \gamma) = (9.68 \pm 0.31)\%$.

$\Gamma(\phi \phi)/\Gamma_{\text{total}}$ Γ_{56}/Γ

VALUE (units 10^{-3})	DOCUMENT ID
0.80 ± 0.07 OUR FIT	

$\Gamma(\phi \phi \eta)/\Gamma_{\text{total}}$ Γ_{57}/Γ

VALUE (units 10^{-4})	EVTS	DOCUMENT ID	TECN	COMMENT
$8.4 \pm 0.7 \pm 0.6$	186.6	¹ ABLIKIM	20B BES3	$\psi(2S) \rightarrow \gamma \phi \phi \eta$

¹ ABLIKIM 20B reports $(8.41 \pm 0.74 \pm 0.62) \times 10^{-4}$ from a measurement of $[\Gamma(\chi_{c0}(1P) \rightarrow \phi \phi \eta)/\Gamma_{\text{total}}] \times [B(\psi(2S) \rightarrow \gamma\chi_{c0}(1P))]$ assuming $B(\psi(2S) \rightarrow \gamma\chi_{c0}(1P)) = (9.79 \pm 0.20) \times 10^{-2}$.

$\Gamma(\rho \bar{\rho})/\Gamma_{\text{total}}$ Γ_{58}/Γ

VALUE (units 10^{-4})	DOCUMENT ID
2.21 ± 0.08 OUR FIT	

$\Gamma(\rho \bar{\rho} \pi^0)/\Gamma_{\text{total}}$ Γ_{59}/Γ

VALUE (units 10^{-3})	DOCUMENT ID	TECN	COMMENT
0.70 ± 0.07 OUR AVERAGE	Error includes scale factor of 1.3.		
$0.73 \pm 0.06 \pm 0.01$	¹ ONYISI	10 CLE3	$\psi(2S) \rightarrow \gamma \rho \bar{\rho} X$
$0.56 \pm 0.12 \pm 0.01$	² ATHAR	07 CLEO	$\psi(2S) \rightarrow \gamma h^+ h^- h^0$

¹ ONYISI 10 reports $(7.76 \pm 0.37 \pm 0.51 \pm 0.39) \times 10^{-4}$ from a measurement of $[\Gamma(\chi_{c0}(1P) \rightarrow \rho \bar{\rho} \pi^0)/\Gamma_{\text{total}}] \times [B(\psi(2S) \rightarrow \gamma\chi_{c0}(1P))]$ assuming $B(\psi(2S) \rightarrow \gamma\chi_{c0}(1P)) = (9.22 \pm 0.11 \pm 0.46) \times 10^{-2}$, which we rescale to our best value $B(\psi(2S) \rightarrow \gamma\chi_{c0}(1P)) = (9.79 \pm 0.20) \times 10^{-2}$. Our first error is their experiment's error and our second error is the systematic error from using our best value.

² ATHAR 07 reports $(0.59 \pm 0.10 \pm 0.08) \times 10^{-3}$ from a measurement of $[\Gamma(\chi_{c0}(1P) \rightarrow \rho \bar{\rho} \pi^0)/\Gamma_{\text{total}}] \times [B(\psi(2S) \rightarrow \gamma\chi_{c0}(1P))]$ assuming $B(\psi(2S) \rightarrow \gamma\chi_{c0}(1P)) = (9.22 \pm 0.11 \pm 0.46) \times 10^{-2}$, which we rescale to our best value $B(\psi(2S) \rightarrow \gamma\chi_{c0}(1P)) = (9.79 \pm 0.20) \times 10^{-2}$. Our first error is their experiment's error and our second error is the systematic error from using our best value.

$\Gamma(\rho \bar{\rho} \eta)/\Gamma_{\text{total}}$ Γ_{60}/Γ

VALUE (units 10^{-3})	DOCUMENT ID	TECN	COMMENT
0.35 ± 0.04 OUR AVERAGE			
$0.35 \pm 0.04 \pm 0.01$	¹ ONYISI	10 CLE3	$\psi(2S) \rightarrow \gamma \rho \bar{\rho} X$
$0.37 \pm 0.11 \pm 0.01$	² ATHAR	07 CLEO	$\psi(2S) \rightarrow \gamma h^+ h^- h^0$

¹ ONYISI 10 reports $(3.73 \pm 0.38 \pm 0.28 \pm 0.19) \times 10^{-4}$ from a measurement of $[\Gamma(\chi_{c0}(1P) \rightarrow \rho \bar{\rho} \eta)/\Gamma_{\text{total}}] \times [B(\psi(2S) \rightarrow \gamma\chi_{c0}(1P))]$ assuming $B(\psi(2S) \rightarrow \gamma\chi_{c0}(1P)) = (9.22 \pm 0.11 \pm 0.46) \times 10^{-2}$, which we rescale to our best value $B(\psi(2S) \rightarrow \gamma\chi_{c0}(1P)) = (9.79 \pm 0.20) \times 10^{-2}$. Our first error is their experiment's error and our second error is the systematic error from using our best value.

² ATHAR 07 reports $(0.39 \pm 0.11 \pm 0.04) \times 10^{-3}$ from a measurement of $[\Gamma(\chi_{c0}(1P) \rightarrow \rho \bar{\rho} \eta)/\Gamma_{\text{total}}] \times [B(\psi(2S) \rightarrow \gamma\chi_{c0}(1P))]$ assuming $B(\psi(2S) \rightarrow \gamma\chi_{c0}(1P)) = (9.22 \pm 0.11 \pm 0.46) \times 10^{-2}$, which we rescale to our best value $B(\psi(2S) \rightarrow \gamma\chi_{c0}(1P)) = (9.79 \pm 0.20) \times 10^{-2}$. Our first error is their experiment's error and our second error is the systematic error from using our best value.

$\Gamma(\rho \bar{\rho} \omega)/\Gamma_{\text{total}}$ Γ_{61}/Γ

VALUE (units 10^{-3})	DOCUMENT ID	TECN	COMMENT
$0.52 \pm 0.06 \pm 0.01$	¹ ONYISI	10 CLE3	$\psi(2S) \rightarrow \gamma \rho \bar{\rho} X$

¹ ONYISI 10 reports $(5.57 \pm 0.48 \pm 0.42 \pm 0.14) \times 10^{-4}$ from a measurement of $[\Gamma(\chi_{c0}(1P) \rightarrow \rho \bar{\rho} \omega)/\Gamma_{\text{total}}] \times [B(\psi(2S) \rightarrow \gamma\chi_{c0}(1P))]$ assuming $B(\psi(2S) \rightarrow \gamma\chi_{c0}(1P)) = (9.22 \pm 0.11 \pm 0.46) \times 10^{-2}$, which we rescale to our best value $B(\psi(2S) \rightarrow \gamma\chi_{c0}(1P)) = (9.79 \pm 0.20) \times 10^{-2}$. Our first error is their experiment's error and our second error is the systematic error from using our best value.

$\Gamma(\rho\bar{p}\phi)/\Gamma_{\text{total}}$		Γ_{62}/Γ	
VALUE (units 10^{-5})	EVTS	DOCUMENT ID	TECN COMMENT
6.0 ± 1.4 ± 0.1	42 ± 8	¹ ABLIKIM	11F BES3 $\psi(2S) \rightarrow \gamma\rho\bar{p}K^+K^-$

¹ ABLIKIM 11F reports $(6.12 \pm 1.18 \pm 0.86) \times 10^{-5}$ from a measurement of $[\Gamma(\chi_{c0}(1P) \rightarrow \rho\bar{p}\phi)/\Gamma_{\text{total}}] \times [B(\psi(2S) \rightarrow \gamma\chi_{c0}(1P))]$ assuming $B(\psi(2S) \rightarrow \gamma\chi_{c0}(1P)) = (9.62 \pm 0.31) \times 10^{-2}$, which we rescale to our best value $B(\psi(2S) \rightarrow \gamma\chi_{c0}(1P)) = (9.79 \pm 0.20) \times 10^{-2}$. Our first error is their experiment's error and our second error is the systematic error from using our best value.

$\Gamma(\rho\bar{p}\pi^+\pi^-)/\Gamma_{\text{total}}$		Γ_{63}/Γ	
VALUE (units 10^{-3})	DOCUMENT ID	TECN	COMMENT
2.1 ± 0.7 OUR EVALUATION	Error includes scale factor of 1.4. Treating systematic error as correlated.		
2.1 ± 1.0 OUR AVERAGE	Error includes scale factor of 2.0.		

1.57 ± 0.21 ± 0.53 ¹ BAI 99B BES $\psi(2S) \rightarrow \gamma\chi_{c0}$
 4.20 ± 1.15 ± 0.18 ¹ TANENBAUM 78 MRK1 $\psi(2S) \rightarrow \gamma\chi_{c0}$
¹ Rescaled by us using $B(\psi(2S) \rightarrow \gamma\chi_{c0}) = (9.4 \pm 0.4)\%$ and $B(\psi(2S) \rightarrow J/\psi(1S)\pi^+\pi^-) = (32.6 \pm 0.5)\%$.

$\Gamma(\rho\bar{p}\pi^0\pi^0)/\Gamma_{\text{total}}$		Γ_{64}/Γ	
VALUE (%)	EVTS	DOCUMENT ID	TECN COMMENT
0.104 ± 0.028 ± 0.002	39.5	¹ HE	08B CLEO $e^+e^- \rightarrow \gamma h^+h^-h^0h^0$

¹ HE 08B reports $0.11 \pm 0.02 \pm 0.02 \pm 0.01\%$ from a measurement of $[\Gamma(\chi_{c0}(1P) \rightarrow \rho\bar{p}\pi^0\pi^0)/\Gamma_{\text{total}}] \times [B(\psi(2S) \rightarrow \gamma\chi_{c0}(1P))]$ assuming $B(\psi(2S) \rightarrow \gamma\chi_{c0}(1P)) = (9.22 \pm 0.11 \pm 0.46) \times 10^{-2}$, which we rescale to our best value $B(\psi(2S) \rightarrow \gamma\chi_{c0}(1P)) = (9.79 \pm 0.20) \times 10^{-2}$. Our first error is their experiment's error and our second error is the systematic error from using our best value.

$\Gamma(\rho\bar{p}K^+K^- \text{ (non-resonant)})/\Gamma_{\text{total}}$		Γ_{65}/Γ	
VALUE (units 10^{-4})	EVTS	DOCUMENT ID	TECN COMMENT
1.22 ± 0.26 ± 0.02	48 ± 8	¹ ABLIKIM	11F BES3 $\psi(2S) \rightarrow \gamma\rho\bar{p}K^+K^-$

¹ ABLIKIM 11F reports $(1.24 \pm 0.20 \pm 0.18) \times 10^{-4}$ from a measurement of $[\Gamma(\chi_{c0}(1P) \rightarrow \rho\bar{p}K^+K^- \text{ (non-resonant)})/\Gamma_{\text{total}}] \times [B(\psi(2S) \rightarrow \gamma\chi_{c0}(1P))]$ assuming $B(\psi(2S) \rightarrow \gamma\chi_{c0}(1P)) = (9.62 \pm 0.31) \times 10^{-2}$, which we rescale to our best value $B(\psi(2S) \rightarrow \gamma\chi_{c0}(1P)) = (9.79 \pm 0.20) \times 10^{-2}$. Our first error is their experiment's error and our second error is the systematic error from using our best value.

$\Gamma(\rho\bar{p}K_S^0K_S^0)/\Gamma_{\text{total}}$		Γ_{66}/Γ	
VALUE (units 10^{-4})	CL%	DOCUMENT ID	TECN COMMENT
< 8.8	90	¹ ABLIKIM	06D BES2 $\psi(2S) \rightarrow \chi_{c0}\gamma$

¹ Using $B(\psi(2S) \rightarrow \chi_{c0}\gamma) = (9.2 \pm 0.5)\%$

$\Gamma(\rho\bar{p}\pi^-)/\Gamma_{\text{total}}$		Γ_{67}/Γ	
VALUE (units 10^{-4})	EVTS	DOCUMENT ID	TECN COMMENT
12.7 ± 1.1 OUR AVERAGE	Error includes scale factor of 1.3.		

12.9 ± 1.1 ± 0.3 5150 ¹ ABLIKIM 12J BES3 $\psi(2S) \rightarrow \gamma\rho\bar{p}\pi^-$
 11.2 ± 3.1 ± 0.2 ² ABLIKIM 06I BES2 $\psi(2S) \rightarrow \gamma\rho\pi^-X$
¹ ABLIKIM 12J reports $[\Gamma(\chi_{c0}(1P) \rightarrow \rho\bar{p}\pi^-)/\Gamma_{\text{total}}] \times [B(\psi(2S) \rightarrow \gamma\chi_{c0}(1P))] = (1.26 \pm 0.02 \pm 0.11) \times 10^{-4}$ which we divide by our best value $B(\psi(2S) \rightarrow \gamma\chi_{c0}(1P)) = (9.79 \pm 0.20) \times 10^{-2}$. Our first error is their experiment's error and our second error is the systematic error from using our best value.
² ABLIKIM 06I reports $[\Gamma(\chi_{c0}(1P) \rightarrow \rho\bar{p}\pi^-)/\Gamma_{\text{total}}] \times [B(\psi(2S) \rightarrow \gamma\chi_{c0}(1P))] = (1.10 \pm 0.24 \pm 0.18) \times 10^{-4}$ which we divide by our best value $B(\psi(2S) \rightarrow \gamma\chi_{c0}(1P)) = (9.79 \pm 0.20) \times 10^{-2}$. Our first error is their experiment's error and our second error is the systematic error from using our best value.

$\Gamma(\bar{p}n\pi^+)/\Gamma_{\text{total}}$		Γ_{68}/Γ	
VALUE (units 10^{-4})	EVTS	DOCUMENT ID	TECN COMMENT
13.7 ± 1.2 ± 0.3	5808	¹ ABLIKIM	12J BES3 $\psi(2S) \rightarrow \gamma\bar{p}n\pi^+$

¹ ABLIKIM 12J reports $[\Gamma(\chi_{c0}(1P) \rightarrow \bar{p}n\pi^+)/\Gamma_{\text{total}}] \times [B(\psi(2S) \rightarrow \gamma\chi_{c0}(1P))] = (1.34 \pm 0.03 \pm 0.11) \times 10^{-4}$ which we divide by our best value $B(\psi(2S) \rightarrow \gamma\chi_{c0}(1P)) = (9.79 \pm 0.20) \times 10^{-2}$. Our first error is their experiment's error and our second error is the systematic error from using our best value.

$\Gamma(\rho\bar{p}\pi^-\pi^0)/\Gamma_{\text{total}}$		Γ_{69}/Γ	
VALUE (units 10^{-4})	EVTS	DOCUMENT ID	TECN COMMENT
23.4 ± 2.0 ± 0.5	2480	¹ ABLIKIM	12J BES3 $\psi(2S) \rightarrow \gamma\rho\bar{p}\pi^-\pi^0$

¹ ABLIKIM 12J reports $[\Gamma(\chi_{c0}(1P) \rightarrow \rho\bar{p}\pi^-\pi^0)/\Gamma_{\text{total}}] \times [B(\psi(2S) \rightarrow \gamma\chi_{c0}(1P))] = (2.29 \pm 0.08 \pm 0.18) \times 10^{-4}$ which we divide by our best value $B(\psi(2S) \rightarrow \gamma\chi_{c0}(1P)) = (9.79 \pm 0.20) \times 10^{-2}$. Our first error is their experiment's error and our second error is the systematic error from using our best value.

$\Gamma(\bar{p}n\pi^+\pi^0)/\Gamma_{\text{total}}$		Γ_{70}/Γ	
VALUE (units 10^{-4})	EVTS	DOCUMENT ID	TECN COMMENT
22.1 ± 1.8 ± 0.5	2757	¹ ABLIKIM	12J BES3 $\psi(2S) \rightarrow \gamma\bar{p}n\pi^+\pi^0$

¹ ABLIKIM 12J reports $[\Gamma(\chi_{c0}(1P) \rightarrow \bar{p}n\pi^+\pi^0)/\Gamma_{\text{total}}] \times [B(\psi(2S) \rightarrow \gamma\chi_{c0}(1P))] = (2.16 \pm 0.07 \pm 0.16) \times 10^{-4}$ which we divide by our best value $B(\psi(2S) \rightarrow \gamma\chi_{c0}(1P)) = (9.79 \pm 0.20) \times 10^{-2}$. Our first error is their experiment's error and our second error is the systematic error from using our best value.

$\Gamma(\Lambda\bar{\Lambda})/\Gamma_{\text{total}}$		Γ_{71}/Γ	
VALUE (units 10^{-4})	DOCUMENT ID	TECN	COMMENT
3.27 ± 0.24 OUR FIT			

$\Gamma(\Lambda\bar{\Lambda}\pi^+\pi^-)/\Gamma_{\text{total}}$		Γ_{72}/Γ	
VALUE (units 10^{-5})	CL%	EVTS	DOCUMENT ID
118 ± 12 ± 2	426	¹ ABLIKIM	12I BES3 $\psi(2S) \rightarrow \gamma\Lambda\bar{\Lambda}\pi^+\pi^-$

••• We do not use the following data for averages, fits, limits, etc. **••••**
 <400 90 ² ABLIKIM 06D BES2 $\psi(2S) \rightarrow \chi_{c0}\gamma$
¹ ABLIKIM 12I reports $(119.0 \pm 6.4 \pm 11.4) \times 10^{-5}$ from a measurement of $[\Gamma(\chi_{c0}(1P) \rightarrow \Lambda\bar{\Lambda}\pi^+\pi^-)/\Gamma_{\text{total}}] \times [B(\psi(2S) \rightarrow \gamma\chi_{c0}(1P))]$ assuming $B(\psi(2S) \rightarrow \gamma\chi_{c0}(1P)) = (9.68 \pm 0.31) \times 10^{-2}$, which we rescale to our best value $B(\psi(2S) \rightarrow \gamma\chi_{c0}(1P)) = (9.79 \pm 0.20) \times 10^{-2}$. Our first error is their experiment's error and our second error is the systematic error from using our best value.
² Using $B(\psi(2S) \rightarrow \chi_{c0}\gamma) = (9.2 \pm 0.5)\%$

$\Gamma(\Lambda\bar{\Lambda}\pi^+\pi^- \text{ (non-resonant)})/\Gamma_{\text{total}}$		Γ_{73}/Γ	
VALUE (units 10^{-5})	CL%	DOCUMENT ID	TECN COMMENT
< 50	90	¹ ABLIKIM	12I BES3 $\psi(2S) \rightarrow \gamma\Lambda\bar{\Lambda}\pi^+\pi^-$

¹ ABLIKIM 12I reports $< 54 \times 10^{-5}$ from a measurement of $[\Gamma(\chi_{c0}(1P) \rightarrow \Lambda\bar{\Lambda}\pi^+\pi^- \text{ (non-resonant)})/\Gamma_{\text{total}}] \times [B(\psi(2S) \rightarrow \gamma\chi_{c0}(1P))]$ assuming $B(\psi(2S) \rightarrow \gamma\chi_{c0}(1P)) = (9.68 \pm 0.31) \times 10^{-2}$, which we rescale to our best value $B(\psi(2S) \rightarrow \gamma\chi_{c0}(1P)) = (9.79 \pm 0.20) \times 10^{-2}$.

$\Gamma(\Sigma(1385)^+\bar{\Lambda}\pi^- + \text{c.c.})/\Gamma_{\text{total}}$		Γ_{74}/Γ	
VALUE (units 10^{-5})	CL%	DOCUMENT ID	TECN COMMENT
< 50	90	¹ ABLIKIM	12I BES3 $\psi(2S) \rightarrow \gamma\Sigma(1385)^+\bar{\Lambda}\pi^-$

¹ ABLIKIM 12I reports $< 55 \times 10^{-5}$ from a measurement of $[\Gamma(\chi_{c0}(1P) \rightarrow \Sigma(1385)^+\bar{\Lambda}\pi^- + \text{c.c.})/\Gamma_{\text{total}}] \times [B(\psi(2S) \rightarrow \gamma\chi_{c0}(1P))]$ assuming $B(\psi(2S) \rightarrow \gamma\chi_{c0}(1P)) = (9.68 \pm 0.31) \times 10^{-2}$, which we rescale to our best value $B(\psi(2S) \rightarrow \gamma\chi_{c0}(1P)) = (9.79 \pm 0.20) \times 10^{-2}$.

$\Gamma(\Sigma(1385)^-\bar{\Lambda}\pi^+ + \text{c.c.})/\Gamma_{\text{total}}$		Γ_{75}/Γ	
VALUE (units 10^{-5})	CL%	DOCUMENT ID	TECN COMMENT
< 50	90	¹ ABLIKIM	12I BES3 $\psi(2S) \rightarrow \gamma\Sigma(1385)^-\bar{\Lambda}\pi^+$

¹ ABLIKIM 12I reports $< 50 \times 10^{-5}$ from a measurement of $[\Gamma(\chi_{c0}(1P) \rightarrow \Sigma(1385)^-\bar{\Lambda}\pi^+ + \text{c.c.})/\Gamma_{\text{total}}] \times [B(\psi(2S) \rightarrow \gamma\chi_{c0}(1P))]$ assuming $B(\psi(2S) \rightarrow \gamma\chi_{c0}(1P)) = (9.68 \pm 0.31) \times 10^{-2}$, which we rescale to our best value $B(\psi(2S) \rightarrow \gamma\chi_{c0}(1P)) = (9.79 \pm 0.20) \times 10^{-2}$.

$\Gamma(K^+\bar{p}\Lambda + \text{c.c.})/\Gamma_{\text{total}}$		Γ_{76}/Γ	
VALUE (units 10^{-3})	EVTS	DOCUMENT ID	TECN COMMENT
1.25 ± 0.12 OUR AVERAGE	Error includes scale factor of 1.3.		

1.30 ± 0.09 ± 0.03 9k ^{1,2} ABLIKIM 13D BES3 $\psi(2S) \rightarrow \gamma\Lambda\bar{p}K^+$
 1.01 ± 0.19 ± 0.02 ³ ATHAR 07 CLEO $\psi(2S) \rightarrow \gamma h^+h^-h^0$
¹ ABLIKIM 13D reports $(1.32 \pm 0.03 \pm 0.10) \times 10^{-3}$ from a measurement of $[\Gamma(\chi_{c0}(1P) \rightarrow K^+\bar{p}\Lambda + \text{c.c.})/\Gamma_{\text{total}}] \times [B(\psi(2S) \rightarrow \gamma\chi_{c0}(1P))]$ assuming $B(\psi(2S) \rightarrow \gamma\chi_{c0}(1P)) = (9.68 \pm 0.31) \times 10^{-2}$, which we rescale to our best value $B(\psi(2S) \rightarrow \gamma\chi_{c0}(1P)) = (9.79 \pm 0.20) \times 10^{-2}$. Our first error is their experiment's error and our second error is the systematic error from using our best value.
² Using $B(\Lambda \rightarrow p\pi^-) = 63.9\%$.
³ ATHAR 07 reports $(1.07 \pm 0.17 \pm 0.12) \times 10^{-3}$ from a measurement of $[\Gamma(\chi_{c0}(1P) \rightarrow K^+\bar{p}\Lambda + \text{c.c.})/\Gamma_{\text{total}}] \times [B(\psi(2S) \rightarrow \gamma\chi_{c0}(1P))]$ assuming $B(\psi(2S) \rightarrow \gamma\chi_{c0}(1P)) = (9.22 \pm 0.11 \pm 0.46) \times 10^{-2}$, which we rescale to our best value $B(\psi(2S) \rightarrow \gamma\chi_{c0}(1P)) = (9.79 \pm 0.20) \times 10^{-2}$. Our first error is their experiment's error and our second error is the systematic error from using our best value.

$\Gamma(K^*(892)^+\bar{p}\Lambda + \text{c.c.})/\Gamma_{\text{total}}$		Γ_{77}/Γ	
VALUE (units 10^{-4})	EVTS	DOCUMENT ID	TECN COMMENT
4.8 ± 0.9 ± 0.1	254	¹ ABLIKIM	19AU BES3 $\psi(2S) \rightarrow \gamma K^{*+}\bar{p}\Lambda$

¹ ABLIKIM 19AU reports $[\Gamma(\chi_{c0}(1P) \rightarrow K^*(892)^+\bar{p}\Lambda + \text{c.c.})/\Gamma_{\text{total}}] \times [B(\psi(2S) \rightarrow \gamma\chi_{c0}(1P))] = (4.7 \pm 0.7 \pm 0.5) \times 10^{-4}$ which we divide by our best value $B(\psi(2S) \rightarrow \gamma\chi_{c0}(1P)) = (9.79 \pm 0.20) \times 10^{-2}$. Our first error is their experiment's error and our second error is the systematic error from using our best value.

$\Gamma(K^+\bar{p}\Lambda(1520) + \text{c.c.})/\Gamma_{\text{total}}$		Γ_{78}/Γ	
VALUE (units 10^{-4})	EVTS	DOCUMENT ID	TECN COMMENT
2.9 ± 0.7 ± 0.1	62 ± 12	¹ ABLIKIM	11F BES3 $\psi(2S) \rightarrow \gamma\rho\bar{p}K^+K^-$

¹ ABLIKIM 11F reports $(3.00 \pm 0.58 \pm 0.50) \times 10^{-4}$ from a measurement of $[\Gamma(\chi_{c0}(1P) \rightarrow K^+\bar{p}\Lambda(1520) + \text{c.c.})/\Gamma_{\text{total}}] \times [B(\psi(2S) \rightarrow \gamma\chi_{c0}(1P))]$ assuming $B(\psi(2S) \rightarrow \gamma\chi_{c0}(1P)) = (9.62 \pm 0.31) \times 10^{-2}$, which we rescale to our best value $B(\psi(2S) \rightarrow \gamma\chi_{c0}(1P)) = (9.79 \pm 0.20) \times 10^{-2}$. Our first error is their experiment's error and our second error is the systematic error from using our best value.

Meson Particle Listings

$\chi_{c0}(1P)$

$\Gamma(\Lambda(1520)\bar{\Lambda}(1520))/\Gamma_{total}$ Γ_{79}/Γ

VALUE (units 10^{-4})	EVTS	DOCUMENT ID	TECN	COMMENT
3.1 ± 1.2 ± 0.1	28 ± 10	¹ ABLIKIM	11F BES3	$\psi(2S) \rightarrow \gamma \rho^0 K^+ K^-$

¹ ABLIKIM 11F reports $(3.18 \pm 1.11 \pm 0.53) \times 10^{-4}$ from a measurement of $[\Gamma(\chi_{c0}(1P) \rightarrow \Lambda(1520)\bar{\Lambda}(1520))/\Gamma_{total}] \times [B(\psi(2S) \rightarrow \gamma \chi_{c0}(1P))]$ assuming $B(\psi(2S) \rightarrow \gamma \chi_{c0}(1P)) = (9.62 \pm 0.31) \times 10^{-2}$, which we rescale to our best value $B(\psi(2S) \rightarrow \gamma \chi_{c0}(1P)) = (9.79 \pm 0.20) \times 10^{-2}$. Our first error is their experiment's error and our second error is the systematic error from using our best value.

$\Gamma(\Sigma^0 \bar{\Sigma}^0)/\Gamma_{total}$ Γ_{80}/Γ

VALUE (units 10^{-4})	EVTS	DOCUMENT ID	TECN	COMMENT
4.68 ± 0.32 OUR AVERAGE				
4.82 ± 0.34 ± 0.10	1046	¹ ABLIKIM	18V BES3	$\psi(2S) \rightarrow \gamma \Sigma^0 \bar{\Sigma}^0$
4.2 ± 0.7 ± 0.1	78 ± 10	² NAIK	08 CLEO	$\psi(2S) \rightarrow \gamma \Sigma^0 \bar{\Sigma}^0$
4.7 ± 0.5 ± 0.1	243	^{3,4} ABLIKIM	13H BES3	$\psi(2S) \rightarrow \gamma \Sigma^0 \bar{\Sigma}^0$

¹ ABLIKIM 18V reports $[\Gamma(\chi_{c0}(1P) \rightarrow \Sigma^0 \bar{\Sigma}^0)/\Gamma_{total}] \times [B(\psi(2S) \rightarrow \gamma \chi_{c0}(1P))] = (4.72 \pm 0.18 \pm 0.28) \times 10^{-5}$ which we divide by our best value $B(\psi(2S) \rightarrow \gamma \chi_{c0}(1P)) = (9.79 \pm 0.20) \times 10^{-2}$. Our first error is their experiment's error and our second error is the systematic error from using our best value.

² NAIK 08 reports $(4.41 \pm 0.56 \pm 0.47) \times 10^{-4}$ from a measurement of $[\Gamma(\chi_{c0}(1P) \rightarrow \Sigma^0 \bar{\Sigma}^0)/\Gamma_{total}] \times [B(\psi(2S) \rightarrow \gamma \chi_{c0}(1P))]$ assuming $B(\psi(2S) \rightarrow \gamma \chi_{c0}(1P)) = (9.22 \pm 0.11 \pm 0.46) \times 10^{-2}$, which we rescale to our best value $B(\psi(2S) \rightarrow \gamma \chi_{c0}(1P)) = (9.79 \pm 0.20) \times 10^{-2}$. Our first error is their experiment's error and our second error is the systematic error from using our best value.

³ ABLIKIM 13H reports $(4.78 \pm 0.34 \pm 0.39) \times 10^{-4}$ from a measurement of $[\Gamma(\chi_{c0}(1P) \rightarrow \Sigma^0 \bar{\Sigma}^0)/\Gamma_{total}] \times [B(\psi(2S) \rightarrow \gamma \chi_{c0}(1P))]$ assuming $B(\psi(2S) \rightarrow \gamma \chi_{c0}(1P)) = (9.62 \pm 0.31) \times 10^{-2}$, which we rescale to our best value $B(\psi(2S) \rightarrow \gamma \chi_{c0}(1P)) = (9.79 \pm 0.20) \times 10^{-2}$. Our first error is their experiment's error and our second error is the systematic error from using our best value.

⁴ Superseded by ABLIKIM 18V

$\Gamma(\Sigma^+ \bar{\Sigma}^-)/\Gamma_{total}$ Γ_{82}/Γ

VALUE (units 10^{-4})	EVTS	DOCUMENT ID	TECN	COMMENT
4.6 ± 0.8 OUR AVERAGE				Error includes scale factor of 2.6.
5.10 ± 0.35 ± 0.10	747	¹ ABLIKIM	18V BES3	$\psi(2S) \rightarrow \gamma \Sigma^+ \bar{\Sigma}^-$
3.1 ± 0.7 ± 0.1	39 ± 7	² NAIK	08 CLEO	$\psi(2S) \rightarrow \gamma \Sigma^+ \bar{\Sigma}^-$

¹ ABLIKIM 18V reports $[\Gamma(\chi_{c0}(1P) \rightarrow \Sigma^+ \bar{\Sigma}^-)/\Gamma_{total}] \times [B(\psi(2S) \rightarrow \gamma \chi_{c0}(1P))] = (4.99 \pm 0.24 \pm 0.24) \times 10^{-5}$ which we divide by our best value $B(\psi(2S) \rightarrow \gamma \chi_{c0}(1P)) = (9.79 \pm 0.20) \times 10^{-2}$. Our first error is their experiment's error and our second error is the systematic error from using our best value.

² NAIK 08 reports $(3.25 \pm 0.57 \pm 0.43) \times 10^{-4}$ from a measurement of $[\Gamma(\chi_{c0}(1P) \rightarrow \Sigma^+ \bar{\Sigma}^-)/\Gamma_{total}] \times [B(\psi(2S) \rightarrow \gamma \chi_{c0}(1P))]$ assuming $B(\psi(2S) \rightarrow \gamma \chi_{c0}(1P)) = (9.22 \pm 0.11 \pm 0.46) \times 10^{-2}$, which we rescale to our best value $B(\psi(2S) \rightarrow \gamma \chi_{c0}(1P)) = (9.79 \pm 0.20) \times 10^{-2}$. Our first error is their experiment's error and our second error is the systematic error from using our best value.

³ ABLIKIM 13H reports $(4.54 \pm 0.42 \pm 0.30) \times 10^{-4}$ from a measurement of $[\Gamma(\chi_{c0}(1P) \rightarrow \Sigma^+ \bar{\Sigma}^-)/\Gamma_{total}] \times [B(\psi(2S) \rightarrow \gamma \chi_{c0}(1P))]$ assuming $B(\psi(2S) \rightarrow \gamma \chi_{c0}(1P)) = (9.62 \pm 0.31) \times 10^{-2}$, which we rescale to our best value $B(\psi(2S) \rightarrow \gamma \chi_{c0}(1P)) = (9.79 \pm 0.20) \times 10^{-2}$. Our first error is their experiment's error and our second error is the systematic error from using our best value.

⁴ Superseded by ABLIKIM 18V

$\Gamma(\Sigma(1385)^+ \bar{\Sigma}(1385)^-)/\Gamma_{total}$ Γ_{83}/Γ

VALUE (units 10^{-5})	EVTS	DOCUMENT ID	TECN	COMMENT
16.2 ± 5.8 ± 0.3	27	¹ ABLIKIM	12I BES3	$\psi(2S) \rightarrow \gamma \Lambda \bar{\Lambda} \pi^+ \pi^-$

¹ ABLIKIM 12I reports $(16.4 \pm 5.7 \pm 1.6) \times 10^{-5}$ from a measurement of $[\Gamma(\chi_{c0}(1P) \rightarrow \Sigma(1385)^+ \bar{\Sigma}(1385)^-)/\Gamma_{total}] \times [B(\psi(2S) \rightarrow \gamma \chi_{c0}(1P))]$ assuming $B(\psi(2S) \rightarrow \gamma \chi_{c0}(1P)) = (9.68 \pm 0.31) \times 10^{-2}$, which we rescale to our best value $B(\psi(2S) \rightarrow \gamma \chi_{c0}(1P)) = (9.79 \pm 0.20) \times 10^{-2}$. Our first error is their experiment's error and our second error is the systematic error from using our best value.

$\Gamma(\Sigma(1385)^- \bar{\Sigma}(1385)^+)/\Gamma_{total}$ Γ_{84}/Γ

VALUE (units 10^{-5})	EVTS	DOCUMENT ID	TECN	COMMENT
23.2 ± 6.5 ± 0.5	33	¹ ABLIKIM	12I BES3	$\psi(2S) \rightarrow \gamma \Lambda \bar{\Lambda} \pi^+ \pi^-$

¹ ABLIKIM 12I reports $(23.5 \pm 6.2 \pm 2.3) \times 10^{-5}$ from a measurement of $[\Gamma(\chi_{c0}(1P) \rightarrow \Sigma(1385)^- \bar{\Sigma}(1385)^+)/\Gamma_{total}] \times [B(\psi(2S) \rightarrow \gamma \chi_{c0}(1P))]$ assuming $B(\psi(2S) \rightarrow \gamma \chi_{c0}(1P)) = (9.68 \pm 0.31) \times 10^{-2}$, which we rescale to our best value $B(\psi(2S) \rightarrow \gamma \chi_{c0}(1P)) = (9.79 \pm 0.20) \times 10^{-2}$. Our first error is their experiment's error and our second error is the systematic error from using our best value.

$\Gamma(K^- \Lambda \bar{\Xi}^+ + c.c.)/\Gamma_{total}$ Γ_{85}/Γ

VALUE (units 10^{-4})	EVTS	DOCUMENT ID	TECN	COMMENT
1.94 ± 0.35 ± 0.04	57	¹ ABLIKIM	15I BES3	$\psi(2S) \rightarrow \gamma K^- \Lambda \bar{\Xi}^+ + c.c.$

¹ ABLIKIM 15I reports $[\Gamma(\chi_{c0}(1P) \rightarrow K^- \Lambda \bar{\Xi}^+ + c.c.)/\Gamma_{total}] \times [B(\psi(2S) \rightarrow \gamma \chi_{c0}(1P))] = (1.90 \pm 0.30 \pm 0.16) \times 10^{-5}$ which we divide by our best value $B(\psi(2S) \rightarrow \gamma \chi_{c0}(1P)) = (9.79 \pm 0.20) \times 10^{-2}$. Our first error is their experiment's error and our second error is the systematic error from using our best value.

$\Gamma(\Xi^0 \bar{\Xi}^0)/\Gamma_{total}$ Γ_{86}/Γ

VALUE (units 10^{-4})	EVTS	DOCUMENT ID	TECN	COMMENT
3.1 ± 0.8 ± 0.1	23.3 ± 4.9	¹ NAIK	08 CLEO	$\psi(2S) \rightarrow \gamma \Xi^0 \bar{\Xi}^0$

¹ NAIK 08 reports $(3.34 \pm 0.70 \pm 0.48) \times 10^{-4}$ from a measurement of $[\Gamma(\chi_{c0}(1P) \rightarrow \Xi^0 \bar{\Xi}^0)/\Gamma_{total}] \times [B(\psi(2S) \rightarrow \gamma \chi_{c0}(1P))]$ assuming $B(\psi(2S) \rightarrow \gamma \chi_{c0}(1P)) = (9.22 \pm 0.11 \pm 0.46) \times 10^{-2}$, which we rescale to our best value $B(\psi(2S) \rightarrow \gamma \chi_{c0}(1P)) = (9.79 \pm 0.20) \times 10^{-2}$. Our first error is their experiment's error and our second error is the systematic error from using our best value.

$\Gamma(\Xi^- \bar{\Xi}^+)/\Gamma_{total}$ Γ_{87}/Γ

VALUE (units 10^{-4})	CL%	EVTS	DOCUMENT ID	TECN	COMMENT
4.8 ± 0.7 ± 0.1		95 ± 11	¹ NAIK	08 CLEO	$\psi(2S) \rightarrow \gamma \Xi^- \bar{\Xi}^+$
<10.3	90		² ABLIKIM	06D BES2	$\psi(2S) \rightarrow \chi_{c0} \gamma$

¹ NAIK 08 reports $(5.14 \pm 0.60 \pm 0.47) \times 10^{-4}$ from a measurement of $[\Gamma(\chi_{c0}(1P) \rightarrow \Xi^- \bar{\Xi}^+)/\Gamma_{total}] \times [B(\psi(2S) \rightarrow \gamma \chi_{c0}(1P))]$ assuming $B(\psi(2S) \rightarrow \gamma \chi_{c0}(1P)) = (9.22 \pm 0.11 \pm 0.46) \times 10^{-2}$, which we rescale to our best value $B(\psi(2S) \rightarrow \gamma \chi_{c0}(1P)) = (9.79 \pm 0.20) \times 10^{-2}$. Our first error is their experiment's error and our second error is the systematic error from using our best value.

² Using $B(\psi(2S) \rightarrow \chi_{c0} \gamma) = (9.2 \pm 0.5)\%$

$\Gamma(\eta_c \pi^+ \pi^-)/\Gamma_{total}$ Γ_{88}/Γ

VALUE	CL%	DOCUMENT ID	TECN	COMMENT
< 7 × 10⁻⁴	90	^{1,2} ABLIKIM	13B BES3	$e^+ e^- \rightarrow \psi(2S) \rightarrow \gamma \chi_{c0}$
<41 × 10 ⁻⁴	90	^{1,3} ABLIKIM	13B BES3	$e^+ e^- \rightarrow \psi(2S) \rightarrow \gamma \chi_{c0}$

¹ Using 1.06×10^8 $\psi(2S)$ mesons and $B(\psi(2S) \rightarrow \chi_{c0} \gamma) = (9.68 \pm 0.31)\%$.

² From the $\eta_c \rightarrow K_S^0 K^{\pm} \pi^{\mp}$ decays.

³ From the $\eta_c \rightarrow K^+ K^- \pi^0$ decays.

$\Gamma(\rho^0 \bar{\rho}^0)/\Gamma_{total} \times \Gamma(\pi^+ \pi^-)/\Gamma_{total}$ $\Gamma_{58}/\Gamma \times \Gamma_{32}/\Gamma$

VALUE (units 10^{-7})	DOCUMENT ID	TECN	COMMENT
18.8 ± 1.0 OUR FIT			
15.3 ± 2.4 ± 0.8	¹ ANDREOTTI	03 E835	$\bar{p} p \rightarrow \chi_{c0} \rightarrow \pi^0 \pi^0$

¹ We have multiplied $B(\rho^0 \bar{\rho}^0) \cdot B(\pi^0 \pi^0)$ measurement by 3 to obtain $B(\rho^0 \bar{\rho}^0) \cdot B(\pi^0 \pi^0)$.

$\Gamma(\rho^0 \bar{\rho}^0)/\Gamma_{total} \times \Gamma(\pi^0 \eta)/\Gamma_{total}$ $\Gamma_{58}/\Gamma \times \Gamma_{33}/\Gamma$

VALUE (units 10^{-7})	DOCUMENT ID	TECN	COMMENT
<0.4	ANDREOTTI	05c E835	$\bar{p} p \rightarrow \pi^0 \eta$

$\Gamma(\rho^0 \bar{\rho}^0)/\Gamma_{total} \times \Gamma(\pi^0 \eta')/\Gamma_{total}$ $\Gamma_{58}/\Gamma \times \Gamma_{34}/\Gamma$

VALUE (units 10^{-7})	DOCUMENT ID	TECN	COMMENT
<2.5	ANDREOTTI	05c E835	$\bar{p} p \rightarrow \pi^0 \eta$

$\Gamma(\rho^0 \bar{\rho}^0)/\Gamma_{total} \times \Gamma(\eta \eta)/\Gamma_{total}$ $\Gamma_{58}/\Gamma \times \Gamma_{36}/\Gamma$

VALUE (units 10^{-7})	DOCUMENT ID	TECN	COMMENT
6.7 ± 0.5 OUR FIT			
4.0 ± 1.2 ± 0.5	ANDREOTTI	05c E835	$\bar{p} p \rightarrow \eta \eta$

$\Gamma(\rho^0 \bar{\rho}^0)/\Gamma_{total} \times \Gamma(\eta \eta')/\Gamma_{total}$ $\Gamma_{58}/\Gamma \times \Gamma_{37}/\Gamma$

VALUE (units 10^{-6})	DOCUMENT ID	TECN	COMMENT
2.1 ± 2.3	ANDREOTTI	05c E835	$\bar{p} p \rightarrow \pi^0 \eta$
-1.5			

RADIATIVE DECAYS

$\Gamma(\gamma J/\psi(1S))/\Gamma_{total}$ Γ_{89}/Γ

VALUE (units 10^{-2})	EVTS	DOCUMENT ID	TECN	COMMENT
1.40 ± 0.05 OUR FIT				

¹ We do not use the following data for averages, fits, limits, etc. **•••**

0.25 ± 0.16 ± 2.15	12k	¹ ABLIKIM	17U BES3	$e^+ e^- \rightarrow \gamma X$
2.0 ± 0.2 ± 0.2		² ADAM	05A CLEO	$e^+ e^- \rightarrow \psi(2S) \rightarrow \gamma \chi_{c0}$

¹ Not independent from $B(\psi(2S) \rightarrow \gamma \chi_{c0}(1P))$ and the product $B(\psi(2S) \rightarrow \gamma \chi_{c0}(1P)) \times B(\chi_{c0}(1P) \rightarrow \gamma J/\psi(1S))$ also measured in ABLIKIM 17U.

² Uses $B(\psi(2S) \rightarrow \gamma \chi_{c0}) \rightarrow \gamma J/\psi$ from ADAM 05A and $B(\psi(2S) \rightarrow \gamma \chi_{c0})$ from ATHAR 04.

$\Gamma(\gamma \rho^0)/\Gamma_{total}$ Γ_{90}/Γ

VALUE (units 10^{-6})	CL%	EVTS	DOCUMENT ID	TECN	COMMENT
< 9	90	1.2 ± 4.5	¹ BENNETT	08A CLEO	$\psi(2S) \rightarrow \gamma \gamma \rho^0$
<10	90	6 ± 12	² ABLIKIM	11E BES3	$\psi(2S) \rightarrow \gamma \gamma \rho^0$

¹ BENNETT 08A reports $< 9.6 \times 10^{-6}$ from a measurement of $[\Gamma(\chi_{c0}(1P) \rightarrow \gamma \rho^0)/\Gamma_{total}] \times [B(\psi(2S) \rightarrow \gamma \chi_{c0}(1P))]$ assuming $B(\psi(2S) \rightarrow \gamma \chi_{c0}(1P)) = (9.2 \pm 0.4) \times 10^{-2}$, which we rescale to our best value $B(\psi(2S) \rightarrow \gamma \chi_{c0}(1P)) = 9.79 \times 10^{-2}$.

² ABLIKIM 11E reports $< 10.5 \times 10^{-6}$ from a measurement of $[\Gamma(\chi_{c0}(1P) \rightarrow \gamma \rho^0)/\Gamma_{total}] \times [B(\psi(2S) \rightarrow \gamma \chi_{c0}(1P))]$ assuming $B(\psi(2S) \rightarrow \gamma \chi_{c0}(1P)) = (9.62 \pm 0.31) \times 10^{-2}$, which we rescale to our best value $B(\psi(2S) \rightarrow \gamma \chi_{c0}(1P)) = 9.79 \times 10^{-2}$.

$\Gamma(\gamma\omega)/\Gamma_{total}$ Γ_{91}/Γ

VALUE (units 10 ⁻⁶)	CL%	EVTS	DOCUMENT ID	TECN	COMMENT
< 8	90	0.0 ± 2.8	¹ BENNETT 08A	CLEO	$\psi(2S) \rightarrow \gamma\gamma\omega$
••• We do not use the following data for averages, fits, limits, etc. •••					
<13	90	5 ± 11	² ABLIKIM 11E	BES3	$\psi(2S) \rightarrow \gamma\gamma\omega$
¹ BENNETT 08A reports < 8.8 × 10 ⁻⁶ from a measurement of $[\Gamma(\chi_{c0}(1P) \rightarrow \gamma\omega)/\Gamma_{total}] \times [B(\psi(2S) \rightarrow \gamma\chi_{c0}(1P))]$ assuming $B(\psi(2S) \rightarrow \gamma\chi_{c0}(1P)) = (9.2 \pm 0.4) \times 10^{-2}$, which we rescale to our best value $B(\psi(2S) \rightarrow \gamma\chi_{c0}(1P)) = 9.79 \times 10^{-2}$. ² ABLIKIM 11E reports < 12.9 × 10 ⁻⁶ from a measurement of $[\Gamma(\chi_{c0}(1P) \rightarrow \gamma\omega)/\Gamma_{total}] \times [B(\psi(2S) \rightarrow \gamma\chi_{c0}(1P))]$ assuming $B(\psi(2S) \rightarrow \gamma\chi_{c0}(1P)) = (9.62 \pm 0.31) \times 10^{-2}$, which we rescale to our best value $B(\psi(2S) \rightarrow \gamma\chi_{c0}(1P)) = 9.79 \times 10^{-2}$.					

$\Gamma(\gamma\phi)/\Gamma_{total}$ Γ_{92}/Γ

VALUE (units 10 ⁻⁶)	CL%	EVTS	DOCUMENT ID	TECN	COMMENT
< 6	90	0.1 ± 1.6	¹ BENNETT 08A	CLEO	$\psi(2S) \rightarrow \gamma\gamma\phi$
••• We do not use the following data for averages, fits, limits, etc. •••					
<16	90	15 ± 7	² ABLIKIM 11E	BES3	$\psi(2S) \rightarrow \gamma\gamma\phi$
¹ BENNETT 08A reports < 6.4 × 10 ⁻⁶ from a measurement of $[\Gamma(\chi_{c0}(1P) \rightarrow \gamma\phi)/\Gamma_{total}] \times [B(\psi(2S) \rightarrow \gamma\chi_{c0}(1P))]$ assuming $B(\psi(2S) \rightarrow \gamma\chi_{c0}(1P)) = (9.2 \pm 0.4) \times 10^{-2}$, which we rescale to our best value $B(\psi(2S) \rightarrow \gamma\chi_{c0}(1P)) = 9.79 \times 10^{-2}$. ² ABLIKIM 11E reports < 16.2 × 10 ⁻⁶ from a measurement of $[\Gamma(\chi_{c0}(1P) \rightarrow \gamma\phi)/\Gamma_{total}] \times [B(\psi(2S) \rightarrow \gamma\chi_{c0}(1P))]$ assuming $B(\psi(2S) \rightarrow \gamma\chi_{c0}(1P)) = (9.62 \pm 0.31) \times 10^{-2}$, which we rescale to our best value $B(\psi(2S) \rightarrow \gamma\chi_{c0}(1P)) = 9.79 \times 10^{-2}$.					

$\Gamma(\gamma\eta)/\Gamma_{total}$ Γ_{93}/Γ

VALUE (units 10 ⁻⁴)	CL%	DOCUMENT ID	TECN	COMMENT
2.04 ± 0.09 OUR FIT				
••• We do not use the following data for averages, fits, limits, etc. •••				
<7	90	¹ WICHT 08	BELL	$B^{\pm} \rightarrow K^{\pm}\gamma\eta$
¹ WICHT 08 reports $[\Gamma(\chi_{c0}(1P) \rightarrow \gamma\eta)/\Gamma_{total}] \times [B(B^{\pm} \rightarrow \chi_{c0} K^{\pm})] < 0.11 \times 10^{-6}$ which we divide by our best value $B(B^{\pm} \rightarrow \chi_{c0} K^{\pm}) = 1.50 \times 10^{-4}$.				

$\Gamma(e^{+}e^{-}J/\psi(1S))/\Gamma_{total}$ Γ_{94}/Γ

VALUE (units 10 ⁻⁴)	EVTS	DOCUMENT ID	TECN	COMMENT
1.54 ± 0.33 ± 0.03	56	^{1,2} ABLIKIM 17I	BES3	$\psi(2S) \rightarrow \gamma e^{+}e^{-}J/\psi$
¹ ABLIKIM 17I reports $(1.51 \pm 0.30 \pm 0.13) \times 10^{-4}$ from a measurement of $[\Gamma(\chi_{c0}(1P) \rightarrow e^{+}e^{-}J/\psi(1S))/\Gamma_{total}] \times [B(\psi(2S) \rightarrow \gamma\chi_{c0}(1P))]$ assuming $B(\psi(2S) \rightarrow \gamma\chi_{c0}(1P)) = (9.99 \pm 0.27) \times 10^{-2}$, which we rescale to our best value $B(\psi(2S) \rightarrow \gamma\chi_{c0}(1P)) = (9.79 \pm 0.20) \times 10^{-2}$. Our first error is their experiment's error and our second error is the systematic error from using our best value. ² Not independent from other measurements reported by ABLIKIM 17I				

$\Gamma(e^{+}e^{-}J/\psi(1S))/\Gamma(\gamma J/\psi(1S))$ Γ_{94}/Γ_{89}

VALUE (units 10 ⁻³)	EVTS	DOCUMENT ID	TECN	COMMENT
9.5 ± 1.9 ± 0.7	56	¹ ABLIKIM 17I	BES3	$\psi(2S) \rightarrow e^{+}e^{-}\gamma J/\psi$
¹ Uses $B(\psi(2S) \rightarrow \gamma\chi_{c0}(1P)) \times B(\chi_{c0}(1P) \rightarrow \gamma J/\psi(1S)) = (15.8 \pm 0.3 \pm 0.6) \times 10^{-4}$ from ABLIKIM 17N and accounts for common systematic errors.				

$\Gamma(\mu^{+}\mu^{-}J/\psi(1S))/\Gamma(e^{+}e^{-}J/\psi(1S))$ Γ_{95}/Γ_{94}

VALUE	CL%	EVTS	DOCUMENT ID	TECN	COMMENT
<0.14	90	<9.5	ABLIKIM 19Z	BES3	$\psi(2S) \rightarrow \gamma\chi_{c0} \rightarrow \gamma(\mu^{+}\mu^{-}J/\psi)$

$\Gamma(\gamma\eta)/\Gamma(\gamma J/\psi(1S))$ Γ_{93}/Γ_{89}

VALUE (units 10 ⁻²)	DOCUMENT ID	TECN	COMMENT
1.45 ± 0.08 OUR FIT			
2.0 ± 0.4 OUR AVERAGE			
2.2 ± 0.4 ± 0.1 ± 0.2	¹ ANDREOTTI 04	E835	$p\bar{p} \rightarrow \chi_{c0} \rightarrow \gamma\eta$
1.45 ± 0.74	² AMBROGIANI 00B	E835	$p\bar{p} \rightarrow \chi_{c2} \rightarrow \gamma\eta, \gamma J/\psi$
¹ The values of $B(p\bar{p})B(\gamma\eta)$ and $B(\gamma\eta)B(\gamma J/\psi)$ measured by ANDREOTTI 04 are not independent. The latter is used in the fit because of smaller systematics. ² Calculated by us using $B(J/\psi(1S) \rightarrow e^{+}e^{-}) = 0.0593 \pm 0.0010$.			

$\Gamma(p\bar{p})/\Gamma_{total} \times \Gamma(\gamma J/\psi(1S))/\Gamma_{total}$ $\Gamma_{58}/\Gamma \times \Gamma_{89}/\Gamma$

VALUE (units 10 ⁻⁷)	EVTS	DOCUMENT ID	TECN	COMMENT
31.1 ± 1.5 OUR FIT				
28.2 ± 2.1 OUR AVERAGE				
28.0 ± 1.9 ± 1.3	392	^{1,2,3} BAGNASCO 02	E835	$p\bar{p} \rightarrow \chi_{c0} \rightarrow J/\psi\gamma$
29.3 ± 5.7 ± 1.5	89	^{1,2} AMBROGIANI 99B		$p\bar{p} \rightarrow \chi_{c0} \rightarrow J/\psi\gamma$
¹ Values in $(\Gamma(p\bar{p}) \times \Gamma(\gamma J/\psi(1S))/\Gamma_{total})$ and $(\Gamma(p\bar{p})/\Gamma_{total} \times \Gamma(\gamma J/\psi(1S))/\Gamma_{total})$ are not independent. The latter is used in the fit since it is less correlated to the total width. ² Calculated by us using $B(J/\psi(1S) \rightarrow e^{+}e^{-}) = 0.0593 \pm 0.0010$. ³ Recalculated by ANDREOTTI 05A.				

$\Gamma(p\bar{p})/\Gamma_{total} \times \Gamma(\gamma\gamma)/\Gamma_{total}$ $\Gamma_{58}/\Gamma \times \Gamma_{93}/\Gamma$

VALUE (units 10 ⁻⁸)	DOCUMENT ID	TECN	COMMENT
4.52 ± 0.27 OUR FIT			
••• We do not use the following data for averages, fits, limits, etc. •••			
6.52 ± 1.18 ± 0.48 ± 0.72	¹ ANDREOTTI 04	E835	$p\bar{p} \rightarrow \chi_{c0} \rightarrow \gamma\gamma$
¹ The values of $B(p\bar{p})B(\gamma\gamma)$ and $B(\gamma\gamma)B(\gamma J/\psi)$ measured by ANDREOTTI 04 are not independent. The latter is used in the fit because of smaller systematics.			

$\chi_{c0}(1P)$ CROSS-PARTICLE BRANCHING RATIOS

$\Gamma(\chi_{c0}(1P) \rightarrow p\bar{p})/\Gamma_{total} \times \Gamma(\psi(2S) \rightarrow \gamma\chi_{c0}(1P))/\Gamma_{total}$

VALUE (units 10 ⁻⁶)	EVTS	DOCUMENT ID	TECN	COMMENT
21.7 ± 0.9 OUR FIT				
23.7 ± 1.0 OUR AVERAGE				
23.7 ± 0.8 ± 0.9	1222	ABLIKIM 13V	BES3	$\psi(2S) \rightarrow \gamma p\bar{p}$
23.7 ± 1.4 ± 1.4	383 ± 22	¹ NAIK 08	CLEO	$\psi(2S) \rightarrow \gamma p\bar{p}$
23.6 ± 3.7 ± 3.4	89.5 ± 14 ± 13	BAI	04F	BES $\psi(2S) \rightarrow \gamma\chi_{c0}(1P) \rightarrow \gamma p\bar{p}$

¹ Calculated by us. NAIK 08 reports $B(\chi_{c0} \rightarrow p\bar{p}) = (25.7 \pm 1.5 \pm 1.5 \pm 1.3) \times 10^{-5}$ using $B(\psi(2S) \rightarrow \gamma\chi_{c0}) = (9.22 \pm 0.11 \pm 0.46)\%$.

$\Gamma(\chi_{c0}(1P) \rightarrow p\bar{p})/\Gamma_{total} \times \Gamma(\psi(2S) \rightarrow \gamma\chi_{c0}(1P))/\Gamma(\psi(2S) \rightarrow J/\psi(1S)\pi^{+}\pi^{-})$

VALUE (units 10 ⁻⁵)	DOCUMENT ID	TECN	COMMENT
6.25 ± 0.26 OUR FIT			
4.6 ± 1.9	¹ BAI	98I	BES $\psi(2S) \rightarrow \gamma\chi_{c0} \rightarrow \gamma p\bar{p}$

¹ Calculated by us. The value for $B(\chi_{c0} \rightarrow p\bar{p})$ reported in BAI 98I is derived using $B(\psi(2S) \rightarrow \gamma\chi_{c0}) = (9.3 \pm 0.8)\%$ and $B(\psi(2S) \rightarrow J/\psi(1S)\pi^{+}\pi^{-}) = (32.4 \pm 2.6)\%$ [BAI 98d].

$\Gamma(\chi_{c0}(1P) \rightarrow \Lambda\bar{\Lambda})/\Gamma_{total} \times \Gamma(\psi(2S) \rightarrow \gamma\chi_{c0}(1P))/\Gamma_{total}$

VALUE (units 10 ⁻⁶)	EVTS	DOCUMENT ID	TECN	COMMENT
32.0 ± 2.3 OUR FIT				
31.7 ± 2.3 OUR AVERAGE				
32.0 ± 1.9 ± 2.2	369	¹ ABLIKIM 13H	BES3	$\psi(2S) \rightarrow \gamma\Lambda\bar{\Lambda}$
31.2 ± 3.3 ± 2.0	131 ± 12	² NAIK 08	CLEO	$\psi(2S) \rightarrow \gamma\Lambda\bar{\Lambda}$

¹ Calculated by us. ABLIKIM 13H reports $B(\chi_{c0} \rightarrow \Lambda\bar{\Lambda}) = (33.3 \pm 2.0 \pm 2.6) \times 10^{-5}$ from a measurement of $B(\chi_{c0} \rightarrow \Lambda\bar{\Lambda}) \times B(\psi(2S) \rightarrow \gamma\chi_{c0})$ assuming $B(\psi(2S) \rightarrow \gamma\chi_{c0}) = (9.62 \pm 0.31)\%$.

² Calculated by us. NAIK 08 reports $B(\chi_{c0} \rightarrow \Lambda\bar{\Lambda}) = (33.8 \pm 3.6 \pm 2.2 \pm 1.7) \times 10^{-5}$ using $B(\psi(2S) \rightarrow \gamma\chi_{c0}) = (9.22 \pm 0.11 \pm 0.46)\%$.

$\Gamma(\chi_{c0}(1P) \rightarrow \Lambda\bar{\Lambda})/\Gamma_{total} \times \Gamma(\psi(2S) \rightarrow \gamma\chi_{c0}(1P))/\Gamma(\psi(2S) \rightarrow J/\psi(1S)\pi^{+}\pi^{-})$

VALUE (units 10 ⁻⁵)	EVTS	DOCUMENT ID	TECN	COMMENT
9.2 ± 0.7 OUR FIT				
13.0 ± 3.6 ± 2.5	15.2 ± 4.2 ± 4.0	¹ BAI	03E	BES $\psi(2S) \rightarrow \gamma\Lambda\bar{\Lambda}$

¹ BAI 03E reports $[B(\chi_{c0} \rightarrow \Lambda\bar{\Lambda})B(\psi(2S) \rightarrow \gamma\chi_{c0})/B(\psi(2S) \rightarrow J/\psi\pi^{+}\pi^{-})] \times [B^2(\Lambda \rightarrow \pi^{-}p)/B(J/\psi \rightarrow p\bar{p})] = (2.45^{+0.68}_{-0.65} \pm 0.46)\%$. We calculate from this measurement the presented value using $B(\Lambda \rightarrow \pi^{-}p) = (63.9 \pm 0.5)\%$ and $B(J/\psi \rightarrow p\bar{p}) = (2.17 \pm 0.07) \times 10^{-3}$.

$\Gamma(\chi_{c0}(1P) \rightarrow \gamma J/\psi(1S))/\Gamma_{total} \times \Gamma(\psi(2S) \rightarrow \gamma\chi_{c0}(1P))/\Gamma_{total}$

VALUE (units 10 ⁻²)	EVTS	DOCUMENT ID	TECN	COMMENT
0.138 ± 0.005 OUR FIT				
0.147 ± 0.029 OUR AVERAGE				
0.158 ± 0.003 ± 0.006	4.8k	¹ ABLIKIM 17N	BES3	$\psi(2S) \rightarrow \gamma\gamma J/\psi$
0.024 ± 0.015 ± 0.205	12k	ABLIKIM 17U	BES3	$e^{+}e^{-} \rightarrow \gamma\chi$
0.069 ± 0.018		² OREGLIA 82	CBAL	$\psi(2S) \rightarrow \gamma\chi_{c0}$
0.4 ± 0.3		³ BRANDELIC 79B	DASP	$\psi(2S) \rightarrow \gamma\chi_{c0}$
0.16 ± 0.11		³ BARTEL 78B	CNTR	$\psi(2S) \rightarrow \gamma\chi_{c0}$
3.3 ± 1.7		⁴ BIDDICK 77	CNTR	$e^{+}e^{-} \rightarrow \gamma\chi$
••• We do not use the following data for averages, fits, limits, etc. •••				
0.151 ± 0.003 ± 0.010	4.3k	⁵ ABLIKIM 12O	BES3	$\psi(2S) \rightarrow \gamma\chi_{c0}$
0.125 ± 0.007 ± 0.013	560	⁶ MENDEZ 08	CLEO	$\psi(2S) \rightarrow \gamma\chi_{c0}$
0.18 ± 0.01 ± 0.02	172	⁷ ADAM 05A	CLEO	Repl. by MENDEZ 08

¹ Uses $B(J/\psi \rightarrow e^{+}e^{-}) = (5.971 \pm 0.032)\%$ and $B(J/\psi \rightarrow \mu^{+}\mu^{-}) = (5.961 \pm 0.033)\%$.
² Recalculated by us using $B(J/\psi(1S) \rightarrow \ell^{+}\ell^{-}) = 0.1181 \pm 0.0020$.
³ Recalculated by us using $B(J/\psi(1S) \rightarrow \mu^{+}\mu^{-}) = 0.0588 \pm 0.0010$.
⁴ Assumes isotropic gamma distribution.
⁵ Superseded by ABLIKIM 17N.
⁶ Not independent from other measurements of MENDEZ 08.
⁷ Not independent from other values reported by ADAM 05A.

Meson Particle Listings

 $\chi_{c0}(1P)$

$$\Gamma(\chi_{c0}(1P) \rightarrow \gamma J/\psi(1S))/\Gamma_{\text{total}} \times \Gamma(\psi(2S) \rightarrow \gamma \chi_{c0}(1P))/\Gamma(\psi(2S) \rightarrow J/\psi(1S) \text{ anything})$$

$$\frac{\Gamma_{89}/\Gamma \times \Gamma_{153}^{\psi(2S)}/\Gamma_{9}^{\psi(2S)}}{\Gamma_{89}/\Gamma \times \Gamma_{153}^{\psi(2S)}/\Gamma_{9}^{\psi(2S)} + \Gamma_{11}^{\psi(2S)} + \Gamma_{12}^{\psi(2S)} + \Gamma_{13}^{\psi(2S)} + 0.343\Gamma_{154}^{\psi(2S)} + 0.190\Gamma_{155}^{\psi(2S)}}$$

VALUE (units 10^{-2}) EVTS DOCUMENT ID TECN COMMENT
0.224±0.009 OUR FIT

• • • We do not use the following data for averages, fits, limits, etc. • • •

0.201±0.011±0.021 560 ¹ MENDEZ 08 CLEO $\psi(2S) \rightarrow \gamma \chi_{c0}$
 0.31 ± 0.02 ± 0.03 172 ADAM 05A CLEO Repl. by MENDEZ 08

¹ Not independent from other measurements of MENDEZ 08.

$$\Gamma(\chi_{c0}(1P) \rightarrow \gamma J/\psi(1S))/\Gamma_{\text{total}} \times \Gamma(\psi(2S) \rightarrow \gamma \chi_{c0}(1P))/\Gamma(\psi(2S) \rightarrow J/\psi(1S) \pi^+ \pi^-)$$

$$\frac{\Gamma_{89}/\Gamma \times \Gamma_{153}^{\psi(2S)}/\Gamma_{11}^{\psi(2S)}}{\Gamma_{89}/\Gamma \times \Gamma_{153}^{\psi(2S)}/\Gamma_{11}^{\psi(2S)} + \Gamma_{12}^{\psi(2S)} + \Gamma_{13}^{\psi(2S)} + 0.343\Gamma_{154}^{\psi(2S)} + 0.190\Gamma_{155}^{\psi(2S)}}$$

VALUE (units 10^{-2}) EVTS DOCUMENT ID TECN COMMENT
0.397±0.015 OUR FIT
0.358±0.020±0.037

• • • We do not use the following data for averages, fits, limits, etc. • • •

0.55 ± 0.04 ± 0.06 172 ¹ ADAM 05A CLEO Repl. by MENDEZ 08

¹ Not independent from other values reported by ADAM 05A.

$$\Gamma(\chi_{c0}(1P) \rightarrow \gamma \gamma)/\Gamma_{\text{total}} \times \Gamma(\psi(2S) \rightarrow \gamma \chi_{c0}(1P))/\Gamma_{\text{total}}$$

$$\frac{\Gamma_{93}/\Gamma \times \Gamma_{153}^{\psi(2S)}/\Gamma_{\psi(2S)}}{\Gamma_{93}/\Gamma \times \Gamma_{153}^{\psi(2S)}/\Gamma_{\psi(2S)} + \Gamma_{12}^{\psi(2S)} + \Gamma_{13}^{\psi(2S)} + 0.343\Gamma_{154}^{\psi(2S)} + 0.190\Gamma_{155}^{\psi(2S)}}$$

VALUE (units 10^{-5}) EVTS DOCUMENT ID TECN COMMENT
2.00±0.08 OUR FIT
1.95±0.09 OUR AVERAGE

1.93±0.08±0.05 3.5k ABLIKIM 17Ae BES3 $\psi(2S) \rightarrow \gamma \chi_{c0} \rightarrow 3\gamma$
 2.17±0.32±0.10 0.2k ECKLUND 08A CLEO $\psi(2S) \rightarrow \gamma \chi_{c0} \rightarrow 3\gamma$
 3.7 ± 1.8 ± 1.0 LEE 85 CBAL $\psi(2S) \rightarrow \gamma \chi_{c0}$

• • • We do not use the following data for averages, fits, limits, etc. • • •

2.17±0.17±0.12 0.8k ¹ ABLIKIM 12A BES3 $\psi(2S) \rightarrow \gamma \chi_{c0} \rightarrow 3\gamma$

¹ Superseded by ABLIKIM 17Ae.

$$\Gamma(\chi_{c0}(1P) \rightarrow \pi \pi)/\Gamma_{\text{total}} \times \Gamma(\psi(2S) \rightarrow \gamma \chi_{c0}(1P))/\Gamma_{\text{total}}$$

$$\frac{\Gamma_{32}/\Gamma \times \Gamma_{153}^{\psi(2S)}/\Gamma_{\psi(2S)}}{\Gamma_{32}/\Gamma \times \Gamma_{153}^{\psi(2S)}/\Gamma_{\psi(2S)} + \Gamma_{12}^{\psi(2S)} + \Gamma_{13}^{\psi(2S)} + 0.343\Gamma_{154}^{\psi(2S)} + 0.190\Gamma_{155}^{\psi(2S)}}$$

VALUE (units 10^{-4}) EVTS DOCUMENT ID TECN COMMENT
8.34±0.29 OUR FIT
8.80±0.34 OUR AVERAGE

9.11±0.08±0.65 17k ¹ ABLIKIM 10A BES3 $e^+e^- \rightarrow \psi(2S) \rightarrow \gamma \chi_{c0}$
 8.81±0.11±0.43 8.9k ² ASNER 09 CLEO $\psi(2S) \rightarrow \gamma \pi^+ \pi^-$
 8.13±0.19±0.89 2.8k ³ ASNER 09 CLEO $\psi(2S) \rightarrow \gamma \pi^0 \pi^0$

¹ Calculated by us. ABLIKIM 10A reports $B(\chi_{c0} \rightarrow \pi^0 \pi^0) = (3.23 \pm 0.03 \pm 0.23 \pm 0.14) \times 10^{-3}$ using $B(\psi(2S) \rightarrow \gamma \chi_{c0}) = (9.4 \pm 0.4)\%$. We have multiplied the $\pi^0 \pi^0$ measurement by 3 to obtain $\pi \pi$.

² Calculated by us. ASNER 09 reports $B(\chi_{c0} \rightarrow \pi^+ \pi^-) = (6.37 \pm 0.08 \pm 0.31 \pm 0.32) \times 10^{-3}$ using $B(\psi(2S) \rightarrow \gamma \chi_{c0}) = (9.22 \pm 0.11 \pm 0.46)\%$. We have multiplied the $\pi^+ \pi^-$ measurement by 3/2 to obtain $\pi \pi$.

³ Calculated by us. ASNER 09 reports $B(\chi_{c0} \rightarrow \pi^0 \pi^0) = (2.94 \pm 0.07 \pm 0.32 \pm 0.15) \times 10^{-3}$ using $B(\psi(2S) \rightarrow \gamma \chi_{c0}) = (9.22 \pm 0.11 \pm 0.46)\%$. We have multiplied the $\pi^0 \pi^0$ measurement by 3 to obtain $\pi \pi$.

$$\Gamma(\chi_{c0}(1P) \rightarrow \pi \pi)/\Gamma_{\text{total}} \times \Gamma(\psi(2S) \rightarrow \gamma \chi_{c0}(1P))/\Gamma(\psi(2S) \rightarrow J/\psi(1S) \pi^+ \pi^-)$$

$$\frac{\Gamma_{32}/\Gamma \times \Gamma_{153}^{\psi(2S)}/\Gamma_{11}^{\psi(2S)}}{\Gamma_{32}/\Gamma \times \Gamma_{153}^{\psi(2S)}/\Gamma_{11}^{\psi(2S)} + \Gamma_{12}^{\psi(2S)} + \Gamma_{13}^{\psi(2S)} + 0.343\Gamma_{154}^{\psi(2S)} + 0.190\Gamma_{155}^{\psi(2S)}}$$

VALUE (units 10^{-4}) EVTS DOCUMENT ID TECN COMMENT
24.0±0.8 OUR FIT
20.7±1.7 OUR AVERAGE

23.9±2.7±4.1 97 ± 11 ¹ BAI 03c BES $\psi(2S) \rightarrow \gamma \chi_{c0} \rightarrow \gamma \pi^0 \pi^0$
 20.2±1.1±1.5 720 ± 32 ² BAI 98i BES $\psi(2S) \rightarrow \gamma \chi_{c0} \rightarrow \gamma \pi^+ \pi^-$

¹ We have multiplied $\pi^0 \pi^0$ measurement by 3 to obtain $\pi \pi$.

² Calculated by us. The value for $B(\chi_{c0} \rightarrow \pi^+ \pi^-)$ reported in BAI 98i is derived using $B(\psi' \rightarrow \gamma \chi_{c0}) = (9.3 \pm 0.8)\%$ and $B(\psi' \rightarrow J/\psi \pi^+ \pi^-) = (32.4 \pm 2.6)\%$ [BAI 98b]. We have multiplied $\pi^+ \pi^-$ measurement by 3/2 to obtain $\pi \pi$.

$$\Gamma(\chi_{c0}(1P) \rightarrow \eta \eta)/\Gamma_{\text{total}} \times \Gamma(\psi(2S) \rightarrow \gamma \chi_{c0}(1P))/\Gamma_{\text{total}}$$

$$\frac{\Gamma_{36}/\Gamma \times \Gamma_{153}^{\psi(2S)}/\Gamma_{\psi(2S)}}{\Gamma_{36}/\Gamma \times \Gamma_{153}^{\psi(2S)}/\Gamma_{\psi(2S)} + \Gamma_{12}^{\psi(2S)} + \Gamma_{13}^{\psi(2S)} + 0.343\Gamma_{154}^{\psi(2S)} + 0.190\Gamma_{155}^{\psi(2S)}}$$

VALUE (units 10^{-4}) EVTS DOCUMENT ID TECN COMMENT
2.95±0.18 OUR FIT
3.12±0.19 OUR AVERAGE

3.23±0.09±0.23 2132 ¹ ABLIKIM 10A BES3 $e^+e^- \rightarrow \psi(2S) \rightarrow \gamma \chi_{c0}$
 2.93±0.12±0.29 0.9k ² ASNER 09 CLEO $\psi(2S) \rightarrow \gamma \eta \eta$

• • • We do not use the following data for averages, fits, limits, etc. • • •

2.86±0.46±0.37 48 ³ ADAMS 07 CLEO $\psi(2S) \rightarrow \gamma \chi_{c0}$

¹ Calculated by us. ABLIKIM 10A reports $B(\chi_{c0} \rightarrow \eta \eta) = (3.44 \pm 0.10 \pm 0.24 \pm 0.13) \times 10^{-3}$ using $B(\psi(2S) \rightarrow \gamma \chi_{c0}) = (9.4 \pm 0.4)\%$.

² Calculated by us. ASNER 09 reports $B(\chi_{c0} \rightarrow \eta \eta) = (3.18 \pm 0.13 \pm 0.31 \pm 0.16) \times 10^{-3}$ using $B(\psi(2S) \rightarrow \gamma \chi_{c0}) = (9.22 \pm 0.11 \pm 0.46)\%$.

³ Superseded by ASNER 09. Calculated by us. The value of $B(\chi_{c0}(1P) \rightarrow \eta \eta)$ reported by ADAMS 07 was derived using $B(\psi(2S) \rightarrow \gamma \chi_{c0}(1P)) = (9.22 \pm 0.11 \pm 0.46)\%$ (ATHAR 04).

$$\Gamma(\chi_{c0}(1P) \rightarrow \eta \eta)/\Gamma_{\text{total}} \times \Gamma(\psi(2S) \rightarrow \gamma \chi_{c0}(1P))/\Gamma(\psi(2S) \rightarrow J/\psi(1S) \pi^+ \pi^-)$$

$$\frac{\Gamma_{36}/\Gamma \times \Gamma_{153}^{\psi(2S)}/\Gamma_{11}^{\psi(2S)}}{\Gamma_{36}/\Gamma \times \Gamma_{153}^{\psi(2S)}/\Gamma_{11}^{\psi(2S)} + \Gamma_{12}^{\psi(2S)} + \Gamma_{13}^{\psi(2S)} + 0.343\Gamma_{154}^{\psi(2S)} + 0.190\Gamma_{155}^{\psi(2S)}}$$

VALUE (units 10^{-3}) DOCUMENT ID TECN COMMENT
0.85 ± 0.05 OUR FIT
0.578±0.241±0.158

BAI 03c BES $\psi(2S) \rightarrow \gamma \eta \eta$

$$\Gamma(\chi_{c0}(1P) \rightarrow K^+ K^-)/\Gamma_{\text{total}} \times \Gamma(\psi(2S) \rightarrow \gamma \chi_{c0}(1P))/\Gamma_{\text{total}}$$

$$\frac{\Gamma_{42}/\Gamma \times \Gamma_{153}^{\psi(2S)}/\Gamma_{\psi(2S)}}{\Gamma_{42}/\Gamma \times \Gamma_{153}^{\psi(2S)}/\Gamma_{\psi(2S)} + \Gamma_{12}^{\psi(2S)} + \Gamma_{13}^{\psi(2S)} + 0.343\Gamma_{154}^{\psi(2S)} + 0.190\Gamma_{155}^{\psi(2S)}}$$

VALUE (units 10^{-4}) EVTS DOCUMENT ID TECN COMMENT
5.92±0.28 OUR FIT
5.97±0.07±0.32

8.1k ¹ ASNER 09 CLEO $\psi(2S) \rightarrow \gamma K^+ K^-$

¹ Calculated by us. ASNER 09 reports $B(\chi_{c0} \rightarrow K^+ K^-) = (6.47 \pm 0.08 \pm 0.35 \pm 0.32) \times 10^{-3}$ using $B(\psi(2S) \rightarrow \gamma \chi_{c0}) = (9.22 \pm 0.11 \pm 0.46)\%$.

$$\Gamma(\chi_{c0}(1P) \rightarrow K^+ K^-)/\Gamma_{\text{total}} \times \Gamma(\psi(2S) \rightarrow \gamma \chi_{c0}(1P))/\Gamma(\psi(2S) \rightarrow J/\psi(1S) \pi^+ \pi^-)$$

$$\frac{\Gamma_{42}/\Gamma \times \Gamma_{153}^{\psi(2S)}/\Gamma_{11}^{\psi(2S)}}{\Gamma_{42}/\Gamma \times \Gamma_{153}^{\psi(2S)}/\Gamma_{11}^{\psi(2S)} + \Gamma_{12}^{\psi(2S)} + \Gamma_{13}^{\psi(2S)} + 0.343\Gamma_{154}^{\psi(2S)} + 0.190\Gamma_{155}^{\psi(2S)}}$$

VALUE (units 10^{-3}) EVTS DOCUMENT ID TECN COMMENT
1.71±0.08 OUR FIT
1.63±0.10±0.15

774 ± 38 ¹ BAI 98i BES $\psi(2S) \rightarrow \gamma K^+ K^-$

¹ Calculated by us. The value for $B(\chi_{c0} \rightarrow K^+ K^-)$ reported by BAI 98i is derived using $B(\psi(2S) \rightarrow \gamma \chi_{c0}) = (9.3 \pm 0.8)\%$ and $B(\psi(2S) \rightarrow J/\psi \pi^+ \pi^-) = (32.4 \pm 2.6)\%$ [BAI 98d].

$$\Gamma(\chi_{c0}(1P) \rightarrow K_S^0 K_S^0)/\Gamma_{\text{total}} \times \Gamma(\psi(2S) \rightarrow \gamma \chi_{c0}(1P))/\Gamma_{\text{total}}$$

$$\frac{\Gamma_{43}/\Gamma \times \Gamma_{153}^{\psi(2S)}/\Gamma_{\psi(2S)}}{\Gamma_{43}/\Gamma \times \Gamma_{153}^{\psi(2S)}/\Gamma_{\psi(2S)} + \Gamma_{12}^{\psi(2S)} + \Gamma_{13}^{\psi(2S)} + 0.343\Gamma_{154}^{\psi(2S)} + 0.190\Gamma_{155}^{\psi(2S)}}$$

VALUE (units 10^{-4}) EVTS DOCUMENT ID TECN COMMENT
3.10±0.16 OUR FIT
3.18±0.17 OUR AVERAGE

3.22±0.07±0.17 2.1k ¹ ASNER 09 CLEO $\psi(2S) \rightarrow \gamma K_S^0 K_S^0$
 3.02±0.19±0.33 322 ABLIKIM 05o BES2 $\psi(2S) \rightarrow \gamma K_S^0 K_S^0$

¹ Calculated by us. ASNER 09 reports $B(\chi_{c0} \rightarrow K_S^0 K_S^0) = (3.49 \pm 0.08 \pm 0.18 \pm 0.17) \times 10^{-3}$ using $B(\psi(2S) \rightarrow \gamma \chi_{c0}) = (9.22 \pm 0.11 \pm 0.46)\%$.

$$\Gamma(\chi_{c0}(1P) \rightarrow K_S^0 K_S^0)/\Gamma_{\text{total}} \times \Gamma(\psi(2S) \rightarrow \gamma \chi_{c0}(1P))/\Gamma(\psi(2S) \rightarrow J/\psi(1S) \pi^+ \pi^-)$$

$$\frac{\Gamma_{43}/\Gamma \times \Gamma_{153}^{\psi(2S)}/\Gamma_{11}^{\psi(2S)}}{\Gamma_{43}/\Gamma \times \Gamma_{153}^{\psi(2S)}/\Gamma_{11}^{\psi(2S)} + \Gamma_{12}^{\psi(2S)} + \Gamma_{13}^{\psi(2S)} + 0.343\Gamma_{154}^{\psi(2S)} + 0.190\Gamma_{155}^{\psi(2S)}}$$

VALUE (units 10^{-4}) EVTS DOCUMENT ID TECN COMMENT
8.9±0.5 OUR FIT
5.6±0.8±1.3

¹ BAI 99b BES $\psi(2S) \rightarrow \gamma K_S^0 K_S^0$

¹ Calculated by us. The value of $B(\chi_{c0} \rightarrow K_S^0 K_S^0)$ reported by BAI 99b was derived using $B(\psi(2S) \rightarrow \gamma \chi_{c0}(1P)) = (9.3 \pm 0.8)\%$ and $B(\psi(2S) \rightarrow J/\psi \pi^+ \pi^-) = (32.4 \pm 2.6)\%$ [BAI 98d].

$$\Gamma(\chi_{c0}(1P) \rightarrow 2(\pi^+ \pi^-))/\Gamma_{\text{total}} \times \Gamma(\psi(2S) \rightarrow \gamma \chi_{c0}(1P))/\Gamma(\psi(2S) \rightarrow J/\psi(1S) \pi^+ \pi^-)$$

$$\frac{\Gamma_{11}/\Gamma \times \Gamma_{153}^{\psi(2S)}/\Gamma_{11}^{\psi(2S)}}{\Gamma_{11}/\Gamma \times \Gamma_{153}^{\psi(2S)}/\Gamma_{11}^{\psi(2S)} + \Gamma_{12}^{\psi(2S)} + \Gamma_{13}^{\psi(2S)} + 0.343\Gamma_{154}^{\psi(2S)} + 0.190\Gamma_{155}^{\psi(2S)}}$$

VALUE (units 10^{-3}) DOCUMENT ID TECN COMMENT
6.6±0.5 OUR FIT
6.9±2.4 OUR AVERAGE Error includes scale factor of 3.8.

4.4±0.1±0.9 ¹ BAI 99b BES $\psi(2S) \rightarrow \gamma \chi_{c0}$
 9.3±0.9 ² TANENBAUM 78 MRK1 $\psi(2S) \rightarrow \gamma \chi_{c0}$

¹ Calculated by us. The value for $B(\chi_{c0} \rightarrow 2\pi^+ 2\pi^-)$ reported in BAI 99b is derived using $B(\psi(2S) \rightarrow \gamma \chi_{c0}) = (9.3 \pm 0.8)\%$ and $B(\psi(2S) \rightarrow J/\psi(1S) \pi^+ \pi^-) = (32.4 \pm 2.6)\%$ [BAI 98d].

² The value $B(\psi(1S) \rightarrow \gamma \chi_{c0}) \times B(\chi_{c0} \rightarrow 2\pi^+ 2\pi^-)$ reported in TANENBAUM 78 is derived using $B(\psi(2S) \rightarrow J/\psi(1S) \pi^+ \pi^-) \times B(J/\psi(1S) \rightarrow \ell^+ \ell^-) = (4.6 \pm 0.7)\%$. Calculated by us using $B(J/\psi(1S) \rightarrow \ell^+ \ell^-) = 0.1181 \pm 0.0020$.

$$\Gamma(\chi_{c0}(1P) \rightarrow \pi^+ \pi^- K^+ K^-)/\Gamma_{\text{total}} \times \Gamma(\psi(2S) \rightarrow \gamma \chi_{c0}(1P))/\Gamma_{\text{total}}$$

$$\frac{\Gamma_{8}/\Gamma \times \Gamma_{153}^{\psi(2S)}/\Gamma_{\psi(2S)}}{\Gamma_{8}/\Gamma \times \Gamma_{153}^{\psi(2S)}/\Gamma_{\psi(2S)} + \Gamma_{12}^{\psi(2S)} + \Gamma_{13}^{\psi(2S)} + 0.343\Gamma_{154}^{\psi(2S)} + 0.190\Gamma_{155}^{\psi(2S)}}$$

VALUE (units 10^{-3}) DOCUMENT ID TECN COMMENT
1.78±0.14 OUR FIT
1.64±0.05±0.2

ABLIKIM 05q BES2 $\psi(2S) \rightarrow \gamma \chi_{c0}$

$$\Gamma(\chi_{c0}(1P) \rightarrow \pi^+ \pi^- K^+ K^-)/\Gamma_{\text{total}} \times \Gamma(\psi(2S) \rightarrow \gamma \chi_{c0}(1P))/\Gamma(\psi(2S) \rightarrow J/\psi(1S) \pi^+ \pi^-)$$

$$\frac{\Gamma_{8}/\Gamma \times \Gamma_{153}^{\psi(2S)}/\Gamma_{11}^{\psi(2S)}}{\Gamma_{8}/\Gamma \times \Gamma_{153}^{\psi(2S)}/\Gamma_{11}^{\psi(2S)} + \Gamma_{12}^{\psi(2S)} + \Gamma_{13}^{\psi(2S)} + 0.343\Gamma_{154}^{\psi(2S)} + 0.190\Gamma_{155}^{\psi(2S)}}$$

VALUE (units 10^{-3}) DOCUMENT ID TECN COMMENT
5.1 ± 0.4 OUR FIT
5.8 ± 1.6 OUR AVERAGE Error includes scale factor of 2.3.

4.22±0.20±0.97 BAI 99b BES $\psi(2S) \rightarrow \gamma \chi_{c0}$
 7.4 ± 1.0 ¹ TANENBAUM 78 MRK1 $\psi(2S) \rightarrow \gamma \chi_{c0}$

¹ The reported value is derived using $B(\psi(2S) \rightarrow \pi^+ \pi^- J/\psi) \times B(J/\psi \rightarrow \ell^+ \ell^-) = (4.6 \pm 0.7)\%$. Calculated by us using $B(J/\psi \rightarrow \ell^+ \ell^-) = 0.1181 \pm 0.0020$.

$$\Gamma(\chi_{c0}(1P) \rightarrow K^+ K^- K^+ K^-)/\Gamma_{\text{total}} \times \Gamma(\psi(2S) \rightarrow \gamma \chi_{c0}(1P))/\Gamma_{\text{total}}$$

$$\frac{\Gamma_{51}/\Gamma \times \Gamma_{153}^{\psi(2S)}/\Gamma_{\psi(2S)}}{\Gamma_{51}/\Gamma \times \Gamma_{153}^{\psi(2S)}/\Gamma_{\psi(2S)} + \Gamma_{12}^{\psi(2S)} + \Gamma_{13}^{\psi(2S)} + 0.343\Gamma_{154}^{\psi(2S)} + 0.190\Gamma_{155}^{\psi(2S)}}$$

VALUE (units 10^{-4}) EVTS DOCUMENT ID TECN COMMENT
2.76±0.28 OUR FIT
3.20±0.11±0.41

278 ¹ ABLIKIM 06t BES2 $\psi(2S) \rightarrow \gamma 2K^+ 2K^-$

¹ Calculated by us. The value of $B(\chi_{c0} \rightarrow 2K^+ 2K^-)$ reported by ABLIKIM 06t was derived using $B(\psi(2S) \rightarrow \gamma \chi_{c0}(1P)) = (9.2 \pm 0.4)\%$.

See key on page 999

Meson Particle Listings

$\chi_{c0}(1P), \chi_{c1}(1P)$

$\Gamma(\chi_{c0}(1P) \rightarrow K^+K^-K^+K^-)/\Gamma_{total} \times \Gamma(\psi(2S) \rightarrow \gamma\chi_{c0}(1P))/\Gamma(\psi(2S) \rightarrow J/\psi(1S)\pi^+\pi^-)$

Table with columns: VALUE (units 10^-4), DOCUMENT ID, TECN, COMMENT. Row 1: 8.0 ± 0.8 OUR FIT. Row 2: 6.1 ± 0.8 ± 0.9. Row 3: 1 BAI 99B BES $\psi(2S) \rightarrow \gamma 2K^+ 2K^-$

1 Calculated by us. The value of $B(\chi_{c0} \rightarrow 2K^+ 2K^-)$ reported by BAI 99B was derived using $B(\psi(2S) \rightarrow \gamma\chi_{c0}(1P)) = (9.3 \pm 0.8)\%$ and $B(\psi(2S) \rightarrow J/\psi\pi^+\pi^-) = (32.4 \pm 2.6)\%$ [BAI 98d].

$\Gamma(\chi_{c0}(1P) \rightarrow \phi\phi)/\Gamma_{total} \times \Gamma(\psi(2S) \rightarrow \gamma\chi_{c0}(1P))/\Gamma_{total}$

Table with columns: VALUE (units 10^-4), EVTS, DOCUMENT ID, TECN, COMMENT. Row 1: 0.78 ± 0.07 OUR FIT. Row 2: 0.78 ± 0.08 OUR AVERAGE. Row 3: 0.77 ± 0.03 ± 0.08. Row 4: 0.86 ± 0.19 ± 0.12

1 Calculated by us. The value of $B(\chi_{c0} \rightarrow \phi\phi)$ reported by ABLIKIM 11K was derived using $B(\psi(2S) \rightarrow \gamma\chi_{c0}(1P)) = (9.62 \pm 0.31)\%$.

2 Calculated by us. The value of $B(\chi_{c0} \rightarrow \phi\phi)$ reported by ABLIKIM 06T was derived using $B(\psi(2S) \rightarrow \gamma\chi_{c0}(1P)) = (9.2 \pm 0.4)\%$.

$\Gamma(\chi_{c0}(1P) \rightarrow \phi\phi)/\Gamma_{total} \times \Gamma(\psi(2S) \rightarrow \gamma\chi_{c0}(1P))/\Gamma(\psi(2S) \rightarrow J/\psi(1S)\pi^+\pi^-)$

Table with columns: VALUE (units 10^-4), DOCUMENT ID, TECN, COMMENT. Row 1: 2.25 ± 0.21 OUR FIT. Row 2: 2.6 ± 1.0 ± 1.1. Row 3: 1 BAI 99B BES $\psi(2S) \rightarrow \gamma 2K^+ 2K^-$

1 Calculated by us. The value of $B(\chi_{c0} \rightarrow \phi\phi)$ reported by BAI 99B was derived using $B(\psi(2S) \rightarrow \gamma\chi_{c0}(1P)) = (9.3 \pm 0.8)\%$ and $B(\psi(2S) \rightarrow J/\psi\pi^+\pi^-) = (32.4 \pm 2.6)\%$ [BAI 98d].

$\Gamma(\chi_{c0}(1P) \rightarrow \Sigma^+ \bar{p} K_S^0 + c.c.)/\Gamma_{total} \times \Gamma(\psi(2S) \rightarrow \gamma\chi_{c0}(1P))/\Gamma_{total}$

Table with columns: VALUE (units 10^-5), EVTS, DOCUMENT ID, TECN, COMMENT. Row 1: 3.45 ± 0.17 ± 0.19. Row 2: 493. Row 3: 1 ABLIKIM 19BB BES3 $\psi(2S) \rightarrow \gamma \Sigma^+ \bar{p} K_S^0 + c.c.$

1 Calculated by us. ABLIKIM 19BB reports $B(\chi_{c0} \rightarrow \Sigma^+ \bar{p} K_S^0 + c.c.) = (3.52 \pm 0.19 \pm 0.21) \times 10^{-4}$ using $B(\psi(2S) \rightarrow \gamma\chi_{c0}(1P)) = (9.79 \pm 0.20)\%$ and other branching fractions from PDG 18.

$\chi_{c0}(1P)$ REFERENCES

Table of references for $\chi_{c0}(1P)$ with columns: AUTHOR, YEAR, DOCUMENT ID, TECN, COMMENT. Includes entries like ABLIKIM 20B, ABLIKIM 19A, ABLIKIM 19AU, etc.

Table of references for $\chi_{c1}(1P)$ with columns: AUTHOR, YEAR, DOCUMENT ID, TECN, COMMENT. Includes entries like ANDREOTTI 05A, NAKAZAWA 05C, ABE 04G, etc.

$\chi_{c1}(1P)$

$J^G(J^{PC}) = 0^+(1^+ +)$

See the Review on " $\psi(2S)$ and χ_c branching ratios" before the $\chi_{c0}(1P)$ Listings.

$\chi_{c1}(1P)$ MASS

Table of $\chi_{c1}(1P)$ mass measurements with columns: VALUE (MeV), EVTS, DOCUMENT ID, TECN, COMMENT. Includes entries like 3510.67 ± 0.05 OUR AVERAGE, 3508.4 ± 1.9 ± 0.7, 3510.71 ± 0.04 ± 0.09, etc.

••• We do not use the following data for averages, fits, limits, etc. •••

- 1 From a fit of the $\phi\phi$ invariant mass with the width of $\chi_{c1}(1P)$ fixed to the PDG 16 value.
- 2 AAIJ 17B1 reports also $m(\chi_{c2}) - m(\chi_{c1}) = 45.39 \pm 0.07 \pm 0.03$ MeV.
- 3 Recalculated by ANDREOTTI 05A, using the value of $\psi(2S)$ mass from AULCHENKO 03.
- 4 Using mass of $\psi(2S) = 3686.0$ MeV.
- 5 $J/\psi(1S)$ mass constrained to 3097 MeV.
- 6 Mass value shifted by us by amount appropriate for $\psi(2S)$ mass = 3686 MeV and $J/\psi(1S)$ mass = 3097 MeV.
- 7 From a simultaneous fit to radiative and hadronic decay channels.

$\chi_{c1}(1P)$ WIDTH

Table of $\chi_{c1}(1P)$ width measurements with columns: VALUE (MeV), CL%, EVTS, DOCUMENT ID, TECN, COMMENT. Includes entries like 0.84 ± 0.04 OUR FIT, 0.88 ± 0.05 OUR AVERAGE, 1.39 +0.40 -0.38 -0.77, etc.

••• We do not use the following data for averages, fits, limits, etc. •••

1 Recalculated by ANDREOTTI 05A.

$\chi_{c1}(1P)$ DECAY MODES

Table of $\chi_{c1}(1P)$ decay modes with columns: Mode, Fraction (Γ_i/Γ), Scale factor/Confidence level. Includes entries like Hadronic decays, $3(\pi^+\pi^-)$, $2(\pi^+\pi^0)$, $\pi^+\pi^-\pi^0\pi^0$.

Meson Particle Listings

$\chi_{c1}(1P)$

Γ_4	$\rho^+ \pi^- \pi^0 + c.c.$	(1.45±0.24) %	
Γ_5	$\rho^0 \pi^+ \pi^-$	(3.9 ±3.5) × 10 ⁻³	
Γ_6	$4\pi^0$	(5.4 ±0.8) × 10 ⁻⁴	
Γ_7	$\pi^+ \pi^- K^+ K^-$	(4.5 ±1.0) × 10 ⁻³	
Γ_8	$K^+ K^- \pi^0 \pi^0$	(1.12±0.27) × 10 ⁻³	
Γ_9	$K^+ K^- \pi^+ \pi^- \pi^0$	(1.15±0.13) %	
Γ_{10}	$K_S^0 K_S^+ \pi^+ \pi^- \pi^0$	(7.5 ±0.8) × 10 ⁻³	
Γ_{11}	$K^+ \pi^- \bar{K}^0 \pi^0 + c.c.$	(8.6 ±1.4) × 10 ⁻³	
Γ_{12}	$\rho^- K^+ \bar{K}^0 + c.c.$	(5.0 ±1.2) × 10 ⁻³	
Γ_{13}	$K^*(892)^0 \bar{K}^0 \pi^0 \rightarrow$ $K^+ \pi^- \bar{K}^0 \pi^0 + c.c.$	(2.3 ±0.6) × 10 ⁻³	
Γ_{14}	$K^+ K^- \eta \pi^0$	(1.12±0.34) × 10 ⁻³	
Γ_{15}	$\pi^+ \pi^- K_S^0 K_S^0$	(6.9 ±2.9) × 10 ⁻⁴	
Γ_{16}	$K^+ K^- \eta$	(3.2 ±1.0) × 10 ⁻⁴	
Γ_{17}	$\bar{K}^0 K^+ \pi^- + c.c.$	(7.0 ±0.6) × 10 ⁻³	
Γ_{18}	$K^*(892)^0 \bar{K}^0 + c.c.$	(10 ±4) × 10 ⁻⁴	
Γ_{19}	$K^*(892)^+ K^- + c.c.$	(1.4 ±0.6) × 10 ⁻³	
Γ_{20}	$K_J^*(1430)^0 \bar{K}^0 + c.c. \rightarrow$ $K_S^0 K^+ \pi^- + c.c.$	< 8 × 10 ⁻⁴	CL=90%
Γ_{21}	$K_J^*(1430)^+ K^- + c.c. \rightarrow$ $K_S^0 K^+ \pi^- + c.c.$	< 2.1 × 10 ⁻³	CL=90%
Γ_{22}	$K^+ K^- \pi^0$	(1.81±0.24) × 10 ⁻³	
Γ_{23}	$\eta \pi^+ \pi^-$	(4.62±0.23) × 10 ⁻³	
Γ_{24}	$a_0(980)^+ \pi^- + c.c. \rightarrow \eta \pi^+ \pi^-$	(3.2 ±0.4) × 10 ⁻³	S=2.2
Γ_{25}	$a_2(1320)^+ \pi^- + c.c. \rightarrow \eta \pi^+ \pi^-$	(1.76±0.24) × 10 ⁻⁴	
Γ_{26}	$a_2(1700)^+ \pi^- + c.c. \rightarrow \eta \pi^+ \pi^-$	(4.6 ±0.7) × 10 ⁻⁵	
Γ_{27}	$f_2(1270) \eta \rightarrow \eta \pi^+ \pi^-$	(3.5 ±0.6) × 10 ⁻⁴	
Γ_{28}	$f_4(2050) \eta \rightarrow \eta \pi^+ \pi^-$	(2.5 ±0.9) × 10 ⁻⁵	
Γ_{29}	$\pi_1(1400)^+ \pi^- + c.c. \rightarrow \eta \pi^+ \pi^-$	< 5 × 10 ⁻⁵	CL=90%
Γ_{30}	$\pi_1(1600)^+ \pi^- + c.c. \rightarrow \eta \pi^+ \pi^-$	< 1.5 × 10 ⁻⁵	CL=90%
Γ_{31}	$\pi_1(2015)^+ \pi^- + c.c. \rightarrow \eta \pi^+ \pi^-$	< 8 × 10 ⁻⁶	CL=90%
Γ_{32}	$f_2(1270) \eta$	(6.7 ±1.1) × 10 ⁻⁴	
Γ_{33}	$\pi^+ \pi^- \eta'$	(2.2 ±0.4) × 10 ⁻³	
Γ_{34}	$K^+ K^- \eta'(958)$	(8.8 ±0.9) × 10 ⁻⁴	
Γ_{35}	$K_0^*(1430)^+ K^- + c.c.$	(6.4 $\begin{smallmatrix} +2.2 \\ -2.8 \end{smallmatrix}$) × 10 ⁻⁴	
Γ_{36}	$f_0(980) \eta'(958)$	(1.6 $\begin{smallmatrix} +1.4 \\ -0.7 \end{smallmatrix}$) × 10 ⁻⁴	
Γ_{37}	$f_0(1710) \eta'(958)$	(7 $\begin{smallmatrix} +7 \\ -5 \end{smallmatrix}$) × 10 ⁻⁵	
Γ_{38}	$f_2'(1525) \eta'(958)$	(9 ±6) × 10 ⁻⁵	
Γ_{39}	$\pi^0 f_0(980) \rightarrow \pi^0 \pi^+ \pi^-$	(3.5 ±0.9) × 10 ⁻⁷	
Γ_{40}	$K^+ \bar{K}^*(892)^0 \pi^- + c.c.$	(3.2 ±2.1) × 10 ⁻³	
Γ_{41}	$K^*(892)^0 \bar{K}^*(892)^0$	(1.4 ±0.4) × 10 ⁻³	
Γ_{42}	$K^+ K^- K_S^0 K_S^0$	< 4 × 10 ⁻⁴	CL=90%
Γ_{43}	$K_S^0 K_S^0 K_S^0 K_S^0$	(3.5 ±1.0) × 10 ⁻⁵	
Γ_{44}	$K^+ K^- K^+ K^-$	(5.4 ±1.1) × 10 ⁻⁴	
Γ_{45}	$K^+ K^- \phi$	(4.1 ±1.5) × 10 ⁻⁴	
Γ_{46}	$\bar{K}^0 K^+ \pi^- \phi + c.c.$	(3.3 ±0.5) × 10 ⁻³	
Γ_{47}	$K^+ K^- \pi^0 \phi$	(1.62±0.30) × 10 ⁻³	
Γ_{48}	$\phi \pi^+ \pi^- \pi^0$	(7.5 ±1.0) × 10 ⁻⁴	
Γ_{49}	$\omega \omega$	(5.7 ±0.7) × 10 ⁻⁴	
Γ_{50}	$\omega K^+ K^-$	(7.8 ±0.9) × 10 ⁻⁴	
Γ_{51}	$\omega \phi$	(2.7 ±0.4) × 10 ⁻⁵	
Γ_{52}	$\phi \phi$	(4.2 ±0.5) × 10 ⁻⁴	
Γ_{53}	$\phi \phi \eta$	(3.0 ±0.5) × 10 ⁻⁴	
Γ_{54}	$p\bar{p}$	(7.60±0.34) × 10 ⁻⁵	
Γ_{55}	$p\bar{p} \pi^0$	(1.55±0.18) × 10 ⁻⁴	
Γ_{56}	$p\bar{p} \eta$	(1.45±0.25) × 10 ⁻⁴	
Γ_{57}	$p\bar{p} \omega$	(2.12±0.31) × 10 ⁻⁴	
Γ_{58}	$p\bar{p} \phi$	< 1.7 × 10 ⁻⁵	CL=90%
Γ_{59}	$p\bar{p} \pi^+ \pi^-$	(5.0 ±1.9) × 10 ⁻⁴	
Γ_{60}	$p\bar{p} \pi^0 \pi^0$	< 5 × 10 ⁻⁴	CL=90%
Γ_{61}	$p\bar{p} K^+ K^-$ (non-resonant)	(1.27±0.22) × 10 ⁻⁴	
Γ_{62}	$p\bar{p} K_S^0 K_S^0$	< 4.5 × 10 ⁻⁴	CL=90%
Γ_{63}	$p\bar{p} \pi^-$	(3.8 ±0.5) × 10 ⁻⁴	
Γ_{64}	$p\bar{p} \pi^+$	(3.9 ±0.5) × 10 ⁻⁴	
Γ_{65}	$p\bar{p} \pi^- \pi^0$	(1.03±0.12) × 10 ⁻³	
Γ_{66}	$p\bar{p} \pi^+ \pi^0$	(1.01±0.12) × 10 ⁻³	
Γ_{67}	$\Lambda \bar{\Lambda}$	(1.14±0.11) × 10 ⁻⁴	
Γ_{68}	$\Lambda \bar{\Lambda} \pi^+ \pi^-$	(2.9 ±0.5) × 10 ⁻⁴	
Γ_{69}	$\Lambda \bar{\Lambda} \pi^+ \pi^-$ (non-resonant)	(2.5 ±0.6) × 10 ⁻⁴	
Γ_{70}	$\Sigma(1385)^+ \bar{\Lambda} \pi^- + c.c.$	< 1.3 × 10 ⁻⁴	CL=90%
Γ_{71}	$\Sigma(1385)^- \bar{\Lambda} \pi^+ + c.c.$	< 1.3 × 10 ⁻⁴	CL=90%
Γ_{72}	$K^+ \bar{p} \Lambda + c.c.$	(4.2 ±0.4) × 10 ⁻⁴	S=1.2
Γ_{73}	$K^*(892)^+ \bar{p} \Lambda + c.c.$	(4.9 ±0.7) × 10 ⁻⁴	

Γ_{74}	$K^+ \bar{p} \Lambda(1520) + c.c.$	(1.7 ±0.4) × 10 ⁻⁴	
Γ_{75}	$\Lambda(1520) \bar{\Lambda}(1520)$	< 9 × 10 ⁻⁵	CL=90%
Γ_{76}	$\Sigma^0 \bar{\Sigma}^0$	(4.2 ±0.6) × 10 ⁻⁵	
Γ_{77}	$\Sigma^+ \bar{p} K_S^0 + c.c.$	(1.53±0.12) × 10 ⁻⁴	
Γ_{78}	$\Sigma^+ \bar{\Sigma}^-$	(3.6 ±0.7) × 10 ⁻⁵	
Γ_{79}	$\Sigma(1385)^+ \bar{\Sigma}(1385)^-$	< 9 × 10 ⁻⁵	CL=90%
Γ_{80}	$\Sigma(1385)^- \bar{\Sigma}(1385)^+$	< 5 × 10 ⁻⁵	CL=90%
Γ_{81}	$K^- \Lambda \bar{\Xi}^+ + c.c.$	(1.35±0.24) × 10 ⁻⁴	
Γ_{82}	$\Xi^0 \Xi^0$	< 6 × 10 ⁻⁵	CL=90%
Γ_{83}	$\Xi^- \Xi^+$	(8.0 ±2.1) × 10 ⁻⁵	
Γ_{84}	$\pi^+ \pi^- + K^+ K^-$	< 2.1 × 10 ⁻³	
Γ_{85}	$K_S^0 K_S^0$	< 6 × 10 ⁻⁵	CL=90%
Γ_{86}	$\eta_c \pi^+ \pi^-$	< 3.2 × 10 ⁻³	CL=90%

Radiative decays

Γ_{87}	$\gamma J/\psi(1S)$	(34.3 ±1.0) %	
Γ_{88}	$\gamma \rho^0$	(2.16±0.17) × 10 ⁻⁴	
Γ_{89}	$\gamma \omega$	(6.8 ±0.8) × 10 ⁻⁵	
Γ_{90}	$\gamma \phi$	(2.4 ±0.5) × 10 ⁻⁵	
Γ_{91}	$\gamma \gamma$	< 6.3 × 10 ⁻⁶	CL=90%
Γ_{92}	$e^+ e^- J/\psi(1S)$	(3.46±0.22) × 10 ⁻³	
Γ_{93}	$\mu^+ \mu^- J/\psi(1S)$	(2.33±0.29) × 10 ⁻⁴	

CONSTRAINED FIT INFORMATION

A multiparticle fit to $\chi_{c1}(1P)$, $\chi_{c0}(1P)$, $\chi_{c2}(1P)$, and $\psi(2S)$ with 4 total widths, a partial width, 25 combinations of partial widths obtained from integrated cross section, and 84 branching ratios uses 248 measurements to determine 49 parameters. The overall fit has a $\chi^2 = 378.1$ for 199 degrees of freedom.

The following *off-diagonal* array elements are the correlation coefficients $\langle \delta p_i \delta p_j \rangle / (\delta p_i \delta p_j)$, in percent, from the fit to parameters p_i , including the branching fractions, $x_i \equiv \Gamma_i / \Gamma_{total}$.

x_{44}	3				
x_{54}	4	2			
x_{67}	7	3	4		
x_{87}	23	9	2	20	
Γ	-12	-5	-63	-10	-41
	x_{17}	x_{44}	x_{54}	x_{67}	x_{87}

$\chi_{c1}(1P)$ PARTIAL WIDTHS

$\chi_{c1}(1P) \Gamma(i) \Gamma(\gamma J/\psi(1S)) / \Gamma_{total}$				$\Gamma_{54} \Gamma_{87} / \Gamma$
$\Gamma(p\bar{p}) \times \Gamma(\gamma J/\psi(1S)) / \Gamma_{total}$	VALUE (eV)	DOCUMENT ID	TECN	COMMENT
21.9±0.8 OUR FIT				
21.4±0.9 OUR AVERAGE				
21.5±0.5±0.8		¹ ANDREOTTI 05A	E835	$p\bar{p} \rightarrow e^+ e^- \gamma$
21.4±1.5±2.2		^{1,2} ARMSTRONG 92	E760	$p\bar{p} \rightarrow e^+ e^- \gamma$
19.9 $\begin{smallmatrix} +4.4 \\ -4.0 \end{smallmatrix}$		¹ BAGLIN 86B	SPEC	$p\bar{p} \rightarrow e^+ e^- X$
¹ Calculated by us using $B(J/\psi(1S) \rightarrow e^+ e^-) = 0.0593 \pm 0.0010$.				
² Recalculated by ANDREOTTI 05A.				

$\chi_{c1}(1P)$ BRANCHING RATIOS

HADRONIC DECAYS

$\Gamma(3(\pi^+ \pi^-)) / \Gamma_{total}$	Γ_1 / Γ		
VALUE (units 10 ⁻³)	DOCUMENT ID	TECN	COMMENT
5.8±1.4 OUR EVALUATION Error includes scale factor of 1.2. Treating systematic error as correlated.			
5.8±1.1 OUR AVERAGE			
5.4±0.7±0.9	¹ BAI	99B	BES $\psi(2S) \rightarrow \gamma \chi_{c1}$
16.0±5.9±0.8	¹ TANENBAUM 78	MRK1	$\psi(2S) \rightarrow \gamma \chi_{c1}$
¹ Rescaled by us using $B(\psi(2S) \rightarrow \gamma \chi_{c1}) = (8.8 \pm 0.4)\%$ and $B(\psi(2S) \rightarrow J/\psi(1S) \pi^+ \pi^-) = (32.6 \pm 0.5)\%$.			
$\Gamma(2(\pi^+ \pi^-)) / \Gamma_{total}$	Γ_2 / Γ		
VALUE (units 10 ⁻³)	DOCUMENT ID	TECN	COMMENT
7.6±2.6 OUR EVALUATION Treating systematic error as correlated.			
8 ±4 OUR AVERAGE Error includes scale factor of 1.5.			
4.6±2.1±2.6	¹ BAI	99B	BES $\psi(2S) \rightarrow \gamma \chi_{c1}$
12.5±4.2±0.6	¹ TANENBAUM 78	MRK1	$\psi(2S) \rightarrow \gamma \chi_{c1}$
¹ Rescaled by us using $B(\psi(2S) \rightarrow \gamma \chi_{c1}) = (8.8 \pm 0.4)\%$ and $B(\psi(2S) \rightarrow J/\psi(1S) \pi^+ \pi^-) = (32.6 \pm 0.5)\%$.			

$\Gamma(\pi^+\pi^-\pi^0\pi^0)/\Gamma_{total}$					Γ_3/Γ
VALUE (%)	EVTS	DOCUMENT ID	TECN	COMMENT	

1.19±0.15±0.03 604.7 ¹HE 08B CLEO $e^+e^- \rightarrow \gamma h^+h^-h^0h^0$
¹HE 08B reports $1.28 \pm 0.06 \pm 0.15 \pm 0.08$ % from a measurement of $[\Gamma(\chi_{c1}(1P) \rightarrow \pi^+\pi^-\pi^0\pi^0)/\Gamma_{total}] \times [B(\psi(2S) \rightarrow \gamma\chi_{c1}(1P))]$ assuming $B(\psi(2S) \rightarrow \gamma\chi_{c1}(1P)) = (9.07 \pm 0.11 \pm 0.54) \times 10^{-2}$, which we rescale to our best value $B(\psi(2S) \rightarrow \gamma\chi_{c1}(1P)) = (9.75 \pm 0.24) \times 10^{-2}$. Our first error is their experiment's error and our second error is the systematic error from using our best value.

$\Gamma(\rho^+\pi^-\pi^0 + c.c.)/\Gamma_{total}$					Γ_4/Γ
VALUE (%)	EVTS	DOCUMENT ID	TECN	COMMENT	

1.45±0.24±0.04 712.3 ^{1,2}HE 08B CLEO $e^+e^- \rightarrow \gamma h^+h^-h^0h^0$
¹HE 08B reports $1.56 \pm 0.13 \pm 0.22 \pm 0.10$ % from a measurement of $[\Gamma(\chi_{c1}(1P) \rightarrow \rho^+\pi^-\pi^0 + c.c.)/\Gamma_{total}] \times [B(\psi(2S) \rightarrow \gamma\chi_{c1}(1P))]$ assuming $B(\psi(2S) \rightarrow \gamma\chi_{c1}(1P)) = (9.07 \pm 0.11 \pm 0.54) \times 10^{-2}$, which we rescale to our best value $B(\psi(2S) \rightarrow \gamma\chi_{c1}(1P)) = (9.75 \pm 0.24) \times 10^{-2}$. Our first error is their experiment's error and our second error is the systematic error from using our best value.
²Calculated by us. We have added the values from HE 08B for $\rho^+\pi^-\pi^0$ and $\rho^-\pi^+\pi^0$ decays assuming uncorrelated statistical and fully correlated systematic uncertainties.

$\Gamma(\rho^0\pi^+\pi^-)/\Gamma_{total}$					Γ_5/Γ
VALUE (units 10^{-3})	EVTS	DOCUMENT ID	TECN	COMMENT	

3.9±3.5 ¹TANENBAUM 78 MRK1 $\psi(2S) \rightarrow \gamma\chi_{c1}$
¹Estimated using $B(\psi(2S) \rightarrow \gamma\chi_{c1}(1P)) = 0.087$. The errors do not contain the uncertainty in the $\psi(2S)$ decay.

$\Gamma(4\pi^0)/\Gamma_{total}$					Γ_6/Γ
VALUE (units 10^{-4})	EVTS	DOCUMENT ID	TECN	COMMENT	

5.4±0.8±0.1 608 ¹ABLIKIM 11A BES3 $e^+e^- \rightarrow \psi(2S) \rightarrow \gamma\chi_{c1}$
¹ABLIKIM 11A reports $(0.57 \pm 0.03 \pm 0.08) \times 10^{-3}$ from a measurement of $[\Gamma(\chi_{c1}(1P) \rightarrow 4\pi^0)/\Gamma_{total}] \times [B(\psi(2S) \rightarrow \gamma\chi_{c1}(1P))]$ assuming $B(\psi(2S) \rightarrow \gamma\chi_{c1}(1P)) = (9.2 \pm 0.4) \times 10^{-2}$, which we rescale to our best value $B(\psi(2S) \rightarrow \gamma\chi_{c1}(1P)) = (9.75 \pm 0.24) \times 10^{-2}$. Our first error is their experiment's error and our second error is the systematic error from using our best value.

$\Gamma(\pi^+\pi^-K^+K^-)/\Gamma_{total}$					Γ_7/Γ
VALUE (units 10^{-3})	EVTS	DOCUMENT ID	TECN	COMMENT	

4.5±1.0 OUR EVALUATION Treating systematic error as correlated.
4.5±0.9 OUR AVERAGE
 4.2±0.4±0.9 ¹BAI 99B BES $\psi(2S) \rightarrow \gamma\chi_{c1}$
 7.3±3.0±0.4 ¹TANENBAUM 78 MRK1 $\psi(2S) \rightarrow \gamma\chi_{c1}$
¹Rescaled by us using $B(\psi(2S) \rightarrow \gamma\chi_{c1}) = (8.8 \pm 0.4)\%$ and $B(\psi(2S) \rightarrow J/\psi(1S)\pi^+\pi^-) = (32.6 \pm 0.5)\%$.

$\Gamma(K^+K^-\pi^0\pi^0)/\Gamma_{total}$					Γ_8/Γ
VALUE (units 10^{-3})	EVTS	DOCUMENT ID	TECN	COMMENT	

1.12±0.27±0.03 45.1 ¹HE 08B CLEO $e^+e^- \rightarrow \gamma h^+h^-h^0h^0$
¹HE 08B reports $(0.12 \pm 0.02 \pm 0.02 \pm 0.01) \times 10^{-2}$ from a measurement of $[\Gamma(\chi_{c1}(1P) \rightarrow K^+K^-\pi^0\pi^0)/\Gamma_{total}] \times [B(\psi(2S) \rightarrow \gamma\chi_{c1}(1P))]$ assuming $B(\psi(2S) \rightarrow \gamma\chi_{c1}(1P)) = (9.07 \pm 0.11 \pm 0.54) \times 10^{-2}$, which we rescale to our best value $B(\psi(2S) \rightarrow \gamma\chi_{c1}(1P)) = (9.75 \pm 0.24) \times 10^{-2}$. Our first error is their experiment's error and our second error is the systematic error from using our best value.

$\Gamma(K^+K^-\pi^+\pi^-)/\Gamma_{total}$					Γ_9/Γ
VALUE (units 10^{-3})	EVTS	DOCUMENT ID	TECN	COMMENT	

11.46±0.12±1.29 12k ¹ABLIKIM 13B BES3 $e^+e^- \rightarrow \psi(2S) \rightarrow \gamma\chi_{c1}$
¹Using 1.06×10^8 $\psi(2S)$ mesons and $B(\psi(2S) \rightarrow \chi_{c1}\gamma) = (9.2 \pm 0.4)\%$.

$\Gamma(K_S^0K^\pm\pi^\mp\pi^\pm\pi^-)/\Gamma_{total}$					Γ_{10}/Γ
VALUE (units 10^{-3})	EVTS	DOCUMENT ID	TECN	COMMENT	

7.5±0.11±0.79 5.1k ¹ABLIKIM 13B BES3 $e^+e^- \rightarrow \psi(2S) \rightarrow \gamma\chi_{c1}$
¹Using 1.06×10^8 $\psi(2S)$ mesons and $B(\psi(2S) \rightarrow \chi_{c1}\gamma) = (9.2 \pm 0.4)\%$.

$\Gamma(K^+\pi^-\bar{K}^0\pi^0 + c.c.)/\Gamma_{total}$					Γ_{11}/Γ
VALUE (%)	EVTS	DOCUMENT ID	TECN	COMMENT	

0.86±0.13±0.02 141.3 ¹HE 08B CLEO $e^+e^- \rightarrow \gamma h^+h^-h^0h^0$
¹HE 08B reports $0.92 \pm 0.09 \pm 0.11 \pm 0.06$ % from a measurement of $[\Gamma(\chi_{c1}(1P) \rightarrow K^+\pi^-\bar{K}^0\pi^0 + c.c.)/\Gamma_{total}] \times [B(\psi(2S) \rightarrow \gamma\chi_{c1}(1P))]$ assuming $B(\psi(2S) \rightarrow \gamma\chi_{c1}(1P)) = (9.07 \pm 0.11 \pm 0.54) \times 10^{-2}$, which we rescale to our best value $B(\psi(2S) \rightarrow \gamma\chi_{c1}(1P)) = (9.75 \pm 0.24) \times 10^{-2}$. Our first error is their experiment's error and our second error is the systematic error from using our best value.

$\Gamma(\rho^-K^+\bar{K}^0 + c.c.)/\Gamma_{total}$					Γ_{12}/Γ
VALUE (%)	EVTS	DOCUMENT ID	TECN	COMMENT	

0.50±0.12±0.01 141.3 ¹HE 08B CLEO $e^+e^- \rightarrow \gamma h^+h^-h^0h^0$
¹HE 08B reports $0.54 \pm 0.11 \pm 0.07 \pm 0.03$ % from a measurement of $[\Gamma(\chi_{c1}(1P) \rightarrow \rho^-K^+\bar{K}^0 + c.c.)/\Gamma_{total}] \times [B(\psi(2S) \rightarrow \gamma\chi_{c1}(1P))]$ assuming $B(\psi(2S) \rightarrow \gamma\chi_{c1}(1P)) = (9.07 \pm 0.11 \pm 0.54) \times 10^{-2}$, which we rescale to our best value $B(\psi(2S) \rightarrow \gamma\chi_{c1}(1P)) = (9.75 \pm 0.24) \times 10^{-2}$. Our first error is their experiment's error and our second error is the systematic error from using our best value.

$\Gamma(K^*(892)^0\bar{K}^0\pi^0 \rightarrow K^+\pi^-\bar{K}^0\pi^0 + c.c.)/\Gamma_{total}$					Γ_{13}/Γ
VALUE (%)	EVTS	DOCUMENT ID	TECN	COMMENT	

0.23±0.06±0.01 141.3 ¹HE 08B CLEO $e^+e^- \rightarrow \gamma h^+h^-h^0h^0$
¹HE 08B reports $0.25 \pm 0.06 \pm 0.03 \pm 0.02$ % from a measurement of $[\Gamma(\chi_{c1}(1P) \rightarrow K^*(892)^0\bar{K}^0\pi^0 \rightarrow K^+\pi^-\bar{K}^0\pi^0 + c.c.)/\Gamma_{total}] \times [B(\psi(2S) \rightarrow \gamma\chi_{c1}(1P))]$ assuming $B(\psi(2S) \rightarrow \gamma\chi_{c1}(1P)) = (9.07 \pm 0.11 \pm 0.54) \times 10^{-2}$, which we rescale to our best value $B(\psi(2S) \rightarrow \gamma\chi_{c1}(1P)) = (9.75 \pm 0.24) \times 10^{-2}$. Our first error is their experiment's error and our second error is the systematic error from using our best value.

$\Gamma(K^+K^-\eta\pi^0)/\Gamma_{total}$					Γ_{14}/Γ
VALUE (%)	EVTS	DOCUMENT ID	TECN	COMMENT	

0.112±0.034±0.003 141.3 ¹HE 08B CLEO $e^+e^- \rightarrow \gamma h^+h^-h^0h^0$
¹HE 08B reports $0.12 \pm 0.03 \pm 0.02 \pm 0.01$ % from a measurement of $[\Gamma(\chi_{c1}(1P) \rightarrow K^+K^-\eta\pi^0)/\Gamma_{total}] \times [B(\psi(2S) \rightarrow \gamma\chi_{c1}(1P))]$ assuming $B(\psi(2S) \rightarrow \gamma\chi_{c1}(1P)) = (9.07 \pm 0.11 \pm 0.54) \times 10^{-2}$, which we rescale to our best value $B(\psi(2S) \rightarrow \gamma\chi_{c1}(1P)) = (9.75 \pm 0.24) \times 10^{-2}$. Our first error is their experiment's error and our second error is the systematic error from using our best value.

$\Gamma(\pi^+\pi^-K_S^0K_S^0)/\Gamma_{total}$					Γ_{15}/Γ
VALUE (units 10^{-4})	EVTS	DOCUMENT ID	TECN	COMMENT	

6.9±2.9±0.2 19.8±7.7 ¹ABLIKIM 05o BES2 $\psi(2S) \rightarrow \chi_{c1}\gamma$
¹ABLIKIM 05o reports $[\Gamma(\chi_{c1}(1P) \rightarrow \pi^+\pi^-K_S^0K_S^0)/\Gamma_{total}] \times [B(\psi(2S) \rightarrow \gamma\chi_{c1}(1P))]$ = $(0.67 \pm 0.26 \pm 0.11) \times 10^{-4}$ which we divide by our best value $B(\psi(2S) \rightarrow \gamma\chi_{c1}(1P)) = (9.75 \pm 0.24) \times 10^{-2}$. Our first error is their experiment's error and our second error is the systematic error from using our best value.

$\Gamma(K^+K^-\eta)/\Gamma_{total}$					Γ_{16}/Γ
VALUE (units 10^{-4})	EVTS	DOCUMENT ID	TECN	COMMENT	

3.2±1.0±0.1 ¹ATHAR 07 CLEO $\psi(2S) \rightarrow \gamma h^+h^-h^0$
¹ATHAR 07 reports $(0.34 \pm 0.10 \pm 0.04) \times 10^{-3}$ from a measurement of $[\Gamma(\chi_{c1}(1P) \rightarrow K^+K^-\eta)/\Gamma_{total}] \times [B(\psi(2S) \rightarrow \gamma\chi_{c1}(1P))]$ assuming $B(\psi(2S) \rightarrow \gamma\chi_{c1}(1P)) = 0.0907 \pm 0.0011 \pm 0.0054$, which we rescale to our best value $B(\psi(2S) \rightarrow \gamma\chi_{c1}(1P)) = (9.75 \pm 0.24) \times 10^{-2}$. Our first error is their experiment's error and our second error is the systematic error from using our best value.

$\Gamma(\bar{K}^0K^+\pi^- + c.c.)/\Gamma_{total}$					Γ_{17}/Γ
VALUE (units 10^{-3})	EVTS	DOCUMENT ID	TECN	COMMENT	

7.0±0.6 OUR FIT

$\Gamma(K^*(892)^0\bar{K}^0 + c.c.)/\Gamma_{total}$					Γ_{18}/Γ
VALUE (units 10^{-3})	EVTS	DOCUMENT ID	TECN	COMMENT	

0.98±0.37±0.02 22 ¹ABLIKIM 06R BES2 $\psi(2S) \rightarrow \gamma\chi_{c1}$
¹ABLIKIM 06R reports $(1.1 \pm 0.4 \pm 0.1) \times 10^{-3}$ from a measurement of $[\Gamma(\chi_{c1}(1P) \rightarrow K^*(892)^0\bar{K}^0 + c.c.)/\Gamma_{total}] \times [B(\psi(2S) \rightarrow \gamma\chi_{c1}(1P))]$ assuming $B(\psi(2S) \rightarrow \gamma\chi_{c1}(1P)) = (8.7 \pm 0.4) \times 10^{-2}$, which we rescale to our best value $B(\psi(2S) \rightarrow \gamma\chi_{c1}(1P)) = (9.75 \pm 0.24) \times 10^{-2}$. Our first error is their experiment's error and our second error is the systematic error from using our best value.

$\Gamma(K^*(892)^+K^- + c.c.)/\Gamma_{total}$					Γ_{19}/Γ
VALUE (units 10^{-3})	EVTS	DOCUMENT ID	TECN	COMMENT	

1.43±0.65±0.03 27 ¹ABLIKIM 06R BES2 $\psi(2S) \rightarrow \gamma\chi_{c1}$
¹ABLIKIM 06R reports $(1.6 \pm 0.7 \pm 0.2) \times 10^{-3}$ from a measurement of $[\Gamma(\chi_{c1}(1P) \rightarrow K^*(892)^+K^- + c.c.)/\Gamma_{total}] \times [B(\psi(2S) \rightarrow \gamma\chi_{c1}(1P))]$ assuming $B(\psi(2S) \rightarrow \gamma\chi_{c1}(1P)) = (8.7 \pm 0.4) \times 10^{-2}$, which we rescale to our best value $B(\psi(2S) \rightarrow \gamma\chi_{c1}(1P)) = (9.75 \pm 0.24) \times 10^{-2}$. Our first error is their experiment's error and our second error is the systematic error from using our best value.

$\Gamma(K_S^*(1430)^0\bar{K}^0 + c.c. \rightarrow K_S^0K^+\pi^- + c.c.)/\Gamma_{total}$					Γ_{20}/Γ
VALUE	CL%	DOCUMENT ID	TECN	COMMENT	

<8 × 10⁻⁴ 90 ¹ABLIKIM 06R BES2 $\psi(2S) \rightarrow \gamma\chi_{c1}$
¹ABLIKIM 06R reports $< 0.9 \times 10^{-3}$ from a measurement of $[\Gamma(\chi_{c1}(1P) \rightarrow K_S^*(1430)^0\bar{K}^0 + c.c. \rightarrow K_S^0K^+\pi^- + c.c.)/\Gamma_{total}] \times [B(\psi(2S) \rightarrow \gamma\chi_{c1}(1P))]$ assuming $B(\psi(2S) \rightarrow \gamma\chi_{c1}(1P)) = (8.7 \pm 0.4) \times 10^{-2}$, which we rescale to our best value $B(\psi(2S) \rightarrow \gamma\chi_{c1}(1P)) = 9.75 \times 10^{-2}$.

$\Gamma(K_S^*(1430)^+K^- + c.c. \rightarrow K_S^0K^+\pi^- + c.c.)/\Gamma_{total}$					Γ_{21}/Γ
VALUE	CL%	DOCUMENT ID	TECN	COMMENT	

<2.1 × 10⁻³ 90 ¹ABLIKIM 06R BES2 $\psi(2S) \rightarrow \gamma\chi_{c1}$
¹ABLIKIM 06R reports $< 2.4 \times 10^{-3}$ from a measurement of $[\Gamma(\chi_{c1}(1P) \rightarrow K_S^*(1430)^+K^- + c.c. \rightarrow K_S^0K^+\pi^- + c.c.)/\Gamma_{total}] \times [B(\psi(2S) \rightarrow \gamma\chi_{c1}(1P))]$ assuming $B(\psi(2S) \rightarrow \gamma\chi_{c1}(1P)) = (8.7 \pm 0.4) \times 10^{-2}$, which we rescale to our best value $B(\psi(2S) \rightarrow \gamma\chi_{c1}(1P)) = 9.75 \times 10^{-2}$.

$\Gamma(K^+K^-\pi^0)/\Gamma_{total}$					Γ_{22}/Γ
VALUE (units 10^{-3})	EVTS	DOCUMENT ID	TECN	COMMENT	

1.81±0.24±0.04 ¹ATHAR 07 CLEO $\psi(2S) \rightarrow \gamma h^+h^-h^0$
¹ATHAR 07 reports $(1.95 \pm 0.16 \pm 0.23) \times 10^{-3}$ from a measurement of $[\Gamma(\chi_{c1}(1P) \rightarrow K^+K^-\pi^0)/\Gamma_{total}] \times [B(\psi(2S) \rightarrow \gamma\chi_{c1}(1P))]$ assuming $B(\psi(2S) \rightarrow \gamma\chi_{c1}(1P)) = 0.0907 \pm 0.0011 \pm 0.0054$, which we rescale to our best value $B(\psi(2S) \rightarrow \gamma\chi_{c1}(1P)) = (9.75 \pm 0.24) \times 10^{-2}$. Our first error is their experiment's error and our second error is the systematic error from using our best value.

Meson Particle Listings

$\chi_{c1}(1P)$

$\Gamma(\eta\pi^+\pi^-)/\Gamma_{total}$		Γ_{23}/Γ			
VALUE (units 10^{-3})	EVTS	DOCUMENT ID	TECN	COMMENT	
4.62±0.23 OUR AVERAGE					

4.56±0.23±0.11		1,2 ABLIKIM	17k BES3	$\psi(2S) \rightarrow \gamma\eta\pi^+\pi^-$	
4.7 ±0.5 ±0.1		3 ATHAR	07 CLEO	$\psi(2S) \rightarrow \gamma h^+ h^- h^0$	
5.3 ±0.9 ±0.1	222	4 ABLIKIM	06R BES2	$\psi(2S) \rightarrow \gamma\chi_{c1}$	

¹ From an amplitude analysis using an isobar model.
² ABLIKIM 17k reports $(4.67 \pm 0.03 \pm 0.23 \pm 0.16) \times 10^{-3}$ from a measurement of $[\Gamma(\chi_{c1}(1P) \rightarrow \eta\pi^+\pi^-)/\Gamma_{total}] \times [B(\psi(2S) \rightarrow \gamma\chi_{c1}(1P))]$ assuming $B(\psi(2S) \rightarrow \gamma\chi_{c1}(1P)) = (9.55 \pm 0.31) \times 10^{-2}$, which we rescale to our best value $B(\psi(2S) \rightarrow \gamma\chi_{c1}(1P)) = (9.75 \pm 0.24) \times 10^{-2}$. Our first error is their experiment's error and our second error is the systematic error from using our best value.

³ ATHAR 07 reports $(5.0 \pm 0.3 \pm 0.5) \times 10^{-3}$ from a measurement of $[\Gamma(\chi_{c1}(1P) \rightarrow \eta\pi^+\pi^-)/\Gamma_{total}] \times [B(\psi(2S) \rightarrow \gamma\chi_{c1}(1P))]$ assuming $B(\psi(2S) \rightarrow \gamma\chi_{c1}(1P)) = 0.0907 \pm 0.0011 \pm 0.0054$, which we rescale to our best value $B(\psi(2S) \rightarrow \gamma\chi_{c1}(1P)) = (9.75 \pm 0.24) \times 10^{-2}$. Our first error is their experiment's error and our second error is the systematic error from using our best value.

⁴ ABLIKIM 06R reports $(5.9 \pm 0.7 \pm 0.8) \times 10^{-3}$ from a measurement of $[\Gamma(\chi_{c1}(1P) \rightarrow \eta\pi^+\pi^-)/\Gamma_{total}] \times [B(\psi(2S) \rightarrow \gamma\chi_{c1}(1P))]$ assuming $B(\psi(2S) \rightarrow \gamma\chi_{c1}(1P)) = (8.7 \pm 0.4) \times 10^{-2}$, which we rescale to our best value $B(\psi(2S) \rightarrow \gamma\chi_{c1}(1P)) = (9.75 \pm 0.24) \times 10^{-2}$. Our first error is their experiment's error and our second error is the systematic error from using our best value.

$\Gamma(a_0(980)^+\pi^- + c.c. \rightarrow \eta\pi^+\pi^-)/\Gamma_{total}$		Γ_{24}/Γ			
VALUE (units 10^{-3})	EVTS	DOCUMENT ID	TECN	COMMENT	
3.2 ±0.4 OUR AVERAGE				Error includes scale factor of 2.2.	

3.33±0.19±0.08		1,2 ABLIKIM	17k BES3	$\psi(2S) \rightarrow \gamma\eta\pi^+\pi^-$	
1.79±0.63±0.04	58	3 ABLIKIM	06R BES2	$\psi(2S) \rightarrow \gamma\chi_{c1}$	

¹ From an amplitude analysis using an isobar model.
² ABLIKIM 17k reports $(3.40 \pm 0.03 \pm 0.19 \pm 0.11) \times 10^{-3}$ from a measurement of $[\Gamma(\chi_{c1}(1P) \rightarrow a_0(980)^+\pi^- + c.c. \rightarrow \eta\pi^+\pi^-)/\Gamma_{total}] \times [B(\psi(2S) \rightarrow \gamma\chi_{c1}(1P))]$ assuming $B(\psi(2S) \rightarrow \gamma\chi_{c1}(1P)) = (9.55 \pm 0.31) \times 10^{-2}$, which we rescale to our best value $B(\psi(2S) \rightarrow \gamma\chi_{c1}(1P)) = (9.75 \pm 0.24) \times 10^{-2}$. Our first error is their experiment's error and our second error is the systematic error from using our best value.

³ ABLIKIM 06R reports $(2.0 \pm 0.5 \pm 0.5) \times 10^{-3}$ from a measurement of $[\Gamma(\chi_{c1}(1P) \rightarrow a_0(980)^+\pi^- + c.c. \rightarrow \eta\pi^+\pi^-)/\Gamma_{total}] \times [B(\psi(2S) \rightarrow \gamma\chi_{c1}(1P))]$ assuming $B(\psi(2S) \rightarrow \gamma\chi_{c1}(1P)) = (8.7 \pm 0.4) \times 10^{-2}$, which we rescale to our best value $B(\psi(2S) \rightarrow \gamma\chi_{c1}(1P)) = (9.75 \pm 0.24) \times 10^{-2}$. Our first error is their experiment's error and our second error is the systematic error from using our best value.

$\Gamma(a_2(1320)^+\pi^- + c.c. \rightarrow \eta\pi^+\pi^-)/\Gamma_{total}$		Γ_{25}/Γ			
VALUE (units 10^{-3})		DOCUMENT ID	TECN	COMMENT	
0.176±0.023±0.004		1,2 ABLIKIM	17k BES3	$\psi(2S) \rightarrow \gamma\eta\pi^+\pi^-$	

¹ From an amplitude analysis using an isobar model.
² ABLIKIM 17k reports $(0.18 \pm 0.01 \pm 0.02 \pm 0.01) \times 10^{-3}$ from a measurement of $[\Gamma(\chi_{c1}(1P) \rightarrow a_2(1320)^+\pi^- + c.c. \rightarrow \eta\pi^+\pi^-)/\Gamma_{total}] \times [B(\psi(2S) \rightarrow \gamma\chi_{c1}(1P))]$ assuming $B(\psi(2S) \rightarrow \gamma\chi_{c1}(1P)) = (9.55 \pm 0.31) \times 10^{-2}$, which we rescale to our best value $B(\psi(2S) \rightarrow \gamma\chi_{c1}(1P)) = (9.75 \pm 0.24) \times 10^{-2}$. Our first error is their experiment's error and our second error is the systematic error from using our best value.

$\Gamma(a_2(1700)^+\pi^- + c.c. \rightarrow \eta\pi^+\pi^-)/\Gamma_{total}$		Γ_{26}/Γ			
VALUE (units 10^{-5})		DOCUMENT ID	TECN	COMMENT	
4.6 ±0.7 ±0.1		1,2 ABLIKIM	17k BES3	$\psi(2S) \rightarrow \gamma\eta\pi^+\pi^-$	

¹ From an amplitude analysis using an isobar model.
² ABLIKIM 17k reports $(4.7 \pm 0.4 \pm 0.6 \pm 0.2) \times 10^{-5}$ from a measurement of $[\Gamma(\chi_{c1}(1P) \rightarrow a_2(1700)^+\pi^- + c.c. \rightarrow \eta\pi^+\pi^-)/\Gamma_{total}] \times [B(\psi(2S) \rightarrow \gamma\chi_{c1}(1P))]$ assuming $B(\psi(2S) \rightarrow \gamma\chi_{c1}(1P)) = (9.55 \pm 0.31) \times 10^{-2}$, which we rescale to our best value $B(\psi(2S) \rightarrow \gamma\chi_{c1}(1P)) = (9.75 \pm 0.24) \times 10^{-2}$. Our first error is their experiment's error and our second error is the systematic error from using our best value.

$\Gamma(f_2(1270)\eta \rightarrow \eta\pi^+\pi^-)/\Gamma_{total}$		Γ_{27}/Γ			
VALUE (units 10^{-4})		DOCUMENT ID	TECN	COMMENT	
3.5 ±0.6 ±0.1		1,2 ABLIKIM	17k BES3	$\psi(2S) \rightarrow \gamma\eta\pi^+\pi^-$	

¹ From an amplitude analysis using an isobar model.
² ABLIKIM 17k reports $(0.36 \pm 0.01 \pm 0.06 \pm 0.01) \times 10^{-3}$ from a measurement of $[\Gamma(\chi_{c1}(1P) \rightarrow f_2(1270)\eta \rightarrow \eta\pi^+\pi^-)/\Gamma_{total}] \times [B(\psi(2S) \rightarrow \gamma\chi_{c1}(1P))]$ assuming $B(\psi(2S) \rightarrow \gamma\chi_{c1}(1P)) = (9.55 \pm 0.31) \times 10^{-2}$, which we rescale to our best value $B(\psi(2S) \rightarrow \gamma\chi_{c1}(1P)) = (9.75 \pm 0.24) \times 10^{-2}$. Our first error is their experiment's error and our second error is the systematic error from using our best value.

$\Gamma(f_4(2050)\eta \rightarrow \eta\pi^+\pi^-)/\Gamma_{total}$		Γ_{28}/Γ			
VALUE (units 10^{-5})		DOCUMENT ID	TECN	COMMENT	
2.5 ±0.9 ±0.1		1,2 ABLIKIM	17k BES3	$\psi(2S) \rightarrow \gamma\eta\pi^+\pi^-$	

¹ From an amplitude analysis using an isobar model.
² ABLIKIM 17k reports $(2.6 \pm 0.4 \pm 0.8 \pm 0.1) \times 10^{-5}$ from a measurement of $[\Gamma(\chi_{c1}(1P) \rightarrow f_4(2050)\eta \rightarrow \eta\pi^+\pi^-)/\Gamma_{total}] \times [B(\psi(2S) \rightarrow \gamma\chi_{c1}(1P))]$ assuming $B(\psi(2S) \rightarrow \gamma\chi_{c1}(1P)) = (9.55 \pm 0.31) \times 10^{-2}$, which we rescale to our best value $B(\psi(2S) \rightarrow \gamma\chi_{c1}(1P)) = (9.75 \pm 0.24) \times 10^{-2}$. Our first error is their experiment's error and our second error is the systematic error from using our best value.

$\Gamma(\pi_1(1400)^+\pi^- + c.c. \rightarrow \eta\pi^+\pi^-)/\Gamma_{total}$		Γ_{29}/Γ			
VALUE	CL%	DOCUMENT ID	TECN	COMMENT	
<5 × 10⁻⁵	90	1,2 ABLIKIM	17k BES3	$\psi(2S) \rightarrow \gamma\eta\pi^+\pi^-$	

¹ From an amplitude analysis using an isobar model.
² ABLIKIM 17k reports $< 4.6 \times 10^{-5}$ from a measurement of $[\Gamma(\chi_{c1}(1P) \rightarrow \pi_1(1400)^+\pi^- + c.c. \rightarrow \eta\pi^+\pi^-)/\Gamma_{total}] \times [B(\psi(2S) \rightarrow \gamma\chi_{c1}(1P))]$ assuming $B(\psi(2S) \rightarrow \gamma\chi_{c1}(1P)) = (9.55 \pm 0.31) \times 10^{-2}$, which we rescale to our best value $B(\psi(2S) \rightarrow \gamma\chi_{c1}(1P)) = 9.75 \times 10^{-2}$.

$\Gamma(\pi_1(1600)^+\pi^- + c.c. \rightarrow \eta\pi^+\pi^-)/\Gamma_{total}$		Γ_{30}/Γ			
VALUE	CL%	DOCUMENT ID	TECN	COMMENT	
<1.5 × 10⁻⁵	90	1,2 ABLIKIM	17k BES3	$\psi(2S) \rightarrow \gamma\eta\pi^+\pi^-$	

¹ From an amplitude analysis using an isobar model.
² ABLIKIM 17k reports $< 1.5 \times 10^{-5}$ from a measurement of $[\Gamma(\chi_{c1}(1P) \rightarrow \pi_1(1600)^+\pi^- + c.c. \rightarrow \eta\pi^+\pi^-)/\Gamma_{total}] \times [B(\psi(2S) \rightarrow \gamma\chi_{c1}(1P))]$ assuming $B(\psi(2S) \rightarrow \gamma\chi_{c1}(1P)) = (9.55 \pm 0.31) \times 10^{-2}$, which we rescale to our best value $B(\psi(2S) \rightarrow \gamma\chi_{c1}(1P)) = 9.75 \times 10^{-2}$.

$\Gamma(\pi_1(2015)^+\pi^- + c.c. \rightarrow \eta\pi^+\pi^-)/\Gamma_{total}$		Γ_{31}/Γ			
VALUE	CL%	DOCUMENT ID	TECN	COMMENT	
<8 × 10⁻⁶	90	1,2 ABLIKIM	17k BES3	$\psi(2S) \rightarrow \gamma\eta\pi^+\pi^-$	

¹ From an amplitude analysis using an isobar model.
² ABLIKIM 17k reports $< 8 \times 10^{-6}$ from a measurement of $[\Gamma(\chi_{c1}(1P) \rightarrow \pi_1(2015)^+\pi^- + c.c. \rightarrow \eta\pi^+\pi^-)/\Gamma_{total}] \times [B(\psi(2S) \rightarrow \gamma\chi_{c1}(1P))]$ assuming $B(\psi(2S) \rightarrow \gamma\chi_{c1}(1P)) = (9.55 \pm 0.31) \times 10^{-2}$, which we rescale to our best value $B(\psi(2S) \rightarrow \gamma\chi_{c1}(1P)) = 9.75 \times 10^{-2}$.

$\Gamma(f_2(1270)\eta)/\Gamma_{total}$		Γ_{32}/Γ			
VALUE (units 10^{-3})	EVTS	DOCUMENT ID	TECN	COMMENT	
0.67±0.11 OUR AVERAGE					

0.63±0.11±0.02		1,2 ABLIKIM	17k BES3	$\psi(2S) \rightarrow \gamma\eta\pi^+\pi^-$	
2.7 ±0.8 ±0.1	53	3 ABLIKIM	06R BES2	$\psi(2S) \rightarrow \gamma\chi_{c1}$	

¹ ABLIKIM 17k reports $(6.4 \pm 1.1) \times 10^{-4}$ from a measurement of $[\Gamma(\chi_{c1}(1P) \rightarrow f_2(1270)\eta)/\Gamma_{total}] \times [B(\psi(2S) \rightarrow \gamma\chi_{c1}(1P))]$ assuming $B(\psi(2S) \rightarrow \gamma\chi_{c1}(1P)) = (9.55 \pm 0.31) \times 10^{-2}$, which we rescale to our best value $B(\psi(2S) \rightarrow \gamma\chi_{c1}(1P)) = (9.75 \pm 0.24) \times 10^{-2}$. Our first error is their experiment's error and our second error is the systematic error from using our best value.

² From an amplitude analysis using an isobar model.
³ ABLIKIM 06R reports $(3.0 \pm 0.7 \pm 0.5) \times 10^{-3}$ from a measurement of $[\Gamma(\chi_{c1}(1P) \rightarrow f_2(1270)\eta)/\Gamma_{total}] \times [B(\psi(2S) \rightarrow \gamma\chi_{c1}(1P))]$ assuming $B(\psi(2S) \rightarrow \gamma\chi_{c1}(1P)) = (8.7 \pm 0.4) \times 10^{-2}$, which we rescale to our best value $B(\psi(2S) \rightarrow \gamma\chi_{c1}(1P)) = (9.75 \pm 0.24) \times 10^{-2}$. Our first error is their experiment's error and our second error is the systematic error from using our best value.

$\Gamma(\pi^+\pi^-\eta)/\Gamma_{total}$		Γ_{33}/Γ			
VALUE (units 10^{-3})		DOCUMENT ID	TECN	COMMENT	
2.2 ±0.4 ±0.1		1 ATHAR	07 CLEO	$\psi(2S) \rightarrow \gamma h^+ h^- h^0$	

¹ ATHAR 07 reports $(2.4 \pm 0.4 \pm 0.3) \times 10^{-3}$ from a measurement of $[\Gamma(\chi_{c1}(1P) \rightarrow \pi^+\pi^-\eta)/\Gamma_{total}] \times [B(\psi(2S) \rightarrow \gamma\chi_{c1}(1P))]$ assuming $B(\psi(2S) \rightarrow \gamma\chi_{c1}(1P)) = 0.0907 \pm 0.0011 \pm 0.0054$, which we rescale to our best value $B(\psi(2S) \rightarrow \gamma\chi_{c1}(1P)) = (9.75 \pm 0.24) \times 10^{-2}$. Our first error is their experiment's error and our second error is the systematic error from using our best value.

$\Gamma(K^+K^-\eta'(958))/\Gamma_{total}$		Γ_{34}/Γ			
VALUE (units 10^{-4})	EVTS	DOCUMENT ID	TECN	COMMENT	
8.75±0.87	310	1 ABLIKIM	14J BES3	$\psi(2S) \rightarrow \gamma K^+K^-\eta'(958)$	

¹ Derived using $B(\psi(2S) \rightarrow \gamma\chi_{c1}) = (9.2 \pm 0.4)\%$. Uncertainty includes both statistical and systematic contributions combined in quadrature.

$\Gamma(K_0^*(1430)^+K^- + c.c.)/\Gamma_{total}$		Γ_{35}/Γ			
VALUE (units 10^{-4})		DOCUMENT ID	TECN	COMMENT	
6.41±0.57±^{2.09}_{-2.71}		1 ABLIKIM	14J BES3	$\psi(2S) \rightarrow \gamma K^+K^-\eta'(958)$	

¹ Normalized to $B(\chi_{c1} \rightarrow K^+K^-\eta'(958))$ branching fraction.

$\Gamma(f_0(980)\eta'(958))/\Gamma_{total}$		Γ_{36}/Γ			
VALUE (units 10^{-4})		DOCUMENT ID	TECN	COMMENT	
1.65±0.47±^{1.32}_{-0.56}		1 ABLIKIM	14J BES3	$\psi(2S) \rightarrow \gamma K^+K^-\eta'(958)$	

¹ Normalized to $B(\chi_{c1} \rightarrow K^+K^-\eta'(958))$ branching fraction.

$\Gamma(f_0(1710)\eta'(958))/\Gamma_{total}$		Γ_{37}/Γ			
VALUE (units 10^{-4})		DOCUMENT ID	TECN	COMMENT	
0.71±0.22±^{0.68}_{-0.48}		1 ABLIKIM	14J BES3	$\psi(2S) \rightarrow \gamma K^+K^-\eta'(958)$	

¹ Normalized to $B(\chi_{c1} \rightarrow K^+K^-\eta'(958))$ branching fraction.

$\Gamma(f_2'(1525)\eta'(958))/\Gamma_{total}$		Γ_{38}/Γ			
VALUE (units 10^{-4})		DOCUMENT ID	TECN	COMMENT	
0.92±0.23±^{0.55}_{-0.51}		1 ABLIKIM	14J BES3	$\psi(2S) \rightarrow \gamma K^+K^-\eta'(958)$	

¹ Normalized to $B(\chi_{c1} \rightarrow K^+K^-\eta'(958))$ branching fraction.

Meson Particle Listings

$\chi_{c1}(1P)$

$\Gamma(e^+e^- J/\psi(1S))/\Gamma_{total}$ VALUE (units 10^{-3})	EVTS	DOCUMENT ID	TECN	COMMENT	Γ_{92}/Γ
--	------	-------------	------	---------	----------------------

• • • We do not use the following data for averages, fits, limits, etc. • • •

3.65 ± 0.23 ± 0.09 1.9k 1,2 ABLIKIM 17I BES3 $\psi(2S) \rightarrow \gamma e^+ e^- J/\psi$

¹ ABLIKIM 17I reports (3.73 ± 0.09 ± 0.25) × 10⁻³ from a measurement of $[\Gamma(\chi_{c1}(1P) \rightarrow e^+ e^- J/\psi(1S))/\Gamma_{total}] \times [B(\psi(2S) \rightarrow \gamma \chi_{c1}(1P))]$ assuming $B(\psi(2S) \rightarrow \gamma \chi_{c1}(1P)) = (9.55 \pm 0.31) \times 10^{-2}$, which we rescale to our best value $B(\psi(2S) \rightarrow \gamma \chi_{c1}(1P)) = (9.75 \pm 0.24) \times 10^{-2}$. Our first error is their experiment's error and our second error is the systematic error from using our best value.

² Not independent from other measurements reported by ABLIKIM 17I

$\Gamma(e^+e^- J/\psi(1S))/\Gamma(\gamma J/\psi(1S))$ VALUE (units 10^{-3})	EVTS	DOCUMENT ID	TECN	COMMENT	Γ_{92}/Γ_{87}
---	------	-------------	------	---------	---------------------------

10.1 ± 0.3 ± 0.5 1.9k 1 ABLIKIM 17I BES3 $\psi(2S) \rightarrow e^+ e^- \gamma J/\psi$

¹ Uses $B(\psi(2S) \rightarrow \gamma \chi_{c1}(1P)) \times B(\chi_{c1}(1P) \rightarrow \gamma J/\psi(1S)) = (351.8 \pm 1.0 \pm 12.0) \times 10^{-4}$ from ABLIKIM 17N and accounts for common systematic errors.

$\Gamma(\mu^+ \mu^- J/\psi(1S))/\Gamma(e^+ e^- J/\psi(1S))$ VALUE (units 10^{-2})	EVTS	DOCUMENT ID	TECN	COMMENT	Γ_{93}/Γ_{92}
---	------	-------------	------	---------	---------------------------

6.73 ± 0.51 ± 0.50 222 ABLIKIM 19Z BES3 $\psi(2S) \rightarrow \gamma \chi_C \rightarrow \gamma(\mu^+ \mu^- J/\psi)$

$\chi_{c1}(1P)$ CROSS-PARTICLE BRANCHING RATIOS

$\Gamma(\chi_{c1}(1P) \rightarrow p\bar{p})/\Gamma_{total} \times \Gamma(\psi(2S) \rightarrow \gamma \chi_{c1}(1P))/\Gamma(\psi(2S) \rightarrow J/\psi(1S) \pi^+ \pi^-)$ VALUE (units 10^{-5})	DOCUMENT ID	TECN	COMMENT	$\Gamma_{54}/\Gamma \times \Gamma_{154}^{\psi(2S)}/\Gamma_{11}^{\psi(2S)}$
--	-------------	------	---------	--

2.14 ± 0.10 OUR FIT

1.1 ± 0.1 1 BAI 98I BES $\psi(2S) \rightarrow \gamma \chi_{c1} \rightarrow \gamma p\bar{p}$

¹ Calculated by us. The value for $B(\chi_{c1} \rightarrow p\bar{p})$ reported in BAI 98I is derived using $B(\psi(2S) \rightarrow \gamma \chi_{c1}) = (8.7 \pm 0.8)\%$ and $B(\psi(2S) \rightarrow J/\psi(1S) \pi^+ \pi^-) = (32.4 \pm 2.6)\%$ [BAI 98b].

$\Gamma(\chi_{c1}(1P) \rightarrow \Lambda\bar{\Lambda})/\Gamma_{total} \times \Gamma(\psi(2S) \rightarrow \gamma \chi_{c1}(1P))/\Gamma_{total}$ VALUE (units 10^{-6})	EVTS	DOCUMENT ID	TECN	COMMENT	$\Gamma_{67}/\Gamma \times \Gamma_{154}^{\psi(2S)}/\Gamma_{11}^{\psi(2S)}$
---	------	-------------	------	---------	--

11.1 ± 1.1 OUR FIT

10.9 ± 1.1 OUR AVERAGE

11.2 ± 1.0 ± 0.9 136 1 ABLIKIM 13H BES3 $\psi(2S) \rightarrow \gamma \Lambda\bar{\Lambda}$

10.5 ± 1.6 ± 0.6 46 ± 7 2 NAIK 08 CLEO $\psi(2S) \rightarrow \gamma \Lambda\bar{\Lambda}$

¹ Calculated by us. ABLIKIM 13H reports $B(\chi_{c1} \rightarrow \Lambda\bar{\Lambda}) = (12.2 \pm 1.1 \pm 1.1) \times 10^{-5}$ from a measurement of $B(\chi_{c1} \rightarrow \Lambda\bar{\Lambda}) \times B(\psi(2S) \rightarrow \gamma \chi_{c1})$ assuming $B(\psi(2S) \rightarrow \gamma \chi_{c1}) = (9.2 \pm 0.4)\%$.

² Calculated by us. NAIK 08 reports $B(\chi_{c1} \rightarrow \Lambda\bar{\Lambda}) = (11.6 \pm 1.8 \pm 0.7 \pm 0.7) \times 10^{-5}$ using $B(\psi(2S) \rightarrow \gamma \chi_{c1}) = (9.07 \pm 0.11 \pm 0.54)\%$.

$\Gamma(\chi_{c1}(1P) \rightarrow \Lambda\bar{\Lambda})/\Gamma_{total} \times \Gamma(\psi(2S) \rightarrow \gamma \chi_{c1}(1P))/\Gamma(\psi(2S) \rightarrow J/\psi(1S) \pi^+ \pi^-)$ VALUE (units 10^{-5})	EVTS	DOCUMENT ID	TECN	COMMENT	$\Gamma_{67}/\Gamma \times \Gamma_{154}^{\psi(2S)}/\Gamma_{11}^{\psi(2S)}$
--	------	-------------	------	---------	--

3.20 ± 0.30 OUR FIT

7.1 ± 2.8 ± 1.3 9.0 ± 3.5 3.1 1 BAI 03E BES $\psi(2S) \rightarrow \gamma \Lambda\bar{\Lambda}$

¹ BAI 03E reports $[B(\chi_{c1} \rightarrow \Lambda\bar{\Lambda}) B(\psi(2S) \rightarrow \gamma \chi_{c1}) / B(\psi(2S) \rightarrow J/\psi \pi^+ \pi^-)] \times [B^2(\Lambda \rightarrow \pi^- p) / B(J/\psi \rightarrow p\bar{p})] = (1.33 \pm 0.52 \pm 0.25)\%$. We calculate from this measurement the presented value using $B(\Lambda \rightarrow \pi^- p) = (63.9 \pm 0.5)\%$ and $B(J/\psi \rightarrow p\bar{p}) = (2.17 \pm 0.07) \times 10^{-3}$.

$\Gamma(\chi_{c1}(1P) \rightarrow \gamma J/\psi(1S))/\Gamma_{total} \times \Gamma(\psi(2S) \rightarrow \gamma \chi_{c1}(1P))/\Gamma_{total}$ VALUE (units 10^{-2})	EVTS	DOCUMENT ID	TECN	COMMENT	$\Gamma_{87}/\Gamma \times \Gamma_{154}^{\psi(2S)}/\Gamma_{11}^{\psi(2S)}$
--	------	-------------	------	---------	--

3.34 ± 0.06 OUR FIT

3.24 ± 0.16 OUR AVERAGE

3.518 ± 0.010 ± 0.120 143k 1 ABLIKIM 17N BES3 $\psi(2S) \rightarrow \gamma \gamma J/\psi$

3.442 ± 0.010 ± 0.132 1.9M ABLIKIM 17U BES3 $e^+ e^- \rightarrow \gamma X$

2.81 ± 0.05 ± 0.23 13k BAI 04I BES2 $\psi(2S) \rightarrow J/\psi \gamma \gamma$

2.56 ± 0.12 ± 0.20 GAISER 86 CBAL $\psi(2S) \rightarrow \gamma X$

2.78 ± 0.30 2 OREGLIA 82 CBAL $\psi(2S) \rightarrow \gamma \chi_{c1}$

2.2 ± 0.5 3 BRANDELIK 79B DASP $\psi(2S) \rightarrow \gamma \chi_{c1}$

2.9 ± 0.5 3 BARTEL 78B CNTR $\psi(2S) \rightarrow \gamma \chi_{c1}$

5.0 ± 1.5 4 BIDDICK 77 CNTR $e^+ e^- \rightarrow \gamma X$

2.8 ± 0.9 2 WHITAKER 76 MRK1 $e^+ e^-$

• • • We do not use the following data for averages, fits, limits, etc. • • •

3.377 ± 0.009 ± 0.183 142k 5 ABLIKIM 12o BES3 $\psi(2S) \rightarrow \gamma \chi_{c1}$

3.56 ± 0.03 ± 0.12 24.9k 6 MENDEZ 08 CLEO $\psi(2S) \rightarrow \gamma \chi_{c1}$

3.44 ± 0.06 ± 0.13 3.7k 7 ADAM 05A CLEO Repl. by MENDEZ 08

¹ Uses $B(J/\psi \rightarrow e^+ e^-) = (5.971 \pm 0.032)\%$ and $B(J/\psi \rightarrow \mu^+ \mu^-) = (5.961 \pm 0.033)\%$.

² Recalculated by us using $B(J/\psi(1S) \rightarrow \ell^+ \ell^-) = 0.1181 \pm 0.0020$.

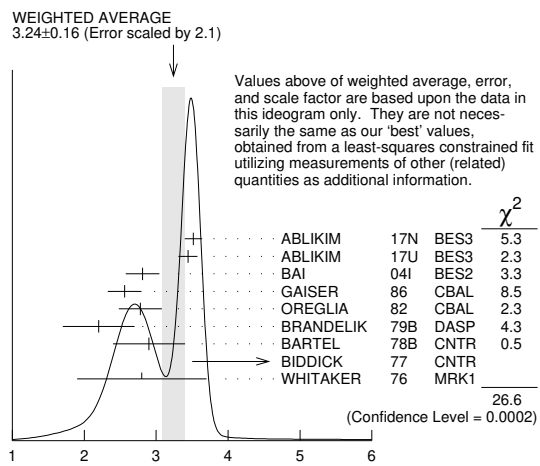
³ Recalculated by us using $B(J/\psi(1S) \rightarrow \mu^+ \mu^-) = 0.0588 \pm 0.0010$.

⁴ Assumes isotropic gamma distribution.

⁵ Superseded by ABLIKIM 17N.

⁶ Not independent from other measurements of MENDEZ 08.

⁷ Not independent from other values reported by ADAM 05A.



$\Gamma(\chi_{c1}(1P) \rightarrow \gamma J/\psi(1S))/\Gamma_{total} \times \Gamma(\psi(2S) \rightarrow \gamma \chi_{c1}(1P))/\Gamma_{total}$ (units 10^{-2})

$\Gamma(\chi_{c1}(1P) \rightarrow \gamma J/\psi(1S))/\Gamma_{total} \times \Gamma(\psi(2S) \rightarrow \gamma \chi_{c1}(1P))/\Gamma(\psi(2S) \rightarrow J/\psi(1S) \text{ anything})$ VALUE (units 10^{-2})	EVTS	DOCUMENT ID	TECN	COMMENT	$\Gamma_{87}/\Gamma \times \Gamma_{154}^{\psi(2S)}/\Gamma_{9}^{\psi(2S)}$
--	------	-------------	------	---------	---

9.63 ± 0.17 OUR FIT

10.15 ± 0.28 OUR AVERAGE

10.17 ± 0.07 ± 0.27 24.9k MENDEZ 08 CLEO $\psi(2S) \rightarrow \gamma \chi_{c1}$

12.6 ± 0.3 ± 3.8 3k 1 ABLIKIM 04B BES $\psi(2S) \rightarrow J/\psi X$

8.5 ± 2.1 2 HIMEL 80 MRK2 $\psi(2S) \rightarrow \gamma \chi_{c1}$

• • • We do not use the following data for averages, fits, limits, etc. • • •

10.24 ± 0.17 ± 0.23 3.7k 3 ADAM 05A CLEO Repl. by MENDEZ 08

¹ From a fit to the J/ψ recoil mass spectra.

² The value for $B(\psi(2S) \rightarrow \gamma \chi_{c1}) \times B(\chi_{c1} \rightarrow \gamma J/\psi(1S))$ quoted in HIMEL 80 is derived using $B(\psi(2S) \rightarrow J/\psi(1S) \pi^+ \pi^-) = (33 \pm 3)\%$ and $B(J/\psi(1S) \rightarrow \ell^+ \ell^-) = 0.138 \pm 0.018$. Calculated by us using $B(J/\psi(1S) \rightarrow \ell^+ \ell^-) = 0.1181 \pm 0.0020$.

$\Gamma(\chi_{c1}(1P) \rightarrow \gamma J/\psi(1S))/\Gamma_{total} \times \Gamma(\psi(2S) \rightarrow \gamma \chi_{c1}(1P))/\Gamma(\psi(2S) \rightarrow J/\psi(1S) \pi^+ \pi^-)$ VALUE (units 10^{-2})	EVTS	DOCUMENT ID	TECN	COMMENT	$\Gamma_{87}/\Gamma \times \Gamma_{154}^{\psi(2S)}/\Gamma_{11}^{\psi(2S)}$
---	------	-------------	------	---------	--

9.63 ± 0.17 OUR FIT

10.15 ± 0.28 OUR AVERAGE

10.17 ± 0.07 ± 0.27 24.9k MENDEZ 08 CLEO $\psi(2S) \rightarrow \gamma \chi_{c1}$

12.6 ± 0.3 ± 3.8 3k 1 ABLIKIM 04B BES $\psi(2S) \rightarrow J/\psi X$

8.5 ± 2.1 2 HIMEL 80 MRK2 $\psi(2S) \rightarrow \gamma \chi_{c1}$

• • • We do not use the following data for averages, fits, limits, etc. • • •

10.24 ± 0.17 ± 0.23 3.7k 3 ADAM 05A CLEO Repl. by MENDEZ 08

¹ From a fit to the J/ψ recoil mass spectra.

² The value for $B(\psi(2S) \rightarrow \gamma \chi_{c1}) \times B(\chi_{c1} \rightarrow \gamma J/\psi(1S))$ quoted in HIMEL 80 is derived using $B(\psi(2S) \rightarrow J/\psi(1S) \pi^+ \pi^-) = (33 \pm 3)\%$ and $B(J/\psi(1S) \rightarrow \ell^+ \ell^-) = 0.138 \pm 0.018$. Calculated by us using $B(J/\psi(1S) \rightarrow \ell^+ \ell^-) = 0.1181 \pm 0.0020$.

³ Not independent from other values reported by ADAM 05A.

$\Gamma(\chi_{c1}(1P) \rightarrow \bar{K}^0 K^+ \pi^- + \text{c.c.})/\Gamma_{total} \times \Gamma(\psi(2S) \rightarrow \gamma \chi_{c1}(1P))/\Gamma_{total}$ VALUE (units 10^{-4})	DOCUMENT ID	TECN	COMMENT	$\Gamma_{17}/\Gamma \times \Gamma_{154}^{\psi(2S)}/\Gamma_{11}^{\psi(2S)}$
--	-------------	------	---------	--

6.8 ± 0.5 OUR FIT

7.2 ± 0.6 OUR AVERAGE

7.3 ± 0.5 ± 0.5 1 ATHAR 07 CLEO $\psi(2S) \rightarrow \gamma K_S^0 K^+ \pi^-$

7.0 ± 0.5 ± 0.9 2 ABLIKIM 06R BES2 $\psi(2S) \rightarrow \gamma \chi_{c1}$

¹ Calculated by us. The value of $B(\chi_{c1} \rightarrow \bar{K}^0 K^+ \pi^- + \text{c.c.})$ reported by ATHAR 07 was derived using $B(\psi(2S) \rightarrow \gamma \chi_{c1}(1P)) = (9.07 \pm 0.11 \pm 0.54)\%$.

² Calculated by us. ABLIKIM 06R reports $B(\chi_{c1} \rightarrow K_S^0 K^+ \pi^-) = (4.0 \pm 0.3 \pm 0.5) \times 10^{-3}$. We use $B(\psi(2S) \rightarrow \gamma \chi_{c1}) = (8.7 \pm 0.4) \times 10^{-2}$.

$\Gamma(\chi_{c1}(1P) \rightarrow \bar{K}^0 K^+ \pi^- + \text{c.c.})/\Gamma_{total} \times \Gamma(\psi(2S) \rightarrow \gamma \chi_{c1}(1P))/\Gamma(\psi(2S) \rightarrow J/\psi(1S) \pi^+ \pi^-)$
VALUE (units 10^{-4})

19.6 ± 1.6 OUR FIT

13.2 ± 2.4 ± 3.2 1 BAI 99B BES $\psi(2S) \rightarrow \gamma K_S^0 K^+ \pi^-$

¹ Calculated by us. The value of $B(\chi_{c1} \rightarrow K_S^0 K^+ \pi^-)$ reported by BAI 99B was derived using $B(\psi(2S) \rightarrow \gamma \chi_{c1}(1P)) = (8.7 \pm 0.8)\%$ and $B(\psi(2S) \rightarrow J/\psi \pi^+ \pi^-) = (32.4 \pm 2.6)\%$ [BAI 98b].

Meson Particle Listings

$\chi_{c1}(1P), h_c(1P)$

BAI	04I	PR D70 012006	J.Z. Bai <i>et al.</i>	(BES Collab.)
AULCHENKO	03	PL B573 63	V.M. Aulchenko <i>et al.</i>	(KEDR Collab.)
BAI	03E	PR D67 112001	J.Z. Bai <i>et al.</i>	(BES Collab.)
AMBROGIANI	02	PR D65 052002	M. Ambrogiani <i>et al.</i>	(FNAL E835 Collab.)
BAI	99B	PR D60 072001	J.Z. Bai <i>et al.</i>	(BES Collab.)
BAI	98D	PR D58 092006	J.Z. Bai <i>et al.</i>	(BES Collab.)
BAI	98I	PRL 81 3091	J.Z. Bai <i>et al.</i>	(BES Collab.)
ARMSTRONG	92	NP B373 35	T.A. Armstrong <i>et al.</i>	(FNAL, FERR, GENO+)
Also		PRL 69 1468	T.A. Armstrong <i>et al.</i>	(FNAL, FERR, GENO+)
BAGLIN	86B	PL B172 455	C. Baglin	(LAPP, CERN, GENO, LYON, OSLO+)
GAISER	86	PR D34 711	J. Gaiser <i>et al.</i>	(Crystal Ball Collab.)
LEM OIGNE	82	PL 113B 509	Y. Lemoigne <i>et al.</i>	(SACL, LOIC, SHMP+)
OREGLIA	82	PR D25 2259	M.J. Oreglia <i>et al.</i>	(SLAC, CIT, HARV+)
Also		Private Comm.	M.J. Oreglia	(EFI)
HIMEL	80	PRL 44 920	T. Himel <i>et al.</i>	(LBL, SLAC)
Also		Private Comm.	C. Trilling	(LBL, UCB)
BRANDELIC	79B	NP B160 426	R. Brandelik <i>et al.</i>	(DASP Collab.)
BARTEL	78B	PL 79B 492	W. Bartel <i>et al.</i>	(DESY, HEIDP)
TANENBAUM	78	PR D17 1731	W.M. Tanenbaum <i>et al.</i>	(SLAC, LBL)
Also		Private Comm.	G. Trilling	(LBL, UCB)
BIDDICK	77	PRL 38 1324	C.J. Biddick <i>et al.</i>	(UCSD, UMD, PAVI+)
FELDMAN	77	PRPL 33C 285	G.J. Feldman, M.L. Perl	(LBL, SLAC)
YAMADA	77	Hamburg Conf. 69	S. Yamada	(DASP Collab.)
WHITAKER	76	PRL 37 1596	J.S. Whitaker <i>et al.</i>	(SLAC, LBL)
TANENBAUM	75	PRL 35 1323	W.M. Tanenbaum <i>et al.</i>	(LBL, SLAC)

$h_c(1P)$

$$J^{PC} = 0^-(1^{+-})$$

Quantum numbers are quark model prediction, $C = -$ established by $\eta_c \gamma$ decay.

$h_c(1P)$ MASS

VALUE (MeV)	EVTS	DOCUMENT ID	TECN	COMMENT
3525.38 ± 0.11 OUR AVERAGE				
3525.31 ± 0.11 ± 0.14	832	¹ ABLIKIM	12N BES3	$\psi(2S) \rightarrow \pi^0 \gamma$ hadrons
3525.40 ± 0.13 ± 0.18	3679	ABLIKIM	10B BES3	$\psi(2S) \rightarrow \pi^0 \gamma \eta_c$
3525.20 ± 0.18 ± 0.12	1282	² DOBBS	08A CLEO	$\psi(2S) \rightarrow \pi^0 \gamma \eta_c$
3525.8 ± 0.2 ± 0.2	13	ANDREOTTI	05B E835	$\bar{p}p \rightarrow \eta_c \gamma$
●●● We do not use the following data for averages, fits, limits, etc. ●●●				
3525.6 ± 0.5	92 ± ²³ / ₂₂	ADAMS	09 CLEO	$\psi(2S) \rightarrow 2(\pi^+ \pi^- \pi^0)$
3524.4 ± 0.6 ± 0.4	168 ± 40	³ ROSNER	05 CLEO	$\psi(2S) \rightarrow \pi^0 \eta_c \gamma$
3527 ± 8	42	ANTONIAZZI	94 E705	300 $\pi^\pm, \rho L \rightarrow J/\psi \pi^0 X$
3526.28 ± 0.18 ± 0.19	59	⁴ ARMSTRONG	92D E760	$\bar{p}p \rightarrow J/\psi \pi^0$
3525.4 ± 0.8 ± 0.4	5	BAGLIN	86 SPEC	$\bar{p}p \rightarrow J/\psi X$

¹ With floating width.
² Combination of exclusive and inclusive analyses for the reaction $\psi(2S) \rightarrow \pi^0 h_c \rightarrow \pi^0 \eta_c \gamma$. This result is the average of DOBBS 08A and ROSNER 05.
³ Superseded by DOBBS 08A.
⁴ Mass central value and systematic error recalculated by us according to Eq. (16) in ARMSTRONG 93B, using the value for the $\psi(2S)$ mass from AULCHENKO 03.

$h_c(1P)$ WIDTH

VALUE (MeV)	CL%	EVTS	DOCUMENT ID	TECN	COMMENT
0.70 ± 0.28 ± 0.22		832	¹ ABLIKIM	12N BES3	$\psi(2S) \rightarrow \pi^0 \gamma$ hadrons
●●● We do not use the following data for averages, fits, limits, etc. ●●●					
< 1.44	90	3679	² ABLIKIM	10B BES3	$\psi(2S) \rightarrow \pi^0 \gamma \eta_c$
< 1		13	ANDREOTTI	05B E835	$\bar{p}p \rightarrow \eta_c \gamma$
< 1.1	90	59	ARMSTRONG	92D E760	$\bar{p}p \rightarrow J/\psi \pi^0$
¹ With floating mass. ² The central value is $\Gamma = 0.73 \pm 0.45 \pm 0.28$ MeV.					

$h_c(1P)$ DECAY MODES

Mode	Fraction (Γ_i/Γ)	Confidence level
Γ_1 $J/\psi(1S) \pi^0$		
Γ_2 $J/\psi(1S) \pi \pi$	not seen	
Γ_3 $J/\psi(1S) \pi^+ \pi^-$	< 2.3 × 10 ⁻³	90%
Γ_4 $\rho \bar{\rho}$	< 1.5 × 10 ⁻⁴	90%
Γ_5 $\rho \bar{\rho} \pi^+ \pi^-$	(2.9 ± 0.6) × 10 ⁻³	
Γ_6 $\pi^+ \pi^- \pi^0$	(1.6 ± 0.5) × 10 ⁻³	
Γ_7 $2\pi^+ 2\pi^- \pi^0$	(8.1 ± 1.8) × 10 ⁻³	
Γ_8 $3\pi^+ 3\pi^- \pi^0$	< 9 × 10 ⁻³	90%
Γ_9 $K^+ K^- \pi^+ \pi^-$	< 6 × 10 ⁻⁴	90%
Radiative decays		
Γ_{10} $\gamma \eta$	(4.7 ± 2.1) × 10 ⁻⁴	
Γ_{11} $\gamma \eta'(958)$	(1.5 ± 0.4) × 10 ⁻³	
Γ_{12} $\gamma \eta_c(1S)$	(51 ± 6) %	

$h_c(1P)$ PARTIAL WIDTHS

$h_c(1P) \Gamma(i)\Gamma(\bar{p}p)/\Gamma(\text{total})$

VALUE (eV)	EVTS	DOCUMENT ID	TECN	COMMENT
$\Gamma(\gamma \eta_c(1S)) \times \Gamma(\bar{p}p)/\Gamma_{\text{total}}$				$\Gamma_2 \Gamma_4/\Gamma$
12.0 ± 4.5	13	¹ ANDREOTTI	05B E835	$\bar{p}p \rightarrow \eta_c \gamma$
¹ Assuming $\Gamma = 1$ MeV.				

$h_c(1P)$ BRANCHING RATIOS

$\Gamma(J/\psi(1S) \pi \pi)/\Gamma(J/\psi(1S) \pi^0)$ Γ_2/Γ_1

VALUE	CL%	DOCUMENT ID	TECN	COMMENT
< 0.18	90	ARMSTRONG	92D E760	$\bar{p}p \rightarrow J/\psi \pi^0$

$\Gamma(J/\psi(1S) \pi^+ \pi^-)/\Gamma_{\text{total}}$ Γ_3/Γ

VALUE	CL%	DOCUMENT ID	TECN	COMMENT
< 2.3 × 10⁻³	90	¹ ABLIKIM	18M BES3	$\psi(2S) \rightarrow \pi^0 \pi^+ \pi^- J/\psi$
¹ ABLIKIM 18M reports [$\Gamma(h_c(1P) \rightarrow J/\psi(1S) \pi^+ \pi^-)/\Gamma_{\text{total}}$] × [B($\psi(2S) \rightarrow \pi^0 h_c(1P)$)] < 2.0 × 10 ⁻⁶ which we divide by our best value B($\psi(2S) \rightarrow \pi^0 h_c(1P)$) = 8.6 × 10 ⁻⁴ .				

$\Gamma(\pi^+ \pi^- \pi^0)/\Gamma_{\text{total}}$ Γ_6/Γ

VALUE (units 10 ⁻³)	CL%	EVTS	DOCUMENT ID	TECN	COMMENT
1.6 ± 0.5 ± 0.2	101		¹ ABLIKIM	19AG BES3	$\psi(2S) \rightarrow \pi^0 h_c(1P)$
●●● We do not use the following data for averages, fits, limits, etc. ●●●					
< 2.2	90		² ADAMS	09 CLEO	$\psi(2S) \rightarrow \pi^0 \gamma \eta_c$
¹ ABLIKIM 19AG reports [$\Gamma(h_c(1P) \rightarrow \pi^+ \pi^- \pi^0)/\Gamma_{\text{total}}$] × [B($\psi(2S) \rightarrow \pi^0 h_c(1P)$)] = (1.38 ± 0.35 ± 0.17) × 10 ⁻⁶ which we divide by our best value B($\psi(2S) \rightarrow \pi^0 h_c(1P)$) = (8.6 ± 1.3) × 10 ⁻⁴ . Our first error is their experiment's error and our second error is the systematic error from using our best value. ² ADAMS 09 reports [$\Gamma(h_c(1P) \rightarrow \pi^+ \pi^- \pi^0)/\Gamma_{\text{total}}$] × [B($\psi(2S) \rightarrow \pi^0 h_c(1P)$)] < 0.19 × 10 ⁻⁵ which we divide by our best value B($\psi(2S) \rightarrow \pi^0 h_c(1P)$) = 8.6 × 10 ⁻⁴ .					

$\Gamma(2\pi^+ 2\pi^- \pi^0)/\Gamma_{\text{total}}$ Γ_7/Γ

VALUE (units 10 ⁻²)	CL%	EVTS	DOCUMENT ID	TECN	COMMENT
0.81 ± 0.18 OUR AVERAGE					
0.74 ± 0.14 ± 0.11	254		¹ ABLIKIM	19AG BES3	$\psi(2S) \rightarrow \pi^0 h_c(1P)$
2.2 ± ^{0.8} / _{0.6} ± 0.3	92		² ADAMS	09 CLEO	$\psi(2S) \rightarrow \pi^0 \gamma \eta_c$

¹ ABLIKIM 19AG reports [$\Gamma(h_c(1P) \rightarrow 2\pi^+ 2\pi^- \pi^0)/\Gamma_{\text{total}}$] × [B($\psi(2S) \rightarrow \pi^0 h_c(1P)$)] = (6.40 ± 0.81 ± 0.87) × 10⁻⁶ which we divide by our best value B($\psi(2S) \rightarrow \pi^0 h_c(1P)$) = (8.6 ± 1.3) × 10⁻⁴. Our first error is their experiment's error and our second error is the systematic error from using our best value.
² ADAMS 09 reports [$\Gamma(h_c(1P) \rightarrow 2\pi^+ 2\pi^- \pi^0)/\Gamma_{\text{total}}$] × [B($\psi(2S) \rightarrow \pi^0 h_c(1P)$)] = (1.88 ± ^{0.48 + 0.47}/_{0.45 - 0.36}) × 10⁻⁵ which we divide by our best value B($\psi(2S) \rightarrow \pi^0 h_c(1P)$) = (8.6 ± 1.3) × 10⁻⁴. Our first error is their experiment's error and our second error is the systematic error from using our best value.

$\Gamma(3\pi^+ 3\pi^- \pi^0)/\Gamma_{\text{total}}$ Γ_8/Γ

VALUE	CL%	DOCUMENT ID	TECN	COMMENT
< 9 × 10 ⁻³	90	¹ ABLIKIM	19AG BES3	$\psi(2S) \rightarrow \pi^0 h_c(1P)$
●●● We do not use the following data for averages, fits, limits, etc. ●●●				
< 0.029	90	² ADAMS	09 CLEO	$\psi(2S) \rightarrow \pi^0 \gamma \eta_c$
¹ ABLIKIM 19AG reports [$\Gamma(h_c(1P) \rightarrow 3\pi^+ 3\pi^- \pi^0)/\Gamma_{\text{total}}$] × [B($\psi(2S) \rightarrow \pi^0 h_c(1P)$)] < 7.5 × 10 ⁻⁶ which we divide by our best value B($\psi(2S) \rightarrow \pi^0 h_c(1P)$) = 8.6 × 10 ⁻⁴ . ² ADAMS 09 reports [$\Gamma(h_c(1P) \rightarrow 3\pi^+ 3\pi^- \pi^0)/\Gamma_{\text{total}}$] × [B($\psi(2S) \rightarrow \pi^0 h_c(1P)$)] < 2.5 × 10 ⁻⁵ which we divide by our best value B($\psi(2S) \rightarrow \pi^0 h_c(1P)$) = 8.6 × 10 ⁻⁴ .				

$\Gamma(\rho \bar{\rho} \pi^+ \pi^-)/\Gamma_{\text{total}}$ Γ_5/Γ

VALUE (units 10 ⁻³)	EVTS	DOCUMENT ID	TECN	COMMENT
2.9 ± 0.5 ± 0.4	230	¹ ABLIKIM	19AG BES3	$\psi(2S) \rightarrow \pi^0 h_c(1P)$
¹ ABLIKIM 19AG reports [$\Gamma(h_c(1P) \rightarrow \rho \bar{\rho} \pi^+ \pi^-)/\Gamma_{\text{total}}$] × [B($\psi(2S) \rightarrow \pi^0 h_c(1P)$)] = (2.49 ± 0.27 ± 0.28) × 10 ⁻⁶ which we divide by our best value B($\psi(2S) \rightarrow \pi^0 h_c(1P)$) = (8.6 ± 1.3) × 10 ⁻⁴ . Our first error is their experiment's error and our second error is the systematic error from using our best value.				

$\Gamma(K^+ K^- \pi^+ \pi^-)/\Gamma_{\text{total}}$ Γ_9/Γ

VALUE	CL%	DOCUMENT ID	TECN	COMMENT
< 6 × 10 ⁻⁴	90	¹ ABLIKIM	19AG BES3	$\psi(2S) \rightarrow \pi^0 h_c(1P)$
¹ ABLIKIM 19AG reports [$\Gamma(h_c(1P) \rightarrow K^+ K^- \pi^+ \pi^-)/\Gamma_{\text{total}}$] × [B($\psi(2S) \rightarrow \pi^0 h_c(1P)$)] < 0.5 × 10 ⁻⁶ which we divide by our best value B($\psi(2S) \rightarrow \pi^0 h_c(1P)$) = 8.6 × 10 ⁻⁴ .				

Meson Particle Listings

$\chi_{c2}(1P)$

Γ_{35}	$K^*(892)^0 \bar{K}^0 + c.c.$	$(1.24 \pm 0.27) \times 10^{-4}$	
Γ_{36}	$K_S^*(1430)^\pm K^\mp$	$(1.48 \pm 0.12) \times 10^{-3}$	
Γ_{37}	$K_S^*(1430)^0 \bar{K}^0 + c.c.$	$(1.24 \pm 0.17) \times 10^{-3}$	
Γ_{38}	$K_S^*(1780)^\pm K^\mp$	$(5.2 \pm 0.8) \times 10^{-4}$	
Γ_{39}	$K_S^*(1780)^0 \bar{K}^0 + c.c.$	$(5.6 \pm 2.1) \times 10^{-4}$	
Γ_{40}	$a_2(1320)^0 \pi^0$	$(1.29 \pm 0.34) \times 10^{-3}$	
Γ_{41}	$a_2(1320)^\pm \pi^\mp$	$(1.8 \pm 0.6) \times 10^{-3}$	
Γ_{42}	$\bar{K}^0 K^+ \pi^- + c.c.$	$(1.28 \pm 0.18) \times 10^{-3}$	
Γ_{43}	$K^+ K^- \pi^0$	$(3.0 \pm 0.8) \times 10^{-4}$	
Γ_{44}	$K^+ K^- \eta$	$< 3.2 \times 10^{-4}$	90%
Γ_{45}	$K^+ K^- \eta'(958)$	$(1.94 \pm 0.34) \times 10^{-4}$	
Γ_{46}	$\eta \eta'$	$(2.2 \pm 0.5) \times 10^{-5}$	
Γ_{47}	$\eta' \eta'$	$(4.6 \pm 0.6) \times 10^{-5}$	
Γ_{48}	$\pi^+ \pi^- K_S^0 K_S^0$	$(2.2 \pm 0.5) \times 10^{-3}$	
Γ_{49}	$K^+ K^- K_S^0 K_S^0$	$< 4 \times 10^{-4}$	90%
Γ_{50}	$K_S^0 K_S^0 K_S^0 K_S^0$	$(1.13 \pm 0.18) \times 10^{-4}$	
Γ_{51}	$K^+ K^- K^+ K^-$	$(1.65 \pm 0.20) \times 10^{-3}$	
Γ_{52}	$K^+ K^- \phi$	$(1.42 \pm 0.29) \times 10^{-3}$	
Γ_{53}	$\bar{K}^0 K^+ \pi^- \phi + c.c.$	$(4.8 \pm 0.7) \times 10^{-3}$	
Γ_{54}	$K^+ K^- \pi^0 \phi$	$(2.7 \pm 0.5) \times 10^{-3}$	
Γ_{55}	$\phi \pi^+ \pi^- \pi^0$	$(9.3 \pm 1.2) \times 10^{-4}$	
Γ_{56}	$\rho \bar{\rho}$	$(7.33 \pm 0.33) \times 10^{-5}$	
Γ_{57}	$\rho \bar{\rho} \pi^0$	$(4.7 \pm 0.4) \times 10^{-4}$	
Γ_{58}	$\rho \bar{\rho} \eta$	$(1.74 \pm 0.25) \times 10^{-4}$	
Γ_{59}	$\rho \bar{\rho} \omega$	$(3.6 \pm 0.4) \times 10^{-4}$	
Γ_{60}	$\rho \bar{\rho} \phi$	$(2.8 \pm 0.9) \times 10^{-5}$	
Γ_{61}	$\rho \bar{\rho} \pi^+ \pi^-$	$(1.32 \pm 0.34) \times 10^{-3}$	
Γ_{62}	$\rho \bar{\rho} \pi^0 \pi^0$	$(7.8 \pm 2.3) \times 10^{-4}$	
Γ_{63}	$\rho \bar{\rho} K^+ K^-$ (non-resonant)	$(1.91 \pm 0.32) \times 10^{-4}$	
Γ_{64}	$\rho \bar{\rho} K_S^0 K_S^0$	$< 7.9 \times 10^{-4}$	90%
Γ_{65}	$\rho \bar{\rho} \pi^-$	$(8.5 \pm 0.9) \times 10^{-4}$	
Γ_{66}	$\bar{\rho} \pi \pi^+$	$(8.9 \pm 0.8) \times 10^{-4}$	
Γ_{67}	$\rho \bar{\rho} \pi^- \pi^0$	$(2.17 \pm 0.18) \times 10^{-3}$	
Γ_{68}	$\bar{\rho} \pi \pi^+ \pi^0$	$(2.11 \pm 0.18) \times 10^{-3}$	
Γ_{69}	$\Lambda \bar{\Lambda}$	$(1.84 \pm 0.15) \times 10^{-4}$	
Γ_{70}	$\Lambda \bar{\Lambda} \pi^+ \pi^-$	$(1.25 \pm 0.15) \times 10^{-3}$	
Γ_{71}	$\Lambda \bar{\Lambda} \pi^+ \pi^-$ (non-resonant)	$(6.6 \pm 1.5) \times 10^{-4}$	
Γ_{72}	$\Sigma(1385)^+ \bar{\Lambda} \pi^- + c.c.$	$< 4 \times 10^{-4}$	90%
Γ_{73}	$\Sigma(1385)^- \bar{\Lambda} \pi^+ + c.c.$	$< 6 \times 10^{-4}$	90%
Γ_{74}	$K^+ \bar{\rho} \Lambda + c.c.$	$(7.8 \pm 0.5) \times 10^{-4}$	
Γ_{75}	$K^*(892) \bar{\rho} \Lambda + c.c.$	$(8.2 \pm 1.1) \times 10^{-4}$	
Γ_{76}	$K^+ \bar{\rho} \Lambda(1520) + c.c.$	$(2.8 \pm 0.7) \times 10^{-4}$	
Γ_{77}	$\Lambda(1520) \bar{\Lambda}(1520)$	$(4.6 \pm 1.5) \times 10^{-4}$	
Γ_{78}	$\Sigma^0 \bar{\Sigma}^0$	$(3.7 \pm 0.6) \times 10^{-5}$	
Γ_{79}	$\Sigma^+ \bar{\rho} K_S^0 + c.c.$	$(8.2 \pm 0.9) \times 10^{-5}$	
Γ_{80}	$\Sigma^+ \bar{\Sigma}^-$	$(3.4 \pm 0.7) \times 10^{-5}$	
Γ_{81}	$\Sigma(1385)^+ \bar{\Sigma}(1385)^-$	$< 1.6 \times 10^{-4}$	90%
Γ_{82}	$\Sigma(1385)^- \bar{\Sigma}(1385)^+$	$< 8 \times 10^{-5}$	90%
Γ_{83}	$K^- \bar{\Lambda} \Xi^+ + c.c.$	$(1.76 \pm 0.32) \times 10^{-4}$	
Γ_{84}	$\Xi^0 \bar{\Xi}^0$	$< 1.0 \times 10^{-4}$	90%
Γ_{85}	$\Xi^- \bar{\Xi}^+$	$(1.42 \pm 0.32) \times 10^{-4}$	
Γ_{86}	$J/\psi(1S) \pi^+ \pi^- \pi^0$	$< 1.5 \%$	90%
Γ_{87}	$\pi^0 \eta_c$	$< 3.2 \times 10^{-3}$	90%
Γ_{88}	$\eta_c(1S) \pi^+ \pi^-$	$< 5.4 \times 10^{-3}$	90%

Radiative decays

Γ_{89}	$\gamma J/\psi(1S)$	$(19.0 \pm 0.5) \%$	
Γ_{90}	$\gamma \rho^0$	$< 1.9 \times 10^{-5}$	90%
Γ_{91}	$\gamma \omega$	$< 6 \times 10^{-6}$	90%
Γ_{92}	$\gamma \phi$	$< 7 \times 10^{-6}$	90%
Γ_{93}	$\gamma \gamma$	$(2.85 \pm 0.10) \times 10^{-4}$	
Γ_{94}	$e^+ e^- J/\psi(1S)$	$(2.15 \pm 0.14) \times 10^{-3}$	
Γ_{95}	$\mu^+ \mu^- J/\psi(1S)$	$(2.02 \pm 0.33) \times 10^{-4}$	

CONSTRAINED FIT INFORMATION

A multiparticle fit to $\chi_{c1}(1P)$, $\chi_{c0}(1P)$, $\chi_{c2}(1P)$, and $\psi(2S)$ with 4 total widths, a partial width, 25 combinations of partial widths obtained from integrated cross section, and 84 branching ratios uses 248 measurements to determine 49 parameters. The overall fit has a $\chi^2 = 378.1$ for 199 degrees of freedom.

The following off-diagonal array elements are the correlation coefficients $\langle \delta p_i \delta p_j \rangle / (\delta p_i \delta p_j)$, in percent, from the fit to parameters p_i , including the branching fractions, $x_i \equiv \Gamma_i / \Gamma_{total}$.

x_{14}	7																		
x_{17}	2	21																	
x_{18}	4	3	1																
x_{20}	7	5	1	3															
x_{25}	7	6	1	4	10														
x_{26}	18	2	0	1	1	1													
x_{31}	3	3	1	2	5	12	1												
x_{32}	5	4	1	3	7	15	1	8											
x_{33}	5	4	1	2	6	13	1	7	8										
x_{42}	2	2	0	1	3	7	0	3	4	4									
x_{51}	4	3	1	2	4	7	1	4	5	4									
x_{56}	10	9	2	5	9	11	2	5	8	7									
x_{69}	3	3	1	2	5	13	1	7	8	7									
x_{89}	12	10	2	6	15	34	2	18	22	18									
x_{93}	-6	-4	-1	-2	2	20	-2	12	12	10									
Γ	-23	-19	-4	-11	-19	-25	-5	-12	-18	-15									
	x_1	x_{14}	x_{17}	x_{18}	x_{20}	x_{25}	x_{26}	x_{31}	x_{32}	x_{33}									

x_{51}	2																		
x_{56}	4	5																	
x_{69}	4	4	6																
x_{89}	10	11	4	18															
x_{93}	5	4	18	12	34														
Γ	-8	-11	-45	-12	-46	-43													
	x_{42}	x_{51}	x_{56}	x_{69}	x_{89}	x_{93}													

$\chi_{c2}(1P)$ PARTIAL WIDTHS

$$\chi_{c2}(1P) \Gamma(i) \Gamma(\gamma J/\psi(1S)) / \Gamma_{total}$$

$\Gamma(\rho \bar{\rho}) \times \Gamma(\gamma J/\psi(1S)) / \Gamma_{total}$	DOCUMENT ID	TECN	COMMENT	$\Gamma_{56} \Gamma_{89} / \Gamma$
27.5 ± 1.2 OUR FIT				
27.5 ± 1.5 OUR AVERAGE				
27.0 ± 1.5 ± 1.1	¹ ANDREOTTI 05A	E835	$\rho \bar{\rho} \rightarrow e^+ e^- \gamma$	
27.7 ± 1.5 ± 2.0	^{1,2} ARMSTRONG 92	E760	$\bar{p} p \rightarrow e^+ e^- \gamma$	
36 ± 8	¹ BAGLIN 86B	SPEC	$\bar{p} p \rightarrow e^+ e^- X$	

¹ Calculated by us using $B(J/\psi(1S) \rightarrow e^+ e^-) = 0.0593 \pm 0.0010$.
² Recalculated by ANDREOTTI 05A.

$\Gamma(\gamma \gamma) \times \Gamma(\gamma J/\psi(1S)) / \Gamma_{total}$	DOCUMENT ID	TECN	COMMENT	$\Gamma_{93} \Gamma_{89} / \Gamma$
107 ± 5 OUR FIT				
117 ± 10 OUR AVERAGE				
111 ± 12 ± 9	¹ DOBBS 06	CLE3	$10.4 e^+ e^- \rightarrow e^+ e^- \chi_{c2}$	
114 ± 11 ± 9	^{1,2} ABE 02T	BELL	$e^+ e^- \rightarrow e^+ e^- \chi_{c2}$	
139 ± 55 ± 21	^{1,3} ACCIARRI 99E	L3	$e^+ e^- \rightarrow e^+ e^- \chi_{c2}$	
242 ± 65 ± 51	^{1,4} ACKER.,K... 98	OPAL	$e^+ e^- \rightarrow e^+ e^- \chi_{c2}$	
150 ± 42 ± 36	^{1,5} DOMINICK 94	CLE2	$e^+ e^- \rightarrow e^+ e^- \chi_{c2}$	
470 ± 240 ± 120	^{1,6} BAUER 93	TPC	$e^+ e^- \rightarrow e^+ e^- \chi_{c2}$	

¹ Calculated by us using $B(J/\psi \rightarrow \ell^+ \ell^-) = 0.1187 \pm 0.0008$.
² All systematic errors added in quadrature.
³ The value for $\Gamma(\chi_{c2} \rightarrow \gamma \gamma)$ reported in ACCIARRI 99E is derived using $B(\chi_{c2} \rightarrow \gamma J/\psi(1S)) \times B(J/\psi(1S) \rightarrow \ell^+ \ell^-) = 0.0162 \pm 0.0014$.
⁴ The value for $\Gamma(\chi_{c2} \rightarrow \gamma \gamma)$ reported in ACKERSTAFF, K 98 is derived using $B(\chi_{c2} \rightarrow \gamma J/\psi(1S)) = 0.135 \pm 0.011$ and $B(J/\psi(1S) \rightarrow \ell^+ \ell^-) = 0.1203 \pm 0.0038$.
⁵ The value for $\Gamma(\chi_{c2} \rightarrow \gamma \gamma)$ reported in DOMINICK 94 is derived using $B(\chi_{c2} \rightarrow \gamma J/\psi(1S)) = 0.135 \pm 0.011$, $B(J/\psi(1S) \rightarrow e^+ e^-) = 0.0627 \pm 0.0020$, and $B(J/\psi(1S) \rightarrow \mu^+ \mu^-) = 0.0597 \pm 0.0025$.
⁶ The value for $\Gamma(\chi_{c2} \rightarrow \gamma \gamma)$ reported in BAUER 93 is derived using $B(\chi_{c2} \rightarrow \gamma J/\psi(1S)) = 0.135 \pm 0.011$, $B(J/\psi(1S) \rightarrow e^+ e^-) = 0.0627 \pm 0.0020$, and $B(J/\psi(1S) \rightarrow \mu^+ \mu^-) = 0.0597 \pm 0.0025$.

$\chi_{c2}(1P) \Gamma(i) \Gamma(\gamma \gamma) / \Gamma_{total}$

$\Gamma(2\pi^+ \pi^-) \times \Gamma(\gamma \gamma) / \Gamma_{total}$	DOCUMENT ID	TECN	COMMENT	$\Gamma_1 \Gamma_{93} / \Gamma$
5.7 ± 0.5 OUR FIT				
5.2 ± 0.7 OUR AVERAGE				
5.01 ± 0.44 ± 0.55	UEHARA 08	BELL	$\gamma \gamma \rightarrow \chi_{c2} \rightarrow 2(\pi^+ \pi^-)$	
6.4 ± 1.8 ± 0.8	EISENSTEIN 01	CLE2	$e^+ e^- \rightarrow e^+ e^- \chi_{c2}$	

$\Gamma(\rho \rho) \times \Gamma(\gamma \gamma) / \Gamma_{total}$	DOCUMENT ID	TECN	COMMENT	$\Gamma_2 \Gamma_{93} / \Gamma$
5.7 ± 0.5 OUR FIT				
5.2 ± 0.7 OUR AVERAGE				
5.01 ± 0.44 ± 0.55	UEHARA 08	BELL	$\gamma \gamma \rightarrow \chi_{c2} \rightarrow 2(\pi^+ \pi^-)$	
6.4 ± 1.8 ± 0.8	EISENSTEIN 01	CLE2	$e^+ e^- \rightarrow e^+ e^- \chi_{c2}$	

••• We do not use the following data for averages, fits, limits, etc. •••
 < 7.8 90 < 598 UEHARA 08 BELL $\gamma \gamma \rightarrow \chi_{c2} \rightarrow 2(\pi^+ \pi^-)$

$\Gamma(K^+ K^- \pi^+ \pi^-) \times \Gamma(\gamma\gamma)/\Gamma_{\text{total}}$					$\Gamma_{14} \Gamma_{93}/\Gamma$
VALUE (eV)	EVTS	DOCUMENT ID	TECN	COMMENT	

4.7 ± 0.5 OUR FIT					
4.42 ± 0.42 ± 0.53	780 ± 74	UEHARA	08 BELL	$\gamma\gamma \rightarrow \chi_{c2} \rightarrow K^+ K^- \pi^+ \pi^-$	

$\Gamma(K^+ K^- \pi^+ \pi^- \pi^0) \times \Gamma(\gamma\gamma)/\Gamma_{\text{total}}$					$\Gamma_{15} \Gamma_{93}/\Gamma$
VALUE (eV)	EVTS	DOCUMENT ID	TECN	COMMENT	

6.5 ± 0.9 ± 1.5	1250	DEL-AMO-SA...11M	BABR	$\gamma\gamma \rightarrow K^+ K^- \pi^+ \pi^- \pi^0$	
------------------------	------	------------------	------	--	--

$\Gamma(K^*(892)^0 \bar{K}^*(892)^0) \times \Gamma(\gamma\gamma)/\Gamma_{\text{total}}$					$\Gamma_{18} \Gamma_{93}/\Gamma$
VALUE (eV)	EVTS	DOCUMENT ID	TECN	COMMENT	

1.26 ± 0.24 OUR FIT					
0.8 ± 0.17 ± 0.27	151 ± 30	UEHARA	08 BELL	$\gamma\gamma \rightarrow \chi_{c2} \rightarrow K^+ K^- \pi^+ \pi^-$	

$\Gamma(\phi\phi) \times \Gamma(\gamma\gamma)/\Gamma_{\text{total}}$					$\Gamma_{20} \Gamma_{93}/\Gamma$
VALUE (eV)	EVTS	DOCUMENT ID	TECN	COMMENT	

0.60 ± 0.05 OUR FIT					
0.62 ± 0.07 ± 0.05	89 ± 11	¹ LIU	12B BELL	$\gamma\gamma \rightarrow 2(K^+ K^-)$	

• • • We do not use the following data for averages, fits, limits, etc. • • •

0.58 ± 0.18 ± 0.16	26.5 ± 8.1	UEHARA	08 BELL	$\gamma\gamma \rightarrow \chi_{c2} \rightarrow 2(K^+ K^-)$	
--------------------	------------	--------	---------	---	--

¹ Supersedes UEHARA 08. Using $B(\phi \rightarrow K^+ K^-) = (48.9 \pm 0.5)\%$.

$\Gamma(\omega\omega) \times \Gamma(\gamma\gamma)/\Gamma_{\text{total}}$					$\Gamma_{22} \Gamma_{93}/\Gamma$
VALUE (eV)	CL%	DOCUMENT ID	TECN	COMMENT	

• • • We do not use the following data for averages, fits, limits, etc. • • •

<0.64	90	¹ LIU	12B BELL	$\gamma\gamma \rightarrow 2(\pi^+ \pi^- \pi^0)$	
-------	----	------------------	----------	---	--

¹ Using $B(\omega \rightarrow \pi^+ \pi^- \pi^0) = (89.2 \pm 0.7)\%$.

$\Gamma(\omega\phi) \times \Gamma(\gamma\gamma)/\Gamma_{\text{total}}$					$\Gamma_{24} \Gamma_{93}/\Gamma$
VALUE (eV)	CL%	DOCUMENT ID	TECN	COMMENT	

• • • We do not use the following data for averages, fits, limits, etc. • • •

<0.04	90	¹ LIU	12B BELL	$\gamma\gamma \rightarrow K^+ K^- \pi^+ \pi^- \pi^0$	
-------	----	------------------	----------	--	--

¹ Using $B(\phi \rightarrow K^+ K^-) = (48.9 \pm 0.5)\%$ and $B(\omega \rightarrow \pi^+ \pi^- \pi^0) = (89.2 \pm 0.7)\%$.

$\Gamma(\pi\pi) \times \Gamma(\gamma\gamma)/\Gamma_{\text{total}}$					$\Gamma_{25} \Gamma_{93}/\Gamma$
VALUE (eV)	EVTS	DOCUMENT ID	TECN	COMMENT	

1.25 ± 0.07 OUR FIT					
1.18 ± 0.25 OUR AVERAGE					

1.44 ± 0.54 ± 0.47	34 ± 13	¹ UEHARA	09 BELL	$10.6 e^+ e^- \rightarrow e^+ e^- \pi^0 \pi^0$	
--------------------	---------	---------------------	---------	--	--

1.14 ± 0.21 ± 0.17	54 ± 10	² NAKAZAWA	05 BELL	$10.6 e^+ e^- \rightarrow e^+ e^- \pi^+ \pi^-$	
--------------------	---------	-----------------------	---------	--	--

¹ We multiplied the measurement by 3 to convert from $\pi^0 \pi^0$ to $\pi\pi$. Interference with the continuum included.
² We have multiplied $\pi^+ \pi^-$ measurement by 3/2 to obtain $\pi\pi$.

$\Gamma(\rho^0 \pi^+ \pi^-) \times \Gamma(\gamma\gamma)/\Gamma_{\text{total}}$					$\Gamma_{26} \Gamma_{93}/\Gamma$
VALUE (eV)	EVTS	DOCUMENT ID	TECN	COMMENT	

2.1 ± 0.9 OUR FIT					
3.2 ± 1.9 ± 0.5	986 ± 578	UEHARA	08 BELL	$\gamma\gamma \rightarrow \chi_{c2} \rightarrow 2(\pi^+ \pi^-)$	

$\Gamma(\eta\eta) \times \Gamma(\gamma\gamma)/\Gamma_{\text{total}}$					$\Gamma_{31} \Gamma_{93}/\Gamma$
VALUE (eV)	EVTS	DOCUMENT ID	TECN	COMMENT	

0.53 ± 0.22 ± 0.09	8	¹ UEHARA	10A BELL	$10.6 e^+ e^- \rightarrow e^+ e^- \eta\eta$	
---------------------------	---	---------------------	----------	---	--

¹ Interference with the continuum not included.

$\Gamma(K^+ K^-) \times \Gamma(\gamma\gamma)/\Gamma_{\text{total}}$					$\Gamma_{32} \Gamma_{93}/\Gamma$
VALUE (eV)	EVTS	DOCUMENT ID	TECN	COMMENT	

0.56 ± 0.04 OUR FIT					
0.44 ± 0.11 ± 0.07	33 ± 8	NAKAZAWA	05 BELL	$10.6 e^+ e^- \rightarrow e^+ e^- K^+ K^-$	

$\Gamma(K_S^0 \bar{K}_S^0) \times \Gamma(\gamma\gamma)/\Gamma_{\text{total}}$					$\Gamma_{33} \Gamma_{93}/\Gamma$
VALUE (eV)	EVTS	DOCUMENT ID	TECN	COMMENT	

0.294 ± 0.025 OUR FIT					
0.27 ± 0.07 ± 0.03	53	¹ UEHARA	13 BELL	$\gamma\gamma \rightarrow K_S^0 \bar{K}_S^0$	

• • • We do not use the following data for averages, fits, limits, etc. • • •

0.31 ± 0.05 ± 0.03	38 ± 7	CHEN	07B BELL	$e^+ e^- \rightarrow e^+ e^- \chi_{c2}$	
--------------------	--------	------	----------	---	--

¹ Supersedes CHEN 07B.

$\Gamma(\bar{K}^0 K^+ \pi^- + \text{c.c.}) \times \Gamma(\gamma\gamma)/\Gamma_{\text{total}}$					$\Gamma_{42} \Gamma_{93}/\Gamma$
VALUE (eV)	EVTS	DOCUMENT ID	TECN	COMMENT	

0.72 ± 0.11 OUR FIT					
1.20 ± 0.33 ± 0.13	126	¹ DEL-AMO-SA...11M	BABR	$\gamma\gamma \rightarrow K_S^0 K^+ \pi^-$	

¹ We have multiplied $\bar{K} K \pi$ by 2/3 to obtain $\bar{K}^0 K^+ \pi^- + \text{c.c.}$

$\Gamma(K^+ K^- K^+ K^-) \times \Gamma(\gamma\gamma)/\Gamma_{\text{total}}$					$\Gamma_{51} \Gamma_{93}/\Gamma$
VALUE (eV)	EVTS	DOCUMENT ID	TECN	COMMENT	

0.93 ± 0.11 OUR FIT					
1.10 ± 0.21 ± 0.15	126 ± 24	UEHARA	08 BELL	$\gamma\gamma \rightarrow \chi_{c2} \rightarrow 2(K^+ K^-)$	

$\Gamma(\eta_c(1S) \pi^+ \pi^-) \times \Gamma(\gamma\gamma)/\Gamma_{\text{total}}$					$\Gamma_{88} \Gamma_{93}/\Gamma$
VALUE (eV)	CL%	DOCUMENT ID	TECN	COMMENT	

<15.7	90	LEES	12AE BABR	$e^+ e^- \rightarrow e^+ e^- \pi^+ \pi^- \eta_c$	
-------	----	------	-----------	--	--

 $\chi_{c2}(1P)$ BRANCHING RATIOS

HADRONIC DECAYS

$\Gamma(2(\pi^+ \pi^-))/\Gamma_{\text{total}}$		Γ_1/Γ
VALUE	DOCUMENT ID	

0.0102 ± 0.0009 OUR FIT		
--------------------------------	--	--

$\Gamma(\rho^0 \pi^+ \pi^-)/\Gamma(2(\pi^+ \pi^-))$		Γ_{26}/Γ_1
VALUE	DOCUMENT ID	TECN

0.36 ± 0.15 OUR FIT		
0.31 ± 0.17	TANENBAUM	78 MRK1

$\Gamma(\pi^+ \pi^- \pi^0 \pi^0)/\Gamma_{\text{total}}$		Γ_3/Γ
VALUE (%)	EVTS	DOCUMENT ID

1.83 ± 0.23 ± 0.04	903.5	¹ HE
---------------------------	-------	-----------------

¹ HE 08B reports $1.87 \pm 0.07 \pm 0.22 \pm 0.13\%$ from a measurement of $[\Gamma(\chi_{c2}(1P) \rightarrow \pi^+ \pi^- \pi^0 \pi^0)/\Gamma_{\text{total}}] \times [B(\psi(2S) \rightarrow \gamma\chi_{c2}(1P))]$ assuming $B(\psi(2S) \rightarrow \gamma\chi_{c2}(1P)) = (9.33 \pm 0.14 \pm 0.61) \times 10^{-2}$, which we rescale to our best value $B(\psi(2S) \rightarrow \gamma\chi_{c2}(1P)) = (9.52 \pm 0.20) \times 10^{-2}$. Our first error is their experiment's error and our second error is the systematic error from using our best value.

² Calculated by us. We have added the values from HE 08B for $\rho^+ \pi^- \pi^0$ and $\rho^- \pi^+ \pi^0$ decays assuming uncorrelated statistical and fully correlated systematic uncertainties.

$\Gamma(\rho^+ \pi^- \pi^0 + \text{c.c.})/\Gamma_{\text{total}}$		Γ_4/Γ
VALUE (%)	EVTS	DOCUMENT ID

2.19 ± 0.34 ± 0.05	1031.9	^{1,2} HE
---------------------------	--------	-------------------

¹ HE 08B reports $2.23 \pm 0.11 \pm 0.32 \pm 0.16\%$ from a measurement of $[\Gamma(\chi_{c2}(1P) \rightarrow \rho^+ \pi^- \pi^0 + \text{c.c.})/\Gamma_{\text{total}}] \times [B(\psi(2S) \rightarrow \gamma\chi_{c2}(1P))]$ assuming $B(\psi(2S) \rightarrow \gamma\chi_{c2}(1P)) = (9.33 \pm 0.14 \pm 0.61) \times 10^{-2}$, which we rescale to our best value $B(\psi(2S) \rightarrow \gamma\chi_{c2}(1P)) = (9.52 \pm 0.20) \times 10^{-2}$. Our first error is their experiment's error and our second error is the systematic error from using our best value.

² Calculated by us. We have added the values from HE 08B for $\rho^+ \pi^- \pi^0$ and $\rho^- \pi^+ \pi^0$ decays assuming uncorrelated statistical and fully correlated systematic uncertainties.

$\Gamma(4\pi^0)/\Gamma_{\text{total}}$		Γ_5/Γ
VALUE (units 10^{-3})	EVTS	DOCUMENT ID

1.11 ± 0.15 ± 0.02	1164	¹ ABLIKIM
---------------------------	------	----------------------

¹ ABLIKIM 11A reports $(1.21 \pm 0.05 \pm 0.16) \times 10^{-3}$ from a measurement of $[\Gamma(\chi_{c2}(1P) \rightarrow 4\pi^0)/\Gamma_{\text{total}}] \times [B(\psi(2S) \rightarrow \gamma\chi_{c2}(1P))]$ assuming $B(\psi(2S) \rightarrow \gamma\chi_{c2}(1P)) = (8.74 \pm 0.35) \times 10^{-2}$, which we rescale to our best value $B(\psi(2S) \rightarrow \gamma\chi_{c2}(1P)) = (9.52 \pm 0.20) \times 10^{-2}$. Our first error is their experiment's error and our second error is the systematic error from using our best value.

$\Gamma(K^+ K^- \pi^0 \pi^0)/\Gamma_{\text{total}}$		Γ_6/Γ
VALUE (%)	EVTS	DOCUMENT ID

0.206 ± 0.040 ± 0.004	76.9	¹ HE
------------------------------	------	-----------------

¹ HE 08B reports $0.21 \pm 0.03 \pm 0.03 \pm 0.01\%$ from a measurement of $[\Gamma(\chi_{c2}(1P) \rightarrow K^+ K^- \pi^0 \pi^0)/\Gamma_{\text{total}}] \times [B(\psi(2S) \rightarrow \gamma\chi_{c2}(1P))]$ assuming $B(\psi(2S) \rightarrow \gamma\chi_{c2}(1P)) = (9.33 \pm 0.14 \pm 0.61) \times 10^{-2}$, which we rescale to our best value $B(\psi(2S) \rightarrow \gamma\chi_{c2}(1P)) = (9.52 \pm 0.20) \times 10^{-2}$. Our first error is their experiment's error and our second error is the systematic error from using our best value.

$\Gamma(K^+ \pi^- \bar{K}^0 \pi^0 + \text{c.c.})/\Gamma_{\text{total}}$		Γ_7/Γ
VALUE (%)	EVTS	DOCUMENT ID

1.38 ± 0.19 ± 0.03	211.6	¹ HE
---------------------------	-------	-----------------

¹ HE 08B reports $1.41 \pm 0.11 \pm 0.16 \pm 0.10\%$ from a measurement of $[\Gamma(\chi_{c2}(1P) \rightarrow K^+ \pi^- \bar{K}^0 \pi^0 + \text{c.c.})/\Gamma_{\text{total}}] \times [B(\psi(2S) \rightarrow \gamma\chi_{c2}(1P))]$ assuming $B(\psi(2S) \rightarrow \gamma\chi_{c2}(1P)) = (9.33 \pm 0.14 \pm 0.61) \times 10^{-2}$, which we rescale to our best value $B(\psi(2S) \rightarrow \gamma\chi_{c2}(1P)) = (9.52 \pm 0.20) \times 10^{-2}$. Our first error is their experiment's error and our second error is the systematic error from using our best value.

$\Gamma(K^+ \pi^- \bar{K}^0 \pi^0 + \text{c.c.})/\Gamma_{\text{total}}$		Γ_8/Γ
VALUE (%)	EVTS	DOCUMENT ID

0.41 ± 0.12 ± 0.01	62.9	¹ HE
---------------------------	------	-----------------

¹ HE 08B reports $0.42 \pm 0.11 \pm 0.06 \pm 0.03\%$ from a measurement of $[\Gamma(\chi_{c2}(1P) \rightarrow \rho^- K^+ \bar{K}^0 \pi^0 + \text{c.c.})/\Gamma_{\text{total}}] \times [B(\psi(2S) \rightarrow \gamma\chi_{c2}(1P))]$ assuming $B(\psi(2S) \rightarrow \gamma\chi_{c2}(1P)) = (9.33 \pm 0.14 \pm 0.61) \times 10^{-2}$, which we rescale to our best value $B(\psi(2S) \rightarrow \gamma\chi_{c2}(1P)) = (9.52 \pm 0.20) \times 10^{-2}$. Our first error is their experiment's error and our second error is the systematic error from using our best value.

$\Gamma(K^*(892)^0 K^- \pi^+ \rightarrow K^- \pi^+ K^0 \pi^0 + \text{c.c.})/\Gamma_{\text{total}}$		Γ_9/Γ
VALUE (%)	EVTS	DOCUMENT ID

0.29 ± 0.08 ± 0.01	38.7	¹ HE
---------------------------	------	-----------------

¹ HE 08B reports $0.30 \pm 0.07 \pm 0.04 \pm 0.02\%$ from a measurement of $[\Gamma(\chi_{c2}(1P) \rightarrow K^*(892)^0 K^- \pi^+ \rightarrow K^- \pi^+ K^0 \pi^0 + \text{c.c.})/\Gamma_{\text{total}}] \times [B(\psi(2S) \rightarrow \gamma\chi_{c2}(1P))]$ assuming $B(\psi(2S) \rightarrow \gamma\chi_{c2}(1P)) = (9.33 \pm 0.14 \pm 0.61) \times 10^{-2}$, which we rescale to our best value $B(\psi(2S) \rightarrow \gamma\chi_{c2}(1P)) = (9.52 \pm 0.20) \times 10^{-2}$. Our first error is their experiment's error and our second error is the systematic error from using our best value.

$\Gamma(K^*(892)^0 K^- \pi^+ \rightarrow K^- \pi^+ K^0 \pi^0 + \text{c.c.})/\Gamma_{\text{total}}$		Γ_9/Γ
VALUE (%)	EVTS	DOCUMENT ID

0.29 ± 0.08 ± 0.01	38.7	¹ HE
---------------------------	------	-----------------

¹ HE 08B reports $0.30 \pm 0.07 \pm 0.04 \pm 0.02\%$ from a measurement of $[\Gamma(\chi_{c2}(1P) \rightarrow K^*(892)^0 K^- \pi^+ \rightarrow K^- \pi^+ K^0 \pi^0 + \text{c.c.})/\Gamma_{\text{total}}] \times [B(\psi(2S) \rightarrow \gamma\chi_{c2}(1P))]$ assuming $B(\psi(2S) \rightarrow \gamma\chi_{c2}(1P)) = (9.33 \pm 0.14 \pm 0.61) \times 10^{-2}$, which we rescale to our best value $B(\psi(2S) \rightarrow \gamma\chi_{c2}(1P)) = (9.52 \pm 0.20) \times 10^{-2}$. Our first error is their experiment's error and our second error is the systematic error from using our best value.

$\Gamma(K^*(892)^0 K^- \pi^+ \rightarrow K^- \pi^+ K^0 \pi^0 + \text{c.c.})/\Gamma_{\text{total}}$		Γ_9/Γ
VALUE (%)	EVTS	DOCUMENT ID

0.29 ± 0.08 ± 0.01	38.7	¹ HE
---------------------------	------	-----------------

¹ HE 08B reports $0.30 \pm 0.07 \pm 0.04 \pm 0.02\%$ from a measurement of $[\Gamma(\chi_{c2}(1P) \rightarrow K^*(892)^0 K^- \pi^+ \rightarrow K^- \pi^+ K^0 \pi^0 + \text{c.c.})/\Gamma_{\text{total}}] \times [B(\psi(2S) \rightarrow \gamma\chi_{c2}(1P))]$ assuming $B(\psi(2S) \rightarrow \gamma\chi_{c2}(1P)) = (9.33 \pm 0.14 \pm 0.61) \times 10^{-2}$, which we rescale to our best value $B(\psi(2S) \rightarrow \gamma\chi_{c2}(1P)) = (9.52 \pm 0.20) \times 10^{-2}$. Our first error is their experiment's error and our second error is the systematic error from using our best value.

$\Gamma(K^*(892)^0 K^- \pi^+ \rightarrow K^- \pi^+ K^0 \pi^0 + \text{c.c.})/\Gamma_{\text{total}}$		Γ_9/Γ
VALUE (%)	EVTS	DOCUMENT ID

0.29 ± 0.08 ± 0.01	38.7	¹ HE
---------------------------	------	-----------------

¹ HE 08B reports $0.30 \pm 0.07 \pm 0.04 \pm$

Meson Particle Listings

$\chi_{c2}(1P)$

$\Gamma(K^*(892)^0 \bar{K}^0 \pi^0 \rightarrow K^+ \pi^- \bar{K}^0 \pi^0 + c.c.) / \Gamma_{total}$					Γ_{10} / Γ
VALUE (%)	EVTS	DOCUMENT ID	TECN	COMMENT	
0.38 ± 0.09 ± 0.01	63.0	¹ HE	08B CLEO	$e^+ e^- \rightarrow \gamma h^+ h^- h^0 h^0$	

¹HE 08B reports $0.39 \pm 0.07 \pm 0.05 \pm 0.03$ % from a measurement of $[\Gamma(\chi_{c2}(1P) \rightarrow K^*(892)^0 \bar{K}^0 \pi^0 \rightarrow K^+ \pi^- \bar{K}^0 \pi^0 + c.c.) / \Gamma_{total}] \times [B(\psi(2S) \rightarrow \gamma \chi_{c2}(1P))]$ assuming $B(\psi(2S) \rightarrow \gamma \chi_{c2}(1P)) = (9.33 \pm 0.14 \pm 0.61) \times 10^{-2}$, which we rescale to our best value $B(\psi(2S) \rightarrow \gamma \chi_{c2}(1P)) = (9.52 \pm 0.20) \times 10^{-2}$. Our first error is their experiment's error and our second error is the systematic error from using our best value.

$\Gamma(K^*(892)^- K^+ \pi^0 \rightarrow K^+ \pi^- \bar{K}^0 \pi^0 + c.c.) / \Gamma_{total}$					Γ_{11} / Γ
VALUE (%)	EVTS	DOCUMENT ID	TECN	COMMENT	
0.37 ± 0.08 ± 0.01	51.1	¹ HE	08B CLEO	$e^+ e^- \rightarrow \gamma h^+ h^- h^0 h^0$	

¹HE 08B reports $0.38 \pm 0.07 \pm 0.04 \pm 0.03$ % from a measurement of $[\Gamma(\chi_{c2}(1P) \rightarrow K^*(892)^- K^+ \pi^0 \rightarrow K^+ \pi^- \bar{K}^0 \pi^0 + c.c.) / \Gamma_{total}] \times [B(\psi(2S) \rightarrow \gamma \chi_{c2}(1P))]$ assuming $B(\psi(2S) \rightarrow \gamma \chi_{c2}(1P)) = (9.33 \pm 0.14 \pm 0.61) \times 10^{-2}$, which we rescale to our best value $B(\psi(2S) \rightarrow \gamma \chi_{c2}(1P)) = (9.52 \pm 0.20) \times 10^{-2}$. Our first error is their experiment's error and our second error is the systematic error from using our best value.

$\Gamma(K^*(892)^+ \bar{K}^0 \pi^- \rightarrow K^+ \pi^- \bar{K}^0 \pi^0 + c.c.) / \Gamma_{total}$					Γ_{12} / Γ
VALUE (%)	EVTS	DOCUMENT ID	TECN	COMMENT	
0.29 ± 0.08 ± 0.01	39.3	¹ HE	08B CLEO	$e^+ e^- \rightarrow \gamma h^+ h^- h^0 h^0$	

¹HE 08B reports $0.30 \pm 0.07 \pm 0.04 \pm 0.02$ % from a measurement of $[\Gamma(\chi_{c2}(1P) \rightarrow K^*(892)^+ \bar{K}^0 \pi^- \rightarrow K^+ \pi^- \bar{K}^0 \pi^0 + c.c.) / \Gamma_{total}] \times [B(\psi(2S) \rightarrow \gamma \chi_{c2}(1P))]$ assuming $B(\psi(2S) \rightarrow \gamma \chi_{c2}(1P)) = (9.33 \pm 0.14 \pm 0.61) \times 10^{-2}$, which we rescale to our best value $B(\psi(2S) \rightarrow \gamma \chi_{c2}(1P)) = (9.52 \pm 0.20) \times 10^{-2}$. Our first error is their experiment's error and our second error is the systematic error from using our best value.

$\Gamma(K^+ K^- \eta \pi^0) / \Gamma_{total}$					Γ_{13} / Γ
VALUE (%)	EVTS	DOCUMENT ID	TECN	COMMENT	
0.127 ± 0.044 ± 0.003	22.9	¹ HE	08B CLEO	$e^+ e^- \rightarrow \gamma h^+ h^- h^0 h^0$	

¹HE 08B reports $0.13 \pm 0.04 \pm 0.02 \pm 0.01$ % from a measurement of $[\Gamma(\chi_{c2}(1P) \rightarrow K^+ K^- \eta \pi^0) / \Gamma_{total}] \times [B(\psi(2S) \rightarrow \gamma \chi_{c2}(1P))]$ assuming $B(\psi(2S) \rightarrow \gamma \chi_{c2}(1P)) = (9.33 \pm 0.14 \pm 0.61) \times 10^{-2}$, which we rescale to our best value $B(\psi(2S) \rightarrow \gamma \chi_{c2}(1P)) = (9.52 \pm 0.20) \times 10^{-2}$. Our first error is their experiment's error and our second error is the systematic error from using our best value.

$\Gamma(K^+ K^- \pi^+ \pi^-) / \Gamma_{total}$					Γ_{14} / Γ
VALUE (units 10^{-3})	DOCUMENT ID	TECN	COMMENT		
8.4 ± 0.9 OUR FIT					

$\Gamma(K^+ K^- \pi^+ \pi^- \pi^0) / \Gamma_{total}$					Γ_{15} / Γ
VALUE (units 10^{-3})	EVTS	DOCUMENT ID	TECN	COMMENT	
11.69 ± 0.13 ± 1.31	11k	¹ ABLIKIM	13B BES3	$e^+ e^- \rightarrow \psi(2S) \rightarrow \gamma \chi_{c2}$	

¹Using 1.06×10^8 $\psi(2S)$ mesons and $B(\psi(2S) \rightarrow \chi_{c2} \gamma) = (8.72 \pm 0.34)$ %.

$\Gamma(K_S^0 K^\pm \pi^\mp \pi^+ \pi^-) / \Gamma_{total}$					Γ_{16} / Γ
VALUE (units 10^{-3})	EVTS	DOCUMENT ID	TECN	COMMENT	
7.30 ± 0.11 ± 0.75	4.5k	¹ ABLIKIM	13B BES3	$e^+ e^- \rightarrow \psi(2S) \rightarrow \gamma \chi_{c2}$	

¹Using 1.06×10^8 $\psi(2S)$ mesons and $B(\psi(2S) \rightarrow \chi_{c2} \gamma) = (8.72 \pm 0.34)$ %.

$\Gamma(K^+ \bar{K}^*(892)^0 \pi^- + c.c.) / \Gamma(K^+ K^- \pi^+ \pi^-)$				$\Gamma_{17} / \Gamma_{14}$
VALUE	DOCUMENT ID	TECN	COMMENT	
0.25 ± 0.13 OUR FIT				
0.25 ± 0.13	TANENBAUM 78	MRK1	$\psi(2S) \rightarrow \gamma \chi_{c2}$	

$\Gamma(K^+ \bar{K}^*(892)^0 \pi^- + c.c.) / \Gamma_{total}$				Γ_{17} / Γ
VALUE (units 10^{-4})	DOCUMENT ID	TECN	COMMENT	
21 ± 11 OUR FIT				

$\Gamma(K^*(892)^0 \bar{K}^*(892)^0) / \Gamma_{total}$					Γ_{18} / Γ
VALUE (units 10^{-3})	DOCUMENT ID	TECN	COMMENT		
2.3 ± 0.4 OUR FIT					

$\Gamma(3(\pi^+ \pi^-)) / \Gamma_{total}$					Γ_{19} / Γ
VALUE (units 10^{-3})	DOCUMENT ID	TECN	COMMENT		
8.6 ± 1.8 OUR EVALUATION	Treating systematic error as correlated.				
8.6 ± 1.8 OUR AVERAGE					

¹Rescaled by us using $B(\psi(2S) \rightarrow \gamma \chi_{c2}) = (8.3 \pm 0.4)$ % and $B(\psi(2S) \rightarrow J/\psi(1S) \pi^+ \pi^-) = (32.6 \pm 0.5)$ %. Multiplied by a factor of 2 to convert from $K_S^0 K^+ \pi^-$ to $K^0 K^+ \pi^-$ decay.

$\Gamma(\phi \phi) / \Gamma_{total}$					Γ_{20} / Γ
VALUE (units 10^{-3})	DOCUMENT ID	TECN	COMMENT		
1.06 ± 0.09 OUR FIT					

$\Gamma(\phi \phi \eta) / \Gamma_{total}$					Γ_{21} / Γ
VALUE (units 10^{-4})	EVTS	DOCUMENT ID	TECN	COMMENT	
5.3 ± 0.5 ± 0.4	143.6	¹ ABLIKIM	20B BES3	$\psi(2S) \rightarrow \gamma \phi \phi \eta$	

¹ABLIKIM 20B reports $(5.33 \pm 0.52 \pm 0.39) \times 10^{-4}$ from a measurement of $[\Gamma(\chi_{c2}(1P) \rightarrow \phi \phi \eta) / \Gamma_{total}] \times [B(\psi(2S) \rightarrow \gamma \chi_{c2}(1P))]$ assuming $B(\psi(2S) \rightarrow \gamma \chi_{c2}(1P)) = (9.52 \pm 0.20) \times 10^{-2}$.

$\Gamma(\omega \omega) / \Gamma_{total}$					Γ_{22} / Γ
VALUE (units 10^{-3})	EVTS	DOCUMENT ID	TECN	COMMENT	
0.84 ± 0.10 OUR AVERAGE					
0.82 ± 0.10 ± 0.02	762	¹ ABLIKIM	11K BES3	$\psi(2S) \rightarrow \gamma$ hadrons	
1.73 ± 0.57 ± 0.04	27.7 ± 7.4	² ABLIKIM	05N BES2	$\psi(2S) \rightarrow \gamma \chi_{c2} \rightarrow \gamma 6\pi$	

¹ABLIKIM 11K reports $(8.9 \pm 0.3 \pm 1.1) \times 10^{-4}$ from a measurement of $[\Gamma(\chi_{c2}(1P) \rightarrow \omega \omega) / \Gamma_{total}] \times [B(\psi(2S) \rightarrow \gamma \chi_{c2}(1P))]$ assuming $B(\psi(2S) \rightarrow \gamma \chi_{c2}(1P)) = (8.74 \pm 0.35) \times 10^{-2}$, which we rescale to our best value $B(\psi(2S) \rightarrow \gamma \chi_{c2}(1P)) = (9.52 \pm 0.20) \times 10^{-2}$. Our first error is their experiment's error and our second error is the systematic error from using our best value.

²ABLIKIM 05N reports $[\Gamma(\chi_{c2}(1P) \rightarrow \omega \omega) / \Gamma_{total}] \times [B(\psi(2S) \rightarrow \gamma \chi_{c2}(1P))]$ = $(0.165 \pm 0.044 \pm 0.032) \times 10^{-3}$ which we divide by our best value $B(\psi(2S) \rightarrow \gamma \chi_{c2}(1P)) = (9.52 \pm 0.20) \times 10^{-2}$. Our first error is their experiment's error and our second error is the systematic error from using our best value.

$\Gamma(\omega K^+ K^-) / \Gamma_{total}$					Γ_{23} / Γ
VALUE (units 10^{-3})	EVTS	DOCUMENT ID	TECN	COMMENT	
0.73 ± 0.04 ± 0.08	512	¹ ABLIKIM	13B BES3	$e^+ e^- \rightarrow \psi(2S) \rightarrow \gamma \chi_{c2}$	

¹Using 1.06×10^8 $\psi(2S)$ mesons and $B(\psi(2S) \rightarrow \chi_{c2} \gamma) = (8.72 \pm 0.34)$ %.

$\Gamma(\omega \phi) / \Gamma_{total}$					Γ_{24} / Γ
VALUE (units 10^{-6})	CL%	EVTS	DOCUMENT ID	TECN	COMMENT
9.6 ± 2.7 ± 0.2	33	¹ ABLIKIM	19J BES3	$\psi(2S) \rightarrow \gamma$ hadrons	
<18	90	^{2,3} ABLIKIM	11K BES3	$\psi(2S) \rightarrow \gamma$ hadrons	

• • • We do not use the following data for averages, fits, limits, etc. • • •

¹ABLIKIM 19J reports $[\Gamma(\chi_{c2}(1P) \rightarrow \omega \phi) / \Gamma_{total}] \times [B(\psi(2S) \rightarrow \gamma \chi_{c2}(1P))]$ = $(0.91 \pm 0.23 \pm 0.12) \times 10^{-6}$ which we divide by our best value $B(\psi(2S) \rightarrow \gamma \chi_{c2}(1P)) = (9.52 \pm 0.20) \times 10^{-2}$. Our first error is their experiment's error and our second error is the systematic error from using our best value.

²ABLIKIM 11K reports $< 2 \times 10^{-5}$ from a measurement of $[\Gamma(\chi_{c2}(1P) \rightarrow \omega \phi) / \Gamma_{total}] \times [B(\psi(2S) \rightarrow \gamma \chi_{c2}(1P))]$ assuming $B(\psi(2S) \rightarrow \gamma \chi_{c2}(1P)) = (8.74 \pm 0.35) \times 10^{-2}$, which we rescale to our best value $B(\psi(2S) \rightarrow \gamma \chi_{c2}(1P)) = 9.52 \times 10^{-2}$.

³Superseded by ABLIKIM 19J.

$\Gamma(\pi \pi) / \Gamma_{total}$					Γ_{25} / Γ
VALUE (units 10^{-3})	DOCUMENT ID	TECN	COMMENT		
2.23 ± 0.09 OUR FIT					

$\Gamma(\rho^0 \pi^+ \pi^-) / \Gamma_{total}$					Γ_{26} / Γ
VALUE (units 10^{-4})	DOCUMENT ID	TECN	COMMENT		
37 ± 16 OUR FIT					

$\Gamma(\pi^+ \pi^- \pi^0 \text{ (non-resonant)}) / \Gamma_{total}$					Γ_{27} / Γ
VALUE (units 10^{-5})	EVTS	DOCUMENT ID	TECN	COMMENT	
2.01 ± 0.42 ± 0.04	64	¹ ABLIKIM	17AG BES3	$\psi(2S) \rightarrow \gamma \pi^+ \pi^- \pi^0$	

¹ABLIKIM 17AG reports $(2.1 \pm 0.4 \pm 0.2) \times 10^{-5}$ from a measurement of $[\Gamma(\chi_{c2}(1P) \rightarrow \pi^+ \pi^- \pi^0 \text{ (non-resonant)}) / \Gamma_{total}] \times [B(\psi(2S) \rightarrow \gamma \chi_{c2}(1P))]$ assuming $B(\psi(2S) \rightarrow \gamma \chi_{c2}(1P)) = (9.11 \pm 0.31) \times 10^{-2}$, which we rescale to our best value $B(\psi(2S) \rightarrow \gamma \chi_{c2}(1P)) = (9.52 \pm 0.20) \times 10^{-2}$. Our first error is their experiment's error and our second error is the systematic error from using our best value.

$\Gamma(\rho(770)^\pm \pi^\mp) / \Gamma_{total}$					Γ_{28} / Γ
VALUE (units 10^{-5})	EVTS	DOCUMENT ID	TECN	COMMENT	
0.61 ± 0.38 ± 0.01	15	¹ ABLIKIM	17AG BES3	$\psi(2S) \rightarrow \gamma \pi^+ \pi^- \pi^0$	

¹ABLIKIM 17AG reports $(0.64 \pm 0.39 \pm 0.07) \times 10^{-5}$ from a measurement of $[\Gamma(\chi_{c2}(1P) \rightarrow \rho(770)^\pm \pi^\mp) / \Gamma_{total}] \times [B(\psi(2S) \rightarrow \gamma \chi_{c2}(1P))]$ assuming $B(\psi(2S) \rightarrow \gamma \chi_{c2}(1P)) = (9.11 \pm 0.31) \times 10^{-2}$, which we rescale to our best value $B(\psi(2S) \rightarrow \gamma \chi_{c2}(1P)) = (9.52 \pm 0.20) \times 10^{-2}$. Our first error is their experiment's error and our second error is the systematic error from using our best value.

$\Gamma(\pi^+ \pi^- \eta) / \Gamma_{total}$					Γ_{29} / Γ
VALUE (units 10^{-3})	CL%	DOCUMENT ID	TECN	COMMENT	
0.48 ± 0.13 ± 0.01		¹ ATHAR	07 CLEO	$\psi(2S) \rightarrow \gamma h^+ h^- h^0$	
<1.4	90	² ABLIKIM	06R BES2	$\psi(2S) \rightarrow \gamma \chi_{c2}$	

• • • We do not use the following data for averages, fits, limits, etc. • • •

¹ATHAR 07 reports $(0.49 \pm 0.12 \pm 0.06) \times 10^{-3}$ from a measurement of $[\Gamma(\chi_{c2}(1P) \rightarrow \pi^+ \pi^- \eta) / \Gamma_{total}] \times [B(\psi(2S) \rightarrow \gamma \chi_{c2}(1P))]$ assuming $B(\psi(2S) \rightarrow \gamma \chi_{c2}(1P)) = (9.33 \pm 0.14 \pm 0.61) \times 10^{-2}$, which we rescale to our best value $B(\psi(2S) \rightarrow \gamma \chi_{c2}(1P)) = (9.52 \pm 0.20) \times 10^{-2}$. Our first error is their experiment's error and our second error is the systematic error from using our best value.

²ABLIKIM 06R reports $< 1.7 \times 10^{-3}$ from a measurement of $[\Gamma(\chi_{c2}(1P) \rightarrow \pi^+ \pi^- \eta) / \Gamma_{total}] \times [B(\psi(2S) \rightarrow \gamma \chi_{c2}(1P))]$ assuming $B(\psi(2S) \rightarrow \gamma \chi_{c2}(1P)) = (8.1 \pm 0.4) \times 10^{-2}$, which we rescale to our best value $B(\psi(2S) \rightarrow \gamma \chi_{c2}(1P)) = 9.52 \times 10^{-2}$.

See key on page 999

Meson Particle Listings

$\chi_{c2}(1P)$

$\Gamma(\pi^+\pi^-\eta')/\Gamma_{total}$	Γ_{30}/Γ
VALUE (units 10^{-3})	DOCUMENT ID TECN COMMENT
0.50±0.18±0.01	¹ ATHAR 07 CLEO $\psi(2S) \rightarrow \gamma h^+ h^- h^0$

¹ ATHAR 07 reports $(0.51 \pm 0.18 \pm 0.06) \times 10^{-3}$ from a measurement of $[\Gamma(\chi_{c2}(1P) \rightarrow \pi^+\pi^-\eta')/\Gamma_{total}] \times [B(\psi(2S) \rightarrow \gamma\chi_{c2}(1P))]$ assuming $B(\psi(2S) \rightarrow \gamma\chi_{c2}(1P)) = (9.33 \pm 0.14 \pm 0.61) \times 10^{-2}$, which we rescale to our best value $B(\psi(2S) \rightarrow \gamma\chi_{c2}(1P)) = (9.52 \pm 0.20) \times 10^{-2}$. Our first error is their experiment's error and our second error is the systematic error from using our best value.

$\Gamma(\eta\eta)/\Gamma_{total}$	Γ_{31}/Γ
VALUE (units 10^{-4})	DOCUMENT ID
5.4±0.4 OUR FIT	

$\Gamma(K^+K^-)/\Gamma_{total}$	Γ_{32}/Γ
VALUE (units 10^{-3})	DOCUMENT ID
1.01±0.06 OUR FIT	

$\Gamma(K_S^0 K_S^0)/\Gamma_{total}$	Γ_{33}/Γ
VALUE (units 10^{-3})	DOCUMENT ID
0.52±0.04 OUR FIT	

$\Gamma(K_S^0 K_S^0)/\Gamma(\pi\pi)$	Γ_{33}/Γ_{25}
VALUE	DOCUMENT ID TECN COMMENT
0.235±0.019 OUR FIT	

• • • We do not use the following data for averages, fits, limits, etc. • • •
 0.27 ± 0.07 ± 0.04 ^{1,2} CHEN 07B BELL $e^+e^- \rightarrow e^+e^-\chi_{c2}$
¹ Using $\Gamma(\pi\pi) \times \Gamma(\gamma\gamma)/\Gamma_{total}$ from the $\pi^+\pi^-$ measurement of NAKAZAWA 05 rescaled by $\sqrt{2}$ to convert to $\pi\pi$.
² Not independent from other measurements.

$\Gamma(K_S^0 K_S^0)/\Gamma(K^+K^-)$	Γ_{33}/Γ_{32}
VALUE	DOCUMENT ID TECN COMMENT
0.52±0.05 OUR FIT	

• • • We do not use the following data for averages, fits, limits, etc. • • •
 0.70±0.21±0.12 ^{1,2} CHEN 07B BELL $e^+e^- \rightarrow e^+e^-\chi_{c2}$
¹ Using $\Gamma(K^+K^-) \times \Gamma(\gamma\gamma)/\Gamma_{total}$ from NAKAZAWA 05.
² Not independent from other measurements.

$\Gamma(K^*(892^\pm K^\mp)/\Gamma_{total}$	Γ_{34}/Γ
VALUE (units 10^{-4})	DOCUMENT ID TECN COMMENT
1.44±0.21±0.03	¹ ABLIKIM 17AG BES3 $\psi(2S) \rightarrow \gamma K \bar{K} \pi$

• • • We do not use the following data for averages, fits, limits, etc. • • •
 1.72±0.26±0.04 ² ABLIKIM 17AG BES3 $\psi(2S) \rightarrow \gamma K^+ K^- \pi^0$
 1.34±0.27±0.03 ³ ABLIKIM 17AG BES3 $\psi(2S) \rightarrow \gamma K_S^0 K^\pm \pi^\mp$

¹ ABLIKIM 17AG reports $(1.5 \pm 0.1 \pm 0.2) \times 10^{-4}$ from a measurement of $[\Gamma(\chi_{c2}(1P) \rightarrow K^*(892^\pm K^\mp)/\Gamma_{total}) \times [B(\psi(2S) \rightarrow \gamma\chi_{c2}(1P))]]$ assuming $B(\psi(2S) \rightarrow \gamma\chi_{c2}(1P)) = (9.11 \pm 0.31) \times 10^{-2}$, which we rescale to our best value $B(\psi(2S) \rightarrow \gamma\chi_{c2}(1P)) = (9.52 \pm 0.20) \times 10^{-2}$. Our first error is their experiment's error and our second error is the systematic error from using our best value.

² ABLIKIM 17AG reports $(1.8 \pm 0.2 \pm 0.2) \times 10^{-4}$ from a measurement of $[\Gamma(\chi_{c2}(1P) \rightarrow K^*(892^\pm K^\mp)/\Gamma_{total}) \times [B(\psi(2S) \rightarrow \gamma\chi_{c2}(1P))]]$ assuming $B(\psi(2S) \rightarrow \gamma\chi_{c2}(1P)) = (9.11 \pm 0.31) \times 10^{-2}$, which we rescale to our best value $B(\psi(2S) \rightarrow \gamma\chi_{c2}(1P)) = (9.52 \pm 0.20) \times 10^{-2}$. Our first error is their experiment's error and our second error is the systematic error from using our best value.

³ ABLIKIM 17AG reports $(1.4 \pm 0.2 \pm 0.2) \times 10^{-4}$ from a measurement of $[\Gamma(\chi_{c2}(1P) \rightarrow K^*(892^\pm K^\mp)/\Gamma_{total}) \times [B(\psi(2S) \rightarrow \gamma\chi_{c2}(1P))]]$ assuming $B(\psi(2S) \rightarrow \gamma\chi_{c2}(1P)) = (9.11 \pm 0.31) \times 10^{-2}$, which we rescale to our best value $B(\psi(2S) \rightarrow \gamma\chi_{c2}(1P)) = (9.52 \pm 0.20) \times 10^{-2}$. Our first error is their experiment's error and our second error is the systematic error from using our best value.

$\Gamma(K^*(892^0 \bar{K}^0 + c.c.)/\Gamma_{total}$	Γ_{35}/Γ
VALUE (units 10^{-4})	DOCUMENT ID TECN COMMENT
1.24±0.27±0.03	¹ ABLIKIM 17AG BES3 $\psi(2S) \rightarrow \gamma K_S^0 K^\pm \pi^\mp$

¹ ABLIKIM 17AG reports $(1.3 \pm 0.2 \pm 0.2) \times 10^{-4}$ from a measurement of $[\Gamma(\chi_{c2}(1P) \rightarrow K^*(892^0 \bar{K}^0 + c.c.)/\Gamma_{total}) \times [B(\psi(2S) \rightarrow \gamma\chi_{c2}(1P))]]$ assuming $B(\psi(2S) \rightarrow \gamma\chi_{c2}(1P)) = (9.11 \pm 0.31) \times 10^{-2}$, which we rescale to our best value $B(\psi(2S) \rightarrow \gamma\chi_{c2}(1P)) = (9.52 \pm 0.20) \times 10^{-2}$. Our first error is their experiment's error and our second error is the systematic error from using our best value.

$\Gamma(K_2^*(1430^\pm K^\mp)/\Gamma_{total}$	Γ_{36}/Γ
VALUE (units 10^{-4})	DOCUMENT ID TECN COMMENT
14.8±1.2±0.3	¹ ABLIKIM 17AG BES3 $\psi(2S) \rightarrow \gamma K \bar{K} \pi$

• • • We do not use the following data for averages, fits, limits, etc. • • •
 17.4±1.6±0.4 ² ABLIKIM 17AG BES3 $\psi(2S) \rightarrow \gamma K^+ K^- \pi^0$
 13.0±1.5±0.3 ³ ABLIKIM 17AG BES3 $\psi(2S) \rightarrow \gamma K_S^0 K^\pm \pi^\mp$

¹ ABLIKIM 17AG reports $(15.5 \pm 0.6 \pm 1.2) \times 10^{-4}$ from a measurement of $[\Gamma(\chi_{c2}(1P) \rightarrow K_2^*(1430^\pm K^\mp)/\Gamma_{total}) \times [B(\psi(2S) \rightarrow \gamma\chi_{c2}(1P))]]$ assuming $B(\psi(2S) \rightarrow \gamma\chi_{c2}(1P)) = (9.11 \pm 0.31) \times 10^{-2}$, which we rescale to our best value $B(\psi(2S) \rightarrow \gamma\chi_{c2}(1P)) = (9.52 \pm 0.20) \times 10^{-2}$. Our first error is their experiment's error and our second error is the systematic error from using our best value.

² ABLIKIM 17AG reports $(18.2 \pm 0.8 \pm 1.6) \times 10^{-4}$ from a measurement of $[\Gamma(\chi_{c2}(1P) \rightarrow K_2^*(1430^\pm K^\mp)/\Gamma_{total}) \times [B(\psi(2S) \rightarrow \gamma\chi_{c2}(1P))]]$ assuming $B(\psi(2S) \rightarrow \gamma\chi_{c2}(1P)) = (9.11 \pm 0.31) \times 10^{-2}$, which we rescale to our best value $B(\psi(2S) \rightarrow \gamma\chi_{c2}(1P)) = (9.52 \pm 0.20) \times 10^{-2}$. Our first error is their experiment's error and our second error is the systematic error from using our best value.

³ ABLIKIM 17AG reports $(13.6 \pm 0.8 \pm 1.4) \times 10^{-4}$ from a measurement of $[\Gamma(\chi_{c2}(1P) \rightarrow K_2^*(1430^\pm K^\mp)/\Gamma_{total}) \times [B(\psi(2S) \rightarrow \gamma\chi_{c2}(1P))]]$ assuming $B(\psi(2S) \rightarrow \gamma\chi_{c2}(1P)) = (9.11 \pm 0.31) \times 10^{-2}$, which we rescale to our best value $B(\psi(2S) \rightarrow \gamma\chi_{c2}(1P)) = (9.52 \pm 0.20) \times 10^{-2}$. Our first error is their experiment's error and our second error is the systematic error from using our best value.

$\Gamma(K_2^*(1430^0 \bar{K}^0 + c.c.)/\Gamma_{total}$	Γ_{37}/Γ
VALUE (units 10^{-4})	DOCUMENT ID TECN COMMENT
12.4±1.7±0.3	¹ ABLIKIM 17AG BES3 $\psi(2S) \rightarrow \gamma K_S^0 K^\pm \pi^\mp$

¹ ABLIKIM 17AG reports $(13.0 \pm 1.0 \pm 1.5) \times 10^{-4}$ from a measurement of $[\Gamma(\chi_{c2}(1P) \rightarrow K_2^*(1430^0 \bar{K}^0 + c.c.)/\Gamma_{total}) \times [B(\psi(2S) \rightarrow \gamma\chi_{c2}(1P))]]$ assuming $B(\psi(2S) \rightarrow \gamma\chi_{c2}(1P)) = (9.11 \pm 0.31) \times 10^{-2}$, which we rescale to our best value $B(\psi(2S) \rightarrow \gamma\chi_{c2}(1P)) = (9.52 \pm 0.20) \times 10^{-2}$. Our first error is their experiment's error and our second error is the systematic error from using our best value.

$\Gamma(K_3^*(1780^\pm K^\mp)/\Gamma_{total}$	Γ_{38}/Γ
VALUE (units 10^{-4})	DOCUMENT ID TECN COMMENT
5.2±0.8±0.1	¹ ABLIKIM 17AG BES3 $\psi(2S) \rightarrow \gamma K \bar{K} \pi$

• • • We do not use the following data for averages, fits, limits, etc. • • •
 5.1±1.0±0.1 ² ABLIKIM 17AG BES3 $\psi(2S) \rightarrow \gamma K^+ K^- \pi^0$
 5.6±1.8±0.1 ³ ABLIKIM 17AG BES3 $\psi(2S) \rightarrow \gamma K_S^0 K^\pm \pi^\mp$

¹ ABLIKIM 17AG reports $(5.4 \pm 0.5 \pm 0.7) \times 10^{-4}$ from a measurement of $[\Gamma(\chi_{c2}(1P) \rightarrow K_3^*(1780^\pm K^\mp)/\Gamma_{total}) \times [B(\psi(2S) \rightarrow \gamma\chi_{c2}(1P))]]$ assuming $B(\psi(2S) \rightarrow \gamma\chi_{c2}(1P)) = (9.11 \pm 0.31) \times 10^{-2}$, which we rescale to our best value $B(\psi(2S) \rightarrow \gamma\chi_{c2}(1P)) = (9.52 \pm 0.20) \times 10^{-2}$. Our first error is their experiment's error and our second error is the systematic error from using our best value.

² ABLIKIM 17AG reports $(5.3 \pm 0.5 \pm 0.9) \times 10^{-4}$ from a measurement of $[\Gamma(\chi_{c2}(1P) \rightarrow K_3^*(1780^\pm K^\mp)/\Gamma_{total}) \times [B(\psi(2S) \rightarrow \gamma\chi_{c2}(1P))]]$ assuming $B(\psi(2S) \rightarrow \gamma\chi_{c2}(1P)) = (9.11 \pm 0.31) \times 10^{-2}$, which we rescale to our best value $B(\psi(2S) \rightarrow \gamma\chi_{c2}(1P)) = (9.52 \pm 0.20) \times 10^{-2}$. Our first error is their experiment's error and our second error is the systematic error from using our best value.

³ ABLIKIM 17AG reports $(5.9 \pm 1.1 \pm 1.5) \times 10^{-4}$ from a measurement of $[\Gamma(\chi_{c2}(1P) \rightarrow K_3^*(1780^\pm K^\mp)/\Gamma_{total}) \times [B(\psi(2S) \rightarrow \gamma\chi_{c2}(1P))]]$ assuming $B(\psi(2S) \rightarrow \gamma\chi_{c2}(1P)) = (9.11 \pm 0.31) \times 10^{-2}$, which we rescale to our best value $B(\psi(2S) \rightarrow \gamma\chi_{c2}(1P)) = (9.52 \pm 0.20) \times 10^{-2}$. Our first error is their experiment's error and our second error is the systematic error from using our best value.

$\Gamma(K_3^*(1780^0 \bar{K}^0 + c.c.)/\Gamma_{total}$	Γ_{39}/Γ
VALUE (units 10^{-4})	DOCUMENT ID TECN COMMENT
5.6±2.1±0.1	¹ ABLIKIM 17AG BES3 $\psi(2S) \rightarrow \gamma K_S^0 K^\pm \pi^\mp$

¹ ABLIKIM 17AG reports $(5.9 \pm 1.6 \pm 1.5) \times 10^{-4}$ from a measurement of $[\Gamma(\chi_{c2}(1P) \rightarrow K_3^*(1780^0 \bar{K}^0 + c.c.)/\Gamma_{total}) \times [B(\psi(2S) \rightarrow \gamma\chi_{c2}(1P))]]$ assuming $B(\psi(2S) \rightarrow \gamma\chi_{c2}(1P)) = (9.11 \pm 0.31) \times 10^{-2}$, which we rescale to our best value $B(\psi(2S) \rightarrow \gamma\chi_{c2}(1P)) = (9.52 \pm 0.20) \times 10^{-2}$. Our first error is their experiment's error and our second error is the systematic error from using our best value.

$\Gamma(a_2(1320^0 \pi^0)/\Gamma_{total}$	Γ_{40}/Γ
VALUE (units 10^{-4})	DOCUMENT ID TECN COMMENT
12.9±3.4±0.3	¹ ABLIKIM 17AG BES3 $\psi(2S) \rightarrow \gamma K^+ K^- \pi^0$

¹ ABLIKIM 17AG reports $(13.5 \pm 1.6 \pm 3.2) \times 10^{-4}$ from a measurement of $[\Gamma(\chi_{c2}(1P) \rightarrow a_2(1320^0 \pi^0)/\Gamma_{total}) \times [B(\psi(2S) \rightarrow \gamma\chi_{c2}(1P))]]$ assuming $B(\psi(2S) \rightarrow \gamma\chi_{c2}(1P)) = (9.11 \pm 0.31) \times 10^{-2}$, which we rescale to our best value $B(\psi(2S) \rightarrow \gamma\chi_{c2}(1P)) = (9.52 \pm 0.20) \times 10^{-2}$. Our first error is their experiment's error and our second error is the systematic error from using our best value.

$\Gamma(a_2(1320^\pm \pi^\mp)/\Gamma_{total}$	Γ_{41}/Γ
VALUE (units 10^{-4})	DOCUMENT ID TECN COMMENT
17.6±6.1±0.4	¹ ABLIKIM 17AG BES3 $\psi(2S) \rightarrow \gamma K_S^0 K^\pm \pi^\mp$

¹ ABLIKIM 17AG reports $(18.4 \pm 3.3 \pm 5.5) \times 10^{-4}$ from a measurement of $[\Gamma(\chi_{c2}(1P) \rightarrow a_2(1320^\pm \pi^\mp)/\Gamma_{total}) \times [B(\psi(2S) \rightarrow \gamma\chi_{c2}(1P))]]$ assuming $B(\psi(2S) \rightarrow \gamma\chi_{c2}(1P)) = (9.11 \pm 0.31) \times 10^{-2}$, which we rescale to our best value $B(\psi(2S) \rightarrow \gamma\chi_{c2}(1P)) = (9.52 \pm 0.20) \times 10^{-2}$. Our first error is their experiment's error and our second error is the systematic error from using our best value.

$\Gamma(K^+ K^- \pi^0)/\Gamma_{total}$	Γ_{43}/Γ
VALUE (units 10^{-3})	DOCUMENT ID TECN COMMENT
0.30±0.08±0.01	¹ ATHAR 07 CLEO $\psi(2S) \rightarrow \gamma h^+ h^- h^0$

¹ ATHAR 07 reports $(0.31 \pm 0.07 \pm 0.04) \times 10^{-3}$ from a measurement of $[\Gamma(\chi_{c2}(1P) \rightarrow K^+ K^- \pi^0)/\Gamma_{total}] \times [B(\psi(2S) \rightarrow \gamma\chi_{c2}(1P))]$ assuming $B(\psi(2S) \rightarrow \gamma\chi_{c2}(1P)) = (9.33 \pm 0.14 \pm 0.61) \times 10^{-2}$, which we rescale to our best value $B(\psi(2S) \rightarrow \gamma\chi_{c2}(1P)) = (9.52 \pm 0.20) \times 10^{-2}$. Our first error is their experiment's error and our second error is the systematic error from using our best value.

Meson Particle Listings

 $\chi_{c2}(1P)$

$\Gamma(K^+ K^- \eta)/\Gamma_{\text{total}}$		Γ_{44}/Γ
VALUE (units 10^{-3})	CL%	DOCUMENT ID

<0.32 90 ¹ATHAR 07 CLEO $\psi(2S) \rightarrow \gamma h^+ h^- h^0$
¹ATHAR 07 reports $< 0.33 \times 10^{-3}$ from a measurement of $[\Gamma(\chi_{c2}(1P) \rightarrow K^+ K^- \eta)/\Gamma_{\text{total}}] \times [B(\psi(2S) \rightarrow \gamma \chi_{c2}(1P))]$ assuming $B(\psi(2S) \rightarrow \gamma \chi_{c2}(1P)) = (9.33 \pm 0.14 \pm 0.61) \times 10^{-2}$, which we rescale to our best value $B(\psi(2S) \rightarrow \gamma \chi_{c2}(1P)) = 9.52 \times 10^{-2}$.

$\Gamma(K^+ K^- \eta'(958))/\Gamma_{\text{total}}$		Γ_{45}/Γ
VALUE (units 10^{-4})	EVTS	DOCUMENT ID

1.94 ± 0.34 107 ¹ABLIKIM 14J BES3 $\psi(2S) \rightarrow \gamma K^+ K^- \eta'(958)$
¹Derived using $B(\psi(2S) \rightarrow \gamma \chi_{c2}) = (8.72 \pm 0.34)\%$. Uncertainty includes both statistical and systematic contributions combined in quadrature.

$\Gamma(\eta \eta')/\Gamma_{\text{total}}$		Γ_{46}/Γ
VALUE (units 10^{-5})	CL%	EVTS

2.17 ± 0.47 ± 0.05 20 ¹ABLIKIM 17AI BES3 $\psi(2S) \rightarrow \gamma \eta' \eta$
 • • • We do not use the following data for averages, fits, limits, etc. • • •
 < 6 90 3.3 ± 8.0 ²ASNER 09 CLEO $\psi(2S) \rightarrow \gamma \eta \eta'$
 <23 90 ³ADAMS 07 CLEO $\psi(2S) \rightarrow \gamma \chi_{c2}$

¹ABLIKIM 17AI reports $(2.27 \pm 0.43 \pm 0.25) \times 10^{-5}$ from a measurement of $[\Gamma(\chi_{c2}(1P) \rightarrow \eta \eta')/\Gamma_{\text{total}}] \times [B(\psi(2S) \rightarrow \gamma \chi_{c2}(1P))]$ assuming $B(\psi(2S) \rightarrow \gamma \chi_{c2}(1P)) = (9.11 \pm 0.31) \times 10^{-2}$, which we rescale to our best value $B(\psi(2S) \rightarrow \gamma \chi_{c2}(1P)) = (9.52 \pm 0.20) \times 10^{-2}$. Our first error is their experiment's error and our second error is the systematic error from using our best value.
²ASNER 09 reports $< 0.6 \times 10^{-4}$ from a measurement of $[\Gamma(\chi_{c2}(1P) \rightarrow \eta \eta')/\Gamma_{\text{total}}] \times [B(\psi(2S) \rightarrow \gamma \chi_{c2}(1P))]$ assuming $B(\psi(2S) \rightarrow \gamma \chi_{c2}(1P)) = (9.33 \pm 0.14 \pm 0.61) \times 10^{-2}$, which we rescale to our best value $B(\psi(2S) \rightarrow \gamma \chi_{c2}(1P)) = 9.52 \times 10^{-2}$.
³Superseded by ASNER 09. ADAMS 07 reports $< 2.3 \times 10^{-4}$ from a measurement of $[\Gamma(\chi_{c2}(1P) \rightarrow \eta \eta')/\Gamma_{\text{total}}] \times [B(\psi(2S) \rightarrow \gamma \chi_{c2}(1P))]$ assuming $B(\psi(2S) \rightarrow \gamma \chi_{c2}(1P)) = 0.0933 \pm 0.0014 \pm 0.0061$, which we rescale to our best value $B(\psi(2S) \rightarrow \gamma \chi_{c2}(1P)) = 9.52 \times 10^{-2}$.

$\Gamma(\eta' \eta')/\Gamma_{\text{total}}$		Γ_{47}/Γ
VALUE (units 10^{-5})	CL%	EVTS

4.6 ± 0.6 ± 0.1 60 ¹ABLIKIM 17AI BES3 $\psi(2S) \rightarrow \gamma \eta' \eta'$
 • • • We do not use the following data for averages, fits, limits, etc. • • •
 < 10 90 12 ± 7 ²ASNER 09 CLEO $\psi(2S) \rightarrow \gamma \eta' \eta'$
 <30 90 ³ADAMS 07 CLEO $\psi(2S) \rightarrow \gamma \chi_{c2}$

¹ABLIKIM 17AI reports $(4.76 \pm 0.56 \pm 0.38) \times 10^{-5}$ from a measurement of $[\Gamma(\chi_{c2}(1P) \rightarrow \eta' \eta')/\Gamma_{\text{total}}] \times [B(\psi(2S) \rightarrow \gamma \chi_{c2}(1P))]$ assuming $B(\psi(2S) \rightarrow \gamma \chi_{c2}(1P)) = (9.11 \pm 0.31) \times 10^{-2}$, which we rescale to our best value $B(\psi(2S) \rightarrow \gamma \chi_{c2}(1P)) = (9.52 \pm 0.20) \times 10^{-2}$. Our first error is their experiment's error and our second error is the systematic error from using our best value.
²ASNER 09 reports $< 1.0 \times 10^{-4}$ from a measurement of $[\Gamma(\chi_{c2}(1P) \rightarrow \eta' \eta')/\Gamma_{\text{total}}] \times [B(\psi(2S) \rightarrow \gamma \chi_{c2}(1P))]$ assuming $B(\psi(2S) \rightarrow \gamma \chi_{c2}(1P)) = (9.33 \pm 0.14 \pm 0.61) \times 10^{-2}$, which we rescale to our best value $B(\psi(2S) \rightarrow \gamma \chi_{c2}(1P)) = 9.52 \times 10^{-2}$.
³Superseded by ASNER 09. ADAMS 07 reports $< 3.1 \times 10^{-4}$ from a measurement of $[\Gamma(\chi_{c2}(1P) \rightarrow \eta' \eta')/\Gamma_{\text{total}}] \times [B(\psi(2S) \rightarrow \gamma \chi_{c2}(1P))]$ assuming $B(\psi(2S) \rightarrow \gamma \chi_{c2}(1P)) = 0.0933 \pm 0.0014 \pm 0.0061$, which we rescale to our best value $B(\psi(2S) \rightarrow \gamma \chi_{c2}(1P)) = 9.52 \times 10^{-2}$.

$\Gamma(\pi^+ \pi^- K_S^0 K_S^0)/\Gamma_{\text{total}}$		Γ_{48}/Γ
VALUE (units 10^{-3})	EVTS	DOCUMENT ID

2.17 ± 0.54 ± 0.05 57 ± 11 ¹ABLIKIM 05O BES2 $\psi(2S) \rightarrow \gamma \chi_{c2}$
¹ABLIKIM 05O reports $[\Gamma(\chi_{c2}(1P) \rightarrow \pi^+ \pi^- K_S^0 K_S^0)/\Gamma_{\text{total}}] \times [B(\psi(2S) \rightarrow \gamma \chi_{c2}(1P))]$ = $(0.207 \pm 0.039 \pm 0.033) \times 10^{-3}$ which we divide by our best value $B(\psi(2S) \rightarrow \gamma \chi_{c2}(1P)) = (9.52 \pm 0.20) \times 10^{-2}$. Our first error is their experiment's error and our second error is the systematic error from using our best value.

$\Gamma(K^+ K^- K_S^0 K_S^0)/\Gamma_{\text{total}}$		Γ_{49}/Γ
VALUE (units 10^{-4})	CL%	EVTS

<4 90 2.3 ± 2.2 ¹ABLIKIM 05O BES2 $e^+ e^- \rightarrow \chi_{c2} \gamma$
¹ABLIKIM 05O reports $[\Gamma(\chi_{c2}(1P) \rightarrow K^+ K^- K_S^0 K_S^0)/\Gamma_{\text{total}}] \times [B(\psi(2S) \rightarrow \gamma \chi_{c2}(1P))]$ < 3.5×10^{-5} which we divide by our best value $B(\psi(2S) \rightarrow \gamma \chi_{c2}(1P)) = 9.52 \times 10^{-2}$.

$\Gamma(K_S^0 K_S^0 K_S^0 K_S^0)/\Gamma_{\text{total}}$		Γ_{50}/Γ
VALUE (units 10^{-4})	EVTS	DOCUMENT ID

1.13 ± 0.18 ± 0.02 68 ¹ABLIKIM 19AA BES3 $\psi(2S) \rightarrow \gamma 4K_S^0$
¹Using $B(K_S^0 \rightarrow \pi^+ \pi^-) = (69.20 \pm 0.05)\%$. ABLIKIM 19AA reports $[\Gamma(\chi_{c2}(1P) \rightarrow K_S^0 K_S^0 K_S^0 K_S^0)/\Gamma_{\text{total}}] \times [B(\psi(2S) \rightarrow \gamma \chi_{c2}(1P))]$ = $(10.8 \pm 1.5 \pm 0.8) \times 10^{-6}$ which we divide by our best value $B(\psi(2S) \rightarrow \gamma \chi_{c2}(1P)) = (9.52 \pm 0.20) \times 10^{-2}$. Our first error is their experiment's error and our second error is the systematic error from using our best value..

$\Gamma(K^+ K^- K^+ K^-)/\Gamma_{\text{total}}$		Γ_{51}/Γ
VALUE (units 10^{-3})	DOCUMENT ID	

1.65 ± 0.20 OUR FIT

$\Gamma(K^+ K^- \phi)/\Gamma_{\text{total}}$		Γ_{52}/Γ
VALUE (units 10^{-3})	EVTS	DOCUMENT ID

1.42 ± 0.29 ± 0.03 52 ¹ABLIKIM 06T BES2 $\psi(2S) \rightarrow \gamma 2K^+ 2K^-$
¹ABLIKIM 06T reports $(1.67 \pm 0.26 \pm 0.24) \times 10^{-3}$ from a measurement of $[\Gamma(\chi_{c2}(1P) \rightarrow K^+ K^- \phi)/\Gamma_{\text{total}}] \times [B(\psi(2S) \rightarrow \gamma \chi_{c2}(1P))]$ assuming $B(\psi(2S) \rightarrow \gamma \chi_{c2}(1P)) = (8.1 \pm 0.4) \times 10^{-2}$, which we rescale to our best value $B(\psi(2S) \rightarrow \gamma \chi_{c2}(1P)) = (9.52 \pm 0.20) \times 10^{-2}$. Our first error is their experiment's error and our second error is the systematic error from using our best value.

$\Gamma(K^0 K^+ \pi^- \phi + \text{c.c.})/\Gamma_{\text{total}}$		Γ_{53}/Γ
VALUE (units 10^{-3})	DOCUMENT ID	TECN

4.83 ± 0.32 ± 0.66 ABLIKIM 15M BES3 $\psi(2S) \rightarrow \gamma \chi_{c2}$

$\Gamma(K^+ K^- \pi^0 \phi)/\Gamma_{\text{total}}$		Γ_{54}/Γ
VALUE (units 10^{-3})	DOCUMENT ID	TECN

2.74 ± 0.16 ± 0.44 ABLIKIM 15M BES3 $\psi(2S) \rightarrow \gamma \chi_{c2}$

$\Gamma(\phi \pi^+ \pi^- \pi^0)/\Gamma_{\text{total}}$		Γ_{55}/Γ
VALUE (units 10^{-3})	EVTS	DOCUMENT ID

0.93 ± 0.06 ± 0.10 408 ¹ABLIKIM 13B BES3 $e^+ e^- \rightarrow \psi(2S) \rightarrow \gamma \chi_{c2}$
¹Using 1.06×10^8 $\psi(2S)$ mesons and $B(\psi(2S) \rightarrow \chi_{c2} \gamma) = (8.72 \pm 0.34)\%$.

$\Gamma(p\bar{p})/\Gamma_{\text{total}}$		Γ_{56}/Γ
VALUE (units 10^{-4})	DOCUMENT ID	

0.733 ± 0.033 OUR FIT

$\Gamma(p\bar{p}\pi^0)/\Gamma_{\text{total}}$		Γ_{57}/Γ
VALUE (units 10^{-3})	DOCUMENT ID	TECN

0.47 ± 0.04 OUR AVERAGE
 0.47 ± 0.04 ± 0.01 ¹ONYISI 10 CLE3 $\psi(2S) \rightarrow \gamma p\bar{p}\chi$
 0.43 ± 0.09 ± 0.01 ²ATHAR 07 CLEO $\psi(2S) \rightarrow \gamma h^+ h^- h^0$

¹ONYISI 10 reports $(4.83 \pm 0.25 \pm 0.35 \pm 0.31) \times 10^{-4}$ from a measurement of $[\Gamma(\chi_{c2}(1P) \rightarrow p\bar{p}\pi^0)/\Gamma_{\text{total}}] \times [B(\psi(2S) \rightarrow \gamma \chi_{c2}(1P))]$ assuming $B(\psi(2S) \rightarrow \gamma \chi_{c2}(1P)) = (9.33 \pm 0.14 \pm 0.61) \times 10^{-2}$, which we rescale to our best value $B(\psi(2S) \rightarrow \gamma \chi_{c2}(1P)) = (9.52 \pm 0.20) \times 10^{-2}$. Our first error is their experiment's error and our second error is the systematic error from using our best value.
²ATHAR 07 reports $(0.44 \pm 0.08 \pm 0.05) \times 10^{-3}$ from a measurement of $[\Gamma(\chi_{c2}(1P) \rightarrow p\bar{p}\pi^0)/\Gamma_{\text{total}}] \times [B(\psi(2S) \rightarrow \gamma \chi_{c2}(1P))]$ assuming $B(\psi(2S) \rightarrow \gamma \chi_{c2}(1P)) = (9.33 \pm 0.14 \pm 0.61) \times 10^{-2}$, which we rescale to our best value $B(\psi(2S) \rightarrow \gamma \chi_{c2}(1P)) = (9.52 \pm 0.20) \times 10^{-2}$. Our first error is their experiment's error and our second error is the systematic error from using our best value.

$\Gamma(p\bar{p}\eta)/\Gamma_{\text{total}}$		Γ_{58}/Γ
VALUE (units 10^{-3})	DOCUMENT ID	TECN

0.174 ± 0.025 OUR AVERAGE
 0.172 ± 0.026 ± 0.004 ¹ONYISI 10 CLE3 $\psi(2S) \rightarrow \gamma p\bar{p}\chi$
 0.186 ± 0.070 ± 0.004 ²ATHAR 07 CLEO $\psi(2S) \rightarrow \gamma h^+ h^- h^0$

¹ONYISI 10 reports $(1.76 \pm 0.23 \pm 0.14 \pm 0.11) \times 10^{-4}$ from a measurement of $[\Gamma(\chi_{c2}(1P) \rightarrow p\bar{p}\eta)/\Gamma_{\text{total}}] \times [B(\psi(2S) \rightarrow \gamma \chi_{c2}(1P))]$ assuming $B(\psi(2S) \rightarrow \gamma \chi_{c2}(1P)) = (9.33 \pm 0.14 \pm 0.61) \times 10^{-2}$, which we rescale to our best value $B(\psi(2S) \rightarrow \gamma \chi_{c2}(1P)) = (9.52 \pm 0.20) \times 10^{-2}$. Our first error is their experiment's error and our second error is the systematic error from using our best value.
²ATHAR 07 reports $(0.19 \pm 0.07 \pm 0.02) \times 10^{-3}$ from a measurement of $[\Gamma(\chi_{c2}(1P) \rightarrow p\bar{p}\eta)/\Gamma_{\text{total}}] \times [B(\psi(2S) \rightarrow \gamma \chi_{c2}(1P))]$ assuming $B(\psi(2S) \rightarrow \gamma \chi_{c2}(1P)) = (9.33 \pm 0.14 \pm 0.61) \times 10^{-2}$, which we rescale to our best value $B(\psi(2S) \rightarrow \gamma \chi_{c2}(1P)) = (9.52 \pm 0.20) \times 10^{-2}$. Our first error is their experiment's error and our second error is the systematic error from using our best value.

$\Gamma(p\bar{p}\omega)/\Gamma_{\text{total}}$		Γ_{59}/Γ
VALUE (units 10^{-3})	DOCUMENT ID	TECN

0.36 ± 0.04 ± 0.01 ¹ONYISI 10 CLE3 $\psi(2S) \rightarrow \gamma p\bar{p}\chi$
¹ONYISI 10 reports $(3.68 \pm 0.35 \pm 0.26 \pm 0.24) \times 10^{-4}$ from a measurement of $[\Gamma(\chi_{c2}(1P) \rightarrow p\bar{p}\omega)/\Gamma_{\text{total}}] \times [B(\psi(2S) \rightarrow \gamma \chi_{c2}(1P))]$ assuming $B(\psi(2S) \rightarrow \gamma \chi_{c2}(1P)) = (9.33 \pm 0.14 \pm 0.61) \times 10^{-2}$, which we rescale to our best value $B(\psi(2S) \rightarrow \gamma \chi_{c2}(1P)) = (9.52 \pm 0.20) \times 10^{-2}$. Our first error is their experiment's error and our second error is the systematic error from using our best value.

$\Gamma(p\bar{p}\phi)/\Gamma_{\text{total}}$		Γ_{60}/Γ
VALUE (units 10^{-3})	EVTS	DOCUMENT ID

2.8 ± 0.9 ± 0.1 24 ± 7 ¹ABLIKIM 11F BES3 $\psi(2S) \rightarrow \gamma p\bar{p}K^+ K^-$
¹ABLIKIM 11F reports $(3.04 \pm 0.85 \pm 0.43) \times 10^{-5}$ from a measurement of $[\Gamma(\chi_{c2}(1P) \rightarrow p\bar{p}\phi)/\Gamma_{\text{total}}] \times [B(\psi(2S) \rightarrow \gamma \chi_{c2}(1P))]$ assuming $B(\psi(2S) \rightarrow \gamma \chi_{c2}(1P)) = (8.74 \pm 0.35) \times 10^{-2}$, which we rescale to our best value $B(\psi(2S) \rightarrow \gamma \chi_{c2}(1P)) = (9.52 \pm 0.20) \times 10^{-2}$. Our first error is their experiment's error and our second error is the systematic error from using our best value.

$\Gamma(p\bar{p}\pi^+\pi^-)/\Gamma_{total}$ Γ_{61}/Γ

VALUE (units 10 ⁻³)	DOCUMENT ID	TECN	COMMENT
1.32 ± 0.34 OUR EVALUATION	Treating systematic error as correlated.		
1.3 ± 0.4 OUR AVERAGE	Error includes scale factor of 1.3.		
1.17 ± 0.19 ± 0.30	¹ BAI	99B BES	$\psi(2S) \rightarrow \gamma\chi_{c2}$
2.64 ± 1.03 ± 0.14	¹ TANENBAUM	78 MRK1	$\psi(2S) \rightarrow \gamma\chi_{c2}$

¹Rescaled by us using $B(\psi(2S) \rightarrow \gamma\chi_{c2}) = (8.3 \pm 0.4)\%$ and $B(\psi(2S) \rightarrow J/\psi(1S)\pi^+\pi^-) = (32.6 \pm 0.5)\%$. Multiplied by a factor of 2 to convert from $K_S^0 K^+\pi^-$ to $K^0 K^+\pi^-$ decay.

$\Gamma(p\bar{p}\pi^0\pi^0)/\Gamma_{total}$ Γ_{62}/Γ

VALUE (%)	EVTS	DOCUMENT ID	TECN	COMMENT
0.078 ± 0.023 ± 0.002	29.2	¹ HE	08B CLEO	$e^+e^- \rightarrow \gamma h^+ h^- h^0 h^0$

¹HE 08B reports $0.08 \pm 0.02 \pm 0.01 \pm 0.01\%$ from a measurement of $[\Gamma(\chi_{c2}(1P) \rightarrow p\bar{p}\pi^0\pi^0)/\Gamma_{total}] \times [B(\psi(2S) \rightarrow \gamma\chi_{c2}(1P))]$ assuming $B(\psi(2S) \rightarrow \gamma\chi_{c2}(1P)) = (9.33 \pm 0.14 \pm 0.61) \times 10^{-2}$, which we rescale to our best value $B(\psi(2S) \rightarrow \gamma\chi_{c2}(1P)) = (9.52 \pm 0.20) \times 10^{-2}$. Our first error is their experiment's error and our second error is the systematic error from using our best value.

$\Gamma(p\bar{p}K^+K^- \text{ (non-resonant)})/\Gamma_{total}$ Γ_{63}/Γ

VALUE (units 10 ⁻⁴)	EVTS	DOCUMENT ID	TECN	COMMENT
1.91 ± 0.32 ± 0.04	131 ± 12	¹ ABLIKIM	11F BES3	$\psi(2S) \rightarrow \gamma p\bar{p}K^+K^-$

¹ABLIKIM 11F reports $(2.08 \pm 0.19 \pm 0.30) \times 10^{-4}$ from a measurement of $[\Gamma(\chi_{c2}(1P) \rightarrow p\bar{p}K^+K^- \text{ (non-resonant)})/\Gamma_{total}] \times [B(\psi(2S) \rightarrow \gamma\chi_{c2}(1P))]$ assuming $B(\psi(2S) \rightarrow \gamma\chi_{c2}(1P)) = (8.74 \pm 0.35) \times 10^{-2}$, which we rescale to our best value $B(\psi(2S) \rightarrow \gamma\chi_{c2}(1P)) = (9.52 \pm 0.20) \times 10^{-2}$. Our first error is their experiment's error and our second error is the systematic error from using our best value.

$\Gamma(p\bar{p}K_S^0 K_S^0)/\Gamma_{total}$ Γ_{64}/Γ

VALUE (units 10 ⁻⁴)	CL%	DOCUMENT ID	TECN	COMMENT
<7.9	90	¹ ABLIKIM	06D BES2	$\psi(2S) \rightarrow \chi_{c2}\gamma$

¹Using $B(\psi(2S) \rightarrow \chi_{c2}\gamma) = (9.3 \pm 0.6)\%$.

$\Gamma(p\bar{p}\pi^-\pi^-)/\Gamma_{total}$ Γ_{65}/Γ

VALUE (units 10 ⁻⁴)	EVTS	DOCUMENT ID	TECN	COMMENT
8.5 ± 0.9 OUR AVERAGE				
8.4 ± 1.0 ± 0.2	3309	¹ ABLIKIM	12J BES3	$\psi(2S) \rightarrow \gamma p\bar{p}\pi^-\pi^-$
10.2 ± 3.4 ± 0.2		² ABLIKIM	06I BES2	$\psi(2S) \rightarrow \gamma p\pi^- X$

¹ABLIKIM 12J reports $[\Gamma(\chi_{c2}(1P) \rightarrow p\bar{p}\pi^-\pi^-)/\Gamma_{total}] \times [B(\psi(2S) \rightarrow \gamma\chi_{c2}(1P))] = (0.80 \pm 0.02 \pm 0.09) \times 10^{-4}$ which we divide by our best value $B(\psi(2S) \rightarrow \gamma\chi_{c2}(1P)) = (9.52 \pm 0.20) \times 10^{-2}$. Our first error is their experiment's error and our second error is the systematic error from using our best value.

²ABLIKIM 06I reports $[\Gamma(\chi_{c2}(1P) \rightarrow p\bar{p}\pi^-\pi^-)/\Gamma_{total}] \times [B(\psi(2S) \rightarrow \gamma\chi_{c2}(1P))] = (0.97 \pm 0.20 \pm 0.26) \times 10^{-4}$ which we divide by our best value $B(\psi(2S) \rightarrow \gamma\chi_{c2}(1P)) = (9.52 \pm 0.20) \times 10^{-2}$. Our first error is their experiment's error and our second error is the systematic error from using our best value.

$\Gamma(p\bar{p}n\pi^+)/\Gamma_{total}$ Γ_{66}/Γ

VALUE (units 10 ⁻⁴)	EVTS	DOCUMENT ID	TECN	COMMENT
8.9 ± 0.8 ± 0.2	3732	¹ ABLIKIM	12J BES3	$\psi(2S) \rightarrow \gamma p\bar{p}n\pi^+$

¹ABLIKIM 12J reports $[\Gamma(\chi_{c2}(1P) \rightarrow p\bar{p}n\pi^+)/\Gamma_{total}] \times [B(\psi(2S) \rightarrow \gamma\chi_{c2}(1P))] = (0.85 \pm 0.02 \pm 0.07) \times 10^{-4}$ which we divide by our best value $B(\psi(2S) \rightarrow \gamma\chi_{c2}(1P)) = (9.52 \pm 0.20) \times 10^{-2}$. Our first error is their experiment's error and our second error is the systematic error from using our best value.

$\Gamma(p\bar{p}\pi^-\pi^0)/\Gamma_{total}$ Γ_{67}/Γ

VALUE (units 10 ⁻⁴)	EVTS	DOCUMENT ID	TECN	COMMENT
21.7 ± 1.7 ± 0.5	2128	¹ ABLIKIM	12J BES3	$\psi(2S) \rightarrow \gamma p\bar{p}\pi^-\pi^0$

¹ABLIKIM 12J reports $[\Gamma(\chi_{c2}(1P) \rightarrow p\bar{p}\pi^-\pi^0)/\Gamma_{total}] \times [B(\psi(2S) \rightarrow \gamma\chi_{c2}(1P))] = (2.07 \pm 0.06 \pm 0.15) \times 10^{-4}$ which we divide by our best value $B(\psi(2S) \rightarrow \gamma\chi_{c2}(1P)) = (9.52 \pm 0.20) \times 10^{-2}$. Our first error is their experiment's error and our second error is the systematic error from using our best value.

$\Gamma(p\bar{p}n\pi^+\pi^0)/\Gamma_{total}$ Γ_{68}/Γ

VALUE (units 10 ⁻⁴)	EVTS	DOCUMENT ID	TECN	COMMENT
21.1 ± 1.8 ± 0.4	2352	¹ ABLIKIM	12J BES3	$\psi(2S) \rightarrow \gamma p\bar{p}n\pi^+\pi^0$

¹ABLIKIM 12J reports $[\Gamma(\chi_{c2}(1P) \rightarrow p\bar{p}n\pi^+\pi^0)/\Gamma_{total}] \times [B(\psi(2S) \rightarrow \gamma\chi_{c2}(1P))] = (2.01 \pm 0.06 \pm 0.16) \times 10^{-4}$ which we divide by our best value $B(\psi(2S) \rightarrow \gamma\chi_{c2}(1P)) = (9.52 \pm 0.20) \times 10^{-2}$. Our first error is their experiment's error and our second error is the systematic error from using our best value.

$\Gamma(\Lambda\bar{\Lambda})/\Gamma_{total}$ Γ_{69}/Γ

VALUE (units 10 ⁻⁴)	DOCUMENT ID
1.84 ± 0.15 OUR FIT	

$\Gamma(\Lambda\bar{\Lambda}\pi^+\pi^-)/\Gamma_{total}$ Γ_{70}/Γ

VALUE (units 10 ⁻⁵)	CL%	EVTS	DOCUMENT ID	TECN	COMMENT
125 ± 15 ± 3		371	¹ ABLIKIM	12I BES3	$\psi(2S) \rightarrow \gamma\Lambda\bar{\Lambda}\pi^+\pi^-$

• • • We do not use the following data for averages, fits, limits, etc. • • •

<350 90 ²ABLIKIM 06D BES2 $\psi(2S) \rightarrow \chi_{c2}\gamma$
¹ABLIKIM 12I reports $(137.0 \pm 7.6 \pm 15.7) \times 10^{-5}$ from a measurement of $[\Gamma(\chi_{c2}(1P) \rightarrow \Lambda\bar{\Lambda}\pi^+\pi^-)/\Gamma_{total}] \times [B(\psi(2S) \rightarrow \gamma\chi_{c2}(1P))]$ assuming $B(\psi(2S) \rightarrow \gamma\chi_{c2}(1P)) = (8.72 \pm 0.34) \times 10^{-2}$, which we rescale to our best value $B(\psi(2S) \rightarrow \gamma\chi_{c2}(1P)) = (9.52 \pm 0.20) \times 10^{-2}$. Our first error is their experiment's error and our second error is the systematic error from using our best value.
²Using $B(\psi(2S) \rightarrow \chi_{c2}\gamma) = (9.3 \pm 0.6)\%$.

$\Gamma(\Lambda\bar{\Lambda}\pi^+\pi^- \text{ (non-resonant)})/\Gamma_{total}$ Γ_{71}/Γ

VALUE (units 10 ⁻⁵)	EVTS	DOCUMENT ID	TECN	COMMENT
66 ± 15 ± 1	36	¹ ABLIKIM	12I BES3	$\psi(2S) \rightarrow \gamma\Lambda\bar{\Lambda}\pi^+\pi^-$

¹ABLIKIM 12I reports $(71.8 \pm 14.5 \pm 8.2) \times 10^{-5}$ from a measurement of $[\Gamma(\chi_{c2}(1P) \rightarrow \Lambda\bar{\Lambda}\pi^+\pi^- \text{ (non-resonant)})/\Gamma_{total}] \times [B(\psi(2S) \rightarrow \gamma\chi_{c2}(1P))]$ assuming $B(\psi(2S) \rightarrow \gamma\chi_{c2}(1P)) = (8.72 \pm 0.34) \times 10^{-2}$, which we rescale to our best value $B(\psi(2S) \rightarrow \gamma\chi_{c2}(1P)) = (9.52 \pm 0.20) \times 10^{-2}$. Our first error is their experiment's error and our second error is the systematic error from using our best value.

$\Gamma(\Sigma(1385)^+\bar{\Lambda}\pi^- + c.c.)/\Gamma_{total}$ Γ_{72}/Γ

VALUE (units 10 ⁻⁵)	CL%	DOCUMENT ID	TECN	COMMENT
<40	90	¹ ABLIKIM	12I BES3	$\psi(2S) \rightarrow \gamma\Sigma(1385)^+\bar{\Lambda}\pi^-$

¹ABLIKIM 12I reports $< 42 \times 10^{-5}$ from a measurement of $[\Gamma(\chi_{c2}(1P) \rightarrow \Sigma(1385)^+\bar{\Lambda}\pi^- + c.c.)/\Gamma_{total}] \times [B(\psi(2S) \rightarrow \gamma\chi_{c2}(1P))]$ assuming $B(\psi(2S) \rightarrow \gamma\chi_{c2}(1P)) = (8.72 \pm 0.34) \times 10^{-2}$, which we rescale to our best value $B(\psi(2S) \rightarrow \gamma\chi_{c2}(1P)) = 9.52 \times 10^{-2}$.

$\Gamma(\Sigma(1385)^-\bar{\Lambda}\pi^+ + c.c.)/\Gamma_{total}$ Γ_{73}/Γ

VALUE (units 10 ⁻⁵)	CL%	DOCUMENT ID	TECN	COMMENT
<60	90	¹ ABLIKIM	12I BES3	$\psi(2S) \rightarrow \gamma\Sigma(1385)^-\bar{\Lambda}\pi^+$

¹ABLIKIM 12I reports $< 61 \times 10^{-5}$ from a measurement of $[\Gamma(\chi_{c2}(1P) \rightarrow \Sigma(1385)^-\bar{\Lambda}\pi^+ + c.c.)/\Gamma_{total}] \times [B(\psi(2S) \rightarrow \gamma\chi_{c2}(1P))]$ assuming $B(\psi(2S) \rightarrow \gamma\chi_{c2}(1P)) = (8.72 \pm 0.34) \times 10^{-2}$, which we rescale to our best value $B(\psi(2S) \rightarrow \gamma\chi_{c2}(1P)) = 9.52 \times 10^{-2}$.

$\Gamma(K^+\bar{p}\Lambda + c.c.)/\Gamma_{total}$ Γ_{74}/Γ

VALUE (units 10 ⁻⁴)	EVTS	DOCUMENT ID	TECN	COMMENT
7.8 ± 0.5 OUR AVERAGE				
7.7 ± 0.5 ± 0.2	5k	^{1,2} ABLIKIM	13D BES3	$\psi(2S) \rightarrow \gamma\Lambda\bar{p}K^+$
8.3 ± 1.6 ± 0.2		³ ATHAR	07 CLEO	$\psi(2S) \rightarrow \gamma h^+ h^- h^0$

¹ABLIKIM 13D reports $(8.4 \pm 0.3 \pm 0.6) \times 10^{-4}$ from a measurement of $[\Gamma(\chi_{c2}(1P) \rightarrow K^+\bar{p}\Lambda + c.c.)/\Gamma_{total}] \times [B(\psi(2S) \rightarrow \gamma\chi_{c2}(1P))]$ assuming $B(\psi(2S) \rightarrow \gamma\chi_{c2}(1P)) = (8.72 \pm 0.34) \times 10^{-2}$, which we rescale to our best value $B(\psi(2S) \rightarrow \gamma\chi_{c2}(1P)) = (9.52 \pm 0.20) \times 10^{-2}$. Our first error is their experiment's error and our second error is the systematic error from using our best value.
²Using $B(\Lambda \rightarrow p\pi^-) = 63.9\%$.
³ATHAR 07 reports $(8.5 \pm 1.4 \pm 1.0) \times 10^{-4}$ from a measurement of $[\Gamma(\chi_{c2}(1P) \rightarrow K^+\bar{p}\Lambda + c.c.)/\Gamma_{total}] \times [B(\psi(2S) \rightarrow \gamma\chi_{c2}(1P))]$ assuming $B(\psi(2S) \rightarrow \gamma\chi_{c2}(1P)) = (9.33 \pm 0.14 \pm 0.61) \times 10^{-2}$, which we rescale to our best value $B(\psi(2S) \rightarrow \gamma\chi_{c2}(1P)) = (9.52 \pm 0.20) \times 10^{-2}$. Our first error is their experiment's error and our second error is the systematic error from using our best value.

$\Gamma(K^*(892)^+\bar{p}\Lambda + c.c.)/\Gamma_{total}$ Γ_{75}/Γ

VALUE (units 10 ⁻⁴)	EVTS	DOCUMENT ID	TECN	COMMENT
8.2 ± 1.1 ± 0.2	476	¹ ABLIKIM	19AU BES3	$\psi(2S) \rightarrow \gamma K^*\bar{p}\Lambda$

¹ABLIKIM 19AU reports $[\Gamma(\chi_{c2}(1P) \rightarrow K^*(892)^+\bar{p}\Lambda + c.c.)/\Gamma_{total}] \times [B(\psi(2S) \rightarrow \gamma\chi_{c2}(1P))] = (7.8 \pm 0.9 \pm 0.6) \times 10^{-5}$ which we divide by our best value $B(\psi(2S) \rightarrow \gamma\chi_{c2}(1P)) = (9.52 \pm 0.20) \times 10^{-2}$. Our first error is their experiment's error and our second error is the systematic error from using our best value.

$\Gamma(K^+\bar{p}\Lambda(1520) + c.c.)/\Gamma_{total}$ Γ_{76}/Γ

VALUE (units 10 ⁻⁴)	EVTS	DOCUMENT ID	TECN	COMMENT
2.8 ± 0.7 ± 0.1	79 ± 13	¹ ABLIKIM	11F BES3	$\psi(2S) \rightarrow \gamma p\bar{p}K^+K^-$

¹ABLIKIM 11F reports $(3.06 \pm 0.50 \pm 0.54) \times 10^{-4}$ from a measurement of $[\Gamma(\chi_{c2}(1P) \rightarrow K^+\bar{p}\Lambda(1520) + c.c.)/\Gamma_{total}] \times [B(\psi(2S) \rightarrow \gamma\chi_{c2}(1P))]$ assuming $B(\psi(2S) \rightarrow \gamma\chi_{c2}(1P)) = (8.74 \pm 0.35) \times 10^{-2}$, which we rescale to our best value $B(\psi(2S) \rightarrow \gamma\chi_{c2}(1P)) = (9.52 \pm 0.20) \times 10^{-2}$. Our first error is their experiment's error and our second error is the systematic error from using our best value.

$\Gamma(\Lambda(1520)\bar{\Lambda}(1520))/\Gamma_{total}$ Γ_{77}/Γ

VALUE (units 10 ⁻⁴)	EVTS	DOCUMENT ID	TECN	COMMENT
4.6 ± 1.4 ± 0.1	29 ± 7	¹ ABLIKIM	11F BES3	$\psi(2S) \rightarrow \gamma p\bar{p}K^+K^-$

¹ABLIKIM 11F reports $(5.05 \pm 1.29 \pm 0.93) \times 10^{-4}$ from a measurement of $[\Gamma(\chi_{c2}(1P) \rightarrow \Lambda(1520)\bar{\Lambda}(1520))/\Gamma_{total}] \times [B(\psi(2S) \rightarrow \gamma\chi_{c2}(1P))]$ assuming $B(\psi(2S) \rightarrow \gamma\chi_{c2}(1P)) = (8.74 \pm 0.35) \times 10^{-2}$, which we rescale to our best value $B(\psi(2S) \rightarrow \gamma\chi_{c2}(1P)) = (9.52 \pm 0.20) \times 10^{-2}$. Our first error is their experiment's error and our second error is the systematic error from using our best value.

Meson Particle Listings

 $\chi_{c2}(1P)$ $\Gamma(\Sigma^0 \bar{\Sigma}^0)/\Gamma_{\text{total}}$ Γ_{78}/Γ

VALUE (units 10^{-5})	CL%	EVTS	DOCUMENT ID	TECN	COMMENT
$3.7 \pm 0.6 \pm 0.1$		91	¹ ABLIKIM	18v BES3	$\psi(2S) \rightarrow \gamma \Sigma^0 \bar{\Sigma}^0$

• • • We do not use the following data for averages, fits, limits, etc. • • •

<6	90		² ABLIKIM	13h BES3	$\psi(2S) \rightarrow \gamma \Sigma^0 \bar{\Sigma}^0$
<7	90	7.5 ± 3.4	³ NAIK	08 CLEO	$\psi(2S) \rightarrow \gamma \Sigma^0 \bar{\Sigma}^0$

¹ ABLIKIM 18v reports $[\Gamma(\chi_{c2}(1P) \rightarrow \Sigma^0 \bar{\Sigma}^0)/\Gamma_{\text{total}}] \times [B(\psi(2S) \rightarrow \gamma \chi_{c2}(1P))] = (0.35 \pm 0.05 \pm 0.02) \times 10^{-5}$ which we divide by our best value $B(\psi(2S) \rightarrow \gamma \chi_{c2}(1P)) = (9.52 \pm 0.20) \times 10^{-2}$. Our first error is their experiment's error and our second error is the systematic error from using our best value.

² ABLIKIM 13h reports $< 0.65 \times 10^{-4}$ from a measurement of $[\Gamma(\chi_{c2}(1P) \rightarrow \Sigma^0 \bar{\Sigma}^0)/\Gamma_{\text{total}}] \times [B(\psi(2S) \rightarrow \gamma \chi_{c2}(1P))]$ assuming $B(\psi(2S) \rightarrow \gamma \chi_{c2}(1P)) = (8.74 \pm 0.35) \times 10^{-2}$, which we rescale to our best value $B(\psi(2S) \rightarrow \gamma \chi_{c2}(1P)) = 9.52 \times 10^{-2}$.

³ NAIK 08 reports $< 0.75 \times 10^{-4}$ from a measurement of $[\Gamma(\chi_{c2}(1P) \rightarrow \Sigma^0 \bar{\Sigma}^0)/\Gamma_{\text{total}}] \times [B(\psi(2S) \rightarrow \gamma \chi_{c2}(1P))]$ assuming $B(\psi(2S) \rightarrow \gamma \chi_{c2}(1P)) = (9.33 \pm 0.14 \pm 0.61) \times 10^{-2}$, which we rescale to our best value $B(\psi(2S) \rightarrow \gamma \chi_{c2}(1P)) = 9.52 \times 10^{-2}$.

 $\Gamma(\Sigma^+ \bar{\Sigma}^-)/\Gamma_{\text{total}}$ Γ_{80}/Γ

VALUE (units 10^{-5})	CL%	EVTS	DOCUMENT ID	TECN	COMMENT
$3.4 \pm 0.7 \pm 0.1$		55	¹ ABLIKIM	18v BES3	$\psi(2S) \rightarrow \gamma \Sigma^+ \bar{\Sigma}^-$

• • • We do not use the following data for averages, fits, limits, etc. • • •

<8	90		² ABLIKIM	13h BES3	$\psi(2S) \rightarrow \gamma \Sigma^+ \bar{\Sigma}^-$
<7	90	4.0 ± 3.5	³ NAIK	08 CLEO	$\psi(2S) \rightarrow \gamma \Sigma^+ \bar{\Sigma}^-$

¹ ABLIKIM 18v reports $[\Gamma(\chi_{c2}(1P) \rightarrow \Sigma^+ \bar{\Sigma}^-)/\Gamma_{\text{total}}] \times [B(\psi(2S) \rightarrow \gamma \chi_{c2}(1P))] = (0.32 \pm 0.06 \pm 0.03) \times 10^{-5}$ which we divide by our best value $B(\psi(2S) \rightarrow \gamma \chi_{c2}(1P)) = (9.52 \pm 0.20) \times 10^{-2}$. Our first error is their experiment's error and our second error is the systematic error from using our best value.

² ABLIKIM 13h reports $< 0.88 \times 10^{-4}$ from a measurement of $[\Gamma(\chi_{c2}(1P) \rightarrow \Sigma^+ \bar{\Sigma}^-)/\Gamma_{\text{total}}] \times [B(\psi(2S) \rightarrow \gamma \chi_{c2}(1P))]$ assuming $B(\psi(2S) \rightarrow \gamma \chi_{c2}(1P)) = (8.74 \pm 0.35) \times 10^{-2}$, which we rescale to our best value $B(\psi(2S) \rightarrow \gamma \chi_{c2}(1P)) = 9.52 \times 10^{-2}$.

³ NAIK 08 reports $< 0.67 \times 10^{-4}$ from a measurement of $[\Gamma(\chi_{c2}(1P) \rightarrow \Sigma^+ \bar{\Sigma}^-)/\Gamma_{\text{total}}] \times [B(\psi(2S) \rightarrow \gamma \chi_{c2}(1P))]$ assuming $B(\psi(2S) \rightarrow \gamma \chi_{c2}(1P)) = (9.33 \pm 0.14 \pm 0.61) \times 10^{-2}$, which we rescale to our best value $B(\psi(2S) \rightarrow \gamma \chi_{c2}(1P)) = 9.52 \times 10^{-2}$.

 $\Gamma(\Sigma(1385)^+ \bar{\Sigma}(1385)^-)/\Gamma_{\text{total}}$ Γ_{81}/Γ

VALUE (units 10^{-5})	CL%	DOCUMENT ID	TECN	COMMENT
<16	90	¹ ABLIKIM	12i BES3	$\psi(2S) \rightarrow \gamma \Sigma(1385)^+ \bar{\Sigma}(1385)^-$

¹ ABLIKIM 12i reports $< 17 \times 10^{-5}$ from a measurement of $[\Gamma(\chi_{c2}(1P) \rightarrow \Sigma(1385)^+ \bar{\Sigma}(1385)^-)/\Gamma_{\text{total}}] \times [B(\psi(2S) \rightarrow \gamma \chi_{c2}(1P))]$ assuming $B(\psi(2S) \rightarrow \gamma \chi_{c2}(1P)) = (8.72 \pm 0.34) \times 10^{-2}$, which we rescale to our best value $B(\psi(2S) \rightarrow \gamma \chi_{c2}(1P)) = 9.52 \times 10^{-2}$.

 $\Gamma(\Sigma(1385)^- \bar{\Sigma}(1385)^+)/\Gamma_{\text{total}}$ Γ_{82}/Γ

VALUE (units 10^{-5})	CL%	DOCUMENT ID	TECN	COMMENT
<8	90	¹ ABLIKIM	12i BES3	$\psi(2S) \rightarrow \gamma \Sigma(1385)^- \bar{\Sigma}(1385)^+$

¹ ABLIKIM 12i reports $< 8.5 \times 10^{-5}$ from a measurement of $[\Gamma(\chi_{c2}(1P) \rightarrow \Sigma(1385)^- \bar{\Sigma}(1385)^+)/\Gamma_{\text{total}}] \times [B(\psi(2S) \rightarrow \gamma \chi_{c2}(1P))]$ assuming $B(\psi(2S) \rightarrow \gamma \chi_{c2}(1P)) = (8.72 \pm 0.34) \times 10^{-2}$, which we rescale to our best value $B(\psi(2S) \rightarrow \gamma \chi_{c2}(1P)) = 9.52 \times 10^{-2}$.

 $\Gamma(K^- \Lambda \bar{\Sigma}^+ + \text{c.c.})/\Gamma_{\text{total}}$ Γ_{83}/Γ

VALUE (units 10^{-4})	EVTS	DOCUMENT ID	TECN	COMMENT
$1.76 \pm 0.32 \pm 0.04$	51	¹ ABLIKIM	15i BES3	$\psi(2S) \rightarrow \gamma K^- \Lambda \bar{\Sigma}^+ + \text{c.c.}$

¹ ABLIKIM 15i reports $[\Gamma(\chi_{c2}(1P) \rightarrow K^- \Lambda \bar{\Sigma}^+ + \text{c.c.})/\Gamma_{\text{total}}] \times [B(\psi(2S) \rightarrow \gamma \chi_{c2}(1P))] = (1.68 \pm 0.26 \pm 0.15) \times 10^{-5}$ which we divide by our best value $B(\psi(2S) \rightarrow \gamma \chi_{c2}(1P)) = (9.52 \pm 0.20) \times 10^{-2}$. Our first error is their experiment's error and our second error is the systematic error from using our best value.

 $\Gamma(\Xi^0 \bar{\Xi}^0)/\Gamma_{\text{total}}$ Γ_{84}/Γ

VALUE (units 10^{-4})	CL%	EVTS	DOCUMENT ID	TECN	COMMENT
<1.0	90	2.9 ± 1.7	¹ NAIK	08 CLEO	$\psi(2S) \rightarrow \gamma \Xi^0 \bar{\Xi}^0$

¹ NAIK 08 reports $< 1.06 \times 10^{-4}$ from a measurement of $[\Gamma(\chi_{c2}(1P) \rightarrow \Xi^0 \bar{\Xi}^0)/\Gamma_{\text{total}}] \times [B(\psi(2S) \rightarrow \gamma \chi_{c2}(1P))]$ assuming $B(\psi(2S) \rightarrow \gamma \chi_{c2}(1P)) = (9.33 \pm 0.14 \pm 0.61) \times 10^{-2}$, which we rescale to our best value $B(\psi(2S) \rightarrow \gamma \chi_{c2}(1P)) = 9.52 \times 10^{-2}$.

 $\Gamma(\Xi^- \bar{\Xi}^+)/\Gamma_{\text{total}}$ Γ_{85}/Γ

VALUE (units 10^{-4})	CL%	EVTS	DOCUMENT ID	TECN	COMMENT
$1.42 \pm 0.31 \pm 0.03$		29 ± 5	¹ NAIK	08 CLEO	$\psi(2S) \rightarrow \gamma \Xi^- \bar{\Xi}^+$

• • • We do not use the following data for averages, fits, limits, etc. • • •

< 3.7	90		² ABLIKIM	06d BES2	$\psi(2S) \rightarrow \chi_{c2} \gamma$
-------	----	--	----------------------	----------	---

¹ NAIK 08 reports $(1.45 \pm 0.30 \pm 0.15) \times 10^{-4}$ from a measurement of $[\Gamma(\chi_{c2}(1P) \rightarrow \Xi^- \bar{\Xi}^+)/\Gamma_{\text{total}}] \times [B(\psi(2S) \rightarrow \gamma \chi_{c2}(1P))]$ assuming $B(\psi(2S) \rightarrow \gamma \chi_{c2}(1P)) = (9.33 \pm 0.14 \pm 0.61) \times 10^{-2}$, which we rescale to our best value $B(\psi(2S) \rightarrow \gamma \chi_{c2}(1P)) = (9.52 \pm 0.20) \times 10^{-2}$. Our first error is their experiment's error and our second error is the systematic error from using our best value.

² Using $B(\psi(2S) \rightarrow \chi_{c2} \gamma) = (9.3 \pm 0.6)\%$.

 $\Gamma(J/\psi(1S) \pi^+ \pi^- \pi^0)/\Gamma_{\text{total}}$ Γ_{86}/Γ

VALUE	CL%	DOCUMENT ID	TECN	COMMENT
<0.015	90	BARATE	81 SPEC	190 GeV $\pi^- \text{Be} \rightarrow 2\pi 2\mu$

 $\Gamma(\pi^0 \eta_c)/\Gamma_{\text{total}}$ Γ_{87}/Γ

VALUE	CL%	DOCUMENT ID	TECN	COMMENT
< 3.2×10^{-3}	90	¹ ABLIKIM	15N BES3	$\psi(2S) e^+ e^- \rightarrow \gamma \pi^0 \eta_c$

¹ Using $B(\eta_c \rightarrow K_S^0 K^\pm \pi^\mp) \times B(K_S^0 \rightarrow \pi^+ \pi^-) \times B(\pi^0 \rightarrow \gamma\gamma) = (1.66 \pm 0.11) \times 10^{-2}$.

 $\Gamma(\eta_c(1S) \pi^+ \pi^-)/\Gamma_{\text{total}}$ Γ_{88}/Γ

VALUE	CL%	DOCUMENT ID	TECN	COMMENT
< 0.54×10^{-2}	90	^{1,2} ABLIKIM	13B BES3	$e^+ e^- \rightarrow \psi(2S) \rightarrow \gamma \chi_{c2}$

• • • We do not use the following data for averages, fits, limits, etc. • • •

< 1.2×10^{-2}	90	^{1,3} ABLIKIM	13B BES3	$e^+ e^- \rightarrow \psi(2S) \rightarrow \gamma \chi_{c2}$
------------------------	----	------------------------	----------	---

¹ Using $1.06 \times 10^8 \psi(2S)$ mesons and $B(\psi(2S) \rightarrow \chi_{c2} \gamma) = (8.72 \pm 0.34)\%$.

² From the $\eta_c \rightarrow K_S^0 K^\pm \pi^\mp$ decays.

³ From the $\eta_c \rightarrow K^+ K^- \pi^0$ decays.

 $\Gamma(\eta_c(1S) \pi^+ \pi^-)/\Gamma(K^0 K^+ \pi^- + \text{c.c.})$ Γ_{88}/Γ_{42}

VALUE	CL%	DOCUMENT ID	TECN	COMMENT
<16.4	90	¹ LEES	12AE BABR	$e^+ e^- \rightarrow e^+ e^- \pi^+ \pi^- \eta_c$

¹ We divided the reported limit by 2 to take into account the $K_L^0 K^+ \pi^-$ mode.

RADIATIVE DECAYS

 $\Gamma(\gamma J/\psi(1S))/\Gamma_{\text{total}}$ Γ_{89}/Γ

VALUE (units 10^{-2})	EVTS	DOCUMENT ID	TECN	COMMENT
19.0 ± 0.5		OUR FIT		

• • • We do not use the following data for averages, fits, limits, etc. • • •

18.64 ± 0.08 ± 1.69	1.0M	¹ ABLIKIM	17u BES3	$e^+ e^- \rightarrow \gamma X$
19.9 ± 0.5 ± 1.2		² ADAM	05A CLEO	$e^+ e^- \rightarrow \psi(2S) \rightarrow \gamma \chi_{c2}$

¹ Not independent from $B(\psi(2S) \rightarrow \gamma \chi_{c2}(1P))$ and the product $B(\psi(2S) \rightarrow \gamma \chi_{c2}(1P)) \times B(\chi_{c2}(1P) \rightarrow \gamma J/\psi(1S))$ also measured in ABLIKIM 17u.

² Uses $B(\psi(2S) \rightarrow \gamma \chi_{c2} \rightarrow \gamma J/\psi)$ from ADAM 05A and $B(\psi(2S) \rightarrow \gamma \chi_{c2})$ from ATHAR 04.

 $\Gamma(\gamma \rho^0)/\Gamma_{\text{total}}$ Γ_{90}/Γ

VALUE (units 10^{-6})	CL%	EVTS	DOCUMENT ID	TECN	COMMENT
<19	90	13 ± 11	¹ ABLIKIM	11E BES3	$\psi(2S) \rightarrow \gamma \rho^0$

• • • We do not use the following data for averages, fits, limits, etc. • • •

<40	90	17.2 ± 6.8	² BENNETT	08A CLEO	$\psi(2S) \rightarrow \gamma \rho^0$
-----	----	------------	----------------------	----------	--------------------------------------

¹ ABLIKIM 11E reports $< 20.8 \times 10^{-6}$ from a measurement of $[\Gamma(\chi_{c2}(1P) \rightarrow \gamma \rho^0)/\Gamma_{\text{total}}] \times [B(\psi(2S) \rightarrow \gamma \chi_{c2}(1P))]$ assuming $B(\psi(2S) \rightarrow \gamma \chi_{c2}(1P)) = (8.74 \pm 0.35) \times 10^{-2}$, which we rescale to our best value $B(\psi(2S) \rightarrow \gamma \chi_{c2}(1P)) = 9.52 \times 10^{-2}$.

² BENNETT 08A reports $< 50 \times 10^{-6}$ from a measurement of $[\Gamma(\chi_{c2}(1P) \rightarrow \gamma \rho^0)/\Gamma_{\text{total}}] \times [B(\psi(2S) \rightarrow \gamma \chi_{c2}(1P))]$ assuming $B(\psi(2S) \rightarrow \gamma \chi_{c2}(1P)) = (8.1 \pm 0.4) \times 10^{-2}$, which we rescale to our best value $B(\psi(2S) \rightarrow \gamma \chi_{c2}(1P)) = 9.52 \times 10^{-2}$.

 $\Gamma(\gamma \omega)/\Gamma_{\text{total}}$ Γ_{91}/Γ

VALUE (units 10^{-6})	CL%	EVTS	DOCUMENT ID	TECN	COMMENT
<6	90	1 ± 6	¹ ABLIKIM	11E BES3	$\psi(2S) \rightarrow \gamma \gamma \omega$

• • • We do not use the following data for averages, fits, limits, etc. • • •

<6	90	0.0 ± 1.8	² BENNETT	08A CLEO	$\psi(2S) \rightarrow \gamma \gamma \omega$
----	----	-----------	----------------------	----------	---

¹ ABLIKIM 11E reports $< 6.1 \times 10^{-6}$ from a measurement of $[\Gamma(\chi_{c2}(1P) \rightarrow \gamma \omega)/\Gamma_{\text{total}}] \times [B(\psi(2S) \rightarrow \gamma \chi_{c2}(1P))]$ assuming $B(\psi(2S) \rightarrow \gamma \chi_{c2}(1P)) = (8.74 \pm 0.35) \times 10^{-2}$, which we rescale to our best value $B(\psi(2S) \rightarrow \gamma \chi_{c2}(1P)) = 9.52 \times 10^{-2}$.

² BENNETT 08A reports $< 7.0 \times 10^{-6}$ from a measurement of $[\Gamma(\chi_{c2}(1P) \rightarrow \gamma \omega)/\Gamma_{\text{total}}] \times [B(\psi(2S) \rightarrow \gamma \chi_{c2}(1P))]$ assuming $B(\psi(2S) \rightarrow \gamma \chi_{c2}(1P)) = (8.1 \pm 0.4) \times 10^{-2}$, which we rescale to our best value $B(\psi(2S) \rightarrow \gamma \chi_{c2}(1P)) = 9.52 \times 10^{-2}$.

 $\Gamma(\gamma \phi)/\Gamma_{\text{total}}$ Γ_{92}/Γ

VALUE (units 10^{-6})	CL%	EVTS	DOCUMENT ID	TECN	COMMENT
< 7	90	5 ± 5	¹ ABLIKIM	11E BES3	$\psi(2S) \rightarrow \gamma \gamma \phi$

• • • We do not use the following data for averages, fits, limits, etc. • • •

<11	90	1.3 ± 2.5	² BENNETT	08A CLEO	$\psi(2S) \rightarrow \gamma \gamma \phi$
-----	----	-----------	----------------------	----------	---

¹ ABLIKIM 11E reports $< 8.1 \times 10^{-6}$ from a measurement of $[\Gamma(\chi_{c2}(1P) \rightarrow \gamma \phi)/\Gamma_{\text{total}}] \times [B(\psi(2S) \rightarrow \gamma \chi_{c2}(1P))]$ assuming $B(\psi(2S) \rightarrow \gamma \chi_{c2}(1P)) = (8.74 \pm 0.35) \times 10^{-2}$, which we rescale to our best value $B(\psi(2S) \rightarrow \gamma \chi_{c2}(1P)) = 9.52 \times 10^{-2}$.

² BENNETT 08A reports $< 13 \times 10^{-6}$ from a measurement of $[\Gamma(\chi_{c2}(1P) \rightarrow \gamma \phi)/\Gamma_{\text{total}}] \times [B(\psi(2S) \rightarrow \gamma \chi_{c2}(1P))]$ assuming $B(\psi(2S) \rightarrow \gamma \chi_{c2}(1P)) = (8.1 \pm 0.4) \times 10^{-2}$, which we rescale to our best value $B(\psi(2S) \rightarrow \gamma \chi_{c2}(1P)) = 9.52 \times 10^{-2}$.

 $\Gamma(\gamma \gamma)/\Gamma_{\text{total}}$ Γ_{93}/Γ

VALUE (units 10^{-4})	DOCUMENT ID
2.85 ± 0.10	OUR FIT

$\Gamma(e^+e^- J/\psi(1S))/\Gamma_{total}$		Γ_{94}/Γ	
VALUE (units 10^{-3})	EVTS	DOCUMENT ID	TECN COMMENT

••• We do not use the following data for averages, fits, limits, etc. •••

2.37±0.15±0.05 1.3k 1,2 ABLIKIM 17i BES3 $\psi(2S) \rightarrow \gamma e^+e^- J/\psi$

¹ ABLIKIM 17i reports $(2.48 \pm 0.08 \pm 0.16) \times 10^{-3}$ from a measurement of $[\Gamma(\chi_{c2}(1P) \rightarrow e^+e^- J/\psi(1S))/\Gamma_{total}] \times [B(\psi(2S) \rightarrow \gamma \chi_{c2}(1P))]$ assuming $B(\psi(2S) \rightarrow \gamma \chi_{c2}(1P)) = (9.11 \pm 0.31) \times 10^{-2}$, which we rescale to our best value $B(\psi(2S) \rightarrow \gamma \chi_{c2}(1P)) = (9.52 \pm 0.20) \times 10^{-2}$. Our first error is their experiment's error and our second error is the systematic error from using our best value.

² Not independent from other measurements reported by ABLIKIM 17i

$\Gamma(e^+e^- J/\psi(1S))/\Gamma(\gamma J/\psi(1S))$		Γ_{94}/Γ_{89}	
VALUE (units 10^{-3})	EVTS	DOCUMENT ID	TECN COMMENT

11.3±0.4±0.5 1.3k 1 ABLIKIM 17i BES3 $\psi(2S) \rightarrow e^+e^- \gamma J/\psi$

¹ Uses $B(\psi(2S) \rightarrow \gamma \chi_{c2}(1P)) \times B(\chi_{c2}(1P) \rightarrow \gamma J/\psi(1S)) = (199.6 \pm 0.8 \pm 7.0) \times 10^{-4}$ from ABLIKIM 17i and accounts for common systematic errors.

$\Gamma(\mu^+\mu^- J/\psi(1S))/\Gamma(e^+e^- J/\psi(1S))$		Γ_{95}/Γ_{94}	
VALUE (units 10^{-2})	EVTS	DOCUMENT ID	TECN COMMENT

9.40±0.79±1.15 219 ABLIKIM 19z BES3 $\psi(2S) \rightarrow \gamma \chi_{c2} \rightarrow \gamma(\mu^+\mu^- J/\psi)$

$\Gamma(\gamma\gamma)/\Gamma(\gamma J/\psi(1S))$		Γ_{93}/Γ_{89}	
VALUE (units 10^{-3})	EVTS	DOCUMENT ID	TECN COMMENT

1.50±0.05 OUR FIT
0.99±0.18

1 AMBROGIANI 00b E835 $\bar{p}p \rightarrow \chi_{c2} \rightarrow \gamma\gamma, \gamma J/\psi$

¹ Calculated by us using $B(J/\psi(1S) \rightarrow e^+e^-) = 0.0593 \pm 0.0010$.

$\Gamma(\gamma\gamma)/\Gamma_{total} \times \Gamma(\bar{p}\bar{p})/\Gamma_{total}$		$\Gamma_{93}/\Gamma \times \Gamma_{56}/\Gamma$	
VALUE (units 10^{-8})	EVTS	DOCUMENT ID	TECN COMMENT

2.09±0.13 OUR FIT
1.7 ± 0.4 OUR AVERAGE

1.60±0.42 ARMSTRONG 93 E760 $\bar{p}p \rightarrow \gamma\gamma X$
9.9 ± 4.5 BAGLIN 87b SPEC $\bar{p}p \rightarrow \gamma\gamma X$

$\chi_{c2}(1P)$ CROSS-PARTICLE BRANCHING RATIOS

$\Gamma(\chi_{c2}(1P) \rightarrow K^+K^-\pi^+\pi^-)/\Gamma_{total} \times \Gamma(\psi(2S) \rightarrow \gamma \chi_{c2}(1P))/\Gamma(\psi(2S) \rightarrow J/\psi(1S)\pi^+\pi^-)$		$\Gamma_{14}/\Gamma \times \Gamma_{155}^{\psi(2S)}/\Gamma_{11}^{\psi(2S)}$	
VALUE (units 10^{-3})	EVTS	DOCUMENT ID	TECN COMMENT

2.31±0.26 OUR FIT
2.5 ± 0.9 OUR AVERAGE Error includes scale factor of 2.3.

1.90±0.14±0.44 BAI 99b BES $\psi(2S) \rightarrow \gamma \chi_{c2}$
3.8 ± 0.67 1 TANENBAUM 78 MRK1 $\psi(2S) \rightarrow \gamma \chi_{c2}$

¹ The reported value is derived using $B(\psi(2S) \rightarrow \pi^+\pi^- J/\psi) \times B(J/\psi \rightarrow \ell^+\ell^-) = (4.6 \pm 0.7)\%$. Calculated by us using $B(J/\psi \rightarrow \ell^+\ell^-) = 0.1181 \pm 0.0020$.

$\Gamma(\chi_{c2}(1P) \rightarrow K^*(892)^0 \bar{K}^*(892)^0)/\Gamma_{total} \times \Gamma(\psi(2S) \rightarrow \gamma \chi_{c2}(1P))/\Gamma_{total}$		$\Gamma_{18}/\Gamma \times \Gamma_{155}^{\psi(2S)}/\Gamma_{155}^{\psi(2S)}$	
VALUE (units 10^{-4})	EVTS	DOCUMENT ID	TECN COMMENT

2.1 ± 0.4 OUR FIT
3.11±0.36±0.48

ABLIKIM 04h BES2 $\psi(2S) \rightarrow \gamma \chi_{c2}$

$\Gamma(\chi_{c2}(1P) \rightarrow \rho\bar{\rho})/\Gamma_{total} \times \Gamma(\psi(2S) \rightarrow \gamma \chi_{c2}(1P))/\Gamma(\psi(2S) \rightarrow J/\psi(1S)\pi^+\pi^-)$		$\Gamma_{56}/\Gamma \times \Gamma_{155}^{\psi(2S)}/\Gamma_{11}^{\psi(2S)}$	
VALUE (units 10^{-5})	EVTS	DOCUMENT ID	TECN COMMENT

2.01±0.09 OUR FIT
1.4 ± 1.1

1 BAI 98i BES $\psi(2S) \rightarrow \gamma \chi_{c2} \rightarrow \gamma \bar{\rho}\rho$

¹ Calculated by us. The value for $B(\chi_{c2} \rightarrow \rho\bar{\rho})$ reported in BAI 98i is derived using $B(\psi(2S) \rightarrow \gamma \chi_{c2}) = (7.8 \pm 0.8)\%$ and $B(\psi(2S) \rightarrow J/\psi(1S)\pi^+\pi^-) = (32.4 \pm 2.6)\%$ [BAI 98d].

$\Gamma(\chi_{c2}(1P) \rightarrow \rho\bar{\rho})/\Gamma_{total} \times \Gamma(\psi(2S) \rightarrow \gamma \chi_{c2}(1P))/\Gamma_{total}$		$\Gamma_{56}/\Gamma \times \Gamma_{155}^{\psi(2S)}/\Gamma_{155}^{\psi(2S)}$	
VALUE (units 10^{-6})	EVTS	DOCUMENT ID	TECN COMMENT

6.98±0.32 OUR FIT
7.1 ± 0.5 OUR AVERAGE Error includes scale factor of 1.2.

7.3 ± 0.4 ± 0.3 405 ABLIKIM 13v BES3 $\psi(2S) \rightarrow \gamma \rho\bar{\rho}$
7.2 ± 0.7 ± 0.4 121 ± 12 1 NAIK 08 CLEO $\psi(2S) \rightarrow \gamma \rho\bar{\rho}$
4.4 +1.6 ± 0.6 14.3 +5.2 -1.4 ± 0.6 BAI 04f BES $\psi(2S) \rightarrow \gamma \chi_{c2}(1P) \rightarrow \gamma \bar{\rho}\rho$

¹ Calculated by us. NAIK 08 reports $B(\chi_{c2} \rightarrow \rho\bar{\rho}) = (7.7 \pm 0.8 \pm 0.4 \pm 0.5) \times 10^{-5}$ using $B(\psi(2S) \rightarrow \gamma \chi_{c2}) = (9.33 \pm 0.14 \pm 0.61)\%$.

$\Gamma(\chi_{c2}(1P) \rightarrow \Lambda\bar{\Lambda})/\Gamma_{total} \times \Gamma(\psi(2S) \rightarrow \gamma \chi_{c2}(1P))/\Gamma_{total}$		$\Gamma_{69}/\Gamma \times \Gamma_{155}^{\psi(2S)}/\Gamma_{155}^{\psi(2S)}$	
VALUE (units 10^{-6})	EVTS	DOCUMENT ID	TECN COMMENT

17.5±1.3 OUR FIT
17.4±1.4 OUR AVERAGE

18.2±1.4±0.9 207 1 ABLIKIM 13h BES3 $\psi(2S) \rightarrow \gamma \Lambda\bar{\Lambda}$
15.9±2.1±1.0 71 ± 9 2 NAIK 08 CLEO $\psi(2S) \rightarrow \gamma \Lambda\bar{\Lambda}$

¹ Calculated by us. ABLIKIM 13h reports $B(\chi_{c2} \rightarrow \Lambda\bar{\Lambda}) = (20.8 \pm 1.6 \pm 2.3) \times 10^{-5}$ from a measurement of $B(\chi_{c2} \rightarrow \Lambda\bar{\Lambda}) \times B(\psi(2S) \rightarrow \gamma \chi_{c2})$ assuming $B(\psi(2S) \rightarrow \gamma \chi_{c2}) = (8.74 \pm 0.35)\%$.

² Calculated by us. NAIK 08 reports $B(\chi_{c2} \rightarrow \Lambda\bar{\Lambda}) = (17.0 \pm 2.2 \pm 1.1 \pm 1.1) \times 10^{-5}$ using $B(\psi(2S) \rightarrow \gamma \chi_{c2}) = (9.33 \pm 0.14 \pm 0.61)\%$.

$\Gamma(\chi_{c2}(1P) \rightarrow \Lambda\bar{\Lambda})/\Gamma_{total} \times \Gamma(\psi(2S) \rightarrow \gamma \chi_{c2}(1P))/\Gamma(\psi(2S) \rightarrow J/\psi(1S)\pi^+\pi^-)$		$\Gamma_{69}/\Gamma \times \Gamma_{155}^{\psi(2S)}/\Gamma_{11}^{\psi(2S)}$	
VALUE (units 10^{-5})	EVTS	DOCUMENT ID	TECN COMMENT

5.1±0.4 OUR FIT
7.1 +3.1 -2.9 ± 1.3 8.3 +3.7 -3.4 1 BAI 03E BES $\psi(2S) \rightarrow \gamma \Lambda\bar{\Lambda}$

¹ BAI 03E reports $[B(\chi_{c2} \rightarrow \Lambda\bar{\Lambda}) B(\psi(2S) \rightarrow \gamma \chi_{c2}) / B(\psi(2S) \rightarrow J/\psi\pi^+\pi^-)] \times [B^2(\Lambda \rightarrow \pi^-\rho) / B(J/\psi \rightarrow \rho\bar{\rho})] = (1.33 +0.59 -0.55 \pm 0.25)\%$. We calculate from this measurement the presented value using $B(\Lambda \rightarrow \pi^-\rho) = (63.9 \pm 0.5)\%$ and $B(J/\psi \rightarrow \rho\bar{\rho}) = (2.17 \pm 0.07) \times 10^{-3}$.

$\Gamma(\chi_{c2}(1P) \rightarrow \pi\pi)/\Gamma_{total} \times \Gamma(\psi(2S) \rightarrow \gamma \chi_{c2}(1P))/\Gamma_{total}$		$\Gamma_{25}/\Gamma \times \Gamma_{155}^{\psi(2S)}/\Gamma_{155}^{\psi(2S)}$	
VALUE (units 10^{-4})	EVTS	DOCUMENT ID	TECN COMMENT

2.12±0.08 OUR FIT
2.17±0.09 OUR AVERAGE

2.19±0.05±0.15 4.5k 1 ABLIKIM 10A BES3 $e^+e^- \rightarrow \psi(2S) \rightarrow \gamma \chi_{c2}$
2.23±0.06±0.10 2.5k 2 ASNER 09 CLEO $\psi(2S) \rightarrow \gamma \pi^+\pi^-$
1.90±0.08±0.20 0.8k 3 ASNER 09 CLEO $\psi(2S) \rightarrow \gamma \pi^0\pi^0$

¹ Calculated by us. ABLIKIM 10A reports $B(\chi_{c2} \rightarrow \pi^0\pi^0) = (0.88 \pm 0.02 \pm 0.06 \pm 0.04) \times 10^{-3}$ using $B(\psi(2S) \rightarrow \gamma \chi_{c2}) = (8.3 \pm 0.4)\%$. We have multiplied the $\pi^0\pi^0$ measurement by 3 to obtain $\pi\pi$.

² Calculated by us. ASNER 09 reports $B(\chi_{c2} \rightarrow \pi^+\pi^-) = (1.59 \pm 0.04 \pm 0.07 \pm 0.10) \times 10^{-3}$ using $B(\psi(2S) \rightarrow \gamma \chi_{c2}) = (9.33 \pm 0.14 \pm 0.61)\%$. We have multiplied the $\pi^+\pi^-$ measurement by 3/2 to obtain $\pi\pi$.

³ Calculated by us. ASNER 09 reports $B(\chi_{c2} \rightarrow \pi^0\pi^0) = (0.68 \pm 0.03 \pm 0.07 \pm 0.04) \times 10^{-3}$ using $B(\psi(2S) \rightarrow \gamma \chi_{c2}) = (9.33 \pm 0.14 \pm 0.61)\%$. We have multiplied the $\pi^0\pi^0$ measurement by 3 to obtain $\pi\pi$.

$\Gamma(\chi_{c2}(1P) \rightarrow \pi\pi)/\Gamma_{total} \times \Gamma(\psi(2S) \rightarrow \gamma \chi_{c2}(1P))/\Gamma(\psi(2S) \rightarrow J/\psi(1S)\pi^+\pi^-)$		$\Gamma_{25}/\Gamma \times \Gamma_{155}^{\psi(2S)}/\Gamma_{11}^{\psi(2S)}$	
VALUE (units 10^{-3})	EVTS	DOCUMENT ID	TECN COMMENT

0.612±0.023 OUR FIT
0.54 ± 0.06 OUR AVERAGE

0.66 ± 0.18 ± 0.37 21 ± 6 1 BAI 03c BES $\psi(2S) \rightarrow \gamma \pi^0\pi^0$
0.54 ± 0.05 ± 0.04 185 ± 16 2 BAI 98i BES $\psi(2S) \rightarrow \gamma \pi^+\pi^-$

¹ We have multiplied $\pi^0\pi^0$ measurement by 3 to obtain $\pi\pi$.

² Calculated by us. The value for $B(\chi_{c2} \rightarrow \pi^+\pi^-)$ reported by BAI 98i is derived using $B(\psi(2S) \rightarrow \gamma \chi_{c2}) = (7.8 \pm 0.8)\%$ and $B(\psi(2S) \rightarrow J/\psi\pi^+\pi^-) = (32.4 \pm 2.6)\%$ [BAI 98d]. We have multiplied $\pi^+\pi^-$ measurement by 3/2 to obtain $\pi\pi$.

$\Gamma(\chi_{c2}(1P) \rightarrow \eta\eta)/\Gamma_{total} \times \Gamma(\psi(2S) \rightarrow \gamma \chi_{c2}(1P))/\Gamma_{total}$		$\Gamma_{31}/\Gamma \times \Gamma_{155}^{\psi(2S)}/\Gamma_{155}^{\psi(2S)}$	
VALUE (units 10^{-4})	CL% EVTS	DOCUMENT ID	TECN COMMENT

0.52±0.04 OUR FIT
0.52±0.04 OUR AVERAGE

0.54±0.03±0.04 386 1 ABLIKIM 10A BES3 $e^+e^- \rightarrow \psi(2S) \rightarrow \gamma \chi_{c2}$
0.47±0.05±0.05 156 ASNER 09 CLEO $\psi(2S) \rightarrow \gamma \eta\eta$

••• We do not use the following data for averages, fits, limits, etc. •••

< 0.44 90 2 ADAMS 07 CLEO $\psi(2S) \rightarrow \gamma \chi_{c2}$
< 3 90 BAI 03c BES $\psi(2S) \rightarrow \gamma \eta\eta \rightarrow 5\gamma$
0.62±0.31±0.19 LEE 85 CBAL $\psi(2S) \rightarrow \text{photons}$

¹ Calculated by us. ABLIKIM 10A reports $B(\chi_{c2} \rightarrow \eta\eta) = (0.65 \pm 0.04 \pm 0.05 \pm 0.03) \times 10^{-3}$ using $B(\psi(2S) \rightarrow \gamma \chi_{c2}) = (8.3 \pm 0.4)\%$.

² Superseded by ASNER 09.

$\Gamma(\chi_{c2}(1P) \rightarrow K^+K^-)/\Gamma_{total} \times \Gamma(\psi(2S) \rightarrow \gamma \chi_{c2}(1P))/\Gamma_{total}$		$\Gamma_{32}/\Gamma \times \Gamma_{155}^{\psi(2S)}/\Gamma_{155}^{\psi(2S)}$	
VALUE (units 10^{-5})	EVTS	DOCUMENT ID	TECN COMMENT

9.6±0.6 OUR FIT
10.5±0.3±0.6 1.6k 1 ASNER 09 CLEO $\psi(2S) \rightarrow \gamma K^+K^-$

¹ Calculated by us. ASNER 09 reports $B(\chi_{c2} \rightarrow K^+K^-) = (1.13 \pm 0.03 \pm 0.06 \pm 0.07) \times 10^{-3}$ using $B(\psi(2S) \rightarrow \gamma \chi_{c2}) = (9.33 \pm 0.14 \pm 0.61)\%$.

Meson Particle Listings

$\chi_{c2}(1P)$

$$\Gamma(\chi_{c2}(1P) \rightarrow K^+ K^-) / \Gamma_{\text{total}} \times \Gamma(\psi(2S) \rightarrow \gamma \chi_{c2}(1P)) / \Gamma(\psi(2S) \rightarrow J/\psi(1S) \pi^+ \pi^-) / \Gamma_{\text{total}} \times \Gamma(\psi(2S) \rightarrow \gamma \chi_{c2}(1P)) / \Gamma(\psi(2S) \rightarrow J/\psi(1S) \pi^+ \pi^-)$$

VALUE (units 10^{-3})	EVTS	DOCUMENT ID	TECN	COMMENT
--------------------------	------	-------------	------	---------

0.276 ± 0.017 OUR FIT
0.190 ± 0.034 ± 0.019 115 ± 13 1 BAI 98i BES $\psi(2S) \rightarrow \gamma K^+ K^-$
 1 Calculated by us. The value for $B(\chi_{c2} \rightarrow K^+ K^-)$ reported by BAI 98i is derived using $B(\psi(2S) \rightarrow \gamma \chi_{c2}) = (7.8 \pm 0.8)\%$ and $B(\psi(2S) \rightarrow J/\psi \pi^+ \pi^-) = (32.4 \pm 2.6)\%$ [BAI 98d].

$$\Gamma(\chi_{c2}(1P) \rightarrow K_S^0 K_S^0) / \Gamma_{\text{total}} \times \Gamma(\psi(2S) \rightarrow \gamma \chi_{c2}(1P)) / \Gamma(\psi(2S) \rightarrow J/\psi(1S) \pi^+ \pi^-) / \Gamma_{\text{total}} \times \Gamma(\psi(2S) \rightarrow \gamma \chi_{c2}(1P)) / \Gamma(\psi(2S) \rightarrow J/\psi(1S) \pi^+ \pi^-)$$

VALUE (units 10^{-5})	EVTS	DOCUMENT ID	TECN	COMMENT
--------------------------	------	-------------	------	---------

5.0 ± 0.4 OUR FIT
5.0 ± 0.4 OUR AVERAGE
 4.9 ± 0.3 ± 0.3 373 ± 20 1 ASNER 09 CLEO $\psi(2S) \rightarrow \gamma K_S^0 K_S^0$
 5.72 ± 0.76 ± 0.63 65 ABLIKIM 05o BES2 $\psi(2S) \rightarrow \gamma K_S^0 K_S^0$
 1 Calculated by us. ASNER 09 reports $B(\chi_{c2} \rightarrow K_S^0 K_S^0) = (0.53 \pm 0.03 \pm 0.03 \pm 0.03) \times 10^{-3}$ using $B(\psi(2S) \rightarrow \gamma \chi_{c2}) = (9.33 \pm 0.14 \pm 0.61)\%$.

$$\Gamma(\chi_{c2}(1P) \rightarrow K_S^0 K_S^0) / \Gamma_{\text{total}} \times \Gamma(\psi(2S) \rightarrow \gamma \chi_{c2}(1P)) / \Gamma(\psi(2S) \rightarrow J/\psi(1S) \pi^+ \pi^-) / \Gamma_{\text{total}} \times \Gamma(\psi(2S) \rightarrow \gamma \chi_{c2}(1P)) / \Gamma(\psi(2S) \rightarrow J/\psi(1S) \pi^+ \pi^-)$$

VALUE (units 10^{-5})	DOCUMENT ID	TECN	COMMENT
--------------------------	-------------	------	---------

14.4 ± 1.1 OUR FIT
14.7 ± 4.1 ± 3.3 1 BAI 99b BES $\psi(2S) \rightarrow \gamma K_S^0 K_S^0$
 1 Calculated by us. The value of $B(\chi_{c2} \rightarrow K_S^0 K_S^0)$ reported by BAI 99b was derived using $B(\psi(2S) \rightarrow \gamma \chi_{c2}(1P)) = (7.8 \pm 0.8)\%$ and $B(\psi(2S) \rightarrow J/\psi \pi^+ \pi^-) = (32.4 \pm 2.6)\%$ [BAI 98d].

$$\Gamma(\chi_{c2}(1P) \rightarrow \bar{K}^0 K^+ \pi^- + \text{c.c.}) / \Gamma_{\text{total}} \times \Gamma(\psi(2S) \rightarrow \gamma \chi_{c2}(1P)) / \Gamma(\psi(2S) \rightarrow J/\psi(1S) \pi^+ \pi^-) / \Gamma_{\text{total}} \times \Gamma(\psi(2S) \rightarrow \gamma \chi_{c2}(1P)) / \Gamma(\psi(2S) \rightarrow J/\psi(1S) \pi^+ \pi^-)$$

VALUE (units 10^{-4})	EVTS	DOCUMENT ID	TECN	COMMENT
--------------------------	------	-------------	------	---------

1.22 ± 0.17 OUR FIT
1.15 ± 0.18 OUR AVERAGE
 1.21 ± 0.19 ± 0.09 37 1 ATHAR 07 CLEO $\psi(2S) \rightarrow \gamma K_S^0 K^{\pm} \pi^{\mp}$
 0.97 ± 0.32 ± 0.13 28 2 ABLIKIM 06R BES2 $\psi(2S) \rightarrow \gamma K_S^0 K^{\pm} \pi^{\mp}$
 1 Calculated by us. ATHAR 07 reports $B(\chi_{c2} \rightarrow \bar{K}^0 K^+ \pi^- + \text{c.c.}) = (1.3 \pm 0.2 \pm 0.1 \pm 0.1) \times 10^{-3}$ using $B(\psi(2S) \rightarrow \gamma \chi_{c2}) = (9.33 \pm 0.14 \pm 0.61)\%$.
 2 Calculated by us. ABLIKIM 06R reports $B(\chi_{c2} \rightarrow K_S^0 K^{\pm} \pi^{\mp}) = (0.6 \pm 0.2 \pm 0.1) \times 10^{-3}$ using $B(\psi(2S) \rightarrow \gamma \chi_{c2}) = (8.1 \pm 0.6)\%$. We have multiplied by 2 to obtain $\bar{K}^0 K^+ \pi^- + \text{c.c.}$ from $K_S^0 K^{\pm} \pi^{\mp}$.

$$\Gamma(\chi_{c2}(1P) \rightarrow 2(\pi^+ \pi^-)) / \Gamma_{\text{total}} \times \Gamma(\psi(2S) \rightarrow \gamma \chi_{c2}(1P)) / \Gamma(\psi(2S) \rightarrow J/\psi(1S) \pi^+ \pi^-) / \Gamma_{\text{total}} \times \Gamma(\psi(2S) \rightarrow \gamma \chi_{c2}(1P)) / \Gamma(\psi(2S) \rightarrow J/\psi(1S) \pi^+ \pi^-)$$

VALUE (units 10^{-3})	DOCUMENT ID	TECN	COMMENT
--------------------------	-------------	------	---------

2.79 ± 0.26 OUR FIT
3.1 ± 1.0 OUR AVERAGE Error includes scale factor of 2.5.
 2.3 ± 0.1 ± 0.5 1 BAI 99b BES $\psi(2S) \rightarrow \gamma \chi_{c2}$
 4.3 ± 0.6 2 TANENBAUM 78 MRK1 $\psi(2S) \rightarrow \gamma \chi_{c2}$
 1 Calculated by us. The value for $B(\chi_{c2} \rightarrow 2\pi^+ 2\pi^-)$ reported in BAI 99b is derived using $B(\psi(2S) \rightarrow \gamma \chi_{c2}) = (7.8 \pm 0.8)\%$ and $B(\psi(2S) \rightarrow J/\psi(1S) \pi^+ \pi^-) = (32.4 \pm 2.6)\%$ [BAI 98d].
 2 The value for $B(\psi(2S) \rightarrow \gamma \chi_{c2}) \times B(\chi_{c2} \rightarrow 2\pi^+ \pi^-)$ reported in TANENBAUM 78 is derived using $B(\psi(2S) \rightarrow J/\psi(1S) \pi^+ \pi^-) \times B(J/\psi(1S) \ell^+ \ell^-) = (4.6 \pm 0.7)\%$. Calculated by us using $B(J/\psi(1S) \rightarrow \ell^+ \ell^-) = 0.1181 \pm 0.0020$.

$$\Gamma(\chi_{c2}(1P) \rightarrow K^+ K^- K^+ K^-) / \Gamma_{\text{total}} \times \Gamma(\psi(2S) \rightarrow \gamma \chi_{c2}(1P)) / \Gamma(\psi(2S) \rightarrow J/\psi(1S) \pi^+ \pi^-) / \Gamma_{\text{total}} \times \Gamma(\psi(2S) \rightarrow \gamma \chi_{c2}(1P)) / \Gamma(\psi(2S) \rightarrow J/\psi(1S) \pi^+ \pi^-)$$

VALUE (units 10^{-4})	EVTS	DOCUMENT ID	TECN	COMMENT
--------------------------	------	-------------	------	---------

1.57 ± 0.19 OUR FIT
1.76 ± 0.16 ± 0.24 160 1 ABLIKIM 06T BES2 $\psi(2S) \rightarrow \gamma 2K^+ 2K^-$
 1 Calculated by us. The value of $B(\chi_{c2} \rightarrow 2K^+ 2K^-)$ reported by ABLIKIM 06T was derived using $B(\psi(2S) \rightarrow \gamma \chi_{c2}(1P)) = (8.1 \pm 0.4)\%$.

$$\Gamma(\chi_{c2}(1P) \rightarrow K^+ K^- K^+ K^-) / \Gamma_{\text{total}} \times \Gamma(\psi(2S) \rightarrow \gamma \chi_{c2}(1P)) / \Gamma(\psi(2S) \rightarrow J/\psi(1S) \pi^+ \pi^-) / \Gamma_{\text{total}} \times \Gamma(\psi(2S) \rightarrow \gamma \chi_{c2}(1P)) / \Gamma(\psi(2S) \rightarrow J/\psi(1S) \pi^+ \pi^-)$$

VALUE (units 10^{-4})	DOCUMENT ID	TECN	COMMENT
--------------------------	-------------	------	---------

4.5 ± 0.5 OUR FIT
3.6 ± 0.6 ± 0.6 1 BAI 99b BES $\psi(2S) \rightarrow \gamma 2K^+ 2K^-$
 1 Calculated by us. The value of $B(\chi_{c2} \rightarrow 2K^+ 2K^-)$ reported by BAI 99b was derived using $B(\psi(2S) \rightarrow \gamma \chi_{c2}(1P)) = (7.8 \pm 0.8)\%$ and $B(\psi(2S) \rightarrow J/\psi \pi^+ \pi^-) = (32.4 \pm 2.6)\%$ [BAI 98d].

$$\Gamma(\chi_{c2}(1P) \rightarrow \phi \phi) / \Gamma_{\text{total}} \times \Gamma(\psi(2S) \rightarrow \gamma \chi_{c2}(1P)) / \Gamma(\psi(2S) \rightarrow J/\psi(1S) \pi^+ \pi^-) / \Gamma_{\text{total}} \times \Gamma(\psi(2S) \rightarrow \gamma \chi_{c2}(1P)) / \Gamma(\psi(2S) \rightarrow J/\psi(1S) \pi^+ \pi^-)$$

VALUE (units 10^{-4})	EVTS	DOCUMENT ID	TECN	COMMENT
--------------------------	------	-------------	------	---------

1.01 ± 0.08 OUR FIT
0.98 ± 0.13 OUR AVERAGE Error includes scale factor of 1.3.
 0.94 ± 0.03 ± 0.10 849 1 ABLIKIM 11k BES3 $\psi(2S) \rightarrow \gamma$ hadrons
 1.38 ± 0.24 ± 0.23 41 2 ABLIKIM 06T BES2 $\psi(2S) \rightarrow \gamma 2K^+ 2K^-$
 1 Calculated by us. The value of $B(\chi_{c2} \rightarrow \phi \phi)$ reported by ABLIKIM 11k was derived using $B(\psi(2S) \rightarrow \gamma \chi_{c2}(1P)) = (8.74 \pm 0.35)\%$.
 2 Calculated by us. The value of $B(\chi_{c2} \rightarrow \phi \phi)$ reported by ABLIKIM 06T was derived using $B(\psi(2S) \rightarrow \gamma \chi_{c2}(1P)) = (8.1 \pm 0.4)\%$.

$$\Gamma(\chi_{c2}(1P) \rightarrow \phi \phi) / \Gamma_{\text{total}} \times \Gamma(\psi(2S) \rightarrow \gamma \chi_{c2}(1P)) / \Gamma(\psi(2S) \rightarrow J/\psi(1S) \pi^+ \pi^-) / \Gamma_{\text{total}} \times \Gamma(\psi(2S) \rightarrow \gamma \chi_{c2}(1P)) / \Gamma(\psi(2S) \rightarrow J/\psi(1S) \pi^+ \pi^-)$$

VALUE (units 10^{-4})	DOCUMENT ID	TECN	COMMENT
--------------------------	-------------	------	---------

2.92 ± 0.24 OUR FIT
4.8 ± 1.3 ± 1.3 1 BAI 99b BES $\psi(2S) \rightarrow \gamma 2K^+ 2K^-$
 1 Calculated by us. The value of $B(\chi_{c2} \rightarrow \phi \phi)$ reported by BAI 99b was derived using $B(\psi(2S) \rightarrow \gamma \chi_{c2}(1P)) = (7.8 \pm 0.8)\%$ and $B(\psi(2S) \rightarrow J/\psi \pi^+ \pi^-) = (32.4 \pm 2.6)\%$ [BAI 98d].

$$\Gamma(\chi_{c2}(1P) \rightarrow \Sigma^+ \bar{p} K_S^0 + \text{c.c.}) / \Gamma_{\text{total}} \times \Gamma(\psi(2S) \rightarrow \gamma \chi_{c2}(1P)) / \Gamma(\psi(2S) \rightarrow J/\psi(1S) \pi^+ \pi^-) / \Gamma_{\text{total}} \times \Gamma(\psi(2S) \rightarrow \gamma \chi_{c2}(1P)) / \Gamma(\psi(2S) \rightarrow J/\psi(1S) \pi^+ \pi^-)$$

VALUE (units 10^{-6})	EVTS	DOCUMENT ID	TECN	COMMENT
--------------------------	------	-------------	------	---------

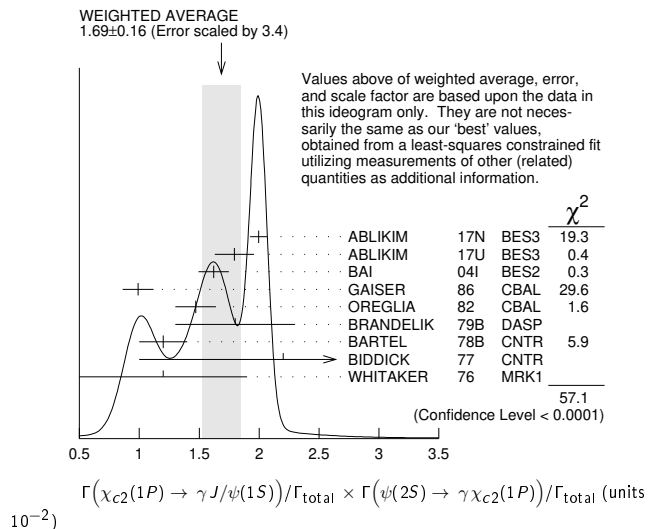
7.85 ± 0.77 ± 0.44 129 1 ABLIKIM 19bB BES3 $\psi(2S) \rightarrow \gamma \Sigma^+ \bar{p} K_S^0 + \text{c.c.}$
 1 Calculated by us. ABLIKIM 19bB reports $B(\chi_{c2} \rightarrow \Sigma^+ \bar{p} K_S^0 + \text{c.c.}) = (8.25 \pm 0.83 \pm 0.49) \times 10^{-5}$ using $B(\psi(2S) \rightarrow \gamma \chi_{c2}) = (9.52 \pm 0.20)\%$ and other branching fractions from PDG 18.

$$\Gamma(\chi_{c2}(1P) \rightarrow \gamma J/\psi(1S)) / \Gamma_{\text{total}} \times \Gamma(\psi(2S) \rightarrow \gamma \chi_{c2}(1P)) / \Gamma(\psi(2S) \rightarrow J/\psi(1S) \pi^+ \pi^-) / \Gamma_{\text{total}} \times \Gamma(\psi(2S) \rightarrow \gamma \chi_{c2}(1P)) / \Gamma(\psi(2S) \rightarrow J/\psi(1S) \pi^+ \pi^-)$$

VALUE (units 10^{-2})	EVTS	DOCUMENT ID	TECN	COMMENT
--------------------------	------	-------------	------	---------

1.81 ± 0.04 OUR FIT
1.69 ± 0.16 OUR AVERAGE Error includes scale factor of 3.4. See the ideogram below.
 1.996 ± 0.008 ± 0.070 81k 1 ABLIKIM 17N BES3 $\psi(2S) \rightarrow \gamma \gamma J/\psi$
 1.793 ± 0.008 ± 0.163 1.0M ABLIKIM 17U BES3 $e^+ e^- \rightarrow \gamma X$
 1.62 ± 0.04 ± 0.12 5.8k BAI 04i BES2 $\psi(2S) \rightarrow J/\psi \gamma \gamma$
 0.99 ± 0.10 ± 0.08 GAISER 86 CBAL $\psi(2S) \rightarrow \gamma X$
 1.47 ± 0.17 2 OREGLIA 82 CBAL $\psi(2S) \rightarrow \gamma \chi_{c2}$
 1.8 ± 0.5 3 BRANDELIK 79B DASP $\psi(2S) \rightarrow \gamma \chi_{c2}$
 1.2 ± 0.2 3 BARTEL 78B CNTR $\psi(2S) \rightarrow \gamma \chi_{c2}$
 2.2 ± 1.2 4 BIDDICK 77 CNTR $e^+ e^- \rightarrow \gamma X$
 1.2 ± 0.7 2 WHITAKER 76 MRK1 $e^+ e^-$
 • • • We do not use the following data for averages, fits, limits, etc. • • •
 1.874 ± 0.007 ± 0.102 76k 5 ABLIKIM 12o BES3 $\psi(2S) \rightarrow \gamma \chi_{c2}$
 1.95 ± 0.02 ± 0.07 12.4k 6 MENDEZ 08 CLEO $\psi(2S) \rightarrow \gamma \chi_{c2}$
 1.85 ± 0.04 ± 0.07 1.9k 7 ADAM 05A CLEO Repl. by MENDEZ 08

1 Uses $B(J/\psi \rightarrow e^+ e^-) = (5.971 \pm 0.032)\%$ and $B(J/\psi \rightarrow \mu^+ \mu^-) = (5.961 \pm 0.033)\%$.
 2 Recalculated by us using $B(J/\psi(1S) \rightarrow \ell^+ \ell^-) = 0.1181 \pm 0.0020$.
 3 Recalculated by us using $B(J/\psi(1S) \rightarrow \mu^+ \mu^-) = 0.0588 \pm 0.0010$.
 4 Assumes isotropic gamma distribution.
 5 Superseded by ABLIKIM 17N.
 6 Not independent from other measurements of MENDEZ 08.
 7 Not independent from other values reported by ADAM 05A.



$$\Gamma(\chi_{c2}(1P) \rightarrow \gamma J/\psi(1S))/\Gamma_{\text{total}} \times \Gamma(\psi(2S) \rightarrow \gamma \chi_{c2}(1P))/\Gamma(\psi(2S) \rightarrow J/\psi(1S) \text{ anything})$$

$$\frac{\Gamma_{89}/\Gamma \times \Gamma_{155}^{\psi(2S)}/\Gamma_9^{\psi(2S)}}{\Gamma_{89}/\Gamma \times \Gamma_{155}^{\psi(2S)}/\Gamma_9^{\psi(2S)} + \Gamma_{11}^{\psi(2S)} + \Gamma_{12}^{\psi(2S)} + \Gamma_{13}^{\psi(2S)} + 0.343\Gamma_{154}^{\psi(2S)} + 0.190\Gamma_{155}^{\psi(2S)}}$$

VALUE (units 10^{-2})	EVTS	DOCUMENT ID	TECN	COMMENT
2.95 ± 0.06 OUR FIT				
• • • We do not use the following data for averages, fits, limits, etc. • • •				
3.12 ± 0.03 ± 0.09	12.4k	¹ MENDEZ	08 CLEO	$\psi(2S) \rightarrow \gamma \chi_{c2}$
3.11 ± 0.07 ± 0.07	1.9k	ADAM	05A CLEO	Repl. by MENDEZ 08
¹ Not independent from other measurements of MENDEZ 08.				

$$\Gamma(\chi_{c2}(1P) \rightarrow \gamma J/\psi(1S))/\Gamma_{\text{total}} \times \Gamma(\psi(2S) \rightarrow \gamma \chi_{c2}(1P))/\Gamma(\psi(2S) \rightarrow J/\psi(1S) \pi^+ \pi^-)$$

$$\frac{\Gamma_{89}/\Gamma \times \Gamma_{155}^{\psi(2S)}/\Gamma_{11}^{\psi(2S)}}{\Gamma_{89}/\Gamma \times \Gamma_{155}^{\psi(2S)}/\Gamma_{11}^{\psi(2S)} + \Gamma_{11}^{\psi(2S)}}$$

VALUE (units 10^{-2})	EVTS	DOCUMENT ID	TECN	COMMENT
5.22 ± 0.11 OUR FIT				
5.53 ± 0.17 OUR AVERAGE				
5.56 ± 0.05 ± 0.16	12.4k	MENDEZ	08 CLEO	$\psi(2S) \rightarrow \gamma \chi_{c2}$
6.0 ± 2.8	1.3k	¹ ABLIKIM	04B BES	$\psi(2S) \rightarrow J/\psi X$
3.9 ± 1.2		² HIMEL	80 MRK2	$\psi(2S) \rightarrow \gamma \chi_{c2}$
• • • We do not use the following data for averages, fits, limits, etc. • • •				
5.52 ± 0.13 ± 0.13	1.9k	³ ADAM	05A CLEO	Repl. by MENDEZ 08

¹ From a fit to the J/ψ recoil mass spectra.
² The value for $B(\psi(2S) \rightarrow \gamma \chi_{c2}) \times B(\chi_{c2} \rightarrow \gamma J/\psi(1S))$ reported in HIMEL 80 is derived using $B(\psi(2S) \rightarrow J/\psi(1S) \pi^+ \pi^-) = (33 \pm 3)\%$ and $B(J/\psi(1S) \rightarrow \ell^+ \ell^-) = 0.138 \pm 0.018$. Calculated by us using $B(J/\psi(1S) \rightarrow \ell^+ \ell^-) = (0.1181 \pm 0.0020)$.
³ Not independent from other values reported by ADAM 05A.

$$\Gamma(\chi_{c2}(1P) \rightarrow \gamma \gamma)/\Gamma_{\text{total}} \times \Gamma(\psi(2S) \rightarrow \gamma \chi_{c2}(1P))/\Gamma_{\text{total}}$$

$$\frac{\Gamma_{93}/\Gamma \times \Gamma_{155}^{\psi(2S)}/\Gamma_{\psi(2S)}}{\Gamma_{93}/\Gamma \times \Gamma_{155}^{\psi(2S)}/\Gamma_{\psi(2S)} + \Gamma_{\psi(2S)}}$$

VALUE (units 10^{-5})	EVTS	DOCUMENT ID	TECN	COMMENT
2.71 ± 0.08 OUR FIT				
2.82 ± 0.10 OUR AVERAGE				
2.83 ± 0.08 ± 0.06	5k	¹ ABLIKIM	17AE BES3	$\psi(2S) \rightarrow \gamma \chi_{c2} \rightarrow 3\gamma$
2.68 ± 0.28 ± 0.15	0.3k	ECKLUND	08A CLEO	$\psi(2S) \rightarrow \gamma \chi_{c2} \rightarrow 3\gamma$
7.0 ± 2.1 ± 2.0		LEE	85 CBAL	$\psi(2S) \rightarrow \gamma \chi_{c2}$
• • • We do not use the following data for averages, fits, limits, etc. • • •				
2.81 ± 0.17 ± 0.15	1.1k	² ABLIKIM	12A BES3	$\psi(2S) \rightarrow \gamma \chi_{c2} \rightarrow 3\gamma$

¹ ABLIKIM 17AE measures the ratio of two-photon partial widths for the helicity $\lambda = 0$ and helicity $\lambda = 2$ components to be $f_{0/2} = \Gamma_{\gamma\gamma}^{\lambda=0} / \Gamma_{\gamma\gamma}^{\lambda=2} = 0.000 \pm 0.006 \pm 0.012$.
² ABLIKIM 12A measures the ratio of two-photon partial widths for the helicity $\lambda = 0$ and helicity $\lambda = 2$ components to be $f_{0/2} = \Gamma_{\gamma\gamma}^{\lambda=0} / \Gamma_{\gamma\gamma}^{\lambda=2} = 0.00 \pm 0.02 \pm 0.02$. Superseded by ABLIKIM 17AE.

$$\Gamma(\chi_{c2}(1P) \rightarrow \gamma \gamma)/\Gamma(\chi_{c0}(1P) \rightarrow \gamma \gamma)$$

$$\frac{\Gamma_{93}/\Gamma_{93}^{\chi_{c0}(1P)}}{\Gamma_{93}/\Gamma_{93}^{\chi_{c0}(1P)}}$$

VALUE	EVTS	DOCUMENT ID	TECN	COMMENT
0.292 ± 0.028 OUR AVERAGE				
0.295 ± 0.014 ± 0.028	8k	¹ ABLIKIM	17AE BES3	$\psi(2S) \rightarrow \gamma \chi_{cJ} \rightarrow 3\gamma$
0.278 ± 0.050 ± 0.036	0.5k	¹ ECKLUND	08A CLEO	$\psi(2S) \rightarrow \gamma \chi_{cJ} \rightarrow 3\gamma$
• • • We do not use the following data for averages, fits, limits, etc. • • •				
0.271 ± 0.029 ± 0.030	1.9k	^{1,2} ABLIKIM	12A BES3	$\psi(2S) \rightarrow \gamma \chi_{cJ} \rightarrow 3\gamma$

¹ Not independent from the values of $\Gamma(\chi_{c0}, \chi_{c2})$ and $B(\psi(2S) \rightarrow \chi_{c0}, \chi_{c2})$.
² Superseded by ABLIKIM 17AE.

MULTIPOLE AMPLITUDES IN $\chi_{c2}(1P) \rightarrow \gamma J/\psi(1S)$ RADIATIVE DECAY

$a_2 = M_2/\sqrt{E_1^2 + M_2^2 + E_3^2}$ Magnetic quadrupole fractional transition amplitude

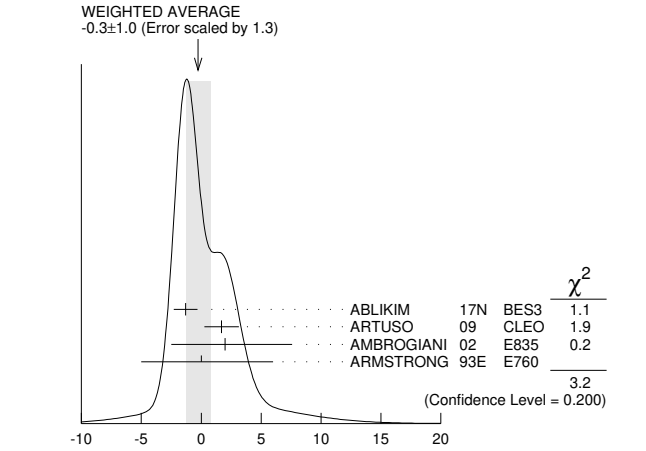
VALUE (units 10^{-2})	EVTS	DOCUMENT ID	TECN	COMMENT
-11.0 ± 1.0 OUR AVERAGE				
-12.0 ± 1.3 ± 0.4	89k	¹ ABLIKIM	17N BES3	$\psi(2S) \rightarrow \gamma \gamma \ell^+ \ell^-$
-9.3 ± 1.6 ± 0.3	19.8k	² ARTUSO	09 CLEO	$\psi(2S) \rightarrow \gamma \gamma \ell^+ \ell^-$
-9.3 ± 3.9 ± 0.6	5.9k	³ AMBROGIANI	02 E835	$p\bar{p} \rightarrow \chi_{c2} \rightarrow J/\psi \gamma$
-14 ± 6	1.9k	³ ARMSTRONG	93E E760	$p\bar{p} \rightarrow \chi_{c2} \rightarrow J/\psi \gamma$
-33.3 ± 11.6 ± 29.2	441	³ OREGLIA	82 CBAL	$\psi(2S) \rightarrow \chi_{c1} \gamma \rightarrow J/\psi \gamma \gamma$

• • • We do not use the following data for averages, fits, limits, etc. • • •
 -7.9 ± 1.9 ± 0.3 19.8k ⁴ ARTUSO 09 CLEO $\psi(2S) \rightarrow \gamma \gamma \ell^+ \ell^-$
¹ Correlated with $a_3, b_2,$ and b_3 with correlation coefficients $\rho_{a_2 a_3} = 0.733, \rho_{a_2 b_2} = -0.605,$ and $\rho_{a_2 b_3} = -0.095$.
² From a fit with floating M_2 amplitudes a_2 and $b_2,$ and fixed E_3 amplitudes $a_3 = b_3 = 0$.
³ Assuming $a_3 = 0$.
⁴ From a fit with floating M_2 and E_3 amplitudes $a_2, b_2,$ and $a_3,$ and b_3 .

$a_3 = E_3/\sqrt{E_1^2 + M_2^2 + E_3^2}$ Electric octupole fractional transition amplitude

VALUE (units 10^{-2})	EVTS	DOCUMENT ID	TECN	COMMENT
-0.3 ± 1.0 OUR AVERAGE				Error includes scale factor of 1.3. See the ideogram below.
-1.3 ± 0.9 ± 0.4	89k	¹ ABLIKIM	17N BES3	$\psi(2S) \rightarrow \gamma \gamma \ell^+ \ell^-$
1.7 ± 1.4 ± 0.3	19.8k	² ARTUSO	09 CLEO	$\psi(2S) \rightarrow \gamma \gamma \ell^+ \ell^-$
2.0 ± 5.5 ± 4.4 ± 0.9	5908	AMBROGIANI	02 E835	$p\bar{p} \rightarrow \chi_{c2} \rightarrow J/\psi \gamma$
0 ± 6	1904	ARMSTRONG	93E E760	$p\bar{p} \rightarrow \chi_{c2} \rightarrow J/\psi \gamma$

¹ Correlated with $a_2, b_2,$ and b_3 with correlation coefficients $\rho_{a_2 a_3} = 0.733, \rho_{a_3 b_2} = -0.422,$ and $\rho_{a_3 b_3} = -0.024$.
² From a fit with floating M_2 and E_3 amplitudes $a_2, b_2,$ and $a_3,$ and b_3 .



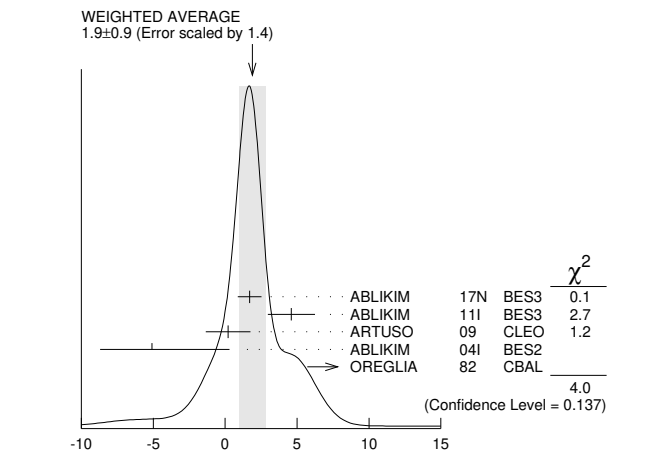
$a_3 = E_3/\sqrt{E_1^2 + M_2^2 + E_3^2}$ Electric octupole fractional transition amplitude (units 10^{-2})

MULTIPOLE AMPLITUDES IN $\psi(2S) \rightarrow \gamma \chi_{c2}(1P)$ RADIATIVE DECAY

$b_2 = M_2/\sqrt{E_1^2 + M_2^2 + E_3^2}$ Magnetic quadrupole fractional transition amplitude

VALUE (units 10^{-2})	EVTS	DOCUMENT ID	TECN	COMMENT
1.9 ± 0.9 OUR AVERAGE				Error includes scale factor of 1.4. See the ideogram below.
1.7 ± 0.8 ± 0.2	89k	¹ ABLIKIM	17N BES3	$\psi(2S) \rightarrow \gamma \gamma \ell^+ \ell^-$
4.6 ± 1.0 ± 1.3	13.8k	² ABLIKIM	11I BES3	$\psi(2S) \rightarrow \gamma \pi^+ \pi^-, \gamma K^+ K^-$
0.2 ± 1.5 ± 0.4	19.8k	³ ARTUSO	09 CLEO	$\psi(2S) \rightarrow \gamma \gamma \ell^+ \ell^-$
-5.1 ± 5.4 ± 3.6	721	² ABLIKIM	04I BES2	$\psi(2S) \rightarrow \gamma \pi^+ \pi^-, \gamma K^+ K^-$
13.2 ± 9.8 ± 7.5	441	⁴ OREGLIA	82 CBAL	$\psi(2S) \rightarrow \gamma \gamma \ell^+ \ell^-$

• • • We do not use the following data for averages, fits, limits, etc. • • •
 1.0 ± 1.3 ± 0.3 19.8k ⁴ ARTUSO 09 CLEO $\psi(2S) \rightarrow \gamma \gamma \ell^+ \ell^-$
¹ Correlated with $a_2, a_3,$ and b_3 with correlation coefficients $\rho_{a_2 b_2} = -0.605, \rho_{a_3 b_2} = -0.422,$ and $\rho_{b_2 b_3} = 0.384$.
² From a fit with floating M_2 and E_3 amplitudes b_2 and b_3 .
³ From a fit with floating M_2 and E_3 amplitudes $a_2, b_2,$ and $a_3,$ and b_3 .
⁴ From a fit with floating M_2 amplitudes a_2 and $b_2,$ and fixed E_3 amplitudes $a_3 = b_3 = 0$.



$b_2 = M_2/\sqrt{E_1^2 + M_2^2 + E_3^2}$ Magnetic quadrupole fractional transition amplitude (units 10^{-2})

Meson Particle Listings

$\chi_{c2}(1P), \eta_c(2S)$

$b_3 = E3/\sqrt{E1^2 + M2^2 + E3^2}$ Electric octupole fractional transition amplitude

VALUE (units 10^{-2})	EVTS	DOCUMENT ID	TECN	COMMENT
-1.0 ± 0.6	OUR AVERAGE			
$-1.4 \pm 0.7 \pm 0.4$	89k	1 ABLIKIM 17N BES3		$\psi(2S) \rightarrow \gamma\gamma\ell^+\ell^-$
$1.5 \pm 0.8 \pm 1.8$	13.8k	2 ABLIKIM 111 BES3		$\psi(2S) \rightarrow \gamma\pi^+\pi^-, \gamma K^+ K^-$
$-0.8 \pm 1.2 \pm 0.2$	19.8k	ARTUSO 09 CLEO		$\psi(2S) \rightarrow \gamma\gamma\ell^+\ell^-$
$-2.7^{+4.3}_{-2.9}$	721	2 ABLIKIM 041 BES2		$\psi(2S) \rightarrow \gamma\pi^+\pi^-, \gamma K^+ K^-$

¹ Correlated with $a_2, a_3,$ and b_2 with correlation coefficients $\rho_{a_2 b_3} = -0.095, \rho_{a_3 b_3} = -0.024,$ and $\rho_{b_2 b_3} = 0.384.$

² From a fit with floating $M2$ and $E3$ amplitudes b_2 and $b_3.$

MULTIPOLE AMPLITUDE RATIOS IN RADIATIVE DECAYS $\psi(2S) \rightarrow \gamma\chi_{c2}(1P)$ and $\chi_{c2} \rightarrow \gamma J/\psi(1S)$

b_2/a_2 Magnetic quadrupole transition amplitude ratio

VALUE (units 10^{-2})	EVTS	DOCUMENT ID	TECN	COMMENT
-11^{+14}_{-15}	19.8k	1 ARTUSO 09	CLEO	$\psi(2S) \rightarrow \gamma\gamma\ell^+\ell^-$

¹ Statistical and systematic errors combined. From a fit with floating $M2$ amplitudes a_2 and $b_2,$ and fixed $E3$ amplitudes $a_3 = b_3 = 0.$ Not independent of values for $a_2(\chi_{c2}(1P))$ and $b_2(\chi_{c2}(1P))$ from ARTUSO 09.

$\chi_{c2}(1P)$ REFERENCES

ABLIKIM	20B	PR D101 012012	M. Ablikim et al.	(BESIII Collab.)
ABLIKIM	19AA	PR D99 052008	M. Ablikim et al.	(BESIII Collab.)
ABLIKIM	19AU	PR D100 052010	M. Ablikim et al.	(BESIII Collab.)
ABLIKIM	19BB	PR D100 092006	M. Ablikim et al.	(BESIII Collab.)
ABLIKIM	19J	PR D99 012015	M. Ablikim et al.	(BESIII Collab.)
ABLIKIM	19Z	PR D99 051101	M. Ablikim et al.	(BESIII Collab.)
ABLIKIM	18V	PR D97 052011	M. Ablikim et al.	(BESIII Collab.)
PDG	18	PR D98 030001	M. Tanabashi et al.	(PDG Collab.)
AAIJ	17BB	EPL C77 409	R. Aaij et al.	(LHCb Collab.)
AAIJ	17BI	PRL 119 221801	R. Aaij et al.	(LHCb Collab.)
ABLIKIM	17AE	PR D96 092007	M. Ablikim et al.	(BESIII Collab.)
ABLIKIM	17AG	PR D96 111102	M. Ablikim et al.	(BESIII Collab.)
ABLIKIM	17AI	PR D96 112006	M. Ablikim et al.	(BESIII Collab.)
ABLIKIM	17I	PRL 118 221802	M. Ablikim et al.	(BESIII Collab.)
ABLIKIM	17N	PR D95 072004	M. Ablikim et al.	(BESIII Collab.)
ABLIKIM	17U	PR D96 032001	M. Ablikim et al.	(BESIII Collab.)
PDG	16	C40 100001	C. Patrignani et al.	(PDG Collab.)
ABLIKIM	15I	PR D91 092006	M. Ablikim et al.	(BESIII Collab.)
ABLIKIM	15M	PR D91 112008	M. Ablikim et al.	(BESIII Collab.)
ABLIKIM	15N	PR D91 112018	M. Ablikim et al.	(BESIII Collab.)
ABLIKIM	14J	PR D89 074030	M. Ablikim et al.	(BESIII Collab.)
ABLIKIM	13B	PR D87 012002	M. Ablikim et al.	(BESIII Collab.)
ABLIKIM	13D	PR D87 012007	M. Ablikim et al.	(BESIII Collab.)
ABLIKIM	13H	PR D87 032007	M. Ablikim et al.	(BESIII Collab.)
ABLIKIM	13V	PR D88 112001	M. Ablikim et al.	(BESIII Collab.)
UEHARA	13	PTEP 2013 123C01	S. Uehara et al.	(BELLE Collab.)
ABLIKIM	12A	PR D85 112008	M. Ablikim et al.	(BESIII Collab.)
ABLIKIM	12I	PR D86 052004	M. Ablikim et al.	(BESIII Collab.)
ABLIKIM	12J	PR D86 052011	M. Ablikim et al.	(BESIII Collab.)
ABLIKIM	12O	PRL 109 172002	M. Ablikim et al.	(BESIII Collab.)
LEES	12AE	PR D86 092005	J.P. Lees et al.	(BABAR Collab.)
LIU	12B	PRL 108 232001	Z.Q. Liu et al.	(BELLE Collab.)
ABLIKIM	11A	PR D83 012006	M. Ablikim et al.	(BESIII Collab.)
ABLIKIM	11E	PR D83 112005	M. Ablikim et al.	(BESIII Collab.)
ABLIKIM	11F	PR D83 112009	M. Ablikim et al.	(BESIII Collab.)
ABLIKIM	11I	PR D84 092006	M. Ablikim et al.	(BESIII Collab.)
ABLIKIM	11K	PRL 107 092001	M. Ablikim et al.	(BESIII Collab.)
DEL-AMO-SA... 11M	PR D84 012004	P. del Amo Sanchez et al.	(BABAR Collab.)	
ABLIKIM	10A	PR D81 052005	M. Ablikim et al.	(BESIII Collab.)
ONYISI	10	PR D82 011103	P.U.E. Onyisi et al.	(CLEO Collab.)
UEHARA	10A	PR D82 114031	S. Uehara et al.	(BELLE Collab.)
ARTUSO	09	PR D80 112003	M. Artuso et al.	(CLEO Collab.)
ASNER	09	PR D79 072007	D.H. Asner et al.	(CLEO Collab.)
UEHARA	09	PR D79 052009	S. Uehara et al.	(BELLE Collab.)
BENNETT	08A	PRL 101 151801	J.V. Bennett et al.	(CLEO Collab.)
ECKLUND	08A	PR D78 091501	K.M. Ecklund et al.	(CLEO Collab.)
HE	08B	PR D78 092004	Q. He et al.	(CLEO Collab.)
MENDEZ	08	PR D78 011102	H. Mendez et al.	(CLEO Collab.)
NAIK	08	PR D78 031101	P. Naik et al.	(CLEO Collab.)
UEHARA	08	EPJ C53 1	S. Uehara et al.	(BELLE Collab.)
ADAMS	07	PR D75 071101	G.S. Adams et al.	(CLEO Collab.)
ATHAR	07	PR D75 032002	S.B. Athar et al.	(CLEO Collab.)
CHEN	07B	PL B651 15	W.T. Chen et al.	(BELLE Collab.)
ABLIKIM	06D	PR D73 052006	M. Ablikim et al.	(CLEO Collab.)
ABLIKIM	06I	PR D74 012004	M. Ablikim et al.	(BES Collab.)
ABLIKIM	06R	PR D74 072001	M. Ablikim et al.	(BES Collab.)
ABLIKIM	06T	PL B642 197	M. Ablikim et al.	(BES Collab.)
DOBBS	06	PR D73 071101	S. Dobbs et al.	(CLEO Collab.)
ABLIKIM	05G	PR D71 092002	M. Ablikim et al.	(BES Collab.)
ABLIKIM	05N	PL B630 7	M. Ablikim et al.	(BES Collab.)
ABLIKIM	05O	PL B630 21	M. Ablikim et al.	(BES Collab.)
ADAM	05A	PRL 94 232002	N.E. Adam et al.	(CLEO Collab.)
ANDREOTTI	05A	NP B717 34	M. Andreotti et al.	(FNAL E835 Collab.)
NAKAZAWA	05	PL B615 39	H. Nakazawa et al.	(BELLE Collab.)
ABLIKIM	04B	PR D70 012003	M. Ablikim et al.	(BES Collab.)
ABLIKIM	04H	PR D70 092003	M. Ablikim et al.	(BES Collab.)
ABLIKIM	04I	PR D70 092004	M. Ablikim et al.	(BES Collab.)
ATHAR	04	PR D70 112002	S.B. Athar et al.	(CLEO Collab.)
BAI	04F	PR D69 092001	J.Z. Bai et al.	(BES Collab.)
BAI	04I	PR D70 012006	J.Z. Bai et al.	(BES Collab.)
AULCHENKO	03	PL B573 63	V.M. Aulchenko et al.	(KEDR Collab.)
BAI	03C	PR D67 032004	J.Z. Bai et al.	(BES Collab.)
BAI	03E	PR D67 112001	J.Z. Bai et al.	(BES Collab.)
ABE	02T	PL B540 33	K. Abe et al.	(BELLE Collab.)
AMBROGIANI	02	PR D65 052002	M. Ambrogiani et al.	(FNAL E835 Collab.)
EISENSTEIN	01	PRL 87 061801	B.J. Eisenstein et al.	(CLEO Collab.)
AMBROGIANI	00B	PR D62 052002	M. Ambrogiani et al.	(FNAL E835 Collab.)
ACCIARI	99E	PL B453 73	M. Acciari et al.	(L3 Collab.)
BAI	99B	PR D60 072001	J.Z. Bai et al.	(BES Collab.)
ACKER...K...	98	PL B439 197	K. Ackerstaff et al.	(OPAL Collab.)
BAI	98D	PR D58 092006	J.Z. Bai et al.	(BES Collab.)
BAI	98I	PRL 81 30191	J.Z. Bai et al.	(BES Collab.)
DOMINICK	94	PR D50 4265	J. Dominick et al.	(CLEO Collab.)

ARMSTRONG	93	PRL 70 2988	T.A. Armstrong et al.	(FNAL E760 Collab.)
ARMSTRONG	93E	PR D48 3037	T.A. Armstrong et al.	(FNAL-E760 Collab.)
BAUER	93	PL B302 345	D.A. Bauer et al.	(TPC Collab.)
ARMSTRONG	92	NP B373 35	T.A. Armstrong et al.	(FNAL, FERR, GENO+)
Also		PRL 68 1468	T.A. Armstrong et al.	(FNAL, FERR, GENO+)
BAGLIN	87B	PL B187 191	C. Baglin et al.	(R704 Collab.)
BAGLIN	86B	PL B172 455	C. Baglin (LAPP, CERN, GENO, OSLO+)	
GAISER	86	PR D34 711	J. Gaiser et al.	(Crystal Ball Collab.)
LEE	85	SLAC 282	R.A. Lee	(SLAC)
LEMIGNON	82	PL 113B 509	Y. Lemoigne et al.	(SACL, LOIC, SHMP+)
OREGLIA	82	PR D25 2259	M.J. Oreglia et al.	(SLAC, CIT, HARV+)
Also		Private Comm.	M.J. Oreglia	(EFI)
BARATE	81	PR D24 2994	R. Barate et al.	(SACL, LOIC, SHMP, CERN+)
HIMEL	80	PRL 44 920	T. Himel et al.	(LBL, SLAC)
Also		Private Comm.	G. Trilling	(LBL, UCB)
BRANDELIC	79B	NP B160 426	R. Brandelik et al.	(DASP Collab.)
BARTEL	78B	PL 79B 492	W. Bartel et al.	(DESY, HEIDP)
TANENBAUM	78	PR D17 1731	W.M. Tanenbaum et al.	(SLAC, LBL)
Also		Private Comm.	G. Trilling	(LBL, UCB)
BIDDICK	77	PRL 38 1324	C.J. Biddick et al.	(UCSD, UMD, PAV+)
WHITAKER	76	PRL 37 1596	J.S. Whitaker et al.	(SLAC, LBL)

$\eta_c(2S)$

$$I^G(J^{PC}) = 0^+(0^-)$$

Quantum numbers are quark model predictions.

$\eta_c(2S)$ MASS

VALUE (MeV)	EVTS	DOCUMENT ID	TECN	COMMENT
3637.5 ± 1.1	OUR AVERAGE	Error includes scale factor of 1.2.		
$3635.1 \pm 3.7 \pm 2.9$	106	XU	18	BELL $e^+e^- \rightarrow e^+e^- \eta/\pi^+\pi^-$
$3633.6 \pm 1.7 \pm 0.6$	106	1 AAJ	17A	dLHCB $p\bar{p} \rightarrow B^+X \rightarrow p\bar{p}K^+X$
$3636.4 \pm 4.1 \pm 0.7$	365	2 AAJ	17B	bLHCB $p\bar{p} \rightarrow b\bar{b}X \rightarrow 2(K^+K^-)X$
$3637.0 \pm 5.7 \pm 3.4$	178	3,4	LEES	14E BABR $\gamma\gamma \rightarrow K^+K^-\pi^0$
$3635.1 \pm 5.8 \pm 2.1$	47	3,5	LEES	14E BABR $\gamma\gamma \rightarrow K^+K^-\eta$
$3646.9 \pm 1.6 \pm 3.6$	57 \pm 17	ABLIKIM	13K	BES3 $\psi(2S) \rightarrow \gamma K_S^0 K^\pm \pi^\mp \pi^\pm \pi^-$
$3637.6 \pm 2.9 \pm 1.6$	127 \pm 18	6	ABLIKIM	12G BES3 $\psi(2S) \rightarrow \gamma K^0 K \pi, K K \pi^0$
$3638.5 \pm 1.5 \pm 0.8$	624	3	DEL-AMO-SA...11M	BABR $\gamma\gamma \rightarrow K^\pm K^\pm \pi^\mp$
$3640.5 \pm 3.2 \pm 2.5$	1201	3	DEL-AMO-SA...11M	BABR $\gamma\gamma \rightarrow K^+K^-\pi^+\pi^-\pi^0$
$3636.1^{+3.9+0.7}_{-4.2-2.0}$	128	7	VINOKUROVA	11 BELL $B^\pm \rightarrow K^\pm(K_S^0 K^\pm \pi^\mp)$
$3626 \pm 5 \pm 6$	311	8	ABE	07 BELL $e^+e^- \rightarrow J/\psi(c\bar{c})$
$3645.0 \pm 5.5 \pm 4.9$	121 \pm 27	AUBERT	05c	BABR $e^+e^- \rightarrow J/\psi c\bar{c}$
$3642.9 \pm 3.1 \pm 1.5$	61	ASNER	04	CLEO $\gamma\gamma \rightarrow \eta_c \rightarrow K_S^0 K^\pm \pi^\mp$

- • •** We do not use the following data for averages, fits, limits, etc. **• • •**
 - 3639 \pm 7 98 \pm 52 ⁹ AUBERT 06E BABR $B^\pm \rightarrow K^\pm X_{c\bar{c}}$
 - 3630.8 \pm 3.4 \pm 1.0 112 \pm 24 ¹⁰ AUBERT 04D BABR $\gamma\gamma \rightarrow \eta_c(2S) \rightarrow K\bar{K}\pi$
 - 3654 \pm 6 \pm 8 39 \pm 11 ¹¹ CHOI 02 BELL $B \rightarrow K K_S^0 K^-\pi^+$
 - 3594 \pm 5 ¹² EDWARDS 82c CBAL $e^+e^- \rightarrow \gamma X$
- ¹ AAJ 17AD report $m_{\psi(2S)} - m_{\eta_c(2S)} = 52.5 \pm 1.7 \pm 0.6$ MeV. We use the current value $m_{\psi(2S)} = 3686.097 \pm 0.025$ MeV to obtain the quoted mass.
 - ² From a fit of the $\phi\phi$ invariant mass with the width of $\eta_c(2S)$ fixed to the PDG 16 value.
 - ³ Ignoring possible interference with continuum.
 - ⁴ With a width fixed to 11.3 MeV.
 - ⁵ With a width fixed to 11.3 MeV. Using both $\eta \rightarrow \gamma\gamma$ and $\eta \rightarrow \pi^+\pi^-\pi^0$ decays.
 - ⁶ From a simultaneous fit to $K_S^0 K^\pm \pi^\mp$ and $K^+ K^-\pi^0$ decay modes.
 - ⁷ Accounts for interference with non-resonant continuum.
 - ⁸ From a fit of the J/ψ recoil mass spectrum. Supersedes ABE, K 02 and ABE 04c.
 - ⁹ From the fit of the kaon momentum spectrum. Systematic errors not evaluated.
 - ¹⁰ Superseded by DEL-AMO-SANCHEZ 11M.
 - ¹¹ Superseded by VINOKUROVA 11.
 - ¹² Assuming mass of $\psi(2S) = 3686$ MeV.

$\eta_c(2S)$ WIDTH

VALUE (MeV)	CL%	EVTS	DOCUMENT ID	TECN	COMMENT
$11.3^{+3.2}_{-2.9}$	OUR AVERAGE				
$9.9 \pm 4.8 \pm 2.9$		57 \pm 17	ABLIKIM	13k	BES3 $\psi(2S) \rightarrow \gamma K_S^0 K^\pm \pi^\mp \pi^\pm \pi^-$
$16.9 \pm 6.4 \pm 4.8$		127 \pm 18	13	ABLIKIM	12G BES3 $\psi(2S) \rightarrow \gamma K^0 K \pi, K K \pi^0$
$13.4 \pm 4.6 \pm 3.2$		624	14	DEL-AMO-SA...11M	BABR $\gamma\gamma \rightarrow K_S^0 K^\pm \pi^\mp$
$6.6^{+8.4+2.6}_{-5.1-0.9}$		128	15	VINOKUROVA	11 BELL $B^\pm \rightarrow K^\pm(K_S^0 K^\pm \pi^\mp)$
$6.3 \pm 12.4 \pm 4.0$		61	ASNER	04	CLEO $\gamma\gamma \rightarrow \eta_c \rightarrow K_S^0 K^\pm \pi^\mp$

• • • We do not use the following data for averages, fits, limits, etc. **• • •**

< 23	90	98 \pm 52	16	AUBERT	06E BABR $B^\pm \rightarrow K^\pm X_{c\bar{c}}$
22 \pm 14	121 \pm 27	AUBERT	05c	BABR $e^+e^- \rightarrow J/\psi c\bar{c}$	
17.0 \pm 8.3 \pm 2.5	112 \pm 24	17	AUBERT	04D BABR $\gamma\gamma \rightarrow \eta_c(2S) \rightarrow K\bar{K}\pi$	

$\eta_c(2S)$

<55	90	39 ± 11	¹⁸ CHOI	02	BELL	$B \rightarrow K K_S K^- \pi^+$
<8.0	95		¹⁹ EDWARDS	82c	CBAL	$e^+ e^- \rightarrow \gamma X$

¹³ From a simultaneous fit to $K_S^0 K^\pm \pi^\mp$ and $K^+ K^- \pi^0$ decay modes.
¹⁴ Ignoring possible interference with continuum.
¹⁵ Accounts for interference with non-resonant continuum.
¹⁶ From the fit of the kaon momentum spectrum. Systematic errors not evaluated.
¹⁷ Superseded by DEL-AMO-SANCHEZ 11M.
¹⁸ For a mass value of 3654 ± 6 MeV. Superseded by VINOKUROVA 11.
¹⁹ For a mass value of 3594 ± 5 MeV

$\eta_c(2S)$ DECAY MODES

Mode	Fraction (Γ_i/Γ)	Confidence level
Γ_1 hadrons	not seen	
Γ_2 $K \bar{K} \pi$	(1.9 ± 1.2) %	
Γ_3 $K \bar{K} \eta$	(5 ± 4) × 10 ⁻³	
Γ_4 $2\pi^+ 2\pi^-$	not seen	
Γ_5 $\rho^0 \rho^0$	not seen	
Γ_6 $3\pi^+ 3\pi^-$	not seen	
Γ_7 $K^+ K^- \pi^+ \pi^-$	not seen	
Γ_8 $K^{*0} \bar{K}^{*0}$	not seen	
Γ_9 $K^+ K^- \pi^+ \pi^- \pi^0$	(1.4 ± 1.0) %	
Γ_{10} $K^+ K^- 2\pi^+ 2\pi^-$	not seen	
Γ_{11} $K_S^0 K^- 2\pi^+ \pi^- + c.c.$	seen	
Γ_{12} $2K^+ 2K^-$	not seen	
Γ_{13} $\phi \phi$	not seen	
Γ_{14} $p \bar{p}$	seen	
Γ_{15} $p \bar{p} \pi^+ \pi^-$	seen	
Γ_{16} $\gamma \gamma$	(1.9 ± 1.3) × 10 ⁻⁴	
Γ_{17} $\gamma J/\psi(1S)$	< 1.4 %	90%
Γ_{18} $\pi^+ \pi^- \eta$	not seen	
Γ_{19} $\pi^+ \pi^- \eta'$	not seen	
Γ_{20} $\pi^+ \pi^- \eta_c(1S)$	< 25 %	90%

$\eta_c(2S)$ PARTIAL WIDTHS

$\Gamma(\gamma\gamma)$	VALUE (keV)	EVTs	DOCUMENT ID	TECN	COMMENT	Γ_{16}
	0.44 ± 0.14	106	20 XU	18	BELL $e^+ e^- \rightarrow e^+ e^- \eta' \pi^+ \pi^-$	
	1.3 ± 0.6		21 ASNER	04	CLEO $\gamma\gamma \rightarrow \eta_c \rightarrow K_S^0 K^\pm \pi^\mp$	

²⁰ Assuming that the branching fraction into $\eta' \pi^+ \pi^-$ is the same as for $\eta_c(1S)$.
²¹ They measure $\Gamma(\eta_c(2S) \gamma\gamma) B(\eta_c(2S) \rightarrow K \bar{K} \pi) = (0.18 \pm 0.05 \pm 0.02) \Gamma(\eta_c(1S) \gamma\gamma) B(\eta_c(1S) \rightarrow K \bar{K} \pi)$. The value for $\Gamma(\eta_c(2S) \rightarrow \gamma\gamma)$ is derived assuming that the branching fractions for $\eta_c(2S)$ and $\eta_c(1S)$ decays to $K_S K \pi$ are equal and using $\Gamma(\eta_c(1S) \rightarrow \gamma\gamma) = 7.4 \pm 0.4 \pm 2.3$ keV.

$\Gamma(\gamma\gamma) \times \Gamma(\pi^+ \pi^- \eta')/\Gamma_{total}$	VALUE (eV)	EVTs	DOCUMENT ID	TECN	COMMENT	$\Gamma_{16} \Gamma_{19}/\Gamma$
	5.6 ^{+1.2} _{-1.1} ± 1.1	106	XU	18	BELL $e^+ e^- \rightarrow e^+ e^- \eta' \pi^+ \pi^-$	

$\eta_c(2S)$ $\Gamma(i)\Gamma(\gamma\gamma)/\Gamma(total)$

$\Gamma(2\pi^+ 2\pi^-) \times \Gamma(\gamma\gamma)/\Gamma_{total}$	VALUE (eV)	CL%	DOCUMENT ID	TECN	COMMENT	$\Gamma_4 \Gamma_{16}/\Gamma$
	< 6.5	90	UEHARA	08	BELL $\gamma\gamma \rightarrow \eta_c(2S) \rightarrow 2(\pi^+ \pi^-)$	

$\Gamma(K \bar{K} \pi) \times \Gamma(\gamma\gamma)/\Gamma_{total}$	VALUE (eV)	EVTs	DOCUMENT ID	TECN	COMMENT	$\Gamma_2 \Gamma_{16}/\Gamma$
	41 ± 4 ± 6	624	22 DEL-AMO-SA..11M	BABR	$\gamma\gamma \rightarrow K_S^0 K^\pm \pi^\mp$	

²² Not independent from other measurements reported in DEL-AMO-SANCHEZ 11M.

$\Gamma(K^+ K^- \pi^+ \pi^-) \times \Gamma(\gamma\gamma)/\Gamma_{total}$	VALUE (eV)	CL%	DOCUMENT ID	TECN	COMMENT	$\Gamma_7 \Gamma_{16}/\Gamma$
	< 5.0	90	UEHARA	08	BELL $\gamma\gamma \rightarrow \eta_c(2S) \rightarrow K^+ K^- \pi^+ \pi^-$	

$\Gamma(K^+ K^- \pi^+ \pi^- \pi^0) \times \Gamma(\gamma\gamma)/\Gamma_{total}$	VALUE (eV)	EVTs	DOCUMENT ID	TECN	COMMENT	$\Gamma_9 \Gamma_{16}/\Gamma$
	30 ± 6 ± 5	1201	23 DEL-AMO-SA..11M	BABR	$\gamma\gamma \rightarrow K^+ K^- \pi^+ \pi^- \pi^0$	

²³ Not independent from other measurements reported in DEL-AMO-SANCHEZ 11M.

$\Gamma(2K^+ 2K^-) \times \Gamma(\gamma\gamma)/\Gamma_{total}$	VALUE (eV)	CL%	DOCUMENT ID	TECN	COMMENT	$\Gamma_{12} \Gamma_{16}/\Gamma$
	< 2.9	90	UEHARA	08	BELL $\gamma\gamma \rightarrow \eta_c(2S) \rightarrow 2(K^+ K^-)$	

$\Gamma(\pi^+ \pi^- \eta_c(1S)) \times \Gamma(\gamma\gamma)/\Gamma_{total}$	VALUE (eV)	CL%	DOCUMENT ID	TECN	COMMENT	$\Gamma_{20} \Gamma_{16}/\Gamma$
	< 133	90	LEES	12AE	BABR $e^+ e^- \rightarrow e^+ e^- \pi^+ \pi^- \eta_c$	

$\eta_c(2S)$ $\Gamma(i)\Gamma(\gamma\gamma)/\Gamma^2(total)$

$\Gamma(p \bar{p})/\Gamma_{total} \times \Gamma(\gamma\gamma)/\Gamma_{total}$	VALUE (units 10 ⁻⁸)	CL%	DOCUMENT ID	TECN	COMMENT	$\Gamma_{14}/\Gamma \times \Gamma_{16}/\Gamma$
	< 5.6	90 ^{24,25,26}	AMBROGIANI 01	E835	$p \bar{p} \rightarrow \gamma\gamma$	
• • • We do not use the following data for averages, fits, limits, etc. • • •						
	< 8.0	90 ^{24,25,27}	AMBROGIANI 01	E835	$p \bar{p} \rightarrow \gamma\gamma$	
	< 12.0	90	25,27	AMBROGIANI 01	E835	$p \bar{p} \rightarrow \gamma\gamma$

²⁴ Including the measurements of ARMSTRONG 95F in the AMBROGIANI 01 analysis.
²⁵ For a total width $\Gamma = 5$ MeV.
²⁶ For the resonance mass region 3589–3599 MeV/c².
²⁷ For the resonance mass region 3575–3660 MeV/c².

$\eta_c(2S)$ BRANCHING RATIOS

$\Gamma(hadrons)/\Gamma_{total}$	VALUE	DOCUMENT ID	TECN	COMMENT	Γ_1/Γ
	not seen	ABREU	98o	DLPH $e^+ e^- \rightarrow e^+ e^- + hadrons$	
• • • We do not use the following data for averages, fits, limits, etc. • • •					
	seen	28	EDWARDS	82c	CBAL $e^+ e^- \rightarrow \gamma X$

²⁸ For a mass value of 3594 ± 5 MeV

$\Gamma(K \bar{K} \pi)/\Gamma_{total}$	VALUE (units 10 ⁻²)	EVTs	DOCUMENT ID	TECN	COMMENT	Γ_2/Γ
	1.9 ± 0.4 ± 1.1	59 ± 12	29	AUBERT	08AB	BABR $B \rightarrow \eta_c(2S) K \rightarrow K \bar{K} \pi$
• • • We do not use the following data for averages, fits, limits, etc. • • •						
	seen	127 ± 18	ABLIKIM	13k	BES3 $\psi(2S) \rightarrow \gamma K \bar{K} \pi$	
	seen	39 ± 11	30	CHOI	02	BELL $B \rightarrow K K_S K^- \pi^+$

²⁹ Derived from a measurement of $[B(B^+ \rightarrow \eta_c(2S) K^+) \times B(\eta_c(2S) \rightarrow K \bar{K} \pi)] / [B(B^+ \rightarrow \eta_c K^+) \times B(\eta_c \rightarrow K \bar{K} \pi)] = (9.6^{+2.0}_{-1.9} \pm 2.5)\%$ and using $B(B^+ \rightarrow \eta_c(2S) K^+) = (3.4 \pm 1.8) \times 10^{-4}$, and $[B(B^+ \rightarrow \eta_c K^+) \times B(\eta_c \rightarrow K \bar{K} \pi)] = (6.88 \pm 0.77^{+0.55}_{-0.66}) \times 10^{-5}$.
³⁰ For a mass value of 3654 ± 6 MeV

$\Gamma(K \bar{K} \eta)/\Gamma(K \bar{K} \pi)$	VALUE (units 10 ⁻²)	EVTs	DOCUMENT ID	TECN	COMMENT	Γ_3/Γ_2
	27.3 ± 7.0 ± 9.0	225	31	LEES	14E	BABR $\gamma\gamma \rightarrow K^+ K^- \gamma\gamma$

³¹ LEES 14E reports $B(\eta_c(2S) \rightarrow K^+ K^- \eta)/B(\eta_c(2S) \rightarrow K^+ K^- \pi^0) = 0.82 \pm 0.21 \pm 0.27$, which we divide by 3 to account for isospin symmetry.

$\Gamma(2\pi^+ 2\pi^-)/\Gamma_{total}$	VALUE	DOCUMENT ID	TECN	COMMENT	Γ_4/Γ
	not seen	UEHARA	08	BELL $\gamma\gamma \rightarrow \eta_c(2S)$	

$\Gamma(\rho^0 \rho^0)/\Gamma_{total}$	VALUE	DOCUMENT ID	TECN	COMMENT	Γ_5/Γ
	not seen	ABLIKIM	11H	BES3 $\psi(2S) \rightarrow \gamma 2\pi^+ 2\pi^-$	

$\Gamma(K^+ K^- \pi^+ \pi^-)/\Gamma_{total}$	VALUE	DOCUMENT ID	TECN	COMMENT	Γ_7/Γ
	not seen	UEHARA	08	BELL $\gamma\gamma \rightarrow \eta_c(2S)$	

$\Gamma(K^+ K^- \pi^+ \pi^- \pi^0)/\Gamma(K \bar{K} \pi)$	VALUE	EVTs	DOCUMENT ID	TECN	COMMENT	Γ_9/Γ_2
	0.73 ± 0.17 ± 0.17	1201	32	DEL-AMO-SA..11M	BABR $\gamma\gamma \rightarrow K^+ K^- \pi^+ \pi^- \pi^0$	

³² We have multiplied the value of $\Gamma(K^+ K^- \pi^+ \pi^- \pi^0)/\Gamma(K_S^0 K^\pm \pi^\mp)$ reported in DEL-AMO-SANCHEZ 11M by a factor 1/3 to obtain $\Gamma(K^+ K^- \pi^+ \pi^- \pi^0)/\Gamma(K \bar{K} \pi)$. Not independent from other measurements reported in DEL-AMO-SANCHEZ 11M.

$\Gamma(K^{*0} \bar{K}^{*0})/\Gamma_{total}$	VALUE	DOCUMENT ID	TECN	COMMENT	Γ_8/Γ
	not seen	ABLIKIM	11H	BES3 $\psi(2S) \rightarrow \gamma K^+ K^- \pi^+ \pi^-$	

$\Gamma(K_S^0 K^- 2\pi^+ \pi^- + c.c.)/\Gamma_{total}$	VALUE	EVTs	DOCUMENT ID	TECN	COMMENT	Γ_{11}/Γ
	seen	57 ± 17	ABLIKIM	13k	BES3 $\psi(2S) \rightarrow \gamma K_S^0 K^\pm \pi^\mp \pi^\pm \pi^-$	

$\Gamma(2K^+ 2K^-)/\Gamma_{total}$	VALUE	DOCUMENT ID	TECN	COMMENT	Γ_{12}/Γ
	not seen	UEHARA	08	BELL $\gamma\gamma \rightarrow \eta_c(2S)$	

$\Gamma(\phi\phi)/\Gamma_{total}$	VALUE	DOCUMENT ID	TECN	COMMENT	Γ_{13}/Γ
	not seen	ABLIKIM	11H	BES3 $\psi(2S) \rightarrow \gamma K^+ K^- K^+ K^-$	

Meson Particle Listings

$\eta_c(2S)$

$\Gamma(p\bar{p})/\Gamma_{total}$					Γ_{14}/Γ
VALUE	CL%	DOCUMENT ID	TECN	COMMENT	
seen	106	33 AAIJ	17AD LHCB	$p\bar{p} \rightarrow B^+ X \rightarrow p\bar{p}K^+ X$	
33 AAIJ 17AD report a 6.4 standard deviation signal, with $B(B^+ \rightarrow \eta_c(2S)K^+ \rightarrow p\bar{p}K^+)/B(B^+ \rightarrow J/\psi K^+ \rightarrow p\bar{p}K^+) = (1.58 \pm 0.33 \pm 0.09) \times 10^{-2}$.					

$\Gamma(p\bar{p}\pi^+\pi^-)/\Gamma_{total}$					Γ_{15}/Γ
VALUE	CL%	DOCUMENT ID	TECN	COMMENT	
seen	110	34 CHILIKIN	19 BELL	$e^+e^- \rightarrow \Upsilon(4S)$	
34 CHILIKIN 19 reports signals in $B^+ \rightarrow \eta_c(2S)K^+$ and $B^0 \rightarrow \eta_c(2S)K_S^0$ with 12.3 and 5.9 standard deviations, respectively.					

$\Gamma(\gamma\gamma)/\Gamma_{total}$					Γ_{16}/Γ
VALUE	CL%	DOCUMENT ID	TECN	COMMENT	
••• We do not use the following data for averages, fits, limits, etc. •••					
$<4 \times 10^{-4}$	90	35 WICHT	08 BELL	$B^\pm \rightarrow K^\pm \gamma\gamma$	
not seen		AMBROGIANI	01 E835	$\bar{p}p \rightarrow \gamma\gamma$	
<0.01	90	LEE	85 CBAL	$\psi' \rightarrow$ photons	
35 WICHT 08 reports $[\Gamma(\eta_c(2S) \rightarrow \gamma\gamma)/\Gamma_{total}] \times [B(B^+ \rightarrow \eta_c(2S)K^+)] < 0.18 \times 10^{-6}$ which we divide by our best value $B(B^+ \rightarrow \eta_c(2S)K^+) = 4.4 \times 10^{-4}$.					

$\Gamma(\pi^+\pi^-\eta_c(1S))/\Gamma(K\bar{K}\pi)$					Γ_{20}/Γ_2
VALUE	CL%	DOCUMENT ID	TECN	COMMENT	
<3.33	90	36 LEES	12AE BABR	$e^+e^- \rightarrow e^+e^-\pi^+\pi^-\eta_c$	
36 We divided the reported limit by 3 to take into account isospin relations.					

$\eta_c(2S)$ CROSS-PARTICLE BRANCHING RATIOS

$\Gamma(\eta_c(2S) \rightarrow K\bar{K}\eta)/\Gamma_{total} \times \Gamma(\psi(2S) \rightarrow \gamma\eta_c(2S))/\Gamma_{total}$					$\Gamma_3/\Gamma \times \Gamma_{157}^{\psi(2S)}/\Gamma_{\psi(2S)}$
VALUE	CL%	DOCUMENT ID	TECN	COMMENT	
••• We do not use the following data for averages, fits, limits, etc. •••					
$<11.8 \times 10^{-6}$	90	37 CRONIN-HEN..10	CLEO	$\psi(2S) \rightarrow \gamma K^+ K^- \eta$	
37 CRONIN-HENNESSY 10 reports a limit of $< 5.9 \times 10^{-6}$ for the decay $\eta_c(2S) \rightarrow K^+ K^- \eta$ which we multiply by 2 account for isospin symmetry. It assumes $\Gamma(\eta_c(2S)) = 14$ MeV. It also gives the analytic dependence of limits on width.					

$\Gamma(\eta_c(2S) \rightarrow 2\pi^+ 2\pi^-)/\Gamma_{total} \times \Gamma(\psi(2S) \rightarrow \gamma\eta_c(2S))/\Gamma_{total}$					$\Gamma_4/\Gamma \times \Gamma_{157}^{\psi(2S)}/\Gamma_{\psi(2S)}$
VALUE	CL%	DOCUMENT ID	TECN	COMMENT	
$<14.6 \times 10^{-6}$	90	38 CRONIN-HEN..10	CLEO	$\psi(2S) \rightarrow \gamma 2\pi^+ 2\pi^-$	
38 Assuming $\Gamma(\eta_c(2S)) = 14$ MeV. CRONIN-HENNESSY 10 gives the analytic dependence of limits on width.					

$\Gamma(\eta_c(2S) \rightarrow \rho^0 \rho^0)/\Gamma_{total} \times \Gamma(\psi(2S) \rightarrow \gamma\eta_c(2S))/\Gamma_{total}$					$\Gamma_5/\Gamma \times \Gamma_{157}^{\psi(2S)}/\Gamma_{\psi(2S)}$
VALUE	CL%	DOCUMENT ID	TECN	COMMENT	
$<12.7 \times 10^{-7}$	90	ABLIKIM	11H BES3	$\psi(2S) \rightarrow \gamma 2\pi^+ 2\pi^-$	

$\Gamma(\eta_c(2S) \rightarrow 3\pi^+ 3\pi^-)/\Gamma_{total} \times \Gamma(\psi(2S) \rightarrow \gamma\eta_c(2S))/\Gamma_{total}$					$\Gamma_6/\Gamma \times \Gamma_{157}^{\psi(2S)}/\Gamma_{\psi(2S)}$
VALUE	CL%	DOCUMENT ID	TECN	COMMENT	
$<13.2 \times 10^{-6}$	90	39 CRONIN-HEN..10	CLEO	$\psi(2S) \rightarrow \gamma 3\pi^+ 3\pi^-$	
39 Assuming $\Gamma(\eta_c(2S)) = 14$ MeV. CRONIN-HENNESSY 10 gives the analytic dependence of limits on width.					

$\Gamma(\eta_c(2S) \rightarrow K^+ K^- \pi^+ \pi^-)/\Gamma_{total} \times \Gamma(\psi(2S) \rightarrow \gamma\eta_c(2S))/\Gamma_{total}$					$\Gamma_7/\Gamma \times \Gamma_{157}^{\psi(2S)}/\Gamma_{\psi(2S)}$
VALUE	CL%	DOCUMENT ID	TECN	COMMENT	
$<9.6 \times 10^{-6}$	90	40 CRONIN-HEN..10	CLEO	$\psi(2S) \rightarrow \gamma K^+ K^- \pi^+ \pi^-$	
40 Assuming $\Gamma(\eta_c(2S)) = 14$ MeV. CRONIN-HENNESSY 10 gives the analytic dependence of limits on width.					

$\Gamma(\eta_c(2S) \rightarrow K^{*0} \bar{K}^{*0})/\Gamma_{total} \times \Gamma(\psi(2S) \rightarrow \gamma\eta_c(2S))/\Gamma_{total}$					$\Gamma_8/\Gamma \times \Gamma_{157}^{\psi(2S)}/\Gamma_{\psi(2S)}$
VALUE	CL%	DOCUMENT ID	TECN	COMMENT	
$<19.6 \times 10^{-7}$	90	ABLIKIM	11H BES3	$\psi(2S) \rightarrow \gamma K^+ K^- \pi^+ \pi^-$	

$\Gamma(\eta_c(2S) \rightarrow K^+ K^- \pi^+ \pi^- \pi^0)/\Gamma_{total} \times \Gamma(\psi(2S) \rightarrow \gamma\eta_c(2S))/\Gamma_{total}$					$\Gamma_9/\Gamma \times \Gamma_{157}^{\psi(2S)}/\Gamma_{\psi(2S)}$
VALUE	CL%	DOCUMENT ID	TECN	COMMENT	
$<43.0 \times 10^{-6}$	90	41 CRONIN-HEN..10	CLEO	$\psi(2S) \rightarrow \gamma K^+ K^- \pi^+ \pi^- \pi^0$	
41 Assuming $\Gamma(\eta_c(2S)) = 14$ MeV. CRONIN-HENNESSY 10 gives the analytic dependence of limits on width.					

$\Gamma(\eta_c(2S) \rightarrow K^+ K^- 2\pi^+ 2\pi^-)/\Gamma_{total} \times \Gamma(\psi(2S) \rightarrow \gamma\eta_c(2S))/\Gamma_{total}$					$\Gamma_{10}/\Gamma \times \Gamma_{157}^{\psi(2S)}/\Gamma_{\psi(2S)}$
VALUE	CL%	DOCUMENT ID	TECN	COMMENT	
$<9.7 \times 10^{-6}$	90	42 CRONIN-HEN..10	CLEO	$\psi(2S) \rightarrow \gamma K^+ K^- 2\pi^+ 2\pi^-$	
42 Assuming $\Gamma(\eta_c(2S)) = 14$ MeV. CRONIN-HENNESSY 10 gives the analytic dependence of limits on width.					

$\Gamma(\eta_c(2S) \rightarrow K_S^0 K^- 2\pi^+ \pi^- + c.c.)/\Gamma_{total} \times \Gamma(\psi(2S) \rightarrow \gamma\eta_c(2S))/\Gamma_{total}$					$\Gamma_{11}/\Gamma \times \Gamma_{157}^{\psi(2S)}/\Gamma_{\psi(2S)}$
VALUE (units 10^{-6})	CL%	DOCUMENT ID	TECN	COMMENT	
$7.03 \pm 2.10 \pm 0.7$	60	ABLIKIM	13k BES3	$\psi(2S) \rightarrow \gamma K_S^0 K^- 2\pi^+ \pi^- + c.c.$	
••• We do not use the following data for averages, fits, limits, etc. •••					
<15.2	90	43 CRONIN-HEN..10	CLEO	$\psi(2S) \rightarrow \gamma K_S^0 K^- 2\pi^+ \pi^- + c.c.$	
43 Assuming $\Gamma(\eta_c(2S)) = 14$ MeV. CRONIN-HENNESSY 10 gives the analytic dependence of limits on width.					

$\Gamma(\eta_c(2S) \rightarrow \phi\phi)/\Gamma_{total} \times \Gamma(\psi(2S) \rightarrow \gamma\eta_c(2S))/\Gamma_{total}$					$\Gamma_{13}/\Gamma \times \Gamma_{157}^{\psi(2S)}/\Gamma_{\psi(2S)}$
VALUE	CL%	DOCUMENT ID	TECN	COMMENT	
$<7.8 \times 10^{-7}$	90	ABLIKIM	11H BES3	$\psi(2S) \rightarrow \gamma K^+ K^- K^+ K^-$	

$\Gamma(\eta_c(2S) \rightarrow \rho\bar{\rho})/\Gamma_{total} \times \Gamma(\psi(2S) \rightarrow \gamma\eta_c(2S))/\Gamma_{total}$					$\Gamma_{14}/\Gamma \times \Gamma_{157}^{\psi(2S)}/\Gamma_{\psi(2S)}$
VALUE	CL%	DOCUMENT ID	TECN	COMMENT	
$<1.4 \times 10^{-6}$	90	ABLIKIM	13v BES3	$\psi(2S) \rightarrow \gamma \rho\bar{\rho}$	

$\Gamma(\eta_c(2S) \rightarrow \gamma J/\psi(1S))/\Gamma_{total} \times \Gamma(\psi(2S) \rightarrow \gamma\eta_c(2S))/\Gamma_{total}$					$\Gamma_{17}/\Gamma \times \Gamma_{157}^{\psi(2S)}/\Gamma_{\psi(2S)}$
VALUE	CL%	EVTS	DOCUMENT ID	TECN	COMMENT
$<9.7 \times 10^{-6}$	90	33	44 ABLIKIM	17N BES3	$\psi(2S) \rightarrow \gamma\gamma J/\psi$
44 Uses $B(J/\psi \rightarrow e^+e^-) = (5.971 \pm 0.032)\%$ and $B(J/\psi \rightarrow \mu^+\mu^-) = (5.961 \pm 0.033)\%$.					

$\Gamma(\eta_c(2S) \rightarrow \pi^+ \pi^- \eta)/\Gamma_{total} \times \Gamma(\psi(2S) \rightarrow \gamma\eta_c(2S))/\Gamma_{total}$					$\Gamma_{18}/\Gamma \times \Gamma_{157}^{\psi(2S)}/\Gamma_{\psi(2S)}$
VALUE	CL%	DOCUMENT ID	TECN	COMMENT	
$<4.3 \times 10^{-6}$	90	45 CRONIN-HEN..10	CLEO	$\psi(2S) \rightarrow \gamma \pi^+ \pi^- \eta$	
45 Assuming $\Gamma(\eta_c(2S)) = 14$ MeV. CRONIN-HENNESSY 10 gives the analytic dependence of limits on width.					

$\Gamma(\eta_c(2S) \rightarrow \pi^+ \pi^- \eta')/\Gamma_{total} \times \Gamma(\psi(2S) \rightarrow \gamma\eta_c(2S))/\Gamma_{total}$					$\Gamma_{19}/\Gamma \times \Gamma_{157}^{\psi(2S)}/\Gamma_{\psi(2S)}$
VALUE	CL%	DOCUMENT ID	TECN	COMMENT	
$<14.2 \times 10^{-6}$	90	46 CRONIN-HEN..10	CLEO	$\psi(2S) \rightarrow \gamma \pi^+ \pi^- \eta'$	
46 Assuming $\Gamma(\eta_c(2S)) = 14$ MeV. CRONIN-HENNESSY 10 gives the analytic dependence of limits on width.					

$\Gamma(\eta_c(2S) \rightarrow \pi^+ \pi^- \eta_c(1S))/\Gamma_{total} \times \Gamma(\psi(2S) \rightarrow \gamma\eta_c(2S))/\Gamma_{total}$					$\Gamma_{20}/\Gamma \times \Gamma_{157}^{\psi(2S)}/\Gamma_{\psi(2S)}$
VALUE	CL%	DOCUMENT ID	TECN	COMMENT	
$<1.7 \times 10^{-4}$	90	47 CRONIN-HEN..10	CLEO	$\psi(2S) \rightarrow \gamma \pi^+ \pi^- \eta_c(1S)$	
47 Assuming $\Gamma(\eta_c(2S)) = 14$ MeV. CRONIN-HENNESSY 10 gives the analytic dependence of limits on width.					

$\eta_c(2S)$ REFERENCES

CHILIKIN	19	PR D100 012001	K. Chilikin <i>et al.</i>	(BELLE Collab.)
XU	18	PR D98 072001	Q.N. Xu <i>et al.</i>	(BELLE Collab.)
AAIJ	17AD	PL B769 305	R. Aaij <i>et al.</i>	(LHCb Collab.)
AAIJ	17BB	EPJ C77 609	R. Aaij <i>et al.</i>	(LHCb Collab.)
ABLIKIM	17N	PR D95 072004	M. Ablikim <i>et al.</i>	(BESIII Collab.)
PDC	16	CP C40 100001	C. Patrignani <i>et al.</i>	(PDG Collab.)
LEES	14E	PR D89 112004	J.P. Lees <i>et al.</i>	(BABAR Collab.)
ABLIKIM	13K	PR D87 052005	M. Ablikim <i>et al.</i>	(BESIII Collab.)
ABLIKIM	13V	PR D88 112001	M. Ablikim <i>et al.</i>	(BESIII Collab.)
ABLIKIM	12G	PRL 109 042003	M. Ablikim <i>et al.</i>	(BESIII Collab.)
LEES	12AE	PR D86 092005	J.P. Lees <i>et al.</i>	(BABAR Collab.)
ABLIKIM	11H	PR D84 091102	M. Ablikim <i>et al.</i>	(BESIII Collab.)
DEL-AMO-SA...	11M	PR D84 012004	P. del Amo Sanchez <i>et al.</i>	(BABAR Collab.)
VINOKUROVA	11	PL B706 139	A. Vinokurova <i>et al.</i>	(BELLE Collab.)
CRONIN-HEN..10	10	PR D81 052002	D. Cronin-Hennessey <i>et al.</i>	(CLEO Collab.)
AUBERT	08AB	PR D78 012006	B. Aubert <i>et al.</i>	(BABAR Collab.)
UEHARA	08	EPJ C53 1	S. Uehara <i>et al.</i>	(BELLE Collab.)
WICHT	08	PL B662 323	J. Wicht <i>et al.</i>	(BELLE Collab.)
ABE	07	PRL 98 082001	K. Abe <i>et al.</i>	(BELLE Collab.)
AUBERT	06E	PRL 96 052002	B. Aubert <i>et al.</i>	(BABAR Collab.)
AUBERT	05C	PR D72 031101	B. Aubert <i>et al.</i>	(BABAR Collab.)
ABE	04G	PR D70 071102	K. Abe <i>et al.</i>	(BELLE Collab.)
ASNER	04	PRL 92 142001	D.M. Asner <i>et al.</i>	(BESIII Collab.)
AUBERT	04D	PRL 92 142002	B. Aubert <i>et al.</i>	(BABAR Collab.)
ABE,K	02	PRL 89 142001	K. Abe <i>et al.</i>	(BELLE Collab.)
CHOI	02	PRL 89 102001	S.-K. Choi <i>et al.</i>	(BELLE Collab.)
AMBROGIANI	01	PR D64 052003	M. Ambrogiani <i>et al.</i>	(FNAL E835 Collab.)
ABREU	98O	PL B44 1479	P. Abreu <i>et al.</i>	(DELPHI Collab.)
ARMSTRONG	95F	PR D52 4839	T.A. Armstrong <i>et al.</i>	(FNAL, FERR, GENO+)
LEE	85	SLAC 282	R.A. Lee	(SLAC)
EDWARDS	82C	PRL 48 70	C. Edwards <i>et al.</i>	(CIT, HARV, PRIN+)

$\psi(2S)$

$$I^G(J^{PC}) = 0^-(1^{--})$$

See the Review on " $\psi(2S)$ and χ_c branching ratios" before the $\chi_{c0}(1P)$ Listings.

$\psi(2S)$ MASS

OUR FIT includes measurements of $m_{\psi(2S)}$, $m_{\psi(3770)}$, and $m_{\psi(3770)} - m_{\psi(2S)}$.

VALUE (MeV)	EVTS	DOCUMENT ID	TECN	COMMENT
3686.10 ± 0.06 OUR FIT				Error includes scale factor of 5.9.
3686.097 ± 0.010 OUR AVERAGE				
3686.099 ± 0.004 ± 0.009		¹ ANASHIN 15	KEDR	$e^+e^- \rightarrow$ hadrons
3686.12 ± 0.06 ± 0.10	4k	AAIJ 12H	LHCB	$pp \rightarrow J/\psi \pi^+ \pi^- X$
3685.95 ± 0.10	413	² ARTAMONOV 00	OLYA	$e^+e^- \rightarrow$ hadrons
3685.98 ± 0.09 ± 0.04		³ ARMSTRONG 93B	E760	$\bar{p}p \rightarrow e^+e^-$
3686.114 ± 0.007 ^{+0.011} _{-0.016}		⁴ ANASHIN 12	KEDR	$e^+e^- \rightarrow$ hadrons
3686.111 ± 0.025 ± 0.009		AULCHENKO 03	KEDR	$e^+e^- \rightarrow$ hadrons
3686.00 ± 0.10	413	⁵ ZHOLENTZ 80	OLYA	e^+e^-

¹ Supersedes AULCHENKO 03 and ANASHIN 12.
² Reanalysis of ZHOLENTZ 80 using new electron mass (COHEN 87) and radiative corrections (KURAEV 85).
³ Mass central value and systematic error recalculated by us according to Eq. (16) in ARMSTRONG 93B, using the value for the $J/\psi(1S)$ mass from AULCHENKO 03.
⁴ From the scans in 2004 and 2006. ANASHIN 12 reports the value $3686.114 \pm 0.007 \pm 0.011 \pm 0.002$ MeV, where the third uncertainty is due to assumptions on the interference between the resonance and hadronic continuum. We combined the two systematic uncertainties.
⁵ Superseded by ARTAMONOV 00.

$m_{\psi(2S)} - m_{J/\psi(1S)}$

VALUE (MeV)	DOCUMENT ID	TECN	COMMENT
589.188 ± 0.028 OUR AVERAGE			
589.194 ± 0.027 ± 0.011	¹ AULCHENKO 03	KEDR	$e^+e^- \rightarrow$ hadrons
589.7 ± 1.2	LEMOIGNE 82	GOLI	$185 \pi^- \text{Be} \rightarrow \gamma \mu^+ \mu^- A$
589.07 ± 0.13	¹ ZHOLENTZ 80	OLYA	e^+e^-
588.7 ± 0.8	LUTH 75	MRK1	
588 ± 1	² BAI 98E	BES	e^+e^-

¹ Redundant with data in mass above.
² Systematic errors not evaluated.

$\psi(2S)$ WIDTH

VALUE (keV)	EVTS	DOCUMENT ID	TECN	COMMENT
294 ± 8 OUR FIT				
286 ± 16 OUR AVERAGE				
358 ± 8 ± 4		ABLIKIM 08B	BES2	$e^+e^- \rightarrow$ hadrons
290 ± 25 ± 4	2.7k	ANDREOTTI 07	E835	$p\bar{p} \rightarrow e^+e^-, J/\psi X$
331 ± 5 ± 2		ABLIKIM 06L	BES2	$e^+e^- \rightarrow$ hadrons
264 ± 27		¹ BAI 02B	BES2	e^+e^-
287 ± 37 ± 16		² ARMSTRONG 93B	E760	$\bar{p}p \rightarrow e^+e^-$

¹ From a simultaneous fit to the hadronic and $\mu^+ \mu^-$ cross section, assuming $\Gamma = \Gamma_h + \Gamma_e + \Gamma_\mu + \Gamma_\tau$ and lepton universality. Does not include vacuum polarization correction.
² The initial-state radiation correction reevaluated by ANDREOTTI 07 in its Ref. [4].

$\psi(2S)$ DECAY MODES

Mode	Fraction (Γ_i/Γ)	Scale factor/ Confidence level
Γ_1 hadrons	(97.85 ± 0.13) %	
Γ_2 virtual $\gamma \rightarrow$ hadrons	(1.73 ± 0.14) %	S=1.5
Γ_3 ggg	(10.6 ± 1.6) %	
Γ_4 γgg	(1.03 ± 0.29) %	
Γ_5 light hadrons	(15.4 ± 1.5) %	
Γ_6 e^+e^-	(7.93 ± 0.17) × 10 ⁻³	
Γ_7 $\mu^+ \mu^-$	(8.0 ± 0.6) × 10 ⁻³	
Γ_8 $\tau^+ \tau^-$	(3.1 ± 0.4) × 10 ⁻³	

Decays into $J/\psi(1S)$ and anything

Γ_9 $J/\psi(1S)$ anything	(61.4 ± 0.6) %
Γ_{10} $J/\psi(1S)$ neutrals	(25.38 ± 0.32) %
Γ_{11} $J/\psi(1S) \pi^+ \pi^-$	(34.68 ± 0.30) %
Γ_{12} $J/\psi(1S) \pi^0 \pi^0$	(18.24 ± 0.31) %
Γ_{13} $J/\psi(1S) \eta$	(3.37 ± 0.05) %
Γ_{14} $J/\psi(1S) \pi^0$	(1.268 ± 0.032) × 10 ⁻³

Hadronic decays

Γ_{15} $\pi^0 h_c(1P)$	(8.6 ± 1.3) × 10 ⁻⁴	
Γ_{16} $3(\pi^+ \pi^-) \pi^0$	(3.5 ± 1.6) × 10 ⁻³	
Γ_{17} $2(\pi^+ \pi^-) \pi^0$	(2.9 ± 1.0) × 10 ⁻³	S=4.7
Γ_{18} $\rho \partial_2(1320)$	(2.6 ± 0.9) × 10 ⁻⁴	
Γ_{19} $\pi^+ \pi^- \pi^0 \pi^0 \pi^0$	(5.3 ± 0.9) × 10 ⁻³	
Γ_{20} $\rho^\pm \pi^\mp \pi^0 \pi^0$	< 2.7 × 10 ⁻³	CL=90%
Γ_{21} $p\bar{p}$	(2.94 ± 0.08) × 10 ⁻⁴	
Γ_{22} $n\bar{n}$	(3.06 ± 0.15) × 10 ⁻⁴	
Γ_{23} $\Delta^{++} \bar{\Delta}^{--}$	(1.28 ± 0.35) × 10 ⁻⁴	
Γ_{24} $\Lambda \bar{\Lambda} \pi^0$	< 2.9 × 10 ⁻⁶	CL=90%
Γ_{25} $\Lambda \bar{\Lambda} \eta$	(2.5 ± 0.4) × 10 ⁻⁵	
Γ_{26} $\Lambda \bar{\Lambda} K^+$	(1.00 ± 0.14) × 10 ⁻⁴	
Γ_{27} $K^*(892)^+ \bar{p} \Lambda + \text{c.c.}$	(6.3 ± 0.7) × 10 ⁻⁵	
Γ_{28} $\Lambda \bar{\Lambda} K^+ \pi^+ \pi^-$	(1.8 ± 0.4) × 10 ⁻⁴	
Γ_{29} $\Lambda \bar{\Lambda} \pi^+ \pi^-$	(2.8 ± 0.6) × 10 ⁻⁴	
Γ_{30} $\Lambda \bar{\Lambda}$	(3.81 ± 0.13) × 10 ⁻⁴	S=1.4
Γ_{31} $\Lambda \bar{\Sigma}^+ \pi^- + \text{c.c.}$	(1.40 ± 0.13) × 10 ⁻⁴	
Γ_{32} $\Lambda \bar{\Sigma}^- \pi^+ + \text{c.c.}$	(1.54 ± 0.14) × 10 ⁻⁴	
Γ_{33} $\Lambda \bar{\Sigma}^0$	(1.23 ± 0.24) × 10 ⁻⁵	
Γ_{34} $\Sigma^0 \bar{p} K^+ + \text{c.c.}$	(1.67 ± 0.18) × 10 ⁻⁵	
Γ_{35} $\Sigma^+ \bar{\Sigma}^-$	(2.32 ± 0.12) × 10 ⁻⁴	
Γ_{36} $\Sigma^0 \bar{\Sigma}^0$	(2.35 ± 0.09) × 10 ⁻⁴	S=1.1
Γ_{37} $\Sigma(1385)^+ \bar{\Sigma}(1385)^-$	(8.5 ± 0.7) × 10 ⁻⁵	
Γ_{38} $\Sigma(1385)^- \bar{\Sigma}(1385)^+$	(8.5 ± 0.8) × 10 ⁻⁵	
Γ_{39} $\Sigma(1385)^0 \bar{\Sigma}(1385)^0$	(6.9 ± 0.7) × 10 ⁻⁵	
Γ_{40} $\Xi^- \bar{\Xi}^+$	(2.87 ± 0.11) × 10 ⁻⁴	S=1.1
Γ_{41} $\Xi^0 \bar{\Xi}^0$	(2.3 ± 0.4) × 10 ⁻⁴	S=4.2
Γ_{42} $\Xi(1530)^0 \bar{\Xi}(1530)^0$	(5.2 ± 3.2 _{-1.2}) × 10 ⁻⁵	
Γ_{43} $K^- \Lambda \bar{\Xi}^+ + \text{c.c.}$	(3.9 ± 0.4) × 10 ⁻⁵	
Γ_{44} $\Xi(1530)^- \bar{\Xi}(1530)^+$	(1.15 ± 0.07) × 10 ⁻⁴	
Γ_{45} $\Xi(1530)^- \bar{\Xi}^+$	(7.0 ± 1.2) × 10 ⁻⁶	
Γ_{46} $\Xi(1690)^- \bar{\Xi}^+ \rightarrow K^- \Lambda \bar{\Xi}^+ + \text{c.c.}$	(5.2 ± 1.6) × 10 ⁻⁶	
Γ_{47} $\Xi(1820)^- \bar{\Xi}^+ \rightarrow K^- \Lambda \bar{\Xi}^+ + \text{c.c.}$	(1.20 ± 0.32) × 10 ⁻⁵	
Γ_{48} $K^- \Sigma^0 \bar{\Xi}^+ + \text{c.c.}$	(3.7 ± 0.4) × 10 ⁻⁵	
Γ_{49} $\Omega^- \bar{\Omega}^+$	(5.2 ± 0.4) × 10 ⁻⁵	
Γ_{50} $\pi^0 p\bar{p}$	(1.53 ± 0.07) × 10 ⁻⁴	
Γ_{51} $N(940) \bar{p} + \text{c.c.} \rightarrow \pi^0 p\bar{p}$	(6.4 ± 1.8 _{-1.3}) × 10 ⁻⁵	
Γ_{52} $N(1440) \bar{p} + \text{c.c.} \rightarrow \pi^0 p\bar{p}$	(7.3 ± 1.7 _{-1.5}) × 10 ⁻⁵	S=2.5
Γ_{53} $N(1520) \bar{p} + \text{c.c.} \rightarrow \pi^0 p\bar{p}$	(6.4 ± 2.3 _{-1.8}) × 10 ⁻⁶	
Γ_{54} $N(1535) \bar{p} + \text{c.c.} \rightarrow \pi^0 p\bar{p}$	(2.5 ± 1.0) × 10 ⁻⁵	
Γ_{55} $N(1650) \bar{p} + \text{c.c.} \rightarrow \pi^0 p\bar{p}$	(3.8 ± 1.4 _{-1.7}) × 10 ⁻⁵	
Γ_{56} $N(1720) \bar{p} + \text{c.c.} \rightarrow \pi^0 p\bar{p}$	(1.79 ± 0.26 _{-0.70}) × 10 ⁻⁵	
Γ_{57} $N(2300) \bar{p} + \text{c.c.} \rightarrow \pi^0 p\bar{p}$	(2.6 ± 1.2 _{-0.7}) × 10 ⁻⁵	
Γ_{58} $N(2570) \bar{p} + \text{c.c.} \rightarrow \pi^0 p\bar{p}$	(2.13 ± 0.40 _{-0.31}) × 10 ⁻⁵	
Γ_{59} $\pi^0 f_0(2100) \rightarrow \pi^0 p\bar{p}$	(1.1 ± 0.4) × 10 ⁻⁵	
Γ_{60} $\eta p\bar{p}$	(6.0 ± 0.4) × 10 ⁻⁵	
Γ_{61} $\eta f_0(2100) \rightarrow \eta p\bar{p}$	(1.2 ± 0.4) × 10 ⁻⁵	
Γ_{62} $N(1535) \bar{p} \rightarrow \eta p\bar{p}$	(4.4 ± 0.7) × 10 ⁻⁵	
Γ_{63} $\omega p\bar{p}$	(6.9 ± 2.1) × 10 ⁻⁵	
Γ_{64} $\eta' p\bar{p}$	(1.10 ± 0.13) × 10 ⁻⁵	
Γ_{65} $\phi p\bar{p}$	(6.1 ± 0.6) × 10 ⁻⁶	
Γ_{66} $\phi X(1835) \rightarrow \phi p\bar{p}$	< 1.82 × 10 ⁻⁷	CL=90%
Γ_{67} $\pi^+ \pi^- p\bar{p}$	(6.0 ± 0.4) × 10 ⁻⁴	
Γ_{68} $p\bar{p} \pi^-$ or c.c.	(2.48 ± 0.17) × 10 ⁻⁴	
Γ_{69} $p\bar{p} \pi^- \pi^0$	(3.2 ± 0.7) × 10 ⁻⁴	
Γ_{70} $2(\pi^+ \pi^- \pi^0)$	(4.8 ± 1.5) × 10 ⁻³	
Γ_{71} $\eta \pi^+ \pi^-$	< 1.6 × 10 ⁻⁴	CL=90%
Γ_{72} $\eta \pi^+ \pi^- \pi^0$	(9.5 ± 1.7) × 10 ⁻⁴	
Γ_{73} $2(\pi^+ \pi^-) \eta$	(1.2 ± 0.6) × 10 ⁻³	
Γ_{74} $\pi^+ \pi^- \pi^0 \pi^0 \eta$	< 4 × 10 ⁻⁴	CL=90%
Γ_{75} $\eta' \pi^+ \pi^- \pi^0$	(4.5 ± 2.1) × 10 ⁻⁴	
Γ_{76} $\omega \pi^+ \pi^-$	(7.3 ± 1.2) × 10 ⁻⁴	S=2.1
Γ_{77} $b_1^\pm \pi^\mp$	(4.0 ± 0.6) × 10 ⁻⁴	S=1.1
Γ_{78} $b_1^0 \pi^0$	(2.4 ± 0.6) × 10 ⁻⁴	
Γ_{79} $\omega f_2(1270)$	(2.2 ± 0.4) × 10 ⁻⁴	
Γ_{80} $\omega \pi^0 \pi^0$	(1.11 ± 0.35) × 10 ⁻³	
Γ_{81} $\pi^0 \pi^0 K^+ K^-$	(2.6 ± 1.3) × 10 ⁻⁴	
Γ_{82} $\pi^+ \pi^- K^+ K^-$	(7.3 ± 0.5) × 10 ⁻⁴	

Meson Particle Listings

$\psi(2S)$

Γ_{83}	$\pi^0 \pi^0 K_S^0 K_L^0$	$(1.3 \pm 0.6) \times 10^{-3}$		Γ_{150}	$\bar{\Theta}(1540) K_S^0 p \rightarrow K_S^0 p K^- \bar{n}$	< 6.0	$\times 10^{-6}$	CL=90%
Γ_{84}	$\rho^0 K^+ K^-$	$(2.2 \pm 0.4) \times 10^{-4}$		Γ_{151}	$K_S^0 K_S^0$	< 4.6	$\times 10^{-6}$	
Γ_{85}	$K^*(892)^0 \bar{K}_2^*(1430)^0$	$(1.9 \pm 0.5) \times 10^{-4}$		Γ_{152}	$\Lambda_c^+ \bar{p} e^+ e^- + c.c.$	< 1.7	$\times 10^{-6}$	CL=90%
Γ_{86}	$K^+ K^- \pi^+ \pi^- \eta$	$(1.3 \pm 0.7) \times 10^{-3}$		Radiative decays				
Γ_{87}	$K^+ K^- 2(\pi^+ \pi^-) \pi^0$	$(1.00 \pm 0.31) \times 10^{-3}$		Γ_{153}	$\gamma \chi_{c0}(1P)$	$(9.79 \pm 0.20) \%$		
Γ_{88}	$K^+ K^- 2(\pi^+ \pi^-)$	$(1.9 \pm 0.9) \times 10^{-3}$		Γ_{154}	$\gamma \chi_{c1}(1P)$	$(9.75 \pm 0.24) \%$		
Γ_{89}	$K_1(1270)^\pm K^\mp$	$(1.00 \pm 0.28) \times 10^{-3}$		Γ_{155}	$\gamma \chi_{c2}(1P)$	$(9.52 \pm 0.20) \%$		
Γ_{90}	$K_S^0 K_S^0 \pi^+ \pi^-$	$(2.2 \pm 0.4) \times 10^{-4}$		Γ_{156}	$\gamma \eta_c(1S)$	$(3.4 \pm 0.5) \times 10^{-3}$	S=1.3	
Γ_{91}	$\rho^0 p \bar{p}$	$(5.0 \pm 2.2) \times 10^{-5}$		Γ_{157}	$\gamma \eta_c(2S)$	$(7 \pm 5) \times 10^{-4}$		
Γ_{92}	$K^+ \bar{K}^*(892)^0 \pi^- + c.c.$	$(6.7 \pm 2.5) \times 10^{-4}$		Γ_{158}	$\gamma \pi^0$	$(1.04 \pm 0.22) \times 10^{-6}$	S=1.4	
Γ_{93}	$2(\pi^+ \pi^-)$	$(2.4 \pm 0.6) \times 10^{-4}$	S=2.2	Γ_{159}	$\gamma \eta'(958)$	$(1.24 \pm 0.04) \times 10^{-4}$		
Γ_{94}	$\rho^0 \pi^+ \pi^-$	$(2.2 \pm 0.6) \times 10^{-4}$	S=1.4	Γ_{160}	$\gamma f_2(1270)$	$(2.73^{+0.29}_{-0.25}) \times 10^{-4}$	S=1.8	
Γ_{95}	$K^+ K^- \pi^+ \pi^- \pi^0$	$(1.26 \pm 0.09) \times 10^{-3}$		Γ_{161}	$\gamma f_0(1370) \rightarrow \gamma K \bar{K}$	$(3.1 \pm 1.7) \times 10^{-5}$		
Γ_{96}	$\omega f_0(1710) \rightarrow \omega K^+ K^-$	$(5.9 \pm 2.2) \times 10^{-5}$		Γ_{162}	$\gamma f_0(1500)$	$(9.3 \pm 1.9) \times 10^{-5}$		
Γ_{97}	$K^*(892)^0 K^- \pi^+ \pi^0 + c.c.$	$(8.6 \pm 2.2) \times 10^{-4}$		Γ_{163}	$\gamma f_2'(1525)$	$(3.3 \pm 0.8) \times 10^{-5}$		
Γ_{98}	$K^*(892)^+ K^- \pi^+ \pi^- + c.c.$	$(9.6 \pm 2.8) \times 10^{-4}$		Γ_{164}	$\gamma f_0(1710)$			
Γ_{99}	$K^*(892)^+ K^- \rho^0 + c.c.$	$(7.3 \pm 2.6) \times 10^{-4}$		Γ_{165}	$\gamma f_0(1710) \rightarrow \gamma \pi \pi$	$(3.5 \pm 0.6) \times 10^{-5}$		
Γ_{100}	$K^*(892)^0 K^- \rho^+ + c.c.$	$(6.1 \pm 1.8) \times 10^{-4}$		Γ_{166}	$\gamma f_0(1710) \rightarrow \gamma K \bar{K}$	$(6.6 \pm 0.7) \times 10^{-5}$		
Γ_{101}	$\eta K^+ K^-$, no $\eta \phi$	$(3.1 \pm 0.4) \times 10^{-5}$		Γ_{167}	$\gamma f_0(2100) \rightarrow \gamma \pi \pi$	$(4.8 \pm 1.0) \times 10^{-6}$		
Γ_{102}	$\omega K^+ K^-$	$(1.62 \pm 0.11) \times 10^{-4}$	S=1.1	Γ_{168}	$\gamma f_0(2200) \rightarrow \gamma K \bar{K}$	$(3.2 \pm 1.0) \times 10^{-6}$		
Γ_{103}	$\omega K^*(892)^+ K^- + c.c.$	$(2.07 \pm 0.26) \times 10^{-4}$		Γ_{169}	$\gamma f_j(2220) \rightarrow \gamma \pi \pi$	< 5.8	$\times 10^{-6}$	CL=90%
Γ_{104}	$\omega K_2^*(1430)^+ K^- + c.c.$	$(6.1 \pm 1.2) \times 10^{-5}$		Γ_{170}	$\gamma f_j(2220) \rightarrow \gamma K \bar{K}$	< 9.5	$\times 10^{-6}$	CL=90%
Γ_{105}	$\omega \bar{K}^*(892)^0 K^0$	$(1.68 \pm 0.30) \times 10^{-4}$		Γ_{171}	$\gamma \gamma$	< 1.5	$\times 10^{-4}$	CL=90%
Γ_{106}	$\omega \bar{K}_2^*(1430)^0 K^0$	$(5.8 \pm 2.2) \times 10^{-5}$		Γ_{172}	$\gamma \eta$	$(9.2 \pm 1.8) \times 10^{-7}$		
Γ_{107}	$\omega X(1440) \rightarrow \omega K_S^0 K^- \pi^+ + c.c.$	$(1.6 \pm 0.4) \times 10^{-5}$		Γ_{173}	$\gamma \eta \pi^+ \pi^-$	$(8.7 \pm 2.1) \times 10^{-4}$		
Γ_{108}	$\omega X(1440) \rightarrow \omega K^+ K^- \pi^0$	$(1.09 \pm 0.26) \times 10^{-5}$		Γ_{174}	$\gamma \eta(1405)$			
Γ_{109}	$\omega f_1(1285) \rightarrow \omega K_S^0 K^- \pi^+ + c.c.$	$(3.0 \pm 1.0) \times 10^{-6}$		Γ_{175}	$\gamma \eta(1405) \rightarrow \gamma K \bar{K} \pi$	< 9	$\times 10^{-5}$	CL=90%
Γ_{110}	$\omega f_1(1285) \rightarrow \omega K^+ K^- \pi^0$	$(1.2 \pm 0.7) \times 10^{-6}$		Γ_{176}	$\gamma \eta(1405) \rightarrow \eta \pi^+ \pi^-$	$(3.6 \pm 2.5) \times 10^{-5}$		
Γ_{111}	$3(\pi^+ \pi^-)$	$(3.5 \pm 2.0) \times 10^{-4}$	S=2.8	Γ_{177}	$\gamma \eta(1405) \rightarrow \gamma f_0(980) \pi^0 \rightarrow \gamma \pi^+ \pi^- \pi^0$	< 5.0	$\times 10^{-7}$	CL=90%
Γ_{112}	$p \bar{p} \pi^+ \pi^- \pi^0$	$(7.3 \pm 0.7) \times 10^{-4}$		Γ_{178}	$\gamma \eta(1475)$			
Γ_{113}	$K^+ K^-$	$(7.5 \pm 0.5) \times 10^{-5}$		Γ_{179}	$\gamma \eta(1475) \rightarrow K \bar{K} \pi$	< 1.4	$\times 10^{-4}$	CL=90%
Γ_{114}	$K_S^0 K_L^0$	$(5.34 \pm 0.33) \times 10^{-5}$		Γ_{180}	$\gamma \eta(1475) \rightarrow \eta \pi^+ \pi^-$	< 8.8	$\times 10^{-5}$	CL=90%
Γ_{115}	$\pi^+ \pi^- \pi^0$	$(2.01 \pm 0.17) \times 10^{-4}$	S=1.7	Γ_{181}	$\gamma 2(\pi^+ \pi^-)$	$(4.0 \pm 0.6) \times 10^{-4}$		
Γ_{116}	$\rho(2150) \pi \rightarrow \pi^+ \pi^- \pi^0$	$(1.9^{+1.2}_{-0.4}) \times 10^{-4}$		Γ_{182}	$\gamma K^{*0} K^+ \pi^- + c.c.$	$(3.7 \pm 0.9) \times 10^{-4}$		
Γ_{117}	$\rho(770) \pi \rightarrow \pi^+ \pi^- \pi^0$	$(3.2 \pm 1.2) \times 10^{-5}$	S=1.8	Γ_{183}	$\gamma K^{*0} \bar{K}^{*0}$	$(2.4 \pm 0.7) \times 10^{-4}$		
Γ_{118}	$\pi^+ \pi^-$	$(7.8 \pm 2.6) \times 10^{-6}$		Γ_{184}	$\gamma K_S^0 K^+ \pi^- + c.c.$	$(2.6 \pm 0.5) \times 10^{-4}$		
Γ_{119}	$K_1(1400)^\pm K^\mp$	< 3.1	CL=90%	Γ_{185}	$\gamma K^+ K^- \pi^+ \pi^-$	$(1.9 \pm 0.5) \times 10^{-4}$		
Γ_{120}	$K_2^*(1430)^\pm K^\mp$	$(7.1^{+1.3}_{-0.9}) \times 10^{-5}$		Γ_{186}	$\gamma p \bar{p}$	$(3.9 \pm 0.5) \times 10^{-5}$	S=2.0	
Γ_{121}	$K^+ K^- \pi^0$	$(4.07 \pm 0.31) \times 10^{-5}$		Γ_{187}	$\gamma f_2(1950) \rightarrow \gamma p \bar{p}$	$(1.20 \pm 0.22) \times 10^{-5}$		
Γ_{122}	$K_S^0 K_L^0 \pi^0$	< 3.0	CL=90%	Γ_{188}	$\gamma f_2(2150) \rightarrow \gamma p \bar{p}$	$(7.2 \pm 1.8) \times 10^{-6}$		
Γ_{123}	$K_S^0 K_L^0 \eta$	$(1.3 \pm 0.5) \times 10^{-3}$		Γ_{189}	$\gamma X(1835) \rightarrow \gamma p \bar{p}$	$(4.6^{+1.8}_{-4.0}) \times 10^{-6}$		
Γ_{124}	$K^+ K^*(892)^- + c.c.$	$(2.9 \pm 0.4) \times 10^{-5}$	S=1.2	Γ_{190}	$\gamma X \rightarrow \gamma p \bar{p}$	$[a] < 2$	$\times 10^{-6}$	CL=90%
Γ_{125}	$K^*(892)^0 \bar{K}^0 + c.c.$	$(1.09 \pm 0.20) \times 10^{-4}$		Γ_{191}	$\gamma \pi^+ \pi^- p \bar{p}$	$(2.8 \pm 1.4) \times 10^{-5}$		
Γ_{126}	$\phi \pi^+ \pi^-$	$(1.18 \pm 0.26) \times 10^{-4}$	S=1.5	Γ_{192}	$\gamma 2(\pi^+ \pi^-) K^+ K^-$	< 2.2	$\times 10^{-4}$	CL=90%
Γ_{127}	$\phi f_0(980) \rightarrow \pi^+ \pi^-$	$(7.5 \pm 3.3) \times 10^{-5}$	S=1.6	Γ_{193}	$\gamma 3(\pi^+ \pi^-)$	< 1.7	$\times 10^{-4}$	CL=90%
Γ_{128}	$2(K^+ K^-)$	$(6.3 \pm 1.3) \times 10^{-5}$		Γ_{194}	$\gamma K^+ K^- K^+ K^-$	< 4	$\times 10^{-5}$	CL=90%
Γ_{129}	$\phi K^+ K^-$	$(7.0 \pm 1.6) \times 10^{-5}$		Γ_{195}	$\gamma \gamma J/\psi$	$(3.1^{+1.0}_{-1.2}) \times 10^{-4}$		
Γ_{130}	$2(K^+ K^-) \pi^0$	$(1.10 \pm 0.28) \times 10^{-4}$		Γ_{196}	$e^+ e^- \eta'$	$(1.90 \pm 0.26) \times 10^{-6}$		
Γ_{131}	$\phi \eta$	$(3.10 \pm 0.31) \times 10^{-5}$		Γ_{197}	$e^+ e^- \chi_{c0}(1P)$	$(1.06 \pm 0.24) \times 10^{-3}$		
Γ_{132}	$\eta \phi(2170)$, $\phi(2170) \rightarrow \phi f_0(980)$, $f_0 \rightarrow \pi^+ \pi^-$	< 2.2	CL=90%	Γ_{198}	$e^+ e^- \chi_{c1}(1P)$	$(8.5 \pm 0.6) \times 10^{-4}$		
Γ_{133}	$\phi \eta'$	$(1.54 \pm 0.20) \times 10^{-5}$		Γ_{199}	$e^+ e^- \chi_{c2}(1P)$	$(7.0 \pm 0.8) \times 10^{-4}$		
Γ_{134}	$\phi f_1(1285)$	$(3.0 \pm 1.3) \times 10^{-5}$		Weak decays				
Γ_{135}	$\phi \eta(1405) \rightarrow \phi \pi^+ \pi^- \eta$	$(8.5 \pm 1.7) \times 10^{-6}$		Γ_{200}	$D^0 e^+ e^- + c.c.$	< 1.4	$\times 10^{-7}$	CL=90%
Γ_{136}	$\omega \eta'$	$(3.2^{+2.5}_{-2.1}) \times 10^{-5}$		Other decays				
Γ_{137}	$\omega \pi^0$	$(2.1 \pm 0.6) \times 10^{-5}$		Γ_{201}	invisible	< 1.6	$\%$	CL=90%
Γ_{138}	$\rho \eta'$	$(1.9^{+1.7}_{-1.2}) \times 10^{-5}$		[a] For a narrow resonance in the range $2.2 < M(X) < 2.8$ GeV.				
Γ_{139}	$\rho \eta$	$(2.2 \pm 0.6) \times 10^{-5}$	S=1.1	CONSTRAINED FIT INFORMATION				
Γ_{140}	$\omega \eta$	< 1.1	CL=90%	A multiparticle fit to $\chi_{c1}(1P)$, $\chi_{c0}(1P)$, $\chi_{c2}(1P)$, and $\psi(2S)$ with 4 total widths, a partial width, 25 combinations of partial widths obtained from integrated cross section, and 84 branching ratios uses 248 measurements to determine 49 parameters. The overall fit has a $\chi^2 = 378.1$ for 199 degrees of freedom.				
Γ_{141}	$\phi \pi^0$	< 4	CL=90%	The following off-diagonal array elements are the correlation coefficients $\langle \delta p_i \delta p_j \rangle / (\delta p_i \delta p_j)$, in percent, from the fit to parameters p_i , including the branching fractions, $x_i \equiv \Gamma_i / \Gamma_{\text{total}}$.				
Γ_{142}	$\eta_c \pi^+ \pi^- \pi^0$	< 1.0	CL=90%					
Γ_{143}	$p \bar{p} K^+ K^-$	$(2.7 \pm 0.7) \times 10^{-5}$						
Γ_{144}	$\bar{\Lambda} n K_S^0 + c.c.$	$(8.1 \pm 1.8) \times 10^{-5}$						
Γ_{145}	$\phi f_2'(1525)$	$(4.4 \pm 1.6) \times 10^{-5}$						
Γ_{146}	$\Theta(1540) \bar{\Theta}(1540) \rightarrow K_S^0 p K^- \bar{n} + c.c.$	< 8.8	CL=90%					
Γ_{147}	$\Theta(1540) K^- \bar{n} \rightarrow K_S^0 p K^- \bar{n}$	< 1.0	CL=90%					
Γ_{148}	$\Theta(1540) K_S^0 \bar{p} \rightarrow K_S^0 \bar{p} K^+ n$	< 7.0	CL=90%					
Γ_{149}	$\bar{\Theta}(1540) K^+ n \rightarrow K_S^0 \bar{p} K^+ n$	< 2.6	CL=90%					

x_7	3									
x_8	1	0								
x_{11}	29	11	2							
x_{12}	28	6	1	48						
x_{13}	13	4	1	36	15					
x_{21}	0	0	0	4	3	2				
x_{153}	1	0	0	2	1	1	0			
x_{154}	1	0	0	2	1	1	0	0		
x_{155}	1	0	0	3	1	1	0	0	0	
Γ	-81	-4	-1	-38	-34	-16	-7	-1	-1	-1
	x_6	x_7	x_8	x_{11}	x_{12}	x_{13}	x_{21}	x_{153}	x_{154}	x_{155}

$\psi(2S)$ PARTIAL WIDTHS

$\Gamma(\text{hadrons})$

VALUE (keV)	DOCUMENT ID	TECN	COMMENT
258±26	BAI	02B	BES2 e^+e^-
224±56	LUTH	75	MRK1 e^+e^-

$\Gamma(e^+e^-)$

VALUE (keV)	DOCUMENT ID	TECN	COMMENT
2.33 ± 0.04 OUR FIT			
2.29 ± 0.06 OUR AVERAGE			
2.23 ± 0.10 ± 0.02	¹ ABLIKIM	15v	BES3 4.0-4.4 $e^+e^- \rightarrow \pi^+\pi^- J/\psi$
2.338±0.037±0.096	ABLIKIM	08B	BES2 $e^+e^- \rightarrow$ hadrons
2.330±0.036±0.110	ABLIKIM	06L	BES2 $e^+e^- \rightarrow$ hadrons
2.44 ± 0.21	² BAI	02B	BES2 e^+e^-
2.14 ± 0.21	ALEXANDER	89	RVUE See Υ mini-review
2.279±0.015±0.042	³ ANASHIN	18	KEDR e^+e^-
2.282±0.015±0.042	⁴ ANASHIN	18	KEDR e^+e^-
2.0 ± 0.3	BRANDELIK	79c	DASP e^+e^-
2.1 ± 0.3	⁵ LUTH	75	MRK1 e^+e^-

¹ ABLIKIM 15v reports 2.213 ± 0.018 ± 0.099 keV from a measurement of $[\Gamma(\psi(2S) \rightarrow e^+e^-)] \times [B(\psi(2S) \rightarrow J/\psi(1S)\pi^+\pi^-)]$ assuming $B(\psi(2S) \rightarrow J/\psi(1S)\pi^+\pi^-) = (34.95 \pm 0.45) \times 10^{-2}$, which we rescale to our best value $B(\psi(2S) \rightarrow J/\psi(1S)\pi^+\pi^-) = (34.68 \pm 0.30) \times 10^{-2}$. Our first error is their experiment's error and our second error is the systematic error from using our best value.

² From a simultaneous fit to e^+e^- , $\mu^+\mu^-$, and hadronic channel, assuming $\Gamma_e = \Gamma_\mu = \Gamma_\tau/0.38847$.

³ Combining $\Gamma_{e^+e^-} \cdot B(\mu^+\mu^-)$ from ANASHIN 18 with $\Gamma_{e^+e^-} \cdot B(\text{hadrons})$ from ANASHIN 12 and assuming lepton universality.

⁴ From the sum of $\Gamma_{e^+e^-} \cdot B(\text{hadrons})$ from ANASHIN 12, $\Gamma_{e^+e^-} \cdot B(e^+e^-)$ and $\Gamma_{e^+e^-} \cdot B(\mu^+\mu^-)$ from ANASHIN 18, and $\Gamma_{e^+e^-} \cdot B(\tau^+\tau^-)$ from ANASHIN 07.

⁵ From a simultaneous fit to e^+e^- , $\mu^+\mu^-$, and hadronic channels assuming $\Gamma(e^+e^-) = \Gamma(\mu^+\mu^-)$.

$\Gamma(\gamma\gamma)$

VALUE (eV)	CL%	DOCUMENT ID	TECN	COMMENT
<43	90	BRANDELIK	79c	DASP e^+e^-

$\psi(2S) \Gamma(i)\Gamma(e^+e^-)/\Gamma(\text{total})$

This combination of a partial width with the partial width into e^+e^- and with the total width is obtained from the integrated cross section into channel(i) in the e^+e^- annihilation. We list only data that have not been used to determine the partial width $\Gamma(i)$ or the branching ratio $\Gamma(i)/\text{total}$.

$\Gamma(\text{hadrons}) \times \Gamma(e^+e^-)/\Gamma_{\text{total}}$

VALUE (keV)	DOCUMENT ID	TECN	COMMENT
2.233±0.015±0.042	¹ ANASHIN	12	KEDR $e^+e^- \rightarrow$ hadrons
2.2 ± 0.4	ABRAMS	75	MRK1 e^+e^-

¹ ANASHIN 12 reports the value 2.233 ± 0.015 ± 0.037 ± 0.020 keV, where the third uncertainty is due to assumptions on the interference between the resonance and hadronic continuum. We combined the two systematic uncertainties.

$\Gamma(e^+e^-) \times \Gamma(e^+e^-)/\Gamma_{\text{total}}$

VALUE (eV)	DOCUMENT ID	TECN	COMMENT
21.2±0.7±1.2	¹ ANASHIN	18	KEDR e^+e^-

¹ From the average of nine scans of the $\psi(2S)$.

$\Gamma(\mu^+\mu^-) \times \Gamma(e^+e^-)/\Gamma_{\text{total}}$

VALUE (eV)	DOCUMENT ID	TECN	COMMENT
19.3±0.3±0.5	¹ ANASHIN	18	KEDR $\psi(2S) \rightarrow \mu^+\mu^-$

¹ From the average of nine scans of the $\psi(2S)$.

$\Gamma(\tau^+\tau^-) \times \Gamma(e^+e^-)/\Gamma_{\text{total}}$

VALUE (eV)	EVTs	DOCUMENT ID	TECN	COMMENT
9.0±2.6	79	¹ ANASHIN	07	KEDR $e^+e^- \rightarrow \psi(2S) \rightarrow \tau^+\tau^-$

¹ Using $\psi(2S)$ total width of 337 ± 13 keV. Systematic errors not evaluated.

$\Gamma(J/\psi(1S)\pi^+\pi^-) \times \Gamma(e^+e^-)/\Gamma_{\text{total}}$

VALUE (keV)	EVTs	DOCUMENT ID	TECN	COMMENT
0.808±0.013 OUR FIT				
0.837±0.025 OUR AVERAGE				Error includes scale factor of 1.3. See the ideogram below.
0.837±0.028±0.005		¹ LEES	12E	BABR 10.6 $e^+e^- \rightarrow 2\pi^+2\pi^-\gamma$
0.852±0.010±0.026	19.5k	ADAM	06	CLEO 3.773 $e^+e^- \rightarrow \gamma\psi(2S)$
0.68 ± 0.09		² BAI	98E	BES e^+e^-
0.88 ± 0.08 ± 0.03	256	³ AUBERT	07AU	BABR 10.6 $e^+e^- \rightarrow J/\psi\pi^+\pi^-\gamma$
0.755±0.048±0.004	544	⁴ AUBERT	05D	BABR 10.6 $e^+e^- \rightarrow \pi^+\pi^-\mu^+\mu^-\gamma$

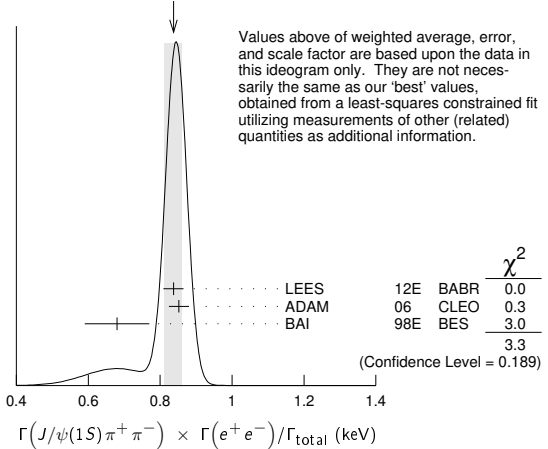
¹ LEES 12E reports $[\Gamma(\psi(2S) \rightarrow J/\psi(1S)\pi^+\pi^-) \times \Gamma(\psi(2S) \rightarrow e^+e^-)/\Gamma_{\text{total}}] \times [B(J/\psi(1S) \rightarrow \mu^+\mu^-)] = (49.9 \pm 1.3 \pm 1.0) \times 10^{-3}$ keV which we divide by our best value $B(J/\psi(1S) \rightarrow \mu^+\mu^-) = (5.961 \pm 0.033) \times 10^{-2}$. Our first error is their experiment's error and our second error is the systematic error from using our best value.

² The value of $\Gamma(e^+e^-)$ quoted in BAI 98E is derived using $B(\psi(2S) \rightarrow J/\psi(1S)\pi^+\pi^-) = (32.4 \pm 2.6) \times 10^{-2}$ and $B(J/\psi(1S) \rightarrow \ell^+\ell^-) = 0.1203 \pm 0.0038$. Recalculated by us using $B(J/\psi(1S) \rightarrow \ell^+\ell^-) = 0.1181 \pm 0.0020$.

³ AUBERT 07AU reports $[\Gamma(\psi(2S) \rightarrow J/\psi(1S)\pi^+\pi^-) \times \Gamma(\psi(2S) \rightarrow e^+e^-)/\Gamma_{\text{total}}] \times [B(J/\psi(1S) \rightarrow \pi^+\pi^-\pi^0)] = 0.0186 \pm 0.0012 \pm 0.0011$ keV which we divide by our best value $B(J/\psi(1S) \rightarrow \pi^+\pi^-\pi^0) = (2.10 \pm 0.08) \times 10^{-2}$. Our first error is their experiment's error and our second error is the systematic error from using our best value.

⁴ AUBERT 05D reports $[\Gamma(\psi(2S) \rightarrow J/\psi(1S)\pi^+\pi^-) \times \Gamma(\psi(2S) \rightarrow e^+e^-)/\Gamma_{\text{total}}] \times [B(J/\psi(1S) \rightarrow \mu^+\mu^-)] = 0.0450 \pm 0.0018 \pm 0.0022$ keV which we divide by our best value $B(J/\psi(1S) \rightarrow \mu^+\mu^-) = (5.961 \pm 0.033) \times 10^{-2}$. Our first error is their experiment's error and our second error is the systematic error from using our best value. Superseded by LEES 12E.

WEIGHTED AVERAGE
0.837±0.025 (Error scaled by 1.3)



$\Gamma(J/\psi(1S)\pi^0\pi^0) \times \Gamma(e^+e^-)/\Gamma_{\text{total}}$

VALUE (keV)	EVTs	DOCUMENT ID	TECN	COMMENT
0.425±0.009 OUR FIT				
0.411±0.008±0.018	3.6k	ADAM	06	CLEO 3.773 $e^+e^- \rightarrow \gamma\psi(2S)$
0.48 ± 0.09 ± 0.02	142	¹ LEES	18E	BABR 10.6 $e^+e^- \rightarrow J/\psi\pi^0\pi^0\gamma$

¹ LEES 18E reports $[\Gamma(\psi(2S) \rightarrow J/\psi(1S)\pi^0\pi^0) \times \Gamma(\psi(2S) \rightarrow e^+e^-)/\Gamma_{\text{total}}] \times [B(J/\psi(1S) \rightarrow \pi^+\pi^-\pi^0)] = 0.0101 \pm 0.0015 \pm 0.0011$ keV which we divide by our best value $B(J/\psi(1S) \rightarrow \pi^+\pi^-\pi^0) = (2.10 \pm 0.08) \times 10^{-2}$. Our first error is their experiment's error and our second error is the systematic error from using our best value.

$\Gamma(J/\psi(1S)\eta) \times \Gamma(e^+e^-)/\Gamma_{\text{total}}$

VALUE (eV)	EVTs	DOCUMENT ID	TECN	COMMENT
78.6± 1.6 OUR FIT				
87 ± 9 OUR AVERAGE				
83 ± 25 ± 5	14	¹ AUBERT	07AU	BABR 10.6 $e^+e^- \rightarrow J/\psi\pi^+\pi^-\pi^0\gamma$
88 ± 6 ± 7	291 ± 24	ADAM	06	CLEO 3.773 $e^+e^- \rightarrow \gamma\psi(2S)$
		¹ AUBERT	07AU	quotes $\Gamma_{ee}^{\psi(2S)} \cdot B(\psi(2S) \rightarrow J/\psi\eta) \cdot B(J/\psi \rightarrow \mu^+\mu^-) \cdot B(\eta \rightarrow \pi^+\pi^-\pi^0) = 1.11 \pm 0.33 \pm 0.07$ eV.

$\Gamma(J/\psi(1S)\pi^0) \times \Gamma(e^+e^-)/\Gamma_{\text{total}}$

VALUE (eV)	CL%	EVTs	DOCUMENT ID	TECN	COMMENT
<8	90	<37	ADAM	06	CLEO 3.773 $e^+e^- \rightarrow \gamma\psi(2S)$

Meson Particle Listings

 $\psi(2S)$ $\Gamma(p\bar{p}) \times \Gamma(e^+e^-)/\Gamma_{\text{total}}$ $\Gamma_{21}\Gamma_6/\Gamma$

VALUE (eV)	EVTS	DOCUMENT ID	TECN	COMMENT
0.686 ± 0.019 OUR FIT				
0.63 ± 0.05 OUR AVERAGE				Error includes scale factor of 1.2.
0.67 ± 0.12 ± 0.02	43	¹ LEES	130	BABR $e^+e^- \rightarrow p\bar{p}\gamma$
0.74 ± 0.07 ± 0.04	142	² LEES	13V	BABR $e^+e^- \rightarrow p\bar{p}\gamma$
0.579 ± 0.038 ± 0.036	2.7k	ANDREOTTI	07	E835 $p\bar{p} \rightarrow e^+e^-, J/\psi X$
• • •				We do not use the following data for averages, fits, limits, etc. • • •
0.70 ± 0.17 ± 0.03	22	³ AUBERT	06B	BABR $e^+e^- \rightarrow p\bar{p}\gamma$

¹ISR photon reconstructed in the detector
²ISR photon undetected
³Superseded by LEES 130

 $\Gamma(\Lambda\bar{\Lambda}) \times \Gamma(e^+e^-)/\Gamma_{\text{total}}$ $\Gamma_{30}\Gamma_6/\Gamma$

VALUE (eV)	DOCUMENT ID	TECN	COMMENT
1.5 ± 0.4 ± 0.1	AUBERT	07BD	BABR 10.6 $e^+e^- \rightarrow \Lambda\bar{\Lambda}\gamma$

 $\Gamma(2(\pi^+\pi^-\pi^0)) \times \Gamma(e^+e^-)/\Gamma_{\text{total}}$ $\Gamma_{70}\Gamma_6/\Gamma$

VALUE (eV)	EVTS	DOCUMENT ID	TECN	COMMENT
11.2 ± 3.3 ± 1.3	43	AUBERT	06D	BABR 10.6 $e^+e^- \rightarrow 2(\pi^+\pi^-\pi^0)\gamma$

 $\Gamma(\pi^0\pi^0K^+K^-) \times \Gamma(e^+e^-)/\Gamma_{\text{total}}$ $\Gamma_{81}\Gamma_6/\Gamma$

VALUE (eV)	EVTS	DOCUMENT ID	TECN	COMMENT
0.60 ± 0.31 ± 0.03	17	LEES	12F	BABR 10.6 $e^+e^- \rightarrow \pi^0\pi^0K^+K^-\gamma$

 $\Gamma(K^+K^-\pi^+\pi^-) \times \Gamma(e^+e^-)/\Gamma_{\text{total}}$ $\Gamma_{88}\Gamma_6/\Gamma$

VALUE (eV)	EVTS	DOCUMENT ID	TECN	COMMENT
4.4 ± 2.1 ± 0.3	26	AUBERT	06D	BABR 10.6 $e^+e^- \rightarrow K^+K^-\pi^+\pi^-\gamma$

 $\Gamma(\pi^+\pi^-K^+K^-) \times \Gamma(e^+e^-)/\Gamma_{\text{total}}$ $\Gamma_{82}\Gamma_6/\Gamma$

VALUE (eV)	EVTS	DOCUMENT ID	TECN	COMMENT
1.92 ± 0.30 ± 0.06	133	LEES	12F	BABR 10.6 $e^+e^- \rightarrow \pi^+\pi^-K^+K^-\gamma$
• • •				We do not use the following data for averages, fits, limits, etc. • • •
2.56 ± 0.42 ± 0.16	85	¹ AUBERT	07AK	BABR 10.6 $e^+e^- \rightarrow \pi^+\pi^-K^+K^-\gamma$
¹ Superseded by LEES 12F.				

 $\Gamma(\pi^0\pi^0K_S^0K_L^0) \times \Gamma(e^+e^-)/\Gamma_{\text{total}}$ $\Gamma_{83}\Gamma_6/\Gamma$

VALUE (eV)	EVTS	DOCUMENT ID	TECN	COMMENT
2.92 ± 1.27 ± 0.15	14	LEES	17A	BABR $e^+e^- \rightarrow K_S^0K_L^0\pi^0\pi^0\gamma$

 $\Gamma(K_S^0K_L^0\pi^0) \times \Gamma(e^+e^-)/\Gamma_{\text{total}}$ $\Gamma_{122}\Gamma_6/\Gamma$

VALUE (eV)	CL%	EVTS	DOCUMENT ID	TECN	COMMENT
<0.7	90	8	LEES	17A	BABR $e^+e^- \rightarrow K_S^0K_L^0\pi^0\gamma$

 $\Gamma(K_S^0K_L^0\eta) \times \Gamma(e^+e^-)/\Gamma_{\text{total}}$ $\Gamma_{123}\Gamma_6/\Gamma$

VALUE (eV)	EVTS	DOCUMENT ID	TECN	COMMENT
3.14 ± 1.08 ± 0.16	16	LEES	17A	BABR $e^+e^- \rightarrow K_S^0K_L^0\eta\gamma$

 $\Gamma(\phi_0(980) \rightarrow \pi^+\pi^-) \times \Gamma(e^+e^-)/\Gamma_{\text{total}}$ $\Gamma_{127}\Gamma_6/\Gamma$

VALUE (eV)	EVTS	DOCUMENT ID	TECN	COMMENT
0.345 ± 0.128 ± 0.004	12	¹ LEES	12F	BABR 10.6 $e^+e^- \rightarrow \pi^+\pi^-K^+K^-\gamma$

• • • We do not use the following data for averages, fits, limits, etc. • • •
0.345 ± 0.168 ± 0.004 6 ± 3 ² AUBERT 07AK BABR 10.6 $e^+e^- \rightarrow \pi^+\pi^-K^+K^-\gamma$

¹ LEES 12F reports $[\Gamma(\psi(2S) \rightarrow \phi_0(980) \rightarrow \pi^+\pi^-) \times \Gamma(\psi(2S) \rightarrow e^+e^-)/\Gamma_{\text{total}}] \times [B(\phi(1020) \rightarrow K^+K^-)] = 0.17 \pm 0.06 \pm 0.02$ eV which we divide by our best value $B(\phi(1020) \rightarrow K^+K^-) = (49.2 \pm 0.5) \times 10^{-2}$. Our first error is their experiment's error and our second error is the systematic error from using our best value.

² Superseded by LEES 12F. AUBERT 07AK reports $[\Gamma(\psi(2S) \rightarrow \phi_0(980) \rightarrow \pi^+\pi^-) \times \Gamma(\psi(2S) \rightarrow e^+e^-)/\Gamma_{\text{total}}] \times [B(\phi(1020) \rightarrow K^+K^-)] = 0.17 \pm 0.08 \pm 0.02$ eV which we divide by our best value $B(\phi(1020) \rightarrow K^+K^-) = (49.2 \pm 0.5) \times 10^{-2}$. Our first error is their experiment's error and our second error is the systematic error from using our best value.

 $\Gamma(2(K^+K^-)) \times \Gamma(e^+e^-)/\Gamma_{\text{total}}$ $\Gamma_{128}\Gamma_6/\Gamma$

VALUE (eV)	EVTS	DOCUMENT ID	TECN	COMMENT
0.22 ± 0.10 ± 0.02	13	LEES	12F	BABR 10.6 $e^+e^- \rightarrow K^+K^-K^+K^-\gamma$

 $\Gamma(\phi\pi^+\pi^-) \times \Gamma(e^+e^-)/\Gamma_{\text{total}}$ $\Gamma_{126}\Gamma_6/\Gamma$

VALUE (eV)	EVTS	DOCUMENT ID	TECN	COMMENT
0.55 ± 0.19 ± 0.01	19	¹ LEES	12F	BABR 10.6 $e^+e^- \rightarrow K^+K^-\pi^+\pi^-\gamma$
• • •				We do not use the following data for averages, fits, limits, etc. • • •
0.57 ± 0.23 ± 0.01	10	² AUBERT, BE	06D	BABR 10.6 $e^+e^- \rightarrow K^+K^-\pi^+\pi^-\gamma$

¹ LEES 12F reports $[\Gamma(\psi(2S) \rightarrow \phi\pi^+\pi^-) \times \Gamma(\psi(2S) \rightarrow e^+e^-)/\Gamma_{\text{total}}] \times [B(\phi(1020) \rightarrow K^+K^-)] = 0.27 \pm 0.09 \pm 0.02$ eV which we divide by our best value $B(\phi(1020) \rightarrow K^+K^-) = (49.2 \pm 0.5) \times 10^{-2}$. Our first error is their experiment's error and our second error is the systematic error from using our best value.

² Superseded by LEES 12F. AUBERT, BE 06D reports $[\Gamma(\psi(2S) \rightarrow \phi\pi^+\pi^-) \times \Gamma(\psi(2S) \rightarrow e^+e^-)/\Gamma_{\text{total}}] \times [B(\phi(1020) \rightarrow K^+K^-)] = 0.28 \pm 0.11 \pm 0.02$ eV which we divide by our best value $B(\phi(1020) \rightarrow K^+K^-) = (49.2 \pm 0.5) \times 10^{-2}$. Our first error is their experiment's error and our second error is the systematic error from using our best value.

 $\Gamma(2(\pi^+\pi^-\pi^0)) \times \Gamma(e^+e^-)/\Gamma_{\text{total}}$ $\Gamma_{17}\Gamma_6/\Gamma$

VALUE (eV)	EVTS	DOCUMENT ID	TECN	COMMENT
29.7 ± 2.2 ± 1.8	410	AUBERT	07AU	BABR 10.6 $e^+e^- \rightarrow 2(\pi^+\pi^-\pi^0)\gamma$

 $\Gamma(\pi^+\pi^-\pi^0\pi^0) \times \Gamma(e^+e^-)/\Gamma_{\text{total}}$ $\Gamma_{19}\Gamma_6/\Gamma$

VALUE (eV)	EVTS	DOCUMENT ID	TECN	COMMENT
12.4 ± 1.8 ± 1.2	177	LEES	18E	BABR 10.6 $e^+e^- \rightarrow \pi^+\pi^-\pi^0\pi^0\gamma$

 $\Gamma(\rho^\pm\pi^\mp\pi^0) \times \Gamma(e^+e^-)/\Gamma_{\text{total}}$ $\Gamma_{20}\Gamma_6/\Gamma$

VALUE (eV)	CL%	DOCUMENT ID	TECN	COMMENT
<6.2	90	LEES	18E	BABR 10.6 $e^+e^- \rightarrow \pi^+\pi^-\pi^0\gamma$

 $\Gamma(\omega\pi^+\pi^-) \times \Gamma(e^+e^-)/\Gamma_{\text{total}}$ $\Gamma_{76}\Gamma_6/\Gamma$

VALUE (eV)	EVTS	DOCUMENT ID	TECN	COMMENT
3.01 ± 0.84 ± 0.02	37	¹ AUBERT	07AU	BABR 10.6 $e^+e^- \rightarrow \omega\pi^+\pi^-\gamma$

¹ AUBERT 07AU reports $[\Gamma(\psi(2S) \rightarrow \omega\pi^+\pi^-) \times \Gamma(\psi(2S) \rightarrow e^+e^-)/\Gamma_{\text{total}}] \times [B(\omega(782) \rightarrow \pi^+\pi^-\pi^0)] = 2.69 \pm 0.73 \pm 0.16$ eV which we divide by our best value $B(\omega(782) \rightarrow \pi^+\pi^-\pi^0) = (89.3 \pm 0.6) \times 10^{-2}$. Our first error is their experiment's error and our second error is the systematic error from using our best value.

 $\Gamma(\omega\pi^0\pi^0) \times \Gamma(e^+e^-)/\Gamma_{\text{total}}$ $\Gamma_{80}\Gamma_6/\Gamma$

VALUE (eV)	EVTS	DOCUMENT ID	TECN	COMMENT
2.58 ± 0.82 ± 0.02	33	¹ LEES	18E	BABR 10.6 $e^+e^- \rightarrow \pi^+\pi^-\pi^0\pi^0\gamma$

¹ LEES 18E reports $[\Gamma(\psi(2S) \rightarrow \omega\pi^0\pi^0) \times \Gamma(\psi(2S) \rightarrow e^+e^-)/\Gamma_{\text{total}}] \times [B(\omega(782) \rightarrow \pi^+\pi^-\pi^0)] = 2.3 \pm 0.7 \pm 0.2$ eV which we divide by our best value $B(\omega(782) \rightarrow \pi^+\pi^-\pi^0) = (89.3 \pm 0.6) \times 10^{-2}$. Our first error is their experiment's error and our second error is the systematic error from using our best value.

 $\Gamma(2(\pi^+\pi^-\eta)) \times \Gamma(e^+e^-)/\Gamma_{\text{total}}$ $\Gamma_{73}\Gamma_6/\Gamma$

VALUE (eV)	EVTS	DOCUMENT ID	TECN	COMMENT
2.87 ± 1.41 ± 0.01	16	¹ AUBERT	07AU	BABR 10.6 $e^+e^- \rightarrow 2(\pi^+\pi^-\eta)\gamma$

¹ AUBERT 07AU reports $[\Gamma(\psi(2S) \rightarrow 2(\pi^+\pi^-\eta)) \times \Gamma(\psi(2S) \rightarrow e^+e^-)/\Gamma_{\text{total}}] \times [B(\eta \rightarrow 2\gamma)] = 1.13 \pm 0.55 \pm 0.08$ eV which we divide by our best value $B(\eta \rightarrow 2\gamma) = (39.41 \pm 0.20) \times 10^{-2}$. Our first error is their experiment's error and our second error is the systematic error from using our best value.

 $\Gamma(\pi^+\pi^-\pi^0\eta) \times \Gamma(e^+e^-)/\Gamma_{\text{total}}$ $\Gamma_{74}\Gamma_6/\Gamma$

VALUE (eV)	CL%	DOCUMENT ID	TECN	COMMENT
<0.85	90	LEES	18E	BABR 10.6 $e^+e^- \rightarrow \pi^+\pi^-\pi^0\eta\gamma$

 $\Gamma(K^+K^-\pi^+\pi^-) \times \Gamma(e^+e^-)/\Gamma_{\text{total}}$ $\Gamma_{95}\Gamma_6/\Gamma$

VALUE (eV)	EVTS	DOCUMENT ID	TECN	COMMENT
4.4 ± 1.3 ± 0.3	32	AUBERT	07AU	BABR 10.6 $e^+e^- \rightarrow K^+K^-\pi^+\pi^-\gamma$

 $\Gamma(K^+K^-\pi^+\pi^-) \times \Gamma(e^+e^-)/\Gamma_{\text{total}}$ $\Gamma_{86}\Gamma_6/\Gamma$

VALUE (eV)	EVTS	DOCUMENT ID	TECN	COMMENT
3.04 ± 1.79 ± 0.02	7	¹ AUBERT	07AU	BABR 10.6 $e^+e^- \rightarrow K^+K^-\pi^+\pi^-\gamma$

¹ AUBERT 07AU reports $[\Gamma(\psi(2S) \rightarrow K^+K^-\pi^+\pi^-) \times \Gamma(\psi(2S) \rightarrow e^+e^-)/\Gamma_{\text{total}}] \times [B(\eta \rightarrow 2\gamma)] = 1.2 \pm 0.7 \pm 0.1$ eV which we divide by our best value $B(\eta \rightarrow 2\gamma) = (39.41 \pm 0.20) \times 10^{-2}$. Our first error is their experiment's error and our second error is the systematic error from using our best value.

 $\Gamma(K^+K^-) \times \Gamma(e^+e^-)/\Gamma_{\text{total}}$ $\Gamma_{113}\Gamma_6/\Gamma$

VALUE (eV)	EVTS	DOCUMENT ID	TECN	COMMENT
• • •				We do not use the following data for averages, fits, limits, etc. • • •
0.147 ± 0.035 ± 0.005	66	¹ LEES	15J	BABR $e^+e^- \rightarrow K^+K^-\gamma$
0.197 ± 0.035 ± 0.005	66	² LEES	15J	BABR $e^+e^- \rightarrow K^+K^-\gamma$
0.35 ± 0.14 ± 0.03	11	³ LEES	13Q	BABR $e^+e^- \rightarrow K^+K^-\gamma$

¹ $\sin\phi > 0$.

² $\sin\phi < 0$.

³ Interference with non-resonant K^+K^- production not taken into account.

 $\psi(2S)$ BRANCHING RATIOS $\Gamma(\text{hadrons})/\Gamma_{\text{total}}$ Γ_1/Γ

VALUE	DOCUMENT ID	TECN	COMMENT
0.9785 ± 0.0013 OUR AVERAGE			
0.9779 ± 0.0015	¹ BAI	02B	BES2 e^+e^-
0.981 ± 0.003	¹ LUTH	75	MRK1 e^+e^-

¹ Includes cascade decay into $J/\psi(1S)$.

 $\Gamma(\text{virtual}\gamma \rightarrow \text{hadrons})/\Gamma_{\text{total}}$ Γ_2/Γ

VALUE	DOCUMENT ID	TECN	COMMENT
0.0173 ± 0.0014 OUR AVERAGE			Error includes scale factor of 1.5.
0.0166 ± 0.0010	^{1,2} SETH	04	RVUE e^+e^-
0.0199 ± 0.0019	¹ BAI	02B	BES2 e^+e^-

• • • We do not use the following data for averages, fits, limits, etc. • • •

0.029 ± 0.004 ¹ LUTH 75 MRK1 e^+e^-

¹ Included in $\Gamma(\text{hadrons})/\Gamma_{\text{total}}$.

² Using $B(\psi(2S) \rightarrow \ell^+\ell^-) = (0.73 \pm 0.04)\%$ from RPP-2002 and $R = 2.28 \pm 0.04$ determined by a fit to data from BAI 00 and BAI 02c.

$\Gamma(ggg)/\Gamma_{total}$ Γ_3/Γ

VALUE (units 10^{-2})	EVTS	DOCUMENT ID	TECN	COMMENT
10.58 ± 0.162	2.9 M	¹ LIBBY 09	CLEO	$\psi(2S) \rightarrow$ hadrons

¹ Calculated using $\Gamma(\gamma gg)/\Gamma(ggg) = 0.097 \pm 0.026 \pm 0.016$ from LIBBY 09, $B(\psi(2S) \rightarrow X J/\psi)$ relative and absolute branching fractions from MENDEZ 08, $B(\psi(2S) \rightarrow \gamma \eta_c)$ from MITCHELL 09, and $B(\psi(2S) \rightarrow$ virtual $\gamma \rightarrow$ hadrons), $B(\psi(2S) \rightarrow \gamma \chi_{cJ})$, and $B(\psi(2S) \rightarrow \ell^+ \ell^-)$ from PDG 08. The statistical error is negligible and the systematic error is largely uncorrelated with that of $\Gamma(\gamma gg)/\Gamma_{total}$ LIBBY 09 measurement.

$\Gamma(\gamma gg)/\Gamma_{total}$ Γ_4/Γ

VALUE (units 10^{-2})	EVTS	DOCUMENT ID	TECN	COMMENT
1.025 ± 0.288	200 k	¹ LIBBY 09	CLEO	$\psi(2S) \rightarrow \gamma +$ hadrons

¹ Calculated using $\Gamma(\gamma gg)/\Gamma(ggg) = 0.097 \pm 0.026 \pm 0.016$ from LIBBY 09. The statistical error is negligible and the systematic error is largely uncorrelated with that of $\Gamma(ggg)/\Gamma_{total}$ LIBBY 09 measurement.

$\Gamma(\gamma gg)/\Gamma(ggg)$ Γ_4/Γ_3

VALUE (units 10^{-2})	EVTS	DOCUMENT ID	TECN	COMMENT
9.7 ± 2.6 ± 1.6	2.9 M	LIBBY 09	CLEO	$\psi(2S) \rightarrow (\gamma +)$ hadrons

$\Gamma(\text{light hadrons})/\Gamma_{total}$ Γ_5/Γ

VALUE	DOCUMENT ID	TECN	COMMENT
0.154 ± 0.015	¹ MENDEZ 08	CLEO	$e^+ e^- \rightarrow \psi(2S)$

• • • We do not use the following data for averages, fits, limits, etc. • • •
 0.169 ± 0.026 ² ADAM 05A CLEO $e^+ e^- \rightarrow \psi(2S)$
¹ Uses $B(\psi(2S) \rightarrow J/\psi X)$ from MENDEZ 08 and other branching fractions from PDG 07.
² Uses $B(J/\psi X)$ from ADAM 05A, $B(\chi_{cJ} \gamma)$, $B(\eta_c \gamma)$ from ATHAR 04 and $B(\ell^+ \ell^-)$ from PDG 04. Superseded by MENDEZ 08.

$\Gamma(e^+ e^-)/\Gamma_{total}$ Γ_6/Γ

VALUE (units 10^{-4})	DOCUMENT ID	TECN	COMMENT
79.3 ± 1.7 OUR FIT			

• • • We do not use the following data for averages, fits, limits, etc. • • •
 88 ± 13 ¹ FELDMAN 77 RVUE $e^+ e^-$
¹ From an overall fit assuming equal partial widths for $e^+ e^-$ and $\mu^+ \mu^-$. For a measurement of the ratio see the entry $\Gamma(\mu^+ \mu^-)/\Gamma(e^+ e^-)$ below. Includes LUTH 75, HILGER 75, BURMESTER 77.

$\Gamma(\mu^+ \mu^-)/\Gamma_{total}$ Γ_7/Γ

VALUE (units 10^{-4})	DOCUMENT ID	TECN	COMMENT
80 ± 6 OUR FIT			

$\Gamma(\mu^+ \mu^-)/\Gamma(e^+ e^-)$ Γ_7/Γ_6

VALUE	DOCUMENT ID	TECN	COMMENT
1.00 ± 0.08 OUR FIT			

• • • We do not use the following data for averages, fits, limits, etc. • • •
 0.89 ± 0.16 BOYARSKI 75c MRK1 $e^+ e^-$

$\Gamma(\tau^+ \tau^-)/\Gamma_{total}$ Γ_8/Γ

VALUE (units 10^{-4})	DOCUMENT ID	TECN	COMMENT
31 ± 4 OUR FIT			

30.8 ± 2.1 ± 3.8 ¹ ABLIKIM 06w BES $e^+ e^- \rightarrow \psi(2S)$
¹ Computed using PDG 02 value of $B(\psi(2S) \rightarrow$ hadrons) = 0.9810 ± 0.0030 to estimate the total number of $\psi(2S)$ events.

DECAYS INTO $J/\psi(1S)$ AND ANYTHING

$\Gamma(J/\psi(1S) \text{ anything})/\Gamma_{total}$ Γ_9/Γ

VALUE	EVTS	DOCUMENT ID	TECN	COMMENT
0.614 ± 0.006 OUR FIT				
0.55 ± 0.07 OUR AVERAGE				

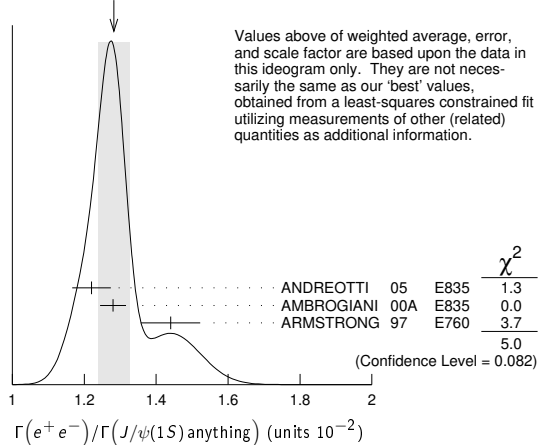
0.51 ± 0.12 BRANDELIK 79c DASP $e^+ e^- \rightarrow \mu^+ \mu^- X$
 0.57 ± 0.08 ABRAMS 75b MRK1 $e^+ e^- \rightarrow \mu^+ \mu^- X$
 • • • We do not use the following data for averages, fits, limits, etc. • • •
 0.6254 ± 0.0016 ± 0.0155 1.1M ¹ MENDEZ 08 CLEO $\psi(2S) \rightarrow \ell^+ \ell^- X$
 0.5950 ± 0.0015 ± 0.0190 151k ADAM 05A CLEO Repl. by MENDEZ 08
¹ Not independent from other measurements of MENDEZ 08.

$\Gamma(e^+ e^-)/\Gamma(J/\psi(1S) \text{ anything})$
 $\Gamma_6/\Gamma_9 = \Gamma_6/(\Gamma_{11} + \Gamma_{12} + \Gamma_{13} + 0.343\Gamma_{154} + 0.190\Gamma_{155})$

VALUE (units 10^{-2})	EVTS	DOCUMENT ID	TECN	COMMENT
1.291 ± 0.026 OUR FIT				
1.28 ± 0.04 OUR AVERAGE				

1.22 ± 0.02 ± 0.05 5097 ± 73 ¹ ANDREOTTI 05 E835 $\rho \bar{p} \rightarrow \psi(2S) \rightarrow e^+ e^-$
 1.28 ± 0.03 ± 0.02 ¹ AMBROGIANI 00A E835 $\rho \bar{p} \rightarrow \psi(2S)$
 1.44 ± 0.08 ± 0.02 ¹ ARMSTRONG 97 E760 $\bar{p} p \rightarrow \psi(2S)$
¹ Using $B(J/\psi(1S) \rightarrow e^+ e^-) = 0.0593 \pm 0.0010$.

WEIGHTED AVERAGE
 1.28 ± 0.04 (Error scaled by 1.6)



$\Gamma(\mu^+ \mu^-)/\Gamma(J/\psi(1S) \text{ anything})$
 $\Gamma_7/\Gamma_9 = \Gamma_7/(\Gamma_{11} + \Gamma_{12} + \Gamma_{13} + 0.343\Gamma_{154} + 0.190\Gamma_{155})$

VALUE	DOCUMENT ID	TECN	COMMENT
0.0130 ± 0.0010 OUR FIT			
0.014 ± 0.003	HILGER 75	SPEC	$e^+ e^-$

$\Gamma(J/\psi(1S) \text{ neutrals})/\Gamma_{total}$ Γ_{10}/Γ

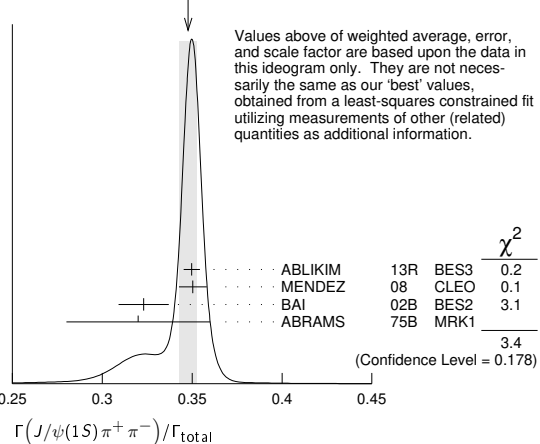
VALUE	DOCUMENT ID	TECN	COMMENT
0.2538 ± 0.0032 OUR FIT			

$\Gamma(J/\psi(1S) \pi^+ \pi^-)/\Gamma_{total}$ Γ_{11}/Γ

VALUE	EVTS	DOCUMENT ID	TECN	COMMENT
0.3468 ± 0.0030 OUR FIT				
0.348 ± 0.005 OUR AVERAGE				

Error includes scale factor of 1.3. See the ideogram below.
 0.3498 ± 0.0002 ± 0.0045 20M ABLIKIM 13R BES3 $\psi(2S) \rightarrow J/\psi \pi^+ \pi^-$
 0.3504 ± 0.0007 ± 0.0077 565k MENDEZ 08 CLEO $\psi(2S) \rightarrow \ell^+ \ell^- \pi^+ \pi^-$
 0.323 ± 0.014 BAI 02B BES2 $e^+ e^-$
 0.32 ± 0.04 ABRAMS 75B MRK1 $e^+ e^- \rightarrow J/\psi \pi^+ \pi^-$
 • • • We do not use the following data for averages, fits, limits, etc. • • •
 0.3354 ± 0.0014 ± 0.0110 60k ¹ ADAM 05A CLEO Repl. by MENDEZ 08
¹ Not independent from other values reported by ADAM 05A.

WEIGHTED AVERAGE
 0.348 ± 0.005 (Error scaled by 1.3)



$\Gamma(e^+ e^-)/\Gamma(J/\psi(1S) \pi^+ \pi^-)$ Γ_6/Γ_{11}

VALUE	DOCUMENT ID	TECN	COMMENT
0.0229 ± 0.0005 OUR FIT			
0.0252 ± 0.0028 ± 0.0011	¹ AUBERT 02B	BABR	$e^+ e^-$

¹ Using $B(J/\psi(1S) \rightarrow e^+ e^-) = 0.0593 \pm 0.0010$.

$\Gamma(\mu^+ \mu^-)/\Gamma(J/\psi(1S) \pi^+ \pi^-)$ Γ_7/Γ_{11}

VALUE	DOCUMENT ID	TECN	COMMENT
0.0230 ± 0.0017 OUR FIT			
0.0228 ± 0.0018 OUR AVERAGE			

0.0230 ± 0.0020 ± 0.0012 ¹ AAJ 16Y LHCb $\Lambda_b^0 \rightarrow \psi(2S) X$
 0.0216 ± 0.0026 ± 0.0014 ² AUBERT 02B BABR $e^+ e^-$
 0.0327 ± 0.0077 ± 0.0072 ² GRIBUSHIN 96 FMPS 515 $\pi^- Be \rightarrow 2\mu X$
¹ Using $B(J/\psi(1S) \rightarrow \mu^+ \mu^-) = (5.961 \pm 0.033) \times 10^{-2}$.
² Using $B(J/\psi(1S) \rightarrow \mu^+ \mu^-) = (5.88 \pm 0.10) \times 10^{-2}$.

Meson Particle Listings

 $\psi(2S)$ $\Gamma(\tau^+\tau^-)/\Gamma(J/\psi(1S)\pi^+\pi^-)$ Γ_8/Γ_{11}

VALUE (units 10^{-3})	DOCUMENT ID	TECN	COMMENT
8.8 ± 1.1 OUR FIT			
8.73 ± 1.39 ± 1.57	BAI	02	BES e^+e^-

 $\Gamma(J/\psi(1S)\pi^+\pi^-)/\Gamma(J/\psi(1S)\text{anything})$ Γ_{11}/Γ_9

VALUE	EVTs	DOCUMENT ID	TECN	COMMENT
0.5645 ± 0.0026 OUR FIT				
0.554 ± 0.008 OUR AVERAGE				Error includes scale factor of 1.3. See the ideogram below.

0.5604 ± 0.0009 ± 0.0062	565k	MENDEZ	08	CLEO $\psi(2S) \rightarrow \ell^+\ell^-\pi^+\pi^-$
0.525 ± 0.009 ± 0.022	4k	ANDREOTTI	05	E835 $\psi(2S) \rightarrow J/\psi X$
0.536 ± 0.007 ± 0.016	20k	^{1,2} ABLIKIM	04B	BES $\psi(2S) \rightarrow J/\psi X$
0.496 ± 0.037		ARMSTRONG	97	E760 $\bar{p}p \rightarrow \psi(2S)$

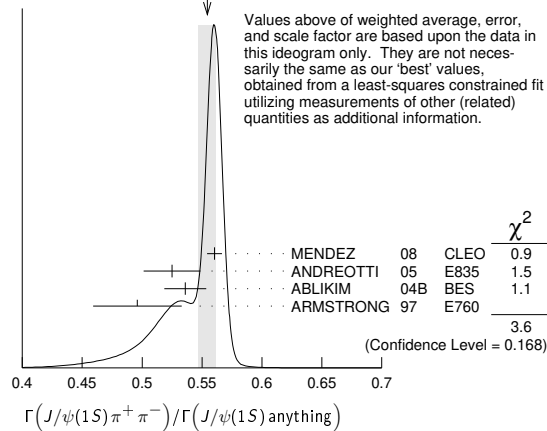
• • • We do not use the following data for averages, fits, limits, etc. • • •

0.5637 ± 0.0027 ± 0.0046 60k ADAM 05A CLEO Repl. by MENDEZ 08

¹ From a fit to the J/ψ recoil mass spectra.

² ABLIKIM 04B quotes $B(\psi(2S) \rightarrow J/\psi X) / B(\psi(2S) \rightarrow J/\psi\pi^+\pi^-)$.

WEIGHTED AVERAGE
0.554 ± 0.008 (Error scaled by 1.3)

 $\Gamma(J/\psi(1S)\text{neutrals})/\Gamma(J/\psi(1S)\pi^+\pi^-)$ $\Gamma_{10}/\Gamma_{11} = (0.9761\Gamma_{12} + 0.719\Gamma_{13} + 0.343\Gamma_{154} + 0.190\Gamma_{155})/\Gamma_{11}$

VALUE	DOCUMENT ID	TECN	COMMENT
0.732 ± 0.008 OUR FIT			
0.73 ± 0.09	TANENBAUM 76	MRK1	e^+e^-

 $\Gamma(J/\psi(1S)\pi^0\pi^0)/\Gamma_{\text{total}}$ Γ_{12}/Γ

VALUE	EVTs	DOCUMENT ID	TECN	COMMENT
0.1824 ± 0.0031 OUR FIT				

• • • We do not use the following data for averages, fits, limits, etc. • • •

0.1769 ± 0.0008 ± 0.0053 61k ¹MENDEZ 08 CLEO $\psi(2S) \rightarrow \ell^+\ell^-2\pi^0$

0.1652 ± 0.0014 ± 0.0058 13.4k ²ADAM 05A CLEO Repl. by MENDEZ 08

¹ Not independent from other measurements of MENDEZ 08.

² Not independent from other values reported by ADAM 05A.

 $\Gamma(J/\psi(1S)\pi^0\pi^0)/\Gamma(J/\psi(1S)\text{anything})$ Γ_{12}/Γ_9

VALUE	EVTs	DOCUMENT ID	TECN	COMMENT
0.2968 ± 0.0031 OUR FIT				
0.320 ± 0.012 OUR AVERAGE				

0.300 ± 0.008 ± 0.022	1655 ± 44	ANDREOTTI 05	E835	$\psi(2S) \rightarrow J/\psi X$
0.328 ± 0.013 ± 0.008		AMBROGIANI 00A	E835	$p\bar{p} \rightarrow \psi(2S)$
0.323 ± 0.033		ARMSTRONG 97	E760	$\bar{p}p \rightarrow \psi(2S)$

• • • We do not use the following data for averages, fits, limits, etc. • • •

0.2829 ± 0.0012 ± 0.0056 61k MENDEZ 08 CLEO $\psi(2S) \rightarrow \ell^+\ell^-2\pi^0$

0.2776 ± 0.0025 ± 0.0043 13.4k ADAM 05A CLEO Repl. by MENDEZ 08

 $\Gamma(J/\psi(1S)\pi^0\pi^0)/\Gamma(J/\psi(1S)\pi^+\pi^-)$ Γ_{12}/Γ_{11}

VALUE	EVTs	DOCUMENT ID	TECN	COMMENT
0.526 ± 0.008 OUR FIT				
0.513 ± 0.022 OUR AVERAGE				Error includes scale factor of 2.2.

0.5047 ± 0.0022 ± 0.0102	61k	MENDEZ	08	CLEO $\psi(2S) \rightarrow \ell^+\ell^-2\pi^0$
0.570 ± 0.009 ± 0.026	14k	¹ ABLIKIM	04B	BES $\psi(2S) \rightarrow J/\psi X$

• • • We do not use the following data for averages, fits, limits, etc. • • •

0.4924 ± 0.0047 ± 0.0086 73k ^{2,3}ADAM 05A CLEO Repl. by MENDEZ 08

0.571 ± 0.018 ± 0.044 ⁴ANDREOTTI 05 E835 $\psi(2S) \rightarrow J/\psi X$

0.53 ± 0.06 TANENBAUM 76 MRK1 e^+e^-

0.64 ± 0.15 ⁵HILGER 75 SPEC e^+e^-

¹ From a fit to the J/ψ recoil mass spectra.

² Not independent from other values reported by ADAM 05A.

³ Using 13,217 $J/\psi\pi^0\pi^0$ and 60,010 $J/\psi\pi^+\pi^-$ events.

⁴ Not independent from other values reported by ANDREOTTI 05.

⁵ Ignoring the $J/\psi(1S)\eta$ and $J/\psi(1S)\gamma\gamma$ decays.

 $\Gamma(J/\psi(1S)\eta)/\Gamma_{\text{total}}$ Γ_{13}/Γ

VALUE (units 10^{-3})	EVTs	DOCUMENT ID	TECN	COMMENT
33.9 ± 0.5 OUR FIT				
32.9 ± 1.7 OUR AVERAGE				Error includes scale factor of 2.1. See the ideogram below.

33.75 ± 0.17 ± 0.86	68.2k	ABLIKIM	12M	BES3 $e^+e^- \rightarrow \ell^+\ell^-2\gamma$
29.8 ± 0.9 ± 2.3	5.7k	BAI	04I	BES2 $\psi(2S) \rightarrow J/\psi\gamma\gamma$
25.5 ± 2.9	386	¹ OREGLIA	80	CBAL $e^+e^- \rightarrow J/\psi 2\gamma$
45 ± 12	17	² BRANDELIK	79B	DASP $e^+e^- \rightarrow J/\psi 2\gamma$
42 ± 6	164	² BARTEL	78B	CNTR e^+e^-

• • • We do not use the following data for averages, fits, limits, etc. • • •

34.3 ± 0.4 ± 0.9 18.4k ³MENDEZ 08 CLEO $\psi(2S) \rightarrow \ell^+\ell^-\eta$

32.5 ± 0.6 ± 1.1 2.8k ⁴ADAM 05A CLEO Repl. by MENDEZ 08

43 ± 8 44 TANENBAUM 76 MRK1 e^+e^-

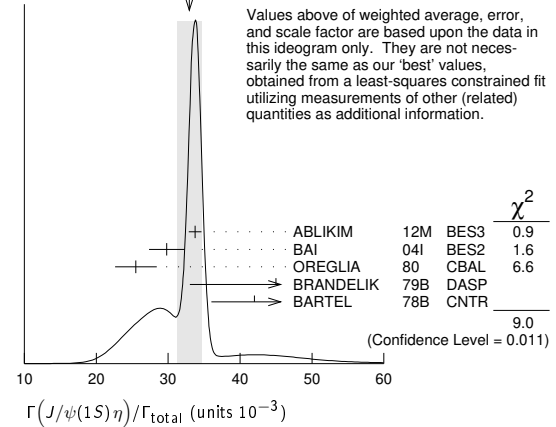
¹ Recalculated by us using $B(J/\psi(1S) \rightarrow \ell^+\ell^-) = 0.1181 \pm 0.0020$.

² Recalculated by us using $B(J/\psi(1S) \rightarrow \mu^+\mu^-) = 0.0588 \pm 0.0010$.

³ Not independent from other measurements of MENDEZ 08.

⁴ Not independent from other values reported by ADAM 05A.

WEIGHTED AVERAGE
32.9 ± 1.7 (Error scaled by 2.1)

 $\Gamma(J/\psi(1S)\eta)/\Gamma(J/\psi(1S)\text{anything})$ Γ_{13}/Γ_9

VALUE	EVTs	DOCUMENT ID	TECN	COMMENT
0.0549 ± 0.0008 OUR FIT				
0.058 ± 0.007 OUR AVERAGE				Error includes scale factor of 1.4. See the ideogram below.

0.050 ± 0.006 ± 0.003	298 ± 20	ANDREOTTI 05	E835	$\psi(2S) \rightarrow J/\psi X$
0.072 ± 0.009		AMBROGIANI 00A	E835	$p\bar{p} \rightarrow \psi(2S)$
0.061 ± 0.015		ARMSTRONG 97	E760	$\bar{p}p \rightarrow \psi(2S)$

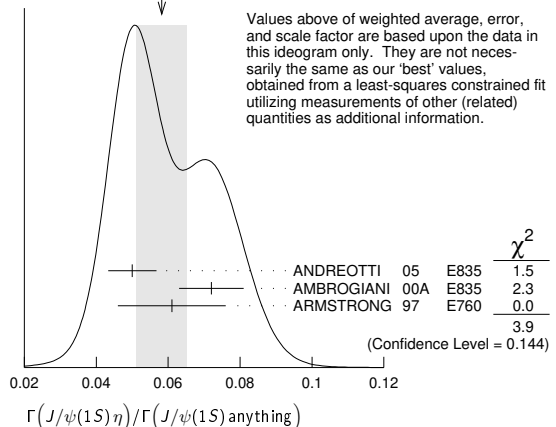
• • • We do not use the following data for averages, fits, limits, etc. • • •

0.0549 ± 0.0006 ± 0.0009 18.4k ¹MENDEZ 08 CLEO $\psi(2S) \rightarrow \ell^+\ell^-\eta$

0.0546 ± 0.0010 ± 0.0007 2.8k ADAM 05A CLEO Repl. by MENDEZ 08

¹ Not independent from other measurements of MENDEZ 08.

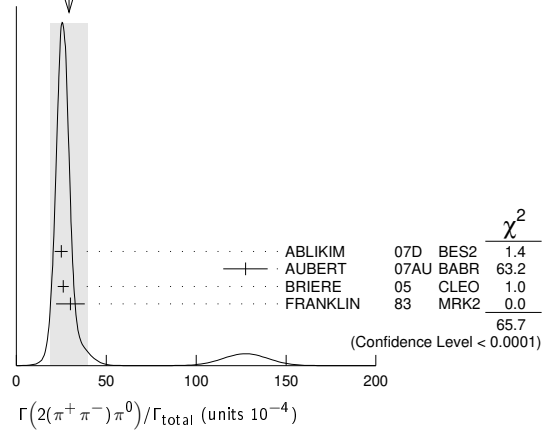
WEIGHTED AVERAGE
0.058 ± 0.007 (Error scaled by 1.4)



$\Gamma(J/\psi(1S)\eta)/\Gamma(J/\psi(1S)\pi^+\pi^-)$ Γ_{13}/Γ_{11}

VALUE	EVTs	DOCUMENT ID	TECN	COMMENT
0.0972 ± 0.0014 OUR FIT				
0.0979 ± 0.0018 OUR AVERAGE				
0.0979 ± 0.0010 ± 0.0015	18.4k	MENDEZ	08	CLEO $\psi(2S) \rightarrow \ell^+ \ell^- \eta$
0.098 ± 0.005 ± 0.010	2k	¹ ABLIKIM	04b	BES $\psi(2S) \rightarrow J/\psi X$
0.091 ± 0.021		² HIMEL	80	MRK2 $e^+ e^- \rightarrow \psi(2S) X$
• • • We do not use the following data for averages, fits, limits, etc. • • •				
0.0968 ± 0.0019 ± 0.0013	2.8k	³ ADAM	05A	CLEO Repl. by MENDEZ 08
0.095 ± 0.007 ± 0.007		⁴ ANDREOTTI	05	E835 $\psi(2S) \rightarrow J/\psi X$
¹ From a fit to the J/ψ recoil mass spectra.				
² The value for $B(\psi(2S) \rightarrow J/\psi(1S)\eta)$ reported in HIMEL 80 is derived using $B(\psi(2S) \rightarrow J/\psi(1S)\pi^+\pi^-) = (33 \pm 3)\%$ and $B(J/\psi(1S) \rightarrow \ell^+ \ell^-) = 0.138 \pm 0.018$. Calculated by us using $B(J/\psi(1S) \rightarrow \ell^+ \ell^-) = (0.1181 \pm 0.0020)$.				
³ Not independent from other values reported by ADAM 05A.				
⁴ Not independent from other values reported by ANDREOTTI 05.				

WEIGHTED AVERAGE
 29 ± 10 (Error scaled by 4.7)



$\Gamma(J/\psi(1S)\pi^0)/\Gamma_{total}$ Γ_{14}/Γ

VALUE (units 10^{-4})	EVTs	DOCUMENT ID	TECN	COMMENT
12.68 ± 0.32 OUR AVERAGE				
12.6 ± 0.2 ± 0.3	4.1k	ABLIKIM	12M	BES3 $e^+ e^- \rightarrow \ell^+ \ell^- 2\gamma$
13.3 ± 0.8 ± 0.3	530	MENDEZ	08	CLEO $\psi(2S) \rightarrow \ell^+ \ell^- 2\gamma$
14.3 ± 1.4 ± 1.2	280	BAI	04I	BES2 $\psi(2S) \rightarrow J/\psi \gamma \gamma$
14 ± 6	7	HIMEL	80	MRK2 $e^+ e^-$
9 ± 2 ± 1	23	¹ OREGLIA	80	CBAL $\psi(2S) \rightarrow J/\psi 2\gamma$
• • • We do not use the following data for averages, fits, limits, etc. • • •				
13 ± 1 ± 1	88	ADAM	05A	CLEO Repl. by MENDEZ 08
¹ Recalculated by us using $B(J/\psi(1S) \rightarrow \ell^+ \ell^-) = 0.1181 \pm 0.0020$.				

$\Gamma(\rho_{22}(1320))/\Gamma_{total}$ Γ_{18}/Γ

VALUE (units 10^{-4})	CL%	EVTs	DOCUMENT ID	TECN	COMMENT
2.55 ± 0.73 ± 0.47		112 ± 31	BAI	04c	BES2 $\psi(2S) \rightarrow 2(\pi^+\pi^-)\pi^0$
• • • We do not use the following data for averages, fits, limits, etc. • • •					
< 2.3		90	BAI	98J	BES $e^+ e^-$

$\Gamma(J/\psi(1S)\pi^0)/\Gamma(J/\psi(1S)\text{ anything})$
 $\Gamma_{14}/\Gamma_9 = \Gamma_{14}/(\Gamma_{11} + \Gamma_{12} + \Gamma_{13} + 0.343\Gamma_{154} + 0.190\Gamma_{155})$

VALUE (units 10^{-2})	EVTs	DOCUMENT ID	TECN	COMMENT
• • • We do not use the following data for averages, fits, limits, etc. • • •				
0.213 ± 0.012 ± 0.003	527	¹ MENDEZ	08	CLEO $e^+ e^- \rightarrow J/\psi \gamma \gamma$
0.22 ± 0.02 ± 0.01		² ADAM	05A	CLEO $e^+ e^- \rightarrow \psi(2S) \rightarrow J/\psi \gamma \gamma$
¹ Not independent from other values reported by MENDEZ 08. Supersedes ADAM 05A.				
² Not independent from other values reported by ADAM 05A.				

$\Gamma(\rho\bar{\rho})/\Gamma_{total}$ Γ_{21}/Γ

VALUE (units 10^{-4})	EVTs	DOCUMENT ID	TECN	COMMENT
2.94 ± 0.08 OUR FIT				
3.02 ± 0.08 OUR AVERAGE				
3.05 ± 0.02 ± 0.12	19k	ABLIKIM	18T	BES3 $e^+ e^- \rightarrow \psi(2S) \rightarrow \rho\bar{\rho}$
3.08 ± 0.05 ± 0.18	4.5k	¹ DOBBS	14	$e^+ e^- \rightarrow \psi(2S) \rightarrow \rho\bar{\rho}$
3.36 ± 0.09 ± 0.25	1.6k	ABLIKIM	07c	BES $e^+ e^- \rightarrow \psi(2S) \rightarrow \rho\bar{\rho}$
2.87 ± 0.12 ± 0.15	557	PEDLAR	05	CLEO $e^+ e^- \rightarrow \psi(2S) \rightarrow \rho\bar{\rho}$
1.4 ± 0.8	4	BRANDELIK	79c	DASP $e^+ e^- \rightarrow \psi(2S) \rightarrow \rho\bar{\rho}$
2.3 ± 0.7		FELDMAN	77	MRK1 $e^+ e^- \rightarrow \psi(2S) \rightarrow \rho\bar{\rho}$
¹ Using CLEO-c data but not authored by the CLEO Collaboration.				

$\Gamma(J/\psi(1S)\pi^0)/\Gamma(J/\psi(1S)\pi^+\pi^-)$ Γ_{14}/Γ_{11}

VALUE (units 10^{-2})	EVTs	DOCUMENT ID	TECN	COMMENT
• • • We do not use the following data for averages, fits, limits, etc. • • •				
0.380 ± 0.022 ± 0.005	527	¹ MENDEZ	08	CLEO $e^+ e^- \rightarrow J/\psi \gamma \gamma$
0.39 ± 0.04 ± 0.01		² ADAM	05A	CLEO $e^+ e^- \rightarrow \psi(2S) \rightarrow J/\psi \gamma \gamma$
¹ Not independent from other values reported by MENDEZ 08. Supersedes ADAM 05A.				
² Not independent from other values reported by ADAM 05A.				

$\Gamma(\rho\bar{\rho})/\Gamma(J/\psi(1S)\pi^+\pi^-)$ Γ_{21}/Γ_{11}

VALUE (units 10^{-4})	DOCUMENT ID	TECN	COMMENT
8.49 ± 0.23 OUR FIT			
6.98 ± 0.49 ± 0.97	BAI	01	BES $e^+ e^- \rightarrow \psi(2S) \rightarrow \rho\bar{\rho}$

HADRONIC DECAYS

$\Gamma(\pi^0 h_c(1P))/\Gamma_{total}$ Γ_{15}/Γ

VALUE (units 10^{-4})	EVTs	DOCUMENT ID	TECN	COMMENT
8.6 ± 1.3 OUR AVERAGE				
9.0 ± 1.5 ± 1.3	3k	¹ GE	11	CLEO $\psi(2S) \rightarrow \pi^0$ anything
8.4 ± 1.3 ± 1.0	11k	ABLIKIM	10b	BES3 $\psi(2S) \rightarrow \pi^0 h_c$
• • • We do not use the following data for averages, fits, limits, etc. • • •				
seen	92 ± 23	ADAMS	09	CLEO $\psi(2S) \rightarrow 2\pi^+ 2\pi^- 2\pi^0$
seen	1282	DOBBS	08A	CLEO $\psi(2S) \rightarrow \pi^0 \eta_c \gamma$
seen	168 ± 40	ROSNER	05	CLEO $\psi(2S) \rightarrow \pi^0 \eta_c \gamma$
¹ Assuming a width $\Gamma(h_c(1P)) = 0.86 \text{ MeV} \equiv \Gamma_0$, a measured dependence of the central value of $B = (7.6 \pm 1.4 \times \Gamma(h_c(1P))/\Gamma_0) \times 10^{-4}$, and with a systematic error that accounts for the width variation range 0.43–1.29 MeV.				

$\Gamma(n\bar{n})/\Gamma_{total}$ Γ_{22}/Γ

VALUE (units 10^{-4})	EVTs	DOCUMENT ID	TECN	COMMENT
3.06 ± 0.06 ± 0.14	6k	ABLIKIM	18T	BES3 $e^+ e^- \rightarrow \psi(2S) \rightarrow n\bar{n}$

$\Gamma(\Delta^{++}\bar{\Delta}^{--})/\Gamma_{total}$ Γ_{23}/Γ

VALUE (units 10^{-5})	EVTs	DOCUMENT ID	TECN	COMMENT
12.8 ± 1.0 ± 3.4	157	¹ BAI	01	BES $e^+ e^- \rightarrow \psi(2S) \rightarrow$ hadrons
¹ Estimated using $B(\psi(2S) \rightarrow J/\psi \pi^+ \pi^-) = 0.310 \pm 0.028$.				

$\Gamma(3(\pi^+\pi^-)\pi^0)/\Gamma_{total}$ Γ_{16}/Γ

VALUE (units 10^{-4})	EVTs	DOCUMENT ID	TECN	COMMENT
35 ± 16	6	FRANKLIN	83	MRK2 $e^+ e^- \rightarrow$ hadrons

$\Gamma(\Lambda\bar{\Lambda}\pi^0)/\Gamma_{total}$ Γ_{24}/Γ

VALUE (units 10^{-5})	CL%	EVTs	DOCUMENT ID	TECN	COMMENT
< 0.29	90	¹ ABLIKIM	13F	BES3 $\psi(2S) \rightarrow p\bar{p}\pi^+\pi^-\gamma\gamma$	
• • • We do not use the following data for averages, fits, limits, etc. • • •					
< 12	90	² ABLIKIM	07H	BES2 $e^+ e^- \rightarrow \psi(2S)$	
¹ Using $B(\Lambda \rightarrow \pi^- p) = 63.9\%$ and $B(\pi^0 \rightarrow \gamma\gamma) = 98.8\%$.					
² Using $B(\Lambda \rightarrow \pi^- p) = 63.9\%$ and $B(\eta \rightarrow \gamma\gamma) = 39.4\%$.					

$\Gamma(2(\pi^+\pi^-)\pi^0)/\Gamma_{total}$ Γ_{17}/Γ

VALUE (units 10^{-4})	EVTs	DOCUMENT ID	TECN	COMMENT
29 ± 10 OUR AVERAGE				
Error includes scale factor of 4.7. See the ideogram below.				
24.9 ± 0.7 ± 3.6	2173	ABLIKIM	07D	BES2 $e^+ e^- \rightarrow \psi(2S)$
127 ± 12 ± 2	410	¹ AUBERT	07AU	BABR 10.6 $e^+ e^- \rightarrow 2(\pi^+\pi^-)\pi^0 \gamma$
26.1 ± 0.7 ± 3.0	1703	BRIERE	05	CLEO $e^+ e^- \rightarrow \psi(2S) \rightarrow 2(\pi^+\pi^-)\pi^0$
30 ± 8	42	FRANKLIN	83	MRK2 $e^+ e^-$
¹ AUBERT 07AU reports $[\Gamma(\psi(2S) \rightarrow 2(\pi^+\pi^-)\pi^0)/\Gamma_{total}] \times [\Gamma(\psi(2S) \rightarrow e^+ e^-)] = (297 \pm 22 \pm 18) \times 10^{-4} \text{ keV}$ which we divide by our best value $\Gamma(\psi(2S) \rightarrow e^+ e^-) = 2.33 \pm 0.04 \text{ keV}$. Our first error is their experiment's error and our second error is the systematic error from using our best value.				

$\Gamma(\Lambda\bar{\Lambda}K^+)/\Gamma_{total}$ Γ_{25}/Γ

VALUE (units 10^{-5})	CL%	EVTs	DOCUMENT ID	TECN	COMMENT
2.46 ± 0.34 ± 0.19	60	¹ ABLIKIM	13F	BES3 $\psi(2S) \rightarrow p\bar{p}\pi^+\pi^-\gamma\gamma$	
• • • We do not use the following data for averages, fits, limits, etc. • • •					
< 4.9	90	² ABLIKIM	07H	BES2 $e^+ e^- \rightarrow \psi(2S)$	
¹ Using $B(\Lambda \rightarrow \pi^- p) = 63.9\%$ and $B(\eta \rightarrow \gamma\gamma) = 39.31\%$.					
² Using $B(\Lambda \rightarrow \pi^- p) = 63.9\%$.					

$\Gamma(\Lambda\bar{\Lambda}K^+)/\Gamma_{total}$ Γ_{26}/Γ

VALUE (units 10^{-4})	EVTs	DOCUMENT ID	TECN	COMMENT
1.0 ± 0.1 ± 0.1	74.0	BRIERE	05	CLEO $e^+ e^- \rightarrow \psi(2S) \rightarrow p\bar{p}K^+\pi^-$

$\Gamma(K^*(892)^+\bar{p}\Lambda + \text{c.c.})/\Gamma_{total}$ Γ_{27}/Γ

VALUE (units 10^{-5})	EVTs	DOCUMENT ID	TECN	COMMENT
6.3 ± 0.5 ± 0.5	1011	ABLIKIM	19AU	BES3 $e^+ e^- \rightarrow \psi(2S)$

Meson Particle Listings

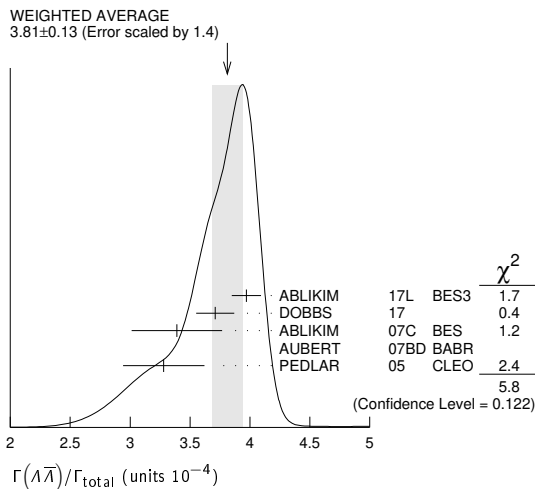
$\psi(2S)$

$\Gamma(\Lambda\bar{p}K^+\pi^+\pi^-)/\Gamma_{total}$		Γ_{28}/Γ	
VALUE (units 10^{-4})	EVTS	DOCUMENT ID	TECN COMMENT
1.8 ± 0.3 ± 0.3	45.8	BRIERE 05	CLEO $e^+e^- \rightarrow \psi(2S) \rightarrow p\bar{p}K^+\pi^+\pi^-$

$\Gamma(\Lambda\bar{\Lambda}\pi^+\pi^-)/\Gamma_{total}$		Γ_{29}/Γ	
VALUE (units 10^{-4})	EVTS	DOCUMENT ID	TECN COMMENT
2.8 ± 0.4 ± 0.5	73.4	BRIERE 05	CLEO $e^+e^- \rightarrow \psi(2S) \rightarrow p\bar{p}2(\pi^+\pi^-)$

$\Gamma(\Lambda\bar{\Lambda})/\Gamma_{total}$		Γ_{30}/Γ	
VALUE (units 10^{-4})	CL% EVTS	DOCUMENT ID	TECN COMMENT
3.81 ± 0.13 OUR AVERAGE		Error includes scale factor of 1.4. See the ideogram below.	
3.97 ± 0.02 ± 0.12	31k	ABLIKIM 17L	BES3 $e^+e^- \rightarrow \Lambda\bar{\Lambda}$
3.71 ± 0.05 ± 0.15	6.5k	¹ DOBBS 17	$e^+e^- \rightarrow \Lambda\bar{\Lambda}$
3.39 ± 0.20 ± 0.32	337	ABLIKIM 07c	BES $e^+e^- \rightarrow \psi(2S) \rightarrow \text{hadrons}$
6.4 ± 1.8 ± 0.1		² AUBERT 07BD	BABR 10.6 $e^+e^- \rightarrow \Lambda\bar{\Lambda}\gamma$
3.28 ± 0.23 ± 0.25	208	PEDLAR 05	CLEO $e^+e^- \rightarrow \psi(2S) \rightarrow \text{hadrons}$
• • • We do not use the following data for averages, fits, limits, etc. • • •			
3.75 ± 0.09 ± 0.23	1.9k	^{1,3} DOBBS 14	$e^+e^- \rightarrow \Lambda\bar{\Lambda}$
1.81 ± 0.20 ± 0.27	80	⁴ BAI 01	BES $e^+e^- \rightarrow \psi(2S) \rightarrow \text{hadrons}$
< 4	90	FELDMAN 77	MRK1 $e^+e^- \rightarrow \psi(2S) \rightarrow \text{hadrons}$

¹ Using CLEO-c data but not authored by the CLEO Collaboration.
² AUBERT 07BD reports $[\Gamma(\psi(2S) \rightarrow \Lambda\bar{\Lambda})/\Gamma_{total}] \times [\Gamma(\psi(2S) \rightarrow e^+e^-)] = (15 \pm 4) \times 10^{-4}$ keV which we divide by our best value $\Gamma(\psi(2S) \rightarrow e^+e^-) = 2.33 \pm 0.04$ keV. Our first error is their experiment's error and our second error is the systematic error from using our best value.
³ Superseded by DOBBS 17.
⁴ Estimated using $B(\psi(2S) \rightarrow J/\psi\pi^+\pi^-) = 0.310 \pm 0.028$.



$\Gamma(\Lambda\Sigma^+\pi^- + c.c.)/\Gamma_{total}$		Γ_{31}/Γ	
VALUE (units 10^{-4})	EVTS	DOCUMENT ID	TECN COMMENT
1.40 ± 0.03 ± 0.13	2.8k	ABLIKIM 13W	BES3 $\psi(2S) \rightarrow \text{hadrons}$

$\Gamma(\Lambda\Sigma^-\pi^+ + c.c.)/\Gamma_{total}$		Γ_{32}/Γ	
VALUE (units 10^{-4})	EVTS	DOCUMENT ID	TECN COMMENT
1.54 ± 0.04 ± 0.13	2.8k	ABLIKIM 13W	BES3 $\psi(2S) \rightarrow \text{hadrons}$

$\Gamma(\Lambda\Sigma^0)/\Gamma_{total}$		Γ_{33}/Γ	
VALUE (units 10^{-5})	EVTS	DOCUMENT ID	COMMENT
1.23 ± 0.23 ± 0.08	30	¹ DOBBS 17	$e^+e^- \rightarrow \psi(2S) \rightarrow \text{hadrons}$
¹ Using CLEO-c data but not authored by the CLEO Collaboration.			

$\Gamma(\Sigma^0\bar{p}K^+ + c.c.)/\Gamma_{total}$		Γ_{34}/Γ	
VALUE (units 10^{-5})	EVTS	DOCUMENT ID	COMMENT
1.67 ± 0.13 ± 0.12	276	¹ ABLIKIM 13D	BES3 $\psi(2S) \rightarrow \gamma\Lambda\bar{p}K^+$
¹ Using $B(\Lambda \rightarrow p\pi^-) = 63.9\%$, and $B(\Sigma^0 \rightarrow \Lambda\gamma) = 100\%$.			

$\Gamma(\Sigma^+\bar{\Sigma}^-)/\Gamma_{total}$		Γ_{35}/Γ	
VALUE (units 10^{-4})	EVTS	DOCUMENT ID	COMMENT
2.32 ± 0.12 OUR AVERAGE			
2.31 ± 0.06 ± 0.10	1.9k	¹ DOBBS 17	$e^+e^- \rightarrow \psi(2S) \rightarrow \text{hadrons}$
2.57 ± 0.44 ± 0.68	35	PEDLAR 05	CLEO $e^+e^- \rightarrow \psi(2S) \rightarrow \text{hadrons}$
• • • We do not use the following data for averages, fits, limits, etc. • • •			
2.51 ± 0.15 ± 0.16	281	^{1,2} DOBBS 14	$e^+e^- \rightarrow \psi(2S) \rightarrow \text{hadrons}$
¹ Using CLEO-c data but not authored by the CLEO Collaboration.			
² Superseded by DOBBS 17.			

$\Gamma(\Sigma^0\bar{\Sigma}^0)/\Gamma_{total}$		Γ_{36}/Γ	
VALUE (units 10^{-4})	EVTS	DOCUMENT ID	TECN COMMENT
2.35 ± 0.09 OUR AVERAGE		Error includes scale factor of 1.1.	
2.44 ± 0.03 ± 0.11	7k	ABLIKIM 17L	BES3 $e^+e^- \rightarrow \psi(2S) \rightarrow \text{hadrons}$
2.22 ± 0.05 ± 0.11	2.6k	¹ DOBBS 17	$e^+e^- \rightarrow \psi(2S) \rightarrow \text{hadrons}$
2.35 ± 0.36 ± 0.32	59	ABLIKIM 07c	BES $e^+e^- \rightarrow \psi(2S) \rightarrow \text{hadrons}$
2.63 ± 0.35 ± 0.21	58	PEDLAR 05	CLEO $e^+e^- \rightarrow \psi(2S) \rightarrow \text{hadrons}$
• • • We do not use the following data for averages, fits, limits, etc. • • •			
2.25 ± 0.11 ± 0.16	439	^{1,2} DOBBS 14	$e^+e^- \rightarrow \psi(2S) \rightarrow \text{hadrons}$
1.2 ± 0.4 ± 0.4	8	³ BAI 01	BES $e^+e^- \rightarrow \psi(2S) \rightarrow \text{hadrons}$
¹ Using CLEO-c data but not authored by the CLEO Collaboration.			
² Superseded by DOBBS 17.			
³ Estimated using $B(\psi(2S) \rightarrow J/\psi\pi^+\pi^-) = 0.310 \pm 0.028$.			

$\Gamma(\Sigma(1385)^+\bar{\Sigma}(1385)^-)/\Gamma_{total}$		Γ_{37}/Γ	
VALUE (units 10^{-5})	EVTS	DOCUMENT ID	TECN COMMENT
8.5 ± 0.7 OUR AVERAGE			
8.4 ± 0.5 ± 0.5	1.5k	ABLIKIM 16L	BES3 $\psi(2S) \rightarrow \Sigma(1385)^+\bar{\Sigma}(1385)^-$
11 ± 3 ± 3	14	¹ BAI 01	BES $e^+e^- \rightarrow \psi(2S) \rightarrow \text{hadrons}$
¹ Estimated using $B(\psi(2S) \rightarrow J/\psi\pi^+\pi^-) = 0.310 \pm 0.028$.			

$\Gamma(\Sigma(1385)^-\bar{\Sigma}(1385)^+)/\Gamma_{total}$		Γ_{38}/Γ	
VALUE (units 10^{-5})	EVTS	DOCUMENT ID	TECN COMMENT
8.5 ± 0.6 ± 0.6	1.4k	ABLIKIM 16L	BES3 $\psi(2S) \rightarrow \Sigma(1385)^-\bar{\Sigma}(1385)^+$

$\Gamma(\Sigma(1385)^0\bar{\Sigma}(1385)^0)/\Gamma_{total}$		Γ_{39}/Γ	
VALUE (units 10^{-4})	EVTS	DOCUMENT ID	TECN COMMENT
0.69 ± 0.05 ± 0.05	2.2k	ABLIKIM 17E	BES3 $e^+e^- \rightarrow \psi(2S) \rightarrow \text{hadrons}$

$\Gamma(\Xi^-\bar{\Xi}^+)/\Gamma_{total}$		Γ_{40}/Γ	
VALUE (units 10^{-4})	CL% EVTS	DOCUMENT ID	TECN COMMENT
2.87 ± 0.11 OUR AVERAGE		Error includes scale factor of 1.1.	
3.03 ± 0.05 ± 0.14	3.6k	¹ DOBBS 17	$e^+e^- \rightarrow \psi(2S) \rightarrow \text{hadrons}$
2.78 ± 0.05 ± 0.14	5k	ABLIKIM 16L	BES3 $\psi(2S) \rightarrow \Xi^-\bar{\Xi}^+$
3.03 ± 0.40 ± 0.32	67	ABLIKIM 07c	BES $e^+e^- \rightarrow \psi(2S) \rightarrow \text{hadrons}$
2.38 ± 0.30 ± 0.21	63	PEDLAR 05	CLEO $e^+e^- \rightarrow \psi(2S) \rightarrow \text{hadrons}$
• • • We do not use the following data for averages, fits, limits, etc. • • •			
2.66 ± 0.12 ± 0.20	548	^{1,2} DOBBS 14	$e^+e^- \rightarrow \psi(2S) \rightarrow \text{hadrons}$
0.94 ± 0.27 ± 0.15	12	³ BAI 01	BES $e^+e^- \rightarrow \psi(2S) \rightarrow \text{hadrons}$
< 2	90	FELDMAN 77	MRK1 $e^+e^- \rightarrow \psi(2S) \rightarrow \text{hadrons}$
¹ Using CLEO-c data but not authored by the CLEO Collaboration.			
² Superseded by DOBBS 17.			
³ Estimated using $B(\psi(2S) \rightarrow J/\psi\pi^+\pi^-) = 0.310 \pm 0.028$.			

$\Gamma(\Xi^0\bar{\Xi}^0)/\Gamma_{total}$		Γ_{41}/Γ	
VALUE (units 10^{-4})	EVTS	DOCUMENT ID	TECN COMMENT
2.3 ± 0.4 OUR AVERAGE		Error includes scale factor of 4.2.	
2.73 ± 0.03 ± 0.13	11k	ABLIKIM 17E	BES3 $e^+e^- \rightarrow \psi(2S) \rightarrow \text{hadrons}$
1.97 ± 0.06 ± 0.11	1.2k	¹ DOBBS 17	$e^+e^- \rightarrow \psi(2S) \rightarrow \text{hadrons}$
2.75 ± 0.64 ± 0.61	19	PEDLAR 05	CLEO $e^+e^- \rightarrow \psi(2S) \rightarrow \text{hadrons}$
• • • We do not use the following data for averages, fits, limits, etc. • • •			
2.02 ± 0.19 ± 0.15	112	^{1,2} DOBBS 14	$e^+e^- \rightarrow \psi(2S) \rightarrow \text{hadrons}$
¹ Using CLEO-c data but not authored by the CLEO Collaboration.			
² Superseded by DOBBS 17.			

$\Gamma(\Xi(1530)^0\bar{\Xi}(1530)^0)/\Gamma_{total}$		Γ_{42}/Γ	
VALUE (units 10^{-5})	CL% EVTS	DOCUMENT ID	TECN COMMENT
5.2 ± 0.3 ± 3.2 ± 1.2	527	¹ ABLIKIM 13S	BES3 $\psi(2S) \rightarrow \eta\rho\bar{p}$
• • • We do not use the following data for averages, fits, limits, etc. • • •			
< 32	90	PEDLAR 05	CLEO $e^+e^- \rightarrow \psi(2S) \rightarrow \text{hadrons}$
< 8.1	90	² BAI 01	BES $e^+e^- \rightarrow \psi(2S) \rightarrow \text{hadrons}$
¹ With $N(1535)$ decaying to $p\eta$.			
² Estimated using $B(\psi(2S) \rightarrow J/\psi\pi^+\pi^-) = 0.310 \pm 0.028$.			

$\Gamma(\Xi(1530)^-\bar{\Xi}(1530)^+)/\Gamma_{total}$		Γ_{44}/Γ	
VALUE (units 10^{-5})	EVTS	DOCUMENT ID	TECN COMMENT
11.45 ± 0.40 ± 0.59	5k	ABLIKIM 19AT	BES3 $e^+e^- \rightarrow \psi(2S) \rightarrow \text{hadrons}$

$\Gamma(\Xi(1530)^-\bar{\Xi}^+)/\Gamma_{total}$		Γ_{45}/Γ	
VALUE (units 10^{-6})	EVTS	DOCUMENT ID	TECN COMMENT
7.0 ± 1.1 ± 0.4	399	ABLIKIM 19AT	BES3 $e^+e^- \rightarrow \psi(2S) \rightarrow \text{hadrons}$

$\Gamma(K^-\Lambda\bar{\Xi}^+ + c.c.)/\Gamma_{total}$		Γ_{43}/Γ	
VALUE (units 10^{-5})	EVTS	DOCUMENT ID	TECN COMMENT
3.86 ± 0.27 ± 0.32	236	ABLIKIM 15I	BES3 $e^+e^- \rightarrow \psi(2S) \rightarrow K^-\Lambda\bar{\Xi}^+ + c.c.$

$\Gamma(\Xi(1690)^-\Xi^+\rightarrow K^-\Lambda\Xi^++\text{c.c.})/\Gamma_{\text{total}}$					Γ_{46}/Γ
VALUE (units 10^{-6})	EVTS	DOCUMENT ID	TECN	COMMENT	
$5.21\pm 1.48\pm 0.57$	74	ABLIKIM	15i	BES3 $e^+e^-\rightarrow\psi(2S)\rightarrow K^-\Lambda\Xi^++\text{c.c.}$	

$\Gamma(\Xi(1820)^-\Xi^+\rightarrow K^-\Lambda\Xi^++\text{c.c.})/\Gamma_{\text{total}}$					Γ_{47}/Γ
VALUE (units 10^{-6})	EVTS	DOCUMENT ID	TECN	COMMENT	
$12.03\pm 2.94\pm 1.22$	136	ABLIKIM	15i	BES3 $e^+e^-\rightarrow\psi(2S)\rightarrow K^-\Lambda\Xi^++\text{c.c.}$	

$\Gamma(K^-\Sigma^0\Xi^++\text{c.c.})/\Gamma_{\text{total}}$					Γ_{48}/Γ
VALUE (units 10^{-5})	EVTS	DOCUMENT ID	TECN	COMMENT	
$3.67\pm 0.33\pm 0.28$	142	ABLIKIM	15i	BES3 $e^+e^-\rightarrow\psi(2S)\rightarrow K^-\Sigma^0\Xi^++\text{c.c.}$	

$\Gamma(\Omega^-\bar{\Omega}^+)/\Gamma_{\text{total}}$					Γ_{49}/Γ
VALUE (units 10^{-4})	CL%	EVTS	DOCUMENT ID	TECN	COMMENT
$0.52\pm 0.03\pm 0.03$		326	¹ DOBBS	17	$e^+e^-\rightarrow\psi(2S)\rightarrow$ hadrons

• • • We do not use the following data for averages, fits, limits, etc. • • •					
$0.47\pm 0.09\pm 0.05$	27	^{1,2} DOBBS	14		$e^+e^-\rightarrow\psi(2S)\rightarrow$ hadrons
<1.5	90	ABLIKIM	12Q	BES2	$e^+e^-\rightarrow\psi(2S)\rightarrow$ hadrons
<1.6	90	PEDLAR	05	CLEO	$e^+e^-\rightarrow\psi(2S)\rightarrow$ hadrons
<0.73	90	³ BAI	01	BES	$e^+e^-\rightarrow\psi(2S)\rightarrow$ hadrons

¹ Using CLEO-c data but not authored by the CLEO Collaboration.

² Superseded by DOBBS 17.

³ Estimated using $B(\psi(2S)\rightarrow J/\psi\pi^+\pi^-)=0.310\pm 0.028$.

$\Gamma(\pi^0\rho\bar{\rho})/\Gamma_{\text{total}}$					Γ_{50}/Γ
VALUE (units 10^{-4})	EVTS	DOCUMENT ID	TECN	COMMENT	
1.53 ± 0.07 OUR AVERAGE					
$1.65\pm 0.03\pm 0.15$	4.5k	ABLIKIM	13A	BES3 $\psi(2S)\rightarrow\rho\bar{\rho}\pi^0$	
$1.54\pm 0.06\pm 0.06$	948	ALEXANDER	10	CLEO $\psi(2S)\rightarrow\pi^0\rho\bar{\rho}$	
$1.32\pm 0.10\pm 0.15$	256	¹ ABLIKIM	05E	BES2 $e^+e^-\rightarrow\psi(2S)\rightarrow\rho\bar{\rho}\gamma\gamma$	
1.4 ± 0.5	9	FRANKLIN	83	MRK2 e^+e^-	

¹ Computed using $B(\pi^0\rightarrow\gamma\gamma)=(98.80\pm 0.03)\%$.

$\Gamma(N(940)\bar{\rho}+ \text{c.c.}\rightarrow\pi^0\rho\bar{\rho})/\Gamma_{\text{total}}$					Γ_{51}/Γ
VALUE (units 10^{-5})	EVTS	DOCUMENT ID	TECN	COMMENT	
$6.42\pm 0.20\pm 1.78$	1.9k	¹ ABLIKIM	13A	BES3 $\psi(2S)\rightarrow\rho\bar{\rho}\pi^0$	

¹ From a fit of $\pi^0\rho\bar{\rho}$ data to eight distinct intermediate $N\bar{\rho}$ resonant states.

$\Gamma(N(1440)\bar{\rho}+ \text{c.c.}\rightarrow\pi^0\rho\bar{\rho})/\Gamma_{\text{total}}$					Γ_{52}/Γ
VALUE (units 10^{-5})	EVTS	DOCUMENT ID	TECN	COMMENT	
7.3 ± 1.7 OUR AVERAGE				Error includes scale factor of 2.5.	
$3.58\pm 0.25\pm 1.59$	1.1k	¹ ABLIKIM	13A	BES3 $\psi(2S)\rightarrow\rho\bar{\rho}\pi^0$	
$8.1\pm 0.7\pm 0.3$	474	² ALEXANDER	10	CLEO $\psi(2S)\rightarrow\pi^0\rho\bar{\rho}$	

¹ From a fit of $\pi^0\rho\bar{\rho}$ data to eight distinct intermediate $N\bar{\rho}$ resonant states.

² From a fit of the $\rho\bar{\rho}$ and π^0 mass distributions to a combination of $N(1440)\bar{\rho}$, $\pi^0 f_0(2100)$, and two other broad, unestablished resonances.

$\Gamma(N(1520)\bar{\rho}+ \text{c.c.}\rightarrow\pi^0\rho\bar{\rho})/\Gamma_{\text{total}}$					Γ_{53}/Γ
VALUE (units 10^{-5})	EVTS	DOCUMENT ID	TECN	COMMENT	
$0.64\pm 0.05\pm 0.22$	0.2k	¹ ABLIKIM	13A	BES3 $\psi(2S)\rightarrow\rho\bar{\rho}\pi^0$	

¹ From a fit of $\pi^0\rho\bar{\rho}$ data to eight distinct intermediate $N\bar{\rho}$ resonant states.

$\Gamma(N(1535)\bar{\rho}+ \text{c.c.}\rightarrow\pi^0\rho\bar{\rho})/\Gamma_{\text{total}}$					Γ_{54}/Γ
VALUE (units 10^{-5})	EVTS	DOCUMENT ID	TECN	COMMENT	
$2.47\pm 0.28\pm 0.99$	0.7k	¹ ABLIKIM	13A	BES3 $\psi(2S)\rightarrow\rho\bar{\rho}\pi^0$	

¹ From a fit of $\pi^0\rho\bar{\rho}$ data to eight distinct intermediate $N\bar{\rho}$ resonant states.

$\Gamma(N(1650)\bar{\rho}+ \text{c.c.}\rightarrow\pi^0\rho\bar{\rho})/\Gamma_{\text{total}}$					Γ_{55}/Γ
VALUE (units 10^{-5})	EVTS	DOCUMENT ID	TECN	COMMENT	
$3.76\pm 0.28\pm 1.37$	1.1k	¹ ABLIKIM	13A	BES3 $\psi(2S)\rightarrow\rho\bar{\rho}\pi^0$	

¹ From a fit of $\pi^0\rho\bar{\rho}$ data to eight distinct intermediate $N\bar{\rho}$ resonant states.

$\Gamma(N(1720)\bar{\rho}+ \text{c.c.}\rightarrow\pi^0\rho\bar{\rho})/\Gamma_{\text{total}}$					Γ_{56}/Γ
VALUE (units 10^{-5})	EVTS	DOCUMENT ID	TECN	COMMENT	
$1.79\pm 0.10\pm 0.24$	0.5k	¹ ABLIKIM	13A	BES3 $\psi(2S)\rightarrow\rho\bar{\rho}\pi^0$	

¹ From a fit of $\pi^0\rho\bar{\rho}$ data to eight distinct intermediate $N\bar{\rho}$ resonant states.

$\Gamma(N(2300)\bar{\rho}+ \text{c.c.}\rightarrow\pi^0\rho\bar{\rho})/\Gamma_{\text{total}}$					Γ_{57}/Γ
VALUE (units 10^{-5})	EVTS	DOCUMENT ID	TECN	COMMENT	
$2.62\pm 0.28\pm 1.12$	0.9k	¹ ABLIKIM	13A	BES3 $\psi(2S)\rightarrow\rho\bar{\rho}\pi^0$	

¹ From a fit of $\pi^0\rho\bar{\rho}$ data to eight distinct intermediate $N\bar{\rho}$ resonant states.

$\Gamma(N(2570)\bar{\rho}+ \text{c.c.}\rightarrow\pi^0\rho\bar{\rho})/\Gamma_{\text{total}}$					Γ_{58}/Γ
VALUE (units 10^{-5})	EVTS	DOCUMENT ID	TECN	COMMENT	
$2.13\pm 0.08\pm 0.40$	0.8k	¹ ABLIKIM	13A	BES3 $\psi(2S)\rightarrow\rho\bar{\rho}\pi^0$	

¹ From a fit of $\pi^0\rho\bar{\rho}$ data to eight distinct intermediate $N\bar{\rho}$ resonant states.

$\Gamma(\pi^0 f_0(2100)\rightarrow\pi^0\rho\bar{\rho})/\Gamma_{\text{total}}$					Γ_{59}/Γ
VALUE (units 10^{-5})	EVTS	DOCUMENT ID	TECN	COMMENT	
$1.1\pm 0.4\pm 0.1$	76	¹ ALEXANDER	10	CLEO $\psi(2S)\rightarrow\pi^0\rho\bar{\rho}$	

¹ From a fit of the $\rho\bar{\rho}$ and π^0 mass distributions to a combination of $N_1^*(1440)\bar{\rho}$, $\pi^0 f_0(2100)$, and two other broad, unestablished resonances.

$\Gamma(\eta\rho\bar{\rho})/\Gamma_{\text{total}}$					Γ_{60}/Γ
VALUE (units 10^{-5})	EVTS	DOCUMENT ID	TECN	COMMENT	
6.0 ± 0.4 OUR AVERAGE					
$6.4\pm 0.2\pm 0.6$	679	¹ ABLIKIM	13s	BES3 $\psi(2S)\rightarrow\eta\rho\bar{\rho}$	
$5.6\pm 0.6\pm 0.3$	154	¹ ALEXANDER	10	CLEO $\psi(2S)\rightarrow\eta\rho\bar{\rho}$	
$5.8\pm 1.1\pm 0.7$	44.8 ± 8.5	² ABLIKIM	05E	BES2 $e^+e^-\rightarrow\psi(2S)\rightarrow$ $\rho\bar{\rho}\gamma\gamma$	
$8\pm 3\pm 3$	9.8	BRIERE	05	CLEO $e^+e^-\rightarrow\psi(2S)\rightarrow$ $\rho\bar{\rho}\pi^+\pi^-\pi^0$	

¹ With $N(1535)$ decaying to $\rho\eta$.

² Computed using $B(\eta\rightarrow\gamma\gamma)=(39.43\pm 0.26)\%$.

$\Gamma(\eta f_0(2100)\rightarrow\eta\rho\bar{\rho})/\Gamma_{\text{total}}$					Γ_{61}/Γ
VALUE (units 10^{-5})	EVTS	DOCUMENT ID	TECN	COMMENT	
$1.2\pm 0.4\pm 0.1$	31	¹ ALEXANDER	10	CLEO $\psi(2S)\rightarrow\eta\rho\bar{\rho}$	

¹ From a fit of the $\rho\bar{\rho}$ and η distributions to a combination of $N^*(1535)\bar{\rho}$ and $\eta f_0(2100)$.

$\Gamma(N(1535)\bar{\rho}\rightarrow\eta\rho\bar{\rho})/\Gamma_{\text{total}}$					Γ_{62}/Γ
VALUE (units 10^{-5})	EVTS	DOCUMENT ID	TECN	COMMENT	
$4.4\pm 0.6\pm 0.3$	123	¹ ALEXANDER	10	CLEO $\psi(2S)\rightarrow\eta\rho\bar{\rho}$	

¹ From a fit of the $\rho\bar{\rho}$ and η distributions to a combination of $N^*(1535)\bar{\rho}$ and $\eta f_0(2100)$.

$\Gamma(\omega\rho\bar{\rho})/\Gamma_{\text{total}}$					Γ_{63}/Γ
VALUE (units 10^{-4})	EVTS	DOCUMENT ID	TECN	COMMENT	
0.69 ± 0.21 OUR AVERAGE					
$0.6\pm 0.2\pm 0.2$	21.2	BRIERE	05	CLEO $e^+e^-\rightarrow\psi(2S)\rightarrow$ $\rho\bar{\rho}\pi^+\pi^-\pi^0$	
$0.8\pm 0.3\pm 0.1$	14.9 ± 0.1	¹ BAI	03B	BES $\psi(2S)\rightarrow\rho\bar{\rho}\pi^+\pi^-\pi^0$	

¹ Normalized to $B(\psi(2S)\rightarrow J/\psi\pi^+\pi^-)=0.305\pm 0.016$.

$\Gamma(\eta'\rho\bar{\rho})/\Gamma_{\text{total}}$					Γ_{64}/Γ
VALUE (units 10^{-5})	EVTS	DOCUMENT ID	TECN	COMMENT	
$1.10\pm 0.10\pm 0.08$	491	¹ ABLIKIM	19N	BES3 $\psi(2S)\rightarrow\eta'\rho\bar{\rho}$	

¹ From the combination of $\rho\bar{\rho}\eta'\rightarrow\rho\bar{\rho}\pi^+\pi^-\eta$ and $\rho\bar{\rho}\eta'\rightarrow\rho\bar{\rho}\pi^+\pi^-\gamma$ channels.

$\Gamma(\rho\bar{\rho})/\Gamma_{\text{total}}$					Γ_{65}/Γ
VALUE (units 10^{-6})	CL%	EVTS	DOCUMENT ID	TECN	COMMENT
$6.06\pm 0.38\pm 0.48$		753	ABLIKIM	19A0	BES3 $e^+e^-\rightarrow\psi(2S)\rightarrow$ $\rho\bar{\rho}K^+K^-$
<24		90	BRIERE	05	CLEO $e^+e^-\rightarrow\psi(2S)\rightarrow$ $\rho\bar{\rho}K^+K^-$
<26		90	¹ BAI	03B	BES $\psi(2S)\rightarrow$ $K^+K^-\rho\bar{\rho}$

¹ Normalized to $B(\psi(2S)\rightarrow J/\psi\pi^+\pi^-)=0.305\pm 0.016$.

$\Gamma(\phi X(1835)\rightarrow\phi\rho\bar{\rho})/\Gamma_{\text{total}}$					Γ_{66}/Γ
VALUE	CL%	DOCUMENT ID	TECN	COMMENT	
<1.82 × 10 ⁻⁷	90	ABLIKIM	19A0	BES3 $e^+e^-\rightarrow\psi(2S)\rightarrow$ $\rho\bar{\rho}K^+K^-$	

$\Gamma(\pi^+\pi^-\rho\bar{\rho})/\Gamma_{\text{total}}$					Γ_{67}/Γ
VALUE (units 10^{-4})	EVTS	DOCUMENT ID	TECN	COMMENT	
6.0 ± 0.4 OUR AVERAGE					
$5.9\pm 0.2\pm 0.4$	904.5	BRIERE	05	CLEO $e^+e^-\rightarrow\psi(2S)\rightarrow$ $\rho\bar{\rho}\pi^+\pi^-$	
8 ± 2		¹ TANENBAUM	78	MRK1 e^+e^-	

¹ Assuming entirely strong decay.

$\Gamma(\rho\bar{\rho}\pi^-\text{ or c.c.})/\Gamma_{\text{total}}$					Γ_{68}/Γ
VALUE (units 10^{-4})	EVTS	DOCUMENT ID	TECN	COMMENT	
2.48 ± 0.17 OUR AVERAGE					
$2.45\pm 0.11\pm 0.21$	851	ABLIKIM	06i	BES2 $e^+e^-\rightarrow\rho\pi^-X$	
$2.52\pm 0.12\pm 0.22$	849	ABLIKIM	06i	BES2 $e^+e^-\rightarrow\bar{\rho}\pi^+X$	

Meson Particle Listings

$\psi(2S)$

$\Gamma(\rho^0 \pi^+ \pi^- \pi^0)/\Gamma_{total}$			Γ_{69}/Γ		
VALUE (units 10^{-4})	EVTS	DOCUMENT ID	TECN	COMMENT	
$3.18 \pm 0.50 \pm 0.50$	135 ± 21	ABLIKIM	06i	BES2	$e^+ e^- \rightarrow \rho \pi^- \pi^0 X$

$\Gamma(\eta \pi^+ \pi^-)/\Gamma_{total}$			Γ_{71}/Γ		
VALUE (units 10^{-4})	CL%	DOCUMENT ID	TECN	COMMENT	
<1.6	90	BRIERE	05	CLEO	$e^+ e^- \rightarrow \psi(2S) \rightarrow 2(\pi^+ \pi^-) \pi^0$

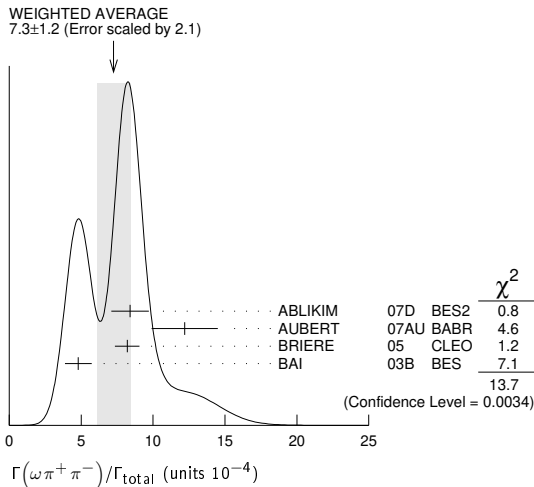
$\Gamma(\eta \pi^+ \pi^- \pi^0)/\Gamma_{total}$			Γ_{72}/Γ		
VALUE (units 10^{-4})	EVTS	DOCUMENT ID	TECN	COMMENT	
$9.5 \pm 0.7 \pm 1.5$		¹ BRIERE	05	CLEO	$e^+ e^- \rightarrow \psi(2S) \rightarrow \text{hadr}$
• • • We do not use the following data for averages, fits, limits, etc. • • •					
$10.3 \pm 0.8 \pm 1.4$	201.7	² BRIERE	05	CLEO	$e^+ e^- \rightarrow \psi(2S) \rightarrow \eta 3\pi(\eta \rightarrow \gamma\gamma)$
$8.1 \pm 1.4 \pm 1.6$	50.0	² BRIERE	05	CLEO	$e^+ e^- \rightarrow \psi(2S) \rightarrow \eta 3\pi(\eta \rightarrow 3\pi)$

¹ Average of $\eta \rightarrow \gamma\gamma$ and $\eta \rightarrow 3\pi$.
² Not independent from other values reported by BRIERE 05.

$\Gamma(2(\pi^+ \pi^-) \eta)/\Gamma_{total}$			Γ_{73}/Γ		
VALUE (units 10^{-3})	EVTS	DOCUMENT ID	TECN	COMMENT	
$1.2 \pm 0.6 \pm 0.1$	16	¹ AUBERT	07AU	BABR	$10.6 e^+ e^- \rightarrow 2(\pi^+ \pi^-) \eta \gamma$
¹ AUBERT 07AU quotes $\Gamma_{ee}^{\psi(2S)} \cdot B(\psi(2S) \rightarrow 2(\pi^+ \pi^-) \eta) \cdot B(\eta \rightarrow \gamma\gamma) = 1.2 \pm 0.7 \pm 0.1 \text{ eV}$.					

$\Gamma(\eta' \pi^+ \pi^- \pi^0)/\Gamma_{total}$			Γ_{75}/Γ		
VALUE (units 10^{-4})	EVTS	DOCUMENT ID	TECN	COMMENT	
$4.5 \pm 1.6 \pm 1.3$	12.8	BRIERE	05	CLEO	$e^+ e^- \rightarrow \psi(2S) \rightarrow \text{hadr}$

$\Gamma(\omega \pi^+ \pi^-)/\Gamma_{total}$			Γ_{76}/Γ		
VALUE (units 10^{-4})	EVTS	DOCUMENT ID	TECN	COMMENT	
7.3 ± 1.2 OUR AVERAGE		Error includes scale factor of 2.1. See the ideogram below.			
$8.4 \pm 0.5 \pm 1.2$	386	ABLIKIM	07D	BES2	$e^+ e^- \rightarrow \psi(2S)$
$12.2 \pm 2.2 \pm 0.7$	37	¹ AUBERT	07AU	BABR	$10.6 e^+ e^- \rightarrow \omega \pi^+ \pi^- \gamma$
$8.2 \pm 0.5 \pm 0.7$	391	BRIERE	05	CLEO	$e^+ e^- \rightarrow \psi(2S) \rightarrow 2(\pi^+ \pi^-) \pi^0$
$4.8 \pm 0.6 \pm 0.7$	100 ± 22	² BAI	03B	BES	$\psi(2S) \rightarrow 2(\pi^+ \pi^-) \pi^0$
¹ AUBERT 07AU quotes $\Gamma_{ee}^{\psi(2S)} \cdot B(\psi(2S) \rightarrow \omega \pi^+ \pi^-) \cdot B(\omega \rightarrow 3\pi) = 2.69 \pm 0.73 \pm 0.16 \text{ eV}$.					
² Normalized to $B(\psi(2S) \rightarrow J/\psi \pi^+ \pi^-) = 0.305 \pm 0.016$.					



$\Gamma(b_1^\pm \pi^\mp)/\Gamma_{total}$			Γ_{77}/Γ		
VALUE (units 10^{-4})	EVTS	DOCUMENT ID	TECN	COMMENT	
4.0 ± 0.6 OUR AVERAGE		Error includes scale factor of 1.1.			
$5.1 \pm 0.6 \pm 0.8$	202	ABLIKIM	07D	BES2	$e^+ e^- \rightarrow \psi(2S)$
$4.18^{+0.43}_{-0.42} \pm 0.92$	170	ADAM	05	CLEO	$e^+ e^- \rightarrow \psi(2S)$
$3.2 \pm 0.6 \pm 0.5$	61 ± 11	^{1,2} BAI	03B	BES	$\psi(2S) \rightarrow 2(\pi^+ \pi^-) \pi^0$
• • • We do not use the following data for averages, fits, limits, etc. • • •					
$5.2 \pm 0.8 \pm 1.0$		¹ BAI	99c	BES	Repl. by BAI 03B
¹ Assuming $B(b_1 \rightarrow \omega \pi) = 1$.					
² Normalized to $B(\psi(2S) \rightarrow J/\psi \pi^+ \pi^-) = 0.305 \pm 0.016$.					

$\Gamma(b_1^0 \pi^0)/\Gamma_{total}$			Γ_{78}/Γ		
VALUE (units 10^{-4})	EVTS	DOCUMENT ID	TECN	COMMENT	
$2.35^{+0.47}_{-0.42} \pm 0.40$	45	ADAM	05	CLEO	$e^+ e^- \rightarrow \psi(2S)$

$\Gamma(\omega f_2(1270))/\Gamma_{total}$			Γ_{79}/Γ			
VALUE (units 10^{-4})	CL%	EVTS	DOCUMENT ID	TECN	COMMENT	
2.2 ± 0.4 OUR AVERAGE						
$2.3 \pm 0.5 \pm 0.4$		57	ABLIKIM	07D	BES2	$e^+ e^- \rightarrow \psi(2S)$
$2.05 \pm 0.41 \pm 0.38$		62 ± 12	BAI	04c	BES2	$\psi(2S) \rightarrow 2(\pi^+ \pi^-) \pi^0$

• • • We do not use the following data for averages, fits, limits, etc. • • •

<1.5	90	¹ BAI	03B	BES	$\psi(2S) \rightarrow 2(\pi^+ \pi^-) \pi^0$
<1.7	90	BAI	98J	BES	Repl. by BAI 03B

¹ Normalized to $B(\psi(2S) \rightarrow J/\psi \pi^+ \pi^-) = 0.305 \pm 0.016$.

$\Gamma(\pi^+ \pi^- K^+ K^-)/\Gamma_{total}$			Γ_{82}/Γ		
VALUE (units 10^{-4})	EVTS	DOCUMENT ID	TECN	COMMENT	
7.3 ± 0.5 OUR AVERAGE					
$8.1 \pm 1.3 \pm 0.3$	133	LEES	12F	BABR	$10.6 e^+ e^- \rightarrow \pi^+ \pi^- K^+ K^- \gamma$
$7.1 \pm 0.3 \pm 0.4$	817.2	BRIERE	05	CLEO	$e^+ e^- \rightarrow \psi(2S) \rightarrow K^+ K^- \pi^+ \pi^-$
16 ± 4		¹ TANENBAUM	78	MRK1	$e^+ e^-$
• • • We do not use the following data for averages, fits, limits, etc. • • •					
$11.0 \pm 1.9 \pm 0.2$	85	² AUBERT	07AK	BABR	$10.6 e^+ e^- \rightarrow \pi^+ \pi^- K^+ K^- \gamma$

¹ Assuming entirely strong decay.
² Superseded by LEES 12F. AUBERT 07AK reports $[\Gamma(\psi(2S) \rightarrow \pi^+ \pi^- K^+ K^-)/\Gamma_{total}] \times [\Gamma(\psi(2S) \rightarrow e^+ e^-)] = (2.56 \pm 0.42 \pm 0.16) \times 10^{-3} \text{ keV}$ which we divide by our best value $\Gamma(\psi(2S) \rightarrow e^+ e^-) = 2.33 \pm 0.04 \text{ keV}$. Our first error is their experiment's error and our second error is the systematic error from using our best value.

$\Gamma(\rho^0 K^+ K^-)/\Gamma_{total}$			Γ_{84}/Γ		
VALUE (units 10^{-4})	EVTS	DOCUMENT ID	TECN	COMMENT	
$2.2 \pm 0.2 \pm 0.4$	223.8	BRIERE	05	CLEO	$e^+ e^- \rightarrow \psi(2S) \rightarrow K^+ K^- \pi^+ \pi^-$

$\Gamma(K^*(892)^0 \bar{K}_S^0(1430)^0)/\Gamma_{total}$			Γ_{85}/Γ			
VALUE (units 10^{-4})	CL%	EVTS	DOCUMENT ID	TECN	COMMENT	
$1.86 \pm 0.32 \pm 0.43$		93 ± 16	BAI	04c	$\psi(2S) \rightarrow K^+ K^- \pi^+ \pi^-$	
• • • We do not use the following data for averages, fits, limits, etc. • • •						
<1.2	90		BAI	98J	BES	$e^+ e^-$

$\Gamma(K^+ K^- \pi^+ \pi^- \eta)/\Gamma_{total}$			Γ_{86}/Γ		
VALUE (units 10^{-3})	EVTS	DOCUMENT ID	TECN	COMMENT	
$1.3 \pm 0.7 \pm 0.1$	7	¹ AUBERT	07AU	BABR	$10.6 e^+ e^- \rightarrow K^+ K^- \pi^+ \pi^- \eta \gamma$
¹ AUBERT 07AU quotes $\Gamma_{ee}^{\psi(2S)} \cdot B(\psi(2S) \rightarrow 2(\pi^+ \pi^-) \eta) \cdot B(\eta \rightarrow \gamma\gamma) = 1.2 \pm 0.7 \pm 0.1 \text{ eV}$.					

$\Gamma(K^+ K^- 2(\pi^+ \pi^-) \pi^0)/\Gamma_{total}$			Γ_{87}/Γ		
VALUE (units 10^{-4})	EVTS	DOCUMENT ID	TECN	COMMENT	
$10.0 \pm 2.5 \pm 1.8$	65	ABLIKIM	07D	BES2	$e^+ e^- \rightarrow \psi(2S)$

$\Gamma(K_1(1270)^\pm K^\mp)/\Gamma_{total}$			Γ_{89}/Γ		
VALUE (units 10^{-4})	EVTS	DOCUMENT ID	TECN	COMMENT	
$10.0 \pm 1.8 \pm 2.1$		¹ BAI	99c	BES	$e^+ e^-$
¹ Assuming $B(K_1(1270) \rightarrow K \rho) = 0.42 \pm 0.06$					

$\Gamma(K_S^0 K_S^0 \pi^+ \pi^-)/\Gamma_{total}$			Γ_{90}/Γ		
VALUE (units 10^{-4})	EVTS	DOCUMENT ID	TECN	COMMENT	
$2.20 \pm 0.25 \pm 0.37$	83 ± 9	ABLIKIM	05o	BES2	$e^+ e^- \rightarrow \psi(2S)$

$\Gamma(\rho^0 p \bar{p})/\Gamma_{total}$			Γ_{91}/Γ		
VALUE (units 10^{-4})	EVTS	DOCUMENT ID	TECN	COMMENT	
$0.5 \pm 0.1 \pm 0.2$	61.1	BRIERE	05	CLEO	$e^+ e^- \rightarrow \psi(2S) \rightarrow p \bar{p} \pi^+ \pi^-$

$\Gamma(K^+ \bar{K}^*(892)^0 \pi^- + c.c.)/\Gamma_{total}$			Γ_{92}/Γ		
VALUE (units 10^{-4})	EVTS	DOCUMENT ID	TECN	COMMENT	
6.7 ± 2.5		TANENBAUM	78	MRK1	$e^+ e^-$

$\Gamma(2(\pi^+ \pi^-))/\Gamma_{total}$			Γ_{93}/Γ		
VALUE (units 10^{-4})	EVTS	DOCUMENT ID	TECN	COMMENT	
2.4 ± 0.6 OUR AVERAGE		Error includes scale factor of 2.2.			
$2.2 \pm 0.2 \pm 0.2$	308	BRIERE	05	CLEO	$e^+ e^- \rightarrow \psi(2S) \rightarrow 2(\pi^+ \pi^-)$
4.5 ± 1.0		TANENBAUM	78	MRK1	$e^+ e^-$

$\Gamma(\rho^0 \pi^+ \pi^-)/\Gamma_{total}$			Γ_{94}/Γ		
VALUE (units 10^{-4})	EVTS	DOCUMENT ID	TECN	COMMENT	
2.2 ± 0.6 OUR AVERAGE		Error includes scale factor of 1.4.			
$2.0 \pm 0.2 \pm 0.4$	285.5	BRIERE	05	CLEO	$e^+ e^- \rightarrow \psi(2S) \rightarrow 2(\pi^+ \pi^-)$
4.2 ± 1.5		TANENBAUM	78	MRK1	$e^+ e^-$

See key on page 999

Meson Particle Listings

$\psi(2S)$

$\Gamma(K^+ K^- \pi^+ \pi^- \pi^0)/\Gamma_{total}$ Γ_{95}/Γ

VALUE (units 10^{-4})	EVTS	DOCUMENT ID	TECN	COMMENT
12.6 ± 0.9 OUR AVERAGE				
18.9 ± 5.7 ± 0.3	32	¹ AUBERT	07AU BABR	10.6 $e^+ e^- \rightarrow K^+ K^- \pi^+ \pi^- \pi^0 \gamma$
11.7 ± 1.0 ± 1.5	597	ABLIKIM	06G BES2	$\psi(2S) \rightarrow K^+ K^- \pi^+ \pi^- \pi^0$
12.7 ± 0.5 ± 1.0	711.6	BRIERE	05 CLEO	$e^+ e^- \rightarrow \psi(2S) \rightarrow K^+ K^- \pi^+ \pi^- \pi^0$

¹AUBERT 07AU reports $[\Gamma(\psi(2S) \rightarrow K^+ K^- \pi^+ \pi^- \pi^0)/\Gamma_{total}] \times [\Gamma(\psi(2S) \rightarrow e^+ e^-)] = (44 \pm 13 \pm 3) \times 10^{-4}$ keV which we divide by our best value $\Gamma(\psi(2S) \rightarrow e^+ e^-) = 2.33 \pm 0.04$ keV. Our first error is their experiment's error and our second error is the systematic error from using our best value.

$\Gamma(\omega f_0(1710) \rightarrow \omega K^+ K^-)/\Gamma_{total}$ Γ_{96}/Γ

VALUE (units 10^{-5})	EVTS	DOCUMENT ID	TECN	COMMENT
5.9 ± 2.0 ± 0.9	19	ABLIKIM	06G BES2	$\psi(2S) \rightarrow K^+ K^- \pi^+ \pi^- \pi^0$

$\Gamma(K^*(892)^0 K^- \pi^+ \pi^0 + c.c.)/\Gamma_{total}$ Γ_{97}/Γ

VALUE (units 10^{-4})	EVTS	DOCUMENT ID	TECN	COMMENT
8.6 ± 1.3 ± 1.8	238	ABLIKIM	06G BES2	$\psi(2S) \rightarrow K^+ K^- \pi^+ \pi^- \pi^0$

$\Gamma(K^*(892)^+ K^- \pi^+ \pi^- + c.c.)/\Gamma_{total}$ Γ_{98}/Γ

VALUE (units 10^{-4})	EVTS	DOCUMENT ID	TECN	COMMENT
9.6 ± 2.2 ± 1.7	133	ABLIKIM	06G BES2	$\psi(2S) \rightarrow K^+ K^- \pi^+ \pi^- \pi^0$

$\Gamma(K^*(892)^+ K^- \rho^0 + c.c.)/\Gamma_{total}$ Γ_{99}/Γ

VALUE (units 10^{-4})	EVTS	DOCUMENT ID	TECN	COMMENT
7.3 ± 2.2 ± 1.4	78	ABLIKIM	06G BES2	$\psi(2S) \rightarrow K^+ K^- \pi^+ \pi^- \pi^0$

$\Gamma(K^*(892)^0 K^- \rho^+ + c.c.)/\Gamma_{total}$ Γ_{100}/Γ

VALUE (units 10^{-4})	EVTS	DOCUMENT ID	TECN	COMMENT
6.1 ± 1.3 ± 1.2	125	ABLIKIM	06G BES2	$\psi(2S) \rightarrow K^+ K^- \pi^+ \pi^- \pi^0$

$\Gamma(\eta K^+ K^-, \text{no } \eta\phi)/\Gamma_{total}$ Γ_{101}/Γ

VALUE (units 10^{-5})	CL%	EVTS	DOCUMENT ID	TECN	COMMENT
3.08 ± 0.29 ± 0.25	0.3k		¹ ABLIKIM	12L BES3	$\psi(2S) \rightarrow K^+ K^- \gamma \gamma$
<13	90		BRIERE	05 CLEO	$e^+ e^- \rightarrow \psi(2S) \rightarrow K^+ K^- \pi^+ \pi^- \pi^0$

• • • We do not use the following data for averages, fits, limits, etc. • • •

¹Excluding $\eta\phi$.

$\Gamma(\omega K^+ K^-)/\Gamma_{total}$ Γ_{102}/Γ

VALUE (units 10^{-4})	EVTS	DOCUMENT ID	TECN	COMMENT
1.62 ± 0.11 OUR AVERAGE				Error includes scale factor of 1.1.
1.56 ± 0.04 ± 0.11	2.8k	ABLIKIM	14G BES3	$\psi(2S) \rightarrow K^+ K^- \pi^+ \pi^- \pi^0$
2.38 ± 0.37 ± 0.29	78	ABLIKIM	06G BES2	$\psi(2S) \rightarrow K^+ K^- \pi^+ \pi^- \pi^0$
1.9 ± 0.3 ± 0.3	76.8	BRIERE	05 CLEO	$e^+ e^- \rightarrow \psi(2S) \rightarrow K^+ K^- \pi^+ \pi^- \pi^0$
1.5 ± 0.3 ± 0.2	23	¹ BAI	03B BES	$\psi(2S) \rightarrow K^+ K^- \pi^+ \pi^- \pi^0$

¹Normalized to $B(\psi(2S) \rightarrow J/\psi \pi^+ \pi^-) = 0.305 \pm 0.016$.

$\Gamma(\omega K^*(892)^+ K^- + c.c.)/\Gamma_{total}$ Γ_{103}/Γ

VALUE (units 10^{-5})	EVTS	DOCUMENT ID	TECN	COMMENT
20.7 ± 2.6 OUR AVERAGE				
18.9 ± 2.9 ± 2.2	396	ABLIKIM	13M BES3	$\psi(2S) \rightarrow \omega K_S^0 K^- \pi^+$
22.6 ± 3.0 ± 2.4	535	ABLIKIM	13M BES3	$\psi(2S) \rightarrow \omega K^+ K^- \pi^0$

$\Gamma(\omega K_S^0(1430)^+ K^- + c.c.)/\Gamma_{total}$ Γ_{104}/Γ

VALUE (units 10^{-5})	EVTS	DOCUMENT ID	TECN	COMMENT
6.1 ± 1.2 OUR AVERAGE				
6.39 ± 1.50 ± 0.78	128	ABLIKIM	13M BES3	$\psi(2S) \rightarrow \omega K_S^0 K^- \pi^+$
5.86 ± 1.61 ± 0.83	143	ABLIKIM	13M BES3	$\psi(2S) \rightarrow \omega K^+ K^- \pi^0$

$\Gamma(\omega \bar{K}^*(892)^0 K^0)/\Gamma_{total}$ Γ_{105}/Γ

VALUE (units 10^{-5})	EVTS	DOCUMENT ID	TECN	COMMENT
16.8 ± 2.5 ± 1.6	356	ABLIKIM	13M BES3	$\psi(2S) \rightarrow \omega K_S^0 K^- \pi^+$

$\Gamma(\omega \bar{K}_S^0(1430)^0 K^0)/\Gamma_{total}$ Γ_{106}/Γ

VALUE (units 10^{-5})	EVTS	DOCUMENT ID	TECN	COMMENT
5.82 ± 2.08 ± 0.72	116	ABLIKIM	13M BES3	$\psi(2S) \rightarrow \omega K_S^0 K^- \pi^+$

$\Gamma(\omega X(1440) \rightarrow \omega K_S^0 K^- \pi^+ + c.c.)/\Gamma_{total}$ Γ_{107}/Γ

VALUE (units 10^{-5})	EVTS	DOCUMENT ID	TECN	COMMENT
1.60 ± 0.27 ± 0.24	109	¹ ABLIKIM	13M BES3	$\psi(2S) \rightarrow \omega K_S^0 K^- \pi^+$

¹X(1440) compatible with $\eta(1405)$ and $\eta(1475)$. A $f_1(1420)$ is also possible.

$\Gamma(\omega X(1440) \rightarrow \omega K^+ K^- \pi^0)/\Gamma_{total}$ Γ_{108}/Γ

VALUE (units 10^{-5})	EVTS	DOCUMENT ID	TECN	COMMENT
1.09 ± 0.20 ± 0.16	82	¹ ABLIKIM	13M BES3	$\psi(2S) \rightarrow \omega K^+ K^- \pi^0$

¹X(1440) compatible with $\eta(1405)$ and $\eta(1475)$. A $f_1(1420)$ is also possible.

$\Gamma(\omega f_1(1285) \rightarrow \omega K_S^0 K^- \pi^+ + c.c.)/\Gamma_{total}$ Γ_{109}/Γ

VALUE (units 10^{-5})	EVTS	DOCUMENT ID	TECN	COMMENT
0.302 ± 0.098 ± 0.027	22	¹ ABLIKIM	13M BES3	$\psi(2S) \rightarrow \omega K_S^0 K^- \pi^+$

¹Statistical significance 4.5 σ . This measurement is equivalent to a limit of $< 0.478 \times 10^{-5}$ at 90% C.L.

$\Gamma(\omega f_1(1285) \rightarrow \omega K^+ K^- \pi^0)/\Gamma_{total}$ Γ_{110}/Γ

VALUE (units 10^{-5})	EVTS	DOCUMENT ID	TECN	COMMENT
0.125 ± 0.070 ± 0.013	10	¹ ABLIKIM	13M BES3	$\psi(2S) \rightarrow \omega K^+ K^- \pi^0$

¹Statistical significance 3.2 σ . This measurement is equivalent to a limit of $< 0.221 \times 10^{-5}$ at 90% C.L.

$\Gamma(3(\pi^+ \pi^-))/\Gamma_{total}$ Γ_{111}/Γ

VALUE (units 10^{-4})	EVTS	DOCUMENT ID	TECN	COMMENT
3.5 ± 2.0 OUR AVERAGE				Error includes scale factor of 2.8.
5.45 ± 0.42 ± 0.87	671	ABLIKIM	05H BES2	$e^+ e^- \rightarrow \psi(2S) \rightarrow 3(\pi^+ \pi^-)$
1.5 ± 1.0		¹ TANENBAUM	78 MRK1	$e^+ e^-$

¹Assuming entirely strong decay.

$\Gamma(\rho \bar{\rho} \pi^+ \pi^- \pi^0)/\Gamma_{total}$ Γ_{112}/Γ

VALUE (units 10^{-4})	EVTS	DOCUMENT ID	TECN	COMMENT
7.3 ± 0.4 ± 0.6	434.9	BRIERE	05 CLEO	$e^+ e^- \rightarrow \psi(2S) \rightarrow \rho \bar{\rho} \pi^+ \pi^- \pi^0$

$\Gamma(K^+ K^-)/\Gamma_{total}$ Γ_{113}/Γ

VALUE (units 10^{-5})	CL%	EVTS	DOCUMENT ID	TECN	COMMENT
7.48 ± 0.23 ± 0.39		1.3k	¹ METREVELI	12	$\psi(2S) \rightarrow K^+ K^-$
• • • We do not use the following data for averages, fits, limits, etc. • • •					
6.2 ± 1.5 ± 0.2		66	^{2,3} LEES	15J BABR	$e^+ e^- \rightarrow K^+ K^- \gamma$
8.3 ± 1.5 ± 0.2		66	^{3,4} LEES	15J BABR	$e^+ e^- \rightarrow K^+ K^- \gamma$
6.3 ± 0.6 ± 0.3			⁵ DOBBS	06A CLEO	$e^+ e^-$
10 ± 7			⁵ BRANDELK	79C DASP	$e^+ e^-$
< 5		90	FELDMAN	77 MRK1	$e^+ e^-$

¹Obtained by analyzing CLEO-c data but not authored by the CLEO Collaboration.
² $\sin\phi > 0$.
³Using $\Gamma(\psi(2S) \rightarrow e^+ e^-) = (2.37 \pm 0.04)$ keV.
⁴ $\sin\phi < 0$.
⁵Interference with non-resonant $K^+ K^-$ production not taken into account.

$\Gamma(K_S^0 K_L^0)/\Gamma_{total}$ Γ_{114}/Γ

VALUE (units 10^{-5})	EVTS	DOCUMENT ID	TECN	COMMENT
5.34 ± 0.33 OUR AVERAGE				
5.28 ± 0.25 ± 0.34	478 ± 23	¹ METREVELI	12	$\psi(2S) \rightarrow K_S^0 K_L^0$
5.8 ± 0.8 ± 0.4		DOBBS	06A CLEO	$e^+ e^-$
5.24 ± 0.47 ± 0.48	156 ± 14	² BAI	04B BES2	$\psi(2S) \rightarrow K_S^0 K_L^0 \rightarrow \pi^+ \pi^- X$

¹Obtained by analyzing CLEO-c data but not authored by the CLEO Collaboration.
²Using $B(K_S^0 \rightarrow \pi^+ \pi^-) = 0.6860 \pm 0.0027$.

$\Gamma(\pi^+ \pi^- \pi^0)/\Gamma_{total}$ Γ_{115}/Γ

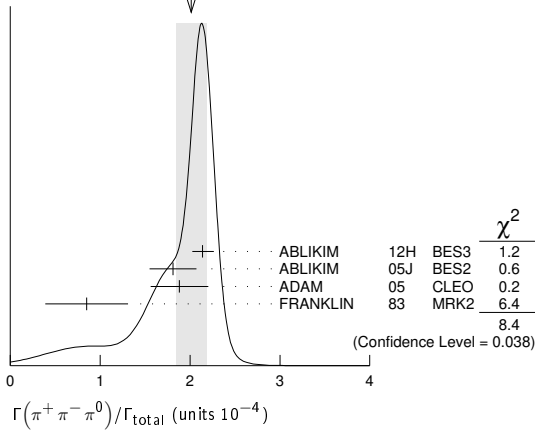
VALUE (units 10^{-4})	EVTS	DOCUMENT ID	TECN	COMMENT
2.01 ± 0.17 OUR AVERAGE				Error includes scale factor of 1.7. See the ideogram below.
2.14 ± 0.03 ± 0.12 ± 0.11	7k	¹ ABLIKIM	12H BES3	$e^+ e^- \rightarrow \psi(2S)$
1.81 ± 0.18 ± 0.19	260 ± 19	² ABLIKIM	05J BES2	$e^+ e^- \rightarrow \psi(2S)$
1.88 ± 0.16 ± 0.28 ± 0.15	194	ADAM	05 CLEO	$e^+ e^- \rightarrow \psi(2S)$
0.85 ± 0.46	4	FRANKLIN	83 MRK2	$e^+ e^- \rightarrow \text{hadrons}$

¹From $\psi(2S) \rightarrow \pi^+ \pi^- \pi^0$ events directly. The quoted systematic error includes a contribution of 4% (added in quadrature) from the uncertainty on the number of $\psi(2S)$ events.
²From a PW analysis of $\psi(2S) \rightarrow \pi^+ \pi^- \pi^0$.

Meson Particle Listings

$\psi(2S)$

WEIGHTED AVERAGE
2.01±0.17 (Error scaled by 1.7)



$\Gamma(\rho(2150)\pi \rightarrow \pi^+\pi^-\pi^0)/\Gamma_{total}$ Γ_{116}/Γ

VALUE (units 10^{-4})	DOCUMENT ID	TECN	COMMENT
1.94 ± 0.25 ± 1.15	1 ABLIKIM	05J	BES2 $\psi(2S) \rightarrow \rho(2150)\pi \rightarrow \pi^+\pi^-\pi^0$

¹ From a PW analysis of $\psi(2S) \rightarrow \pi^+\pi^-\pi^0$.

$\Gamma(\rho(770)\pi \rightarrow \pi^+\pi^-\pi^0)/\Gamma_{total}$ Γ_{117}/Γ

VALUE (units 10^{-4})	CL%	EVTS	DOCUMENT ID	TECN	COMMENT
0.32 ± 0.12	OUR AVERAGE	Error includes scale factor of 1.8.			
0.51 ± 0.07 ± 0.11			¹ ABLIKIM	05J	BES2 $\psi(2S) \rightarrow \rho(770)\pi \rightarrow \pi^+\pi^-\pi^0$
0.24 ± 0.08 ± 0.02		22	ADAM	05	CLEO $e^+e^- \rightarrow \psi(2S)$

• • • We do not use the following data for averages, fits, limits, etc. • • •

<0.83	90	1	FRANKLIN	83	MRK2 e^+e^-
<10	90		BARTEL	76	CNTR e^+e^-
<10	90		² ABRAMS	75	MRK1 e^+e^-

¹ From a PW analysis of $\psi(2S) \rightarrow \pi^+\pi^-\pi^0$.
² Final state $\rho^0\pi^0$.

$\Gamma(\pi^+\pi^-)/\Gamma_{total}$ Γ_{118}/Γ

VALUE (units 10^{-5})	CL%	EVTS	DOCUMENT ID	TECN	COMMENT
0.78 ± 0.26	OUR AVERAGE				
0.76 ± 0.25 ± 0.06		30	¹ METREVELI	12	$\psi(2S) \rightarrow \pi^+\pi^-$
8 ± 5			BRANDELIK	79c	DASP e^+e^-

• • • We do not use the following data for averages, fits, limits, etc. • • •

<2.1	90		DOBBS	06A	CLEO $e^+e^- \rightarrow \psi(2S)$
<5	90		FELDMAN	77	MRK1 e^+e^-

¹ Obtained by analyzing CLEO-c data but not authored by the CLEO Collaboration. Using $\psi(3770) \rightarrow \pi^+\pi^-$ for continuum subtraction.

$\Gamma(K_1(1400)^\pm K^\mp)/\Gamma_{total}$ Γ_{119}/Γ

VALUE (units 10^{-4})	CL%	DOCUMENT ID	TECN	COMMENT
<3.1	90	¹ BAI	99c	BES e^+e^-

¹ Assuming $B(K_1(1400) \rightarrow K^*\pi) = 0.94 \pm 0.06$

$\Gamma(K_2^*(1430)^\pm K^\mp)/\Gamma_{total}$ Γ_{120}/Γ

VALUE (units 10^{-5})	EVTS	DOCUMENT ID	TECN	COMMENT
7.12 ± 0.62 ± 1.13	251 ± 22	ABLIKIM	12L	BES3 $e^+e^- \rightarrow \psi(2S)$

$\Gamma(K^+K^-\pi^0)/\Gamma_{total}$ Γ_{121}/Γ

VALUE (units 10^{-5})	CL%	EVTS	DOCUMENT ID	TECN	COMMENT
4.07 ± 0.16 ± 0.26	0.9k	ABLIKIM	12L	BES3 $e^+e^- \rightarrow \psi(2S)$	

• • • We do not use the following data for averages, fits, limits, etc. • • •

<8.9	90	1	FRANKLIN	83	MRK2 $e^+e^- \rightarrow \text{hadrons}$
------	----	---	----------	----	--

$\Gamma(K^+K^*(892)^- + c.c.)/\Gamma_{total}$ Γ_{124}/Γ

VALUE (units 10^{-5})	CL%	EVTS	DOCUMENT ID	TECN	COMMENT
2.9 ± 0.4	OUR AVERAGE	Error includes scale factor of 1.2.			
3.18 ± 0.30 ± 0.26		0.2k	ABLIKIM	12L	BES3 $e^+e^- \rightarrow \psi(2S)$
2.9 ± 1.3 ± 1.7		9.6 ± 4.2	ABLIKIM	05i	BES2 $e^+e^- \rightarrow \psi(2S)$
1.3 ± 1.0 ± 0.7		7	ADAM	05	CLEO $e^+e^- \rightarrow \psi(2S)$

• • • We do not use the following data for averages, fits, limits, etc. • • •

<5.4	90		FRANKLIN	83	MRK2 $e^+e^- \rightarrow \text{hadrons}$
------	----	--	----------	----	--

$\Gamma(K^*(892)^0\bar{K}^0 + c.c.)/\Gamma_{total}$ Γ_{125}/Γ

VALUE (units 10^{-5})	EVTS	DOCUMENT ID	TECN	COMMENT
10.9 ± 2.0	OUR AVERAGE			
13.3 ± 2.4 ± 2.8	65.6 ± 9.0	ABLIKIM	05i	BES2 $e^+e^- \rightarrow \psi(2S)$
9.2 ± 2.7 ± 2.2	25	ADAM	05	CLEO $e^+e^- \rightarrow \psi(2S)$

$\Gamma(K^+K^*(892)^- + c.c.)/\Gamma(K^*(892)^0\bar{K}^0 + c.c.)$ $\Gamma_{124}/\Gamma_{125}$

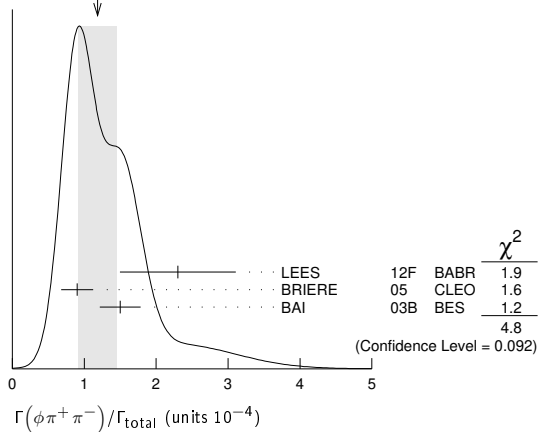
VALUE	DOCUMENT ID	TECN	COMMENT
0.16 ± 0.06	OUR AVERAGE		
0.22 ± 0.10 ± 0.14	ABLIKIM	05i	BES2 $e^+e^- \rightarrow \psi(2S)$
0.14 ± 0.08 ± 0.06	ADAM	05	CLEO $e^+e^- \rightarrow \psi(2S)$

$\Gamma(\phi\pi^+\pi^-)/\Gamma_{total}$ Γ_{126}/Γ

VALUE (units 10^{-4})	EVTS	DOCUMENT ID	TECN	COMMENT
1.18 ± 0.26	OUR AVERAGE	Error includes scale factor of 1.5. See the ideogram below.		
2.3 ± 0.8 ± 0.1	19 ± 6	LEES	12F	BABR $10.6 e^+e^- \rightarrow \pi^+\pi^-K^+K^-\gamma$
0.9 ± 0.2 ± 0.1	47.6	BRIERE	05	CLEO $e^+e^- \rightarrow \psi(2S) \rightarrow K^+K^-\pi^+\pi^-$
1.5 ± 0.2 ± 0.2	51.5 ± 8.3	¹ BAI	03B	BES $\psi(2S) \rightarrow K^+K^-\pi^+\pi^-$
2.45 ± 0.96 ± 0.04	10 ± 4	^{2,3} AUBERT	07AK	BABR $10.6 e^+e^- \rightarrow \pi^+\pi^-K^+K^-\gamma$

¹ Normalized to $B(\psi(2S) \rightarrow J/\psi\pi^+\pi^-) = 0.305 \pm 0.016$.
² Superseded by LEES 12F. AUBERT 07AK reports $[\Gamma(\psi(2S) \rightarrow \phi\pi^+\pi^-)/\Gamma_{total}] \times [\Gamma(\psi(2S) \rightarrow e^+e^-)] = (0.57 \pm 0.22 \pm 0.04) \times 10^{-3}$ keV which we divide by our best value $\Gamma(\psi(2S) \rightarrow e^+e^-) = 2.33 \pm 0.04$ keV. Our first error is their experiment's error and our second error is the systematic error from using our best value.
³ Using $B(\phi \rightarrow K^+K^-) = (49.3 \pm 0.6)\%$.

WEIGHTED AVERAGE
1.18±0.26 (Error scaled by 1.5)



$\Gamma(\phi f_0(980) \rightarrow \pi^+\pi^-)/\Gamma_{total}$ Γ_{127}/Γ

VALUE (units 10^{-4})	EVTS	DOCUMENT ID	TECN	COMMENT
0.75 ± 0.33	OUR AVERAGE	Error includes scale factor of 1.6.		
1.5 ± 0.5 ± 0.1	12 ± 4	LEES	12F	BABR $10.6 e^+e^- \rightarrow \pi^+\pi^-K^+K^-\gamma$
0.6 ± 0.2 ± 0.1	18.4 ± 6.4	¹ BAI	03B	BES $\psi(2S) \rightarrow K^+K^-\pi^+\pi^-$
1.46 ± 0.71 ± 0.02	6 ± 3	^{2,3} AUBERT	07AK	BABR $10.6 e^+e^- \rightarrow \pi^+\pi^-K^+K^-\gamma$

¹ Normalized to $B(\psi(2S) \rightarrow J/\psi\pi^+\pi^-) = 0.305 \pm 0.016$.
² Superseded by LEES 12F. AUBERT 07AK reports $[\Gamma(\psi(2S) \rightarrow \phi f_0(980) \rightarrow \pi^+\pi^-)/\Gamma_{total}] \times [\Gamma(\psi(2S) \rightarrow e^+e^-)] = (0.34 \pm 0.16 \pm 0.04) \times 10^{-3}$ keV which we divide by our best value $\Gamma(\psi(2S) \rightarrow e^+e^-) = 2.33 \pm 0.04$ keV. Our first error is their experiment's error and our second error is the systematic error from using our best value.
³ Using $B(\phi \rightarrow K^+K^-) = (49.3 \pm 0.6)\%$.

$\Gamma(2(K^+K^-))/\Gamma_{total}$ Γ_{128}/Γ

VALUE (units 10^{-4})	EVTS	DOCUMENT ID	TECN	COMMENT
0.63 ± 0.13	OUR AVERAGE			
0.9 ± 0.4 ± 0.1	13	LEES	12F	BABR $10.6 e^+e^- \rightarrow 2(K^+K^-)\gamma$
0.6 ± 0.1 ± 0.1	59.2	BRIERE	05	CLEO $e^+e^- \rightarrow \psi(2S) \rightarrow 2(K^+K^-)$

$\Gamma(\phi K^+ K^-)/\Gamma_{total}$		Γ_{129}/Γ	
VALUE (units 10^{-4})	EVTS	DOCUMENT ID	TECN COMMENT
0.70 ± 0.16 OUR AVERAGE			
0.8 ± 0.2 ± 0.1	36.8	BRIERE	05 CLEO $e^+e^- \rightarrow \psi(2S) \rightarrow 2(K^+K^-)$

0.6 ± 0.2 ± 0.1	16.1 ± 5.0	¹ BAI	03B BES $\psi(2S) \rightarrow 2(K^+K^-)$
¹ Normalized to $B(\psi(2S) \rightarrow J/\psi\pi^+\pi^-) = 0.305 \pm 0.016$.			

$\Gamma(2(K^+K^-)\pi^0)/\Gamma_{total}$		Γ_{130}/Γ	
VALUE (units 10^{-4})	EVTS	DOCUMENT ID	TECN COMMENT
1.1 ± 0.2 ± 0.2	44.7	BRIERE	05 CLEO $e^+e^- \rightarrow \psi(2S) \rightarrow 2(K^+K^-)\pi^0$

$\Gamma(\phi\eta)/\Gamma_{total}$		Γ_{131}/Γ	
VALUE (units 10^{-5})	EVTS	DOCUMENT ID	TECN COMMENT
3.10 ± 0.31 OUR AVERAGE			
3.14 ± 0.23 ± 0.23	0.2k	ABLIKIM	12L BES3 $e^+e^- \rightarrow \psi(2S)$
2.0 ^{+1.5} _{-1.1} ± 0.4	6	ADAM	05 CLEO $e^+e^- \rightarrow \psi(2S)$
3.3 ± 1.1 ± 0.5	17	ABLIKIM	04k BES $e^+e^- \rightarrow \psi(2S)$

$\Gamma(\eta\phi(2170), \phi(2170) \rightarrow \phi f_0(980), f_0 \rightarrow \pi^+\pi^-)/\Gamma_{total}$		Γ_{132}/Γ	
VALUE	CL%	DOCUMENT ID	TECN COMMENT
<2.2 × 10⁻⁶	90	ABLIKIM	19i BES3 $e^+e^- \rightarrow \eta\phi f_0(980)$

$\Gamma(\phi\eta')/\Gamma_{total}$		Γ_{133}/Γ	
VALUE (units 10^{-5})	EVTS	DOCUMENT ID	TECN COMMENT
1.54 ± 0.20 OUR AVERAGE			
1.51 ± 0.16 ± 0.12	201	ABLIKIM	19BA BES3 $e^+e^- \rightarrow \psi(2S)$
3.1 ± 1.4 ± 0.7	8	¹ ABLIKIM	04k BES $e^+e^- \rightarrow \psi(2S)$
¹ Calculated combining $\eta' \rightarrow \gamma\rho$ and $\eta\pi^+\pi^-$ channels.			

$\Gamma(\omega\eta')/\Gamma_{total}$		Γ_{136}/Γ	
VALUE (units 10^{-5})	EVTS	DOCUMENT ID	TECN COMMENT
3.2 ^{+2.4}_{-2.0} ± 0.7	4	¹ ABLIKIM	04k BES $e^+e^- \rightarrow \psi(2S)$
¹ Calculated combining $\eta' \rightarrow \gamma\rho$ and $\eta\pi^+\pi^-$ channels.			

$\Gamma(\omega\pi^0)/\Gamma_{total}$		Γ_{137}/Γ	
VALUE (units 10^{-5})	EVTS	DOCUMENT ID	TECN COMMENT
2.1 ± 0.6 OUR AVERAGE			
2.5 ^{+1.2} _{-1.0} ± 0.2	14	ADAM	05 CLEO $e^+e^- \rightarrow \psi(2S)$
1.87 ^{+0.68} _{-0.62} ± 0.28	14	ABLIKIM	04L BES $e^+e^- \rightarrow \psi(2S)$

$\Gamma(\rho\eta')/\Gamma_{total}$		Γ_{138}/Γ	
VALUE (units 10^{-5})	EVTS	DOCUMENT ID	TECN COMMENT
1.87 ^{+1.64}_{-1.11} ± 0.33	2	ABLIKIM	04L BES $e^+e^- \rightarrow \psi(2S)$
• • • We do not use the following data for averages, fits, limits, etc. • • •			
1.02 ± 0.11 ± 0.24	143	¹ ABLIKIM	17AK BES3 $e^+e^- \rightarrow \psi(2S)$
0.569 ± 0.128 ± 0.236	80	² ABLIKIM	17AK BES3 $e^+e^- \rightarrow \psi(2S)$

¹Destructive-interference solution of a partial wave analysis of the decay $\psi(2S) \rightarrow \pi^+\pi^-\eta'$.
²Constructive-interference solution of a partial wave analysis of the decay $\psi(2S) \rightarrow \pi^+\pi^-\eta'$.

$\Gamma(\rho\eta)/\Gamma_{total}$		Γ_{139}/Γ	
VALUE (units 10^{-5})	EVTS	DOCUMENT ID	TECN COMMENT
2.2 ± 0.6 OUR AVERAGE	Error includes scale factor of 1.1.		
3.0 ^{+1.1} _{-0.9} ± 0.2	18	ADAM	05 CLEO $e^+e^- \rightarrow \psi(2S)$
1.78 ^{+0.67} _{-0.62} ± 0.17	13	ABLIKIM	04L BES $e^+e^- \rightarrow \psi(2S)$

$\Gamma(\omega\eta)/\Gamma_{total}$		Γ_{140}/Γ	
VALUE (units 10^{-5})	CL%	DOCUMENT ID	TECN COMMENT
<1.1	90	ADAM	05 CLEO $e^+e^- \rightarrow \psi(2S)$
• • • We do not use the following data for averages, fits, limits, etc. • • •			
<3.1	90	ABLIKIM	04k BES $e^+e^- \rightarrow \psi(2S)$

$\Gamma(\phi\pi^0)/\Gamma_{total}$		Γ_{141}/Γ	
VALUE (units 10^{-5})	CL%	DOCUMENT ID	TECN COMMENT
<0.04	90	ABLIKIM	12L BES3 $e^+e^- \rightarrow \psi(2S)$
• • • We do not use the following data for averages, fits, limits, etc. • • •			
<0.7	90	ADAM	05 CLEO $e^+e^- \rightarrow \psi(2S)$
<0.4	90	ABLIKIM	04k BES $e^+e^- \rightarrow \psi(2S)$

$\Gamma(\eta_c\pi^+\pi^-)/\Gamma_{total}$		Γ_{142}/Γ	
VALUE (units 10^{-3})	CL%	DOCUMENT ID	TECN COMMENT
<1.0	90	PEDLAR	07 CLEO $e^+e^- \rightarrow \psi(2S)$

$\Gamma(\rho\bar{\rho}K^+K^-)/\Gamma_{total}$		Γ_{143}/Γ	
VALUE (units 10^{-5})	EVTS	DOCUMENT ID	TECN COMMENT
2.7 ± 0.6 ± 0.4	30.1	BRIERE	05 CLEO $e^+e^- \rightarrow \psi(2S) \rightarrow \rho\bar{\rho}K^+K^-$

$\Gamma(\bar{\Lambda}nK_S^0 + c.c.)/\Gamma_{total}$		Γ_{144}/Γ	
VALUE (units 10^{-4})	EVTS	DOCUMENT ID	TECN COMMENT
0.81 ± 0.11 ± 0.14	50	¹ ABLIKIM	08c BES2 $e^+e^- \rightarrow J/\psi$
¹ Using $B(\bar{\Lambda} \rightarrow \bar{p}\pi^+) = 63.9\%$ and $B(K_S^0 \rightarrow \pi^+\pi^-) = 69.2\%$.			

$\Gamma(\phi f_2'(1525))/\Gamma_{total}$		Γ_{145}/Γ	
VALUE (units 10^{-4})	CL%	DOCUMENT ID	TECN COMMENT
0.44 ± 0.12 ± 0.11	20 ± 6	BAI	04c $\psi(2S) \rightarrow 2(K^+K^-)$
• • • We do not use the following data for averages, fits, limits, etc. • • •			
<0.45	90	BAI	98J BES $e^+e^- \rightarrow 2(K^+K^-)$

$\Gamma(\phi f_1(1285))/\Gamma_{total}$		Γ_{134}/Γ	
VALUE (units 10^{-5})	EVTS	DOCUMENT ID	TECN COMMENT
3.0 ± 0.4 ± 1.3	234	¹ ABLIKIM	19BA BES3 $e^+e^- \rightarrow \psi(2S)$
¹ ABLIKIM 19BA reports $[\Gamma(\psi(2S) \rightarrow \phi f_1(1285))/\Gamma_{total}] \times [B(f_1(1285) \rightarrow \eta\pi^+\pi^-)] = (1.03 \pm 0.10 \pm 0.09) \times 10^{-5}$ which we divide by our best value $B(f_1(1285) \rightarrow \eta\pi^+\pi^-) = (35 \pm 15) \times 10^{-2}$. Our first error is their experiment's error and our second error is the systematic error from using our best value.			

$\Gamma(\phi\eta(1405) \rightarrow \phi\pi^+\pi^-\eta)/\Gamma_{total}$		Γ_{135}/Γ	
VALUE (units 10^{-6})	EVTS	DOCUMENT ID	TECN COMMENT
8.46 ± 1.37 ± 0.92	195	ABLIKIM	19BA BES3 $e^+e^- \rightarrow \psi(2S)$

$\Gamma(\Theta(1540)\bar{\Theta}(1540) \rightarrow K_S^0\rho K^-\bar{\pi} + c.c.)/\Gamma_{total}$		Γ_{146}/Γ	
VALUE (units 10^{-5})	CL%	DOCUMENT ID	TECN COMMENT
<0.88	90	BAI	04G BES2 e^+e^-

$\Gamma(\Theta(1540)K^-\bar{\pi} \rightarrow K_S^0\rho K^-\bar{\pi})/\Gamma_{total}$		Γ_{147}/Γ	
VALUE (units 10^{-5})	CL%	DOCUMENT ID	TECN COMMENT
<1.0	90	BAI	04G BES2 e^+e^-

$\Gamma(\Theta(1540)K_S^0\bar{p} \rightarrow K_S^0\bar{p}K^+n)/\Gamma_{total}$		Γ_{148}/Γ	
VALUE (units 10^{-5})	CL%	DOCUMENT ID	TECN COMMENT
<0.70	90	BAI	04G BES2 e^+e^-

$\Gamma(\bar{\Theta}(1540)K^+n \rightarrow K_S^0\bar{p}K^+n)/\Gamma_{total}$		Γ_{149}/Γ	
VALUE (units 10^{-5})	CL%	DOCUMENT ID	TECN COMMENT
<2.6	90	BAI	04G BES2 e^+e^-

$\Gamma(\bar{\Theta}(1540)K_S^0\rho \rightarrow K_S^0\rho K^-\bar{\pi})/\Gamma_{total}$		Γ_{150}/Γ	
VALUE (units 10^{-5})	CL%	DOCUMENT ID	TECN COMMENT
<0.60	90	BAI	04G BES2 e^+e^-

$\Gamma(K_S^0K_S^0)/\Gamma_{total}$		Γ_{151}/Γ	
VALUE (units 10^{-4})	DOCUMENT ID	TECN	COMMENT
<0.046	¹ BAI	04D	BES e^+e^-
¹ Forbidden by CP.			

$\Gamma(\Lambda_c^+\bar{p}e^+ + c.c.)/\Gamma_{total}$		Γ_{152}/Γ	
VALUE	CL% EVTS	DOCUMENT ID	TECN COMMENT
<1.7 × 10⁻⁶	90 450M	ABLIKIM	18q BES3 $e^+e^- \rightarrow \psi(2S)$

RADIATIVE DECAYS

$\Gamma(\gamma\chi_{c0}(1P))/\Gamma_{total}$		Γ_{153}/Γ	
VALUE (units 10^{-2})	EVTS	DOCUMENT ID	TECN COMMENT
9.79 ± 0.20 OUR FIT			
9.33 ± 0.26 OUR AVERAGE			
9.389 ± 0.014 ± 0.332	4.7M	ABLIKIM	17U BES3 $e^+e^- \rightarrow \gamma X$
9.22 ± 0.11 ± 0.46	72k	ATHAR	04 CLEO $e^+e^- \rightarrow \gamma X$
9.9 ± 0.5 ± 0.8		¹ GAISER	86 CBAL $e^+e^- \rightarrow \gamma X$
7.2 ± 2.3		¹ BIDDICK	77 CNTR $e^+e^- \rightarrow \gamma X$
7.5 ± 2.6		¹ WHITAKER	76 MRK1 e^+e^-
¹ Angular distribution $(1+\cos^2\theta)$ assumed.			

$\Gamma(\gamma\chi_{c1}(1P))/\Gamma_{total}$		Γ_{154}/Γ	
VALUE (units 10^{-2})	EVTS	DOCUMENT ID	TECN COMMENT
9.75 ± 0.24 OUR FIT			
9.54 ± 0.29 OUR AVERAGE			
9.905 ± 0.011 ± 0.353	5.0M	ABLIKIM	17U BES3 $e^+e^- \rightarrow \gamma X$
9.07 ± 0.11 ± 0.54	76k	ATHAR	04 CLEO $e^+e^- \rightarrow \gamma X$
9.0 ± 0.5 ± 0.7		¹ GAISER	86 CBAL $e^+e^- \rightarrow \gamma X$
7.1 ± 1.9		² BIDDICK	77 CNTR $e^+e^- \rightarrow \gamma X$
¹ Angular distribution $(1-0.189\cos^2\theta)$ assumed.			
² Valid for isotropic distribution of the photon.			

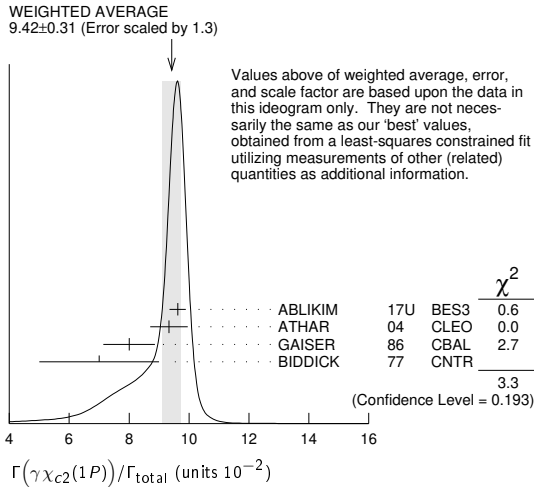
Meson Particle Listings

$\psi(2S)$

$\Gamma(\gamma\chi_{c2}(1P))/\Gamma_{total}$

VALUE (units 10^{-2})	EVTS	DOCUMENT ID	TECN	COMMENT
9.52 ± 0.20 OUR FIT				
9.42 ± 0.31 OUR AVERAGE				Error includes scale factor of 1.3. See the ideogram below.
9.621 ± 0.013 ± 0.272	4.2M	ABLIKIM	17U	BES3 $e^+e^- \rightarrow \gamma X$
9.33 ± 0.14 ± 0.61	79k	ATHAR	04	CLEO $e^+e^- \rightarrow \gamma X$
8.0 ± 0.5 ± 0.7		¹ GAISER	86	CBAL $e^+e^- \rightarrow \gamma X$
7.0 ± 2.0		² BIDDICK	77	CNTR $e^+e^- \rightarrow \gamma X$

¹ Angular distribution $(1-0.052 \cos^2\theta)$ assumed.
² Valid for isotropic distribution of the photon.



$[\Gamma(\gamma\chi_{c0}(1P)) + \Gamma(\gamma\chi_{c1}(1P)) + \Gamma(\gamma\chi_{c2}(1P))]/\Gamma_{total}$

VALUE	DOCUMENT ID	TECN	COMMENT
7 ± 2 ± 4			

••• We do not use the following data for averages, fits, limits, etc. •••
 27.6 ± 0.3 ± 2.0 ¹ ATHAR 04 CLEO $e^+e^- \rightarrow \gamma X$
¹ Not independent from ATHAR 04 measurements of $B(\gamma\chi_{cJ})$.

$\Gamma(\gamma\chi_{c0}(1P))/\Gamma(\gamma\chi_{c1}(1P))$

VALUE	DOCUMENT ID	TECN	COMMENT
1.02 ± 0.01 ± 0.07			
1.03 ± 0.04 ± 0.03	¹ ATHAR	04	CLEO $e^+e^- \rightarrow \gamma X$

¹ Not independent from ATHAR 04 measurements of $B(\gamma\chi_{cJ})$.

$\Gamma(\gamma\chi_{c2}(1P))/\Gamma(\gamma\chi_{c1}(1P))$

VALUE	DOCUMENT ID	TECN	COMMENT
1.03 ± 0.02 ± 0.03			
1.03 ± 0.04 ± 0.03	¹ ATHAR	04	CLEO $e^+e^- \rightarrow \gamma X$

¹ Not independent from ATHAR 04 measurements of $B(\gamma\chi_{cJ})$.

$\Gamma(\gamma\chi_{c0}(1P))/\Gamma(\gamma\chi_{c2}(1P))$

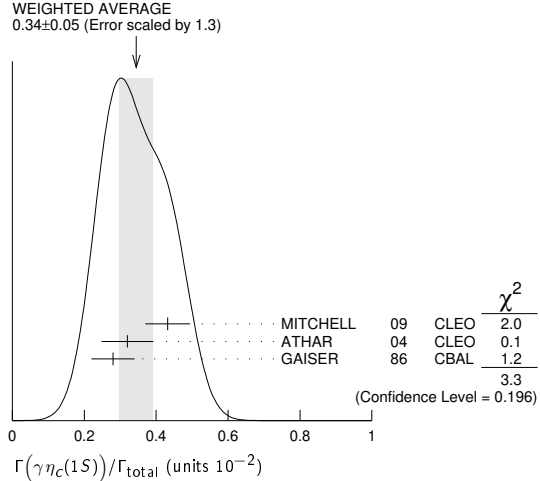
VALUE	DOCUMENT ID	TECN	COMMENT
0.99 ± 0.02 ± 0.08			
0.99 ± 0.02 ± 0.08	¹ ATHAR	04	CLEO $e^+e^- \rightarrow \gamma X$

¹ Not independent from ATHAR 04 measurements of $B(\gamma\chi_{cJ})$.

$\Gamma(\gamma\eta_c(1S))/\Gamma_{total}$

VALUE (units 10^{-2})	EVTS	DOCUMENT ID	TECN	COMMENT
0.34 ± 0.05 OUR AVERAGE				Error includes scale factor of 1.3. See the ideogram below.
0.432 ± 0.016 ± 0.060		MITCHELL	09	CLEO $e^+e^- \rightarrow \gamma X$
0.32 ± 0.04 ± 0.06	2.5k	¹ ATHAR	04	CLEO $e^+e^- \rightarrow \gamma X$
0.28 ± 0.06		² GAISER	86	CBAL $e^+e^- \rightarrow \gamma X$

¹ ATHAR 04 used $\Gamma_{\eta_c(1S)} = 24.8 \pm 4.9$ MeV to obtain this result.
² GAISER 86 used $\Gamma_{\eta_c(1S)} = 11.5 \pm 4.5$ MeV to obtain this result.



$\Gamma(\gamma\eta_c(2S))/\Gamma_{total}$

VALUE (units 10^{-4})	CL%	DOCUMENT ID	TECN	COMMENT
7 ± 2 ± 4				
< 8	90	² CRONIN-HENNESSY 10	CLEO	$\psi(2S) \rightarrow \gamma K \bar{K} \pi$
< 20	90	ATHAR	04	CLEO $e^+e^- \rightarrow \gamma X$
20-130	95	EDWARDS	82c	CBAL $e^+e^- \rightarrow \gamma X$

••• We do not use the following data for averages, fits, limits, etc. •••
¹ ABLIKIM 12G reports $[\Gamma(\psi(2S) \rightarrow \gamma\eta_c(2S))/\Gamma_{total}] \times [B(\eta_c(2S) \rightarrow K \bar{K} \pi)] = (1.30 \pm 0.20 \pm 0.30) \times 10^{-5}$ which we divide by our best value $B(\eta_c(2S) \rightarrow K \bar{K} \pi) = (1.9 \pm 1.2) \times 10^{-2}$. Our first error is their experiment's error and our second error is the systematic error from using our best value.
² CRONIN-HENNESSY 10 reports $[\Gamma(\psi(2S) \rightarrow \gamma\eta_c(2S))/\Gamma_{total}] \times [B(\eta_c(2S) \rightarrow K \bar{K} \pi)] < 14.5 \times 10^{-6}$ which we divide by our best value $B(\eta_c(2S) \rightarrow K \bar{K} \pi) = 1.9 \times 10^{-2}$. This measurement assumes $\Gamma(\eta_c(2S)) = 14$ MeV. CRONIN-HENNESSY 10 gives the analytic dependence of limits on width.

$\Gamma(\gamma\pi^0)/\Gamma_{total}$

VALUE (units 10^{-6})	CL%	EVTS	DOCUMENT ID	TECN	COMMENT
1.04 ± 0.22 OUR AVERAGE					Error includes scale factor of 1.4.
0.95 ± 0.16 ± 0.05	423		ABLIKIM	17X	BES3 $\psi(2S) \rightarrow \gamma\pi^0$
1.58 ± 0.40 ± 0.13	37		ABLIKIM	10F	BES3 $\psi(2S) \rightarrow \gamma\pi^0$
< 5	90		PEDLAR	09	CLE3 $\psi(2S) \rightarrow \gamma X$
< 5400	95		¹ LIBERMAN	75	SPEC e^+e^-
< 1×10^4	90		WIJK	75	DASP e^+e^-

••• We do not use the following data for averages, fits, limits, etc. •••
¹ Restated by us using $B(\psi(2S) \rightarrow \mu^+\mu^-) = 0.0077$.

$\Gamma(\gamma\eta'(958))/\Gamma_{total}$

VALUE (units 10^{-4})	CL%	EVTS	DOCUMENT ID	TECN	COMMENT
1.24 ± 0.04 OUR AVERAGE					
1.251 ± 0.022 ± 0.062	56K		ABLIKIM	17X	BES3 $\psi(2S) \rightarrow \gamma\pi^+\pi^-\eta, \gamma\pi^0\pi^0\eta$
1.26 ± 0.03 ± 0.08	2226		¹ ABLIKIM	10F	BES3 $\psi(2S) \rightarrow 3\gamma\pi^+\pi^-, 2\gamma\pi^+\pi^-$
1.19 ± 0.08 ± 0.03			PEDLAR	09	CLE3 $\psi(2S) \rightarrow \gamma X$
1.24 ± 0.27 ± 0.15	23		ABLIKIM	06R	BES2 $e^+e^- \rightarrow \psi(2S)$
1.54 ± 0.31 ± 0.20	~ 43		BAI	98F	BES $\psi(2S) \rightarrow \pi^+\pi^-\pi^0, \pi^+\pi^-\pi^+\pi^0$

••• We do not use the following data for averages, fits, limits, etc. •••
 < 60 90 ² BRAUNSCH... 77 DASP e^+e^-
 < 11 90 ³ BARTEL 76 CNTR e^+e^-
¹ Combining the results from $\eta' \rightarrow \pi^+\pi^-\eta$ and $\eta' \rightarrow \pi^+\pi^-\gamma$ decay modes.
² Restated by us using total decay width 228 keV.
³ The value is normalized to the branching ratio for $\Gamma(J/\psi(1S)\eta)/\Gamma_{total}$.

$\Gamma(\gamma f_2(1270))/\Gamma_{total}$

VALUE (units 10^{-4})	EVTS	DOCUMENT ID	TECN	COMMENT
2.73 ± 0.29 OUR AVERAGE				Error includes scale factor of 1.8.
2.84 ± 0.15 ± 0.03	1.9k	^{1,2} DOBBS	15	$\psi(2S) \rightarrow \gamma\pi\pi$
2.12 ± 0.19 ± 0.32		^{3,4} BAI	03c	BES $\psi(2S) \rightarrow \gamma\pi\pi$
2.08 ± 0.19 ± 0.33	200.6 ± 18.8	³ BAI	03c	BES $\psi(2S) \rightarrow \gamma\pi^+\pi^-$
2.90 ± 1.08 ± 1.07	29.9 ± 11.1	³ BAI	03c	BES $\psi(2S) \rightarrow \gamma\pi^0\pi^0$

••• We do not use the following data for averages, fits, limits, etc. •••
¹ Using CLEO-c data but not authored by the CLEO Collaboration.
² DOBBS 15 reports $[\Gamma(\psi(2S) \rightarrow \gamma f_2(1270))/\Gamma_{total}] \times [B(f_2(1270) \rightarrow \pi\pi)] = (2.39 \pm 0.09 \pm 0.09) \times 10^{-4}$ which we divide by our best value $B(f_2(1270) \rightarrow \pi\pi) = (84.2 \pm 2.9 \pm 0.9) \times 10^{-2}$. Our first error is their experiment's error and our second error is the systematic error from using our best value.
³ Normalized to $B(\psi(2S) \rightarrow J/\psi\pi^+\pi^-) = 0.305 \pm 0.016$.
⁴ Combining the results from $\pi^+\pi^-$ and $\pi^0\pi^0$ decay modes.

$\Gamma(\gamma f_0(1370) \rightarrow \gamma K \bar{K})/\Gamma_{\text{total}}$ Γ_{161}/Γ

VALUE (units 10^{-5})	EVTS	DOCUMENT ID	COMMENT
3.1 ± 1.0 ± 1.4	175	¹ DOBBS 15	$\psi(2S) \rightarrow \gamma K \bar{K}$

¹ Using CLEO-c data but not authored by the CLEO Collaboration.

$\Gamma(\gamma f_0(1500))/\Gamma_{\text{total}}$ Γ_{162}/Γ

VALUE (units 10^{-5})	EVTS	DOCUMENT ID	COMMENT
9.3 ± 1.8 ± 0.6	274	^{1,2} DOBBS 15	$\psi(2S) \rightarrow \gamma \pi \pi$

¹ DOBBS 15 reports $[\Gamma(\psi(2S) \rightarrow \gamma f_0(1500))/\Gamma_{\text{total}}] \times [B(f_0(1500) \rightarrow \pi\pi)] = (3.2 \pm 0.6 \pm 0.2) \times 10^{-5}$ which we divide by our best value $B(f_0(1500) \rightarrow \pi\pi) = (34.5 \pm 2.2) \times 10^{-2}$. Our first error is their experiment's error and our second error is the systematic error from using our best value.

² Using CLEO-c data but not authored by the CLEO Collaboration.

$\Gamma(\gamma f'_2(1525))/\Gamma_{\text{total}}$ Γ_{163}/Γ

VALUE (units 10^{-5})	EVTS	DOCUMENT ID	COMMENT
3.3 ± 0.8 ± 0.1	136	^{1,2} DOBBS 15	$\psi(2S) \rightarrow \gamma K \bar{K}$

¹ DOBBS 15 reports $[\Gamma(\psi(2S) \rightarrow \gamma f'_2(1525))/\Gamma_{\text{total}}] \times [B(f'_2(1525) \rightarrow K \bar{K})] = (2.9 \pm 0.6 \pm 0.3) \times 10^{-5}$ which we divide by our best value $B(f'_2(1525) \rightarrow K \bar{K}) = (87.6 \pm 2.2) \times 10^{-2}$. Our first error is their experiment's error and our second error is the systematic error from using our best value.

² Using CLEO-c data but not authored by the CLEO Collaboration.

$\Gamma(\gamma f_0(1710) \rightarrow \gamma \pi \pi)/\Gamma_{\text{total}}$ Γ_{165}/Γ

VALUE (units 10^{-5})	EVTS	DOCUMENT ID	TECN	COMMENT
3.5 ± 0.6 OUR AVERAGE				
3.6 ± 0.4 ± 0.5	290	¹ DOBBS 15		$\psi(2S) \rightarrow \gamma \pi \pi$
3.01 ± 0.41 ± 1.24	35.6 ± 4.8	² BAI 03c	BES	$\psi(2S) \rightarrow \gamma \pi^+ \pi^-$

¹ Using CLEO-c data but not authored by the CLEO Collaboration.

² Normalized to $B(\psi(2S) \rightarrow J/\psi \pi^+ \pi^-) = 0.305 \pm 0.016$.

$\Gamma(\gamma f_0(1710) \rightarrow \gamma K \bar{K})/\Gamma_{\text{total}}$ Γ_{166}/Γ

VALUE (units 10^{-5})	CL%	EVTS	DOCUMENT ID	TECN	COMMENT
6.6 ± 0.7 OUR AVERAGE					
6.7 ± 0.6 ± 0.6		375	¹ DOBBS 15		$\psi(2S) \rightarrow \gamma K \bar{K}$
6.04 ± 0.90 ± 1.32		39.6 ± 5.9	^{2,3} BAI 03c	BES	$\psi(2S) \rightarrow \gamma K^+ K^-$

• • • We do not use the following data for averages, fits, limits, etc. • • •

< 15.6	90	6.8 ± 3.1	^{2,3} BAI 03c	BES	$\psi(2S) \rightarrow \gamma K_S^0 K_S^0$
--------	----	-----------	------------------------	-----	---

¹ Using CLEO-c data but not authored by the CLEO Collaboration.

² Includes unknown branching fractions to $K^+ K^-$ or $K_S^0 K_S^0$. We have multiplied the $K^+ K^-$ result by a factor of 2 and the $K_S^0 K_S^0$ result by a factor of 4 to obtain the $K \bar{K}$ result.

³ Normalized to $B(\psi(2S) \rightarrow J/\psi \pi^+ \pi^-) = 0.305 \pm 0.016$.

$\Gamma(\gamma f_0(2100) \rightarrow \gamma \pi \pi)/\Gamma_{\text{total}}$ Γ_{167}/Γ

VALUE (units 10^{-6})	EVTS	DOCUMENT ID	COMMENT
4.8 ± 0.5 ± 0.9	373	¹ DOBBS 15	$\psi(2S) \rightarrow \gamma \pi \pi$

¹ Using CLEO-c data but not authored by the CLEO Collaboration.

$\Gamma(\gamma f_0(2200) \rightarrow \gamma K \bar{K})/\Gamma_{\text{total}}$ Γ_{168}/Γ

VALUE (units 10^{-6})	EVTS	DOCUMENT ID	COMMENT
3.2 ± 0.6 ± 0.8	207	¹ DOBBS 15	$\psi(2S) \rightarrow \gamma K \bar{K}$

¹ Using CLEO-c data but not authored by the CLEO Collaboration.

$\Gamma(\gamma f_2(2220) \rightarrow \gamma \pi \pi)/\Gamma_{\text{total}}$ Γ_{169}/Γ

VALUE	CL%	DOCUMENT ID	COMMENT
< 5.8 × 10⁻⁶	90	^{1,2} DOBBS 15	$\psi(2S) \rightarrow \gamma \pi \pi$

¹ Using CLEO-c data but not authored by the CLEO Collaboration.

² For $\Gamma = 20/50$ MeV, the 90% CL upper limits for $\pi^+ \pi^-$ and $\pi^0 \pi^0$ are $3.2/4.3 \times 10^{-6}$ and $2.6/4.0 \times 10^{-6}$, respectively.

$\Gamma(\gamma f_2(2220) \rightarrow \gamma K \bar{K})/\Gamma_{\text{total}}$ Γ_{170}/Γ

VALUE	CL%	DOCUMENT ID	COMMENT
< 9.5 × 10⁻⁶	90	^{1,2} DOBBS 15	$\psi(2S) \rightarrow \gamma K \bar{K}$

¹ Using CLEO-c data but not authored by the CLEO Collaboration.

² For $\Gamma = 20/50$ MeV, the 90% CL upper limits for $K^+ K^-$ and $K_S^0 K_S^0$ are $2.1/4.3 \times 10^{-6}$ and $3.7/5.5 \times 10^{-6}$, respectively.

$\Gamma(\gamma \eta)/\Gamma_{\text{total}}$ Γ_{172}/Γ

VALUE (units 10^{-6})	CL%	EVTS	DOCUMENT ID	TECN	COMMENT
0.92 ± 0.18 OUR AVERAGE					
0.85 ± 0.18 ± 0.04		382	¹ ABLIKIM 17x	BES3	$\psi(2S) \rightarrow \gamma \pi^+ \pi^- \pi^0$, $\gamma 3\pi^0$
1.38 ± 0.48 ± 0.09		13	¹ ABLIKIM 10f	BES3	$\psi(2S) \rightarrow \gamma \pi^+ \pi^- \pi^0$, $\gamma 3\pi^0$

• • • We do not use the following data for averages, fits, limits, etc. • • •

< 2	90	PEDLAR 09	CLE3		$\psi(2S) \rightarrow \gamma X$
< 90	90	BAI 98f	BES		$\psi(2S) \rightarrow \pi^+ \pi^- 3\gamma$
< 200	90	YAMADA 77	DASP		$e^+ e^- \rightarrow 3\gamma$

¹ Combining the results from $\eta \rightarrow \pi^+ \pi^- \pi^0$ and $\eta \rightarrow 3\pi^0$ decay modes.

$\Gamma(\gamma \eta \pi^+ \pi^-)/\Gamma_{\text{total}}$ Γ_{173}/Γ

VALUE (units 10^{-4})	EVTS	DOCUMENT ID	TECN	COMMENT
8.71 ± 1.25 ± 1.64	418	ABLIKIM 06r	BES2	$\psi(2S) \rightarrow \gamma \eta \pi^+ \pi^-$

$\Gamma(\gamma \eta(1405) \rightarrow \gamma K \bar{K} \pi)/\Gamma_{\text{total}}$ Γ_{175}/Γ

VALUE (units 10^{-4})	CL%	DOCUMENT ID	TECN	COMMENT
< 0.9	90	ABLIKIM 06r	BES2	$\psi(2S) \rightarrow \gamma K_S^0 K^+ \pi^- + \text{c.c.}$
< 1.3	90	ABLIKIM 06r	BES2	$\psi(2S) \rightarrow \gamma K^+ K^- \pi^0$
< 1.2	90	¹ SCHARRE 80	MRK1	$e^+ e^-$

• • • We do not use the following data for averages, fits, limits, etc. • • •

¹ Includes unknown branching fraction $\eta(1405) \rightarrow K \bar{K} \pi$.

$\Gamma(\gamma \eta(1405) \rightarrow \eta \pi^+ \pi^-)/\Gamma_{\text{total}}$ Γ_{176}/Γ

VALUE (units 10^{-4})	EVTS	DOCUMENT ID	TECN	COMMENT
0.36 ± 0.25 ± 0.05	10	ABLIKIM 06r	BES2	$\psi(2S) \rightarrow \gamma \eta \pi^+ \pi^-$

$\Gamma(\gamma \eta(1405) \rightarrow \gamma f_0(980) \pi^0 \rightarrow \gamma \pi^+ \pi^- \pi^0)/\Gamma_{\text{total}}$ Γ_{177}/Γ

VALUE	CL%	DOCUMENT ID	TECN	COMMENT
< 5.0 × 10⁻⁷	90	ABLIKIM 17AJ	BES3	$\psi(2S) \rightarrow \gamma \pi^+ \pi^- \pi^0$

$\Gamma(\gamma \eta(1475) \rightarrow K \bar{K} \pi)/\Gamma_{\text{total}}$ Γ_{179}/Γ

VALUE (units 10^{-4})	CL%	DOCUMENT ID	TECN	COMMENT
< 1.4	90	ABLIKIM 06r	BES2	$\psi(2S) \rightarrow \gamma K^+ K^- \pi^0$

• • • We do not use the following data for averages, fits, limits, etc. • • •

< 1.5	90	ABLIKIM 06r	BES2	$\psi(2S) \rightarrow \gamma K_S^0 K^+ \pi^- + \text{c.c.}$
-------	----	-------------	------	---

$\Gamma(\gamma \eta(1475) \rightarrow \eta \pi^+ \pi^-)/\Gamma_{\text{total}}$ Γ_{180}/Γ

VALUE (units 10^{-4})	CL%	DOCUMENT ID	TECN	COMMENT
< 0.88	90	ABLIKIM 06r	BES2	$\psi(2S) \rightarrow \gamma \eta \pi^+ \pi^-$

$\Gamma(\gamma 2(\pi^+ \pi^-))/\Gamma_{\text{total}}$ Γ_{181}/Γ

VALUE (units 10^{-5})	EVTS	DOCUMENT ID	TECN	COMMENT
39.6 ± 2.8 ± 5.0	583	ABLIKIM 07D	BES2	$e^+ e^- \rightarrow \psi(2S)$

$\Gamma(\gamma K^{*0} K^+ \pi^- + \text{c.c.})/\Gamma_{\text{total}}$ Γ_{182}/Γ

VALUE (units 10^{-5})	EVTS	DOCUMENT ID	TECN	COMMENT
37.0 ± 6.1 ± 7.2	237	ABLIKIM 07D	BES2	$e^+ e^- \rightarrow \psi(2S)$

$\Gamma(\gamma K^{*0} \bar{K}^{*0})/\Gamma_{\text{total}}$ Γ_{183}/Γ

VALUE (units 10^{-5})	EVTS	DOCUMENT ID	TECN	COMMENT
24.0 ± 4.5 ± 5.0	41	ABLIKIM 07D	BES2	$e^+ e^- \rightarrow \psi(2S)$

$\Gamma(\gamma K_S^0 K^+ \pi^- + \text{c.c.})/\Gamma_{\text{total}}$ Γ_{184}/Γ

VALUE (units 10^{-5})	EVTS	DOCUMENT ID	TECN	COMMENT
25.6 ± 3.6 ± 3.6	115	ABLIKIM 07D	BES2	$e^+ e^- \rightarrow \psi(2S)$

$\Gamma(\gamma K^+ K^- \pi^+ \pi^-)/\Gamma_{\text{total}}$ Γ_{185}/Γ

VALUE (units 10^{-5})	EVTS	DOCUMENT ID	TECN	COMMENT
19.1 ± 2.7 ± 4.3	132	ABLIKIM 07D	BES2	$e^+ e^- \rightarrow \psi(2S)$

$\Gamma(\gamma \rho \bar{\rho})/\Gamma_{\text{total}}$ Γ_{186}/Γ

VALUE (units 10^{-5})	EVTS	DOCUMENT ID	TECN	COMMENT
3.9 ± 0.5 OUR AVERAGE				Error includes scale factor of 2.0.
4.18 ± 0.26 ± 0.18	348	¹ ALEXANDER 10	CLEO	$\psi(2S) \rightarrow \gamma \rho \bar{\rho}$
2.9 ± 0.4 ± 0.4	142	ABLIKIM 07D	BES2	$e^+ e^- \rightarrow \psi(2S)$

¹ From a fit of the $\rho \bar{\rho}$ mass distribution to a combination of $\gamma f_2(1950)$, $\gamma f_2(2150)$, and $\gamma \rho \bar{\rho}$ phase space, for $M(\rho \bar{\rho}) < 2.85$ GeV, and accounting for backgrounds from $\psi(2S) \rightarrow \pi^0 \rho \bar{\rho}$ and continuum.

$\Gamma(\gamma f_2(1950) \rightarrow \gamma \rho \bar{\rho})/\Gamma_{\text{total}}$ Γ_{187}/Γ

VALUE (units 10^{-5})	EVTS	DOCUMENT ID	TECN	COMMENT
1.2 ± 0.2 ± 0.1	111	¹ ALEXANDER 10	CLEO	$\psi(2S) \rightarrow \gamma \rho \bar{\rho}$

¹ From a fit of the $\rho \bar{\rho}$ mass distribution to a combination of $\gamma f_2(1950)$, $\gamma f_2(2150)$, and $\gamma \rho \bar{\rho}$ phase space, for $M(\rho \bar{\rho}) < 2.85$ GeV, and accounting for backgrounds from $\psi(2S) \rightarrow \pi^0 \rho \bar{\rho}$ and continuum.

$\Gamma(\gamma f_2(2150) \rightarrow \gamma \rho \bar{\rho})/\Gamma_{\text{total}}$ Γ_{188}/Γ

VALUE (units 10^{-5})	EVTS	DOCUMENT ID	TECN	COMMENT
0.72 ± 0.18 ± 0.03	73	¹ ALEXANDER 10	CLEO	$\psi(2S) \rightarrow \gamma \rho \bar{\rho}$

¹ From a fit of the $\rho \bar{\rho}$ mass distribution to a combination of $\gamma f_2(1950)$, $\gamma f_2(2150)$, and $\gamma \rho \bar{\rho}$ phase space, for $M(\rho \bar{\rho}) < 2.85$ GeV, and accounting for backgrounds from $\psi(2S) \rightarrow \pi^0 \rho \bar{\rho}$ and continuum.

$\Gamma(\gamma X(1835) \rightarrow \gamma \rho \bar{\rho})/\Gamma_{\text{total}}$ Γ_{189}/Γ

VALUE (units 10^{-6})	CL%	DOCUMENT ID	TECN	COMMENT
4.57 ± 0.36 ± 4.26		ABLIKIM 12D	BES3	$J/\psi \rightarrow \gamma \rho \bar{\rho}$

• • • We do not use the following data for averages, fits, limits, etc. • • •

< 1.6	90	ALEXANDER 10	CLEO	$\psi(2S) \rightarrow \gamma \rho \bar{\rho}$
< 5.4	90	ABLIKIM 07D	BES	$\psi(2S) \rightarrow \gamma \rho \bar{\rho}$

Meson Particle Listings

$\psi(2S)$

$\Gamma(\gamma X \rightarrow \gamma p \bar{p})/\Gamma_{\text{total}}$ Γ_{190}/Γ

For a narrow resonance in the range $2.2 < M(X) < 2.8$ GeV.

VALUE (units 10^{-6})	CL%	DOCUMENT ID	TECN	COMMENT
<2	90	ALEXANDER	10	CLEO $\psi(2S) \rightarrow \gamma p \bar{p}$

$\Gamma(\gamma \pi^+ \pi^- p \bar{p})/\Gamma_{\text{total}}$ Γ_{191}/Γ

VALUE (units 10^{-5})	EVTS	DOCUMENT ID	TECN	COMMENT
$2.8 \pm 1.2 \pm 0.7$	17	ABLIKIM	07D	BES2 $e^+ e^- \rightarrow \psi(2S)$

$\Gamma(\gamma 2(\pi^+ \pi^-) K^+ K^-)/\Gamma_{\text{total}}$ Γ_{192}/Γ

VALUE (units 10^{-5})	CL%	DOCUMENT ID	TECN	COMMENT
<22	90	ABLIKIM	07D	BES2 $e^+ e^- \rightarrow \psi(2S)$

$\Gamma(\gamma 3(\pi^+ \pi^-))/\Gamma_{\text{total}}$ Γ_{193}/Γ

VALUE (units 10^{-5})	CL%	DOCUMENT ID	TECN	COMMENT
<17	90	ABLIKIM	07D	BES2 $e^+ e^- \rightarrow \psi(2S)$

$\Gamma(\gamma K^+ K^- K^+ K^-)/\Gamma_{\text{total}}$ Γ_{194}/Γ

VALUE (units 10^{-5})	CL%	DOCUMENT ID	TECN	COMMENT
<4	90	ABLIKIM	07D	BES2 $e^+ e^- \rightarrow \psi(2S)$

$\Gamma(\gamma \gamma J/\psi)/\Gamma_{\text{total}}$ Γ_{195}/Γ

VALUE (units 10^{-4})	EVTS	DOCUMENT ID	TECN	COMMENT
$3.1 \pm 0.6 \pm 1.0$	1.1k	ABLIKIM	12o	BES3 $e^+ e^- \rightarrow \psi(2S)$

• • • We do not use the following data for averages, fits, limits, etc. • • •

3.2 ± 0.6 1.1k 1 ABLIKIM 17N BES3 $\psi(2S) \rightarrow \gamma \gamma J/\psi$

¹ Uses $B(J/\psi \rightarrow e^+ e^-) = (5.971 \pm 0.032)\%$ and $B(J/\psi \rightarrow \mu^+ \mu^-) = (5.961 \pm 0.033)\%$. No systematic error estimation.

$\Gamma(e^+ e^- \eta')/\Gamma_{\text{total}}$ Γ_{196}/Γ

VALUE (units 10^{-6})	EVTS	DOCUMENT ID	TECN	COMMENT
1.90 ± 0.26 OUR AVERAGE				
$1.99 \pm 0.33 \pm 0.12$	57	ABLIKIM	18Z	BES3 $\psi(2S) \rightarrow \eta' e^+ e^-$,

$\eta' \rightarrow \gamma \pi^+ \pi^-$

$1.79 \pm 0.38 \pm 0.11$ 20 ABLIKIM 18Z BES3 $\psi(2S) \rightarrow \eta' e^+ e^-$,

$\eta' \rightarrow \eta \pi^+ \pi^-$

$\Gamma(e^+ e^- \chi_{c0}(1P))/\Gamma_{\text{total}}$ Γ_{197}/Γ

VALUE (units 10^{-4})	EVTS	DOCUMENT ID	TECN	COMMENT
$10.6 \pm 2.4 \pm 0.4$	48	1 ABLIKIM	17i	BES3 $\psi(2S) \rightarrow e^+ e^- \gamma J/\psi$

¹ ABLIKIM 17i reports $(11.7 \pm 2.5 \pm 1.0) \times 10^{-4}$ from a measurement of $[\Gamma(\psi(2S) \rightarrow e^+ e^- \chi_{c0}(1P))/\Gamma_{\text{total}}] \times [B(\chi_{c0}(1P) \rightarrow \gamma J/\psi(1S))]$ assuming $B(\chi_{c0}(1P) \rightarrow \gamma J/\psi(1S)) = (1.27 \pm 0.06) \times 10^{-2}$, which we rescale to our best value $B(\chi_{c0}(1P) \rightarrow \gamma J/\psi(1S)) = (1.40 \pm 0.05) \times 10^{-2}$. Our first error is their experiment's error and our second error is the systematic error from using our best value.

$\Gamma(e^+ e^- \chi_{c1}(1P))/\Gamma_{\text{total}}$ Γ_{198}/Γ

VALUE (units 10^{-4})	EVTS	DOCUMENT ID	TECN	COMMENT
$8.5 \pm 0.6 \pm 0.2$	873	1 ABLIKIM	17i	BES3 $\psi(2S) \rightarrow e^+ e^- \gamma J/\psi$

¹ ABLIKIM 17i reports $(8.6 \pm 0.3 \pm 0.6) \times 10^{-4}$ from a measurement of $[\Gamma(\psi(2S) \rightarrow e^+ e^- \chi_{c1}(1P))/\Gamma_{\text{total}}] \times [B(\chi_{c1}(1P) \rightarrow \gamma J/\psi(1S))]$ assuming $B(\chi_{c1}(1P) \rightarrow \gamma J/\psi(1S)) = (33.9 \pm 1.2) \times 10^{-2}$, which we rescale to our best value $B(\chi_{c1}(1P) \rightarrow \gamma J/\psi(1S)) = (34.3 \pm 1.0) \times 10^{-2}$. Our first error is their experiment's error and our second error is the systematic error from using our best value.

$\Gamma(e^+ e^- \chi_{c2}(1P))/\Gamma_{\text{total}}$ Γ_{199}/Γ

VALUE (units 10^{-4})	EVTS	DOCUMENT ID	TECN	COMMENT
$7.0 \pm 0.7 \pm 0.2$	227	1 ABLIKIM	17i	BES3 $\psi(2S) \rightarrow e^+ e^- \gamma J/\psi$

¹ ABLIKIM 17i reports $(6.9 \pm 0.5 \pm 0.6) \times 10^{-4}$ from a measurement of $[\Gamma(\psi(2S) \rightarrow e^+ e^- \chi_{c2}(1P))/\Gamma_{\text{total}}] \times [B(\chi_{c2}(1P) \rightarrow \gamma J/\psi(1S))]$ assuming $B(\chi_{c2}(1P) \rightarrow \gamma J/\psi(1S)) = (19.2 \pm 0.7) \times 10^{-2}$, which we rescale to our best value $B(\chi_{c2}(1P) \rightarrow \gamma J/\psi(1S)) = (19.0 \pm 0.5) \times 10^{-2}$. Our first error is their experiment's error and our second error is the systematic error from using our best value.

$\Gamma(e^+ e^- \chi_{c0}(1P))/\Gamma(\gamma \chi_{c0}(1P))$ $\Gamma_{197}/\Gamma_{153}$

VALUE (units 10^{-3})	EVTS	DOCUMENT ID	TECN	COMMENT
$9.4 \pm 1.9 \pm 0.6$	48	1 ABLIKIM	17i	BES3 $\psi(2S) \rightarrow e^+ e^- \gamma J/\psi$

¹ Uses $B(\psi(2S) \rightarrow \gamma \chi_{c0}(1P)) \times B(\chi_{c0}(1P) \rightarrow \gamma J/\psi(1S)) = (15.8 \pm 0.3 \pm 0.6) \times 10^{-4}$ from ABLIKIM 17N and accounts for common systematic errors.

$\Gamma(e^+ e^- \chi_{c1}(1P))/\Gamma(\gamma \chi_{c1}(1P))$ $\Gamma_{198}/\Gamma_{154}$

VALUE (units 10^{-3})	EVTS	DOCUMENT ID	TECN	COMMENT
$8.3 \pm 0.3 \pm 0.4$	873	1 ABLIKIM	17i	BES3 $\psi(2S) \rightarrow e^+ e^- \gamma J/\psi$

¹ Uses $B(\psi(2S) \rightarrow \gamma \chi_{c1}(1P)) \times B(\chi_{c1}(1P) \rightarrow \gamma J/\psi(1S)) = (351.8 \pm 1.0 \pm 12.0) \times 10^{-4}$ from ABLIKIM 17N and accounts for common systematic errors.

$\Gamma(e^+ e^- \chi_{c2}(1P))/\Gamma(\gamma \chi_{c2}(1P))$ $\Gamma_{199}/\Gamma_{155}$

VALUE (units 10^{-3})	EVTS	DOCUMENT ID	TECN	COMMENT
$6.6 \pm 0.5 \pm 0.4$	227	1 ABLIKIM	17i	BES3 $\psi(2S) \rightarrow e^+ e^- \gamma J/\psi$

¹ Uses $B(\psi(2S) \rightarrow \gamma \chi_{c2}(1P)) \times B(\chi_{c2}(1P) \rightarrow \gamma J/\psi(1S)) = (199.6 \pm 0.8 \pm 7.0) \times 10^{-4}$ from ABLIKIM 17N and accounts for common systematic errors.

WEAK DECAYS

$\Gamma(D^0 e^+ e^- + \text{c.c.})/\Gamma_{\text{total}}$ Γ_{200}/Γ

VALUE	CL%	DOCUMENT ID	TECN	COMMENT
< 1.4×10^{-7}	90	1 ABLIKIM	17AF	BES3 $e^+ e^- \rightarrow \psi(2S)$

¹ Using D^0 decays to $K^- \pi^+$, $K^- \pi^+ \pi^0$, and $K^- \pi^+ \pi^+ \pi^-$.

OTHER DECAYS

$\Gamma(\text{invisible})/\Gamma(e^+ e^-)$ Γ_{201}/Γ_6

VALUE	CL%	DOCUMENT ID	TECN	COMMENT
<2.0	90	LEES	13i	BABR $B \rightarrow K^{(*)} \psi(2S)$

$\psi(2S)$ CROSS-PARTICLE BRANCHING RATIOS

For measurements involving $B(\psi(2S) \rightarrow \gamma \chi_{cJ}(1P)) \times B(\chi_{cJ}(1P) \rightarrow X)$ see the corresponding entries in the $\chi_{cJ}(1P)$ sections.

MULTIPOLE AMPLITUDE RATIOS IN RADIATIVE DECAYS

$\psi(2S) \rightarrow \gamma \chi_{cJ}(1P)$ and $\chi_{cJ} \rightarrow \gamma J/\psi(1S)$

$a_2(\chi_{c1})/a_2(\chi_{c2})$ Magnetic quadrupole transition amplitude ratio

VALUE (units 10^{-2})	EVTS	DOCUMENT ID	TECN	COMMENT
63 ± 7 OUR AVERAGE				
61.7 ± 8.3	253k	1 ABLIKIM	17N	BES3 $\psi(2S) \rightarrow \gamma \gamma \ell^+ \ell^-$

67 ± 19 59k 2 ARTUSO 09 CLEO $\psi(2S) \rightarrow \gamma \gamma \ell^+ \ell^-$

-13

¹ Statistical and systematic errors combined.

² Statistical and systematic errors combined. Using values from fits with floating $M2$ amplitudes $a_2(\chi_{c1})$, $a_2(\chi_{c2})$, $b_2(\chi_{c1})$, $b_2(\chi_{c2})$ and fixed $E3$ amplitudes of $a_3(\chi_{c2}) = b_3(\chi_{c2}) = 0$. Not independent of values for $a_2(\chi_{c1}(1P))$ and $a_2(\chi_{c2}(1P))$ from ARTUSO 09.

$b_2(\chi_{c2})/b_2(\chi_{c1})$ Magnetic quadrupole transition amplitude ratio

VALUE (units 10^{-2})	EVTS	DOCUMENT ID	TECN	COMMENT
60 ± 31 OUR AVERAGE				
74 ± 40	253k	1 ABLIKIM	17N	BES3 $\psi(2S) \rightarrow \gamma \gamma \ell^+ \ell^-$

37 ± 53 59k 2 ARTUSO 09 CLEO $\psi(2S) \rightarrow \gamma \gamma \ell^+ \ell^-$

-47

¹ Statistical and systematic errors combined. Derived from the reported measurement of $b_2(\chi_{c1})/b_2(\chi_{c2}) = 1.35 \pm 0.72$.

² Statistical and systematic errors combined. Using values from fits with floating $M2$ amplitudes $a_3(\chi_{c1})$, $a_3(\chi_{c2})$, $b_3(\chi_{c1})$, $b_3(\chi_{c2})$ and fixed $E3$ amplitudes of $a_2(\chi_{c2}) = b_2(\chi_{c2}) = 0$. Not independent of values for $b_2(\chi_{c1}(1P))$ and $b_2(\chi_{c2}(1P))$ from ARTUSO 09.

$\psi(2S)$ REFERENCES

ABLIKIM	19A0	PR	D99	112010	M. Ablikim et al.	(BESIII Collab.)
ABLIKIM	19AT	PR	D100	051101	M. Ablikim et al.	(BESIII Collab.)
ABLIKIM	19AU	PR	D100	052010	M. Ablikim et al.	(BESIII Collab.)
ABLIKIM	19BA	PR	D100	092003	M. Ablikim et al.	(BESIII Collab.)
ABLIKIM	19I	PR	D99	012014	M. Ablikim et al.	(BESIII Collab.)
ABLIKIM	19N	PR	D99	032006	M. Ablikim et al.	(BESIII Collab.)
ABLIKIM	18Q	PR	D97	091102	M. Ablikim et al.	(BESIII Collab.)
ABLIKIM	18T	PR	D98	032006	M. Ablikim et al.	(BESIII Collab.)
ABLIKIM	18Z	PL	B783	452	M. Ablikim et al.	(BESIII Collab.)
ANASHIN	18	PL	B781	174	V.V. Anashin et al.	(KEDR Collab.)
LEES	18E	PR	D98	112015	J.P. Lees et al.	(BABAR Collab.)
ABLIKIM	17AF	PR	D96	111101	M. Ablikim et al.	(BESIII Collab.)
ABLIKIM	17AJ	PR	D96	112008	M. Ablikim et al.	(BESIII Collab.)
ABLIKIM	17AK	PR	D96	112012	M. Ablikim et al.	(BESIII Collab.)
ABLIKIM	17E	PL	B770	217	M. Ablikim et al.	(BESIII Collab.)
ABLIKIM	17I	PRL	118	221802	M. Ablikim et al.	(BESIII Collab.)
ABLIKIM	17L	PR	D95	052003	M. Ablikim et al.	(BESIII Collab.)
ABLIKIM	17N	PR	D95	072004	M. Ablikim et al.	(BESIII Collab.)
ABLIKIM	17U	PR	D96	032001	M. Ablikim et al.	(BESIII Collab.)
ABLIKIM	17X	PR	D96	052003	M. Ablikim et al.	(BESIII Collab.)
DOBBS	17	PR	D96	092004	S. Dobbs et al.	(NWES, WAYN)
LEES	17A	PR	D95	052001	J.P. Lees et al.	(BABAR Collab.)
AAIJ	16Y	JHEP	1605	132	R. Aaij et al.	(LHCb Collab.)
ABLIKIM	16L	PR	D93	072003	M. Ablikim et al.	(BESIII Collab.)
ABLIKIM	15I	PR	D91	092006	M. Ablikim et al.	(BESIII Collab.)
ABLIKIM	15V	PL	B749	414	M. Ablikim et al.	(BESIII Collab.)
ANASHIN	15	PL	B749	50	V.V. Anashin et al.	(KEDR Collab.)
DOBBS	15	PR	D91	052006	S. Dobbs et al.	(NWES)
LEES	15J	PR	D92	072008	J.P. Lees et al.	(BABAR Collab.)
ABLIKIM	14G	PR	D89	112006	M. Ablikim et al.	(BESIII Collab.)
DOBBS	14	PL	B739	90	S. Dobbs et al.	(NWES, WAYN)
ABLIKIM	13A	PRL	110	022001	M. Ablikim et al.	(BESIII Collab.)
ABLIKIM	13D	PR	D87	012007	M. Ablikim et al.	(BESIII Collab.)
ABLIKIM	13F	PR	D87	052007	M. Ablikim et al.	(BESIII Collab.)
ABLIKIM	13M	PR	D87	092006	M. Ablikim et al.	(BESIII Collab.)
ABLIKIM	13R	PR	D88	032007	M. Ablikim et al.	(BESIII Collab.)
ABLIKIM	13S	PR	D88	032010	M. Ablikim et al.	(BESIII Collab.)
ABLIKIM	13W	PR	D88	112007	M. Ablikim et al.	(BESIII Collab.)
LEES	13I	PR	D87	112005	J.P. Lees et al.	(BABAR Collab.)
LEES	13O	PR	D87	092005	J.P. Lees et al.	(BABAR Collab.)
LEES	13Q	PR	D88	032013	J.P. Lees et al.	(BABAR Collab.)
LEES	13Y	PR	D88	072009	J.P. Lees et al.	(BABAR Collab.)
AAIJ	12H	EPJ	C72	1972	R. Aaij et al.	(LHCb Collab.)
ABLIKIM	12D	PRL	108	112003	M. Ablikim et al.	(BESIII Collab.)
ABLIKIM	12G	PRL	109	042003	M. Ablikim et al.	(BESIII Collab.)

See key on page 999

Meson Particle Listings

$\psi(2S), \psi(3770)$

ABLIKIM	12H	PL B710 594	M. Ablikim et al.	(BESIII Collab.)
ABLIKIM	12L	PR D86 072011	M. Ablikim et al.	(BESIII Collab.)
ABLIKIM	12M	PR D86 092008	M. Ablikim et al.	(BESIII Collab.)
ABLIKIM	12O	PRL 109 172002	M. Ablikim et al.	(BESIII Collab.)
ABLIKIM	12Q	CP C36 1040	M. Ablikim et al.	(BES II Collab.)
ANASHIN	12	PL B711 280	V.V. Anashin et al.	(KEDR Collab.)
LEES	12E	PR D85 112009	J.P. Lees et al.	(BABAR Collab.)
LEES	12F	PR D86 012008	J.P. Lees et al.	(BABAR Collab.)
METREVELI	12	PR D85 092007	Z. Metreveli et al.	(NWES, FLOR, WAYN+)
GE	11	PR D84 032008	J.Y. Ge et al.	(CLEO Collab.)
ABLIKIM	10B	PRL 104 132002	M. Ablikim et al.	(BESIII Collab.)
ABLIKIM	10F	PRL 105 241801	M. Ablikim et al.	(BESIII Collab.)
ALEXANDER	10	PR D82 092002	D.P. Alexander et al.	(CLEO Collab.)
CRONIN-HEN.	10	PR D81 052002	D. Cronin-Hennessey et al.	(CLEO Collab.)
ADAMS	09	PR D80 051106	G.S. Adams et al.	(CLEO Collab.)
ARTUSO	09	PR D80 112003	M. Artuso et al.	(CLEO Collab.)
LIBBY	09	PR D80 072002	J. Libby et al.	(CLEO Collab.)
MITCHELL	09	PRL 102 011801	R.E. Mitchell et al.	(CLEO Collab.)
PEDLAR	09	PR D79 111101	T.K. Pedlar et al.	(CLEO Collab.)
ABLIKIM	08B	PL B659 74	M. Ablikim et al.	(BES Collab.)
ABLIKIM	08C	PL B659 789	M. Ablikim et al.	(BES Collab.)
DOBBS	08A	PRL 101 182003	S. Dobbs et al.	(CLEO Collab.)
MENDEZ	08	PR D78 011102	H. Mendez et al.	(CLEO Collab.)
PDG	08	PL B667 1	C. Amisler et al.	(PDG Collab.)
ABLIKIM	07C	PL B648 149	M. Ablikim et al.	(BES Collab.)
ABLIKIM	07D	PRL 99 011802	M. Ablikim et al.	(BES II Collab.)
ABLIKIM	07H	PR D76 092003	M. Ablikim et al.	(BES Collab.)
ANASHIN	07	JETPL 85 347	V.V. Anashin et al.	(KEDR Collab.)
ANDREOTTI	07	PL B654 74	M. Andreotti et al.	(Femilab E835 Collab.)
AUBERT	07AK	PR D76 012008	B. Aubert et al.	(BABAR Collab.)
AUBERT	07AU	PR D76 092005	B. Aubert et al.	(BABAR Collab.)
Also	07	PR D77 119902E (errata)	B. Aubert et al.	(BABAR Collab.)
AUBERT	07BD	PR D76 092006	B. Aubert et al.	(BABAR Collab.)
PDG	07	Unofficial 2007 WWW edition		(PDG Collab.)
PEDLAR	07	PR D75 011102	T.K. Pedlar et al.	(CLEO Collab.)
ABLIKIM	06G	PR D73 052004	M. Ablikim et al.	(BES Collab.)
ABLIKIM	06I	PR D74 012004	M. Ablikim et al.	(BES Collab.)
ABLIKIM	06L	PRL 97 121801	M. Ablikim et al.	(BES Collab.)
ABLIKIM	06R	PR D74 072001	M. Ablikim et al.	(BES Collab.)
ABLIKIM	06W	PR D74 112003	M. Ablikim et al.	(BES Collab.)
ADAM	06	PRL 96 082004	N.E. Adam et al.	(CLEO Collab.)
AUBERT	06B	PR D73 012005	B. Aubert et al.	(BABAR Collab.)
AUBERT	06D	PR D73 052003	B. Aubert et al.	(BABAR Collab.)
AUBERT, BE	06D	PR D74 091103	B. Aubert et al.	(BABAR Collab.)
DOBBS	06A	PR D74 011105	S. Dobbs et al.	(CLEO Collab.)
ABLIKIM	05E	PR D71 072006	M. Ablikim et al.	(BES Collab.)
ABLIKIM	05H	PR D72 012002	M. Ablikim et al.	(BES Collab.)
ABLIKIM	05I	PL B614 37	M. Ablikim et al.	(BES Collab.)
ABLIKIM	05J	PL B619 247	M. Ablikim et al.	(BES Collab.)
ABLIKIM	05O	PL B630 21	M. Ablikim et al.	(BES Collab.)
ADAM	05	PRL 94 012005	N.E. Adam et al.	(CLEO Collab.)
ADAM	05A	PRL 94 232002	N.E. Adam et al.	(CLEO Collab.)
ANDREOTTI	05	PR D71 032006	M. Andreotti et al.	(FNAL E835 Collab.)
AUBERT	05D	PR D71 052001	B. Aubert et al.	(BABAR Collab.)
BRIERE	05	PRL 95 062001	R.A. Briere et al.	(CLEO Collab.)
PEDLAR	05	PR D72 051108	T.K. Pedlar et al.	(CLEO Collab.)
ROSNER	05	PRL 95 102003	J.L. Rosner et al.	(CLEO Collab.)
ABLIKIM	04B	PR D70 012003	M. Ablikim et al.	(BES Collab.)
ABLIKIM	04K	PR D70 112003	M. Ablikim et al.	(BES Collab.)
ABLIKIM	04L	PR D70 112007	M. Ablikim et al.	(BES Collab.)
ATHAR	04	PR D70 112002	S.B. Athar et al.	(CLEO Collab.)
BAI	04B	PRL 92 052001	J.Z. Bai et al.	(BES Collab.)
BAI	04C	PR D69 072001	J.Z. Bai et al.	(BES Collab.)
BAI	04D	PL B589 7	J.Z. Bai et al.	(BES Collab.)
BAI	04G	PR D70 012004	J.Z. Bai et al.	(BES Collab.)
BAI	04I	PR D70 012006	J.Z. Bai et al.	(BES Collab.)
PDG	04	PL B592 1	S. Edelman et al.	(PDG Collab.)
SETH	04	PR D69 097503	K.K. Seth	(CLEO Collab.)
AULCHENKO	03	PL B573 63	V.M. Aulchenko et al.	(KEDR Collab.)
BAI	03B	PR D67 052002	J.Z. Bai et al.	(BES Collab.)
BAI	03C	PR D67 032004	J.Z. Bai et al.	(BES Collab.)
AUBERT	02B	PR D65 031101	B. Aubert et al.	(BABAR Collab.)
BAI	02	PR D65 052004	J.Z. Bai et al.	(BES Collab.)
BAI	02B	PL B550 24	J.Z. Bai et al.	(BES Collab.)
BAI	02C	PRL 88 101802	J.Z. Bai et al.	(BES Collab.)
PDG	02	PR D66 010001	K. Hagiwara et al.	(PDG Collab.)
BAI	01	PR D63 032002	J.Z. Bai et al.	(BES Collab.)
AMBROGIANI	00A	PR D62 032004	M. Ambrogiani et al.	(FNAL E835 Collab.)
ARTAMONOV	00	PL B474 427	A.S. Artamonov et al.	(NOVO)
BAI	00	PRL 84 594	J.Z. Bai et al.	(BES Collab.)
BAI	99C	PRL 83 1918	J.Z. Bai et al.	(BES Collab.)
BAI	98E	PR D57 3854	J.Z. Bai et al.	(BES Collab.)
BAI	98F	PR D58 097101	J.Z. Bai et al.	(BES Collab.)
BAI	98J	PRL 81 5080	J.Z. Bai et al.	(BES Collab.)
ARMSTRONG	97	PR D55 1153	T.A. Armstrong et al.	(E764 Collab.)
GRIBUSHIN	96	PR D53 4723	A. Gribushin et al.	(E672 and E706 Collab.)
ARMSTRONG	93B	PR D47 772	T.A. Armstrong et al.	(FNAL E760 Collab.)
ALEXANDER	89	NP B320 45	J.P. Alexander et al.	(LBL, MICH, SLAC)
COHEN	87	RMP 59 1121	E.R. Cohen, B.N. Taylor	(RIS C, NBS)
GAISER	86	PR D34 711	J. Gaiser et al.	(Crystal Ball Collab.)
KURAEV	85	SJNP 41 466	E.A. Kuraev, V.S. Fadin	(NOVO)
FRANKLIN	83	PRL 51 963	M.E.B. Franklin et al.	(LBL, SLAC)
EDWARDS	82C	PRL 48 70	C. Edwards et al.	(CIT, HARV, PRIB)
LEM OIGNE	82	PL 113B 509	Y. Lemoigne et al.	(SACL, LOIC, SHMP+)
HIMEL	80	PRL 44 920	T. Himel et al.	(LBL, SLAC)
OREGLIA	80	PRL 45 959	M.J. Oreglia et al.	(SLAC, CIT, HARV+)
SCHARRE	80	PL 97B 329	D.L. Scharre et al.	(SLAC, LBL)
ZHOLENTZ	80	PL 96B 214	A.A. Zholents et al.	(NOVO)
Also	80	SJNP 34 814	A.A. Zholents et al.	(NOVO)
BRANDELK	79B	NP B160 426	R. Brandelik et al.	(DASP Collab.)
BRANDELK	79C	ZPHY C1 233	R. Brandelik et al.	(DASP Collab.)
BARTEL	78B	PL 79B 492	W. Bartel et al.	(SLAC, HEIDP)
TANENBAUM	78	PR D17 1731	W.M. Tanenbaum et al.	(SLAC, LBL)
BIDDICK	77	PRL 38 1324	C.J. Biddick et al.	(UCSD, UMD, PAVI+)
BRUNSCHEWIG	77	PL 67B 249	W. Braunschweig et al.	(DASP Collab.)
BURMESTER	77	PL 66B 395	J. Burmester et al.	(DESY, HAMB, SIEG+)
FELDMAN	77	PRPL 33C 285	G.J. Feldman, M.L. Perl	(LBL, SLAC)
YAMADA	77	Hamburg Conf. 69	S. Yamada	(DASP Collab.)
BARTEL	76	PL 64B 483	W. Bartel et al.	(DESY, HEIDP)
TANENBAUM	76	PRL 36 402	W.M. Tanenbaum et al.	(SLAC, LBL) IG
WHITAKER	76	PR 37 1596	J.S. Whitaker et al.	(SLAC, LBL)
ABRAMS	75	Stanford Symp. 25	G.S. Abrams	(LBL)
ABRAMS	75B	PRL 34 1181	G.S. Abrams et al.	(LBL, SLAC)
BOYARSKI	75C	Palermo Conf. 54	A.M. Boyarski et al.	(SLAC, LBL)
HILGER	75	PRL 35 625	E. Hilger et al.	(STAN, PENN)
LIBERMAN	75	Stanford Symp. 55	A.D. Liberman	(STAN)
LUTH	75	PRL 35 1124	V. Luth et al.	(SLAC, LBL) JPC
WIJK	75	Stanford Symp. 69	B.H. Wiik	(DESY)

$\psi(3770)$

$$J^{PC} = 0^{-}(1^{-}-)$$

$\psi(3770)$ MASS (MeV)

OUR FIT includes measurements of $m_{\psi(2S)}$, $m_{\psi(3770)}$, and $m_{\psi(3770)} - m_{\psi(2S)}$.

VALUE (MeV)	EVTs	DOCUMENT ID	TECN	COMMENT
3773.7 ± 0.4 OUR FIT		Error includes scale factor of 1.4.		
3778.1 ± 0.7 OUR AVERAGE				
3778.1 ± 0.7 ± 0.6		¹ AAIJ	19M LHCb	$pp \rightarrow D\bar{D} + \text{anything}$
3779.2 ^{+1.8+0.6} _{-1.7-0.8}		² ANASHIN	12A KEDR	$e^+e^- \rightarrow D\bar{D}$
3775.5 ± 2.4 ± 0.5	57	AUBERT	08B BABR	$B \rightarrow D\bar{D}K$
3776 ± 5 ± 4	68	BRODZICKA	08B BELL	$B^+ \rightarrow D^0\bar{D}^0K^+$
3778.8 ± 1.9 ± 0.9		AUBERT	07BE BABR	$e^+e^- \rightarrow D\bar{D}\gamma$
3779.8 ± 0.6		³ SHAMOV	17 RVUE	$e^+e^- \rightarrow D\bar{D}$, hadrons
3772.0 ± 1.9		^{4,5} ABLIKIM	08D BES2	$e^+e^- \rightarrow \text{hadrons}$
3778.4 ± 3.0 ± 1.3	34	CHISTOV	04 BELL	Sup. by BRODZICKA 08

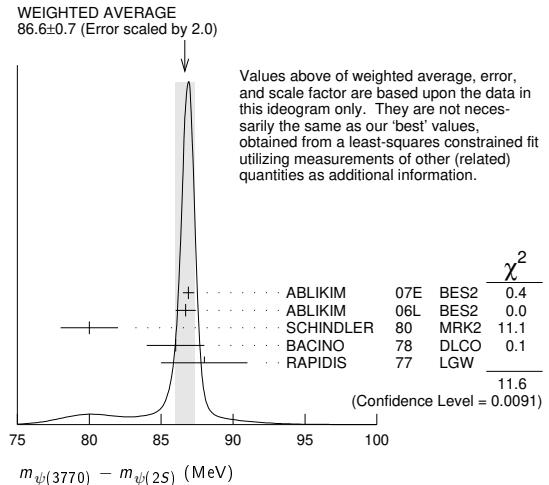
- • • We do not use the following data for averages, fits, limits, etc. • • •
- ¹ Measured in prompt hadroproduction.
- ² Taking into account interference between the resonant and non-resonant $D\bar{D}$ production.
- ³ From the joint analysis of the data on the $D\bar{D}$ and inclusive hadronic cross sections in the $\psi(3770)$ region from BaBar, Belle, BES-II, CLEO and KEDR.
- ⁴ Reanalysis of data presented in BAI 02c. From a global fit over the center-of-mass energy region 3.7–5.0 GeV covering the $\psi(3770)$, $\psi(4040)$, $\psi(4160)$, and $\psi(4415)$ resonances. Phase angle fixed in the fit to $\delta = 0^\circ$.
- ⁵ Interference between the resonant and non-resonant $D\bar{D}$ production not taken into account.

$m_{\psi(3770)} - m_{\psi(2S)}$

OUR FIT includes measurements of $m_{\psi(2S)}$, $m_{\psi(3770)}$, and $m_{\psi(3770)} - m_{\psi(2S)}$.

VALUE (MeV)	DOCUMENT ID	TECN	COMMENT
86.6 ± 0.4 OUR FIT	Error includes scale factor of 1.4.		
86.6 ± 0.7 OUR AVERAGE	Error includes scale factor of 2.0. See the ideogram below.		
86.9 ± 0.4	¹ ABLIKIM	07E BES2	$e^+e^- \rightarrow \text{hadrons}$
86.7 ± 0.7	ABLIKIM	06L BES2	$e^+e^- \rightarrow \text{hadrons}$
80 ± 2	SCHINDLER	80 MRK2	$e^+e^- \rightarrow \text{hadrons}$
86 ± 2	² BACINO	78 DLCO	$e^+e^- \rightarrow \text{hadrons}$
88 ± 3	RAPIDIS	77 LGW	$e^+e^- \rightarrow \text{hadrons}$

- ¹ BES-II $\psi(2S)$ mass subtracted (see ABLIKIM 06L).
- ² SPEAR $\psi(2S)$ mass subtracted (see SCHINDLER 80).



$\psi(3770)$ WIDTH

VALUE (MeV)	EVTs	DOCUMENT ID	TECN	COMMENT
27.2 ± 1.0 OUR FIT				
27.5 ± 0.9 OUR AVERAGE				
24.9 ^{+4.6+0.5} _{-4.0-1.1}		¹ ANASHIN	12A KEDR	$e^+e^- \rightarrow D\bar{D}$
30.4 ± 8.5		^{2,3} ABLIKIM	08D BES2	$e^+e^- \rightarrow \text{hadrons}$
27 ± 10 ± 5	68	BRODZICKA	08B BELL	$B^+ \rightarrow D^0\bar{D}^0K^+$
28.5 ± 1.2 ± 0.2		³ ABLIKIM	07E BES2	$e^+e^- \rightarrow \text{hadrons}$
23.5 ± 3.7 ± 0.9		AUBERT	07BE BABR	$e^+e^- \rightarrow D\bar{D}\gamma$
26.9 ± 2.4 ± 0.3		³ ABLIKIM	06L BES2	$e^+e^- \rightarrow \text{hadrons}$
24 ± 5		³ SCHINDLER	80 MRK2	$e^+e^- \rightarrow \text{hadrons}$
24 ± 5		³ BACINO	78 DLCO	$e^+e^- \rightarrow \text{hadrons}$
28 ± 5		³ RAPIDIS	77 LGW	$e^+e^- \rightarrow \text{hadrons}$

- • • We do not use the following data for averages, fits, limits, etc. • • •

Meson Particle Listings

 $\psi(3770)$ 25.8 ± 1.3 4 SHAMOV 17 RVUE $e^+e^- \rightarrow D\bar{D}$, hadrons¹ Taking into account interference between the resonant and non-resonant $D\bar{D}$ production.² Reanalysis of data presented in BAI 02c. From a global fit over the center-of-mass energy region 3.7–5.0 GeV covering the $\psi(3770)$, $\psi(4040)$, $\psi(4160)$, and $\psi(4415)$ resonances. Phase angle fixed in the fit to $\delta = 0^\circ$.³ Interference between the resonant and non-resonant $D\bar{D}$ production not taken into account.⁴ From the joint analysis of the data on the $D\bar{D}$ and inclusive hadronic cross sections in the $\psi(3770)$ region from BaBar, Belle, BES-II, CLEO and KEDR. **$\psi(3770)$ DECAY MODES**

In addition to the dominant decay mode to $D\bar{D}$, $\psi(3770)$ was found to decay into the final states containing the J/ψ (BAI 05, ADAM 06). ADAMS 06 and HUANG 06a searched for various decay modes with light hadrons and found a statistically significant signal for the decay to $\phi\eta$ only (ADAMS 06).

Mode	Fraction (Γ_i/Γ)	Scale factor/ Confidence level
Γ_1 $D\bar{D}$	(93 $\frac{+8}{-9}$) %	S=2.0
Γ_2 $D^0\bar{D}^0$	(52 $\frac{+4}{-5}$) %	S=2.0
Γ_3 D^+D^-	(41 ± 4) %	S=2.0
Γ_4 $J/\psi\pi^+\pi^-$	(1.93 ± 0.28) × 10 ⁻³	
Γ_5 $J/\psi\pi^0\pi^0$	(8.0 ± 3.0) × 10 ⁻⁴	
Γ_6 $J/\psi\eta$	(9 ± 4) × 10 ⁻⁴	
Γ_7 $J/\psi\pi^0$	< 2.8 × 10 ⁻⁴	CL=90%
Γ_8 e^+e^-	(9.6 ± 0.7) × 10 ⁻⁶	S=1.3

Decays to light hadrons

Γ_9 $b_1(1235)\pi$	< 1.4 × 10 ⁻⁵	CL=90%
Γ_{10} $\phi\eta'$	< 7 × 10 ⁻⁴	CL=90%
Γ_{11} $\omega\eta'$	< 4 × 10 ⁻⁴	CL=90%
Γ_{12} $\rho^0\eta'$	< 6 × 10 ⁻⁴	CL=90%
Γ_{13} $\phi\eta$	(3.1 ± 0.7) × 10 ⁻⁴	
Γ_{14} $\omega\eta$	< 1.4 × 10 ⁻⁵	CL=90%
Γ_{15} $\rho^0\eta$	< 5 × 10 ⁻⁴	CL=90%
Γ_{16} $\phi\pi^0$	< 3 × 10 ⁻⁵	CL=90%
Γ_{17} $\omega\pi^0$	< 6 × 10 ⁻⁴	CL=90%
Γ_{18} $\pi^+\pi^-\pi^0$	< 5 × 10 ⁻⁶	CL=90%
Γ_{19} $\rho\pi$	< 5 × 10 ⁻⁶	CL=90%
Γ_{20} K^+K^-		
Γ_{21} $K^*(892)^+K^- + c.c.$	< 1.4 × 10 ⁻⁵	CL=90%
Γ_{22} $K^*(892)^0\bar{K}^0 + c.c.$	< 1.2 × 10 ⁻³	CL=90%
Γ_{23} $K_S^0 K_L^0$	< 1.2 × 10 ⁻⁵	CL=90%
Γ_{24} $2(\pi^+\pi^-)$	< 1.12 × 10 ⁻³	CL=90%
Γ_{25} $2(\pi^+\pi^-)\pi^0$	< 1.06 × 10 ⁻³	CL=90%
Γ_{26} $2(\pi^+\pi^-\pi^0)$	< 5.85 %	CL=90%
Γ_{27} $\omega\pi^+\pi^-$	< 6.0 × 10 ⁻⁴	CL=90%
Γ_{28} $3(\pi^+\pi^-)$	< 9.1 × 10 ⁻³	CL=90%
Γ_{29} $3(\pi^+\pi^-)\pi^0$	< 1.37 %	CL=90%
Γ_{30} $3(\pi^+\pi^-)2\pi^0$	< 11.74 %	CL=90%
Γ_{31} $\eta\pi^+\pi^-$	< 1.24 × 10 ⁻³	CL=90%
Γ_{32} $\pi^+\pi^-2\pi^0$	< 8.9 × 10 ⁻³	CL=90%
Γ_{33} $\rho^0\pi^+\pi^-$	< 6.9 × 10 ⁻³	CL=90%
Γ_{34} $\eta3\pi$	< 1.34 × 10 ⁻³	CL=90%
Γ_{35} $\eta2(\pi^+\pi^-)$	< 2.43 %	CL=90%
Γ_{36} $\eta\rho^0\pi^+\pi^-$	< 1.45 %	CL=90%
Γ_{37} $\eta'3\pi$	< 2.44 × 10 ⁻³	CL=90%
Γ_{38} $K^+K^-\pi^+\pi^-$	< 9.0 × 10 ⁻⁴	CL=90%
Γ_{39} $\phi\pi^+\pi^-$	< 4.1 × 10 ⁻⁴	CL=90%
Γ_{40} $K^+K^-2\pi^0$	< 4.2 × 10 ⁻³	CL=90%
Γ_{41} $4(\pi^+\pi^-)$	< 1.67 %	CL=90%
Γ_{42} $4(\pi^+\pi^-)\pi^0$	< 3.06 %	CL=90%
Γ_{43} $\phi f_0(980)$	< 4.5 × 10 ⁻⁴	CL=90%
Γ_{44} $K^+K^-\pi^+\pi^-\pi^0$	< 2.36 × 10 ⁻³	CL=90%
Γ_{45} $K^+K^-\rho^0\pi^0$	< 8 × 10 ⁻⁴	CL=90%
Γ_{46} $K^+K^-\rho^+\pi^-$	< 1.46 %	CL=90%
Γ_{47} ωK^+K^-	< 3.4 × 10 ⁻⁴	CL=90%
Γ_{48} $\phi\pi^+\pi^-\pi^0$	< 3.8 × 10 ⁻³	CL=90%
Γ_{49} $K^{*0}K^-\pi^+\pi^0 + c.c.$	< 1.62 %	CL=90%
Γ_{50} $K^{*+}K^-\pi^+\pi^- + c.c.$	< 3.23 %	CL=90%
Γ_{51} $K^+K^-\pi^+\pi^-2\pi^0$	< 2.67 %	CL=90%
Γ_{52} $K^+K^-2(\pi^+\pi^-)$	< 1.03 %	CL=90%
Γ_{53} $K^+K^-2(\pi^+\pi^-)\pi^0$	< 3.60 %	CL=90%
Γ_{54} ηK^+K^-	< 4.1 × 10 ⁻⁴	CL=90%
Γ_{55} $\eta K^+K^-\pi^+\pi^-$	< 1.24 %	CL=90%
Γ_{56} $\rho^0 K^+K^-$	< 5.0 × 10 ⁻³	CL=90%

Γ_{57} $2(K^+K^-)$	< 6.0 × 10 ⁻⁴	CL=90%
Γ_{58} ϕK^+K^-	< 7.5 × 10 ⁻⁴	CL=90%
Γ_{59} $2(K^+K^-)\pi^0$	< 2.9 × 10 ⁻⁴	CL=90%
Γ_{60} $2(K^+K^-)\pi^+\pi^-$	< 3.2 × 10 ⁻³	CL=90%
Γ_{61} $K_S^0 K^- \pi^+$	< 3.2 × 10 ⁻³	CL=90%
Γ_{62} $K_S^0 K^- \pi^+\pi^0$	< 1.33 %	CL=90%
Γ_{63} $K_S^0 K^- \rho^+$	< 6.6 × 10 ⁻³	CL=90%
Γ_{64} $K_S^0 K^- 2\pi^+\pi^-$	< 8.7 × 10 ⁻³	CL=90%
Γ_{65} $K_S^0 K^- \pi^+\rho^0$	< 1.6 %	CL=90%
Γ_{66} $K_S^0 K^- \pi^+\eta$	< 1.3 %	CL=90%
Γ_{67} $K_S^0 K^- 2\pi^+\pi^-\pi^0$	< 4.18 %	CL=90%
Γ_{68} $K_S^0 K^- 2\pi^+\pi^-\eta$	< 4.8 %	CL=90%
Γ_{69} $K_S^0 K^- \pi^+ 2(\pi^+\pi^-)$	< 1.22 %	CL=90%
Γ_{70} $K_S^0 K^- \pi^+ 2\pi^0$	< 2.65 %	CL=90%
Γ_{71} $K_S^0 K^- K^+ K^- \pi^+$	< 4.9 × 10 ⁻³	CL=90%
Γ_{72} $K_S^0 K^- K^+ K^- \pi^+\pi^0$	< 3.0 %	CL=90%
Γ_{73} $K_S^0 K^- K^+ K^- \pi^+\eta$	< 2.2 %	CL=90%
Γ_{74} $K^{*0} K^- \pi^+ + c.c.$	< 9.7 × 10 ⁻³	CL=90%
Γ_{75} $\rho\bar{\rho}$		
Γ_{76} $\rho\bar{\rho}\pi^0$	< 4 × 10 ⁻⁵	CL=90%
Γ_{77} $\rho\bar{\rho}\pi^+\pi^-$	< 5.8 × 10 ⁻⁴	CL=90%
Γ_{78} $\Lambda\bar{\Lambda}$	< 1.2 × 10 ⁻⁴	CL=90%
Γ_{79} $\rho\bar{\rho}\pi^+\pi^-\pi^0$	< 1.85 × 10 ⁻³	CL=90%
Γ_{80} $\omega\rho\bar{\rho}$	< 2.9 × 10 ⁻⁴	CL=90%
Γ_{81} $\Lambda\bar{\Lambda}\pi^0$	< 7 × 10 ⁻⁵	CL=90%
Γ_{82} $\rho\bar{\rho}2(\pi^+\pi^-)$	< 2.6 × 10 ⁻³	CL=90%
Γ_{83} $\eta\rho\bar{\rho}$	< 5.4 × 10 ⁻⁴	CL=90%
Γ_{84} $\eta\rho\bar{\rho}\pi^+\pi^-$	< 3.3 × 10 ⁻³	CL=90%
Γ_{85} $\rho^0\rho\bar{\rho}$	< 1.7 × 10 ⁻³	CL=90%
Γ_{86} $\rho\bar{\rho}K^+K^-$	< 3.2 × 10 ⁻⁴	CL=90%
Γ_{87} $\eta\rho\bar{\rho}K^+K^-$	< 6.9 × 10 ⁻³	CL=90%
Γ_{88} $\pi^0\rho\bar{\rho}K^+K^-$	< 1.2 × 10 ⁻³	CL=90%
Γ_{89} $\phi\rho\bar{\rho}$	< 1.3 × 10 ⁻⁴	CL=90%
Γ_{90} $\Lambda\bar{\Lambda}\pi^+\pi^-$	< 2.5 × 10 ⁻⁴	CL=90%
Γ_{91} $\Lambda\bar{\rho}K^+$	< 2.8 × 10 ⁻⁴	CL=90%
Γ_{92} $\Lambda\bar{\rho}K^+\pi^+\pi^-$	< 6.3 × 10 ⁻⁴	CL=90%
Γ_{93} $\Lambda\bar{\Lambda}\eta$	< 1.9 × 10 ⁻⁴	CL=90%
Γ_{94} $\Sigma^+\Sigma^-$	< 1.0 × 10 ⁻⁴	CL=90%
Γ_{95} $\Sigma^0\Sigma^0$	< 4 × 10 ⁻⁵	CL=90%
Γ_{96} $\Xi^+\Xi^-$	< 1.5 × 10 ⁻⁴	CL=90%
Γ_{97} $\Xi^0\Xi^0$	< 1.4 × 10 ⁻⁴	CL=90%

Radiative decays

Γ_{98} $\gamma\chi_{c2}$	< 6.4 × 10 ⁻⁴	CL=90%
Γ_{99} $\gamma\chi_{c1}$	(2.49 ± 0.23) × 10 ⁻³	
Γ_{100} $\gamma\chi_{c0}$	(6.9 ± 0.6) × 10 ⁻³	
Γ_{101} $\gamma\eta_c$	< 7 × 10 ⁻⁴	CL=90%
Γ_{102} $\gamma\eta_c(2S)$	< 9 × 10 ⁻⁴	CL=90%
Γ_{103} $\gamma\eta'$	< 1.8 × 10 ⁻⁴	CL=90%
Γ_{104} $\gamma\eta$	< 1.5 × 10 ⁻⁴	CL=90%
Γ_{105} $\gamma\pi^0$	< 2 × 10 ⁻⁴	CL=90%

CONSTRAINED FIT INFORMATION

An overall fit to the total width, a partial width, and 3 branching ratios uses 23 measurements and one constraint to determine 5 parameters. The overall fit has a $\chi^2 = 20.1$ for 19 degrees of freedom.

The following *off-diagonal* array elements are the correlation coefficients $\langle \delta p_i \delta p_j \rangle / (\delta p_i \delta p_j)$, in percent, from the fit to parameters p_i , including the branching fractions, $x_i \equiv \Gamma_i / \Gamma_{\text{total}}$. The fit constrains the x_i whose labels appear in this array to sum to one.

x_3	99		
x_8	0	0	
Γ	0	0	-44
	x_2	x_3	x_8

Mode	Rate (MeV)	Scale factor
Γ_2 $D^0\bar{D}^0$	14.0 ± 1.4	1.8
Γ_3 D^+D^-	11.2 ± 1.1	1.7
Γ_8 e^+e^-	(2.62 ± 0.18) × 10 ⁻⁴	1.4

$\psi(3770)$ PARTIAL WIDTHS

$\Gamma(e^+e^-)$					Γ_8
VALUE (keV)	EVTS	DOCUMENT ID	TECN	COMMENT	
0.262 ± 0.018 OUR FIT	Error	includes scale factor of 1.4.			$D\bar{D}$
0.256 ± 0.016 OUR AVERAGE	Error	includes scale factor of 1.2.			
0.154 + 0.079 + 0.021 - 0.058 - 0.027		1,2 ANASHIN	12A KEDR	$e^+e^- \rightarrow D\bar{D}$	
0.22 ± 0.05		3,4 ABLIKIM	08D BES2	$e^+e^- \rightarrow$ hadrons	
0.277 ± 0.011 ± 0.013		4 ABLIKIM	07E BES2	$e^+e^- \rightarrow$ hadrons	
0.203 ± 0.003 + 0.041 - 0.027	1.4M	4,5 BESSON	06 CLEO	$e^+e^- \rightarrow$ hadrons	
0.276 ± 0.050		4 SCHINDLER	80 MRK2	e^+e^-	
0.18 ± 0.06		4 BACINO	78 DLCO	e^+e^-	
••• We do not use the following data for averages, fits, limits, etc. •••					
0.196 ± 0.018		6 SHAMOV	17 RVUE	$e^+e^- \rightarrow D\bar{D}$, hadrons	
0.414 + 0.072 + 0.093 - 0.080 - 0.028		2,7 ANASHIN	12A KEDR	$e^+e^- \rightarrow D\bar{D}$	
0.37 ± 0.09		8 RAPIDIS	77 LGW	e^+e^-	

1 Solution I of the two solutions.
 2 Taking into account interference between the resonant and non-resonant $D\bar{D}$ production.
 3 Reanalysis of data presented in BAI 02C. From a global fit over the center-of-mass energy region 3.7–5.0 GeV covering the $\psi(3770)$, $\psi(4040)$, $\psi(4160)$, and $\psi(4415)$ resonances. Phase angle fixed in the fit to $\delta = 0^\circ$.
 4 Interference between the resonant and non-resonant $D\bar{D}$ production not taken into account.
 5 BESSON 06 (as corrected in BESSON 10) measure $\sigma(e^+e^- \rightarrow \psi(3770) \rightarrow$ hadrons) = $6.36 \pm 0.08 + 0.41 - 0.30$ nb at $\sqrt{s} = 3773 \pm 1$ MeV, and obtain Γ_{ee} from the Born-level cross section calculated using $\psi(3770)$ mass and width from our 2004 edition, PDG 04.
 6 From the joint analysis of the data on the $D\bar{D}$ and inclusive hadronic cross sections in the $\psi(3770)$ region from BaBar, Belle, BES-II, CLEO and KEDR.
 7 Solution II of the two solutions.
 8 See also $\Gamma(e^+e^-)/\Gamma_{total}$ below.

$\psi(3770)$ BRANCHING RATIOS

$\Gamma(D\bar{D})/\Gamma_{total}$					$\Gamma_1/\Gamma = (\Gamma_2 + \Gamma_3)/\Gamma$
VALUE	EVTS	DOCUMENT ID	TECN	COMMENT	
0.93 ± 0.08 - 0.09 OUR FIT	Error	includes scale factor of 2.0.			$non-D\bar{D}$
0.93 ± 0.08 - 0.09 OUR AVERAGE	Error	includes scale factor of 2.1.			
0.849 ± 0.056 ± 0.018		1 ABLIKIM	08B BES2	$e^+e^- \rightarrow non-D\bar{D}$	
1.033 ± 0.014 + 0.048 - 0.066	1.427M	2 BESSON	06 CLEO	$e^+e^- \rightarrow$ hadrons	
••• We do not use the following data for averages, fits, limits, etc. •••					
0.836 ± 0.049		3 SHAMOV	17 RVUE	$e^+e^- \rightarrow D\bar{D}$, hadrons	
0.866 ± 0.050 ± 0.036		4,5 ABLIKIM	07K BES2	$e^+e^- \rightarrow non-D\bar{D}$	
0.836 ± 0.073 ± 0.042		5 ABLIKIM	06L BES2	$e^+e^- \rightarrow D\bar{D}$	
0.855 ± 0.017 ± 0.058		5,6 ABLIKIM	06N BES2	$e^+e^- \rightarrow D\bar{D}$	

1 Neglecting interference.
 2 Obtained by comparing a measurement of the total cross section (corrected in BESSON 10) with that of $D\bar{D}$ reported by CLEO in DOBBS 07.
 3 From the joint analysis of the data on the $D\bar{D}$ and inclusive hadronic cross sections in the $\psi(3770)$ region from BaBar, Belle, BES-II, CLEO and KEDR.
 4 Using $\sigma_{obs} = 7.07 \pm 0.58$ nb and neglecting interference.
 5 Not independent of ABLIKIM 08B.
 6 From a measurement of $\sigma(e^+e^- \rightarrow D\bar{D})$ at $\sqrt{s} = 3773$ MeV, using the $\psi(3770)$ resonance parameters measured by ABLIKIM 06L.

$\Gamma(D^0\bar{D}^0)/\Gamma_{total}$					Γ_2/Γ
VALUE	EVTS	DOCUMENT ID	TECN	COMMENT	
0.52 ± 0.04 - 0.05 OUR FIT	Error	includes scale factor of 2.0.			$D^0\bar{D}^0$
0.467 ± 0.047 ± 0.023		ABLIKIM 06L BES2 $e^+e^- \rightarrow D^0\bar{D}^0$			
0.499 ± 0.013 ± 0.038		1 ABLIKIM	06N BES2	$e^+e^- \rightarrow D^0\bar{D}^0$	

1 From a measurement of $\sigma(e^+e^- \rightarrow D\bar{D})$ at $\sqrt{s} = 3773$ MeV, using the $\psi(3770)$ resonance parameters measured by ABLIKIM 06L.

$\Gamma(D^+D^-)/\Gamma_{total}$					Γ_3/Γ
VALUE	EVTS	DOCUMENT ID	TECN	COMMENT	
0.41 ± 0.04 OUR FIT	Error	includes scale factor of 2.0.			D^+D^-
0.369 ± 0.037 ± 0.028		ABLIKIM 06L BES2 $e^+e^- \rightarrow D^+D^-$			
0.357 ± 0.011 ± 0.034		1 ABLIKIM	06N BES2	$e^+e^- \rightarrow D^+D^-$	

1 From a measurement of $\sigma(e^+e^- \rightarrow D\bar{D})$ at $\sqrt{s} = 3773$ MeV, using the $\psi(3770)$ resonance parameters measured by ABLIKIM 06L.

$\Gamma(D^0\bar{D}^0)/\Gamma(D^+D^-)$					Γ_2/Γ_3
VALUE	EVTS	DOCUMENT ID	TECN	COMMENT	
1.253 ± 0.016 OUR FIT					$D\bar{D}$
1.253 ± 0.016 OUR AVERAGE					
1.252 ± 0.009 ± 0.013	5.3M	BONVICINI	14 CLEO	$e^+e^- \rightarrow D\bar{D}$	
1.39 ± 0.31 ± 0.12		PAKHOVA	08 BELL	$10.6 e^+e^- \rightarrow D\bar{D}\gamma$	
1.78 ± 0.33 ± 0.24		AUBERT	07BE BABR	$e^+e^- \rightarrow D\bar{D}\gamma$	
1.27 ± 0.12 ± 0.08		ABLIKIM	06L BES2	$e^+e^- \rightarrow D\bar{D}$	
2.43 ± 1.50 ± 0.43	34	1 CHISTOV	04 BELL	$B^+ \rightarrow \psi(3770) K^+$	

••• We do not use the following data for averages, fits, limits, etc. •••

1.258 ± 0.016 ± 0.014	2 DOBBS	07 CLEO	$e^+e^- \rightarrow D\bar{D}$
-----------------------	---------	---------	-------------------------------

1 See ADLER 88c for older measurements of this quantity.
 2 Superseded by BONVICINI 14.

$\Gamma(J/\psi\pi^+\pi^-)/\Gamma_{total}$					Γ_4/Γ
VALUE (units 10 ⁻³)	EVTS	DOCUMENT ID	TECN	COMMENT	
1.93 ± 0.28 OUR AVERAGE					$\psi(3770)$
1.89 ± 0.20 ± 0.20	231 ± 33	ADAM	06 CLEO	$e^+e^- \rightarrow \psi(3770)$	
3.4 ± 1.4 ± 0.9	17.8 ± 4.8	BAI	05 BES2	$e^+e^- \rightarrow \psi(3770)$	

$\Gamma(J/\psi\pi^0\pi^0)/\Gamma_{total}$					Γ_5/Γ
VALUE (units 10 ⁻²)	EVTS	DOCUMENT ID	TECN	COMMENT	
0.080 ± 0.025 ± 0.016	39 ± 14	ADAM	06 CLEO	$e^+e^- \rightarrow \psi(3770)$	

$\Gamma(J/\psi\eta)/\Gamma_{total}$					Γ_6/Γ
VALUE (units 10 ⁻⁵)	EVTS	DOCUMENT ID	TECN	COMMENT	
87 ± 33 ± 22	22 ± 10	ADAM	06 CLEO	$e^+e^- \rightarrow \psi(3770)$	

$\Gamma(J/\psi\pi^0)/\Gamma_{total}$					Γ_7/Γ
VALUE (units 10 ⁻⁵)	CL%	EVTS	DOCUMENT ID	TECN	
<28	90	<10	ADAM	06 CLEO	$e^+e^- \rightarrow \psi(3770)$

$\Gamma(e^+e^-)/\Gamma_{total}$					Γ_8/Γ
VALUE (units 10 ⁻⁵)	EVTS	DOCUMENT ID	TECN	COMMENT	
0.96 ± 0.07 OUR FIT	Error	includes scale factor of 1.3.			e^+e^-
1.3 ± 0.2		RAPIDIS	77 LGW	e^+e^-	

DECAYS TO LIGHT HADRONS

$\Gamma(b_1(1235)\pi)/\Gamma_{total}$					Γ_9/Γ
VALUE (units 10 ⁻⁵)	CL%	DOCUMENT ID	TECN	COMMENT	
<1.4	90	1 ADAMS	06 CLEO	$e^+e^- \rightarrow \psi(3770)$	

1 Comparing cross sections at $\sqrt{s} = 3.773$ GeV and $\sqrt{s} = 3.671$ GeV, neglecting interference, and using $\sigma(\psi(3770) \rightarrow D\bar{D}) = 6.39 \pm 0.20$ nb.

$\Gamma(\phi\eta)/\Gamma_{total}$					Γ_{10}/Γ
VALUE (units 10 ⁻⁴)	CL%	DOCUMENT ID	TECN	COMMENT	
<7	90	1 ADAMS	06 CLEO	$e^+e^- \rightarrow \psi(3770)$	

1 Comparing cross sections at $\sqrt{s} = 3.773$ GeV and $\sqrt{s} = 3.671$ GeV, neglecting interference, and using $\sigma(\psi(3770) \rightarrow D\bar{D}) = 6.39 \pm 0.20$ nb.

$\Gamma(\omega\eta)/\Gamma_{total}$					Γ_{11}/Γ
VALUE (units 10 ⁻⁴)	CL%	DOCUMENT ID	TECN	COMMENT	
<4	90	1 ADAMS	06 CLEO	$e^+e^- \rightarrow \psi(3770)$	

1 Comparing cross sections at $\sqrt{s} = 3.773$ GeV and $\sqrt{s} = 3.671$ GeV, neglecting interference, and using $\sigma(\psi(3770) \rightarrow D\bar{D}) = 6.39 \pm 0.20$ nb.

$\Gamma(\rho^0\eta)/\Gamma_{total}$					Γ_{12}/Γ
VALUE (units 10 ⁻⁴)	CL%	DOCUMENT ID	TECN	COMMENT	
<6	90	1 ADAMS	06 CLEO	$e^+e^- \rightarrow \psi(3770)$	

1 Comparing cross sections at $\sqrt{s} = 3.773$ GeV and $\sqrt{s} = 3.671$ GeV, neglecting interference, and using $\sigma(\psi(3770) \rightarrow D\bar{D}) = 6.39 \pm 0.20$ nb.

$\Gamma(\phi\eta)/\Gamma_{total}$					Γ_{13}/Γ
VALUE (units 10 ⁻⁴)	CL%	DOCUMENT ID	TECN	COMMENT	
3.1 ± 0.6 ± 0.3		1 ADAMS	06 CLEO	$3.773 e^+e^- \rightarrow \phi\eta$	

••• We do not use the following data for averages, fits, limits, etc. •••

<19	90	2 ABLIKIM	07B BES2	$e^+e^- \rightarrow \psi(3770)$
-----	----	-----------	----------	---------------------------------

1 Comparing cross sections at $\sqrt{s} = 3.773$ GeV and $\sqrt{s} = 3.671$ GeV, neglecting interference, and using $\sigma(\psi(3770) \rightarrow D\bar{D}) = 6.39 \pm 0.20$ nb.
 2 Assuming that interference effects between resonance and continuum can be neglected and using $\sigma_{obs}(e^+e^- \rightarrow \psi(3770)) = 7.15 \pm 0.38$ nb.

$\Gamma(\omega\eta)/\Gamma_{total}$					Γ_{14}/Γ
VALUE (units 10 ⁻⁵)	CL%	DOCUMENT ID	TECN	COMMENT	
<1.4	90	1 ADAMS	06 CLEO	$e^+e^- \rightarrow \psi(3770)$	

1 Comparing cross sections at $\sqrt{s} = 3.773$ GeV and $\sqrt{s} = 3.671$ GeV, neglecting interference, and using $\sigma(\psi(3770) \rightarrow D\bar{D}) = 6.39 \pm 0.20$ nb.

$\Gamma(\rho^0\eta)/\Gamma_{total}$					Γ_{15}/Γ
VALUE (units 10 ⁻⁴)	CL%	DOCUMENT ID	TECN	COMMENT	
<5	90	1 ADAMS	06 CLEO	$e^+e^- \rightarrow \psi(3770)$	

1 Comparing cross sections at $\sqrt{s} = 3.773$ GeV and $\sqrt{s} = 3.671$ GeV, neglecting interference, and using $\sigma(\psi(3770) \rightarrow D\bar{D}) = 6.39 \pm 0.20$ nb.

$\Gamma(\phi\pi^0)/\Gamma_{total}$					Γ_{16}/Γ
VALUE (units 10 ⁻⁵)	CL%	DOCUMENT ID	TECN	COMMENT	
<3	90	1 ADAMS	06 CLEO	$e^+e^- \rightarrow \psi(3770)$	

Meson Particle Listings

$\psi(3770)$

• • • We do not use the following data for averages, fits, limits, etc. • • •
 <50 90 2 ABLIKIM 07B BES2 $e^+e^- \rightarrow \psi(3770)$

- 1 Comparing cross sections at $\sqrt{s} = 3.773$ GeV and $\sqrt{s} = 3.671$ GeV, neglecting interference, and using $\sigma(\psi(3770) \rightarrow D\bar{D}) = 6.39 \pm 0.20$ nb.
- 2 Assuming that interference effects between resonance and continuum can be neglected and using $\sigma^{obs}(e^+e^- \rightarrow \psi(3770)) = 7.15 \pm 0.38$ nb.

$\Gamma(\omega\pi^0)/\Gamma_{total}$ Γ_{17}/Γ

VALUE (units 10^{-4})	CL%	DOCUMENT ID	TECN	COMMENT
<6	90	1 ADAMS 06	CLEO	$e^+e^- \rightarrow \psi(3770)$

- 1 Comparing cross sections at $\sqrt{s} = 3.773$ GeV and $\sqrt{s} = 3.671$ GeV, neglecting interference, and using $\sigma(\psi(3770) \rightarrow D\bar{D}) = 6.39 \pm 0.20$ nb.

$\Gamma(\pi^+\pi^-\pi^0)/\Gamma_{total}$ Γ_{18}/Γ

VALUE (units 10^{-6})	CL%	DOCUMENT ID	TECN	COMMENT
<5	90	1,2 ADAMS 06	CLEO	$e^+e^- \rightarrow \psi(3770)$

- 1 Data suggest possible destructive interference with continuum.
- 2 Comparing cross sections at $\sqrt{s} = 3.773$ GeV and $\sqrt{s} = 3.671$ GeV, neglecting interference, and using $\sigma(\psi(3770) \rightarrow D\bar{D}) = 6.39 \pm 0.20$ nb.

$\Gamma(\rho\pi)/\Gamma_{total}$ Γ_{19}/Γ

VALUE (units 10^{-6})	CL%	DOCUMENT ID	TECN	COMMENT
<5	90	1,2 ADAMS 06	CLEO	$e^+e^- \rightarrow \psi(3770)$

- 1 Comparing cross sections at $\sqrt{s} = 3.773$ GeV and $\sqrt{s} = 3.671$ GeV, neglecting interference, and using $\sigma(\psi(3770) \rightarrow D\bar{D}) = 6.39 \pm 0.20$ nb.
- 2 Data suggest possible destructive interference with continuum.

$\Gamma(K^+K^-)/\Gamma_{total}$ Γ_{20}/Γ

VALUE	DOCUMENT ID	TECN	COMMENT
$\sim 10^{-5}$	1 DRUZHININ 15	RVUE	$e^+e^- \rightarrow \psi(3770)$

- 1 DRUZHININ 15 uses BABAR and CLEO data takitaking into account interference of the processes $e^+e^- \rightarrow K^+K^-$ and $e^+e^- \rightarrow K_S^0 K_L^0$.

$\Gamma(K^*(892)^+K^- + c.c.)/\Gamma_{total}$ Γ_{21}/Γ

VALUE (units 10^{-5})	CL%	DOCUMENT ID	TECN	COMMENT
<1.4	90	1 ADAMS 06	CLEO	$e^+e^- \rightarrow \psi(3770)$

- 1 Comparing cross sections at $\sqrt{s} = 3.773$ GeV and $\sqrt{s} = 3.671$ GeV, neglecting interference, and using $\sigma(\psi(3770) \rightarrow D\bar{D}) = 6.39 \pm 0.20$ nb.

$\Gamma(K^*(892)^0\bar{K}^0 + c.c.)/\Gamma_{total}$ Γ_{22}/Γ

VALUE (units 10^{-3})	CL%	DOCUMENT ID	TECN	COMMENT
<1.2	90	1 ADAMS 06	CLEO	$e^+e^- \rightarrow \psi(3770)$

- 1 Comparing cross sections at $\sqrt{s} = 3.773$ GeV and $\sqrt{s} = 3.671$ GeV, neglecting interference, and using $\sigma(\psi(3770) \rightarrow D\bar{D}) = 6.39 \pm 0.20$ nb.

$\Gamma(K_S^0 K_L^0)/\Gamma_{total}$ Γ_{23}/Γ

VALUE (units 10^{-5})	CL%	DOCUMENT ID	TECN	COMMENT
< 1.2	90	1 CRONIN-HEN..06	CLEO	$e^+e^- \rightarrow \psi(3770)$

• • • We do not use the following data for averages, fits, limits, etc. • • •

<21 90 2 ABLIKIM 04F BES $e^+e^- \rightarrow \psi(3770)$

1 Using $\sigma(e^+e^- \rightarrow \psi(3770) \rightarrow \text{hadrons}) = (6.38 \pm 0.08_{-0.30}^{+0.41})$ nb from BESSON 06 and $B(K_S^0 \rightarrow \pi^+\pi^-) = 0.6895 \pm 0.0014$.

2 Using $B(K_S^0 \rightarrow \pi^+\pi^-) = 0.6860 \pm 0.0027$.

$\Gamma(2(\pi^+\pi^-))/\Gamma_{total}$ Γ_{24}/Γ

VALUE (units 10^{-4})	CL%	DOCUMENT ID	TECN	COMMENT
<11.2	90	1 HUANG 06A	CLEO	$e^+e^- \rightarrow \psi(3770)$

• • • We do not use the following data for averages, fits, limits, etc. • • •

<48 90 2 ABLIKIM 07B BES2 $e^+e^- \rightarrow \psi(3770)$

1 Using $\sigma_{tot}(e^+e^- \rightarrow \psi(3770)) = 7.9 \pm 0.6$ nb at the resonance.

2 Assuming that interference effects between resonance and continuum can be neglected and using $\sigma^{obs}(e^+e^- \rightarrow \psi(3770)) = 7.15 \pm 0.38$ nb.

$\Gamma(2(\pi^+\pi^-\pi^0))/\Gamma_{total}$ Γ_{25}/Γ

VALUE (units 10^{-4})	CL%	DOCUMENT ID	TECN	COMMENT
<10.6	90	1 HUANG 06A	CLEO	$e^+e^- \rightarrow \psi(3770)$

• • • We do not use the following data for averages, fits, limits, etc. • • •

<62 90 2 ABLIKIM 07B BES2 $e^+e^- \rightarrow \psi(3770)$

1 Using $\sigma_{tot}(e^+e^- \rightarrow \psi(3770)) = 7.9 \pm 0.6$ nb at the resonance.

2 Assuming that interference effects between resonance and continuum can be neglected and using $\sigma^{obs}(e^+e^- \rightarrow \psi(3770)) = 7.15 \pm 0.38$ nb.

$\Gamma(2(\pi^+\pi^-\pi^0))/\Gamma_{total}$ Γ_{26}/Γ

VALUE (units 10^{-3})	CL%	EVTS	DOCUMENT ID	TECN	COMMENT
<58.5	90	305	ABLIKIM 08N	BES2	$e^+e^- \rightarrow \psi(3770)$

$\Gamma(\omega\pi^+\pi^-)/\Gamma_{total}$ Γ_{27}/Γ

VALUE (units 10^{-4})	CL%	DOCUMENT ID	TECN	COMMENT
< 6.0	90	1 HUANG 06A	CLEO	$e^+e^- \rightarrow \psi(3770)$

• • • We do not use the following data for averages, fits, limits, etc. • • •

<55 90 2 ABLIKIM 07i BES2 $3.77 e^+e^-$

1 Using $\sigma_{tot}(e^+e^- \rightarrow \psi(3770)) = 7.9 \pm 0.6$ nb at the resonance.

2 Assuming that interference effects between resonance and continuum can be neglected and using $\sigma^{obs}(e^+e^- \rightarrow \psi(3770)) = 7.15 \pm 0.38$ nb.

$\Gamma(3(\pi^+\pi^-))/\Gamma_{total}$ Γ_{28}/Γ

VALUE (units 10^{-4})	CL%	DOCUMENT ID	TECN	COMMENT
<91	90	1 ABLIKIM 07B	BES2	$e^+e^- \rightarrow \psi(3770)$

- 1 Assuming that interference effects between resonance and continuum can be neglected and using $\sigma^{obs}(e^+e^- \rightarrow \psi(3770)) = 7.15 \pm 0.38$ nb.

$\Gamma(3(\pi^+\pi^-\pi^0))/\Gamma_{total}$ Γ_{29}/Γ

VALUE (units 10^{-4})	CL%	DOCUMENT ID	TECN	COMMENT
<137	90	1 ABLIKIM 07B	BES2	$e^+e^- \rightarrow \psi(3770)$

- 1 Assuming that interference effects between resonance and continuum can be neglected and using $\sigma^{obs}(e^+e^- \rightarrow \psi(3770)) = 7.15 \pm 0.38$ nb.

$\Gamma(3(\pi^+\pi^-)2\pi^0)/\Gamma_{total}$ Γ_{30}/Γ

VALUE (units 10^{-3})	CL%	EVTS	DOCUMENT ID	TECN	COMMENT
<117.4	90	59	ABLIKIM 08N	BES2	$e^+e^- \rightarrow \psi(3770)$

$\Gamma(\eta\pi^+\pi^-)/\Gamma_{total}$ Γ_{31}/Γ

VALUE (units 10^{-3})	CL%	DOCUMENT ID	TECN	COMMENT
<1.24	90	1 HUANG 06A	CLEO	$e^+e^- \rightarrow \psi(3770)$

• • • We do not use the following data for averages, fits, limits, etc. • • •

<2.3 90 2 ABLIKIM 10D BES2 $e^+e^- \rightarrow \psi(3770)$

1 Using $\sigma_{tot}(e^+e^- \rightarrow \psi(3770)) = 7.9 \pm 0.6$ nb at the resonance.

2 Assuming that interference effects between resonance and continuum can be neglected and using $\sigma^{obs}(e^+e^- \rightarrow \psi(3770)) = 7.15 \pm 0.38$ nb.

$\Gamma(\pi^+\pi^-2\pi^0)/\Gamma_{total}$ Γ_{32}/Γ

VALUE (units 10^{-3})	CL%	EVTS	DOCUMENT ID	TECN	COMMENT
<8.9	90	218	ABLIKIM 08N	BES2	$e^+e^- \rightarrow \psi(3770)$

$\Gamma(\rho^0\pi^+\pi^-)/\Gamma_{total}$ Γ_{33}/Γ

VALUE (units 10^{-3})	CL%	DOCUMENT ID	TECN	COMMENT
<6.9	90	1 ABLIKIM 07F	BES2	$e^+e^- \rightarrow \psi(3770)$

- 1 Assuming that interference effects between resonance and continuum can be neglected and using $\sigma^{obs}(e^+e^- \rightarrow \psi(3770)) = 7.15 \pm 0.38$ nb.

$\Gamma(\eta3\pi)/\Gamma_{total}$ Γ_{34}/Γ

VALUE (units 10^{-4})	CL%	DOCUMENT ID	TECN	COMMENT
<13.4	90	1 HUANG 06A	CLEO	$e^+e^- \rightarrow \psi(3770)$

- 1 Using $\sigma_{tot}(e^+e^- \rightarrow \psi(3770)) = 7.9 \pm 0.6$ nb at the resonance.

$\Gamma(\eta2(\pi^+\pi^-))/\Gamma_{total}$ Γ_{35}/Γ

VALUE (units 10^{-4})	CL%	DOCUMENT ID	TECN	COMMENT
<243	90	1 ABLIKIM 07B	BES2	$e^+e^- \rightarrow \psi(3770)$

- 1 Assuming that interference effects between resonance and continuum can be neglected and using $\sigma^{obs}(e^+e^- \rightarrow \psi(3770)) = 7.15 \pm 0.38$ nb.

$\Gamma(\eta\rho^0\pi^+\pi^-)/\Gamma_{total}$ Γ_{36}/Γ

VALUE (units 10^{-2})	CL%	DOCUMENT ID	TECN	COMMENT
<1.45	90	1 ABLIKIM 10D	BES2	$e^+e^- \rightarrow \psi(3770)$

- 1 Assuming that interference effects between resonance and continuum can be neglected and using $\sigma^{obs}(e^+e^- \rightarrow \psi(3770)) = 7.15 \pm 0.38$ nb.

$\Gamma(\eta'3\pi)/\Gamma_{total}$ Γ_{37}/Γ

VALUE (units 10^{-4})	CL%	DOCUMENT ID	TECN	COMMENT
<24.4	90	1 HUANG 06A	CLEO	$e^+e^- \rightarrow \psi(3770)$

- 1 Using $\sigma_{tot}(e^+e^- \rightarrow \psi(3770)) = 7.9 \pm 0.6$ nb at the resonance.

$\Gamma(K^+K^-\pi^+\pi^-)/\Gamma_{total}$ Γ_{38}/Γ

VALUE (units 10^{-4})	CL%	DOCUMENT ID	TECN	COMMENT
< 9.0	90	1 HUANG 06A	CLEO	$e^+e^- \rightarrow \psi(3770)$

• • • We do not use the following data for averages, fits, limits, etc. • • •

<48 90 2 ABLIKIM 07B BES2 $e^+e^- \rightarrow \psi(3770)$

1 Using $\sigma_{tot}(e^+e^- \rightarrow \psi(3770)) = 7.9 \pm 0.6$ nb at the resonance.

2 Assuming that interference effects between resonance and continuum can be neglected and using $\sigma^{obs}(e^+e^- \rightarrow \psi(3770)) = 7.15 \pm 0.38$ nb.

$\Gamma(\phi\pi^+\pi^-)/\Gamma_{total}$ Γ_{39}/Γ

VALUE (units 10^{-4})	CL%	DOCUMENT ID	TECN	COMMENT
< 4.1	90	¹ HUANG 06A	CLEO	$e^+e^- \rightarrow \psi(3770)$

• • • We do not use the following data for averages, fits, limits, etc. • • •

<16	90	² ABLIKIM 07B	BES2	$e^+e^- \rightarrow \psi(3770)$
-----	----	--------------------------	------	---------------------------------

¹ Using $\sigma_{tot}(e^+e^- \rightarrow \psi(3770)) = 7.9 \pm 0.6$ nb at the resonance.
² Assuming that interference effects between resonance and continuum can be neglected and using $\sigma^{obs}(e^+e^- \rightarrow \psi(3770)) = 7.15 \pm 0.38$ nb.

$\Gamma(K^+K^-2\pi^0)/\Gamma_{total}$ Γ_{40}/Γ

VALUE (units 10^{-3})	CL%	EVTS	DOCUMENT ID	TECN	COMMENT
<4.2	90	14	ABLIKIM 08N	BES2	$e^+e^- \rightarrow \psi(3770)$

$\Gamma(4(\pi^+\pi^-))/\Gamma_{total}$ Γ_{41}/Γ

VALUE (units 10^{-3})	CL%	DOCUMENT ID	TECN	COMMENT
<16.7	90	¹ ABLIKIM 07F	BES2	$e^+e^- \rightarrow \psi(3770)$

¹ Assuming that interference effects between resonance and continuum can be neglected and using $\sigma^{obs}(e^+e^- \rightarrow \psi(3770)) = 7.15 \pm 0.38$ nb.

$\Gamma(4(\pi^+\pi^-\pi^0))/\Gamma_{total}$ Γ_{42}/Γ

VALUE (units 10^{-3})	CL%	DOCUMENT ID	TECN	COMMENT
<30.6	90	¹ ABLIKIM 07F	BES2	$e^+e^- \rightarrow \psi(3770)$

¹ Assuming that interference effects between resonance and continuum can be neglected and using $\sigma^{obs}(e^+e^- \rightarrow \psi(3770)) = 7.15 \pm 0.38$ nb.

$\Gamma(\phi f_0(980))/\Gamma_{total}$ Γ_{43}/Γ

VALUE (units 10^{-4})	CL%	DOCUMENT ID	TECN	COMMENT
<4.5	90	¹ HUANG 06A	CLEO	$e^+e^- \rightarrow \psi(3770)$

¹ Using $\sigma_{tot}(e^+e^- \rightarrow \psi(3770)) = 7.9 \pm 0.6$ nb at the resonance.

$\Gamma(K^+K^-\pi^+\pi^-\pi^0)/\Gamma_{total}$ Γ_{44}/Γ

VALUE (units 10^{-4})	CL%	DOCUMENT ID	TECN	COMMENT
< 23.6	90	¹ HUANG 06A	CLEO	$e^+e^- \rightarrow \psi(3770)$

• • • We do not use the following data for averages, fits, limits, etc. • • •

<111	90	² ABLIKIM 07B	BES2	$e^+e^- \rightarrow \psi(3770)$
------	----	--------------------------	------	---------------------------------

¹ Using $\sigma_{tot}(e^+e^- \rightarrow \psi(3770)) = 7.9 \pm 0.6$ nb at the resonance.
² Assuming that interference effects between resonance and continuum can be neglected and using $\sigma^{obs}(e^+e^- \rightarrow \psi(3770)) = 7.15 \pm 0.38$ nb.

$\Gamma(K^+K^-\rho^0\pi^0)/\Gamma_{total}$ Γ_{45}/Γ

VALUE (units 10^{-4})	CL%	DOCUMENT ID	TECN	COMMENT
<8	90	¹ ABLIKIM 07I	BES2	$3.77 e^+e^-$

¹ Assuming that interference effects between resonance and continuum can be neglected and using $\sigma^{obs}(e^+e^- \rightarrow \psi(3770)) = 7.15 \pm 0.38$ nb.

$\Gamma(K^+K^-\rho^+\pi^-)/\Gamma_{total}$ Γ_{46}/Γ

VALUE (units 10^{-4})	CL%	DOCUMENT ID	TECN	COMMENT
<146	90	¹ ABLIKIM 07I	BES2	$3.77 e^+e^-$

¹ Assuming that interference effects between resonance and continuum can be neglected and using $\sigma^{obs}(e^+e^- \rightarrow \psi(3770)) = 7.15 \pm 0.38$ nb.

$\Gamma(\omega K^+K^-)/\Gamma_{total}$ Γ_{47}/Γ

VALUE (units 10^{-4})	CL%	DOCUMENT ID	TECN	COMMENT
< 3.4	90	¹ HUANG 06A	CLEO	$e^+e^- \rightarrow \psi(3770)$

• • • We do not use the following data for averages, fits, limits, etc. • • •

<66	90	² ABLIKIM 07I	BES2	$3.77 e^+e^-$
-----	----	--------------------------	------	---------------

¹ Using $\sigma_{tot}(e^+e^- \rightarrow \psi(3770)) = 7.9 \pm 0.6$ nb at the resonance.
² Assuming that interference effects between resonance and continuum can be neglected and using $\sigma^{obs}(e^+e^- \rightarrow \psi(3770)) = 7.15 \pm 0.38$ nb.

$\Gamma(\phi\pi^+\pi^-\pi^0)/\Gamma_{total}$ Γ_{48}/Γ

VALUE (units 10^{-4})	CL%	DOCUMENT ID	TECN	COMMENT
<38	90	¹ ABLIKIM 07I	BES2	$3.77 e^+e^-$

¹ Assuming that interference effects between resonance and continuum can be neglected and using $\sigma^{obs}(e^+e^- \rightarrow \psi(3770)) = 7.15 \pm 0.38$ nb.

$\Gamma(K^{*0}K^-\pi^+\pi^0 + c.c.)/\Gamma_{total}$ Γ_{49}/Γ

VALUE (units 10^{-4})	CL%	DOCUMENT ID	TECN	COMMENT
<162	90	¹ ABLIKIM 07I	BES2	$3.77 e^+e^-$

¹ Assuming that interference effects between resonance and continuum can be neglected and using $\sigma^{obs}(e^+e^- \rightarrow \psi(3770)) = 7.15 \pm 0.38$ nb.

$\Gamma(K^{*+}K^-\pi^+\pi^- + c.c.)/\Gamma_{total}$ Γ_{50}/Γ

VALUE (units 10^{-4})	CL%	DOCUMENT ID	TECN	COMMENT
<323	90	¹ ABLIKIM 07I	BES2	$3.77 e^+e^-$

¹ Assuming that interference effects between resonance and continuum can be neglected and using $\sigma^{obs}(e^+e^- \rightarrow \psi(3770)) = 7.15 \pm 0.38$ nb.

$\Gamma(K^+K^-\pi^+\pi^-2\pi^0)/\Gamma_{total}$ Γ_{51}/Γ

VALUE (units 10^{-3})	CL%	EVTS	DOCUMENT ID	TECN	COMMENT
<26.7	90	24	ABLIKIM 08N	BES2	$e^+e^- \rightarrow \psi(3770)$

$\Gamma(K^+K^-2(\pi^+\pi^-))/\Gamma_{total}$ Γ_{52}/Γ

VALUE (units 10^{-3})	CL%	DOCUMENT ID	TECN	COMMENT
<10.3	90	¹ ABLIKIM 07F	BES2	$e^+e^- \rightarrow \psi(3770)$

¹ Assuming that interference effects between resonance and continuum can be neglected and using $\sigma^{obs}(e^+e^- \rightarrow \psi(3770)) = 7.15 \pm 0.38$ nb.

$\Gamma(K^+K^-2(\pi^+\pi^-\pi^0))/\Gamma_{total}$ Γ_{53}/Γ

VALUE (units 10^{-3})	CL%	DOCUMENT ID	TECN	COMMENT
<36.0	90	¹ ABLIKIM 07F	BES2	$e^+e^- \rightarrow \psi(3770)$

¹ Assuming that interference effects between resonance and continuum can be neglected and using $\sigma^{obs}(e^+e^- \rightarrow \psi(3770)) = 7.15 \pm 0.38$ nb.

$\Gamma(\eta K^+K^-)/\Gamma_{total}$ Γ_{54}/Γ

VALUE (units 10^{-4})	CL%	DOCUMENT ID	TECN	COMMENT
< 4.1	90	¹ HUANG 06A	CLEO	$e^+e^- \rightarrow \psi(3770)$

• • • We do not use the following data for averages, fits, limits, etc. • • •

<31	90	² ABLIKIM 10D	BES2	$e^+e^- \rightarrow \psi(3770)$
-----	----	--------------------------	------	---------------------------------

¹ Using $\sigma_{tot}(e^+e^- \rightarrow \psi(3770)) = 7.9 \pm 0.6$ nb at the resonance.
² Assuming that interference effects between resonance and continuum can be neglected and using $\sigma^{obs}(e^+e^- \rightarrow \psi(3770)) = 7.15 \pm 0.38$ nb.

$\Gamma(\eta K^+K^-\pi^+\pi^-)/\Gamma_{total}$ Γ_{55}/Γ

VALUE (units 10^{-2})	CL%	DOCUMENT ID	TECN	COMMENT
<1.24	90	¹ ABLIKIM 10D	BES2	$e^+e^- \rightarrow \psi(3770)$

¹ Assuming that interference effects between resonance and continuum can be neglected and using $\sigma^{obs}(e^+e^- \rightarrow \psi(3770)) = 7.15 \pm 0.38$ nb.

$\Gamma(\rho^0 K^+K^-)/\Gamma_{total}$ Γ_{56}/Γ

VALUE (units 10^{-3})	CL%	DOCUMENT ID	TECN	COMMENT
<5.0	90	¹ ABLIKIM 07F	BES2	$e^+e^- \rightarrow \psi(3770)$

¹ Assuming that interference effects between resonance and continuum can be neglected and using $\sigma^{obs}(e^+e^- \rightarrow \psi(3770)) = 7.15 \pm 0.38$ nb.

$\Gamma(2(K^+K^-))/\Gamma_{total}$ Γ_{57}/Γ

VALUE (units 10^{-4})	CL%	DOCUMENT ID	TECN	COMMENT
< 6.0	90	¹ HUANG 06A	CLEO	$e^+e^- \rightarrow \psi(3770)$

• • • We do not use the following data for averages, fits, limits, etc. • • •

<17	90	² ABLIKIM 07B	BES2	$e^+e^- \rightarrow \psi(3770)$
-----	----	--------------------------	------	---------------------------------

¹ Using $\sigma_{tot}(e^+e^- \rightarrow \psi(3770)) = 7.9 \pm 0.6$ nb at the resonance.
² Assuming that interference effects between resonance and continuum can be neglected and using $\sigma^{obs}(e^+e^- \rightarrow \psi(3770)) = 7.15 \pm 0.38$ nb.

$\Gamma(\phi K^+K^-)/\Gamma_{total}$ Γ_{58}/Γ

VALUE (units 10^{-4})	CL%	DOCUMENT ID	TECN	COMMENT
< 7.5	90	¹ HUANG 06A	CLEO	$e^+e^- \rightarrow \psi(3770)$

• • • We do not use the following data for averages, fits, limits, etc. • • •

<24	90	² ABLIKIM 07B	BES2	$e^+e^- \rightarrow \psi(3770)$
-----	----	--------------------------	------	---------------------------------

¹ Using $\sigma_{tot}(e^+e^- \rightarrow \psi(3770)) = 7.9 \pm 0.6$ nb at the resonance.
² Assuming that interference effects between resonance and continuum can be neglected and using $\sigma^{obs}(e^+e^- \rightarrow \psi(3770)) = 7.15 \pm 0.38$ nb.

$\Gamma(2(K^+K^-)\pi^0)/\Gamma_{total}$ Γ_{59}/Γ

VALUE (units 10^{-4})	CL%	DOCUMENT ID	TECN	COMMENT
< 2.9	90	¹ HUANG 06A	CLEO	$e^+e^- \rightarrow \psi(3770)$

• • • We do not use the following data for averages, fits, limits, etc. • • •

<46	90	² ABLIKIM 07B	BES2	$e^+e^- \rightarrow \psi(3770)$
-----	----	--------------------------	------	---------------------------------

¹ Using $\sigma_{tot}(e^+e^- \rightarrow \psi(3770)) = 7.9 \pm 0.6$ nb at the resonance.
² Assuming that interference effects between resonance and continuum can be neglected and using $\sigma^{obs}(e^+e^- \rightarrow \psi(3770)) = 7.15 \pm 0.38$ nb.

$\Gamma(2(K^+K^-)\pi^+\pi^-)/\Gamma_{total}$ Γ_{60}/Γ

VALUE (units 10^{-3})	CL%	DOCUMENT ID	TECN	COMMENT
<3.2	90	¹ ABLIKIM 07F	BES2	$e^+e^- \rightarrow \psi(3770)$

¹ Assuming that interference effects between resonance and continuum can be neglected and using $\sigma^{obs}(e^+e^- \rightarrow \psi(3770)) = 7.15 \pm 0.38$ nb.

$\Gamma(K_S^0 K^-\pi^+)/\Gamma_{total}$ Γ_{61}/Γ

VALUE (units 10^{-3})	CL%	EVTS	DOCUMENT ID	TECN	COMMENT
<3.2	90	18	ABLIKIM 08M	BES2	$e^+e^- \rightarrow \psi(3770)$

$\Gamma(K_S^0 K^-\pi^+\pi^0)/\Gamma_{total}$ Γ_{62}/Γ

VALUE (units 10^{-3})	CL%	EVTS	DOCUMENT ID	TECN	COMMENT
<13.3	90	40	ABLIKIM 08M	BES2	$e^+e^- \rightarrow \psi(3770)$

Meson Particle Listings

 $\psi(3770)$

$\Gamma(K_S^0 K^- \rho^+)/\Gamma_{\text{total}}$	Γ_{63}/Γ
VALUE (units 10^{-3}) CL% <6.6 90	DOCUMENT ID TECN COMMENT ABLIKIM 09c BES2 $e^+ e^- \rightarrow \psi(3770)$

$\Gamma(K_S^0 K^- 2\pi^+ \pi^-)/\Gamma_{\text{total}}$	Γ_{64}/Γ
VALUE (units 10^{-3}) CL% EVTS <8.7 90 39	DOCUMENT ID TECN COMMENT ABLIKIM 08M BES2 $e^+ e^- \rightarrow \psi(3770)$

$\Gamma(K_S^0 K^- \pi^+ \rho^0)/\Gamma_{\text{total}}$	Γ_{65}/Γ
VALUE (units 10^{-2}) CL% <1.6 90	DOCUMENT ID TECN COMMENT ABLIKIM 09c BES2 $e^+ e^- \rightarrow \psi(3770)$

$\Gamma(K_S^0 K^- \pi^+ \eta)/\Gamma_{\text{total}}$	Γ_{66}/Γ
VALUE (units 10^{-2}) CL% <1.3 90	DOCUMENT ID TECN COMMENT ABLIKIM 09c BES2 $e^+ e^- \rightarrow \psi(3770)$

$\Gamma(K_S^0 K^- 2\pi^+ \pi^- \pi^0)/\Gamma_{\text{total}}$	Γ_{67}/Γ
VALUE (units 10^{-3}) CL% EVTS <41.8 90 23	DOCUMENT ID TECN COMMENT ABLIKIM 08M BES2 $e^+ e^- \rightarrow \psi(3770)$

$\Gamma(K_S^0 K^- 2\pi^+ \pi^- \eta)/\Gamma_{\text{total}}$	Γ_{68}/Γ
VALUE (units 10^{-2}) CL% <4.8 90	DOCUMENT ID TECN COMMENT ABLIKIM 09c BES2 $e^+ e^- \rightarrow \psi(3770)$

$\Gamma(K_S^0 K^- \pi^+ 2(\pi^+ \pi^-))/\Gamma_{\text{total}}$	Γ_{69}/Γ
VALUE (units 10^{-3}) CL% EVTS <12.2 90 4	DOCUMENT ID TECN COMMENT ABLIKIM 08M BES2 $e^+ e^- \rightarrow \psi(3770)$

$\Gamma(K_S^0 K^- \pi^+ 2\pi^0)/\Gamma_{\text{total}}$	Γ_{70}/Γ
VALUE (units 10^{-3}) CL% EVTS <26.5 90 17	DOCUMENT ID TECN COMMENT ABLIKIM 08M BES2 $e^+ e^- \rightarrow \psi(3770)$

$\Gamma(K_S^0 K^- K^+ K^- \pi^+)/\Gamma_{\text{total}}$	Γ_{71}/Γ
VALUE (units 10^{-3}) CL% <4.9 90	DOCUMENT ID TECN COMMENT ABLIKIM 09c BES2 $e^+ e^- \rightarrow \psi(3770)$

$\Gamma(K_S^0 K^- K^+ K^- \pi^+ \pi^0)/\Gamma_{\text{total}}$	Γ_{72}/Γ
VALUE (units 10^{-2}) CL% <3.0 90	DOCUMENT ID TECN COMMENT ABLIKIM 09c BES2 $e^+ e^- \rightarrow \psi(3770)$

$\Gamma(K_S^0 K^- K^+ K^- \pi^+ \eta)/\Gamma_{\text{total}}$	Γ_{73}/Γ
VALUE (units 10^{-2}) CL% <2.2 90	DOCUMENT ID TECN COMMENT ABLIKIM 09c BES2 $e^+ e^- \rightarrow \psi(3770)$

$\Gamma(K^*0 K^- \pi^+ + c.c.)/\Gamma_{\text{total}}$	Γ_{74}/Γ
VALUE (units 10^{-3}) CL% <9.7 90	DOCUMENT ID TECN COMMENT 1 ABLIKIM 07F BES2 $e^+ e^- \rightarrow \psi(3770)$

¹ Assuming that interference effects between resonance and continuum can be neglected and using $\sigma_{\text{obs}}(e^+ e^- \rightarrow \psi(3770)) = 7.15 \pm 0.38$ nb.

$\Gamma(\rho\bar{\rho})/\Gamma_{\text{total}}$	Γ_{75}/Γ
VALUE (units 10^{-6}) EVTS ••• We do not use the following data for averages, fits, limits, etc. •••	DOCUMENT ID TECN COMMENT

not seen	1 AAIJ 17AD LHCb $pp \rightarrow B^+ X \rightarrow \rho\bar{\rho} K^+ X$
$7.1^+_{-2.9}$ 684	2 ABLIKIM 14L BES3 $e^+ e^- \rightarrow \psi(3770)$
310 ± 30 684	3 ABLIKIM 14L BES3 $e^+ e^- \rightarrow \psi(3770)$

¹ AAIJ 17AD reports $B(B^+ \rightarrow \psi(3770) K^+ \rightarrow \rho\bar{\rho} K^+)/B(B^+ \rightarrow J/\psi K^+ \rightarrow \rho\bar{\rho} K^+) < 0.09$ (0.10) at 90% (95%) CL.

² Solution I of two equivalent solutions in a fit with a resonance interfering with continuum.
³ Solution II of two equivalent solutions in a fit with a resonance interfering with continuum.

$\Gamma(\rho\bar{\rho}\pi^0)/\Gamma_{\text{total}}$	Γ_{76}/Γ
VALUE (units 10^{-4}) CL% < 0.4 90	DOCUMENT ID TECN COMMENT 1,2 ABLIKIM 14o BES3 $e^+ e^- \rightarrow \psi(3770)$

••• We do not use the following data for averages, fits, limits, etc. •••	
$59^+_{-2} \pm 5$	1,3 ABLIKIM 14o BES3 $e^+ e^- \rightarrow \psi(3770)$
<12	4 ABLIKIM 07B BES2 $e^+ e^- \rightarrow \psi(3770)$

¹ Calculated by the authors using $\sigma(e^+ e^- \rightarrow \psi(3770) \rightarrow \text{hadrons}) = 6.36 \pm 0.08^{+0.41}_{-0.30}$ nb from BESSON 10.

² Solution I of two equivalent solutions in a fit with a resonance interfering with continuum.
³ Solution II of two equivalent solutions in a fit with a resonance interfering with continuum.

⁴ Assuming that interference effects between resonance and continuum can be neglected and using $\sigma_{\text{obs}}(e^+ e^- \rightarrow \psi(3770)) = 7.15 \pm 0.38$ nb.

$\Gamma(\rho\bar{\rho}\pi^+ \pi^-)/\Gamma_{\text{total}}$	Γ_{77}/Γ
VALUE (units 10^{-4}) CL% < 5.8 90	DOCUMENT ID TECN COMMENT 1 HUANG 06A CLEO $e^+ e^- \rightarrow \psi(3770)$

••• We do not use the following data for averages, fits, limits, etc. •••

<16 90 2 ABLIKIM 07B BES2 $e^+ e^- \rightarrow \psi(3770)$

¹ Using $\sigma_{\text{tot}}(e^+ e^- \rightarrow \psi(3770)) = 7.9 \pm 0.6$ nb at the resonance.
² Assuming that interference effects between resonance and continuum can be neglected and using $\sigma_{\text{obs}}(e^+ e^- \rightarrow \psi(3770)) = 7.15 \pm 0.38$ nb.

$\Gamma(\Lambda\bar{\Lambda})/\Gamma_{\text{total}}$	Γ_{78}/Γ
VALUE (units 10^{-4}) CL% <1.2 90	DOCUMENT ID TECN COMMENT 1 HUANG 06A CLEO $e^+ e^- \rightarrow \psi(3770)$

••• We do not use the following data for averages, fits, limits, etc. •••

<4 90 2 ABLIKIM 07F BES2 $e^+ e^- \rightarrow \psi(3770)$

¹ Using $\sigma_{\text{tot}}(e^+ e^- \rightarrow \psi(3770)) = 7.9 \pm 0.6$ nb at the resonance.
² Assuming that interference effects between resonance and continuum can be neglected and using $\sigma_{\text{obs}}(e^+ e^- \rightarrow \psi(3770)) = 7.15 \pm 0.38$ nb.

$\Gamma(\rho\bar{\rho}\pi^+ \pi^- \pi^0)/\Gamma_{\text{total}}$	Γ_{79}/Γ
VALUE (units 10^{-4}) CL% <18.5 90	DOCUMENT ID TECN COMMENT 1 HUANG 06A CLEO $e^+ e^- \rightarrow \psi(3770)$

••• We do not use the following data for averages, fits, limits, etc. •••

<73 90 2 ABLIKIM 07B BES2 $e^+ e^- \rightarrow \psi(3770)$

¹ Using $\sigma_{\text{tot}}(e^+ e^- \rightarrow \psi(3770)) = 7.9 \pm 0.6$ nb at the resonance.
² Assuming that interference effects between resonance and continuum can be neglected and using $\sigma_{\text{obs}}(e^+ e^- \rightarrow \psi(3770)) = 7.15 \pm 0.38$ nb.

$\Gamma(\omega\rho\bar{\rho})/\Gamma_{\text{total}}$	Γ_{80}/Γ
VALUE (units 10^{-4}) CL% < 2.9 90	DOCUMENT ID TECN COMMENT 1 HUANG 06A CLEO $e^+ e^- \rightarrow \psi(3770)$

••• We do not use the following data for averages, fits, limits, etc. •••

<30 90 2 ABLIKIM 07i BES2 $3.77 e^+ e^-$

¹ Using $\sigma_{\text{tot}}(e^+ e^- \rightarrow \psi(3770)) = 7.9 \pm 0.6$ nb at the resonance.
² Using $\sigma_{\text{obs}} = 7.15 \pm 0.27 \pm 0.27$ nb and neglecting interference.

$\Gamma(\Lambda\bar{\Lambda}\pi^0)/\Gamma_{\text{total}}$	Γ_{81}/Γ
VALUE (units 10^{-4}) CL% < 0.7 90	DOCUMENT ID TECN COMMENT 1 ABLIKIM 13Q BES3 $e^+ e^- \rightarrow \psi(3770)$

••• We do not use the following data for averages, fits, limits, etc. •••

<12 90 2 ABLIKIM 07i BES2 $3.77 e^+ e^-$

¹ Assuming that interference effects between resonance and continuum can be neglected.
² Assuming that interference effects between resonance and continuum can be neglected and using $\sigma_{\text{obs}}(e^+ e^- \rightarrow \psi(3770)) = 7.15 \pm 0.38$ nb.

$\Gamma(\rho\bar{\rho}2(\pi^+ \pi^-))/\Gamma_{\text{total}}$	Γ_{82}/Γ
VALUE (units 10^{-3}) CL% <2.6 90	DOCUMENT ID TECN COMMENT 1 ABLIKIM 07F BES2 $e^+ e^- \rightarrow \psi(3770)$

¹ Assuming that interference effects between resonance and continuum can be neglected and using $\sigma_{\text{obs}}(e^+ e^- \rightarrow \psi(3770)) = 7.15 \pm 0.38$ nb.

$\Gamma(\eta\rho\bar{\rho})/\Gamma_{\text{total}}$	Γ_{83}/Γ
VALUE (units 10^{-4}) CL% < 5.4 90	DOCUMENT ID TECN COMMENT 1 HUANG 06A CLEO $e^+ e^- \rightarrow \psi(3770)$

••• We do not use the following data for averages, fits, limits, etc. •••

<11 90 2 ABLIKIM 10D BES2 $e^+ e^- \rightarrow \psi(3770)$

¹ Using $\sigma_{\text{tot}}(e^+ e^- \rightarrow \psi(3770)) = 7.9 \pm 0.6$ nb at the resonance.
² Assuming that interference effects between resonance and continuum can be neglected and using $\sigma_{\text{obs}}(e^+ e^- \rightarrow \psi(3770)) = 7.15 \pm 0.38$ nb.

$\Gamma(\eta\rho\bar{\rho}\pi^+ \pi^-)/\Gamma_{\text{total}}$	Γ_{84}/Γ
VALUE (units 10^{-3}) CL% <3.3 90	DOCUMENT ID TECN COMMENT 1 ABLIKIM 10D BES2 $e^+ e^- \rightarrow \psi(3770)$

¹ Assuming that interference effects between resonance and continuum can be neglected and using $\sigma_{\text{obs}}(e^+ e^- \rightarrow \psi(3770)) = 7.15 \pm 0.38$ nb.

$\Gamma(\rho^0\rho\bar{\rho})/\Gamma_{\text{total}}$	Γ_{85}/Γ
VALUE (units 10^{-3}) CL% <1.7 90	DOCUMENT ID TECN COMMENT 1 ABLIKIM 07F BES2 $e^+ e^- \rightarrow \psi(3770)$

¹ Assuming that interference effects between resonance and continuum can be neglected and using $\sigma_{\text{obs}}(e^+ e^- \rightarrow \psi(3770)) = 7.15 \pm 0.38$ nb.

$\Gamma(\rho\bar{\rho}K^+ K^-)/\Gamma_{\text{total}}$	Γ_{86}/Γ
VALUE (units 10^{-4}) CL% < 3.2 90	DOCUMENT ID TECN COMMENT 1 HUANG 06A CLEO $e^+ e^- \rightarrow \psi(3770)$

••• We do not use the following data for averages, fits, limits, etc. •••

<11 90 2 ABLIKIM 07B BES2 $e^+ e^- \rightarrow \psi(3770)$

¹ Using $\sigma_{\text{tot}}(e^+ e^- \rightarrow \psi(3770)) = 7.9 \pm 0.6$ nb at the resonance.
² Assuming that interference effects between resonance and continuum can be neglected and using $\sigma_{\text{obs}}(e^+ e^- \rightarrow \psi(3770)) = 7.15 \pm 0.38$ nb.

$\Gamma(\eta\rho\bar{p}K^+K^-)/\Gamma_{total}$ Γ_{87}/Γ

VALUE (units 10^{-3})	CL%	DOCUMENT ID	TECN	COMMENT
<6.9	90	1 ABLIKIM 10D BES2		$e^+e^- \rightarrow \psi(3770)$

¹ Assuming that interference effects between resonance and continuum can be neglected and using $\sigma^{obs}(e^+e^- \rightarrow \psi(3770)) = 7.15 \pm 0.38$ nb.

$\Gamma(\pi^0\rho\bar{p}K^+K^-)/\Gamma_{total}$ Γ_{88}/Γ

VALUE (units 10^{-3})	CL%	DOCUMENT ID	TECN	COMMENT
<1.2	90	1 ABLIKIM 10D BES2		$e^+e^- \rightarrow \psi(3770)$

¹ Assuming that interference effects between resonance and continuum can be neglected and using $\sigma^{obs}(e^+e^- \rightarrow \psi(3770)) = 7.15 \pm 0.38$ nb.

$\Gamma(\phi\rho\bar{p})/\Gamma_{total}$ Γ_{89}/Γ

VALUE (units 10^{-4})	CL%	DOCUMENT ID	TECN	COMMENT
<1.3	90	1 HUANG 06A CLEO		$e^+e^- \rightarrow \psi(3770)$

• • • We do not use the following data for averages, fits, limits, etc. • • •

¹ Using $\sigma_{tot}(e^+e^- \rightarrow \psi(3770)) = 7.9 \pm 0.6$ nb at the resonance.
² Assuming that interference effects between resonance and continuum can be neglected and using $\sigma^{obs}(e^+e^- \rightarrow \psi(3770)) = 7.15 \pm 0.38$ nb.

$\Gamma(\Lambda\bar{\Lambda}\pi^+\pi^-)/\Gamma_{total}$ Γ_{90}/Γ

VALUE (units 10^{-4})	CL%	DOCUMENT ID	TECN	COMMENT
< 2.5	90	1 HUANG 06A CLEO		$e^+e^- \rightarrow \psi(3770)$

• • • We do not use the following data for averages, fits, limits, etc. • • •

¹ Using $\sigma_{tot}(e^+e^- \rightarrow \psi(3770)) = 7.9 \pm 0.6$ nb at the resonance.
² Assuming that interference effects between resonance and continuum can be neglected.
³ Assuming that interference effects between resonance and continuum can be neglected and using $\sigma^{obs}(e^+e^- \rightarrow \psi(3770)) = 7.15 \pm 0.38$ nb.

$\Gamma(\Lambda\bar{p}K^+)/\Gamma_{total}$ Γ_{91}/Γ

VALUE (units 10^{-4})	CL%	DOCUMENT ID	TECN	COMMENT
<2.8	90	1 HUANG 06A CLEO		$e^+e^- \rightarrow \psi(3770)$

¹ Using $\sigma_{tot}(e^+e^- \rightarrow \psi(3770)) = 7.9 \pm 0.6$ nb at the resonance.

$\Gamma(\Lambda\bar{p}K^+\pi^+\pi^-)/\Gamma_{total}$ Γ_{92}/Γ

VALUE (units 10^{-4})	CL%	DOCUMENT ID	TECN	COMMENT
<6.3	90	1 HUANG 06A CLEO		$e^+e^- \rightarrow \psi(3770)$

¹ Using $\sigma_{tot}(e^+e^- \rightarrow \psi(3770)) = 7.9 \pm 0.6$ nb at the resonance.

$\Gamma(\Lambda\bar{\Lambda}\eta)/\Gamma_{total}$ Γ_{93}/Γ

VALUE (units 10^{-4})	CL%	DOCUMENT ID	TECN	COMMENT
<1.9	90	1 ABLIKIM 13Q BES3		$e^+e^- \rightarrow \psi(3770)$

¹ Assuming that interference effects between resonance and continuum can be neglected.

$\Gamma(\Sigma^+\bar{\Sigma}^-)/\Gamma_{total}$ Γ_{94}/Γ

VALUE (units 10^{-4})	CL%	DOCUMENT ID	TECN	COMMENT
<1.0	90	1 ABLIKIM 13Q BES3		$e^+e^- \rightarrow \psi(3770)$

¹ Assuming that interference effects between resonance and continuum can be neglected.

$\Gamma(\Sigma^0\bar{\Sigma}^0)/\Gamma_{total}$ Γ_{95}/Γ

VALUE (units 10^{-4})	CL%	DOCUMENT ID	TECN	COMMENT
<0.4	90	1 ABLIKIM 13Q BES3		$e^+e^- \rightarrow \psi(3770)$

¹ Assuming that interference effects between resonance and continuum can be neglected.

$\Gamma(\Xi^+\bar{\Xi}^-)/\Gamma_{total}$ Γ_{96}/Γ

VALUE (units 10^{-4})	CL%	DOCUMENT ID	TECN	COMMENT
<1.5	90	1 ABLIKIM 13Q BES3		$e^+e^- \rightarrow \psi(3770)$

¹ Assuming that interference effects between resonance and continuum can be neglected.

$\Gamma(\Xi^0\bar{\Xi}^0)/\Gamma_{total}$ Γ_{97}/Γ

VALUE (units 10^{-4})	CL%	DOCUMENT ID	TECN	COMMENT
<1.4	90	1 ABLIKIM 13Q BES3		$e^+e^- \rightarrow \psi(3770)$

¹ Assuming that interference effects between resonance and continuum can be neglected.

RADIATIVE DECAYS

$\Gamma(\gamma\chi_{c2})/\Gamma_{total}$ Γ_{98}/Γ

VALUE (units 10^{-3})	CL%	DOCUMENT ID	TECN	COMMENT
<0.64	90	1 ABLIKIM 15J BES3		$e^+e^- \rightarrow \psi(3770) \rightarrow \gamma\gamma J/\psi$

• • • We do not use the following data for averages, fits, limits, etc. • • •

¹ This limit is equivalent to $(0.25 \pm 0.21 \pm 0.18) \times 10^{-3}$ branching fraction value.
² Uses $B(\psi(2S) \rightarrow \gamma\chi_{c2}) = 9.22 \pm 0.11 \pm 0.46\%$ from ATHAR 04, $\psi(2S)$ mass and width from PDG 04, and $\Gamma_{ee}(\psi(2S)) = 2.54 \pm 0.03 \pm 0.11$ keV from ADAM 06.
³ Using $\Gamma_{ee}(\psi(2S)) = (2.54 \pm 0.03 \pm 0.11)$ keV from ADAM 06 and taking $\sigma(e^+e^- \rightarrow D\bar{D})$ from HE 05 for $\sigma(e^+e^- \rightarrow \psi(3770))$.

$\Gamma(\gamma\chi_{c1})/\Gamma_{total}$ Γ_{99}/Γ

VALUE (units 10^{-3})	EVTS	DOCUMENT ID	TECN	COMMENT
2.49 ± 0.23 OUR AVERAGE				
1.98 ± 0.78 ± 0.05	202	1 ABLIKIM 16B BES3		$e^+e^- \rightarrow \psi(3770) \rightarrow \gamma + \text{hadrons}$
2.48 ± 0.15 ± 0.23	0.6k	ABLIKIM 15J BES3		$e^+e^- \rightarrow \psi(3770) \rightarrow \gamma\gamma J/\psi$
2.4 ± 0.8 ± 0.2		2 ABLIKIM 14H BES3		$e^+e^- \rightarrow \psi(3770) \rightarrow K_S^0 K^\pm \pi^\mp$
2.9 ± 0.5 ± 0.4		3 BRIERE 06 CLEO		$e^+e^- \rightarrow \psi(3770) \rightarrow \gamma + \text{hadrons}, \gamma\gamma J/\psi$
3.9 ± 1.4 ± 0.6	54	4 BRIERE 06 CLEO		$e^+e^- \rightarrow \psi(3770) \rightarrow \gamma + \text{hadrons}$
2.8 ± 0.5 ± 0.4	53	5 COAN 06A CLEO		$e^+e^- \rightarrow \psi(3770) \rightarrow \gamma\gamma J/\psi$

• • • We do not use the following data for averages, fits, limits, etc. • • •

¹ ABLIKIM 16B reports $(1.94 \pm 0.42 \pm 0.64) \times 10^{-3}$ from a measurement of $[\Gamma(\psi(3770) \rightarrow \gamma\chi_{c1})/\Gamma_{total}] / [B(\psi(2S) \rightarrow \gamma\chi_{c1}(1P))]$ assuming $B(\psi(2S) \rightarrow \gamma\chi_{c1}(1P)) = (9.55 \pm 0.31) \times 10^{-2}$, which we rescale to our best value $B(\psi(2S) \rightarrow \gamma\chi_{c1}(1P)) = (9.75 \pm 0.24) \times 10^{-2}$. Our first error is their experiment's error and our second error is the systematic error from using our best value.

² ABLIKIM 14H reports $[\Gamma(\psi(3770) \rightarrow \gamma\chi_{c1})/\Gamma_{total}] \times [B(\chi_{c1}(1P) \rightarrow K_S^0 K^\pm \pi^\mp)] = (8.51 \pm 2.39 \pm 1.42) \times 10^{-6}$ which we divide by our best value $B(\chi_{c1}(1P) \rightarrow K_S^0 K^\pm \pi^\mp) = 0.00349 \pm 0.00029$. Our first error is their experiment's error and our second error is the systematic error from using our best value. We have calculated the best value of $B(\chi_{c1}(1P) \rightarrow K_S^0 K^\pm \pi^\mp)$ as 1/2 of $B(\chi_{c1}(1P) \rightarrow \bar{K}^0 K^+ \pi^- + c.c.) = (7.0 \pm 0.6) \times 10^{-3}$.

³ Averages the two measurements from COAN 06A and BRIERE 06.

⁴ Uses $B(\psi(2S) \rightarrow \gamma\chi_{c1}) = 9.07 \pm 0.11 \pm 0.54\%$ from ATHAR 04, $\psi(2S)$ mass and width from PDG 04, and $\Gamma_{ee}(\psi(2S)) = 2.54 \pm 0.03 \pm 0.11$ keV from ADAM 06.

⁵ Using $\Gamma_{ee}(\psi(2S)) = (2.54 \pm 0.03 \pm 0.11)$ keV from ADAM 06 and taking $\sigma(e^+e^- \rightarrow D\bar{D})$ from HE 05 for $\sigma(e^+e^- \rightarrow \psi(3770))$.

$\Gamma(\gamma\chi_{c1})/\Gamma(J/\psi\pi^+\pi^-)$ Γ_{99}/Γ_4

VALUE	EVTS	DOCUMENT ID	TECN	COMMENT
1.49 ± 0.31 ± 0.26	53 ± 10	1 COAN 06A CLEO		$e^+e^- \rightarrow \psi(3770) \rightarrow \gamma\gamma J/\psi$

¹ Using $B(\psi(3770) \rightarrow J/\psi\pi^+\pi^-) = (1.89 \pm 0.20 \pm 0.20) \times 10^{-3}$ from ADAM 06.

$\Gamma(\gamma\chi_{c0})/\Gamma_{total}$ Γ_{100}/Γ

VALUE (units 10^{-3})	CL%	EVTS	DOCUMENT ID	TECN	COMMENT
6.9 ± 0.6 OUR AVERAGE					
6.7 ± 0.7 ± 0.1		2.2K	1 ABLIKIM 16B BES3		$e^+e^- \rightarrow \psi(3770) \rightarrow \gamma + \text{hadrons}$
7.3 ± 0.7 ± 0.6		274	BRIERE 06 CLEO		$e^+e^- \rightarrow \psi(3770) \rightarrow \gamma + \text{hadrons}$
< 44	90		2 COAN 06A CLEO		$e^+e^- \rightarrow \psi(3770) \rightarrow \gamma\gamma J/\psi$

• • • We do not use the following data for averages, fits, limits, etc. • • •

¹ ABLIKIM 16B reports $(6.88 \pm 0.28 \pm 0.67) \times 10^{-3}$ from a measurement of $[\Gamma(\psi(3770) \rightarrow \gamma\chi_{c0})/\Gamma_{total}] / [B(\psi(2S) \rightarrow \gamma\chi_{c0}(1P))]$ assuming $B(\psi(2S) \rightarrow \gamma\chi_{c0}(1P)) = (9.99 \pm 0.27) \times 10^{-2}$, which we rescale to our best value $B(\psi(2S) \rightarrow \gamma\chi_{c0}(1P)) = (9.79 \pm 0.20) \times 10^{-2}$. Our first error is their experiment's error and our second error is the systematic error from using our best value.

² Using $\Gamma_{ee}(\psi(2S)) = (2.54 \pm 0.03 \pm 0.11)$ keV from ADAM 06 and taking $\sigma(e^+e^- \rightarrow D\bar{D})$ from HE 05 for $\sigma(e^+e^- \rightarrow \psi(3770))$.

$\Gamma(\gamma\chi_{c0})/\Gamma(\gamma\chi_{c2})$ Γ_{100}/Γ_{98}

VALUE	CL%	DOCUMENT ID	TECN	COMMENT
>8	90	1 BRIERE 06 CLEO		$e^+e^- \rightarrow \psi(3770)$

¹ Not independent of other results in BRIERE 06.

$\Gamma(\gamma\chi_{c0})/\Gamma(\gamma\chi_{c1})$ Γ_{100}/Γ_{99}

VALUE	DOCUMENT ID	TECN	COMMENT
2.5 ± 0.6	1 BRIERE 06 CLEO		$e^+e^- \rightarrow \psi(3770)$

¹ Not independent of other results in BRIERE 06.

$\Gamma(\gamma\eta_c)/\Gamma_{total}$ Γ_{101}/Γ

VALUE	CL%	DOCUMENT ID	TECN	COMMENT
<7 × 10 ⁻⁴	90	1 ABLIKIM 14H BES3		

¹ ABLIKIM 14H reports $[\Gamma(\psi(3770) \rightarrow \gamma\eta_c)/\Gamma_{total}] \times [B(\eta_c(1S) \rightarrow K_S^0 K^\pm \pi^\mp)] < 16 \times 10^{-6}$ which we divide by our best value $B(\eta_c(1S) \rightarrow K_S^0 K^\pm \pi^\mp) = 2.43 \times 10^{-2}$. We have calculated the best value of $B(\eta_c(1S) \rightarrow K_S^0 K^\pm \pi^\mp)$ as 1/3 of $B(\eta_c(1S) \rightarrow K\bar{K}\pi) = 7.3 \times 10^{-2}$.

Meson Particle Listings

 $\psi(3770)$, $\psi_2(3823)$, $\psi_3(3842)$ $\Gamma(\gamma\eta_c(2S))/\Gamma_{\text{total}}$

VALUE	CL%	DOCUMENT ID	TECN
$<9 \times 10^{-4}$	90	¹ ABLIKIM	14H BES3

¹ ABLIKIM 14H reports $[\Gamma(\psi(3770) \rightarrow \gamma\eta_c(2S))/\Gamma_{\text{total}}] \times [B(\eta_c(2S) \rightarrow K_S^0 K^\pm \pi^\mp)] < 5.6 \times 10^{-6}$ which we divide by our best value $B(\eta_c(2S) \rightarrow K_S^0 K^\pm \pi^\mp) = 6 \times 10^{-3}$. We have calculated the best value of $B(\eta_c(2S) \rightarrow K_S^0 K^\pm \pi^\mp)$ as $1/3$ of $B(\eta_c(2S) \rightarrow K \bar{K} \pi) = 1.9 \times 10^{-2}$.

 $\Gamma(\gamma\eta)/\Gamma_{\text{total}}$

VALUE (units 10^{-4})	CL%	DOCUMENT ID	TECN	COMMENT
<1.8	90	¹ PEDLAR	09 CLE3	$\psi(2S) \rightarrow \gamma X$

¹ Assuming maximal destructive interference between $\psi(3770)$ and continuum sources.

 $\Gamma(\gamma\eta)/\Gamma_{\text{total}}$

VALUE (units 10^{-4})	CL%	DOCUMENT ID	TECN	COMMENT
<1.5	90	¹ PEDLAR	09 CLE3	$\psi(2S) \rightarrow \gamma X$

¹ Assuming maximal destructive interference between $\psi(3770)$ and continuum sources.

 $\Gamma(\gamma\pi^0)/\Gamma_{\text{total}}$

VALUE (units 10^{-4})	CL%	DOCUMENT ID	TECN	COMMENT
<2	90	PEDLAR	09 CLE3	$\psi(2S) \rightarrow \gamma X$

 $\psi(3770)$ REFERENCES

AAIJ	19M	JHEP 1907 035	R. Aaij <i>et al.</i>	(LHCb Collab.)
AAIJ	17AD	PL B769 305	R. Aaij <i>et al.</i>	(LHCb Collab.)
SHAMOV	17	PL B769 187	A.G. Shamov, K.Yu. Todyshev	
ABLIKIM	16B	PL B753 103	M. Ablikim <i>et al.</i>	(BESIII Collab.)
ABLIKIM	15J	PR D91 092009	M. Ablikim <i>et al.</i>	(BESIII Collab.)
DRUZHININ	15	PR D92 054024	V.P. Druzhinin	(NOVO)
ABLIKIM	14H	PR D89 112005	M. Ablikim <i>et al.</i>	(BESIII Collab.)
ABLIKIM	14L	PL B735 101	M. Ablikim <i>et al.</i>	(BESIII Collab.)
ABLIKIM	14O	PR D90 032007	M. Ablikim <i>et al.</i>	(BESIII Collab.)
BONVICINI	14	PR D89 072002	G. Bonvicini <i>et al.</i>	(CLEO Collab.)
ABLIKIM	13Q	PR D87 112011	Ablikim M. <i>et al.</i>	(BESIII Collab.)
ANASHIN	12A	PL B711 292	V.V. Anashin <i>et al.</i>	(KEDR Collab.)
ABLIKIM	10D	EPJ C66 11	M. Ablikim <i>et al.</i>	(BES II Collab.)
BESSON	10	PRL 104 159901 (errata)	D. Besson <i>et al.</i>	(CLEO Collab.)
ABLIKIM	09C	EPJ C64 243	M. Ablikim <i>et al.</i>	(BES Collab.)
PEDLAR	09	PR D79 111101	T.K. Pedlar <i>et al.</i>	(CLEO Collab.)
ABLIKIM	08B	PL B659 74	M. Ablikim <i>et al.</i>	(BES Collab.)
ABLIKIM	08D	PL B660 315	M. Ablikim <i>et al.</i>	(BES Collab.)
ABLIKIM	08M	PL B670 179	M. Ablikim <i>et al.</i>	(BES Collab.)
ABLIKIM	08N	PL B670 184	M. Ablikim <i>et al.</i>	(BES Collab.)
AUBERT	08B	PR D77 011102	B. Aubert <i>et al.</i>	(BABAR Collab.)
BRODZICKA	08	PRL 100 092001	J. Brodzicka <i>et al.</i>	(BELLE Collab.)
PAKHOVA	08	PR D77 011103	G. Pakhlova <i>et al.</i>	(BELLE Collab.)
ABLIKIM	07B	PL B650 111	M. Ablikim <i>et al.</i>	(BES Collab.)
ABLIKIM	07E	PL B652 238	M. Ablikim <i>et al.</i>	(BES Collab.)
ABLIKIM	07F	PL B656 30	M. Ablikim <i>et al.</i>	(BES Collab.)
ABLIKIM	07I	EPJ C52 805	M. Ablikim <i>et al.</i>	(BES Collab.)
ABLIKIM	07K	PR D76 122002	M. Ablikim <i>et al.</i>	(BES Collab.)
AUBERT	07BE	PR D76 111105	B. Aubert <i>et al.</i>	(BABAR Collab.)
DOBBS	07	PR D76 112001	S. Dobbs <i>et al.</i>	(CLEO Collab.)
ABLIKIM	06L	PRL 97 121801	M. Ablikim <i>et al.</i>	(BES Collab.)
ABLIKIM	06N	PL B641 145	M. Ablikim <i>et al.</i>	(BES Collab.)
ADAM	06	PRL 96 082004	N.E. Adam <i>et al.</i>	(CLEO Collab.)
ADAMS	06	PR D73 012002	G.S. Adams <i>et al.</i>	(CLEO Collab.)
BESSON	06	PRL 96 092002	D. Besson <i>et al.</i>	(CLEO Collab.)
Also		PRL 104 159901 (errata)	D. Besson <i>et al.</i>	(CLEO Collab.)
BRIERE	06	PR D74 031106	R.A. Briere <i>et al.</i>	(CLEO Collab.)
COAN	06A	PRL 96 182002	T.E. Coan <i>et al.</i>	(CLEO Collab.)
CRONIN-HENNESSY	06	PR D74 012005	D. Cronin-Hennessy <i>et al.</i>	(CLEO Collab.)
HUANG	06A	PRL 96 032003	G.S. Huang <i>et al.</i>	(CLEO Collab.)
BAI	05	PL B605 63	J.Z. Bai <i>et al.</i>	(BES Collab.)
HE	05	PRL 95 121801	Q. He <i>et al.</i>	(CLEO Collab.)
Also		PRL 96 199903 (errata)	Q. He <i>et al.</i>	(CLEO Collab.)
ABLIKIM	04F	PR D70 077101	M. Ablikim <i>et al.</i>	(BES Collab.)
ATHAR	04	PR D70 112002	S.B. Athar <i>et al.</i>	(CLEO Collab.)
CHISTOV	04	PRL 93 051803	R. Chistov <i>et al.</i>	(BELLE Collab.)
PDG	04	PL B592 1	S. Eidelman <i>et al.</i>	(PDG Collab.)
BAI	02C	PRL 88 101802	J.Z. Bai <i>et al.</i>	(BES Collab.)
ADLER	85C	PR 60 89	J. Adler <i>et al.</i>	(Mark III Collab.)
SCHINDLER	80	PR D21 2716	R.H. Schindler <i>et al.</i>	(Mark II Collab.)
BACINO	78	PRL 40 671	W.J. Bacino <i>et al.</i>	(SLAC, UCLA, UCI)
RAPIDIS	77	PRL 39 526	P.A. Rapidis <i>et al.</i>	(LGW Collab.)

 $\psi_2(3823)$

$$I^G(J^{PC}) = 0^-(2^{--})$$

I, J, P need confirmation.

was $\psi(3823)$, $X(3823)$

Seen by BHARDWAJ 13 in $B \rightarrow \chi_{c1} \gamma K$ and ABLIKIM 15S in $e^+ e^- \rightarrow \pi^+ \pi^- \gamma \chi_{c1}$ decays as a narrow peak in the invariant mass distribution of the $\chi_{c1} \gamma$ system. Properties consistent with the $\psi_2(1^3 D_2) c \bar{c}$ state.

 $\psi_2(3823)$ MASS

VALUE (MeV)	EVTs	DOCUMENT ID	TECN	COMMENT
3822.2 ± 1.2 OUR AVERAGE				
3821.7 ± 1.3 ± 0.7	19 ± 5	¹ ABLIKIM	15s BES3	$e^+ e^- \rightarrow \pi^+ \pi^- \chi_{c1} \gamma$
3823.1 ± 1.8 ± 0.7	33 ± 10	² BHARDWAJ	13 BELL	$B \rightarrow \chi_{c1} \gamma K$

¹ From a simultaneous unbinned maximum likelihood fit of $e^+ e^- \rightarrow \pi^+ \pi^- \chi_{c1} \gamma$ data (the $\pi^+ \pi^-$ recoil mass) taken at \sqrt{s} values of 4.23, 4.26, 4.36, 4.42, and 4.60 GeV to simulated events including both $\psi(2S) \rightarrow \chi_{c1} \gamma$ and $\psi_2(3823) \rightarrow \chi_{c1} \gamma$ together, with floating mass scale offset for $\psi(2S)$, floating $\psi_2(3823)$ mass, and zero $\psi_2(3823)$ width, resulting in a significance of 5.9 σ when including systematic uncertainties.

² From a simultaneous fit to $B^\pm \rightarrow (\chi_{c1} \gamma) K^\pm$ and $B^0 \rightarrow (\chi_{c1} \gamma) K_S^0$ with significance 4.0 σ including systematics. Corrected for the measured $\psi(2S)$ mass using $B \rightarrow \psi(2S) K \rightarrow (\gamma \chi_{c1}) K$ decays.

 $\psi_2(3823)$ WIDTH

VALUE (MeV)	CL%	DOCUMENT ID	TECN	COMMENT
<16	90	¹ ABLIKIM	15s BES3	$e^+ e^- \rightarrow \pi^+ \pi^- \chi_{c1} \gamma$
<24	90	² BHARDWAJ	13 BELL	$B \rightarrow \chi_{c1} \gamma K$

¹ From a fit of $e^+ e^- \rightarrow \pi^+ \pi^- \chi_{c1} \gamma$ data (the $\pi^+ \pi^-$ recoil mass) taken at \sqrt{s} values of 4.23, 4.26, 4.36, 4.42, and 4.60 GeV to a Breit-Wigner function with the mass fixed from the likelihood fit above, Gaussian resolution smearing, and floating width.

² From a simultaneous fit to $B^\pm \rightarrow (\chi_{c1} \gamma) K^\pm$ and $B^0 \rightarrow (\chi_{c1} \gamma) K_S^0$ with significance 4.0 σ including systematics.

 $\psi_2(3823)$ DECAY MODES

Mode	Fraction (Γ_i/Γ)
$\Gamma_1 \quad \chi_{c1} \gamma$	seen
$\Gamma_2 \quad \chi_{c2} \gamma$	not seen

 $\psi_2(3823)$ BRANCHING RATIOS

$\Gamma(\chi_{c1} \gamma)/\Gamma_{\text{total}}$	Γ_1/Γ			
VALUE	EVTs	DOCUMENT ID	TECN	COMMENT
seen	33 ± 10	¹ BHARDWAJ	13 BELL	$B^+ \rightarrow \chi_{c1} \gamma K^+$

¹ Reported $B(B^\pm \rightarrow \psi_2(3823) K^\pm) \times B(\psi_2(3823) \rightarrow \gamma \chi_{c1}) = (9.7 \pm 2.8 \pm 1.1) \times 10^{-6}$ with statistical significance 3.8 σ .

 $\Gamma(\chi_{c2} \gamma)/\Gamma_{\text{total}}$

VALUE	DOCUMENT ID	TECN	COMMENT
not seen	¹ ABLIKIM	15s BES3	$e^+ e^- \rightarrow \pi^+ \pi^- \chi_{c2} \gamma$
not seen	² BHARDWAJ	13 BELL	$B^+ \rightarrow \chi_{c2} \gamma K^+$

¹ From a simultaneous unbinned maximum likelihood fit of $e^+ e^- \rightarrow \pi^+ \pi^- \chi_{c2} \gamma$ data (the $\pi^+ \pi^-$ recoil mass) taken at \sqrt{s} values of 4.23, 4.26, 4.36, 4.42, and 4.60 GeV to simulated events including both $\psi(2S) \rightarrow \chi_{c2} \gamma$ and $\psi_2(3823) \rightarrow \chi_{c2} \gamma$ together, with floating mass scale offset for $\psi(2S)$, $\psi_2(3823)$ mass floating (fixed to that above), and zero $\psi_2(3823)$ width.

² Reported $B(B^\pm \rightarrow \psi_2(3823) K^\pm) \times B(\psi_2(3823) \rightarrow \gamma \chi_{c2}) < 3.6 \times 10^{-6}$ at 90% CL.

 $\Gamma(\chi_{c2} \gamma)/\Gamma(\chi_{c1} \gamma)$

VALUE	CL%	DOCUMENT ID	TECN	COMMENT
<0.41	90	BHARDWAJ	13 BELL	$B^+ \rightarrow \chi_{c1} \gamma K^+$

$\bullet \bullet \bullet$ We do not use the following data for averages, fits, limits, etc. $\bullet \bullet \bullet$

<0.42 90 ¹ ABLIKIM 15s BES3 $e^+ e^- \rightarrow \pi^+ \pi^- \chi_{c1} \gamma$

¹ From a simultaneous unbinned maximum likelihood fit of $e^+ e^- \rightarrow \pi^+ \pi^- \chi_{c1} \gamma$ data (the $\pi^+ \pi^-$ recoil mass) taken at \sqrt{s} values of 4.23, 4.26, 4.36, 4.42, and 4.60 GeV to simulated events including both $\psi(2S) \rightarrow \chi_{c1} \gamma$ and $\psi_2(3823) \rightarrow \chi_{c1} \gamma$ together, with floating mass scale offset for $\psi(2S)$, $\psi_2(3823)$ mass floating (fixed to that above), and zero $\psi_2(3823)$ width.

 $\psi_2(3823)$ REFERENCES

ABLIKIM	15S	PRL 115 011803	M. Ablikim <i>et al.</i>	(BESIII Collab.)
BHARDWAJ	13	PRL 111 032001	V. Bhardwaj <i>et al.</i>	(BELLE Collab.)

 $\psi_3(3842)$

$$I^G(J^{PC}) = 0^-(3^{--})$$

J, P need confirmation.

J^P has not been measured, 3^- is the quark model prediction.

 $\psi_3(3842)$ MASS

VALUE (MeV)	DOCUMENT ID	TECN	COMMENT
3842.71 ± 0.16 ± 0.12	AAIJ	19M LHCb	$p p \rightarrow D \bar{D} + \text{anything}$

 $\psi_3(3842)$ WIDTH

VALUE (MeV)	DOCUMENT ID	TECN	COMMENT
2.79 ± 0.51 ± 0.35	AAIJ	19M LHCb	$p p \rightarrow D \bar{D} + \text{anything}$

 $\psi_3(3842)$ DECAY MODES

Mode	Fraction (Γ_i/Γ)
$\Gamma_1 \quad D^+ D^-$	seen
$\Gamma_2 \quad D^0 \bar{D}^0$	seen

See key on page 999

Meson Particle Listings

$\psi_3(3842)$, $\chi_{c0}(3860)$, $\chi_{c1}(3872)$

$\psi_3(3842)$ BRANCHING RATIOS

$\Gamma(D^+ D^-)/\Gamma_{total}$				Γ_1/Γ
VALUE	DOCUMENT ID	TECN	COMMENT	
seen	AAIJ	19M LHCb	$pp \rightarrow D\bar{D} + \text{anything}$	

$\Gamma(D^0 \bar{D}^0)/\Gamma_{total}$				Γ_2/Γ
VALUE	DOCUMENT ID	TECN	COMMENT	
seen	AAIJ	19M LHCb	$pp \rightarrow D\bar{D} + \text{anything}$	

$\psi_3(3842)$ REFERENCES

AAIJ 19M JHEP 1907 035 R. Aaij et al. (LHCb Collab.)

$\chi_{c0}(3860) \quad I^G(J^{PC}) = 0^+(0^{++})$

OMITTED FROM SUMMARY TABLE

The assignment $J^P = 0^+$ is preferred over 2^+ by 2.5 sigma.

Observed by CHILIKIN 17 using full amplitude analysis of the process $e^+ e^- \rightarrow J/\psi D\bar{D}$, where $D = D^0, D^+$.

$\chi_{c0}(3860)$ MASS

VALUE (MeV)	DOCUMENT ID	TECN	COMMENT
3862^{+26+40}_{-32-13}	CHILIKIN	17 BELL	$e^+ e^- \rightarrow J/\psi D\bar{D}$

$\chi_{c0}(3860)$ WIDTH

VALUE (MeV)	DOCUMENT ID	TECN	COMMENT
$201^{+154+88}_{-67-82}$	CHILIKIN	17 BELL	$e^+ e^- \rightarrow J/\psi D\bar{D}$

$\chi_{c0}(3860)$ DECAY MODES

Mode	Fraction (Γ_i/Γ)
$\Gamma_1 \quad D^0 \bar{D}^0$	seen
$\Gamma_2 \quad D^+ D^-$	seen

$\chi_{c0}(3860)$ BRANCHING RATIOS

$\Gamma(D^0 \bar{D}^0)/\Gamma_{total}$				Γ_1/Γ
VALUE	DOCUMENT ID	TECN	COMMENT	
seen	CHILIKIN	17 BELL	$e^+ e^- \rightarrow J/\psi D^0 \bar{D}^0$	

$\Gamma(D^+ D^-)/\Gamma_{total}$				Γ_2/Γ
VALUE	DOCUMENT ID	TECN	COMMENT	
seen	CHILIKIN	17 BELL	$e^+ e^- \rightarrow J/\psi D^+ D^-$	

$\chi_{c0}(3860)$ REFERENCES

CHILIKIN 17 PR D95 112003 K. Chilikin et al. (BELLE Collab.) JPC

$\chi_{c1}(3872) \quad I^G(J^{PC}) = 0^+(1^{++})$

also known as $X(3872)$

This state shows properties different from a conventional $q\bar{q}$ state. A candidate for an exotic structure. See the review on non- $q\bar{q}$ states.

First observed by CHOI 03 in $B \rightarrow K\pi^+\pi^- J/\psi(1S)$ decays as a narrow peak in the invariant mass distribution of the $\pi^+\pi^- J/\psi(1S)$ final state. Isovector hypothesis excluded by AUBERT 05B and CHOI 11.

AAIJ 13Q perform a full five-dimensional amplitude analysis of the angular correlations between the decay products in $B^+ \rightarrow \chi_{c1}(3872) K^+$ decays, where $\chi_{c1}(3872) \rightarrow J/\psi\pi^+\pi^-$ and $J/\psi \rightarrow \mu^+\mu^-$, which unambiguously gives the $J^{PC} = 1^{++}$ assignment under the assumption that the $\pi^+\pi^-$ and J/ψ are in an S-wave. AAJ 15AO extend this analysis with more data to limit D-wave contributions to < 4% at 95% CL.

See the review on "Spectroscopy of Mesons Containing Two Heavy Quarks."

$\chi_{c1}(3872)$ MASS FROM $J/\psi X$ MODE

VALUE (MeV)	EVTS	DOCUMENT ID	TECN	COMMENT
3871.69 ± 0.17	OUR AVERAGE			
$3871.9 \pm 0.7 \pm 0.2$	20 ± 5	ABLIKIM 14	BES3	$e^+ e^- \rightarrow J/\psi\pi^+\pi^-\gamma$
$3871.95 \pm 0.48 \pm 0.12$	$0.6k$	AAIJ 12H	LHCb	$pp \rightarrow J/\psi\pi^+\pi^- X$
$3871.85 \pm 0.27 \pm 0.19$	~ 170	¹ CHOI 11	BELL	$B \rightarrow K\pi^+\pi^- J/\psi$
$3873^{+1.8}_{-1.6} \pm 1.3$	27 ± 8	² DEL-AMO-SA.10B	BABR	$B \rightarrow \omega J/\psi K$
$3871.61 \pm 0.16 \pm 0.19$	$6k$	^{2,3} AALTONEN 09AU	CDF2	$p\bar{p} \rightarrow J/\psi\pi^+\pi^- X$
$3871.4 \pm 0.6 \pm 0.1$	93.4	AUBERT 08Y	BABR	$B^+ \rightarrow K^+ J/\psi\pi^+\pi^-$
$3868.7 \pm 1.5 \pm 0.4$	9.4	AUBERT 08Y	BABR	$B^0 \rightarrow K_S^0 J/\psi\pi^+\pi^-$
$3871.8 \pm 3.1 \pm 3.0$	522	^{2,4} ABAZOV 04F	D0	$p\bar{p} \rightarrow J/\psi\pi^+\pi^- X$
• • • We do not use the following data for averages, fits, limits, etc. • • •				
$3873.3 \pm 1.1 \pm 1.0$	45	⁵ ABLIKIM 19V	BES	$e^+ e^- \rightarrow \gamma\omega J/\psi$
3860.0 ± 10.4	13.6	^{2,6} AGHASYAN 18A	COMP	$\gamma^* N \rightarrow X\pi^\pm N'$
$3868.6 \pm 1.2 \pm 0.2$	8	⁷ AUBERT 06	BABR	$B^0 \rightarrow K_S^0 J/\psi\pi^+\pi^-$
$3871.3 \pm 0.6 \pm 0.1$	61	⁷ AUBERT 06	BABR	$B^- \rightarrow K^- J/\psi\pi^+\pi^-$
3873.4 ± 1.4	25	⁸ AUBERT 05R	BABR	$B^+ \rightarrow K^+ J/\psi\pi^+\pi^-$
$3871.3 \pm 0.7 \pm 0.4$	730	^{2,9} ACOSTA 04	CDF2	$p\bar{p} \rightarrow J/\psi\pi^+\pi^- X$
$3872.0 \pm 0.6 \pm 0.5$	36	¹⁰ CHOI 03	BELL	$B \rightarrow K\pi^+\pi^- J/\psi$
3836 ± 13	58	^{2,11} ANTONIAZZI 94	E705	$300 \pi^\pm Li \rightarrow J/\psi\pi^+\pi^- X$

- The mass difference for the $\chi_{c1}(3872)$ produced in B^+ and B^0 decays is $(-0.71 \pm 0.96 \pm 0.19)$ MeV.
- Width consistent with detector resolution.
- A possible equal mixture of two states with a mass difference greater than 3.6 MeV/c² is excluded at 95% CL.
- Calculated from the corresponding $m_{\chi_{c1}(3872)} - m_{J/\psi}$ using $m_{J/\psi} = 3096.916$ MeV.
- Fit with fixed width and including two resonances, X(3915) and X(3960).
- Could be a different state.
- Calculated from the corresponding $m_{\chi_{c1}(3872)} - m_{\psi(2S)}$ using $m_{\psi(2S)} = 3686.093$ MeV. Superseded by AUBERT 08Y.
- Calculated from the corresponding $m_{\chi_{c1}(3872)} - m_{\psi(2S)}$ using $m_{\psi(2S)} = 3685.96$ MeV. Superseded by AUBERT 06.
- Superseded by AALTONEN 09AU.
- Superseded by CHOI 11.
- A lower mass value can be due to an incorrect momentum scale for soft pions.

$\chi_{c1}(3872)$ MASS FROM $\bar{D}^{*0} D^0$ MODE

VALUE (MeV)	EVTS	DOCUMENT ID	TECN	COMMENT
$3872.9^{+0.6+0.4}_{-0.4-0.5}$	50	^{1,2} AUSHEV 10	BELL	$B \rightarrow \bar{D}^{*0} D^0 K$
$3875.1^{+0.7}_{-0.5} \pm 0.5$	33 ± 6	² AUBERT 08B	BABR	$B \rightarrow \bar{D}^{*0} D^0 K$
$3875.2 \pm 0.7^{+0.9}_{-1.8}$	24 ± 6	^{2,3} GOKHROO 06	BELL	$B \rightarrow D^0 \bar{D}^0 \pi^0 K$

- Calculated from the measured $m_{\chi_{c1}(3872)} - m_{D^{*0}} - m_{D^0} = 1.1^{+0.6+0.1}_{-0.4-0.3}$ MeV.
- Experiments report $D^{*0} \bar{D}^0$ invariant mass above $D^{*0} \bar{D}^0$ threshold because D^{*0} decay products are kinematically constrained to the D^{*0} mass, even though the D^{*0} may decay off-shell.
- Superseded by AUSHEV 10.

$m_{\chi_{c1}(3872)} - m_{J/\psi}$

VALUE (MeV)	EVTS	DOCUMENT ID	TECN	COMMENT
$774.9 \pm 3.1 \pm 3.0$	522	ABAZOV 04F	D0	$p\bar{p} \rightarrow J/\psi\pi^+\pi^- X$

$m_{\chi_{c1}(3872)} - m_{\psi(2S)}$

VALUE (MeV)	EVTS	DOCUMENT ID	TECN	COMMENT
187.4 ± 1.4	25	¹ AUBERT 05R	BABR	$B^+ \rightarrow K^+ J/\psi\pi^+\pi^-$

¹ Superseded by AUBERT 06.

$\chi_{c1}(3872)$ WIDTH

VALUE (MeV)	CL%	EVTS	DOCUMENT ID	TECN	COMMENT
<1.2	90		CHOI 11	BELL	$B \rightarrow K\pi^+\pi^- J/\psi$
• • • We do not use the following data for averages, fits, limits, etc. • • •					
<2.4	90		ABLIKIM 14	BES3	$e^+ e^- \rightarrow J/\psi\pi^+\pi^- \gamma$
<3.3	90		AUBERT 08Y	BABR	$B^+ \rightarrow K^+ J/\psi\pi^+\pi^-$
<4.1	90	69	AUBERT 06	BABR	$B \rightarrow K\pi^+\pi^- J/\psi$
<2.3	90	36	¹ CHOI 03	BELL	$B \rightarrow K\pi^+\pi^- J/\psi$

- Superseded by CHOI 11.

Meson Particle Listings

$\chi_{c1}(3872)$

$\chi_{c1}(3872)$ WIDTH FROM $\bar{D}^{*0} D^0$ MODE

VALUE (MeV)	EVTS	DOCUMENT ID	TECN	COMMENT
$3.9^{+2.8+0.2}_{-1.4-1.1}$	50	¹ AUSHEV	10	BELL $B \rightarrow \bar{D}^{*0} D^0 K$
$3.0^{+1.9}_{-1.4} \pm 0.9$	33 ± 6	AUBERT	08B	BABR $B \rightarrow \bar{D}^{*0} D^0 K$

¹With a measured value of $B(B \rightarrow \chi_{c1}(3872) K) \times B(\chi_{c1}(3872) \rightarrow D^{*0} \bar{D}^0) = (0.80 \pm 0.20 \pm 0.10) \times 10^{-4}$, assumed to be equal for both charged and neutral modes.

$\chi_{c1}(3872)$ DECAY MODES

Mode	Fraction (Γ_i/Γ)
Γ_1 $e^+ e^-$	
Γ_2 $\pi^+ \pi^- J/\psi(1S)$	$> 3.2\%$
Γ_3 $\rho^0 J/\psi(1S)$	
Γ_4 $\omega J/\psi(1S)$	$> 2.3\%$
Γ_5 $D^0 \bar{D}^0 \pi^0$	$> 40\%$
Γ_6 $\bar{D}^{*0} D^0$	$> 30\%$
Γ_7 $\gamma \gamma$	
Γ_8 $D^0 \bar{D}^0$	
Γ_9 $D^+ D^-$	
Γ_{10} $\gamma \chi_{c1}$	
Γ_{11} $\gamma \chi_{c2}$	
Γ_{12} $\pi^0 \chi_{c2}$	
Γ_{13} $\pi^0 \chi_{c1}$	$> 2.8\%$
Γ_{14} $\pi^0 \chi_{c0}$	
Γ_{15} $\gamma J/\psi$	$> 7 \times 10^{-3}$
Γ_{16} $\gamma \psi(2S)$	$> 4\%$
Γ_{17} $\pi^+ \pi^- \eta_c(1S)$	not seen
Γ_{18} $\pi^+ \pi^- \chi_{c1}$	not seen
Γ_{19} $p \bar{p}$	not seen
Γ_{20} $\eta J/\psi$	

C-violating decays

$\chi_{c1}(3872)$ PARTIAL WIDTHS

$\Gamma(e^+ e^-)$					Γ_1
VALUE (eV)	CL%	DOCUMENT ID	TECN	COMMENT	
< 4.3	90	¹ ABLIKIM	15V	BES3	$4.0-4.4 e^+ e^- \rightarrow \pi^+ \pi^- J/\psi$
< 280	90	² YUAN	04	RVUE	$e^+ e^- \rightarrow \pi^+ \pi^- J/\psi$

¹ABLIKIM 15V reports this limit from the measurement of $\Gamma(\chi_{c1}(3872) \rightarrow \pi^+ \pi^- J/\psi(1S)) \times \Gamma(\chi_{c1}(3872) \rightarrow e^+ e^-) / \Gamma < 0.13$ eV using $\Gamma(\chi_{c1}(3872) \rightarrow \pi^+ \pi^- J/\psi(1S)) / \Gamma = 3\%$.

²Using BAI 98E data on $e^+ e^- \rightarrow \pi^+ \pi^- \ell^+ \ell^-$. Assuming that $\Gamma(\pi^+ \pi^- J/\psi)$ of $\chi_{c1}(3872)$ is the same as that of $\psi(2S)$ (85.4 keV).

$\chi_{c1}(3872)$ $\Gamma(i)\Gamma(e^+ e^-) / \Gamma(\text{total})$

$\Gamma(\pi^+ \pi^- J/\psi(1S)) \times \Gamma(e^+ e^-) / \Gamma(\text{total})$					$\Gamma_2 \Gamma_1 / \Gamma$
VALUE (eV)	CL%	DOCUMENT ID	TECN	COMMENT	
< 0.13	90	ABLIKIM	15V	BES3	$4.0-4.4 e^+ e^- \rightarrow \pi^+ \pi^- J/\psi$
< 6.2	90	^{1,2} AUBERT	05D	BABR	$10.6 e^+ e^- \rightarrow K^+ K^- \pi^+ \pi^- \gamma$
< 8.3	90	² DOBBS	05	CLE3	$e^+ e^- \rightarrow \pi^+ \pi^- J/\psi$
< 10	90	³ YUAN	04	RVUE	$e^+ e^- \rightarrow \pi^+ \pi^- J/\psi$

¹Using $B(\chi_{c1}(3872) \rightarrow J/\psi \pi^+ \pi^-) \cdot B(J/\psi \rightarrow \mu^+ \mu^-) \cdot \Gamma(\chi_{c1}(3872) \rightarrow e^+ e^-) < 0.37$ eV from AUBERT 05D and $B(J/\psi \rightarrow \mu^+ \mu^-) = 0.0588 \pm 0.0010$ from the PDG 04.

²Assuming $\chi_{c1}(3872)$ has $J^{PC} = 1^{--}$.

³Using BAI 98E data on $e^+ e^- \rightarrow \pi^+ \pi^- \ell^+ \ell^-$. From theoretical calculation of the production cross section and using $B(J/\psi \rightarrow \mu^+ \mu^-) = (5.88 \pm 0.10)\%$.

$\chi_{c1}(3872)$ $\Gamma(i)\Gamma(\gamma\gamma) / \Gamma(\text{total})$

$\Gamma(\pi^+ \pi^- J/\psi(1S)) \times \Gamma(\gamma\gamma) / \Gamma(\text{total})$					$\Gamma_2 \Gamma_7 / \Gamma$
VALUE (eV)	CL%	DOCUMENT ID	TECN	COMMENT	
< 12.9	90	¹ DOBBS	05	CLE3	$e^+ e^- \rightarrow \pi^+ \pi^- J/\psi \gamma$

¹Assuming $\chi_{c1}(3872)$ has positive C parity and spin 0.

$\Gamma(\omega J/\psi(1S)) \times \Gamma(\gamma\gamma) / \Gamma(\text{total})$					$\Gamma_4 \Gamma_7 / \Gamma$
VALUE (eV)	CL%	DOCUMENT ID	TECN	COMMENT	
< 1.7	90	¹ LEES	12AD	BABR	$e^+ e^- \rightarrow e^+ e^- \omega J/\psi$

¹Assuming $\chi_{c1}(3872)$ has spin 2.

$\Gamma(\pi^+ \pi^- \eta_c(1S)) \times \Gamma(\gamma\gamma) / \Gamma(\text{total})$					$\Gamma_{17} \Gamma_7 / \Gamma$
VALUE (eV)	CL%	DOCUMENT ID	TECN	COMMENT	
< 11.1	90	LEES	12AE	BABR	$e^+ e^- \rightarrow e^+ e^- \pi^+ \pi^- \eta_c$

$\chi_{c1}(3872)$ BRANCHING RATIOS

$\Gamma(\pi^+ \pi^- J/\psi(1S)) / \Gamma(\text{total})$					Γ_2 / Γ
VALUE	EVTS	DOCUMENT ID	TECN	COMMENT	
> 0.032	93 ± 17	¹ AUBERT	08Y	BABR	$B \rightarrow \chi_{c1}(3872) K$
seen	151	² BALA	15	BELL	$B \rightarrow \chi_{c1}(3872) K \pi$
> 0.05	30	³ AUBERT	05R	BABR	$B^+ \rightarrow K^+ \pi^+ \pi^- J/\psi$
> 0.05	36 ± 7	⁴ CHOI	03	BELL	$B^+ \rightarrow K^+ \pi^+ \pi^- J/\psi$

¹AUBERT 08Y reports $[\Gamma(\chi_{c1}(3872) \rightarrow \pi^+ \pi^- J/\psi(1S)) / \Gamma(\text{total})] \times [B(B^+ \rightarrow \chi_{c1}(3872) K^+)] = (8.4 \pm 1.5 \pm 0.7) \times 10^{-6}$ which we divide by our best value $B(B^+ \rightarrow \chi_{c1}(3872) K^+) < 2.6 \times 10^{-4}$.

²BALA 15 reports $B(\chi_{c1}(3872) \rightarrow \pi^+ \pi^- J/\psi) \times B(B^0 \rightarrow \chi_{c1}(3872) K^+ \pi^-) = (7.9 \pm 1.3 \pm 0.4) \times 10^{-6}$ and $B(\chi_{c1}(3872) \rightarrow \pi^+ \pi^- J/\psi) \times B(B^+ \rightarrow \chi_{c1}(3872) K^0 \pi^+) = (10.6 \pm 3.0 \pm 0.9) \times 10^{-6}$.

³Superseded by AUBERT 08Y. AUBERT 05R reports $[\Gamma(\chi_{c1}(3872) \rightarrow \pi^+ \pi^- J/\psi(1S)) / \Gamma(\text{total})] \times [B(B^+ \rightarrow \chi_{c1}(3872) K^+)] = (1.28 \pm 0.41) \times 10^{-5}$ which we divide by our best value $B(B^+ \rightarrow \chi_{c1}(3872) K^+) < 2.6 \times 10^{-4}$.

⁴CHOI 03 reports $[\Gamma(\chi_{c1}(3872) \rightarrow \pi^+ \pi^- J/\psi(1S)) / \Gamma(\text{total})] \times [B(B^+ \rightarrow \chi_{c1}(3872) K^+) / [B(B^+ \rightarrow \psi(2S) K^+) / [B(\psi(2S) \rightarrow J/\psi(1S) \pi^+ \pi^-)]] = 0.063 \pm 0.012 \pm 0.007$ which we multiply or divide by our best values $B(B^+ \rightarrow \chi_{c1}(3872) K^+) < 2.6 \times 10^{-4}$, $B(B^+ \rightarrow \psi(2S) K^+) = (6.19 \pm 0.22) \times 10^{-4}$, $B(\psi(2S) \rightarrow J/\psi(1S) \pi^+ \pi^-) = (34.68 \pm 0.30) \times 10^{-2}$.

$\Gamma(\omega J/\psi(1S)) / \Gamma(\text{total})$					Γ_4 / Γ
VALUE	EVTS	DOCUMENT ID	TECN	COMMENT	
> 0.023	21 ± 7	¹ DEL-AMO-SA...	10B	BABR	$B^+ \rightarrow \omega J/\psi K^+$

¹DEL-AMO-SANCHEZ 10B reports $[\Gamma(\chi_{c1}(3872) \rightarrow \omega J/\psi(1S)) / \Gamma(\text{total})] \times [B(B^+ \rightarrow \chi_{c1}(3872) K^+)] = (6 \pm 2 \pm 1) \times 10^{-6}$ which we divide by our best value $B(B^+ \rightarrow \chi_{c1}(3872) K^+) < 2.6 \times 10^{-4}$. DEL-AMO-SANCHEZ 10B also reports $B(B^0 \rightarrow \chi_{c1}(3872) K^0) \times B(\chi_{c1}(3872) \rightarrow J/\psi \omega) = (6 \pm 3 \pm 1) \times 10^{-6}$.

$\Gamma(\omega J/\psi(1S)) / \Gamma(\pi^+ \pi^- J/\psi(1S))$					Γ_4 / Γ_2
VALUE	DOCUMENT ID	TECN	COMMENT		
1.1 ± 0.4 OUR AVERAGE	Error includes scale factor of 1.7.				
$1.6^{+0.4}_{-0.3} \pm 0.2$	¹ ABLIKIM	19V	BES	$e^+ e^- \rightarrow \gamma \omega J/\psi$	
0.8 ± 0.3	² DEL-AMO-SA...	10B	BABR	$B \rightarrow \omega J/\psi K$	

¹Fit with fixed width and including two resonances, X(3915) and X(3960).

²Statistical and systematic errors added in quadrature. Uses the values of $B(B \rightarrow \chi_{c1}(3872) K) \times B(\chi_{c1}(3872) \rightarrow J/\psi \pi^+ \pi^-)$ reported in AUBERT 08Y, taking into account the common systematics.

$\Gamma(D^0 \bar{D}^0 \pi^0) / \Gamma(\text{total})$					Γ_5 / Γ
VALUE	EVTS	DOCUMENT ID	TECN	COMMENT	
> 0.4	17 ± 5	¹ GOKHROO	06	BELL	$B^+ \rightarrow D^0 \bar{D}^0 \pi^0 K^+$

¹GOKHROO 06 reports $[\Gamma(\chi_{c1}(3872) \rightarrow D^0 \bar{D}^0 \pi^0) / \Gamma(\text{total})] \times [B(B^+ \rightarrow \chi_{c1}(3872) K^+)] = (1.02 \pm 0.31^{+0.21}_{-0.29}) \times 10^{-4}$ which we divide by our best value $B(B^+ \rightarrow \chi_{c1}(3872) K^+) < 2.6 \times 10^{-4}$.

$\Gamma(D^0 \bar{D}^0 \pi^0) / \Gamma(\pi^+ \pi^- J/\psi(1S))$					Γ_5 / Γ_2
VALUE	DOCUMENT ID	TECN	COMMENT		
seen	¹ GOKHROO	06	BELL	$B \rightarrow D^0 \bar{D}^0 \pi^0 K$	
seen	AUSHEV	10	BELL	$B \rightarrow D^0 \bar{D}^0 \pi^0 K$	

¹May not necessarily be the same state as that observed in the $J/\psi \pi^+ \pi^-$ mode. Supersedes CHISTOV 04.

$\Gamma(\bar{D}^{*0} D^0) / \Gamma(\text{total})$					Γ_6 / Γ
VALUE	EVTS	DOCUMENT ID	TECN	COMMENT	
> 0.30	$41 \pm \frac{9}{8}$	¹ AUSHEV	10	BELL	$B^+ \rightarrow D^{*0} \bar{D}^0 K^+$
> 0.6	27 ± 6	² AUBERT	08B	BABR	$B^+ \rightarrow \bar{D}^{*0} D^0 K^+$

¹AUSHEV 10 reports $[\Gamma(\chi_{c1}(3872) \rightarrow \bar{D}^{*0} D^0) / \Gamma(\text{total})] \times [B(B^+ \rightarrow \chi_{c1}(3872) K^+)] = (0.77 \pm 0.16 \pm 0.10) \times 10^{-4}$ which we divide by our best value $B(B^+ \rightarrow \chi_{c1}(3872) K^+) < 2.6 \times 10^{-4}$.

²AUBERT 08B reports $[\Gamma(\chi_{c1}(3872) \rightarrow \bar{D}^{*0} D^0) / \Gamma(\text{total})] \times [B(B^+ \rightarrow \chi_{c1}(3872) K^+)] = (1.67 \pm 0.36 \pm 0.47) \times 10^{-4}$ which we divide by our best value $B(B^+ \rightarrow \chi_{c1}(3872) K^+) < 2.6 \times 10^{-4}$.

$\Gamma(D^0 \bar{D}^0) / \Gamma(\pi^+ \pi^- J/\psi(1S))$					Γ_8 / Γ_2
VALUE	DOCUMENT ID	TECN	COMMENT		
not seen	CHISTOV	04	BELL	$B \rightarrow K D^0 \bar{D}^0$	

$\Gamma(D^+ D^-)/\Gamma(\pi^+ \pi^- J/\psi(1S))$ Γ_9/Γ_2

VALUE	DOCUMENT ID	TECN	COMMENT
not seen	CHISTOV 04	BELL	$B \rightarrow K D^+ D^-$

$\Gamma(\gamma \chi_{c1})/\Gamma(\pi^+ \pi^- J/\psi(1S))$ Γ_{10}/Γ_2

VALUE	CL%	DOCUMENT ID	TECN	COMMENT
not seen		¹ BHARDWAJ 13	BELL	$B^+ \rightarrow \chi_{c1} \gamma K^+$
<0.89	90	CHOI 03	BELL	$B \rightarrow K \pi^+ \pi^- J/\psi$

¹ Reported $B(B^\pm \rightarrow \chi_{c1}(3872) K^\pm) \times B(\chi_{c1}(3872) \rightarrow \gamma \chi_{c1}) < 1.9 \times 10^{-6}$ at 90% CL.

$\Gamma(\gamma \chi_{c2})/\Gamma(\pi^+ \pi^- J/\psi(1S))$ Γ_{11}/Γ_2

VALUE	DOCUMENT ID	TECN	COMMENT
not seen	¹ BHARDWAJ 13	BELL	$B^\pm \rightarrow \chi_{c2} \gamma K^\pm$

¹ Reported $B(B^\pm \rightarrow \chi_{c1}(3872) K^\pm) \times B(\chi_{c1}(3872) \rightarrow \gamma \chi_{c2}) < 6.7 \times 10^{-6}$ at 90% CL.

$\Gamma(\gamma J/\psi)/\Gamma_{total}$ Γ_{15}/Γ

VALUE	EVTS	DOCUMENT ID	TECN	COMMENT
>7	$\times 10^{-3}$	¹ BHARDWAJ 11	BELL	$B^\pm \rightarrow \gamma J/\psi K^\pm$

••• We do not use the following data for averages, fits, limits, etc. •••

VALUE	EVTS	DOCUMENT ID	TECN	COMMENT
>0.011	20	² AUBERT 09B	BABR	$B^+ \rightarrow \gamma J/\psi K^+$
>0.013	19	³ AUBERT, BE 06M	BABR	$B^+ \rightarrow \gamma J/\psi K^+$

¹ BHARDWAJ 11 reports $[\Gamma(\chi_{c1}(3872) \rightarrow \gamma J/\psi)/\Gamma_{total}] \times [B(B^+ \rightarrow \chi_{c1}(3872) K^+)] = (1.78^{+0.48}_{-0.44} \pm 0.12) \times 10^{-6}$ which we divide by our best value $B(B^+ \rightarrow \chi_{c1}(3872) K^+) < 2.6 \times 10^{-4}$.

² AUBERT 09B reports $[\Gamma(\chi_{c1}(3872) \rightarrow \gamma J/\psi)/\Gamma_{total}] \times [B(B^+ \rightarrow \chi_{c1}(3872) K^+)] = (2.8 \pm 0.8 \pm 0.1) \times 10^{-6}$ which we divide by our best value $B(B^+ \rightarrow \chi_{c1}(3872) K^+) < 2.6 \times 10^{-4}$.

³ Superseded by AUBERT 09B. AUBERT, BE 06M reports $[\Gamma(\chi_{c1}(3872) \rightarrow \gamma J/\psi)/\Gamma_{total}] \times [B(B^+ \rightarrow \chi_{c1}(3872) K^+)] = (3.3 \pm 1.0 \pm 0.3) \times 10^{-6}$ which we divide by our best value $B(B^+ \rightarrow \chi_{c1}(3872) K^+) < 2.6 \times 10^{-4}$.

$\Gamma(\gamma \psi(2S))/\Gamma_{total}$ Γ_{16}/Γ

VALUE	EVTS	DOCUMENT ID	TECN	COMMENT
seen	36 ± 9	¹ AAIJ 14AH	LHCB	$B^+ \rightarrow \gamma \psi(2S) K^+$
>0.04	25 ± 7	² AUBERT 09B	BABR	$B^+ \rightarrow \gamma \psi(2S) K^+$

••• We do not use the following data for averages, fits, limits, etc. •••

VALUE	EVTS	DOCUMENT ID	TECN	COMMENT
not seen		³ BHARDWAJ 11	BELL	$B^+ \rightarrow \gamma \psi(2S) K^+$

¹ From 36.4 ± 9.0 events of $\chi_{c1}(3872) \rightarrow J/\psi \gamma$ decays with a statistical significance of 4.4σ.

² AUBERT 09B reports $[\Gamma(\chi_{c1}(3872) \rightarrow \gamma \psi(2S))/\Gamma_{total}] \times [B(B^+ \rightarrow \chi_{c1}(3872) K^+)] = (9.5 \pm 2.7 \pm 0.6) \times 10^{-6}$ which we divide by our best value $B(B^+ \rightarrow \chi_{c1}(3872) K^+) < 2.6 \times 10^{-4}$.

³ BHARDWAJ 11 reports $B(B^+ \rightarrow K^+ \chi_{c1}(3872)) \times B(\chi_{c1} \rightarrow \gamma \psi(2S)) < 3.45 \times 10^{-6}$ at 90% CL.

$\Gamma(\gamma \psi(2S))/\Gamma(\gamma J/\psi)$ Γ_{16}/Γ_{15}

VALUE	CL%	EVTS	DOCUMENT ID	TECN	COMMENT
2.6 ± 0.6					OUR AVERAGE
2.46 ± 0.64 ± 0.29		36 ± 9	¹ AAIJ 14AH	LHCB	$B^+ \rightarrow \gamma \psi(2S) K^+$
3.4 ± 1.4			AUBERT 09B	BABR	$B^+ \rightarrow \gamma c \bar{c} K'$

••• We do not use the following data for averages, fits, limits, etc. •••

VALUE	CL%	DOCUMENT ID	TECN	COMMENT
<2.1	90	BHARDWAJ 11	BELL	$B^+ \rightarrow \gamma \psi(2S) K^+$

¹ From 36.4 ± 9.0 events of $\chi_{c1}(3872) \rightarrow J/\psi \gamma$ decays with a statistical significance of 4.4σ.

$\Gamma(\pi^+ \pi^- \chi_{c1})/\Gamma_{total}$ Γ_{18}/Γ

VALUE	DOCUMENT ID	TECN	COMMENT
not seen	¹ BHARDWAJ 16	BELL	$B^+ \rightarrow \pi^+ \pi^- \chi_{c1} K^+$

¹ BHARDWAJ 16 quotes $B(B^+ \rightarrow \chi_{c1}(3872) K^+) \cdot B(\chi_{c1}(3872) \rightarrow \pi^+ \pi^- \chi_{c1}) < 1.5 \times 10^{-6}$ at 90% CL.

$\Gamma(p\bar{p})/\Gamma_{total}$ Γ_{19}/Γ

VALUE	DOCUMENT ID	TECN	COMMENT
not seen	¹ AAIJ 17AD	LHCB	$p p \rightarrow B^+ X \rightarrow p \bar{p} K^+ X$

¹ AAIJ 17AD reports $B(B^+ \rightarrow \chi_{c1}(3872) K^+) \cdot B(\chi_{c1}(3872) \rightarrow p \bar{p} K^+) < 2.0 (2.5) \times 10^{-3}$ at 90% (95%) CL.

$\Gamma(p\bar{p})/\Gamma(\pi^+ \pi^- J/\psi(1S))$ Γ_{19}/Γ_2

VALUE	CL%	DOCUMENT ID	TECN	COMMENT
<2.0 × 10⁻³	95	¹ AAIJ 13S	LHCB	$B^+ \rightarrow p \bar{p} K^+$

¹ AAIJ 13S reports $[\Gamma(\chi_{c1}(3872) \rightarrow p \bar{p})/\Gamma(\chi_{c1}(3872) \rightarrow \pi^+ \pi^- J/\psi(1S))] \times [B(B^+ \rightarrow \chi_{c1}(3872) K^+), \chi_{c1} \rightarrow J/\psi \pi^+ \pi^-] < 1.7 \times 10^{-8}$ which we divide by our best value $B(B^+ \rightarrow \chi_{c1}(3872) K^+), \chi_{c1} \rightarrow J/\psi \pi^+ \pi^- = 8.6 \times 10^{-6}$.

$\Gamma(\pi^0 \chi_{c0})/\Gamma(\pi^+ \pi^- J/\psi(1S))$ Γ_{14}/Γ_2

VALUE	CL%	DOCUMENT ID	TECN	COMMENT
<19	90	ABLIKIM 19U	BES3	$e^+ e^- \rightarrow \gamma \chi_{c1}(3872)$

$\Gamma(\pi^0 \chi_{c1})/\Gamma(\pi^+ \pi^- J/\psi(1S))$ Γ_{13}/Γ_2

VALUE (units 10 ⁻²)	CL%	EVTS	DOCUMENT ID	TECN	COMMENT
88 ± 33 ± 10		10.8	ABLIKIM 19U	BES3	$e^+ e^- \rightarrow \gamma \chi_{c1}(3872)$

••• We do not use the following data for averages, fits, limits, etc. •••

VALUE	CL%	DOCUMENT ID	TECN	COMMENT
<97	90	¹ BHARDWAJ 19	BELL	$B^\pm \rightarrow \chi_{c1} \pi^0 K^\pm$

¹ BHARDWAJ 19 reports $B(B^\pm \rightarrow \chi_{c1}(3872) K^\pm) \times B(\chi_{c1}(3872) \rightarrow \pi^0 \chi_{c1}) < 8.1 \times 10^{-6}$ at 90% CL which was divided by $B(B^\pm \rightarrow \chi_{c1}(3872) K^\pm) \times B(\chi_{c1}(3872) \rightarrow J/\psi \pi^+ \pi^-) = (8.63 \pm 0.97) \times 10^{-6}$ from CHOI 11.

$\Gamma(\pi^0 \chi_{c2})/\Gamma(\pi^+ \pi^- J/\psi(1S))$ Γ_{12}/Γ_2

VALUE	CL%	DOCUMENT ID	TECN	COMMENT
<1.1	90	ABLIKIM 19U	BES3	$e^+ e^- \rightarrow \gamma \chi_{c1}(3872)$

C-violating decays

$\Gamma(\eta J/\psi)/\Gamma(\pi^+ \pi^- J/\psi(1S))$ Γ_{20}/Γ_2

VALUE	CL%	DOCUMENT ID	TECN	COMMENT
<0.4	90	^{1,2} IWASHITA 14	BELL	$B \rightarrow K \eta J/\psi$

••• We do not use the following data for averages, fits, limits, etc. •••

VALUE	CL%	DOCUMENT ID	TECN	COMMENT
<0.6	90	AUBERT 04Y	BABR	$B \rightarrow K \eta J/\psi$

¹ IWASHITA 14 reports $[\Gamma(\chi_{c1}(3872) \rightarrow \eta J/\psi)/\Gamma(\chi_{c1}(3872) \rightarrow \pi^+ \pi^- J/\psi(1S))] \times [B(B^+ \rightarrow \chi_{c1}(3872) K^+), \chi_{c1} \rightarrow J/\psi \pi^+ \pi^-] < 3.8 \times 10^{-6}$ which we divide by our best value $B(B^+ \rightarrow \chi_{c1}(3872) K^+), \chi_{c1} \rightarrow J/\psi \pi^+ \pi^- = 8.6 \times 10^{-6}$.

² IWASHITA 14 also scans the $\eta J/\psi$ mass range 3.8–4.75 GeV and sets upper limits for $B(B^\pm \rightarrow \chi_{c1}(3872) K^\pm) \times B(\chi_{c1}(3872) \rightarrow \eta J/\psi)$ in 5 MeV intervals.

$\chi_{c1}(3872)$ REFERENCES

ABLIKIM 19U	PRL 122 202001	M. Ablikim <i>et al.</i>	(BESIII Collab.)
ABLIKIM 19V	PRL 122 232002	M. Ablikim <i>et al.</i>	(BESIII Collab.)
BHARDWAJ 19A	PR D 99 111101	V. Bhardwaj <i>et al.</i>	(BELLE Collab.)
AGHASYAN 18A	PL B783 334	M. Aghasyan <i>et al.</i>	(COMPASS Collab.)
AAIJ 17AD	PL B779 305	R. Aaij <i>et al.</i>	(LHCb Collab.)
BHARDWAJ 16	PR D 93 052016	V. Bhardwaj <i>et al.</i>	(BELLE Collab.)
AAIJ 15AO	PR D 92 011102	R. Aaij <i>et al.</i>	(LHCb Collab.)
ABLIKIM 15V	PL B749 414	M. Ablikim <i>et al.</i>	(BESIII Collab.)
BALA 15	PR D 91 051101	A. Bala <i>et al.</i>	(BELLE Collab.)
AAIJ 14AH	NP B886 665	R. Aaij <i>et al.</i>	(LHCb Collab.)
ABLIKIM 14	PRL 112 092001	M. Ablikim <i>et al.</i>	(BESIII Collab.)
IWASHITA 14	PTEP 2014 043C01	T. Iwashita <i>et al.</i>	(BELLE Collab.)
AAIJ 13Q	PRL 110 222001	R. Aaij <i>et al.</i>	(LHCb Collab.) JP
AAIJ 13S	EPJ C73 2462	R. Aaij <i>et al.</i>	(LHCb Collab.)
BHARDWAJ 13	PRL 111 032001	V. Bhardwaj <i>et al.</i>	(BELLE Collab.)
AAIJ 12H	EPJ C72 1972	R. Aaij <i>et al.</i>	(LHCb Collab.)
LEES 12AD	PR D 86 072002	J.P. Lees <i>et al.</i>	(BABAR Collab.)
LEES 12AE	PR D 86 092005	J.P. Lees <i>et al.</i>	(BABAR Collab.)
BHARDWAJ 11	PRL 107 091803	V. Bhardwaj <i>et al.</i>	(BELLE Collab.)
CHOI 11	PR D 84 052004	S.-K. Choi <i>et al.</i>	(BELLE Collab.)
AUSHEV 10	PR D 81 031103	T. Aushev <i>et al.</i>	(BELLE Collab.)
DEL-AMO-SALAZAR 10B	PR D 82 011101	P. del Amo Sanchez <i>et al.</i>	(BABAR Collab.)
AALTONEN 09AU	PRL 103 152001	T. Aaltonen <i>et al.</i>	(CDF Collab.)
AUBERT 09B	PRL 102 132001	B. Aubert <i>et al.</i>	(BABAR Collab.)
AUBERT 08B	PR D 77 011102	B. Aubert <i>et al.</i>	(BABAR Collab.)
AUBERT 08Y	PR D 77 111101	B. Aubert <i>et al.</i>	(BABAR Collab.)
AUBERT 06	PR D 73 011101	B. Aubert <i>et al.</i>	(BABAR Collab.)
AUBERT, BE 06M	PR D 74 071101	B. Aubert <i>et al.</i>	(BABAR Collab.)
GOKHROO 05	PRL 97 162002	G. Gokhroo <i>et al.</i>	(BELLE Collab.)
AUBERT 05B	PR D 71 031501	B. Aubert <i>et al.</i>	(BABAR Collab.)
AUBERT 05D	PR D 71 052001	B. Aubert <i>et al.</i>	(BABAR Collab.)
AUBERT 05R	PR D 71 071103	B. Aubert <i>et al.</i>	(BABAR Collab.)
DOBBS 05	PRL 94 032004	S. Dobbs <i>et al.</i>	(CLEO Collab.)
ABAZOV 04F	PRL 93 162002	V.M. Abazov <i>et al.</i>	(DO Collab.)
ACOSTA 04	PRL 93 072001	D. Acosta <i>et al.</i>	(CDF Collab.)
AUBERT 04Y	PRL 93 041801	B. Aubert <i>et al.</i>	(BABAR Collab.)
CHISTOV 04	PRL 93 051803	R. Chistov <i>et al.</i>	(BELLE Collab.)
PDG 04	PL B592 1	S. Edelman <i>et al.</i>	(PDG Collab.)
YUAN 04	PL B579 74	C.Z. Yuan <i>et al.</i>	(BELLE Collab.)
CHOI 03	PRL 91 262001	S.-K. Choi <i>et al.</i>	(BELLE Collab.)
BAI 98E	PR D 57 3854	J.Z. Bai <i>et al.</i>	(BES Collab.)
ANTONIAZZI 94	PR D 50 4258	L. Antoniazzi <i>et al.</i>	(E705 Collab.)

$Z_c(3900)$

$I^G(J^{PC}) = 1^+(1^+ -)$

was $X(3900)$

Properties incompatible with a $q\bar{q}$ structure (exotic state). See the review on non- $q\bar{q}$ states.

Charged $Z_c(3900)$ seen as a peak in the invariant mass distribution of the $J/\psi \pi^\pm$ system by BES III (ABLIKIM 13T) in $e^+ e^- \rightarrow \pi^+ \pi^- J/\psi$ at c.m. energy of 4.26 GeV and by radiative return from $e^+ e^-$ collisions at \sqrt{s} from 9.46 to 10.86 GeV at Belle (LIU 13B). Partial wave analysis of ABLIKIM 17J determines $J^P = 1^+$ with more than 7σ significance. Neutral $Z_c(3900)$ seen in the $J/\psi \pi^0$ invariant mass distribution in $e^+ e^- \rightarrow \pi^0 \pi^0 J/\psi$ at c.m. energies of 4.23, 4.26, and 4.36 GeV by BES III (ABLIKIM 15U) and at 4.17 GeV by XIAO 13A. Peaks in $(D^*)^{0,\pm}$ reported by BES III (ABLIKIM 14A, ABLIKIM 15AB) are assumed to be related.

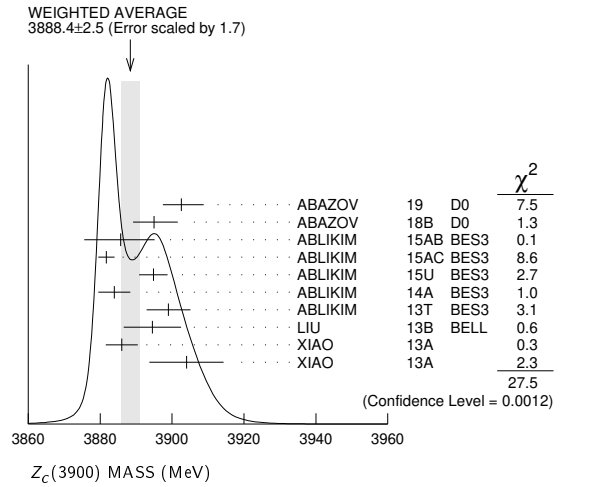
Meson Particle Listings

Z_c(3900)

Z_c(3900) MASS

VALUE (MeV)	EVTS	DOCUMENT ID	TECN	CHG	COMMENT
3888.4 ± 2.5 OUR AVERAGE Error includes scale factor of 1.7. See the ideogram below.					
3902.6 ^{+5.2+3.3} _{-5.0-1.4}		1 ABAZOV	19 D0		1.96 TeV p \bar{p} → J/ψπ ⁺ π ⁻ X
3895.0 ± 5.2 ^{+4.0} _{-2.7}	502	2 ABAZOV	18B D0		1.96 TeV p \bar{p} → J/ψπ ⁺ π ⁻ X
3885.7 ^{+4.3} _{-5.7} ± 8.4		3 ABLIKIM	15AB BES3	0	e ⁺ e ⁻ → π ⁰ (D \bar{D}^*) ⁰
3881.7 ± 1.6 ± 1.6	1.2k	3 ABLIKIM	15AC BES3	±	e ⁺ e ⁻ → π [±] (D \bar{D}^*) \mp
3894.8 ± 2.3 ± 3.2	356	3 ABLIKIM	15U BES3	0	e ⁺ e ⁻ → π ⁰ π ⁰ J/ψ
3883.9 ± 1.5 ± 4.2	1.2k	3 ABLIKIM	14A BES3	±	e ⁺ e ⁻ → π [±] (D \bar{D}^*) \mp
3899.0 ± 3.6 ± 4.9	307	3 ABLIKIM	13T BES3	±	e ⁺ e ⁻ → π ⁺ π ⁻ J/ψ
3894.5 ± 6.6 ± 4.5	159	3 LIU	13B BELL	±	e ⁺ e ⁻ → γπ ⁺ π ⁻ J/ψ
3886 ± 4 ± 2	81	3,4 XIAO	13A	±	4.17 e ⁺ e ⁻ → π ⁺ π ⁻ J/ψ
3904 ± 9 ± 5	25	3,4 XIAO	13A	0	4.17 e ⁺ e ⁻ → π ⁰ π ⁰ J/ψ

- • • We do not use the following data for averages, fits, limits, etc. • • •
- 3881.2 ± 4.2 ± 52.7 6k 5 ABLIKIM 17J BES3 ± e⁺e⁻ → π⁺π⁻J/ψ
- ¹ Measured in weak decays of b-flavored hadrons (nonprompt).
- ² The signal of the Z_c(3900) is correlated with a parent J/ψπ⁺π⁻ system in the invariant mass range 4.2–4.7 GeV.
- ³ Neglecting interference between the Z_c(3900) and non-resonant continuum.
- ⁴ For M²(π⁺π⁻) < 0.65 GeV². Obtained by analyzing CLEO-c data but not authored by the CLEO Collaboration.
- ⁵ Pole mass obtained from a fit to a Flatte-like formula.



Z_c(3900) WIDTH

VALUE (MeV)	EVTS	DOCUMENT ID	TECN	CHG	COMMENT
28.3 ± 2.5 OUR AVERAGE					
32 ⁺²⁸ ₋₂₁ ± 26 ₋₇		1 ABAZOV	19 D0		1.96 TeV p \bar{p} → π ⁺ π ⁻ J/ψX (nonprompt)
51.8 ± 4.6 ± 36.0	6 k	2 ABLIKIM	17J BES3	±	e ⁺ e ⁻ → π ⁺ π ⁻ J/ψ
35 ⁺¹¹ ₋₁₂ ± 15		3 ABLIKIM	15AB BES3	0	e ⁺ e ⁻ → π ⁰ (D \bar{D}^*) ⁰
26.6 ± 2.0 ± 2.1	1248	3 ABLIKIM	15AC BES3	±	e ⁺ e ⁻ → π [±] (D \bar{D}^*) \mp
29.6 ± 8.2 ± 8.2	356	3 ABLIKIM	15U BES3	0	e ⁺ e ⁻ → π ⁰ π ⁰ J/ψ
24.8 ± 3.3 ± 11.0	1212	3 ABLIKIM	14A BES3	±	e ⁺ e ⁻ → π [±] (D \bar{D}^*) \mp
46 ± 10 ± 20	307	3 ABLIKIM	13T BES3	±	e ⁺ e ⁻ → π ⁺ π ⁻ J/ψ
63 ± 24 ± 26	159	3 LIU	13B BELL	±	e ⁺ e ⁻ → γπ ⁺ π ⁻ J/ψ
37 ± 4 ± 8	81	3,4 XIAO	13A	±	4.17 e ⁺ e ⁻ → π ⁺ π ⁻ J/ψ

- ¹ Measured in weak decays of b-flavored hadrons (nonprompt).
- ² Pole width obtained from a fit to a Flatte-like formula.
- ³ Neglecting interference between the Z_c(3900) and non-resonant continuum.
- ⁴ For M²(π⁺π⁻) < 0.65 GeV². Obtained by analyzing CLEO-c data but not authored by the CLEO Collaboration.

Z_c(3900) DECAY MODES

Mode	Fraction (Γ _i /Γ)
Γ ₁ J/ψπ	seen
Γ ₂ h _c π [±]	not seen
Γ ₃ η _c π ⁺ π ⁻	not seen
Γ ₄ η _c (1S)ρ(770) [±]	
Γ ₅ (D \bar{D}^*) [±]	seen

Γ ₆ D ⁰ D ^{*-} + c.c.	seen
Γ ₇ ωπ [±]	seen
Γ ₈ ωπ [±]	not seen
Γ ₉ J/ψη	not seen
Γ ₁₀ D ⁺ D ^{*-} + c.c.	seen
Γ ₁₁ D ⁰ D ^{*0} + c.c.	seen

Z_c(3900) BRANCHING RATIOS

Γ(J/ψπ)/Γ _{total}	Γ ₁ /Γ				
VALUE	CL% EVTS	DOCUMENT ID	TECN	CHG	COMMENT
seen	356	ABLIKIM	15U BES3	0	e ⁺ e ⁻ → π ⁰ π ⁰ J/ψ
seen	307	ABLIKIM	13T BES3	±	e ⁺ e ⁻ → π ⁺ π ⁻ J/ψ
seen	25	1 XIAO	13A	0	4.17 e ⁺ e ⁻ → π ⁰ π ⁰ J/ψ
• • • We do not use the following data for averages, fits, limits, etc. • • •					
not seen		2 ABAZOV	19 D0		1.96 TeV p \bar{p} → π ⁺ π ⁻ J/ψX (prompt)
not seen	90	3 ADOLPH	15D COMP	±	γN → J/ψπ [±] N
¹ Obtained by analyzing CLEO-c data but not authored by the CLEO Collaboration.					
² Upper limit for the prompt production is set: N _{prompt} /N _{nonprompt} < 0.70, CL = 95%.					
³ ADOLPH 15D measure B(Z _c (3900) [±] → J/ψπ [±])σ(γN → Z _c (3900) [±] N)/σ(γN → J/ψN) < 3.7 × 10 ⁻³ at 90% CL.					

Γ(h _c π [±])/Γ _{total}	Γ ₂ /Γ			
VALUE	DOCUMENT ID	TECN	CHG	COMMENT
not seen	ABLIKIM	13X BES3	±	e ⁺ e ⁻ → h _c π ⁺ π ⁻

Γ(η _c π ⁺ π ⁻)/Γ _{total}	Γ ₃ /Γ			
VALUE	DOCUMENT ID	TECN	CHG	COMMENT
not seen	1 VINOKUROVA	15 BELL	0	B ⁺ → K ⁺ η _c π ⁺ π ⁻
¹ VINOKUROVA 15 reports B(B ⁺ → K ⁺ Z _c (3900) ⁰) × B(X → η _c π ⁺ π ⁻) < 4.7 × 10 ⁻⁵ at 90% CL.				

Γ((D \bar{D}^*) [±])/Γ(J/ψπ)	Γ ₅ /Γ ₁			
VALUE	DOCUMENT ID	TECN	CHG	COMMENT
6.2 ± 1.1 ± 2.7	1 ABLIKIM	14A BES3	±	e ⁺ e ⁻ → π [±] (D \bar{D}^*) \mp
¹ Assuming the same origin of the (D \bar{D}^*) [±] and π [±] J/ψ decay modes.				

Γ(D ⁰ D ^{*-} + c.c.)/Γ _{total}	Γ ₆ /Γ			
VALUE	DOCUMENT ID	TECN	CHG	COMMENT
seen	ABLIKIM	15AC BES3	±	e ⁺ e ⁻ → π ⁺ D ⁰ D ^{*-} + c.c.
seen	ABLIKIM	14A BES3	±	e ⁺ e ⁻ → π ⁺ D ⁰ D ^{*-} + c.c.

Γ(D ⁻ D ^{*0} + c.c.)/Γ _{total}	Γ ₇ /Γ			
VALUE	DOCUMENT ID	TECN	CHG	COMMENT
seen	ABLIKIM	15AC BES3	±	e ⁺ e ⁻ → π ⁺ D ⁻ D ^{*0} + c.c.
seen	ABLIKIM	14A BES3	±	e ⁺ e ⁻ → π ⁺ D ⁻ D ^{*0} + c.c.

Γ(ωπ [±])/Γ _{total}	Γ ₈ /Γ			
VALUE	DOCUMENT ID	TECN	CHG	COMMENT
not seen	ABLIKIM	15R BES3	±	e ⁺ e ⁻ → ωπ ⁺ π ⁻

Γ(J/ψη)/Γ _{total}	Γ ₉ /Γ			
VALUE	DOCUMENT ID	TECN	CHG	COMMENT
not seen	ABLIKIM	15Q BES3	0	4.0–4.6 e ⁺ e ⁻ → J/ψηπ ⁰

Γ(J/ψη)/Γ(J/ψπ)	Γ ₉ /Γ ₁				
VALUE	CL%	DOCUMENT ID	TECN	CHG	COMMENT
<0.15	90	ABLIKIM	15Q BES3	0	4.226 e ⁺ e ⁻ → J/ψηπ ⁰
• • • We do not use the following data for averages, fits, limits, etc. • • •					
<0.65	90	ABLIKIM	15Q BES3	0	4.257 e ⁺ e ⁻ → J/ψηπ ⁰

Γ(η _c (1S)ρ(770) [±])/Γ(J/ψπ)	Γ ₄ /Γ ₁			
VALUE	EVTS	DOCUMENT ID	TECN	COMMENT
2.3 ± 0.8	332	1 ABLIKIM	19Bc BES3	e ⁺ e ⁻ → π ⁺ π ⁻ π ⁰ η _c (1S)
¹ Using e ⁺ e ⁻ → π [±] (Z _c (3900) [±] → J/ψπ [±]) cross section at 4.23 and 4.26 GeV from ABLIKIM 17I.				

Γ(D ⁺ D ^{*-} + c.c.)/Γ _{total}	Γ ₁₀ /Γ			
VALUE	DOCUMENT ID	TECN	CHG	COMMENT
seen	ABLIKIM	15AB BES3	0	e ⁺ e ⁻ → π ⁰ (D \bar{D}^*) ⁰

Γ(D ⁰ D ^{*0} + c.c.)/Γ _{total}	Γ ₁₁ /Γ			
VALUE	DOCUMENT ID	TECN	CHG	COMMENT
seen	ABLIKIM	15AB BES3	0	e ⁺ e ⁻ → π ⁰ (D \bar{D}^*) ⁰

Γ(D ⁺ D ^{*-} + c.c.)/Γ(D ⁰ D ^{*0} + c.c.)	Γ ₁₀ /Γ ₁₁			
VALUE	DOCUMENT ID	TECN	CHG	COMMENT
0.96 ± 0.18 ± 0.12	ABLIKIM	15AB BES3	0	e ⁺ e ⁻ → π ⁰ (D \bar{D}^*) ⁰

Meson Particle Listings

Z_c(3900), X(3915), χ_{c2}(3930)

Z_c(3900) REFERENCES

Author	Year	Ref	Collab
ABAZOV	19	PR D100 012005	V.M. Abazov et al. (D0 Collab.)
ABLIKIM	19BC	PR D100 111102	M. Ablikim et al. (BESIII Collab.)
ABAZOV	18B	PR D98 052010	V.M. Abazov et al. (D0 Collab.)
ABLIKIM	17J	PRL 119 072001	M. Ablikim et al. (BESIII Collab.)
ABLIKIM	15AB	PRL 115 222002	M. Ablikim et al. (BESIII Collab.)
ABLIKIM	15AC	PR D92 092006	M. Ablikim et al. (BESIII Collab.) JP
ABLIKIM	15Q	PR D92 012008	M. Ablikim et al. (BESIII Collab.)
ABLIKIM	15R	PR D92 032009	M. Ablikim et al. (BESIII Collab.)
ABLIKIM	15U	PRL 115 112003	M. Ablikim et al. (BESIII Collab.)
ADOLPH	15D	PL B742 330	C. Adolph et al. (COMPASS Collab.)
VINOKUROVA	15	JHEP 1506 132	A. Vinokurova et al. (BELLE Collab.)
Also		JHEP 1702 088 (errat.)	A. Vinokurova et al. (BELLE Collab.)
ABLIKIM	14A	PRL 112 022001	M. Ablikim et al. (BESIII Collab.) JP
ABLIKIM	13T	PRL 110 252001	M. Ablikim et al. (BESIII Collab.)
ABLIKIM	13X	PRL 111 242001	M. Ablikim et al. (BESIII Collab.)
LIU	13B	PRL 110 252002	Z.Q. Liu et al. (BELLE Collab.)
XIAO	13A	PL B727 366	T. Xiao et al. (NWES)

VALUE (eV)	CL%	DOCUMENT ID	TECN	COMMENT	Γ ₃ Γ ₇ /Γ
<16	90	LEES	12AE	BABR	e ⁺ e ⁻ → e ⁺ e ⁻ π ⁺ π ⁻ η _c

VALUE (eV)	CL%	DOCUMENT ID	TECN	COMMENT	Γ ₆ Γ ₇ /Γ
<1.96	90	UEHARA	13	BELL	γγ → K _S ⁰ K _S ⁰

X(3915) BRANCHING RATIOS

VALUE	DOCUMENT ID	TECN	COMMENT	Γ ₁ /Γ
seen	7 DEL-AMO-SA...10B	BABR	B → ωJ/ψK	
seen	8 CHOI	05	BELL	B → ωJ/ψK

7 DEL-AMO-SANCHEZ 10B reports B(B[±] → X(3915)K[±]) × B(X(3915) → J/ψω) = (3.0^{+0.7+0.5}_{-0.6-0.3}) × 10⁻⁵ and B(B⁰ → X(3915)K⁰) × B(X(3915) → J/ψω) = (2.1 ± 0.9 ± 0.3) × 10⁻⁵.
8 CHOI 05 reports B(B → X(3915)K) × B(X(3915) → J/ψω) = (7.1 ± 1.3 ± 3.1) × 10⁻⁵.

VALUE	CL%	DOCUMENT ID	TECN	COMMENT	Γ ₁ /Γ ₂
>0.71	90	9 AUSHEV	10	BELL	B → D ^{*0} D ⁰ K

9 By combining the upper limit B(B → X(3915)K) × B(X(3915) → D^{*0}D⁰) < 0.67 × 10⁻⁴ from AUSHEV 10 with the average of CHOI 05 and AUBERT 08w measurements B(B → X(3915)K) × B(X(3915) → ωJ/ψ) = (0.51 ± 0.11) × 10⁻⁴.

VALUE	DOCUMENT ID	TECN	COMMENT	Γ ₄ /Γ
not seen	10 VINOKUROVA 15	BELL	B ⁺ → K ⁺ η _c η	
	10 VINOKUROVA 15	reports	B(B ⁺ → K ⁺ X(3915) ⁰) × B(X → η _c η) < 3.3 × 10 ⁻⁵ at 90% CL.	

10 VINOKUROVA 15 reports B(B⁺ → K⁺X(3915)⁰) × B(X → η_cη) < 3.3 × 10⁻⁵ at 90% CL.

VALUE	DOCUMENT ID	TECN	COMMENT	Γ ₅ /Γ
not seen	11 VINOKUROVA 15	BELL	B ⁺ → K ⁺ η _c π ⁰	
	11 VINOKUROVA 15	reports	B(B ⁺ → K ⁺ X(3915) ⁰) × B(X → η _c π ⁰) < 1.8 × 10 ⁻⁵ at 90% CL.	

11 VINOKUROVA 15 reports B(B⁺ → K⁺X(3915)⁰) × B(X → η_cπ⁰) < 1.8 × 10⁻⁵ at 90% CL.

VALUE	EVTs	DOCUMENT ID	TECN	COMMENT	Γ ₇ /Γ
seen	59 ± 10	LEES	12AD	BABR	e ⁺ e ⁻ → e ⁺ e ⁻ ωJ/ψ
seen		UEHARA	10	BELL	10.6 e ⁺ e ⁻ → e ⁺ e ⁻ ωJ/ψ

VALUE	EVTs	DOCUMENT ID	TECN	COMMENT	Γ ₈ /Γ
not seen	42 ± 14	12 BHARDWAJ 19	BELL	B [±] → χ _{c1} π ⁰ K [±]	
		12 BHARDWAJ 19	reports	B(B ⁺ → K ⁺ X(3915)) × B(X(3915) → χ _{c1} π ⁰) < 3.8 × 10 ⁻⁵ at 90% CL. A signal significance 2.3 standard deviations.	

X(3915) REFERENCES

Author	Year	Ref	Collab
ABLIKIM	19V	PRL 122 232002	M. Ablikim et al. (BESIII Collab.)
BHARDWAJ	19	PR D99 111101	V. Bhardwaj et al. (BELLE Collab.)
VINOKUROVA	15	JHEP 1506 132	A. Vinokurova et al. (BELLE Collab.)
Also		JHEP 1702 088 (errat.)	A. Vinokurova et al. (BELLE Collab.)
ZHOU	15C	PRL 115 022001	Z.-Y. Zhou, Z. Xiao, H.-Q. Zhou (BEIJT, NANJ)
UEHARA	13	PTEP 2013 123C01	S. Uehara et al. (BELLE Collab.)
LEES	12AD	PR D86 072002	J.P. Lees et al. (BABAR Collab.)
LEES	12AE	PR D86 092005	J.P. Lees et al. (BABAR Collab.)
AUSHEV	10	PR D81 031103	T. Aushev et al. (BELLE Collab.)
DEL-AMO-SA...10B	PR D82 011101		P. del Amo Sanchez et al. (BABAR Collab.)
UEHARA	10	PRL 104 092001	S. Uehara et al. (BELLE Collab.)
AUBERT	08W	PRL 101 082001	B. Aubert et al. (BABAR Collab.)
CHOI	05	PRL 94 182002	S.-K. Choi et al. (BELLE Collab.)

χ _{c2} (3930)	J ^{PC}
	0 ⁺ (2 ⁺ +)

χ_{c2}(3930) MASS

VALUE (MeV)	EVTs	DOCUMENT ID	TECN	COMMENT	
3922.2 ± 1.0 OUR AVERAGE				Error includes scale factor of 1.6.	
3921.9 ± 0.6 ± 0.2		1 AAIJ	19M	LHCB	pp → D ⁰ D ⁺ + anything
3926.7 ± 2.7 ± 1.1	76 ± 17	AUBERT	10G	BABR	10.6 e ⁺ e ⁻ → e ⁺ e ⁻ D ⁰ D ⁺
3929 ± 5 ± 2	64	UEHARA	06	BELL	10.6 e ⁺ e ⁻ → e ⁺ e ⁻ D ⁰ D ⁺

1 Measured in prompt hadroproduction.

X(3915) $I^G(J^{PC}) = 0^+(0 \text{ or } 2^+ +)$

was χ_{c0}(3915)

The experimental analysis prefers J^{PC} = 0⁺⁺. However, a re-analysis presented in ZHOU 15C shows that if helicity-2 dominance assumption is abandoned and a sizable helicity-0 component is allowed, a J^{PC} = 2⁺⁺ assignment is possible.

X(3915) MASS

VALUE (MeV)	EVTs	DOCUMENT ID	TECN	COMMENT	
3918.4 ± 1.9 OUR AVERAGE				Error includes scale factor of 1.1.	
3919.4 ± 2.2 ± 1.6	59 ± 10	LEES	12AD	BABR	e ⁺ e ⁻ → e ⁺ e ⁻ ωJ/ψ
3919.1 ^{+3.8} _{-3.4} ± 2.0		DEL-AMO-SA...10B	BABR	B → ωJ/ψK	
3915 ± 3 ± 2	49 ± 15	UEHARA	10	BELL	10.6 e ⁺ e ⁻ → e ⁺ e ⁻ ωJ/ψ
3943 ± 11 ± 13	58 ± 11	1 CHOI	05	BELL	B → ωJ/ψK
• • • We do not use the following data for averages, fits, limits, etc. • • •					
3926.4 ± 2.2 ± 1.2		2 ABLIKIM	19v	BES	e ⁺ e ⁻ → γωJ/ψ
3914.6 ^{+3.8} _{-3.4} ± 2.0		1 AUBERT	08w	BABR	Superseded by DEL-AMO-SANCHEZ 10B

¹ ωJ/ψ threshold enhancement fitted as an S-wave Breit-Wigner resonance.
² Could also be X(3940). Significance 3.1σ. Fit with additional resonance at 3963.7 ± 5.7 MeV, significance 3.4σ.

X(3915) WIDTH

VALUE (MeV)	EVTs	DOCUMENT ID	TECN	COMMENT	
20 ± 5 OUR AVERAGE				Error includes scale factor of 1.1.	
13 ± 6 ± 3	59	LEES	12AD	BABR	e ⁺ e ⁻ → e ⁺ e ⁻ ωJ/ψ
31 ⁺¹⁰ ₋₈ ± 5		DEL-AMO-SA...10B	BABR	B → ωJ/ψK	
17 ± 10 ± 3	49	UEHARA	10	BELL	10.6 e ⁺ e ⁻ → e ⁺ e ⁻ ωJ/ψ
87 ± 22 ± 26	58	3 CHOI	05	BELL	B → ωJ/ψK
• • • We do not use the following data for averages, fits, limits, etc. • • •					
3.8 ± 7.5 ± 2.6		4 ABLIKIM	19v	BES	e ⁺ e ⁻ → γωJ/ψ
34 ⁺¹² ₋₈ ± 5		3 AUBERT	08w	BABR	Superseded by DEL-AMO-SANCHEZ 10B

³ ωJ/ψ threshold enhancement fitted as an S-wave Breit-Wigner resonance.
⁴ Could also be X(3940). Significance 3.1σ. Fit with additional resonance at 3963.7 ± 5.7 MeV, significance 3.4σ.

X(3915) DECAY MODES

Mode	Fraction (Γ _i /Γ)
Γ ₁ ωJ/ψ	seen
Γ ₂ D ^{*0} D ⁰	
Γ ₃ π ⁺ π ⁻ η _c (1S)	not seen
Γ ₄ η _c η	not seen
Γ ₅ η _c π ⁰	not seen
Γ ₆ KK	not seen
Γ ₇ γγ	seen
Γ ₈ π ⁰ χ _{c1}	

X(3915) Γ(i)Γ(γγ)/Γ(total)

VALUE (eV)	EVTs	DOCUMENT ID	TECN	COMMENT	Γ ₁ Γ ₇ /Γ
54 ± 9 OUR AVERAGE					
52 ± 10 ± 3	59 ± 10	5 LEES	12AD	BABR	e ⁺ e ⁻ → e ⁺ e ⁻ ωJ/ψ
61 ± 17 ± 8	49 ± 15	5 UEHARA	10	BELL	10.6 e ⁺ e ⁻ → e ⁺ e ⁻ ωJ/ψ
• • • We do not use the following data for averages, fits, limits, etc. • • •					
18 ± 5 ± 2	49 ± 15	6 UEHARA	10	BELL	10.6 e ⁺ e ⁻ → e ⁺ e ⁻ ωJ/ψ

⁵ For J^P = 0⁺.
⁶ For J^P = 2⁺, helicity-2.

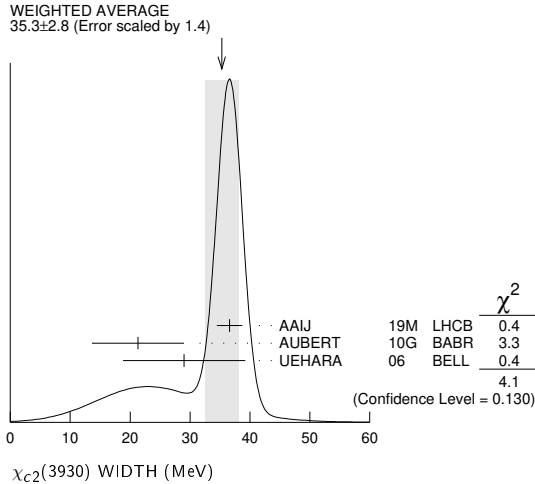
Meson Particle Listings

$\chi_{c2}(3930)$, $X(3940)$

$\chi_{c2}(3930)$ WIDTH

VALUE (MeV)	EVTS	DOCUMENT ID	TECN	COMMENT
35.3 ± 2.8 OUR AVERAGE		Error includes scale factor of 1.4. See the ideogram below.		
36.6 ± 1.9 ± 0.9		² AAIJ	19M LHCb	$pp \rightarrow D\bar{D} + \text{anything}$
21.3 ± 6.8 ± 3.6	76 ± 17	AUBERT	10G BABR	10.6 $e^+e^- \rightarrow e^+e^- D\bar{D}$
29 ± 10 ± 2	64	UEHARA	06 BELL	10.6 $e^+e^- \rightarrow e^+e^- D\bar{D}$

² Measured in prompt hadroproduction.



$\chi_{c2}(3930)$ DECAY MODES

Mode	Fraction (Γ_i/Γ)
Γ_1 $\gamma\gamma$	seen
Γ_2 $K\bar{K}\pi$	
Γ_3 $K^+K^-\pi^+\pi^-\pi^0$	
Γ_4 $D\bar{D}$	seen
Γ_5 D^+D^-	seen
Γ_6 $D^0\bar{D}^0$	seen
Γ_7 $\pi^+\pi^-\eta_c(1S)$	not seen
Γ_8 $K\bar{K}$	not seen

$\chi_{c2}(3930)$ PARTIAL WIDTHS

$\chi_{c2}(3930)$ $\Gamma(i)\Gamma(\gamma\gamma)/\Gamma(\text{total})$

VALUE (eV)	CL%	DOCUMENT ID	TECN	COMMENT	$\Gamma_2\Gamma_1/\Gamma$
<2.1	90	DEL-AMO-SA..11M	BABR	$\gamma\gamma \rightarrow K_S^0 K^\pm \pi^\mp$	

VALUE (eV)	CL%	DOCUMENT ID	TECN	COMMENT	$\Gamma_3\Gamma_1/\Gamma$
<3.4	90	DEL-AMO-SA..11M	BABR	$\gamma\gamma \rightarrow K^+K^-\pi^+\pi^-\pi^0$	

VALUE (keV)	EVTS	DOCUMENT ID	TECN	COMMENT	$\Gamma_4\Gamma_1/\Gamma$
0.21 ± 0.04 OUR AVERAGE					
0.24 ± 0.05 ± 0.04	76 ± 17	AUBERT	10G BABR	10.6 $e^+e^- \rightarrow e^+e^- D\bar{D}$	
0.18 ± 0.05 ± 0.03	64	³ UEHARA	06 BELL	10.6 $e^+e^- \rightarrow e^+e^- D\bar{D}$	

³ Assuming $B(D^+D^-) = 0.89 B(D^0\bar{D}^0)$.

VALUE (eV)	CL%	DOCUMENT ID	TECN	COMMENT	$\Gamma_7\Gamma_1/\Gamma$
<18	90	LEES	12AE BABR	$e^+e^- \rightarrow e^+e^-\pi^+\pi^-\eta_c$	

VALUE (eV)	CL%	DOCUMENT ID	TECN	COMMENT	$\Gamma_8\Gamma_1/\Gamma$
<0.256	90	UEHARA	13 BELL	$\gamma\gamma \rightarrow K_S^0 K_S^0$	

$\chi_{c2}(3930)$ BRANCHING RATIOS

VALUE	EVTS	DOCUMENT ID	TECN	COMMENT	Γ_5/Γ_6
0.74 ± 0.43 ± 0.16	64	UEHARA	06 BELL	10.6 $e^+e^- \rightarrow e^+e^- D\bar{D}$	

$\chi_{c2}(3930)$ REFERENCES

AAIJ	19M	JHEP 1907 035	R. Aaij et al.	(LHCb Collab.)
UEHARA	13	PTEP 2013 123C01	S. Uehara et al.	(BELLE Collab.)
LEES	12AE	PR D86 092005	J.P. Lees et al.	(BABAR Collab.)
DEL-AMO-SA...	11M	PR D84 012004	P. del Amo Sanchez et al.	(BABAR Collab.)
AUBERT	10G	PR D81 092003	B. Aubert et al.	(BABAR Collab.)
UEHARA	06	PRL 96 082003	S. Uehara et al.	(BELLE Collab.)

$X(3940)$

$$J^G(J^PC) = ?^?(?^??)$$

OMITTED FROM SUMMARY TABLE

Reported by ABE 07, observed in $e^+e^- \rightarrow J/\psi X$.

$X(3940)$ MASS

VALUE (MeV)	EVTS	DOCUMENT ID	TECN	COMMENT
3942 ± 7 ± 6	52	PAKHOLOV	08 BELL	$e^+e^- \rightarrow J/\psi X$
• • • We do not use the following data for averages, fits, limits, etc. • • •				
3943 ± 6 ± 6	25	¹ ABE	07 BELL	$e^+e^- \rightarrow J/\psi X$
3936 ± 14	266	² ABE	07 BELL	$e^+e^- \rightarrow J/\psi(c\bar{c})$

¹ From a fit to $D^{*+}D^-$ and $D^{*0}\bar{D}^0$ events.
² From the inclusive fit. Not independent of the exclusive measurement by ABE 07.

$X(3940)$ WIDTH

VALUE (MeV)	CL%	EVTS	DOCUMENT ID	TECN	COMMENT
37 ± 26 ± 15 ± 8		52	PAKHOLOV	08 BELL	$e^+e^- \rightarrow J/\psi X$
• • • We do not use the following data for averages, fits, limits, etc. • • •					
<52	90	25	ABE	07 BELL	$e^+e^- \rightarrow J/\psi X$

$X(3940)$ DECAY MODES

Mode	Fraction (Γ_i/Γ)
Γ_1 $D\bar{D}^* + c.c.$	seen
Γ_2 $D\bar{D}$	not seen
Γ_3 $J/\psi\omega$	not seen

$X(3940)$ BRANCHING RATIOS

VALUE	CL%	EVTS	DOCUMENT ID	TECN	COMMENT	Γ_1/Γ
>0.45	90	25	^{1,2} ABE	07 BELL	$e^+e^- \rightarrow J/\psi X$	

¹ For $X(3940)$ decaying to final states with more than two tracks.
² PAKHOLOV 08 finds that the inclusive peak near 3940 MeV/c² may consist of several states.

VALUE	CL%	DOCUMENT ID	TECN	COMMENT	Γ_2/Γ
<0.41	90	^{1,2} ABE	07 BELL	$e^+e^- \rightarrow J/\psi X$	

¹ For $X(3940)$ decaying to final states with more than two tracks.
² PAKHOLOV 08 finds that the inclusive peak near 3940 MeV/c² may consist of several states.

VALUE	CL%	DOCUMENT ID	TECN	COMMENT	Γ_3/Γ
<0.26	90	^{1,2} ABE	07 BELL	$e^+e^- \rightarrow J/\psi X$	

¹ For $X(3940)$ decaying to final states with more than two tracks.
² PAKHOLOV 08 finds that the inclusive peak near 3940 MeV/c² may consist of several states.

$X(3940)$ REFERENCES

PAKHOLOV	08	PRL 100 202001	P. Pakhlov et al.	(BELLE Collab.)
ABE	07	PRL 98 082001	K. Abe et al.	(BELLE Collab.)

See key on page 999

Meson Particle Listings

$X(4020)^\pm, \psi(4040)$

$X(4020)^\pm$

$$I^G(J^{PC}) = 1^+(?^{?^-})$$

Properties incompatible with a $q\bar{q}$ structure (exotic state). See the review on non- $q\bar{q}$ states.

Charged $X(4020)$ seen by ABLIKIM 13X from $e^+e^- \rightarrow \pi^+\pi^-h_c(1P)$ at c.m. energy from 3.90 to 4.42 GeV as a peak in the invariant mass distribution of the $\pi^\pm h_c(1P)$ system, and by ABLIKIM 14B from $e^+e^- \rightarrow (D^*\bar{D}^*)^\pm\pi^\mp$ events in $(D^*\bar{D}^*)^\pm$ mass. A neutral $X(4020)$ seen by ABLIKIM 14P at three c.m. energies in the same range in $e^+e^- \rightarrow \pi^0\pi^0 h_c(1P)$ as a peak in the larger of the two masses recoiling against a π^0 . ABLIKIM 15AA observes a 5.9σ signal in $(D^*\bar{D}^*)^0$ in $e^+e^- \rightarrow (D^*\bar{D}^*)^0\pi^0$ events using collisions at two c.m. energies. Production rates and mass values support grouping neutral and charged $X(4020)$ together as manifestations of a single $l = 1$ particle.

$X(4020)^\pm$ MASS

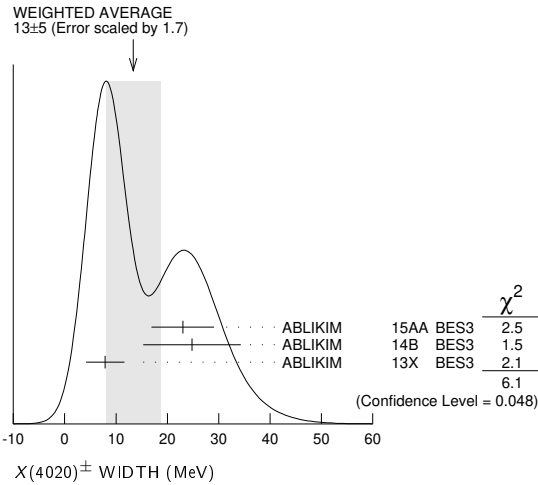
VALUE (MeV)	EVTS	DOCUMENT ID	TECN	CHG	COMMENT
4024.1 ± 1.9 OUR AVERAGE					
4025.5 ^{+2.0} _{-4.7} ± 3.1	116	¹ ABLIKIM 15AA	BES3	0	$e^+e^- \rightarrow (D^*\bar{D}^*)^0\pi^0$
4026.3 ± 2.6 ± 3.7	401	¹ ABLIKIM 14B	BES3	±	$e^+e^- \rightarrow (D^*\bar{D}^*)^\pm\pi^\mp$
4023.9 ± 2.2 ± 3.8	61	^{1,2} ABLIKIM 14P	BES3	0	$e^+e^- \rightarrow \pi^0\pi^0 h_c$
4022.9 ± 0.8 ± 2.7	253	¹ ABLIKIM 13X	BES3	±	$e^+e^- \rightarrow \pi^+\pi^- h_c$

¹ Neglecting interference between the $X(4020)$ and non-resonant continuum.
² Assuming $J^P = 1^+$ and width of 7.9 ± 2.6 MeV.

$X(4020)^\pm$ WIDTH

VALUE (MeV)	EVTS	DOCUMENT ID	TECN	CHG	COMMENT
13 ± 5 OUR AVERAGE					Error includes scale factor of 1.7. See the ideogram below.
23.0 ± 6.0 ± 1.0	116	¹ ABLIKIM 15AA	BES3	0	$e^+e^- \rightarrow (D^*\bar{D}^*)^0\pi^0$
24.8 ± 5.6 ± 7.7	401	¹ ABLIKIM 14B	BES3	±	$e^+e^- \rightarrow (D^*\bar{D}^*)^\pm\pi^\mp$
7.9 ± 2.7 ± 2.6	253	¹ ABLIKIM 13X	BES3	±	$e^+e^- \rightarrow \pi^+\pi^- h_c$

¹ Neglecting interference between the $X(4020)$ and non-resonant continuum.



$X(4020)^\pm$ DECAY MODES

Mode	Fraction (Γ_i/Γ)
Γ_1 $h_c(1P)\pi$	seen
Γ_2 $D^*\bar{D}^*$	seen
Γ_3 $D\bar{D}^* + c.c.$	not seen
Γ_4 $\eta_c\pi^+\pi^-$	not seen
Γ_5 $\eta_c(1S)\rho(770)^\pm$	
Γ_6 $J/\psi(1S)\pi^\pm$	not seen

$X(4020)^\pm$ BRANCHING RATIOS

$\Gamma(h_c(1P)\pi)/\Gamma_{total}$	VALUE	EVTS	DOCUMENT ID	TECN	CHG	COMMENT
seen	61		ABLIKIM 14P	BES3	0	$e^+e^- \rightarrow \pi^0\pi^0 h_c$
seen	253		ABLIKIM 13X	BES3	±	$e^+e^- \rightarrow \pi^+\pi^- h_c$

$\Gamma(D^*\bar{D}^*)/\Gamma_{total}$

VALUE	EVTS	DOCUMENT ID	TECN	CHG	COMMENT
seen	116	¹ ABLIKIM 15AA	BES3	0	$e^+e^- \rightarrow (D^*\bar{D}^*)^0\pi^0$
seen	401	¹ ABLIKIM 14B	BES3	±	$e^+e^- \rightarrow (D^*\bar{D}^*)^\pm\pi^\mp$

¹ Neglecting interference between the $X(4020)$ and non-resonant continuum.

$\Gamma(D\bar{D}^* + c.c.)/\Gamma_{total}$

VALUE	DOCUMENT ID	TECN	CHG	COMMENT
not seen	ABLIKIM 15AC	BES3	±	$e^+e^- \rightarrow \pi^\pm(D\bar{D}^*)^\mp$

$\Gamma(\eta_c\pi^+\pi^-)/\Gamma_{total}$

VALUE	DOCUMENT ID	TECN	COMMENT
not seen	¹ VINOKUROVA 15	BELL	$B^+ \rightarrow K^+\eta_c\pi^+\pi^-$

¹ VINOKUROVA 15 reports $B(B^+ \rightarrow K^+X(4020)^0) \times B(X \rightarrow \eta_c\pi^+\pi^-) < 1.6 \times 10^{-5}$ at 90% CL.

$\Gamma(\eta_c(1S)\rho(770)^\pm)/\Gamma(h_c(1P)\pi)$

VALUE	CL%	DOCUMENT ID	TECN	COMMENT
<1.2	90	¹ ABLIKIM 19Bc	BES3	$e^+e^- \rightarrow \pi^+\pi^-\eta_c(1S)$

¹ Using $e^+e^- \rightarrow \pi^\mp(Z_c(4020)^\pm \rightarrow h_c(1P)\pi^\pm)$ cross section at 4.23, 4.26 and 4.36 GeV from ABLIKIM 13x.

$\Gamma(J/\psi(1S)\pi^\pm)/\Gamma_{total}$

VALUE	DOCUMENT ID	TECN	COMMENT
not seen	¹ ABLIKIM 17J	BES3	$e^+e^- \rightarrow \pi^+\pi^-J/\psi$

¹ From Partial Wave Analysis assuming $J^P = 1^+$.

$X(4020)^\pm$ REFERENCES

ABLIKIM 19BC	PR D100 111102	M. Ablikim <i>et al.</i>	(BESIII Collab.)
ABLIKIM 17J	PRL 119 072001	M. Ablikim <i>et al.</i>	(BESIII Collab.)
ABLIKIM 15AA	PRL 115 182002	M. Ablikim <i>et al.</i>	(BESIII Collab.)
ABLIKIM 15AC	PR D92 092006	M. Ablikim <i>et al.</i>	(BESIII Collab.)
VINOKUROVA 15	JHEP 1506 132	A. Vinokurova <i>et al.</i>	(BELLE Collab.)
Also	JHEP 1702 088 (err.)	A. Vinokurova <i>et al.</i>	(BELLE Collab.)
ABLIKIM 14B	PRL 112 132001	M. Ablikim <i>et al.</i>	(BESIII Collab.)
ABLIKIM 14P	PRL 113 212002	M. Ablikim <i>et al.</i>	(BESIII Collab.)
ABLIKIM 13X	PRL 111 242001	M. Ablikim <i>et al.</i>	(BESIII Collab.)

$\psi(4040)$

$$I^G(J^{PC}) = 0^-(1^{--})$$

$\psi(4040)$ MASS

VALUE (MeV)	DOCUMENT ID	TECN	COMMENT
4039 ± 1 OUR ESTIMATE			
4039.6 ± 4.3	¹ ABLIKIM 08D	BES2	$e^+e^- \rightarrow$ hadrons
4034 ± 6	² MO 10	RVUE	$e^+e^- \rightarrow$ hadrons
4037 ± 2	³ SETH 05A	RVUE	$e^+e^- \rightarrow$ hadrons
4040 ± 1	⁴ SETH 05A	RVUE	$e^+e^- \rightarrow$ hadrons
4040 ± 10	BRANDELIK 78c	DASP	e^+e^-

¹ Reanalysis of data presented in BAI 02c. From a global fit over the center-of-mass energy region 3.7–5.0 GeV covering the $\psi(3770)$, $\psi(4040)$, $\psi(4160)$, and $\psi(4415)$ resonances. Phase angle fixed in the fit to $\delta = (130 \pm 46)^\circ$.
² Reanalysis of data presented in BAI 00 and BAI 02c. From a global fit over the center-of-mass energy 3.8–4.8 GeV covering the $\psi(4040)$, $\psi(4160)$ and $\psi(4415)$ resonances and including interference effects.
³ From a fit to Crystal Ball (OSTERHELD 86) data.
⁴ From a fit to BES (BAI 02c) data.

$\psi(4040)$ WIDTH

VALUE (MeV)	DOCUMENT ID	TECN	COMMENT
80 ± 10 OUR ESTIMATE			
84.5 ± 12.3	⁵ ABLIKIM 08D	BES2	$e^+e^- \rightarrow$ hadrons
87 ± 11	⁶ MO 10	RVUE	$e^+e^- \rightarrow$ hadrons
85 ± 10	⁷ SETH 05A	RVUE	$e^+e^- \rightarrow$ hadrons
89 ± 6	⁸ SETH 05A	RVUE	$e^+e^- \rightarrow$ hadrons
52 ± 10	BRANDELIK 78c	DASP	e^+e^-

⁵ Reanalysis of data presented in BAI 02c. From a global fit over the center-of-mass energy region 3.7–5.0 GeV covering the $\psi(3770)$, $\psi(4040)$, $\psi(4160)$, and $\psi(4415)$ resonances. Phase angle fixed in the fit to $\delta = (130 \pm 46)^\circ$.
⁶ Reanalysis of data presented in BAI 00 and BAI 02c. From a global fit over the center-of-mass energy 3.8–4.8 GeV covering the $\psi(4040)$, $\psi(4160)$ and $\psi(4415)$ resonances and including interference effects.
⁷ From a fit to Crystal Ball (OSTERHELD 86) data.
⁸ From a fit to BES (BAI 02c) data.

Meson Particle Listings

$\psi(4040)$

$\psi(4040)$ DECAY MODES

Due to the complexity of the $c\bar{c}$ threshold region, in this listing, “seen” (“not seen”) means that a cross section for the mode in question has been measured at effective \sqrt{s} near this particle’s central mass value, more (less) than 2σ above zero, without regard to any peaking behavior in \sqrt{s} or absence thereof. See mode listing(s) for details and references.

Mode	Fraction (Γ_i/Γ)	Confidence level
Γ_1 e^+e^-	$(1.07 \pm 0.16) \times 10^{-5}$	
Γ_2 $D\bar{D}$	seen	
Γ_3 $D^0\bar{D}^0$	seen	
Γ_4 D^+D^-	seen	
Γ_5 $D^*\bar{D}^+$ + c.c.	seen	
Γ_6 $D^*(2007)^0\bar{D}^0$ + c.c.	seen	
Γ_7 $D^*(2010)^+D^-$ + c.c.	seen	
Γ_8 $D^*\bar{D}^*$	seen	
Γ_9 $D^*(2007)^0\bar{D}^*(2007)^0$	seen	
Γ_{10} $D^*(2010)^+D^*(2010)^-$	seen	
Γ_{11} $D\bar{D}\pi$ (excl. $D^*\bar{D}$)		
Γ_{12} $D^0D^-\pi^+$ + c.c. (excl. $D^*(2007)^0\bar{D}^0$ + c.c., $D^*(2010)^+D^-$ + c.c.)	not seen	
Γ_{13} $D\bar{D}^*\pi$ (excl. $D^*\bar{D}^*$)	not seen	
Γ_{14} $D^0\bar{D}^*\pi^+$ + c.c. (excl. $D^*(2010)^+D^*(2010)^-$)	seen	
Γ_{15} $D_s^+D_s^-$	seen	
Γ_{16} $J/\psi(1S)$ hadrons		
Γ_{17} $J/\psi\pi^+\pi^-$	$< 4 \times 10^{-3}$	90%
Γ_{18} $J/\psi\pi^0\pi^0$	$< 2 \times 10^{-3}$	90%
Γ_{19} $J/\psi\eta$	$(5.2 \pm 0.7) \times 10^{-3}$	
Γ_{20} $J/\psi\pi^0$	$< 2.8 \times 10^{-4}$	90%
Γ_{21} $J/\psi\pi^+\pi^-\pi^0$	$< 2 \times 10^{-3}$	90%
Γ_{22} $\chi_{c1}\gamma$	$< 3.4 \times 10^{-3}$	90%
Γ_{23} $\chi_{c2}\gamma$	$< 5 \times 10^{-3}$	90%
Γ_{24} $\chi_{c1}\pi^+\pi^-\pi^0$	$< 1.1\%$	90%
Γ_{25} $\chi_{c2}\pi^+\pi^-\pi^0$	$< 3.2\%$	90%
Γ_{26} $h_c(1P)\pi^+\pi^-$	$< 3 \times 10^{-3}$	90%
Γ_{27} $\phi\pi^+\pi^-$	$< 3 \times 10^{-3}$	90%
Γ_{28} $\Lambda\bar{\Lambda}\pi^+\pi^-$	$< 2.9 \times 10^{-4}$	90%
Γ_{29} $\Lambda\bar{\Lambda}\pi^0$	$< 9 \times 10^{-5}$	90%
Γ_{30} $\Lambda\bar{\Lambda}\eta$	$< 3.0 \times 10^{-4}$	90%
Γ_{31} $\Sigma^+\Sigma^-$	$< 1.3 \times 10^{-4}$	90%
Γ_{32} $\Sigma^0\Sigma^0$	$< 7 \times 10^{-5}$	90%
Γ_{33} $\Xi^+\Xi^-$	$< 1.6 \times 10^{-4}$	90%
Γ_{34} $\Xi^0\Xi^0$	$< 1.8 \times 10^{-4}$	90%
Γ_{35} $\mu^+\mu^-$		

$\psi(4040)$ PARTIAL WIDTHS

$\Gamma(e^+e^-)$	Γ_1
VALUE (keV)	DOCUMENT ID TECN COMMENT
0.86 ± 0.07 OUR ESTIMATE	
0.83 ± 0.20	⁹ ABLIKIM 08D BES2 $e^+e^- \rightarrow$ hadrons
0.6 to 1.4	¹⁰ MO 10 RVUE $e^+e^- \rightarrow$ hadrons
0.88 ± 0.11	¹¹ SETH 05A RVUE $e^+e^- \rightarrow$ hadrons
0.91 ± 0.13	¹² SETH 05A RVUE $e^+e^- \rightarrow$ hadrons
0.75 ± 0.15	BRANDELIK 78c DASP e^+e^-

⁹ Reanalysis of data presented in BAI 02c. From a global fit over the center-of-mass energy region 3.7–5.0 GeV covering the $\psi(3770)$, $\psi(4040)$, $\psi(4160)$, and $\psi(4415)$ resonances. Phase angle fixed in the fit to $\delta = (130 \pm 46)^\circ$.
¹⁰ Reanalysis of data presented in BAI 00 and BAI 02c. From a global fit over the center-of-mass energy 3.8–4.8 GeV covering the $\psi(4040)$, $\psi(4160)$ and $\psi(4415)$ resonances and including interference effects. Four sets of solutions are obtained with the same fit quality, mass and total width, but with different e^+e^- partial widths. We quote only the range of values.
¹¹ From a fit to Crystal Ball (OSTERHELD 86) data.
¹² From a fit to BES (BAI 02c) data.

$\psi(4040)$ $\Gamma(i) \times \Gamma(e^+e^-)/\Gamma(\text{total})$

$\Gamma(\chi_{c1}\gamma) \times \Gamma(e^+e^-)/\Gamma_{\text{total}}$	$\Gamma_{22}\Gamma_1/\Gamma$
VALUE (eV) CL%	DOCUMENT ID TECN COMMENT
< 2.9	¹³ HAN 15 BELL $10.58 e^+e^- \rightarrow \chi_{c1}\gamma$

¹³ Using $B(\eta \rightarrow \gamma\gamma) = (39.41 \pm 0.21)\%$.

$\Gamma(\chi_{c2}\gamma) \times \Gamma(e^+e^-)/\Gamma_{\text{total}}$	$\Gamma_{23}\Gamma_1/\Gamma$
VALUE (eV) CL%	DOCUMENT ID TECN COMMENT
< 4.6	¹⁴ HAN 15 BELL $10.58 e^+e^- \rightarrow \chi_{c2}\gamma$

¹⁴ Using $B(\eta \rightarrow \gamma\gamma) = (39.41 \pm 0.21)\%$.

$\psi(4040)$ $\Gamma(i) \times \Gamma(e^+e^-)/\Gamma^2(\text{total})$

$\Gamma(J/\psi\eta)/\Gamma_{\text{total}} \times \Gamma(e^+e^-)/\Gamma_{\text{total}}$	$\Gamma_{19}/\Gamma \times \Gamma_1/\Gamma$
VALUE (units 10^{-8})	DOCUMENT ID TECN COMMENT
$5.1 \pm 1.4 \pm 1.5$	¹⁵ WANG 13B BELL $e^+e^- \rightarrow J/\psi\eta\gamma$
$12.8 \pm 2.1 \pm 1.9$	¹⁶ WANG 13B BELL $e^+e^- \rightarrow J/\psi\eta\gamma$

$\bullet \bullet \bullet$ We do not use the following data for averages, fits, limits, etc. $\bullet \bullet \bullet$
¹⁵ Solution I of two equivalent solutions in a fit using two interfering resonances. Mass and width fixed at 4039 MeV and 80 MeV, respectively.
¹⁶ Solution II of two equivalent solutions in a fit using two interfering resonances. Mass and width fixed at 4039 MeV and 80 MeV, respectively.

$\psi(4040)$ BRANCHING RATIOS

$\Gamma(e^+e^-)/\Gamma_{\text{total}}$	Γ_1/Γ
VALUE (units 10^{-5})	DOCUMENT ID TECN COMMENT
~ 1.0	FELDMAN 77 MRK1 e^+e^-

$\bullet \bullet \bullet$ We do not use the following data for averages, fits, limits, etc. $\bullet \bullet \bullet$

$\Gamma(D^0\bar{D}^0)/\Gamma_{\text{total}}$	Γ_3/Γ
VALUE	DOCUMENT ID TECN COMMENT
seen	AUBERT 09M BABR $e^+e^- \rightarrow D^0\bar{D}^0\gamma$
seen	CRONIN-HEN..09 CLEO $e^+e^- \rightarrow D^0\bar{D}^0$
seen	PAKHLOVA 08 BELL $e^+e^- \rightarrow D^0\bar{D}^0\gamma$

$\Gamma(D^+D^-)/\Gamma_{\text{total}}$	Γ_4/Γ
VALUE	DOCUMENT ID TECN COMMENT
seen	AUBERT 09M BABR $e^+e^- \rightarrow D^+D^-\gamma$
seen	CRONIN-HEN..09 CLEO $e^+e^- \rightarrow D^+D^-$
seen	PAKHLOVA 08 BELL $e^+e^- \rightarrow D^+D^-\gamma$

$\Gamma(D\bar{D})/\Gamma(D^*\bar{D} + \text{c.c.})$	Γ_2/Γ_5
VALUE	DOCUMENT ID TECN COMMENT
$0.24 \pm 0.05 \pm 0.12$	AUBERT 09M BABR $e^+e^- \rightarrow \gamma D^{(*)}\bar{D}$

$\Gamma(D^0\bar{D}^0)/\Gamma(D^*(2007)^0\bar{D}^0 + \text{c.c.})$	Γ_3/Γ_6
VALUE	DOCUMENT ID TECN COMMENT
0.05 ± 0.03	¹⁷ GOLDHABER 77 MRK1 e^+e^-

¹⁷ Phase-space factor (p^3) explicitly removed.

$\Gamma(D^*(2007)^0\bar{D}^0 + \text{c.c.})/\Gamma_{\text{total}}$	Γ_6/Γ
VALUE	DOCUMENT ID TECN COMMENT
seen	AUBERT 09M BABR $e^+e^- \rightarrow D^{*0}\bar{D}^0\gamma$
seen	CRONIN-HEN..09 CLEO $e^+e^- \rightarrow D^{*0}\bar{D}^0$

$\Gamma(D^*(2010)^+D^- + \text{c.c.})/\Gamma_{\text{total}}$	Γ_7/Γ
VALUE	DOCUMENT ID TECN COMMENT
seen	¹⁸ ZHUKOVA 18 BELL $e^+e^- \rightarrow D^{*+}D^-\gamma$
seen	AUBERT 09M BABR $e^+e^- \rightarrow D^{*+}D^-\gamma$
seen	CRONIN-HEN..09 CLEO $e^+e^- \rightarrow D^{*+}D^-$

$\bullet \bullet \bullet$ We do not use the following data for averages, fits, limits, etc. $\bullet \bullet \bullet$
¹⁸ Supersedes PAKHLOVA 07.

$\Gamma(D^*(2010)^+D^- + \text{c.c.})/\Gamma(D^*(2007)^0\bar{D}^0 + \text{c.c.})$	Γ_7/Γ_6
VALUE	DOCUMENT ID TECN COMMENT
$0.95 \pm 0.09 \pm 0.10$	AUBERT 09M BABR $e^+e^- \rightarrow \gamma D^*\bar{D}$

$\Gamma(D^*\bar{D}^*)/\Gamma(D^*\bar{D} + \text{c.c.})$	Γ_8/Γ_5
VALUE	DOCUMENT ID TECN COMMENT
$0.18 \pm 0.14 \pm 0.03$	AUBERT 09M BABR $e^+e^- \rightarrow \gamma D^{(*)}\bar{D}^{(*)}$

$\Gamma(D^*(2007)^0\bar{D}^*(2007)^0)/\Gamma_{\text{total}}$	Γ_9/Γ
VALUE	DOCUMENT ID TECN COMMENT
seen	AUBERT 09M BABR $e^+e^- \rightarrow D^{*0}\bar{D}^{*0}\gamma$
seen	CRONIN-HEN..09 CLEO $e^+e^- \rightarrow D^{*0}\bar{D}^{*0}$

$\Gamma(D^*(2007)^0\bar{D}^*(2007)^0)/\Gamma(D^*(2007)^0\bar{D}^0 + \text{c.c.})$	Γ_9/Γ_6
VALUE	DOCUMENT ID TECN COMMENT
32.0 ± 12.0	¹⁹ GOLDHABER 77 MRK1 e^+e^-

¹⁹ Phase-space factor (p^3) explicitly removed.

See key on page 999

Meson Particle Listings

$\psi(4040), X(4050)^\pm$

$\Gamma(D^*(2010)^+ D^*(2010)^-)/\Gamma_{total}$				Γ_{10}/Γ
VALUE	DOCUMENT ID	TECN	COMMENT	
seen	20 ZHUKOVA	18 BELL	$e^+ e^- \rightarrow D^{*+} D^{*-} \gamma$	
seen	AUBERT 09M	BABR	$e^+ e^- \rightarrow D^{*+} D^{*-} \gamma$	
seen	CRONIN-HEN..09	CLEO	$e^+ e^- \rightarrow D^{*+} D^{*-}$	
• • • We do not use the following data for averages, fits, limits, etc. • • •				
seen	PAKHLOVA 07	BELL	$e^+ e^- \rightarrow D^{*+} D^{*-} \gamma$	
20 Supersedes PAKHLOVA 07.				

$\Gamma(D^0 D^- \pi^+ + c.c. (excl. D^*(2007)^0 \bar{D}^0 + c.c., D^*(2010)^+ D^- + c.c.))/\Gamma_{total}$				Γ_{12}/Γ
VALUE	DOCUMENT ID	TECN	COMMENT	
not seen	PAKHLOVA 08A	BELL	$e^+ e^- \rightarrow D^0 D^- \pi^+ \gamma$	

$\Gamma(D \bar{D}^* \pi (excl. D^* \bar{D}^*))/\Gamma_{total}$				Γ_{13}/Γ
VALUE	DOCUMENT ID	TECN	COMMENT	
not seen	CRONIN-HEN..09	CLEO	$e^+ e^- \rightarrow D \bar{D}^* \pi$	

$\Gamma(D^0 \bar{D}^{*-} \pi^+ + c.c. (excl. D^*(2010)^+ D^*(2010)^-))/\Gamma_{total}$				Γ_{14}/Γ
VALUE	DOCUMENT ID	TECN	COMMENT	
seen	PAKHLOVA 09	BELL	$e^+ e^- \rightarrow D^0 D^{*-} \pi^+ \gamma$	

$\Gamma(D_s^+ D_s^-)/\Gamma_{total}$				Γ_{15}/Γ
VALUE	DOCUMENT ID	TECN	COMMENT	
seen	PAKHLOVA 11	BELL	$e^+ e^- \rightarrow D_s^+ D_s^- \gamma$	
seen	DEL-AMO-SA..10N	BABR	$e^+ e^- \rightarrow D_s^+ D_s^- \gamma$	
seen	CRONIN-HEN..09	CLEO	$e^+ e^- \rightarrow D_s^+ D_s^-$	

$\Gamma(J/\psi \pi^+ \pi^-)/\Gamma_{total}$				Γ_{17}/Γ
VALUE (units 10^{-3})	CL%	DOCUMENT ID	TECN	COMMENT
<4	90	COAN 06	CLEO	3.97-4.06 $e^+ e^- \rightarrow$ hadrons

$\Gamma(J/\psi \pi^0 \pi^0)/\Gamma_{total}$				Γ_{18}/Γ
VALUE (units 10^{-3})	CL%	DOCUMENT ID	TECN	COMMENT
<2	90	COAN 06	CLEO	3.97-4.06 $e^+ e^- \rightarrow$ hadrons

$\Gamma(J/\psi \eta)/\Gamma_{total}$				Γ_{19}/Γ
VALUE (units 10^{-3})	CL%	DOCUMENT ID	TECN	COMMENT
$5.2 \pm 0.5 \pm 0.5$		21 ABLIKIM 12k	BES3	$e^+ e^- \rightarrow \ell^+ \ell^- 2\gamma$
• • • We do not use the following data for averages, fits, limits, etc. • • •				
<7	90	COAN 06	CLEO	3.97-4.06 $e^+ e^- \rightarrow$ hadrons
21 ABLIKIM 12k measure $\sigma(e^+ e^- \rightarrow J/\psi \eta) = 32.1 \pm 2.8 \pm 1.3$ pb. They assume the η J/ψ fully originates from $\psi(4040)$ decays.				

$\Gamma(J/\psi \pi^0 \pi^0)/\Gamma_{total}$				Γ_{20}/Γ
VALUE (units 10^{-3})	CL%	DOCUMENT ID	TECN	COMMENT
<0.28	90	22 ABLIKIM 12k	BES3	$e^+ e^- \rightarrow \ell^+ \ell^- 2\gamma$
• • • We do not use the following data for averages, fits, limits, etc. • • •				
<2	90	COAN 06	CLEO	3.97-4.06 $e^+ e^- \rightarrow$ hadrons
22 ABLIKIM 12k measure $\sigma(e^+ e^- \rightarrow J/\psi \pi^0 \pi^0) < 1.6$ pb. They assume the η J/ψ fully originates from $\psi(4040)$ decays.				

$\Gamma(J/\psi \pi^+ \pi^- \pi^0)/\Gamma_{total}$				Γ_{21}/Γ
VALUE (units 10^{-3})	CL%	DOCUMENT ID	TECN	COMMENT
<2	90	COAN 06	CLEO	3.97-4.06 $e^+ e^- \rightarrow$ hadrons

$\Gamma(\chi_{c1} \gamma)/\Gamma_{total}$				Γ_{22}/Γ
VALUE (units 10^{-3})	CL%	DOCUMENT ID	TECN	COMMENT
• • • We do not use the following data for averages, fits, limits, etc. • • •				
<11	90	COAN 06	CLEO	3.97-4.06 $e^+ e^- \rightarrow$ hadrons

$\Gamma(\chi_{c2} \gamma)/\Gamma_{total}$				Γ_{23}/Γ
VALUE (units 10^{-3})	CL%	DOCUMENT ID	TECN	COMMENT
• • • We do not use the following data for averages, fits, limits, etc. • • •				
<17	90	COAN 06	CLEO	3.97-4.06 $e^+ e^- \rightarrow$ hadrons

$\Gamma(\chi_{c1} \pi^+ \pi^- \pi^0)/\Gamma_{total}$				Γ_{24}/Γ
VALUE (units 10^{-3})	CL%	DOCUMENT ID	TECN	COMMENT
<11	90	COAN 06	CLEO	3.97-4.06 $e^+ e^- \rightarrow$ hadrons

$\Gamma(\chi_{c2} \pi^+ \pi^- \pi^0)/\Gamma_{total}$				Γ_{25}/Γ
VALUE (units 10^{-3})	CL%	DOCUMENT ID	TECN	COMMENT
<32	90	COAN 06	CLEO	3.97-4.06 $e^+ e^- \rightarrow$ hadrons

$\Gamma(h_c(1P) \pi^+ \pi^-)/\Gamma_{total}$				Γ_{26}/Γ
VALUE (units 10^{-3})	CL%	DOCUMENT ID	TECN	COMMENT
<3	90	23 PEDLAR 11	CLEO	$e^+ e^- \rightarrow h_c(1P) \pi^+ \pi^-$

23 From several values of \sqrt{s} near the peak of the $\psi(4040)$, PEDLAR 11 measures $\sigma(e^+ e^- \rightarrow h_c(1P) \pi^+ \pi^-) = 1.0 \pm 8.0 \pm 5.4 \pm 0.2$ pb, where the errors are statistical, systematic, and due to uncertainty in $B(\psi(2S) \rightarrow \pi^0 h_c(1P))$, respectively.

$\Gamma(\phi \pi^+ \pi^-)/\Gamma_{total}$				Γ_{27}/Γ
VALUE (units 10^{-3})	CL%	DOCUMENT ID	TECN	COMMENT
<3	90	COAN 06	CLEO	3.97-4.06 $e^+ e^- \rightarrow$ hadrons

$\Gamma(\Lambda \bar{\Lambda} \pi^+ \pi^-)/\Gamma_{total}$				Γ_{28}/Γ
VALUE (units 10^{-4})	CL%	DOCUMENT ID	TECN	COMMENT
<2.9	90	24 ABLIKIM 13Q	BES3	$e^+ e^- \rightarrow \psi(4040)$
24 Assuming that interference effects between resonance and continuum can be neglected.				

$\Gamma(\Lambda \bar{\Lambda} \pi^0)/\Gamma_{total}$				Γ_{29}/Γ
VALUE (units 10^{-4})	CL%	DOCUMENT ID	TECN	COMMENT
<0.9	90	25 ABLIKIM 13Q	BES3	$e^+ e^- \rightarrow \psi(4040)$
25 Assuming that interference effects between resonance and continuum can be neglected.				

$\Gamma(\Lambda \bar{\Lambda} \eta)/\Gamma_{total}$				Γ_{30}/Γ
VALUE (units 10^{-4})	CL%	DOCUMENT ID	TECN	COMMENT
<3.0	90	26 ABLIKIM 13Q	BES3	$e^+ e^- \rightarrow \psi(4040)$
26 Assuming that interference effects between resonance and continuum can be neglected.				

$\Gamma(\Sigma^+ \bar{\Sigma}^-)/\Gamma_{total}$				Γ_{31}/Γ
VALUE (units 10^{-4})	CL%	DOCUMENT ID	TECN	COMMENT
<1.3	90	27 ABLIKIM 13Q	BES3	$e^+ e^- \rightarrow \psi(4040)$
27 Assuming that interference effects between resonance and continuum can be neglected.				

$\Gamma(\Sigma^0 \bar{\Sigma}^0)/\Gamma_{total}$				Γ_{32}/Γ
VALUE (units 10^{-4})	CL%	DOCUMENT ID	TECN	COMMENT
<0.7	90	28 ABLIKIM 13Q	BES3	$e^+ e^- \rightarrow \psi(4040)$
28 Assuming that interference effects between resonance and continuum can be neglected.				

$\Gamma(\Xi^+ \bar{\Xi}^-)/\Gamma_{total}$				Γ_{33}/Γ
VALUE (units 10^{-4})	CL%	DOCUMENT ID	TECN	COMMENT
<1.6	90	29 ABLIKIM 13Q	BES3	$e^+ e^- \rightarrow \psi(4040)$
29 Assuming that interference effects between resonance and continuum can be neglected.				

$\Gamma(\Xi^0 \bar{\Xi}^0)/\Gamma_{total}$				Γ_{34}/Γ
VALUE (units 10^{-4})	CL%	DOCUMENT ID	TECN	COMMENT
<1.8	90	30 ABLIKIM 13Q	BES3	$e^+ e^- \rightarrow \psi(4040)$
30 Assuming that interference effects between resonance and continuum can be neglected.				

$\psi(4040)$ REFERENCES

ZHUKOVA 18	PR D97 012002	V. Zhukova et al.	(BELLE Collab.)
HAN 15	PR D92 012011	Y.L. Han et al.	(BELLE Collab.)
ABLIKIM 13Q	PR D87 112011	Ablikim M. et al.	(BESIII Collab.)
WANG 13B	PR D87 051101	X.L. Wang et al.	(BELLE Collab.)
ABLIKIM 12K	PR D86 071101	M. Ablikim et al.	(BESIII Collab.)
PAKHLOVA 11	PR D83 011101	G. Pakhlova et al.	(BELLE Collab.)
PEDLAR 11	PRL 107 041803	T. Pedlar et al.	(CLEO Collab.)
DEL-AMO-SA...10N	PR D82 052004	P. del Amo Sanchez et al.	(BABAR Collab.)
MO 10	PR D82 077501	X.H. Mo, C.Z. Yuan, P. Wang	(BHEP)
AUBERT 09M	PR D79 092001	B. Aubert et al.	(BABAR Collab.)
CRONIN-HEN...09	PR D80 072001	D. Cronin-Hennessy et al.	(CLEO Collab.)
PAKHLOVA 09	PR D80 091101	G. Pakhlova et al.	(BELLE Collab.)
ABLIKIM 08D	PL B660 315	M. Ablikim et al.	(BES Collab.)
PAKHLOVA 08A	PR D77 011103	G. Pakhlova et al.	(BELLE Collab.)
PAKHLOVA 08A	PRL 100 062001	G. Pakhlova et al.	(BELLE Collab.)
PAKHLOVA 07	PRL 98 092001	G. Pakhlova et al.	(BELLE Collab.)
COAN 06	PRL 96 162003	T.E. Coan et al.	(CLEO Collab.)
SETH 05A	PR D72 017501	K.K. Seth	
BAI 02C	PRL 88 101802	J.Z. Bai et al.	(BES Collab.)
BAI 00	PRL 84 594	J.Z. Bai et al.	(BES Collab.)
OSTERHELD 86	SLAC-PUB-4160	A. Osterheld et al.	(SLAC Crystal Ball Collab.)
BRANDELK 78C	PL 76B 361	R. Brandelik et al.	(DASP Collab.)
Also	ZPHY C1 233	R. Brandelik et al.	(DASP Collab.)
FELDMAN 77	PRPL 33C 285	G.J. Feldman, M.L. Perl	(LBL, SLAC)
GOLDBABER 77	PL 69B 503	G. Goldhaber et al.	(Mark I Collab.)

$X(4050)^\pm$

$I^G(J^{PC}) = 1^-(?^?+)$
 I, G, C need confirmation.

OMITTED FROM SUMMARY TABLE

Properties incompatible with a $q\bar{q}$ structure (exotic state). See the review on non- $q\bar{q}$ states.

Observed by MIZUK 08 in the $\pi^+ \chi_{c1}(1P)$ invariant mass distribution in $\bar{B}^0 \rightarrow K^- \pi^+ \chi_{c1}(1P)$ decays. Not seen by LEES 12B in this same mode after accounting for K π resonant mass and angular structure.

$X(4050)^\pm$ MASS

VALUE (MeV)	DOCUMENT ID	TECN	COMMENT
$4051 \pm 14 \pm 20$	1 MIZUK 08	BELL	$\bar{B}^0 \rightarrow K^- \pi^+ \chi_{c1}(1P)$

1 From a Dalitz plot analysis with two Breit-Wigner amplitudes.

Meson Particle Listings

 $X(4050)^\pm$, $X(4055)^\pm$, $X(4100)^\pm$ $X(4050)^\pm$ WIDTH

VALUE (MeV)	DOCUMENT ID	TECN	COMMENT
82^{+21+47}_{-17-22}	¹ MIZUK 08 BELL		$\overline{B}^0 \rightarrow K^- \pi^+ \chi_{c1}(1P)$

¹ From a Dalitz plot analysis with two Breit-Wigner amplitudes.

 $X(4050)^\pm$ DECAY MODES

Mode	Fraction (Γ_i/Γ)
Γ_1 $\pi^+ \chi_{c1}(1P)$	seen
Γ_2 $\pi^\pm \psi(3770)$	not seen

 $X(4050)^\pm$ BRANCHING RATIOS

$\Gamma(\pi^+ \chi_{c1}(1P))/\Gamma_{\text{total}}$	VALUE	DOCUMENT ID	TECN	COMMENT	Γ_1/Γ
seen		¹ MIZUK 08 BELL		$\overline{B}^0 \rightarrow K^- \pi^+ \chi_{c1}(1P)$	
not seen		² LEES 12B BABR		$B \rightarrow K \pi \chi_{c1}(1P)$	

¹ With a product branching fraction measurement of $B(\overline{B}^0 \rightarrow K^- X(4050)^+) \times B(X(4050)^+ \rightarrow \pi^+ \chi_{c1}(1P)) = (3.0^{+1.5+3.7}_{-0.8-1.6}) \times 10^{-5}$.

² With a product branching fraction limit of $B(\overline{B}^0 \rightarrow X(4050)^+ K^-) \times B(X(4050)^+ \rightarrow \chi_{c1} \pi^+) < 1.8 \times 10^{-5}$ at 90% CL.

$\Gamma(\pi^\pm \psi(3770))/\Gamma_{\text{total}}$	VALUE	DOCUMENT ID	TECN	COMMENT	Γ_2/Γ
not seen		¹ ABLIKIM 19AR BES3		$e^+ e^- \rightarrow \pi^+ \pi^- D \overline{D}$	

¹ From a measurement of $\sigma(e^+ e^- \rightarrow \pi^+ \pi^- D \overline{D})$ between $\sqrt{s} = 4.08$ and 4.6 GeV.

 $X(4050)^\pm$ REFERENCES

ABLIKIM	19AR	PR D100 032005	M. Ablikim <i>et al.</i>	(BESIII Collab.)
LEES	12B	PR D85 052003	J.P. Lees <i>et al.</i>	(BABAR Collab.)
MIZUK	08	PR D78 072004	R. Mizuk <i>et al.</i>	(BELLE Collab.)

 $X(4055)^\pm$

$$J^G(J^{PC}) = 1^+(?^2-)$$

I, G, C need confirmation.

OMITTED FROM SUMMARY TABLE

Properties incompatible with a $q\overline{q}$ structure (exotic state). See the review on non- $q\overline{q}$ states.

Needs confirmation. Seen by WANG 15A in the $\psi(2S)\pi^+$ invariant mass distribution in $\psi(4360) \rightarrow \psi(2S)\pi^+\pi^-$ decay.

 $X(4055)^\pm$ MASS

VALUE (MeV)	DOCUMENT ID	TECN	COMMENT
$4054 \pm 3 \pm 1$	¹ WANG 15A BELL		$10.58 e^+ e^- \rightarrow \gamma \pi^+ \pi^- \psi(2S)$
4039.3 ± 6.0	² ABLIKIM 18K BES3		$e^+ e^- \rightarrow \pi^0 \pi^0 \psi(2S)$
4032.1 ± 2.4	³ ABLIKIM 17V BES3		$e^+ e^- \rightarrow \pi^+ \pi^- \psi(2S)$

- • • We do not use the following data for averages, fits, limits, etc. • • •
- ¹ Statistical significance of 3.5 σ .
- ² Statistical error only, with significance of 5.9 σ (from a fit with a 19% CL). Identified as the same structure observed in ABLIKIM 17V in $e^+ e^- \rightarrow \pi^+ \pi^- \psi(2S)$ decays.
- ³ Statistical error only, with significance of 9.2 σ . From an unbinned maximum likelihood fit of the $\pi^+ \pi^- \psi(2S)$ Dalitz plot from data collected at $\sqrt{s} = 4.416$ GeV for a $J^C = 1^+$ state. The fit does not match the detailed structure of the data, having a C.L. of only 8%.

 $X(4055)^\pm$ WIDTH

VALUE (MeV)	DOCUMENT ID	TECN	COMMENT
$45 \pm 11 \pm 6$	¹ WANG 15A BELL		$10.58 e^+ e^- \rightarrow \gamma \pi^+ \pi^- \psi(2S)$
31.9 ± 14.8	² ABLIKIM 18K BES3		$e^+ e^- \rightarrow \pi^0 \pi^0 \psi(2S)$
26.1 ± 5.3	³ ABLIKIM 17V BES3		$e^+ e^- \rightarrow \pi^+ \pi^- \psi(2S)$

- • • We do not use the following data for averages, fits, limits, etc. • • •
- ¹ Statistical significance of 3.5 σ .
- ² Statistical error only, with significance of 5.9 σ (from a fit with a 19% CL). Identified as the same structure observed in ABLIKIM 17V in $e^+ e^- \rightarrow \pi^+ \pi^- \psi(2S)$ decays.
- ³ Statistical error only, with significance of 9.2 σ . From an unbinned maximum likelihood fit of the $\pi^+ \pi^- \psi(2S)$ Dalitz plot from data collected at $\sqrt{s} = 4.416$ GeV for a $J^C = 1^+$ state. The fit does not match the detailed structure of the data, having a C.L. of only 8%.

 $X(4055)^\pm$ DECAY MODES

Mode	Fraction (Γ_i/Γ)
Γ_1 $\pi^+ \psi(2S)$	seen
Γ_2 $\pi^\pm \psi(3770)$	not seen

 $X(4055)^\pm$ BRANCHING RATIOS

$\Gamma(\pi^+ \psi(2S))/\Gamma_{\text{total}}$	VALUE	DOCUMENT ID	TECN	COMMENT	Γ_1/Γ
seen		¹ WANG 15A BELL		$10.58 e^+ e^- \rightarrow \gamma \pi^+ \pi^- \psi(2S)$	

¹ Statistical significance of 3.5 σ .

$\Gamma(\pi^\pm \psi(3770))/\Gamma_{\text{total}}$	VALUE	DOCUMENT ID	TECN	COMMENT	Γ_2/Γ
not seen		¹ ABLIKIM 19AR BES3		$e^+ e^- \rightarrow \pi^+ \pi^- D \overline{D}$	

¹ From a measurement of $\sigma(e^+ e^- \rightarrow \pi^+ \pi^- D \overline{D})$ between $\sqrt{s} = 4.08$ and 4.6 GeV.

 $X(4055)^\pm$ REFERENCES

ABLIKIM	19AR	PR D100 032005	M. Ablikim <i>et al.</i>	(BESIII Collab.)
ABLIKIM	18K	PR D97 052001	M. Ablikim <i>et al.</i>	(BESIII Collab.)
ABLIKIM	17V	PR D96 032004	M. Ablikim <i>et al.</i>	(BESIII Collab.)
Also		PR D99 019903 (errata.)	M. Ablikim <i>et al.</i>	(BESIII Collab.)
WANG	15A	PR D91 112007	X.L. Wang <i>et al.</i>	(BELLE Collab.)

 $X(4100)^\pm$

$$J^G(J^{PC}) = 1^-(???)$$

OMITTED FROM SUMMARY TABLE

Properties incompatible with a $q\overline{q}$ structure (exotic state). See the review on non- $q\overline{q}$ states.

Reported by AAIJ 18AN in the $\eta_c(1S)\pi^-$ invariant mass distribution in $B^0 \rightarrow \eta_c(1S)K^+\pi^-$ decays with a significance of 3.4 σ . $J^P = 0^+$ or 1^- assignment consistent with data.

 $X(4100)^\pm$ MASS

VALUE (MeV)	DOCUMENT ID	TECN	COMMENT
$4096 \pm 20^{+18}_{-22}$	AAIJ 18AN LHCB		$B^0 \rightarrow \eta_c(1S)K^+\pi^-$

 $X(4100)^\pm$ WIDTH

VALUE (MeV)	DOCUMENT ID	TECN	COMMENT
$152 \pm 5 \pm 60_{-35}$	AAIJ 18AN LHCB		$B^0 \rightarrow \eta_c(1S)K^+\pi^-$

 $X(4100)^\pm$ DECAY MODES

Mode	Fraction (Γ_i/Γ)
Γ_1 $\eta_c(1S)\pi^-$	seen
Γ_2 $\pi^\pm \psi(3770)$	not seen

 $X(4100)^\pm$ BRANCHING RATIOS

$\Gamma(\eta_c(1S)\pi^-)/\Gamma_{\text{total}}$	VALUE	DOCUMENT ID	TECN	COMMENT	Γ_1/Γ
seen		¹ AAIJ 18AN LHCB		$B^0 \rightarrow \eta_c(1S)K^+\pi^-$	

¹ AAIJ 18AN quotes a fit fraction for $B^0 \rightarrow X(4100)^- K^+ \rightarrow \eta_c(1S)\pi^- K^+$ of $(3.3 \pm 1.1^{+1.2}_{-1.1})\%$ from an amplitude analysis.

$\Gamma(\pi^\pm \psi(3770))/\Gamma_{\text{total}}$	VALUE	DOCUMENT ID	TECN	COMMENT	Γ_2/Γ
not seen		¹ ABLIKIM 19AR BES3		$e^+ e^- \rightarrow \pi^+ \pi^- D \overline{D}$	

¹ From a measurement of $\sigma(e^+ e^- \rightarrow \pi^+ \pi^- D \overline{D})$ between $\sqrt{s} = 4.08$ and 4.6 GeV.

 $X(4100)^\pm$ REFERENCES

ABLIKIM	19AR	PR D100 032005	M. Ablikim <i>et al.</i>	(BESIII Collab.)
AAIJ	18AN	EPJ C78 1019	R. Aaij <i>et al.</i>	(LHCb Collab.)

See key on page 999

Meson Particle Listings

$\chi_{c1}(4140), \psi(4160)$

$\chi_{c1}(4140)$

$I^G(J^{PC}) = 0^+(1^{++})$

was $X(4140)$

This state shows properties different from a conventional $q\bar{q}$ state. A candidate for an exotic structure. See the review on non- $q\bar{q}$ states.

Seen by AALTONEN 09AH, ABAZOV 14A, CHATRCHYAN 14M, AAIJ 17C in $B^+ \rightarrow \chi_{c1} K^+$, $\chi_{c1} \rightarrow J/\psi\phi$, and by ABAZOV 15M separately in both prompt (4.7 σ) and non-prompt (5.6 σ) production in $p\bar{p} \rightarrow J/\psi\phi + \text{anything}$. Not seen by SHEN 10 in $\gamma\gamma \rightarrow J/\psi\phi$ and ABLIKIM 15 in $e^+e^- \rightarrow \gamma J/\psi\phi$ at $\sqrt{s} = 4.23, 4.26, 4.36$ GeV.

$\chi_{c1}(4140)$ MASS

VALUE (MeV)	EVTs	DOCUMENT ID	TECN	COMMENT
4146.8 ± 2.4 OUR AVERAGE		Error includes scale factor of 1.1.		
4146.5 ± 4.5 ^{+4.6} _{-2.8}	4289	¹ AAIJ	17c LHCb	$B^+ \rightarrow J/\psi\phi K^+$
4143.4 ± 2.9 ^{+2.9} _{-3.0} ± 0.6	19	² AALTONEN	17 CDF	$B^+ \rightarrow J/\psi\phi K^+$
4152.5 ± 1.7 ^{+6.2} _{-5.4}	616	³ ABAZOV	15M D0	$p\bar{p} \rightarrow J/\psi\phi + \text{anything}$
4159.0 ± 4.3 ± 6.6	52	⁴ ABAZOV	14A D0	$B^+ \rightarrow J/\psi\phi K^+$
4148.0 ± 2.4 ± 6.3	0.3k	⁵ CHATRCHYAN 14M	CMS	$B^+ \rightarrow J/\psi\phi K^+$
• • • We do not use the following data for averages, fits, limits, etc. • • •				
4143.0 ± 2.9 ± 1.2	14	^{6,7} AALTONEN	09AH CDF	$B^+ \rightarrow J/\psi\phi K^+$

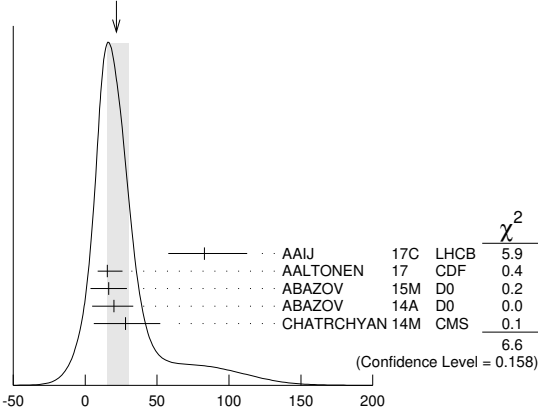
- ¹ From an amplitude analysis of the decay $B^+ \rightarrow J/\psi\phi K^+$ with a significance of 8.4 σ .
- ² Statistical significance of more than 5 σ .
- ³ Statistical significance of more than 6 σ .
- ⁴ Statistical significance of 3.1 σ .
- ⁵ From a fit assuming an S-wave relativistic Breit-Wigner shape above a three-body phase-space non-resonant component with statistical significance of more than 5 σ .
- ⁶ Statistical significance of 3.8 σ .
- ⁷ Superseded by AALTONEN 17.

$\chi_{c1}(4140)$ WIDTH

VALUE (MeV)	EVTs	DOCUMENT ID	TECN	COMMENT
22 ± 8 OUR AVERAGE		Error includes scale factor of 1.3. See the ideogram below.		
83 ± 21 ± 21 ⁺⁸ ₋₁₄	4289	¹ AAIJ	17c LHCb	$B^+ \rightarrow J/\psi\phi K^+$
15.3 ± 10.4 ± 6.1 ± 2.5	19	² AALTONEN	17 CDF	$B^+ \rightarrow J/\psi\phi K^+$
16.3 ± 5.6 ± 11.4	616	³ ABAZOV	15M D0	$p\bar{p} \rightarrow J/\psi\phi + \text{anything}$
20 ± 13 ± 3 ⁺³ ₋₈	52	⁴ ABAZOV	14A D0	$B^+ \rightarrow J/\psi\phi K^+$
28 ± 15 ± 11 ± 19	0.3k	⁵ CHATRCHYAN 14M	CMS	$B^+ \rightarrow J/\psi\phi K^+$
• • • We do not use the following data for averages, fits, limits, etc. • • •				
11.7 ± 8.3 ± 5.0 ± 3.7	14	^{6,7} AALTONEN	09AH CDF	$B^+ \rightarrow J/\psi\phi K^+$

- ¹ From an amplitude analysis of the decay $B^+ \rightarrow J/\psi\phi K^+$ with a significance of 8.4 σ .
- ² Statistical significance of more than 5 σ .
- ³ Statistical significance of more than 6 σ .
- ⁴ Statistical significance of 3.1 σ .
- ⁵ From a fit assuming an S-wave relativistic Breit-Wigner shape above a three-body phase-space non-resonant component with statistical significance of more than 5 σ .
- ⁶ Statistical significance of 3.8 σ .
- ⁷ Superseded by AALTONEN 17.

WEIGHTED AVERAGE
22±8.7 (Error scaled by 1.3)



$\chi_{c1}(4140)$ DECAY MODES

Mode	Fraction (Γ_i/Γ)
Γ_1 $J/\psi\phi$	seen
Γ_2 $\gamma\gamma$	not seen

$\chi_{c1}(4140)$ $\Gamma(i)\Gamma(\gamma\gamma)/\Gamma(\text{total})$

VALUE (eV)	CL%	DOCUMENT ID	TECN	COMMENT	$\Gamma_2\Gamma_1/\Gamma$
<41	90	¹ SHEN	10 BELL	$10.6 e^+e^- \rightarrow e^+e^- J/\psi\phi$	
• • • We do not use the following data for averages, fits, limits, etc. • • •					
< 6	90	² SHEN	10 BELL	$10.6 e^+e^- \rightarrow e^+e^- J/\psi\phi$	

- ¹ For $J^P = 0^+$.
- ² For $J^P = 2^+$.

$\chi_{c1}(4140)$ BRANCHING RATIOS

$\Gamma(J/\psi\phi)/\Gamma_{\text{total}}$	EVTs	DOCUMENT ID	TECN	COMMENT	Γ_1/Γ
seen	4289	¹ AAIJ	17c LHCb	$B^+ \rightarrow J/\psi\phi K^+$	
seen	616	² ABAZOV	15M D0	$p\bar{p} \rightarrow J/\psi\phi + \text{anything}$	
seen	52	³ ABAZOV	14A D0	$B^+ \rightarrow J/\psi\phi K^+$	
seen	0.3k	⁴ CHATRCHYAN 14M	CMS	$B^+ \rightarrow J/\psi\phi K^+$	
seen	14	⁵ AALTONEN	09AH CDF	$B^+ \rightarrow J/\psi\phi K^+$	
• • • We do not use the following data for averages, fits, limits, etc. • • •					
not seen		⁶ ABLIKIM	15 BES3	$e^+e^- \rightarrow \gamma\phi J/\psi$	
not seen		⁷ AAIJ	12AA LHCb	$p\bar{p} \rightarrow B^+ X$ at 7 TeV	

- ¹ From an amplitude analysis of the decay $B^+ \rightarrow J/\psi\phi K^+$ with a significance of 8.4 σ .
- ² Statistical significance of more than 6 σ .
- ³ ABAZOV 14A reports $B(B^+ \rightarrow \chi_{c1}(4140) K^+ \rightarrow J/\psi\phi K^+)/B(B^+ \rightarrow J/\psi\phi K^+) = (19 \pm 7 \pm 4)\%$ with 3.1 σ significance.
- ⁴ From a fit assuming an S-wave relativistic Breit-Wigner shape above a three-body phase-space non-resonant component with statistical significance of more than 5 σ .
- ⁵ Statistical significance of 3.8 σ .
- ⁶ Reported $\sigma(e^+e^- \rightarrow \gamma\chi_{c1}(4140)) \cdot B(\chi_{c1}(4140) \rightarrow J/\psi\phi) < 0.35, 0.28,$ and 0.33 pb at 4.23, 4.26, and 4.36 GeV, respectively, at 90% CL.
- ⁷ Reported $B(B^+ \rightarrow \chi_{c1}(4140) K^+) \cdot B(\chi_{c1}(4140) \rightarrow J/\psi\phi)/B(B^+ \rightarrow J/\psi\phi K^+) < 0.07$ at 90% CL.

$\Gamma(\gamma\gamma)/\Gamma_{\text{total}}$	DOCUMENT ID	TECN	COMMENT	Γ_2/Γ
not seen	SHEN	10 BELL	$10.6 e^+e^- \rightarrow e^+e^- J/\psi\phi$	

$\chi_{c1}(4140)$ REFERENCES

AAIJ	17C	PRL 118 022003	R. Aaij et al.	(LHCb Collab.) JP
Also		PR D95 012002	R. Aaij et al.	(LHCb Collab.)
AALTONEN	17	MPL A32 1750139	T. Aaltonen et al.	(CDF Collab.)
ABAZOV	15M	PRL 115 232001	V.M. Abazov et al.	(D0 Collab.)
ABLIKIM	15	PR D91 032002	M. Ablikim et al.	(BESIII Collab.)
ABAZOV	14A	PR D89 012004	V.M. Abazov et al.	(D0 Collab.)
CHATRCHYAN	14M	PL B734 261	S. Chatrchyan et al.	(CMS Collab.)
AAIJ	12AA	PR D85 091103	R. Aaij et al.	(LHCb Collab.)
SHEN	10	PRL 104 112004	C.P. Shen et al.	(BELLE Collab.)
AALTONEN	09AH	PRL 102 242002	T. Aaltonen et al.	(CDF Collab.)

$\psi(4160)$

$I^G(J^{PC}) = 0^-(1^{--})$

$\psi(4160)$ MASS

VALUE (MeV)	DOCUMENT ID	TECN	COMMENT
4191 ± 5 OUR AVERAGE			
4191 ± 9 ⁺⁹ ₋₈	AAIJ	13Bc LHCb	$B^+ \rightarrow K^+ \mu^+ \mu^-$
4191.7 ± 6.5	¹ ABLIKIM	08D BES2	$e^+e^- \rightarrow \text{hadrons}$
• • • We do not use the following data for averages, fits, limits, etc. • • •			
4193 ± 7	² MO	10 RVUE	$e^+e^- \rightarrow \text{hadrons}$
4151 ± 4	³ SETH	05A RVUE	$e^+e^- \rightarrow \text{hadrons}$
4155 ± 5	⁴ SETH	05A RVUE	$e^+e^- \rightarrow \text{hadrons}$
4159 ± 20	BRANDELIK	78c DASP	e^+e^-

- ¹ Reanalysis of data presented in BAI 02c. From a global fit over the center-of-mass energy region 3.7–5.0 GeV covering the $\psi(3770), \psi(4040), \psi(4160),$ and $\psi(4415)$ resonances. Phase angle fixed in the fit to $\delta = (293 \pm 57)^\circ$.
- ² Reanalysis of data presented in BAI 00 and BAI 02c. From a global fit over the center-of-mass energy 3.8–4.8 GeV covering the $\psi(4040), \psi(4160)$ and $\psi(4415)$ resonances and including interference effects.
- ³ From a fit to Crystal Ball (OSTERHELD 86) data.
- ⁴ From a fit to BES (BAI 02c) data.

Meson Particle Listings

 $\psi(4160)$ $\psi(4160)$ WIDTH

VALUE (MeV)	DOCUMENT ID	TECN	COMMENT
70 ± 10 OUR AVERAGE			
65 ⁺²² ₋₁₆	AAIJ	13Bc LHCB	$B^+ \rightarrow K^+ \mu^+ \mu^-$
71.8 ± 12.3	¹ ABLIKIM	08D BES2	$e^+ e^- \rightarrow \text{hadrons}$
• • • We do not use the following data for averages, fits, limits, etc. • • •			
79 ± 14	² MO	10 RVUE	$e^+ e^- \rightarrow \text{hadrons}$
107 ± 10	³ SETH	05A RVUE	$e^+ e^- \rightarrow \text{hadrons}$
107 ± 16	⁴ SETH	05A RVUE	$e^+ e^- \rightarrow \text{hadrons}$
78 ± 20	BRANDELIK	78c DASP	$e^+ e^-$

¹ Reanalysis of data presented in BAI 02c. From a global fit over the center-of-mass energy region 3.7–5.0 GeV covering the $\psi(3770)$, $\psi(4040)$, $\psi(4160)$, and $\psi(4415)$ resonances. Phase angle fixed in the fit to $\delta = (293 \pm 57)^\circ$.

² Reanalysis of data presented in BAI 00 and BAI 02c. From a global fit over the center-of-mass energy 3.8–4.8 GeV covering the $\psi(4040)$, $\psi(4160)$ and $\psi(4415)$ resonances and including interference effects.

³ From a fit to Crystal Ball (OSTERHELD 86) data.

⁴ From a fit to BES (BAI 02c) data.

 $\psi(4160)$ DECAY MODES

Due to the complexity of the $c\bar{c}$ threshold region, in this listing, “seen” (“not seen”) means that a cross section for the mode in question has been measured at effective \sqrt{s} near this particle’s central mass value, more (less) than 2σ above zero, without regard to any peaking behavior in \sqrt{s} or absence thereof. See mode listing(s) for details and references.

Mode	Fraction (Γ_i/Γ)	Confidence level
Γ_1 $e^+ e^-$	$(6.9 \pm 3.3) \times 10^{-6}$	
Γ_2 $\mu^+ \mu^-$	seen	
Γ_3 $D\bar{D}$	seen	
Γ_4 $D^0 \bar{D}^0$	seen	
Γ_5 $D^+ D^-$	seen	
Γ_6 $D^* \bar{D}^+ + \text{c.c.}$	seen	
Γ_7 $D^*(2007)^0 \bar{D}^0 + \text{c.c.}$	seen	
Γ_8 $D^*(2010)^+ D^- + \text{c.c.}$	seen	
Γ_9 $D^* \bar{D}^*$	seen	
Γ_{10} $D^*(2007)^0 \bar{D}^*(2007)^0$	seen	
Γ_{11} $D^*(2010)^+ D^*(2010)^-$	seen	
Γ_{12} $D^0 D^- \pi^+ + \text{c.c. (excl. } D^*(2007)^0 \bar{D}^0 + \text{c.c., } D^*(2010)^+ D^- + \text{c.c.)}$	not seen	
Γ_{13} $D\bar{D}^* \pi + \text{c.c. (excl. } D^* \bar{D}^*)$	seen	
Γ_{14} $D^0 D^* \pi^+ + \text{c.c. (excl. } D^*(2010)^+ D^*(2010)^-)$	not seen	
Γ_{15} $D_s^+ D_s^-$	not seen	
Γ_{16} $D_s^+ D_s^- + \text{c.c.}$	seen	
Γ_{17} $J/\psi \pi^+ \pi^-$	< 3	$\times 10^{-3}$ 90%
Γ_{18} $J/\psi \pi^0 \pi^0$	< 3	$\times 10^{-3}$ 90%
Γ_{19} $J/\psi K^+ K^-$	< 2	$\times 10^{-3}$ 90%
Γ_{20} $J/\psi \eta$	< 8	$\times 10^{-3}$ 90%
Γ_{21} $J/\psi \pi^0$	< 1	$\times 10^{-3}$ 90%
Γ_{22} $J/\psi \eta'$	< 5	$\times 10^{-3}$ 90%
Γ_{23} $J/\psi \pi^+ \pi^- \pi^0$	< 1	$\times 10^{-3}$ 90%
Γ_{24} $\psi(2S) \pi^+ \pi^-$	< 4	$\times 10^{-3}$ 90%
Γ_{25} $\chi_{c1} \gamma$	< 5	$\times 10^{-3}$ 90%
Γ_{26} $\chi_{c2} \gamma$	< 1.3	% 90%
Γ_{27} $\chi_{c1} \pi^+ \pi^- \pi^0$	< 2	$\times 10^{-3}$ 90%
Γ_{28} $\chi_{c2} \pi^+ \pi^- \pi^0$	< 8	$\times 10^{-3}$ 90%
Γ_{29} $h_c(1P) \pi^+ \pi^-$	< 5	$\times 10^{-3}$ 90%
Γ_{30} $h_c(1P) \pi^0 \pi^0$	< 2	$\times 10^{-3}$ 90%
Γ_{31} $h_c(1P) \eta$	< 2	$\times 10^{-3}$ 90%
Γ_{32} $h_c(1P) \pi^0$	< 4	$\times 10^{-4}$ 90%
Γ_{33} $\phi \pi^+ \pi^-$	< 2	$\times 10^{-3}$ 90%
Γ_{34} $\gamma \chi_{c1}(3872) \rightarrow \gamma J/\psi \pi^+ \pi^-$	< 6.8	$\times 10^{-5}$ 90%
Γ_{35} $\gamma X(3915) \rightarrow \gamma J/\psi \pi^+ \pi^-$	< 1.36	$\times 10^{-4}$ 90%
Γ_{36} $\gamma X(3930) \rightarrow \gamma J/\psi \pi^+ \pi^-$	< 1.18	$\times 10^{-4}$ 90%
Γ_{37} $\gamma X(3940) \rightarrow \gamma J/\psi \pi^+ \pi^-$	< 1.47	$\times 10^{-4}$ 90%
Γ_{38} $\gamma \chi_{c1}(3872) \rightarrow \gamma \gamma J/\psi$	< 1.05	$\times 10^{-4}$ 90%
Γ_{39} $\gamma X(3915) \rightarrow \gamma \gamma J/\psi$	< 1.26	$\times 10^{-4}$ 90%
Γ_{40} $\gamma X(3930) \rightarrow \gamma \gamma J/\psi$	< 8.8	$\times 10^{-5}$ 90%
Γ_{41} $\gamma X(3940) \rightarrow \gamma \gamma J/\psi$	< 1.79	$\times 10^{-4}$ 90%
Γ_{42} $K^+ K^-$		
Γ_{43} $K_S^0 K^\pm \pi^\mp$		

 $\psi(4160)$ PARTIAL WIDTHS

$\Gamma(e^+ e^-)$	DOCUMENT ID	TECN	COMMENT	Γ_1
0.48 ± 0.22	¹ ABLIKIM	08D BES2	$e^+ e^- \rightarrow \text{hadrons}$	
• • • We do not use the following data for averages, fits, limits, etc. • • •				
0.4 to 1.1	² MO	10 RVUE	$e^+ e^- \rightarrow \text{hadrons}$	
0.83 ± 0.08	³ SETH	05A RVUE	$e^+ e^- \rightarrow \text{hadrons}$	
0.84 ± 0.13	⁴ SETH	05A RVUE	$e^+ e^- \rightarrow \text{hadrons}$	
0.77 ± 0.23	BRANDELIK	78c DASP	$e^+ e^-$	

¹ Reanalysis of data presented in BAI 02c. From a global fit over the center-of-mass energy region 3.7–5.0 GeV covering the $\psi(3770)$, $\psi(4040)$, $\psi(4160)$, and $\psi(4415)$ resonances. Phase angle fixed in the fit to $\delta = (293 \pm 57)^\circ$.

² Reanalysis of data presented in BAI 00 and BAI 02c. From a global fit over the center-of-mass energy 3.8–4.8 GeV covering the $\psi(4040)$, $\psi(4160)$ and $\psi(4415)$ resonances and including interference effects. Four sets of solutions are obtained with the same fit quality, mass and total width, but with different $e^+ e^-$ partial widths. We quote only the range of values.

³ From a fit to Crystal Ball (OSTERHELD 86) data.

⁴ From a fit to BES (BAI 02c) data.

 $\psi(4160)$ $\Gamma(i) \times \Gamma(e^+ e^-)/\Gamma(\text{total})$

$\Gamma(J/\psi \eta) \times \Gamma(e^+ e^-)/\Gamma(\text{total})$	VALUE (eV)	EVTS	DOCUMENT ID	TECN	COMMENT	$\Gamma_{22}\Gamma_1/\Gamma$
• • • We do not use the following data for averages, fits, limits, etc. • • •						
0.17 ± 0.04	86	^{1,2}	ABLIKIM	20A BES3	$e^+ e^- \rightarrow \eta' J/\psi$	
1.07 ± 0.09	86	^{1,3}	ABLIKIM	20A BES3	$e^+ e^- \rightarrow \eta' J/\psi$	

¹ Based on a fit to $\sigma(e^+ e^- \rightarrow \eta' J/\psi)$ from $\sqrt{s} = 4.18$ to 4.60 GeV assuming interfering $\psi(4160)$ and $\psi(4260)$ contributions. At $\sqrt{s} = 4.18$ GeV, $\sigma(e^+ e^- \rightarrow \eta' J/\psi) = 2.4 \pm 0.3 \pm 0.2$ pb.

² Solution I of the fit, corresponding to a phase of -0.03 ± 0.44 rad.

³ Solution II of the fit, corresponding to a phase of 2.54 ± 0.04 rad.

$\Gamma(\chi_{c1} \gamma) \times \Gamma(e^+ e^-)/\Gamma(\text{total})$	VALUE (eV)	CL%	DOCUMENT ID	TECN	COMMENT	$\Gamma_{25}\Gamma_1/\Gamma$
< 2.2	90		¹ HAN	15 BELL	$10.58 e^+ e^- \rightarrow \chi_{c1} \gamma$	

¹ Using $B(\eta \rightarrow \gamma \gamma) = (39.41 \pm 0.21)\%$.

$\Gamma(\chi_{c2} \gamma) \times \Gamma(e^+ e^-)/\Gamma(\text{total})$	VALUE (eV)	CL%	DOCUMENT ID	TECN	COMMENT	$\Gamma_{26}\Gamma_1/\Gamma$
• • • We do not use the following data for averages, fits, limits, etc. • • •						
< 6.1	90		¹ HAN	15 BELL	$10.58 e^+ e^- \rightarrow \chi_{c2} \gamma$	

¹ Using $B(\eta \rightarrow \gamma \gamma) = (39.41 \pm 0.21)\%$.

$\Gamma(K_S^0 K^\pm \pi^\mp) \times \Gamma(e^+ e^-)/\Gamma(\text{total})$	VALUE (eV)	DOCUMENT ID	TECN	COMMENT	$\Gamma_{43}\Gamma_1/\Gamma$
• • • We do not use the following data for averages, fits, limits, etc. • • •					
2.71 ± 0.13 ± 0.12		¹ ABLIKIM	19A BES3	$e^+ e^- \rightarrow K_S^0 K^\pm \pi^\mp$	
0.0095 ± 0.0088 ± 0.0004		² ABLIKIM	19A BES3	$e^+ e^- \rightarrow K_S^0 K^\pm \pi^\mp$	

¹ Solution I of the fit including the $\psi(4160)$ with mass 4191 ± 5 MeV and width 70 ± 10 MeV from PDG 16 and the $\psi(4230)$ with mass $4219.6 \pm 3.3 \pm 5.1$ MeV and width $56.0 \pm 3.6 \pm 6.9$ MeV from GAO 17.

² Solution II of the fit including the $\psi(4160)$ with mass 4191 ± 5 MeV and width 70 ± 10 MeV from PDG 16 and the $\psi(4230)$ with mass $4219.6 \pm 3.3 \pm 5.1$ MeV and width $56.0 \pm 3.6 \pm 6.9$ MeV from GAO 17.

 $\psi(4160)$ $\Gamma(i) \times \Gamma(e^+ e^-)/\Gamma^2(\text{total})$

$\Gamma(J/\psi \eta)/\Gamma(\text{total}) \times \Gamma(e^+ e^-)/\Gamma(\text{total})$	VALUE (units 10^{-8})	DOCUMENT ID	TECN	COMMENT	$\Gamma_{20}/\Gamma \times \Gamma_1/\Gamma$
• • • We do not use the following data for averages, fits, limits, etc. • • •					
2.8 ± 0.9 ± 0.9		¹ WANG	13B BELL	$e^+ e^- \rightarrow J/\psi \eta \gamma$	
12.8 ± 1.7 ± 2.0		² WANG	13B BELL	$e^+ e^- \rightarrow J/\psi \eta \gamma$	

¹ Solution I of two equivalent solutions in a fit using two interfering resonances. Mass and width fixed at 4153 MeV and 103 MeV, respectively.

² Solution II of two equivalent solutions in a fit using two interfering resonances. Mass and width fixed at 4153 MeV and 103 MeV, respectively.

 $\psi(4160)$ BRANCHING RATIOS

$\Gamma(\mu^+ \mu^-)/\Gamma(\text{total})$	DOCUMENT ID	TECN	COMMENT	Γ_2/Γ
seen	¹ AAIJ	13Bc LHCB	$B^+ \rightarrow K^+ \mu^+ \mu^-$	

¹ AAIJ 13Bc report $B(B^+ \rightarrow K^+ \psi(4160)) B(\psi(4160) \rightarrow \mu^+ \mu^-) = (3.5^{+0.9}_{-0.8}) \times 10^{-9}$.

$\Gamma(D\bar{D})/\Gamma(D^* \bar{D}^*)$	DOCUMENT ID	TECN	COMMENT	Γ_3/Γ_9
0.02 ± 0.03 ± 0.02	AUBERT	09M BABR	$e^+ e^- \rightarrow \gamma D^*(*) \bar{D}^*(*)$	

$\Gamma(D^0\bar{D}^0)/\Gamma_{total}$ Γ_4/Γ

VALUE	DOCUMENT ID	TECN	COMMENT
seen	CRONIN-HEN..09	CLEO	$e^+e^- \rightarrow D^0\bar{D}^0$
seen	PAKHLOVA 08	BELL	$e^+e^- \rightarrow D^0\bar{D}^0\gamma$
••• We do not use the following data for averages, fits, limits, etc. •••			
not seen	AUBERT 09M	BABR	$e^+e^- \rightarrow D^0\bar{D}^0\gamma$

$\Gamma(D^+D^-)/\Gamma_{total}$ Γ_5/Γ

VALUE	DOCUMENT ID	TECN	COMMENT
seen	CRONIN-HEN..09	CLEO	$e^+e^- \rightarrow D^+D^-$
seen	PAKHLOVA 08	BELL	$e^+e^- \rightarrow D^+D^-\gamma$
••• We do not use the following data for averages, fits, limits, etc. •••			
not seen	AUBERT 09M	BABR	$e^+e^- \rightarrow D^+D^-\gamma$

$\Gamma(D^*(2007)^0\bar{D}^0 + c.c.)/\Gamma_{total}$ Γ_7/Γ

VALUE	DOCUMENT ID	TECN	COMMENT
seen	AUBERT 09M	BABR	$e^+e^- \rightarrow D^{*0}\bar{D}^0\gamma$
seen	CRONIN-HEN..09	CLEO	$e^+e^- \rightarrow D^{*0}\bar{D}^0$

$\Gamma(D^*(2010)^+D^- + c.c.)/\Gamma_{total}$ Γ_8/Γ

VALUE	DOCUMENT ID	TECN	COMMENT
seen	¹ ZHUKOVA 18	BELL	$e^+e^- \rightarrow D^{*+}D^-\gamma$
seen	AUBERT 09M	BABR	$e^+e^- \rightarrow D^{*+}D^-\gamma$
seen	CRONIN-HEN..09	CLEO	$e^+e^- \rightarrow D^{*+}D^-$
••• We do not use the following data for averages, fits, limits, etc. •••			
seen	PAKHLOVA 07	BELL	$e^+e^- \rightarrow D^{*+}D^-\gamma$
¹ Supersedes PAKHLOVA 07.			

$\Gamma(D^*\bar{D}^+ + c.c.)/\Gamma(D^*\bar{D}^*)$ Γ_6/Γ_9

VALUE	DOCUMENT ID	TECN	COMMENT
0.34 ± 0.14 ± 0.05	AUBERT 09M	BABR	$e^+e^- \rightarrow \gamma D^{(*)}\bar{D}^{(*)}$

$\Gamma(D^*(2007)^0\bar{D}^*(2007)^0)/\Gamma_{total}$ Γ_{10}/Γ

VALUE	DOCUMENT ID	TECN	COMMENT
seen	AUBERT 09M	BABR	$e^+e^- \rightarrow D^{*0}\bar{D}^{*0}\gamma$
seen	CRONIN-HEN..09	CLEO	$e^+e^- \rightarrow D^{*0}\bar{D}^{*0}$

$\Gamma(D^*(2010)^+D^*(2010)^-)/\Gamma_{total}$ Γ_{11}/Γ

VALUE	DOCUMENT ID	TECN	COMMENT
seen	¹ ZHUKOVA 18	BELL	$e^+e^- \rightarrow D^{*+}D^{*-}\gamma$
seen	AUBERT 09M	BABR	$e^+e^- \rightarrow D^{*+}D^{*-}\gamma$
seen	CRONIN-HEN..09	CLEO	$e^+e^- \rightarrow D^{*+}D^{*-}$
••• We do not use the following data for averages, fits, limits, etc. •••			
seen	PAKHLOVA 07	BELL	$e^+e^- \rightarrow D^{*+}D^{*-}\gamma$
¹ Supersedes PAKHLOVA 07.			

$\Gamma(D^0D^-\pi^+ + c.c. (excl. D^*(2007)^0\bar{D}^0 + c.c., D^*(2010)^+D^-\pi^+ + c.c.))/\Gamma_{total}$ Γ_{12}/Γ

VALUE	DOCUMENT ID	TECN	COMMENT
not seen	PAKHLOVA 08A	BELL	$e^+e^- \rightarrow D^0D^-\pi^+\gamma$

$\Gamma(D\bar{D}^*\pi + c.c. (excl. D^*\bar{D}^*))/\Gamma_{total}$ Γ_{13}/Γ

VALUE	DOCUMENT ID	TECN	COMMENT
seen	CRONIN-HEN..09	CLEO	$e^+e^- \rightarrow D\bar{D}^*\pi$

$\Gamma(D^0D^{*-}\pi^+ + c.c. (excl. D^*(2010)^+D^*(2010)^-))/\Gamma_{total}$ Γ_{14}/Γ

VALUE	DOCUMENT ID	TECN	COMMENT
not seen	PAKHLOVA 09	BELL	$e^+e^- \rightarrow D^0D^{*-}\pi^+\gamma$

$\Gamma(D_s^+D_s^-)/\Gamma_{total}$ Γ_{15}/Γ

VALUE	DOCUMENT ID	TECN	COMMENT
not seen	PAKHLOVA 11	BELL	$e^+e^- \rightarrow D_s^+D_s^-\gamma$
not seen	DEL-AMO-SA..10N	BABR	$e^+e^- \rightarrow D_s^+D_s^-\gamma$
not seen	CRONIN-HEN..09	CLEO	$e^+e^- \rightarrow D_s^+D_s^-$

$\Gamma(D_s^{*+}D_s^- + c.c.)/\Gamma_{total}$ Γ_{16}/Γ

VALUE	DOCUMENT ID	TECN	COMMENT
seen	PAKHLOVA 11	BELL	$e^+e^- \rightarrow D_s^{*+}D_s^-\gamma$
seen	DEL-AMO-SA..10N	BABR	$e^+e^- \rightarrow D_s^{*+}D_s^-\gamma$
seen	CRONIN-HEN..09	CLEO	$e^+e^- \rightarrow D_s^{*+}D_s^-$

$\Gamma(J/\psi\pi^+\pi^-)/\Gamma_{total}$ Γ_{17}/Γ

VALUE (units 10 ⁻³)	CL%	DOCUMENT ID	TECN	COMMENT
<3	90	COAN 06	CLEO	4.12-4.2 e ⁺ e ⁻ → hadrons

$\Gamma(J/\psi\pi^0\pi^0)/\Gamma_{total}$ Γ_{18}/Γ

VALUE (units 10 ⁻³)	CL%	DOCUMENT ID	TECN	COMMENT
<3	90	COAN 06	CLEO	4.12-4.2 e ⁺ e ⁻ → hadrons

$\Gamma(J/\psi K^+K^-)/\Gamma_{total}$ Γ_{19}/Γ

VALUE (units 10 ⁻³)	CL%	DOCUMENT ID	TECN	COMMENT
<2	90	COAN 06	CLEO	4.12-4.2 e ⁺ e ⁻ → hadrons

$\Gamma(J/\psi\eta)/\Gamma_{total}$ Γ_{20}/Γ

VALUE (units 10 ⁻³)	CL%	DOCUMENT ID	TECN	COMMENT
<8	90	COAN 06	CLEO	4.12-4.2 e ⁺ e ⁻ → hadrons
••• We do not use the following data for averages, fits, limits, etc. •••				
possibly seen		¹ ABLIKIM 15L	BES3	$e^+e^- \rightarrow J/\psi\eta$
seen		WANG 13B	BELL	$e^+e^- \rightarrow J/\psi\eta\gamma$
¹ An enhancement around 4.2 GeV is observed.				

$\Gamma(J/\psi\pi^0)/\Gamma_{total}$ Γ_{21}/Γ

VALUE (units 10 ⁻³)	CL%	DOCUMENT ID	TECN	COMMENT
<1	90	COAN 06	CLEO	4.12-4.2 e ⁺ e ⁻ → hadrons

$\Gamma(J/\psi\eta)/\Gamma_{total}$ Γ_{22}/Γ

VALUE (units 10 ⁻³)	CL%	DOCUMENT ID	TECN	COMMENT
<5	90	COAN 06	CLEO	4.12-4.2 e ⁺ e ⁻ → hadrons

$\Gamma(J/\psi\pi^+\pi^-\pi^0)/\Gamma_{total}$ Γ_{23}/Γ

VALUE (units 10 ⁻³)	CL%	DOCUMENT ID	TECN	COMMENT
<1	90	COAN 06	CLEO	4.12-4.2 e ⁺ e ⁻ → hadrons

$\Gamma(\psi(2S)\pi^+\pi^-)/\Gamma_{total}$ Γ_{24}/Γ

VALUE (units 10 ⁻³)	CL%	DOCUMENT ID	TECN	COMMENT
<4	90	COAN 06	CLEO	4.12-4.2 e ⁺ e ⁻ → hadrons

$\Gamma(\chi_{c1}\gamma)/\Gamma_{total}$ Γ_{25}/Γ

VALUE (units 10 ⁻³)	CL%	DOCUMENT ID	TECN	COMMENT
<7	90	COAN 06	CLEO	4.12-4.2 e ⁺ e ⁻ → hadrons
••• We do not use the following data for averages, fits, limits, etc. •••				

$\Gamma(\chi_{c2}\gamma)/\Gamma_{total}$ Γ_{26}/Γ

VALUE (units 10 ⁻³)	CL%	DOCUMENT ID	TECN	COMMENT
<13	90	COAN 06	CLEO	4.12-4.2 e ⁺ e ⁻ → hadrons

$\Gamma(\chi_{c1}\pi^+\pi^-\pi^0)/\Gamma_{total}$ Γ_{27}/Γ

VALUE (units 10 ⁻³)	CL%	DOCUMENT ID	TECN	COMMENT
<2	90	COAN 06	CLEO	4.12-4.2 e ⁺ e ⁻ → hadrons

$\Gamma(\chi_{c2}\pi^+\pi^-\pi^0)/\Gamma_{total}$ Γ_{28}/Γ

VALUE (units 10 ⁻³)	CL%	DOCUMENT ID	TECN	COMMENT
<8	90	COAN 06	CLEO	4.12-4.2 e ⁺ e ⁻ → hadrons

$\Gamma(h_c(1P)\pi^+\pi^-)/\Gamma_{total}$ Γ_{29}/Γ

VALUE (units 10 ⁻³)	CL%	DOCUMENT ID	TECN	COMMENT
<5	90	¹ PEDLAR 11	CLEO	$e^+e^- \rightarrow h_c(1P)\pi^+\pi^-$
¹ At $\sqrt{s} = 4170$ MeV, PEDLAR 11 measures $\sigma(e^+e^- \rightarrow h_c(1P)\pi^+\pi^-) = 15.6 \pm 2.3 \pm 1.9 \pm 3.0$ pb, where the errors are statistical, systematic, and due to uncertainty in $B(\psi(2S) \rightarrow \pi^0 h_c(1P))$, respectively.				

$\Gamma(h_c(1P)\pi^0\pi^0)/\Gamma_{total}$ Γ_{30}/Γ

VALUE (units 10 ⁻³)	CL%	DOCUMENT ID	TECN	COMMENT
<2	90	¹ PEDLAR 11	CLEO	$e^+e^- \rightarrow h_c(1P)\pi^0\pi^0$
¹ At $\sqrt{s} = 4170$ MeV, PEDLAR 11 measures $\sigma(e^+e^- \rightarrow h_c(1P)\pi^0\pi^0) = 3.0 \pm 3.3 \pm 1.1 \pm 0.6$ pb, where the errors are statistical, systematic, and due to uncertainty in $B(\psi(2S) \rightarrow \pi^0 h_c(1P))$, respectively.				

$\Gamma(h_c(1P)\eta)/\Gamma_{total}$ Γ_{31}/Γ

VALUE (units 10 ⁻³)	CL%	EVTS	DOCUMENT ID	TECN	COMMENT
<2	90		¹ PEDLAR 11	CLEO	$e^+e^- \rightarrow h_c(1P)\eta$
••• We do not use the following data for averages, fits, limits, etc. •••					
possibly seen		41	² ABLIKIM 17R	BES3	$e^+e^- \rightarrow h_c(1P)\eta$
¹ At $\sqrt{s} = 4170$ MeV, PEDLAR 11 measures $\sigma(e^+e^- \rightarrow h_c(1P)\eta) = 4.7 \pm 1.7 \pm 1.0 \pm 0.9$ pb, where the errors are statistical, systematic, and due to uncertainty in $B(\psi(2S) \rightarrow \pi^0 h_c(1P))$, respectively.					
² An enhancement around 4.2 GeV is observed.					

$\Gamma(h_c(1P)\pi^0)/\Gamma_{total}$ Γ_{32}/Γ

VALUE (units 10 ⁻³)	CL%	DOCUMENT ID	TECN	COMMENT
<0.4	90	¹ PEDLAR 11	CLEO	$e^+e^- \rightarrow h_c(1P)\pi^0$
¹ At $\sqrt{s} = 4170$ MeV, PEDLAR 11 measures $\sigma(e^+e^- \rightarrow h_c(1P)\pi^0) = -0.7 \pm 1.8 \pm 0.7 \pm 0.1$ pb, where the errors are statistical, systematic, and due to uncertainty in $B(\psi(2S) \rightarrow \pi^0 h_c(1P))$, respectively.				

$\Gamma(\phi\pi^+\pi^-)/\Gamma_{total}$ Γ_{33}/Γ

VALUE (units 10 ⁻³)	CL%	DOCUMENT ID	TECN	COMMENT
<2	90	COAN 06	CLEO	4.12-4.2 e ⁺ e ⁻ → hadrons

Meson Particle Listings

$\psi(4160)$, $X(4160)$, $Z_c(4200)$, $\psi(4230)$

$\Gamma(\gamma\chi_{c1}(3872) \rightarrow \gamma J/\psi\pi^+\pi^-)/\Gamma_{\text{total}}$				Γ_{34}/Γ
VALUE	CL%	DOCUMENT ID	COMMENT	
$<0.68 \times 10^{-4}$	90	¹ XIAO 13	$\psi(4160) \rightarrow \gamma J/\psi\pi^+\pi^-$	

¹ Obtained by analyzing CLEO data but not authored by the CLEO Collaboration.

$\Gamma(\gamma X(3915) \rightarrow \gamma J/\psi\pi^+\pi^-)/\Gamma_{\text{total}}$				Γ_{35}/Γ
VALUE	CL%	DOCUMENT ID	COMMENT	
$<1.36 \times 10^{-4}$	90	¹ XIAO 13	$\psi(4160) \rightarrow \gamma J/\psi\pi^+\pi^-$	

¹ Obtained by analyzing CLEO data but not authored by the CLEO Collaboration.

$\Gamma(\gamma X(3930) \rightarrow \gamma J/\psi\pi^+\pi^-)/\Gamma_{\text{total}}$				Γ_{36}/Γ
VALUE	CL%	DOCUMENT ID	COMMENT	
$<1.18 \times 10^{-4}$	90	¹ XIAO 13	$\psi(4160) \rightarrow \gamma J/\psi\pi^+\pi^-$	

¹ Obtained by analyzing CLEO data but not authored by the CLEO Collaboration.

$\Gamma(\gamma X(3940) \rightarrow \gamma J/\psi\pi^+\pi^-)/\Gamma_{\text{total}}$				Γ_{37}/Γ
VALUE	CL%	DOCUMENT ID	COMMENT	
$<1.47 \times 10^{-4}$	90	¹ XIAO 13	$\psi(4160) \rightarrow \gamma J/\psi\pi^+\pi^-$	

¹ Obtained by analyzing CLEO data but not authored by the CLEO Collaboration.

$\Gamma(\gamma\chi_{c1}(3872) \rightarrow \gamma\gamma J/\psi)/\Gamma_{\text{total}}$				Γ_{38}/Γ
VALUE	CL%	DOCUMENT ID	COMMENT	
$<1.05 \times 10^{-4}$	90	¹ XIAO 13	$\psi(4160) \rightarrow \gamma\gamma J/\psi$	

¹ Obtained by analyzing CLEO data but not authored by the CLEO Collaboration.

$\Gamma(\gamma X(3915) \rightarrow \gamma\gamma J/\psi)/\Gamma_{\text{total}}$				Γ_{39}/Γ
VALUE	CL%	DOCUMENT ID	COMMENT	
$<1.26 \times 10^{-4}$	90	¹ XIAO 13	$\psi(4160) \rightarrow \gamma\gamma J/\psi$	

¹ Obtained by analyzing CLEO data but not authored by the CLEO Collaboration.

$\Gamma(\gamma X(3930) \rightarrow \gamma\gamma J/\psi)/\Gamma_{\text{total}}$				Γ_{40}/Γ
VALUE	CL%	DOCUMENT ID	COMMENT	
$<0.88 \times 10^{-4}$	90	¹ XIAO 13	$\psi(4160) \rightarrow \gamma\gamma J/\psi$	

¹ Obtained by analyzing CLEO data but not authored by the CLEO Collaboration.

$\Gamma(\gamma X(3940) \rightarrow \gamma\gamma J/\psi)/\Gamma_{\text{total}}$				Γ_{41}/Γ
VALUE	CL%	DOCUMENT ID	COMMENT	
$<1.79 \times 10^{-4}$	90	¹ XIAO 13	$\psi(4160) \rightarrow \gamma\gamma J/\psi$	

¹ Obtained by analyzing CLEO data but not authored by the CLEO Collaboration.

$\Gamma(K^+K^-)/\Gamma_{\text{total}}$					Γ_{42}/Γ
VALUE	CL%	DOCUMENT ID	TECN	COMMENT	
$<2 \times 10^{-5}$	90	¹ DRUZHININ 15	RVUE	$e^+e^- \rightarrow \psi(3770)$	

• • • We do not use the following data for averages, fits, limits, etc. • • •

¹ DRUZHININ 15 uses BABAR and CLEO data takitaking into account interference of the processes $e^+e^- \rightarrow K^+K^-$ and $e^+e^- \rightarrow K_S^0 K_L^0$.

$\psi(4160)$ REFERENCES

ABLIKIM 20A	PR D101 012008	M. Ablikim et al.	(BESIII Collab.)
ABLIKIM 19AE	PR D99 072005	M. Ablikim et al.	(BESIII Collab.)
ZHUKOVA 18	PR D97 012002	V. Zhukova et al.	(BELLE Collab.)
ABLIKIM 17R	PR D96 012001	M. Ablikim et al.	(BESIII Collab.)
GAO 17	PR D95 092007	X.Y. Gao, C.P. Shen, C.Z. Yuan	(PDG Collab.)
PDG 16	CP C40 100001	C. Patrignani et al.	(BESIII Collab.)
ABLIKIM 15L	PR D91 112005	M. Ablikim et al.	(NOVO Collab.)
DRUZHININ 15	PR D92 054024	V.P. Druzhinin	(NOVO Collab.)
HAN 15	PR D92 012011	Y.L. Han et al.	(BELLE Collab.)
AAIJ 13BC	PRL 111 112003	R. Aaij et al.	(LHCb Collab.)
WANG 13B	PR D87 051101	X.L. Wang et al.	(BELLE Collab.)
XIAO 13	PR D87 057501	T. Xiao et al.	(NWES, WAYN Collab.)
PAKHOVA 11	PR D83 011101	G. Pakhlova et al.	(BELLE Collab.)
PEDLAR 11	PRL 107 041803	T. Pedlar et al.	(CLEO Collab.)
DEL-AMO-SA... 10N	PR D82 052004	P. del Amo Sanchez et al.	(BABAR Collab.)
MO 10	PR D82 077501	X.H. Mo, C.Z. Yuan, P. Wang	(BHEP Collab.)
AUBERT 09M	PR D79 092001	B. Aubert et al.	(BABAR Collab.)
CRONIN-HEN... 09	PR D80 072001	D. Cronin-Hennessy et al.	(CLEO Collab.)
PAKHOVA 09	PR D80 091101	G. Pakhlova et al.	(BELLE Collab.)
ABLIKIM 08D	PL B660 315	M. Ablikim et al.	(BES Collab.)
PAKHOVA 08	PR D77 011103	G. Pakhlova et al.	(BELLE Collab.)
PAKHOVA 08A	PRL 100 062001	G. Pakhlova et al.	(BELLE Collab.)
PAKHOVA 07	PRL 98 092001	G. Pakhlova et al.	(BELLE Collab.)
COAN 06	PRL 96 162003	T.E. Coan et al.	(CLEO Collab.)
SETH 05A	PR D72 017501	K.K. Seth	(CLEO Collab.)
BAI 02C	PRL 88 101802	J.Z. Bai et al.	(BES Collab.)
BAI 00	PRL 84 594	J.Z. Bai et al.	(BES Collab.)
OSTERHELD 86	SLAC-PUB-4160	A. Osterheld et al.	(SLAC Crystal Ball Collab.)
BRANDELIK 78C	PL 76B 361	R. Brandelik et al.	(DASP Collab.)

X(4160) $I^G(J^{PC}) = ?^?(?^?)$

OMITTED FROM SUMMARY TABLE

Seen by PAKHOVA 08 in $e^+e^- \rightarrow J/\psi X$, $X \rightarrow D^*\bar{D}^*$

X(4160) MASS

VALUE (MeV)	EVTS	DOCUMENT ID	TECN	COMMENT
$4156^{+25}_{-20} \pm 15$	24	PAKHOVA 08	BELL	$e^+e^- \rightarrow J/\psi X$

X(4160) WIDTH

VALUE (MeV)	EVTS	DOCUMENT ID	TECN	COMMENT
$139^{+111}_{-61} \pm 21$	24	PAKHOVA 08	BELL	$e^+e^- \rightarrow J/\psi X$

X(4160) DECAY MODES

Mode	Fraction (Γ_i/Γ)
Γ_1 $D\bar{D}$	not seen
Γ_2 $D^*\bar{D} + \text{c.c.}$	not seen
Γ_3 $D^*\bar{D}^*$	seen

X(4160) BRANCHING RATIOS

$\Gamma(D\bar{D})/\Gamma(D^*\bar{D}^*)$				Γ_1/Γ_3
VALUE	CL%	DOCUMENT ID	TECN	COMMENT
<0.09	90	PAKHOVA 08	BELL	$e^+e^- \rightarrow J/\psi X$

$\Gamma(D^*\bar{D} + \text{c.c.})/\Gamma(D^*\bar{D}^*)$				Γ_2/Γ_3
VALUE	CL%	DOCUMENT ID	TECN	COMMENT
<0.22	90	PAKHOVA 08	BELL	$e^+e^- \rightarrow J/\psi X$

X(4160) REFERENCES

PAKHOVA 08	PRL 100 202001	P. Pakhlov et al.	(BELLE Collab.)
------------	----------------	-------------------	-----------------

Z_c(4200) $I^G(J^{PC}) = 1^+(1^+ -)$
 I, G, C need confirmation.

OMITTED FROM SUMMARY TABLE

was X(4200)[±]

This state shows properties different from a conventional $q\bar{q}$ state. A candidate for an exotic structure. See the review on non- $q\bar{q}$ states.

Reported by CHILIKIN 14 in $J/\psi\pi^+$ at a significance of 6.2 σ . Assignments of 0⁻, 1⁻, 2⁻, and 2⁺ excluded at 6.1 σ , 7.4 σ , 4.4 σ , and 7.0 σ level, respectively. Needs confirmation.

Z_c(4200) MASS

VALUE (MeV)	DOCUMENT ID	TECN	COMMENT
4196^{+31+17}_{-29-13}	CHILIKIN 14	BELL	$\bar{B}^0 \rightarrow J/\psi K^- \pi^+$

Z_c(4200) WIDTH

VALUE (MeV)	DOCUMENT ID	TECN	COMMENT
$370 \pm 70^{+70}_{-132}$	CHILIKIN 14	BELL	$\bar{B}^0 \rightarrow J/\psi K^- \pi^+$

Z_c(4200) DECAY MODES

Mode	Fraction (Γ_i/Γ)
Γ_1 $J/\psi\pi^+$	seen

Z_c(4200) BRANCHING RATIOS

$\Gamma(J/\psi\pi^+)/\Gamma_{\text{total}}$				Γ_1/Γ
VALUE	DOCUMENT ID	TECN	COMMENT	
seen	CHILIKIN 14	BELL	$\bar{B}^0 \rightarrow J/\psi K^- \pi^+$	

• • • We do not use the following data for averages, fits, limits, etc. • • •

possibly seen ¹AAIJ 19R LHCb $B^0 \rightarrow K^+\pi^- J/\psi + \text{c.c.}$

¹ From a model-independent analysis.

Z_c(4200) REFERENCES

AAIJ 19R	PRL 122 152002	R. Aaij et al.	(LHCb Collab.)
CHILIKIN 14	PR D90 112009	K. Chilikin et al.	(BELLE Collab.)

$\psi(4230)$ $I^G(J^{PC}) = 0^-(1^- -)$

also known as Y(4230); was X(4230)

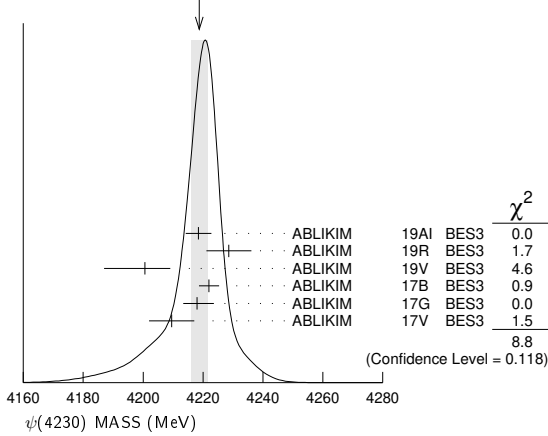
The recent measurement of $e^+e^- \rightarrow J/\psi\pi\pi$ (ABLIKIM 17B) led to a downward shift in the mass of the $\psi(4260)$, also known as Y(4260), such that a distinction between the $\psi(4260)$ and $\psi(4230)$ no longer appears justified. Therefore, starting from this edition, we include the data of ABLIKIM 17B in this node and have listed the $\psi(4230)$ in the summary tables instead of the $\psi(4260)$.

$\psi(4230)$ MASS

VALUE (MeV)	EVTS	DOCUMENT ID	TECN	COMMENT
4220 ± 15	OUR ESTIMATE			
4218.7 ± 2.8	OUR AVERAGE			Error includes scale factor of 1.3. See the ideogram below.
4218.5 ± 1.6 ± 4.0		¹ ABLIKIM	19A1 BES3	$e^+e^- \rightarrow \omega\chi_{c0}$
4228.6 ± 4.1 ± 6.3		ABLIKIM	19R BES3	$e^+e^- \rightarrow \pi^+D^0D^{*-} + c.c.$
4200.6 + 7.9 - 13.3 ± 3.0		² ABLIKIM	19V BES3	$e^+e^- \rightarrow \gamma\chi_{c1}(3872)$
4222.0 ± 3.1 ± 1.4		³ ABLIKIM	17B BES3	$e^+e^- \rightarrow \pi^+\pi^-J/\psi$
4218 + 5.5 - 4.5 ± 0.9		ABLIKIM	17G BES3	$e^+e^- \rightarrow \pi^+\pi^-h_c$
4209.5 ± 7.4 ± 1.4		⁴ ABLIKIM	17V BES3	$e^+e^- \rightarrow \pi^+\pi^-\psi(2S)$
4230 ± 8 ± 6	180	⁵ ABLIKIM	15c BES3	$e^+e^- \rightarrow \omega\chi_{c0}$

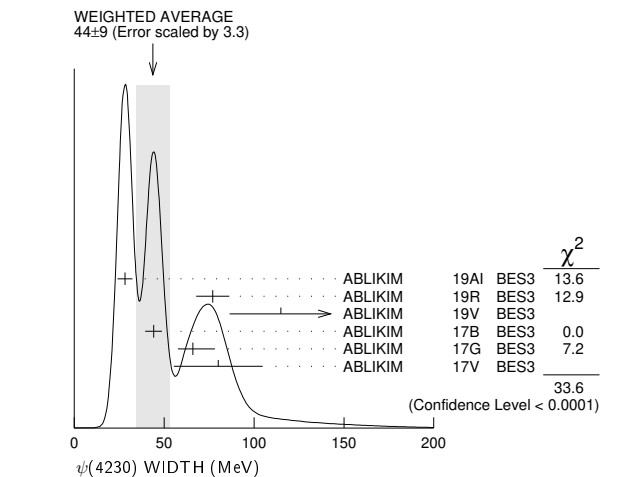
- ¹ From a fit of the measured cross section from $\sqrt{s} = 4.178-4.278$ GeV. Supersedes ABLIKIM 15c.
- ² Simultaneous fit to $\chi_{c1} \rightarrow \omega J/\psi$ and $\chi_{c1} \rightarrow \pi^+\pi^-J/\psi$.
- ³ From a three-resonance fit.
- ⁴ From a fit to the cross section for $e^+e^- \rightarrow \pi^+\pi^-\psi(2S) \rightarrow 2(\pi^+\pi^-)\ell^+\ell^-$ obtained from 16 center-of-mass energies between 4.008 and 4.600 GeV and comprising 5.1 fb⁻¹.
- ⁵ From a 3-parameter fit of measured cross sections from $\sqrt{s} = 4.21-4.42$ GeV to a phase-space modified Breit-Wigner function, using the decays $\chi_{c0} \rightarrow \pi^+\pi^-$, $\chi_{c0} \rightarrow K^+K^-$, and $\omega \rightarrow \pi^+\pi^-\pi^0$.

WEIGHTED AVERAGE
4218.7 ± 2.8 (Error scaled by 1.3)



$\psi(4230)$ WIDTH

VALUE (MeV)	EVTS	DOCUMENT ID	TECN	COMMENT
20 to 100	OUR ESTIMATE			
44 ± 9	OUR AVERAGE			Error includes scale factor of 3.3. See the ideogram below.
28.2 ± 3.9 ± 1.6		¹ ABLIKIM	19A1 BES3	$e^+e^- \rightarrow \omega\chi_{c0}$
77.0 ± 6.8 ± 6.3		ABLIKIM	19R BES3	$e^+e^- \rightarrow \pi^+D^0D^{*-} + c.c.$
115 + 38 - 26 ± 12		² ABLIKIM	19V BES3	$e^+e^- \rightarrow \gamma\chi_{c1}(3872)$
44.1 ± 4.3 ± 2.0		³ ABLIKIM	17B BES3	$e^+e^- \rightarrow \pi^+\pi^-J/\psi$
66.0 + 12.3 - 8.3 ± 0.4		ABLIKIM	17G BES3	$e^+e^- \rightarrow \pi^+\pi^-h_c$
80.1 ± 24.6 ± 2.9		⁴ ABLIKIM	17V BES3	$e^+e^- \rightarrow \pi^+\pi^-\psi(2S)$
38 ± 12 ± 2	180	⁵ ABLIKIM	15c BES3	$e^+e^- \rightarrow \omega\chi_{c0}$



- ¹ From a fit of the measured cross section from $\sqrt{s} = 4.178-4.278$ GeV. Supersedes ABLIKIM 15c.

- ² Simultaneous fit to $\chi_{c1} \rightarrow \omega J/\psi$ and $\chi_{c1} \rightarrow \pi^+\pi^-J/\psi$.
- ³ From a three-resonance fit.
- ⁴ From a fit to the cross section for $e^+e^- \rightarrow \pi^+\pi^-\psi(2S) \rightarrow 2(\pi^+\pi^-)\ell^+\ell^-$ obtained from 16 center-of-mass energies between 4.008 and 4.600 GeV and comprising 5.1 fb⁻¹.
- ⁵ From a 3-parameter fit of measured cross sections from $\sqrt{s} = 4.21-4.42$ GeV to a phase-space modified Breit-Wigner function, using the decays $\chi_{c0} \rightarrow \pi^+\pi^-$, $\chi_{c0} \rightarrow K^+K^-$, and $\omega \rightarrow \pi^+\pi^-\pi^0$.

$\psi(4230)$ DECAY MODES

Mode	Fraction (Γ_i/Γ)
Γ_1 e^+e^-	
Γ_2 $\omega\chi_{c0}$	seen
Γ_3 $\pi^+\pi^-h_c$	seen
Γ_4 $\pi^+\pi^-J/\psi$	seen
Γ_5 $\pi^+\pi^-\psi(2S)$	seen
Γ_6 $\pi^+D^0D^{*-} + c.c.$	seen
Γ_7 $\Xi^-\Xi^+$	
Γ_8 $\gamma\chi_{c1}(3872)$	seen

$\psi(4230)$ $\Gamma(i)\Gamma(e^+e^-)/\Gamma(\text{total})$

VALUE (eV)	EVTS	DOCUMENT ID	TECN	COMMENT	$\Gamma_2\Gamma_1/\Gamma$
2.5 ± 0.2 ± 0.3		¹ ABLIKIM	19A1 BES3	$e^+e^- \rightarrow \omega\chi_{c0}$	
• • •				We do not use the following data for averages, fits, limits, etc. • • •	
2.7 ± 0.5 ± 0.4	180	² ABLIKIM	15c BES3	$e^+e^- \rightarrow \omega\chi_{c0}$	

- ¹ From a fit of the measured cross section from $\sqrt{s} = 4.178-4.278$ GeV. Supersedes ABLIKIM 15c.
- ² From a 3-parameter fit of measured cross sections from $\sqrt{s} = 4.21-4.42$ GeV to a phase-space modified Breit-Wigner function, using the decays $\chi_{c0} \rightarrow \pi^+\pi^-$, $\chi_{c0} \rightarrow K^+K^-$, and $\omega \rightarrow \pi^+\pi^-\pi^0$.

$\Gamma(\pi^+\pi^-\psi(2S)) \times \Gamma(e^+e^-)/\Gamma(\text{total})$

VALUE (eV)	DOCUMENT ID	TECN	COMMENT	$\Gamma_5\Gamma_1/\Gamma$
• • •			We do not use the following data for averages, fits, limits, etc. • • •	
1.6 ± 1.3	¹ ABLIKIM	19K BES3	$e^+e^- \rightarrow \pi^+\pi^-\psi(2S)$	
1.8 ± 1.4	² ABLIKIM	19K BES3	$e^+e^- \rightarrow \pi^+\pi^-\psi(2S)$	

- ¹ Solution I of two equivalent solutions in a fit using two interfering resonances.
- ² Solution II of two equivalent solutions in a fit using two interfering resonances.

$\Gamma(\Xi^-\Xi^+) \times \Gamma(e^+e^-)/\Gamma(\text{total})$

VALUE (eV)	CL%	DOCUMENT ID	TECN	COMMENT	$\Gamma_7\Gamma_1/\Gamma$
< 3.3 × 10⁻⁴	90	ABLIKIM	20c BES3	$e^+e^- \rightarrow \Xi^-\Xi^+$	

$\psi(4230)$ BRANCHING RATIOS

$\Gamma(\omega\chi_{c0})/\Gamma(\text{total})$

VALUE	EVTS	DOCUMENT ID	TECN	COMMENT	Γ_2/Γ
seen	180	¹ ABLIKIM	15c BES3	$e^+e^- \rightarrow \omega\chi_{c0}$	

- ¹ From a 3-parameter fit of measured cross sections from $\sqrt{s} = 4.21-4.42$ GeV to a phase-space modified Breit-Wigner function, using the decays $\chi_{c0} \rightarrow \pi^+\pi^-$, $\chi_{c0} \rightarrow K^+K^-$, and $\omega \rightarrow \pi^+\pi^-\pi^0$.

$\Gamma(\pi^+\pi^-h_c)/\Gamma(\text{total})$

VALUE	DOCUMENT ID	TECN	COMMENT	Γ_3/Γ
seen	ABLIKIM	17G BES3	$e^+e^- \rightarrow \pi^+\pi^-h_c$	

$\Gamma(\pi^+\pi^-J/\psi)/\Gamma(\text{total})$

VALUE	DOCUMENT ID	TECN	COMMENT	Γ_4/Γ
seen	ABLIKIM	17B BES3	$e^+e^- \rightarrow \pi^+\pi^-J/\psi$	

$\Gamma(\pi^+\pi^-\psi(2S))/\Gamma(\text{total})$

VALUE	DOCUMENT ID	TECN	COMMENT	Γ_5/Γ
seen	¹ ABLIKIM	17V BES3	$e^+e^- \rightarrow \pi^+\pi^-\psi(2S)$	

- ¹ From a fit to the cross section for $e^+e^- \rightarrow \pi^+\pi^-\psi(2S) \rightarrow 2(\pi^+\pi^-)\ell^+\ell^-$ obtained from 16 center-of-mass energies between 4.008 and 4.600 GeV and comprising 5.1 fb⁻¹.

$\Gamma(\pi^+D^0D^{*-} + c.c.)/\Gamma(\text{total})$

VALUE	DOCUMENT ID	TECN	COMMENT	Γ_6/Γ
seen	ABLIKIM	19R BES3	$e^+e^- \rightarrow \pi^+D^0D^{*-} + c.c.$	

$\Gamma(\gamma\chi_{c1}(3872))/\Gamma(\text{total})$

VALUE	DOCUMENT ID	TECN	COMMENT	Γ_8/Γ
seen	ABLIKIM	19V BES3	$e^+e^- \rightarrow \gamma\chi_{c1}(3872)$	

Meson Particle Listings

 $\psi(4230)$, $R_{c0}(4240)$, $X(4250)^\pm$, $\psi(4260)$ $\psi(4230)$ REFERENCES

ABLIKIM	20C	PRL 124 032002	M. Ablikim <i>et al.</i>	(BESIII Collab.)
ABLIKIM	19AI	PR D99 091103	M. Ablikim <i>et al.</i>	(BESIII Collab.)
ABLIKIM	19K	PR D99 019903 (errata.)	M. Ablikim <i>et al.</i>	(BESIII Collab.)
ABLIKIM	19R	PRL 122 102002	M. Ablikim <i>et al.</i>	(BESIII Collab.)
ABLIKIM	19V	PRL 122 232002	M. Ablikim <i>et al.</i>	(BESIII Collab.)
ABLIKIM	17B	PRL 118 092001	M. Ablikim <i>et al.</i>	(BESIII Collab.)
ABLIKIM	17G	PRL 118 092002	M. Ablikim <i>et al.</i>	(BESIII Collab.)
ABLIKIM	17V	PR D96 032004	M. Ablikim <i>et al.</i>	(BESIII Collab.)
Also		PR D99 019903 (errata.)	M. Ablikim <i>et al.</i>	(BESIII Collab.)
ABLIKIM	15C	PRL 114 092003	M. Ablikim <i>et al.</i>	(BESIII Collab.)

 $R_{c0}(4240)$

$$J^G(J^{PC}) = 1^+(0^{- -})$$

I, G, C need confirmation.

OMITTED FROM SUMMARY TABLE
was $X(4240)^\pm$

Properties incompatible with a $q\bar{q}$ structure (exotic state). See the review on non- $q\bar{q}$ states.

Spin and parity assignment $J^P = 0^-$ is favored over $1^-, 2^-$, and 2^+ by 8σ and over 1^+ by 1σ , according to the four-dimensional amplitude analysis of AAIJ 14AG.

 $R_{c0}(4240)$ MASS

VALUE (MeV)	DOCUMENT ID	TECN	COMMENT
$4239 \pm 18^{+45}_{-10}$	1 AAIJ	14AG LHCB	$B^0 \rightarrow K^+ \pi^- \psi(2S)$

¹ From a 4-dimensional analysis when a second, lower mass resonance is allowed in the $Z_c(4430)$ fit, with significance 6σ including systematic variations.

 $R_{c0}(4240)$ WIDTH

VALUE (MeV)	DOCUMENT ID	TECN	COMMENT
$220 \pm 47^{+108}_{-74}$	1 AAIJ	14AG LHCB	$B^0 \rightarrow K^+ \pi^- \psi(2S)$

¹ From a 4-dimensional analysis when a second, lower mass resonance is allowed in the $Z_c(4430)$ fit, with significance 6σ including systematic variations.

 $R_{c0}(4240)$ DECAY MODES

Mode	Fraction (Γ_i/Γ)
$\Gamma_1 \pi^- \psi(2S)$	seen

 $R_{c0}(4240)$ BRANCHING RATIOS

$\Gamma(\pi^- \psi(2S))/\Gamma_{\text{total}}$	Γ_1/Γ
seen	seen

¹ From a 4-dimensional analysis when a second, lower mass resonance is allowed in the $Z_c(4430)$ fit. No partial branching fraction quoted.

 $R_{c0}(4240)$ REFERENCES

AAIJ	14AG PRL 112 222002	R. Aaij <i>et al.</i>	(LHCb Collab.)
------	---------------------	-----------------------	----------------

 $X(4250)^\pm$

$$J^G(J^{PC}) = 1^-(?^{?+})$$

I, G, C need confirmation.

OMITTED FROM SUMMARY TABLE

Properties incompatible with a $q\bar{q}$ structure (exotic state). See the review on non- $q\bar{q}$ states.

Observed by MIZUK 08 in the $\pi^+ \chi_{c1}(1P)$ invariant mass distribution in $\bar{B}^0 \rightarrow K^- \pi^+ \chi_{c1}(1P)$ decays. Not seen by LEES 12B in this same mode after accounting for $K\pi$ resonant mass and angular structure.

 $X(4250)^\pm$ MASS

VALUE (MeV)	DOCUMENT ID	TECN	COMMENT
$4248^{+44+180}_{-29-35}$	1 MIZUK	08 BELL	$\bar{B}^0 \rightarrow K^- \pi^+ \chi_{c1}(1P)$

¹ From a Dalitz plot analysis with two Breit-Wigner amplitudes.

 $X(4250)^\pm$ WIDTH

VALUE (MeV)	DOCUMENT ID	TECN	COMMENT
$177^{+54+316}_{-39-61}$	1 MIZUK	08 BELL	$\bar{B}^0 \rightarrow K^- \pi^+ \chi_{c1}(1P)$

¹ From a Dalitz plot analysis with two Breit-Wigner amplitudes.

 $X(4250)^\pm$ DECAY MODES

Mode	Fraction (Γ_i/Γ)
$\Gamma_1 \pi^+ \chi_{c1}(1P)$	seen

 $X(4250)^\pm$ BRANCHING RATIOS

$\Gamma(\pi^+ \chi_{c1}(1P))/\Gamma_{\text{total}}$	Γ_1/Γ
seen	seen

¹ MIZUK 08 BELL $\bar{B}^0 \rightarrow K^- \pi^+ \chi_{c1}(1P)$

• • • We do not use the following data for averages, fits, limits, etc. • • •

not seen ² LEES 12B BABR $B \rightarrow K \pi \chi_{c1}(1P)$

¹ With a product branching fraction measurement of $B(\bar{B}^0 \rightarrow K^- X(4250)^+) \times B(X(4250)^+ \rightarrow \pi^+ \chi_{c1}(1P)) = (4.0^{+2.3+19.7}_{-0.9-0.5}) \times 10^{-5}$.

² With a product branching fraction limit of $B(\bar{B}^0 \rightarrow X(4250)^+ K^-) \times B(X(4250)^+ \rightarrow \chi_{c1} \pi^+) < 4.0 \times 10^{-5}$ at 90% CL.

 $X(4250)^\pm$ REFERENCES

LEES	12B	PR D85 052003	J.P. Lees <i>et al.</i>	(BABAR Collab.)
MIZUK	08	PR D78 072004	R. Mizuk <i>et al.</i>	(BELLE Collab.)

 $\psi(4260)$

$$J^G(J^{PC}) = 0^-(1^{- -})$$

OMITTED FROM SUMMARY TABLE
also known as $Y(4260)$; was $X(4260)$

The state $\psi(4260)$ received its mass label from a Breit-Wigner (BW) fit to the $J/\psi\pi\pi$ data listed below. The symmetric BW placed the mass unavoidably into the center of the distribution. The most recent measurement in the 4260 MeV mass range in the same channel (ABLIKIM 17B), however, revealed that the distribution is asymmetric and that the state has a much lower mass consistent with the entry for particle $\psi(4230)$. Thus, in this edition we merged the measurement of ABLIKIM 17B with the $\psi(4230)$ node and labeled the older measurements of this node as not used. For details see the review on "Spectroscopy of mesons containing two heavy quarks."

 $\psi(4260)$ MASS

VALUE (MeV)	EVS	DOCUMENT ID	TECN	COMMENT
$4209.1 \pm 6.8 \pm 7.0$	¹	ZHANG	17B RVUE	$e^+e^- \rightarrow \pi^+ \pi^- \psi(2S)$
$4223.3 \pm 1.6 \pm 2.5$	²	ZHANG	17c RVUE	$e^+e^- \rightarrow \pi^+ \pi^- J/\psi$ or $\psi(2S)$
$4258.6 \pm 8.3 \pm 12.1$	³	LIU	13B BELL	$e^+e^- \rightarrow \gamma \pi^+ \pi^- J/\psi$
$4245 \pm 5 \pm 4$	⁴	LEES	12AC BABR	$10.58 e^+e^- \rightarrow \gamma \pi^+ \pi^- J/\psi$
$4247 \pm 12^{+17}_{-32}$	^{3,5}	YUAN	07 BELL	$10.58 e^+e^- \rightarrow \gamma \pi^+ \pi^- J/\psi$
$4284^{+17}_{-16} \pm 413.6$	HE	06B CLEO	9.4-10.6	$e^+e^- \rightarrow \gamma \pi^+ \pi^- J/\psi$
$4259 \pm 8 \pm 125$	⁶	AUBERT,B	05i BABR	$10.58 e^+e^- \rightarrow \gamma \pi^+ \pi^- J/\psi$

¹ From a three-resonance fit.
² From a combined fit of BELLE, BABAR and BES3 $e^+e^- \rightarrow \pi^+ \pi^- J/\psi$ and $e^+e^- \rightarrow \pi^+ \pi^- \psi(2S)$ data.
³ From a two-resonance fit.
⁴ From a single-resonance fit. Supersedes AUBERT,B 05i.
⁵ Superseded by LIU 13B.
⁶ From a single-resonance fit. Two interfering resonances are not excluded. Superseded by LEES 12AC.

 $\psi(4260)$ WIDTH

VALUE (MeV)	EVS	DOCUMENT ID	TECN	COMMENT
$76.6 \pm 14.2 \pm 2.4$	¹	ZHANG	17B RVUE	$e^+e^- \rightarrow \pi^+ \pi^- \psi(2S)$
$54.2 \pm 2.6 \pm 1.0$	²	ZHANG	17c RVUE	$e^+e^- \rightarrow \pi^+ \pi^- J/\psi$ or $\psi(2S)$
$134.1 \pm 16.4 \pm 5.5$	³	LIU	13B BELL	$e^+e^- \rightarrow \gamma \pi^+ \pi^- J/\psi$
$114^{+16}_{-15} \pm 7$	⁴	LEES	12AC BABR	$10.58 e^+e^- \rightarrow \gamma \pi^+ \pi^- J/\psi$
$108 \pm 19 \pm 10$	^{3,5}	YUAN	07 BELL	$10.58 e^+e^- \rightarrow \gamma \pi^+ \pi^- J/\psi$
$73^{+39}_{-25} \pm 5$	13.6	HE	06B CLEO	$9.4-10.6 e^+e^- \rightarrow \gamma \pi^+ \pi^- J/\psi$
$88 \pm 23 \pm 6^{+4}_{-4} 125$	⁶	AUBERT,B	05i BABR	$10.58 e^+e^- \rightarrow \gamma \pi^+ \pi^- J/\psi$

¹ From a three-resonance fit.
² From a combined fit of BELLE, BABAR and BES3 $e^+e^- \rightarrow \pi^+ \pi^- J/\psi$ and $e^+e^- \rightarrow \pi^+ \pi^- \psi(2S)$ data.
³ From a two-resonance fit.
⁴ From a single-resonance fit. Supersedes AUBERT,B 05i.
⁵ Superseded by LIU 13B.
⁶ From a single-resonance fit. Two interfering resonances are not excluded. Superseded by LEES 12AC.

$\psi(4260)$ DECAY MODES

Mode	Fraction (Γ_i/Γ)
Γ_1 $e^+ e^-$	
Γ_2 $J/\psi \pi^+ \pi^-$	seen
Γ_3 $J/\psi f_0(980), f_0(980) \rightarrow \pi^+ \pi^-$	seen
Γ_4 $Z_c(3900)^\pm \pi^\mp, Z_c^\pm \rightarrow J/\psi \pi^\pm$	seen
Γ_5 $J/\psi \pi^0 \pi^0$	seen
Γ_6 $J/\psi K^+ K^-$	seen
Γ_7 $J/\psi K_S^0 K_S^0$	not seen
Γ_8 $J/\psi \eta$	not seen
Γ_9 $J/\psi \pi^0$	not seen
Γ_{10} $J/\psi \eta'$	not seen
Γ_{11} $J/\psi \pi^+ \pi^- \pi^0$	not seen
Γ_{12} $J/\psi \eta \pi^0$	not seen
Γ_{13} $J/\psi \eta \eta$	not seen
Γ_{14} $\psi(2S) \pi^+ \pi^-$	not seen
Γ_{15} $\psi(2S) \eta$	not seen
Γ_{16} $\chi_{c0} \omega$	not seen
Γ_{17} $\chi_{c1} \pi^+ \pi^- \pi^0$	not seen
Γ_{18} $\chi_{c2} \pi^+ \pi^- \pi^0$	not seen
Γ_{19} $h_c(1P) \pi^+ \pi^-$	not seen
Γ_{20} $\phi \pi^+ \pi^-$	not seen
Γ_{21} $\phi f_0(980) \rightarrow \phi \pi^+ \pi^-$	not seen
Γ_{22} $D \bar{D}$	not seen
Γ_{23} $D^0 \bar{D}^0$	not seen
Γ_{24} $D^+ D^-$	not seen
Γ_{25} $D^* \bar{D} + c.c.$	not seen
Γ_{26} $D^*(2007)^0 \bar{D}^0 + c.c.$	not seen
Γ_{27} $D^*(2010)^+ D^- + c.c.$	not seen
Γ_{28} $D^* \bar{D}^*$	not seen
Γ_{29} $D^*(2007)^0 \bar{D}^*(2007)^0$	not seen
Γ_{30} $D^*(2010)^+ D^*(2010)^-$	not seen
Γ_{31} $D \bar{D} \pi + c.c.$	
Γ_{32} $D^0 D^- \pi^+ + c.c. (excl. D^*(2007)^0 \bar{D}^{*0} + c.c., D^*(2010)^+ D^- + c.c.)$	not seen
Γ_{33} $D \bar{D}^* \pi + c.c. (excl. D^* \bar{D}^*)$	not seen
Γ_{34} $D^0 D^* \pi^+ + c.c. (excl. D^*(2010)^+ D^*(2010)^-)$	not seen
Γ_{35} $D^0 D^*(2010)^- \pi^+ + c.c.$	not seen
Γ_{36} $D_1(2420) \bar{D} + c.c.$	not seen
Γ_{37} $D^* \bar{D}^* \pi$	not seen
Γ_{38} $D_s^+ D_s^-$	not seen
Γ_{39} $D_s^{*+} D_s^- + c.c.$	not seen
Γ_{40} $D_s^{*+} D_s^{*-}$	not seen
Γ_{41} $\rho \bar{\rho}$	not seen
Γ_{42} $\rho \bar{\rho} \pi^0$	not seen
Γ_{43} $\Xi^- \Xi^+$	
Γ_{44} $K_S^0 K^\pm \pi^\mp$	not seen
Γ_{45} $K_S^0 K^\pm \pi^\mp \pi^0$	
Γ_{46} $K_S^0 K^\pm \pi^\mp \eta$	
Γ_{47} $K^+ K^- \pi^0$	not seen
Radiative decays	
Γ_{48} $\eta_c(1S) \gamma$	possibly seen
Γ_{49} $\chi_{c1} \gamma$	not seen
Γ_{50} $\chi_{c2} \gamma$	not seen
Γ_{51} $\chi_{c1}(3872) \gamma$	seen

$\psi(4260) \Gamma(i) \times \Gamma(e^+ e^-)/\Gamma(\text{total})$

$\Gamma(J/\psi \pi^+ \pi^-) \times \Gamma(e^+ e^-)/\Gamma(\text{total})$	$\Gamma_2 \Gamma_1/\Gamma$
VALUE (eV) EVTS DOCUMENT ID TECN COMMENT	
9.2±1.0 OUR AVERAGE	
9.2±0.8±0.7	¹ LEES 12Ac BABR 10.58 e ⁺ e ⁻ → $\gamma \pi^+ \pi^- J/\psi$
8.9 ^{+3.9} _{-3.1} ±1.8	8.1 HE 06B CLEO 9.4-10.6 e ⁺ e ⁻ → $\gamma \pi^+ \pi^- J/\psi$
••• We do not use the following data for averages, fits, limits, etc. •••	
6.4±0.8±0.6	² LIU 13B BELL e ⁺ e ⁻ → $\gamma \pi^+ \pi^- J/\psi$
20.5±1.4±2.0	³ LIU 13B BELL e ⁺ e ⁻ → $\gamma \pi^+ \pi^- J/\psi$
6.0±1.2 ^{+4.7} _{-0.5}	2.4 YUAN 07 BELL 10.58 e ⁺ e ⁻ → $\gamma \pi^+ \pi^- J/\psi$
20.6±2.3 ^{+9.1} _{-1.7}	3.4 YUAN 07 BELL 10.58 e ⁺ e ⁻ → $\gamma \pi^+ \pi^- J/\psi$
5.5±1.0 ^{+9.8} _{-0.7}	125 ⁵ AUBERT,B 05i BABR 10.58 e ⁺ e ⁻ → $\gamma \pi^+ \pi^- J/\psi$

¹ From a single-resonance fit. Supersedes AUBERT,B 05i.

² Solution I of two equivalent solutions in a fit using two interfering resonances.
³ Solution II of two equivalent solutions in a fit using two interfering resonances.
⁴ Superseded by LIU 13B.
⁵ From a single-resonance fit. Two interfering resonances are not excluded. Superseded by LEES 12Ac.

$\Gamma(J/\psi K^+ K^-) \times \Gamma(e^+ e^-)/\Gamma(\text{total})$ $\Gamma_6 \Gamma_1/\Gamma$

VALUE (eV) CL% DOCUMENT ID TECN COMMENT	
<1.7	90 ¹ SHEN 14 BELL 9.4-10.9 e ⁺ e ⁻ → $\gamma K^+ K^- J/\psi$
••• We do not use the following data for averages, fits, limits, etc. •••	
<1.2	90 ² YUAN 08 BELL e ⁺ e ⁻ → $\gamma K^+ K^- J/\psi$

¹ From a fit of the broad $K^+ K^- J/\psi$ enhancement including a coherent $\psi(4260)$ amplitude with mass and width from LIU 13B. Supersedes YUAN 08. The shape of the cross section observed by ABLIKIM 18W between 2.2 and 2.3 GeV is incompatible with that of e⁺e⁻ → $\pi^+ \pi^- J/\psi$ in ABLIKIM 13T and ABLIKIM 17B. They also observe a broad enhancement around 2.5 GeV.
² From a fit of the broad $K^+ K^- J/\psi$ enhancement including a coherent $\psi(4260)$ amplitude with mass and width from YUAN 07.

$\Gamma(J/\psi K_S^0 K_S^0) \times \Gamma(e^+ e^-)/\Gamma(\text{total})$ $\Gamma_7 \Gamma_1/\Gamma$

VALUE (eV) CL% DOCUMENT ID TECN COMMENT	
<0.85	90 ¹ SHEN 14 BELL 9.4-10.9 e ⁺ e ⁻ → $\gamma K_S^0 K_S^0 J/\psi$

¹ From a fit of the $K_S^0 K_S^0 J/\psi$ mass range from 4.4 to 5.5 GeV including a coherent $\psi(4260)$ amplitude with mass and width from LIU 13B.

$\Gamma(J/\psi \eta) \times \Gamma(e^+ e^-)/\Gamma(\text{total})$ $\Gamma_8 \Gamma_1/\Gamma$

VALUE (eV) CL% DOCUMENT ID TECN COMMENT	
<14.2	90 WANG 13B BELL e ⁺ e ⁻ → $J/\psi \eta \eta$

$\Gamma(J/\psi \eta') \times \Gamma(e^+ e^-)/\Gamma(\text{total})$ $\Gamma_{10} \Gamma_1/\Gamma$

VALUE (eV) EVTS DOCUMENT ID TECN COMMENT	
0.06±0.03	46 ^{1,2} ABLIKIM 20A BES3 e ⁺ e ⁻ → $\eta' J/\psi$
1.38±0.11	46 ^{1,3} ABLIKIM 20A BES3 e ⁺ e ⁻ → $\eta' J/\psi$

¹ Based on a fit to $\sigma(e^+ e^- \rightarrow \eta' J/\psi)$ from $\sqrt{s} = 4.18$ to 4.60 GeV assuming interfering $\psi(4160)$ and $\psi(4260)$ contributions. At $\sqrt{s} = 4.23$ GeV, $\sigma(e^+ e^- \rightarrow \eta' J/\psi) = 3.6 \pm 0.6 \pm 0.3$ pb.
² Solution I of the fit, corresponding to a phase of -0.03 ± 0.44 rad.
³ Solution II of the fit, corresponding to a phase of 2.54 ± 0.04 rad.

$\Gamma(\psi(2S) \pi^+ \pi^-) \times \Gamma(e^+ e^-)/\Gamma(\text{total})$ $\Gamma_{14} \Gamma_1/\Gamma$

VALUE (eV) CL% DOCUMENT ID TECN COMMENT	
<4.3	90 ¹ LIU 08H RVUE 10.58 e ⁺ e ⁻ → $\psi(2S) \pi^+ \pi^- \gamma$
7.4 ^{+2.1} _{-1.7}	² LIU 08H RVUE 10.58 e ⁺ e ⁻ → $\psi(2S) \pi^+ \pi^- \gamma$

¹ For constructive interference with the $\psi(4360)$ in a combined fit of AUBERT 07s and WANG 07b data with three resonances.
² For destructive interference with the $\psi(4360)$ in a combined fit of AUBERT 07s and WANG 07b data with three resonances.

$\Gamma(\phi \pi^+ \pi^-) \times \Gamma(e^+ e^-)/\Gamma(\text{total})$ $\Gamma_{20} \Gamma_1/\Gamma$

VALUE (eV) CL% DOCUMENT ID TECN COMMENT	
<0.4	90 AUBERT,BE 06d BABR 10.6 e ⁺ e ⁻ → $K^+ K^- \pi^+ \pi^- \gamma$

$\Gamma(\phi f_0(980) \rightarrow \phi \pi^+ \pi^-) \times \Gamma(e^+ e^-)/\Gamma(\text{total})$ $\Gamma_{21} \Gamma_1/\Gamma$

VALUE (eV) CL% DOCUMENT ID TECN COMMENT	
<0.28	90 ¹ AUBERT 07AK BABR 10.6 e ⁺ e ⁻ → $\pi^+ \pi^- K^+ K^- \gamma$

¹ AUBERT 07AK reports $[\Gamma(\psi(4260) \rightarrow \phi f_0(980) \rightarrow \phi \pi^+ \pi^-) \times \Gamma(\psi(4260) \rightarrow e^+ e^-)/\Gamma(\text{total})] \times [B(\phi(1020) \rightarrow K^+ K^-)] < 0.14$ eV which we divide by our best value $B(\phi(1020) \rightarrow K^+ K^-) = 49.2 \times 10^{-2}$.

$\Gamma(\Xi^- \Xi^+) \times \Gamma(e^+ e^-)/\Gamma(\text{total})$ $\Gamma_{43} \Gamma_1/\Gamma$

VALUE (eV) CL% DOCUMENT ID TECN COMMENT	
<2.7 × 10 ⁻⁴	90 ABLIKIM 20c BES3 e ⁺ e ⁻ → $\Xi^- \Xi^+$

$\Gamma(K_S^0 K^\pm \pi^\mp) \times \Gamma(e^+ e^-)/\Gamma(\text{total})$ $\Gamma_{44} \Gamma_1/\Gamma$

VALUE (eV) DOCUMENT ID TECN COMMENT			
••• We do not use the following data for averages, fits, limits, etc. •••			
2.04 ± 0.19 ± 0.09	¹ ABLIKIM 19AE BES3 e ⁺ e ⁻ → $K_S^0 K^\pm \pi^\mp$		
0.0027 ± 0.0023 ± 0.0001	² ABLIKIM 19AE BES3 e ⁺ e ⁻ → $K_S^0 K^\pm \pi^\mp$		
< 0.5 at 90% CL	AUBERT 08s BABR 10.6 e ⁺ e ⁻ → $K_S^0 K^\pm \pi^\mp \gamma$		

¹ Solution I of the fit including the $\psi(4160)$ with mass 4191 ± 5 MeV and width 70 ± 10 MeV from PDG 16 and the $\psi(4230)$ with mass 4219.6 ± 3.3 ± 5.1 MeV and width 56.0 ± 3.6 ± 6.9 MeV from GAO 17.
² Solution II of the fit including the $\psi(4160)$ with mass 4191 ± 5 MeV and width 70 ± 10 MeV from PDG 16 and the $\psi(4230)$ with mass 4219.6 ± 3.3 ± 5.1 MeV and width 56.0 ± 3.6 ± 6.9 MeV from GAO 17.

Meson Particle Listings

 $\psi(4260)$

$\Gamma(K_S^0 K^\pm \pi^\mp \pi^0) \times \Gamma(e^+ e^-)/\Gamma_{\text{total}}$					Γ_{45}/Γ
VALUE (eV)	CL%	DOCUMENT ID	TECN	COMMENT	
<0.05	90	ABLIKIM	19	BES3 $e^+ e^- \rightarrow K_S^0 K^\pm \pi^\mp \pi^0$	

$\Gamma(K_S^0 K^\pm \pi^\mp \eta) \times \Gamma(e^+ e^-)/\Gamma_{\text{total}}$					Γ_{46}/Γ
VALUE (eV)	CL%	DOCUMENT ID	TECN	COMMENT	
<0.19	90	ABLIKIM	19	BES3 $e^+ e^- \rightarrow K_S^0 K^\pm \pi^\mp \eta$	

$\Gamma(K^+ K^- \pi^0) \times \Gamma(e^+ e^-)/\Gamma_{\text{total}}$					Γ_{47}/Γ
VALUE (eV)	CL%	DOCUMENT ID	TECN	COMMENT	
<0.6	90	AUBERT	08s	BABR $10.6 e^+ e^- \rightarrow K^+ K^- \pi^0 \gamma$	
• • • We do not use the following data for averages, fits, limits, etc. • • •					

$\Gamma(\chi_{c1} \gamma) \times \Gamma(e^+ e^-)/\Gamma_{\text{total}}$					Γ_{49}/Γ
VALUE (eV)	CL%	DOCUMENT ID	TECN	COMMENT	
<1.4	90	¹ HAN	15	BELL $10.58 e^+ e^- \rightarrow \chi_{c1} \gamma$	
¹ Using $B(\eta \rightarrow \gamma\gamma) = (39.41 \pm 0.21)\%$.					

$\Gamma(\chi_{c2} \gamma) \times \Gamma(e^+ e^-)/\Gamma_{\text{total}}$					Γ_{50}/Γ
VALUE (eV)	CL%	DOCUMENT ID	TECN	COMMENT	
<4.0	90	¹ HAN	15	BELL $10.58 e^+ e^- \rightarrow \chi_{c2} \gamma$	
¹ Using $B(\eta \rightarrow \gamma\gamma) = (39.41 \pm 0.21)\%$.					

 $\psi(4260)$ BRANCHING RATIOS

$\Gamma(J/\psi f_0(980), f_0(980) \rightarrow \pi^+ \pi^-)/\Gamma(J/\psi \pi^+ \pi^-)$					Γ_3/Γ_2
VALUE	DOCUMENT ID	TECN	COMMENT		
0.17 ± 0.13	¹ LEES	12Ac	BABR	$10.58 e^+ e^- \rightarrow \gamma \pi^+ \pi^- J/\psi$	
¹ Systematic uncertainties not estimated.					

$\Gamma(Z_c(3900)^\pm \pi^\mp, Z_c^\pm \rightarrow J/\psi \pi^\pm)/\Gamma(J/\psi \pi^+ \pi^-)$					Γ_4/Γ_2
VALUE	DOCUMENT ID	TECN	COMMENT		
$0.215 \pm 0.033 \pm 0.075$	¹ ABLIKIM	13T	BES3	$e^+ e^- \rightarrow \pi^+ \pi^- J/\psi$	
• • • We do not use the following data for averages, fits, limits, etc. • • •					
0.29 ± 0.08	² LIU	13b	BELL	$e^+ e^- \rightarrow \gamma \pi^+ \pi^- J/\psi$	
¹ Assuming that the cross section of $e^+ e^- \rightarrow \pi^+ \pi^- J/\psi$ is fully due to the $\psi(4260)$.					
² Systematic error not evaluated.					

$\Gamma(J/\psi K_S^0 K_S^0)/\Gamma_{\text{total}}$					Γ_7/Γ
VALUE	DOCUMENT ID	TECN	COMMENT		
not seen	SHEN	14	BELL	$9.4\text{--}10.9 e^+ e^- \rightarrow \gamma K_S^0 K_S^0 J/\psi$	

$\Gamma(J/\psi \eta \pi^0)/\Gamma_{\text{total}}$					Γ_{12}/Γ
VALUE	DOCUMENT ID	TECN	COMMENT		
not seen	ABLIKIM	15q	BES3	$4.0\text{--}4.6 e^+ e^- \rightarrow J/\psi \eta \pi^0$	

$\Gamma(\psi(2S) \pi^+ \pi^-)/\Gamma(J/\psi \pi^+ \pi^-)$					Γ_{14}/Γ_2
VALUE	DOCUMENT ID	TECN	COMMENT		
(0.11 ± 0.03 ± 0.03) to (0.55 ± 0.18 ± 0.19)	¹ ZHANG	17c	RVUE	$e^+ e^- \rightarrow \pi^+ \pi^- J/\psi$ or $\psi(2S)$	
¹ From a combined fit of BELLE, BABAR and BES3 $e^+ e^- \rightarrow \pi^+ \pi^- J/\psi$ and $e^+ e^- \rightarrow \pi^+ \pi^- \psi(2S)$ data.					

$\Gamma(h_c(1P) \pi^+ \pi^-)/\Gamma(J/\psi \pi^+ \pi^-)$					Γ_{19}/Γ_2
VALUE	CL%	DOCUMENT ID	TECN	COMMENT	
<1.0	90	¹ PEDLAR	11	CLEO $e^+ e^- \rightarrow h_c(1P) \pi^+ \pi^-$	
¹ At $\sqrt{s} = 4260$ MeV, PEDLAR 11 measures $\sigma(e^+ e^- \rightarrow h_c(1P) \pi^+ \pi^-) = 32 \pm 17 \pm 6 \pm 6$ pb, where the errors are statistical, systematic, and due to uncertainty in $B(\psi(2S) \rightarrow \pi^0 h_c(1P))$, respectively.					

$\Gamma(D\bar{D})/\Gamma(J/\psi \pi^+ \pi^-)$					Γ_{22}/Γ_2
VALUE	CL%	DOCUMENT ID	TECN	COMMENT	
<1.0	90	¹ AUBERT	07bE	BABR $e^+ e^- \rightarrow D\bar{D} \gamma$	
• • • We do not use the following data for averages, fits, limits, etc. • • •					
<4.0	90	CRONIN-HEN..09	CLEO	$e^+ e^-$	
¹ Using 4259 ± 10 MeV for the mass and 88 ± 24 MeV for the width of $\psi(4260)$.					

$\Gamma(D^0 \bar{D}^0)/\Gamma_{\text{total}}$					Γ_{23}/Γ
VALUE	DOCUMENT ID	TECN	COMMENT		
not seen	CRONIN-HEN..09	CLEO	$e^+ e^- \rightarrow D^0 \bar{D}^0$		
• • • We do not use the following data for averages, fits, limits, etc. • • •					
not seen	AUBERT	09M	BABR	$e^+ e^- \rightarrow D^0 \bar{D}^0 \gamma$	
not seen	PAKHLOVA	08	BELL	$e^+ e^- \rightarrow D^0 \bar{D}^0 \gamma$	

$\Gamma(D^+ D^-)/\Gamma_{\text{total}}$					Γ_{24}/Γ
VALUE	DOCUMENT ID	TECN	COMMENT		
not seen	CRONIN-HEN..09	CLEO	$e^+ e^- \rightarrow D^+ D^-$		
• • • We do not use the following data for averages, fits, limits, etc. • • •					
not seen	AUBERT	09M	BABR	$e^+ e^- \rightarrow D^+ D^- \gamma$	
not seen	PAKHLOVA	08	BELL	$e^+ e^- \rightarrow D^+ D^- \gamma$	

$\Gamma(D^* \bar{D} + \text{c.c.})/\Gamma(J/\psi \pi^+ \pi^-)$					Γ_{25}/Γ_2
VALUE	CL%	DOCUMENT ID	TECN	COMMENT	
<34	90	AUBERT	09M	BABR $e^+ e^- \rightarrow \gamma D^* \bar{D}$	
• • • We do not use the following data for averages, fits, limits, etc. • • •					
<45	90	CRONIN-HEN..09	CLEO	$e^+ e^-$	

$\Gamma(D^*(2007)^0 \bar{D}^0 + \text{c.c.})/\Gamma_{\text{total}}$					Γ_{26}/Γ
VALUE	DOCUMENT ID	TECN	COMMENT		
not seen	CRONIN-HEN..09	CLEO	$e^+ e^- \rightarrow D^{*0} \bar{D}^0$		
• • • We do not use the following data for averages, fits, limits, etc. • • •					
not seen	AUBERT	09M	BABR	$e^+ e^- \rightarrow D^{*0} \bar{D}^0 \gamma$	

$\Gamma(D^*(2010)^+ D^- + \text{c.c.})/\Gamma_{\text{total}}$					Γ_{27}/Γ
VALUE	DOCUMENT ID	TECN	COMMENT		
not seen	CRONIN-HEN..09	CLEO	$e^+ e^- \rightarrow D^{*+} D^-$		
not seen	PAKHLOVA	07	BELL	$e^+ e^- \rightarrow D^{*+} D^- \gamma$	
• • • We do not use the following data for averages, fits, limits, etc. • • •					
not seen	AUBERT	09M	BABR	$e^+ e^- \rightarrow D^{*+} D^- \gamma$	

$\Gamma(D^* \bar{D}^*)/\Gamma(J/\psi \pi^+ \pi^-)$					Γ_{28}/Γ_2
VALUE	CL%	DOCUMENT ID	TECN	COMMENT	
<11	90	CRONIN-HEN..09	CLEO	$e^+ e^-$	
• • • We do not use the following data for averages, fits, limits, etc. • • •					
<40	90	AUBERT	09M	BABR $e^+ e^- \rightarrow \gamma D^* \bar{D}^*$	

$\Gamma(D^*(2007)^0 \bar{D}^*(2007)^0)/\Gamma_{\text{total}}$					Γ_{29}/Γ
VALUE	DOCUMENT ID	TECN	COMMENT		
not seen	CRONIN-HEN..09	CLEO	$e^+ e^- \rightarrow D^{*0} \bar{D}^{*0}$		
• • • We do not use the following data for averages, fits, limits, etc. • • •					
not seen	AUBERT	09M	BABR	$e^+ e^- \rightarrow D^{*0} \bar{D}^{*0} \gamma$	

$\Gamma(D^*(2010)^+ D^*(2010)^-)/\Gamma_{\text{total}}$					Γ_{30}/Γ
VALUE	DOCUMENT ID	TECN	COMMENT		
not seen	CRONIN-HEN..09	CLEO	$e^+ e^- \rightarrow D^{*+} D^{*-}$		
not seen	PAKHLOVA	07	BELL	$e^+ e^- \rightarrow D^{*+} D^{*-} \gamma$	
• • • We do not use the following data for averages, fits, limits, etc. • • •					
not seen	AUBERT	09M	BABR	$e^+ e^- \rightarrow D^{*+} D^{*-} \gamma$	

$\Gamma(D^0 D^- \pi^+ + \text{c.c. (excl. } D^*(2007)^0 \bar{D}^{*0} + \text{c.c., } D^*(2010)^+ D^- + \text{c.c.})/\Gamma_{\text{total}}$					Γ_{32}/Γ
VALUE	DOCUMENT ID	TECN	COMMENT		
not seen	PAKHLOVA	08a	BELL	$10.6 e^+ e^- \rightarrow D^0 D^- \pi^+ \gamma$	

$\Gamma(D\bar{D}^* \pi + \text{c.c. (excl. } D^* \bar{D}^*)/\Gamma_{\text{total}}$					Γ_{33}/Γ
VALUE	DOCUMENT ID	TECN	COMMENT		
not seen	CRONIN-HEN..09	CLEO	$e^+ e^- \rightarrow D^* \bar{D} \pi$		

$\Gamma(D\bar{D}^* \pi + \text{c.c. (excl. } D^* \bar{D}^*)/\Gamma(J/\psi \pi^+ \pi^-)$					Γ_{33}/Γ_2
VALUE	CL%	DOCUMENT ID	TECN	COMMENT	
<15	90	CRONIN-HEN..09	CLEO	$e^+ e^-$	

$\Gamma(D^0 D^{*-} \pi^+ + \text{c.c. (excl. } D^*(2010)^+ D^*(2010)^-)/\Gamma_{\text{total}}$					Γ_{34}/Γ
VALUE	DOCUMENT ID	TECN	COMMENT		
not seen	PAKHLOVA	09	BELL	$e^+ e^- \rightarrow D^0 D^{*-} \pi^+ \gamma$	

$\Gamma(D^0 D^*(2010)^- \pi^+ + \text{c.c.})/\Gamma(J/\psi \pi^+ \pi^-)$					Γ_{35}/Γ_2
VALUE	CL%	DOCUMENT ID	TECN	COMMENT	
<9	90	PAKHLOVA	09	BELL $e^+ e^- \rightarrow D^0 D^{*-} \pi^+$	

$\Gamma(D^0 D^*(2010)^- \pi^+ + \text{c.c.})/\Gamma_{\text{total}} \times \Gamma(e^+ e^-)/\Gamma_{\text{total}}$					$\Gamma_{35}/\Gamma \times \Gamma_1/\Gamma$
VALUE	CL%	DOCUMENT ID	TECN	COMMENT	
<0.42 × 10 ⁻⁶	90	¹ PAKHLOVA	09	BELL $e^+ e^- \rightarrow D^0 D^{*-} \pi^+$	
¹ Using 4263 ⁺⁸ / ₋₉ MeV for the mass of $\psi(4260)$.					

$\Gamma(D^* \bar{D}^* \pi)/\Gamma_{\text{total}}$					Γ_{37}/Γ
VALUE	DOCUMENT ID	TECN	COMMENT		
not seen	CRONIN-HEN..09	CLEO	$e^+ e^- \rightarrow D^* \bar{D}^* \pi$		

$\Gamma(D^* \bar{D}^* \pi)/\Gamma(J/\psi \pi^+ \pi^-)$					Γ_{37}/Γ_2
VALUE	CL%	DOCUMENT ID	TECN	COMMENT	
<8.2	90	CRONIN-HEN..09	CLEO	$e^+ e^-$	

$\Gamma(D_1(2420)\bar{D} + c.c.)/\Gamma_{total}$ Γ_{36}/Γ

Table with columns: VALUE, DOCUMENT ID, TECN, COMMENT. Row 1: not seen, 1 ABLIKIM 19AR BES3 e+e- -> pi+ pi- D D-bar. Includes a note about the measurement of sigma(e+e- -> D1(2420) D-bar + c.c.) between sqrt(s) = 4.3 and 4.6 GeV.

$\Gamma(D_s^+ D_s^-)/\Gamma_{total}$ Γ_{38}/Γ

Table with columns: VALUE, DOCUMENT ID, TECN, COMMENT. Row 1: not seen, DEL-AMO-SA...10N BABR e+e- -> D_s^+ D_s^- gamma. Row 2: not seen, CRONIN-HEN..09 CLEO e+e- -> D_s^+ D_s^-.

$\Gamma(D_s^+ D_s^-)/\Gamma(J/\psi\pi^+\pi^-)$ Γ_{38}/Γ_2

Table with columns: VALUE, CL%, DOCUMENT ID, TECN, COMMENT. Row 1: <0.7, 95, DEL-AMO-SA...10N BABR 10.6 e+e-.

$\Gamma(D_s^+ D_s^- + c.c.)/\Gamma_{total}$ Γ_{39}/Γ

Table with columns: VALUE, DOCUMENT ID, TECN, COMMENT. Row 1: not seen, DEL-AMO-SA...10N BABR e+e- -> D_s^{*+} D_s^-.

$\Gamma(D_s^{*+} D_s^- + c.c.)/\Gamma(J/\psi\pi^+\pi^-)$ Γ_{39}/Γ_2

Table with columns: VALUE, CL%, DOCUMENT ID, TECN, COMMENT. Row 1: <0.8, 90, CRONIN-HEN..09 CLEO e+e-.

$\Gamma(D_s^{*+} D_s^{*-})/\Gamma_{total}$ Γ_{40}/Γ

Table with columns: VALUE, DOCUMENT ID, TECN, COMMENT. Row 1: not seen, CRONIN-HEN..09 CLEO e+e- -> D_s^{*+} D_s^{*-}.

$\Gamma(D_s^{*+} D_s^{*-})/\Gamma(J/\psi\pi^+\pi^-)$ Γ_{40}/Γ_2

Table with columns: VALUE, CL%, DOCUMENT ID, TECN, COMMENT. Row 1: <9.5, 90, CRONIN-HEN..09 CLEO e+e-.

$\Gamma(p\bar{p})/\Gamma(J/\psi\pi^+\pi^-)$ Γ_{41}/Γ_2

Table with columns: VALUE, CL%, DOCUMENT ID, TECN, COMMENT. Row 1: <0.13, 90, 1 AUBERT 06B BABR e+e- -> p p-bar gamma. Includes a note about mass and width of psi(4260).

$\Gamma(p\bar{p}\pi^0)/\Gamma(J/\psi\pi^+\pi^-)$ Γ_{42}/Γ_2

Table with columns: VALUE, CL%, DOCUMENT ID, TECN, COMMENT. Row 1: <2 x 10^-4, 90, ABLIKIM 17F BES3 e+e- -> psi(4260) -> hadrons.

Radiative decays

$\Gamma(\eta_c(1S)\gamma)/\Gamma_{total}$ Γ_{48}/Γ

Table with columns: VALUE, DOCUMENT ID, COMMENT. Row 1: possibly seen, 1 ABLIKIM 17W e+e- -> gamma eta_c(1S). Includes a note about significance ranges.

$\Gamma(\chi_{c1}(3872)\gamma)/\Gamma_{total}$ Γ_{51}/Γ

Table with columns: VALUE, EVTS, DOCUMENT ID, TECN, COMMENT. Row 1: seen, 20 +/- 5, ABLIKIM 14 BES3 e+e- -> J/psi pi+ pi- gamma.

psi(4260) REFERENCES

Table of references for psi(4260) with columns: Author, Year, Journal, Comment.

Table of references for chi_c1(4274) with columns: Author, Year, Journal, Comment.

chi_c1(4274) $I^G(J^{PC}) = 0^+(1^{++})$

was X(4274) This state shows properties different from a conventional q q-bar state. A candidate for an exotic structure. See the review on non-q q-bar states. Seen by AAJ 17C in B+ -> chi_c1 K+, chi_c1 -> J/psi phi using an amplitude analysis of B+ -> J/psi phi K+ with a significance (accounting for systematic uncertainties) of 6.0 sigma.

chi_c1(4274) MASS

Table with columns: VALUE (MeV), EVTS, DOCUMENT ID, TECN, COMMENT. Row 1: 4274 +/- 8/-6 OUR AVERAGE. Row 2: 4273.3 +/- 8.3 +/- 17.2/3.6, 4289, 1 AAJ 17c LHCB B+ -> J/psi phi K+.

chi_c1(4274) WIDTH

Table with columns: VALUE (MeV), EVTS, DOCUMENT ID, TECN, COMMENT. Row 1: 49 +/- 12 OUR AVERAGE. Row 2: 56 +/- 11 +/- 8/-11, 4289, 1 AAJ 17c LHCB B+ -> J/psi phi K+.

chi_c1(4274) DECAY MODES

Table with columns: Mode, Fraction (Gamma_i/Gamma). Row 1: Gamma_1 J/psi phi, seen.

chi_c1(4274) BRANCHING RATIOS

Table with columns: Gamma(J/psi phi)/Gamma_total, EVTS, DOCUMENT ID, TECN, COMMENT, Gamma_1/Gamma. Row 1: seen, 4289, 1 AAJ 17c LHCB B+ -> J/psi phi K+.

chi_c1(4274) REFERENCES

Table of references for chi_c1(4274) with columns: Author, Year, Journal, Comment.

X(4350) $I^G(J^{PC}) = 0^+(?^{?+})$

OMITTED FROM SUMMARY TABLE Seen by SHEN 10 in the gamma gamma -> J/psi phi. Needs confirmation.

X(4350) MASS

Table with columns: VALUE (MeV), EVTS, DOCUMENT ID, TECN, COMMENT. Row 1: 4350.6 +/- 4.6 +/- 5.1 +/- 0.7, 8.8 +/- 4.2/-3.2, 1 SHEN 10 BELL 10.6 e+e- -> e+e- J/psi phi. Includes a note about statistical significance.

Downloaded from https://academic.oup.com/ptep/article/2020/8/083C01/5891211 by guest on 20 August 2020

Meson Particle Listings

X(4350), $\psi(4360)$

X(4350) WIDTH

VALUE (MeV)	EVTs	DOCUMENT ID	TECN	COMMENT
$13^{+18}_{-9} \pm 4$	$8.8^{+4.2}_{-3.2}$	1 SHEN	10 BELL	$10.6 e^+ e^- \rightarrow e^+ e^- J/\psi \phi$

¹ Statistical significance of 3.2 σ .

X(4350) DECAY MODES

Mode	Fraction (Γ_i/Γ)
Γ_1 $J/\psi \phi$	seen
Γ_2 $\gamma \gamma$	seen

X(4350) $\Gamma(i)\Gamma(\gamma\gamma)/\Gamma(\text{total})$

$\Gamma(\gamma\gamma) \times \Gamma(J/\psi\phi)/\Gamma_{\text{total}}$	VALUE (eV)	EVTs	DOCUMENT ID	TECN	COMMENT	$\Gamma_2\Gamma_1/\Gamma$
$6.7^{+3.2}_{-2.4} \pm 1.1$	$8.8^{+4.2}_{-3.2}$	1 SHEN	10 BELL	10.6 $e^+ e^- \rightarrow e^+ e^- J/\psi \phi$		
$1.5^{+0.7}_{-0.6} \pm 0.3$	$8.8^{+4.2}_{-3.2}$	2 SHEN	10 BELL	10.6 $e^+ e^- \rightarrow e^+ e^- J/\psi \phi$		

• • • We do not use the following data for averages, fits, limits, etc. • • •
¹ For $J^P = 0^+$. Statistical significance of 3.2 σ .
² For $J^P = 2^+$. Statistical significance of 3.2 σ .

X(4350) BRANCHING RATIOS

$\Gamma(J/\psi\phi)/\Gamma_{\text{total}}$	VALUE	DOCUMENT ID	TECN	COMMENT	Γ_1/Γ
seen	1 SHEN	10 BELL	10.6 $e^+ e^- \rightarrow e^+ e^- J/\psi \phi$		

¹ Statistical significance of 3.2 σ .

$\Gamma(\gamma\gamma)/\Gamma_{\text{total}}$	VALUE	DOCUMENT ID	TECN	COMMENT	Γ_2/Γ
seen	1 SHEN	10 BELL	10.6 $e^+ e^- \rightarrow e^+ e^- J/\psi \phi$		

¹ Statistical significance of 3.2 σ .

X(4350) REFERENCES

SHEN 10 PRL 104 112004 C.P. Shen et al. (BELLE Collab.)

$\psi(4360) \quad I^G(J^{PC}) = 0^-(1^{--})$

also known as $Y(4360)$; was X(4360)
 This state shows properties different from a conventional $q\bar{q}$ state. A candidate for an exotic structure. See the review on non- $q\bar{q}$ states.

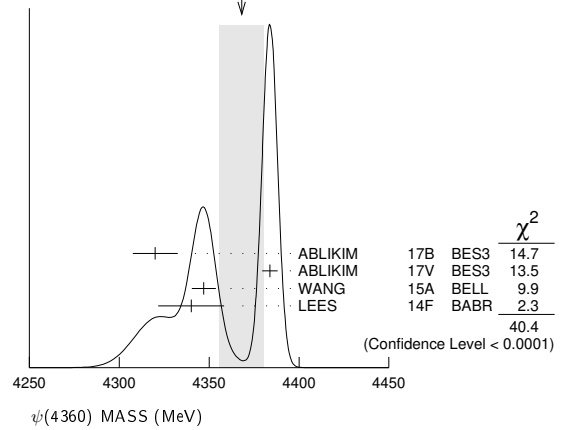
Seen in radiative return from $e^+ e^-$ collisions at $\sqrt{s} = 9.54\text{--}10.58$ GeV by AUBERT 07s, WANG 07D, and LEES 14F. See also the review on "Spectroscopy of mesons containing two heavy quarks."

$\psi(4360)$ MASS

VALUE (MeV)	EVTs	DOCUMENT ID	TECN	COMMENT
4368 \pm 13 OUR AVERAGE				Error includes scale factor of 3.7. See the ideogram below.
$4320.0 \pm 10.4 \pm 7.0$		1 ABLIKIM	17B BES3	$e^+ e^- \rightarrow \pi^+ \pi^- J/\psi$
$4383.8 \pm 4.2 \pm 0.8$		2 ABLIKIM	17V BES3	$e^+ e^- \rightarrow \pi^+ \pi^- \psi(2S)$
$4347 \pm 6 \pm 3$	279	3 WANG	15A BELL	$10.58 e^+ e^- \rightarrow \gamma \pi^+ \pi^- \psi(2S)$
$4340 \pm 16 \pm 9$	37	4 LEES	14F BABR	$10.58 e^+ e^- \rightarrow \gamma \pi^+ \pi^- \psi(2S)$
$4383.7 \pm 2.9 \pm 6.2$		5 ZHANG	17B RVUE	$e^+ e^- \rightarrow \pi^+ \pi^- \psi(2S)$
$4386.4 \pm 2.1 \pm 6.4$		6 ZHANG	17C RVUE	$e^+ e^- \rightarrow \pi^+ \pi^- J/\psi$ or $\psi(2S)$
$4355^{+9}_{-10} \pm 9$	74	7 LIU	08H RVUE	$10.58 e^+ e^- \rightarrow \gamma \pi^+ \pi^- \psi(2S)$
4324 ± 24		8 AUBERT	07s BABR	$10.58 e^+ e^- \rightarrow \gamma \pi^+ \pi^- \psi(2S)$
$4361 \pm 9 \pm 9$	47	4 WANG	07D BELL	$10.58 e^+ e^- \rightarrow \gamma \pi^+ \pi^- \psi(2S)$

• • • We do not use the following data for averages, fits, limits, etc. • • •
¹ From a three-resonance fit.
² From a fit to the cross section for $e^+ e^- \rightarrow \pi^+ \pi^- \psi(2S) \rightarrow 2(\pi^+ \pi^-) \ell^+ \ell^-$ obtained from 16 center-of-mass energies between 4.008 and 4.600 GeV and comprising 5.1 fb⁻¹.
³ From a two-resonance fit. Supersedes WANG 07D.
⁴ From a two-resonance fit.
⁵ From a three-resonance fit.
⁶ From a combined fit of BELLE, BABAR and BES3 $e^+ e^- \rightarrow \pi^+ \pi^- J/\psi$ and $e^+ e^- \rightarrow \pi^+ \pi^- \psi(2S)$ data.
⁷ From a combined fit of AUBERT 07s and WANG 07D data with two resonances.
⁸ From a single-resonance fit. Systematic errors not estimated.

WEIGHTED AVERAGE
 4368 \pm 13 (Error scaled by 3.7)



$\psi(4360)$ WIDTH

VALUE (MeV)	EVTs	DOCUMENT ID	TECN	COMMENT
96 \pm 7 OUR AVERAGE				
$101.4^{+25.3}_{-19.7} \pm 10.2$		1 ABLIKIM	17B BES3	$e^+ e^- \rightarrow \pi^+ \pi^- J/\psi$
$84.2 \pm 12.5 \pm 2.1$		2 ABLIKIM	17V BES3	$e^+ e^- \rightarrow \pi^+ \pi^- \psi(2S)$
$103 \pm 9 \pm 5$	279	3 WANG	15A BELL	$10.58 e^+ e^- \rightarrow \gamma \pi^+ \pi^- \psi(2S)$
$94 \pm 32 \pm 13$	37	4 LEES	14F BABR	$10.58 e^+ e^- \rightarrow \gamma \pi^+ \pi^- \psi(2S)$
$94.2 \pm 7.3 \pm 2.0$		5 ZHANG	17B RVUE	$e^+ e^- \rightarrow \pi^+ \pi^- \psi(2S)$
$96.0 \pm 6.7 \pm 2.7$		6 ZHANG	17C RVUE	$e^+ e^- \rightarrow \pi^+ \pi^- J/\psi$ or $\psi(2S)$
$103^{+17}_{-15} \pm 11$	74	7 LIU	08H RVUE	$10.58 e^+ e^- \rightarrow \gamma \pi^+ \pi^- \psi(2S)$
172 ± 33		8 AUBERT	07s BABR	$10.58 e^+ e^- \rightarrow \gamma \pi^+ \pi^- \psi(2S)$
$74 \pm 15 \pm 10$	47	4 WANG	07D BELL	$10.58 e^+ e^- \rightarrow \gamma \pi^+ \pi^- \psi(2S)$

• • • We do not use the following data for averages, fits, limits, etc. • • •
¹ From a three-resonance fit.
² From a fit to the cross section for $e^+ e^- \rightarrow \pi^+ \pi^- \psi(2S) \rightarrow 2(\pi^+ \pi^-) \ell^+ \ell^-$ obtained from 16 center-of-mass energies between 4.008 and 4.600 GeV and comprising 5.1 fb⁻¹.
³ From a two-resonance fit. Supersedes WANG 07D.
⁴ From a two-resonance fit.
⁵ From a three-resonance fit.
⁶ From a combined fit of BELLE, BABAR and BES3 $e^+ e^- \rightarrow \pi^+ \pi^- J/\psi$ and $e^+ e^- \rightarrow \pi^+ \pi^- \psi(2S)$ data.
⁷ From a combined fit of AUBERT 07s and WANG 07D data with two resonances.
⁸ From a single-resonance fit. Systematic errors not estimated.

$\psi(4360)$ DECAY MODES

Mode	Fraction (Γ_i/Γ)
Γ_1 $e^+ e^-$	
Γ_2 $J/\psi \pi^+ \pi^-$	
Γ_3 $\psi(2S) \pi^+ \pi^-$	seen
Γ_4 $\psi_2(3823) \pi^+ \pi^-$	possibly seen
Γ_5 $J/\psi \eta$	
Γ_6 $D^0 D^{*-} \pi^+$	
Γ_7 $D_1(2420) \bar{D}^+ + \text{c.c.}$	possibly seen
Γ_8 $\chi_{c1} \gamma$	
Γ_9 $\chi_{c2} \gamma$	

$\psi(4360)$ $\Gamma(i) \times \Gamma(e^+ e^-)/\Gamma(\text{total})$

$\Gamma(\psi(2S)\pi^+\pi^-) \times \Gamma(e^+ e^-)/\Gamma_{\text{total}}$	VALUE (eV)	EVTs	DOCUMENT ID	TECN	COMMENT	$\Gamma_3\Gamma_1/\Gamma$
7.3 ± 2.8			1 ABLIKIM	19K BES3	$e^+ e^- \rightarrow \pi^+ \pi^- \psi(2S)$	
11.0 ± 3.8			2 ABLIKIM	19K BES3	$e^+ e^- \rightarrow \pi^+ \pi^- \psi(2S)$	
$9.2 \pm 0.6 \pm 0.6$	279		3 WANG	15A BELL	$10.58 e^+ e^- \rightarrow \gamma \pi^+ \pi^- \psi(2S)$	
$10.9 \pm 0.6 \pm 0.7$	279		4 WANG	15A BELL	$10.58 e^+ e^- \rightarrow \gamma \pi^+ \pi^- \psi(2S)$	
$6.0 \pm 1.0 \pm 0.5$	37		1 LEES	14F BABR	$10.58 e^+ e^- \rightarrow \gamma \pi^+ \pi^- \psi(2S)$	
$7.2 \pm 1.0 \pm 0.6$	37		2 LEES	14F BABR	$10.58 e^+ e^- \rightarrow \gamma \pi^+ \pi^- \psi(2S)$	
$11.1^{+1.3}_{-1.2}$	74		5 LIU	08H RVUE	$10.58 e^+ e^- \rightarrow \gamma \pi^+ \pi^- \psi(2S)$	

• • • We do not use the following data for averages, fits, limits, etc. • • •

See key on page 999

Meson Particle Listings

$\psi(4360)$, $\psi(4390)$, $\psi(4415)$

12.3±1.2	74	⁶ LIU	08H RVUE	10.58 e ⁺ e ⁻ → $\gamma\pi^+\pi^-\psi(2S)$
10.4±1.7±1.5	47	¹ WANG	07D BELL	10.58 e ⁺ e ⁻ → $\gamma\pi^+\pi^-\psi(2S)$
11.8±1.8±1.4	47	² WANG	07D BELL	10.58 e ⁺ e ⁻ → $\gamma\pi^+\pi^-\psi(2S)$

- ¹ Solution I of two equivalent solutions in a fit using two interfering resonances.
- ² Solution II of two equivalent solutions in a fit using two interfering resonances.
- ³ Solution I of two equivalent solutions from a fit using two interfering resonances. Supercedes WANG 07D.
- ⁴ Solution II of two equivalent solutions from a fit using two interfering resonances. Supercedes WANG 07D.
- ⁵ Solution I in a combined fit of AUBERT 07s and WANG 07D data with two resonances.
- ⁶ Solution II in a combined fit of AUBERT 07s and WANG 07D data with two resonances.

$\Gamma(J/\psi\eta) \times \Gamma(e^+e^-)/\Gamma_{\text{total}}$		Γ_5/Γ			
VALUE (eV)	CL%	DOCUMENT ID	TECN	COMMENT	

• • • We do not use the following data for averages, fits, limits, etc. • • •
 <6.8 90 WANG 13B BELL e⁺e⁻ → J/ψηγ

$\Gamma(\chi_{c1}\gamma) \times \Gamma(e^+e^-)/\Gamma_{\text{total}}$		Γ_8/Γ			
VALUE (eV)	CL%	DOCUMENT ID	TECN	COMMENT	

<0.57 90 ¹HAN 15 BELL 10.58 e⁺e⁻ → χ_{c1}γ
¹ Using B(η → γγ) = (39.41 ± 0.21)%.

$\Gamma(\chi_{c2}\gamma) \times \Gamma(e^+e^-)/\Gamma_{\text{total}}$		Γ_9/Γ			
VALUE (eV)	CL%	DOCUMENT ID	TECN	COMMENT	

<1.9 90 ¹HAN 15 BELL 10.58 e⁺e⁻ → χ_{c2}γ
¹ Using B(η → γγ) = (39.41 ± 0.21)%.

$\psi(4360)$ BRANCHING RATIOS

$\Gamma(D^0 D^{*-} \pi^+)/\Gamma(\psi(2S)\pi^+\pi^-)$		Γ_6/Γ_3			
VALUE	CL%	DOCUMENT ID	TECN	COMMENT	

<8 90 PAKHLOVA 09 BELL e⁺e⁻ → ψ(4360) → D⁰D^{*-}π⁺

$\Gamma(\psi(2S)\pi^+\pi^-)/\Gamma_{\text{total}}$		Γ_3/Γ			
VALUE		DOCUMENT ID	TECN	COMMENT	

seen ¹ ABLIKIM 17V BES3 e⁺e⁻ → π⁺π⁻ψ(2S)
¹ From a fit to the cross section for e⁺e⁻ → π⁺π⁻ψ(2S) → 2(π⁺π⁻)ℓ⁺ℓ⁻ obtained from 16 center-of-mass energies between 4.008 and 4.600 GeV and comprising 5.1 fb⁻¹.

$\Gamma(\psi(2S)\pi^+\pi^-)/\Gamma(J/\psi\pi^+\pi^-)$		Γ_3/Γ_2			
VALUE		DOCUMENT ID	TECN	COMMENT	

• • • We do not use the following data for averages, fits, limits, etc. • • •
 (0.81 ± 0.12 ± 0.13) to (42 ± 15 ± 15) ¹ZHANG 17C RVUE e⁺e⁻ → π⁺π⁻J/ψ or ψ(2S)
¹ From a combined fit of BELLE, BABAR and BES3 e⁺e⁻ → π⁺π⁻J/ψ and e⁺e⁻ → π⁺π⁻ψ(2S) data.

$\Gamma(\psi_2(3823)\pi^+\pi^-)/\Gamma_{\text{total}}$		Γ_4/Γ			
VALUE	EVTs	DOCUMENT ID	TECN	COMMENT	

possibly seen 19 ¹ ABLIKIM 15S BES3 e⁺e⁻ → π⁺π⁻χ_{c1}γ
¹ From a fit of e⁺e⁻ → π⁺π⁻ψ₂(3823), ψ₂(3823) → χ_{c1}γ cross sections taken at √s values of 4.23, 4.26, 4.36, 4.42, and 4.60 GeV to the ψ(4360) line shape.

$\Gamma(D^0 D^{*-} \pi^+)/\Gamma_{\text{total}} \times \Gamma(e^+e^-)/\Gamma_{\text{total}}$		$\Gamma_6/\Gamma \times \Gamma_1/\Gamma$			
VALUE	CL%	DOCUMENT ID	TECN	COMMENT	

<0.72 × 10⁻⁶ 90 ¹ PAKHLOVA 09 BELL e⁺e⁻ → ψ(4360) → D⁰D^{*-}π⁺
¹ Using 4355⁺⁹₋₁₀ ± 9 MeV for the mass of ψ(4360).

$\Gamma(D_1(2420)\bar{D} + c.c.)/\Gamma_{\text{total}}$		Γ_7/Γ			
VALUE		DOCUMENT ID	TECN	COMMENT	

possibly seen ¹ ABLIKIM 19AR BES3 e⁺e⁻ → π⁺π⁻D⁰
¹ Evidence for e⁺e⁻ → D₁(2420)D̄ + c.c. between √s = 4.3 and 4.6 GeV, not necessarily resonant.

$\psi(4360)$ REFERENCES

ABLIKIM 19AR PR D100 032005	M. Ablikim et al.	(BESIII Collab.)
ABLIKIM 19K PR D99 019903 (errata)	M. Ablikim et al.	(BESIII Collab.)
ABLIKIM 17B PRL 118 092001	M. Ablikim et al.	(BESIII Collab.)
ABLIKIM 17V PR D96 032004	M. Ablikim et al.	(BESIII Collab.)
Also PR D99 019903 (errata)	M. Ablikim et al.	(BESIII Collab.)
ZHANG 17B PR D96 054008	J. Zhang, J. Zhang	
ZHANG 17C EPJ C77 727	J. Zhang, L. Yuan	
ABLIKIM 15S PRL 115 011803	M. Ablikim et al.	(BESIII Collab.)
HAN 15 PR D92 012011	Y.L. Han et al.	(BELLE Collab.)
WANG 15A PR D91 112007	X.L. Wang et al.	(BELLE Collab.)
LEES 14F PR D89 111103	J.P. Lees et al.	(BABAR Collab.)
WANG 13B PR D87 051101	X.L. Wang et al.	(BELLE Collab.)
PAKHOVA 09 PR D80 091101	G. Pakhlova et al.	(BELLE Collab.)
LIU 08H PR D78 014032	Z.Q. Liu, X.S. Qin, C.Z. Yuan	
AUBERT 07S PRL 98 212001	B. Aubert et al.	(BABAR Collab.)
WANG 07D PRL 99 142002	X.L. Wang et al.	(BELLE Collab.)

$\psi(4390)$

$I^G(J^{PC}) = 0^-(1^{--})$
 I needs confirmation.

OMITTED FROM SUMMARY TABLE
 was X(4390)

This state shows properties different from a conventional q \bar{q} state. A candidate for an exotic structure. See the review on non-q \bar{q} states.

$\psi(4390)$ MASS

VALUE (MeV)	DOCUMENT ID	TECN	COMMENT
-------------	-------------	------	---------

4391.5^{+6.3}_{-6.8} ± 1.0 ABLIKIM 17G BES3 e⁺e⁻ → π⁺π⁻h_c

$\psi(4390)$ WIDTH

VALUE (MeV)	DOCUMENT ID	TECN	COMMENT
-------------	-------------	------	---------

139.5^{+16.2}_{-20.6} ± 0.6 ABLIKIM 17G BES3 e⁺e⁻ → π⁺π⁻h_c

$\psi(4390)$ DECAY MODES

Mode	Fraction (Γ _i /Γ)
Γ ₁ π ⁺ π ⁻ h _c	seen
Γ ₂ π ⁺ π ⁻ ψ(3770)	possibly seen

$\psi(4390)$ BRANCHING RATIOS

$\Gamma(\pi^+\pi^-\bar{h}_c)/\Gamma_{\text{total}}$		Γ_1/Γ			
VALUE		DOCUMENT ID	TECN	COMMENT	

seen ABLIKIM 17G BES3 e⁺e⁻ → π⁺π⁻h_c

$\Gamma(\pi^+\pi^-\psi(3770))/\Gamma_{\text{total}}$		Γ_2/Γ			
VALUE		DOCUMENT ID	TECN	COMMENT	

possibly seen ¹ ABLIKIM 19AR BES3 e⁺e⁻ → π⁺π⁻D⁰
¹ Observe e⁺e⁻ → π⁺π⁻ψ(3770) at √s = 4.26, 4.36, and 4.42 GeV but cannot establish if continuum or resonant.

$\psi(4390)$ REFERENCES

ABLIKIM 19AR PR D100 032005	M. Ablikim et al.	(BESIII Collab.)
ABLIKIM 17G PRL 118 092002	M. Ablikim et al.	(BESIII Collab.)

$\psi(4415)$

$I^G(J^{PC}) = 0^-(1^{--})$

$\psi(4415)$ MASS

VALUE (MeV)	DOCUMENT ID	TECN	COMMENT
-------------	-------------	------	---------

4421 ± 4 OUR ESTIMATE
 4415.1 ± 7.9 ¹ ABLIKIM 08D BES2 e⁺e⁻ → hadrons

- • • We do not use the following data for averages, fits, limits, etc. • • •
- 4412 ± 15 ² MO 10 RVUE e⁺e⁻ → hadrons
- 4411 ± 7 ³ PAKHOVA 08A BELL 10.6 e⁺e⁻ → D⁰D⁻π⁺γ
- 4425 ± 6 ⁴ SETH 05A RVUE e⁺e⁻ → hadrons
- 4429 ± 9 ⁵ SETH 05A RVUE e⁺e⁻ → hadrons
- 4417 ± 10 BRANDELIC 78C DASP e⁺e⁻
- 4414 ± 7 SIEGRIST 76 MRK1 e⁺e⁻

- ¹ Reanalysis of data presented in BAI 02c. From a global fit over the center-of-mass energy region 3.7–5.0 GeV covering the ψ(3770), ψ(4040), ψ(4160), and ψ(4415) resonances. Phase angle fixed in the fit to δ = (234 ± 88)°.
- ² Reanalysis of data presented in BAI 00 and BAI 02c. From a global fit over the center-of-mass energy 3.8–4.8 GeV covering the ψ(4040), ψ(4160) and ψ(4415) resonances and including interference effects.
- ³ Systematic uncertainties not estimated.
- ⁴ From a fit to Crystal Ball (OSTERHELD 86) data.
- ⁵ From a fit to BES (BAI 02c) data.

$\psi(4415)$ WIDTH

VALUE (MeV)	DOCUMENT ID	TECN	COMMENT
-------------	-------------	------	---------

62 ± 20 OUR ESTIMATE
 71.5 ± 19.0 ⁶ ABLIKIM 08D BES2 e⁺e⁻ → hadrons

- • • We do not use the following data for averages, fits, limits, etc. • • •
- 118 ± 32 ⁷ MO 10 RVUE e⁺e⁻ → hadrons
- 77 ± 20 ⁸ PAKHOVA 08A BELL 10.6 e⁺e⁻ → D⁰D⁻π⁺γ
- 119 ± 16 ⁹ SETH 05A RVUE e⁺e⁻ → hadrons
- 118 ± 35 ¹⁰ SETH 05A RVUE e⁺e⁻ → hadrons
- 66 ± 15 BRANDELIC 78C DASP e⁺e⁻

Meson Particle Listings

 $\psi(4415)$ 33 ± 10 SIEGRIST 76 MRK1 e^+e^-

⁶ Reanalysis of data presented in BAI 02c. From a global fit over the center-of-mass energy region 3.7–5.0 GeV covering the $\psi(3770)$, $\psi(4040)$, $\psi(4160)$, and $\psi(4415)$ resonances. Phase angle fixed in the fit to $\delta = (234 \pm 88)^\circ$.

⁷ Reanalysis of data presented in BAI 00 and BAI 02c. From a global fit over the center-of-mass energy 3.8–4.8 GeV covering the $\psi(4040)$, $\psi(4160)$ and $\psi(4415)$ resonances and including interference effects.

⁸ Systematic uncertainties not estimated.

⁹ From a fit to Crystal Ball (OSTERHELD 86) data.

¹⁰ From a fit to BES (BAI 02c) data.

 $\psi(4415)$ DECAY MODES

Due to the complexity of the $c\bar{c}$ threshold region, in this listing, “seen” (“not seen”) means that a cross section for the mode in question has been measured at effective \sqrt{s} near this particle's central mass value, more (less) than 2σ above zero, without regard to any peaking behavior in \sqrt{s} or absence thereof. See mode listing(s) for details and references.

Mode	Fraction (Γ_i/Γ)	Confidence level
Γ_1 $D\bar{D}$	seen	
Γ_2 $D^0\bar{D}^0$	seen	
Γ_3 D^+D^-	seen	
Γ_4 $D^*\bar{D} + c.c.$	seen	
Γ_5 $D^*(2007)^0\bar{D}^0 + c.c.$	seen	
Γ_6 $D^*(2010)^+D^- + c.c.$	seen	
Γ_7 $D^*\bar{D}^*$	seen	
Γ_8 $D^*(2007)^0\bar{D}^*(2007)^0 + c.c.$	seen	
Γ_9 $D^*(2010)^+D^*(2010)^- + c.c.$	seen	
Γ_{10} $D^0D^-\pi^+$ (excl. $D^*(2007)^0\bar{D}^0$ + c.c., $D^*(2010)^+D^- + c.c.$)	< 2.3 %	90%
Γ_{11} $D\bar{D}_2^*(2460) \rightarrow D^0D^-\pi^+ + c.c.$	(10 \pm 4) %	
Γ_{12} $D^0\bar{D}^*\pi^+ + c.c.$	< 11 %	90%
Γ_{13} $D_1(2420)\bar{D} + c.c.$	possibly seen	
Γ_{14} $D_s^+D_s^-$	not seen	
Γ_{15} $\omega\chi_{c2}$	possibly seen	
Γ_{16} $D_s^{*+}D_s^- + c.c.$	seen	
Γ_{17} $D_s^+D_s^{*-}$	not seen	
Γ_{18} $\psi_2(3823)\pi^+\pi^-$	possibly seen	
Γ_{19} $\psi(3770)\pi^+\pi^-$	possibly seen	
Γ_{20} $J/\psi\eta$	< 6 $\times 10^{-3}$	90%
Γ_{21} $\chi_{c1}\gamma$	< 8 $\times 10^{-4}$	90%
Γ_{22} $\chi_{c2}\gamma$	< 4 $\times 10^{-3}$	90%
Γ_{23} e^+e^-	(9.4 \pm 3.2) $\times 10^{-6}$	

 $\psi(4415)$ PARTIAL WIDTHS

$\Gamma(e^+e^-)$	Γ_{23}
VALUE (keV)	DOCUMENT ID TECN COMMENT
0.58 \pm 0.07 OUR ESTIMATE	
0.35 \pm 0.12	11 ABLIKIM 08D BES2 $e^+e^- \rightarrow$ hadrons
• • • We do not use the following data for averages, fits, limits, etc. • • •	
0.4 to 0.8	12 MO 10 RVUE $e^+e^- \rightarrow$ hadrons
0.72 \pm 0.11	13 SETH 05A RVUE $e^+e^- \rightarrow$ hadrons
0.64 \pm 0.23	14 SETH 05A RVUE $e^+e^- \rightarrow$ hadrons
0.49 \pm 0.13	BRADELNIK 78C DASP e^+e^-
0.44 \pm 0.14	SIEGRIST 76 MRK1 e^+e^-

¹¹ Reanalysis of data presented in BAI 00 and BAI 02c. From a global fit over the center-of-mass energy region 3.7–5.0 GeV covering the $\psi(3770)$, $\psi(4040)$, $\psi(4160)$, and $\psi(4415)$ resonances. Phase angle fixed in the fit to $\delta = (234 \pm 88)^\circ$.

¹² Reanalysis of data presented in BAI 00 and BAI 02c. From a global fit over the center-of-mass energy 3.8–4.8 GeV covering the $\psi(4040)$, $\psi(4160)$ and $\psi(4415)$ resonances and including interference effects. Four sets of solutions are obtained with the same fit quality, mass and total width, but with different e^+e^- partial widths. We quote only the range of values.

¹³ From a fit to Crystal Ball (OSTERHELD 86) data.

¹⁴ From a fit to BES (BAI 02c) data.

 $\psi(4415)$ $\Gamma(i) \times \Gamma(e^+e^-)/\Gamma(\text{total})$

$\Gamma(J/\psi\eta) \times \Gamma(e^+e^-)/\Gamma(\text{total})$	$\Gamma_{20}\Gamma_{23}/\Gamma$
VALUE (eV) CL%	DOCUMENT ID TECN COMMENT
<3.6	90 WANG 13B BELL $e^+e^- \rightarrow J/\psi\eta\gamma$

$\Gamma(\chi_{c1}\gamma) \times \Gamma(e^+e^-)/\Gamma(\text{total})$	$\Gamma_{21}\Gamma_{23}/\Gamma$
VALUE (eV) CL%	DOCUMENT ID TECN COMMENT
<0.47	90 15 HAN 15 BELL 10.58 $e^+e^- \rightarrow \chi_{c1}\gamma$

¹⁵ Using $B(\eta \rightarrow \gamma\gamma) = (39.41 \pm 0.21)\%$.

$\Gamma(\chi_{c2}\gamma) \times \Gamma(e^+e^-)/\Gamma(\text{total})$	$\Gamma_{22}\Gamma_{23}/\Gamma$
VALUE (eV) CL%	DOCUMENT ID TECN COMMENT
<2.3	90 16 HAN 15 BELL 10.58 $e^+e^- \rightarrow \chi_{c2}\gamma$

¹⁶ Using $B(\eta \rightarrow \gamma\gamma) = (39.41 \pm 0.21)\%$.

 $\psi(4415)$ BRANCHING RATIOS

$\Gamma(D^0\bar{D}^0)/\Gamma(\text{total})$	Γ_2/Γ
VALUE	DOCUMENT ID TECN COMMENT
seen	PAKHOVA 08 BELL $e^+e^- \rightarrow D^0\bar{D}^0\gamma$
• • • We do not use the following data for averages, fits, limits, etc. • • •	
not seen	AUBERT 09M BABR $e^+e^- \rightarrow D^0\bar{D}^0\gamma$

$\Gamma(D^+D^-)/\Gamma(\text{total})$	Γ_3/Γ
VALUE	DOCUMENT ID TECN COMMENT
seen	PAKHOVA 08 BELL $e^+e^- \rightarrow D^+D^-\gamma$
• • • We do not use the following data for averages, fits, limits, etc. • • •	
not seen	AUBERT 09M BABR $e^+e^- \rightarrow D^+D^-\gamma$

$\Gamma(D\bar{D})/\Gamma(D^*\bar{D}^*)$	Γ_1/Γ_7
VALUE	DOCUMENT ID TECN COMMENT
0.14 \pm 0.12 \pm 0.03	AUBERT 09M BABR $e^+e^- \rightarrow \gamma D^{(*)}\bar{D}^{(*)}$

$\Gamma(D^*(2007)^0\bar{D}^0 + c.c.)/\Gamma(\text{total})$	Γ_5/Γ
VALUE	DOCUMENT ID TECN COMMENT
seen	AUBERT 09M BABR $e^+e^- \rightarrow D^{*0}\bar{D}^0\gamma$

$\Gamma(D^*(2010)^+D^- + c.c.)/\Gamma(\text{total})$	Γ_6/Γ
VALUE	DOCUMENT ID TECN COMMENT
seen	17 ZHUKOVA 18 BELL $e^+e^- \rightarrow D^{*+}D^-\gamma$
seen	AUBERT 09M BABR $e^+e^- \rightarrow D^{*+}D^-\gamma$
• • • We do not use the following data for averages, fits, limits, etc. • • •	
seen	PAKHOVA 07 BELL $e^+e^- \rightarrow D^{*+}D^-\gamma$

¹⁷ Supersedes PAKHOVA 07.

$\Gamma(D^*\bar{D} + c.c.)/\Gamma(D^*\bar{D}^*)$	Γ_4/Γ_7
VALUE	DOCUMENT ID TECN COMMENT
0.17 \pm 0.25 \pm 0.03	AUBERT 09M BABR $e^+e^- \rightarrow \gamma D^{(*)}\bar{D}^{(*)}$

$\Gamma(D^*(2007)^0\bar{D}^*(2007)^0 + c.c.)/\Gamma(\text{total})$	Γ_8/Γ
VALUE	DOCUMENT ID TECN COMMENT
seen	AUBERT 09M BABR $e^+e^- \rightarrow D^{*0}\bar{D}^{*0}\gamma$

$\Gamma(D^*(2010)^+D^*(2010)^- + c.c.)/\Gamma(\text{total})$	Γ_9/Γ
VALUE	DOCUMENT ID TECN COMMENT
seen	18 ZHUKOVA 18 BELL $e^+e^- \rightarrow D^{*+}D^{*-}\gamma$
seen	AUBERT 09M BABR $e^+e^- \rightarrow D^{*+}D^{*-}\gamma$
• • • We do not use the following data for averages, fits, limits, etc. • • •	
seen	PAKHOVA 07 BELL $e^+e^- \rightarrow D^{*+}D^{*-}\gamma$

¹⁸ Supersedes PAKHOVA 07.

$\Gamma(D\bar{D}_2^*(2460) \rightarrow D^0D^-\pi^+ + c.c.)/\Gamma(\text{total})$	Γ_{11}/Γ
VALUE (units 10^{-2})	DOCUMENT ID TECN COMMENT
10.5 \pm 2.4 \pm 3.8	19 PAKHOVA 08A BELL 10.6 $e^+e^- \rightarrow D^0D^-\pi^+\gamma$

¹⁹ Using 4421 \pm 4 MeV for the mass and 62 \pm 20 MeV for the width of $\psi(4415)$.

$\Gamma(D^0D^-\pi^+ \text{ (excl. } D^*(2007)^0\bar{D}^0 + c.c., D^*(2010)^+D^- + c.c.)/\Gamma(D\bar{D}_2^*(2460) \rightarrow D^0D^-\pi^+ + c.c.)$	Γ_{10}/Γ_{11}
VALUE CL%	DOCUMENT ID TECN COMMENT
<0.22	90 20 PAKHOVA 08A BELL 10.6 $e^+e^- \rightarrow D^0D^-\pi^+\gamma$

²⁰ Using 4421 \pm 4 MeV for the mass and 62 \pm 20 MeV for the width of $\psi(4415)$.

$\Gamma(D^0D^{*-}\pi^+ + c.c.)/\Gamma(\text{total}) \times \Gamma(e^+e^-)/\Gamma(\text{total})$	$\Gamma_{12}/\Gamma \times \Gamma_{23}/\Gamma$
VALUE CL%	DOCUMENT ID TECN COMMENT
<0.99 $\times 10^{-6}$	90 21 PAKHOVA 09 BELL $e^+e^- \rightarrow D^0D^{*-}\pi^+$

²¹ Using 4421 \pm 4 MeV for the mass of $\psi(4415)$.

$\Gamma(D_1(2420)\bar{D} + c.c.)/\Gamma(\text{total})$	Γ_{13}/Γ
VALUE	DOCUMENT ID TECN COMMENT
possibly seen	22 ABLIKIM 19AR BES3 $e^+e^- \rightarrow \pi^+\pi^-\bar{D}\bar{D}$

²² Evidence for $e^+e^- \rightarrow D_1(2420)\bar{D} + c.c.$ between $\sqrt{s} = 4.3$ and 4.6 GeV, not necessarily resonant.

$\Gamma(D_s^+D_s^-)/\Gamma(\text{total})$	Γ_{14}/Γ
VALUE	DOCUMENT ID TECN COMMENT
not seen	PAKHOVA 11 BELL $e^+e^- \rightarrow D_s^+D_s^-\gamma$
not seen	DEL-AMO-SA...10N BABR $e^+e^- \rightarrow D_s^+D_s^-\gamma$

$\Gamma(\omega\chi_{c2})/\Gamma(\text{total})$	Γ_{15}/Γ
VALUE	DOCUMENT ID TECN COMMENT
possibly seen	ABLIKIM 16A BES3 $e^+e^- \rightarrow \gamma\pi^+\pi^-\pi^0\ell^+\ell^-$

See key on page 999

Meson Particle Listings

$\psi(4415)$, $Z_c(4430)$, $\chi_{c0}(4500)$

$\Gamma(D_s^{*+} D_s^- + c.c.) / \Gamma_{total}$				Γ_{16} / Γ
VALUE	DOCUMENT ID	TECN	COMMENT	
seen	PAKHOVA 11	BELL	$e^+ e^- \rightarrow D_s^{*+} D_s^- \gamma$	
seen	DEL-AMO-SA...10N	BABR	$e^+ e^- \rightarrow D_s^{*+} D_s^- \gamma$	

$\Gamma(D_s^{*+} D_s^{*-}) / \Gamma_{total}$				Γ_{17} / Γ
VALUE	DOCUMENT ID	TECN	COMMENT	
not seen	PAKHOVA 11	BELL	$e^+ e^- \rightarrow D_s^{*+} D_s^{*-} \gamma$	
not seen	DEL-AMO-SA...10N	BABR	$e^+ e^- \rightarrow D_s^{*+} D_s^{*-} \gamma$	

$\Gamma(\psi(3770) \pi^+ \pi^-) / \Gamma_{total}$				Γ_{19} / Γ
VALUE	DOCUMENT ID	TECN	COMMENT	
possibly seen	23 ABLIKIM 19AR	BES3	$e^+ e^- \rightarrow \pi^+ \pi^- D \bar{D}$	

²³ Observe $e^+ e^- \rightarrow \pi^+ \pi^- \psi(3770)$ at $\sqrt{s} = 4.26, 4.36, \text{ and } 4.42$ GeV but cannot establish if continuum or resonant.

$\Gamma(\psi_2(3823) \pi^+ \pi^-) / \Gamma_{total}$				Γ_{18} / Γ
VALUE	EVTS	DOCUMENT ID	TECN	COMMENT
possibly seen	19	24 ABLIKIM 15s	BES3	$e^+ e^- \rightarrow \pi^+ \pi^- \chi_{c1} \gamma$

²⁴ From a fit of $e^+ e^- \rightarrow \pi^+ \pi^- \psi_2(3823)$, $\psi_2(3823) \rightarrow \chi_{c1} \gamma$ cross sections taken at \sqrt{s} values of 4.23, 4.26, 4.36, 4.42, and 4.60 GeV to the $\psi(4415)$ line shape.

$\psi(4415)$ REFERENCES

ABLIKIM 19AR	PR D100 032005	M. Ablikim et al.	(BESIII Collab.)
ZHUKOVA 18	PR D97 012002	V. Zhukova et al.	(BELLE Collab.)
ABLIKIM 16A	PR D93 011102	M. Ablikim et al.	(BESIII Collab.)
ABLIKIM 15S	PRL 115 011803	M. Ablikim et al.	(BESIII Collab.)
HAN 15	PR D92 012011	Y.L. Han et al.	(BELLE Collab.)
WANG 13B	PR D87 051101	X.L. Wang et al.	(BELLE Collab.)
PAKHOVA 11	PR D83 011101	G. Pakhlova et al.	(BELLE Collab.)
DEL-AMO-SA...10N	PR D82 052004	P. del Amo Sanchez et al.	(BABAR Collab.)
MO 10	PR D82 077501	X.H. Mo, C.Z. Yuan, P. Wang	(BHEP)
AUBERT 09M	PR D79 092001	B. Aubert et al.	(BABAR Collab.)
PAKHOVA 09	PR D80 091301	G. Pakhlova et al.	(BELLE Collab.)
ABLIKIM 08D	PL B660 315	M. Ablikim et al.	(BES Collab.)
PAKHOVA 08	PR D77 011103	G. Pakhlova et al.	(BELLE Collab.)
PAKHOVA 08A	PRL 100 062001	G. Pakhlova et al.	(BELLE Collab.)
PAKHOVA 07	PRL 98 092001	G. Pakhlova et al.	(BELLE Collab.)
SETH 05A	PR D72 017501	K.K. Seth	(BES Collab.)
BAI 02C	PRL 88 101802	J.Z. Bai et al.	(BES Collab.)
BAI 00	PRL 84 594	J.Z. Bai et al.	(BES Collab.)
OSTERHELD 86	SLAC-PUB-4160	A. Osterheld et al.	(SLAC Crystal Ball Collab.)
BRANDELIK 78C	PL 76B 361	R. Brandelik et al.	(DASP Collab.)
SIEGRIST 76	PRL 36 700	J.L. Siegrist et al.	(LBL, SLAC)

$Z_c(4430)$

$$I^G(J^{PC}) = 1^+(1^{+-})$$

G, C need confirmation.

was $X(4430)^\pm$
 Properties incompatible with a $q\bar{q}$ structure (exotic state). See the review on non- $q\bar{q}$ states.

First seen by CHOI 08 in $B \rightarrow K\pi^+\psi(2S)$ decays, confirmed by AAIJ 14AG, and confirmed in a model-independent way by AAIJ 15BH. Also seen by CHILIKIN 14 in $B \rightarrow K^+\pi J/\psi$ decays. J^P was determined by CHILIKIN 13 and AAIJ 14AG.

$Z_c(4430)$ MASS

VALUE (MeV)	DOCUMENT ID	TECN	COMMENT
$4478 \pm^{+15}_{-18}$ OUR AVERAGE			
$4475 \pm 7^{+15}_{-25}$	¹ AAIJ 14AG	LHCB	$B^0 \rightarrow K^+\pi^-\psi(2S)$
$4485 \pm 22^{+28}_{-11}$	¹ CHILIKIN 13	BELL	$B^0 \rightarrow K^+\pi^-\psi(2S)$
$4443 \pm^{+15}_{-12} \pm^{+19}_{-13}$	² MIZUK 09	BELL	$B \rightarrow K\pi^+\psi(2S)$
$4433 \pm 4 \pm 2$	³ CHOI 08	BELL	$B \rightarrow K\pi^+\psi(2S)$

¹ From a four-dimensional amplitude analysis.
² From a Dalitz plot analysis. Superseded by CHILIKIN 13.
³ Superseded by MIZUK 09 and CHILIKIN 13.

$Z_c(4430)$ WIDTH

VALUE (MeV)	DOCUMENT ID	TECN	COMMENT
181 ± 31 OUR AVERAGE			
$172 \pm 13^{+37}_{-34}$	¹ AAIJ 14AG	LHCB	$B^0 \rightarrow K^+\pi^-\psi(2S)$
$200 \pm 41^{+26}_{-46} \pm 26^{+35}_{-35}$	¹ CHILIKIN 13	BELL	$B^0 \rightarrow K^+\pi^-\psi(2S)$
$107 \pm 86^{+74}_{-43} \pm 56$	² MIZUK 09	BELL	$B \rightarrow K\pi^+\psi(2S)$
$45 \pm 18^{+30}_{-13} \pm 13$	³ CHOI 08	BELL	$B \rightarrow K\pi^+\psi(2S)$

¹ From a four-dimensional amplitude analysis.
² From a Dalitz plot analysis. Superseded by CHILIKIN 13.
³ Superseded by MIZUK 09 and CHILIKIN 13.

$Z_c(4430)$ DECAY MODES

Mode	Fraction (Γ_i/Γ)
$\Gamma_1 \pi^+ \psi(2S)$	seen
$\Gamma_2 \pi^+ J/\psi$	seen

$Z_c(4430)$ BRANCHING RATIOS

$\Gamma(\pi^+ \psi(2S)) / \Gamma_{total}$	Γ_1 / Γ		
VALUE	DOCUMENT ID	TECN	COMMENT
seen	¹ AAIJ 14AG	LHCB	$B^0 \rightarrow K^+\pi^-\psi(2S)$
seen	² CHILIKIN 13	BELL	$B^0 \rightarrow K^+\pi^-\psi(2S)$
not seen	³ AUBERT 09AA	BABR	$B \rightarrow K\pi^+\psi(2S)$
seen	⁴ MIZUK 09	BELL	$B \rightarrow K\pi^+\psi(2S)$

• • • We do not use the following data for averages, fits, limits, etc. • • •

¹ From a four-dimensional amplitude analysis. No product of branching fractions quoted.
² From a four-dimensional amplitude analysis. Measured a product of branching fractions $B(B^0 \rightarrow Z_c(4430)^- K^+) \times B(Z_c(4430)^- \rightarrow \psi(2S) \pi^-) = (6.0 \pm^{+2.5}_{-2.0} -^{+1.4}_{-1.4}) \times 10^{-5}$.
³ AUBERT 09AA quotes $B(B^+ \rightarrow \bar{K}^0 Z_c(4430)^+) \times B(Z_c(4430)^+ \rightarrow \pi^+\psi(2S)) < 4.7 \times 10^{-5}$ and $B(\bar{B}^0 \rightarrow K^- Z_c(4430)^+) \times B(Z_c(4430)^+ \rightarrow \pi^+\psi(2S)) < 3.1 \times 10^{-5}$ at 95% CL.
⁴ Measured a product of branching fractions $B(\bar{B}^0 \rightarrow K^- Z_c(4430)^+) \times B(Z_c(4430)^+ \rightarrow \pi^+\psi(2S)) = (3.2 \pm^{+1.8+5.3}_{-0.9-1.6}) \times 10^{-5}$. Superseded by CHILIKIN 13.

$\Gamma(\pi^+ J/\psi) / \Gamma_{total}$

VALUE	DOCUMENT ID	TECN	COMMENT
seen	^{1,2} CHILIKIN 14	BELL	$\bar{B}^0 \rightarrow K^-\pi^+ J/\psi$
not seen	³ AUBERT 09AA	BABR	$B \rightarrow K\pi^+ J/\psi$

• • • We do not use the following data for averages, fits, limits, etc. • • •

¹ CHILIKIN 14 reports $B(\bar{B}^0 \rightarrow Z_c(4430)^+ K^-) \times B(Z_c(4430)^+ \rightarrow J/\psi \pi^+) = (5.4 \pm^{+4.0+1.1}_{-1.0-0.9}) \times 10^{-6}$.
² A broad enhancement seen by AAIJ 19R in the decays $B^0 \rightarrow J/\psi \pi^+ K^-$ at 4600 MeV can be due to an interplay of $Z_c(4430)$, $Z_c(4200)$ and the fitting polynomials.
³ AUBERT 09AA quotes $B(B^+ \rightarrow \bar{K}^0 Z_c(4430)^+) \times B(Z_c(4430)^+ \rightarrow \pi^+ J/\psi) < 1.5 \times 10^{-5}$ and $B(\bar{B}^0 \rightarrow K^- Z_c(4430)^+) \times B(Z_c(4430)^+ \rightarrow \pi^+ J/\psi) < 0.4 \times 10^{-5}$ at 95% CL.

$Z_c(4430)$ REFERENCES

AAIJ 19R	PRL 122 152002	R. Aaij et al.	(LHCb Collab.)
AAIJ 15BH	PR D92 112009	R. Aaij et al.	(LHCb Collab.)
AAIJ 14AG	PRL 112 222002	R. Aaij et al.	(LHCb Collab.) JP
CHILIKIN 14	PR D90 112009	K. Chilikin et al.	(BELLE Collab.)
CHILIKIN 13	PR D88 074026	K. Chilikin et al.	(BELLE Collab.) JP
AUBERT 09AA	PR D79 112001	B. Aubert et al.	(BABAR Collab.)
MIZUK 09	PR D80 031104	R. Mizuk et al.	(BELLE Collab.)
CHOI 08	PRL 100 142001	S.-K. Choi et al.	(BELLE Collab.)

$\chi_{c0}(4500)$

$$I^G(J^{PC}) = 0^+(0^{++})$$

OMITTED FROM SUMMARY TABLE
 was $X(4500)$

This state shows properties different from a conventional $q\bar{q}$ state. A candidate for an exotic structure. See the review on non- $q\bar{q}$ states.
 Seen by AAIJ 17C in $B^+ \rightarrow \chi_{c0} K^+$, $\chi_{c0} \rightarrow J/\psi \phi$ using an amplitude analysis of $B^+ \rightarrow J/\psi \phi K^+$ with a significance (accounting for systematic uncertainties) of 6.1 σ .

$\chi_{c0}(4500)$ MASS

VALUE (MeV)	EVTS	DOCUMENT ID	TECN	COMMENT
$4506 \pm 11^{+12}_{-15}$	4289	¹ AAIJ 17C	LHCB	$B^+ \rightarrow J/\psi \phi K^+$

¹ From an amplitude analysis of the decay $B^+ \rightarrow J/\psi \phi K^+$ with a significance of 6.1 σ .

$\chi_{c0}(4500)$ WIDTH

VALUE (MeV)	EVTS	DOCUMENT ID	TECN	COMMENT
$92 \pm 21^{+21}_{-20}$	4289	¹ AAIJ 17C	LHCB	$B^+ \rightarrow J/\psi \phi K^+$

¹ From an amplitude analysis of the decay $B^+ \rightarrow J/\psi \phi K^+$ with a significance of 6.1 σ .

$\chi_{c0}(4500)$ DECAY MODES

Mode	Fraction (Γ_i/Γ)
$\Gamma_1 J/\psi \phi$	seen

Meson Particle Listings

$\chi_{c0}(4500), \psi(4660)$

$\chi_{c0}(4500)$ BRANCHING RATIOS

$\Gamma(J/\psi\phi)/\Gamma_{total}$	VALUE	EVTS	DOCUMENT ID	TECN	COMMENT	Γ_1/Γ
seen		4289	¹ AAIJ	17c	LHCB $B^+ \rightarrow J/\psi\phi K^+$	

¹ From an amplitude analysis of the decay $B^+ \rightarrow J/\psi\phi K^+$ with a significance of 6.1 σ .

$\chi_{c0}(4500)$ REFERENCES

AAIJ	17C	PRL 118 022003	R. Aaij <i>et al.</i>	(LHCb Collab.) JP
Also		PR D95 012002	R. Aaij <i>et al.</i>	(LHCb Collab.)

$\psi(4660)$

$$J^G(J^{PC}) = 0^-(1^{--})$$

also known as $Y(4660)$; was $X(4660)$

This state shows properties different from a conventional $q\bar{q}$ state. A candidate for an exotic structure. See the review on non- $q\bar{q}$ states.

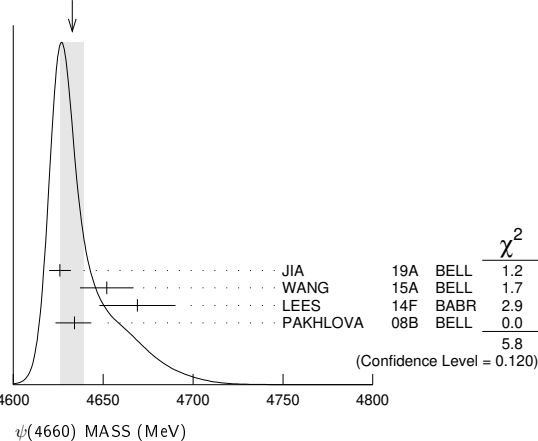
Seen in radiative return from e^+e^- collisions at $\sqrt{s} = 9.54\text{--}10.58$ GeV by WANG 07D. Also obtained in a combined fit of WANG 07D, AUBERT 07s, and LEES 14F. See also the review on "Spectroscopy of mesons containing two heavy quarks."

$\psi(4660)$ MASS

VALUE (MeV)	EVTS	DOCUMENT ID	TECN	COMMENT
4633 ± 7 OUR AVERAGE				Error includes scale factor of 1.4. See the ideogram below.
4625.9 ^{+6.2} _{-6.0} ± 0.4	89	¹ JIA	19A	BELL $e^+e^- \rightarrow \gamma D_s^+ D_{s1}^-(2536)^-$
4652 ± 10 ± 11	279	² WANG	15A	BELL $10.58 e^+e^- \rightarrow \gamma \pi^+ \pi^- \psi(2S)$
4669 ± 21 ± 3	37	³ LEES	14F	BABR $10.58 e^+e^- \rightarrow \gamma \pi^+ \pi^- \psi(2S)$
4634 ⁺⁸ ₋₇ ± 5 ₈	142	⁴ PAKHLOVA	08B	BELL $e^+e^- \rightarrow \Lambda_c^+ \Lambda_c^-$
4652.5 ± 3.4 ± 1.1		⁵ DAI	17	RVUE $e^+e^- \rightarrow \Lambda_c^+ \Lambda_c^-$
4645.2 ± 9.5 ± 6.0		⁶ ZHANG	17B	RVUE $e^+e^- \rightarrow \pi^+ \pi^- \psi(2S)$
4646.4 ± 9.7 ± 4.8		⁷ ZHANG	17C	RVUE $e^+e^- \rightarrow \pi^+ \pi^- J/\psi$ or $\psi(2S)$
4661 ⁺⁹ ₋₈ ± 6	44	⁸ LIU	08H	RVUE $10.58 e^+e^- \rightarrow \gamma \pi^+ \pi^- \psi(2S)$
4664 ± 11 ± 5	44	WANG	07D	BELL $10.58 e^+e^- \rightarrow \gamma \pi^+ \pi^- \psi(2S)$

- • • We do not use the following data for averages, fits, limits, etc. • • •
- ¹ From a fit of a Breit-Wigner convolved with a Gaussian.
- ² From a two-resonance fit. Supersedes WANG 07D.
- ³ From a two-resonance fit.
- ⁴ The $\pi^+ \pi^- \psi(2S)$ and $\Lambda_c^+ \Lambda_c^-$ states are not necessarily the same.
- ⁵ The pole parameters are extracted from the speed plot.
- ⁶ From a three-resonance fit.
- ⁷ From a combined fit of BELLE, BABAR and BES3 $e^+e^- \rightarrow \pi^+ \pi^- J/\psi$ and $e^+e^- \rightarrow \pi^+ \pi^- \psi(2S)$ data.
- ⁸ From a combined fit of AUBERT 07s and WANG 07D data with two resonances.

WEIGHTED AVERAGE
4633±7 (Error scaled by 1.4)



$\psi(4660)$ WIDTH

VALUE (MeV)	EVTS	DOCUMENT ID	TECN	COMMENT
64 ± 9 OUR AVERAGE				
49.8 ^{+13.9} _{-11.5} ± 4.0	89	¹ JIA	19A	BELL $e^+e^- \rightarrow \gamma D_s^+ D_{s1}^-(2536)^-$
68 ± 11 ± 5	279	² WANG	15A	BELL $10.58 e^+e^- \rightarrow \gamma \pi^+ \pi^- \psi(2S)$
104 ± 48 ± 10	37	³ LEES	14F	BABR $10.58 e^+e^- \rightarrow \gamma \pi^+ \pi^- \psi(2S)$
92 ⁺⁴⁰ ₋₂₄ ± 10 ₂₁	142	⁴ PAKHLOVA	08B	BELL $e^+e^- \rightarrow \Lambda_c^+ \Lambda_c^-$

• • • We do not use the following data for averages, fits, limits, etc. • • •

62.6 ± 5.6 ± 4.3		⁵ DAI	17	RVUE $e^+e^- \rightarrow \Lambda_c^+ \Lambda_c^-$
113.8 ± 18.1 ± 3.4		⁶ ZHANG	17B	RVUE $e^+e^- \rightarrow \pi^+ \pi^- \psi(2S)$
103.5 ± 15.6 ± 4.0		⁷ ZHANG	17C	RVUE $e^+e^- \rightarrow \pi^+ \pi^- J/\psi$ or $\psi(2S)$
42 ⁺¹⁷ ₋₁₂ ± 6	44	⁸ LIU	08H	RVUE $10.58 e^+e^- \rightarrow \gamma \pi^+ \pi^- \psi(2S)$
48 ± 15 ± 3	44	WANG	07D	BELL $10.58 e^+e^- \rightarrow \gamma \pi^+ \pi^- \psi(2S)$

- ¹ From a fit of a Breit-Wigner convolved with a Gaussian.
- ² From a two-resonance fit. Supersedes WANG 07D.
- ³ From a two-resonance fit.
- ⁴ The $\pi^+ \pi^- \psi(2S)$ and $\Lambda_c^+ \Lambda_c^-$ states are not necessarily the same.
- ⁵ The pole parameters are extracted from the speed plot.
- ⁶ From a three-resonance fit.
- ⁷ From a combined fit of BELLE, BABAR and BES3 $e^+e^- \rightarrow \pi^+ \pi^- J/\psi$ and $e^+e^- \rightarrow \pi^+ \pi^- \psi(2S)$ data.
- ⁸ From a combined fit of AUBERT 07s and WANG 07D data with two resonances.

$\psi(4660)$ DECAY MODES

Mode	Fraction (Γ_i/Γ)
Γ_1 e^+e^-	not seen
Γ_2 $\psi(2S)\pi^+\pi^-$	seen
Γ_3 $J/\psi\eta$	not seen
Γ_4 $D^0 D^{*0}\pi^+$	not seen
Γ_5 $\chi_{c1}\gamma$	not seen
Γ_6 $\chi_{c2}\gamma$	not seen
Γ_7 $\Lambda_c^+ \Lambda_c^-$	seen
Γ_8 $D_s^+ D_{s1}^-(2536)^-$	seen

$\psi(4660)$ $\Gamma(i) \times \Gamma(e^+e^-)/\Gamma(total)$

VALUE (eV)	EVTS	DOCUMENT ID	TECN	COMMENT	$\Gamma_2\Gamma_1/\Gamma$
2.0 ± 0.3 ± 0.2	279	¹ WANG	15A	BELL $10.58 e^+e^- \rightarrow \gamma \pi^+ \pi^- \psi(2S)$	
8.1 ± 1.1 ± 1.0	279	² WANG	15A	BELL $10.58 e^+e^- \rightarrow \gamma \pi^+ \pi^- \psi(2S)$	
2.7 ± 1.3 ± 0.5	37	³ LEES	14F	BABR $10.58 e^+e^- \rightarrow \gamma \pi^+ \pi^- \psi(2S)$	
7.5 ± 1.7 ± 0.7	37	⁴ LEES	14F	BABR $10.58 e^+e^- \rightarrow \gamma \pi^+ \pi^- \psi(2S)$	
2.2 ^{+0.7} _{-0.6}	44	⁵ LIU	08H	RVUE $10.58 e^+e^- \rightarrow \gamma \pi^+ \pi^- \psi(2S)$	
5.9 ± 1.6	44	⁶ LIU	08H	RVUE $10.58 e^+e^- \rightarrow \gamma \pi^+ \pi^- \psi(2S)$	
3.0 ± 0.9 ± 0.3	44	³ WANG	07D	BELL $10.58 e^+e^- \rightarrow \gamma \pi^+ \pi^- \psi(2S)$	
7.6 ± 1.8 ± 0.8	44	⁴ WANG	07D	BELL $10.58 e^+e^- \rightarrow \gamma \pi^+ \pi^- \psi(2S)$	

- • • We do not use the following data for averages, fits, limits, etc. • • •
- ¹ Solution I of two equivalent solutions from a fit using two interfering resonances. Supersedes WANG 07D.
- ² Solution II of two equivalent solutions from a fit using two interfering resonances. Supersedes WANG 07D.
- ³ Solution I of two equivalent solutions in a fit using two interfering resonances.
- ⁴ Solution II of two equivalent solutions in a fit using two interfering resonances.
- ⁵ Solution I in a combined fit of AUBERT 07s and WANG 07D data with two resonances.
- ⁶ Solution II in a combined fit of AUBERT 07s and WANG 07D data with two resonances.

VALUE (eV)	CL%	DOCUMENT ID	TECN	COMMENT	$\Gamma_3\Gamma_1/\Gamma$
<0.94	90	WANG	13B	BELL $e^+e^- \rightarrow J/\psi\eta\gamma$	

• • • We do not use the following data for averages, fits, limits, etc. • • •

VALUE (eV)	CL%	DOCUMENT ID	TECN	COMMENT	$\Gamma_5\Gamma_1/\Gamma$
<0.45	90	¹ HAN	15	BELL $10.58 e^+e^- \rightarrow \chi_{c1}\gamma$	

¹ Using $B(\eta \rightarrow \gamma\gamma) = (39.41 \pm 0.21)\%$.

VALUE (eV)	CL%	DOCUMENT ID	TECN	COMMENT	$\Gamma_6\Gamma_1/\Gamma$
<2.1	90	¹ HAN	15	BELL $10.58 e^+e^- \rightarrow \chi_{c2}\gamma$	

¹ Using $B(\eta \rightarrow \gamma\gamma) = (39.41 \pm 0.21)\%$.

VALUE (eV)	EVTS	DOCUMENT ID	TECN	COMMENT	$\Gamma_8\Gamma_1/\Gamma$
14.3^{+2.8}_{-2.6} ± 1.5	89	¹ JIA	19A	BELL $e^+e^- \rightarrow \gamma D_s^+ D_{s1}^-(2536)^-$	

¹ Using $D_{s1}^-(2536)^- \rightarrow \bar{D}^{*0} K^-$.

See key on page 999

Meson Particle Listings

$\psi(4660), \chi_{c0}(4700)$

$\psi(4660)$ BRANCHING RATIOS

$\Gamma(D^0 D^{*-} \pi^+)/\Gamma(\psi(2S)\pi^+\pi^-)$					Γ_4/Γ_2
VALUE	CL%	DOCUMENT ID	TECN	COMMENT	
<10	90	PAKHOLOVA 09	BELL	$e^+e^- \rightarrow D^0 D^{*-} \pi^+$	

$\Gamma(D^0 D^{*-} \pi^+)/\Gamma_{\text{total}} \times \Gamma(e^+e^-)/\Gamma_{\text{total}}$					$\Gamma_4/\Gamma \times \Gamma_1/\Gamma$
VALUE	CL%	DOCUMENT ID	TECN	COMMENT	
<0.37 $\times 10^{-6}$	90	¹ PAKHOLOVA 09	BELL	$e^+e^- \rightarrow D^0 D^{*-} \pi^+$	

¹ Using $4664 \pm 11 \pm 5$ MeV for the mass of $\psi(4660)$.

$\Gamma(\Lambda_c^+ \Lambda_c^-)/\Gamma_{\text{total}} \times \Gamma(e^+e^-)/\Gamma_{\text{total}}$					$\Gamma_7/\Gamma \times \Gamma_1/\Gamma$
VALUE (units 10^{-6})	EVTS	DOCUMENT ID	TECN	COMMENT	
0.68 $\pm 0.16 + 0.29$ -0.15 -0.30	142	¹ PAKHOLOVA 08B	BELL	$e^+e^- \rightarrow \Lambda_c^+ \Lambda_c^-$	

¹ The $\pi^+\pi^-\psi(2S)$ and $\Lambda_c^+ \Lambda_c^-$ states are not necessarily the same.

$\psi(4660)$ REFERENCES

JIA	19A	PR D100 111103	S. Jia <i>et al.</i>	(BELLE Collab.)
DAI	17	PR D96 116001	L.-Y. Dai, J. Haidenbauer, U.-G. Meissner	(JULI+)
ZHANG	17B	PR D96 054008	J. Zhang, J. Zhang	
ZHANG	17C	EPJ C77 727	J. Zhang, L. Yuan	
HAN	15	PR D92 012011	Y.L. Han <i>et al.</i>	(BELLE Collab.)
WANG	15A	PR D91 112007	X.L. Wang <i>et al.</i>	(BELLE Collab.)
LEES	14F	PR D89 111103	J.P. Lees <i>et al.</i>	(BABAR Collab.)
WANG	13B	PR D87 051101	X.L. Wang <i>et al.</i>	(BELLE Collab.)
PAKHOLOVA	09	PR D80 091101	G. Pakhlova <i>et al.</i>	(BELLE Collab.)
LIU	08H	PR D78 014032	Z.Q. Liu, X.S. Qin, C.Z. Yuan	
PAKHOLOVA	08B	PRL 101 172001	C. Pakhlova <i>et al.</i>	(BELLE Collab.)
AUBERT	07S	PRL 98 212001	B. Aubert <i>et al.</i>	(BABAR Collab.)
WANG	07D	PRL 99 142002	X.L. Wang <i>et al.</i>	(BELLE Collab.)

$\chi_{c0}(4700)$

$$I^G(J^{PC}) = 0^+(0^{++})$$

OMITTED FROM SUMMARY TABLE
was X(4700)

This state shows properties different from a conventional $q\bar{q}$ state. A candidate for an exotic structure. See the review on non- $q\bar{q}$ states.

Seen by AAIJ 17C in $B^+ \rightarrow \chi_{c0} K^+, \chi_{c0} \rightarrow J/\psi\phi$ using an amplitude analysis of $B^+ \rightarrow J/\psi\phi K^+$ with a significance (accounting for systematic uncertainties) of 5.6σ .

$\chi_{c0}(4700)$ MASS

VALUE (MeV)	EVTS	DOCUMENT ID	TECN	COMMENT
4704 $\pm 10 + 14$ -24	4289	¹ AAIJ	17c	LHCB $B^+ \rightarrow J/\psi\phi K^+$

¹ From an amplitude analysis of the decay $B^+ \rightarrow J/\psi\phi K^+$ with a significance of 5.6σ .

$\chi_{c0}(4700)$ WIDTH

VALUE (MeV)	EVTS	DOCUMENT ID	TECN	COMMENT
120 $\pm 31 + 42$ -33	4289	¹ AAIJ	17c	LHCB $B^+ \rightarrow J/\psi\phi K^+$

¹ From an amplitude analysis of the decay $B^+ \rightarrow J/\psi\phi K^+$ with a significance of 5.6σ .

$\chi_{c0}(4700)$ DECAY MODES

Mode	Fraction (Γ_i/Γ)
Γ_1 $J/\psi\phi$	seen

$\chi_{c0}(4700)$ BRANCHING RATIOS

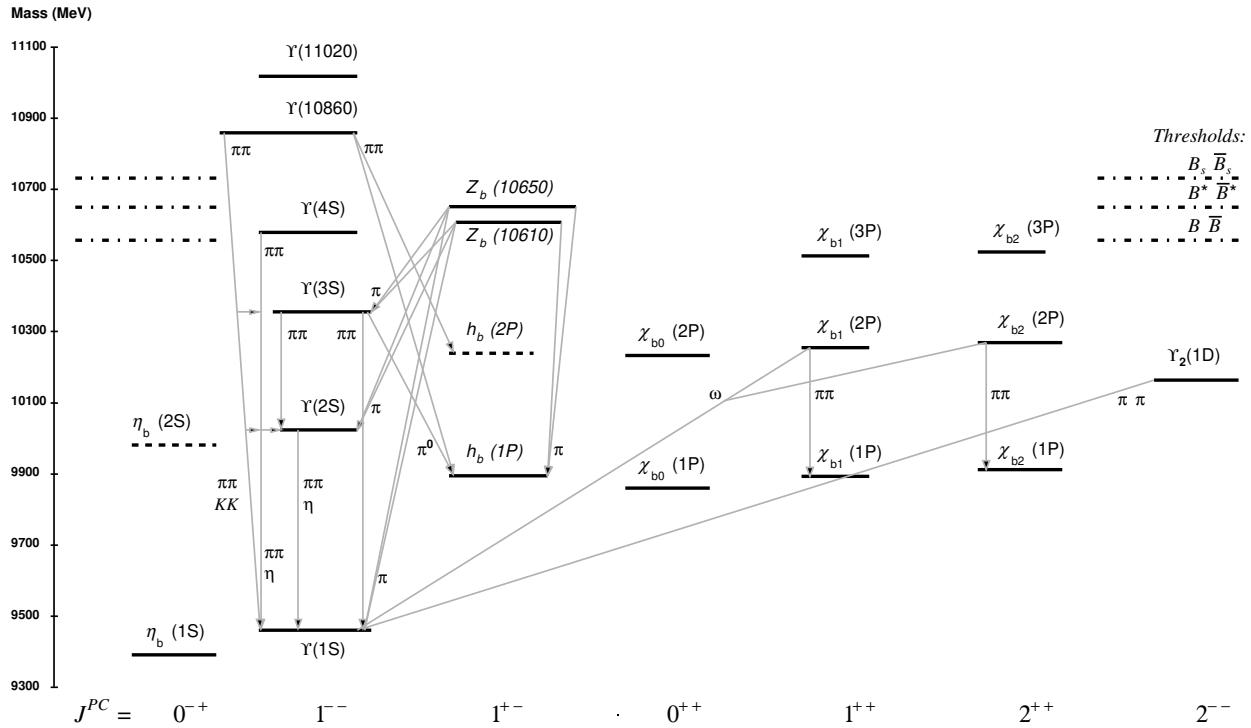
$\Gamma(J/\psi\phi)/\Gamma_{\text{total}}$					Γ_1/Γ
VALUE	EVTS	DOCUMENT ID	TECN	COMMENT	
seen	4289	¹ AAIJ	17c	LHCB $B^+ \rightarrow J/\psi\phi K^+$	

¹ From an amplitude analysis of the decay $B^+ \rightarrow J/\psi\phi K^+$ with a significance of 5.6σ .

$\chi_{c0}(4700)$ REFERENCES

AAIJ	17C	PRL 118 022003	R. Aaij <i>et al.</i>	(LHCb Collab.) JP
Also		PR D95 012002	R. Aaij <i>et al.</i>	(LHCb Collab.)

$b\bar{b}$ MESONS (including possibly non- $q\bar{q}$ states)



The level scheme of meson states containing a minimal quark content of $b\bar{b}$. The name of a state is determined by its quantum numbers $I^G J^{PC}$ (see the review “Naming Scheme for Hadrons”). States included in the Summary Tables are shown with solid lines; those requiring confirmation are shown with dotted lines. The arrows indicate the most dominant hadronic transitions. Single photon transitions, including $\Upsilon(nS) \rightarrow \gamma\eta_b(mS)$, $\Upsilon(nS) \rightarrow \gamma\chi_{bJ}(mP)$, and $\chi_{bJ}(nP) \rightarrow \gamma\Upsilon(mS)$, are omitted for clarity. For orientation, the location of the thresholds related to a pair of ground state open bottom mesons is indicated in the figure.

WIDTH DETERMINATIONS OF THE Υ STATES

As is the case for the $J/\psi(1S)$ and $\psi(2S)$, the full widths of the $b\bar{b}$ states $\Upsilon(1S)$, $\Upsilon(2S)$, and $\Upsilon(3S)$ are not directly measurable, since they are much narrower than the energy resolution of the e^+e^- storage rings where these states are produced. The common indirect method to determine Γ starts from

$$\Gamma = \Gamma_{\ell\ell}/B_{\ell\ell}, \quad (1)$$

where $\Gamma_{\ell\ell}$ is one leptonic partial width and $B_{\ell\ell}$ is the corresponding branching fraction ($\ell = e, \mu, \text{ or } \tau$). One then assumes $e-\mu-\tau$ universality and uses

$$\begin{aligned} \Gamma_{\ell\ell} &= \Gamma_{ee} \\ B_{\ell\ell} &= \text{average of } B_{ee}, B_{\mu\mu}, \text{ and } B_{\tau\tau}. \end{aligned} \quad (2)$$

The electronic partial width Γ_{ee} is also not directly measurable at e^+e^- storage rings, only in the combination $\Gamma_{ee}\Gamma_{\text{had}}/\Gamma$, where Γ_{had} is the hadronic partial width and

$$\Gamma_{\text{had}} + 3\Gamma_{ee} = \Gamma. \quad (3)$$

This combination is obtained experimentally from the energy-integrated hadronic cross section

$$\begin{aligned} &\int_{\text{resonance}} \sigma(e^+e^- \rightarrow \Upsilon \rightarrow \text{hadrons})dE \\ &= \frac{6\pi^2 \Gamma_{ee}\Gamma_{\text{had}}}{M^2 \Gamma} C_r = \frac{6\pi^2 \Gamma_{ee}^{(0)}\Gamma_{\text{had}}}{M^2 \Gamma} C_r^{(0)}, \end{aligned} \quad (4)$$

where M is the Υ mass, and C_r and $C_r^{(0)}$ are radiative correction factors. C_r is used for obtaining Γ_{ee} as defined in Eq. (1), and contains corrections from all orders of QED for describing $(b\bar{b}) \rightarrow e^+e^-$. The lowest order QED value $\Gamma_{ee}^{(0)}$, relevant for comparison with potential-model calculations, is defined by the lowest order QED graph (Born term) alone, and is about 7% lower than Γ_{ee} .

The Listings give experimental results on B_{ee} , $B_{\mu\mu}$, $B_{\tau\tau}$, and $\Gamma_{ee}\Gamma_{\text{had}}/\Gamma$. The entries of the last quantity have been re-evaluated consistently using the correction procedure of KURAEV 85 [1]. The partial width Γ_{ee} is obtained from the average values for $\Gamma_{ee}\Gamma_{\text{had}}/\Gamma$ and $B_{\ell\ell}$ using

$$\Gamma_{ee} = \frac{\Gamma_{ee}\Gamma_{\text{had}}}{\Gamma(1-3B_{\ell\ell})}. \quad (5)$$

See key on page 999

Meson Particle Listings

Bottomonium, $\eta_b(1S)$

The total width Γ is then obtained from Eq. (1). We do not list Γ_{ee} and Γ values of individual experiments. The Γ_{ee} values in the Meson Summary Table are also those defined in Eq. (1).

References

- E.A. Kuraev, V.S. Fadin, Sov. J. Nucl. Phys. **41**, 466 (1985).

$\eta_b(1S)$

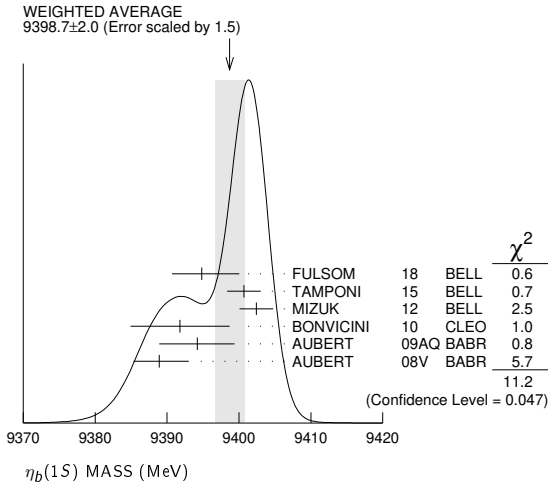
$$J^{PC} = 0^+(0^{-+})$$

Quantum numbers shown are quark-model predictions. Observed in radiative decay of the $\Upsilon(3S)$, therefore $C = +$.

$\eta_b(1S)$ MASS

VALUE (MeV)	EVTS	DOCUMENT ID	TECN	COMMENT
9398.7 ± 2.0 OUR AVERAGE				Error includes scale factor of 1.5. See the ideogram below.
9394.8 ^{+2.7+4.5} _{-3.1-2.7}	29K	FULSOM	18	BELL $\Upsilon(2S) \rightarrow \gamma X$
9400.7 ± 1.7 ± 1.6	33.1k	TAMPONI	15	BELL $e^+e^- \rightarrow \gamma\eta + \text{hadrons}$
9402.4 ± 1.5 ± 1.8	34k	¹ MIZUK	12	BELL $e^+e^- \rightarrow \gamma\pi^+\pi^- + \text{hadrons}$
9391.8 ± 6.6 ± 2.0	2.3k	² BONVICINI	10	CLEO $\Upsilon(3S) \rightarrow \gamma X$
9394.2 ^{+4.8+2.0} _{-4.9-2.0}	13k	² AUBERT	09AQ BABR	$\Upsilon(2S) \rightarrow \gamma X$
9388.9 ^{+3.1+2.7} _{-2.3-2.7}	19k	² AUBERT	08V BABR	$\Upsilon(3S) \rightarrow \gamma X$
9393.2 ± 3.4 ± 2.3	10	^{2,3} DOBBS	12	$\Upsilon(2S) \rightarrow \gamma \text{hadrons}$
9300 ± 20 ± 20		HEISTER	02D ALEP	181-209 e^+e^-

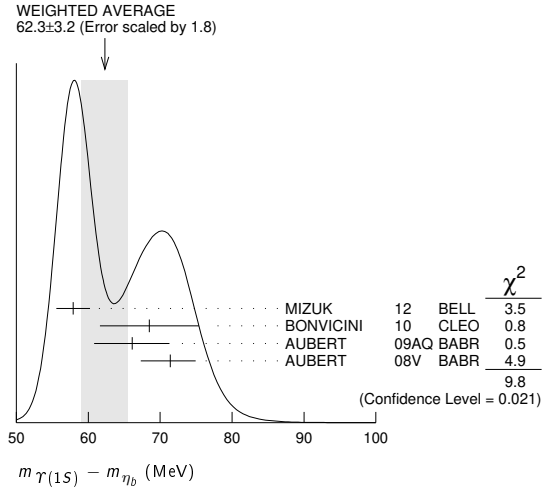
- • • We do not use the following data for averages, fits, limits, etc. • • •
- ¹ With floating width. Not independent of the corresponding mass difference measurement.
- ² Assuming $\Gamma_{\eta_b(1S)} = 10$ MeV. Not independent of the corresponding γ energy or mass difference measurements.
- ³ Obtained by analyzing CLEO III data but not authored by the CLEO Collaboration.



$m\Upsilon(1S) - m\eta_b$

VALUE (MeV)	EVTS	DOCUMENT ID	TECN	COMMENT
62.3 ± 3.2 OUR AVERAGE				Error includes scale factor of 1.8. See the ideogram below.
57.9 ± 1.5 ± 1.8	34k	¹ MIZUK	12	BELL $e^+e^- \rightarrow \gamma\pi^+\pi^- + \text{hadrons}$
68.5 ± 6.6 ± 2.0	2.3 ± 0.5k	² BONVICINI	10	CLEO $\Upsilon(3S) \rightarrow \gamma X$
66.1 ^{+4.8+2.0} _{-4.9-2.0}	13 ± 5k	² AUBERT	09AQ BABR	$\Upsilon(2S) \rightarrow \gamma X$
71.4 ^{+2.3+2.7} _{-3.1-2.7}	19 ± 3k	² AUBERT	08V BABR	$\Upsilon(3S) \rightarrow \gamma X$
67.1 ± 3.4 ± 2.3	10 ⁺⁵ ₋₄	^{2,3} DOBBS	12	$\Upsilon(2S) \rightarrow \gamma \text{hadrons}$

- • • We do not use the following data for averages, fits, limits, etc. • • •
- ¹ With floating width. Not independent of the corresponding mass measurement.
- ² Assuming $\Gamma_{\eta_b(1S)} = 10$ MeV. Not independent of the corresponding γ energy or mass measurements.
- ³ Obtained by analyzing CLEO III data but not authored by the CLEO Collaboration.



γ ENERGY IN $\Upsilon(3S)$ DECAY

VALUE (MeV)	EVTS	DOCUMENT ID	TECN	COMMENT
920.6 ± 2.8 OUR AVERAGE				
918.6 ± 6.0 ± 1.9	2.3 ± 0.5k	¹ BONVICINI	10	CLEO $\Upsilon(3S) \rightarrow \gamma X$
921.2 ^{+2.1+2.4} _{-2.8-2.4}	19 ± 3k	¹ AUBERT	08V BABR	$\Upsilon(3S) \rightarrow \gamma X$

- ¹ Assuming $\Gamma_{\eta_b(1S)} = 10$ MeV. Not independent of the corresponding mass or mass difference measurements.

γ ENERGY IN $\Upsilon(2S)$ DECAY

VALUE (MeV)	EVTS	DOCUMENT ID	TECN	COMMENT
609.3 ± 4.6 OUR AVERAGE	13 ± 5k	¹ AUBERT	09AQ BABR	$\Upsilon(2S) \rightarrow \gamma X$

- ¹ Assuming $\Gamma_{\eta_b(1S)} = 10$ MeV. Not independent of the corresponding mass or mass difference measurements.

$\eta_b(1S)$ WIDTH

VALUE (MeV)	EVTS	DOCUMENT ID	TECN	COMMENT
10⁺⁵₋₄ OUR AVERAGE				
8 ⁺⁶ ₋₅ ± 5	33.1k	¹ TAMPONI	15	BELL $e^+e^- \rightarrow \gamma\eta + \text{hadrons}$
10.8 ^{+4.0+4.5} _{-3.7-2.0}	34k	¹ MIZUK	12	BELL $e^+e^- \rightarrow \gamma\pi^+\pi^- + \text{hadrons}$

- ¹ With floating mass.

$\eta_b(1S)$ DECAY MODES

Mode	Fraction (Γ_i/Γ)	Confidence level
Γ_1 hadrons	seen	
Γ_2 $3h^+3h^-$	not seen	
Γ_3 $2h^+2h^-$	not seen	
Γ_4 $4h^+4h^-$	not seen	
Γ_5 $\gamma\gamma$	not seen	
Γ_6 $\mu^+\mu^-$	$< 9 \times 10^{-3}$	90%
Γ_7 $\tau^+\tau^-$	$< 8\%$	90%

$\eta_b(1S)$ $\Gamma(i)\Gamma(\gamma\gamma)/\Gamma(\text{total})$

VALUE (eV)	CL%	DOCUMENT ID	TECN	COMMENT	$\Gamma_2\Gamma_5/\Gamma$
< 470	95	ABDALLAH	06	DLPH 161-209 e^+e^-	
< 132	95	HEISTER	02D	ALEP 181-209 e^+e^-	

- • • We do not use the following data for averages, fits, limits, etc. • • •

VALUE (eV)	CL%	DOCUMENT ID	TECN	COMMENT	$\Gamma_3\Gamma_5/\Gamma$
< 190	95	ABDALLAH	06	DLPH 161-209 e^+e^-	
< 48	95	HEISTER	02D	ALEP 181-209 e^+e^-	

- • • We do not use the following data for averages, fits, limits, etc. • • •

Meson Particle Listings

$\eta_b(1S), \Upsilon(1S)$

$\Gamma(4h^+4h^-) \times \Gamma(\gamma\gamma)/\Gamma_{total}$					$\Gamma_4\Gamma_5/\Gamma$
VALUE (eV)	CL%	DOCUMENT ID	TECN	COMMENT	
<660	95	ABDALLAH	06	DLPH	161-209 e^+e^-

••• We do not use the following data for averages, fits, limits, etc. •••

$\eta_b(1S)$ BRANCHING RATIOS

$\Gamma(\text{hadrons})/\Gamma_{total}$					Γ_1/Γ
VALUE	EVTS	DOCUMENT ID	TECN	COMMENT	
seen	34k	MIZUK	12	BELL	$e^+e^- \rightarrow \gamma\pi^+\pi^- + \text{hadrons}$

$\Gamma(\mu^+\mu^-)/\Gamma_{total}$					Γ_6/Γ
VALUE	CL%	DOCUMENT ID	TECN	COMMENT	
$<9 \times 10^{-3}$	90	¹ AUBERT	09Z	BABR	$e^+e^- \rightarrow \Upsilon(2S,3S) \rightarrow \gamma\eta_b$
¹ Obtained using $B(\Upsilon(2S) \rightarrow \gamma\eta_b) = (4.2^{+1.1}_{-1.0} \pm 0.9) \times 10^{-4}$ and $B(\Upsilon(3S) \rightarrow \gamma\eta_b) = (4.8 \pm 0.5 \pm 0.6) \times 10^{-4}$. This limit is equivalent to $B(\eta_b \rightarrow \mu^+\mu^-) = (-0.25 \pm 0.51 \pm 0.33)\%$ measurement.					

$\Gamma(\tau^+\tau^-)/\Gamma_{total}$					Γ_7/Γ
VALUE	CL%	DOCUMENT ID	TECN	COMMENT	
$<8 \times 10^{-2}$	90	AUBERT	09P	BABR	$e^+e^- \rightarrow \gamma\tau^+\tau^-$

$\eta_b(1S)$ REFERENCES

FULSOM	18	PRL 121 232001	B. G. Fulsom <i>et al.</i>	(BELLE Collab.)
TAMPONI	15	PRL 115 142001	U. Tamponi <i>et al.</i>	(BELLE Collab.)
DOBBS	12	PRL 109 082001	S. Dobbs <i>et al.</i>	
MIZUK	12	PRL 109 232002	R. Mizuk <i>et al.</i>	(BELLE Collab.)
BONVICINI	10	PR D81 031104	G. Bonvicini <i>et al.</i>	(CLEO Collab.)
AUBERT	09AQ	PRL 103 161801	B. Aubert <i>et al.</i>	(BABAR Collab.)
AUBERT	09P	PRL 103 181801	B. Aubert <i>et al.</i>	(BABAR Collab.)
AUBERT	09Z	PRL 103 081803	B. Aubert <i>et al.</i>	(BABAR Collab.)
AUBERT	08V	PRL 101 071801	B. Aubert <i>et al.</i>	(BABAR Collab.)
ABDALLAH	06	PL B634 340	J.M. Abdallah <i>et al.</i>	(DELPHI Collab.)
HEISTER	02D	PL B530 56	A. Heister <i>et al.</i>	(ALEPH Collab.)

$\Upsilon(1S)$

$$I^G(J^{PC}) = 0^-(1^{--})$$

$\Upsilon(1S)$ MASS

VALUE (MeV)	DOCUMENT ID	TECN	COMMENT
9460.30 ± 0.26 OUR AVERAGE	Error includes scale factor of 3.3.		
9460.51 ± 0.09 ± 0.05	¹ ARTAMONOV 00	MD1	$e^+e^- \rightarrow \text{hadrons}$
9459.97 ± 0.11 ± 0.07	MACKAY	84	REDE $e^+e^- \rightarrow \text{hadrons}$
••• We do not use the following data for averages, fits, limits, etc. •••			
9460.60 ± 0.09 ± 0.05	^{2,3} BARU	92B	REDE $e^+e^- \rightarrow \text{hadrons}$
9460.59 ± 0.12	BARU	86	REDE $e^+e^- \rightarrow \text{hadrons}$
9460.6 ± 0.4	^{3,4} ARTAMONOV 84	REDE	$e^+e^- \rightarrow \text{hadrons}$

¹ Reanalysis of BARU 92B and ARTAMONOV 84 using new electron mass (COHEN 87).
² Superseding BARU 86.
³ Superseded by ARTAMONOV 00.
⁴ Value includes data of ARTAMONOV 82.

$\Upsilon(1S)$ WIDTH

VALUE (keV)	DOCUMENT ID
54.02 ± 1.25 OUR EVALUATION	See the Note on "Width Determinations of the Υ States"

$\Upsilon(1S)$ DECAY MODES

Mode	Fraction (Γ_i/Γ)	Scale factor/ Confidence level
Γ_1 $\tau^+\tau^-$	(2.60 ± 0.10) %	
Γ_2 e^+e^-	(2.38 ± 0.11) %	
Γ_3 $\mu^+\mu^-$	(2.48 ± 0.05) %	
Hadronic decays		
Γ_4 ggg	(81.7 ± 0.7) %	
Γ_5 γgg	(2.2 ± 0.6) %	
Γ_6 $\eta'(958)$ anything	(2.94 ± 0.24) %	
Γ_7 $J/\psi(1S)$ anything	(5.4 ± 0.4) × 10 ⁻⁴	S=1.4
Γ_8 $J/\psi(1S)\eta_c$	< 2.2	× 10 ⁻⁶ CL=90%
Γ_9 $J/\psi(1S)\chi_{c0}$	< 3.4	× 10 ⁻⁶ CL=90%
Γ_{10} $J/\psi(1S)\chi_{c1}$	(3.9 ± 1.2) × 10 ⁻⁶	
Γ_{11} $J/\psi(1S)\chi_{c2}$	< 1.4	× 10 ⁻⁶ CL=90%
Γ_{12} $J/\psi(1S)\eta_c(2S)$	< 2.2	× 10 ⁻⁶ CL=90%
Γ_{13} $J/\psi(1S)X(3940)$	< 5.4	× 10 ⁻⁶ CL=90%
Γ_{14} $J/\psi(1S)X(4160)$	< 5.4	× 10 ⁻⁶ CL=90%
Γ_{15} $X(4350)$ anything, $X \rightarrow J/\psi(1S)\phi$	< 8.1	× 10 ⁻⁶ CL=90%

Γ_{16}	$Z_c(3900)^\pm$ anything, $Z_c \rightarrow J/\psi(1S)\pi^\pm$	< 1.3	× 10 ⁻⁵	CL=90%
Γ_{17}	$Z_c(4200)^\pm$ anything, $Z_c \rightarrow J/\psi(1S)\pi^\pm$	< 6.0	× 10 ⁻⁵	CL=90%
Γ_{18}	$Z_c(4430)^\pm$ anything, $Z_c \rightarrow J/\psi(1S)\pi^\pm$	< 4.9	× 10 ⁻⁵	CL=90%
Γ_{19}	X_{cs}^\pm anything, $X \rightarrow J/\psi K^\pm$	< 5.7	× 10 ⁻⁶	CL=90%
Γ_{20}	$\chi_{c1}(3872)$ anything, $\chi_{c1} \rightarrow J/\psi(1S)\pi^+\pi^-$	< 9.5	× 10 ⁻⁶	CL=90%
Γ_{21}	$\psi(4260)$ anything, $\psi \rightarrow J/\psi(1S)\pi^+\pi^-$	< 3.8	× 10 ⁻⁵	CL=90%
Γ_{22}	$\psi(4260)$ anything, $\psi \rightarrow J/\psi(1S)K^+K^-$	< 7.5	× 10 ⁻⁶	CL=90%
Γ_{23}	$\chi_{c1}(4140)$ anything, $\chi_{c1} \rightarrow J/\psi(1S)\phi$	< 5.2	× 10 ⁻⁶	CL=90%
Γ_{24}	χ_{c0} anything	< 4	× 10 ⁻³	CL=90%
Γ_{25}	χ_{c1} anything	(1.90 ± 0.35) × 10 ⁻⁴		
Γ_{26}	$\chi_{c1}(1P)X_{tetra}$	< 3.78	× 10 ⁻⁵	CL=90%
Γ_{27}	χ_{c2} anything	(2.8 ± 0.8) × 10 ⁻⁴		
Γ_{28}	$\psi(2S)$ anything	(1.23 ± 0.20) × 10 ⁻⁴		
Γ_{29}	$\psi(2S)\eta_c$	< 3.6	× 10 ⁻⁶	CL=90%
Γ_{30}	$\psi(2S)\chi_{c0}$	< 6.5	× 10 ⁻⁶	CL=90%
Γ_{31}	$\psi(2S)\chi_{c1}$	< 4.5	× 10 ⁻⁶	CL=90%
Γ_{32}	$\psi(2S)\chi_{c2}$	< 2.1	× 10 ⁻⁶	CL=90%
Γ_{33}	$\psi(2S)\eta_c(2S)$	< 3.2	× 10 ⁻⁶	CL=90%
Γ_{34}	$\psi(2S)X(3940)$	< 2.9	× 10 ⁻⁶	CL=90%
Γ_{35}	$\psi(2S)X(4160)$	< 2.9	× 10 ⁻⁶	CL=90%
Γ_{36}	$\psi(4260)$ anything, $\psi \rightarrow \psi(2S)\pi^+\pi^-$	< 7.9	× 10 ⁻⁵	CL=90%
Γ_{37}	$\psi(4360)$ anything, $\psi \rightarrow \psi(2S)\pi^+\pi^-$	< 5.2	× 10 ⁻⁵	CL=90%
Γ_{38}	$\psi(4660)$ anything, $\psi \rightarrow \psi(2S)\pi^+\pi^-$	< 2.2	× 10 ⁻⁵	CL=90%
Γ_{39}	$X(4050)^\pm$ anything, $X \rightarrow \psi(2S)\pi^\pm$	< 8.8	× 10 ⁻⁵	CL=90%
Γ_{40}	$Z_c(4430)^\pm$ anything, $Z_c \rightarrow \psi(2S)\pi^\pm$	< 6.7	× 10 ⁻⁵	CL=90%
Γ_{41}	$Z_c(4200)^+Z_c(4200)^-$	< 2.23	× 10 ⁻⁵	CL=90%
Γ_{42}	$Z_c(3900)^\pm Z_c(4200)^\mp$	< 8.1	× 10 ⁻⁶	CL=90%
Γ_{43}	$Z_c(3900)^+Z_c(3900)^-$	< 1.8	× 10 ⁻⁶	CL=90%
Γ_{44}	$X(4050)^+X(4050)^-$	< 1.58	× 10 ⁻⁵	CL=90%
Γ_{45}	$X(4250)^+X(4250)^-$	< 2.66	× 10 ⁻⁵	CL=90%
Γ_{46}	$X(4050)^\pm X(4250)^\mp$	< 4.42	× 10 ⁻⁵	CL=90%
Γ_{47}	$Z_c(4430)^+Z_c(4430)^-$	< 2.03	× 10 ⁻⁵	CL=90%
Γ_{48}	$X(4055)^\pm X(4055)^\mp$	< 2.33	× 10 ⁻⁵	CL=90%
Γ_{49}	$X(4055)^\pm Z_c(4430)^\mp$	< 4.55	× 10 ⁻⁵	CL=90%
Γ_{50}	$\rho\pi$	< 3.68	× 10 ⁻⁶	CL=90%
Γ_{51}	$\omega\pi^0$	< 3.90	× 10 ⁻⁶	CL=90%
Γ_{52}	$\pi^+\pi^-$	< 5	× 10 ⁻⁴	CL=90%
Γ_{53}	K^+K^-	< 5	× 10 ⁻⁴	CL=90%
Γ_{54}	$\rho\bar{\rho}$	< 5	× 10 ⁻⁴	CL=90%
Γ_{55}	$\pi^+\pi^-\pi^0$	(2.1 ± 0.8) × 10 ⁻⁶		
Γ_{56}	ϕK^+K^-	(2.4 ± 0.5) × 10 ⁻⁶		
Γ_{57}	$\omega\pi^+\pi^-$	(4.5 ± 1.0) × 10 ⁻⁶		
Γ_{58}	$K^*(892)^0 K^- \pi^+ + c.c.$	(4.4 ± 0.8) × 10 ⁻⁶		
Γ_{59}	$\phi f_2'(1525)$	< 1.63	× 10 ⁻⁶	CL=90%
Γ_{60}	$\omega f_2(1270)$	< 1.79	× 10 ⁻⁶	CL=90%
Γ_{61}	$\rho(770)a_2(1320)$	< 2.24	× 10 ⁻⁶	CL=90%
Γ_{62}	$K^*(892)^0 \bar{K}_2^*(1430)^0 + c.c.$	(3.0 ± 0.8) × 10 ⁻⁶		
Γ_{63}	$K_1(1270)^\pm K^\mp$	< 2.41	× 10 ⁻⁶	CL=90%
Γ_{64}	$K_1(1400)^\pm K^\mp$	(1.0 ± 0.4) × 10 ⁻⁶		
Γ_{65}	$b_1(1235)^\pm \pi^\mp$	< 1.25	× 10 ⁻⁶	CL=90%
Γ_{66}	$\pi^+\pi^-\pi^0$	(1.28 ± 0.30) × 10 ⁻⁵		
Γ_{67}	$K_S^0 K^+\pi^- + c.c.$	(1.6 ± 0.4) × 10 ⁻⁶		
Γ_{68}	$K^*(892)^0 \bar{K}^0 + c.c.$	(2.9 ± 0.9) × 10 ⁻⁶		
Γ_{69}	$K^*(892)^- K^+ + c.c.$	< 1.11	× 10 ⁻⁶	CL=90%
Γ_{70}	$f_1(1285)$ anything	(4.6 ± 3.1) × 10 ⁻³		
Γ_{71}	$D^*(2010)^\pm$ anything	(2.52 ± 0.20) %		
Γ_{72}	$f_1(1285)X_{tetra}$	< 6.24	× 10 ⁻⁵	CL=90%
Γ_{73}	2H anything	(2.85 ± 0.25) × 10 ⁻⁵		
Γ_{74}	Sum of 100 exclusive modes	(1.200 ± 0.017) %		
Radiative decays				
Γ_{75}	$\gamma\pi^+\pi^-$	(6.3 ± 1.8) × 10 ⁻⁵		
Γ_{76}	$\gamma\pi^0\pi^0$	(1.7 ± 0.7) × 10 ⁻⁵		
Γ_{77}	$\gamma\pi\pi$ (S-wave)	(4.6 ± 0.7) × 10 ⁻⁵		

Υ_{78}	$\gamma\pi^0\eta$	< 2.4	$\times 10^{-6}$	CL=90%
Υ_{79}	$\gamma K^+ K^-$	[a] (1.14 ± 0.13)	$\times 10^{-5}$	
Υ_{80}	$\gamma p\bar{p}$	[b] < 6	$\times 10^{-6}$	CL=90%
Υ_{81}	$\gamma 2h^+ 2h^-$	(7.0 ± 1.5)	$\times 10^{-4}$	
Υ_{82}	$\gamma 3h^+ 3h^-$	(5.4 ± 2.0)	$\times 10^{-4}$	
Υ_{83}	$\gamma 4h^+ 4h^-$	(7.4 ± 3.5)	$\times 10^{-4}$	
Υ_{84}	$\gamma\pi^+\pi^- K^+ K^-$	(2.9 ± 0.9)	$\times 10^{-4}$	
Υ_{85}	$\gamma 2\pi^+ 2\pi^-$	(2.5 ± 0.9)	$\times 10^{-4}$	
Υ_{86}	$\gamma 3\pi^+ 3\pi^-$	(2.5 ± 1.2)	$\times 10^{-4}$	
Υ_{87}	$\gamma 2\pi^+ 2\pi^- K^+ K^-$	(2.4 ± 1.2)	$\times 10^{-4}$	
Υ_{88}	$\gamma\pi^+\pi^- p\bar{p}$	(1.5 ± 0.6)	$\times 10^{-4}$	
Υ_{89}	$\gamma 2\pi^+ 2\pi^- p\bar{p}$	(4 ± 6)	$\times 10^{-5}$	
Υ_{90}	$\gamma 2K^+ 2K^-$	(2.0 ± 2.0)	$\times 10^{-5}$	
Υ_{91}	$\gamma\eta'(958)$	< 1.9	$\times 10^{-6}$	CL=90%
Υ_{92}	$\gamma\eta$	< 1.0	$\times 10^{-6}$	CL=90%
Υ_{93}	$\gamma f_0(980)$	< 3	$\times 10^{-5}$	CL=90%
Υ_{94}	$\gamma f_2'(1525)$	(2.9 ± 0.6)	$\times 10^{-5}$	
Υ_{95}	$\gamma f_2(1270)$	(1.01 ± 0.06)	$\times 10^{-4}$	
Υ_{96}	$\gamma\eta(1405)$	< 8.2	$\times 10^{-5}$	CL=90%
Υ_{97}	$\gamma f_0(1500)$	< 1.5	$\times 10^{-5}$	CL=90%
Υ_{98}	$\gamma f_0(1500) \rightarrow \gamma K^+ K^-$	(1.0 ± 0.4)	$\times 10^{-5}$	
Υ_{99}	$\gamma f_0(1710)$	< 2.6	$\times 10^{-4}$	CL=90%
Υ_{100}	$\gamma f_0(1710) \rightarrow \gamma K^+ K^-$	(1.01 ± 0.32)	$\times 10^{-5}$	
Υ_{101}	$\gamma f_0(1710) \rightarrow \gamma\pi^+\pi^-$	(5.3 ± 2.0)	$\times 10^{-6}$	
Υ_{102}	$\gamma f_0(1710) \rightarrow \gamma\pi^0\pi^0$	< 1.4	$\times 10^{-6}$	CL=90%
Υ_{103}	$\gamma f_0(1710) \rightarrow \gamma\eta\eta$	< 1.8	$\times 10^{-6}$	CL=90%
Υ_{104}	$\gamma f_4(2050)$	< 5.3	$\times 10^{-5}$	CL=90%
Υ_{105}	$\gamma f_0(2200) \rightarrow \gamma K^+ K^-$	< 2	$\times 10^{-4}$	CL=90%
Υ_{106}	$\gamma f_2(2220) \rightarrow \gamma K^+ K^-$	< 8	$\times 10^{-7}$	CL=90%
Υ_{107}	$\gamma f_2(2220) \rightarrow \gamma\pi^+\pi^-$	< 6	$\times 10^{-7}$	CL=90%
Υ_{108}	$\gamma f_2(2220) \rightarrow \gamma p\bar{p}$	< 1.1	$\times 10^{-6}$	CL=90%
Υ_{109}	$\gamma\eta(2225) \rightarrow \gamma\phi\phi$	< 3	$\times 10^{-3}$	CL=90%
Υ_{110}	$\gamma\eta_c(1S)$	< 5.7	$\times 10^{-5}$	CL=90%
Υ_{111}	$\gamma\chi_{c0}$	< 6.5	$\times 10^{-4}$	CL=90%
Υ_{112}	$\gamma\chi_{c1}$	< 2.3	$\times 10^{-5}$	CL=90%
Υ_{113}	$\gamma\chi_{c2}$	< 7.6	$\times 10^{-6}$	CL=90%
Υ_{114}	$\gamma\chi_{c1}(3872) \rightarrow \pi^+\pi^- J/\psi$	< 1.6	$\times 10^{-6}$	CL=90%
Υ_{115}	$\gamma\chi_{c1}(3872) \rightarrow \pi^+\pi^-\pi^0 J/\psi$	< 2.8	$\times 10^{-6}$	CL=90%
Υ_{116}	$\gamma X(3915) \rightarrow \omega J/\psi$	< 3.0	$\times 10^{-6}$	CL=90%
Υ_{117}	$\gamma\chi_{c1}(4140) \rightarrow \phi J/\psi$	< 2.2	$\times 10^{-6}$	CL=90%
Υ_{118}	γX	[c] < 4.5	$\times 10^{-6}$	CL=90%
Υ_{119}	$\gamma X\bar{X}(m_X < 3.1 \text{ GeV})$	[d] < 1	$\times 10^{-3}$	CL=90%
Υ_{120}	$\gamma X\bar{X}(m_X < 4.5 \text{ GeV})$	[e] < 2.4	$\times 10^{-4}$	CL=90%
Υ_{121}	$\gamma X \rightarrow \gamma + \geq 4 \text{ prongs}$	[f] < 1.78	$\times 10^{-4}$	CL=95%
Υ_{122}	$\gamma a_1^0 \rightarrow \gamma\mu^+\mu^-$	[g] < 9	$\times 10^{-6}$	CL=90%
Υ_{123}	$\gamma a_1^0 \rightarrow \gamma\tau^+\tau^-$	[a] < 1.30	$\times 10^{-4}$	CL=90%
Υ_{124}	$\gamma a_1^0 \rightarrow \gamma g g$	[h] < 1	%	CL=90%
Υ_{125}	$\gamma a_1^0 \rightarrow \gamma 5\pi$	[h] < 1	$\times 10^{-3}$	CL=90%

Lepton Family number (LF) violating modes

Υ_{126}	$\mu^+ \tau^\mp$	LF	< 6.0	$\times 10^{-6}$	CL=95%
------------------	------------------	----	---------	------------------	--------

Other decays

Υ_{127}	invisible	< 3.0	$\times 10^{-4}$	CL=90%
------------------	-----------	---------	------------------	--------

- [a] $2m_\tau < M(\tau^+\tau^-) < 9.2 \text{ GeV}$
- [b] $2 \text{ GeV} < m_{K^+K^-} < 3 \text{ GeV}$
- [c] $X = \text{scalar with } m < 8.0 \text{ GeV}$
- [d] $X\bar{X} = \text{vectors with } m < 3.1 \text{ GeV}$
- [e] $X \text{ and } \bar{X} = \text{zero spin with } m < 4.5 \text{ GeV}$
- [f] $1.5 \text{ GeV} < m_X < 5.0 \text{ GeV}$
- [g] $201 \text{ MeV} < M(\mu^+\mu^-) < 3565 \text{ MeV}$
- [h] $0.5 \text{ GeV} < m_X < 9.0 \text{ GeV}$, where m_X is the invariant mass of the hadronic final state.

$\Upsilon(1S) \Gamma(i)\Gamma(e^+e^-)/\Gamma(\text{total})$

$\Gamma(e^+e^-) \times \Gamma(\mu^+\mu^-)/\Gamma(\text{total})$	$\Gamma_2\Gamma_3/\Gamma$
VALUE (eV)	DOCUMENT ID TECN COMMENT
31.2±1.6±1.7	KOBEL 92 CBAL $e^+e^- \rightarrow \mu^+\mu^-$

$\Gamma(\text{hadrons}) \times \Gamma(e^+e^-)/\Gamma(\text{total})$	$\Gamma_0\Gamma_2/\Gamma$
VALUE (keV)	DOCUMENT ID TECN COMMENT
1.240±0.016 OUR AVERAGE	
1.252±0.004±0.019	¹ ROSNER 06 CLEO 9.5 $e^+e^- \rightarrow \text{hadrons}$
1.187±0.023±0.031	¹ BARU 92B MD1 $e^+e^- \rightarrow \text{hadrons}$

1.23 ± 0.02 ± 0.05	¹ JAKUBOWSKI 88 CBAL $e^+e^- \rightarrow \text{hadrons}$
1.37 ± 0.06 ± 0.09	² GILES 84B CLEO $e^+e^- \rightarrow \text{hadrons}$
1.23 ± 0.08 ± 0.04	² ALBRECHT 82 DASP $e^+e^- \rightarrow \text{hadrons}$
1.13 ± 0.07 ± 0.11	² NICZYPORUK 82 LENA $e^+e^- \rightarrow \text{hadrons}$
1.09 ± 0.25	² BOCK 80 CNTR $e^+e^- \rightarrow \text{hadrons}$
1.35 ± 0.14	³ BERGER 79 PLUT $e^+e^- \rightarrow \text{hadrons}$

- ¹Radiative corrections evaluated following KURAEV 85.
- ²Radiative corrections reevaluated by BUCHMUELLER 88 following KURAEV 85.
- ³Radiative corrections reevaluated by ALEXANDER 89 using $B(\mu\mu) = 0.026$.

$\Upsilon(1S)$ PARTIAL WIDTHS

$\Gamma(e^+e^-)$	Γ_2
VALUE (keV)	DOCUMENT ID
1.340±0.018 OUR EVALUATION	

$\Upsilon(1S)$ BRANCHING RATIOS

$\Gamma(\tau^+\tau^-)/\Gamma(\text{total})$	Γ_1/Γ
VALUE (units 10^{-2}) EVTS	DOCUMENT ID TECN COMMENT
2.60±0.10 OUR AVERAGE	

2.53±0.13±0.05	60k	¹ BESSON 07 CLEO $e^+e^- \rightarrow \Upsilon(1S) \rightarrow \tau^+\tau^-$
2.61±0.12 $^{+0.09}_{-0.13}$	25k	CINABRO 94B CLE2 $e^+e^- \rightarrow \tau^+\tau^-$
2.7 ± 0.4 ± 0.2		² ALBRECHT 85C ARG $\Upsilon(2S) \rightarrow \pi^+\pi^-\tau^+\tau^-$
3.4 ± 0.4 ± 0.4		GILES 83 CLEO $e^+e^- \rightarrow \tau^+\tau^-$

- ¹ BESSON 07 reports $[\Gamma(\Upsilon(1S) \rightarrow \tau^+\tau^-)/\Gamma(\text{total})] / [B(\Upsilon(1S) \rightarrow \mu^+\mu^-)] = 1.02 \pm 0.02 \pm 0.05$ which we multiply by our best value $B(\Upsilon(1S) \rightarrow \mu^+\mu^-) = (2.48 \pm 0.05) \times 10^{-2}$. Our first error is their experiment's error and our second error is the systematic error from using our best value.
- ² Using $B(\Upsilon(1S) \rightarrow ee) = B(\Upsilon(1S) \rightarrow \mu\mu) = 0.0256$; not used for width evaluations.

$\Gamma(e^+e^-)/\Gamma(\text{total})$	Γ_2/Γ
VALUE (units 10^{-2}) EVTS	DOCUMENT ID TECN COMMENT
2.38±0.11 OUR AVERAGE	

2.29±0.08±0.11		ALEXANDER 98 CLE2 $\Upsilon(2S) \rightarrow \pi^+\pi^-e^+e^-$
2.42±0.14±0.14	307	ALBRECHT 87 ARG $\Upsilon(2S) \rightarrow \pi^+\pi^-e^+e^-$
2.8 ± 0.3 ± 0.2	826	BESSON 84 CLEO $\Upsilon(2S) \rightarrow \pi^+\pi^-e^+e^-$
5.1 ± 3.0		BERGER 80c PLUT $e^+e^- \rightarrow e^+e^-$

$\Gamma(\mu^+\mu^-)/\Gamma(\text{total})$	Γ_3/Γ
VALUE EVTS	DOCUMENT ID TECN COMMENT
0.0248±0.0005 OUR AVERAGE	

0.0249±0.0002±0.0007	345k	ADAMS 05 CLEO $e^+e^- \rightarrow \mu^+\mu^-$
0.0249±0.0008±0.0013		ALEXANDER 98 CLE2 $\Upsilon(2S) \rightarrow \pi^+\pi^-\mu^+\mu^-$
0.0212±0.0020±0.0010		¹ BARU 92 MD1 $e^+e^- \rightarrow \mu^+\mu^-$
0.0231±0.0012±0.0010		¹ KOBEL 92 CBAL $e^+e^- \rightarrow \mu^+\mu^-$
0.0252±0.0007±0.0007		CHEN 89B CLEO $e^+e^- \rightarrow \mu^+\mu^-$
0.0261±0.0009±0.0011		KAARSBERG 89 CSB2 $e^+e^- \rightarrow \mu^+\mu^-$
0.0230±0.0025±0.0013	86	ALBRECHT 87 ARG $\Upsilon(2S) \rightarrow \pi^+\pi^-\mu^+\mu^-$
0.029 ± 0.003 ± 0.002	864	BESSON 84 CLEO $\Upsilon(2S) \rightarrow \pi^+\pi^-\mu^+\mu^-$
0.027 ± 0.003 ± 0.003		ANDREWS 83 CLEO $e^+e^- \rightarrow \mu^+\mu^-$
0.032 ± 0.013 ± 0.003		ALBRECHT 82 DASP $e^+e^- \rightarrow \mu^+\mu^-$
0.038 ± 0.015 ± 0.002		NICZYPORUK 82 LENA $e^+e^- \rightarrow \mu^+\mu^-$
0.014 + 0.034 - 0.014		BOCK 80 CNTR $e^+e^- \rightarrow \mu^+\mu^-$
0.022 ± 0.020		BERGER 79 PLUT $e^+e^- \rightarrow \mu^+\mu^-$

- ¹ Taking into account interference between the resonance and continuum.

$\Gamma(\tau^+\tau^-)/\Gamma(\mu^+\mu^-)$	Γ_1/Γ_3
VALUE EVTS	DOCUMENT ID TECN COMMENT
1.008±0.023 OUR AVERAGE	

1.005 ± 0.013 ± 0.022	0.7M	¹ DEL-AMO-SA...10c BABR $\Upsilon(3S) \rightarrow \pi^+\pi^-\Upsilon(1S)$
1.02 ± 0.02 ± 0.05	60k	BESSON 07 CLEO $e^+e^- \rightarrow \Upsilon(1S)$

- ¹ Allows any number of extra photons with total energy < 500 MeV.

$\Gamma(g g g)/\Gamma(\text{total})$	Γ_4/Γ
VALUE (units 10^{-2}) EVTS	DOCUMENT ID TECN COMMENT
81.7±0.7	20M ¹ BESSON 06A CLEO $\Upsilon(1S) \rightarrow \text{hadrons}$

- ¹ Calculated using the value $\Gamma(\gamma g g)/\Gamma(g g g) = (2.70 \pm 0.01 \pm 0.13 \pm 0.24)\%$ from BESSON 06A and PDG 08 values of $B(\mu^+\mu^-) = (2.48 \pm 0.05)\%$ and $R_{\text{hadrons}} = 3.51$. The statistical error is negligible and the systematic error is partially correlated with that of $\Gamma(\gamma g g)/\Gamma(\text{total})$ measurement of BESSON 06A.

$\Gamma(\gamma g g)/\Gamma(\text{total})$	Γ_5/Γ
VALUE (units 10^{-2}) EVTS	DOCUMENT ID TECN COMMENT
2.20±0.60	400k ¹ BESSON 06A CLEO $\Upsilon(1S) \rightarrow \gamma + \text{hadrons}$

- ¹ Calculated using BESSON 06A values of $\Gamma(\gamma g g)/\Gamma(g g g) = (2.70 \pm 0.01 \pm 0.13 \pm 0.24)\%$ and $\Gamma(g g g)/\Gamma(\text{total})$. The statistical error is negligible and the systematic error is partially correlated with that of $\Gamma(g g g)/\Gamma(\text{total})$ measurement of BESSON 06A.

Meson Particle Listings

 $\Upsilon(1S)$ $\Gamma(\Upsilon g g)/\Gamma(g g g)$

VALUE (units 10^{-2})	EVTS	DOCUMENT ID	TECN	COMMENT
$2.70 \pm 0.01 \pm 0.27$	20M	BESSON	06A CLEO	$\Upsilon(1S) \rightarrow (\gamma^+)$ hadrons

 Γ_5/Γ_4 $\Gamma(\eta'(958) \text{ anything})/\Gamma_{\text{total}}$

VALUE	DOCUMENT ID	TECN	COMMENT
0.0294 ± 0.0024 OUR FIT			
0.0294 ± 0.0024 OUR AVERAGE			
0.030 $\pm 0.002 \pm 0.002$	AQUINES	06A CLE3	$\Upsilon(1S) \rightarrow \eta'$ anything
0.028 $\pm 0.004 \pm 0.002$	ARTUSO	03 CLE2	$\Upsilon(1S) \rightarrow \eta'$ anything

 Γ_6/Γ $\Gamma(J/\psi(1S) \text{ anything})/\Gamma_{\text{total}}$

VALUE (units 10^{-4})	CL%	EVTS	DOCUMENT ID	TECN	COMMENT
5.4 ± 0.4 OUR FIT					Error includes scale factor of 1.4.
5.4 ± 0.4 OUR AVERAGE					Error includes scale factor of 1.5.
5.25 $\pm 0.13 \pm 0.25$	3k		SHEN	16 BELL	$e^+e^- \rightarrow J/\psi X$
6.4 $\pm 0.4 \pm 0.6$	730		BRIERE	04 CLEO	$e^+e^- \rightarrow J/\psi X$
11 $\pm 4 \pm 2$			¹ FULTON	89 CLEO	$e^+e^- \rightarrow \mu^+\mu^- X$
• • • We do not use the following data for averages, fits, limits, etc. • • •					
<6.8	90		ALBRECHT	92J ARG	$e^+e^- \rightarrow e^+e^- X$, $\mu^+\mu^- X$
<17	90		MASCHMANN	90 CBAL	$e^+e^- \rightarrow$ hadrons
<200	90		NICZYPORUK	83 LENA	

¹ Using $B(J/\psi \rightarrow \mu^+\mu^-) = (6.9 \pm 0.9)\%$.

 $\Gamma(J/\psi(1S)\eta_c)/\Gamma_{\text{total}}$

VALUE	CL%	DOCUMENT ID	TECN	COMMENT
$<2.2 \times 10^{-6}$	90	YANG	14 BELL	$e^+e^- \rightarrow J/\psi X$

 Γ_8/Γ $\Gamma(J/\psi(1S)\chi_{c0})/\Gamma_{\text{total}}$

VALUE	CL%	DOCUMENT ID	TECN	COMMENT
$<3.4 \times 10^{-6}$	90	YANG	14 BELL	$e^+e^- \rightarrow J/\psi X$

 Γ_9/Γ $\Gamma(J/\psi(1S)\chi_{c1})/\Gamma_{\text{total}}$

VALUE (units 10^{-6})	EVTS	DOCUMENT ID	TECN	COMMENT
$3.90 \pm 1.21 \pm 0.23$	20	YANG	14 BELL	$e^+e^- \rightarrow J/\psi X$

 Γ_{10}/Γ $\Gamma(J/\psi(1S)\chi_{c2})/\Gamma_{\text{total}}$

VALUE	CL%	DOCUMENT ID	TECN	COMMENT
$<1.4 \times 10^{-6}$	90	YANG	14 BELL	$e^+e^- \rightarrow J/\psi X$

 Γ_{11}/Γ $\Gamma(J/\psi(1S)\eta_c(2S))/\Gamma_{\text{total}}$

VALUE	CL%	DOCUMENT ID	TECN	COMMENT
$<2.2 \times 10^{-6}$	90	YANG	14 BELL	$e^+e^- \rightarrow J/\psi X$

 Γ_{12}/Γ $\Gamma(J/\psi(1S)X(3940))/\Gamma_{\text{total}}$

VALUE	CL%	DOCUMENT ID	TECN	COMMENT
$<5.4 \times 10^{-6}$	90	YANG	14 BELL	$e^+e^- \rightarrow J/\psi X$

 Γ_{13}/Γ $\Gamma(J/\psi(1S)X(4160))/\Gamma_{\text{total}}$

VALUE	CL%	DOCUMENT ID	TECN	COMMENT
$<5.4 \times 10^{-6}$	90	YANG	14 BELL	$e^+e^- \rightarrow J/\psi X$

 Γ_{14}/Γ $\Gamma(X(4350) \text{ anything}, X \rightarrow J/\psi(1S)\phi)/\Gamma_{\text{total}}$

VALUE	CL%	DOCUMENT ID	TECN	COMMENT
$<8.1 \times 10^{-6}$	90	SHEN	16 BELL	$\Upsilon(1S) \rightarrow J/\psi K^+ K^- X$

 Γ_{15}/Γ $\Gamma(Z_c(3900)^\pm \text{ anything}, Z_c \rightarrow J/\psi(1S)\pi^\pm)/\Gamma_{\text{total}}$

VALUE	CL%	DOCUMENT ID	TECN	COMMENT
$<1.3 \times 10^{-5}$	90	SHEN	16 BELL	$\Upsilon(1S) \rightarrow J/\psi \pi^\pm X$

 Γ_{16}/Γ $\Gamma(Z_c(4200)^\pm \text{ anything}, Z_c \rightarrow J/\psi(1S)\pi^\pm)/\Gamma_{\text{total}}$

VALUE	CL%	DOCUMENT ID	TECN	COMMENT
$<6.0 \times 10^{-5}$	90	SHEN	16 BELL	$\Upsilon(1S) \rightarrow J/\psi \pi^\pm X$

 Γ_{17}/Γ $\Gamma(Z_c(4430)^\pm \text{ anything}, Z_c \rightarrow J/\psi(1S)\pi^\pm)/\Gamma_{\text{total}}$

VALUE	CL%	DOCUMENT ID	TECN	COMMENT
$<4.9 \times 10^{-5}$	90	SHEN	16 BELL	$\Upsilon(1S) \rightarrow J/\psi \pi^\pm X$

 Γ_{18}/Γ $\Gamma(X_{cb}^\pm \text{ anything}, X \rightarrow J/\psi K^\pm)/\Gamma_{\text{total}}$

VALUE	CL%	DOCUMENT ID	TECN	COMMENT
$<5.7 \times 10^{-6}$	90	SHEN	16 BELL	$\Upsilon(1S) \rightarrow J/\psi K^- X$

 Γ_{19}/Γ $\Gamma(\chi_{c1}(3872) \text{ anything}, \chi_{c1} \rightarrow J/\psi(1S)\pi^+\pi^-)/\Gamma_{\text{total}}$

VALUE	CL%	DOCUMENT ID	TECN	COMMENT
$<9.5 \times 10^{-6}$	90	SHEN	16 BELL	$\Upsilon(1S) \rightarrow J/\psi \pi^+\pi^- X$

 Γ_{20}/Γ $\Gamma(\psi(4260) \text{ anything}, \psi \rightarrow J/\psi(1S)\pi^+\pi^-)/\Gamma_{\text{total}}$

VALUE	CL%	DOCUMENT ID	TECN	COMMENT
$<3.8 \times 10^{-5}$	90	SHEN	16 BELL	$\Upsilon(1S) \rightarrow J/\psi \pi^+\pi^- X$

 Γ_{21}/Γ $\Gamma(\psi(4260) \text{ anything}, \psi \rightarrow J/\psi(1S)K^+K^-)/\Gamma_{\text{total}}$

VALUE	CL%	DOCUMENT ID	TECN	COMMENT
$<7.5 \times 10^{-6}$	90	SHEN	16 BELL	$\Upsilon(1S) \rightarrow J/\psi K^+ K^- X$

 Γ_{22}/Γ $\Gamma(\chi_{c1}(4140) \text{ anything}, \chi_{c1} \rightarrow J/\psi(1S)\phi)/\Gamma_{\text{total}}$

VALUE	CL%	DOCUMENT ID	TECN	COMMENT
$<5.2 \times 10^{-6}$	90	SHEN	16 BELL	$\Upsilon(1S) \rightarrow J/\psi K^+ K^- X$

 Γ_{23}/Γ $\Gamma(\chi_{c0} \text{ anything})/\Gamma(J/\psi(1S) \text{ anything})$

VALUE	CL%	DOCUMENT ID	TECN	COMMENT
<7.4	90	BRIERE	04 CLEO	$e^+e^- \rightarrow J/\psi X$

 Γ_{24}/Γ_7 $\Gamma(\chi_{c1} \text{ anything})/\Gamma_{\text{total}}$

VALUE (units 10^{-4})	EVTS	DOCUMENT ID	TECN	COMMENT
1.90 ± 0.35 OUR FIT				
$1.90 \pm 0.43 \pm 0.14$	215	JIA	17 BELL	$\Upsilon(1S) \rightarrow \gamma J/\psi(1S)$

 Γ_{25}/Γ $\Gamma(\chi_{c1} \text{ anything})/\Gamma(J/\psi(1S) \text{ anything})$

VALUE	CL%	DOCUMENT ID	TECN	COMMENT
0.35 ± 0.07 OUR FIT				
$0.35 \pm 0.08 \pm 0.06$	52 ± 12	BRIERE	04 CLEO	$e^+e^- \rightarrow J/\psi X$

 Γ_{25}/Γ_7 $\Gamma(\chi_{c1}(1P)X_{tetra})/\Gamma_{\text{total}}$

VALUE	CL%	DOCUMENT ID	TECN	COMMENT
$<37.8 \times 10^{-6}$	90	¹ JIA	17A BELL	$e^+e^- \rightarrow$ hadrons

 Γ_{26}/Γ

¹ For a tetraquark state X_{tetra} , with mass in the range 1.16–2.46 GeV and width in the range 0–0.3 GeV. Measured 90% CL limits as a function of X_{tetra} mass and width range from 4.4×10^{-6} to 37.8×10^{-6} .

 $\Gamma(\chi_{c2} \text{ anything})/\Gamma(J/\psi(1S) \text{ anything})$

VALUE	EVTS	DOCUMENT ID	TECN	COMMENT
$0.52 \pm 0.12 \pm 0.09$	47 ± 11	BRIERE	04 CLEO	$e^+e^- \rightarrow J/\psi X$

 Γ_{27}/Γ_7 $\Gamma(\psi(2S) \text{ anything})/\Gamma_{\text{total}}$

VALUE (units 10^{-4})	EVTS	DOCUMENT ID	TECN	COMMENT
$1.23 \pm 0.17 \pm 0.11$	215	SHEN	16 BELL	$e^+e^- \rightarrow \psi(2S) X$

 Γ_{28}/Γ $\Gamma(\psi(2S) \text{ anything})/\Gamma(J/\psi(1S) \text{ anything})$

VALUE	EVTS	DOCUMENT ID	TECN	COMMENT
$0.41 \pm 0.11 \pm 0.08$	42 ± 11	BRIERE	04 CLEO	$e^+e^- \rightarrow J/\psi \pi^+ \pi^- X$

 Γ_{28}/Γ_7 $\Gamma(\psi(2S)\eta_c)/\Gamma_{\text{total}}$

VALUE	CL%	DOCUMENT ID	TECN	COMMENT
$<3.6 \times 10^{-6}$	90	YANG	14 BELL	$e^+e^- \rightarrow \psi(2S) X$

 Γ_{29}/Γ $\Gamma(\psi(2S)\chi_{c0})/\Gamma_{\text{total}}$

VALUE	CL%	DOCUMENT ID	TECN	COMMENT
$<6.5 \times 10^{-6}$	90	YANG	14 BELL	$e^+e^- \rightarrow \psi(2S) X$

 Γ_{30}/Γ $\Gamma(\psi(2S)\chi_{c1})/\Gamma_{\text{total}}$

VALUE	CL%	DOCUMENT ID	TECN	COMMENT
$<4.5 \times 10^{-6}$	90	YANG	14 BELL	$e^+e^- \rightarrow \psi(2S) X$

 Γ_{31}/Γ $\Gamma(\psi(2S)\chi_{c2})/\Gamma_{\text{total}}$

VALUE	CL%	DOCUMENT ID	TECN	COMMENT
$<2.1 \times 10^{-6}$	90	YANG	14 BELL	$e^+e^- \rightarrow \psi(2S) X$

 Γ_{32}/Γ $\Gamma(\psi(2S)\eta_c(2S))/\Gamma_{\text{total}}$

VALUE	CL%	DOCUMENT ID	TECN	COMMENT
$<3.2 \times 10^{-6}$	90	YANG	14 BELL	$e^+e^- \rightarrow \psi(2S) X$

 Γ_{33}/Γ $\Gamma(\psi(2S)X(3940))/\Gamma_{\text{total}}$

VALUE	CL%	DOCUMENT ID	TECN	COMMENT
$<2.9 \times 10^{-6}$	90	YANG	14 BELL	$e^+e^- \rightarrow \psi(2S) X$

 Γ_{34}/Γ $\Gamma(\psi(2S)X(4160))/\Gamma_{\text{total}}$

VALUE	CL%	DOCUMENT ID	TECN	COMMENT
$<2.9 \times 10^{-6}$	90	YANG	14 BELL	$e^+e^- \rightarrow \psi(2S) X$

 Γ_{35}/Γ $\Gamma(\psi(4260) \text{ anything}, \psi \rightarrow \psi(2S)\pi^+\pi^-)/\Gamma_{\text{total}}$

VALUE	CL%	DOCUMENT ID	TECN	COMMENT
$<7.9 \times 10^{-5}$	90	SHEN	16 BELL	$\Upsilon(1S) \rightarrow \psi(2S)\pi^+\pi^- X$

 Γ_{36}/Γ $\Gamma(\psi(4360) \text{ anything}, \psi \rightarrow \psi(2S)\pi^+\pi^-)/\Gamma_{\text{total}}$

VALUE	CL%	DOCUMENT ID	TECN	COMMENT
$<5.2 \times 10^{-5}$	90	SHEN	16 BELL	$\Upsilon(1S) \rightarrow \psi(2S)\pi^+\pi^- X$

 Γ_{37}/Γ $\Gamma(\psi(4660) \text{ anything}, \psi \rightarrow \psi(2S)\pi^+\pi^-)/\Gamma_{\text{total}}$

VALUE	CL%	DOCUMENT ID	TECN	COMMENT
$<2.2 \times 10^{-5}$	90	SHEN	16 BELL	$\Upsilon(1S) \rightarrow \psi(2S)\pi^+\pi^- X$

 Γ_{38}/Γ $\Gamma(X(4050)^\pm \text{ anything}, X \rightarrow \psi(2S)\pi^\pm)/\Gamma_{\text{total}}$

VALUE	CL%	DOCUMENT ID	TECN	COMMENT
$<8.8 \times 10^{-5}$	90	SHEN	16 BELL	$\Upsilon(1S) \rightarrow \psi(2S)\pi^\pm X$

 Γ_{39}/Γ

See key on page 999

Meson Particle Listings

$\Upsilon(1S)$

$\Gamma(Z_c(4430)^\pm \text{ anything}, Z_c \rightarrow \psi(2S)\pi^\pm)/\Gamma_{\text{total}}$					Γ_{40}/Γ
VALUE	CL%	DOCUMENT ID	TECN	COMMENT	
$<6.7 \times 10^{-5}$	90	SHEN	16	BELL $\Upsilon(1S) \rightarrow \psi(2S)\pi^\pm X$	

$\Gamma(Z_c(4200)^+ Z_c(4200)^-)/\Gamma_{\text{total}}$					Γ_{41}/Γ
VALUE	CL%	DOCUMENT ID	TECN	COMMENT	
$<22.3 \times 10^{-6}$	90	¹ JIA	18	BELL $\Upsilon(1S) \rightarrow J/\psi\pi^\pm X$	
¹ Assuming $B(Z_c(4200)^\pm \rightarrow J/\psi\pi^\pm) = 1$.					

$\Gamma(Z_c(3900)^\pm Z_c(4200)^\mp)/\Gamma_{\text{total}}$					Γ_{42}/Γ
VALUE	CL%	DOCUMENT ID	TECN	COMMENT	
$<8.1 \times 10^{-6}$	90	¹ JIA	18	BELL $\Upsilon(1S) \rightarrow J/\psi\pi^\pm X$	
¹ Assuming $B(Z_c(4200)^\pm \rightarrow J/\psi\pi^\pm) = 1 = B(Z_c(3900)^\pm \rightarrow J/\psi\pi^\pm)$.					

$\Gamma(Z_c(3900)^+ Z_c(3900)^-)/\Gamma_{\text{total}}$					Γ_{43}/Γ
VALUE	CL%	DOCUMENT ID	TECN	COMMENT	
$<1.8 \times 10^{-6}$	90	¹ JIA	18	BELL $\Upsilon(1S) \rightarrow J/\psi\pi^\pm X$	
¹ Assuming $B(Z_c(3900)^\pm \rightarrow J/\psi\pi^\pm) = 1$					

$\Gamma(X(4050)^+ X(4050)^-)/\Gamma_{\text{total}}$					Γ_{44}/Γ
VALUE	CL%	DOCUMENT ID	TECN	COMMENT	
$<15.8 \times 10^{-6}$	90	¹ JIA	18	BELL $\Upsilon(1S) \rightarrow \chi_{c1}(1P)\pi^\pm X$	
¹ Assuming $B(X(4050)^\pm \rightarrow \chi_{c1}(1P)\pi^\pm) = 1$					

$\Gamma(X(4250)^+ X(4250)^-)/\Gamma_{\text{total}}$					Γ_{45}/Γ
VALUE	CL%	DOCUMENT ID	TECN	COMMENT	
$<26.6 \times 10^{-6}$	90	¹ JIA	18	BELL $\Upsilon(1S) \rightarrow \chi_{c1}(1P)\pi^\pm X$	
¹ Assuming $B(X(4250)^\pm \rightarrow \chi_{c1}(1P)\pi^\pm) = 1$					

$\Gamma(X(4050)^\pm X(4250)^\mp)/\Gamma_{\text{total}}$					Γ_{46}/Γ
VALUE	CL%	DOCUMENT ID	TECN	COMMENT	
$<44.2 \times 10^{-6}$	90	¹ JIA	18	BELL $\Upsilon(1S) \rightarrow \chi_{c1}(1P)\pi^\pm X$	
¹ Assuming $B(X(4050)^\pm \rightarrow \chi_{c1}(1P)\pi^\pm) = 1 = B(X(4250)^\pm \rightarrow \chi_{c1}(1P)\pi^\pm)$					

$\Gamma(Z_c(4430)^+ Z_c(4430)^-)/\Gamma_{\text{total}}$					Γ_{47}/Γ
VALUE	CL%	DOCUMENT ID	TECN	COMMENT	
$<20.3 \times 10^{-6}$	90	¹ JIA	18	BELL $\Upsilon(2S) \rightarrow \psi(2S)\pi^\pm X$	
¹ Assuming $B(Z_c(4430)^\pm \rightarrow \psi(2S)\pi^\pm) = 1$					

$\Gamma(X(4055)^\pm X(4055)^\mp)/\Gamma_{\text{total}}$					Γ_{48}/Γ
VALUE	CL%	DOCUMENT ID	TECN	COMMENT	
$<23.3 \times 10^{-6}$	90	¹ JIA	18	BELL $\Upsilon(1S) \rightarrow \psi(2S)\pi^\pm X$	
¹ Assuming $B(X(4055)^\pm \rightarrow \psi(2S)\pi^\pm) = 1$					

$\Gamma(X(4055)^\pm Z_c(4430)^\mp)/\Gamma_{\text{total}}$					Γ_{49}/Γ
VALUE	CL%	DOCUMENT ID	TECN	COMMENT	
$<45.5 \times 10^{-6}$	90	¹ JIA	18	BELL $\Upsilon(1S) \rightarrow \psi(2S)\pi^\pm X$	
¹ Assuming $B(X(4055)^\pm \rightarrow \psi(2S)\pi^\pm) = 1 = B(Z_c(4430)^\pm \rightarrow \psi(2S)\pi^\pm)$					

$\Gamma(\rho\pi)/\Gamma_{\text{total}}$					Γ_{50}/Γ
VALUE (units 10^{-6})	CL%	DOCUMENT ID	TECN	COMMENT	
<3.68	90	SHEN	13	BELL $\Upsilon(1S) \rightarrow \pi^+\pi^-\pi^0$	
••• We do not use the following data for averages, fits, limits, etc. •••					
$<1 \times 10^3$	90	BLINOV	90	MD1 $\Upsilon(1S) \rightarrow \rho^0\pi^0$	
$<2 \times 10^2$	90	FULTON	90B	$\Upsilon(1S) \rightarrow \rho^0\pi^0$	
$<2.1 \times 10^3$	90	NICZYPORUK	83	LENA $\Upsilon(1S) \rightarrow \rho^0\pi^0$	

$\Gamma(\omega\pi^0)/\Gamma_{\text{total}}$					Γ_{51}/Γ
VALUE (units 10^{-6})	CL%	DOCUMENT ID	TECN	COMMENT	
<3.90	90	SHEN	13	BELL $\Upsilon(1S) \rightarrow \pi^+\pi^-\pi^0\pi^0$	

$\Gamma(\pi^+\pi^-)/\Gamma_{\text{total}}$					Γ_{52}/Γ
VALUE (units 10^{-4})	CL%	DOCUMENT ID	TECN	COMMENT	
<5	90	BARU	92	MD1 $\Upsilon(1S) \rightarrow \pi^+\pi^-$	

$\Gamma(K^+K^-)/\Gamma_{\text{total}}$					Γ_{53}/Γ
VALUE (units 10^{-4})	CL%	DOCUMENT ID	TECN	COMMENT	
<5	90	BARU	92	MD1 $\Upsilon(1S) \rightarrow K^+K^-$	

$\Gamma(\rho\bar{\rho})/\Gamma_{\text{total}}$					Γ_{54}/Γ
VALUE (units 10^{-4})	CL%	DOCUMENT ID	TECN	COMMENT	
<5	90	¹ BARU	96	MD1 $\Upsilon(1S) \rightarrow \rho\bar{\rho}$	
¹ Supersedes BARU 92 in this node.					

$\Gamma(\pi^+\pi^-\pi^0)/\Gamma_{\text{total}}$					Γ_{55}/Γ
VALUE (units 10^{-6})	CL%	EVTs	DOCUMENT ID	TECN	COMMENT
$2.14 \pm 0.72 \pm 0.34$		26 ± 9	SHEN	13	BELL $\Upsilon(1S) \rightarrow \pi^+\pi^-\pi^0$
••• We do not use the following data for averages, fits, limits, etc. •••					
<18.4	90		ANASTASSOV	99	CLE2 $e^+e^- \rightarrow \text{hadrons}$

$\Gamma(\phi K^+K^-)/\Gamma_{\text{total}}$					Γ_{56}/Γ
VALUE (units 10^{-6})	EVTs	DOCUMENT ID	TECN	COMMENT	
$2.36 \pm 0.37 \pm 0.29$	56	SHEN	12A	BELL $\Upsilon(1S) \rightarrow 2(K^+K^-)$	

$\Gamma(\omega\pi^+\pi^-)/\Gamma_{\text{total}}$					Γ_{57}/Γ
VALUE (units 10^{-6})	EVTs	DOCUMENT ID	TECN	COMMENT	
$4.46 \pm 0.67 \pm 0.72$	64	SHEN	12A	BELL $\Upsilon(1S) \rightarrow 2(\pi^+\pi^-)\pi^0$	

$\Gamma(K^*(892)^0 K^-\pi^+ + c.c.)/\Gamma_{\text{total}}$					Γ_{58}/Γ
VALUE (units 10^{-6})	EVTs	DOCUMENT ID	TECN	COMMENT	
$4.42 \pm 0.50 \pm 0.58$	173	SHEN	12A	BELL $\Upsilon(1S) \rightarrow K^+K^-\pi^+\pi^-$	

$\Gamma(\phi f_2'(1525))/\Gamma_{\text{total}}$					Γ_{59}/Γ
VALUE (units 10^{-6})	CL%	DOCUMENT ID	TECN	COMMENT	
<1.63	90	SHEN	12A	BELL $\Upsilon(1S) \rightarrow 2(K^+K^-)$	

$\Gamma(\omega f_2(1270))/\Gamma_{\text{total}}$					Γ_{60}/Γ
VALUE (units 10^{-6})	CL%	DOCUMENT ID	TECN	COMMENT	
<1.79	90	SHEN	12A	BELL $\Upsilon(1S) \rightarrow 2(\pi^+\pi^-)\pi^0$	

$\Gamma(\rho(770) a_2(1320))/\Gamma_{\text{total}}$					Γ_{61}/Γ
VALUE (units 10^{-6})	CL%	DOCUMENT ID	TECN	COMMENT	
<2.24	90	SHEN	12A	BELL $\Upsilon(1S) \rightarrow 2(\pi^+\pi^-)\pi^0$	

$\Gamma(K^*(892)^0 \bar{K}_2^0(1430)^0 + c.c.)/\Gamma_{\text{total}}$					Γ_{62}/Γ
VALUE (units 10^{-6})	EVTs	DOCUMENT ID	TECN	COMMENT	
$3.02 \pm 0.68 \pm 0.34$	42	SHEN	12A	BELL $\Upsilon(1S) \rightarrow K^+K^-\pi^+\pi^-$	

$\Gamma(K_1(1270)^\pm K^\mp)/\Gamma_{\text{total}}$					Γ_{63}/Γ
VALUE (units 10^{-6})	CL%	DOCUMENT ID	TECN	COMMENT	
<2.41	90	SHEN	12A	BELL $\Upsilon(1S) \rightarrow K^+K^-\pi^+\pi^-$	

$\Gamma(K_1(1400)^\pm K^\mp)/\Gamma_{\text{total}}$					Γ_{64}/Γ
VALUE (units 10^{-6})	EVTs	DOCUMENT ID	TECN	COMMENT	
$1.02 \pm 0.35 \pm 0.22$	24	SHEN	12A	BELL $\Upsilon(1S) \rightarrow K^+K^-\pi^+\pi^-$	

$\Gamma(b_1(1235)^\pm \pi^\mp)/\Gamma_{\text{total}}$					Γ_{65}/Γ
VALUE (units 10^{-6})	CL%	DOCUMENT ID	TECN	COMMENT	
<1.25	90	SHEN	12A	BELL $\Upsilon(1S) \rightarrow 2(\pi^+\pi^-)\pi^0$	

$\Gamma(\pi^+\pi^-\pi^0\pi^0)/\Gamma_{\text{total}}$					Γ_{66}/Γ
VALUE (units 10^{-6})	EVTs	DOCUMENT ID	TECN	COMMENT	
$12.8 \pm 2.0 \pm 2.3$	143 ± 22	SHEN	13	BELL $\Upsilon(1S) \rightarrow \pi^+\pi^-\pi^0\pi^0$	

$\Gamma(K_S^0 K^+\pi^- + c.c.)/\Gamma_{\text{total}}$					Γ_{67}/Γ
VALUE (units 10^{-6})	CL%	EVTs	DOCUMENT ID	TECN	COMMENT
$1.59 \pm 0.33 \pm 0.18$		37 ± 8	SHEN	13	BELL $\Upsilon(1S) \rightarrow K_S^0 K^-\pi^+$
••• We do not use the following data for averages, fits, limits, etc. •••					
<3.4	90		¹ DOBBS	12A	$\Upsilon(1S) \rightarrow K_S^0 K^-\pi^+$
¹ Obtained by analyzing CLEO III data but not authored by the CLEO Collaboration.					

$\Gamma(K^*(892)^0 \bar{K}^0 + c.c.)/\Gamma_{\text{total}}$					Γ_{68}/Γ
VALUE (units 10^{-6})	EVTs	DOCUMENT ID	TECN	COMMENT	
$2.92 \pm 0.85 \pm 0.37$	16 ± 5	SHEN	13	BELL $\Upsilon(1S) \rightarrow K_S^0 K^-\pi^+$	

$\Gamma(K^*(892)^- K^+ + c.c.)/\Gamma_{\text{total}}$					Γ_{69}/Γ
VALUE (units 10^{-6})	CL%	DOCUMENT ID	TECN	COMMENT	
<1.11	90	SHEN	13	BELL $\Upsilon(1S) \rightarrow K_S^0 K^-\pi^+$	

$\Gamma(f_1(1285) \text{ anything})/\Gamma_{\text{total}}$					Γ_{70}/Γ
VALUE (units 10^{-3})	EVTs	DOCUMENT ID	TECN	COMMENT	
$4.6 \pm 2.8 \pm 1.3$	3.1k	JIA	17A	BELL $e^+e^- \rightarrow \text{hadrons}$	

$\Gamma(D^*(2010)^\pm \text{ anything})/\Gamma_{\text{total}}$					Γ_{71}/Γ
VALUE (units 10^{-3})	CL%	EVTs	DOCUMENT ID	TECN	COMMENT
$25.2 \pm 1.3 \pm 1.5$		$\approx 2k$	¹ AUBERT	10c	BABR $\Upsilon(2S) \rightarrow \pi^+\pi^-\Upsilon(1S)$
••• We do not use the following data for averages, fits, limits, etc. •••					
<19	90		² ALBRECHT	92J	ARG $e^+e^- \rightarrow D^0\pi^\pm X$
¹ For $x_p > 0.1$.					
² For $x_p > 0.2$.					

Meson Particle Listings

 $\Upsilon(1S)$

$\Gamma(f_1(1285)X_{tetra})/\Gamma_{total}$ Γ_{72}/Γ

VALUE	CL%	DOCUMENT ID	TECN	COMMENT
$<62.4 \times 10^{-6}$	90	¹ JIA	17A	BELL $e^+e^- \rightarrow$ hadrons

¹ For a tetraquark state X_{tetra} , with mass in the range 1.16–2.46 GeV and width in the range 0–0.3 GeV. Measured 90% CL limits as a function of X_{tetra} mass and width range from 4.6×10^{-6} to 62.4×10^{-6} .

$\Gamma(2\overline{H} \text{ anything})/\Gamma_{total}$ Γ_{73}/Γ

VALUE (units 10^{-5})	EVTS	DOCUMENT ID	TECN	COMMENT
2.85 ± 0.25 OUR AVERAGE				
$2.81 \pm 0.49^{+0.20}_{-0.24}$		LEES	14G	BABR $e^+e^- \rightarrow 2\overline{H} X$
$2.86 \pm 0.19 \pm 0.21$	455	ASNER	07	CLEO $e^+e^- \rightarrow 2\overline{H} X$

$\Gamma(\text{Sum of 100 exclusive modes})/\Gamma_{total}$ Γ_{74}/Γ

VALUE (units 10^{-2})	DOCUMENT ID	TECN	COMMENT
1.200 ± 0.017	^{1,2} DOBBS	12A	$\Upsilon(1S) \rightarrow$ hadrons

¹ DOBBS 12A presents individual exclusive branching fractions or upper limits for 100 modes of four to ten pions, kaons, or protons.

² Obtained by analyzing CLEO III data but not authored by the CLEO Collaboration.

$\Gamma(ggg, \gamma g g \rightarrow \overline{d} \text{ anything})/\Gamma(ggg, \gamma g g \rightarrow \text{anything})$ Γ_{75}/Γ

VALUE (units 10^{-5})	EVTS	DOCUMENT ID	TECN	COMMENT
$3.36 \pm 0.23 \pm 0.25$	455	ASNER	07	CLEO $e^+e^- \rightarrow \overline{d} X$

$\Gamma(\gamma\pi^+\pi^-)/\Gamma_{total}$ Γ_{75}/Γ

VALUE (units 10^{-5})	DOCUMENT ID	TECN	COMMENT
$6.3 \pm 1.2 \pm 1.3$	¹ ANASTASSOV	99	CLE2 $e^+e^- \rightarrow$ hadrons

¹ For $m_{\pi\pi} > 1$ GeV.

$\Gamma(\gamma\pi^0\pi^0)/\Gamma_{total}$ Γ_{76}/Γ

VALUE (units 10^{-5})	DOCUMENT ID	TECN	COMMENT
$1.7 \pm 0.6 \pm 0.3$	¹ ANASTASSOV	99	CLE2 $e^+e^- \rightarrow$ hadrons

¹ For $m_{\pi\pi} > 1$ GeV.

$\Gamma(\gamma\pi\pi(S\text{-wave}))/\Gamma_{total}$ Γ_{77}/Γ

VALUE (units 10^{-5})	DOCUMENT ID	TECN	COMMENT
$4.63 \pm 0.56 \pm 0.48$	LEES	18A	BABR $\Upsilon(1S) \rightarrow \gamma\pi^+\pi^-$

$\Gamma(\gamma\pi^0\eta)/\Gamma_{total}$ Γ_{78}/Γ

VALUE (units 10^{-6})	CL%	DOCUMENT ID	TECN	COMMENT
<2.4	90	¹ BESSON	07A	CLEO $e^+e^- \rightarrow \Upsilon(1S)$

¹ BESSON 07A obtained this limit for $0.7 < m_{\pi^0\eta} < 3$ GeV.

$\Gamma(\gamma K^+ K^-)/\Gamma_{total}$ Γ_{79}/Γ

($2 < m_{K^+K^-} < 3$ GeV)

VALUE (units 10^{-5})	CL%	DOCUMENT ID	TECN	COMMENT
$1.14 \pm 0.08 \pm 0.10$	90	ATHAR	06	CLE3 $\Upsilon(1S) \rightarrow \gamma K^+ K^-$

$\Gamma(\gamma\rho\overline{\rho})/\Gamma_{total}$ Γ_{80}/Γ

($2 < m_{\rho\overline{\rho}} < 3$ GeV)

VALUE (units 10^{-5})	CL%	DOCUMENT ID	TECN	COMMENT
<0.6	90	ATHAR	06	CLE3 $\Upsilon(1S) \rightarrow \gamma\rho\overline{\rho}$

$\Gamma(\gamma 2h^+ 2h^-)/\Gamma_{total}$ Γ_{81}/Γ

VALUE (units 10^{-4})	EVTS	DOCUMENT ID	TECN	COMMENT
$7.0 \pm 1.1 \pm 1.0$	80 ± 12	FULTON	90B	CLEO $e^+e^- \rightarrow$ hadrons

$\Gamma(\gamma 3h^+ 3h^-)/\Gamma_{total}$ Γ_{82}/Γ

VALUE (units 10^{-4})	EVTS	DOCUMENT ID	TECN	COMMENT
$5.4 \pm 1.5 \pm 1.3$	39 ± 11	FULTON	90B	CLEO $e^+e^- \rightarrow$ hadrons

$\Gamma(\gamma 4h^+ 4h^-)/\Gamma_{total}$ Γ_{83}/Γ

VALUE (units 10^{-4})	EVTS	DOCUMENT ID	TECN	COMMENT
$7.4 \pm 2.5 \pm 2.5$	36 ± 12	FULTON	90B	CLEO $e^+e^- \rightarrow$ hadrons

$\Gamma(\gamma\pi^+\pi^-K^+K^-)/\Gamma_{total}$ Γ_{84}/Γ

VALUE (units 10^{-4})	EVTS	DOCUMENT ID	TECN	COMMENT
$2.9 \pm 0.7 \pm 0.6$	29 ± 8	FULTON	90B	CLEO $e^+e^- \rightarrow$ hadrons

$\Gamma(\gamma 2\pi^+ 2\pi^-)/\Gamma_{total}$ Γ_{85}/Γ

VALUE (units 10^{-4})	EVTS	DOCUMENT ID	TECN	COMMENT
$2.5 \pm 0.7 \pm 0.5$	26 ± 7	FULTON	90B	CLEO $e^+e^- \rightarrow$ hadrons

$\Gamma(\gamma 3\pi^+ 3\pi^-)/\Gamma_{total}$ Γ_{86}/Γ

VALUE (units 10^{-4})	EVTS	DOCUMENT ID	TECN	COMMENT
$2.5 \pm 0.9 \pm 0.8$	17 ± 5	FULTON	90B	CLEO $e^+e^- \rightarrow$ hadrons

$\Gamma(\gamma 2\pi^+ 2\pi^- K^+ K^-)/\Gamma_{total}$ Γ_{87}/Γ

VALUE (units 10^{-4})	EVTS	DOCUMENT ID	TECN	COMMENT
$2.4 \pm 0.9 \pm 0.8$	18 ± 7	FULTON	90B	CLEO $e^+e^- \rightarrow$ hadrons

$\Gamma(\gamma\pi^+\pi^-\rho\overline{\rho})/\Gamma_{total}$ Γ_{88}/Γ

VALUE (units 10^{-4})	EVTS	DOCUMENT ID	TECN	COMMENT
$1.5 \pm 0.5 \pm 0.3$	22 ± 6	FULTON	90B	CLEO $e^+e^- \rightarrow$ hadrons

$\Gamma(\gamma 2\pi^+ 2\pi^- \rho\overline{\rho})/\Gamma_{total}$ Γ_{89}/Γ

VALUE (units 10^{-4})	EVTS	DOCUMENT ID	TECN	COMMENT
$0.4 \pm 0.4 \pm 0.4$	7 ± 6	FULTON	90B	CLEO $e^+e^- \rightarrow$ hadrons

$\Gamma(\gamma 2K^+ 2K^-)/\Gamma_{total}$ Γ_{90}/Γ

VALUE (units 10^{-4})	EVTS	DOCUMENT ID	TECN	COMMENT
0.2 ± 0.2	2 ± 2	FULTON	90B	CLEO $e^+e^- \rightarrow$ hadrons

$\Gamma(\gamma\eta(958))/\Gamma_{total}$ Γ_{91}/Γ

VALUE (units 10^{-6})	CL%	DOCUMENT ID	TECN	COMMENT
< 1.9	90	ATHAR	07A	CLEO $\Upsilon(1S) \rightarrow \gamma\eta' \rightarrow \gamma\pi^+\pi^-\eta, \gamma\rho$
< 16	90	RICCHICI	01B	CLE2 $\Upsilon(1S) \rightarrow \gamma\eta' \rightarrow \gamma\eta\pi^+\pi^-$

• • • We do not use the following data for averages, fits, limits, etc. • • •

$\Gamma(\gamma\eta)/\Gamma_{total}$ Γ_{92}/Γ

VALUE (units 10^{-6})	CL%	DOCUMENT ID	TECN	COMMENT
< 1.0	90	ATHAR	07A	CLEO $\Upsilon(1S) \rightarrow \gamma\eta \rightarrow \gamma\gamma\gamma, \gamma\pi^+\pi^-\pi^0, \gamma 3\pi^0$
< 21	90	MASEK	02	CLEO $\Upsilon(1S) \rightarrow \gamma\eta$

• • • We do not use the following data for averages, fits, limits, etc. • • •

$\Gamma(\gamma f_0(980))/\Gamma_{total}$ Γ_{93}/Γ

VALUE (units 10^{-5})	CL%	DOCUMENT ID	TECN	COMMENT
< 3	90	¹ ATHAR	06	CLE3 $\Upsilon(1S) \rightarrow \gamma\pi^+\pi^-$

¹ Assuming $B(f_0(980) \rightarrow \pi\pi) = 1$.

$\Gamma(\gamma f_2'(1525))/\Gamma_{total}$ Γ_{94}/Γ

VALUE (units 10^{-5})	CL%	EVTS	DOCUMENT ID	TECN	COMMENT
2.9 ± 0.6 OUR AVERAGE					
$2.13 \pm 0.28 \pm 0.72$			¹ LEES	18A	BABR $\Upsilon(1S) \rightarrow \gamma K^+ K^-$
$4.1 \pm 1.4 \pm 0.1$		17	² BESSON	11	CLEO $\Upsilon(1S) \rightarrow K_S^0 K_S^0$
$3.7^{+0.9}_{-0.7} \pm 0.8$			ATHAR	06	CLE3 $\Upsilon(1S) \rightarrow \gamma K^+ K^-$

• • • We do not use the following data for averages, fits, limits, etc. • • •

< 14	90	³ FULTON	90B	CLEO $\Upsilon(1S) \rightarrow \gamma K^+ K^-$
< 19.4	90	³ ALBRECHT	89	ARG $\Upsilon(1S) \rightarrow \gamma K^+ K^-$

¹ Using $B(f_2'(1525) \rightarrow K\overline{K}) = 0.887 \pm 0.022$ and $B(K^0\overline{K}^0) = 1/2 B(K\overline{K})$.

² BESSON 11 reports $(4.0 \pm 1.3 \pm 0.6) \times 10^{-5}$ from a measurement of $[\Gamma(\Upsilon(1S) \rightarrow f_2'(1525))/\Gamma_{total}] \times [B(f_2'(1525) \rightarrow K\overline{K})]$ assuming $B(f_2'(1525) \rightarrow K\overline{K}) = (88.8 \pm 3.1) \times 10^{-2}$, which we rescale to our best value $B(f_2'(1525) \rightarrow K\overline{K}) = (87.6 \pm 2.2) \times 10^{-2}$. Our first error is their experiment's error and our second error is the systematic error from using our best value. The result also assumes $B(K_S^0 \rightarrow \pi^+\pi^-) = (69.20 \pm 0.05)\%$ and $B(f_2'(1525) \rightarrow K\overline{K}) = 4 B(f_2'(1525) \rightarrow K_S^0 K_S^0)$.

³ Assuming $B(f_2'(1525) \rightarrow K\overline{K}) = 0.71$.

$\Gamma(\gamma f_2(1270))/\Gamma_{total}$ Γ_{95}/Γ

VALUE (units 10^{-5})	CL%	DOCUMENT ID	TECN	COMMENT
10.1 ± 0.6 OUR AVERAGE				
$10.15 \pm 0.59^{+0.54}_{-0.43}$		¹ LEES	18A	BABR $\Upsilon(1S) \rightarrow \gamma\pi^+\pi^-$
$10.5 \pm 1.6^{+1.9}_{-1.8}$		² BESSON	07A	CLE3 $\Upsilon(1S) \rightarrow \gamma\pi^0\pi^0$
$10.2 \pm 0.8 \pm 0.7$		ATHAR	06	CLE3 $\Upsilon(1S) \rightarrow \gamma\pi^+\pi^-$
$8.1 \pm 2.3^{+2.9}_{-2.7}$		³ ANASTASSOV	99	CLE2 $e^+e^- \rightarrow$ hadrons

• • • We do not use the following data for averages, fits, limits, etc. • • •

< 21	90	³ FULTON	90B	CLEO $\Upsilon(1S) \rightarrow \gamma\pi^+\pi^-$
< 13	90	³ ALBRECHT	89	ARG $\Upsilon(1S) \rightarrow \gamma\pi^+\pi^-$
< 81	90	SCHMITT	88	CBAL $\Upsilon(1S) \rightarrow \gamma X$

¹ Using $B(f_2(1270) \rightarrow \pi^0\pi^0) = 1/3 B(f_2(1270) \rightarrow \pi\pi)$ and $B(f_2(1270) \rightarrow \pi\pi) = (84.2^{+2.9}_{-0.9})\%$.

² Using $B(f_2(1270) \rightarrow \pi^0\pi^0) = B(f_2(1270) \rightarrow \pi\pi)/3$ and $B(f_2(1270) \rightarrow \pi\pi) = (84.7^{+2.5}_{-1.2})\%$.

³ Using $B(f_2(1270) \rightarrow \pi\pi) = 0.84$.

$\Gamma(\gamma\eta(1405))/\Gamma_{total}$ Γ_{96}/Γ

VALUE (units 10^{-5})	CL%	DOCUMENT ID	TECN	COMMENT
< 8.2	90	¹ FULTON	90B	CLEO $\Upsilon(1S) \rightarrow \gamma K^\pm \pi^\mp K_S^0$

¹ Includes unknown branching ratio of $\eta(1405) \rightarrow K^\pm \pi^\mp K_S^0$.

Meson Particle Listings
T(1S)

$\Gamma(\gamma f_0(1500))/\Gamma_{total}$ Γ_{97}/Γ
VALUE (units 10^{-5}) CL% DOCUMENT ID TECN COMMENT

<1.5 90 1 BESSON 07A CLEO $e^+e^- \rightarrow T(1S) \rightarrow \gamma\pi^0\pi^0$
• • • We do not use the following data for averages, fits, limits, etc. • • •
<6.1 90 2 BESSON 07A CLEO $e^+e^- \rightarrow T(1S) \rightarrow \gamma\eta\eta$
1 Using $B(f_0(1500) \rightarrow \pi^0\pi^0) = B(f_0(1500) \rightarrow \pi\pi)/3$ and $B(f_0(1500) \rightarrow \pi\pi) = (0.349 \pm 0.023)\%$.
2 Calculated by us using $B(f_0(1500) \rightarrow \eta\eta) = (5.1 \pm 0.9)\%$.

$\Gamma(\gamma f_0(1500) \rightarrow \gamma K^+ K^-)/\Gamma_{total}$ Γ_{98}/Γ
VALUE (units 10^{-5}) CL% DOCUMENT ID TECN COMMENT

1.04 ± 0.14 ± 0.33 1 LEES 18A BABR $e^+e^- \rightarrow T(1S) \rightarrow \gamma K^+ K^-$
1 LEES 18A quotes $B(T(1S) \rightarrow \gamma f_0(1500) \rightarrow \gamma K\bar{K}) = (2.08 \pm 0.27 \pm 0.65) \times 10^{-5}$ assuming $B(K^0\bar{K}^0) = 1/2 B(K\bar{K})$.

$\Gamma(\gamma f_0(1710))/\Gamma_{total}$ Γ_{99}/Γ
VALUE (units 10^{-4}) CL% DOCUMENT ID TECN COMMENT

< 2.6 90 1 ALBRECHT 89 ARG $T(1S) \rightarrow \gamma K^+ K^-$
• • • We do not use the following data for averages, fits, limits, etc. • • •
< 6.3 90 1 FULTON 90B CLEO $T(1S) \rightarrow \gamma K^+ K^-$
<19 90 1 FULTON 90B CLEO $T(1S) \rightarrow \gamma K_S^0 K_S^0$
< 8 90 2 ALBRECHT 89 ARG $T(1S) \rightarrow \gamma\pi^+\pi^-$
<24 90 3 SCHMITT 88 CBAL $T(1S) \rightarrow \gamma X$
1 Assuming $B(f_0(1710) \rightarrow K\bar{K}) = 0.38$.
2 Assuming $B(f_0(1710) \rightarrow \pi\pi) = 0.04$.
3 Assuming $B(f_0(1710) \rightarrow \eta\eta) = 0.18$.

$\Gamma(\gamma f_0(1710) \rightarrow \gamma K^+ K^-)/\Gamma_{total}$ Γ_{100}/Γ
VALUE (units 10^{-5}) CL% DOCUMENT ID TECN COMMENT

1.01 ± 0.26 ± 0.18 1 LEES 18A BABR $e^+e^- \rightarrow T(1S) \rightarrow \gamma K^+ K^-$
• • • We do not use the following data for averages, fits, limits, etc. • • •
<0.7 90 ATHAR 06 CLEO $e^+e^- \rightarrow T(1S) \rightarrow \gamma K^+ K^-$
1 LEES 18A quotes $B(T(1S) \rightarrow \gamma f_0(1710) \rightarrow \gamma K\bar{K}) = (2.02 \pm 0.51 \pm 0.35) \times 10^{-5}$ assuming $B(K^0\bar{K}^0) = 1/2 B(K\bar{K})$.

$\Gamma(\gamma f_0(1710) \rightarrow \gamma\pi^+\pi^-)/\Gamma_{total}$ Γ_{101}/Γ
VALUE (units 10^{-5}) CL% DOCUMENT ID TECN COMMENT

0.53 ± 0.17 ± 0.11 1 LEES 18A BABR $T(1S) \rightarrow \gamma\pi^+\pi^-$
1 LEES 18A quotes $B(T(1S) \rightarrow \gamma f_0(1710) \rightarrow \gamma\pi\pi) = (0.79 \pm 0.26 \pm 0.17) \times 10^{-5}$ assuming $B(\pi^0\pi^0) = 1/3 B(\pi\pi)$.

$\Gamma(\gamma f_0(1710) \rightarrow \gamma\pi^0\pi^0)/\Gamma_{total}$ Γ_{102}/Γ
VALUE (units 10^{-6}) CL% DOCUMENT ID TECN COMMENT

<1.4 90 BESSON 07A CLEO $e^+e^- \rightarrow T(1S) \rightarrow \gamma\pi^0\pi^0$

$\Gamma(\gamma f_0(1710) \rightarrow \gamma\eta\eta)/\Gamma_{total}$ Γ_{103}/Γ
VALUE (units 10^{-6}) CL% DOCUMENT ID TECN COMMENT

<1.8 90 BESSON 07A CLEO $e^+e^- \rightarrow T(1S) \rightarrow \gamma\eta\eta$

$\Gamma(\gamma f_4(2050))/\Gamma_{total}$ Γ_{104}/Γ
VALUE (units 10^{-5}) CL% DOCUMENT ID TECN COMMENT

<5.3 90 1 ATHAR 06 CLE3 $T(1S) \rightarrow \gamma\pi^+\pi^-$
1 Assuming $B(f_4(2050) \rightarrow \pi\pi) = 0.17$.

$\Gamma(\gamma f_0(2200) \rightarrow \gamma K^+ K^-)/\Gamma_{total}$ Γ_{105}/Γ
VALUE CL% DOCUMENT ID TECN COMMENT

<0.0002 90 BARU 89 MD1 $T(1S) \rightarrow \gamma K^+ K^-$

$\Gamma(\gamma f_2(2220) \rightarrow \gamma K^+ K^-)/\Gamma_{total}$ Γ_{106}/Γ
VALUE (units 10^{-7}) CL% DOCUMENT ID TECN COMMENT

< 8 90 ATHAR 06 CLE3 $T(1S) \rightarrow \gamma K^+ K^-$
• • • We do not use the following data for averages, fits, limits, etc. • • •
< 160 90 MASEK 02 CLEO $T(1S) \rightarrow \gamma K^+ K^-$
< 150 90 FULTON 90B CLEO $T(1S) \rightarrow \gamma K^+ K^-$
< 290 90 ALBRECHT 89 ARG $T(1S) \rightarrow \gamma K^+ K^-$
<2000 90 BARU 89 MD1 $T(1S) \rightarrow \gamma K^+ K^-$

$\Gamma(\gamma f_2(2220) \rightarrow \gamma\pi^+\pi^-)/\Gamma_{total}$ Γ_{107}/Γ
VALUE (units 10^{-7}) CL% DOCUMENT ID TECN COMMENT

< 6 90 ATHAR 06 CLE3 $T(1S) \rightarrow \gamma\pi^+\pi^-$
• • • We do not use the following data for averages, fits, limits, etc. • • •
<120 90 MASEK 02 CLEO $T(1S) \rightarrow \gamma\pi^+\pi^-$

$\Gamma(\gamma f_2(2220) \rightarrow \gamma\rho\bar{\rho})/\Gamma_{total}$ Γ_{108}/Γ
VALUE (units 10^{-7}) CL% DOCUMENT ID TECN COMMENT

< 11 90 ATHAR 06 CLE3 $T(1S) \rightarrow \gamma\rho\bar{\rho}$
• • • We do not use the following data for averages, fits, limits, etc. • • •
<160 90 MASEK 02 CLEO $T(1S) \rightarrow \gamma\rho\bar{\rho}$

$\Gamma(\gamma\eta(2225) \rightarrow \gamma\phi\phi)/\Gamma_{total}$ Γ_{109}/Γ
VALUE CL% DOCUMENT ID TECN COMMENT

<0.003 90 BARU 89 MD1 $T(1S) \rightarrow \gamma K^+ K^- K^+ K^-$

$\Gamma(\gamma\eta_c(1S))/\Gamma_{total}$ Γ_{110}/Γ
VALUE (units 10^{-5}) CL% DOCUMENT ID TECN COMMENT

<5.7 90 SHEN 10A BELL $T(1S) \rightarrow \gamma X$

$\Gamma(\gamma\chi_{c0})/\Gamma_{total}$ Γ_{111}/Γ
VALUE (units 10^{-4}) CL% DOCUMENT ID TECN COMMENT

<6.5 90 SHEN 10A BELL $T(1S) \rightarrow \gamma X$

$\Gamma(\gamma\chi_{c1})/\Gamma_{total}$ Γ_{112}/Γ
VALUE (units 10^{-5}) CL% DOCUMENT ID TECN COMMENT

<2.3 90 SHEN 10A BELL $T(1S) \rightarrow \gamma X$

$\Gamma(\gamma\chi_{c2})/\Gamma_{total}$ Γ_{113}/Γ
VALUE (units 10^{-6}) CL% DOCUMENT ID TECN COMMENT

<7.6 90 SHEN 10A BELL $T(1S) \rightarrow \gamma X$

$\Gamma(\gamma\chi_{c1}(3872) \rightarrow \pi^+\pi^-J/\psi)/\Gamma_{total}$ Γ_{114}/Γ
VALUE (units 10^{-6}) CL% DOCUMENT ID TECN COMMENT

<1.6 90 SHEN 10A BELL $T(1S) \rightarrow \gamma X$

$\Gamma(\gamma\chi_{c1}(3872) \rightarrow \pi^+\pi^-\pi^0J/\psi)/\Gamma_{total}$ Γ_{115}/Γ
VALUE (units 10^{-6}) CL% DOCUMENT ID TECN COMMENT

<2.8 90 SHEN 10A BELL $T(1S) \rightarrow \gamma X$

$\Gamma(\gamma X(3915) \rightarrow \omega J/\psi)/\Gamma_{total}$ Γ_{116}/Γ
VALUE (units 10^{-6}) CL% DOCUMENT ID TECN COMMENT

<3.0 90 SHEN 10A BELL $T(1S) \rightarrow \gamma X$

$\Gamma(\gamma\chi_{c1}(4140) \rightarrow \phi J/\psi)/\Gamma_{total}$ Γ_{117}/Γ
VALUE (units 10^{-6}) CL% DOCUMENT ID TECN COMMENT

<2.2 90 SHEN 10A BELL $T(1S) \rightarrow \gamma X$

$\Gamma(\gamma X)/\Gamma_{total}$ Γ_{118}/Γ
(X = scalar with $m < 8.0$ GeV)

< 4.5 90 1 DEL-AMO-SA...11J BABR $e^+e^- \rightarrow \gamma + X$

• • • We do not use the following data for averages, fits, limits, etc. • • •
<30 90 2 BALEST 95 CLEO $e^+e^- \rightarrow \gamma + X$

1 For a noninteracting scalar X with mass $m < 8.0$ GeV.
2 For a noninteracting pseudoscalar X with mass < 7.2 GeV.

$\Gamma(\gamma X\bar{X}(m_X < 3.1 \text{ GeV}))/\Gamma_{total}$ Γ_{119}/Γ
($X\bar{X}$ = vectors with $m < 3.1$ GeV)

VALUE (units 10^{-3}) CL% DOCUMENT ID TECN COMMENT

<1 90 1 BALEST 95 CLEO $e^+e^- \rightarrow \gamma + X\bar{X}$

1 For a noninteracting vector X with mass < 3.1 GeV.

$\Gamma(\gamma X\bar{X}(m_X < 4.5 \text{ GeV}))/\Gamma_{total}$ Γ_{120}/Γ
X and \bar{X} = zero spin with $m < 4.5$ GeV

VALUE (units 10^{-5}) CL% DOCUMENT ID TECN COMMENT

<24 90 1 DEL-AMO-SA...11J BABR $e^+e^- \rightarrow \gamma + X\bar{X}$

1 For a noninteracting scalar X with mass $m < 4.5$ GeV.

$\Gamma(\gamma X \rightarrow \gamma + \geq 4 \text{ prongs})/\Gamma_{total}$ Γ_{121}/Γ
(1.5 GeV $< m_X < 5.0$ GeV)

VALUE (units 10^{-4}) CL% DOCUMENT ID TECN COMMENT

<1.78 95 ROSNER 07A CLEO $e^+e^- \rightarrow \gamma X$

$\Gamma(\gamma a_1^0 \rightarrow \gamma\mu^+\mu^-)/\Gamma_{total}$ Γ_{122}/Γ
($201 < M(\mu^+\mu^-) < 3565$ MeV)

VALUE (units 10^{-6}) CL% DOCUMENT ID TECN COMMENT

<9 90 1 LOVE 08 CLEO $e^+e^- \rightarrow \gamma a_1^0 \rightarrow \gamma\mu^+\mu^-$

• • • We do not use the following data for averages, fits, limits, etc. • • •
<9.7 90 2 LEES 13c BABR $e^+e^- \rightarrow \gamma a_1^0 \rightarrow \gamma\mu^+\mu^-$

1 For a narrow scalar or pseudoscalar a_1^0 with $201 < M(\mu^+\mu^-) < 3565$ MeV, excluding J/ψ . Measured 90% CL limits as a function of $M(\mu^+\mu^-)$ range from $1-9 \times 10^{-6}$.
2 For a narrow scalar or pseudoscalar a_1^0 with mass in the range $212-9200$ MeV, excluding J/ψ and $\psi(2S)$. Measured 90% CL limits as a function of $m_{a_1^0}$ range from $0.28-9.7 \times 10^{-6}$.

$\Gamma(\gamma a_1^0 \rightarrow \gamma\tau^+\tau^-)/\Gamma_{total}$ Γ_{123}/Γ
($2m_\tau < M(\tau^+\tau^-) < 9.2$ GeV)

VALUE (units 10^{-6}) CL% DOCUMENT ID TECN COMMENT

<130 90 1 LEES 13R BABR $T(2S) \rightarrow \gamma\tau^+\tau^-\pi^+\pi^-$

Meson Particle Listings

$\Upsilon(1S), \chi_{b0}(1P)$

••• We do not use the following data for averages, fits, limits, etc. •••

< 50 90 2 LOVE 08 CLEO $e^+e^- \rightarrow \gamma a_1^0 \rightarrow \gamma \tau^+ \tau^-$

¹ For a narrow scalar a_1^0 with $2m_\tau < M(a_1^0) < 9.2$ GeV, which result in a 90% CL upper limits of 0.9×10^{-5} at $M(a_1^0) = 2m_\tau$, $\approx 1.5 \times 10^{-5}$ at $M(a_1^0) = 7.5$ GeV, and 13×10^{-5} at $M(a_1^0) = 9.2$ GeV.

² For a narrow scalar or pseudoscalar a_1^0 with $2m_\tau < M(a_1^0) < 7.5$ GeV, which result in a 90% CL limits ranging from 1×10^{-5} at $M(a_1^0) = 2m_\tau$ to 5×10^{-5} at $M(a_1^0) = 7.5$ GeV.

$\Gamma(\gamma a_1^0 \rightarrow \gamma \mathcal{E})/\Gamma_{\text{total}}$ Γ_{124}/Γ
(0.5 GeV < m < 9.0 GeV)

VALUE	CL%	DOCUMENT ID	TECN	COMMENT
< 1×10^{-2}	90	1 LEES	13L BABR	$\Upsilon(1S) \rightarrow \gamma X$

¹ For a narrow, CP-odd pseudoscalar a_1^0 searched for in 26 hadronic decay modes with invariant mass $0.5 \text{ GeV} < m_X < 9.0 \text{ GeV}$. Measured 90% CL limit as a function of m_X range from 10^{-6} to 10^{-2} .

$\Gamma(\gamma a_1^0 \rightarrow \gamma s \bar{s})/\Gamma_{\text{total}}$ Γ_{125}/Γ
(0.5 GeV < m < 9.0 GeV)

VALUE	CL%	DOCUMENT ID	TECN	COMMENT
< 1×10^{-3}	90	1 LEES	13L BABR	$\Upsilon(1S) \rightarrow \gamma X$

¹ For a narrow, CP-odd pseudoscalar a_1^0 searched for in 14 hadronic decay modes with invariant mass $1.5 \text{ GeV} < m_X < 9.0 \text{ GeV}$. Measured 90% CL limit as a function of m_X range from 10^{-5} to 10^{-3} .

LEPTON FAMILY NUMBER (LF) VIOLATING MODES

$\Gamma(\mu^\pm \tau^\mp)/\Gamma_{\text{total}}$ Γ_{126}/Γ

VALUE (units 10^{-6})	CL%	DOCUMENT ID	TECN	COMMENT
< 6.0	95	LOVE	08A CLEO	$e^+e^- \rightarrow \mu^\pm \tau^\mp$

OTHER DECAYS

$\Gamma(\text{invisible})/\Gamma_{\text{total}}$ Γ_{127}/Γ

VALUE (units 10^{-4})	CL%	DOCUMENT ID	TECN	COMMENT
< 3.0	90	AUBERT	09AX BABR	$\Upsilon(3S) \rightarrow \pi^+ \pi^- \Upsilon(1S)$

••• We do not use the following data for averages, fits, limits, etc. •••

< 39 90 RUBIN 07 CLEO $\Upsilon(2S) \rightarrow \pi^+ \pi^- \Upsilon(1S)$

< 25 90 TA JIMA 07 BELL $\Upsilon(3S) \rightarrow \pi^+ \pi^- \Upsilon(1S)$

$\Upsilon(1S)$ REFERENCES

JIA	18	PR D97 112004	S. Jia et al.	(BELLE Collab.)
LEES	18A	PR D97 112006	J.P. Lees et al.	(BABAR Collab.)
JIA	17	PR D95 012001	S. Jia et al.	(BELLE Collab.)
JIA	17A	PR D96 112002	S. Jia et al.	(BELLE Collab.)
SHEN	16	PR D93 112013	C.P. Shen et al.	(BELLE Collab.)
LEES	14G	PR D89 111102	J.P. Lees et al.	(BABAR Collab.)
YANG	14	PR D90 112008	S.D. Yang et al.	(BELLE Collab.)
LEES	13C	PR D87 031102	J.P. Lees et al.	(BABAR Collab.)
LEES	13L	PR D88 031701	J.P. Lees et al.	(BABAR Collab.)
LEES	13R	PR D88 071102	J.P. Lees et al.	(BABAR Collab.)
SHEN	13	PR D88 011102	C.P. Shen et al.	(BELLE Collab.)
DOBBS	12A	PR D86 052003	S. Dobbs et al.	(BELLE Collab.)
SHEN	12A	PR D86 031102	C.P. Shen et al.	(BELLE Collab.)
BESSON	11	PR D83 037101	D. Besson et al.	(CLEO Collab.)
DEL-AMO-SA...	11J	PRL 107 021804	P. del Amo Sanchez et al.	(BABAR Collab.)
AUBERT	10C	PR D81 011102	B. Aubert et al.	(BABAR Collab.)
DEL-AMO-SA...	10C	PRL 104 191801	P. del Amo Sanchez et al.	(BABAR Collab.)
SHEN	10A	PR D82 051504	C.P. Shen et al.	(BELLE Collab.)
AUBERT	09AX	PRL 103 251801	B. Aubert et al.	(BABAR Collab.)
LOVE	08	PRL 101 151802	W. Love et al.	(CLEO Collab.)
LOVE	08A	PRL 101 201601	W. Love et al.	(CLEO Collab.)
PDG	08	PL B667 1	C. Amstler et al.	(PDG Collab.)
ASNER	07	PR D75 012009	D.M. Asner et al.	(CLEO Collab.)
ATHAR	07A	PR D76 072003	S.B. Athar et al.	(CLEO Collab.)
BESSON	07	PRL 98 052002	D. Besson et al.	(CLEO Collab.)
BESSON	07A	PR D75 072001	D. Besson et al.	(CLEO Collab.)
ROSNER	07A	PR D76 17102	J.L. Rosner et al.	(CLEO Collab.)
RUBIN	07	PR D75 031104	P. Rubin et al.	(CLEO Collab.)
TAJIMA	07	PRL 98 132001	O. Tajima et al.	(BELLE Collab.)
AQUINES	06A	PR D74 092006	O. Aquines et al.	(CLEO Collab.)
ATHAR	06	PR D73 032001	S.B. Athar et al.	(CLEO Collab.)
BESSON	06A	PR D74 012003	D. Besson et al.	(CLEO Collab.)
ROSNER	06	PRL 96 092003	J.L. Rosner et al.	(CLEO Collab.)
ADAMS	05	PRL 94 012001	G.S. Adams et al.	(CLEO Collab.)
BRIERE	04	PR D70 072001	R.A. Briere et al.	(CLEO Collab.)
ARTUSO	03	PR D67 052003	M. Artuso et al.	(CLEO Collab.)
MASEK	02	PR D65 072002	G. Masek et al.	(CLEO Collab.)
RICHICHI	01B	PRL 87 141801	S.J. Richichi et al.	(CLEO Collab.)
ARTAMONOV	00	PL B474 427	A.S. Artamonov et al.	(CLEO Collab.)
ANASTASSOV	99	PRL 82 286	A. Anastassov et al.	(CLEO Collab.)
ALEXANDER	98	PR D58 052004	J.P. Alexander et al.	(CLEO Collab.)
BARU	96	PRPL 267 71	S.E. Baru et al.	(NOVO)
BALEST	95	PR D51 2053	R. Balest et al.	(CLEO Collab.)
CINABRO	94B	PL B340 129	D. Cinabro et al.	(CLEO Collab.)
ALBRECHT	92J	ZPHY C55 25	H. Albrecht et al.	(ARGUS Collab.)
BARU	92	ZPHY C54 229	S.E. Baru et al.	(NOVO)
BARU	92B	ZPHY C56 547	S.E. Baru et al.	(NOVO)
KOBEL	92	ZPHY C53 193	M. Kobel et al.	(Crystal Ball Collab.)
BLINOV	90	PL B245 311	A.E. Blinov et al.	(NOVO)
FULTON	90B	PR D41 1401	R. Fulton et al.	(CLEO Collab.)
MASCHMANN	90	ZPHY C46 555	W.S. Maschmann et al.	(Crystal Ball Collab.)
ALBRECHT	89	ZPHY C42 349	H. Albrecht et al.	(ARGUS Collab.)
ALEXANDER	89	NP B320 45	J.P. Alexander et al.	(LBL, MICH, SLAC)
BARU	89	ZPHY C42 505	S.E. Baru et al.	(NOVO)
CHEN	89B	PR D39 3528	W.Y. Chen et al.	(CLEO Collab.)
FULTON	89	PL B224 445	R. Fulton et al.	(CLEO Collab.)
KAARSBERG	89	PRL 62 2077	T.M. Kaarsberg et al.	(CUSB Collab.)

BUCHMUELL...	88	HE e^+e^- Physics 412	W. Buchmueller, S. Cooper	(HANN, DESY, MIT)
Editors:		A. Ali and P. Soeding, World Scientific, Singapore		
JAKUBOWSKI	88	ZPHY C40 49	Z. Jakubowski et al.	(Crystal Ball Collab.)
SCHMITT	88	ZPHY C40 199	P. Schmitt et al.	(Crystal Ball Collab.)
ALBRECHT	87	ZPHY C35 283	H. Albrecht et al.	(ARGUS Collab.)
COHEN	87	RMP 59 1121	E.R. Cohen, B.N. Taylor	(RISC, NBS)
BARU	86	ZPHY C30 651	S.E. Baru et al.	(NOVO)
ALBRECHT	85C	PL 154B 452	H. Albrecht et al.	(ARGUS Collab.)
KURAEV	85	SJNP 41 466	E.A. Kurayev, V.S. Fadin	(NOVO)
		Translated from YAF 41 733.		
ARTAMONOV	84	PL 137B 272	A.S. Artamonov et al.	(NOVO)
BESSON	84	PR D30 1433	D. Besson et al.	(CLEO Collab.)
GILES	84B	PR D29 1285	R. Giles et al.	(CLEO Collab.)
MACKAY	84	PR D29 2483	W.W. Mackay et al.	(CUSB Collab.)
ANDREWS	83	PRL 50 807	D.E. Andrews et al.	(CLEO Collab.)
GILES	83	PRL 50 877	R. Giles et al.	(HARV, OSU, ROCH, RUTG+)
NICZYPORUK	83	ZPHY C17 197	B. Niczyporuk et al.	(LENA Collab.)
ALBRECHT	82	PL 116B 383	H. Albrecht et al.	(DESY, DORT, HEIDH+)
ARTAMONOV	82	PL 118B 225	A.S. Artamonov et al.	(NOVO)
NICZYPORUK	82	ZPHY C15 299	B. Niczyporuk et al.	(LENA Collab.)
BERGER	80C	PL 93B 497	C. Berger et al.	(PLUTO Collab.)
BOCK	80	ZPHY C6 125	P. Bock et al.	(HEIDP, MPIM, DESY, HAMB)
BERGER	79	ZPHY C1 343	C. Berger et al.	(PLUTO Collab.)

$\chi_{b0}(1P)$

$I^G(J^{PC}) = 0^+(0^+)$
J needs confirmation.

Observed in radiative decay of the $\Upsilon(2S)$, therefore $C = +$. Branching ratio requires E1 transition, M1 is strongly disfavored, therefore $P = +$.

$\chi_{b0}(1P)$ MASS

VALUE (MeV)	DOCUMENT ID
9859.44 ± 0.42 ± 0.31 OUR EVALUATION	From average γ energy below, using $\Upsilon(2S)$ mass = 10023.26 ± 0.31 MeV

$m_{\chi_{b1}(1P)} - m_{\chi_{b0}(1P)}$

VALUE (MeV)	DOCUMENT ID	TECN	COMMENT
32.49 ± 0.93	LEES	14M BABR	$\Upsilon(2S) \rightarrow \gamma \gamma \mu^+ \mu^-$

γ ENERGY IN $\Upsilon(2S)$ DECAY

VALUE (MeV)	DOCUMENT ID	TECN	COMMENT
162.5 ± 0.4 OUR AVERAGE			
162.56 ± 0.19 ± 0.42	ARTUSO	05	CLEO $\Upsilon(2S) \rightarrow \gamma X$
162.0 ± 0.8 ± 1.2	EDWARDS	99	CLE2 $\Upsilon(2S) \rightarrow \gamma \chi(1P)$
162.1 ± 0.5 ± 1.4	ALBRECHT	85E	ARG $\Upsilon(2S) \rightarrow \text{conv. } \gamma X$
163.8 ± 1.6 ± 2.7	NERNST	85	CBAL $\Upsilon(2S) \rightarrow \gamma X$
158.0 ± 7 ± 1	HAAS	84	CLEO $\Upsilon(2S) \rightarrow \text{conv. } \gamma X$
••• We do not use the following data for averages, fits, limits, etc. •••			
149.4 ± 0.7 ± 5.0	KLOPFEN...	83	CUSB $\Upsilon(2S) \rightarrow \gamma X$

$\chi_{b0}(1P)$ DECAY MODES

Mode	Fraction (Γ_i/Γ)	Confidence level
Γ_1 $\gamma \Upsilon(1S)$	(1.94 ± 0.27) %	
Γ_2 $D^0 X$	< 10.4 %	90%
Γ_3 $\pi^+ \pi^- K^+ K^- \pi^0$	< 1.6 $\times 10^{-4}$	90%
Γ_4 $2\pi^+ \pi^- K^- K_S^0$	< 5 $\times 10^{-5}$	90%
Γ_5 $2\pi^+ \pi^- K^- K_S^0 2\pi^0$	< 5 $\times 10^{-4}$	90%
Γ_6 $2\pi^+ 2\pi^- 2\pi^0$	< 2.1 $\times 10^{-4}$	90%
Γ_7 $2\pi^+ 2\pi^- K^+ K^-$	(1.1 ± 0.6) $\times 10^{-4}$	
Γ_8 $2\pi^+ 2\pi^- K^+ K^- \pi^0$	< 2.7 $\times 10^{-4}$	90%
Γ_9 $2\pi^+ 2\pi^- K^+ K^- 2\pi^0$	< 5 $\times 10^{-4}$	90%
Γ_{10} $3\pi^+ 2\pi^- K^- K_S^0 \pi^0$	< 1.6 $\times 10^{-4}$	90%
Γ_{11} $3\pi^+ 3\pi^-$	< 8 $\times 10^{-5}$	90%
Γ_{12} $3\pi^+ 3\pi^- 2\pi^0$	< 6 $\times 10^{-4}$	90%
Γ_{13} $3\pi^+ 3\pi^- K^+ K^-$	(2.4 ± 1.2) $\times 10^{-4}$	
Γ_{14} $3\pi^+ 3\pi^- K^+ K^- \pi^0$	< 1.0 $\times 10^{-3}$	90%
Γ_{15} $4\pi^+ 4\pi^-$	< 8 $\times 10^{-5}$	90%
Γ_{16} $4\pi^+ 4\pi^- 2\pi^0$	< 2.1 $\times 10^{-3}$	90%
Γ_{17} $J/\psi J/\psi$	< 7 $\times 10^{-5}$	90%
Γ_{18} $J/\psi \psi(2S)$	< 1.2 $\times 10^{-4}$	90%
Γ_{19} $\psi(2S) \psi(2S)$	< 3.1 $\times 10^{-5}$	90%
Γ_{20} $J/\psi(1S)$ anything	< 2.3 $\times 10^{-3}$	90%

$\chi_{b0}(1P)$ BRANCHING RATIOS

$\Gamma(\gamma \Upsilon(1S))/\Gamma_{\text{total}}$	VALUE (%)	CL%	EVTS	DOCUMENT ID	TECN	COMMENT	Γ_1/Γ
	1.94 ± 0.27 OUR AVERAGE						
	2.07 ± 0.24 ± 0.21			1,2 LEES	14M BABR	$\Upsilon(2S) \rightarrow \gamma \gamma \mu^+ \mu^-$	
	1.76 ± 0.30 ± 0.18		87	3,4 KORNICER	11 CLEO	$e^+e^- \rightarrow \gamma \gamma e^+ e^-$	

• • • We do not use the following data for averages, fits, limits, etc. • • •

- < 4.6 90 5 LEES 11J BABR $\Upsilon(2S) \rightarrow X\gamma$
 - < 6 90 WALK 86 CBAL $\Upsilon(2S) \rightarrow \gamma\gamma\ell^+\ell^-$
 - <11 90 PAUSS 83 CUSB $\Upsilon(2S) \rightarrow \gamma\gamma\ell^+\ell^-$
- ¹ LEES 14M quotes $\Gamma(\chi_{b0}(1P) \rightarrow \gamma\Upsilon(1S))/\Gamma_{\text{total}} \times \Gamma(\Upsilon(2S) \rightarrow \gamma\chi_{b0}(1P))/\Gamma_{\text{total}}$ = $(7.75 \pm 0.91) \times 10^{-4}$ combining the results from samples of $\Upsilon(2S) \rightarrow \gamma\gamma\mu^+\mu^-$ with and without converted photons. Assumes $B(\Upsilon(1S) \rightarrow \mu^+\mu^-) = (2.48 \pm 0.05)\%$.
- ² LEES 14M reports $[\Gamma(\chi_{b0}(1P) \rightarrow \gamma\Upsilon(1S))/\Gamma_{\text{total}}] \times [B(\Upsilon(2S) \rightarrow \gamma\chi_{b0}(1P))] = (7.75 \pm 0.91) \times 10^{-4}$ which we divide by our best value $B(\Upsilon(2S) \rightarrow \gamma\chi_{b0}(1P)) = (3.8 \pm 0.4) \times 10^{-2}$. Our first error is their experiment's error and our second error is the systematic error from using our best value.
- ³ Assuming $B(\Upsilon(1S) \rightarrow \ell^+\ell^-) = (2.48 \pm 0.05)\%$.
- ⁴ KORNICER 11 reports $[\Gamma(\chi_{b0}(1P) \rightarrow \gamma\Upsilon(1S))/\Gamma_{\text{total}}] \times [B(\Upsilon(2S) \rightarrow \gamma\chi_{b0}(1P))] = (6.59 \pm 0.96 \pm 0.60) \times 10^{-4}$ which we divide by our best value $B(\Upsilon(2S) \rightarrow \gamma\chi_{b0}(1P)) = (3.8 \pm 0.4) \times 10^{-2}$. Our first error is their experiment's error and our second error is the systematic error from using our best value.
- ⁵ LEES 11J quotes a central value of $\Gamma(\chi_{b0}(1P) \rightarrow \gamma\Upsilon(1S))/\Gamma_{\text{total}} \times \Gamma(\Upsilon(2S) \rightarrow \gamma\chi_{b0}(1P))/\Gamma_{\text{total}} = (8.3 \pm 5.6^{+3.7}_{-2.6}) \times 10^{-4}$.

$\Gamma(D^0 X)/\Gamma_{\text{total}} \quad \Gamma_2/\Gamma$

VALUE (units 10^{-4})	CL%	DOCUMENT ID	TECN	COMMENT
<10.4 × 10 ⁻²	90	6,7 BRIERE	08	CLEO $\Upsilon(2S) \rightarrow \gamma D^0 X$

⁶ For $p_{D^0} > 2.5$ GeV/c.
⁷ The authors also present their result as $(5.6 \pm 3.6 \pm 0.5) \times 10^{-2}$.

$\Gamma(\pi^+ \pi^- K^+ K^- \pi^0)/\Gamma_{\text{total}} \quad \Gamma_3/\Gamma$

VALUE (units 10^{-4})	CL%	DOCUMENT ID	TECN	COMMENT
<1.6	90	8 ASNER	08A	CLEO $\Upsilon(2S) \rightarrow \gamma\pi^+\pi^-K^+K^-\pi^0$

⁸ ASNER 08A reports $[\Gamma(\chi_{b0}(1P) \rightarrow \pi^+\pi^-K^+K^-\pi^0)/\Gamma_{\text{total}}] \times [B(\Upsilon(2S) \rightarrow \gamma\chi_{b0}(1P))] < 6 \times 10^{-6}$ which we divide by our best value $B(\Upsilon(2S) \rightarrow \gamma\chi_{b0}(1P)) = 3.8 \times 10^{-2}$.

$\Gamma(2\pi^+ \pi^- K^- K_S^0)/\Gamma_{\text{total}} \quad \Gamma_4/\Gamma$

VALUE (units 10^{-4})	CL%	DOCUMENT ID	TECN	COMMENT
<0.5	90	9 ASNER	08A	CLEO $\Upsilon(2S) \rightarrow \gamma 2\pi^+\pi^-K^-K_S^0$

⁹ ASNER 08A reports $[\Gamma(\chi_{b0}(1P) \rightarrow 2\pi^+\pi^-K^-K_S^0)/\Gamma_{\text{total}}] \times [B(\Upsilon(2S) \rightarrow \gamma\chi_{b0}(1P))] < 2 \times 10^{-6}$ which we divide by our best value $B(\Upsilon(2S) \rightarrow \gamma\chi_{b0}(1P)) = 3.8 \times 10^{-2}$.

$\Gamma(2\pi^+ \pi^- K^- K_S^0 2\pi^0)/\Gamma_{\text{total}} \quad \Gamma_5/\Gamma$

VALUE (units 10^{-4})	CL%	DOCUMENT ID	TECN	COMMENT
<5	90	10 ASNER	08A	CLEO $\Upsilon(2S) \rightarrow \gamma 2\pi^+\pi^-K^-2\pi^0$

¹⁰ ASNER 08A reports $[\Gamma(\chi_{b0}(1P) \rightarrow 2\pi^+\pi^-K^-K_S^0 2\pi^0)/\Gamma_{\text{total}}] \times [B(\Upsilon(2S) \rightarrow \gamma\chi_{b0}(1P))] < 18 \times 10^{-6}$ which we divide by our best value $B(\Upsilon(2S) \rightarrow \gamma\chi_{b0}(1P)) = 3.8 \times 10^{-2}$.

$\Gamma(2\pi^+ 2\pi^- 2\pi^0)/\Gamma_{\text{total}} \quad \Gamma_6/\Gamma$

VALUE (units 10^{-4})	CL%	DOCUMENT ID	TECN	COMMENT
<2.1	90	11 ASNER	08A	CLEO $\Upsilon(2S) \rightarrow \gamma 2\pi^+ 2\pi^- 2\pi^0$

¹¹ ASNER 08A reports $[\Gamma(\chi_{b0}(1P) \rightarrow 2\pi^+ 2\pi^- 2\pi^0)/\Gamma_{\text{total}}] \times [B(\Upsilon(2S) \rightarrow \gamma\chi_{b0}(1P))] < 8 \times 10^{-6}$ which we divide by our best value $B(\Upsilon(2S) \rightarrow \gamma\chi_{b0}(1P)) = 3.8 \times 10^{-2}$.

$\Gamma(2\pi^+ 2\pi^- K^+ K^-)/\Gamma_{\text{total}} \quad \Gamma_7/\Gamma$

VALUE (units 10^{-4})	EVTS	DOCUMENT ID	TECN	COMMENT
1.1 ± 0.6 ± 0.1	7	12 ASNER	08A	CLEO $\Upsilon(2S) \rightarrow \gamma 2\pi^+ 2\pi^- K^+ K^-$

¹² ASNER 08A reports $[\Gamma(\chi_{b0}(1P) \rightarrow 2\pi^+ 2\pi^- K^+ K^-)/\Gamma_{\text{total}}] \times [B(\Upsilon(2S) \rightarrow \gamma\chi_{b0}(1P))] = (4 \pm 2 \pm 1) \times 10^{-6}$ which we divide by our best value $B(\Upsilon(2S) \rightarrow \gamma\chi_{b0}(1P)) = (3.8 \pm 0.4) \times 10^{-2}$. Our first error is their experiment's error and our second error is the systematic error from using our best value.

$\Gamma(2\pi^+ 2\pi^- K^+ K^- \pi^0)/\Gamma_{\text{total}} \quad \Gamma_8/\Gamma$

VALUE (units 10^{-4})	CL%	DOCUMENT ID	TECN	COMMENT
<2.7	90	13 ASNER	08A	CLEO $\Upsilon(2S) \rightarrow \gamma 2\pi^+ 2\pi^- K^+ K^- \pi^0$

¹³ ASNER 08A reports $[\Gamma(\chi_{b0}(1P) \rightarrow 2\pi^+ 2\pi^- K^+ K^- \pi^0)/\Gamma_{\text{total}}] \times [B(\Upsilon(2S) \rightarrow \gamma\chi_{b0}(1P))] < 10 \times 10^{-6}$ which we divide by our best value $B(\Upsilon(2S) \rightarrow \gamma\chi_{b0}(1P)) = 3.8 \times 10^{-2}$.

$\Gamma(2\pi^+ 2\pi^- K^+ K^- 2\pi^0)/\Gamma_{\text{total}} \quad \Gamma_9/\Gamma$

VALUE (units 10^{-4})	CL%	DOCUMENT ID	TECN	COMMENT
<5	90	14 ASNER	08A	CLEO $\Upsilon(2S) \rightarrow \gamma 2\pi^+ 2\pi^- K^+ K^- 2\pi^0$

¹⁴ ASNER 08A reports $[\Gamma(\chi_{b0}(1P) \rightarrow 2\pi^+ 2\pi^- K^+ K^- 2\pi^0)/\Gamma_{\text{total}}] \times [B(\Upsilon(2S) \rightarrow \gamma\chi_{b0}(1P))] < 20 \times 10^{-6}$ which we divide by our best value $B(\Upsilon(2S) \rightarrow \gamma\chi_{b0}(1P)) = 3.8 \times 10^{-2}$.

$\Gamma(3\pi^+ 2\pi^- K^- K_S^0 \pi^0)/\Gamma_{\text{total}} \quad \Gamma_{10}/\Gamma$

VALUE (units 10^{-4})	CL%	DOCUMENT ID	TECN	COMMENT
<1.6	90	15 ASNER	08A	CLEO $\Upsilon(2S) \rightarrow \gamma 3\pi^+ 2\pi^- K^- K_S^0 \pi^0$

¹⁵ ASNER 08A reports $[\Gamma(\chi_{b0}(1P) \rightarrow 3\pi^+ 2\pi^- K^- K_S^0 \pi^0)/\Gamma_{\text{total}}] \times [B(\Upsilon(2S) \rightarrow \gamma\chi_{b0}(1P))] < 6 \times 10^{-6}$ which we divide by our best value $B(\Upsilon(2S) \rightarrow \gamma\chi_{b0}(1P)) = 3.8 \times 10^{-2}$.

$\Gamma(3\pi^+ 3\pi^-)/\Gamma_{\text{total}} \quad \Gamma_{11}/\Gamma$

VALUE (units 10^{-4})	CL%	DOCUMENT ID	TECN	COMMENT
<0.8	90	16 ASNER	08A	CLEO $\Upsilon(2S) \rightarrow \gamma 3\pi^+ 3\pi^-$

¹⁶ ASNER 08A reports $[\Gamma(\chi_{b0}(1P) \rightarrow 3\pi^+ 3\pi^-)/\Gamma_{\text{total}}] \times [B(\Upsilon(2S) \rightarrow \gamma\chi_{b0}(1P))] < 3 \times 10^{-6}$ which we divide by our best value $B(\Upsilon(2S) \rightarrow \gamma\chi_{b0}(1P)) = 3.8 \times 10^{-2}$.

$\Gamma(3\pi^+ 3\pi^- 2\pi^0)/\Gamma_{\text{total}} \quad \Gamma_{12}/\Gamma$

VALUE (units 10^{-4})	CL%	DOCUMENT ID	TECN	COMMENT
<6	90	17 ASNER	08A	CLEO $\Upsilon(2S) \rightarrow \gamma 3\pi^+ 3\pi^- 2\pi^0$

¹⁷ ASNER 08A reports $[\Gamma(\chi_{b0}(1P) \rightarrow 3\pi^+ 3\pi^- 2\pi^0)/\Gamma_{\text{total}}] \times [B(\Upsilon(2S) \rightarrow \gamma\chi_{b0}(1P))] < 22 \times 10^{-6}$ which we divide by our best value $B(\Upsilon(2S) \rightarrow \gamma\chi_{b0}(1P)) = 3.8 \times 10^{-2}$.

$\Gamma(3\pi^+ 3\pi^- K^+ K^-)/\Gamma_{\text{total}} \quad \Gamma_{13}/\Gamma$

VALUE (units 10^{-4})	EVTS	DOCUMENT ID	TECN	COMMENT
2.4 ± 1.2 ± 0.2	9	18 ASNER	08A	CLEO $\Upsilon(2S) \rightarrow \gamma 3\pi^+ 3\pi^- K^+ K^-$

¹⁸ ASNER 08A reports $[\Gamma(\chi_{b0}(1P) \rightarrow 3\pi^+ 3\pi^- K^+ K^-)/\Gamma_{\text{total}}] \times [B(\Upsilon(2S) \rightarrow \gamma\chi_{b0}(1P))] = (9 \pm 4 \pm 2) \times 10^{-6}$ which we divide by our best value $B(\Upsilon(2S) \rightarrow \gamma\chi_{b0}(1P)) = (3.8 \pm 0.4) \times 10^{-2}$. Our first error is their experiment's error and our second error is the systematic error from using our best value.

$\Gamma(3\pi^+ 3\pi^- K^+ K^- \pi^0)/\Gamma_{\text{total}} \quad \Gamma_{14}/\Gamma$

VALUE (units 10^{-4})	CL%	DOCUMENT ID	TECN	COMMENT
<10	90	19 ASNER	08A	CLEO $\Upsilon(2S) \rightarrow \gamma 3\pi^+ 3\pi^- K^+ K^- \pi^0$

¹⁹ ASNER 08A reports $[\Gamma(\chi_{b0}(1P) \rightarrow 3\pi^+ 3\pi^- K^+ K^- \pi^0)/\Gamma_{\text{total}}] \times [B(\Upsilon(2S) \rightarrow \gamma\chi_{b0}(1P))] < 37 \times 10^{-6}$ which we divide by our best value $B(\Upsilon(2S) \rightarrow \gamma\chi_{b0}(1P)) = 3.8 \times 10^{-2}$.

$\Gamma(4\pi^+ 4\pi^-)/\Gamma_{\text{total}} \quad \Gamma_{15}/\Gamma$

VALUE (units 10^{-4})	CL%	DOCUMENT ID	TECN	COMMENT
<0.8	90	20 ASNER	08A	CLEO $\Upsilon(2S) \rightarrow \gamma 4\pi^+ 4\pi^-$

²⁰ ASNER 08A reports $[\Gamma(\chi_{b0}(1P) \rightarrow 4\pi^+ 4\pi^-)/\Gamma_{\text{total}}] \times [B(\Upsilon(2S) \rightarrow \gamma\chi_{b0}(1P))] < 3 \times 10^{-6}$ which we divide by our best value $B(\Upsilon(2S) \rightarrow \gamma\chi_{b0}(1P)) = 3.8 \times 10^{-2}$.

$\Gamma(4\pi^+ 4\pi^- 2\pi^0)/\Gamma_{\text{total}} \quad \Gamma_{16}/\Gamma$

VALUE (units 10^{-4})	CL%	DOCUMENT ID	TECN	COMMENT
<21	90	21 ASNER	08A	CLEO $\Upsilon(2S) \rightarrow \gamma 4\pi^+ 4\pi^- 2\pi^0$

²¹ ASNER 08A reports $[\Gamma(\chi_{b0}(1P) \rightarrow 4\pi^+ 4\pi^- 2\pi^0)/\Gamma_{\text{total}}] \times [B(\Upsilon(2S) \rightarrow \gamma\chi_{b0}(1P))] < 77 \times 10^{-6}$ which we divide by our best value $B(\Upsilon(2S) \rightarrow \gamma\chi_{b0}(1P)) = 3.8 \times 10^{-2}$.

$\Gamma(J/\psi J/\psi)/\Gamma_{\text{total}} \quad \Gamma_{17}/\Gamma$

VALUE (units 10^{-5})	CL%	DOCUMENT ID	TECN	COMMENT
<7	90	22 SHEN	12	BELL $\Upsilon(2S) \rightarrow \gamma\psi X$

²² SHEN 12 reports $< 7.1 \times 10^{-5}$ from a measurement of $[\Gamma(\chi_{b0}(1P) \rightarrow J/\psi J/\psi)/\Gamma_{\text{total}}] \times [B(\Upsilon(2S) \rightarrow \gamma\chi_{b0}(1P))]$ assuming $B(\Upsilon(2S) \rightarrow \gamma\chi_{b0}(1P)) = (3.8 \pm 0.4) \times 10^{-2}$.

$\Gamma(J/\psi\psi(2S))/\Gamma_{\text{total}} \quad \Gamma_{18}/\Gamma$

VALUE (units 10^{-5})	CL%	DOCUMENT ID	TECN	COMMENT
<12	90	23 SHEN	12	BELL $\Upsilon(2S) \rightarrow \gamma\psi X$

²³ SHEN 12 reports $< 12 \times 10^{-5}$ from a measurement of $[\Gamma(\chi_{b0}(1P) \rightarrow J/\psi\psi(2S))/\Gamma_{\text{total}}] \times [B(\Upsilon(2S) \rightarrow \gamma\chi_{b0}(1P))]$ assuming $B(\Upsilon(2S) \rightarrow \gamma\chi_{b0}(1P)) = (3.8 \pm 0.4) \times 10^{-2}$.

$\Gamma(\psi(2S)\psi(2S))/\Gamma_{\text{total}} \quad \Gamma_{19}/\Gamma$

VALUE (units 10^{-5})	CL%	DOCUMENT ID	TECN	COMMENT
<3.1	90	24 SHEN	12	BELL $\Upsilon(2S) \rightarrow \gamma\psi X$

²⁴ SHEN 12 reports $< 3.1 \times 10^{-5}$ from a measurement of $[\Gamma(\chi_{b0}(1P) \rightarrow \psi(2S)\psi(2S))/\Gamma_{\text{total}}] \times [B(\Upsilon(2S) \rightarrow \gamma\chi_{b0}(1P))]$ assuming $B(\Upsilon(2S) \rightarrow \gamma\chi_{b0}(1P)) = (3.8 \pm 0.4) \times 10^{-2}$.

$\Gamma(J/\psi(1S) \text{ anything})/\Gamma_{\text{total}} \quad \Gamma_{20}/\Gamma$

VALUE	CL%	DOCUMENT ID	TECN	COMMENT
<2.3 × 10 ⁻³	90	JIA	17A	BELL $e^+e^- \rightarrow \text{hadrons}$

$\chi_{b0}(1P)$ CROSS-PARTICLE BRANCHING RATIOS

$\Gamma(\chi_{b0}(1P) \rightarrow \gamma\Upsilon(1S))/\Gamma_{\text{total}} \times \Gamma(\Upsilon(2S) \rightarrow \gamma\chi_{b0}(1P))/\Gamma_{\text{total}} \quad \Gamma_1/\Gamma \times \Gamma_6/\Gamma$

VALUE	CL%	DOCUMENT ID	TECN	COMMENT
<1.7 × 10 ⁻³	90	25 LEES	11J	BABR $\Upsilon(2S) \rightarrow X\gamma$

²⁵ LEES 11J quotes a central value of $\Gamma(\chi_{b0}(1P) \rightarrow \gamma\Upsilon(1S))/\Gamma_{\text{total}} \times \Gamma(\Upsilon(2S) \rightarrow \gamma\chi_{b0}(1P))/\Gamma_{\text{total}} = (8.3 \pm 5.6^{+3.7}_{-2.6}) \times 10^{-4}$ and derives a 90% CL upper limit of $\Gamma(\gamma\Upsilon(1S))/\Gamma_{\text{total}} < 4.6\%$ using $B(\Upsilon(2S) \rightarrow \gamma\chi_{b0}(1P)) = (3.8 \pm 0.4)\%$.

Meson Particle Listings

$\chi_{b0}(1P), \chi_{b1}(1P)$

$B(\chi_{b0}(1P) \rightarrow \gamma T(1S)) \times B(T(2S) \rightarrow \gamma \chi_{b0}(1P)) \times B(T(1S) \rightarrow \ell^+ \ell^-)$

VALUE (units 10^{-5})	EVTS	DOCUMENT ID	TECN	COMMENT
1.67 ± 0.28 OUR AVERAGE				
2.9 ^{+1.7} _{-1.4} ± 0.1 ^{+0.1} _{-0.8}		²⁶ LEES	14M BABR	$T(2S) \rightarrow \gamma \gamma \mu^+ \mu^-$
1.63 ± 0.24 ± 0.15	87	KORNICER	11 CLEO	$e^+ e^- \rightarrow \gamma \gamma \ell^+ \ell^-$

$[B(\chi_{b0}(1P) \rightarrow \gamma T(1S)) \times B(T(2S) \rightarrow \gamma \chi_{b0}(1P))] / [B(\chi_{b1}(1P) \rightarrow \gamma T(1S)) \times B(T(2S) \rightarrow \gamma \chi_{b1}(1P))]$

VALUE (%)	DOCUMENT ID	TECN	COMMENT
3.28 ± 0.37			
	²⁷ LEES	14M BABR	$T(2S) \rightarrow \gamma \gamma \mu^+ \mu^-$

²⁷ From a sample of $T(2S) \rightarrow \gamma \gamma \mu^+ \mu^-$ without converted photons.

$\chi_{b0}(1P)$ REFERENCES

JIA	17A	PR D96 112002	S. Jia et al.	(BELLE Collab.)
LEES	14M	PR D90 112010	J.P. Lees et al.	(BABAR Collab.)
SHEN	12	PR D85 071102	C.P. Shen et al.	(BELLE Collab.)
KORNICER	11	PR D83 054003	M. Kornicer et al.	(CLEO Collab.)
LEES	11J	PR D84 072002	J.P. Lees et al.	(BABAR Collab.)
ASNER	08A	PR D78 091103	D.M. Asner et al.	(CLEO Collab.)
BRIERE	08	PR D78 092007	R.A. Briere et al.	(CLEO Collab.)
ARTUSO	05	PRL 94 032001	M. Artuso et al.	(CLEO Collab.)
EDWARDS	99	PR D59 032003	K.W. Edwards et al.	(CLEO Collab.)
WALK	86	PR D34 2611	W.S. Walk et al.	(Crystal Ball Collab.)
ALBRECHT	85E	PL 160B 331	H. Albrecht et al.	(ARGUS Collab.)
NERNST	85	PRL 54 2195	R. Nernst et al.	(Crystal Ball Collab.)
HAAS	84	PRL 52 799	J. Haas et al.	(CLEO Collab.)
KLOPFEN...	83	PRL 51 160	C. Klopfenstein et al.	(CUSB Collab.)
PAUSS	83	PL 130B 439	F. Pauss et al.	(MPIM, COLU, CORN, LSU+)

$\chi_{b1}(1P)$

$$J^G(JPC) = 0^+(1^{++})$$

J needs confirmation.

Observed in radiative decay of the $T(2S)$, therefore $C = +$. Branching ratio requires E1 transition, M1 is strongly disfavored, therefore $P = +$. $J = 1$ from SKWARNICKI 87.

$\chi_{b1}(1P)$ MASS

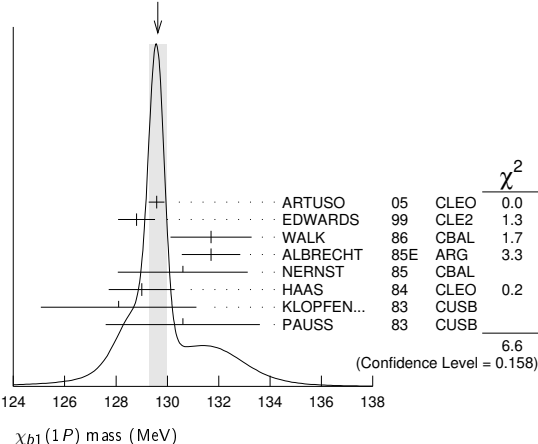
VALUE (MeV)	DOCUMENT ID
9892.78 ± 0.26 ± 0.31 OUR EVALUATION	

From average γ energy below, using $T(2S)$ mass = 10023.26 ± 0.31 MeV

γ ENERGY IN $T(2S)$ DECAY

VALUE (MeV)	DOCUMENT ID	TECN	COMMENT
129.63 ± 0.33 OUR AVERAGE			
129.58 ± 0.09 ± 0.29	ARTUSO 05	CLEO	$T(2S) \rightarrow \gamma X$
128.8 ± 0.4 ± 0.6	EDWARDS 99	CLE2	$T(2S) \rightarrow \gamma \chi(1P)$
131.7 ± 0.9 ± 1.3	WALK 86	CBAL	$T(2S) \rightarrow \gamma \gamma \ell^+ \ell^-$
131.7 ± 0.3 ± 1.1	ALBRECHT 85E	ARG	$T(2S) \rightarrow \text{conv. } \gamma X$
130.6 ± 0.8 ± 2.4	NERNST 85	CBAL	$T(2S) \rightarrow \gamma X$
129 ± 0.8 ± 1	HAAS 84	CLEO	$T(2S) \rightarrow \text{conv. } \gamma X$
128.1 ± 0.4 ± 3.0	KLOPFEN... 83	CUSB	$T(2S) \rightarrow \gamma X$
130.6 ± 3.0	PAUSS 83	CUSB	$T(2S) \rightarrow \gamma \gamma \ell^+ \ell^-$

WEIGHTED AVERAGE
129.63 ± 0.33 (Error scaled by 1.3)



$\chi_{b1}(1P)$ DECAY MODES

Mode	Fraction (Γ_i/Γ)	Confidence level
Γ_1 $\gamma T(1S)$	(35.2 ± 2.0) %	
Γ_2 $D^0 X$	(12.6 ± 2.2) %	
Γ_3 $\pi^+ \pi^- K^+ K^- \pi^0$	(2.0 ± 0.6) × 10 ⁻⁴	
Γ_4 $2\pi^+ \pi^- K^- K_S^0$	(1.3 ± 0.5) × 10 ⁻⁴	
Γ_5 $2\pi^+ \pi^- K^- K_S^0 2\pi^0$	< 6 × 10 ⁻⁴	90%
Γ_6 $2\pi^+ 2\pi^- 2\pi^0$	(8.0 ± 2.5) × 10 ⁻⁴	
Γ_7 $2\pi^+ 2\pi^- K^+ K^-$	(1.5 ± 0.5) × 10 ⁻⁴	
Γ_8 $2\pi^+ 2\pi^- K^+ K^- \pi^0$	(3.5 ± 1.2) × 10 ⁻⁴	
Γ_9 $2\pi^+ 2\pi^- K^+ K^- 2\pi^0$	(8.6 ± 3.2) × 10 ⁻⁴	
Γ_{10} $3\pi^+ 2\pi^- K^- K_S^0 \pi^0$	(9.3 ± 3.3) × 10 ⁻⁴	
Γ_{11} $3\pi^+ 3\pi^-$	(1.9 ± 0.6) × 10 ⁻⁴	
Γ_{12} $3\pi^+ 3\pi^- 2\pi^0$	(1.7 ± 0.5) × 10 ⁻³	
Γ_{13} $3\pi^+ 3\pi^- K^+ K^-$	(2.6 ± 0.8) × 10 ⁻⁴	
Γ_{14} $3\pi^+ 3\pi^- K^+ K^- \pi^0$	(7.5 ± 2.6) × 10 ⁻⁴	
Γ_{15} $4\pi^+ 4\pi^-$	(2.6 ± 0.9) × 10 ⁻⁴	
Γ_{16} $4\pi^+ 4\pi^- 2\pi^0$	(1.4 ± 0.6) × 10 ⁻³	
Γ_{17} ω anything	(4.9 ± 1.4) %	
Γ_{18} ωX_{tetra}	< 4.44 × 10 ⁻⁴	90%
Γ_{19} $J/\psi J/\psi$	< 2.7 × 10 ⁻⁵	90%
Γ_{20} $J/\psi \psi(2S)$	< 1.7 × 10 ⁻⁵	90%
Γ_{21} $\psi(2S) \psi(2S)$	< 6 × 10 ⁻⁵	90%
Γ_{22} $J/\psi(1S)$ anything	< 1.1 × 10 ⁻³	90%
Γ_{23} $J/\psi(1S) X_{tetra}$	< 2.27 × 10 ⁻⁴	90%

$\chi_{b1}(1P)$ BRANCHING RATIOS

VALUE	EVTS	DOCUMENT ID	TECN	COMMENT	Γ_1/Γ
0.352 ± 0.020 OUR AVERAGE					
0.356 ^{+0.016} _{-0.022} ± 0.019	964k	¹ FULSOM	18 BELL	$T(2S) \rightarrow \gamma X$	
0.364 ± 0.017 ± 0.019		^{2,3,4} LEES	14M BABR	$T(2S) \rightarrow \gamma \gamma \mu^+ \mu^-$	
0.331 ± 0.018 ± 0.017	3222	^{4,5} KORNICER	11 CLEO	$e^+ e^- \rightarrow \gamma \gamma \ell^+ \ell^-$	
0.350 ± 0.023 ± 0.018	13k	⁶ LEES	11J BABR	$T(2S) \rightarrow \gamma X$	
0.34 ± 0.07 ± 0.02	53	^{4,7,8} WALK	86 CBAL	$T(2S) \rightarrow \gamma \gamma \ell^+ \ell^-$	
0.47 ± 0.18			83 CUSB	$T(2S) \rightarrow \gamma \gamma \ell^+ \ell^-$	

- FULSOM 18 reports $[\Gamma(\chi_{b1}(1P) \rightarrow \gamma T(1S))/\Gamma_{total}] \times [B(T(2S) \rightarrow \gamma \chi_{b1}(1P))] = (2.45 \pm 0.02 \pm 0.11) \times 10^{-2}$ which we divide by our best value $B(T(2S) \rightarrow \gamma \chi_{b1}(1P)) = (6.9 \pm 0.4) \times 10^{-2}$. Our first error is their experiment's error and our second error is the systematic error from using our best value.
- LEES 14M quotes $\Gamma(\chi_{b1}(1P) \rightarrow \gamma T(1S))/\Gamma_{total} \times \Gamma(T(2S) \rightarrow \gamma \chi_{b1}(1P))/\Gamma_{total} = (2.51 \pm 0.12) \%$ combining the results from samples of $T(2S) \rightarrow \gamma \gamma \mu^+ \mu^-$ with and without converted photons.
- LEES 14M reports $[\Gamma(\chi_{b1}(1P) \rightarrow \gamma T(1S))/\Gamma_{total}] \times [B(T(2S) \rightarrow \gamma \chi_{b1}(1P))] = (2.51 \pm 0.12) \times 10^{-2}$ which we divide by our best value $B(T(2S) \rightarrow \gamma \chi_{b1}(1P)) = (6.9 \pm 0.4) \times 10^{-2}$. Our first error is their experiment's error and our second error is the systematic error from using our best value.
- Assuming $B(T(1S) \rightarrow \mu^+ \mu^-) = (2.48 \pm 0.05) \%$.
- KORNICER 11 reports $[\Gamma(\chi_{b1}(1P) \rightarrow \gamma T(1S))/\Gamma_{total}] \times [B(T(2S) \rightarrow \gamma \chi_{b1}(1P))] = (22.8 \pm 0.4 \pm 1.2) \times 10^{-3}$ which we divide by our best value $B(T(2S) \rightarrow \gamma \chi_{b1}(1P)) = (6.9 \pm 0.4) \times 10^{-2}$. Our first error is their experiment's error and our second error is the systematic error from using our best value.
- LEES 11J reports $[\Gamma(\chi_{b1}(1P) \rightarrow \gamma T(1S))/\Gamma_{total}] \times [B(T(2S) \rightarrow \gamma \chi_{b1}(1P))] = (24.1 \pm 0.6 \pm 1.5) \times 10^{-3}$ which we divide by our best value $B(T(2S) \rightarrow \gamma \chi_{b1}(1P)) = (6.9 \pm 0.4) \times 10^{-2}$. Our first error is their experiment's error and our second error is the systematic error from using our best value.
- WALK 86 quotes $B(T(2S) \rightarrow \gamma \chi_{b1}(1P)) \times B(\chi_{b1}(1P) \rightarrow \gamma T(1S)) \times B(T(1S) \rightarrow \ell^+ \ell^-) = (5.8 \pm 0.9 \pm 0.7) \%$.
- WALK 86 reports $[\Gamma(\chi_{b1}(1P) \rightarrow \gamma T(1S))/\Gamma_{total}] \times [B(T(2S) \rightarrow \gamma \chi_{b1}(1P))] = (23.4 \pm 3.63 \pm 2.82) \times 10^{-3}$ which we divide by our best value $B(T(2S) \rightarrow \gamma \chi_{b1}(1P)) = (6.9 \pm 0.4) \times 10^{-2}$. Our first error is their experiment's error and our second error is the systematic error from using our best value.

VALUE (units 10^{-2})	EVTS	DOCUMENT ID	TECN	COMMENT	Γ_2/Γ
12.6 ± 1.9 ± 1.1					
	2310	¹ BRIERE	08 CLEO	$T(2S) \rightarrow \gamma D^0 X$	

¹ For $p_{D^0} > 2.5$ GeV/c.

VALUE (units 10^{-4})	EVTS	DOCUMENT ID	TECN	COMMENT	Γ_3/Γ
2.0 ± 0.6 ± 0.1					
	18	¹ ASNER	08A CLEO	$T(2S) \rightarrow \gamma \pi^+ \pi^- K^+ K^- \pi^0$	

- ASNER 08A reports $[\Gamma(\chi_{b1}(1P) \rightarrow \pi^+ \pi^- K^+ K^- \pi^0)/\Gamma_{total}] \times [B(T(2S) \rightarrow \gamma \chi_{b1}(1P))] = (14 \pm 3 \pm 3) \times 10^{-6}$ which we divide by our best value $B(T(2S) \rightarrow \gamma \chi_{b1}(1P)) = (6.9 \pm 0.4) \times 10^{-2}$. Our first error is their experiment's error and our second error is the systematic error from using our best value.

See key on page 999

Meson Particle Listings

$\chi_{b1}(1P)$

$\Gamma(2\pi^+\pi^-K^-K_S^0)/\Gamma_{total}$ Γ_4/Γ

VALUE (units 10^{-4})	EVTS	DOCUMENT ID	TECN	COMMENT
1.3 ± 0.5 ± 0.1	11	¹ ASNER	08A CLEO	$\Upsilon(2S) \rightarrow \gamma 2\pi^+\pi^-K^-K_S^0$
¹ ASNER 08A reports $[\Gamma(\chi_{b1}(1P) \rightarrow 2\pi^+\pi^-K^-K_S^0)/\Gamma_{total}] \times [B(\Upsilon(2S) \rightarrow \gamma\chi_{b1}(1P))]$ = $(9 \pm 3 \pm 2) \times 10^{-6}$ which we divide by our best value $B(\Upsilon(2S) \rightarrow \gamma\chi_{b1}(1P)) = (6.9 \pm 0.4) \times 10^{-2}$. Our first error is their experiment's error and our second error is the systematic error from using our best value.				

$\Gamma(2\pi^+\pi^-K^-K_S^0 2\pi^0)/\Gamma_{total}$ Γ_5/Γ

VALUE (units 10^{-4})	CL%	DOCUMENT ID	TECN	COMMENT
<6	90	¹ ASNER	08A CLEO	$\Upsilon(2S) \rightarrow \gamma 2\pi^+\pi^-K^-2\pi^0$
¹ ASNER 08A reports $[\Gamma(\chi_{b1}(1P) \rightarrow 2\pi^+\pi^-K^-K_S^0 2\pi^0)/\Gamma_{total}] \times [B(\Upsilon(2S) \rightarrow \gamma\chi_{b1}(1P))]$ = 42×10^{-6} which we divide by our best value $B(\Upsilon(2S) \rightarrow \gamma\chi_{b1}(1P)) = 6.9 \times 10^{-2}$.				

$\Gamma(2\pi^+2\pi^-2\pi^0)/\Gamma_{total}$ Γ_6/Γ

VALUE (units 10^{-4})	EVTS	DOCUMENT ID	TECN	COMMENT
8.0 ± 2.4 ± 0.4	46	¹ ASNER	08A CLEO	$\Upsilon(2S) \rightarrow \gamma 2\pi^+2\pi^-2\pi^0$
¹ ASNER 08A reports $[\Gamma(\chi_{b1}(1P) \rightarrow 2\pi^+2\pi^-2\pi^0)/\Gamma_{total}] \times [B(\Upsilon(2S) \rightarrow \gamma\chi_{b1}(1P))]$ = $(55 \pm 9 \pm 14) \times 10^{-6}$ which we divide by our best value $B(\Upsilon(2S) \rightarrow \gamma\chi_{b1}(1P)) = (6.9 \pm 0.4) \times 10^{-2}$. Our first error is their experiment's error and our second error is the systematic error from using our best value.				

$\Gamma(2\pi^+2\pi^-K^+K^-)/\Gamma_{total}$ Γ_7/Γ

VALUE (units 10^{-4})	EVTS	DOCUMENT ID	TECN	COMMENT
1.5 ± 0.5 ± 0.1	18	¹ ASNER	08A CLEO	$\Upsilon(2S) \rightarrow \gamma 2\pi^+2\pi^-K^+K^-$
¹ ASNER 08A reports $[\Gamma(\chi_{b1}(1P) \rightarrow 2\pi^+2\pi^-K^+K^-)/\Gamma_{total}] \times [B(\Upsilon(2S) \rightarrow \gamma\chi_{b1}(1P))]$ = $(10 \pm 3 \pm 2) \times 10^{-6}$ which we divide by our best value $B(\Upsilon(2S) \rightarrow \gamma\chi_{b1}(1P)) = (6.9 \pm 0.4) \times 10^{-2}$. Our first error is their experiment's error and our second error is the systematic error from using our best value.				

$\Gamma(2\pi^+2\pi^-K^+K^-\pi^0)/\Gamma_{total}$ Γ_8/Γ

VALUE (units 10^{-4})	EVTS	DOCUMENT ID	TECN	COMMENT
3.5 ± 1.2 ± 0.2	22	¹ ASNER	08A CLEO	$\Upsilon(2S) \rightarrow \gamma 2\pi^+2\pi^-K^+K^-\pi^0$
¹ ASNER 08A reports $[\Gamma(\chi_{b1}(1P) \rightarrow 2\pi^+2\pi^-K^+K^-\pi^0)/\Gamma_{total}] \times [B(\Upsilon(2S) \rightarrow \gamma\chi_{b1}(1P))]$ = $(24 \pm 6 \pm 6) \times 10^{-6}$ which we divide by our best value $B(\Upsilon(2S) \rightarrow \gamma\chi_{b1}(1P)) = (6.9 \pm 0.4) \times 10^{-2}$. Our first error is their experiment's error and our second error is the systematic error from using our best value.				

$\Gamma(2\pi^+2\pi^-K^+K^-2\pi^0)/\Gamma_{total}$ Γ_9/Γ

VALUE (units 10^{-4})	EVTS	DOCUMENT ID	TECN	COMMENT
8.6 ± 3.2 ± 0.4	26	¹ ASNER	08A CLEO	$\Upsilon(2S) \rightarrow \gamma 2\pi^+2\pi^-K^+K^-2\pi^0$
¹ ASNER 08A reports $[\Gamma(\chi_{b1}(1P) \rightarrow 2\pi^+2\pi^-K^+K^-2\pi^0)/\Gamma_{total}] \times [B(\Upsilon(2S) \rightarrow \gamma\chi_{b1}(1P))]$ = $(59 \pm 14 \pm 17) \times 10^{-6}$ which we divide by our best value $B(\Upsilon(2S) \rightarrow \gamma\chi_{b1}(1P)) = (6.9 \pm 0.4) \times 10^{-2}$. Our first error is their experiment's error and our second error is the systematic error from using our best value.				

$\Gamma(3\pi^+2\pi^-K^-K_S^0\pi^0)/\Gamma_{total}$ Γ_{10}/Γ

VALUE (units 10^{-4})	EVTS	DOCUMENT ID	TECN	COMMENT
9.3 ± 3.3 ± 0.5	21	¹ ASNER	08A CLEO	$\Upsilon(2S) \rightarrow \gamma 3\pi^+2\pi^-K^-K_S^0\pi^0$
¹ ASNER 08A reports $[\Gamma(\chi_{b1}(1P) \rightarrow 3\pi^+2\pi^-K^-K_S^0\pi^0)/\Gamma_{total}] \times [B(\Upsilon(2S) \rightarrow \gamma\chi_{b1}(1P))]$ = $(64 \pm 16 \pm 16) \times 10^{-6}$ which we divide by our best value $B(\Upsilon(2S) \rightarrow \gamma\chi_{b1}(1P)) = (6.9 \pm 0.4) \times 10^{-2}$. Our first error is their experiment's error and our second error is the systematic error from using our best value.				

$\Gamma(3\pi^+3\pi^-)/\Gamma_{total}$ Γ_{11}/Γ

VALUE (units 10^{-4})	EVTS	DOCUMENT ID	TECN	COMMENT
1.9 ± 0.6 ± 0.1	25	¹ ASNER	08A CLEO	$\Upsilon(2S) \rightarrow \gamma 3\pi^+3\pi^-$
¹ ASNER 08A reports $[\Gamma(\chi_{b1}(1P) \rightarrow 3\pi^+3\pi^-)/\Gamma_{total}] \times [B(\Upsilon(2S) \rightarrow \gamma\chi_{b1}(1P))]$ = $(13 \pm 3 \pm 3) \times 10^{-6}$ which we divide by our best value $B(\Upsilon(2S) \rightarrow \gamma\chi_{b1}(1P)) = (6.9 \pm 0.4) \times 10^{-2}$. Our first error is their experiment's error and our second error is the systematic error from using our best value.				

$\Gamma(3\pi^+3\pi^-2\pi^0)/\Gamma_{total}$ Γ_{12}/Γ

VALUE (units 10^{-4})	EVTS	DOCUMENT ID	TECN	COMMENT
17 ± 5 ± 1	56	¹ ASNER	08A CLEO	$\Upsilon(2S) \rightarrow \gamma 3\pi^+3\pi^-2\pi^0$
¹ ASNER 08A reports $[\Gamma(\chi_{b1}(1P) \rightarrow 3\pi^+3\pi^-2\pi^0)/\Gamma_{total}] \times [B(\Upsilon(2S) \rightarrow \gamma\chi_{b1}(1P))]$ = $(119 \pm 18 \pm 32) \times 10^{-6}$ which we divide by our best value $B(\Upsilon(2S) \rightarrow \gamma\chi_{b1}(1P)) = (6.9 \pm 0.4) \times 10^{-2}$. Our first error is their experiment's error and our second error is the systematic error from using our best value.				

$\Gamma(3\pi^+3\pi^-K^+K^-)/\Gamma_{total}$ Γ_{13}/Γ

VALUE (units 10^{-4})	EVTS	DOCUMENT ID	TECN	COMMENT
2.6 ± 0.8 ± 0.1	21	¹ ASNER	08A CLEO	$\Upsilon(2S) \rightarrow \gamma 3\pi^+3\pi^-K^+K^-$
¹ ASNER 08A reports $[\Gamma(\chi_{b1}(1P) \rightarrow 3\pi^+3\pi^-K^+K^-)/\Gamma_{total}] \times [B(\Upsilon(2S) \rightarrow \gamma\chi_{b1}(1P))]$ = $(18 \pm 4 \pm 4) \times 10^{-6}$ which we divide by our best value $B(\Upsilon(2S) \rightarrow \gamma\chi_{b1}(1P)) = (6.9 \pm 0.4) \times 10^{-2}$. Our first error is their experiment's error and our second error is the systematic error from using our best value.				

$\Gamma(3\pi^+3\pi^-K^+K^-\pi^0)/\Gamma_{total}$ Γ_{14}/Γ

VALUE (units 10^{-4})	EVTS	DOCUMENT ID	TECN	COMMENT
7.5 ± 2.6 ± 0.4	28	¹ ASNER	08A CLEO	$\Upsilon(2S) \rightarrow \gamma 3\pi^+3\pi^-K^+K^-\pi^0$
¹ ASNER 08A reports $[\Gamma(\chi_{b1}(1P) \rightarrow 3\pi^+3\pi^-K^+K^-\pi^0)/\Gamma_{total}] \times [B(\Upsilon(2S) \rightarrow \gamma\chi_{b1}(1P))]$ = $(52 \pm 11 \pm 14) \times 10^{-6}$ which we divide by our best value $B(\Upsilon(2S) \rightarrow \gamma\chi_{b1}(1P)) = (6.9 \pm 0.4) \times 10^{-2}$. Our first error is their experiment's error and our second error is the systematic error from using our best value.				

$\Gamma(4\pi^+4\pi^-)/\Gamma_{total}$ Γ_{15}/Γ

VALUE (units 10^{-4})	EVTS	DOCUMENT ID	TECN	COMMENT
2.6 ± 0.9 ± 0.1	24	¹ ASNER	08A CLEO	$\Upsilon(2S) \rightarrow \gamma 4\pi^+4\pi^-$
¹ ASNER 08A reports $[\Gamma(\chi_{b1}(1P) \rightarrow 4\pi^+4\pi^-)/\Gamma_{total}] \times [B(\Upsilon(2S) \rightarrow \gamma\chi_{b1}(1P))]$ = $(18 \pm 4 \pm 5) \times 10^{-6}$ which we divide by our best value $B(\Upsilon(2S) \rightarrow \gamma\chi_{b1}(1P)) = (6.9 \pm 0.4) \times 10^{-2}$. Our first error is their experiment's error and our second error is the systematic error from using our best value.				

$\Gamma(4\pi^+4\pi^-2\pi^0)/\Gamma_{total}$ Γ_{16}/Γ

VALUE (units 10^{-4})	EVTS	DOCUMENT ID	TECN	COMMENT
14 ± 5 ± 1	26	¹ ASNER	08A CLEO	$\Upsilon(2S) \rightarrow \gamma 4\pi^+4\pi^-2\pi^0$
¹ ASNER 08A reports $[\Gamma(\chi_{b1}(1P) \rightarrow 4\pi^+4\pi^-2\pi^0)/\Gamma_{total}] \times [B(\Upsilon(2S) \rightarrow \gamma\chi_{b1}(1P))]$ = $(96 \pm 24 \pm 29) \times 10^{-6}$ which we divide by our best value $B(\Upsilon(2S) \rightarrow \gamma\chi_{b1}(1P)) = (6.9 \pm 0.4) \times 10^{-2}$. Our first error is their experiment's error and our second error is the systematic error from using our best value.				

$\Gamma(\omega \text{ anything})/\Gamma_{total}$ Γ_{17}/Γ

VALUE (units 10^{-2})	EVTS	DOCUMENT ID	TECN	COMMENT
4.9 ± 1.3 ± 0.6	51k	JIA	17A BELL	$e^+e^- \rightarrow \text{hadrons}$

$\Gamma(\omega X_{tetra})/\Gamma_{total}$ Γ_{18}/Γ

VALUE	CL%	DOCUMENT ID	TECN	COMMENT
<44.4 × 10⁻⁵	90	¹ JIA	17A BELL	$e^+e^- \rightarrow \text{hadrons}$
¹ For a tetraquark state X_{tetra} , with mass in the range 1.16–2.46 GeV and width in the range 0–0.3 GeV. Measured 90% CL limits as a function of X_{tetra} mass and width range from 3.3×10^{-5} to 44.4×10^{-5} .				

$\Gamma(J/\psi J/\psi)/\Gamma_{total}$ Γ_{19}/Γ

VALUE (units 10^{-5})	CL%	DOCUMENT ID	TECN	COMMENT
<2.7	90	¹ SHEN	12 BELL	$\Upsilon(2S) \rightarrow \gamma\psi X$
¹ SHEN 12 reports $< 2.7 \times 10^{-5}$ from a measurement of $[\Gamma(\chi_{b1}(1P) \rightarrow J/\psi J/\psi)/\Gamma_{total}] \times [B(\Upsilon(2S) \rightarrow \gamma\chi_{b1}(1P))]$ assuming $B(\Upsilon(2S) \rightarrow \gamma\chi_{b1}(1P)) = (6.9 \pm 0.4) \times 10^{-2}$.				

$\Gamma(J/\psi\psi(2S))/\Gamma_{total}$ Γ_{20}/Γ

VALUE (units 10^{-5})	CL%	DOCUMENT ID	TECN	COMMENT
<1.7	90	¹ SHEN	12 BELL	$\Upsilon(2S) \rightarrow \gamma\psi X$
¹ SHEN 12 reports $< 1.7 \times 10^{-5}$ from a measurement of $[\Gamma(\chi_{b1}(1P) \rightarrow J/\psi\psi(2S))/\Gamma_{total}] \times [B(\Upsilon(2S) \rightarrow \gamma\chi_{b1}(1P))]$ assuming $B(\Upsilon(2S) \rightarrow \gamma\chi_{b1}(1P)) = (6.9 \pm 0.4) \times 10^{-2}$.				

$\Gamma(\psi(2S)\psi(2S))/\Gamma_{total}$ Γ_{21}/Γ

VALUE (units 10^{-5})	CL%	DOCUMENT ID	TECN	COMMENT
<6	90	¹ SHEN	12 BELL	$\Upsilon(2S) \rightarrow \gamma\psi X$
¹ SHEN 12 reports $< 6.2 \times 10^{-5}$ from a measurement of $[\Gamma(\chi_{b1}(1P) \rightarrow \psi(2S)\psi(2S))/\Gamma_{total}] \times [B(\Upsilon(2S) \rightarrow \gamma\chi_{b1}(1P))]$ assuming $B(\Upsilon(2S) \rightarrow \gamma\chi_{b1}(1P)) = (6.9 \pm 0.4) \times 10^{-2}$.				

$\Gamma(J/\psi(1S) \text{ anything})/\Gamma_{total}$ Γ_{22}/Γ

VALUE	CL%	DOCUMENT ID	TECN	COMMENT
<1.1 × 10⁻³	90	JIA	17A BELL	$e^+e^- \rightarrow \text{hadrons}$

$\Gamma(J/\psi(1S) X_{tetra})/\Gamma_{total}$ Γ_{23}/Γ

VALUE	CL%	DOCUMENT ID	TECN	COMMENT
<22.7 × 10⁻⁵	90	¹ JIA	17A BELL	$e^+e^- \rightarrow \text{hadrons}$
¹ For a tetraquark state X_{tetra} , with mass in the range 1.16–2.46 GeV and width in the range 0–0.3 GeV. Measured 90% CL limits as a function of X_{tetra} mass and width range from 1.8×10^{-5} to 22.7×10^{-5} .				

$\chi_{b1}(1P)$ Cross-Particle Branching Ratios

$\Gamma(\chi_{b1}(1P) \rightarrow \gamma \Upsilon(1S))/\Gamma_{total} \times \Gamma(\Upsilon(2S) \rightarrow \gamma\chi_{b1}(1P))/\Gamma_{total}$ $\Gamma_{1/\Gamma} \times \Gamma_{59}^{\Upsilon(2S)}/\Gamma_{\Upsilon(2S)}$

VALUE (units 10^{-3})	EVTS	DOCUMENT ID	TECN	COMMENT
24.1 ± 0.6 ± 1.5	13k	LEES	11 BABR	$\Upsilon(2S) \rightarrow X\gamma$

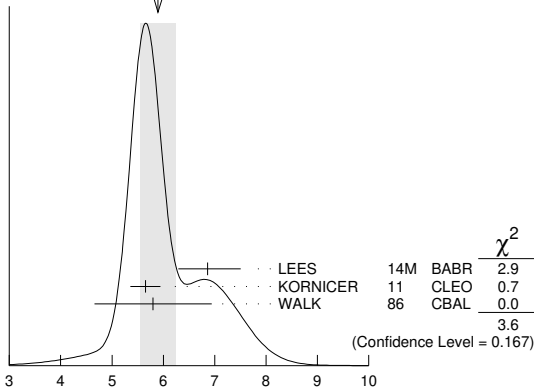
$B(\chi_{b1}(1P) \rightarrow \gamma \Upsilon(1S)) \times B(\Upsilon(2S) \rightarrow \gamma\chi_{b1}(1P)) \times B(\Upsilon(1S) \rightarrow \ell^+\ell^-)$

VALUE (units 10^{-4})	EVTS	DOCUMENT ID	TECN	COMMENT
5.90 ± 0.34 OUR AVERAGE		Error includes scale factor of 1.3. See the ideogram below.		
$6.86^{+0.47+0.44}_{-0.45-0.35}$		¹ LEES	14M BABR	$\Upsilon(2S) \rightarrow \gamma\gamma\mu^+\mu^-$
$5.65 \pm 0.11 \pm 0.27$	3222	KORNICER	11 CLEO	$e^+e^- \rightarrow \gamma\gamma\ell^+\ell^-$
$5.8 \pm 0.9 \pm 0.7$	53	WALK	86 CBAL	$\Upsilon(2S) \rightarrow \gamma\gamma\ell^+\ell^-$
¹ From a sample of $\Upsilon(2S) \rightarrow \gamma\gamma\mu^+\mu^-$ with one converted photon.				

Meson Particle Listings

$\chi_{b1}(1P), h_b(1P), \chi_{b2}(1P)$

WEIGHTED AVERAGE
5.90±0.34 (Error scaled by 1.3)



$$B(\chi_{b1}(1P) \rightarrow \gamma \Upsilon(1S)) \times B(\Upsilon(2S) \rightarrow \gamma \chi_{b1}(1P)) \times B(\Upsilon(1S) \rightarrow \ell^+ \ell^-)$$

(units 10^{-4})

$$B(\chi_{b1}(1P) \rightarrow \gamma \Upsilon(1S)) \times B(\Upsilon(3S) \rightarrow \gamma \chi_{b1}(1P)) \times B(\Upsilon(1S) \rightarrow \ell^+ \ell^-)$$

VALUE (units 10^{-5})	EVTS	DOCUMENT ID	TECN	COMMENT
1.30±0.34 OUR AVERAGE				

1.16 ^{+0.78+0.14} _{-0.67-0.16}		¹ LEES	14M BABR	$\Upsilon(3S) \rightarrow \gamma \gamma \mu^+ \mu^-$
--	--	-------------------	----------	--

1.33±0.30±0.23	50	KORNICER	11 CLEO	$e^+ e^- \rightarrow \gamma \gamma \ell^+ \ell^-$
----------------	----	----------	---------	---

¹ From a sample of $\Upsilon(3S) \rightarrow \gamma \gamma \mu^+ \mu^-$ with converted photons.

$$B(\chi_{b1}(1P) \rightarrow \rho X + \bar{\rho} X) / B(\chi_{b1}(1P) \rightarrow \rho X + \bar{\rho} X)$$

VALUE	DOCUMENT ID	TECN	COMMENT
1.068±0.010±0.040	BRIERE 07	CLEO	$\Upsilon(2S) \rightarrow \gamma \chi_{bJ}(1P)$

$$B(\chi_{b0}(1P) \rightarrow \rho X + \bar{\rho} X) / B(\chi_{b1}(1P) \rightarrow \rho X + \bar{\rho} X)$$

VALUE	DOCUMENT ID	TECN	COMMENT
1.11±0.15±0.20	BRIERE 07	CLEO	$\Upsilon(2S) \rightarrow \gamma \chi_{bJ}(1P)$

$\chi_{b1}(1P)$ REFERENCES

FULSOM 18	PRL 121 232001	B. G. Fulsom et al.	(BELLE Collab.)
JIA 17A	PR D96 112002	S. Jia et al.	(BELLE Collab.)
LEES 14M	PR D90 112010	J.P. Lees et al.	(BABAR Collab.)
SHEN 12	PR D85 071102	C.P. Shen et al.	(BELLE Collab.)
KORNICER 11	PR D83 054003	M. Kornicer et al.	(CLEO Collab.)
LEES 11J	PR D84 072002	J.P. Lees et al.	(BABAR Collab.)
ASNER 08A	PR D78 091103	D.M. Asner et al.	(CLEO Collab.)
BRIERE 08B	PR D78 092007	R.A. Briere et al.	(CLEO Collab.)
BRIERE 07	PR D76 012005	R.A. Briere et al.	(CLEO Collab.)
ARTUSO 05	PRL 94 032001	M. Artuso et al.	(CLEO Collab.)
EDWARDS 99	PR D59 032003	K.W. Edwards et al.	(CLEO Collab.)
SKWARNICKI 87	PRL 58 972	T. Skwarnicki et al.	(Crystal Ball Collab.) ^J
WALK 86	PR D34 2611	W.S. Walk et al.	(Crystal Ball Collab.)
ALBRECHT 85E	PL 160B 331	H. Albrecht et al.	(ARGUS Collab.)
NERNST 85	PL 54 2195	R. Nernst et al.	(Crystal Ball Collab.)
HAAS 84	PRL 52 739	J. Haas et al.	(CLEO Collab.)
KLOPFEN... 83	PRL 51 160	C. Klopfenstein et al.	(CUSP Collab.)
PAUSS 83	PL 130B 439	F. Pauss et al.	(MPIM, COLU, CORN, LSU+)

$h_b(1P)$

$$J^G(J^{PC}) = 0^-(1^{+-})$$

Quantum numbers are quark model predictions, $C = -$ established by $\eta_b \gamma$ decay.

$h_b(1P)$ MASS

VALUE (MeV)	EVTS	DOCUMENT ID	TECN	COMMENT
9899.3±0.8 OUR AVERAGE				

9899.3±0.4±1.0	112k	TAMPONI 15	BELL	$e^+ e^- \rightarrow \gamma \eta + \text{hadrons}$
----------------	------	------------	------	--

9899.1±0.4±1.0	70k	MIZUK 12	BELL	$e^+ e^- \rightarrow \pi^+ \pi^- \text{hadrons}$
----------------	-----	----------	------	--

9902 ± 4 ± 2	10.8k	LEES 11K	BABR	$\Upsilon(3S) \rightarrow \eta_b \gamma \pi^0$
--------------	-------	----------	------	--

• • • We do not use the following data for averages, fits, limits, etc. • • •

9898.2 ^{+1.1+1.0} _{-1.0-1.1}	50.0k	¹ ADACHI 12	BELL	10.86 $e^+ e^- \rightarrow \pi^+ \pi^- \text{MM}$
--	-------	------------------------	------	---

¹ Superseded by MIZUK 12.

$h_b(1P)$ DECAY MODES

Mode	Fraction (Γ_i/Γ)
$\Gamma_1 \eta_b(1S) \gamma$	(52 ⁺⁶ ₋₅) %

$h_b(1P)$ BRANCHING RATIOS

$\Gamma(\eta_b(1S)\gamma)/\Gamma_{\text{total}}$	VALUE (units 10^{-2})	EVTS	DOCUMENT ID	TECN	COMMENT	Γ_i/Γ
--	--------------------------	------	-------------	------	---------	-------------------

52⁺⁶₋₅ OUR AVERAGE

56 ± 8 ± 4	33.1k	¹ TAMPONI 15	BELL	$e^+ e^- \rightarrow \gamma \eta + \text{hadrons}$
------------	-------	-------------------------	------	--

49.2±5.7 ^{+5.6} _{-3.3}	24k	MIZUK 12	BELL	$e^+ e^- \rightarrow (\gamma) \pi^+ \pi^- \text{hadrons}$
--	-----	----------	------	---

• • • We do not use the following data for averages, fits, limits, etc. • • •

seen 10.8k	LEES 11K	BABR	$\Upsilon(3S) \rightarrow \eta_b \gamma \pi^0$
------------	----------	------	--

¹ Using $B(\eta \rightarrow 2\gamma) = (39.41 \pm 0.20)\%$.

$h_b(1P)$ REFERENCES

TAMPONI 15	PRL 115 142001	U. Tamponi et al.	(BELLE Collab.)
ADACHI 12	PRL 108 032001	I. Adachi et al.	(BELLE Collab.)
MIZUK 12	PRL 109 232002	R. Mizuk et al.	(BELLE Collab.)
LEES 11K	PR D84 091101	J.P. Lees et al.	(BABAR Collab.)

$\chi_{b2}(1P)$

$$J^G(J^{PC}) = 0^+(2^{++})$$

J needs confirmation.

Observed in radiative decay of the $\Upsilon(2S)$, therefore $C = +$. Branching ratio requires E1 transition, M1 is strongly disfavored, therefore $P = +$. $J = 2$ from SKWARNICKI 87.

$\chi_{b2}(1P)$ MASS

VALUE (MeV)	DOCUMENT ID
9912.21±0.26±0.31 OUR EVALUATION	From average γ energy below, using $\Upsilon(2S)$ mass = 10023.26 ± 0.31 MeV

$m_{\chi_{b2}(1P)} - m_{\chi_{b1}(1P)}$

VALUE (MeV)	DOCUMENT ID	TECN	COMMENT
19.10±0.25 OUR AVERAGE	Error includes scale factor of 1.1.		
19.81±0.65±0.20	¹ AAIJ 14B6	LHCB	$pp \rightarrow \gamma \mu^+ \mu^- X$
19.01±0.24	LEES	14M BABR	$\Upsilon(2S) \rightarrow \gamma \gamma \mu^+ \mu^-$

¹ From the $\chi_{bJ}(1P) \rightarrow \Upsilon(1S) \gamma$ transition.

γ ENERGY IN $\Upsilon(2S)$ DECAY

VALUE (MeV)	DOCUMENT ID	TECN	COMMENT
110.44±0.29 OUR AVERAGE	Error includes scale factor of 1.1.		
110.58±0.08±0.30	ARTUSO 05	CLEO	$\Upsilon(2S) \rightarrow \gamma X$
110.8 ± 0.3 ± 0.6	EDWARDS 99	CLE2	$\Upsilon(2S) \rightarrow \gamma \chi(1P)$
107.0 ± 1.1 ± 1.3	WALK 86	CBAL	$\Upsilon(2S) \rightarrow \gamma \gamma \ell^+ \ell^-$
110.6 ± 0.3 ± 0.9	ALBRECHT 85E	ARG	$\Upsilon(2S) \rightarrow \text{conv. } \gamma X$
110.4 ± 0.8 ± 2.2	NERNST 85	CBAL	$\Upsilon(2S) \rightarrow \gamma X$
109.5 ± 0.7 ± 1.0	HAAS 84	CLEO	$\Upsilon(2S) \rightarrow \text{conv. } \gamma X$
108.2 ± 0.3 ± 2.0	KLOPFEN... 83	CUSB	$\Upsilon(2S) \rightarrow \gamma X$
108.8 ± 4.0	PAUSS 83	CUSB	$\Upsilon(2S) \rightarrow \gamma \gamma \ell^+ \ell^-$

$\chi_{b2}(1P)$ DECAY MODES

Mode	Fraction (Γ_i/Γ)	Confidence level
$\Gamma_1 \gamma \Upsilon(1S)$	(18.0±1.0) %	
$\Gamma_2 D^0 X$	< 7.9 %	90%
$\Gamma_3 \pi^+ \pi^- K^+ K^- \pi^0$	(8 ± 5) × 10 ⁻⁵	
$\Gamma_4 2\pi^+ \pi^- K^- K_S^0$	< 1.0 × 10 ⁻⁴	90%
$\Gamma_5 2\pi^+ \pi^- K^- K_S^0 2\pi^0$	(5.3±2.4) × 10 ⁻⁴	
$\Gamma_6 2\pi^+ 2\pi^- 2\pi^0$	(3.5±1.4) × 10 ⁻⁴	
$\Gamma_7 2\pi^+ 2\pi^- K^+ K^-$	(1.1±0.4) × 10 ⁻⁴	
$\Gamma_8 2\pi^+ 2\pi^- K^+ K^- \pi^0$	(2.1±0.9) × 10 ⁻⁴	
$\Gamma_9 2\pi^+ 2\pi^- K^+ K^- 2\pi^0$	(3.9±1.8) × 10 ⁻⁴	
$\Gamma_{10} 3\pi^+ 2\pi^- K^- K_S^0 \pi^0$	< 5 × 10 ⁻⁴	90%
$\Gamma_{11} 3\pi^+ 3\pi^-$	(7.0±3.1) × 10 ⁻⁵	
$\Gamma_{12} 3\pi^+ 3\pi^- 2\pi^0$	(1.0±0.4) × 10 ⁻³	
$\Gamma_{13} 3\pi^+ 3\pi^- K^+ K^-$	< 8 × 10 ⁻⁵	90%
$\Gamma_{14} 3\pi^+ 3\pi^- K^+ K^- \pi^0$	(3.6±1.5) × 10 ⁻⁴	
$\Gamma_{15} 4\pi^+ 4\pi^-$	(8 ± 4) × 10 ⁻⁵	
$\Gamma_{16} 4\pi^+ 4\pi^- 2\pi^0$	(1.8±0.7) × 10 ⁻³	
$\Gamma_{17} J/\psi J/\psi$	< 4 × 10 ⁻⁵	90%
$\Gamma_{18} J/\psi \psi(2S)$	< 5 × 10 ⁻⁵	90%
$\Gamma_{19} \psi(2S) \psi(2S)$	< 1.6 × 10 ⁻⁵	90%
$\Gamma_{20} J/\psi(1S) \text{anything}$	(1.5±0.4) × 10 ⁻³	

See key on page 999

Meson Particle Listings

 $\chi_{b2}(1P)$ $\chi_{b2}(1P)$ BRANCHING RATIOS

$\Gamma(\gamma \mathcal{T}(1S))/\Gamma_{\text{total}}$					Γ_1/Γ
VALUE	EVTS	DOCUMENT ID	TECN	COMMENT	

0.180 ± 0.010 OUR AVERAGE

0.164 ^{+0.009} _{-0.016} ± 0.008	503k	¹ FULSOM	18 BELL	$\mathcal{T}(2S) \rightarrow \gamma X$	
0.185 ± 0.008 ± 0.009	2,3,4	LEES	14M BABR	$\mathcal{T}(2S) \rightarrow \gamma \gamma \mu^+ \mu^-$	
0.186 ± 0.011 ± 0.009	1770	^{4,5} KORNICER	11 CLEO	$e^+ e^- \rightarrow \gamma \gamma \ell^+ \ell^-$	
0.194 ^{+0.014} _{-0.017} ± 0.009	8k	⁶ LEES	11J BABR	$\mathcal{T}(2S) \rightarrow X \gamma$	
0.25 ± 0.06 ± 0.01	35	^{4,7,8} WALK	86 CBAL	$\mathcal{T}(2S) \rightarrow \gamma \gamma \ell^+ \ell^-$	
0.20 ± 0.05		KLOPFEN...	83 CUSB	$\mathcal{T}(2S) \rightarrow \gamma \gamma \ell^+ \ell^-$	

¹ FULSOM 18 reports $[\Gamma(\chi_{b2}(1P) \rightarrow \gamma \mathcal{T}(1S))/\Gamma_{\text{total}}] \times [B(\mathcal{T}(2S) \rightarrow \gamma \chi_{b2}(1P))] = (1.17 \pm 0.01 \pm 0.09) \times 10^{-2}$ which we divide by our best value $B(\mathcal{T}(2S) \rightarrow \gamma \chi_{b2}(1P)) = (7.15 \pm 0.35) \times 10^{-2}$. Our first error is their experiment's error and our second error is the systematic error from using our best value.

² LEES 14M quotes $\Gamma(\chi_{b2}(1P) \rightarrow \gamma \mathcal{T}(1S))/\Gamma_{\text{total}} \times \Gamma(\mathcal{T}(2S) \rightarrow \gamma \chi_{b2}(1P))/\Gamma_{\text{total}} = (1.32 \pm 0.06)\%$ combining the results from samples of $\mathcal{T}(2S) \rightarrow \gamma \gamma \mu^+ \mu^-$ with and without converted photons.

³ LEES 14M reports $[\Gamma(\chi_{b2}(1P) \rightarrow \gamma \mathcal{T}(1S))/\Gamma_{\text{total}}] \times [B(\mathcal{T}(2S) \rightarrow \gamma \chi_{b2}(1P))] = (1.32 \pm 0.06) \times 10^{-2}$ which we divide by our best value $B(\mathcal{T}(2S) \rightarrow \gamma \chi_{b2}(1P)) = (7.15 \pm 0.35) \times 10^{-2}$. Our first error is their experiment's error and our second error is the systematic error from using our best value.

⁴ Assuming $B(\mathcal{T}(1S) \rightarrow \mu^+ \mu^-) = (2.48 \pm 0.05)\%$.

⁵ KORNICER 11 reports $[\Gamma(\chi_{b2}(1P) \rightarrow \gamma \mathcal{T}(1S))/\Gamma_{\text{total}}] \times [B(\mathcal{T}(2S) \rightarrow \gamma \chi_{b2}(1P))] = (1.33 \pm 0.04 \pm 0.07) \times 10^{-2}$ which we divide by our best value $B(\mathcal{T}(2S) \rightarrow \gamma \chi_{b2}(1P)) = (7.15 \pm 0.35) \times 10^{-2}$. Our first error is their experiment's error and our second error is the systematic error from using our best value.

⁶ LEES 11J reports $[\Gamma(\chi_{b2}(1P) \rightarrow \gamma \mathcal{T}(1S))/\Gamma_{\text{total}}] \times [B(\mathcal{T}(2S) \rightarrow \gamma \chi_{b2}(1P))] = (13.9 \pm 0.5 \pm 0.9) \times 10^{-3}$ which we divide by our best value $B(\mathcal{T}(2S) \rightarrow \gamma \chi_{b2}(1P)) = (7.15 \pm 0.35) \times 10^{-2}$. Our first error is their experiment's error and our second error is the systematic error from using our best value.

⁷ WALK 86 quotes $B(\mathcal{T}(2S) \rightarrow \gamma \chi_{b2}(1P)) \times B(\chi_{b2}(1P) \rightarrow \gamma \mathcal{T}(1S)) \times B(\mathcal{T}(1S) \rightarrow \ell^+ \ell^-) = (4.4 \pm 0.9 \pm 0.5)\%$.

⁸ WALK 86 reports $[\Gamma(\chi_{b2}(1P) \rightarrow \gamma \mathcal{T}(1S))/\Gamma_{\text{total}}] \times [B(\mathcal{T}(2S) \rightarrow \gamma \chi_{b2}(1P))] = (17.7 \pm 3.6 \pm 2.0) \times 10^{-3}$ which we divide by our best value $B(\mathcal{T}(2S) \rightarrow \gamma \chi_{b2}(1P)) = (7.15 \pm 0.35) \times 10^{-2}$. Our first error is their experiment's error and our second error is the systematic error from using our best value.

$\Gamma(D^0 X)/\Gamma_{\text{total}}$					Γ_2/Γ
VALUE	CL%	DOCUMENT ID	TECN	COMMENT	

<7.9 × 10⁻²

¹ For $p_{D^0} > 2.5$ GeV/c.

² The authors also present their result as $(5.4 \pm 1.9 \pm 0.5) \times 10^{-2}$.

$\Gamma(\pi^+ \pi^- K^+ K^- \pi^0)/\Gamma_{\text{total}}$					Γ_3/Γ
VALUE (units 10 ⁻⁴)	EVTS	DOCUMENT ID	TECN	COMMENT	

0.84 ± 0.50 ± 0.04

¹ ASNER 08A reports $[\Gamma(\chi_{b2}(1P) \rightarrow \pi^+ \pi^- K^+ K^- \pi^0)/\Gamma_{\text{total}}] \times [B(\mathcal{T}(2S) \rightarrow \gamma \chi_{b2}(1P))] = (6 \pm 3 \pm 2) \times 10^{-6}$ which we divide by our best value $B(\mathcal{T}(2S) \rightarrow \gamma \chi_{b2}(1P)) = (7.15 \pm 0.35) \times 10^{-2}$. Our first error is their experiment's error and our second error is the systematic error from using our best value.

$\Gamma(2\pi^+ \pi^- K^- K_S^0)/\Gamma_{\text{total}}$					Γ_4/Γ
VALUE (units 10 ⁻⁴)	CL%	DOCUMENT ID	TECN	COMMENT	

<1.0

¹ ASNER 08A reports $[\Gamma(\chi_{b2}(1P) \rightarrow 2\pi^+ \pi^- K^- K_S^0)/\Gamma_{\text{total}}] \times [B(\mathcal{T}(2S) \rightarrow \gamma \chi_{b2}(1P))] < 7 \times 10^{-6}$ which we divide by our best value $B(\mathcal{T}(2S) \rightarrow \gamma \chi_{b2}(1P)) = 7.15 \times 10^{-2}$.

$\Gamma(2\pi^+ \pi^- K^- K_S^0 2\pi^0)/\Gamma_{\text{total}}$					Γ_5/Γ
VALUE (units 10 ⁻⁴)	EVTS	DOCUMENT ID	TECN	COMMENT	

5.3 ± 2.4 ± 0.3

¹ ASNER 08A reports $[\Gamma(\chi_{b2}(1P) \rightarrow 2\pi^+ \pi^- K^- K_S^0 2\pi^0)/\Gamma_{\text{total}}] \times [B(\mathcal{T}(2S) \rightarrow \gamma \chi_{b2}(1P))] = (38 \pm 14 \pm 10) \times 10^{-6}$ which we divide by our best value $B(\mathcal{T}(2S) \rightarrow \gamma \chi_{b2}(1P)) = (7.15 \pm 0.35) \times 10^{-2}$. Our first error is their experiment's error and our second error is the systematic error from using our best value.

$\Gamma(2\pi^+ 2\pi^- 2\pi^0)/\Gamma_{\text{total}}$					Γ_6/Γ
VALUE (units 10 ⁻⁴)	EVTS	DOCUMENT ID	TECN	COMMENT	

3.5 ± 1.4 ± 0.2

¹ ASNER 08A reports $[\Gamma(\chi_{b2}(1P) \rightarrow 2\pi^+ 2\pi^- 2\pi^0)/\Gamma_{\text{total}}] \times [B(\mathcal{T}(2S) \rightarrow \gamma \chi_{b2}(1P))] = (25 \pm 8 \pm 6) \times 10^{-6}$ which we divide by our best value $B(\mathcal{T}(2S) \rightarrow \gamma \chi_{b2}(1P)) = (7.15 \pm 0.35) \times 10^{-2}$. Our first error is their experiment's error and our second error is the systematic error from using our best value.

$\Gamma(2\pi^+ 2\pi^- K^+ K^-)/\Gamma_{\text{total}}$					Γ_7/Γ
VALUE (units 10 ⁻⁴)	EVTS	DOCUMENT ID	TECN	COMMENT	

1.1 ± 0.4 ± 0.1

¹ ASNER 08A reports $[\Gamma(\chi_{b2}(1P) \rightarrow 2\pi^+ 2\pi^- K^+ K^-)/\Gamma_{\text{total}}] \times [B(\mathcal{T}(2S) \rightarrow \gamma \chi_{b2}(1P))] = (8 \pm 2 \pm 2) \times 10^{-6}$ which we divide by our best value $B(\mathcal{T}(2S) \rightarrow \gamma \chi_{b2}(1P)) = (7.15 \pm 0.35) \times 10^{-2}$. Our first error is their experiment's error and our second error is the systematic error from using our best value.

$\Gamma(2\pi^+ 2\pi^- K^+ K^- \pi^0)/\Gamma_{\text{total}}$					Γ_8/Γ
VALUE (units 10 ⁻⁴)	EVTS	DOCUMENT ID	TECN	COMMENT	

2.1 ± 0.9 ± 0.1

¹ ASNER 08A reports $[\Gamma(\chi_{b2}(1P) \rightarrow 2\pi^+ 2\pi^- K^+ K^- \pi^0)/\Gamma_{\text{total}}] \times [B(\mathcal{T}(2S) \rightarrow \gamma \chi_{b2}(1P))] = (15 \pm 5 \pm 4) \times 10^{-6}$ which we divide by our best value $B(\mathcal{T}(2S) \rightarrow \gamma \chi_{b2}(1P)) = (7.15 \pm 0.35) \times 10^{-2}$. Our first error is their experiment's error and our second error is the systematic error from using our best value.

$\Gamma(2\pi^+ 2\pi^- K^+ K^- 2\pi^0)/\Gamma_{\text{total}}$					Γ_9/Γ
VALUE (units 10 ⁻⁴)	EVTS	DOCUMENT ID	TECN	COMMENT	

3.9 ± 1.8 ± 0.2

¹ ASNER 08A reports $[\Gamma(\chi_{b2}(1P) \rightarrow 2\pi^+ 2\pi^- K^+ K^- 2\pi^0)/\Gamma_{\text{total}}] \times [B(\mathcal{T}(2S) \rightarrow \gamma \chi_{b2}(1P))] = (28 \pm 11 \pm 7) \times 10^{-6}$ which we divide by our best value $B(\mathcal{T}(2S) \rightarrow \gamma \chi_{b2}(1P)) = (7.15 \pm 0.35) \times 10^{-2}$. Our first error is their experiment's error and our second error is the systematic error from using our best value.

$\Gamma(3\pi^+ 2\pi^- K^- K_S^0 \pi^0)/\Gamma_{\text{total}}$					Γ_{10}/Γ
VALUE (units 10 ⁻⁴)	CL%	DOCUMENT ID	TECN	COMMENT	

<5

¹ ASNER 08A reports $[\Gamma(\chi_{b2}(1P) \rightarrow 3\pi^+ 2\pi^- K^- K_S^0 \pi^0)/\Gamma_{\text{total}}] \times [B(\mathcal{T}(2S) \rightarrow \gamma \chi_{b2}(1P))] < 36 \times 10^{-6}$ which we divide by our best value $B(\mathcal{T}(2S) \rightarrow \gamma \chi_{b2}(1P)) = 7.15 \times 10^{-2}$.

$\Gamma(3\pi^+ 3\pi^-)/\Gamma_{\text{total}}$					Γ_{11}/Γ
VALUE (units 10 ⁻⁴)	EVTS	DOCUMENT ID	TECN	COMMENT	

0.70 ± 0.31 ± 0.03

¹ ASNER 08A reports $[\Gamma(\chi_{b2}(1P) \rightarrow 3\pi^+ 3\pi^-)/\Gamma_{\text{total}}] \times [B(\mathcal{T}(2S) \rightarrow \gamma \chi_{b2}(1P))] = (5 \pm 2 \pm 1) \times 10^{-6}$ which we divide by our best value $B(\mathcal{T}(2S) \rightarrow \gamma \chi_{b2}(1P)) = (7.15 \pm 0.35) \times 10^{-2}$. Our first error is their experiment's error and our second error is the systematic error from using our best value.

$\Gamma(3\pi^+ 3\pi^- 2\pi^0)/\Gamma_{\text{total}}$					Γ_{12}/Γ
VALUE (units 10 ⁻⁴)	EVTS	DOCUMENT ID	TECN	COMMENT	

10.2 ± 3.6 ± 0.5

¹ ASNER 08A reports $[\Gamma(\chi_{b2}(1P) \rightarrow 3\pi^+ 3\pi^- 2\pi^0)/\Gamma_{\text{total}}] \times [B(\mathcal{T}(2S) \rightarrow \gamma \chi_{b2}(1P))] = (73 \pm 16 \pm 20) \times 10^{-6}$ which we divide by our best value $B(\mathcal{T}(2S) \rightarrow \gamma \chi_{b2}(1P)) = (7.15 \pm 0.35) \times 10^{-2}$. Our first error is their experiment's error and our second error is the systematic error from using our best value.

$\Gamma(3\pi^+ 3\pi^- K^+ K^-)/\Gamma_{\text{total}}$					Γ_{13}/Γ
VALUE (units 10 ⁻⁴)	CL%	DOCUMENT ID	TECN	COMMENT	

<0.8

¹ ASNER 08A reports $[\Gamma(\chi_{b2}(1P) \rightarrow 3\pi^+ 3\pi^- K^+ K^-)/\Gamma_{\text{total}}] \times [B(\mathcal{T}(2S) \rightarrow \gamma \chi_{b2}(1P))] < 6 \times 10^{-6}$ which we divide by our best value $B(\mathcal{T}(2S) \rightarrow \gamma \chi_{b2}(1P)) = 7.15 \times 10^{-2}$.

$\Gamma(3\pi^+ 3\pi^- K^+ K^- \pi^0)/\Gamma_{\text{total}}$					Γ_{14}/Γ
VALUE (units 10 ⁻⁴)	EVTS	DOCUMENT ID	TECN	COMMENT	

3.6 ± 1.5 ± 0.2

¹ ASNER 08A reports $[\Gamma(\chi_{b2}(1P) \rightarrow 3\pi^+ 3\pi^- K^+ K^- \pi^0)/\Gamma_{\text{total}}] \times [B(\mathcal{T}(2S) \rightarrow \gamma \chi_{b2}(1P))] = (26 \pm 8 \pm 7) \times 10^{-6}$ which we divide by our best value $B(\mathcal{T}(2S) \rightarrow \gamma \chi_{b2}(1P)) = (7.15 \pm 0.35) \times 10^{-2}$. Our first error is their experiment's error and our second error is the systematic error from using our best value.

$\Gamma(4\pi^+ 4\pi^-)/\Gamma_{\text{total}}$					Γ_{15}/Γ
VALUE (units 10 ⁻⁴)	EVTS	DOCUMENT ID	TECN	COMMENT	

0.84 ± 0.40 ± 0.04

¹ ASNER 08A reports $[\Gamma(\chi_{b2}(1P) \rightarrow 4\pi^+ 4\pi^-)/\Gamma_{\text{total}}] \times [B(\mathcal{T}(2S) \rightarrow \gamma \chi_{b2}(1P))] = (6 \pm 2 \pm 2) \times 10^{-6}$ which we divide by our best value $B(\mathcal{T}(2S) \rightarrow \gamma \chi_{b2}(1P)) = (7.15 \pm 0.35) \times 10^{-2}$. Our first error is their experiment's error and our second error is the systematic error from using our best value.

$\Gamma(4\pi^+ 4\pi^- 2\pi^0)/\Gamma_{\text{total}}$					Γ_{16}/Γ
VALUE (units 10 ⁻⁴)	EVTS	DOCUMENT ID	TECN	COMMENT	

18 ± 7 ± 1

¹ ASNER 08A reports $[\Gamma(\chi_{b2}(1P) \rightarrow 4\pi^+ 4\pi^- 2\pi^0)/\Gamma_{\text{total}}] \times [B(\mathcal{T}(2S) \rightarrow \gamma \chi_{b2}(1P))] = (132 \pm 31 \pm 40) \times 10^{-6}$ which we divide by our best value $B(\mathcal{T}(2S) \rightarrow \gamma \chi_{b2}(1P)) = (7.15 \pm 0.35) \times 10^{-2}$. Our first error is their experiment's error and our second error is the systematic error from using our best value.

Meson Particle Listings

$\chi_{b2}(1P), \eta_b(2S), \Upsilon(2S)$

$\Gamma(J/\psi J/\psi)/\Gamma_{total}$				Γ_{17}/Γ
VALUE (units 10^{-5})	CL%	DOCUMENT ID	TECN	COMMENT
<5	90	¹ SHEN	12 BELL	$\Upsilon(2S) \rightarrow \gamma\psi X$

¹ SHEN 12 reports $< 4.5 \times 10^{-5}$ from a measurement of $[\Gamma(\chi_{b2}(1P) \rightarrow J/\psi J/\psi)/\Gamma_{total}] \times [B(\Upsilon(2S) \rightarrow \gamma\chi_{b2}(1P))]$ assuming $B(\Upsilon(2S) \rightarrow \gamma\chi_{b2}(1P)) = (7.15 \pm 0.35) \times 10^{-2}$.

$\Gamma(J/\psi\psi(2S))/\Gamma_{total}$				Γ_{18}/Γ
VALUE (units 10^{-5})	CL%	DOCUMENT ID	TECN	COMMENT
<5	90	¹ SHEN	12 BELL	$\Upsilon(2S) \rightarrow \gamma\psi X$

¹ SHEN 12 reports $< 4.9 \times 10^{-5}$ from a measurement of $[\Gamma(\chi_{b2}(1P) \rightarrow J/\psi\psi(2S))/\Gamma_{total}] \times [B(\Upsilon(2S) \rightarrow \gamma\chi_{b2}(1P))]$ assuming $B(\Upsilon(2S) \rightarrow \gamma\chi_{b2}(1P)) = (7.15 \pm 0.35) \times 10^{-2}$.

$\Gamma(\psi(2S)\psi(2S))/\Gamma_{total}$				Γ_{19}/Γ
VALUE (units 10^{-5})	CL%	DOCUMENT ID	TECN	COMMENT
<1.6	90	¹ SHEN	12 BELL	$\Upsilon(2S) \rightarrow \gamma\psi X$

¹ SHEN 12 reports $< 1.6 \times 10^{-5}$ from a measurement of $[\Gamma(\chi_{b2}(1P) \rightarrow \psi(2S)\psi(2S))/\Gamma_{total}] \times [B(\Upsilon(2S) \rightarrow \gamma\chi_{b2}(1P))]$ assuming $B(\Upsilon(2S) \rightarrow \gamma\chi_{b2}(1P)) = (7.15 \pm 0.35) \times 10^{-2}$.

$\Gamma(J/\psi(1S) \text{ anything})/\Gamma_{total}$				Γ_{20}/Γ
VALUE (units 10^{-3})	EVTS	DOCUMENT ID	TECN	COMMENT
1.50 ± 0.34 ± 0.22	462	JIA	17A BELL	$e^+e^- \rightarrow \text{hadrons}$

$\chi_{b2}(1P)$ Cross-Particle Branching Ratios

$\Gamma(\chi_{b2}(1P) \rightarrow \gamma \Upsilon(1S))/\Gamma_{total} \times \Gamma(\Upsilon(2S) \rightarrow \gamma\chi_{b2}(1P))/\Gamma_{total}$				$\Gamma_{1}/\Gamma \times \Gamma_{60}^{\Upsilon(2S)}/\Gamma \Upsilon(2S)$
VALUE (units 10^{-3})	EVTS	DOCUMENT ID	TECN	COMMENT
13.9 ± 0.5 ± 0.9	8k	LEES	11J BABR	$\Upsilon(2S) \rightarrow X\gamma$

¹ From a sample of $\Upsilon(2S) \rightarrow \gamma\gamma\mu^+\mu^-$ with converted photons.

$B(\chi_{b2}(1P) \rightarrow \gamma \Upsilon(1S)) \times B(\Upsilon(2S) \rightarrow \gamma\chi_{b2}(1P)) \times B(\Upsilon(1S) \rightarrow \ell^+\ell^-)$				
VALUE (units 10^{-4})	EVTS	DOCUMENT ID	TECN	COMMENT
3.38 ± 0.16 OUR AVERAGE				

$3.63^{+0.36+0.18}_{-0.34-0.19}$		¹ LEES	14M BABR	$\Upsilon(2S) \rightarrow \gamma\gamma\mu^+\mu^-$
$3.29 \pm 0.09 \pm 0.16$	1770	KORNICER	11 CLEO	$e^+e^- \rightarrow \gamma\gamma\ell^+\ell^-$
$4.4 \pm 0.9 \pm 0.5$	35	WALK	86 CBAL	$\Upsilon(2S) \rightarrow \gamma\gamma\ell^+\ell^-$

¹ From a sample of $\Upsilon(2S) \rightarrow \gamma\gamma\mu^+\mu^-$ with converted photons.

$[B(\chi_{b2}(1P) \rightarrow \gamma \Upsilon(1S)) \times B(\Upsilon(2S) \rightarrow \gamma\chi_{b2}(1P))] / [B(\chi_{b1}(1P) \rightarrow \gamma \Upsilon(1S)) \times B(\Upsilon(2S) \rightarrow \gamma\chi_{b1}(1P))]$				
VALUE (%)	DOCUMENT ID	TECN	COMMENT	
55.6 ± 1.6	¹ LEES	14M BABR	$\Upsilon(2S) \rightarrow \gamma\gamma\mu^+\mu^-$	

¹ From a sample of $\Upsilon(2S) \rightarrow \gamma\gamma\mu^+\mu^-$ events without converted photons.

$B(\chi_{b2}(1P) \rightarrow \gamma \Upsilon(1S)) \times B(\Upsilon(3S) \rightarrow \gamma\chi_{b2}(1P)) \times B(\Upsilon(1S) \rightarrow \ell^+\ell^-)$				
VALUE (units 10^{-5})	EVTS	DOCUMENT ID	TECN	COMMENT
3.8 ± 0.5 OUR AVERAGE				

$4.68^{+0.99}_{-0.92} \pm 0.37$		¹ LEES	14M BABR	$\Upsilon(3S) \rightarrow \gamma\gamma\mu^+\mu^-$
$3.56 \pm 0.40 \pm 0.41$	126	KORNICER	11 CLEO	$e^+e^- \rightarrow \gamma\gamma\ell^+\ell^-$

¹ From a sample of $\Upsilon(3S) \rightarrow \gamma\gamma\mu^+\mu^-$ with converted photons.

$\chi_{b2}(1P)$ REFERENCES

FULSOM	18	PRL 121 232001	B.G. Fulsom et al.	(BELLE Collab.)
JIA	17A	PR D96 112002	S. Jia et al.	(BELLE Collab.)
AJAJ	14BG	JHEP 1410 088	R. Aaij et al.	(LHCb Collab.)
LEES	14M	PR D90 112010	J.P. Lees et al.	(BABAR Collab.)
SHEN	12	PR D85 071102	C.P. Shen et al.	(BELLE Collab.)
KORNICER	11	PR D83 054003	M. Kornicer et al.	(CLEO Collab.)
LEES	11J	PR D84 072002	J.P. Lees et al.	(BABAR Collab.)
ASNER	08A	PR D78 091103	D.M. Asner et al.	(CLEO Collab.)
BRIERE	08	PR D78 092007	R.A. Briere et al.	(CLEO Collab.)
ARTUSO	05	PR 94 032001	M. Artuso et al.	(CLEO Collab.)
EDWARDS	99	PR D59 032003	K.W. Edwards et al.	(CLEO Collab.)
SKWARNICKI	87	PRL 58 972	T. Skwarnicki et al.	(Crystal Ball Collab.)
WALK	86	PR D34 2611	W.S. Walk et al.	(Crystal Ball Collab.)
ALBRECHT	85E	PL 160B 331	H. Albrecht et al.	(ARGUS Collab.)
NERNST	85	PRL 54 2195	R. Nernst et al.	(Crystal Ball Collab.)
HAAS	84	PRL 52 799	J. Haas et al.	(CLEO Collab.)
KLOPFEN...	83	PRL 51 160	C. Klopffenstein et al.	(CUSB Collab.)
PAUSS	83	PL 130B 439	F. Pauss et al.	(MPIM, COLU, CORN, LSU+)

$\eta_b(2S)$

$$J^G(J^{PC}) = 0^+(0^-+)$$

OMITTED FROM SUMMARY TABLE

Quantum numbers shown are quark-model predictions.

$\eta_b(2S)$ MASS

VALUE (MeV)	EVTS	DOCUMENT ID	TECN	COMMENT
9999.0 ± 3.5 ± 1.9	26k	¹ MIZUK	12 BELL	$e^+e^- \rightarrow \gamma\pi^+\pi^- + \text{hadrons}$

••• We do not use the following data for averages, fits, limits, etc. •••

9974.6 ± 2.3 ± 2.1	11 ± 4	^{2,3,4} DOBBS	12	$\Upsilon(2S) \rightarrow \gamma \text{ hadrons}$
--------------------	--------	------------------------	----	---

¹ Assuming $\Gamma_{\eta_b(2S)} = 4.9$ MeV. Not independent of the corresponding mass difference measurement.

² SANDILYA 13 (Belle Collab.) search for such a state reconstructed in the same 26 exclusive hadronic final states as DOBBS 12 using a sample of $(157.8 \pm 3.6) \times 10^6 \Upsilon(2S)$ decays or about 17 times larger and find no evidence for a signal. Their 90% C.L. upper limit on the branching fraction $B(\Upsilon(2S) \rightarrow \eta_b(2S)\gamma) \times \sum_i B(\eta_b(2S) \rightarrow X_i) < 4.9 \times 10^{-6}$, summed over the exclusive hadronic final states X_i , is an order of magnitude smaller than that reported by DOBBS 12.

³ Obtained by analyzing CLEO III data but not authored by the CLEO Collaboration.

⁴ Assuming $\Gamma_{\eta_b(2S)} = 5$ MeV. Not independent of the corresponding mass difference measurement.

$m_{\Upsilon(2S)} - m_{\eta_b(2S)}$

VALUE (MeV)	EVTS	DOCUMENT ID	TECN	COMMENT
24.3 ± 3.5 ± 2.8	26k	⁵ MIZUK	12 BELL	$e^+e^- \rightarrow \gamma\pi^+\pi^- + \text{hadrons}$

••• We do not use the following data for averages, fits, limits, etc. •••

48.7 ± 2.3 ± 2.1	11 ± 4	^{6,7,8} DOBBS	12	$\Upsilon(2S) \rightarrow \gamma \text{ hadrons}$
------------------	--------	------------------------	----	---

⁵ Assuming $\Gamma_{\eta_b(2S)} = 4.9$ MeV. Not independent of the corresponding mass measurement.

⁶ SANDILYA 13 (Belle Collab.) search for such a state reconstructed in the same 26 exclusive hadronic final states as DOBBS 12 using a sample of $(157.8 \pm 3.6) \times 10^6 \Upsilon(2S)$ decays or about 17 times larger and find no evidence for a signal. Their 90% C.L. upper limit on the branching fraction $B(\Upsilon(2S) \rightarrow \eta_b(2S)\gamma) \times \sum_i B(\eta_b(2S) \rightarrow X_i) < 4.9 \times 10^{-6}$, summed over the exclusive hadronic final states X_i , is an order of magnitude smaller than that reported by DOBBS 12.

⁷ Obtained by analyzing CLEO III data but not authored by the CLEO Collaboration.

⁸ Assuming $\Gamma_{\eta_b(2S)} = 5$ MeV. Not independent of the corresponding mass measurement.

$\eta_b(2S)$ WIDTH

VALUE (MeV)	CL%	DOCUMENT ID	TECN	COMMENT
<24	90	MIZUK	12 BELL	$e^+e^- \rightarrow \gamma\pi^+\pi^- \text{ hadrons}$

$\eta_b(2S)$ DECAY MODES

Mode	Fraction (Γ_i/Γ)
Γ_1 hadrons	seen

$\eta_b(2S)$ BRANCHING RATIOS

$\Gamma(\text{hadrons})/\Gamma_{total}$				Γ_1/Γ
VALUE	EVTS	DOCUMENT ID	TECN	COMMENT
seen	26k	MIZUK	12 BELL	$e^+e^- \rightarrow \gamma\pi^+\pi^- \text{ hadrons}$

••• We do not use the following data for averages, fits, limits, etc. •••

seen	9.10	DOBBS	12	$\Upsilon(2S) \rightarrow \gamma \text{ hadrons}$
------	------	-------	----	---

⁹ SANDILYA 13 (Belle Collab.) search for such a state reconstructed in the same 26 exclusive hadronic final states as DOBBS 12 using a sample of $(157.8 \pm 3.6) \times 10^6 \Upsilon(2S)$ decays or about 17 times larger and find no evidence for a signal. Their 90% C.L. upper limit on the branching fraction $B(\Upsilon(2S) \rightarrow \eta_b(2S)\gamma) \times \sum_i B(\eta_b(2S) \rightarrow X_i) < 4.9 \times 10^{-6}$, summed over the exclusive hadronic final states X_i , is an order of magnitude smaller than that reported by DOBBS 12.

¹⁰ Obtained by analyzing CLEO III data but not authored by the CLEO Collaboration.

$\eta_b(2S)$ REFERENCES

SANDILYA	13	PRL 111 112001	S. Sandilya et al.	(BELLE Collab.)
DOBBS	12	PRL 109 082001	S. Dobbs et al.	
MIZUK	12	PRL 109 232002	R. Mizuk et al.	(BELLE Collab.)

$\Upsilon(2S)$

$$J^G(J^{PC}) = 0^-(1^{--})$$

$\Upsilon(2S)$ MASS

VALUE (MeV)	DOCUMENT ID	TECN	COMMENT
10023.26 ± 0.31 OUR AVERAGE			

10023.5 ± 0.5	¹ ARTA MONOV	00 MD1	$e^+e^- \rightarrow \text{hadrons}$
10023.1 ± 0.4	BARBER	84 REDE	$e^+e^- \rightarrow \text{hadrons}$

••• We do not use the following data for averages, fits, limits, etc. •••

10023.6 ± 0.5	^{2,3} BARU	86B REDE	$e^+e^- \rightarrow \text{hadrons}$
---------------	---------------------	----------	-------------------------------------

¹ Reanalysis of BARU 86B using new electron mass (COHEN 87).

² Reanalysis of ARTAMONOV 84.

³ Superseded by ARTAMONOV 00.

$m_{\Upsilon(3S)} - m_{\Upsilon(2S)}$

VALUE (MeV)	DOCUMENT ID	TECN	COMMENT
331.50 ± 0.02 ± 0.13	LEES	11c	BABR $e^+e^- \rightarrow \pi^+\pi^-X$

$\Upsilon(2S)$ WIDTH

VALUE (keV)	DOCUMENT ID	COMMENT
31.98 ± 2.63 OUR EVALUATION	See the Note on "Width Determinations of the Υ States"	

$\Upsilon(2S)$ DECAY MODES

Mode	Fraction (Γ_i/Γ)	Scale factor / Confidence level
Γ_1 $\Upsilon(1S)\pi^+\pi^-$	(17.85 ± 0.26) %	
Γ_2 $\Upsilon(1S)\pi^0\pi^0$	(8.6 ± 0.4) %	
Γ_3 $\tau^+\tau^-$	(2.00 ± 0.21) %	
Γ_4 $\mu^+\mu^-$	(1.93 ± 0.17) %	S=2.2
Γ_5 e^+e^-	(1.91 ± 0.16) %	
Γ_6 $\Upsilon(1S)\pi^0$	< 4 × 10 ⁻⁵	CL=90%
Γ_7 $\Upsilon(1S)\eta$	(2.9 ± 0.4) × 10 ⁻⁴	S=2.0
Γ_8 $J/\psi(1S)$ anything	< 6 × 10 ⁻³	CL=90%
Γ_9 $J/\psi(1S)\eta_c$	< 5.4 × 10 ⁻⁶	CL=90%
Γ_{10} $J/\psi(1S)\chi_{c0}$	< 3.4 × 10 ⁻⁶	CL=90%
Γ_{11} $J/\psi(1S)\chi_{c1}$	< 1.2 × 10 ⁻⁶	CL=90%
Γ_{12} $J/\psi(1S)\chi_{c2}$	< 2.0 × 10 ⁻⁶	CL=90%
Γ_{13} $J/\psi(1S)\eta_c(2S)$	< 2.5 × 10 ⁻⁶	CL=90%
Γ_{14} $J/\psi(1S)X(3940)$	< 2.0 × 10 ⁻⁶	CL=90%
Γ_{15} $J/\psi(1S)X(4160)$	< 2.0 × 10 ⁻⁶	CL=90%
Γ_{16} χ_{c1} anything	(2.2 ± 0.5) × 10 ⁻⁴	
Γ_{17} $\chi_{c1}(1P)^0 X_{tetra}$	< 3.67 × 10 ⁻⁵	CL=90%
Γ_{18} χ_{c2} anything	(2.3 ± 0.8) × 10 ⁻⁴	
Γ_{19} $\psi(2S)\eta_c$	< 5.1 × 10 ⁻⁶	CL=90%
Γ_{20} $\psi(2S)\chi_{c0}$	< 4.7 × 10 ⁻⁶	CL=90%
Γ_{21} $\psi(2S)\chi_{c1}$	< 2.5 × 10 ⁻⁶	CL=90%
Γ_{22} $\psi(2S)\chi_{c2}$	< 1.9 × 10 ⁻⁶	CL=90%
Γ_{23} $\psi(2S)\eta_c(2S)$	< 3.3 × 10 ⁻⁶	CL=90%
Γ_{24} $\psi(2S)X(3940)$	< 3.9 × 10 ⁻⁶	CL=90%
Γ_{25} $\psi(2S)X(4160)$	< 3.9 × 10 ⁻⁶	CL=90%
Γ_{26} $Z_c(3900)^+ Z_c(3900)^-$	< 1.0 × 10 ⁻⁶	CL=90%
Γ_{27} $Z_c(4200)^+ Z_c(4200)^-$	< 1.67 × 10 ⁻⁵	CL=90%
Γ_{28} $Z_c(3900)^{\pm} Z_c(4200)^{\mp}$	< 7.3 × 10 ⁻⁶	CL=90%
Γ_{29} $X(4050)^+ X(4050)^-$	< 1.35 × 10 ⁻⁵	CL=90%
Γ_{30} $X(4250)^+ X(4250)^-$	< 2.67 × 10 ⁻⁵	CL=90%
Γ_{31} $X(4050)^{\pm} X(4250)^{\mp}$	< 2.72 × 10 ⁻⁵	CL=90%
Γ_{32} $Z_c(4430)^+ Z_c(4430)^-$	< 2.03 × 10 ⁻⁵	CL=90%
Γ_{33} $X(4055)^{\pm} X(4055)^{\mp}$	< 1.11 × 10 ⁻⁵	CL=90%
Γ_{34} $X(4055)^{\pm} Z_c(4430)^{\mp}$	< 2.11 × 10 ⁻⁵	CL=90%
Γ_{35} 2H anything	(2.78 ± 0.30 / 0.26) × 10 ⁻⁵	S=1.2
Γ_{36} hadrons	(94 ± 11) %	
Γ_{37} ggg	(58.8 ± 1.2) %	
Γ_{38} γgg	(1.87 ± 0.28) %	
Γ_{39} $\phi K^+ K^-$	(1.6 ± 0.4) × 10 ⁻⁶	
Γ_{40} $\omega\pi^+\pi^-$	< 2.58 × 10 ⁻⁶	CL=90%
Γ_{41} $K^*(892)^0 K^- \pi^+ + c.c.$	(2.3 ± 0.7) × 10 ⁻⁶	
Γ_{42} $\phi f_2'(1525)$	< 1.33 × 10 ⁻⁶	CL=90%
Γ_{43} $\omega f_2'(1270)$	< 5.7 × 10 ⁻⁷	CL=90%
Γ_{44} $\rho(770) a_2(1320)$	< 8.8 × 10 ⁻⁷	CL=90%
Γ_{45} $K^*(892)^0 K_2^*(1430)^0 + c.c.$	(1.5 ± 0.6) × 10 ⁻⁶	
Γ_{46} $K_1(1270)^{\pm} K^{\mp}$	< 3.22 × 10 ⁻⁶	CL=90%
Γ_{47} $K_1(1400)^{\pm} K^{\mp}$	< 8.3 × 10 ⁻⁷	CL=90%
Γ_{48} $b_1(1235)^{\pm} \pi^{\mp}$	< 4.0 × 10 ⁻⁷	CL=90%
Γ_{49} $\rho\pi$	< 1.16 × 10 ⁻⁶	CL=90%
Γ_{50} $\pi^+\pi^-\pi^0$	< 8.0 × 10 ⁻⁷	CL=90%
Γ_{51} $\omega\pi^0$	< 1.63 × 10 ⁻⁶	CL=90%
Γ_{52} $\pi^+\pi^-\pi^0\pi^0$	(1.30 ± 0.28) × 10 ⁻⁵	
Γ_{53} $K_S^0 K^+ \pi^- + c.c.$	(1.14 ± 0.33) × 10 ⁻⁶	
Γ_{54} $K^*(892)^0 \bar{K}^0 + c.c.$	< 4.22 × 10 ⁻⁶	CL=90%
Γ_{55} $K^*(892)^- K^+ + c.c.$	< 1.45 × 10 ⁻⁶	CL=90%
Γ_{56} $f_1(1285)$ anything	(2.2 ± 1.6) × 10 ⁻³	
Γ_{57} $f_1(1285) X_{tetra}$	< 6.47 × 10 ⁻⁵	CL=90%
Γ_{58} Sum of 100 exclusive modes	(2.90 ± 0.30) × 10 ⁻³	

Radiative decays

Γ_{59} $\gamma\chi_{b1}(1P)$	(6.9 ± 0.4) %	
Γ_{60} $\gamma\chi_{b2}(1P)$	(7.15 ± 0.35) %	
Γ_{61} $\gamma\chi_{b0}(1P)$	(3.8 ± 0.4) %	
Γ_{62} $\gamma f_0(1710)$	< 5.9 × 10 ⁻⁴	CL=90%
Γ_{63} $\gamma f_2'(1525)$	< 5.3 × 10 ⁻⁴	CL=90%
Γ_{64} $\gamma f_2'(1270)$	< 2.41 × 10 ⁻⁴	CL=90%
Γ_{65} $\gamma f_3(2220)$		
Γ_{66} $\gamma\eta_c(1S)$	< 2.7 × 10 ⁻⁵	CL=90%
Γ_{67} $\gamma\chi_{c0}$	< 1.0 × 10 ⁻⁴	CL=90%
Γ_{68} $\gamma\chi_{c1}$	< 3.6 × 10 ⁻⁶	CL=90%
Γ_{69} $\gamma\chi_{c2}$	< 1.5 × 10 ⁻⁵	CL=90%
Γ_{70} $\gamma\chi_{c1}(3872) \rightarrow \pi^+\pi^-J/\psi$	< 8 × 10 ⁻⁷	CL=90%
Γ_{71} $\gamma\chi_{c1}(3872) \rightarrow \pi^+\pi^-\pi^0 J/\psi$	< 2.4 × 10 ⁻⁶	CL=90%
Γ_{72} $\gamma X(3915) \rightarrow \omega J/\psi$	< 2.8 × 10 ⁻⁶	CL=90%
Γ_{73} $\gamma\chi_{c1}(4140) \rightarrow \phi J/\psi$	< 1.2 × 10 ⁻⁶	CL=90%
Γ_{74} $\gamma X(4350) \rightarrow \phi J/\psi$	< 1.3 × 10 ⁻⁶	CL=90%
Γ_{75} $\gamma\eta_b(1S)$	(5.5 ± 1.1 / 0.9) × 10 ⁻⁴	S=1.2
Γ_{76} $\gamma\eta_b(1S) \rightarrow \gamma$ Sum of 26 exclusive modes	< 3.7 × 10 ⁻⁶	CL=90%
Γ_{77} $\gamma X_{b\bar{b}} \rightarrow \gamma$ Sum of 26 exclusive modes	< 4.9 × 10 ⁻⁶	CL=90%
Γ_{78} $\gamma X \rightarrow \gamma + \geq 4$ prongs	[a] < 1.95 × 10 ⁻⁴	CL=95%
Γ_{79} $\gamma A^0 \rightarrow \gamma$ hadrons	< 8 × 10 ⁻⁵	CL=90%
Γ_{80} $\gamma a_1^0 \rightarrow \gamma\mu^+\mu^-$	< 8.3 × 10 ⁻⁶	CL=90%

Lepton Family number (LF) violating modes

Γ_{81} $e^{\pm}\tau^{\mp}$	LF	< 3.2 × 10 ⁻⁶	CL=90%
Γ_{82} $\mu^{\pm}\tau^{\mp}$	LF	< 3.3 × 10 ⁻⁶	CL=90%

[a] 1.5 GeV < m_X < 5.0 GeV

CONSTRAINED FIT INFORMATION

An overall fit to 3 branching ratios uses 13 measurements and one constraint to determine 3 parameters. The overall fit has a $\chi^2 = 11.8$ for 11 degrees of freedom.

The following off-diagonal array elements are the correlation coefficients $\langle \delta x_i \delta x_j \rangle / (\delta x_i \delta x_j)$, in percent, from the fit to the branching fractions, $x_i \equiv \Gamma_i/\Gamma_{total}$. The fit constrains the x_i whose labels appear in this array to sum to one.

$$x_7 \begin{matrix} \text{---} 2 \\ | \\ \text{---} x_1 \end{matrix}$$

$\Upsilon(2S)$ $\Gamma(i)\Gamma(e^+e^-)/\Gamma(total)$

$\Gamma(\mu^+\mu^-) \times \Gamma(e^+e^-)/\Gamma_{total}$	DOCUMENT ID	TECN	COMMENT	$\Gamma_4\Gamma_5/\Gamma$
6.5 ± 1.5 ± 1.0	KOBEL	92	CBAL $e^+e^- \rightarrow \mu^+\mu^-$	

$\Gamma(\Upsilon(1S)\pi^+\pi^-) \times \Gamma(e^+e^-)/\Gamma_{total}$	DOCUMENT ID	TECN	COMMENT	$\Gamma_1\Gamma_5/\Gamma$
105.4 ± 1.0 ± 4.2	11.8K	1	AUBERT 08BP BABR 10.58 $e^+e^- \rightarrow \gamma\pi^+\pi^-\ell^+\ell^-$	
			¹ Using $B(\Upsilon(1S) \rightarrow e^+e^-) = (2.38 \pm 0.11)\%$ and $B(\Upsilon(1S) \rightarrow \mu^+\mu^-) = (2.48 \pm 0.05)\%$.	

$\Gamma(hadrons) \times \Gamma(e^+e^-)/\Gamma_{total}$	DOCUMENT ID	TECN	COMMENT	$\Gamma_{36}\Gamma_5/\Gamma$
0.577 ± 0.009 OUR AVERAGE				
0.581 ± 0.004 ± 0.009	1	ROSNER	06 CLEO 10.0 $e^+e^- \rightarrow$ hadrons	
0.552 ± 0.031 ± 0.017	1	BARU	96 MD1 $e^+e^- \rightarrow$ hadrons	
0.54 ± 0.04 ± 0.02	1	JAKUBOWSKI	88 CBAL $e^+e^- \rightarrow$ hadrons	
0.58 ± 0.03 ± 0.04	2	GILES	84B CLEO $e^+e^- \rightarrow$ hadrons	
0.60 ± 0.12 ± 0.07	2	ALBRECHT	82 DASP $e^+e^- \rightarrow$ hadrons	
0.54 ± 0.07 ± 0.09 / -0.05	2	NICZYPORUK	81c LENA $e^+e^- \rightarrow$ hadrons	
0.41 ± 0.18	2	BOCK	80 CNTR $e^+e^- \rightarrow$ hadrons	

¹ Radiative corrections evaluated following KURAEV 85.
² Radiative corrections reevaluated by BUCHMUELLER 88 following KURAEV 85.

$\Upsilon(2S)$ PARTIAL WIDTHS

$\Gamma(e^+e^-)$	DOCUMENT ID	Γ_5
0.612 ± 0.011 OUR EVALUATION		

Meson Particle Listings

$\Upsilon(2S)$

$\Upsilon(2S)$ BRANCHING RATIOS

$\Gamma(\Upsilon(1S)\pi^+\pi^-)/\Gamma_{total}$ Γ_1/Γ
 Abbreviation MM in the COMMENT field below stands for missing mass.

VALUE (units 10^{-2})	EVTS	DOCUMENT ID	TECN	COMMENT
17.85 ± 0.26 OUR FIT				
17.92 ± 0.26 OUR AVERAGE				
16.8 ± 1.1 ± 1.3	906k	¹ LEES	11C	BABR $e^+e^- \rightarrow \pi^+\pi^- X$
17.80 ± 0.05 ± 0.37	170k	² LEES	11L	BABR $\Upsilon(2S) \rightarrow \pi^+\pi^-\mu^+\mu^-$
18.02 ± 0.02 ± 0.61	851k	³ BHARI	09	CLEO $e^+e^- \rightarrow \pi^+\pi^- MM$
17.22 ± 0.17 ± 0.75	11.8k	⁴ AUBERT	08BP	BABR $e^+e^- \rightarrow \gamma\pi^+\pi^-\ell^+\ell^-$
19.2 ± 0.2 ± 1.0	52.6k	⁵ ALEXANDER	98	CLE2 $\pi^+\pi^-\ell^+\ell^-, \pi^+\pi^- MM$
18.1 ± 0.5 ± 1.0	11.6k	ALBRECHT	87	ARG $e^+e^- \rightarrow \pi^+\pi^- MM$
16.9 ± 4.0		GELPHMAN	85	CBAL $e^+e^- \rightarrow e^+e^-\pi^+\pi^-$
19.1 ± 1.2 ± 0.6		BESSON	84	CLEO $\pi^+\pi^- MM$
18.9 ± 2.6		FONSECA	84	CUSB $e^+e^- \rightarrow \ell^+\ell^-\pi^+\pi^-$
21 ± 7	7	NICZYPORUK	81B	LENA $e^+e^- \rightarrow \ell^+\ell^-\pi^+\pi^-$

¹ LEES 11c reports $[\Gamma(\Upsilon(2S) \rightarrow \Upsilon(1S)\pi^+\pi^-)/\Gamma_{total}] \times [B(\Upsilon(3S) \rightarrow \Upsilon(2S)\text{anything})] = (1.78 \pm 0.02 \pm 0.11) \times 10^{-2}$ which we divide by our best value $B(\Upsilon(3S) \rightarrow \Upsilon(2S)\text{anything}) = (10.6 \pm 0.8) \times 10^{-2}$. Our first error is their experiment's error and our second error is the systematic error from using our best value.
² Using $B(\Upsilon(1S) \rightarrow \mu^+\mu^-) = (2.48 \pm 0.05)\%$.
³ A weighted average of the inclusive and exclusive results.
⁴ Using $B(\Upsilon(2S) \rightarrow e^+e^-) = (1.91 \pm 0.16)\%$, $B(\Upsilon(2S) \rightarrow \mu^+\mu^-) = (1.93 \pm 0.17)\%$ and $\Gamma_{ee}(\Upsilon(2S)) = 0.612 \pm 0.011$ keV.
⁵ Using $B(\Upsilon(1S) \rightarrow e^+e^-) = (2.52 \pm 0.17)\%$ and $B(\Upsilon(1S) \rightarrow \mu^+\mu^-) = (2.48 \pm 0.07)\%$.

$\Gamma(\Upsilon(1S)\pi^0\pi^0)/\Gamma_{total}$ Γ_2/Γ

VALUE (units 10^{-2})	EVTS	DOCUMENT ID	TECN	COMMENT
8.6 ± 0.4 OUR AVERAGE				
8.43 ± 0.16 ± 0.42	38k	¹ BHARI	09	CLEO $e^+e^- \rightarrow \pi^0\pi^0\ell^+\ell^-$
9.2 ± 0.6 ± 0.8	275	² ALEXANDER	98	CLE2 $e^+e^- \rightarrow \pi^0\pi^0\ell^+\ell^-$
9.5 ± 1.9 ± 1.9	25	ALBRECHT	87	ARG $e^+e^- \rightarrow \pi^0\pi^0\ell^+\ell^-$
8.0 ± 1.5		GELPHMAN	85	CBAL $e^+e^- \rightarrow \pi^0\pi^0\ell^+\ell^-$
10.3 ± 2.3		FONSECA	84	CUSB $e^+e^- \rightarrow \pi^0\pi^0\ell^+\ell^-$

¹ Authors assume $B(\Upsilon(1S) \rightarrow e^+e^-) + B(\Upsilon(1S) \rightarrow \mu^+\mu^-) = 4.96\%$.
² Using $B(\Upsilon(1S) \rightarrow e^+e^-) = (2.52 \pm 0.17)\%$ and $B(\Upsilon(1S) \rightarrow \mu^+\mu^-) = (2.48 \pm 0.07)\%$.

$\Gamma(\Upsilon(1S)\pi^0\pi^0)/\Gamma(\Upsilon(1S)\pi^+\pi^-)$ Γ_2/Γ_1

VALUE	DOCUMENT ID	TECN	COMMENT
0.462 ± 0.037	¹ BHARI 09	CLEO	$e^+e^- \rightarrow \Upsilon(2S)$

¹ Not independent of other values reported by BHARI 09.

$\Gamma(\tau^+\tau^-)/\Gamma_{total}$ Γ_3/Γ

VALUE (units 10^{-2})	EVTS	DOCUMENT ID	TECN	COMMENT
2.00 ± 0.21 OUR AVERAGE				
2.00 ± 0.12 ± 0.18	22k	¹ BESSON	07	CLEO $e^+e^- \rightarrow \Upsilon(2S) \rightarrow \tau^+\tau^-$
1.7 ± 1.5 ± 0.6		HAAS	84B	CLEO $e^+e^- \rightarrow \tau^+\tau^-$

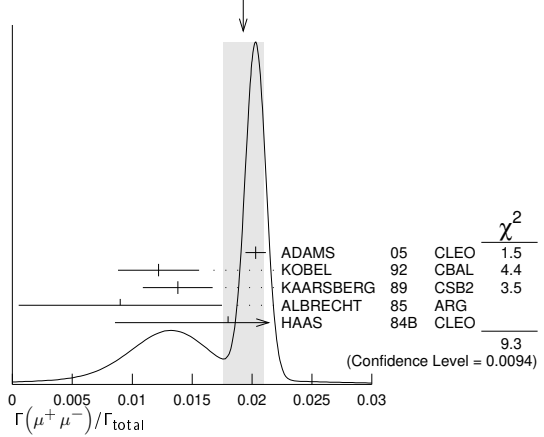
¹ BESSON 07 reports $[\Gamma(\Upsilon(2S) \rightarrow \tau^+\tau^-)/\Gamma_{total}] / [B(\Upsilon(2S) \rightarrow \mu^+\mu^-)] = 1.04 \pm 0.04 \pm 0.05$ which we multiply by our best value $B(\Upsilon(2S) \rightarrow \mu^+\mu^-) = (1.93 \pm 0.17) \times 10^{-2}$. Our first error is their experiment's error and our second error is the systematic error from using our best value.

$\Gamma(\mu^+\mu^-)/\Gamma_{total}$ Γ_4/Γ

VALUE	CL%	EVTS	DOCUMENT ID	TECN	COMMENT
0.0193 ± 0.0017 OUR AVERAGE					Error includes scale factor of 2.2. See the ideogram below.
0.0203 ± 0.0003 ± 0.0008		120k	ADAMS	05	CLEO $e^+e^- \rightarrow \mu^+\mu^-$
0.0122 ± 0.0028 ± 0.0019			¹ KOBEL	92	CBAL $e^+e^- \rightarrow \mu^+\mu^-$
0.0138 ± 0.0025 ± 0.0015			KAARSBERG	89	CSB2 $e^+e^- \rightarrow \mu^+\mu^-$
0.009 ± 0.006 ± 0.006			² ALBRECHT	85	ARG $e^+e^- \rightarrow \mu^+\mu^-$
0.018 ± 0.008 ± 0.005			HAAS	84B	CLEO $e^+e^- \rightarrow \mu^+\mu^-$
< 0.038		90	NICZYPORUK	81c	LENA $e^+e^- \rightarrow \mu^+\mu^-$

¹ Taking into account interference between the resonance and continuum.
² Re-evaluated using $B(\Upsilon(1S) \rightarrow \mu^+\mu^-) = 0.026$.

WEIGHTED AVERAGE
 0.0193 ± 0.0017 (Error scaled by 2.2)



$\Gamma(\tau^+\tau^-)/\Gamma(\mu^+\mu^-)$ Γ_3/Γ_4

VALUE	EVTS	DOCUMENT ID	TECN	COMMENT
1.04 ± 0.04 ± 0.05	22k	BESSON	07	CLEO $e^+e^- \rightarrow \Upsilon(2S)$

$\Gamma(\Upsilon(1S)\pi^0)/\Gamma_{total}$ Γ_6/Γ

VALUE (units 10^{-5})	CL%	DOCUMENT ID	TECN	COMMENT
< 4	90	¹ TAMPONI	13	BELL $e^+e^- \rightarrow \Upsilon(1S)\pi^0$
< 18	90	² HE	08A	CLEO $e^+e^- \rightarrow \ell^+\ell^-\gamma\gamma$
< 110	90	ALEXANDER	98	CLE2 $e^+e^- \rightarrow \ell^+\ell^-\gamma\gamma$
< 800	90	LURZ	87	CBAL $e^+e^- \rightarrow \ell^+\ell^-\gamma\gamma$

¹ TAMPONI 13 reports $[\Gamma(\Upsilon(2S) \rightarrow \Upsilon(1S)\pi^0)/\Gamma_{total}] / [B(\Upsilon(2S) \rightarrow \Upsilon(1S)\pi^+\pi^-)] < 2.3 \times 10^{-4}$ which we multiply by our best value $B(\Upsilon(2S) \rightarrow \Upsilon(1S)\pi^+\pi^-) = 17.85 \times 10^{-2}$.
² Authors assume $B(\Upsilon(1S) \rightarrow e^+e^-) + B(\Upsilon(1S) \rightarrow \mu^+\mu^-) = 4.96\%$.

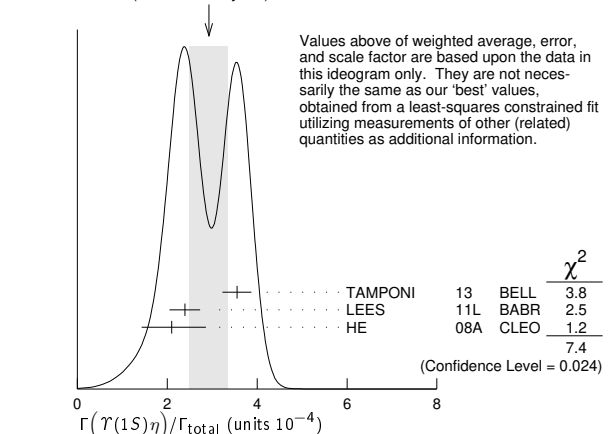
$\Gamma(\Upsilon(1S)\pi^0)/\Gamma(\Upsilon(1S)\pi^+\pi^-)$ Γ_6/Γ_1

VALUE (units 10^{-4})	CL%	DOCUMENT ID	TECN	COMMENT
< 2.3	90	TAMPONI	13	BELL $e^+e^- \rightarrow \Upsilon(1S)\pi^0$

$\Gamma(\Upsilon(1S)\eta)/\Gamma_{total}$ Γ_7/Γ

VALUE (units 10^{-4})	CL%	EVTS	DOCUMENT ID	TECN	COMMENT
2.9 ± 0.4 OUR FIT					Error includes scale factor of 2.0.
2.9 ± 0.4 OUR AVERAGE					Error includes scale factor of 1.9. See the ideogram below.
2.39 ± 0.31 ± 0.14		112	¹ LEES	11L	BABR $\Upsilon(2S) \rightarrow \ell^+\ell^-\eta$
2.1 $^{+0.7}_{-0.6}$ ± 0.3		14	² HE	08A	CLEO $e^+e^- \rightarrow \ell^+\ell^-\eta$
3.55 ± 0.32 ± 0.05		241	³ TAMPONI	13	BELL $e^+e^- \rightarrow \Upsilon(1S)\eta$
< 9	90	^{1,4} AUBERT	08BP	BABR $e^+e^- \rightarrow \gamma\pi^+\pi^-\pi^0\ell^+\ell^-$	
< 28	90	ALEXANDER	98	CLE2 $e^+e^- \rightarrow \ell^+\ell^-\eta$	
< 50	90	ALBRECHT	87	ARG $e^+e^- \rightarrow \pi^+\pi^-\ell^+\ell^- MM$	
< 70	90	LURZ	87	CBAL $e^+e^- \rightarrow \ell^+\ell^-(\gamma\gamma, 3\pi^0)$	
< 100	90	BESSON	84	CLEO $e^+e^- \rightarrow \pi^+\pi^-\ell^+\ell^- MM$	
< 20	90	FONSECA	84	CUSB $e^+e^- \rightarrow \ell^+\ell^-(\gamma\gamma, \pi^+\pi^-\pi^0)$	

WEIGHTED AVERAGE
 2.9 ± 0.4 (Error scaled by 1.9)



¹ Using $B(\Upsilon(1S) \rightarrow e^+e^-) = (2.38 \pm 0.11)\%$ and $B(\Upsilon(1S) \rightarrow \mu^+\mu^-) = (2.48 \pm 0.05)\%$.

Meson Particle Listings
T(2S)

² Authors assume $B(T(1S) \rightarrow e^+e^-) + B(T(1S) \rightarrow \mu^+\mu^-) = 4.96\%$.

³ TAMPONI 13 reports $[\Gamma(T(2S) \rightarrow T(1S)\eta)/\Gamma_{total}] / [B(T(2S) \rightarrow T(1S)\pi^+\pi^-)] = (1.99 \pm 0.14 \pm 0.11) \times 10^{-3}$ which we multiply by our best value $B(T(2S) \rightarrow T(1S)\pi^+\pi^-) = (17.85 \pm 0.26) \times 10^{-2}$. Our first error is their experiment's error and our second error is the systematic error from using our best value.

⁴ Using $\Gamma_{ee}(T(2S)) = 0.612 \pm 0.011$ keV.

$\Gamma(T(1S)\eta)/\Gamma(T(1S)\pi^+\pi^-)$ Γ_7/Γ_1

VALUE (units 10^{-3}) CL% EVTS DOCUMENT ID TECN COMMENT
1.64 ± 0.25 OUR FIT Error includes scale factor of 2.0.

1.99 ± 0.14 ± 0.11 241 TAMPONI 13 BELL $e^+e^- \rightarrow T(1S)\eta$
• • • We do not use the following data for averages, fits, limits, etc. • • •
1.35 ± 0.17 ± 0.08 ¹ LEES 11L BABR $T(2S) \rightarrow (\pi^+\pi^-)(\gamma\gamma)\mu^+\mu^-$
< 5.2 90 ² AUBERT 08BP BABR $e^+e^- \rightarrow \gamma\pi^+\pi^-(\pi^0)\ell^+\ell^-$

¹ Not independent of other values reported by LEES 11L.

² Not independent of other values reported by AUBERT 08BP.

$\Gamma(T(1S)\pi^0)/\Gamma(T(1S)\eta)$ Γ_6/Γ_7

VALUE CL% DOCUMENT ID TECN COMMENT
• • • We do not use the following data for averages, fits, limits, etc. • • •

< 0.13 90 TAMPONI 13 BELL $e^+e^- \rightarrow T(1S)\pi^0$

$\Gamma(J/\psi(1S) \text{ anything})/\Gamma_{total}$ Γ_8/Γ

VALUE CL% DOCUMENT ID TECN COMMENT
< 0.006 90 MASCHMANN 90 CBAL $e^+e^- \rightarrow$ hadrons

$\Gamma(J/\psi(1S)\eta_c)/\Gamma_{total}$ Γ_9/Γ

VALUE CL% DOCUMENT ID TECN COMMENT
< 5.4 × 10⁻⁶ 90 YANG 14 BELL $e^+e^- \rightarrow J/\psi X$

$\Gamma(J/\psi(1S)\chi_{c0})/\Gamma_{total}$ Γ_{10}/Γ

VALUE CL% DOCUMENT ID TECN COMMENT
< 3.4 × 10⁻⁶ 90 YANG 14 BELL $e^+e^- \rightarrow J/\psi X$

$\Gamma(J/\psi(1S)\chi_{c1})/\Gamma_{total}$ Γ_{11}/Γ

VALUE CL% DOCUMENT ID TECN COMMENT
< 1.2 × 10⁻⁶ 90 YANG 14 BELL $e^+e^- \rightarrow J/\psi X$

$\Gamma(J/\psi(1S)\chi_{c2})/\Gamma_{total}$ Γ_{12}/Γ

VALUE CL% DOCUMENT ID TECN COMMENT
< 2.0 × 10⁻⁶ 90 YANG 14 BELL $e^+e^- \rightarrow J/\psi X$

$\Gamma(J/\psi(1S)\eta_c(2S))/\Gamma_{total}$ Γ_{13}/Γ

VALUE CL% DOCUMENT ID TECN COMMENT
< 2.5 × 10⁻⁶ 90 YANG 14 BELL $e^+e^- \rightarrow J/\psi X$

$\Gamma(J/\psi(1S)X(3940))/\Gamma_{total}$ Γ_{14}/Γ

VALUE CL% DOCUMENT ID TECN COMMENT
< 2.0 × 10⁻⁶ 90 YANG 14 BELL $e^+e^- \rightarrow J/\psi X$

$\Gamma(J/\psi(1S)X(4160))/\Gamma_{total}$ Γ_{15}/Γ

VALUE CL% DOCUMENT ID TECN COMMENT
< 2.0 × 10⁻⁶ 90 YANG 14 BELL $e^+e^- \rightarrow J/\psi X$

$\Gamma(\chi_{c1} \text{ anything})/\Gamma_{total}$ Γ_{16}/Γ

VALUE (units 10^{-4}) EVTS DOCUMENT ID TECN COMMENT
2.24 ± 0.44 ± 0.20 376 JIA 17 BELL $T(2S) \rightarrow \gamma J/\psi(1S)$

$\Gamma(\chi_{c1}(1P)^0 X_{tetra})/\Gamma_{total}$ Γ_{17}/Γ

VALUE CL% DOCUMENT ID TECN COMMENT
< 36.7 × 10⁻⁶ 90 ¹ JIA 17A BELL $e^+e^- \rightarrow$ hadrons

¹ For a tetraquark state X_{tetra} , with mass in the range 1.16–2.46 GeV and width in the range 0–0.3 GeV. Measured 90% CL limits as a function of X_{tetra} mass and width range from 4.4×10^{-6} to 36.7×10^{-6} .

$\Gamma(\chi_{c2} \text{ anything})/\Gamma_{total}$ Γ_{18}/Γ

VALUE (units 10^{-4}) DOCUMENT ID TECN COMMENT
2.28 ± 0.73 ± 0.34 JIA 17 BELL $T(2S) \rightarrow \gamma J/\psi(1S)$

$\Gamma(\psi(2S)\eta_c)/\Gamma_{total}$ Γ_{19}/Γ

VALUE CL% DOCUMENT ID TECN COMMENT
< 5.1 × 10⁻⁶ 90 YANG 14 BELL $e^+e^- \rightarrow \psi(2S) X$

$\Gamma(\psi(2S)\chi_{c0})/\Gamma_{total}$ Γ_{20}/Γ

VALUE CL% DOCUMENT ID TECN COMMENT
< 4.7 × 10⁻⁶ 90 YANG 14 BELL $e^+e^- \rightarrow \psi(2S) X$

$\Gamma(\psi(2S)\chi_{c1})/\Gamma_{total}$ Γ_{21}/Γ

VALUE CL% DOCUMENT ID TECN COMMENT
< 2.5 × 10⁻⁶ 90 YANG 14 BELL $e^+e^- \rightarrow \psi(2S) X$

$\Gamma(\psi(2S)\chi_{c2})/\Gamma_{total}$ Γ_{22}/Γ

VALUE CL% DOCUMENT ID TECN COMMENT
< 1.9 × 10⁻⁶ 90 YANG 14 BELL $e^+e^- \rightarrow \psi(2S) X$

$\Gamma(\psi(2S)\eta_c(2S))/\Gamma_{total}$ Γ_{23}/Γ

VALUE CL% DOCUMENT ID TECN COMMENT
< 3.3 × 10⁻⁶ 90 YANG 14 BELL $e^+e^- \rightarrow \psi(2S) X$

$\Gamma(\psi(2S)X(3940))/\Gamma_{total}$ Γ_{24}/Γ

VALUE CL% DOCUMENT ID TECN COMMENT
< 3.9 × 10⁻⁶ 90 YANG 14 BELL $e^+e^- \rightarrow \psi(2S) X$

$\Gamma(\psi(2S)X(4160))/\Gamma_{total}$ Γ_{25}/Γ

VALUE CL% DOCUMENT ID TECN COMMENT
< 3.9 × 10⁻⁶ 90 YANG 14 BELL $e^+e^- \rightarrow \psi(2S) X$

$\Gamma(Z_c(3900)^+ Z_c(3900)^-)/\Gamma_{total}$ Γ_{26}/Γ

VALUE CL% DOCUMENT ID TECN COMMENT
< 1.0 × 10⁻⁶ 90 ¹ JIA 18 BELL $T(2S) \rightarrow J/\psi\pi^\pm X$
¹ Assuming $B(Z_c(3900)^\pm) \rightarrow J/\psi\pi^\pm = 1$.

$\Gamma(Z_c(4200)^+ Z_c(4200)^-)/\Gamma_{total}$ Γ_{27}/Γ

VALUE CL% DOCUMENT ID TECN COMMENT
< 16.7 × 10⁻⁶ 90 ¹ JIA 18 BELL $T(1S) \rightarrow J/\psi\pi^\pm X$
¹ Assuming $B(Z_c(4200)^\pm) \rightarrow J/\psi\pi^\pm = 1$

$\Gamma(Z_c(3900)^\pm Z_c(4200)^\mp)/\Gamma_{total}$ Γ_{28}/Γ

VALUE CL% DOCUMENT ID TECN COMMENT
< 7.3 × 10⁻⁶ 90 ¹ JIA 18 BELL $T(2S) \rightarrow J/\psi\pi^\pm X$
¹ Assuming $B(Z_c(4200)^\pm) \rightarrow J/\psi\pi^\pm = 1 = B(Z_c(3900)^\pm) \rightarrow J/\psi\pi^\pm$.

$\Gamma(X(4050)^+ X(4050)^-)/\Gamma_{total}$ Γ_{29}/Γ

VALUE CL% DOCUMENT ID TECN COMMENT
< 13.5 × 10⁻⁶ 90 ¹ JIA 18 BELL $T(2S) \rightarrow \chi_{c1}(1P)\pi^\pm X$
¹ Assuming $B(X(4050)^\pm) \rightarrow \chi_{c1}(1P)\pi^\pm$

$\Gamma(X(4250)^+ X(4250)^-)/\Gamma_{total}$ Γ_{30}/Γ

VALUE CL% DOCUMENT ID TECN COMMENT
< 26.7 × 10⁻⁶ 90 ¹ JIA 18 BELL $T(2S) \rightarrow \chi_{c1}(1P)\pi^\pm X$
¹ Assuming $B(X(4250)^\pm) \rightarrow \chi_{c1}(1P)\pi^\pm = 1$

$\Gamma(X(4050)^\pm X(4250)^\mp)/\Gamma_{total}$ Γ_{31}/Γ

VALUE CL% DOCUMENT ID TECN COMMENT
< 27.2 × 10⁻⁶ 90 ¹ JIA 18 BELL $T(2S) \rightarrow \chi_{c1}(1P)\pi^\pm X$
¹ Assuming $B(X(4050)^\pm) \rightarrow \chi_{c1}(1P)\pi^\pm = 1 = B(X(4250)^\pm) \rightarrow \chi_{c1}(1P)\pi^\pm$

$\Gamma(Z_c(4430)^+ Z_c(4430)^-)/\Gamma_{total}$ Γ_{32}/Γ

VALUE CL% DOCUMENT ID TECN COMMENT
< 20.3 × 10⁻⁶ 90 ¹ JIA 18 BELL $T(2S) \rightarrow \psi(2S)\pi^\pm X$
¹ Assuming $B(Z_c(4430)^\pm) \rightarrow \psi(2P)\pi^\pm = 1$

$\Gamma(X(4055)^\pm X(4055)^\mp)/\Gamma_{total}$ Γ_{33}/Γ

VALUE CL% DOCUMENT ID TECN COMMENT
< 11.1 × 10⁻⁶ 90 ¹ JIA 18 BELL $T(2S) \rightarrow \psi(2S)\pi^\pm X$
¹ Assuming $B(X(4055)^\pm) \rightarrow \psi(2S)\pi^\pm = 1$

$\Gamma(X(4055)^\pm Z_c(4430)^\mp)/\Gamma_{total}$ Γ_{34}/Γ

VALUE CL% DOCUMENT ID TECN COMMENT
< 21.1 × 10⁻⁶ 90 ¹ JIA 18 BELL $T(2S) \rightarrow \psi(2S)\pi^\pm X$
¹ Assuming $B(X(4055)^\pm) \rightarrow \psi(2S)\pi^\pm = 1 = B(Z_c(4430)^\pm) \rightarrow \psi(2S)\pi^\pm$

$\Gamma(\overline{2}H \text{ anything})/\Gamma_{total}$ Γ_{35}/Γ

VALUE (units 10^{-5}) EVTS DOCUMENT ID TECN COMMENT
2.78 ^{+0.30} -0.26 OUR AVERAGE Error includes scale factor of 1.2.
2.64 ± 0.11 ^{+0.26} -0.21 LEES 14G BABR $e^+e^- \rightarrow \overline{2}H X$
3.37 ± 0.50 ± 0.25 58 ASNER 07 CLEO $e^+e^- \rightarrow \overline{2}H X$

$\Gamma(g g g)/\Gamma_{total}$ Γ_{37}/Γ

VALUE (units 10^{-2}) EVTS DOCUMENT ID TECN COMMENT
58.8 ± 1.2 6M ¹ BESSON 06A CLEO $T(2S) \rightarrow$ hadrons

¹ Calculated using the value $\Gamma(\gamma g g)/\Gamma(g g g) = (3.18 \pm 0.04 \pm 0.22 \pm 0.41)\%$ from BESSON 06A and PDG 08 values of $B(\pi^+\pi^- T(1S)) = (18.1 \pm 0.4)\%$, $B(\pi^0\pi^0 T(1S)) = (8.6 \pm 0.4)\%$, $B(\mu^+\mu^-) = (1.93 \pm 0.17)\%$, and $R_{hadrons} = 3.51$. The statistical error is negligible and the systematic error is partially correlated with that of $\Gamma(\gamma g g)/\Gamma_{total}$ measurement of BESSON 06A.

Meson Particle Listings

 $\Upsilon(2S)$

$\Gamma(\gamma g g)/\Gamma(g g g)$				Γ_{38}/Γ_{37}		
VALUE (units 10^{-2})	EVTS	DOCUMENT ID	TECN	COMMENT		
$3.18 \pm 0.04 \pm 0.47$	6M	BESSON	06A	CLEO	$\Upsilon(2S) \rightarrow (\gamma +) \text{ hadrons}$	
$\Gamma(\phi K^+ K^-)/\Gamma_{\text{total}}$				Γ_{39}/Γ		
VALUE (units 10^{-6})	EVTS	DOCUMENT ID	TECN	COMMENT		
$1.58 \pm 0.33 \pm 0.18$	58	SHEN	12A	BELL	$\Upsilon(1S) \rightarrow 2(K^+ K^-)$	
$\Gamma(\omega \pi^+ \pi^-)/\Gamma_{\text{total}}$				Γ_{40}/Γ		
VALUE (units 10^{-6})	CL%	DOCUMENT ID	TECN	COMMENT		
<2.58	90	SHEN	12A	BELL	$\Upsilon(1S) \rightarrow 2(\pi^+ \pi^-) \pi^0$	
$\Gamma(K^*(892)^0 K^- \pi^+ + \text{c.c.})/\Gamma_{\text{total}}$				Γ_{41}/Γ		
VALUE (units 10^{-6})	EVTS	DOCUMENT ID	TECN	COMMENT		
$2.32 \pm 0.40 \pm 0.54$	135	SHEN	12A	BELL	$\Upsilon(1S) \rightarrow K^+ K^- \pi^+ \pi^-$	
$\Gamma(\phi f_2'(1525))/\Gamma_{\text{total}}$				Γ_{42}/Γ		
VALUE (units 10^{-6})	CL%	DOCUMENT ID	TECN	COMMENT		
<1.33	90	SHEN	12A	BELL	$\Upsilon(1S) \rightarrow 2(K^+ K^-)$	
$\Gamma(\omega f_2(1270))/\Gamma_{\text{total}}$				Γ_{43}/Γ		
VALUE (units 10^{-6})	CL%	DOCUMENT ID	TECN	COMMENT		
<0.57	90	SHEN	12A	BELL	$\Upsilon(1S) \rightarrow 2(\pi^+ \pi^-) \pi^0$	
$\Gamma(\rho(770) \rho_2(1320))/\Gamma_{\text{total}}$				Γ_{44}/Γ		
VALUE (units 10^{-6})	CL%	DOCUMENT ID	TECN	COMMENT		
<0.88	90	SHEN	12A	BELL	$\Upsilon(1S) \rightarrow 2(\pi^+ \pi^-) \pi^0$	
$\Gamma(K^*(892)^0 \bar{K}_2^0(1430)^0 + \text{c.c.})/\Gamma_{\text{total}}$				Γ_{45}/Γ		
VALUE (units 10^{-6})	EVTS	DOCUMENT ID	TECN	COMMENT		
$1.53 \pm 0.52 \pm 0.19$	32	SHEN	12A	BELL	$\Upsilon(1S) \rightarrow K^+ K^- \pi^+ \pi^-$	
$\Gamma(K_1(1270)^\pm K^\mp)/\Gamma_{\text{total}}$				Γ_{46}/Γ		
VALUE (units 10^{-6})	CL%	DOCUMENT ID	TECN	COMMENT		
<3.22	90	SHEN	12A	BELL	$\Upsilon(1S) \rightarrow K^+ K^- \pi^+ \pi^-$	
$\Gamma(K_1(1400)^\pm K^\mp)/\Gamma_{\text{total}}$				Γ_{47}/Γ		
VALUE (units 10^{-6})	CL%	DOCUMENT ID	TECN	COMMENT		
<0.83	90	SHEN	12A	BELL	$\Upsilon(1S) \rightarrow K^+ K^- \pi^+ \pi^-$	
$\Gamma(b_1(1235)^\pm \pi^\mp)/\Gamma_{\text{total}}$				Γ_{48}/Γ		
VALUE (units 10^{-6})	CL%	DOCUMENT ID	TECN	COMMENT		
<0.40	90	SHEN	12A	BELL	$\Upsilon(1S) \rightarrow 2(\pi^+ \pi^-) \pi^0$	
$\Gamma(\rho\pi)/\Gamma_{\text{total}}$				Γ_{49}/Γ		
VALUE (units 10^{-6})	CL%	DOCUMENT ID	TECN	COMMENT		
<1.16	90	SHEN	13	BELL	$\Upsilon(2S) \rightarrow \pi^+ \pi^- \pi^0$	
$\Gamma(\pi^+ \pi^- \pi^0)/\Gamma_{\text{total}}$				Γ_{50}/Γ		
VALUE (units 10^{-6})	CL%	DOCUMENT ID	TECN	COMMENT		
<0.80	90	SHEN	13	BELL	$\Upsilon(2S) \rightarrow \pi^+ \pi^- \pi^0$	
$\Gamma(\omega \pi^0)/\Gamma_{\text{total}}$				Γ_{51}/Γ		
VALUE (units 10^{-6})	CL%	DOCUMENT ID	TECN	COMMENT		
<1.63	90	SHEN	13	BELL	$\Upsilon(2S) \rightarrow \pi^+ \pi^- \pi^0 \pi^0$	
$\Gamma(\pi^+ \pi^- \pi^0 \pi^0)/\Gamma_{\text{total}}$				Γ_{52}/Γ		
VALUE (units 10^{-6})	EVTS	DOCUMENT ID	TECN	COMMENT		
$13.0 \pm 1.9 \pm 2.1$	261 \pm 37	SHEN	13	BELL	$\Upsilon(2S) \rightarrow \pi^+ \pi^- \pi^0 \pi^0$	
$\Gamma(K_S^0 K^+ \pi^- + \text{c.c.})/\Gamma_{\text{total}}$				Γ_{53}/Γ		
VALUE (units 10^{-6})	CL%	EVTS	DOCUMENT ID	TECN	COMMENT	
$1.14 \pm 0.30 \pm 0.13$		40 \pm 10	SHEN	13	BELL	$\Upsilon(2S) \rightarrow K_S^0 K^- \pi^+$
• • • We do not use the following data for averages, fits, limits, etc. • • •						
<3.2	90		¹ DOBBS	12A	$\Upsilon(2S) \rightarrow K_S^0 K^- \pi^+$	
¹ Obtained by analyzing CLEO III data but not authored by the CLEO Collaboration.						
$\Gamma(K^*(892)^0 \bar{K}^0 + \text{c.c.})/\Gamma_{\text{total}}$				Γ_{54}/Γ		
VALUE (units 10^{-6})	CL%	DOCUMENT ID	TECN	COMMENT		
<4.22	90	SHEN	13	BELL	$\Upsilon(2S) \rightarrow K_S^0 K^- \pi^+$	
$\Gamma(K^*(892)^- K^+ + \text{c.c.})/\Gamma_{\text{total}}$				Γ_{55}/Γ		
VALUE (units 10^{-6})	CL%	DOCUMENT ID	TECN	COMMENT		
<1.45	90	SHEN	13	BELL	$\Upsilon(2S) \rightarrow K_S^0 K^- \pi^+$	
$\Gamma(f_1(1285) \text{ anything})/\Gamma_{\text{total}}$				Γ_{56}/Γ		
VALUE (units 10^{-3})	EVTS	DOCUMENT ID	TECN	COMMENT		
$2.20 \pm 1.50 \pm 0.63$	2.9k	JIA	17A	BELL	$e^+ e^- \rightarrow \text{hadrons}$	
$\Gamma(f_1(1285) X_{tetra})/\Gamma_{\text{total}}$				Γ_{57}/Γ		
VALUE	CL%	DOCUMENT ID	TECN	COMMENT		
$<64.7 \times 10^{-6}$	90	¹ JIA	17A	BELL	$e^+ e^- \rightarrow \text{hadrons}$	
¹ For a tetraquark state X_{tetra} , with mass in the range 1.16–2.46 GeV and width in the range 0–0.3 GeV. Measured 90% CL limits as a function of X_{tetra} mass and width range from 7.8×10^{-6} to 64.7×10^{-6} .						
$\Gamma(\text{Sum of 100 exclusive modes})/\Gamma_{\text{total}}$				Γ_{58}/Γ		
VALUE (units 10^{-2})	DOCUMENT ID	TECN	COMMENT			
0.29 ± 0.03	^{1,2} DOBBS	12A	$\Upsilon(2S) \rightarrow \text{hadrons}$			
¹ DOBBS 12A presents individual exclusive branching fractions or upper limits for 100 modes of four to ten pions, kaons, or protons.						
² Obtained by analyzing CLEO III data but not authored by the CLEO Collaboration.						
$\Gamma(\gamma \chi_{b1}(1P))/\Gamma_{\text{total}}$				Γ_{59}/Γ		
VALUE	EVTS	DOCUMENT ID	TECN	COMMENT		
0.069 ± 0.004	OUR AVERAGE					
0.0693 \pm 0.0012 \pm 0.0041	407k	ARTUSO	05	CLEO	$e^+ e^- \rightarrow \gamma X$	
0.069 \pm 0.005 \pm 0.009		EDWARDS	99	CLE2	$\Upsilon(2S) \rightarrow \gamma \chi(1P)$	
0.091 \pm 0.018 \pm 0.022		ALBRECHT	85E	ARG	$e^+ e^- \rightarrow \gamma \text{conv. } X$	
0.065 \pm 0.007 \pm 0.012		NERNST	85	CBAL	$e^+ e^- \rightarrow \gamma X$	
0.080 \pm 0.017 \pm 0.016		HAAS	84	CLEO	$e^+ e^- \rightarrow \gamma \text{conv. } X$	
0.059 \pm 0.014		KLOPFEN...	83	CUSB	$e^+ e^- \rightarrow \gamma X$	
$\Gamma(\gamma \chi_{b2}(1P))/\Gamma_{\text{total}}$				Γ_{60}/Γ		
VALUE	EVTS	DOCUMENT ID	TECN	COMMENT		
0.0715 ± 0.0035	OUR AVERAGE					
0.0724 \pm 0.0011 \pm 0.0040	410k	ARTUSO	05	CLEO	$e^+ e^- \rightarrow \gamma X$	
0.074 \pm 0.005 \pm 0.008		EDWARDS	99	CLE2	$\Upsilon(2S) \rightarrow \gamma \chi(1P)$	
0.098 \pm 0.021 \pm 0.024		ALBRECHT	85E	ARG	$e^+ e^- \rightarrow \gamma \text{conv. } X$	
0.058 \pm 0.007 \pm 0.010		NERNST	85	CBAL	$e^+ e^- \rightarrow \gamma X$	
0.102 \pm 0.018 \pm 0.021		HAAS	84	CLEO	$e^+ e^- \rightarrow \gamma \text{conv. } X$	
0.061 \pm 0.014		KLOPFEN...	83	CUSB	$e^+ e^- \rightarrow \gamma X$	
$\Gamma(\gamma \chi_{b0}(1P))/\Gamma_{\text{total}}$				Γ_{61}/Γ		
VALUE	EVTS	DOCUMENT ID	TECN	COMMENT		
0.038 ± 0.004	OUR AVERAGE					
0.0375 \pm 0.0012 \pm 0.0047	198k	ARTUSO	05	CLEO	$e^+ e^- \rightarrow \gamma X$	
0.034 \pm 0.005 \pm 0.006		EDWARDS	99	CLE2	$\Upsilon(2S) \rightarrow \gamma \chi(1P)$	
0.064 \pm 0.014 \pm 0.016		ALBRECHT	85E	ARG	$e^+ e^- \rightarrow \gamma \text{conv. } X$	
0.036 \pm 0.008 \pm 0.009		NERNST	85	CBAL	$e^+ e^- \rightarrow \gamma X$	
0.044 \pm 0.023 \pm 0.009		HAAS	84	CLEO	$e^+ e^- \rightarrow \gamma \text{conv. } X$	
• • • We do not use the following data for averages, fits, limits, etc. • • •						
0.035 \pm 0.014		KLOPFEN...	83	CUSB	$e^+ e^- \rightarrow \gamma X$	
$\Gamma(\gamma f_0(1710))/\Gamma_{\text{total}}$				Γ_{62}/Γ		
VALUE (units 10^{-5})	CL%	DOCUMENT ID	TECN	COMMENT		
<5.9	90	¹ ALBRECHT	89	ARG	$\Upsilon(2S) \rightarrow \gamma K^+ K^-$	
• • • We do not use the following data for averages, fits, limits, etc. • • •						
< 5.9	90	² ALBRECHT	89	ARG	$\Upsilon(2S) \rightarrow \gamma \pi^+ \pi^-$	
¹ Re-evaluated assuming $B(f_0(1710) \rightarrow K^+ K^-) = 0.19$.						
² Includes unknown branching ratio of $f_0(1710) \rightarrow \pi^+ \pi^-$.						
$\Gamma(\gamma f_2'(1525))/\Gamma_{\text{total}}$				Γ_{63}/Γ		
VALUE (units 10^{-5})	CL%	DOCUMENT ID	TECN	COMMENT		
<53	90	¹ ALBRECHT	89	ARG	$\Upsilon(2S) \rightarrow \gamma K^+ K^-$	
¹ Re-evaluated assuming $B(f_2'(1525) \rightarrow K \bar{K}) = 0.71$.						
$\Gamma(\gamma f_2(1270))/\Gamma_{\text{total}}$				Γ_{64}/Γ		
VALUE (units 10^{-5})	CL%	DOCUMENT ID	TECN	COMMENT		
<24.1	90	¹ ALBRECHT	89	ARG	$\Upsilon(2S) \rightarrow \gamma \pi^+ \pi^-$	
¹ Using $B(f_2(1270) \rightarrow \pi \pi) = 0.84$.						
$\Gamma(\gamma f_J(2220))/\Gamma_{\text{total}}$				Γ_{65}/Γ		
VALUE (units 10^{-5})	CL%	DOCUMENT ID	TECN	COMMENT		
<6.8	90	¹ ALBRECHT	89	ARG	$\Upsilon(2S) \rightarrow \gamma K^+ K^-$	
• • • We do not use the following data for averages, fits, limits, etc. • • •						
¹ Includes unknown branching ratio of $f_J(2220) \rightarrow K^+ K^-$.						
$\Gamma(\gamma \eta_c(1S))/\Gamma_{\text{total}}$				Γ_{66}/Γ		
VALUE	CL%	DOCUMENT ID	TECN	COMMENT		
$<2.7 \times 10^{-5}$	90	WANG	11B	BELL	$\Upsilon(2S) \rightarrow \gamma X$	
$\Gamma(\gamma \chi_{c0})/\Gamma_{\text{total}}$				Γ_{67}/Γ		
VALUE	CL%	DOCUMENT ID	TECN	COMMENT		
$<1.0 \times 10^{-4}$	90	WANG	11B	BELL	$\Upsilon(2S) \rightarrow \gamma X$	
$\Gamma(\gamma \chi_{c1})/\Gamma_{\text{total}}$				Γ_{68}/Γ		
VALUE	CL%	DOCUMENT ID	TECN	COMMENT		
$<3.6 \times 10^{-6}$	90	WANG	11B	BELL	$\Upsilon(2S) \rightarrow \gamma X$	

See key on page 999

Meson Particle Listings

$\Upsilon(2S), \Upsilon_2(1D)$

$\Gamma(\gamma\chi_{c2})/\Gamma_{total}$					Γ_{69}/Γ
VALUE	CL%	DOCUMENT ID	TECN	COMMENT	
$<1.5 \times 10^{-5}$	90	WANG	11B	BELL	$\Upsilon(2S) \rightarrow \gamma X$

$\Gamma(\gamma\chi_{c1}(3872) \rightarrow \pi^+ \pi^- J/\psi)/\Gamma_{total}$					Γ_{70}/Γ
VALUE	CL%	DOCUMENT ID	TECN	COMMENT	
$<0.8 \times 10^{-6}$	90	WANG	11B	BELL	$\Upsilon(2S) \rightarrow \gamma X$

$\Gamma(\gamma\chi_{c1}(3872) \rightarrow \pi^+ \pi^- \pi^0 J/\psi)/\Gamma_{total}$					Γ_{71}/Γ
VALUE	CL%	DOCUMENT ID	TECN	COMMENT	
$<2.4 \times 10^{-6}$	90	WANG	11B	BELL	$\Upsilon(2S) \rightarrow \gamma X$

$\Gamma(\gamma X(3915) \rightarrow \omega J/\psi)/\Gamma_{total}$					Γ_{72}/Γ
VALUE	CL%	DOCUMENT ID	TECN	COMMENT	
$<2.8 \times 10^{-6}$	90	WANG	11B	BELL	$\Upsilon(2S) \rightarrow \gamma X$

$\Gamma(\gamma\chi_{c1}(4140) \rightarrow \phi J/\psi)/\Gamma_{total}$					Γ_{73}/Γ
VALUE	CL%	DOCUMENT ID	TECN	COMMENT	
$<1.2 \times 10^{-6}$	90	WANG	11B	BELL	$\Upsilon(2S) \rightarrow \gamma X$

$\Gamma(\gamma X(4350) \rightarrow \phi J/\psi)/\Gamma_{total}$					Γ_{74}/Γ
VALUE	CL%	DOCUMENT ID	TECN	COMMENT	
$<1.3 \times 10^{-6}$	90	WANG	11B	BELL	$\Upsilon(2S) \rightarrow \gamma X$

$\Gamma(\gamma\eta_b(1S))/\Gamma_{total}$					Γ_{75}/Γ
VALUE (units 10^{-4})	CL%	EVTS	DOCUMENT ID	TECN	COMMENT
5.5 ± 1.1	0.9		OUR AVERAGE Error includes scale factor of 1.2.		
$6.1 \pm 0.6 + 0.9$		29k	FULSOM	18	BELL $\Upsilon(2S) \rightarrow \gamma X$
$3.9 \pm 1.1 + 1.1$		$13 \pm 5k$	¹ AUBERT	09AQ	BABR $\Upsilon(2S) \rightarrow \gamma X$

- • • We do not use the following data for averages, fits, limits, etc. • • •
- <21 90 LEES 11J BABR $\Upsilon(2S) \rightarrow X\gamma$
- < 8.4 90 ¹BONVICINI 10 CLEO $\Upsilon(2S) \rightarrow \gamma X$
- < 5.1 90 ²ARTUSO 05 CLEO $e^+e^- \rightarrow \gamma X$

¹ Assuming $\Gamma_{\eta_b(1S)} = 10$ MeV.
² Superseded by BONVICINI 10.

$\Gamma(\gamma\eta_b(1S) \rightarrow \gamma \text{Sum of 26 exclusive modes})/\Gamma_{total}$					Γ_{76}/Γ
VALUE	CL%	DOCUMENT ID	TECN	COMMENT	
$<3.7 \times 10^{-6}$		SANDILYA	13	BELL	$\Upsilon(2S) \rightarrow \gamma$ hadrons

$\Gamma(\gamma X_{b\bar{b}} \rightarrow \gamma \text{Sum of 26 exclusive modes})/\Gamma_{total}$					Γ_{77}/Γ
VALUE (units 10^{-6})	CL%	EVTS	DOCUMENT ID	TECN	COMMENT
< 4.9	90		SANDILYA	13	BELL $\Upsilon(2S) \rightarrow \gamma$ hadrons

- • • We do not use the following data for averages, fits, limits, etc. • • •
- $46.2 \pm 29.7 \pm 10.6$ 10 ¹DOBBS 12 $\Upsilon(2S) \rightarrow \gamma$ hadrons

¹ Obtained by analyzing CLEO III data but not authored by the CLEO Collaboration.

$\Gamma(\gamma X \rightarrow \gamma + \geq 4 \text{ prongs})/\Gamma_{total}$					Γ_{78}/Γ
(1.5 GeV $< m_X < 5.0$ GeV)					
VALUE (units 10^{-4})	CL%	DOCUMENT ID	TECN	COMMENT	
<1.95	95	ROSNER	07A	CLEO	$e^+e^- \rightarrow \gamma X$

$\Gamma(\gamma A^0 \rightarrow \gamma \text{ hadrons})/\Gamma_{total}$					Γ_{79}/Γ
(0.3 GeV $< m_{A^0} < 7$ GeV)					
VALUE	CL%	DOCUMENT ID	TECN	COMMENT	
$<8 \times 10^{-5}$	90	¹ LEES	11H	BABR	$\Upsilon(2S) \rightarrow \gamma$ hadrons

¹ For a narrow scalar or pseudoscalar A^0 , excluding known resonances, with mass in the range 0.3–7 GeV. Measured 90% CL limits as a function of m_{A^0} range from 1×10^{-6} to 8×10^{-5} .

$\Gamma(\gamma a_1^0 \rightarrow \gamma \mu^+ \mu^-)/\Gamma_{total}$					Γ_{80}/Γ
VALUE (units 10^{-6})	CL%	DOCUMENT ID	TECN	COMMENT	
<8.3	90	¹ AUBERT	09Z	BABR	$e^+e^- \rightarrow \gamma a_1^0 \rightarrow \gamma \mu^+ \mu^-$

¹ For a narrow scalar or pseudoscalar a_1^0 with mass in the range 212–9300 MeV, excluding J/ψ and $\psi(2S)$. Measured 90% CL limits as a function of $m_{a_1^0}$ range from 0.26–8.3 $\times 10^{-6}$.

LEPTON FAMILY NUMBER (LF) VIOLATING MODES

$\Gamma(e^\pm \tau^\mp)/\Gamma_{total}$					Γ_{81}/Γ
VALUE (units 10^{-6})	CL%	DOCUMENT ID	TECN	COMMENT	
<3.2	90	LEES	10B	BABR	$e^+e^- \rightarrow e^\pm \tau^\mp$

$\Gamma(\mu^\pm \tau^\mp)/\Gamma_{total}$					Γ_{82}/Γ
VALUE (units 10^{-6})	CL%	DOCUMENT ID	TECN	COMMENT	
< 3.3	90	LEES	10B	BABR	$e^+e^- \rightarrow \mu^\pm \tau^\mp$

- • • We do not use the following data for averages, fits, limits, etc. • • •
- <14.4 95 LOVE 08A CLEO $e^+e^- \rightarrow \mu^\pm \tau^\mp$

$\Upsilon(2S)$ Cross-Particle Branching Ratios				
$B(\Upsilon(2S) \rightarrow \pi^+ \pi^-) \times B(\Upsilon(3S) \rightarrow \Upsilon(2S) X)$				
VALUE (units 10^{-2})	EVTS	DOCUMENT ID	TECN	COMMENT
$1.78 \pm 0.02 \pm 0.11$	906k	LEES	11C	BABR $e^+e^- \rightarrow \pi^+ \pi^- X$

$\Upsilon(2S)$ REFERENCES

FULSOM 18 PRL 121 232001	B. G. Fulsom et al.	(BELLE Collab.)
JIA 18 PR D97 112004	S. Jia et al.	(BELLE Collab.)
JIA 17 PR D95 012001	S. Jia et al.	(BELLE Collab.)
JIA 17A PR D96 112002	S. Jia et al.	(BELLE Collab.)
LEES 14G PR D89 111102	J.P. Lees et al.	(BABAR Collab.)
YANG 14 PR D90 112008	S.D. Yang et al.	(BELLE Collab.)
SANDILYA 13 PRL 111 112001	S. Sandilya et al.	(BELLE Collab.)
SHEN 13 PR D88 011102	C.P. Shen et al.	(BELLE Collab.)
TAMPONI 13 PR D87 011104	U. Tamponi et al.	(BELLE Collab.)
DOBBS 12 PRL 109 082001	S. Dobbs et al.	(BELLE Collab.)
DOBBS 12A PR D86 052003	S. Dobbs et al.	(BELLE Collab.)
SHEN 12A PR D86 031102	C.P. Shen et al.	(BELLE Collab.)
LEES 11C PR D84 011104	J.P. Lees et al.	(BABAR Collab.)
LEES 11H PRL 107 221803	J.P. Lees et al.	(BABAR Collab.)
LEES 11J PR D84 072002	J.P. Lees et al.	(BABAR Collab.)
LEES 11L PR D84 092003	J.P. Lees et al.	(BABAR Collab.)
WANG 11B PR D84 071107	X.L. Wang et al.	(BELLE Collab.)
BONVICINI 10 PR D81 031104	G. Bonvicini et al.	(CLEO Collab.)
LEES 10B PRL 104 151802	J.P. Lees et al.	(BABAR Collab.)
AUBERT 09A0 PR 103 161801	B. Aubert et al.	(BABAR Collab.)
AUBERT 09Z PRL 103 081803	B. Aubert et al.	(BABAR Collab.)
BHARI 09Z PR D79 011103	S.R. Bhari et al.	(CLEO Collab.)
AUBERT 08BP PR D78 112002	B. Aubert et al.	(BABAR Collab.)
HE 08A PRL 101 192001	Q. He et al.	(CLEO Collab.)
LOVE 08A PRL 101 201601	W. Love et al.	(CLEO Collab.)
PDG 08 PL B667 1	C. Amsler et al.	(PDG Collab.)
ASNER 07 PR D75 012009	D.M. Asner et al.	(CLEO Collab.)
BESSON 07 PRL 98 052002	D. Besson et al.	(CLEO Collab.)
ROSNER 07A PR D76 117102	J.L. Rosner et al.	(CLEO Collab.)
BESSON 06A PR D74 012003	D. Besson et al.	(CLEO Collab.)
ROSNER 06 PRL 96 092003	J.L. Rosner et al.	(CLEO Collab.)
ADAMS 05 PRL 94 012001	G.S. Adams et al.	(CLEO Collab.)
ARTUSO 05 PRL 94 032001	M. Artuso et al.	(CLEO Collab.)
ARTAMONOV 00 PL B474 427	A.S. Artamonov et al.	(CLEO Collab.)
EDWARDS 99 PR D59 032003	K.W. Edwards et al.	(CLEO Collab.)
ALEXANDER 98 PR D58 052004	J.P. Alexander et al.	(CLEO Collab.)
BARU 96 PRPL 267 71	S.E. Baru et al.	(NOVO)
KOBEL 92 ZPHY C53 193	M. Kobel et al.	(Crystal Ball Collab.)
MASCHMANN 90 ZPHY C46 555	W.S. Maschmann et al.	(Crystal Ball Collab.)
ALBRECHT 89 ZPHY C42 349	H. Albrecht et al.	(ARGUS Collab.)
KAARSBERG 89 PRL 62 2077	T.M. Kaarsberg et al.	(CUSB Collab.)
BUCHMUEL... 88 HE e^+e^- Physics 412	W. Buchmueller, S. Cooper	(HANM, DESY, MIT)
Editors: A. Ali and P. Soering, World Scientific, Singapore		
JAKUBOWSKI 88 ZPHY C40 49	Z. Jakubowski et al.	(Crystal Ball Collab.)
ALBRECHT 87 ZPHY C35 283	H. Albrecht et al.	(ARGUS Collab.)
COHEN 87 RMP 59 1121	E.R. Cohen, B.N. Taylor	(RIS C, NBS)
LURZ 87 ZPHY C36 383	B. Lurz et al.	(Crystal Ball Collab.)
BARU 86B ZPHY C32 622 (erratum)	S.E. Baru et al.	(NOVO)
ALBRECHT 85 ZPHY C28 45	H. Albrecht et al.	(ARGUS Collab.)
ALBRECHT 85E PL 160B 331	H. Albrecht et al.	(ARGUS Collab.)
GELPHIMAN 85 PR D32 2893	D. Gelphiman et al.	(Crystal Ball Collab.)
KURAEV 85 SJNP 41 466	E.A. Kuraev, V.S. Fadin	(NOVO)
Translated from YAF 41 733.		
NERNST 85 PRL 54 2195	R. Nernst et al.	(Crystal Ball Collab.)
ARTAMONOV 84 PL 137B 272	A.S. Artamonov et al.	(NOVO)
BARBER 84 PL 135B 498	D.P. Barber et al.	(CLEO Collab.)
BESSON 84 PR D30 1433	D. Besson et al.	(CLEO Collab.)
FONSECA 84 NP B242 31	V. Fonseca et al.	(CUSB Collab.)
GILES 84B PR D29 1285	R. Giles et al.	(CLEO Collab.)
HAAS 84 PRL 52 799	J. Haas et al.	(CLEO Collab.)
HAAS 84B PR D30 1996	J. Haas et al.	(CLEO Collab.)
KLOPFEN... 83 PRL 51 160	C. Klopffenstein et al.	(CUSB Collab.)
ALBRECHT 82 PL 116B 383	H. Albrecht et al.	(HEIDP, MPIM)
NICZYPORUK 81B PL 100B 95	B. Niczyporuk et al.	(LENA Collab.)
NICZYPORUK 81C PL 99B 169	B. Niczyporuk et al.	(LENA Collab.)
BOCK 80 ZPHY C6 125	P. Bock et al.	(HEIDP, MPIM, DESY, HAMB)

$\Upsilon_2(1D)$

$I_G(J^{PC}) = 0^-(2^{--})$

was $\Upsilon(1D)$

First observed by BONVICINI 04 in the decay $\gamma\gamma \Upsilon(1S)$ and confirmed by DEL-AMO-SANCHEZ 10R in the decay $\pi^+ \pi^- \Upsilon(1S)$. Data consistent with $J^P = 2^-$. The states with $J = 1$ and 3 also possibly seen, but need confirmation.

$\Upsilon_2(1D)$ MASS

VALUE (MeV)	EVTS	DOCUMENT ID	TECN	COMMENT
10163.7 ± 1.4		OUR AVERAGE Error includes scale factor of 1.7.		
$10164.5 \pm 0.8 \pm 0.5$		DEL-AMO-SA...10R	BABR	$\Upsilon(3S) \rightarrow \gamma\gamma \pi^+ \pi^- \ell^+ \ell^-$
$10161.1 \pm 0.6 \pm 1.6$	38	BONVICINI	04	CLE3 $\Upsilon(3S) \rightarrow 4\gamma \ell^+ \ell^-$

$\Upsilon_2(1D)$ DECAY MODES

Mode	Fraction (Γ_i/Γ)
$\Gamma_1 \gamma\gamma \Upsilon(1S)$	seen
$\Gamma_2 \gamma\chi_{bJ}(1P)$	seen
$\Gamma_3 \eta \Upsilon(1S)$	not seen
$\Gamma_4 \pi^+ \pi^- \Upsilon(1S)$	$(6.6 \pm 1.6) \times 10^{-3}$

Meson Particle Listings

$\Upsilon_2(1D), \chi_{b0}(2P)$

$\Upsilon_2(1D)$ BRANCHING RATIOS

$\Gamma(\eta \Upsilon(1S))/\Gamma(\gamma\gamma \Upsilon(1S))$					Γ_3/Γ_1
VALUE	CL%	DOCUMENT ID	TECN	COMMENT	
<0.25	90	BONVICINI	04	CLE3	$\Upsilon(3S) \rightarrow 4\gamma\ell^+\ell^-$

$\Gamma(\pi^+\pi^-\Upsilon(1S))/\Gamma_{\text{total}}$					Γ_4/Γ
VALUE (units 10^{-2})	CL%	DOCUMENT ID	TECN	COMMENT	
$0.66^{+0.15}_{-0.14} \pm 0.06$		¹ DEL-AMO-SA...10R	BABR	$\Upsilon(3S) \rightarrow \gamma\gamma\pi^+\pi^-\ell^+\ell^-$	

¹ Using theoretical predictions for $B(\chi_{bJ}(2P) \rightarrow \gamma \Upsilon_2(1D))$.

$\Gamma(\pi^+\pi^-\Upsilon(1S))/\Gamma(\gamma\gamma \Upsilon(1S))$					Γ_4/Γ_1
VALUE	CL%	DOCUMENT ID	TECN	COMMENT	
<1.2	90	² BONVICINI	04	CLE3	$\Upsilon(3S) \rightarrow 4\gamma\ell^+\ell^-$

² Assuming $J = 2$.

$\Upsilon_2(1D)$ REFERENCES

DEL-AMO-SA...10R	PR D82 111102	P. del Amo Sanchez et al.	(BABAR Collab.)
BONVICINI 04	PR D70 032001	G. Bonvicini et al.	(CLEO Collab.)

$\chi_{b0}(2P)$

$I^G(J^{PC}) = 0^+(0^{++})$
 J needs confirmation.

Observed in radiative decay of the $\Upsilon(3S)$, therefore $C = +$. Branching ratio requires E1 transition, M1 is strongly disfavored, therefore $P = +$.

$\chi_{b0}(2P)$ MASS

VALUE (MeV)	DOCUMENT ID
$10232.5 \pm 0.4 \pm 0.5$ OUR EVALUATION	From γ energy below, using $\Upsilon(3S)$ mass = 10355.2 ± 0.5 MeV

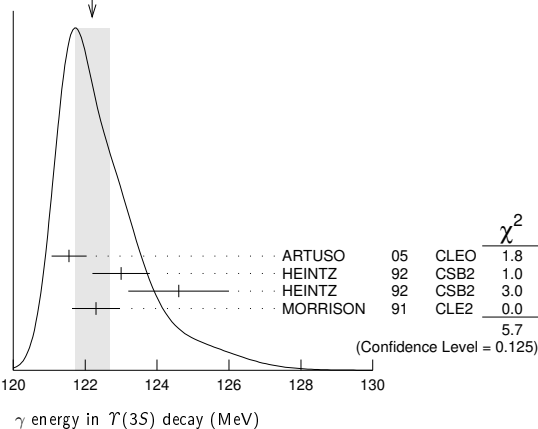
$m_{\chi_{b1}(2P)} - m_{\chi_{b0}(2P)}$				
VALUE (MeV)	DOCUMENT ID	TECN	COMMENT	
23.8 ± 1.7	LEES	14M	BABR $\Upsilon(3S) \rightarrow \gamma\gamma\mu^+\mu^-$	

γ ENERGY IN $\Upsilon(3S)$ DECAY

VALUE (MeV)	EVTS	DOCUMENT ID	TECN	COMMENT
121.9 ± 0.4 OUR EVALUATION		Treating systematic errors as correlated		
122.2 ± 0.5 OUR AVERAGE		Error includes scale factor of 1.4. See the ideogram below.		
$121.55 \pm 0.16 \pm 0.46$		ARTUSO	05	CLEO $\Upsilon(3S) \rightarrow \gamma X$
123.0 ± 0.8	4959	¹ HEINTZ	92	CSB2 $e^+e^- \rightarrow \gamma X$
124.6 ± 1.4	17	² HEINTZ	92	CSB2 $e^+e^- \rightarrow \ell^+\ell^-\gamma\gamma$
$122.3 \pm 0.3 \pm 0.6$	9903	MORRISON	91	CLE2 $e^+e^- \rightarrow \gamma X$

¹ A systematic uncertainty on the energy scale of 0.9% not included. Supersedes NARAIN 91.
² A systematic uncertainty on the energy scale of 0.9% not included. Supersedes HEINTZ 91.

WEIGHTED AVERAGE
 122.2 ± 0.5 (Error scaled by 1.4)



$\chi_{b0}(2P)$ DECAY MODES

Mode	Fraction (Γ_i/Γ)	Confidence level
Γ_1 $\gamma \Upsilon(2S)$	$(1.38 \pm 0.30)\%$	
Γ_2 $\gamma \Upsilon(1S)$	$(3.8 \pm 1.7) \times 10^{-3}$	
Γ_3 $D^0 X$	< 8.2	90%
Γ_4 $\pi^+\pi^-K^+K^-\pi^0$	$< 3.4 \times 10^{-5}$	90%
Γ_5 $2\pi^+\pi^-K^+K^-\pi^0$	$< 5 \times 10^{-5}$	90%
Γ_6 $2\pi^+\pi^-K^+K^-\pi^0$	$< 2.2 \times 10^{-4}$	90%
Γ_7 $2\pi^+2\pi^-2\pi^0$	$< 2.4 \times 10^{-4}$	90%
Γ_8 $2\pi^+2\pi^-K^+K^-$	$< 1.5 \times 10^{-4}$	90%
Γ_9 $2\pi^+2\pi^-K^+K^-\pi^0$	$< 2.2 \times 10^{-4}$	90%
Γ_{10} $2\pi^+2\pi^-K^+K^-\pi^0$	$< 1.1 \times 10^{-3}$	90%
Γ_{11} $3\pi^+2\pi^-K^+K^-\pi^0$	$< 7 \times 10^{-4}$	90%
Γ_{12} $3\pi^+3\pi^-$	$< 7 \times 10^{-5}$	90%
Γ_{13} $3\pi^+3\pi^-2\pi^0$	$< 1.2 \times 10^{-3}$	90%
Γ_{14} $3\pi^+3\pi^-K^+K^-$	$< 1.5 \times 10^{-4}$	90%
Γ_{15} $3\pi^+3\pi^-K^+K^-\pi^0$	$< 7 \times 10^{-4}$	90%
Γ_{16} $4\pi^+4\pi^-$	$< 1.7 \times 10^{-4}$	90%
Γ_{17} $4\pi^+4\pi^-2\pi^0$	$< 6 \times 10^{-4}$	90%

$\chi_{b0}(2P)$ BRANCHING RATIOS

$\Gamma(\gamma \Upsilon(2S))/\Gamma_{\text{total}}$					Γ_1/Γ
VALUE (%)	CL%	DOCUMENT ID	TECN	COMMENT	

1.38 ± 0.30 OUR AVERAGE				
$1.31 \pm 0.27^{+0.13}_{-0.12}$		^{3,4} LEES	14M	BABR $\Upsilon(3S) \rightarrow \gamma\gamma\mu^+\mu^-$
$3.6 \pm 1.6 \pm 0.3$		^{3,5} HEINTZ	92	CSB2 $e^+e^- \rightarrow \ell^+\ell^-\gamma\gamma$
< 2.8	90	⁶ LEES	11J	BABR $\Upsilon(3S) \rightarrow X\gamma$
< 8.9	90	⁷ CRAWFORD	92B	CLE2 $e^+e^- \rightarrow \ell^+\ell^-\gamma\gamma$

••• We do not use the following data for averages, fits, limits, etc. •••
³ Assuming $B(\Upsilon(2S) \rightarrow \mu^+\mu^-) = (1.93 \pm 0.17)\%$.
⁴ LEES 14M reports $[\Gamma(\chi_{b0}(2P) \rightarrow \gamma \Upsilon(2S))/\Gamma_{\text{total}}] \times [B(\Upsilon(3S) \rightarrow \gamma \chi_{b0}(2P))]$ = $(7.7 \pm 1.6) \times 10^{-4}$ which we divide by our best value $B(\Upsilon(3S) \rightarrow \gamma \chi_{b0}(2P)) = (5.9 \pm 0.6) \times 10^{-2}$. Our first error is their experiment's error and our second error is the systematic error from using our best value.
⁵ Recalculated by us. HEINTZ 92 quotes $B(\Upsilon(3S) \rightarrow \gamma \chi_{b0}(2P)) \times B(\chi_{b0}(2P) \rightarrow \gamma \Upsilon(2S)) = (0.28 \pm 0.12 \pm 0.03)\%$ using $B(\Upsilon(2S) \rightarrow \mu^+\mu^-) = (1.44 \pm 0.10)\%$. Supersedes HEINTZ 91.
⁶ LEES 11J quotes a central value of $\Gamma(\chi_{b0}(2P) \rightarrow \gamma \Upsilon(2S))/\Gamma_{\text{total}} \times \Gamma(\Upsilon(3S) \rightarrow \gamma \chi_{b0}(2P))/\Gamma_{\text{total}} = (-0.3 \pm 0.2^{+0.5}_{-0.4})\%$.
⁷ Using $B(\Upsilon(2S) \rightarrow \mu^+\mu^-) = (1.37 \pm 0.26)\%$, $B(\Upsilon(3S) \rightarrow \gamma\gamma \Upsilon(2S)) \times 2 B(\Upsilon(2S) \rightarrow \mu^+\mu^-) < 1.19 \times 10^{-4}$, and $B(\Upsilon(3S) \rightarrow \chi_{b0}(2P)\gamma) = 0.049$.

$\Gamma(\gamma \Upsilon(1S))/\Gamma_{\text{total}}$					Γ_2/Γ
VALUE (%)	CL%	DOCUMENT ID	TECN	COMMENT	

0.38 ± 0.17 OUR AVERAGE				
$0.36 \pm 0.17 \pm 0.03$		^{8,9,10} LEES	14M	BABR $\Upsilon(3S) \rightarrow \gamma\gamma\mu^+\mu^-$
$0.9 \pm 0.7 \pm 0.1$		^{9,11} HEINTZ	92	CSB2 $e^+e^- \rightarrow \ell^+\ell^-\gamma\gamma$
< 1.2	90	¹² LEES	11J	BABR $\Upsilon(3S) \rightarrow X\gamma$
< 2.5	90	¹³ CRAWFORD	92B	CLE2 $e^+e^- \rightarrow \ell^+\ell^-\gamma\gamma$

••• We do not use the following data for averages, fits, limits, etc. •••
⁸ LEES 14M quotes $\Gamma(\chi_{b0}(2P) \rightarrow \gamma \Upsilon(1S))/\Gamma_{\text{total}} \times \Gamma(\Upsilon(3S) \rightarrow \gamma \chi_{b0}(2P))/\Gamma_{\text{total}} = (2.1 \pm 1.0) \times 10^{-4}$ combining the results from $\Upsilon(3S) \rightarrow \gamma\gamma\mu^+\mu^-$ samples with and without photon conversions.
⁹ Assuming $B(\Upsilon(1S) \rightarrow \mu^+\mu^-) = (2.48 \pm 0.05)\%$.
¹⁰ LEES 14M reports $[\Gamma(\chi_{b0}(2P) \rightarrow \gamma \Upsilon(1S))/\Gamma_{\text{total}}] \times [B(\Upsilon(3S) \rightarrow \gamma \chi_{b0}(2P))]$ = $(2.1 \pm 1.0) \times 10^{-4}$ which we divide by our best value $B(\Upsilon(3S) \rightarrow \gamma \chi_{b0}(2P)) = (5.9 \pm 0.6) \times 10^{-2}$. Our first error is their experiment's error and our second error is the systematic error from using our best value.
¹¹ Recalculated by us. HEINTZ 92 quotes $B(\Upsilon(3S) \rightarrow \gamma \chi_{b0}(2P)) \times B(\chi_{b0}(2P) \rightarrow \gamma \Upsilon(1S)) = (0.05 \pm 0.04 \pm 0.01)\%$ using $B(\Upsilon(1S) \rightarrow \mu^+\mu^-) = (2.57 \pm 0.05)\%$. Supersedes HEINTZ 91.
¹² LEES 11J quotes a central value of $\Gamma(\chi_{b0}(2P) \rightarrow \gamma \Upsilon(1S))/\Gamma_{\text{total}} \times \Gamma(\Upsilon(3S) \rightarrow \gamma \chi_{b0}(2P))/\Gamma_{\text{total}} = (3.9 \pm 2.2^{+1.2}_{-0.6}) \times 10^{-4}$.
¹³ Using $B(\Upsilon(1S) \rightarrow \mu^+\mu^-) = (2.57 \pm 0.07)\%$, $B(\Upsilon(3S) \rightarrow \gamma\gamma \Upsilon(1S)) \times 2 B(\Upsilon(1S) \rightarrow \mu^+\mu^-) < 0.63 \times 10^{-4}$, and $B(\Upsilon(3S) \rightarrow \chi_{b0}(2P)\gamma) = 0.049$.

$\Gamma(D^0 X)/\Gamma_{\text{total}}$					Γ_3/Γ
VALUE	CL%	DOCUMENT ID	TECN	COMMENT	

$< 8.2 \times 10^{-2}$	90	^{14,15} BRIERE	08	CLEO $\Upsilon(3S) \rightarrow \gamma D^0 X$
---	----	-------------------------	----	--

¹⁴ For $p_{D^0} > 2.5$ GeV/c.
¹⁵ The authors also present their result as $(4.1 \pm 3.0 \pm 0.4) \times 10^{-2}$.

$\Gamma(\pi^+\pi^-K^+K^-\pi^0)/\Gamma_{\text{total}}$					Γ_4/Γ
VALUE (units 10^{-4})	CL%	DOCUMENT ID	TECN	COMMENT	

<0.34	90	¹⁶ ASNER	08A	CLEO $\Upsilon(3S) \rightarrow \gamma\pi^+\pi^-K^+K^-\pi^0$
-----------------	----	---------------------	-----	---

¹⁶ ASNER 08A reports $[\Gamma(\chi_{b0}(2P) \rightarrow \pi^+\pi^-K^+K^-\pi^0)/\Gamma_{\text{total}}] \times [B(\Upsilon(3S) \rightarrow \gamma \chi_{b0}(2P))]$ = 2×10^{-6} which we divide by our best value $B(\Upsilon(3S) \rightarrow \gamma \chi_{b0}(2P)) = 5.9 \times 10^{-2}$.

$\Gamma(2\pi^+\pi^-K^-K_S^0)/\Gamma_{\text{total}}$					Γ_5/Γ
VALUE (units 10^{-4})	CL%	DOCUMENT ID	TECN	COMMENT	
<0.5	90	17 ASNER	08A CLEO	$\Upsilon(3S) \rightarrow \gamma 2\pi^+\pi^-K^-K_S^0$	
17 ASNER 08A reports $[\Gamma(\chi_{b0}(2P) \rightarrow 2\pi^+\pi^-K^-K_S^0)/\Gamma_{\text{total}}] \times [B(\Upsilon(3S) \rightarrow \gamma\chi_{b0}(2P))] < 3 \times 10^{-6}$ which we divide by our best value $B(\Upsilon(3S) \rightarrow \gamma\chi_{b0}(2P)) = 5.9 \times 10^{-2}$.					

$\Gamma(2\pi^+\pi^-K^-K_S^0 2\pi^0)/\Gamma_{\text{total}}$					Γ_6/Γ
VALUE (units 10^{-4})	CL%	DOCUMENT ID	TECN	COMMENT	
<2.2	90	18 ASNER	08A CLEO	$\Upsilon(3S) \rightarrow \gamma 2\pi^+\pi^-K^-2\pi^0$	
18 ASNER 08A reports $[\Gamma(\chi_{b0}(2P) \rightarrow 2\pi^+\pi^-K^-K_S^0 2\pi^0)/\Gamma_{\text{total}}] \times [B(\Upsilon(3S) \rightarrow \gamma\chi_{b0}(2P))] < 13 \times 10^{-6}$ which we divide by our best value $B(\Upsilon(3S) \rightarrow \gamma\chi_{b0}(2P)) = 5.9 \times 10^{-2}$.					

$\Gamma(2\pi^+2\pi^-2\pi^0)/\Gamma_{\text{total}}$					Γ_7/Γ
VALUE (units 10^{-4})	CL%	DOCUMENT ID	TECN	COMMENT	
<2.4	90	19 ASNER	08A CLEO	$\Upsilon(3S) \rightarrow \gamma 2\pi^+2\pi^-2\pi^0$	
19 ASNER 08A reports $[\Gamma(\chi_{b0}(2P) \rightarrow 2\pi^+2\pi^-2\pi^0)/\Gamma_{\text{total}}] \times [B(\Upsilon(3S) \rightarrow \gamma\chi_{b0}(2P))] < 14 \times 10^{-6}$ which we divide by our best value $B(\Upsilon(3S) \rightarrow \gamma\chi_{b0}(2P)) = 5.9 \times 10^{-2}$.					

$\Gamma(2\pi^+2\pi^-K^+K^-)/\Gamma_{\text{total}}$					Γ_8/Γ
VALUE (units 10^{-4})	CL%	DOCUMENT ID	TECN	COMMENT	
<1.5	90	20 ASNER	08A CLEO	$\Upsilon(3S) \rightarrow \gamma 2\pi^+2\pi^-K^+K^-$	
20 ASNER 08A reports $[\Gamma(\chi_{b0}(2P) \rightarrow 2\pi^+2\pi^-K^+K^-)/\Gamma_{\text{total}}] \times [B(\Upsilon(3S) \rightarrow \gamma\chi_{b0}(2P))] < 9 \times 10^{-6}$ which we divide by our best value $B(\Upsilon(3S) \rightarrow \gamma\chi_{b0}(2P)) = 5.9 \times 10^{-2}$.					

$\Gamma(2\pi^+2\pi^-K^+K^-\pi^0)/\Gamma_{\text{total}}$					Γ_9/Γ
VALUE (units 10^{-4})	CL%	DOCUMENT ID	TECN	COMMENT	
<2.2	90	21 ASNER	08A CLEO	$\Upsilon(3S) \rightarrow \gamma 2\pi^+2\pi^-K^+K^-\pi^0$	
21 ASNER 08A reports $[\Gamma(\chi_{b0}(2P) \rightarrow 2\pi^+2\pi^-K^+K^-\pi^0)/\Gamma_{\text{total}}] \times [B(\Upsilon(3S) \rightarrow \gamma\chi_{b0}(2P))] < 13 \times 10^{-6}$ which we divide by our best value $B(\Upsilon(3S) \rightarrow \gamma\chi_{b0}(2P)) = 5.9 \times 10^{-2}$.					

$\Gamma(2\pi^+2\pi^-K^+K^-2\pi^0)/\Gamma_{\text{total}}$					Γ_{10}/Γ
VALUE (units 10^{-4})	CL%	DOCUMENT ID	TECN	COMMENT	
<11	90	22 ASNER	08A CLEO	$\Upsilon(3S) \rightarrow \gamma 2\pi^+2\pi^-K^+K^-2\pi^0$	
22 ASNER 08A reports $[\Gamma(\chi_{b0}(2P) \rightarrow 2\pi^+2\pi^-K^+K^-2\pi^0)/\Gamma_{\text{total}}] \times [B(\Upsilon(3S) \rightarrow \gamma\chi_{b0}(2P))] < 63 \times 10^{-6}$ which we divide by our best value $B(\Upsilon(3S) \rightarrow \gamma\chi_{b0}(2P)) = 5.9 \times 10^{-2}$.					

$\Gamma(3\pi^+2\pi^-K^-K_S^0\pi^0)/\Gamma_{\text{total}}$					Γ_{11}/Γ
VALUE (units 10^{-4})	CL%	DOCUMENT ID	TECN	COMMENT	
<7	90	23 ASNER	08A CLEO	$\Upsilon(3S) \rightarrow \gamma 3\pi^+2\pi^-K^-K_S^0\pi^0$	
23 ASNER 08A reports $[\Gamma(\chi_{b0}(2P) \rightarrow 3\pi^+2\pi^-K^-K_S^0\pi^0)/\Gamma_{\text{total}}] \times [B(\Upsilon(3S) \rightarrow \gamma\chi_{b0}(2P))] < 39 \times 10^{-6}$ which we divide by our best value $B(\Upsilon(3S) \rightarrow \gamma\chi_{b0}(2P)) = 5.9 \times 10^{-2}$.					

$\Gamma(3\pi^+3\pi^-)/\Gamma_{\text{total}}$					Γ_{12}/Γ
VALUE (units 10^{-4})	CL%	DOCUMENT ID	TECN	COMMENT	
<0.7	90	24 ASNER	08A CLEO	$\Upsilon(3S) \rightarrow \gamma 3\pi^+3\pi^-$	
24 ASNER 08A reports $[\Gamma(\chi_{b0}(2P) \rightarrow 3\pi^+3\pi^-)/\Gamma_{\text{total}}] \times [B(\Upsilon(3S) \rightarrow \gamma\chi_{b0}(2P))] < 4 \times 10^{-6}$ which we divide by our best value $B(\Upsilon(3S) \rightarrow \gamma\chi_{b0}(2P)) = 5.9 \times 10^{-2}$.					

$\Gamma(3\pi^+3\pi^-2\pi^0)/\Gamma_{\text{total}}$					Γ_{13}/Γ
VALUE (units 10^{-4})	CL%	DOCUMENT ID	TECN	COMMENT	
<12	90	25 ASNER	08A CLEO	$\Upsilon(3S) \rightarrow \gamma 3\pi^+3\pi^-2\pi^0$	
25 ASNER 08A reports $[\Gamma(\chi_{b0}(2P) \rightarrow 3\pi^+3\pi^-2\pi^0)/\Gamma_{\text{total}}] \times [B(\Upsilon(3S) \rightarrow \gamma\chi_{b0}(2P))] < 72 \times 10^{-6}$ which we divide by our best value $B(\Upsilon(3S) \rightarrow \gamma\chi_{b0}(2P)) = 5.9 \times 10^{-2}$.					

$\Gamma(3\pi^+3\pi^-K^+K^-)/\Gamma_{\text{total}}$					Γ_{14}/Γ
VALUE (units 10^{-4})	CL%	DOCUMENT ID	TECN	COMMENT	
<1.5	90	26 ASNER	08A CLEO	$\Upsilon(3S) \rightarrow \gamma 3\pi^+3\pi^-K^+K^-$	
26 ASNER 08A reports $[\Gamma(\chi_{b0}(2P) \rightarrow 3\pi^+3\pi^-K^+K^-)/\Gamma_{\text{total}}] \times [B(\Upsilon(3S) \rightarrow \gamma\chi_{b0}(2P))] < 9 \times 10^{-6}$ which we divide by our best value $B(\Upsilon(3S) \rightarrow \gamma\chi_{b0}(2P)) = 5.9 \times 10^{-2}$.					

$\Gamma(3\pi^+3\pi^-K^+K^-\pi^0)/\Gamma_{\text{total}}$					Γ_{15}/Γ
VALUE (units 10^{-4})	CL%	DOCUMENT ID	TECN	COMMENT	
<7	90	27 ASNER	08A CLEO	$\Upsilon(3S) \rightarrow \gamma 3\pi^+3\pi^-K^+K^-\pi^0$	
27 ASNER 08A reports $[\Gamma(\chi_{b0}(2P) \rightarrow 3\pi^+3\pi^-K^+K^-\pi^0)/\Gamma_{\text{total}}] \times [B(\Upsilon(3S) \rightarrow \gamma\chi_{b0}(2P))] < 43 \times 10^{-6}$ which we divide by our best value $B(\Upsilon(3S) \rightarrow \gamma\chi_{b0}(2P)) = 5.9 \times 10^{-2}$.					

$\Gamma(4\pi^+4\pi^-)/\Gamma_{\text{total}}$					Γ_{16}/Γ
VALUE (units 10^{-4})	CL%	DOCUMENT ID	TECN	COMMENT	
<1.7	90	28 ASNER	08A CLEO	$\Upsilon(3S) \rightarrow \gamma 4\pi^+4\pi^-$	
28 ASNER 08A reports $[\Gamma(\chi_{b0}(2P) \rightarrow 4\pi^+4\pi^-)/\Gamma_{\text{total}}] \times [B(\Upsilon(3S) \rightarrow \gamma\chi_{b0}(2P))] < 10 \times 10^{-6}$ which we divide by our best value $B(\Upsilon(3S) \rightarrow \gamma\chi_{b0}(2P)) = 5.9 \times 10^{-2}$.					

$\Gamma(4\pi^+4\pi^-2\pi^0)/\Gamma_{\text{total}}$					Γ_{17}/Γ
VALUE (units 10^{-4})	CL%	DOCUMENT ID	TECN	COMMENT	
<6	90	29 ASNER	08A CLEO	$\Upsilon(3S) \rightarrow \gamma 4\pi^+4\pi^-2\pi^0$	
29 ASNER 08A reports $[\Gamma(\chi_{b0}(2P) \rightarrow 4\pi^+4\pi^-2\pi^0)/\Gamma_{\text{total}}] \times [B(\Upsilon(3S) \rightarrow \gamma\chi_{b0}(2P))] < 38 \times 10^{-6}$ which we divide by our best value $B(\Upsilon(3S) \rightarrow \gamma\chi_{b0}(2P)) = 5.9 \times 10^{-2}$.					

$\Gamma(\chi_{b0}(2P) \rightarrow \gamma\Upsilon(1S))/\Gamma_{\text{total}} \times \Gamma(\Upsilon(3S) \rightarrow \gamma\chi_{b0}(2P))/\Gamma_{\text{total}}$					$\Gamma_2/\Gamma \times \Gamma_{22}^{(\Upsilon(3S))}/\Gamma\Upsilon(3S)$
VALUE (units 10^{-4})	CL%	DOCUMENT ID	TECN	COMMENT	
<8.2	90	30 LEES	11J BABR	$\Upsilon(3S) \rightarrow X\gamma$	
30 LEES 11J quotes a central value of $\Gamma(\chi_{b0}(2P) \rightarrow \gamma\Upsilon(1S))/\Gamma_{\text{total}} \times \Gamma(\Upsilon(3S) \rightarrow \gamma\chi_{b0}(2P))/\Gamma_{\text{total}} = (3.9 \pm 2.2^{+1.2}_{-0.6}) \times 10^{-4}$ and derives a 90% CL upper limit of $B(\chi_{b0}(2P) \rightarrow \gamma\Upsilon(1S)) < 1.2\%$ using $B(\Upsilon(3S) \rightarrow \gamma\chi_{b0}(2P)) = (5.9 \pm 0.6)\%$.					

$B(\chi_{b0}(2P) \rightarrow \gamma\Upsilon(1S)) \times B(\Upsilon(3S) \rightarrow \gamma\chi_{b0}(2P)) \times B(\Upsilon(1S) \rightarrow \ell^+\ell^-)$					
VALUE (units 10^{-5})	DOCUMENT ID	TECN	COMMENT		
1.4 ± 0.9 OUR AVERAGE					
1.7 ± 1.5 + 0.1 -1.4 - 1.2	31 LEES	14M BABR	$\Upsilon(3S) \rightarrow \gamma\gamma\mu^+\mu^-$		
1.3 ± 1.0 ± 0.3	32 HEINTZ	92 CSB2	$\Upsilon(3S) \rightarrow \gamma\gamma\ell^+\ell^-$		
31 From a sample of $\Upsilon(3S) \rightarrow \gamma\gamma\mu^+\mu^-$ with one converted photon. 32 Calculated by us. HEINTZ 92 quotes $B(\Upsilon(3S) \rightarrow \gamma\chi_{b0}(2P)) \times B(\chi_{b0}(2P) \rightarrow \gamma\Upsilon(1S)) = (0.05 \pm 0.04 \pm 0.01)\%$ using $B(\Upsilon(1S) \rightarrow \mu^+\mu^-) = (2.57 \pm 0.05)\%$.					

$[B(\chi_{b0}(2P) \rightarrow \gamma\Upsilon(1S)) \times B(\Upsilon(3S) \rightarrow \gamma\chi_{b0}(2P))] / [B(\chi_{b1}(2P) \rightarrow \gamma\Upsilon(1S)) \times B(\Upsilon(3S) \rightarrow \gamma\chi_{b1}(2P))]$					
VALUE (%)	DOCUMENT ID	TECN	COMMENT		
1.71 ± 0.80	33 LEES	14M BABR	$\Upsilon(3S) \rightarrow \gamma\gamma\mu^+\mu^-$		
33 From a sample of $\Upsilon(3S) \rightarrow \gamma\gamma\mu^+\mu^-$ without converted photons.					

$\Gamma(\chi_{b0}(2P) \rightarrow \gamma\Upsilon(2S))/\Gamma_{\text{total}} \times \Gamma(\Upsilon(3S) \rightarrow \gamma\chi_{b0}(2P))/\Gamma_{\text{total}}$					$\Gamma_1/\Gamma \times \Gamma_{22}^{(\Upsilon(3S))}/\Gamma\Upsilon(3S)$
VALUE (units 10^{-3})	CL%	DOCUMENT ID	TECN	COMMENT	
<1.6	90	34 LEES	11J BABR	$\Upsilon(3S) \rightarrow X\gamma$	
34 LEES 11J quotes a central value of $\Gamma(\chi_{b0}(2P) \rightarrow \gamma\Upsilon(2S))/\Gamma_{\text{total}} \times \Gamma(\Upsilon(3S) \rightarrow \gamma\chi_{b0}(2P))/\Gamma_{\text{total}} = (-0.3 \pm 0.2^{+0.3}_{-0.4})\%$ and derives a 90% CL upper limit of $B(\chi_{b0}(2P) \rightarrow \gamma\Upsilon(2S)) < 2.8\%$ using $B(\Upsilon(3S) \rightarrow \gamma\chi_{b0}(2P)) = (5.9 \pm 0.6)\%$.					

$B(\chi_{b0}(2P) \rightarrow \gamma\Upsilon(2S)) \times B(\Upsilon(3S) \rightarrow \gamma\chi_{b0}(2P)) \times B(\Upsilon(2S) \rightarrow \ell^+\ell^-)$					
VALUE (units 10^{-5})	DOCUMENT ID	TECN	COMMENT		
4.4 ± 1.6 OUR AVERAGE					
6.6 ± 4.9 + 2.0 -4.0 - 0.3	35 LEES	14M BABR	$\Upsilon(3S) \rightarrow \gamma\gamma\mu^+\mu^-$		
4.0 ± 1.7 ± 0.3	36 HEINTZ	92 CSB2	$\Upsilon(3S) \rightarrow \gamma\gamma\ell^+\ell^-$		
35 From a sample of $\Upsilon(3S) \rightarrow \gamma\gamma\mu^+\mu^-$ with one converted photon. 36 Calculated by us. HEINTZ 92 quotes $B(\Upsilon(3S) \rightarrow \gamma\chi_{b0}(2P)) \times B(\chi_{b0}(2P) \rightarrow \gamma\Upsilon(2S)) = (0.28 \pm 0.12 \pm 0.03)\%$ using $B(\Upsilon(2S) \rightarrow \mu^+\mu^-) = (1.44 \pm 0.10)\%$.					

$[B(\chi_{b0}(2P) \rightarrow \gamma\Upsilon(2S)) \times B(\Upsilon(3S) \rightarrow \gamma\chi_{b0}(2P))] / [B(\chi_{b1}(2P) \rightarrow \gamma\Upsilon(2S)) \times B(\Upsilon(3S) \rightarrow \gamma\chi_{b1}(2P))]$					
VALUE (%)	DOCUMENT ID	TECN	COMMENT		
3.31 ± 0.56	37 LEES	14M BABR	$\Upsilon(3S) \rightarrow \gamma\gamma\mu^+\mu^-$		
37 From a sample of $\Upsilon(3S) \rightarrow \gamma\gamma\mu^+\mu^-$ without converted photons.					

$\chi_{b0}(2P)$ REFERENCES

LEES	14M	PR D90 112010	J.P. Lees et al.	(BABAR Collab.)
LEES	11J	PR D84 072002	J.P. Lees et al.	(BABAR Collab.)
ASNER	08A	PR D78 091103	D.M. Asner et al.	(CLEO Collab.)
BRIERE	08	PR D78 092007	R.A. Briere et al.	(CLEO Collab.)
ARTUSO	05	PRL 94 032001	M. Artuso et al.	(CLEO Collab.)
CRAWFORD	92B	PL B294 139	G. Crawford et al.	(CLEO Collab.)
HEINTZ	92	PR D46 1928	U. Heintz et al.	(CUSB II Collab.)
HEINTZ	91	PRL 66 1563	U. Heintz et al.	(CUSB Collab.)
MORRISON	91	PRL 67 1696	R.J. Morrison et al.	(CLEO Collab.)
NARAIN	91	PRL 66 3113	M. Narain et al.	(CUSB Collab.)

$\chi_{b1}(2P)$

$J^PC = 0^+(1^+)$
J needs confirmation.

Observed in radiative decay of the $\Upsilon(3S)$, therefore $C = +$. Branching ratio requires E1 transition, M1 is strongly disfavored, therefore $P = +$.

Meson Particle Listings

$\chi_{b1}(2P)$

$\chi_{b1}(2P)$ MASS

VALUE (MeV)	DOCUMENT ID	TECN	COMMENT
10295.46 ± 0.22 ± 0.50 OUR EVALUATION			From γ energy below, using $\Upsilon(3S)$ mass = 10355.2 ± 0.5 MeV

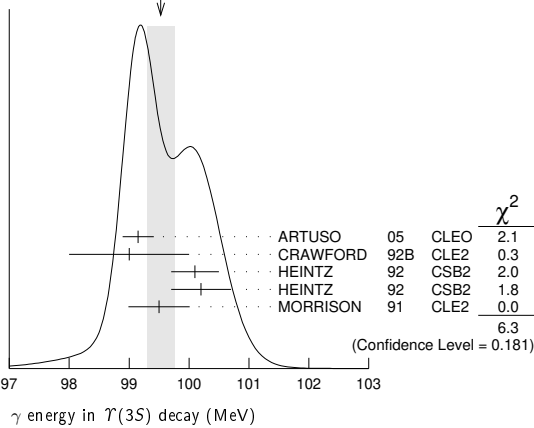
$m_{\chi_{b1}(2P)} - m_{\chi_{b0}(2P)}$

VALUE (MeV)	DOCUMENT ID	TECN	COMMENT
23.5 ± 0.7 ± 0.7	1 HEINTZ	92 CSB2	$e^+e^- \rightarrow \gamma X, \ell^+\ell^-\gamma\gamma$
1 From the average photon energy for inclusive and exclusive events. Supersedes NARAIN 91.			

γ ENERGY IN $\Upsilon(3S)$ DECAY

VALUE (MeV)	EVTS	DOCUMENT ID	TECN	COMMENT
99.26 ± 0.22 OUR EVALUATION				Treating systematic errors as correlated
99.53 ± 0.23 OUR AVERAGE				Error includes scale factor of 1.3. See the ideogram below.
99.15 ± 0.07 ± 0.25		ARTUSO 05	CLEO	$\Upsilon(3S) \rightarrow \gamma X$
99 ± 1	169	CRAWFORD 92B	CLE2	$e^+e^- \rightarrow \ell^+\ell^-\gamma\gamma$
100.1 ± 0.4	11147	2 HEINTZ 92	CSB2	$e^+e^- \rightarrow \gamma X$
100.2 ± 0.5	223	3 HEINTZ 92	CSB2	$e^+e^- \rightarrow \ell^+\ell^-\gamma\gamma$
99.5 ± 0.1 ± 0.5	25759	MORRISON 91	CLE2	$e^+e^- \rightarrow \gamma X$
2 A systematic uncertainty on the energy scale of 0.9% not included. Supersedes NARAIN 91.				
3 A systematic uncertainty on the energy scale of 0.9% not included. Supersedes HEINTZ 91.				

WEIGHTED AVERAGE
99.53 ± 0.23 (Error scaled by 1.3)



$\chi_{b1}(2P)$ DECAY MODES

Mode	Fraction (Γ_i/Γ)
Γ_1 $\omega \Upsilon(1S)$	(1.63 ^{+0.40} _{-0.34}) %
Γ_2 $\gamma \Upsilon(2S)$	(18.1 ± 1.9) %
Γ_3 $\gamma \Upsilon(1S)$	(9.9 ± 1.0) %
Γ_4 $\pi\pi \chi_{b1}(1P)$	(9.1 ± 1.3) × 10 ⁻³
Γ_5 $D^0 X$	(8.8 ± 1.7) %
Γ_6 $\pi^+\pi^- K^+ K^- \pi^0$	(3.1 ± 1.0) × 10 ⁻⁴
Γ_7 $2\pi^+\pi^- K^- K_S^0$	(1.1 ± 0.5) × 10 ⁻⁴
Γ_8 $2\pi^+\pi^- K^- K_S^0 2\pi^0$	(7.7 ± 3.2) × 10 ⁻⁴
Γ_9 $2\pi^+ 2\pi^- 2\pi^0$	(5.9 ± 2.0) × 10 ⁻⁴
Γ_{10} $2\pi^+ 2\pi^- K^+ K^-$	(10 ± 4) × 10 ⁻⁵
Γ_{11} $2\pi^+ 2\pi^- K^+ K^- \pi^0$	(5.5 ± 1.8) × 10 ⁻⁴
Γ_{12} $2\pi^+ 2\pi^- K^+ K^- 2\pi^0$	(10 ± 4) × 10 ⁻⁴
Γ_{13} $3\pi^+ 2\pi^- K^- K_S^0 \pi^0$	(6.7 ± 2.6) × 10 ⁻⁴
Γ_{14} $3\pi^+ 3\pi^-$	(1.2 ± 0.4) × 10 ⁻⁴
Γ_{15} $3\pi^+ 3\pi^- 2\pi^0$	(1.2 ± 0.4) × 10 ⁻³
Γ_{16} $3\pi^+ 3\pi^- K^+ K^-$	(2.0 ± 0.8) × 10 ⁻⁴
Γ_{17} $3\pi^+ 3\pi^- K^+ K^- \pi^0$	(6.1 ± 2.2) × 10 ⁻⁴
Γ_{18} $4\pi^+ 4\pi^-$	(1.7 ± 0.6) × 10 ⁻⁴
Γ_{19} $4\pi^+ 4\pi^- 2\pi^0$	(1.9 ± 0.7) × 10 ⁻³

$\chi_{b1}(2P)$ BRANCHING RATIOS

$\Gamma(\omega \Upsilon(1S))/\Gamma_{total}$	VALUE (units 10 ⁻²)	EVTS	DOCUMENT ID	TECN	COMMENT
1.63 ± 0.35 ± 0.16					
	32.6 ^{+6.9} _{-6.1}	4	CRONIN-HEN..04	CLE3	$\Upsilon(3S) \rightarrow \gamma\omega \Upsilon(1S)$
4 Using $B(\Upsilon(3S) \rightarrow \gamma \chi_{b1}(2P)) = (11.3 \pm 0.6)\%$ and $B(\Upsilon(1S) \rightarrow \ell^+\ell^-) = 2 B(\Upsilon(1S) \rightarrow \mu^+\mu^-) = 2(2.48 \pm 0.06)\%$.					

$\Gamma(\gamma \Upsilon(2S))/\Gamma_{total}$

VALUE	EVTS	DOCUMENT ID	TECN	COMMENT
0.181 ± 0.019 OUR AVERAGE				
0.211 ± 0.017 ± 0.019		5,6,7 LEES	14M BABR	$\Upsilon(3S) \rightarrow \gamma\gamma\mu^+\mu^-$
0.190 ± 0.018 ± 0.017	4.3k	8 LEES	11J BABR	$\Upsilon(3S) \rightarrow X\gamma$
0.206 ± 0.035 ± 0.019		5,9 CRAWFORD	92B CLE2	$e^+e^- \rightarrow \ell^+\ell^-\gamma\gamma$
0.132 ± 0.018 ± 0.012		5,10 HEINTZ	92 CSB2	$e^+e^- \rightarrow \ell^+\ell^-\gamma\gamma$

5 Assuming $B(\Upsilon(2S) \rightarrow \mu^+\mu^-) = (1.93 \pm 0.17)\%$.

6 LEES 14M quotes $\Gamma(\chi_{b1}(2P) \rightarrow \gamma \Upsilon(2S))/\Gamma_{total} \times \Gamma(\Upsilon(3S) \rightarrow \gamma \chi_{b1}(2P))/\Gamma_{total} = (2.66 \pm 0.22)\%$ combining the results from $\Upsilon(3S) \rightarrow \gamma\gamma\mu^+\mu^-$ samples with and without photon conversions.

7 LEES 14M reports $[\Gamma(\chi_{b1}(2P) \rightarrow \gamma \Upsilon(2S))/\Gamma_{total}] \times [B(\Upsilon(3S) \rightarrow \gamma \chi_{b1}(2P))]$ = (2.66 ± 0.22) × 10⁻² which we divide by our best value $B(\Upsilon(3S) \rightarrow \gamma \chi_{b1}(2P)) = (12.6 \pm 1.2) \times 10^{-2}$. Our first error is their experiment's error and our second error is the systematic error from using our best value.

8 LEES 11J reports $[\Gamma(\chi_{b1}(2P) \rightarrow \gamma \Upsilon(2S))/\Gamma_{total}] \times [B(\Upsilon(3S) \rightarrow \gamma \chi_{b1}(2P))]$ = (2.4 ± 0.1 ± 0.2) × 10⁻² which we divide by our best value $B(\Upsilon(3S) \rightarrow \gamma \chi_{b1}(2P)) = (12.6 \pm 1.2) \times 10^{-2}$. Our first error is their experiment's error and our second error is the systematic error from using our best value.

9 CRAWFORD 92B quotes $B(\Upsilon(3S) \rightarrow \gamma \chi_{b1}(2P)) \times B(\chi_{b1}(2P) \rightarrow \gamma \Upsilon(2S)) \times 2 B(\Upsilon(2S) \rightarrow \ell^+\ell^-) = (10.23 \pm 1.20 \pm 1.26) 10^{-4}$.

10 Recalculated by us. HEINTZ 92 quotes $B(\Upsilon(3S) \rightarrow \gamma \chi_{b1}(2P)) \times B(\chi_{b1}(2P) \rightarrow \gamma \Upsilon(2S)) = (2.29 \pm 0.23 \pm 0.21) \%$ using $B(\Upsilon(2S) \rightarrow \mu^+\mu^-) = (1.44 \pm 0.10)\%$. Supersedes HEINTZ 91.

$\Gamma(\gamma \Upsilon(1S))/\Gamma_{total}$

VALUE	EVTS	DOCUMENT ID	TECN	COMMENT
0.099 ± 0.010 OUR AVERAGE				
0.107 ± 0.006 ± 0.010	11,12,13	LEES	14M BABR	$\Upsilon(3S) \rightarrow \gamma\gamma\mu^+\mu^-$
0.098 ± 0.005 ± 0.009	15k	14 LEES	11J BABR	$\Upsilon(3S) \rightarrow X\gamma$
0.103 ± 0.023 ± 0.009		11,15 CRAWFORD	92B CLE2	$e^+e^- \rightarrow \ell^+\ell^-\gamma\gamma$
0.075 ± 0.010 ± 0.007		11,16 HEINTZ	92 CSB2	$e^+e^- \rightarrow \ell^+\ell^-\gamma\gamma$

11 Assuming $B(\Upsilon(1S) \rightarrow \mu^+\mu^-) = (2.48 \pm 0.05)\%$.

12 LEES 14M quotes $\Gamma(\chi_{b1}(2P) \rightarrow \gamma \Upsilon(1S))/\Gamma_{total} \times \Gamma(\Upsilon(3S) \rightarrow \gamma \chi_{b1}(2P))/\Gamma_{total} = (13.48 \pm 0.72) \times 10^{-3}$ combining the results from samples of $\Upsilon(3S) \rightarrow \gamma\gamma\mu^+\mu^-$ with and without converted photons.

13 LEES 14M reports $[\Gamma(\chi_{b1}(2P) \rightarrow \gamma \Upsilon(1S))/\Gamma_{total}] \times [B(\Upsilon(3S) \rightarrow \gamma \chi_{b1}(2P))]$ = (13.48 ± 0.72) × 10⁻³ which we divide by our best value $B(\Upsilon(3S) \rightarrow \gamma \chi_{b1}(2P)) = (12.6 \pm 1.2) \times 10^{-2}$. Our first error is their experiment's error and our second error is the systematic error from using our best value.

14 LEES 11J reports $[\Gamma(\chi_{b1}(2P) \rightarrow \gamma \Upsilon(1S))/\Gamma_{total}] \times [B(\Upsilon(3S) \rightarrow \gamma \chi_{b1}(2P))]$ = (12.4 ± 0.3 ± 0.6) × 10⁻³ which we divide by our best value $B(\Upsilon(3S) \rightarrow \gamma \chi_{b1}(2P)) = (12.6 \pm 1.2) \times 10^{-2}$. Our first error is their experiment's error and our second error is the systematic error from using our best value.

15 CRAWFORD 92B quotes $B(\Upsilon(3S) \rightarrow \gamma \chi_{b1}(2P)) \times B(\chi_{b1}(2P) \rightarrow \gamma \Upsilon(1S)) \times 2 B(\Upsilon(1S) \rightarrow \ell^+\ell^-) = (6.47 \pm 1.12 \pm 0.82) 10^{-4}$.

16 Recalculated by us. HEINTZ 92 quotes $B(\Upsilon(3S) \rightarrow \gamma \chi_{b1}(2P)) \times B(\chi_{b1}(2P) \rightarrow \gamma \Upsilon(1S)) = (0.91 \pm 0.11 \pm 0.06)\%$ using $B(\Upsilon(1S) \rightarrow \mu^+\mu^-) = (2.57 \pm 0.05)\%$. Supersedes HEINTZ 91.

$\Gamma(\pi\pi \chi_{b1}(1P))/\Gamma_{total}$

VALUE (units 10 ⁻³)	EVTS	DOCUMENT ID	TECN	COMMENT
9.1 ± 1.3 OUR AVERAGE				
9.2 ± 1.1 ± 0.8	31k	17 LEES	11c BABR	$e^+e^- \rightarrow \pi^+\pi^- X$
8.6 ± 2.3 ± 2.1		18 CAWLFIELD	06 CLE3	$\Upsilon(3S) \rightarrow 2(\gamma\pi\ell)$

17 LEES 11c measures $B(\Upsilon(3S) \rightarrow \chi_{b1}(2P) X) \times B(\chi_{b1}(2P) \rightarrow \chi_{b1}(1P)\pi^+\pi^-) = (1.16 \pm 0.07 \pm 0.12) \times 10^{-3}$. We derive the value assuming $B(\Upsilon(3S) \rightarrow \chi_{b1}(2P) X) = B(\Upsilon(3S) \rightarrow \chi_{b1}(2P) \gamma) = (12.6 \pm 1.2) \times 10^{-2}$.

18 CAWLFIELD 06 quote $\Gamma(\chi_b(2P) \rightarrow \pi\pi \chi_b(1P)) = 0.83 \pm 0.22 \pm 0.08 \pm 0.19$ keV assuming l-spin conservation, no D-wave contribution, $\Gamma(\chi_{b1}(2P)) = 96 \pm 16$ keV, and $\Gamma(\chi_{b2}(2P)) = 138 \pm 19$ keV.

$\Gamma(D^0 X)/\Gamma_{total}$

VALUE (units 10 ⁻²)	EVTS	DOCUMENT ID	TECN	COMMENT
8.8 ± 1.5 ± 0.8	2243	19 BRIERE	08 CLEO	$\Upsilon(3S) \rightarrow \gamma D^0 X$

19 For $p_{D^0} > 2.5$ GeV/c.

$\Gamma(\pi^+\pi^- K^+ K^- \pi^0)/\Gamma_{total}$

VALUE (units 10 ⁻⁴)	EVTS	DOCUMENT ID	TECN	COMMENT
3.1 ± 1.0 ± 0.3	30	20 ASNER	08A CLEO	$\Upsilon(3S) \rightarrow \gamma\pi^+\pi^- K^+ K^- \pi^0$
20 ASNER 08A reports $[\Gamma(\chi_{b1}(2P) \rightarrow \pi^+\pi^- K^+ K^- \pi^0)/\Gamma_{total}] \times [B(\Upsilon(3S) \rightarrow \gamma \chi_{b1}(2P))] = (39 \pm 8 \pm 9) \times 10^{-6}$ which we divide by our best value $B(\Upsilon(3S) \rightarrow \gamma \chi_{b1}(2P)) = (12.6 \pm 1.2) \times 10^{-2}$. Our first error is their experiment's error and our second error is the systematic error from using our best value.				

$\Gamma(2\pi^+\pi^- K^- K_S^0)/\Gamma_{total}$

VALUE (units 10 ⁻⁴)	EVTS	DOCUMENT ID	TECN	COMMENT
1.1 ± 0.5 ± 0.1	10	21 ASNER	08A CLEO	$\Upsilon(3S) \rightarrow \gamma 2\pi^+\pi^- K^- K_S^0$
21 ASNER 08A reports $[\Gamma(\chi_{b1}(2P) \rightarrow 2\pi^+\pi^- K^- K_S^0)/\Gamma_{total}] \times [B(\Upsilon(3S) \rightarrow \gamma \chi_{b1}(2P))] = (14 \pm 5 \pm 3) \times 10^{-6}$ which we divide by our best value $B(\Upsilon(3S) \rightarrow \gamma \chi_{b1}(2P)) = (12.6 \pm 1.2) \times 10^{-2}$. Our first error is their experiment's error and our second error is the systematic error from using our best value.				

See key on page 999

Meson Particle Listings

$\chi_{b1}(2P)$

$\Gamma(2\pi^+\pi^-K^-K_S^0 2\pi^0)/\Gamma_{total}$ Γ_8/Γ

VALUE (units 10^{-4})	EVTS	DOCUMENT ID	TECN	COMMENT
$7.7 \pm 3.1 \pm 0.7$	15	22 ASNER	08A CLEO	$\Upsilon(3S) \rightarrow \gamma 2\pi^+\pi^-K^-2\pi^0$
22 ASNER 08A reports $[\Gamma(\chi_{b1}(2P) \rightarrow 2\pi^+\pi^-K^-K_S^0 2\pi^0)/\Gamma_{total}] \times [B(\Upsilon(3S) \rightarrow \gamma \chi_{b1}(2P))]$ = $(97 \pm 30 \pm 26) \times 10^{-6}$ which we divide by our best value $B(\Upsilon(3S) \rightarrow \gamma \chi_{b1}(2P)) = (12.6 \pm 1.2) \times 10^{-2}$. Our first error is their experiment's error and our second error is the systematic error from using our best value.				

$\Gamma(2\pi^+2\pi^-2\pi^0)/\Gamma_{total}$ Γ_9/Γ

VALUE (units 10^{-4})	EVTS	DOCUMENT ID	TECN	COMMENT
$5.9 \pm 2.0 \pm 0.5$	36	23 ASNER	08A CLEO	$\Upsilon(3S) \rightarrow \gamma 2\pi^+2\pi^-2\pi^0$
23 ASNER 08A reports $[\Gamma(\chi_{b1}(2P) \rightarrow 2\pi^+2\pi^-2\pi^0)/\Gamma_{total}] \times [B(\Upsilon(3S) \rightarrow \gamma \chi_{b1}(2P))]$ = $(74 \pm 16 \pm 19) \times 10^{-6}$ which we divide by our best value $B(\Upsilon(3S) \rightarrow \gamma \chi_{b1}(2P)) = (12.6 \pm 1.2) \times 10^{-2}$. Our first error is their experiment's error and our second error is the systematic error from using our best value.				

$\Gamma(2\pi^+2\pi^-K^+K^-)/\Gamma_{total}$ Γ_{10}/Γ

VALUE (units 10^{-4})	EVTS	DOCUMENT ID	TECN	COMMENT
$1.0 \pm 0.4 \pm 0.1$	12	24 ASNER	08A CLEO	$\Upsilon(3S) \rightarrow \gamma 2\pi^+2\pi^-K^+K^-$
24 ASNER 08A reports $[\Gamma(\chi_{b1}(2P) \rightarrow 2\pi^+2\pi^-K^+K^-)/\Gamma_{total}] \times [B(\Upsilon(3S) \rightarrow \gamma \chi_{b1}(2P))]$ = $(12 \pm 4 \pm 3) \times 10^{-6}$ which we divide by our best value $B(\Upsilon(3S) \rightarrow \gamma \chi_{b1}(2P)) = (12.6 \pm 1.2) \times 10^{-2}$. Our first error is their experiment's error and our second error is the systematic error from using our best value.				

$\Gamma(2\pi^+2\pi^-K^+K^-\pi^0)/\Gamma_{total}$ Γ_{11}/Γ

VALUE (units 10^{-4})	EVTS	DOCUMENT ID	TECN	COMMENT
$5.5 \pm 1.7 \pm 0.5$	38	25 ASNER	08A CLEO	$\Upsilon(3S) \rightarrow \gamma 2\pi^+2\pi^-K^+K^-\pi^0$
25 ASNER 08A reports $[\Gamma(\chi_{b1}(2P) \rightarrow 2\pi^+2\pi^-K^+K^-\pi^0)/\Gamma_{total}] \times [B(\Upsilon(3S) \rightarrow \gamma \chi_{b1}(2P))]$ = $(69 \pm 13 \pm 17) \times 10^{-6}$ which we divide by our best value $B(\Upsilon(3S) \rightarrow \gamma \chi_{b1}(2P)) = (12.6 \pm 1.2) \times 10^{-2}$. Our first error is their experiment's error and our second error is the systematic error from using our best value.				

$\Gamma(2\pi^+2\pi^-K^+K^-2\pi^0)/\Gamma_{total}$ Γ_{12}/Γ

VALUE (units 10^{-4})	EVTS	DOCUMENT ID	TECN	COMMENT
$9.6 \pm 3.5 \pm 0.9$	27	26 ASNER	08A CLEO	$\Upsilon(3S) \rightarrow \gamma 2\pi^+2\pi^-K^+K^-2\pi^0$
26 ASNER 08A reports $[\Gamma(\chi_{b1}(2P) \rightarrow 2\pi^+2\pi^-K^+K^-2\pi^0)/\Gamma_{total}] \times [B(\Upsilon(3S) \rightarrow \gamma \chi_{b1}(2P))]$ = $(121 \pm 29 \pm 33) \times 10^{-6}$ which we divide by our best value $B(\Upsilon(3S) \rightarrow \gamma \chi_{b1}(2P)) = (12.6 \pm 1.2) \times 10^{-2}$. Our first error is their experiment's error and our second error is the systematic error from using our best value.				

$\Gamma(3\pi^+2\pi^-K^-K_S^0\pi^0)/\Gamma_{total}$ Γ_{13}/Γ

VALUE (units 10^{-4})	EVTS	DOCUMENT ID	TECN	COMMENT
$6.7 \pm 2.5 \pm 0.6$	17	27 ASNER	08A CLEO	$\Upsilon(3S) \rightarrow \gamma 3\pi^+2\pi^-K^-K_S^0\pi^0$
27 ASNER 08A reports $[\Gamma(\chi_{b1}(2P) \rightarrow 3\pi^+2\pi^-K^-K_S^0\pi^0)/\Gamma_{total}] \times [B(\Upsilon(3S) \rightarrow \gamma \chi_{b1}(2P))]$ = $(85 \pm 23 \pm 22) \times 10^{-6}$ which we divide by our best value $B(\Upsilon(3S) \rightarrow \gamma \chi_{b1}(2P)) = (12.6 \pm 1.2) \times 10^{-2}$. Our first error is their experiment's error and our second error is the systematic error from using our best value.				

$\Gamma(3\pi^+3\pi^-)/\Gamma_{total}$ Γ_{14}/Γ

VALUE (units 10^{-4})	EVTS	DOCUMENT ID	TECN	COMMENT
$1.2 \pm 0.4 \pm 0.1$	18	28 ASNER	08A CLEO	$\Upsilon(3S) \rightarrow \gamma 3\pi^+3\pi^-$
28 ASNER 08A reports $[\Gamma(\chi_{b1}(2P) \rightarrow 3\pi^+3\pi^-)/\Gamma_{total}] \times [B(\Upsilon(3S) \rightarrow \gamma \chi_{b1}(2P))]$ = $(15 \pm 4 \pm 3) \times 10^{-6}$ which we divide by our best value $B(\Upsilon(3S) \rightarrow \gamma \chi_{b1}(2P)) = (12.6 \pm 1.2) \times 10^{-2}$. Our first error is their experiment's error and our second error is the systematic error from using our best value.				

$\Gamma(3\pi^+3\pi^-2\pi^0)/\Gamma_{total}$ Γ_{15}/Γ

VALUE (units 10^{-4})	EVTS	DOCUMENT ID	TECN	COMMENT
$12 \pm 4 \pm 1$	44	29 ASNER	08A CLEO	$\Upsilon(3S) \rightarrow \gamma 3\pi^+3\pi^-2\pi^0$
29 ASNER 08A reports $[\Gamma(\chi_{b1}(2P) \rightarrow 3\pi^+3\pi^-2\pi^0)/\Gamma_{total}] \times [B(\Upsilon(3S) \rightarrow \gamma \chi_{b1}(2P))]$ = $(150 \pm 30 \pm 40) \times 10^{-6}$ which we divide by our best value $B(\Upsilon(3S) \rightarrow \gamma \chi_{b1}(2P)) = (12.6 \pm 1.2) \times 10^{-2}$. Our first error is their experiment's error and our second error is the systematic error from using our best value.				

$\Gamma(3\pi^+3\pi^-K^+K^-)/\Gamma_{total}$ Γ_{16}/Γ

VALUE (units 10^{-4})	EVTS	DOCUMENT ID	TECN	COMMENT
$2.0 \pm 0.7 \pm 0.2$	16	30 ASNER	08A CLEO	$\Upsilon(3S) \rightarrow \gamma 3\pi^+3\pi^-K^+K^-$
30 ASNER 08A reports $[\Gamma(\chi_{b1}(2P) \rightarrow 3\pi^+3\pi^-K^+K^-)/\Gamma_{total}] \times [B(\Upsilon(3S) \rightarrow \gamma \chi_{b1}(2P))]$ = $(25 \pm 7 \pm 6) \times 10^{-6}$ which we divide by our best value $B(\Upsilon(3S) \rightarrow \gamma \chi_{b1}(2P)) = (12.6 \pm 1.2) \times 10^{-2}$. Our first error is their experiment's error and our second error is the systematic error from using our best value.				

$\Gamma(3\pi^+3\pi^-K^+K^-\pi^0)/\Gamma_{total}$ Γ_{17}/Γ

VALUE (units 10^{-4})	EVTS	DOCUMENT ID	TECN	COMMENT
$6.1 \pm 2.1 \pm 0.6$	25	31 ASNER	08A CLEO	$\Upsilon(3S) \rightarrow \gamma 3\pi^+3\pi^-K^+K^-\pi^0$
31 ASNER 08A reports $[\Gamma(\chi_{b1}(2P) \rightarrow 3\pi^+3\pi^-K^+K^-\pi^0)/\Gamma_{total}] \times [B(\Upsilon(3S) \rightarrow \gamma \chi_{b1}(2P))]$ = $(77 \pm 17 \pm 21) \times 10^{-6}$ which we divide by our best value $B(\Upsilon(3S) \rightarrow \gamma \chi_{b1}(2P)) = (12.6 \pm 1.2) \times 10^{-2}$. Our first error is their experiment's error and our second error is the systematic error from using our best value.				

$\Gamma(4\pi^+4\pi^-)/\Gamma_{total}$ Γ_{18}/Γ

VALUE (units 10^{-4})	EVTS	DOCUMENT ID	TECN	COMMENT
$1.7 \pm 0.6 \pm 0.2$	16	32 ASNER	08A CLEO	$\Upsilon(3S) \rightarrow \gamma 4\pi^+4\pi^-$
32 ASNER 08A reports $[\Gamma(\chi_{b1}(2P) \rightarrow 4\pi^+4\pi^-)/\Gamma_{total}] \times [B(\Upsilon(3S) \rightarrow \gamma \chi_{b1}(2P))]$ = $(22 \pm 6 \pm 5) \times 10^{-6}$ which we divide by our best value $B(\Upsilon(3S) \rightarrow \gamma \chi_{b1}(2P)) = (12.6 \pm 1.2) \times 10^{-2}$. Our first error is their experiment's error and our second error is the systematic error from using our best value.				

$\Gamma(4\pi^+4\pi^-2\pi^0)/\Gamma_{total}$ Γ_{19}/Γ

VALUE (units 10^{-4})	EVTS	DOCUMENT ID	TECN	COMMENT
$19 \pm 7 \pm 2$	41	33 ASNER	08A CLEO	$\Upsilon(3S) \rightarrow \gamma 4\pi^+4\pi^-2\pi^0$
33 ASNER 08A reports $[\Gamma(\chi_{b1}(2P) \rightarrow 4\pi^+4\pi^-2\pi^0)/\Gamma_{total}] \times [B(\Upsilon(3S) \rightarrow \gamma \chi_{b1}(2P))]$ = $(241 \pm 47 \pm 72) \times 10^{-6}$ which we divide by our best value $B(\Upsilon(3S) \rightarrow \gamma \chi_{b1}(2P)) = (12.6 \pm 1.2) \times 10^{-2}$. Our first error is their experiment's error and our second error is the systematic error from using our best value.				

$\chi_{b1}(2P)$ Cross-Particle Branching Ratios

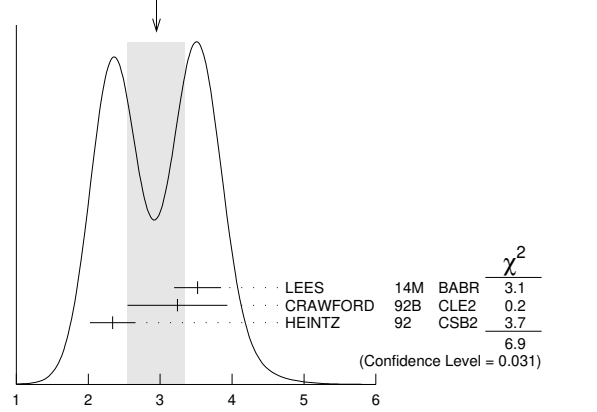
$\Gamma(\chi_{b1}(2P) \rightarrow \gamma \Upsilon(1S))/\Gamma_{total} \times \Gamma(\Upsilon(3S) \rightarrow \gamma \chi_{b1}(2P))/\Gamma_{total}$
 $\Gamma_3/\Gamma \times \Gamma_{21}^{(3S)}/\Gamma \Upsilon(3S)$

VALUE (units 10^{-3})	EVTS	DOCUMENT ID	TECN	COMMENT
$12.4 \pm 0.3 \pm 0.6$	15k	LEES	11J BABR	$\Upsilon(3S) \rightarrow X \gamma$

$B(\chi_{b1}(2P) \rightarrow \gamma \Upsilon(1S)) \times B(\Upsilon(3S) \rightarrow \gamma \chi_{b1}(2P)) \times B(\Upsilon(1S) \rightarrow \ell^+\ell^-)$

VALUE (units 10^{-4})	EVTS	DOCUMENT ID	TECN	COMMENT
2.9 ± 0.4 OUR AVERAGE				Error includes scale factor of 1.9. See the ideogram below.
$3.52_{-0.27}^{+0.28+0.17}$		34 LEES	14M BABR	$\Upsilon(3S) \rightarrow \gamma \gamma \mu^+ \mu^-$
$3.24 \pm 0.56 \pm 0.41$	58	35 CRAWFORD	92B CLE2	$\Upsilon(3S) \rightarrow \gamma \gamma \ell^+ \ell^-$
$2.34 \pm 0.28 \pm 0.15$		36 HEINTZ	92 CSB2	$\Upsilon(3S) \rightarrow \gamma \gamma \ell^+ \ell^-$
34 From a sample of $\Upsilon(3S) \rightarrow \gamma \gamma \mu^+ \mu^-$ with one converted photon.				
35 CRAWFORD 92b quotes $2 \times B(\Upsilon(3S) \rightarrow \gamma \chi_{bJ}(2P)) B(\chi_{bJ}(2P) \rightarrow \gamma \Upsilon(nS))$				
$B(\Upsilon(nS) \rightarrow \ell^+ \ell^-)$.				
36 Calculated by us. HEINTZ 92 quotes $B(\Upsilon(3S) \rightarrow \gamma \chi_{b1}(2P)) \times B(\chi_{b1}(2P) \rightarrow \gamma \Upsilon(1S)) = (0.91 \pm 0.11 \pm 0.06)\%$ using $B(\Upsilon(1S) \rightarrow \mu^+ \mu^-) = (2.57 \pm 0.05)\%$.				

WEIGHTED AVERAGE
2.9±0.4 (Error scaled by 1.9)



$B(\chi_{b1}(2P) \rightarrow \gamma \Upsilon(1S)) \times B(\Upsilon(3S) \rightarrow \gamma \chi_{b1}(2P)) \times B(\Upsilon(1S) \rightarrow \ell^+\ell^-)$
(units 10^{-4})

$\Gamma(\chi_{b1}(2P) \rightarrow \gamma \Upsilon(2S))/\Gamma_{total} \times \Gamma(\Upsilon(3S) \rightarrow \gamma \chi_{b1}(2P))/\Gamma_{total}$
 $\Gamma_2/\Gamma \times \Gamma_{21}^{(3S)}/\Gamma \Upsilon(3S)$

VALUE (units 10^{-2})	EVTS	DOCUMENT ID	TECN	COMMENT
$2.4 \pm 0.1 \pm 0.2$	4.3k	LEES	11J BABR	$\Upsilon(3S) \rightarrow X \gamma$

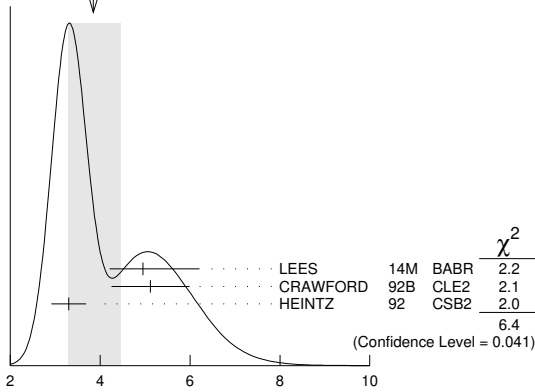
$B(\chi_{b1}(2P) \rightarrow \gamma \Upsilon(2S)) \times B(\Upsilon(3S) \rightarrow \gamma \chi_{b1}(2P)) \times B(\Upsilon(2S) \rightarrow \ell^+\ell^-)$

VALUE (units 10^{-4})	EVTS	DOCUMENT ID	TECN	COMMENT
3.8 ± 0.6 OUR AVERAGE				Error includes scale factor of 1.8. See the ideogram below.
$4.95_{-0.70}^{+0.75+1.01}$		37 LEES	14M BABR	$\Upsilon(3S) \rightarrow \gamma \gamma \mu^+ \mu^-$
$5.12 \pm 0.60 \pm 0.63$	111	38 CRAWFORD	92B CLE2	$\Upsilon(3S) \rightarrow \gamma \gamma \ell^+ \ell^-$
$3.30 \pm 0.33 \pm 0.20$		39 HEINTZ	92 CSB2	$\Upsilon(3S) \rightarrow \gamma \gamma \ell^+ \ell^-$
37 From a sample of $\Upsilon(3S) \rightarrow \gamma \gamma \mu^+ \mu^-$ with one converted photon.				
38 CRAWFORD 92b quotes $2 \times B(\Upsilon(3S) \rightarrow \gamma \chi_{bJ}(2P)) B(\chi_{bJ}(2P) \rightarrow \gamma \Upsilon(nS))$				
$B(\Upsilon(nS) \rightarrow \ell^+ \ell^-)$.				
39 Calculated by us. HEINTZ 92 quotes $B(\Upsilon(3S) \rightarrow \gamma \chi_{b1}(2P)) \times B(\chi_{b1}(2P) \rightarrow \gamma \Upsilon(2S)) = (2.29 \pm 0.23 \pm 0.21)\%$ using $B(\Upsilon(2S) \rightarrow \mu^+ \mu^-) = (1.44 \pm 0.10)\%$.				

Meson Particle Listings

$\chi_{b1}(2P), h_b(2P), \chi_{b2}(2P)$

WEIGHTED AVERAGE
3.8±0.6 (Error scaled by 1.8)



$B(\chi_{b1}(2P) \rightarrow \gamma T(2S)) \times B(T(3S) \rightarrow \gamma \chi_{b1}(2P)) \times B(T(2S) \rightarrow \ell^+ \ell^-)$
(units 10^{-4})

VALUE (units 10^{-3})	EVTS	DOCUMENT ID	TECN	COMMENT
1.16 ± 0.07 ± 0.12	31k	LEES	11c	BABR $e^+e^- \rightarrow \pi^+\pi^-X$

VALUE	DOCUMENT ID	TECN	COMMENT
1.109 ± 0.007 ± 0.040	BRIERE 07	CLEO	$T(3S) \rightarrow \gamma \chi_{b1}(2P)$

VALUE	DOCUMENT ID	TECN	COMMENT
1.082 ± 0.025 ± 0.060	BRIERE 07	CLEO	$T(3S) \rightarrow \gamma \chi_{b1}(2P)$

$\chi_{b1}(2P)$ REFERENCES

LEES 14M PR D90 112010	J.P. Lees et al.	(BABAR Collab.)
LEES 11C PR D84 011104	J.P. Lees et al.	(BABAR Collab.)
LEES 11J PR D84 072002	J.P. Lees et al.	(BABAR Collab.)
ASNER 08A PR D78 091103	D.M. Asner et al.	(CLEO Collab.)
BRIERE 08 PR D78 092007	R.A. Briere et al.	(CLEO Collab.)
BRIERE 07 PR D76 012005	R.A. Briere et al.	(CLEO Collab.)
CRAWFIELD 06 PR D73 012003	C. Crawford et al.	(CLEO Collab.)
ARTUSO 05 PRL 94 032001	M. Artuso et al.	(CLEO Collab.)
CRONIN-HEN. 04 PRL 92 222002	D. Cronin-Hennessy et al.	(CLEO Collab.)
CRAWFORD 92B PL B294 139	G. Crawford et al.	(CLEO Collab.)
HEINTZ 92 PR D46 1928	U. Heintz et al.	(CUSB II Collab.)
HEINTZ 91 PRL 66 1563	U. Heintz et al.	(CUSB Collab.)
MORRISON 91 PRL 67 1696	R.J. Morrison et al.	(CLEO Collab.)
NARAIN 91 PRL 66 3113	M. Narain et al.	(CUSB Collab.)

$h_b(2P)$

$$J^{G(JPC)} = 0^-(1^{+-})$$

OMITTED FROM SUMMARY TABLE

Quantum numbers are quark model predictions.

$h_b(2P)$ MASS

VALUE (MeV)	EVTS	DOCUMENT ID	TECN	COMMENT
10259.8 ± 0.5 ± 1.1	90k	MIZUK	12	BELL $e^+e^- \rightarrow \pi^+\pi^-$ hadrons

••• We do not use the following data for averages, fits, limits, etc. •••

10259.8 ± 0.6 ^{+1.4} _{-1.0}	83.9k	¹ ADACHI	12	BELL 10.86 $e^+e^- \rightarrow \pi^+\pi^-$ MM
---	-------	---------------------	----	---

¹ Superseded by MIZUK 12.

$h_b(2P)$ DECAY MODES

Mode	Fraction (Γ_i/Γ)
Γ_1 hadrons	not seen
Γ_2 $\eta_b(1S)\gamma$	(22 ± 5) %
Γ_3 $\eta_b(2S)\gamma$	(48 ± 13) %

$h_b(2P)$ BRANCHING RATIOS

$\Gamma(\text{hadrons})/\Gamma_{\text{total}}$	Γ_1/Γ
not seen	83.9k
ADACHI 12 BELL 10.86 $e^+e^- \rightarrow \pi^+\pi^-$ MM	

$\Gamma(\eta_b(1S)\gamma)/\Gamma_{\text{total}}$	Γ_2/Γ
22.3 ± 3.8 ± 3.1	10k
MIZUK 12 BELL $e^+e^- \rightarrow (\gamma)\pi^+\pi^-$ hadrons	

$\Gamma(\eta_b(2S)\gamma)/\Gamma_{\text{total}}$	Γ_3/Γ
47.5 ± 10.5 ± 6.8 _{-7.7}	26k
MIZUK 12 BELL $e^+e^- \rightarrow (\gamma)\pi^+\pi^-$ hadrons	

$h_b(2P)$ REFERENCES

ADACHI 12 PRL 108 032001	I. Adachi et al.	(BELLE Collab.)
MIZUK 12 PRL 109 232002	R. Mizuk et al.	(BELLE Collab.)

$\chi_{b2}(2P)$

$$J^{G(JPC)} = 0^+(2^{++})$$

J needs confirmation.

Observed in radiative decay of the $T(3S)$, therefore $C = +$. Branching ratio requires E1 transition, M1 is strongly disfavored, therefore $P = +$.

$\chi_{b2}(2P)$ MASS

VALUE (MeV)	DOCUMENT ID
10268.65 ± 0.22 ± 0.50 OUR EVALUATION	From γ energy below, using $T(3S)$ mass = 10355.2 ± 0.5 MeV

$m_{\chi_{b2}(2P)} - m_{\chi_{b1}(2P)}$

VALUE (MeV)	DOCUMENT ID	TECN	COMMENT
13.10 ± 0.24 OUR AVERAGE			
12.3 ± 2.6 ± 0.6	¹ AAIJ 14B6 LHCB		$pp \rightarrow \gamma\mu^+\mu^-X$
13.04 ± 0.26	LEES 14M BABR		$T(3S) \rightarrow \gamma\gamma\mu^+\mu^-$
13.5 ± 0.4 ± 0.5	² HEINTZ 92 CSB2		$e^+e^- \rightarrow \gamma X, \ell^+\ell^-\gamma\gamma$

¹ From the $\chi_{b1}(2P) \rightarrow T(1S)\gamma$ transition.

² From the average photon energy for inclusive and exclusive events. Supersedes NARAIN 91.

γ ENERGY IN $T(3S)$ DECAY

VALUE (MeV)	EVTS	DOCUMENT ID	TECN	COMMENT
86.19 ± 0.22 OUR EVALUATION				Treating systematic errors as correlated
86.40 ± 0.18 OUR AVERAGE				
86.04 ± 0.06 ± 0.27		ARTUSO 05 CLEO		$T(3S) \rightarrow \gamma X$
86 ± 1	101	CRAWFORD 92B CLE2		$e^+e^- \rightarrow \ell^+\ell^-\gamma\gamma$
86.7 ± 0.4	10319	³ HEINTZ 92 CSB2		$e^+e^- \rightarrow \gamma X$
86.9 ± 0.4	157	⁴ HEINTZ 92 CSB2		$e^+e^- \rightarrow \ell^+\ell^-\gamma\gamma$
86.4 ± 0.1 ± 0.4	30741	MORRISON 91 CLE2		$e^+e^- \rightarrow \gamma X$

³ A systematic uncertainty on the energy scale of 0.9% not included. Supersedes NARAIN 91.

⁴ A systematic uncertainty on the energy scale of 0.9% not included. Supersedes HEINTZ 91.

$\chi_{b2}(2P)$ DECAY MODES

Mode	Fraction (Γ_i/Γ)	Confidence level
Γ_1 $\omega T(1S)$	(1.10 ^{+0.34} _{-0.30}) %	
Γ_2 $\gamma T(2S)$	(8.9 ± 1.2) %	
Γ_3 $\gamma T(1S)$	(6.6 ± 0.8) %	
Γ_4 $\pi\pi\chi_{b2}(1P)$	(5.1 ± 0.9) × 10 ⁻³	
Γ_5 $D^0 X$	< 2.4 %	90%
Γ_6 $\pi^+\pi^-K^+K^-\pi^0$	< 1.1 × 10 ⁻⁴	90%
Γ_7 $2\pi^+\pi^-K^-K_S^0$	< 9 × 10 ⁻⁵	90%
Γ_8 $2\pi^+\pi^-K^-K_S^0 2\pi^0$	< 7 × 10 ⁻⁴	90%
Γ_9 $2\pi^+2\pi^-2\pi^0$	(3.9 ± 1.6) × 10 ⁻⁴	
Γ_{10} $2\pi^+2\pi^-K^+K^-$	(9 ± 4) × 10 ⁻⁵	
Γ_{11} $2\pi^+2\pi^-K^+K^-\pi^0$	(2.4 ± 1.1) × 10 ⁻⁴	
Γ_{12} $2\pi^+2\pi^-K^+K^-2\pi^0$	(4.7 ± 2.3) × 10 ⁻⁴	
Γ_{13} $3\pi^+2\pi^-K^-K_S^0\pi^0$	< 4 × 10 ⁻⁴	90%
Γ_{14} $3\pi^+3\pi^-$	(9 ± 4) × 10 ⁻⁵	
Γ_{15} $3\pi^+3\pi^-2\pi^0$	(1.2 ± 0.4) × 10 ⁻³	
Γ_{16} $3\pi^+3\pi^-K^+K^-$	(1.4 ± 0.7) × 10 ⁻⁴	
Γ_{17} $3\pi^+3\pi^-K^+K^-\pi^0$	(4.2 ± 1.7) × 10 ⁻⁴	
Γ_{18} $4\pi^+4\pi^-$	(9 ± 5) × 10 ⁻⁵	
Γ_{19} $4\pi^+4\pi^-2\pi^0$	(1.3 ± 0.5) × 10 ⁻³	

$\chi_{b2}(2P)$ BRANCHING RATIOS

$\Gamma(\omega T(1S))/\Gamma_{\text{total}}$	Γ_1/Γ
1.10 ± 0.32 ± 0.11 _{-0.28 - 0.10}	20.1 ^{+5.8} _{-5.1} ⁵ CRONIN-HEN..04 CLE3 $T(3S) \rightarrow \gamma\omega T(1S)$

⁵ Using $B(T(3S) \rightarrow \gamma\chi_{b2}(2P)) = (11.4 ± 0.8)\%$ and $B(T(1S) \rightarrow \ell^+\ell^-) = 2$ $B(T(1S) \rightarrow \mu^+\mu^-) = 2(2.48 ± 0.06)\%$.

See key on page 999

Meson Particle Listings

$\chi_{b2}(2P)$

$\Gamma(\gamma T(2S))/\Gamma_{total}$					Γ_2/Γ
VALUE	EVTS	DOCUMENT ID	TECN	COMMENT	
0.089±0.012 OUR AVERAGE					
0.085±0.010±0.010		6,7,8 LEES	14M BABR	$T(3S) \rightarrow \gamma\gamma\mu^+\mu^-$	
0.084±0.011±0.010	2.5k	9 LEES	11J BABR	$T(3S) \rightarrow X\gamma$	
0.096±0.022±0.012		7,10 CRAWFORD	92B CLE2	$e^+e^- \rightarrow \ell^+\ell^-\gamma\gamma$	
0.106±0.016±0.013		7,11 HEINTZ	92 CSB2	$e^+e^- \rightarrow \ell^+\ell^-\gamma\gamma$	

⁶ LEES 14M quotes $\Gamma(\chi_{b2}(2P) \rightarrow \gamma T(2S))/\Gamma_{total} \times \Gamma(T(3S) \rightarrow \gamma\gamma\mu^+\mu^-)/\Gamma_{total} = (1.12 \pm 0.13)\%$ combining the results from samples of $T(3S) \rightarrow \gamma\gamma\mu^+\mu^-$ with and without converted photons.
⁷ Assuming $B(T(2S) \rightarrow \mu^+\mu^-) = (1.93 \pm 0.17)\%$.
⁸ LEES 14M reports $[\Gamma(\chi_{b2}(2P) \rightarrow \gamma T(2S))/\Gamma_{total}] \times [B(T(3S) \rightarrow \gamma\chi_{b2}(2P))] = (1.12 \pm 0.13) \times 10^{-2}$ which we divide by our best value $B(T(3S) \rightarrow \gamma\chi_{b2}(2P)) = (13.1 \pm 1.6) \times 10^{-2}$. Our first error is their experiment's error and our second error is the systematic error from using our best value.
⁹ LEES 11J reports $[\Gamma(\chi_{b2}(2P) \rightarrow \gamma T(2S))/\Gamma_{total}] \times [B(T(3S) \rightarrow \gamma\chi_{b2}(2P))] = (1.1 \pm 0.1 \pm 0.1) \times 10^{-2}$ which we divide by our best value $B(T(3S) \rightarrow \gamma\chi_{b2}(2P)) = (13.1 \pm 1.6) \times 10^{-2}$. Our first error is their experiment's error and our second error is the systematic error from using our best value.
¹⁰ CRAWFORD 92B quotes $B(T(3S) \rightarrow \gamma\chi_{b1}(2P)) \times B(\chi_{b2}(2P) \rightarrow \gamma T(2S)) \times 2 B(T(2S) \rightarrow \ell^+\ell^-) = (4.98 \pm 0.94 \pm 0.62) 10^{-4}$.
¹¹ Recalculated by us. HEINTZ 92 quotes $B(T(3S) \rightarrow \gamma\chi_{b2}(2P)) \times B(\chi_{b2}(2P) \rightarrow \gamma T(2S)) = (1.90 \pm 0.23 \pm 0.18) \%$ using $B(T(2S) \rightarrow \mu^+\mu^-) = (1.44 \pm 0.10)\%$. Supersedes HEINTZ 91.

$\Gamma(\gamma T(1S))/\Gamma_{total}$					Γ_3/Γ
VALUE	EVTS	DOCUMENT ID	TECN	COMMENT	
0.066±0.008 OUR AVERAGE					
0.061±0.004±0.007		12,13,14 LEES	14M BABR	$T(3S) \rightarrow \gamma\gamma\mu^+\mu^-$	
0.070±0.004±0.008	11k	15 LEES	11J BABR	$T(3S) \rightarrow X\gamma$	
0.077±0.018±0.009		13,16 CRAWFORD	92B CLE2	$e^+e^- \rightarrow \ell^+\ell^-\gamma\gamma$	
0.061±0.009±0.007		13,17 HEINTZ	92 CSB2	$e^+e^- \rightarrow \ell^+\ell^-\gamma\gamma$	

¹² LEES 14M quotes $\Gamma(\chi_{b2}(2P) \rightarrow \gamma T(1S))/\Gamma_{total} \times \Gamma(T(3S) \rightarrow \gamma\gamma\mu^+\mu^-)/\Gamma_{total} = (8.03 \pm 0.50) \times 10^{-3}$ combining the results from samples of $T(3S) \rightarrow \gamma\gamma\mu^+\mu^-$ with and without converted photons.
¹³ Assuming $B(T(1S) \rightarrow \mu^+\mu^-) = (2.48 \pm 0.05)\%$.
¹⁴ LEES 14M reports $[\Gamma(\chi_{b2}(2P) \rightarrow \gamma T(1S))/\Gamma_{total}] \times [B(T(3S) \rightarrow \gamma\chi_{b2}(2P))] = (8.03 \pm 0.50) \times 10^{-3}$ which we divide by our best value $B(T(3S) \rightarrow \gamma\chi_{b2}(2P)) = (13.1 \pm 1.6) \times 10^{-2}$. Our first error is their experiment's error and our second error is the systematic error from using our best value.
¹⁵ LEES 11J reports $[\Gamma(\chi_{b2}(2P) \rightarrow \gamma T(1S))/\Gamma_{total}] \times [B(T(3S) \rightarrow \gamma\chi_{b2}(2P))] = (9.2 \pm 0.3 \pm 0.4) \times 10^{-3}$ which we divide by our best value $B(T(3S) \rightarrow \gamma\chi_{b2}(2P)) = (13.1 \pm 1.6) \times 10^{-2}$. Our first error is their experiment's error and our second error is the systematic error from using our best value.
¹⁶ CRAWFORD 92B quotes $B(T(3S) \rightarrow \gamma\chi_{b2}(2P)) \times B(\chi_{b2}(2P) \rightarrow \gamma T(1S)) \times 2 B(T(1S) \rightarrow \ell^+\ell^-) = (5.03 \pm 0.94 \pm 0.63) 10^{-4}$.
¹⁷ Recalculated by us. HEINTZ 92 quotes $B(T(3S) \rightarrow \gamma\chi_{b2}(2P)) \times B(\chi_{b2}(2P) \rightarrow \gamma T(1S)) = (0.77 \pm 0.11 \pm 0.05)\%$ using $B(T(1S) \rightarrow \mu^+\mu^-) = (2.57 \pm 0.05)\%$. Supersedes HEINTZ 91.

$\Gamma(\pi\pi\chi_{b2}(1P))/\Gamma_{total}$					Γ_4/Γ
VALUE (units 10^{-3})	EVTS	DOCUMENT ID	TECN	COMMENT	
5.1±0.9 OUR AVERAGE					
4.9±0.7±0.6	17k	18 LEES	11C BABR	$e^+e^- \rightarrow \pi^+\pi^-X$	
6.0±1.6±1.4		19 CRAWFIELD	06 CLE3	$T(3S) \rightarrow 2(\gamma\pi\ell)$	

¹⁸ $(0.64 \pm 0.05 \pm 0.08) \times 10^{-3}$. We derive the value assuming $B(T(3S) \rightarrow \chi_{b2}(2P)X) = B(T(3S) \rightarrow \chi_{b2}(2P)\gamma) = (13.1 \pm 1.6) \times 10^{-2}$.
¹⁹ CRAWFIELD 06 quote $\Gamma(\chi_b(2P) \rightarrow \pi\pi\chi_b(1P)) = 0.83 \pm 0.22 \pm 0.08 \pm 0.19$ keV assuming l-spin conservation, no D-wave contribution, $\Gamma(\chi_{b1}(2P)) = 96 \pm 16$ keV, and $\Gamma(\chi_{b2}(2P)) = 138 \pm 19$ keV.

$\Gamma(D^0 X)/\Gamma_{total}$					Γ_5/Γ
VALUE	CL%	DOCUMENT ID	TECN	COMMENT	
<2.4 × 10⁻²					
	90	20,21 BRIERE	08 CLEO	$T(3S) \rightarrow \gamma D^0 X$	

²⁰ For $p_{D^0} > 2.5$ GeV/c.
²¹ The authors also present their result as $(0.2 \pm 1.4 \pm 0.1) \times 10^{-2}$.

$\Gamma(\pi^+\pi^-K^+K^-\pi^0)/\Gamma_{total}$					Γ_6/Γ
VALUE (units 10^{-4})	CL%	DOCUMENT ID	TECN	COMMENT	
<1.1					
	90	22 ASNER	08A CLEO	$T(3S) \rightarrow \gamma\pi^+\pi^-K^+K^-\pi^0$	

²² ASNER 08A reports $[\Gamma(\chi_{b2}(2P) \rightarrow \pi^+\pi^-K^+K^-\pi^0)/\Gamma_{total}] \times [B(T(3S) \rightarrow \gamma\chi_{b2}(2P))] < 14 \times 10^{-6}$ which we divide by our best value $B(T(3S) \rightarrow \gamma\chi_{b2}(2P)) = 13.1 \times 10^{-2}$.

$\Gamma(2\pi^+\pi^-K^-K_S^0)/\Gamma_{total}$					Γ_7/Γ
VALUE (units 10^{-4})	CL%	DOCUMENT ID	TECN	COMMENT	
<0.9					
	90	23 ASNER	08A CLEO	$T(3S) \rightarrow \gamma 2\pi^+\pi^-K^-K_S^0$	

²³ ASNER 08A reports $[\Gamma(\chi_{b2}(2P) \rightarrow 2\pi^+\pi^-K^-K_S^0)/\Gamma_{total}] \times [B(T(3S) \rightarrow \gamma\chi_{b2}(2P))] < 12 \times 10^{-6}$ which we divide by our best value $B(T(3S) \rightarrow \gamma\chi_{b2}(2P)) = 13.1 \times 10^{-2}$.

$\Gamma(2\pi^+\pi^-K^-K_S^0 2\pi^0)/\Gamma_{total}$					Γ_8/Γ
VALUE (units 10^{-4})	CL%	DOCUMENT ID	TECN	COMMENT	
<7					
	90	24 ASNER	08A CLEO	$T(3S) \rightarrow \gamma 2\pi^+\pi^-K^-K_S^0 2\pi^0$	

²⁴ ASNER 08A reports $[\Gamma(\chi_{b2}(2P) \rightarrow 2\pi^+\pi^-K^-K_S^0 2\pi^0)/\Gamma_{total}] \times [B(T(3S) \rightarrow \gamma\chi_{b2}(2P))] < 87 \times 10^{-6}$ which we divide by our best value $B(T(3S) \rightarrow \gamma\chi_{b2}(2P)) = 13.1 \times 10^{-2}$.

$\Gamma(2\pi^+2\pi^-2\pi^0)/\Gamma_{total}$					Γ_9/Γ
VALUE (units 10^{-4})	EVTS	DOCUMENT ID	TECN	COMMENT	
3.9±1.6±0.5					
	23	25 ASNER	08A CLEO	$T(3S) \rightarrow \gamma 2\pi^+2\pi^-2\pi^0$	

²⁵ ASNER 08A reports $[\Gamma(\chi_{b2}(2P) \rightarrow 2\pi^+2\pi^-2\pi^0)/\Gamma_{total}] \times [B(T(3S) \rightarrow \gamma\chi_{b2}(2P))] = (51 \pm 16 \pm 13) \times 10^{-6}$ which we divide by our best value $B(T(3S) \rightarrow \gamma\chi_{b2}(2P)) = (13.1 \pm 1.6) \times 10^{-2}$. Our first error is their experiment's error and our second error is the systematic error from using our best value.

$\Gamma(2\pi^+2\pi^-K^+K^-)/\Gamma_{total}$					Γ_{10}/Γ
VALUE (units 10^{-4})	EVTS	DOCUMENT ID	TECN	COMMENT	
0.9±0.4±0.1					
	11	26 ASNER	08A CLEO	$T(3S) \rightarrow \gamma 2\pi^+2\pi^-K^+K^-$	

²⁶ ASNER 08A reports $[\Gamma(\chi_{b2}(2P) \rightarrow 2\pi^+2\pi^-K^+K^-)/\Gamma_{total}] \times [B(T(3S) \rightarrow \gamma\chi_{b2}(2P))] = (12 \pm 4 \pm 3) \times 10^{-6}$ which we divide by our best value $B(T(3S) \rightarrow \gamma\chi_{b2}(2P)) = (13.1 \pm 1.6) \times 10^{-2}$. Our first error is their experiment's error and our second error is the systematic error from using our best value.

$\Gamma(2\pi^+2\pi^-K^+K^-\pi^0)/\Gamma_{total}$					Γ_{11}/Γ
VALUE (units 10^{-4})	EVTS	DOCUMENT ID	TECN	COMMENT	
2.4±1.0±0.3					
	16	27 ASNER	08A CLEO	$T(3S) \rightarrow \gamma 2\pi^+2\pi^-K^+K^-\pi^0$	

²⁷ ASNER 08A reports $[\Gamma(\chi_{b2}(2P) \rightarrow 2\pi^+2\pi^-K^+K^-\pi^0)/\Gamma_{total}] \times [B(T(3S) \rightarrow \gamma\chi_{b2}(2P))] = (32 \pm 11 \pm 8) \times 10^{-6}$ which we divide by our best value $B(T(3S) \rightarrow \gamma\chi_{b2}(2P)) = (13.1 \pm 1.6) \times 10^{-2}$. Our first error is their experiment's error and our second error is the systematic error from using our best value.

$\Gamma(2\pi^+2\pi^-K^+K^-2\pi^0)/\Gamma_{total}$					Γ_{12}/Γ
VALUE (units 10^{-4})	EVTS	DOCUMENT ID	TECN	COMMENT	
4.7±2.2±0.6					
	14	28 ASNER	08A CLEO	$T(3S) \rightarrow \gamma 2\pi^+2\pi^-K^+K^-2\pi^0$	

²⁸ ASNER 08A reports $[\Gamma(\chi_{b2}(2P) \rightarrow 2\pi^+2\pi^-K^+K^-2\pi^0)/\Gamma_{total}] \times [B(T(3S) \rightarrow \gamma\chi_{b2}(2P))] = (62 \pm 23 \pm 17) \times 10^{-6}$ which we divide by our best value $B(T(3S) \rightarrow \gamma\chi_{b2}(2P)) = (13.1 \pm 1.6) \times 10^{-2}$. Our first error is their experiment's error and our second error is the systematic error from using our best value.

$\Gamma(3\pi^+2\pi^-K^-K_S^0\pi^0)/\Gamma_{total}$					Γ_{13}/Γ
VALUE (units 10^{-4})	CL%	DOCUMENT ID	TECN	COMMENT	
<4					
	90	29 ASNER	08A CLEO	$T(3S) \rightarrow \gamma 3\pi^+2\pi^-K^-K_S^0\pi^0$	

²⁹ ASNER 08A reports $[\Gamma(\chi_{b2}(2P) \rightarrow 3\pi^+2\pi^-K^-K_S^0\pi^0)/\Gamma_{total}] \times [B(T(3S) \rightarrow \gamma\chi_{b2}(2P))] < 58 \times 10^{-6}$ which we divide by our best value $B(T(3S) \rightarrow \gamma\chi_{b2}(2P)) = 13.1 \times 10^{-2}$.

$\Gamma(3\pi^+3\pi^-)/\Gamma_{total}$					Γ_{14}/Γ
VALUE (units 10^{-4})	EVTS	DOCUMENT ID	TECN	COMMENT	
0.9±0.4±0.1					
	14	30 ASNER	08A CLEO	$T(3S) \rightarrow \gamma 3\pi^+3\pi^-$	

³⁰ ASNER 08A reports $[\Gamma(\chi_{b2}(2P) \rightarrow 3\pi^+3\pi^-)/\Gamma_{total}] \times [B(T(3S) \rightarrow \gamma\chi_{b2}(2P))] = (12 \pm 4 \pm 3) \times 10^{-6}$ which we divide by our best value $B(T(3S) \rightarrow \gamma\chi_{b2}(2P)) = (13.1 \pm 1.6) \times 10^{-2}$. Our first error is their experiment's error and our second error is the systematic error from using our best value.

$\Gamma(3\pi^+3\pi^-2\pi^0)/\Gamma_{total}$					Γ_{15}/Γ
VALUE (units 10^{-4})	EVTS	DOCUMENT ID	TECN	COMMENT	
12±4±1					
	45	31 ASNER	08A CLEO	$T(3S) \rightarrow \gamma 3\pi^+3\pi^-2\pi^0$	

³¹ ASNER 08A reports $[\Gamma(\chi_{b2}(2P) \rightarrow 3\pi^+3\pi^-2\pi^0)/\Gamma_{total}] \times [B(T(3S) \rightarrow \gamma\chi_{b2}(2P))] = (159 \pm 33 \pm 43) \times 10^{-6}$ which we divide by our best value $B(T(3S) \rightarrow \gamma\chi_{b2}(2P)) = (13.1 \pm 1.6) \times 10^{-2}$. Our first error is their experiment's error and our second error is the systematic error from using our best value.

$\Gamma(3\pi^+3\pi^-K^+K^-)/\Gamma_{total}$					Γ_{16}/Γ
VALUE (units 10^{-4})	EVTS	DOCUMENT ID	TECN	COMMENT	
1.4±0.7±0.2					
	12	32 ASNER	08A CLEO	$T(3S) \rightarrow \gamma 3\pi^+3\pi^-K^+K^-$	

³² ASNER 08A reports $[\Gamma(\chi_{b2}(2P) \rightarrow 3\pi^+3\pi^-K^+K^-)/\Gamma_{total}] \times [B(T(3S) \rightarrow \gamma\chi_{b2}(2P))] = (19 \pm 7 \pm 5) \times 10^{-6}$ which we divide by our best value $B(T(3S) \rightarrow \gamma\chi_{b2}(2P)) = (13.1 \pm 1.6) \times 10^{-2}$. Our first error is their experiment's error and our second error is the systematic error from using our best value.

$\Gamma(3\pi^+3\pi^-K^+K^-\pi^0)/\Gamma_{total}$					Γ_{17}/Γ
VALUE (units 10^{-4})	EVTS	DOCUMENT ID	TECN	COMMENT	
4.2±1.7±0.5					
	16	33 ASNER	08A CLEO	$T(3S) \rightarrow \gamma 3\pi^+3\pi^-K^+K^-\pi^0$	

³³ ASNER 08A reports $[\Gamma(\chi_{b2}(2P) \rightarrow 3\pi^+3\pi^-K^+K^-\pi^0)/\Gamma_{total}] \times [B(T(3S) \rightarrow \gamma\chi_{b2}(2P))] = (55 \pm 16 \pm 15) \times 10^{-6}$ which we divide by our best value $B(T(3S) \rightarrow \gamma\chi_{b2}(2P)) = (13.1 \pm 1.6) \times 10^{-2}$. Our first error is their experiment's error and our second error is the systematic error from using our best value.

Meson Particle Listings

$\chi_{b2}(2P), \Upsilon(3S)$

$\Gamma(4\pi^+4\pi^-)/\Gamma_{\text{total}}$					Γ_{18}/Γ
VALUE (units 10^{-4})	EVTS	DOCUMENT ID	TECN	COMMENT	
$0.9 \pm 0.4 \pm 0.1$	9	³⁴ ASNER	08A CLEO	$\Upsilon(3S) \rightarrow \gamma 4\pi^+ 4\pi^-$	
³⁴ ASNER 08A reports $[\Gamma(\chi_{b2}(2P) \rightarrow 4\pi^+ 4\pi^-)/\Gamma_{\text{total}}] \times [B(\Upsilon(3S) \rightarrow \gamma \chi_{b2}(2P))]$ = $(12 \pm 5 \pm 3) \times 10^{-6}$ which we divide by our best value $B(\Upsilon(3S) \rightarrow \gamma \chi_{b2}(2P))$ = $(13.1 \pm 1.6) \times 10^{-2}$. Our first error is their experiment's error and our second error is the systematic error from using our best value.					

$\Gamma(4\pi^+4\pi^-2\pi^0)/\Gamma_{\text{total}}$					Γ_{19}/Γ
VALUE (units 10^{-4})	EVTS	DOCUMENT ID	TECN	COMMENT	
$13 \pm 5 \pm 2$	27	³⁵ ASNER	08A CLEO	$\Upsilon(3S) \rightarrow \gamma 4\pi^+ 4\pi^- 2\pi^0$	
³⁵ ASNER 08A reports $[\Gamma(\chi_{b2}(2P) \rightarrow 4\pi^+ 4\pi^- 2\pi^0)/\Gamma_{\text{total}}] \times [B(\Upsilon(3S) \rightarrow \gamma \chi_{b2}(2P))]$ = $(165 \pm 46 \pm 50) \times 10^{-6}$ which we divide by our best value $B(\Upsilon(3S) \rightarrow \gamma \chi_{b2}(2P))$ = $(13.1 \pm 1.6) \times 10^{-2}$. Our first error is their experiment's error and our second error is the systematic error from using our best value.					

$\chi_{b2}(2P)$ Cross-Particle Branching Ratios

$\Gamma(\chi_{b2}(2P) \rightarrow \gamma \Upsilon(1S))/\Gamma_{\text{total}} \times \Gamma(\Upsilon(3S) \rightarrow \gamma \chi_{b2}(2P))/\Gamma_{\text{total}}$				
$\Gamma_3/\Gamma \times \Gamma_{20}^{\Upsilon(3S)}/\Gamma_{\Upsilon(3S)}$				
VALUE (units 10^{-3})	EVTS	DOCUMENT ID	TECN	COMMENT
$9.2 \pm 0.3 \pm 0.4$	11k	LEES	11J BABR	$\Upsilon(3S) \rightarrow X \gamma$

$\Gamma(\chi_{b2}(2P) \rightarrow \gamma \Upsilon(2S))/\Gamma_{\text{total}} \times \Gamma(\Upsilon(3S) \rightarrow \gamma \chi_{b2}(2P))/\Gamma_{\text{total}}$				
$\Gamma_2/\Gamma \times \Gamma_{20}^{\Upsilon(3S)}/\Gamma_{\Upsilon(3S)}$				
VALUE (units 10^{-2})	EVTS	DOCUMENT ID	TECN	COMMENT
$1.1 \pm 0.1 \pm 0.1$	2.5k	LEES	11J BABR	$\Upsilon(3S) \rightarrow X \gamma$

$B(\chi_{b2}(2P) \rightarrow \chi_{b2}(1P)\pi^+\pi^-) \times B(\Upsilon(3S) \rightarrow \chi_{b2}(2P)X)$				
VALUE (units 10^{-3})	EVTS	DOCUMENT ID	TECN	COMMENT
$0.6 \pm 0.05 \pm 0.08$	17k	LEES	11c BABR	$e^+e^- \rightarrow \pi^+\pi^-X$

$B(\chi_{b2}(2P) \rightarrow \gamma \Upsilon(1S)) \times B(\Upsilon(3S) \rightarrow \gamma \chi_{b2}(2P)) \times B(\Upsilon(1S) \rightarrow \ell^+\ell^-)$				
VALUE (units 10^{-4})	EVTS	DOCUMENT ID	TECN	COMMENT
2.02 ± 0.18 OUR AVERAGE				

$1.95^{+0.22+0.10}_{-0.21-0.16}$		³⁶ LEES	14M BABR	$\Upsilon(3S) \rightarrow \gamma \gamma \mu^+ \mu^-$
$2.52 \pm 0.47 \pm 0.32$	48	³⁷ CRAWFORD	92B CLE2	$\Upsilon(3S) \rightarrow \gamma \gamma \ell^+ \ell^-$
$1.98 \pm 0.28 \pm 0.12$		³⁸ HEINTZ	92 CSB2	$\Upsilon(3S) \rightarrow \gamma \gamma \ell^+ \ell^-$

³⁶ From a sample of $\Upsilon(3S) \rightarrow \gamma \gamma \mu^+ \mu^-$ with converted photons.
³⁷ CRAWFORD 92b quotes $2 \times B(\Upsilon(3S) \rightarrow \gamma \chi_{bJ}(2P)) B(\chi_{bJ}(2P) \rightarrow \gamma \Upsilon(nS))$
 $B(\Upsilon(nS) \rightarrow \ell^+ \ell^-)$.
³⁸ Calculated by us. HEINTZ 92 quotes $B(\Upsilon(3S) \rightarrow \gamma \chi_{b2}(2P)) \times B(\chi_{b2}(2P) \rightarrow \gamma \Upsilon(1S)) = (0.77 \pm 0.11 \pm 0.05)\%$ using $B(\Upsilon(1S) \rightarrow \mu^+ \mu^-) = (2.57 \pm 0.05)\%$.

$[B(\chi_{b2}(2P) \rightarrow \gamma \Upsilon(1S)) \times B(\Upsilon(3S) \rightarrow \gamma \chi_{b2}(2P))] / [B(\chi_{b1}(2P) \rightarrow \gamma \Upsilon(1S)) \times B(\Upsilon(3S) \rightarrow \gamma \chi_{b1}(2P))]$				
VALUE (%)	DOCUMENT ID	TECN	COMMENT	
66.6 ± 3.0	³⁹ LEES	14M BABR	$\Upsilon(3S) \rightarrow \gamma \gamma \mu^+ \mu^-$	

³⁹ From a sample of $\Upsilon(3S) \rightarrow \gamma \gamma \mu^+ \mu^-$ events without converted photons.

$B(\chi_{b2}(2P) \rightarrow \gamma \Upsilon(2S)) \times B(\Upsilon(3S) \rightarrow \gamma \chi_{b2}(2P)) \times B(\Upsilon(2S) \rightarrow \ell^+\ell^-)$				
VALUE (units 10^{-4})	EVTS	DOCUMENT ID	TECN	COMMENT
2.74 ± 0.29 OUR AVERAGE				

$3.22^{+0.58+0.16}_{-0.53-0.71}$		40 LEES	14M BABR	$\Upsilon(3S) \rightarrow \gamma \gamma \mu^+ \mu^-$
$2.49 \pm 0.47 \pm 0.31$	53	⁴¹ CRAWFORD	92B CLE2	$\Upsilon(3S) \rightarrow \gamma \gamma \ell^+ \ell^-$
$2.74 \pm 0.33 \pm 0.18$		⁴² HEINTZ	92 CSB2	$\Upsilon(3S) \rightarrow \gamma \gamma \ell^+ \ell^-$

⁴⁰ From a sample of $\Upsilon(3S) \rightarrow \gamma \gamma \mu^+ \mu^-$ with converted photons.
⁴¹ CRAWFORD 92b quotes $2 \times B(\Upsilon(3S) \rightarrow \gamma \chi_{bJ}(2P)) B(\chi_{bJ}(2P) \rightarrow \gamma \Upsilon(nS))$
 $B(\Upsilon(nS) \rightarrow \ell^+ \ell^-)$.
⁴² Calculated by us. HEINTZ 92 quotes $B(\Upsilon(3S) \rightarrow \gamma \chi_{b2}(2P)) \times B(\chi_{b2}(2P) \rightarrow \gamma \Upsilon(2S)) = (1.90 \pm 0.23 \pm 0.18)\%$ using $B(\Upsilon(2S) \rightarrow \mu^+ \mu^-) = (1.44 \pm 0.10)\%$.

$[B(\chi_{b2}(2P) \rightarrow \gamma \Upsilon(2S)) \times B(\Upsilon(3S) \rightarrow \gamma \chi_{b2}(2P))] / [B(\chi_{b1}(2P) \rightarrow \gamma \Upsilon(2S)) \times B(\Upsilon(3S) \rightarrow \gamma \chi_{b1}(2P))]$				
VALUE (%)	DOCUMENT ID	TECN	COMMENT	
46.9 ± 2.0	⁴³ LEES	14M BABR	$\Upsilon(3S) \rightarrow \gamma \gamma \mu^+ \mu^-$	

⁴³ From a sample of $\Upsilon(3S) \rightarrow \gamma \gamma \mu^+ \mu^-$ without converted photons.

$\chi_{b2}(2P)$ REFERENCES

AJLI	14BG	JHEP 1410 088	R. Ajai et al.	(LHCb Collab.)
LEES	14M	PR D90 112010	J.P. Lees et al.	(BABAR Collab.)
LEES	11C	PR D84 011104	J.P. Lees et al.	(BABAR Collab.)
LEES	11J	PR D84 072002	J.P. Lees et al.	(BABAR Collab.)
ASNER	08A	PR D78 091103	D.M. Asner et al.	(CLEO Collab.)
BRIERE	08	PR D78 092007	R.A. Briere et al.	(CLEO Collab.)
CRAWFIELD	06	PR D73 012003	C. Cawfield et al.	(CLEO Collab.)
ARTUSO	05	PRL 94 032001	M. Artuso et al.	(CLEO Collab.)
CRONIN-HENNESSY	04	PRL 92 222002	D. Cronin-Hennessy et al.	(CLEO Collab.)
CRAWFORD	92B	PL B294 139	G. Crawford et al.	(CLEO Collab.)
HEINTZ	92	PR D46 1928	U. Heintz et al.	(CUSB II Collab.)
HEINTZ	91	PRL 66 1563	U. Heintz et al.	(CUSB Collab.)
MORRISON	91	PRL 67 1696	R.J. Morrison et al.	(CLEO Collab.)
NARAIN	91	PRL 66 3113	M. Narain et al.	(CUSB Collab.)

$\Upsilon(3S)$ $J^{PC} = 0^-(1^{--})$

$\Upsilon(3S)$ MASS

VALUE (MeV)	DOCUMENT ID	TECN	COMMENT
10355.2 ± 0.5	¹ ARTA MONOV 00	MD1	$e^+e^- \rightarrow$ hadrons
• • • We do not use the following data for averages, fits, limits, etc. • • •			
10355.3 ± 0.5	^{2,3} BARU	86B REDE	$e^+e^- \rightarrow$ hadrons
¹ Reanalysis of BARU 86B using new electron mass (COHEN 87). ² Reanalysis of ARTAMONOV 84. ³ Superseded by ARTAMONOV 00.			

$m_{\Upsilon(3S)} - m_{\Upsilon(2S)}$

VALUE (MeV)	DOCUMENT ID	TECN	COMMENT
$331.50 \pm 0.02 \pm 0.13$	LEES	11c BABR	$e^+e^- \rightarrow \pi^+\pi^-X$

$\Upsilon(3S)$ WIDTH

VALUE (keV)	DOCUMENT ID	COMMENT
20.32 ± 1.85 OUR EVALUATION		See the Note on "Width Determinations of the Υ States"

$\Upsilon(3S)$ DECAY MODES

Mode	Fraction (Γ_i/Γ)	Scale factor/ Confidence level
Γ_1 $\Upsilon(2S)$ anything	$(10.6 \pm 0.8)\%$	
Γ_2 $\Upsilon(2S)\pi^+\pi^-$	$(2.82 \pm 0.18)\%$	S=1.6
Γ_3 $\Upsilon(2S)\pi^0\pi^0$	$(1.85 \pm 0.14)\%$	
Γ_4 $\Upsilon(2S)\gamma\gamma$	$(5.0 \pm 0.7)\%$	
Γ_5 $\Upsilon(2S)\pi^0$	< 5.1	$\times 10^{-4}$ CL=90%
Γ_6 $\Upsilon(1S)\pi^+\pi^-$	$(4.37 \pm 0.08)\%$	
Γ_7 $\Upsilon(1S)\pi^0\pi^0$	$(2.20 \pm 0.13)\%$	
Γ_8 $\Upsilon(1S)\eta$	< 1	$\times 10^{-4}$ CL=90%
Γ_9 $\Upsilon(1S)\pi^0$	< 7	$\times 10^{-5}$ CL=90%
Γ_{10} $h_b(1P)\pi^0$	< 1.2	$\times 10^{-3}$ CL=90%
Γ_{11} $h_b(1P)\pi^0 \rightarrow \gamma h_b(1S)\pi^0$	$(4.3 \pm 1.4) \times 10^{-4}$	
Γ_{12} $h_b(1P)\pi^+\pi^-$	< 1.2	$\times 10^{-4}$ CL=90%
Γ_{13} $\tau^+\tau^-$	$(2.29 \pm 0.30)\%$	
Γ_{14} $\mu^+\mu^-$	$(2.18 \pm 0.21)\%$	S=2.1
Γ_{15} e^+e^-	$(2.18 \pm 0.20)\%$	
Γ_{16} hadrons	$(93 \pm 12)\%$	
Γ_{17} ggg	$(35.7 \pm 2.6)\%$	
Γ_{18} γgg	$(9.7 \pm 1.8) \times 10^{-3}$	
Γ_{19} 2H anything	$(2.33 \pm 0.33) \times 10^{-5}$	

Radiative decays

Γ_{20} $\gamma \chi_{b2}(2P)$	$(13.1 \pm 1.6)\%$	S=3.4
Γ_{21} $\gamma \chi_{b1}(2P)$	$(12.6 \pm 1.2)\%$	S=2.4
Γ_{22} $\gamma \chi_{b0}(2P)$	$(5.9 \pm 0.6)\%$	S=1.4
Γ_{23} $\gamma \chi_{b2}(1P)$	$(10.0 \pm 1.0) \times 10^{-3}$	S=1.7
Γ_{24} $\gamma \chi_{b1}(1P)$	$(9 \pm 5) \times 10^{-4}$	S=1.8
Γ_{25} $\gamma \chi_{b0}(1P)$	$(2.7 \pm 0.4) \times 10^{-3}$	
Γ_{26} $\gamma h_b(2S)$	< 6.2	$\times 10^{-4}$ CL=90%
Γ_{27} $\gamma h_b(1S)$	$(5.1 \pm 0.7) \times 10^{-4}$	
Γ_{28} $\gamma A^0 \rightarrow \gamma$ hadrons	< 8	$\times 10^{-5}$ CL=90%
Γ_{29} $\gamma X \rightarrow \gamma + \geq 4$ prongs	[a] < 2.2	$\times 10^{-4}$ CL=95%
Γ_{30} $\gamma a_0^0 \rightarrow \gamma \mu^+ \mu^-$	< 5.5	$\times 10^{-6}$ CL=90%
Γ_{31} $\gamma a_1^0 \rightarrow \gamma \tau^+ \tau^-$	[b] < 1.6	$\times 10^{-4}$ CL=90%

Lepton Family number (LF) violating modes

Γ_{32} $e^\pm \tau^\mp$	LF	< 4.2	$\times 10^{-6}$ CL=90%
Γ_{33} $\mu^\pm \tau^\mp$	LF	< 3.1	$\times 10^{-6}$ CL=90%

[a] $1.5 \text{ GeV} < m_X < 5.0 \text{ GeV}$

[b] For $m_{\tau^+\tau^-}$ in the ranges 4.03–9.52 and 9.61–10.10 GeV.

$\Upsilon(3S)$ $\Gamma(i)\Gamma(e^+e^-)/\Gamma(\text{total})$

VALUE (keV)	DOCUMENT ID	TECN	COMMENT
0.414 ± 0.007 OUR AVERAGE			
$0.413 \pm 0.004 \pm 0.006$	ROSNER	06 CLEO	$10.4 e^+e^- \rightarrow$ hadrons
$0.45 \pm 0.03 \pm 0.03$	⁴ GILES	84B CLEO	$e^+e^- \rightarrow$ hadrons

⁴ Radiative corrections reevaluated by BUCHMUELLER 88 following KURAEV 85.

Meson Particle Listings

$\Upsilon(3S)$

$\Gamma(\Upsilon(1S)\pi^+\pi^-) \times \Gamma(e^+e^-)/\Gamma_{total}$					Γ_6/Γ
VALUE (eV)	EVTS	DOCUMENT ID	TECN	COMMENT	
18.46 ± 0.27 ± 0.77	6.4K	⁵ AUBERT	08BP BABR	$e^+e^- \rightarrow \gamma\pi^+\pi^-\ell^+\ell^-$	
⁵ Using $B(\Upsilon(1S) \rightarrow e^+e^-) = (2.38 \pm 0.11)\%$ and $B(\Upsilon(1S) \rightarrow \mu^+\mu^-) = (2.48 \pm 0.05)\%$.					

$\Gamma(\Upsilon(2S)\gamma\gamma)/\Gamma_{total}$					Γ_4/Γ
VALUE	DOCUMENT ID	TECN	COMMENT		
0.0502 ± 0.0069	¹⁸ BUTLER	94B	CLE2	$e^+e^- \rightarrow \ell^+\ell^-2\gamma$	
¹⁸ From the exclusive mode.					

$\Upsilon(3S)$ PARTIAL WIDTHS

$\Gamma(e^+e^-)$		Γ_{15}
VALUE (keV)	DOCUMENT ID	
0.443 ± 0.008 OUR EVALUATION		

$\Gamma(\Upsilon(2S)\pi^0)/\Gamma_{total}$					Γ_5/Γ
VALUE (units 10^{-3})	CL%	DOCUMENT ID	TECN	COMMENT	
<0.51	90	¹⁹ HE	08A	CLEO	$e^+e^- \rightarrow \ell^+\ell^-\gamma\gamma$
¹⁹ Authors assume $B(\Upsilon(2S) \rightarrow e^+e^-) + B(\Upsilon(1S) \rightarrow \mu^+\mu^-) = 4.06\%$.					

$\Upsilon(3S)$ BRANCHING RATIOS

$\Gamma(\Upsilon(2S)\text{anything})/\Gamma_{total}$					Γ_1/Γ
VALUE	EVTS	DOCUMENT ID	TECN	COMMENT	
0.106 ± 0.008 OUR AVERAGE					
0.1023 ± 0.0105	4625	^{6,7,8} BUTLER	94B	CLE2	$e^+e^- \rightarrow \ell^+\ell^-X$
0.111 ± 0.012	4891	^{7,8,9} BROCK	91	CLEO	$e^+e^- \rightarrow \pi^+\pi^-\ell^+\ell^-$

$\Gamma(\Upsilon(1S)\pi^+\pi^-)/\Gamma_{total}$					Γ_6/Γ
VALUE (units 10^{-2})	EVTS	DOCUMENT ID	TECN	COMMENT	
4.37 ± 0.08 OUR AVERAGE					
4.32 ± 0.07 ± 0.13	90k	²⁰ LEES	11L	BABR	$\Upsilon(3S) \rightarrow \pi^+\pi^-\ell^+\ell^-$
4.46 ± 0.01 ± 0.13	190k	²¹ BHARI	09	CLEO	$e^+e^- \rightarrow \pi^+\pi^-MM$
4.17 ± 0.06 ± 0.19	6.4K	²² AUBERT	08BP	BABR	$10.58 e^+e^- \rightarrow \gamma\pi^+\pi^-\ell^+\ell^-$
4.52 ± 0.35	11830	²³ BUTLER	94B	CLE2	$e^+e^- \rightarrow \pi^+\pi^-X$
4.46 ± 0.34 ± 0.50	451	²³ WU	93	CUSB	$\Upsilon(3S) \rightarrow \pi^+\pi^-\ell^+\ell^-$
4.46 ± 0.30	11221	²³ BROCK	91	CLEO	$e^+e^- \rightarrow \pi^+\pi^-X$

⁶ Using $B(\Upsilon(2S) \rightarrow \Upsilon(1S)\gamma\gamma) = (0.038 \pm 0.007)\%$, and $B(\Upsilon(2S) \rightarrow \Upsilon(1S)\pi^0\pi^0) = (1/2)B(\Upsilon(2S) \rightarrow \Upsilon(1S)\pi^+\pi^-)$.

⁷ Using $B(\Upsilon(1S) \rightarrow \mu^+\mu^-) = (2.48 \pm 0.06)\%$. With the assumption of $e\mu$ universality.

⁸ Using $B(\Upsilon(2S) \rightarrow \Upsilon(1S)\pi^+\pi^-) = (18.5 \pm 0.8)\%$.

⁹ Using $B(\Upsilon(2S) \rightarrow \mu^+\mu^-) = (1.31 \pm 0.21)\%$, $B(\Upsilon(2S) \rightarrow \Upsilon(1S)\gamma\gamma) \times 2B(\Upsilon(1S) \rightarrow \mu^+\mu^-) = (0.188 \pm 0.035)\%$, and $B(\Upsilon(2S) \rightarrow \Upsilon(1S)\pi^0\pi^0) \times 2B(\Upsilon(1S) \rightarrow \mu^+\mu^-) = (0.436 \pm 0.056)\%$. With the assumption of $e\mu$ universality.

••• We do not use the following data for averages, fits, limits, etc. •••

4.9 ± 1.0 ²² GREEN 82 CLEO $\Upsilon(3S) \rightarrow \pi^+\pi^-\ell^+\ell^-$

3.9 ± 1.3 ²⁶ MAGERAS 82 CUSB $\Upsilon(3S) \rightarrow \pi^+\pi^-\ell^+\ell^-$

²⁰ Using $B(\Upsilon(1S) \rightarrow e^+e^-) = (2.38 \pm 0.11)\%$ and $B(\Upsilon(1S) \rightarrow \mu^+\mu^-) = (2.48 \pm 0.05)\%$.

²¹ A weighted average of the inclusive and exclusive results.

²² Using $B(\Upsilon(2S) \rightarrow e^+e^-) = (1.91 \pm 0.16)\%$, $B(\Upsilon(2S) \rightarrow \mu^+\mu^-) = (1.93 \pm 0.17)\%$, and $\Gamma_{ee}(\Upsilon(3S)) = 0.443 \pm 0.008$ keV.

²³ Using $B(\Upsilon(1S) \rightarrow \mu^+\mu^-) = (2.48 \pm 0.06)\%$. With the assumption of $e\mu$ universality.

$\Gamma(\Upsilon(2S)\pi^+\pi^-)/\Gamma_{total}$					Γ_2/Γ
VALUE (units 10^{-2})	EVTS	DOCUMENT ID	TECN	COMMENT	
2.82 ± 0.18 OUR AVERAGE					
3.00 ± 0.02 ± 0.14	543k	LEES	11C	BABR	$e^+e^- \rightarrow \pi^+\pi^-X$
2.40 ± 0.10 ± 0.26	800	¹⁰ AUBERT	08BP	BABR	$e^+e^- \rightarrow \gamma\pi^+\pi^-e^+e^-$
3.12 ± 0.49	980	^{11,12} BUTLER	94B	CLE2	$e^+e^- \rightarrow \pi^+\pi^-\ell^+\ell^-$
2.13 ± 0.38	974	¹³ BROCK	91	CLEO	$e^+e^- \rightarrow \pi^+\pi^-X$

$\Gamma(\Upsilon(2S)\pi^+\pi^-)/\Gamma(\Upsilon(1S)\pi^+\pi^-)$					Γ_2/Γ_6
VALUE	EVTS	DOCUMENT ID	TECN	COMMENT	
0.577 ± 0.026 ± 0.060	800	²⁴ AUBERT	08BP	BABR	$e^+e^- \rightarrow \gamma\pi^+\pi^-\ell^+\ell^-$
²⁴ Using $B(\Upsilon(1S) \rightarrow e^+e^-) = (2.38 \pm 0.11)\%$, $B(\Upsilon(1S) \rightarrow \mu^+\mu^-) = (2.48 \pm 0.05)\%$, $B(\Upsilon(2S) \rightarrow e^+e^-) = (1.91 \pm 0.16)\%$, and $B(\Upsilon(2S) \rightarrow \mu^+\mu^-) = (1.93 \pm 0.17)\%$. Not independent of other values reported by AUBERT 08BP.					

••• We do not use the following data for averages, fits, limits, etc. •••

4.82 ± 0.65 ± 0.53 ¹³ WU 93 CUSB $\Upsilon(3S) \rightarrow \pi^+\pi^-\ell^+\ell^-$

3.1 ± 2.0 ⁵ MAGERAS 82 CUSB $\Upsilon(3S) \rightarrow \pi^+\pi^-\ell^+\ell^-$

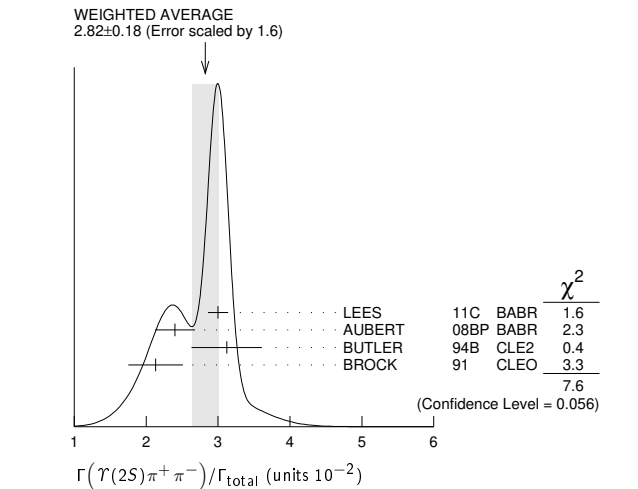
¹⁰ Using $B(\Upsilon(1S) \rightarrow e^+e^-) = (2.38 \pm 0.11)\%$, $B(\Upsilon(1S) \rightarrow \mu^+\mu^-) = (2.48 \pm 0.05)\%$, and $\Gamma_{ee}(\Upsilon(3S)) = 0.443 \pm 0.008$ keV.

¹¹ From the exclusive mode.

¹² Using $B(\Upsilon(2S) \rightarrow \Upsilon(1S)\gamma\gamma) = (0.038 \pm 0.007)\%$, and $B(\Upsilon(2S) \rightarrow \Upsilon(1S)\pi^0\pi^0) = (1/2)B(\Upsilon(2S) \rightarrow \Upsilon(1S)\pi^+\pi^-)$.

¹³ Using $B(\Upsilon(2S) \rightarrow \mu^+\mu^-) = (1.31 \pm 0.21)\%$, $B(\Upsilon(2S) \rightarrow \Upsilon(1S)\gamma\gamma) \times 2B(\Upsilon(1S) \rightarrow \mu^+\mu^-) = (0.188 \pm 0.035)\%$, and $B(\Upsilon(2S) \rightarrow \Upsilon(1S)\pi^0\pi^0) \times 2B(\Upsilon(1S) \rightarrow \mu^+\mu^-) = (0.436 \pm 0.056)\%$. With the assumption of $e\mu$ universality.

$\Gamma(\Upsilon(1S)\pi^0\pi^0)/\Gamma_{total}$					Γ_7/Γ
VALUE (units 10^{-2})	EVTS	DOCUMENT ID	TECN	COMMENT	
2.20 ± 0.13 OUR AVERAGE					
2.24 ± 0.09 ± 0.11	6584	²⁵ BHARI	09	CLEO	$e^+e^- \rightarrow \pi^0\pi^0\ell^+\ell^-$
1.99 ± 0.34	56	²⁶ BUTLER	94B	CLE2	$e^+e^- \rightarrow \pi^0\pi^0\ell^+\ell^-$
2.2 ± 0.4 ± 0.3	33	²⁷ HEINTZ	92	CSB2	$e^+e^- \rightarrow \pi^0\pi^0\ell^+\ell^-$



$\Gamma(\Upsilon(1S)\pi^0\pi^0)/\Gamma(\Upsilon(1S)\pi^+\pi^-)$					Γ_7/Γ_6
VALUE	DOCUMENT ID	TECN	COMMENT		
0.501 ± 0.043	²⁸ BHARI	09	CLEO	$e^+e^- \rightarrow \Upsilon(3S)$	
²⁸ Not independent of other values reported by BHARI 09.					

$\Gamma(\Upsilon(2S)\pi^0\pi^0)/\Gamma_{total}$					Γ_3/Γ
VALUE (units 10^{-2})	EVTS	DOCUMENT ID	TECN	COMMENT	
1.85 ± 0.14 OUR AVERAGE					
1.82 ± 0.09 ± 0.12	4391	¹⁴ BHARI	09	CLEO	$e^+e^- \rightarrow \pi^0\pi^0\ell^+\ell^-$
2.16 ± 0.39		^{15,16} BUTLER	94B	CLE2	$e^+e^- \rightarrow \pi^0\pi^0\ell^+\ell^-$
1.7 ± 0.5 ± 0.2	10	¹⁷ HEINTZ	92	CSB2	$e^+e^- \rightarrow \pi^0\pi^0\ell^+\ell^-$

$\Gamma(\Upsilon(1S)\eta)/\Gamma_{total}$					Γ_8/Γ
VALUE (units 10^{-3})	CL%	DOCUMENT ID	TECN	COMMENT	
<0.1	90	²⁹ LEES	11L	BABR	$\Upsilon(3S) \rightarrow (\pi^+\pi^-)(\gamma\gamma)\ell^+\ell^-$
••• We do not use the following data for averages, fits, limits, etc. •••					
<0.8	90	^{29,30} AUBERT	08BP	BABR	$e^+e^- \rightarrow \gamma\pi^+\pi^-\pi^0\ell^+\ell^-$
<0.18	90	³¹ HE	08A	CLEO	$e^+e^- \rightarrow \ell^+\ell^-\eta$
<2.2	90	BROCK	91	CLEO	$e^+e^- \rightarrow \ell^+\ell^-\eta$

¹⁴ Authors assume $B(\Upsilon(1S) \rightarrow e^+e^-) + B(\Upsilon(1S) \rightarrow \mu^+\mu^-) = 4.06\%$.

¹⁵ $B(\Upsilon(2S) \rightarrow \mu^+\mu^-) = (1.31 \pm 0.21)\%$ and assuming $e\mu$ universality.

¹⁶ From the exclusive mode.

¹⁷ $B(\Upsilon(2S) \rightarrow \mu^+\mu^-) = (1.44 \pm 0.10)\%$ and assuming $e\mu$ universality. Supersedes HEINTZ 91.

$\Gamma(\Upsilon(1S)\eta)/\Gamma(\Upsilon(1S)\pi^+\pi^-)$					Γ_8/Γ_6
VALUE (units 10^{-2})	CL%	DOCUMENT ID	TECN	COMMENT	
<0.23	90	³² LEES	11L	BABR	$\Upsilon(3S) \rightarrow (\pi^+\pi^-)(\gamma\gamma)\ell^+\ell^-$
••• We do not use the following data for averages, fits, limits, etc. •••					
<1.9	90	³³ AUBERT	08BP	BABR	$e^+e^- \rightarrow \gamma\pi^+\pi^-(\pi^0)\ell^+\ell^-$

$\Gamma(\Upsilon(1S)\pi^0)/\Gamma_{total}$					Γ_9/Γ
VALUE (units 10^{-3})	CL%	DOCUMENT ID	TECN	COMMENT	
<0.07	90	³⁴ HE	08A	CLEO	$e^+e^- \rightarrow \ell^+\ell^-\gamma\gamma$
³⁴ Authors assume $B(\Upsilon(1S) \rightarrow e^+e^-) + B(\Upsilon(1S) \rightarrow \mu^+\mu^-) = 4.96\%$.					

Meson Particle Listings

$\Upsilon(3S)$

$\Gamma(h_b(1P)\pi^0)/\Gamma_{total}$					Γ_{10}/Γ
VALUE	CL%	DOCUMENT ID	TECN	COMMENT	
$<1.2 \times 10^{-3}$	90	35 GE	11	CLEO $\Upsilon(3S) \rightarrow \pi^0$ anything	
³⁵ Assuming $M(h_b(1P)) = 9900$ MeV and $\Gamma(h_b(1P)) = 0$ MeV, and allowing $B(h_b(1P) \rightarrow \gamma\eta_b(1S))$ to vary from 0-100%.					

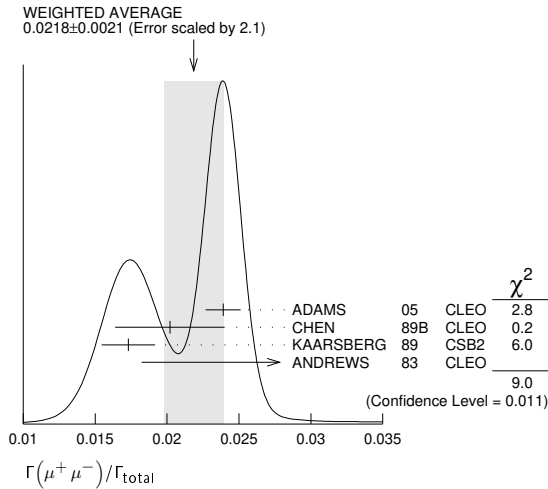
$\Gamma(h_b(1P)\pi^0 \rightarrow \gamma\eta_b(1S)\pi^0)/\Gamma_{total}$					Γ_{11}/Γ
VALUE (units 10^{-4})	DOCUMENT ID	TECN	COMMENT		
$4.3 \pm 1.1 \pm 0.9$	LEES	11k	BABR	$\Upsilon(3S) \rightarrow \eta_b \gamma \pi^0$	

$\Gamma(h_b(1P)\pi^+\pi^-)/\Gamma_{total}$					Γ_{12}/Γ
VALUE (units 10^{-4})	CL%	DOCUMENT ID	TECN	COMMENT	
< 1.2	90	36 LEES	11c	BABR $e^+e^- \rightarrow \pi^+\pi^- X$	
••• We do not use the following data for averages, fits, limits, etc. •••					
<18		36 BUTLER	94b	CLE2 $e^+e^- \rightarrow \pi^+\pi^- X$	
<15		36 BROCK	91	CLEO $e^+e^- \rightarrow \pi^+\pi^- X$	
³⁶ For $M(h_b(1P)) = 9900$ MeV.					

$\Gamma(\tau^+\tau^-)/\Gamma_{total}$					Γ_{13}/Γ
VALUE (units 10^{-2})	EVTS	DOCUMENT ID	TECN	COMMENT	
$2.29 \pm 0.21 \pm 0.22$	15k	37 BESSON	07	CLEO $e^+e^- \rightarrow \Upsilon(3S) \rightarrow \tau^+\tau^-$	
³⁷ BESSON 07 reports $[\Gamma(\Upsilon(3S) \rightarrow \tau^+\tau^-)/\Gamma_{total}] / [B(\Upsilon(3S) \rightarrow \mu^+\mu^-)] = 1.05 \pm 0.08 \pm 0.05$ which we multiply by our best value $B(\Upsilon(3S) \rightarrow \mu^+\mu^-) = (2.18 \pm 0.21) \times 10^{-2}$. Our first error is their experiment's error and our second error is the systematic error from using our best value.					

$\Gamma(\tau^+\tau^-)/\Gamma(\mu^+\mu^-)$					Γ_{13}/Γ_{14}
VALUE	EVTS	DOCUMENT ID	TECN	COMMENT	
$1.05 \pm 0.08 \pm 0.05$	15k	BESSON	07	CLEO $e^+e^- \rightarrow \Upsilon(3S)$	

$\Gamma(\mu^+\mu^-)/\Gamma_{total}$					Γ_{14}/Γ
VALUE	EVTS	DOCUMENT ID	TECN	COMMENT	
0.0218 ± 0.0021 OUR AVERAGE				Error includes scale factor of 2.1. See the ideogram below.	
$0.0239 \pm 0.0007 \pm 0.0010$	81k	ADAMS	05	CLEO $e^+e^- \rightarrow \mu^+\mu^-$	
$0.0202 \pm 0.0019 \pm 0.0033$		CHEN	89b	CLEO $e^+e^- \rightarrow \mu^+\mu^-$	
$0.0173 \pm 0.0015 \pm 0.0011$		KAARSBERG	89	CSB2 $e^+e^- \rightarrow \mu^+\mu^-$	
$0.033 \pm 0.013 \pm 0.007$	1096	ANDREWS	83	CLEO $e^+e^- \rightarrow \mu^+\mu^-$	



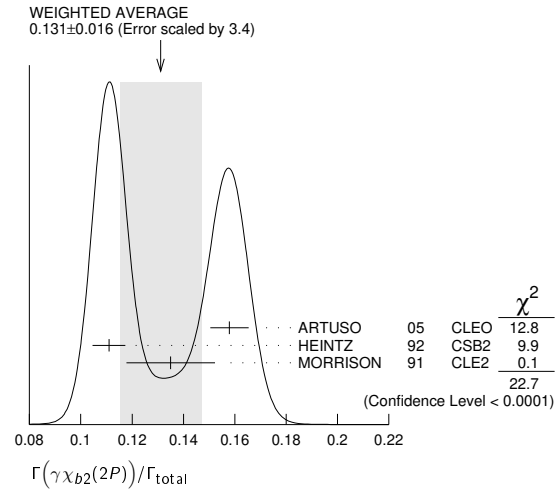
$\Gamma(ggg)/\Gamma_{total}$					Γ_{17}/Γ
VALUE (units 10^{-2})	EVTS	DOCUMENT ID	TECN	COMMENT	
35.7 ± 2.6	3M	38 BESSON	06a	CLEO $\Upsilon(3S) \rightarrow$ hadrons	
³⁸ Calculated using BESSON 06a value of $\Gamma(\gamma gg)/\Gamma(ggg) = (2.72 \pm 0.06 \pm 0.32 \pm 0.37)\%$ and the PDG 08 values of $B(\Upsilon(2S) + \text{anything}) = (10.6 \pm 0.8)\%$, $B(\pi^+\pi^-\Upsilon(1S)) = (4.40 \pm 0.10)\%$, $B(\pi^0\pi^0\Upsilon(1S)) = (2.20 \pm 0.13)\%$, $B(\gamma\chi_{b2}(2P)) = (13.1 \pm 1.6)\%$, $B(\gamma\chi_{b1}(2P)) = (12.6 \pm 1.2)\%$, $B(\gamma\chi_{b0}(2P)) = (5.9 \pm 0.6)\%$, $B(\gamma\chi_{b0}(1P)) = (0.30 \pm 0.11)\%$, $B(\mu^+\mu^-) = (2.18 \pm 0.21)\%$, and $R_{\text{hadrons}} = 3.51$. The statistical error is negligible and the systematic error is partially correlated with $\Gamma(\gamma gg)/\Gamma_{total}$ BESSON 06a value.					

$\Gamma(\gamma gg)/\Gamma_{total}$					Γ_{18}/Γ
VALUE (units 10^{-2})	EVTS	DOCUMENT ID	TECN	COMMENT	
0.97 ± 0.18	60k	39 BESSON	06a	CLEO $\Upsilon(3S) \rightarrow \gamma +$ hadrons	
³⁹ Calculated using BESSON 06a values of $\Gamma(\gamma gg)/\Gamma(ggg) = (2.72 \pm 0.06 \pm 0.32 \pm 0.37)\%$ and $\Gamma(ggg)/\Gamma_{total}$. The statistical error is negligible and the systematic error is partially correlated with $\Gamma(ggg)/\Gamma_{total}$ BESSON 06a value.					

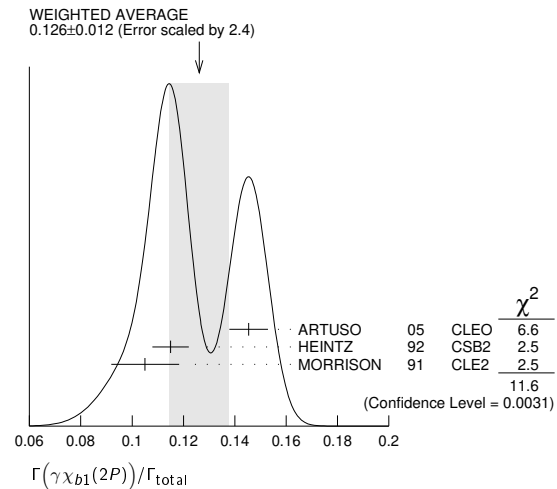
$\Gamma(\gamma gg)/\Gamma(ggg)$					Γ_{18}/Γ_{17}
VALUE (units 10^{-2})	EVTS	DOCUMENT ID	TECN	COMMENT	
$2.72 \pm 0.06 \pm 0.49$	3M	BESSON	06a	CLEO $\Upsilon(3S) \rightarrow (\gamma +)$ hadrons	

$\Gamma(2H \text{ anything})/\Gamma_{total}$					Γ_{19}/Γ
VALUE (units 10^{-5})	DOCUMENT ID	TECN	COMMENT		
$2.33 \pm 0.15 \pm 0.31$ -0.28	LEES	14g	BABR	$e^+e^- \rightarrow 2H X$	

$\Gamma(\gamma\chi_{b2}(2P))/\Gamma_{total}$					Γ_{20}/Γ
VALUE	EVTS	DOCUMENT ID	TECN	COMMENT	
0.131 ± 0.016 OUR AVERAGE				Error includes scale factor of 3.4. See the ideogram below.	
$0.1579 \pm 0.0017 \pm 0.0073$	568k	ARTUSO	05	CLEO $e^+e^- \rightarrow \gamma X$	
$0.111 \pm 0.005 \pm 0.004$	10319	40 HEINTZ	92	CSB2 $e^+e^- \rightarrow \gamma X$	
$0.135 \pm 0.003 \pm 0.017$	30741	MORRISON	91	CLE2 $e^+e^- \rightarrow \gamma X$	
⁴⁰ Supersedes NARAIN 91.					

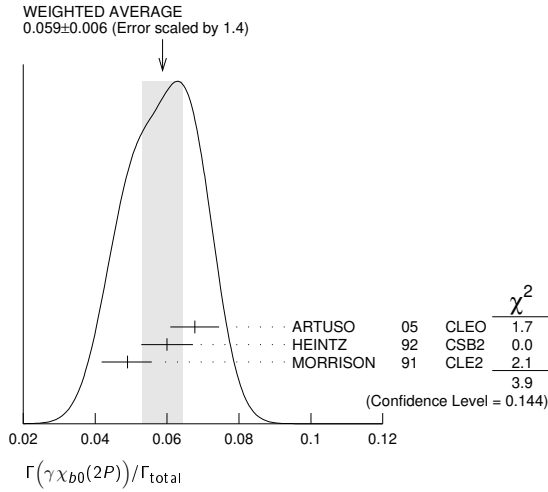


$\Gamma(\gamma\chi_{b1}(2P))/\Gamma_{total}$					Γ_{21}/Γ
VALUE	EVTS	DOCUMENT ID	TECN	COMMENT	
0.126 ± 0.012 OUR AVERAGE				Error includes scale factor of 2.4. See the ideogram below.	
$0.1454 \pm 0.0018 \pm 0.0073$	537k	ARTUSO	05	CLEO $e^+e^- \rightarrow \gamma X$	
$0.115 \pm 0.005 \pm 0.005$	11147	41 HEINTZ	92	CSB2 $e^+e^- \rightarrow \gamma X$	
$0.105 \pm 0.003 \pm 0.013$	25759	MORRISON	91	CLE2 $e^+e^- \rightarrow \gamma X$	
⁴¹ Supersedes NARAIN 91.					



$\Gamma(\gamma\chi_{b0}(2P))/\Gamma_{total}$					Γ_{22}/Γ
VALUE	EVTS	DOCUMENT ID	TECN	COMMENT	
0.059 ± 0.006 OUR AVERAGE				Error includes scale factor of 1.4. See the ideogram below.	
$0.0677 \pm 0.0020 \pm 0.0065$	225k	ARTUSO	05	CLEO $e^+e^- \rightarrow \gamma X$	
$0.060 \pm 0.004 \pm 0.006$	4959	42 HEINTZ	92	CSB2 $e^+e^- \rightarrow \gamma X$	
$0.049 \pm 0.003 \pm 0.006$	9903	MORRISON	91	CLE2 $e^+e^- \rightarrow \gamma X$	

⁴² Supersedes NARAIN 91.



$\Gamma(\gamma\chi_{b2}(1P))/\Gamma_{total}$ Γ_{23}/Γ

VALUE (units 10^{-3})	CL%	EVTS	DOCUMENT ID	TECN	COMMENT
10.0 ± 1.0 OUR AVERAGE			Error includes scale factor of 1.7.		
8.0 ± 1.3 ± 0.4	126	43,44	KORNICER 11	CLEO	$e^+e^- \rightarrow \gamma\gamma\ell^+\ell^-$
10.5 ± 0.3 ± 0.7	9.7k		LEES 11J	BABR	$\Upsilon(3S) \rightarrow X\gamma$
• • • We do not use the following data for averages, fits, limits, etc. • • •					
<19	90		45 ASNER 08A	CLEO	$\Upsilon(3S) \rightarrow \gamma + \text{hadrons}$
seen			46 HEINTZ 92	CSB2	$e^+e^- \rightarrow \gamma\gamma\ell^+\ell^-$

⁴³ Assuming $B(\Upsilon(1S) \rightarrow \ell^+\ell^-) = (2.48 \pm 0.05)\%$.

⁴⁴ KORNICER 11 reports $[\Gamma(\Upsilon(3S) \rightarrow \gamma\chi_{b2}(1P))/\Gamma_{total}] \times [B(\chi_{b2}(1P) \rightarrow \gamma\Upsilon(1S))] = (1.435 \pm 0.162 \pm 0.169) \times 10^{-3}$ which we divide by our best value $B(\chi_{b2}(1P) \rightarrow \gamma\Upsilon(1S)) = (18.0 \pm 1.0) \times 10^{-2}$. Our first error is their experiment's error and our second error is the systematic error from using our best value.

⁴⁵ ASNER 08A reports $[\Gamma(\Upsilon(3S) \rightarrow \gamma\chi_{b2}(1P))/\Gamma_{total}] / [B(\Upsilon(2S) \rightarrow \gamma\chi_{b2}(1P))] < 27.1 \times 10^{-2}$ which we multiply by our best value $B(\Upsilon(2S) \rightarrow \gamma\chi_{b2}(1P)) = 7.15 \times 10^{-2}$.

⁴⁶ HEINTZ 92, while unable to distinguish between different J states, measures $\sum_J B(\Upsilon(3S) \rightarrow \gamma\chi_{bJ}) \times B(\chi_{bJ} \rightarrow \gamma\Upsilon(1S)) = (1.7 \pm 0.4 \pm 0.6) \times 10^{-3}$ for $J = 0, 1, 2$ using inclusive $\Upsilon(1S)$ decays and $(1.2^{+0.4}_{-0.3} \pm 0.09) \times 10^{-3}$ for $J = 1, 2$ using $\Upsilon(1S) \rightarrow \ell^+\ell^-$.

$\Gamma(\gamma\chi_{b1}(1P))/\Gamma_{total}$ Γ_{24}/Γ

VALUE (units 10^{-3})	CL%	EVTS	DOCUMENT ID	TECN	COMMENT
0.9 ± 0.5 OUR AVERAGE			Error includes scale factor of 1.8.		
1.5 ± 0.4 ± 0.1	50	47,48	KORNICER 11	CLEO	$e^+e^- \rightarrow \gamma\gamma\ell^+\ell^-$
0.5 ± 0.3 ± 0.2			LEES 11J	BABR	$\Upsilon(3S) \rightarrow X\gamma$
0.1 ± 0.1	90		49 ASNER 08A	CLEO	$\Upsilon(3S) \rightarrow \gamma + \text{hadrons}$
seen			50 HEINTZ 92	CSB2	$e^+e^- \rightarrow \gamma\gamma\ell^+\ell^-$

⁴⁷ Assuming $B(\Upsilon(1S) \rightarrow \ell^+\ell^-) = (2.48 \pm 0.05)\%$.

⁴⁸ KORNICER 11 reports $[\Gamma(\Upsilon(3S) \rightarrow \gamma\chi_{b1}(1P))/\Gamma_{total}] \times [B(\chi_{b1}(1P) \rightarrow \gamma\Upsilon(1S))] = (5.38 \pm 1.20 \pm 0.95) \times 10^{-4}$ which we divide by our best value $B(\chi_{b1}(1P) \rightarrow \gamma\Upsilon(1S)) = (35.2 \pm 2.0) \times 10^{-2}$. Our first error is their experiment's error and our second error is the systematic error from using our best value.

⁴⁹ ASNER 08A reports $[\Gamma(\Upsilon(3S) \rightarrow \gamma\chi_{b1}(1P))/\Gamma_{total}] / [B(\Upsilon(2S) \rightarrow \gamma\chi_{b1}(1P))] < 2.5 \times 10^{-2}$ which we multiply by our best value $B(\Upsilon(2S) \rightarrow \gamma\chi_{b1}(1P)) = 6.9 \times 10^{-2}$.

⁵⁰ HEINTZ 92, while unable to distinguish between different J states, measures $\sum_J B(\Upsilon(3S) \rightarrow \gamma\chi_{bJ}) \times B(\chi_{bJ} \rightarrow \gamma\Upsilon(1S)) = (1.7 \pm 0.4 \pm 0.6) \times 10^{-3}$ for $J = 0, 1, 2$ using inclusive $\Upsilon(1S)$ decays and $(1.2^{+0.4}_{-0.3} \pm 0.09) \times 10^{-3}$ for $J = 1, 2$ using $\Upsilon(1S) \rightarrow \ell^+\ell^-$.

$\Gamma(\gamma\chi_{b0}(1P))/\Gamma_{total}$ Γ_{25}/Γ

VALUE (units 10^{-2})	CL%	EVTS	DOCUMENT ID	TECN	COMMENT
0.27 ± 0.04 OUR AVERAGE					
0.27 ± 0.04 ± 0.02	2.3k		LEES 11J	BABR	$\Upsilon(3S) \rightarrow X\gamma$
0.30 ± 0.04 ± 0.10	8.7k		ARTUSO 05	CLEO	$e^+e^- \rightarrow \gamma X$
• • • We do not use the following data for averages, fits, limits, etc. • • •					
<0.8	90		51 ASNER 08A	CLEO	$\Upsilon(3S) \rightarrow \gamma + \text{hadrons}$

⁵¹ ASNER 08A reports $[\Gamma(\Upsilon(3S) \rightarrow \gamma\chi_{b0}(1P))/\Gamma_{total}] / [B(\Upsilon(2S) \rightarrow \gamma\chi_{b0}(1P))] < 21.9 \times 10^{-2}$ which we multiply by our best value $B(\Upsilon(2S) \rightarrow \gamma\chi_{b0}(1P)) = 3.8 \times 10^{-2}$.

$\Gamma(\gamma\eta_b(2S))/\Gamma_{total}$ Γ_{26}/Γ

VALUE (units 10^{-4})	CL%	DOCUMENT ID	TECN	COMMENT
< 6.2	90	ARTUSO 05	CLEO	$e^+e^- \rightarrow \gamma X$
• • • We do not use the following data for averages, fits, limits, etc. • • •				
<19	90	LEES 11J	BABR	$\Upsilon(3S) \rightarrow X\gamma$

$\Gamma(\gamma\eta_b(1S))/\Gamma_{total}$ Γ_{27}/Γ

VALUE (units 10^{-4})	CL%	EVTS	DOCUMENT ID	TECN	COMMENT
5.1 ± 0.7 OUR AVERAGE					
7.1 ± 1.8 ± 1.3	2.3 ± 0.5k		52 BONVICINI 10	CLEO	$\Upsilon(3S) \rightarrow \gamma X$
4.8 ± 0.5 ± 0.6	19 ± 3k		52 AUBERT 09AQ	BABR	$\Upsilon(3S) \rightarrow \gamma X$
• • • We do not use the following data for averages, fits, limits, etc. • • •					
<8.5	90		LEES 11J	BABR	$\Upsilon(3S) \rightarrow X\gamma$
4.8 ± 0.5 ± 1.2	19 ± 3k		52,53 AUBERT 08v	BABR	$\Upsilon(3S) \rightarrow \gamma X$
<4.3	90		54 ARTUSO 05	CLEO	$e^+e^- \rightarrow \gamma X$
52 Assuming $\Gamma_{\eta_b(1S)} = 10$ MeV.					
53 Systematic error re-evaluated by AUBERT 09AQ.					
54 Superseded by BONVICINI 10.					

$\Gamma(\gamma A^0 \rightarrow \gamma \text{hadrons})/\Gamma_{total}$ Γ_{28}/Γ

VALUE	CL%	DOCUMENT ID	TECN	COMMENT
< 8 × 10⁻⁵	90	55 LEES 11H	BABR	$\Upsilon(3S) \rightarrow \gamma \text{hadrons}$
55 For a narrow scalar or pseudoscalar A^0 , excluding known resonances, with mass in the range 0.3–7 GeV. Measured 90% CL limits as a function of m_{A^0} range from 1×10^{-6} to 8×10^{-5} .				

$\Gamma(\gamma X \rightarrow \gamma + \geq 4 \text{ prongs})/\Gamma_{total}$ Γ_{29}/Γ

VALUE (units 10^{-4})	CL%	DOCUMENT ID	TECN	COMMENT
< 2.2	95	ROSNER 07A	CLEO	$e^+e^- \rightarrow \gamma X$

$\Gamma(\gamma a_1^0 \rightarrow \gamma \mu^+ \mu^-)/\Gamma_{total}$ Γ_{30}/Γ

VALUE (units 10^{-6})	CL%	DOCUMENT ID	TECN	COMMENT
< 5.5	90	56 AUBERT 09Z	BABR	$e^+e^- \rightarrow \gamma a_1^0 \rightarrow \gamma \mu^+ \mu^-$
56 For a narrow scalar or pseudoscalar a_1^0 with mass in the range 212–9300 MeV, excluding J/ψ and $\psi(2S)$. Measured 90% CL limits as a function of $m_{a_1^0}$ range from 0.27–5.5 × 10 ⁻⁶ .				

$\Gamma(\gamma a_1^0 \rightarrow \gamma \tau^+ \tau^-)/\Gamma_{total}$ Γ_{31}/Γ

VALUE	CL%	DOCUMENT ID	TECN	COMMENT
< 1.6 × 10⁻⁴	90	57 AUBERT 09P	BABR	$e^+e^- \rightarrow \gamma a_1^0 \rightarrow \gamma \tau^+ \tau^-$
57 For a narrow scalar or pseudoscalar a_1^0 with $M(\tau^+ \tau^-)$ in the ranges 4.03–9.52 and 9.61–10.10 GeV. Measured 90% CL limits as a function of $M(\tau^+ \tau^-)$ range from $1.5\text{--}16 \times 10^{-5}$.				

LEPTON FAMILY NUMBER (LF) VIOLATING MODES

$\Gamma(e^\pm \tau^\mp)/\Gamma_{total}$ Γ_{32}/Γ

VALUE (units 10^{-6})	CL%	DOCUMENT ID	TECN	COMMENT
< 4.2	90	LEES 10B	BABR	$e^+e^- \rightarrow e^\pm \tau^\mp$

$\Gamma(\mu^\pm \tau^\mp)/\Gamma_{total}$ Γ_{33}/Γ

VALUE (units 10^{-6})	CL%	DOCUMENT ID	TECN	COMMENT
< 3.1	90	LEES 10B	BABR	$e^+e^- \rightarrow \mu^\pm \tau^\mp$
• • • We do not use the following data for averages, fits, limits, etc. • • •				
<20.3	95	LOVE 08A	CLEO	$e^+e^- \rightarrow \mu^\pm \tau^\mp$

$\Upsilon(3S)$ REFERENCES

LEES 14G	PR D89 111102	J.P. Lees et al.	(BABAR Collab.)
GE 11	PR D84 032008	J.Y. Ge et al.	(CLEO Collab.)
KORNICER 11	PR D83 054003	M. Koricic et al.	(CLEO Collab.)
LEES 11C	PR D84 011104	J.P. Lees et al.	(BABAR Collab.)
LEES 11H	PRL 107 221803	J.P. Lees et al.	(BABAR Collab.)
LEES 11J	PR D84 072002	J.P. Lees et al.	(BABAR Collab.)
LEES 11K	PR D84 091101	J.P. Lees et al.	(BABAR Collab.)
LEES 11L	PR D84 092003	J.P. Lees et al.	(BABAR Collab.)
BONVICINI 10	PR D81 031104	G. Bonvicini et al.	(CLEO Collab.)
LEES 10B	PRL 104 151802	J.P. Lees et al.	(BABAR Collab.)
AUBERT 09AQ	PRL 103 161801	B. Aubert et al.	(BABAR Collab.)
AUBERT 09P	PRL 103 181801	B. Aubert et al.	(BABAR Collab.)
AUBERT 09Z	PRL 103 081803	B. Aubert et al.	(BABAR Collab.)
BHARI 09	PR D79 011103	S.R. Bhari et al.	(CLEO Collab.)
ASNER 08A	PR D78 091103	D.M. Asner et al.	(CLEO Collab.)
AUBERT 08BP	PR D78 112002	B. Aubert et al.	(BABAR Collab.)
AUBERT 08V	PRL 101 071801	B. Aubert et al.	(BABAR Collab.)
HE 08A	PRL 101 192001	Q. He et al.	(CLEO Collab.)
LOVE 08A	PRL 101 201601	W. Love et al.	(CLEO Collab.)
PDG 08	PL B667 1	C. Amisler et al.	(PDG Collab.)
BESSON 07	PRL 98 052002	D. Besson et al.	(CLEO Collab.)
ROSNER 07A	PR D76 117102	J.L. Rosner et al.	(CLEO Collab.)
BESSON 06A	PR D74 012003	D. Besson et al.	(CLEO Collab.)
ROSNER 06	PRL 96 092003	J.L. Rosner et al.	(CLEO Collab.)
ADAMS 05	PRL 94 012001	G.S. Adams et al.	(CLEO Collab.)

Meson Particle Listings

 $\Upsilon(3S)$, $\chi_{b1}(3P)$, $\chi_{b2}(3P)$, $\Upsilon(4S)$

ARTUSO	05	PRL 94 032001	M. Artuso <i>et al.</i>	(CLEO Collab.)
ARTAMONOV	00	PL B474 427	A.S. Artamonov <i>et al.</i>	
BUTLER	94B	PR D49 40	F. Butler <i>et al.</i>	(CLEO Collab.)
WU	93	PL B301 307	Q.W. Wu <i>et al.</i>	(CUSB Collab.)
HEINTZ	92	PR D46 1928	U. Heintz <i>et al.</i>	(CUSB II Collab.)
BROCK	91	PR D43 1448	I.C. Brock <i>et al.</i>	(CLEO Collab.)
HEINTZ	91	PRL 66 1563	U. Heintz <i>et al.</i>	(CUSB Collab.)
MORRISON	91	PRL 67 1696	R.J. Morrison <i>et al.</i>	(CLEO Collab.)
NARAIN	91	PRL 66 3113	M. Narain <i>et al.</i>	(CUSB Collab.)
CHEN	89B	PR D39 3528	W.Y. Chen <i>et al.</i>	(CLEO Collab.)
KAARSBERG	89	PRL 62 2077	T.M. Kaarsberg <i>et al.</i>	(CUSB Collab.)
BUCHMUELLER	88	HE e^+e^- Physics 412	W. Buchmueller, S. Cooper	(HANN, DESY, MIT)
Editors: A. Ali and P. Soeding, World Scientific, Singapore				
COHEN	87	RMP 59 1121	E.R. Cohen, B.N. Taylor	(RIS C, NBS)
BARU	86B	ZPHY C32 622 (erratum)	S.E. Baru <i>et al.</i>	(NOVO)
KURAEV	85	SJNP 41 466	E.A. Kurayev, V.S. Fadin	(NOVO)
Translated from YAF 41 733.				
ARTAMONOV	84	PL 137B 272	A.S. Artamonov <i>et al.</i>	(NOVO)
GILES	84B	PR D29 1285	R. Giles <i>et al.</i>	(CLEO Collab.)
ANDREWS	83	PRL 50 807	D.E. Andrews <i>et al.</i>	(CLEO Collab.)
GREEN	82	PRL 49 617	J. Green <i>et al.</i>	(CLEO Collab.)
MAGERAS	82	PL 118B 453	G. Mageras <i>et al.</i>	(COLU, CORN, LSU+)

 $\chi_{b1}(3P)$

$$I^G(J^{PC}) = 0^+(1^{++})$$

Needs confirmation.

Observed in the radiative decay to $\Upsilon(1S, 2S, 3S)$, therefore $C = +$. J needs confirmation. $\chi_{b1}(3P)$ MASS

VALUE (MeV)	EVTS	DOCUMENT ID	TECN	COMMENT
10513.42 ± 0.41 ± 0.53		¹ SIRUNYAN	18N CMS	$pp \rightarrow \gamma \mu^+ \mu^- X$
••• We do not use the following data for averages, fits, limits, etc. •••				
10515.7 ± 2.2 + 1.5 - 3.9 - 2.1	169	² AAIJ	14BG LHCB	$pp \rightarrow \gamma \mu^+ \mu^- X$
10512.1 ± 2.1 ± 0.9	351	³ AAIJ	14BG LHCB	$pp \rightarrow \gamma \mu^+ \mu^- X$
10511.3 ± 1.7 ± 2.5	182	⁴ AAIJ	14BI LHCB	$pp \rightarrow \gamma \mu^+ \mu^- X$
10530 ± 5 ± 9		⁵ AAD	12A ATLS	$pp \rightarrow \gamma \mu^+ \mu^- X$
10551 ± 14 ± 17		⁵ ABAZOV	12Q D0	$p\bar{p} \rightarrow \gamma \mu^+ \mu^- X$

¹ Systematic error includes an additional 0.5 MeV for the uncertainty on the $\Upsilon(3S)$ mass. Also measures $m_{\chi_{b2}(3P)} - m_{\chi_{b1}(3P)} = 10.60 \pm 0.64 \pm 0.17$ MeV. A total of 372 $\chi_{b1}(3P)$ and $\chi_{b2}(3P)$ events was observed.

² From $\chi_{b1}(3P) \rightarrow \Upsilon(1S, 2S)\gamma$ transitions assuming $m_{\chi_{b2}(3P)} - m_{\chi_{b1}(3P)} = 10.5 \pm 1.5$ MeV and allowing for $\pm 30\%$ variation in the $\chi_{b2}(3P)$ production rate relative to that of $\chi_{b1}(3P)$.

³ The mass of the $\chi_{b1}(3P)$ state obtained by combining the results of AAIJ 14BG with that of AAIJ 14BI. The first uncertainty is experimental and the second attributable to the unknown mass splitting, assumed to be $m_{\chi_{b2}(3P)} - m_{\chi_{b1}(3P)} = 10.5 \pm 1.5$ MeV.

⁴ From $\chi_{b1}(3P) \rightarrow \Upsilon(3S)\gamma$ transition assuming $m_{\chi_{b2}(3P)} - m_{\chi_{b1}(3P)} = 10.5 \pm 1.5$ MeV.

⁵ The mass barycenter of the merged lineshapes from the $J = 1$ and 2 states.

 $\chi_{b1}(3P)$ DECAY MODES

Mode	Fraction (Γ_i/Γ)
Γ_1 $\Upsilon(1S)\gamma$	seen
Γ_2 $\Upsilon(2S)\gamma$	seen
Γ_3 $\Upsilon(3S)\gamma$	seen

 $\chi_{b1}(3P)$ BRANCHING RATIOS

$\Gamma(\Upsilon(1S)\gamma)/\Gamma_{\text{total}}$	Γ_1/Γ			
VALUE	EVTS	DOCUMENT ID	TECN	COMMENT
seen	169	¹ AAIJ	14BG LHCB	$pp \rightarrow \gamma \mu^+ \mu^- X$
••• We do not use the following data for averages, fits, limits, etc. •••				
seen		AAD	12A ATLS	$pp \rightarrow \gamma \mu^+ \mu^- X$
seen		ABAZOV	12Q D0	$p\bar{p} \rightarrow \gamma \mu^+ \mu^- X$

¹ From $\chi_{b1}(3P) \rightarrow \Upsilon(1S, 2S)\gamma$ transitions assuming $m_{\chi_{b2}(3P)} - m_{\chi_{b1}(3P)} = 10.5 \pm 1.5$ MeV and allowing for $\pm 30\%$ variation in the $\chi_{b2}(3P)$ production rate relative to that of $\chi_{b1}(3P)$.

$\Gamma(\Upsilon(2S)\gamma)/\Gamma_{\text{total}}$	Γ_2/Γ			
VALUE	EVTS	DOCUMENT ID	TECN	COMMENT
seen	169	¹ AAIJ	14BG LHCB	$pp \rightarrow \gamma \mu^+ \mu^- X$
••• We do not use the following data for averages, fits, limits, etc. •••				
seen		AAD	12A ATLS	$pp \rightarrow \gamma \mu^+ \mu^- X$

¹ From $\chi_{b1}(3P) \rightarrow \Upsilon(1S, 2S)\gamma$ transitions assuming $m_{\chi_{b2}(3P)} - m_{\chi_{b1}(3P)} = 10.5 \pm 1.5$ MeV and allowing for $\pm 30\%$ variation in the $\chi_{b2}(3P)$ production rate relative to that of $\chi_{b1}(3P)$.

$\Gamma(\Upsilon(3S)\gamma)/\Gamma_{\text{total}}$	Γ_3/Γ			
VALUE	EVTS	DOCUMENT ID	TECN	COMMENT
seen		SIRUNYAN	18N CMS	$pp \rightarrow \gamma \mu^+ \mu^- X$
seen	182	AAIJ	14BI LHCB	$pp \rightarrow \gamma \mu^+ \mu^- X$

 $\chi_{b1}(3P)$ REFERENCES

SIRUNYAN	18N	PRL 121 092002	A.M. Sirunyan <i>et al.</i>	(CMS Collab.)
AAIJ	14BG	JHEP 1410 089	R. Aaij <i>et al.</i>	(LHCb Collab.)
AAIJ	14BI	EPJ C74 3092	R. Aaij <i>et al.</i>	(LHCb Collab.)
AAD	12A	PRL 108 152001	G. Aad <i>et al.</i>	(ATLAS Collab.)
ABAZOV	12Q	PR D86 031103	V.M. Abazov <i>et al.</i>	(D0 Collab.)

 $\chi_{b2}(3P)$

$$I^G(J^{PC}) = 0^+(2^{++})$$

Needs confirmation.

Observed in the radiative decay to $\Upsilon(3S)$, therefore $C = +$. J needs confirmation. $\chi_{b2}(3P)$ MASS

VALUE (MeV)	DOCUMENT ID	TECN	COMMENT
10524.02 ± 0.57 ± 0.53	¹ SIRUNYAN	18N CMS	$pp \rightarrow \gamma \mu^+ \mu^- X$
••• We do not use the following data for averages, fits, limits, etc. •••			
10530 ± 5 ± 9	² AAD	12A ATLS	$pp \rightarrow \gamma \mu^+ \mu^- X$

¹ Systematic error includes an additional 0.5 MeV for the uncertainty on the $\Upsilon(3S)$ mass. Also measures $m_{\chi_{b2}(3P)} - m_{\chi_{b1}(3P)} = 10.60 \pm 0.64 \pm 0.17$ MeV. A total of 372 $\chi_{b1}(3P)$ and $\chi_{b2}(3P)$ events was observed.

² The mass barycenter of the merged lineshapes from the $J = 1$ and 2 states.

 $\chi_{b2}(3P)$ DECAY MODES

Mode	Fraction (Γ_i/Γ)
Γ_1 $\Upsilon(3S)\gamma$	seen

 $\chi_{b2}(3P)$ BRANCHING RATIOS

$\Gamma(\Upsilon(3S)\gamma)/\Gamma_{\text{total}}$	Γ_1/Γ		
VALUE	DOCUMENT ID	TECN	COMMENT
seen	SIRUNYAN	18N CMS	$pp \rightarrow \gamma \mu^+ \mu^- X$

 $\chi_{b2}(3P)$ REFERENCES

SIRUNYAN	18N	PRL 121 092002	A.M. Sirunyan <i>et al.</i>	(CMS Collab.)
AAD	12A	PRL 108 152001	G. Aad <i>et al.</i>	(ATLAS Collab.)

 $\Upsilon(4S)$

$$I^G(J^{PC}) = 0^-(1^{--})$$

also known as $\Upsilon(10580)$ $\Upsilon(4S)$ MASS

VALUE (MeV)	DOCUMENT ID	TECN	COMMENT
10579.4 ± 1.2 OUR AVERAGE			
10579.3 ± 0.4 ± 1.2	AUBERT	05Q BABR	$e^+e^- \rightarrow$ hadrons
10580.0 ± 3.5	¹ BEBEK	87 CLEO	$e^+e^- \rightarrow$ hadrons
••• We do not use the following data for averages, fits, limits, etc. •••			
10577.4 ± 1.0	² LOVELOCK	85 CUSB	$e^+e^- \rightarrow$ hadrons

¹ Reanalysis of BESSON 85.

² No systematic error given.

 $\Upsilon(4S)$ WIDTH

VALUE (MeV)	DOCUMENT ID	TECN	COMMENT
20.5 ± 2.5 OUR AVERAGE			
20.7 ± 1.6 ± 2.5	AUBERT	05Q BABR	$e^+e^- \rightarrow$ hadrons
20 ± 2 ± 4	BESSON	85 CLEO	$e^+e^- \rightarrow$ hadrons
••• We do not use the following data for averages, fits, limits, etc. •••			
25 ± 2.5	LOVELOCK	85 CUSB	$e^+e^- \rightarrow$ hadrons

 $\Upsilon(4S)$ DECAY MODES

Mode	Fraction (Γ_i/Γ)	Confidence level
Γ_1 $B\bar{B}$	> 96	%
Γ_2 B^+B^-	(51.4 ± 0.6)	%
Γ_3 $D_s^+ \text{ anything} + \text{ c.c.}$	(17.8 ± 2.6)	%
Γ_4 $B^0\bar{B}^0$	(48.6 ± 0.6)	%
Γ_5 $J/\psi K_S^0 + (J/\psi, \eta_c) K_S^0$	< 4	$\times 10^{-7}$
Γ_6 non- $B\bar{B}$	< 4	%
Γ_7 e^+e^-	(1.57 ± 0.08)	$\times 10^{-5}$
Γ_8 $\rho^+\rho^-$	< 5.7	$\times 10^{-6}$
Γ_9 $K^*(892)^0\bar{K}^0$	< 2.0	$\times 10^{-6}$
Γ_{10} $J/\psi(1S)$ anything	< 1.9	$\times 10^{-4}$

Meson Particle Listings
 $\Upsilon(4S)$

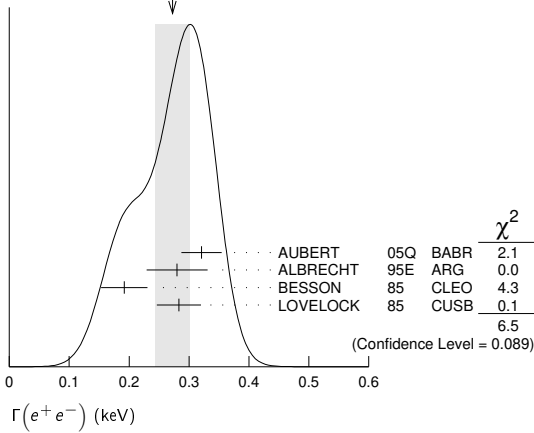
Γ_{11}	D^{*+} anything + c.c.	< 7.4	%	90%
Γ_{12}	ϕ anything	(7.1 \pm 0.6)	%	
Γ_{13}	$\phi\eta$	< 1.8	$\times 10^{-6}$	90%
Γ_{14}	$\phi\eta'$	< 4.3	$\times 10^{-6}$	90%
Γ_{15}	$\rho\eta$	< 1.3	$\times 10^{-6}$	90%
Γ_{16}	$\rho\eta'$	< 2.5	$\times 10^{-6}$	90%
Γ_{17}	$\Upsilon(1S)$ anything	< 4	$\times 10^{-3}$	90%
Γ_{18}	$\Upsilon(1S)\pi^+\pi^-$	(8.2 \pm 0.4)	$\times 10^{-5}$	
Γ_{19}	$\Upsilon(1S)\eta$	(1.81 \pm 0.18)	$\times 10^{-4}$	
Γ_{20}	$\Upsilon(1S)\eta'$	(3.4 \pm 0.9)	$\times 10^{-5}$	
Γ_{21}	$\Upsilon(2S)\pi^+\pi^-$	(8.2 \pm 0.8)	$\times 10^{-5}$	
Γ_{22}	$h_b(1P)\pi^+\pi^-$	not seen		
Γ_{23}	$h_b(1P)\eta$	(2.18 \pm 0.21)	$\times 10^{-3}$	
Γ_{24}	2H anything	< 1.3	$\times 10^{-5}$	90%
Double Radiative Decays				
Γ_{25}	$\gamma\gamma \Upsilon(D) \rightarrow \gamma\gamma\eta \Upsilon(1S)$	< 2.3	$\times 10^{-5}$	90%

$\Upsilon(4S)$ PARTIAL WIDTHS

$\Gamma(e^+e^-)$				Γ_7
VALUE (keV)	DOCUMENT ID	TECN	COMMENT	
0.272 \pm 0.029 OUR AVERAGE	Error includes scale factor of 1.5.		See the ideogram below.	
0.321 \pm 0.017 \pm 0.029	AUBERT 05Q	BABR	$e^+e^- \rightarrow$ hadrons	
0.28 \pm 0.05 \pm 0.01	¹ ALBRECHT 95E	ARG	$e^+e^- \rightarrow$ hadrons	
0.192 \pm 0.007 \pm 0.038	BESSION 85	CLEO	$e^+e^- \rightarrow$ hadrons	
0.283 \pm 0.037	LOVELOCK 85	CUSB	$e^+e^- \rightarrow$ hadrons	

¹Using LEYAOUANC 77 parametrization of $\Gamma(s)$.

WEIGHTED AVERAGE
 0.272 \pm 0.029 (Error scaled by 1.5)



$\Upsilon(4S)$ BRANCHING RATIOS

$B\bar{B}$ DECAYS

The ratio of branching fraction to charged and neutral B mesons is often derived assuming isospin invariance in the decays, and relies on the knowledge of the B^+/B^0 lifetime ratio. "OUR EVALUATION" is obtained based on averages of rescaled data listed below. The average and rescaling were performed by the Heavy Flavor Averaging Group (HFLAV) and are described at <https://hflav.web.cern.ch/>. The averaging/rescaling procedure takes into account the common dependence of the measurement on the value of the lifetime ratio.

$\Gamma(B^+B^-)/\Gamma_{total}$				Γ_2/Γ
VALUE	DOCUMENT ID	TECN	COMMENT	
0.514 \pm 0.006 OUR EVALUATION	Assuming $B(\Upsilon(4S) \rightarrow B\bar{B}) = 1$			

$\Gamma(D_s^+ \text{ anything + c.c.})/\Gamma_{total}$				Γ_3/Γ
VALUE	DOCUMENT ID	TECN	COMMENT	
0.178 \pm 0.021 \pm 0.016	¹ ARTUSO 05B	CLE3	$e^+e^- \rightarrow D_X X$	

¹ARTUSO 05B reports $[\Gamma(\Upsilon(4S) \rightarrow D_s^+ \text{ anything + c.c.})/\Gamma_{total}] \times [B(D_s^+ \rightarrow \phi\pi^+)] = (8.0 \pm 0.2 \pm 0.9) \times 10^{-3}$ which we divide by our best value $B(D_s^+ \rightarrow \phi\pi^+) = (4.5 \pm 0.4) \times 10^{-2}$. Our first error is their experiment's error and our second error is the systematic error from using our best value.

$\Gamma(B^0\bar{B}^0)/\Gamma_{total}$				Γ_4/Γ
---------------------------------------	--	--	--	-------------------

VALUE DOCUMENT ID TECN COMMENT
0.486 \pm 0.006 OUR EVALUATION Assuming $B(\Upsilon(4S) \rightarrow B\bar{B}) = 1$
 ••• We do not use the following data for averages, fits, limits, etc. •••
 0.487 \pm 0.010 \pm 0.008 ¹AUBERT,B 05H BABR $\Upsilon(4S) \rightarrow \bar{B}B \rightarrow D^*\ell\nu_\ell$
¹ Direct measurement. This value is averaged with the value extracted from the $\Gamma(B^+B^-) / \Gamma(B^0\bar{B}^0)$ measurements.

$\Gamma(B^+B^-)/\Gamma(B^0\bar{B}^0)$				Γ_2/Γ_4
---------------------------------------	--	--	--	---------------------

VALUE DOCUMENT ID TECN COMMENT
1.058 \pm 0.024 OUR EVALUATION
 1.006 \pm 0.036 \pm 0.031 ¹AUBERT 04F BABR $\Upsilon(4S) \rightarrow B\bar{B} \rightarrow J/\psi K$
 1.01 \pm 0.03 \pm 0.09 ¹HASTINGS 03 BELL $\Upsilon(4S) \rightarrow B\bar{B} \rightarrow$ dileptons
 1.058 \pm 0.084 \pm 0.136 ²ATHAR 02 CLEO $\Upsilon(4S) \rightarrow B\bar{B} \rightarrow D^*\ell\nu$
 1.10 \pm 0.06 \pm 0.05 ³AUBERT 02 BABR $\Upsilon(4S) \rightarrow B\bar{B} \rightarrow (c\bar{c})K^*$
 1.04 \pm 0.07 \pm 0.04 ⁴ALEXANDER 01 CLEO $\Upsilon(4S) \rightarrow B\bar{B} \rightarrow J/\psi K^*$
¹HASTINGS 03 and AUBERT 04F assume $\tau(B^+) / \tau(B^0) = 1.083 \pm 0.017$.
²ATHAR 02 assumes $\tau(B^+) / \tau(B^0) = 1.074 \pm 0.028$. Supersedes BARISH 95.
³AUBERT 02 assumes $\tau(B^+) / \tau(B^0) = 1.062 \pm 0.029$.
⁴ALEXANDER 01 assumes $\tau(B^+) / \tau(B^0) = 1.066 \pm 0.024$.

$[\Gamma(J/\psi K_S^0) + \Gamma(J/\psi, \eta_c) K_S^0]/\Gamma_{total}$				Γ_5/Γ
--	--	--	--	-------------------

Forbidden by CP invariance.
 VALUE (units 10^{-7}) CL% DOCUMENT ID TECN COMMENT
<4 90 ¹TAJIMA 07A BELL $\Upsilon(4S) \rightarrow B^0\bar{B}^0$
¹ $\Upsilon(4S)$ with $CP = +1$ decays to the final state with $CP = -1$.

non- $B\bar{B}$ DECAYS

$\Gamma(\text{non-}B\bar{B})/\Gamma_{total}$				Γ_6/Γ
--	--	--	--	-------------------

VALUE CL% DOCUMENT ID TECN COMMENT
<0.04 95 BARISH 96B CLEO e^+e^-

$\Gamma(e^+e^-)/\Gamma_{total}$				Γ_7/Γ
---------------------------------	--	--	--	-------------------

VALUE (units 10^{-5}) DOCUMENT ID TECN COMMENT
1.57 \pm 0.08 OUR AVERAGE
 1.55 \pm 0.04 \pm 0.07 AUBERT 05Q BABR $e^+e^- \rightarrow$ hadrons
 2.77 \pm 0.50 \pm 0.49 ¹ALBRECHT 95E ARG $e^+e^- \rightarrow$ hadrons
¹Using LEYAOUANC 77 parametrization of $\Gamma(s)$.

$\Gamma(\rho^+\rho^-)/\Gamma_{total}$				Γ_8/Γ
---------------------------------------	--	--	--	-------------------

VALUE CL% DOCUMENT ID TECN COMMENT
<5.7 $\times 10^{-6}$ 90 AUBERT 08B BABR $e^+e^- \rightarrow \pi^+\pi^-\pi^0$

$\Gamma(K^*(892)^0\bar{K}^0)/\Gamma_{total}$				Γ_9/Γ
--	--	--	--	-------------------

VALUE CL% DOCUMENT ID TECN COMMENT
<2.0 $\times 10^{-6}$ 90 SHEN 13A BELL $e^+e^- \rightarrow K^*(892)^0\bar{K}^0$

$\Gamma(J/\psi(1S) \text{ anything})/\Gamma_{total}$				Γ_{10}/Γ
--	--	--	--	----------------------

VALUE (units 10^{-4}) CL% DOCUMENT ID TECN COMMENT
<1.9 95 ¹ABE 02D BELL $e^+e^- \rightarrow J/\psi X \rightarrow \ell^+\ell^-X$
 ••• We do not use the following data for averages, fits, limits, etc. •••
 <4.7 90 ¹AUBERT 01c BABR $e^+e^- \rightarrow J/\psi X \rightarrow \ell^+\ell^-X$
¹Uses $B(J/\psi \rightarrow e^+e^-) = 0.0593 \pm 0.0010$ and $B(J/\psi \rightarrow \mu^+\mu^-) = 0.0588 \pm 0.0010$.

$\Gamma(D^{*+} \text{ anything + c.c.})/\Gamma_{total}$				Γ_{11}/Γ
---	--	--	--	----------------------

VALUE CL% DOCUMENT ID TECN COMMENT
<0.074 90 ¹ALEXANDER 90c CLEO e^+e^-
¹For $x > 0.473$.

$\Gamma(\phi \text{ anything})/\Gamma_{total}$				Γ_{12}/Γ
--	--	--	--	----------------------

VALUE (units 10^{-2}) CL% DOCUMENT ID TECN COMMENT
7.1 \pm 0.1 \pm 0.6 HUANG 07 CLEO $\Upsilon(4S) \rightarrow \phi X$
 ••• We do not use the following data for averages, fits, limits, etc. •••
 <0.23 90 ¹ALEXANDER 90c CLEO e^+e^-
¹For $x > 0.52$.

$\Gamma(\phi\eta)/\Gamma_{total}$				Γ_{13}/Γ
-----------------------------------	--	--	--	----------------------

VALUE (units 10^{-6}) CL% DOCUMENT ID TECN COMMENT
<1.8 90 ¹BELOUS 09 BELL $e^+e^- \rightarrow \phi\eta$
 ••• We do not use the following data for averages, fits, limits, etc. •••
 <2.5 90 AUBERT,BE 06F BABR $e^+e^- \rightarrow \phi\eta$
¹Using all intermediate branching fraction values from PDG 08.

$\Gamma(\phi\eta')/\Gamma_{total}$				Γ_{14}/Γ
------------------------------------	--	--	--	----------------------

VALUE (units 10^{-6}) CL% DOCUMENT ID TECN COMMENT
<4.3 90 ¹BELOUS 09 BELL $e^+e^- \rightarrow \phi\eta'$
¹Using all intermediate branching fraction values from PDG 08.

Meson Particle Listings

$\Upsilon(4S)$, $Z_b(10610)$

$\Gamma(\rho\eta)/\Gamma_{total}$					Γ_{15}/Γ
VALUE (units 10^{-6})	CL%	DOCUMENT ID	TECN	COMMENT	
<1.3	90	¹ BELOUS	09 BELL	$e^+e^- \rightarrow \rho\eta$	

¹ Using all intermedite branching fraction values from PDG 08.

$\Gamma(\rho\eta')/\Gamma_{total}$					Γ_{16}/Γ
VALUE (units 10^{-6})	CL%	DOCUMENT ID	TECN	COMMENT	
<2.5	90	¹ BELOUS	09 BELL	$e^+e^- \rightarrow \rho\eta'$	

¹ Using all intermedite branching fraction values from PDG 08.

$\Gamma(\Upsilon(1S) \text{ anything})/\Gamma_{total}$					Γ_{17}/Γ
VALUE	CL%	DOCUMENT ID	TECN	COMMENT	
<0.004	90	ALEXANDER	90c CLEO	e^+e^-	

$\Gamma(\Upsilon(1S)\pi^+\pi^-)/\Gamma_{total}$					Γ_{18}/Γ
VALUE (units 10^{-5})	CL%	EVTS	DOCUMENT ID	TECN	COMMENT
8.2 ± 0.4 OUR AVERAGE					
8.2 ± 0.5 ± 0.4		515	GUIDO 17 BELL	$\Upsilon(4S) \rightarrow \pi^+\pi^-\mu^+\mu^-$	
8.5 ± 1.3 ± 0.2		113 ± 16	¹ SOKOLOV 09 BELL	$e^+e^- \rightarrow \pi^+\pi^-\mu^+\mu^-$	
8.00 ± 0.64 ± 0.27		430	² AUBERT 08BP BABR	$\Upsilon(4S) \rightarrow \pi^+\pi^-\ell^+\ell^-$	

• • • We do not use the following data for averages, fits, limits, etc. • • •

17.8 ± 4.0 ± 0.3			^{3,4} SOKOLOV 07 BELL	$e^+e^- \rightarrow \pi^+\pi^-\mu^+\mu^-$	
9.0 ± 1.5 ± 0.2		167 ± 19	⁵ AUBERT 06R BABR	$e^+e^- \rightarrow \pi^+\pi^-\mu^+\mu^-$	
<12		90	GLENN 99 CLE2	e^+e^-	

¹ SOKOLOV 09 reports $[\Gamma(\Upsilon(4S) \rightarrow \Upsilon(1S)\pi^+\pi^-)/\Gamma_{total}] \times [B(\Upsilon(1S) \rightarrow \mu^+\mu^-)] = (0.211 \pm 0.030 \pm 0.014) \times 10^{-5}$ which we divide by our best value $B(\Upsilon(1S) \rightarrow \mu^+\mu^-) = (2.48 \pm 0.05) \times 10^{-2}$. Our first error is their experiment's error and our second error is the systematic error from using our best value.

² Using $B(\Upsilon(1S) \rightarrow e^+e^-) = (2.38 \pm 0.11)\%$ and $B(\Upsilon(1S) \rightarrow \mu^+\mu^-) = (2.48 \pm 0.05)\%$.

³ SOKOLOV 07 reports $[\Gamma(\Upsilon(4S) \rightarrow \Upsilon(1S)\pi^+\pi^-)/\Gamma_{total}] \times [B(\Upsilon(1S) \rightarrow \mu^+\mu^-)] = (4.42 \pm 0.81 \pm 0.56) \times 10^{-6}$ which we divide by our best value $B(\Upsilon(1S) \rightarrow \mu^+\mu^-) = (2.48 \pm 0.05) \times 10^{-2}$. Our first error is their experiment's error and our second error is the systematic error from using our best value.

⁴ According to the authors, systematic errors were underestimated.

⁵ Superseded by AUBERT 08BP. AUBERT 06R reports $[\Gamma(\Upsilon(4S) \rightarrow \Upsilon(1S)\pi^+\pi^-)/\Gamma_{total}] \times [B(\Upsilon(1S) \rightarrow \mu^+\mu^-)] = (2.23 \pm 0.25 \pm 0.27) \times 10^{-6}$ which we divide by our best value $B(\Upsilon(1S) \rightarrow \mu^+\mu^-) = (2.48 \pm 0.05) \times 10^{-2}$. Our first error is their experiment's error and our second error is the systematic error from using our best value.

$\Gamma(\Upsilon(1S)\eta)/\Gamma_{total}$					Γ_{19}/Γ
VALUE (units 10^{-4})	CL%	EVTS	DOCUMENT ID	TECN	COMMENT
1.81 ± 0.18 OUR AVERAGE					
1.70 ± 0.23 ± 0.08		49	GUIDO 17 BELL	$\Upsilon(4S) \rightarrow \pi^+\pi^-\pi^0\mu^+\mu^-$	
1.96 ± 0.26 ± 0.09		56	¹ AUBERT 08BP BABR	$\Upsilon(4S) \rightarrow \pi^+\pi^-\pi^0\ell^+\ell^-$	

• • • We do not use the following data for averages, fits, limits, etc. • • •

<2.7		90	² TAMPONI 15 BELL	$e^+e^- \rightarrow \gamma\eta + \text{hadrons}$	
------	--	----	------------------------------	--	--

¹ Using $B(\Upsilon(1S) \rightarrow e^+e^-) = (2.38 \pm 0.11)\%$ and $B(\Upsilon(1S) \rightarrow \mu^+\mu^-) = (2.48 \pm 0.05)\%$.

² Using $B(\eta \rightarrow 2\gamma) = (39.41 \pm 0.20)\%$.

$\Gamma(\Upsilon(1S)\eta')/\Gamma_{total}$					Γ_{20}/Γ
VALUE (units 10^{-5})	EVTS	DOCUMENT ID	TECN	COMMENT	
3.43 ± 0.88 ± 0.21	27	GUIDO 18 BELL	$\Upsilon(4S) \rightarrow (\rho^0\gamma, \pi^+\pi^-\eta)\mu^+\mu^-$		

$\Gamma(\Upsilon(1S)\eta)/\Gamma(\Upsilon(1S)\pi^+\pi^-)$					Γ_{19}/Γ_{18}
VALUE	EVTS	DOCUMENT ID	TECN	COMMENT	
2.41 ± 0.40 ± 0.12	56	¹ AUBERT 08BP BABR	$\Upsilon(4S) \rightarrow \pi^+\pi^-(\pi^0)\ell^+\ell^-$		

• • • We do not use the following data for averages, fits, limits, etc. • • •

¹ Not independent of other values reported by AUBERT 08BP.

$\Gamma(\Upsilon(2S)\pi^+\pi^-)/\Gamma_{total}$					Γ_{21}/Γ
VALUE (units 10^{-5})	CL%	EVTS	DOCUMENT ID	TECN	COMMENT
8.2 ± 0.8 OUR AVERAGE					
7.9 ± 1.0 ± 0.4		181	GUIDO 17 BELL	$\Upsilon(4S) \rightarrow \pi^+\pi^-\mu^+\mu^-$	
8.6 ± 1.1 ± 0.7		220	¹ AUBERT 08BP BABR	$\Upsilon(4S) \rightarrow \pi^+\pi^-\ell^+\ell^-$	

• • • We do not use the following data for averages, fits, limits, etc. • • •

8.8 ± 1.7 ± 0.8		97 ± 15	² AUBERT 06R BABR	$e^+e^- \rightarrow \pi^+\pi^-\mu^+\mu^-$	
<3.9		90	GLENN 99 CLE2	e^+e^-	

¹ Using $B(\Upsilon(2S) \rightarrow e^+e^-) = (1.91 \pm 0.16)\%$ and $B(\Upsilon(2S) \rightarrow \mu^+\mu^-) = (1.93 \pm 0.17)\%$.

² Superseded by AUBERT 08BP. AUBERT 06R reports $[\Gamma(\Upsilon(4S) \rightarrow \Upsilon(2S)\pi^+\pi^-)/\Gamma_{total}] \times [B(\Upsilon(2S) \rightarrow \mu^+\mu^-)] = (1.69 \pm 0.26 \pm 0.20) \times 10^{-6}$ which we divide by our best value $B(\Upsilon(2S) \rightarrow \mu^+\mu^-) = (1.93 \pm 0.17) \times 10^{-2}$. Our first error is their experiment's error and our second error is the systematic error from using our best value.

$\Gamma(\Upsilon(2S)\pi^+\pi^-)/\Gamma(\Upsilon(1S)\pi^+\pi^-)$					Γ_{21}/Γ_{18}
VALUE	EVTS	DOCUMENT ID	TECN	COMMENT	

• • • We do not use the following data for averages, fits, limits, etc. • • •

1.16 ± 0.16 ± 0.14		220	¹ AUBERT 08BP BABR	$\Upsilon(4S) \rightarrow \pi^+\pi^-\ell^+\ell^-$	
--------------------	--	-----	-------------------------------	---	--

¹ Using $B(\Upsilon(1S) \rightarrow e^+e^-) = (2.38 \pm 0.11)\%$, $B(\Upsilon(1S) \rightarrow \mu^+\mu^-) = (2.48 \pm 0.05)\%$, $B(\Upsilon(2S) \rightarrow e^+e^-) = (1.91 \pm 0.16)\%$, and $B(\Upsilon(2S) \rightarrow \mu^+\mu^-) = (1.93 \pm 0.17)\%$. Not independent of other values reported by AUBERT 08BP.

$\Gamma(h_b(1P)\pi^+\pi^-)/\Gamma_{total}$					Γ_{22}/Γ
VALUE	EVTS	DOCUMENT ID	TECN	COMMENT	
not seen	$(35^{+32}_{-26})k$	¹ ADACHI 12 BELL	10.58 $e^+e^- \rightarrow h_b(1P)\pi^+\pi^-$		

¹ From the upper limit on the ratio of $\sigma(e^+e^- \rightarrow h_b(1P)\pi^+\pi^-)$ at the $\Upsilon(4S)$ to that at the $\Upsilon(5S)$ of 0.27.

$\Gamma(h_b(1P)\eta)/\Gamma_{total}$					Γ_{23}/Γ
VALUE (units 10^{-3})	EVTS	DOCUMENT ID	TECN	COMMENT	
2.18 ± 0.11 ± 0.18	112k	¹ TAMPONI 15 BELL	$e^+e^- \rightarrow h_b(1P)\eta$		

¹ Using $B(\eta \rightarrow 2\gamma) = (39.41 \pm 0.20)\%$.

$\Gamma(\overline{2H} \text{ anything})/\Gamma_{total}$					Γ_{24}/Γ
VALUE (units 10^{-5})	CL%	DOCUMENT ID	TECN	COMMENT	
<1.3	90	ASNER 07 CLEO	$e^+e^- \rightarrow \overline{2}X$		

Double Radiative Decays

$\Gamma(\gamma\gamma \Upsilon(D) \rightarrow \gamma\gamma\eta\Upsilon(1S))/\Gamma_{total}$					Γ_{25}/Γ
VALUE	CL%	DOCUMENT ID	TECN	COMMENT	
<2.3 × 10⁻⁵	90	GUIDO 17 BELL	$\Upsilon(4S) \rightarrow \gamma\gamma\pi^+\pi^-\pi^0\mu^+\mu^-$		

$\Upsilon(4S)$ REFERENCES

GUIDO 18	PRL 121 062001	E. Guido et al.	(BELLE Collab.)
GUIDO 17	PR D96 052005	E. Guido et al.	(BELLE Collab.)
TAMPONI 15	PRL 115 142001	U. Tamponi et al.	(BELLE Collab.)
SHEN 13A	PR D88 052019	C.P. Shen et al.	(BELLE Collab.)
ADACHI 12	PRL 108 032001	I. Adachi et al.	(BELLE Collab.)
BELOUS 09	PL B681 400	K. Belous et al.	(BELLE Collab.)
SOKOLOV 09	PR D79 051103	A. Sokolov et al.	(BELLE Collab.)
AUBERT 08BP	PR D78 071103	B. Aubert et al.	(BABAR Collab.)
AUBERT 08BP	PR D78 112002	B. Aubert et al.	(BABAR Collab.)
PDG 08	PL B667 1	C. Anisler et al.	(PDG Collab.)
ASNER 07	PR D75 012009	D.M. Asner et al.	(CLEO Collab.)
HUANG 07	PR D75 012002	G.S. Huang et al.	(CLEO Collab.)
SOKOLOV 07	PR D75 071103	A. Sokolov et al.	(BELLE Collab.)
TAJIMA 07A	PRL 99 211601	O. Tajima et al.	(BELLE Collab.)
AUBERT 06R	PRL 96 232001	B. Aubert et al.	(BABAR Collab.)
AUBERT, BE 06F	PR D74 111103	B. Aubert et al.	(BABAR Collab.)
ARTUSO 05B	PRL 95 261801	M. Artuso et al.	(CLEO Collab.)
AUBERT 05Q	PR D72 032005	B. Aubert et al.	(BABAR Collab.)
AUBERT, B 05H	PRL 95 042001	B. Aubert et al.	(BABAR Collab.)
AUBERT 04F	PR D69 071101	B. Aubert et al.	(BABAR Collab.)
HASTINGS 03	PR D67 052004	M.C. Hastings et al.	(BELLE Collab.)
ABE 02D	PRL 88 052001	K. Abe et al.	(BELLE Collab.)
ATHAR 02	PR D66 052003	S.B. Athar et al.	(CLEO Collab.)
AUBERT 02	PR D65 032001	B. Aubert et al.	(BABAR Collab.)
ALEXANDER 01	PRL 86 2737	J.P. Alexander et al.	(CLEO Collab.)
AUBERT 01C	PRL 87 162002	B. Aubert et al.	(BABAR Collab.)
GLENN 99	PR D59 052003	S. Glenn et al.	(CLEO Collab.)
BARISH 96B	PRL 76 1570	B.C. Barish et al.	(CLEO Collab.)
ALBRECHT 95E	ZPHY C65 619	H. Albrecht et al.	(ARGUS Collab.)
BARISH 95	PR D51 1014	B.C. Barish et al.	(CLEO Collab.)
ALEXANDER 90C	PRL 64 2226	J. Alexander et al.	(CLEO Collab.)
BEBEK 87	PR D36 1389	C. Bebek et al.	(CLEO Collab.)
BESSON 85	PRL 54 381	D. Besson et al.	(CLEO Collab.)
LOVELOCK 85	PRL 54 377	D.M.J. Lovelock et al.	(CUSB Collab.)
LEYAOUANC 77	PL B71 397	A. Le Yaouanc et al.	(ORSAY)

$Z_b(10610)$

$$I^G(J^{PC}) = 1^+(1^+ -)$$

was $X(10610)$

Properties incompatible with a $q\bar{q}$ structure (exotic state). See the review on non- $q\bar{q}$ states.

Observed by BONDAR 12 in $\Upsilon(5S)$ decays to $\Upsilon(nS)\pi^+\pi^-$ ($n = 1, 2, 3$) and $h_b(mP)\pi^+\pi^-$ ($m = 1, 2$). $J^P = 1^+$ is favored from angular analyses.

$Z_b(10610)^\pm$ MASS

VALUE (MeV)	DOCUMENT ID	TECN	COMMENT
10607.2 ± 2.0	¹ BONDAR 12 BELL	$e^+e^- \rightarrow \text{hadrons}$	
• • • We do not use the following data for averages, fits, limits, etc. • • •			
10608.5 ± 3.4 ^{+3.7} _{-1.4}	² GARMASH 15 BELL	$e^+e^- \rightarrow \Upsilon(1S)\pi^+\pi^-$	
10608.1 ± 1.2 ^{+1.5} _{-0.2}	² GARMASH 15 BELL	$e^+e^- \rightarrow \Upsilon(2S)\pi^+\pi^-$	
10607.4 ± 1.5 ^{+0.8} _{-0.2}	² GARMASH 15 BELL	$e^+e^- \rightarrow \Upsilon(3S)\pi^+\pi^-$	
10611 ± 4 ± 3	³ BONDAR 12 BELL	$e^+e^- \rightarrow \Upsilon(1S)\pi^+\pi^-$	
10609 ± 2 ± 3	³ BONDAR 12 BELL	$e^+e^- \rightarrow \Upsilon(2S)\pi^+\pi^-$	
10608 ± 2 ± 3	³ BONDAR 12 BELL	$e^+e^- \rightarrow \Upsilon(3S)\pi^+\pi^-$	

See key on page 999

Meson Particle Listings

$Z_b(10610)$

10605	$\pm 2 \begin{smallmatrix} +3 \\ -1 \end{smallmatrix}$	³ BONDAR	12	BELL	$e^+e^- \rightarrow h_b(1P)\pi^+\pi^-$
10599	$\begin{smallmatrix} +6 \\ -3 \end{smallmatrix} \begin{smallmatrix} +5 \\ -4 \end{smallmatrix}$	³ BONDAR	12	BELL	$e^+e^- \rightarrow h_b(2P)\pi^+\pi^-$

¹ Average of the BONDAR 12 measurements in separate channels.
² Correlated with the corresponding result from BONDAR 12.
³ Superseded by the average measurement of BONDAR 12.

$Z_b(10610)^0$ MASS

VALUE (MeV)	DOCUMENT ID	TECN	COMMENT
10609 ± 4 ± 4	¹ KROKOVNY	13	BELL $e^+e^- \rightarrow \Upsilon(2S)/\Upsilon(3S)\pi^0\pi^0$

¹ From a simultaneous fit to the KROKOVNY 13 Dalitz analysis of $e^+e^- \rightarrow \Upsilon(2S)/\Upsilon(3S)\pi^0\pi^0$ decays with fixed width $\Gamma(Z_b(10610)^0) = 18.4$ MeV.

$Z_b(10610)^\pm$ WIDTH

VALUE (MeV)	DOCUMENT ID	TECN	COMMENT
18.4 ± 2.4	¹ BONDAR	12	BELL $e^+e^- \rightarrow$ hadrons
••• We do not use the following data for averages, fits, limits, etc. •••			
18.5 ± 5.3 $\begin{smallmatrix} +6.1 \\ -2.3 \end{smallmatrix}$	² GARMASH	15	BELL $e^+e^- \rightarrow \Upsilon(1S)\pi^+\pi^-$
20.8 ± 2.5 $\begin{smallmatrix} +0.3 \\ -2.1 \end{smallmatrix}$	² GARMASH	15	BELL $e^+e^- \rightarrow \Upsilon(2S)\pi^+\pi^-$
18.7 ± 3.4 $\begin{smallmatrix} +2.5 \\ -1.3 \end{smallmatrix}$	² GARMASH	15	BELL $e^+e^- \rightarrow \Upsilon(3S)\pi^+\pi^-$
22.3 ± 7.7 $\begin{smallmatrix} +3.0 \\ -4.0 \end{smallmatrix}$	³ BONDAR	12	BELL $e^+e^- \rightarrow \Upsilon(1S)\pi^+\pi^-$
24.2 ± 3.1 $\begin{smallmatrix} +2.0 \\ -3.0 \end{smallmatrix}$	³ BONDAR	12	BELL $e^+e^- \rightarrow \Upsilon(2S)\pi^+\pi^-$
17.6 ± 3.0 ± 3.0	³ BONDAR	12	BELL $e^+e^- \rightarrow \Upsilon(3S)\pi^+\pi^-$
11.4 $\begin{smallmatrix} +4.5 \\ -3.9 \end{smallmatrix} \begin{smallmatrix} +2.1 \\ -1.2 \end{smallmatrix}$	³ BONDAR	12	BELL $e^+e^- \rightarrow h_b(1P)\pi^+\pi^-$
13 $\begin{smallmatrix} +10 \\ -8 \end{smallmatrix} \begin{smallmatrix} +9 \\ -7 \end{smallmatrix}$	³ BONDAR	12	BELL $e^+e^- \rightarrow h_b(2P)\pi^+\pi^-$

¹ Average of the BONDAR 12 measurements in separate channels.
² Correlated with the corresponding result from BONDAR 12.
³ Superseded by the average measurement of BONDAR 12.

$Z_b(10610)$ DECAY MODES

Mode	Fraction (Γ_i/Γ)
Γ_1 $\Upsilon(1S)\pi^+$	$(5.4 \begin{smallmatrix} +1.9 \\ -1.5 \end{smallmatrix}) \times 10^{-3}$
Γ_2 $\Upsilon(1S)\pi^0$	not seen
Γ_3 $\Upsilon(2S)\pi^+$	$(3.6 \begin{smallmatrix} +1.1 \\ -0.8 \end{smallmatrix}) \%$
Γ_4 $\Upsilon(2S)\pi^0$	seen
Γ_5 $\Upsilon(3S)\pi^+$	$(2.1 \begin{smallmatrix} +0.8 \\ -0.6 \end{smallmatrix}) \%$
Γ_6 $\Upsilon(3S)\pi^0$	seen
Γ_7 $h_b(1P)\pi^+$	$(3.5 \begin{smallmatrix} +1.2 \\ -0.9 \end{smallmatrix}) \%$
Γ_8 $h_b(2P)\pi^+$	$(4.7 \begin{smallmatrix} +1.7 \\ -1.3 \end{smallmatrix}) \%$
Γ_9 $B^+\bar{B}^0$	not seen
Γ_{10} $B^+\bar{B}^{*0} + B^{*+}\bar{B}^0$	$(85.6 \begin{smallmatrix} +2.1 \\ -2.9 \end{smallmatrix}) \%$

$Z_b(10610)$ BRANCHING RATIOS

$\Gamma(\Upsilon(1S)\pi^+)/\Gamma_{total}$	DOCUMENT ID	TECN	COMMENT	Γ_1/Γ
5.4 $\begin{smallmatrix} +1.6 \\ -1.3 \end{smallmatrix} \begin{smallmatrix} +1.1 \\ -0.8 \end{smallmatrix}$	¹ GARMASH	16	BELL $e^+e^- \rightarrow \pi^-B^+\bar{B}^{*0}, \pi^-\bar{B}^0B^{*+}$	

••• We do not use the following data for averages, fits, limits, etc. •••
 seen GARMASH 15 BELL $e^+e^- \rightarrow \Upsilon(1S)\pi^+\pi^-$
 seen BONDAR 12 BELL $e^+e^- \rightarrow \Upsilon(1S)\pi^+\pi^-$

¹ Assuming the $Z_b(10610)$ decay width is saturated by the channels $\pi^+\Upsilon(1S, 2S, 3S)$, $\pi^+h_b(1P, 2P)$, and $B^+\bar{B}^{*0} + \bar{B}^0B^{*+}$, and using the results from BONDAR 12 and MIZUK 16.

$\Gamma(\Upsilon(1S)\pi^0)/\Gamma_{total}$	DOCUMENT ID	TECN	COMMENT	Γ_2/Γ
not seen	KROKOVNY	13	BELL $e^+e^- \rightarrow \Upsilon(1S)\pi^0\pi^0$	

$\Gamma(\Upsilon(2S)\pi^+)/\Gamma_{total}$	DOCUMENT ID	TECN	COMMENT	Γ_3/Γ
3.62 $\begin{smallmatrix} +0.76 \\ -0.59 \end{smallmatrix} \begin{smallmatrix} +0.79 \\ -0.53 \end{smallmatrix}$	¹ GARMASH	16	BELL $e^+e^- \rightarrow \pi^-B^+\bar{B}^{*0}, \pi^-\bar{B}^0B^{*+}$	

••• We do not use the following data for averages, fits, limits, etc. •••
 seen GARMASH 15 BELL $e^+e^- \rightarrow \Upsilon(2S)\pi^+\pi^-$
 seen BONDAR 12 BELL $e^+e^- \rightarrow \Upsilon(2S)\pi^+\pi^-$

¹ Assuming the $Z_b(10610)$ decay width is saturated by the channels $\pi^+\Upsilon(1S, 2S, 3S)$, $\pi^+h_b(1P, 2P)$, and $B^+\bar{B}^{*0} + \bar{B}^0B^{*+}$, and using the results from BONDAR 12 and MIZUK 16.

$\Gamma(\Upsilon(2S)\pi^0)/\Gamma_{total}$	DOCUMENT ID	TECN	COMMENT	Γ_4/Γ
not seen	¹ KROKOVNY	13	BELL $e^+e^- \rightarrow \Upsilon(2S)\pi^0\pi^0$	

¹ Combined significance in $e^+e^- \rightarrow \Upsilon(2S)/\Upsilon(3S)\pi^0\pi^0$, including systematics, of 6.5 σ .

$\Gamma(\Upsilon(3S)\pi^+)/\Gamma_{total}$	DOCUMENT ID	TECN	COMMENT	Γ_5/Γ
2.15 $\begin{smallmatrix} +0.55 \\ -0.42 \end{smallmatrix} \begin{smallmatrix} +0.60 \\ -0.43 \end{smallmatrix}$	¹ GARMASH	16	BELL $e^+e^- \rightarrow \pi^-B^+\bar{B}^{*0}, \pi^-\bar{B}^0B^{*+}$	

••• We do not use the following data for averages, fits, limits, etc. •••
 seen GARMASH 15 BELL $e^+e^- \rightarrow \Upsilon(3S)\pi^+\pi^-$
 seen BONDAR 12 BELL $e^+e^- \rightarrow \Upsilon(3S)\pi^+\pi^-$

¹ Assuming the $Z_b(10610)$ decay width is saturated by the channels $\pi^+\Upsilon(1S, 2S, 3S)$, $\pi^+h_b(1P, 2P)$, and $B^+\bar{B}^{*0} + \bar{B}^0B^{*+}$, and using the results from BONDAR 12 and MIZUK 16.

$\Gamma(\Upsilon(3S)\pi^0)/\Gamma_{total}$	DOCUMENT ID	TECN	COMMENT	Γ_6/Γ
not seen	¹ KROKOVNY	13	BELL $e^+e^- \rightarrow \Upsilon(3S)\pi^0\pi^0$	

¹ Combined significance in $e^+e^- \rightarrow \Upsilon(2S)/\Upsilon(3S)\pi^0\pi^0$, including systematics, of 6.5 σ .

$\Gamma(h_b(1P)\pi^+)/\Gamma_{total}$	DOCUMENT ID	TECN	COMMENT	Γ_7/Γ
3.45 $\begin{smallmatrix} +0.87 \\ -1.00 \end{smallmatrix} \begin{smallmatrix} +0.86 \\ -0.89 \end{smallmatrix}$	¹ GARMASH	16	BELL $e^+e^- \rightarrow \pi^-B^+\bar{B}^{*0}, \pi^-\bar{B}^0B^{*+}$	

••• We do not use the following data for averages, fits, limits, etc. •••
 possibly seen ² MIZUK 16 BELL $e^+e^- \rightarrow h_b(1P)\pi^+\pi^-$
 seen ³ BONDAR 12 BELL $e^+e^- \rightarrow h_b(1P)\pi^+\pi^-$

¹ Assuming the $Z_b(10610)$ decay width is saturated by the channels $\pi^+\Upsilon(1S, 2S, 3S)$, $\pi^+h_b(1P, 2P)$, and $B^+\bar{B}^{*0} + \bar{B}^0B^{*+}$, and using the results from BONDAR 12 and MIZUK 16.
² Using e^+e^- energies near the $\Upsilon(11020)$.
³ Using e^+e^- energies near the $\Upsilon(10860)$.

$\Gamma(h_b(2P)\pi^+)/\Gamma_{total}$	DOCUMENT ID	TECN	COMMENT	Γ_8/Γ
4.67 $\begin{smallmatrix} +1.24 \\ -1.00 \end{smallmatrix} \begin{smallmatrix} +1.18 \\ -0.89 \end{smallmatrix}$	¹ GARMASH	16	BELL $e^+e^- \rightarrow \pi^-B^+\bar{B}^{*0}, \pi^-\bar{B}^0B^{*+}$	

••• We do not use the following data for averages, fits, limits, etc. •••
 possibly seen ² MIZUK 16 BELL $e^+e^- \rightarrow h_b(2P)\pi^+\pi^-$
 seen ³ BONDAR 12 BELL $e^+e^- \rightarrow h_b(2P)\pi^+\pi^-$

¹ Assuming the $Z_b(10610)$ decay width is saturated by the channels $\pi^+\Upsilon(1S, 2S, 3S)$, $\pi^+h_b(1P, 2P)$, and $B^+\bar{B}^{*0} + \bar{B}^0B^{*+}$, and using the results from BONDAR 12 and MIZUK 16.
² Using e^+e^- energies near the $\Upsilon(11020)$.
³ Using e^+e^- energies near the $\Upsilon(10860)$.

$\Gamma(B^+\bar{B}^0)/\Gamma_{total}$	DOCUMENT ID	TECN	COMMENT	Γ_9/Γ
not seen	GARMASH	16	BELL $e^+e^- \rightarrow \pi^-B^+\bar{B}^0$	

$[\Gamma(B^+\bar{B}^{*0}) + \Gamma(B^{*+}\bar{B}^0)]/\Gamma_{total}$	EVTS	DOCUMENT ID	TECN	COMMENT	Γ_{10}/Γ
85.6 $\begin{smallmatrix} +1.5 \\ -2.0 \end{smallmatrix} \begin{smallmatrix} +1.5 \\ -2.1 \end{smallmatrix}$	357	¹ GARMASH	16	BELL $e^+e^- \rightarrow \pi^-B^+\bar{B}^{*0}, \pi^-\bar{B}^0B^{*+}$	

¹ Assuming the $Z_b(10610)$ decay width is saturated by the channels $\pi^+\Upsilon(1S, 2S, 3S)$, $\pi^+h_b(1P, 2P)$, and $B^+\bar{B}^{*0} + B^{*+}\bar{B}^0$, and using the results from BONDAR 12 and MIZUK 16. Using the mass and width of the $Z_b(10610)$ from BONDAR 12.

$[\Gamma(B^+\bar{B}^{*0}) + \Gamma(B^{*+}\bar{B}^0)] / [\Gamma(\Upsilon(1S)\pi^+) + \Gamma(\Upsilon(2S)\pi^+) + \Gamma(\Upsilon(3S)\pi^+) + \Gamma(h_b(1P)\pi^+) + \Gamma(h_b(2P)\pi^+)]$	EVTS	DOCUMENT ID	TECN	COMMENT	$\Gamma_{10}/(\Gamma_1 + \Gamma_3 + \Gamma_5 + \Gamma_7 + \Gamma_8)$
5.93 $\begin{smallmatrix} +0.99 \\ -0.69 \end{smallmatrix} \begin{smallmatrix} +1.01 \\ -0.73 \end{smallmatrix}$	357	¹ GARMASH	16	BELL $e^+e^- \rightarrow \pi^-B^+\bar{B}^{*0}, \pi^-\bar{B}^0B^{*+}$	

••• We do not use the following data for averages, fits, limits, etc. •••
¹ Combined with the results of BONDAR 12 and MIZUK 16. Not independent from $Z_b(10610)$ branching fractions to $\pi^+\Upsilon(1S, 2S, 3S)$, $\pi^+h_b(1P, 2P)$, and $B^+\bar{B}^{*0} + \bar{B}^0B^{*+}$.

$Z_b(10610)$ REFERENCES

GARMASH	16	PRL 116 212001	A. Garmash <i>et al.</i>	(BELLE Collab.)
MIZUK	16	PRL 117 142001	R. Mizuk <i>et al.</i>	(BELLE Collab.)
GARMASH	15	PR D91 072003	A. Garmash <i>et al.</i>	(BELLE Collab.)
KROKOVNY	13	PR D88 052016	P. Krokovny <i>et al.</i>	(BELLE Collab.)
BONDAR	12	PRL 108 122001	A. Bondar <i>et al.</i>	(BELLE Collab.)

Meson Particle Listings

 $Z_b(10650)$ **$Z_b(10650)$** was $X(10650)^\pm$ Properties incompatible with a $q\bar{q}$ structure (exotic state). See the review on non- $q\bar{q}$ states.Observed by BONDAR 12 in $\Upsilon(5S)$ decays to $\Upsilon(nS)\pi^+\pi^-$ ($n = 1, 2, 3$) and $h_b(mP)\pi^+\pi^-$ ($m = 1, 2$). $J^P = 1^+$ is favored from angular analyses. $I^G(J^{PC}) = 1^+(1^+ -)$
 I, G, C need confirmation. **$Z_b(10650)$ MASS**

VALUE (MeV)	DOCUMENT ID	TECN	COMMENT
10652.2 ± 1.5	¹ BONDAR 12	BELL	$e^+e^- \rightarrow$ hadrons
$10656.7 \pm 5.0^{+1.1}_{-3.1}$	² GARMASH 15	BELL	$e^+e^- \rightarrow \Upsilon(1S)\pi^+\pi^-$
$10650.7 \pm 1.5^{+0.5}_{-0.2}$	² GARMASH 15	BELL	$e^+e^- \rightarrow \Upsilon(2S)\pi^+\pi^-$
$10651.2 \pm 1.0^{+0.4}_{-0.3}$	² GARMASH 15	BELL	$e^+e^- \rightarrow \Upsilon(3S)\pi^+\pi^-$
$10657 \pm 6 \pm 3$	³ BONDAR 12	BELL	$e^+e^- \rightarrow \Upsilon(1S)\pi^+\pi^-$
$10651 \pm 2 \pm 3$	³ BONDAR 12	BELL	$e^+e^- \rightarrow \Upsilon(2S)\pi^+\pi^-$
$10652 \pm 1 \pm 2$	³ BONDAR 12	BELL	$e^+e^- \rightarrow \Upsilon(3S)\pi^+\pi^-$
$10654 \pm 3 \pm 1$	³ BONDAR 12	BELL	$e^+e^- \rightarrow h_b(1P)\pi^+\pi^-$
$10651 \pm 2 \pm 3$	³ BONDAR 12	BELL	$e^+e^- \rightarrow h_b(2P)\pi^+\pi^-$

¹ Average of the BONDAR 12 measurements in separate channels.² Correlated with the corresponding result from BONDAR 12.³ Superseded by the average measurement of BONDAR 12. **$Z_b(10650)$ WIDTH**

VALUE (MeV)	DOCUMENT ID	TECN	COMMENT
11.5 ± 2.2	⁴ BONDAR 12	BELL	$e^+e^- \rightarrow$ hadrons
$12.1 \pm 11.3 \pm 2.7$ 4.8 ± 0.6	⁵ GARMASH 15	BELL	$e^+e^- \rightarrow \Upsilon(1S)\pi^+\pi^-$
$14.2 \pm 3.7 \pm 0.9$ 0.4	⁵ GARMASH 15	BELL	$e^+e^- \rightarrow \Upsilon(2S)\pi^+\pi^-$
$9.3 \pm 2.2 \pm 0.3$ 0.5	⁵ GARMASH 15	BELL	$e^+e^- \rightarrow \Upsilon(3S)\pi^+\pi^-$
$16.3 \pm 9.8 \pm 6.0$ 2.0	⁶ BONDAR 12	BELL	$e^+e^- \rightarrow \Upsilon(1S)\pi^+\pi^-$
$13.3 \pm 3.3 \pm 4.0$ 3.0	⁶ BONDAR 12	BELL	$e^+e^- \rightarrow \Upsilon(2S)\pi^+\pi^-$
$8.4 \pm 2.0 \pm 2.0$	⁶ BONDAR 12	BELL	$e^+e^- \rightarrow \Upsilon(3S)\pi^+\pi^-$
$20.9 \pm 5.4 \pm 2.1$ 4.7 ± 5.7	⁶ BONDAR 12	BELL	$e^+e^- \rightarrow h_b(1P)\pi^+\pi^-$
$19 \pm 7 \pm 11$ 7	⁶ BONDAR 12	BELL	$e^+e^- \rightarrow h_b(2P)\pi^+\pi^-$

⁴ Average of the BONDAR 12 measurements in separate channels.⁵ Correlated with the corresponding result from BONDAR 12.⁶ Superseded by the average measurement of BONDAR 12. **$Z_b(10650)^+$ DECAY MODES** $Z_b(10650)^-$ decay modes are charge conjugates of the modes below.

Mode	Fraction (Γ_j/Γ)
Γ_1 $\Upsilon(1S)\pi^+$	$(1.7^{+0.8}_{-0.6}) \times 10^{-3}$
Γ_2 $\Upsilon(2S)\pi^+$	$(1.4^{+0.6}_{-0.4}) \%$
Γ_3 $\Upsilon(3S)\pi^+$	$(1.6^{+0.7}_{-0.5}) \%$
Γ_4 $h_b(1P)\pi^+$	$(8.4^{+2.9}_{-2.4}) \%$
Γ_5 $h_b(2P)\pi^+$	$(15 \pm 4) \%$
Γ_6 $B^+\bar{B}^0$	not seen
Γ_7 $B^+\bar{B}^{*0} + B^{*+}\bar{B}^0$	not seen
Γ_8 $B^{*+}\bar{B}^{*0}$	$(74 \pm 4) \%$

 $Z_b(10650)$ BRANCHING RATIOS

$\Gamma(\Upsilon(1S)\pi^+)/\Gamma_{\text{total}}$	DOCUMENT ID	TECN	COMMENT	Γ_1/Γ
$1.7^{+0.7+0.3}_{-0.6-0.2}$	⁷ GARMASH 16	BELL	$e^+e^- \rightarrow \pi^-B^{*+}\bar{B}^{*0}$	
seen	GARMASH 15	BELL	$e^+e^- \rightarrow \Upsilon(1S)\pi^+\pi^-$	
seen	BONDAR 12	BELL	$e^+e^- \rightarrow \Upsilon(1S)\pi^+\pi^-$	

⁷ Assuming the $Z_b(10650)$ decay width is saturated by the channels $\pi^+\Upsilon(1S, 2S, 3S)$, $\pi^+h_b(1P, 2P)$, and $B^{*+}\bar{B}^{*0}$, and using the results from BONDAR 12 and MIZUK 16. $\Gamma(\Upsilon(2S)\pi^+)/\Gamma_{\text{total}}$ Γ_2/Γ

VALUE (units 10^{-2})	DOCUMENT ID	TECN	COMMENT
$1.39^{+0.48+0.34}_{-0.38-0.23}$	⁸ GARMASH 16	BELL	$e^+e^- \rightarrow \pi^-B^{*+}\bar{B}^{*0}$
$\bullet \bullet \bullet$ We do not use the following data for averages, fits, limits, etc. $\bullet \bullet \bullet$			
seen	GARMASH 15	BELL	$e^+e^- \rightarrow \Upsilon(2S)\pi^+\pi^-$
seen	BONDAR 12	BELL	$e^+e^- \rightarrow \Upsilon(2S)\pi^+\pi^-$

⁸ Assuming the $Z_b(10650)$ decay width is saturated by the channels $\pi^+\Upsilon(1S, 2S, 3S)$, $\pi^+h_b(1P, 2P)$, and $B^{*+}\bar{B}^{*0}$, and using the results from BONDAR 12 and MIZUK 16. $\Gamma(\Upsilon(3S)\pi^+)/\Gamma_{\text{total}}$ Γ_3/Γ

VALUE (units 10^{-2})	DOCUMENT ID	TECN	COMMENT
$1.63^{+0.53+0.39}_{-0.42-0.28}$	⁹ GARMASH 16	BELL	$e^+e^- \rightarrow \pi^-B^{*+}\bar{B}^{*0}$
$\bullet \bullet \bullet$ We do not use the following data for averages, fits, limits, etc. $\bullet \bullet \bullet$			
seen	GARMASH 15	BELL	$e^+e^- \rightarrow \Upsilon(3S)\pi^+\pi^-$
seen	BONDAR 12	BELL	$e^+e^- \rightarrow \Upsilon(3S)\pi^+\pi^-$

⁹ Assuming the $Z_b(10650)$ decay width is saturated by the channels $\pi^+\Upsilon(1S, 2S, 3S)$, $\pi^+h_b(1P, 2P)$, and $B^{*+}\bar{B}^{*0}$, and using the results from BONDAR 12 and MIZUK 16. $\Gamma(h_b(1P)\pi^+)/\Gamma_{\text{total}}$ Γ_4/Γ

VALUE (units 10^{-2})	DOCUMENT ID	TECN	COMMENT
$8.41^{+2.43+1.49}_{-2.12-1.06}$	¹⁰ GARMASH 16	BELL	$e^+e^- \rightarrow \pi^-B^{*+}\bar{B}^{*0}$
$\bullet \bullet \bullet$ We do not use the following data for averages, fits, limits, etc. $\bullet \bullet \bullet$			
seen	¹¹ MIZUK 16	BELL	$e^+e^- \rightarrow h_b(1P)\pi^+\pi^-$
seen	¹² BONDAR 12	BELL	$e^+e^- \rightarrow h_b(1P)\pi^+\pi^-$

¹⁰ Assuming the $Z_b(10650)$ decay width is saturated by the channels $\pi^+\Upsilon(1S, 2S, 3S)$, $\pi^+h_b(1P, 2P)$, and $B^{*+}\bar{B}^{*0}$, and using the results from BONDAR 12 and MIZUK 16.¹¹ Using e^+e^- energies near the $\Upsilon(11020)$.¹² Using e^+e^- energies near the $\Upsilon(10860)$. $\Gamma(h_b(2P)\pi^+)/\Gamma_{\text{total}}$ Γ_5/Γ

VALUE (units 10^{-2})	DOCUMENT ID	TECN	COMMENT
$14.7^{+3.2+2.8}_{-2.8-2.3}$	¹³ GARMASH 16	BELL	$e^+e^- \rightarrow \pi^-B^{*+}\bar{B}^{*0}$
$\bullet \bullet \bullet$ We do not use the following data for averages, fits, limits, etc. $\bullet \bullet \bullet$			
possibly seen	¹⁴ MIZUK 16	BELL	$e^+e^- \rightarrow h_b(2P)\pi^+\pi^-$
seen	¹⁵ BONDAR 12	BELL	$e^+e^- \rightarrow h_b(2P)\pi^+\pi^-$

¹³ Assuming the $Z_b(10650)$ decay width is saturated by the channels $\pi^+\Upsilon(1S, 2S, 3S)$, $\pi^+h_b(1P, 2P)$, and $B^{*+}\bar{B}^{*0}$, and using the results from BONDAR 12 and MIZUK 16.¹⁴ Using e^+e^- energies near the $\Upsilon(11020)$.¹⁵ Using e^+e^- energies near the $\Upsilon(10860)$. $\Gamma(B^+\bar{B}^0)/\Gamma_{\text{total}}$ Γ_6/Γ

VALUE	DOCUMENT ID	TECN	COMMENT
not seen	GARMASH 16	BELL	$e^+e^- \rightarrow \pi^-B^+\bar{B}^0$

 $[\Gamma(B^+\bar{B}^{*0}) + \Gamma(B^{*+}\bar{B}^0)]/\Gamma_{\text{total}}$ Γ_7/Γ

VALUE	DOCUMENT ID	TECN	COMMENT
not seen	GARMASH 16	BELL	$e^+e^- \rightarrow \pi^-B^+\bar{B}^{*0}, \pi^-B^0\bar{B}^{*+}$

 $\Gamma(B^{*+}\bar{B}^{*0})/\Gamma_{\text{total}}$ Γ_8/Γ

VALUE (units 10^{-2})	EVTS	DOCUMENT ID	TECN	COMMENT
$73.7^{+3.4+2.7}_{-4.4-3.5}$	161	¹⁶ GARMASH 16	BELL	$e^+e^- \rightarrow \pi^-B^{*+}\bar{B}^{*0}$

¹⁶ Assuming the $Z_b(10650)$ decay width is saturated by the channels $\pi^+\Upsilon(1S, 2S, 3S)$, $\pi^+h_b(1P, 2P)$, and $B^{*+}\bar{B}^{*0}$, and using the results from BONDAR 12 and MIZUK 16. Using the mass and width of the $Z_b(10650)$ from BONDAR 12. $\Gamma(B^{*+}\bar{B}^{*0})/[\Gamma(\Upsilon(1S)\pi^+) + \Gamma(\Upsilon(2S)\pi^+) + \Gamma(\Upsilon(3S)\pi^+) + \Gamma(h_b(1P)\pi^+) + \Gamma(h_b(2P)\pi^+)]$ $\Gamma_8/(\Gamma_1+\Gamma_2+\Gamma_3+\Gamma_4+\Gamma_5)$

VALUE (units 10^{-2})	EVTS	DOCUMENT ID	TECN	COMMENT
$\bullet \bullet \bullet$ We do not use the following data for averages, fits, limits, etc. $\bullet \bullet \bullet$				

VALUE	DOCUMENT ID	TECN	COMMENT
$2.80^{+0.69+0.54}_{-0.40-0.36}$	161	¹⁷ GARMASH 16	BELL $e^+e^- \rightarrow \pi^-B^{*+}\bar{B}^{*0}$

¹⁷ Combined with the results of BONDAR 12 and MIZUK 16. Not independent from $Z_b(10650)$ branching fractions to $\pi^+\Upsilon(1S, 2S, 3S)$, $\pi^+h_b(1P, 2P)$, and $B^{*+}\bar{B}^{*0}$. **$Z_b(10650)$ REFERENCES**

GARMASH 16	PRL 116 212001	A. Garmash et al.	(BELLE Collab.)
MIZUK 16	PRL 117 142001	R. Mizuk et al.	(BELLE Collab.)
GARMASH 15	PR D91 072003	A. Garmash et al.	(BELLE Collab.)
BONDAR 12	PRL 108 122001	A. Bondar et al.	(BELLE Collab.)

$\Upsilon(10753)$ $I^G(J^{PC}) = ?^?(1^{--})$

OMITTED FROM SUMMARY TABLE
A candidate for $\Upsilon(3D)$ state or an exotic structure.

Seen by MIZUK 19 in $e^+e^- \rightarrow \Upsilon(nS)\pi^+\pi^-$ ($n=1,2,3$) with a significance of 5.2σ .

$\Upsilon(10753)$ MASS

VALUE (MeV)	DOCUMENT ID	TECN	COMMENT
10752.7 ± 5.9^{+0.7}_{-1.1}	1 MIZUK	19	BELL $e^+e^- \rightarrow \Upsilon(nS)\pi^+\pi^-$

¹ From a simultaneous fit to the $\Upsilon(nS)\pi^+\pi^-$, $n = 1, 2, 3$, cross sections at 28 energy points within $\sqrt{s} = 10.63$ –11.02 GeV, including the initial-state radiation at $\Upsilon(10860)$.

$\Upsilon(10753)$ WIDTH

VALUE (MeV)	DOCUMENT ID	TECN	COMMENT
35.5 ± 17.6 + 3.9^{+3.3}_{-1.3}	1 MIZUK	19	BELL $e^+e^- \rightarrow \Upsilon(nS)\pi^+\pi^-$

¹ From a simultaneous fit to the $\Upsilon(nS)\pi^+\pi^-$, $n = 1, 2, 3$, cross sections at 28 energy points within $\sqrt{s} = 10.63$ –11.02 GeV, including the initial-state radiation at $\Upsilon(10860)$.

$\Upsilon(10753)$ DECAY MODES

Mode
$\Gamma_1 \quad \Upsilon(1S)\pi^+\pi^-$
$\Gamma_2 \quad \Upsilon(2S)\pi^+\pi^-$
$\Gamma_3 \quad \Upsilon(3S)\pi^+\pi^-$
$\Gamma_4 \quad e^+e^-$

$\Upsilon(10753)$ $\Gamma(i)\Gamma(e^+e^-)/\Gamma(\text{total})$

$\Gamma(\Upsilon(1S)\pi^+\pi^-) \times \Gamma(e^+e^-)/\Gamma_{\text{total}}$	DOCUMENT ID	TECN	COMMENT	$\Gamma_1\Gamma_4/\Gamma$
0.295 ± 0.175	1,2 MIZUK	19	BELL $e^+e^- \rightarrow \Upsilon(nS)\pi^+\pi^-$	

¹ From a simultaneous fit to the $\Upsilon(nS)\pi^+\pi^-$, $n = 1, 2, 3$, cross sections at 28 energy points within $\sqrt{s} = 10.63$ –11.02 GeV, including the initial-state radiation at $\Upsilon(10860)$.

² Reported as the range 0.12–0.47 eV obtained from multiple solutions of an amplitude fit within a model composed as a sum of Breit-Wigner functions.

$\Gamma(\Upsilon(2S)\pi^+\pi^-) \times \Gamma(e^+e^-)/\Gamma_{\text{total}}$	DOCUMENT ID	TECN	COMMENT	$\Gamma_2\Gamma_4/\Gamma$
0.875 ± 0.345	1,2 MIZUK	19	BELL $e^+e^- \rightarrow \Upsilon(nS)\pi^+\pi^-$	

¹ From a simultaneous fit to the $\Upsilon(nS)\pi^+\pi^-$, $n = 1, 2, 3$, cross sections at 28 energy points within $\sqrt{s} = 10.63$ –11.02 GeV, including the initial-state radiation at $\Upsilon(10860)$.

² Reported as the range 0.53–1.22 eV obtained from multiple solutions of an amplitude fit within a model composed as a sum of Breit-Wigner functions.

$\Gamma(\Upsilon(3S)\pi^+\pi^-) \times \Gamma(e^+e^-)/\Gamma_{\text{total}}$	DOCUMENT ID	TECN	COMMENT	$\Gamma_3\Gamma_4/\Gamma$
0.235 ± 0.025	1,2 MIZUK	19	BELL $e^+e^- \rightarrow \Upsilon(nS)\pi^+\pi^-$	

¹ From a simultaneous fit to the $\Upsilon(nS)\pi^+\pi^-$, $n = 1, 2, 3$, cross sections at 28 energy points within $\sqrt{s} = 10.63$ –11.02 GeV, including the initial-state radiation at $\Upsilon(10860)$.

² Reported as the range 0.21–0.26 eV obtained from multiple solutions of an amplitude fit within a model composed as a sum of Breit-Wigner functions.

$\Upsilon(10753)$ REFERENCES

MIZUK 19 JHEP 1910 220 R. Mizuk et al. (BELLE Collab.)

$\Upsilon(10860)$ $I^G(J^{PC}) = 0^-(1^{--})$

$\Upsilon(10860)$ MASS

VALUE (MeV)	DOCUMENT ID	TECN	COMMENT
10885.2 ± 2.6 OUR AVERAGE			
10885.3 ± 1.5 ± 2.2 ^{+2.2} _{-0.9}	1 MIZUK	19	BELL $e^+e^- \rightarrow \Upsilon(nS)\pi^+\pi^-$
10884.7 ± 3.6 + 8.9 ^{+8.9} _{-3.4} - 1.0	2 MIZUK	16	BELL $e^+e^- \rightarrow h_b(1P, 2P)\pi^+\pi^-$

••• We do not use the following data for averages, fits, limits, etc. •••

10881.8 ± 1.0 ± 1.2 ^{+1.2} _{-1.1}	3,4 SANTEL	16	BELL $e^+e^- \rightarrow \text{hadrons}$
10891.1 ± 3.2 ± 1.2 ^{+1.2} _{-2.0}	5,6 SANTEL	16	BELL $e^+e^- \rightarrow \Upsilon(1S, 2S, 3S)\pi^+\pi^-$
10879 ± 3	7,8 CHEN	10	BELL $e^+e^- \rightarrow \text{hadrons}$
10888.4 ± 2.7 ± 1.2 ^{+2.7} _{-2.6}	9 CHEN	10	BELL $e^+e^- \rightarrow \Upsilon(1S, 2S, 3S)\pi^+\pi^-$
10876 ± 2	7 AUBERT	09E	BABR $e^+e^- \rightarrow \text{hadrons}$
10869 ± 2	10 AUBERT	09E	BABR $e^+e^- \rightarrow \text{hadrons}$
10868 ± 6 ± 5	11 BESSON	85	CLEO $e^+e^- \rightarrow \text{hadrons}$
10845 ± 20	12 LOVELOCK	85	CUSB $e^+e^- \rightarrow \text{hadrons}$

¹ From a simultaneous fit to the $\Upsilon(nS)\pi^+\pi^-$, $n = 1, 2, 3$, cross sections at 28 energy points within $\sqrt{s} = 10.6$ –11.05 GeV, including the initial-state radiation at $\Upsilon(10860)$.

² From a simultaneous fit to the $h_b(nP)\pi^+\pi^-$, $n = 1, 2$ cross sections at 22 energy points within $\sqrt{s} = 10.77$ –11.02 GeV to a pair of interfering Breit-Wigner amplitudes modified by phase space factors, with eight resonance parameters (a mass and width for each of $\Upsilon(10860)$ and $\Upsilon(11020)$, a single relative phase, a single relative amplitude, and two overall normalization factors, one for each n). The systematic error estimate is dominated by possible interference with a small nonresonant continuum amplitude.

³ From a fit to the total hadronic cross sections measured at 60 energy points within $\sqrt{s} = 10.82$ –11.05 GeV to a pair of interfering Breit-Wigner amplitudes and two floating continuum amplitudes with $1/\sqrt{s}$ dependence, one coherent with the resonances and one incoherent, with six resonance parameters (a mass, width, and an amplitude for each of $\Upsilon(10860)$ and $\Upsilon(11020)$, one relative phase, and one decoherence coefficient).
⁴ Not including uncertain and potentially large systematic errors due to assumed continuum amplitude $1/\sqrt{s}$ dependence and related interference contributions.

⁵ From a simultaneous fit to the $\Upsilon(nS)\pi^+\pi^-$, $n = 1, 2, 3$, cross sections at 25energy points within $\sqrt{s} = 10.6$ –11.05 GeV to a pair of interfering Breit-Wigner amplitudes modified by phase space factors, with fourteen resonance parameters (a mass, width, and three amplitudes for each of $\Upsilon(10860)$ and $\Upsilon(11020)$, a single universal relative phase, and three decoherence coefficients, one for each n). Continuum contributions were measured (and therefore fixed) to be zero.

⁶ Superseded by MIZUK 19.

⁷ In a model where a flat non-resonant $b\bar{b}$ -continuum is incoherently added to a second flat component interfering with two Breit-Wigner resonances. Systematic uncertainties not estimated.

⁸ The parameters of the $\Upsilon(11020)$ are fixed to those in AUBERT 09E.

⁹ In a model where a flat nonresonant $\Upsilon(1S, 2S, 3S)\pi^+\pi^-$ continuum interferes with a single Breit-Wigner resonance.

¹⁰ In a model where a non-resonant $b\bar{b}$ -continuum represented by a threshold function at $\sqrt{s} = 2m_B$ is incoherently added to a flat component interfering with two Breit-Wigner resonances. Not independent of other AUBERT 09E results. Systematic uncertainties not estimated.

¹¹ Assuming four Gaussians with radiative tails and a single step in R .

¹² In a coupled-channel model with three resonances and a smooth step in R .

$\Upsilon(10860)$ WIDTH

VALUE (MeV)	DOCUMENT ID	TECN	COMMENT
37 ± 4 OUR AVERAGE			
36.6 ± 4.5 + 0.5 ^{+0.5} _{-3.9} - 1.1	1 MIZUK	19	BELL $e^+e^- \rightarrow \Upsilon(nS)\pi^+\pi^-$
40.6 ± 12.7 + 1.1 ^{+1.1} _{-8.0} - 19.1	2 MIZUK	16	BELL $e^+e^- \rightarrow h_b(1P, 2P)\pi^+\pi^-$

••• We do not use the following data for averages, fits, limits, etc. •••

48.5 ± 1.9 + 2.0 ^{+2.0} _{-1.8} - 2.8	3,4 SANTEL	16	BELL $e^+e^- \rightarrow \text{hadrons}$
53.7 ± 7.1 + 1.3 ^{+1.3} _{-5.6} - 5.4	5,6 SANTEL	16	BELL $e^+e^- \rightarrow \Upsilon(1S, 2S, 3S)\pi^+\pi^-$
46 ± 9	7,8 CHEN	10	BELL $e^+e^- \rightarrow \text{hadrons}$
30.7 ± 8.3 ± 3.1 ^{+8.3} _{-7.0}	9 CHEN	10	BELL $e^+e^- \rightarrow \Upsilon(1S, 2S, 3S)\pi^+\pi^-$
43 ± 4	7 AUBERT	09E	BABR $e^+e^- \rightarrow \text{hadrons}$
74 ± 4	10 AUBERT	09E	BABR $e^+e^- \rightarrow \text{hadrons}$
112 ± 17 ± 23	11 BESSON	85	CLEO $e^+e^- \rightarrow \text{hadrons}$
110 ± 15	12 LOVELOCK	85	CUSB $e^+e^- \rightarrow \text{hadrons}$

¹ From a simultaneous fit to the $\Upsilon(nS)\pi^+\pi^-$, $n = 1, 2, 3$, cross sections at 28 energy points within $\sqrt{s} = 10.6$ –11.05 GeV, including the initial-state radiation at $\Upsilon(10860)$.

² From a simultaneous fit to the $h_b(nP)\pi^+\pi^-$, $n = 1, 2$ cross sections at 22 energy points within $\sqrt{s} = 10.77$ –11.02 GeV to a pair of interfering Breit-Wigner amplitudes modified by phase space factors, with eight resonance parameters (a mass and width for each of $\Upsilon(10860)$ and $\Upsilon(11020)$, a single relative phase, a single relative amplitude, and two overall normalization factors, one for each n). The systematic error estimate is dominated by possible interference with a small nonresonant continuum amplitude.

³ From a fit to the total hadronic cross sections measured at 60 energy points within $\sqrt{s} = 10.82$ –11.05 GeV to a pair of interfering Breit-Wigner amplitudes and two floating continuum amplitudes with $1/\sqrt{s}$ dependence, one coherent with the resonances and one incoherent, with six resonance parameters (a mass, width, and an amplitude for each of $\Upsilon(10860)$ and $\Upsilon(11020)$, one relative phase, and one decoherence coefficient).
⁴ Not including uncertain and potentially large systematic errors due to assumed continuum amplitude $1/\sqrt{s}$ dependence and related interference contributions.

⁵ From a simultaneous fit to the $\Upsilon(nS)\pi^+\pi^-$, $n = 1, 2, 3$, cross sections at 25energy points within $\sqrt{s} = 10.6$ –11.05 GeV to a pair of interfering Breit-Wigner amplitudes modified by phase space factors, with fourteen resonance parameters (a mass, width, and three amplitudes for each of $\Upsilon(10860)$ and $\Upsilon(11020)$, a single universal relative phase, and three decoherence coefficients, one for each n). Continuum contributions were measured (and therefore fixed) to be zero.

⁶ Superseded by MIZUK 19.

⁷ In a model where a flat non-resonant $b\bar{b}$ -continuum is incoherently added to a second flat component interfering with two Breit-Wigner resonances. Systematic uncertainties not estimated.

⁸ The parameters of the $\Upsilon(11020)$ are fixed to those in AUBERT 09E.

Meson Particle Listings

$\Upsilon(10860)$

⁹In a model where a flat nonresonant $\Upsilon(1S, 2S, 3S)\pi^+\pi^-$ continuum interferes with a single Breit-Wigner resonance.
¹⁰In a model where a non-resonant $b\bar{b}$ -continuum represented by a threshold function at $\sqrt{s}=2m_B$ is incoherently added to a flat component interfering with two Breit-Wigner resonances. Not independent of other AUBERT 09E results. Systematic uncertainties not estimated.
¹¹Assuming four Gaussians with radiative tails and a single step in R .
¹²In a coupled-channel model with three resonances and a smooth step in R .

$\Upsilon(10860)$ DECAY MODES

Mode	Fraction (Γ_i/Γ)	Confidence level
Γ_1 $B\bar{B}X$	(76.2 \pm 2.7 $\overline{-4.0}$) %	
Γ_2 $B\bar{B}$	(5.5 \pm 1.0) %	
Γ_3 $B\bar{B}^* + \text{c.c.}$	(13.7 \pm 1.6) %	
Γ_4 $B^*\bar{B}^*$	(38.1 \pm 3.4) %	
Γ_5 $B\bar{B}^*\pi$	< 19.7 %	90%
Γ_6 $B\bar{B}\pi$	(0.0 \pm 1.2) %	
Γ_7 $B^*\bar{B}\pi + B\bar{B}^*\pi$	(7.3 \pm 2.3) %	
Γ_8 $B^*\bar{B}^*\pi$	(1.0 \pm 1.4) %	
Γ_9 $B\bar{B}\pi\pi$	< 8.9 %	90%
Γ_{10} $B_s^{(*)}\bar{B}_s^{(*)}$	(20.1 \pm 3.1) %	
Γ_{11} $B_s\bar{B}_s$	(5. \pm 5) $\times 10^{-3}$	
Γ_{12} $B_s\bar{B}_s^* + \text{c.c.}$	(1.35 \pm 0.32) %	
Γ_{13} $B_s^*\bar{B}_s^*$	(17.6 \pm 2.7) %	
Γ_{14} no open-bottom	(3.8 \pm 5.0 $\overline{-0.5}$) %	
Γ_{15} e^+e^-	(8.3 \pm 2.1) $\times 10^{-6}$	
Γ_{16} $K^*(892)^0\bar{K}^0$	< 1.0 $\times 10^{-5}$	90%
Γ_{17} $\Upsilon(1S)\pi^+\pi^-$	(5.3 \pm 0.6) $\times 10^{-3}$	
Γ_{18} $\Upsilon(2S)\pi^+\pi^-$	(7.8 \pm 1.3) $\times 10^{-3}$	
Γ_{19} $\Upsilon(3S)\pi^+\pi^-$	(4.8 \pm 1.9 $\overline{-1.7}$) $\times 10^{-3}$	
Γ_{20} $\Upsilon(1S)K^+K^-$	(6.1 \pm 1.8) $\times 10^{-4}$	
Γ_{21} $\eta\Upsilon_J(1D)$	(4.8 \pm 1.1) $\times 10^{-3}$	
Γ_{22} $h_b(1P)\pi^+\pi^-$	(3.5 \pm 1.0 $\overline{-1.3}$) $\times 10^{-3}$	
Γ_{23} $h_b(2P)\pi^+\pi^-$	(5.7 \pm 1.7 $\overline{-2.1}$) $\times 10^{-3}$	
Γ_{24} $\chi_{bJ}(1P)\pi^+\pi^-\pi^0$	(2.5 \pm 2.3) $\times 10^{-3}$	
Γ_{25} $\chi_{b0}(1P)\pi^+\pi^-\pi^0$	< 6.3 $\times 10^{-3}$	90%
Γ_{26} $\chi_{b0}(1P)\omega$	< 3.9 $\times 10^{-3}$	90%
Γ_{27} $\chi_{b0}(1P)(\pi^+\pi^-\pi^0)_{\text{non-}\omega}$	< 4.8 $\times 10^{-3}$	90%
Γ_{28} $\chi_{b1}(1P)\pi^+\pi^-\pi^0$	(1.85 \pm 0.33) $\times 10^{-3}$	
Γ_{29} $\chi_{b1}(1P)\omega$	(1.57 \pm 0.30) $\times 10^{-3}$	
Γ_{30} $\chi_{b1}(1P)(\pi^+\pi^-\pi^0)_{\text{non-}\omega}$	(5.2 \pm 1.9) $\times 10^{-4}$	
Γ_{31} $\chi_{b2}(1P)\pi^+\pi^-\pi^0$	(1.17 \pm 0.30) $\times 10^{-3}$	
Γ_{32} $\chi_{b2}(1P)\omega$	(6.0 \pm 2.7) $\times 10^{-4}$	
Γ_{33} $\chi_{b2}(1P)(\pi^+\pi^-\pi^0)_{\text{non-}\omega}$	(6 \pm 4) $\times 10^{-4}$	
Γ_{34} $\gamma\chi_b \rightarrow \gamma\Upsilon(1S)\omega$	< 3.8 $\times 10^{-5}$	90%

Inclusive Decays.

These decay modes are submodes of one or more of the decay modes above.

Γ_{35} ϕ anything	(13.8 \pm 2.4 $\overline{-1.7}$) %
Γ_{36} D^0 anything + c.c.	(108 \pm 8) %
Γ_{37} D_s anything + c.c.	(46 \pm 6) %
Γ_{38} J/ψ anything	(2.06 \pm 0.21) %
Γ_{39} B^0 anything + c.c.	(77 \pm 8) %
Γ_{40} B^+ anything + c.c.	(72 \pm 6) %

$\Upsilon(10860)$ PARTIAL WIDTHS

$\Gamma(e^+e^-)$		Γ_{15}
VALUE (keV)	DOCUMENT ID	TECN COMMENT
0.31 \pm 0.07 OUR AVERAGE	Error includes scale factor of 1.3.	
0.22 \pm 0.05 \pm 0.07	BESSON 85	CLEO $e^+e^- \rightarrow$ hadrons
0.365 \pm 0.070	LOVELOCK 85	CUSB $e^+e^- \rightarrow$ hadrons

$\Gamma(e^+e^-) \times \Gamma(\Upsilon(1S)\pi^+\pi^-)/\Gamma_{\text{total}}$		$\Gamma_{15}\Gamma_{17}/\Gamma$
VALUE (eV)	DOCUMENT ID	TECN COMMENT
••• We do not use the following data for averages, fits, limits, etc. ••••		
1.09 \pm 0.34	^{1,2} MIZUK 19	BELL $e^+e^- \rightarrow \Upsilon(nS)\pi^+\pi^-$

¹From a simultaneous fit to the $\Upsilon(nS)\pi^+\pi^-$, $n = 1, 2, 3$, cross sections at 28 energy points within $\sqrt{s} = 10.6$ –11.05 GeV, including the initial-state radiation at $\Upsilon(10860)$.
²Reported as the range 0.75–1.43 eV obtained from multiple solutions of an amplitude fit within a model composed as a sum of Breit-Wigner functions.

$\Gamma(e^+e^-) \times \Gamma(\Upsilon(2S)\pi^+\pi^-)/\Gamma_{\text{total}}$		$\Gamma_{15}\Gamma_{18}/\Gamma$
VALUE (eV)	DOCUMENT ID	TECN COMMENT
••• We do not use the following data for averages, fits, limits, etc. ••••		
2.58 \pm 1.22	^{1,2} MIZUK 19	BELL $e^+e^- \rightarrow \Upsilon(nS)\pi^+\pi^-$

¹From a simultaneous fit to the $\Upsilon(nS)\pi^+\pi^-$, $n = 1, 2, 3$, cross sections at 28 energy points within $\sqrt{s} = 10.6$ –11.05 GeV, including the initial-state radiation at $\Upsilon(10860)$.
²Reported as the range 1.35–3.80 eV obtained from multiple solutions of an amplitude fit within a model composed as a sum of Breit-Wigner functions.

$\Gamma(e^+e^-) \times \Gamma(\Upsilon(3S)\pi^+\pi^-)/\Gamma_{\text{total}}$		$\Gamma_{15}\Gamma_{19}/\Gamma$
VALUE (eV)	DOCUMENT ID	TECN COMMENT
••• We do not use the following data for averages, fits, limits, etc. ••••		
0.73 \pm 0.30	^{1,2} MIZUK 19	BELL $e^+e^- \rightarrow \Upsilon(nS)\pi^+\pi^-$

¹From a simultaneous fit to the $\Upsilon(nS)\pi^+\pi^-$, $n = 1, 2, 3$, cross sections at 28 energy points within $\sqrt{s} = 10.6$ –11.05 GeV, including the initial-state radiation at $\Upsilon(10860)$.
²Reported as the range 0.43–1.03 eV obtained from multiple solutions of an amplitude fit within a model composed as a sum of Breit-Wigner functions.

$\Upsilon(10860)$ BRANCHING RATIOS

“OUR EVALUATION” is obtained based on averages of rescaled data listed below. The averages and rescaling were performed by the Heavy Flavor Averaging Group (HFLAV) and are described at <https://hflav.web.cern.ch/>.

$\Gamma(B\bar{B}X)/\Gamma_{\text{total}}$		Γ_1/Γ	
VALUE	EVTS	DOCUMENT ID	TECN COMMENT
0.762 \pm 0.027 $\overline{-0.043}$ OUR EVALUATION			
0.71 \pm 0.06 OUR AVERAGE			
0.737 \pm 0.032 \pm 0.051	1063	¹ DRUTSKOY 10	BELL $\Upsilon(5S) \rightarrow B^+X, B^0X$
0.589 \pm 0.100 \pm 0.092		² HUANG 07	CLEO $\Upsilon(5S) \rightarrow$ hadrons

¹Not independent of DRUTSKOY 10 values for $\Upsilon(5S) \rightarrow B^\pm, 0$ anything.
²Using measurements or limits from AQUINES 06.

$\Gamma(B\bar{B})/\Gamma_{\text{total}}$		Γ_2/Γ	
VALUE (units 10^{-2})	CL%	DOCUMENT ID	TECN COMMENT
5.5 \pm 1.0 $\overline{-0.9} \pm 0.4$		¹ DRUTSKOY 10	BELL $\Upsilon(5S) \rightarrow B^+X, B^0X$

••• We do not use the following data for averages, fits, limits, etc. **••••**

<13.8	90	² HUANG 07	CLEO $\Upsilon(5S) \rightarrow$ hadrons
-------	----	-----------------------	---

¹Assuming isospin conservation.
²Using measurements or limits from AQUINES 06.

$\Gamma(B\bar{B})/\Gamma(B\bar{B}X)$		Γ_2/Γ_1	
VALUE	CL%	DOCUMENT ID	TECN COMMENT
<0.22	90	AQUINES 06	CLE3 $\Upsilon(5S) \rightarrow$ hadrons

$\Gamma(B\bar{B}^* + \text{c.c.})/\Gamma_{\text{total}}$		Γ_3/Γ
VALUE	DOCUMENT ID	TECN COMMENT
0.137 \pm 0.016 OUR AVERAGE		
0.137 \pm 0.013 \pm 0.011	¹ DRUTSKOY 10	BELL $\Upsilon(5S) \rightarrow B^+X, B^0X$
0.143 \pm 0.053 \pm 0.027	² HUANG 07	CLEO $\Upsilon(5S) \rightarrow$ hadrons

¹Assuming isospin conservation.
²Using measurements or limits from AQUINES 06.

$\Gamma(B\bar{B}^* + \text{c.c.})/\Gamma(B\bar{B}X)$		Γ_3/Γ_1	
VALUE	EVTS	DOCUMENT ID	TECN COMMENT
0.24 \pm 0.09 \pm 0.03	10	AQUINES 06	CLE3 $\Upsilon(5S) \rightarrow$ hadrons

$\Gamma(B^*\bar{B}^*)/\Gamma_{\text{total}}$		Γ_4/Γ
VALUE	DOCUMENT ID	TECN COMMENT
0.381 \pm 0.034 OUR AVERAGE		
0.375 \pm 0.021 $\overline{-0.019} \pm 0.030$	¹ DRUTSKOY 10	BELL $\Upsilon(5S) \rightarrow B^+X, B^0X$
0.436 \pm 0.083 \pm 0.072	² HUANG 07	CLEO $\Upsilon(5S) \rightarrow$ hadrons

¹Assuming isospin conservation.
²Using measurements or limits from AQUINES 06.

$\Gamma(B^*\bar{B}^*)/\Gamma(B\bar{B}X)$		Γ_4/Γ_1	
VALUE	EVTS	DOCUMENT ID	TECN COMMENT
0.74 \pm 0.15 \pm 0.08	31	AQUINES 06	CLE3 $\Upsilon(5S) \rightarrow$ hadrons

$\Gamma(B\bar{B}^*(\pi))/\Gamma_{\text{total}}$		Γ_5/Γ	
VALUE	CL%	DOCUMENT ID	TECN COMMENT
<0.197	90	¹ HUANG 07	CLEO $\Upsilon(5S) \rightarrow$ hadrons

¹Using measurements or limits from AQUINES 06.

$\Gamma(B\bar{B}^*(\pi))/\Gamma(B\bar{B}X)$		Γ_5/Γ_1	
VALUE	CL%	DOCUMENT ID	TECN COMMENT
<0.32	90	AQUINES 06	CLE3 $\Upsilon(5S) \rightarrow$ hadrons

$\Gamma(B\bar{B}\pi)/\Gamma_{\text{total}}$		Γ_6/Γ	
VALUE (units 10^{-2})	EVTS	DOCUMENT ID	TECN COMMENT
0.0 \pm 1.2 \pm 0.3	0	¹ DRUTSKOY 10	BELL $\Upsilon(5S) \rightarrow B^+, 0\pi^-X$

¹Assuming isospin conservation.

- ¹ From a simultaneous fit to the $\Upsilon(nS)\pi^+\pi^-$, $n = 1, 2, 3$, cross sections at 28 energy points within $\sqrt{s} = 10.6\text{--}11.05$ GeV, including the initial-state radiation at $\Upsilon(10860)$.
- ² From a simultaneous fit to the $h_b(nP)\pi^+\pi^-$, $n = 1, 2$ cross sections at 22 energy points within $\sqrt{s} = 10.77\text{--}11.02$ GeV to a pair of interfering Breit-Wigner amplitudes modified by phase space factors, with eight resonance parameters (a mass and width for each of $\Upsilon(10860)$ and $\Upsilon(11020)$, a single relative phase, a single relative amplitude, and two overall normalization factors, one for each n). The systematic error estimate is dominated by possible interference with a small nonresonant continuum amplitude.
- ³ From a fit to the total hadronic cross sections measured at 60 energy points within $\sqrt{s} = 10.82\text{--}11.05$ GeV to a pair of interfering Breit-Wigner amplitudes and two floating continuum amplitudes with $1/\sqrt{s}$ dependence, one coherent with the resonances and one incoherent, with six resonance parameters (a mass, width, and an amplitude for each of $\Upsilon(10860)$ and $\Upsilon(11020)$, one relative phase, and one decoherence coefficient).
- ⁴ Not including uncertain and potentially large systematic errors due to assumed continuum amplitude $1/\sqrt{s}$ dependence and related interference contributions.
- ⁵ From a simultaneous fit to the $\Upsilon(nS)\pi^+\pi^-$, $n = 1, 2, 3$, cross sections at 25 energy points within $\sqrt{s} = 10.6\text{--}11.05$ GeV to a pair of interfering Breit-Wigner amplitudes modified by phase space factors, with fourteen resonance parameters (a mass, width, and three amplitudes for each of $\Upsilon(10860)$ and $\Upsilon(11020)$, a single universal relative phase, and three decoherence coefficients, one for each n). Continuum contributions were measured (and therefore fixed) to be zero.
- ⁶ Superseded by MIZUK 19.
- ⁷ In a model where a flat non-resonant $b\bar{b}$ -continuum is incoherently added to a second flat component interfering with two Breit-Wigner resonances. Systematic uncertainties not estimated.

$\Upsilon(11020)$ DECAY MODES

Mode	Fraction (Γ_j/Γ)
Γ_1 e^+e^-	$(5.4^{+1.9}_{-2.1}) \times 10^{-6}$
Γ_2 $\Upsilon(1S)\pi^+\pi^-$	
Γ_3 $\Upsilon(2S)\pi^+\pi^-$	
Γ_4 $\Upsilon(3S)\pi^+\pi^-$	
Γ_5 $\chi_{bJ}(1P)\pi^+\pi^-\pi^0$	$(9^{+9}_{-8}) \times 10^{-3}$
Γ_6 $\chi_{b1}(1P)\pi^+\pi^-\pi^0$	seen
Γ_7 $\chi_{b2}(1P)\pi^+\pi^-\pi^0$	seen

$\Upsilon(11020)$ PARTIAL WIDTHS

$\Gamma(e^+e^-)$	DOCUMENT ID	TECN	COMMENT	Γ_1
0.130 ± 0.030 OUR AVERAGE				
$0.095 \pm 0.03 \pm 0.035$	BESSION	85	CLEO $e^+e^- \rightarrow$ hadrons	
0.156 ± 0.040	LOVELOCK	85	CUSB $e^+e^- \rightarrow$ hadrons	

$\Gamma(e^+e^-) \times \Gamma(\Upsilon(1S)\pi^+\pi^-)/\Gamma_{\text{total}}$	DOCUMENT ID	TECN	COMMENT	$\Gamma_1\Gamma_2/\Gamma$
0.46 ± 0.08	^{1,2} MIZUK	19	BELL $e^+e^- \rightarrow \Upsilon(nS)\pi^+\pi^-$	

- ¹ From a simultaneous fit to the $\Upsilon(nS)\pi^+\pi^-$, $n = 1, 2, 3$, cross sections at 28 energy points within $\sqrt{s} = 10.6\text{--}11.05$ GeV, including the initial-state radiation at $\Upsilon(10860)$.
- ² Reported as the range $0.38\text{--}0.54$ eV obtained from multiple solutions of an amplitude fit within a model composed as a sum of Breit-Wigner functions.

$\Gamma(e^+e^-) \times \Gamma(\Upsilon(2S)\pi^+\pi^-)/\Gamma_{\text{total}}$	DOCUMENT ID	TECN	COMMENT	$\Gamma_1\Gamma_3/\Gamma$
0.65 ± 0.52	^{1,2} MIZUK	19	BELL $e^+e^- \rightarrow \Upsilon(nS)\pi^+\pi^-$	

- • • We do not use the following data for averages, fits, limits, etc. • • •
- ¹ From a simultaneous fit to the $\Upsilon(nS)\pi^+\pi^-$, $n = 1, 2, 3$, cross sections at 28 energy points within $\sqrt{s} = 10.6\text{--}11.05$ GeV, including the initial-state radiation at $\Upsilon(10860)$.
- ² Reported as the range $0.13\text{--}1.16$ eV obtained from multiple solutions of an amplitude fit within a model composed as a sum of Breit-Wigner functions.

$\Gamma(e^+e^-) \times \Gamma(\Upsilon(3S)\pi^+\pi^-)/\Gamma_{\text{total}}$	DOCUMENT ID	TECN	COMMENT	$\Gamma_1\Gamma_4/\Gamma$
0.33 ± 0.16	^{1,2} MIZUK	19	BELL $e^+e^- \rightarrow \Upsilon(nS)\pi^+\pi^-$	

- • • We do not use the following data for averages, fits, limits, etc. • • •
- ¹ From a simultaneous fit to the $\Upsilon(nS)\pi^+\pi^-$, $n = 1, 2, 3$, cross sections at 28 energy points within $\sqrt{s} = 10.6\text{--}11.05$ GeV, including the initial-state radiation at $\Upsilon(10860)$.
- ² Reported as the range $0.17\text{--}0.49$ eV obtained from multiple solutions of an amplitude fit within a model composed as a sum of Breit-Wigner functions.

$\Gamma(\chi_{bJ}(1P)\pi^+\pi^-\pi^0)/\Gamma_{\text{total}}$	DOCUMENT ID	TECN	COMMENT	Γ_5/Γ
$8.7 \pm 4.3^{+7.6}_{-6.6}$	YIN	18	BELL $e^+e^- \rightarrow$ hadrons	

$\Gamma(\chi_{b1}(1P)\pi^+\pi^-\pi^0)/\Gamma_{\text{total}}$	DOCUMENT ID	TECN	COMMENT	Γ_6/Γ
seen	YIN	18	BELL $e^+e^- \rightarrow$ hadrons	

$\Gamma(\chi_{b2}(1P)\pi^+\pi^-\pi^0)/\Gamma_{\text{total}}$	DOCUMENT ID	TECN	COMMENT	Γ_7/Γ
seen	YIN	18	BELL $e^+e^- \rightarrow$ hadrons	

$\Gamma(\chi_{b2}(1P)\pi^+\pi^-\pi^0)/\Gamma(\chi_{b1}(1P)\pi^+\pi^-\pi^0)$	DOCUMENT ID	TECN	COMMENT	Γ_7/Γ_6
0.4 ± 0.2	YIN	18	BELL $e^+e^- \rightarrow$ hadrons	

$\Upsilon(11020)$ REFERENCES

MIZUK	19	JHEP 1910 220	R. Mizuk <i>et al.</i>	(BELLE Collab.)
YIN	18	PR D98 091102	J.H. Yin <i>et al.</i>	(BELLE Collab.)
MIZUK	16	PRL 117 142001	R. Mizuk <i>et al.</i>	(BELLE Collab.)
SANTELE	16	PR D93 011101	D. Santel <i>et al.</i>	(BELLE Collab.)
AUBERT	09E	PRL 102 012001	B. Aubert <i>et al.</i>	(BABAR Collab.)
BESSION	85	PRL 54 381	D. Besson <i>et al.</i>	(CLEO Collab.)
LOVELOCK	85	PRL 54 377	D.M.J. Lovelock <i>et al.</i>	(CUSB Collab.)

<i>N</i> BARYONS (<i>S</i> = 0, <i>I</i> = 1/2)	
<i>p</i>	1825
<i>n</i>	1834
<i>N</i> resonances	1839
Δ BARYONS (<i>S</i> = 0, <i>I</i> = 3/2)	
Δ resonances	1878
Λ BARYONS (<i>S</i> = -1, <i>I</i> = 0)	
Λ	1902
Λ resonances	1905
Σ BARYONS (<i>S</i> = -1, <i>I</i> = 1)	
Σ^+	1927
Σ^0	1929
Σ^-	1930
Σ resonances	1932
Ξ BARYONS (<i>S</i> = -2, <i>I</i> = 1/2)	
Ξ^0	1959
Ξ^-	1961
Ξ resonances	1964
Ω BARYONS (<i>S</i> = -3, <i>I</i> = 0)	
Ω^-	1971
Ω resonances	1973
CHARMED BARYONS (<i>C</i> = +1)	
Λ_c^+	1974
$\Lambda_c(2595)^+$	1980
$\Lambda_c(2625)^+$	1981
$\Lambda_c(2765)^+$	1982
$\Lambda_c(2860)^+$	1982
$\Lambda_c(2880)^+$	1982
$\Lambda_c(2940)^+$	1983
$\Sigma_c(2455)$	1983
$\Sigma_c(2520)$	1984
$\Sigma_c(2800)$	1985
Ξ_c^+	1985
Ξ_c^0	1987
$\Xi_c^{'+}$	1988
Ξ_c^0	1989
$\Xi_c(2645)$	1989
$\Xi_c(2790)$	1989
$\Xi_c(2815)$	1990
$\Xi_c(2930)$	1990
$\Xi_c(2970)$ was $\Xi_c(2980)$	1991
$\Xi_c(3055)$	1992
$\Xi_c(3080)$	1992
$\Xi_c(3123)$	1992
Ω_c^0	1993
$\Omega_c(2770)^0$	1994
$\Omega_c(3000)^0$	1994
$\Omega_c(3050)^0$	1994
$\Omega_c(3065)^0$	1994
$\Omega_c(3090)^0$	1995
$\Omega_c(3120)^0$	1995

DOUBLY-CHARMED BARYONS (<i>C</i> = +2)	
Ξ_{cc}^{++}	1996
BOTTOM (BEAUTY) BARYONS (<i>B</i> = -1)	
Λ_b^0	1997
$\Lambda_b(5912)^0$	2005
$\Lambda_b(5920)^0$	2005
$\Lambda_b(6146)^0$	2005
$\Lambda_b(6152)^0$	2005
Σ_b	2006
$\Sigma_b(6097)^+$	2007
$\Sigma_b(6097)^-$	2007
Σ_b^*	2006
Ξ_b^0, Ξ_b^-	2007
$\Xi_b'(5935)^-$	2009
$\Xi_b(5945)^0$	2010
$\Xi_b(5955)^-$	2010
$\Xi_b(6227)$	2010
Ω_b^-	2011
<i>b</i> -baryon ADMIXTURE ($\Lambda_b, \Xi_b, \Omega_b$)	2011
EXOTIC BARYONS	
$P_c(4312)^+$	2014
$P_c(4440)^+$	2014
$P_c(4380)^+$	2014
$P_c(4457)^+$ was $P_c(4450)$	2014

Notes in the Listings

$\Sigma(1670)$ region	1938
Radiative hyperon decays	1960
Ξ resonances	1964

Related Reviews in Volume 1

79. Baryon decay parameters	868
80. <i>N</i> and Δ resonances (rev.)	869
81. Baryon magnetic moments	874
82. Λ and Σ resonances (rev.)	875
83. Pole structure of the $\Lambda(1405)$ region (rev.)	878
84. Charmed baryons (rev.)	879
85. Pentaquarks (rev.)	881



N BARYONS
(S = 0, I = 1/2)
 $p, N^+ = uud; \quad n, N^0 = udd$

$I(J^P) = \frac{1}{2}(\frac{1}{2}^+)$ Status: * * * *

p MASS (atomic mass units u)

The mass is known much more precisely in u (atomic mass units) than in MeV. See the next data block.

VALUE (u)	DOCUMENT ID	TECN	COMMENT
1.00727646662 ± 0.0000000009	OUR AVERAGE	Error includes scale factor of 3.1.	
1.007276466583 ± 0.00000000032	¹ HEISSE	17	SPEC Penning trap
1.007276466879 ± 0.00000000091	MOHR	16	RVUE 2014 CODATA value
• • • We do not use the following data for averages, fits, limits, etc. • • •			
1.007276466812 ± 0.00000000090	MOHR	12	RVUE 2010 CODATA value
1.00727646677 ± 0.00000000010	MOHR	08	RVUE 2006 CODATA value
1.00727646688 ± 0.00000000013	MOHR	05	RVUE 2002 CODATA value
1.00727646688 ± 0.00000000013	MOHR	99	RVUE 1998 CODATA value
1.007276470 ± 0.0000000012	COHEN	87	RVUE 1986 CODATA value

¹ The statistical and systematic errors are 15 and 29 in the last two places of the value. The value disagrees with the MOHR 16 value by over 3 standard deviations.

p MASS (MeV)

The mass is known much more precisely in u (atomic mass units) than in MeV. The conversion from u to MeV, $1 u = 931.494 0054(57) \text{ MeV}/c^2$ (MOHR 16, the 2014 CODATA value), involves the relatively poorly known electronic charge.

VALUE (MeV)	DOCUMENT ID	TECN	COMMENT
938.2720813 ± 0.0000058	MOHR	16	RVUE 2014 CODATA value
• • • We do not use the following data for averages, fits, limits, etc. • • •			
938.272046 ± 0.000021	MOHR	12	RVUE 2010 CODATA value
938.272013 ± 0.000023	MOHR	08	RVUE 2006 CODATA value
938.272029 ± 0.000080	MOHR	05	RVUE 2002 CODATA value
938.271998 ± 0.000038	MOHR	99	RVUE 1998 CODATA value
938.27231 ± 0.00028	COHEN	87	RVUE 1986 CODATA value
938.2796 ± 0.0027	COHEN	73	RVUE 1973 CODATA value

$|m_p - m_{\bar{p}}|/m_p$

A test of CPT invariance. Note that the comparison of the \bar{p} and p charge-to-mass ratio, given in the next data block, is much better determined.

VALUE	CL%	DOCUMENT ID	TECN	COMMENT
<7 × 10⁻¹⁰	90	¹ HORI	11	SPEC $\bar{p}e^-$ He atom
• • • We do not use the following data for averages, fits, limits, etc. • • •				
<2 × 10 ⁻⁹	90	¹ HORI	06	SPEC $\bar{p}e^-$ He atom
<1.0 × 10 ⁻⁸	90	¹ HORI	03	SPEC $\bar{p}e^-$ ⁴ He, $\bar{p}e^-$ ³ He
<6 × 10 ⁻⁸	90	¹ HORI	01	SPEC $\bar{p}e^-$ He atom
<5 × 10 ⁻⁷		² TORII	99	SPEC $\bar{p}e^-$ He atom

¹ HORI 01, HORI 03, HORI 06, and HORI 11 use the more-precisely-known constraint on the \bar{p} charge-to-mass ratio of GABRIELSE 99 (see below) to get their results. Their results are not independent of the HORI 01, HORI 03, HORI 06, and HORI 11 values for $|q_p + q_{\bar{p}}|/e$, below.

² TORII 99 uses the more-precisely-known constraint on the \bar{p} charge-to-mass ratio of GABRIELSE 95 (see below) to get this result. This is not independent of the TORII 99 value for $|q_p + q_{\bar{p}}|/e$, below.

\bar{p}/p CHARGE-TO-MASS RATIO, $|\frac{q_{\bar{p}}}{m_{\bar{p}}} - \frac{q_p}{m_p}|$

A test of CPT invariance. Listed here are measurements involving the inertial masses. For a discussion of what may be inferred about the ratio of \bar{p} and p gravitational masses, see ERICSON 90; they obtain an upper bound of 10⁻⁶-10⁻⁷ for violation of the equivalence principle for \bar{p} 's.

VALUE	DOCUMENT ID	TECN	COMMENT
1.00000000001 ± 0.00000000069	ULMER	15	TRAP Penning trap
• • • We do not use the following data for averages, fits, limits, etc. • • •			
0.99999999991 ± 0.0000000009	GABRIELSE	99	TRAP Penning trap
1.0000000015 ± 0.0000000011	¹ GABRIELSE	95	TRAP Penning trap
1.0000000023 ± 0.0000000042	² GABRIELSE	90	TRAP Penning trap

¹ Equation (2) of GABRIELSE 95 should read $M(\bar{p})/M(p) = 0.999 999 9985(11)$ (G. Gabrielse, private communication).

² GABRIELSE 90 also measures $m_{\bar{p}}/m_{e^-} = 1836.152660 ± 0.000083$ and $m_p/m_{e^-} = 1836.152680 ± 0.000088$. Both are completely consistent with the 1986 CODATA (COHEN 87) value for m_p/m_{e^-} of 1836.152701 ± 0.000037.

$(\frac{q_{\bar{p}}}{m_{\bar{p}}} - \frac{q_p}{m_p})/\frac{q_p}{m_p}$

A test of CPT invariance. Taken from the \bar{p}/p charge-to-mass ratio, above.

VALUE	DOCUMENT ID
(0.1 ± 6.9) × 10⁻¹¹	OUR EVALUATION

$|q_p + q_{\bar{p}}|/e$

A test of CPT invariance. Note that the comparison of the \bar{p} and p charge-to-mass ratios given above is much better determined. See also a similar test involving the electron.

VALUE	CL%	DOCUMENT ID	TECN	COMMENT
<7 × 10⁻¹⁰	90	¹ HORI	11	SPEC $\bar{p}e^-$ He atom
• • • We do not use the following data for averages, fits, limits, etc. • • •				
<2 × 10 ⁻⁹	90	¹ HORI	06	SPEC $\bar{p}e^-$ He atom
<1.0 × 10 ⁻⁸	90	¹ HORI	03	SPEC $\bar{p}e^-$ ⁴ He, $\bar{p}e^-$ ³ He
<6 × 10 ⁻⁸	90	¹ HORI	01	SPEC $\bar{p}e^-$ He atom
<5 × 10 ⁻⁷		² TORII	99	SPEC $\bar{p}e^-$ He atom
<2 × 10 ⁻⁵		³ HUGHES	92	RVUE

¹ HORI 01, HORI 03, HORI 06, and HORI 11 use the more-precisely-known constraint on the \bar{p} charge-to-mass ratio of GABRIELSE 99 (see above) to get their results. Their results are not independent of the HORI 01, HORI 03, HORI 06, and HORI 11 values for $|m_p - m_{\bar{p}}|/m_p$, above.

² TORII 99 uses the more-precisely-known constraint on the \bar{p} charge-to-mass ratio of GABRIELSE 95 (see above) to get this result. This is not independent of the TORII 99 value for $|m_p - m_{\bar{p}}|/m_p$, above.

³ HUGHES 92 uses recent measurements of Rydberg-energy and cyclotron-frequency ratios.

$|q_p + q_e|/e$

See BRESSI 11 for a summary of experiments on the neutrality of matter. See also "n CHARGE" in the neutron Listings.

VALUE	DOCUMENT ID	COMMENT
<1 × 10⁻²¹	¹ BRESSI	11 Neutrality of SF ₆
• • • We do not use the following data for averages, fits, limits, etc. • • •		
<3.2 × 10 ⁻²⁰	² SENGUPTA	00 binary pulsar
<0.8 × 10 ⁻²¹	MARINELLI	84 Magnetic levitation
<1.0 × 10 ⁻²¹	¹ DYLLA	73 Neutrality of SF ₆

¹ BRESSI 11 uses the method of DYLLA 73 but finds serious errors in that experiment that greatly reduce its accuracy. The BRESSI 11 limit assumes that $n \rightarrow p e^- \nu_e$ conserves charge. Thus the limit applies equally to the charge of the neutron.

² SENGUPTA 00 uses the difference between the observed rate of rotational energy loss by the binary pulsar PSR B1913+16 and the rate predicted by general relativity to set this limit. See the paper for assumptions.

p MAGNETIC MOMENT

See the "Note on Baryon Magnetic Moments" in the Λ Listings.

VALUE (μ_N)	DOCUMENT ID	TECN	COMMENT
2.79284734462 ± 0.00000000082	SCHNEIDER	17	TRAP Double Penning trap
• • • We do not use the following data for averages, fits, limits, etc. • • •			
2.7928473508 ± 0.00000000085	MOHR	16	RVUE 2014 CODATA value
2.792847356 ± 0.0000000023	MOHR	12	RVUE 2010 CODATA value
2.792847356 ± 0.0000000023	MOHR	08	RVUE 2006 CODATA value
2.792847351 ± 0.0000000028	MOHR	05	RVUE 2002 CODATA value
2.792847337 ± 0.0000000029	MOHR	99	RVUE 1998 CODATA value
2.792847386 ± 0.0000000063	COHEN	87	RVUE 1986 CODATA value

\bar{p} MAGNETIC MOMENT

A few early results have been omitted.

VALUE (μ_N)	DOCUMENT ID	TECN	COMMENT
-2.7928473441 ± 0.00000000042	SMORRA	17	TRAP Hot/cold \bar{p} frequencies, Penning traps
• • • We do not use the following data for averages, fits, limits, etc. • • •			
-2.7928465 ± 0.0000023	NAGAHAMA	17	TRAP Single \bar{p} , Penning trap
-2.792845 ± 0.000012	DISCIACCA	13	TRAP Single \bar{p} , Penning trap
-2.7862 ± 0.0083	PASK	09	CNTR \bar{p} He ⁺ hyperfine structure
-2.8005 ± 0.0090	KREISSL	88	CNTR \bar{p} ²⁰⁸ Pb 11 → 10 X-ray
-2.817 ± 0.048	ROBERTS	78	CNTR
-2.791 ± 0.021	HU	75	CNTR Exotic atoms

Baryon Particle Listings

ρ

$$(\mu_p + \mu_{\bar{p}}) / \mu_p$$

A test of *CPT* invariance.

VALUE (units 10^{-6})	DOCUMENT ID	TECN	COMMENT
0.002 ± 0.004	SMORRA 17	TRAP	Hot/cold \bar{p} frequencies, Penning traps

• • • We do not use the following data for averages, fits, limits, etc. • • •

0.3 ± 0.8	NAGAHAMA 17	TRAP	Single \bar{p} , Penning trap
0 ± 5	DISCIACCA 13	TRAP	Single \bar{p} , Penning trap

ρ ELECTRIC DIPOLE MOMENT

A nonzero value is forbidden by both *T* invariance and *P* invariance.

VALUE (10^{-23} e cm)	DOCUMENT ID	TECN	COMMENT
< 0.021	1 SAHOO 17		Theory plus ^{199}Hg atom EDM

• • • We do not use the following data for averages, fits, limits, etc. • • •

< 0.54	1 DMITRIEV 03		Theory plus ^{199}Hg atom EDM
- 3.7 ± 6.3	CHO 89	NMR	TI F molecules
< 400	DZUBA 85	THEO	Uses ^{129}Xe moment
130 ± 200	2 WILKENING 84		
900 ± 1400	3 WILKENING 84		
700 ± 900	HARRISON 69	MBR	Molecular beam

- 1 SAHOO 17 and DMITRIEV 03 are not direct measurements of the proton electric dipole moment. They use theory to calculate this limit from the limit on the electric dipole moment of the ^{199}Hg atom.
 2 This WILKENING 84 value includes a finite-size effect and a magnetic effect.
 3 This WILKENING 84 value is more cautious than the other and excludes the finite-size effect, which relies on uncertain nuclear integrals.

ρ ELECTRIC POLARIZABILITY α_p

For a very complete review of the "polarizability of the nucleon and Compton scattering," see SCHUMACHER 05. His recommended values for the proton are $\alpha_p = (12.0 \pm 0.6) \times 10^{-4} \text{ fm}^3$ and $\beta_p = (1.9 \mp 0.6) \times 10^{-4} \text{ fm}^3$, almost exactly our averages.

VALUE (10^{-4} fm^3)	DOCUMENT ID	TECN	COMMENT
11.2 ± 0.4 OUR AVERAGE			
10.65 ± 0.35 ± 0.36	MCGOVERN 13	RVUE	$\chi\text{EFT} + \text{Compton scattering}$
12.1 ± 1.1 ± 0.5	1 BEANE 03	EF	$\text{EFT} + \gamma p$
11.82 ± 0.98 ± 0.52 - 0.98	2 BLANPIED 01	LEGS	$\rho(\vec{\gamma}, \gamma), \rho(\vec{\gamma}, \pi^0), \rho(\vec{\gamma}, \pi^+)$
11.9 ± 0.5 ± 1.3	3 OLMOSDEL... 01	CNTR	γp Compton scattering
12.1 ± 0.8 ± 0.5	4 MACGIBBON 95	RVUE	global average

• • • We do not use the following data for averages, fits, limits, etc. • • •

11.7 ± 0.8 ± 0.7	5 BARANOV 01	RVUE	Global average
12.5 ± 0.6 ± 0.9	MACGIBBON 95	CNTR	γp Compton scattering
9.8 ± 0.4 ± 1.1	HALLIN 93	CNTR	γp Compton scattering
10.62 ± 1.25 ± 1.07 - 1.19 - 1.03	ZIEGER 92	CNTR	γp Compton scattering
10.9 ± 2.2 ± 1.3	6 FEDERSPIEL 91	CNTR	γp Compton scattering

- 1 BEANE 03 uses effective field theory and low-energy γp and γd Compton-scattering data. It also gets for the isoscalar polarizabilities (see the erratum) $\alpha_N = (13.0 \pm 1.9 \pm 3.9) \times 10^{-4} \text{ fm}^3$ and $\beta_N = (-1.8 \pm 1.9 \pm 2.1) \times 10^{-4} \text{ fm}^3$.
 2 BLANPIED 01 gives $\alpha_p + \beta_p$ and $\alpha_p - \beta_p$. The separate α_p and β_p are provided to us by A. Sandorfi. The first error above is statistics plus systematics; the second is from the model.
 3 This OLMOSDELEON 01 result uses the TAPS data alone, and does not use the (re-evaluated) sum-rule constraint that $\alpha + \beta = (13.8 \pm 0.4) \times 10^{-4} \text{ fm}^3$. See the paper for a discussion.
 4 MACGIBBON 95 combine the results of ZIEGER 92, FEDERSPIEL 91, and their own experiment to get a "global average" in which model errors and systematic errors are treated in a consistent way. See MACGIBBON 95 for a discussion.
 5 BARANOV 01 combines the results of 10 experiments from 1958 through 1995 to get a global average that takes into account both systematic and model errors and does not use the theoretical constraint on the sum $\alpha_p + \beta_p$.
 6 FEDERSPIEL 91 obtains for the (static) electric polarizability α_p , defined in terms of the induced electric dipole moment by $\mathbf{D} = 4\pi\epsilon_0\alpha_p\mathbf{E}$, the value $(7.0 \pm 2.2 \pm 1.3) \times 10^{-4} \text{ fm}^3$.

ρ MAGNETIC POLARIZABILITY β_p

The electric and magnetic polarizabilities are subject to a dispersion sum-rule constraint $\bar{\alpha} + \bar{\beta} = (14.2 \pm 0.5) \times 10^{-4} \text{ fm}^3$. Errors here are anticorrelated with those on $\bar{\alpha}_p$ due to this constraint.

VALUE (10^{-4} fm^3)	DOCUMENT ID	TECN	COMMENT
2.5 ± 0.4 OUR AVERAGE			Error includes scale factor of 1.2.
3.15 ± 0.35 ± 0.36	MCGOVERN 13	RVUE	$\chi\text{EFT} + \text{Compton scattering}$
3.4 ± 1.1 ± 0.1	1 BEANE 03		$\text{EFT} + \gamma p$
1.43 ± 0.98 ± 0.52 - 0.98	2 BLANPIED 01	LEGS	$\rho(\vec{\gamma}, \gamma), \rho(\vec{\gamma}, \pi^0), \rho(\vec{\gamma}, \pi^+)$
1.2 ± 0.7 ± 0.5	3 OLMOSDEL... 01	CNTR	γp Compton scattering
2.1 ± 0.8 ± 0.5	4 MACGIBBON 95	RVUE	global average

• • • We do not use the following data for averages, fits, limits, etc. • • •

2.3 ± 0.9 ± 0.7	5 BARANOV 01	RVUE	Global average
1.7 ± 0.6 ± 0.9	MACGIBBON 95	CNTR	γp Compton scattering
4.4 ± 0.4 ± 1.1	HALLIN 93	CNTR	γp Compton scattering
3.58 ± 1.19 ± 1.03 - 1.25 - 1.07	ZIEGER 92	CNTR	γp Compton scattering
3.3 ± 2.2 ± 1.3	FEDERSPIEL 91	CNTR	γp Compton scattering

- 1 BEANE 03 uses effective field theory and low-energy γp and γd Compton-scattering data. It also gets for the isoscalar polarizabilities (see the erratum) $\alpha_N = (13.0 \pm 1.9 \pm 3.9) \times 10^{-4} \text{ fm}^3$ and $\beta_N = (-1.8 \pm 1.9 \pm 2.1) \times 10^{-4} \text{ fm}^3$.
 2 BLANPIED 01 gives $\alpha_p + \beta_p$ and $\alpha_p - \beta_p$. The separate α_p and β_p are provided to us by A. Sandorfi. The first error above is statistics plus systematics; the second is from the model.
 3 This OLMOSDELEON 01 result uses the TAPS data alone, and does not use the (re-evaluated) sum-rule constraint that $\alpha + \beta = (13.8 \pm 0.4) \times 10^{-4} \text{ fm}^3$. See the paper for a discussion.
 4 MACGIBBON 95 combine the results of ZIEGER 92, FEDERSPIEL 91, and their own experiment to get a "global average" in which model errors and systematic errors are treated in a consistent way. See MACGIBBON 95 for a discussion.
 5 BARANOV 01 combines the results of 10 experiments from 1958 through 1995 to get a global average that takes into account both systematic and model errors and does not use the theoretical constraint on the sum $\alpha_p + \beta_p$.

ρ CHARGE RADIUS

This is the rms electric charge radius, $\sqrt{\langle r_E^2 \rangle}$.

There are three kinds of measurements of the proton radius: via transitions in atomic hydrogen; via electron scattering off hydrogen; and via muonic hydrogen Lamb shift. Most measurements of the radius of the proton involve electron-proton interactions, the most recent of which is the electron scattering measurement $r_p = 0.831(14) \text{ fm}$ (XIONG 19), and the atomic-hydrogen value, $r_p = 0.833(10) \text{ fm}$ (BEZGINOV 19). These agree well with another recent atomic-hydrogen value $r_p = 0.8335(95) \text{ fm}$ (BEYER 17), and with the best measurement using muonic hydrogen $r_p = 0.84087(39) \text{ fm}$ (ANTOGNINI 13), that is far more precise.

The MOHR 16 value (2014 CODATA), obtained from the electronic results available at the time, was 0.8751(61) fm. This differs by 5.6 standard deviations from the muonic hydrogen value, leading to the so-called proton charge radius puzzle. See our 2018 edition (Physical Review D98 030001 (2018)) for a further discussion of interpretations of this puzzle. However, reflecting the new electronic measurements, the 2018 CODATA recommended value is 0.8414(19) fm, and the puzzle appears to be resolved.

See our 2014 edition (Chinese Physics C38 070001 (2014)) for values published before 2003.

VALUE (fm)	DOCUMENT ID	TECN	COMMENT
0.8409 ± 0.0004 OUR AVERAGE			
0.833 ± 0.010	1 BEZGINOV 19	LASR	2S-2P transition in H
0.831 ± 0.007 ± 0.012	2 XIONG 19	SPEC	$e p \rightarrow e p$ form factor
0.84087 ± 0.00026 ± 0.00029	ANTOGNINI 13	LASR	μp -atom Lamb shift

• • • We do not use the following data for averages, fits, limits, etc. • • •

0.877 ± 0.013	3 FLEURBAEY 18	LASR	1S-3S transition in H
0.8335 ± 0.0095	4 BEYER 17	LASR	2S-4P transition in H
0.8751 ± 0.0061	MOHR 16	RVUE	2014 CODATA value
0.895 ± 0.014 ± 0.014	5 LEE 15	SPEC	Just 2010 Mainz data
0.916 ± 0.024	LEE 15	SPEC	World data, no Mainz
0.8775 ± 0.0051	MOHR 12	RVUE	2010 CODATA, $e p$ data
0.875 ± 0.008 ± 0.006	ZHAN 11	SPEC	Recoil polarimetry
0.879 ± 0.005 ± 0.006	BERNAUER 10	SPEC	$e p \rightarrow e p$ form factor
0.912 ± 0.009 ± 0.007	BORISYUK 10	SPEC	reanalyzes old $e p$ data
0.871 ± 0.009 ± 0.003	HILL 10	SPEC	z-expansion reanalysis
0.84184 ± 0.00036 ± 0.00056	POHL 10	LASR	See ANTOGNINI 13
0.8768 ± 0.0069	MOHR 08	RVUE	2006 CODATA value
0.844 ± 0.008 - 0.004	BELUSHKIN 07		Dispersion analysis
0.897 ± 0.018	BLUNDEN 05		SICK 03 + 2γ correction
0.8750 ± 0.0068	MOHR 05	RVUE	2002 CODATA value
0.895 ± 0.010 ± 0.013	SICK 03		$e p \rightarrow e p$ reanalysis

- 1 BEZGINOV 19 measures the $2S_{1/2}$ to $2P_{1/2}$ transition frequency in atomic hydrogen using the frequency-offset separated oscillatory field (FOSOF) technique. The result agrees well with the muonic hydrogen Lamb shift value.
 2 The XIONG 19 value from $e p \rightarrow e p$ scattering and supports the muonic hydrogen Lamb shift value.
 3 FLEURBAEY 18 measures the 1S-3S transition frequency in hydrogen and in combination with the 1S-2S transition frequency deduces the proton radius and the Rydberg constant.
 4 The BEYER 17 result is 3.3 combined standard deviations below the MOHR 16 (2014 CODATA) value. The experiment measures the 2S-4P transition in hydrogen and gets the proton radius and the Rydberg constant.
 5 Authors also provide values for combinations of all available data.

p MAGNETIC RADIUS

This is the rms magnetic radius, $\sqrt{\langle r_M^2 \rangle}$.

VALUE (fm)	DOCUMENT ID	TECN	COMMENT
0.851 ± 0.026	¹ LEE 15		Combination of world and Mainz data
0.87 ± 0.02	EPSTEIN 14		Using $e p, e n, \pi \pi$ data
0.867 ± 0.009 ± 0.018	ZHAN 11	SPEC	Recoil polarimetry
0.777 ± 0.013 ± 0.010	BERNAUER 10	SPEC	$e p \rightarrow e p$ form factor
0.876 ± 0.010 ± 0.016	BORISYUK 10		Reanalyzes old $e p \rightarrow e p$ data
0.854 ± 0.005	BELUSHKIN 07		Dispersion analysis

• • • We do not use the following data for averages, fits, limits, etc. • • •

¹In a consistent reanalysis LEE 2015 extract values separately for the Mainz 2010 data only (0.776+0.034+-0.017) fm and for the world data without Mainz data (0.914+-0.035) fm. The quoted value is a simple combination of the two, which ignores possible discrepancies and unknown correlations and should be considered with caution.

p MEAN LIFE

A test of baryon conservation. See the "p Partial Mean Lives" section below for limits for identified final states. The limits here are to "anything" or are for "disappearance" modes of a bound proton (p) or (n). See also the 3ν modes in the "Partial Mean Lives" section. Table 1 of BACK 03 is a nice summary.

LIMIT (years)	PARTICLE	CL%	DOCUMENT ID	TECN	COMMENT
> 3.6 × 10²⁹	p	90	¹ ANDERSON 19A	SNO+	p → invisible
> 5.8 × 10²⁹	n	90	² ARAKI 06	KLND	n → invisible
• • • We do not use the following data for averages, fits, limits, etc. • • •					
> 2.5 × 10 ²⁹	n	90	¹ ANDERSON 19A	SNO+	n → invisible
> 2.1 × 10 ²⁹	p	90	¹ AHMED 04	SNO	p → invisible
> 1.9 × 10 ²⁹	n	90	¹ AHMED 04	SNO	n → invisible
> 1.8 × 10 ²⁵	n	90	³ BACK 03	BORX	
> 1.1 × 10 ²⁶	p	90	³ BACK 03	BORX	
> 3.5 × 10 ²⁸	p	90	⁴ ZDESENKO 03		p → invisible
> 1 × 10 ²⁸	p	90	⁵ AHMAD 02	SNO	p → invisible
> 4 × 10 ²³	p	95	⁶ TRETYAK 01		d → n + ?
> 1.9 × 10 ²⁴	p	90	⁶ BERNABEI 00B	DAMA	
> 1.6 × 10 ²⁵	p, n		^{7,8} EVANS 77		
> 3 × 10 ²³	p		⁸ DIX 70	CNTR	
> 3 × 10 ²³	p, n		^{8,9} FLEROV 58		

¹AHMED 04 and ANDERSON 19A look for γ rays from the de-excitation of a residual ¹⁵O* or ¹⁵N* following the disappearance of a neutron or proton in ¹⁶O.
²ARAKI 06 looks for signs of de-excitation of the residual nucleus after disappearance of a neutron from the s shell of ¹²C.
³BACK 03 looks for decays of unstable nuclides left after N decays of parent ¹²C, ¹³C, ¹⁶O nuclei. These are "invisible channel" limits.
⁴ZDESENKO 03 gets this limit on proton disappearance in deuterium by analyzing SNO data in AHMAD 02.
⁵AHMAD 02 (see its footnote 7) looks for neutrons left behind after the disappearance of the proton in deuterons.
⁶BERNABEI 00B looks for the decay of a ¹²⁸I nucleus following the disappearance of a proton in the otherwise-stable ¹²⁹Xe nucleus.
⁷EVANS 77 looks for the daughter nuclide ¹²⁹Xe from possible ¹³⁰Te decays in ancient Te ore samples.
⁸This mean-life limit has been obtained from a half-life limit by dividing the latter by ln(2) = 0.693.
⁹FLEROV 58 looks for the spontaneous fission of a ²³²Th nucleus after the disappearance of one of its nucleons.

p̄ MEAN LIFE

Of the two astrophysical limits here, that of GEER 00D involves considerably more refinements in its modeling. The other limits come from direct observations of stored antiprotons. See also "p̄ Partial Mean Lives" after "p Partial Mean Lives," below, for exclusive-mode limits. The best (lifetime/branching fraction) limit there is 7 × 10⁵ years, for p̄ → e⁻γ. We advance only the exclusive-mode limits to our Summary Tables.

LIMIT (years)	CL%	EVTs	DOCUMENT ID	TECN	COMMENT
• • • We do not use the following data for averages, fits, limits, etc. • • •					
> 5.0	90		SELLNER 17	TRAP	Penning trap
> 8 × 10 ⁵	90		¹ GEER 00D		p̄/p ratio, cosmic rays
> 0.28			GABRIELSE 90	TRAP	Penning trap
> 0.08	90	1	BELL 79	CNTR	Storage ring
> 1 × 10 ⁷			GOLDEN 79	SPEC	p̄/p ratio, cosmic rays
> 3.7 × 10 ⁻³			BREGMAN 78	CNTR	Storage ring

¹GEER 00D uses agreement between a model of galactic p̄ production and propagation and the observed p̄/p cosmic-ray spectrum to set this limit.

p DECAY MODES

See the "Note on Nucleon Decay" in our 1994 edition (Phys. Rev. D50, 1173) for a short review.

The "partial mean life" limits tabulated here are the limits on τ/B_j , where τ is the total mean life and B_j is the branching fraction for the mode in question. For N decays, p and n indicate proton and neutron partial lifetimes.

Mode	Partial mean life (10 ³⁰ years)	Confidence level
Antilepton + meson		
τ_1 N → e ⁺ π	> 5300 (n), > 16000 (p)	90%
τ_2 N → μ ⁺ π	> 3500 (n), > 7700 (p)	90%
τ_3 N → νπ	> 1100 (n), > 390 (p)	90%
τ_4 p → e ⁺ η	> 10000	90%
τ_5 p → μ ⁺ η	> 4700	90%
τ_6 n → νη	> 158	90%
τ_7 N → e ⁺ ρ	> 217 (n), > 720 (p)	90%
τ_8 N → μ ⁺ ρ	> 228 (n), > 570 (p)	90%
τ_9 N → νρ	> 19 (n), > 162 (p)	90%
τ_{10} p → e ⁺ ω	> 1600	90%
τ_{11} p → μ ⁺ ω	> 2800	90%
τ_{12} n → νω	> 108	90%
τ_{13} N → e ⁺ K	> 17 (n), > 1000 (p)	90%
τ_{14} p → e ⁺ K _S ⁰		
τ_{15} p → e ⁺ K _L ⁰		
τ_{16} N → μ ⁺ K	> 26 (n), > 1600 (p)	90%
τ_{17} p → μ ⁺ K _S ⁰		
τ_{18} p → μ ⁺ K _L ⁰		
τ_{19} N → νK	> 86 (n), > 5900 (p)	90%
τ_{20} n → νK _S ⁰	> 260	90%
τ_{21} p → e ⁺ K*(892) ⁰	> 84	90%
τ_{22} N → νK*(892)	> 78 (n), > 51 (p)	90%
Antilepton + mesons		
τ_{23} p → e ⁺ π ⁺ π ⁻	> 82	90%
τ_{24} p → e ⁺ π ⁰ π ⁰	> 147	90%
τ_{25} n → e ⁺ π ⁻ π ⁰	> 52	90%
τ_{26} p → μ ⁺ π ⁺ π ⁻	> 133	90%
τ_{27} p → μ ⁺ π ⁰ π ⁰	> 101	90%
τ_{28} n → μ ⁺ π ⁻ π ⁰	> 74	90%
τ_{29} n → e ⁺ K ⁰ π ⁻	> 18	90%
Lepton + meson		
τ_{30} n → e ⁻ π ⁺	> 65	90%
τ_{31} n → μ ⁻ π ⁺	> 49	90%
τ_{32} n → e ⁻ ρ ⁺	> 62	90%
τ_{33} n → μ ⁻ ρ ⁺	> 7	90%
τ_{34} n → e ⁻ K ⁺	> 32	90%
τ_{35} n → μ ⁻ K ⁺	> 57	90%
Lepton + mesons		
τ_{36} p → e ⁻ π ⁺ π ⁺	> 30	90%
τ_{37} n → e ⁻ π ⁺ π ⁰	> 29	90%
τ_{38} p → μ ⁻ π ⁺ π ⁺	> 17	90%
τ_{39} n → μ ⁻ π ⁺ π ⁰	> 34	90%
τ_{40} p → e ⁻ π ⁺ K ⁺	> 75	90%
τ_{41} p → μ ⁻ π ⁺ K ⁺	> 245	90%
Antilepton + photon(s)		
τ_{42} p → e ⁺ γ	> 670	90%
τ_{43} p → μ ⁺ γ	> 478	90%
τ_{44} n → νγ	> 550	90%
τ_{45} p → e ⁺ γγ	> 100	90%
τ_{46} n → νγγ	> 219	90%
Antilepton + single massless		
τ_{47} p → e ⁺ X	> 790	90%
τ_{48} p → μ ⁺ X	> 410	90%
Three (or more) leptons		
τ_{49} p → e ⁺ e ⁺ e ⁻	> 793	90%
τ_{50} p → e ⁺ μ ⁺ μ ⁻	> 359	90%
τ_{51} p → e ⁺ νν	> 170	90%
τ_{52} n → e ⁺ e ⁻ ν	> 257	90%
τ_{53} n → μ ⁺ e ⁻ ν	> 83	90%
τ_{54} n → μ ⁺ μ ⁻ ν	> 79	90%
τ_{55} p → μ ⁺ e ⁺ e ⁻	> 529	90%
τ_{56} p → μ ⁺ μ ⁺ μ ⁻	> 675	90%

See key on page 999

Baryon Particle Listings

p

> 200	<i>p</i>	90	5	3.3	HAINES	86	IMB
> 64	<i>p</i>	90	0	<0.8	ARISAKA	85	KAMI
> 64	<i>p</i> (free)	90	5	6.5	BLEWITT	85	IMB
> 200	<i>p</i>	90	5	4.7	BLEWITT	85	IMB
> 1.2	<i>p</i>	90	2		¹ CHERRY	81	HOME

¹ We have converted 2 possible events to 90% CL limit.

$\tau(p \rightarrow \mu^+ \eta)$ τ_5

LIMIT (10^{30} years)	PARTICLE	CL%	EVTs	BKGD EST	DOCUMENT ID	TECN
>4700	<i>p</i>	90	2	0.85	ABE	17D SKAM
•••	We do not use the following data for averages, fits, limits, etc. •••					
>1300	<i>p</i>	90	2	0.49	NISHINO	12 SKAM
> 89	<i>p</i>	90	0	1.6	WALL	00B SOU2
> 126	<i>p</i>	90	3	2.8	MCGREW	99 IMB3
> 26	<i>p</i>	90	1	0.8	BERGER	91 FREJ
> 69	<i>p</i>	90	1	<0.08	HIRATA	89C KAMI
> 1.3	<i>p</i>	90	0	0.7	PHILLIPS	89 HPW
> 34	<i>p</i>	90	1	1.5	SEIDEL	88 IMB
> 46	<i>p</i>	90	7	6	HAINES	86 IMB
> 26	<i>p</i>	90	1	<0.8	ARISAKA	85 KAMI
> 17	<i>p</i> (free)	90	6	6	BLEWITT	85 IMB
> 46	<i>p</i>	90	7	8	BLEWITT	85 IMB

$\tau(n \rightarrow \nu \eta)$ τ_6

LIMIT (10^{30} years)	PARTICLE	CL%	EVTs	BKGD EST	DOCUMENT ID	TECN
>158	<i>n</i>	90	0	1.2	MCGREW	99 IMB3
•••	We do not use the following data for averages, fits, limits, etc. •••					
> 71	<i>n</i>	90	2	3.7	WALL	00B SOU2
> 29	<i>n</i>	90	0	0.9	BERGER	89 FREJ
> 54	<i>n</i>	90	2	0.9	HIRATA	89C KAMI
> 16	<i>n</i>	90	3	2.1	SEIDEL	88 IMB
> 25	<i>n</i>	90	7	6	HAINES	86 IMB
> 30	<i>n</i>	90	0	0.4	KAJITA	86 KAMI
> 18	<i>n</i>	90	4	3	PARK	85 IMB
> 0.6	<i>n</i>	90	2		¹ CHERRY	81 HOME

¹ We have converted 2 possible events to 90% CL limit.

$\tau(N \rightarrow e^+ \rho)$ τ_7

LIMIT (10^{30} years)	PARTICLE	CL%	EVTs	BKGD EST	DOCUMENT ID	TECN
>720	<i>p</i>	90	2	0.64	ABE	17D SKAM
>217	<i>n</i>	90	4	4.8	MCGREW	99 IMB3
•••	We do not use the following data for averages, fits, limits, etc. •••					
> 30	<i>n</i>	90	4	0.87	ABE	17D SKAM
>710	<i>p</i>	90	0	0.35	NISHINO	12 SKAM
> 70	<i>n</i>	90	1	0.38	NISHINO	12 SKAM
> 29	<i>p</i>	90	0	2.2	BERGER	91 FREJ
> 41	<i>n</i>	90	0	1.4	BERGER	91 FREJ
> 75	<i>p</i>	90	2	2.7	HIRATA	89C KAMI
> 58	<i>n</i>	90	0	1.9	HIRATA	89C KAMI
> 38	<i>n</i>	90	2	4.1	SEIDEL	88 IMB
> 1.2	<i>p</i>	90	0		BARTELT	87 SOUD
> 1.5	<i>n</i>	90	0		BARTELT	87 SOUD
> 17	<i>p</i>	90	7	7	HAINES	86 IMB
> 14	<i>n</i>	90	9	4	HAINES	86 IMB
> 12	<i>p</i>	90	0	<1.2	ARISAKA	85 KAMI
> 6	<i>n</i>	90	2	<1	ARISAKA	85 KAMI
> 6.7	<i>p</i> (free)	90	6	6	BLEWITT	85 IMB
> 17	<i>p</i>	90	7	7	BLEWITT	85 IMB
> 12	<i>n</i>	90	4	2	PARK	85 IMB
> 0.6	<i>n</i>	90	1	0.3	¹ BARTELT	83 SOUD
> 0.5	<i>p</i>	90	1	0.3	¹ BARTELT	83 SOUD
> 9.8	<i>p</i>	90	1		² KRISHNA...	82 KOLR
> 0.8	<i>p</i>	90	2		³ CHERRY	81 HOME

¹ Limit based on zero events.

² We have calculated 90% CL limit from 0 confined events.

³ We have converted 2 possible events to 90% CL limit.

$\tau(N \rightarrow \mu^+ \rho)$ τ_8

LIMIT (10^{30} years)	PARTICLE	CL%	EVTs	BKGD EST	DOCUMENT ID	TECN
>570	<i>p</i>	90	1	1.30	ABE	17D SKAM
>228	<i>n</i>	90	3	9.5	MCGREW	99 IMB3
•••	We do not use the following data for averages, fits, limits, etc. •••					
> 60	<i>n</i>	90	1	0.96	ABE	17D SKAM
>160	<i>p</i>	90	1	0.42	NISHINO	12 SKAM
> 36	<i>n</i>	90	0	0.29	NISHINO	12 SKAM
> 12	<i>p</i>	90	0	0.5	BERGER	91 FREJ
> 22	<i>n</i>	90	0	1.1	BERGER	91 FREJ
>110	<i>p</i>	90	0	1.7	HIRATA	89C KAMI
> 23	<i>n</i>	90	1	1.8	HIRATA	89C KAMI
> 4.3	<i>p</i>	90	0	0.7	PHILLIPS	89 HPW
> 30	<i>p</i>	90	0	0.5	SEIDEL	88 IMB

> 11	<i>n</i>	90	1	1.1	SEIDEL	88 IMB
> 16	<i>p</i>	90	4	4.5	HAINES	86 IMB
> 7	<i>n</i>	90	6	5	HAINES	86 IMB
> 12	<i>p</i>	90	0	<0.7	ARISAKA	85 KAMI
> 5	<i>n</i>	90	1	<1.2	ARISAKA	85 KAMI
> 5.5	<i>p</i> (free)	90	4	5	BLEWITT	85 IMB
> 16	<i>p</i>	90	4	5	BLEWITT	85 IMB
> 9	<i>n</i>	90	1	2	PARK	85 IMB

$\tau(N \rightarrow \nu \rho)$ τ_9

LIMIT (10^{30} years)	PARTICLE	CL%	EVTs	BKGD EST	DOCUMENT ID	TECN
>162	<i>p</i>	90	18	21.7	MCGREW	99 IMB3
> 19	<i>n</i>	90	0	0.5	SEIDEL	88 IMB
•••	We do not use the following data for averages, fits, limits, etc. •••					
> 9	<i>n</i>	90	4	2.4	BERGER	89 FREJ
> 24	<i>p</i>	90	0	0.9	BERGER	89 FREJ
> 27	<i>p</i>	90	5	1.5	HIRATA	89C KAMI
> 13	<i>n</i>	90	4	3.6	HIRATA	89C KAMI
> 13	<i>p</i>	90	1	1.1	SEIDEL	88 IMB
> 8	<i>p</i>	90	6	5	HAINES	86 IMB
> 2	<i>n</i>	90	15	10	HAINES	86 IMB
> 11	<i>p</i>	90	2	1	KAJITA	86 KAMI
> 4	<i>n</i>	90	2	2	KAJITA	86 KAMI
> 4.1	<i>p</i> (free)	90	6	7	BLEWITT	85 IMB
> 8.4	<i>p</i>	90	6	5	BLEWITT	85 IMB
> 2	<i>n</i>	90	7	3	PARK	85 IMB
> 0.9	<i>p</i>	90	2		¹ CHERRY	81 HOME
> 0.6	<i>n</i>	90	2		¹ CHERRY	81 HOME

¹ We have converted 2 possible events to 90% CL limit.

$\tau(p \rightarrow e^+ \omega)$ τ_{10}

LIMIT (10^{30} years)	PARTICLE	CL%	EVTs	BKGD EST	DOCUMENT ID	TECN
>1600	<i>p</i>	90	1	1.35	ABE	17D SKAM
•••	We do not use the following data for averages, fits, limits, etc. •••					
> 320	<i>p</i>	90	1	0.53	NISHINO	12 SKAM
> 107	<i>p</i>	90	7	10.8	MCGREW	99 IMB3
> 17	<i>p</i>	90	0	1.1	BERGER	91 FREJ
> 45	<i>p</i>	90	2	1.45	HIRATA	89C KAMI
> 26	<i>p</i>	90	1	1.0	SEIDEL	88 IMB
> 1.5	<i>p</i>	90	0		BARTELT	87 SOUD
> 37	<i>p</i>	90	6	5.3	HAINES	86 IMB
> 25	<i>p</i>	90	1	<1.4	ARISAKA	85 KAMI
> 12	<i>p</i> (free)	90	6	7.5	BLEWITT	85 IMB
> 37	<i>p</i>	90	6	5.7	BLEWITT	85 IMB
> 0.6	<i>p</i>	90	1	0.3	¹ BARTELT	83 SOUD
> 9.8	<i>p</i>	90	1		² KRISHNA...	82 KOLR
> 2.8	<i>p</i>	90	2		³ CHERRY	81 HOME

¹ Limit based on zero events.

² We have calculated 90% CL limit from 0 confined events.

³ We have converted 2 possible events to 90% CL limit.

$\tau(p \rightarrow \mu^+ \omega)$ τ_{11}

LIMIT (10^{30} years)	PARTICLE	CL%	EVTs	BKGD EST	DOCUMENT ID	TECN
>2800	<i>p</i>	90	0	1.09	ABE	17D SKAM
•••	We do not use the following data for averages, fits, limits, etc. •••					
> 780	<i>p</i>	90	0	0.48	NISHINO	12 SKAM
> 117	<i>p</i>	90	11	12.1	MCGREW	99 IMB3
> 11	<i>p</i>	90	0	1.0	BERGER	91 FREJ
> 57	<i>p</i>	90	2	1.9	HIRATA	89C KAMI
> 4.4	<i>p</i>	90	0	0.7	PHILLIPS	89 HPW
> 10	<i>p</i>	90	2	1.3	SEIDEL	88 IMB
> 23	<i>p</i>	90	2	1	HAINES	86 IMB
> 6.5	<i>p</i> (free)	90	9	8.7	BLEWITT	85 IMB
> 23	<i>p</i>	90	8	7	BLEWITT	85 IMB

$\tau(n \rightarrow \nu \omega)$ τ_{12}

LIMIT (10^{30} years)	PARTICLE	CL%	EVTs	BKGD EST	DOCUMENT ID	TECN
>108	<i>n</i>	90	12	22.5	MCGREW	99 IMB3
•••	We do not use the following data for averages, fits, limits, etc. •••					
> 17	<i>n</i>	90	1	0.7	BERGER	89 FREJ
> 43	<i>n</i>	90	3	2.7	HIRATA	89C KAMI
> 6	<i>n</i>	90	2	1.3	SEIDEL	88 IMB
> 12	<i>n</i>	90	6	6	HAINES	86 IMB
> 18	<i>n</i>	90	2	2	KAJITA	86 KAMI
> 16	<i>n</i>	90	1	2	PARK	85 IMB
> 2.0	<i>n</i>	90	2		¹ CHERRY	81 HOME

¹ We have converted 2 possible events to 90% CL limit.

$\tau(N \rightarrow e^+ K)$ τ_{13}

LIMIT (10^{30} years)	PARTICLE	CL%	EVTs	BKGD EST	DOCUMENT ID	TECN
>1000	<i>p</i>	90	6	4.7	KOBAYASHI	05 SKAM
> 17	<i>n</i>	90	35	29.4	MCGREW	99 IMB3

••• We do not use the following data for averages, fits, limits, etc. •••

> 17	<i>p</i>	90	1	2.6	BERGER	91	FREJ
> 3.3	<i>p</i>	90	0	0.7	PHILLIPS	89	HPW

$\tau(p \rightarrow \mu^+ \pi^0 \pi^0)$ 727

LIMIT (10 ³⁰ years)	PARTICLE	CL%	EVTs	BKGD EST	DOCUMENT ID	TECN
>101	<i>p</i>	90	3	1.6	MCGREW	99 IMB3

••• We do not use the following data for averages, fits, limits, etc. •••

> 33	<i>p</i>	90	1	0.9	BERGER	91	FREJ
------	----------	----	---	-----	--------	----	------

$\tau(n \rightarrow \mu^+ \pi^- \pi^0)$ 728

LIMIT (10 ³⁰ years)	PARTICLE	CL%	EVTs	BKGD EST	DOCUMENT ID	TECN
>74	<i>n</i>	90	17	20.8	MCGREW	99 IMB3

••• We do not use the following data for averages, fits, limits, etc. •••

>33	<i>n</i>	90	0	1.1	BERGER	91	FREJ
-----	----------	----	---	-----	--------	----	------

$\tau(n \rightarrow e^+ K^0 \pi^-)$ 729

LIMIT (10 ³⁰ years)	PARTICLE	CL%	EVTs	BKGD EST	DOCUMENT ID	TECN	
>18	<i>n</i>	90	1	0.2	BERGER	91	FREJ

———— Lepton + meson ————

$\tau(n \rightarrow e^- \pi^+)$ 730

LIMIT (10 ³⁰ years)	PARTICLE	CL%	EVTs	BKGD EST	DOCUMENT ID	TECN
>65	<i>n</i>	90	0	1.6	SEIDEL	88 IMB

••• We do not use the following data for averages, fits, limits, etc. •••

>55	<i>n</i>	90	0	1.09	BERGER	91B	FREJ
>16	<i>n</i>	90	9	7	HAINES	86	IMB
>25	<i>n</i>	90	2	4	PARK	85	IMB

$\tau(n \rightarrow \mu^- \pi^+)$ 731

LIMIT (10 ³⁰ years)	PARTICLE	CL%	EVTs	BKGD EST	DOCUMENT ID	TECN
>49	<i>n</i>	90	0	0.5	SEIDEL	88 IMB

••• We do not use the following data for averages, fits, limits, etc. •••

>33	<i>n</i>	90	0	1.40	BERGER	91B	FREJ
> 2.7	<i>n</i>	90	0	0.7	PHILLIPS	89	HPW
>25	<i>n</i>	90	7	6	HAINES	86	IMB
>27	<i>n</i>	90	2	3	PARK	85	IMB

$\tau(n \rightarrow e^- \rho^+)$ 732

LIMIT (10 ³⁰ years)	PARTICLE	CL%	EVTs	BKGD EST	DOCUMENT ID	TECN
>62	<i>n</i>	90	2	4.1	SEIDEL	88 IMB

••• We do not use the following data for averages, fits, limits, etc. •••

>12	<i>n</i>	90	13	6	HAINES	86	IMB
>12	<i>n</i>	90	5	3	PARK	85	IMB

$\tau(n \rightarrow \mu^- \rho^+)$ 733

LIMIT (10 ³⁰ years)	PARTICLE	CL%	EVTs	BKGD EST	DOCUMENT ID	TECN
>7	<i>n</i>	90	1	1.1	SEIDEL	88 IMB

••• We do not use the following data for averages, fits, limits, etc. •••

>2.6	<i>n</i>	90	0	0.7	PHILLIPS	89	HPW
>9	<i>n</i>	90	7	5	HAINES	86	IMB
>9	<i>n</i>	90	2	2	PARK	85	IMB

$\tau(n \rightarrow e^- K^+)$ 734

LIMIT (10 ³⁰ years)	PARTICLE	CL%	EVTs	BKGD EST	DOCUMENT ID	TECN	
>32	<i>n</i>	90	3	2.96	BERGER	91B	FREJ

••• We do not use the following data for averages, fits, limits, etc. •••

> 0.23	<i>n</i>	90	0	0.7	PHILLIPS	89	HPW
--------	----------	----	---	-----	----------	----	-----

$\tau(n \rightarrow \mu^- K^+)$ 735

LIMIT (10 ³⁰ years)	PARTICLE	CL%	EVTs	BKGD EST	DOCUMENT ID	TECN	
>57	<i>n</i>	90	0	2.18	BERGER	91B	FREJ

••• We do not use the following data for averages, fits, limits, etc. •••

> 4.7	<i>n</i>	90	0	0.7	PHILLIPS	89	HPW
-------	----------	----	---	-----	----------	----	-----

———— Lepton + mesons ————

$\tau(p \rightarrow e^- \pi^+ \pi^+)$ 736

LIMIT (10 ³⁰ years)	PARTICLE	CL%	EVTs	BKGD EST	DOCUMENT ID	TECN	
>30	<i>p</i>	90	1	2.50	BERGER	91B	FREJ

••• We do not use the following data for averages, fits, limits, etc. •••

> 2.0	<i>p</i>	90	0	0.7	PHILLIPS	89	HPW
-------	----------	----	---	-----	----------	----	-----

$\tau(n \rightarrow e^- \pi^+ \pi^0)$ 737

LIMIT (10 ³⁰ years)	PARTICLE	CL%	EVTs	BKGD EST	DOCUMENT ID	TECN	
>29	<i>n</i>	90	1	0.78	BERGER	91B	FREJ

$\tau(p \rightarrow \mu^- \pi^+ \pi^+)$ 738

LIMIT (10 ³⁰ years)	PARTICLE	CL%	EVTs	BKGD EST	DOCUMENT ID	TECN	
>17	<i>p</i>	90	1	1.72	BERGER	91B	FREJ

••• We do not use the following data for averages, fits, limits, etc. •••

> 7.8	<i>p</i>	90	0	0.7	PHILLIPS	89	HPW
-------	----------	----	---	-----	----------	----	-----

$\tau(n \rightarrow \mu^- \pi^+ \pi^0)$ 739

LIMIT (10 ³⁰ years)	PARTICLE	CL%	EVTs	BKGD EST	DOCUMENT ID	TECN	
>34	<i>n</i>	90	0	0.78	BERGER	91B	FREJ

$\tau(p \rightarrow e^- \pi^+ K^+)$ 740

LIMIT (10 ³⁰ years)	PARTICLE	CL%	EVTs	BKGD EST	DOCUMENT ID	TECN
>75	<i>p</i>	90	81	127.2	MCGREW	99 IMB3

••• We do not use the following data for averages, fits, limits, etc. •••

>20	<i>p</i>	90	3	2.50	BERGER	91B	FREJ
-----	----------	----	---	------	--------	-----	------

$\tau(p \rightarrow \mu^- \pi^+ K^+)$ 741

LIMIT (10 ³⁰ years)	PARTICLE	CL%	EVTs	BKGD EST	DOCUMENT ID	TECN
>245	<i>p</i>	90	3	4.0	MCGREW	99 IMB3

••• We do not use the following data for averages, fits, limits, etc. •••

> 5	<i>p</i>	90	2	0.78	BERGER	91B	FREJ
-----	----------	----	---	------	--------	-----	------

———— Antilepton + photon(s) ————

$\tau(p \rightarrow e^+ \gamma)$ 742

LIMIT (10 ³⁰ years)	PARTICLE	CL%	EVTs	BKGD EST	DOCUMENT ID	TECN
>670	<i>p</i>	90	0	0.1	MCGREW	99 IMB3

••• We do not use the following data for averages, fits, limits, etc. •••

>133	<i>p</i>	90	0	0.3	BERGER	91	FREJ
>460	<i>p</i>	90	0	0.6	SEIDEL	88	IMB
>360	<i>p</i>	90	0	0.3	HAINES	86	IMB
> 87	<i>p</i> (free)	90	0	0.2	BLEWITT	85	IMB
>360	<i>p</i>	90	0	0.2	BLEWITT	85	IMB
> 0.1	<i>p</i>	90			¹ GURR	67	CNTR

¹ We have converted half-life to 90% CL mean life.

$\tau(p \rightarrow \mu^+ \gamma)$ 743

LIMIT (10 ³⁰ years)	PARTICLE	CL%	EVTs	BKGD EST	DOCUMENT ID	TECN
>478	<i>p</i>	90	0	0.1	MCGREW	99 IMB3

••• We do not use the following data for averages, fits, limits, etc. •••

>155	<i>p</i>	90	0	0.1	BERGER	91	FREJ
>380	<i>p</i>	90	0	0.5	SEIDEL	88	IMB
> 97	<i>p</i>	90	3	2	HAINES	86	IMB
> 61	<i>p</i> (free)	90	0	0.2	BLEWITT	85	IMB
>280	<i>p</i>	90	0	0.6	BLEWITT	85	IMB
> 0.3	<i>p</i>	90			¹ GURR	67	CNTR

¹ We have converted half-life to 90% CL mean life.

$\tau(n \rightarrow \nu \gamma)$ 744

LIMIT (10 ³⁰ years)	PARTICLE	CL%	EVTs	BKGD EST	DOCUMENT ID	TECN
>550	<i>n</i>	90			TAKHISTOV	15 SKAM

••• We do not use the following data for averages, fits, limits, etc. •••

> 28	<i>n</i>	90	163	144.7	MCGREW	99 IMB3	
> 24	<i>n</i>	90	10	6.86	BERGER	91B	FREJ
> 9	<i>n</i>	90	73	60	HAINES	86	IMB
> 11	<i>n</i>	90	28	19	PARK	85	IMB

$\tau(p \rightarrow e^+ \gamma \gamma)$ 745

LIMIT (10 ³⁰ years)	PARTICLE	CL%	EVTs	BKGD EST	DOCUMENT ID	TECN	
>100	<i>p</i>	90	1	0.8	BERGER	91	FREJ

$\tau(n \rightarrow \nu \gamma \gamma)$ 746

LIMIT (10 ³⁰ years)	PARTICLE	CL%	EVTs	BKGD EST	DOCUMENT ID	TECN
>219	<i>n</i>	90	5	7.5	MCGREW	99 IMB3

———— Antilepton + single massless ————

$\tau(p \rightarrow e^+ X)$ 747

VALUE (10 ³⁰ years)	CL%	DOCUMENT ID	TECN
>790	90	TAKHISTOV	15 SKAM

Baryon Particle Listings

p

$\tau(p \rightarrow \mu^+ X)$		748	
VALUE (10^{30} years)	CL%	DOCUMENT ID	TECN
>410	90	TAKHISTOV 15	SKAM

Three (or more) leptons

$\tau(p \rightarrow e^+ e^+ e^-)$		749	
LIMIT (10^{30} years)	PARTICLE	CL%	EVTs BKGD EST
>793	p	90	0 0.5
••• We do not use the following data for averages, fits, limits, etc. •••			
>147	p	90	0 0.1
>510	p	90	0 0.3
> 89	p (free)	90	0 0.5
>510	p	90	0 0.7

$\tau(p \rightarrow e^+ \mu^+ \mu^-)$		750	
LIMIT (10^{30} years)	PARTICLE	CL%	EVTs BKGD EST
>359	p	90	1 0.9
••• We do not use the following data for averages, fits, limits, etc. •••			
> 81	p	90	0 0.16
> 5.0	p	90	0 0.7

$\tau(p \rightarrow e^+ \nu \nu)$		751	
LIMIT (10^{30} years)	PARTICLE	CL%	EVTs BKGD EST
>170	p	90	1 0.9
••• We do not use the following data for averages, fits, limits, etc. •••			
> 17	p	90	152 153.7
> 11	p	90	11 6.08

¹ Allowed events at 90% CL are 459.

$\tau(n \rightarrow e^+ e^- \nu)$		752	
LIMIT (10^{30} years)	PARTICLE	CL%	EVTs BKGD EST
>257	n	90	5 7.5
••• We do not use the following data for averages, fits, limits, etc. •••			
> 74	n	90	0 < 0.1
> 45	n	90	5 5
> 26	n	90	4 3

$\tau(n \rightarrow \mu^+ e^- \nu)$		753	
LIMIT (10^{30} years)	PARTICLE	CL%	EVTs BKGD EST
>83	n	90	25 29.4
••• We do not use the following data for averages, fits, limits, etc. •••			
>47	n	90	0 < 0.1

$\tau(n \rightarrow \mu^+ \mu^- \nu)$		754	
LIMIT (10^{30} years)	PARTICLE	CL%	EVTs BKGD EST
>79	n	90	100 145
••• We do not use the following data for averages, fits, limits, etc. •••			
>42	n	90	0 1.4
> 5.1	n	90	0 0.7
>16	n	90	14 7
>19	n	90	4 7

$\tau(p \rightarrow \mu^+ e^+ e^-)$		755	
LIMIT (10^{30} years)	PARTICLE	CL%	EVTs BKGD EST
>529	p	90	0 1.0
••• We do not use the following data for averages, fits, limits, etc. •••			
> 91	p	90	0 \leq 0.1

$\tau(p \rightarrow \mu^+ \mu^+ \mu^-)$		756	
LIMIT (10^{30} years)	PARTICLE	CL%	EVTs BKGD EST
>675	p	90	0 0.3
••• We do not use the following data for averages, fits, limits, etc. •••			
>119	p	90	0 0.2
> 10.5	p	90	0 0.7
>190	p	90	1 0.1
> 44	p (free)	90	1 0.7
>190	p	90	1 0.9
> 2.1	p	90	1

¹ We have converted 1 possible event to 90% CL limit.

$\tau(p \rightarrow \mu^+ \nu \nu)$		757	
LIMIT (10^{30} years)	PARTICLE	CL%	EVTs BKGD EST
>220	p	90	7 11.23
••• We do not use the following data for averages, fits, limits, etc. •••			
> 21	p	90	7 11.23

¹ Allowed events at 90% CL are 286.

$\tau(p \rightarrow e^- \mu^+ \mu^+)$		758	
LIMIT (10^{30} years)	PARTICLE	CL%	EVTs BKGD EST
>6.0	p	90	0 0.7

$\tau(n \rightarrow 3\nu)$		759	
LIMIT (10^{30} years)	PARTICLE	CL%	EVTs BKGD EST
>0.0049	n	90	2 2
••• We do not use the following data for averages, fits, limits, etc. •••			
>0.0023	n	90	0
>0.00003	n	90	11 6.1
>0.00012	n	90	7 11.2
>0.0005	n	90	0

See also the "to anything" and "disappearance" limits for bound nucleons in the "p Mean Life" data block just in front of the list of possible p decay modes. Such modes could of course be to three (or five) neutrinos, and the limits are stronger, but we do not repeat them here.

¹ The SUZUKI 93B limit applies to any of $\nu_e \nu_e \bar{\nu}_e$, $\nu_\mu \nu_\mu \bar{\nu}_\mu$, or $\nu_\tau \nu_\tau \bar{\nu}_\tau$.

² GLICENSTEIN 97 uses Kamioka data and the idea that the disappearance of the neutron's magnetic moment should produce radiation.

³ The first BERGER 91B limit is for $n \rightarrow \nu_e \nu_e \bar{\nu}_e$, the second is for $n \rightarrow \nu_\mu \nu_\mu \bar{\nu}_\mu$.

$\tau(n \rightarrow 5\nu)$		760	
LIMIT (10^{30} years)	PARTICLE	CL%	EVTs BKGD EST
>0.0017	n	90	0

See the note on $\tau(n \rightarrow 3\nu)$ on the previous data block.

$\tau(N \rightarrow e^+ \text{ anything})$		761	
LIMIT (10^{30} years)	PARTICLE	CL%	EVTs BKGD EST
>0.6	p, n	90	0
••• We do not use the following data for averages, fits, limits, etc. •••			
>0.0017	n	90	0

¹ GLICENSTEIN 97 uses Kamioka data and the idea that the disappearance of the neutron's magnetic moment should produce radiation.

Inclusive modes

$\tau(N \rightarrow \mu^+ \text{ anything})$		762	
LIMIT (10^{30} years)	PARTICLE	CL%	EVTs BKGD EST
>12	p, n	90	2
••• We do not use the following data for averages, fits, limits, etc. •••			
> 1.8	p, n	90	0
> 6	p, n	90	0

¹ We have converted 2 possible events to 90% CL limit.
² The muon may be primary or secondary.

$\tau(N \rightarrow \nu \text{ anything})$		763	
LIMIT (10^{30} years)	PARTICLE	CL%	EVTs BKGD EST
>0.0002	p, n	90	0
••• We do not use the following data for averages, fits, limits, etc. •••			

Anything = π, ρ, K , etc.

$\tau(N \rightarrow e^+ \pi^0 \text{ anything})$		764	
LIMIT (10^{30} years)	PARTICLE	CL%	EVTs BKGD EST
>0.6	p, n	90	0
••• We do not use the following data for averages, fits, limits, etc. •••			

$\tau(N \rightarrow 2 \text{ bodies, } \nu\text{-free})$		765	
LIMIT (10^{30} years)	PARTICLE	CL%	EVTs BKGD EST
>1.3	p, n	90	0
••• We do not use the following data for averages, fits, limits, etc. •••			

$\Delta B = 2$ dinucleon modes

$\tau(pp \rightarrow \pi^+ \pi^+)$		766	
LIMIT (10^{30} years)	CL%	EVTs BKGD EST	DOCUMENT ID TECN COMMENT
>72.2	90	2 4.45	GUSTAFSON 15 SKAM per oxygen nucleus
••• We do not use the following data for averages, fits, limits, etc. •••			
> 0.7	90	4 2.34	BERGER 91B FREJ per iron nucleus

$\tau(pn \rightarrow \pi^+ \pi^0)$		767	
LIMIT (10^{30} years)	CL%	EVTs BKGD EST	DOCUMENT ID TECN COMMENT
>170	90	0 0.31	GUSTAFSON 15 SKAM per oxygen nucleus
••• We do not use the following data for averages, fits, limits, etc. •••			
> 2.0	90	0 0.31	BERGER 91B FREJ per iron nucleus

$\tau(nn \rightarrow \pi^+ \pi^-)$ **768**

LIMIT (10^{30} years)	CL%	EVTs	BKGD EST	DOCUMENT ID	TECN	COMMENT
>0.7	90	4	2.18	BERGER	91B	FREJ τ per iron nucleus

$\tau(nn \rightarrow \pi^0 \pi^0)$ **769**

LIMIT (10^{30} years)	CL%	EVTs	BKGD EST	DOCUMENT ID	TECN	COMMENT
>404	90			GUSTAFSON	15	SKAM per oxygen nucleus
••• We do not use the following data for averages, fits, limits, etc. •••						
> 3.4	90	0	0.78	BERGER	91B	FREJ per iron nucleus

$\tau(pp \rightarrow K^+ K^+)$ **770**

LIMIT (10^{30} years)	CL%	EVTs	BKGD EST	DOCUMENT ID	TECN	COMMENT
>170	90	0	0.28	LITOS	14	SKAM τ per oxygen nucleus

$\tau(pp \rightarrow e^+ e^+)$ **771**

LIMIT (10^{30} years)	CL%	EVTs	BKGD EST	DOCUMENT ID	TECN	COMMENT
>5.8	90	0	<0.1	BERGER	91B	FREJ τ per iron nucleus

$\tau(pp \rightarrow e^+ \mu^+)$ **772**

LIMIT (10^{30} years)	CL%	EVTs	BKGD EST	DOCUMENT ID	TECN	COMMENT
>3.6	90	0	<0.1	BERGER	91B	FREJ τ per iron nucleus

$\tau(pp \rightarrow \mu^+ \mu^+)$ **773**

LIMIT (10^{30} years)	CL%	EVTs	BKGD EST	DOCUMENT ID	TECN	COMMENT
>1.7	90	0	0.62	BERGER	91B	FREJ τ per iron nucleus

$\tau(pn \rightarrow e^+ \bar{\nu})$ **774**

LIMIT (10^{30} years)	CL%	EVTs	BKGD EST	DOCUMENT ID	TECN	COMMENT
>260	90			TAKHISTOV	15	SKAM
••• We do not use the following data for averages, fits, limits, etc. •••						
> 2.8	90	5	9.67	BERGER	91B	FREJ τ per iron nucleus

$\tau(pn \rightarrow \mu^+ \bar{\nu})$ **775**

LIMIT (10^{30} years)	CL%	EVTs	BKGD EST	DOCUMENT ID	TECN	COMMENT
>200	90			TAKHISTOV	15	SKAM
••• We do not use the following data for averages, fits, limits, etc. •••						
> 1.6	90	4	4.37	BERGER	91B	FREJ τ per iron nucleus

$\tau(pn \rightarrow \tau^+ \bar{\nu}_\tau)$ **776**

LIMIT (10^{30} years)	CL%	EVTs	BKGD EST	DOCUMENT ID	TECN	COMMENT
>29	90			TAKHISTOV	15	SKAM
••• We do not use the following data for averages, fits, limits, etc. •••						
> 1	90			1 BRYMAN	14	CHER
1 BRYMAN 14 uses a MCGREW 99 limit on the $p \rightarrow e^+ \nu \nu$ lifetime to extract this value.						

$\tau(nn \rightarrow \nu_e \bar{\nu}_e)$ **777**

We include "invisible" modes here.

LIMIT (10^{30} years)	CL%	EVTs	BKGD EST	DOCUMENT ID	TECN	COMMENT
>1.4	90			1 ARAKI	06	KLND $nn \rightarrow$ invisible
••• We do not use the following data for averages, fits, limits, etc. •••						
>0.013	90			2 ANDERSON	19A	SNO+ $nn \rightarrow$ invisible
>0.000042	90			3 TRETYAK	04	CNTR $nn \rightarrow$ invisible
>0.000049	90			4 BACK	03	BORX $nn \rightarrow$ invisible
>0.000012	90			5 BERNABEI	00B	DAMA $nn \rightarrow$ invisible
>0.000012	90	5	9.7	BERGER	91B	FREJ τ per iron nucleus

1 ARAKI 06 looks for signs of de-excitation of the residual nucleus after disappearance of two neutrons from the s shell of ^{12}C .
 2 ANDERSON 19A looks for γ rays from the de-excitation of a residual $^{14}\text{O}^*$ following the disappearance of nn in ^{16}O .
 3 TRETYAK 04 uses data from an old Homestake-mine radiochemical experiment on limits for invisible decays of ^{39}K to ^{37}Ar .
 4 BACK 03 looks for decays of unstable nuclides left after NN decays of parent ^{12}C , ^{13}C , ^{16}O nuclei. These are "invisible channel" limits.
 5 BERNABEI 00b looks for the decay of a ^{127}Te nucleus following the disappearance of an nn pair in the otherwise-stable ^{129}Xe nucleus. The limit here applies as well to $nn \rightarrow \nu_\mu \bar{\nu}_\mu$, $nn \rightarrow \nu_\tau \bar{\nu}_\tau$, or any "disappearance" mode.

$\tau(nn \rightarrow \nu_\mu \bar{\nu}_\mu)$ **778**

See the preceding data block. "Invisible modes" would include any multi-neutrino mode.

LIMIT (10^{30} years)	CL%	EVTs	BKGD EST	DOCUMENT ID	TECN	COMMENT
> 1.4 (CL=90%)	OUR LIMIT					
••• We do not use the following data for averages, fits, limits, etc. •••						
>0.000006	90	4	4.4	BERGER	91B	FREJ τ per iron nucleus

$\tau(pn \rightarrow \text{invisible})$ **779**

This violates charge conservation as well as baryon number conservation.

VALUE (10^{30} years)	CL%	DOCUMENT ID	TECN
>0.026	90	1 ANDERSON	19A SNO+
>0.000021	90	2 TRETYAK	04 CNTR

1 ANDERSON 19A looks for γ rays from the de-excitation of a residual $^{14}\text{N}^*$ following the disappearance of pn in ^{16}O .
 2 TRETYAK 04 uses data from an old Homestake-mine radiochemical experiment on limits for invisible decays of ^{39}K to ^{37}Ar .

$\tau(pp \rightarrow \text{invisible})$ **780**

This violates charge conservation as well as baryon number conservation.

LIMIT (10^{30} years)	CL%	EVTs	BKGD EST	DOCUMENT ID	TECN
>0.047	90			1 ANDERSON	19A SNO+
••• We do not use the following data for averages, fits, limits, etc. •••					
>0.000005	90			2 BACK	03 BORX
>0.00000055	90			3 BERNABEI	00B DAMA

1 ANDERSON 19A looks for γ rays from the de-excitation of a residual $^{14}\text{C}^*$ following the disappearance of pp in ^{16}O .
 2 BACK 03 looks for decays of unstable nuclides left after NN decays of parent ^{12}C , ^{13}C , ^{16}O nuclei. These are "invisible channel" limits.
 3 BERNABEI 00b looks for the decay of a ^{127}Te nucleus following the disappearance of a pp pair in the otherwise-stable ^{129}Xe nucleus.

\bar{p} PARTIAL MEAN LIVES

The "partial mean life" limits tabulated here are the limits on $\bar{\tau}/B_j$, where $\bar{\tau}$ is the total mean life for the antiproton and B_j is the branching fraction for the mode in question.

$\tau(\bar{p} \rightarrow e^- \gamma)$ **781**

VALUE (years)	CL%	DOCUMENT ID	TECN	COMMENT
> 7×10^5	90	GEER	00	APEX 8.9 GeV/c \bar{p} beam
••• We do not use the following data for averages, fits, limits, etc. •••				
>1848	95	GEER	94	CALO 8.9 GeV/c \bar{p} beam

$\tau(\bar{p} \rightarrow \mu^- \gamma)$ **782**

VALUE (years)	CL%	DOCUMENT ID	TECN	COMMENT
> 5×10^4	90	GEER	00	APEX 8.9 GeV/c \bar{p} beam
••• We do not use the following data for averages, fits, limits, etc. •••				
> 5.0×10^4	90	HU	98B	APEX 8.9 GeV/c \bar{p} beam

$\tau(\bar{p} \rightarrow e^- \pi^0)$ **783**

VALUE (years)	CL%	DOCUMENT ID	TECN	COMMENT
> 4×10^5	90	GEER	00	APEX 8.9 GeV/c \bar{p} beam
••• We do not use the following data for averages, fits, limits, etc. •••				
>554	95	GEER	94	CALO 8.9 GeV/c \bar{p} beam

$\tau(\bar{p} \rightarrow \mu^- \pi^0)$ **784**

VALUE (years)	CL%	DOCUMENT ID	TECN	COMMENT
> 5×10^4	90	GEER	00	APEX 8.9 GeV/c \bar{p} beam
••• We do not use the following data for averages, fits, limits, etc. •••				
> 4.8×10^4	90	HU	98B	APEX 8.9 GeV/c \bar{p} beam

$\tau(\bar{p} \rightarrow e^- \eta)$ **785**

VALUE (years)	CL%	DOCUMENT ID	TECN	COMMENT
> 2×10^4	90	GEER	00	APEX 8.9 GeV/c \bar{p} beam
••• We do not use the following data for averages, fits, limits, etc. •••				
>171	95	GEER	94	CALO 8.9 GeV/c \bar{p} beam

$\tau(\bar{p} \rightarrow \mu^- \eta)$ **786**

VALUE (years)	CL%	DOCUMENT ID	TECN	COMMENT
> 8×10^3	90	GEER	00	APEX 8.9 GeV/c \bar{p} beam
••• We do not use the following data for averages, fits, limits, etc. •••				
> 7.9×10^3	90	HU	98B	APEX 8.9 GeV/c \bar{p} beam

$\tau(\bar{p} \rightarrow e^- K_S^0)$ **787**

VALUE (years)	CL%	DOCUMENT ID	TECN	COMMENT
>900	90	GEER	00	APEX 8.9 GeV/c \bar{p} beam
••• We do not use the following data for averages, fits, limits, etc. •••				
> 29	95	GEER	94	CALO 8.9 GeV/c \bar{p} beam

$\tau(\bar{p} \rightarrow \mu^- K_S^0)$ **788**

VALUE (years)	CL%	DOCUMENT ID	TECN	COMMENT
> 4×10^3	90	GEER	00	APEX 8.9 GeV/c \bar{p} beam
••• We do not use the following data for averages, fits, limits, etc. •••				
> 4.3×10^3	90	HU	98B	APEX 8.9 GeV/c \bar{p} beam

Baryon Particle Listings

p, n

$\tau(\bar{p} \rightarrow e^- K_L^0)$ 789

VALUE (years)	CL%	DOCUMENT ID	TECN	COMMENT
$>9 \times 10^3$	90	GEER 00	APEX	8.9 GeV/c \bar{p} beam
••• We do not use the following data for averages, fits, limits, etc. •••				
>9	95	GEER 94	CALO	8.9 GeV/c \bar{p} beam

$\tau(\bar{p} \rightarrow \mu^- K_L^0)$ 790

VALUE (years)	CL%	DOCUMENT ID	TECN	COMMENT
$>7 \times 10^3$	90	GEER 00	APEX	8.9 GeV/c \bar{p} beam
••• We do not use the following data for averages, fits, limits, etc. •••				
$>6.5 \times 10^3$	90	HU 98b	APEX	8.9 GeV/c \bar{p} beam

$\tau(\bar{p} \rightarrow e^- \gamma \gamma)$ 791

VALUE (years)	CL%	DOCUMENT ID	TECN	COMMENT
$>2 \times 10^4$	90	GEER 00	APEX	8.9 GeV/c \bar{p} beam

$\tau(\bar{p} \rightarrow \mu^- \gamma \gamma)$ 792

VALUE (years)	CL%	DOCUMENT ID	TECN	COMMENT
$>2 \times 10^4$	90	GEER 00	APEX	8.9 GeV/c \bar{p} beam
••• We do not use the following data for averages, fits, limits, etc. •••				
$>2.3 \times 10^4$	90	HU 98b	APEX	8.9 GeV/c \bar{p} beam

$\tau(\bar{p} \rightarrow e^- \omega)$ 793

VALUE (years)	CL%	DOCUMENT ID	TECN	COMMENT
>200	90	GEER 00	APEX	8.9 GeV/c \bar{p} beam

p REFERENCES

ANDERSON 19A PR D99 032008
 BEZGINOV 19 SCI 365 1007
 XIONG 19 NAT 575 147
 FLEURBAEY 18 PRL 120 183001
 PDG 18 PR D98 030001
 ABE 17 PR D95 012004
 ABE 17D PR D96 012003
 BEYER 17 SCI 358 79
 HEISSE 17 PRL 119 033001
 NAGAHAMA 17 NATC 8 14084
 SAHOO 17 PR D95 013002
 SCHNEIDER 17 SCI 358 1081
 SELLNER 17 NJP 19 083023
 SMORRA 17 NAT 550 371
 MOHR 16 RMP 88 035009
 ASAKURA 15 PR D92 052006
 GUSTAFSON 15 PR D91 072009
 LEE 15 PR D92 013013
 TAKHISTOV 15 PRL 115 121803
 ULMER 15 NAT 524 196
 ABE 14E PRL 113 121802
 ABE 14G PR D90 072005
 BRYMAN 14 PL B733 190
 EPSTEIN 14 PR D90 074027
 LITOS 14 PRL 112 131803
 PDG 14 CP C38 070001
 TAKHISTOV 14 PRL 113 101801
 ANTÖGNINI 13 SCI 339 417
 DIS CIACCA 13 PRL 110 130801
 MCGOVERN 13 EPJ A49 12
 MOHR 12 RMP 84 1527
 NISHINO 12 PR D85 112001
 REGIS 12 PR D86 012006
 BRESSI 11 PR AB3 052101
 HORI 11 NAT 475 484
 ZHAN 11 PL B705 59
 BERNAUER 10 PRL 105 242001
 Also PR C90 015206
 BORISYUK 10 NP A843 59
 HILL 10 PR D82 113005
 POHL 10 NAT 466 213
 NISHINO 09 PRL 102 141801
 PASK 09 PL B678 55
 MOHR 08 RMP 80 633
 BELUSHKIN 07 PR C75 035202
 ARAKI 06 PRL 96 101802
 HORI 06 PRL 96 243401
 BLUNDEN 05 PR C72 057601
 KOBAYASHI 05 PR D72 052007
 MOHR 05 RMP 77 1
 SCHUMACHER 05 PPNP 55 567
 AHMAD 04 PRL 92 102004
 TRETAYAK 04 JETPL 79 106
 Translated from ZETFP 79 136
 BACK 03 PL B563 23
 BEANE 03 PL B567 200
 Also PL B607 320 (err.)
 DMITRIEV 03 PRL 91 212303
 HORI 03 PRL 91 123401
 SICK 03 PL B576 62
 ZDESENKO 03 PL B553 135
 AHMAD 02 PRL 89 011301
 BARANOV 01 PPN 32 376
 Translated from FCAY 32 699
 BLANPIED 01 PR C64 025203
 HORI 01 PRL 87 093401
 OLMOSDEL... 01 EPJ A10 207
 TRETAYAK 01 PL B505 59
 BERNABEI 00B PL B493 12
 GEER 00 PRL 84 590
 Also PR D62 052004
 Also PRL 85 3546 (err.)
 GEER 00D APJ 532 648
 SENGUPTA 00 PL B484 275
 WALL 00 PR D61 072004
 WALL 00B PR D62 092003
 GABRIELSE 99 PRL 82 3198
 HAYATO 99 PRL 83 1529
 MCGREW 99 PR D59 052004

MOHR 99 JPCRD 28 1713
 Also RMP 72 351
 TORII 99 PR A59 223
 ALLISON 98 PL B427 217
 HU 98B PR D58 111101
 SHIOZAWA 98 PRL 81 3319
 GLICENSTEIN 97 PL B411 326
 GABRIELSE 95 PRL 74 3544
 MACGIBBON 95 PR C52 2097
 GEER 94 PRL 72 1596
 HALLIN 93 PR C48 1497
 SUZUKI 93B PL B311 357
 HUGHES 92 PRL 69 578
 ZIEGER 92 PL B278 34
 Also PL B281 417 (erratum)
 BERGER 91 ZPHY C50 385
 BERGER 91B PL B269 227
 FEDERSPIEL 91 PRL 67 1511
 BECKER-SZ... 90 PR D42 2974
 ERICSON 90 EPL 11 295
 GABRIELSE 90 PRL 65 1317
 BERGER 89 NP B313 509
 CHO 89 PRL 63 2559
 HIRATA 89C PL B220 308
 PHILLIPS 89 PL B224 348
 KREISSL 88 ZPHY C37 557
 SEIDEL 88 PRL 61 2522
 BARTELT 87 PR D36 1990
 Also PR D40 1701 (erratum)
 COHEN 87 RMP 59 1121
 HAINES 86 PRL 57 1906
 KAJITA 86 JPSJ 55 711
 ARISAKA 85 JPSJ 54 3213
 BLEWITT 85 PRL 55 2114
 DZUBA 85 PL 154B 93
 PARK 85 PRL 54 22
 BATTISTONI 84 PL 133B 454
 MARINELLI 84 PL 137B 439
 WILKENING 84 PR A29 425
 BARTELT 83 PRL 50 651
 BATTISTONI 82 PL 118B 461
 KRISHNA... 82 PL 115B 349
 ALEKSEEV 81 JETPL 33 651
 Translated from ZETFP 33 664
 CHERY 81 PRL 47 1507
 COWSIK 80 PR D22 2204
 BELL 79 PL 86B 215
 GOLDEN 79 PRL 43 1196
 LEARNED 79 PRL 43 907
 BREGMAN 78 PL 76B 374
 ROBERTS 78 PR D17 358
 EVANS 77 SCI 197 989
 HU 75 NP A254 403
 COHEN 73 JPCRD 2 664
 DYLLA 73 PR A7 1224
 DIX 70 Thesis Case
 HARRISON 69 PRL 22 1263
 GURR 67 PR 158 1321
 FLEROV 58 DOKL 3 79

P.J. Mohr, B.N. Taylor (NIST)
 P.J. Mohr, B.N. Taylor (NIST)
 H.A. Torii et al. (CERN PS-205 Collab.)
 W.W.M. Allison et al. (Soudan-2 Collab.)
 M. Hu et al. (FNAL APEX Collab.)
 M. Shiozawa et al. (Super-Kamiokande Collab.)
 J.F. Glicenstein (SACL)
 G. Gabrielse et al. (HARV, MANZ, SEOUL)
 B.E. MacGibbon et al. (ILL, SASK, INRM)
 S. Geer et al. (FNAL, UCLA, PSU)
 E.L. Hallin et al. (SASK, BOST, ILL)
 Y. Suzuki et al. (Kamiokande Collab.)
 R.J. Hughes, B.I. Deutch (LANL, AARH)
 A. Zieger et al. (MPCM)
 A. Zieger et al. (MPCM)
 C. Berger et al. (FREJUS Collab.)
 C. Berger et al. (FREJUS Collab.)
 F.J. Federspiel et al. (ILL)
 R.A. Becker-Szendy et al. (IMB-3 Collab.)
 T.E.O. Ericson, A. Richter (CERN, DARM)
 G. Gabrielse et al. (HARV, MANZ, WASH+)
 C. Berger et al. (FREJUS Collab.)
 D. Cho, K. Sangster, E.A. Hinds (YALE)
 K.S. Hirata et al. (Kamiokande Collab.)
 T.J. Phillips et al. (HPW Collab.)
 A. Kreissl et al. (CERN PS176 Collab.)
 S. Seidel et al. (IMB Collab.)
 J.E. Bartelt et al. (Soudan Collab.)
 J.E. Bartelt et al. (Soudan Collab.)
 E.R. Cohen, B.N. Taylor (FRIS, NBS)
 T.J. Haines et al. (IMB Collab.)
 T. Kajita et al. (Kamiokande Collab.)
 K. Arisaka et al. (Kamiokande Collab.)
 G.B. Blewitt et al. (IMB Collab.)
 V.A. Dzuba, V.V. Flambaum, P.G. Silvestrov (NOVO)
 H.S. Park et al. (IMB Collab.)
 G. Battistoni et al. (NUSEX Collab.)
 M. Marinelli, G. Morpurgo (GENO)
 D.A. Wilkening, N.F. Ramsey, D.J. Larson (HARV+)
 J.E. Bartelt et al. (MINN, ANL)
 G. Battistoni et al. (NUSEX Collab.)
 M.R. Krishnaswamy et al. (TATA, OSK+)
 E.N. Alekseev et al. (PNPI)

n $I(J^P) = \frac{1}{2}(1^+)$ Status: * * * *

We have omitted some results that have been superseded by later experiments. See our earlier editions.

Anyone interested in the neutron should look at these two review articles: D. Dubbers and M.G. Schmidt, "The neutron and its role in cosmology and particle physics," *Reviews of Modern Physics* **83** 1111 (2011); and F.E. Wietfeldt and G.L. Greene, "The neutron lifetime," *Reviews of Modern Physics* **83** 1173 (2011).

n MASS (atomic mass units u)

The mass is known much more precisely in u (atomic mass units) than in MeV. See the next data block.

VALUE (u)	DOCUMENT ID	TECN	COMMENT
1.00866491588 ± 0.0000000049	MOHR 16	RVUE	2014 CODATA value
••• We do not use the following data for averages, fits, limits, etc. •••			
1.00866491600 ± 0.0000000043	MOHR 12	RVUE	2010 CODATA value
1.00866491597 ± 0.0000000043	MOHR 08	RVUE	2006 CODATA value
1.00866491560 ± 0.0000000055	MOHR 05	RVUE	2002 CODATA value
1.00866491578 ± 0.0000000055	MOHR 99	RVUE	1998 CODATA value
1.008665904 ± 0.000000014	COHEN 87	RVUE	1986 CODATA value

n MASS (MeV)

The mass is known much more precisely in u (atomic mass units) than in MeV. The conversion from u to MeV, $1 u = 931.494 005 4(57)$ MeV/c² (MOHR 16, the 2014 CODATA value), involves the relatively poorly known electronic charge.

VALUE (MeV)	DOCUMENT ID	TECN	COMMENT
939.5654133 ± 0.0000058	MOHR 16	RVUE	2014 CODATA value
••• We do not use the following data for averages, fits, limits, etc. •••			
939.565379 ± 0.000021	MOHR 12	RVUE	2010 CODATA value
939.565346 ± 0.000023	MOHR 08	RVUE	2006 CODATA value
939.565360 ± 0.000081	MOHR 05	RVUE	2002 CODATA value
939.565331 ± 0.000037	1 KESSLER 99	SPEC	$np \rightarrow d\gamma$
939.565330 ± 0.000038	MOHR 99	RVUE	1998 CODATA value
939.56565 ± 0.00028	2,3 DIFILIPPO 94	TRAP	Penning trap
939.56563 ± 0.00028	COHEN 87	RVUE	1986 CODATA value
939.56564 ± 0.00028	3,4 GREENE 86	SPEC	$np \rightarrow d\gamma$
939.5731 ± 0.0027	3 COHEN 73	RVUE	1973 CODATA value

- ¹ We use the 1998 CODATA *u*-to-MeV conversion factor (see the heading above) to get this mass in MeV from the much more precisely measured KESSLER 99 value of $1.00866491637 \pm 0.0000000082$ u.
- ² The mass is known much more precisely in *u*: $m = 1.0086649235 \pm 0.0000000023$ u. We use the 1986 CODATA conversion factor to get the mass in MeV.
- ³ These determinations are not independent of the $m_n - m_p$ measurements below.
- ⁴ The mass is known much more precisely in *u*: $m = 1.008664919 \pm 0.000000014$ u.

\bar{n} MASS

VALUE (MeV)	EVTS	DOCUMENT ID	TECN	COMMENT
939.485 ± 0.051	59	¹ CRESTI	86	HBC $\bar{p}p \rightarrow \bar{\pi}n$

¹ This is a corrected result (see the erratum). The error is statistical. The maximum systematic error is 0.029 MeV.

$(m_n - m_{\bar{n}}) / m_n$

A test of *CPT* invariance. Calculated from the *n* and \bar{n} masses, above.

VALUE	DOCUMENT ID
(9 ± 6) × 10⁻⁵ OUR EVALUATION	

$m_n - m_p$

VALUE (MeV)	DOCUMENT ID	TECN	COMMENT
1.29333205 ± 0.00000051	¹ MOHR	16	RVUE 2014 CODATA value
••• We do not use the following data for averages, fits, limits, etc. •••			
1.29333217 ± 0.00000042	² MOHR	12	RVUE 2010 CODATA value
1.29333214 ± 0.00000043	³ MOHR	08	RVUE 2006 CODATA value
1.2933317 ± 0.00000005	⁴ MOHR	05	RVUE 2002 CODATA value
1.2933318 ± 0.00000005	⁵ MOHR	99	RVUE 1998 CODATA value
1.293318 ± 0.0000009	⁶ COHEN	87	RVUE 1986 CODATA value
1.2933328 ± 0.0000072	GREENE	86	SPEC <i>np</i> → <i>dγ</i>
1.293429 ± 0.000036	COHEN	73	RVUE 1973 CODATA value

- ¹ The 2014 CODATA mass difference in *u* is $m_n - m_p = 1.00138844900(51) \times 10^{-3}$ u.
- ² The 2010 CODATA mass difference in *u* is $m_n - m_p = 1.38844919(45) \times 10^{-3}$ u.
- ³ Calculated by us from the MOHR 08 ratio $m_n/m_p = 1.00137841918(46)$. In *u*, $m_n - m_p = 1.38844920(46) \times 10^{-3}$ u.
- ⁴ Calculated by us from the MOHR 05 ratio $m_n/m_p = 1.00137841870 \pm 0.00000000058$. In *u*, $m_n - m_p = (1.3884487 \pm 0.00000006) \times 10^{-3}$ u.
- ⁵ Calculated by us from the MOHR 99 ratio $m_n/m_p = 1.00137841887 \pm 0.00000000058$. In *u*, $m_n - m_p = (1.3884489 \pm 0.00000006) \times 10^{-3}$ u.
- ⁶ Calculated by us from the COHEN 87 ratio $m_n/m_p = 1.001378404 \pm 0.000000009$. In *u*, $m_n - m_p = 0.001388434 \pm 0.000000009$ u.

***n* MEAN LIFE**

Limits on lifetimes for *bound* neutrons are given in the section “p PARTIAL MEAN LIVES.”

We average seven of the best eight measurements, those made with ultracold neutrons (UCN’s). If we include the one in-beam measurement with a comparable error (YUE 13), we get 879.6 ± 0.8 s, where the scale factor is now 2.0.

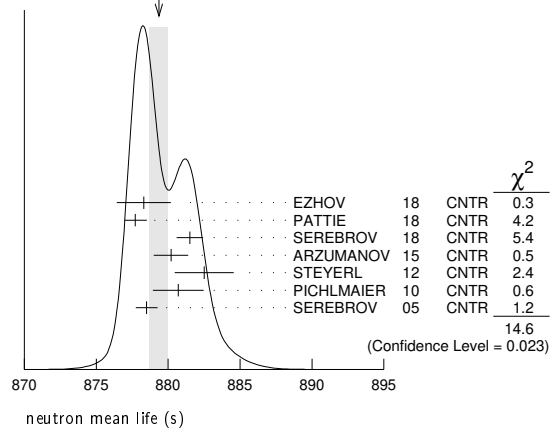
For a recent discussion of the long-standing disagreement between in-beam and UCN results, see CZARNECKI 18 (Physical Review Letters **120** 202002 (2018)). For a full review of all matters concerning the neutron lifetime until about 2010, see WIETFELDT 11, F.E. Wietfeldt and G.L. Greene, “The neutron lifetime,” Reviews of Modern Physics **83** 1173 (2011).

VALUE (s)	DOCUMENT ID	TECN	COMMENT
879.4 ± 0.6 OUR AVERAGE	Error includes scale factor of 1.6. See the ideogram below.		
878.3 ± 1.6 ± 1.0	EZHOV	18	CNTR UCN magneto-gravit. trap
877.7 ± 0.7 ± 0.4	¹ PATTIE	18	CNTR UCN asym. magnetic trap
881.5 ± 0.7 ± 0.6	SEREBROV	18	CNTR UCN gravitational trap
880.2 ± 1.2	² ARZUMANOV	15	CNTR UCN double bottle
882.5 ± 1.4 ± 1.5	³ STEYERL	12	CNTR UCN material bottle
880.7 ± 1.3 ± 1.2	PICHLMAIER	10	CNTR UCN material bottle
878.5 ± 0.7 ± 0.3	SEREBROV	05	CNTR UCN gravitational trap
••• We do not use the following data for averages, fits, limits, etc. •••			
887.7 ± 1.2 ± 1.9	⁴ YUE	13	CNTR In-beam <i>n</i> , trapped <i>p</i>
881.6 ± 0.8 ± 1.9	⁵ ARZUMANOV	12	CNTR See ARZUMANOV 15
886.3 ± 1.2 ± 3.2	NICO	05	CNTR See YUE 13
886.8 ± 1.2 ± 3.2	DEWEY	03	CNTR See NICO 05
885.4 ± 0.9 ± 0.4	ARZUMANOV	00	CNTR See ARZUMANOV 12
889.2 ± 3.0 ± 3.8	BYRNE	96	CNTR Penning trap
882.6 ± 2.7	⁶ MAMPE	93	CNTR UCN material bottle
888.4 ± 3.1 ± 1.1	⁷ NESVIZHEV...	92	CNTR UCN material bottle
888.4 ± 2.9	ALFIMENKOV	90	CNTR See NESVIZHEVSKII 92
893.6 ± 3.8 ± 3.7	BYRNE	90	CNTR See BYRNE 96
878 ± 27 ± 14	KOSSAKOW...	89	TPC Pulsed beam

887.6 ± 3.0	MAMPE	89	CNTR See STEYERL 12
877 ± 10	PAUL	89	CNTR Magnetic storage ring
876 ± 10 ± 19	LAST	88	SPEC Pulsed beam
891 ± 9	SPIVAK	88	CNTR Beam
903 ± 13	KOSVINTSEV	86	CNTR UCN material bottle
937 ± 18	⁸ BYRNE	80	CNTR
875 ± 95	KOSVINTSEV	80	CNTR
881 ± 8	BONDAREN...	78	CNTR See SPIVAK 88
918 ± 14	CHRISTENSEN72	CNTR	

- ¹ PATTIE 18 uses a new technique, with a semi-toroidal magneto-gravitational asymmetric trap and a novel in situ *n*-detector.
- ² ARZUMANOV 15 is a reanalysis of their 2008–2010 dataset, with improved systematic corrections of ARZUMANOV 00 and ARZUMANOV 12.
- ³ STEYERL 12 is a detailed reanalysis of neutron storage loss corrections to the raw data of MAMPE 89, and it replaces that value.
- ⁴ YUE 13 differs from NICO 05 in that a different and better method was used to measure the neutron density in the fiducial volume. This shifted the lifetime by +1.4 seconds and reduced the previously largest source of systematic uncertainty by a factor of five.
- ⁵ ARZUMANOV 12 reanalyzes its systematic corrections in ARZUMANOV 00 and obtains this corrected value.
- ⁶ IGNATOVICH 95 calls into question some of the corrections and averaging procedures used by MAMPE 93. The response, BONDARENKO 96, denies the validity of the criticisms.
- ⁷ The NESVIZHEVSKII 92 measurement has been withdrawn by A. Serebrov.
- ⁸ The BYRNE 80 measurement has been withdrawn (J. Byrne, private communication, 1990).

WEIGHTED AVERAGE
879.4 ± 0.6 (Error scaled by 1.6)



***n* MAGNETIC MOMENT**

See the “Note on Baryon Magnetic Moments” in the *A* Listings.

VALUE (μ _N)	DOCUMENT ID	TECN	COMMENT
−1.91304273 ± 0.00000045	MOHR	16	RVUE 2014 CODATA value
••• We do not use the following data for averages, fits, limits, etc. •••			
−1.91304272 ± 0.00000045	MOHR	12	RVUE 2010 CODATA value
−1.91304273 ± 0.00000045	MOHR	08	RVUE 2006 CODATA value
−1.91304273 ± 0.00000045	MOHR	05	RVUE 2002 CODATA value
−1.91304272 ± 0.00000045	MOHR	99	RVUE 1998 CODATA value
−1.91304275 ± 0.00000045	COHEN	87	RVUE 1986 CODATA value
−1.91304277 ± 0.00000048	¹ GREENE	82	MRS

¹ GREENE 82 measures the moment to be $(1.04187564 \pm 0.00000026) \times 10^{-3}$ Bohr magnetons. The value above is obtained by multiplying this by $m_p/m_e = 1836.152701 \pm 0.000037$ (the 1986 CODATA value from COHEN 87).

***n* ELECTRIC DIPOLE MOMENT**

A nonzero value is forbidden by both *T* invariance and *P* invariance. A number of early results have been omitted. See RAMSEY 90, GOLUB 94, and LAMOREAUX 09 for reviews.

The results are upper limits on $|d_n|$.

VALUE (10 ^{−25} ecm)	CL%	DOCUMENT ID	TECN	COMMENT
< 0.18	90	¹ ABEL	20	MRS UCN
••• We do not use the following data for averages, fits, limits, etc. •••				
< 0.22	95	² SAHOO	17	¹⁹⁹ Hg atom EDM + theory
< 0.16	95	GRANER	16	MRS ¹⁹⁹ Hg atom EDM + theory
< 0.30	90	³ PENDLEBURY	15	MRS Superseded by ABEL 20
< 0.55	90	SEREBROV	15	MRS UCN’s, $h\nu = 2\mu_n B \pm 2d_n E$
< 0.55	90	⁴ SEREBROV	14	MRS See SEREBROV 15
< 0.29	90	⁵ BAKER	06	MRS See PENDLEBURY 15
< 0.63	90	⁶ HARRIS	99	MRS $d = (-0.1 \pm 0.36) \times 10^{-25}$

Baryon Particle Listings

n

< 0.97	90	ALTAREV	96	MRS	See SEREBROV 14
< 1.1	95	ALTAREV	92	MRS	See ALTAREV 96
< 1.2	95	SMITH	90	MRS	See HARRIS 99
< 2.6	95	ALTAREV	86	MRS	$d = (-1.4 \pm 0.6) \times 10^{-25}$
0.3 ± 4.8		PENDLEBURY	84	MRS	Ultracold neutrons
< 6	90	ALTAREV	81	MRS	$d = (2.1 \pm 2.4) \times 10^{-25}$
< 16	90	ALTAREV	79	MRS	$d = (4.0 \pm 7.5) \times 10^{-25}$

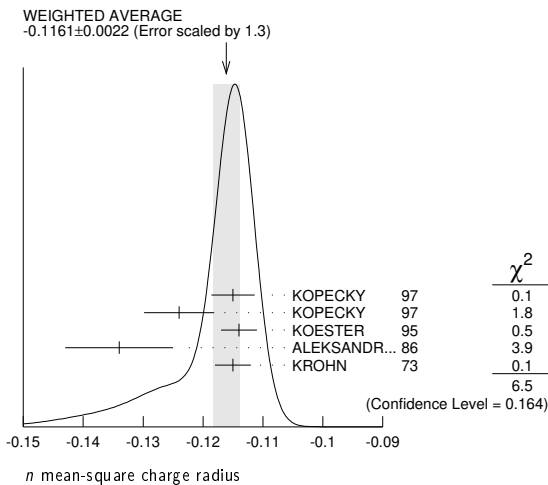
- ABEL 20 reports $d = (0.0 \pm 1.1 \pm 0.2) \times 10^{-26}$ e cm value corresponding to the listed limit.
- SAHOO 17 develops theory to calculate this limit from the measured limit by GRANER 16 of the ^{199}Hg atom EDM.
- PENDLEBURY 15 reports $d = (-0.21 \pm 1.82) \times 10^{-26}$ e cm value corresponding to the listed limit.
- SEREBROV 14 includes the data of ALTAREV 96.
- LAMOREAUX 07 faults BAKER 06 for not including in the estimate of systematic error an effect due to the Earth's rotation. BAKER 07 replies (1) that the effect was included implicitly in the analysis and (2) that further analysis confirms that the BAKER 06 limit is correct as is. See also SILENKO 07.
- This HARRIS 99 result includes the result of SMITH 90. However, the averaging of the results of these two experiments has been criticized by LAMOREAUX 00.

n MEAN-SQUARE CHARGE RADIUS

The mean-square charge radius of the neutron, $\langle r_n^2 \rangle$, is related to the neutron-electron scattering length b_{ne} by $\langle r_n^2 \rangle = 3(m_e a_0 / m_n) b_{ne}$, where m_e and m_n are the masses of the electron and neutron, and a_0 is the Bohr radius. Numerically, $\langle r_n^2 \rangle = 86.34 b_{ne}$, if we use a_0 for a nucleus with infinite mass.

VALUE (fm ²)	DOCUMENT ID	COMMENT
-0.1161 ± 0.0022 OUR AVERAGE		Error includes scale factor of 1.3. See the ideogram below.
-0.115 ± 0.002 ± 0.003	KOPECKY 97	<i>ne</i> scattering (Pb)
-0.124 ± 0.003 ± 0.005	KOPECKY 97	<i>ne</i> scattering (Bi)
-0.114 ± 0.003	KOESTER 95	<i>ne</i> scattering (Pb, Bi)
-0.134 ± 0.009	ALEKSANDR...86	<i>ne</i> scattering (Bi)
-0.115 ± 0.003	1 KROHN 73	<i>ne</i> scattering (Ne, Ar, Kr, Xe)
• • • We do not use the following data for averages, fits, limits, etc. • • •		
-0.117 + 0.007 -0.011	BELUSHKIN 07	Dispersion analysis
-0.113 ± 0.003 ± 0.004	KOPECKY 95	<i>ne</i> scattering (Pb)
-0.114 ± 0.003	KOESTER 86	<i>ne</i> scattering (Pb, Bi)
-0.118 ± 0.002	KOESTER 76	<i>ne</i> scattering (Pb)
-0.120 ± 0.002	KOESTER 76	<i>ne</i> scattering (Bi)
-0.116 ± 0.003	KROHN 66	<i>ne</i> scattering (Ne, Ar, Kr, Xe)

¹ This value is as corrected by KOESTER 76.



n MAGNETIC RADIUS

This is the rms magnetic radius, $\sqrt{\langle r_M^2 \rangle}$.

VALUE (fm)	DOCUMENT ID	COMMENT
0.864 ± 0.009 -0.008 OUR AVERAGE		
0.89 ± 0.03	EPSTEIN 14	Using <i>ep</i> , <i>en</i> , $\pi\pi$ data
0.862 ± 0.009 -0.008	BELUSHKIN 07	Dispersion analysis

n ELECTRIC POLARIZABILITY α_n

Following is the electric polarizability α_n defined in terms of the induced electric dipole moment by $\mathbf{D} = 4\pi\epsilon_0\alpha_n\mathbf{E}$. For a review, see SCHMIED-MAYER 89.

For very complete reviews of the polarizability of the nucleon and Compton scattering, see SCHUMACHER 05 and GRIESSHAMMER 12.

VALUE (10^{-4} fm ³)	DOCUMENT ID	TECN	COMMENT
11.8 ± 1.1 OUR AVERAGE			
11.55 ± 1.25 ± 0.8	MYERS 14	CNTR	$\gamma d \rightarrow \gamma d$
12.5 ± 1.8 +1.6 -1.3	1 KOSSERT 03	CNTR	$\gamma d \rightarrow \gamma p n$
12.0 ± 1.5 ± 2.0	SCHMIEDM... 91	CNTR	<i>n</i> Pb transmission
10.7 + 3.3 -10.7	ROSE 90b	CNTR	$\gamma d \rightarrow \gamma n p$
• • • We do not use the following data for averages, fits, limits, etc. • • •			
8.8 ± 2.4 ± 3.0	2 LUNDIN 03	CNTR	$\gamma d \rightarrow \gamma d$
13.6	3 KOLB 00	CNTR	$\gamma d \rightarrow \gamma n p$
0.0 ± 5.0	4 KOESTER 95	CNTR	<i>n</i> Pb, <i>n</i> Bi transmission
11.7 + 4.3 -11.7	ROSE 90	CNTR	See ROSE 90b
8 ± 10	KOESTER 88	CNTR	<i>n</i> Pb, <i>n</i> Bi transmission
12 ± 10	SCHMIEDM... 88	CNTR	<i>n</i> Pb, <i>n</i> C transmission

- KOSSERT 03 gets $\alpha_n - \beta_n = (9.8 \pm 3.6 + 2.1 - 1.1 \pm 2.2) \times 10^{-4}$ fm³, and uses $\alpha_n + \beta_n = (15.2 \pm 0.5) \times 10^{-4}$ fm³ from LEVCHUK 00. Thus the errors on α_n and β_n are anti-correlated.
- LUNDIN 03 measures $\alpha_N - \beta_N = (6.4 \pm 2.4) \times 10^{-4}$ fm³ and uses accurate values for α_p and α_p and a precise sum-rule result for $\alpha_n + \beta_n$. The second error is a model uncertainty, and errors on α_n and β_n are anticorrelated. The data from this paper are included in the analysis of MYERS 14.
- KOLB 00 obtains this value with a lower limit of 7.6×10^{-4} fm³ but no upper limit from this experiment alone. Combined with results of ROSE 90, the 1- σ range is $(7.6-14.0) \times 10^{-4}$ fm³.
- KOESTER 95 uses natural Pb and the isotopes 208, 207, and 206. See this paper for a discussion of methods used by various groups to extract α_n from data.

n MAGNETIC POLARIZABILITY β_n

VALUE (10^{-4} fm ³)	DOCUMENT ID	TECN	COMMENT
3.7 ± 1.2 OUR AVERAGE			
3.65 ± 1.25 ± 0.8	MYERS 14	CNTR	$\gamma d \rightarrow \gamma d$
2.7 ± 1.8 +1.3 -1.6	1 KOSSERT 03	CNTR	$\gamma d \rightarrow \gamma p n$
6.5 ± 2.4 ± 3.0	2 LUNDIN 03	CNTR	$\gamma d \rightarrow \gamma d$
• • • We do not use the following data for averages, fits, limits, etc. • • •			
1.6	3 KOLB 00	CNTR	$\gamma d \rightarrow \gamma n p$

- KOSSERT 03 gets $\alpha_n - \beta_n = (9.8 \pm 3.6 + 2.1 - 1.1 \pm 2.2) \times 10^{-4}$ fm³, and uses $\alpha_n + \beta_n = (15.2 \pm 0.5) \times 10^{-4}$ fm³ from LEVCHUK 00. Thus the errors on α_n and β_n are anti-correlated.
- LUNDIN 03 measures $\alpha_N - \beta_N = (6.4 \pm 2.4) \times 10^{-4}$ fm³ and uses accurate values for α_p and α_p and a precise sum-rule result for $\alpha_n + \beta_n$. The second error is a model uncertainty, and errors on α_n and β_n are anticorrelated.
- KOLB 00 obtains this value with an upper limit of 7.6×10^{-4} fm³ but no lower limit from this experiment alone. Combined with results of ROSE 90, the 1- σ range is $(1.2-7.6) \times 10^{-4}$ fm³.

n CHARGE

See also $|q_p + q_e|/e$ in the proton Listings.

VALUE (10^{-21} e)	DOCUMENT ID	TECN	COMMENT
-0.2 ± 0.8 OUR AVERAGE			
-0.1 ± 1.1	1 BRESSI 11		Neutrality of SF ₆
-0.4 ± 1.1	2 BAUMANN 88		Cold <i>n</i> deflection
• • • We do not use the following data for averages, fits, limits, etc. • • •			
-15 ± 22	3 GAEHLER 82	CNTR	Cold <i>n</i> deflection

- As a limit, this BRESSI 11 value is $< 1 \times 10^{-21}$ e.
- The BAUMANN 88 error ± 1.1 gives the 68% CL limits about the the value -0.4.
- The GAEHLER 82 error ± 22 gives the 90% CL limits about the the value -15.

LIMIT ON *n*π OSCILLATIONS

Mean Time for *n*π Transition in Vacuum

A test of $\Delta B=2$ baryon number nonconservation. MOHAPATRA 80 and MOHAPATRA 89 discuss the theoretical motivations for looking for *n*π oscillations. DOVER 83 and DOVER 85 give phenomenological analyses. The best limits come from looking for the decay of neutrons bound in nuclei. However, these analyses require model-dependent corrections for nuclear effects. See KABIR 83, DOVER 89, ALBERICO 91, and GAL 00 for discussions. Direct searches for $n \rightarrow \bar{n}$ transitions using reactor neutrons are cleaner but give somewhat poorer limits. We include limits for both free and bound neutrons in the Summary Table. See MOHAPATRA 09 and PHILLIPS 16 for recent reviews.

VALUE (s)	CL%	DOCUMENT ID	TECN	COMMENT
>2.7 × 10⁸	90	ABE	15c	CNTR <i>n</i> bound in oxygen
>8.6 × 10⁷	90	BALDO...	94	CNTR Reactor (free) neutrons

See key on page 999

Baryon Particle Listings

n

• • • We do not use the following data for averages, fits, limits, etc. • • •

>1.37 × 10 ⁸	90	¹ AHARMIM	17	SNO	<i>n</i> bound in deuteron
>1.3 × 10 ⁸	90	CHUNG	02B	SOU2	<i>n</i> bound in iron
>1 × 10 ⁷	90	BALDO-...	90	CNTR	See BALDO-CEOLIN 94
>1.2 × 10 ⁸	90	BERGER	90	FREJ	<i>n</i> bound in iron
>4.9 × 10 ⁵	90	BRESSI	90	CNTR	Reactor neutrons
>4.7 × 10 ⁵	90	BRESSI	89	CNTR	See BRESSI 90
>1.2 × 10 ⁸	90	TAKITA	86	CNTR	<i>n</i> bound in oxygen
>1 × 10 ⁶	90	FIDECARO	85	CNTR	Reactor neutrons
>8.8 × 10 ⁷	90	PARK	85B	CNTR	
>3 × 10 ⁷		BATTISTONI	84	NUSX	
> 0.27-1.1 × 10 ⁸		JONES	84	CNTR	
>2 × 10 ⁷		CHERRY	83	CNTR	

¹ The AHARMIM 17 value is an unbounded limit (it does not assume a positive lifetime). The bounded limit is 1.23 × 10⁸ sec.

LIMIT ON *nn'* OSCILLATIONS

Lee and Yang (LEE 56) proposed the existence of mirror world in an attempt to restore global parity symmetry. A possible candidate for dark matter. Limits depend on assumptions about fields *B* and *B'*. See the papers for details. See BEREZHIANI 18 for a recent discussion.

VALUE (s)	CL%	DOCUMENT ID	TECN	COMMENT
>448	90	SEREBROV 09A	CNTR	Assumes <i>B'</i> < 100 nT

• • • We do not use the following data for averages, fits, limits, etc. • • •

> 17	95	¹ BEREZHIANI 18	CNTR	UCN, scan of <i>B</i> field
> 12	95	² ALTAREV 09A	CNTR	UCN, scan 0 ≤ <i>B</i> ≤ 12.5 μT
>414	90	SEREBROV 08	CNTR	UCN, <i>B</i> field on & off
>103	95	BAN 07	CNTR	UCN, <i>B</i> field on & off

¹ The *B* field was set to (0.09, 0.12, 0.21) G. Limits on oscillation time are valid for any mirror field *B'* in (0.08-0.17) G, and for aligned fields *B* and *B'*. For larger values of *B'*, the limits are significantly reduced.
² Losses of neutrons due to oscillations to mirror neutrons would be maximal when the magnetic fields *B* and *B'* in the two worlds were equal. Hence the scan over *B* by ALTAREV 09A: the limit applies for any *B'* over the given range. At *B'* = 0, the limit is 141 s (95% CL).

n DECAY MODES

Mode	Fraction (Γ _{<i>i</i>} /Γ)	Confidence level
Γ ₁ <i>p e</i> ⁻ $\bar{\nu}_e$	100 %	
Γ ₂ <i>p e</i> ⁻ $\bar{\nu}_e \gamma$	[a] (9.2±0.7) × 10 ⁻³	
Γ ₃ hydrogen-atom $\bar{\nu}_e$	< 2.7 × 10 ⁻³	95%

Charge conservation (*Q*) violating mode

Γ ₄ <i>p ν_e ν_e</i>	<i>Q</i> < 8 × 10 ⁻²⁷	68%
---	----------------------------------	-----

Baryon number violating decay

Γ ₅ <i>e</i> ⁺ <i>e</i> ⁻ invisible		
--	--	--

[a] This limit is for γ energies between 0.4 and 782 keV.

n BRANCHING RATIOS

Γ(<i>p e</i> ⁻ $\bar{\nu}_e \gamma$)/Γ _{total}	Γ ₂ /Γ			
VALUE (units 10 ⁻³)	CL%	DOCUMENT ID	TECN	COMMENT
9.17±0.24±0.64		¹ BALES 16	RDk2	Two different set-ups

• • • We do not use the following data for averages, fits, limits, etc. • • •

3.09±0.11±0.30		² COOPER 10	CNTR	See BALES 16
3.13±0.11±0.33		NICO 06	CNTR	See COOPER 10
<6.9	90	³ BECK 02	CNTR	γ, p, e^- coincidence

¹ BALES 16 gets a branching fraction of (5.82 ± 0.23 ± 0.62) × 10⁻³ for a photon energy range 0.4 to 14.0 keV, and with a different detector array, (3.35 ± 0.05 ± 0.15) × 10⁻³ for 14.1 to 782 keV. Our result above is the sum; the error on the sum is completely dominated by the error on the lower range.
² This COOPER 10 result is for γ energies between 15 and 340 keV.
³ This BECK 02 limit is for γ energies between 35 and 100 keV.

Γ(hydrogen-atom $\bar{\nu}_e$)/Γ _{total}	Γ ₃ /Γ			
VALUE	CL%	DOCUMENT ID	TECN	COMMENT
<0.27 × 10 ⁻²	95	¹ CZARNECKI 18		Lifetime analysis

• • • We do not use the following data for averages, fits, limits, etc. • • •

<3 × 10 ⁻²	95	² GREEN 90	RVUE	
-----------------------	----	-----------------------	------	--

¹ CZARNECKI 18 limit from an analysis of experimental discrepancies on the neutron lifetime and axial coupling applies as well to other possible exotic neutron decays.
² GREEN 90 infers that $\tau(\text{hydrogen-atom } \bar{\nu}_e) > 3 \times 10^4$ s by comparing neutron lifetime measurements made in storage experiments with those made in β -decay experiments. However, the result depends sensitively on the lifetime measurements, and does not of course take into account more recent measurements of same.

Γ(<i>p ν_e ν_e</i>)/Γ _{total}	Γ ₄ /Γ			
Forbidden by charge conservation.				
VALUE	CL%	DOCUMENT ID	TECN	COMMENT
<8 × 10 ⁻²⁷	68	¹ NORMAN 96	RVUE	⁷¹ Ga → ⁷¹ Ge neutrals

• • • We do not use the following data for averages, fits, limits, etc. • • •

<9.7 × 10 ⁻¹⁸	90	ROY 83	CNTR	¹¹³ Cd → ^{113m} In neut.
<7.9 × 10 ⁻²¹		VAIDYA 83	CNTR	⁸⁷ Rb → ^{87m} Sr neut.
<9 × 10 ⁻²⁴	90	BARABANOV 80	CNTR	⁷¹ Ga → ⁷¹ GeX
<3 × 10 ⁻¹⁹		NORMAN 79	CNTR	⁸⁷ Rb → ^{87m} Sr neut.

¹ NORMAN 96 gets this limit by attributing SAGE and GALLEX counting rates to the charge-nonconserving transition ⁷¹Ga → ⁷¹Ge+neutrals rather than to solar-neutrino reactions.

Γ(<i>e</i> ⁺ <i>e</i> ⁻ invisible)/Γ _{total}	Γ ₅ /Γ			
Baryon number violating decay				
VALUE	CL%	DOCUMENT ID	TECN	COMMENT
<0.01	90	¹ KLOPF 19	CNTR	re-interpretation of MUND 13
<1 × 10 ⁻⁴	90	² SUN 18	SPEC	Ultracold <i>n</i> , polarized

• • • We do not use the following data for averages, fits, limits, etc. • • •

¹ KLOPF 19 value is for baryon number violating decay of neutron to electrons plus an invisible state, χ . The limit is valid for KE(*e*⁺ *e*⁻) range between 32 keV and 664 keV, strengthening to few × 10⁻⁴ above approximately 100 keV.
² SUN 18 value is for baryon number violating decay of neutron to electrons plus an invisible state, χ . The limit is valid for 644 keV > KE(*e*⁺ *e*⁻) > 100 keV. Assuming this decay $\chi e e$ is the only allowed χ decay channel, a 0.01 BR is ruled out for 644 keV > E(*e*⁺ *e*⁻) > 100 keV at over 5 σ .

See the related review(s):
 Baryon Decay Parameters

n → *p e*⁻ $\bar{\nu}_e$ DECAY PARAMETERS

See the above "Note on Baryon Decay Parameters." For discussions of recent results, see the references cited at the beginning of the section on the neutron mean life. For discussions of the values of the weak coupling constants *g_A* and *g_V* obtained using the neutron lifetime and asymmetry parameter *A*, comparisons with other methods of obtaining these constants, and implications for particle physics and for astrophysics, see DUBBERS 91 and WOOLCOCK 91. For tests of the *V-A* theory of neutron decay, see EROZOLIMSKII 91B, MOSTOVOI 96, NICO 05, SEVERIJS 06, and ABELE 08.

λ ≡ <i>g_A</i> / <i>g_V</i>	DOCUMENT ID	TECN	COMMENT
VALUE			
-1.2756 ± 0.0013 OUR AVERAGE			Error includes scale factor of 2.6. See the ideogram below.
-1.27641 ± 0.00045 ± 0.00033	¹ MAERKISCH 19	SPEC	pulsed cold <i>n</i> , polarized
-1.2772 ± 0.0020	² BROWN 18	UCNA	Ultracold <i>n</i> , polarized
-1.284 ± 0.014	³ DARIUS 17	SPEC	Cold <i>n</i> , unpolarized
-1.2748 ± 0.0008 +0.0010 -0.0011	⁴ MUND 13	SPEC	Cold <i>n</i> , polarized
-1.275 ± 0.006 ± 0.015	SCHUMANN 08	CNTR	Cold <i>n</i> , polarized
-1.2686 ± 0.0046 ± 0.0007	⁵ MOSTOVOI 01	CNTR	<i>A</i> and <i>B</i> × polarizations
-1.266 ± 0.004	LIAUD 97	TPC	Cold <i>n</i> , polarized, <i>A</i>
-1.2594 ± 0.0038	⁶ YEROZLIM... 97	CNTR	Cold <i>n</i> , polarized, <i>A</i>
-1.262 ± 0.005	BOPP 86	SPEC	Cold <i>n</i> , polarized, <i>A</i>
-1.2755 ± 0.0030	⁷ MENDENHALL 13	UCNA	See BROWN 18
-1.27590 ± 0.00239 ± 0.00331 -0.00377	⁸ PLASTER 12	UCNA	See MENDENHALL 13
-1.27590 +0.00409 -0.00445	LIU 10	UCNA	See PLASTER 12
-1.2739 ± 0.0019	⁹ ABELE 02	SPEC	See MUND 13
-1.274 ± 0.003	ABELE 97D	SPEC	Cold <i>n</i> , polarized, <i>A</i>
-1.266 ± 0.004	SCHRECK... 95	TPC	See LIAUD 97
-1.2544 ± 0.0036	EROZOLIM... 91	CNTR	See YEROZOLIMSKY 97
-1.226 ± 0.042	MOSTOVOY 83	RVUE	
-1.261 ± 0.012	EROZOLIM... 79	CNTR	Cold <i>n</i> , polarized, <i>A</i>
-1.259 ± 0.017	STRATOWA 78	CNTR	<i>p</i> recoil spectrum, <i>a</i>
-1.263 ± 0.015	EROZOLIM... 77	CNTR	See EROZOLIMSKII 79
-1.250 ± 0.036	¹⁰ DOBROZE... 75	CNTR	See STRATOWA 78
-1.258 ± 0.015	11 KROHN 75	CNTR	Cold <i>n</i> , polarized, <i>A</i>
-1.263 ± 0.016	¹² KROPF 74	RVUE	<i>n</i> decay alone
-1.250 ± 0.009	¹² KROPF 74	RVUE	<i>n</i> decay + nuclear ft

¹ MAERKISCH 19 gets *A* = -0.11985 ± 0.00017 ± 0.00012.
² BROWN 18 gets *A* = -0.12054 ± 0.00044 ± 0.00068 and $\lambda = -1.2783 \pm 0.0022$. We quote the combined values that include the earlier UCNA measurements (MENDENHALL 13).
³ DARIUS 17 calculates this value from the measurement of the *a* parameter (see below).
⁴ This MUND 13 value includes earlier PERKEO II measurements (ABELE 02 and ABELE 97D).
⁵ MOSTOVOI 01 measures the two *P*-odd correlations *A* and *B*, or rather *SA* and *SB*, where *S* is the *n* polarization, in free neutron decay.
⁶ YEROZOLIMSKY 97 makes a correction to the EROZOLIMSKII 91 value.

Baryon Particle Listings

n

⁷ MENDENHALL 13 gets $A = -0.11954 \pm 0.00055 \pm 0.00098$ and $\lambda = -1.2756 \pm 0.0030$. We quote the nearly identical values that include the earlier UCNA measurement (PLASTER 12), with a correction to that result.

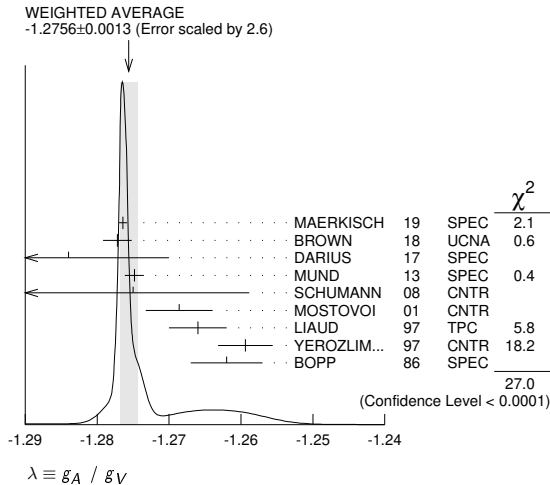
⁸ This PLASTER 12 value is identical with that given in LIU 10, but the experiment is now described in detail.

⁹ This is the combined result of ABELE 02 and ABELE 97d.

¹⁰ These experiments measure the absolute value of g_A/g_V only.

¹¹ KROHN 75 includes events of CHRISTENSEN 70.

¹² KROPP 74 reviews all data through 1972.

**e⁻ ASYMMETRY PARAMETER A**

This is the neutron-spin electron-momentum correlation coefficient. Unless otherwise noted, the values are corrected for radiative effects and weak magnetism. In the Standard Model, A is related to $\lambda \equiv g_A/g_V$ by $A = -2\lambda(\lambda+1)/(1+3\lambda^2)$; this assumes that g_A and g_V are real.

VALUE	DOCUMENT ID	TECN	COMMENT
-0.11958 ± 0.00021 OUR AVERAGE	Error includes scale factor of 1.2.		
-0.11985 ± 0.00017 ± 0.00012	¹ MAERKISCH 19	SPEC	pulsed cold n , polarized
-0.12015 ± 0.00034 ± 0.00063	² BROWN 18	UCNA	Ultracold n , polarized
-0.11926 ± 0.00031 ± 0.00036 ± 0.00042	³ MUND 13	SPEC	Cold n , polarized
-0.1160 ± 0.0009 ± 0.0012	LIAUD 97	TPC	Cold n , polarized
-0.1135 ± 0.0014	⁴ YEROZLIM... 97	CNTR	Cold n , polarized
-0.1146 ± 0.0019	BOPP 86	SPEC	Cold n , polarized
••• We do not use the following data for averages, fits, limits, etc. •••			
-0.11952 ± 0.00110	⁵ MENDENHALL 13	UCNA	See BROWN 18
-0.11966 ± 0.00089 ± 0.00123 ± 0.00140	⁶ PLASTER 12	UCNA	See MENDENHALL 13
-0.11966 ± 0.00089 ± 0.00123 ± 0.00140	LIU 10	UCNA	See PLASTER 12
-0.1138 ± 0.0046 ± 0.0021	PATTIE 09	SPEC	Ultracold n , polarized
-0.1189 ± 0.0007	⁷ ABELE 02	SPEC	See MUND 13
-0.1168 ± 0.0017	⁸ MOSTOVOI 01	CNTR	Inferred
-0.1189 ± 0.0012	ABELE 97d	SPEC	Cold n , polarized
-0.1160 ± 0.0009 ± 0.0011	SCHRECK... 95	TPC	See LIAUD 97
-0.1116 ± 0.0014	EROZOLIM... 91	CNTR	See YEROZOLIM-SKY 97
-0.114 ± 0.005	⁹ EROZOLIM... 79	CNTR	Cold n , polarized
-0.113 ± 0.006	⁹ KROHN 75	CNTR	Cold n , polarized

¹ MAERKISCH 19 further derive a value for the CKM-element $|V_{ud}| = 0.97351 \pm 0.00060$, using $\tau_n = 879.7(8)$ sec and the relation from CZARNECKI 18.

² BROWN 18 gets $A = -0.12054 \pm 0.00044 \pm 0.00068$ and $\lambda = -1.2783 \pm 0.0022$. We quote the combined values that include the earlier UCNA measurements (MENDENHALL 13).

³ This MUND 13 value includes earlier PERKEO II measurements (ABELE 02 and ABELE 97d), with a correction to those results.

⁴ YEROZOLIMSKY 97 makes a correction to the EROZOLIMSKII 91 value.

⁵ MENDENHALL 13 gets $A = -0.11954 \pm 0.00055 \pm 0.00098$ and $\lambda = -1.2756 \pm 0.0030$. We quote the nearly identical values that include the earlier UCNA measurement (PLASTER 12), with a correction to that result.

⁶ This PLASTER 12 value is identical with that given in LIU 10, but the experiment is now described in detail.

⁷ This is the combined result of ABELE 02 and ABELE 97d.

⁸ MOSTOVOI 01 calculates this from its measurement of $\lambda = g_A/g_V$ above.

⁹ These results are not corrected for radiative effects and weak magnetism, but the corrections are small compared to the errors.

 $\bar{\nu}_e$ ASYMMETRY PARAMETER B

This is the neutron-spin antineutrino-momentum correlation coefficient. In the Standard Model, B is related to $\lambda \equiv g_A/g_V$ by $B = 2\lambda(\lambda-1)/(1+3\lambda^2)$; this assumes that g_A and g_V are real.

VALUE	DOCUMENT ID	TECN	COMMENT
0.9807 ± 0.0030 OUR AVERAGE			
0.9802 ± 0.0034 ± 0.0036	SCHUMANN 07	CNTR	Cold n , polarized
0.967 ± 0.006 ± 0.010	KREUZ 05	CNTR	Cold n , polarized
0.9801 ± 0.0046	SEREBROV 98	CNTR	Cold n , polarized

0.9894 ± 0.0083 KUZNETSOV 95 CNTR Cold n , polarized
 1.00 ± 0.05 CHRISTENSEN70 CNTR Cold n , polarized
 0.995 ± 0.034 EROZOLIM... 70c CNTR Cold n , polarized

••• We do not use the following data for averages, fits, limits, etc. •••

0.9876 ± 0.0004 ¹ MOSTOVOI 01 CNTR Inferred

¹ MOSTOVOI 01 calculates this from its measurement of $\lambda = g_A/g_V$ above.

PROTON ASYMMETRY PARAMETER C

Describes the correlation between the neutron spin and the proton momentum. In the Standard Model, C is related to $\lambda \equiv g_A/g_V$ by $C = -x_c(A+B) = x_c 4\lambda/(1+3\lambda^2)$, where $x_c = 0.27484$ is a kinematic factor; this assumes that g_A and g_V are real.

VALUE	DOCUMENT ID	TECN	COMMENT
-0.2377 ± 0.0010 ± 0.0024	SCHUMANN 08	CNTR	Cold n , polarized

e⁻ $\bar{\nu}_e$ ANGULAR CORRELATION COEFFICIENT a

For a review of past experiments and plans for future measurements of the a parameter, see WIETFELDT 05. In the Standard Model, a is related to $\lambda \equiv g_A/g_V$ by $a = (1 - \lambda^2)/(1 + 3\lambda^2)$; this assumes that g_A and g_V are real.

VALUE	DOCUMENT ID	TECN	COMMENT
-0.1059 ± 0.0028 OUR AVERAGE			

-0.1090 ± 0.0030 ± 0.0028 ¹ DARIUS 17 SPEC Cold n , unpolarized

-0.1054 ± 0.0055 BYRNE 02 SPEC Proton recoil spectrum

-0.1017 ± 0.0051 STRATOWA 78 CNTR Proton recoil spectrum

-0.091 ± 0.039 GRIGOREV 68 SPEC Proton recoil spectrum

••• We do not use the following data for averages, fits, limits, etc. •••

-0.1045 ± 0.0014 ² MOSTOVOI 01 CNTR Inferred

¹ DARIUS 17 exploits a "wishbone" correlation, where the p time of flight is correlated with the momentum of the electron in delayed coincidence.

² MOSTOVOI 01 calculates this from its measurement of $\lambda = g_A/g_V$ above.

 ϕ_{AV} PHASE OF g_A RELATIVE TO g_V

Time reversal invariance requires this to be 0 or 180°. This is related to D given in the next data block and $\lambda \equiv g_A/g_V$ by $\sin(\phi_{AV}) \equiv D(1+3\lambda^2)/2|\lambda|$; this assumes that g_A and g_V are real.

VALUE (°)	CL%	DOCUMENT ID	TECN	COMMENT
180.017 ± 0.026 OUR AVERAGE				

180.012 ± 0.028 68 CHUPP 12 CNTR Cold n , polarized > 91%

180.04 ± 0.09 SOLDNER 04 CNTR Cold n , polarized

180.08 ± 0.13 LISING 00 CNTR Polarized > 93%

••• We do not use the following data for averages, fits, limits, etc. •••

180.013 ± 0.028 MUMM 11 CNTR See CHUPP 12

179.71 ± 0.39 EROZOLIM... 78 CNTR Cold n , polarized

180.35 ± 0.43 EROZOLIM... 74 CNTR Cold n , polarized

181.1 ± 1.3 ¹ KROPP 74 RVUE n decay

180.14 ± 0.22 STEINBERG 74 CNTR Cold n , polarized

¹ KROPP 74 reviews all data through 1972.

TRIPLE CORRELATION COEFFICIENT D

These are measurements of the component of n spin perpendicular to the decay plane in β decay. Should be zero if T invariance is not violated.

VALUE (units 10 ⁻⁴)	DOCUMENT ID	TECN	COMMENT
-1.2 ± 2.0 OUR AVERAGE			

-0.94 ± 1.89 ± 0.97 CHUPP 12 CNTR Cold n , polarized > 91%

-2.8 ± 6.4 ± 3.0 SOLDNER 04 CNTR Cold n , polarized

-6 ± 12 ± 5 LISING 00 CNTR Polarized > 93%

••• We do not use the following data for averages, fits, limits, etc. •••

-0.96 ± 1.89 ± 1.01 MUMM 11 CNTR See CHUPP 12

+22 ± 30 EROZOLIM... 78 CNTR Cold n , polarized

-27 ± 50 ¹ EROZOLIM... 74 CNTR Cold n , polarized

-11 ± 17 STEINBERG 74 CNTR Cold n , polarized

¹ EROZOLIMSKII 78 says asymmetric proton losses and nonuniform beam polarization may give a systematic error up to 30×10^{-4} , thus increasing the EROZOLIMSKII 74 error to 50×10^{-4} . STEINBERG 74 and STEINBERG 76 estimate these systematic errors to be insignificant in their experiment.

TRIPLE CORRELATION COEFFICIENT R

Another test of time-reversal invariance. R measures the polarization of the electron in the direction perpendicular to the plane defined by the neutron spin and the electron momentum. $R = 0$ for T invariance.

VALUE	DOCUMENT ID	TECN	COMMENT
+0.004 ± 0.012 ± 0.005	¹ KOZELA 12	CNTR	Mott polarimeter

••• We do not use the following data for averages, fits, limits, etc. •••

+0.008 ± 0.015 ± 0.005 KOZELA 09 CNTR See KOZELA 12

¹ KOZELA 12 also measures the polarization of the electron along the direction of the neutron spin. This is nonzero in the Standard Model; the correlation coefficient is $N = +0.067 \pm 0.011 \pm 0.004$.

n REFERENCES

We have omitted some papers that have been superseded by later experiments. See our earlier editions.

ABEL 20	PRL 124 081803	C. Abel et al.	(nEDM Collab.)
KLOPP 19	PRL 122 222503	M. Klopff et al.	(PERKEO II Collab.)
MAERKISCH 19	PRL 122 242501	B. Maerksich et al.	(TUM, ILL, +)
BEREZHIANI 18	EPJ C78 717	Z. Berezhiani et al.	(AQU, INFN, ILLG+)
BROWN 18	PR C97 035505	M.A.-P. Brown et al.	(UCNA Collab.)
CZARNECKI 18	PRL 120 202002	A. Czarnecki, W.J. Marciano, A. Sifflin	(ALB+)

See key on page 999

Baryon Particle Listings
n, N's and Δ's, N(1440)

Table listing baryon particles with columns for particle name, mass, and various identifiers. Includes sub-sections for EROZOLIM... and N(1440) POLE POSITION.

Downloaded from https://academic.oup.com/ptep/article/2020/8/083C01/5891211 by guest on 20 August 2020

See the related review(s):
N and Δ Resonances

N(1440) 1/2+ (J^P) = 1/2(1/2+) Status: ***

Older and obsolete values are listed and referenced in the 2014 edition, Chinese Physics C38 070001 (2014).

N(1440) POLE POSITION table with columns: REAL VALUE (MeV), DOCUMENT ID, TECN, COMMENT. Includes rows for 1360 to 1380 (OUR ESTIMATE) and 1369 ± 3, 1363 ± 2 ± 2, 1375 ± 30.

Baryon Particle Listings

 $N(1440)$

••• We do not use the following data for averages, fits, limits, etc. •••

VALUE (MeV)	DOCUMENT ID	TECN	COMMENT
1360	HUNT	19	DPWA Multichannel
1355	ROENCHEN	15A	DPWA Multichannel
1386	SHKLYAR	13	DPWA Multichannel
1370 ± 4	ANISOVICH	12A	DPWA Multichannel
1363 ± 11	BATINIC	10	DPWA $\pi N \rightarrow N\pi, N\eta$
1359	ARNDT	06	DPWA $\pi N \rightarrow \pi N, \eta N$
1383	VRANA	00	DPWA Multichannel
1385	HOEHLER	93	SPED $\pi N \rightarrow \pi N$

¹ Fit to the amplitudes of HOEHLER 79.

-2xIMAGINARY PART

VALUE (MeV)	DOCUMENT ID	TECN	COMMENT
160 to 190 (≈ 175) OUR ESTIMATE			
189 ± 5	SOKHOYAN	15A	DPWA Multichannel
180 ± 4 ± 5	¹ SVARC	14	L+P $\pi N \rightarrow \pi N$
180 ± 40	CUTKOSKY	80	IPWA $\pi N \rightarrow \pi N$

••• We do not use the following data for averages, fits, limits, etc. •••

VALUE (MeV)	DOCUMENT ID	TECN	COMMENT
186	HUNT	19	DPWA Multichannel
215	ROENCHEN	15A	DPWA Multichannel
277	SHKLYAR	13	DPWA Multichannel
190 ± 7	ANISOVICH	12A	DPWA Multichannel
151 ± 13	BATINIC	10	DPWA $\pi N \rightarrow N\pi, N\eta$
162	ARNDT	06	DPWA $\pi N \rightarrow \pi N, \eta N$
316	VRANA	00	DPWA Multichannel
164	HOEHLER	93	SPED $\pi N \rightarrow \pi N$

¹ Fit to the amplitudes of HOEHLER 79.

 $N(1440)$ ELASTIC POLE RESIDUEMODULUS $|r|$

VALUE (MeV)	DOCUMENT ID	TECN	COMMENT
46 to 54 (≈ 50) OUR ESTIMATE			
49 ± 3	SOKHOYAN	15A	DPWA Multichannel
50 ± 1 ± 2	¹ SVARC	14	L+P $\pi N \rightarrow \pi N$
52 ± 5	CUTKOSKY	80	IPWA $\pi N \rightarrow \pi N$

••• We do not use the following data for averages, fits, limits, etc. •••

VALUE (MeV)	DOCUMENT ID	TECN	COMMENT
62	ROENCHEN	15A	DPWA Multichannel
126	SHKLYAR	13	DPWA Multichannel
48 ± 3	ANISOVICH	12A	DPWA Multichannel
44	BATINIC	10	DPWA $\pi N \rightarrow N\pi, N\eta$
38	ARNDT	06	DPWA $\pi N \rightarrow \pi N, \eta N$
40	HOEHLER	93	SPED $\pi N \rightarrow \pi N$

¹ Fit to the amplitudes of HOEHLER 79.

PHASE θ

VALUE (°)	DOCUMENT ID	TECN	COMMENT
-100 to -80 (≈ -90) OUR ESTIMATE			
-82 ± 5	SOKHOYAN	15A	DPWA Multichannel
-88 ± 1 ± 2	¹ SVARC	14	L+P $\pi N \rightarrow \pi N$
-100 ± 35	CUTKOSKY	80	IPWA $\pi N \rightarrow \pi N$

••• We do not use the following data for averages, fits, limits, etc. •••

VALUE (°)	DOCUMENT ID	TECN	COMMENT
-98	ROENCHEN	15A	DPWA Multichannel
-60	SHKLYAR	13	DPWA Multichannel
-78 ± 4	ANISOVICH	12A	DPWA Multichannel
-88	BATINIC	10	DPWA $\pi N \rightarrow N\pi, N\eta$
-98	ARNDT	06	DPWA $\pi N \rightarrow \pi N, \eta N$

¹ Fit to the amplitudes of HOEHLER 79.

 $N(1440)$ INELASTIC POLE RESIDUE

The "normalized residue" is the residue divided by $\Gamma_{pole}/2$.

Normalized residue in $N\pi \rightarrow N(1440) \rightarrow N\eta$

MODULUS	PHASE (°)	DOCUMENT ID	TECN	COMMENT
0.078	-27	ROENCHEN	15A	DPWA Multichannel

••• We do not use the following data for averages, fits, limits, etc. •••

Normalized residue in $N\pi \rightarrow N(1440) \rightarrow \Delta\pi, P$ -wave

MODULUS	PHASE (°)	DOCUMENT ID	TECN	COMMENT
0.27 ± 0.02	38 ± 5	SOKHOYAN	15A	DPWA Multichannel

••• We do not use the following data for averages, fits, limits, etc. •••

MODULUS	PHASE (°)	DOCUMENT ID	TECN	COMMENT
0.27 ± 0.02	40 ± 5	ANISOVICH	12A	DPWA Multichannel

Normalized residue in $N\pi \rightarrow N(1440) \rightarrow \Lambda K$

MODULUS	PHASE (°)	DOCUMENT ID	TECN	COMMENT
0.016	145	ROENCHEN	15A	DPWA Multichannel

••• We do not use the following data for averages, fits, limits, etc. •••

Normalized residue in $N\pi \rightarrow N(1440) \rightarrow \Sigma K$

MODULUS	PHASE (°)	DOCUMENT ID	TECN	COMMENT
0.027	113	ROENCHEN	15A	DPWA Multichannel

••• We do not use the following data for averages, fits, limits, etc. •••

Normalized residue in $N\pi \rightarrow N(1440) \rightarrow N(\pi\pi)_{S=0}^{I=0}$

MODULUS	PHASE (°)	DOCUMENT ID	TECN	COMMENT
0.21 ± 0.04	-136 ± 4	SOKHOYAN	15A	DPWA Multichannel

••• We do not use the following data for averages, fits, limits, etc. •••

MODULUS	PHASE (°)	DOCUMENT ID	TECN	COMMENT
0.21 ± 0.05	-135 ± 7	ANISOVICH	12A	DPWA Multichannel

 $N(1440)$ BREIT-WIGNER MASS

VALUE (MeV)	DOCUMENT ID	TECN	COMMENT
1410 to 1470 (≈ 1440) OUR ESTIMATE			
1417 ± 4	¹ HUNT	19	DPWA Multichannel
1430 ± 10	SOKHOYAN	15A	DPWA Multichannel
1515 ± 15	¹ SHKLYAR	13	DPWA Multichannel
1485.0 ± 1.2	¹ ARNDT	06	DPWA $\pi N \rightarrow \pi N, N\eta$
1440 ± 30	CUTKOSKY	80	IPWA $\pi N \rightarrow \pi N$
1410 ± 12	HOEHLER	79	IPWA $\pi N \rightarrow \pi N$

••• We do not use the following data for averages, fits, limits, etc. •••

VALUE (MeV)	DOCUMENT ID	TECN	COMMENT
1430 ± 8	ANISOVICH	12A	DPWA Multichannel
1412 ± 2	¹ SHRESTHA	12A	DPWA Multichannel
1439 ± 19	BATINIC	10	DPWA $\pi N \rightarrow N\pi, N\eta$
1518 ± 5	PENNER	02c	DPWA Multichannel
1479 ± 80	VRANA	00	DPWA Multichannel

¹ Statistical error only.

 $N(1440)$ BREIT-WIGNER WIDTH

VALUE (MeV)	DOCUMENT ID	TECN	COMMENT
250 to 450 (≈ 350) OUR ESTIMATE			
257 ± 11	¹ HUNT	19	DPWA Multichannel
360 ± 30	SOKHOYAN	15A	DPWA Multichannel
605 ± 90	¹ SHKLYAR	13	DPWA Multichannel
284 ± 18	¹ ARNDT	06	DPWA $\pi N \rightarrow \pi N, \eta N$
340 ± 70	CUTKOSKY	80	IPWA $\pi N \rightarrow \pi N$
135 ± 10	HOEHLER	79	IPWA $\pi N \rightarrow \pi N$

••• We do not use the following data for averages, fits, limits, etc. •••

VALUE (MeV)	DOCUMENT ID	TECN	COMMENT
365 ± 35	ANISOVICH	12A	DPWA Multichannel
248 ± 5	¹ SHRESTHA	12A	DPWA Multichannel
437 ± 141	BATINIC	10	DPWA $\pi N \rightarrow N\pi, N\eta$
668 ± 41	PENNER	02c	DPWA Multichannel
490 ± 120	VRANA	00	DPWA Multichannel

¹ Statistical error only.

 $N(1440)$ DECAY MODES

The following branching fractions are our estimates, not fits or averages.

Mode	Fraction (Γ_i/Γ)
Γ_1 $N\pi$	55-75 %
Γ_2 $N\eta$	<1 %
Γ_3 $N\pi\pi$	17-50 %
Γ_4 $\Delta(1232)\pi, P$ -wave	6-27 %
Γ_5 $N\sigma$	11-23 %
Γ_6 $p\gamma$, helicity=1/2	0.035-0.048 %
Γ_7 $n\gamma$, helicity=1/2	0.02-0.04 %

 $N(1440)$ BRANCHING RATIOS

$\Gamma(N\pi)/\Gamma_{total}$	Γ_1/Γ		
55 to 75 (≈ 65) OUR ESTIMATE			
59 ± 2	¹ HUNT	19	DPWA Multichannel
63 ± 2	SOKHOYAN	15A	DPWA Multichannel
56 ± 2	¹ SHKLYAR	13	DPWA Multichannel
78.7 ± 1.6	¹ ARNDT	06	DPWA $\pi N \rightarrow \pi N, \eta N$
68 ± 4	CUTKOSKY	80	IPWA $\pi N \rightarrow \pi N$
51 ± 5	HOEHLER	79	IPWA $\pi N \rightarrow \pi N$

••• We do not use the following data for averages, fits, limits, etc. •••

VALUE (%)	DOCUMENT ID	TECN	COMMENT
62 ± 3	ANISOVICH	12A	DPWA Multichannel
64.8 ± 0.9	¹ SHRESTHA	12A	DPWA Multichannel
62 ± 4	BATINIC	10	DPWA $\pi N \rightarrow N\pi, N\eta$
57 ± 1	PENNER	02c	DPWA Multichannel
72 ± 5	VRANA	00	DPWA Multichannel

¹ Statistical error only.

$\Gamma(N\eta)/\Gamma_{total}$	Γ_2/Γ		
0 ± 1	VRANA	00	DPWA Multichannel

••• We do not use the following data for averages, fits, limits, etc. •••

Baryon Particle Listings
N(1440), N(1520)

$\Gamma(\Delta(1232)\pi, P\text{-wave})/\Gamma_{\text{total}}$

VALUE (%)	DOCUMENT ID	TECN	COMMENT
6 to 27 (≈ 15) OUR ESTIMATE			
22 ± 4	¹ HUNT	19	DPWA Multichannel
12 $^{+5}_{-3}$	SHKLYAR	16	DPWA Multichannel
20 ± 7	SOKHOYAN	15A	DPWA Multichannel
••• We do not use the following data for averages, fits, limits, etc. •••			
21 ± 8	ANISOVICH	12A	DPWA Multichannel
6.5 ± 0.8	¹ SHRESTHA	12A	DPWA Multichannel
16 ± 1	VRANA	00	DPWA Multichannel

¹ Statistical error only.

$\Gamma(N\sigma)/\Gamma_{\text{total}}$

VALUE (%)	DOCUMENT ID	TECN	COMMENT
16 ± 3	¹ HUNT	19	DPWA Multichannel
27 $^{+4}_{-9}$	SHKLYAR	16	DPWA Multichannel
17 ± 6	SOKHOYAN	15A	DPWA Multichannel
••• We do not use the following data for averages, fits, limits, etc. •••			
17 ± 7	ANISOVICH	12A	DPWA Multichannel
27 ± 1	¹ SHRESTHA	12A	DPWA Multichannel
12 ± 1	VRANA	00	DPWA Multichannel

¹ Statistical error only.

N(1440) PHOTON DECAY AMPLITUDES AT THE POLE

N(1440) $\rightarrow p\gamma$, helicity-1/2 amplitude $A_{1/2}$

MODULUS ($\text{GeV}^{-1/2}$)	PHASE ($^\circ$)	DOCUMENT ID	TECN	COMMENT
-0.044 ± 0.005	-40 ± 8	SOKHOYAN	15A	DPWA Multichannel
-0.054 $^{+0.004}_{-0.003}$	5 $^{+2}_{-5}$	ROENCHEN	14	DPWA

••• We do not use the following data for averages, fits, limits, etc. •••

-0.060	-23	ROENCHEN	15A	DPWA Multichannel
--------	-----	----------	-----	-------------------

N(1440) BREIT-WIGNER PHOTON DECAY AMPLITUDES

N(1440) $\rightarrow p\gamma$, helicity-1/2 amplitude $A_{1/2}$

VALUE ($\text{GeV}^{-1/2}$)	DOCUMENT ID	TECN	COMMENT
-0.080 to -0.050 (≈ -0.065) OUR ESTIMATE			
-0.091 ± 0.007	¹ HUNT	19	DPWA Multichannel
-0.061 ± 0.006	SOKHOYAN	15A	DPWA Multichannel
-0.085 ± 0.003	¹ SHKLYAR	13	DPWA Multichannel
-0.056 ± 0.001	¹ WORKMAN	12A	DPWA $\gamma N \rightarrow N\pi$
-0.051 ± 0.002	¹ DUGGER	07	DPWA $\gamma N \rightarrow \pi N$
••• We do not use the following data for averages, fits, limits, etc. •••			
-0.061 ± 0.008	ANISOVICH	12A	DPWA Multichannel
-0.084 ± 0.003	¹ SHRESTHA	12A	DPWA Multichannel
-0.061	DRECHSEL	07	DPWA $\gamma N \rightarrow \pi N$
-0.087	PENNER	02D	DPWA Multichannel

¹ Statistical error only.

N(1440) $\rightarrow n\gamma$, helicity-1/2 amplitude $A_{1/2}$

VALUE ($\text{GeV}^{-1/2}$)	DOCUMENT ID	TECN	COMMENT
0.035 to 0.055 (≈ 0.045) OUR ESTIMATE			
0.013 ± 0.012	¹ HUNT	19	DPWA Multichannel
0.043 ± 0.012	ANISOVICH	13B	DPWA Multichannel
0.048 ± 0.004	¹ CHEN	12A	DPWA $\gamma N \rightarrow \pi N$
••• We do not use the following data for averages, fits, limits, etc. •••			
0.040 ± 0.005	¹ SHRESTHA	12A	DPWA Multichannel
0.054	DRECHSEL	07	DPWA $\gamma N \rightarrow \pi N$
0.121	PENNER	02D	DPWA Multichannel

¹ Statistical error only.

N(1440) REFERENCES

For early references, see Physics Letters **111B** 1 (1982).

HUNT	19	PR C99 055205	B.C. Hunt, D.M. Manley	
SHKLYAR	16	PR C93 045206	V. Shklyar, H. Lenseke, U. Mosel	(GIES)
ROENCHEN	15A	EPJ A51 70	D. Roenchen <i>et al.</i>	
SOKHOYAN	15A	EPJ A51 95	V. Sokhoyan <i>et al.</i>	(CBELSA/TAPS Collab.)
PDG	14	CP C38 070001	K. Olive <i>et al.</i>	(PDG Collab.)
ROENCHEN	14	EPJ A50 101	D. Roenchen <i>et al.</i>	
Also		EPJ A51 63 (errata.)	D. Roenchen <i>et al.</i>	
SVARC	14	PR C89 045205	A. Svarc <i>et al.</i>	(RBI Zagreb, UNI Tuzla)
ANISOVICH	13B	EPJ A49 67	A.V. Anisovich <i>et al.</i>	
SHKLYAR	13	PR C87 015201	V. Shklyar, H. Lenseke, U. Mosel	(GIES)
ANISOVICH	12A	EPJ A48 15	A.V. Anisovich <i>et al.</i>	(BONN, PNPI)
CHEN	12A	PR C86 015206	W. Chen <i>et al.</i>	(DUKE, GWU, MSST, ITEP+)
SHRESTHA	12A	PR C86 055203	M. Shrestha, D.M. Manley	(KSU)
WORKMAN	12A	PR C86 015202	R. Workman <i>et al.</i>	(GWU)
BATINIC	10	PR C82 038203	M. Batinic <i>et al.</i>	(ZAGR)
DRECHSEL	07	EPJ A34 69	D. Drechsel, S.S. Kamalov, L. Tiator	(MAINZ, JINR)
DUGGER	07	PR C76 025211	D. Dugger <i>et al.</i>	(JLab CLAS Collab.)
ARNDT	06	PR C74 045205	R.A. Arndt <i>et al.</i>	(GWU)
PENNER	02C	PR C66 055211	G. Penner, U. Mosel	(GIES)
PENNER	02D	PR C66 055212	G. Penner, U. Mosel	(GIES)

VRANA	00	PRPL 328 181	T.P. Vrana, S.A. Dytman, T.-S.H. Lee	(PITT, ANL)
HOEHLER	93	πN Newsletter 9 1	G. Hohlner	(KARL)
CUTKOSKY	80	Toronto Conf. 19	R.E. Cutkosky <i>et al.</i>	(CMU, LBL) IJP
Also		PR D20 2839	R.E. Cutkosky <i>et al.</i>	(CMU, LBL) IJP
HOEHLER	79	PDAT 12-1	G. Hohlner <i>et al.</i>	(KARLT) IJP
Also		Toronto Conf. 3	R. Koch	(KARLT) IJP

N(1520) 3/2⁻

$I(J^P) = \frac{1}{2}(\frac{3}{2}^-)$ Status: * * * *

Older and obsolete values are listed and referenced in the 2014 edition, Chinese Physics **C38** 070001 (2014).

N(1520) POLE POSITION

REAL PART

VALUE (MeV)	DOCUMENT ID	TECN	COMMENT
1505 to 1515 (≈ 1510) OUR ESTIMATE			
1507 ± 2	SOKHOYAN	15A	DPWA Multichannel
1506 $\pm 1 \pm 1$	¹ SVARC	14	L+P $\pi N \rightarrow \pi N$
1510 ± 5	CUTKOSKY	80	IPWA $\pi N \rightarrow \pi N$
••• We do not use the following data for averages, fits, limits, etc. •••			
1500	HUNT	19	DPWA Multichannel
1512	ROENCHEN	15A	DPWA Multichannel
1492	SHKLYAR	13	DPWA Multichannel
1507 ± 3	ANISOVICH	12A	DPWA Multichannel
1506 ± 9	BATINIC	10	DPWA $\pi N \rightarrow N\pi, N\eta$
1515	ARNDT	06	DPWA $\pi N \rightarrow \pi N, \eta N$
1504	VRANA	00	DPWA Multichannel
1510	HOEHLER	93	ARGD $\pi N \rightarrow \pi N$

¹ Fit to the amplitudes of HOEHLER 79.

-2xIMAGINARY PART

VALUE (MeV)	DOCUMENT ID	TECN	COMMENT
105 to 120 (≈ 110) OUR ESTIMATE			
111 ± 3	SOKHOYAN	15A	DPWA Multichannel
115 $\pm 2 \pm 1$	¹ SVARC	14	L+P $\pi N \rightarrow \pi N$
114 ± 10	CUTKOSKY	80	IPWA $\pi N \rightarrow \pi N$
••• We do not use the following data for averages, fits, limits, etc. •••			
117	HUNT	19	DPWA Multichannel
89	ROENCHEN	15A	DPWA Multichannel
94	SHKLYAR	13	DPWA Multichannel
111 ± 5	ANISOVICH	12A	DPWA Multichannel
122 ± 9	BATINIC	10	DPWA $\pi N \rightarrow N\pi, N\eta$
113	ARNDT	06	DPWA $\pi N \rightarrow \pi N, \eta N$
112	VRANA	00	DPWA Multichannel
120	HOEHLER	93	ARGD $\pi N \rightarrow \pi N$

¹ Fit to the amplitudes of HOEHLER 79.

N(1520) ELASTIC POLE RESIDUE

MODULUS $|r|$

VALUE (MeV)	DOCUMENT ID	TECN	COMMENT
32 to 38 (≈ 35) OUR ESTIMATE			
36 ± 2	SOKHOYAN	15A	DPWA Multichannel
33 $\pm 1 \pm 1$	¹ SVARC	14	L+P $\pi N \rightarrow \pi N$
35 ± 2	CUTKOSKY	80	IPWA $\pi N \rightarrow \pi N$
••• We do not use the following data for averages, fits, limits, etc. •••			
37	ROENCHEN	15A	DPWA Multichannel
27	SHKLYAR	13	DPWA Multichannel
36 ± 3	ANISOVICH	12A	DPWA Multichannel
35	BATINIC	10	DPWA $\pi N \rightarrow N\pi, N\eta$
38	ARNDT	06	DPWA $\pi N \rightarrow \pi N, \eta N$
32	HOEHLER	93	ARGD $\pi N \rightarrow \pi N$

¹ Fit to the amplitudes of HOEHLER 79.

PHASE θ

VALUE ($^\circ$)	DOCUMENT ID	TECN	COMMENT
-15 to -5 (≈ -10) OUR ESTIMATE			
-14 ± 3	SOKHOYAN	15A	DPWA Multichannel
-15 $\pm 1 \pm 1$	¹ SVARC	14	L+P $\pi N \rightarrow \pi N$
-12 ± 5	CUTKOSKY	80	IPWA $\pi N \rightarrow \pi N$
••• We do not use the following data for averages, fits, limits, etc. •••			
-6	ROENCHEN	15A	DPWA Multichannel
-35	SHKLYAR	13	DPWA Multichannel
-14 ± 3	ANISOVICH	12A	DPWA Multichannel
-7	BATINIC	10	DPWA $\pi N \rightarrow N\pi, N\eta$
-5	ARNDT	06	DPWA $\pi N \rightarrow \pi N, \eta N$
-8	HOEHLER	93	ARGD $\pi N \rightarrow \pi N$

¹ Fit to the amplitudes of HOEHLER 79.

Baryon Particle Listings

 $N(1520)$ $N(1520)$ INELASTIC POLE RESIDUE

The "normalized residue" is the residue divided by $\Gamma_{pole}/2$.

Normalized residue in $N\pi \rightarrow N(1520) \rightarrow \Delta\pi, S\text{-wave}$

MODULUS	PHASE ($^\circ$)	DOCUMENT ID	TECN	COMMENT
0.33 ± 0.04	155 ± 15	SOKHOYAN 15A	DPWA	Multichannel
•••				We do not use the following data for averages, fits, limits, etc. •••
0.33 ± 0.05	150 ± 20	ANISOVICH 12A	DPWA	Multichannel

Normalized residue in $N\pi \rightarrow N(1520) \rightarrow \Delta\pi, D\text{-wave}$

MODULUS	PHASE ($^\circ$)	DOCUMENT ID	TECN	COMMENT
0.25 ± 0.03	105 ± 18	SOKHOYAN 15A	DPWA	Multichannel
•••				We do not use the following data for averages, fits, limits, etc. •••
0.25 ± 0.03	100 ± 20	ANISOVICH 12A	DPWA	Multichannel

Normalized residue in $N\pi \rightarrow N(1520) \rightarrow N\eta$

MODULUS	PHASE ($^\circ$)	DOCUMENT ID	TECN	COMMENT
•••				We do not use the following data for averages, fits, limits, etc. •••
0.026	95	ROENCHEN 15A	DPWA	Multichannel

Normalized residue in $N\pi \rightarrow N(1520) \rightarrow \Lambda K$

MODULUS	PHASE ($^\circ$)	DOCUMENT ID	TECN	COMMENT
•••				We do not use the following data for averages, fits, limits, etc. •••
0.069	158	ROENCHEN 15A	DPWA	Multichannel

Normalized residue in $N\pi \rightarrow N(1520) \rightarrow \Sigma K$

MODULUS	PHASE ($^\circ$)	DOCUMENT ID	TECN	COMMENT
•••				We do not use the following data for averages, fits, limits, etc. •••
0.049	-41	ROENCHEN 15A	DPWA	Multichannel

Normalized residue in $N\pi \rightarrow N(1520) \rightarrow N\sigma$

MODULUS	PHASE ($^\circ$)	DOCUMENT ID	TECN	COMMENT
0.08 ± 0.03	-45 ± 25	SOKHOYAN 15A	DPWA	Multichannel

 $N(1520)$ BREIT-WIGNER MASS

VALUE (MeV)	DOCUMENT ID	TECN	COMMENT
1510 to 1520 (≈ 1515) OUR ESTIMATE			
1512.0 ± 1.5	¹ HUNT 19	DPWA	Multichannel
1516 ± 2	SOKHOYAN 15A	DPWA	Multichannel
1505 ± 4	¹ SHKLYAR 13	DPWA	Multichannel
1514.5 ± 0.2	¹ ARNDT 06	DPWA	$\pi N \rightarrow \pi N, \eta N$
1525 ± 10	CUTKOSKY 80	IPWA	$\pi N \rightarrow \pi N$
1519 ± 4	HOEHLER 79	IPWA	$\pi N \rightarrow \pi N$
•••			We do not use the following data for averages, fits, limits, etc. •••
1517 ± 3	ANISOVICH 12A	DPWA	Multichannel
1512.6 ± 0.5	¹ SHRESTHA 12A	DPWA	Multichannel
1522 ± 8	BATINIC 10	DPWA	$\pi N \rightarrow N\pi, N\eta$
1509 ± 1	PENNER 02c	DPWA	Multichannel
1518 ± 3	VRANA 00	DPWA	Multichannel

¹ Statistical error only.

 $N(1520)$ BREIT-WIGNER WIDTH

VALUE (MeV)	DOCUMENT ID	TECN	COMMENT
100 to 120 (≈ 110) OUR ESTIMATE			
121 ± 3	¹ HUNT 19	DPWA	Multichannel
113 ± 4	SOKHOYAN 15A	DPWA	Multichannel
100 ± 2	¹ SHKLYAR 13	DPWA	Multichannel
103.6 ± 0.4	¹ ARNDT 06	DPWA	$\pi N \rightarrow \pi N, \eta N$
120 ± 15	CUTKOSKY 80	IPWA	$\pi N \rightarrow \pi N$
114 ± 7	HOEHLER 79	IPWA	$\pi N \rightarrow \pi N$
•••			We do not use the following data for averages, fits, limits, etc. •••
114 ± 5	ANISOVICH 12A	DPWA	Multichannel
117 ± 1	¹ SHRESTHA 12A	DPWA	Multichannel
132 ± 11	BATINIC 10	DPWA	$\pi N \rightarrow N\pi, N\eta$
100 ± 2	PENNER 02c	DPWA	Multichannel
124 ± 4	VRANA 00	DPWA	Multichannel

¹ Statistical error only.

 $N(1520)$ DECAY MODES

The following branching fractions are our estimates, not fits or averages.

Mode	Fraction (Γ_i/Γ)
Γ_1 $N\pi$	55–65 %
Γ_2 $N\eta$	0.07–0.09 %
Γ_3 $N\pi\pi$	25–35 %
Γ_4 $\Delta(1232)\pi$	22–34 %
Γ_5 $\Delta(1232)\pi, S\text{-wave}$	15–23 %
Γ_6 $\Delta(1232)\pi, D\text{-wave}$	7–11 %

Γ_7 $N\sigma$	< 2 %
Γ_8 $p\gamma$	0.31–0.52 %
Γ_9 $p\gamma, \text{ helicity}=1/2$	0.01–0.02 %
Γ_{10} $p\gamma, \text{ helicity}=3/2$	0.30–0.50 %
Γ_{11} $n\gamma$	0.30–0.53 %
Γ_{12} $n\gamma, \text{ helicity}=1/2$	0.04–0.10 %
Γ_{13} $n\gamma, \text{ helicity}=3/2$	0.25–0.45 %

 $N(1520)$ BRANCHING RATIOS

$\Gamma(N\pi)/\Gamma_{total}$	DOCUMENT ID	TECN	COMMENT	Γ_1/Γ
55 to 65 (≈ 60) OUR ESTIMATE				
58.3 ± 1.5	¹ HUNT 19	DPWA	Multichannel	
61 ± 2	SOKHOYAN 15A	DPWA	Multichannel	
57 ± 2	¹ SHKLYAR 13	DPWA	Multichannel	
63.2 ± 0.1	¹ ARNDT 06	DPWA	$\pi N \rightarrow \pi N, \eta N$	
58 ± 3	CUTKOSKY 80	IPWA	$\pi N \rightarrow \pi N$	
54 ± 3	HOEHLER 79	IPWA	$\pi N \rightarrow \pi N$	
•••			We do not use the following data for averages, fits, limits, etc. •••	
62 ± 3	ANISOVICH 12A	DPWA	Multichannel	
62.7 ± 0.5	¹ SHRESTHA 12A	DPWA	Multichannel	
55 ± 5	BATINIC 10	DPWA	$\pi N \rightarrow N\pi, N\eta$	
56 ± 1	PENNER 02c	DPWA	Multichannel	
63 ± 2	VRANA 00	DPWA	Multichannel	

¹ Statistical error only.

$\Gamma(N\eta)/\Gamma_{total}$	DOCUMENT ID	TECN	COMMENT	Γ_2/Γ
0.03 \pm 0.01	¹ HUNT 19	DPWA	Multichannel	
<1	SHKLYAR 13	DPWA	Multichannel	
0.08 ± 0.01	TIATOR 99	DPWA	$\gamma p \rightarrow p\eta$	
•••			We do not use the following data for averages, fits, limits, etc. •••	
0.1 ± 0.1	BATINIC 10	DPWA	$\pi N \rightarrow N\pi, N\eta$	
0.2 ± 0.1	THOMA 08	DPWA	Multichannel	
$0.08 \text{ to } 0.12$	ARNDT 05	DPWA	Multichannel	
0.23 ± 0.04	PENNER 02c	DPWA	Multichannel	
0 ± 1	VRANA 00	DPWA	Multichannel	

¹ Statistical error only.

$\Gamma(\Delta(1232)\pi, S\text{-wave})/\Gamma_{total}$	DOCUMENT ID	TECN	COMMENT	Γ_5/Γ
21 \pm 2	¹ HUNT 19	DPWA	Multichannel	
19 ± 4	SOKHOYAN 15A	DPWA	Multichannel	
•••			We do not use the following data for averages, fits, limits, etc. •••	
19 ± 4	ANISOVICH 12A	DPWA	Multichannel	
9.3 ± 0.7	¹ SHRESTHA 12A	DPWA	Multichannel	
15 ± 2	VRANA 00	DPWA	Multichannel	

¹ Statistical error only.

$\Gamma(\Delta(1232)\pi, D\text{-wave})/\Gamma_{total}$	DOCUMENT ID	TECN	COMMENT	Γ_6/Γ
6 \pm 1	¹ HUNT 19	DPWA	Multichannel	
9 ± 2	SOKHOYAN 15A	DPWA	Multichannel	
•••			We do not use the following data for averages, fits, limits, etc. •••	
9 ± 2	ANISOVICH 12A	DPWA	Multichannel	
6.3 ± 0.5	¹ SHRESTHA 12A	DPWA	Multichannel	
11 ± 2	VRANA 00	DPWA	Multichannel	

¹ Statistical error only.

$\Gamma(N\sigma)/\Gamma_{total}$	DOCUMENT ID	TECN	COMMENT	Γ_7/Γ
<0.7	¹ HUNT 19	DPWA	Multichannel	
<2	SOKHOYAN 15A	DPWA	Multichannel	
•••			We do not use the following data for averages, fits, limits, etc. •••	
<1	¹ SHRESTHA 12A	DPWA	Multichannel	
<4	THOMA 08	DPWA	Multichannel	
1 ± 1	VRANA 00	DPWA	Multichannel	

¹ Statistical error only.

 $N(1520)$ PHOTON DECAY AMPLITUDES AT THE POLE $N(1520) \rightarrow p\gamma, \text{ helicity}=1/2$ amplitude $A_{1/2}$

MODULUS ($\text{GeV}^{-1/2}$)	PHASE ($^\circ$)	DOCUMENT ID	TECN	COMMENT
-0.023 ± 0.004	-6 ± 5	SOKHOYAN 15A	DPWA	Multichannel
$-0.024^{+0.008}_{-0.003}$	-17^{+16}_{-6}	ROENCHEN 14	DPWA	
•••				We do not use the following data for averages, fits, limits, etc. •••
-0.031	-17	ROENCHEN 15A	DPWA	Multichannel

See key on page 999

Baryon Particle Listings

$N(1520)$, $N(1535)$

$N(1520) \rightarrow p\gamma$, helicity-3/2 amplitude $A_{3/2}$

MODULUS ($\text{GeV}^{-1/2}$)	PHASE ($^\circ$)	DOCUMENT ID	TECN	COMMENT
0.131 ± 0.006	4 ± 4	SOKHOYAN	15A	DPWA Multichannel
$0.117^{+0.006}_{-0.010}$	26 ± 2	ROENCHEN	14	DPWA
0.075	1.7	ROENCHEN	15A	DPWA Multichannel

• • • We do not use the following data for averages, fits, limits, etc. • • •

$N(1520)$ BREIT-WIGNER PHOTON DECAY AMPLITUDES

$N(1520) \rightarrow p\gamma$, helicity-1/2 amplitude $A_{1/2}$

VALUE ($\text{GeV}^{-1/2}$)	DOCUMENT ID	TECN	COMMENT
-0.030 to -0.015 (≈ -0.025) OUR ESTIMATE			
-0.034 ± 0.003	1 HUNT	19	DPWA Multichannel
-0.024 ± 0.004	SOKHOYAN	15A	DPWA Multichannel
-0.015 ± 0.001	1 SHKLYAR	13	DPWA Multichannel
-0.019 ± 0.002	1 WORKMAN	12A	DPWA $\gamma N \rightarrow N\pi$
-0.028 ± 0.002	1 DUGGER	07	DPWA $\gamma N \rightarrow \pi N$
-0.038 ± 0.003	1 AHRENS	02	DPWA $\gamma N \rightarrow \pi N$
• • • We do not use the following data for averages, fits, limits, etc. • • •			
-0.022 ± 0.004	ANISOVICH	12A	DPWA Multichannel
-0.034 ± 0.001	1 SHRESTHA	12A	DPWA Multichannel
-0.027	DRECHSEL	07	DPWA $\gamma N \rightarrow \pi N$
-0.003	PENNER	02D	DPWA Multichannel
$-0.052 \pm 0.010 \pm 0.007$	1 MUKHOPAD...	98	$\gamma p \rightarrow \eta p$
1 Statistical error only.			

$N(1520) \rightarrow n\gamma$, helicity-3/2 amplitude $A_{3/2}$

VALUE ($\text{GeV}^{-1/2}$)	DOCUMENT ID	TECN	COMMENT
0.135 to 0.145 (≈ 0.140) OUR ESTIMATE			
0.142 ± 0.003	1 HUNT	19	DPWA Multichannel
0.130 ± 0.006	SOKHOYAN	15A	DPWA Multichannel
0.146 ± 0.001	1 SHKLYAR	13	DPWA Multichannel
0.141 ± 0.002	1 WORKMAN	12A	DPWA $\gamma N \rightarrow N\pi$
0.143 ± 0.002	1 DUGGER	07	DPWA $\gamma N \rightarrow \pi N$
0.147 ± 0.010	1 AHRENS	02	DPWA $\gamma N \rightarrow \pi N$
• • • We do not use the following data for averages, fits, limits, etc. • • •			
0.131 ± 0.010	ANISOVICH	12A	DPWA Multichannel
0.127 ± 0.003	1 SHRESTHA	12A	DPWA Multichannel
0.161	DRECHSEL	07	DPWA $\gamma N \rightarrow \pi N$
0.151	PENNER	02D	DPWA Multichannel
$0.130 \pm 0.020 \pm 0.015$	1 MUKHOPAD...	98	$\gamma p \rightarrow \eta p$
1 Statistical error only.			

$N(1520) \rightarrow n\gamma$, helicity-1/2 amplitude $A_{1/2}$

VALUE ($\text{GeV}^{-1/2}$)	DOCUMENT ID	TECN	COMMENT
-0.055 to -0.040 (≈ -0.050) OUR ESTIMATE			
-0.072 ± 0.003	1 HUNT	19	DPWA Multichannel
-0.049 ± 0.008	ANISOVICH	13B	DPWA Multichannel
-0.046 ± 0.006	1 CHEN	12A	DPWA $\gamma N \rightarrow \pi N$
• • • We do not use the following data for averages, fits, limits, etc. • • •			
-0.038 ± 0.003	1 SHRESTHA	12A	DPWA Multichannel
-0.077	DRECHSEL	07	DPWA $\gamma N \rightarrow \pi N$
-0.084	PENNER	02D	DPWA Multichannel
1 Statistical error only.			

$N(1520) \rightarrow n\gamma$, helicity-3/2 amplitude $A_{3/2}$

VALUE ($\text{GeV}^{-1/2}$)	DOCUMENT ID	TECN	COMMENT
-0.120 to -0.100 (≈ -0.115) OUR ESTIMATE			
-0.123 ± 0.006	1 HUNT	19	DPWA Multichannel
-0.113 ± 0.012	ANISOVICH	13B	DPWA Multichannel
-0.115 ± 0.005	1 CHEN	12A	DPWA $\gamma N \rightarrow \pi N$
• • • We do not use the following data for averages, fits, limits, etc. • • •			
-0.101 ± 0.004	1 SHRESTHA	12A	DPWA Multichannel
-0.154	DRECHSEL	07	DPWA $\gamma N \rightarrow \pi N$
-0.159	PENNER	02D	DPWA Multichannel
1 Statistical error only.			

$N(1520)$ REFERENCES

For early references, see Physics Letters **111B** 1 (1982). For very early references, see Reviews of Modern Physics **37** 633 (1965).

HUNT	19	PR C99 055205	B. C. Hunt, D.M. Manley
ROENCHEN	15A	EPJ A51 70	D. Roenchen et al.
SOKHOYAN	15A	EPJ A51 95	V. Sokhoyan et al.
PDG	14	CP C38 070001	K. Olive et al.
ROENCHEN	14	EPJ A50 101	D. Roenchen et al.
Also		EPJ A51 63 (err.)	D. Roenchen et al.
SVARC	14	PR C89 045205	A. Svarc et al.
ANISOVICH	13B	EPJ A49 67	A.V. Anisovich et al.
SHKLYAR	13	PR C87 015201	V. Shklyar, H. Lenske, U. Mosel
ANISOVICH	12A	EPJ A48 15	A.V. Anisovich et al.
CHEN	12A	PR C86 015206	W. Chen et al.
SHRESTHA	12A	PR C86 055203	M. Shrestha, D.M. Manley
WORKMAN	12A	PR C86 015202	R. Workman et al.
BATINIC	10	PR C82 038203	M. Batinic et al.

THOMA	08	PL B659 87	U. Thoma et al.
DRECHSEL	07	EPJ A34 69	D. Drechsel, S.S. Kamalov, L. Tiator
DUGGER	07	PR C74 025211	M. Dugger et al.
ARNDT	06	PR C74 045205	R.A. Arndt et al.
ARNDT	05	PR C72 045202	R.A. Arndt et al.
AHRENS	02C	PRL 88 232002	J. Ahrens et al.
PENNER	02C	PR C66 055211	G. Penner, U. Mosel
PENNER	02D	PR C66 055212	G. Penner, U. Mosel
VRANA	00	PRPL 320 181	T.P. Vrana, S.A. Dytman, T.-S.H. Lee
TIATOR	99	PR C60 035210	L. Tiator et al.
MUKHOPAD...	98	PL B444 7	N. C. Mukhopadhyay, N. Mathur
HOEHLER	93	πN Newsletter 9 1	G. Hoehler
CUTKOSKY	80	Toronto Conf. 19	R.E. Cutkosky et al.
Also		PR D20 2839	R.E. Cutkosky et al.
HOEHLER	79	PDAT 12-1	G. Hoehler et al.
Also		Toronto Conf. 3	R. Koch

$N(1535) 1/2^-$

$$I(J^P) = \frac{1}{2}(\frac{1}{2}^-) \text{ Status: } ***$$

Older and obsolete values are listed and referenced in the 2014 edition, Chinese Physics **C38** 070001 (2014).

$N(1535)$ POLE POSITION

REAL PART

VALUE (MeV)	DOCUMENT ID	TECN	COMMENT
1500 to 1520 (≈ 1510) OUR ESTIMATE			
1500 ± 4	SOKHOYAN	15A	DPWA Multichannel
$1509 \pm 4 \pm 2$	1 SVARC	14	L+P $\pi N \rightarrow \pi N$
1510 ± 50	CUTKOSKY	80	IPWA $\pi N \rightarrow \pi N$
• • • We do not use the following data for averages, fits, limits, etc. • • •			
1496	HUNT	19	DPWA Multichannel
1499	ROENCHEN	15A	DPWA Multichannel
1490	SHKLYAR	13	DPWA Multichannel
1501 ± 4	ANISOVICH	12A	DPWA Multichannel
1521 ± 14	BATINIC	10	DPWA $\pi N \rightarrow N\pi, N\eta$
1502	ARNDT	06	DPWA $\pi N \rightarrow \pi N, \eta N$
1525	VRANA	00	DPWA Multichannel
1487	HOEHLER	93	SPED $\pi N \rightarrow \pi N$
1 Fit to the amplitudes of HOEHLER 79.			

-2xIMAGINARY PART

VALUE (MeV)	DOCUMENT ID	TECN	COMMENT
110 to 150 (≈ 130) OUR ESTIMATE			
128 ± 9	SOKHOYAN	15A	DPWA Multichannel
$118 \pm 9 \pm 2$	2 SVARC	14	L+P $\pi N \rightarrow \pi N$
260 ± 80	CUTKOSKY	80	IPWA $\pi N \rightarrow \pi N$
• • • We do not use the following data for averages, fits, limits, etc. • • •			
119	HUNT	19	DPWA Multichannel
104	ROENCHEN	15A	DPWA Multichannel
100	SHKLYAR	13	DPWA Multichannel
134 ± 11	ANISOVICH	12A	DPWA Multichannel
190 ± 28	BATINIC	10	DPWA $\pi N \rightarrow N\pi, N\eta$
95	ARNDT	06	DPWA $\pi N \rightarrow \pi N, \eta N$
102	VRANA	00	DPWA Multichannel
2 Fit to the amplitudes of HOEHLER 79.			

$N(1535)$ ELASTIC POLE RESIDUE

MODULUS $|r|$

VALUE (MeV)	DOCUMENT ID	TECN	COMMENT
15 to 35 (≈ 25) OUR ESTIMATE			
29 ± 4	SOKHOYAN	15A	DPWA Multichannel
$22 \pm 2 \pm 0.4$	3 SVARC	14	L+P $\pi N \rightarrow \pi N$
120 ± 40	CUTKOSKY	80	IPWA $\pi N \rightarrow \pi N$
• • • We do not use the following data for averages, fits, limits, etc. • • •			
22	ROENCHEN	15A	DPWA Multichannel
15	SHKLYAR	13	DPWA Multichannel
31 ± 4	ANISOVICH	12A	DPWA Multichannel
68	BATINIC	10	DPWA $\pi N \rightarrow N\pi, N\eta$
16	ARNDT	06	DPWA $\pi N \rightarrow \pi N, \eta N$
3 Fit to the amplitudes of HOEHLER 79.			

PHASE θ

VALUE ($^\circ$)	DOCUMENT ID	TECN	COMMENT
-30 to 0 (≈ -15) OUR ESTIMATE			
-20 ± 10	SOKHOYAN	15A	DPWA Multichannel
$-5 \pm 5 \pm 3$	4 SVARC	14	L+P $\pi N \rightarrow \pi N$
$+15 \pm 45$	CUTKOSKY	80	IPWA $\pi N \rightarrow \pi N$
• • • We do not use the following data for averages, fits, limits, etc. • • •			
-46	ROENCHEN	15A	DPWA Multichannel
-51	SHKLYAR	13	DPWA Multichannel
-29 ± 5	ANISOVICH	12A	DPWA Multichannel
12	BATINIC	10	DPWA $\pi N \rightarrow N\pi, N\eta$
-16	ARNDT	06	DPWA $\pi N \rightarrow \pi N, \eta N$
4 Fit to the amplitudes of HOEHLER 79.			

Baryon Particle Listings

 $N(1535)$ $N(1535)$ INELASTIC POLE RESIDUE

The "normalized residue" is the residue divided by $\Gamma_{pole}/2$.

Normalized residue in $N\pi \rightarrow N(1535) \rightarrow N\eta$

MODULUS	PHASE ($^\circ$)	DOCUMENT ID	TECN	COMMENT
0.43 ± 0.03	-76 ± 5	ANISOVICH 12A	DPWA	Multichannel
••• We do not use the following data for averages, fits, limits, etc. •••				
0.51	112	ROENCHEN 15A	DPWA	Multichannel

Normalized residue in $N\pi \rightarrow N(1535) \rightarrow \Lambda K$

MODULUS	PHASE ($^\circ$)	DOCUMENT ID	TECN	COMMENT
••• We do not use the following data for averages, fits, limits, etc. •••				
0.05	32	ROENCHEN 15A	DPWA	Multichannel

Normalized residue in $N\pi \rightarrow N(1535) \rightarrow \Sigma K$

MODULUS	PHASE ($^\circ$)	DOCUMENT ID	TECN	COMMENT
••• We do not use the following data for averages, fits, limits, etc. •••				
0.05	-69	ROENCHEN 15A	DPWA	Multichannel

Normalized residue in $N\pi \rightarrow N(1535) \rightarrow \Delta\pi, D\text{-wave}$

MODULUS	PHASE ($^\circ$)	DOCUMENT ID	TECN	COMMENT
0.11 ± 0.02	160 ± 20	SOKHOYAN 15A	DPWA	Multichannel
••• We do not use the following data for averages, fits, limits, etc. •••				
0.12 ± 0.03	145 ± 17	ANISOVICH 12A	DPWA	Multichannel

Normalized residue in $N\pi \rightarrow N(1535) \rightarrow N\sigma$

MODULUS	PHASE ($^\circ$)	DOCUMENT ID	TECN	COMMENT
0.16 ± 0.07	25 ± 40	SOKHOYAN 15A	DPWA	Multichannel

Normalized residue in $N\pi \rightarrow N(1535) \rightarrow N(1440)\pi$

MODULUS	PHASE ($^\circ$)	DOCUMENT ID	TECN	COMMENT
0.21 ± 0.14	-45 ± 50	SOKHOYAN 15A	DPWA	Multichannel

 $N(1535)$ BREIT-WIGNER MASS

VALUE (MeV)	DOCUMENT ID	TECN	COMMENT
1515 to 1545 (≈ 1530) OUR ESTIMATE			
1525 ± 2	⁵ HUNT 19	DPWA	Multichannel
1528 ± 6	KASHEVAROV 17	DPWA	$\gamma p \rightarrow \eta p, \eta' p$
1517 ± 4	SOKHOYAN 15A	DPWA	Multichannel
1526 ± 2	⁵ SHKLYAR 13	DPWA	Multichannel
1547.0 ± 0.7	⁵ ARNDT 06	DPWA	$\pi N \rightarrow \pi N, N\eta$
1550 ± 40	CUTKOSKY 80	IPWA	$\pi N \rightarrow \pi N$
1526 ± 7	HOEHLER 79	IPWA	$\pi N \rightarrow \pi N$
••• We do not use the following data for averages, fits, limits, etc. •••			
1519 ± 5	ANISOVICH 12A	DPWA	Multichannel
1538 ± 1	⁵ SHRESTHA 12A	DPWA	Multichannel
1553 ± 8	BATINIC 10	DPWA	$\pi N \rightarrow N\pi, N\eta$
1546.7 ± 2.2	ARNDT 04	DPWA	$\pi N \rightarrow \pi N, N\eta$
1526 ± 2	PENNER 02c	DPWA	Multichannel
1530 ± 10	BAI 01B	BES	$J/\psi \rightarrow p\bar{p}\eta$
1522 ± 11	THOMPSON 01	CLAS	$\gamma^* p \rightarrow p\eta$
1542 ± 3	VRANA 00	DPWA	Multichannel
1532 ± 5	ARMSTRONG 99B	DPWA	$\gamma^* p \rightarrow p\eta$
⁵ Statistical error only.			

 $N(1535)$ BREIT-WIGNER WIDTH

VALUE (MeV)	DOCUMENT ID	TECN	COMMENT
125 to 175 (≈ 150) OUR ESTIMATE			
147 ± 5	⁶ HUNT 19	DPWA	Multichannel
163 ± 25	KASHEVAROV 17	DPWA	$\gamma p \rightarrow \eta p, \eta' p$
120 ± 10	SOKHOYAN 15A	DPWA	Multichannel
131 ± 12	⁶ SHKLYAR 13	DPWA	Multichannel
188.4 ± 3.8	⁶ ARNDT 06	DPWA	$\pi N \rightarrow \pi N, N\eta$
240 ± 80	CUTKOSKY 80	IPWA	$\pi N \rightarrow \pi N$
120 ± 20	HOEHLER 79	IPWA	$\pi N \rightarrow \pi N$
••• We do not use the following data for averages, fits, limits, etc. •••			
128 ± 14	ANISOVICH 12A	DPWA	Multichannel
141 ± 4	⁶ SHRESTHA 12A	DPWA	Multichannel
182 ± 25	BATINIC 10	DPWA	$\pi N \rightarrow N\pi, N\eta$
129 ± 8	PENNER 02c	DPWA	Multichannel
95 ± 25	BAI 01B	BES	$J/\psi \rightarrow p\bar{p}\eta$
143 ± 18	THOMPSON 01	CLAS	$\gamma^* p \rightarrow p\eta$
112 ± 19	VRANA 00	DPWA	Multichannel
154 ± 20	ARMSTRONG 99B	DPWA	$\gamma^* p \rightarrow p\eta$
⁶ Statistical error only.			

 $N(1535)$ DECAY MODES

The following branching fractions are our estimates, not fits or averages.

Mode	Fraction (Γ_i/Γ)
Γ_1 $N\pi$	32-52 %
Γ_2 $N\eta$	30-55 %
Γ_3 $N\pi\pi$	3-14 %
Γ_4 $\Delta(1232)\pi$	
Γ_5 $\Delta(1232)\pi, D\text{-wave}$	1-4 %
Γ_6 $N\rho$	
Γ_7 $N\rho, S=1/2$	
Γ_8 $N\rho, S=3/2, D\text{-wave}$	
Γ_9 $N\sigma$	2-10 %
Γ_{10} $N(1440)\pi$	5-12 %
Γ_{11} $p\gamma, \text{helicity}=1/2$	0.15-0.30 %
Γ_{12} $n\gamma, \text{helicity}=1/2$	0.01-0.25 %

 $N(1535)$ BRANCHING RATIOS

$\Gamma(N\pi)/\Gamma_{total}$	DOCUMENT ID	TECN	COMMENT	Γ_1/Γ
32 to 52 (≈ 42) OUR ESTIMATE				
42 ± 2	⁷ HUNT 19	DPWA	Multichannel	
52 ± 5	SOKHOYAN 15A	DPWA	Multichannel	
35 ± 3	⁷ SHKLYAR 13	DPWA	Multichannel	
35.5 ± 0.2	⁷ ARNDT 06	DPWA	$\pi N \rightarrow \pi N, N\eta$	
50 ± 10	CUTKOSKY 80	IPWA	$\pi N \rightarrow \pi N$	
38 ± 4	HOEHLER 79	IPWA	$\pi N \rightarrow \pi N$	
••• We do not use the following data for averages, fits, limits, etc. •••				
54 ± 5	ANISOVICH 12A	DPWA	Multichannel	
37 ± 1	⁷ SHRESTHA 12A	DPWA	Multichannel	
46 ± 7	BATINIC 10	DPWA	$\pi N \rightarrow N\pi, N\eta$	
36 ± 1	PENNER 02c	DPWA	Multichannel	
35 ± 8	VRANA 00	DPWA	Multichannel	
⁷ Statistical error only.				

$\Gamma(N\eta)/\Gamma_{total}$	DOCUMENT ID	TECN	COMMENT	Γ_2/Γ
30 to 55 (≈ 42) OUR ESTIMATE				
43 ± 3	⁸ HUNT 19	DPWA	Multichannel	
41 ± 4	⁹ KASHEVAROV 17	DPWA	$\gamma p \rightarrow \eta p, \eta' p$	
58 ± 4	⁸ SHKLYAR 13	DPWA	Multichannel	
33 ± 5	ANISOVICH 12A	DPWA	Multichannel	
53 ± 1	PENNER 02c	DPWA	Multichannel	
51 ± 5	VRANA 00	DPWA	Multichannel	
••• We do not use the following data for averages, fits, limits, etc. •••				
41 ± 2	⁸ SHRESTHA 12A	DPWA	Multichannel	
50 ± 7	BATINIC 10	DPWA	$\pi N \rightarrow N\pi, N\eta$	
⁸ Statistical error only.				
⁹ Assuming $A_{1/2} = 0.115 \text{ GeV}^{-1/2}$.				

$\Gamma(N\eta)/\Gamma(N\pi)$	DOCUMENT ID	TECN	COMMENT	Γ_2/Γ_1
••• We do not use the following data for averages, fits, limits, etc. •••				
0.95 ± 0.03	AZNAURYAN 09	CLAS	π, η electroproduction	

$\Gamma(\Delta(1232)\pi, D\text{-wave})/\Gamma_{total}$	DOCUMENT ID	TECN	COMMENT	Γ_5/Γ
30 to 55 (≈ 42) OUR ESTIMATE				
<1.1	¹⁰ HUNT 19	DPWA	Multichannel	
2.5 ± 1.5	SOKHOYAN 15A	DPWA	Multichannel	
••• We do not use the following data for averages, fits, limits, etc. •••				
2.5 ± 1.5	ANISOVICH 12A	DPWA	Multichannel	
1.8 ± 0.8	¹⁰ SHRESTHA 12A	DPWA	Multichannel	
1 ± 1	VRANA 00	DPWA	Multichannel	
¹⁰ Statistical error only.				

$\Gamma(N\rho, S=1/2)/\Gamma_{total}$	DOCUMENT ID	TECN	COMMENT	Γ_7/Γ
30 to 55 (≈ 42) OUR ESTIMATE				
14 ± 2	¹¹ HUNT 19	DPWA	Multichannel	
¹¹ Statistical error only.				

$\Gamma(N\rho, S=3/2, D\text{-wave})/\Gamma_{total}$	DOCUMENT ID	TECN	COMMENT	Γ_8/Γ
30 to 55 (≈ 42) OUR ESTIMATE				
<0.3	¹² HUNT 19	DPWA	Multichannel	
¹² Statistical error only.				

$\Gamma(N\sigma)/\Gamma_{total}$

VALUE (%)	DOCUMENT ID	TECN	COMMENT
<1	13 HUNT 19	DPWA	Multichannel
6 ± 4	SOKHOYAN 15A	DPWA	Multichannel
1.5 ± 0.5	13 SHRESTHA 12A	DPWA	Multichannel
2 ± 1	VRANA 00	DPWA	Multichannel

• • • We do not use the following data for averages, fits, limits, etc. • • •

13 Statistical error only.

$\Gamma(N(1440)\pi)/\Gamma_{total}$

VALUE (%)	DOCUMENT ID	TECN	COMMENT
< 0.01	14 HUNT 19	DPWA	Multichannel
12 ± 8	SOKHOYAN 15A	DPWA	Multichannel
8 ± 2	14 STAROSTIN 03		$\pi^- p \rightarrow n3\pi^0$
< 1	14 SHRESTHA 12A	DPWA	Multichannel
10 ± 9	VRANA 00	DPWA	Multichannel

• • • We do not use the following data for averages, fits, limits, etc. • • •

14 This value is an estimate made using simplest assumptions.

N(1535) PHOTON DECAY AMPLITUDES AT THE POLE

$N(1535) \rightarrow p\gamma$, helicity-1/2 amplitude $A_{1/2}$

MODULUS ($\text{GeV}^{-1/2}$)	PHASE ($^\circ$)	DOCUMENT ID	TECN	COMMENT
0.093 ± 0.009	8 ± 4	ANISOVICH 17D	DPWA	Multichannel
0.050 ± 0.004	-14 ± 10	15 ROENCHEN 14	DPWA	
0.114 ± 0.008	10 ± 5	ANISOVICH 15A	DPWA	Multichannel
0.106	5.2	ROENCHEN 15A	DPWA	Multichannel
0.114 ± 0.008	10 ± 5	SOKHOYAN 15A	DPWA	Multichannel

• • • We do not use the following data for averages, fits, limits, etc. • • •

15 T-Matrix amplitude

$N(1535) \rightarrow n\gamma$, helicity-1/2 amplitude $A_{1/2}$

MODULUS ($\text{GeV}^{-1/2}$)	PHASE ($^\circ$)	DOCUMENT ID	TECN	COMMENT
-0.088 ± 0.004	5 ± 4	ANISOVICH 17D	DPWA	Multichannel
-0.095 ± 0.006	8 ± 5	ANISOVICH 15A	DPWA	Multichannel

• • • We do not use the following data for averages, fits, limits, etc. • • •

N(1535) BREIT-WIGNER PHOTON DECAY AMPLITUDES

$N(1535) \rightarrow p\gamma$, helicity-1/2 amplitude $A_{1/2}$

VALUE ($\text{GeV}^{-1/2}$)	DOCUMENT ID	TECN	COMMENT
0.090 to 0.120 (≈ 0.105) OUR ESTIMATE	16 HUNT 19	DPWA	Multichannel
0.107 ± 0.003	SOKHOYAN 15A	DPWA	Multichannel
0.101 ± 0.007	16 SHKLYAR 13	DPWA	Multichannel
0.091 ± 0.004	16 WORKMAN 12A	DPWA	$\gamma N \rightarrow N\pi$
0.128 ± 0.004	16 DUGGER 07	DPWA	$\gamma N \rightarrow \pi N$
0.091 ± 0.002	ANISOVICH 12A	DPWA	Multichannel
0.105 ± 0.010	16 SHRESTHA 12A	DPWA	Multichannel
0.059 ± 0.003	DRECHSEL 07	DPWA	$\gamma N \rightarrow \pi N$
0.066	PENNER 02D	DPWA	Multichannel
0.090			

• • • We do not use the following data for averages, fits, limits, etc. • • •

16 Statistical error only.

$N(1535) \rightarrow n\gamma$, helicity-1/2 amplitude $A_{1/2}$

VALUE ($\text{GeV}^{-1/2}$)	DOCUMENT ID	TECN	COMMENT
-0.095 to -0.055 (≈ -0.075) OUR ESTIMATE	17 HUNT 19	DPWA	Multichannel
-0.055 ± 0.006	ANISOVICH 13B	DPWA	Multichannel
-0.093 ± 0.011	17 CHEN 12A	DPWA	$\gamma N \rightarrow \pi N$
-0.058 ± 0.006	SHRESTHA 12A	DPWA	Multichannel
-0.049 ± 0.003	DRECHSEL 07	DPWA	$\gamma N \rightarrow \pi N$
-0.051	PENNER 02D	DPWA	Multichannel
-0.024			

• • • We do not use the following data for averages, fits, limits, etc. • • •

17 Statistical error only.

$N(1535) \rightarrow N\gamma$, ratio $A_{1/2}^n/A_{1/2}^p$

VALUE ($\text{GeV}^{-1/2}$)	DOCUMENT ID	TECN	COMMENT
-0.84 ± 0.15	MUKHOPAD... 95B	IPWA	

N(1535) REFERENCES

For early references, see Physics Letters **111B 1** (1982).

HUNT 19	PR C99 055205	B.C. Hunt, D.M. Manley	
ANISOVICH 17D	PR C95 035211	A.V. Anisovich et al.	
KASHEVAROV 17	PRL 118 212001	V.L. Kashevarov et al.	(A2/MAMI Collab.)
ANISOVICH 15A	EPJ A51 72	A.V. Anisovich et al.	
ROENCHEN 15A	EPJ A51 70	D. Roenchen et al.	
SOKHOYAN 15A	EPJ A51 95	V. Sokhoyan et al.	(CBELSA/TAPS Collab.)

PDG	14	CP C38 070001	K. Olive et al.	(PDG Collab.)
ROENCHEN	14	EPJ A50 101	D. Roenchen et al.	
Also		EPJ A51 63 (errat.)	D. Roenchen et al.	
SVARC	14	PR C89 045205	A. Svarc et al.	(RBI Zagreb, UNI Tuzla)
ANISOVICH 13B	EPJ A49 67		A.V. Anisovich et al.	
SHKLYAR	13	PR C87 015201	V. Shklyar, H. Lenske, U. Mosel	(GIES)
ANISOVICH 12A	EPJ A48 15		A.V. Anisovich et al.	(BONN, PNPI)
CHEN	12A	PR C86 015206	W. Chen et al.	(DUKE, GWU, MSST, ITP+)
SHRESTHA	12A	PR C86 055203	M. Shrestha, D.M. Manley	(KSU)
WORKMAN	12A	PR C86 015202	R. Workman et al.	(GWU)
BATINIC	10	PR C82 038203	M. Batinic et al.	(ZAGR)
AZNAURYAN	09	PR C80 055203	I.G. Aznauryan et al.	(JLab CLAS Collab.)
DRECHSEL	07	EPJ A34 69	D. Drechsel, S.S. Kamalov, L. Tiator	(MAINZ, JINR)
DUGGER	07	PR C76 025211	M. Dugger et al.	(JLab CLAS Collab.)
ARNDT	06	PR C74 045205	R.A. Arndt et al.	(GWU)
ARNDT	04	PR C69 035213	R.A. Arndt et al.	(GWU, TRIU)
STAROSTIN	03	PR C67 068201	A. Starostin et al.	(BNL Crystal Ball Collab.)
PENNER	02C	PR C66 055211	G. Penner, U. Mosel	(GIES)
PENNER	02D	PR C66 055212	G. Penner, U. Mosel	(GIES)
BAI	01B	PL B510 75	J.Z. Bai et al.	(BES Collab.)
THOMPSON	01	PRL 86 1702	R. Thompson et al.	(JLab CLAS Collab.)
VRANA	00	PRPL 328 181	T.P. Vrana, S.A. Dytman, T.-S.H. Lee	(JLab CLAS Collab.)
ARMSTRONG	99B	PR D60 052004	C.S. Armstrong et al.	(PITT, ANL)
MUKHOPAD... 95B	PL B364 1		N.C. Mukhopadhyay, J.F. Zhang, M. Benmerrouche	
HOEHLER	93	πN Newsletter 9 1	G. Hohlner	(KARL)
CUTKOSKY	80	Toronto Conf. 19	R.E. Cutkosky et al.	(CMU, LBL) IJP
Also		PR D20 2839	R.E. Cutkosky et al.	(CMU, LBL) IJP
HOEHLER	79	PDAT 12-1	G. Hohlner et al.	(KARLT) IJP
Also		Toronto Conf. 3	R. Koch	(KARLT) IJP

N(1650) 1/2⁻ $I(J^P) = \frac{1}{2}(\frac{1}{2}^-)$ Status: * * * *

Older and obsolete values are listed and referenced in the 2014 edition, Chinese Physics **C38 070001** (2014).

N(1650) POLE POSITION

REAL PART

VALUE (MeV)	DOCUMENT ID	TECN	COMMENT
1640 to 1670 (≈ 1655) OUR ESTIMATE			
1658 ± 10	ANISOVICH 17A	DPWA	Multichannel
1660 ± 5	1 ANISOVICH 17A	L+P	$\gamma p, \pi^- p \rightarrow K\Lambda$
1660 ± 3.5 ± 1	2 SVARC 14	L+P	$\pi N \rightarrow \pi N$
1640 ± 20	CUTKOSKY 80	IPWA	$\pi N \rightarrow \pi N$
1656	HUNT 19	DPWA	Multichannel
1672	ROENCHEN 15A	DPWA	Multichannel
1652 ± 7	SOKHOYAN 15A	DPWA	Multichannel
1650	SHKLYAR 13	DPWA	Multichannel
1647 ± 6	ANISOVICH 12A	DPWA	Multichannel
1646 ± 8	BATINIC 10	DPWA	$\pi N \rightarrow N\pi, N\eta$
1648	ARNDT 06	DPWA	$\pi N \rightarrow \pi N, \eta N$
1663	VRANA 00	DPWA	Multichannel
1670	HOEHLER 93	ARGD	$\pi N \rightarrow \pi N$

1 Statistical error only.
2 Fit to the amplitudes of HOEHLER 79.

-2xIMAGINARY PART

VALUE (MeV)	DOCUMENT ID	TECN	COMMENT
100 to 170 (≈ 135) OUR ESTIMATE			
102 ± 8	ANISOVICH 17A	DPWA	Multichannel
59 ± 16	1 ANISOVICH 17A	L+P	$\gamma p, \pi^- p \rightarrow K\Lambda$
167 ± 8 ± 2	2 SVARC 14	L+P	$\pi N \rightarrow \pi N$
150 ± 30	CUTKOSKY 80	IPWA	$\pi N \rightarrow \pi N$
130	HUNT 19	DPWA	Multichannel
137	ROENCHEN 15A	DPWA	Multichannel
102 ± 8	SOKHOYAN 15A	DPWA	Multichannel
89	SHKLYAR 13	DPWA	Multichannel
103 ± 8	ANISOVICH 12A	DPWA	Multichannel
204 ± 17	BATINIC 10	DPWA	$\pi N \rightarrow N\pi, N\eta$
80	ARNDT 06	DPWA	$\pi N \rightarrow \pi N, \eta N$
240	VRANA 00	DPWA	Multichannel
163	HOEHLER 93	ARGD	$\pi N \rightarrow \pi N$

1 Statistical error only.
2 Fit to the amplitudes of HOEHLER 79.

N(1650) ELASTIC POLE RESIDUE

MODULUS |r|

VALUE (MeV)	DOCUMENT ID	TECN	COMMENT
25 to 55 (≈ 45) OUR ESTIMATE			
27 ± 6	SOKHOYAN 15A	DPWA	Multichannel
47 ± 3 ± 1	1 SVARC 14	L+P	$\pi N \rightarrow \pi N$
60 ± 10	CUTKOSKY 80	IPWA	$\pi N \rightarrow \pi N$
37	ROENCHEN 15A	DPWA	Multichannel
19	SHKLYAR 13	DPWA	Multichannel
24 ± 3	ANISOVICH 12A	DPWA	Multichannel
100	BATINIC 10	DPWA	$\pi N \rightarrow N\pi, N\eta$
14	ARNDT 06	DPWA	$\pi N \rightarrow \pi N, \eta N$
39	HOEHLER 93	ARGD	$\pi N \rightarrow \pi N$

1 Fit to the amplitudes of HOEHLER 79.

Baryon Particle Listings

 $N(1650)$ PHASE θ

VALUE ($^{\circ}$)	DOCUMENT ID	TECN	COMMENT
-80 to -50 (≈ -70) OUR ESTIMATE			
-60 \pm 20	SOKHOYAN 15A	DPWA	Multichannel
-47 \pm 3 \pm 1	¹ SVARC 14	L+P	$\pi N \rightarrow \pi N$
-75 \pm 25	CUTKOSKY 80	IPWA	$\pi N \rightarrow \pi N$
••• We do not use the following data for averages, fits, limits, etc. •••			
-59	ROENCHEN 15A	DPWA	Multichannel
-46	SHKLYAR 13	DPWA	Multichannel
-75 \pm 12	ANISOVICH 12A	DPWA	Multichannel
-65	BATINIC 10	DPWA	$\pi N \rightarrow N\pi, N\eta$
-69	ARNDT 06	DPWA	$\pi N \rightarrow \pi N, \eta N$
-37	HOEHLER 93	ARGD	$\pi N \rightarrow \pi N$

¹ Fit to the amplitudes of HOEHLER 79. $N(1650)$ INELASTIC POLE RESIDUEThe "normalized residue" is the residue divided by $\Gamma_{pole}/2$.Normalized residue in $N\pi \rightarrow N(1650) \rightarrow N\eta$

MODULUS	PHASE ($^{\circ}$)	DOCUMENT ID	TECN	COMMENT
0.29 \pm 0.03	134 \pm 10	ANISOVICH 12A	DPWA	Multichannel
••• We do not use the following data for averages, fits, limits, etc. •••				
0.21	48	ROENCHEN 15A	DPWA	Multichannel

Normalized residue in $N\pi \rightarrow N(1650) \rightarrow \Lambda K$

MODULUS	PHASE ($^{\circ}$)	DOCUMENT ID	TECN	COMMENT
0.26 \pm 0.10	110 \pm 20	ANISOVICH 17A	DPWA	Multichannel
0.10 \pm 0.10	95 \pm 33	¹ ANISOVICH 17A	L+P	$\gamma p, \pi^- p \rightarrow \Lambda K$
••• We do not use the following data for averages, fits, limits, etc. •••				
0.20	-54	ROENCHEN 15A	DPWA	Multichannel
0.23 \pm 0.09	85 \pm 9	ANISOVICH 12A	DPWA	Multichannel

¹ Statistical error only.Normalized residue in $N\pi \rightarrow N(1650) \rightarrow \Sigma K$

MODULUS	PHASE ($^{\circ}$)	DOCUMENT ID	TECN	COMMENT
••• We do not use the following data for averages, fits, limits, etc. •••				
0.026	-74	ROENCHEN 15A	DPWA	Multichannel

Normalized residue in $N\pi \rightarrow N(1650) \rightarrow \Delta\pi, D\text{-wave}$

MODULUS	PHASE ($^{\circ}$)	DOCUMENT ID	TECN	COMMENT
0.19 \pm 0.06	-30 \pm 20	SOKHOYAN 15A	DPWA	Multichannel
••• We do not use the following data for averages, fits, limits, etc. •••				
0.23 \pm 0.04	-30 \pm 20	ANISOVICH 12A	DPWA	Multichannel

Normalized residue in $N\pi \rightarrow N(1650) \rightarrow N\sigma$

MODULUS	PHASE ($^{\circ}$)	DOCUMENT ID	TECN	COMMENT
0.20 \pm 0.15	undefined	SOKHOYAN 15A	DPWA	Multichannel

Normalized residue in $N\pi \rightarrow N(1650) \rightarrow N(1440)\pi$

MODULUS	PHASE ($^{\circ}$)	DOCUMENT ID	TECN	COMMENT
0.30 \pm 0.17	undefined	SOKHOYAN 15A	DPWA	Multichannel

 $N(1650)$ BREIT-WIGNER MASS

VALUE (MeV)	DOCUMENT ID	TECN	COMMENT
1635 to 1665 (≈ 1650) OUR ESTIMATE			
1657 \pm 6	GOLOVATCH 19	DPWA	$\gamma p \rightarrow \pi^+ \pi^- p$
1666 \pm 3	¹ HUNT 19	DPWA	Multichannel
1634 \pm 5	KASHEVAROV 17	DPWA	$\gamma p \rightarrow \eta p, \eta' p$
1654 \pm 6	SOKHOYAN 15A	DPWA	Multichannel
1665 \pm 2	¹ SHKLYAR 13	DPWA	Multichannel
1634.7 \pm 1.1	¹ ARNDT 06	DPWA	$\pi N \rightarrow \pi N, \eta N$
1650 \pm 30	CUTKOSKY 80	IPWA	$\pi N \rightarrow \pi N$
1670 \pm 8	HOEHLER 79	IPWA	$\pi N \rightarrow \pi N$
••• We do not use the following data for averages, fits, limits, etc. •••			
1651 \pm 6	ANISOVICH 12A	DPWA	Multichannel
1664 \pm 2	¹ SHRESTHA 12A	DPWA	Multichannel
1652 \pm 9	BATINIC 10	DPWA	$\pi N \rightarrow N\pi, N\eta$
1665 \pm 2	PENNER 02c	DPWA	Multichannel
1647 \pm 20	BAI 01b	BES	$J/\psi \rightarrow p\bar{p}\eta$
1689 \pm 12	VRANA 00	DPWA	Multichannel

¹ Statistical error only. $N(1650)$ BREIT-WIGNER WIDTH

VALUE (MeV)	DOCUMENT ID	TECN	COMMENT
100 to 150 (≈ 125) OUR ESTIMATE			
154 \pm 28	GOLOVATCH 19	DPWA	$\gamma p \rightarrow \pi^+ \pi^- p$
133 \pm 7	¹ HUNT 19	DPWA	Multichannel
128 \pm 16	KASHEVAROV 17	DPWA	$\gamma p \rightarrow \eta p, \eta' p$
102 \pm 8	SOKHOYAN 15A	DPWA	Multichannel
147 \pm 14	¹ SHKLYAR 13	DPWA	Multichannel
115.4 \pm 2.8	¹ ARNDT 06	DPWA	$\pi N \rightarrow \pi N, \eta N$
150 \pm 40	CUTKOSKY 80	IPWA	$\pi N \rightarrow \pi N$
180 \pm 20	HOEHLER 79	IPWA	$\pi N \rightarrow \pi N$

••• We do not use the following data for averages, fits, limits, etc. •••

104 \pm 10	ANISOVICH 12A	DPWA	Multichannel
126 \pm 3	¹ SHRESTHA 12A	DPWA	Multichannel
202 \pm 16	BATINIC 10	DPWA	$\pi N \rightarrow N\pi, N\eta$
138 \pm 7	PENNER 02c	DPWA	Multichannel
145 \pm 80	BAI 01b	BES	$J/\psi \rightarrow p\bar{p}\eta$
202 \pm 40	VRANA 00	DPWA	Multichannel

¹ Statistical error only. $N(1650)$ DECAY MODES

The following branching fractions are our estimates, not fits or averages.

Mode	Fraction (Γ_i/Γ)
Γ_1 $N\pi$	50-70 %
Γ_2 $N\eta$	15-35 %
Γ_3 ΛK	5-15 %
Γ_4 $N\pi\pi$	8-36 %
Γ_5 $\Delta(1232)\pi$	
Γ_6 $\Delta(1232)\pi, D\text{-wave}$	6-18 %
Γ_7 $N\rho$	
Γ_8 $N\rho, S=1/2$	
Γ_9 $N\rho, S=3/2, D\text{-wave}$	
Γ_{10} $N\sigma$	2-18 %
Γ_{11} $N(1440)\pi$	6-26 %
Γ_{12} $p\gamma, \text{helicity}=1/2$	0.04-0.20 %
Γ_{13} $n\gamma, \text{helicity}=1/2$	0.003-0.17 %

 $N(1650)$ BRANCHING RATIOS

$\Gamma(N\pi)/\Gamma_{total}$	DOCUMENT ID	TECN	COMMENT	Γ_1/Γ
50 to 70 (≈ 60) OUR ESTIMATE				
64 \pm 4	¹ HUNT 19	DPWA	Multichannel	
51 \pm 4	SOKHOYAN 15A	DPWA	Multichannel	
74 \pm 3	¹ SHKLYAR 13	DPWA	Multichannel	
65 \pm 10	CUTKOSKY 80	IPWA	$\pi N \rightarrow \pi N$	
61 \pm 4	HOEHLER 79	IPWA	$\pi N \rightarrow \pi N$	
••• We do not use the following data for averages, fits, limits, etc. •••				
51 \pm 4	ANISOVICH 12A	DPWA	Multichannel	
57 \pm 2	¹ SHRESTHA 12A	DPWA	Multichannel	
79 \pm 6	BATINIC 10	DPWA	$\pi N \rightarrow N\pi, N\eta$	
100	ARNDT 06	DPWA	$\pi N \rightarrow \pi N, \eta N$	
65 \pm 4	PENNER 02c	DPWA	Multichannel	
74 \pm 2	VRANA 00	DPWA	Multichannel	

¹ Statistical error only.

$\Gamma(N\eta)/\Gamma_{total}$	DOCUMENT ID	TECN	COMMENT	Γ_2/Γ
15 to 35 (≈ 25) OUR ESTIMATE				
0.8 \pm 0.6	¹ HUNT 19	DPWA	Multichannel	
28 \pm 11	² KASHEVAROV 17	DPWA	$\gamma p \rightarrow \eta p, \eta' p$	
< 3	SHKLYAR 13	DPWA	Multichannel	
18 \pm 4	ANISOVICH 12A	DPWA	Multichannel	
••• We do not use the following data for averages, fits, limits, etc. •••				
21 \pm 2	¹ SHRESTHA 12A	DPWA	Multichannel	
13 \pm 5	BATINIC 10	DPWA	$\pi N \rightarrow N\pi, N\eta$	
1.0 \pm 0.6	PENNER 02c	DPWA	Multichannel	
6 \pm 1	VRANA 00	DPWA	Multichannel	

¹ Statistical error only.² Assuming $A_{1/2} = 0.045 \text{ GeV}^{-1/2}$.

$\Gamma(\Lambda K)/\Gamma_{total}$	DOCUMENT ID	TECN	COMMENT	Γ_3/Γ
5 to 15 (≈ 10) OUR ESTIMATE				
3.5 \pm 0.2	¹ HUNT 19	DPWA	Multichannel	
10 \pm 5	ANISOVICH 12A	DPWA	Multichannel	
4 \pm 1	¹ SHKLYAR 05	DPWA	Multichannel	
••• We do not use the following data for averages, fits, limits, etc. •••				
8 \pm 1	¹ SHRESTHA 12A	DPWA	Multichannel	
2.7 \pm 0.4	PENNER 02c	DPWA	Multichannel	

¹ Statistical error only.

$\Gamma(N\pi\pi)/\Gamma_{total}$	DOCUMENT ID	TECN	COMMENT	Γ_4/Γ
0.12 \pm 0.02	GOLOVATCH 19	DPWA	$\gamma p \rightarrow \pi^+ \pi^- p$	

$\Gamma(\Delta(1232)\pi, D\text{-wave})/\Gamma_{\text{total}}$

VALUE (%)	DOCUMENT ID	TECN	COMMENT
< 0.2	¹ HUNT 19	DPWA	Multichannel
12 ± 6	SOKHOYAN 15A	DPWA	Multichannel
••• We do not use the following data for averages, fits, limits, etc. •••			
19 ± 9	ANISOVICH 12A	DPWA	Multichannel
7 ± 2	¹ SHRESTHA 12A	DPWA	Multichannel
2 ± 1	VRANA 00	DPWA	Multichannel

¹ Statistical error only.

$\Gamma(N\rho, S=1/2)/\Gamma_{\text{total}}$

VALUE (%)	DOCUMENT ID	TECN	COMMENT
1.8 ± 1.7	¹ HUNT 19	DPWA	Multichannel

¹ Statistical error only.

$\Gamma(N\rho, S=3/2, D\text{-wave})/\Gamma_{\text{total}}$

VALUE (%)	DOCUMENT ID	TECN	COMMENT
15 ± 3	¹ HUNT 19	DPWA	Multichannel

¹ Statistical error only.

$\Gamma(N\sigma)/\Gamma_{\text{total}}$

VALUE (%)	DOCUMENT ID	TECN	COMMENT
12 ± 4	¹ HUNT 19	DPWA	Multichannel
10 ± 8	SOKHOYAN 15A	DPWA	Multichannel
••• We do not use the following data for averages, fits, limits, etc. •••			
< 1	¹ SHRESTHA 12A	DPWA	Multichannel
1 ± 1	VRANA 00	DPWA	Multichannel

¹ Statistical error only.

$\Gamma(N(1440)\pi)/\Gamma_{\text{total}}$

VALUE (%)	DOCUMENT ID	TECN	COMMENT
2 ± 1	¹ HUNT 19	DPWA	Multichannel
16 ± 10	SOKHOYAN 15A	DPWA	Multichannel
••• We do not use the following data for averages, fits, limits, etc. •••			
< 1	¹ SHRESTHA 12A	DPWA	Multichannel
3 ± 1	VRANA 00	DPWA	Multichannel

¹ Statistical error only.

$N(1650)$ PHOTON DECAY AMPLITUDES AT THE POLE

$N(1650) \rightarrow p\gamma$, helicity-1/2 amplitude $A_{1/2}$

MODULUS ($\text{GeV}^{-1/2}$)	PHASE ($^\circ$)	DOCUMENT ID	TECN	COMMENT
0.032 ± 0.006	7 ± 7	ANISOVICH 17D	DPWA	Multichannel
0.023 + 0.003 - 0.008	6 + 28 - 15	ROENCHEN 14	DPWA	
••• We do not use the following data for averages, fits, limits, etc. •••				
0.032 ± 0.007	-2 ± 11	ANISOVICH 15A	DPWA	Multichannel
0.059	-14	ROENCHEN 15A	DPWA	Multichannel
0.032 ± 0.006	-2 ± 11	SOKHOYAN 15A	DPWA	Multichannel

$N(1650) \rightarrow n\gamma$, helicity-1/2 amplitude $A_{1/2}$

MODULUS ($\text{GeV}^{-1/2}$)	PHASE ($^\circ$)	DOCUMENT ID	TECN	COMMENT
0.016 ± 0.004	-28 ± 10	ANISOVICH 17D	DPWA	Multichannel
••• We do not use the following data for averages, fits, limits, etc. •••				
0.019 ± 0.006	0 ± 15	ANISOVICH 15A	DPWA	Multichannel

$N(1650)$ BREIT-WIGNER PHOTON DECAY AMPLITUDES

$N(1650) \rightarrow p\gamma$, helicity-1/2 amplitude $A_{1/2}$

VALUE ($\text{GeV}^{-1/2}$)	DOCUMENT ID	TECN	COMMENT
0.035 to 0.055 (≈ 0.045) OUR ESTIMATE			
0.0605 ± 0.0077	GOLOVATCH 19	DPWA	$\gamma p \rightarrow \pi^+ \pi^- p$
0.048 ± 0.003	¹ HUNT 19	DPWA	Multichannel
0.032 ± 0.006	SOKHOYAN 15A	DPWA	Multichannel
0.063 ± 0.006	¹ SHKLYAR 13	DPWA	Multichannel
0.055 ± 0.030	¹ WORKMAN 12A	DPWA	$\gamma N \rightarrow N\pi$
0.022 ± 0.007	¹ DUGGER 07	DPWA	$\gamma N \rightarrow \pi N$
••• We do not use the following data for averages, fits, limits, etc. •••			
0.033 ± 0.007	ANISOVICH 12A	DPWA	Multichannel
0.030 ± 0.003	¹ SHRESTHA 12A	DPWA	Multichannel
0.033	DRECHSEL 07	DPWA	$\gamma N \rightarrow \pi N$
0.049	PENNER 02D	DPWA	Multichannel

¹ Statistical error only.

$N(1650) \rightarrow n\gamma$, helicity-1/2 amplitude $A_{1/2}$

VALUE ($\text{GeV}^{-1/2}$)	DOCUMENT ID	TECN	COMMENT
-0.040 to 0.030 (≈ -0.010) OUR ESTIMATE			
0.001 ± 0.006	¹ HUNT 19	DPWA	Multichannel
0.025 ± 0.020	ANISOVICH 13B	DPWA	Multichannel
-0.040 ± 0.010	¹ CHEN 12A	DPWA	$\gamma N \rightarrow \pi N$

••• We do not use the following data for averages, fits, limits, etc. •••

0.011 ± 0.002	¹ SHRESTHA 12A	DPWA	Multichannel
0.009	DRECHSEL 07	DPWA	$\gamma N \rightarrow \pi N$
-0.011	PENNER 02D	DPWA	Multichannel

¹ Statistical error only.

$N(1650)$ REFERENCES

For early references, see Physics Letters **111B** 1 (1982).

GOLOVATCH 19	PL B788 371	E. Golovatch et al.	(CLAS Collab.)
HUNT 19	PR C99 055205	B.C. Hunt, D.M. Manley	
ANISOVICH 17A	PRL 119 062004	A.V. Anisovich et al.	
ANISOVICH 17D	PR C95 035211	A.V. Anisovich et al.	
KASHEVAROV 17	PRL 118 212001	V.L. Kashevarov et al.	(A2/MAMI Collab.)
ANISOVICH 15A	EPJ A51 72	A.V. Anisovich et al.	
ROENCHEN 15A	EPJ A51 70	D. Roenchen et al.	
SOKHOYAN 15A	EPJ A51 95	V. Sokhoyan et al.	(CBELSA/TAPS Collab.)
PDG 14	CP C38 070001	K. Olive et al.	(PDG Collab.)
ROENCHEN 14	EPJ A50 101	D. Roenchen et al.	
Also	EPJ A51 63 (errata.)	D. Roenchen et al.	
SVARC 14	PR C89 045205	A. Svarc et al.	(RBI Zagreb, UNI Tuzla)
ANISOVICH 13B	EPJ A49 67	A.V. Anisovich et al.	
SHKLYAR 13	PR C87 015201	V. Shklyar, H. Lenske, U. Mosel	(GIES)
ANISOVICH 12A	EPJ A48 15	A.V. Anisovich et al.	(BONN, PNPI)
CHEN 12A	PR C86 015206	W. Chen et al.	(DUKE, GWU, MSST, ITEP+)
SHRESTHA 12A	PR C86 055203	M. Shrestha, D.M. Manley	(KSU)
WORKMAN 12A	PR C86 015202	R. Workman et al.	(GWU)
BATINIC 10	PR C82 038203	M. Batinic et al.	(ZAGR)
DRECHSEL 07	EPJ A34 69	D. Drechsel, S.S. Kamalov, L. Tiator	(MAINZ, JINR)
DUGGER 07	PR C76 025211	M. Dugger et al.	(JLab CLAS Collab.)
ARNDT 06	PR C74 045205	R.A. Arndt et al.	(GWU)
SHKLYAR 05	PR C72 015210	V. Shklyar, H. Lenske, U. Mosel	(GIES)
PENNER 02C	PR C66 055211	G. Penner, U. Mosel	(GIES)
PENNER 02D	PR C66 055212	G. Penner, U. Mosel	(GIES)
BAI 01B	PL B510 75	J.Z. Bai et al.	(BES Collab.)
VRANA 00	PRPL 328 181	T.P. Vrana, S.A. Dytman, T.-S.H. Lee	(PITT, ANL)
HOEHLER 93	πN Newsletter 9 1	G. Hoehler	(KARL)
CUTKOSKY 80	Toronto Conf. 19	R.E. Cutkosky et al.	(CMU, LBL) IJP
Also	PR D20 2839	R.E. Cutkosky et al.	(CMU, LBL) IJP
HOEHLER 79	PDAT 12-1	G. Hoehler et al.	(KARLT) IJP
Also	Toronto Conf. 3	R. Koch	(KARLT) IJP

$N(1675) 5/2^-$ $I(J^P) = \frac{1}{2}(\frac{5}{2}^-)$ Status: ***

Older and obsolete values are listed and referenced in the 2014 edition, Chinese Physics **C38** 070001 (2014).

$N(1675)$ POLE POSITION

REAL PART

VALUE (MeV)	DOCUMENT ID	TECN	COMMENT
1655 to 1665 (≈ 1660) OUR ESTIMATE			
1655 ± 4	SOKHOYAN 15A	DPWA	Multichannel
1654 ± 2	¹ SVARC 14	L+P	$\pi N \rightarrow \pi N$
1660 ± 10	CUTKOSKY 80	IPWA	$\pi N \rightarrow \pi N$
••• We do not use the following data for averages, fits, limits, etc. •••			
1646	HUNT 19	DPWA	Multichannel
1646	ROENCHEN 15A	DPWA	Multichannel
1640	SHKLYAR 13	DPWA	Multichannel
1654 ± 4	ANISOVICH 12A	DPWA	Multichannel
1658 ± 9	BATINIC 10	DPWA	$\pi N \rightarrow N\pi, N\eta$
1657	ARNDT 06	DPWA	$\pi N \rightarrow \pi N, \eta N$
1674	VRANA 00	DPWA	Multichannel
1656	HOEHLER 93	ARGD	$\pi N \rightarrow \pi N$

¹ Fit to the amplitudes of HOEHLER 79.

-2xIMAGINARY PART

VALUE (MeV)	DOCUMENT ID	TECN	COMMENT
125 to 150 (≈ 135) OUR ESTIMATE			
147 ± 5	SOKHOYAN 15A	DPWA	Multichannel
125 ± 3 ± 1	¹ SVARC 14	L+P	$\pi N \rightarrow \pi N$
140 ± 10	CUTKOSKY 80	IPWA	$\pi N \rightarrow \pi N$
••• We do not use the following data for averages, fits, limits, etc. •••			
146	HUNT 19	DPWA	Multichannel
125	ROENCHEN 15A	DPWA	Multichannel
108	SHKLYAR 13	DPWA	Multichannel
151 ± 5	ANISOVICH 12A	DPWA	Multichannel
137 ± 7	BATINIC 10	DPWA	$\pi N \rightarrow N\pi, N\eta$
139	ARNDT 06	DPWA	$\pi N \rightarrow \pi N, \eta N$
120	VRANA 00	DPWA	Multichannel
126	HOEHLER 93	ARGD	$\pi N \rightarrow \pi N$

¹ Fit to the amplitudes of HOEHLER 79.

$N(1675)$ ELASTIC POLE RESIDUE

MODULUS $|r|$

VALUE (MeV)	DOCUMENT ID	TECN	COMMENT
23 to 33 (≈ 28) OUR ESTIMATE			
28 ± 1	SOKHOYAN 15A	DPWA	Multichannel
23 ± 1	¹ SVARC 14	L+P	$\pi N \rightarrow \pi N$
31 ± 5	CUTKOSKY 80	IPWA	$\pi N \rightarrow \pi N$

Baryon Particle Listings

 $N(1675)$

••• We do not use the following data for averages, fits, limits, etc. •••

24	ROENCHEN	15A	DPWA	Multichannel
20	SHKLYAR	13	DPWA	Multichannel
28±1	ANISOVICH	12A	DPWA	Multichannel
25	BATINIC	10	DPWA	$\pi N \rightarrow N\pi, N\eta$
27	ARNDT	06	DPWA	$\pi N \rightarrow \pi N, \eta N$
23	HOEHLER	93	ARGD	$\pi N \rightarrow \pi N$

¹ Fit to the amplitudes of HOEHLER 79.

PHASE θ

VALUE (°)	DOCUMENT ID	TECN	COMMENT
-----------	-------------	------	---------

-30 to -20 (≈ -25) OUR ESTIMATE

-24 ± 4	SOKHOYAN	15A	DPWA	Multichannel
-25 ± 2	¹ SVARC	14	L+P	$\pi N \rightarrow \pi N$
-30±10	CUTKOSKY	80	IPWA	$\pi N \rightarrow \pi N$

••• We do not use the following data for averages, fits, limits, etc. •••

-22	ROENCHEN	15A	DPWA	Multichannel
-49	SHKLYAR	13	DPWA	Multichannel
-26 ± 4	ANISOVICH	12A	DPWA	Multichannel
-16	BATINIC	10	DPWA	$\pi N \rightarrow N\pi, N\eta$
-21	ARNDT	06	DPWA	$\pi N \rightarrow \pi N, \eta N$
-22	HOEHLER	93	ARGD	$\pi N \rightarrow \pi N$

¹ Fit to the amplitudes of HOEHLER 79.

 $N(1675)$ INELASTIC POLE RESIDUE

The "normalized residue" is the residue divided by $\Gamma_{pole}/2$.

Normalized residue in $N\pi \rightarrow N(1675) \rightarrow \Delta\pi, D\text{-wave}$

MODULUS	PHASE (°)	DOCUMENT ID	TECN	COMMENT
---------	-----------	-------------	------	---------

0.33±0.04	90 ± 15	SOKHOYAN	15A	DPWA	Multichannel
-----------	---------	----------	-----	------	--------------

••• We do not use the following data for averages, fits, limits, etc. •••

0.33±0.05	82 ± 10	ANISOVICH	12A	DPWA	Multichannel
-----------	---------	-----------	-----	------	--------------

Normalized residue in $N\pi \rightarrow N(1675) \rightarrow N\eta$

MODULUS	PHASE (°)	DOCUMENT ID	TECN	COMMENT
---------	-----------	-------------	------	---------

••• We do not use the following data for averages, fits, limits, etc. •••

0.044	-43	ROENCHEN	15A	DPWA	Multichannel
-------	-----	----------	-----	------	--------------

Normalized residue in $N\pi \rightarrow N(1675) \rightarrow \Lambda K$

MODULUS	PHASE (°)	DOCUMENT ID	TECN	COMMENT
---------	-----------	-------------	------	---------

••• We do not use the following data for averages, fits, limits, etc. •••

0.001	100	ROENCHEN	15A	DPWA	Multichannel
-------	-----	----------	-----	------	--------------

Normalized residue in $N\pi \rightarrow N(1675) \rightarrow \Sigma K$

MODULUS	PHASE (°)	DOCUMENT ID	TECN	COMMENT
---------	-----------	-------------	------	---------

••• We do not use the following data for averages, fits, limits, etc. •••

0.031	-175	ROENCHEN	15A	DPWA	Multichannel
-------	------	----------	-----	------	--------------

Normalized residue in $N\pi \rightarrow N(1675) \rightarrow N\sigma$

MODULUS	PHASE (°)	DOCUMENT ID	TECN	COMMENT
---------	-----------	-------------	------	---------

••• We do not use the following data for averages, fits, limits, etc. •••

0.15±0.04	132 ± 18	ANISOVICH	12A	DPWA	Multichannel
-----------	----------	-----------	-----	------	--------------

 $N(1675)$ BREIT-WIGNER MASS

VALUE (MeV)	DOCUMENT ID	TECN	COMMENT
-------------	-------------	------	---------

1665 to 1680 (≈ 1675) OUR ESTIMATE

1669 ± 2	¹ HUNT	19	DPWA	Multichannel
1663 ± 4	SOKHOYAN	15A	DPWA	Multichannel
1666 ± 2	¹ SHKLYAR	13	DPWA	Multichannel
1674.1 ± 0.2	¹ ARNDT	06	DPWA	$\pi N \rightarrow \pi N, \eta N$
1675 ± 10	CUTKOSKY	80	IPWA	$\pi N \rightarrow \pi N$
1679 ± 8	HOEHLER	79	IPWA	$\pi N \rightarrow \pi N$

••• We do not use the following data for averages, fits, limits, etc. •••

1664 ± 5	ANISOVICH	12A	DPWA	Multichannel
1679 ± 1	¹ SHRESTHA	12A	DPWA	Multichannel
1679 ± 9	BATINIC	10	DPWA	$\pi N \rightarrow N\pi, N\eta$
1685 ± 4	VRANA	00	DPWA	Multichannel

¹ Statistical error only.

 $N(1675)$ BREIT-WIGNER WIDTH

VALUE (MeV)	DOCUMENT ID	TECN	COMMENT
-------------	-------------	------	---------

130 to 160 (≈ 145) OUR ESTIMATE

161 ± 8	¹ HUNT	19	DPWA	Multichannel
146 ± 6	SOKHOYAN	15A	DPWA	Multichannel
148 ± 1	¹ SHKLYAR	13	DPWA	Multichannel
146.5 ± 1.0	¹ ARNDT	06	DPWA	$\pi N \rightarrow \pi N, \eta N$
160 ± 20	CUTKOSKY	80	IPWA	$\pi N \rightarrow \pi N$
120 ± 15	HOEHLER	79	IPWA	$\pi N \rightarrow \pi N$

••• We do not use the following data for averages, fits, limits, etc. •••

152 ± 7	ANISOVICH	12A	DPWA	Multichannel
145 ± 4	¹ SHRESTHA	12A	DPWA	Multichannel
152 ± 8	BATINIC	10	DPWA	$\pi N \rightarrow N\pi, N\eta$
131 ± 10	VRANA	00	DPWA	Multichannel

¹ Statistical error only.

 $N(1675)$ DECAY MODES

The following branching fractions are our estimates, not fits or averages.

Mode	Fraction (Γ_i/Γ)
Γ_1 $N\pi$	38-42 %
Γ_2 $N\eta$	< 1 %
Γ_3 ΛK	
Γ_4 $N\pi\pi$	25-45 %
Γ_5 $\Delta(1232)\pi$	
Γ_6 $\Delta(1232)\pi, D\text{-wave}$	23-37 %
Γ_7 $N\rho$	
Γ_8 $N\rho, S=1/2$	
Γ_9 $N\rho, S=3/2, D\text{-wave}$	
Γ_{10} $N\sigma$	3-7 %
Γ_{11} $p\gamma$	0-0.02 %
Γ_{12} $p\gamma, \text{ helicity}=1/2$	0-0.01 %
Γ_{13} $p\gamma, \text{ helicity}=3/2$	0-0.01 %
Γ_{14} $n\gamma$	0-0.15 %
Γ_{15} $n\gamma, \text{ helicity}=1/2$	0-0.05 %
Γ_{16} $n\gamma, \text{ helicity}=3/2$	0-0.10 %

 $N(1675)$ BRANCHING RATIOS

$\Gamma(N\pi)/\Gamma_{total}$	VALUE (%)	DOCUMENT ID	TECN	COMMENT	Γ_1/Γ
-------------------------------	-----------	-------------	------	---------	-------------------

38 to 42 (≈ 40) OUR ESTIMATE

33 ± 1	¹ HUNT	19	DPWA	Multichannel
41 ± 2	SOKHOYAN	15A	DPWA	Multichannel
41 ± 1	¹ SHKLYAR	13	DPWA	Multichannel
39.3±0.1	¹ ARNDT	06	DPWA	$\pi N \rightarrow \pi N, \eta N$
38 ± 5	CUTKOSKY	80	IPWA	$\pi N \rightarrow \pi N$
38 ± 3	HOEHLER	79	IPWA	$\pi N \rightarrow \pi N$

••• We do not use the following data for averages, fits, limits, etc. •••

40 ± 3	ANISOVICH	12A	DPWA	Multichannel
38.6±0.6	¹ SHRESTHA	12A	DPWA	Multichannel
35 ± 4	BATINIC	10	DPWA	$\pi N \rightarrow N\pi, N\eta$
35 ± 1	VRANA	00	DPWA	Multichannel

¹ Statistical error only.

$\Gamma(N\eta)/\Gamma_{total}$	VALUE (%)	DOCUMENT ID	TECN	COMMENT	Γ_2/Γ
--------------------------------	-----------	-------------	------	---------	-------------------

2.0 to 0.3 OUR ESTIMATE

2.0±0.3	¹ HUNT	19	DPWA	Multichannel
<1	SHKLYAR	13	DPWA	Multichannel
<1	¹ SHRESTHA	12A	DPWA	Multichannel
0.1±0.1	BATINIC	10	DPWA	$\pi N \rightarrow N\pi, N\eta$
3 ± 3	THOMA	08	DPWA	Multichannel
0 ± 1	VRANA	00	DPWA	Multichannel

¹ Statistical error only.

$\Gamma(\Lambda K)/\Gamma_{total}$	VALUE (%)	DOCUMENT ID	TECN	COMMENT	Γ_3/Γ
------------------------------------	-----------	-------------	------	---------	-------------------

<0.04 OUR ESTIMATE

<0.04	¹ HUNT	19	DPWA	Multichannel
-------	-------------------	----	------	--------------

¹ Statistical error only.

$\Gamma(\Delta(1232)\pi, D\text{-wave})/\Gamma_{total}$	VALUE (%)	DOCUMENT ID	TECN	COMMENT	Γ_6/Γ
---	-----------	-------------	------	---------	-------------------

58.3±0.2	¹ HUNT	19	DPWA	Multichannel
30 ± 7	SOKHOYAN	15A	DPWA	Multichannel
33 ± 8	ANISOVICH	12A	DPWA	Multichannel
46 ± 1	¹ SHRESTHA	12A	DPWA	Multichannel
63 ± 2	VRANA	00	DPWA	Multichannel

••• We do not use the following data for averages, fits, limits, etc. •••

¹ Statistical error only.

$\Gamma(N\rho, S=1/2)/\Gamma_{total}$	VALUE (%)	DOCUMENT ID	TECN	COMMENT	Γ_8/Γ
---------------------------------------	-----------	-------------	------	---------	-------------------

<0.2	¹ HUNT	19	DPWA	Multichannel
------	-------------------	----	------	--------------

¹ Statistical error only.

$\Gamma(N\rho, S=3/2, D\text{-wave})/\Gamma_{\text{total}}$ Γ_9/Γ

VALUE (%)	DOCUMENT ID	TECN	COMMENT
0.4 ± 0.3	¹ HUNT 19	DPWA	Multichannel

¹ Statistical error only.

$\Gamma(N\sigma)/\Gamma_{\text{total}}$ Γ_{10}/Γ

VALUE (%)	DOCUMENT ID	TECN	COMMENT
5 ± 2	SOKHOYAN 15A	DPWA	Multichannel
7 ± 3	ANISOVICH 12A	DPWA	Multichannel

• • • We do not use the following data for averages, fits, limits, etc. • • •

N(1675) PHOTON DECAY AMPLITUDES AT THE POLE

N(1675) → pγ, helicity-1/2 amplitude A_{1/2}

MODULUS (GeV ^{-1/2})	PHASE (°)	DOCUMENT ID	TECN	COMMENT
0.022 ± 0.003	-12 ± 7	SOKHOYAN 15A	DPWA	Multichannel
0.022 ± 0.004 -0.007	49 ⁺⁵ ₋₂	ROENCHEN 14	DPWA	
0.032	36	ROENCHEN 15A	DPWA	Multichannel

• • • We do not use the following data for averages, fits, limits, etc. • • •

N(1675) → pγ, helicity-3/2 amplitude A_{3/2}

MODULUS (GeV ^{-1/2})	PHASE (°)	DOCUMENT ID	TECN	COMMENT
0.028 ± 0.006	-17 ± 6	SOKHOYAN 15A	DPWA	Multichannel
0.036 ± 0.004 -0.005	-30 ± 4	ROENCHEN 14	DPWA	
0.051	-9.3	ROENCHEN 15A	DPWA	Multichannel

• • • We do not use the following data for averages, fits, limits, etc. • • •

N(1675) BREIT-WIGNER PHOTON DECAY AMPLITUDES

N(1675) → pγ, helicity-1/2 amplitude A_{1/2}

VALUE (GeV ^{-1/2})	DOCUMENT ID	TECN	COMMENT
0.010 to 0.025 (≈ 0.018) OUR ESTIMATE			
0.026 ± 0.002	¹ HUNT 19	DPWA	Multichannel
0.022 ± 0.003	SOKHOYAN 15A	DPWA	Multichannel
0.009 ± 0.001	¹ SHKLYAR 13	DPWA	Multichannel
0.013 ± 0.001	¹ WORKMAN 12A	DPWA	γN → Nπ
0.018 ± 0.002	¹ DUGGER 07	DPWA	γN → πN
• • • We do not use the following data for averages, fits, limits, etc. • • •			
0.024 ± 0.003	ANISOVICH 12A	DPWA	Multichannel
0.011 ± 0.001	¹ SHRESTHA 12A	DPWA	Multichannel
0.015	DRECHSEL 07	DPWA	γN → πN

¹ Statistical error only.

N(1675) → pγ, helicity-3/2 amplitude A_{3/2}

VALUE (GeV ^{-1/2})	DOCUMENT ID	TECN	COMMENT
0.015 to 0.030 (≈ 0.022) OUR ESTIMATE			
0.005 ± 0.002	¹ HUNT 19	DPWA	Multichannel
0.027 ± 0.006	SOKHOYAN 15A	DPWA	Multichannel
0.021 ± 0.001	¹ SHKLYAR 13	DPWA	Multichannel
0.016 ± 0.001	¹ WORKMAN 12A	DPWA	γN → Nπ
0.021 ± 0.001	¹ DUGGER 07	DPWA	γN → πN
• • • We do not use the following data for averages, fits, limits, etc. • • •			
0.025 ± 0.007	ANISOVICH 12A	DPWA	Multichannel
0.020 ± 0.001	¹ SHRESTHA 12A	DPWA	Multichannel
0.022	DRECHSEL 07	DPWA	γN → πN

¹ Statistical error only.

N(1675) → nγ, helicity-1/2 amplitude A_{1/2}

VALUE (GeV ^{-1/2})	DOCUMENT ID	TECN	COMMENT
-0.065 to -0.055 (≈ -0.060) OUR ESTIMATE			
-0.069 ± 0.005	¹ HUNT 19	DPWA	Multichannel
-0.060 ± 0.007	ANISOVICH 13B	DPWA	Multichannel
-0.058 ± 0.002	¹ CHEN 12A	DPWA	γN → πN
• • • We do not use the following data for averages, fits, limits, etc. • • •			
-0.040 ± 0.004	¹ SHRESTHA 12A	DPWA	Multichannel
-0.062	DRECHSEL 07	DPWA	γN → πN

¹ Statistical error only.

N(1675) → nγ, helicity-3/2 amplitude A_{3/2}

VALUE (GeV ^{-1/2})	DOCUMENT ID	TECN	COMMENT
-0.095 to -0.075 (≈ -0.085) OUR ESTIMATE			
-0.031 ± 0.005	¹ HUNT 19	DPWA	Multichannel
-0.088 ± 0.010	ANISOVICH 13B	DPWA	Multichannel
-0.080 ± 0.005	¹ CHEN 12A	DPWA	γN → πN
• • • We do not use the following data for averages, fits, limits, etc. • • •			
-0.068 ± 0.004	¹ SHRESTHA 12A	DPWA	Multichannel
-0.084	DRECHSEL 07	DPWA	γN → πN

¹ Statistical error only.

N(1675) REFERENCES

For early references, see Physics Letters **111B** 1 (1982).

HUNT 19	PR C99 055205	B.C. Hunt, D.M. Manley
ROENCHEN 15A	EPJ A51 70	D. Roenchen <i>et al.</i>
SOKHOYAN 15A	EPJ A51 95	V. Sokhoyan <i>et al.</i> (CBELSA/TAPS Collab.)
PDC 14	CP C38 070001	K. Olive <i>et al.</i> (PDG Collab.)
ROENCHEN 14	EPJ A50 101	D. Roenchen <i>et al.</i>
Also	EPJ A51 63 (errat.)	D. Roenchen <i>et al.</i>
SVARC 14	PR C89 045205	A. Svarc <i>et al.</i> (RBI Zagreb, UNI Tuzla)
ANISOVICH 13B	EPJ A49 67	A.V. Anisovich <i>et al.</i>
SHKLYAR 13	PR C87 015201	V. Shklyar, H. Lenske, U. Mosel (GIES)
ANISOVICH 12A	EPJ A48 15	A.V. Anisovich <i>et al.</i> (BONN, PNPI)
CHEN 12A	PR C86 015206	W. Chen <i>et al.</i> (DUKE, GWU, MSST, ITEP+)
SHRESTHA 12A	PR C86 055203	M. Shrestha, D.M. Manley (KSU)
WORKMAN 12A	PR C86 015202	R. Workman <i>et al.</i> (GWU)
BATINIC 10	PR C82 038203	M. Batinic <i>et al.</i> (ZAGR)
THOMA 08	PL B659 87	U. Thoma <i>et al.</i> (CB-ELSA Collab.)
DRECHSEL 07	EPJ A34 69	D. Drechsel, S.S. Kamalov, L. Tiator (MAINZ, JINR)
DUGGER 07	PR C76 025211	M. Dugger <i>et al.</i> (JLab CLAS Collab.)
ARNDT 06	PR C74 045205	R.A. Arndt <i>et al.</i> (GWU)
VRANA 00	PRPL 328 181	T.P. Vrana, S.A. Dytman, T.-S.H. Lee (PITT, ANL)
HOEHLER 93	πN Newsletter 9 1	G. Hoehler (KARL)
CUTKOSKY 80	Toronto Conf. 19	R.E. Cutkosky <i>et al.</i> (CMU, LBL) IJP
Also	PR D20 2839	R.E. Cutkosky <i>et al.</i> (CMU, LBL) IJP
HOEHLER 79	PDAT 12-1	G. Hoehler <i>et al.</i> (KARLT) IJP
Also	Toronto Conf. 3	R. Koch (KARLT) IJP

N(1680) 5/2⁺

$I(J^P) = \frac{1}{2}(5_2^+)$ Status: * * * *

Older and obsolete values are listed and referenced in the 2014 edition, Chinese Physics **C38** 070001 (2014).

N(1680) POLE POSITION

REAL PART

VALUE (MeV)	DOCUMENT ID	TECN	COMMENT
1665 to 1680 (≈ 1675) OUR ESTIMATE			
1678 ± 5	SOKHOYAN 15A	DPWA	Multichannel
1674 ± 2 ± 1	¹ SVARC 14	L+P	πN → πN
1667 ± 5	CUTKOSKY 80	IPWA	πN → πN
• • • We do not use the following data for averages, fits, limits, etc. • • •			
1668	HUNT 19	DPWA	Multichannel
1669	ROENCHEN 15A	DPWA	Multichannel
1660	SHKLYAR 13	DPWA	Multichannel
1676 ± 6	ANISOVICH 12A	DPWA	Multichannel
1666 ± 8	BATINIC 10	DPWA	πN → Nπ, Nη
1674	ARNDT 06	DPWA	πN → πN, ηN
1667	VRANA 00	DPWA	Multichannel
1673	HOEHLER 93	ARGD	πN → πN

¹ Fit to the amplitudes of HOEHLER 79.

-2×IMAGINARY PART

VALUE (MeV)	DOCUMENT ID	TECN	COMMENT
110 to 135 (≈ 120) OUR ESTIMATE			
113 ± 4	SOKHOYAN 15A	DPWA	Multichannel
129 ± 3 ± 1	¹ SVARC 14	L+P	πN → πN
110 ± 10	CUTKOSKY 80	IPWA	πN → πN
• • • We do not use the following data for averages, fits, limits, etc. • • •			
118	HUNT 19	DPWA	Multichannel
100	ROENCHEN 15A	DPWA	Multichannel
98	SHKLYAR 13	DPWA	Multichannel
113 ± 4	ANISOVICH 12A	DPWA	Multichannel
135 ± 6	BATINIC 10	DPWA	πN → Nπ, Nη
115	ARNDT 06	DPWA	πN → πN, ηN
122	VRANA 00	DPWA	Multichannel
135	HOEHLER 93	ARGD	πN → πN

¹ Fit to the amplitudes of HOEHLER 79.

N(1680) ELASTIC POLE RESIDUE

MODULUS |r|

VALUE (MeV)	DOCUMENT ID	TECN	COMMENT
35 to 45 (≈ 40) OUR ESTIMATE			
45 ± 4	SOKHOYAN 15A	DPWA	Multichannel
44 ± 1 ± 1	¹ SVARC 14	L+P	πN → πN
34 ± 2	CUTKOSKY 80	IPWA	πN → πN
• • • We do not use the following data for averages, fits, limits, etc. • • •			
34	ROENCHEN 15A	DPWA	Multichannel
33	SHKLYAR 13	DPWA	Multichannel
43 ± 4	ANISOVICH 12A	DPWA	Multichannel
44	BATINIC 10	DPWA	πN → Nπ, Nη
42	ARNDT 06	DPWA	πN → πN, ηN
44	HOEHLER 93	ARGD	πN → πN

¹ Fit to the amplitudes of HOEHLER 79.

Baryon Particle Listings

 $N(1680)$ PHASE θ

VALUE ($^{\circ}$)	DOCUMENT ID	TECN	COMMENT
-20 to 10 (≈ -5) OUR ESTIMATE			
5 \pm 10	SOKHOYAN 15A	DPWA	Multichannel
-16 \pm 1 \pm 1	¹ SVARC 14	L+P	$\pi N \rightarrow \pi N$
-25 \pm 5	CUTKOSKY 80	IPWA	$\pi N \rightarrow \pi N$
••• We do not use the following data for averages, fits, limits, etc. •••			
-19	ROENCHEN 15A	DPWA	Multichannel
-32	SHKLYAR 13	DPWA	Multichannel
-2 \pm 10	ANISOVICH 12A	DPWA	Multichannel
-19	BATINIC 10	DPWA	$\pi N \rightarrow N\pi, N\eta$
-4	ARNDT 06	DPWA	$\pi N \rightarrow \pi N, \eta N$
-17	HOEHLER 93	ARGD	$\pi N \rightarrow \pi N$

¹ Fit to the amplitudes of HOEHLER 79.

 $N(1680)$ INELASTIC POLE RESIDUE

The "normalized residue" is the residue divided by $\Gamma_{pole}/2$.

Normalized residue in $N\pi \rightarrow N(1680) \rightarrow \Delta\pi, P$ -wave

MODULUS	PHASE ($^{\circ}$)	DOCUMENT ID	TECN	COMMENT
0.15 \pm 0.03	-60 \pm 30	SOKHOYAN 15A	DPWA	Multichannel
••• We do not use the following data for averages, fits, limits, etc. •••				
0.15 \pm 0.03	-70 \pm 45	ANISOVICH 12A	DPWA	Multichannel

Normalized residue in $N\pi \rightarrow N(1680) \rightarrow \Delta\pi, F$ -wave

MODULUS	PHASE ($^{\circ}$)	DOCUMENT ID	TECN	COMMENT
0.23 \pm 0.04	90 \pm 12	SOKHOYAN 15A	DPWA	Multichannel
••• We do not use the following data for averages, fits, limits, etc. •••				
0.23 \pm 0.04	85 \pm 15	ANISOVICH 12A	DPWA	Multichannel

Normalized residue in $N\pi \rightarrow N(1680) \rightarrow N\eta$

MODULUS	PHASE ($^{\circ}$)	DOCUMENT ID	TECN	COMMENT
••• We do not use the following data for averages, fits, limits, etc. •••				
0.027	136	ROENCHEN 15A	DPWA	Multichannel

Normalized residue in $N\pi \rightarrow N(1680) \rightarrow \Lambda K$

MODULUS	PHASE ($^{\circ}$)	DOCUMENT ID	TECN	COMMENT
••• We do not use the following data for averages, fits, limits, etc. •••				
0.001	90	ROENCHEN 15A	DPWA	Multichannel

Normalized residue in $N\pi \rightarrow N(1680) \rightarrow \Sigma K$

MODULUS	PHASE ($^{\circ}$)	DOCUMENT ID	TECN	COMMENT
••• We do not use the following data for averages, fits, limits, etc. •••				
0.004	148	ROENCHEN 15A	DPWA	Multichannel

Normalized residue in $N\pi \rightarrow N(1680) \rightarrow N(\pi\pi)_{S=0}^{I=0}$

MODULUS	PHASE ($^{\circ}$)	DOCUMENT ID	TECN	COMMENT
0.29 \pm 0.06	-45 \pm 15	SOKHOYAN 15A	DPWA	Multichannel
••• We do not use the following data for averages, fits, limits, etc. •••				
0.26 \pm 0.04	-56 \pm 15	ANISOVICH 12A	DPWA	Multichannel

 $N(1680)$ BREIT-WIGNER MASS

VALUE (MeV)	DOCUMENT ID	TECN	COMMENT
1680 to 1690 (≈ 1685) OUR ESTIMATE			
1686 \pm 5	GOLOVATCH 19	DPWA	$\gamma p \rightarrow \pi^+ \pi^- p$
1681.0 \pm 0.1	¹ HUNT 19	DPWA	Multichannel
1690 \pm 5	SOKHOYAN 15A	DPWA	Multichannel
1676 \pm 2	¹ SHKLYAR 13	DPWA	Multichannel
1680.1 \pm 0.2	¹ ARNDT 06	DPWA	$\pi N \rightarrow \pi N, \eta N$
1680 \pm 10	CUTKOSKY 80	IPWA	$\pi N \rightarrow \pi N$
1684 \pm 3	HOEHLER 79	IPWA	$\pi N \rightarrow \pi N$
••• We do not use the following data for averages, fits, limits, etc. •••			
1689 \pm 6	ANISOVICH 12A	DPWA	Multichannel
1682.7 \pm 0.5	¹ SHRESTHA 12A	DPWA	Multichannel
1680 \pm 7	BATINIC 10	DPWA	$\pi N \rightarrow N\pi, N\eta$
1679 \pm 3	VRANA 00	DPWA	Multichannel

¹ Statistical error only.

 $N(1680)$ BREIT-WIGNER WIDTH

VALUE (MeV)	DOCUMENT ID	TECN	COMMENT
115 to 130 (≈ 120) OUR ESTIMATE			
118 \pm 20	GOLOVATCH 19	DPWA	$\gamma p \rightarrow \pi^+ \pi^- p$
123 \pm 3	¹ HUNT 19	DPWA	Multichannel
119 \pm 4	SOKHOYAN 15A	DPWA	Multichannel
115 \pm 1	¹ SHKLYAR 13	DPWA	Multichannel
128.0 \pm 1.1	¹ ARNDT 06	DPWA	$\pi N \rightarrow \pi N, \eta N$
120 \pm 10	CUTKOSKY 80	IPWA	$\pi N \rightarrow \pi N$
128 \pm 8	HOEHLER 79	IPWA	$\pi N \rightarrow \pi N$

••• We do not use the following data for averages, fits, limits, etc. •••

118 \pm 6	ANISOVICH 12A	DPWA	Multichannel
126 \pm 1	¹ SHRESTHA 12A	DPWA	Multichannel
142 \pm 7	BATINIC 10	DPWA	$\pi N \rightarrow N\pi, N\eta$
128 \pm 9	VRANA 00	DPWA	Multichannel

¹ Statistical error only.

 $N(1680)$ DECAY MODES

The following branching fractions are our estimates, not fits or averages.

Mode	Fraction (Γ_i/Γ)
Γ_1 $N\pi$	60-70 %
Γ_2 $N\eta$	<1 %
Γ_3 ΛK	
Γ_4 $N\pi\pi$	20-40 %
Γ_5 $\Delta(1232)\pi$	11-23 %
Γ_6 $\Delta(1232)\pi, P$ -wave	4-10 %
Γ_7 $\Delta(1232)\pi, F$ -wave	1-13 %
Γ_8 $N\rho$	
Γ_9 $N\rho, S=3/2, P$ -wave	
Γ_{10} $N\rho, S=3/2, F$ -wave	
Γ_{11} $N\sigma$	9-19 %
Γ_{12} $p\gamma$	0.21-0.32 %
Γ_{13} $p\gamma, \text{helicity}=1/2$	0.001-0.011 %
Γ_{14} $p\gamma, \text{helicity}=3/2$	0.20-0.32 %
Γ_{15} $n\gamma$	0.021-0.046 %
Γ_{16} $n\gamma, \text{helicity}=1/2$	0.004-0.029 %
Γ_{17} $n\gamma, \text{helicity}=3/2$	0.01-0.024 %

 $N(1680)$ BRANCHING RATIOS

$\Gamma(N\pi)/\Gamma_{total}$	VALUE (%)	DOCUMENT ID	TECN	COMMENT	Γ_1/Γ
60 to 70 (≈ 65) OUR ESTIMATE					
68.0 \pm 0.1	¹ HUNT 19	DPWA	Multichannel		
62 \pm 4	SOKHOYAN 15A	DPWA	Multichannel		
68 \pm 1	¹ SHKLYAR 13	DPWA	Multichannel		
70.1 \pm 0.1	¹ ARNDT 06	DPWA	$\pi N \rightarrow \pi N, \eta N$		
62 \pm 5	CUTKOSKY 80	IPWA	$\pi N \rightarrow \pi N$		
65 \pm 2	HOEHLER 79	IPWA	$\pi N \rightarrow \pi N$		
••• We do not use the following data for averages, fits, limits, etc. •••					
64 \pm 5	ANISOVICH 12A	DPWA	Multichannel		
68.0 \pm 0.5	¹ SHRESTHA 12A	DPWA	Multichannel		
67 \pm 3	BATINIC 10	DPWA	$\pi N \rightarrow N\pi, N\eta$		
69 \pm 2	VRANA 00	DPWA	Multichannel		

¹ Statistical error only.

$\Gamma(N\eta)/\Gamma_{total}$	VALUE (%)	DOCUMENT ID	TECN	COMMENT	Γ_2/Γ
0.09 \pm 0.02	¹ HUNT 19	DPWA	Multichannel		
<1	SHKLYAR 13	DPWA	Multichannel		
0.15 $^{+0.35}_{-0.10}$	TIATOR 99	DPWA	$\gamma p \rightarrow p\eta$		
••• We do not use the following data for averages, fits, limits, etc. •••					
1.0 \pm 0.3	¹ SHRESTHA 12A	DPWA	Multichannel		
0.4 \pm 0.2	BATINIC 10	DPWA	$\pi N \rightarrow N\pi, N\eta$		
<1	THOMA 08	DPWA	Multichannel		
0 \pm 1	VRANA 00	DPWA	Multichannel		

¹ Statistical error only.

$\Gamma(\Lambda K)/\Gamma_{total}$	VALUE (%)	DOCUMENT ID	TECN	COMMENT	Γ_3/Γ
0.24 \pm 0.04					
0.24 \pm 0.04	GOLOVATCH 19	DPWA	$\gamma p \rightarrow \pi^+ \pi^- p$		

$\Gamma(\Delta(1232)\pi, P\text{-wave})/\Gamma_{total}$	VALUE (%)	DOCUMENT ID	TECN	COMMENT	Γ_6/Γ
13 \pm 1	¹ HUNT 19	DPWA	Multichannel		
7 \pm 3	SOKHOYAN 15A	DPWA	Multichannel		
••• We do not use the following data for averages, fits, limits, etc. •••					
5 \pm 3	ANISOVICH 12A	DPWA	Multichannel		
10.5 \pm 0.9	¹ SHRESTHA 12A	DPWA	Multichannel		
14 \pm 3	VRANA 00	DPWA	Multichannel		

¹ Statistical error only.

$\Gamma(\Delta(1232)\pi, F\text{-wave})/\Gamma_{total}$	VALUE (%)	DOCUMENT ID	TECN	COMMENT	Γ_7/Γ
< 0.3	¹ HUNT 19	DPWA	Multichannel		
10 \pm 3	SOKHOYAN 15A	DPWA	Multichannel		

See key on page 999

Baryon Particle Listings

$N(1680)$, $N(1700)$

••• We do not use the following data for averages, fits, limits, etc. •••

10 ± 3	ANISOVICH	12A	DPWA	Multichannel
1.0 ± 0.1	¹ SHRESTHA	12A	DPWA	Multichannel
1 ± 1	VRANA	00	DPWA	Multichannel

¹ Statistical error only. $\Gamma(N\rho, S=3/2, P\text{-wave})/\Gamma_{\text{total}}$ Γ_9/Γ

VALUE (%)	DOCUMENT ID	TECN	COMMENT
7 ± 1	¹ HUNT	19	DPWA Multichannel

¹ Statistical error only. $\Gamma(N\rho, S=3/2, F\text{-wave})/\Gamma_{\text{total}}$ Γ_{10}/Γ

VALUE (%)	DOCUMENT ID	TECN	COMMENT
2.4 ± 0.4	¹ HUNT	19	DPWA Multichannel

¹ Statistical error only. $\Gamma(N\sigma)/\Gamma_{\text{total}}$ Γ_{11}/Γ

VALUE (%)	DOCUMENT ID	TECN	COMMENT
8.7 ± 1.5	¹ HUNT	19	DPWA Multichannel
14 ± 5	SOKHOYAN	15A	DPWA Multichannel

••• We do not use the following data for averages, fits, limits, etc. •••

14 ± 7	ANISOVICH	12A	DPWA	Multichannel
9.4 ± 0.8	¹ SHRESTHA	12A	DPWA	Multichannel
9 ± 1	VRANA	00	DPWA	Multichannel

¹ Statistical error only. **$N(1680)$ PHOTON DECAY AMPLITUDES AT THE POLE** $N(1680) \rightarrow p\gamma$, helicity-1/2 amplitude $A_{1/2}$

MODULUS (GeV ^{-1/2})	PHASE (°)	DOCUMENT ID	TECN	COMMENT
-0.013 ± 0.003	-20 ± 17	SOKHOYAN	15A	DPWA Multichannel
-0.013 ± 0.002	-42 ⁺⁹ ₋₁₈	ROENCHEN	14	DPWA

••• We do not use the following data for averages, fits, limits, etc. •••

-0.022	-28	ROENCHEN	15A	DPWA Multichannel
--------	-----	----------	-----	-------------------

 $N(1680) \rightarrow p\gamma$, helicity-3/2 amplitude $A_{3/2}$

MODULUS (GeV ^{-1/2})	PHASE (°)	DOCUMENT ID	TECN	COMMENT
0.135 ± 0.005	1 ± 3	SOKHOYAN	15A	DPWA Multichannel
0.126 ± 0.001	-7 ⁺³ ₋₂	ROENCHEN	14	DPWA

••• We do not use the following data for averages, fits, limits, etc. •••

0.102	-11	ROENCHEN	15A	DPWA Multichannel
-------	-----	----------	-----	-------------------

 $N(1680)$ BREIT-WIGNER PHOTON DECAY AMPLITUDES $N(1680) \rightarrow p\gamma$, helicity-1/2 amplitude $A_{1/2}$

VALUE (GeV ^{-1/2})	DOCUMENT ID	TECN	COMMENT
-0.018 to -0.005 (≈ -0.010) OUR ESTIMATE			

-0.0278 ± 0.0036	GOLOVATCH	19	DPWA	$\gamma p \rightarrow \pi^+ \pi^- p$
-0.026 ± 0.004	¹ HUNT	19	DPWA	Multichannel
-0.015 ± 0.002	SOKHOYAN	15A	DPWA	Multichannel
0.003 ± 0.001	¹ SHKLYAR	13	DPWA	Multichannel
-0.007 ± 0.002	¹ WORKMAN	12A	DPWA	$\gamma N \rightarrow N\pi$
-0.017 ± 0.001	¹ DUGGER	07	DPWA	$\gamma N \rightarrow \pi N$

••• We do not use the following data for averages, fits, limits, etc. •••

-0.013 ± 0.003	ANISOVICH	12A	DPWA	Multichannel
-0.017 ± 0.001	¹ SHRESTHA	12A	DPWA	Multichannel
-0.025	DRECHSEL	07	DPWA	$\gamma N \rightarrow \pi N$

¹ Statistical error only. $N(1680) \rightarrow p\gamma$, helicity-3/2 amplitude $A_{3/2}$

VALUE (GeV ^{-1/2})	DOCUMENT ID	TECN	COMMENT
0.130 to 0.140 (≈ 0.135) OUR ESTIMATE			

0.128 ± 0.011	GOLOVATCH	19	DPWA	$\gamma p \rightarrow \pi^+ \pi^- p$
0.112 ± 0.005	¹ HUNT	19	DPWA	Multichannel
0.136 ± 0.005	SOKHOYAN	15A	DPWA	Multichannel
0.116 ± 0.001	¹ SHKLYAR	13	DPWA	Multichannel
0.140 ± 0.002	¹ WORKMAN	12A	DPWA	$\gamma N \rightarrow N\pi$
0.134 ± 0.002	¹ DUGGER	07	DPWA	$\gamma N \rightarrow \pi N$

••• We do not use the following data for averages, fits, limits, etc. •••

0.135 ± 0.006	ANISOVICH	12A	DPWA	Multichannel
0.136 ± 0.001	¹ SHRESTHA	12A	DPWA	Multichannel
0.134	DRECHSEL	07	DPWA	$\gamma N \rightarrow \pi N$

¹ Statistical error only. **$N(1680) \rightarrow n\gamma$, helicity-1/2 amplitude $A_{1/2}$**

VALUE (GeV ^{-1/2})	DOCUMENT ID	TECN	COMMENT
0.020 to 0.040 (≈ 0.030) OUR ESTIMATE			

0.005 ± 0.004	¹ HUNT	19	DPWA Multichannel
0.034 ± 0.006	ANISOVICH	13B	DPWA Multichannel
0.026 ± 0.004	¹ CHEN	12A	DPWA $\gamma N \rightarrow \pi N$

••• We do not use the following data for averages, fits, limits, etc. •••

0.029 ± 0.002	¹ SHRESTHA	12A	DPWA Multichannel
0.028	DRECHSEL	07	DPWA $\gamma N \rightarrow \pi N$

¹ Statistical error only. **$N(1680) \rightarrow n\gamma$, helicity-3/2 amplitude $A_{3/2}$**

VALUE (GeV ^{-1/2})	DOCUMENT ID	TECN	COMMENT
-0.050 to -0.025 (≈ -0.035) OUR ESTIMATE			

-0.061 ± 0.004	¹ HUNT	19	DPWA Multichannel
-0.044 ± 0.009	ANISOVICH	13B	DPWA Multichannel
-0.029 ± 0.002	¹ CHEN	12A	DPWA $\gamma N \rightarrow \pi N$

••• We do not use the following data for averages, fits, limits, etc. •••

-0.059 ± 0.002	¹ SHRESTHA	12A	DPWA Multichannel
-0.038	DRECHSEL	07	DPWA $\gamma N \rightarrow \pi N$

¹ Statistical error only. **$N(1680)$ REFERENCES**

For early references, see Physics Letters **111B** 1 (1982). For very early references, see Reviews of Modern Physics **37** 633 (1965).

GOLOVATCH	19	PL B788 371	E. Golovatch <i>et al.</i>	(CLAS Collab.)
HUNT	19	PR C99 055205	B.C. Hunt, D.M. Manley	
ROENCHEN	15A	EPJ A51 70	D. Roenchen <i>et al.</i>	
SOKHOYAN	15A	EPJ A51 95	V. Sokhoyan <i>et al.</i>	(CBELSA/TAPS Collab.)
PDG	14	CP C38 070001	K. Olive <i>et al.</i>	(PDG Collab.)
ROENCHEN	14	EPJ A50 101	D. Roenchen <i>et al.</i>	
Also		EPJ A51 63 (errata.)	D. Roenchen <i>et al.</i>	
SVARC	14	PR C89 045205	A. Svarc <i>et al.</i>	(RBI Zagreb, UNI Tuzla)
ANISOVICH	13B	EPJ A49 67	A.V. Anisovich <i>et al.</i>	
SHKLYAR	13	PR C87 015201	V. Shklyar, H. Lenske, U. Mosel	(GIES)
ANISOVICH	12A	EPJ A48 15	A.V. Anisovich <i>et al.</i>	(BONN, PNPI)
CHEN	12A	PR C86 015206	W. Chen <i>et al.</i>	(DUKE, GWU, MSST, ITP+)
SHRESTHA	12A	PR C86 055203	M. Shrestha, D.M. Manley	(KSU)
WORKMAN	12A	PR C86 015202	R. Workman <i>et al.</i>	(GWU)
BATINIC	10	PR C82 038203	M. Batinic <i>et al.</i>	(ZAGR)
THOMA	08	PL B659 87	U. Thoma <i>et al.</i>	(CB-ELSA Collab.)
DRECHSEL	07	EPJ A34 69	D. Drechsel, S.S. Kamalov, L. Tiator	(MAINZ, JINR)
DUGGER	07	PR C76 025211	M. Dugger <i>et al.</i>	(JLab CLAS Collab.)
ARNDT	06	PR C74 045205	R.A. Arndt <i>et al.</i>	(GWU)
VRANA	00	PRPL 328 181	T.P. Vrana, S.A. Dytman, T.-S.H. Lee	(PITT, ANL)
TIATOR	99	PR C60 035210	L. Tiator <i>et al.</i>	
HOEHLER	93	πN Newsletter 9 1	G. Hoehler	(KARL)
CUTKOSKY	80	Toronto Conf. 19	R.E. Cutkosky <i>et al.</i>	(CMU, LBL) IJP
Also		PR D20 2839	R.E. Cutkosky <i>et al.</i>	(CMU, LBL) IJP
HOEHLER	79	PDAT 12-1	G. Hoehler <i>et al.</i>	(KARLT) IJP
Also		Toronto Conf. 3	R. Koch	(KARLT) IJP

 $N(1700)$ 3/2⁻

$$I(J^P) = \frac{1}{2} \left(\frac{3}{2}^-\right) \text{ Status: } ** *$$

Older and obsolete values are listed and referenced in the 2014 edition, Chinese Physics **C38** 070001 (2014).

 $N(1700)$ POLE POSITION**REAL PART**

VALUE (MeV)	DOCUMENT ID	TECN	COMMENT
1650 to 1750 (≈ 1700) OUR ESTIMATE			

1780 ± 35	SOKHOYAN	15A	DPWA Multichannel
1757 ± 4 ± 1	¹ SVARC	14	L+P $\pi N \rightarrow \pi N$
1660 ± 30	CUTKOSKY	80	IPWA $\pi N \rightarrow \pi N$

••• We do not use the following data for averages, fits, limits, etc. •••

1647	HUNT	19	DPWA Multichannel
1770 ± 40	ANISOVICH	12A	DPWA Multichannel
1806 ± 23	BATINIC	10	DPWA $\pi N \rightarrow N\pi, N\eta$
1704	VRANA	00	DPWA Multichannel
1700	HOEHLER	93	SPED $\pi N \rightarrow \pi N$

¹ Fit to the amplitudes of HOEHLER 79.**-2xIMAGINARY PART**

VALUE (MeV)	DOCUMENT ID	TECN	COMMENT
100 to 300 (≈ 200) OUR ESTIMATE			

420 ± 140	SOKHOYAN	15A	DPWA Multichannel
136 ± 7 ± 4	¹ SVARC	14	L+P $\pi N \rightarrow \pi N$
90 ± 40	CUTKOSKY	80	IPWA $\pi N \rightarrow \pi N$

••• We do not use the following data for averages, fits, limits, etc. •••

79	HUNT	19	DPWA Multichannel
420 ± 180	ANISOVICH	12A	DPWA Multichannel
129 ± 33	BATINIC	10	DPWA $\pi N \rightarrow N\pi, N\eta$
156	VRANA	00	DPWA Multichannel
120	HOEHLER	93	SPED $\pi N \rightarrow \pi N$

¹ Fit to the amplitudes of HOEHLER 79.

Baryon Particle Listings

 $N(1700)$ $N(1700)$ ELASTIC POLE RESIDUEMODULUS $|r|$

VALUE (MeV)	DOCUMENT ID	TECN	COMMENT
5 to 50 (≈ 10) OUR ESTIMATE			
60 ± 30	SOKHOYAN	15A	DPWA Multichannel
7 ± 1 ± 1	¹ SVARC	14	L+P $\pi N \rightarrow \pi N$
6 ± 3	CUTKOSKY	80	IPWA $\pi N \rightarrow \pi N$
• • • We do not use the following data for averages, fits, limits, etc. • • •			
50 ± 40	ANISOVICH	12A	DPWA Multichannel
7	BATINIC	10	DPWA $\pi N \rightarrow N\pi, N\eta$
5	HOEHLER	93	SPED $\pi N \rightarrow \pi N$

¹ Fit to the amplitudes of HOEHLER 79.PHASE θ

VALUE (°)	DOCUMENT ID	TECN	COMMENT
-120 to 0 (≈ -90) OUR ESTIMATE			
-115 ± 30	SOKHOYAN	15A	DPWA Multichannel
-113 ± 4 ± 2	¹ SVARC	14	L+P $\pi N \rightarrow \pi N$
0 ± 50	CUTKOSKY	80	IPWA $\pi N \rightarrow \pi N$
• • • We do not use the following data for averages, fits, limits, etc. • • •			
-100 ± 40	ANISOVICH	12A	DPWA Multichannel
-34	BATINIC	10	DPWA $\pi N \rightarrow N\pi, N\eta$

¹ Fit to the amplitudes of HOEHLER 79. $N(1700)$ INELASTIC POLE RESIDUEThe "normalized residue" is the residue divided by $\Gamma_{pole}/2$.Normalized residue in $N\pi \rightarrow N(1700) \rightarrow \Delta\pi, S$ -wave

MODULUS	PHASE (°)	DOCUMENT ID	TECN	COMMENT
0.33 ± 0.10	-70 ± 25	SOKHOYAN	15A	DPWA Multichannel
• • • We do not use the following data for averages, fits, limits, etc. • • •				
0.34 ± 0.21	-60 ± 40	ANISOVICH	12A	DPWA Multichannel

Normalized residue in $N\pi \rightarrow N(1700) \rightarrow \Delta\pi, D$ -wave

MODULUS	PHASE (°)	DOCUMENT ID	TECN	COMMENT
0.10 ± 0.06	75 ± 30	SOKHOYAN	15A	DPWA Multichannel
• • • We do not use the following data for averages, fits, limits, etc. • • •				
0.08 ± 0.06	90 ± 35	ANISOVICH	12A	DPWA Multichannel

Normalized residue in $N\pi \rightarrow N(1700) \rightarrow N\sigma$

MODULUS	PHASE (°)	DOCUMENT ID	TECN	COMMENT
0.13 ± 0.08	-100 ± 35	SOKHOYAN	15A	DPWA Multichannel

Normalized residue in $N\pi \rightarrow N(1700) \rightarrow N(1440)\pi$

MODULUS	PHASE (°)	DOCUMENT ID	TECN	COMMENT
0.13 ± 0.05	40 ± 35	SOKHOYAN	15A	DPWA Multichannel

Normalized residue in $N\pi \rightarrow N(1700) \rightarrow N(1520)\pi, P$ -wave

MODULUS	PHASE (°)	DOCUMENT ID	TECN	COMMENT
0.07 ± 0.03	160 ± 45	SOKHOYAN	15A	DPWA Multichannel

 $N(1700)$ BREIT-WIGNER MASS

VALUE (MeV)	DOCUMENT ID	TECN	COMMENT
1650 to 1800 (≈ 1720) OUR ESTIMATE			
1653 ± 5	¹ HUNT	19	DPWA Multichannel
1800 ± 35	SOKHOYAN	15A	DPWA Multichannel
1675 ± 25	CUTKOSKY	80	IPWA $\pi N \rightarrow \pi N$
1731 ± 15	HOEHLER	79	IPWA $\pi N \rightarrow \pi N$
• • • We do not use the following data for averages, fits, limits, etc. • • •			
1790 ± 40	ANISOVICH	12A	DPWA Multichannel
1665 ± 3	¹ SHRESTHA	12A	DPWA Multichannel
1817 ± 22	BATINIC	10	DPWA $\pi N \rightarrow N\pi, N\eta$
1736 ± 33	VRANA	00	DPWA Multichannel

¹ Statistical error only. $N(1700)$ BREIT-WIGNER WIDTH

VALUE (MeV)	DOCUMENT ID	TECN	COMMENT
100 to 300 (≈ 200) OUR ESTIMATE			
81 ± 13	¹ HUNT	19	DPWA Multichannel
400 ± 100	SOKHOYAN	15A	DPWA Multichannel
90 ± 40	CUTKOSKY	80	IPWA $\pi N \rightarrow \pi N$
110 ± 30	HOEHLER	79	IPWA $\pi N \rightarrow \pi N$
• • • We do not use the following data for averages, fits, limits, etc. • • •			
390 ± 140	ANISOVICH	12A	DPWA Multichannel
56 ± 8	¹ SHRESTHA	12A	DPWA Multichannel
134 ± 37	BATINIC	10	DPWA $\pi N \rightarrow N\pi, N\eta$
175 ± 133	VRANA	00	DPWA Multichannel

¹ Statistical error only. $N(1700)$ DECAY MODES

The following branching fractions are our estimates, not fits or averages.

Mode	Fraction (Γ_i/Γ)
Γ_1 $N\pi$	7-17 %
Γ_2 $N\eta$	seen
Γ_3 $N\omega$	10-34 %
Γ_4 ΛK	
Γ_5 $N\pi\pi$	60-90 %
Γ_6 $\Delta(1232)\pi$	55-85 %
Γ_7 $\Delta(1232)\pi, S$ -wave	50-80 %
Γ_8 $\Delta(1232)\pi, D$ -wave	4-14 %
Γ_9 $N(1440)\pi$	3-11 %
Γ_{10} $N(1520)\pi$	<4 %
Γ_{11} $N\rho, S=3/2, S$ -wave	32-44 %
Γ_{12} $N\sigma$	2-14 %
Γ_{13} $p\gamma$	0.01-0.05 %
Γ_{14} $p\gamma, \text{helicity}=1/2$	
Γ_{15} $p\gamma, \text{helicity}=3/2$	0.002-0.026 %
Γ_{16} $n\gamma$	0.01-0.13 %
Γ_{17} $n\gamma, \text{helicity}=1/2$	0.0-0.09 %
Γ_{18} $n\gamma, \text{helicity}=3/2$	0.01-0.05 %

 $N(1700)$ BRANCHING RATIOS $\Gamma(N\pi)/\Gamma_{\text{total}}$ Γ_1/Γ

VALUE (%)	DOCUMENT ID	TECN	COMMENT
7 to 17 (≈ 12) OUR ESTIMATE			
3.7 ± 0.1	¹ HUNT	19	DPWA Multichannel
15 ± 6	SOKHOYAN	15A	DPWA Multichannel
11 ± 5	CUTKOSKY	80	IPWA $\pi N \rightarrow \pi N$
8 ± 3	HOEHLER	79	IPWA $\pi N \rightarrow \pi N$
• • • We do not use the following data for averages, fits, limits, etc. • • •			
12 ± 5	ANISOVICH	12A	DPWA Multichannel
2.8 ± 0.5	¹ SHRESTHA	12A	DPWA Multichannel
9 ± 6	BATINIC	10	DPWA $\pi N \rightarrow N\pi, N\eta$
4 ± 2	VRANA	00	DPWA Multichannel

¹ Statistical error only. $\Gamma(N\eta)/\Gamma_{\text{total}}$ Γ_2/Γ

VALUE (%)	DOCUMENT ID	TECN	COMMENT
1.1 ± 0.6	¹ HUNT	19	DPWA Multichannel
• • • We do not use the following data for averages, fits, limits, etc. • • •			
14 ± 5	BATINIC	10	DPWA $\pi N \rightarrow N\pi, N\eta$
10 ± 5	THOMA	08	DPWA Multichannel
0 ± 1	VRANA	00	DPWA Multichannel

¹ Statistical error only. $\Gamma(N\omega)/\Gamma_{\text{total}}$ Γ_3/Γ

VALUE (%)	DOCUMENT ID	TECN	COMMENT
22 ± 12	DENISENKO	16	DPWA Multichannel

 $\Gamma(\Lambda K)/\Gamma_{\text{total}}$ Γ_4/Γ

VALUE (%)	DOCUMENT ID	TECN	COMMENT
1.3 ± 0.7	¹ HUNT	19	DPWA Multichannel

¹ Statistical error only. $\Gamma(\Delta(1232)\pi, S\text{-wave})/\Gamma_{\text{total}}$ Γ_7/Γ

VALUE (%)	DOCUMENT ID	TECN	COMMENT
11 ± 8	¹ HUNT	19	DPWA Multichannel
65 ± 15	SOKHOYAN	15A	DPWA Multichannel
• • • We do not use the following data for averages, fits, limits, etc. • • •			
72 ± 23	ANISOVICH	12A	DPWA Multichannel
31 ± 9	¹ SHRESTHA	12A	DPWA Multichannel
11 ± 1	VRANA	00	DPWA Multichannel

¹ Statistical error only. $\Gamma(\Delta(1232)\pi, D\text{-wave})/\Gamma_{\text{total}}$ Γ_8/Γ

VALUE (%)	DOCUMENT ID	TECN	COMMENT
13 ± 5	¹ HUNT	19	DPWA Multichannel
9 ± 5	SOKHOYAN	15A	DPWA Multichannel
• • • We do not use the following data for averages, fits, limits, etc. • • •			
<10	ANISOVICH	12A	DPWA Multichannel
3 ± 2	¹ SHRESTHA	12A	DPWA Multichannel
79 ± 56	VRANA	00	DPWA Multichannel

¹ Statistical error only. $\Gamma(N(1440)\pi)/\Gamma_{\text{total}}$ Γ_9/Γ

VALUE (%)	DOCUMENT ID	TECN	COMMENT
7 ± 4	SOKHOYAN	15A	DPWA Multichannel

See key on page 999

Baryon Particle Listings

$N(1700)$, $N(1710)$

$\Gamma(N(1520)\pi)/\Gamma_{total}$	DOCUMENT ID	TECN	COMMENT	Γ_{10}/Γ
VALUE (%)				
<4	SOKHOYAN	15A	DPWA Multichannel	

$\Gamma(N\rho, S=3/2, S\text{-wave})/\Gamma_{total}$	DOCUMENT ID	TECN	COMMENT	Γ_{11}/Γ
VALUE (%)				
7.5 ± 3.6	¹ HUNT	19	DPWA Multichannel	
••• We do not use the following data for averages, fits, limits, etc. •••				
38 ± 6	¹ SHRESTHA	12A	DPWA Multichannel	
7 ± 1	VRANA	00	DPWA Multichannel	
¹ Statistical error only.				

$\Gamma(N\sigma)/\Gamma_{total}$	DOCUMENT ID	TECN	COMMENT	Γ_{12}/Γ
VALUE (%)				
62 ± 9	¹ HUNT	19	DPWA Multichannel	
8 ± 6	SOKHOYAN	15A	DPWA Multichannel	
••• We do not use the following data for averages, fits, limits, etc. •••				
24 ± 6	¹ SHRESTHA	12A	DPWA Multichannel	
18 ± 12	THOMA	08	DPWA Multichannel	
0 ± 1	VRANA	00	DPWA Multichannel	
¹ Statistical error only.				

$N(1700)$ PHOTON DECAY AMPLITUDES AT THE POLE

$N(1700) \rightarrow \rho\gamma$, helicity-1/2 amplitude $A_{1/2}$

MODULUS ($\text{GeV}^{-1/2}$)	PHASE ($^\circ$)	DOCUMENT ID	TECN	COMMENT
0.047 ± 0.016	75 ± 30	SOKHOYAN	15A	DPWA Multichannel

$N(1700) \rightarrow \rho\gamma$, helicity-3/2 amplitude $A_{3/2}$

MODULUS ($\text{GeV}^{-1/2}$)	PHASE ($^\circ$)	DOCUMENT ID	TECN	COMMENT
-0.041 ± 0.014	0 ± 20	SOKHOYAN	15A	DPWA Multichannel

$N(1700)$ BREIT-WIGNER PHOTON DECAY AMPLITUDES

$N(1700) \rightarrow \rho\gamma$, helicity-1/2 amplitude $A_{1/2}$

VALUE ($\text{GeV}^{-1/2}$)	DOCUMENT ID	TECN	COMMENT
0.032 ± 0.005	¹ HUNT	19	DPWA Multichannel
0.041 ± 0.017	ANISOVICH	12A	DPWA Multichannel
••• We do not use the following data for averages, fits, limits, etc. •••			
0.021 ± 0.005	¹ SHRESTHA	12A	DPWA Multichannel
¹ Statistical error only.			

$N(1700) \rightarrow \rho\gamma$, helicity-3/2 amplitude $A_{3/2}$

VALUE ($\text{GeV}^{-1/2}$)	DOCUMENT ID	TECN	COMMENT
0.034 ± 0.006	¹ HUNT	19	DPWA Multichannel
-0.037 ± 0.014	SOKHOYAN	15A	DPWA Multichannel
••• We do not use the following data for averages, fits, limits, etc. •••			
-0.034 ± 0.013	ANISOVICH	12A	DPWA Multichannel
0.050 ± 0.009	¹ SHRESTHA	12A	DPWA Multichannel
¹ Statistical error only.			

$N(1700) \rightarrow n\gamma$, helicity-1/2 amplitude $A_{1/2}$

VALUE ($\text{GeV}^{-1/2}$)	DOCUMENT ID	TECN	COMMENT
0.005 ± 0.011	¹ HUNT	19	DPWA Multichannel
0.025 ± 0.010	ANISOVICH	13B	DPWA Multichannel
••• We do not use the following data for averages, fits, limits, etc. •••			
-0.049 ± 0.008	¹ SHRESTHA	12A	DPWA Multichannel
¹ Statistical error only.			

$N(1700) \rightarrow n\gamma$, helicity-3/2 amplitude $A_{3/2}$

VALUE ($\text{GeV}^{-1/2}$)	DOCUMENT ID	TECN	COMMENT
-0.094 ± 0.017	¹ HUNT	19	DPWA Multichannel
-0.032 ± 0.018	ANISOVICH	13B	DPWA Multichannel
••• We do not use the following data for averages, fits, limits, etc. •••			
-0.092 ± 0.014	¹ SHRESTHA	12A	DPWA Multichannel
¹ Statistical error only.			

$N(1700)$ REFERENCES

For early references, see Physics Letters **111B** 1 (1982).

HUNT	19	PR C99 055205	B.C. Hunt, D.M. Manley
DENISENKO	16	PL B755 97	I. Denisenko et al.
SOKHOYAN	15A	EPJ A51 95	V. Sokhoyan et al.
PDG	14	CP C38 070001	K. Olive et al. (PDG Collab.)
SVARC	14	PR C89 045205	A. Svarc et al. (RBI Zagreb, UNI Tuzla)
ANISOVICH	13B	EPJ A49 67	A.V. Anisovich et al.
ANISOVICH	12A	EPJ A48 15	A.V. Anisovich et al. (BONN, PNPI)
SHRESTHA	12A	PR C86 055203	M. Shrestha, D.M. Manley (KSU)
BATINIC	10	PR C82 038203	M. Batinic et al. (ZAGR)
THOMA	08	PL B659 87	U. Thoma et al. (CB-ELSA Collab.)
VRANA	00	PRPL 328 181	T.P. Vrana, S.A. Dytman, T.-S.H. Lee (PITT, ANL)
HOEHLER	93	π -N Newsletter 9 1	G. Hohlner (KARL)
CUTKOSKY	80	Toronto Conf. 19	R.E. Cutkosky et al. (CMU, LBL) IUP
Also		PR D20 2839	R.E. Cutkosky et al. (CMU, LBL) IUP
HOEHLER	79	PDAT 12-1	G. Hohlner et al. (KARLT) IUP
Also		Toronto Conf. 3	R. Koch (KARLT) IUP

$N(1710) 1/2^+$

$$I(J^P) = \frac{1}{2}(\frac{1}{2}^+) \text{ Status: } ****$$

Older and obsolete values are listed and referenced in the 2014 edition, Chinese Physics **C38** 070001 (2014).

$N(1710)$ POLE POSITION

REAL PART	DOCUMENT ID	TECN	COMMENT
VALUE (MeV)			
1680 to 1720 (≈ 1700) OUR ESTIMATE			
1690 ± 15	ANISOVICH	17A	DPWA Multichannel
1697 ± 23	¹ ANISOVICH	17A	L+P $\gamma p, \pi^- p \rightarrow K A$
$1770 \pm 5 \pm 2$	² SVARC	14	L+P $\pi N \rightarrow \pi N$
1690 ± 20	CUTKOSKY	80	IPWA $\pi N \rightarrow \pi N$
••• We do not use the following data for averages, fits, limits, etc. •••			
1615	HUNT	19	DPWA Multichannel
1651	ROENCHEN	15A	DPWA Multichannel
1690 ± 15	SOKHOYAN	15A	DPWA Multichannel
1690 ± 15	GUTZ	14	DPWA Multichannel
1670	SHKLYAR	13	DPWA Multichannel
1687 ± 17	ANISOVICH	12A	DPWA Multichannel
1711 ± 15	³ BATINIC	10	DPWA $\pi N \rightarrow N\pi, N\eta$
1679	VRANA	00	DPWA Multichannel
1690	HOEHLER	93	SPED $\pi N \rightarrow \pi N$
1698	CUTKOSKY	90	IPWA $\pi N \rightarrow \pi N$

- ¹ Statistical error only.
- ² Fit to the amplitudes of HOEHLER 79.
- ³ BATINIC 10 finds evidence for a second P_{11} state with all parameters except for the phase of the pole residue very similar to the parameters we give here.

$-2\times$ IMAGINARY PART

VALUE (MeV)	DOCUMENT ID	TECN	COMMENT
80 to 160 (≈ 120) OUR ESTIMATE			
155 ± 25	ANISOVICH	17A	DPWA Multichannel
84 ± 34	¹ ANISOVICH	17A	L+P $\gamma p, \pi^- p \rightarrow K A$
$98 \pm 8 \pm 5$	² SVARC	14	L+P $\pi N \rightarrow \pi N$
80 ± 20	CUTKOSKY	80	IPWA $\pi N \rightarrow \pi N$
••• We do not use the following data for averages, fits, limits, etc. •••			
169	HUNT	19	DPWA Multichannel
121	ROENCHEN	15A	DPWA Multichannel
170 ± 20	SOKHOYAN	15A	DPWA Multichannel
170 ± 20	GUTZ	14	DPWA Multichannel
159	SHKLYAR	13	DPWA Multichannel
200 ± 25	ANISOVICH	12A	DPWA Multichannel
174 ± 16	³ BATINIC	10	DPWA $\pi N \rightarrow N\pi, N\eta$
132	VRANA	00	DPWA Multichannel
200	HOEHLER	93	SPED $\pi N \rightarrow \pi N$
88	CUTKOSKY	90	IPWA $\pi N \rightarrow \pi N$

- ¹ Statistical error only.
- ² Fit to the amplitudes of HOEHLER 79.
- ³ BATINIC 10 finds evidence for a second P_{11} state with all parameters except for the phase of the pole residue very similar to the parameters we give here.

$N(1710)$ ELASTIC POLE RESIDUE

MODULUS $ r $	DOCUMENT ID	TECN	COMMENT
VALUE (MeV)			
4 to 10 (≈ 7) OUR ESTIMATE			
6 ± 3	SOKHOYAN	15A	DPWA Multichannel
$5 \pm 1 \pm 1$	¹ SVARC	14	L+P $\pi N \rightarrow \pi N$
8 ± 2	CUTKOSKY	80	IPWA $\pi N \rightarrow \pi N$
••• We do not use the following data for averages, fits, limits, etc. •••			
3.2	ROENCHEN	15A	DPWA Multichannel
6 ± 3	GUTZ	14	DPWA Multichannel
11	SHKLYAR	13	DPWA Multichannel
6 ± 4	ANISOVICH	12A	DPWA Multichannel
24	² BATINIC	10	DPWA $\pi N \rightarrow N\pi, N\eta$
15	HOEHLER	93	SPED $\pi N \rightarrow \pi N$
9	CUTKOSKY	90	IPWA $\pi N \rightarrow \pi N$

- ¹ Fit to the amplitudes of HOEHLER 79.
- ² BATINIC 10 finds evidence for a second P_{11} state with all parameters except for the phase of the pole residue very similar to the parameters we give here.

PHASE θ	DOCUMENT ID	TECN	COMMENT
VALUE ($^\circ$)			
120 to 260 (≈ 190) OUR ESTIMATE			
130 ± 35	SOKHOYAN	15A	DPWA Multichannel
$-104 \pm 7 \pm 3$	¹ SVARC	14	L+P $\pi N \rightarrow \pi N$
175 ± 35	CUTKOSKY	80	IPWA $\pi N \rightarrow \pi N$
••• We do not use the following data for averages, fits, limits, etc. •••			
55	ROENCHEN	15A	DPWA Multichannel
120 ± 45	GUTZ	14	DPWA Multichannel
9	SHKLYAR	13	DPWA Multichannel
120 ± 70	ANISOVICH	12A	DPWA Multichannel
20	² BATINIC	10	DPWA $\pi N \rightarrow N\pi, N\eta$
-167	CUTKOSKY	90	IPWA $\pi N \rightarrow \pi N$

Baryon Particle Listings

 $N(1710)$ ¹ Fit to the amplitudes of HOEHLER 79.² BATINIC 10 finds evidence for a second P_{11} state with all parameters except for the phase of the pole residue very similar to the parameters we give here. **$N(1710)$ INELASTIC POLE RESIDUE**The "normalized residue" is the residue divided by $\Gamma_{pole}/2$.**Normalized residue in $N\pi \rightarrow N(1710) \rightarrow N\eta$**

MODULUS	PHASE (°)	DOCUMENT ID	TECN	COMMENT
0.12 ± 0.04	0 ± 45	ANISOVICH 12A	DPWA	Multichannel
• • • We do not use the following data for averages, fits, limits, etc. • • •				
0.16	-180	ROENCHEN 15A	DPWA	Multichannel

Normalized residue in $N\pi \rightarrow N(1710) \rightarrow \Lambda K$

MODULUS	PHASE (°)	DOCUMENT ID	TECN	COMMENT
0.16 ± 0.05	-160 ± 25	ANISOVICH 17A	DPWA	Multichannel
$0.12^{+0.24}_{-0.12}$	-119 ± 83	¹ ANISOVICH 17A	L+P	$\gamma p, \pi^- p \rightarrow K\Lambda$
• • • We do not use the following data for averages, fits, limits, etc. • • •				
0.12	-32	ROENCHEN 15A	DPWA	Multichannel
0.17 ± 0.06	-110 ± 20	ANISOVICH 12A	DPWA	Multichannel

¹ Statistical error only.**Normalized residue in $N\pi \rightarrow N(1710) \rightarrow \Sigma K$**

MODULUS	PHASE (°)	DOCUMENT ID	TECN	COMMENT
• • • We do not use the following data for averages, fits, limits, etc. • • •				
0.004	-43	ROENCHEN 15A	DPWA	Multichannel

Normalized residue in $N\pi \rightarrow N(1710) \rightarrow N(1535)\pi$

MODULUS	PHASE (°)	DOCUMENT ID	TECN	COMMENT
0.10 ± 0.04	140 ± 40	GUTZ 14	DPWA	Multichannel

 $N(1710)$ BREIT-WIGNER MASS

VALUE (MeV)	DOCUMENT ID	TECN	COMMENT
1680 to 1740 (≈ 1710) OUR ESTIMATE			
1648 ± 16	¹ HUNT 19	DPWA	Multichannel
1715 ± 20	SOKHOYAN 15A	DPWA	Multichannel
1737 ± 17	¹ SHKLYAR 13	DPWA	Multichannel
1700 ± 50	CUTKOSKY 80	IPWA	$\pi N \rightarrow \pi N$
1723 ± 9	HOEHLER 79	IPWA	$\pi N \rightarrow \pi N$
• • • We do not use the following data for averages, fits, limits, etc. • • •			
1715 ± 20	GUTZ 14	DPWA	Multichannel
1710 ± 20	ANISOVICH 12A	DPWA	Multichannel
1662 ± 7	¹ SHRESTHA 12A	DPWA	Multichannel
1729 ± 16	² BATINIC 10	DPWA	$\pi N \rightarrow N\pi, N\eta$
1752 ± 3	PENNER 02c	DPWA	Multichannel
1699 ± 65	VRANA 00	DPWA	Multichannel

¹ Statistical error only.² BATINIC 10 finds evidence for a second P_{11} state with all parameters except for the phase of the pole residue very similar to the parameters we give here. **$N(1710)$ BREIT-WIGNER WIDTH**

VALUE (MeV)	DOCUMENT ID	TECN	COMMENT
80 to 200 (≈ 140) OUR ESTIMATE			
195 ± 46	¹ HUNT 19	DPWA	Multichannel
175 ± 15	SOKHOYAN 15A	DPWA	Multichannel
368 ± 120	¹ SHKLYAR 13	DPWA	Multichannel
93 ± 30	CUTKOSKY 90	IPWA	$\pi N \rightarrow \pi N$
90 ± 30	CUTKOSKY 80	IPWA	$\pi N \rightarrow \pi N$
120 ± 15	HOEHLER 79	IPWA	$\pi N \rightarrow \pi N$
• • • We do not use the following data for averages, fits, limits, etc. • • •			
175 ± 15	GUTZ 14	DPWA	Multichannel
200 ± 18	ANISOVICH 12A	DPWA	Multichannel
116 ± 17	¹ SHRESTHA 12A	DPWA	Multichannel
180 ± 17	² BATINIC 10	DPWA	$\pi N \rightarrow N\pi, N\eta$
386 ± 59	PENNER 02c	DPWA	Multichannel
143 ± 100	VRANA 00	DPWA	Multichannel

¹ Statistical error only.² BATINIC 10 finds evidence for a second P_{11} state with all parameters except for the phase of the pole residue very similar to the parameters we give here. **$N(1710)$ DECAY MODES**

The following branching fractions are our estimates, not fits or averages.

Mode	Fraction (Γ_i/Γ)
Γ_1 $N\pi$	5–20 %
Γ_2 $N\eta$	10–50 %
Γ_3 $N\omega$	1–5 %
Γ_4 ΛK	5–25 %

Γ_5 ΣK	seen
Γ_6 $N\pi\pi$	seen
Γ_7 $\Delta(1232)\pi$	
Γ_8 $\Delta(1232)\pi, P$ -wave	3–9 %
Γ_9 $N(1535)\pi$	9–21 %
Γ_{10} $N\rho$	
Γ_{11} $N\rho, S=1/2, P$ -wave	11–23 %
Γ_{12} $N\sigma$	
Γ_{13} $\rho\gamma, \text{helicity}=1/2$	0.002–0.08 %
Γ_{14} $n\gamma, \text{helicity}=1/2$	0.0–0.02 %

 $N(1710)$ BRANCHING RATIOS

$\Gamma(N\pi)/\Gamma_{total}$	DOCUMENT ID	TECN	COMMENT	Γ_1/Γ	
VALUE (%)					
5 to 20 (≈ 10) OUR ESTIMATE					
12 ± 6	¹ HUNT 19	DPWA	Multichannel		
5 ± 3	SOKHOYAN 15A	DPWA	Multichannel		
2 ± 2	¹ SHKLYAR 13	PWA	Multichannel		
20 ± 4	CUTKOSKY 80	IPWA	$\pi N \rightarrow \pi N$		
12 ± 4	HOEHLER 79	IPWA	$\pi N \rightarrow \pi N$		
• • • We do not use the following data for averages, fits, limits, etc. • • •					
5 ± 3	GUTZ 14	DPWA	Multichannel		
5 ± 4	ANISOVICH 12A	DPWA	Multichannel		
15 ± 4	¹ SHRESTHA 12A	DPWA	Multichannel		
22 ± 24	² BATINIC 10	DPWA	$\pi N \rightarrow N\pi, N\eta$		
14 ± 8	PENNER 02c	DPWA	Multichannel		
27 ± 13	VRANA 00	DPWA	Multichannel		

¹ Statistical error only.² BATINIC 10 finds evidence for a second P_{11} state with all parameters except for the phase of the pole residue very similar to the parameters we give here.

$\Gamma(N\eta)/\Gamma_{total}$	DOCUMENT ID	TECN	COMMENT	Γ_2/Γ	
VALUE (%)					
10 to 50 (≈ 30) OUR ESTIMATE					
17 ± 8	¹ HUNT 19	DPWA	Multichannel		
45 ± 4	¹ SHKLYAR 13	DPWA	Multichannel		
17 ± 10	ANISOVICH 12A	DPWA	Multichannel		
• • • We do not use the following data for averages, fits, limits, etc. • • •					
11 ± 7	¹ SHRESTHA 12A	DPWA	Multichannel		
6 ± 8	² BATINIC 10	DPWA	$\pi N \rightarrow N\pi, N\eta$		
36 ± 11	PENNER 02c	DPWA	Multichannel		
6 ± 1	VRANA 00	DPWA	Multichannel		

¹ Statistical error only.² BATINIC 10 finds evidence for a second P_{11} state with all parameters except for the phase of the pole residue very similar to the parameters we give here.

$\Gamma(N\omega)/\Gamma_{total}$	DOCUMENT ID	TECN	COMMENT	Γ_3/Γ	
VALUE (%)					
1 to 5 (≈ 3) OUR ESTIMATE					
2 ± 2	DENISENKO 16	DPWA	Multichannel		
3 ± 2	¹ SHKLYAR 13	DPWA	Multichannel		
• • • We do not use the following data for averages, fits, limits, etc. • • •					
13 ± 2	PENNER 02c	DPWA	Multichannel		

¹ Statistical error only.

$\Gamma(\Lambda K)/\Gamma_{total}$	DOCUMENT ID	TECN	COMMENT	Γ_4/Γ	
VALUE (%)					
5 to 25 (≈ 15) OUR ESTIMATE					
1.8 ± 1.5	¹ HUNT 19	DPWA	Multichannel		
23 ± 7	ANISOVICH 12A	DPWA	Multichannel		
5 ± 3	SHKLYAR 05	DPWA	Multichannel		
• • • We do not use the following data for averages, fits, limits, etc. • • •					
8 ± 4	¹ SHRESTHA 12A	DPWA	Multichannel		
5 ± 2	PENNER 02c	DPWA	Multichannel		
10 ± 10	VRANA 00	DPWA	Multichannel		

¹ Statistical error only.

$\Gamma(\Sigma K)/\Gamma_{total}$	DOCUMENT ID	TECN	COMMENT	Γ_5/Γ
VALUE (%)				
• • • We do not use the following data for averages, fits, limits, etc. • • •				
7 ± 7	PENNER 02c	DPWA	Multichannel	

$\Gamma(\Delta(1232)\pi, P$ -wave)/ Γ_{total}	DOCUMENT ID	TECN	COMMENT	Γ_8/Γ
VALUE (%)				
• • • We do not use the following data for averages, fits, limits, etc. • • •				
28 ± 9	¹ HUNT 19	DPWA	Multichannel	
6 ± 3	¹ SHRESTHA 12A	DPWA	Multichannel	
39 ± 8	VRANA 00	DPWA	Multichannel	

¹ Statistical error only.

See key on page 999

Baryon Particle Listings

$N(1710), N(1720)$

$\Gamma(N(1535)\pi)/\Gamma_{total}$	DOCUMENT ID	TECN	COMMENT
15 ± 6	GUTZ	14	DPWA Multichannel

$\Gamma(N\rho, S=1/2, P\text{-wave})/\Gamma_{total}$	DOCUMENT ID	TECN	COMMENT
17 ± 9	¹ HUNT	19	DPWA Multichannel

••• We do not use the following data for averages, fits, limits, etc. •••

17 ± 6	¹ SHRESTHA	12A	DPWA Multichannel
17 ± 1	VRANA	00	DPWA Multichannel

¹ Statistical error only.

$\Gamma(N\sigma)/\Gamma_{total}$	DOCUMENT ID	TECN	COMMENT
<16	¹ HUNT	19	DPWA Multichannel

¹ Statistical error only.

N(1710) PHOTON DECAY AMPLITUDES AT THE POLE

MODULUS (GeV ^{-1/2})	PHASE (°)	DOCUMENT ID	TECN	COMMENT
0.028 ± 0.009	103 ± 20	ROENCHEN	14	DPWA
-0.050 ± 0.002	-6			

••• We do not use the following data for averages, fits, limits, etc. •••

0.020	-83	ROENCHEN	15A	DPWA Multichannel
-------	-----	----------	-----	-------------------

N(1710) BREIT-WIGNER PHOTON DECAY AMPLITUDES

VALUE (GeV ^{-1/2})	DOCUMENT ID	TECN	COMMENT
0.014 ± 0.008	¹ HUNT	19	DPWA Multichannel
0.050 ± 0.010	SOKHOYAN	15A	DPWA Multichannel
-0.050 ± 0.001	¹ SHKLYAR	13	DPWA Multichannel

••• We do not use the following data for averages, fits, limits, etc. •••

0.05 ± 0.01	GUTZ	14	DPWA Multichannel
0.052 ± 0.015	ANISOVICH	12A	DPWA Multichannel
-0.008 ± 0.003	¹ SHRESTHA	12A	DPWA Multichannel
0.044	PENNER	02D	DPWA Multichannel

¹ Statistical error only.

VALUE (GeV ^{-1/2})	DOCUMENT ID	TECN	COMMENT
0.0053 ± 0.0003	¹ HUNT	19	DPWA Multichannel
-0.040 ± 0.020	ANISOVICH	13B	DPWA Multichannel

••• We do not use the following data for averages, fits, limits, etc. •••

0.017 ± 0.003	¹ SHRESTHA	12A	DPWA Multichannel
-0.024	PENNER	02D	DPWA Multichannel

¹ Statistical error only.

N(1710) REFERENCES

For early references, see Physics Letters **111B 1** (1982).

HUNT	19	PR C99 055205	B. C. Hunt, D. M. Manley
ANISOVICH	17A	PRL 119 062004	A. V. Anisovich et al.
DENISENKO	16	PL B75 97	I. Denisenko et al.
ROENCHEN	15A	EPJ A51 70	D. Roenchen et al.
SOKHOYAN	15A	EPJ A51 95	V. Sokhoyan et al. (CBELSA/TAPS Collab.)
GUTZ	14	EPJ A50 74	E. Gutz et al. (CBELSA/TAPS Collab.)
PDG	14	CP C38 070001	K. Olive et al. (PDG Collab.)
ROENCHEN	14	EPJ A50 101	D. Roenchen et al.
Also		EPJ A51 63 (errata.)	D. Roenchen et al.
SVARC	14	PR C89 045205	A. Svarc et al. (RBI Zagreb, UNI Tuzla)
ANISOVICH	13B	EPJ A49 67	A. V. Anisovich et al.
SHKLYAR	13	PR C87 015201	V. Shklyar, H. Lenske, U. Mosel (GIES)
ANISOVICH	12A	EPJ A48 15	A. V. Anisovich et al. (BONN, PHPI)
SHRESTHA	12A	PR C86 055203	M. Shrestha, D. M. Manley (KSU)
BATINIC	10	PR C82 038203	M. Batinic et al. (ZAGR)
SHKLYAR	05	PR C72 015210	V. Shklyar, H. Lenske, U. Mosel (GIES)
PENNER	02C	PR C66 055211	G. Penner, U. Mosel (GIES)
PENNER	02D	PR C66 055212	G. Penner, U. Mosel (GIES)
VRANA	00	PRPL 326 181	T. P. Vrana, S. A. Dytman, T.-S. H. Lee (PITT, ANL)
HOEHLER	93	πN Newsletter 9 1	G. Hohlner (KARL)
CUTKOSKY	90	PR D42 235	R. E. Cutkosky, S. Wang (CMU)
CUTKOSKY	80	Toronto Conf. 19	R. E. Cutkosky et al. (CMU, LBL) JJP
Also		PR D20 2839	R. E. Cutkosky et al. (KARLT) JJP
HOEHLER	79	PDAT 12-1	G. Hohlner et al. (KARLT) JJP
Also		Toronto Conf. 3	R. Koch (KARLT) JJP

$N(1720) 3/2^+$

$J(P) = \frac{1}{2}(3/2^+)$ Status: * * * *

Older and obsolete values are listed and referenced in the 2014 edition, Chinese Physics **C38** 070001 (2014).

N(1720) POLE POSITION

REAL PART	DOCUMENT ID	TECN	COMMENT
1660 ± 25	SOKHOYAN	15A	DPWA Multichannel
1677 ± 4 ± 1	¹ SVARC	14	L+P $\pi N \rightarrow \pi N$
1680 ± 30	CUTKOSKY	80	IPWA $\pi N \rightarrow \pi N$

••• We do not use the following data for averages, fits, limits, etc. •••

1654	HUNT	19	DPWA Multichannel
1710	ROENCHEN	15A	DPWA Multichannel
1670	SHKLYAR	13	DPWA Multichannel
1660 ± 30	ANISOVICH	12A	DPWA Multichannel
1691 ± 23	BATINIC	10	DPWA $\pi N \rightarrow N\pi, N\eta$
1666	ARNDT	06	DPWA $\pi N \rightarrow \pi N, \eta N$
1692	VRANA	00	DPWA Multichannel
1686	HOEHLER	93	SPED $\pi N \rightarrow \pi N$

¹ Fit to the amplitudes of HOEHLER 79.

-2xIMAGINARY PART

VALUE (MeV)	DOCUMENT ID	TECN	COMMENT
150 to 400 (≈ 250) OUR ESTIMATE			
430 ± 100	SOKHOYAN	15A	DPWA Multichannel
184 ± 8 ± 1	¹ SVARC	14	L+P $\pi N \rightarrow \pi N$
120 ± 40	CUTKOSKY	80	IPWA $\pi N \rightarrow \pi N$

••• We do not use the following data for averages, fits, limits, etc. •••

100	HUNT	19	DPWA Multichannel
219	ROENCHEN	15A	DPWA Multichannel
118	SHKLYAR	13	DPWA Multichannel
450 ± 100	ANISOVICH	12A	DPWA Multichannel
233 ± 23	BATINIC	10	DPWA $\pi N \rightarrow N\pi, N\eta$
355	ARNDT	06	DPWA $\pi N \rightarrow \pi N, \eta N$
94	VRANA	00	DPWA Multichannel
187	HOEHLER	93	SPED $\pi N \rightarrow \pi N$

¹ Fit to the amplitudes of HOEHLER 79.

N(1720) ELASTIC POLE RESIDUE

MODULUS r	DOCUMENT ID	TECN	COMMENT
10 to 25 (≈ 15) OUR ESTIMATE			
26 ± 10	SOKHOYAN	15A	DPWA Multichannel
13 ± 1	¹ SVARC	14	L+P $\pi N \rightarrow \pi N$
8 ± 2	CUTKOSKY	80	IPWA $\pi N \rightarrow \pi N$

••• We do not use the following data for averages, fits, limits, etc. •••

4.2	ROENCHEN	15A	DPWA Multichannel
12	SHKLYAR	13	DPWA Multichannel
22 ± 8	ANISOVICH	12A	DPWA Multichannel
20	BATINIC	10	DPWA $\pi N \rightarrow N\pi, N\eta$
25	ARNDT	06	DPWA $\pi N \rightarrow \pi N, \eta N$
15	HOEHLER	93	SPED $\pi N \rightarrow \pi N$

¹ Fit to the amplitudes of HOEHLER 79.

PHASE θ

VALUE (°)	DOCUMENT ID	TECN	COMMENT
-160 to -100 (≈ -130) OUR ESTIMATE			
-100 ± 25	SOKHOYAN	15A	DPWA Multichannel
-115 ± 3 ± 2	¹ SVARC	14	L+P $\pi N \rightarrow \pi N$
-160 ± 30	CUTKOSKY	80	IPWA $\pi N \rightarrow \pi N$

••• We do not use the following data for averages, fits, limits, etc. •••

-47	ROENCHEN	15A	DPWA Multichannel
-45	SHKLYAR	13	DPWA Multichannel
-115 ± 30	ANISOVICH	12A	DPWA Multichannel
-109	BATINIC	10	DPWA $\pi N \rightarrow N\pi, N\eta$
-94	ARNDT	06	DPWA $\pi N \rightarrow \pi N, \eta N$

¹ Fit to the amplitudes of HOEHLER 79.

N(1720) INELASTIC POLE RESIDUE

The "normalized residue" is the residue divided by $\Gamma_{pole}/2$.

Normalized residue in $N\pi \rightarrow N(1720) \rightarrow N\eta$	DOCUMENT ID	TECN	COMMENT
0.03 ± 0.02	ANISOVICH	12A	DPWA Multichannel
0.007	ROENCHEN	15A	DPWA Multichannel

••• We do not use the following data for averages, fits, limits, etc. •••

Normalized residue in $N\pi \rightarrow N(1720) \rightarrow \Lambda K$	DOCUMENT ID	TECN	COMMENT
0.06 ± 0.04	ANISOVICH	12A	DPWA Multichannel
0.011	ROENCHEN	15A	DPWA Multichannel

••• We do not use the following data for averages, fits, limits, etc. •••

Baryon Particle Listings

 $N(1720)$ Normalized residue in $N\pi \rightarrow N(1720) \rightarrow \Sigma K$

MODULUS	PHASE (°)	DOCUMENT ID	TECN	COMMENT
0.002	79	ROENCHEN 15A	DPWA	Multichannel

• • • We do not use the following data for averages, fits, limits, etc. • • •

Normalized residue in $N\pi \rightarrow N(1720) \rightarrow \Delta\pi, P\text{-wave}$

MODULUS	PHASE (°)	DOCUMENT ID	TECN	COMMENT
0.28±0.09	95 ± 30	SOKHOYAN 15A	DPWA	Multichannel
0.29±0.08	80 ± 40	ANISOVICH 12A	DPWA	Multichannel

• • • We do not use the following data for averages, fits, limits, etc. • • •

Normalized residue in $N\pi \rightarrow N(1720) \rightarrow \Delta\pi, F\text{-wave}$

MODULUS	PHASE (°)	DOCUMENT ID	TECN	COMMENT
0.07±0.05		SOKHOYAN 15A	DPWA	Multichannel
0.03±0.03		ANISOVICH 12A	DPWA	Multichannel

• • • We do not use the following data for averages, fits, limits, etc. • • •

Normalized residue in $N\pi \rightarrow N(1720) \rightarrow N\sigma$

MODULUS	PHASE (°)	DOCUMENT ID	TECN	COMMENT
0.08±0.04	-110 ± 35	SOKHOYAN 15A	DPWA	Multichannel

Normalized residue in $N\pi \rightarrow N(1720) \rightarrow N(1520)\pi, S\text{-wave}$

MODULUS	PHASE (°)	DOCUMENT ID	TECN	COMMENT
0.05±0.04	undefined	SOKHOYAN 15A	DPWA	Multichannel

 $N(1720)$ BREIT-WIGNER MASS

VALUE (MeV)	DOCUMENT ID	TECN	COMMENT
1680 to 1750 (≈ 1720) OUR ESTIMATE			
1745 ± 6	GOLOVATCH 19	DPWA	$\gamma p \rightarrow \pi^+ \pi^- p$
1711 ± 4	¹ HUNT 19	DPWA	Multichannel
1690 ± 30	SOKHOYAN 15A	DPWA	Multichannel
1700 ± 10	¹ SHKLYAR 13	DPWA	Multichannel
1763.8 ± 4.6	ARNDT 06	DPWA	$\pi N \rightarrow \pi N, \eta N$
1700 ± 50	CUTKOSKY 80	IPWA	$\pi N \rightarrow \pi N$
1710 ± 20	HOEHLER 79	IPWA	$\pi N \rightarrow \pi N$
• • • We do not use the following data for averages, fits, limits, etc. • • •			
1690 + 70 - 35	ANISOVICH 12A	DPWA	Multichannel
1720 ± 5	¹ SHRESTHA 12A	DPWA	Multichannel
1720 ± 18	BATINIC 10	DPWA	$\pi N \rightarrow N\pi, N\eta$
1705 ± 10	PENNER 02c	DPWA	Multichannel
1716 ± 112	VRANA 00	DPWA	Multichannel

¹ Statistical error only.

 $N(1720)$ BREIT-WIGNER WIDTH

VALUE (MeV)	DOCUMENT ID	TECN	COMMENT
150 to 400 (≈ 250) OUR ESTIMATE			
116 ± 27	GOLOVATCH 19	DPWA	$\gamma p \rightarrow \pi^+ \pi^- p$
229 ± 22	¹ HUNT 19	DPWA	Multichannel
420 ± 80	SOKHOYAN 15A	DPWA	Multichannel
152 ± 2	¹ SHKLYAR 13	DPWA	Multichannel
210 ± 22	ARNDT 06	DPWA	$\pi N \rightarrow \pi N, \eta N$
125 ± 70	CUTKOSKY 80	IPWA	$\pi N \rightarrow \pi N$
190 ± 30	HOEHLER 79	IPWA	$\pi N \rightarrow \pi N$
• • • We do not use the following data for averages, fits, limits, etc. • • •			
420±100	ANISOVICH 12A	DPWA	Multichannel
200 ± 20	¹ SHRESTHA 12A	DPWA	Multichannel
244 ± 28	BATINIC 10	DPWA	$\pi N \rightarrow N\pi, N\eta$
237 ± 73	PENNER 02c	DPWA	Multichannel
121 ± 39	VRANA 00	DPWA	Multichannel

¹ Statistical error only.

 $N(1720)$ DECAY MODES

The following branching fractions are our estimates, not fits or averages.

Mode	Fraction (Γ_j/Γ)
Γ_1 $N\pi$	8–14 %
Γ_2 $N\eta$	1–5 %
Γ_3 $N\omega$	12–40 %
Γ_4 ΛK	4–5 %
Γ_5 $N\pi\pi$	50–90 %
Γ_6 $\Delta(1232)\pi$	47–89 %
Γ_7 $\Delta(1232)\pi, P\text{-wave}$	47–77 %
Γ_8 $\Delta(1232)\pi, F\text{-wave}$	<12 %
Γ_9 $N\rho$	
Γ_{10} $N\rho, S=1/2, P\text{-wave}$	1–2 %
Γ_{11} $N\sigma$	2–14 %

Γ_{12} $N(1440)\pi$	<2 %
Γ_{13} $N(1520)\pi, S\text{-wave}$	1–5 %
Γ_{14} $\rho\gamma$	0.05–0.25 %
Γ_{15} $\rho\gamma, \text{helicity}=1/2$	0.05–0.15 %
Γ_{16} $\rho\gamma, \text{helicity}=3/2$	0.002–0.16 %
Γ_{17} $n\gamma$	0.0–0.016 %
Γ_{18} $n\gamma, \text{helicity}=1/2$	0.0–0.01 %
Γ_{19} $n\gamma, \text{helicity}=3/2$	0.0–0.015 %

 $N(1720)$ BRANCHING RATIOS

$\Gamma(N\pi)/\Gamma_{\text{total}}$	DOCUMENT ID	TECN	COMMENT	Γ_1/Γ
8 to 14 (≈ 11) OUR ESTIMATE				
18 ± 2	¹ HUNT 19	DPWA	Multichannel	
11 ± 4	SOKHOYAN 15A	DPWA	Multichannel	
17 ± 2	¹ SHKLYAR 13	DPWA	Multichannel	
9.4±0.5	ARNDT 06	DPWA	$\pi N \rightarrow \pi N, \eta N$	
10 ± 4	CUTKOSKY 80	IPWA	$\pi N \rightarrow \pi N$	
14 ± 3	HOEHLER 79	IPWA	$\pi N \rightarrow \pi N$	
• • • We do not use the following data for averages, fits, limits, etc. • • •				
10 ± 5	ANISOVICH 12A	DPWA	Multichannel	
13.6±0.6	¹ SHRESTHA 12A	DPWA	Multichannel	
18 ± 3	BATINIC 10	DPWA	$\pi N \rightarrow N\pi, N\eta$	
17 ± 2	PENNER 02c	DPWA	Multichannel	
5 ± 5	VRANA 00	DPWA	Multichannel	

¹ Statistical error only.

$\Gamma(N\eta)/\Gamma_{\text{total}}$	DOCUMENT ID	TECN	COMMENT	Γ_2/Γ
1 to 5 (≈ 3) OUR ESTIMATE				
3.8±0.5	¹ HUNT 19	DPWA	Multichannel	
< 1	SHKLYAR 13	DPWA	Multichannel	
3 ± 2	ANISOVICH 12A	DPWA	Multichannel	
• • • We do not use the following data for averages, fits, limits, etc. • • •				
< 1	¹ SHRESTHA 12A	DPWA	Multichannel	
0 ± 1	BATINIC 10	DPWA	$\pi N \rightarrow N\pi, N\eta$	
10 ± 7	THOMA 08	DPWA	Multichannel	
0.2±0.2	PENNER 02c	DPWA	Multichannel	
4 ± 1	VRANA 00	DPWA	Multichannel	

¹ Statistical error only.

$\Gamma(N\omega)/\Gamma_{\text{total}}$	DOCUMENT ID	TECN	COMMENT	Γ_3/Γ
26±14	DENISENKO 16	DPWA	Multichannel	

$\Gamma(\Lambda K)/\Gamma_{\text{total}}$	DOCUMENT ID	TECN	COMMENT	Γ_4/Γ
16 ± 3	¹ HUNT 19	DPWA	Multichannel	
4.3±0.4	SHKLYAR 05	DPWA	Multichannel	
• • • We do not use the following data for averages, fits, limits, etc. • • •				
2.8±0.4	¹ SHRESTHA 12A	DPWA	Multichannel	
12 ± 9	THOMA 08	DPWA	Multichannel	
9 ± 3	PENNER 02c	DPWA	Multichannel	

¹ Statistical error only.

$\Gamma(N\pi\pi)/\Gamma_{\text{total}}$	DOCUMENT ID	TECN	COMMENT	Γ_5/Γ
0.84±0.16	GOLOVATCH 19	DPWA	$\gamma p \rightarrow \pi^+ \pi^- p$	

$\Gamma(\Delta(1232)\pi, P\text{-wave})/\Gamma_{\text{total}}$	DOCUMENT ID	TECN	COMMENT	Γ_7/Γ
62±15	SOKHOYAN 15A	DPWA	Multichannel	
• • • We do not use the following data for averages, fits, limits, etc. • • •				
75±15	ANISOVICH 12A	DPWA	Multichannel	

$\Gamma(\Delta(1232)\pi, F\text{-wave})/\Gamma_{\text{total}}$	DOCUMENT ID	TECN	COMMENT	Γ_8/Γ
6±6	SOKHOYAN 15A	DPWA	Multichannel	

$\Gamma(N\rho, S=1/2, P\text{-wave})/\Gamma_{\text{total}}$	DOCUMENT ID	TECN	COMMENT	Γ_{10}/Γ
1.4±0.5	¹ SHRESTHA 12A	DPWA	Multichannel	
• • • We do not use the following data for averages, fits, limits, etc. • • •				
91 ± 1	VRANA 00	DPWA	Multichannel	

¹ Statistical error only.

$\Gamma(N\sigma)/\Gamma_{\text{total}}$	DOCUMENT ID	TECN	COMMENT	Γ_{11}/Γ
8±6	SOKHOYAN 15A	DPWA	Multichannel	

See key on page 999

Baryon Particle Listings

$N(1720)$, $N(1860)$

$\Gamma(N(1440)\pi)/\Gamma_{total}$				Γ_{12}/Γ
VALUE (%)	DOCUMENT ID	TECN	COMMENT	
<2	SOKHOYAN	15A	DPWA	Multichannel

$\Gamma(N(1520)\pi, S\text{-wave})/\Gamma_{total}$				Γ_{13}/Γ
VALUE (%)	DOCUMENT ID	TECN	COMMENT	
3±2	SOKHOYAN	15A	DPWA	Multichannel

$N(1720)$ PHOTON DECAY AMPLITUDES AT THE POLE

$N(1720) \rightarrow \rho\gamma$, helicity-1/2 amplitude $A_{1/2}$				
MODULUS ($\text{GeV}^{-1/2}$)	PHASE ($^\circ$)	DOCUMENT ID	TECN	COMMENT
0.115 ± 0.045	0 ± 35	SOKHOYAN	15A	DPWA Multichannel
0.051 ± 0.005	57 ± 9	ROENCHEN	14	DPWA
0.051 ± 0.004	57 ± 4	ROENCHEN	14	DPWA
• • • We do not use the following data for averages, fits, limits, etc. • • •				
0.039	5.3	ROENCHEN	15A	DPWA Multichannel

$N(1720) \rightarrow \rho\gamma$, helicity-3/2 amplitude $A_{3/2}$				
MODULUS ($\text{GeV}^{-1/2}$)	PHASE ($^\circ$)	DOCUMENT ID	TECN	COMMENT
0.140 ± 0.040	65 ± 35	SOKHOYAN	15A	DPWA Multichannel
0.014 + 0.009	102 + 29	ROENCHEN	14	DPWA
0.014 - 0.003	102 - 59	ROENCHEN	14	DPWA
• • • We do not use the following data for averages, fits, limits, etc. • • •				
0.032	66	ROENCHEN	15A	DPWA Multichannel

$N(1720)$ BREIT-WIGNER PHOTON DECAY AMPLITUDES

$N(1720) \rightarrow \rho\gamma$, helicity-1/2 amplitude $A_{1/2}$				
VALUE ($\text{GeV}^{-1/2}$)	DOCUMENT ID	TECN	COMMENT	
0.080 to 0.120 (≈ 0.100) OUR ESTIMATE				
0.0809 ± 0.0115	GOLOVATCH	19	DPWA	$\gamma p \rightarrow \pi^+ \pi^- p$
0.068 ± 0.004	HUNT	19	DPWA	Multichannel
0.115 ± 0.045	SOKHOYAN	15A	DPWA	Multichannel
-0.065 ± 0.002	SHKLYAR	13	DPWA	Multichannel
0.095 ± 0.002	WORKMAN	12A	DPWA	$\gamma N \rightarrow N\pi$
• • • We do not use the following data for averages, fits, limits, etc. • • •				
0.110 ± 0.045	ANISOVICH	12A	DPWA	Multichannel
0.057 ± 0.003	SHRESTHA	12A	DPWA	Multichannel
0.073	DRECHSEL	07	DPWA	$\gamma N \rightarrow \pi N$
0.097 ± 0.003	DUGGER	07	DPWA	$\gamma N \rightarrow \pi N$
-0.053	PENNER	02D	DPWA	Multichannel
¹ Statistical error only.				

$N(1720) \rightarrow \rho\gamma$, helicity-3/2 amplitude $A_{3/2}$				
VALUE ($\text{GeV}^{-1/2}$)	DOCUMENT ID	TECN	COMMENT	
-0.034 ± 0.0076	GOLOVATCH	19	DPWA	$\gamma p \rightarrow \pi^+ \pi^- p$
0.028 ± 0.003	HUNT	19	DPWA	Multichannel
0.135 ± 0.040	SOKHOYAN	15A	DPWA	Multichannel
0.035 ± 0.002	SHKLYAR	13	DPWA	Multichannel
-0.048 ± 0.002	WORKMAN	12A	DPWA	$\gamma N \rightarrow N\pi$
• • • We do not use the following data for averages, fits, limits, etc. • • •				
0.150 ± 0.030	ANISOVICH	12A	DPWA	Multichannel
-0.019 ± 0.002	SHRESTHA	12A	DPWA	Multichannel
-0.011	DRECHSEL	07	DPWA	$\gamma N \rightarrow \pi N$
-0.039 ± 0.003	DUGGER	07	DPWA	$\gamma N \rightarrow \pi N$
0.027	PENNER	02D	DPWA	Multichannel
¹ Statistical error only.				

$N(1720) \rightarrow n\gamma$, helicity-1/2 amplitude $A_{1/2}$				
VALUE ($\text{GeV}^{-1/2}$)	DOCUMENT ID	TECN	COMMENT	
-0.064 ± 0.006	HUNT	19	DPWA	Multichannel
-0.080 ± 0.050	ANISOVICH	13B	DPWA	Multichannel
• • • We do not use the following data for averages, fits, limits, etc. • • •				
-0.002 ± 0.001	SHRESTHA	12A	DPWA	Multichannel
-0.003	DRECHSEL	07	DPWA	$\gamma N \rightarrow \pi N$
-0.004	PENNER	02D	DPWA	Multichannel
¹ Statistical error only.				

$N(1720) \rightarrow n\gamma$, helicity-3/2 amplitude $A_{3/2}$				
VALUE ($\text{GeV}^{-1/2}$)	DOCUMENT ID	TECN	COMMENT	
-0.004 ± 0.006	HUNT	19	DPWA	Multichannel
-0.140 ± 0.065	ANISOVICH	13B	DPWA	Multichannel
• • • We do not use the following data for averages, fits, limits, etc. • • •				
-0.001 ± 0.002	SHRESTHA	12A	DPWA	Multichannel
-0.031	DRECHSEL	07	DPWA	$\gamma N \rightarrow \pi N$
0.003	PENNER	02D	DPWA	Multichannel
¹ Statistical error only.				

$N(1720)$ REFERENCES

For early references, see Physics Letters **111B** 1 (1982).

GOLOVATCH	19	PL B788 371	E. Golovatch <i>et al.</i>	(CLAS Collab.)
HUNT	19	PR C39 055205	B.C. Hunt, D.M. Manley	
DENISEWKO	16	PL B755 97	I. Denisenko <i>et al.</i>	
ROENCHEN	15A	EPJ A51 70	D. Roenchen <i>et al.</i>	
SOKHOYAN	15A	EPJ A51 95	V. Sokhoyan <i>et al.</i>	(CBELSA/TAPS Collab.)
PDG	14	CP C38 070001	K. Olive <i>et al.</i>	(PDG Collab.)
ROENCHEN	14	EPJ A50 101	D. Roenchen <i>et al.</i>	
Also		EPJ A51 63 (errata.)	D. Roenchen <i>et al.</i>	
SVARC	14	PR C89 045205	A. Svarc <i>et al.</i>	(RBI Zagreb, UNI Tuzla)
ANISOVICH	13B	EPJ A49 67	A.V. Anisovich <i>et al.</i>	
SHKLYAR	13	PR C87 015201	V. Shklyar, H. Lenske, U. Mosel	(GIES)
ANISOVICH	12A	EPJ A48 15	A.V. Anisovich <i>et al.</i>	(BONN, PNPI)
SHRESTHA	12A	PR C86 055203	M. Shrestha, D.M. Manley	(KSU)
WORKMAN	12A	PR C86 015202	R. Workman <i>et al.</i>	(GWU)
BATINIC	10	PR C82 038203	M. Batinic <i>et al.</i>	(ZAGR)
THOMA	08	PL B659 87	U. Thoma <i>et al.</i>	(CB-ELSA Collab.)
DRECHSEL	07	EPJ A34 69	D. Drechsel, S.S. Kamalov, L. Tiator	(MAINZ, JINR)
DUGGER	07	PR C76 025211	M. Dugger <i>et al.</i>	(JLab CLAS Collab.)
ARNDT	06	PR C74 045205	R.A. Arndt <i>et al.</i>	(GWU)
SHKLYAR	05	PR C72 015210	V. Shklyar, H. Lenske, U. Mosel	(GIES)
PENNER	02C	PR C66 055211	G. Penner, U. Mosel	(GIES)
PENNER	02D	PR C66 055212	G. Penner, U. Mosel	(GIES)
VRANA	00	PRPL 328 181	T.P. Vrana, S.A. Dytman, T.-S.H. Lee	(PITT, ANL)
HOEHLER	93	πN Newsletter 9 1	G. Hoehler	(KARL)
CUTKOSKY	80	Toronto Conf. 19	R.E. Cutkosky <i>et al.</i>	(CMU, LBL) IJP
Also		PR D20 2839	R.E. Cutkosky <i>et al.</i>	(CMU, LBL) IJP
HOEHLER	79	PDAT 12-1	G. Hoehler <i>et al.</i>	(KARLT) IJP
Also		Toronto Conf. 3	R. Koch	(KARLT) IJP

$N(1860) 5/2^+$

$$I(J^P) = \frac{1}{2}(\frac{5}{2}^+) \text{ Status: } **$$

OMITTED FROM SUMMARY TABLE

Before the 2012 Review, all the evidence for a $J^P = 5/2^+$ state with a mass above 1800 MeV was filed under a two-star $N(2000)$. There is now some evidence from ANISOVICH 12A for two $5/2^+$ states in this region, so we have split the older data (according to mass) between two two-star $5/2^+$ states, an $N(1860)$ and an $N(2000)$.

$N(1860)$ POLE POSITION

REAL PART				
VALUE (MeV)	DOCUMENT ID	TECN	COMMENT	
1834 ± 19 ± 6	SVARC	14	L+P	$\pi N \rightarrow \pi N$
1830 + 120	ANISOVICH	12A	DPWA	Multichannel
- 60				
• • • We do not use the following data for averages, fits, limits, etc. • • •				
1871	HUNT	19	DPWA	Multichannel
1807	ARNDT	06	DPWA	$\pi N \rightarrow \pi N, \eta N$
¹ Fit to the amplitudes of HOEHLER 79.				

-2xIMAGINARY PART

VALUE (MeV)				
VALUE (MeV)	DOCUMENT ID	TECN	COMMENT	
122 ± 34 ± 7	SVARC	14	L+P	$\pi N \rightarrow \pi N$
250 + 150	ANISOVICH	12A	DPWA	Multichannel
- 50				
• • • We do not use the following data for averages, fits, limits, etc. • • •				
337	HUNT	19	DPWA	Multichannel
109	ARNDT	06	DPWA	$\pi N \rightarrow \pi N, \eta N$
² Fit to the amplitudes of HOEHLER 79.				

$N(1860)$ ELASTIC POLE RESIDUE

MODULUS $ r $				
VALUE (MeV)	DOCUMENT ID	TECN	COMMENT	
4 ± 1 ± 1	SVARC	14	L+P	$\pi N \rightarrow \pi N$
50 ± 20	ANISOVICH	12A	DPWA	Multichannel
• • • We do not use the following data for averages, fits, limits, etc. • • •				
60	ARNDT	06	DPWA	$\pi N \rightarrow \pi N, \eta N$
³ Fit to the amplitudes of HOEHLER 79.				

PHASE θ

VALUE ($^\circ$)				
VALUE ($^\circ$)	DOCUMENT ID	TECN	COMMENT	
-39 ± 18 ± 9	SVARC	14	L+P	$\pi N \rightarrow \pi N$
-80 ± 40	ANISOVICH	12A	DPWA	Multichannel
• • • We do not use the following data for averages, fits, limits, etc. • • •				
-67	ARNDT	06	DPWA	$\pi N \rightarrow \pi N, \eta N$
⁴ Fit to the amplitudes of HOEHLER 79.				

$N(1860)$ BREIT-WIGNER MASS

VALUE (MeV)				
VALUE (MeV)	DOCUMENT ID	TECN	COMMENT	
1928 ± 21	HUNT	19	DPWA	Multichannel
1860 + 120	ANISOVICH	12A	DPWA	Multichannel
- 60				
1882 ± 10	HOEHLER	79	IPWA	$\pi N \rightarrow \pi N$
• • • We do not use the following data for averages, fits, limits, etc. • • •				
1900 ± 7	SHRESTHA	12A	DPWA	Multichannel
1817.7	ARNDT	06	DPWA	$\pi N \rightarrow \pi N, \eta N$

Baryon Particle Listings

 $N(1860)$, $N(1875)$ ⁵ Statistical error only. $N(1860)$ BREIT-WIGNER WIDTH

VALUE (MeV)	DOCUMENT ID	TECN	COMMENT
376 ± 58	⁶ HUNT	19	DPWA Multichannel
270 ± 140 50	ANISOVICH	12A	DPWA Multichannel
95 ± 20	HOEHLER	79	IPWA $\pi N \rightarrow \pi N$
••• We do not use the following data for averages, fits, limits, etc. •••			
219 ± 23	⁶ SHRESTHA	12A	DPWA Multichannel
117.6	ARNDT	06	DPWA $\pi N \rightarrow \pi N, \eta N$

⁶ Statistical error only. $N(1860)$ DECAY MODES

Mode	Fraction (Γ_i/Γ)
Γ_1 $N\pi$	4–20 %
Γ_2 $N\eta$	2–6 %
Γ_3 ΛK	
Γ_4 $N\pi\pi$	
Γ_5 $\Delta\pi$	
Γ_6 $\Delta\pi$, P -wave	
Γ_7 $\Delta\pi$, F -wave	
Γ_8 $N\rho$	
Γ_9 $N\rho$, $S=3/2$, P -wave	
Γ_{10} $N\rho$, $S=3/2$, F -wave	
Γ_{11} $N\sigma$	35–47 %
Γ_{12} $\rho\gamma$	
Γ_{13} $\rho\gamma$, helicity=1/2	seen
Γ_{14} $\rho\gamma$, helicity=3/2	seen
Γ_{15} $n\gamma$	0.0017–0.062 %
Γ_{16} $n\gamma$, helicity=1/2	0.0003–0.019 %
Γ_{17} $n\gamma$, helicity=3/2	0.0014–0.043 %

 $N(1860)$ BRANCHING RATIOS

$\Gamma(N\pi)/\Gamma_{\text{total}}$	DOCUMENT ID	TECN	COMMENT	Γ_1/Γ
8.0±0.1	⁷ HUNT	19	DPWA Multichannel	
20 ± 6	ANISOVICH	12A	DPWA Multichannel	
4 ± 2	HOEHLER	79	IPWA $\pi N \rightarrow \pi N$	
••• We do not use the following data for averages, fits, limits, etc. •••				
17 ± 1	⁷ SHRESTHA	12A	DPWA Multichannel	
12.7	ARNDT	06	DPWA $\pi N \rightarrow \pi N, \eta N$	

⁷ Statistical error only.

$\Gamma(N\eta)/\Gamma_{\text{total}}$	DOCUMENT ID	TECN	COMMENT	Γ_2/Γ
0.11±0.09	⁸ HUNT	19	DPWA Multichannel	
••• We do not use the following data for averages, fits, limits, etc. •••				
4 ± 2	⁸ SHRESTHA	12A	DPWA Multichannel	

⁸ Statistical error only.

$\Gamma(\Lambda K)/\Gamma_{\text{total}}$	DOCUMENT ID	TECN	COMMENT	Γ_3/Γ
<0.01	⁹ HUNT	19	DPWA Multichannel	

⁹ Statistical error only.

$\Gamma(\Delta\pi, P\text{-wave})/\Gamma_{\text{total}}$	DOCUMENT ID	TECN	COMMENT	Γ_6/Γ
10±6	¹⁰ HUNT	19	DPWA Multichannel	

¹⁰ Statistical error only.

$\Gamma(\Delta\pi, F\text{-wave})/\Gamma_{\text{total}}$	DOCUMENT ID	TECN	COMMENT	Γ_7/Γ
27±11	¹¹ HUNT	19	DPWA Multichannel	

¹¹ Statistical error only.

$\Gamma(N\rho, S=3/2, P\text{-wave})/\Gamma_{\text{total}}$	DOCUMENT ID	TECN	COMMENT	Γ_9/Γ
<8.5	¹² HUNT	19	DPWA Multichannel	

¹² Statistical error only.

$\Gamma(N\rho, S=3/2, F\text{-wave})/\Gamma_{\text{total}}$	DOCUMENT ID	TECN	COMMENT	Γ_{10}/Γ
<0.1	¹³ HUNT	19	DPWA Multichannel	

¹³ Statistical error only.

$\Gamma(N\sigma)/\Gamma_{\text{total}}$	DOCUMENT ID	TECN	COMMENT	Γ_{11}/Γ
51±10	¹⁴ HUNT	19	DPWA Multichannel	
••• We do not use the following data for averages, fits, limits, etc. •••				
41 ± 6	¹⁴ SHRESTHA	12A	DPWA Multichannel	
¹⁴ Statistical error only.				

 $N(1860)$ BREIT-WIGNER PHOTON DECAY AMPLITUDES

$N(1860) \rightarrow \rho\gamma$, helicity-1/2 amplitude $A_{1/2}$	DOCUMENT ID	TECN	COMMENT
–0.022±0.020	¹⁵ HUNT	19	DPWA Multichannel
••• We do not use the following data for averages, fits, limits, etc. •••			
–0.017±0.003	¹⁵ SHRESTHA	12A	DPWA Multichannel
¹⁵ Statistical error only.			

$N(1860) \rightarrow \rho\gamma$, helicity-3/2 amplitude $A_{3/2}$	DOCUMENT ID	TECN	COMMENT
–0.032±0.034	¹⁶ HUNT	19	DPWA Multichannel
••• We do not use the following data for averages, fits, limits, etc. •••			
0.029±0.004	¹⁶ SHRESTHA	12A	DPWA Multichannel
¹⁶ Statistical error only.			

$N(1860) \rightarrow n\gamma$, helicity-1/2 amplitude $A_{1/2}$	DOCUMENT ID	TECN	COMMENT
0.021 ± 0.029	¹⁷ HUNT	19	DPWA Multichannel
0.021 ± 0.013	ANISOVICH	13B	DPWA Multichannel
••• We do not use the following data for averages, fits, limits, etc. •••			
0.010 ± 0.005	¹⁷ SHRESTHA	12A	DPWA Multichannel
¹⁷ Statistical error only.			

$N(1860) \rightarrow n\gamma$, helicity-3/2 amplitude $A_{3/2}$	DOCUMENT ID	TECN	COMMENT
0.070 ± 0.035	¹⁸ HUNT	19	DPWA Multichannel
0.034 ± 0.017	ANISOVICH	13B	DPWA Multichannel
••• We do not use the following data for averages, fits, limits, etc. •••			
–0.009 ± 0.005	¹⁸ SHRESTHA	12A	DPWA Multichannel
¹⁸ Statistical error only.			

 $N(1860)$ REFERENCES

HUNT	19	PR C99 055205	B.C. Hunt, D.M. Manley	
SVARC	14	PR C89 045205	A. Svarc et al.	(RBI Zagreb, UNI Tuzla)
ANISOVICH	13B	EPJ A49 57	A.V. Anisovich et al.	
ANISOVICH	12A	EPJ A48 15	A.V. Anisovich et al.	(BONN, PNPI)
SHRESTHA	12A	PR C86 055203	M. Shrestha, D.M. Manley	(KSU)
ARNDT	06	PR C74 045205	R.A. Arndt et al.	(GWU)
HOEHLER	79	PDAT 12-1	G. Hohler et al.	(KARLT)

 $N(1875) 3/2^-$

$$I(J^P) = \frac{1}{2} \left(\frac{3}{2}^-\right) \text{ Status: } ** *$$

Before the 2012 Review, all the evidence for a $J^P = 3/2^-$ state with a mass above 1800 MeV was filed under a two-star $N(2080)$.

There is now evidence from ANISOVICH 12A for two $3/2^-$ states in this region, so we have split the older data (according to mass) between a three-star $N(1875)$ and a two-star $N(2120)$.

 $N(1875)$ POLE POSITION

REAL PART	DOCUMENT ID	TECN	COMMENT
1870 ± 20	SOKHOYAN	15A	DPWA Multichannel
1880 ± 100	CUTKOSKY	80	IPWA $\pi N \rightarrow \pi N$ (lower m)
••• We do not use the following data for averages, fits, limits, etc. •••			
1993	HUNT	19	DPWA Multichannel
1810	SHKLYAR	13	DPWA Multichannel
1860 ± 25	ANISOVICH	12A	DPWA Multichannel
1957 ± 49	BATINIC	10	DPWA $\pi N \rightarrow N\pi, N\eta$
1824	VRANA	00	DPWA Multichannel

–2×IMAGINARY PART

VALUE (MeV)	DOCUMENT ID	TECN	COMMENT
100 to 220 (≈ 160) OUR ESTIMATE			
200 ± 15	SOKHOYAN	15A	DPWA Multichannel
160 ± 80	CUTKOSKY	80	IPWA $\pi N \rightarrow \pi N$ (lower m)
••• We do not use the following data for averages, fits, limits, etc. •••			
319	HUNT	19	DPWA Multichannel
98	SHKLYAR	13	DPWA Multichannel
200 ± 20	ANISOVICH	12A	DPWA Multichannel
467 ± 106	BATINIC	10	DPWA $\pi N \rightarrow N\pi, N\eta$
614	VRANA	00	DPWA Multichannel

N(1875) ELASTIC POLE RESIDUE

MODULUS |r|

VALUE (MeV)	DOCUMENT ID	TECN	COMMENT
3 to 12 (≈ 10) OUR ESTIMATE			
3 ± 1.5	SOKHOYAN 15A	DPWA	Multichannel
10 ± 5	CUTKOSKY 80	IPWA	$\pi N \rightarrow \pi N$ (lower <i>m</i>)
• • • We do not use the following data for averages, fits, limits, etc. • • •			
3	SHKLYAR 13	DPWA	Multichannel
2.5 ± 1.0	ANISOVICH 12A	DPWA	Multichannel
53	BATINIC 10	DPWA	$\pi N \rightarrow N\pi, N\eta$

PHASE θ

VALUE (°)	DOCUMENT ID	TECN	COMMENT
50 to 200 (≈ 100) OUR ESTIMATE			
160 ± 50	SOKHOYAN 15A	DPWA	Multichannel
100 ± 80	CUTKOSKY 80	IPWA	$\pi N \rightarrow \pi N$ (lower <i>m</i>)
• • • We do not use the following data for averages, fits, limits, etc. • • •			
- 76	SHKLYAR 13	DPWA	Multichannel
- 65	BATINIC 10	DPWA	$\pi N \rightarrow N\pi, N\eta$

N(1875) INELASTIC POLE RESIDUE

The "normalized residue" is the residue divided by $\Gamma_{pole}/2$.

Normalized residue in $N\pi \rightarrow N(1875) \rightarrow \Lambda K$

MODULUS	PHASE (°)	DOCUMENT ID	TECN	COMMENT
0.015 ± 0.005		ANISOVICH 12A	DPWA	Multichannel

Normalized residue in $N\pi \rightarrow N(1875) \rightarrow \Sigma K$

MODULUS	PHASE (°)	DOCUMENT ID	TECN	COMMENT
0.04 ± 0.02		ANISOVICH 12A	DPWA	Multichannel

Normalized residue in $N\pi \rightarrow N(1875) \rightarrow N\sigma$

MODULUS	PHASE (°)	DOCUMENT ID	TECN	COMMENT
0.09 ± 0.03	-175 ± 45	SOKHOYAN 15A	DPWA	Multichannel
• • • We do not use the following data for averages, fits, limits, etc. • • •				
0.08 ± 0.03	-170 ± 65	ANISOVICH 12A	DPWA	Multichannel

Normalized residue in $N\pi \rightarrow N(1875) \rightarrow \Delta(1232)\pi, S\text{-wave}$

MODULUS	PHASE (°)	DOCUMENT ID	TECN	COMMENT
0.05 ± 0.03	undefined	SOKHOYAN 15A	DPWA	Multichannel

Normalized residue in $N\pi \rightarrow N(1875) \rightarrow \Delta(1232)\pi, D\text{-wave}$

MODULUS	PHASE (°)	DOCUMENT ID	TECN	COMMENT
0.04 ± 0.02	undefined	SOKHOYAN 15A	DPWA	Multichannel

Normalized residue in $N\pi \rightarrow N(1875) \rightarrow N(1440)\pi$

MODULUS	PHASE (°)	DOCUMENT ID	TECN	COMMENT
0.03 ± 0.02	undefined	SOKHOYAN 15A	DPWA	Multichannel

N(1875) BREIT-WIGNER MASS

VALUE (MeV)	DOCUMENT ID	TECN	COMMENT
1850 to 1920 (≈ 1875) OUR ESTIMATE			
2005 ± 12	¹ HUNT 19	DPWA	Multichannel
1875 ± 20	SOKHOYAN 15A	DPWA	Multichannel
1934 ± 10	¹ SHKLYAR 13	DPWA	Multichannel
1880 ± 100	CUTKOSKY 80	IPWA	$\pi N \rightarrow \pi N$
• • • We do not use the following data for averages, fits, limits, etc. • • •			
1880 ± 20	ANISOVICH 12A	DPWA	Multichannel
1951 ± 27	¹ SHRESTHA 12A	DPWA	Multichannel
2048 ± 65	BATINIC 10	DPWA	$\pi N \rightarrow N\pi, N\eta$
1946 ± 1	PENNER 02c	DPWA	Multichannel
1895	MART 00	DPWA	$\gamma p \rightarrow \Lambda K^+$
2003 ± 18	VRANA 00	DPWA	Multichannel
¹ Statistical error only.			

N(1875) BREIT-WIGNER WIDTH

VALUE (MeV)	DOCUMENT ID	TECN	COMMENT
120 to 250 (≈ 200) OUR ESTIMATE			
321 ± 21	¹ HUNT 19	DPWA	Multichannel
200 ± 25	SOKHOYAN 15A	DPWA	Multichannel
857 ± 100	¹ SHKLYAR 13	DPWA	Multichannel
180 ± 60	CUTKOSKY 80	IPWA	$\pi N \rightarrow \pi N$ (lower <i>m</i>)
• • • We do not use the following data for averages, fits, limits, etc. • • •			
200 ± 25	ANISOVICH 12A	DPWA	Multichannel
500 ± 45	¹ SHRESTHA 12A	DPWA	Multichannel
529 ± 128	BATINIC 10	DPWA	$\pi N \rightarrow N\pi, N\eta$
859 ± 7	PENNER 02c	DPWA	Multichannel
372	MART 00	DPWA	$\gamma p \rightarrow \Lambda K^+$
1070 ± 858	VRANA 00	DPWA	Multichannel
¹ Statistical error only.			

N(1875) DECAY MODES

Mode	Fraction (Γ_i/Γ)
Γ_1 $N\pi$	3-11 %
Γ_2 $N\eta$	<1 %
Γ_3 $N\omega$	15-25 %
Γ_4 ΛK	seen
Γ_5 ΣK	seen
Γ_6 $N\pi\pi$	
Γ_7 $\Delta(1232)\pi$	10-35 %
Γ_8 $\Delta(1232)\pi, S\text{-wave}$	7-21 %
Γ_9 $\Delta(1232)\pi, D\text{-wave}$	2-12 %
Γ_{10} $N\rho, S=3/2, S\text{-wave}$	seen
Γ_{11} $\Lambda K^*(892)$	
Γ_{12} $N\sigma$	30-60 %
Γ_{13} $N(1440)\pi$	2-8 %
Γ_{14} $N(1520)\pi$	<2 %
Γ_{15} $p\gamma$	0.001-0.025 %
Γ_{16} $p\gamma, \text{helicity}=1/2$	0.001-0.021 %
Γ_{17} $p\gamma, \text{helicity}=3/2$	<0.003 %
Γ_{18} $n\gamma$	<0.040 %
Γ_{19} $n\gamma, \text{helicity}=1/2$	<0.007 %
Γ_{20} $n\gamma, \text{helicity}=3/2$	<0.033 %

N(1875) BRANCHING RATIOS

$\Gamma(N\pi)/\Gamma_{total}$	VALUE (%)	DOCUMENT ID	TECN	COMMENT	Γ_1/Γ
3 to 11 (≈ 7) OUR ESTIMATE					
	7.5 ± 0.1	¹ HUNT 19	DPWA	Multichannel	
	4 ± 2	SOKHOYAN 15A	DPWA	Multichannel	
	11 ± 1	¹ SHKLYAR 13	DPWA	Multichannel	
	10 ± 4	CUTKOSKY 80	IPWA	$\pi N \rightarrow \pi N$ (lower <i>m</i>)	
• • • We do not use the following data for averages, fits, limits, etc. • • •					
	3 ± 2	ANISOVICH 12A	DPWA	Multichannel	
	7 ± 2	¹ SHRESTHA 12A	DPWA	Multichannel	
	17 ± 7	BATINIC 10	DPWA	$\pi N \rightarrow N\pi, N\eta$	
	12 ± 2	PENNER 02c	DPWA	Multichannel	
	13 ± 3	VRANA 00	DPWA	Multichannel	
¹ Statistical error only.					

$\Gamma(N\eta)/\Gamma_{total}$	VALUE (%)	DOCUMENT ID	TECN	COMMENT	Γ_2/Γ
	3.3 ± 0.8	¹ HUNT 19	DPWA	Multichannel	
	<1	SHKLYAR 13	DPWA	Multichannel	
• • • We do not use the following data for averages, fits, limits, etc. • • •					
	8 ± 3	BATINIC 10	DPWA	$\pi N \rightarrow N\pi, N\eta$	
	7 ± 2	PENNER 02c	DPWA	Multichannel	
	0 ± 2	VRANA 00	DPWA	Multichannel	
¹ Statistical error only.					

$\Gamma(N\omega)/\Gamma_{total}$	VALUE (%)	DOCUMENT ID	TECN	COMMENT	Γ_3/Γ
	13 ± 7	DENISENKO 16	DPWA	Multichannel	
	20 ± 5	¹ SHKLYAR 13	DPWA	Multichannel	
• • • We do not use the following data for averages, fits, limits, etc. • • •					
	21 ± 7	PENNER 02c	DPWA	Multichannel	
¹ Statistical error only.					

$\Gamma(\Lambda K)/\Gamma_{total}$	VALUE (%)	DOCUMENT ID	TECN	COMMENT	Γ_4/Γ
	1.1 ± 0.4	¹ HUNT 19	DPWA	Multichannel	
• • • We do not use the following data for averages, fits, limits, etc. • • •					
	0.2 ± 0.2	PENNER 02c	DPWA	Multichannel	
¹ Statistical error only.					

$\Gamma(\Sigma K)/\Gamma_{total}$	VALUE (%)	DOCUMENT ID	TECN	COMMENT	Γ_5/Γ
	0.7 ± 0.4	PENNER 02c	DPWA	Multichannel	

$\Gamma(\Delta(1232)\pi, S\text{-wave})/\Gamma_{total}$	VALUE (%)	DOCUMENT ID	TECN	COMMENT	Γ_8/Γ
	< 2	¹ HUNT 19	DPWA	Multichannel	
	14 ± 7	SOKHOYAN 15A	DPWA	Multichannel	
• • • We do not use the following data for averages, fits, limits, etc. • • •					
	87 ± 3	¹ SHRESTHA 12A	DPWA	Multichannel	
	40 ± 10	VRANA 00	DPWA	Multichannel	
¹ Statistical error only.					

Baryon Particle Listings

 $N(1875)$, $N(1880)$ $\Gamma(\Delta(1232)\pi, D\text{-wave})/\Gamma_{\text{total}}$

VALUE (%)	DOCUMENT ID	TECN	COMMENT
17 ± 6	¹ HUNT 19	DPWA	Multichannel
7 ± 5	SOKHOYAN 15A	DPWA	Multichannel
••• We do not use the following data for averages, fits, limits, etc. •••			
< 6	¹ SHRESTHA 12A	DPWA	Multichannel
17 ± 10	VRANA 00	DPWA	Multichannel
¹ Statistical error only.			

 $\Gamma(N\rho, S=3/2, S\text{-wave})/\Gamma_{\text{total}}$

VALUE (%)	DOCUMENT ID	TECN	COMMENT
46 ± 10	¹ HUNT 19	DPWA	Multichannel
••• We do not use the following data for averages, fits, limits, etc. •••			
< 5	¹ SHRESTHA 12A	DPWA	Multichannel
6 ± 6	VRANA 00	DPWA	Multichannel
¹ Statistical error only.			

 $\Gamma(\Lambda K^*(892))/\Gamma_{\text{total}}$

VALUE	DOCUMENT ID	TECN	COMMENT
< 0.002	ANISOVICH 17B	DPWA	Multichannel

 $\Gamma(N\sigma)/\Gamma_{\text{total}}$

VALUE (%)	DOCUMENT ID	TECN	COMMENT
24.3 ± 8.6	¹ HUNT 19	DPWA	Multichannel
45 ± 15	SOKHOYAN 15A	DPWA	Multichannel
••• We do not use the following data for averages, fits, limits, etc. •••			
< 4	¹ SHRESTHA 12A	DPWA	Multichannel
24 ± 24	VRANA 00	DPWA	Multichannel
¹ Statistical error only.			

 $\Gamma(N(1440)\pi)/\Gamma_{\text{total}}$

VALUE (%)	DOCUMENT ID	TECN	COMMENT
5 ± 3	SOKHOYAN 15A	DPWA	Multichannel

 $\Gamma(N(1520)\pi)/\Gamma_{\text{total}}$

VALUE (%)	DOCUMENT ID	TECN	COMMENT
< 2	SOKHOYAN 15A	DPWA	Multichannel

N(1875) PHOTON DECAY AMPLITUDES AT THE POLE

 $N(1875) \rightarrow p\gamma$, helicity-1/2 amplitude $A_{1/2}$

MODULUS ($\text{GeV}^{-1/2}$)	PHASE ($^\circ$)	DOCUMENT ID	TECN	COMMENT
0.017 ± 0.009	-110 ± 40	SOKHOYAN 15A	DPWA	Multichannel

 $N(1875) \rightarrow p\gamma$, helicity-3/2 amplitude $A_{3/2}$

MODULUS ($\text{GeV}^{-1/2}$)	PHASE ($^\circ$)	DOCUMENT ID	TECN	COMMENT
0.008 ± 0.004	180 ± 40	SOKHOYAN 15A	DPWA	Multichannel

N(1875) BREIT-WIGNER PHOTON DECAY AMPLITUDES

 $N(1875) \rightarrow p\gamma$, helicity-1/2 amplitude $A_{1/2}$

VALUE ($\text{GeV}^{-1/2}$)	DOCUMENT ID	TECN	COMMENT
0.010 to 0.025 (≈ 0.015) OUR ESTIMATE			
-0.013 ± 0.008	¹ HUNT 19	DPWA	Multichannel
0.011 ± 0.001	¹ SHKLYAR 13	DPWA	Multichannel
0.018 ± 0.010	ANISOVICH 12A	DPWA	Multichannel
••• We do not use the following data for averages, fits, limits, etc. •••			
0.007 ± 0.008	¹ SHRESTHA 12A	DPWA	Multichannel
0.012	PENNER 02D	DPWA	Multichannel
¹ Statistical error only.			

 $N(1875) \rightarrow p\gamma$, helicity-3/2 amplitude $A_{3/2}$

VALUE ($\text{GeV}^{-1/2}$)	DOCUMENT ID	TECN	COMMENT
-0.010 to 0.025 (≈ -0.005) OUR ESTIMATE			
-0.093 ± 0.009	¹ HUNT 19	DPWA	Multichannel
-0.007 ± 0.004	SOKHOYAN 15A	DPWA	Multichannel
0.026 ± 0.001	¹ SHKLYAR 13	DPWA	Multichannel
••• We do not use the following data for averages, fits, limits, etc. •••			
-0.009 ± 0.005	ANISOVICH 12A	DPWA	Multichannel
0.043 ± 0.022	¹ SHRESTHA 12A	DPWA	Multichannel
-0.010	PENNER 02D	DPWA	Multichannel
¹ Statistical error only.			

 $N(1875) \rightarrow n\gamma$, helicity-1/2 amplitude $A_{1/2}$

VALUE ($\text{GeV}^{-1/2}$)	DOCUMENT ID	TECN	COMMENT
0.050 ± 0.009	¹ HUNT 19	DPWA	Multichannel
0.010 ± 0.006	ANISOVICH 13B	DPWA	Multichannel
••• We do not use the following data for averages, fits, limits, etc. •••			
0.055 ± 0.021	¹ SHRESTHA 12A	DPWA	Multichannel
0.023	PENNER 02D	DPWA	Multichannel
¹ Statistical error only.			

 Γ_9/Γ $N(1875) \rightarrow n\gamma$, helicity-3/2 amplitude $A_{3/2}$

VALUE ($\text{GeV}^{-1/2}$)	DOCUMENT ID	TECN	COMMENT
0.141 ± 0.022	¹ HUNT 19	DPWA	Multichannel
-0.020 ± 0.015	ANISOVICH 13B	DPWA	Multichannel
••• We do not use the following data for averages, fits, limits, etc. •••			
-0.085 ± 0.031	¹ SHRESTHA 12A	DPWA	Multichannel
-0.009	PENNER 02D	DPWA	Multichannel
¹ Statistical error only.			

N(1875) REFERENCES

For early references, see Physics Letters **111B** 1 (1982).

HUNT 19	PR C99 055205	B.C. Hunt, D.M. Manley	
ANISOVICH 17B	PL B771 142	A.V. Anisovich <i>et al.</i>	
DENISENKO 16	PL B755 97	I. Denisenko <i>et al.</i>	
SOKHOYAN 15A	EPJ A51 95	V. Sokhoyan <i>et al.</i>	(CBELSA/TAPS Collab.)
ANISOVICH 13B	EPJ A49 67	A.V. Anisovich <i>et al.</i>	
SHKLYAR 13	PR C87 015201	V. Shklyar, H. Lenske, U. Mosel	(GIES)
ANISOVICH 12A	EPJ A48 15	A.V. Anisovich <i>et al.</i>	(BONN, PNPI)
SHRESTHA 12A	PR C86 055203	M. Shrestha, D.M. Manley	(KSU)
BATINIC 10	PR C82 038203	M. Batinic <i>et al.</i>	(ZAGR)
PENNER 02C	PR C66 055211	G. Penner, U. Mosel	(GIES)
PENNER 02D	PR C66 055212	G. Penner, U. Mosel	(GIES)
MART 00	PR C61 012201	T. Mart, C. Bennhold	
VRANA 00	PRPL 328 181	T.P. Vrana, S.A. Dytman, T.-S.H. Lee	(PITT, ANL)
CUTKOSKY 80	Toronto Conf. 19	R.E. Cutkosky <i>et al.</i>	(CMU, LBL) IJP
Also	PR D20 2839	R.E. Cutkosky <i>et al.</i>	(CMU, LBL) IJP

 $N(1880) 1/2^+$ $I(J^P) = \frac{1}{2}(\frac{1}{2}^+)$ Status: ***

N(1880) POLE POSITION

REAL PART

VALUE (MeV)	DOCUMENT ID	TECN	COMMENT
1820 to 1900 (≈ 1860) OUR ESTIMATE			
1860 ± 40	ANISOVICH 17A	DPWA	Multichannel
••• We do not use the following data for averages, fits, limits, etc. •••			
1880	HUNT 19	DPWA	Multichannel
1875 ± 11	¹ ANISOVICH 17A	L+P	$\gamma p, \pi^- p \rightarrow K\Lambda$
1870 ± 40	SOKHOYAN 15A	DPWA	Multichannel
1870 ± 40	GUTZ 14	DPWA	Multichannel
1860 ± 35	ANISOVICH 12A	DPWA	Multichannel
¹ Statistical error only.			

-2xIMAGINARY PART

VALUE (MeV)	DOCUMENT ID	TECN	COMMENT
180 to 280 (≈ 230) OUR ESTIMATE			
230 ± 50	ANISOVICH 17A	DPWA	Multichannel
••• We do not use the following data for averages, fits, limits, etc. •••			
429	HUNT 19	DPWA	Multichannel
33 ± 9	² ANISOVICH 17A	L+P	$\gamma p, \pi^- p \rightarrow K\Lambda$
220 ± 50	SOKHOYAN 15A	DPWA	Multichannel
220 ± 50	GUTZ 14	DPWA	Multichannel
250 ± 70	ANISOVICH 12A	DPWA	Multichannel
² Statistical error only.			

N(1880) ELASTIC POLE RESIDUE

MODULUS $|r|$

VALUE (MeV)	DOCUMENT ID	TECN	COMMENT
6 ± 4	SOKHOYAN 15A	DPWA	Multichannel
••• We do not use the following data for averages, fits, limits, etc. •••			
6 ± 4	GUTZ 14	DPWA	Multichannel
6 ± 4	ANISOVICH 12A	DPWA	Multichannel

PHASE θ

VALUE ($^\circ$)	DOCUMENT ID	TECN	COMMENT
70 ± 60	SOKHOYAN 15A	DPWA	Multichannel
••• We do not use the following data for averages, fits, limits, etc. •••			
70 ± 60	GUTZ 14	DPWA	Multichannel
80 ± 65	ANISOVICH 12A	DPWA	Multichannel

N(1880) INELASTIC POLE RESIDUE

The "normalized residue" is the residue divided by $\Gamma_{\text{pole}}/2$.Normalized residue in $N\pi \rightarrow N(1880) \rightarrow N\eta$

MODULUS	PHASE ($^\circ$)	DOCUMENT ID	TECN	COMMENT
0.11 ± 0.07	-75 ± 55	ANISOVICH 12A	DPWA	Multichannel

Normalized residue in $N\pi \rightarrow N(1880) \rightarrow \Lambda K$

MODULUS	PHASE ($^\circ$)	DOCUMENT ID	TECN	COMMENT
0.05 ± 0.02	27 ± 30	ANISOVICH 17A	DPWA	$\gamma p, \pi^- p \rightarrow K\Lambda$

See key on page 999

Baryon Particle Listings
N(1880)

••• We do not use the following data for averages, fits, limits, etc. •••
 0.3 ± 0.1 82 ± 9 ³ ANISOVICH 17A L+P $\gamma p, \pi^- p \rightarrow K \Lambda$
 0.03 ± 0.02 40 ± 40 ANISOVICH 12A DPWA Multichannel
³ Statistical error only.

Normalized residue in $N\pi \rightarrow N(1880) \rightarrow \Sigma K$

MODULUS	PHASE (°)	DOCUMENT ID	TECN	COMMENT
0.11 ± 0.06	95 ± 40	ANISOVICH	12A	DPWA Multichannel

••• We do not use the following data for averages, fits, limits, etc. •••

Normalized residue in $N\pi \rightarrow N(1880) \rightarrow \Delta\pi, P\text{-wave}$

MODULUS	PHASE (°)	DOCUMENT ID	TECN	COMMENT
0.14 ± 0.08	-150 ± 55	SOKHOYAN	15A	DPWA Multichannel
0.20 ± 0.08	-150 ± 50	ANISOVICH	12A	DPWA Multichannel

••• We do not use the following data for averages, fits, limits, etc. •••

Normalized residue in $N\pi \rightarrow N(1880) \rightarrow N(1535)\pi$

MODULUS	PHASE (°)	DOCUMENT ID	TECN	COMMENT
0.09 ± 0.05	130 ± 60	GUTZ	14	DPWA Multichannel

Normalized residue in $N\pi \rightarrow N(1880) \rightarrow N a_0(980)$

MODULUS	PHASE (°)	DOCUMENT ID	TECN	COMMENT
0.04 ± 0.03	40 ± 65	GUTZ	14	DPWA Multichannel

Normalized residue in $N\pi \rightarrow N(1880) \rightarrow N\sigma$

MODULUS	PHASE (°)	DOCUMENT ID	TECN	COMMENT
0.10 ± 0.05	-140 ± 55	SOKHOYAN	15A	DPWA Multichannel

N(1880) BREIT-WIGNER MASS

VALUE (MeV)	DOCUMENT ID	TECN	COMMENT
1830 to 1930 (≈ 1880) OUR ESTIMATE			
1967 ± 20	⁴ HUNT	19	DPWA Multichannel
1875 ± 40	SOKHOYAN	15A	DPWA Multichannel
••• We do not use the following data for averages, fits, limits, etc. •••			
1875 ± 40	GUTZ	14	DPWA Multichannel
1870 ± 35	ANISOVICH	12A	DPWA Multichannel
1900 ± 36	⁴ SHRESTHA	12A	DPWA Multichannel
⁴ Statistical error only.			

N(1880) BREIT-WIGNER WIDTH

VALUE (MeV)	DOCUMENT ID	TECN	COMMENT
200 to 400 (≈ 300) OUR ESTIMATE			
500 ± 77	⁵ HUNT	19	DPWA Multichannel
230 ± 50	SOKHOYAN	15A	DPWA Multichannel
••• We do not use the following data for averages, fits, limits, etc. •••			
230 ± 50	GUTZ	14	DPWA Multichannel
235 ± 65	ANISOVICH	12A	DPWA Multichannel
485 ± 142	⁵ SHRESTHA	12A	DPWA Multichannel
⁵ Statistical error only.			

N(1880) DECAY MODES

Mode	Fraction (Γ_i/Γ)
Γ_1 $N\pi$	3-9 %
Γ_2 $N\eta$	5-55 %
Γ_3 $N\omega$	12-28 %
Γ_4 ΛK	12-28 %
Γ_5 ΣK	10-24 %
Γ_6 $N\pi\pi$	30-80 %
Γ_7 $\Delta(1232)\pi$	18-42 %
Γ_8 $N\rho, S=1/2$	
Γ_9 $N\sigma$	10-40 %
Γ_{10} $N(1535)\pi$	4-12 %
Γ_{11} $N a_0(980)$	1-5 %
Γ_{12} $\Lambda K^*(892)$	0.5-1 %
Γ_{13} $p\gamma, \text{helicity}=1/2$	seen
Γ_{14} $n\gamma, \text{helicity}=1/2$	0.002-0.63 %

N(1880) BRANCHING RATIOS

$\Gamma(N\pi)/\Gamma_{\text{total}}$	DOCUMENT ID	TECN	COMMENT	Γ_1/Γ
25 ± 6	⁶ HUNT	19	DPWA Multichannel	
6 ± 3	SOKHOYAN	15A	DPWA Multichannel	
••• We do not use the following data for averages, fits, limits, etc. •••				
6 ± 3	GUTZ	14	DPWA Multichannel	
5 ± 3	ANISOVICH	12A	DPWA Multichannel	
15 ± 5	⁶ SHRESTHA	12A	DPWA Multichannel	
⁶ Statistical error only.				

$\Gamma(N\eta)/\Gamma_{\text{total}}$

VALUE (%)	DOCUMENT ID	TECN	COMMENT	Γ_2/Γ
2 ± 1	⁷ HUNT	19	DPWA Multichannel	
25 \pm 30	ANISOVICH	12A	DPWA Multichannel	
16 ± 7	⁷ SHRESTHA	12A	DPWA Multichannel	
⁷ Statistical error only.				

$\Gamma(N\omega)/\Gamma_{\text{total}}$

VALUE (%)	DOCUMENT ID	TECN	COMMENT	Γ_3/Γ
20 ± 8	DENISENKO	16	DPWA Multichannel	

$\Gamma(\Lambda K)/\Gamma_{\text{total}}$

VALUE (%)	DOCUMENT ID	TECN	COMMENT	Γ_4/Γ
2 ± 1	⁸ HUNT	19	DPWA Multichannel	
2 ± 1	ANISOVICH	12A	DPWA Multichannel	
32 ± 10	⁸ SHRESTHA	12A	DPWA Multichannel	
⁸ Statistical error only.				

$\Gamma(\Sigma K)/\Gamma_{\text{total}}$

VALUE (%)	DOCUMENT ID	TECN	COMMENT	Γ_5/Γ
17 ± 7	ANISOVICH	12A	DPWA Multichannel	

$\Gamma(\Delta(1232)\pi)/\Gamma_{\text{total}}$

VALUE (%)	DOCUMENT ID	TECN	COMMENT	Γ_7/Γ
11 ± 6	⁹ HUNT	19	DPWA Multichannel	
30 ± 12	SOKHOYAN	15A	DPWA Multichannel	
29 ± 12	ANISOVICH	12A	DPWA Multichannel	
< 2	⁹ SHRESTHA	12A	DPWA Multichannel	
⁹ Statistical error only.				

$\Gamma(N\rho, S=1/2)/\Gamma_{\text{total}}$

VALUE (%)	DOCUMENT ID	TECN	COMMENT	Γ_8/Γ
32 ± 13	¹⁰ HUNT	19	DPWA Multichannel	
¹⁰ Statistical error only.				

$\Gamma(N\sigma)/\Gamma_{\text{total}}$

VALUE (%)	DOCUMENT ID	TECN	COMMENT	Γ_9/Γ
< 9	¹¹ HUNT	19	DPWA Multichannel	
25 ± 15	SOKHOYAN	15A	DPWA Multichannel	
8 ± 5	¹¹ SHRESTHA	12A	DPWA Multichannel	
¹¹ Statistical error only.				

$\Gamma(N(1535)\pi)/\Gamma_{\text{total}}$

VALUE (%)	DOCUMENT ID	TECN	COMMENT	Γ_{10}/Γ
8 ± 4	GUTZ	14	DPWA Multichannel	

$\Gamma(N a_0(980))/\Gamma_{\text{total}}$

VALUE (%)	DOCUMENT ID	TECN	COMMENT	Γ_{11}/Γ
3 ± 2	GUTZ	14	DPWA Multichannel	

$\Gamma(\Lambda K^*(892))/\Gamma_{\text{total}}$

VALUE	DOCUMENT ID	TECN	COMMENT	Γ_{12}/Γ
0.008 ± 0.003	ANISOVICH	17B	DPWA Multichannel	

N(1880) BREIT-WIGNER PHOTON DECAY AMPLITUDES

N(1880) → pγ, helicity-1/2 amplitude A_{1/2}

VALUE (GeV ^{-1/2})	DOCUMENT ID	TECN	COMMENT
0.119 ± 0.015	¹² HUNT	19	DPWA Multichannel
••• We do not use the following data for averages, fits, limits, etc. •••			
0.021 ± 0.006	¹² SHRESTHA	12A	DPWA Multichannel
¹² Statistical error only.			

N(1880) → nγ, helicity-1/2 amplitude A_{1/2}

VALUE (GeV ^{-1/2})	DOCUMENT ID	TECN	COMMENT
0.016 ± 0.010	¹³ HUNT	19	DPWA Multichannel
-0.060 ± 0.050	ANISOVICH	13B	DPWA Multichannel
0.014 ± 0.007	¹³ SHRESTHA	12A	DPWA Multichannel
••• We do not use the following data for averages, fits, limits, etc. •••			
¹³ Statistical error only.			

N(1880) REFERENCES

HUNT	19	PR C99 055205	B.C. Hunt, D.M. Manley
ANISOVICH	17A	PRL 119 062004	A.V. Anisovich et al.
ANISOVICH	17B	PL B771 142	A.V. Anisovich et al.
DENISENKO	16	PL B755 97	I. Denisenko et al.

Baryon Particle Listings

 $N(1880)$, $N(1895)$

SOKHOYAN 15A	EPJ A51 95	V. Sokhoyan et al.	(CBELSA/TAPS Collab.)
GUTZ 14	EPJ A50 74	E. Gutz et al.	(CBELSA/TAPS Collab.)
ANISOVICH 13B	EPJ A49 67	A.V. Anisovich et al.	
ANISOVICH 12A	EPJ A48 15	A.V. Anisovich et al.	(BONN, PNPI)
SHRESTHA 12A	PR C86 055203	M. Shrestha, D.M. Manley	(KSU)

 $N(1895) 1/2^-$

$$I(J^P) = \frac{1}{2}(\frac{1}{2}^-) \text{ Status: } ***$$

Before our 2012 Review, this state appeared in our Listings as the $N(2090)$. Any structure in the S_{11} wave above 1800 MeV is listed here. A few early results that are now obsolete have been omitted.

 $N(1895)$ POLE POSITION

REAL PART

VALUE (MeV)	DOCUMENT ID	TECN	COMMENT
1890 to 1930 (≈ 1910) OUR ESTIMATE			
1895 \pm 15	ANISOVICH 17A	DPWA	Multichannel
1906 \pm 17	¹ ANISOVICH 17A	L+P	$\gamma p, \pi^- p \rightarrow K \Lambda$
1917 \pm 19 \pm 1	² SVARC 14	L+P	$\pi N \rightarrow \pi N$
• • • We do not use the following data for averages, fits, limits, etc. • • •			
1956	HUNT 19	DPWA	Multichannel
1907 \pm 10	ANISOVICH 17C	DPWA	Multichannel
1907 \pm 10	SOKHOYAN 15A	DPWA	Multichannel
1900 \pm 15	ANISOVICH 12A	DPWA	Multichannel
1797 \pm 26	BATINIC 10	DPWA	$\pi N \rightarrow N\pi, N\eta$
1795	VRANA 00	DPWA	Multichannel
2150 \pm 70	CUTKOSKY 80	IPWA	$\pi N \rightarrow \pi N$

¹ Statistical error only.

² Fit to the amplitudes of HOEHLER 79.

-2xIMAGINARY PART

VALUE (MeV)	DOCUMENT ID	TECN	COMMENT
80 to 140 (≈ 110) OUR ESTIMATE			
132 \pm 30	ANISOVICH 17A	DPWA	Multichannel
100 \pm 10	¹ ANISOVICH 17A	L+P	$\gamma p, \pi^- p \rightarrow K \Lambda$
101 \pm 36 \pm 1	^{1,2} SVARC 14	L+P	$\pi N \rightarrow \pi N$
• • • We do not use the following data for averages, fits, limits, etc. • • •			
449	HUNT 19	DPWA	Multichannel
100 \pm 40	ANISOVICH 17C	DPWA	Multichannel
100 \pm 40	SOKHOYAN 15A	DPWA	Multichannel
100 \pm 15	ANISOVICH 12A	DPWA	Multichannel
90 \pm 30	ANISOVICH 12A	DPWA	Multichannel
420 \pm 45	BATINIC 10	DPWA	$\pi N \rightarrow N\pi, N\eta$
220	VRANA 00	DPWA	Multichannel
350 \pm 100	CUTKOSKY 80	IPWA	$\pi N \rightarrow \pi N$

¹ Statistical error only.

² Fit to the amplitudes of HOEHLER 79.

 $N(1895)$ ELASTIC POLE RESIDUEMODULUS $|r|$

VALUE (MeV)	DOCUMENT ID	TECN	COMMENT
1 to 5 (≈ 3) OUR ESTIMATE			
3 \pm 2	SOKHOYAN 15A	DPWA	Multichannel
3.1 \pm 1.4	¹ SVARC 14	L+P	$\pi N \rightarrow \pi N$
• • • We do not use the following data for averages, fits, limits, etc. • • •			
1 \pm 1	ANISOVICH 12A	DPWA	Multichannel
60	BATINIC 10	DPWA	$\pi N \rightarrow N\pi, N\eta$
40 \pm 20	CUTKOSKY 80	IPWA	$\pi N \rightarrow \pi N$
• • • We do not use the following data for averages, fits, limits, etc. • • •			
-164	BATINIC 10	DPWA	$\pi N \rightarrow N\pi, N\eta$

¹ Fit to the amplitudes of HOEHLER 79.

PHASE θ

VALUE ($^\circ$)	DOCUMENT ID	TECN	COMMENT
125 \pm 45	SOKHOYAN 15A	DPWA	Multichannel
-107 \pm 23 \pm 2	¹ SVARC 14	L+P	$\pi N \rightarrow \pi N$
0 \pm 90	CUTKOSKY 80	IPWA	$\pi N \rightarrow \pi N$
• • • We do not use the following data for averages, fits, limits, etc. • • •			
-164	BATINIC 10	DPWA	$\pi N \rightarrow N\pi, N\eta$

¹ Fit to the amplitudes of HOEHLER 79.

 $N(1895)$ INELASTIC POLE RESIDUE

The "normalized residue" is the residue divided by $\Gamma_{pole}/2$.

Normalized residue in $N\pi \rightarrow N(1895) \rightarrow \Lambda K$

MODULUS	PHASE ($^\circ$)	DOCUMENT ID	TECN	COMMENT
0.09 \pm 0.03	8 \pm 30	ANISOVICH 17A	DPWA	Multichannel
0.06 \pm 0.02	87 \pm 27	¹ ANISOVICH 17A	L+P	$\gamma p, \pi^- p \rightarrow K \Lambda$
• • • We do not use the following data for averages, fits, limits, etc. • • •				
0.05 \pm 0.02	-90 \pm 30	ANISOVICH 12A	DPWA	Multichannel

¹ Statistical error only.

Normalized residue in $N\pi \rightarrow N(1895) \rightarrow \Sigma K$

MODULUS	PHASE ($^\circ$)	DOCUMENT ID	TECN	COMMENT
0.06 \pm 0.02	40 \pm 30	ANISOVICH 12A	DPWA	Multichannel

Normalized residue in $N\pi \rightarrow N(1895) \rightarrow \Delta(1232)\pi$

MODULUS	PHASE ($^\circ$)	DOCUMENT ID	TECN	COMMENT
0.05 \pm 0.025	-100 \pm 45	SOKHOYAN 15A	DPWA	Multichannel

Normalized residue in $N\pi \rightarrow N(1895) \rightarrow N(1440)\pi$

MODULUS	PHASE ($^\circ$)	DOCUMENT ID	TECN	COMMENT
0.05 \pm 0.025	-100 \pm 45	SOKHOYAN 15A	DPWA	Multichannel

 $N(1895)$ BREIT-WIGNER MASS

VALUE (MeV)	DOCUMENT ID	TECN	COMMENT
1870 to 1920 (≈ 1895) OUR ESTIMATE			
2000 \pm 29	¹ HUNT 19	DPWA	Multichannel
1890 \pm 9	KASHEVAROV 17	DPWA	$\gamma p \rightarrow \eta p, \eta' p$
1890 \pm 23	SOKHOYAN 15A	DPWA	Multichannel
1905 \pm 12	HOEHLER 79	IPWA	$\pi N \rightarrow \pi N$
1880 \pm 20	HOEHLER 79	IPWA	$\pi N \rightarrow \pi N$
• • • We do not use the following data for averages, fits, limits, etc. • • •			
1895 \pm 15	ANISOVICH 12A	DPWA	Multichannel
1910 \pm 15	¹ SHRESTHA 12A	DPWA	Multichannel
1812 \pm 25	BATINIC 10	DPWA	$\pi N \rightarrow N\pi, N\eta$
1822 \pm 43	VRANA 00	DPWA	Multichannel
2180 \pm 80	CUTKOSKY 80	IPWA	$\pi N \rightarrow \pi N$

¹ Statistical error only.

 $N(1895)$ BREIT-WIGNER WIDTH

VALUE (MeV)	DOCUMENT ID	TECN	COMMENT
80 to 200 (≈ 120) OUR ESTIMATE			
466 \pm 72	¹ HUNT 19	DPWA	Multichannel
150 \pm 57	KASHEVAROV 17	DPWA	$\gamma p \rightarrow \eta p, \eta' p$
100 \pm 30	SOKHOYAN 15A	DPWA	Multichannel
100 \pm 10	SOKHOYAN 15A	DPWA	Multichannel
95 \pm 30	HOEHLER 79	IPWA	$\pi N \rightarrow \pi N$
• • • We do not use the following data for averages, fits, limits, etc. • • •			
90 \pm 30	ANISOVICH 12A	DPWA	Multichannel
90 \pm 15	ANISOVICH 12A	DPWA	Multichannel
502 \pm 47	¹ SHRESTHA 12A	DPWA	Multichannel
405 \pm 40	BATINIC 10	DPWA	$\pi N \rightarrow N\pi, N\eta$
248 \pm 185	VRANA 00	DPWA	Multichannel
350 \pm 100	CUTKOSKY 80	IPWA	$\pi N \rightarrow \pi N$

¹ Statistical error only.

 $N(1895)$ DECAY MODES

Mode	Fraction (Γ_i/Γ)
Γ_1 $N\pi$	2-18 %
Γ_2 $N\eta$	15-40 %
Γ_3 $N\eta'$	10-40 %
Γ_4 $N\omega$	16-40 %
Γ_5 ΛK	13-23 %
Γ_6 ΣK	6-20 %
Γ_7 $N\pi\pi$	
Γ_8 $\Delta(1232)\pi$	
Γ_9 $\Delta(1232)\pi, D$ -wave	3-11 %
Γ_{10} $N\rho$	
Γ_{11} $N\rho, S=1/2, S$ -wave	seen
Γ_{12} $N\rho, S=3/2, D$ -wave	3-12 %
Γ_{13} $\Lambda K^*(892)$	4-9 %
Γ_{14} $N\sigma$	seen
Γ_{15} $N(1440)\pi$	1-4 %
Γ_{16} $p\gamma, \text{ helicity}=1/2$	0.01-0.06 %
Γ_{17} $n\gamma, \text{ helicity}=1/2$	0.003-0.05 %

 $N(1895)$ BRANCHING RATIOS

$\Gamma(N\pi)/\Gamma_{total}$	DOCUMENT ID	TECN	COMMENT	Γ_1/Γ
2 to 18 (≈ 10) OUR ESTIMATE				
8 \pm 4	¹ HUNT 19	DPWA	Multichannel	
2.5 \pm 1.5	SOKHOYAN 15A	DPWA	Multichannel	
9 \pm 5	HOEHLER 79	IPWA	$\pi N \rightarrow \pi N$	
• • • We do not use the following data for averages, fits, limits, etc. • • •				
2 \pm 1	ANISOVICH 12A	DPWA	Multichannel	
17 \pm 2	¹ SHRESTHA 12A	DPWA	Multichannel	
32 \pm 6	BATINIC 10	DPWA	$\pi N \rightarrow N\pi, N\eta$	
17 \pm 3	VRANA 00	DPWA	Multichannel	
18 \pm 8	CUTKOSKY 80	IPWA	$\pi N \rightarrow \pi N$	

¹ Statistical error only.

See key on page 999

Baryon Particle Listings

$N(1895)$, $N(1900)$

$\Gamma(N\eta)/\Gamma_{total}$ Γ_2/Γ

VALUE (%)	DOCUMENT ID	TECN	COMMENT
15 to 40 (≈ 25) OUR ESTIMATE			
37 ± 9	¹ HUNT 19	DPWA	Multichannel
10 ± 5	ANISOVICH 17c	DPWA	Multichannel
20 ± 6	² KASHEVAROV 17	DPWA	$\gamma p \rightarrow \eta p, \eta' p$
• • • We do not use the following data for averages, fits, limits, etc. • • •			
21 ± 6	ANISOVICH 12A	DPWA	Multichannel
40 ± 4	¹ SHRESTHA 12A	DPWA	Multichannel
22 ± 10	BATINIC 10	DPWA	$\pi N \rightarrow N\pi, N\eta$
41 ± 4	VRANA 00	DPWA	Multichannel

¹ Statistical error only.
² Assuming $A_{1/2} = -0.030 \text{ GeV}^{-1/2}$.

$\Gamma(N\eta')/\Gamma_{total}$ Γ_3/Γ

VALUE (%)	DOCUMENT ID	TECN	COMMENT
0.10 to 0.40 (≈ 0.20) OUR ESTIMATE			
0.13 ± 0.05	ANISOVICH 17c	DPWA	Multichannel
0.38 ± 0.20	¹ KASHEVAROV 17	DPWA	$\gamma p \rightarrow \eta p, \eta' p$
• • • We do not use the following data for averages, fits, limits, etc. • • •			
0.012 ± 0.006	¹ SHRESTHA 12A	DPWA	Multichannel

¹ Assuming $A_{1/2} = -0.030 \text{ GeV}^{-1/2}$.

$\Gamma(N\omega)/\Gamma_{total}$ Γ_4/Γ

VALUE (%)	DOCUMENT ID	TECN	COMMENT
28 ± 12	DENISENKO 16	DPWA	Multichannel

$\Gamma(\Lambda K)/\Gamma_{total}$ Γ_5/Γ

VALUE (%)	DOCUMENT ID	TECN	COMMENT
7 ± 4	¹ HUNT 19	DPWA	Multichannel
18 ± 5	ANISOVICH 12A	DPWA	Multichannel
• • • We do not use the following data for averages, fits, limits, etc. • • •			
1.8 ± 0.8	¹ SHRESTHA 12A	DPWA	Multichannel

¹ Statistical error only.

$\Gamma(\Sigma K)/\Gamma_{total}$ Γ_6/Γ

VALUE (%)	DOCUMENT ID	TECN	COMMENT
13 ± 7	ANISOVICH 12A	DPWA	Multichannel

$\Gamma(\Delta(1232)\pi, D\text{-wave})/\Gamma_{total}$ Γ_9/Γ

VALUE (%)	DOCUMENT ID	TECN	COMMENT
< 10	¹ HUNT 19	DPWA	Multichannel
7 ± 4	SOKHOYAN 15A	DPWA	Multichannel
• • • We do not use the following data for averages, fits, limits, etc. • • •			
7 ± 3	¹ SHRESTHA 12A	DPWA	Multichannel
1 ± 1	VRANA 00	DPWA	Multichannel

¹ Statistical error only.

$\Gamma(N\rho, S=1/2, S\text{-wave})/\Gamma_{total}$ Γ_{11}/Γ

VALUE (%)	DOCUMENT ID	TECN	COMMENT
< 18	¹ HUNT 19	DPWA	Multichannel
• • • We do not use the following data for averages, fits, limits, etc. • • •			
< 2	¹ SHRESTHA 12A	DPWA	Multichannel
36 ± 1	VRANA 00	DPWA	Multichannel

¹ Statistical error only.

$\Gamma(N\rho, S=3/2, D\text{-wave})/\Gamma_{total}$ Γ_{12}/Γ

VALUE (%)	DOCUMENT ID	TECN	COMMENT
23 ± 9	¹ HUNT 19	DPWA	Multichannel
• • • We do not use the following data for averages, fits, limits, etc. • • •			
9 ± 3	¹ SHRESTHA 12A	DPWA	Multichannel
1 ± 1	VRANA 00	DPWA	Multichannel

¹ Statistical error only.

$\Gamma(\Lambda K^*(892))/\Gamma_{total}$ Γ_{13}/Γ

VALUE (%)	DOCUMENT ID	TECN	COMMENT
0.063 ± 0.025	ANISOVICH 17b	DPWA	Multichannel

$\Gamma(N\sigma)/\Gamma_{total}$ Γ_{14}/Γ

VALUE (%)	DOCUMENT ID	TECN	COMMENT
< 13	¹ HUNT 19	DPWA	Multichannel
• • • We do not use the following data for averages, fits, limits, etc. • • •			
< 2	¹ SHRESTHA 12A	DPWA	Multichannel
2 ± 1	VRANA 00	DPWA	Multichannel

¹ Statistical error only.

$\Gamma(N(1440)\pi)/\Gamma_{total}$ Γ_{15}/Γ

VALUE (%)	DOCUMENT ID	TECN	COMMENT
7 ± 5	¹ HUNT 19	DPWA	Multichannel
2.5 ± 1.5	SOKHOYAN 15A	DPWA	Multichannel
• • • We do not use the following data for averages, fits, limits, etc. • • •			
24 ± 4	¹ SHRESTHA 12A	DPWA	Multichannel
2 ± 1	VRANA 00	DPWA	Multichannel

¹ Statistical error only.

$N(1895)$ PHOTON DECAY AMPLITUDES AT THE POLE

$N(1895) \rightarrow p\gamma$, helicity-1/2 amplitude $A_{1/2}$

MODULUS ($\text{GeV}^{-1/2}$)	PHASE ($^\circ$)	DOCUMENT ID	TECN	COMMENT
-0.015 ± 0.006	-35 ± 35	ANISOVICH 17c	DPWA	Multichannel
• • • We do not use the following data for averages, fits, limits, etc. • • •				
0.015 ± 0.006	145 ± 35	SOKHOYAN 15A	DPWA	Multichannel

$N(1895)$ BREIT-WIGNER PHOTON DECAY AMPLITUDES

$N(1895) \rightarrow p\gamma$, helicity-1/2 amplitude $A_{1/2}$

VALUE ($\text{GeV}^{-1/2}$)	DOCUMENT ID	TECN	COMMENT
0.017 ± 0.005	¹ HUNT 19	DPWA	Multichannel
-0.016 ± 0.006	SOKHOYAN 15A	DPWA	Multichannel
• • • We do not use the following data for averages, fits, limits, etc. • • •			
0.012 ± 0.006	¹ SHRESTHA 12A	DPWA	Multichannel

¹ Statistical error only.

$N(1895) \rightarrow n\gamma$, helicity-1/2 amplitude $A_{1/2}$

VALUE ($\text{GeV}^{-1/2}$)	DOCUMENT ID	TECN	COMMENT
0.002 ± 0.013	¹ HUNT 19	DPWA	Multichannel
0.013 ± 0.006	ANISOVICH 13b	DPWA	Multichannel
• • • We do not use the following data for averages, fits, limits, etc. • • •			
0.003 ± 0.007	¹ SHRESTHA 12A	DPWA	Multichannel

¹ Statistical error only.

$N(1895)$ REFERENCES

HUNT 19	PR C99 055205	B.C. Hunt, D.M. Manley
ANISOVICH 17A	PRL 119 062004	A.V. Anisovich et al.
ANISOVICH 17B	PL B771 142	A.V. Anisovich et al.
ANISOVICH 17C	PL B772 247	A.V. Anisovich et al.
KASHEVAROV 17	PRL 118 212001	V.L. Kashevarov et al. (A2/MAMI Collab.)
DENISENKO 16	PL B755 97	I. Denisenko et al.
SOKHOYAN 15A	EPJ A51 95	V. Sokhoyan et al. (CBELSA/TAPS Collab.)
SVARC 14	PR C89 049205	A. Svarc et al. (RBI Zagreb, UNI Tuzla)
ANISOVICH 13B	EPJ A49 67	A.V. Anisovich et al.
ANISOVICH 12A	EPJ A48 15	A.V. Anisovich et al. (BONN, PNPI)
SHRESTHA 12A	PR C86 055203	M. Shrestha, D.M. Manley (KSU)
BATINIC 10	PR C82 038203	M. Batinic et al. (ZAGR)
VRANA 00	PRPL 328 181	T.P. Vrana, S.A. Dytman, T.-S.H. Lee (PITT, ANL)
CUTKOSKY 80	Toronto Conf. 19	R.E. Cutkosky et al. (CMU, LBL) IJP
Also	PR D20 2839	R.E. Cutkosky et al. (CMU, LBL)
HOEHLER 79	PDAT 12-1	G. Hoehler et al. (KARLT) IJP
Also	Toronto Conf. 3	R. Koch (KARLT) IJP

$$N(1900) \ 3/2^+$$

$$I(J^P) = \frac{1}{2}(\frac{3}{2}^+) \text{ Status: } ***$$

$N(1900)$ POLE POSITION

REAL PART

VALUE (MeV)	DOCUMENT ID	TECN	COMMENT
1900 to 1940 (≈ 1920) OUR ESTIMATE			
1945 ± 35	ANISOVICH 17A	DPWA	Multichannel
1928 ± 18 ± 2	¹ SVARC 14	L+P	$\pi N \rightarrow \pi N$
• • • We do not use the following data for averages, fits, limits, etc. • • •			
1856	HUNT 19	DPWA	Multichannel
1912 ± 30	² ANISOVICH 17A	L+P	$\gamma p, \pi^- p \rightarrow K\Lambda$
1910 ± 30	SOKHOYAN 15A	DPWA	Multichannel
1910 ± 30	GUTZ 14	DPWA	Multichannel
1910	SHKLYAR 13	DPWA	Multichannel
1900 ± 30	ANISOVICH 12A	DPWA	Multichannel

¹ Fit to the amplitudes of HOEHLER 79.

² Statistical error only.

-2xIMAGINARY PART

VALUE (MeV)	DOCUMENT ID	TECN	COMMENT
100 to 200 (≈ 150) OUR ESTIMATE			
135 ± $\frac{70}{30}$	ANISOVICH 17A	DPWA	Multichannel
152 ± 40 ± 9	¹ SVARC 14	L+P	$\pi N \rightarrow \pi N$
• • • We do not use the following data for averages, fits, limits, etc. • • •			
241	HUNT 19	DPWA	Multichannel
166 ± 30	² ANISOVICH 17A	L+P	$\gamma p, \pi^- p \rightarrow K\Lambda$
280 ± 50	SOKHOYAN 15A	DPWA	Multichannel
280 ± 50	GUTZ 14	DPWA	Multichannel
173	SHKLYAR 13	DPWA	Multichannel
200 ± $\frac{100}{60}$	ANISOVICH 12A	DPWA	Multichannel

¹ Fit to the amplitudes of HOEHLER 79.

² Statistical error only.

Baryon Particle Listings

 $N(1900)$ $N(1900)$ ELASTIC POLE RESIDUEMODULUS $|r|$

VALUE (MeV)	DOCUMENT ID	TECN	COMMENT
-------------	-------------	------	---------

2 to 6 (≈ 4) OUR ESTIMATE

4 ± 2	SOKHOYAN	15A	DPWA Multichannel
4 ± 1 ± 1	¹ SVARC	14	L+P $\pi N \rightarrow \pi N$

• • • We do not use the following data for averages, fits, limits, etc. • • •

4 ± 2	GUTZ	14	DPWA Multichannel
10	SHKLYAR	13	DPWA Multichannel
3 ± 2	ANISOVICH	12A	DPWA Multichannel

¹ Fit to the amplitudes of HOEHLER 79.

PHASE θ

VALUE (°)	DOCUMENT ID	TECN	COMMENT
-----------	-------------	------	---------

-50 to 10 (≈ -20) OUR ESTIMATE

-10 ± 40	SOKHOYAN	15A	DPWA Multichannel
-29 ± 15 ± 2	¹ SVARC	14	L+P $\pi N \rightarrow \pi N$

• • • We do not use the following data for averages, fits, limits, etc. • • •

-10 ± 40	GUTZ	14	DPWA Multichannel
-64	SHKLYAR	13	DPWA Multichannel
10 ± 35	ANISOVICH	12A	DPWA Multichannel

¹ Fit to the amplitudes of HOEHLER 79.

 $N(1900)$ INELASTIC POLE RESIDUE

The "normalized residue" is the residue divided by $\Gamma_{pole}/2$.

Normalized residue in $N\pi \rightarrow N(1900) \rightarrow N\eta$

MODULUS	PHASE (°)	DOCUMENT ID	TECN	COMMENT
0.05 ± 0.02	70 ± 60	ANISOVICH	12A	DPWA Multichannel

Normalized residue in $N\pi \rightarrow N(1900) \rightarrow \Lambda K$

MODULUS	PHASE (°)	DOCUMENT ID	TECN	COMMENT
0.03 ± 0.02	90 ± 40	ANISOVICH	17A	DPWA Multichannel

• • • We do not use the following data for averages, fits, limits, etc. • • •

0.07 ± 0.03	135 ± 25	ANISOVICH	12A	DPWA Multichannel
-------------	----------	-----------	-----	-------------------

Normalized residue in $N\pi \rightarrow N(1900) \rightarrow \Sigma K$

MODULUS	PHASE (°)	DOCUMENT ID	TECN	COMMENT
0.04 ± 0.02	110 ± 30	ANISOVICH	12A	DPWA Multichannel

Normalized residue in $N\pi \rightarrow N(1900) \rightarrow N(1535)\pi$

MODULUS	PHASE (°)	DOCUMENT ID	TECN	COMMENT
0.04 ± 0.01	170 ± 30	GUTZ	14	DPWA Multichannel

Normalized residue in $N\pi \rightarrow N(1900) \rightarrow \Delta(1232)\pi, P\text{-wave}$

MODULUS	PHASE (°)	DOCUMENT ID	TECN	COMMENT
0.07 ± 0.04	-65 ± 30	SOKHOYAN	15A	DPWA Multichannel

Normalized residue in $N\pi \rightarrow N(1900) \rightarrow \Delta(1232)\pi, F\text{-wave}$

MODULUS	PHASE (°)	DOCUMENT ID	TECN	COMMENT
0.10 ± 0.05	80 ± 30	SOKHOYAN	15A	DPWA Multichannel

Normalized residue in $N\pi \rightarrow N(1900) \rightarrow N(1520)\pi$

MODULUS	PHASE (°)	DOCUMENT ID	TECN	COMMENT
0.07 ± 0.04	-105 ± 35	SOKHOYAN	15A	DPWA Multichannel

Normalized residue in $N\pi \rightarrow N(1900) \rightarrow N\sigma$

MODULUS	PHASE (°)	DOCUMENT ID	TECN	COMMENT
0.03 ± 0.02	-110 ± 35	SOKHOYAN	15A	DPWA Multichannel

 $N(1900)$ BREIT-WIGNER MASS

VALUE (MeV)	DOCUMENT ID	TECN	COMMENT
-------------	-------------	------	---------

190 to 1950 (≈ 1920) OUR ESTIMATE

1911 ± 6	¹ HUNT	19	DPWA Multichannel
1910 ± 30	SOKHOYAN	15A	DPWA Multichannel
1998 ± 3	¹ SHKLYAR	13	DPWA Multichannel

• • • We do not use the following data for averages, fits, limits, etc. • • •

1910 ± 30	GUTZ	14	DPWA Multichannel
1905 ± 30	ANISOVICH	12A	DPWA Multichannel
1900 ± 8	¹ SHRESTHA	12A	DPWA Multichannel
1951 ± 53	PENNER	02C	DPWA Multichannel

¹ Statistical error only.

 $N(1900)$ BREIT-WIGNER WIDTH

VALUE (MeV)	DOCUMENT ID	TECN	COMMENT
-------------	-------------	------	---------

100 to 320 (≈ 200) OUR ESTIMATE

292 ± 16	¹ HUNT	19	DPWA Multichannel
270 ± 50	SOKHOYAN	15A	DPWA Multichannel
359 ± 10	¹ SHKLYAR	13	DPWA Multichannel

• • • We do not use the following data for averages, fits, limits, etc. • • •

270 ± 50	GUTZ	14	DPWA Multichannel
----------	------	----	-------------------

250 ⁺¹²⁰ ₋₅₀	ANISOVICH	12A	DPWA Multichannel
------------------------------------	-----------	-----	-------------------

101 ± 15	¹ SHRESTHA	12A	DPWA Multichannel
----------	-----------------------	-----	-------------------

622 ± 42	PENNER	02C	DPWA Multichannel
----------	--------	-----	-------------------

¹ Statistical error only.

 $N(1900)$ DECAY MODES

Mode	Fraction (Γ_i/Γ)
Γ_1 $N\pi$	1-20 %
Γ_2 $N\eta$	2-14 %
Γ_3 $N\eta'$	4-8 %
Γ_4 $N\omega$	7-13 %
Γ_5 ΛK	2-20 %
Γ_6 ΣK	3-7 %
Γ_7 $N\pi\pi$	40-80 %
Γ_8 $\Delta(1232)\pi$	30-70 %
Γ_9 $\Delta(1232)\pi, P\text{-wave}$	9-25 %
Γ_{10} $\Delta(1232)\pi, F\text{-wave}$	21-45 %
Γ_{11} $N\rho$	
Γ_{12} $N\rho, S=1/2$	
Γ_{13} $\Lambda K^*(892)$	< 0.2 %
Γ_{14} $N\sigma$	1-7 %
Γ_{15} $N(1520)\pi$	7-23 %
Γ_{16} $N(1535)\pi$	4-10 %
Γ_{17} $p\gamma$	0.001-0.025 %
Γ_{18} $p\gamma, \text{helicity}=1/2$	0.001-0.021 %
Γ_{19} $p\gamma, \text{helicity}=3/2$	< 0.003 %
Γ_{20} $n\gamma$	< 0.040 %
Γ_{21} $n\gamma, \text{helicity}=1/2$	< 0.007 %
Γ_{22} $n\gamma, \text{helicity}=3/2$	< 0.033 %

 $N(1900)$ BRANCHING RATIOS

$\Gamma(N\pi)/\Gamma_{total}$	VALUE (%)	DOCUMENT ID	TECN	COMMENT	Γ_1/Γ
2 to 20 (≈ 10) OUR ESTIMATE					
	1.9 ± 0.1	¹ HUNT	19	DPWA Multichannel	
	3 ± 2	SOKHOYAN	15A	DPWA Multichannel	
	25 ± 1	¹ SHKLYAR	13	DPWA Multichannel	
	• • • We do not use the following data for averages, fits, limits, etc. • • •				
	3 ± 2	GUTZ	14	DPWA Multichannel	
	3 ± 2	ANISOVICH	12A	DPWA Multichannel	
	7 ± 4	¹ SHRESTHA	12A	DPWA Multichannel	
	16 ± 2	PENNER	02C	DPWA Multichannel	
	¹ Statistical error only.				

$\Gamma(N\eta)/\Gamma_{total}$	VALUE (%)	DOCUMENT ID	TECN	COMMENT	Γ_2/Γ
	1.3 ± 0.5	¹ HUNT	19	DPWA Multichannel	
	2 ± 2	¹ SHKLYAR	13	DPWA Multichannel	
	10 ± 4	ANISOVICH	12A	DPWA Multichannel	
	• • • We do not use the following data for averages, fits, limits, etc. • • •				
	< 1	¹ SHRESTHA	12A	DPWA Multichannel	
	14 ± 5	PENNER	02C	DPWA Multichannel	
	¹ Statistical error only.				

$\Gamma(N\eta')/\Gamma_{total}$	VALUE (%)	DOCUMENT ID	TECN	COMMENT	Γ_3/Γ
	0.06 ± 0.02	ANISOVICH	17C	DPWA Multichannel	

$\Gamma(N\omega)/\Gamma_{total}$	VALUE (%)	DOCUMENT ID	TECN	COMMENT	Γ_4/Γ
	15 ± 8	DENISENKO	16	DPWA Multichannel	
	10 ± 3	¹ SHKLYAR	13	DPWA Multichannel	
	• • • We do not use the following data for averages, fits, limits, etc. • • •				
	39 ± 9	PENNER	02C	DPWA Multichannel	
	¹ Statistical error only.				

$\Gamma(\Lambda K)/\Gamma_{total}$	VALUE (%)	DOCUMENT ID	TECN	COMMENT	Γ_5/Γ
	13.7 ± 0.3	¹ HUNT	19	DPWA Multichannel	
	16 ± 5	ANISOVICH	12A	DPWA Multichannel	
	2.4 ± 0.3	¹ SHKLYAR	05	DPWA Multichannel	
	• • • We do not use the following data for averages, fits, limits, etc. • • •				
	14 ± 5	¹ SHRESTHA	12A	DPWA Multichannel	
	5 to 15	NIKONOV	08	DPWA Multichannel	
	0.1 ± 0.1	PENNER	02C	DPWA Multichannel	
	¹ Statistical error only.				

See key on page 999

Baryon Particle Listings

$N(1900)$, $N(1990)$

$\Gamma(\Sigma K)/\Gamma_{\text{total}}$ Γ_6/Γ

VALUE (%)	DOCUMENT ID	TECN	COMMENT
5 ± 2	ANISOVICH 12A	DPWA	Multichannel
••• We do not use the following data for averages, fits, limits, etc. •••			
1 ± 1	PENNER 02C	DPWA	Multichannel

$\Gamma(\Lambda K^*(892))/\Gamma_{\text{total}}$ Γ_{13}/Γ

VALUE (%)	DOCUMENT ID	TECN	COMMENT
< 0.002	ANISOVICH 17B	DPWA	Multichannel

$\Gamma(N\rho, S=1/2)/\Gamma_{\text{total}}$ Γ_{12}/Γ

VALUE (%)	DOCUMENT ID	TECN	COMMENT
32 ± 7	¹ HUNT 19	DPWA	Multichannel
¹ Statistical error only.			

$\Gamma(N\sigma)/\Gamma_{\text{total}}$ Γ_{14}/Γ

VALUE (%)	DOCUMENT ID	TECN	COMMENT
4 ± 3	SOKHOYAN 15A	DPWA	Multichannel

$\Gamma(N(1520)\pi)/\Gamma_{\text{total}}$ Γ_{15}/Γ

VALUE (%)	DOCUMENT ID	TECN	COMMENT
15 ± 8	SOKHOYAN 15A	DPWA	Multichannel

$\Gamma(N(1535)\pi)/\Gamma_{\text{total}}$ Γ_{16}/Γ

VALUE (%)	DOCUMENT ID	TECN	COMMENT
7 ± 3	GUTZ 14	DPWA	Multichannel

$\Gamma(\Delta(1232)\pi, P\text{-wave})/\Gamma_{\text{total}}$ Γ_9/Γ

VALUE (%)	DOCUMENT ID	TECN	COMMENT
17 ± 8	SOKHOYAN 15A	DPWA	Multichannel

$\Gamma(\Delta(1232)\pi, F\text{-wave})/\Gamma_{\text{total}}$ Γ_{10}/Γ

VALUE (%)	DOCUMENT ID	TECN	COMMENT
33 ± 12	SOKHOYAN 15A	DPWA	Multichannel

$N(1900)$ PHOTON DECAY AMPLITUDES AT THE POLE

$N(1900) \rightarrow p\gamma$, helicity-1/2 amplitude $A_{1/2}$

MODULUS ($\text{GeV}^{-1/2}$)	PHASE ($^\circ$)	DOCUMENT ID	TECN	COMMENT
0.026 ± 0.014	60 ± 35	SOKHOYAN 15A	DPWA	Multichannel

$N(1900) \rightarrow p\gamma$, helicity-3/2 amplitude $A_{3/2}$

MODULUS ($\text{GeV}^{-1/2}$)	PHASE ($^\circ$)	DOCUMENT ID	TECN	COMMENT
-0.070 ± 0.030	70 ± 50	SOKHOYAN 15A	DPWA	Multichannel

$N(1900)$ BREIT-WIGNER PHOTON DECAY AMPLITUDES

$N(1900) \rightarrow p\gamma$, helicity-1/2 amplitude $A_{1/2}$

VALUE ($\text{GeV}^{-1/2}$)	DOCUMENT ID	TECN	COMMENT
0.040 ± 0.004	¹ HUNT 19	DPWA	Multichannel
0.024 ± 0.014	SOKHOYAN 15A	DPWA	Multichannel
-0.008 ± 0.001	¹ SHKLYAR 13	DPWA	Multichannel

••• We do not use the following data for averages, fits, limits, etc. •••

VALUE ($\text{GeV}^{-1/2}$)	DOCUMENT ID	TECN	COMMENT
0.024 ± 0.014	GUTZ 14	DPWA	Multichannel
0.026 ± 0.015	ANISOVICH 12A	DPWA	Multichannel
0.041 ± 0.008	¹ SHRESTHA 12A	DPWA	Multichannel
-0.017	PENNER 02D	DPWA	Multichannel

¹ Statistical error only.

$N(1900) \rightarrow p\gamma$, helicity-3/2 amplitude $A_{3/2}$

VALUE ($\text{GeV}^{-1/2}$)	DOCUMENT ID	TECN	COMMENT
-0.094 ± 0.007	¹ HUNT 19	DPWA	Multichannel
-0.067 ± 0.030	SOKHOYAN 15A	DPWA	Multichannel
< 0.001	SHKLYAR 13	DPWA	Multichannel
••• We do not use the following data for averages, fits, limits, etc. •••			
-0.067 ± 0.030	GUTZ 14	DPWA	Multichannel
-0.065 ± 0.030	ANISOVICH 12A	DPWA	Multichannel
-0.004 ± 0.006	¹ SHRESTHA 12A	DPWA	Multichannel
0.031	PENNER 02D	DPWA	Multichannel

¹ Statistical error only.

$N(1900) \rightarrow n\gamma$, helicity-1/2 amplitude $A_{1/2}$

VALUE ($\text{GeV}^{-1/2}$)	DOCUMENT ID	TECN	COMMENT
0.007 ± 0.014	¹ HUNT 19	DPWA	Multichannel
0.000 ± 0.030	ANISOVICH 13B	DPWA	Multichannel
••• We do not use the following data for averages, fits, limits, etc. •••			
-0.010 ± 0.004	¹ SHRESTHA 12A	DPWA	Multichannel
-0.016	PENNER 02D	DPWA	Multichannel

¹ Statistical error only.

$N(1900) \rightarrow n\gamma$, helicity-3/2 amplitude $A_{3/2}$

VALUE ($\text{GeV}^{-1/2}$)	DOCUMENT ID	TECN	COMMENT
0.007 ± 0.011	¹ HUNT 19	DPWA	Multichannel
-0.060 ± 0.045	ANISOVICH 13B	DPWA	Multichannel
••• We do not use the following data for averages, fits, limits, etc. •••			
-0.011 ± 0.007	¹ SHRESTHA 12A	DPWA	Multichannel
-0.002	PENNER 02D	DPWA	Multichannel

¹ Statistical error only.

$N(1900)$ REFERENCES

HUNT 19	PR C99 055205	B.C. Hunt, D.M. Manley
ANISOVICH 17A	PRL 119 062004	A.V. Anisovich et al.
ANISOVICH 17B	PL B771 142	A.V. Anisovich et al.
ANISOVICH 17C	PL B772 247	A.V. Anisovich et al.
DENISENKO 16	PL B755 97	I. Denisenko et al.
SOKHOYAN 15A	EPJ A51 95	V. Sokhoyan et al. (CBELSA/TAPS Collab.)
GUTZ 14	EPJ A50 74	E. Gutz et al. (CBELSA/TAPS Collab.)
SVARC 14	PR C89 045205	A. Svarc et al. (RBI Zagreb, UNI-Tuzla)
ANISOVICH 13B	EPJ A49 67	A.V. Anisovich et al.
SHKLYAR 13	PR C87 015201	V. Shklyar, H. Lenske, U. Mosel (GIES)
ANISOVICH 12A	EPJ A48 15	A.V. Anisovich et al. (BONN, PNPI)
SHRESTHA 12A	PR C86 055203	M. Shrestha, D.M. Manley (KSU)
NIKONOV 08	PL B662 245	V.A. Nikonov et al. (Bonn, Gatchina)
SHKLYAR 05	PR C72 015210	V. Shklyar, H. Lenske, U. Mosel (GIES)
PENNER 02C	PR C66 055211	G. Penner, U. Mosel (GIES)
PENNER 02D	PR C66 055212	G. Penner, U. Mosel (GIES)
HOEHLER 79	PDAT 12-1	G. Hohler et al. (KARLT)

$N(1900) 7/2^+$

$I(J^P) = \frac{1}{2}(7^+)$ Status: **

OMITTED FROM SUMMARY TABLE

Older and obsolete values are listed and referenced in the 2014 edition, Chinese Physics C38 070001 (2014).

$N(1990)$ POLE POSITION

REAL PART

VALUE (MeV)	DOCUMENT ID	TECN	COMMENT
2030 ± 65	ANISOVICH 12A	DPWA	Multichannel
1900 ± 30	CUTKOSKY 80	IPWA	$\pi N \rightarrow \pi N$
••• We do not use the following data for averages, fits, limits, etc. •••			
1913	HUNT 19	DPWA	Multichannel
1738	ROENCHEN 15A	DPWA	Multichannel
2301	VRANA 00	DPWA	Multichannel

-2xIMAGINARY PART

VALUE (MeV)	DOCUMENT ID	TECN	COMMENT
240 ± 60	ANISOVICH 12A	DPWA	Multichannel
260 ± 60	CUTKOSKY 80	IPWA	$\pi N \rightarrow \pi N$
••• We do not use the following data for averages, fits, limits, etc. •••			
163	HUNT 19	DPWA	Multichannel
188	ROENCHEN 15A	DPWA	Multichannel
202	VRANA 00	DPWA	Multichannel

$N(1990)$ ELASTIC POLE RESIDUE

MODULUS $|r|$

VALUE (MeV)	DOCUMENT ID	TECN	COMMENT
2 ± 1	ANISOVICH 12A	DPWA	Multichannel
9 ± 3	CUTKOSKY 80	IPWA	$\pi N \rightarrow \pi N$
••• We do not use the following data for averages, fits, limits, etc. •••			
4.3	ROENCHEN 15A	DPWA	Multichannel

PHASE θ

VALUE ($^\circ$)	DOCUMENT ID	TECN	COMMENT
125 ± 65	ANISOVICH 12A	DPWA	Multichannel
-60 ± 30	CUTKOSKY 80	IPWA	$\pi N \rightarrow \pi N$
••• We do not use the following data for averages, fits, limits, etc. •••			
-70	ROENCHEN 15A	DPWA	Multichannel

$\Delta(1990)$ INELASTIC POLE RESIDUE

The "normalized residue" is the residue divided by $\Gamma_{\text{pole}}/2$.

Normalized residue in $N\pi \rightarrow N(1990) \rightarrow N\eta$

MODULUS	PHASE ($^\circ$)	DOCUMENT ID	TECN	COMMENT
••• We do not use the following data for averages, fits, limits, etc. •••				
0.013	-82	ROENCHEN 15A	DPWA	Multichannel

Normalized residue in $N\pi \rightarrow N(1990) \rightarrow \Lambda K$

MODULUS	PHASE ($^\circ$)	DOCUMENT ID	TECN	COMMENT
••• We do not use the following data for averages, fits, limits, etc. •••				
0.022	-111	ROENCHEN 15A	DPWA	Multichannel

Baryon Particle Listings

$N(1990)$, $N(2000)$

Normalized residue in $N\pi \rightarrow N(1990) \rightarrow \Sigma K$

MODULUS	PHASE (°)	DOCUMENT ID	TECN	COMMENT
0.005	24	ROENCHEN	15A	DPWA Multichannel

$N(1990)$ BREIT-WIGNER MASS

VALUE (MeV)	DOCUMENT ID	TECN	COMMENT
1950 to 2100 (≈ 2020) OUR ESTIMATE			
2028 ± 19	¹ HUNT	19	DPWA Multichannel
2060 ± 65	ANISOVICH	12A	DPWA Multichannel
1970 ± 50	CUTKOSKY	80	IPWA $\pi N \rightarrow \pi N$
2005 ± 150	HOEHLER	79	IPWA $\pi N \rightarrow \pi N$
• • • We do not use the following data for averages, fits, limits, etc. • • •			
1990 ± 45	¹ SHRESTHA	12A	DPWA Multichannel
2311 ± 16	VRANA	00	DPWA Multichannel
¹ Statistical error only.			

$N(1990)$ BREIT-WIGNER WIDTH

VALUE (MeV)	DOCUMENT ID	TECN	COMMENT
200 to 400 (≈ 300) OUR ESTIMATE			
490 ± 110	¹ HUNT	19	DPWA Multichannel
240 ± 50	ANISOVICH	12A	DPWA Multichannel
350 ± 120	CUTKOSKY	80	IPWA $\pi N \rightarrow \pi N$
350 ± 100	HOEHLER	79	IPWA $\pi N \rightarrow \pi N$
• • • We do not use the following data for averages, fits, limits, etc. • • •			
203 ± 161	¹ SHRESTHA	12A	DPWA Multichannel
205 ± 72	VRANA	00	DPWA Multichannel
¹ Statistical error only.			

$N(1990)$ DECAY MODES

Mode	Fraction (Γ_i/Γ)
Γ_1 $N\pi$	2–6 %
Γ_2 $N\eta$	
Γ_3 ΛK	
Γ_4 $p\gamma$	0.01–0.12 %
Γ_5 $p\gamma$, helicity=1/2	0.003–0.042 %
Γ_6 $p\gamma$, helicity=3/2	0.009–0.075 %
Γ_7 $n\gamma$	0.01–0.16 %
Γ_8 $n\gamma$, helicity=1/2	0.003–0.066 %
Γ_9 $n\gamma$, helicity=3/2	0.003–0.098 %

$N(1990)$ BRANCHING RATIOS

$\Gamma(N\pi)/\Gamma_{total}$	DOCUMENT ID	TECN	COMMENT	Γ_1/Γ
2 to 6 (≈ 4) OUR ESTIMATE				
1.9 ± 0.4	¹ HUNT	19	DPWA Multichannel	
2 ± 1	ANISOVICH	12A	DPWA Multichannel	
6 ± 2	CUTKOSKY	80	IPWA $\pi N \rightarrow \pi N$	
4 ± 2	HOEHLER	79	IPWA $\pi N \rightarrow \pi N$	
• • • We do not use the following data for averages, fits, limits, etc. • • •				
2 ± 1	¹ SHRESTHA	12A	DPWA Multichannel	
22 ± 11	VRANA	00	DPWA Multichannel	
¹ Statistical error only.				

$\Gamma(N\eta)/\Gamma_{total}$	DOCUMENT ID	TECN	COMMENT	Γ_2/Γ
1.7 ± 0.9	¹ HUNT	19	DPWA Multichannel	
¹ Statistical error only.				

$\Gamma(\Lambda K)/\Gamma_{total}$	DOCUMENT ID	TECN	COMMENT	Γ_3/Γ
6.0 ± 0.1	¹ HUNT	19	DPWA Multichannel	
¹ Statistical error only.				

$N(1990)$ PHOTON DECAY AMPLITUDES AT THE POLE

$N(1990) \rightarrow p\gamma$, helicity-1/2 amplitude $A_{1/2}$

MODULUS (GeV ^{-1/2})	PHASE (°)	DOCUMENT ID	TECN	COMMENT
0.010 + 0.011 – 0.006	–103 + 108 – 155	ROENCHEN	14	DPWA
• • • We do not use the following data for averages, fits, limits, etc. • • •				
0.029	67	ROENCHEN	15A	DPWA Multichannel

$N(1990) \rightarrow p\gamma$, helicity-3/2 amplitude $A_{3/2}$

MODULUS (GeV ^{-1/2})	PHASE (°)	DOCUMENT ID	TECN	COMMENT
0.053 + 0.023 – 0.028	36 + 17 – 4	ROENCHEN	14	DPWA
• • • We do not use the following data for averages, fits, limits, etc. • • •				
0.033	39	ROENCHEN	15A	DPWA Multichannel

$N(1990)$ BREIT-WIGNER PHOTON DECAY AMPLITUDES

$N(1990) \rightarrow p\gamma$, helicity-1/2 amplitude $A_{1/2}$

VALUE (GeV ^{-1/2})	DOCUMENT ID	TECN	COMMENT
0.006 ± 0.003	¹ HUNT	19	DPWA Multichannel
0.040 ± 0.012	ANISOVICH	12A	DPWA Multichannel
¹ Statistical error only.			

$N(1990) \rightarrow p\gamma$, helicity-3/2 amplitude $A_{3/2}$

VALUE (GeV ^{-1/2})	DOCUMENT ID	TECN	COMMENT
– 0.055 ± 0.008	¹ HUNT	19	DPWA Multichannel
0.057 ± 0.012	ANISOVICH	12A	DPWA Multichannel
¹ Statistical error only.			

$N(1990) \rightarrow n\gamma$, helicity-1/2 amplitude $A_{1/2}$

VALUE (GeV ^{-1/2})	DOCUMENT ID	TECN	COMMENT
– 0.027 ± 0.024	¹ HUNT	19	DPWA Multichannel
– 0.045 ± 0.020	ANISOVICH	13B	DPWA Multichannel
¹ Statistical error only.			

$N(1990) \rightarrow n\gamma$, helicity-3/2 amplitude $A_{3/2}$

VALUE (GeV ^{-1/2})	DOCUMENT ID	TECN	COMMENT
0.051 ± 0.020	¹ HUNT	19	DPWA Multichannel
– 0.052 ± 0.027	ANISOVICH	13B	DPWA Multichannel
¹ Statistical error only.			

$N(1990)$ REFERENCES

For early references, see Physics Letters **111B** 1 (1982).

HUNT	19	PR C99 055205	B.C. Hunt, D.M. Manley
ROENCHEN	15A	EPJ A51 70	D. Roenchen et al.
PDG	14	CP C38 070001	K. Olive et al. (PDG Collab.)
ROENCHEN	14	EPJ A50 101	D. Roenchen et al.
Also		EPJ A51 63 (errat.)	D. Roenchen et al.
ANISOVICH	13B	EPJ A49 67	A.V. Anisovich et al.
ANISOVICH	12A	EPJ A48 15	A.V. Anisovich et al. (BONN, PNPI)
SHRESTHA	12A	PR C86 055203	M. Shrestha, D.M. Manley (KSU)
VRANA	00	PRPL 328 181	T.P. Vrana, S.A. Dytman, T.-S.H. Lee (PITT, ANL)
CUTKOSKY	80	Toronto Conf. 19	R.E. Cutkosky et al. (CMU, LBL) IJP
Also		PR D20 2839	R.E. Cutkosky et al. (CMU, LBL) IJP
HOEHLER	79	PDAT 12-1	G. Hoehler et al. (KARLT) IJP
Also		Toronto Conf. 3	R. Koch (KARLT) IJP

$N(2000) 5/2^+$

$$I(J^P) = \frac{1}{2}(\frac{5}{2}^+) \text{ Status: **}$$

OMITTED FROM SUMMARY TABLE

Before the 2012 Review, all the evidence for a $J^P = 5/2^+$ state with a mass above 1800 MeV was filed under a two-star $N(2000)$. There is now some evidence from ANISOVICH 12A for two $5/2^+$ states in this region, so we have split the older data (according to mass) between two two-star $5/2^+$ states, an $N(1860)$ and an $N(2000)$.

$N(2000)$ POLE POSITION

REAL PART

VALUE (MeV)	DOCUMENT ID	TECN	COMMENT
2030 ± 40	SOKHOYAN	15A	DPWA Multichannel
• • • We do not use the following data for averages, fits, limits, etc. • • •			
1900	SHKLYAR	13	DPWA Multichannel
2030 ± 110	ANISOVICH	12A	DPWA Multichannel

–2xIMAGINARY PART

VALUE (MeV)	DOCUMENT ID	TECN	COMMENT
380 ± 60	SOKHOYAN	15A	DPWA Multichannel
• • • We do not use the following data for averages, fits, limits, etc. • • •			
123	SHKLYAR	13	DPWA Multichannel
480 ± 100	ANISOVICH	12A	DPWA Multichannel

$N(2000)$ ELASTIC POLE RESIDUE

MODULUS $|r|$

VALUE (MeV)	DOCUMENT ID	TECN	COMMENT
18 ± 8	SOKHOYAN	15A	DPWA Multichannel
• • • We do not use the following data for averages, fits, limits, etc. • • •			
11	SHKLYAR	13	DPWA Multichannel
35 + 80 – 15	ANISOVICH	12A	DPWA Multichannel

PHASE θ

VALUE (°)	DOCUMENT ID	TECN	COMMENT
-150±40	SOKHOYAN 15A	DPWA	Multichannel
••• We do not use the following data for averages, fits, limits, etc. •••			
-6	SHKLYAR 13	DPWA	Multichannel
-100±40	ANISOVICH 12A	DPWA	Multichannel

N(2000) INELASTIC POLE RESIDUE

The "normalized residue" is the residue divided by $\Gamma_{pole}/2$.

Normalized residue in $N\pi \rightarrow N(2000) \rightarrow \Delta(1232)\pi, P\text{-wave}$

MODULUS	PHASE (°)	DOCUMENT ID	TECN	COMMENT
0.16±0.06	100±50	SOKHOYAN 15A	DPWA	Multichannel

Normalized residue in $N\pi \rightarrow N(2000) \rightarrow \Delta(1232)\pi, F\text{-wave}$

MODULUS	PHASE (°)	DOCUMENT ID	TECN	COMMENT
0.20±0.10	-20±45	SOKHOYAN 15A	DPWA	Multichannel

Normalized residue in $N\pi \rightarrow N(2000) \rightarrow N\sigma$

MODULUS	PHASE (°)	DOCUMENT ID	TECN	COMMENT
0.12±0.06	80±40	SOKHOYAN 15A	DPWA	Multichannel

Normalized residue in $N\pi \rightarrow N(2000) \rightarrow N(1520)\pi, D\text{-wave}$

MODULUS	PHASE (°)	DOCUMENT ID	TECN	COMMENT
0.17±0.09	-60±35	SOKHOYAN 15A	DPWA	Multichannel

N(2000) BREIT-WIGNER MASS

VALUE (MeV)	DOCUMENT ID	TECN	COMMENT
2060±30	SOKHOYAN 15A	DPWA	Multichannel
1946±4	¹ SHKLYAR 13	DPWA	Multichannel
••• We do not use the following data for averages, fits, limits, etc. •••			
2090±120	ANISOVICH 12A	DPWA	Multichannel

¹ Statistical error only.

N(2000) BREIT-WIGNER WIDTH

VALUE (MeV)	DOCUMENT ID	TECN	COMMENT
390±55	SOKHOYAN 15A	DPWA	Multichannel
198±2	² SHKLYAR 13	DPWA	Multichannel
••• We do not use the following data for averages, fits, limits, etc. •••			
460±100	ANISOVICH 12A	DPWA	Multichannel

² Statistical error only.

N(2000) DECAY MODES

Mode	Fraction (Γ_i/Γ)
Γ_1 $N\pi$	6-10 %
Γ_2 $N\eta$	<4 %
Γ_3 $N\omega$	<2 %
Γ_4 $N\pi\pi$	35-90 %
Γ_5 $\Delta(1232)\pi$	30-80 %
Γ_6 $\Delta(1232)\pi, P\text{-wave}$	12-32 %
Γ_7 $\Delta(1232)\pi, F\text{-wave}$	19-49 %
Γ_8 $\Lambda K^*(892)$	(2.2±1.0) %
Γ_9 $N\sigma$	5-15 %
Γ_{10} $N(1520)\pi, D\text{-wave}$	11-31 %
Γ_{11} $N(1680)\pi, P\text{-wave}$	17-25 %
Γ_{12} $\rho\gamma$	0.01-0.08 %
Γ_{13} $\rho\gamma, \text{helicity}=1/2$	0.003-0.031 %
Γ_{14} $\rho\gamma, \text{helicity}=3/2$	0.008-0.048 %
Γ_{15} $n\gamma$	0.002-0.07 %
Γ_{16} $n\gamma, \text{helicity}=1/2$	<0.017 %
Γ_{17} $n\gamma, \text{helicity}=3/2$	0.001-0.056 %

N(2000) BRANCHING RATIOS

$\Gamma(N\pi)/\Gamma_{total}$

VALUE (%)	DOCUMENT ID	TECN	COMMENT
6 to 10 (≈ 8) OUR ESTIMATE			
8±4	SOKHOYAN 15A	DPWA	Multichannel
10±1	³ SHKLYAR 13	DPWA	Multichannel
••• We do not use the following data for averages, fits, limits, etc. •••			
9±4	ANISOVICH 12A	DPWA	Multichannel

³ Statistical error only.

$\Gamma(N\eta)/\Gamma_{total}$

VALUE (%)	DOCUMENT ID	TECN	COMMENT
2±2	⁴ SHKLYAR 13	DPWA	Multichannel

⁴ Statistical error only.

$\Gamma(N\omega)/\Gamma_{total}$

VALUE (%)	DOCUMENT ID	TECN	COMMENT
18±8	DENISENKO 16	DPWA	Multichannel
1±1	⁵ SHKLYAR 13	DPWA	Multichannel

⁵ Statistical error only.

$\Gamma(\Delta(1232)\pi, P\text{-wave})/\Gamma_{total}$

VALUE (%)	DOCUMENT ID	TECN	COMMENT
22±10	SOKHOYAN 15A	DPWA	Multichannel

$\Gamma(\Delta(1232)\pi, F\text{-wave})/\Gamma_{total}$

VALUE (%)	DOCUMENT ID	TECN	COMMENT
34±15	SOKHOYAN 15A	DPWA	Multichannel

$\Gamma(\Lambda K^*(892))/\Gamma_{total}$

VALUE (%)	DOCUMENT ID	TECN	COMMENT
0.022±0.010	ANISOVICH 17B	DPWA	Multichannel

$\Gamma(N\sigma)/\Gamma_{total}$

VALUE (%)	DOCUMENT ID	TECN	COMMENT
10±5	SOKHOYAN 15A	DPWA	Multichannel

$\Gamma(N(1520)\pi, D\text{-wave})/\Gamma_{total}$

VALUE (%)	DOCUMENT ID	TECN	COMMENT
21±10	SOKHOYAN 15A	DPWA	Multichannel

$\Gamma(N(1680)\pi, P\text{-wave})/\Gamma_{total}$

VALUE (%)	DOCUMENT ID	TECN	COMMENT
16±9	SOKHOYAN 15A	DPWA	Multichannel

N(2000) PHOTON DECAY AMPLITUDES AT THE POLE

$N(2000) \rightarrow \rho\gamma, \text{helicity-1/2 amplitude } A_{1/2}$

MODULUS ($\text{GeV}^{-1/2}$)	PHASE (°)	DOCUMENT ID	TECN	COMMENT
0.033±0.010	15±25	SOKHOYAN 15A	DPWA	Multichannel

$N(2000) \rightarrow \rho\gamma, \text{helicity-3/2 amplitude } A_{3/2}$

MODULUS ($\text{GeV}^{-1/2}$)	PHASE (°)	DOCUMENT ID	TECN	COMMENT
0.045±0.008	-140±25	SOKHOYAN 15A	DPWA	Multichannel

N(2000) BREIT-WIGNER PHOTON DECAY AMPLITUDES

$N(2000) \rightarrow \rho\gamma, \text{helicity-1/2 amplitude } A_{1/2}$

VALUE ($\text{GeV}^{-1/2}$)	DOCUMENT ID	TECN	COMMENT
0.031±0.010	SOKHOYAN 15A	DPWA	Multichannel
0.011±0.001	⁶ SHKLYAR 13	DPWA	Multichannel

⁶ Statistical error only.

$N(2000) \rightarrow \rho\gamma, \text{helicity-3/2 amplitude } A_{3/2}$

VALUE ($\text{GeV}^{-1/2}$)	DOCUMENT ID	TECN	COMMENT
-0.043±0.008	SOKHOYAN 15A	DPWA	Multichannel
0.025±0.001	⁷ SHKLYAR 13	DPWA	Multichannel

⁷ Statistical error only.

$N(2000) \rightarrow n\gamma, \text{helicity-1/2 amplitude } A_{1/2}$

VALUE ($\text{GeV}^{-1/2}$)	DOCUMENT ID	TECN	COMMENT
-0.018±0.012	ANISOVICH 13B	DPWA	Multichannel

$N(2000) \rightarrow n\gamma, \text{helicity-3/2 amplitude } A_{3/2}$

VALUE ($\text{GeV}^{-1/2}$)	DOCUMENT ID	TECN	COMMENT
-0.035±0.020	ANISOVICH 13B	DPWA	Multichannel

N(2000) REFERENCES

ANISOVICH 17B PL B771 142 A.V. Anisovich et al.
 DENISENKO 16 PL B755 97 I. Denisenko et al.
 SOKHOYAN 15A EPJ A51 95 V. Sokhoyan et al. (CBELSA/TAPS Collab.)
 ANISOVICH 13B EPJ A49 67 A.V. Anisovich et al.
 SHKLYAR 13 PR C87 015201 V. Shklyar, H. Lenske, U. Mosel (GIES)
 ANISOVICH 12A EPJ A48 15 A.V. Anisovich et al. (BONN, PNPI)

N(2040) 3/2⁺

$J^P = \frac{3}{2}^+$ Status: *

OMITTED FROM SUMMARY TABLE

N(2040) MASS

VALUE (MeV)	DOCUMENT ID	TECN	COMMENT
2040 ⁺ ₋₄ ±25	ABLIKIM 09B	BES2	$J/\psi \rightarrow p\bar{p}\pi^0$
2068±3 ⁺¹⁵ ₋₄₀	ABLIKIM 06K	BES2	$J/\psi \rightarrow p\bar{n}\pi^-, n\bar{p}\pi^+$
••• We do not use the following data for averages, fits, limits, etc. •••			
2244±30	^{1,2} HUNT 19	DPWA	Multichannel

Baryon Particle Listings

 $N(2040)$, $N(2060)$ ¹ Statistical error only.² We list here candidates for high-mass $3/2^+$ states. $N(2040)$ WIDTH

VALUE (MeV)	DOCUMENT ID	TECN	COMMENT
$230 \pm 8 \pm 52$	ABLIKIM 09B	BES2	$J/\psi \rightarrow p\bar{p}\pi^0$
$165 \pm 14 \pm 40$	ABLIKIM 06K	BES2	$J/\psi \rightarrow p\bar{n}\pi^-, n\bar{p}\pi^+$
530 ± 89	^{3,4} HUNT 19	DPWA	Multichannel

³ Statistical error only.⁴ We list here candidates for high-mass $3/2^+$ states. $N(2040)$ REFERENCES

HUNT 19	PR C99 055205	B. C. Hunt, D.M. Manley	
ABLIKIM 09B	PR D80 052004	M. Ablilikim et al.	(BES II Collab.)
ABLIKIM 06K	PRL 97 062001	M. Ablilikim et al.	(BES II Collab.)

 $N(2060) 5/2^-$

$$I(J^P) = \frac{1}{2}(\frac{5}{2}^-) \text{ Status: } ***$$

Before our 2012 Review, this state appeared in our Listings as the $N(2200)$.

 $N(2060)$ POLE POSITION

REAL PART

VALUE (MeV)	DOCUMENT ID	TECN	COMMENT
2020 to 2130 (≈ 2070) OUR ESTIMATE			
2030 ± 15	SOKHOYAN 15A	DPWA	Multichannel
$2119 \pm 11 \pm 1$	¹ SVARC 14	L+P	$\pi N \rightarrow \pi N$
2100 ± 60	CUTKOSKY 80	IPWA	$\pi N \rightarrow \pi N$
2010	HUNT 19	DPWA	Multichannel
2040 ± 15	ANISOVICH 12A	DPWA	Multichannel
2144 ± 31	BATINIC 10	DPWA	$\pi N \rightarrow N\pi, N\eta$

¹ Fit to the amplitudes of HOEHLER 79. $-2 \times$ IMAGINARY PART

VALUE (MeV)	DOCUMENT ID	TECN	COMMENT
350 to 430 (≈ 400) OUR ESTIMATE			
400 ± 35	SOKHOYAN 15A	DPWA	Multichannel
$370 \pm 20 \pm 5$	¹ SVARC 14	L+P	$\pi N \rightarrow \pi N$
360 ± 80	CUTKOSKY 80	IPWA	$\pi N \rightarrow \pi N$
395	HUNT 19	DPWA	Multichannel
390 ± 25	ANISOVICH 12A	DPWA	Multichannel
438 ± 13	BATINIC 10	DPWA	$\pi N \rightarrow N\pi, N\eta$

¹ Fit to the amplitudes of HOEHLER 79. $N(2060)$ ELASTIC POLE RESIDUEMODULUS $|r|$

VALUE (MeV)	DOCUMENT ID	TECN	COMMENT
15 to 30 (≈ 20) OUR ESTIMATE			
25 ± 8	SOKHOYAN 15A	DPWA	Multichannel
$19 \pm 1 \pm 1$	¹ SVARC 14	L+P	$\pi N \rightarrow \pi N$
20 ± 10	CUTKOSKY 80	IPWA	$\pi N \rightarrow \pi N$
19 ± 5	ANISOVICH 12A	DPWA	Multichannel
26	BATINIC 10	DPWA	$\pi N \rightarrow N\pi, N\eta$

¹ Fit to the amplitudes of HOEHLER 79.PHASE θ

VALUE ($^\circ$)	DOCUMENT ID	TECN	COMMENT
-130 to -90 (≈ -110) OUR ESTIMATE			
-130 ± 20	SOKHOYAN 15A	DPWA	Multichannel
$-94 \pm 5 \pm 1$	¹ SVARC 14	L+P	$\pi N \rightarrow \pi N$
-90 ± 50	CUTKOSKY 80	IPWA	$\pi N \rightarrow \pi N$
-125 ± 20	ANISOVICH 12A	DPWA	Multichannel
-71	BATINIC 10	DPWA	$\pi N \rightarrow N\pi, N\eta$

¹ Fit to the amplitudes of HOEHLER 79. $N(2060)$ INELASTIC POLE RESIDUE

The "normalized residue" is the residue divided by $\Gamma_{pole}/2$.

Normalized residue in $N\pi \rightarrow N(2060) \rightarrow N\eta$

MODULUS	PHASE ($^\circ$)	DOCUMENT ID	TECN	COMMENT
0.05 ± 0.03	40 ± 25	ANISOVICH 12A	DPWA	Multichannel

Normalized residue in $N\pi \rightarrow N(2060) \rightarrow \Lambda K$

MODULUS	DOCUMENT ID	TECN	COMMENT
0.01 ± 0.005	ANISOVICH 12A	DPWA	Multichannel

Normalized residue in $N\pi \rightarrow N(2060) \rightarrow \Sigma K$

MODULUS	PHASE ($^\circ$)	DOCUMENT ID	TECN	COMMENT
0.04 ± 0.02	-70 ± 30	ANISOVICH 12A	DPWA	Multichannel

Normalized residue in $N\pi \rightarrow N(2060) \rightarrow \Delta(1232)\pi, D\text{-wave}$

MODULUS	PHASE ($^\circ$)	DOCUMENT ID	TECN	COMMENT
0.06 ± 0.03	-90 ± 40	SOKHOYAN 15A	DPWA	Multichannel

Normalized residue in $N\pi \rightarrow N(2060) \rightarrow N\sigma$

MODULUS	PHASE ($^\circ$)	DOCUMENT ID	TECN	COMMENT
0.12 ± 0.06	80 ± 40	SOKHOYAN 15A	DPWA	Multichannel

Normalized residue in $N\pi \rightarrow N(2060) \rightarrow N(1440)\pi$

MODULUS	PHASE ($^\circ$)	DOCUMENT ID	TECN	COMMENT
0.17 ± 0.09	-60 ± 35	SOKHOYAN 15A	DPWA	Multichannel

Normalized residue in $N\pi \rightarrow N(2060) \rightarrow N(1520)\pi, P\text{-wave}$

MODULUS	PHASE ($^\circ$)	DOCUMENT ID	TECN	COMMENT
0.14 ± 0.06	-45 ± 15	SOKHOYAN 15A	DPWA	Multichannel

 $N(2060)$ BREIT-WIGNER MASS

VALUE (MeV)	DOCUMENT ID	TECN	COMMENT
2030 to 2200 (≈ 2100) OUR ESTIMATE			
2111 ± 17	¹ HUNT 19	DPWA	Multichannel
2045 ± 15	SOKHOYAN 15A	DPWA	Multichannel
2180 ± 80	CUTKOSKY 80	IPWA	$\pi N \rightarrow \pi N$
2228 ± 30	HOEHLER 79	IPWA	$\pi N \rightarrow \pi N$
2060 ± 15	ANISOVICH 12A	DPWA	Multichannel
2116 ± 21	¹ SHRESTHA 12A	DPWA	Multichannel
2217 ± 27	BATINIC 10	DPWA	$\pi N \rightarrow N\pi, N\eta$

¹ Statistical error only. $N(2060)$ BREIT-WIGNER WIDTH

VALUE (MeV)	DOCUMENT ID	TECN	COMMENT
300 to 450 (≈ 400) OUR ESTIMATE			
499 ± 70	¹ HUNT 19	DPWA	Multichannel
420 ± 30	SOKHOYAN 15A	DPWA	Multichannel
400 ± 100	CUTKOSKY 80	IPWA	$\pi N \rightarrow \pi N$
310 ± 50	HOEHLER 79	IPWA	$\pi N \rightarrow \pi N$
375 ± 25	ANISOVICH 12A	DPWA	Multichannel
307 ± 112	¹ SHRESTHA 12A	DPWA	Multichannel
481 ± 17	BATINIC 10	DPWA	$\pi N \rightarrow N\pi, N\eta$

¹ Statistical error only. $N(2060)$ DECAY MODES

Mode	Fraction (Γ_i/Γ)
Γ_1 $N\pi$	7–12 %
Γ_2 $N\eta$	2–6 %
Γ_3 $N\omega$	1–7 %
Γ_4 ΛK	seen
Γ_5 ΣK	1–5 %
Γ_6 $N\pi\pi$	7–19 %
Γ_7 $\Delta(1232)\pi$	
Γ_8 $\Delta(1232)\pi, D\text{-wave}$	4–10 %
Γ_9 $N\rho$	
Γ_{10} $N\rho, S=1/2, P\text{-wave}$	seen
Γ_{11} $N\rho, S=3/2, D\text{-wave}$	
Γ_{12} $\Lambda K^*(892)$	0.3–1.3 %
Γ_{13} $N\sigma$	3–9 %
Γ_{14} $N(1440)\pi$	4–14 %
Γ_{15} $N(1520)\pi, P\text{-wave}$	9–21 %
Γ_{16} $N(1680)\pi, S\text{-wave}$	8–22 %
Γ_{17} $p\gamma$	0.03–0.19 %
Γ_{18} $p\gamma, \text{helicity}=1/2$	0.02–0.08 %
Γ_{19} $p\gamma, \text{helicity}=3/2$	0.01–0.10 %
Γ_{20} $n\gamma$	0.003–0.07 %
Γ_{21} $n\gamma, \text{helicity}=1/2$	0.001–0.02 %
Γ_{22} $n\gamma, \text{helicity}=3/2$	0.002–0.05 %

N(2060) BRANCHING RATIOS

$\Gamma(N\pi)/\Gamma_{total}$	DOCUMENT ID	TECN	COMMENT	Γ_1/Γ
VALUE (%)				
7 to 12 (≈ 10) OUR ESTIMATE				
5.3 \pm 1.4	¹ HUNT	19	DPWA	Multichannel
11 \pm 2	SOKHOYAN	15A	DPWA	Multichannel
10 \pm 3	CUTKOSKY	80	IPWA	$\pi N \rightarrow \pi N$
7 \pm 2	HOEHLER	79	IPWA	$\pi N \rightarrow \pi N$
••• We do not use the following data for averages, fits, limits, etc. •••				
8 \pm 2	ANISOVICH	12A	DPWA	Multichannel
9 \pm 2	¹ SHRESTHA	12A	DPWA	Multichannel
13 \pm 4	BATINIC	10	DPWA	$\pi N \rightarrow N\pi, N\eta$

¹ Statistical error only.

$\Gamma(N\eta)/\Gamma_{total}$	DOCUMENT ID	TECN	COMMENT	Γ_2/Γ
VALUE (%)				
30 \pm 8	¹ HUNT	19	DPWA	Multichannel
4 \pm 2	ANISOVICH	12A	DPWA	Multichannel
••• We do not use the following data for averages, fits, limits, etc. •••				
< 1	¹ SHRESTHA	12A	DPWA	Multichannel
0.2 \pm 1.0	BATINIC	10	DPWA	$\pi N \rightarrow N\pi, N\eta$

¹ Statistical error only.

$\Gamma(N\omega)/\Gamma_{total}$	DOCUMENT ID	TECN	COMMENT	Γ_3/Γ
VALUE (%)				
4 \pm 3	DENISENKO	16	DPWA	Multichannel

$\Gamma(\Lambda K)/\Gamma_{total}$	DOCUMENT ID	TECN	COMMENT	Γ_4/Γ
VALUE (%)				
15 \pm 5	¹ HUNT	19	DPWA	Multichannel

¹ Statistical error only.

$\Gamma(\Sigma K)/\Gamma_{total}$	DOCUMENT ID	TECN	COMMENT	Γ_5/Γ
VALUE (%)				
3 \pm 2	ANISOVICH	12A	DPWA	Multichannel

$\Gamma(\Delta(1232)\pi, D\text{-wave})/\Gamma_{total}$	DOCUMENT ID	TECN	COMMENT	Γ_8/Γ
VALUE (%)				
15 \pm 6	¹ HUNT	19	DPWA	Multichannel
7 \pm 3	SOKHOYAN	15A	DPWA	Multichannel
••• We do not use the following data for averages, fits, limits, etc. •••				
40 \pm 13	¹ SHRESTHA	12A	DPWA	Multichannel

¹ Statistical error only.

$\Gamma(N\rho, S=1/2, P\text{-wave})/\Gamma_{total}$	DOCUMENT ID	TECN	COMMENT	Γ_{10}/Γ
VALUE (%)				
<10	¹ HUNT	19	DPWA	Multichannel
••• We do not use the following data for averages, fits, limits, etc. •••				
21 \pm 15	¹ SHRESTHA	12A	DPWA	Multichannel

¹ Statistical error only.

$\Gamma(N\rho, S=3/2, D\text{-wave})/\Gamma_{total}$	DOCUMENT ID	TECN	COMMENT	Γ_{11}/Γ
VALUE (%)				
14 \pm 9	¹ HUNT	19	DPWA	Multichannel

¹ Statistical error only.

$\Gamma(\Lambda K^*(892))/\Gamma_{total}$	DOCUMENT ID	TECN	COMMENT	Γ_{12}/Γ
VALUE				
0.008 \pm 0.005	ANISOVICH	17B	DPWA	Multichannel

$\Gamma(N\sigma)/\Gamma_{total}$	DOCUMENT ID	TECN	COMMENT	Γ_{13}/Γ
VALUE (%)				
6 \pm 3	SOKHOYAN	15A	DPWA	Multichannel

$\Gamma(N(1440)\pi)/\Gamma_{total}$	DOCUMENT ID	TECN	COMMENT	Γ_{14}/Γ
VALUE (%)				
9 \pm 5	SOKHOYAN	15A	DPWA	Multichannel

$\Gamma(N(1520)\pi, P\text{-wave})/\Gamma_{total}$	DOCUMENT ID	TECN	COMMENT	Γ_{15}/Γ
VALUE (%)				
15 \pm 6	SOKHOYAN	15A	DPWA	Multichannel

$\Gamma(N(1680)\pi, S\text{-wave})/\Gamma_{total}$	DOCUMENT ID	TECN	COMMENT	Γ_{16}/Γ
VALUE (%)				
15 \pm 7	SOKHOYAN	15A	DPWA	Multichannel

N(2060) PHOTON DECAY AMPLITUDES AT THE POLE

N(2060) $\rightarrow p\gamma$, helicity-1/2 amplitude $A_{1/2}$

MODULUS (GeV ^{-1/2})	PHASE (°)	DOCUMENT ID	TECN	COMMENT
0.064 \pm 0.010	12 \pm 8	SOKHOYAN	15A	DPWA Multichannel

N(2060) $\rightarrow p\gamma$, helicity-3/2 amplitude $A_{3/2}$

MODULUS (GeV ^{-1/2})	PHASE (°)	DOCUMENT ID	TECN	COMMENT
0.060 \pm 0.020	13 \pm 10	SOKHOYAN	15A	DPWA Multichannel

N(2060) BREIT-WIGNER PHOTON DECAY AMPLITUDES

N(2060) $\rightarrow p\gamma$, helicity-1/2 amplitude $A_{1/2}$

VALUE (GeV ^{-1/2})	DOCUMENT ID	TECN	COMMENT
-0.019 \pm 0.005	¹ HUNT	19	DPWA Multichannel
0.062 \pm 0.010	SOKHOYAN	15A	DPWA Multichannel
••• We do not use the following data for averages, fits, limits, etc. •••			
0.018 \pm 0.004	¹ SHRESTHA	12A	DPWA Multichannel

¹ Statistical error only.

N(2060) $\rightarrow p\gamma$, helicity-3/2 amplitude $A_{3/2}$

VALUE (GeV ^{-1/2})	DOCUMENT ID	TECN	COMMENT
0.039 \pm 0.005	¹ HUNT	19	DPWA Multichannel
0.062 \pm 0.020	SOKHOYAN	15A	DPWA Multichannel
••• We do not use the following data for averages, fits, limits, etc. •••			
0.010 \pm 0.004	¹ SHRESTHA	12A	DPWA Multichannel

¹ Statistical error only.

N(2060) $\rightarrow n\gamma$, helicity-1/2 amplitude $A_{1/2}$

VALUE (GeV ^{-1/2})	DOCUMENT ID	TECN	COMMENT
0.069 \pm 0.017	¹ HUNT	19	DPWA Multichannel
0.025 \pm 0.011	ANISOVICH	13B	DPWA Multichannel
••• We do not use the following data for averages, fits, limits, etc. •••			
-0.012 \pm 0.017	¹ SHRESTHA	12A	DPWA Multichannel

¹ Statistical error only.

N(2060) $\rightarrow n\gamma$, helicity-3/2 amplitude $A_{3/2}$

VALUE (GeV ^{-1/2})	DOCUMENT ID	TECN	COMMENT
-0.023 \pm 0.020	¹ HUNT	19	DPWA Multichannel
-0.037 \pm 0.017	ANISOVICH	13B	DPWA Multichannel
••• We do not use the following data for averages, fits, limits, etc. •••			
-0.023 \pm 0.023	¹ SHRESTHA	12A	DPWA Multichannel

¹ Statistical error only.

N(2060) REFERENCES

HUNT	19	PR C99 055205	B.C. Hunt, D.M. Manley
ANISOVICH	17B	PL B771 142	A.V. Anisovich et al.
DENISENKO	16	PL B755 37	I. Denisenko et al.
SOKHOYAN	15A	EPJ A51 95	V. Sokhoyan et al.
SVARC	14	PR C89 045205	A. Svarc et al.
ANISOVICH	13B	EPJ A49 67	A.V. Anisovich et al.
ANISOVICH	12A	EPJ A48 15	A.V. Anisovich et al.
SHRESTHA	12A	PR C86 055203	M. Shrestha, D.M. Manley
BATINIC	10	PR C82 038203	M. Batinic et al.
CUTKOSKY	80	Toronto Conf. 19	R.E. Cutkosky et al.
Also		PR D20 2839	R.E. Cutkosky et al.
HOEHLER	79	PDAT 12-1	G. Hoehler et al.
Also		Toronto Conf. 3	R. Koch

N(2100) 1/2⁺

$I(J^P) = \frac{1}{2}(\frac{1}{2}^+)$ Status: ***

N(2100) POLE POSITION

REAL PART

VALUE (MeV)	DOCUMENT ID	TECN	COMMENT
2050 to 2150 (≈ 2100) OUR ESTIMATE			
2120 \pm 25	SOKHOYAN	15A	DPWA Multichannel
2052 \pm 6 \pm 3	¹ SVARC	14	L+P $\pi N \rightarrow \pi N$
2120 \pm 40	CUTKOSKY	80	IPWA $\pi N \rightarrow \pi N$
••• We do not use the following data for averages, fits, limits, etc. •••			
2217	HUNT	19	DPWA Multichannel
2120 \pm 47	BATINIC	10	DPWA $\pi N \rightarrow N\pi, N\eta$
1810	VRANA	00	DPWA Multichannel

¹ Fit to the amplitudes of HOEHLER 79.

-2xIMAGINARY PART

VALUE (MeV)	DOCUMENT ID	TECN	COMMENT
240 to 340 (≈ 300) OUR ESTIMATE			
290 \pm 30	SOKHOYAN	15A	DPWA Multichannel
337 \pm 10 \pm 4	¹ SVARC	14	L+P $\pi N \rightarrow \pi N$
240 \pm 80	CUTKOSKY	80	IPWA $\pi N \rightarrow \pi N$
••• We do not use the following data for averages, fits, limits, etc. •••			
545	HUNT	19	DPWA Multichannel
346 \pm 80	BATINIC	10	DPWA $\pi N \rightarrow N\pi, N\eta$
622	VRANA	00	DPWA Multichannel

¹ Fit to the amplitudes of HOEHLER 79.

Baryon Particle Listings

 $N(2100)$ $N(2100)$ ELASTIC POLE RESIDUEMODULUS $|r|$

VALUE (MeV)	DOCUMENT ID	TECN	COMMENT
15 to 30 (≈ 20) OUR ESTIMATE			
23 \pm 5	SOKHOYAN	15A	DPWA Multichannel
30 \pm 1 \pm 1	¹ SVARC	14	L+P $\pi N \rightarrow \pi N$
14 \pm 7	CUTKOSKY	80	IPWA $\pi N \rightarrow \pi N$
••• We do not use the following data for averages, fits, limits, etc. •••			
33	BATINIC	10	DPWA $\pi N \rightarrow N\pi, N\eta$
¹ Fit to the amplitudes of HOEHLER 79.			

PHASE θ

VALUE ($^\circ$)	DOCUMENT ID	TECN	COMMENT
-100 to -60 (≈ -80) OUR ESTIMATE			
-70 \pm 25	SOKHOYAN	15A	DPWA Multichannel
-92 \pm 3 \pm 2	¹ SVARC	14	L+P $\pi N \rightarrow \pi N$
35 \pm 25	CUTKOSKY	80	IPWA $\pi N \rightarrow \pi N$
••• We do not use the following data for averages, fits, limits, etc. •••			
-59	BATINIC	10	DPWA $\pi N \rightarrow N\pi, N\eta$
¹ Fit to the amplitudes of HOEHLER 79.			

 $N(2100)$ INELASTIC POLE RESIDUENormalized residue in $N\pi \rightarrow N(2100) \rightarrow \Delta(1232)\pi$

MODULUS	PHASE ($^\circ$)	DOCUMENT ID	TECN	COMMENT
0.11 \pm 0.05	20 \pm 60	SOKHOYAN	15A	DPWA Multichannel

Normalized residue in $N\pi \rightarrow N(2100) \rightarrow N\sigma$

MODULUS	PHASE ($^\circ$)	DOCUMENT ID	TECN	COMMENT
0.18 \pm 0.06	125 \pm 25	SOKHOYAN	15A	DPWA Multichannel

Normalized residue in $N\pi \rightarrow N(2100) \rightarrow N(1535)\pi$

MODULUS	PHASE ($^\circ$)	DOCUMENT ID	TECN	COMMENT
0.22 \pm 0.06	-40 \pm 25	SOKHOYAN	15A	DPWA Multichannel

 $N(2100)$ BREIT-WIGNER MASS

VALUE (MeV)	DOCUMENT ID	TECN	COMMENT
2050 to 2150 (≈ 2100) OUR ESTIMATE			
2221 \pm 92	¹ HUNT	19	DPWA Multichannel
2115 \pm 20	SOKHOYAN	15A	DPWA Multichannel
2125 \pm 75	CUTKOSKY	80	IPWA $\pi N \rightarrow \pi N$
2050 \pm 20	HOEHLER	79	IPWA $\pi N \rightarrow \pi N$
••• We do not use the following data for averages, fits, limits, etc. •••			
2157 \pm 42	BATINIC	10	DPWA $\pi N \rightarrow N\pi, N\eta$
2068 \pm 3 \pm 15	ABLIKIM	06K	BES2 $J/\psi \rightarrow (p\pi^-)\bar{\pi}$
2084 \pm 93	VRANA	00	DPWA Multichannel
¹ Statistical error only.			

 $N(2100)$ BREIT-WIGNER WIDTH

VALUE (MeV)	DOCUMENT ID	TECN	COMMENT
200 to 320 (≈ 260) OUR ESTIMATE			
545 \pm 170	¹ HUNT	19	DPWA Multichannel
290 \pm 20	SOKHOYAN	15A	DPWA Multichannel
260 \pm 100	CUTKOSKY	80	IPWA $\pi N \rightarrow \pi N$
200 \pm 30	HOEHLER	79	IPWA $\pi N \rightarrow \pi N$
••• We do not use the following data for averages, fits, limits, etc. •••			
355 \pm 88	BATINIC	10	DPWA $\pi N \rightarrow N\pi, N\eta$
165 \pm 14 \pm 40	ABLIKIM	06K	BES2 $J/\psi \rightarrow (p\pi^-)\bar{\pi}$
1077 \pm 643	VRANA	00	DPWA Multichannel
¹ Statistical error only.			

 $N(2100)$ DECAY MODES

Mode	Fraction (Γ_i/Γ)
Γ_1 $N\pi$	8-18 %
Γ_2 $N\eta$	seen
Γ_3 $N\eta'$	5-11 %
Γ_4 $N\omega$	10-25 %
Γ_5 ΛK	seen
Γ_6 $N\pi\pi$	20-40 %
Γ_7 $\Delta(1232)\pi$	
Γ_8 $\Delta(1232)\pi, P\text{-wave}$	6-14 %
Γ_9 $N\rho$	
Γ_{10} $N\rho, S=1/2, P\text{-wave}$	seen
Γ_{11} $\Lambda K^*(892)$	3-11 %
Γ_{12} $N\sigma$	14-26 %
Γ_{13} $N(1535)\pi$	26-34 %
Γ_{14} $N\gamma, \text{helicity}=1/2$	0.001-0.012 %

 $N(2100)$ BRANCHING RATIOS $\Gamma(N\pi)/\Gamma_{\text{total}}$

VALUE (%)	DOCUMENT ID	TECN	COMMENT
8 to 18 (≈ 12) OUR ESTIMATE			
21 \pm 11	¹ HUNT	19	DPWA Multichannel
16 \pm 5	SOKHOYAN	15A	DPWA Multichannel
12 \pm 3	CUTKOSKY	80	IPWA $\pi N \rightarrow \pi N$
10 \pm 4	HOEHLER	79	IPWA $\pi N \rightarrow \pi N$
••• We do not use the following data for averages, fits, limits, etc. •••			
16 \pm 5	BATINIC	10	DPWA $\pi N \rightarrow N\pi, N\eta$
2 \pm 5	VRANA	00	DPWA Multichannel
¹ Statistical error only.			

 $\Gamma(N\eta)/\Gamma_{\text{total}}$

VALUE (%)	DOCUMENT ID	TECN	COMMENT
< 4.7			
••• We do not use the following data for averages, fits, limits, etc. •••			
83 \pm 5	BATINIC	10	DPWA $\pi N \rightarrow N\pi, N\eta$
61 \pm 61	VRANA	00	DPWA Multichannel
¹ Statistical error only.			

 $\Gamma(N\eta')/\Gamma_{\text{total}}$

VALUE	DOCUMENT ID	TECN	COMMENT
0.08 \pm 0.03	ANISOVICH	17C	DPWA Multichannel

 $\Gamma(N\omega)/\Gamma_{\text{total}}$

VALUE (%)	DOCUMENT ID	TECN	COMMENT
15 \pm 10	DENISENKO	16	DPWA Multichannel

 $\Gamma(\Lambda K)/\Gamma_{\text{total}}$

VALUE (%)	DOCUMENT ID	TECN	COMMENT
< 1.0			
••• We do not use the following data for averages, fits, limits, etc. •••			
21 \pm 20	VRANA	00	DPWA Multichannel
¹ Statistical error only.			

 $\Gamma(\Delta(1232)\pi, P\text{-wave})/\Gamma_{\text{total}}$

VALUE (%)	DOCUMENT ID	TECN	COMMENT
< 7.5			
10 \pm 4	¹ HUNT	19	DPWA Multichannel
••• We do not use the following data for averages, fits, limits, etc. •••			
2 \pm 1	VRANA	00	DPWA Multichannel
¹ Statistical error only.			

 $\Gamma(N\rho, S=1/2, P\text{-wave})/\Gamma_{\text{total}}$

VALUE (%)	DOCUMENT ID	TECN	COMMENT
52 \pm 19	¹ HUNT	19	DPWA Multichannel
••• We do not use the following data for averages, fits, limits, etc. •••			
4 \pm 1	VRANA	00	DPWA Multichannel
¹ Statistical error only.			

 $\Gamma(\Lambda K^*(892))/\Gamma_{\text{total}}$

VALUE	DOCUMENT ID	TECN	COMMENT
0.07 \pm 0.04	ANISOVICH	17B	DPWA Multichannel

 $\Gamma(N\sigma)/\Gamma_{\text{total}}$

VALUE (%)	DOCUMENT ID	TECN	COMMENT
< 35			
20 \pm 6	¹ HUNT	19	DPWA Multichannel
••• We do not use the following data for averages, fits, limits, etc. •••			
10 \pm 1	VRANA	00	DPWA Multichannel
¹ Statistical error only.			

 $\Gamma(N(1535)\pi)/\Gamma_{\text{total}}$

VALUE (%)	DOCUMENT ID	TECN	COMMENT
30 \pm 4	SOKHOYAN	15A	DPWA Multichannel

 $N(2100)$ PHOTON DECAY AMPLITUDES AT THE POLE $N(2100) \rightarrow p\gamma, \text{helicity-1/2 amplitude } A_{1/2}$

MODULUS ($\text{GeV}^{-1/2}$)	PHASE ($^\circ$)	DOCUMENT ID	TECN	COMMENT
0.011 \pm 0.004	65 \pm 30	SOKHOYAN	15A	DPWA Multichannel

 $N(2100)$ BREIT-WIGNER PHOTON DECAY AMPLITUDES $N(2100) \rightarrow p\gamma, \text{helicity-1/2 amplitude } A_{1/2}$

VALUE ($\text{GeV}^{-1/2}$)	DOCUMENT ID	TECN	COMMENT
0.032 \pm 0.014	¹ HUNT	19	DPWA Multichannel
0.010 \pm 0.004	SOKHOYAN	15A	DPWA Multichannel
¹ Statistical error only.			

See key on page 999

Baryon Particle Listings

$N(2100)$, $N(2120)$

$N(2100) \rightarrow n\gamma$, helicity-1/2 amplitude $A_{1/2}$

VALUE (GeV ^{-1/2})	DOCUMENT ID	TECN	COMMENT
0.026 ± 0.013	¹ HUNT	19	DPWA Multichannel

¹ Statistical error only.

$N(2100)$ REFERENCES

HUNT	19	PR C99 055205	B.C. Hunt, D.M. Manley
ANISOVICH	17B	PL B771 142	A.V. Anisovich et al.
ANISOVICH	17C	PL B772 247	A.V. Anisovich et al.
DENISENKO	16	PL B755 97	I. Denisenko et al.
SOKHOYAN	15A	EPJ A51 95	V. Sokhoyan et al. (CBELSA/TAPS Collab.)
SVARC	14	PR C89 045205	A. Svarc et al. (RBI Zagreb, UNI Tuzla)
BATINIC	10	PR C82 038203	M. Batinic et al. (ZAGR)
ABLIKIM	06K	PRL 97 062001	M. Ablikim et al. (BES II Collab.)
VRANA	00	PRPL 328 181	T.P. Vrana, S.A. Dytman, T.-S.H. Lee (PITT, ANL)
CUTKOSKY	80	Toronto Conf. 19	R.E. Cutkosky et al. (CMU, LBL) IJP
Also		PR D20 2839	R.E. Cutkosky et al. (CMU, LBL)
HOEHLER	79	PDAT 12-1	G. Hoehler et al. (KARLT) IJP
Also		Toronto Conf. 3	R. Koch (KARLT) IJP

$N(2120) 3/2^-$

$$J(P) = \frac{1}{2}(3/2^-) \text{ Status: } ***$$

Before the 2012 Review, all the evidence for a $J^P = 3/2^-$ state with a mass above 1800 MeV was filed under a two-star $N(2080)$. There is now evidence from ANISOVICH 12A for two $3/2^-$ states in this region, so we have split the older data (according to mass) between a three-star $N(1875)$ and a two-star $N(2120)$.

$N(2120)$ POLE POSITION

REAL PART

VALUE (MeV)	DOCUMENT ID	TECN	COMMENT
2050 to 2150 (≈ 2100) OUR ESTIMATE			
2115 ± 40	SOKHOYAN	15A	DPWA Multichannel
2094 ± 7 ± 11	SVARC	14	L+P $\pi N \rightarrow \pi N$
2050 ± 70	CUTKOSKY	80	IPWA $\pi N \rightarrow \pi N$ (higher m)
• • • We do not use the following data for averages, fits, limits, etc. • • •			
2357	HUNT	19	DPWA Multichannel
2115 ± 40	GUTZ	14	DPWA Multichannel
2110 ± 50	ANISOVICH	12A	DPWA Multichannel

-2xIMAGINARY PART

VALUE (MeV)	DOCUMENT ID	TECN	COMMENT
200 to 360 (≈ 280) OUR ESTIMATE			
345 ± 35	SOKHOYAN	15A	DPWA Multichannel
296 ± 15 ± 4	SVARC	14	L+P $\pi N \rightarrow \pi N$
200 ± 80	CUTKOSKY	80	IPWA $\pi N \rightarrow \pi N$ (higher m)
• • • We do not use the following data for averages, fits, limits, etc. • • •			
503	HUNT	19	DPWA Multichannel
345 ± 35	GUTZ	14	DPWA Multichannel
340 ± 45	ANISOVICH	12A	DPWA Multichannel

$N(2120)$ ELASTIC POLE RESIDUE

MODULUS $|r|$

VALUE (MeV)	DOCUMENT ID	TECN	COMMENT
10 to 30 (≈ 20) OUR ESTIMATE			
11 ± 6	SOKHOYAN	15A	DPWA Multichannel
13 ± 1 ± 1	SVARC	14	L+P $\pi N \rightarrow \pi N$
30 ± 20	CUTKOSKY	80	IPWA $\pi N \rightarrow \pi N$ (higher m)
• • • We do not use the following data for averages, fits, limits, etc. • • •			
11 ± 6	GUTZ	14	DPWA Multichannel
13 ± 3	ANISOVICH	12A	DPWA Multichannel

PHASE θ

VALUE (°)	DOCUMENT ID	TECN	COMMENT
-40 to 20 (≈ -10) OUR ESTIMATE			
-30 ± 20	SOKHOYAN	15A	DPWA Multichannel
-2 ± 4 ± 9	SVARC	14	L+P $\pi N \rightarrow \pi N$
0 ± 100	CUTKOSKY	80	IPWA $\pi N \rightarrow \pi N$ (higher m)
• • • We do not use the following data for averages, fits, limits, etc. • • •			
-30 ± 20	GUTZ	14	DPWA Multichannel
-20 ± 10	ANISOVICH	12A	DPWA Multichannel

$N(2120)$ INELASTIC POLE RESIDUE

The "normalized residue" is the residue divided by $\Gamma_{pole}/2$.

Normalized residue in $N\pi \rightarrow N(2120) \rightarrow \Lambda K$

MODULUS	PHASE (°)	DOCUMENT ID	TECN	COMMENT
0.03 ± 0.01	100 ± 30	ANISOVICH	12A	DPWA Multichannel

Normalized residue in $N\pi \rightarrow N(2120) \rightarrow \Sigma K$

MODULUS	PHASE (°)	DOCUMENT ID	TECN	COMMENT
0.02 ± 0.015	-50 ± 40	ANISOVICH	12A	DPWA Multichannel

Normalized residue in $N\pi \rightarrow N(2120) \rightarrow N(1535)\pi$

MODULUS	PHASE (°)	DOCUMENT ID	TECN	COMMENT
0.15 ± 0.08	-90 ± 40	GUTZ	14	DPWA Multichannel

Normalized residue in $N\pi \rightarrow N(2120) \rightarrow \Delta(1232)\pi$, S-wave

MODULUS	PHASE (°)	DOCUMENT ID	TECN	COMMENT
0.25 ± 0.10	undefined	SOKHOYAN	15A	DPWA Multichannel

Normalized residue in $N\pi \rightarrow N(2120) \rightarrow \Delta(1232)\pi$, D-wave

MODULUS	PHASE (°)	DOCUMENT ID	TECN	COMMENT
0.15 ± 0.06	-35 ± 30	SOKHOYAN	15A	DPWA Multichannel

Normalized residue in $N\pi \rightarrow N(2120) \rightarrow N\sigma$

MODULUS	PHASE (°)	DOCUMENT ID	TECN	COMMENT
0.09 ± 0.05	-80 ± 50	SOKHOYAN	15A	DPWA Multichannel

$N(2120)$ BREIT-WIGNER MASS

VALUE (MeV)	DOCUMENT ID	TECN	COMMENT
2060 to 2160 (≈ 2120) OUR ESTIMATE			
2353 ± 29	¹ HUNT	19	DPWA Multichannel
2120 ± 45	SOKHOYAN	15A	DPWA Multichannel
2060 ± 80	CUTKOSKY	80	IPWA $\pi N \rightarrow \pi N$
2081 ± 20	HOEHLER	79	IPWA $\pi N \rightarrow \pi N$
• • • We do not use the following data for averages, fits, limits, etc. • • •			
2120 ± 35	GUTZ	14	DPWA Multichannel
2150 ± 60	ANISOVICH	12A	DPWA Multichannel

¹ Statistical error only.

$N(2120)$ BREIT-WIGNER WIDTH

VALUE (MeV)	DOCUMENT ID	TECN	COMMENT
260 to 360 (≈ 300) OUR ESTIMATE			
503 ± 62	¹ HUNT	19	DPWA Multichannel
340 ± 35	SOKHOYAN	15A	DPWA Multichannel
300 ± 100	CUTKOSKY	80	IPWA $\pi N \rightarrow \pi N$ (higher m)
265 ± 40	HOEHLER	79	IPWA $\pi N \rightarrow \pi N$
• • • We do not use the following data for averages, fits, limits, etc. • • •			
340 ± 35	GUTZ	14	DPWA Multichannel
330 ± 45	ANISOVICH	12A	DPWA Multichannel

¹ Statistical error only.

$N(2120)$ DECAY MODES

Mode	Fraction (Γ_i/Γ)
Γ_1 $N\pi$	5-15 %
Γ_2 $N\eta$	
Γ_3 $N\eta'$	2-6 %
Γ_4 $N\omega$	4-20 %
Γ_5 ΛK	
Γ_6 $N\pi\pi$	50-95 %
Γ_7 $\Delta(1232)\pi$	40-90 %
Γ_8 $\Delta(1232)\pi$, S-wave	30-70 %
Γ_9 $\Delta(1232)\pi$, D-wave	8-32 %
Γ_{10} $N\rho$	
Γ_{11} $N\rho$, $S=3/2$, S-wave	
Γ_{12} $\Lambda K^*(892)$	< 0.2 %
Γ_{13} $N\sigma$	7-15 %
Γ_{14} $N(1535)\pi$	7-23 %
Γ_{15} $p\gamma$	0.16-2.1 %
Γ_{16} $p\gamma$, helicity=1/2	0.07-0.80 %
Γ_{17} $p\gamma$, helicity=3/2	0.09-1.3 %
Γ_{18} $n\gamma$	0.04-0.72 %
Γ_{19} $n\gamma$, helicity=1/2	0.04-0.60 %
Γ_{20} $n\gamma$, helicity=3/2	0.001-0.12 %

$N(2120)$ BRANCHING RATIOS

$\Gamma(N\pi)/\Gamma_{total}$	VALUE (%)	DOCUMENT ID	TECN	COMMENT	Γ_1/Γ
5 to 15 (≈ 10) OUR ESTIMATE					
	19 ± 2	¹ HUNT	19	DPWA Multichannel	
	5 ± 3	SOKHOYAN	15A	DPWA Multichannel	
	14 ± 7	CUTKOSKY	80	IPWA $\pi N \rightarrow \pi N$ (higher m)	
	6 ± 2	HOEHLER	79	IPWA $\pi N \rightarrow \pi N$	
• • • We do not use the following data for averages, fits, limits, etc. • • •					
	5 ± 3	GUTZ	14	DPWA Multichannel	
	6 ± 2	ANISOVICH	12A	DPWA Multichannel	

¹ Statistical error only.

Baryon Particle Listings

 $N(2120)$, $N(2190)$ $\Gamma(N\eta)/\Gamma_{\text{total}}$

VALUE (%)	DOCUMENT ID	TECN	COMMENT
3.1 ± 2.4	¹ HUNT 19	DPWA	Multichannel

¹ Statistical error only. $\Gamma(N\eta')/\Gamma_{\text{total}}$

VALUE (%)	DOCUMENT ID	TECN	COMMENT
0.04 ± 0.02	ANISOVICH 17C	DPWA	Multichannel

 $\Gamma(N\omega)/\Gamma_{\text{total}}$

VALUE (%)	DOCUMENT ID	TECN	COMMENT
12 ± 8	DENISENKO 16	DPWA	Multichannel

 $\Gamma(\Lambda K)/\Gamma_{\text{total}}$

VALUE (%)	DOCUMENT ID	TECN	COMMENT
8.5 ± 2.5	¹ HUNT 19	DPWA	Multichannel

¹ Statistical error only. $\Gamma(\Delta(1232)\pi, S\text{-wave})/\Gamma_{\text{total}}$

VALUE (%)	DOCUMENT ID	TECN	COMMENT
25 ± 11	¹ HUNT 19	DPWA	Multichannel
50 ± 20	SOKHOYAN 15A	DPWA	Multichannel

¹ Statistical error only. $\Gamma(\Delta(1232)\pi, D\text{-wave})/\Gamma_{\text{total}}$

VALUE (%)	DOCUMENT ID	TECN	COMMENT
34 ± 11	¹ HUNT 19	DPWA	Multichannel
20 ± 12	SOKHOYAN 15A	DPWA	Multichannel

¹ Statistical error only. $\Gamma(N\rho, S=3/2, S\text{-wave})/\Gamma_{\text{total}}$

VALUE (%)	DOCUMENT ID	TECN	COMMENT
< 3	¹ HUNT 19	DPWA	Multichannel

¹ Statistical error only. $\Gamma(\Lambda K^*(892))/\Gamma_{\text{total}}$

VALUE (%)	DOCUMENT ID	TECN	COMMENT
< 0.002	ANISOVICH 17B	DPWA	Multichannel

 $\Gamma(N\sigma)/\Gamma_{\text{total}}$

VALUE (%)	DOCUMENT ID	TECN	COMMENT
9 ± 5	¹ HUNT 19	DPWA	Multichannel
11 ± 4	SOKHOYAN 15A	DPWA	Multichannel

¹ Statistical error only. $\Gamma(N(1535)\pi)/\Gamma_{\text{total}}$

VALUE (%)	DOCUMENT ID	TECN	COMMENT
15 ± 8	GUTZ 14	DPWA	Multichannel

 $N(2120)$ PHOTON DECAY AMPLITUDES AT THE POLE $N(2120) \rightarrow p\gamma$, helicity-1/2 amplitude $A_{1/2}$

MODULUS ($\text{GeV}^{-1/2}$)	PHASE ($^\circ$)	DOCUMENT ID	TECN	COMMENT
0.130 ± 0.045	-40 ± 25	SOKHOYAN 15A	DPWA	Multichannel

 $N(2120) \rightarrow p\gamma$, helicity-3/2 amplitude $A_{3/2}$

MODULUS ($\text{GeV}^{-1/2}$)	PHASE ($^\circ$)	DOCUMENT ID	TECN	COMMENT
0.160 ± 0.060	-30 ± 15	SOKHOYAN 15A	DPWA	Multichannel

 $N(2120)$ BREIT-WIGNER PHOTON DECAY AMPLITUDES $N(2120) \rightarrow p\gamma$, helicity-1/2 amplitude $A_{1/2}$

VALUE ($\text{GeV}^{-1/2}$)	DOCUMENT ID	TECN	COMMENT
0.047 ± 0.009	¹ HUNT 19	DPWA	Multichannel
0.130 ± 0.050	SOKHOYAN 15A	DPWA	Multichannel

• • • We do not use the following data for averages, fits, limits, etc. • • •

VALUE ($\text{GeV}^{-1/2}$)	DOCUMENT ID	TECN	COMMENT
0.130 ± 0.050	GUTZ 14	DPWA	Multichannel

¹ Statistical error only. $N(2120) \rightarrow p\gamma$, helicity-3/2 amplitude $A_{3/2}$

VALUE ($\text{GeV}^{-1/2}$)	DOCUMENT ID	TECN	COMMENT
0.001 ± 0.007	¹ HUNT 19	DPWA	Multichannel
0.160 ± 0.065	SOKHOYAN 15A	DPWA	Multichannel

• • • We do not use the following data for averages, fits, limits, etc. • • •

VALUE ($\text{GeV}^{-1/2}$)	DOCUMENT ID	TECN	COMMENT
0.160 ± 0.065	GUTZ 14	DPWA	Multichannel

¹ Statistical error only. $N(2120) \rightarrow n\gamma$, helicity-1/2 amplitude $A_{1/2}$

VALUE ($\text{GeV}^{-1/2}$)	DOCUMENT ID	TECN	COMMENT
-0.020 ± 0.013	¹ HUNT 19	DPWA	Multichannel
0.110 ± 0.045	ANISOVICH 13B	DPWA	Multichannel

¹ Statistical error only. $N(2120) \rightarrow n\gamma$, helicity-3/2 amplitude $A_{3/2}$

VALUE ($\text{GeV}^{-1/2}$)	DOCUMENT ID	TECN	COMMENT
-0.00 ± 0.02	¹ HUNT 19	DPWA	Multichannel
0.040 ± 0.030	ANISOVICH 13B	DPWA	Multichannel

¹ Statistical error only. **$N(2120)$ REFERENCES**

HUNT 19	PR C99 055205	B.C. Hunt, D.M. Manley
ANISOVICH 17B	PL B771 142	A.V. Anisovich et al.
ANISOVICH 17C	PL B772 247	A.V. Anisovich et al.
DENISENKO 16	PL B755 97	I. Denisenko et al.
SOKHOYAN 15A	EPJ A51 95	V. Sokhoyan et al. (CBELSA/TAPS Collab.)
GUTZ 14	EPJ A50 74	E. Gutz et al. (CBELSA/TAPS Collab.)
SVARC 14	PR C89 045205	A. Svarc et al. (RBI Zagreb, UNI Tuzla)
ANISOVICH 13B	EPJ A49 67	A.V. Anisovich et al.
ANISOVICH 12A	EPJ A48 15	A.V. Anisovich et al. (BONN, PNPI)
CUTKOSKY 80	Toronto Conf. 19	R.E. Cutkosky et al. (CMU, LBL)
HOEHLER 79	PDAT 12-1	G. Hoehler et al. (KARLT)

 $N(2190) 7/2^-$ $I(J^P) = \frac{1}{2}(7_2^-)$ Status: * * * *

Older and obsolete values are listed and referenced in the 2014 edition, Chinese Physics C38 070001 (2014).

 $N(2190)$ POLE POSITION**REAL PART**

VALUE (MeV)	DOCUMENT ID	TECN	COMMENT
-------------	-------------	------	---------

2050 to 2150 (≈ 2100) OUR ESTIMATE

2150 ± 25	SOKHOYAN 15A	DPWA	Multichannel
---------------	--------------	------	--------------

$2079 \pm 4 \pm 9$	¹ SVARC 14	L+P	$\pi N \rightarrow \pi N$
--------------------	-----------------------	-----	---------------------------

2100 ± 50	CUTKOSKY 80	IPWA	$\pi N \rightarrow \pi N$
---------------	-------------	------	---------------------------

• • • We do not use the following data for averages, fits, limits, etc. • • •

2162	HUNT 19	DPWA	Multichannel
------	---------	------	--------------

2074	ROENCHEN 15A	DPWA	Multichannel
------	--------------	------	--------------

2150 ± 25	ANISOVICH 12A	DPWA	Multichannel
---------------	---------------	------	--------------

2063 ± 32	BATINIC 10	DPWA	$\pi N \rightarrow N\pi, N\eta$
---------------	------------	------	---------------------------------

2070	ARNDT 06	DPWA	$\pi N \rightarrow \pi N, \eta N$
------	----------	------	-----------------------------------

2107	VRANA 00	DPWA	Multichannel
------	----------	------	--------------

2042	HOEHLER 93	SPED	$\pi N \rightarrow \pi N$
------	------------	------	---------------------------

¹ Fit to the amplitudes of HOEHLER 79.**-2xIMAGINARY PART**

VALUE (MeV)	DOCUMENT ID	TECN	COMMENT
-------------	-------------	------	---------

300 to 500 (≈ 400) OUR ESTIMATE

325 ± 25	SOKHOYAN 15A	DPWA	Multichannel
--------------	--------------	------	--------------

$509 \pm 7 \pm 16$	¹ SVARC 14	L+P	$\pi N \rightarrow \pi N$
--------------------	-----------------------	-----	---------------------------

400 ± 160	CUTKOSKY 80	IPWA	$\pi N \rightarrow \pi N$
---------------	-------------	------	---------------------------

• • • We do not use the following data for averages, fits, limits, etc. • • •

407	HUNT 19	DPWA	Multichannel
-----	---------	------	--------------

327	ROENCHEN 15A	DPWA	Multichannel
-----	--------------	------	--------------

330 ± 30	ANISOVICH 12A	DPWA	Multichannel
--------------	---------------	------	--------------

330 ± 101	BATINIC 10	DPWA	$\pi N \rightarrow N\pi, N\eta$
---------------	------------	------	---------------------------------

520	ARNDT 06	DPWA	$\pi N \rightarrow \pi N, \eta N$
-----	----------	------	-----------------------------------

380	VRANA 00	DPWA	Multichannel
-----	----------	------	--------------

482	HOEHLER 93	SPED	$\pi N \rightarrow \pi N$
-----	------------	------	---------------------------

¹ Fit to the amplitudes of HOEHLER 79. **$N(2190)$ ELASTIC POLE RESIDUE****MODULUS $|r|$**

VALUE (MeV)	DOCUMENT ID	TECN	COMMENT
-------------	-------------	------	---------

25 to 70 (≈ 50) OUR ESTIMATE

30 ± 4	SOKHOYAN 15A	DPWA	Multichannel
------------	--------------	------	--------------

$54 \pm 1 \pm 3$	¹ SVARC 14	L+P	$\pi N \rightarrow \pi N$
------------------	-----------------------	-----	---------------------------

25 ± 10	CUTKOSKY 80	IPWA	$\pi N \rightarrow \pi N$
-------------	-------------	------	---------------------------

• • • We do not use the following data for averages, fits, limits, etc. • • •

35	ROENCHEN 15A	DPWA	Multichannel
----	--------------	------	--------------

30 ± 5	ANISOVICH 12A	DPWA	Multichannel
------------	---------------	------	--------------

34	BATINIC 10	DPWA	$\pi N \rightarrow N\pi, N\eta$
----	------------	------	---------------------------------

72	ARNDT 06	DPWA	$\pi N \rightarrow \pi N, \eta N$
----	----------	------	-----------------------------------

45	HOEHLER 93	SPED	$\pi N \rightarrow \pi N$
----	------------	------	---------------------------

¹ Fit to the amplitudes of HOEHLER 79.

PHASE θ

VALUE (°)	DOCUMENT ID	TECN	COMMENT
-30 to 30 (≈ 0) OUR ESTIMATE			
28 ± 10	SOKHOYAN 15A	DPWA	Multichannel
-18 ± 1 ± 3	¹ SVARC 14	L+P	$\pi N \rightarrow \pi N$
-30 ± 50	CUTKOSKY 80	IPWA	$\pi N \rightarrow \pi N$
• • • We do not use the following data for averages, fits, limits, etc. • • •			
-40	ROENCHEN 15A	DPWA	Multichannel
30 ± 10	ANISOVICH 12A	DPWA	Multichannel
-19	BATINIC 10	DPWA	$\pi N \rightarrow N\pi, N\eta$
-32	ARNDT 06	DPWA	$\pi N \rightarrow \pi N, \eta N$

¹ Fit to the amplitudes of HOEHLER 79.

N(2190) INELASTIC POLE RESIDUE

The "normalized residue" is the residue divided by $\Gamma_{pole}/2$.

Normalized residue in $N\pi \rightarrow N(2190) \rightarrow \Lambda K$

MODULUS	PHASE (°)	DOCUMENT ID	TECN	COMMENT
0.03 ± 0.01	20 ± 15	ANISOVICH 12A	DPWA	Multichannel
• • • We do not use the following data for averages, fits, limits, etc. • • •				
0.005	-51	ROENCHEN 15A	DPWA	Multichannel

Normalized residue in $N\pi \rightarrow N(2190) \rightarrow \Sigma K$

MODULUS	PHASE (°)	DOCUMENT ID	TECN	COMMENT
• • • We do not use the following data for averages, fits, limits, etc. • • •				
0.013	-69	ROENCHEN 15A	DPWA	Multichannel

Normalized residue in $N\pi \rightarrow N(2190) \rightarrow N\eta$

MODULUS	PHASE (°)	DOCUMENT ID	TECN	COMMENT
• • • We do not use the following data for averages, fits, limits, etc. • • •				
0.016	129	ROENCHEN 15A	DPWA	Multichannel

Normalized residue in $N\pi \rightarrow N(2190) \rightarrow \Delta(1232)\pi, D\text{-wave}$

MODULUS	PHASE (°)	DOCUMENT ID	TECN	COMMENT
0.27 ± 0.04	-165 ± 20	SOKHOYAN 15A	DPWA	Multichannel

Normalized residue in $N\pi \rightarrow N(2190) \rightarrow N\sigma$

MODULUS	PHASE (°)	DOCUMENT ID	TECN	COMMENT
0.13 ± 0.05	50 ± 15	SOKHOYAN 15A	DPWA	Multichannel

N(2190) BREIT-WIGNER MASS

VALUE (MeV)	DOCUMENT ID	TECN	COMMENT
2140 to 2220 (≈ 2180) OUR ESTIMATE			
2222 ± 15	¹ HUNT 19	DPWA	Multichannel
2205 ± 18	SOKHOYAN 15A	DPWA	Multichannel
2152.4 ± 1.4	¹ ARNDT 06	DPWA	$\pi N \rightarrow \pi N, \eta N$
2200 ± 70	CUTKOSKY 80	IPWA	$\pi N \rightarrow \pi N$
2140 ± 12	HOEHLER 79	IPWA	$\pi N \rightarrow \pi N$
• • • We do not use the following data for averages, fits, limits, etc. • • •			
2180 ± 20	ANISOVICH 12A	DPWA	Multichannel
2150 ± 26	¹ SHRESTHA 12A	DPWA	Multichannel
2125 ± 61	BATINIC 10	DPWA	$\pi N \rightarrow N\pi, N\eta$
2168 ± 18	VRANA 00	DPWA	Multichannel

¹ Statistical error only.

N(2190) BREIT-WIGNER WIDTH

VALUE (MeV)	DOCUMENT ID	TECN	COMMENT
300 to 500 (≈ 400) OUR ESTIMATE			
442 ± 40	¹ HUNT 19	DPWA	Multichannel
355 ± 30	SOKHOYAN 15A	DPWA	Multichannel
484 ± 13	¹ ARNDT 06	DPWA	$\pi N \rightarrow \pi N, \eta N$
500 ± 150	CUTKOSKY 80	IPWA	$\pi N \rightarrow \pi N$
390 ± 30	HOEHLER 79	IPWA	$\pi N \rightarrow \pi N$
• • • We do not use the following data for averages, fits, limits, etc. • • •			
335 ± 40	ANISOVICH 12A	DPWA	Multichannel
500 ± 74	¹ SHRESTHA 12A	DPWA	Multichannel
381 ± 160	BATINIC 10	DPWA	$\pi N \rightarrow N\pi, N\eta$
453 ± 101	VRANA 00	DPWA	Multichannel

¹ Statistical error only.

N(2190) DECAY MODES

The following branching fractions are our estimates, not fits or averages.

Mode	Fraction (Γ_j/Γ)
Γ_1 $N\pi$	10–20 %
Γ_2 $N\eta$	1–3 %
Γ_3 $N\omega$	8–20 %

Γ_4 ΛK	
Γ_5 $N\pi\pi$	
Γ_6 $\Delta(1232)\pi$	
Γ_7 $\Delta(1232)\pi, D\text{-wave}$	19–31 %
Γ_8 $N\rho$	
Γ_9 $N\rho, S=3/2, D\text{-wave}$	seen
Γ_{10} $\Lambda K^*(892)$	0.2–0.8 %
Γ_{11} $N\sigma$	3–9 %
Γ_{12} $p\gamma$	0.014–0.077 %
Γ_{13} $p\gamma, \text{helicity}=1/2$	
Γ_{14} $p\gamma, \text{helicity}=3/2$	
Γ_{15} $n\gamma$	<0.04 %
Γ_{16} $n\gamma, \text{helicity}=1/2$	
Γ_{17} $n\gamma, \text{helicity}=3/2$	<0.03 %

N(2190) BRANCHING RATIOS

$\Gamma(N\pi)/\Gamma_{total}$	DOCUMENT ID	TECN	COMMENT	Γ_1/Γ
10 to 20 (≈ 15) OUR ESTIMATE				
22.9 ± 0.6	¹ HUNT 19	DPWA	Multichannel	
16 ± 2	SOKHOYAN 15A	DPWA	Multichannel	
23.8 ± 0.1	¹ ARNDT 06	DPWA	$\pi N \rightarrow \pi N, \eta N$	
12 ± 6	CUTKOSKY 80	IPWA	$\pi N \rightarrow \pi N$	
14 ± 2	HOEHLER 79	IPWA	$\pi N \rightarrow \pi N$	
• • • We do not use the following data for averages, fits, limits, etc. • • •				
16 ± 2	ANISOVICH 12A	DPWA	Multichannel	
20 ± 1	¹ SHRESTHA 12A	DPWA	Multichannel	
18 ± 12	BATINIC 10	DPWA	$\pi N \rightarrow N\pi, N\eta$	
20 ± 4	VRANA 00	DPWA	Multichannel	

¹ Statistical error only.

$\Gamma(N\eta)/\Gamma_{total}$	DOCUMENT ID	TECN	COMMENT	Γ_2/Γ
10 to 20 (≈ 15) OUR ESTIMATE				
2.7 ± 2.2	¹ HUNT 19	DPWA	Multichannel	
• • • We do not use the following data for averages, fits, limits, etc. • • •				
2 ± 1	¹ SHRESTHA 12A	DPWA	Multichannel	
0.1 ± 0.3	BATINIC 10	DPWA	$\pi N \rightarrow N\pi, N\eta$	
0 ± 1	VRANA 00	DPWA	Multichannel	

¹ Statistical error only.

$\Gamma(N\omega)/\Gamma_{total}$	DOCUMENT ID	TECN	COMMENT	Γ_3/Γ
10 to 20 (≈ 15) OUR ESTIMATE				
14 ± 6	DENISENKO 16	DPWA	Multichannel	
• • • We do not use the following data for averages, fits, limits, etc. • • •				
seen	WILLIAMS 09	IPWA	$\gamma p \rightarrow p\omega$	

¹ Statistical error only.

$\Gamma(\Lambda K)/\Gamma_{total}$	DOCUMENT ID	TECN	COMMENT	Γ_4/Γ
10 to 20 (≈ 15) OUR ESTIMATE				
0.6 ± 0.1	¹ HUNT 19	DPWA	Multichannel	
0.5 ± 0.3	ANISOVICH 12A	DPWA	Multichannel	
• • • We do not use the following data for averages, fits, limits, etc. • • •				
<1	¹ SHRESTHA 12A	DPWA	Multichannel	

¹ Statistical error only.

$\Gamma(\Delta(1232)\pi, D\text{-wave})/\Gamma_{total}$	DOCUMENT ID	TECN	COMMENT	Γ_7/Γ
10 to 20 (≈ 15) OUR ESTIMATE				
25 ± 6	SOKHOYAN 15A	DPWA	Multichannel	

¹ Statistical error only.

$\Gamma(N\rho, S=3/2, D\text{-wave})/\Gamma_{total}$	DOCUMENT ID	TECN	COMMENT	Γ_9/Γ
10 to 20 (≈ 15) OUR ESTIMATE				
<11	¹ HUNT 19	DPWA	Multichannel	
• • • We do not use the following data for averages, fits, limits, etc. • • •				
29 ± 28	VRANA 00	DPWA	Multichannel	

¹ Statistical error only.

$\Gamma(\Lambda K^*(892))/\Gamma_{total}$	DOCUMENT ID	TECN	COMMENT	Γ_{10}/Γ
10 to 20 (≈ 15) OUR ESTIMATE				
0.005 ± 0.003	ANISOVICH 17B	DPWA	Multichannel	

¹ Statistical error only.

$\Gamma(N\sigma)/\Gamma_{total}$	DOCUMENT ID	TECN	COMMENT	Γ_{11}/Γ
10 to 20 (≈ 15) OUR ESTIMATE				
6 ± 3	SOKHOYAN 15A	DPWA	Multichannel	

N(2190) PHOTON DECAY AMPLITUDES AT THE POLE

N(2190) $\rightarrow p\gamma, \text{helicity}=1/2$ amplitude $A_{1/2}$

MODULUS ($\text{GeV}^{-1/2}$)	PHASE (°)	DOCUMENT ID	TECN	COMMENT
0.068 ± 0.005	-170 ± 12	SOKHOYAN 15A	DPWA	Multichannel
-0.083 ± 0.007	-11 ± 6	ROENCHEN 14	DPWA	
• • • We do not use the following data for averages, fits, limits, etc. • • •				
-0.041	-21	ROENCHEN 15A	DPWA	Multichannel

Baryon Particle Listings

$N(2190)$, $N(2220)$

$N(2190) \rightarrow p\gamma$, helicity-3/2 amplitude $A_{3/2}$

MODULUS ($\text{GeV}^{-1/2}$)	PHASE ($^\circ$)	DOCUMENT ID	TECN	COMMENT
0.025 ± 0.010	22 ± 10	SOKHOYAN 15A	DPWA	Multichannel
$0.095^{+0.013}_{-0.010}$	-3^{+3}_{-5}	ROENCHEN 14	DPWA	
0.085	-22	ROENCHEN 15A	DPWA	Multichannel

••• We do not use the following data for averages, fits, limits, etc. •••

$N(2190)$ BREIT-WIGNER PHOTON DECAY AMPLITUDES

$N(2190) \rightarrow p\gamma$, helicity-1/2 amplitude $A_{1/2}$

VALUE ($\text{GeV}^{-1/2}$)	DOCUMENT ID	TECN	COMMENT
0.001 ± 0.002	¹ HUNT 19	DPWA	Multichannel
-0.071 ± 0.006	SOKHOYAN 15A	DPWA	Multichannel
-0.065 ± 0.008	ANISOVICH 12A	DPWA	Multichannel

••• We do not use the following data for averages, fits, limits, etc. •••

¹ Statistical error only.

$N(2190) \rightarrow p\gamma$, helicity-3/2 amplitude $A_{3/2}$

VALUE ($\text{GeV}^{-1/2}$)	DOCUMENT ID	TECN	COMMENT
0.015 ± 0.003	¹ HUNT 19	DPWA	Multichannel
0.027 ± 0.010	SOKHOYAN 15A	DPWA	Multichannel
0.035 ± 0.017	ANISOVICH 12A	DPWA	Multichannel

••• We do not use the following data for averages, fits, limits, etc. •••

¹ Statistical error only.

$N(2190) \rightarrow p\gamma$, ratio of helicity amplitudes $A_{3/2}/A_{1/2}$

VALUE	DOCUMENT ID	TECN	COMMENT
-0.17 ± 0.15	WILLIAMS 09	IPWA	$\gamma p \rightarrow p\omega$

$N(2190) \rightarrow n\gamma$, helicity-1/2 amplitude $A_{1/2}$

VALUE ($\text{GeV}^{-1/2}$)	DOCUMENT ID	TECN	COMMENT
-0.01 ± 0.02	¹ HUNT 19	DPWA	Multichannel
-0.015 ± 0.013	ANISOVICH 13B	DPWA	Multichannel

¹ Statistical error only.

$N(2190) \rightarrow n\gamma$, helicity-3/2 amplitude $A_{3/2}$

VALUE ($\text{GeV}^{-1/2}$)	DOCUMENT ID	TECN	COMMENT
-0.023 ± 0.022	¹ HUNT 19	DPWA	Multichannel
-0.034 ± 0.022	ANISOVICH 13B	DPWA	Multichannel

¹ Statistical error only.

$N(2190)$ REFERENCES

For early references, see Physics Letters **111B** 1 (1982).

HUNT 19	PR C99 055205	B. C. Hunt, D.M. Manley
ANISOVICH 17B	PL B771 142	A.V. Anisovich et al.
DENISENKO 16	PL B755 97	I. Denisenko et al.
ROENCHEN 15A	EPJ A51 70	D. Roenchen et al.
SOKHOYAN 15A	EPJ A51 95	V. Sokhoyan et al. (CBELSA/TAPS Collab.)
PDG 14	CP C38 070001	K. Olive et al. (PDG Collab.)
ROENCHEN 14	EPJ A50 101	D. Roenchen et al.
Also	EPJ A51 63 (errata.)	D. Roenchen et al.
SVARC 14	PR C89 045205	A. Svarc et al. (RBI Zagreb, UNI Tuzla)
ANISOVICH 13B	EPJ A49 67	A.V. Anisovich et al.
ANISOVICH 12A	EPJ A48 15	A.V. Anisovich et al. (BONN, PNPI)
SHRESTHA 12A	PR C86 055203	M. Shrestha, D.M. Manley (KSU)
BATINIC 10	PR C82 038203	M. Batinic et al. (ZAGR)
WILLIAMS 09	PR C80 065209	M. Williams et al. (JLab CLAS Collab.)
ARNDT 06	PR C74 045205	R.A. Arndt et al. (GVU)
VRANA 00	PRPL 328 181	T.P. Vrana, S.A. Dytman, T.-S.H. Lee (PITT, ANL)
HOEHLER 93	πN Newsletter 9 1	G. Hoehler (KARL)
CUTKOSKY 80	Toronto Conf. 19	R.E. Cutkosky et al. (CMU, LBL) IJP
Also	PR D20 2839	R.E. Cutkosky et al. (CMU, LBL) IJP
HOEHLER 79	PDAT 12-1	G. Hoehler et al. (KARLT) IJP
Also	Toronto Conf. 3	R. Koch (KARLT) IJP

$N(2220) 9/2^+$

 $I(J^P) = \frac{1}{2}(9/2^+)$ Status: ***

Older and obsolete values are listed and referenced in the 2014 edition, Chinese Physics **C38** 070001 (2014).

$N(2220)$ POLE POSITION

REAL PART

VALUE (MeV)	DOCUMENT ID	TECN	COMMENT
2130 to 2200 (≈ 2170) OUR ESTIMATE			
$2127 \pm 3 \pm 24$	¹ SVARC 14	L+P	$\pi N \rightarrow \pi N$
2150 ± 35	ANISOVICH 12A	DPWA	Multichannel
2160 ± 80	CUTKOSKY 80	IPWA	$\pi N \rightarrow \pi N$

••• We do not use the following data for averages, fits, limits, etc. •••

2171	ROENCHEN 15A	DPWA	Multichannel
2199	ARNDT 06	DPWA	$\pi N \rightarrow \pi N, \eta N$
2135	HOEHLER 93	ARGD	$\pi N \rightarrow \pi N$

¹ Fit to the amplitudes of HOEHLER 79.

-2xIMAGINARY PART

VALUE (MeV)	DOCUMENT ID	TECN	COMMENT
360 to 480 (≈ 400) OUR ESTIMATE			
$380 \pm 7 \pm 22$	¹ SVARC 14	L+P	$\pi N \rightarrow \pi N$
440 ± 40	ANISOVICH 12A	DPWA	Multichannel
480 ± 100	CUTKOSKY 80	IPWA	$\pi N \rightarrow \pi N$
••• We do not use the following data for averages, fits, limits, etc. •••			
593	ROENCHEN 15A	DPWA	Multichannel
372	ARNDT 06	DPWA	$\pi N \rightarrow \pi N, \eta N$
400	HOEHLER 93	ARGD	$\pi N \rightarrow \pi N$

¹ Fit to the amplitudes of HOEHLER 79.

$N(2220)$ ELASTIC POLE RESIDUE

MODULUS $|r|$

VALUE (MeV)	DOCUMENT ID	TECN	COMMENT
35 to 60 (≈ 45) OUR ESTIMATE			
$38 \pm 1 \pm 5$	¹ SVARC 14	L+P	$\pi N \rightarrow \pi N$
60 ± 12	ANISOVICH 12A	DPWA	Multichannel
45 ± 20	CUTKOSKY 80	IPWA	$\pi N \rightarrow \pi N$
••• We do not use the following data for averages, fits, limits, etc. •••			
62	ROENCHEN 15A	DPWA	Multichannel
33	ARNDT 06	DPWA	$\pi N \rightarrow \pi N, \eta N$
40	HOEHLER 93	ARGD	$\pi N \rightarrow \pi N$

¹ Fit to the amplitudes of HOEHLER 79.

PHASE θ

VALUE ($^\circ$)	DOCUMENT ID	TECN	COMMENT
-60 to -30 (≈ -50) OUR ESTIMATE			
$-52 \pm 1 \pm 14$	¹ SVARC 14	L+P	$\pi N \rightarrow \pi N$
-58 ± 12	ANISOVICH 12A	DPWA	Multichannel
-45 ± 25	CUTKOSKY 80	IPWA	$\pi N \rightarrow \pi N$
••• We do not use the following data for averages, fits, limits, etc. •••			
-59	ROENCHEN 15A	DPWA	Multichannel
-33	ARNDT 06	DPWA	$\pi N \rightarrow \pi N, \eta N$
-50	HOEHLER 93	ARGD	$\pi N \rightarrow \pi N$

¹ Fit to the amplitudes of HOEHLER 79.

$N(2220)$ INELASTIC POLE RESIDUE

The "normalized residue" is the residue divided by $\Gamma_{pole}/2$.

Normalized residue in $N\pi \rightarrow N(2220) \rightarrow N\eta$

MODULUS	PHASE ($^\circ$)	DOCUMENT ID	TECN	COMMENT
0.004	-101	ROENCHEN 15A	DPWA	Multichannel

Normalized residue in $N\pi \rightarrow N(2220) \rightarrow \Lambda K$

MODULUS	PHASE ($^\circ$)	DOCUMENT ID	TECN	COMMENT
0.007	62	ROENCHEN 15A	DPWA	Multichannel

Normalized residue in $N\pi \rightarrow N(2220) \rightarrow \Sigma K$

MODULUS	PHASE ($^\circ$)	DOCUMENT ID	TECN	COMMENT
0.009	-128	ROENCHEN 15A	DPWA	Multichannel

$N(2220)$ BREIT-WIGNER MASS

VALUE (MeV)	DOCUMENT ID	TECN	COMMENT
2200 to 2300 (≈ 2250) OUR ESTIMATE			
2316.3 ± 2.9	¹ ARNDT 06	DPWA	$\pi N \rightarrow \pi N, \eta N$
2230 ± 80	CUTKOSKY 80	IPWA	$\pi N \rightarrow \pi N$
2205 ± 10	HOEHLER 79	IPWA	$\pi N \rightarrow \pi N$

¹ Statistical error only.

$N(2220)$ BREIT-WIGNER WIDTH

VALUE (MeV)	DOCUMENT ID	TECN	COMMENT
350 to 500 (≈ 400) OUR ESTIMATE			
633 ± 17	¹ ARNDT 06	DPWA	$\pi N \rightarrow \pi N, \eta N$
500 ± 150	CUTKOSKY 80	IPWA	$\pi N \rightarrow \pi N$
365 ± 30	HOEHLER 79	IPWA	$\pi N \rightarrow \pi N$

¹ Statistical error only.

N(2220) DECAY MODES

The following branching fractions are our estimates, not fits or averages.

Mode	Fraction (Γ_i/Γ)
Γ_1 $N\pi$	15–30 %

N(2220) BRANCHING RATIOS

$\Gamma(N\pi)/\Gamma_{total}$	DOCUMENT ID	TECN	COMMENT	Γ_1/Γ
15 to 30 (≈ 25) OUR ESTIMATE				
24 ± 5	ANISOVICH	12A	DPWA	Multichannel
24.6 ± 0.1	¹ ARNDT	06	DPWA	$\pi N \rightarrow \pi N, \eta N$
15 ± 3	CUTKOSKY	80	IPWA	$\pi N \rightarrow \pi N$
18.0 ± 1.5	HOEHLER	79	IPWA	$\pi N \rightarrow \pi N$

¹ Statistical error only.

N(2220) PHOTON DECAY AMPLITUDES AT THE POLE

N(2220) → pγ, helicity-1/2 amplitude A_{1/2}

MODULUS (GeV ^{-1/2})	PHASE (°)	DOCUMENT ID	TECN	COMMENT
-0.233 ^{+0.084} _{-0.044}	-47 ⁺¹⁰ ₋₆	ROENCHEN	14	DPWA
0.135	114	ROENCHEN	15A	DPWA Multichannel

• • • We do not use the following data for averages, fits, limits, etc. • • •

N(2220) → pγ, helicity-3/2 amplitude A_{3/2}

MODULUS (GeV ^{-1/2})	PHASE (°)	DOCUMENT ID	TECN	COMMENT
0.162 ^{+0.041} _{-0.038}	-27 ⁺²⁶ ₋₁₃	ROENCHEN	14	DPWA
0.082	-41	ROENCHEN	15A	DPWA Multichannel

• • • We do not use the following data for averages, fits, limits, etc. • • •

N(2220) REFERENCES

For early references, see Physics Letters **111B** 1 (1982).

ROENCHEN 15A	EPJ A51 70	D. Roenchen et al.	
PDG 14	CP C39 070001	K. Olive et al.	(PDG Collab.)
ROENCHEN 14	EPJ A50 101	D. Roenchen et al.	
Also	EPJ A51 63 (errata.)	D. Roenchen et al.	
SVARC 14	PR C89 045205	A. Svarc et al.	(RBI Zagreb, UNI Tuzla)
ANISOVICH 12A	EPJ A48 15	A.V. Anisovich et al.	(BONN, PNPI)
ARNDT 06	PR C74 045205	R.A. Arndt et al.	(GWU)
HOEHLER 93	πN Newsletter 9 1	G. Hohlner	(KARL)
CUTKOSKY 80	Toronto Conf. 19	R.E. Cutkosky et al.	(CMU, LBL) IJP
Also	PR D20 2839	R.E. Cutkosky et al.	(CMU, LBL) IJP
HOEHLER 79	PDAT 12-1	G. Hohlner et al.	(KARLT) IJP
Also	Toronto Conf. 3	R. Koch	(KARLT) IJP

N(2250) 9/2⁻ $I(J^P) = \frac{1}{2}(9/2^-)$ Status: * * * *

Older and obsolete values are listed and referenced in the 2014 edition, Chinese Physics **C38** 070001 (2014).

N(2250) POLE POSITION

REAL PART

VALUE (MeV)	DOCUMENT ID	TECN	COMMENT
2150 to 2250 (≈ 2200) OUR ESTIMATE			
2157 ± 3 ± 14	¹ SVARC	14	L+P $\pi N \rightarrow \pi N$
2195 ± 45	ANISOVICH	12A	DPWA Multichannel
2150 ± 50	CUTKOSKY	80	IPWA $\pi N \rightarrow \pi N$
• • •	We do not use the following data for averages, fits, limits, etc. • • •		
2127	HUNT	19	DPWA Multichannel
2062	ROENCHEN	15A	DPWA Multichannel
2217	ARNDT	06	DPWA $\pi N \rightarrow \pi N, \eta N$
2187	HOEHLER	93	SPED $\pi N \rightarrow \pi N$

¹ Fit to the amplitudes of HOEHLER 79.

-2xIMAGINARY PART

VALUE (MeV)	DOCUMENT ID	TECN	COMMENT
350 to 500 (≈ 420) OUR ESTIMATE			
412 ± 7 ± 44	¹ SVARC	14	L+P $\pi N \rightarrow \pi N$
470 ± 50	ANISOVICH	12A	DPWA Multichannel
360 ± 100	CUTKOSKY	80	IPWA $\pi N \rightarrow \pi N$
• • •	We do not use the following data for averages, fits, limits, etc. • • •		
262	HUNT	19	DPWA Multichannel
403	ROENCHEN	15A	DPWA Multichannel
431	ARNDT	06	DPWA $\pi N \rightarrow \pi N, \eta N$
388	HOEHLER	93	SPED $\pi N \rightarrow \pi N$

¹ Fit to the amplitudes of HOEHLER 79.

N(2250) ELASTIC POLE RESIDUE

MODULUS |r|

VALUE (MeV)	DOCUMENT ID	TECN	COMMENT
20 to 30 (≈ 25) OUR ESTIMATE			
24 ± 1 ± 5	¹ SVARC	14	L+P $\pi N \rightarrow \pi N$
26 ± 5	ANISOVICH	12A	DPWA Multichannel
20 ± 6	CUTKOSKY	80	IPWA $\pi N \rightarrow \pi N$
• • •	We do not use the following data for averages, fits, limits, etc. • • •		
8.2	ROENCHEN	15A	DPWA Multichannel
21	ARNDT	06	DPWA $\pi N \rightarrow \pi N, \eta N$
21	HOEHLER	93	SPED $\pi N \rightarrow \pi N$

¹ Fit to the amplitudes of HOEHLER 79.

PHASE θ

VALUE (°)	DOCUMENT ID	TECN	COMMENT
-60 to -20 (≈ -40) OUR ESTIMATE			
-62 ± 1 ± 11	¹ SVARC	14	L+P $\pi N \rightarrow \pi N$
-38 ± 25	ANISOVICH	12A	DPWA Multichannel
-50 ± 20	CUTKOSKY	80	IPWA $\pi N \rightarrow \pi N$
• • •	We do not use the following data for averages, fits, limits, etc. • • •		
-64	ROENCHEN	15A	DPWA Multichannel
-20	ARNDT	06	DPWA $\pi N \rightarrow \pi N, \eta N$

¹ Fit to the amplitudes of HOEHLER 79.

N(2250) INELASTIC POLE RESIDUE

The "normalized residue" is the residue divided by $\Gamma_{pole}/2$.

Normalized residue in $N\pi \rightarrow N(2250) \rightarrow N\eta$

MODULUS	PHASE (°)	DOCUMENT ID	TECN	COMMENT
0.017	-89	ROENCHEN	15A	DPWA Multichannel

• • • We do not use the following data for averages, fits, limits, etc. • • •

Normalized residue in $N\pi \rightarrow N(2250) \rightarrow \Lambda K$

MODULUS	PHASE (°)	DOCUMENT ID	TECN	COMMENT
0.006	-101	ROENCHEN	15A	DPWA Multichannel

• • • We do not use the following data for averages, fits, limits, etc. • • •

Normalized residue in $N\pi \rightarrow N(2250) \rightarrow \Sigma K$

MODULUS	PHASE (°)	DOCUMENT ID	TECN	COMMENT
0.002	70	ROENCHEN	15A	DPWA Multichannel

• • • We do not use the following data for averages, fits, limits, etc. • • •

N(2250) BREIT-WIGNER MASS

VALUE (MeV)	DOCUMENT ID	TECN	COMMENT
2250 to 2320 (≈ 2280) OUR ESTIMATE			
2200 ± 10	¹ HUNT	19	DPWA Multichannel
2280 ± 40	ANISOVICH	12A	DPWA Multichannel
2302 ± 6	¹ ARNDT	06	DPWA $\pi N \rightarrow \pi N, \eta N$
2250 ± 80	CUTKOSKY	80	IPWA $\pi N \rightarrow \pi N$
2268 ± 15	HOEHLER	79	IPWA $\pi N \rightarrow \pi N$

¹ Statistical error only.

N(2250) BREIT-WIGNER WIDTH

VALUE (MeV)	DOCUMENT ID	TECN	COMMENT
300 to 600 (≈ 500) OUR ESTIMATE			
343 ± 51	¹ HUNT	19	DPWA Multichannel
520 ± 50	ANISOVICH	12A	DPWA Multichannel
628 ± 28	¹ ARNDT	06	DPWA $\pi N \rightarrow \pi N, \eta N$
480 ± 120	CUTKOSKY	80	IPWA $\pi N \rightarrow \pi N$
300 ± 40	HOEHLER	79	IPWA $\pi N \rightarrow \pi N$

¹ Statistical error only.

N(2250) DECAY MODES

The following branching fractions are our estimates, not fits or averages.

Mode	Fraction (Γ_i/Γ)
Γ_1 $N\pi$	0.05 to 0.15 (≈ 0.10)
Γ_2 $N\eta$	
Γ_3 ΛK	

Baryon Particle Listings

 $N(2250)$, $N(2300)$, $N(2570)$, $N(2600)$, $N(2700)$ $N(2250)$ BRANCHING RATIOS

$\Gamma(N\pi)/\Gamma_{\text{total}}$	DOCUMENT ID	TECN	COMMENT	Γ_1/Γ
5 to 15 (≈ 10) OUR ESTIMATE				
8.5 \pm 0.4	¹ HUNT	19	DPWA Multichannel	
12 \pm 4	ANISOVICH	12A	DPWA Multichannel	
8.9 \pm 0.1	¹ ARNDT	06	DPWA $\pi N \rightarrow \pi N, \eta N$	
10 \pm 2	CUTKOSKY	80	IPWA $\pi N \rightarrow \pi N$	
10 \pm 2	HOEHLER	79	IPWA $\pi N \rightarrow \pi N$	
¹ Statistical error only.				
$\Gamma(N\eta)/\Gamma_{\text{total}}$	DOCUMENT ID	TECN	COMMENT	Γ_2/Γ
<5	¹ HUNT	19	DPWA Multichannel	
¹ Statistical error only.				
$\Gamma(\Lambda K)/\Gamma_{\text{total}}$	DOCUMENT ID	TECN	COMMENT	Γ_3/Γ
2.0 \pm 0.6	¹ HUNT	19	DPWA Multichannel	
¹ Statistical error only.				

 $N(2250)$ PHOTON DECAY AMPLITUDES AT THE POLE

$N(2250) \rightarrow p\gamma$, helicity-1/2 amplitude $A_{1/2}$	DOCUMENT ID	TECN	COMMENT
MODULUS ($\text{GeV}^{-1/2}$)	PHASE ($^\circ$)		
-0.090 \pm 0.025 -0.022	-49 \pm 17 -11	ROENCHEN	14 DPWA
••• We do not use the following data for averages, fits, limits, etc. •••			
0.026	-26	ROENCHEN	15A DPWA Multichannel
$N(2250) \rightarrow p\gamma$, helicity-3/2 amplitude $A_{3/2}$	DOCUMENT ID	TECN	COMMENT
MODULUS ($\text{GeV}^{-1/2}$)	PHASE ($^\circ$)		
0.049 \pm 0.031 -0.019	171 \pm 36 -43	ROENCHEN	14 DPWA
••• We do not use the following data for averages, fits, limits, etc. •••			
0.119	-42	ROENCHEN	15A DPWA Multichannel

 $N(2250)$ BREIT-WIGNER PHOTON DECAY AMPLITUDES

$N(2250) \rightarrow p\gamma$, helicity-1/2 amplitude $A_{1/2}$	DOCUMENT ID	TECN	COMMENT
VALUE ($\text{GeV}^{-1/2}$)			
0.0006 \pm 0.0037	¹ HUNT	19	DPWA Multichannel
¹ Statistical error only.			
$N(2250) \rightarrow p\gamma$, helicity-3/2 amplitude $A_{3/2}$	DOCUMENT ID	TECN	COMMENT
VALUE ($\text{GeV}^{-1/2}$)			
0.013 \pm 0.004	¹ HUNT	19	DPWA Multichannel
¹ Statistical error only.			

 $N(2250)$ REFERENCES

HUNT	19	PR C99 055205	B. C. Hunt, D.M. Manley	
ROENCHEN	15A	EPJ A51 70	D. Roenchen et al.	
PDG	14	CP C38 070001	K. Olive et al.	(PDG Collab.)
ROENCHEN	14	EPJ A50 101	D. Roenchen et al.	
Also		EPJ A51 63 (errata.)	D. Roenchen et al.	
SVARC	14	PR C89 045205	A. Svarc et al.	(RBI Zagreb, UNI Tuzla)
ANISOVICH	12A	EPJ A48 15	A.V. Anisovich et al.	(BONN, PNPI)
ARNDT	06	PR C74 045205	R.A. Arndt et al.	(GWU)
HOEHLER	93	πN Newsletter 9 1	G. Hohler	(KARL)
CUTKOSKY	80	Toronto Conf. 19	R.E. Cutkosky et al.	(CMU, LBL) IJP
Also		PR D20 2839	R.E. Cutkosky et al.	(CMU, LBL) IJP
HOEHLER	79	PDAT 12-1	G. Hohler et al.	(KARLT) IJP
Also		Toronto Conf. 3	R. Koch	(KARLT) IJP

$N(2300)$ 1/2⁺ $I(J^P) = \frac{1}{2}(\frac{1}{2}^+)$ Status: **

OMITTED FROM SUMMARY TABLE

 $N(2300)$ MASS

VALUE (MeV)	DOCUMENT ID	TECN	COMMENT
2300 \pm 40 \pm 109 -30 - 0	ABLIKIM	13A	BES3 $\psi(2S) \rightarrow p\bar{p}\pi^0$

 $N(2300)$ WIDTH

VALUE (MeV)	DOCUMENT ID	TECN	COMMENT
340 \pm 30 \pm 110 58	ABLIKIM	13A	BES3 $\psi(2S) \rightarrow p\bar{p}\pi^0$

 $N(2300)$ REFERENCES

ABLIKIM	13A	PRL 110 022001	M. Ablikim et al.	(BESIII Collab.)
---------	-----	----------------	-------------------	------------------

$N(2570)$ 5/2⁻ $I(J^P) = \frac{1}{2}(\frac{5}{2}^-)$ Status: **

OMITTED FROM SUMMARY TABLE

 $N(2570)$ MASS

VALUE (MeV)	DOCUMENT ID	TECN	COMMENT
2570 \pm 14 \pm 34 -24 - 10	ABLIKIM	13A	BES3 $\psi(2S) \rightarrow p\bar{p}\pi^0$

 $N(2570)$ WIDTH

VALUE (MeV)	DOCUMENT ID	TECN	COMMENT
250 \pm 14 \pm 69 -24 - 21	ABLIKIM	13A	BES3 $\psi(2S) \rightarrow p\bar{p}\pi^0$

 $N(2570)$ REFERENCES

ABLIKIM	13A	PRL 110 022001	M. Ablikim et al.	(BESIII Collab.)
---------	-----	----------------	-------------------	------------------

$N(2600)$ 11/2⁻ $I(J^P) = \frac{1}{2}(\frac{11}{2}^-)$ Status: ***

 $N(2600)$ BREIT-WIGNER MASS

VALUE (MeV)	DOCUMENT ID	TECN	COMMENT
2550 to 2750 (≈ 2600) OUR ESTIMATE			
2623 \pm 197	ARNDT	06	DPWA $\pi N \rightarrow \pi N, \eta N$
2577 \pm 50	HOEHLER	79	IPWA $\pi N \rightarrow \pi N$

 $N(2600)$ BREIT-WIGNER WIDTH

VALUE (MeV)	DOCUMENT ID	TECN	COMMENT
500 to 800 (≈ 650) OUR ESTIMATE			
1311 \pm 996	ARNDT	06	DPWA $\pi N \rightarrow \pi N, \eta N$
400 \pm 100	HOEHLER	79	IPWA $\pi N \rightarrow \pi N$

 $N(2600)$ DECAY MODES

Mode	Fraction (Γ_i/Γ)
Γ_1 $N\pi$	3-8 %

 $N(2600)$ BRANCHING RATIOS

$\Gamma(N\pi)/\Gamma_{\text{total}}$	DOCUMENT ID	TECN	COMMENT	Γ_1/Γ
3 to 8 (≈ 5) OUR ESTIMATE				
5.0 \pm 1.8	ARNDT	06	DPWA $\pi N \rightarrow \pi N, \eta N$	
5 \pm 1	HOEHLER	79	IPWA $\pi N \rightarrow \pi N$	

 $N(2600)$ REFERENCES

ARNDT	06	PR C74 045205	R.A. Arndt et al.	(GWU)
HOEHLER	79	PDAT 12-1	G. Hohler et al.	(KARLT) IJP
Also		Toronto Conf. 3	R. Koch	(KARLT) IJP

$N(2700)$ 13/2⁺ $I(J^P) = \frac{1}{2}(\frac{13}{2}^+)$ Status: **

OMITTED FROM SUMMARY TABLE

 $N(2700)$ BREIT-WIGNER MASS

VALUE (MeV)	DOCUMENT ID	TECN	COMMENT
2612 \pm 45	HOEHLER	79	IPWA $\pi N \rightarrow \pi N$

 $N(2700)$ BREIT-WIGNER WIDTH

VALUE (MeV)	DOCUMENT ID	TECN	COMMENT
350 \pm 50	HOEHLER	79	IPWA $\pi N \rightarrow \pi N$

 $N(2700)$ DECAY MODES

Mode	Fraction (Γ_i/Γ)
Γ_1 $N\pi$	3-5 %

See key on page 999

Baryon Particle Listings
 $N(2700)$, $N(\sim 3000)$

$N(2700)$ BRANCHING RATIOS

$\Gamma(N\pi)/\Gamma_{\text{total}}$	DOCUMENT ID	TECN	COMMENT	Γ_1/Γ
4±1	HOEHLER	79	IPWA $\pi N \rightarrow \pi N$	

$N(2700)$ REFERENCES

HOEHLER	79	PDAT 12-1	G. Hohler et al.	(KARLT) IJP
Also		Toronto Conf. 3	R. Koch	(KARLT) IJP

**$N(\sim 3000)$ Region
 Partial-Wave Analyses**

OMITTED FROM SUMMARY TABLE

We list here miscellaneous high-mass candidates for isospin-1/2 resonances found in partial-wave analyses.

Our 1982 edition had an $N(3245)$, an $N(3690)$, and an $N(3755)$, each a narrow peak seen in a production experiment. Since nothing has been heard from them since the 1960's, we declare them to be dead. There was also an $N(3030)$, deduced from total cross-section and 180° elastic cross-section measurements; it is the KOCH 80 $L_{1,15}$ state below.

$N(\sim 3000)$ BREIT-WIGNER MASS

VALUE (MeV)	DOCUMENT ID	TECN	COMMENT
≈ 3000 OUR ESTIMATE			
2600	KOCH	80	IPWA $\pi N \rightarrow \pi N D_{13}$
3100	KOCH	80	IPWA $\pi N \rightarrow \pi N L_{1,15}$ wave
3500	KOCH	80	IPWA $\pi N \rightarrow \pi N M_{1,17}$ wave
3500 to 4000	KOCH	80	IPWA $\pi N \rightarrow \pi N N_{1,19}$ wave
3500±200	HENDRY	78	MPWA $\pi N \rightarrow \pi N L_{1,15}$ wave
3800±200	HENDRY	78	MPWA $\pi N \rightarrow \pi N M_{1,17}$ wave
4100±200	HENDRY	78	MPWA $\pi N \rightarrow \pi N N_{1,19}$ wave

$N(\sim 3000)$ BREIT-WIGNER WIDTH

VALUE (MeV)	DOCUMENT ID	TECN	COMMENT
1300±200	HENDRY	78	MPWA $\pi N \rightarrow \pi N L_{1,15}$ wave
1600±200	HENDRY	78	MPWA $\pi N \rightarrow \pi N M_{1,17}$ wave
1900±300	HENDRY	78	MPWA $\pi N \rightarrow \pi N N_{1,19}$ wave

$N(\sim 3000)$ DECAY MODES

Mode
$\Gamma_1 N\pi$

$N(\sim 3000)$ BRANCHING RATIOS

$\Gamma(N\pi)/\Gamma_{\text{total}}$	DOCUMENT ID	TECN	COMMENT	Γ_1/Γ
6 ± 2	HENDRY	78	MPWA $\pi N \rightarrow \pi N L_{1,15}$ wave	
4.0±1.5	HENDRY	78	MPWA $\pi N \rightarrow \pi N M_{1,17}$ wave	
3.0±1.5	HENDRY	78	MPWA $\pi N \rightarrow \pi N N_{1,19}$ wave	

$N(\sim 3000)$ REFERENCES

KOCH	80	Toronto Conf. 3	R. Koch	(KARLT) IJP
HENDRY	78	PRL 41 222	A.W. Hendry	(IND, LBL) IJP
Also		ANP 136 1	A.W. Hendry	(IND) IJP

Baryon Particle Listings

 $\Delta(1232)$ **Δ BARYONS**
($S = 0, I = 3/2$)

$$\Delta^{++} = uuu, \Delta^+ = uud, \Delta^0 = udd, \Delta^- = ddd$$

 $\Delta(1232) 3/2^+$

$$I(J^P) = \frac{3}{2}(\frac{3}{2}^+) \text{ Status: } ****$$

Older and obsolete values are listed and referenced in the 2014 edition, Chinese Physics C38 070001 (2014).

 $\Delta(1232)$ POLE POSITIONS**REAL PART, MIXED CHARGES**

VALUE (MeV)	DOCUMENT ID	TECN	COMMENT
1209 to 1211 (≈ 1210) OUR ESTIMATE			
1211 $\pm 1 \pm 1$	¹ SVARC 14	L+P	$\pi N \rightarrow \pi N$
1210.5 ± 1.0	ANISOVICH 12A	DPWA	Multichannel
1210 ± 1	CUTKOSKY 80	IPWA	$\pi N \rightarrow \pi N$
••• We do not use the following data for averages, fits, limits, etc. •••			
1212.4	HUNT 19	DPWA	Multichannel
1218	ROENCHEN 15A	DPWA	Multichannel
1211 ± 1	ANISOVICH 10	DPWA	Multichannel
1211	ARNDT 06	DPWA	$\pi N \rightarrow \pi N, \eta N$
1210	ARNDT 04	DPWA	$\pi N \rightarrow \pi N, \eta N$
1209	² HOEHLER 93	ARGD	$\pi N \rightarrow \pi N$

¹ Fit to the amplitudes of HOEHLER 79.

² See HOEHLER 93 for a detailed discussion of the evidence for and the pole parameters of N and Δ resonances as determined from Argand diagrams of πN elastic partial-wave amplitudes and from plots of the speeds with which the amplitudes traverse the diagrams.

 $-2\times$ IMAGINARY PART, MIXED CHARGES

VALUE (MeV)	DOCUMENT ID	TECN	COMMENT
98 to 102 (≈ 100) OUR ESTIMATE			
98 $\pm 2 \pm 1$	¹ SVARC 14	L+P	$\pi N \rightarrow \pi N$
99 ± 2	ANISOVICH 12A	DPWA	Multichannel
100 ± 2	CUTKOSKY 80	IPWA	$\pi N \rightarrow \pi N$
••• We do not use the following data for averages, fits, limits, etc. •••			
96.8	HUNT 19	DPWA	Multichannel
92	ROENCHEN 15A	DPWA	Multichannel
100 ± 2	ANISOVICH 10	DPWA	Multichannel
99	ARNDT 06	DPWA	$\pi N \rightarrow \pi N, \eta N$
100	ARNDT 04	DPWA	$\pi N \rightarrow \pi N, \eta N$
100	² HOEHLER 93	ARGD	$\pi N \rightarrow \pi N$

¹ Fit to the amplitudes of HOEHLER 79.

² See HOEHLER 93 for a detailed discussion of the evidence for and the pole parameters of N and Δ resonances as determined from Argand diagrams of πN elastic partial-wave amplitudes and from plots of the speeds with which the amplitudes traverse the diagrams.

REAL PART, $\Delta(1232)^{++}$

VALUE (MeV)	DOCUMENT ID	COMMENT
••• We do not use the following data for averages, fits, limits, etc. •••		
1212.50 ± 0.24	BERNICHIA 96	Fit to PEDRONI 78

 $-2\times$ IMAGINARY PART, $\Delta(1232)^{++}$

VALUE (MeV)	DOCUMENT ID	COMMENT
••• We do not use the following data for averages, fits, limits, etc. •••		
97.37 ± 0.42	BERNICHIA 96	Fit to PEDRONI 78

REAL PART, $\Delta(1232)^+$

VALUE (MeV)	DOCUMENT ID	TECN	COMMENT
••• We do not use the following data for averages, fits, limits, etc. •••			
1211 ± 1 to 1212 ± 1	HANSTEIN 96	DPWA	$\gamma N \rightarrow \pi N$
1206.9 ± 0.9 to 1210.5 ± 1.8	MIROSHNIC... 79		Fit photoproduction

 $-2\times$ IMAGINARY PART, $\Delta(1232)^+$

VALUE (MeV)	DOCUMENT ID	TECN	COMMENT
••• We do not use the following data for averages, fits, limits, etc. •••			
102 ± 2 to 99 ± 2	¹ HANSTEIN 96	DPWA	$\gamma N \rightarrow \pi N$
111.2 ± 2.0 to 116.6 ± 2.2	MIROSHNIC... 79		Fit photoproduction

¹ The second (lower) value of HANSTEIN 96 here goes with the second (higher) value of the real part in the preceding data block.

REAL PART, $\Delta(1232)^0$

VALUE (MeV)	DOCUMENT ID	COMMENT
••• We do not use the following data for averages, fits, limits, etc. •••		
1213.20 ± 0.66	BERNICHIA 96	Fit to PEDRONI 78

 $-2\times$ IMAGINARY PART, $\Delta(1232)^0$

VALUE (MeV)	DOCUMENT ID	COMMENT
••• We do not use the following data for averages, fits, limits, etc. •••		
104.10 ± 1.01	BERNICHIA 96	Fit to PEDRONI 78

 $\Delta(1232)$ ELASTIC POLE RESIDUES**ABSOLUTE VALUE, MIXED CHARGES**

VALUE (MeV)	DOCUMENT ID	TECN	COMMENT
49 to 52 (≈ 50) OUR ESTIMATE			
50 $\pm 1 \pm 1$	¹ SVARC 14	L+P	$\pi N \rightarrow \pi N$
51.6 ± 0.6	ANISOVICH 12A	DPWA	Multichannel
53 ± 2	CUTKOSKY 80	IPWA	$\pi N \rightarrow \pi N$
••• We do not use the following data for averages, fits, limits, etc. •••			
46	ROENCHEN 15A	DPWA	Multichannel
52	ARNDT 06	DPWA	$\pi N \rightarrow \pi N, \eta N$
53	ARNDT 04	DPWA	$\pi N \rightarrow \pi N, \eta N$
50	HOEHLER 93	ARGD	$\pi N \rightarrow \pi N$

PHASE, MIXED CHARGES

VALUE ($^\circ$)	DOCUMENT ID	TECN	COMMENT
-48 to -45 (≈ -46) OUR ESTIMATE			
-46 $\pm 1 \pm 1$	¹ SVARC 14	L+P	$\pi N \rightarrow \pi N$
-46 ± 1	ANISOVICH 12A	DPWA	Multichannel
-47 ± 1	CUTKOSKY 80	IPWA	$\pi N \rightarrow \pi N$
••• We do not use the following data for averages, fits, limits, etc. •••			
-36	ROENCHEN 15A	DPWA	Multichannel
-47	ARNDT 06	DPWA	$\pi N \rightarrow \pi N, \eta N$
-47	ARNDT 04	DPWA	$\pi N \rightarrow \pi N, \eta N$
-48	HOEHLER 93	ARGD	$\pi N \rightarrow \pi N$

¹ Fit to the amplitudes of HOEHLER 79.

 $\Delta(1232)$ BREIT-WIGNER MASSES**MIXED CHARGES**

VALUE (MeV)	DOCUMENT ID	TECN	COMMENT
1230 to 1234 (≈ 1232) OUR ESTIMATE			
1230.8 ± 0.4	¹ HUNT 19	DPWA	Multichannel
1228 ± 2	ANISOVICH 12A	DPWA	Multichannel
1233.4 ± 0.4	¹ ARNDT 06	DPWA	$\pi N \rightarrow \pi N, \eta N$
1232 ± 3	CUTKOSKY 80	IPWA	$\pi N \rightarrow \pi N$
1233 ± 2	HOEHLER 79	IPWA	$\pi N \rightarrow \pi N$
••• We do not use the following data for averages, fits, limits, etc. •••			
1231.1 ± 0.2	¹ SHRESTHA 12A	DPWA	Multichannel
1230 ± 2	ANISOVICH 10	DPWA	Multichannel
1232.9 ± 1.2	ARNDT 04	DPWA	$\pi N \rightarrow \pi N, \eta N$
1228 ± 1	PENNER 02c	DPWA	Multichannel

¹ Statistical error only.

 $\Delta(1232)^{++}$ MASS

VALUE (MeV)	DOCUMENT ID	TECN	COMMENT
••• We do not use the following data for averages, fits, limits, etc. •••			
1230.55 ± 0.20	GRIDNEV 06	DPWA	$\pi N \rightarrow \pi N$
1231.88 ± 0.29	BERNICHIA 96		Fit to PEDRONI 78
1230.5 ± 0.2	ABAEV 95	IPWA	$\pi N \rightarrow \pi N$
1230.9 ± 0.3	KOCH 80b	IPWA	$\pi N \rightarrow \pi N$
1231.1 ± 0.2	PEDRONI 78		$\pi N \rightarrow \pi N$ 70-370 MeV

 $\Delta(1232)^+$ MASS

VALUE (MeV)	DOCUMENT ID	COMMENT
••• We do not use the following data for averages, fits, limits, etc. •••		
1234.9 ± 1.4	MIROSHNIC... 79	Fit photoproduction

 $\Delta(1232)^0$ MASS

VALUE (MeV)	DOCUMENT ID	TECN	COMMENT
••• We do not use the following data for averages, fits, limits, etc. •••			
1231.3 ± 0.6	BREITSCHOP...06	CNTR	Using new CHEX data
1233.40 ± 0.22	GRIDNEV 06	DPWA	$\pi N \rightarrow \pi N$
1234.35 ± 0.75	BERNICHIA 96		Fit to PEDRONI 78
1233.1 ± 0.3	ABAEV 95	IPWA	$\pi N \rightarrow \pi N$
1233.6 ± 0.5	KOCH 80b	IPWA	$\pi N \rightarrow \pi N$
1233.8 ± 0.2	PEDRONI 78		$\pi N \rightarrow \pi N$ 70-370 MeV

 $m_{\Delta^0} - m_{\Delta^{++}}$

VALUE (MeV)	DOCUMENT ID	TECN	COMMENT
••• We do not use the following data for averages, fits, limits, etc. •••			
2.86 ± 0.30	GRIDNEV 06	DPWA	$\pi N \rightarrow \pi N$
2.25 ± 0.68	BERNICHIA 96		Fit to PEDRONI 78
2.6 ± 0.4	ABAEV 95	IPWA	$\pi N \rightarrow \pi N$
2.7 ± 0.3	¹ PEDRONI 78		See the masses

¹ Using $\pi^\pm d$ as well, PEDRONI 78 determine $(M^- - M^{++}) + (M^0 - M^+)/3 = 4.6 \pm 0.2$ MeV.

$\Delta(1232)$ BREIT-WIGNER WIDTHS

MIXED CHARGES

VALUE (MeV)	DOCUMENT ID	TECN	COMMENT
114 to 120 (≈ 117) OUR ESTIMATE			
110.9 \pm 0.8	¹ HUNT 19	DPWA	Multichannel
110 \pm 3	ANISOVICH 12A	DPWA	Multichannel
118.7 \pm 0.6	¹ ARNDT 06	DPWA	$\pi N \rightarrow \pi N, \eta N$
120 \pm 5	CUTKOSKY 80	IPWA	$\pi N \rightarrow \pi N$
116 \pm 5	HOEHLER 79	IPWA	$\pi N \rightarrow \pi N$
••• We do not use the following data for averages, fits, limits, etc. •••			
113.0 \pm 0.5	¹ SHRESTHA 12A	DPWA	Multichannel
112 \pm 4	ANISOVICH 10	DPWA	Multichannel
118.0 \pm 2.2	ARNDT 04	DPWA	$\pi N \rightarrow \pi N, \eta N$
106 \pm 1	PENNER 02c	DPWA	Multichannel

¹ Statistical error only.

$\Delta(1232)^{++}$ WIDTH

VALUE (MeV)	DOCUMENT ID	TECN	COMMENT
••• We do not use the following data for averages, fits, limits, etc. •••			
112.2 \pm 0.7	GRIDNEV 06	DPWA	$\pi N \rightarrow \pi N$
109.07 \pm 0.48	BERNICHIA 96		Fit to PEDRONI 78
111.0 \pm 1.0	KOCH 80b	IPWA	$\pi N \rightarrow \pi N$
111.3 \pm 0.5	PEDRONI 78		$\pi N \rightarrow \pi N$ 70–370 MeV

$\Delta(1232)^+$ WIDTH

VALUE (MeV)	DOCUMENT ID	COMMENT
••• We do not use the following data for averages, fits, limits, etc. •••		
131.1 \pm 2.4	MIROSHNIC... 79	Fit photoproduction

$\Delta(1232)^0$ WIDTH

VALUE (MeV)	DOCUMENT ID	TECN	COMMENT
••• We do not use the following data for averages, fits, limits, etc. •••			
112.5 \pm 1.9	BREITSHOP..06	CNTR	Using new CHEX data
116.9 \pm 0.7	GRIDNEV 06	DPWA	$\pi N \rightarrow \pi N$
117.58 \pm 1.16	BERNICHIA 96		Fit to PEDRONI 78
113.0 \pm 1.5	KOCH 80b	IPWA	$\pi N \rightarrow \pi N$
117.9 \pm 0.9	PEDRONI 78		$\pi N \rightarrow \pi N$ 70–370 MeV

Δ^0 - Δ^{++} WIDTH DIFFERENCE

VALUE (MeV)	DOCUMENT ID	TECN	COMMENT
••• We do not use the following data for averages, fits, limits, etc. •••			
4.66 \pm 1.0	GRIDNEV 06	DPWA	$\pi N \rightarrow \pi N$
8.45 \pm 1.11	BERNICHIA 96		Fit to PEDRONI 78
5.1 \pm 1.0	ABAEV 95	IPWA	$\pi N \rightarrow \pi N$
6.6 \pm 1.0	PEDRONI 78		See the widths

$\Delta(1232)$ DECAY MODES

The following branching fractions are our estimates, not fits or averages.

Mode	Fraction (Γ_j/Γ)
Γ_1 $N\pi$	99.4 %
Γ_2 $N\gamma$	0.55–0.65 %
Γ_3 $N\gamma$, helicity=1/2	0.11–0.13 %
Γ_4 $N\gamma$, helicity=3/2	0.44–0.52 %
Γ_5 pe^+e^-	(4.2 \pm 0.7) $\times 10^{-5}$

$\Delta(1232)$ BRANCHING RATIOS

$\Gamma(N\pi)/\Gamma_{total}$	DOCUMENT ID	TECN	COMMENT	Γ_1/Γ
0.994 OUR ESTIMATE				
0.9939 \pm 0.0001	¹ HUNT 19	DPWA	Multichannel	
1.00	ARNDT 06	DPWA	$\pi N \rightarrow \pi N, \eta N$	
1.0	CUTKOSKY 80	IPWA	$\pi N \rightarrow \pi N$	
1.0	HOEHLER 79	IPWA	$\pi N \rightarrow \pi N$	
••• We do not use the following data for averages, fits, limits, etc. •••				
0.994	SHRESTHA 12A	DPWA	Multichannel	
1.0	ANISOVICH 10	DPWA	Multichannel	
1.000	ARNDT 04	DPWA	$\pi N \rightarrow \pi N, \eta N$	
1.00	PENNER 02c	DPWA	Multichannel	

¹ Statistical error only.

$\Gamma(pe^+e^-)/\Gamma_{total}$	DOCUMENT ID	COMMENT	Γ_5/Γ
4.19\pm0.34\pm0.62	¹ ADAMCZEV...17		

¹ The systematic uncertainty includes the model dependence.

$\Delta(1232)$ PHOTON DECAY AMPLITUDES AT THE POLE

$\Delta(1232) \rightarrow N\gamma$, helicity-1/2 amplitude $A_{1/2}$

MODULUS ($\text{GeV}^{-1/2}$)	PHASE ($^\circ$)	DOCUMENT ID	TECN	COMMENT
-0.114 ^{+0.010} _{-0.003}	-9 ⁺⁴ ₋₂	ROENCHEN 14	DPWA	
••• We do not use the following data for averages, fits, limits, etc. •••				
-0.117	-6.6	ROENCHEN 15A	DPWA	Multichannel

$\Delta(1232) \rightarrow N\gamma$, helicity-3/2 amplitude $A_{3/2}$

MODULUS ($\text{GeV}^{-1/2}$)	PHASE ($^\circ$)	DOCUMENT ID	TECN	COMMENT
-0.229 ^{+0.003} _{-0.004}	3 ^{+0.3} _{-0.4}	ROENCHEN 14	DPWA	
••• We do not use the following data for averages, fits, limits, etc. •••				
-0.226	2.8	ROENCHEN 15A	DPWA	Multichannel

$\Delta(1232)$ BREIT-WIGNER PHOTON DECAY AMPLITUDES

Papers on γN amplitudes predating 1981 may be found in our 2006 edition, Journal of Physics **G33** 1 (2006).

$\Delta(1232) \rightarrow N\gamma$, helicity-1/2 amplitude $A_{1/2}$

VALUE ($\text{GeV}^{-1/2}$)	DOCUMENT ID	TECN	COMMENT
-0.142 to -0.129 (≈ -0.135) OUR ESTIMATE			
-0.146 \pm 0.002	¹ HUNT 19	DPWA	Multichannel
-0.131 \pm 0.004	ANISOVICH 12A	DPWA	Multichannel
-0.139 \pm 0.002	¹ WORKMAN 12A	DPWA	$\gamma N \rightarrow N\pi$
-0.139 \pm 0.004	¹ DUGGER 07	DPWA	$\gamma N \rightarrow \pi N$
-0.137 \pm 0.005	AHRENS 04A	DPWA	$\tilde{\gamma}\tilde{p} \rightarrow N\pi$
-0.1357 \pm 0.0013 \pm 0.0037	BLANPIED 01	LEGS	$\gamma p \rightarrow p\gamma, p\pi^0, n\pi^+$
-0.131 \pm 0.001	¹ BECK 00	IPWA	$\tilde{\gamma}p \rightarrow p\pi^0, n\pi^+$
-0.140 \pm 0.005	KAMALOV 99	DPWA	$\gamma N \rightarrow \pi N$
-0.1294 \pm 0.0013	HANSTEIN 98	IPWA	$\gamma N \rightarrow \pi N$
-0.1278 \pm 0.0012	DAVIDSON 97	DPWA	$\gamma N \rightarrow \pi N$
••• We do not use the following data for averages, fits, limits, etc. •••			
-0.137 \pm 0.001	¹ SHRESTHA 12A	DPWA	Multichannel
-0.136 \pm 0.005	ANISOVICH 10	DPWA	Multichannel
-0.140	DRECHSEL 07	DPWA	$\gamma N \rightarrow \pi N$
-0.129 \pm 0.001	ARNDT 02	DPWA	$\gamma p \rightarrow N\pi$
-0.128	PENNER 02D	DPWA	Multichannel
-0.1312	HANSTEIN 98	DPWA	$\gamma N \rightarrow \pi N$

¹ Statistical error only.

$\Delta(1232) \rightarrow N\gamma$, helicity-3/2 amplitude $A_{3/2}$

VALUE ($\text{GeV}^{-1/2}$)	DOCUMENT ID	TECN	COMMENT
-0.262 to -0.248 (≈ -0.255) OUR ESTIMATE			
-0.250 \pm 0.002	¹ HUNT 19	DPWA	Multichannel
-0.254 \pm 0.005	ANISOVICH 12A	DPWA	Multichannel
-0.262 \pm 0.003	WORKMAN 12A	DPWA	$\gamma N \rightarrow N\pi$
-0.258 \pm 0.005	DUGGER 07	DPWA	$\gamma N \rightarrow \pi N$
-0.256 \pm 0.003	AHRENS 04A	DPWA	$\tilde{\gamma}\tilde{p} \rightarrow N\pi$
-0.2669 \pm 0.0016 \pm 0.0078	BLANPIED 01	LEGS	$\gamma p \rightarrow p\gamma, p\pi^0, n\pi^+$
-0.251 \pm 0.001	BECK 00	IPWA	$\tilde{\gamma}p \rightarrow p\pi^0, n\pi^+$
-0.258 \pm 0.006	KAMALOV 99	DPWA	$\gamma N \rightarrow \pi N$
-0.2466 \pm 0.0013	HANSTEIN 98	IPWA	$\gamma N \rightarrow \pi N$
-0.2524 \pm 0.0013	DAVIDSON 97	DPWA	$\gamma N \rightarrow \pi N$
••• We do not use the following data for averages, fits, limits, etc. •••			
-0.251 \pm 0.001	¹ SHRESTHA 12A	DPWA	Multichannel
-0.267 \pm 0.008	ANISOVICH 10	DPWA	Multichannel
-0.265	DRECHSEL 07	DPWA	$\gamma N \rightarrow \pi N$
-0.243 \pm 0.001	ARNDT 02	DPWA	$\gamma p \rightarrow N\pi$
-0.247	PENNER 02D	DPWA	Multichannel
-0.2522	HANSTEIN 98	DPWA	$\gamma N \rightarrow \pi N$

¹ Statistical error only.

$\Delta(1232) \rightarrow N\gamma$, E_2/M_1 ratio

VALUE	DOCUMENT ID	TECN	COMMENT
-0.030 to -0.020 (≈ -0.025) OUR ESTIMATE			
-0.0274 \pm 0.0003 \pm 0.0030	AHRENS 04A	DPWA	$\tilde{\gamma}\tilde{p} \rightarrow N\pi$
-0.020 \pm 0.002	ARNDT 02	DPWA	$\gamma p \rightarrow N\pi$
-0.0307 \pm 0.0026 \pm 0.0024	BLANPIED 01	LEGS	$\gamma p \rightarrow p\gamma, p\pi^0, n\pi^+$
-0.016 \pm 0.004 \pm 0.002	GALLER 01	DPWA	$\gamma p \rightarrow \gamma p$
-0.025 \pm 0.001 \pm 0.002	BECK 00	IPWA	$\tilde{\gamma}p \rightarrow p\pi^0, n\pi^+$
-0.0233 \pm 0.0017	HANSTEIN 98	IPWA	$\gamma N \rightarrow \pi N$
-0.015 \pm 0.005	¹ ARNDT 97	IPWA	$\gamma N \rightarrow \pi N$
-0.0319 \pm 0.0024	DAVIDSON 97	DPWA	$\gamma N \rightarrow \pi N$
••• We do not use the following data for averages, fits, limits, etc. •••			
-0.022	DRECHSEL 07	DPWA	$\gamma N \rightarrow \pi N$
-0.026	PENNER 02D	DPWA	Multichannel
-0.0254 \pm 0.0010	HANSTEIN 98	DPWA	$\gamma N \rightarrow \pi N$
-0.025 \pm 0.002 \pm 0.002	BECK 97	IPWA	$\gamma N \rightarrow \pi N$
-0.030 \pm 0.003 \pm 0.002	BLANPIED 97	DPWA	$\gamma N \rightarrow \pi N, \gamma N$

¹ This ARNDT 97 value is very sensitive to the database being fitted. The result is from a fit to the full pion photoproduction database, apart from the BLANPIED 97 cross-section measurements.

Baryon Particle Listings

 $\Delta(1232), \Delta(1600)$ $\Delta(1232) \rightarrow N\gamma$, absolute value of E_2/M_1 ratio at pole

VALUE	DOCUMENT ID	TECN	COMMENT
0.065 ± 0.007	ARNDT 97	DPWA	$\gamma N \rightarrow \pi N$
0.058	HANSTEIN 96	DPWA	$\gamma N \rightarrow \pi N$

 $\Delta(1232) \rightarrow N\gamma$, phase of E_2/M_1 ratio at pole

VALUE	DOCUMENT ID	TECN	COMMENT
-122 ± 5	ARNDT 97	DPWA	$\gamma N \rightarrow \pi N$
-127.2	HANSTEIN 96	DPWA	$\gamma N \rightarrow \pi N$

 $\Delta(1232)$ MAGNETIC MOMENTS $\Delta(1232)^{++}$ MAGNETIC MOMENT

The values are extracted from UCLA and SIN data on $\pi^+ p$ bremsstrahlung using a variety of different theoretical approximations and methods. Our estimate is only a rough guess of the range we expect the moment to lie within.

VALUE (μ_N)	DOCUMENT ID	TECN	COMMENT
6.14 ± 0.51	LOPEZCAST... 01	DPWA	$\pi^+ p \rightarrow \pi^+ p \gamma$
4.52 ± 0.50 ± 0.45	BOSSHARD 91		$\pi^+ p \rightarrow \pi^+ p \gamma$ (SIN data)
3.7 to 4.2	LIN 91B		$\pi^+ p \rightarrow \pi^+ p \gamma$ (from UCLA data)
4.6 to 4.9	LIN 91B		$\pi^+ p \rightarrow \pi^+ p \gamma$ (from SIN data)
5.6 to 7.5	WITTMAN 88		$\pi^+ p \rightarrow \pi^+ p \gamma$ (from UCLA data)
6.9 to 9.8	HELLER 87		$\pi^+ p \rightarrow \pi^+ p \gamma$ (from UCLA data)
4.7 to 6.7	NEFKENS 78		$\pi^+ p \rightarrow \pi^+ p \gamma$ (UCLA data)

 $\Delta(1232)^+$ MAGNETIC MOMENT

VALUE (μ_N)	DOCUMENT ID	COMMENT
2.7 ± 1.0 1.3 ± 1.5 ± 3	¹ KOTULLA 02	$\gamma p \rightarrow \rho \pi^0 \gamma'$

¹ The second error is systematic, the third is an estimate of theoretical uncertainties.

 $\Delta(1232)$ REFERENCES

For early references, see Physics Letters **111B** 1 (1982).

HUNT 19	PR C99 055205	B. C. Hunt, D.M. Manley	
ADAMCZEW... 17	PR C95 065205	J. Adamczewski-Musch et al.	(HADES Collab.)
ROENCHEN 15A	EPJ A51 70	D. Roenchen et al.	
PDG 14	CP C38 070001	K. Olive et al.	(PDG Collab.)
ROENCHEN 14	EPJ A50 101	D. Roenchen et al.	
Also	EPJ A51 63 (errata.)	D. Roenchen et al.	
SVARC 14	PR C89 045205	A. Svarc et al.	(RBI Zagreb, UNI Tuzla)
ANISOVICH 12A	EPJ A48 15	A.V. Anisovich et al.	(BONN, PNPI)
SHRESTHA 12A	PR C86 055203	M. Shrestha, D.M. Manley	(KSU)
WORKMAN 12A	PR C86 015202	R. Workman et al.	(GWU)
ANISOVICH 10	EPJ A44 203	A.V. Anisovich et al.	(BONN, PNPI)
DRECHSEL 07	EPJ A34 69	D. Drechsel, S.S. Kamalov, L. Tiator	(MAINZ, JINR)
DUGGER 07	PR C76 025211	M. Dugger et al.	(JLab CLAS Collab.)
ARNDT 06	PR C74 045205	R.A. Arndt et al.	(GWU)
BREITSCHOP... 06	PL B639 424	J. Breitschopf et al.	(TUBIN, HEBR, CSUS)
GRIDNEV 06	PAN 69 1542	A.B. Gridnev et al.	(PNPI, BONN, GWU)
PDG 06	JP G33 1	W.-M. Yao et al.	(PDG Collab.)
AHRENS 04A	EPJ A21 323	J. Ahrens et al.	(A2 Collab.)
ARNDT 04	PR C69 035213	R.A. Arndt et al.	(GWU, TRIU)
ARNDT 02	PR C66 055213	R.A. Arndt et al.	(GWU)
KOTULLA 02	PRL 89 272001	M. Kotulla et al.	(MAMI TAPS Collab.)
PENNER 02C	PR C64 055211	G. Penner, U. Mosel	(GIES)
PENNER 02D	PR C66 055212	G. Penner, U. Mosel	(GIES)
BLANPIED 01	PR C64 025203	G. Blanpied et al.	(BNL LEGS Collab.)
GALLER 01	PL B503 245	G. Galler et al.	(Mainz LARA Collab.)
LOPEZCAST... 01	PL B517 339	G. Lopez Castro, A. Mariano	
Also	NP A697 440	G. Lopez Castro, A. Mariano	
BECK 00	PR C61 035204	R. Beck et al.	(Mainz Microtron DAPHNE Col.)
KAMALOV 99	PRL 83 4494	S.S. Kamalov, S.N. Yang	(Taiwan U.)
HANSTEIN 98	NP A632 561	O. Hanstein, D. Drechsel, L. Tiator	
ARNDT 97	PR C56 577	R.A. Arndt, I.I. Strakovsky, R.L. Workman	(VPI)
BECK 97	PRL 79 606	R. Beck et al.	(MANZ, SACL, PAVI, GLAS)
Also	PRL 79 4510	R.L. Beck, H.P. Krahn	(MANZ)
Also	PRL 79 4512	R.L. Beck, H.P. Krahn	(MANZ)
Also	PRL 79 4515 (erratum)	R.L. Beck et al.	(MANZ, SACL, PAVI, GLAS)
BLANPIED 97	PRL 79 4337	G.S. Blanpied et al.	(LEGS Collab.)
DAVIDSON 97	PRL 79 4509	R.M. Davidson, N.C.A. Mukhopadhyay	(RPI)
BERNICHIA 96	NP A597 623	A. Bernichia, G. Lopez Castro, J. Pestieau	(LOUV+)
HANSTEIN 96	PL B385 45	O. Hanstein, D. Drechsel, L. Tiator	(MANZ)
ABAEV 95	ZPHY A352 85	V.V. Abaev, S.P. Kruglov	(PNPI)
HOEHLER 93	πN Newsletter 9 1	G. Hoehler	(KARL)
BOSSHARD 91	PR D44 1362	A. Boshard et al.	(ZURI, LBL, VILL+)
Also	PRL 64 2619	A. Boshard et al.	(CATH, LAUS, LBL+)
LIN 91B	PR C44 1819	D.H. Lin, M.K. Liou, Z.M. Ding	(CUINY, CSOK)
Also	PR C43 R930	D. Lin, M.K. Liou	(CUINY)
WITTMAN 88	PR C37 2075	R. Wittman	(TRIU)
HELLER 87	PR C35 718	L. Heller et al.	(LANL, MIT, ILL)
CUTKOSKY 80	Toronto Conf. 19	R.E. Cutkosky et al.	(CMU, LBL) IJP
Also	PR D20 2839	R.E. Cutkosky et al.	(CMU, LBL)
KOCH 80B	NP A336 331	R. Koch, E. Pietarinen	(KARLT) IJP
HOEHLER 79	PDAT 12-1	G. Hoehler et al.	(KARLT) IJP
Also	Toronto Conf. 3	R. Koch	(KARLT) IJP
MIROSHNIC... 79	SJNP 29 94	I.I. Miroshnichenko et al.	(KFTI) IJP
Also	Translated from YAF 29 188		
NEFKENS 78	PR D18 3911	B.M.K. Nefkens et al.	(UCLA, CATH) IJP
PEDRONI 78	NP A300 321	E. Pedroni et al.	(SIN, ISNG, KARLE+) IJP

 $\Delta(1600) 3/2^+$

$$I(J^P) = \frac{3}{2}(\frac{3}{2}^+) \text{ Status: } ***$$

Older and obsolete values are listed and referenced in the 2014 edition, Chinese Physics **C38** 070001 (2014).

 $\Delta(1600)$ POLE POSITION

REAL PART

VALUE (MeV)	DOCUMENT ID	TECN	COMMENT
1460 to 1560 (≈ 1510) OUR ESTIMATE			
1515 ± 20	SOKHOYAN 15A	DPWA	Multichannel
1469 ± 10 ± 5	¹ SVARC 14	L+P	$\pi N \rightarrow \pi N$
1550 ± 40	CUTKOSKY 80	IPWA	$\pi N \rightarrow \pi N$
• • • We do not use the following data for averages, fits, limits, etc. • • •			
1619	HUNT 19	DPWA	Multichannel
1552	ROENCHEN 15A	DPWA	Multichannel
1498 ± 25	ANISOVICH 12A	DPWA	Multichannel
1457	ARNDT 06	DPWA	$\pi N \rightarrow \pi N, \eta N$
1599	VRANA 00	DPWA	Multichannel
1550	HOEHLER 93	SPED	$\pi N \rightarrow \pi N$

¹ Fit to the amplitudes of HOEHLER 79.

-2xIMAGINARY PART

VALUE (MeV)	DOCUMENT ID	TECN	COMMENT
200 to 340 (≈ 270) OUR ESTIMATE			
250 ± 30	SOKHOYAN 15A	DPWA	Multichannel
314 ± 18 ± 8	¹ SVARC 14	L+P	$\pi N \rightarrow \pi N$
200 ± 60	CUTKOSKY 80	IPWA	$\pi N \rightarrow \pi N$
• • • We do not use the following data for averages, fits, limits, etc. • • •			
295	HUNT 19	DPWA	Multichannel
350	ROENCHEN 15A	DPWA	Multichannel
230 ± 50	ANISOVICH 12A	DPWA	Multichannel
400	ARNDT 06	DPWA	$\pi N \rightarrow \pi N, \eta N$
312	VRANA 00	DPWA	Multichannel

¹ Fit to the amplitudes of HOEHLER 79.

 $\Delta(1600)$ ELASTIC POLE RESIDUEMODULUS $|r|$

VALUE (MeV)	DOCUMENT ID	TECN	COMMENT
10 to 40 (≈ 25) OUR ESTIMATE			
13 ± 3	SOKHOYAN 15A	DPWA	Multichannel
38 ± 2 ± 2	¹ SVARC 14	L+P	$\pi N \rightarrow \pi N$
17 ± 4	CUTKOSKY 80	IPWA	$\pi N \rightarrow \pi N$
• • • We do not use the following data for averages, fits, limits, etc. • • •			
23	ROENCHEN 15A	DPWA	Multichannel
11 ± 6	ANISOVICH 12A	DPWA	Multichannel
44	ARNDT 06	DPWA	$\pi N \rightarrow \pi N, \eta N$

¹ Fit to the amplitudes of HOEHLER 79.

PHASE θ

VALUE (°)	DOCUMENT ID	TECN	COMMENT
150 to 210 (≈ 180) OUR ESTIMATE			
-155 ± 20	SOKHOYAN 15A	DPWA	Multichannel
-173 ± 5 ± 5	¹ SVARC 14	L+P	$\pi N \rightarrow \pi N$
-150 ± 30	CUTKOSKY 80	IPWA	$\pi N \rightarrow \pi N$
• • • We do not use the following data for averages, fits, limits, etc. • • •			
-155	ROENCHEN 15A	DPWA	Multichannel
-160 ± 33	ANISOVICH 12A	DPWA	Multichannel
+147	ARNDT 06	DPWA	$\pi N \rightarrow \pi N, \eta N$

¹ Fit to the amplitudes of HOEHLER 79.

 $\Delta(1600)$ INELASTIC POLE RESIDUE

The "normalized residue" is the residue divided by $\Gamma_{pole}/2$.

Normalized residue in $N\pi \rightarrow \Delta(1600) \rightarrow \Delta\pi, P$ -wave

MODULUS	PHASE (°)	DOCUMENT ID	TECN	COMMENT
0.15 ± 0.04	30 ± 35	SOKHOYAN 15A	DPWA	Multichannel
• • • We do not use the following data for averages, fits, limits, etc. • • •				
0.31	31	ROENCHEN 15A	DPWA	Multichannel
0.14 ± 0.10	154 ± 40	ANISOVICH 12A	DPWA	Multichannel

Normalized residue in $N\pi \rightarrow \Delta(1600) \rightarrow \Delta\pi, F$ -wave

MODULUS	PHASE (°)	DOCUMENT ID	TECN	COMMENT
0.010 ± 0.005		SOKHOYAN 15A	DPWA	Multichannel
• • • We do not use the following data for averages, fits, limits, etc. • • •				
0.013	29	ROENCHEN 15A	DPWA	Multichannel
0.010 ± 0.005		ANISOVICH 12A	DPWA	Multichannel

Normalized residue in $N\pi \rightarrow \Delta(1600) \rightarrow \Sigma K$

MODULUS	PHASE (°)	DOCUMENT ID	TECN	COMMENT
0.13	-5.6	ROENCHEN 15A	DPWA	Multichannel

$\Delta(1600)$ BREIT-WIGNER MASS

VALUE (MeV)	DOCUMENT ID	TECN	COMMENT
1500 to 1640 (≈ 1570) OUR ESTIMATE			
1664 ± 16	¹ HUNT 19	DPWA	Multichannel
1520 ± 20	SOKHOYAN 15A	DPWA	Multichannel
1600 ± 50	CUTKOSKY 80	IPWA	$\pi N \rightarrow \pi N$
1522 ± 13	HOEHLER 79	IPWA	$\pi N \rightarrow \pi N$
••• We do not use the following data for averages, fits, limits, etc. •••			
1510 ± 20	ANISOVICH 12A	DPWA	Multichannel
1626 ± 8	¹ SHRESTHA 12A	DPWA	Multichannel
1667 ± 1	PENNER 02C	DPWA	Multichannel
1687 ± 44	VRANA 00	DPWA	Multichannel

¹ Statistical error only.

$\Delta(1600)$ BREIT-WIGNER WIDTH

VALUE (MeV)	DOCUMENT ID	TECN	COMMENT
200 to 300 (≈ 250) OUR ESTIMATE			
322 ± 46	¹ HUNT 19	DPWA	Multichannel
235 ± 30	SOKHOYAN 15A	DPWA	Multichannel
300 ± 100	CUTKOSKY 80	IPWA	$\pi N \rightarrow \pi N$
220 ± 40	HOEHLER 79	IPWA	$\pi N \rightarrow \pi N$
••• We do not use the following data for averages, fits, limits, etc. •••			
220 ± 45	ANISOVICH 12A	DPWA	Multichannel
225 ± 18	¹ SHRESTHA 12A	DPWA	Multichannel
397 ± 10	PENNER 02C	DPWA	Multichannel
493 ± 75	VRANA 00	DPWA	Multichannel

¹ Statistical error only.

$\Delta(1600)$ DECAY MODES

The following branching fractions are our estimates, not fits or averages.

Mode	Fraction (Γ_j/Γ)
Γ_1 $N\pi$	8-24 %
Γ_2 $N\pi\pi$	75-90 %
Γ_3 $\Delta(1232)\pi$	73-83 %
Γ_4 $\Delta(1232)\pi, P$ -wave	72-82 %
Γ_5 $\Delta(1232)\pi, F$ -wave	<2 %
Γ_6 $N(1440)\pi$	
Γ_7 $N(1440)\pi, P$ -wave	15-25 %
Γ_8 $N\gamma$	0.001-0.035 %
Γ_9 $N\gamma, \text{helicity}=1/2$	0.0-0.02 %
Γ_{10} $N\gamma, \text{helicity}=3/2$	0.001-0.015 %

$\Delta(1600)$ BRANCHING RATIOS

$\Gamma(N\pi)/\Gamma_{\text{total}}$	DOCUMENT ID	TECN	COMMENT	Γ_1/Γ
8 to 24 (≈ 16) OUR ESTIMATE				
10.7 ± 1.9	¹ HUNT 19	DPWA	Multichannel	
14 ± 4	SOKHOYAN 15A	DPWA	Multichannel	
18 ± 4	CUTKOSKY 80	IPWA	$\pi N \rightarrow \pi N$	
21 ± 6	HOEHLER 79	IPWA	$\pi N \rightarrow \pi N$	
••• We do not use the following data for averages, fits, limits, etc. •••				
12 ± 5	ANISOVICH 12A	DPWA	Multichannel	
8 ± 2	¹ SHRESTHA 12A	DPWA	Multichannel	
13 ± 1	PENNER 02C	DPWA	Multichannel	
28 ± 5	VRANA 00	DPWA	Multichannel	

¹ Statistical error only.

$\Gamma(\Delta(1232)\pi, P\text{-wave})/\Gamma_{\text{total}}$

VALUE (%)	DOCUMENT ID	TECN	COMMENT	Γ_4/Γ
64 ± 6	¹ HUNT 19	DPWA	Multichannel	
77 ± 5	SOKHOYAN 15A	DPWA	Multichannel	
••• We do not use the following data for averages, fits, limits, etc. •••				
78 ± 6	ANISOVICH 12A	DPWA	Multichannel	
70 ± 3	¹ SHRESTHA 12A	DPWA	Multichannel	
59 ± 10	VRANA 00	DPWA	Multichannel	

¹ Statistical error only.

$\Gamma(\Delta(1232)\pi, F\text{-wave})/\Gamma_{\text{total}}$

VALUE (%)	DOCUMENT ID	TECN	COMMENT	Γ_5/Γ
<2	SOKHOYAN 15A	DPWA	Multichannel	

$\Gamma(N(1440)\pi)/\Gamma_{\text{total}}$

VALUE (%)	DOCUMENT ID	TECN	COMMENT	Γ_6/Γ
22 ± 5	¹ HUNT 19	DPWA	Multichannel	
••• We do not use the following data for averages, fits, limits, etc. •••				
22 ± 3	¹ SHRESTHA 12A	DPWA	Multichannel	
13 ± 4	VRANA 00	DPWA	Multichannel	

¹ Statistical error only.

$\Delta(1600)$ PHOTON DECAY AMPLITUDES AT THE POLE

$\Delta(1600) \rightarrow N\gamma, \text{helicity-1/2 amplitude } A_{1/2}$

MODULUS ($\text{GeV}^{-1/2}$)	PHASE (°)	DOCUMENT ID	TECN	COMMENT
0.053 ± 0.010	130 ± 15	SOKHOYAN 15A	DPWA	Multichannel
0.193 ^{+0.023} _{-0.024}	151 ⁺⁹ ₋₁₅	ROENCHEN 14	DPWA	
••• We do not use the following data for averages, fits, limits, etc. •••				
-0.230	-42	ROENCHEN 15A	DPWA	Multichannel

$\Delta(1600) \rightarrow N\gamma, \text{helicity-3/2 amplitude } A_{3/2}$

MODULUS ($\text{GeV}^{-1/2}$)	PHASE (°)	DOCUMENT ID	TECN	COMMENT
0.055 ± 0.010	152 ± 15	SOKHOYAN 15A	DPWA	Multichannel
-0.254 ^{+0.085} _{-0.086}	110 ⁺¹⁰ ₋₆	ROENCHEN 14	DPWA	
••• We do not use the following data for averages, fits, limits, etc. •••				
0.332	-71	ROENCHEN 15A	DPWA	Multichannel

$\Delta(1600)$ BREIT-WIGNER PHOTON DECAY AMPLITUDES

$\Delta(1600) \rightarrow N\gamma, \text{helicity-1/2 amplitude } A_{1/2}$

VALUE ($\text{GeV}^{-1/2}$)	DOCUMENT ID	TECN	COMMENT
-0.060 to -0.030 (≈ -0.045) OUR ESTIMATE			
0.0082 ± 0.0014	¹ HUNT 19	DPWA	Multichannel
-0.051 ± 0.010	SOKHOYAN 15A	DPWA	Multichannel
-0.018 ± 0.015	¹ ARNDT 96	IPWA	$\gamma N \rightarrow \pi N$
••• We do not use the following data for averages, fits, limits, etc. •••			
-0.050 ± 0.009	ANISOVICH 12A	DPWA	Multichannel
0.006 ± 0.005	¹ SHRESTHA 12A	DPWA	Multichannel
0.0	PENNER 02D	DPWA	Multichannel

¹ Statistical error only.

$\Delta(1600) \rightarrow N\gamma, \text{helicity-3/2 amplitude } A_{3/2}$

VALUE ($\text{GeV}^{-1/2}$)	DOCUMENT ID	TECN	COMMENT
-0.050 to -0.020 (≈ -0.035) OUR ESTIMATE			
0.048 ± 0.014	¹ HUNT 19	DPWA	Multichannel
-0.055 ± 0.010	SOKHOYAN 15A	DPWA	Multichannel
-0.025 ± 0.015	¹ ARNDT 96	IPWA	$\gamma N \rightarrow \pi N$
••• We do not use the following data for averages, fits, limits, etc. •••			
-0.040 ± 0.012	ANISOVICH 12A	DPWA	Multichannel
0.052 ± 0.008	¹ SHRESTHA 12A	DPWA	Multichannel
-0.024	PENNER 02D	DPWA	Multichannel

¹ Statistical error only.

$\Delta(1600)$ REFERENCES

For early references, see Physics Letters **111B** 1 (1982).

HUNT 19	PR C99 055205	B. C. Hunt, D. M. Manley
ROENCHEN 15A	EPJ A51 70	D. Roenchen <i>et al.</i>
SOKHOYAN 15A	EPJ A51 95	V. Sokhoyan <i>et al.</i> (CBELSA/TAPS Collab.)
PDG 14	CP C38 070001	K. Olive <i>et al.</i> (PDG Collab.)
ROENCHEN 14	EPJ A50 101	D. Roenchen <i>et al.</i>
Also	EPJ A51 63 (errata.)	D. Roenchen <i>et al.</i>
SVARC 14	PR C89 045205	A. Svarc <i>et al.</i> (RBI Zagreb, UNI Tuzla)
ANISOVICH 12A	EPJ A48 15	A.V. Anisovich <i>et al.</i> (BONN, PNPI)
SHRESTHA 12A	PR C86 055203	M. Shrestha, D.M. Manley (KSU)
ARNDT 06	PR C74 045205	R.A. Arndt <i>et al.</i> (GWU)
PENNER 02C	PR C66 055211	G. Penner, U. Mosel (GIES)
PENNER 02D	PR C66 055212	G. Penner, U. Mosel (GIES)
VRANA 00	PRPL 328 181	T.P. Vrana, S.A. Dytman, T.-S.H. Lee (PITT, ANL)
ARNDT 96	PR C53 430	R.A. Arndt, I.I. Strakovsky, R.L. Workman (VPI)
HOEHLER 93	πN Newsletter 9 1	G. Hohlner (KARL)
CUTKOSKY 80	Toronto Conf. 19	R.E. Cutkosky <i>et al.</i> (CMU, LBL) IJP
Also	PR D20 2839	R.E. Cutkosky <i>et al.</i> (CMU, LBL) IJP
HOEHLER 79	PDAT 12-1	G. Hohlner <i>et al.</i> (KARL) IJP
Also	Toronto Conf. 3	R. Koch (KARL) IJP

$\Delta(1620) 1/2^-$

$I(J^P) = \frac{3}{2}(\frac{1}{2}^-)$ Status: ***

Older and obsolete values are listed and referenced in the 2014 edition, Chinese Physics **C38** 070001 (2014).

$\Delta(1620)$ POLE POSITION

REAL PART

VALUE (MeV)	DOCUMENT ID	TECN	COMMENT
1590 to 1610 (≈ 1600) OUR ESTIMATE			
1597 ± 5	SOKHOYAN 15A	DPWA	Multichannel
1603 ± 7 ± 2	¹ SVARC 14	L+P	$\pi N \rightarrow \pi N$
1600 ± 15	CUTKOSKY 80	IPWA	$\pi N \rightarrow \pi N$

Baryon Particle Listings

 $\Delta(1620)$

••• We do not use the following data for averages, fits, limits, etc. •••

1577	HUNT	19	DPWA	Multichannel
1600	ROENCHEN	15A	DPWA	Multichannel
1597 ± 4	ANISOVICH	12A	DPWA	Multichannel
1595	ARNDT	06	DPWA	$\pi N \rightarrow \pi N, \eta N$
1607	VRANA	00	DPWA	Multichannel
1608	HOEHLER	93	SPED	$\pi N \rightarrow \pi N$

¹ Fit to the amplitudes of HOEHLER 79.

-2xIMAGINARY PART

VALUE (MeV)	DOCUMENT ID	TECN	COMMENT
-------------	-------------	------	---------

100 to 140 (≈ 120) OUR ESTIMATE

134 ± 8	SOKHOYAN	15A	DPWA	Multichannel
114 ± 12 ± 4	¹ SVARC	14	L+P	$\pi N \rightarrow \pi N$
120 ± 20	CUTKOSKY	80	IPWA	$\pi N \rightarrow \pi N$

••• We do not use the following data for averages, fits, limits, etc. •••

101	HUNT	19	DPWA	Multichannel
65	ROENCHEN	15A	DPWA	Multichannel
130 ± 9	ANISOVICH	12A	DPWA	Multichannel
135	ARNDT	06	DPWA	$\pi N \rightarrow \pi N, \eta N$
148	VRANA	00	DPWA	Multichannel
116	HOEHLER	93	SPED	$\pi N \rightarrow \pi N$

¹ Fit to the amplitudes of HOEHLER 79.

 $\Delta(1620)$ ELASTIC POLE RESIDUEMODULUS $|r|$

VALUE (MeV)	DOCUMENT ID	TECN	COMMENT
-------------	-------------	------	---------

15 to 20 (≈ 17) OUR ESTIMATE

20 ± 3	SOKHOYAN	15A	DPWA	Multichannel
17 ± 2 ± 1	¹ SVARC	14	L+P	$\pi N \rightarrow \pi N$
15 ± 2	CUTKOSKY	80	IPWA	$\pi N \rightarrow \pi N$

••• We do not use the following data for averages, fits, limits, etc. •••

16	ROENCHEN	15A	DPWA	Multichannel
18 ± 2	ANISOVICH	12A	DPWA	Multichannel
15	ARNDT	06	DPWA	$\pi N \rightarrow \pi N, \eta N$
19	HOEHLER	93	SPED	$\pi N \rightarrow \pi N$

¹ Fit to the amplitudes of HOEHLER 79.

PHASE θ

VALUE (°)	DOCUMENT ID	TECN	COMMENT
-----------	-------------	------	---------

-120 to -80 (≈ -100) OUR ESTIMATE

-90 ± 15	SOKHOYAN	15A	DPWA	Multichannel
-106 ± 10 ± 4	¹ SVARC	14	L+P	$\pi N \rightarrow \pi N$
-110 ± 20	CUTKOSKY	80	IPWA	$\pi N \rightarrow \pi N$

••• We do not use the following data for averages, fits, limits, etc. •••

-104	ROENCHEN	15A	DPWA	Multichannel
-100 ± 5	ANISOVICH	12A	DPWA	Multichannel
-92	ARNDT	06	DPWA	$\pi N \rightarrow \pi N, \eta N$
-95	HOEHLER	93	SPED	$\pi N \rightarrow \pi N$

¹ Fit to the amplitudes of HOEHLER 79.

 $\Delta(1620)$ INELASTIC POLE RESIDUE

The "normalized residue" is the residue divided by $\Gamma_{pole}/2$.

Normalized residue in $N\pi \rightarrow \Delta(1620) \rightarrow \Delta\pi, D\text{-wave}$

MODULUS	PHASE (°)	DOCUMENT ID	TECN	COMMENT
---------	-----------	-------------	------	---------

0.42 ± 0.06	-90 ± 20	SOKHOYAN	15A	DPWA	Multichannel
-------------	----------	----------	-----	------	--------------

••• We do not use the following data for averages, fits, limits, etc. •••

0.57	105	ROENCHEN	15A	DPWA	Multichannel
0.38 ± 0.09	-85 ± 30	ANISOVICH	12A	DPWA	Multichannel

Normalized residue in $N\pi \rightarrow \Delta(1620) \rightarrow \Sigma K$

MODULUS	PHASE (°)	DOCUMENT ID	TECN	COMMENT
---------	-----------	-------------	------	---------

••• We do not use the following data for averages, fits, limits, etc. •••

0.22	-105	ROENCHEN	15A	DPWA	Multichannel
------	------	----------	-----	------	--------------

Normalized residue in $N\pi \rightarrow \Delta(1620) \rightarrow N(1440)\pi$

MODULUS	PHASE (°)	DOCUMENT ID	TECN	COMMENT
---------	-----------	-------------	------	---------

0.10 ± 0.06	-65 ± 30	SOKHOYAN	15A	DPWA	Multichannel
-------------	----------	----------	-----	------	--------------

 $\Delta(1620)$ BREIT-WIGNER MASS

VALUE (MeV)	DOCUMENT ID	TECN	COMMENT
-------------	-------------	------	---------

1590 to 1630 (≈ 1610) OUR ESTIMATE

1635 ± 8	GOLOVATCH	19	DPWA	$\gamma p \rightarrow \pi^+ \pi^- p$
1589 ± 3	¹ HUNT	19	DPWA	Multichannel
1595 ± 8	SOKHOYAN	15A	DPWA	Multichannel
1615.2 ± 0.4	¹ ARNDT	06	DPWA	$\pi N \rightarrow \pi N, \eta N$
1620 ± 20	CUTKOSKY	80	IPWA	$\pi N \rightarrow \pi N$
1610 ± 7	HOEHLER	79	IPWA	$\pi N \rightarrow \pi N$

••• We do not use the following data for averages, fits, limits, etc. •••

1600 ± 8	ANISOVICH	12A	DPWA	Multichannel
1600 ± 1	¹ SHRESTHA	12A	DPWA	Multichannel
1612 ± 2	PENNER	02c	DPWA	Multichannel
1617 ± 15	VRANA	00	DPWA	Multichannel

¹ Statistical error only.

 $\Delta(1620)$ BREIT-WIGNER WIDTH

VALUE (MeV)	DOCUMENT ID	TECN	COMMENT
-------------	-------------	------	---------

110 to 150 (≈ 130) OUR ESTIMATE

144 ± 16	GOLOVATCH	19	DPWA	$\gamma p \rightarrow \pi^+ \pi^- p$
107 ± 7	¹ HUNT	19	DPWA	Multichannel
135 ± 9	SOKHOYAN	15A	DPWA	Multichannel
146.9 ± 1.9	¹ ARNDT	06	DPWA	$\pi N \rightarrow \pi N, \eta N$
140 ± 20	CUTKOSKY	80	IPWA	$\pi N \rightarrow \pi N$
139 ± 18	HOEHLER	79	IPWA	$\pi N \rightarrow \pi N$

••• We do not use the following data for averages, fits, limits, etc. •••

130 ± 11	ANISOVICH	12A	DPWA	Multichannel
112 ± 2	¹ SHRESTHA	12A	DPWA	Multichannel
202 ± 7	PENNER	02c	DPWA	Multichannel
143 ± 42	VRANA	00	DPWA	Multichannel

¹ Statistical error only.

 $\Delta(1620)$ DECAY MODES

The following branching fractions are our estimates, not fits or averages.

Mode	Fraction (Γ_i/Γ)
Γ_1 $N\pi$	25–35 %
Γ_2 $N\pi\pi$	55–80 %
Γ_3 $\Delta(1232)\pi$	
Γ_4 $\Delta(1232)\pi, D\text{-wave}$	52–72 %
Γ_5 $N\rho$	
Γ_6 $N\rho, S=1/2, S\text{-wave}$	seen
Γ_7 $N\rho, S=3/2, D\text{-wave}$	seen
Γ_8 $N(1440)\pi$	3–9 %
Γ_9 $N\gamma, \text{helicity}=1/2$	0.03–0.10 %

 $\Delta(1620)$ BRANCHING RATIOS

$\Gamma(N\pi)/\Gamma_{total}$	Γ_1/Γ
-------------------------------	-------------------

VALUE (%)	DOCUMENT ID	TECN	COMMENT
-----------	-------------	------	---------

25 to 35 (≈ 30) OUR ESTIMATE

24 ± 2	¹ HUNT	19	DPWA	Multichannel
28 ± 3	SOKHOYAN	15A	DPWA	Multichannel
31.5 ± 0.1	¹ ARNDT	06	DPWA	$\pi N \rightarrow \pi N, \eta N$
25 ± 3	CUTKOSKY	80	IPWA	$\pi N \rightarrow \pi N$
35 ± 6	HOEHLER	79	IPWA	$\pi N \rightarrow \pi N$

••• We do not use the following data for averages, fits, limits, etc. •••

28 ± 3	ANISOVICH	12A	DPWA	Multichannel
33 ± 2	¹ SHRESTHA	12A	DPWA	Multichannel
34 ± 1	PENNER	02c	DPWA	Multichannel
45 ± 5	VRANA	00	DPWA	Multichannel

¹ Statistical error only.

$\Gamma(N\pi\pi)/\Gamma_{total}$	Γ_2/Γ
----------------------------------	-------------------

VALUE	DOCUMENT ID	TECN	COMMENT
-------	-------------	------	---------

0.90 ± 0.10	GOLOVATCH	19	DPWA	$\gamma p \rightarrow \pi^+ \pi^- p$
-------------	-----------	----	------	--------------------------------------

$\Gamma(\Delta(1232)\pi, D\text{-wave})/\Gamma_{total}$	Γ_4/Γ
---	-------------------

VALUE (%)	DOCUMENT ID	TECN	COMMENT
-----------	-------------	------	---------

48 ± 4	¹ HUNT	19	DPWA	Multichannel
62 ± 10	SOKHOYAN	15A	DPWA	Multichannel

••• We do not use the following data for averages, fits, limits, etc. •••

60 ± 17	ANISOVICH	12A	DPWA	Multichannel
32 ± 2	¹ SHRESTHA	12A	DPWA	Multichannel
39 ± 2	VRANA	00	DPWA	Multichannel

¹ Statistical error only.

$\Gamma(N\rho, S=1/2, S\text{-wave})/\Gamma_{total}$	Γ_6/Γ
--	-------------------

VALUE (%)	DOCUMENT ID	TECN	COMMENT
-----------	-------------	------	---------

27 ± 4	¹ HUNT	19	DPWA	Multichannel
--------	-------------------	----	------	--------------

••• We do not use the following data for averages, fits, limits, etc. •••

26 ± 2	¹ SHRESTHA	12A	DPWA	Multichannel
14 ± 3	VRANA	00	DPWA	Multichannel

¹ Statistical error only.

$\Gamma(N\rho, S=3/2, D\text{-wave})/\Gamma_{\text{total}}$ Γ_7/Γ

VALUE (%)	DOCUMENT ID	TECN	COMMENT
<0.04	¹ HUNT 19	DPWA	Multichannel
••• We do not use the following data for averages, fits, limits, etc. •••			
2 ±1	VRANA 00	DPWA	Multichannel
¹ Statistical error only.			

$\Gamma(N(1440)\pi)/\Gamma_{\text{total}}$ Γ_8/Γ

VALUE (%)	DOCUMENT ID	TECN	COMMENT
<0.02	¹ HUNT 19	DPWA	Multichannel
6 ±3	SOKHOYAN 15A	DPWA	Multichannel
••• We do not use the following data for averages, fits, limits, etc. •••			
9 ±1	¹ SHRESTHA 12A	DPWA	Multichannel
0 ±1	VRANA 00	DPWA	Multichannel
¹ Statistical error only.			

$\Delta(1620)$ PHOTON DECAY AMPLITUDES AT THE POLE

$\Delta(1620) \rightarrow N\gamma$, helicity-1/2 amplitude $A_{1/2}$

MODULUS (GeV ^{-1/2})	PHASE (°)	DOCUMENT ID	TECN	COMMENT
0.054 ± 0.007	-6 ± 7	SOKHOYAN 15A	DPWA	Multichannel
-0.028 ± 0.006	-166 ⁺¹ ₋₄	ROENCHEN 14	DPWA	
••• We do not use the following data for averages, fits, limits, etc. •••				
0.014	26	ROENCHEN 15A	DPWA	Multichannel

$\Delta(1620)$ BREIT-WIGNER PHOTON DECAY AMPLITUDES

$\Delta(1620) \rightarrow N\gamma$, helicity-1/2 amplitude $A_{1/2}$

VALUE (GeV ^{-1/2})	DOCUMENT ID	TECN	COMMENT
0.030 to 0.060 (≈ 0.050) OUR ESTIMATE			
0.029 ± 0.0062	GOLOVATCH 19	DPWA	$\gamma p \rightarrow \pi^+ \pi^- p$
0.0124 ± 0.0007	¹ HUNT 19	DPWA	Multichannel
0.055 ± 0.007	SOKHOYAN 15A	DPWA	Multichannel
0.029 ± 0.003	¹ WORKMAN 12A	DPWA	$\gamma N \rightarrow N\pi$
0.050 ± 0.002	¹ DUGGER 07	DPWA	$\gamma N \rightarrow \pi N$
••• We do not use the following data for averages, fits, limits, etc. •••			
0.052 ± 0.005	ANISOVICH 12A	DPWA	Multichannel
-0.003 ± 0.003	¹ SHRESTHA 12A	DPWA	Multichannel
0.066	DRECHSEL 07	DPWA	$\gamma N \rightarrow \pi N$
-0.050	PENNER 02D	DPWA	Multichannel
¹ Statistical error only.			

$\Delta(1620)$ REFERENCES

For early references, see Physics Letters **111B** 1 (1982).

GOLOVATCH 19	PL B788 371	E. Golovatch et al.	(CLAS Collab.)
HUNT 19	PR C99 055205	B. C. Hunt, D.M. Manley	
ROENCHEN 15A	EPJ A51 70	D. Roenchen et al.	
SOKHOYAN 15A	EPJ A51 95	V. Sokhoyan et al.	(CBELSA/TAPS Collab.)
PDC 14	CP C38 070001	K. Olive et al.	(PDG Collab.)
ROENCHEN 14	EPJ A50 101	D. Roenchen et al.	
Also	EPJ A51 63 (errata.)	D. Roenchen et al.	
SVARC 14	PR C89 045205	A. Svarc et al.	(RBI Zagreb, UNI Tuzla)
ANISOVICH 12A	EPJ A48 15	A.V. Anisovich et al.	(BONN, PNPI)
SHRESTHA 12A	PR C86 055203	M. Shrestha, D.M. Manley	(KSU)
WORKMAN 12A	PR C86 015202	R. Workman et al.	(GWU)
DRECHSEL 07	EPJ A34 69	D. Drechsel, S.S. Kamalov, L. Tiator	(MAINZ, JINR)
DUGGER 07	PR C76 025211	M. Dugger et al.	(JLab CLAS Collab.)
ARNDT 06	PR C74 045205	R.A. Arndt et al.	(GWU)
PENNER 02C	PR C66 055211	G. Penner, U. Mosel	(GIES)
PENNER 02D	PR C66 055212	G. Penner, U. Mosel	(GIES)
VRANA 00	PRL 328 181	T.P. Vrana, S.A. Dytman, T.-S.H. Lee	(PITT, ANL)
HOEHLER 93	πN Newsletter 9 1	G. Hohler	(KARL)
CUTKOSKY 80	Toronto Conf. 19	R.E. Cutkosky et al.	(CMU, LBL) IJP
Also	PR D20 2839	R.E. Cutkosky et al.	(CMU, LBL) IJP
HOEHLER 79	PDAT 12-1	G. Hohler et al.	(KARLT) IJP
Also	Toronto Conf. 3	R. Koch	(KARLT) IJP

$\Delta(1700) 3/2^-$

$I(J^P) = \frac{3}{2}(\frac{3}{2}^-)$ Status: ***

Older and obsolete values are listed and referenced in the 2014 edition, Chinese Physics **C38** 070001 (2014).

$\Delta(1700)$ POLE POSITION

REAL PART	DOCUMENT ID	TECN	COMMENT
1640 to 1690 (≈ 1665) OUR ESTIMATE			
1685 ± 10	SOKHOYAN 15A	DPWA	Multichannel
1643 ± 6 ± 3	¹ SVARC 14	L+P	$\pi N \rightarrow \pi N$
1675 ± 25	CUTKOSKY 80	IPWA	$\pi N \rightarrow \pi N$

••• We do not use the following data for averages, fits, limits, etc. •••

1693	HUNT 19	DPWA	Multichannel
1677	ROENCHEN 15A	DPWA	Multichannel
1685 ± 10	GUTZ 14	DPWA	Multichannel
1680 ± 10	ANISOVICH 12A	DPWA	Multichannel
1632	ARNDT 06	DPWA	$\pi N \rightarrow \pi N, \eta N$
1726	VRANA 00	DPWA	Multichannel
1651	HOEHLER 93	SPED	$\pi N \rightarrow \pi N$

¹ Fit to the amplitudes of HOEHLER 79.

-2xIMAGINARY PART

VALUE (MeV)	DOCUMENT ID	TECN	COMMENT
200 to 300 (≈ 250) OUR ESTIMATE			
300 ± 15	SOKHOYAN 15A	DPWA	Multichannel
217 ± 10 ± 8	¹ SVARC 14	L+P	$\pi N \rightarrow \pi N$
220 ± 40	CUTKOSKY 80	IPWA	$\pi N \rightarrow \pi N$
••• We do not use the following data for averages, fits, limits, etc. •••			
213	HUNT 19	DPWA	Multichannel
305	ROENCHEN 15A	DPWA	Multichannel
300 ± 15	GUTZ 14	DPWA	Multichannel
305 ± 15	ANISOVICH 12A	DPWA	Multichannel
253	ARNDT 06	DPWA	$\pi N \rightarrow \pi N, \eta N$
118	VRANA 00	DPWA	Multichannel
159	HOEHLER 93	SPED	$\pi N \rightarrow \pi N$

¹ Fit to the amplitudes of HOEHLER 79.

$\Delta(1700)$ ELASTIC POLE RESIDUE

MODULUS |r|

VALUE (MeV)	DOCUMENT ID	TECN	COMMENT
10 to 40 (≈ 25) OUR ESTIMATE			
40 ± 6	SOKHOYAN 15A	DPWA	Multichannel
13 ± 1 ± 1	¹ SVARC 14	L+P	$\pi N \rightarrow \pi N$
13 ± 3	CUTKOSKY 80	IPWA	$\pi N \rightarrow \pi N$
••• We do not use the following data for averages, fits, limits, etc. •••			
24	ROENCHEN 15A	DPWA	Multichannel
40 ± 6	GUTZ 14	DPWA	Multichannel
42 ± 7	ANISOVICH 12A	DPWA	Multichannel
18	ARNDT 06	DPWA	$\pi N \rightarrow \pi N, \eta N$
10	HOEHLER 93	SPED	$\pi N \rightarrow \pi N$

¹ Fit to the amplitudes of HOEHLER 79.

PHASE θ

VALUE (°)	DOCUMENT ID	TECN	COMMENT
-40 to 0 (≈ -20) OUR ESTIMATE			
-1 ± 10	SOKHOYAN 15A	DPWA	Multichannel
-30 ± 4 ± 3	¹ SVARC 14	L+P	$\pi N \rightarrow \pi N$
-40	ARNDT 06	DPWA	$\pi N \rightarrow \pi N, \eta N$
-20 ± 25	CUTKOSKY 80	IPWA	$\pi N \rightarrow \pi N$
••• We do not use the following data for averages, fits, limits, etc. •••			
-7.3	ROENCHEN 15A	DPWA	Multichannel
-1 ± 10	GUTZ 14	DPWA	Multichannel
-3 ± 15	ANISOVICH 12A	DPWA	Multichannel

¹ Fit to the amplitudes of HOEHLER 79.

$\Delta(1700)$ INELASTIC POLE RESIDUE

The "normalized residue" is the residue divided by $\Gamma_{\text{pole}}/2$.

Normalized residue in $N\pi \rightarrow \Delta(1700) \rightarrow \Delta\eta$

MODULUS	PHASE (°)	DOCUMENT ID	TECN	COMMENT
0.12 ± 0.02	-60 ± 12	GUTZ 14	DPWA	Multichannel
••• We do not use the following data for averages, fits, limits, etc. •••				
0.12 ± 0.03	-60 ± 15	ANISOVICH 12A	DPWA	Multichannel

Normalized residue in $N\pi \rightarrow \Delta(1700) \rightarrow \Sigma K$

MODULUS	PHASE (°)	DOCUMENT ID	TECN	COMMENT
••• We do not use the following data for averages, fits, limits, etc. •••				
0.011	-147	ROENCHEN 15A	DPWA	Multichannel

Normalized residue in $N\pi \rightarrow \Delta(1700) \rightarrow N(1535)\pi$

MODULUS	PHASE (°)	DOCUMENT ID	TECN	COMMENT
0.035 ± 0.015	-75 ± 30	GUTZ 14	DPWA	Multichannel

Normalized residue in $N\pi \rightarrow \Delta(1700) \rightarrow \Delta(1232)\pi, S\text{-wave}$

MODULUS	PHASE (°)	DOCUMENT ID	TECN	COMMENT
0.25 ± 0.12	135 ± 45	SOKHOYAN 15A	DPWA	Multichannel
••• We do not use the following data for averages, fits, limits, etc. •••				
0.39	151	ROENCHEN 15A	DPWA	Multichannel

Normalized residue in $N\pi \rightarrow \Delta(1700) \rightarrow \Delta(1232)\pi, D\text{-wave}$

MODULUS	PHASE (°)	DOCUMENT ID	TECN	COMMENT
0.12 ± 0.06	-160 ± 30	SOKHOYAN 15A	DPWA	Multichannel
••• We do not use the following data for averages, fits, limits, etc. •••				
0.054	166	ROENCHEN 15A	DPWA	Multichannel

Baryon Particle Listings

 $\Delta(1700)$ Normalized residue in $N\pi \rightarrow \Delta(1700) \rightarrow N(1520)\pi, P\text{-wave}$

MODULUS	PHASE (°)	DOCUMENT ID	TECN	COMMENT
0.10 ± 0.03	-10 ± 20	SOKHOYAN 15A	DPWA	Multichannel

 $\Delta(1700)$ BREIT-WIGNER MASS

VALUE (MeV)	DOCUMENT ID	TECN	COMMENT
1690 to 1730 (≈ 1710) OUR ESTIMATE			
1704 ± 8	GOLOVATCH 19	DPWA	$\gamma p \rightarrow \pi^+ \pi^- p$
1720 ± 5	¹ HUNT 19	DPWA	Multichannel
1715 ± 20	SOKHOYAN 15A	DPWA	Multichannel
1695.0 ± 1.3	¹ ARNDT 06	DPWA	$\pi N \rightarrow \pi N, \eta N$
1710 ± 30	CUTKOSKY 80	IPWA	$\pi N \rightarrow \pi N$
1680 ± 70	HOEHLER 79	IPWA	$\pi N \rightarrow \pi N$
• • • We do not use the following data for averages, fits, limits, etc. • • •			
1715 ± 20	GUTZ 14	DPWA	Multichannel
1715 +30 -15	ANISOVICH 12A	DPWA	Multichannel
1691 ± 4	¹ SHRESTHA 12A	DPWA	Multichannel
1678 ± 1	PENNER 02c	DPWA	Multichannel
1732 ± 23	VRANA 00	DPWA	Multichannel

¹ Statistical error only. $\Delta(1700)$ BREIT-WIGNER WIDTH

VALUE (MeV)	DOCUMENT ID	TECN	COMMENT
220 to 380 (≈ 300) OUR ESTIMATE			
295 ± 35	GOLOVATCH 19	DPWA	$\gamma p \rightarrow \pi^+ \pi^- p$
226 ± 14	¹ HUNT 19	DPWA	Multichannel
300 ± 25	SOKHOYAN 15A	DPWA	Multichannel
375.5 ± 7.0	¹ ARNDT 06	DPWA	$\pi N \rightarrow \pi N, \eta N$
280 ± 80	CUTKOSKY 80	IPWA	$\pi N \rightarrow \pi N$
230 ± 80	HOEHLER 79	IPWA	$\pi N \rightarrow \pi N$
• • • We do not use the following data for averages, fits, limits, etc. • • •			
300 ± 25	GUTZ 14	DPWA	Multichannel
310 +40 -15	ANISOVICH 12A	DPWA	Multichannel
248 ± 9	¹ SHRESTHA 12A	DPWA	Multichannel
606 ± 15	PENNER 02c	DPWA	Multichannel
119 ± 70	VRANA 00	DPWA	Multichannel

¹ Statistical error only. $\Delta(1700)$ DECAY MODES

The following branching fractions are our estimates, not fits or averages.

Mode	Fraction (Γ_i/Γ)
Γ_1 $N\pi$	10–20 %
Γ_2 $N\pi\pi$	10–55 %
Γ_3 $\Delta(1232)\pi$	10–50 %
Γ_4 $\Delta(1232)\pi, S\text{-wave}$	5–35 %
Γ_5 $\Delta(1232)\pi, D\text{-wave}$	4–16 %
Γ_6 $N\rho$	
Γ_7 $N\rho, S=3/2, S\text{-wave}$	seen
Γ_8 $N(1520)\pi, P\text{-wave}$	1–5 %
Γ_9 $N(1535)\pi$	0.5–1.5 %
Γ_{10} $\Delta(1232)\eta$	3–7 %
Γ_{11} $N\gamma$	0.22–0.60 %
Γ_{12} $N\gamma, \text{helicity}=1/2$	0.12–0.30 %
Γ_{13} $N\gamma, \text{helicity}=3/2$	0.10–0.30 %

 $\Delta(1700)$ BRANCHING RATIOS

$\Gamma(N\pi)/\Gamma_{\text{total}}$	DOCUMENT ID	TECN	COMMENT	Γ_1/Γ
10 to 20 OUR ESTIMATE				
15 ± 2	¹ HUNT 19	DPWA	Multichannel	
22 ± 4	SOKHOYAN 15A	DPWA	Multichannel	
15.6 ± 0.1	¹ ARNDT 06	DPWA	$\pi N \rightarrow \pi N, \eta N$	
12 ± 3	CUTKOSKY 80	IPWA	$\pi N \rightarrow \pi N$	
20 ± 3	HOEHLER 79	IPWA	$\pi N \rightarrow \pi N$	
• • • We do not use the following data for averages, fits, limits, etc. • • •				
22 ± 4	GUTZ 14	DPWA	Multichannel	
22 ± 4	ANISOVICH 12A	DPWA	Multichannel	
14 ± 1	¹ SHRESTHA 12A	DPWA	Multichannel	
14 ± 1	PENNER 02c	DPWA	Multichannel	
5 ± 1	VRANA 00	DPWA	Multichannel	

¹ Statistical error only.

$\Gamma(N\pi\pi)/\Gamma_{\text{total}}$	DOCUMENT ID	TECN	COMMENT	Γ_2/Γ
0.89 ± 0.11	GOLOVATCH 19	DPWA	$\gamma p \rightarrow \pi^+ \pi^- p$	

 $\Gamma(\Delta(1232)\pi, S\text{-wave})/\Gamma_{\text{total}}$

VALUE (%)	DOCUMENT ID	TECN	COMMENT	Γ_4/Γ
49 ± 5	¹ HUNT 19	DPWA	Multichannel	
20 ± 15	SOKHOYAN 15A	DPWA	Multichannel	
• • • We do not use the following data for averages, fits, limits, etc. • • •				
20 +25 -13	ANISOVICH 12A	DPWA	Multichannel	
54 ± 3	¹ SHRESTHA 12A	DPWA	Multichannel	
90 ± 2	VRANA 00	DPWA	Multichannel	

¹ Statistical error only. $\Gamma(\Delta(1232)\pi, D\text{-wave})/\Gamma_{\text{total}}$

VALUE (%)	DOCUMENT ID	TECN	COMMENT	Γ_5/Γ
7.6 ± 0.3	¹ HUNT 19	DPWA	Multichannel	
10 ± 6	SOKHOYAN 15A	DPWA	Multichannel	
• • • We do not use the following data for averages, fits, limits, etc. • • •				
12 +14 -7	ANISOVICH 12A	DPWA	Multichannel	
1 ± 1	¹ SHRESTHA 12A	DPWA	Multichannel	
4 ± 1	VRANA 00	DPWA	Multichannel	

¹ Statistical error only. $\Gamma(N\rho, S=3/2, S\text{-wave})/\Gamma_{\text{total}}$

VALUE (%)	DOCUMENT ID	TECN	COMMENT	Γ_7/Γ
27 ± 5	¹ HUNT 19	DPWA	Multichannel	
• • • We do not use the following data for averages, fits, limits, etc. • • •				
30 ± 3	¹ SHRESTHA 12A	DPWA	Multichannel	
1 ± 1	VRANA 00	DPWA	Multichannel	

¹ Statistical error only. $\Gamma(N(1520)\pi, P\text{-wave})/\Gamma_{\text{total}}$

VALUE (%)	DOCUMENT ID	TECN	COMMENT	Γ_8/Γ
3 ± 2	SOKHOYAN 15A	DPWA	Multichannel	

 $\Gamma(N(1535)\pi)/\Gamma_{\text{total}}$

VALUE (%)	DOCUMENT ID	TECN	COMMENT	Γ_9/Γ
1.0 ± 0.5	GUTZ 14	DPWA	Multichannel	
• • • We do not use the following data for averages, fits, limits, etc. • • •				
4 ± 2	HORN 08A	DPWA	Multichannel	

 $\Gamma(\Delta(1232)\eta)/\Gamma_{\text{total}}$

VALUE (%)	DOCUMENT ID	TECN	COMMENT	Γ_{10}/Γ
5 ± 2	GUTZ 14	DPWA	Multichannel	
• • • We do not use the following data for averages, fits, limits, etc. • • •				
5 ± 2	ANISOVICH 12A	DPWA	Multichannel	

 $\Gamma(N(1535)\pi)/\Gamma(\Delta(1232)\eta)$

VALUE	DOCUMENT ID	TECN	COMMENT	Γ_9/Γ_{10}
• • • We do not use the following data for averages, fits, limits, etc. • • •				
0.67	KASHEVAROV 09	CBAL	$\gamma p \rightarrow p \pi^0 \eta$	

 $\Delta(1700)$ PHOTON DECAY AMPLITUDES AT THE POLE $\Delta(1700) \rightarrow N\gamma, \text{helicity-1/2 amplitude } A_{1/2}$

MODULUS (GeV ^{-1/2})	PHASE (°)	DOCUMENT ID	TECN	COMMENT
0.175 ± 0.020	50 ± 10	SOKHOYAN 15A	DPWA	Multichannel
0.109 ± 0.010	-21 +12 -6	ROENCHEN 14	DPWA	
• • • We do not use the following data for averages, fits, limits, etc. • • •				
0.123	1.1	ROENCHEN 15A	DPWA	Multichannel

 $\Delta(1700) \rightarrow N\gamma, \text{helicity-3/2 amplitude } A_{3/2}$

MODULUS (GeV ^{-1/2})	PHASE (°)	DOCUMENT ID	TECN	COMMENT
0.180 ± 0.020	45 ± 10	SOKHOYAN 15A	DPWA	Multichannel
0.111 +0.027 -0.006	12 +9 -11	ROENCHEN 14	DPWA	
• • • We do not use the following data for averages, fits, limits, etc. • • •				
0.124	22	ROENCHEN 15A	DPWA	Multichannel

 $\Delta(1700)$ BREIT-WIGNER PHOTON DECAY AMPLITUDES $\Delta(1700) \rightarrow N\gamma, \text{helicity-1/2 amplitude } A_{1/2}$

VALUE (GeV ^{-1/2})	DOCUMENT ID	TECN	COMMENT
0.100 to 0.160 (≈ 0.130) OUR ESTIMATE			
0.0872 ± 0.0189	GOLOVATCH 19	DPWA	$\gamma p \rightarrow \pi^+ \pi^- p$
0.156 ± 0.017	¹ HUNT 19	DPWA	Multichannel
0.165 ± 0.020	SOKHOYAN 15A	DPWA	Multichannel
0.132 ± 0.005	¹ DUGGER 13	DPWA	$\gamma N \rightarrow \pi N$
0.105 ± 0.005	¹ WORKMAN 12A	DPWA	$\gamma N \rightarrow \pi N$

See key on page 999

Baryon Particle Listings

$\Delta(1700)$, $\Delta(1750)$, $\Delta(1900)$

••• We do not use the following data for averages, fits, limits, etc. •••

0.165 ± 0.020	GUTZ	14	DPWA	Multichannel
0.160 ± 0.020	ANISOVICH	12A	DPWA	Multichannel
0.058 ± 0.010	¹ SHRESTHA	12A	DPWA	Multichannel
0.226	DRECHSEL	07	DPWA	$\gamma N \rightarrow \pi N$
0.125 ± 0.003	DUGGER	07	DPWA	$\gamma N \rightarrow \pi N$
0.096	PENNER	02D	DPWA	Multichannel

¹ Statistical error only.

$\Delta(1700) \rightarrow N\gamma$, helicity-3/2 amplitude $A_{3/2}$

VALUE (GeV ^{-1/2})	DOCUMENT ID	TECN	COMMENT
0.090 to 0.170 (≈ 0.130) OUR ESTIMATE			
0.0872 ± 0.0164	GOLOVATCH	19	DPWA $\gamma p \rightarrow \pi^+ \pi^- p$
0.0125 ± 0.0016	¹ HUNT	19	DPWA Multichannel
0.170 ± 0.025	SOKHOYAN	15A	DPWA Multichannel
0.108 ± 0.005	¹ DUGGER	13	DPWA $\gamma N \rightarrow \pi N$
0.092 ± 0.004	¹ WORKMAN	12A	DPWA $\gamma N \rightarrow \pi N$
••• We do not use the following data for averages, fits, limits, etc. •••			
0.170 ± 0.025	GUTZ	14	DPWA Multichannel
0.165 ± 0.025	ANISOVICH	12A	DPWA Multichannel
0.097 ± 0.008	¹ SHRESTHA	12A	DPWA Multichannel
0.210	DRECHSEL	07	DPWA $\gamma N \rightarrow \pi N$
0.105 ± 0.003	DUGGER	07	DPWA $\gamma N \rightarrow \pi N$
0.154	PENNER	02D	DPWA Multichannel

¹ Statistical error only.

$\Delta(1700)$ REFERENCES

For early references, see Physics Letters **111B** 1 (1982).

GOLOVATCH	19	PL B788 371	E. Golovatch <i>et al.</i>	(CLAS Collab.)
HUNT	19	PR C9 055205	B. C. Hunt, D.M. Manley	
ROENCHEN	15A	EPJ A51 70	D. Roenchen <i>et al.</i>	
SOKHOYAN	15A	EPJ A51 95	V. Sokhoyan <i>et al.</i>	(CBELSA/TAPS Collab.)
GUTZ	14	EPJ A50 74	E. Gutz <i>et al.</i>	(CBELSA/TAPS Collab.)
PDG	14	CP C38 070001	K. Olive <i>et al.</i>	(PDG Collab.)
ROENCHEN	14	EPJ A50 101	D. Roenchen <i>et al.</i>	
Also		EPJ A51 63 (errata.)	D. Roenchen <i>et al.</i>	
SVARC	14	PR C89 045205	A. Svarc <i>et al.</i>	(RBI Zagreb, UNI Tuzla)
DUGGER	13	PR C80 065203	M. Dugger <i>et al.</i>	(JLab CLAS Collab.)
ANISOVICH	12A	EPJ A48 15	A.V. Anisovich <i>et al.</i>	(BONN, PNPI)
SHRESTHA	12A	PR C86 055203	M. Shrestha, D.M. Manley	(KSU)
WORKMAN	12A	PR C86 015202	R. Workman <i>et al.</i>	(GWU)
KASHEVAROV	09	EPJ A42 141	V.L. Kashevarov <i>et al.</i>	(MAMI Crystal Ball/TAPS)
HORN	08A	EPJ A38 173	I. Horn <i>et al.</i>	(CB-ELSA Collab.)
Also		PRL 101 202002	I. Horn <i>et al.</i>	(CB-ELSA Collab.)
DRECHSEL	07	EPJ A34 69	D. Drechsel, S.S. Kamalov, L. Tiator	(MAINZ, JINR)
DUGGER	07	PR C76 025211	M. Dugger <i>et al.</i>	(JLab CLAS Collab.)
ARNDT	06	PR C74 045205	R.A. Arndt <i>et al.</i>	(GWU)
PENNER	02C	PR C66 055211	G. Penner, U. Mosel	(GIES)
PENNER	02D	PR C66 055212	G. Penner, U. Mosel	(GIES)
VRANA	00	PRPL 328 181	T.P. Vrana, S.A. Dytman, T.-S.H. Lee	(PITT, ANL)
HOEHLER	93	πN Newsletter 9 1	G. Hoehler	(KARL)
CUTKOSKY	80	Toronto Conf. 19	R.E. Cutkosky <i>et al.</i>	(CMU, LBL) IJP
Also		PR D20 2839	R.E. Cutkosky <i>et al.</i>	(CMU, LBL) IJP
HOEHLER	79	PDAT 12-1	G. Hoehler <i>et al.</i>	(KARLT) IJP
Also		Toronto Conf. 3	R. Koch	(KARLT) IJP

$\Delta(1750) 1/2^+$

$$I(J^P) = \frac{3}{2}(\frac{1}{2}^+) \text{ Status: } *$$

OMITTED FROM SUMMARY TABLE

$\Delta(1750)$ POLE POSITION

REAL PART

VALUE (MeV)	DOCUMENT ID	TECN	COMMENT
••• We do not use the following data for averages, fits, limits, etc. •••			
1748	ARNDT	04	DPWA $\pi N \rightarrow \pi N, \eta N$
1714	VRANA	00	DPWA Multichannel

-2xIMAGINARY PART

VALUE (MeV)	DOCUMENT ID	TECN	COMMENT
••• We do not use the following data for averages, fits, limits, etc. •••			
524	ARNDT	04	DPWA $\pi N \rightarrow \pi N, \eta N$
68	VRANA	00	DPWA Multichannel

$\Delta(1750)$ ELASTIC POLE RESIDUE

MODULUS $|r|$

VALUE (MeV)	DOCUMENT ID	TECN	COMMENT
••• We do not use the following data for averages, fits, limits, etc. •••			
48	ARNDT	04	DPWA $\pi N \rightarrow \pi N, \eta N$

PHASE θ

VALUE (°)	DOCUMENT ID	TECN	COMMENT
••• We do not use the following data for averages, fits, limits, etc. •••			
158	ARNDT	04	DPWA $\pi N \rightarrow \pi N, \eta N$

$\Delta(1750)$ BREIT-WIGNER MASS

VALUE (MeV)	DOCUMENT ID	TECN	COMMENT
••• We do not use the following data for averages, fits, limits, etc. •••			
1712 ± 1	PENNER	02C	DPWA Multichannel
1721 ± 61	VRANA	00	DPWA Multichannel

$\Delta(1750)$ BREIT-WIGNER WIDTH

VALUE (MeV)	DOCUMENT ID	TECN	COMMENT
••• We do not use the following data for averages, fits, limits, etc. •••			
643 ± 17	PENNER	02C	DPWA Multichannel
70 ± 5.0	VRANA	00	DPWA Multichannel

$\Delta(1750)$ DECAY MODES

Mode	Fraction (Γ_i/Γ)
Γ_1 $N\pi$	seen
Γ_2 $N\pi\pi$	
Γ_3 $N(1440)\pi$	seen
Γ_4 ΣK	seen

$\Delta(1750)$ BRANCHING RATIOS

$\Gamma(N\pi)/\Gamma_{total}$	DOCUMENT ID	TECN	COMMENT	Γ_1/Γ
••• We do not use the following data for averages, fits, limits, etc. •••				
1 ± 1	PENNER	02C	DPWA Multichannel	
6 ± 9	VRANA	00	DPWA Multichannel	

$\Gamma(N(1440)\pi)/\Gamma_{total}$	DOCUMENT ID	TECN	COMMENT	Γ_3/Γ
••• We do not use the following data for averages, fits, limits, etc. •••				
83 ± 1	VRANA	00	DPWA Multichannel	

$\Gamma(\Sigma K)/\Gamma_{total}$	DOCUMENT ID	TECN	COMMENT	Γ_4/Γ
••• We do not use the following data for averages, fits, limits, etc. •••				
0.1 ± 0.1	PENNER	02C	DPWA Multichannel	

$\Delta(1750)$ BREIT-WIGNER PHOTON DECAY AMPLITUDES

Papers on γN amplitudes predating 1981 may be found in our 2006 edition, Journal of Physics **G33** 1 (2006).

$\Delta(1750) \rightarrow N\gamma$, helicity-1/2 amplitude $A_{1/2}$

VALUE (GeV ^{-1/2})	DOCUMENT ID	TECN	COMMENT
••• We do not use the following data for averages, fits, limits, etc. •••			
0.053	PENNER	02D	DPWA Multichannel

$\Delta(1750)$ REFERENCES

PDG	06	JP G33 1	W.-M. Yao <i>et al.</i>	(PDG Collab.)
ARNDT	04	PR C69 035213	R.A. Arndt <i>et al.</i>	(GWU, TRIU)
PENNER	02C	PR C66 055211	G. Penner, U. Mosel	(GIES)
PENNER	02D	PR C66 055212	G. Penner, U. Mosel	(GIES)
VRANA	00	PRPL 328 181	T.P. Vrana, S.A. Dytman, T.-S.H. Lee	(PITT, ANL)

$\Delta(1900) 1/2^-$

$$I(J^P) = \frac{3}{2}(\frac{1}{2}^-) \text{ Status: } ***$$

Older and obsolete values are listed and referenced in the 2014 edition, Chinese Physics **C38** 070001 (2014).

$\Delta(1900)$ POLE POSITION

REAL PART

VALUE (MeV)	DOCUMENT ID	TECN	COMMENT
1830 to 1900 (≈ 1865) OUR ESTIMATE			
1845 ± 20	SOKHOYAN	15A	DPWA Multichannel
1865 ± 35 ± 19	¹ SVARC	14	L+P $\pi N \rightarrow \pi N$
1870 ± 40	CUTKOSKY	80	IPWA $\pi N \rightarrow \pi N$
••• We do not use the following data for averages, fits, limits, etc. •••			
1957	HUNT	19	DPWA Multichannel
1845 ± 20	GUTZ	14	DPWA Multichannel
1845 ± 25	ANISOVICH	12A	DPWA Multichannel
1795	VRANA	00	DPWA Multichannel
1780	HOEHLER	93	SPED $\pi N \rightarrow \pi N$

¹ Fit to the amplitudes of HOEHLER 79.

Baryon Particle Listings

 $\Delta(1900)$ **-2xIMAGINARY PART**

VALUE (MeV)	DOCUMENT ID	TECN	COMMENT
180 to 300 (≈ 240) OUR ESTIMATE			
295 \pm 35	SOKHOYAN	15A DPWA	Multichannel
187 \pm 5.0 \pm 19	¹ SVARC	14 L+P	$\pi N \rightarrow \pi N$
180 \pm 5.0	CUTKOSKY	80 IPWA	$\pi N \rightarrow \pi N$
••• We do not use the following data for averages, fits, limits, etc. •••			
447	HUNT	19 DPWA	Multichannel
295 \pm 35	GUTZ	14 DPWA	Multichannel
300 \pm 45	ANISOVICH	12A DPWA	Multichannel
58	VRANA	00 DPWA	Multichannel

¹ Fit to the amplitudes of HOEHLER 79. **$\Delta(1900)$ ELASTIC POLE RESIDUE****MODULUS $|r|$**

VALUE (MeV)	DOCUMENT ID	TECN	COMMENT
8 to 14 (≈ 11) OUR ESTIMATE			
11 \pm 2	SOKHOYAN	15A DPWA	Multichannel
11 \pm 4 \pm 2	¹ SVARC	14 L+P	$\pi N \rightarrow \pi N$
10 \pm 3	CUTKOSKY	80 IPWA	$\pi N \rightarrow \pi N$
••• We do not use the following data for averages, fits, limits, etc. •••			
11 \pm 2	GUTZ	14 DPWA	Multichannel
10 \pm 3	ANISOVICH	12A DPWA	Multichannel

¹ Fit to the amplitudes of HOEHLER 79.**PHASE θ**

VALUE ($^\circ$)	DOCUMENT ID	TECN	COMMENT
-115 \pm 20	SOKHOYAN	15A DPWA	Multichannel
20 \pm 27 \pm 19	¹ SVARC	14 L+P	$\pi N \rightarrow \pi N$
+ 20 \pm 40	CUTKOSKY	80 IPWA	$\pi N \rightarrow \pi N$
••• We do not use the following data for averages, fits, limits, etc. •••			
-115 \pm 20	GUTZ	14 DPWA	Multichannel
-125 \pm 20	ANISOVICH	12A DPWA	Multichannel

¹ Fit to the amplitudes of HOEHLER 79. **$\Delta(1900)$ INELASTIC POLE RESIDUE**The "normalized residue" is the residue divided by $\Gamma_{pole}/2$.**Normalized residue in $N\pi \rightarrow \Delta(1900) \rightarrow \Sigma K$**

MODULUS	PHASE ($^\circ$)	DOCUMENT ID	TECN	COMMENT
0.07 \pm 0.02	-50 \pm 30	ANISOVICH	12A DPWA	Multichannel

Normalized residue in $N\pi \rightarrow \Delta(1900) \rightarrow \Delta\pi, D$ -wave

MODULUS	PHASE ($^\circ$)	DOCUMENT ID	TECN	COMMENT
0.18 \pm 0.10	105 \pm 25	SOKHOYAN	15A DPWA	Multichannel
••• We do not use the following data for averages, fits, limits, etc. •••				
0.12 $^{+0.08}_{-0.05}$	110 \pm 20	ANISOVICH	12A DPWA	Multichannel

Normalized residue in $N\pi \rightarrow \Delta(1900) \rightarrow \Delta(1232)\eta$

MODULUS	PHASE ($^\circ$)	DOCUMENT ID	TECN	COMMENT
0.013 \pm 0.006	undefined	GUTZ	14 DPWA	Multichannel

Normalized residue in $N\pi \rightarrow \Delta(1900) \rightarrow N(1440)\pi$

MODULUS	PHASE ($^\circ$)	DOCUMENT ID	TECN	COMMENT
0.11 \pm 0.06	115 \pm 30	SOKHOYAN	15A DPWA	Multichannel

Normalized residue in $N\pi \rightarrow \Delta(1900) \rightarrow N(1520)\pi$

MODULUS	PHASE ($^\circ$)	DOCUMENT ID	TECN	COMMENT
0.06 \pm 0.03	undefined	SOKHOYAN	15A DPWA	Multichannel

 $\Delta(1900)$ BREIT-WIGNER MASS

VALUE (MeV)	DOCUMENT ID	TECN	COMMENT
1840 to 1920 (≈ 1860) OUR ESTIMATE			
1989 \pm 22	¹ HUNT	19 DPWA	Multichannel
1840 \pm 20	SOKHOYAN	15A DPWA	Multichannel
1890 \pm 50	CUTKOSKY	80 IPWA	$\pi N \rightarrow \pi N$
1908 \pm 30	HOEHLER	79 IPWA	$\pi N \rightarrow \pi N$
••• We do not use the following data for averages, fits, limits, etc. •••			
1840 \pm 20	GUTZ	14 DPWA	Multichannel
1840 \pm 30	ANISOVICH	12A DPWA	Multichannel
1868 \pm 12	¹ SHRESTHA	12A DPWA	Multichannel
1802 \pm 87	VRANA	00 DPWA	Multichannel

¹ Statistical error only. **$\Delta(1900)$ BREIT-WIGNER WIDTH**

VALUE (MeV)	DOCUMENT ID	TECN	COMMENT
180 to 320 (≈ 250) OUR ESTIMATE			
457 \pm 60	¹ HUNT	19 DPWA	Multichannel
295 \pm 30	SOKHOYAN	15A DPWA	Multichannel
170 \pm 50	CUTKOSKY	80 IPWA	$\pi N \rightarrow \pi N$
140 \pm 40	HOEHLER	79 IPWA	$\pi N \rightarrow \pi N$

••• We do not use the following data for averages, fits, limits, etc. •••

295 \pm 30	GUTZ	14 DPWA	Multichannel
300 \pm 45	ANISOVICH	12A DPWA	Multichannel
234 \pm 27	¹ SHRESTHA	12A DPWA	Multichannel
48 \pm 45	VRANA	00 DPWA	Multichannel

¹ Statistical error only. **$\Delta(1900)$ DECAY MODES**

The following branching fractions are our estimates, not fits or averages.

Mode	Fraction (Γ_i/Γ)
Γ_1 $N\pi$	4-12 %
Γ_2 ΣK	seen
Γ_3 $N\pi\pi$	45-85 %
Γ_4 $\Delta(1232)\pi$	
Γ_5 $\Delta(1232)\pi, D$ -wave	30-70 %
Γ_6 $N\rho$	
Γ_7 $N\rho, S=1/2, S$ -wave	8-16 %
Γ_8 $N\rho, S=3/2, D$ -wave	18-28 %
Γ_9 $N(1440)\pi$	8-32 %
Γ_{10} $N(1520)\pi$	2-10 %
Γ_{11} $\Delta(1232)\eta$	0-2 %
Γ_{12} $N\gamma, \text{ helicity}=1/2$	0.06-0.43 %

 $\Delta(1900)$ BRANCHING RATIOS

$\Gamma(N\pi)/\Gamma_{total}$	DOCUMENT ID	TECN	COMMENT	Γ_1/Γ
4 to 12 (≈ 8) OUR ESTIMATE				
3.7 \pm 0.8	¹ HUNT	19 DPWA	Multichannel	
7 \pm 2	SOKHOYAN	15A DPWA	Multichannel	
10 \pm 3	CUTKOSKY	80 IPWA	$\pi N \rightarrow \pi N$	
8 \pm 4	HOEHLER	79 IPWA	$\pi N \rightarrow \pi N$	
••• We do not use the following data for averages, fits, limits, etc. •••				
7 \pm 2	GUTZ	14 DPWA	Multichannel	
7 \pm 3	ANISOVICH	12A DPWA	Multichannel	
8 \pm 1	¹ SHRESTHA	12A DPWA	Multichannel	
33 \pm 10	VRANA	00 DPWA	Multichannel	

¹ Statistical error only.

$\Gamma(\Delta(1232)\pi, D$ -wave)/ Γ_{total}	DOCUMENT ID	TECN	COMMENT	Γ_5/Γ
4 to 12 (≈ 8) OUR ESTIMATE				
42 \pm 8	¹ HUNT	19 DPWA	Multichannel	
50 \pm 20	SOKHOYAN	15A DPWA	Multichannel	
••• We do not use the following data for averages, fits, limits, etc. •••				
15 $^{+50}_{-10}$	ANISOVICH	12A DPWA	Multichannel	
56 \pm 6	¹ SHRESTHA	12A DPWA	Multichannel	
28 \pm 1	VRANA	00 DPWA	Multichannel	

¹ Statistical error only.

$\Gamma(N\rho, S=1/2, S$ -wave)/ Γ_{total}	DOCUMENT ID	TECN	COMMENT	Γ_7/Γ
4 to 12 (≈ 8) OUR ESTIMATE				
23 \pm 12	¹ HUNT	19 DPWA	Multichannel	
••• We do not use the following data for averages, fits, limits, etc. •••				
12 \pm 4	¹ SHRESTHA	12A DPWA	Multichannel	
30 \pm 2	VRANA	00 DPWA	Multichannel	

¹ Statistical error only.

$\Gamma(N\rho, S=3/2, D$ -wave)/ Γ_{total}	DOCUMENT ID	TECN	COMMENT	Γ_8/Γ
4 to 12 (≈ 8) OUR ESTIMATE				
18 \pm 7	¹ HUNT	19 DPWA	Multichannel	
••• We do not use the following data for averages, fits, limits, etc. •••				
23 \pm 5	¹ SHRESTHA	12A DPWA	Multichannel	
5 \pm 1	VRANA	00 DPWA	Multichannel	

¹ Statistical error only.

$\Gamma(N(1440)\pi)/\Gamma_{total}$	DOCUMENT ID	TECN	COMMENT	Γ_9/Γ
4 to 12 (≈ 8) OUR ESTIMATE				
12 \pm 9	¹ HUNT	19 DPWA	Multichannel	
20 \pm 12	SOKHOYAN	15A DPWA	Multichannel	
••• We do not use the following data for averages, fits, limits, etc. •••				
< 1	¹ SHRESTHA	12A DPWA	Multichannel	
4 \pm 1	VRANA	00 DPWA	Multichannel	

¹ Statistical error only.

$\Gamma(N(1520)\pi)/\Gamma_{total}$	DOCUMENT ID	TECN	COMMENT	Γ_{10}/Γ
4 to 12 (≈ 8) OUR ESTIMATE				
6 \pm 4	SOKHOYAN	15A DPWA	Multichannel	

See key on page 999

Baryon Particle Listings

$\Delta(1900)$, $\Delta(1905)$

$\Gamma(\Delta(1232)\eta)/\Gamma_{total}$	DOCUMENT ID	TECN	COMMENT	Γ_{11}/Γ
VALUE (%)				
1±1	GUTZ	14	DPWA	Multichannel

$\Delta(1900)$ PHOTON DECAY AMPLITUDES AT THE POLE

$\Delta(1900) \rightarrow N\gamma$, helicity-1/2 amplitude $A_{1/2}$

MODULUS (GeV ^{-1/2})	PHASE (°)	DOCUMENT ID	TECN	COMMENT
0.064±0.015	60 ± 20	SOKHOYAN	15A	DPWA Multichannel

$\Delta(1900)$ BREIT-WIGNER PHOTON DECAY AMPLITUDES

$\Delta(1900) \rightarrow N\gamma$, helicity-1/2 amplitude $A_{1/2}$

VALUE (GeV ^{-1/2})	DOCUMENT ID	TECN	COMMENT
0.212±0.029	¹ HUNT	19	DPWA Multichannel
0.065±0.015	SOKHOYAN	15A	DPWA Multichannel
0.057±0.014	GUTZ	14	DPWA Multichannel
-0.082±0.009	¹ SHRESTHA	12A	DPWA Multichannel

••• We do not use the following data for averages, fits, limits, etc. •••

¹ Statistical error only.

$\Delta(1900)$ REFERENCES

For early references, see Physics Letters **111B** 1 (1982).

HUNT	19	PR C99 055205	B. C. Hunt, D.M. Manley	
SOKHOYAN	15A	EPJ A51 95	V. Sokhoyan et al.	(CBELSA/TAPS Collab.)
GUTZ	14	EPJ A50 74	E. Gutz et al.	(CBELSA/TAPS Collab.)
PDG	14	CP C38 070001	K. Olive et al.	(PDG Collab.)
SVARC	14	PR C89 045205	A. Svarc et al.	(RBI Zagreb, UNI Tuzla)
ANISOVICH	12A	EPJ A48 15	A.V. Anisovich et al.	(BONN, PNPI)
SHRESTHA	12A	PR C86 055203	M. Shrestha, D.M. Manley	(KSU)
VRANA	00	PRPL 328 181	T.P. Vrana, S.A. Dytman, T.-S.H. Lee	(PITT, ANL)
HOEHLER	93	π N Newsletter 9 1	G. Hohlner	(KARL)
CUTKOSKY	80	Toronto Conf. 19	R.E. Cutkosky et al.	(CMU, LBL) IJP
		Also PR D20 2839	R.E. Cutkosky et al.	(CMU, LBL) IJP
HOEHLER	79	PDAT 12-1	G. Hohlner et al.	(KARLT) IJP
		Also Toronto Conf. 3	R. Koch	(KARLT) IJP

$\Delta(1905) 5/2^+$

 $I(J^P) = \frac{3}{2}(\frac{5}{2}^+)$ Status: * * * *

Older and obsolete values are listed and referenced in the 2014 edition, Chinese Physics **C38** 070001 (2014).

$\Delta(1905)$ POLE POSITION

REAL PART

VALUE (MeV)	DOCUMENT ID	TECN	COMMENT
1770 to 1830 (≈ 1800) OUR ESTIMATE			
1800 ± 6	SOKHOYAN	15A	DPWA Multichannel
1752 ± 3 ± 2	¹ SVARC	14	L+P $\pi N \rightarrow \pi N$
1830 ± 40	CUTKOSKY	80	IPWA $\pi N \rightarrow \pi N$
••• We do not use the following data for averages, fits, limits, etc. •••			
1819	HUNT	19	DPWA Multichannel
1795	ROENCHEN	15A	DPWA Multichannel
1800 ± 6	GUTZ	14	DPWA Multichannel
1805 ± 10	ANISOVICH	12A	DPWA Multichannel
1819	ARNDT	06	DPWA $\pi N \rightarrow \pi N, \eta N$
1793	VRANA	00	DPWA Multichannel
1829	HOEHLER	93	SPED $\pi N \rightarrow \pi N$

¹ Fit to the amplitudes of HOEHLER 79.

-2xIMAGINARY PART

VALUE (MeV)	DOCUMENT ID	TECN	COMMENT
260 to 340 (≈ 300) OUR ESTIMATE			
290±15	SOKHOYAN	15A	DPWA Multichannel
346 ± 6 ± 2	¹ SVARC	14	L+P $\pi N \rightarrow \pi N$
280±60	CUTKOSKY	80	IPWA $\pi N \rightarrow \pi N$
••• We do not use the following data for averages, fits, limits, etc. •••			
253	HUNT	19	DPWA Multichannel
247	ROENCHEN	15A	DPWA Multichannel
290±15	GUTZ	14	DPWA Multichannel
300±15	ANISOVICH	12A	DPWA Multichannel
247	ARNDT	06	DPWA $\pi N \rightarrow \pi N, \eta N$
302	VRANA	00	DPWA Multichannel
303	HOEHLER	93	SPED $\pi N \rightarrow \pi N$

¹ Fit to the amplitudes of HOEHLER 79.

$\Delta(1905)$ ELASTIC POLE RESIDUE

MODULUS |r|

VALUE (MeV)	DOCUMENT ID	TECN	COMMENT
15 to 25 (≈ 20) OUR ESTIMATE			
19 ± 2	SOKHOYAN	15A	DPWA Multichannel
24 ± 1 ± 1	¹ SVARC	14	L+P $\pi N \rightarrow \pi N$
25 ± 8	CUTKOSKY	80	IPWA $\pi N \rightarrow \pi N$

¹ Statistical error only.

••• We do not use the following data for averages, fits, limits, etc. •••

5.3	ROENCHEN	15A	DPWA Multichannel
19 ± 2	GUTZ	14	DPWA Multichannel
20 ± 2	ANISOVICH	12A	DPWA Multichannel
15	ARNDT	06	DPWA $\pi N \rightarrow \pi N, \eta N$
25	HOEHLER	93	SPED $\pi N \rightarrow \pi N$

¹ Fit to the amplitudes of HOEHLER 79.

PHASE θ

VALUE (°)	DOCUMENT ID	TECN	COMMENT
-120 to -30 (≈ -50) OUR ESTIMATE			
-45 ± 4	SOKHOYAN	15A	DPWA Multichannel
-114 ± 1 ± 2	¹ SVARC	14	L+P $\pi N \rightarrow \pi N$
-50 ± 20	CUTKOSKY	80	IPWA $\pi N \rightarrow \pi N$
••• We do not use the following data for averages, fits, limits, etc. •••			
-89	ROENCHEN	15A	DPWA Multichannel
-45 ± 4	GUTZ	14	DPWA Multichannel
-44 ± 5	ANISOVICH	12A	DPWA Multichannel
-30	ARNDT	06	DPWA $\pi N \rightarrow \pi N, \eta N$

¹ Fit to the amplitudes of HOEHLER 79.

$\Delta(1905)$ INELASTIC POLE RESIDUE

The "normalized residue" is the residue divided by $\Gamma_{pole}/2$.

Normalized residue in $N\pi \rightarrow \Delta(1905) \rightarrow \Delta\pi, P$ -wave

MODULUS	PHASE (°)	DOCUMENT ID	TECN	COMMENT
0.19 ± 0.07	10 ± 30	SOKHOYAN	15A	DPWA Multichannel
••• We do not use the following data for averages, fits, limits, etc. •••				
0.0870	72	ROENCHEN	15A	DPWA Multichannel
0.25 ± 0.06	0 ± 15	ANISOVICH	12A	DPWA Multichannel

Normalized residue in $N\pi \rightarrow \Delta(1905) \rightarrow \Delta\pi, F$ -wave

MODULUS	PHASE (°)	DOCUMENT ID	TECN	COMMENT
••• We do not use the following data for averages, fits, limits, etc. •••				
0.009	64	ROENCHEN	15A	DPWA Multichannel

Normalized residue in $N\pi \rightarrow \Delta(1905) \rightarrow \Sigma K$

MODULUS	PHASE (°)	DOCUMENT ID	TECN	COMMENT
••• We do not use the following data for averages, fits, limits, etc. •••				
0.001	-155	ROENCHEN	15A	DPWA Multichannel

Normalized residue in $N\pi \rightarrow \Delta(1905) \rightarrow N(1535)\pi$

MODULUS	PHASE (°)	DOCUMENT ID	TECN	COMMENT
0.025 ± 0.010	130 ± 35	GUTZ	14	DPWA Multichannel

Normalized residue in $N\pi \rightarrow \Delta(1905) \rightarrow \Delta(1232)\eta$

MODULUS	PHASE (°)	DOCUMENT ID	TECN	COMMENT
0.07 ± 0.02	40 ± 20	GUTZ	14	DPWA Multichannel

$\Delta(1905)$ BREIT-WIGNER MASS

VALUE (MeV)	DOCUMENT ID	TECN	COMMENT
1855 to 1910 (≈ 1880) OUR ESTIMATE			
1883 ± 19	GOLOVATCH	19	DPWA $\gamma p \rightarrow \pi^+ \pi^- p$
1866 ± 9	¹ HUNT	19	DPWA Multichannel
1856 ± 6	SOKHOYAN	15A	DPWA Multichannel
1857.8 ± 1.6	¹ ARNDT	06	DPWA $\pi N \rightarrow \pi N, \eta N$
1910 ± 30	CUTKOSKY	80	IPWA $\pi N \rightarrow \pi N$
1905 ± 20	HOEHLER	79	IPWA $\pi N \rightarrow \pi N$
••• We do not use the following data for averages, fits, limits, etc. •••			
1856 ± 6	GUTZ	14	DPWA Multichannel
1861 ± 6	ANISOVICH	12A	DPWA Multichannel
1818 ± 8	¹ SHRESTHA	12A	DPWA Multichannel
1873 ± 77	VRANA	00	DPWA Multichannel

¹ Statistical error only.

$\Delta(1905)$ BREIT-WIGNER WIDTH

VALUE (MeV)	DOCUMENT ID	TECN	COMMENT
270 to 400 (≈ 330) OUR ESTIMATE			
327 ± 69	GOLOVATCH	19	DPWA $\gamma p \rightarrow \pi^+ \pi^- p$
289 ± 20	¹ HUNT	19	DPWA Multichannel
325 ± 15	SOKHOYAN	15A	DPWA Multichannel
320.6 ± 8.6	¹ ARNDT	06	DPWA $\pi N \rightarrow \pi N, \eta N$
400 ± 100	CUTKOSKY	80	IPWA $\pi N \rightarrow \pi N$
260 ± 20	HOEHLER	79	IPWA $\pi N \rightarrow \pi N$
••• We do not use the following data for averages, fits, limits, etc. •••			
325 ± 15	GUTZ	14	DPWA Multichannel
335 ± 18	ANISOVICH	12A	DPWA Multichannel
278 ± 18	¹ SHRESTHA	12A	DPWA Multichannel
461 ± 111	VRANA	00	DPWA Multichannel

¹ Statistical error only.

Baryon Particle Listings

 $\Delta(1905)$, $\Delta(1910)$ $\Delta(1905)$ DECAY MODES

The following branching fractions are our estimates, not fits or averages.

Mode	Fraction (Γ_i/Γ)
Γ_1 $N\pi$	9–15 %
Γ_2 $N\pi\pi$	
Γ_3 $\Delta(1232)\pi$	80–100 %
Γ_4 $\Delta(1232)\pi$, P -wave	23–43 %
Γ_5 $\Delta(1232)\pi$, F -wave	56–72 %
Γ_6 $N\rho$	
Γ_7 $N\rho$, $S=3/2$, P -wave	seen
Γ_8 $N(1535)\pi$	< 1 %
Γ_9 $N(1680)\pi$, P -wave	5–15 %
Γ_{10} $\Delta(1232)\eta$	2–6 %
Γ_{11} $N\gamma$	0.012–0.036 %
Γ_{12} $N\gamma$, helicity=1/2	0.002–0.006 %
Γ_{13} $N\gamma$, helicity=3/2	0.01–0.03 %

 $\Delta(1905)$ BRANCHING RATIOS

$\Gamma(N\pi)/\Gamma_{\text{total}}$				Γ_1/Γ
VALUE (%)	DOCUMENT ID	TECN	COMMENT	
9 to 15 (≈ 12) OUR ESTIMATE				
17 \pm 1	¹ HUNT	19	DPWA Multichannel	
13 \pm 2	SOKHOYAN	15A	DPWA Multichannel	
12.2 \pm 0.1	¹ ARNDT	06	DPWA $\pi N \rightarrow \pi N$, ηN	
8 \pm 3	CUTKOSKY	80	IPWA $\pi N \rightarrow \pi N$	
15 \pm 2	HOEHLER	79	IPWA $\pi N \rightarrow \pi N$	
••• We do not use the following data for averages, fits, limits, etc. •••				
13 \pm 2	GUTZ	14	DPWA Multichannel	
13 \pm 2	ANISOVICH	12A	DPWA Multichannel	
6 \pm 1	¹ SHRESTHA	12A	DPWA Multichannel	
9 \pm 1	VRANA	00	DPWA Multichannel	
¹ Statistical error only.				

$\Gamma(N\pi\pi)/\Gamma_{\text{total}}$				Γ_2/Γ
VALUE	DOCUMENT ID	TECN	COMMENT	
0.85 \pm 0.15	GOLOVATCH	19	DPWA $\gamma p \rightarrow \pi^+ \pi^- p$	

$\Gamma(\Delta(1232)\pi, P\text{-wave})/\Gamma_{\text{total}}$				Γ_4/Γ
VALUE (%)	DOCUMENT ID	TECN	COMMENT	
8.4 \pm 0.5	¹ HUNT	19	DPWA Multichannel	
33 \pm 10	SOKHOYAN	15A	DPWA Multichannel	
••• We do not use the following data for averages, fits, limits, etc. •••				
45 \pm 14	ANISOVICH	12A	DPWA Multichannel	
28 \pm 7	¹ SHRESTHA	12A	DPWA Multichannel	
23 \pm 1	VRANA	00	DPWA Multichannel	
¹ Statistical error only.				

$\Gamma(\Delta(1232)\pi, F\text{-wave})/\Gamma_{\text{total}}$				Γ_5/Γ
VALUE (%)	DOCUMENT ID	TECN	COMMENT	
49 \pm 9	¹ HUNT	19	DPWA Multichannel	
••• We do not use the following data for averages, fits, limits, etc. •••				
64 \pm 8	¹ SHRESTHA	12A	DPWA Multichannel	
44 \pm 1	VRANA	00	DPWA Multichannel	
¹ Statistical error only.				

$\Gamma(N\rho, S=3/2, P\text{-wave})/\Gamma_{\text{total}}$				Γ_7/Γ
VALUE (%)	DOCUMENT ID	TECN	COMMENT	
26 \pm 9	¹ HUNT	19	DPWA Multichannel	
••• We do not use the following data for averages, fits, limits, etc. •••				
< 6	¹ SHRESTHA	12A	DPWA Multichannel	
24 \pm 1	VRANA	00	DPWA Multichannel	
¹ Statistical error only.				

$\Gamma(N(1535)\pi)/\Gamma_{\text{total}}$				Γ_8/Γ
VALUE (%)	DOCUMENT ID	TECN	COMMENT	
< 1	GUTZ	14	DPWA Multichannel	

$\Gamma(N(1680)\pi, P\text{-wave})/\Gamma_{\text{total}}$				Γ_9/Γ
VALUE (%)	DOCUMENT ID	TECN	COMMENT	
10 \pm 5	SOKHOYAN	15A	DPWA Multichannel	

$\Gamma(\Delta(1232)\eta)/\Gamma_{\text{total}}$				Γ_{10}/Γ
VALUE (%)	DOCUMENT ID	TECN	COMMENT	
4 \pm 2	GUTZ	14	DPWA Multichannel	

 $\Delta(1905)$ PHOTON DECAY AMPLITUDES AT THE POLE $\Delta(1905) \rightarrow N\gamma$, helicity-1/2 amplitude $A_{1/2}$

MODULUS ($\text{GeV}^{-1/2}$)	PHASE ($^\circ$)	DOCUMENT ID	TECN	COMMENT
0.025 \pm 0.005	-28 ± 12	SOKHOYAN	15A	DPWA Multichannel
0.013 $^{+0.013}_{-0.005}$	64^{+72}_{-36}	ROENCHEN	14	DPWA
••• We do not use the following data for averages, fits, limits, etc. •••				
0.053	89	ROENCHEN	15A	DPWA Multichannel

 $\Delta(1905) \rightarrow N\gamma$, helicity-3/2 amplitude $A_{3/2}$

MODULUS ($\text{GeV}^{-1/2}$)	PHASE ($^\circ$)	DOCUMENT ID	TECN	COMMENT
-0.050 ± 0.004	5 ± 10	SOKHOYAN	15A	DPWA Multichannel
0.072 \pm 0.016	113^{+13}_{-7}	ROENCHEN	14	DPWA
••• We do not use the following data for averages, fits, limits, etc. •••				
-0.030	80	ROENCHEN	15A	DPWA Multichannel

 $\Delta(1905)$ BREIT-WIGNER PHOTON DECAY AMPLITUDES $\Delta(1905) \rightarrow N\gamma$, helicity-1/2 amplitude $A_{1/2}$

VALUE ($\text{GeV}^{-1/2}$)	DOCUMENT ID	TECN	COMMENT
0.017 to 0.027 (≈ 0.022) OUR ESTIMATE			
0.019 \pm 0.0076	GOLOVATCH	19	DPWA $\gamma p \rightarrow \pi^+ \pi^- p$
0.077 \pm 0.010	¹ HUNT	19	DPWA Multichannel
0.025 \pm 0.005	SOKHOYAN	15A	DPWA Multichannel
0.020 \pm 0.002	¹ DUGGER	13	DPWA $\gamma N \rightarrow \pi N$
0.019 \pm 0.002	¹ WORKMAN	12A	DPWA $\gamma N \rightarrow \pi N$
••• We do not use the following data for averages, fits, limits, etc. •••			
0.025 \pm 0.005	GUTZ	14	DPWA Multichannel
0.025 \pm 0.004	ANISOVICH	12A	DPWA Multichannel
0.066 \pm 0.018	¹ SHRESTHA	12A	DPWA Multichannel
0.018	DRECHSEL	07	DPWA $\gamma N \rightarrow \pi N$
¹ Statistical error only.			

 $\Delta(1905) \rightarrow N\gamma$, helicity-3/2 amplitude $A_{3/2}$

VALUE ($\text{GeV}^{-1/2}$)	DOCUMENT ID	TECN	COMMENT
-0.055 to -0.035 (≈ -0.045) OUR ESTIMATE			
-0.0432 ± 0.0173	GOLOVATCH	19	DPWA $\gamma p \rightarrow \pi^+ \pi^- p$
-0.053 ± 0.029	¹ HUNT	19	DPWA Multichannel
-0.050 ± 0.005	SOKHOYAN	15A	DPWA Multichannel
-0.049 ± 0.005	¹ DUGGER	13	DPWA $\gamma N \rightarrow \pi N$
-0.038 ± 0.004	WORKMAN	12A	DPWA $\gamma N \rightarrow \pi N$
••• We do not use the following data for averages, fits, limits, etc. •••			
-0.050 ± 0.005	GUTZ	14	DPWA Multichannel
-0.049 ± 0.004	ANISOVICH	12A	DPWA Multichannel
-0.223 ± 0.029	¹ SHRESTHA	12A	DPWA Multichannel
-0.028	DRECHSEL	07	DPWA $\gamma N \rightarrow \pi N$
¹ Statistical error only.			

 $\Delta(1905)$ REFERENCES

For early references, see Physics Letters **111B** 1 (1982).

GOLOVATCH	19	PL B788 371	E. Golovatch <i>et al.</i>	(CLAS Collab.)
HUNT	19	PR C99 055205	B.C. Hunt, D.M. Manley	
ROENCHEN	15A	EPJ A51 70	D. Roenchen <i>et al.</i>	
SOKHOYAN	15A	EPJ A51 95	V. Sokhoyan <i>et al.</i>	(CBELSA/TAPS Collab.)
GUTZ	14	EPJ A50 74	E. Gutz <i>et al.</i>	(CBELSA/TAPS Collab.)
PDG	14	CP C38 070001	K. Olive <i>et al.</i>	(PDG Collab.)
ROENCHEN	14	EPJ A50 101	D. Roenchen <i>et al.</i>	
Also		EPJ A51 63 (errat.)	D. Roenchen <i>et al.</i>	
SVARC	14	PR C89 045205	A. Svarc <i>et al.</i>	(RBI Zagreb, UNI Tuzla)
DUGGER	13	PR C88 065203	M. Dugger <i>et al.</i>	(JLab CLAS Collab.)
ANISOVICH	12A	EPJ A48 15	A.V. Anisovich <i>et al.</i>	(BONN, PNPI)
SHRESTHA	12A	PR C86 055203	M. Shrestha, D.M. Manley	(KSU)
WORKMAN	12A	PR C86 015202	R. Workman <i>et al.</i>	(GWU)
DRECHSEL	07	EPJ A34 69	D. Drechsel, S.S. Kamalov, L. Tiator	(MAINZ, JINR)
ARNDT	06	PR C74 045205	R.A. Arndt <i>et al.</i>	(GWU)
VRANA	00	PRPL 328 181	T.P. Vrana, S.A. Dytmann, T.-S.H. Lee	(PITT, ANL)
HOEHLER	93	πN Newsletter 9 1	G. Hohlner	(KARL)
CUTKOSKY	80	Toronto Conf. 19	R.E. Cutkosky <i>et al.</i>	(CMU, LBL) IJP
Also		PR D20 2839	R.E. Cutkosky <i>et al.</i>	(CMU, LBL) IJP
HOEHLER	79	PDAT 12-1	G. Hohlner <i>et al.</i>	(KARLT) IJP
Also		Toronto Conf. 3	R. Koch	(KARLT) IJP

 $\Delta(1910) 1/2^+$

$$I(J^P) = \frac{3}{2}(\frac{1}{2}^+) \text{ Status: } ***$$

Older and obsolete values are listed and referenced in the 2014 edition, Chinese Physics **C38** 070001 (2014).

 $\Delta(1910)$ POLE POSITION

REAL PART				
VALUE (MeV)	DOCUMENT ID	TECN	COMMENT	
1830 to 1890 (≈ 1860) OUR ESTIMATE				
1840 \pm 40	SOKHOYAN	15A	DPWA Multichannel	
1896 \pm 11	¹ SVARC	14	L+P $\pi N \rightarrow \pi N$	
1880 \pm 30	CUTKOSKY	80	IPWA $\pi N \rightarrow \pi N$	

••• We do not use the following data for averages, fits, limits, etc. •••

1801	HUNT	19	DPWA	Multichannel
1799	ROENCHEN	15A	DPWA	Multichannel
1840 ± 40	GUTZ	14	DPWA	Multichannel
1850 ± 40	ANISOVICH	12A	DPWA	Multichannel
1771	ARNDT	06	DPWA	$\pi N \rightarrow \pi N, \eta N$
1880	VRANA	00	DPWA	Multichannel
1874	HOEHLER	93	SPED	$\pi N \rightarrow \pi N$

¹ Fit to the amplitudes of HOEHLER 79.

-2xIMAGINARY PART

VALUE (MeV)	DOCUMENT ID	TECN	COMMENT
-------------	-------------	------	---------

200 to 400 (≈ 300) OUR ESTIMATE

370 ± 60	SOKHOYAN	15A	DPWA	Multichannel
302 ± 22	¹ SVARC	14	L+P	$\pi N \rightarrow \pi N$
200 ± 40	CUTKOSKY	80	IPWA	$\pi N \rightarrow \pi N$

••• We do not use the following data for averages, fits, limits, etc. •••

224	HUNT	19	DPWA	Multichannel
648	ROENCHEN	15A	DPWA	Multichannel
370 ± 60	GUTZ	14	DPWA	Multichannel
350 ± 45	ANISOVICH	12A	DPWA	Multichannel
479	ARNDT	06	DPWA	$\pi N \rightarrow \pi N, \eta N$
496	VRANA	00	DPWA	Multichannel
283	HOEHLER	93	SPED	$\pi N \rightarrow \pi N$

¹ Fit to the amplitudes of HOEHLER 79.

$\Delta(1910)$ ELASTIC POLE RESIDUE

MODULUS |r|

VALUE (MeV)	DOCUMENT ID	TECN	COMMENT
-------------	-------------	------	---------

20 to 30 (≈ 25) OUR ESTIMATE

25 ± 6	SOKHOYAN	15A	DPWA	Multichannel
29 ± 2	¹ SVARC	14	L+P	$\pi N \rightarrow \pi N$
20 ± 4	CUTKOSKY	80	IPWA	$\pi N \rightarrow \pi N$

••• We do not use the following data for averages, fits, limits, etc. •••

90	ROENCHEN	15A	DPWA	Multichannel
25 ± 6	GUTZ	14	DPWA	Multichannel
24 ± 6	ANISOVICH	12A	DPWA	Multichannel
45	ARNDT	06	DPWA	$\pi N \rightarrow \pi N, \eta N$
38	HOEHLER	93	SPED	$\pi N \rightarrow \pi N$

¹ Fit to the amplitudes of HOEHLER 79.

PHASE θ

VALUE (°)	DOCUMENT ID	TECN	COMMENT
-----------	-------------	------	---------

-180 to -80 (≈ -130) OUR ESTIMATE

-155 ± 30	SOKHOYAN	15A	DPWA	Multichannel
- 83 ± 4 ± 1	¹ SVARC	14	L+P	$\pi N \rightarrow \pi N$
- 90 ± 30	CUTKOSKY	80	IPWA	$\pi N \rightarrow \pi N$
- 83	ROENCHEN	15A	DPWA	Multichannel
-155 ± 30	GUTZ	14	DPWA	Multichannel
-145 ± 30	ANISOVICH	12A	DPWA	Multichannel
+172	ARNDT	06	DPWA	$\pi N \rightarrow \pi N, \eta N$

¹ Fit to the amplitudes of HOEHLER 79.

$\Delta(1910)$ INELASTIC POLE RESIDUE

The "normalized residue" is the residue divided by $\Gamma_{pole}/2$.

Normalized residue in $N\pi \rightarrow \Delta(1910) \rightarrow \Sigma K$

MODULUS	PHASE (°)	DOCUMENT ID	TECN	COMMENT
---------	-----------	-------------	------	---------

0.07 ± 0.02	-110 ± 30	ANISOVICH	12A	DPWA Multichannel
-------------	-----------	-----------	-----	-------------------

••• We do not use the following data for averages, fits, limits, etc. •••

0.019	-123	ROENCHEN	15A	DPWA Multichannel
-------	------	----------	-----	-------------------

Normalized residue in $N\pi \rightarrow \Delta(1910) \rightarrow \Delta\pi, P$ -wave

MODULUS	PHASE (°)	DOCUMENT ID	TECN	COMMENT
---------	-----------	-------------	------	---------

0.24 ± 0.10	85 ± 35	SOKHOYAN	15A	DPWA Multichannel
-------------	---------	----------	-----	-------------------

••• We do not use the following data for averages, fits, limits, etc. •••

0.58	131	ROENCHEN	15A	DPWA Multichannel
0.16 ± 0.09	95 ± 40	ANISOVICH	12A	DPWA Multichannel

Normalized residue in $N\pi \rightarrow \Delta(1910) \rightarrow \Delta(1232)\eta$

MODULUS	PHASE (°)	DOCUMENT ID	TECN	COMMENT
---------	-----------	-------------	------	---------

0.11 ± 0.04	-150 ± 50	GUTZ	14	DPWA Multichannel
-------------	-----------	------	----	-------------------

Normalized residue in $N\pi \rightarrow \Delta(1910) \rightarrow N(1440)\pi$

MODULUS	PHASE (°)	DOCUMENT ID	TECN	COMMENT
---------	-----------	-------------	------	---------

0.06 ± 0.03	170 ± 45	SOKHOYAN	15A	DPWA Multichannel
-------------	----------	----------	-----	-------------------

$\Delta(1910)$ BREIT-WIGNER MASS

VALUE (MeV)	DOCUMENT ID	TECN	COMMENT
-------------	-------------	------	---------

1850 to 1950 (≈ 1900) OUR ESTIMATE

1846 ± 18	¹ HUNT	19	DPWA	Multichannel
1845 ± 40	SOKHOYAN	15A	DPWA	Multichannel
2067.9 ± 1.7	¹ ARNDT	06	DPWA	$\pi N \rightarrow \pi N, \eta N$
1910 ± 40	CUTKOSKY	80	IPWA	$\pi N \rightarrow \pi N$
1888 ± 20	HOEHLER	79	IPWA	$\pi N \rightarrow \pi N$

••• We do not use the following data for averages, fits, limits, etc. •••

1845 ± 40	GUTZ	14	DPWA	Multichannel
1860 ± 40	ANISOVICH	12A	DPWA	Multichannel
1934 ± 5	¹ SHRESTHA	12A	DPWA	Multichannel
1995 ± 12	VRANA	00	DPWA	Multichannel

¹ Statistical error only.

$\Delta(1910)$ BREIT-WIGNER WIDTH

VALUE (MeV)	DOCUMENT ID	TECN	COMMENT
-------------	-------------	------	---------

200 to 400 (≈ 300) OUR ESTIMATE

260 ± 57	¹ HUNT	19	DPWA	Multichannel
360 ± 60	SOKHOYAN	15A	DPWA	Multichannel
543 ± 10	¹ ARNDT	06	DPWA	$\pi N \rightarrow \pi N, \eta N$
225 ± 50	CUTKOSKY	80	IPWA	$\pi N \rightarrow \pi N$
280 ± 50	HOEHLER	79	IPWA	$\pi N \rightarrow \pi N$

••• We do not use the following data for averages, fits, limits, etc. •••

360 ± 60	GUTZ	14	DPWA	Multichannel
350 ± 55	ANISOVICH	12A	DPWA	Multichannel
211 ± 11	¹ SHRESTHA	12A	DPWA	Multichannel
713 ± 465	VRANA	00	DPWA	Multichannel

¹ Statistical error only.

$\Delta(1910)$ DECAY MODES

The following branching fractions are our estimates, not fits or averages.

Mode	Fraction (Γ_i/Γ)
Γ_1 $N\pi$	15-30 %
Γ_2 ΣK	4-14 %
Γ_3 $N\pi\pi$	
Γ_4 $\Delta(1232)\pi$	34-66 %
Γ_5 $N(1440)\pi$	3-9 %
Γ_6 $\Delta(1232)\eta$	5-13 %
Γ_7 $N\gamma$, helicity=1/2	0.0-0.02 %

$\Delta(1910)$ BRANCHING RATIOS

$\Gamma(N\pi)/\Gamma_{total}$	DOCUMENT ID	TECN	COMMENT	Γ_1/Γ
-------------------------------	-------------	------	---------	-------------------

15 to 30 (≈ 20) OUR ESTIMATE

13 ± 3	¹ HUNT	19	DPWA	Multichannel
12 ± 3	SOKHOYAN	15A	DPWA	Multichannel
23.9 ± 0.1	¹ ARNDT	06	DPWA	$\pi N \rightarrow \pi N, \eta N$
19 ± 3	CUTKOSKY	80	IPWA	$\pi N \rightarrow \pi N$
24 ± 6	HOEHLER	79	IPWA	$\pi N \rightarrow \pi N$

••• We do not use the following data for averages, fits, limits, etc. •••

12 ± 3	GUTZ	14	DPWA	Multichannel
12 ± 3	ANISOVICH	12A	DPWA	Multichannel
17 ± 1	¹ SHRESTHA	12A	DPWA	Multichannel
29 ± 21	VRANA	00	DPWA	Multichannel

¹ Statistical error only.

$\Gamma(\Sigma K)/\Gamma_{total}$	DOCUMENT ID	TECN	COMMENT	Γ_2/Γ
-----------------------------------	-------------	------	---------	-------------------

9 ± 5	ANISOVICH	12A	DPWA	Multichannel
-------	-----------	-----	------	--------------

$\Gamma(\Delta(1232)\pi)/\Gamma_{total}$	DOCUMENT ID	TECN	COMMENT	Γ_4/Γ
--	-------------	------	---------	-------------------

50 ± 16	SOKHOYAN	15A	DPWA	Multichannel
---------	----------	-----	------	--------------

••• We do not use the following data for averages, fits, limits, etc. •••

60 ± 28	ANISOVICH	12A	DPWA	Multichannel
---------	-----------	-----	------	--------------

$\Gamma(N(1440)\pi)/\Gamma_{total}$	DOCUMENT ID	TECN	COMMENT	Γ_5/Γ
-------------------------------------	-------------	------	---------	-------------------

33 ± 12	¹ HUNT	19	DPWA	Multichannel
6 ± 3	SOKHOYAN	15A	DPWA	Multichannel

••• We do not use the following data for averages, fits, limits, etc. •••

47 ± 6	¹ SHRESTHA	12A	DPWA	Multichannel
56 ± 7	VRANA	00	DPWA	Multichannel

¹ Statistical error only.

Baryon Particle Listings

$\Delta(1910)$, $\Delta(1920)$

$\Gamma(\Delta(1232)\eta)/\Gamma_{\text{total}}$	DOCUMENT ID	TECN	COMMENT
VALUE (%)			
9±4	GUTZ	14	DPWA Multichannel

Γ_6/Γ

$\Delta(1910)$ PHOTON DECAY AMPLITUDES AT THE POLE

$\Delta(1910) \rightarrow N\gamma$, helicity-1/2 amplitude $A_{1/2}$

MODULUS (GeV ^{-1/2})	PHASE (°)	DOCUMENT ID	TECN	COMMENT
0.027±0.009	-30±60	SOKHOYAN	15A	DPWA Multichannel
-0.246 ^{+0.024} _{-0.047}	159 ⁺⁹ ₋₄	ROENCHEN	14	DPWA
0.321	39	ROENCHEN	15A	DPWA Multichannel

••• We do not use the following data for averages, fits, limits, etc. •••

$\Delta(1910)$ BREIT-WIGNER PHOTON DECAY AMPLITUDES

$\Delta(1910) \rightarrow N\gamma$, helicity-1/2 amplitude $A_{1/2}$

VALUE (GeV ^{-1/2})	DOCUMENT ID	TECN	COMMENT
0.010 to 0.030 (≈ 0.020) OUR ESTIMATE			
0.203±0.056	¹ HUNT	19	DPWA Multichannel
0.026±0.008	SOKHOYAN	15A	DPWA Multichannel
-0.002±0.008	¹ ARNDT	96	IPWA $\gamma N \rightarrow \pi N$
0.026±0.008	GUTZ	14	DPWA Multichannel
0.022±0.009	ANISOVICH	12A	DPWA Multichannel
0.030±0.002	¹ SHRESTHA	12A	DPWA Multichannel

¹ Statistical error only.

$\Delta(1910)$ REFERENCES

For early references, see Physics Letters **111B** 1 (1982).

HUNT	19	PR C99 055205	B. C. Hunt, D.M. Manley
ROENCHEN	15A	EPJ A51 70	D. Roenchen et al.
SOKHOYAN	15A	EPJ A51 95	V. Sokhoyan et al. (CBELSA/TAPS Collab.)
GUTZ	14	EPJ A50 74	E. Gutz et al. (CBELSA/TAPS Collab.)
PDG	14	CP C38 070001	K. Olive et al. (PDG Collab.)
ROENCHEN	14	EPJ A50 101	D. Roenchen et al.
Also		EPJ A51 63 (errat.)	D. Roenchen et al.
SVARC	14	PR C89 045205	A. Svarc et al. (RBI Zagreb, UNI Tuzla)
ANISOVICH	12A	EPJ A48 15	A.V. Anisovich et al. (BONN, PNPI)
SHRESTHA	12A	PR C86 055203	M. Shrestha, D.M. Manley (KSU)
ARNDT	06	PR C74 045205	R.A. Arndt et al. (GWU)
VRANA	00	PRPL 328 181	T.P. Vrana, S.A. Dytman, T.-S.H. Lee (PITT, ANL)
ARNDT	96	PR C53 430	R.A. Arndt, I.I. Strakovsky, R.L. Workman (VPI)
HOEHLER	93	πN Newsletter 9 1	G. Hoehler (KARL)
CUTKOSKY	80	Toronto Conf. 19	R.E. Cutkosky et al. (CMU, LBL) IJP
Also		PR D20 2839	R.E. Cutkosky et al. (CMU, LBL) IJP
HOEHLER	79	PDAT 12-1	G. Hoehler et al. (KARL) IJP
Also		Toronto Conf. 3	R. Koch (KARL) IJP

$\Delta(1920)$ 3/2⁺

$$J(P) = \frac{3}{2}(\frac{3}{2}^+) \text{ Status: } ***$$

Older and obsolete values are listed and referenced in the 2014 edition, Chinese Physics **C38** 070001 (2014).

$\Delta(1920)$ POLE POSITION

REAL PART

VALUE (MeV)	DOCUMENT ID	TECN	COMMENT
1850 to 1950 (≈ 1900) OUR ESTIMATE			
1875±30	SOKHOYAN	15A	DPWA Multichannel
1906±10±2	¹ SVARC	14	L+P $\pi N \rightarrow \pi N$
1900±80	CUTKOSKY	80	IPWA $\pi N \rightarrow \pi N$
1910	HUNT	19	DPWA Multichannel
1715	ROENCHEN	15A	DPWA Multichannel
1875±30	GUTZ	14	DPWA Multichannel
1890±30	ANISOVICH	12A	DPWA Multichannel
1880	VRANA	00	DPWA Multichannel
1900	HOEHLER	93	SPED $\pi N \rightarrow \pi N$

¹ Fit to the amplitudes of HOEHLER 79.

-2xIMAGINARY PART

VALUE (MeV)	DOCUMENT ID	TECN	COMMENT
200 to 400 (≈ 300) OUR ESTIMATE			
300±40	SOKHOYAN	15A	DPWA Multichannel
310±20±11	¹ SVARC	14	L+P $\pi N \rightarrow \pi N$
300±100	CUTKOSKY	80	IPWA $\pi N \rightarrow \pi N$
472	HUNT	19	DPWA Multichannel
882	ROENCHEN	15A	DPWA Multichannel
300±40	GUTZ	14	DPWA Multichannel
300±60	ANISOVICH	12A	DPWA Multichannel
120	VRANA	00	DPWA Multichannel

¹ Fit to the amplitudes of HOEHLER 79.

$\Delta(1920)$ ELASTIC POLE RESIDUE

MODULUS $|r|$

VALUE (MeV)	DOCUMENT ID	TECN	COMMENT
8 to 24 (≈ 16) OUR ESTIMATE			
16±6	SOKHOYAN	15A	DPWA Multichannel
26±3±2	¹ SVARC	14	L+P $\pi N \rightarrow \pi N$
24±4	CUTKOSKY	80	IPWA $\pi N \rightarrow \pi N$
38	ROENCHEN	15A	DPWA Multichannel
16±6	GUTZ	14	DPWA Multichannel
17±8	ANISOVICH	12A	DPWA Multichannel

••• We do not use the following data for averages, fits, limits, etc. •••

¹ Fit to the amplitudes of HOEHLER 79.

PHASE θ

VALUE (°)	DOCUMENT ID	TECN	COMMENT
-150 to -50 (≈ -100) OUR ESTIMATE			
-50±25	SOKHOYAN	15A	DPWA Multichannel
-130±5±3	¹ SVARC	14	L+P $\pi N \rightarrow \pi N$
-150±30	CUTKOSKY	80	IPWA $\pi N \rightarrow \pi N$
146	ROENCHEN	15A	DPWA Multichannel
-50±25	GUTZ	14	DPWA Multichannel
-40±20	ANISOVICH	12A	DPWA Multichannel

••• We do not use the following data for averages, fits, limits, etc. •••

¹ Fit to the amplitudes of HOEHLER 79.

$\Delta(1920)$ INELASTIC POLE RESIDUE

The "normalized residue" is the residue divided by $\Gamma_{\text{pole}}/2$.

Normalized residue in $N\pi \rightarrow \Delta(1920) \rightarrow \Delta\eta$

MODULUS	PHASE (°)	DOCUMENT ID	TECN	COMMENT
0.15±0.04	70±20	GUTZ	14	DPWA Multichannel
0.17±0.08	70±20	ANISOVICH	12A	DPWA Multichannel

••• We do not use the following data for averages, fits, limits, etc. •••

Normalized residue in $N\pi \rightarrow \Delta(1920) \rightarrow \Sigma K$

MODULUS	PHASE (°)	DOCUMENT ID	TECN	COMMENT
0.09±0.03	80±40	ANISOVICH	12A	DPWA Multichannel
0.17	-35	ROENCHEN	15A	DPWA Multichannel

••• We do not use the following data for averages, fits, limits, etc. •••

Normalized residue in $N\pi \rightarrow \Delta(1920) \rightarrow \Delta\pi, P\text{-wave}$

MODULUS	PHASE (°)	DOCUMENT ID	TECN	COMMENT
0.20±0.08	-105±25	SOKHOYAN	15A	DPWA Multichannel
0.069	131	ROENCHEN	15A	DPWA Multichannel
0.20±0.12	-120±30	ANISOVICH	12A	DPWA Multichannel

••• We do not use the following data for averages, fits, limits, etc. •••

Normalized residue in $N\pi \rightarrow \Delta(1920) \rightarrow \Delta\pi, F\text{-wave}$

MODULUS	PHASE (°)	DOCUMENT ID	TECN	COMMENT
0.37±0.10	-90±20	SOKHOYAN	15A	DPWA Multichannel
0.013	-115	ROENCHEN	15A	DPWA Multichannel
0.28±0.07	-95±35	ANISOVICH	12A	DPWA Multichannel

••• We do not use the following data for averages, fits, limits, etc. •••

Normalized residue in $N\pi \rightarrow \Delta(1920) \rightarrow N(1535)\pi$

MODULUS	PHASE (°)	DOCUMENT ID	TECN	COMMENT
0.03±0.02	35±45	GUTZ	14	DPWA Multichannel

Normalized residue in $N\pi \rightarrow \Delta(1920) \rightarrow N\eta_0(980)$

MODULUS	PHASE (°)	DOCUMENT ID	TECN	COMMENT
0.03±0.02	-85±45	GUTZ	14	DPWA Multichannel

Normalized residue in $N\pi \rightarrow \Delta(1920) \rightarrow N(1440)\pi$

MODULUS	PHASE (°)	DOCUMENT ID	TECN	COMMENT
0.04±0.03	undefined	SOKHOYAN	15A	DPWA Multichannel

Normalized residue in $N\pi \rightarrow \Delta(1920) \rightarrow N(1520)\pi, S\text{-wave}$

MODULUS	PHASE (°)	DOCUMENT ID	TECN	COMMENT
0.05±0.05	undefined	SOKHOYAN	15A	DPWA Multichannel

$\Delta(1920)$ BREIT-WIGNER MASS

VALUE (MeV)	DOCUMENT ID	TECN	COMMENT
1870 to 1970 (≈ 1920) OUR ESTIMATE			
1976±49	HUNT	19	DPWA Multichannel
1880±30	SOKHOYAN	15A	DPWA Multichannel
2146±32	¹ SHRESTHA	12A	DPWA Multichannel
1920±80	CUTKOSKY	80	IPWA $\pi N \rightarrow \pi N$
1868±10	HOEHLER	79	IPWA $\pi N \rightarrow \pi N$

See key on page 999

Baryon Particle Listings

$\Delta(1920)$

••• We do not use the following data for averages, fits, limits, etc. •••

1880 ± 30	GUTZ	14	DPWA	Multichannel
1900 ± 30	ANISOVICH	12A	DPWA	Multichannel
2057 ± 1	PENNER	02c	DPWA	Multichannel
1889 ± 100	VRANA	00	DPWA	Multichannel

¹ Statistical error only.

$\Delta(1920)$ BREIT-WIGNER WIDTH

VALUE (MeV)	DOCUMENT ID	TECN	COMMENT
240 to 360 (≈ 300) OUR ESTIMATE			
509 ± 170	HUNT	19	DPWA Multichannel
300 ± 40	SOKHOYAN	15A	DPWA Multichannel
400 ± 80	¹ SHRESTHA	12A	DPWA Multichannel
300 ± 100	CUTKOSKY	80	IPWA $\pi N \rightarrow \pi N$
220 ± 80	HOEHLER	79	IPWA $\pi N \rightarrow \pi N$
••• We do not use the following data for averages, fits, limits, etc. •••			
300 ± 40	GUTZ	14	DPWA Multichannel
310 ± 60	ANISOVICH	12A	DPWA Multichannel
525 ± 32	PENNER	02c	DPWA Multichannel
123 ± 53	VRANA	00	DPWA Multichannel

¹ Statistical error only.

$\Delta(1920)$ DECAY MODES

The following branching fractions are our estimates, not fits or averages.

Mode	Fraction (Γ_j/Γ)
Γ_1 $N\pi$	5–20 %
Γ_2 ΣK	2–6 %
Γ_3 $N\pi\pi$	
Γ_4 $\Delta(1232)\pi$	50–90 %
Γ_5 $\Delta(1232)\pi$, P -wave	8–28 %
Γ_6 $\Delta(1232)\pi$, F -wave	44–72 %
Γ_7 $N(1440)\pi$, P -wave	< 4 %
Γ_8 $N(1520)\pi$, S -wave	< 5 %
Γ_9 $N(1535)\pi$	< 2 %
Γ_{10} $N_{a_0}(980)$	seen
Γ_{11} $\Delta(1232)\eta$	5–17 %

$\Delta(1920)$ BRANCHING RATIOS

$\Gamma(N\pi)/\Gamma_{total}$	DOCUMENT ID	TECN	COMMENT	Γ_1/Γ
5 to 20 (≈ 12) OUR ESTIMATE				
10.5 ± 3.0	¹ HUNT	19	DPWA Multichannel	
8 ± 4	SOKHOYAN	15A	DPWA Multichannel	
20 ± 5	CUTKOSKY	80	IPWA $\pi N \rightarrow \pi N$	
14 ± 4	HOEHLER	79	IPWA $\pi N \rightarrow \pi N$	
••• We do not use the following data for averages, fits, limits, etc. •••				
8 ± 4	GUTZ	14	DPWA Multichannel	
8 ± 4	ANISOVICH	12A	DPWA Multichannel	
16 ± 4	¹ SHRESTHA	12A	DPWA Multichannel	
15 ± 1	PENNER	02c	DPWA Multichannel	
5 ± 4	VRANA	00	DPWA Multichannel	

¹ Statistical error only.

$\Gamma(\Sigma K)/\Gamma_{total}$	DOCUMENT ID	TECN	COMMENT	Γ_2/Γ
4 ± 2	ANISOVICH	12A	DPWA Multichannel	
••• We do not use the following data for averages, fits, limits, etc. •••				
2.1 ± 0.3	PENNER	02c	DPWA Multichannel	

$\Gamma(\Delta(1232)\pi, P\text{-wave})/\Gamma_{total}$	DOCUMENT ID	TECN	COMMENT	Γ_5/Γ
VALUE (%)				
< 1.6	¹ HUNT	19	DPWA Multichannel	
18 ± 10	SOKHOYAN	15A	DPWA Multichannel	
••• We do not use the following data for averages, fits, limits, etc. •••				
22 ± 12	ANISOVICH	12A	DPWA Multichannel	
7 ± 5	¹ SHRESTHA	12A	DPWA Multichannel	
41 ± 3	VRANA	00	DPWA Multichannel	

¹ Statistical error only.

$\Gamma(\Delta(1232)\pi, F\text{-wave})/\Gamma_{total}$	DOCUMENT ID	TECN	COMMENT	Γ_6/Γ
VALUE (%)				
58 ± 14	SOKHOYAN	15A	DPWA Multichannel	
••• We do not use the following data for averages, fits, limits, etc. •••				
45 ± 20	ANISOVICH	12A	DPWA Multichannel	

$\Gamma(N(1440)\pi, P\text{-wave})/\Gamma_{total}$	DOCUMENT ID	TECN	COMMENT	Γ_7/Γ
VALUE (%)				
77 ± 9	¹ HUNT	19	DPWA Multichannel	
< 4	SOKHOYAN	15A	DPWA Multichannel	
••• We do not use the following data for averages, fits, limits, etc. •••				
< 20	¹ SHRESTHA	12A	DPWA Multichannel	
53 ± 8	VRANA	00	DPWA Multichannel	

¹ Statistical error only.

$\Gamma(N(1520)\pi, S\text{-wave})/\Gamma_{total}$	DOCUMENT ID	TECN	COMMENT	Γ_8/Γ
VALUE (%)				
< 5	SOKHOYAN	15A	DPWA Multichannel	

$\Gamma(N(1535)\pi)/\Gamma_{total}$	DOCUMENT ID	TECN	COMMENT	Γ_9/Γ
VALUE (%)				
< 2	GUTZ	14	DPWA Multichannel	

$\Gamma(N_{a_0}(980))/\Gamma_{total}$	DOCUMENT ID	TECN	COMMENT	Γ_{10}/Γ
VALUE (%)				
••• We do not use the following data for averages, fits, limits, etc. •••				
4 ± 2	HORN	08A	DPWA Multichannel	

$\Gamma(\Delta(1232)\eta)/\Gamma_{total}$	DOCUMENT ID	TECN	COMMENT	Γ_{11}/Γ
VALUE (%)				
11 ± 6	GUTZ	14	DPWA Multichannel	
••• We do not use the following data for averages, fits, limits, etc. •••				
15 ± 8	ANISOVICH	12A	DPWA Multichannel	

$\Delta(1920)$ PHOTON DECAY AMPLITUDES AT THE POLE

$\Delta(1920) \rightarrow N\gamma$, helicity-1/2 amplitude $A_{1/2}$

MODULUS (GeV ^{-1/2})	PHASE (°)	DOCUMENT ID	TECN	COMMENT
0.110 ± 0.030	-50 ± 20	SOKHOYAN	15A	DPWA Multichannel
0.190 ^{+0.050} _{-0.022}	-160 ⁺²⁴ ₋₁₁	ROENCHEN	14	DPWA
••• We do not use the following data for averages, fits, limits, etc. •••				
-0.192	46	ROENCHEN	15A	DPWA Multichannel

$\Delta(1920) \rightarrow N\gamma$, helicity-3/2 amplitude $A_{3/2}$

MODULUS (GeV ^{-1/2})	PHASE (°)	DOCUMENT ID	TECN	COMMENT
-0.100 ± 0.040	0 ± 20	SOKHOYAN	15A	DPWA Multichannel
-0.398 ^{+0.070} _{-0.067}	-110 ⁺⁴ ₋₅	ROENCHEN	14	DPWA
••• We do not use the following data for averages, fits, limits, etc. •••				
0.522	67	ROENCHEN	15A	DPWA Multichannel

$\Delta(1920)$ BREIT-WIGNER PHOTON DECAY AMPLITUDES

$\Delta(1920) \rightarrow N\gamma$, helicity-1/2 amplitude $A_{1/2}$

VALUE (GeV ^{-1/2})	DOCUMENT ID	TECN	COMMENT
-0.028 ± 0.010	¹ HUNT	19	DPWA Multichannel
0.110 ± 0.030	SOKHOYAN	15A	DPWA Multichannel
••• We do not use the following data for averages, fits, limits, etc. •••			
0.110 ± 0.030	GUTZ	14	DPWA Multichannel
0.130 ^{+0.030} _{-0.060}	ANISOVICH	12A	DPWA Multichannel
0.051 ± 0.010	¹ SHRESTHA	12A	DPWA Multichannel
-0.007	PENNER	02D	DPWA Multichannel

¹ Statistical error only.

$\Delta(1920) \rightarrow N\gamma$, helicity-3/2 amplitude $A_{3/2}$

VALUE (GeV ^{-1/2})	DOCUMENT ID	TECN	COMMENT
-0.043 ± 0.014	¹ HUNT	19	DPWA Multichannel
-0.105 ± 0.035	SOKHOYAN	15A	DPWA Multichannel
••• We do not use the following data for averages, fits, limits, etc. •••			
-0.105 ± 0.035	GUTZ	14	DPWA Multichannel
-0.115 ^{+0.025} _{-0.050}	ANISOVICH	12A	DPWA Multichannel
0.017 ± 0.015	¹ SHRESTHA	12A	DPWA Multichannel
-0.001	PENNER	02D	DPWA Multichannel

¹ Statistical error only.

$\Delta(1920)$ REFERENCES

For early references, see Physics Letters **111B** 1 (1982).

HUNT	19	PR C99 055205	B.C. Hunt, D.M. Manley
ROENCHEN	15A	EPJ A51 70	D. Roenchen <i>et al.</i>
SOKHOYAN	15A	EPJ A51 95	V. Sokhoyan <i>et al.</i>
GUTZ	14	EPJ A50 74	E. Gutz <i>et al.</i>
PDG	14	CP C38 070001	K. Olive <i>et al.</i>
			(CBELSA/TAPS Collab.)
			(CBELSA/TAPS Collab.)
			(PDG Collab.)

Baryon Particle Listings

 $\Delta(1920), \Delta(1930)$

ROENCHEN	14	EPJ A50 101	D. Roenchen <i>et al.</i>	
Also		EPJ A51 63 (errat.)	D. Roenchen <i>et al.</i>	
SVARC	14	PR C89 045205	A. Svarc <i>et al.</i>	(RBI Zagreb, UNI Tuzla)
ANISOVICH	12A	EPJ A48 15	A.V. Anisovich <i>et al.</i>	(BOONN, PNPI)
SHRESTHA	12A	PR C86 055203	M. Shrestha, D.M. Manley	(KSU)
HORN	08A	EPJ A38 173	I. Horn <i>et al.</i>	(CB-ELSA Collab.)
Also		PRL 101 202002	I. Horn <i>et al.</i>	(CB-ELSA Collab.)
PENNER	02C	PR C66 055211	G. Penner, U. Mosel	(GIES)
PENNER	02D	PR C66 055212	G. Penner, U. Mosel	(GIES)
VRANA	00	PRPL 320 181	T.P. Vrana, S.A. Dytman, T.-S.H. Lee	(PITT, ANL)
HOEHLER	93	πN Newsletter 9 1	G. Hoehler	(KARL)
CUTKOSKY	80	Toronto Conf. 19	R.E. Cutkosky <i>et al.</i>	(CMU, LBL) IJP
Also		PR D20 2839	R.E. Cutkosky <i>et al.</i>	(CMU, LBL) IJP
HOEHLER	79	PDAT 12-1	G. Hoehler <i>et al.</i>	(KARLT) IJP
Also		Toronto Conf. 3	R. Koch	(KARLT) IJP

 $\Delta(1930) 5/2^-$

$$I(J^P) = \frac{3}{2}(\frac{5}{2}^-) \text{ Status: } **$$

Older and obsolete values are listed and referenced in the 2014 edition, Chinese Physics C38 070001 (2014).

 $\Delta(1930)$ POLE POSITION

REAL PART

VALUE (MeV)	DOCUMENT ID	TECN	COMMENT
1840 to 1920 (≈ 1880) OUR ESTIMATE			
1848 \pm 9 \pm 19	¹ SVARC 14	L+P	$\pi N \rightarrow \pi N$
1890 \pm 50	CUTKOSKY 80	IPWA	$\pi N \rightarrow \pi N$
••• We do not use the following data for averages, fits, limits, etc. •••			
1863	HUNT 19	DPWA	Multichannel
1836	ROENCHEN 15A	DPWA	Multichannel
2001	ARNDT 06	DPWA	$\pi N \rightarrow \pi N, \eta N$
1883	VRANA 00	DPWA	Multichannel
1850	HOEHLER 93	SPED	$\pi N \rightarrow \pi N$

¹ Fit to the amplitudes of HOEHLER 79.

-2xIMAGINARY PART

VALUE (MeV)	DOCUMENT ID	TECN	COMMENT
230 to 330 (≈ 280) OUR ESTIMATE			
321 \pm 17 \pm 7	¹ SVARC 14	L+P	$\pi N \rightarrow \pi N$
260 \pm 60	CUTKOSKY 80	IPWA	$\pi N \rightarrow \pi N$
••• We do not use the following data for averages, fits, limits, etc. •••			
260	HUNT 19	DPWA	Multichannel
724	ROENCHEN 15A	DPWA	Multichannel
387	ARNDT 06	DPWA	$\pi N \rightarrow \pi N, \eta N$
250	VRANA 00	DPWA	Multichannel
180	HOEHLER 93	SPED	$\pi N \rightarrow \pi N$

¹ Fit to the amplitudes of HOEHLER 79.

 $\Delta(1930)$ ELASTIC POLE RESIDUEMODULUS $|r|$

VALUE (MeV)	DOCUMENT ID	TECN	COMMENT
8 to 20 (≈ 14) OUR ESTIMATE			
9 \pm 1 \pm 1	¹ SVARC 14	L+P	$\pi N \rightarrow \pi N$
18 \pm 6	CUTKOSKY 80	IPWA	$\pi N \rightarrow \pi N$
••• We do not use the following data for averages, fits, limits, etc. •••			
34	ROENCHEN 15A	DPWA	Multichannel
7	ARNDT 06	DPWA	$\pi N \rightarrow \pi N, \eta N$
20	HOEHLER 93	SPED	$\pi N \rightarrow \pi N$

¹ Fit to the amplitudes of HOEHLER 79.

PHASE θ

VALUE ($^\circ$)	DOCUMENT ID	TECN	COMMENT
-40 to -10 (≈ -30) OUR ESTIMATE			
-37 \pm 3 \pm 7	¹ SVARC 14	L+P	$\pi N \rightarrow \pi N$
-20 \pm 40	CUTKOSKY 80	IPWA	$\pi N \rightarrow \pi N$
••• We do not use the following data for averages, fits, limits, etc. •••			
-155	ROENCHEN 15A	DPWA	Multichannel
-12	ARNDT 06	DPWA	$\pi N \rightarrow \pi N, \eta N$

¹ Fit to the amplitudes of HOEHLER 79.

 $\Delta(1930)$ INELASTIC POLE RESIDUE

The "normalized residue" is the residue divided by $\Gamma_{pole}/2$.

Normalized residue in $N\pi \rightarrow \Delta(1930) \rightarrow \Sigma K$

MODULUS	PHASE ($^\circ$)	DOCUMENT ID	TECN	COMMENT
••• We do not use the following data for averages, fits, limits, etc. •••				
0.043	-0.5	ROENCHEN 15A	DPWA	Multichannel

Normalized residue in $N\pi \rightarrow \Delta(1930) \rightarrow \Delta\pi, D\text{-wave}$

MODULUS	PHASE ($^\circ$)	DOCUMENT ID	TECN	COMMENT
••• We do not use the following data for averages, fits, limits, etc. •••				
0.15	30	ROENCHEN 15A	DPWA	Multichannel

Normalized residue in $N\pi \rightarrow \Delta(1930) \rightarrow \Delta\pi, G\text{-wave}$

MODULUS	PHASE ($^\circ$)	DOCUMENT ID	TECN	COMMENT
••• We do not use the following data for averages, fits, limits, etc. •••				
0.009	121	ROENCHEN 15A	DPWA	Multichannel

 $\Delta(1930)$ BREIT-WIGNER MASS

VALUE (MeV)	DOCUMENT ID	TECN	COMMENT
1900 to 2000 (≈ 1950) OUR ESTIMATE			
1988 \pm 32	¹ HUNT 19	DPWA	Multichannel
2233 \pm 53	¹ ARNDT 06	DPWA	$\pi N \rightarrow \pi N, \eta N$
1940 \pm 30	CUTKOSKY 80	IPWA	$\pi N \rightarrow \pi N$
1901 \pm 15	HOEHLER 79	IPWA	$\pi N \rightarrow \pi N$
••• We do not use the following data for averages, fits, limits, etc. •••			
1930 \pm 12	¹ SHRESTHA 12A	DPWA	Multichannel
1932 \pm 100	VRANA 00	DPWA	Multichannel

¹ Statistical error only.

 $\Delta(1930)$ BREIT-WIGNER WIDTH

VALUE (MeV)	DOCUMENT ID	TECN	COMMENT
200 to 400 (≈ 300) OUR ESTIMATE			
500 \pm 160	¹ HUNT 19	DPWA	Multichannel
773 \pm 187	ARNDT 06	DPWA	$\pi N \rightarrow \pi N, \eta N$
320 \pm 60	CUTKOSKY 80	IPWA	$\pi N \rightarrow \pi N$
195 \pm 60	HOEHLER 79	IPWA	$\pi N \rightarrow \pi N$
••• We do not use the following data for averages, fits, limits, etc. •••			
235 \pm 39	¹ SHRESTHA 12A	DPWA	Multichannel
316 \pm 237	VRANA 00	DPWA	Multichannel

¹ Statistical error only.

 $\Delta(1930)$ DECAY MODES

The following branching fractions are our estimates, not fits or averages.

Mode	Fraction (Γ_i/Γ)
Γ_1 $N\pi$	5-15 %
Γ_2 $N\gamma$	0.0-0.01 %
Γ_3 $N\gamma$, helicity=1/2	0.0-0.005 %
Γ_4 $N\gamma$, helicity=3/2	0.0-0.004 %

 $\Delta(1930)$ BRANCHING RATIOS

$\Gamma(N\pi)/\Gamma_{total}$	DOCUMENT ID	TECN	COMMENT	Γ_1/Γ
5 to 15 (≈ 10) OUR ESTIMATE				
9.5 \pm 0.1	¹ HUNT 19	DPWA	Multichannel	
8.1 \pm 1.2	¹ ARNDT 06	DPWA	$\pi N \rightarrow \pi N, \eta N$	
14 \pm 4	CUTKOSKY 80	IPWA	$\pi N \rightarrow \pi N$	
4 \pm 3	HOEHLER 79	IPWA	$\pi N \rightarrow \pi N$	
••• We do not use the following data for averages, fits, limits, etc. •••				
7.9 \pm 0.4	¹ SHRESTHA 12A	DPWA	Multichannel	
9 \pm 8	VRANA 00	DPWA	Multichannel	

¹ Statistical error only.

 $\Delta(1930)$ PHOTON DECAY AMPLITUDES AT THE POLE $\Delta(1930) \rightarrow N\gamma$, helicity-1/2 amplitude $A_{1/2}$

MODULUS ($\text{GeV}^{-1/2}$)	PHASE ($^\circ$)	DOCUMENT ID	TECN	COMMENT
0.130 $^{+0.073}_{-0.096}$	-50 $^{+77}_{-26}$	ROENCHEN 14	DPWA	
••• We do not use the following data for averages, fits, limits, etc. •••				
-0.270	33	ROENCHEN 15A	DPWA	Multichannel

 $\Delta(1930) \rightarrow N\gamma$, helicity-3/2 amplitude $A_{3/2}$

MODULUS ($\text{GeV}^{-1/2}$)	PHASE ($^\circ$)	DOCUMENT ID	TECN	COMMENT
-0.056 $^{+0.003}_{-0.151}$	168 $^{+72}_{-76}$	ROENCHEN 14	DPWA	
••• We do not use the following data for averages, fits, limits, etc. •••				
0.153	81	ROENCHEN 15A	DPWA	Multichannel

 $\Delta(1930)$ BREIT-WIGNER PHOTON DECAY AMPLITUDES $\Delta(1930) \rightarrow N\gamma$, helicity-1/2 amplitude $A_{1/2}$

VALUE ($\text{GeV}^{-1/2}$)	DOCUMENT ID	TECN	COMMENT
-0.043 \pm 0.008	¹ HUNT 19	DPWA	Multichannel
-0.007 \pm 0.010	¹ ARNDT 96	IPWA	$\gamma N \rightarrow \pi N$
••• We do not use the following data for averages, fits, limits, etc. •••			
0.011 \pm 0.003	¹ SHRESTHA 12A	DPWA	Multichannel

¹ Statistical error only.

$\Delta(1930) \rightarrow N\gamma$, helicity-3/2 amplitude $A_{3/2}$

VALUE (GeV ^{-1/2})	DOCUMENT ID	TECN	COMMENT
-0.020 ± 0.017	¹ HUNT 19	DPWA	Multichannel
0.005 ± 0.010	¹ ARNDT 96	IPWA	$\gamma N \rightarrow \pi N$
• • • We do not use the following data for averages, fits, limits, etc. • • •			
0.002 ± 0.002	¹ SHRESTHA 12A	DPWA	Multichannel
¹ Statistical error only.			

$\Delta(1930)$ REFERENCES

For early references, see Physics Letters **111B** 1 (1982).

HUNT 19	PR C99 055205	B. C. Hunt, D.M. Manley	
ROENCHEN 15A	EPJ A51 70	D. Roenchen et al.	
PDG 14	CP C38 070001	K. Olive et al.	(PDG Collab.)
ROENCHEN 14	EPJ A50 101	D. Roenchen et al.	
Also	EPJ A51 63 (errata.)	D. Roenchen et al.	
SVARC 14	PR C89 045205	A. Svarc et al.	(RBI Zagreb, UNI Tuzla)
SHRESTHA 12A	PR C86 055203	M. Shrestha, D.M. Manley	(KSU)
ARNDT 06	PR C74 045203	R.A. Arndt et al.	(GWU)
VRANA 00	PRPL 328 181	T.P. Vrana, S.A. Dytman, T.-S.H. Lee	(PITT, ANL)
ARNDT 96	PR C53 430	R.A. Arndt, I.I. Strakovsky, R.L. Workman	(VPI)
HOEHLER 93	πN Newsletter 9 1	G. Hoehler	(KARL)
CUTKOSKY 80	Toronto Conf. 19	R.E. Cutkosky et al.	(CMU, LBL) IJP
Also	PR D20 2839	R.E. Cutkosky et al.	(CMU, LBL) IJP
HOEHLER 79	PDAT 12-1	G. Hoehler et al.	(KARLT) IJP
Also	Toronto Conf. 3	R. Koch	(KARLT) IJP

$\Delta(1940) 3/2^-$

 $I(J^P) = \frac{3}{2}(\frac{3}{2}^-)$ Status: **
 OMITTED FROM SUMMARY TABLE

$\Delta(1940)$ POLE POSITION

REAL PART

VALUE (MeV)	DOCUMENT ID	TECN	COMMENT
1850 to 2050 (≈ 1950) OUR ESTIMATE			
2040 ± 50	SOKHOYAN 15A	DPWA	Multichannel
1878 ± 11 ± 5.5	¹ SVARC 14	L+P	$\pi N \rightarrow \pi N$
1900 ± 100	CUTKOSKY 80	IPWA	$\pi N \rightarrow \pi N$
• • • We do not use the following data for averages, fits, limits, etc. • • •			
2139	HUNT 19	DPWA	Multichannel
2040 ± 50	GUTZ 14	DPWA	Multichannel
1990 ± ¹⁰⁰ / ₅₀	ANISOVICH 12A	DPWA	Multichannel
¹ Fit to the amplitudes of HOEHLER 79.			

-2xIMAGINARY PART

VALUE (MeV)	DOCUMENT ID	TECN	COMMENT
200 to 500 (≈ 350) OUR ESTIMATE			
450 ± 90	SOKHOYAN 15A	DPWA	Multichannel
212 ± 21 ± 6	¹ SVARC 14	L+P	$\pi N \rightarrow \pi N$
200 ± 60	CUTKOSKY 80	IPWA	$\pi N \rightarrow \pi N$
• • • We do not use the following data for averages, fits, limits, etc. • • •			
400	HUNT 19	DPWA	Multichannel
450 ± 90	GUTZ 14	DPWA	Multichannel
450 ± 90	ANISOVICH 12A	DPWA	Multichannel
¹ Fit to the amplitudes of HOEHLER 79.			

$\Delta(1940)$ ELASTIC POLE RESIDUE

MODULUS |r|

VALUE (MeV)	DOCUMENT ID	TECN	COMMENT
4 to 10 (≈ 7) OUR ESTIMATE			
6 ± 3	SOKHOYAN 15A	DPWA	Multichannel
9 ± 1 ± 1	¹ SVARC 14	L+P	$\pi N \rightarrow \pi N$
8 ± 3	CUTKOSKY 80	IPWA	$\pi N \rightarrow \pi N$
• • • We do not use the following data for averages, fits, limits, etc. • • •			
4 ± 3	GUTZ 14	DPWA	Multichannel
4 ± 4	ANISOVICH 12A	DPWA	Multichannel
¹ Fit to the amplitudes of HOEHLER 79.			

PHASE θ

VALUE (°)	DOCUMENT ID	TECN	COMMENT
150 to 250 (≈ 200) OUR ESTIMATE			
- 90 ± 35	SOKHOYAN 15A	DPWA	Multichannel
140 ± 7 ± 7	¹ SVARC 14	L+P	$\pi N \rightarrow \pi N$
135 ± 45	CUTKOSKY 80	IPWA	$\pi N \rightarrow \pi N$
• • • We do not use the following data for averages, fits, limits, etc. • • •			
- 50 ± 35	GUTZ 14	DPWA	Multichannel
¹ Fit to the amplitudes of HOEHLER 79.			

$\Delta(1940)$ INELASTIC POLE RESIDUE

The "normalized residue" is the residue divided by $\Gamma_{pole}/2$.

Normalized residue in $N\pi \rightarrow \Delta(1940) \rightarrow \Delta(1232)\eta$

MODULUS	PHASE (°)	DOCUMENT ID	TECN	COMMENT
<0.01	undefined	GUTZ 14	DPWA	Multichannel

Normalized residue in $N\pi \rightarrow \Delta(1940) \rightarrow N(1535)\pi$

MODULUS	PHASE (°)	DOCUMENT ID	TECN	COMMENT
<0.03	undefined	GUTZ 14	DPWA	Multichannel

Normalized residue in $N\pi \rightarrow \Delta(1940) \rightarrow \Delta(1232)\pi$, S-wave

MODULUS	PHASE (°)	DOCUMENT ID	TECN	COMMENT
0.12 ± 0.06	120 ± 45	SOKHOYAN 15A	DPWA	Multichannel

Normalized residue in $N\pi \rightarrow \Delta(1940) \rightarrow \Delta(1232)\pi$, D-wave

MODULUS	PHASE (°)	DOCUMENT ID	TECN	COMMENT
0.06 ± 0.04	- 80 ± 35	SOKHOYAN 15A	DPWA	Multichannel

$\Delta(1940)$ BREIT-WIGNER MASS

VALUE (MeV)	DOCUMENT ID	TECN	COMMENT
1940 to 2060 (≈ 2000) OUR ESTIMATE			
2137 ± 13	¹ HUNT 19	DPWA	Multichannel
2050 ± 40	SOKHOYAN 15A	DPWA	Multichannel
1940 ± 100	CUTKOSKY 80	IPWA	$\pi N \rightarrow \pi N$
• • • We do not use the following data for averages, fits, limits, etc. • • •			
2050 ± 40	GUTZ 14	DPWA	Multichannel
1995 ± ¹⁰⁵ / ₆₀	ANISOVICH 12A	DPWA	Multichannel
¹ Statistical error only.			

$\Delta(1940)$ BREIT-WIGNER WIDTH

VALUE (MeV)	DOCUMENT ID	TECN	COMMENT
300 to 500 (≈ 400) OUR ESTIMATE			
400 ± 43	¹ HUNT 19	DPWA	Multichannel
450 ± 70	SOKHOYAN 15A	DPWA	Multichannel
200 ± 100	CUTKOSKY 80	IPWA	$\pi N \rightarrow \pi N$
• • • We do not use the following data for averages, fits, limits, etc. • • •			
450 ± 70	GUTZ 14	DPWA	Multichannel
450 ± 100	ANISOVICH 12A	DPWA	Multichannel
¹ Statistical error only.			

$\Delta(1940)$ DECAY MODES

Mode	Fraction (Γ_i/Γ)
Γ_1 $N\pi$	1-7 %
Γ_2 $N\pi\pi$	
Γ_3 $\Delta(1232)\pi$	30-85 %
Γ_4 $\Delta(1232)\pi$, S-wave	25-65 %
Γ_5 $\Delta(1232)\pi$, D-wave	5-20 %
Γ_6 $N\rho$	
Γ_7 $N\rho$, S=3/2, S-wave	
Γ_8 $N(1535)\pi$	2-14 %
Γ_9 $N a_0(980)$	seen
Γ_{10} $\Delta(1232)\eta$	4-16 %
Γ_{11} $N\gamma$, helicity=1/2	seen
Γ_{12} $N\gamma$, helicity=3/2	seen

$\Delta(1940)$ BRANCHING RATIOS

$\Gamma(N\pi)/\Gamma_{total}$	DOCUMENT ID	TECN	COMMENT	Γ_1/Γ
1 to 7 (≈ 4) OUR ESTIMATE				
16 ± 4	¹ HUNT 19	DPWA	Multichannel	
2 ± 1	SOKHOYAN 15A	DPWA	Multichannel	
5 ± 2	CUTKOSKY 80	IPWA	$\pi N \rightarrow \pi N$	
• • • We do not use the following data for averages, fits, limits, etc. • • •				
2 ± 1	GUTZ 14	DPWA	Multichannel	
¹ Statistical error only.				

$\Gamma(\Delta(1232)\pi, S\text{-wave})/\Gamma_{total}$	DOCUMENT ID	TECN	COMMENT	Γ_4/Γ
1 to 7 (≈ 4) OUR ESTIMATE				
< 0.9	¹ HUNT 19	DPWA	Multichannel	
46 ± 20	SOKHOYAN 15A	DPWA	Multichannel	
¹ Statistical error only.				

Baryon Particle Listings

$\Delta(1940), \Delta(1950)$

$\Gamma(\Delta(1232)\pi, D\text{-wave})/\Gamma_{\text{total}}$				Γ_5/Γ
VALUE (%)	DOCUMENT ID	TECN	COMMENT	
< 6.3	¹ HUNT	19	DPWA Multichannel	
12 ± 7	SOKHOYAN	15A	DPWA Multichannel	
¹ Statistical error only.				
$\Gamma(N\rho, S=3/2, S\text{-wave})/\Gamma_{\text{total}}$				Γ_7/Γ
VALUE (%)	DOCUMENT ID	TECN	COMMENT	
80 ± 5	¹ HUNT	19	DPWA Multichannel	
¹ Statistical error only.				
$\Gamma(N(1535)\pi)/\Gamma_{\text{total}}$				Γ_8/Γ
VALUE (%)	DOCUMENT ID	TECN	COMMENT	
8 ± 6	GUTZ	14	DPWA Multichannel	
••• We do not use the following data for averages, fits, limits, etc. •••				
2 ± 1	HORN	08A	DPWA Multichannel	
$\Gamma(N\pi_0(980))/\Gamma_{\text{total}}$				Γ_9/Γ
VALUE (%)	DOCUMENT ID	TECN	COMMENT	
••• We do not use the following data for averages, fits, limits, etc. •••				
2 ± 1	HORN	08A	DPWA Multichannel	
$\Gamma(\Delta(1232)\eta)/\Gamma_{\text{total}}$				Γ_{10}/Γ
VALUE (%)	DOCUMENT ID	TECN	COMMENT	
10 ± 6	GUTZ	14	DPWA Multichannel	
••• We do not use the following data for averages, fits, limits, etc. •••				
4 ± 2	HORN	08A	DPWA Multichannel	

$\Delta(1940)$ PHOTON DECAY AMPLITUDES AT THE POLE

$\Delta(1940) \rightarrow N\gamma, \text{ helicity-1/2 amplitude } A_{1/2}$				
MODULUS ($\text{GeV}^{-1/2}$)	PHASE ($^\circ$)	DOCUMENT ID	TECN	COMMENT
0.170 \pm $\begin{smallmatrix} +0.120 \\ -0.100 \end{smallmatrix}$	-10 ± 30	SOKHOYAN	15A	DPWA Multichannel
$\Delta(1940) \rightarrow N\gamma, \text{ helicity-3/2 amplitude } A_{3/2}$				
MODULUS ($\text{GeV}^{-1/2}$)	PHASE ($^\circ$)	DOCUMENT ID	TECN	COMMENT
0.150 ± 0.080	-10 ± 30	SOKHOYAN	15A	DPWA Multichannel

$\Delta(1940)$ BREIT-WIGNER PHOTON DECAY AMPLITUDES

$\Delta(1940) \rightarrow N\gamma, \text{ helicity-1/2 amplitude } A_{1/2}$				
VALUE ($\text{GeV}^{-1/2}$)	DOCUMENT ID	TECN	COMMENT	
0.1614 ± 0.0031	¹ HUNT	19	DPWA Multichannel	
0.170 \pm $\begin{smallmatrix} +0.110 \\ -0.080 \end{smallmatrix}$	SOKHOYAN	15A	DPWA Multichannel	
••• We do not use the following data for averages, fits, limits, etc. •••				
0.170 \pm $\begin{smallmatrix} +0.110 \\ -0.080 \end{smallmatrix}$	GUTZ	14	DPWA Multichannel	
¹ Statistical error only.				
$\Delta(1940) \rightarrow N\gamma, \text{ helicity-3/2 amplitude } A_{3/2}$				
VALUE ($\text{GeV}^{-1/2}$)	DOCUMENT ID	TECN	COMMENT	
-0.209 ± 0.023	¹ HUNT	19	DPWA Multichannel	
0.150 ± 0.080	SOKHOYAN	15A	DPWA Multichannel	
••• We do not use the following data for averages, fits, limits, etc. •••				
0.150 ± 0.080	GUTZ	14	DPWA Multichannel	
¹ Statistical error only.				

$\Delta(1940)$ REFERENCES

HUNT	19	PR C99 055205	B. C. Hunt, D.M. Manley
SOKHOYAN	15A	EPJ A51 95	V. Sokhoyan et al.
GUTZ	14	EPJ A50 74	E. Gutz et al.
SVARC	14	PR C89 045205	A. V. Svarc et al.
ANISOVICH	12A	EPJ A48 15	A.V. Anisovich et al.
HORN	08A	EPJ A38 173	I. Horn et al.
		PRL 101 202002	(CB-ELSA Collab.)
CUTKOSKY	80	Toronto Conf. 19	R.E. Cutkosky et al.
		PR D20 2839	R.E. Cutkosky et al.
HOEHLER	79	PDAT 12-1	G. Hoehler et al.
			(CMU, LBL) IJP (CB-ELSA Collab.) (CMU, LBL) (KARLT)

$\Delta(1950) 7/2^+$

$$I(J^P) = \frac{3}{2}(7/2^+) \text{ Status: } ****$$

Older and obsolete values are listed and referenced in the 2014 edition, Chinese Physics C38 070001 (2014).

$\Delta(1950)$ POLE POSITION

REAL PART

VALUE (MeV)	DOCUMENT ID	TECN	COMMENT
1870 to 1890 (\approx 1880) OUR ESTIMATE			
1888 ± 4	SOKHOYAN	15A	DPWA Multichannel
1877 ± 2 ± 1	¹ SVARC	14	L+P $\pi N \rightarrow \pi N$
1890 ± 15	CUTKOSKY	80	IPWA $\pi N \rightarrow \pi N$
••• We do not use the following data for averages, fits, limits, etc. •••			
1871	HUNT	19	DPWA Multichannel
1874	ROENCHEN	15A	DPWA Multichannel
1888 ± 4	GUTZ	14	DPWA Multichannel
1890 ± 4	ANISOVICH	12A	DPWA Multichannel
1876	ARNDT	06	DPWA $\pi N \rightarrow \pi N, \eta N$
1910	VRANA	00	DPWA Multichannel
1878	HOEHLER	93	ARGD $\pi N \rightarrow \pi N$
¹ Fit to the amplitudes of HOEHLER 79.			
-2xIMAGINARY PART			
VALUE (MeV)	DOCUMENT ID	TECN	COMMENT
220 to 260 (\approx 240) OUR ESTIMATE			
245 ± 8	SOKHOYAN	15A	DPWA Multichannel
223 ± 4 ± 1	¹ SVARC	14	L+P $\pi N \rightarrow \pi N$
260 ± 40	CUTKOSKY	80	IPWA $\pi N \rightarrow \pi N$
••• We do not use the following data for averages, fits, limits, etc. •••			
206	HUNT	19	DPWA Multichannel
239	ROENCHEN	15A	DPWA Multichannel
245 ± 8	GUTZ	14	DPWA Multichannel
243 ± 8	ANISOVICH	12A	DPWA Multichannel
227	ARNDT	06	DPWA $\pi N \rightarrow \pi N, \eta N$
230	VRANA	00	DPWA Multichannel
230	HOEHLER	93	ARGD $\pi N \rightarrow \pi N$
¹ Fit to the amplitudes of HOEHLER 79.			

$\Delta(1950)$ ELASTIC POLE RESIDUE

MODULUS $ r $				
VALUE (MeV)	DOCUMENT ID	TECN	COMMENT	
44 to 60 (\approx 52) OUR ESTIMATE				
58 ± 2	SOKHOYAN	15A	DPWA Multichannel	
44 ± 1	¹ SVARC	14	L+P $\pi N \rightarrow \pi N$	
50 ± 7	CUTKOSKY	80	IPWA $\pi N \rightarrow \pi N$	
••• We do not use the following data for averages, fits, limits, etc. •••				
56	ROENCHEN	15A	DPWA Multichannel	
58 ± 2	GUTZ	14	DPWA Multichannel	
58 ± 2	ANISOVICH	12A	DPWA Multichannel	
53	ARNDT	06	DPWA $\pi N \rightarrow \pi N, \eta N$	
47	HOEHLER	93	ARGD $\pi N \rightarrow \pi N$	
¹ Fit to the amplitudes of HOEHLER 79.				
PHASE θ				
VALUE ($^\circ$)	DOCUMENT ID	TECN	COMMENT	
-40 to -24 (\approx -32) OUR ESTIMATE				
-24 ± 3	SOKHOYAN	15A	DPWA Multichannel	
-39 ± 1 ± 1	¹ SVARC	14	L+P $\pi N \rightarrow \pi N$	
-33 ± 8	CUTKOSKY	80	IPWA $\pi N \rightarrow \pi N$	
••• We do not use the following data for averages, fits, limits, etc. •••				
-33	ROENCHEN	15A	DPWA Multichannel	
-24 ± 3	GUTZ	14	DPWA Multichannel	
-24 ± 3	ANISOVICH	12A	DPWA Multichannel	
-31	ARNDT	06	DPWA $\pi N \rightarrow \pi N, \eta N$	
-32	HOEHLER	93	ARGD $\pi N \rightarrow \pi N$	
¹ Fit to the amplitudes of HOEHLER 79.				

$\Delta(1950)$ INELASTIC POLE RESIDUE

The "normalized residue" is the residue divided by $\Gamma_{\text{pole}}/2$.

Normalized residue in $N\pi \rightarrow \Delta(1950) \rightarrow \Sigma K$				
MODULUS	PHASE ($^\circ$)	DOCUMENT ID	TECN	COMMENT
0.05 ± 0.01	-65 ± 25	ANISOVICH	12A	DPWA Multichannel
••• We do not use the following data for averages, fits, limits, etc. •••				
0.031	-87	ROENCHEN	15A	DPWA Multichannel
Normalized residue in $N\pi \rightarrow \Delta(1950) \rightarrow \Delta\pi, F\text{-wave}$				
MODULUS	PHASE ($^\circ$)	DOCUMENT ID	TECN	COMMENT
0.12 ± 0.04	undefined	SOKHOYAN	15A	DPWA Multichannel
••• We do not use the following data for averages, fits, limits, etc. •••				
0.54	131	ROENCHEN	15A	DPWA Multichannel
0.12 ± 0.04	12 ± 10	ANISOVICH	12A	DPWA Multichannel
Normalized residue in $N\pi \rightarrow \Delta(1950) \rightarrow \Delta\pi, H\text{-wave}$				
MODULUS	PHASE ($^\circ$)	DOCUMENT ID	TECN	COMMENT
••• We do not use the following data for averages, fits, limits, etc. •••				
0.033	-97	ROENCHEN	15A	DPWA Multichannel

$\Delta(1950)$

Normalized residue in $N\pi \rightarrow \Delta(1950) \rightarrow \Delta(1232)\eta$

MODULUS	PHASE ($^\circ$)	DOCUMENT ID	TECN	COMMENT
0.035 ± 0.005	90 ± 25	GUTZ	14	DPWA Multichannel

$\Delta(1950)$ BREIT-WIGNER MASS

VALUE (MeV)	DOCUMENT ID	TECN	COMMENT
1915 to 1950 (\approx 1930) OUR ESTIMATE			
1943 ± 18	GOLOVATCH 19	DPWA	$\gamma p \rightarrow \pi^+ \pi^- p$
1913 ± 4	¹ HUNT 19	DPWA	Multichannel
1917 ± 4	ANISOVICH 17	DPWA	Multichannel
1921.3 ± 0.2	¹ ARNDT 06	DPWA	$\pi N \rightarrow \pi N, \eta N$
1950 ± 15	CUTKOSKY 80	IPWA	$\pi N \rightarrow \pi N$
1913 ± 8	HOEHLER 79	IPWA	$\pi N \rightarrow \pi N$
• • • We do not use the following data for averages, fits, limits, etc. • • •			
1917 ± 4	SOKHOYAN 15A	DPWA	Multichannel
1917 ± 4	GUTZ 14	DPWA	Multichannel
1915 ± 6	ANISOVICH 12A	DPWA	Multichannel
1918 ± 1	¹ SHRESTHA 12A	DPWA	Multichannel
1936 ± 5	VRANA 00	DPWA	Multichannel

¹ Statistical error only.

$\Delta(1950)$ BREIT-WIGNER WIDTH

VALUE (MeV)	DOCUMENT ID	TECN	COMMENT
235 to 335 (\approx 285) OUR ESTIMATE			
230 ± 88	GOLOVATCH 19	DPWA	$\gamma p \rightarrow \pi^+ \pi^- p$
241 ± 10	¹ HUNT 19	DPWA	Multichannel
251 ± 8	ANISOVICH 17	DPWA	Multichannel
271.1 ± 1.1	¹ ARNDT 06	DPWA	$\pi N \rightarrow \pi N, \eta N$
340 ± 5.0	CUTKOSKY 80	IPWA	$\pi N \rightarrow \pi N$
224 ± 10	HOEHLER 79	IPWA	$\pi N \rightarrow \pi N$
• • • We do not use the following data for averages, fits, limits, etc. • • •			
251 ± 8	SOKHOYAN 15A	DPWA	Multichannel
251 ± 8	GUTZ 14	DPWA	Multichannel
246 ± 10	ANISOVICH 12A	DPWA	Multichannel
259 ± 4	¹ SHRESTHA 12A	DPWA	Multichannel
245 ± 12	VRANA 00	DPWA	Multichannel

¹ Statistical error only.

$\Delta(1950)$ DECAY MODES

The following branching fractions are our estimates, not fits or averages.

Mode	Fraction (Γ_i/Γ)
Γ_1 $N\pi$	35–45 %
Γ_2 ΣK	0.3–0.5 %
Γ_3 $N\pi\pi$	
Γ_4 $\Delta(1232)\pi, F\text{-wave}$	1–9 %
Γ_5 $N(1680)\pi, P\text{-wave}$	3–9 %
Γ_6 $\Delta(1232)\eta$	< 0.6 %

$\Delta(1950)$ BRANCHING RATIOS

$\Gamma(N\pi)/\Gamma_{\text{total}}$

VALUE (%)	DOCUMENT ID	TECN	COMMENT
35 to 45 (\approx 40) OUR ESTIMATE			
38 ± 2	¹ HUNT 19	DPWA	Multichannel
46 ± 2	ANISOVICH 17	DPWA	Multichannel
47.1 ± 0.1	¹ ARNDT 06	DPWA	$\pi N \rightarrow \pi N, \eta N$
39 ± 4	CUTKOSKY 80	IPWA	$\pi N \rightarrow \pi N$
38 ± 2	HOEHLER 79	IPWA	$\pi N \rightarrow \pi N$
• • • We do not use the following data for averages, fits, limits, etc. • • •			
0.046 ± 0.002	SOKHOYAN 15A	DPWA	Multichannel
46 ± 2	GUTZ 14	DPWA	Multichannel
45 ± 2	ANISOVICH 12A	DPWA	Multichannel
45.6 ± 0.4	¹ SHRESTHA 12A	DPWA	Multichannel
44 ± 1	VRANA 00	DPWA	Multichannel

¹ Statistical error only.

$\Gamma(N\pi\pi)/\Gamma_{\text{total}}$

VALUE (%)	DOCUMENT ID	TECN	COMMENT
0.57 ± 0.20	GOLOVATCH 19	DPWA	$\gamma p \rightarrow \pi^+ \pi^- p$

$\Gamma(\Sigma K)/\Gamma_{\text{total}}$

VALUE (%)	DOCUMENT ID	TECN	COMMENT
0.6 ± 0.2	ANISOVICH 17	DPWA	Multichannel

• • • We do not use the following data for averages, fits, limits, etc. • • •

VALUE (%)	DOCUMENT ID	TECN	COMMENT
0.4 ± 0.1	ANISOVICH 12A	DPWA	Multichannel

$\Gamma(\Delta(1232)\pi, F\text{-wave})/\Gamma_{\text{total}}$

VALUE (%)	DOCUMENT ID	TECN	COMMENT
5 ± 3	ANISOVICH 17	DPWA	Multichannel
8 ± 1	¹ SHRESTHA 12A	DPWA	Multichannel

• • • We do not use the following data for averages, fits, limits, etc. • • •

5 ± 4	SOKHOYAN 15A	DPWA	Multichannel
2.8 ± 1.4	ANISOVICH 12A	DPWA	Multichannel
36 ± 1	VRANA 00	DPWA	Multichannel

¹ Statistical error only.

$\Gamma(N(1680)\pi, P\text{-wave})/\Gamma_{\text{total}}$

VALUE (%)	DOCUMENT ID	TECN	COMMENT
6 ± 3	SOKHOYAN 15A	DPWA	Multichannel

$\Gamma(\Delta(1232)\eta)/\Gamma_{\text{total}}$

VALUE (%)	DOCUMENT ID	TECN	COMMENT
0.3 ± 0.3	ANISOVICH 17	DPWA	Multichannel

• • • We do not use the following data for averages, fits, limits, etc. • • •

< 1	GUTZ 14	DPWA	Multichannel
-----	---------	------	--------------

$\Delta(1950)$ PHOTON DECAY AMPLITUDES AT THE POLE

$\Delta(1950) \rightarrow N\gamma, \text{helicity-1/2 amplitude } A_{1/2}$

MODULUS ($\text{GeV}^{-1/2}$)	PHASE ($^\circ$)	DOCUMENT ID	TECN	COMMENT
-0.067 ± 0.004	-10 ± 5	SOKHOYAN 15A	DPWA	Multichannel
-0.071 ± 0.004	-14 ± 2	ROENCHEN 14	DPWA	

• • • We do not use the following data for averages, fits, limits, etc. • • •

-0.068	-19	ROENCHEN 15A	DPWA	Multichannel
--------	-----	--------------	------	--------------

$\Delta(1950) \rightarrow N\gamma, \text{helicity-3/2 amplitude } A_{3/2}$

MODULUS ($\text{GeV}^{-1/2}$)	PHASE ($^\circ$)	DOCUMENT ID	TECN	COMMENT
-0.095 ± 0.004	-10 ± 5	SOKHOYAN 15A	DPWA	Multichannel
-0.089 ± 0.008	-10 ± 3	ROENCHEN 14	DPWA	

• • • We do not use the following data for averages, fits, limits, etc. • • •

-0.084	-19	ROENCHEN 15A	DPWA	Multichannel
--------	-----	--------------	------	--------------

$\Delta(1950)$ BREIT-WIGNER PHOTON DECAY AMPLITUDES

$\Delta(1950) \rightarrow N\gamma, \text{helicity-1/2 amplitude } A_{1/2}$

VALUE ($\text{GeV}^{-1/2}$)	DOCUMENT ID	TECN	COMMENT
-0.075 to -0.065 (\approx -0.070) OUR ESTIMATE			
-0.0698 ± 0.0141	GOLOVATCH 19	DPWA	$\gamma p \rightarrow \pi^+ \pi^- p$
-0.047 ± 0.002	¹ HUNT 19	DPWA	Multichannel
-0.067 ± 0.005	ANISOVICH 17	DPWA	Multichannel
-0.083 ± 0.004	WORKMAN 12A	DPWA	$\gamma N \rightarrow N\pi$
• • • We do not use the following data for averages, fits, limits, etc. • • •			
-0.067 ± 0.005	SOKHOYAN 15A	DPWA	Multichannel
-0.067 ± 0.005	GUTZ 14	DPWA	Multichannel
-0.071 ± 0.004	ANISOVICH 12A	DPWA	Multichannel
-0.065 ± 0.001	¹ SHRESTHA 12A	DPWA	Multichannel
-0.094	DRECHSEL 07	DPWA	$\gamma N \rightarrow \pi N$

¹ Statistical error only.

$\Delta(1950) \rightarrow N\gamma, \text{helicity-3/2 amplitude } A_{3/2}$

VALUE ($\text{GeV}^{-1/2}$)	DOCUMENT ID	TECN	COMMENT
-0.100 to -0.080 (\approx -0.090) OUR ESTIMATE			
-0.1181 ± 0.0193	GOLOVATCH 19	DPWA	$\gamma p \rightarrow \pi^+ \pi^- p$
-0.074 ± 0.002	¹ HUNT 19	DPWA	Multichannel
-0.094 ± 0.004	ANISOVICH 17	DPWA	Multichannel
-0.096 ± 0.004	WORKMAN 12A	DPWA	$\gamma N \rightarrow N\pi$
• • • We do not use the following data for averages, fits, limits, etc. • • •			
-0.094 ± 0.004	SOKHOYAN 15A	DPWA	Multichannel
-0.094 ± 0.004	GUTZ 14	DPWA	Multichannel
-0.094 ± 0.005	ANISOVICH 12A	DPWA	Multichannel
-0.083 ± 0.001	¹ SHRESTHA 12A	DPWA	Multichannel
-0.121	DRECHSEL 07	DPWA	$\gamma N \rightarrow \pi N$

¹ Statistical error only.

$\Delta(1950)$ REFERENCES

GOLOVATCH 19	PL B788 371	E. Golovatch <i>et al.</i>	(CLAS Collab.)
HUNT 19	PR C99 055205	B.C. Hunt, D.M. Manley	
ANISOVICH 17	PL B766 357	A.V. Anisovich <i>et al.</i>	
ROENCHEN 15A	EPJ A51 70	D. Roenchen <i>et al.</i>	
SOKHOYAN 15A	EPJ A51 95	V. Sokhoyan <i>et al.</i>	(CBELSA/TAPS Collab.)
GUTZ 14	EPJ A50 74	E. Gutz <i>et al.</i>	(CBELSA/TAPS Collab.)
PDG 14	CP C39 070001	K. Olive <i>et al.</i>	(PDG Collab.)
ROENCHEN 14	EPJ A50 101	D. Roenchen <i>et al.</i>	
Also	EPJ A51 63 (errata.)	D. Roenchen <i>et al.</i>	
SVARC 14	PR C89 045205	A. Svarc <i>et al.</i>	(RBI Zagreb, UNI Tuzla)

Baryon Particle Listings

 $\Delta(1950)$, $\Delta(2000)$, $\Delta(2150)$

ANISOVICH	12A	EPJ A48 15	A.V. Anisovich et al.	(BONN, PNPI)
SHRESTHA	12A	PR C86 055203	M. Shrestha, D.M. Manley	(KSU)
WORKMAN	12A	PR C86 015202	R. Workman et al.	(GWU)
DRECHSEL	07	EPJ A34 69	D. Drechsel, S.S. Kamalov, L. Tiator	(MAINZ, JINR)
ARNDT	06	PR C74 045205	R.A. Arndt et al.	(GWU)
VRANA	00	PRPL 328 181	T.P. Vrana, S.A. Dytman, T.-S.H. Lee	(PITT, ANL)
HOEHLER	93	πN Newsletter 9 1	G. Hohlner	(KARL)
CUTKOSKY	80	Toronto Conf. 19	R.E. Cutkosky et al.	(CMU, LBL) JJP
Also		PR D20 2839	R.E. Cutkosky et al.	(CMU, LBL) JJP
HOEHLER	79	PDAT 12-1	G. Hohlner et al.	(KARLT) JJP
Also		Toronto Conf. 3	R. Koch	(KARLT) JJP

 $\Delta(2000) 5/2^+$ $I(J^P) = \frac{3}{2}(\frac{5}{2}^+)$ Status: **

OMITTED FROM SUMMARY TABLE

 $\Delta(2000)$ POLE POSITION

REAL PART

VALUE (MeV)	DOCUMENT ID	TECN	COMMENT
$1998 \pm 4 \pm 4$	¹ SVARC 14	L+P	$\pi N \rightarrow \pi N$
1976	SHRESTHA 12A	DPWA	Multichannel
2150 ± 100	CUTKOSKY 80	IPWA	$\pi N \rightarrow \pi N$
••• We do not use the following data for averages, fits, limits, etc. •••			
1697	VRANA 00	DPWA	Multichannel

¹ Fit to the amplitudes of HOEHLER 79.

-2xIMAGINARY PART

VALUE (MeV)	DOCUMENT ID	TECN	COMMENT
$404 \pm 10 \pm 4$	¹ SVARC 14	L+P	$\pi N \rightarrow \pi N$
350 ± 100	CUTKOSKY 80	IPWA	$\pi N \rightarrow \pi N$
••• We do not use the following data for averages, fits, limits, etc. •••			
488	SHRESTHA 12A	DPWA	Multichannel
112	VRANA 00	DPWA	Multichannel

¹ Fit to the amplitudes of HOEHLER 79. $\Delta(2000)$ ELASTIC POLE RESIDUEMODULUS $|r|$

VALUE (MeV)	DOCUMENT ID	TECN	COMMENT
$34 \pm 1 \pm 1$	¹ SVARC 14	L+P	$\pi N \rightarrow \pi N$
16 ± 5	CUTKOSKY 80	IPWA	$\pi N \rightarrow \pi N$

¹ Fit to the amplitudes of HOEHLER 79.PHASE θ

VALUE (°)	DOCUMENT ID	TECN	COMMENT
$110 \pm 1 \pm 3$	¹ SVARC 14	L+P	$\pi N \rightarrow \pi N$
150 ± 90	CUTKOSKY 80	IPWA	$\pi N \rightarrow \pi N$

¹ Fit to the amplitudes of HOEHLER 79. $\Delta(2000)$ BREIT-WIGNER MASS

VALUE (MeV)	DOCUMENT ID	TECN	COMMENT
2015 ± 24	¹ SHRESTHA 12A	DPWA	Multichannel
2200 ± 125	CUTKOSKY 80	IPWA	$\pi N \rightarrow \pi N$
••• We do not use the following data for averages, fits, limits, etc. •••			
1724 ± 61	VRANA 00	DPWA	Multichannel
1752 ± 32	MANLEY 92	IPWA	$\pi N \rightarrow \pi N$ & $N\pi\pi$

¹ Statistical error only. $\Delta(2000)$ BREIT-WIGNER WIDTH

VALUE (MeV)	DOCUMENT ID	TECN	COMMENT
500 ± 52	¹ SHRESTHA 12A	DPWA	Multichannel
400 ± 125	CUTKOSKY 80	IPWA	$\pi N \rightarrow \pi N$
••• We do not use the following data for averages, fits, limits, etc. •••			
138 ± 68	VRANA 00	DPWA	Multichannel
251 ± 93	MANLEY 92	IPWA	$\pi N \rightarrow \pi N$ & $N\pi\pi$

¹ Statistical error only. $\Delta(2000)$ DECAY MODES

Mode	Fraction (Γ_i/Γ)
Γ_1 $N\pi$	3-11 %
Γ_2 $N\pi\pi$	
Γ_3 $\Delta(1232)\pi$, P-wave	seen
Γ_4 $\Delta(1232)\pi$, F-wave	seen
Γ_5 $N\rho$, S=3/2, P-wave	seen
Γ_6 $N\gamma$	
Γ_7 $N\gamma$, helicity=1/2	seen
Γ_8 $N\gamma$, helicity=3/2	seen

 $\Delta(2000)$ BRANCHING RATIOS

$\Gamma(N\pi)/\Gamma_{total}$	VALUE (%)	DOCUMENT ID	TECN	COMMENT	Γ_1/Γ
7 ± 1		¹ SHRESTHA 12A	DPWA	Multichannel	
7 ± 4		CUTKOSKY 80	IPWA	$\pi N \rightarrow \pi N$	
••• We do not use the following data for averages, fits, limits, etc. •••					
0 ± 1		VRANA 00	DPWA	Multichannel	
2 ± 1		MANLEY 92	IPWA	$\pi N \rightarrow \pi N$ & $N\pi\pi$	

¹ Statistical error only.

$\Gamma(\Delta(1232)\pi, P\text{-wave})/\Gamma_{total}$	VALUE (%)	DOCUMENT ID	TECN	COMMENT	Γ_3/Γ
3 ± 3		¹ SHRESTHA 12A	DPWA	Multichannel	
••• We do not use the following data for averages, fits, limits, etc. •••					
0 ± 1		VRANA 00	DPWA	Multichannel	

¹ Statistical error only.

$\Gamma(\Delta(1232)\pi, F\text{-wave})/\Gamma_{total}$	VALUE (%)	DOCUMENT ID	TECN	COMMENT	Γ_4/Γ
< 3		SHRESTHA 12A	DPWA	Multichannel	
••• We do not use the following data for averages, fits, limits, etc. •••					
40 ± 1		VRANA 00	DPWA	Multichannel	

$\Gamma(N\rho, S=3/2, P\text{-wave})/\Gamma_{total}$	VALUE (%)	DOCUMENT ID	TECN	COMMENT	Γ_5/Γ
90 ± 3		¹ SHRESTHA 12A	DPWA	Multichannel	
••• We do not use the following data for averages, fits, limits, etc. •••					
60 ± 60		VRANA 00	DPWA	Multichannel	

¹ Statistical error only. $\Delta(2000)$ BREIT-WIGNER PHOTON DECAY AMPLITUDES $\Delta(2000) \rightarrow p\gamma$, helicity-1/2 amplitude $A_{1/2}$

VALUE ($\text{GeV}^{-1/2}$)	DOCUMENT ID	TECN	COMMENT
-0.061 ± 0.018	¹ SHRESTHA 12A	DPWA	Multichannel

¹ Statistical error only. $\Delta(2000) \rightarrow p\gamma$, helicity-3/2 amplitude $A_{3/2}$

VALUE ($\text{GeV}^{-1/2}$)	DOCUMENT ID	TECN	COMMENT
0.158 ± 0.032	¹ SHRESTHA 12A	DPWA	Multichannel

¹ Statistical error only. $\Delta(2000)$ REFERENCES

SVARC	14	PR C89 045205	A. Svarc et al.	(RBI Zagreb, UNI Tuzla)
SHRESTHA	12A	PR C86 055203	M. Shrestha, D.M. Manley	(KSU)
VRANA	00	PRPL 328 181	T.P. Vrana, S.A. Dytman, T.-S.H. Lee	(PITT, ANL)
MANLEY	92	PR D30 904	D.M. Manley, E.M. Saleski	(KSA) IJP
Also			D.M. Manley et al.	(VPI)
CUTKOSKY	80	Toronto Conf. 19	R.E. Cutkosky et al.	(CMU, LBL)
Also		PR D20 2839	R.E. Cutkosky et al.	(CMU, LBL)
HOEHLER	79	PDAT 12-1	G. Hohlner et al.	(KARLT)

 $\Delta(2150) 1/2^-$ $I(J^P) = \frac{3}{2}(\frac{1}{2}^-)$ Status: *

OMITTED FROM SUMMARY TABLE

 $\Delta(2150)$ POLE POSITION

REAL PART

VALUE (MeV)	DOCUMENT ID	TECN	COMMENT
2140 ± 80	CUTKOSKY 80	IPWA	$\pi N \rightarrow \pi N$

-2xIMAGINARY PART

VALUE (MeV)	DOCUMENT ID	TECN	COMMENT
200 ± 80	CUTKOSKY 80	IPWA	$\pi N \rightarrow \pi N$

 $\Delta(2150)$ ELASTIC POLE RESIDUE

MODULUS $ r $	VALUE (MeV)	DOCUMENT ID	TECN	COMMENT
7 ± 2		CUTKOSKY 80	IPWA	$\pi N \rightarrow \pi N$

PHASE θ

VALUE (°)	DOCUMENT ID	TECN	COMMENT
-60 ± 90	CUTKOSKY 80	IPWA	$\pi N \rightarrow \pi N$

See key on page 999

Baryon Particle Listings
 $\Delta(2150)$, $\Delta(2200)$

$\Delta(2150)$ BREIT-WIGNER MASS

VALUE (MeV)	DOCUMENT ID	TECN	COMMENT
2150 ± 100	CUTKOSKY 80	IPWA	$\pi N \rightarrow \pi N$

$\Delta(2150)$ BREIT-WIGNER WIDTH

VALUE (MeV)	DOCUMENT ID	TECN	COMMENT
200 ± 100	CUTKOSKY 80	IPWA	$\pi N \rightarrow \pi N$

$\Delta(2150)$ DECAY MODES

Mode	Fraction (Γ_i/Γ)
Γ_1 $N\pi$	6–10 %

$\Delta(2150)$ BRANCHING RATIOS

$\Gamma(N\pi)/\Gamma_{total}$	DOCUMENT ID	TECN	COMMENT	Γ_1/Γ
8 ± 2	CUTKOSKY 80	IPWA	$\pi N \rightarrow \pi N$	

$\Delta(2150)$ REFERENCES

CUTKOSKY 80	Toronto Conf. 19	R.E. Cutkosky et al.	(CMU, LBL) IJP
Also	PR D20 2839	R.E. Cutkosky et al.	(CMU, LBL)

$\Delta(2200) 7/2^-$

$$I(J^P) = \frac{3}{2}(\frac{7}{2}^-) \text{ Status: } ***$$

$\Delta(2200)$ POLE POSITION

REAL PART

VALUE (MeV)	DOCUMENT ID	TECN	COMMENT
2050 to 2150 (≈ 2100) OUR ESTIMATE			
2100 ± 50	CUTKOSKY 80	IPWA	$\pi N \rightarrow \pi N$
••• We do not use the following data for averages, fits, limits, etc. •••			
2142	ROENCHEN 15A	DPWA	Multichannel

–2xIMAGINARY PART

VALUE (MeV)	DOCUMENT ID	TECN	COMMENT
260 to 420 (≈ 340) OUR ESTIMATE			
340 ± 80	CUTKOSKY 80	IPWA	$\pi N \rightarrow \pi N$
••• We do not use the following data for averages, fits, limits, etc. •••			
486	ROENCHEN 15A	DPWA	Multichannel

$\Delta(2200)$ ELASTIC POLE RESIDUE

MODULUS $|r|$

VALUE (MeV)	DOCUMENT ID	TECN	COMMENT
8 ± 3	CUTKOSKY 80	IPWA	$\pi N \rightarrow \pi N$
••• We do not use the following data for averages, fits, limits, etc. •••			
17	ROENCHEN 15A	DPWA	Multichannel

PHASE θ

VALUE (°)	DOCUMENT ID	TECN	COMMENT
–70 ± 40	CUTKOSKY 80	IPWA	$\pi N \rightarrow \pi N$
••• We do not use the following data for averages, fits, limits, etc. •••			
–56	ROENCHEN 15A	DPWA	Multichannel

$\Delta(2200)$ INELASTIC POLE RESIDUE

The "normalized residue" is the residue divided by $\Gamma_{pole}/2$.

Normalized residue in $N\pi \rightarrow \Delta(2200) \rightarrow \Sigma K$

MODULUS	PHASE (°)	DOCUMENT ID	TECN	COMMENT
••• We do not use the following data for averages, fits, limits, etc. •••				
0.005	–103	ROENCHEN 15A	DPWA	Multichannel

Normalized residue in $N\pi \rightarrow \Delta(2200) \rightarrow \Delta\pi, D\text{-wave}$

MODULUS	PHASE (°)	DOCUMENT ID	TECN	COMMENT
••• We do not use the following data for averages, fits, limits, etc. •••				
0.23	107	ROENCHEN 15A	DPWA	Multichannel

Normalized residue in $N\pi \rightarrow \Delta(2200) \rightarrow \Delta\pi, G\text{-wave}$

MODULUS	PHASE (°)	DOCUMENT ID	TECN	COMMENT
••• We do not use the following data for averages, fits, limits, etc. •••				
0.022	–151	ROENCHEN 15A	DPWA	Multichannel

$\Delta(2200)$ BREIT-WIGNER MASS

VALUE (MeV)	DOCUMENT ID	TECN	COMMENT
2150 to 2250 (≈ 2200) OUR ESTIMATE			
2176 ± 40	ANISOVICH 17	DPWA	Multichannel
2200 ± 80	CUTKOSKY 80	IPWA	$\pi N \rightarrow \pi N$
2215 ± 60	HOEHLER 79	IPWA	$\pi N \rightarrow \pi N$

$\Delta(2200)$ BREIT-WIGNER WIDTH

VALUE (MeV)	DOCUMENT ID	TECN	COMMENT
200 to 500 (≈ 350) OUR ESTIMATE			
210 ± 70	ANISOVICH 17	DPWA	Multichannel
450 ± 100	CUTKOSKY 80	IPWA	$\pi N \rightarrow \pi N$
400 ± 100	HOEHLER 79	IPWA	$\pi N \rightarrow \pi N$

$\Delta(2200)$ DECAY MODES

Mode	Fraction (Γ_i/Γ)
Γ_1 $N\pi$	2–8 %
Γ_2 ΣK	1–7 %
Γ_3 $\Delta\pi, D\text{-wave}$	40–100 %
Γ_4 $\Delta\pi, G\text{-wave}$	5–25 %
Γ_5 $\Delta\eta, D\text{-wave}$	seen

$\Delta(2200)$ BRANCHING RATIOS

$\Gamma(N\pi)/\Gamma_{total}$	DOCUMENT ID	TECN	COMMENT	Γ_1/Γ
2 to 8 (≈ 5) OUR ESTIMATE				
3.5 ± 1.5	ANISOVICH 17	DPWA	Multichannel	
6 ± 2	CUTKOSKY 80	IPWA	$\pi N \rightarrow \pi N$	
5 ± 2	HOEHLER 79	IPWA	$\pi N \rightarrow \pi N$	

$\Gamma(\Sigma K)/\Gamma_{total}$	DOCUMENT ID	TECN	COMMENT	Γ_2/Γ
0.04 ± 0.03	ANISOVICH 17	DPWA	Multichannel	

$\Gamma(\Delta\pi, D\text{-wave})/\Gamma_{total}$	DOCUMENT ID	TECN	COMMENT	Γ_3/Γ
0.70 ± 0.30	ANISOVICH 17	DPWA	Multichannel	

$\Gamma(\Delta\pi, G\text{-wave})/\Gamma_{total}$	DOCUMENT ID	TECN	COMMENT	Γ_4/Γ
0.15 ± 0.10	ANISOVICH 17	DPWA	Multichannel	

$\Gamma(\Delta\eta, D\text{-wave})/\Gamma_{total}$	DOCUMENT ID	TECN	COMMENT	Γ_5/Γ
~ 0.01	ANISOVICH 17	DPWA	Multichannel	

$\Delta(2200)$ PHOTON DECAY AMPLITUDES AT THE POLE

$\Delta(2200) \rightarrow N\gamma, \text{ helicity-1/2 amplitude } A_{1/2}$

MODULUS ($\text{GeV}^{-1/2}$)	PHASE (°)	DOCUMENT ID	TECN	COMMENT
0.107 ^{+0.011} _{–0.020}	–36 ± 5	ROENCHEN 14	DPWA	
••• We do not use the following data for averages, fits, limits, etc. •••				
0.106	–23	ROENCHEN 15A	DPWA	Multichannel

$\Delta(2200) \rightarrow N\gamma, \text{ helicity-3/2 amplitude } A_{3/2}$

MODULUS ($\text{GeV}^{-1/2}$)	PHASE (°)	DOCUMENT ID	TECN	COMMENT
–0.131 ^{+0.024} _{–0.009}	113 ⁺⁹ _{–5}	ROENCHEN 14	DPWA	
••• We do not use the following data for averages, fits, limits, etc. •••				
0.157	–60	ROENCHEN 15A	DPWA	Multichannel

$\Delta(2200)$ REFERENCES

ANISOVICH 17	PL B766 357	A.V. Anisovich et al.	
ROENCHEN 15A	EPJ A51 70	D. Roenchen et al.	
ROENCHEN 14	EPJ A50 101	D. Roenchen et al.	
Also	EPJ A51 63 (errat.)	D. Roenchen et al.	
CUTKOSKY 80	Toronto Conf. 19	R.E. Cutkosky et al.	(CMU, LBL) IJP
Also	PR D20 2839	R.E. Cutkosky et al.	(CMU, LBL) IJP
HOEHLER 79	PDAT 12-1	G. Hoehler et al.	(KARLT) IJP
Also	Toronto Conf. 3	R. Koch	(KARLT) IJP

Baryon Particle Listings

 $\Delta(2300)$, $\Delta(2350)$, $\Delta(2390)$

$$\Delta(2300) \ 9/2^+$$

$$I(J^P) = \frac{3}{2}(\frac{9}{2}^+) \text{ Status: } **$$

OMITTED FROM SUMMARY TABLE

 $\Delta(2300)$ POLE POSITION

REAL PART

VALUE (MeV)	DOCUMENT ID	TECN	COMMENT
2370 ± 80	CUTKOSKY 80	IPWA	$\pi N \rightarrow \pi N$

-2xIMAGINARY PART

VALUE (MeV)	DOCUMENT ID	TECN	COMMENT
420 ± 160	CUTKOSKY 80	IPWA	$\pi N \rightarrow \pi N$

 $\Delta(2300)$ ELASTIC POLE RESIDUEMODULUS $|r|$

VALUE (MeV)	DOCUMENT ID	TECN	COMMENT
10 ± 4	CUTKOSKY 80	IPWA	$\pi N \rightarrow \pi N$

PHASE θ

VALUE (°)	DOCUMENT ID	TECN	COMMENT
-20 ± 30	CUTKOSKY 80	IPWA	$\pi N \rightarrow \pi N$

 $\Delta(2300)$ BREIT-WIGNER MASS

VALUE (MeV)	DOCUMENT ID	TECN	COMMENT
2400 ± 125	CUTKOSKY 80	IPWA	$\pi N \rightarrow \pi N$
2217 ± 80	HOEHLER 79	IPWA	$\pi N \rightarrow \pi N$

 $\Delta(2300)$ BREIT-WIGNER WIDTH

VALUE (MeV)	DOCUMENT ID	TECN	COMMENT
425 ± 150	CUTKOSKY 80	IPWA	$\pi N \rightarrow \pi N$
300 ± 100	HOEHLER 79	IPWA	$\pi N \rightarrow \pi N$

 $\Delta(2300)$ DECAY MODES

Mode	Fraction (Γ_i/Γ)
$\Gamma_1 \ N \pi$	1-8 %

 $\Delta(2300)$ BRANCHING RATIOS

$\Gamma(N\pi)/\Gamma_{\text{total}}$	DOCUMENT ID	TECN	COMMENT	Γ_1/Γ
6 ± 2	CUTKOSKY 80	IPWA	$\pi N \rightarrow \pi N$	
3 ± 2	HOEHLER 79	IPWA	$\pi N \rightarrow \pi N$	

 $\Delta(2300)$ REFERENCES

CUTKOSKY 80	Toronto Conf. 19	R.E. Cutkosky <i>et al.</i>	(CMU, LBL) IJP
Also	PR D20 2839	R.E. Cutkosky <i>et al.</i>	(CMU, LBL)
HOEHLER 79	PDAT 12-1	G. Hoehler <i>et al.</i>	(KARLT) IJP
Also	Toronto Conf. 3	R. Koch	(KARLT) IJP

$$\Delta(2350) \ 5/2^-$$

$$I(J^P) = \frac{3}{2}(\frac{5}{2}^-) \text{ Status: } *$$

OMITTED FROM SUMMARY TABLE

 $\Delta(2350)$ POLE POSITION

REAL PART

VALUE (MeV)	DOCUMENT ID	TECN	COMMENT
2400 ± 125	CUTKOSKY 80	IPWA	$\pi N \rightarrow \pi N$

••• We do not use the following data for averages, fits, limits, etc. •••

2427	VRANA 00	DPWA	Multichannel
------	----------	------	--------------

-2xIMAGINARY PART

VALUE (MeV)	DOCUMENT ID	TECN	COMMENT
400 ± 150	CUTKOSKY 80	IPWA	$\pi N \rightarrow \pi N$

••• We do not use the following data for averages, fits, limits, etc. •••

458	VRANA 00	DPWA	Multichannel
-----	----------	------	--------------

 $\Delta(2350)$ ELASTIC POLE RESIDUEMODULUS $|r|$

VALUE (MeV)	DOCUMENT ID	TECN	COMMENT
15 ± 8	CUTKOSKY 80	IPWA	$\pi N \rightarrow \pi N$

PHASE θ

VALUE (°)	DOCUMENT ID	TECN	COMMENT
-70 ± 70	CUTKOSKY 80	IPWA	$\pi N \rightarrow \pi N$

 $\Delta(2350)$ BREIT-WIGNER MASS

VALUE (MeV)	DOCUMENT ID	TECN	COMMENT
2400 ± 125	CUTKOSKY 80	IPWA	$\pi N \rightarrow \pi N$
2305 ± 26	HOEHLER 79	IPWA	$\pi N \rightarrow \pi N$

••• We do not use the following data for averages, fits, limits, etc. •••

2459 ± 100	VRANA 00	DPWA	Multichannel
------------	----------	------	--------------

 $\Delta(2350)$ BREIT-WIGNER WIDTH

VALUE (MeV)	DOCUMENT ID	TECN	COMMENT
400 ± 150	CUTKOSKY 80	IPWA	$\pi N \rightarrow \pi N$
300 ± 70	HOEHLER 79	IPWA	$\pi N \rightarrow \pi N$

••• We do not use the following data for averages, fits, limits, etc. •••

480 ± 360	VRANA 00	DPWA	Multichannel
-----------	----------	------	--------------

 $\Delta(2350)$ DECAY MODES

Mode	Fraction (Γ_i/Γ)
$\Gamma_1 \ N \pi$	4-30 %

 $\Delta(2350)$ BRANCHING RATIOS

$\Gamma(N\pi)/\Gamma_{\text{total}}$	DOCUMENT ID	TECN	COMMENT	Γ_1/Γ
20 ± 10	CUTKOSKY 80	IPWA	$\pi N \rightarrow \pi N$	
4 ± 2	HOEHLER 79	IPWA	$\pi N \rightarrow \pi N$	

••• We do not use the following data for averages, fits, limits, etc. •••

7 ± 14	VRANA 00	DPWA	Multichannel
--------	----------	------	--------------

 $\Delta(2350)$ REFERENCES

VRANA 00	PRPL 328 181	T.P. Vrana, S.A. Dytman, T.-S.H. Lee	(PITT, ANL)
CUTKOSKY 80	Toronto Conf. 19	R.E. Cutkosky <i>et al.</i>	(CMU, LBL) IJP
Also	PR D20 2839	R.E. Cutkosky <i>et al.</i>	(CMU, LBL)
HOEHLER 79	PDAT 12-1	G. Hoehler <i>et al.</i>	(KARLT) IJP
Also	Toronto Conf. 3	R. Koch	(KARLT) IJP

$$\Delta(2390) \ 7/2^+$$

$$I(J^P) = \frac{3}{2}(\frac{7}{2}^+) \text{ Status: } *$$

OMITTED FROM SUMMARY TABLE

 $\Delta(2390)$ POLE POSITION

REAL PART

VALUE (MeV)	DOCUMENT ID	TECN	COMMENT
2223 ± 15 ± 19	¹ SVARC 14	L+P	$\pi N \rightarrow \pi N$
2350 ± 100	CUTKOSKY 80	IPWA	$\pi N \rightarrow \pi N$

-2xIMAGINARY PART

VALUE (MeV)	DOCUMENT ID	TECN	COMMENT
431 ± 26 ± 7	¹ SVARC 14	L+P	$\pi N \rightarrow \pi N$
260 ± 100	CUTKOSKY 80	IPWA	$\pi N \rightarrow \pi N$

 $\Delta(2390)$ ELASTIC POLE RESIDUEMODULUS $|r|$

VALUE (MeV)	DOCUMENT ID	TECN	COMMENT
26 ± 2 ± 1	¹ SVARC 14	L+P	$\pi N \rightarrow \pi N$
12 ± 6	CUTKOSKY 80	IPWA	$\pi N \rightarrow \pi N$

PHASE θ

VALUE (°)	DOCUMENT ID	TECN	COMMENT
-160 ± 5 ± 11	¹ SVARC 14	L+P	$\pi N \rightarrow \pi N$
-90 ± 60	CUTKOSKY 80	IPWA	$\pi N \rightarrow \pi N$

 $\Delta(2390)$ BREIT-WIGNER MASS

VALUE (MeV)	DOCUMENT ID	TECN	COMMENT
2350 ± 100	CUTKOSKY 80	IPWA	$\pi N \rightarrow \pi N$
2425 ± 60	HOEHLER 79	IPWA	$\pi N \rightarrow \pi N$

 $\Delta(2390)$ BREIT-WIGNER WIDTH

VALUE (MeV)	DOCUMENT ID	TECN	COMMENT
300 ± 100	CUTKOSKY 80	IPWA	$\pi N \rightarrow \pi N$
300 ± 80	HOEHLER 79	IPWA	$\pi N \rightarrow \pi N$

See key on page 999

Baryon Particle Listings

$\Delta(2390)$, $\Delta(2400)$, $\Delta(2420)$

$\Delta(2390)$ DECAY MODES

Mode	Fraction (Γ_i/Γ)
Γ_1 $N\pi$	3–12 %

$\Delta(2390)$ BRANCHING RATIOS

$\Gamma(N\pi)/\Gamma_{total}$	DOCUMENT ID	TECN	COMMENT	Γ_1/Γ
8±4	CUTKOSKY 80	IPWA	$\pi N \rightarrow \pi N$	
7±4	HOEHLER 79	IPWA	$\pi N \rightarrow \pi N$	

$\Delta(2390)$ FOOTNOTES

¹ Fit to the amplitudes of HOEHLER 79.

$\Delta(2390)$ REFERENCES

SVARC 14	PR C89 045205	A. Svarc et al.	(RBI Zagreb, UNI Tuzla)
CUTKOSKY 80	Toronto Conf. 19	R.E. Cutkosky et al.	(CMU, LBL) IJP
Also	PR D20 2839	R.E. Cutkosky et al.	(CMU, LBL)
HOEHLER 79	PDAT 12-1	G. Hohlner et al.	(KARLT) IJP
Also	Toronto Conf. 3	R. Koch	(KARLT) IJP

$\Delta(2400) 9/2^-$

 $I(J^P) = \frac{3}{2}(\frac{9}{2}^-)$ Status: **

OMITTED FROM SUMMARY TABLE

$\Delta(2400)$ POLE POSITION

REAL PART

VALUE (MeV)	DOCUMENT ID	TECN	COMMENT
2260±60	CUTKOSKY 80	IPWA	$\pi N \rightarrow \pi N$
•••	We do not use the following data for averages, fits, limits, etc. •••		
1931	ROENCHEN 15A	DPWA	Multichannel
1983	ARNDT 06	DPWA	$\pi N \rightarrow \pi N, \eta N$

-2xIMAGINARY PART

VALUE (MeV)	DOCUMENT ID	TECN	COMMENT
320±160	CUTKOSKY 80	IPWA	$\pi N \rightarrow \pi N$
•••	We do not use the following data for averages, fits, limits, etc. •••		
442	ROENCHEN 15A	DPWA	Multichannel
878	ARNDT 06	DPWA	$\pi N \rightarrow \pi N, \eta N$

$\Delta(2400)$ ELASTIC POLE RESIDUE

MODULUS |r|

VALUE (MeV)	DOCUMENT ID	TECN	COMMENT
8±4	CUTKOSKY 80	IPWA	$\pi N \rightarrow \pi N$
•••	We do not use the following data for averages, fits, limits, etc. •••		
13	ROENCHEN 15A	DPWA	Multichannel
24	ARNDT 06	DPWA	$\pi N \rightarrow \pi N, \eta N$

PHASE θ

VALUE (°)	DOCUMENT ID	TECN	COMMENT
-25±15	CUTKOSKY 80	IPWA	$\pi N \rightarrow \pi N$
•••	We do not use the following data for averages, fits, limits, etc. •••		
-96	ROENCHEN 15A	DPWA	Multichannel
-139	ARNDT 06	DPWA	$\pi N \rightarrow \pi N, \eta N$

$\Delta(2400)$ INELASTIC POLE RESIDUE

The "normalized residue" is the residue divided by $\Gamma_{pole}/2$.

Normalized residue in $N\pi \rightarrow \Delta(2400) \rightarrow \Sigma K$

MODULUS	PHASE (°)	DOCUMENT ID	TECN	COMMENT
•••	We do not use the following data for averages, fits, limits, etc. •••			
0.009	25	ROENCHEN 15A	DPWA	Multichannel

Normalized residue in $N\pi \rightarrow \Delta(2400) \rightarrow \Delta\pi, G$ -wave

MODULUS	PHASE (°)	DOCUMENT ID	TECN	COMMENT
•••	We do not use the following data for averages, fits, limits, etc. •••			
0.18	-110	ROENCHEN 15A	DPWA	Multichannel

Normalized residue in $N\pi \rightarrow \Delta(2400) \rightarrow \Delta\pi, F$ -wave

MODULUS	PHASE (°)	DOCUMENT ID	TECN	COMMENT
•••	We do not use the following data for averages, fits, limits, etc. •••			
0.012	-1.0	ROENCHEN 15A	DPWA	Multichannel

$\Delta(2400)$ BREIT-WIGNER MASS

VALUE (MeV)	DOCUMENT ID	TECN	COMMENT
2643±141	¹ ARNDT 06	DPWA	$\pi N \rightarrow \pi N, \eta N$
2300±100	CUTKOSKY 80	IPWA	$\pi N \rightarrow \pi N$
2468±50	HOEHLER 79	IPWA	$\pi N \rightarrow \pi N$

¹ Statistical error only.

$\Delta(2400)$ BREIT-WIGNER WIDTH

VALUE (MeV)	DOCUMENT ID	TECN	COMMENT
895±432	² ARNDT 06	DPWA	$\pi N \rightarrow \pi N, \eta N$
330±100	CUTKOSKY 80	IPWA	$\pi N \rightarrow \pi N$
480±100	HOEHLER 79	IPWA	$\pi N \rightarrow \pi N$

² Statistical error only.

$\Delta(2400)$ DECAY MODES

Mode	Fraction (Γ_i/Γ)
Γ_1 $N\pi$	3–9 %

$\Delta(2400)$ BRANCHING RATIOS

$\Gamma(N\pi)/\Gamma_{total}$	DOCUMENT ID	TECN	COMMENT	Γ_1/Γ
6.4±2.2	³ ARNDT 06	DPWA	$\pi N \rightarrow \pi N, \eta N$	
5 ±2	CUTKOSKY 80	IPWA	$\pi N \rightarrow \pi N$	
6 ±3	HOEHLER 79	IPWA	$\pi N \rightarrow \pi N$	

³ Statistical error only.

$\Delta(2400)$ PHOTON DECAY AMPLITUDES AT THE POLE

$\Delta(2400) \rightarrow N\gamma$, helicity-1/2 amplitude $A_{1/2}$

MODULUS ($\text{GeV}^{-1/2}$)	PHASE (°)	DOCUMENT ID	TECN	COMMENT
-0.128 ^{+0.046} _{-0.012}	118 ⁺²⁴ ₋₃	ROENCHEN 14	DPWA	
•••	We do not use the following data for averages, fits, limits, etc. •••			
-0.034	63	ROENCHEN 15A	DPWA	Multichannel

$\Delta(2400) \rightarrow N\gamma$, helicity-3/2 amplitude $A_{3/2}$

MODULUS ($\text{GeV}^{-1/2}$)	PHASE (°)	DOCUMENT ID	TECN	COMMENT
-0.115 ^{+0.042} _{-0.024}	140 ⁺¹⁷ ₋₂₈	ROENCHEN 14	DPWA	
•••	We do not use the following data for averages, fits, limits, etc. •••			
0.054	-75	ROENCHEN 15A	DPWA	Multichannel

$\Delta(2400)$ REFERENCES

ROENCHEN 15A	EPJ A51 70	D. Roenchen et al.
ROENCHEN 14	EPJ A50 101	D. Roenchen et al.
Also	EPJ A51 63 (errat.)	D. Roenchen et al.
ARNDT 06	PR C74 045205	R.A. Arndt et al.
CUTKOSKY 80	Toronto Conf. 19	R.E. Cutkosky et al.
Also	PR D20 2839	R.E. Cutkosky et al.
HOEHLER 79	PDAT 12-1	G. Hohlner et al.
Also	Toronto Conf. 3	R. Koch

$\Delta(2420) 11/2^+$

 $I(J^P) = \frac{3}{2}(\frac{11}{2}^+)$ Status: ***

Older and obsolete values are listed and referenced in the 2014 edition, Chinese Physics C38 070001 (2014).

$\Delta(2420)$ POLE POSITION

REAL PART

VALUE (MeV)	DOCUMENT ID	TECN	COMMENT
2300 to 2500 (≈ 2400) OUR ESTIMATE			
2454 ± 4±11	¹ SVARC 14	L+P	$\pi N \rightarrow \pi N$
2360±100	CUTKOSKY 80	IPWA	$\pi N \rightarrow \pi N$
•••	We do not use the following data for averages, fits, limits, etc. •••		
2529	ARNDT 06	DPWA	$\pi N \rightarrow \pi N, \eta N$
2300	HOEHLER 93	ARGD	$\pi N \rightarrow \pi N$

¹ Fit to the amplitudes of HOEHLER 79.

-2xIMAGINARY PART

VALUE (MeV)	DOCUMENT ID	TECN	COMMENT
350 to 550 (≈ 450) OUR ESTIMATE			
462 ± 8±50	¹ SVARC 14	L+P	$\pi N \rightarrow \pi N$
420±100	CUTKOSKY 80	IPWA	$\pi N \rightarrow \pi N$
•••	We do not use the following data for averages, fits, limits, etc. •••		
621	ARNDT 06	DPWA	$\pi N \rightarrow \pi N, \eta N$
620	HOEHLER 93	ARGD	$\pi N \rightarrow \pi N$

¹ Fit to the amplitudes of HOEHLER 79.

Baryon Particle Listings

 $\Delta(2420)$, $\Delta(2750)$, $\Delta(2950)$, $\Delta(\sim 3000)$ $\Delta(2420)$ ELASTIC POLE RESIDUEMODULUS $|r|$

VALUE (MeV)	DOCUMENT ID	TECN	COMMENT
20 to 40 (≈ 30) OUR ESTIMATE			
$30 \pm 1 \pm 7$	¹ SVARC	14	L+P $\pi N \rightarrow \pi N$
18 ± 6	CUTKOSKY	80	IPWA $\pi N \rightarrow \pi N$
••• We do not use the following data for averages, fits, limits, etc. •••			
33	ARNDT	06	DPWA $\pi N \rightarrow \pi N, \eta N$
39	HOEHLER	93	ARGD $\pi N \rightarrow \pi N$

¹ Fit to the amplitudes of HOEHLER 79.PHASE θ

VALUE (°)	DOCUMENT ID	TECN	COMMENT
-60 to 20 (≈ -20) OUR ESTIMATE			
$11 \pm 1 \pm 8$	¹ SVARC	14	L+P $\pi N \rightarrow \pi N$
-30 ± 40	CUTKOSKY	80	IPWA $\pi N \rightarrow \pi N$
••• We do not use the following data for averages, fits, limits, etc. •••			
-45	ARNDT	06	DPWA $\pi N \rightarrow \pi N, \eta N$
-60	HOEHLER	93	ARGD $\pi N \rightarrow \pi N$

¹ Fit to the amplitudes of HOEHLER 79. $\Delta(2420)$ BREIT-WIGNER MASS

VALUE (MeV)	DOCUMENT ID	TECN	COMMENT
2300 to 2600 (≈ 2450) OUR ESTIMATE			
2633 ± 29	¹ ARNDT	06	DPWA $\pi N \rightarrow \pi N, \eta N$
2400 ± 125	CUTKOSKY	80	IPWA $\pi N \rightarrow \pi N$
2416 ± 17	HOEHLER	79	IPWA $\pi N \rightarrow \pi N$

¹ Statistical error only. $\Delta(2420)$ BREIT-WIGNER WIDTH

VALUE (MeV)	DOCUMENT ID	TECN	COMMENT
300 to 700 (≈ 500) OUR ESTIMATE			
692 ± 47	¹ ARNDT	06	DPWA $\pi N \rightarrow \pi N, \eta N$
450 ± 150	CUTKOSKY	80	IPWA $\pi N \rightarrow \pi N$
340 ± 28	HOEHLER	79	IPWA $\pi N \rightarrow \pi N$

¹ Statistical error only. $\Delta(2420)$ DECAY MODES

The following branching fractions are our estimates, not fits or averages.

Mode	Fraction (Γ_i/Γ)
Γ_1 $N\pi$	5-10 %

 $\Delta(2420)$ BRANCHING RATIOS

$\Gamma(N\pi)/\Gamma_{\text{total}}$	DOCUMENT ID	TECN	COMMENT	Γ_1/Γ
5 to 10 (≈ 8) OUR ESTIMATE				
8.5 ± 0.8	¹ ARNDT	06	DPWA $\pi N \rightarrow \pi N, \eta N$	
8 ± 3	CUTKOSKY	80	IPWA $\pi N \rightarrow \pi N$	
8.0 ± 1.5	HOEHLER	79	IPWA $\pi N \rightarrow \pi N$	

¹ Statistical error only. $\Delta(2420)$ REFERENCES

PDG	14	CP C38 070001	K. Olive <i>et al.</i>	(PDG Collab.)
SVARC	14	PR C89 045205	A. Svarc <i>et al.</i>	(RBI Zagreb, UNI Tuzla)
ARNDT	06	PR C74 045205	R.A. Arndt <i>et al.</i>	(GWU)
HOEHLER	93	πN Newsletter 9 1	G. Höhler	(KARL)
CUTKOSKY	80	Toronto Conf. 19	R.E. Cutkosky <i>et al.</i>	(CMU, LBL) IJP
Also		PR D20 2839	R.E. Cutkosky <i>et al.</i>	(CMU, LBL)
HOEHLER	79	PDAT 12-1	G. Höhler <i>et al.</i>	(KARLT) IJP
Also		Toronto Conf. 3	R. Koch	(KARLT) IJP

$$\Delta(2750) 13/2^- \quad I(J^P) = \frac{3}{2}(\frac{13}{2}^-) \text{Status: } **$$

OMITTED FROM SUMMARY TABLE

 $\Delta(2750)$ BREIT-WIGNER MASS

VALUE (MeV)	DOCUMENT ID	TECN	COMMENT
2794 ± 80	HOEHLER	79	IPWA $\pi N \rightarrow \pi N$

 $\Delta(2750)$ BREIT-WIGNER WIDTH

VALUE (MeV)	DOCUMENT ID	TECN	COMMENT
350 ± 100	HOEHLER	79	IPWA $\pi N \rightarrow \pi N$

 $\Delta(2750)$ DECAY MODES

Mode	Fraction (Γ_i/Γ)
Γ_1 $N\pi$	2-6 %

 $\Delta(2750)$ BRANCHING RATIOS

$\Gamma(N\pi)/\Gamma_{\text{total}}$	DOCUMENT ID	TECN	COMMENT	Γ_1/Γ
VALUE (%)				
4.0 ± 1.5	HOEHLER	79	IPWA $\pi N \rightarrow \pi N$	

 $\Delta(2750)$ REFERENCES

HOEHLER	79	PDAT 12-1	G. Höhler <i>et al.</i>	(KARLT) IJP
Also		Toronto Conf. 3	R. Koch	(KARLT) IJP

$$\Delta(2950) 15/2^+ \quad I(J^P) = \frac{3}{2}(\frac{15}{2}^+) \text{Status: } **$$

OMITTED FROM SUMMARY TABLE

 $\Delta(2950)$ BREIT-WIGNER MASS

VALUE (MeV)	DOCUMENT ID	TECN	COMMENT
2990 ± 100	HOEHLER	79	IPWA $\pi N \rightarrow \pi N$

 $\Delta(2950)$ BREIT-WIGNER WIDTH

VALUE (MeV)	DOCUMENT ID	TECN	COMMENT
330 ± 100	HOEHLER	79	IPWA $\pi N \rightarrow \pi N$

 $\Delta(2950)$ DECAY MODES

Mode	Fraction (Γ_i/Γ)
Γ_1 $N\pi$	2-6 %

 $\Delta(2950)$ BRANCHING RATIOS

$\Gamma(N\pi)/\Gamma_{\text{total}}$	DOCUMENT ID	TECN	COMMENT	Γ_1/Γ
VALUE (%)				
4 ± 2	HOEHLER	79	IPWA $\pi N \rightarrow \pi N$	

 $\Delta(2950)$ REFERENCES

HOEHLER	79	PDAT 12-1	G. Höhler <i>et al.</i>	(KARLT) IJP
Also		Toronto Conf. 3	R. Koch	(KARLT) IJP

$$\Delta(\sim 3000 \text{ Region}) \text{ Partial-Wave Analyses}$$

OMITTED FROM SUMMARY TABLE

We list here miscellaneous high-mass candidates for isospin-3/2 resonances found in partial-wave analyses.

Our 1982 edition also had a $\Delta(2850)$ and a $\Delta(3230)$. The evidence for them was deduced from total cross-section and 180° elastic cross-section measurements. The $\Delta(2850)$ has been resolved into the $\Delta(2750) \frac{1}{2}^-$ and $\Delta(2950) \frac{3}{2}^-$. The $\Delta(3230)$ is perhaps related to the $K_{3,13}$ of HENDRY 78 and to the $L_{3,17}$ of KOCH 80.

 $\Delta(\sim 3000)$ BREIT-WIGNER MASS

VALUE (MeV)	DOCUMENT ID	TECN	COMMENT
3300	¹ KOCH	80	IPWA $\pi N \rightarrow \pi N$ $L_{3,17}$ wave
3500	¹ KOCH	80	IPWA $\pi N \rightarrow \pi N$ $M_{3,19}$ wave
2850 ± 150	HENDRY	78	MPWA $\pi N \rightarrow \pi N$ $I_{3,11}$ wave
3200 ± 200	HENDRY	78	MPWA $\pi N \rightarrow \pi N$ $K_{3,13}$ wave
3300 ± 200	HENDRY	78	MPWA $\pi N \rightarrow \pi N$ $L_{3,17}$ wave
3700 ± 200	HENDRY	78	MPWA $\pi N \rightarrow \pi N$ $M_{3,19}$ wave
4100 ± 300	HENDRY	78	MPWA $\pi N \rightarrow \pi N$ $N_{3,21}$ wave

 $\Delta(\sim 3000)$ BREIT-WIGNER WIDTH

VALUE (MeV)	DOCUMENT ID	TECN	COMMENT
700 ± 200	HENDRY	78	MPWA $\pi N \rightarrow \pi N$ $I_{3,11}$ wave
1000 ± 300	HENDRY	78	MPWA $\pi N \rightarrow \pi N$ $K_{3,13}$ wave
1100 ± 300	HENDRY	78	MPWA $\pi N \rightarrow \pi N$ $L_{3,17}$ wave
1300 ± 400	HENDRY	78	MPWA $\pi N \rightarrow \pi N$ $M_{3,19}$ wave
1600 ± 500	HENDRY	78	MPWA $\pi N \rightarrow \pi N$ $N_{3,21}$ wave

See key on page 999

Baryon Particle Listings

 $\Delta(\sim 3000)$ $\Delta(\sim 3000)$ DECAY MODES

Mode	Fraction (Γ_i/Γ)
Γ_1 $N\pi$	seen

 $\Delta(\sim 3000)$ BRANCHING RATIOS

$\Gamma(N\pi)/\Gamma_{\text{total}}$ VALUE (%)	DOCUMENT ID	TECN	COMMENT	Γ_1/Γ
6 ± 2	HENDRY	78	MPWA $\pi N \rightarrow \pi N I_{3,11}$ wave	
5 ± 2	HENDRY	78	MPWA $\pi N \rightarrow \pi N K_{3,13}$ wave	
3 ± 1	HENDRY	78	MPWA $\pi N \rightarrow \pi N L_{3,17}$ wave	
3 ± 1	HENDRY	78	MPWA $\pi N \rightarrow \pi N M_{3,19}$ wave	
2 ± 1	HENDRY	78	MPWA $\pi N \rightarrow \pi N N_{3,21}$ wave	

 $\Delta(\sim 3000)$ FOOTNOTES

¹In addition, KOCH 80 reports some evidence for an S_{31} $\Delta(2700)$ and a P_{33} $\Delta(2800)$.

 $\Delta(\sim 3000)$ REFERENCES

KOCH	80	Toronto Conf. 3	R. Koch	(KARLT) IJP
HENDRY	78	PRL 41 222	A.W. Hendry	(IND, LBL) IJP
Also		ANP 136 1	A.W. Hendry	(IND)

Baryon Particle Listings

Λ

Λ BARYONS

$(S = -1, I = 0)$

$\Lambda^0 = uds$

$I(J^P) = 0(\frac{1}{2}^+)$ Status: ****

We have omitted some results that have been superseded by later experiments. See our earlier editions.

Λ MASS

The fit uses Λ , Σ^+ , Σ^0 , Σ^- mass and mass-difference measurements.

VALUE (MeV)	EVTS	DOCUMENT ID	TECN	COMMENT
1115.683 ± 0.006 OUR FIT				
1115.683 ± 0.006 OUR AVERAGE				
1115.678 ± 0.006 ± 0.006	20k	HARTOUNI 94	SPEC	pp 27.5 GeV/c
1115.690 ± 0.008 ± 0.006	18k	¹ HARTOUNI 94	SPEC	pp 27.5 GeV/c
••• We do not use the following data for averages, fits, limits, etc. •••				
1115.59 ± 0.08	935	HYMAN 72	HEBC	
1115.39 ± 0.12	195	MAYEUR 67	EMUL	
1115.6 ± 0.4		LONDON 66	HBC	
1115.65 ± 0.07	488	² SCHMIDT 65	HBC	
1115.44 ± 0.12		³ BHOWMIK 63	RVUE	

- ¹We assume *CPT* invariance: this is the $\bar{\Lambda}$ mass as measured by HARTOUNI 94. See below for the fractional mass difference, testing *CPT*.
- ²The SCHMIDT 65 masses have been reevaluated using our April 1973 proton and K^\pm and π^\pm masses. P. Schmidt, private communication (1974).
- ³The mass has been raised 35 keV to take into account a 46 keV increase in the proton mass and an 11 keV decrease in the π^\pm mass (note added Reviews of Modern Physics **39** 1 (1967)).

$$(m_\Lambda - m_{\bar{\Lambda}}) / m_\Lambda$$

A test of *CPT* invariance.

VALUE (units 10^{-5})	EVTS	DOCUMENT ID	TECN	COMMENT
-0.1 ± 1.1 OUR AVERAGE				Error includes scale factor of 1.6.
+ 1.3 ± 1.2	31k	¹ RYBICKI 96	NA32	π^- Cu, 230 GeV
- 1.08 ± 0.90		HARTOUNI 94	SPEC	pp 27.5 GeV/c
4.5 ± 5.4		CHIEN 66	HBC	6.9 GeV/c $\bar{p}p$
••• We do not use the following data for averages, fits, limits, etc. •••				
-26 ± 13		BADIER 67	HBC	2.4 GeV/c $\bar{p}p$

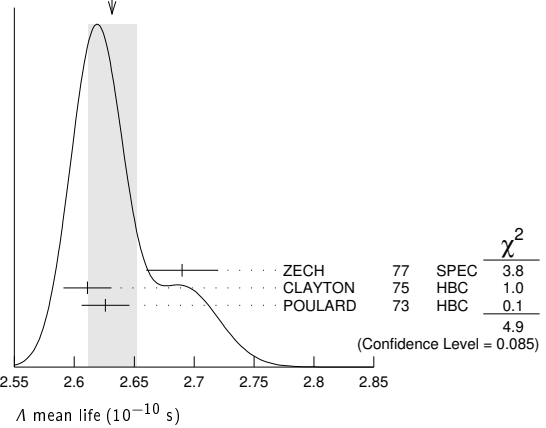
- ¹RYBICKI 96 is an analysis of old ACCMOR (NA32) data.

Λ MEAN LIFE

Measurements with an error $\geq 0.1 \times 10^{-10}$ s have been omitted altogether, and only the latest high-statistics measurements are used for the average.

VALUE (10^{-10} s)	EVTS	DOCUMENT ID	TECN	COMMENT
2.632 ± 0.020 OUR AVERAGE				Error includes scale factor of 1.6. See the ideogram below.
2.69 ± 0.03	53k	ZECH 77	SPEC	Neutral hyperon beam
2.611 ± 0.020	34k	CLAYTON 75	HBC	0.96-1.4 GeV/c $K^- p$
2.626 ± 0.020	36k	POULARD 73	HBC	0.4-2.3 GeV/c $K^- p$
••• We do not use the following data for averages, fits, limits, etc. •••				
2.69 ± 0.05	6582	ALTHOFF 73B	OSPK	$\pi^+ n \rightarrow \Lambda K^+$
2.54 ± 0.04	4572	BALTAY 71B	HBC	$K^- p$ at rest
2.535 ± 0.035	8342	GRIMM 68	HBC	
2.47 ± 0.08	2600	HEPP 68	HBC	
2.35 ± 0.09	916	BURAN 66	HLBC	
2.452 ^{+0.056} _{-0.054}	2213	ENGELMANN 66	HBC	
2.59 ± 0.09	794	HUBBARD 64	HBC	
2.59 ± 0.07	1378	SCHWARTZ 64	HBC	
2.36 ± 0.06	2239	BLOCK 63	HEBC	

WEIGHTED AVERAGE
2.631 ± 0.020 (Error scaled by 1.6)



$$(\tau_\Lambda - \tau_{\bar{\Lambda}}) / \tau_\Lambda$$

A test of *CPT* invariance.

VALUE	DOCUMENT ID	TECN	COMMENT
-0.001 ± 0.009 OUR AVERAGE			
-0.0018 ± 0.0066 ± 0.0056	BARNES 96	CNTR	LEAR $\bar{p}p \rightarrow \bar{\Lambda}\Lambda$
0.044 ± 0.085	BADIER 67	HBC	2.4 GeV/c $\bar{p}p$

See the related review(s):
Baryon Magnetic Moments

Λ MAGNETIC MOMENT

See the "Note on Baryon Magnetic Moments" above. Measurements with an error $\geq 0.15 \mu_N$ have been omitted.

VALUE (μ_N)	EVTS	DOCUMENT ID	TECN	COMMENT
-0.613 ± 0.004 OUR AVERAGE				
-0.606 ± 0.015	200k	COX 81	SPEC	
-0.6138 ± 0.0047	3M	SCHACHIN...	78	SPEC
-0.59 ± 0.07	350k	HELLER 77	SPEC	
-0.57 ± 0.05	1.2M	BUNCE 76	SPEC	
-0.66 ± 0.07	1300	DAHL-JENSEN 71	EMUL	200 kG field

Λ ELECTRIC DIPOLE MOMENT

A nonzero value is forbidden by both *T* invariance and *P* invariance.

VALUE (10^{-16} e-cm)	CL%	DOCUMENT ID	TECN
< 1.5	95	¹ PONDROM 81	SPEC
••• We do not use the following data for averages, fits, limits, etc. •••			
<100	95	² BARONI 71	EMUL
<500	95	GIBSON 66	EMUL
¹ PONDROM 81 measures $(-3.0 \pm 7.4) \times 10^{-17}$ e-cm.			
² BARONI 71 measures $(-5.9 \pm 2.9) \times 10^{-15}$ e-cm.			

Λ DECAY MODES

Mode	Fraction (Γ_i/Γ)	Confidence level
Γ_1 $p\pi^-$	(63.9 ± 0.5) %	
Γ_2 $n\pi^0$	(35.8 ± 0.5) %	
Γ_3 $n\gamma$	(1.75 ± 0.15) × 10 ⁻³	
Γ_4 $p\pi^-\gamma$	[a] (8.4 ± 1.4) × 10 ⁻⁴	
Γ_5 $p e^- \bar{\nu}_e$	(8.32 ± 0.14) × 10 ⁻⁴	
Γ_6 $p\mu^- \bar{\nu}_\mu$	(1.57 ± 0.35) × 10 ⁻⁴	

Lepton (*L*) and/or Baryon (*B*) number violating decay modes

Γ_7 $\pi^+ e^-$	<i>L, B</i>	< 6	× 10 ⁻⁷	90%
Γ_8 $\pi^+ \mu^-$	<i>L, B</i>	< 6	× 10 ⁻⁷	90%
Γ_9 $\pi^- e^+$	<i>L, B</i>	< 4	× 10 ⁻⁷	90%
Γ_{10} $\pi^- \mu^+$	<i>L, B</i>	< 6	× 10 ⁻⁷	90%
Γ_{11} $K^+ e^-$	<i>L, B</i>	< 2	× 10 ⁻⁶	90%
Γ_{12} $K^+ \mu^-$	<i>L, B</i>	< 3	× 10 ⁻⁶	90%
Γ_{13} $K^- e^+$	<i>L, B</i>	< 2	× 10 ⁻⁶	90%
Γ_{14} $K^- \mu^+$	<i>L, B</i>	< 3	× 10 ⁻⁶	90%
Γ_{15} $K_S^0 \nu$	<i>L, B</i>	< 2	× 10 ⁻⁵	90%
Γ_{16} $\bar{p}\pi^+$	<i>B</i>	< 9	× 10 ⁻⁷	90%

[a] See the Listings below for the pion momentum range used in this measurement.

CONSTRAINED FIT INFORMATION

An overall fit to 5 branching ratios uses 20 measurements and one constraint to determine 5 parameters. The overall fit has a $\chi^2 = 10.5$ for 16 degrees of freedom.

The following *off-diagonal* array elements are the correlation coefficients $\langle \delta x_i \delta x_j \rangle / (\delta x_i \delta x_j)$, in percent, from the fit to the branching fractions, $x_i \equiv \Gamma_i / \Gamma_{\text{total}}$. The fit constrains the x_i whose labels appear in this array to sum to one.

x_2	-100			
x_3	-2	-1		
x_5	46	-46	-1	
x_6	0	0	0	0
	x_1	x_2	x_3	x_5

Λ BRANCHING RATIOS

$\Gamma(p\pi^-) / \Gamma(N\pi)$				$\Gamma_1 / (\Gamma_1 + \Gamma_2)$	
VALUE	EVTS	DOCUMENT ID	TECN	COMMENT	
0.641 ± 0.005 OUR FIT					
0.640 ± 0.005 OUR AVERAGE					
0.646 ± 0.008	4572	BALTAY	71B	HBC	$K^- p$ at rest
0.635 ± 0.007	6736	DOYLE	69	HBC	$\pi^- p \rightarrow \Lambda K^0$
0.643 ± 0.016	903	HUMPHREY	62	HBC	
0.624 ± 0.030		CRAWFORD	59B	HBC	$\pi^- p \rightarrow \Lambda K^0$

$\Gamma(n\pi^0) / \Gamma(N\pi)$				$\Gamma_2 / (\Gamma_1 + \Gamma_2)$	
VALUE	EVTS	DOCUMENT ID	TECN	COMMENT	
0.359 ± 0.005 OUR FIT					
0.310 ± 0.028 OUR AVERAGE					
0.35 ± 0.05		BROWN	63	HLBC	
0.291 ± 0.034	75	CHRETIEN	63	HLBC	

$\Gamma(n\gamma) / \Gamma_{\text{total}}$				Γ_3 / Γ	
VALUE (units 10^{-3})	EVTS	DOCUMENT ID	TECN	COMMENT	
1.75 ± 0.15 OUR FIT					
1.75 ± 0.15	1816	LARSON	93	SPEC	$K^- p$ at rest
••• We do not use the following data for averages, fits, limits, etc. •••					
1.78 ± 0.24 ^{+0.14} _{-0.16}	287	NOBLE	92	SPEC	See LARSON 93

$\Gamma(n\gamma) / \Gamma(n\pi^0)$				Γ_3 / Γ_2	
VALUE (units 10^{-3})	EVTS	DOCUMENT ID	TECN	COMMENT	
••• We do not use the following data for averages, fits, limits, etc. •••					
2.86 ± 0.74 ± 0.57	24	BIAGI	86	SPEC	SPS hyperon beam

$\Gamma(p\pi^- \gamma) / \Gamma(p\pi^-)$				Γ_4 / Γ_1	
VALUE (units 10^{-3})	EVTS	DOCUMENT ID	TECN	COMMENT	
1.32 ± 0.22	72	BAGGETT	72c	HBC	$\pi^- < 95$ MeV/c

$\Gamma(p e^- \bar{\nu}_e) / \Gamma(p\pi^-)$				Γ_5 / Γ_1	
VALUE (units 10^{-3})	EVTS	DOCUMENT ID	TECN	COMMENT	
1.301 ± 0.019 OUR FIT					
1.301 ± 0.019 OUR AVERAGE					
1.335 ± 0.056	7111	BOURQUIN	83	SPEC	SPS hyperon beam
1.313 ± 0.024	10k	WISE	80	SPEC	
1.23 ± 0.11	544	LINDQUIST	77	SPEC	$\pi^- p \rightarrow K^0 \Lambda$
1.27 ± 0.07	1089	KATZ	73	HBC	
1.31 ± 0.06	1078	ALTHOFF	71	OSPK	
1.17 ± 0.13	86	1 CANTER	71	HBC	$K^- p$ at rest
1.20 ± 0.12	143	2 MALONEY	69	HBC	
1.17 ± 0.18	120	2 BAGLINI	64	FBC	K^- freon 1.45 GeV/c
1.23 ± 0.20	150	2 ELY	63	FBC	
••• We do not use the following data for averages, fits, limits, etc. •••					
1.32 ± 0.15	218	1 LINDQUIST	71	OSPK	See LINDQUIST 77

¹ Changed by us from $\Gamma(p e^- \bar{\nu}_e) / \Gamma(N\pi)$ assuming the authors used $\Gamma(\Lambda \rightarrow p\pi^-) / \Gamma(\text{total}) = 2/3$.
² Changed by us from $\Gamma(p e^- \bar{\nu}_e) / \Gamma(N\pi)$ because $\Gamma(p e^- \nu) / \Gamma(p\pi^-)$ is the directly measured quantity.

$\Gamma(p\mu^- \bar{\nu}_\mu) / \Gamma(N\pi)$				$\Gamma_6 / (\Gamma_1 + \Gamma_2)$	
VALUE (units 10^{-4})	EVTS	DOCUMENT ID	TECN	COMMENT	
1.57 ± 0.35 OUR FIT					
1.57 ± 0.35 OUR AVERAGE					
1.4 ± 0.5	14	BAGGETT	72B	HBC	$K^- p$ at rest
2.4 ± 0.8	9	CANTER	71B	HBC	$K^- p$ at rest
1.3 ± 0.7	3	LIND	64	RVUE	
1.5 ± 1.2	2	RONNE	64	FBC	

Lepton (L) and/or Baryon (B) number violating decay modes

$\Gamma(\pi^+ e^-) / \Gamma_{\text{total}}$				Γ_7 / Γ	
VALUE	CL%	DOCUMENT ID	TECN	COMMENT	
<6 × 10⁻⁷	90	1 MCCracken	15	CLAS	$\gamma p \rightarrow K^+ \Lambda$
¹ Uses $B(\Lambda \rightarrow p\pi^-) = (63.9 \pm 0.5)\%$ for normalization mode.					

$\Gamma(\pi^+ \mu^-) / \Gamma_{\text{total}}$				Γ_8 / Γ	
VALUE	CL%	DOCUMENT ID	TECN	COMMENT	
<6 × 10⁻⁷	90	1 MCCracken	15	CLAS	$\gamma p \rightarrow K^+ \Lambda$
¹ Uses $B(\Lambda \rightarrow p\pi^-) = (63.9 \pm 0.5)\%$ for normalization mode.					

$\Gamma(\pi^- e^+) / \Gamma_{\text{total}}$				Γ_9 / Γ	
VALUE	CL%	DOCUMENT ID	TECN	COMMENT	
<4 × 10⁻⁷	90	1 MCCracken	15	CLAS	$\gamma p \rightarrow K^+ \Lambda$
¹ Uses $B(\Lambda \rightarrow p\pi^-) = (63.9 \pm 0.5)\%$ for normalization mode.					

$\Gamma(\pi^- \mu^+) / \Gamma_{\text{total}}$				Γ_{10} / Γ	
VALUE	CL%	DOCUMENT ID	TECN	COMMENT	
<6 × 10⁻⁷	90	1 MCCracken	15	CLAS	$\gamma p \rightarrow K^+ \Lambda$
¹ Uses $B(\Lambda \rightarrow p\pi^-) = (63.9 \pm 0.5)\%$ for normalization mode.					

$\Gamma(K^+ e^-) / \Gamma_{\text{total}}$				Γ_{11} / Γ	
VALUE	CL%	DOCUMENT ID	TECN	COMMENT	
<2 × 10⁻⁶	90	1 MCCracken	15	CLAS	$\gamma p \rightarrow K^+ \Lambda$
¹ Uses $B(\Lambda \rightarrow p\pi^-) = (63.9 \pm 0.5)\%$ for normalization mode.					

$\Gamma(K^+ \mu^-) / \Gamma_{\text{total}}$				Γ_{12} / Γ	
VALUE	CL%	DOCUMENT ID	TECN	COMMENT	
<3 × 10⁻⁶	90	1 MCCracken	15	CLAS	$\gamma p \rightarrow K^+ \Lambda$
¹ Uses $B(\Lambda \rightarrow p\pi^-) = (63.9 \pm 0.5)\%$ for normalization mode.					

$\Gamma(K^- e^+) / \Gamma_{\text{total}}$				Γ_{13} / Γ	
VALUE	CL%	DOCUMENT ID	TECN	COMMENT	
<2 × 10⁻⁶	90	1 MCCracken	15	CLAS	$\gamma p \rightarrow K^+ \Lambda$
¹ Uses $B(\Lambda \rightarrow p\pi^-) = (63.9 \pm 0.5)\%$ for normalization mode.					

$\Gamma(K^- \mu^+) / \Gamma_{\text{total}}$				Γ_{14} / Γ	
VALUE	CL%	DOCUMENT ID	TECN	COMMENT	
<3 × 10⁻⁶	90	1 MCCracken	15	CLAS	$\gamma p \rightarrow K^+ \Lambda$
¹ Uses $B(\Lambda \rightarrow p\pi^-) = (63.9 \pm 0.5)\%$ for normalization mode.					

$\Gamma(K_S^0 \nu) / \Gamma_{\text{total}}$				Γ_{15} / Γ	
VALUE	CL%	DOCUMENT ID	TECN	COMMENT	
<2 × 10⁻⁵	90	1 MCCracken	15	CLAS	$\gamma p \rightarrow K^+ \Lambda$
¹ Uses $B(\Lambda \rightarrow p\pi^-) = (63.9 \pm 0.5)\%$ for normalization mode.					

$\Gamma(\bar{p}\pi^+) / \Gamma_{\text{total}}$				Γ_{16} / Γ	
VALUE	CL%	DOCUMENT ID	TECN	COMMENT	
<9 × 10⁻⁷	90	1 MCCracken	15	CLAS	$\gamma p \rightarrow K^+ \Lambda$
¹ Uses $B(\Lambda \rightarrow p\pi^-) = (63.9 \pm 0.5)\%$ for normalization mode.					

Λ DECAY PARAMETERS

See the "Note on Baryon Decay Parameters" in the neutron Listings. Some early results have been omitted.

α_- FOR $\Lambda \rightarrow p\pi^-$					
VALUE	EVTS	DOCUMENT ID	TECN	COMMENT	
0.732 ± 0.014 OUR AVERAGE					Error includes scale factor of 2.3.
0.750 ± 0.009 ± 0.004	420k	ABLIKIM	19Bj	BES3	J/ψ to $\Lambda \bar{\Lambda}$
0.721 ± 0.006 ± 0.005		1 IRELAND	19	CLAS	K production
••• We do not use the following data for averages, fits, limits, etc. •••					
0.584 ± 0.046	8500	ASTBURY	75	SPEC	
0.649 ± 0.023	10325	CLELAND	72	OSPK	
0.67 ± 0.06	3520	DAUBER	69	HBC	From Ξ decay
0.645 ± 0.017	10130	OVERSETH	67	OSPK	Λ from $\pi^- p$
0.62 ± 0.07	1156	CRONIN	63	CNTR	Λ from $\pi^- p$
¹ This is a new analysis based on existing kaon photoproduction data of the CLAS collaboration and using spin algebra constraints.					

α_+ FOR $\bar{\Lambda} \rightarrow \bar{p}\pi^+$					
VALUE	EVTS	DOCUMENT ID	TECN	COMMENT	
-0.758 ± 0.010 ± 0.007	420k	ABLIKIM	19Bj	BES3	J/ψ to $\Lambda \bar{\Lambda}$
••• We do not use the following data for averages, fits, limits, etc. •••					
-0.755 ± 0.083 ± 0.063	≈ 8.7k	ABLIKIM	10	BES	$J/\psi \rightarrow \Lambda \bar{\Lambda}$
-0.63 ± 0.13	770	TIXIER	88	DM2	$J/\psi \rightarrow \Lambda \bar{\Lambda}$

$\bar{\alpha}_0$ FOR $\bar{\Lambda} \rightarrow \bar{\pi}\pi^0$					
VALUE	EVTS	DOCUMENT ID	TECN	COMMENT	
-0.692 ± 0.016 ± 0.006	47k	ABLIKIM	19Bj	BES3	J/ψ to $\Lambda \bar{\Lambda}$

Baryon Particle Listings

Λ , Λ 's and Σ 's,

ϕ ANGLE FOR $\Lambda \rightarrow p\pi^-$

VALUE (°)	EVTs	DOCUMENT ID	TECN	COMMENT
-6.5 ± 3.5 OUR AVERAGE				
-7.0 ± 4.5	10325	CLELAND	72	OSPK Λ from $\pi^- p$
-8.0 ± 6.0	10130	OVERSETH	67	OSPK Λ from $\pi^- p$
13.0 ± 17.0	1156	CRONIN	63	OSPK Λ from $\pi^- p$

$\alpha_0 / \alpha_- = \alpha(\Lambda \rightarrow n\pi^0) / \alpha(\Lambda \rightarrow p\pi^-)$

VALUE	EVTs	DOCUMENT ID	TECN	COMMENT
1.01 ± 0.07 OUR AVERAGE				
1.000 ± 0.068	4760	¹ OLSEN	70	OSPK $\pi^+ n \rightarrow \Lambda K^+$
1.10 ± 0.27		CORK	60	CNTR

¹ OLSEN 70 compares proton and neutron distributions from Λ decay.

$\bar{\alpha}_0 / \alpha_+$ in $\bar{\Lambda} \rightarrow \pi\pi^0, \bar{\Lambda} \rightarrow \bar{p}\pi^+$

VALUE	EVTs	DOCUMENT ID	TECN	COMMENT
$0.913 \pm 0.028 \pm 0.012$	47k	ABLIKIM	19bJ BES3	J/ψ to $\bar{\Lambda}\bar{\Lambda}$

$(\alpha + \bar{\alpha}) / (\alpha - \bar{\alpha})$ in $\Lambda \rightarrow p\pi^-, \bar{\Lambda} \rightarrow \bar{p}\pi^+$

Zero if CP is conserved; α_- and α_+ are the asymmetry parameters for $\Lambda \rightarrow p\pi^-$ and $\bar{\Lambda} \rightarrow \bar{p}\pi^+$ decay. See also the Ξ^- for a similar test involving the decay chain $\Xi^- \rightarrow \Lambda\pi^-, \Lambda \rightarrow p\pi^-$ and the corresponding antiparticle chain.

VALUE	EVTs	DOCUMENT ID	TECN	COMMENT
-0.002 ± 0.012 OUR AVERAGE				
$-0.006 \pm 0.012 \pm 0.007$	420k	ABLIKIM	19bJ BES3	J/ψ to $\bar{\Lambda}\bar{\Lambda}$
$-0.081 \pm 0.055 \pm 0.059$	$\approx 8.7k$	ABLIKIM	10	BES J/ψ to $\bar{\Lambda}\bar{\Lambda}$
$+0.013 \pm 0.022$	96k	BARNES	96	CNTR LEAR $\bar{p}p \rightarrow \bar{\Lambda}\Lambda$
$+0.01 \pm 0.10$	770	TIXIER	88	DM2 $J/\psi \rightarrow \bar{\Lambda}\bar{\Lambda}$
-0.02 ± 0.14	10k	¹ CHAUVAAT	85	CNTR $pp, \bar{p}p$ ISR
-0.07 ± 0.09	4063	BARNES	87	CNTR See BARNES 96

¹ CHAUVAAT 85 actually gives $\alpha_+(\bar{\Lambda})/\alpha_-(\Lambda) = -1.04 \pm 0.29$. Assumes polarization is same in $\bar{p}p \rightarrow \bar{\Lambda}X$ and $pp \rightarrow \Lambda X$. Tests of this assumption, based on C-invariance and fragmentation, are satisfied by the data.

$R = |G_E/G_M|$ in $\Lambda \rightarrow p\pi^-, \bar{\Lambda} \rightarrow \bar{p}\pi^+$

VALUE	DOCUMENT ID	TECN	COMMENT
$0.96 \pm 0.14 \pm 0.02$	¹ ABLIKIM	19bF BES3	$e^+e^- \rightarrow \bar{\Lambda}\Lambda$ at $\sqrt{s} = 2.396$ GeV

¹ Determined using the latest BES-III value on the asymmetry parameter $\alpha = 0.750 \pm 0.010$.

$\Delta\phi = \phi_E - \phi_M$ in $\Lambda \rightarrow p\pi^-, \bar{\Lambda} \rightarrow \bar{p}\pi^+$

VALUE (degrees)	DOCUMENT ID	TECN	COMMENT
$37 \pm 12 \pm 6$	¹ ABLIKIM	19bF BES3	$e^+e^- \rightarrow \bar{\Lambda}\Lambda$ at $\sqrt{s} = 2.396$ GeV

¹ Relative phase between GE and GM, determined using the latest BES-III value on the asymmetry parameter $\alpha = 0.750 \pm 0.010$.

g_A / g_V FOR $\Lambda \rightarrow p e^- \bar{\nu}_e$

Measurements with fewer than 500 events have been omitted. Where necessary, signs have been changed to agree with our conventions, which are given in the "Note on Baryon Decay Parameters" in the neutron Listings. The measurements all assume that the form factor $g_2 = 0$. See also the footnote on DWORKIN 90.

VALUE	EVTs	DOCUMENT ID	TECN	COMMENT
-0.718 ± 0.015 OUR AVERAGE				
$-0.719 \pm 0.016 \pm 0.012$	37k	¹ DWORKIN	90	SPEC $e\nu$ angular corr.
-0.70 ± 0.03	7111	BOURQUIN	83	SPEC $\Xi^- \rightarrow \Lambda\pi^-$
-0.734 ± 0.031	10k	² WISE	81	SPEC $e\nu$ angular correl.
-0.63 ± 0.06	817	ALTHOFF	73	OSPK Polarized Λ

¹ The tabulated result assumes the weak-magnetism coupling $w \equiv g_W(0)/g_V(0)$ to be 0.97, as given by the CVC hypothesis and as assumed by the other listed measurements. However, DWORKIN 90 measures w to be 0.15 ± 0.30 , and then $g_A/g_V = -0.731 \pm 0.016$.

² This experiment measures only the absolute value of g_A/g_V .

REFERENCES

We have omitted some papers that have been superseded by later experiments. See our earlier editions.

ABLIKIM 19bF PRL 123 122003	M. Ablikim et al.	(BESIII Collab.)
ABLIKIM 19bJ NATP 15 631	M. Ablikim et al.	(BESIII Collab.)
IRELAND 19 PRL 123 182301	D.G. Ireland et al.	(GLAS, GWU, JULI+)
MCCRACKEN 15 PR D92 072002	M.E. McCracken et al.	(JLab CLAS Collab.)
ABLIKIM 10 PR D81 012003	M. Ablikim et al.	(BES Collab.)
BARNES 96 PR C54 1877	P.D. Barnes et al.	(CERN PS-185 Collab.)
RYBICKI 96 APP B27 2155	K. Rybicki	
HARTOUNI 94 PRL 72 1322	E.P. Hartouni et al.	(BNL E766 Collab.)
Also PRL 72 2621 (erratum)	E.P. Hartouni et al.	(BNL E766 Collab.)
LARSON 93 PR D47 799	K.D. Larson et al.	(BNL-811 Collab.)
NOBLE 92 PRL 69 414	A.J. Noble et al.	(BIRM, BOST, BRCO+)
DWORKIN 90 PR D41 780	J. Dworkin et al.	(MICH, WISC, RUTG+)
TIXIER 88 PL B212 523	M.H. Tixier et al.	(DM2 Collab.)
BARNES 87 PL B199 147	P.D. Barnes et al.	(CMU, SAcl, LANL+)
BIAGI 86 ZPHY C30 201	S.F. Biagi et al.	(BRIS, CERN, GEVA+)
CHAUVAAT 85 PL 163B 273	P. Chauvat et al.	(CERN, CLER, UCLA+)
BOURQUIN 83 ZPHY C21 1	M.H. Bourquin et al.	(BRIS, GEVA, HEIDP+)
COX 81 PRL 46 877	P.T. Cox et al.	(MICH, WISC, RUTG, MINN+)
PONDROM 81 PR D23 814	L. Pondrom et al.	(WISC, MICH, RUTG+)
WISE 81 PL 90B 123	J.E. Wise et al.	(MASA, BNL)
WISE 80 PL 91B 165	J.E. Wise et al.	(MASA, BNL)
SCHACHIN... 78 PRL 41 1348	L. Schachinger et al.	(MICH, RUTG, WIS)

HELLER 77 PL 68B 480	K. Heller et al.	(MICH, WISC, HEIDH)
LINDQUIST 77 PR D16 2104	J. Lindquist et al.	(EFI, OSU, ANL)
Also JP G2 L211	J. Lindquist et al.	(EFI, WUSL, OSU+)
ZECH 77 NP B124 413	G. Zech et al.	(SIEG, CERN, DORT, HEIDH)
BUNCE 76 PRL 36 1113	G.R.M. Bunce et al.	(WISC, MICH, RUTG)
ASTBURY 75 NP B99 30	P. Astbury et al.	(LOIC, CERN, ETH+)
CLAYTON 75 NP B95 130	E.F. Clayton et al.	(LOIC, RHEL)
ALTHOFF 73 PL 43B 237	K.H. Althoff et al.	(CERN, HEID)
ALTHOFF 73B NP B66 29	K.H. Althoff et al.	(CERN, HEID)
KATZ 73 Thesis MDDP-TR-74-044	C.N. Katz	(UMD)
POULARD 73 PL 46B 135	G. Poulard, A. Givernaud, A.C. Borg	(SAcl)
BAGGETT 72B ZPHY 252 362	M.J. Baggett et al.	(HEID)
BAGGETT 72C PL 42B 379	M.J. Baggett et al.	(HEID)
CLELAND 72 NP B40 221	W.E. Cleland et al.	(CERN, GEVA, LUND)
HYMAN 72 PR D5 1063	L.G. Hyman et al.	(ANL, CMU)
ALTHOFF 71 PL 37B 531	K.H. Althoff et al.	(CERN, HEID)
BALTAY 71B PR D4 670	C. Baltay et al.	(COLU, BINP)
BARONI 71 LNC 2 1256	G. Baroni, S. Petrer, G. Romano	(ROMA)
CANTER 71 PRL 26 868	J. Canter et al.	(STON, COLU)
CANTER 71B PRL 27 59	J. Canter et al.	(STON, COLU)
DAHL-JENSEN 71 NC 3A 1	E. Dahl-Jensen et al.	(CERN, ANKA, LAUS+)
LINDQUIST 71 PRL 27 612	J. Lindquist et al.	(EFI, WUSL, OSU+)
OLSEN 70 PRL 24 843	S.L. Olsen et al.	(WISC, MICH)
DAUBER 69 PR 179 1262	P.M. Dauber et al.	(LRL)
DOYLE 69 Thesis UCLR 18139	J.C. Doyle	(LRL)
MALONEY 69 PRL 23 425	J.E. Maloney, B. Sechi-Zorn	(UMD)
GRIMM 68 NC 54A 187	H.J. Grimm	(HEID)
HEPP 68 ZPHY 214 71	V. Hepp, H. Schleich	(HEID)
BADIER 67 PL 25B 152	J. Badier et al.	(EPOL)
MAYEUR 67 U.Libr.Brx.Bul. 32	C. Mayeur, E. Tompa, J.H. Wickens	(BELG, LOUC)
OVERSETH 67 PRL 19 391	O.E. Overseth, R.F. Roth	(MICH, PRIN)
PDG 67 RMP 39 1	A.H. Rosenfeld et al.	(LRL, CERN, YALE)
BURAN 66 PL 20 318	T. Buran et al.	(OSLO)
CHIEN 66 PR 152 1171	C.Y. Chien et al.	(YALE, BNL)
ENGELMANN 66 NC 45A 1038	R. Engelmann et al.	(HEID, REHO)
GIBSON 66 NC 45A 882	W.M. Gibson, K. Green	(BRIS)
LONDON 66 PR 143 1034	G.V. London et al.	(BNL, SYRA)
SCHMIDT 65 PR 140 B1328	P. Schmidt	(COLU)
BAGLIN 64 NC 35 977	C. Baglin et al.	(EPOL, CERN, LOUC, RHEL+)
HUBBARD 64 PR 135 B183	J.R. Hubbard et al.	(LRL)
LIND 64 PR 135 B1483	V.G. Lind et al.	(WISC)
RONNE 64 PL 13 357	B.E. Ronne et al.	(CERN, EPOL, LOUC+)
SCHWARTZ 64 Thesis UCLR 11360	J.A. Schwartz	(LRL)
BHOWMIK 63 NC 28 1494	B. Bhowmik, D.P. Goyal	(DELH)
BLOCK 63 PR 130 766	M.M. Block et al.	(NWES, BGNA, SYRA+)
BROWN 63 PR 130 769	J.L. Brown et al.	(LRL, MICH)
CHRETIEN 63 PR 131 2208	M. Chretien et al.	(BRAN, BROW, HARY+)
CRONIN 63 PR 129 1795	J.W. Cronin, O.E. Overseth	(PRIN)
ELY 63 PR 131 868	R.P. Ely et al.	(LRL)
HUMPHREY 62 PR 127 1305	W.E. Humphrey, R.R. Ross	(LRL, PRIN, BNL)
CORK 60 PR 120 1000	B. Cork et al.	(LRL, PRIN, BNL)
CRAWFORD 59B PRL 2 266	F.S. Crawford et al.	(LRL)

See the related review(s):

[\$\Lambda\$ and \$\Sigma\$ Resonances](#)

$\Lambda(1380) 1/2^-$

$J^P = \frac{1}{2}^-$

Status: * *

OMITTED FROM SUMMARY TABLE

See the related review on "Pole Structure of the $\Lambda(1405)$ Region."

$\Lambda(1380)$ POLE POSITION

REAL PART

VALUE (MeV)	DOCUMENT ID	TECN
1325 ± 15	¹ MAI	15 DPWA
1330 ± 4	² MAI	15 DPWA
1388 ± 9	GUO	13 DPWA
1381 ± 18	IKEDA	12 DPWA

¹ Solution number 4.
² Solution number 2.

-2xIMAGINARY PART

VALUE (MeV)	DOCUMENT ID	TECN
180 ± 24	¹ MAI	15 DPWA
-36		
112 ± 34	² MAI	15 DPWA
-22		
228 ± 48	GUO	13 DPWA
-50		
162 ± 38	IKEDA	12 DPWA
-16		

¹ Solution number 4.
² Solution number 2.

$\Lambda(1380)$ REFERENCES

MAI 15 EPJ A51 30	M. Mai, U.-G. Meißner	(BONN, JULI)
GUO 13 PR C87 035202	Z.-H. Guo, J. Oller	
IKEDA 12 NP A881 98	Y. Ikeda, T. Hyodo, W. Weise	(MUNT, RIKEN, TINT)

See key on page 999

Baryon Particle Listings

$\Lambda(1405)$

$\Lambda(1405) 1/2^-$

$I(J^P) = 0(\frac{1}{2}^-)$ Status: ****

In the 1998 Note on the $\Lambda(1405)$ in PDG 98, R.H. Dalitz discussed the S-shaped cusp behavior of the intensity at the $N\bar{K}$ threshold observed in THOMAS 73 and HEMINGWAY 85. He commented that this behavior "is characteristic of S-wave coupling; the other below threshold hyperon, the $\Sigma(1385)$, has no such threshold distortion because its $N\bar{K}$ coupling is P-wave. For $\Lambda(1405)$ this asymmetry is the sole direct evidence that $J^P = 1/2^-$."

A recent measurement by the CLAS collaboration, MORIYA 14, definitively established the long-assumed $J^P = 1/2^-$ spin-parity assignment of the $\Lambda(1405)$. The experiment produced the $\Lambda(1405)$ spin-polarized in the photoproduction process $\gamma p \rightarrow K^+ \Lambda(1405)$ and measured the decay of the $\Lambda(1405)$ (polarized) $\rightarrow \Sigma^+$ (polarized) π^- . The observed isotropic decay of $\Lambda(1405)$ is consistent with spin $J = 1/2$. The polarization transfer to the Σ^+ (polarized) direction revealed negative parity, and thus established $J^P = 1/2^-$.

See the related review(s):
[Pole Structure of the \$\Lambda\(1405\)\$ Region](#)

$\Lambda(1405)$ POLE POSITION

REAL PART

VALUE (MeV)	DOCUMENT ID	TECN
••• We do not use the following data for averages, fits, limits, etc. •••		
$1429 \pm \frac{8}{7}$	¹ MAI	15 DPWA
1434 ± 2	² MAI	15 DPWA
$1421 \pm \frac{3}{2}$	GUO	13 DPWA
$1424 \pm \frac{7}{23}$	IKEDA	12 DPWA

¹ Solution number 4.
² Solution number 2.

-2xIMAGINARY PART

VALUE (MeV)	DOCUMENT ID	TECN
••• We do not use the following data for averages, fits, limits, etc. •••		
$24 \pm \frac{4}{6}$	¹ MAI	15 DPWA
$20 \pm \frac{4}{2}$	² MAI	15 DPWA
$38 \pm \frac{16}{10}$	GUO	13 DPWA
$52 \pm \frac{6}{28}$	IKEDA	12 DPWA

¹ Solution number 4.
² Solution number 2.

$\Lambda(1405)$ MASS

PRODUCTION EXPERIMENTS

VALUE (MeV)	EVTS	DOCUMENT ID	TECN	COMMENT
1405.1 \pm $\frac{1.3}{1.0}$ OUR AVERAGE				
$1405 \pm \frac{11}{9}$		HASSANVAND 13	SPEC	$pp \rightarrow p\Lambda(1405) K^+$
$1405 \pm \frac{1.4}{1.0}$		ESMAILI 10	RVUE	$^4\text{He } K^- \rightarrow \Sigma^\pm \pi^\mp X$ at rest
1406.5 ± 4.0		¹ DALITZ 91		M-matrix fit
••• We do not use the following data for averages, fits, limits, etc. •••				
1391 ± 1	700	¹ HEMINGWAY 85	HBC	$K^- p$ 4.2 GeV/c
~ 1405	400	² THOMAS 73	HBC	$\pi^- p$ 1.69 GeV/c
1405	120	BARBARO... 68B	DBC	$K^- d$ 2.1-2.7 GeV/c
1400 ± 5	67	BIRMINGHAM 66	HBC	$K^- p$ 3.5 GeV/c
1382 ± 8		ENGLER 65	HDDB	$\pi^- p, \pi^+ d$ 1.68 GeV/c
1400 ± 24		MUSGRAVE 65	HBC	$\bar{p}p$ 3-4 GeV/c
1410		ALEXANDER 62	HBC	$\pi^- p$ 2.1 GeV/c
1405		ALSTON 62	HBC	$K^- p$ 1.2-0.5 GeV/c
1405		ALSTON 61B	HBC	$K^- p$ 1.15 GeV/c

¹ DALITZ 91 fits the HEMINGWAY 85 data.
² THOMAS 73 data is fit by CHAO 73 (see next section).

EXTRAPOLATIONS BELOW $N\bar{K}$ THRESHOLD

VALUE (MeV)	DOCUMENT ID	TECN	COMMENT
••• We do not use the following data for averages, fits, limits, etc. •••			
1407.56 or 1407.50	¹ KIMURA 00		potential model
1411	² MARTIN 81		K-matrix fit
1406	³ CHAO 73	DPWA	0-range fit (sol. B)
1421	MARTIN 70	RVUE	Constant K-matrix
1416 ± 4	MARTIN 69	HBC	Constant K-matrix
1403 ± 3	KIM 67	HBC	K-matrix fit
1407.5 ± 1.2	⁴ KITTEL 66	HBC	0-effective-range fit
1410.7 ± 1.0	KIM 65	HBC	0-effective-range fit
1409.6 ± 1.7	⁴ SAKITT 65	HBC	0-effective-range fit

- ¹ The KIMURA 00 values are from fits A and B from a coupled-channel potential model using low-energy $\bar{K}N$ and $\Sigma\pi$ data, kaonic-hydrogen x-ray measurements, and our $\Lambda(1405)$ mass and width. The results bear mainly on the nature of the $\Lambda(1405)$: three-quark state or $\bar{K}N$ bound state.
- ² The MARTIN 81 fit includes the $K^\pm p$ forward scattering amplitudes and the dispersion relations they must satisfy.
- ³ See also the accompanying paper of THOMAS 73.
- ⁴ Data of SAKITT 65 are used in the fit by KITTEL 66.

$\Lambda(1405)$ WIDTH

PRODUCTION EXPERIMENTS

VALUE (MeV)	EVTS	DOCUMENT ID	TECN	COMMENT
50.5 \pm 2.0 OUR AVERAGE				
62 ± 10		HASSANVAND 13	SPEC	$pp \rightarrow p\Lambda(1405) K^+$
50 ± 2		¹ DALITZ 91		M-matrix fit
••• We do not use the following data for averages, fits, limits, etc. •••				
$24 \pm \frac{4}{3}$		ESMAILI 10	RVUE	$^4\text{He } K^- \rightarrow \Sigma^\pm \pi^\mp X$ at rest
32 ± 1	700	¹ HEMINGWAY 85	HBC	$K^- p$ 4.2 GeV/c
45 to 55	400	² THOMAS 73	HBC	$\pi^- p$ 1.69 GeV/c
35	120	BARBARO... 68B	DBC	$K^- d$ 2.1-2.7 GeV/c
50 ± 10	67	BIRMINGHAM 66	HBC	$K^- p$ 3.5 GeV/c
89 ± 20		ENGLER 65	HDDB	
60 ± 20		MUSGRAVE 65	HBC	
35 ± 5		ALEXANDER 62	HBC	
50		ALSTON 62	HBC	
20		ALSTON 61B	HBC	

¹ DALITZ 91 fits the HEMINGWAY 85 data.
² THOMAS 73 data is fit by CHAO 73 (see next section).

EXTRAPOLATIONS BELOW $N\bar{K}$ THRESHOLD

VALUE (MeV)	DOCUMENT ID	TECN	COMMENT
••• We do not use the following data for averages, fits, limits, etc. •••			
50.24 or 50.26	¹ KIMURA 00		potential model
30	² MARTIN 81		K-matrix fit
55	^{3,4} CHAO 73	DPWA	0-range fit (sol. B)
20	MARTIN 70	RVUE	Constant K-matrix
29 ± 6	MARTIN 69	HBC	Constant K-matrix
50 ± 5	KIM 67	HBC	K-matrix fit
34.1 ± 4.1	⁵ KITTEL 66	HBC	
37.0 ± 3.2	KIM 65	HBC	
28.2 ± 4.1	⁵ SAKITT 65	HBC	

- ¹ The KIMURA 00 values are from fits A and B from a coupled-channel potential model using low-energy $\bar{K}N$ and $\Sigma\pi$ data, kaonic-hydrogen x-ray measurements, and our $\Lambda(1405)$ mass and width. The results bear mainly on the nature of the $\Lambda(1405)$: three-quark state or $\bar{K}N$ bound state.
- ² The MARTIN 81 fit includes the $K^\pm p$ forward scattering amplitudes and the dispersion relations they must satisfy.
- ³ An asymmetric shape, with $\Gamma/2 = 41$ MeV below resonance, 14 MeV above.
- ⁴ See also the accompanying paper of THOMAS 73.
- ⁵ Data of SAKITT 65 are used in the fit by KITTEL 66.

$\Lambda(1405)$ DECAY MODES

Mode	Fraction (Γ_i/Γ)
$\Gamma_1 \Sigma\pi$	100 %
$\Gamma_2 \Lambda\gamma$	
$\Gamma_3 \Sigma^0\gamma$	
$\Gamma_4 N\bar{K}$	

$\Lambda(1405)$ PARTIAL WIDTHS

$\Gamma(\Lambda\gamma)$	VALUE (keV)	DOCUMENT ID	COMMENT	Γ_2
••• We do not use the following data for averages, fits, limits, etc. •••				
	27 ± 8	BURKHARDT 91	Isobar model fit	
$\Gamma(\Sigma^0\gamma)$	VALUE (keV)	DOCUMENT ID	COMMENT	Γ_3
••• We do not use the following data for averages, fits, limits, etc. •••				
	10 ± 4 or 23 ± 7	BURKHARDT 91	Isobar model fit	

$\Lambda(1405)$ BRANCHING RATIOS

$\Gamma(N\bar{K})/\Gamma(\Sigma\pi)$	VALUE	CL%	DOCUMENT ID	TECN	COMMENT	Γ_4/Γ_1
••• We do not use the following data for averages, fits, limits, etc. •••						
	<3	95	HEMINGWAY 85	HBC	$K^- p$ 4.2 GeV/c	

Baryon Particle Listings

$\Lambda(1405), \Lambda(1520)$

$\Lambda(1405)$ REFERENCES

MAI	15	EPJ A51 30	M. Mai, U.-G. Meissner	(BONN, JULI)
MORIYA	14	PRL 112 082004	K. Moriya et al.	(CLAS Collab.) JP
GUO	13	PR C87 035202	Z.-H. Guo, J. Oller	
HASSANVAND	13	PR C87 055202	M. Hassanvand et al.	
Also		PR C88 019905 (errata)	M. Hassanvand et al.	
IKEDA	12	NP A881 98	Y. Ikeda, T. Hyodo, W. Weise	(MUNT, RIKEN, TINT)
ESMAILI	10	PL B686 23	J. Esmaili, Y. Akaishi, T. Yamazaki	(RIKEN, ISUT+)
KIMURA	00	PR C62 015206	M. Kimura et al.	
PDG	98	EPJ C3 1	C. Caso et al.	(PDG Collab.)
BURKHARDT	91	PR C44 607	H. Burkhardt, J. Lowe	(NOTT, UNM, BIRM)
DALITZ	91	JP G17 289	R.H. Dalitz, A. Deloff	(OXFTP, WINR)
HENNINGWAY	85	NP B253 742	R.J. Hemingway	(CERN J)
MARTIN	81	NP B179 33	A.D. Martin	(DURH)
CHAO	73	NP B56 46	Y.A. Chao et al.	(RHEL, CMU, LOUC)
THOMAS	73	NP B56 15	D.W. Thomas et al.	(CMU) J
MARTIN	70	NP B16 479	A.D. Martin, G.G. Ross	(DURH)
MARTIN	69	PR 183 1352	B.R. Martin, M. Sakitt	(LOUC, BNL)
Also		PR 183 1345	B.R. Martin, M. Sakitt	(LOUC, BNL)
BARBARO...	68B	PRL 21 573	A. Barbaro-Galleri et al.	(LRL, SLAC)
KIM	67	PRL 19 1074	J.K. Kim	(YALE)
BIRMINGHAM	66	PR 152 1148	M. Haque et al.	(BIRM, GLS, LOIC, OXF+)
KITTEL	66	PL 21 349	W. Kittel, G. Otter, I. Wacek	(VIEN)
ENGLER	65	PRL 15 224	A. Engler et al.	(CMU, BNL) J
KIM	65	PR 14 29	J.K. Kim	(COLU)
MUSGRAVE	65	NC 35 735	B. Musgrave et al.	(BIRM, CERN, EPOL+)
SAKITT	65	PR 139 8719	M. Sakitt et al.	(UMD, LRL)
ALEXANDER	62	PRL 8 447	G. Alexander et al.	(LRL) I
ALSTON	62	CERN Conf. 311	M.H. Alston et al.	(LRL) I
ALSTON	61B	PRL 6 698	M.H. Alston et al.	(LRL) I

OTHER RELATED PAPERS

IWASAKI	97	PRL 78 3067	M. Iwasaki et al.	(KEK 228 Collab.)
FINK	90	PR C41 2720	P.J. Fink et al.	(IBMY, ORST, ANSM)
LEINWEBER	90	ANP 198 203	D.B. Leinweber	(MCMS)
MUELLER-GR...	90	NP A513 557	A. Mueller-Groeling, K. Holinde, J. Speth	(JULI)
BARRETT	89	NC 102A 179	R.C. Barrett	(SURR)
BATTY	89	NC 102A 255	C.J. Batty, A. Gal	(RAL, HEBR)
CAPSTICK	89	Excited Baryons 88, p.32	S. Capstick	(GUEL)
LOWE	89	NC 102A 167	J. Lowe	(BIRM)
WHITEHOUSE	89	PRL 63 1352	D.A. Whitehouse et al.	(BIRM, BOST, BRCO+)
SIEGEL	88	PR C38 2221	P.B. Siegel, W. Weise	(REGE)
WORKMAN	88	PR D37 3117	R.L. Workman, H.W. Fearing	(TRIU)
SCHNICK	87	PRL 58 1719	J. Schnick, R.H. Landau	(ORST)
CAPSTICK	86	PR D34 2809	S. Capstick, N. Isgur	(TNTO)
JENNINGS	86	PL B176 229	B.K. Jennings	(TRIU)
MALTMAN	86	PR D34 1372	K. Maltman, N. Isgur	(LANL, TNTO)
ZHONG	86	PL B171 471	Y.S. Zhong et al.	(ADLD, TRIU, SURR)
BURKHARDT	85	NP A440 653	H. Burkhardt, J. Lowe, A.S. Rosenthal	(NOTT+)
DAREWYCH	85	PR D32 1765	J.W. Darewych, R. Koniuk, N. Isgur	(YORKC, TNTO)
VEIT	85	PR D31 1033	E.A. Veit et al.	(TRIU, ADLD, SURR)
KIANG	84	PR C30 1638	D. Kiang et al.	(DALH, MCMS)
MILLER	84	Conference paper	D.J. Miller	(LOUC)
Conf. Intersections between Particle and Nuclear Physics, p. 783				
VANDIJK	84	PR D30 937	W. van Dijk	(MCMS)
VEIT	84	PL 137B 415	E.A. Veit et al.	(TRIU, SURR, CERN)
DALITZ	82	Heid. Conf.	R.H. Dalitz et al.	(OXFTP)
Heidelberg Conf., p. 201				
DALITZ	81	Kaon Conf.	R.H. Dalitz, J.G. McGinley	(OXFTP)
Low and Intermediate Energy Kaon-Nucleon Physics, p.381				
MARTIN	81B	Kaon Conf.	A.D. Martin	(DURH)
Low and Intermediate Energy Kaon-Nucleon Physics, p. 97				
OADES	77	NC 42A 482	G.C. Oades, G. Rasche	(AARH, ZURI)
SHAW	73	Purdue Conf. 417	G.L. Shaw	(UCI)
BARBARO...	72	LBL-555	A. Barbaro-Galleri	(LBL)
DOBSON	72	PR D6 3256	P.N. Dobson, R. McEthaney	(HAWA)
RAJASEKARAN	72	PR D5 610	G. Rajasekaran	(TATA)
Earlier papers also cited in RAJASEKARAN 72.				
CLINE	71	PRL 26 1194	D. Cline, R. Laumann, J. Mapp	(WIS C)
MARTIN	71	PL 35B 62	A.D. Martin, A.D. Martin, G.G. Ross	(DURH, LOUC+)
DALITZ	67	PR 153 1617	R.H. Dalitz, T.C. Wong, G. Rajasekaran	(OXFTP+)
DONALD	66	PL 22 711	R.A. Donald et al.	(LIVP)
KADYK	66	PRL 17 599	J.A. Kadyk et al.	(LRL)
ABRAMS	65	PR 139 B454	G.S. Abrams, B. Sechi-Zorn	(UMD)

$\Lambda(1520) \ 3/2^-$

$\Gamma(J^P) = 0(\frac{3}{2}^-)$ Status: ***

Discovered by FERRO-LUZZI 62; the elaboration in WATSON 63 is the classic paper on the Breit-Wigner analysis of a multichannel resonance.

The measurements of the mass, width, and elasticity published before 1975 are now obsolete and have been omitted. They were last listed in our 1982 edition Physics Letters **111B** 1 (1982).

Production and formation experiments agree quite well, so they are listed together here.

$\Lambda(1520)$ POLE POSITION

REAL PART	VALUE (MeV)	DOCUMENT ID	TECN	COMMENT
1517 to 1518 (≈ 1517.5) OUR ESTIMATE				
1517.5 \pm 0.4 OUR AVERAGE				
1517.5 \pm 0.4		SARANTSEV 19	DPWA	$\bar{K}N$ multichannel
1517 $+4$		¹ KAMANO 15	DPWA	$\bar{K}N$ multichannel
1517 -4				
••• We do not use the following data for averages, fits, limits, etc. •••				
1518		ZHANG 13A	DPWA	$\bar{K}N$ multichannel
1518.8		QIANG 10	SPEC	$e p \rightarrow e' K^+ X$ (fit to X)
¹ From the preferred solution A in KAMANO 15.				

$-2 \times$ IMAGINARY PART

VALUE (MeV)	DOCUMENT ID	TECN	COMMENT
14 to 18 (≈ 16) OUR ESTIMATE			
15.3 \pm 0.9 OUR AVERAGE			
15.3 \pm 0.9		SARANTSEV 19	DPWA $\bar{K}N$ multichannel
15 $+10$		¹ KAMANO 15	DPWA $\bar{K}N$ multichannel
15 -8			
••• We do not use the following data for averages, fits, limits, etc. •••			
16		ZHANG 13A	DPWA $\bar{K}N$ multichannel
17.2		QIANG 10	SPEC $e p \rightarrow e' K^+ X$ (fit to X)
¹ From the preferred solution A in KAMANO 15.			

$\Lambda(1520)$ POLE RESIDUES

The normalized residue is the residue divided by $\Gamma_{pole}/2$.

Normalized residue in $N\bar{K} \rightarrow \Lambda(1520) \rightarrow N\bar{K}$	MODULUS	PHASE ($^\circ$)	DOCUMENT ID	TECN	COMMENT
0.45 \pm 0.01		-10 ± 3			
0.45 \pm 0.01		-10 ± 3	SARANTSEV 19	DPWA	$\bar{K}N$ multichannel
••• We do not use the following data for averages, fits, limits, etc. •••					
0.431		-11	¹ KAMANO 15	DPWA	$\bar{K}N$ multichannel
¹ From the preferred solution A in KAMANO 15.					

Normalized residue in $N\bar{K} \rightarrow \Lambda(1520) \rightarrow \Sigma\pi$	MODULUS	PHASE ($^\circ$)	DOCUMENT ID	TECN	COMMENT
0.44 \pm 0.01		-15 ± 3			
0.44 \pm 0.01		-15 ± 3	SARANTSEV 19	DPWA	$\bar{K}N$ multichannel
••• We do not use the following data for averages, fits, limits, etc. •••					
0.435		-10	¹ KAMANO 15	DPWA	$\bar{K}N$ multichannel
¹ From the preferred solution A in KAMANO 15.					

Normalized residue in $N\bar{K} \rightarrow \Lambda(1520) \rightarrow \Lambda\eta$	MODULUS	PHASE ($^\circ$)	DOCUMENT ID	TECN	COMMENT
0.013 \pm 0.003		116 ± 3			
0.013 \pm 0.003		116 ± 3	SARANTSEV 19	DPWA	$\bar{K}N$ multichannel

Normalized residue in $N\bar{K} \rightarrow \Lambda(1520) \rightarrow \Sigma(1385)\pi, S\text{-wave}$	MODULUS	PHASE ($^\circ$)	DOCUMENT ID	TECN	COMMENT
0.431		-123			
0.431		-123	¹ KAMANO 15	DPWA	$\bar{K}N$ multichannel
¹ From the preferred solution A in KAMANO 15.					

Normalized residue in $N\bar{K} \rightarrow \Lambda(1520) \rightarrow \Sigma(1385)\pi, D\text{-wave}$	MODULUS	PHASE ($^\circ$)	DOCUMENT ID	TECN	COMMENT
0.0141		122			
0.0141		122	¹ KAMANO 15	DPWA	$\bar{K}N$ multichannel
¹ From the preferred solution A in KAMANO 15.					

$\Lambda(1520)$ MASS

VALUE (MeV)	EVTS	DOCUMENT ID	TECN	COMMENT
1518 to 1520 (≈ 1519) OUR ESTIMATE				
1519.42 \pm 0.19 OUR AVERAGE				Error includes scale factor of 1.1.
1518.5 \pm 0.5		SARANTSEV 19	DPWA	$\bar{K}N$ multichannel
1519.6 \pm 0.5		ZHANG 13A	DPWA	$\bar{K}N$ multichannel
1520.4 \pm 0.6 \pm 1.5		QIANG 10	SPEC	$e p \rightarrow e' K^+ X$ (fit to X)
1517.3 \pm 1.5	300	BARBER 80D	SPEC	$\gamma p \rightarrow \Lambda(1520) K^+$
1517.8 \pm 1.2	5k	BARLAG 79	HBC	$K^- p$ 4.2 GeV/c
1520.0 \pm 0.5		ALSTON... 78	DPWA	$\bar{K}N \rightarrow \bar{K}N$
1519.7 \pm 0.3	4k	CAMERON 77	HBC	$K^- p$ 0.96-1.36 GeV/c
1519 \pm 1		GOPAL 77	DPWA	$\bar{K}N$ multichannel
1519.4 \pm 0.3	2000	CORDEN 75	DBC	$K^- d$ 1.4-1.8 GeV/c

$\Lambda(1520)$ WIDTH

VALUE (MeV)	EVTS	DOCUMENT ID	TECN	COMMENT
15 to 17 (≈ 16) OUR ESTIMATE				
15.73 \pm 0.26 OUR AVERAGE				
15.7 \pm 1.0		SARANTSEV 19	DPWA	$\bar{K}N$ multichannel
17 \pm 1		ZHANG 13A	DPWA	$\bar{K}N$ multichannel
18.6 \pm 1.9 \pm 1.0		QIANG 10	SPEC	$e p \rightarrow e' K^+ X$ (fit to X)
16.3 \pm 3.3	300	BARBER 80D	SPEC	$\gamma p \rightarrow \Lambda(1520) K^+$
16 \pm 1		GOPAL 80	DPWA	$\bar{K}N \rightarrow \bar{K}N$
14 \pm 3	677	¹ BARLAG 79	HBC	$K^- p$ 4.2 GeV/c
15.4 \pm 0.5		ALSTON... 78	DPWA	$\bar{K}N \rightarrow \bar{K}N$
16.3 \pm 0.5	4k	CAMERON 77	HBC	$K^- p$ 0.96-1.36 GeV/c
15.0 \pm 0.5		GOPAL 77	DPWA	$\bar{K}N$ multichannel
15.5 \pm 1.6	2000	CORDEN 75	DBC	$K^- d$ 1.4-1.8 GeV/c
¹ From the best-resolution sample of $\Lambda\pi\pi$ events only.				

$\Lambda(1520)$ DECAY MODES

Mode	Fraction (Γ_i/Γ)
Γ_1 $N\bar{K}$	(45 ± 1) %
Γ_2 $\Sigma\pi$	(42 ± 1) %
Γ_3 $\Lambda\pi\pi$	(10 ± 1) %
Γ_4 $\Sigma(1385)\pi, S\text{-wave}$	
Γ_5 $\Sigma(1385)\pi, D\text{-wave}$	
Γ_6 $\Sigma(1385)\pi$	
Γ_7 $\Sigma(1385)\pi(\rightarrow\Lambda\pi\pi)$	
Γ_8 $\Lambda(\pi\pi)_{S\text{-wave}}$	
Γ_9 $\Sigma\pi\pi$	(0.9 ± 0.1) %
Γ_{10} $\Lambda\gamma$	(0.85 ± 0.15) %
Γ_{11} $\Sigma^0\gamma$	

$\Lambda(1520)$ BRANCHING RATIOS

See "Sign conventions for resonance couplings" in the Note on Λ and Σ Resonances.

$\Gamma(N\bar{K})/\Gamma_{\text{total}}$

VALUE	DOCUMENT ID	TECN	COMMENT
0.45 to 0.47 OUR ESTIMATE			
0.45 ± 0.01	SARANTSEV 19	DPWA	$\bar{K}N$ multichannel
0.47 ± 0.04	ZHANG 13A	DPWA	$\bar{K}N$ multichannel
0.47 ± 0.02	GOPAL 80	DPWA	$\bar{K}N \rightarrow \bar{K}N$
0.45 ± 0.03	ALSTON... 78	DPWA	$\bar{K}N \rightarrow \bar{K}N$
0.448 ± 0.014	CORDEN 75	DBC	K^-d 1.4-1.8 GeV/c
••• We do not use the following data for averages, fits, limits, etc. •••			
0.43	¹ KAMANO 15	DPWA	$\bar{K}N$ multichannel
0.47 ± 0.01	GOPAL 77	DPWA	See GOPAL 80
0.42	MAST 76	HBC	$K^-p \rightarrow \bar{K}^0n$

¹ From the preferred solution A in KAMANO 15.

$\Gamma(\Sigma\pi)/\Gamma_{\text{total}}$

VALUE	DOCUMENT ID	TECN	COMMENT
0.42 to 0.46 OUR ESTIMATE			
0.43 ± 0.01	SARANTSEV 19	DPWA	$\bar{K}N$ multichannel
0.47 ± 0.05	ZHANG 13A	DPWA	$\bar{K}N$ multichannel
0.426 ± 0.014	CORDEN 75	DBC	K^-d 1.4-1.8 GeV/c
0.418 ± 0.017	BARBARO... 69B	HBC	K^-p 0.28-0.45 GeV/c
••• We do not use the following data for averages, fits, limits, etc. •••			
0.446	¹ KAMANO 15	DPWA	$\bar{K}N$ multichannel
0.46	KIM 71	DPWA	K-matrix analysis

¹ From the preferred solution A in KAMANO 15.

$\Gamma(\Sigma\pi)/\Gamma(N\bar{K})$

VALUE	DOCUMENT ID	TECN	COMMENT
0.9 to 1.0 OUR ESTIMATE			
0.98 ± 0.03	¹ GOPAL 77	DPWA	$\bar{K}N$ multichannel
0.82 ± 0.08	BURKHARDT 69	HBC	K^-p 0.8-1.2 GeV/c
1.06 ± 0.14	SCHEUER 68	DBC	K^-N 3 GeV/c
0.96 ± 0.20	DAHL 67	HBC	π^-p 1.6-4 GeV/c
0.73 ± 0.11	DAUBER 67	HBC	K^-p 2 GeV/c
••• We do not use the following data for averages, fits, limits, etc. •••			
1.06 ± 0.12	BERTHON 74	HBC	Quasi-2-body σ
1.72 ± 0.78	MUSGRAVE 65	HBC	

¹ The $\bar{K}N \rightarrow \Sigma\pi$ amplitude at resonance is +0.46 ± 0.01.

$\Gamma(\Lambda\pi\pi)/\Gamma_{\text{total}}$

VALUE	DOCUMENT ID	TECN	COMMENT
0.09 to 0.11 OUR ESTIMATE			
0.091 ± 0.006	CORDEN 75	DBC	K^-d 1.4-1.8 GeV/c
0.11 ± 0.01	¹ MAST 73B	IPWA	$K^-p \rightarrow \Lambda\pi\pi$

¹ Assumes $\Gamma(N\bar{K})/\Gamma_{\text{total}} = 0.46 \pm 0.02$.

$\Gamma(\Lambda\pi\pi)/\Gamma(N\bar{K})$

VALUE	DOCUMENT ID	TECN	COMMENT
0.18 to 0.22 OUR ESTIMATE			
0.22 ± 0.03	BURKHARDT 69	HBC	K^-p 0.8-1.2 GeV/c
0.19 ± 0.04	SCHEUER 68	DBC	K^-N 3 GeV/c
0.17 ± 0.05	DAHL 67	HBC	π^-p 1.6-4 GeV/c
0.21 ± 0.18	DAUBER 67	HBC	K^-p 2 GeV/c
••• We do not use the following data for averages, fits, limits, etc. •••			
0.27 ± 0.13	BERTHON 74	HBC	Quasi-2-body σ
0.2	KIM 71	DPWA	K-matrix analysis

$\Gamma(\Sigma\pi)/\Gamma(\Lambda\pi\pi)$

VALUE	DOCUMENT ID	TECN	COMMENT
3.4 to 4.4 OUR ESTIMATE			
3.9 ± 1.0	UHLIG 67	HBC	K^-p 0.9-1.0 GeV/c
3.3 ± 1.1	BIRMINGHAM 66	HBC	K^-p 3.5 GeV/c
4.5 ± 1.0	ARMENTEROS65c	HBC	

$\Gamma(\Sigma(1385)\pi, S\text{-wave})/\Gamma_{\text{total}}$

VALUE	DOCUMENT ID	TECN	COMMENT
••• We do not use the following data for averages, fits, limits, etc. •••			
0.121	¹ KAMANO 15	DPWA	$\bar{K}N$ multichannel

¹ From the preferred solution A in KAMANO 15.

$\Gamma(\Sigma(1385)\pi, D\text{-wave})/\Gamma_{\text{total}}$

VALUE	DOCUMENT ID	TECN	COMMENT
••• We do not use the following data for averages, fits, limits, etc. •••			
0.003	¹ KAMANO 15	DPWA	Multichannel

¹ From the preferred solution A in KAMANO 15.

$\Gamma(\Sigma(1385)\pi)/\Gamma_{\text{total}}$

VALUE	DOCUMENT ID	TECN	COMMENT
0.041 ± 0.005	CHAN 72	HBC	$K^-p \rightarrow \Lambda\pi\pi$

$\Gamma(\Sigma(1385)\pi(\rightarrow\Lambda\pi\pi))/\Gamma(\Lambda\pi\pi)$

The $\Lambda\pi\pi$ mode is largely due to $\Sigma(1385)\pi$. Only the values of $(\Sigma(1385)\pi)/(\Lambda\pi\pi)$ given by MAST 73B and CORDEN 75 are based on real 3-body partial-wave analyses. The discrepancy between the two results is essentially due to the different hypotheses made concerning the shape of the $(\pi\pi)_{S\text{-wave}}$ state.

VALUE	CL%	DOCUMENT ID	TECN	COMMENT
0.58 ± 0.22		CORDEN 75	DBC	K^-d 1.4-1.8 GeV/c
0.82 ± 0.10		¹ MAST 73B	IPWA	$K^-p \rightarrow \Lambda\pi\pi$
••• We do not use the following data for averages, fits, limits, etc. •••				
<0.44	90	WIELAND 11	SPHR	$\gamma p \rightarrow K^+\Lambda(1520)$
0.39 ± 0.10		² BURKHARDT 71	HBC	$K^-p \rightarrow (\Lambda\pi\pi)\pi$

¹ Both $\Sigma(1385)\pi DS_{03}$ and $\Sigma(\pi\pi) DP_{03}$ contribute.
² The central bin (1514-1524 MeV) gives 0.74 ± 0.10 ; other bins are lower by 2-to-5 standard deviations.

$\Gamma(\Lambda(\pi\pi)_{S\text{-wave}})/\Gamma(\Lambda\pi\pi)$

VALUE	DOCUMENT ID	TECN	COMMENT
0.20 ± 0.08	CORDEN 75	DBC	K^-d 1.4-1.8 GeV/c

$\Gamma(\Sigma\pi\pi)/\Gamma_{\text{total}}$

VALUE	DOCUMENT ID	TECN	COMMENT
0.007 to 0.011 OUR ESTIMATE			
0.007 ± 0.002	¹ CORDEN 75	DBC	K^-d 1.4-1.8 GeV/c
0.0085 ± 0.0006	² MAST 73	MPWA	$K^-p \rightarrow \Sigma\pi\pi$
0.010 ± 0.0015	BARBARO... 69B	HBC	K^-p 0.28-0.45 GeV/c

¹ Much of the $\Sigma\pi\pi$ decay proceeds via $\Sigma(1385)\pi$.
² Assumes $\Gamma(N\bar{K})/\Gamma_{\text{total}} = 0.46$.

$\Gamma(\Lambda\gamma)/\Gamma_{\text{total}}$

VALUE (units 10^{-3})	EVTS	DOCUMENT ID	TECN	COMMENT
7 to 11 OUR ESTIMATE				
10.7 ± 2.9 ^{+1.5} _{-0.4}	32	TAYLOR 05	CLAS	$\gamma p \rightarrow K^+\Lambda\gamma$
10.2 ± 2.1 ± 1.5	290	ANTIPOV 04A	SPNX	$pN(C) \rightarrow \Lambda(1520)K^+N(C)$
8.0 ± 1.4	238	MAST 68B	HBC	Using $\Gamma(N\bar{K})/\Gamma_{\text{total}} = 0.45$

$\Gamma(\Sigma^0\gamma)/\Gamma_{\text{total}}$

VALUE	DOCUMENT ID	TECN	COMMENT
0.02 ± 0.0035	¹ MAST 68B	HBC	Not measured; see note

¹ Calculated from $\Gamma(\Lambda\gamma)/\Gamma_{\text{total}}$, assuming SU(3). Needed to constrain the sum of all the branching ratios to be unity.

$\Lambda(1520)$ REFERENCES

SARANTSEV 19	EPJ A55 180	A.V. Sarantsev et al.	(BONN, PNPI)
KAMANO 15	PR C92 025205	H. Kamano et al.	(ANL, OSAK)
ZHANG 13A	PR C88 035205	H. Zhang et al.	(KSU)
WIELAND 11	EPJ A47 47	F. Wieland et al.	(ELSA SAPHIR Collab.)
QIANG 10	PL B694 123	Y. Qiang et al.	(DUKE, JEFF, PNPI, GWU+)
TAYLOR 05	PR C71 054609	S. Taylor et al.	(JLab CLAS Collab.)
Also	PR C72 039902 (errata)	S. Taylor et al.	(JLab CLAS Collab.)
ANTIPOV 04A	PL B604 22	Yu.M. Antipov et al.	(IHEP SPHINX Collab.)
PDG 82	PL 111B 1	M. Roos et al.	(HELS, CIT, CERN)
BARBER 80D	ZPHY C7 17	D.P. Barber et al.	(DARE, LANC, SHEF)
GOPAL 80	Toronto Conf. 159	G.P. Gopal	(RHEL) IUP
BARLAG 79	NP B149 220	S.J.M. Barlag et al.	(AMST, CERN, NIJ+)
ALSTON... 78	PR D18 182	M. Alston-Garnjost et al.	(LBL, MTHO+IUP)
Also	PRL 38 1007	M. Alston-Garnjost et al.	(LBL, MTHO+IUP)
CAMERON 77	NP B131 399	W. Cameron et al.	(RHEL, LOIC IUP)
GOPAL 77	NP B119 362	G.P. Gopal et al.	(RHEL) IUP
MAST 76	PR D14 13	T.S. Mast et al.	(LBL)
CORDEN 75	NP B84 306	M.J. Corden et al.	(BIRM)
BERTHON 74	NC 21A 146	A. Berthon et al.	(CDEF, RHEL, SACL+)
MAST 73	PR D7 3212	T.S. Mast et al.	(LBL) IUP
MAST 73B	PR D7 5	T.S. Mast et al.	(LBL) IUP
CHAN 72	PRL 28 256	S.B. Chan et al.	(MASA, YALE)
BURKHARDT 71	NP B27 64	E. Burkhart et al.	(HEID, CERN, SACL)
KIM 71	PRL 27 356	J.K. Kim	(HARV) IUP
Also	Duke Conf. 161	J.K. Kim	(HARV) IUP
Hyperon Resonances, 1970			
BARBARO... 69B	Lund Conf. 352	A. Barbaro-Galtrieri et al.	(LRL)
Also	Duke Conf. 95	R.D. Tripp	(LRL)
Hyperon Resonances 1970			
BURKHARDT 69	NP B14 106	E. Burkhart et al.	(HEID, EFI, CERN+)
MAST 68B	PRL 21 1715	T.S. Mast et al.	(LRL)
SCHEUER 68	NP B8 503	J.C. Scheuer et al.	(SABRE Collab.)
DAHL 67	PR 163 1377	O.I. Dahl et al.	(LRL)
DAUBER 67	PL 24B 925	P.M. Dauber et al.	(UCLA)

Baryon Particle Listings

 $\Lambda(1520), \Lambda(1600)$

UHLIG 67	PR 155 1448	R.P. Uhlig <i>et al.</i>	(UMD, NRL)
BIRMINGHAM 66	PR 152 1148	M. Haque <i>et al.</i>	(BIRM, GLAS, LOIC, OXF+)
ARMENTEROS 65C	PL 19 338	R. Armenteros <i>et al.</i>	(CERN, HEID, SAFL)
MUSGRAVE 65	NC 35 735	B. Musgrave <i>et al.</i>	(BIRM, CERN, EPOL+)
WATSON 63	PR 131 2248	M.B. Watson, M. Ferro-Luzzi, R.D. Tripp	(LRL) IJP
FERRO-LUZZI 62	PRL 8 28	M. Ferro-Luzzi, R.D. Tripp, M.B. Watson	(LRL) IJP

$$\Lambda(1600) \ 1/2^+$$

$$I(J^P) = 0(\frac{1}{2}^+) \text{ Status: } ****$$

 $\Lambda(1600)$ POLE POSITION

REAL PART

VALUE (MeV)	DOCUMENT ID	TECN	COMMENT
-------------	-------------	------	---------

1540 to 1560 (≈ 1550) OUR ESTIMATE1546 \pm 6 OUR AVERAGE Error includes scale factor of 2.1.1562 \pm 8 SARANTSEV 19 DPWA $\bar{K}N$ multichannel1544 \pm 3 KAMANO 15 DPWA Multichannel

••• We do not use the following data for averages, fits, limits, etc. •••

1572 ZHANG 13A DPWA Multichannel

¹ From the preferred solution A in KAMANO 15.

-2xIMAGINARY PART

VALUE (MeV)	DOCUMENT ID	TECN	COMMENT
-------------	-------------	------	---------

120 to 240 (≈ 180) OUR ESTIMATE159 \pm 12 OUR AVERAGE Error includes scale factor of 6.2.232 \pm 15 SARANTSEV 19 DPWA $\bar{K}N$ multichannel112 \pm 12 KAMANO 15 DPWA Multichannel

••• We do not use the following data for averages, fits, limits, etc. •••

138 ZHANG 13A DPWA Multichannel

¹ From the preferred solution A in KAMANO 15. $\Lambda(1600)$ POLE RESIDUESThe normalized residue is the residue divided by $\Gamma_{pole}/2$.Normalized residue in $N\bar{K} \rightarrow \Lambda(1600) \rightarrow N\bar{K}$

MODULUS	PHASE (°)	DOCUMENT ID	TECN	COMMENT
---------	-----------	-------------	------	---------

0.36 \pm 0.07 -63 \pm 10 SARANTSEV 19 DPWA $\bar{K}N$ multichannel

••• We do not use the following data for averages, fits, limits, etc. •••

0.105 -80 KAMANO 15 DPWA Multichannel

¹ From the preferred solution A in KAMANO 15.Normalized residue in $N\bar{K} \rightarrow \Lambda(1600) \rightarrow \Sigma\pi$

MODULUS	PHASE (°)	DOCUMENT ID	TECN	COMMENT
---------	-----------	-------------	------	---------

0.39 \pm 0.08 148 \pm 10 SARANTSEV 19 DPWA $\bar{K}N$ multichannel

••• We do not use the following data for averages, fits, limits, etc. •••

0.232 108 KAMANO 15 DPWA Multichannel

¹ From the preferred solution A in KAMANO 15.Normalized residue in $N\bar{K} \rightarrow \Lambda(1600) \rightarrow \Lambda\eta$

MODULUS	PHASE (°)	DOCUMENT ID	TECN	COMMENT
---------	-----------	-------------	------	---------

0.22 \pm 0.13 180 \pm 20 SARANTSEV 19 DPWA $\bar{K}N$ multichannelNormalized residue in $N\bar{K} \rightarrow \Lambda(1600) \rightarrow \Lambda\sigma$

MODULUS	PHASE (°)	DOCUMENT ID	TECN	COMMENT
---------	-----------	-------------	------	---------

0.30 \pm 0.06 -70 \pm 10 SARANTSEV 19 DPWA $\bar{K}N$ multichannelNormalized residue in $N\bar{K} \rightarrow \Lambda(1600) \rightarrow \Sigma(1385)\pi$

MODULUS	PHASE (°)	DOCUMENT ID	TECN	COMMENT
---------	-----------	-------------	------	---------

0.37 \pm 0.07 103 \pm 12 SARANTSEV 19 DPWA $\bar{K}N$ multichannel

••• We do not use the following data for averages, fits, limits, etc. •••

0.183 77 KAMANO 15 DPWA Multichannel

¹ From the preferred solution A in KAMANO 15.Normalized residue in $N\bar{K} \rightarrow \Lambda(1600) \rightarrow N\bar{K}^*(892), S=1/2, P\text{-wave}$

MODULUS	PHASE (°)	DOCUMENT ID	TECN	COMMENT
---------	-----------	-------------	------	---------

0.02 \pm 0.01 126 \pm 45 SARANTSEV 19 DPWA $\bar{K}N$ multichannelNormalized residue in $N\bar{K} \rightarrow \Lambda(1600) \rightarrow N\bar{K}^*(892), S=3/2, P\text{-wave}$

MODULUS	PHASE (°)	DOCUMENT ID	TECN	COMMENT
---------	-----------	-------------	------	---------

0.02 \pm 0.01 -135 \pm 45 SARANTSEV 19 DPWA $\bar{K}N$ multichannel $\Lambda(1600)$ MASS

VALUE (MeV)	DOCUMENT ID	TECN	COMMENT
-------------	-------------	------	---------

1570 to 1630 (≈ 1600) OUR ESTIMATE1605 \pm 8 SARANTSEV 19 DPWA $\bar{K}N$ multichannel1592 \pm 10 ZHANG 13A DPWA Multichannel1568 \pm 20 GOPAL 80 DPWA $\bar{K}N \rightarrow \bar{K}N$ 1703 \pm 100 ALSTON... 78 DPWA $\bar{K}N \rightarrow \bar{K}N$ 1573 \pm 25 GOPAL 77 DPWA $\bar{K}N$ multichannel1596 \pm 6 KANE 74 DPWA $K^-p \rightarrow \Sigma\pi$ 1620 \pm 10 LANGBEIN 72 IPWA $\bar{K}N$ multichannel

••• We do not use the following data for averages, fits, limits, etc. •••

1572 or 1617 ¹ MARTIN 77 DPWA $\bar{K}N$ multichannel1646 \pm 7 ² CARROLL 76 DPWA Isospin-0 total σ

KIM 71 DPWA K-matrix analysis

¹ The two MARTIN 77 values are from a T-matrix pole and from a Breit-Wigner fit.² A total cross-section bump with $(J+1/2) \Gamma_{el} / \Gamma_{total} = 0.04$. $\Lambda(1600)$ WIDTH

VALUE (MeV)	DOCUMENT ID	TECN	COMMENT
-------------	-------------	------	---------

150 to 250 (≈ 200) OUR ESTIMATE245 \pm 15 SARANTSEV 19 DPWA $\bar{K}N$ multichannel150 \pm 28 ZHANG 13A DPWA Multichannel116 \pm 20 GOPAL 80 DPWA $\bar{K}N \rightarrow \bar{K}N$ 593 \pm 200 ALSTON... 78 DPWA $\bar{K}N \rightarrow \bar{K}N$ 147 \pm 50 GOPAL 77 DPWA $\bar{K}N$ multichannel175 \pm 20 KANE 74 DPWA $K^-p \rightarrow \Sigma\pi$ 60 \pm 10 LANGBEIN 72 IPWA $\bar{K}N$ multichannel

••• We do not use the following data for averages, fits, limits, etc. •••

247 or 271 ¹ MARTIN 77 DPWA $\bar{K}N$ multichannel20 ² CARROLL 76 DPWA Isospin-0 total σ

50 KIM 71 DPWA K-matrix analysis

¹ The two MARTIN 77 values are from a T-matrix pole and from a Breit-Wigner fit.² A total cross-section bump with $(J+1/2) \Gamma_{el} / \Gamma_{total} = 0.04$. $\Lambda(1600)$ DECAY MODES

Mode	Fraction (Γ_i/Γ)
Γ_1 $N\bar{K}$	15-30 %
Γ_2 $\Sigma\pi$	10-60 %
Γ_3 $\Lambda\sigma$	(19 \pm 4) %
Γ_4 $\Sigma(1385)\pi$	(9 \pm 4) %

 $\Lambda(1600)$ BRANCHING RATIOSSee "Sign conventions for resonance couplings" in the Note on Λ and Σ Resonances.

$\Gamma(N\bar{K})/\Gamma_{total}$	Γ_1/Γ
-----------------------------------	-------------------

VALUE	DOCUMENT ID	TECN	COMMENT
-------	-------------	------	---------

0.14 to 0.28 OUR ESTIMATE

0.29 \pm 0.06 SARANTSEV 19 DPWA $\bar{K}N$ multichannel0.14 \pm 0.04 ZHANG 13A DPWA Multichannel0.23 \pm 0.04 GOPAL 80 DPWA $\bar{K}N \rightarrow \bar{K}N$ 0.14 \pm 0.05 ALSTON... 78 DPWA $\bar{K}N \rightarrow \bar{K}N$ 0.25 \pm 0.15 LANGBEIN 72 IPWA $\bar{K}N$ multichannel

••• We do not use the following data for averages, fits, limits, etc. •••

0.064 ¹ KAMANO 15 DPWA Multichannel0.24 \pm 0.04 GOPAL 77 DPWA See GOPAL 800.30 or 0.29 ² MARTIN 77 DPWA $\bar{K}N$ multichannel¹ From the preferred solution A in KAMANO 15.² The two MARTIN 77 values are from a T-matrix pole and from a Breit-Wigner fit.

$\Gamma(\Sigma\pi)/\Gamma_{total}$	Γ_2/Γ
------------------------------------	-------------------

VALUE	DOCUMENT ID	TECN	COMMENT
-------	-------------	------	---------

0.37 \pm 0.07 SARANTSEV 19 DPWA $\bar{K}N$ multichannel

••• We do not use the following data for averages, fits, limits, etc. •••

0.851 ¹ KAMANO 15 DPWA Multichannel¹ From the preferred solution A in KAMANO 15.

$\Gamma(\Lambda\sigma)/\Gamma_{total}$	Γ_3/Γ
--	-------------------

VALUE	DOCUMENT ID	TECN	COMMENT
-------	-------------	------	---------

0.19 \pm 0.04 SARANTSEV 19 DPWA $\bar{K}N$ multichannel

$\Gamma(\Sigma(1385)\pi)/\Gamma_{total}$	Γ_4/Γ
--	-------------------

VALUE	DOCUMENT ID	TECN	COMMENT
-------	-------------	------	---------

0.09 \pm 0.04 SARANTSEV 19 DPWA $\bar{K}N$ multichannel

••• We do not use the following data for averages, fits, limits, etc. •••

0.085 ¹ KAMANO 15 DPWA Multichannel¹ From the preferred solution A in KAMANO 15.

$(\Gamma_1\Gamma_2)^{1/2}/\Gamma_{total}$ in $N\bar{K} \rightarrow \Lambda(1600) \rightarrow \Sigma\pi$	$(\Gamma_1\Gamma_2)^{1/2}/\Gamma$
---	-----------------------------------

VALUE	DOCUMENT ID	TECN	COMMENT
-------	-------------	------	---------

-0.23 \pm 0.03 ZHANG 13A DPWA Multichannel-0.16 \pm 0.04 GOPAL 77 DPWA $\bar{K}N$ multichannel-0.33 \pm 0.11 KANE 74 DPWA $K^-p \rightarrow \Sigma\pi$ 0.28 \pm 0.09 LANGBEIN 72 IPWA $\bar{K}N$ multichannel

••• We do not use the following data for averages, fits, limits, etc. •••

-0.39 or -0.39 ¹ MARTIN 77 DPWA $\bar{K}N$ multichannelnot seen HEPP 76B DPWA $K^-N \rightarrow \Sigma\pi$ ¹ The two MARTIN 77 values are from a T-matrix pole and from a Breit-Wigner fit.

$\Lambda(1600)$ REFERENCES

SARANTSEV	19	EPJ A55 180	A.V. Sarantsev et al.	(BONN, PNPI)
KAMANO	15	PR C92 025205	H. Kamano et al.	(ANL, OSAK)
ZHANG	13A	PR C88 035205	H. Zhang et al.	(KSU)
GOPAL	80	Toronto Conf. 159	G.P. Gopal	(RHEL) IJP
ALSTON-...	78	PR D18 182	M. Alston-Garnjost et al.	(LBL, MTHO+) IJP
Also		PRL 38 1007	M. Alston-Garnjost et al.	(LBL, MTHO+) IJP
GOPAL	77	NP B119 362	G.P. Gopal et al.	(LOIC, RHEL) IJP
MARTIN	77	NP B127 349	B.R. Martin, M.K. Pldcock, R.G. Moorhouse	(LOUC+) IJP
Also		NP B126 266	B.R. Martin, M.K. Pldcock	(LOUC)
Also		NP B126 285	B.R. Martin, M.K. Pldcock	(LOUC) IJP
CARROLL	76	PRL 37 806	A.S. Carroll et al.	(BNL) I
HEPP	76B	PL 65B 487	V. Hepp et al.	(CERN, HEIDH, MPIM)
KANE	74	LBL-2452	D.F. Kane	(LBL) IJP
LANGBEIN	72	NP B47 477	W. Langbein, F. Wagner	(MPIM) IJP
KIM	71	PRL 27 356	J.K. Kim	(HARV) IJP

$\Lambda(1670) 1/2^-$

 $I(J^P) = 0(\frac{1}{2}^-)$ Status: * * * *

The measurements of the mass, width, and elasticity published before 1974 are now obsolete and have been omitted. They were last listed in our 1982 edition Physics Letters **111B** 1 (1982).

$\Lambda(1670)$ POLE POSITIONS

REAL PART

VALUE (MeV)	DOCUMENT ID	TECN	COMMENT
1670 to 1678 (≈ 1674) OUR ESTIMATE			
1676 ± 2	SARANTSEV 19	DPWA	$\bar{K}N$ multichannel
1669 $+3$ -8	¹ KAMANO 15	DPWA	$\bar{K}N$ multichannel
1677.5 ± 0.8	GARCIA-REC...03	DPWA	$\bar{K}N$ multichannel
••• We do not use the following data for averages, fits, limits, etc. •••			
1667	ZHANG 13A	DPWA	$\bar{K}N$ multichannel
¹ From the preferred solution A in KAMANO 15.			
-2xIMAGINARY PART			
VALUE (MeV)	DOCUMENT ID	TECN	COMMENT
28 to 36 (≈ 32) OUR ESTIMATE			
33 ± 4	SARANTSEV 19	DPWA	$\bar{K}N$ multichannel
19 ± 2	¹ KAMANO 15	DPWA	$\bar{K}N$ multichannel
29.2 ± 1.4	GARCIA-REC...03	DPWA	$\bar{K}N$ multichannel
••• We do not use the following data for averages, fits, limits, etc. •••			
26	ZHANG 13A	DPWA	$\bar{K}N$ multichannel
¹ From the preferred solution A in KAMANO 15.			

$\Lambda(1670)$ POLE RESIDUES

The normalized residue is the residue divided by $\Gamma_{pole}/2$.

Normalized residue in $\bar{K}N \rightarrow \Lambda(1670) \rightarrow \bar{K}N$

MODULUS	PHASE ($^\circ$)	DOCUMENT ID	TECN	COMMENT
0.30 ± 0.06	-145 ± 11	SARANTSEV 19	DPWA	$\bar{K}N$ multichannel
••• We do not use the following data for averages, fits, limits, etc. •••				
0.351	164	¹ KAMANO 15	DPWA	$\bar{K}N$ multichannel
¹ From the preferred solution A in KAMANO 15.				
Normalized residue in $N\bar{K} \rightarrow \Lambda(1670) \rightarrow \Sigma\pi$				
MODULUS	PHASE ($^\circ$)	DOCUMENT ID	TECN	COMMENT
0.19 ± 0.06	145 ± 14	SARANTSEV 19	DPWA	$\bar{K}N$ multichannel
••• We do not use the following data for averages, fits, limits, etc. •••				
0.327	125	¹ KAMANO 15	DPWA	$\bar{K}N$ multichannel
¹ From the preferred solution A in KAMANO 15.				
Normalized residue in $N\bar{K} \rightarrow \Lambda(1670) \rightarrow \Lambda\eta$				
MODULUS	PHASE ($^\circ$)	DOCUMENT ID	TECN	COMMENT
0.26 ± 0.09	104 ± 14	SARANTSEV 19	DPWA	$\bar{K}N$ multichannel
••• We do not use the following data for averages, fits, limits, etc. •••				
0.474	59	¹ KAMANO 15	DPWA	Multichannel
¹ From the preferred solution A in KAMANO 15.				
Normalized residue in $N\bar{K} \rightarrow \Lambda(1670) \rightarrow \Xi K$				
MODULUS	PHASE ($^\circ$)	DOCUMENT ID	TECN	COMMENT
0.02 ± 0.02	100 ± 25	SARANTSEV 19	DPWA	$\bar{K}N$ multichannel
Normalized residue in $N\bar{K} \rightarrow \Lambda(1670) \rightarrow \Lambda\omega, S=1/2, S\text{-wave}$				
MODULUS	PHASE ($^\circ$)	DOCUMENT ID	TECN	COMMENT
0.09 ± 0.04	-60 ± 35	SARANTSEV 19	DPWA	$\bar{K}N$ multichannel
Normalized residue in $N\bar{K} \rightarrow \Lambda(1670) \rightarrow \Lambda\omega, S=3/2, D\text{-wave}$				
MODULUS	PHASE ($^\circ$)	DOCUMENT ID	TECN	COMMENT
0.05 ± 0.04		SARANTSEV 19	DPWA	$\bar{K}N$ multichannel

Normalized residue in $N\bar{K} \rightarrow \Lambda(1670) \rightarrow N\bar{K}^*(892), S=1/2, S\text{-wave}$

MODULUS	PHASE ($^\circ$)	DOCUMENT ID	TECN	COMMENT
0.31 ± 0.14	100 ± 45	SARANTSEV 19	DPWA	$\bar{K}N$ multichannel
Normalized residue in $N\bar{K} \rightarrow \Lambda(1670) \rightarrow N\bar{K}^*(892), S=3/2, D\text{-wave}$				
MODULUS	PHASE ($^\circ$)	DOCUMENT ID	TECN	COMMENT
0.06 ± 0.03	-85 ± 40	SARANTSEV 19	DPWA	$\bar{K}N$ multichannel
Normalized residue in $N\bar{K} \rightarrow \Lambda(1670) \rightarrow \Lambda\sigma$				
MODULUS	PHASE ($^\circ$)	DOCUMENT ID	TECN	COMMENT
0.25 ± 0.08	160 ± 15	SARANTSEV 19	DPWA	$\bar{K}N$ multichannel
Normalized residue in $N\bar{K} \rightarrow \Lambda(1670) \rightarrow \Sigma(1385)\pi$				
MODULUS	PHASE ($^\circ$)	DOCUMENT ID	TECN	COMMENT
0.13 ± 0.06	110 ± 12	SARANTSEV 19	DPWA	$\bar{K}N$ multichannel
••• We do not use the following data for averages, fits, limits, etc. •••				
0.0988	-104	¹ KAMANO 15	DPWA	Multichannel
¹ From the preferred solution A in KAMANO 15.				

$\Lambda(1670)$ MASS

VALUE (MeV)	DOCUMENT ID	TECN	COMMENT
1670 to 1678 (≈ 1674) OUR ESTIMATE			
1677 ± 2	SARANTSEV 19	DPWA	$\bar{K}N$ multichannel
1672 ± 3	ZHANG 13A	DPWA	Multichannel
1670.8 ± 1.7	KOISO 85	DPWA	$K^-p \rightarrow \Sigma\pi$
1667 ± 5	GOPAL 80	DPWA	$\bar{K}N \rightarrow \bar{K}N$
1671 ± 3	ALSTON-... 78	DPWA	$\bar{K}N \rightarrow \bar{K}N$
1675 ± 2	HEPP 76B	DPWA	$K^-N \rightarrow \Sigma\pi$
1679 ± 1	KANE 74	DPWA	$K^-p \rightarrow \Sigma\pi$
1665 ± 5	PREVOST 74	DPWA	$K^-N \rightarrow \Sigma(1385)\pi$
••• We do not use the following data for averages, fits, limits, etc. •••			
1673 ± 2	MANLEY 02	DPWA	$\bar{K}N$ multichannel
1668.9 ± 2.0	ABAEV 96	DPWA	$K^-p \rightarrow \Lambda\eta$
1670 ± 5	GOPAL 77	DPWA	$\bar{K}N$ multichannel
1664	¹ MARTIN 77	DPWA	$\bar{K}N$ multichannel
¹ MARTIN 77 obtains identical resonance parameters from a T-matrix pole and from a Breit-Wigner fit.			

$\Lambda(1670)$ WIDTH

VALUE (MeV)	DOCUMENT ID	TECN	COMMENT
25 to 35 (≈ 30) OUR ESTIMATE			
33 ± 4	SARANTSEV 19	DPWA	$\bar{K}N$ multichannel
29 ± 5	ZHANG 13A	DPWA	$\bar{K}N$ multichannel
34.1 ± 3.7	KOISO 85	DPWA	$K^-p \rightarrow \Sigma\pi$
29 ± 5	GOPAL 80	DPWA	$\bar{K}N \rightarrow \bar{K}N$
29 ± 5	ALSTON-... 78	DPWA	$\bar{K}N \rightarrow \bar{K}N$
46 ± 5	HEPP 76B	DPWA	$K^-N \rightarrow \Sigma\pi$
40 ± 3	KANE 74	DPWA	$K^-p \rightarrow \Sigma\pi$
19 ± 5	PREVOST 74	DPWA	$K^-N \rightarrow \Sigma(1385)\pi$
••• We do not use the following data for averages, fits, limits, etc. •••			
23 ± 6	MANLEY 02	DPWA	$\bar{K}N$ multichannel
21.1 ± 3.6	ABAEV 96	DPWA	$K^-p \rightarrow \Lambda\eta$
45 ± 10	GOPAL 77	DPWA	$\bar{K}N$ multichannel
12	¹ MARTIN 77	DPWA	$\bar{K}N$ multichannel
¹ MARTIN 77 obtains identical resonance parameters from a T-matrix pole and from a Breit-Wigner fit.			

$\Lambda(1670)$ DECAY MODES

Mode	Fraction (Γ_i/Γ)
$\Gamma_1 N\bar{K}$	20-30 %
$\Gamma_2 \Sigma\pi$	25-55 %
$\Gamma_3 \Lambda\eta$	10-25 %
$\Gamma_4 \Sigma(1385)\pi, D\text{-wave}$	(6.0 ± 2.0) %
$\Gamma_5 N\bar{K}^*(892), S=1/2, S\text{-wave}$	
$\Gamma_6 N\bar{K}^*(892), S=3/2, D\text{-wave}$	(5 ± 4) %
$\Gamma_7 \Lambda\sigma$	(20 ± 8) %

$\Lambda(1670)$ BRANCHING RATIOS

See "Sign conventions for resonance couplings" in the Note on Λ and Σ Resonances.

$\Gamma(N\bar{K})/\Gamma_{total}$	DOCUMENT ID	TECN	COMMENT	Γ_1/Γ
0.20 to 0.30 OUR ESTIMATE				
0.33 ± 0.07	SARANTSEV 19	DPWA	$\bar{K}N$ multichannel	
0.26 ± 0.25	ZHANG 13A	DPWA	$\bar{K}N$ multichannel	
0.18 ± 0.03	GOPAL 80	DPWA	$\bar{K}N \rightarrow \bar{K}N$	
0.17 ± 0.03	ALSTON-... 78	DPWA	$\bar{K}N \rightarrow \bar{K}N$	

Baryon Particle Listings

$\Lambda(1670), \Lambda(1690)$

••• We do not use the following data for averages, fits, limits, etc. •••

0.318	1 KAMANO	15	DPWA	$\bar{K}N$ multichannel
0.37 ± 0.07	MANLEY	02	DPWA	$\bar{K}N$ multichannel
0.20 ± 0.03	GOPAL	77	DPWA	See GOPAL 80
0.15	2 MARTIN	77	DPWA	$\bar{K}N$ multichannel

¹ From the preferred solution A in KAMANO 15.

² MARTIN 77 obtains identical resonance parameters from a T-matrix pole and from a Breit-Wigner fit.

$\Gamma(\Sigma\pi)/\Gamma_{total}$ Γ_2/Γ

VALUE	DOCUMENT ID	TECN	COMMENT
0.12 ± 0.03	SARANTSEV	19	DPWA $\bar{K}N$ multichannel

••• We do not use the following data for averages, fits, limits, etc. •••

0.289	1 KAMANO	15	DPWA	Multichannel
-------	----------	----	------	--------------

¹ From the preferred solution A in KAMANO 15.

$\Gamma(\Lambda\eta)/\Gamma_{total}$ Γ_3/Γ

VALUE	DOCUMENT ID	TECN	COMMENT
0.20 ± 0.08	SARANTSEV	19	DPWA $\bar{K}N$ multichannel

••• We do not use the following data for averages, fits, limits, etc. •••

0.373	KAMANO	15	DPWA	Multichannel
0.30 ± 0.08	ABAEV	96	DPWA	$K^-p \rightarrow \Lambda\eta$

$\Gamma(\Sigma(1385)\pi, D\text{-wave})/\Gamma_{total}$ Γ_4/Γ

VALUE	DOCUMENT ID	TECN	COMMENT
0.06 ± 0.02	SARANTSEV	19	DPWA $\bar{K}N$ multichannel

••• We do not use the following data for averages, fits, limits, etc. •••

0.019	KAMANO	15	DPWA	Multi-channel
-------	--------	----	------	---------------

$\Gamma(\Lambda\sigma)/\Gamma_{total}$ Γ_7/Γ

VALUE	DOCUMENT ID	TECN	COMMENT
0.20 ± 0.08	SARANTSEV	19	DPWA $\bar{K}N$ multichannel

$\Gamma(N\bar{K}^*(892), S=1/2, S\text{-wave})/\Gamma_{total}$ Γ_5/Γ

VALUE	DOCUMENT ID	TECN	COMMENT
not seen	1 KAMANO	15	DPWA Multichannel

¹ Not seen in the preferred solution A in KAMANO 15.

$\Gamma(N\bar{K}^*(892), S=3/2, D\text{-wave})/\Gamma_{total}$ Γ_6/Γ

VALUE	DOCUMENT ID	TECN	COMMENT
0.05 ± 0.04	ZHANG	13A	DPWA Multichannel

••• We do not use the following data for averages, fits, limits, etc. •••

not seen	1 KAMANO	15	DPWA Multichannel
----------	----------	----	-------------------

¹ Not seen in the preferred solution A in KAMANO 15.

$(\Gamma_1\Gamma_2)^{1/2}/\Gamma_{total}$ in $N\bar{K} \rightarrow \Lambda(1670) \rightarrow \Sigma\pi$ $(\Gamma_1\Gamma_2)^{1/2}/\Gamma$

VALUE	DOCUMENT ID	TECN	COMMENT
-0.29 ± 0.06	ZHANG	13A	DPWA Multichannel
-0.26 ± 0.02	KOISO	85	DPWA $K^-p \rightarrow \Sigma\pi$
-0.31 ± 0.03	GOPAL	77	DPWA $\bar{K}N$ multichannel
-0.29 ± 0.03	HEPP	76B	DPWA $K^-N \rightarrow \Sigma\pi$
-0.23 ± 0.03	LONDON	75	HLBC $K^-p \rightarrow \Sigma^0\pi^0$
-0.27 ± 0.02	KANE	74	DPWA $K^-p \rightarrow \Sigma\pi$

••• We do not use the following data for averages, fits, limits, etc. •••

-0.38 ± 0.03	MANLEY	02	DPWA $\bar{K}N$ multichannel
-0.13	1 MARTIN	77	DPWA $\bar{K}N$ multichannel

¹ MARTIN 77 obtains identical resonance parameters from a T-matrix pole and from a Breit-Wigner fit.

$(\Gamma_1\Gamma_3)^{1/2}/\Gamma_{total}$ in $N\bar{K} \rightarrow \Lambda(1670) \rightarrow \Lambda\eta$ $(\Gamma_1\Gamma_3)^{1/2}/\Gamma$

VALUE	DOCUMENT ID	TECN	COMMENT
-0.30 ± 0.10	ZHANG	13A	DPWA Multichannel
+0.20 ± 0.05	BAXTER	73	DPWA $K^-p \rightarrow$ neutrals

••• We do not use the following data for averages, fits, limits, etc. •••

+0.24 ± 0.04	MANLEY	02	DPWA $\bar{K}N$ multichannel
0.24	KIM	71	DPWA K-matrix analysis
0.26	ARMENTEROS69c		HBC
0.20 or 0.23	BERLEY	65	HBC

$(\Gamma_1\Gamma_4)^{1/2}/\Gamma_{total}$ in $N\bar{K} \rightarrow \Lambda(1670) \rightarrow \Sigma(1385)\pi, D\text{-wave}$ $(\Gamma_1\Gamma_4)^{1/2}/\Gamma$

VALUE	DOCUMENT ID	TECN	COMMENT
-0.17 ± 0.06	MANLEY	02	DPWA $\bar{K}N$ multichannel
-0.18 ± 0.05	PREVOST	74	DPWA $K^-N \rightarrow \Sigma(1385)\pi$

$\Lambda(1670)$ REFERENCES

SARANTSEV 19	EPJ A55 180	A.V. Sarantsev et al.	(BONN, PNPI)
KAMANO 15	PR C92 025205	H. Kamano et al.	(ANL, OSAK)
ZHANG 13A	PR C88 035205	H. Zhang et al.	(KSU)
GARCIA-REC... 03	PR D67 076009	C. Garcia-Recio et al.	(GRAN, VALE)
MANLEY 02	PRL 88 012002	D.M. Manley et al.	(BNL Crystal Ball Collab.)

ABAEV 96	PR C53 385	V.V. Abaev, B.M.K. Nefkens	(UCLA)
KOISO 85	NP A433 619	H. Koiso et al.	(TOKY, MASA)
PDG 82	PL 111B 1	M. Roos et al.	(HELS, CIT, CERN)
GOPAL 80	Toronto Conf. 159	G.P. Gopal	(RHEL) IJP
ALSTON... 78	PR D18 182	G.P. Gopal et al.	(LBL, MTHO+) IJP
Also	PRL 38 1007	M. Alston-Garnjost et al.	(LBL, MTHO+) IJP
GOPAL 77	NP B119 362	G.P. Gopal et al.	(LOIC, RHEL) IJP
MARTIN 77	NP B127 349	B.R. Martin, M.K. Pidcock, R.G. Moorhouse	(LOUC+) IJP
Also	NP B126 266	B.R. Martin, M.K. Pidcock	(LOUC)
Also	NP B126 285	B.R. Martin, M.K. Pidcock	(LOUC) IJP
HEPP 76B	PL 65B 487	V. Hepp et al.	(CERN, HEIDH, MFIM) IJP
LONDON 75	NP B85 289	G.W. London et al.	(BNL, CERN, EPOL+) IJP
KANE 74	LBL-2452	D.F. Kane	(LBL) IJP
PREVOST 74	NP B69 246	J. Prevost et al.	(SACL, CERN, HEID)
BAXTER 73	NP B67 125	D.F. Baxter et al.	(OXF) IJP
KIM 71	PRL 27 356	J.K. Kim	(HARV) IJP
Also	Duke Conf. 161	J.K. Kim	(HARV) IJP
Hyperon Resonances, 1970			
ARMENTEROS 69C	Lund Paper 229	R. Armenteros et al.	(CERN, HEID, SACL) IJP
Values are quoted in LEVI-SETTI 69.			
BERLEY 65	PRL 15 641	D. Berley et al.	(BNL) IJP

$\Lambda(1690) 3/2^-$

$I(J^P) = 0(\frac{3}{2}^-)$ Status: * * * *

The measurements of the mass, width, and elasticity published before 1974 are now obsolete and have been omitted. They were last listed in our 1982 edition Physics Letters **111B** 1 (1982).

$\Lambda(1690)$ POLE POSITION

REAL PART

VALUE (MeV)	DOCUMENT ID	TECN	COMMENT
-------------	-------------	------	---------

1680 to 1700 (\approx 1690) OUR ESTIMATE

1683 ± 3	SARANTSEV	19	DPWA $\bar{K}N$ multichannel
----------	-----------	----	------------------------------

1697 $^{+6}_{-6}$	1 KAMANO	15	DPWA $\bar{K}N$ multichannel
-------------------	----------	----	------------------------------

••• We do not use the following data for averages, fits, limits, etc. •••

1689	ZHANG	13A	DPWA $\bar{K}N$ multichannel
------	-------	-----	------------------------------

¹ From the preferred solution A in KAMANO 15.

-2xIMAGINARY PART

VALUE (MeV)	DOCUMENT ID	TECN	COMMENT
-------------	-------------	------	---------

60 to 80 (\approx 70) OUR ESTIMATE

72 ± 5	SARANTSEV	19	DPWA $\bar{K}N$ multichannel
--------	-----------	----	------------------------------

65 ± 14	1 KAMANO	15	DPWA $\bar{K}N$ multichannel
---------	----------	----	------------------------------

••• We do not use the following data for averages, fits, limits, etc. •••

53	ZHANG	13A	DPWA $\bar{K}N$ multichannel
----	-------	-----	------------------------------

¹ From the preferred solution A in KAMANO 15.

$\Lambda(1690)$ POLE RESIDUES

The normalized residue is the residue divided by $\Gamma_{pole}/2$.

Normalized residue in $N\bar{K} \rightarrow \Lambda(1690) \rightarrow N\bar{K}$

MODULUS	PHASE (°)	DOCUMENT ID	TECN	COMMENT
---------	-----------	-------------	------	---------

0.24 ± 0.05	-28 ± 5	SARANTSEV	19	DPWA $\bar{K}N$ multichannel
--------------------	----------------	-----------	----	------------------------------

••• We do not use the following data for averages, fits, limits, etc. •••

0.251	3	1 KAMANO	15	DPWA Multichannel
-------	---	----------	----	-------------------

¹ From the preferred solution A in KAMANO 15.

Normalized residue in $N\bar{K} \rightarrow \Lambda(1690) \rightarrow \Sigma\pi$

MODULUS	PHASE (°)	DOCUMENT ID	TECN	COMMENT
---------	-----------	-------------	------	---------

0.35 ± 0.07	175 ± 6	SARANTSEV	19	DPWA $\bar{K}N$ multichannel
--------------------	----------------	-----------	----	------------------------------

••• We do not use the following data for averages, fits, limits, etc. •••

0.315	-173	1 KAMANO	15	DPWA $\bar{K}N$ multichannel
-------	------	----------	----	------------------------------

¹ From the preferred solution A in KAMANO 15.

Normalized residue in $N\bar{K} \rightarrow \Lambda(1690) \rightarrow \Lambda\eta$

MODULUS	PHASE (°)	DOCUMENT ID	TECN	COMMENT
---------	-----------	-------------	------	---------

0.05 ± 0.02	88 ± 8	SARANTSEV	19	DPWA $\bar{K}N$ multichannel
--------------------	---------------	-----------	----	------------------------------

••• We do not use the following data for averages, fits, limits, etc. •••

0.00567	81	1 KAMANO	15	DPWA Multichannel
---------	----	----------	----	-------------------

¹ From the preferred solution A in KAMANO 15.

Normalized residue in $N\bar{K} \rightarrow \Lambda(1690) \rightarrow \Lambda\sigma$

MODULUS	PHASE (°)	DOCUMENT ID	TECN	COMMENT
---------	-----------	-------------	------	---------

0.08 ± 0.02	-10 ± 6	SARANTSEV	19	DPWA $\bar{K}N$ multichannel
--------------------	----------------	-----------	----	------------------------------

Normalized residue in $N\bar{K} \rightarrow \Lambda(1690) \rightarrow \Sigma(1385)\pi, S\text{-wave}$

MODULUS	PHASE (°)	DOCUMENT ID	TECN	COMMENT
---------	-----------	-------------	------	---------

0.11 ± 0.06	170 ± 70	SARANTSEV	19	DPWA $\bar{K}N$ multichannel
--------------------	-----------------	-----------	----	------------------------------

••• We do not use the following data for averages, fits, limits, etc. •••

0.134	168	1 KAMANO	15	DPWA $\bar{K}N$ multichannel
-------	-----	----------	----	------------------------------

¹ From the preferred solution A in KAMANO 15.

See key on page 999

Baryon Particle Listings
 $\Lambda(1690)$

Normalized residue in $N\bar{K} \rightarrow \Lambda(1690) \rightarrow \Sigma(1385)\pi$, D-wave

MODULUS	PHASE (°)	DOCUMENT ID	TECN	COMMENT
0.06 ± 0.04	164 ± 15	SARANTSEV 19	DPWA	$\bar{K}N$ multichannel
0.319	-22	¹ KAMANO 15	DPWA	$\bar{K}N$ multichannel

••• We do not use the following data for averages, fits, limits, etc. •••

¹From the preferred solution A in KAMANO 15.

Normalized residue in $N\bar{K} \rightarrow \Lambda(1690) \rightarrow N\bar{K}^*(892)$, S-wave

VALUE	DOCUMENT ID	TECN	COMMENT
0.05 ± 0.04	SARANTSEV 19	DPWA	$\bar{K}N$ multichannel

Normalized residue in $N\bar{K} \rightarrow \Lambda(1690) \rightarrow N\bar{K}^*(892)$, D-wave

VALUE	DOCUMENT ID	TECN	COMMENT
0.18 ± 0.05 @ -110 ± 45	SARANTSEV 19	DPWA	$\bar{K}N$ multichannel

$\Lambda(1690)$ MASS

VALUE (MeV)	DOCUMENT ID	TECN	COMMENT
1685 to 1695 (≈ 1690) OUR ESTIMATE			
1689 ± 3	SARANTSEV 19	DPWA	$\bar{K}N$ multichannel
1691 ± 3	ZHANG 13A	DPWA	$\bar{K}N$ multichannel
1695.7 ± 2.6	KOISO 85	DPWA	$K^-p \rightarrow \Sigma\pi$
1690 ± 5	GOPAL 80	DPWA	$\bar{K}N \rightarrow \bar{K}N$
1692 ± 5	ALSTON-... 78	DPWA	$\bar{K}N \rightarrow \bar{K}N$
1690 ± 3	HEPP 76B	DPWA	$K^-N \rightarrow \Sigma\pi$
1689 ± 1	KANE 74	DPWA	$K^-p \rightarrow \Sigma\pi$
••• We do not use the following data for averages, fits, limits, etc. •••			
1690 ± 5	GOPAL 77	DPWA	$\bar{K}N$ multichannel
1687 or 1689	¹ MARTIN 77	DPWA	$\bar{K}N$ multichannel
1692 ± 4	CARROLL 76	DPWA	Isospin-0 total σ

¹The two MARTIN 77 values are from a T-matrix pole and from a Breit-Wigner fit. Another $D_{03} \Lambda$ at 1966 MeV is also suggested by MARTIN 77, but is very uncertain.

$\Lambda(1690)$ WIDTH

VALUE (MeV)	DOCUMENT ID	TECN	COMMENT
60 to 80 (≈ 70) OUR ESTIMATE			
75 ± 5	SARANTSEV 19	DPWA	$\bar{K}N$ multichannel
54 ± 5	ZHANG 13A	DPWA	$\bar{K}N$ multichannel
67.2 ± 5.6	KOISO 85	DPWA	$K^-p \rightarrow \Sigma\pi$
61 ± 5	GOPAL 80	DPWA	$\bar{K}N \rightarrow \bar{K}N$
64 ± 10	ALSTON-... 78	DPWA	$\bar{K}N \rightarrow \bar{K}N$
82 ± 8	HEPP 76B	DPWA	$K^-N \rightarrow \Sigma\pi$
60 ± 4	KANE 74	DPWA	$K^-p \rightarrow \Sigma\pi$
••• We do not use the following data for averages, fits, limits, etc. •••			
60 ± 5	GOPAL 77	DPWA	$\bar{K}N$ multichannel
62 or 62	¹ MARTIN 77	DPWA	$\bar{K}N$ multichannel
38	CARROLL 76	DPWA	Isospin-0 total σ

¹The two MARTIN 77 values are from a T-matrix pole and from a Breit-Wigner fit. Another $D_{03} \Lambda$ at 1966 MeV is also suggested by MARTIN 77, but is very uncertain.

$\Lambda(1690)$ DECAY MODES

Mode	Fraction (Γ_i/Γ)
Γ_1 $N\bar{K}$	20-30 %
Γ_2 $\Sigma\pi$	20-40 %
Γ_3 $\Lambda\sigma$	(5.0 ± 2.0) %
Γ_4 $\Lambda\pi\pi$	~ 25 %
Γ_5 $\Sigma\pi\pi$	~ 20 %
Γ_6 $\Lambda\eta$	
Γ_7 $\Sigma(1385)\pi$, S-wave	(9 ± 5) %
Γ_8 $\Sigma(1385)\pi$, D-wave	(3.0 ± 2.0) %
Γ_9 $N\bar{K}^*(892)$, S=1/2, D-wave	
Γ_{10} $N\bar{K}^*(892)$, S=3/2, S-wave	
Γ_{11} $N\bar{K}^*(892)$, S=3/2, D-wave	

$\Lambda(1690)$ BRANCHING RATIOS

$\Gamma(N\bar{K})/\Gamma_{total}$	DOCUMENT ID	TECN	COMMENT
0.20 to 0.28 OUR ESTIMATE			
0.23 ± 0.05	SARANTSEV 19	DPWA	$\bar{K}N$ multichannel
0.25 ± 0.04	ZHANG 13A	DPWA	$\bar{K}N$ multichannel
0.23 ± 0.03	GOPAL 80	DPWA	$\bar{K}N \rightarrow \bar{K}N$
0.22 ± 0.03	ALSTON-... 78	DPWA	$\bar{K}N \rightarrow \bar{K}N$
••• We do not use the following data for averages, fits, limits, etc. •••			
0.239	¹ KAMANO 15	DPWA	$\bar{K}N$ multichannel
0.24 ± 0.03	GOPAL 77	DPWA	See GOPAL 80
0.28 or 0.26	² MARTIN 77	DPWA	$\bar{K}N$ multichannel

¹From the preferred solution A in KAMANO 15.
²The two MARTIN 77 values are from a T-matrix pole and from a Breit-Wigner fit. Another $D_{03} \Lambda$ at 1966 MeV is also suggested by MARTIN 77, but is very uncertain.

$\Gamma(\Sigma\pi)/\Gamma_{total}$

VALUE	DOCUMENT ID	TECN	COMMENT
0.50 ± 0.10	SARANTSEV 19	DPWA	$\bar{K}N$ multichannel
0.387	¹ KAMANO 15	DPWA	$\bar{K}N$ multichannel

••• We do not use the following data for averages, fits, limits, etc. •••

¹From the preferred solution A in KAMANO 15.

$\Gamma(\Lambda\eta)/\Gamma_{total}$

VALUE	DOCUMENT ID	TECN	COMMENT
~ 0.01	SARANTSEV 19	DPWA	$\bar{K}N$ multichannel
not seen	¹ KAMANO 15	DPWA	Multichannel

••• We do not use the following data for averages, fits, limits, etc. •••

¹From the preferred solution A in KAMANO 15.

$\Gamma(\Lambda\sigma)/\Gamma_{total}$

VALUE	DOCUMENT ID	TECN	COMMENT
0.05 ± 0.02	SARANTSEV 19	DPWA	$\bar{K}N$ multichannel

$\Gamma(\Sigma(1385)\pi, S\text{-wave})/\Gamma_{total}$

VALUE	DOCUMENT ID	TECN	COMMENT
0.09 ± 0.05	SARANTSEV 19	DPWA	$\bar{K}N$ multichannel
0.062	¹ KAMANO 15	DPWA	$\bar{K}N$ multichannel

••• We do not use the following data for averages, fits, limits, etc. •••

¹From the preferred solution A in KAMANO 15.

$\Gamma(\Sigma(1385)\pi, D\text{-wave})/\Gamma_{total}$

VALUE	DOCUMENT ID	TECN	COMMENT
0.03 ± 0.02	SARANTSEV 19	DPWA	$\bar{K}N$ multichannel
0.308	¹ KAMANO 15	DPWA	$\bar{K}N$ multichannel

••• We do not use the following data for averages, fits, limits, etc. •••

¹From the preferred solution A in KAMANO 15.

$\Gamma(N\bar{K}^*(892), S=1/2, D\text{-wave})/\Gamma_{total}$

VALUE	DOCUMENT ID	TECN	COMMENT
not seen	SARANTSEV 19	DPWA	$\bar{K}N$ multichannel
not seen	¹ KAMANO 15	DPWA	$\bar{K}N$ multichannel

••• We do not use the following data for averages, fits, limits, etc. •••

¹From the preferred solution A in KAMANO 15.

$\Gamma(N\bar{K}^*(892), S=3/2, S\text{-wave})/\Gamma_{total}$

VALUE	DOCUMENT ID	TECN	COMMENT
0.003	KAMANO 15	DPWA	Multichannel

••• We do not use the following data for averages, fits, limits, etc. •••

$\Gamma(N\bar{K}^*(892), S=3/2, D\text{-wave})/\Gamma_{total}$

VALUE	DOCUMENT ID	TECN	COMMENT
not seen	¹ KAMANO 15	DPWA	Multichannel

••• We do not use the following data for averages, fits, limits, etc. •••

¹From the preferred solution A in KAMANO 15.

$(\Gamma_1\Gamma_7)^{1/2}/\Gamma_{total}$ in $N\bar{K} \rightarrow \Lambda(1690) \rightarrow \Sigma\pi$

VALUE	DOCUMENT ID	TECN	COMMENT
-0.27 ± 0.03	ZHANG 13A	DPWA	Multichannel
-0.34 ± 0.02	KOISO 85	DPWA	$K^-p \rightarrow \Sigma\pi$
-0.25 ± 0.03	GOPAL 77	DPWA	$\bar{K}N$ multichannel
-0.29 ± 0.03	HEPP 76B	DPWA	$K^-N \rightarrow \Sigma\pi$
-0.28 ± 0.03	LONDON 75	HLBC	$K^-p \rightarrow \Sigma^0\pi^0$
-0.28 ± 0.02	KANE 74	DPWA	$K^-p \rightarrow \Sigma\pi$
••• We do not use the following data for averages, fits, limits, etc. •••			
-0.30 or -0.28	¹ MARTIN 77	DPWA	$\bar{K}N$ multichannel

¹The two MARTIN 77 values are from a T-matrix pole and from a Breit-Wigner fit. Another $D_{03} \Lambda$ at 1966 MeV is also suggested by MARTIN 77, but is very uncertain.

$(\Gamma_1\Gamma_7)^{1/2}/\Gamma_{total}$ in $N\bar{K} \rightarrow \Lambda(1690) \rightarrow \Lambda\pi\pi$

VALUE	DOCUMENT ID	TECN	COMMENT
0.25 ± 0.02	¹ BARTLEY 68	HDBC	$K^-p \rightarrow \Lambda\pi\pi$

••• We do not use the following data for averages, fits, limits, etc. •••

¹BARTLEY 68 uses only cross-section data. The enhancement is not seen by PRE-VOST 71.

$(\Gamma_1\Gamma_7)^{1/2}/\Gamma_{total}$ in $N\bar{K} \rightarrow \Lambda(1690) \rightarrow \Sigma\pi\pi$

VALUE	DOCUMENT ID	TECN	COMMENT
0.21	ARMENTEROS68c	HDBC	$K^-N \rightarrow \Sigma\pi\pi$

$(\Gamma_1\Gamma_7)^{1/2}/\Gamma_{total}$ in $N\bar{K} \rightarrow \Lambda(1690) \rightarrow \Lambda\eta$

VALUE	DOCUMENT ID	TECN	COMMENT
0.00 ± 0.03	BAXTER 73	DPWA	$K^-p \rightarrow$ neutrals

Baryon Particle Listings

$\Lambda(1690)$, $\Lambda(1710)$, $\Lambda(1800)$

$(\Gamma_1 \Gamma_2)^{J^P} / \Gamma_{\text{total}}$ in $N\bar{K} \rightarrow \Lambda(1690) \rightarrow \Sigma(1385)\pi$, S-wave				$(\Gamma_1 \Gamma_2)^{J^P} / \Gamma$
VALUE	DOCUMENT ID	TECN	COMMENT	
-0.28 ± 0.06	ZHANG	13A	DPWA	Multichannel
$+0.27 \pm 0.04$	PREVOST	74	DPWA	$K^- N \rightarrow \Sigma(1385)\pi$

$\Lambda(1690)$ REFERENCES

SARANTSEV	19	EPJ A55 180	A.V. Sarantsev et al.	(BONN, PNPI)
KAMANO	15	PR C92 025205	H. Kamano et al.	(ANL, OSAK)
ZHANG	13A	PR C88 035205	H. Zhang et al.	(KSU)
KOISO	85	NP A433 619	H. Koiso et al.	(TOKY, MASA)
PDG	82	PL 111B 1	M. Roos et al.	(HELS, CIT, CERN)
GOPAL	80	Toronto Conf. 159	G.P. Gopal	(RHEL) IJP
ALSTON...	78	PR D18 182	M. Alston-Garnjost et al.	(LBL, MTHO+) IJP
			M. Alston-Garnjost et al.	(LBL, MTHO+) IJP
GOPAL	77	NP B119 362	G.P. Gopal et al.	(LOIC, RHEL) IJP
MARTIN	77	NP B127 349	B.R. Martin, M.K. Pidcock, R.G. Moorhouse	(LOUC+) IJP
			B.R. Martin, M.K. Pidcock	(LOUC) IJP
			B.R. Martin, M.K. Pidcock	(LOUC) IJP
CARROLL	76	PRL 37 806	A.S. Carroll et al.	(BNL) I
HEPP	76B	PL 65B 487	V. Hepp et al.	(CERN, HEIDH, MPIM) IJP
LONDON	75	NP B85 289	G.W. London et al.	(BNL, CERN, EPOL+) IJP
KANE	74	LBL-2452	D.F. Kane	(LBL) IJP
PREVOST	74	NP B69 246	J. Prevost et al.	(SACL, CERN, HEID) IJP
BAXTER	73	NP B67 125	D.F. Baxter et al.	(OXF) IJP
PREVOST	71	Amsterdam Conf.	J. Prevost	(CERN, HEID, SACL) IJP
ARMENTEROS	65C	NP B8 216	R. Armenteros et al.	(CERN, HEID, SACL) I
BARTLEY	68	PRL 21 1111	J.H. Bartley et al.	(TUFTS, FSU, BRAN) I

$\Lambda(1710) 1/2^+$	$I(J^P) = 0(\frac{1}{2}^+)$ Status: *
-----------------------	---------------------------------------

OMITTED FROM SUMMARY TABLE

$\Lambda(1710)$ MASS

VALUE (MeV)	DOCUMENT ID	TECN	COMMENT
1713 ± 13	ZHANG	13A	DPWA Multichannel

$\Lambda(1710)$ WIDTH

VALUE (MeV)	DOCUMENT ID	TECN	COMMENT
180 ± 42	ZHANG	13A	DPWA Multichannel

$\Lambda(1710)$ DECAY MODES

Mode	Fraction (Γ_i / Γ)
Γ_1 $N\bar{K}$	(43 ± 4) %
Γ_2 $\Sigma\pi$	(21 ± 5) %
Γ_3 $\Sigma^*(1385)\pi$, P-wave	(20 ± 8) %
Γ_4 $N\bar{K}^*(892)$	
Γ_5 $N\bar{K}^*(892)$, S=1/2	(5 ± 4) %
Γ_6 $N\bar{K}^*(892)$, S=3/2, P-wave	(10 ± 8) %

$\Lambda(1710)$ BRANCHING RATIOS

$\Gamma(N\bar{K}) / \Gamma_{\text{total}}$				Γ_1 / Γ
VALUE	DOCUMENT ID	TECN	COMMENT	
0.43 ± 0.04	ZHANG	13A	DPWA	Multichannel
$\Gamma(\Sigma\pi) / \Gamma_{\text{total}}$				Γ_2 / Γ
VALUE	DOCUMENT ID	TECN	COMMENT	
0.21 ± 0.05	ZHANG	13A	DPWA	Multichannel
$\Gamma(\Sigma^*(1385)\pi, P\text{-wave}) / \Gamma_{\text{total}}$				Γ_3 / Γ
VALUE	DOCUMENT ID	TECN	COMMENT	
0.20 ± 0.08	ZHANG	13A	DPWA	Multichannel
$\Gamma(N\bar{K}^*(892), S=1/2) / \Gamma_{\text{total}}$				Γ_5 / Γ
VALUE	DOCUMENT ID	TECN	COMMENT	
0.05 ± 0.04	ZHANG	13A	DPWA	Multichannel
$\Gamma(N\bar{K}^*(892), S=3/2, P\text{-wave}) / \Gamma_{\text{total}}$				Γ_6 / Γ
VALUE	DOCUMENT ID	TECN	COMMENT	
0.10 ± 0.08	ZHANG	13A	DPWA	Multichannel

$\Lambda(1710)$ REFERENCES

ZHANG	13A	PR C88 035205	H. Zhang et al.	(KSU)
-------	-----	---------------	-----------------	-------

$\Lambda(1800) 1/2^-$

$I(J^P) = 0(\frac{1}{2}^-)$ Status: ***

$\Lambda(1800)$ POLE POSITION

REAL PART

VALUE (MeV)	DOCUMENT ID	TECN	COMMENT
1809 ± 9	SARANTSEV	19	DPWA $\bar{K}N$ multichannel
1729	ZHANG	13A	DPWA Multichannel

-2xIMAGINARY PART

VALUE (MeV)	DOCUMENT ID	TECN	COMMENT
205 ± 16	SARANTSEV	19	DPWA $\bar{K}N$ multichannel
198	ZHANG	13A	DPWA Multichannel

$\Lambda(1800)$ POLE RESIDUES

The normalized residue is the residue divided by $\Gamma_{\text{pole}}/2$.

Normalized residue in $N\bar{K} \rightarrow \Lambda(1800) \rightarrow N\bar{K}$

MODULUS	PHASE (°)	DOCUMENT ID	TECN	COMMENT
0.34 ± 0.07	103 ± 8	SARANTSEV	19	DPWA $\bar{K}N$ multichannel

Normalized residue in $N\bar{K} \rightarrow \Lambda(1800) \rightarrow \Sigma\pi$

MODULUS	PHASE (°)	DOCUMENT ID	TECN	COMMENT
0.30 ± 0.06	-123 ± 8	SARANTSEV	19	DPWA $\bar{K}N$ multichannel

Normalized residue in $N\bar{K} \rightarrow \Lambda(1800) \rightarrow \Lambda\eta$

MODULUS	PHASE (°)	DOCUMENT ID	TECN	COMMENT
0.06 ± 0.03	75 ± 10	SARANTSEV	19	DPWA $\bar{K}N$ multichannel

Normalized residue in $N\bar{K} \rightarrow \Lambda(1800) \rightarrow \Lambda\sigma$

MODULUS	PHASE (°)	DOCUMENT ID	TECN	COMMENT
0.24 ± 0.05	25 ± 10	SARANTSEV	19	DPWA $\bar{K}N$ multichannel

Normalized residue in $N\bar{K} \rightarrow \Lambda(1800) \rightarrow \Lambda\omega, S=1/2, S\text{-wave}$

MODULUS	PHASE (°)	DOCUMENT ID	TECN	COMMENT
0.12 ± 0.04	-114 ± 30	SARANTSEV	19	DPWA $\bar{K}N$ multichannel

Normalized residue in $N\bar{K} \rightarrow \Lambda(1800) \rightarrow \Lambda\omega, S=3/2, D\text{-wave}$

MODULUS	PHASE (°)	DOCUMENT ID	TECN	COMMENT
0.08 ± 0.03	-90 ± 17	SARANTSEV	19	DPWA $\bar{K}N$ multichannel

Normalized residue in $N\bar{K} \rightarrow \Lambda(1800) \rightarrow \Sigma(1385)\pi$

MODULUS	PHASE (°)	DOCUMENT ID	TECN	COMMENT
0.16 ± 0.06	-140 ± 35	SARANTSEV	19	DPWA $\bar{K}N$ multichannel

Normalized residue in $N\bar{K} \rightarrow \Lambda(1800) \rightarrow N\bar{K}^*(892), S=1/2, S\text{-wave}$

MODULUS	PHASE (°)	DOCUMENT ID	TECN	COMMENT
0.18 ± 0.06	65 ± 40	SARANTSEV	19	DPWA $\bar{K}N$ multichannel

Normalized residue in $N\bar{K} \rightarrow \Lambda(1800) \rightarrow N\bar{K}^*(892), S=3/2, D\text{-wave}$

MODULUS	PHASE (°)	DOCUMENT ID	TECN	COMMENT
0.09 ± 0.07		SARANTSEV	19	DPWA $\bar{K}N$ multichannel

$\Lambda(1800)$ MASS

VALUE (MeV)	DOCUMENT ID	TECN	COMMENT
1750 to 1850 (≈ 1800) OUR ESTIMATE			
1811 ± 10	SARANTSEV	19	DPWA $\bar{K}N$ multichannel
1783 ± 19	ZHANG	13A	DPWA $\bar{K}N$ multichannel
1841 ± 10	GOPAL	80	DPWA $\bar{K}N \rightarrow \bar{K}N$
1725 ± 20	ALSTON...	78	DPWA $\bar{K}N \rightarrow \bar{K}N$
1830 ± 20	LANGBEIN	72	IPWA $\bar{K}N$ multichannel
• • • We do not use the following data for averages, fits, limits, etc. • • •			
1845 ± 10	MANLEY	02	DPWA $\bar{K}N$ multichannel
1825 ± 20	GOPAL	77	DPWA $\bar{K}N$ multichannel
1767 or 1842	MARTIN	77	DPWA $\bar{K}N$ multichannel
1780	KIM	71	DPWA K-matrix analysis
1872 ± 10	BRICMAN	70B	DPWA $\bar{K}N \rightarrow \bar{K}N$

$\Lambda(1800)$ WIDTH

VALUE (MeV)	DOCUMENT ID	TECN	COMMENT
150 to 250 (≈ 200) OUR ESTIMATE			
209 ± 18	SARANTSEV	19	DPWA $\bar{K}N$ multichannel
256 ± 35	ZHANG	13A	DPWA $\bar{K}N$ multichannel
228 ± 20	GOPAL	80	DPWA $\bar{K}N \rightarrow \bar{K}N$
185 ± 20	ALSTON...	78	DPWA $\bar{K}N \rightarrow \bar{K}N$
70 ± 15	LANGBEIN	72	IPWA $\bar{K}N$ multichannel

Baryon Particle Listings

$\Lambda(1800), \Lambda(1810)$

• • • We do not use the following data for averages, fits, limits, etc. • • •

518±84	MANLEY	02	DPWA	$\bar{K}N$ multichannel
230±20	GOPAL	77	DPWA	$\bar{K}N$ multichannel
435 or 473	¹ MARTIN	77	DPWA	$\bar{K}N$ multichannel
40	KIM	71	DPWA	K-matrix analysis
100±20	BRICMAN	70B	DPWA	$\bar{K}N \rightarrow \bar{K}N$

$\Lambda(1800)$ DECAY MODES

Mode	Fraction (Γ_i/Γ)
Γ_1 $N\bar{K}$	25–40 %
Γ_2 $\Sigma\pi$	seen
Γ_3 $\Lambda\sigma$	(15 ± 4) %
Γ_4 $\Sigma(1385)\pi$	seen
Γ_5 $\Lambda\eta$	0.01 to 0.10
Γ_6 $N\bar{K}^*(892)$	seen
Γ_7 $N\bar{K}^*(892), S=1/2, S\text{-wave}$	
Γ_8 $N\bar{K}^*(892), S=3/2, D\text{-wave}$	

$\Lambda(1800)$ BRANCHING RATIOS

See “Sign conventions for resonance couplings” in the Note on Λ and Σ Resonances.

$\Gamma(N\bar{K})/\Gamma_{\text{total}}$

VALUE	DOCUMENT ID	TECN	COMMENT	Γ_1/Γ
0.25 to 0.40 OUR ESTIMATE				
0.35±0.07	SARANTSEV	19	DPWA	$\bar{K}N$ multichannel
0.13±0.06	ZHANG	13A	DPWA	$\bar{K}N$ multichannel
0.36±0.04	GOPAL	80	DPWA	$\bar{K}N \rightarrow \bar{K}N$
0.28±0.05	ALSTON-...	78	DPWA	$\bar{K}N \rightarrow \bar{K}N$
0.35±0.15	LANGBEIN	72	IPWA	$\bar{K}N$ multichannel
• • • We do not use the following data for averages, fits, limits, etc. • • •				
0.24±0.10	MANLEY	02	DPWA	$\bar{K}N$ multichannel
0.37±0.05	GOPAL	77	DPWA	See GOPAL 80
1.21 or 0.70	¹ MARTIN	77	DPWA	$\bar{K}N$ multichannel
0.80	KIM	71	DPWA	K-matrix analysis
0.18±0.02	BRICMAN	70B	DPWA	$\bar{K}N \rightarrow \bar{K}N$

$\Gamma(\Sigma\pi)/\Gamma_{\text{total}}$

VALUE	DOCUMENT ID	TECN	COMMENT	Γ_2/Γ
0.27±0.06	SARANTSEV	19	DPWA	$\bar{K}N$ multichannel

$\Gamma(\Lambda\sigma)/\Gamma_{\text{total}}$

VALUE	DOCUMENT ID	TECN	COMMENT	Γ_3/Γ
0.15±0.04	SARANTSEV	19	DPWA	$\bar{K}N$ multichannel

$\Gamma(\Sigma(1385)\pi)/\Gamma_{\text{total}}$

VALUE	DOCUMENT ID	TECN	COMMENT	Γ_4/Γ
0.09±0.04	SARANTSEV	19	DPWA	$\bar{K}N$ multichannel

$\Gamma(\Lambda\eta)/\Gamma_{\text{total}}$

VALUE	DOCUMENT ID	TECN	COMMENT	Γ_5/Γ
0.01 to 0.10 OUR ESTIMATE				
0.010±0.005	SARANTSEV	19	DPWA	$\bar{K}N$ multichannel
0.06 ± 0.05	ZHANG	13A	DPWA	Multichannel

$(\Gamma_1\Gamma_2)^{1/2}/\Gamma_{\text{total}}$ in $N\bar{K} \rightarrow \Lambda(1800) \rightarrow \Sigma\pi$

VALUE	DOCUMENT ID	TECN	COMMENT	$(\Gamma_1\Gamma_2)^{1/2}/\Gamma$
−0.07±0.02	ZHANG	13A	DPWA	Multichannel
−0.08±0.05	GOPAL	77	DPWA	$\bar{K}N$ multichannel
• • • We do not use the following data for averages, fits, limits, etc. • • •				
−0.74 or −0.43	¹ MARTIN	77	DPWA	$\bar{K}N$ multichannel
0.24	KIM	71	DPWA	K-matrix analysis

$(\Gamma_1\Gamma_4)^{1/2}/\Gamma_{\text{total}}$ in $N\bar{K} \rightarrow \Lambda(1800) \rightarrow \Sigma(1385)\pi$

VALUE	DOCUMENT ID	TECN	COMMENT	$(\Gamma_1\Gamma_4)^{1/2}/\Gamma$
−0.09 ± 0.05	ZHANG	13A	DPWA	Multichannel
+0.056±0.028	² CAMERON	78	DPWA	$K^-p \rightarrow \Sigma(1385)\pi$

$(\Gamma_1\Gamma_7)^{1/2}/\Gamma_{\text{total}}$ in $N\bar{K} \rightarrow \Lambda(1800) \rightarrow N\bar{K}^*(892), S=1/2, S\text{-wave}$

VALUE	DOCUMENT ID	TECN	COMMENT	$(\Gamma_1\Gamma_7)^{1/2}/\Gamma$
−0.13±0.02	ZHANG	13A	DPWA	Multichannel
−0.17±0.03	² CAMERON	78B	DPWA	$K^-p \rightarrow N\bar{K}^*$

$(\Gamma_1\Gamma_8)^{1/2}/\Gamma_{\text{total}}$ in $N\bar{K} \rightarrow \Lambda(1800) \rightarrow N\bar{K}^*(892), S=3/2, D\text{-wave}$

VALUE	DOCUMENT ID	TECN	COMMENT	$(\Gamma_1\Gamma_8)^{1/2}/\Gamma$
−0.13±0.04	CAMERON	78B	DPWA	$K^-p \rightarrow N\bar{K}^*$

$\Lambda(1800)$ FOOTNOTES

¹The two MARTIN 77 values are from a T-matrix pole and from a Breit-Wigner fit.
²The published sign has been changed to be in accord with the baryon-first convention.

$\Lambda(1800)$ REFERENCES

SARANTSEV	19	EPL A55 180	A.V. Sarantsev <i>et al.</i>	(BONN, PNPI)
ZHANG	13A	PR C88 035205	H. Zhang <i>et al.</i>	(KSU)
MANLEY	02	PRL 88 012002	D.M. Manley <i>et al.</i>	(BNL Crystal Ball Collab.)
GOPAL	80	Toronto Conf. 159	G.P. Gopal	(RHEL) IJP
ALSTON-...	78	PR D18 182	M. Alston-Garnjost <i>et al.</i>	(LBL, MTHO+) IJP
Also		PRL 38 1007	M. Alston-Garnjost <i>et al.</i>	(LBL, MTHO+) IJP
CAMERON	78	NP B143 189	W. Cameron <i>et al.</i>	(RHEL, LOIC) IJP
CAMERON	78B	NP B146 327	W. Cameron <i>et al.</i>	(RHEL, LOIC) IJP
GOPAL	77	NP B119 362	G.P. Gopal <i>et al.</i>	(LOIC, RHEL) IJP
MARTIN	77	NP B127 349	B.R. Martin, M.K. Pidcock, R.G. Moorhouse	(LOUC+) IJP
Also		NP B126 266	B.R. Martin, M.K. Pidcock	(LOUC)
Also		NP B126 285	B.R. Martin, M.K. Pidcock	(LOUC) IJP
LANGBEIN	72	NP B47 477	W. Langbein, F. Wagner	(MFM) IJP
KIM	71	PRL 27 356	J.K. Kim	(HARV) IJP
Also		Duke Conf. 161	J.K. Kim	(HARV) IJP
Hyperon Resonances, 1970				
BRICMAN	70B	PL 33B 511	C. Bricman, M. Ferro-Luzzi, J.P. Lagnaux	(CERN) IJP

$$\Lambda(1810) 1/2^+$$

$$I(J^P) = 0(\frac{1}{2}^+) \text{ Status: } ***$$

$\Lambda(1810)$ POLE POSITION

REAL PART

VALUE (MeV)	DOCUMENT ID	TECN	COMMENT
1773±7	SARANTSEV	19	DPWA $\bar{K}N$ multichannel

• • • We do not use the following data for averages, fits, limits, etc. • • •

2097 ⁺⁴⁰ _{−1}	¹ KAMANO	15	DPWA Multichannel
1780	ZHANG	13A	DPWA Multichannel

¹From the preferred solution A in KAMANO 15. Solution B reports $M = 1841 \pm \frac{3}{4}$ MeV.

−2×IMAGINARY PART

VALUE (MeV)	DOCUMENT ID	TECN	COMMENT
38±14	SARANTSEV	19	DPWA $\bar{K}N$ multichannel

• • • We do not use the following data for averages, fits, limits, etc. • • •

166 ⁺⁶⁴ _{−12}	¹ KAMANO	15	DPWA Multichannel
64	ZHANG	13A	DPWA Multichannel

¹From the preferred solution A in KAMANO 15. Solution B Reports $\Gamma = 62 \pm \frac{6}{4}$ MeV.

$\Lambda(1810)$ POLE RESIDUES

The normalized residue is the residue divided by $\Gamma_{\text{pole}}/2$.

Normalized residue in $N\bar{K} \rightarrow \Lambda(1810) \rightarrow N\bar{K}$

MODULUS	PHASE (°)	DOCUMENT ID	TECN	COMMENT
0.018±0.008	65 ± 26	SARANTSEV	19	DPWA $\bar{K}N$ multichannel

• • • We do not use the following data for averages, fits, limits, etc. • • •

0.205	−63	¹ KAMANO	15	DPWA Multichannel
-------	-----	---------------------	----	-------------------

¹From the preferred solution A in KAMANO 15.

Normalized residue in $N\bar{K} \rightarrow \Lambda(1810) \rightarrow \Sigma\pi$

MODULUS	PHASE (°)	DOCUMENT ID	TECN	COMMENT
0.045 ± 0.020	−143 ± 24	SARANTSEV	19	DPWA $\bar{K}N$ multichannel

• • • We do not use the following data for averages, fits, limits, etc. • • •

0.0325	29	¹ KAMANO	15	DPWA Multichannel
--------	----	---------------------	----	-------------------

¹From the preferred solution A in KAMANO 15.

Normalized residue in $N\bar{K} \rightarrow \Lambda(1810) \rightarrow \Lambda\eta$

MODULUS	PHASE (°)	DOCUMENT ID	TECN	COMMENT
0.155	165	¹ KAMANO	15	DPWA Multichannel

• • • We do not use the following data for averages, fits, limits, etc. • • •

¹From the preferred solution A in KAMANO 15.

Normalized residue in $N\bar{K} \rightarrow \Lambda(1810) \rightarrow \Lambda\sigma$

MODULUS	PHASE (°)	DOCUMENT ID	TECN	COMMENT
0.055 ± 0.020	30 ± 16	SARANTSEV	19	DPWA $\bar{K}N$ multichannel

Normalized residue in $N\bar{K} \rightarrow \Lambda(1810) \rightarrow \Xi K$

MODULUS	PHASE (°)	DOCUMENT ID	TECN	COMMENT
0.0937	−64	¹ KAMANO	15	DPWA Multichannel

¹From the preferred solution A in KAMANO 15.

Normalized residue in $N\bar{K} \rightarrow \Lambda(1810) \rightarrow \Sigma(1385)\pi$

MODULUS	PHASE (°)	DOCUMENT ID	TECN	COMMENT
0.08 ± 0.03	−50 ± 30	SARANTSEV	19	DPWA $\bar{K}N$ multichannel

• • • We do not use the following data for averages, fits, limits, etc. • • •

0.244	−10	¹ KAMANO	15	DPWA Multichannel
-------	-----	---------------------	----	-------------------

¹From the preferred solution A in KAMANO 15.

Baryon Particle Listings

$\Lambda(1810)$

Normalized residue in $N\bar{K} \rightarrow \Lambda(1810) \rightarrow N\bar{K}^*(892), S=1/2, P\text{-wave}$

MODULUS	PHASE (°)	DOCUMENT ID	TECN	COMMENT
0.03 ± 0.03		SARANTSEV 19	DPWA	$\bar{K}N$ multichannel
0.159	-97	¹ KAMANO 15	DPWA	Multichannel

••• We do not use the following data for averages, fits, limits, etc. •••

¹ From the preferred solution A in KAMANO 15.

Normalized residue in $N\bar{K} \rightarrow \Lambda(1810) \rightarrow N\bar{K}^*(892), S=3/2, P\text{-wave}$

MODULUS	PHASE (°)	DOCUMENT ID	TECN	COMMENT
0.05 ± 0.04		SARANTSEV 19	DPWA	$\bar{K}N$ multichannel
0.0497	2	¹ KAMANO 15	DPWA	Multichannel

••• We do not use the following data for averages, fits, limits, etc. •••

¹ From the preferred solution A in KAMANO 15.

$\Lambda(1810)$ MASS

VALUE (MeV)	DOCUMENT ID	TECN	COMMENT
1740 to 1840 (≈ 1790) OUR ESTIMATE			
1773 ± 7	SARANTSEV 19	DPWA	$\bar{K}N$ multichannel
1821 ± 10	ZHANG 13A	DPWA	Multichannel
1841 ± 20	GOPAL 80	DPWA	$\bar{K}N \rightarrow \bar{K}N$
1735 ± 5	CARROLL 76	DPWA	Isospin-0 total σ
1746 ± 10	PREVOST 74	DPWA	$K^-N \rightarrow \Sigma(1385)\pi$
1780 ± 20	LANGBEIN 72	IPWA	$\bar{K}N$ multichannel
••• We do not use the following data for averages, fits, limits, etc. •••			
1853 ± 20	GOPAL 77	DPWA	$\bar{K}N$ multichannel
1861 or 1953	¹ MARTIN 77	DPWA	$\bar{K}N$ multichannel
1755	KIM 71	DPWA	K-matrix analysis
1800	ARMENTEROS70	HBC	$\bar{K}N \rightarrow \bar{K}N$
1750	ARMENTEROS70	HBC	$\bar{K}N \rightarrow \Sigma\pi$
1690 ± 10	BARBARO... 70	HBC	$\bar{K}N \rightarrow \Sigma\pi$
1740	BAILEY 69	DPWA	$\bar{K}N \rightarrow \bar{K}N$
1745	ARMENTEROS68B	HBC	$\bar{K}N \rightarrow \bar{K}N$

¹ The two MARTIN 77 values are from a T-matrix pole and from a Breit-Wigner fit.

$\Lambda(1810)$ WIDTH

VALUE (MeV)	DOCUMENT ID	TECN	COMMENT
50 to 170 (≈ 110) OUR ESTIMATE			
39 ± 15	SARANTSEV 19	DPWA	$\bar{K}N$ multichannel
174 ± 5.0	ZHANG 13A	DPWA	Multichannel
164 ± 20	GOPAL 80	DPWA	$\bar{K}N \rightarrow \bar{K}N$
90 ± 20	CAMERON 78B	DPWA	$K^-p \rightarrow N\bar{K}^*$
46 ± 20	PREVOST 74	DPWA	$K^-N \rightarrow \Sigma(1385)\pi$
120 ± 10	LANGBEIN 72	IPWA	$\bar{K}N$ multichannel
••• We do not use the following data for averages, fits, limits, etc. •••			
166 ± 20	GOPAL 77	DPWA	$\bar{K}N$ multichannel
535 or 585	¹ MARTIN 77	DPWA	$\bar{K}N$ multichannel
28	CARROLL 76	DPWA	Isospin-0 total σ
35	KIM 71	DPWA	K-matrix analysis
30	ARMENTEROS70	HBC	$\bar{K}N \rightarrow \bar{K}N$
70	ARMENTEROS70	HBC	$\bar{K}N \rightarrow \Sigma\pi$
22	BARBARO... 70	HBC	$\bar{K}N \rightarrow \Sigma\pi$
300	BAILEY 69	DPWA	$\bar{K}N \rightarrow \bar{K}N$
147	ARMENTEROS68B	HBC	

¹ The two MARTIN 77 values are from a T-matrix pole and from a Breit-Wigner fit.

$\Lambda(1810)$ DECAY MODES

Mode	Fraction (Γ_i/Γ)
Γ_1 $N\bar{K}$	0.05 to 0.35
Γ_2 $\Sigma\pi$	(16 ± 5) %
Γ_3 $\Lambda\eta$	
Γ_4 ΞK	
Γ_5 $\Sigma(1385)\pi$	(40 ± 15) %
Γ_6 $N\bar{K}^*(892)$	30-60 %
Γ_7 $N\bar{K}^*(892), S=1/2, P\text{-wave}$	
Γ_8 $N\bar{K}^*(892), S=3/2, P\text{-wave}$	

$\Lambda(1810)$ BRANCHING RATIOS

$\Gamma(N\bar{K})/\Gamma_{\text{total}}$	DOCUMENT ID	TECN	COMMENT	Γ_1/Γ
0.05 to 0.35 OUR ESTIMATE				
0.025 ± 0.013	SARANTSEV 19	DPWA	$\bar{K}N$ multichannel	
0.19 ± 0.08	ZHANG 13A	DPWA	$\bar{K}N$ multichannel	
0.24 ± 0.04	GOPAL 80	DPWA	$\bar{K}N \rightarrow \bar{K}N$	
0.36 ± 0.05	LANGBEIN 72	IPWA	$\bar{K}N$ multichannel	

••• We do not use the following data for averages, fits, limits, etc. •••

0.225	¹ KAMANO 15	DPWA	$\bar{K}N$ multichannel
0.21 ± 0.04	GOPAL 77	DPWA	See GOPAL 80
0.52 or 0.49	² MARTIN 77	DPWA	$\bar{K}N$ multichannel
0.30	KIM 71	DPWA	K-matrix analysis
0.15	ARMENTEROS70	DPWA	$\bar{K}N \rightarrow \bar{K}N$
0.55	BAILEY 69	DPWA	$\bar{K}N \rightarrow \bar{K}N$
0.4	ARMENTEROS68B	DPWA	$\bar{K}N \rightarrow \bar{K}N$

¹ From the preferred solution A in KAMANO 15.
² The two MARTIN 77 values are from a T-matrix pole and from a Breit-Wigner fit.

$\Gamma(\Sigma\pi)/\Gamma_{\text{total}}$

VALUE	DOCUMENT ID	TECN	COMMENT	Γ_2/Γ
0.16 ± 0.05	SARANTSEV 19	DPWA	$\bar{K}N$ multichannel	
0.009	¹ KAMANO 15	DPWA	Multichannel	

••• We do not use the following data for averages, fits, limits, etc. •••

¹ From the preferred solution A in KAMANO 15.

$\Gamma(\Lambda\eta)/\Gamma_{\text{total}}$

VALUE	DOCUMENT ID	TECN	COMMENT	Γ_3/Γ
0.111	¹ KAMANO 15	DPWA	Multichannel	

••• We do not use the following data for averages, fits, limits, etc. •••

¹ From the preferred solution A in KAMANO 15.

$\Gamma(\Xi K)/\Gamma_{\text{total}}$

VALUE	DOCUMENT ID	TECN	COMMENT	Γ_4/Γ
0.051	¹ KAMANO 15	DPWA	Multichannel	

••• We do not use the following data for averages, fits, limits, etc. •••

¹ From the preferred solution A in KAMANO 15.

$\Gamma(\Sigma(1385)\pi)/\Gamma_{\text{total}}$

VALUE	DOCUMENT ID	TECN	COMMENT	Γ_5/Γ
0.40 ± 0.15	SARANTSEV 19	DPWA	$\bar{K}N$ multichannel	
0.600	¹ KAMANO 15	DPWA	Multichannel	

••• We do not use the following data for averages, fits, limits, etc. •••

¹ From the preferred solution A in KAMANO 15.

$\Gamma(N\bar{K}^*(892), S=1/2, P\text{-wave})/\Gamma_{\text{total}}$

VALUE	DOCUMENT ID	TECN	COMMENT	Γ_7/Γ
0.003	¹ KAMANO 15	DPWA	Multichannel	

••• We do not use the following data for averages, fits, limits, etc. •••

¹ From the preferred solution A in KAMANO 15.

$(\Gamma_1\Gamma_7)^{1/2}/\Gamma_{\text{total}}$ in $N\bar{K} \rightarrow \Lambda(1810) \rightarrow \Sigma\pi$

VALUE	DOCUMENT ID	TECN	COMMENT	$(\Gamma_1\Gamma_2)^{1/2}/\Gamma$
-0.08 ± 0.05	ZHANG 13A	DPWA	Multichannel	
-0.24 ± 0.04	GOPAL 77	DPWA	$\bar{K}N$ multichannel	
••• We do not use the following data for averages, fits, limits, etc. •••				
+0.25 or +0.23	¹ MARTIN 77	DPWA	$\bar{K}N$ multichannel	
< 0.01	LANGBEIN 72	IPWA	$\bar{K}N$ multichannel	
0.17	KIM 71	DPWA	K-matrix analysis	
+0.20	² ARMENTEROS70	DPWA	$\bar{K}N \rightarrow \Sigma\pi$	
-0.13 ± 0.03	BARBARO... 70	DPWA	$\bar{K}N \rightarrow \Sigma\pi$	

¹ The two MARTIN 77 values are from a T-matrix pole and from a Breit-Wigner fit.
² The published sign has been changed to be in accord with the baryon-first convention.

$(\Gamma_1\Gamma_7)^{1/2}/\Gamma_{\text{total}}$ in $N\bar{K} \rightarrow \Lambda(1810) \rightarrow \Sigma(1385)\pi$

VALUE	DOCUMENT ID	TECN	COMMENT	$(\Gamma_1\Gamma_5)^{1/2}/\Gamma$
+0.18 ± 0.10	PREVOST 74	DPWA	$K^-N \rightarrow \Sigma(1385)\pi$	

$(\Gamma_1\Gamma_7)^{1/2}/\Gamma_{\text{total}}$ in $N\bar{K} \rightarrow \Lambda(1810) \rightarrow N\bar{K}^*(892), S=1/2, P\text{-wave}$

VALUE	DOCUMENT ID	TECN	COMMENT	$(\Gamma_1\Gamma_7)^{1/2}/\Gamma$
-0.14 ± 0.03	¹ CAMERON 78B	DPWA	$K^-p \rightarrow N\bar{K}^*$	

¹ The published sign has been changed to be in accord with the baryon-first convention.

$(\Gamma_1\Gamma_7)^{1/2}/\Gamma_{\text{total}}$ in $N\bar{K} \rightarrow \Lambda(1810) \rightarrow N\bar{K}^*(892), S=3/2, P\text{-wave}$

VALUE	DOCUMENT ID	TECN	COMMENT	$(\Gamma_1\Gamma_8)^{1/2}/\Gamma$
+0.38 ± 0.06	ZHANG 13A	DPWA	Multichannel	
+0.35 ± 0.06	CAMERON 78B	DPWA	$K^-p \rightarrow N\bar{K}^*$	

$\Lambda(1810)$ REFERENCES

SARANTSEV 19	EPJ A55 180	A.V. Sarantsev et al.	(BONN, PNPI)
KAMANO 15	PR C92 025205	H. Kamano et al.	(ANL, OSAK)
ZHANG 13A	PR C88 035205	H. Zhang et al.	(KSU)
GOPAL 80	Toronto Conf. 159	G.P. Gopal	(RHEL) IJP
CAMERON 78B	NP B146 327	W. Cameron et al.	(RHEL, LOIC) IJP
GOPAL 77	NP B119 362	G.P. Gopal et al.	(LOIC, RHEL) IJP
MARTIN 77	NP B127 349	B.R. Martin, M.K. Pidcock, R.G. Moorhouse	(LOIC+) IJP
Also	NP B126 266	B.R. Martin, M.K. Pidcock	(LOUC) IJP
Also	NP B126 285	B.R. Martin, M.K. Pidcock	(LOUC) IJP

See key on page 999

Baryon Particle Listings

$\Lambda(1810)$, $\Lambda(1820)$

CARROLL 76	PRL 37 806	A.S. Carroll et al.	(BNL)1
PREVOST 74	NP B69 246	J. Prevost et al.	(SACL, CERN, HEID)
LANGBEIN 72	NP B47 477	W. Langbein, F. Wagner	(MPIM) IJP
KIM 71	PRL 27 356	J.K. Kim	(HARV) IJP
Also Duke Conf. 161		J.K. Kim	(HARV) IJP
Hyperon Resonances, 1970			
ARMENTEROS 70	Duke Conf. 123	R. Armenteros et al.	(CERN, HEID, SACL) IJP
Hyperon Resonances, 1970			
BARBARO... 70	Duke Conf. 173	A. Barbaro-Galtieri	(LRL) IJP
Hyperon Resonances, 1970			
BAILEY 69	Thesis UCRL 50617	J.M. Bailey	(LLL) IJP
ARMENTEROS 68B	NP B8 195	R. Armenteros et al.	(CERN, HEID, SACL) IJP

$\Lambda(1820) \ 5/2^+$

 $I(J^P) = 0(\frac{5}{2}^+)$ Status: ***

This resonance is the cornerstone for all partial-wave analyses in this region. Most of the results published before 1973 are now obsolete and have been omitted. They may be found in our 1982 edition Physics Letters **111B** 1 (1982).

$\Lambda(1820)$ POLE POSITION

REAL PART

VALUE (MeV)	DOCUMENT ID	TECN	COMMENT
1812 to 1825 (\approx 1818) OUR ESTIMATE			
1813 \pm 3	SARANTSEV 19	DPWA	$\bar{K}N$ multichannel
1824 $^{+2}_{-1}$	¹ KAMANO 15	DPWA	$\bar{K}N$ multichannel
••• We do not use the following data for averages, fits, limits, etc. •••			
1814	ZHANG 13A	DPWA	$\bar{K}N$ multichannel
¹ From the preferred solution A in KAMANO 15.			

-2xIMAGINARY PART

VALUE (MeV)	DOCUMENT ID	TECN	COMMENT
75 to 80 (\approx 77) OUR ESTIMATE			
78 \pm 7	SARANTSEV 19	DPWA	$\bar{K}N$ multichannel
77 \pm 2	¹ KAMANO 15	DPWA	$\bar{K}N$ multichannel
••• We do not use the following data for averages, fits, limits, etc. •••			
85	ZHANG 13A	DPWA	$\bar{K}N$ multichannel
¹ From the preferred solution A in KAMANO 15.			

$\Lambda(1820)$ POLE RESIDUES

The normalized residue is the residue divided by $\Gamma_{pole}/2$.

Normalized residue in $N\bar{K} \rightarrow \Lambda(1820) \rightarrow N\bar{K}$

MODULUS	PHASE ($^\circ$)	DOCUMENT ID	TECN	COMMENT
0.60 \pm 0.12	-22 \pm 5	SARANTSEV 19	DPWA	$\bar{K}N$ multichannel
••• We do not use the following data for averages, fits, limits, etc. •••				
0.558	-13	¹ KAMANO 15	DPWA	$\bar{K}N$ multichannel
¹ From the preferred solution A in KAMANO 15.				

Normalized residue in $N\bar{K} \rightarrow \Lambda(1820) \rightarrow \Sigma\pi$

MODULUS	PHASE ($^\circ$)	DOCUMENT ID	TECN	COMMENT
0.34 \pm 0.07	174 \pm 5	SARANTSEV 19	DPWA	$\bar{K}N$ multichannel
••• We do not use the following data for averages, fits, limits, etc. •••				
0.357	168	¹ KAMANO 15	DPWA	$\bar{K}N$ multichannel
¹ From the preferred solution A in KAMANO 15.				

Normalized residue in $N\bar{K} \rightarrow \Lambda(1820) \rightarrow \Lambda\eta$

MODULUS	PHASE ($^\circ$)	DOCUMENT ID	TECN	COMMENT
••• We do not use the following data for averages, fits, limits, etc. •••				
0.0184	-3	¹ KAMANO 15	DPWA	$\bar{K}N$ multichannel
¹ From the preferred solution A in KAMANO 15.				

Normalized residue in $N\bar{K} \rightarrow \Lambda(1820) \rightarrow \Xi K$

MODULUS	PHASE ($^\circ$)	DOCUMENT ID	TECN	COMMENT
~ 0		SARANTSEV 19	DPWA	$\bar{K}N$ multichannel
••• We do not use the following data for averages, fits, limits, etc. •••				
0.00111	70	¹ KAMANO 15	DPWA	$\bar{K}N$ multichannel
¹ From the preferred solution A in KAMANO 15.				

Normalized residue in $N\bar{K} \rightarrow \Lambda(1820) \rightarrow \Sigma(1385)\pi, P$ -wave

MODULUS	PHASE ($^\circ$)	DOCUMENT ID	TECN	COMMENT
0.07 \pm 0.02	-60 \pm 50	SARANTSEV 19	DPWA	$\bar{K}N$ multichannel
••• We do not use the following data for averages, fits, limits, etc. •••				
0.340	161	¹ KAMANO 15	DPWA	$\bar{K}N$ multichannel
¹ From the preferred solution A in KAMANO 15.				

Normalized residue in $N\bar{K} \rightarrow \Lambda(1820) \rightarrow \Sigma(1385)\pi, F$ -wave

MODULUS	PHASE ($^\circ$)	DOCUMENT ID	TECN	COMMENT
0.11 \pm 0.04	5 \pm 45	SARANTSEV 19	DPWA	$\bar{K}N$ multichannel
••• We do not use the following data for averages, fits, limits, etc. •••				
0.201	151	¹ KAMANO 15	DPWA	$\bar{K}N$ multichannel
¹ From the preferred solution A in KAMANO 15.				

Normalized residue in $N\bar{K} \rightarrow \Lambda(1820) \rightarrow N\bar{K}^*(892), S=1/2, F$ -wave

MODULUS	PHASE ($^\circ$)	DOCUMENT ID	TECN	COMMENT
0.02 \pm 0.02		SARANTSEV 19	DPWA	$\bar{K}N$ multichannel
••• We do not use the following data for averages, fits, limits, etc. •••				
0.00750	41	¹ KAMANO 15	DPWA	$\bar{K}N$ multichannel
¹ From the preferred solution A in KAMANO 15.				

Normalized residue in $N\bar{K} \rightarrow \Lambda(1820) \rightarrow N\bar{K}^*(892), S=3/2, P$ -wave

MODULUS	PHASE ($^\circ$)	DOCUMENT ID	TECN	COMMENT
0.35 \pm 0.15	-30 \pm 45	SARANTSEV 19	DPWA	$\bar{K}N$ multichannel
••• We do not use the following data for averages, fits, limits, etc. •••				
0.171	-139	¹ KAMANO 15	DPWA	$\bar{K}N$ multichannel
¹ From the preferred solution A in KAMANO 15.				

Normalized residue in $N\bar{K} \rightarrow \Lambda(1820) \rightarrow N\bar{K}^*(892), S=3/2, F$ -wave

MODULUS	PHASE ($^\circ$)	DOCUMENT ID	TECN	COMMENT
0.02 \pm 0.02		SARANTSEV 19	DPWA	$\bar{K}N$ multichannel
••• We do not use the following data for averages, fits, limits, etc. •••				
0.000517	161	¹ KAMANO 15	DPWA	$\bar{K}N$ multichannel
¹ From the preferred solution A in KAMANO 15.				

$\Lambda(1820)$ MASS

VALUE (MeV)	DOCUMENT ID	TECN	COMMENT
1815 to 1825 (\approx 1820) OUR ESTIMATE			
1822 \pm 4	SARANTSEV 19	DPWA	$\bar{K}N$ multichannel
1823.5 \pm 0.8	ZHANG 13A	DPWA	$\bar{K}N$ multichannel
1823 \pm 3	GOPAL 80	DPWA	$\bar{K}N \rightarrow \bar{K}N$
1819 \pm 2	ALSTON... 78	DPWA	$\bar{K}N \rightarrow \bar{K}N$
1821 \pm 2	KANE 74	DPWA	$K^- p \rightarrow \Sigma\pi$
••• We do not use the following data for averages, fits, limits, etc. •••			
1830	DECLAIS 77	DPWA	$\bar{K}N \rightarrow \bar{K}N$
1822 \pm 2	GOPAL 77	DPWA	$\bar{K}N$ multichannel
1817 or 1819	¹ MARTIN 77	DPWA	$\bar{K}N$ multichannel
¹ The two MARTIN 77 values are from a T-matrix pole and from a Breit-Wigner fit.			

$\Lambda(1820)$ WIDTH

VALUE (MeV)	DOCUMENT ID	TECN	COMMENT
70 to 90 (\approx 80) OUR ESTIMATE			
80 \pm 8	SARANTSEV 19	DPWA	$\bar{K}N$ multichannel
89 \pm 2	ZHANG 13A	DPWA	$\bar{K}N$ multichannel
77 \pm 5	GOPAL 80	DPWA	$\bar{K}N \rightarrow \bar{K}N$
72 \pm 5	ALSTON... 78	DPWA	$\bar{K}N \rightarrow \bar{K}N$
87 \pm 3	KANE 74	DPWA	$K^- p \rightarrow \Sigma\pi$
••• We do not use the following data for averages, fits, limits, etc. •••			
82	DECLAIS 77	DPWA	$\bar{K}N \rightarrow \bar{K}N$
81 \pm 5	GOPAL 77	DPWA	$\bar{K}N$ multichannel
76 or 76	¹ MARTIN 77	DPWA	$\bar{K}N$ multichannel
¹ The two MARTIN 77 values are from a T-matrix pole and from a Breit-Wigner fit.			

$\Lambda(1820)$ DECAY MODES

Mode	Fraction (Γ_i/Γ)
Γ_1 $N\bar{K}$	55-65 %
Γ_2 $\Sigma\pi$	8-14 %
Γ_3 $\Sigma(1385)\pi$	5-10 %
Γ_4 $\Sigma(1385)\pi, P$ -wave	
Γ_5 $\Sigma(1385)\pi, F$ -wave	(2.0 \pm 1.0) %
Γ_6 $\Lambda\eta$	
Γ_7 ΞK	
Γ_8 $\Sigma\pi\pi$	
Γ_9 $N\bar{K}^*(892), S=1/2, F$ -wave	
Γ_{10} $N\bar{K}^*(892), S=3/2, P$ -wave	(3.0 \pm 1.0) %
Γ_{11} $N\bar{K}^*(892), S=3/2, F$ -wave	

$\Lambda(1820)$ BRANCHING RATIOS

Errors quoted do not include uncertainties in the parametrizations used in the partial-wave analyses and are thus too small. See also "Sign conventions for resonance couplings" in the Note on Λ and Σ Resonances.

$\Gamma(N\bar{K})/\Gamma_{total}$	VALUE	DOCUMENT ID	TECN	COMMENT	Γ_i/Γ
0.55 to 0.65 OUR ESTIMATE					
	0.58 \pm 0.12	SARANTSEV 19	DPWA	$\bar{K}N$ multichannel	
	0.54 \pm 0.01	ZHANG 13A	DPWA	$\bar{K}N$ multichannel	
	0.58 \pm 0.02	GOPAL 80	DPWA	$\bar{K}N \rightarrow \bar{K}N$	
	0.60 \pm 0.03	ALSTON... 78	DPWA	$\bar{K}N \rightarrow \bar{K}N$	

Baryon Particle Listings

$\Lambda(1820), \Lambda(1830)$

• • • We do not use the following data for averages, fits, limits, etc. • • •

0.547	1	KAMANO	15	DPWA	$\bar{K}N$ multichannel
0.51		DECLAIS	77	DPWA	$\bar{K}N \rightarrow \bar{K}N$
0.57 ± 0.02		GOPAL	77	DPWA	See GOPAL 80
0.59 or 0.58	2	MARTIN	77	DPWA	$\bar{K}N$ multichannel

¹ From the preferred solution A in KAMANO 15.
² The two MARTIN 77 values are from a T-matrix pole and from a Breit-Wigner fit.

$\Gamma(\Sigma\pi)/\Gamma_{total}$	DOCUMENT ID	TECN	COMMENT	Γ_2/Γ
0.19 ± 0.04	SARANTSEV 19	DPWA	$\bar{K}N$ multichannel	

• • • We do not use the following data for averages, fits, limits, etc. • • •

0.218	1	KAMANO	15	DPWA	$\bar{K}N$ multichannel
-------	---	--------	----	------	-------------------------

¹ From the preferred solution A in KAMANO 15.

$\Gamma(\Sigma(1385)\pi, P\text{-wave})/\Gamma_{total}$	DOCUMENT ID	TECN	COMMENT	Γ_4/Γ
~ 0.01	SARANTSEV 19	DPWA	$\bar{K}N$ multichannel	

• • • We do not use the following data for averages, fits, limits, etc. • • •

0.173	1	KAMANO	15	DPWA	$\bar{K}N$ multichannel
-------	---	--------	----	------	-------------------------

¹ From the preferred solution A in KAMANO 15.

$\Gamma(\Sigma(1385)\pi, F\text{-wave})/\Gamma_{total}$	DOCUMENT ID	TECN	COMMENT	Γ_5/Γ
0.02 ± 0.01	SARANTSEV 19	DPWA	$\bar{K}N$ multichannel	

• • • We do not use the following data for averages, fits, limits, etc. • • •

0.055	1	KAMANO	15	DPWA	$\bar{K}N$ multichannel
-------	---	--------	----	------	-------------------------

¹ From the preferred solution A in KAMANO 15.

$\Gamma(\Lambda\eta)/\Gamma_{total}$	DOCUMENT ID	TECN	COMMENT	Γ_6/Γ	
0.001	1	KAMANO	15	DPWA	Multichannel

¹ From the preferred solution A in KAMANO 15.

$\Gamma(\Xi K)/\Gamma_{total}$	DOCUMENT ID	TECN	COMMENT	Γ_7/Γ	
not seen	1	KAMANO	15	DPWA	Multichannel

¹ From the preferred solution A in KAMANO 15.

$\Gamma(\Sigma\pi\pi)/\Gamma_{total}$	DOCUMENT ID	TECN	COMMENT	Γ_8/Γ
no clear signal	1	ARMENTEROS68C	HD BC $K^-N \rightarrow \Sigma\pi\pi$	

¹ There is a suggestion of a bump, enough to be consistent with what is expected from $\Sigma(1385) \rightarrow \Sigma\pi$ decay.

$\Gamma(N\bar{K}^*(892), S=1/2, F\text{-wave})/\Gamma_{total}$	DOCUMENT ID	TECN	COMMENT	Γ_9/Γ	
not seen	1	KAMANO	15	DPWA	Multichannel

¹ From the preferred solution A in KAMANO 15.

$\Gamma(N\bar{K}^*(892), S=3/2, P\text{-wave})/\Gamma_{total}$	DOCUMENT ID	TECN	COMMENT	Γ_{10}/Γ
0.03 ± 0.01	ZHANG 13A	DPWA	Multichannel	

• • • We do not use the following data for averages, fits, limits, etc. • • •

0.006	1	KAMANO	15	DPWA	Multichannel
-------	---	--------	----	------	--------------

¹ From the preferred solution A in KAMANO 15.

$\Gamma(N\bar{K}^*(892), S=3/2, F\text{-wave})/\Gamma_{total}$	DOCUMENT ID	TECN	COMMENT	Γ_{11}/Γ	
not seen	1	KAMANO	15	DPWA	Multichannel

¹ From the preferred solution A in KAMANO 15.

$(\Gamma_1\Gamma_2)^{1/2}/\Gamma_{total}$ in $N\bar{K} \rightarrow \Lambda(1820) \rightarrow \Sigma\pi$	DOCUMENT ID	TECN	COMMENT	$(\Gamma_1\Gamma_2)^{1/2}/\Gamma$
-0.28 ± 0.01	ZHANG 13A	DPWA	Multichannel	
-0.28 ± 0.03	GOPAL 77	DPWA	$\bar{K}N$ multichannel	
-0.28 ± 0.01	KANE 74	DPWA	$K^-p \rightarrow \Sigma\pi$	

• • • We do not use the following data for averages, fits, limits, etc. • • •

-0.25 or -0.25	1	MARTIN 77	DPWA	$\bar{K}N$ multichannel	
----------------	---	-----------	------	-------------------------	--

¹ The two MARTIN 77 values are from a T-matrix pole and from a Breit-Wigner fit.

$(\Gamma_1\Gamma_2)^{1/2}/\Gamma_{total}$ in $N\bar{K} \rightarrow \Lambda(1820) \rightarrow \Sigma(1385)\pi, P\text{-wave}$	DOCUMENT ID	TECN	COMMENT	$(\Gamma_1\Gamma_4)^{1/2}/\Gamma$
-0.20 ± 0.02	ZHANG 13A	DPWA	Multichannel	
-0.167 ± 0.054	1	CAMERON 78	DPWA $K^-p \rightarrow \Sigma(1385)\pi$	
+0.27 ± 0.03	PREVOST 74	DPWA	$K^-N \rightarrow \Sigma(1385)\pi$	

¹ The published sign has been changed to be in accord with the baryon-first convention.

$(\Gamma_1\Gamma_2)^{1/2}/\Gamma_{total}$ in $N\bar{K} \rightarrow \Lambda(1820) \rightarrow \Sigma(1385)\pi, F\text{-wave}$	DOCUMENT ID	TECN	COMMENT	$(\Gamma_1\Gamma_5)^{1/2}/\Gamma$
+0.065 ± 0.029	1	CAMERON 78	DPWA $K^-p \rightarrow \Sigma(1385)\pi$	

¹ The published sign has been changed to be in accord with the baryon-first convention.

$(\Gamma_1\Gamma_2)^{1/2}/\Gamma_{total}$ in $N\bar{K} \rightarrow \Lambda(1820) \rightarrow \Lambda\eta$	DOCUMENT ID	TECN	COMMENT	$(\Gamma_1\Gamma_6)^{1/2}/\Gamma$
-0.096 ± 0.040 -0.020	RADER 73	MPWA		

$\Lambda(1820)$ REFERENCES

SARANTSEV 19	EPJ A55 180	A.V. Sarantsev <i>et al.</i>	(BONN, PNPI)
KAMANO 15	PR C92 025205	H. Kamano <i>et al.</i>	(ANL, OSAK)
ZHANG 13A	PR C88 035205	H. Zhang <i>et al.</i>	(KSU)
PDG 82	PL 111B 1	M. Roos <i>et al.</i>	(HELS, CIT, CERN)
GOPAL 80	Toronto Conf. 159	G.P. Gopal	(RHEL) IJP
ALSTON... 78	PR D18 182	M. Alston-Garnjost <i>et al.</i>	(LBL, MTHO+) IJP
Also	PRL 38 1007	M. Alston-Garnjost <i>et al.</i>	(LBL, MTHO+) IJP
CAMERON 78	NP B143 189	W. Cameron <i>et al.</i>	(RHEL, LOIC) IJP
DECLAIS 77	CERN 77-16	Y. Declais <i>et al.</i>	(CAEN, CERN) IJP
GOPAL 77	NP B119 362	G.P. Gopal <i>et al.</i>	(LOIC, RHEL) IJP
MARTIN 77	NP B127 349	B.R. Martin, M.K. Pidcock, R.G. Moorhouse	(LOUC+) IJP
Also	NP B126 266	B.R. Martin, M.K. Pidcock	(LOUC)
Also	NP B126 285	B.R. Martin, M.K. Pidcock	(LOUC) IJP
KANE 74	LBL-2452	D.F. Kane	(LBL) IJP
PREVOST 74	NP B69 246	J. Prevost <i>et al.</i>	(SACL, CERN, HEID)
RADER 73	NC 16A 178	R.K. Rader <i>et al.</i>	(SACL, HEID, CERN+)
ARMENTEROS 68C	NP B8 216	R. Armenteros <i>et al.</i>	(CERN, HEID, SACL) I

$\Lambda(1830) 5/2^-$

$I(J^P) = 0(\frac{5}{2}^-)$ Status: * * * *

For results published before 1973 (they are now obsolete), see our 1982 edition Physics Letters **111B** 1 (1982).

The best evidence for this resonance is in the $\Sigma\pi$ channel.

$\Lambda(1830)$ POLE POSITION

REAL PART

VALUE (MeV)	DOCUMENT ID	TECN	COMMENT
1800 to 1860 (≈ 1830) OUR ESTIMATE			
1819.5 ± 3.0	SARANTSEV 19	DPWA	$\bar{K}N$ multichannel
1899 ± 35 -37	1	KAMANO 15	DPWA Multichannel
1766 ± 37 -34	2	KAMANO 15	DPWA Multichannel
1809	ZHANG 13A	DPWA	Multichannel

¹ The preferred solution A in KAMANO 15 reports two poles. This entry is from the preferred solution A.

² From the preferred solution A in KAMANO 15. Not seen in solution B.

-2xIMAGINARY PART

VALUE (MeV)	DOCUMENT ID	TECN	COMMENT
50 to 80 (≈ 65) OUR ESTIMATE			
62 ± 5	SARANTSEV 19	DPWA	$\bar{K}N$ multichannel
80 ± 100 34	1	KAMANO 15	DPWA Multichannel
212 ± 94 62	2	KAMANO 15	DPWA Multichannel
109	ZHANG 13A	DPWA	Multichannel

¹ The preferred solution A in KAMANO 15 reports two poles. This entry is from the preferred solution A.

² From the preferred solution A in KAMANO 15. Not seen in solution B.

$\Lambda(1830)$ POLE RESIDUES

The normalized residue is the residue divided by $\Gamma_{pole}/2$.

Normalized residue in $N\bar{K} \rightarrow \Lambda(1830) \rightarrow N\bar{K}$

MODULUS	PHASE (°)	DOCUMENT ID	TECN	COMMENT
0.055 ± 0.010 20 ± 14		SARANTSEV 19	DPWA	$\bar{K}N$ multichannel
0.00502	-80	1	KAMANO 15	DPWA Multichannel

¹ From the preferred solution A in KAMANO 15.

Normalized residue in $N\bar{K} \rightarrow \Lambda(1830) \rightarrow \Sigma\pi$

MODULUS	PHASE (°)	DOCUMENT ID	TECN	COMMENT
0.15 ± 0.03 180 ± 10		SARANTSEV 19	DPWA	$\bar{K}N$ multichannel
0.00581	179	1	KAMANO 15	DPWA Multichannel

¹ From the preferred solution A in KAMANO 15.

Normalized residue in $N\bar{K} \rightarrow \Lambda(1830) \rightarrow \Lambda\eta$

MODULUS	PHASE (°)	DOCUMENT ID	TECN	COMMENT
0.00941	-65	1	KAMANO 15	DPWA Multichannel

¹ From the preferred solution A in KAMANO 15.

Normalized residue in $N\bar{K} \rightarrow \Lambda(1830) \rightarrow \Xi K$

MODULUS	PHASE (°)	DOCUMENT ID	TECN	COMMENT
0.010 ± 0.005	65 ± 20	SARANTSEV 19	DPWA	$\bar{K}N$ multichannel
0.0477	94	¹ KAMANO 15	DPWA	Multichannel

• • • We do not use the following data for averages, fits, limits, etc. • • •

¹ From the preferred solution A in KAMANO 15.

Normalized residue in $N\bar{K} \rightarrow \Lambda(1830) \rightarrow \Sigma(1385)\pi, D\text{-wave}$

MODULUS	PHASE (°)	DOCUMENT ID	TECN	COMMENT
0.10 ± 0.04	10 ± 25	SARANTSEV 19	DPWA	$\bar{K}N$ multichannel
0.0237	113	¹ KAMANO 15	DPWA	Multichannel

• • • We do not use the following data for averages, fits, limits, etc. • • •

¹ From the preferred solution A in KAMANO 15.

Normalized residue in $N\bar{K} \rightarrow \Lambda(1830) \rightarrow \Sigma(1385)\pi, G\text{-wave}$

MODULUS	PHASE (°)	DOCUMENT ID	TECN	COMMENT
0.03 ± 0.02		SARANTSEV 19	DPWA	$\bar{K}N$ multichannel
0.000726	127	¹ KAMANO 15	DPWA	Multichannel

• • • We do not use the following data for averages, fits, limits, etc. • • •

¹ From the preferred solution A in KAMANO 15.

Normalized residue in $N\bar{K} \rightarrow \Lambda(1830) \rightarrow N\bar{K}^*(892), S=1/2, D\text{-wave}$

MODULUS	PHASE (°)	DOCUMENT ID	TECN	COMMENT
0.0278	-177	¹ KAMANO 15	DPWA	Multichannel

• • • We do not use the following data for averages, fits, limits, etc. • • •

¹ From the preferred solution A in KAMANO 15.

Normalized residue in $N\bar{K} \rightarrow \Lambda(1830) \rightarrow N\bar{K}^*(892), S=3/2, D\text{-wave}$

MODULUS	PHASE (°)	DOCUMENT ID	TECN	COMMENT
0.0255	3	¹ KAMANO 15	DPWA	Multichannel

• • • We do not use the following data for averages, fits, limits, etc. • • •

¹ From the preferred solution A in KAMANO 15.

Normalized residue in $N\bar{K} \rightarrow \Lambda(1830) \rightarrow N\bar{K}^*(892), S=3/2, G\text{-wave}$

MODULUS	PHASE (°)	DOCUMENT ID	TECN	COMMENT
0.00773	-17	¹ KAMANO 15	DPWA	Multichannel

• • • We do not use the following data for averages, fits, limits, etc. • • •

¹ From the preferred solution A in KAMANO 15.

Normalized residue in $N\bar{K} \rightarrow \Lambda(1830) \rightarrow \Lambda\omega, S=1/2, D\text{-wave}$

MODULUS	PHASE (°)	DOCUMENT ID	TECN	COMMENT
0.04 ± 0.03		SARANTSEV 19	DPWA	$\bar{K}N$ multichannel

Normalized residue in $N\bar{K} \rightarrow \Lambda(1830) \rightarrow \Lambda\omega, S=3/2, D\text{-wave}$

MODULUS	PHASE (°)	DOCUMENT ID	TECN	COMMENT
0.05 ± 0.03	-110 ± 35	SARANTSEV 19	DPWA	$\bar{K}N$ multichannel

 $\Lambda(1830)$ MASS

VALUE (MeV)	DOCUMENT ID	TECN	COMMENT
1820 to 1830 (≈ 1825) OUR ESTIMATE			
1821 ± 3	SARANTSEV 19	DPWA	$\bar{K}N$ multichannel
1820 ± 4	ZHANG 13A	DPWA	Multichannel
1831 ± 10	GOPAL 80	DPWA	$\bar{K}N \rightarrow \bar{K}N$
1825 ± 10	GOPAL 77	DPWA	$\bar{K}N$ multichannel
1825 ± 1	KANE 74	DPWA	$K^- p \rightarrow \Sigma\pi$
• • • We do not use the following data for averages, fits, limits, etc. • • •			
1817 or 1818	¹ MARTIN 77	DPWA	$\bar{K}N$ multichannel

¹ The two MARTIN 77 values are from a T-matrix pole and from a Breit-Wigner fit.

 $\Lambda(1830)$ WIDTH

VALUE (MeV)	DOCUMENT ID	TECN	COMMENT
60 to 120 (≈ 90) OUR ESTIMATE			
64 ± 7	SARANTSEV 19	DPWA	$\bar{K}N$ multichannel
114 ± 10	ZHANG 13A	DPWA	Multichannel
100 ± 10	GOPAL 80	DPWA	$\bar{K}N \rightarrow \bar{K}N$
94 ± 10	GOPAL 77	DPWA	$\bar{K}N$ multichannel
119 ± 3	KANE 74	DPWA	$K^- p \rightarrow \Sigma\pi$
• • • We do not use the following data for averages, fits, limits, etc. • • •			
56 or 56	¹ MARTIN 77	DPWA	$\bar{K}N$ multichannel

¹ The two MARTIN 77 values are from a T-matrix pole and from a Breit-Wigner fit.

 $\Lambda(1830)$ DECAY MODES

Mode	Fraction (Γ_i/Γ)	Scale factor
Γ_1 $N\bar{K}$	0.04 to 0.08	
Γ_2 $\Sigma\pi$	35–75 %	
Γ_3 ΞK		
Γ_4 $\Sigma(1385)\pi$	>15 %	
Γ_5 $\Sigma(1385)\pi, D\text{-wave}$	(40 ± 15) %	3.2
Γ_6 $\Sigma(1385)\pi, G\text{-wave}$		
Γ_7 $\Lambda\eta$		
Γ_8 $N\bar{K}^*(892), S=1/2, D\text{-wave}$		
Γ_9 $N\bar{K}^*(892), S=3/2, D\text{-wave}$		
Γ_{10} $N\bar{K}^*(892), S=3/2, G\text{-wave}$		

 $\Lambda(1830)$ BRANCHING RATIOS

See "Sign conventions for resonance couplings" in the Note on Λ and Σ Resonances.

$\Gamma(N\bar{K})/\Gamma_{\text{total}}$	DOCUMENT ID	TECN	COMMENT	Γ_1/Γ
VALUE				
0.04 to 0.08 OUR ESTIMATE				
0.055 ± 0.010	SARANTSEV 19	DPWA	$\bar{K}N$ multichannel	
0.041 ± 0.005	ZHANG 13A	DPWA	Multichannel	
0.08 ± 0.03	GOPAL 80	DPWA	$\bar{K}N \rightarrow \bar{K}N$	
0.02 ± 0.02	ALSTON-... 78	DPWA	$\bar{K}N \rightarrow \bar{K}N$	
• • • We do not use the following data for averages, fits, limits, etc. • • •				
0.006	¹ KAMANO 15	DPWA	Multichannel	
0.04 ± 0.03	GOPAL 77	DPWA	See GOPAL 80	
0.04 or 0.04	² MARTIN 77	DPWA	$\bar{K}N$ multichannel	

¹ From the preferred solution A in KAMANO 15.

² The two MARTIN 77 values are from a T-matrix pole and from a Breit-Wigner fit.

$\Gamma(\Sigma\pi)/\Gamma_{\text{total}}$	DOCUMENT ID	TECN	COMMENT	Γ_2/Γ
VALUE				
0.42 ± 0.08	SARANTSEV 19	DPWA	$\bar{K}N$ multichannel	
• • • We do not use the following data for averages, fits, limits, etc. • • •				
0.017	¹ KAMANO 15	DPWA	Multichannel	

¹ From the preferred solution A in KAMANO 15.

$\Gamma(\Xi K)/\Gamma_{\text{total}}$	DOCUMENT ID	TECN	COMMENT	Γ_3/Γ
VALUE				
• • • We do not use the following data for averages, fits, limits, etc. • • •				
0.562	¹ KAMANO 15	DPWA	Multichannel	

¹ From the preferred solution A in KAMANO 15.

$\Gamma(\Sigma(1385)\pi, D\text{-wave})/\Gamma_{\text{total}}$	DOCUMENT ID	TECN	COMMENT	Γ_5/Γ
VALUE				
0.40 ± 0.15 OUR AVERAGE	Error		includes scale factor of 3.2.	
0.20 ± 0.08	SARANTSEV 19	DPWA	$\bar{K}N$ multichannel	
0.52 ± 0.06	ZHANG 13A	DPWA	Multichannel	
• • • We do not use the following data for averages, fits, limits, etc. • • •				
0.134	¹ KAMANO 15	DPWA	Multichannel	

¹ From the preferred solution A in KAMANO 15.

$\Gamma(\Sigma(1385)\pi, G\text{-wave})/\Gamma_{\text{total}}$	DOCUMENT ID	TECN	COMMENT	Γ_6/Γ
VALUE				
0.020 ± 0.015	SARANTSEV 19	DPWA	$\bar{K}N$ multichannel	

$\Gamma(\Lambda\eta)/\Gamma_{\text{total}}$	DOCUMENT ID	TECN	COMMENT	Γ_7/Γ
VALUE				
• • • We do not use the following data for averages, fits, limits, etc. • • •				
0.024	¹ KAMANO 15	DPWA	Multichannel	

¹ From the preferred solution A in KAMANO 15.

$\Gamma(N\bar{K}^*(892), S=1/2, D\text{-wave})/\Gamma_{\text{total}}$	DOCUMENT ID	TECN	COMMENT	Γ_8/Γ
VALUE				
• • • We do not use the following data for averages, fits, limits, etc. • • •				
0.134	¹ KAMANO 15	DPWA	Multichannel	

¹ From the preferred solution A in KAMANO 15.

$\Gamma(N\bar{K}^*(892), S=3/2, D\text{-wave})/\Gamma_{\text{total}}$	DOCUMENT ID	TECN	COMMENT	Γ_9/Γ
VALUE				
• • • We do not use the following data for averages, fits, limits, etc. • • •				
0.115	¹ KAMANO 15	DPWA	Multichannel	

¹ From the preferred solution A in KAMANO 15.

$\Gamma(N\bar{K}^*(892), S=3/2, G\text{-wave})/\Gamma_{\text{total}}$	DOCUMENT ID	TECN	COMMENT	Γ_{10}/Γ
VALUE				
• • • We do not use the following data for averages, fits, limits, etc. • • •				
0.009	¹ KAMANO 15	DPWA	Multichannel	

¹ From the preferred solution A in KAMANO 15.

Baryon Particle Listings

$\Lambda(1830), \Lambda(1890)$

$(\Gamma_1 \Gamma_2)^{J^P} / \Gamma_{\text{total}}$ in $N\bar{K} \rightarrow \Lambda(1830) \rightarrow \Sigma \pi$ $(\Gamma_1 \Gamma_2)^{J^P} / \Gamma$

VALUE	DOCUMENT ID	TECN	COMMENT
-0.13 ± 0.01	ZHANG	13A	DPWA Multichannel
-0.17 ± 0.03	GOPAL	77	DPWA $\bar{K}N$ multichannel
-0.15 ± 0.01	KANE	74	DPWA $K^- p \rightarrow \Sigma \pi$
••• We do not use the following data for averages, fits, limits, etc. •••			
-0.17 or -0.17	¹ MARTIN	77	DPWA $\bar{K}N$ multichannel

¹The two MARTIN 77 values are from a T-matrix pole and from a Breit-Wigner fit.

$(\Gamma_1 \Gamma_2)^{J^P} / \Gamma_{\text{total}}$ in $N\bar{K} \rightarrow \Lambda(1830) \rightarrow \Sigma(1385)\pi$ $(\Gamma_1 \Gamma_2)^{J^P} / \Gamma$

VALUE	DOCUMENT ID	TECN	COMMENT
0.20 to 0.50 OUR ESTIMATE			
+0.141 ± 0.014	¹ CAMERON	78	DPWA $K^- p \rightarrow \Sigma(1385)\pi$
+0.13 ± 0.03	PREVOST	74	DPWA $K^- N \rightarrow \Sigma(1385)\pi$

¹The CAMERON 78 upper limit on G-wave decay is 0.03. The published sign has been changed to be in accord with the baryon-first convention.

$(\Gamma_1 \Gamma_2)^{J^P} / \Gamma_{\text{total}}$ in $N\bar{K} \rightarrow \Lambda(1830) \rightarrow \Lambda \eta$ $(\Gamma_1 \Gamma_2)^{J^P} / \Gamma$

VALUE	DOCUMENT ID	TECN	COMMENT
-0.044 ± 0.020	RADER	73	MPWA

$\Lambda(1830)$ REFERENCES

SARANTSEV	19	EPJ A55 180	A.V. Sarantsev et al.	(BONN, PNPI)
KAMANO	15	PR C92 025205	H. Kamano et al.	(ANL, OSAK)
ZHANG	13A	PR C88 035205	H. Zhang et al.	(KSU)
PDG	82	PL 111B 1	M. Roos et al.	(HEL5, CIT, CERN)
GOPAL	80	Toronto Conf. 159	G.P. Gopal	(RHEL) IJP
ALSTON-...	78	PR D18 182	M. Alston-Garnjost et al.	(LBL, MTHO+) IJP
Also		PRL 38 1007	M. Alston-Garnjost et al.	(LBL, MTHO+) IJP
CAMERON	78	NP B143 189	W. Cameron et al.	(RHEL, LOIC) IJP
GOPAL	77	NP B119 362	G.P. Gopal et al.	(LOIC, RHEL) IJP
MARTIN	77	NP B127 349	B.R. Martin, M.K. Pidcock, R.G. Moorhouse	(LOUC+) IJP
Also		NP B126 266	B.R. Martin, M.K. Pidcock	(LOUC) IJP
Also		NP B126 285	B.R. Martin, M.K. Pidcock	(LOUC) IJP
KANE	74	LBL-2452	D.F. Kane	(LBL) IJP
PREVOST	74	NP B69 246	J. Prevost et al.	(SACL, CERN, HEID)
RADER	73	NC 16A 178	R.K. Rader et al.	(SACL, HEID, CERN+)

$\Lambda(1890) 3/2^+$

$$I(J^P) = 0(\frac{3}{2}^+) \text{ Status: } ***$$

For results published before 1974 (they are now obsolete), see our 1982 edition Physics Letters **111B** 1 (1982).

$\Lambda(1890)$ POLE POSITION

REAL PART

VALUE (MeV)	DOCUMENT ID	TECN	COMMENT
1872 ± 5	SARANTSEV	19	DPWA $\bar{K}N$ multichannel
••• We do not use the following data for averages, fits, limits, etc. •••			
1859 ⁺⁵ / ₋₇	¹ KAMANO	15	DPWA Multichannel
1876	ZHANG	13A	DPWA Multichannel

¹From the preferred solution A in KAMANO 15, incompatible with solution B.

-2xIMAGINARY PART

VALUE (MeV)	DOCUMENT ID	TECN	COMMENT
101 ± 10	SARANTSEV	19	DPWA $\bar{K}N$ multichannel
••• We do not use the following data for averages, fits, limits, etc. •••			
113 ⁺²⁰ / ₋₄	¹ KAMANO	15	DPWA $\bar{K}N$ multichannel
145	ZHANG	13A	DPWA $\bar{K}N$ multichannel

¹From the preferred solution A in KAMANO 15, incompatible with solution B.

$\Lambda(1890)$ POLE RESIDUE

The "normalized residue" is the residue divided by $\Gamma_{\text{pole}}/2$.

Normalized residue in $KN \rightarrow \Lambda(1890) \rightarrow KN$

MODULUS	PHASE (°)	DOCUMENT ID	TECN	COMMENT
0.30 ± 0.06	0 ± 10	SARANTSEV	19	DPWA $\bar{K}N$ multichannel
••• We do not use the following data for averages, fits, limits, etc. •••				
0.241	-23	¹ KAMANO	15	DPWA $\bar{K}N$ multichannel

¹From the preferred solution A in KAMANO 15.

Normalized residue in $N\bar{K} \rightarrow \Lambda(1890) \rightarrow \Sigma \pi$

MODULUS	PHASE (°)	DOCUMENT ID	TECN	COMMENT
0.14 ± 0.05	148 ± 12	SARANTSEV	19	DPWA $\bar{K}N$ multichannel
••• We do not use the following data for averages, fits, limits, etc. •••				
0.101	104	¹ KAMANO	15	DPWA $\bar{K}N$ multichannel

¹From the preferred solution A in KAMANO 15.

Normalized residue in $N\bar{K} \rightarrow \Lambda(1890) \rightarrow \Lambda \eta$

MODULUS	PHASE (°)	DOCUMENT ID	TECN	COMMENT
••• We do not use the following data for averages, fits, limits, etc. •••				
0.0485	-54	¹ KAMANO	15	DPWA Multichannel

¹From the preferred solution A in KAMANO 15.

Normalized residue in $N\bar{K} \rightarrow \Lambda(1890) \rightarrow \Xi K$

MODULUS	PHASE (°)	DOCUMENT ID	TECN	COMMENT
0.065 ± 0.020	160 ± 30	SARANTSEV	19	DPWA $\bar{K}N$ multichannel
••• We do not use the following data for averages, fits, limits, etc. •••				
0.0562	-85	¹ KAMANO	15	DPWA $\bar{K}N$ multichannel

¹From the preferred solution A in KAMANO 15.

Normalized residue in $N\bar{K} \rightarrow \Lambda(1890) \rightarrow \Sigma(1385)\pi, P$ -wave

MODULUS	PHASE (°)	DOCUMENT ID	TECN	COMMENT
0.11 ± 0.05	-160 ± 45	SARANTSEV	19	DPWA $\bar{K}N$ multichannel
••• We do not use the following data for averages, fits, limits, etc. •••				
0.295	-40	¹ KAMANO	15	DPWA $\bar{K}N$ multichannel

¹From the preferred solution A in KAMANO 15.

Normalized residue in $N\bar{K} \rightarrow \Lambda(1890) \rightarrow \Sigma(1385)\pi, F$ -wave

MODULUS	PHASE (°)	DOCUMENT ID	TECN	COMMENT
0.10 ± 0.04	10 ± 50	SARANTSEV	19	DPWA $\bar{K}N$ multichannel
••• We do not use the following data for averages, fits, limits, etc. •••				
0.064	127	¹ KAMANO	15	DPWA $\bar{K}N$ multichannel

¹From the preferred solution A in KAMANO 15.

Normalized residue in $N\bar{K} \rightarrow \Lambda(1890) \rightarrow N\bar{K}^*(892), S=1/2, P$ -wave

MODULUS	PHASE (°)	DOCUMENT ID	TECN	COMMENT
0.03 ± 0.03		SARANTSEV	19	DPWA $\bar{K}N$ multichannel
••• We do not use the following data for averages, fits, limits, etc. •••				
0.188	-160	¹ KAMANO	15	DPWA $\bar{K}N$ multichannel

¹From the preferred solution A in KAMANO 15.

Normalized residue in $N\bar{K} \rightarrow \Lambda(1890) \rightarrow N\bar{K}^*(892), S=3/2, P$ -wave

MODULUS	PHASE (°)	DOCUMENT ID	TECN	COMMENT
0.05 ± 0.03	180 ± 40	SARANTSEV	19	DPWA $\bar{K}N$ multichannel
••• We do not use the following data for averages, fits, limits, etc. •••				
0.209	15	¹ KAMANO	15	DPWA $\bar{K}N$ multichannel

¹From the preferred solution A in KAMANO 15.

Normalized residue in $N\bar{K} \rightarrow \Lambda(1890) \rightarrow N\bar{K}^*(892), S=3/2, F$ -wave

MODULUS	PHASE (°)	DOCUMENT ID	TECN	COMMENT
••• We do not use the following data for averages, fits, limits, etc. •••				
0.0141	129	¹ KAMANO	15	DPWA Multichannel

¹From the preferred solution A in KAMANO 15.

Normalized residue in $N\bar{K} \rightarrow \Lambda(1890) \rightarrow \Lambda \omega, S=1/2, P$ -wave

MODULUS	PHASE (°)	DOCUMENT ID	TECN	COMMENT
0.24 ± 0.06	15 ± 20	SARANTSEV	19	DPWA $\bar{K}N$ multichannel

Normalized residue in $N\bar{K} \rightarrow \Lambda(1890) \rightarrow \Lambda \omega, S=3/2, P$ -wave

MODULUS	PHASE (°)	DOCUMENT ID	TECN	COMMENT
0.15 ± 0.08	-165 ± 20	SARANTSEV	19	DPWA $\bar{K}N$ multichannel

$\Lambda(1890)$ MASS

VALUE (MeV)	DOCUMENT ID	TECN	COMMENT
1870 to 1910 (≈ 1890) OUR ESTIMATE			
1873 ± 5	SARANTSEV	19	DPWA $\bar{K}N$ multichannel
1900 ± 5	ZHANG	13A	DPWA $\bar{K}N$ multichannel
1897 ± 5	GOPAL	80	DPWA $\bar{K}N \rightarrow \bar{K}N$
1908 ± 10	ALSTON-...	78	DPWA $\bar{K}N \rightarrow \bar{K}N$
1894 ± 10	HEMINGWAY	75	DPWA $K^- p \rightarrow \bar{K}N$
••• We do not use the following data for averages, fits, limits, etc. •••			
1900 ± 5	GOPAL	77	DPWA $\bar{K}N$ multichannel
1856 or 1868	¹ MARTIN	77	DPWA $\bar{K}N$ multichannel
1900	² NAKKASYAN	75	DPWA $K^- p \rightarrow \Lambda \omega$

¹The two MARTIN 77 values are from a T-matrix pole and from a Breit-Wigner fit.
²Found in one of two best solutions.

$\Lambda(1890)$ WIDTH

VALUE (MeV)	DOCUMENT ID	TECN	COMMENT
80 to 160 (≈ 120) OUR ESTIMATE			
103 ± 10	SARANTSEV	19	DPWA $\bar{K}N$ multichannel
161 ± 15	ZHANG	13A	DPWA $\bar{K}N$ multichannel
74 ± 10	GOPAL	80	DPWA $\bar{K}N \rightarrow \bar{K}N$
119 ± 20	ALSTON-...	78	DPWA $\bar{K}N \rightarrow \bar{K}N$
107 ± 10	HEMINGWAY	75	DPWA $K^- p \rightarrow \bar{K}N$

• • • We do not use the following data for averages, fits, limits, etc. • • •

72±10	GOPAL	77	DPWA	$\bar{K}N$ multichannel
191 or 193	¹ MARTIN	77	DPWA	$\bar{K}N$ multichannel
100	² NAKKASYAN	75	DPWA	$K^-p \rightarrow \Lambda\omega$

¹The two MARTIN 77 values are from a T-matrix pole and from a Breit-Wigner fit.
²Found in one of two best solutions.

$\Lambda(1890)$ DECAY MODES

Mode	Fraction (Γ_i/Γ)
Γ_1 $N\bar{K}$	0.24 to 0.36
Γ_2 $\Sigma\pi$	3-10 %
Γ_3 $\Lambda\eta$	
Γ_4 ΞK	
Γ_5 $\Sigma(1385)\pi$	seen
Γ_6 $\Sigma(1385)\pi, P\text{-wave}$	(6.0 ± 3.0) %
Γ_7 $\Sigma(1385)\pi, F\text{-wave}$	(4.0 ± 2.0) %
Γ_8 $N\bar{K}^*(892)$	seen
Γ_9 $N\bar{K}^*(892), S=1/2$	
Γ_{10} $N\bar{K}^*(892), S=1/2, P\text{-wave}$	
Γ_{11} $N\bar{K}^*(892), S=3/2, P\text{-wave}$	
Γ_{12} $N\bar{K}^*(892), S=3/2, F\text{-wave}$	
Γ_{13} $\Lambda\omega$	

$\Lambda(1890)$ BRANCHING RATIOS

See "Sign conventions for resonance couplings" in the Note on Λ and Σ Resonances.

$\Gamma(N\bar{K})/\Gamma_{\text{total}}$

VALUE	DOCUMENT ID	TECN	COMMENT
0.24 to 0.36 OUR ESTIMATE			
0.30 ± 0.06	SARANTSEV 19	DPWA	$\bar{K}N$ multichannel
0.37 ± 0.03	ZHANG 13A	DPWA	$\bar{K}N$ multichannel
0.20 ± 0.02	GOPAL 80	DPWA	$\bar{K}N \rightarrow \bar{K}N$
0.34 ± 0.05	ALSTON-... 78	DPWA	$\bar{K}N \rightarrow \bar{K}N$
0.24 ± 0.04	HEMINGWAY 75	DPWA	$K^-p \rightarrow \bar{K}N$
• • • We do not use the following data for averages, fits, limits, etc. • • •			
0.305	¹ KAMANO 15	DPWA	$\bar{K}N$ multichannel
0.18 ± 0.02	GOPAL 77	DPWA	See GOPAL 80
0.36 or 0.34	² MARTIN 77	DPWA	$\bar{K}N$ multichannel
¹ From the preferred solution A in KAMANO 15. ² The two MARTIN 77 values are from a T-matrix pole and from a Breit-Wigner fit.			

$\Gamma(\Sigma\pi)/\Gamma_{\text{total}}$

VALUE	DOCUMENT ID	TECN	COMMENT
6 ± 2	SARANTSEV 19	DPWA	$\bar{K}N$ multichannel
<0.03	LANGBEIN 72	IPWA	$\bar{K}N$ multichannel
• • • We do not use the following data for averages, fits, limits, etc. • • •			
0.04	¹ KAMANO 15	DPWA	$\bar{K}N$ multichannel
¹ From the preferred solution A in KAMANO 15.			

$\Gamma(\Lambda\eta)/\Gamma_{\text{total}}$

VALUE	DOCUMENT ID	TECN	COMMENT
• • • We do not use the following data for averages, fits, limits, etc. • • •			
0.012	¹ KAMANO 15	DPWA	$\bar{K}N$ multichannel
¹ From the preferred solution A in KAMANO 15.			

$\Gamma(\Xi K)/\Gamma_{\text{total}}$

VALUE	DOCUMENT ID	TECN	COMMENT
~0.01	SARANTSEV 19	DPWA	$\bar{K}N$ multichannel
• • • We do not use the following data for averages, fits, limits, etc. • • •			
0.009	¹ KAMANO 15	DPWA	$\bar{K}N$ multichannel
¹ From the preferred solution A in KAMANO 15.			

$\Gamma(\Sigma(1385)\pi, P\text{-wave})/\Gamma_{\text{total}}$

VALUE	DOCUMENT ID	TECN	COMMENT
0.06 ± 0.03	SARANTSEV 19	DPWA	$\bar{K}N$ multichannel
• • • We do not use the following data for averages, fits, limits, etc. • • •			
0.453	¹ KAMANO 15	DPWA	$\bar{K}N$ multichannel
¹ From the preferred solution A in KAMANO 15.			

$\Gamma(\Sigma(1385)\pi, F\text{-wave})/\Gamma_{\text{total}}$

VALUE	DOCUMENT ID	TECN	COMMENT
0.04 ± 0.02	SARANTSEV 19	DPWA	$\bar{K}N$ multichannel
• • • We do not use the following data for averages, fits, limits, etc. • • •			
0.019	¹ KAMANO 15	DPWA	$\bar{K}N$ multichannel
¹ From the preferred solution A in KAMANO 15.			

$\Gamma(N\bar{K}^*(892), S=1/2, P\text{-wave})/\Gamma_{\text{total}}$

VALUE	DOCUMENT ID	TECN	COMMENT
<0.01	SARANTSEV 19	DPWA	$\bar{K}N$ multichannel
• • • We do not use the following data for averages, fits, limits, etc. • • •			
0.073	¹ KAMANO 15	DPWA	$\bar{K}N$ multichannel
¹ From the preferred solution A in KAMANO 15.			

$\Gamma(N\bar{K}^*(892), S=3/2, P\text{-wave})/\Gamma_{\text{total}}$

VALUE	DOCUMENT ID	TECN	COMMENT
~0.01	SARANTSEV 19	DPWA	$\bar{K}N$ multichannel
• • • We do not use the following data for averages, fits, limits, etc. • • •			
0.088	¹ KAMANO 15	DPWA	$\bar{K}N$ multichannel
¹ From the preferred solution A in KAMANO 15.			

$\Gamma(N\bar{K}^*(892), S=3/2, F\text{-wave})/\Gamma_{\text{total}}$

VALUE	DOCUMENT ID	TECN	COMMENT
• • • We do not use the following data for averages, fits, limits, etc. • • •			
0.001	¹ KAMANO 15	DPWA	$\bar{K}N$ multichannel
¹ From the preferred solution A in KAMANO 15.			

$(\Gamma_1\Gamma_2)^{1/2}/\Gamma_{\text{total}}$ in $N\bar{K} \rightarrow \Lambda(1890) \rightarrow \Sigma\pi$

VALUE	DOCUMENT ID	TECN	COMMENT
-0.09 ± 0.02	ZHANG 13A	DPWA	$\bar{K}N$ multichannel
-0.09 ± 0.03	GOPAL 77	DPWA	$\bar{K}N$ multichannel
• • • We do not use the following data for averages, fits, limits, etc. • • •			
+0.15 or +0.14	¹ MARTIN 77	DPWA	$\bar{K}N$ multichannel
¹ The two MARTIN 77 values are from a T-matrix pole and from a Breit-Wigner fit.			

$(\Gamma_1\Gamma_6)^{1/2}/\Gamma_{\text{total}}$ in $N\bar{K} \rightarrow \Lambda(1890) \rightarrow \Sigma(1385)\pi, P\text{-wave}$

VALUE	DOCUMENT ID	TECN	COMMENT
<0.03	CAMERON 78	DPWA	$K^-p \rightarrow \Sigma(1385)\pi$

$(\Gamma_1\Gamma_7)^{1/2}/\Gamma_{\text{total}}$ in $N\bar{K} \rightarrow \Lambda(1890) \rightarrow \Sigma(1385)\pi, F\text{-wave}$

VALUE	DOCUMENT ID	TECN	COMMENT
-0.31 ± 0.04	ZHANG 13A	DPWA	$\bar{K}N$ multichannel
-0.126 ± 0.055	¹ CAMERON 78	DPWA	$K^-p \rightarrow \Sigma(1385)\pi$
¹ The published sign has been changed to be in accord with the baryon-first convention.			

$(\Gamma_1\Gamma_9)^{1/2}/\Gamma_{\text{total}}$ in $N\bar{K} \rightarrow \Lambda(1890) \rightarrow N\bar{K}^*(892), S=1/2$

VALUE	DOCUMENT ID	TECN	COMMENT
-0.17 ± 0.05	ZHANG 13A	DPWA	$\bar{K}N$ multichannel
-0.07 ± 0.03	^{1,2} CAMERON 78B	DPWA	$K^-p \rightarrow N\bar{K}^*$
¹ Upper limits on the P_3 and F_3 waves are each 0.03. ² The published sign has been changed to be in accord with the baryon-first convention.			

$(\Gamma_1\Gamma_{12})^{1/2}/\Gamma_{\text{total}}$ in $N\bar{K} \rightarrow \Lambda(1890) \rightarrow N\bar{K}^*(892), S=3/2, F\text{-wave}$

VALUE	DOCUMENT ID	TECN	COMMENT
-0.11 ± 0.03	ZHANG 13A	DPWA	$\bar{K}N$ multichannel

$(\Gamma_1\Gamma_{13})^{1/2}/\Gamma_{\text{total}}$ in $N\bar{K} \rightarrow \Lambda(1890) \rightarrow \Lambda\omega$

VALUE	DOCUMENT ID	TECN	COMMENT
seen	BACCARI 77	IPWA	$K^-p \rightarrow \Lambda\omega$
0.032	¹ NAKKASYAN 75	DPWA	$K^-p \rightarrow \Lambda\omega$
¹ Found in one of two best solutions.			

$\Lambda(1890)$ REFERENCES

SARANTSEV 19	EPJ A55 180	A.V. Sarantsev <i>et al.</i>	(BONN, PNPI)
KAMANO 15	PR C92 025205	H. Kamano <i>et al.</i>	(ANL, OSAK)
ZHANG 13A	PR C68 035205	H. Zhang <i>et al.</i>	(KSU)
FDG 82	PL 111B 1	M. Roos <i>et al.</i>	(HELS, CIT, CERN)
GOPAL 80	Toronto Conf. 159	G.P. Gopal	(RHEL) IJP
ALSTON-... 78	PR D18 182	M. Alston-Garnjost <i>et al.</i>	(LBL, MTHO+) IJP
	PRL 38 1007	M. Alston-Garnjost <i>et al.</i>	(LBL, MTHO+) IJP
CAMERON 78	NP B143 189	W. Cameron <i>et al.</i>	(RHEL, LOIC) IJP
CAMERON 78B	NP B146 327	W. Cameron <i>et al.</i>	(RHEL, LOIC) IJP
BACCARI 77	NC 41A 96	B. Baccari <i>et al.</i>	(SACL, CDEF) IJP
GOPAL 77	NP B119 362	G.P. Gopal <i>et al.</i>	(LOIC, RHEL) IJP
MARTIN 77	NP B127 349	B.R. Martin, M.K. Pidcock, R.G. Moorhouse	(LOUC+) IJP
	Also NP B126 266	B.R. Martin, M.K. Pidcock	(LOUC) IJP
	Also NP B126 285	B.R. Martin, M.K. Pidcock	(LOUC) IJP
HEMINGWAY 75	NP B91 12	R.J. Hemingway <i>et al.</i>	(CERN, HEIDH, MPM) IJP
NAKKASYAN 75	NP B93 85	A. Nakkasyan	(CERN) IJP
LANGBEIN 72	NP B47 477	W. Langbein, F. Wagner	(MPIM) IJP

Baryon Particle Listings

 $\Lambda(1890)$, $\Lambda(2000)$, $\Lambda(2050)$, $\Lambda(2070)$ $\Lambda(2000)$ $I(J^P) = 0(\frac{1}{2}^-)$ Status: *

OMITTED FROM SUMMARY TABLE

BARBARO-GALTIERI 70 (in $\Sigma\pi$) and BRANDSTETTER 72 (in $\Lambda\omega$) proposed a state at about this mass. Those analyses are considered to be obsolete, see NAKKASYAN 75 and PDG 18.

 $\Lambda(2000)$ MASS

VALUE (MeV)	DOCUMENT ID	TECN	COMMENT
≈ 2000 OUR ESTIMATE			
2020 \pm 16	ZHANG	13A	DPWA Multichannel
2030 \pm 30	CAMERON	78B	DPWA $K^-p \rightarrow N\bar{K}^*$

 $\Lambda(2000)$ WIDTH

VALUE (MeV)	DOCUMENT ID	TECN	COMMENT
255 \pm 63	ZHANG	13A	DPWA Multichannel
125 \pm 25	CAMERON	78B	DPWA $K^-p \rightarrow N\bar{K}^*$

 $\Lambda(2000)$ DECAY MODES

Mode	Fraction (Γ_i/Γ)
Γ_1 $N\bar{K}$	(27 \pm 6) %
Γ_2 $\Sigma\pi$	
Γ_3 $\Lambda\eta$	(16 \pm 7) %
Γ_4 $N\bar{K}^*(892)$, $S=1/2$, S -wave	
Γ_5 $N\bar{K}^*(892)$, $S=3/2$, D -wave	

 $\Lambda(2000)$ BRANCHING RATIOS

See "Sign conventions for resonance couplings" in the Note on Λ and Σ Resonances.

$\Gamma(N\bar{K})/\Gamma_{\text{total}}$	DOCUMENT ID	TECN	COMMENT	Γ_1/Γ
VALUE				
0.27 ± 0.06	ZHANG	13A	DPWA Multichannel	

$(\Gamma_1\Gamma_2)^{1/2}/\Gamma_{\text{total}}$ in $N\bar{K} \rightarrow \Lambda(2000) \rightarrow \Sigma\pi$	DOCUMENT ID	TECN	COMMENT	$(\Gamma_1\Gamma_2)^{1/2}/\Gamma$
VALUE				
-0.07 ± 0.03	ZHANG	13A	DPWA Multichannel	

$\Gamma(\Lambda\eta)/\Gamma_{\text{total}}$	DOCUMENT ID	TECN	COMMENT	Γ_3/Γ
VALUE				
0.16 ± 0.07	ZHANG	13A	DPWA Multichannel	

$(\Gamma_1\Gamma_3)^{1/2}/\Gamma_{\text{total}}$ in $N\bar{K} \rightarrow \Lambda(2000) \rightarrow N\bar{K}^*(892)$, $S=1/2$, S -wave	DOCUMENT ID	TECN	COMMENT	$(\Gamma_1\Gamma_3)^{1/2}/\Gamma$
VALUE				
-0.12 ± 0.03	¹ CAMERON	78B	DPWA $K^-p \rightarrow N\bar{K}^*$	

¹ The published sign has been changed to be in accord with the baryon-first convention.

$(\Gamma_1\Gamma_5)^{1/2}/\Gamma_{\text{total}}$ in $N\bar{K} \rightarrow \Lambda(2000) \rightarrow N\bar{K}^*(892)$, $S=3/2$, D -wave	DOCUMENT ID	TECN	COMMENT	$(\Gamma_1\Gamma_5)^{1/2}/\Gamma$
VALUE				
$+0.34 \pm 0.05$	ZHANG	13A	DPWA Multichannel	
$+0.09 \pm 0.03$	CAMERON	78B	DPWA $K^-p \rightarrow N\bar{K}^*$	

 $\Lambda(2000)$ REFERENCES

PDG 18	PR D98 030001	M. Tanabashi et al.	(PDG Collab.)
ZHANG 13A	PR C88 035205	H. Zhang et al.	(KSU)
CAMERON 78B	NP B146 327	W. Cameron et al.	(RHEL, LOIC) JUP
NAKKASYAN 75	NP B93 95	A. Nakkasyan	(CERN) JUP
BRANDSTETTER 72	NP B39 13	A.A. Brandstetter et al.	(RHEL, CDF+) JUP
BARBARO-GALTIERI 70	Duke Conf. 173	A. Barbaro-Galvieri	(LRL) JUP

Hyperon Resonances, 1970

 $\Lambda(2050)$ $3/2^-$ $I(J^P) = 0(\frac{3}{2}^-)$ Status: *

OMITTED FROM SUMMARY TABLE

 $\Lambda(2050)$ MASS

VALUE (MeV)	DOCUMENT ID	TECN	COMMENT
2056 ± 22	ZHANG	13A	DPWA Multichannel

 $\Lambda(2050)$ WIDTH

VALUE (MeV)	DOCUMENT ID	TECN	COMMENT
493 ± 61	ZHANG	13A	DPWA Multichannel

 $\Lambda(2050)$ DECAY MODES

Mode	Fraction (Γ_i/Γ)
Γ_1 $N\bar{K}$	(19 \pm 4) %
Γ_2 $\Sigma\pi$	(6.0 \pm 3.0) %
Γ_3 $\Sigma^*(1385)\pi$, S -wave	(8 \pm 6) %
Γ_4 $\Sigma^*(1385)\pi$, D -wave	(4.0 \pm 3.0) %
Γ_5 $N\bar{K}^*(892)$, $S=1/2$	(23 \pm 7) %

 $\Lambda(2050)$ BRANCHING RATIOS

$\Gamma(N\bar{K})/\Gamma_{\text{total}}$	DOCUMENT ID	TECN	COMMENT	Γ_1/Γ
VALUE				
0.19 ± 0.04	ZHANG	13A	DPWA Multichannel	

$\Gamma(\Sigma\pi)/\Gamma_{\text{total}}$	DOCUMENT ID	TECN	COMMENT	Γ_2/Γ
VALUE				
0.06 ± 0.03	ZHANG	13A	DPWA Multichannel	

$\Gamma(\Sigma^*(1385)\pi, S\text{-wave})/\Gamma_{\text{total}}$	DOCUMENT ID	TECN	COMMENT	Γ_3/Γ
VALUE				
0.08 ± 0.06	ZHANG	13A	DPWA Multichannel	

$\Gamma(\Sigma^*(1385)\pi, D\text{-wave})/\Gamma_{\text{total}}$	DOCUMENT ID	TECN	COMMENT	Γ_4/Γ
VALUE				
0.04 ± 0.03	ZHANG	13A	DPWA Multichannel	

$\Gamma(N\bar{K}^*(892), S=1/2)/\Gamma_{\text{total}}$	DOCUMENT ID	TECN	COMMENT	Γ_5/Γ
VALUE				
0.23 ± 0.07	ZHANG	13A	DPWA Multichannel	

 $\Lambda(2050)$ REFERENCES

ZHANG 13A	PR C88 035205	H. Zhang et al.	(KSU)
-----------	---------------	-----------------	-------

 $\Lambda(2070)$ $3/2^+$ $J^P = \frac{3}{2}^+$ Status: *

OMITTED FROM SUMMARY TABLE

 $\Lambda(2070)$ POLE POSITION

REAL PART	DOCUMENT ID	TECN	COMMENT
VALUE (MeV)			
2044 ± 20	SARANTSEV 19	DPWA	$\bar{K}N$ multichannel

$-2 \times$ IMAGINARY PART	DOCUMENT ID	TECN	COMMENT
VALUE (MeV)			
360 ± 45	SARANTSEV 19	DPWA	$\bar{K}N$ multichannel

 $\Lambda(2070)$ POLE RESIDUES

Normalized residue in $N\bar{K} \rightarrow \Lambda(2070) \rightarrow N\bar{K}$	DOCUMENT ID	TECN	COMMENT
MODULUS PHASE ($^\circ$)			
0.15 ± 0.05 -37 ± 10	SARANTSEV 19	DPWA	$\bar{K}N$ multichannel

Normalized residue in $N\bar{K} \rightarrow \Lambda(2070) \rightarrow \Sigma\pi$	DOCUMENT ID	TECN	COMMENT
MODULUS PHASE ($^\circ$)			
0.10 ± 0.03 -47 ± 8	SARANTSEV 19	DPWA	$\bar{K}N$ multichannel

Normalized residue in $N\bar{K} \rightarrow \Lambda(2070) \rightarrow \Xi K$	DOCUMENT ID	TECN	COMMENT
MODULUS PHASE ($^\circ$)			
0.11 ± 0.03 0 ± 25	SARANTSEV 19	DPWA	$\bar{K}N$ multichannel

Normalized residue in $N\bar{K} \rightarrow \Lambda(2070) \rightarrow \Lambda\omega$, $S=1/2$, P -wave	DOCUMENT ID	TECN	COMMENT
MODULUS PHASE ($^\circ$)			
0.10 ± 0.04 150 ± 17	SARANTSEV 19	DPWA	$\bar{K}N$ multichannel

Normalized residue in $N\bar{K} \rightarrow \Lambda(2070) \rightarrow \Lambda\omega$, $S=3/2$, P -wave	DOCUMENT ID	TECN	COMMENT
MODULUS PHASE ($^\circ$)			
0.08 ± 0.04 20 ± 30	SARANTSEV 19	DPWA	$\bar{K}N$ multichannel

Normalized residue in $N\bar{K} \rightarrow \Lambda(2070) \rightarrow \Lambda\omega$, $S=3/2$, F -wave	DOCUMENT ID	TECN	COMMENT
MODULUS PHASE ($^\circ$)			
0.04 ± 0.02 -175 ± 35	SARANTSEV 19	DPWA	$\bar{K}N$ multichannel

Normalized residue in $N\bar{K} \rightarrow \Lambda(2070) \rightarrow \Sigma(1385)\pi$, P -wave	DOCUMENT ID	TECN	COMMENT
MODULUS PHASE ($^\circ$)			
0.12 ± 0.07 -160 ± 55	SARANTSEV 19	DPWA	$\bar{K}N$ multichannel

Normalized residue in $N\bar{K} \rightarrow \Lambda(2070) \rightarrow \Sigma(1385)\pi$, F -wave	DOCUMENT ID	TECN	COMMENT
MODULUS PHASE ($^\circ$)			
0.07 ± 0.04 -145 ± 50	SARANTSEV 19	DPWA	$\bar{K}N$ multichannel

Normalized residue in $N\bar{K} \rightarrow \Lambda(2070) \rightarrow N\bar{K}^*(892), S=1/2, P\text{-wave}$

MODULUS	PHASE (°)	DOCUMENT ID	TECN	COMMENT
0.36 ± 0.07	-45 ± 30	SARANTSEV 19	DPWA	$\bar{K}N$ multichannel

Normalized residue in $N\bar{K} \rightarrow \Lambda(2070) \rightarrow N\bar{K}^*(892), S=3/2, P\text{-wave}$

MODULUS	PHASE (°)	DOCUMENT ID	TECN	COMMENT
0.16 ± 0.05	150 ± 35	SARANTSEV 19	DPWA	$\bar{K}N$ multichannel

Normalized residue in $N\bar{K} \rightarrow \Lambda(2070) \rightarrow N\bar{K}^*(892), S=3/2, F\text{-wave}$

MODULUS	PHASE (°)	DOCUMENT ID	TECN	COMMENT
0.14 ± 0.08	-50 ± 30	SARANTSEV 19	DPWA	$\bar{K}N$ multichannel

$\Lambda(2070)$ MASS

VALUE (MeV)	DOCUMENT ID	TECN	COMMENT
2070 ± 24	SARANTSEV 19	DPWA	$\bar{K}N$ multichannel

$\Lambda(2070)$ WIDTH

VALUE (MeV)	DOCUMENT ID	TECN	COMMENT
370 ± 50	SARANTSEV 19	DPWA	$\bar{K}N$ multichannel

$\Lambda(2070)$ DECAY MODES

Mode	Fraction (Γ_i/Γ)
$\Gamma_1 N\bar{K}$	(12 ± 5) %
$\Gamma_2 \Sigma \pi$	(7.0 ± 3.0) %
$\Gamma_3 \Xi K$	(7.0 ± 3.0) %
$\Gamma_4 \Lambda\omega, S=1/2, P\text{-wave}$	(7 ± 4) %
$\Gamma_5 \Lambda\omega, S=3/2, P\text{-wave}$	(3.0 ± 2.0) %
$\Gamma_6 \Lambda\omega, S=3/2, F\text{-wave}$	(1.0 ± 1.0) %
$\Gamma_7 \Sigma(1385)\pi, P\text{-wave}$	(10 ± 5) %
$\Gamma_8 \Sigma(1385)\pi, F\text{-wave}$	(2.0 ± 2.0) %
$\Gamma_9 N\bar{K}^*(892), S=1/2, P\text{-wave}$	(42 ± 8) %
$\Gamma_{10} N\bar{K}^*(892), S=3/2, P\text{-wave}$	(14 ± 6) %
$\Gamma_{11} N\bar{K}^*(892), S=3/2, F\text{-wave}$	(10 ± 6) %

$\Lambda(2070)$ BRANCHING RATIOS

$\Gamma(N\bar{K})/\Gamma_{\text{total}}$

VALUE	DOCUMENT ID	TECN	COMMENT
0.12 ± 0.05	SARANTSEV 19	DPWA	$\bar{K}N$ multichannel

$\Gamma(\Sigma \pi)/\Gamma_{\text{total}}$

VALUE	DOCUMENT ID	TECN	COMMENT
0.07 ± 0.03	SARANTSEV 19	DPWA	$\bar{K}N$ multichannel

$\Gamma(\Xi K)/\Gamma_{\text{total}}$

VALUE	DOCUMENT ID	TECN	COMMENT
0.07 ± 0.03	SARANTSEV 19	DPWA	$\bar{K}N$ multichannel

$\Gamma(\Lambda\omega, S=1/2, P\text{-wave})/\Gamma_{\text{total}}$

VALUE	DOCUMENT ID	TECN	COMMENT
0.07 ± 0.04	SARANTSEV 19	DPWA	$\bar{K}N$ multichannel

$\Gamma(\Lambda\omega, S=3/2, P\text{-wave})/\Gamma_{\text{total}}$

VALUE	DOCUMENT ID	TECN	COMMENT
0.03 ± 0.02	SARANTSEV 19	DPWA	$\bar{K}N$ multichannel

$\Gamma(\Lambda\omega, S=3/2, F\text{-wave})/\Gamma_{\text{total}}$

VALUE	DOCUMENT ID	TECN	COMMENT
0.01 ± 0.01	SARANTSEV 19	DPWA	$\bar{K}N$ multichannel

$\Gamma(\Sigma(1385)\pi, P\text{-wave})/\Gamma_{\text{total}}$

VALUE	DOCUMENT ID	TECN	COMMENT
0.10 ± 0.05	SARANTSEV 19	DPWA	$\bar{K}N$ multichannel

$\Gamma(\Sigma(1385)\pi, F\text{-wave})/\Gamma_{\text{total}}$

VALUE	DOCUMENT ID	TECN	COMMENT
0.02 ± 0.02	SARANTSEV 19	DPWA	$\bar{K}N$ multichannel

$\Gamma(N\bar{K}^*(892), S=1/2, P\text{-wave})/\Gamma_{\text{total}}$

VALUE	DOCUMENT ID	TECN	COMMENT
0.42 ± 0.08	SARANTSEV 19	DPWA	$\bar{K}N$ multichannel

$\Gamma(N\bar{K}^*(892), S=3/2, P\text{-wave})/\Gamma_{\text{total}}$

VALUE	DOCUMENT ID	TECN	COMMENT
0.14 ± 0.06	SARANTSEV 19	DPWA	$\bar{K}N$ multichannel

$\Gamma(N\bar{K}^*(892), S=3/2, F\text{-wave})/\Gamma_{\text{total}}$

VALUE	DOCUMENT ID	TECN	COMMENT
0.10 ± 0.06	SARANTSEV 19	DPWA	$\bar{K}N$ multichannel

$\Lambda(2070)$ REFERENCES

SARANTSEV 19	EPI A55 180	A.V. Sarantsev et al.	(BONN, PNPI)
--------------	-------------	-----------------------	--------------

$\Lambda(2080) 5/2^-$

$J^P = \frac{5}{2}^-$ Status: *

OMITTED FROM SUMMARY TABLE

$\Lambda(2080)$ POLE POSITION

REAL PART

VALUE (MeV)	DOCUMENT ID	TECN	COMMENT
2070 ± 15	SARANTSEV 19	DPWA	$\bar{K}N$ multichannel

-2xIMAGINARY PART

VALUE (MeV)	DOCUMENT ID	TECN	COMMENT
172 ± 28	SARANTSEV 19	DPWA	$\bar{K}N$ multichannel

$\Lambda(2080)$ POLE RESIDUES

Normalized residue in $N\bar{K} \rightarrow \Lambda(2080) \rightarrow N\bar{K}$

MODULUS	PHASE (°)	DOCUMENT ID	TECN	COMMENT
0.12 ± 0.03	-35 ± 22	SARANTSEV 19	DPWA	$\bar{K}N$ multichannel

Normalized residue in $N\bar{K} \rightarrow \Lambda(2080) \rightarrow \Sigma \pi$

MODULUS	PHASE (°)	DOCUMENT ID	TECN	COMMENT
0.07 ± 0.03	11 ± 16	SARANTSEV 19	DPWA	$\bar{K}N$ multichannel

Normalized residue in $N\bar{K} \rightarrow \Lambda(2080) \rightarrow \Xi K$

MODULUS	PHASE (°)	DOCUMENT ID	TECN	COMMENT
0.06 ± 0.02	115 ± 20	SARANTSEV 19	DPWA	$\bar{K}N$ multichannel

Normalized residue in $N\bar{K} \rightarrow \Lambda(2080) \rightarrow \Lambda\omega, S=1/2, D\text{-wave}$

MODULUS	PHASE (°)	DOCUMENT ID	TECN	COMMENT
0.06 ± 0.03	115 ± 25	SARANTSEV 19	DPWA	$\bar{K}N$ multichannel

Normalized residue in $N\bar{K} \rightarrow \Lambda(2080) \rightarrow \Lambda\omega, S=3/2, D\text{-wave}$

MODULUS	PHASE (°)	DOCUMENT ID	TECN	COMMENT
0.09 ± 0.03	-10 ± 35	SARANTSEV 19	DPWA	$\bar{K}N$ multichannel

Normalized residue in $N\bar{K} \rightarrow \Lambda(2080) \rightarrow \Sigma(1385)\pi, D\text{-wave}$

MODULUS	PHASE (°)	DOCUMENT ID	TECN	COMMENT
0.14 ± 0.04	155 ± 45	SARANTSEV 19	DPWA	$\bar{K}N$ multichannel

Normalized residue in $N\bar{K} \rightarrow \Lambda(2080) \rightarrow \Sigma(1385)\pi, G\text{-wave}$

MODULUS	PHASE (°)	DOCUMENT ID	TECN	COMMENT
0.05 ± 0.03	30 ± 45	SARANTSEV 19	$\bar{K}N$ multichannel	

Normalized residue in $N\bar{K} \rightarrow \Lambda(2080) \rightarrow N\bar{K}^*(892), S=1/2, D\text{-wave}$

MODULUS	PHASE (°)	DOCUMENT ID	TECN	COMMENT
0.16 ± 0.08	-120 ± 50	SARANTSEV 19	DPWA	$\bar{K}N$ multichannel

Normalized residue in $N\bar{K} \rightarrow \Lambda(2080) \rightarrow N\bar{K}^*(892), S=3/2, D\text{-wave}$

MODULUS	PHASE (°)	DOCUMENT ID	TECN	COMMENT
0.20 ± 0.14	60 ± 50	SARANTSEV 19	DPWA	$\bar{K}N$ multichannel

$\Lambda(2080)$ MASS

VALUE (MeV)	DOCUMENT ID	TECN	COMMENT
2082 ± 13	SARANTSEV 19	DPWA	$\bar{K}N$ multichannel

$\Lambda(2080)$ WIDTH

VALUE (MeV)	DOCUMENT ID	TECN	COMMENT
181 ± 29	SARANTSEV 19	DPWA	$\bar{K}N$ multichannel

$\Lambda(2080)$ DECAY MODES

Mode	Fraction (Γ_i/Γ)
$\Gamma_1 N\bar{K}$	(11.0 ± 3.0) %
$\Gamma_2 \Sigma \pi$	(5.0 ± 2.0) %
$\Gamma_3 \Xi K$	(4.0 ± 1.0) %
$\Gamma_4 \Lambda\omega, S=1/2, D\text{-wave}$	(4.0 ± 2.0) %
$\Gamma_5 \Lambda\omega, S=3/2, D\text{-wave}$	(8.0 ± 3.0) %
$\Gamma_6 \Sigma(1385)\pi, D\text{-wave}$	(15 ± 5) %
$\Gamma_7 \Sigma(1385)\pi, G\text{-wave}$	(3.0 ± 2.0) %
$\Gamma_8 N\bar{K}^*(892), S=1/2, D\text{-wave}$	(17 ± 9) %
$\Gamma_9 N\bar{K}^*(892), S=3/2, D\text{-wave}$	(25 ± 16) %

Baryon Particle Listings

$\Lambda(2080), \Lambda(2085)$

$\Lambda(2080)$ BRANCHING RATIOS

$\Gamma(N\bar{K})/\Gamma_{\text{total}}$				Γ_1/Γ
VALUE	DOCUMENT ID	TECN	COMMENT	
0.11 ± 0.03	SARANTSEV 19	DPWA	$\bar{K}N$ multichannel	
$\Gamma(\Sigma\pi)/\Gamma_{\text{total}}$				Γ_2/Γ
VALUE	DOCUMENT ID	TECN	COMMENT	
0.05 ± 0.02	SARANTSEV 19	DPWA	$\bar{K}N$ multichannel	
$\Gamma(\Xi K)/\Gamma_{\text{total}}$				Γ_3/Γ
VALUE	DOCUMENT ID	TECN	COMMENT	
0.04 ± 0.01	SARANTSEV 19	DPWA	$\bar{K}N$ multichannel	
$\Gamma(\Lambda\omega, S=1/2, D\text{-wave})/\Gamma_{\text{total}}$				Γ_4/Γ
VALUE	DOCUMENT ID	TECN	COMMENT	
0.04 ± 0.02	SARANTSEV 19	DPWA	$\bar{K}N$ multichannel	
$\Gamma(\Lambda\omega, S=3/2, D\text{-wave})/\Gamma_{\text{total}}$				Γ_5/Γ
VALUE	DOCUMENT ID	TECN	COMMENT	
0.08 ± 0.03	SARANTSEV 19	DPWA	$\bar{K}N$ multichannel	
$\Gamma(\Sigma(1385)\pi, D\text{-wave})/\Gamma_{\text{total}}$				Γ_6/Γ
VALUE	DOCUMENT ID	TECN	COMMENT	
0.15 ± 0.05	SARANTSEV 19	DPWA	$\bar{K}N$ multichannel	
$\Gamma(\Sigma(1385)\pi, G\text{-wave})/\Gamma_{\text{total}}$				Γ_7/Γ
VALUE	DOCUMENT ID	TECN	COMMENT	
0.03 ± 0.02	SARANTSEV 19	DPWA	$\bar{K}N$ multichannel	
$\Gamma(N\bar{K}^*(892), S=1/2, D\text{-wave})/\Gamma_{\text{total}}$				Γ_8/Γ
VALUE	DOCUMENT ID	TECN	COMMENT	
0.17 ± 0.09	SARANTSEV 19	DPWA	$\bar{K}N$ multichannel	
$\Gamma(N\bar{K}^*(892), S=3/2, D\text{-wave})/\Gamma_{\text{total}}$				Γ_9/Γ
VALUE	DOCUMENT ID	TECN	COMMENT	
0.25 ± 0.16	SARANTSEV 19	DPWA	$\bar{K}N$ multichannel	

$\Lambda(2080)$ REFERENCES

SARANTSEV 19 EPJ A55 180 A.V. Sarantsev et al. (BONN, PNPI)

$\Lambda(2085) 7/2^+$

 $I(J^P) = 0(\frac{7}{2}^+)$ Status: **

OMITTED FROM SUMMARY TABLE was $\Lambda(2020)$

In LITCHFIELD 71, need for the state rests solely on a possibly inconsistent polarization measurement at 1.784 GeV/c. HEMINGWAY 75 does not require this state. GOPAL 77 does not need it in either $N\bar{K}$ or $\Sigma\pi$. With new K^-n angular distributions included, DECLAIS 77 sees it. However, this and other new data are included in GOPAL 80 and the state is not required. BACCARI 77 weakly supports it.

$\Lambda(2085)$ POLE POSITION

REAL PART

VALUE	DOCUMENT ID	TECN	COMMENT
1757	¹ KAMANO 15	DPWA	Multichannel
¹ From the preferred solution A in KAMANO 15. Solution B reports $M = 2041^{+80}_{-82}$ MeV.			

-2xIMAGINARY PART

VALUE	DOCUMENT ID	TECN	COMMENT
146	¹ KAMANO 15	DPWA	Multichannel
¹ From the preferred solution A in KAMANO 15. Solution B reports $M = 238^{+114}_{-34}$ MeV.			

$\Lambda(2085)$ POLE RESIDUES

The normalized residue is the residue divided by $\Gamma_{\text{pole}}/2$.

Normalized residue in $N\bar{K} \rightarrow \Lambda(2085) \rightarrow N\bar{K}$

MODULUS	PHASE (°)	DOCUMENT ID	TECN	COMMENT
0.000145	-77	¹ KAMANO 15	DPWA	Multichannel
¹ From the preferred solution A in KAMANO 15.				

Normalized residue in $N\bar{K} \rightarrow \Lambda(2085) \rightarrow \Sigma\pi$

MODULUS	PHASE (°)	DOCUMENT ID	TECN	COMMENT
0.0112	120	¹ KAMANO 15	DPWA	Multichannel
¹ From the preferred solution A in KAMANO 15.				

Normalized residue in $N\bar{K} \rightarrow \Lambda(2085) \rightarrow \Lambda\eta$

MODULUS	PHASE (°)	DOCUMENT ID	TECN	COMMENT
0.000786	-100	¹ KAMANO 15	DPWA	Multichannel
¹ From the preferred solution A in KAMANO 15.				

Normalized residue in $N\bar{K} \rightarrow \Lambda(2085) \rightarrow \Sigma(1385)\pi, F\text{-wave}$

MODULUS	PHASE (°)	DOCUMENT ID	TECN	COMMENT
0.00451	-82	¹ KAMANO 15	DPWA	Multichannel
¹ From the preferred solution A in KAMANO 15.				

Normalized residue in $N\bar{K} \rightarrow \Lambda(2085) \rightarrow \Sigma(1385)\pi, H\text{-wave}$

MODULUS	PHASE (°)	DOCUMENT ID	TECN	COMMENT
0.0000298	-128	¹ KAMANO 15	DPWA	Multichannel
¹ From the preferred solution A in KAMANO 15.				

$\Lambda(2085)$ MASS

VALUE (MeV)	DOCUMENT ID	TECN	COMMENT
≈ 2020 OUR ESTIMATE			
2043±22	ZHANG 13A	DPWA	Multichannel
2140	BACCARI 77	DPWA	$K^-p \rightarrow \Lambda\omega$
2117	DECLAIS 77	DPWA	$\bar{K}N \rightarrow \bar{K}N$
2100±30	LITCHFIELD 71	DPWA	$K^-p \rightarrow \bar{K}N$
2020±20	BARBARO... 70	DPWA	$K^-p \rightarrow \Sigma\pi$

$\Lambda(2085)$ WIDTH

VALUE (MeV)	DOCUMENT ID	TECN	COMMENT
200±75	ZHANG 13A	DPWA	Multichannel
128	BACCARI 77	DPWA	$K^-p \rightarrow \Lambda\omega$
167	DECLAIS 77	DPWA	$\bar{K}N \rightarrow \bar{K}N$
120±30	LITCHFIELD 71	DPWA	$K^-p \rightarrow \bar{K}N$
160±30	BARBARO... 70	DPWA	$K^-p \rightarrow \Sigma\pi$

$\Lambda(2085)$ DECAY MODES

Mode	Fraction (Γ_i/Γ)
$\Gamma_1 N\bar{K}$	
$\Gamma_2 \Sigma\pi$	
$\Gamma_3 \Lambda\eta$	
$\Gamma_4 \Sigma(1385)\pi, F\text{-wave}$	
$\Gamma_5 \Sigma(1385)\pi, H\text{-wave}$	
$\Gamma_6 N\bar{K}^*(892), S=1/2, F\text{-wave}$	
$\Gamma_7 N\bar{K}^*(892), S=3/2, F\text{-wave}$	
$\Gamma_8 N\bar{K}^*(892), S=3/2, H\text{-wave}$	
$\Gamma_9 \Lambda\omega$	
$\Gamma_{10} N\bar{K}^*(892), S=1/2$	(30±9) %

$\Lambda(2085)$ BRANCHING RATIOS

See "Sign conventions for resonance couplings" in the Note on Λ and Σ Resonances.

$\Gamma(N\bar{K})/\Gamma_{\text{total}}$				Γ_1/Γ
VALUE	DOCUMENT ID	TECN	COMMENT	
0.028±0.005	ZHANG 13A	DPWA	Multichannel	
0.05	DECLAIS 77	DPWA	$\bar{K}N \rightarrow \bar{K}N$	
0.05 ± 0.02	LITCHFIELD 71	DPWA	$K^-p \rightarrow \bar{K}N$	
not seen	¹ KAMANO 15	DPWA	Multichannel	
¹ From the preferred solution A in KAMANO 15.				

$\Gamma(\Sigma\pi)/\Gamma_{\text{total}}$				Γ_2/Γ
VALUE	DOCUMENT ID	TECN	COMMENT	
0.891	¹ KAMANO 15	DPWA	Multichannel	
¹ From the preferred solution A in KAMANO 15.				

Baryon Particle Listings

$\Lambda(2085), \Lambda(2100)$

$\Gamma(\Lambda\eta)/\Gamma_{total}$ Γ_3/Γ

VALUE	DOCUMENT ID	TECN	COMMENT
••• We do not use the following data for averages, fits, limits, etc. •••			
0.002	¹ KAMANO 15	DPWA	Multichannel
	¹ From the preferred solution A in KAMANO 15.		

$\Gamma(\Sigma(1385)\pi, F\text{-wave})/\Gamma_{total}$ Γ_4/Γ

VALUE	DOCUMENT ID	TECN	COMMENT
••• We do not use the following data for averages, fits, limits, etc. •••			
0.105	¹ KAMANO 15	DPWA	Multichannel
	¹ From the preferred solution A in KAMANO 15.		

$\Gamma(\Sigma(1385)\pi, H\text{-wave})/\Gamma_{total}$ Γ_5/Γ

VALUE	DOCUMENT ID	TECN	COMMENT
••• We do not use the following data for averages, fits, limits, etc. •••			
not seen	¹ KAMANO 15	DPWA	Multichannel
	¹ From the preferred solution A in KAMANO 15.		

$\Gamma(N\bar{K}^*(892), S=1/2, F\text{-wave})/\Gamma_{total}$ Γ_6/Γ

VALUE	DOCUMENT ID	TECN	COMMENT
••• We do not use the following data for averages, fits, limits, etc. •••			
not seen	¹ KAMANO 15	DPWA	Multichannel
	¹ From the preferred solution A in KAMANO 15.		

$\Gamma(N\bar{K}^*(892), S=3/2, F\text{-wave})/\Gamma_{total}$ Γ_7/Γ

VALUE	DOCUMENT ID	TECN	COMMENT
••• We do not use the following data for averages, fits, limits, etc. •••			
0.001	¹ KAMANO 15	DPWA	Multichannel
	¹ From the preferred solution A in KAMANO 15.		

$\Gamma(N\bar{K}^*(892), S=3/2, H\text{-wave})/\Gamma_{total}$ Γ_8/Γ

VALUE	DOCUMENT ID	TECN	COMMENT
••• We do not use the following data for averages, fits, limits, etc. •••			
not seen	¹ KAMANO 15	DPWA	Multichannel
	¹ From the preferred solution A in KAMANO 15.		

$\Gamma(N\bar{K}^*(892), S=1/2)/\Gamma_{total}$ Γ_{10}/Γ

VALUE	DOCUMENT ID	TECN	COMMENT
0.30±0.09	ZHANG 13A	DPWA	Multichannel

$(\Gamma_1\Gamma_f)^{1/2}/\Gamma_{total}$ in $N\bar{K} \rightarrow \Lambda(2085) \rightarrow \Sigma\pi$ $(\Gamma_1\Gamma_2)^{1/2}/\Gamma$

VALUE	DOCUMENT ID	TECN	COMMENT
+0.02±0.01	ZHANG 13A	DPWA	Multichannel
-0.15±0.02	BARBARO...	70	DPWA $K^-p \rightarrow \Sigma\pi$

$(\Gamma_1\Gamma_f)^{1/2}/\Gamma_{total}$ in $N\bar{K} \rightarrow \Lambda(2085) \rightarrow \Lambda\omega$ $(\Gamma_1\Gamma_9)^{1/2}/\Gamma$

VALUE	DOCUMENT ID	TECN	COMMENT
<0.05	BACCARI 77	DPWA	$K^-p \rightarrow \Lambda\omega$

$\Lambda(2085)$ REFERENCES

KAMANO 15	PR C92 025205	H. Kamano et al.	(ANL, OSAK)
ZHANG 13A	PR C88 035205	H. Zhang et al.	(KSU)
GOPAL 80	Toronto Conf. 159	G.P. Gopal	(RHEL)
BACCARI 77	NC 41A 96	B. Baccari et al.	(SACL, CDEF) IJP
DECLAIS 77	CERN 77-16	Y. Declais et al.	(CAEN, CERN) IJP
GOPAL 77	NP B119 362	G.P. Gopal et al.	(LOIC, RHEL)
HEMINGWAY 75	NP B91 12	R.J. Hemingway et al.	(CERN, HEIDI, MPIM) IJP
LITCHFIELD 71	NP B30 125	P.J. Litchfield et al.	(RHEL, CDEF, SACL) IJP
BARBARO...	70 Duke Conf. 173	A. Barbaro-Gattieri	(LRL) IJP
Hyperon Resonances, 1970			

$\Lambda(2100) 7/2^-$

 $I(J^P) = 0(\frac{7}{2}^-)$ Status: * * * *

Most of the results published before 1973 are now obsolete and have been omitted. They may be found in our 1982 edition Physics Letters **111B** 1 (1982).

This entry only includes results from partial-wave analyses. Parameters of peaks seen in cross sections and in invariant-mass distributions around 2100 MeV used to be listed in a separate entry immediately following. It may be found in our 1986 edition Physics Letters **170B** 1 (1986).

$\Lambda(2100)$ POLE POSITION

REAL PART

VALUE (MeV)	DOCUMENT ID	TECN	COMMENT
2040±14	SARANTSEV 19	DPWA	$\bar{K}N$ multichannel
••• We do not use the following data for averages, fits, limits, etc. •••			
2023	ZHANG 13A	DPWA	Multichannel

-2xIMAGINARY PART

VALUE (MeV)	DOCUMENT ID	TECN	COMMENT
215±29	SARANTSEV 19	DPWA	$\bar{K}N$ multichannel
••• We do not use the following data for averages, fits, limits, etc. •••			
239	ZHANG 13A	DPWA	Multichannel

$\Lambda(2100)$ POLE RESIDUE

The "normalized residue" is the residue divided by $\Gamma_{pole}/2$.

Normalized residue in $N\bar{K} \rightarrow \Lambda(2100) \rightarrow N\bar{K}$

MODULUS	PHASE (°)	DOCUMENT ID	TECN	COMMENT
0.28±0.06	-40±10	SARANTSEV 19	DPWA	$\bar{K}N$ multichannel

Normalized residue in $N\bar{K} \rightarrow \Lambda(2100) \rightarrow \Sigma\pi$

MODULUS	PHASE (°)	DOCUMENT ID	TECN	COMMENT
0.09±0.02	-35±15	SARANTSEV 19	DPWA	$\bar{K}N$ multichannel

Normalized residue in $N\bar{K} \rightarrow \Lambda(2100) \rightarrow \Sigma(1385)\pi, D\text{-wave}$

MODULUS	PHASE (°)	DOCUMENT ID	TECN	COMMENT
0.04±0.03		SARANTSEV 19	DPWA	$\bar{K}N$ multichannel

Normalized residue in $N\bar{K} \rightarrow \Lambda(2100) \rightarrow \Sigma(1385)\pi, G\text{-wave}$

MODULUS	PHASE (°)	DOCUMENT ID	TECN	COMMENT
0.06±0.03	-45±15	SARANTSEV 19	DPWA	$\bar{K}N$ multichannel

Normalized residue in $N\bar{K} \rightarrow \Lambda(2100) \rightarrow N\bar{K}^*(892), S=3/2, D\text{-wave}$

MODULUS	PHASE (°)	DOCUMENT ID	TECN	COMMENT
0.11±0.06	-30±30	SARANTSEV 19	DPWA	$\bar{K}N$ multichannel

$\Lambda(2100)$ MASS

VALUE (MeV) DOCUMENT ID TECN COMMENT

2090 to 2110 (≈ 2100) OUR ESTIMATE				
2090±15	SARANTSEV 19	DPWA	$\bar{K}N$ multichannel	
2086±6	ZHANG 13A	DPWA	Multichannel	
2104±10	GOPAL 80	DPWA	$\bar{K}N \rightarrow \bar{K}N$	
2106±30	DEBELLEFON 78	DPWA	$\bar{K}N \rightarrow \bar{K}N$	
2110±10	GOPAL 77	DPWA	$\bar{K}N$ multichannel	
2105±10	HEMINGWAY 75	DPWA	$K^-p \rightarrow \bar{K}N$	
2115±10	KANE 74	DPWA	$K^-p \rightarrow \Sigma\pi$	
••• We do not use the following data for averages, fits, limits, etc. •••				
2094	BACCARI 77	DPWA	$K^-p \rightarrow \Lambda\omega$	
2094	DECLAIS 77	DPWA	$\bar{K}N \rightarrow \bar{K}N$	
2110 or 2089	¹ NAKKASYAN 75	DPWA	$K^-p \rightarrow \Lambda\omega$	

$\Lambda(2100)$ WIDTH

VALUE (MeV) DOCUMENT ID TECN COMMENT

100 to 250 (≈ 200) OUR ESTIMATE				
290±30	SARANTSEV 19	DPWA	$\bar{K}N$ multichannel	
305±16	ZHANG 13A	DPWA	Multichannel	
157±40	DEBELLEFON 78	DPWA	$\bar{K}N \rightarrow \bar{K}N$	
250±30	GOPAL 77	DPWA	$\bar{K}N$ multichannel	
241±30	HEMINGWAY 75	DPWA	$K^-p \rightarrow \bar{K}N$	
152±15	KANE 74	DPWA	$K^-p \rightarrow \Sigma\pi$	
••• We do not use the following data for averages, fits, limits, etc. •••				
98	BACCARI 77	DPWA	$K^-p \rightarrow \Lambda\omega$	
250	DECLAIS 77	DPWA	$\bar{K}N \rightarrow \bar{K}N$	
244 or 302	¹ NAKKASYAN 75	DPWA	$K^-p \rightarrow \Lambda\omega$	

$\Lambda(2100)$ DECAY MODES

Mode	Fraction (Γ_i/Γ)
$\Gamma_1 N\bar{K}$	25-35 %
$\Gamma_2 \Sigma\pi$	~5 %
$\Gamma_3 \Lambda\eta$	<3 %
$\Gamma_4 \Xi K$	<3 %
$\Gamma_5 \Lambda\omega$	<8 %
$\Gamma_6 N\bar{K}^*(892)$	10-20 %
$\Gamma_7 \Sigma(1385)\pi, D\text{-wave}$	
$\Gamma_8 \Sigma(1385)\pi, G\text{-wave}$	(1.0±1.0) %
$\Gamma_9 N\bar{K}^*(892), S=3/2, D\text{-wave}$	(4.0±2.0) %
$\Gamma_{10} N\bar{K}^*(892), S=1/2, G\text{-wave}$	
$\Gamma_{11} N\bar{K}^*(892), S=3/2, G\text{-wave}$	

$\Lambda(2100)$ BRANCHING RATIOS

See "Sign conventions for resonance couplings" in the Note on Λ and Σ Resonances.

$\Gamma(N\bar{K})/\Gamma_{total}$ Γ_1/Γ

VALUE DOCUMENT ID TECN COMMENT

0.25 to 0.35 (≈ 0.30) OUR ESTIMATE				
0.24±0.05	SARANTSEV 19	DPWA	$\bar{K}N$ multichannel	
0.23±0.01	ZHANG 13A	DPWA	Multichannel	
0.34±0.03	GOPAL 80	DPWA	$\bar{K}N \rightarrow \bar{K}N$	
0.24±0.06	DEBELLEFON 78	DPWA	$\bar{K}N \rightarrow \bar{K}N$	
0.31±0.03	HEMINGWAY 75	DPWA	$K^-p \rightarrow \bar{K}N$	
••• We do not use the following data for averages, fits, limits, etc. •••				

Baryon Particle Listings

$\Lambda(2100)$, $\Lambda(2110)$

0.29	DECLAIS	77	DPWA	$\bar{K}N \rightarrow \bar{K}N$
0.30±0.03	GOPAL	77	DPWA	See GOPAL 80

$\Gamma(\Sigma\pi)/\Gamma_{\text{total}}$				Γ_2/Γ
VALUE	DOCUMENT ID	TECN	COMMENT	
0.030±0.015	SARANTSEV	19	DPWA	$\bar{K}N$ multichannel

$\Gamma(\Sigma(1385)\pi, D\text{-wave})/\Gamma_{\text{total}}$				Γ_7/Γ
VALUE	DOCUMENT ID	TECN	COMMENT	
<0.01	SARANTSEV	19	DPWA	$\bar{K}N$ multichannel

$\Gamma(\Sigma(1385)\pi, G\text{-wave})/\Gamma_{\text{total}}$				Γ_8/Γ
VALUE	DOCUMENT ID	TECN	COMMENT	
0.01±0.01	SARANTSEV	19	DPWA	$\bar{K}N$ multichannel

$\Gamma(N\bar{K}^*(892), S=3/2, D\text{-wave})/\Gamma_{\text{total}}$				Γ_9/Γ
VALUE	DOCUMENT ID	TECN	COMMENT	
0.04±0.02	SARANTSEV	19	DPWA	$\bar{K}N$ multichannel

$(\Gamma_1\Gamma_f)^{1/2}/\Gamma_{\text{total}}$ in $N\bar{K} \rightarrow \Lambda(2100) \rightarrow \Sigma\pi$				$(\Gamma_1\Gamma_2)^{1/2}/\Gamma$
VALUE	DOCUMENT ID	TECN	COMMENT	
+0.03±0.01	ZHANG	13A	DPWA	Multichannel
+0.12±0.04	GOPAL	77	DPWA	$\bar{K}N$ multichannel
+0.11±0.01	KANE	74	DPWA	$K^-p \rightarrow \Sigma\pi$

$(\Gamma_1\Gamma_f)^{1/2}/\Gamma_{\text{total}}$ in $N\bar{K} \rightarrow \Lambda(2100) \rightarrow \Lambda\eta$				$(\Gamma_1\Gamma_3)^{1/2}/\Gamma$
VALUE	DOCUMENT ID	TECN	COMMENT	
-0.050±0.020	RADER	73	MPWA	$K^-p \rightarrow \Lambda\eta$

$(\Gamma_1\Gamma_f)^{1/2}/\Gamma_{\text{total}}$ in $N\bar{K} \rightarrow \Lambda(2100) \rightarrow \Xi K$				$(\Gamma_1\Gamma_4)^{1/2}/\Gamma$
VALUE	DOCUMENT ID	TECN	COMMENT	
0.035±0.018	LITCHFIELD	71	DPWA	$K^-p \rightarrow \Xi K$
••• We do not use the following data for averages, fits, limits, etc. •••				
0.003	MULLER	69B	DPWA	$K^-p \rightarrow \Xi K$
0.05	TRIPP	67	RVUE	$K^-p \rightarrow \Xi K$

$(\Gamma_1\Gamma_f)^{1/2}/\Gamma_{\text{total}}$ in $N\bar{K} \rightarrow \Lambda(2100) \rightarrow \Lambda\omega$				$(\Gamma_1\Gamma_5)^{1/2}/\Gamma$
VALUE	DOCUMENT ID	TECN	COMMENT	
-0.070	2 BACCARI	77	DPWA	GD_{37} wave
+0.011	2 BACCARI	77	DPWA	GG_{17} wave
+0.008	2 BACCARI	77	DPWA	GG_{37} wave
0.122 or 0.154	1 NAKKASYAN	75	DPWA	$K^-p \rightarrow \Lambda\omega$

$(\Gamma_1\Gamma_f)^{1/2}/\Gamma_{\text{total}}$ in $N\bar{K} \rightarrow \Lambda(2100) \rightarrow N\bar{K}^*(892), S=3/2, D\text{-wave}$				$(\Gamma_1\Gamma_9)^{1/2}/\Gamma$
VALUE	DOCUMENT ID	TECN	COMMENT	
+0.16±0.02	ZHANG	13A	DPWA	Multichannel
+0.21±0.04	CAMERON	78B	DPWA	$K^-p \rightarrow N\bar{K}^*$

$(\Gamma_1\Gamma_f)^{1/2}/\Gamma_{\text{total}}$ in $N\bar{K} \rightarrow \Lambda(2100) \rightarrow N\bar{K}^*(892), S=1/2, G\text{-wave}$				$(\Gamma_1\Gamma_{10})^{1/2}/\Gamma$
VALUE	DOCUMENT ID	TECN	COMMENT	
-0.03±0.02	ZHANG	13A	DPWA	Multichannel
-0.04±0.03	3 CAMERON	78B	DPWA	$K^-p \rightarrow N\bar{K}^*$

$(\Gamma_1\Gamma_f)^{1/2}/\Gamma_{\text{total}}$ in $N\bar{K} \rightarrow \Lambda(2100) \rightarrow N\bar{K}^*(892), S=3/2, G\text{-wave}$				$(\Gamma_1\Gamma_{11})^{1/2}/\Gamma$
VALUE	DOCUMENT ID	TECN	COMMENT	
+0.08±0.02	ZHANG	13A	DPWA	Multichannel

$\Lambda(2100)$ FOOTNOTES

- The NAKKASYAN 75 values are from the two best solutions found. Each has the $\Lambda(2100)$ and one additional resonance (P_3 or F_5).
- Note that the three for BACCARI 77 entries are for three different waves.
- The published sign has been changed to be in accord with the baryon-first convention. The upper limit on the G_3 wave is 0.03.

$\Lambda(2100)$ REFERENCES

SARANTSEV 19	EPJ A55 180	A.V. Sarantsev et al.	(BONN, PNPI)
ZHANG 13A	PR C88 035205	H. Zhang et al.	(KSU)
PDG 86	PL 170B 1	M. Aguilar-Benitez et al.	(CERN, CIT+)
PDG 82	PL 111B 1	M. Roos et al.	(HEL5, CIT, CERN)
GOPAL 80	Toronto Conf. 159	G.P. Gopal	(RHEL) IJP
CAMERON 78B	NP B146 327	W. Cameron et al.	(RHEL, LOIC) IJP
DEBELLEFON 78	NC 42A 403	A. de Bellefon et al.	(CDEF, SACL) IJP
BACCARI 77	NC 41A 96	B. Baccari et al.	(SACL, CDEF) IJP
DECLAIS 77	CERN 77-16	Y. Declais et al.	(CAEN, CERN) IJP
GOPAL 77	NP B119 362	G.P. Gopal et al.	(LOIC, RHEL) IJP
HEMINGWAY 75	NP B91 12	R.J. Hemingway et al.	(CERN, HEIDH, MPIM) IJP
NAKKASYAN 75	NP B93 85	A. Nakkasyan	(CERN) IJP
KANE 74	LBL-2452	D.F. Kane	(LBL) IJP
RADER 73	NC 16A 178	R.K. Rader et al.	(SACL, HEID, CERN+)
LITCHFIELD 71	NP B30 125	P.J. Litchfield et al.	(RHEL, CDEF, SACL) IJP
MULLER 69B	Thesis UCRL 19372	R.A. Muller	(LRL)
TRIPP 67	NP B3 10	R.D. Tripp et al.	(LRL, SLAC, CERN+)

$\Lambda(2110) 5/2^+$

$I(J^P) = 0(\frac{5}{2}^+)$ Status: ***

For results published before 1974 (they are now obsolete), see our 1982 edition Physics Letters **111B** 1 (1982). All the references have been retained.

This resonance is in the Baryon Summary Table, but the evidence for it could be better.

$\Lambda(2110)$ POLE POSITION

REAL PART

VALUE (MeV)	DOCUMENT ID	TECN	COMMENT
2048±10	SARANTSEV	19	DPWA $\bar{K}N$ multichannel
••• We do not use the following data for averages, fits, limits, etc. •••			
1970	ZHANG	13A	DPWA $\bar{K}N$ multichannel

-2xIMAGINARY PART

VALUE (MeV)	DOCUMENT ID	TECN	COMMENT
255±20	SARANTSEV	19	DPWA $\bar{K}N$ multichannel
••• We do not use the following data for averages, fits, limits, etc. •••			
350	ZHANG	13A	DPWA $\bar{K}N$ multichannel

$\Lambda(2110)$ POLE RESIDUE

The "normalized residue" is the residue divided by $\Gamma_{\text{pole}}/2$.

Normalized residue in $N\bar{K} \rightarrow \Lambda(2110) \rightarrow N\bar{K}$

MODULUS	PHASE (°)	DOCUMENT ID	TECN	COMMENT
0.020±0.005	5 ± 15	SARANTSEV	19	DPWA $\bar{K}N$ multichannel

Normalized residue in $N\bar{K} \rightarrow \Lambda(2110) \rightarrow \Sigma\pi$

MODULUS	PHASE (°)	DOCUMENT ID	TECN	COMMENT
0.13±0.03	0 ± 15	SARANTSEV	19	DPWA $\bar{K}N$ multichannel

Normalized residue in $N\bar{K} \rightarrow \Lambda(2110) \rightarrow \Xi K$

MODULUS	PHASE (°)	DOCUMENT ID	TECN	COMMENT
0.005±0.005		SARANTSEV	19	DPWA $\bar{K}N$ multichannel

Normalized residue in $N\bar{K} \rightarrow \Lambda(2110) \rightarrow \Lambda\omega, S=1/2, P\text{-wave}$

MODULUS	PHASE (°)	DOCUMENT ID	TECN	COMMENT
0.01±0.01		SARANTSEV	19	DPWA $\bar{K}N$ multichannel

Normalized residue in $N\bar{K} \rightarrow \Lambda(2110) \rightarrow \Lambda\omega, S=3/2, P\text{-wave}$

MODULUS	PHASE (°)	DOCUMENT ID	TECN	COMMENT
0.03±0.01	-7 ± 16	SARANTSEV	19	DPWA $\bar{K}N$ multichannel

Normalized residue in $N\bar{K} \rightarrow \Lambda(2110) \rightarrow \Lambda\omega, S=3/2, F\text{-wave}$

MODULUS	PHASE (°)	DOCUMENT ID	TECN	COMMENT
0.01±0.01		SARANTSEV	19	DPWA $\bar{K}N$ multichannel

$\Lambda(2110)$ MASS

VALUE (MeV)	DOCUMENT ID	TECN	COMMENT
2050 to 2130 (≈ 2090) OUR ESTIMATE			
2086±12	SARANTSEV	19	DPWA $\bar{K}N$ multichannel
2036±13	ZHANG	13A	DPWA $\bar{K}N$ multichannel
2092±25	GOPAL	80	DPWA $\bar{K}N \rightarrow \bar{K}N$
2125±25	CAMERON	78B	DPWA $K^-p \rightarrow N\bar{K}^*$
2106±50	DEBELLEFON	78	DPWA $\bar{K}N \rightarrow \bar{K}N$
2140±20	DEBELLEFON	77	DPWA $K^-p \rightarrow \Sigma\pi$
2100±50	GOPAL	77	DPWA $\bar{K}N$ multichannel
2112±7	KANE	74	DPWA $K^-p \rightarrow \Sigma\pi$
••• We do not use the following data for averages, fits, limits, etc. •••			
2137	BACCARI	77	DPWA $K^-p \rightarrow \Lambda\omega$
2103	1 NAKKASYAN	75	DPWA $K^-p \rightarrow \Lambda\omega$

$\Lambda(2110)$ WIDTH

VALUE (MeV)	DOCUMENT ID	TECN	COMMENT
200 to 300 (≈ 250) OUR ESTIMATE			
274±25	SARANTSEV	19	DPWA $\bar{K}N$ multichannel
400±38	ZHANG	13A	DPWA $\bar{K}N$ multichannel
245±25	GOPAL	80	DPWA $\bar{K}N \rightarrow \bar{K}N$
160±30	CAMERON	78B	DPWA $K^-p \rightarrow N\bar{K}^*$
251±50	DEBELLEFON	78	DPWA $\bar{K}N \rightarrow \bar{K}N$
140±20	DEBELLEFON	77	DPWA $K^-p \rightarrow \Sigma\pi$
200±50	GOPAL	77	DPWA $\bar{K}N$ multichannel
190±30	KANE	74	DPWA $K^-p \rightarrow \Sigma\pi$
••• We do not use the following data for averages, fits, limits, etc. •••			
132	BACCARI	77	DPWA $K^-p \rightarrow \Lambda\omega$
391	1 NAKKASYAN	75	DPWA $K^-p \rightarrow \Lambda\omega$

Baryon Particle Listings

$\Lambda(2110), \Lambda(2325)$

$\Lambda(2110)$ DECAY MODES

Mode	Fraction (Γ_i/Γ)
Γ_1 $N\bar{K}$	5–25 %
Γ_2 $\Sigma\pi$	10–40 %
Γ_3 $\Lambda\omega$	seen
Γ_4 $\Lambda\omega, S=1/2, P$ -wave	
Γ_5 $\Lambda\omega, S=3/2, P$ -wave	(5.0±2.0) %
Γ_6 $\Lambda\omega, S=3/2, F$ -wave	
Γ_7 ΞK	
Γ_8 $\Sigma(1385)\pi$	seen
Γ_9 $\Sigma(1385)\pi, P$ -wave	
Γ_{10} $N\bar{K}^*(892)$	10–60 %
Γ_{11} $N\bar{K}^*(892), S=1/2$	
Γ_{12} $N\bar{K}^*(892), S=3/2, P$ -wave	

$\Lambda(2110)$ BRANCHING RATIOS

See “Sign conventions for resonance couplings” in the Note on Λ and Σ Resonances.

$\Gamma(N\bar{K})/\Gamma_{\text{total}}$	DOCUMENT ID	TECN	COMMENT	Γ_1/Γ
0.05 to 0.25 OUR ESTIMATE				
0.020±0.005	SARANTSEV 19	DPWA	$\bar{K}N$ multichannel	
0.083±0.005	ZHANG 13A	DPWA	$\bar{K}N$ multichannel	
0.07±0.03	GOPAL 80	DPWA	$\bar{K}N \rightarrow \bar{K}N$	
0.27±0.06	2 DEBELLEFON 78	DPWA	$\bar{K}N \rightarrow \bar{K}N$	
••• We do not use the following data for averages, fits, limits, etc. •••				
0.07±0.03	GOPAL 77	DPWA	See GOPAL 80	

$\Gamma(\Sigma\pi)/\Gamma_{\text{total}}$	DOCUMENT ID	TECN	COMMENT	Γ_2/Γ
0.88±0.20	SARANTSEV 19	DPWA	$\bar{K}N$ multichannel	

$\Gamma(\Lambda\omega, S=1/2, P\text{-wave})/\Gamma_{\text{total}}$	DOCUMENT ID	TECN	COMMENT	Γ_4/Γ
<0.01	SARANTSEV 19	DPWA	$\bar{K}N$ multichannel	

$\Gamma(\Lambda\omega, S=3/2, P\text{-wave})/\Gamma_{\text{total}}$	DOCUMENT ID	TECN	COMMENT	Γ_5/Γ
0.05±0.02	SARANTSEV 19	DPWA	$\bar{K}N$ multichannel	

$\Gamma(\Lambda\omega, S=3/2, F\text{-wave})/\Gamma_{\text{total}}$	DOCUMENT ID	TECN	COMMENT	Γ_6/Γ
<0.01	SARANTSEV 19	DPWA	$\bar{K}N$ multichannel	

$\Gamma(\Xi K)/\Gamma_{\text{total}}$	DOCUMENT ID	TECN	COMMENT	Γ_7/Γ
~0	SARANTSEV 19	DPWA	$\bar{K}N$ multichannel	

$(\Gamma_1\Gamma_2)^{1/2}/\Gamma_{\text{total}}$ in $N\bar{K} \rightarrow \Lambda(2110) \rightarrow \Sigma\pi$	DOCUMENT ID	TECN	COMMENT	$(\Gamma_1\Gamma_2)^{1/2}/\Gamma$
+0.04±0.01	ZHANG 13A	DPWA	Multichannel	
+0.14±0.01	DEBELLEFON 77	DPWA	$K^-p \rightarrow \Sigma\pi$	
+0.20±0.03	KANE 74	DPWA	$K^-p \rightarrow \Sigma\pi$	
••• We do not use the following data for averages, fits, limits, etc. •••				
+0.10±0.03	GOPAL 77	DPWA	$\bar{K}N$ multichannel	

$(\Gamma_1\Gamma_2)^{1/2}/\Gamma_{\text{total}}$ in $N\bar{K} \rightarrow \Lambda(2110) \rightarrow \Lambda\omega$	DOCUMENT ID	TECN	COMMENT	$(\Gamma_1\Gamma_2)^{1/2}/\Gamma$
<0.05	BACCARI 77	DPWA	$K^-p \rightarrow \Lambda\omega$	
0.112	1 NAKKASYAN 75	DPWA	$K^-p \rightarrow \Lambda\omega$	

$(\Gamma_1\Gamma_2)^{1/2}/\Gamma_{\text{total}}$ in $N\bar{K} \rightarrow \Lambda(2110) \rightarrow \Sigma(1385)\pi, P$ -wave	DOCUMENT ID	TECN	COMMENT	$(\Gamma_1\Gamma_2)^{1/2}/\Gamma$
+0.04±0.01	ZHANG 13A	DPWA	Multichannel	
+0.071±0.025	3 CAMERON 78	DPWA	$K^-p \rightarrow \Sigma(1385)\pi$	

$(\Gamma_1\Gamma_2)^{1/2}/\Gamma_{\text{total}}$ in $N\bar{K} \rightarrow \Lambda(2110) \rightarrow N\bar{K}^*(892), S=1/2$	DOCUMENT ID	TECN	COMMENT	$(\Gamma_1\Gamma_2)^{1/2}/\Gamma$
-0.09±0.01	ZHANG 13A	DPWA	Multichannel	
-0.17±0.04	4 CAMERON 78B	DPWA	$K^-p \rightarrow N\bar{K}^*$	

$(\Gamma_1\Gamma_2)^{1/2}/\Gamma_{\text{total}}$ in $N\bar{K} \rightarrow \Lambda(2110) \rightarrow N\bar{K}^*(892), S=3/2, P$ -wave	DOCUMENT ID	TECN	COMMENT	$(\Gamma_1\Gamma_2)^{1/2}/\Gamma$
0.24±0.01	ZHANG 13A	DPWA	Multichannel	

$\Lambda(2110)$ FOOTNOTES

- 1 Found in one of two best solutions.
- 2 The published error of 0.6 was a misprint.
- 3 The CAMERON 78 upper limit on F -wave decay is 0.03. The sign here has been changed to be in accord with the baryon-first convention.
- 4 The published sign has been changed to be in accord with the baryon-first convention. The CAMERON 78B upper limits on the P_3 and F_3 waves are each 0.03.

$\Lambda(2110)$ REFERENCES

SARANTSEV 19	EPJ A55 180	A.V. Sarantsev et al.	(BONN, PNPI)
ZHANG 13A	PR C88 035205	H. Zhang et al.	(KSU)
PDG 82	PL 111B 1	M. Roos et al.	(HELS, CIT, CERN)
GOPAL 80	Toronto Conf. 159	G.P. Gopal	(RHEL) IJP
CAMERON 78	NP B143 189	W. Cameron et al.	(RHEL, LOIC) IJP
CAMERON 78B	NP B146 327	W. Cameron et al.	(RHEL, LOIC) IJP
DEBELLEFON 78	NC 42A 403	A. de Bellefon et al.	(CDEF, SACL) IJP
BACCARI 77	NC 41A 96	B. Baccari et al.	(SACL, CDEF) IJP
DEBELLEFON 77	NC 37A 175	A. de Bellefon et al.	(CDEF, SACL) IJP
GOPAL 77	NP B119 362	G.P. Gopal et al.	(LOIC, RHEL) IJP
NAKKASYAN 75	NP B93 85	A. Nakkasyan	(CERN) IJP
KANE 74	LBL-2452	D.F. Kane	(LBL) IJP

$\Lambda(2325) 3/2^-$

$$I(J^P) = 0(\frac{3}{2}^-) \text{ Status: } *$$

OMITTED FROM SUMMARY TABLE

BACCARI 77 finds this state with either $J^P = 3/2^-$ or $3/2^+$ in a energy-dependent partial-wave analyses of $K^-p \rightarrow \Lambda\omega$ from 2070 to 2436 MeV. A subsequent semi-energy-independent analysis from threshold to 2436 MeV selects $3/2^-$. DEBELLEFON 78 (same group) also sees this state in an energy-dependent partial-wave analysis of $K^-p \rightarrow \bar{K}N$ data, and finds $J^P = 3/2^-$ or $3/2^+$. They again prefer $J^P = 3/2^-$, but only on the basis of model-dependent considerations.

$\Lambda(2325)$ MASS

VALUE (MeV)	DOCUMENT ID	TECN	COMMENT
≈ 2325 OUR ESTIMATE			
2342±30	DEBELLEFON 78	DPWA	$\bar{K}N \rightarrow \bar{K}N$
2327±20	BACCARI 77	DPWA	$K^-p \rightarrow \Lambda\omega$

$\Lambda(2325)$ WIDTH

VALUE (MeV)	DOCUMENT ID	TECN	COMMENT
177±40	DEBELLEFON 78	DPWA	$\bar{K}N \rightarrow \bar{K}N$
160±40	BACCARI 77	IPWA	$K^-p \rightarrow \Lambda\omega$

$\Lambda(2325)$ DECAY MODES

Mode
Γ_1 $N\bar{K}$
Γ_2 $\Lambda\omega$

$\Lambda(2325)$ BRANCHING RATIOS

$\Gamma(N\bar{K})/\Gamma_{\text{total}}$	DOCUMENT ID	TECN	COMMENT	Γ_1/Γ
0.19±0.06	DEBELLEFON 78	DPWA	$\bar{K}N \rightarrow \bar{K}N$	

$(\Gamma_1\Gamma_2)^{1/2}/\Gamma_{\text{total}}$ in $N\bar{K} \rightarrow \Lambda(2325) \rightarrow \Lambda\omega$	DOCUMENT ID	TECN	COMMENT	$(\Gamma_1\Gamma_2)^{1/2}/\Gamma$
0.06±0.02	1 BACCARI 77	IPWA	DS_{33} wave	
0.05±0.02	1 BACCARI 77	DPWA	DD_{13} wave	
0.08±0.03	1 BACCARI 77	DPWA	DD_{33} wave	

$\Lambda(2325)$ FOOTNOTES

- 1 Note that the three BACCARI 77 entries are for three different waves.

$\Lambda(2325)$ REFERENCES

DEBELLEFON 78	NC 42A 403	A. de Bellefon et al.	(CDEF, SACL) IJP
BACCARI 77	NC 41A 96	B. Baccari et al.	(SACL, CDEF) IJP

Baryon Particle Listings

$\Lambda(2325)$, $\Lambda(2350)$, $\Lambda(2585)$ Bumps

$\Lambda(2350) 9/2^+$

$$I(J^P) = 0(\frac{9}{2}^+) \text{ Status: } ***$$

DAUM 68 favors $J^P = 7/2^-$ or $9/2^+$. BRICMAN 70 favors $9/2^+$. LASINSKI 71 suggests three states in this region using a Pomeron + resonances model. There are now also three formation experiments from the College de France-Saclay group, DEBELLEFON 77, BACCARI 77, and DEBELLEFON 78, which find $9/2^+$ in energy-dependent partial-wave analyses of $\bar{K}N \rightarrow \Sigma\pi, \Lambda\omega$, and $N\bar{K}$.

$\Lambda(2350)$ MASS

VALUE (MeV)	DOCUMENT ID	TECN	COMMENT
2340 to 2370 (≈ 2350) OUR ESTIMATE			
2370 \pm 50	DEBELLEFON 78	DPWA	$\bar{K}N \rightarrow \bar{K}N$
2365 \pm 20	DEBELLEFON 77	DPWA	$K^-p \rightarrow \Sigma\pi$
2358 \pm 6	BRICMAN 70	CNTR	Total, charge exchange
• • • We do not use the following data for averages, fits, limits, etc. • • •			
2372	BACCARI 77	DPWA	$K^-p \rightarrow \Lambda\omega$
2344 \pm 15	COOL 70	CNTR	K^-p, K^-d total
2360 \pm 20	LU 70	CNTR	$\gamma p \rightarrow K^+Y^*$
2340 \pm 7	BUGG 68	CNTR	K^-p, K^-d total

$\Lambda(2350)$ WIDTH

VALUE (MeV)	DOCUMENT ID	TECN	COMMENT
100 to 250 (≈ 150) OUR ESTIMATE			
204 \pm 50	DEBELLEFON 78	DPWA	$\bar{K}N \rightarrow \bar{K}N$
110 \pm 20	DEBELLEFON 77	DPWA	$K^-p \rightarrow \Sigma\pi$
324 \pm 30	BRICMAN 70	CNTR	Total, charge exchange
• • • We do not use the following data for averages, fits, limits, etc. • • •			
257	BACCARI 77	DPWA	$K^-p \rightarrow \Lambda\omega$
190	COOL 70	CNTR	K^-p, K^-d total
55	LU 70	CNTR	$\gamma p \rightarrow K^+Y^*$
140 \pm 20	BUGG 68	CNTR	K^-p, K^-d total

$\Lambda(2350)$ DECAY MODES

Mode	Fraction (Γ_i/Γ)
Γ_1 $N\bar{K}$	$\sim 12\%$
Γ_2 $\Sigma\pi$	$\sim 10\%$
Γ_3 $\Lambda\omega$	

$\Lambda(2350)$ BRANCHING RATIOS

See "Sign conventions for resonance couplings" in the Note on Λ and Σ Resonances.

$\Gamma(N\bar{K})/\Gamma_{\text{total}}$	DOCUMENT ID	TECN	COMMENT	Γ_1/Γ
~ 0.12 OUR ESTIMATE				
0.12 \pm 0.04	DEBELLEFON 78	DPWA	$\bar{K}N \rightarrow \bar{K}N$	
$(\Gamma_1\Gamma_2)^{1/2}/\Gamma_{\text{total}}$ in $N\bar{K} \rightarrow \Lambda(2350) \rightarrow \Sigma\pi$				$(\Gamma_1\Gamma_2)^{1/2}/\Gamma$
VALUE	DOCUMENT ID	TECN	COMMENT	
-0.11 \pm 0.02	DEBELLEFON 77	DPWA	$K^-p \rightarrow \Sigma\pi$	
$(\Gamma_1\Gamma_3)^{1/2}/\Gamma_{\text{total}}$ in $N\bar{K} \rightarrow \Lambda(2350) \rightarrow \Lambda\omega$				$(\Gamma_1\Gamma_3)^{1/2}/\Gamma$
VALUE	DOCUMENT ID	TECN	COMMENT	
<0.05	BACCARI 77	DPWA	$K^-p \rightarrow \Lambda\omega$	

$\Lambda(2350)$ REFERENCES

DEBELLEFON 78	NC 42A 403	A. de Bellefon et al.	(CDEF, SACL)JUP
BACCARI 77	NC 41A 96	B. Baccari et al.	(SACL, CDEF)JUP
DEBELLEFON 77	NC 37A 175	A. de Bellefon et al.	(CDEF, SACL)JUP
LASINSKI 71	NP B29 125	T.A. Lasinski	(EFI)JUP
BRICMAN 70	PL 31B 152	C. Bricman et al.	(CERN, CAEN, SACL)
COOL 70	PR D1 1887	R.L. Cool et al.	(BNL)I
Also	PRL 16 1228	R.L. Cool et al.	(BNL)I
LU 70	PR D2 1846	D.C. Lu et al.	(YALE)
BUGG 68	PR 168 1466	D.V. Bugg et al.	(RHEL, BIRM, CAVE)I
DAUM 68	NP B7 19	C. Daum et al.	(CERN)JP

$\Lambda(2585)$ Bumps

$$I(J^P) = 0(?^?) \text{ Status: } **$$

OMITTED FROM SUMMARY TABLE

$\Lambda(2585)$ MASS (BUMPS)

VALUE (MeV)	DOCUMENT ID	TECN	COMMENT
≈ 2585 OUR ESTIMATE			
2585 \pm 45	ABRAMS 70	CNTR	K^-p, K^-d total
2530 \pm 25	LU 70	CNTR	$\gamma p \rightarrow K^+Y^*$

$\Lambda(2585)$ WIDTH (BUMPS)

VALUE (MeV)	DOCUMENT ID	TECN	COMMENT
300	ABRAMS 70	CNTR	K^-p, K^-d total
150	LU 70	CNTR	$\gamma p \rightarrow K^+Y^*$

$\Lambda(2585)$ DECAY MODES (BUMPS)

Mode
Γ_1 $N\bar{K}$

$\Lambda(2585)$ BRANCHING RATIOS (BUMPS)

$$(J+\frac{1}{2}) \times \Gamma(N\bar{K})/\Gamma_{\text{total}} \quad \Gamma_1/\Gamma$$

J is not known, so only $(J+\frac{1}{2}) \times \Gamma(N\bar{K})/\Gamma_{\text{total}}$ can be given.

VALUE	DOCUMENT ID	TECN	COMMENT
1	ABRAMS 70	CNTR	K^-p, K^-d total
0.12 \pm 0.12	¹ BRICMAN 70	CNTR	Total, charge exchange

$\Lambda(2585)$ FOOTNOTES (BUMPS)

¹ The resonance is at the end of the region analyzed — no clear signal.

$\Lambda(2585)$ REFERENCES (BUMPS)

ABRAMS 70	PR D1 1917	R.J. Abrams et al.	(BNL)I
Also	PRL 16 1228	R.L. Cool et al.	(BNL)I
BRICMAN 70	PL 31B 152	C. Bricman et al.	(CERN, CAEN, SACL)
LU 70	PR D2 1846	D.C. Lu et al.	(YALE)

Σ BARYONS

($S = -1, I = 1$)

$\Sigma^+ = uus, \Sigma^0 = uds, \Sigma^- = dds$



$I(J^P) = 1(\frac{1}{2}^+)$ Status: ****

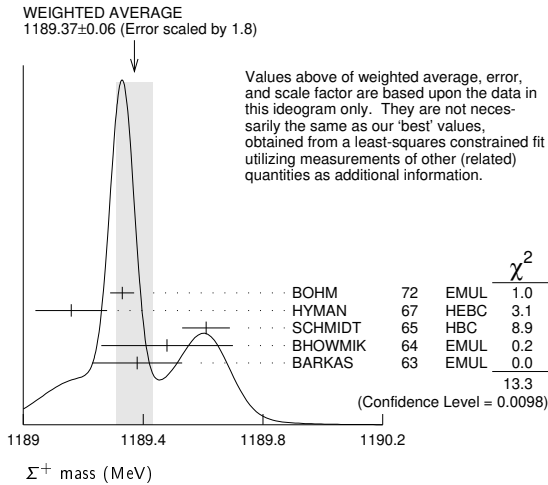
We have omitted some results that have been superseded by later experiments. See our earlier editions.

Σ^+ MASS

The fit uses $\Sigma^+, \Sigma^0, \Sigma^-$, and Λ mass and mass-difference measurements.

VALUE (MeV)	EVTS	DOCUMENT ID	TECN	COMMENT
1189.37 ± 0.07 OUR FIT				Error includes scale factor of 2.2.
1189.37 ± 0.06 OUR AVERAGE				Error includes scale factor of 1.8. See the ideogram below.
1189.33 ± 0.04	607	¹ BOHM	72	EMUL
1189.16 ± 0.12		HYMAN	67	HEBC
1189.61 ± 0.08	4205	SCHMIDT	65	HBC See note with Λ mass
1189.48 ± 0.22	58	² BHOWMIK	64	EMUL
1189.38 ± 0.15	144	² BARKAS	63	EMUL

¹BOHM 72 is updated with our 1973 $K^-, \pi^-,$ and π^0 masses (Reviews of Modern Physics **45** S1 (1973)).
²These masses have been raised 30 keV to take into account a 46 keV increase in the proton mass and a 21 keV decrease in the π^0 mass (note added 1967 edition, Reviews of Modern Physics **39** 1 (1967)).



Σ^+ MEAN LIFE

Measurements with fewer than 1000 events have been omitted.

VALUE (10^{-10} s)	EVTS	DOCUMENT ID	TECN	COMMENT
0.8018 ± 0.0026 OUR AVERAGE				
0.8038 ± 0.0040 ± 0.0014		BARBOSA	00	E761 hyperons, 375 GeV
0.8043 ± 0.0080 ± 0.0014		¹ BARBOSA	00	E761 hyperons, 375 GeV
0.798 ± 0.005	30k	MARRAFFINO	80	HBC $K^-\rho$ 0.42-0.5 GeV/c
0.807 ± 0.013	5719	CONFORTO	76	HBC $K^-\rho$ 1-1.4 GeV/c
0.795 ± 0.010	20k	EISELE	70	HBC $K^-\rho$ at rest
0.803 ± 0.008	10664	BARLOUTAUD	69	HBC $K^-\rho$ 0.4-1.2 GeV/c
0.83 ± 0.032	1300	² CHANG	66	HBC

¹This is a measurement of the Σ^- lifetime. Here we assume CPT invariance; see below for the fractional $\Sigma^+ - \Sigma^-$ lifetime difference obtained by BARBOSA 00.
²We have increased the CHANG 66 error of 0.018; see our 1970 edition, Reviews of Modern Physics **42** 87 (1970).

$(\tau_{\Sigma^+} - \tau_{\Sigma^-}) / \tau_{\Sigma^+}$

A test of CPT invariance.

VALUE	DOCUMENT ID	TECN	COMMENT
$(-6 \pm 12) \times 10^{-4}$	BARBOSA	00	E761 hyperons, 375 GeV

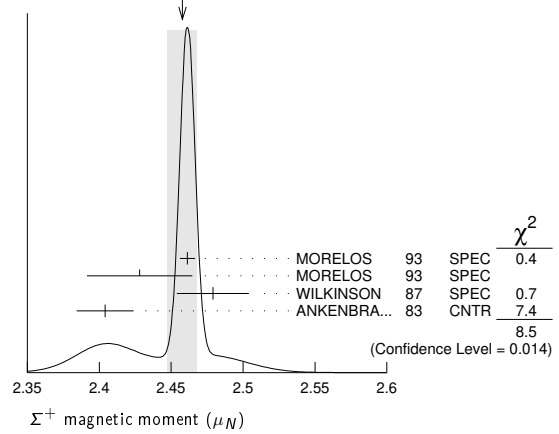
Σ^+ MAGNETIC MOMENT

See the "Note on Baryon Magnetic Moments" in the Λ Listings. Measurements with an error $\geq 0.1 \mu_N$ have been omitted.

VALUE (μ_N)	EVTS	DOCUMENT ID	TECN	COMMENT
2.458 ± 0.010 OUR AVERAGE				Error includes scale factor of 2.1. See the ideogram below.
2.4613 ± 0.0034 ± 0.0040	250k	MORELOS	93	SPEC p Cu 800 GeV
2.428 ± 0.036 ± 0.007	12k	¹ MORELOS	93	SPEC p Cu 800 GeV
2.479 ± 0.012 ± 0.022	137k	WILKINSON	87	SPEC p Be 400 GeV
2.4040 ± 0.0198	44k	² ANKENBRA...	83	CNTR p Cu 400 GeV

¹We assume CPT invariance: this is (minus) the Σ^- magnetic moment as measured by MORELOS 93. See below for the moment difference testing CPT .
²ANKENBRANDT 83 gives the value $2.38 \pm 0.02 \mu_N$. MORELOS 93 uses the same hyperon magnet and channel and claims to determine the field integral better, leading to the revised value given here.

WEIGHTED AVERAGE
2.458 ± 0.010 (Error scaled by 2.1)



$(\mu_{\Sigma^+} + \mu_{\Sigma^-}) / \mu_{\Sigma^+}$

A test of CPT invariance.

VALUE	DOCUMENT ID	TECN	COMMENT
0.014 ± 0.015	¹ MORELOS	93	SPEC p Cu 800 GeV

¹This is our calculation from the MORELOS 93 measurements of the Σ^+ and Σ^- magnetic moments given above. The statistical error on μ_{Σ^-} dominates the error here.

Σ^+ DECAY MODES

Mode	Fraction (Γ_i/Γ)	Confidence level
Γ_1 $p\pi^0$	(51.57 ± 0.30) %	
Γ_2 $n\pi^+$	(48.31 ± 0.30) %	
Γ_3 $p\gamma$	(1.23 ± 0.05) × 10 ⁻³	
Γ_4 $n\pi^+\gamma$	[a] (4.5 ± 0.5) × 10 ⁻⁴	
Γ_5 $\Lambda e^+\nu_e$	(2.0 ± 0.5) × 10 ⁻⁵	

$\Delta S = \Delta Q$ (SQ) violating modes or $\Delta S = 1$ weak neutral current ($S1$) modes

Mode	Fraction	Confidence level
Γ_6 $n e^+ \nu_e$	$SQ < 5 \times 10^{-6}$	90%
Γ_7 $n \mu^+ \nu_\mu$	$SQ < 3.0 \times 10^{-5}$	90%
Γ_8 $p e^+ e^-$	$S1 < 7 \times 10^{-6}$	
Γ_9 $p \mu^+ \mu^-$	$S1 (2.4 \pm 1.7) \times 10^{-8}$	

[a] See the Listings below for the pion momentum range used in this measurement.

CONSTRAINED FIT INFORMATION

An overall fit to 2 branching ratios uses 14 measurements and one constraint to determine 3 parameters. The overall fit has a $\chi^2 = 7.7$ for 12 degrees of freedom.

The following off-diagonal array elements are the correlation coefficients $\langle \delta x_i \delta x_j \rangle / (\delta x_i \delta x_j)$, in percent, from the fit to the branching fractions, $x_i \equiv \Gamma_i / \Gamma_{total}$. The fit constrains the x_i whose labels appear in this array to sum to one.

x_2	-100	
x_3	12	-14
	x_1	x_2

Baryon Particle Listings

 Σ^+ Σ^+ BRANCHING RATIOS $\Gamma(n\pi^+)/\Gamma(N\pi)$

VALUE	EVTS	DOCUMENT ID	TECN	COMMENT	$\Gamma_2/(\Gamma_1+\Gamma_2)$
0.4836 ± 0.0030 OUR FIT					
0.4836 ± 0.0030 OUR AVERAGE					
0.4828 ± 0.0036	10k	¹ MARRAFFINO 80	HBC	$K^- p$ 0.42–0.5 GeV/c	
0.488 ± 0.008	1861	NOWAK 78	HBC		
0.484 ± 0.015	537	TOVEE 71	EMUL		
0.488 ± 0.010	1331	BARLOUTAUD 69	HBC	$K^- p$ 0.4–1.2 GeV/c	
0.46 ± 0.02	534	CHANG 66	HBC		
0.490 ± 0.024	308	HUMPHREY 62	HBC		

¹ MARRAFFINO 80 actually gives $\Gamma(p\pi^0)/\Gamma(\text{total}) = 0.5172 \pm 0.0036$.

 $\Gamma(p\gamma)/\Gamma(p\pi^0)$

VALUE (units 10^{-3})	EVTS	DOCUMENT ID	TECN	COMMENT	Γ_3/Γ_1
2.38 ± 0.10 OUR FIT					
2.38 ± 0.10 OUR AVERAGE					
2.32 ± 0.11 ± 0.10	32k	TIMM 95	E761	Σ^+ 375 GeV	
2.81 ± 0.39 ^{+0.21} _{-0.43}	408	HESSEY 89	CNTR	$K^- p \rightarrow \Sigma^+ \pi^-$ at rest	
2.52 ± 0.28	190	¹ KOBAYASHI 87	CNTR	$\pi^+ p \rightarrow \Sigma^+ K^+$	
2.46 ^{+0.30} _{-0.35}	155	BIAGI 85	CNTR	CERN hyperon beam	
2.11 ± 0.38	46	MANZ 80	HBC	$K^- p \rightarrow \Sigma^+ \pi^-$	
2.1 ± 0.3	45	ANG 69B	HBC	$K^- p$ at rest	
2.76 ± 0.51	31	GERSHWIN 69B	HBC	$K^- p \rightarrow \Sigma^+ \pi^-$	
3.7 ± 0.8	24	BAZIN 65	HBC	$K^- p$ at rest	

¹ KOBAYASHI 87 actually gives $\Gamma(p\gamma)/\Gamma(\text{total}) = (1.30 \pm 0.15) \times 10^{-3}$.

 $\Gamma(n\pi^+\gamma)/\Gamma(n\pi^+)$

VALUE (units 10^{-3})	EVTS	DOCUMENT ID	TECN	COMMENT	Γ_4/Γ_2
0.93 ± 0.10	180	EBENHOH 73	HBC	$\pi^+ < 150$ MeV/c	
••• We do not use the following data for averages, fits, limits, etc. •••					
0.27 ± 0.05	29	ANG 69B	HBC	$\pi^+ < 110$ MeV/c	
~1.8		BAZIN 65B	HBC	$\pi^+ < 116$ MeV/c	

The π^+ momentum cuts differ, so we do not average the results but simply use the latest value in the Summary Table.

 $\Gamma(\Lambda e^+ \nu_e)/\Gamma_{\text{total}}$

VALUE (units 10^{-5})	EVTS	DOCUMENT ID	TECN	COMMENT	Γ_5/Γ
2.0 ± 0.5 OUR AVERAGE					
1.6 ± 0.7	5	BALTAY 69	HBC	$K^- p$ at rest	
2.9 ± 1.0	10	EISELE 69	HBC	$K^- p$ at rest	
2.0 ± 0.8	6	BARASH 67	HBC	$K^- p$ at rest	

 $\Gamma(n e^+ \nu_e)/\Gamma(n\pi^+)$

EFFECTIVE DENOM.	EVTS	DOCUMENT ID	TECN	COMMENT	Γ_6/Γ_2
< 1.1 × 10⁻⁵ OUR LIMIT				Our 90% CL limit = (2.3 events)/(effective denominator sum). [Number of events increased to 2.3 for a 90% confidence level.]	
111000	0	¹ EBENHOH 74	HBC	$K^- p$ at rest	
105000	0	¹ SECHI-ZORN 73	HBC	$K^- p$ at rest	

¹ Effective denominator calculated by us.

 $\Gamma(n\mu^+ \nu_\mu)/\Gamma(n\pi^+)$

EFFECTIVE DENOM.	EVTS	DOCUMENT ID	TECN	COMMENT	Γ_7/Γ_2
< 6.2 × 10⁻⁵ OUR LIMIT				Our 90% CL limit = (6.7 events)/(effective denominator sum). [Number of events increased to 6.7 for a 90% confidence level.]	
33800	0	BAGGETT 69B	HBC		
62000	2	¹ EISELE 69B	HBC		
10150	0	² COURANT 64	HBC		
1710	0	² NAUENBERG 64	HBC		
120	1	GALTIERI 62	EMUL		

¹ Effective denominator calculated by us.

² Effective denominator taken from EISELE 67.

 $\Gamma(pe^+ e^-)/\Gamma_{\text{total}}$

VALUE (units 10^{-6})	DOCUMENT ID	TECN	COMMENT	Γ_8/Γ
< 7	¹ ANG 69B	HBC	$K^- p$ at rest	

¹ ANG 69B found three $pe^+ e^-$ events in agreement with $\gamma \rightarrow e^+ e^-$ conversion from $\Sigma^+ \rightarrow p\gamma$. The limit given here is for neutral currents.

 $\Gamma(p\mu^+ \mu^-)/\Gamma_{\text{total}}$

VALUE (units 10^{-8})	EVTS	DOCUMENT ID	TECN	COMMENT	Γ_9/Γ
2.4 ± 1.7 OUR AVERAGE					
2.2 ^{+0.9} _{-0.8} ± 1.5	10.2	¹ AAIJ 18E	LHCB	pp at 7, 8 TeV	
8.6 ^{+6.6} _{-5.4} ± 5.5	3	² PARK 05	HYCP	p Cu, 800 GeV	

A test for a $\Delta S = 1$ weak neutral current, but also allowed by higher-order electroweak interactions.

¹ AAIJ 18E sees no structure in the dimuon mass distribution, contrary to PARK 05.

² The masses of the three dimuons of PARK 05 are within 1 MeV of one another, perhaps indicating the existence of a new state P^0 with mass 214.3 ± 0.5 MeV. In that case, the decay is $\Sigma^+ \rightarrow pP^0, P^0 \rightarrow \mu^+ \mu^-$, with a branching fraction of $(3.1^{+2.4}_{-1.9} \pm 1.5) \times 10^{-8}$.

 $\Gamma(\Sigma^+ \rightarrow n e^+ \nu_e)/\Gamma(\Sigma^- \rightarrow n e^- \bar{\nu}_e)$

VALUE	CL%	EVTS	DOCUMENT ID	TECN	COMMENT	Γ_6/Γ_3^-
< 0.009 OUR LIMIT					Our 90% CL limit, using $\Gamma(n e^+ \nu_e)/\Gamma(n\pi^+)$ above.	
••• We do not use the following data for averages, fits, limits, etc. •••						
< 0.019	90	0	EBENHOH 74	HBC	$K^- p$ at rest	
< 0.018	90	0	SECHI-ZORN 73	HBC	$K^- p$ at rest	
< 0.12	95	0	COLE 71	HBC	$K^- p$ at rest	
< 0.03	90	0	EISELE 69B	HBC	See EBENHOH 74	

 $\Gamma(\Sigma^+ \rightarrow n\mu^+ \nu_\mu)/\Gamma(\Sigma^- \rightarrow n\mu^- \bar{\nu}_\mu)$

VALUE	EVTS	DOCUMENT ID	TECN	COMMENT	Γ_7/Γ_4^-
< 0.12 OUR LIMIT				Our 90% CL limit, using $\Gamma(n\mu^+ \nu_\mu)/\Gamma(n\pi^+)$ above.	
••• We do not use the following data for averages, fits, limits, etc. •••					
0.06 ^{+0.045} _{-0.03}	2	EISELE 69B	HBC	$K^- p$ at rest	

 $\Gamma(\Sigma^+ \rightarrow n\ell^+ \nu)/\Gamma(\Sigma^- \rightarrow n\ell^- \bar{\nu})$

VALUE	EVTS	DOCUMENT ID	TECN	COMMENT	$(\Gamma_6+\Gamma_7)/(\Gamma_3^-+\Gamma_4^-)$
< 0.043 OUR LIMIT				Our 90% CL limit, using $[\Gamma(\Sigma^+ \rightarrow n\mu^+ \nu_\mu) + \Gamma(\Sigma^+ \rightarrow n e^+ \nu_e)]/\Gamma(\Sigma^+ \rightarrow n\pi^+)$.	
••• We do not use the following data for averages, fits, limits, etc. •••					
< 0.08	1	NORTON 69	HBC		
< 0.034	0	BAGGETT 67	HBC		

 Σ^+ DECAY PARAMETERS

See the "Note on Baryon Decay Parameters" in the neutron Listings. A few early results have been omitted.

 α_0 FOR $\Sigma^+ \rightarrow p\pi^0$

VALUE	EVTS	DOCUMENT ID	TECN	COMMENT
-0.980 ± 0.017 OUR FIT				
-0.980 ± 0.017 OUR AVERAGE				
-0.945 ^{+0.055} _{-0.042}	1259	¹ LIPMAN 73	OSPK	$\pi^+ p \rightarrow \Sigma^+$
-0.940 ± 0.045	16k	BELLAMY 72	ASPK	$\pi^+ p \rightarrow \Sigma^+ K^+$
-0.98 ^{+0.05} _{-0.02}	1335	² HARRIS 70	OSPK	$\pi^+ p \rightarrow \Sigma^+ K^+$
-0.999 ± 0.022	32k	BANGERTER 69	HBC	$K^- p$ 0.4 GeV/c

¹ Decay protons scattered off aluminum.

² Decay protons scattered off carbon.

 ϕ_0 ANGLE FOR $\Sigma^+ \rightarrow p\pi^0$

VALUE (°)	EVTS	DOCUMENT ID	TECN	COMMENT	(tan $\phi_0 = \beta/\gamma$)
36 ± 34 OUR AVERAGE					
38.1 ^{+35.7} _{-37.1}	1259	¹ LIPMAN 73	OSPK	$\pi^+ p \rightarrow \Sigma^+ K^+$	
22 ± 90		² HARRIS 70	OSPK	$\pi^+ p \rightarrow \Sigma^+ K^+$	

¹ Decay proton scattered off aluminum.

² Decay protons scattered off carbon.

 α_+ / α_0

VALUE	EVTS	DOCUMENT ID	TECN	COMMENT
-0.069 ± 0.013 OUR FIT				
-0.073 ± 0.021	23k	MARRAFFINO 80	HBC	$K^- p$ 0.42–0.5 GeV/c

 α_+ FOR $\Sigma^+ \rightarrow n\pi^+$

VALUE	EVTS	DOCUMENT ID	TECN	COMMENT
0.068 ± 0.013 OUR FIT				
0.066 ± 0.016 OUR AVERAGE				
0.037 ± 0.049	4101	BERLEY 70B	HBC	
0.069 ± 0.017	35k	BANGERTER 69	HBC	$K^- p$ 0.4 GeV/c

 ϕ_+ ANGLE FOR $\Sigma^+ \rightarrow n\pi^+$

VALUE (°)	EVTS	DOCUMENT ID	TECN	COMMENT	(tan $\phi_+ = \beta/\gamma$)
167 ± 20 OUR AVERAGE				Error includes scale factor of 1.1.	
184 ± 24	1054	¹ BERLEY 70B	HBC		
143 ± 29	560	BANGERTER 69B	HBC	$K^- p$ 0.4 GeV/c	

¹ Changed from 176 to 184° to agree with our sign convention.

See key on page 999

Baryon Particle Listings

Σ^+ , Σ^0

α_γ FOR $\Sigma^+ \rightarrow p\gamma$

VALUE	EVTS	DOCUMENT ID	TECN	COMMENT
-0.76 ± 0.08 OUR AVERAGE				
-0.720 ± 0.086 ± 0.045	35k	¹ FOUCHER	92 SPEC	$\Sigma^+ 375$ GeV
-0.86 ± 0.13 ± 0.04	190	KOBAYASHI	87 CNTR	$\pi^+ p \rightarrow \Sigma^+ K^+$
-0.53 ^{+0.38} _{-0.36}	46	MANZ	80 HBC	$K^- p \rightarrow \Sigma^+ \pi^-$
-1.03 ^{+0.52} _{-0.42}	61	GERSHWIN	69B HBC	$K^- p \rightarrow \Sigma^+ \pi^-$

¹ See TIMM 95 for a detailed description of the analysis.

Σ^+ REFERENCES

We have omitted some papers that have been superseded by later experiments. See our earlier editions.

AJJI	18E	PRL 120 221803	R. Ajji <i>et al.</i>	(LHCb Collab.)
PARK	05	PRL 94 021801	H.K. Park <i>et al.</i>	(FNAL HyperCP Collab.)
BARBOSA	00	PR D61 031101	R.F. Barbosa <i>et al.</i>	(FNAL E761 Collab.)
TIMM	95	PR D51 4638	S. Timm <i>et al.</i>	(FNAL E761 Collab.)
MORELOS	93	PRL 71 3417	A. Morelos <i>et al.</i>	(FNAL E761 Collab.)
FOUCHER	92	PRL 68 3004	M. Foucher <i>et al.</i>	(FNAL E761 Collab.)
HESSEY	89	ZPHY C42 175	N.P. Hessay <i>et al.</i>	(BNL-811 Collab.)
KOBAYASHI	87	PRL 59 868	M. Kobayashi <i>et al.</i>	(KYOT)
WILKINSON	87	PRL 58 855	C.A. Wilkinson <i>et al.</i>	(WISC, MICH, RUTG+)
BIAGI	85	ZPHY C28 495	S.F. Biagi <i>et al.</i>	(CERN WA62 Collab.)
ANKENBRANDT	83	PRL 51 863	C.M. Ankenbrandt <i>et al.</i>	(FNAL IOWA, ISU+)
MANZ	80	PL 96B 217	A. Manz <i>et al.</i>	(MPIM, VAND)
MARRAFFINO	80	PR D21 2501	J. Marraffino <i>et al.</i>	(VAND, MPIM)
NOWAK	78	NP B139 61	R.J. Nowak <i>et al.</i>	(LOUC, BELG, DURH+)
CONFORTO	76	NP B105 189	B. Conforto <i>et al.</i>	(RHEL, LOIC)
EBENHOH	74	ZPHY 266 367	H. Ebenhoeh <i>et al.</i>	(HEIDT)
EBENHOH	73	ZPHY 264 413	W. Ebenhoeh <i>et al.</i>	(HEIDT)
LIPMAN	73	PL 43B 89	N.H. Lipman <i>et al.</i>	(RHEL, SUSS, LOWC)
PDG	73	RMP 45 51	T.A. Lasinski <i>et al.</i>	(LBL, BRAN, CERN+)
SECHI-ZORN	73	PR D8 12	B. Sechi-Zorn, G.A. Snow	(UMD)
BELLAMY	72	PL 39B 299	E.H. Bellamy <i>et al.</i>	(LOW, RHEL, SUSS)
BOHM	72	NP B48 1	G. Bohm <i>et al.</i>	(BERL, KIDR, BRUX, IASD+)
Also		IHE-73-2 Nov	G. Bohm	(BERL, KIDR, BRUX, IASD, DUUC+)
COLE	71	PR D4 631	J. Cole <i>et al.</i>	(STON, COLU)
TOVEE	71	NP B33 493	D.N. Tovee <i>et al.</i>	(LOUC, KIDR, BERL+)
BERLEY	70B	PR D1 2015	D. Berley <i>et al.</i>	(BNL, MASA, YALE)
EISELE	70	ZPHY 238 372	F. Eisele <i>et al.</i>	(HEID)
HARRIS	70	PRL 24 165	F. Harris <i>et al.</i>	(MICH, WIS C)
PDG	70	RMP 42 87	A. Barbaro-Galsteri <i>et al.</i>	(LRL, BRAN+)
ANG	69B	ZPHY 228 151	G. Ang <i>et al.</i>	(HEID)
BAGGETT	69B	Thesis MDDP-TR-973	N.V. Baggett	(UMD)
BALTAY	69	PRL 22 615	C. Baltay <i>et al.</i>	(COLU, STON)
BANGERTER	69	Thesis UCRL 19244	R.O. Bangertter	(LRL)
BANGERTER	69B	PR 187 1821	R.O. Bangertter <i>et al.</i>	(LRL)
BARLOUTAUD	69	NP B14 153	R. Barloutaud <i>et al.</i>	(SACL, CERN, HEID)
EISELE	69	ZPHY 221 1	F. Eisele <i>et al.</i>	(HEID)
Also		PRL 13 291	W. Willis <i>et al.</i>	(BNL, CERN, HEID, UMD)
EISELE	69B	ZPHY 221 401	F. Eisele <i>et al.</i>	(HEID)
GERSHWIN	69B	PR 189 2077	L.K. Gershwini <i>et al.</i>	(LRL)
Also		Thesis UCRL 19246	L.K. Gershwini	(LRL)
NORTON	69	Thesis Nevis 175	H. Norton	(COLU)
BAGGETT	67	PRL 19 1458	N. Baggett <i>et al.</i>	(UMD)
Also		Vienna Abs. 374	N.V. Baggett, B. Kehoe	(UMD)
Also		Private Comm.	N.V. Baggett	(UMD)
BARASH	67	PRL 19 181	N. Barash <i>et al.</i>	(UMD)
EISELE	67	ZPHY 205 409	F. Eisele <i>et al.</i>	(HEID)
HYMAN	67	PL 25B 376	L.G. Hyman <i>et al.</i>	(ANL, CMU, NWES)
PDG	67	RMP 39 1	A.H. Rosenfeld <i>et al.</i>	(LRL, CERN, YALE)
CHANG	66	PR 151 1081	C.Y. Chang	(COLU)
Also		Thesis Nevis 145	C.Y. Chang	(COLU)
BAZIN	65	PRL 14 154	M. Bazin <i>et al.</i>	(PRIN, COLU)
BAZIN	65B	PR 140 B1358	M. Bazin <i>et al.</i>	(PRIN, RUTG, COLU)
SCHMIDT	65	PR 140 B1328	P. Schmidt	(COLU)
BHOWMIK	64	NP 53 22	B. Bhowmik <i>et al.</i>	(DELH)
COURANT	64	PR 136 B1791	H. Courant <i>et al.</i>	(CERN, HEID, UMD+)
NAUENBERG	64	PRL 12 679	U. Nauenberg <i>et al.</i>	(COLU, RUTG, PRIN)
BARKAS	63	PRL 11 26	W.H. Barkas, J.N. Dyer, H.H. Heckman	(LRL)
Also		Thesis UCRL 9450	J.N. Dyer	(LRL)
GALTIERI	62	PRL 9 26	A. Barbaro-Galsteri <i>et al.</i>	(LRL)
HUMPHREY	62	PR 127 1305	W.E. Humphrey, R.R. Ross	(LRL)



$J(P) = 1(\frac{1}{2}^+)$ Status: * * * *

COURANT 63 and ALFF 65, using $\Sigma^0 \rightarrow \Lambda e^+ e^-$ decays (Dalitz decays), determined the Σ^0 parity to be positive, given that $J = 1/2$ and that certain very reasonable assumptions about form factors are true. The results of experiments involving the Primakoff effect, from which the Σ^0 mean life and $\Sigma^0 \rightarrow \Lambda$ transition magnetic moment come (see below), strongly support $J = 1/2$.

Σ^0 MASS

The fit uses Σ^+ , Σ^0 , Σ^- , and Λ mass and mass-difference measurements.

VALUE (MeV)	EVTS	DOCUMENT ID	TECN	COMMENT
1192.642 ± 0.024 OUR FIT				

• • • We do not use the following data for averages, fits, limits, etc. • • •

1192.65 ± 0.020 ± 0.014	3327	¹ WANG	97 SPEC	$\Sigma^0 \rightarrow \Lambda \gamma \rightarrow (\rho\pi^-)(e^+ e^-)$
-------------------------	------	-------------------	---------	--

¹ This WANG 97 result is redundant with the Σ^0 - Λ mass-difference measurement below.

$m_{\Sigma^-} - m_{\Sigma^0}$

VALUE (MeV)	EVTS	DOCUMENT ID	TECN	COMMENT
4.807 ± 0.035 OUR FIT				Error includes scale factor of 1.1.
4.86 ± 0.08 OUR AVERAGE				Error includes scale factor of 1.2.
4.87 ± 0.12	37	DOSCH	65 HBC	
5.01 ± 0.12	12	SCHMIDT	65 HBC	See note with Λ mass
4.75 ± 0.1	18	BURNSTEIN	64 HBC	

$m_{\Sigma^0} - m_\Lambda$

VALUE (MeV)	EVTS	DOCUMENT ID	TECN	COMMENT
76.959 ± 0.023 OUR FIT				
76.966 ± 0.020 ± 0.013	3327	WANG	97 SPEC	$\Sigma^0 \rightarrow \Lambda \gamma \rightarrow (\rho\pi^-)(e^+ e^-)$
• • •				We do not use the following data for averages, fits, limits, etc. • • •
76.23 ± 0.55	109	COLAS	75 HLBC	$\Sigma^0 \rightarrow \Lambda \gamma$
76.63 ± 0.28	208	SCHMIDT	65 HBC	See note with Λ mass

Σ^0 MEAN LIFE

These lifetimes are deduced from measurements of the cross sections for the Primakoff process $\Lambda \rightarrow \Sigma^0$ in nuclear Coulomb fields. An alternative expression of the same information is the Σ^0 - Λ transition magnetic moment given in the following section. The relation is $(\mu_{\Sigma^0/\mu_N})^2 \tau = 1.92951 \times 10^{-19}$ s (see DEVLIN 86).

VALUE (10^{-20} s)	DOCUMENT ID	TECN	COMMENT
7.4 ± 0.7 OUR EVALUATION			Using μ_{Σ^0/μ_N} (see the above note).
6.5 ^{+1.7} _{-1.1}	² DEVLIN	86 SPEC	Primakoff effect
7.6 ± 0.5 ± 0.7	³ PETERSEN	86 SPEC	Primakoff effect
• • •			We do not use the following data for averages, fits, limits, etc. • • •
5.8 ± 1.3	² DYDAK	77 SPEC	See DEVLIN 86

² DEVLIN 86 is a recalculation of the results of DYDAK 77 removing a numerical approximation made in that work.
³ An additional uncertainty of the Primakoff formalism is estimated to be < 5%.

$|\mu(\Sigma^0 \rightarrow \Lambda)|$ TRANSITION MAGNETIC MOMENT

See the note in the Σ^0 mean-life section above. Also, see the "Note on Baryon Magnetic Moments" in the Λ Listings.

VALUE (μ_N)	DOCUMENT ID	TECN	COMMENT
1.61 ± 0.08 OUR AVERAGE			
1.72 ^{+0.17} _{-0.19}	⁴ DEVLIN	86 SPEC	Primakoff effect
1.59 ± 0.05 ± 0.07	⁵ PETERSEN	86 SPEC	Primakoff effect
• • •			We do not use the following data for averages, fits, limits, etc. • • •
1.82 ^{+0.25} _{-0.18}	⁴ DYDAK	77 SPEC	See DEVLIN 86

⁴ DEVLIN 86 is a recalculation of the results of DYDAK 77 removing a numerical approximation made in that work.
⁵ An additional uncertainty of the Primakoff formalism is estimated to be < 2.5%.

Σ^0 DECAY MODES

Mode	Fraction (Γ_i/Γ)	Confidence level
$\Gamma_1 \Lambda \gamma$	100 %	
$\Gamma_2 \Lambda \gamma \gamma$	< 3 %	90%
$\Gamma_3 \Lambda e^+ e^-$	[a] 5 × 10 ⁻³	

[a] A theoretical value using QED.

Σ^0 BRANCHING RATIOS

$\Gamma(\Lambda \gamma \gamma)/\Gamma_{total}$	CL %	DOCUMENT ID	TECN	Γ_2/Γ
< 0.03	90	COLAS	75 HLBC	

$\Gamma(\Lambda e^+ e^-)/\Gamma_{total}$	COMMENT	Γ_3/Γ
See COURANT 63 and ALFF 65 for measurements of the invariant-mass spectrum of the Dalitz pairs.		

VALUE	DOCUMENT ID	COMMENT
0.00545	FEINBERG	58 Theoretical QED calculation

Σ^0 REFERENCES

WANG	97	PR D56 2544	M.H.L.S. Wang <i>et al.</i>	(BNL-E766 Collab.)
DEVLIN	86	PR D34 1626	T. Devlin, P.C. Petersen, A. Beretvas	(RUTG)
PETERSEN	86	PRL 57 949	P.C. Petersen <i>et al.</i>	(RUTG, WISC, MICH+)
DYDAK	77	NP B118 1	F. Dydak <i>et al.</i>	(CERN, DORT, HEIDH)
COLAS	75	NP B91 253	J. Colas <i>et al.</i>	(ORSAY)
ALFF	65	PR 137 B1105	C. Alff <i>et al.</i>	(COLU, RUTG, BNL)P
DOSCH	65	PL 14 239	H.C. Dosch <i>et al.</i>	(HEID)
SCHMIDT	65	PR 140 B1328	P. Schmidt	(COLU)
BURNSTEIN	64	PRL 13 66	R.A. Burnstein <i>et al.</i>	(UMD)
COURANT	63	PRL 10 409	H. Courant <i>et al.</i>	(CERN, UMD)P
FEINBERG	58	PR 109 1019	G. Feinberg	(BNL)

Baryon Particle Listings

Σ^-



$I(J^P) = 1(\frac{1}{2}^+)$ Status: * * * *

We have omitted some results that have been superseded by later experiments. See our earlier editions.

Σ^- MASS

The fit uses Σ^+ , Σ^0 , Σ^- , and Λ mass and mass-difference measurements.

VALUE (MeV)	EVTS	DOCUMENT ID	TECN	COMMENT
1197.449 ± 0.030 OUR FIT				Error includes scale factor of 1.2.
1197.45 ± 0.04 OUR AVERAGE				Error includes scale factor of 1.2.
1197.417 ± 0.040		GUREV 93	SPEC	Σ^- C atom, crystal diff.
1197.532 ± 0.057		GALL 88	CNTR	Σ^- Pb, Σ^- W atoms
1197.43 ± 0.08	3000	SCHMIDT 65	HBC	See note with Λ mass
• • • We do not use the following data for averages, fits, limits, etc. • • •				
1197.24 ± 0.15		¹ DUGAN 75	CNTR	Exotic atoms
¹ GALL 88 concludes that the DUGAN 75 mass needs to be reevaluated.				

$m_{\Sigma^-} - m_{\Sigma^+}$

VALUE (MeV)	EVTS	DOCUMENT ID	TECN	COMMENT
8.08 ± 0.08 OUR FIT				Error includes scale factor of 1.9.
8.09 ± 0.16 OUR AVERAGE				
7.91 ± 0.23	86	BOHM 72	EMUL	
8.25 ± 0.25	2500	DOSCH 65	HBC	
8.25 ± 0.40	87	BARKAS 63	EMUL	

$m_{\Sigma^-} - m_{\Lambda}$

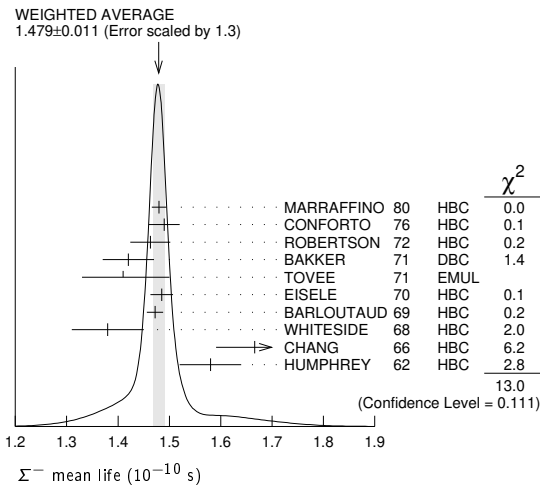
VALUE (MeV)	EVTS	DOCUMENT ID	TECN	COMMENT
81.766 ± 0.030 OUR FIT				Error includes scale factor of 1.2.
81.69 ± 0.07 OUR AVERAGE				
81.64 ± 0.09	2279	HEPP 68	HBC	
81.80 ± 0.13	85	SCHMIDT 65	HBC	See note with Λ mass
81.70 ± 0.19		BURNSTEIN 64	HBC	

Σ^- MEAN LIFE

Measurements with an error $\geq 0.2 \times 10^{-10}$ s have been omitted.

VALUE (10^{-10} s)	EVTS	DOCUMENT ID	TECN	COMMENT
1.479 ± 0.011 OUR AVERAGE				Error includes scale factor of 1.3. See the ideogram below.
1.480 ± 0.014	16k	MARRAFFINO 80	HBC	$K^- p$ 0.42–0.5 GeV/c
1.49 ± 0.03	8437	CONFORTO 76	HBC	$K^- p$ 1–1.4 GeV/c
1.463 ± 0.039	2400	ROBERTSON 72	HBC	$K^- p$ 0.25 GeV/c
1.42 ± 0.05	1383	BAKKER 71	DBC	$K^- N \rightarrow \Sigma^- \pi \pi$
1.41 +0.09 -0.08		TOVEE 71	EMUL	
1.485 ± 0.022	100k	EISELE 70	HBC	$K^- p$ at rest
1.472 ± 0.016	10k	BARLOUTAUD 69	HBC	$K^- p$ 0.4–1.2 GeV/c
1.38 ± 0.07	506	WHITESIDE 68	HBC	$K^- p$ at rest
1.666 ± 0.075	3267	² CHANG 66	HBC	$K^- p$ at rest
1.58 ± 0.06	1208	HUMPHREY 62	HBC	$K^- p$ at rest

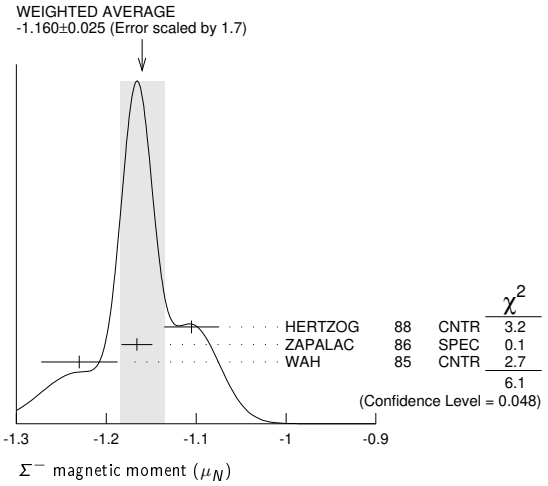
²We have increased the CHANG 66 error of 0.026; see our 1970 edition, Reviews of Modern Physics **42** 87 (1970).



Σ^- MAGNETIC MOMENT

See the "Note on Baryon Magnetic Moments" in the Λ Listings. Measurements with an error $\geq 0.3 \mu_N$ have been omitted.

VALUE (μ_N)	EVTS	DOCUMENT ID	TECN	COMMENT
-1.160 ± 0.025 OUR AVERAGE				Error includes scale factor of 1.7. See the ideogram below.
-1.105 ± 0.029 ± 0.010		HERTZOG 88	CNTR	Σ^- Pb, Σ^- W atoms
-1.166 ± 0.014 ± 0.010	671k	ZAPALAC 86	SPEC	$n e^- \nu, n \pi^-$ decays
-1.23 ± 0.03 ± 0.03		WAH 85	CNTR	p Cu $\rightarrow \Sigma^- X$
• • • We do not use the following data for averages, fits, limits, etc. • • •				
-0.89 ± 0.14	516k	DECK 83	SPEC	p Be $\rightarrow \Sigma^- X$



Σ^- CHARGE RADIUS

VALUE (fm)	DOCUMENT ID	TECN	COMMENT
0.780 ± 0.080 ± 0.060	³ ESCHRICH 01	SELX	$\Sigma^- e \rightarrow \Sigma^- e$
³ ESCHRICH 01 actually gives $\langle r^2 \rangle = (0.61 \pm 0.12 \pm 0.09) \text{ fm}^2$.			

Σ^- DECAY MODES

Mode	Fraction (Γ_i/Γ)
Γ_1 $n \pi^-$	(99.848 ± 0.005) %
Γ_2 $n \pi^- \gamma$	[a] (4.6 ± 0.6) × 10 ⁻⁴
Γ_3 $n e^- \bar{\nu}_e$	(1.017 ± 0.034) × 10 ⁻³
Γ_4 $n \mu^- \bar{\nu}_\mu$	(4.5 ± 0.4) × 10 ⁻⁴
Γ_5 $\Lambda e^- \bar{\nu}_e$	(5.73 ± 0.27) × 10 ⁻⁵

[a] See the Listings below for the pion momentum range used in this measurement.

CONSTRAINED FIT INFORMATION

An overall fit to 3 branching ratios uses 16 measurements and one constraint to determine 4 parameters. The overall fit has a $\chi^2 = 8.7$ for 13 degrees of freedom.

The following *off-diagonal* array elements are the correlation coefficients $\langle \delta x_i \delta x_j \rangle / (\delta x_i \delta x_j)$, in percent, from the fit to the branching fractions, $x_i \equiv \Gamma_i/\Gamma_{\text{total}}$. The fit constrains the x_i whose labels appear in this array to sum to one.

x_3	-64		
x_4	-77	0	
x_5	-5	0	0
	x_1	x_3	x_4

Σ^- BRANCHING RATIOS

$\Gamma(n \pi^- \gamma) / \Gamma(n \pi^-)$ Γ_2 / Γ_1
The π^+ momentum cuts differ, so we do not average the results but simply use the latest value for the Summary Table.

VALUE (units 10^{-3})	EVTS	DOCUMENT ID	TECN	COMMENT
0.46 ± 0.06	292	EBENHOH 73	HBC	π^+ < 150 MeV/c
• • • We do not use the following data for averages, fits, limits, etc. • • •				
0.10 ± 0.02	23	ANG 69b	HBC	π^- < 110 MeV/c
~ 1.1		BAZIN 65b	HBC	π^- < 166 MeV/c

See key on page 999

Baryon Particle Listings

Σ^-

$\Gamma(n e^- \bar{\nu}_e) / \Gamma(n \pi^-)$ Γ_3 / Γ_1

Measurements with an error $\geq 0.2 \times 10^{-3}$ have been omitted.

VALUE (units 10^{-3})	EVTS	DOCUMENT ID	TECN	COMMENT
1.019 ± 0.031 OUR FIT				
1.019 ± 0.031 OUR AVERAGE				
0.96 ± 0.05	2847	BOURQUIN	83c	SPEC SPS hyperon beam
1.09 ^{+0.06} _{-0.08}	601	⁴ EBENHOH	74	HBC $K^- p$ at rest
1.05 ^{+0.07} _{-0.13}	455	⁴ SECHI-ZORN	73	HBC $K^- p$ at rest
0.97 ± 0.15	57	COLE	71	HBC $K^- p$ at rest
1.11 ± 0.09	180	BIERMAN	68	HBC

⁴ An additional negative systematic error is included for internal radiative corrections and latest form factors; see BOURQUIN 83c.

$\Gamma(n \mu^- \bar{\nu}_\mu) / \Gamma(n \pi^-)$ Γ_4 / Γ_1

VALUE (units 10^{-3})	EVTS	DOCUMENT ID	TECN	COMMENT
0.45 ± 0.04 OUR FIT				
0.45 ± 0.04 OUR AVERAGE				
0.38 ± 0.11	13	COLE	71	HBC $K^- p$ at rest
0.43 ± 0.06	72	ANG	69	HBC $K^- p$ at rest
0.43 ± 0.09	56	BAGGETT	69	HBC $K^- p$ at rest
0.56 ± 0.20	11	BAZIN	65B	HBC $K^- p$ at rest
0.66 ± 0.15	22	COURANT	64	HBC

$\Gamma(\Lambda e^- \bar{\nu}_e) / \Gamma(n \pi^-)$ Γ_5 / Γ_1

VALUE (units 10^{-4})	EVTS	DOCUMENT ID	TECN	COMMENT
0.574 ± 0.027 OUR FIT				
0.574 ± 0.027 OUR AVERAGE				
0.561 ± 0.031	1620	⁵ BOURQUIN	82	SPEC SPS hyperon beam
0.63 ± 0.11	114	THOMPSON	80	ASPK Hyperon beam
0.52 ± 0.09	31	BALTAY	69	HBC $K^- p$ at rest
0.69 ± 0.12	31	EISELE	69	HBC $K^- p$ at rest
0.64 ± 0.12	35	BARASH	67	HBC $K^- p$ at rest
0.75 ± 0.28	11	COURANT	64	HBC $K^- p$ at rest

⁵ The value is from BOURQUIN 83B, and includes radiation corrections and new acceptance.

Σ^- DECAY PARAMETERS

See the "Note on Baryon Decay Parameters" in the neutron Listings. Older, outdated results have been omitted.

α_- FOR $\Sigma^- \rightarrow n \pi^-$

VALUE	EVTS	DOCUMENT ID	TECN	COMMENT
-0.068 ± 0.008 OUR AVERAGE				
-0.062 ± 0.024	28k	HANSL	78	HBC $K^- p \rightarrow \Sigma^- \pi^+$
-0.067 ± 0.011	60k	BOGERT	70	HBC $K^- p$ 0.4 GeV/c
-0.071 ± 0.012	51k	BANGERTER	69	HBC $K^- p$ 0.4 GeV/c

ϕ ANGLE FOR $\Sigma^- \rightarrow n \pi^-$ ($\tan \phi = \beta / \gamma$)

VALUE (°)	EVTS	DOCUMENT ID	TECN	COMMENT
10 ± 15 OUR AVERAGE				
+ 5 ± 23	1092	⁶ BERLEY	70B	HBC n rescattering
14 ± 19	1385	BANGERTER	69B	HBC $K^- p$ 0.4 GeV/c

⁶ BERLEY 70B changed from -5 to +5° to agree with our sign convention.

g_A/g_V FOR $\Sigma^- \rightarrow n e^- \bar{\nu}_e$

Measurements with fewer than 500 events have been omitted. Where necessary, signs have been changed to agree with our conventions, which are given in the "Note on Baryon Decay Parameters" in the neutron Listings. What is actually listed is $|g_1/f_1 - 0.237g_2/f_1|$. This reduces to $g_A/g_V \equiv g_1(0)/f_1(0)$ on making the usual assumption that $g_2 = 0$. See also the note on HSUEH 88.

VALUE	EVTS	DOCUMENT ID	TECN	COMMENT
0.340 ± 0.017 OUR AVERAGE				
+0.327 ± 0.007 ± 0.019	50k	⁷ HSUEH	88	SPEC Σ^- 250 GeV
+0.34 ± 0.05	4456	⁸ BOURQUIN	83c	SPEC SPS hyperon beam
0.385 ± 0.037	3507	⁹ TANENBAUM	74	ASPK
• • • We do not use the following data for averages, fits, limits, etc. • • •				
0.29 ± 0.07	25k	HSUEH	85	SPEC See HSUEH 88
0.17 ^{+0.07} _{-0.09}	519	DECAMP	77	ELEC Hyperon beam

⁷ The sign is, with our conventions, unambiguously positive. The value assumes, as usual, that $g_2 = 0$. If g_2 is included in the fit, than (with our sign convention) $g_2 = -0.56 \pm 0.37$, with a corresponding reduction of g_A/g_V to $+0.20 \pm 0.08$.

⁸ BOURQUIN 83c favors the positive sign by at least 2.6 standard deviations.

⁹ TANENBAUM 74 gives 0.435 ± 0.035 , assuming no q^2 dependence in g_A and g_V . The listed result allows q^2 dependence, and is taken from HSUEH 88.

$f_2(0)/f_1(0)$ FOR $\Sigma^- \rightarrow n e^- \bar{\nu}_e$

The signs have been changed to be in accord with our conventions, given in the "Note on Baryon Decay Parameters" in the neutron Listings.

VALUE	EVTS	DOCUMENT ID	TECN	COMMENT
0.97 ± 0.14 OUR AVERAGE				
+0.96 ± 0.07 ± 0.13	50k	HSUEH	88	SPEC Σ^- 250 GeV
+1.02 ± 0.34	4456	BOURQUIN	83c	SPEC SPS hyperon beam

TRIPLE CORRELATION COEFFICIENT D for $\Sigma^- \rightarrow n e^- \bar{\nu}_e$

The coefficient D of the term $D \mathbf{P} \cdot (\mathbf{p}_e \times \mathbf{p}_{\nu})$ in the $\Sigma^- \rightarrow n e^- \bar{\nu}$ decay angular distribution. A nonzero value would indicate a violation of time-reversal invariance.

VALUE	EVTS	DOCUMENT ID	TECN	COMMENT
0.11 ± 0.10	50k	HSUEH	88	SPEC Σ^- 250 GeV

g_V/g_A FOR $\Sigma^- \rightarrow \Lambda e^- \bar{\nu}_e$

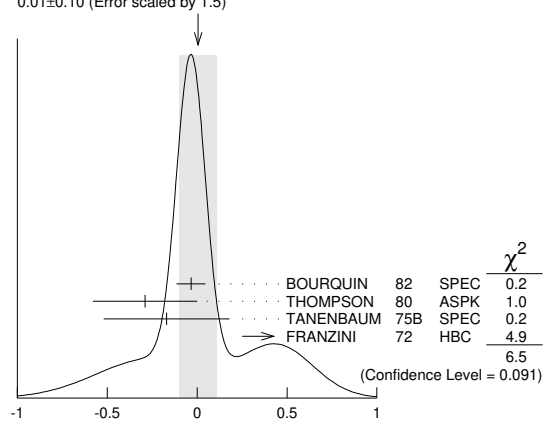
For the sign convention, see the "Note on Baryon Decay Parameters" in the neutron Listings. The value is predicted to be zero by conserved vector current theory. The values averaged assume CVC-SU(3) weak magnetism term.

VALUE	EVTS	DOCUMENT ID	TECN	COMMENT
0.01 ± 0.10 OUR AVERAGE				Error includes scale factor of 1.5. See the ideogram below.
-0.034 ± 0.080	1620	¹⁰ BOURQUIN	82	SPEC SPS hyperon beam
-0.29 ± 0.29	114	THOMPSON	80	ASPK BNL hyperon beam
-0.17 ± 0.35	55	TANENBAUM	75B	SPEC BNL hyperon beam
+0.45 ± 0.20	186	^{10,11} FRANZINI	72	HBC

¹⁰ The sign has been changed to agree with our convention.

¹¹ The FRANZINI 72 value includes the events of earlier papers.

WEIGHTED AVERAGE 0.01 ± 0.10 (Error scaled by 1.5)



g_W/g_A FOR $\Sigma^- \rightarrow \Lambda e^- \bar{\nu}_e$

The values quoted assume the CVC prediction $g_V = 0$.

VALUE	EVTS	DOCUMENT ID	TECN	COMMENT
2.4 ± 1.7 OUR AVERAGE				
1.75 ± 3.5	114	THOMPSON	80	ASPK BNL hyperon beam
3.5 ± 4.5	55	TANENBAUM	75B	SPEC BNL hyperon beam
2.4 ± 2.1	186	FRANZINI	72	HBC

Σ^- REFERENCES

We have omitted some papers that have been superseded by later experiments. See our earlier editions.

ESCHRICH 01	PL B522 233	I. Eschrich et al.	(FNAL SELEX Collab.)
GUREV 93	JETPL 57 400	M.P. Gurev et al.	(PNPI)
	Translated from ZETFP 57 389.		
GALL 88	PRL 60 186	K.P. Gall et al.	(BOST, MIT, WILL, CIT+)
HERTZOG 88	PR D37 1142	D.W. Hertzog et al.	(WILL, BOST, MIT+)
HSUEH 88	PR D38 2056	S.Y. Hsueh et al.	(CHIC, ELMT, FNAL+)
ZAPALAC 86	PRL 57 1526	G. Zapalac et al.	(ERI, ELMT, FNAL+)
HSUEH 85	PRL 54 2399	S.Y. Hsueh et al.	(CHIC, ELMT, FNAL+)
WAH 85	PRL 55 2551	Y.W. Wah et al.	(FNAL, IOWA, ISU)
BOURQUIN 83B	ZPHY C21 27	M.H. Bourquin et al.	(BRIS, GEVA, HEIDP+)
BOURQUIN 83C	ZPHY C21 17	M.H. Bourquin et al.	(BRIS, GEVA, HEIDP+)
DECK 83	PR D28 1	L. Deck et al.	(RUTG, WISC, MICH, MINN)
BOURQUIN 82	ZPHY C12 307	M.H. Bourquin et al.	(BRIS, GEVA, HEIDP+)
MARRAFFINO 80	PR D21 2501	J. Marraffino et al.	(VAND, MPIM)
THOMPSON 80	PR D21 25	J.A. Thompson et al.	(PITT, BNL)
HANSL 78	NP B132 45	T. Hansl et al.	(MPIM, VAND)
DECAMP 77	PL 66B 295	D. Decamp et al.	(LALO, EPOL)
CONFORTO 76	NP B105 189	B. Conforto et al.	(RHEL, LOIC)
DUGAN 75	NP A254 396	G. Dugan et al.	(COLU, YALE)
TANENBAUM 75B	PR D12 1871	W. Tanenbaum et al.	(YALE, FNAL, BNL)
EBENHOH 74	ZPHY 266 367	H. Ebenhoeh et al.	(HEIDT)
TANENBAUM 74	PRL 33 175	W. Tanenbaum et al.	(YALE, FNAL, BNL)
EBENHOH 73	ZPHY 264 413	W. Ebenhoeh et al.	(HEIDT)
SECHI-ZORN 73	PR D8 12	B. Sechi-Zorn, G.A. Snow	(UMD)
BOHM 72	NP B48 1	G. Bohm et al.	(BERL, KIDR, BRUX, IASD+)
FRANZINI 72	PR D6 2417	P. Franzini et al.	(COLU, HEID, UM+)
ROBERTSON 72	Thesis UMI 78-00877	R.M. Robertson	(IIT)
BAKKER 71	LNC 1 37	A.M. Bakker et al.	(SABRE Collab.)
COLE 71	PR D4 431	J. Cole et al.	(STON, COLU)
	Also Thesis Nevis 175	H. Norton	(COLU)
TOVEE 71	NP B33 493	D.N. Tovee et al.	(LOUC, KIDR, BERL+)
BERLEY 70B	PR D1 2015	D. Berley et al.	(BNL, MASA, YALE)
BOGERT 70	PR D2 6	D.V. Bogert et al.	(BNL, MASA, YALE)
EISELE 70	ZPHY 238 372	F. Eisele et al.	(HEID)
PDG 70	RMP 42 87	A. Barbaro-Galtieri et al.	(LRL, BRAN+)
ANG 69	ZPHY 223 103	G. Ang et al.	(HEID)
ANG 69B	ZPHY 228 151	G. Ang et al.	(HEID)
BAGGETT 69	PRL 23 249	N.V. Baggett, B. Kehoe, G.A. Snow	(UMD)
BALTAY 69	PRL 22 615	C. Baltay et al.	(COLU, STON)
BANGERTER 69	Thesis UCRL 19244	R.O. Bangenter	(LRL)
BANGERTER 69B	PR 187 1821	R.O. Bangenter et al.	(LRL)

Baryon Particle Listings

$\Sigma^-, \Sigma(1385)$

BARLOUTAUD 69	NP B14 153	R. Barloutaud <i>et al.</i>	(SACL, CERN, HEID)
EISELE 69	ZPHY 221 1	F. Eisele <i>et al.</i>	(HEID)
BIERMAN 68	PRL 20 1459	E. Bierman <i>et al.</i>	(PRIN)
HEPP 68	ZPHY 214 71	V. Hepp, H. Schleich	(HEID)
WHITESIDE 68	NC 54A 537	H. Whiteside, J. Gottlub	(OBER)
BARASH 67	PRL 19 181	N. Barash <i>et al.</i>	(UMD)
CHANG 66	PR 151 1081	C.Y. Chang	(COLU)
BAZIN 65B	PR 140 B1358	M. Bazin <i>et al.</i>	(PRIN, RUTG, COLU)
DOSCH 65	PL 14 239	H.C. Dosch <i>et al.</i>	(HEID)
Also	PR 151 1081	C.Y. Chang	(COLU)
SCHMIDT 65	PR 140 B1328	P. Schmidt	(COLU)
BURNSTEIN 64	PRL 13 66	R.A. Burnstein <i>et al.</i>	(UMD)
COURANT 64	PR 136 B1791	H. Courant <i>et al.</i>	(CERN, HEID, UMD+)
BARKAS 63	PRL 11 26	W.H. Barkas, J.N. Dyer, H.H. Heckman	(LRL)
HUMPHREY 62	PR 127 1305	W.E. Humphrey, R.R. Ross	(LRL)

$\Sigma(1385) 3/2^+$

$$I(J^P) = 1(\frac{3}{2}^+) \text{ Status: } ****$$

Discovered by ALSTON 60. Early measurements of the mass and width for combined charge states have been omitted. They may be found in our 1984 edition Reviews of Modern Physics 56 S1 (1984).

We average only the most significant determinations. We do not average results from inclusive experiments with large backgrounds or results which are not accompanied by some discussion of experimental resolution. Nevertheless systematic differences between experiments remain. (See the ideograms in the Listings below.) These differences could arise from interference effects that change with production mechanism and/or beam momentum. They can also be accounted for in part by differences in the parametrizations employed. (See BORENSTEIN 74 for a discussion on this point.) Thus BORENSTEIN 74 uses a Breit-Wigner with energy-independent width, since a P -wave was found to give unsatisfactory fits. CAMERON 78 uses the same form. On the other hand HOLMGREN 77 obtains a good fit to their $\Lambda\pi$ spectrum with a P -wave Breit-Wigner, but includes the partial width for the $\Sigma\pi$ decay mode in the parametrization. AGUILAR-BENITEZ 81D gives masses and widths for five different Breit-Wigner shapes. The results vary considerably. Only the best-fit S -wave results are given here.

$\Sigma(1385)$ POLE POSITIONS

$\Sigma(1385)^+$ REAL PART

VALUE	DOCUMENT ID	COMMENT
1379 ± 1	LICHTENBERG74	Extrapolates HABIBI 73

$\Sigma(1385)^+$ -IMAGINARY PART

VALUE	DOCUMENT ID	COMMENT
17.5 ± 1.5	LICHTENBERG74	Extrapolates HABIBI 73

$\Sigma(1385)^-$ REAL PART

VALUE	DOCUMENT ID	COMMENT
1383 ± 1	LICHTENBERG74	Extrapolates HABIBI 73

$\Sigma(1385)^-$ -IMAGINARY PART

VALUE	DOCUMENT ID	COMMENT
22.5 ± 1.5	LICHTENBERG74	Extrapolates HABIBI 73

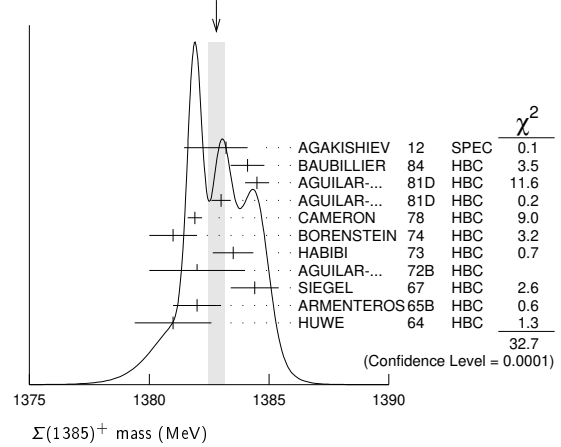
$\Sigma(1385)$ MASSES

$\Sigma(1385)^+$ MASS

VALUE (MeV)	EVTS	DOCUMENT ID	TECN	COMMENT
1382.80 ± 0.35 OUR AVERAGE				Error includes scale factor of 1.9. See the ideogram below.
1383.2 ± 0.9	$^{+0.1}_{-1.5}$	AGAKISHIEV 12	SPEC	$pp \rightarrow \Sigma(1385)^+ K^+ n$, 3.5 GeV
1384.1 ± 0.7	1897	BAUBILLIER 84	HBC	$K^- p \rightarrow 8.25 \text{ GeV}/c$
1384.5 ± 0.5	5256	AGUILAR-... 81D	HBC	$K^- p \rightarrow \Lambda\pi\pi$ 4.2 GeV/c
1383.0 ± 0.4	9361	AGUILAR-... 81D	HBC	$K^- p \rightarrow \Lambda 3\pi$ 4.2 GeV/c
1381.9 ± 0.3	6900	CAMERON 78	HBC	$K^- p$ 0.96-1.36 GeV/c
1381 ± 1	6846	BORENSTEIN 74	HBC	$K^- p$ 2.18 GeV/c
1383.5 ± 0.85	2300	HABIBI 73	HBC	$K^- p \rightarrow \Lambda\pi\pi$
1382 ± 2	400	AGUILAR-... 72B	HBC	$K^- p \rightarrow \Lambda\pi's$
1384.4 ± 1.0	1260	SIEGEL 67	HBC	$K^- p$ 2.1 GeV/c
1382 ± 1	750	ARMENTEROS65B	HBC	$K^- p$ 0.9-1.2 GeV/c
1381.0 ± 1.6	859	HUWE 64	HBC	$K^- p$ 1.22 GeV/c
• • • We do not use the following data for averages, fits, limits, etc. • • •				
1385.1 ± 1.2	600	BAKER 80	HYBR	$\pi^+ p$ 7 GeV/c
1383.2 ± 1.0	750	BAKER 80	HYBR	$K^- p$ 7 GeV/c
1381 ± 2	7k	¹ BAUBILLIER 79B	HBC	$K^- p$ 8.25 GeV/c
1391 ± 2	2k	CAUTIS 79	HYBR	$\pi^+ p/K^- p$ 11.5 GeV
1390 ± 2	100	¹ SUGAHARA 79B	HBC	$\pi^- p$ 6 GeV/c
1385 ± 3	22k	^{1,2} BARREIRO 77B	HBC	$K^- p$ 4.2 GeV/c
1385 ± 1	2594	HOLMGREN 77	HBC	See AGUILAR-BENITEZ 81D
1380 ± 2		¹ BARDADIN-... 75	HBC	$K^- p$ 14.3 GeV/c

1382 ± 1	3740	³ BERTHON 74	HBC	$K^- p$ 1263-1843 MeV/c
1390 ± 6	46	AGUILAR-... 70B	HBC	$K^- p \rightarrow \Sigma\pi's$ 4 GeV/c
1383 ± 8	62	⁴ BIRMINGHAM 66	HBC	$K^- p$ 3.5 GeV/c
1378 ± 5	135	LONDON 66	HBC	$K^- p$ 2.24 GeV/c
1384.3 ± 1.9	250	⁴ SMITH 65	HBC	$K^- p$ 1.8 GeV/c
1382.6 ± 2.1	250	⁴ SMITH 65	HBC	$K^- p$ 1.95 GeV/c
1375.0 ± 3.9	170	COOPER 64	HBC	$K^- p$ 1.45 GeV/c
1376.0 ± 3.9	154	⁴ ELY 61	HLBC	$K^- p$ 1.11 GeV/c

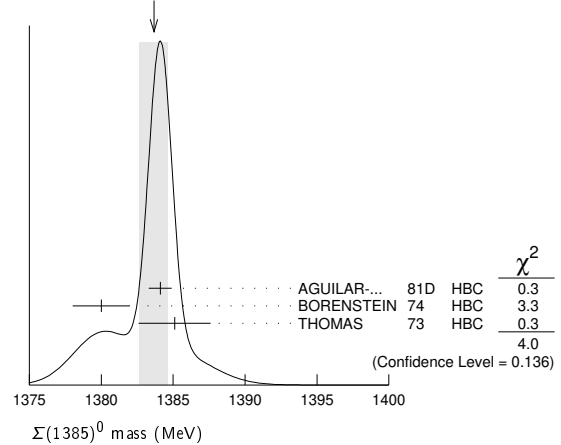
WEIGHTED AVERAGE
1382.80±0.35 (Error scaled by 1.9)



$\Sigma(1385)^0$ MASS

VALUE (MeV)	EVTS	DOCUMENT ID	TECN	COMMENT
1383.7 ± 1.0 OUR AVERAGE				Error includes scale factor of 1.4. See the ideogram below.
1384.1 ± 0.8	5722	AGUILAR-... 81D	HBC	$K^- p \rightarrow \Lambda 3\pi$ 4.2 GeV/c
1380 ± 2	3100	⁵ BORENSTEIN 74	HBC	$K^- p \rightarrow \Lambda 3\pi$ 2.18 GeV/c
1385.1 ± 2.5	240	⁴ THOMAS 73	HBC	$\pi^- p \rightarrow \Lambda\pi^0 K^0$
• • • We do not use the following data for averages, fits, limits, etc. • • •				
1389 ± 3	500	⁶ BAUBILLIER 79B	HBC	$K^- p$ 8.25 GeV/c

WEIGHTED AVERAGE
1383.7±1.0 (Error scaled by 1.4)



$\Sigma(1385)^-$ MASS

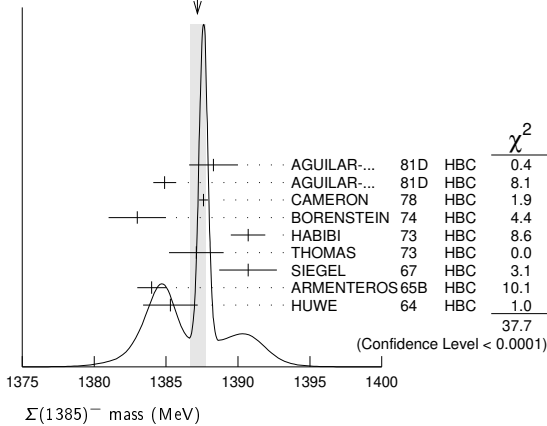
VALUE (MeV)	EVTS	DOCUMENT ID	TECN	COMMENT
1387.2 ± 0.5 OUR AVERAGE				Error includes scale factor of 2.2. See the ideogram below.
1388.3 ± 1.7	620	AGUILAR-... 81D	HBC	$K^- p \rightarrow \Lambda\pi\pi$ 4.2 GeV/c
1384.9 ± 0.8	3346	AGUILAR-... 81D	HBC	$K^- p \rightarrow \Lambda 3\pi$ 4.2 GeV/c
1387.6 ± 0.3	9720	CAMERON 78	HBC	$K^- p$ 0.96-1.36 GeV/c
1383 ± 2	2303	BORENSTEIN 74	HBC	$K^- p$ 2.18 GeV/c
1390.7 ± 1.2	1900	HABIBI 73	HBC	$K^- p \rightarrow \Lambda\pi\pi$
1387.1 ± 1.9	630	⁴ THOMAS 73	HBC	$\pi^- p \rightarrow \Lambda\pi^- K^+$
1390.7 ± 2.0	370	SIEGEL 67	HBC	$K^- p$ 2.1 GeV/c
1384 ± 1	1380	ARMENTEROS65B	HBC	$K^- p$ 0.9-1.2 GeV/c
1385.3 ± 1.9	1086	⁴ HUWE 64	HBC	$K^- p$ 1.15-1.30 GeV/c

Σ(1385)

••• We do not use the following data for averages, fits, limits, etc. •••

Table with columns: Value, CL%, Document ID, TECN, Comment. Lists various experimental data points for Σ(1385) mass and width.

WEIGHTED AVERAGE 1387.2±0.5 (Error scaled by 2.2)



mΣ(1385)- - mΣ(1385)+

Table of mass differences between Σ(1385)- and Σ(1385)+ with columns for Value, CL%, Document ID, TECN, and Comment.

mΣ(1385)0 - mΣ(1385)+

Table of mass differences between Σ(1385)0 and Σ(1385)+ with columns for Value, CL%, Document ID, TECN, and Comment.

mΣ(1385)- - mΣ(1385)0

Table of mass differences between Σ(1385)- and Σ(1385)0 with columns for Value, Document ID, TECN, and Comment.

Σ(1385) WIDTHS

Σ(1385)+ WIDTH

Table of Σ(1385)+ widths with columns for Value, EVTS, Document ID, TECN, and Comment.

••• We do not use the following data for averages, fits, limits, etc. •••

Table with columns: Value, EVTS, Document ID, TECN, Comment. Lists various experimental data points for Σ(1385)0 width.

Σ(1385)0 WIDTH

Table of Σ(1385)0 widths with columns for Value, EVTS, Document ID, TECN, and Comment.

••• We do not use the following data for averages, fits, limits, etc. •••

Table with columns: Value, EVTS, Document ID, TECN, Comment. Lists various experimental data points for Σ(1385)- width.

Σ(1385)- WIDTH

Table of Σ(1385)- widths with columns for Value, EVTS, Document ID, TECN, and Comment.

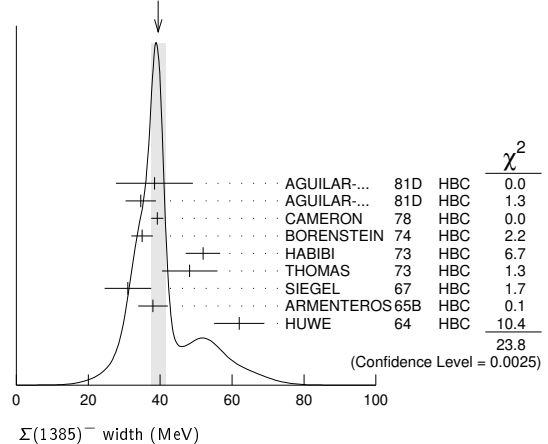
••• We do not use the following data for averages, fits, limits, etc. •••

Table with columns: Value, EVTS, Document ID, TECN, Comment. Lists various experimental data points for Σ(1385)0 width.

••• We do not use the following data for averages, fits, limits, etc. •••

Table with columns: Value, CL%, Document ID, TECN, Comment. Lists various experimental data points for Σ(1385)0 width.

WEIGHTED AVERAGE 39.4±2.1 (Error scaled by 1.7)



Baryon Particle Listings

$\Sigma(1385), \Sigma(1580)$

$\Sigma(1385)$ DECAY MODES

Mode	Fraction (Γ_i/Γ)	Confidence level
$\Gamma_1 \Lambda\pi$	(87.0 \pm 1.5) %	
$\Gamma_2 \Sigma\pi$	(11.7 \pm 1.5) %	
$\Gamma_3 \Lambda\gamma$	(1.25 $^{+0.13}_{-0.12}$) %	
$\Gamma_4 \Sigma^+\gamma$	(7.0 \pm 1.7) $\times 10^{-3}$	
$\Gamma_5 \Sigma^-\gamma$	< 2.4 $\times 10^{-4}$	90%
$\Gamma_6 N\bar{K}$		

$\Sigma(1385)$ BRANCHING RATIOS

$\Gamma(\Sigma\pi)/\Gamma(\Lambda\pi)$	DOCUMENT ID	TECN	CHG	COMMENT	Γ_2/Γ_1
0.135 \pm 0.011 OUR AVERAGE					
0.20 \pm 0.06	DIONISI	78B	HBC	\pm $K^-p \rightarrow Y^*K\bar{K}$	
0.16 \pm 0.03	BERTHON	74	HBC	$+$ K^-p 1.26–1.84 GeV/c	
0.11 \pm 0.02	BERTHON	74	HBC	$-$ K^-p 1.26–1.84 GeV/c	
0.21 \pm 0.05	BORENSTEIN	74	HBC	$+$ $K^-p \rightarrow \Lambda\pi^+\pi^-$, $\Sigma^0\pi^+\pi^-$	
0.18 \pm 0.04	MAST	73	MPWA	\pm $K^-p \rightarrow \Lambda\pi^+\pi^-$, $\Sigma^0\pi^+\pi^-$	
0.10 \pm 0.05	THOMAS	73	HBC	$-$ $\pi^-p \rightarrow \Lambda K\pi, \Sigma K\pi$	
0.16 \pm 0.07	AGUILAR...	72B	HBC	$+$ K^-p 3.9, 4.6 GeV/c	
0.13 \pm 0.04	COLLEY	71B	DBC	-0 K^-N 1.5 GeV/c	
0.13 \pm 0.04	PAN	69	HBC	$+$ $\pi^+p \rightarrow \Lambda K\pi, \Sigma K\pi$	
0.08 \pm 0.06	LONDON	66	HBC	$+$ K^-p 2.24 GeV/c	
0.163 \pm 0.041	ARMENTEROS65B	HBC	\pm K^-p 0.95–1.20 GeV/c		
0.09 \pm 0.04	HUWE	64	HBC	\pm K^-p 1.2–1.7 GeV	
••• We do not use the following data for averages, fits, limits, etc. •••					
<0.04	ALSTON	62	HBC	± 0 K^-p 1.15 GeV/c	
0.04 \pm 0.04	BASTIEN	61	HBC	\pm	

$\Gamma(\Lambda\gamma)/\Gamma(\Lambda\pi)$	EVTS	DOCUMENT ID	TECN	COMMENT	Γ_3/Γ_1
This ratio is of course for $\Sigma(1385)^0 \rightarrow \Lambda\gamma$ and $\Lambda\pi^0$.					
1.43$^{+0.15}_{-0.13}$ OUR AVERAGE					
1.42 \pm 0.12 $^{+0.11}_{-0.07}$	624 \pm 25	KELLER	11	CLAS $\gamma p \rightarrow K^+\Lambda\gamma, E_\gamma$ 1.6–3.8 GeV	
1.53 \pm 0.39 $^{+0.15}_{-0.24}$	61	TAYLOR	05	CLAS $\gamma p \rightarrow K^+\Lambda\gamma$	

$\Gamma(\Sigma^+\gamma)/\Gamma(\Sigma\pi)$	DOCUMENT ID	TECN	COMMENT	Γ_4/Γ_2
This ratio is for $\Sigma(1385)^+ \rightarrow \Sigma^+\gamma$ over $\Sigma(1385)^+ \rightarrow \Sigma\pi$.				
5.98 \pm 1.11 $^{+0.27}_{-0.61}$				
	11	KELLER	12	CLAS $\gamma p \rightarrow K^0\Sigma(1385)^+$

$\Gamma(\Sigma^-\gamma)/\Gamma_{total}$	CL%	DOCUMENT ID	TECN	CHG	COMMENT	Γ_5/Γ
<2.4 $\times 10^{-4}$	90	12	MOLCHANOV	04	SELX $-$ $\Sigma^-Pb \rightarrow \Sigma(1385)^-Pb, 600$ GeV	
••• We do not use the following data for averages, fits, limits, etc. •••						
<6.1 $\times 10^{-4}$	90	13	ARIK	77	SPEC $-$ $\Sigma^-Pb \rightarrow \Sigma(1385)^-Pb, 23$ GeV	

$(\Gamma_i/\Gamma_i)^{1/2}/\Gamma_{total}$ in $N\bar{K} \rightarrow \Sigma(1385) \rightarrow \Lambda\pi$	DOCUMENT ID	CHG	COMMENT	$(\Gamma_6/\Gamma_1)^{1/2}/\Gamma$	
+0.586 \pm 0.319	14	DEVENISH	74B	0	Fixed-t dispersion rel.

$\Sigma(1385)$ FOOTNOTES

- From fit to inclusive $\Lambda\pi$ spectrum.
- Includes data of HOLMGREN 77.
- The errors are statistical only. The resolution is not unfolded.
- The error is enlarged to Γ/\sqrt{N} . See the note on the $K^*(892)$ mass in the 1984 edition.
- From a fit to $\Lambda\pi^0$ with the width fixed at 34 MeV.
- From fit to inclusive $\Lambda\pi^0$ spectrum with the width fixed at 40 MeV.
- Redundant with data in the mass Listings.
- Results from $\Lambda\pi^+\pi^-$ and $\Lambda\pi^+\pi^-\pi^0$ combined by us.
- The error is enlarged to $4\Gamma/\sqrt{N}$. See the note on the $K^*(892)$ mass in the 1984 edition.
- Consistent with +, 0, and - widths equal.
- KELLER 12 gives $\Gamma(\Sigma^+\gamma)/\Gamma(\Sigma^+\pi^0) = (11.95 \pm 2.21 \pm 1.21)\%$, using 1/2 our total $\Sigma(1385) \rightarrow \Sigma\pi$ fraction for $\Sigma^+\pi^0$. We divide the KELLER 12 value by two.
- We calculate this from the MOLCHANOV 04 upper limit of 9.5 keV on the $\Sigma^-\gamma$ width.
- We calculate this from the ARIK 77 upper limit of 24 keV on the $\Sigma^-\gamma$ width.
- An extrapolation of the parametrized amplitude below threshold.

$\Sigma(1385)$ REFERENCES

AGAKISHIEV	12	PR C05 035203	G. Agakishiev et al.	(HADES Collab.)
KELLER	12	PR D85 052004	D. Keller et al.	(JLab CLAS Collab.)
KELLER	11	PR D83 072004	D. Keller et al.	(JLab CLAS Collab.)
TAYLOR	05	PR C71 054609	S. Taylor et al.	(JLab CLAS Collab.)
		Also	PR C72 039902 (errat.)	(JLab CLAS Collab.)
MOLCHANOV	04	PL B590 161	V.V. Molchanov et al.	(FNAL SELEX Collab.)
BAUBILLIER	84	ZPHY C23 213	M. Baubillier et al.	(BIRM, CERN, GLAS+)
PDG	84	RMP 56 51	C.G. Wohl et al.	(LBL, CIT, CERN)
AGUILAR...	81D	AFIS A77 144	M. Aguilar-Benitez, J. Salicio	(MADR)
BAKER	80	NP B166 207	P.A. Baker et al.	(LOIC)
BAUBILLIER	79B	NP B148 18	M. Baubillier et al.	(BIRM, CERN, GLAS+)
CAUTIS	79	NP B156 507	C.V. Cautis et al.	(SLAC)
SUGAHARA	79B	NP B156 237	R. Sugahara et al.	(KEK, OSKC, KINK)
CAMERON	78	NP B143 189	W. Cameron et al.	(RHEL LOIC)
DIONISI	78B	PL 78B 154	C. Dionisi, R. Armenteros, J. Diaz	(CERN, AMST+)
ARIK	77	PRL 38 1000	E. Arik et al.	(PITT, BNL, MASA)
BARREIRO	77B	NP B126 319	F. Barreiro et al.	(CERN, AMST, NIJ)
HOLMGREN	77	NP B119 261	S.O. Holmgren et al.	(CERN, AMST, NIJ)
BARDADIN...	75	NP B98 418	M. Bardadin-Otwinowska et al.	(SACL, EPOL+)
BERTHON	74	NC 21A 146	A. Berthon et al.	(CDEF, RHEL, SACL+)
BORENSTEIN	74	PR D9 3006	S.R. Borenstein et al.	(BNL, MICH)
DEVENISH	74B	NP B81 330	R.C.E. Devenish, C.D. Froggatt, B.R. Martin	(DES+)
LICHTENBERG	74	PR D10 3865	D.B. Lichtenberg	(IND)
		Also	Private Comm.	(IND)
HABIBI	73	Thesis Univ 199	M. Habibi	(COLU)
		Also	Purdue Conf. 387	(COLU, BING)
MAST	73	PR D7 3212	T.S. Mast et al.	(LBL) IJP
		Also	PR D7 5	(LBL) IJP
THOMAS	73	NP B56 15	D.W. Thomas et al.	(CMU) JIP
AGUILAR...	72B	PR D6 29	M. Aguilar-Benitez et al.	(BNL)
COLLEY	71B	NP B31 61	D.C. Colley et al.	(BIRM, EDIN, GLAS+)
AGUILAR...	70B	PRL 25 58	M. Aguilar-Benitez et al.	(BNL, SYRA)
PAN	69	PRL 23 808	Y.L. Pan, F.L. Forman	(PENN) I
SIEGEL	67	Thesis UCRL 18041	D.M. Siegel	(LRL)
BIRMINGHAM	66	PR 152 1148	M. Haque et al.	(BIRM, GLAS, LOIC, OXF+)
LONDON	66	PR 143 1034	G.W. London et al.	(BNL, SYRA) J
ARMENTEROS	65B	PL 19 75	R. Armenteros et al.	(CERN, HEID, SACL)
SMITH	65	Thesis UCLA	L.T. Smith	(UCLA)
COOPER	64	PL 8 365	W.A. Cooper et al.	(CERN, AMST)
HUWE	64	Thesis UCRL 11291	D.O. Huwe	(LRL) JIP
		Also	PR 181 1824	(LRL) J
CURTIS	63	PR 132 1771	L.J. Curtis et al.	(MICH) J
ALSTON	62	CERN Conf. 311	M.H. Alston et al.	(LRL)
BASTIEN	61	PRL 6 702	P.L. Bastien, M. Ferro-Luzzi, A.H. Rosenfeld	(LRL)
DAHL	61	PRL 6 142	O.H. Dahl et al.	(LRL)
ELY	61	PRL 7 461	R.P. Ely et al.	(LRL) J
ALSTON	60	PRL 5 520	M.H. Alston et al.	(LRL) I

$\Sigma(1580) 3/2^-$

$$I(J^P) = 1(\frac{3}{2}^-) \text{ Status: } *$$

OMITTED FROM SUMMARY TABLE

Seen in the isospin-1 $\bar{K}N$ cross section at BNL (LI 73, CARROLL 76) and in a partial-wave analysis of $K^-p \rightarrow \Lambda\pi^0$ for c.m. energies 1560–1600 MeV by LITCHFIELD 74. LITCHFIELD 74 finds $J^P = 3/2^-$. Not seen by ENGLER 78, CAMERON 78C, OLMSTED 04, nor by PRAKHOV 04.

Neither ZHANG 13A nor SARANTSEV 19 see any evidence for this state.

$\Sigma(1580)$ POLE POSITION

REAL PART

VALUE (MeV)	DOCUMENT ID	TECN	COMMENT
••• We do not use the following data for averages, fits, limits, etc. •••			
1607 $^{+13}_{-11}$	1	KAMANO	15 DPWA Multichannel
1 From the preferred solution A in KAMANO 15. Solution B reports $M = 1492^{+4}_{-7}$ MeV.			

-2xIMAGINARY PART

VALUE (MeV)	DOCUMENT ID	TECN	COMMENT
••• We do not use the following data for averages, fits, limits, etc. •••			
253 $^{+30}_{-18}$	2	KAMANO	15 DPWA Multichannel
2 From the preferred solution A in KAMANO 15. Solution B reports $M = 138^{+8}_{-14}$ MeV.			

$\Sigma(1580)$ POLE RESIDUES

The “normalized residue” is the residue divided by $\Gamma_{pole}/2$.

Normalized residue in $N\bar{K} \rightarrow \Sigma(1580) \rightarrow N\bar{K}$

MODULUS	PHASE ($^\circ$)	DOCUMENT ID	TECN	COMMENT
••• We do not use the following data for averages, fits, limits, etc. •••				
0.00778	51	3	KAMANO	15 DPWA Multichannel
3 From the preferred solution A in KAMANO 15.				

Normalized residue in $N\bar{K} \rightarrow \Sigma(1580) \rightarrow \Sigma\pi$

MODULUS	PHASE ($^\circ$)	DOCUMENT ID	TECN	COMMENT
••• We do not use the following data for averages, fits, limits, etc. •••				
0.0625	-6	4	KAMANO	15 DPWA Multichannel
4 From the preferred solution A in KAMANO 15.				

Baryon Particle Listings
 $\Sigma(1580)$, $\Sigma(1620)$

Normalized residue in $N\bar{K} \rightarrow \Sigma(1580) \rightarrow \Lambda\pi$

MODULUS	PHASE (°)	DOCUMENT ID	TECN	COMMENT
0.059	156	⁵ KAMANO	15	DPWA Multichannel

⁵ From the preferred solution A in KAMANO 15.

Normalized residue in $N\bar{K} \rightarrow \Sigma(1580) \rightarrow \Sigma(1385)\pi$, S-wave

MODULUS	PHASE (°)	DOCUMENT ID	TECN	COMMENT
0.0368	-18	⁶ KAMANO	15	DPWA Multichannel

⁶ From the preferred solution A in KAMANO 15.

Normalized residue in $N\bar{K} \rightarrow \Sigma(1580) \rightarrow \Sigma(1385)\pi$, D-wave

MODULUS	PHASE (°)	DOCUMENT ID	TECN	COMMENT
0.0103	123	⁷ KAMANO	15	DPWA Multichannel

⁷ From the preferred solution A in KAMANO 15.

$\Sigma(1580)$ MASS

VALUE (MeV)	DOCUMENT ID	TECN	COMMENT
≈ 1580 OUR ESTIMATE			
1583 ± 4	⁸ CARROLL	76	DPWA Isospin-1 total σ
1582 ± 4	⁹ LITCHFIELD	74	DPWA $K^-p \rightarrow \Lambda\pi^0$

⁸ CARROLL 76 sees a total-cross-section bump with $(J+1/2) \Gamma_{el} / \Gamma_{total} = 0.06$.
⁹ The main effect observed by LITCHFIELD 74 is in the $\Lambda\pi$ final state; the $\bar{K}N$ and $\Sigma\pi$ couplings are estimated from a multichannel fit including total-cross-section data of LI 73.

$\Sigma(1580)$ WIDTH

VALUE (MeV)	DOCUMENT ID	TECN	COMMENT
15	¹⁰ CARROLL	76	DPWA Isospin-1 total σ
11 ± 4	¹¹ LITCHFIELD	74	DPWA $K^-p \rightarrow \Lambda\pi^0$

¹⁰ CARROLL 76 sees a total-cross-section bump with $(J+1/2) \Gamma_{el} / \Gamma_{total} = 0.06$.
¹¹ The main effect observed by LITCHFIELD 74 is in the $\Lambda\pi$ final state; the $\bar{K}N$ and $\Sigma\pi$ couplings are estimated from a multichannel fit including total-cross-section data of LI 73.

$\Sigma(1580)$ DECAY MODES

Mode
Γ_1 $N\bar{K}$
Γ_2 $\Lambda\pi$
Γ_3 $\Sigma\pi$
Γ_4 $\Sigma(1385)\pi$, S-wave
Γ_5 $\Sigma(1385)\pi$, D-wave
Γ_6 $N\bar{K}^*(892)$, $S=1/2$, D-wave
Γ_7 $N\bar{K}^*(892)$, $S=3/2$, S-wave
Γ_8 $N\bar{K}^*(892)$, $S=3/2$, D-wave

$\Sigma(1580)$ BRANCHING RATIOS

See "Sign conventions for resonance couplings" in the Note on Λ and Σ Resonances.

$\Gamma(N\bar{K})/\Gamma_{total}$

VALUE	DOCUMENT ID	TECN	COMMENT
+0.03 ± 0.01	¹² LITCHFIELD	74	DPWA $\bar{K}N$ multichannel

0.003

¹² The main effect observed by LITCHFIELD 74 is in the $\Lambda\pi$ final state; the $\bar{K}N$ and $\Sigma\pi$ couplings are estimated from a multichannel fit including total-cross-section data of LI 73.
¹³ From the preferred solution A in KAMANO 15.

$\Gamma(\Lambda\pi)/\Gamma_{total}$

VALUE	DOCUMENT ID	TECN	COMMENT
0.490	¹⁴ KAMANO	15	DPWA Multichannel

¹⁴ From the preferred solution A in KAMANO 15.

$\Gamma(\Sigma\pi)/\Gamma_{total}$

VALUE	DOCUMENT ID	TECN	COMMENT
0.387	¹⁵ KAMANO	15	DPWA Multichannel

¹⁵ From the preferred solution A in KAMANO 15.

$\Gamma(\Sigma(1385)\pi, S\text{-wave})/\Gamma_{total}$

VALUE	DOCUMENT ID	TECN	COMMENT
0.12	¹⁶ KAMANO	15	DPWA Multichannel

¹⁶ From the preferred solution A in KAMANO 15.

$\Gamma(\Sigma(1385)\pi, D\text{-wave})/\Gamma_{total}$

VALUE	DOCUMENT ID	TECN	COMMENT
0.001	¹⁷ KAMANO	15	DPWA Multichannel

¹⁷ From the preferred solution A in KAMANO 15.

$\Gamma(N\bar{K}^*(892), S=1/2, D\text{-wave})/\Gamma_{total}$

VALUE	DOCUMENT ID	TECN	COMMENT
not seen	¹⁸ KAMANO	15	DPWA Multichannel

¹⁸ From the preferred solution A in KAMANO 15.

$\Gamma(N\bar{K}^*(892), S=3/2, S\text{-wave})/\Gamma_{total}$

VALUE	DOCUMENT ID	TECN	COMMENT
not seen	¹⁹ KAMANO	15	DPWA Multichannel

¹⁹ From the preferred solution A in KAMANO 15.

$\Gamma(N\bar{K}^*(892), S=3/2, D\text{-wave})/\Gamma_{total}$

VALUE	DOCUMENT ID	TECN	COMMENT
not seen	²⁰ KAMANO	15	DPWA Multichannel

²⁰ From the preferred solution A in KAMANO 15.

$(\Gamma_i \Gamma_f)^{1/2} / \Gamma_{total}$ in $N\bar{K} \rightarrow \Sigma(1580) \rightarrow \Lambda\pi$

VALUE	DOCUMENT ID	TECN	COMMENT
not seen	CAMERON	78c	HBC $K_L^0 p \rightarrow \Lambda\pi^+$
not seen	ENGLER	78	HBC $K_L^0 p \rightarrow \Lambda\pi^+$
+0.10 ± 0.02	²¹ LITCHFIELD	74	DPWA $K^-p \rightarrow \Lambda\pi^0$

²¹ The main effect observed by LITCHFIELD 74 is in the $\Lambda\pi$ final state; the $\bar{K}N$ and $\Sigma\pi$ couplings are estimated from a multichannel fit including total-cross-section data of LI 73.

$(\Gamma_i \Gamma_f)^{1/2} / \Gamma_{total}$ in $N\bar{K} \rightarrow \Sigma(1580) \rightarrow \Sigma\pi$

VALUE	DOCUMENT ID	TECN	COMMENT
not seen	CAMERON	78c	HBC $K_L^0 p \rightarrow \Sigma^0 \pi^+$
not seen	ENGLER	78	HBC $K_L^0 p \rightarrow \Sigma^0 \pi^+$
+0.03 ± 0.04	²² LITCHFIELD	74	DPWA $\bar{K}N$ multichannel

²² The main effect observed by LITCHFIELD 74 is in the $\Lambda\pi$ final state; the $\bar{K}N$ and $\Sigma\pi$ couplings are estimated from a multichannel fit including total-cross-section data of LI 73.

$\Sigma(1580)$ REFERENCES

SARANTSEV	19	EPJ A55 180	A.V. Sarantsev et al.	(BONN, PNPI)
KAMANO	15	PR C92 025205	H. Kamano et al.	(ANL, OSAK)
ZHANG	13A	PR C88 035205	H. Zhang et al.	(KSU)
OLMSTED	04	PL B588 29	J. Olmsted et al.	(BNL Crystal Ball Collab.)
PRAKHOV	04	PR C69 042202	S. Prakhov et al.	(BNL Crystal Ball Collab.)
CAMERON	78c	NP B132 189	W. Cameron et al.	(BGNA, EDIN, GLAS+I)
ENGLER	78	PR D18 3061	A. Engler et al.	(CMU, ANL)
CARROLL	76	PRL 37 306	A.S. Carroll et al.	(BNL I)
LITCHFIELD	74	PL 51B 509	P.J. Litchfield	(CERN IUP)
LI	73	Purdue Conf. 283	K.K. Li	(BNL I)

$\Sigma(1620) 1/2^-$

$I(J^P) = 1(\frac{1}{2}^-)$ Status: *

OMITTED FROM SUMMARY TABLE

The S_{11} state at 1697 MeV reported by VANHORN 75 is tentatively listed under the $\Sigma(1750)$. CARROLL 76 sees two bumps in the isospin-1 total cross section near this mass. GAO 12 sees no evidence for this resonance.

Production experiments are listed separately in the next entry.

$\Sigma(1620)$ POLE POSITION

REAL PART

VALUE (MeV)	DOCUMENT ID	TECN	COMMENT
1680 ± 8	SARANTSEV	19	DPWA $\bar{K}N$ multichannel

0.000

¹⁵⁰¹ ZHANG 13A DPWA $\bar{K}N$ multichannel

-2xIMAGINARY PART

VALUE (MeV)	DOCUMENT ID	TECN	COMMENT
39 ± 11	SARANTSEV	19	DPWA $\bar{K}N$ multichannel

0.000

¹⁷¹ ZHANG 13A DPWA $\bar{K}N$ multichannel

Baryon Particle Listings

$\Sigma(1620), \Sigma(1660)$

$\Sigma(1620)$ POLE RESIDUE

The "normalized residue" is the residue divided by $\Gamma_{pole}/2$.

Normalized residue in $N\bar{K} \rightarrow \Sigma(1620) \rightarrow \Sigma\pi$

MODULUS	PHASE (°)	DOCUMENT ID	TECN	COMMENT
0.14±0.03	-90 ± 25	SARANTSEV 19	DPWA	$\bar{K}N$ multichannel

Normalized residue in $N\bar{K} \rightarrow \Sigma(1620) \rightarrow \Lambda\pi$

MODULUS	PHASE (°)	DOCUMENT ID	TECN	COMMENT
0.10±0.03	75 ± 20	SARANTSEV 19	DPWA	$\bar{K}N$ multichannel

Normalized residue in $N\bar{K} \rightarrow \Sigma(1620) \rightarrow \Xi K$

MODULUS	PHASE (°)	DOCUMENT ID	TECN	COMMENT
0.02±0.01	120 ± 20	SARANTSEV 19	DPWA	$\bar{K}N$ multichannel

Normalized residue in $N\bar{K} \rightarrow \Sigma(1620) \rightarrow \Lambda(1520)\pi$

MODULUS	PHASE (°)	DOCUMENT ID	TECN	COMMENT
0.12±0.05	140 ± 40	SARANTSEV 19	DPWA	$\bar{K}N$ multichannel

Normalized residue in $N\bar{K} \rightarrow \Sigma(1620) \rightarrow \Sigma(1385)\pi$

MODULUS	PHASE (°)	DOCUMENT ID	TECN	COMMENT
0.015±0.010	155 ± 40	SARANTSEV 19	DPWA	$\bar{K}N$ multichannel

Normalized residue in $N\bar{K} \rightarrow \Sigma(1620) \rightarrow N\bar{K}^*(892), S\text{-wave}$

MODULUS	PHASE (°)	DOCUMENT ID	TECN	COMMENT
0.05±0.04		SARANTSEV 19	DPWA	$\bar{K}N$ multichannel

Normalized residue in $N\bar{K} \rightarrow \Sigma(1620) \rightarrow N\bar{K}^*(892), D\text{-wave}$

MODULUS	PHASE (°)	DOCUMENT ID	TECN	COMMENT
0.01±0.01		SARANTSEV 19	DPWA	$\bar{K}N$ multichannel

Normalized residue in $N\bar{K} \rightarrow \Sigma(1620) \rightarrow N\bar{K}$

VALUE	DOCUMENT ID	TECN	COMMENT
0.11+0.03@43+-20	SARANTSEV 19	DPWA	$\bar{K}N$ multichannel

$\Sigma(1620)$ MASS

VALUE (MeV)	DOCUMENT ID	TECN	COMMENT
1600 to 1650 (≈ 1620) OUR ESTIMATE			
1681 ± 6	SARANTSEV 19	DPWA	$\bar{K}N$ multichannel
1600 ± 15	ZHANG 13A	DPWA	$\bar{K}N$ multichannel
1600 ± 6	¹ MORRIS 78	DPWA	$K^-n \rightarrow \Lambda\pi^-$
1608 ± 5	² CARROLL 76	DPWA	Isospin-1 total σ
1630 ± 10	LANGBEIN 72	IPWA	$\bar{K}N$ multichannel
1620	KIM 71	DPWA	K-matrix analysis
••• We do not use the following data for averages, fits, limits, etc. •••			
1633 ± 10	³ CARROLL 76	DPWA	Isospin-1 total σ

$\Sigma(1620)$ WIDTH

VALUE (MeV)	DOCUMENT ID	TECN	COMMENT
40 to 100 (≈ 70) OUR ESTIMATE			
40 ± 12	SARANTSEV 19	DPWA	$\bar{K}N$ multichannel
400±152	ZHANG 13A	DPWA	$\bar{K}N$ multichannel
87 ± 19	¹ MORRIS 78	DPWA	$K^-n \rightarrow \Lambda\pi^-$
15	² CARROLL 76	DPWA	Isospin-1 total σ
65 ± 20	LANGBEIN 72	IPWA	$\bar{K}N$ multichannel
40	KIM 71	DPWA	K-matrix analysis
••• We do not use the following data for averages, fits, limits, etc. •••			
10	³ CARROLL 76	DPWA	Isospin-1 total σ

$\Sigma(1620)$ DECAY MODES

Mode	Fraction (Γ_i/Γ)
Γ_1 $N\bar{K}$	0.10 to 0.60
Γ_2 $\Lambda\pi$	(9.0 ± 3.0) %
Γ_3 $\Sigma\pi$	(17 ± 5) %
Γ_4 ΞK	
Γ_5 $\Lambda(1520)\pi$	(10 ± 5) %
Γ_6 $\Sigma(1385)\pi$	

$\Sigma(1620)$ BRANCHING RATIOS

$\Gamma(N\bar{K})/\Gamma_{total}$	DOCUMENT ID	TECN	COMMENT	Γ_1/Γ
0.10 to 0.60 OUR ESTIMATE				
0.11±0.03	SARANTSEV 19	DPWA	$\bar{K}N$ multichannel	
0.59±0.10	ZHANG 13A	DPWA	$\bar{K}N$ multichannel	
0.22±0.02	LANGBEIN 72	IPWA	$\bar{K}N$ multichannel	
0.05	KIM 71	DPWA	K-matrix analysis	

$\Gamma(\Sigma\pi)/\Gamma_{total}$

VALUE	DOCUMENT ID	TECN	COMMENT	Γ_3/Γ
0.17±0.05	SARANTSEV 19	DPWA	$\bar{K}N$ multichannel	

$\Gamma(\Lambda\pi)/\Gamma_{total}$

VALUE	DOCUMENT ID	TECN	COMMENT	Γ_2/Γ
0.09±0.03	SARANTSEV 19	DPWA	$\bar{K}N$ multichannel	

$\Gamma(\Xi K)/\Gamma_{total}$

VALUE	DOCUMENT ID	TECN	COMMENT	Γ_4/Γ
~ 0	SARANTSEV 19	DPWA	$\bar{K}N$ multichannel	

$\Gamma(\Lambda(1520)\pi)/\Gamma_{total}$

VALUE	DOCUMENT ID	TECN	COMMENT	Γ_5/Γ
0.10±0.05	SARANTSEV 19	DPWA	$\bar{K}N$ multichannel	

$\Gamma(\Sigma(1385)\pi)/\Gamma_{total}$

VALUE	DOCUMENT ID	TECN	COMMENT	Γ_6/Γ
<0.01	SARANTSEV 19	DPWA	$\bar{K}N$ multichannel	

$(\Gamma_1\Gamma_2)^{1/2}/\Gamma_{total}$ in $N\bar{K} \rightarrow \Sigma(1620) \rightarrow \Lambda\pi$

VALUE	DOCUMENT ID	TECN	COMMENT	$(\Gamma_1\Gamma_2)^{1/2}/\Gamma$
0.12±0.02	¹ MORRIS 78	DPWA	$K^-n \rightarrow \Lambda\pi^-$	
not seen	BAILLON 75	IPWA	$\bar{K}N \rightarrow \Lambda\pi$	
0.15	KIM 71	DPWA	K-matrix analysis	

$(\Gamma_1\Gamma_3)^{1/2}/\Gamma_{total}$ in $N\bar{K} \rightarrow \Sigma(1620) \rightarrow \Sigma\pi$

VALUE	DOCUMENT ID	TECN	COMMENT	$(\Gamma_1\Gamma_3)^{1/2}/\Gamma$
+0.32±0.03	ZHANG 13A	DPWA	Multichannel	
not seen	HEPP 76B	DPWA	$K^-N \rightarrow \Sigma\pi$	
+0.40±0.06	LANGBEIN 72	IPWA	$\bar{K}N$ multichannel	
+0.08	KIM 71	DPWA	K-matrix analysis	

$\Sigma(1620)$ FOOTNOTES

- ¹MORRIS 78 obtains an equally good fit without including this resonance.
- Total cross-section bump with $(J+1/2) \Gamma_{el} / \Gamma_{total}$ is 0.06 seen by CARROLL 76.
- Total cross-section bump with $(J+1/2) \Gamma_{el} / \Gamma_{total}$ is 0.04 seen by CARROLL 76.

$\Sigma(1620)$ REFERENCES

SARANTSEV 19	EPJ A55 180	A.V. Sarantsev et al.	(BONN, PNPI)
ZHANG 13A	PR C88 035205	H. Zhang et al.	(KSU)
GAO 12	PR C86 025201	P. Gao, J. Shi, B.S. Zou	(BHEP, BEIJT)
	Also NP A567 41	P. Gao, B.S. Zou, A. Sibirtsev	(BHEP, BEIJT+)
MORRIS 78	PR D17 55	W.A. Morris et al.	(FSU) IJP
CARROLL 76	PRL 37 806	A.S. Carroll et al.	(BNL) I
HEPP 76B	PL 65B 487	V. Hepp et al.	(CERN, HEIDH, MPIM) IJP
BAILLON 75	NP B94 39	P.H. Baillon, P.J. Litchfield	(CERN, RHEL) IJP
VANHORN 75	NP B87 145	A.J. van Horn	(LBL) IJP
	Also NP B87 157	A.J. van Horn	(LBL) IJP
LANGBEIN 72	NP B47 477	W. Langbein, F. Wagner	(MPIM) IJP
KIM 71	PRL 27 356	J.K. Kim	(HARV) IJP
	Also Duke Conf. 161	J.K. Kim	(HARV) IJP
	Hyperon Resonances, 1970		

$$\Sigma(1660) 1/2^+$$

$$I(J^P) = 1(\frac{1}{2}^+) \text{ Status: } ***$$

For results published before 1974 (they are now obsolete), see our 1982 edition Physics Letters **111B** 1 (1982).

$\Sigma(1660)$ POLE POSITION

REAL PART

VALUE (MeV)	DOCUMENT ID	TECN	COMMENT
1585 ± 20	SARANTSEV 19	DPWA	$\bar{K}N$ multichannel

••• We do not use the following data for averages, fits, limits, etc. •••

1547 ⁺¹¹¹ ₋₅₉	¹ KAMANO 15	DPWA	$\bar{K}N$ multichannel
¹ From the preferred solution A in KAMANO 15. Solution B reports $M = 1457 \pm 5$ MeV.			

-2xIMAGINARY PART

VALUE (MeV)	DOCUMENT ID	TECN	COMMENT
290 ⁺¹⁴⁰ ₋₄₀	SARANTSEV 19	DPWA	$\bar{K}N$ multichannel

••• We do not use the following data for averages, fits, limits, etc. •••

183 ⁺⁸⁶ ₋₇₈	¹ KAMANO 15	DPWA	$\bar{K}N$ multichannel
¹ From the preferred solution A in KAMANO 15. Solution B reports $\Gamma = 78 \pm 2$ MeV.			

$\Sigma(1660)$ POLE RESIDUES

The normalized residue is the residue divided by $\Gamma_{pole}/2$.

Normalized residue in $N\bar{K} \rightarrow \Sigma(1660) \rightarrow N\bar{K}$

MODULUS	PHASE (°)	DOCUMENT ID	TECN	COMMENT
0.07 ± 0.03	-165 ± 35	SARANTSEV 19	DPWA	$\bar{K}N$ multichannel
••• We do not use the following data for averages, fits, limits, etc. •••				
0.0247	168	¹ KAMANO 15	DPWA	$\bar{K}N$ multichannel
¹ From the preferred solution A in KAMANO 15.				

Normalized residue in $N\bar{K} \rightarrow \Sigma(1660) \rightarrow \Sigma\pi$

MODULUS	PHASE (°)	DOCUMENT ID	TECN	COMMENT
0.17 ± 0.04	150 ± 20	SARANTSEV 19	DPWA	$\bar{K}N$ multichannel
••• We do not use the following data for averages, fits, limits, etc. •••				
0.16	78	¹ KAMANO 15	DPWA	$\bar{K}N$ multichannel
¹ From the preferred solution A in KAMANO 15.				

Normalized residue in $N\bar{K} \rightarrow \Sigma(1660) \rightarrow \Lambda\pi$

MODULUS	PHASE (°)	DOCUMENT ID	TECN	COMMENT
0.16 ± 0.05	0 ± 25	SARANTSEV 19	DPWA	$\bar{K}N$ multichannel
••• We do not use the following data for averages, fits, limits, etc. •••				
0.0614	-84	¹ KAMANO 15	DPWA	$\bar{K}N$ multichannel
¹ From the preferred solution A in KAMANO 15.				

Normalized residue in $N\bar{K} \rightarrow \Sigma(1660) \rightarrow \Sigma\sigma$

MODULUS	PHASE (°)	DOCUMENT ID	TECN	COMMENT
0.14 ± 0.06	-150 ± 30	SARANTSEV 19	DPWA	$\bar{K}N$ multichannel

Normalized residue in $N\bar{K} \rightarrow \Sigma(1660) \rightarrow \Sigma(1385)\pi$

MODULUS	PHASE (°)	DOCUMENT ID	TECN	COMMENT
0.0513	-44	¹ KAMANO 15	DPWA	Multichannel
¹ From the preferred solution A in KAMANO 15.				

Normalized residue in $N\bar{K} \rightarrow \Sigma(1660) \rightarrow \Lambda(1405)\pi$

MODULUS	PHASE (°)	DOCUMENT ID	TECN	COMMENT
0.06 ± 0.03	-90 ± 25	SARANTSEV 19	DPWA	$\bar{K}N$ multichannel

Normalized residue in $N\bar{K} \rightarrow \Sigma(1660) \rightarrow \Lambda(1520)\pi$

MODULUS	PHASE (°)	DOCUMENT ID	TECN	COMMENT
0.04 ± 0.02	5 ± 20	SARANTSEV 19	DPWA	$\bar{K}N$ multichannel

$\Sigma(1660)$ MASS

VALUE (MeV)	DOCUMENT ID	TECN	COMMENT
1640 to 1680 (≈ 1660) OUR ESTIMATE			
1665 ± 20	SARANTSEV 19	DPWA	$\bar{K}N$ multichannel
1633 ± 3	GAO 12	DPWA	$\bar{K}N \rightarrow \Lambda\pi$
1665.1 ± 11.2	¹ KOISO 85	DPWA	$K^-p \rightarrow \Sigma\pi$
1670 ± 10	GOPAL 80	DPWA	$\bar{K}N \rightarrow \bar{K}N$
1679 ± 10	ALSTON-... 78	DPWA	$\bar{K}N \rightarrow \bar{K}N$
1668 ± 25	VANHORN 75	DPWA	$K^-p \rightarrow \Lambda\pi^0$
1670 ± 20	KANE 74	DPWA	$K^-p \rightarrow \Sigma\pi$
••• We do not use the following data for averages, fits, limits, etc. •••			
1676 ± 15	GOPAL 77	DPWA	$\bar{K}N$ multichannel
1565 or 1597	² MARTIN 77	DPWA	$\bar{K}N$ multichannel
1660 ± 30	³ BAILLON 75	IPWA	$\bar{K}N \rightarrow \Lambda\pi$
1671 ± 2	⁴ PONTE 75	DPWA	$K^-p \rightarrow \Lambda\pi^0$

¹The evidence of KOISO 85 is weak.
²The two MARTIN 77 values are from a T-matrix pole and from a Breit-Wigner fit.
³From solution 1 of BAILLON 75; not present in solution 2.
⁴From solution 2 of PONTE 75; not present in solution 1.

$\Sigma(1660)$ WIDTH

VALUE (MeV)	DOCUMENT ID	TECN	COMMENT
100 to 300 (≈ 200) OUR ESTIMATE			
300 +140 -40	SARANTSEV 19	DPWA	$\bar{K}N$ multichannel
121 + 4 - 7	GAO 12	DPWA	$\bar{K}N \rightarrow \Lambda\pi$
81.5 ± 22.2	¹ KOISO 85	DPWA	$K^-p \rightarrow \Sigma\pi$
152 ± 20	GOPAL 80	DPWA	$\bar{K}N \rightarrow \bar{K}N$
38 ± 10	ALSTON-... 78	DPWA	$\bar{K}N \rightarrow \bar{K}N$
230 +165 - 60	VANHORN 75	DPWA	$K^-p \rightarrow \Lambda\pi^0$
250 ± 110	KANE 74	DPWA	$K^-p \rightarrow \Sigma\pi$
••• We do not use the following data for averages, fits, limits, etc. •••			
120 ± 20	GOPAL 77	DPWA	$\bar{K}N$ multichannel
202 or 217	² MARTIN 77	DPWA	$\bar{K}N$ multichannel
80 ± 40	³ BAILLON 75	IPWA	$\bar{K}N \rightarrow \Lambda\pi$
81 ± 10	⁴ PONTE 75	DPWA	$K^-p \rightarrow \Lambda\pi^0$

¹The evidence of KOISO 85 is weak.
²The two MARTIN 77 values are from a T-matrix pole and from a Breit-Wigner fit.
³From solution 1 of BAILLON 75; not present in solution 2.
⁴From solution 2 of PONTE 75; not present in solution 1.

$\Sigma(1660)$ DECAY MODES

Mode	Fraction (Γ_i/Γ)
Γ_1 $N\bar{K}$	0.05 to 0.15 (≈ 010)
Γ_2 $\Lambda\pi$	(35 ± 12) %
Γ_3 $\Sigma\pi$	(37 ± 10) %
Γ_4 $\Sigma\sigma$	(20 ± 8) %
Γ_5 $\Sigma(1385)\pi$	
Γ_6 $\Lambda(1405)\pi$	(4.0 ± 2.0) %
Γ_7 $\Lambda(1520)\pi$	

$\Sigma(1660)$ BRANCHING RATIOS

See "Sign conventions for resonance couplings" in the Note on Λ and Σ Resonances.

$\Gamma(N\bar{K})/\Gamma_{total}$ Γ_1/Γ

VALUE	DOCUMENT ID	TECN	COMMENT
0.05 to 0.15 (≈ 010) OUR ESTIMATE			
0.07 ± 0.03	SARANTSEV 19	DPWA	$\bar{K}N$ multichannel
0.12 ± 0.03	GOPAL 80	DPWA	$\bar{K}N \rightarrow \bar{K}N$
0.10 ± 0.05	ALSTON-... 78	DPWA	$\bar{K}N \rightarrow \bar{K}N$
••• We do not use the following data for averages, fits, limits, etc. •••			
0.005	¹ KAMANO 15	DPWA	$\bar{K}N$ multichannel
<0.04	GOPAL 77	DPWA	See GOPAL 80
0.27 or 0.29	² MARTIN 77	DPWA	$\bar{K}N$ multichannel
¹ From the preferred solution A in KAMANO 15. ² The two MARTIN 77 values are from a T-matrix pole and from a Breit-Wigner fit.			

$\Gamma(\Lambda\pi)/\Gamma_{total}$ Γ_2/Γ

VALUE	DOCUMENT ID	TECN	COMMENT
0.35 ± 0.12	SARANTSEV 19	DPWA	$\bar{K}N$ multichannel
••• We do not use the following data for averages, fits, limits, etc. •••			
0.128	¹ KAMANO 15	DPWA	$\bar{K}N$ multichannel
¹ From the preferred solution A in KAMANO 15.			

$\Gamma(\Sigma\pi)/\Gamma_{total}$ Γ_3/Γ

VALUE	DOCUMENT ID	TECN	COMMENT
0.37 ± 0.10	SARANTSEV 19	DPWA	$\bar{K}N$ multichannel
••• We do not use the following data for averages, fits, limits, etc. •••			
0.865	¹ KAMANO 15	DPWA	$\bar{K}N$ multichannel
¹ From the preferred solution A in KAMANO 15.			

$\Gamma(\Sigma\sigma)/\Gamma_{total}$ Γ_4/Γ

VALUE	DOCUMENT ID	TECN	COMMENT
0.20 ± 0.08	SARANTSEV 19	DPWA	$\bar{K}N$ multichannel

$\Gamma(\Sigma(1385)\pi)/\Gamma_{total}$ Γ_5/Γ

VALUE	DOCUMENT ID	TECN	COMMENT
0.001	¹ KAMANO 15	DPWA	Multichannel
¹ From the preferred solution A in KAMANO 15.			

$\Gamma(\Lambda(1405)\pi)/\Gamma_{total}$ Γ_6/Γ

VALUE	DOCUMENT ID	TECN	COMMENT
0.04 ± 0.02	SARANTSEV 19	DPWA	$\bar{K}N$ multichannel

$\Gamma(\Lambda(1520)\pi)/\Gamma_{total}$ Γ_7/Γ

VALUE	DOCUMENT ID	TECN	COMMENT
<0.01	SARANTSEV 19	DPWA	$\bar{K}N$ multichannel

$(\Gamma_1\Gamma_7)^{1/2}/\Gamma_{total}$ in $N\bar{K} \rightarrow \Sigma(1660) \rightarrow \Lambda\pi$ $(\Gamma_1\Gamma_2)^{1/2}/\Gamma$

VALUE	DOCUMENT ID	TECN	COMMENT
-0.064 + 0.005 - 0.003	GAO 12	DPWA	$\bar{K}N \rightarrow \Lambda\pi$
< 0.04	GOPAL 77	DPWA	$\bar{K}N$ multichannel
0.12 + 0.12 - 0.04	VANHORN 75	DPWA	$K^-p \rightarrow \Lambda\pi^0$

••• We do not use the following data for averages, fits, limits, etc. •••
¹MARTIN 77 values are from a T-matrix pole and from a Breit-Wigner fit.
²BAILLON 75 values are from a T-matrix pole and from a Breit-Wigner fit.
³PONTE 75 values are from a T-matrix pole and from a Breit-Wigner fit.
⁴From solution 2 of PONTE 75; not present in solution 1.

$(\Gamma_1\Gamma_7)^{1/2}/\Gamma_{total}$ in $N\bar{K} \rightarrow \Sigma(1660) \rightarrow \Sigma\pi$ $(\Gamma_1\Gamma_3)^{1/2}/\Gamma$

VALUE	DOCUMENT ID	TECN	COMMENT
-0.13 ± 0.04	¹ KOISO 85	DPWA	$K^-p \rightarrow \Sigma\pi$
-0.16 ± 0.03	GOPAL 77	DPWA	$\bar{K}N$ multichannel
-0.11 ± 0.01	KANE 74	DPWA	$K^-p \rightarrow \Sigma\pi$

Baryon Particle Listings

 $\Sigma(1660)$, $\Sigma(1670)$, $\Sigma(1670)$

••• We do not use the following data for averages, fits, limits, etc. •••
 -0.34 or -0.37 ² MARTIN 77 DPWA $\bar{K}N$ multichannel
 not seen HEPP 76B DPWA $K^-N \rightarrow \Sigma\pi$

¹The evidence of KOISO 85 is weak.

²The two MARTIN 77 values are from a T-matrix pole and from a Breit-Wigner fit.

 $\Sigma(1660)$ REFERENCES

SARANTSEV	19	EPJ A55 180	A.V. Sarantsev <i>et al.</i>	(BONN, PNPI)
KAMANO	15	PR C92 025205	H. Kamano <i>et al.</i>	(ANL, OSAK)
GAO	12	PR C86 025201	P. Gao, J. Shi, B.S. Zou	(BHEP, BEIJT)
Also		NP A867 41	P. Gao, B.S. Zou, A. Sibirtsev	(BHEP, BEIJT+)
KOISO	85	NP A433 619	H. Koiso <i>et al.</i>	(TOKY, MASA)
PDG	82	PL 111B 1	M. Roos <i>et al.</i>	(HELSE, CIT, CERN)
GOPAL	80	Toronto Conf. 159	G.P. Gopal	(RHEL) IJP
ALSTON...	78	PR D38 182	M. Alston-Garnjost <i>et al.</i>	(LBL, MTHO+) IJP
Also		PRL 38 1007	M. Alston-Garnjost <i>et al.</i>	(LBL, MTHO+) IJP
GOPAL	77	NP B119 362	G.P. Gopal <i>et al.</i>	(LOIC, RHEL) IJP
MARTIN	77	NP B127 349	B.R. Martin, M.K. Piddcock, R.G. Moorhouse	(LOUC+) IJP
Also		NP B126 266	B.R. Martin, M.K. Piddcock	(LOUC) IJP
Also		NP B126 285	B.R. Martin, M.K. Piddcock	(LOUC) IJP
HEPP	76B	PL 65B 487	V. Hepp <i>et al.</i>	(CERN, HEIDH, MPIM) IJP
BAILLON	75	NP B94 39	P.H. Baillon, P.J. Litchfield	(CERN, RHEL) IJP
PONTE	75	PR D12 2597	R.A. Ponte <i>et al.</i>	(MASA, TENN, UCR) IJP
VANHORN	75	NP B87 145	A.J. van Horn	(LBL) IJP
Also		NP B87 157	A.J. van Horn	(LBL) IJP
KANE	74	LBL-2452	D.F. Kane	(LBL) IJP

THE $\Sigma(1670)$ REGION

Production experiments: The measured $\Sigma\pi/\Sigma\pi\pi$ branching ratio for the $\Sigma(1670)$ produced in the reaction $K^-p \rightarrow \pi^-\Sigma(1670)^+$ is strongly dependent on momentum transfer. This was first discovered by EBERHARD 69 [1], who suggested that there exist two Σ resonances with the same mass and quantum numbers: one with a large $\Sigma\pi\pi$ (mainly $\Lambda(1405)\pi$) branching fraction produced peripherally, and the other with a large $\Sigma\pi$ branching fraction produced at larger angles. The experimental results have been confirmed by AGUILAR-BENITEZ 70 [2], APSELL 74 [3], ESTES 74 [4], and TIMMERMANS 76 [5]. If, in fact, there are two resonances, the most likely quantum numbers for both the $\Sigma\pi$ and the $\Lambda(1405)\pi$ states are D_{13} . There is also possibly a third Σ in this region, the $\Sigma(1690)$ in the Listings, the main evidence for which is a large $\Lambda\pi/\Sigma\pi$ branching ratio. These topics have been reviewed by EBERHARD 73 [6] and by MILLER 70 [7].

Formation experiments: Two states are also observed near this mass in formation experiments. One of these, the $\Sigma(1670)D_{13}$, has the same quantum numbers as those observed in production and has a large $\Sigma\pi/\Sigma\pi\pi$ branching ratio; it may well be the $\Sigma(1670)$ produced at larger angles (see TIMMERMANS 76 [5]). The other state, the $\Sigma(1660)P_{11}$, has different quantum numbers, its $\Sigma\pi/\Sigma\pi\pi$ branching ratio is unknown, and its relation to the produced $\Sigma(1670)$ states is obscure.

References

1. P.H. Eberhard *et al.*, Phys. Rev. Lett. **22**, 200 (1969).
2. M. Aguilar-Benitez, *et al.*, Phys. Rev. Lett. **25**, 58 (1970).
3. S.P. Apsell, *et al.*, Phys. Rev. **D10**, 1419 (1974).
4. R.D. Estes, Thesis LBL-3827 (1974).
5. J.J.M. Timmermans, *et al.*, Nucl. Phys. **B112**, 77 (1976).
6. P.H. Eberhard, Purdue Conf. 247 (1973).
7. D.H. Miller, Duke Conf. 229 (1970).

 $\Sigma(1670) 3/2^-$

$$I(J^P) = 1(\frac{3}{2}^-) \text{ Status: } ***$$

For most results published before 1974 (they are now obsolete), see our 1982 edition Physics Letters **111B** 1 (1982).

Results from production experiments are listed separately in the next entry.

 $\Sigma(1670)$ POLE POSITION

REAL PART

VALUE (MeV)	DOCUMENT ID	TECN	COMMENT
1655 ± 1675 (≈ 1662) OUR ESTIMATE			
1661 ± 3	SARANTSEV 19	DPWA	$\bar{K}N$ multichannel
1669 \pm $\frac{7}{7}$	¹ KAMANO 15	DPWA	$\bar{K}N$ multichannel

••• We do not use the following data for averages, fits, limits, etc. •••

1674	ZHANG 13A	DPWA	$\bar{K}N$ multichannel
------	-----------	------	-------------------------

¹ From the preferred solution A in KAMANO 15.

-2xIMAGINARY PART

VALUE (MeV)	DOCUMENT ID	TECN	COMMENT
45 to 65 (≈ 55) OUR ESTIMATE			
52 ± 6	SARANTSEV 19	DPWA	$\bar{K}N$ multichannel
64 \pm $\frac{10}{14}$	¹ KAMANO 15	DPWA	$\bar{K}N$ multichannel

••• We do not use the following data for averages, fits, limits, etc. •••

54	ZHANG 13A	DPWA	$\bar{K}N$ multichannel
----	-----------	------	-------------------------

¹ From the preferred solution A in KAMANO 15.

 $\Sigma(1670)$ POLE RESIDUES

The normalized residue is the residue divided by $\Gamma_{pole}/2$.

Normalized residue in $N\bar{K} \rightarrow \Sigma(1670) \rightarrow N\bar{K}$

MODULUS	PHASE (°)	DOCUMENT ID	TECN	COMMENT
0.10 ± 0.02	-31 ± 12	SARANTSEV 19	DPWA	$\bar{K}N$ multichannel
0.129	-20	¹ KAMANO 15	DPWA	$\bar{K}N$ multichannel

¹ From the preferred solution A in KAMANO 15.

Normalized residue in $N\bar{K} \rightarrow \Sigma(1670) \rightarrow \Sigma\pi$

MODULUS	PHASE (°)	DOCUMENT ID	TECN	COMMENT
0.25 ± 0.05	-25 ± 10	SARANTSEV 19	DPWA	$\bar{K}N$ multichannel
0.249	-21	¹ KAMANO 15	DPWA	$\bar{K}N$ multichannel

¹ From the preferred solution A in KAMANO 15.

Normalized residue in $N\bar{K} \rightarrow \Sigma(1670) \rightarrow \Lambda\pi$

MODULUS	PHASE (°)	DOCUMENT ID	TECN	COMMENT
0.09 ± 0.03	-52 ± 12	SARANTSEV 19	DPWA	$\bar{K}N$ multichannel
0.0818	-7	¹ KAMANO 15	DPWA	$\bar{K}N$ multichannel

¹ From the preferred solution A in KAMANO 15.

Normalized residue in $N\bar{K} \rightarrow \Sigma(1670) \rightarrow \Xi K$

MODULUS	PHASE (°)	DOCUMENT ID	TECN	COMMENT
0.02 ± 0.01	160 ± 20	SARANTSEV 19	DPWA	$\bar{K}N$ multichannel

Normalized residue in $N\bar{K} \rightarrow \Sigma(1670) \rightarrow \Sigma\sigma$

MODULUS	PHASE (°)	DOCUMENT ID	TECN	COMMENT
0.08 ± 0.03	-25 ± 15	SARANTSEV 19	DPWA	$\bar{K}N$ multichannel

Normalized residue in $N\bar{K} \rightarrow \Sigma(1670) \rightarrow \Sigma(1385)\pi, S\text{-wave}$

MODULUS	PHASE (°)	DOCUMENT ID	TECN	COMMENT
0.228	167	¹ KAMANO 15	DPWA	$\bar{K}N$ multichannel

¹ From the preferred solution A in KAMANO 15.

Normalized residue in $N\bar{K} \rightarrow \Sigma(1670) \rightarrow \Sigma(1385)\pi, D\text{-wave}$

MODULUS	PHASE (°)	DOCUMENT ID	TECN	COMMENT
0.0915	141	KAMANO 15	DPWA	$\bar{K}N$ multichannel

Normalized residue in $N\bar{K} \rightarrow \Sigma(1670) \rightarrow \Lambda(1405)\pi$

MODULUS	PHASE (°)	DOCUMENT ID	TECN	COMMENT
0.03 ± 0.02	160 ± 15	SARANTSEV 19	DPWA	$\bar{K}N$ multichannel

Normalized residue in $N\bar{K} \rightarrow \Sigma(1670) \rightarrow \Lambda(1520)\pi, P\text{-wave}$

MODULUS	PHASE (°)	DOCUMENT ID	TECN	COMMENT
0.04 ± 0.02	120 ± 20	SARANTSEV 19	DPWA	$\bar{K}N$ multichannel

See key on page 999

Baryon Particle Listings

$\Sigma(1670)$

Normalized residue in $N\bar{K} \rightarrow \Sigma(1670) \rightarrow \Lambda(1520)\pi$, F-wave

MODULUS	PHASE (°)	DOCUMENT ID	TECN	COMMENT
0.01 ± 0.01		SARANTSEV 19	DPWA	$\bar{K}N$ multichannel

Normalized residue in $N\bar{K} \rightarrow \Sigma(1670) \rightarrow \Delta\bar{K}$, S-wave

MODULUS	PHASE (°)	DOCUMENT ID	TECN	COMMENT
0.01 ± 0.01		SARANTSEV 19	DPWA	$\bar{K}N$ multichannel

Normalized residue in $N\bar{K} \rightarrow \Sigma(1670) \rightarrow N\bar{K}^*(892)$, S=3/2, S-wave

VALUE	DOCUMENT ID	TECN	COMMENT
0.05 ± 0.03 @ 50 ± 60	SARANTSEV 19	DPWA	$\bar{K}N$ multichannel

Normalized residue in $N\bar{K} \rightarrow \Sigma(1670) \rightarrow N\bar{K}^*(892)$, S=3/2, D-wave

MODULUS	PHASE (°)	DOCUMENT ID	TECN	COMMENT
0.01 ± 0.01		SARANTSEV 19	DPWA	$\bar{K}N$ multichannel

Normalized residue in $N\bar{K} \rightarrow \Sigma(1670) \rightarrow N\bar{K}^*(892)$, S=1/2, D-wave

MODULUS	PHASE (°)	DOCUMENT ID	TECN	COMMENT
0.03 ± 0.02		SARANTSEV 19	DPWA	$\bar{K}N$ multichannel

$\Sigma(1670)$ MASS

VALUE (MeV)	DOCUMENT ID	TECN	COMMENT
1665 to 1685 (≈ 1675) OUR ESTIMATE			
1665 ± 3	SARANTSEV 19	DPWA	$\bar{K}N$ multichannel
1678 ± 2	ZHANG 13A	DPWA	$\bar{K}N$ multichannel
1673 ± 1	GAO 12	DPWA	$\bar{K}N \rightarrow \Lambda\pi$
1665.1 ± 4.1	KOISO 85	DPWA	$K^-p \rightarrow \Sigma\pi$
1682 ± 5	GOPAL 80	DPWA	$\bar{K}N \rightarrow \bar{K}N$
1679 ± 10	ALSTON-... 78	DPWA	$\bar{K}N \rightarrow \bar{K}N$
1670 ± 5	GOPAL 77	DPWA	$\bar{K}N$ multichannel
1670 ± 6	HEPP 76B	DPWA	$K^-N \rightarrow \Sigma\pi$
1685 ± 20	BAILLON 75	IPWA	$\bar{K}N \rightarrow \Lambda\pi$
1659 ± 12 - 5	VANHORN 75	DPWA	$K^-p \rightarrow \Lambda\pi^0$
1670 ± 2	KANE 74	DPWA	$K^-p \rightarrow \Sigma\pi$
••• We do not use the following data for averages, fits, limits, etc. •••			
1667 or 1668	¹ MARTIN 77	DPWA	$\bar{K}N$ multichannel
1650	DEBELLEFON 76	IPWA	$K^-p \rightarrow \Lambda\pi^0$
1671 ± 3	PONTE 75	DPWA	$K^-p \rightarrow \Lambda\pi^0$ (sol. 1)
1655 ± 2	PONTE 75	DPWA	$K^-p \rightarrow \Lambda\pi^0$ (sol. 2)
¹ The two MARTIN 77 values are from a T-matrix pole and from a Breit-Wigner fit.			

$\Sigma(1670)$ WIDTH

VALUE (MeV)	DOCUMENT ID	TECN	COMMENT
40 to 100 (≈ 70) OUR ESTIMATE			
54 ± 6	SARANTSEV 19	DPWA	$\bar{K}N$ multichannel
55 ± 4	ZHANG 13A	DPWA	$\bar{K}N$ multichannel
52 ± 5 - 2	GAO 12	DPWA	$\bar{K}N \rightarrow \Lambda\pi$
65.0 ± 7.3	KOISO 85	DPWA	$K^-p \rightarrow \Sigma\pi$
79 ± 10	GOPAL 80	DPWA	$\bar{K}N \rightarrow \bar{K}N$
56 ± 20	ALSTON-... 78	DPWA	$\bar{K}N \rightarrow \bar{K}N$
50 ± 5	GOPAL 77	DPWA	$\bar{K}N$ multichannel
56 ± 3	HEPP 76B	DPWA	$K^-N \rightarrow \Sigma\pi$
85 ± 25	BAILLON 75	IPWA	$\bar{K}N \rightarrow \Lambda\pi$
32 ± 11	VANHORN 75	DPWA	$K^-p \rightarrow \Lambda\pi^0$
79 ± 6	KANE 74	DPWA	$K^-p \rightarrow \Sigma\pi$
••• We do not use the following data for averages, fits, limits, etc. •••			
46 or 46	¹ MARTIN 77	DPWA	$\bar{K}N$ multichannel
80	DEBELLEFON 76	IPWA	$K^-p \rightarrow \Lambda\pi^0$
44 ± 11	PONTE 75	DPWA	$K^-p \rightarrow \Lambda\pi^0$ (sol. 1)
76 ± 5	PONTE 75	DPWA	$K^-p \rightarrow \Lambda\pi^0$ (sol. 2)
¹ The two MARTIN 77 values are from a T-matrix pole and from a Breit-Wigner fit.			

$\Sigma(1670)$ DECAY MODES

Mode	Fraction (Γ_i/Γ)
Γ_1 $N\bar{K}$	0.06 to 0.12
Γ_2 $\Lambda\pi$	5–15 %
Γ_3 $\Sigma\pi$	30–60 %
Γ_4 $\Lambda\pi\pi$	
Γ_5 $\Sigma\pi\pi$	
Γ_6 $\Sigma\sigma$	(7.0 ± 3.0) %
Γ_7 $\Sigma(1385)\pi$	
Γ_8 $\Sigma(1385)\pi$, S-wave	
Γ_9 $\Sigma(1385)\pi$, S-wave	
Γ_{10} $\Sigma(1385)\pi$, D-wave	
Γ_{11} $N\bar{K}^*(892)$, S=1/2, D-wave	
Γ_{12} $N\bar{K}^*(892)$, S=3/2, S-wave	
Γ_{13} $N\bar{K}^*(892)$, S=3/2, D-wave	

Γ_{14}	$\Lambda(1405)\pi$
Γ_{15}	$\Lambda(1520)\pi$

$\Sigma(1670)$ BRANCHING RATIOS

See "Sign conventions for resonance couplings" in the Note on Λ and Σ Resonances.

$\Gamma(N\bar{K})/\Gamma_{total}$

VALUE	DOCUMENT ID	TECN	COMMENT
0.06 to 0.12 OUR ESTIMATE			
0.10 ± 0.02	SARANTSEV 19	DPWA	$\bar{K}N$ multichannel
0.062 ± 0.007	ZHANG 13A	DPWA	$\bar{K}N$ multichannel
0.10 ± 0.03	GOPAL 80	DPWA	$\bar{K}N \rightarrow \bar{K}N$
0.11 ± 0.03	ALSTON-... 78	DPWA	$\bar{K}N \rightarrow \bar{K}N$
••• We do not use the following data for averages, fits, limits, etc. •••			
0.121	¹ KAMANO 15	DPWA	$\bar{K}N$ multichannel
0.08 ± 0.03	GOPAL 77	DPWA	See GOPAL 80
0.07 or 0.07	² MARTIN 77	DPWA	$\bar{K}N$ multichannel

¹ From the preferred solution A in KAMANO 15.

² The two MARTIN 77 values are from a T-matrix pole and from a Breit-Wigner fit.

$\Gamma(\Lambda\pi)/\Gamma_{total}$

VALUE	DOCUMENT ID	TECN	COMMENT
0.09 ± 0.02	SARANTSEV 19	DPWA	$\bar{K}N$ multichannel
••• We do not use the following data for averages, fits, limits, etc. •••			
0.058	¹ KAMANO 15	DPWA	$\bar{K}N$ multichannel
¹ From the preferred solution A in KAMANO 15.			

$\Gamma(\Sigma\pi)/\Gamma_{total}$

VALUE	DOCUMENT ID	TECN	COMMENT
0.70 ± 0.15	SARANTSEV 19	DPWA	$\bar{K}N$ multichannel
••• We do not use the following data for averages, fits, limits, etc. •••			
0.465	¹ KAMANO 15	DPWA	$\bar{K}N$ multichannel
¹ From the preferred solution A in KAMANO 15.			

$\Gamma(\Lambda\pi\pi)/\Gamma_{total}$

VALUE	DOCUMENT ID	TECN	COMMENT
••• We do not use the following data for averages, fits, limits, etc. •••			
< 0.11	ARMENTEROS68E HBC		K^-p ($\Gamma_1=0.09$)

$\Gamma(\Sigma\pi\pi)/\Gamma_{total}$

VALUE	DOCUMENT ID	TECN	COMMENT
••• We do not use the following data for averages, fits, limits, etc. •••			
< 0.14	¹ ARMENTEROS68E HBC		K^-p , K^-d ($\Gamma_1=0.09$)
¹ Ratio only for $\Sigma 2\pi$ system in $l=1$, which cannot be $\Sigma(1385)$.			

$\Gamma(\Sigma\sigma)/\Gamma_{total}$

VALUE	DOCUMENT ID	TECN	COMMENT
0.07 ± 0.03	SARANTSEV 19	DPWA	$\bar{K}N$ multichannel

$\Gamma(\Sigma(1385)\pi, S\text{-wave})/\Gamma_{total}$

VALUE	DOCUMENT ID	TECN	COMMENT
••• We do not use the following data for averages, fits, limits, etc. •••			
0.309	¹ KAMANO 15	DPWA	Multichannel
¹ From the preferred solution A in KAMANO 15.			

$\Gamma(\Sigma(1385)\pi, D\text{-wave})/\Gamma_{total}$

VALUE	DOCUMENT ID	TECN	COMMENT
••• We do not use the following data for averages, fits, limits, etc. •••			
0.044	¹ KAMANO 15	DPWA	Multichannel
¹ From the preferred solution A in KAMANO 15.			

$\Gamma(N\bar{K}^*(892), S=1/2, D\text{-wave})/\Gamma_{total}$

VALUE	DOCUMENT ID	TECN	COMMENT
••• We do not use the following data for averages, fits, limits, etc. •••			
0.001	¹ KAMANO 15	DPWA	Multichannel
¹ From the preferred solution A in KAMANO 15.			

$\Gamma(N\bar{K}^*(892), S=3/2, S\text{-wave})/\Gamma_{total}$

VALUE	DOCUMENT ID	TECN	COMMENT
••• We do not use the following data for averages, fits, limits, etc. •••			
0.002	¹ KAMANO 15	DPWA	Multichannel
¹ From the preferred solution A in KAMANO 15.			

$\Gamma(N\bar{K}^*(892), S=3/2, D\text{-wave})/\Gamma_{total}$

VALUE	DOCUMENT ID	TECN	COMMENT
••• We do not use the following data for averages, fits, limits, etc. •••			
0.001	¹ KAMANO 15	DPWA	Multichannel
¹ From the preferred solution A in KAMANO 15.			

Baryon Particle Listings

$\Sigma(1670), \Sigma(1750)$

$\Gamma(\Lambda(1405)\pi)/\Gamma_{\text{total}}$	DOCUMENT ID	TECN	COMMENT	Γ_{14}/Γ
0.01 ± 0.01	SARANTSEV 19	DPWA	$\bar{K}N$ multichannel	
••• We do not use the following data for averages, fits, limits, etc. •••				
<0.06	ARMENTEROS68E	HBC	K^-p, K^-d ($\Gamma_1=0.09$)	

$\Gamma(\Lambda(1405)\pi)/\Gamma(\Sigma(1385)\pi)$	DOCUMENT ID	TECN	COMMENT	Γ_{14}/Γ_7
0.23 ± 0.08	BRUCKER 70	DBC	$K^-N \rightarrow \Sigma\pi\pi$	

$(\Gamma_1\Gamma_7)^{1/2}/\Gamma_{\text{total}}$ in $N\bar{K} \rightarrow \Sigma(1670) \rightarrow \Lambda\pi$	DOCUMENT ID	TECN	COMMENT	$(\Gamma_1\Gamma_7)^{1/2}/\Gamma$
+0.08 ± 0.01	ZHANG 13A	DPWA	Multichannel	
+0.081 ± 0.002	GAO 12	DPWA	$\bar{K}N \rightarrow \Lambda\pi$	
-0.004				
+0.17 ± 0.03	¹ MORRIS 78	DPWA	$K^-n \rightarrow \Lambda\pi^-$	
+0.13 ± 0.02	¹ MORRIS 78	DPWA	$K^-n \rightarrow \Lambda\pi^-$	
+0.10 ± 0.02	GOPAL 77	DPWA	$\bar{K}N$ multichannel	
+0.06 ± 0.02	BAILLON 75	IPWA	$\bar{K}N \rightarrow \Lambda\pi$	
+0.09 ± 0.02	VANHORN 75	DPWA	$K^-p \rightarrow \Lambda\pi^0$	
+0.018 ± 0.060	DEVENISH 74B		Fixed- t dispersion rel.	
••• We do not use the following data for averages, fits, limits, etc. •••				
+0.08 or +0.08	² MARTIN 77	DPWA	$\bar{K}N$ multichannel	
+0.05	DEBELLEFON 76	IPWA	$K^-p \rightarrow \Lambda\pi^0$	
+0.08 ± 0.01	PONTE 75	DPWA	$K^-p \rightarrow \Lambda\pi^0$ (sol. 1)	
+0.17 ± 0.01	PONTE 75	DPWA	$K^-p \rightarrow \Lambda\pi^0$ (sol. 2)	

¹ Results are with and without an S_{11} $\Sigma(1620)$ in the fit.
² The two MARTIN 77 values are from a T-matrix pole and from a Breit-Wigner fit.

$(\Gamma_1\Gamma_7)^{1/2}/\Gamma_{\text{total}}$ in $N\bar{K} \rightarrow \Sigma(1670) \rightarrow \Sigma\pi$	DOCUMENT ID	TECN	COMMENT	$(\Gamma_1\Gamma_3)^{1/2}/\Gamma$
+0.20 ± 0.01	ZHANG 13A	DPWA	Multichannel	
+0.20 ± 0.02	KOISO 85	DPWA	$K^-p \rightarrow \Sigma\pi$	
+0.21 ± 0.02	GOPAL 77	DPWA	$\bar{K}N$ multichannel	
+0.20 ± 0.01	HEPP 76B	DPWA	$K^-N \rightarrow \Sigma\pi$	
+0.21 ± 0.03	KANE 74	DPWA	$K^-p \rightarrow \Sigma\pi$	
••• We do not use the following data for averages, fits, limits, etc. •••				
+0.18 or +0.17	¹ MARTIN 77	DPWA	$\bar{K}N$ multichannel	

¹ The two MARTIN 77 values are from a T-matrix pole and from a Breit-Wigner fit.

$(\Gamma_1\Gamma_7)^{1/2}/\Gamma_{\text{total}}$ in $N\bar{K} \rightarrow \Sigma(1670) \rightarrow \Sigma(1385)\pi, S\text{-wave}$	DOCUMENT ID	TECN	COMMENT	$(\Gamma_1\Gamma_8)^{1/2}/\Gamma$
+0.11 ± 0.03	PREVOST 74	DPWA	$K^-N \rightarrow \Sigma(1385)\pi$	
••• We do not use the following data for averages, fits, limits, etc. •••				
0.17 ± 0.02	¹ SIMS 68	DBC	$K^-N \rightarrow \Lambda\pi\pi$	

$\Gamma_1\Gamma_7/\Gamma_{\text{total}}^2$ in $N\bar{K} \rightarrow \Sigma(1670) \rightarrow \Lambda(1405)\pi$	DOCUMENT ID	TECN	COMMENT	$\Gamma_1\Gamma_{14}/\Gamma^2$
0.007 ± 0.002	¹ BRUCKER 70	DBC	$K^-N \rightarrow \Sigma\pi\pi$	
••• We do not use the following data for averages, fits, limits, etc. •••				
<0.03	BERLEY 69	HBC	K^-p 0.6-0.82 GeV/c	

$(\Gamma_1\Gamma_7)^{1/2}/\Gamma_{\text{total}}$ in $N\bar{K} \rightarrow \Sigma(1670) \rightarrow \Lambda(1520)\pi$	DOCUMENT ID	TECN	COMMENT	$(\Gamma_1\Gamma_{15})^{1/2}/\Gamma$
0.081 ± 0.016	¹ CAMERON 77	DPWA	P-wave decay	

¹ The CAMERON 77 upper limit on F-wave decay is 0.03.

$\Sigma(1670)$ REFERENCES

SARANTSEV 19	EPJ A55 180	A.V. Sarantsev et al.	(BONN, PNPI)
KAMANO 15	PR C92 025205	H. Kamano et al.	(ANL, OSAK)
ZHANG 13A	PR C88 035205	H. Zhang et al.	(KSU)
GAO 12	PR C86 025201	P. Gao, J. Shi, B.S. Zou	(BHEP, BEIJT)
Also	NP A867 41	P. Gao, B.S. Zou, A. Sibirtsev	(BHEP, BEIJT+)
KOISO 85	NP A433 619	H. Koiso et al.	(TOKY, MASA)
PDC 82	PL 111B 1	M. Roos et al.	(HEL5, CIT, CERN)
GOPAL 80	Toronto Conf. 159	G.P. Gopal	(RHEL) IJP
ALSTON... 78	PR D18 182	M. Alston-Garnjost et al.	(LBL, MTHO+) IJP
Also	PRL 38 1007	M. Alston-Garnjost et al.	(LBL, MTHO+) IJP
MORRIS 78	PR D17 55	W.A. Morris et al.	(FSU) IJP
CAMERON 77	NP B131 399	W. Cameron et al.	(RHEL, LOIC) IJP
GOPAL 77	NP B119 362	G.P. Gopal et al.	(LOIC, RHEL) IJP
MARTIN 77	NP B127 349	B.R. Martin, M.K. Piddcock, R.G. Moorhouse	(LOUC+) IJP
Also	NP B126 266	B.R. Martin, M.K. Piddcock	(LOUC) IJP
Also	NP B126 285	B.R. Martin, M.K. Piddcock	(LOUC) IJP
DEBELLEFON 76	NP B109 129	A. de Bellefon, A. Berthon	(CDEF) IJP
HEPP 76B	PL 65B 487	V. Hepp et al.	(CERN, RHEL) IJP
BAILLON 75	NP B94 39	P.H. Baillon, P.J. Litchfield	(CERN, RHEL) IJP
PONTE 75	PR D12 2597	R.A. Ponte et al.	(MASA, TENN, UCR) IJP
VANHORN 75	NP B87 145	A.J. van Horn	(LBL) IJP
Also	NP B87 157	A.J. van Horn	(LBL) IJP
DEVENISH 74B	NP B81 330	R.C.E. Devenish, C.D. Froggatt, B.R. Martin	(DESY+) IJP
KANE 74	LBL-2452	D.F. Kane	(LBL) IJP
PREVOST 74	NP B69 246	J. Prevost et al.	(SACL, CERN, HEID) IJP
BRUCKER 70	Duke Conf. 155	E.B. Brucker et al.	(FSU) I
Hyperon Resonances, 1970			
BERLEY 69	PL 30B 430	D. Berley et al.	(BNL)
ARMENTEROS 65E	PL 28B 521	R. Armenteros et al.	(CERN, HEID, SACL) I
SIMS 68	PRL 21 1413	W.H. Sims et al.	(FSU, TUFTS, BRAN)

$\Sigma(1750) 1/2^-$

$I(J^P) = 1(\frac{1}{2}^-)$ Status: ***

For most results published before 1974 (they are now obsolete), see our 1982 edition Physics Letters **111B** 1 (1982).

There is evidence for this state in many partial-wave analyses, but with wide variations in the mass, width, and couplings. The latest analyses indicated significant couplings to $N\bar{K}$ and $\Lambda\pi$, as well as to $\Sigma\eta$ whose threshold is at 1746 MeV (JONES 74).

$\Sigma(1750)$ POLE POSITION

REAL PART	DOCUMENT ID	TECN	COMMENT
VALUE (MeV)			
1689 ± 11	SARANTSEV 19	DPWA	$\bar{K}N$ multichannel
••• We do not use the following data for averages, fits, limits, etc. •••			
1704 \pm $\frac{3}{6}$	¹ KAMANO 15	DPWA	$\bar{K}N$ multichannel
1708	ZHANG 13A	DPWA	$\bar{K}N$ multichannel
	¹ From the preferred solution A in KAMANO 15. Solution B reports two poles at M = 1551 \pm $\frac{2}{9}$ MeV and 1940 \pm $\frac{2}{2}$ MeV.		

-2xIMAGINARY PART	DOCUMENT ID	TECN	COMMENT
VALUE (MeV)			
206 ± 18	SARANTSEV 19	DPWA	$\bar{K}N$ multichannel
••• We do not use the following data for averages, fits, limits, etc. •••			
86 \pm $\frac{14}{4}$	¹ KAMANO 15	DPWA	$\bar{K}N$ multichannel
158	ZHANG 13A	DPWA	$\bar{K}N$ multichannel
	¹ From the preferred solution A in KAMANO 15. Solution B Reports two poles with $\Gamma = 376 \pm \frac{12}{2}$ and 172 $\pm \frac{4}{4}$ MeV.		

$\Sigma(1750)$ POLE RESIDUES

The normalized residue is the residue divided by $\Gamma_{\text{pole}}/2$.

Normalized residue in $N\bar{K} \rightarrow \Sigma(1750) \rightarrow N\bar{K}$	DOCUMENT ID	TECN	COMMENT
MODULUS PHASE (°)			
0.46 ± 0.09 -144 ± 15	SARANTSEV 19	DPWA	$\bar{K}N$ multichannel
••• We do not use the following data for averages, fits, limits, etc. •••			
0.0982 178	¹ KAMANO 15	DPWA	$\bar{K}N$ multichannel
	¹ From the preferred solution A in KAMANO 15.		

Normalized residue in $N\bar{K} \rightarrow \Sigma(1750) \rightarrow \Sigma\pi$	DOCUMENT ID	TECN	COMMENT
MODULUS PHASE (°)			
0.27 ± 0.05 100 ± 18	SARANTSEV 19	DPWA	$\bar{K}N$ multichannel
••• We do not use the following data for averages, fits, limits, etc. •••			
0.192 137	¹ KAMANO 15	DPWA	Multichannel
	¹ From the preferred solution A in KAMANO 15.		

Normalized residue in $N\bar{K} \rightarrow \Sigma(1750) \rightarrow \Sigma\eta$	DOCUMENT ID	TECN	COMMENT
MODULUS PHASE (°)			
0.05 ± 0.03	SARANTSEV 19	DPWA	$\bar{K}N$ multichannel

Normalized residue in $N\bar{K} \rightarrow \Sigma(1750) \rightarrow \Lambda\pi$	DOCUMENT ID	TECN	COMMENT
MODULUS PHASE (°)			
0.26 ± 0.06 115 ± 15	SARANTSEV 19	DPWA	$\bar{K}N$ multichannel
••• We do not use the following data for averages, fits, limits, etc. •••			
0.207 169	¹ KAMANO 15	DPWA	$\bar{K}N$ multichannel
	¹ From the preferred solution A in KAMANO 15.		

Normalized residue in $N\bar{K} \rightarrow \Sigma(1750) \rightarrow \Xi K$	DOCUMENT ID	TECN	COMMENT
MODULUS PHASE (°)			
0.02 ± 0.02	SARANTSEV 19	DPWA	$\bar{K}N$ multichannel

Normalized residue in $N\bar{K} \rightarrow \Sigma(1750) \rightarrow \Sigma(1385)\pi, D\text{-wave}$	DOCUMENT ID	TECN	COMMENT
MODULUS PHASE (°)			
0.04 ± 0.03	SARANTSEV 19	DPWA	$\bar{K}N$ multichannel
••• We do not use the following data for averages, fits, limits, etc. •••			
0.0536 73	¹ KAMANO 15	DPWA	$\bar{K}N$ multichannel
	¹ From the preferred solution A in KAMANO 15.		

Normalized residue in $N\bar{K} \rightarrow \Sigma(1750) \rightarrow \Lambda(1520)\pi$	DOCUMENT ID	TECN	COMMENT
MODULUS PHASE (°)			
0.15 ± 0.07 -25 ± 40	SARANTSEV 19	DPWA	$\bar{K}N$ multichannel

Normalized residue in $N\bar{K} \rightarrow \Sigma(1750) \rightarrow N\bar{K}^*(892), S=1/2, S\text{-wave}$	DOCUMENT ID	TECN	COMMENT
MODULUS PHASE (°)			
0.05 ± 0.03 -100 ± 35	SARANTSEV 19	DPWA	$\bar{K}N$ multichannel

$\Sigma(1750)$ MASS

VALUE (MeV)	DOCUMENT ID	TECN	COMMENT
1700 to 1800 (≈ 1750) OUR ESTIMATE			
1692 \pm 11	SARANTSEV 19	DPWA	$\bar{K}N$ multichannel
1739 \pm 8	ZHANG 13A	DPWA	$\bar{K}N$ multichannel
1756 \pm 10	GOPAL 80	DPWA	$\bar{K}N \rightarrow \bar{K}N$
1770 \pm 10	ALSTON... 78	DPWA	$\bar{K}N \rightarrow \bar{K}N$
• • • We do not use the following data for averages, fits, limits, etc. • • •			
1770 \pm 15	GOPAL 77	DPWA	$\bar{K}N$ multichannel
1800 or 1813	¹ MARTIN 77	DPWA	$\bar{K}N$ multichannel
1715 \pm 10	² CARROLL 76	DPWA	Isospin-1 total σ
1730	DEBELLEFON 76	IPWA	$K^- p \rightarrow \Lambda\pi^0$
1780 \pm 30	BAILLON 75	IPWA	$\bar{K}N \rightarrow \Lambda\pi$ (sol. 1)
1700 \pm 30	BAILLON 75	IPWA	$\bar{K}N \rightarrow \Lambda\pi$ (sol. 2)
1697 \pm 20 -10	VANHORN 75	DPWA	$K^- p \rightarrow \Lambda\pi^0$
1785 \pm 12	CHU 74	DBC	Fits $\sigma(K^- n \rightarrow \Sigma^- \eta)$
1760 \pm 5	³ JONES 74	HBC	Fits $\sigma(K^- p \rightarrow \Sigma^0 \eta)$
1739 \pm 10	PREVOST 74	DPWA	$K^- N \rightarrow \Sigma(1385)\pi$

¹ The two MARTIN 77 values are from a T-matrix pole and from a Breit-Wigner fit.
² A total cross-section bump with $(J+1/2) \Gamma_{el} / \Gamma_{total} = 0.30$.
³ An S-wave Breit-Wigner fit to the threshold cross section with no background and errors statistical only.

$\Sigma(1750)$ WIDTH

VALUE (MeV)	DOCUMENT ID	TECN	COMMENT
100 to 200 (≈ 150) OUR ESTIMATE			
208 \pm 18	SARANTSEV 19	DPWA	$\bar{K}N$ multichannel
182 \pm 60	ZHANG 13A	DPWA	$\bar{K}N$ multichannel
64 \pm 10	GOPAL 80	DPWA	$\bar{K}N \rightarrow \bar{K}N$
161 \pm 20	ALSTON... 78	DPWA	$\bar{K}N \rightarrow \bar{K}N$
• • • We do not use the following data for averages, fits, limits, etc. • • •			
60 \pm 10	GOPAL 77	DPWA	$\bar{K}N$ multichannel
117 or 119	¹ MARTIN 77	DPWA	$\bar{K}N$ multichannel
10	² CARROLL 76	DPWA	Isospin-1 total σ
110	DEBELLEFON 76	IPWA	$K^- p \rightarrow \Lambda\pi^0$
140 \pm 30	BAILLON 75	IPWA	$\bar{K}N \rightarrow \Lambda\pi$ (sol. 1)
160 \pm 50	BAILLON 75	IPWA	$\bar{K}N \rightarrow \Lambda\pi$ (sol. 2)
66 \pm 14 -12	VANHORN 75	DPWA	$K^- p \rightarrow \Lambda\pi^0$
89 \pm 33	CHU 74	DBC	Fits $\sigma(K^- n \rightarrow \Sigma^- \eta)$
92 \pm 7	³ JONES 74	HBC	Fits $\sigma(K^- p \rightarrow \Sigma^0 \eta)$
108 \pm 20	PREVOST 74	DPWA	$K^- N \rightarrow \Sigma(1385)\pi$

¹ The two MARTIN 77 values are from a T-matrix pole and from a Breit-Wigner fit.
² A total cross-section bump with $(J+1/2) \Gamma_{el} / \Gamma_{total} = 0.30$.
³ An S-wave Breit-Wigner fit to the threshold cross section with no background and errors statistical only.

$\Sigma(1750)$ DECAY MODES

Mode	Fraction (Γ_i/Γ)
Γ_1 $N\bar{K}$	0.06 to 0.12
Γ_2 $\Lambda\pi$	(14 \pm 5) %
Γ_3 $\Sigma\pi$	(16 \pm 4) %
Γ_4 $\Sigma\eta$	15-55 %
Γ_5 $\Sigma(1385)\pi, D$ -wave	< 1 %
Γ_6 $\Lambda(1520)\pi$	(2.0 \pm 1.0) %
Γ_7 $N\bar{K}^*(892), S=1/2$	(8 \pm 4) %
Γ_8 $N\bar{K}^*(892), S=3/2, D$ -wave	

$\Sigma(1750)$ BRANCHING RATIOS

See "Sign conventions for resonance couplings" in the Note on Λ and Σ Resonances.

$\Gamma(N\bar{K})/\Gamma_{total}$	DOCUMENT ID	TECN	COMMENT	Γ_1/Γ
0.06 to 0.12 OUR ESTIMATE				
0.46 \pm 0.09	SARANTSEV 19	DPWA	$\bar{K}N$ multichannel	
0.09 \pm 0.07	ZHANG 13A	DPWA	Multichannel	
0.14 \pm 0.03	GOPAL 80	DPWA	$\bar{K}N \rightarrow \bar{K}N$	
0.33 \pm 0.05	ALSTON... 78	DPWA	$\bar{K}N \rightarrow \bar{K}N$	
• • • We do not use the following data for averages, fits, limits, etc. • • •				
0.154	¹ KAMANO 15	DPWA	Multichannel	
0.15 \pm 0.03	GOPAL 77	DPWA	See GOPAL 80	
0.06 or 0.05	² MARTIN 77	DPWA	$\bar{K}N$ multichannel	

¹ From the preferred solution A in KAMANO 15.
² The two MARTIN 77 values are from a T-matrix pole and from a Breit-Wigner fit.

$\Gamma(\Lambda\pi)/\Gamma_{total}$ Γ_2/Γ

VALUE	DOCUMENT ID	TECN	COMMENT
0.14 \pm 0.05	SARANTSEV 19	DPWA	$\bar{K}N$ multichannel
• • • We do not use the following data for averages, fits, limits, etc. • • •			
0.435	¹ KAMANO 15	DPWA	$\bar{K}N$ multichannel

¹ From the preferred solution A in KAMANO 15.

$\Gamma(\Sigma\pi)/\Gamma_{total}$ Γ_3/Γ

VALUE	DOCUMENT ID	TECN	COMMENT
0.16 \pm 0.04	SARANTSEV 19	DPWA	$\bar{K}N$ multichannel
• • • We do not use the following data for averages, fits, limits, etc. • • •			
0.373	¹ KAMANO 15	DPWA	$\bar{K}N$ multichannel

¹ From the preferred solution A in KAMANO 15.

$\Gamma(\Lambda(1520)\pi)/\Gamma_{total}$ Γ_6/Γ

VALUE	DOCUMENT ID	TECN	COMMENT
0.02 \pm 0.01	SARANTSEV 19	DPWA	$\bar{K}N$ multichannel

$\Gamma(\Sigma(1385)\pi, D$ -wave)/ Γ_{total} Γ_5/Γ

VALUE	DOCUMENT ID	TECN	COMMENT
< 0.01	SARANTSEV 19	DPWA	$\bar{K}N$ multichannel
• • • We do not use the following data for averages, fits, limits, etc. • • •			
0.024	¹ KAMANO 15	DPWA	$\bar{K}N$ multichannel

¹ From the preferred solution A in KAMANO 15.

$\Gamma(N\bar{K}^*(892), S=1/2)/\Gamma_{total}$ Γ_7/Γ

VALUE	DOCUMENT ID	TECN	COMMENT
~ 0 0.08 \pm 0.04	SARANTSEV 19	DPWA	$\bar{K}N$ multichannel
• • • We do not use the following data for averages, fits, limits, etc. • • •			
0.004	¹ KAMANO 15	DPWA	$\bar{K}N$ multichannel

¹ From the preferred solution A in KAMANO 15.

$\Gamma(N\bar{K}^*(892), S=3/2, D$ -wave)/ Γ_{total} Γ_8/Γ

VALUE	DOCUMENT ID	TECN	COMMENT
• • • We do not use the following data for averages, fits, limits, etc. • • •			
0.01	¹ KAMANO 15	DPWA	Multichannel

¹ From the preferred solution A in KAMANO 15.

$(\Gamma_i\Gamma_j)^{1/2}/\Gamma_{total}$ in $N\bar{K} \rightarrow \Sigma(1750) \rightarrow \Lambda\pi$ $(\Gamma_1\Gamma_2)^{1/2}/\Gamma$

VALUE	DOCUMENT ID	TECN	COMMENT
+0.10 \pm 0.04	ZHANG 13A	DPWA	Multichannel
0.04 \pm 0.03	GOPAL 77	DPWA	$\bar{K}N$ multichannel
• • • We do not use the following data for averages, fits, limits, etc. • • •			
-0.10 or -0.09	¹ MARTIN 77	DPWA	$\bar{K}N$ multichannel
-0.12	DEBELLEFON 76	IPWA	$K^- p \rightarrow \Lambda\pi^0$
-0.12 \pm 0.02	BAILLON 75	IPWA	$\bar{K}N \rightarrow \Lambda\pi$ (sol. 1)
-0.13 \pm 0.03	BAILLON 75	IPWA	$\bar{K}N \rightarrow \Lambda\pi$ (sol. 2)
-0.13 \pm 0.04	VANHORN 75	DPWA	$K^- p \rightarrow \Lambda\pi^0$
-0.120 \pm 0.077	DEVENISH 74B		Fixed-t dispersion rel.

¹ The two MARTIN 77 values are from a T-matrix pole and from a Breit-Wigner fit.

$(\Gamma_i\Gamma_j)^{1/2}/\Gamma_{total}$ in $N\bar{K} \rightarrow \Sigma(1750) \rightarrow \Sigma\pi$ $(\Gamma_1\Gamma_3)^{1/2}/\Gamma$

VALUE	DOCUMENT ID	TECN	COMMENT
+0.17 \pm 0.07	ZHANG 13A	DPWA	Multichannel
-0.09 \pm 0.05	GOPAL 77	DPWA	$\bar{K}N$ multichannel
• • • We do not use the following data for averages, fits, limits, etc. • • •			
+0.06 or +0.06	¹ MARTIN 77	DPWA	$\bar{K}N$ multichannel
0.13 \pm 0.02	LANGBEIN 72	IPWA	$\bar{K}N$ multichannel

¹ The two MARTIN 77 values are from a T-matrix pole and from a Breit-Wigner fit.

$(\Gamma_i\Gamma_j)^{1/2}/\Gamma_{total}$ in $N\bar{K} \rightarrow \Sigma(1750) \rightarrow \Sigma\eta$ $(\Gamma_1\Gamma_4)^{1/2}/\Gamma$

VALUE	DOCUMENT ID	TECN	COMMENT
0.23 \pm 0.01	¹ JONES 74	HBC	Fits $\sigma(K^- p \rightarrow \Sigma^0 \eta)$
• • • We do not use the following data for averages, fits, limits, etc. • • •			
seen	CLINE 69	DBC	Threshold bump

¹ An S-wave Breit-Wigner fit to the threshold cross section with no background and errors statistical only.

$(\Gamma_i\Gamma_j)^{1/2}/\Gamma_{total}$ in $N\bar{K} \rightarrow \Sigma(1750) \rightarrow \Sigma(1385)\pi, D$ -wave $(\Gamma_1\Gamma_5)^{1/2}/\Gamma$

VALUE	DOCUMENT ID	TECN	COMMENT
+0.17 \pm 0.07	ZHANG 13A	DPWA	Multichannel
+0.18 \pm 0.15	PREVOST 74	DPWA	$K^- N \rightarrow \Sigma(1385)\pi$

$(\Gamma_i\Gamma_j)^{1/2}/\Gamma_{total}$ in $N\bar{K} \rightarrow \Sigma(1750) \rightarrow \Lambda(1520)\pi$ $(\Gamma_1\Gamma_6)^{1/2}/\Gamma$

VALUE	DOCUMENT ID	TECN	COMMENT
• • • We do not use the following data for averages, fits, limits, etc. • • •			
0.032 \pm 0.021	CAMERON 77	DPWA	P-wave decay

Baryon Particle Listings

$\Sigma(1750), \Sigma(1775)$

$\Sigma(1750)$ REFERENCES

SARANTSEV	19	EPJ A55 180	A.V. Sarantsev <i>et al.</i>	(BONN, PNPI)
KAMANO	15	PR C92 025205	H. Kamano <i>et al.</i>	(ANL, OSAK)
ZHANG	13A	PR C88 035205	H. Zhang <i>et al.</i>	(KSU)
PDG	82	PL 111B 1	M. Roos <i>et al.</i>	(HELS, CIT, CERN)
GOPAL	80	Toronto Conf. 159	G.P. Gopal	(RHEL) IJP
ALSTON-...	78	PR D18 182	M. Alston-Garnjost <i>et al.</i>	(LBL, MTHO+) IJP
Also		PRL 38 1007	M. Alston-Garnjost <i>et al.</i>	(LBL, MTHO+) IJP
CAMERON	77	NP B131 399	W. Cameron <i>et al.</i>	(RHEL, LOIC) IJP
GOPAL	77	NP B119 362	G.P. Gopal <i>et al.</i>	(LOIC, RHEL) IJP
MARTIN	77	NP B127 349	B.R. Martin, M.K. Pldcock, R.G. Moorhouse	(LOUC+) IJP
Also		NP B126 266	B.R. Martin, M.K. Pldcock	(LOUC) IJP
Also		NP B126 285	B.R. Martin, M.K. Pldcock	(LOUC) IJP
CARROLL	76	PRL 37 806	A.S. Carroll <i>et al.</i>	(BNL) I
DEBELLEFON	76	NP B109 129	A. de Bellefon, A. Berthon	(CDEF) IJP
BAILLON	75	NP B94 39	P.H. Baillon, P.J. Litchfield	(CERN, RHEL) IJP
VANHORN	75	NP B87 145	A.J. van Horn	(LBL) IJP
Also		NP B87 157	A.J. van Horn	(LBL) IJP
CHU	74	NC 20A 35	R.Y.L. Chu <i>et al.</i>	(PLAT, TUFTS, BRAN) IJP
DEVENISH	74B	NP B81 330	R.C.E. Devenish, C.D. Froggatt, B.R. Martin	(DESY+) IJP
JONES	74	NP B73 141	M.D. Jones	(CHIC) IJP
PREVOST	74	NP B69 246	J. Prevost <i>et al.</i>	(SACL, CERN, HEID) IJP
LANGBEIN	72	NP B47 477	W. Langbein, F. Wagner	(MPIM) IJP
CLINE	69	LNC 2 407	D. Cline, R. Laumann, J. Mapp	(WISC) IJP

$\Sigma(1775) 5/2^-$

$$I(J^P) = 1(\frac{5}{2}^-) \text{ Status: } ****$$

Discovered by GALTIERI 63, this resonance plays the same role as cornerstone for isospin-1 analyses in this region as the $\Lambda(1820)F_{05}$ does in the isospin-0 channel.

For most results published before 1974 (they are now obsolete), see our 1982 edition Physics Letters **111B** 1 (1982).

$\Sigma(1775)$ POLE POSITION

REAL PART

VALUE (MeV)	DOCUMENT ID	TECN	COMMENT
1760 to 1780 (≈ 1770) OUR ESTIMATE			
1767 ± 4	SARANTSEV 19	DPWA	$\bar{K}N$ multichannel
1767 $^{+2}_{-2}$	¹ KAMANO 15	DPWA	$\bar{K}N$ multichannel
• • • We do not use the following data for averages, fits, limits, etc. • • •			
1759	ZHANG 13A	DPWA	$\bar{K}N$ multichannel
¹ From the preferred solution A in KAMANO 15.			

-2xIMAGINARY PART

VALUE (MeV)	DOCUMENT ID	TECN	COMMENT
45 to 65 (≈ 55) OUR ESTIMATE			
122 ± 8	SARANTSEV 19	DPWA	$\bar{K}N$ multichannel
128 $^{+4}_{-2}$	¹ KAMANO 15	DPWA	$\bar{K}N$ multichannel
• • • We do not use the following data for averages, fits, limits, etc. • • •			
118	ZHANG 13A	DPWA	$\bar{K}N$ multichannel
¹ From the preferred solution A in KAMANO 15.			

$\Sigma(1775)$ POLE RESIDUES

The normalized residue is the residue divided by $\Gamma_{pole}/2$.

Normalized residue in $N\bar{K} \rightarrow \Sigma(1775) \rightarrow N\bar{K}$

MODULUS	PHASE ($^\circ$)	DOCUMENT ID	TECN	COMMENT
0.44 ± 0.09	-17 ± 10	SARANTSEV 19	DPWA	$\bar{K}N$ multichannel
• • • We do not use the following data for averages, fits, limits, etc. • • •				
0.371	-32	¹ KAMANO 15	DPWA	$\bar{K}N$ multichannel
¹ From the preferred solution A in KAMANO 15.				

Normalized residue in $N\bar{K} \rightarrow \Sigma(1775) \rightarrow \Sigma\pi$

MODULUS	PHASE ($^\circ$)	DOCUMENT ID	TECN	COMMENT
0.13 ± 0.03	10 ± 12	SARANTSEV 19	DPWA	$\bar{K}N$ multichannel
• • • We do not use the following data for averages, fits, limits, etc. • • •				
0.115	-24	¹ KAMANO 15	DPWA	$\bar{K}N$ multichannel
¹ From the preferred solution A in KAMANO 15.				

Normalized residue in $N\bar{K} \rightarrow \Sigma(1775) \rightarrow \Lambda\pi$

MODULUS	PHASE ($^\circ$)	DOCUMENT ID	TECN	COMMENT
0.47 ± 0.10	130 ± 15	SARANTSEV 19	DPWA	$\bar{K}N$ multichannel
• • • We do not use the following data for averages, fits, limits, etc. • • •				
0.325	157	¹ KAMANO 15	DPWA	$\bar{K}N$ multichannel
¹ From the preferred solution A in KAMANO 15.				

Normalized residue in $N\bar{K} \rightarrow \Sigma(1775) \rightarrow \Sigma(1385)\pi, D\text{-wave}$

MODULUS	PHASE ($^\circ$)	DOCUMENT ID	TECN	COMMENT
• • • We do not use the following data for averages, fits, limits, etc. • • •				
0.391	137	¹ KAMANO 15	DPWA	$\bar{K}N$ multichannel
¹ From the preferred solution A in KAMANO 15.				

Normalized residue in $N\bar{K} \rightarrow \Sigma(1775) \rightarrow \Sigma(1385)\pi, G\text{-wave}$

MODULUS	PHASE ($^\circ$)	DOCUMENT ID	TECN	COMMENT
• • • We do not use the following data for averages, fits, limits, etc. • • •				
0.0129	-58	¹ KAMANO 15	DPWA	$\bar{K}N$ multichannel
¹ From the preferred solution A in KAMANO 15.				

Normalized residue in $N\bar{K} \rightarrow \Sigma(1775) \rightarrow N\bar{K}^*(892), S=1/2, D\text{-wave}$

MODULUS	PHASE ($^\circ$)	DOCUMENT ID	TECN	COMMENT
0.04 ± 0.02	-100 ± 60	SARANTSEV 19	DPWA	$\bar{K}N$ multichannel

Normalized residue in $N\bar{K} \rightarrow \Sigma(1775) \rightarrow N\bar{K}^*(892), S=3/2, D\text{-wave}$

MODULUS	PHASE ($^\circ$)	DOCUMENT ID	TECN	COMMENT
0.09 ± 0.06	10 ± 50	SARANTSEV 19	DPWA	$\bar{K}N$ multichannel

Normalized residue in $N\bar{K} \rightarrow \Sigma(1775) \rightarrow N\bar{K}^*(892), S=3/2, G\text{-wave}$

MODULUS	PHASE ($^\circ$)	DOCUMENT ID	TECN	COMMENT
0.04 ± 0.02	-100 ± 60	SARANTSEV 19	DPWA	$\bar{K}N$ multichannel

Normalized residue in $N\bar{K} \rightarrow \Sigma(1775) \rightarrow \Xi K$

MODULUS	PHASE ($^\circ$)	DOCUMENT ID	TECN	COMMENT
0.02 ± 0.01	-90 ± 35	SARANTSEV 19	DPWA	$\bar{K}N$ multichannel

Normalized residue in $N\bar{K} \rightarrow \Sigma(1775) \rightarrow \Lambda(1520)\pi, P\text{-wave}$

MODULUS	PHASE ($^\circ$)	DOCUMENT ID	TECN	COMMENT
0.09 ± 0.03	10 ± 30	SARANTSEV 19	DPWA	$\bar{K}N$ multichannel

Normalized residue in $N\bar{K} \rightarrow \Sigma(1775) \rightarrow \Lambda(1520)\pi, F\text{-wave}$

VALUE	DOCUMENT ID	TECN	COMMENT
0.01 ± 0.01	SARANTSEV 19	DPWA	$\bar{K}N$ multichannel

Normalized residue in $N\bar{K} \rightarrow \Sigma(1775) \rightarrow \Delta\bar{K}, D\text{-wave}$

VALUE	DOCUMENT ID	TECN	COMMENT
0.02 ± 0.02	SARANTSEV 19	DPWA	$\bar{K}N$ multichannel

$\Sigma(1775)$ MASS

VALUE (MeV)	DOCUMENT ID	TECN	COMMENT
1770 to 1780 (≈ 1775) OUR ESTIMATE			
1776 ± 4	SARANTSEV 19	DPWA	$\bar{K}N$ multichannel
1778 ± 1	ZHANG 13A	DPWA	$\bar{K}N$ multichannel
1778 ± 5	GOPAL 80	DPWA	$\bar{K}N \rightarrow \bar{K}N$
1777 ± 5	ALSTON-... 78	DPWA	$\bar{K}N \rightarrow \bar{K}N$
1775 ± 10	BAILLON 75	IPWA	$\bar{K}N \rightarrow \Lambda\pi$
1774 ± 10	VANHORN 75	DPWA	$K^- p \rightarrow \Lambda\pi^0$
1772 ± 6	KANE 74	DPWA	$K^- p \rightarrow \Sigma\pi$
• • • We do not use the following data for averages, fits, limits, etc. • • •			
1774 ± 5	GOPAL 77	DPWA	$\bar{K}N$ multichannel
1772 or 1777	¹ MARTIN 77	DPWA	$\bar{K}N$ multichannel
1765	DEBELLEFON 76	IPWA	$K^- p \rightarrow \Lambda\pi^0$
¹ The two MARTIN 77 values are from a T-matrix pole and from a Breit-Wigner fit.			

$\Sigma(1775)$ WIDTH

VALUE (MeV)	DOCUMENT ID	TECN	COMMENT
105 to 135 (≈ 120) OUR ESTIMATE			
124 ± 8	SARANTSEV 19	DPWA	$\bar{K}N$ multichannel
131 ± 3	ZHANG 13A	DPWA	$\bar{K}N$ multichannel
137 ± 10	GOPAL 80	DPWA	$\bar{K}N \rightarrow \bar{K}N$
116 ± 10	ALSTON-... 78	DPWA	$\bar{K}N \rightarrow \bar{K}N$
125 ± 15	BAILLON 75	IPWA	$\bar{K}N \rightarrow \Lambda\pi$
146 ± 18	VANHORN 75	DPWA	$K^- p \rightarrow \Lambda\pi^0$
154 ± 10	KANE 74	DPWA	$K^- p \rightarrow \Sigma\pi$
• • • We do not use the following data for averages, fits, limits, etc. • • •			
130 ± 10	GOPAL 77	DPWA	$\bar{K}N$ multichannel
102 or 103	¹ MARTIN 77	DPWA	$\bar{K}N$ multichannel
120	DEBELLEFON 76	IPWA	$K^- p \rightarrow \Lambda\pi^0$
¹ The two MARTIN 77 values are from a T-matrix pole and from a Breit-Wigner fit.			

$\Sigma(1775)$ DECAY MODES

Mode	Fraction (Γ_i/Γ)
Γ_1 $N\bar{K}$	37-43%
Γ_2 $\Lambda\pi$	14-20%
Γ_3 $\Sigma\pi$	2-5%
Γ_4 $\Sigma(1385)\pi$	8-12%
Γ_5 $\Sigma(1385)\pi, D\text{-wave}$	
Γ_6 $\Sigma(1385)\pi, D\text{-wave}$	
Γ_7 $\Sigma(1385)\pi, G\text{-wave}$	
Γ_8 $\Lambda(1520)\pi, P\text{-wave}$	17-23%
Γ_9 $\Sigma\pi\pi$	

$\Sigma(1775)$

Γ_{10}	$\Delta(1232)\bar{K}$, <i>D</i> -wave
Γ_{11}	$N\bar{K}^*(892)$, <i>S</i> =1/2
Γ_{12}	$N\bar{K}^*(892)$, <i>S</i> =1/2, <i>D</i> -wave
Γ_{13}	$N\bar{K}^*(892)$, <i>S</i> =3/2, <i>D</i> -wave
Γ_{14}	$N\bar{K}^*(892)$, <i>S</i> =3/2, <i>G</i> -wave

$\Sigma(1775)$ BRANCHING RATIOS

See "Sign conventions for resonance couplings" in the Note on Λ and Σ Resonances. Also, the errors quoted do not include uncertainties due to the parametrization used in the partial-wave analyses and are thus too small.

$\Gamma(N\bar{K})/\Gamma_{total}$				Γ_1/Γ
VALUE	DOCUMENT ID	TECN	COMMENT	
0.37 to 0.43 OUR ESTIMATE				
0.43 ± 0.09	SARANTSEV	19	DPWA	$\bar{K}N$ multichannel
0.40 ± 0.01	ZHANG	13A	DPWA	$\bar{K}N$ multichannel
0.40 ± 0.02	GOPAL	80	DPWA	$\bar{K}N \rightarrow \bar{K}N$
0.37 ± 0.03	ALSTON-...	78	DPWA	$\bar{K}N \rightarrow \bar{K}N$
••• We do not use the following data for averages, fits, limits, etc. •••				
0.402	¹ KAMANO	15	DPWA	Multichannel
0.41 ± 0.03	GOPAL	77	DPWA	See GOPAL 80
0.37 or 0.36	² MARTIN	77	DPWA	$\bar{K}N$ multichannel

¹ From the preferred solution A in KAMANO 15.
² The two MARTIN 77 values are from a T-matrix pole and from a Breit-Wigner fit.

$\Gamma(\Lambda\pi)/\Gamma_{total}$				Γ_2/Γ
VALUE	DOCUMENT ID	TECN	COMMENT	
0.49 ± 0.10	SARANTSEV	19	DPWA	$\bar{K}N$ multichannel
••• We do not use the following data for averages, fits, limits, etc. •••				
0.244	¹ KAMANO	15	DPWA	$\bar{K}N$ multichannel

¹ From the preferred solution A in KAMANO 15.

$\Gamma(\Lambda\pi)/\Gamma(N\bar{K})$				Γ_2/Γ_1
VALUE	DOCUMENT ID	TECN	COMMENT	
0.33 ± 0.05	UHLIG	67	HBC	K^-p 0.9 GeV/c

$\Gamma(\Sigma\pi)/\Gamma_{total}$				Γ_3/Γ
VALUE	DOCUMENT ID	TECN	COMMENT	
0.035 ± 0.010	SARANTSEV	19	DPWA	$\bar{K}N$ multichannel
••• We do not use the following data for averages, fits, limits, etc. •••				
0.042	¹ KAMANO	15	DPWA	$\bar{K}N$ multichannel

¹ From the preferred solution A in KAMANO 15.

$\Gamma(\Sigma(1385)\pi)/\Gamma(N\bar{K})$				Γ_4/Γ_1
VALUE	DOCUMENT ID	TECN	COMMENT	
0.25 ± 0.09	UHLIG	67	HBC	K^-p 0.9 GeV/c

$\Gamma(\Sigma(1385)\pi, D\text{-wave})/\Gamma_{total}$				Γ_6/Γ
VALUE	DOCUMENT ID	TECN	COMMENT	
••• We do not use the following data for averages, fits, limits, etc. •••				
0.309	¹ KAMANO	15	DPWA	Multichannel

¹ From the preferred solution A in KAMANO 15.

$\Gamma(\Sigma(1385)\pi, G\text{-wave})/\Gamma_{total}$				Γ_7/Γ
VALUE	DOCUMENT ID	TECN	COMMENT	
••• We do not use the following data for averages, fits, limits, etc. •••				
not seen	¹ KAMANO	15	DPWA	Multichannel

¹ From the preferred solution A in KAMANO 15.

$\Gamma(\Lambda(1520)\pi, P\text{-wave})/\Gamma_{total}$				Γ_8/Γ
VALUE	DOCUMENT ID	TECN	COMMENT	
0.02 ± 0.01	SARANTSEV	19	DPWA	$\bar{K}N$ multichannel

$\Gamma(\Lambda(1520)\pi, P\text{-wave})/\Gamma(N\bar{K})$				Γ_8/Γ_1
VALUE	DOCUMENT ID	TECN	COMMENT	
0.28 ± 0.05	UHLIG	67	HBC	K^-p 0.9 GeV/c

$\Gamma(\Sigma\pi\pi)/\Gamma_{total}$				Γ_9/Γ
VALUE	DOCUMENT ID	TECN	COMMENT	
••• We do not use the following data for averages, fits, limits, etc. •••				
0.12	¹ ARMENTEROS68c	HD8C	$K^-N \rightarrow \Sigma\pi\pi$	

¹ For about 3/4 of this, the $\Sigma\pi$ system has $l = 0$ and is almost entirely $\Lambda(1520)$. For the rest, the $\Sigma\pi$ has $l = 1$, which is about what is expected from the known $\Sigma(1775) \rightarrow \Sigma(1385)\pi$ rate, as seen in $\Lambda\pi\pi$.

$\Gamma(N\bar{K}^*(892), S=1/2, D\text{-wave})/\Gamma_{total}$				Γ_{12}/Γ
VALUE	DOCUMENT ID	TECN	COMMENT	
••• We do not use the following data for averages, fits, limits, etc. •••				
not seen	¹ KAMANO	15	DPWA	Multichannel

¹ From the preferred solution A in KAMANO 15.

$\Gamma(N\bar{K}^*(892), S=3/2, D\text{-wave})/\Gamma_{total}$				Γ_{13}/Γ
VALUE	DOCUMENT ID	TECN	COMMENT	
••• We do not use the following data for averages, fits, limits, etc. •••				
0.003	¹ KAMANO	15	DPWA	Multichannel

¹ From the preferred solution A in KAMANO 15.

$\Gamma(N\bar{K}^*(892), S=3/2, G\text{-wave})/\Gamma_{total}$				Γ_{14}/Γ
VALUE	DOCUMENT ID	TECN	COMMENT	
••• We do not use the following data for averages, fits, limits, etc. •••				
not seen	¹ KAMANO	15	DPWA	Multichannel

¹ From the preferred solution A in KAMANO 15.

$(\Gamma_1\Gamma_7)^{1/2}/\Gamma_{total}$ in $N\bar{K} \rightarrow \Sigma(1775) \rightarrow \Lambda\pi$				$(\Gamma_1\Gamma_2)^{1/2}/\Gamma$
VALUE	DOCUMENT ID	TECN	COMMENT	
-0.31 ± 0.01	ZHANG	13A	DPWA	Multichannel
-0.28 ± 0.03	GOPAL	77	DPWA	$\bar{K}N$ multichannel
-0.25 ± 0.02	BAILLON	75	IPWA	$\bar{K}N \rightarrow \Lambda\pi$
-0.28 ± 0.04	VANHORN	75	DPWA	$K^-p \rightarrow \Lambda\pi^0$
-0.259 ± 0.048	DEVENISH	74B	Fixed- t dispersion rel.	
••• We do not use the following data for averages, fits, limits, etc. •••				
-0.29 or -0.28	¹ MARTIN	77	DPWA	$\bar{K}N$ multichannel
-0.30	DEBELLEFON	76	IPWA	$K^-p \rightarrow \Lambda\pi^0$

¹ The two MARTIN 77 values are from a T-matrix pole and from a Breit-Wigner fit.

$(\Gamma_1\Gamma_7)^{1/2}/\Gamma_{total}$ in $N\bar{K} \rightarrow \Sigma(1775) \rightarrow \Sigma\pi$				$(\Gamma_1\Gamma_3)^{1/2}/\Gamma$
VALUE	DOCUMENT ID	TECN	COMMENT	
+0.08 ± 0.01	ZHANG	13A	DPWA	Multichannel
+0.13 ± 0.02	GOPAL	77	DPWA	$\bar{K}N$ multichannel
0.09 ± 0.01	KANE	74	DPWA	$K^-p \rightarrow \Sigma\pi$
••• We do not use the following data for averages, fits, limits, etc. •••				
+0.08 or +0.08	¹ MARTIN	77	DPWA	$\bar{K}N$ multichannel

¹ The two MARTIN 77 values are from a T-matrix pole and from a Breit-Wigner fit.

$(\Gamma_1\Gamma_7)^{1/2}/\Gamma_{total}$ in $N\bar{K} \rightarrow \Sigma(1775) \rightarrow \Sigma(1385)\pi, D\text{-wave}$				$(\Gamma_1\Gamma_5)^{1/2}/\Gamma$
VALUE	DOCUMENT ID	TECN	COMMENT	
-0.12 ± 0.01	ZHANG	13A	DPWA	Multichannel
-0.184 ± 0.011	¹ CAMERON	78	DPWA	$K^-p \rightarrow \Sigma(1385)\pi$
+0.20 ± 0.02	PREVOST	74	DPWA	$K^-N \rightarrow \Sigma(1385)\pi$
••• We do not use the following data for averages, fits, limits, etc. •••				
0.32 ± 0.06	SIMS	68	DBC	$K^-N \rightarrow \Lambda\pi\pi$
0.24 ± 0.03	ARMENTEROS67c	HBC	$K^-p \rightarrow \Lambda\pi\pi$	

¹ The CAMERON 78 upper limit on G-wave decay is 0.03.

$(\Gamma_1\Gamma_7)^{1/2}/\Gamma_{total}$ in $N\bar{K} \rightarrow \Sigma(1775) \rightarrow \Lambda(1520)\pi, P\text{-wave}$				$(\Gamma_1\Gamma_8)^{1/2}/\Gamma$
VALUE	DOCUMENT ID	TECN	COMMENT	
-0.06 ± 0.01	ZHANG	13A	DPWA	Multichannel
-0.305 ± 0.010	¹ CAMERON	77	DPWA	$K^-p \rightarrow \Lambda(1520)\pi^0$
0.31 ± 0.02	BARLETTA	72	DPWA	$K^-p \rightarrow \Lambda(1520)\pi^0$
0.27 ± 0.03	ARMENTEROS65c	HBC	$K^-p \rightarrow \Lambda(1520)\pi^0$	

¹ This rate combines P-wave- and F-wave decays. The CAMERON 77 results for the separate P-wave- and F-wave decays are -0.303 ± 0.010 and -0.037 ± 0.014 . The published signs have been changed here to be in accord with the baryon-first convention.

$(\Gamma_1\Gamma_7)^{1/2}/\Gamma_{total}$ in $N\bar{K} \rightarrow \Sigma(1775) \rightarrow \Delta(1232)\bar{K}, D\text{-wave}$				$(\Gamma_1\Gamma_{10})^{1/2}/\Gamma$
VALUE	DOCUMENT ID	TECN	COMMENT	
+0.06 ± 0.03	ZHANG	13A	DPWA	Multichannel

$(\Gamma_1\Gamma_7)^{1/2}/\Gamma_{total}$ in $N\bar{K} \rightarrow \Sigma(1775) \rightarrow N\bar{K}^*(892), S=1/2$				$(\Gamma_1\Gamma_{11})^{1/2}/\Gamma$
VALUE	DOCUMENT ID	TECN	COMMENT	
+0.04 ± 0.01	ZHANG	13A	DPWA	Multichannel

$(\Gamma_1\Gamma_7)^{1/2}/\Gamma_{total}$ in $N\bar{K} \rightarrow \Sigma(1775) \rightarrow N\bar{K}^*(892), S=3/2, D\text{-wave}$				$(\Gamma_1\Gamma_{13})^{1/2}/\Gamma$
VALUE	DOCUMENT ID	TECN	COMMENT	
+0.04 ± 0.01	ZHANG	13A	DPWA	Multichannel

$\Sigma(1775)$ REFERENCES

SARANTSEV 19	EPJ A55 180	A.V. Sarantsev et al.	(BONN, PNPI)
KAMANO 15	PR C92 025205	H. Kamano et al.	(ANL, OSAK)
ZHANG 13A	PR C68 035205	H. Zhang et al.	(KSU)
PDC 82	PL 111B 1	M. Roos et al.	(HELS, CIT, CERN)
GOPAL 80	Toronto Conf. 159	G.P. Gopal	(RHEL) IJP
ALSTON-... 78	PR D18 182	M. Alston-Garnjost et al.	(LBL, MTHO+) IJP
Also	PRL 38 1007	M. Alston-Garnjost et al.	(LBL, MTHO+) IJP
CAMERON 78	NP B143 189	W. Cameron et al.	(RHEL, LOIC) IJP
CAMERON 77	NP B131 399	W. Cameron et al.	(RHEL, LOIC) IJP
GOPAL 77	NP B119 362	G.P. Gopal et al.	(LOIC, RHEL) IJP
MARTIN 77	NP B127 349	B.R. Martin, M.K. Pidcock, R.G. Moorhouse	(LOUC+) IJP
Also	NP B126 266	B.R. Martin, M.K. Pidcock	(LOUC) IJP
Also	NP B126 285	B.R. Martin, M.K. Pidcock	(LOUC) IJP
DEBELLEFON 76	NP B109 129	A. de Bellefon, A. Berthon	(CDFE) IJP
BAILLON 75	NP B94 39	P.H. Baillon, P.J. Litchfield	(CERN, RHEL) IJP

Baryon Particle Listings

$\Sigma(1775), \Sigma(1780), \Sigma(1880)$

VANHORN	75	NP B87 145	A.J. van Horn	(LBL) IJP
Also		NP B87 157	A.J. van Horn	(LBL) IJP
DEVENISH	74B	NP B81 330	R.C.E. Devenish, C.D. Froggatt, B.R. Martin	(DESY+)
KANE	74	LBL-2452	D.F. Kane	(LBL) IJP
PREVOST	74	NP B69 246	J. Prevost <i>et al.</i>	(SACL, CERN, HEID)
BARLETTA	72	NP B40 45	W.A. Barletta	(EFI) IJP
Also		PRL 17 841	S. Fenster <i>et al.</i>	(CHIC, ANL, CERN) IJP
ARMENTEROS	68C	NP B8 216	R. Armenteros <i>et al.</i>	(CERN, HEID, SAACL) I
SIMS	68	PRL 21 1413	W.H. Sims <i>et al.</i>	(FSU, TUFTS, BRAN)
ARMENTEROS	67C	ZPHY 202 486	R. Armenteros <i>et al.</i>	(CERN, HEID, SAACL)
UHLIG	67	PR 155 1448	R.P. Uhlig <i>et al.</i>	(UMD, NRL)
ARMENTEROS	65C	PL 19 338	R. Armenteros <i>et al.</i>	(CERN, HEID, SAACL) IJP
GALTIERI	63	PL 6 296	A. Galtieri, A. Hussain, R. Tripp	(LRL) IJ

$\Sigma(1780) 3/2^+$ $I(J^P) = 1(\frac{3}{2}^+)$ Status: *
 OMITTED FROM SUMMARY TABLE
 was $\Sigma(1730)$

$\Sigma(1780)$ MASS

VALUE (MeV)	DOCUMENT ID	TECN	COMMENT
1730 to 1830 (≈ 1780) OUR ESTIMATE			
1727 \pm 27	ZHANG	13A	DPWA Multichannel
1798 or 1802	¹ MARTIN	77	DPWA $\bar{K}N$ multichannel
1720 \pm 30	² BAILLON	75	IPWA $\bar{K}N \rightarrow \Lambda\pi$
1840 \pm 10	LANGBEIN	72	IPWA $\bar{K}N$ multichannel

¹ The two MARTIN 77 values are from a T-matrix pole and from a Breit-Wigner fit.
² From solution 1 of BAILLON 75; not present in solution 2.

$\Sigma(1780)$ WIDTH

VALUE (MeV)	DOCUMENT ID	TECN	COMMENT
100 to 300 (≈ 200) OUR ESTIMATE			
276 \pm 87	ZHANG	13A	DPWA Multichannel
93 or 93	¹ MARTIN	77	DPWA $\bar{K}N$ multichannel
120 \pm 30	² BAILLON	75	IPWA $\bar{K}N \rightarrow \Lambda\pi$
120 \pm 10	LANGBEIN	72	IPWA $\bar{K}N$ multichannel

¹ The two MARTIN 77 values are from a T-matrix pole and from a Breit-Wigner fit.
² From solution 1 of BAILLON 75; not present in solution 2.

$\Sigma(1780)$ DECAY MODES

Mode	Fraction (Γ_i/Γ)
Γ_1 $N\bar{K}$	(2.0 \pm 1.0) %
Γ_2 $\Lambda\pi$	(70 \pm 17) %
Γ_3 $\Sigma\pi$	(12 \pm 6) %

$\Sigma(1780)$ BRANCHING RATIOS

$\Gamma(N\bar{K})/\Gamma_{total}$	DOCUMENT ID	TECN	COMMENT	Γ_1/Γ
0.02 \pm 0.01	ZHANG	13A	DPWA Multichannel	

$\Gamma(\Lambda\pi)/\Gamma_{total}$	DOCUMENT ID	TECN	COMMENT	Γ_2/Γ
0.70 \pm 0.17	ZHANG	13A	DPWA Multichannel	

$\Gamma(\Sigma\pi)/\Gamma_{total}$	DOCUMENT ID	TECN	COMMENT	Γ_3/Γ
0.12 \pm 0.06	ZHANG	13A	DPWA Multichannel	

$\Sigma(1780)$ REFERENCES

ZHANG	13A	PR C88 035205	H. Zhang <i>et al.</i>	(KSU)
MARTIN	77	NP B127 349	B.R. Martin, M.K. Pidcock, R.G. Moorhouse	(LOUC+)
BAILLON	75	NP B94 39	P.H. Baillon, P.J. Litchfield	(CERN, RHEL)
LANGBEIN	72	NP B47 477	W. Langbein, F. Wagner	(MPIM)

$\Sigma(1880) 1/2^+$ $I(J^P) = 1(\frac{1}{2}^+)$ Status: **
 OMITTED FROM SUMMARY TABLE

A P_{11} resonance is suggested by several partial-wave analyses, but with wide variations in the mass and other parameters. We list here all claims which lie well above the P_{11} $\Sigma(1770)$.

$\Sigma(1880)$ POLE POSITION

REAL PART	DOCUMENT ID	TECN	COMMENT
1776	ZHANG	13A	DPWA Multichannel

• • • We do not use the following data for averages, fits, limits, etc. • • •

—2xIMAGINARY PART

VALUE (MeV)	DOCUMENT ID	TECN	COMMENT
• • • We do not use the following data for averages, fits, limits, etc. • • •			
270	ZHANG	13A	DPWA Multichannel

$\Sigma(1880)$ MASS

VALUE (MeV)	DOCUMENT ID	TECN	COMMENT
1820 to 1940 (≈ 1880) OUR ESTIMATE			
1821 \pm 17	ZHANG	13A	DPWA Multichannel
1826 \pm 20	GOPAL	80	DPWA $\bar{K}N \rightarrow \bar{K}N$
1870 \pm 10	CAMERON	78B	DPWA $K^-p \rightarrow N\bar{K}^*$
1847 or 1863	¹ MARTIN	77	DPWA $\bar{K}N$ multichannel
1960 \pm 30	² BAILLON	75	IPWA $\bar{K}N \rightarrow \Lambda\pi$
1985 \pm 50	VANHORN	75	DPWA $K^-p \rightarrow \Lambda\pi^0$
1898	³ LEA	73	DPWA Multichannel K-matrix
~ 1850	ARMENTEROSTO	70	IPWA $\bar{K}N \rightarrow \bar{K}N$
1950 \pm 50	BARBARO...	70	DPWA $K^-N \rightarrow \Lambda\pi$
1920 \pm 30	LITCHFIELD	70	DPWA $K^-N \rightarrow \Lambda\pi$
1850	BAILEY	69	DPWA $\bar{K}N \rightarrow \bar{K}N$
1882 \pm 40	SMART	68	DPWA $K^-N \rightarrow \Lambda\pi$

$\Sigma(1880)$ WIDTH

VALUE (MeV)	DOCUMENT ID	TECN	COMMENT
100 to 300 (≈ 200) OUR ESTIMATE			
300 \pm 59	ZHANG	13A	DPWA Multichannel
86 \pm 15	GOPAL	80	DPWA $\bar{K}N \rightarrow \bar{K}N$
80 \pm 10	CAMERON	78B	DPWA $K^-p \rightarrow N\bar{K}^*$
216 or 220	¹ MARTIN	77	DPWA $\bar{K}N$ multichannel
260 \pm 40	² BAILLON	75	IPWA $\bar{K}N \rightarrow \Lambda\pi$
220 \pm 140	VANHORN	75	DPWA $K^-p \rightarrow \Lambda\pi^0$
222	³ LEA	73	DPWA Multichannel K-matrix
~ 30	ARMENTEROSTO	70	IPWA $\bar{K}N \rightarrow \bar{K}N$
200 \pm 50	BARBARO...	70	DPWA $K^-N \rightarrow \Lambda\pi$
170 \pm 40	LITCHFIELD	70	DPWA $K^-N \rightarrow \Lambda\pi$
200	BAILEY	69	DPWA $\bar{K}N \rightarrow \bar{K}N$
222 \pm 150	SMART	68	DPWA $K^-N \rightarrow \Lambda\pi$

$\Sigma(1880)$ DECAY MODES

Mode	Fraction (Γ_i/Γ)
Γ_1 $N\bar{K}$	0.10 to 0.30 (≈ 0.20)
Γ_2 $\Lambda\pi$	
Γ_3 $\Sigma\pi$	
Γ_4 $\Lambda(1520)\pi, D$ -wave	(2.0 \pm 1.0) %
Γ_5 $N\bar{K}^*(892), S=1/2, P$ -wave	
Γ_6 $N\bar{K}^*(892), S=3/2, P$ -wave	
Γ_7 $\Delta(1232)\bar{K}, P$ -wave	(39 \pm 8) %

$\Sigma(1880)$ BRANCHING RATIOS

See "Sign conventions for resonance couplings" in the Note on Λ and Σ Resonances.

$\Gamma(N\bar{K})/\Gamma_{total}$	DOCUMENT ID	TECN	COMMENT	Γ_1/Γ
0.10 to 0.30 (≈ 0.20) OUR ESTIMATE				
0.10 \pm 0.03	ZHANG	13A	DPWA Multichannel	
0.06 \pm 0.02	GOPAL	80	DPWA $\bar{K}N \rightarrow \bar{K}N$	
0.27 or 0.27	¹ MARTIN	77	DPWA $\bar{K}N$ multichannel	
0.31	³ LEA	73	DPWA Multichannel K-matrix	
0.20	ARMENTEROSTO	70	IPWA $\bar{K}N \rightarrow \bar{K}N$	
0.22	BAILEY	69	DPWA $\bar{K}N \rightarrow \bar{K}N$	

$(\Gamma_1\Gamma_7)^{1/2}/\Gamma_{total}$ in $N\bar{K} \rightarrow \Sigma(1880) \rightarrow \Lambda\pi$	DOCUMENT ID	TECN	COMMENT	$(\Gamma_1\Gamma_2)^{1/2}/\Gamma$
−0.24 or −0.24	¹ MARTIN	77	DPWA $\bar{K}N$ multichannel	
−0.12 \pm 0.02	² BAILLON	75	IPWA $\bar{K}N \rightarrow \Lambda\pi$	
+0.05 \pm 0.07 −0.02	VANHORN	75	DPWA $K^-p \rightarrow \Lambda\pi^0$	
−0.169 \pm 0.119	DEVENISH	74B	Fixed-t dispersion rel.	
−0.30	³ LEA	73	DPWA Multichannel K-matrix	
−0.09 \pm 0.04	BARBARO...	70	DPWA $K^-N \rightarrow \Lambda\pi$	
−0.14 \pm 0.03	LITCHFIELD	70	DPWA $K^-N \rightarrow \Lambda\pi$	
−0.11 \pm 0.03	SMART	68	DPWA $K^-N \rightarrow \Lambda\pi$	

$(\Gamma_1\Gamma_7)^{1/2}/\Gamma_{total}$ in $N\bar{K} \rightarrow \Sigma(1880) \rightarrow \Sigma\pi$	DOCUMENT ID	TECN	COMMENT	$(\Gamma_1\Gamma_3)^{1/2}/\Gamma$
+0.30 or +0.29 not seen	¹ MARTIN	77	DPWA $\bar{K}N$ multichannel	
	³ LEA	73	DPWA Multichannel K-matrix	

See key on page 999

Baryon Particle Listings

$\Sigma(1880), \Sigma(1900)$

$\Gamma(\Lambda(1520)\pi, D\text{-wave})/\Gamma_{\text{total}}$		Γ_4/Γ	
VALUE	DOCUMENT ID	TECN	COMMENT
0.02±0.01	ZHANG	13A	DPWA Multichannel

$(\Gamma_1/\Gamma_7)^{1/2}/\Gamma_{\text{total}}$ in $N\bar{K} \rightarrow \Sigma(1880) \rightarrow N\bar{K}^*(892), S=1/2, P\text{-wave } (\Gamma_1/\Gamma_5)^{1/2}/\Gamma$			
VALUE	DOCUMENT ID	TECN	COMMENT
-0.05±0.03	4 CAMERON	78B	DPWA $K^-p \rightarrow N\bar{K}^*$

$(\Gamma_1/\Gamma_7)^{1/2}/\Gamma_{\text{total}}$ in $N\bar{K} \rightarrow \Sigma(1880) \rightarrow N\bar{K}^*(892), S=3/2, P\text{-wave } (\Gamma_1/\Gamma_6)^{1/2}/\Gamma$			
VALUE	DOCUMENT ID	TECN	COMMENT
+0.11±0.03	CAMERON	78B	DPWA $K^-p \rightarrow N\bar{K}^*$

$\Gamma(\Delta(1232)\bar{K}, P\text{-wave})/\Gamma_{\text{total}}$		Γ_7/Γ	
VALUE	DOCUMENT ID	TECN	COMMENT
0.39±0.08	ZHANG	13A	DPWA Multichannel

$\Sigma(1880)$ FOOTNOTES

- The two MARTIN 77 values are from a T-matrix pole and from a Breit-Wigner fit.
- From solution 1 of BAILLON 75; not present in solution 2.
- Only unconstrained states from table 1 of LEA 73 are listed.
- The published sign has been changed to be in accord with the baryon-first convention.

$\Sigma(1880)$ REFERENCES

ZHANG 13A	PR C88 035205	H. Zhang et al.	(KSU)
GOPAL 80	Toronto Conf. 159	G.P. Gopal	(RHEL) IJP
CAMERON 78B	NP B146 327	W. Cameron et al.	(RHEL, LOIC) IJP
MARTIN 77	NP B127 349	B.R. Martin, M.K. Pidcock, R.G. Moorhouse	(LOUC+) IJP
	Also NP B126 266	B.R. Martin, M.K. Pidcock	(LOUC) IJP
	Also NP B126 285	B.R. Martin, M.K. Pidcock	(LOUC) IJP
BAILLON 75	NP B94 39	P.H. Baillon, P.J. Litchfield	(CERN, RHEL) IJP
VANHORN 75	NP B87 145	A.J. van Horn	(LBL) IJP
	Also NP B87 157	A.J. van Horn	(LBL) IJP
DEVENISH 74B	NP B81 330	R.C.E. Devenish, C.D. Froggatt, B.R. Martin	(DESY+) IJP
LEA 73	NP B56 77	A.T. Lea et al.	(RHEL, LOUC, GLAS, AARH) IJP
ARMENTEROS 70	Duke Conf. 123	R. Armenteros et al.	(CERN, HEID, SACL) IJP
	Hyperon Resonances, 1970		
BARBARO... 70	Duke Conf. 173	A. Barbaro-Galteri	(LRL) IJP
	Hyperon Resonances, 1970		
LITCHFIELD 70	NP B22 269	P.J. Litchfield	(RHEL) IJP
BAILEY 69	Thesis UCRL 50617	J.M. Bailey	(LLL) IJP
SMART 68	PR 169 1330	W.M. Smart	(LRL) IJP

$\Sigma(1900) 1/2^-$

$$I(J^P) = 1(\frac{1}{2}^-) \text{ Status: **}$$

OMITTED FROM SUMMARY TABLE

$\Sigma(1900)$ POLE POSITION

REAL PART			
VALUE	DOCUMENT ID	TECN	COMMENT
1936±10	SARANTSEV	19	DPWA $\bar{K}N$ multichannel
-2×IMAGINARY PART			
VALUE	DOCUMENT ID	TECN	COMMENT
150±25	SARANTSEV	19	DPWA $\bar{K}N$ multichannel

$\Sigma(1900)$ POLE RESIDUES

The normalized residue is the residue divided by $\Gamma_{\text{pole}}/2$.

Normalized residue in $N\bar{K} \rightarrow \Sigma(1900) \rightarrow N\bar{K}$			
MODULUS	PHASE (°)	DOCUMENT ID	TECN
0.45±0.09	90 ± 25	SARANTSEV	19
		DPWA	$\bar{K}N$ multichannel

Normalized residue in $N\bar{K} \rightarrow \Sigma(1900) \rightarrow \Sigma\pi$			
MODULUS	PHASE (°)	DOCUMENT ID	TECN
0.38±0.08	95 ± 20	SARANTSEV	19
		DPWA	$\bar{K}N$ multichannel

Normalized residue in $N\bar{K} \rightarrow \Sigma(1900) \rightarrow \Sigma\eta$			
MODULUS	PHASE (°)	DOCUMENT ID	TECN
0.03±0.01	20 ± 20	SARANTSEV	19
		DPWA	$\bar{K}N$ multichannel

Normalized residue in $N\bar{K} \rightarrow \Sigma(1900) \rightarrow \Lambda\pi$			
MODULUS	PHASE (°)	DOCUMENT ID	TECN
0.14±0.05	-160 ± 50	SARANTSEV	19
		DPWA	$\bar{K}N$ multichannel

Normalized residue in $N\bar{K} \rightarrow \Sigma(1900) \rightarrow \Xi K$			
MODULUS	PHASE (°)	DOCUMENT ID	TECN
0.08±0.05	75 ± 25	SARANTSEV	19
		DPWA	$\bar{K}N$ multichannel

Normalized residue in $N\bar{K} \rightarrow \Sigma(1900) \rightarrow \Sigma(1385)\pi$			
MODULUS	PHASE (°)	DOCUMENT ID	TECN
0.16±0.05	40 ± 30	SARANTSEV	19
		DPWA	$\bar{K}N$ multichannel

Normalized residue in $N\bar{K} \rightarrow \Sigma(1900) \rightarrow \Lambda(1520)\pi$			
MODULUS	PHASE (°)	DOCUMENT ID	TECN
0.04±0.02	-25 ± 40	SARANTSEV	19
		DPWA	$\bar{K}N$ multichannel

Normalized residue in $N\bar{K} \rightarrow \Sigma(1900) \rightarrow \Delta\bar{K}$			
MODULUS	PHASE (°)	DOCUMENT ID	TECN
0.11±0.04	60 ± 30	SARANTSEV	19
		DPWA	$\bar{K}N$ multichannel

Normalized residue in $N\bar{K} \rightarrow \Sigma(1900) \rightarrow N\bar{K}^*(892), S=1/2, S\text{-wave}$			
MODULUS	PHASE (°)	DOCUMENT ID	TECN
0.17±0.06	50 ± 50	SARANTSEV	19
		DPWA	$\bar{K}N$ multichannel

Normalized residue in $N\bar{K} \rightarrow \Sigma(1900) \rightarrow N\bar{K}^*(892), S=3/2, D\text{-wave}$			
MODULUS	PHASE (°)	DOCUMENT ID	TECN
0.05±0.04		SARANTSEV	19
		DPWA	$\bar{K}N$ multichannel

$\Sigma(1900)$ MASS

VALUE (MeV)	DOCUMENT ID	TECN	COMMENT
1900 to 1950 (≈ 1925) OUR ESTIMATE			
1938±12	SARANTSEV	19	DPWA $\bar{K}N$ multichannel
1900±21	ZHANG	13A	DPWA $\bar{K}N$ multichannel
1944±15	GOPAL	80	DPWA $\bar{K}N \rightarrow \bar{K}N$
1755 or 1834	1 MARTIN	77	DPWA $\bar{K}N$ multichannel
2004±40	VANHORN	75	DPWA $K^-p \rightarrow \Lambda\pi^0$
••• We do not use the following data for averages, fits, limits, etc. •••			
1955±15	GOPAL	77	DPWA $\bar{K}N$ multichannel
1 The two MARTIN 77 values are from a T-matrix pole and from a Breit-Wigner fit.			

$\Sigma(1900)$ WIDTH

VALUE (MeV)	DOCUMENT ID	TECN	COMMENT
140 to 190 (≈ 165) OUR ESTIMATE			
155±30	SARANTSEV	19	DPWA $\bar{K}N$ multichannel
191±47	ZHANG	13A	DPWA $\bar{K}N$ multichannel
215±25	GOPAL	80	DPWA $\bar{K}N \rightarrow \bar{K}N$
413 or 450	1 MARTIN	77	DPWA $\bar{K}N$ multichannel
116±40	VANHORN	75	DPWA $K^-p \rightarrow \Lambda\pi^0$
••• We do not use the following data for averages, fits, limits, etc. •••			
170±40	GOPAL	77	DPWA $\bar{K}N$ multichannel
1 The two MARTIN 77 values are from a T-matrix pole and from a Breit-Wigner fit.			

$\Sigma(1900)$ DECAY MODES

Mode	Fraction (Γ_i/Γ)
$\Gamma_1 N\bar{K}$	0.40 to 0.70 (≈ 0.55)
$\Gamma_2 \Sigma\pi$	0.10 to 0.40 (≈ 0.25)
$\Gamma_3 \Sigma\eta$	(1.0 ± 1.0) %
$\Gamma_4 \Lambda\pi$	(6.0 ± 2.0) %
$\Gamma_5 \Xi K$	(3.0 ± 2.0) %
$\Gamma_6 \Sigma(1385)\pi$	(7.0 ± 3.0) %
$\Gamma_7 \Lambda(1520)\pi$	
$\Gamma_8 \Delta\bar{K}$	(2.5 ± 1.0) %
$\Gamma_9 N\bar{K}^*(892), S=1/2, S\text{-wave}$	(7.0 ± 3.0) %
$\Gamma_{10} N\bar{K}^*(892), S=3/2, D\text{-wave}$	

$\Sigma(1900)$ BRANCHING RATIOS

$\Gamma(N\bar{K})/\Gamma_{\text{total}}$		Γ_1/Γ	
VALUE	DOCUMENT ID	TECN	COMMENT
0.40 to 0.70 (≈ 0.55) OUR ESTIMATE			
0.45±0.09	SARANTSEV	19	DPWA $\bar{K}N$ multichannel
0.67±0.17	ZHANG	13A	DPWA $\bar{K}N$ multichannel

$\Gamma(\Sigma\pi)/\Gamma_{\text{total}}$		Γ_2/Γ	
VALUE	DOCUMENT ID	TECN	COMMENT
0.10 to 0.40 (≈ 0.25) OUR ESTIMATE			
0.33±0.07	SARANTSEV	19	DPWA $\bar{K}N$ multichannel
0.10±0.05	ZHANG	13A	DPWA $\bar{K}N$ multichannel

$\Gamma(\Sigma\eta)/\Gamma_{\text{total}}$		Γ_3/Γ	
VALUE	DOCUMENT ID	TECN	COMMENT
0.01±0.01	SARANTSEV	19	DPWA $\bar{K}N$ multichannel

$\Gamma(\Lambda\pi)/\Gamma_{\text{total}}$		Γ_4/Γ	
VALUE	DOCUMENT ID	TECN	COMMENT
0.06±0.02	SARANTSEV	19	DPWA $\bar{K}N$ multichannel

$\Gamma(\Xi K)/\Gamma_{\text{total}}$		Γ_5/Γ	
VALUE	DOCUMENT ID	TECN	COMMENT
0.03±0.02	SARANTSEV	19	DPWA $\bar{K}N$ multichannel

$\Gamma(\Sigma(1385)\pi)/\Gamma_{\text{total}}$		Γ_6/Γ	
VALUE	DOCUMENT ID	TECN	COMMENT
0.07±0.03	SARANTSEV	19	DPWA $\bar{K}N$ multichannel

Baryon Particle Listings

$\Sigma(1900), \Sigma(1910)$

$\Gamma(\Lambda(1520)\pi)/\Gamma_{\text{total}}$				Γ_7/Γ
VALUE	DOCUMENT ID	TECN	COMMENT	
<0.01	SARANTSEV 19	DPWA	$\bar{K}N$ multichannel	

$\Gamma(\Delta\bar{K})/\Gamma_{\text{total}}$				Γ_8/Γ
VALUE	DOCUMENT ID	TECN	COMMENT	
0.025 ± 0.010	SARANTSEV 19	DPWA	$\bar{K}N$ multichannel	

$\Gamma(N\bar{K}^*(892), S=1/2, S\text{-wave})/\Gamma_{\text{total}}$				Γ_9/Γ
VALUE	DOCUMENT ID	TECN	COMMENT	
0.07 ± 0.03	SARANTSEV 19	DPWA	$\bar{K}N$ multichannel	

$\Gamma(N\bar{K}^*(892), S=3/2, D\text{-wave})/\Gamma_{\text{total}}$				Γ_{10}/Γ
VALUE	DOCUMENT ID	TECN	COMMENT	
<0.01	SARANTSEV 19	DPWA	$\bar{K}N$ multichannel	

$\Sigma(1900)$ REFERENCES

SARANTSEV 19	EPJ A55 180	A.V. Sarantsev et al.	(BONN, PNPI)
ZHANG 13A	PR C88 035205	H. Zhang et al.	(KSU)
GOPAL 80	Toronto Conf. 159	G.P. Gopal	(RHEL)
GOPAL 77	NP B119 362	G.P. Gopal et al.	(LOIC, RHEL)
MARTIN 77	NP B127 349	B.R. Martin, M.K. Pittcock, R.G. Moorhouse	(LOUC+)
VANHORN 75	NP B87 145	A.J. van Horn	(LBL)

$\Sigma(1910) 3/2^-$

 $I(J^P) = 1(\frac{3}{2}^-)$ Status: ***

was $\Sigma(1940)$

For results published before 1974 (they are now obsolete), see our 1982 edition Physics Letters **111B** 1 (1982).

Not all analyses require this state. It is not required by the GOYAL 77 analysis of $K^-n \rightarrow (\Sigma\pi)^-$ nor by the GOPAL 80 analysis of $K^-n \rightarrow K^-n$. See also HEMINGWAY 75.

$\Sigma(1910)$ POLE RESIDUES

The normalized residue is the residue divided by $\Gamma_{\text{pole}}/2$.

Normalized residue in $N\bar{K} \rightarrow \Sigma(1910) \rightarrow N\bar{K}$			
MODULUS	PHASE (°)	DOCUMENT ID	TECN COMMENT
0.03 ± 0.02	-95 ± 60	SARANTSEV 19	DPWA $\bar{K}N$ multichannel

Normalized residue in $N\bar{K} \rightarrow \Sigma(1910) \rightarrow \Sigma\pi$			
MODULUS	PHASE (°)	DOCUMENT ID	TECN COMMENT
0.16 ± 0.04	-160 ± 15	SARANTSEV 19	DPWA $\bar{K}N$ multichannel

Normalized residue in $N\bar{K} \rightarrow \Sigma(1910) \rightarrow \Lambda\pi$			
MODULUS	PHASE (°)	DOCUMENT ID	TECN COMMENT
0.04 ± 0.03	25 ± 25	SARANTSEV 19	DPWA $\bar{K}N$ multichannel

Normalized residue in $N\bar{K} \rightarrow \Sigma(1910) \rightarrow \Xi\pi$			
MODULUS	PHASE (°)	DOCUMENT ID	TECN COMMENT
0.01 ± 0.01		SARANTSEV 19	DPWA $\bar{K}N$ multichannel

Normalized residue in $N\bar{K} \rightarrow \Sigma(1910) \rightarrow \Lambda(1520)\pi, P\text{-wave}$			
MODULUS	PHASE (°)	DOCUMENT ID	TECN COMMENT
0.01 ± 0.01		SARANTSEV 19	DPWA $\bar{K}N$ multichannel

Normalized residue in $N\bar{K} \rightarrow \Sigma(1910) \rightarrow \Lambda(1520)\pi, F\text{-wave}$			
MODULUS	PHASE (°)	DOCUMENT ID	TECN COMMENT
~ 0		SARANTSEV 19	DPWA $\bar{K}N$ multichannel

Normalized residue in $N\bar{K} \rightarrow \Sigma(1910) \rightarrow \Delta\bar{K}, S\text{-wave}$			
MODULUS	PHASE (°)	DOCUMENT ID	TECN COMMENT
0.03 ± 0.01	120 ± 20	SARANTSEV 19	DPWA $\bar{K}N$ multichannel

Normalized residue in $N\bar{K} \rightarrow \Sigma(1910) \rightarrow N\bar{K}^*(892), S=3/2, S\text{-wave}$			
MODULUS	PHASE (°)	DOCUMENT ID	TECN COMMENT
0.03 ± 0.02	20 ± 35	SARANTSEV 19	DPWA $\bar{K}N$ multichannel

Normalized residue in $N\bar{K} \rightarrow \Sigma(1910) \rightarrow N\bar{K}^*(892), S=1/2, D\text{-wave}$			
MODULUS	PHASE (°)	DOCUMENT ID	TECN COMMENT
0.02 ± 0.01		SARANTSEV 19	DPWA $\bar{K}N$ multichannel

Normalized residue in $N\bar{K} \rightarrow \Sigma(1910) \rightarrow N\bar{K}^*(892), S=3/2, D\text{-wave}$			
MODULUS	PHASE (°)	DOCUMENT ID	TECN COMMENT
0.01 ± 0.01		SARANTSEV 19	DPWA $\bar{K}N$ multichannel

$\Sigma(1910)$ MASS

1870 to 1950 (≈ 1910) OUR ESTIMATE			
VALUE (MeV)	DOCUMENT ID	TECN	COMMENT
1878 ± 12	SARANTSEV 19	DPWA	$\bar{K}N$ multichannel
1920 ± 50	GOPAL 77	DPWA	$\bar{K}N$ multichannel
1950 ± 30	BAILLON 75	IPWA	$\bar{K}N \rightarrow \Lambda\pi$
1949 +40 -60	VANHORN 75	DPWA	$K^-p \rightarrow \Lambda\pi^0$
1935 ± 80	KANE 74	DPWA	$K^-p \rightarrow \Sigma\pi$
1940 ± 20	LITCHFIELD 74B	DPWA	$K^-p \rightarrow \Lambda(1520)\pi^0$
1950 ± 20	LITCHFIELD 74C	DPWA	$K^-p \rightarrow \Delta(1232)\bar{K}$
••• We do not use the following data for averages, fits, limits, etc. •••			
1886 or 1893	¹ MARTIN 77	DPWA	$\bar{K}N$ multichannel
1940	DEBELLEFON 76	IPWA	$K^-p \rightarrow \Lambda\pi^0, F_{17}$ wave

$\Sigma(1910)$ WIDTH

150 to 300 (≈ 220) OUR ESTIMATE			
VALUE (MeV)	DOCUMENT ID	TECN	COMMENT
224 ± 25	SARANTSEV 19	DPWA	$\bar{K}N$ multichannel
170 ± 25	CAMERON 78B	DPWA	$K^-p \rightarrow N\bar{K}^*$
300 ± 80	GOPAL 77	DPWA	$\bar{K}N$ multichannel
150 ± 75	BAILLON 75	IPWA	$\bar{K}N \rightarrow \Lambda\pi$
160 +70 -40	VANHORN 75	DPWA	$K^-p \rightarrow \Lambda\pi^0$
330 ± 80	KANE 74	DPWA	$K^-p \rightarrow \Sigma\pi$
60 ± 20	LITCHFIELD 74B	DPWA	$K^-p \rightarrow \Lambda(1520)\pi^0$
70 +20 -30	LITCHFIELD 74C	DPWA	$K^-p \rightarrow \Delta(1232)\bar{K}$
••• We do not use the following data for averages, fits, limits, etc. •••			
157 or 159	¹ MARTIN 77	DPWA	$\bar{K}N$ multichannel

$\Sigma(1910)$ DECAY MODES

Mode	Fraction (Γ_i/Γ)
$\Gamma_1 N\bar{K}$	0.01 to 0.05 (≈ 0.02)
$\Gamma_2 \Lambda\pi$	(6 ± 4) %
$\Gamma_3 \Sigma\pi$	(86 ± 21) %
$\Gamma_4 \Sigma(1385)\pi$	seen
$\Gamma_5 \Xi K$	
$\Gamma_6 \Sigma(1385)\pi, S\text{-wave}$	
$\Gamma_7 \Lambda(1520)\pi$	seen
$\Gamma_8 \Lambda(1520)\pi, P\text{-wave}$	
$\Gamma_9 \Lambda(1520)\pi, F\text{-wave}$	
$\Gamma_{10} \Delta(1232)\bar{K}$	(3.0 ± 1.0) %
$\Gamma_{11} \Delta(1232)\bar{K}, S\text{-wave}$	
$\Gamma_{12} \Delta(1232)\bar{K}, D\text{-wave}$	
$\Gamma_{13} N\bar{K}^*(892)$	seen
$\Gamma_{14} N\bar{K}^*(892), S=3/2, S\text{-wave}$	
$\Gamma_{15} N\bar{K}^*(892), S=1/2, D\text{-wave}$	(1.0 ± 1.0) %
$\Gamma_{16} N\bar{K}^*(892), S=3/2, D\text{-wave}$	

$\Sigma(1910)$ BRANCHING RATIOS

See "Sign conventions for resonance couplings" in the Note on Λ and Σ Resonances.

$\Gamma(N\bar{K})/\Gamma_{\text{total}}$				Γ_1/Γ
VALUE	DOCUMENT ID	TECN	COMMENT	
0.01 to 0.05 (≈ 0.02) OUR ESTIMATE				
0.03 ± 0.02	SARANTSEV 19	DPWA	$\bar{K}N$ multichannel	
<0.04	GOPAL 77	DPWA	$\bar{K}N$ multichannel	
0.14 or 0.13	¹ MARTIN 77	DPWA	$\bar{K}N$ multichannel	

$\Gamma(\Lambda\pi)/\Gamma_{\text{total}}$				Γ_2/Γ
VALUE	DOCUMENT ID	TECN	COMMENT	
0.06 ± 0.04	SARANTSEV 19	DPWA	$\bar{K}N$ multichannel	

$\Gamma(\Sigma\pi)/\Gamma_{\text{total}}$				Γ_3/Γ
VALUE	DOCUMENT ID	TECN	COMMENT	
0.86 ± 0.21	SARANTSEV 19	DPWA	$\bar{K}N$ multichannel	

$\Gamma(\Xi K)/\Gamma_{\text{total}}$				Γ_5/Γ
VALUE	DOCUMENT ID	TECN	COMMENT	
~ 0	SARANTSEV 19	DPWA	$\bar{K}N$ multichannel	

$\Gamma(\Lambda(1520)\pi, P\text{-wave})/\Gamma_{\text{total}}$				Γ_8/Γ
VALUE	DOCUMENT ID	TECN	COMMENT	
~ 0	SARANTSEV 19	DPWA	$\bar{K}N$ multichannel	

See key on page 999

Baryon Particle Listings
 $\Sigma(1910), \Sigma(1915)$

$\Gamma(\Lambda(1520)\pi, F\text{-wave})/\Gamma_{\text{total}}$				Γ_9/Γ
VALUE	DOCUMENT ID	TECN	COMMENT	
~ 0	SARANTSEV	19	DPWA $\bar{K}N$ multichannel	
$\Gamma(\Delta(1232)\bar{K})/\Gamma_{\text{total}}$				Γ_{10}/Γ
VALUE	DOCUMENT ID	TECN	COMMENT	
0.03 ± 0.01	SARANTSEV	19	DPWA $\bar{K}N$ multichannel	
$\Gamma(N\bar{K}^*(892))/\Gamma_{\text{total}}$				Γ_{13}/Γ
VALUE	DOCUMENT ID	TECN	COMMENT	
0.03 ± 0.02	SARANTSEV	19	DPWA $\bar{K}N$ multichannel	
$\Gamma(N\bar{K}^*(892), S=1/2, D\text{-wave})/\Gamma_{\text{total}}$				Γ_{15}/Γ
VALUE	DOCUMENT ID	TECN	COMMENT	
0.01 ± 0.01	SARANTSEV	19	DPWA $\bar{K}N$ multichannel	
$\Gamma(N\bar{K}^*(892), S=3/2, D\text{-wave})/\Gamma_{\text{total}}$				Γ_{16}/Γ
VALUE	DOCUMENT ID	TECN	COMMENT	
~ 0	SARANTSEV	19	DPWA $\bar{K}N$ multichannel	
$(\Gamma_1\Gamma_f)^{1/2}/\Gamma_{\text{total}}$ in $N\bar{K} \rightarrow \Sigma(1910) \rightarrow \Lambda\pi$				$(\Gamma_1\Gamma_2)^{1/2}/\Gamma$
VALUE	DOCUMENT ID	TECN	COMMENT	
-0.06 ± 0.03	GOPAL	77	DPWA $\bar{K}N$ multichannel	
-0.04 ± 0.02	BAILLON	75	IPWA $\bar{K}N \rightarrow \Lambda\pi$	
-0.05 ± 0.03	VANHORN	75	DPWA $K^-p \rightarrow \Lambda\pi^0$	
-0.153 ± 0.070	DEVENISH	74B	Fixed- t dispersion rel.	
$\bullet \bullet \bullet$ We do not use the following data for averages, fits, limits, etc. $\bullet \bullet \bullet$				
-0.15 or -0.14	¹ MARTIN	77	DPWA $\bar{K}N$ multichannel	
$(\Gamma_1\Gamma_f)^{1/2}/\Gamma_{\text{total}}$ in $N\bar{K} \rightarrow \Sigma(1910) \rightarrow \Sigma\pi$				$(\Gamma_1\Gamma_3)^{1/2}/\Gamma$
VALUE	DOCUMENT ID	TECN	COMMENT	
-0.08 ± 0.04	GOPAL	77	DPWA $\bar{K}N$ multichannel	
-0.14 ± 0.04	KANE	74	DPWA $K^-p \rightarrow \Sigma\pi$	
$\bullet \bullet \bullet$ We do not use the following data for averages, fits, limits, etc. $\bullet \bullet \bullet$				
$+0.16$ or $+0.16$	¹ MARTIN	77	DPWA $\bar{K}N$ multichannel	
$(\Gamma_1\Gamma_f)^{1/2}/\Gamma_{\text{total}}$ in $N\bar{K} \rightarrow \Sigma(1910) \rightarrow \Sigma(1385)\pi$				$(\Gamma_1\Gamma_4)^{1/2}/\Gamma$
VALUE	DOCUMENT ID	TECN	COMMENT	
$+0.066 \pm 0.025$	² CAMERON	78	DPWA $K^-p \rightarrow \Sigma(1385)\pi$	
$(\Gamma_1\Gamma_f)^{1/2}/\Gamma_{\text{total}}$ in $N\bar{K} \rightarrow \Sigma(1910) \rightarrow \Lambda(1520)\pi, P\text{-wave}$				$(\Gamma_1\Gamma_8)^{1/2}/\Gamma$
VALUE	DOCUMENT ID	TECN	COMMENT	
< 0.03	CAMERON	77	DPWA $K^-p \rightarrow \Lambda(1520)\pi^0$	
-0.11 ± 0.04	LITCHFIELD	74B	DPWA $K^-p \rightarrow \Lambda(1520)\pi^0$	
$(\Gamma_1\Gamma_f)^{1/2}/\Gamma_{\text{total}}$ in $N\bar{K} \rightarrow \Sigma(1910) \rightarrow \Lambda(1520)\pi, F\text{-wave}$				$(\Gamma_1\Gamma_9)^{1/2}/\Gamma$
VALUE	DOCUMENT ID	TECN	COMMENT	
0.062 ± 0.021	CAMERON	77	DPWA $K^-p \rightarrow \Lambda(1520)\pi^0$	
-0.08 ± 0.04	LITCHFIELD	74B	DPWA $K^-p \rightarrow \Lambda(1520)\pi^0$	
$(\Gamma_1\Gamma_f)^{1/2}/\Gamma_{\text{total}}$ in $N\bar{K} \rightarrow \Sigma(1910) \rightarrow \Delta(1232)\bar{K}, S\text{-wave}$				$(\Gamma_1\Gamma_{11})^{1/2}/\Gamma$
VALUE	DOCUMENT ID	TECN	COMMENT	
-0.16 ± 0.05	LITCHFIELD	74C	DPWA $K^-p \rightarrow \Delta(1232)\bar{K}$	
$(\Gamma_1\Gamma_f)^{1/2}/\Gamma_{\text{total}}$ in $N\bar{K} \rightarrow \Sigma(1910) \rightarrow \Delta(1232)\bar{K}, D\text{-wave}$				$(\Gamma_1\Gamma_{12})^{1/2}/\Gamma$
VALUE	DOCUMENT ID	TECN	COMMENT	
-0.14 ± 0.05	LITCHFIELD	74C	DPWA $K^-p \rightarrow \Delta(1232)\bar{K}$	
$(\Gamma_1\Gamma_f)^{1/2}/\Gamma_{\text{total}}$ in $N\bar{K} \rightarrow \Sigma(1910) \rightarrow N\bar{K}^*(892)$				$(\Gamma_1\Gamma_{13})^{1/2}/\Gamma$
VALUE	DOCUMENT ID	TECN	COMMENT	
-0.09 ± 0.02	³ CAMERON	78B	DPWA $K^-p \rightarrow N\bar{K}^*$	

$\Sigma(1910)$ FOOTNOTES

- The two MARTIN 77 values are from a T-matrix pole and from a Breit-Wigner fit.
- The published sign has been changed to be in accord with the baryon-first convention.
- Upper limits on the D_1 and D_3 waves are each 0.03.

$\Sigma(1910)$ REFERENCES

SARANTSEV	19	EPJ A55 180	A.V. Sarantsev et al.	(BONN, PNPI)
PDG	82	PL 111B 1	M. Roos et al.	(HELS, CIT, CERN)
GOPAL	80	Toronto Conf. 159	G.P. Gopal	(RHEL)
CAMERON	78	NP B143 189	W. Cameron et al.	(RHEL, LOIC) IJP
CAMERON	78B	NP B146 327	W. Cameron et al.	(RHEL, LOIC) IJP
CAMERON	77	NP B131 399	W. Cameron et al.	(RHEL, LOIC) IJP
GOPAL	77	NP B119 362	G.P. Gopal et al.	(LOIC, RHEL) IJP
GOYAL	77	PR D16 2746	D.P. Goyal, A.V. Sodhi	(DELH)
MARTIN	77	NP B127 349	B.R. Martin, M.K. Pidcock, R.G. Moorhouse	(LOUC+) IJP
Also		NP B126 266	B.R. Martin, M.K. Pidcock	(LOUC)
Also		NP B126 285	B.R. Martin, M.K. Pidcock	(LOUC) IJP
DEBELLEFON	76	NP B109 129	A. de Bellefon, A. Berthon	(CDEF) IJP
BAILLON	75	NP B9 39	P.H. Baillon, P.J. Litchfield	(CERN, RHEL) IJP
HEMINGWAY	75	NP B91 12	R.J. Hemingway et al.	(CERN, HEIDH, MPIM) IJP
VANHORN	75	NP B87 145	A.J. van Horn	(LBL) IJP
Also		NP B87 157	A.J. van Horn	(LBL) IJP
DEVENISH	74B	NP B81 330	D.F. Kane	(DESY+) IJP
KANE	74	LBL-2452	R.C.E. Devenish, C.D. Froggatt, B.R. Martin	(LBL) IJP
LITCHFIELD	74B	NP B74 19	P.J. Litchfield et al.	(CERN, HEIDH) IJP
LITCHFIELD	74C	NP B74 39	P.J. Litchfield et al.	(CERN, HEIDH) IJP

$\Sigma(1915) 5/2^+$

$I(J^P) = 1(\frac{5}{2}^+)$ Status: * * * *

Discovered by COOL 66. For results published before 1974 (they are now obsolete), see our 1982 edition Physics Letters **111B** 1 (1982).

This entry only includes results from partial-wave analyses. Parameters of peaks seen in cross sections and invariant-mass distributions in this region used to be listed in a separate entry immediately following. They may be found in our 1986 edition Physics Letters **170B** 1 (1986).

$\Sigma(1915)$ POLE POSITION

REAL PART

VALUE (MeV)	DOCUMENT ID	TECN	COMMENT
1885 to 1915 (≈ 1900) OUR ESTIMATE			
1908 ± 7	SARANTSEV	19	DPWA $\bar{K}N$ multichannel
$1890 \pm \frac{3}{2}$	¹ KAMANO	15	DPWA $\bar{K}N$ multichannel
$\bullet \bullet \bullet$ We do not use the following data for averages, fits, limits, etc. $\bullet \bullet \bullet$			
1897	ZHANG	13A	DPWA $\bar{K}N$ multichannel
¹ From the preferred solution A in KAMANO 15.			

-2xIMAGINARY PART

VALUE (MeV)	DOCUMENT ID	TECN	COMMENT
90 to 110 (≈ 100) OUR ESTIMATE			
98 ± 12	SARANTSEV	19	DPWA $\bar{K}N$ multichannel
$97 \pm \frac{4}{6}$	¹ KAMANO	15	DPWA $\bar{K}N$ multichannel
$\bullet \bullet \bullet$ We do not use the following data for averages, fits, limits, etc. $\bullet \bullet \bullet$			
133	ZHANG	13A	DPWA $\bar{K}N$ multichannel
¹ From the preferred solution A in KAMANO 15.			

$\Sigma(1915)$ POLE RESIDUES

The normalized residue is the residue divided by $\Gamma_{\text{pole}}/2$.

Normalized residue in $N\bar{K} \rightarrow \Sigma(1915) \rightarrow N\bar{K}$

MODULUS	PHASE ($^\circ$)	DOCUMENT ID	TECN	COMMENT
0.08 ± 0.02	-33 ± 15	SARANTSEV	19	DPWA $\bar{K}N$ multichannel
$\bullet \bullet \bullet$ We do not use the following data for averages, fits, limits, etc. $\bullet \bullet \bullet$				
0.0391	-15	¹ KAMANO	15	DPWA $\bar{K}N$ multichannel
¹ From the preferred solution A in KAMANO 15.				

Normalized residue in $N\bar{K} \rightarrow \Sigma(1915) \rightarrow \Sigma\pi$

MODULUS	PHASE ($^\circ$)	DOCUMENT ID	TECN	COMMENT
0.09 ± 0.02	180 ± 12	SARANTSEV	19	DPWA $\bar{K}N$ multichannel
$\bullet \bullet \bullet$ We do not use the following data for averages, fits, limits, etc. $\bullet \bullet \bullet$				
0.157	157	¹ KAMANO	15	DPWA $\bar{K}N$ multichannel
¹ From the preferred solution A in KAMANO 15.				

Normalized residue in $N\bar{K} \rightarrow \Sigma(1915) \rightarrow \Lambda\pi$

MODULUS	PHASE ($^\circ$)	DOCUMENT ID	TECN	COMMENT
0.07 ± 0.02	-170 ± 20	SARANTSEV	19	DPWA $\bar{K}N$ multichannel
$\bullet \bullet \bullet$ We do not use the following data for averages, fits, limits, etc. $\bullet \bullet \bullet$				
0.0757	166	¹ KAMANO	15	DPWA $\bar{K}N$ multichannel
¹ From the preferred solution A in KAMANO 15.				

Normalized residue in $N\bar{K} \rightarrow \Sigma(1915) \rightarrow \Xi K$

MODULUS	PHASE ($^\circ$)	DOCUMENT ID	TECN	COMMENT
0.02 ± 0.01	-65 ± 35	SARANTSEV	19	DPWA $\bar{K}N$ multichannel
$\bullet \bullet \bullet$ We do not use the following data for averages, fits, limits, etc. $\bullet \bullet \bullet$				
0.002	-88	¹ KAMANO	15	DPWA $\bar{K}N$ multichannel
¹ From the preferred solution A in KAMANO 15.				

Normalized residue in $N\bar{K} \rightarrow \Lambda(1915) \rightarrow \Sigma(1385)\pi, P\text{-wave}$

MODULUS	PHASE ($^\circ$)	DOCUMENT ID	TECN	COMMENT
0.02 ± 0.02		SARANTSEV	19	DPWA $\bar{K}N$ multichannel
$\bullet \bullet \bullet$ We do not use the following data for averages, fits, limits, etc. $\bullet \bullet \bullet$				
0.0724	161	¹ KAMANO	15	DPWA $\bar{K}N$ multichannel
¹ From the preferred solution A in KAMANO 15.				

Normalized residue in $N\bar{K} \rightarrow \Lambda(1915) \rightarrow \Sigma(1385)\pi, F\text{-wave}$

MODULUS	PHASE ($^\circ$)	DOCUMENT ID	TECN	COMMENT
0.05 ± 0.03	-30 ± 50	SARANTSEV	19	DPWA $\bar{K}N$ multichannel
$\bullet \bullet \bullet$ We do not use the following data for averages, fits, limits, etc. $\bullet \bullet \bullet$				
0.0162	-163	¹ KAMANO	15	DPWA $\bar{K}N$ multichannel
¹ From the preferred solution A in KAMANO 15.				

Normalized residue in $N\bar{K} \rightarrow \Sigma(1915) \rightarrow \Lambda(1520)\pi, D\text{-wave}$

MODULUS	PHASE ($^\circ$)	DOCUMENT ID	TECN	COMMENT
0.08 ± 0.02	-105 ± 50	SARANTSEV	19	DPWA $\bar{K}N$ multichannel

Baryon Particle Listings

 $\Sigma(1915)$ Normalized residue in $N\bar{K} \rightarrow \Sigma(1915) \rightarrow \Delta\bar{K}$, *P*-wave

MODULUS	PHASE (°)	DOCUMENT ID	TECN	COMMENT
0.12 ± 0.03	-10 ± 20	SARANTSEV 19	DPWA	$\bar{K}N$ multichannel

Normalized residue in $N\bar{K} \rightarrow \Sigma(1915) \rightarrow \Delta\bar{K}$, *F*-wave

MODULUS	PHASE (°)	DOCUMENT ID	TECN	COMMENT
0.07 ± 0.02	-35 ± 25	SARANTSEV 19	DPWA	$\bar{K}N$ multichannel

Normalized residue in $N\bar{K} \rightarrow \Sigma(1915) \rightarrow \Lambda(1520)\pi$, *G*-wave

MODULUS	PHASE (°)	DOCUMENT ID	TECN	COMMENT
0.01 ± 0.01		SARANTSEV 19	DPWA	$\bar{K}N$ multichannel

Normalized residue in $N\bar{K} \rightarrow \Sigma(1915) \rightarrow N\bar{K}^*(892)$, *S*=1/2, *F*-wave

MODULUS	PHASE (°)	DOCUMENT ID	TECN	COMMENT
0.07 ± 0.04	-60 ± 45	SARANTSEV 19	DPWA	$\bar{K}N$ multichannel

• • • We do not use the following data for averages, fits, limits, etc. • • •

0.00476	4	¹ KAMANO 15	DPWA	$\bar{K}N$ multichannel
---------	---	------------------------	------	-------------------------

¹ From the preferred solution A in KAMANO 15.

Normalized residue in $N\bar{K} \rightarrow \Sigma(1915) \rightarrow N\bar{K}^*(892)$, *S*=3/2, *P*-wave

MODULUS	PHASE (°)	DOCUMENT ID	TECN	COMMENT
0.0494	51	¹ KAMANO 15	DPWA	$\bar{K}N$ multichannel

• • • We do not use the following data for averages, fits, limits, etc. • • •

¹ From the preferred solution A in KAMANO 15.

Normalized residue in $N\bar{K} \rightarrow \Sigma(1915) \rightarrow N\bar{K}^*(892)$, *S*=3/2, *F*-wave

MODULUS	PHASE (°)	DOCUMENT ID	TECN	COMMENT
0.07 ± 0.03	-40 ± 45	SARANTSEV 19	DPWA	$\bar{K}N$ multichannel

• • • We do not use the following data for averages, fits, limits, etc. • • •

0.000314	16	¹ KAMANO 15	DPWA	$\bar{K}N$ multichannel
----------	----	------------------------	------	-------------------------

¹ From the preferred solution A in KAMANO 15.

 $\Sigma(1915)$ MASS

VALUE (MeV)	DOCUMENT ID	TECN	COMMENT
1900 to 1935 (≈ 1915) OUR ESTIMATE			
1918 ± 6	SARANTSEV 19	DPWA	$\bar{K}N$ multichannel
1920 ± 7	ZHANG 13A	DPWA	$\bar{K}N$ multichannel
1937 ± 20	ALSTON... 78	DPWA	$\bar{K}N \rightarrow \bar{K}N$
1894 ± 5	¹ CORDEN 77c		$K^- n \rightarrow \Sigma\pi$
1909 ± 5	¹ CORDEN 77c		$K^- n \rightarrow \Sigma\pi$
1920 ± 10	GOPAL 77	DPWA	$\bar{K}N$ multichannel
1920 ± 30	BAILLON 75	IPWA	$\bar{K}N \rightarrow \Lambda\pi$
1914 ± 10	HEMINGWAY 75	DPWA	$K^- p \rightarrow \bar{K}N$
1920 ⁺¹⁵ / ₋₂₀	VANHORN 75	DPWA	$K^- p \rightarrow \Lambda\pi^0$
1920 ± 5	KANE 74	DPWA	$K^- p \rightarrow \Sigma\pi$
• • • We do not use the following data for averages, fits, limits, etc. • • •			
not seen	DECLAIS 77	DPWA	$\bar{K}N \rightarrow \bar{K}N$
1925 or 1933	² MARTIN 77	DPWA	$\bar{K}N$ multichannel
1900 ± 4	³ CORDEN 76	DPWA	$K^- n \rightarrow \Lambda\pi^-$
1915	DEBELLEFON 76	IPWA	$K^- p \rightarrow \Lambda\pi^0$

¹ The two entries for CORDEN 77c are from two different acceptable solutions.

² The two MARTIN 77 values are from a T-matrix pole and from a Breit-Wigner fit.

³ Preferred solution 3; see CORDEN 76 for other possibilities.

 $\Sigma(1915)$ WIDTH

VALUE (MeV)	DOCUMENT ID	TECN	COMMENT
80 to 160 (≈ 120) OUR ESTIMATE			
102 ± 12	SARANTSEV 19	DPWA	$\bar{K}N$ multichannel
149 ± 17	ZHANG 13A	DPWA	Multichannel
161 ± 20	ALSTON... 78	DPWA	$\bar{K}N \rightarrow \bar{K}N$
107 ± 14	¹ CORDEN 77c		$K^- n \rightarrow \Sigma\pi$
85 ± 13	¹ CORDEN 77c		$K^- n \rightarrow \Sigma\pi$
130 ± 10	GOPAL 77	DPWA	$\bar{K}N$ multichannel
70 ± 20	BAILLON 75	IPWA	$\bar{K}N \rightarrow \Lambda\pi$
85 ± 15	HEMINGWAY 75	DPWA	$K^- p \rightarrow \bar{K}N$
102 ± 18	VANHORN 75	DPWA	$K^- p \rightarrow \Lambda\pi^0$
162 ± 25	KANE 74	DPWA	$K^- p \rightarrow \Sigma\pi$
• • • We do not use the following data for averages, fits, limits, etc. • • •			
171 or 173	² MARTIN 77	DPWA	$\bar{K}N$ multichannel
75 ± 14	³ CORDEN 76	DPWA	$K^- n \rightarrow \Lambda\pi^-$
60	DEBELLEFON 76	IPWA	$K^- p \rightarrow \Lambda\pi^0$

¹ The two entries for CORDEN 77c are from two different acceptable solutions.

² The two MARTIN 77 values are from a T-matrix pole and from a Breit-Wigner fit.

³ Preferred solution 3; see CORDEN 76 for other possibilities.

 $\Sigma(1915)$ DECAY MODES

Mode	Fraction (Γ_i/Γ)
Γ_1 $N\bar{K}$	0.05 to 0.15
Γ_2 $\Lambda\pi$	(6.0 ± 2.0) %
Γ_3 $\Sigma\pi$	(10.0 ± 2.0) %
Γ_4 ΞK	
Γ_5 $\Sigma(1385)\pi$, <i>P</i> -wave	(2.0 ± 2.0) %
Γ_6 $\Sigma(1385)\pi$, <i>F</i> -wave	(4.0 ± 2.0) %
Γ_7 $\Sigma(1385)\pi$	< 5 %
Γ_8 $\Sigma(1385)\pi$, <i>P</i> -wave	
Γ_9 $\Sigma(1385)\pi$, <i>F</i> -wave	
Γ_{10} $\Lambda(1520)\pi$, <i>D</i> -wave	(8.0 ± 2.0) %
Γ_{11} $\Lambda(1520)\pi$, <i>G</i> -wave	
Γ_{12} $N\bar{K}^*(892)$, <i>S</i> =1/2, <i>F</i> -wave	(5.0 ± 3.0) %
Γ_{13} $N\bar{K}^*(892)$, <i>S</i> =3/2, <i>P</i> -wave	
Γ_{14} $N\bar{K}^*(892)$, <i>S</i> =3/2, <i>F</i> -wave	(5.0 ± 2.0) %
Γ_{15} $\Delta\bar{K}$, <i>P</i> -wave	(16 ± 5) %
Γ_{16} $\Delta\bar{K}$, <i>F</i> -wave	(5.0 ± 3.0) %

 $\Sigma(1915)$ BRANCHING RATIOS

See "Sign conventions for resonance couplings" in the Note on Λ and Σ Resonances.

$\Gamma(N\bar{K})/\Gamma_{\text{total}}$	DOCUMENT ID	TECN	COMMENT	Γ_1/Γ
0.05 to 0.15 OUR ESTIMATE				
0.08 ± 0.02	SARANTSEV 19	DPWA	$\bar{K}N$ multichannel	
0.026 ± 0.004	ZHANG 13A	DPWA	$\bar{K}N$ multichannel	
0.03 ± 0.02	¹ GOPAL 80	DPWA	$\bar{K}N \rightarrow \bar{K}N$	
0.14 ± 0.05	ALSTON... 78	DPWA	$\bar{K}N \rightarrow \bar{K}N$	
0.11 ± 0.04	HEMINGWAY 75	DPWA	$K^- p \rightarrow \bar{K}N$	
• • • We do not use the following data for averages, fits, limits, etc. • • •				
0.036	² KAMANO 15	DPWA	$\bar{K}N$ multichannel	
0.05 ± 0.03	GOPAL 77	DPWA	See GOPAL 80	
0.08 or 0.08	³ MARTIN 77	DPWA	$\bar{K}N$ multichannel	

¹ The mass and width are fixed to the GOPAL 77 values due to the low elasticity.

² From the preferred solution A in KAMANO 15.

³ The two MARTIN 77 values are from a T-matrix pole and from a Breit-Wigner fit.

$\Gamma(\Lambda\pi)/\Gamma_{\text{total}}$	DOCUMENT ID	TECN	COMMENT	Γ_2/Γ
0.06 ± 0.02				
0.127	SARANTSEV 19	DPWA	$\bar{K}N$ multichannel	
• • • We do not use the following data for averages, fits, limits, etc. • • •				
0.127	¹ KAMANO 15	DPWA	$\bar{K}N$ multichannel	

¹ From the preferred solution A in KAMANO 15.

$\Gamma(\Sigma\pi)/\Gamma_{\text{total}}$	DOCUMENT ID	TECN	COMMENT	Γ_3/Γ
0.10 ± 0.02				
0.678	SARANTSEV 19	DPWA	$\bar{K}N$ multichannel	
• • • We do not use the following data for averages, fits, limits, etc. • • •				
0.678	¹ KAMANO 15	DPWA	$\bar{K}N$ multichannel	

¹ From the preferred solution A in KAMANO 15.

$\Gamma(\Xi K)/\Gamma_{\text{total}}$	DOCUMENT ID	TECN	COMMENT	Γ_4/Γ
< 0.01				
< 0.01	SARANTSEV 19	DPWA	$\bar{K}N$ multichannel	
• • • We do not use the following data for averages, fits, limits, etc. • • •				
not seen	¹ KAMANO 15	DPWA	Multichannel	

¹ From the preferred solution A in KAMANO 15.

$\Gamma(\Sigma(1385)\pi, P\text{-wave})/\Gamma_{\text{total}}$	DOCUMENT ID	TECN	COMMENT	Γ_5/Γ
0.02 ± 0.02				
0.112	SARANTSEV 19	DPWA	$\bar{K}N$ multichannel	
• • • We do not use the following data for averages, fits, limits, etc. • • •				
0.112	¹ KAMANO 15	DPWA	$\bar{K}N$ multichannel	

¹ From the preferred solution A in KAMANO 15.

$\Gamma(\Sigma(1385)\pi, F\text{-wave})/\Gamma_{\text{total}}$	DOCUMENT ID	TECN	COMMENT	Γ_6/Γ
0.04 ± 0.02				
0.004	SARANTSEV 19	DPWA	$\bar{K}N$ multichannel	
• • • We do not use the following data for averages, fits, limits, etc. • • •				
0.004	¹ KAMANO 15	DPWA	$\bar{K}N$ multichannel	

¹ From the preferred solution A in KAMANO 15.

$\Gamma(\Lambda(1520)\pi, D\text{-wave})/\Gamma_{\text{total}}$	DOCUMENT ID	TECN	COMMENT	Γ_{10}/Γ
0.08 ± 0.02				
0.08 ± 0.02	SARANTSEV 19	DPWA	$\bar{K}N$ multichannel	

See key on page 999

Baryon Particle Listings

$\Sigma(1915)$, $\Sigma(1940)$, $\Sigma(2010)$

$\Gamma(\Lambda(1520)\pi, G\text{-wave})/\Gamma_{\text{total}}$				Γ_{11}/Γ
VALUE	DOCUMENT ID	TECN	COMMENT	
def 0	SARANTSEV	19	DPWA $\bar{K}N$ multichannel	

$\Gamma(N\bar{K}^*(892), S=1/2, F\text{-wave})/\Gamma_{\text{total}}$				Γ_{12}/Γ
VALUE	DOCUMENT ID	TECN	COMMENT	
0.05 ± 0.03	SARANTSEV	19	DPWA $\bar{K}N$ multichannel	

• • • We do not use the following data for averages, fits, limits, etc. • • •
 0.001 ¹ KAMANO 15 DPWA Multichannel
¹ From the preferred solution A in KAMANO 15.

$\Gamma(N\bar{K}^*(892), S=3/2, P\text{-wave})/\Gamma_{\text{total}}$				Γ_{13}/Γ
VALUE	DOCUMENT ID	TECN	COMMENT	
0.042	¹ KAMANO	15	DPWA Multichannel	

• • • We do not use the following data for averages, fits, limits, etc. • • •
¹ From the preferred solution A in KAMANO 15.

$\Gamma(N\bar{K}^*(892), S=3/2, F\text{-wave})/\Gamma_{\text{total}}$				Γ_{14}/Γ
VALUE	DOCUMENT ID	TECN	COMMENT	
0.05 ± 0.02	SARANTSEV	19	DPWA $\bar{K}N$ multichannel	

• • • We do not use the following data for averages, fits, limits, etc. • • •
 not seen ¹ KAMANO 15 DPWA Multichannel
¹ From the preferred solution A in KAMANO 15.

$\Gamma(\Delta\bar{K}, P\text{-wave})/\Gamma_{\text{total}}$				Γ_{15}/Γ
VALUE	DOCUMENT ID	TECN	COMMENT	
0.16 ± 0.05	SARANTSEV	19	DPWA $\bar{K}N$ multichannel	

$\Gamma(\Delta\bar{K}, F\text{-wave})/\Gamma_{\text{total}}$				Γ_{16}/Γ
VALUE	DOCUMENT ID	TECN	COMMENT	
0.05 ± 0.03	SARANTSEV	19	DPWA $\bar{K}N$ multichannel	

$(\Gamma_1\Gamma_f)^{1/2}/\Gamma_{\text{total}}$ in $N\bar{K} \rightarrow \Sigma(1915) \rightarrow \Lambda\pi$				$(\Gamma_1\Gamma_2)^{1/2}/\Gamma$
VALUE	DOCUMENT ID	TECN	COMMENT	
-0.09 ± 0.03	GOPAL	77	DPWA $\bar{K}N$ multichannel	
-0.10 ± 0.01	¹ CORDEN	76	DPWA $K^-n \rightarrow \Lambda\pi^-$	
-0.06 ± 0.02	BAILLON	75	IPWA $\bar{K}N \rightarrow \Lambda\pi$	
-0.09 ± 0.02	VANHORN	75	DPWA $K^-p \rightarrow \Lambda\pi^0$	
-0.087 ± 0.056	DEVENISH	74B	Fixed-t dispersion rel.	
• • • We do not use the following data for averages, fits, limits, etc. • • •				
-0.09 or -0.09	² MARTIN	77	DPWA $\bar{K}N$ multichannel	
-0.10	DEBELLEFON	76	IPWA $K^-p \rightarrow \Lambda\pi^0$	

¹ Preferred solution 3; see CORDEN 76 for other possibilities.
² The two MARTIN 77 values are from a T-matrix pole and from a Breit-Wigner fit.

$(\Gamma_1\Gamma_f)^{1/2}/\Gamma_{\text{total}}$ in $N\bar{K} \rightarrow \Sigma(1915) \rightarrow \Sigma\pi$				$(\Gamma_1\Gamma_3)^{1/2}/\Gamma$
VALUE	DOCUMENT ID	TECN	COMMENT	
-0.14 ± 0.01	ZHANG	13A	DPWA Multichannel	
-0.17 ± 0.01	¹ CORDEN	77c	$K^-n \rightarrow \Sigma\pi$	
-0.15 ± 0.02	¹ CORDEN	77c	$K^-n \rightarrow \Sigma\pi$	
-0.19 ± 0.03	GOPAL	77	DPWA $\bar{K}N$ multichannel	
-0.16 ± 0.03	KANE	74	DPWA $K^-p \rightarrow \Sigma\pi$	
• • • We do not use the following data for averages, fits, limits, etc. • • •				
-0.05 or -0.05	² MARTIN	77	DPWA $\bar{K}N$ multichannel	

¹ The two entries for CORDEN 77c are from two different acceptable solutions.
² The two MARTIN 77 values are from a T-matrix pole and from a Breit-Wigner fit.

$(\Gamma_1\Gamma_f)^{1/2}/\Gamma_{\text{total}}$ in $N\bar{K} \rightarrow \Sigma(1915) \rightarrow \Sigma(1385)\pi, P\text{-wave}$				$(\Gamma_1\Gamma_8)^{1/2}/\Gamma$
VALUE	DOCUMENT ID	TECN	COMMENT	
<0.01	CAMERON	78	DPWA $K^-p \rightarrow \Sigma(1385)\pi$	

$(\Gamma_1\Gamma_f)^{1/2}/\Gamma_{\text{total}}$ in $N\bar{K} \rightarrow \Sigma(1915) \rightarrow \Sigma(1385)\pi, F\text{-wave}$				$(\Gamma_1\Gamma_9)^{1/2}/\Gamma$
VALUE	DOCUMENT ID	TECN	COMMENT	
+0.06 ± 0.02	ZHANG	13A	DPWA Multichannel	
+0.039 ± 0.009	¹ CAMERON	78	DPWA $K^-p \rightarrow \Sigma(1385)\pi$	

¹ The published sign has been changed to be in accord with the baryon-first convention.

$\Sigma(1915)$ REFERENCES

SARANTSEV	19	EPJ A55 180	A.V. Sarantsev et al.	(BONN, PNPI)
KAMANO	15	PR C92 025205	H. Kamano et al.	(ANL, OSAK)
ZHANG	13A	PR C88 035205	H. Zhang et al.	(KSU)
PDG	86	PL 170B 1	M. Aguilar-Benitez et al.	(CERN, CIT+)
PDG	82	PL 111B 1	M. Roos et al.	(HEL5, CIT, CERN)
GOPAL	80	Toronto Conf. 159	G.P. Gopal et al.	(RHEL) IJP
ALSTON-...	78	PR D18 182	M. Alston-Garnjost et al.	(LBL, MTHO+) IJP
Also		PRL 38 1007	M. Alston-Garnjost et al.	(LBL, MTHO+) IJP
CAMERON	78	NP B143 189	W. Cameron et al.	(RHEL, LOIC) IJP
CORDEN	77C	NP B125 61	M.J. Corden et al.	(BIRM) IJP
DECLAIS	77	CERN 77-16	Y. Declais et al.	(CAEN, CERN) IJP
GOPAL	77	NP B119 362	G.P. Gopal et al.	(LOIC, RHEL) IJP
MARTIN	77	NP B127 349	B.R. Martin, M.K. Pidcock, R.G. Moorhouse	(LOUC+) IJP
Also		NP B126 266	B.R. Martin, M.K. Pidcock	(LOUC) IJP
Also		NP B126 285	B.R. Martin, M.K. Pidcock	(LOUC) IJP

CORDEN	76	NP B104 382	M.J. Corden et al.	(BIRM) IJP
DEBELLEFON	76	NP B109 129	A. de Bellefon, A. Berthon	(CDEF) IJP
BAILLON	75	NP B94 39	P.H. Baillon, P.J. Litchfield	(CERN, RHEL) IJP
HEMINGWAY	75	NP B91 12	R.J. Hemingway et al.	(CERN, HEIDH, MPM) IJP
VANHORN	75	NP B87 145	A.J. van Horn	(LBL) IJP
Also		NP B87 157	A.J. van Horn	(LBL) IJP
DEVENISH	74B	NP B81 330	R.C.E. Devenish, C.D. Froggatt, B.R. Martin	(DESY+) IJP
KANE	74	LBL-2452	D.F. Kane	(LBL) IJP
COOL	66	PRL 16 1228	R.L. Cool et al.	(BNL)

$\Sigma(1940) 3/2^+$

$I(J^P) = 1(\frac{3}{2}^+)$ Status: *

OMITTED FROM SUMMARY TABLE

$\Sigma(1940)$ MASS

VALUE (MeV)	DOCUMENT ID	TECN	COMMENT
1920 to 1960 (\approx 1940) OUR ESTIMATE			
1941 ± 18	ZHANG	13A	DPWA $\bar{K}N$ multichannel
1925 ± 200	VANHORN	75	DPWA $K^-p \rightarrow \Lambda\pi^0$

$\Sigma(1940)$ WIDTH

VALUE (MeV)	DOCUMENT ID	TECN	COMMENT
100 to 400 (\approx 250) OUR ESTIMATE			
400 ± 49	ZHANG	13A	DPWA $\bar{K}N$ multichannel
65 ⁺⁵ ₋₂₀	VANHORN	75	DPWA $K^-p \rightarrow \Lambda\pi^0$

$\Sigma(1940)$ DECAY MODES

Mode	Fraction (Γ_i/Γ)
Γ_1 $N\bar{K}$	(13.0 ± 2.0) %
Γ_2 $\Sigma\pi$	(4.0 ± 2.0) %
Γ_3 $\Sigma(1385)\pi, P\text{-wave}$	(22 ± 7) %
Γ_4 $\Lambda(1520)\pi, S\text{-wave}$	(5.0 ± 2.0) %

$\Sigma(1940)$ BRANCHING RATIOS

$\Gamma(N\bar{K})/\Gamma_{\text{total}}$	Γ_1/Γ		
VALUE	DOCUMENT ID	TECN	COMMENT
0.13 ± 0.02	ZHANG	13A	DPWA $\bar{K}N$ multichannel

$\Gamma(\Sigma\pi)/\Gamma_{\text{total}}$	Γ_2/Γ		
VALUE	DOCUMENT ID	TECN	COMMENT
0.04 ± 0.02	ZHANG	13A	DPWA $\bar{K}N$ multichannel

$\Gamma(\Sigma(1385)\pi, P\text{-wave})/\Gamma_{\text{total}}$	Γ_3/Γ		
VALUE	DOCUMENT ID	TECN	COMMENT
0.22 ± 0.07	ZHANG	13A	DPWA $\bar{K}N$ multichannel

$\Gamma(\Lambda(1520)\pi, S\text{-wave})/\Gamma_{\text{total}}$	Γ_4/Γ		
VALUE	DOCUMENT ID	TECN	COMMENT
0.05 ± 0.02	ZHANG	13A	DPWA $\bar{K}N$ multichannel

$\Sigma(1940)$ REFERENCES

ZHANG	13A	PR C88 035205	H. Zhang et al.	(KSU)
VANHORN	75	NP B87 145	A.J. van Horn	(LBL)

$\Sigma(2010) 3/2^-$

$I(J^P) = 1(\frac{3}{2}^-)$ Status: *

OMITTED FROM SUMMARY TABLE

$\Sigma(2010)$ POLE POSITION

REAL PART	DOCUMENT ID	TECN	COMMENT
VALUE (MeV)			
1995 ± 12	SARANTSEV	19	DPWA $\bar{K}N$ multichannel

-2×IMAGINARY PART	DOCUMENT ID	TECN	COMMENT
VALUE (MeV)			
175 ± 24	SARANTSEV	19	DPWA $\bar{K}N$ multichannel

$\Sigma(2010)$ POLE RESIDUES

The normalized residue is the residue divided by $\Gamma_{\text{pole}}/2$.

Normalized residue in $N\bar{K} \rightarrow \Sigma(2010) \rightarrow N\bar{K}$				
MODULUS	PHASE (°)	DOCUMENT ID	TECN	COMMENT
0.07 ± 0.03	-115 ± 25	SARANTSEV	19	DPWA $\bar{K}N$ multichannel

Baryon Particle Listings

$\Sigma(2010)$, $\Sigma(2030)$

Normalized residue in $N\bar{K} \rightarrow \Sigma(2010) \rightarrow \Sigma\pi$				
MODULUS	PHASE (°)	DOCUMENT ID	TECN	COMMENT
0.04±0.02	130 ± 22	SARANTSEV 19	DPWA	$\bar{K}N$ multichannel
Normalized residue in $N\bar{K} \rightarrow \Sigma(2010) \rightarrow \Lambda\pi$				
MODULUS	PHASE (°)	DOCUMENT ID	TECN	COMMENT
0.06±0.03	170 ± 25	SARANTSEV 19	DPWA	$\bar{K}N$ multichannel
Normalized residue in $N\bar{K} \rightarrow \Sigma(2010) \rightarrow \Xi K$				
MODULUS	PHASE (°)	DOCUMENT ID	TECN	COMMENT
0.04±0.02	-120 ± 45	SARANTSEV 19	DPWA	$\bar{K}N$ multichannel
Normalized residue in $N\bar{K} \rightarrow \Sigma(2010) \rightarrow \Lambda(1520)\pi, P\text{-wave}$				
MODULUS	PHASE (°)	DOCUMENT ID	TECN	COMMENT
0.03±0.02	80 ± 35	SARANTSEV 19	DPWA	$\bar{K}N$ multichannel
Normalized residue in $N\bar{K} \rightarrow \Sigma(2010) \rightarrow \Lambda(1520)\pi, F\text{-wave}$				
MODULUS	PHASE (°)	DOCUMENT ID	TECN	COMMENT
0.08±0.05	150 ± 65	SARANTSEV 19	DPWA	$\bar{K}N$ multichannel
Normalized residue in $N\bar{K} \rightarrow \Sigma(2010) \rightarrow \Sigma(1385)\pi, P\text{-wave}$				
VALUE	DOCUMENT ID	TECN	COMMENT	
0.04+-0.02@25+-45	SARANTSEV 19	DPWA	$\bar{K}N$ multichannel	
Normalized residue in $N\bar{K} \rightarrow \Sigma(2010) \rightarrow \Sigma(1385)\pi, F\text{-wave}$				
VALUE	DOCUMENT ID	TECN	COMMENT	
0.02±0.02	SARANTSEV 19	DPWA	$\bar{K}N$ multichannel	
Normalized residue in $N\bar{K} \rightarrow \Sigma(2010) \rightarrow \Delta\bar{K}, S\text{-wave}$				
MODULUS	PHASE (°)	DOCUMENT ID	TECN	COMMENT
0.08±0.04	0 ± 30	SARANTSEV 19	DPWA	$\bar{K}N$ multichannel
Normalized residue in $N\bar{K} \rightarrow \Sigma(2010) \rightarrow \Delta\bar{K}, D\text{-wave}$				
MODULUS	PHASE (°)	DOCUMENT ID	TECN	COMMENT
0.02±0.02		SARANTSEV 19	DPWA	$\bar{K}N$ multichannel
Normalized residue in $N\bar{K} \rightarrow \Sigma(2010) \rightarrow N\bar{K}^*(892), S\text{-wave}$				
VALUE	DOCUMENT ID	TECN	COMMENT	
0.12+-0.03@60+-60	SARANTSEV 19	DPWA	$\bar{K}N$ multichannel	
Normalized residue in $N\bar{K} \rightarrow \Sigma(2010) \rightarrow N\bar{K}^*(892), S=1/2, D\text{-wave}$				
MODULUS	PHASE (°)	DOCUMENT ID	TECN	COMMENT
0.08±0.04	55 ± 60	SARANTSEV 19	DPWA	$\bar{K}N$ multichannel
Normalized residue in $N\bar{K} \rightarrow \Sigma(2010) \rightarrow N\bar{K}^*(892), S=3/2, D\text{-wave}$				
MODULUS	PHASE (°)	DOCUMENT ID	TECN	COMMENT
0.08±0.04	15 ± 60	SARANTSEV 19	DPWA	$\bar{K}N$ multichannel

$\Sigma(2010)$ MASS

VALUE (MeV)	DOCUMENT ID	TECN	COMMENT
2005±14	SARANTSEV 19	DPWA	$\bar{K}N$ multichannel

$\Sigma(2010)$ WIDTH

VALUE (MeV)	DOCUMENT ID	TECN	COMMENT
178±23	SARANTSEV 19	DPWA	$\bar{K}N$ multichannel

$\Sigma(2010)$ DECAY MODES

Mode	Fraction (Γ_i/Γ)
Γ_1 $N\bar{K}$	(7.0±3.0) %
Γ_2 $\Lambda\pi$	(5.0±2.0) %
Γ_3 $\Sigma\pi$	(3.0±2.0) %
Γ_4 ΞK	(3.0±2.0) %
Γ_5 $\Sigma(1385)\pi, P\text{-wave}$	(3.0±2.0) %
Γ_6 $\Sigma(1385)\pi, F\text{-wave}$	(2.0±2.0) %
Γ_7 $\Lambda(1520)\pi, P\text{-wave}$	(2.0±2.0) %
Γ_8 $\Lambda(1520)\pi, F\text{-wave}$	(12 ± 6) %
Γ_9 $\Delta\bar{K}, S\text{-wave}$	(11 ± 5) %
Γ_{10} $\Delta\bar{K}, D\text{-wave}$	(1.0±1.0) %
Γ_{11} $N\bar{K}^*(892), S=1/2, S\text{-wave}$	(27 ± 7) %
Γ_{12} $N\bar{K}^*(892), S=1/2, D\text{-wave}$	(13 ± 6) %
Γ_{13} $N\bar{K}^*(892), S=3/2, D\text{-wave}$	(13 ± 6) %

$\Sigma(2010)$ BRANCHING RATIOS

See "Sign conventions for resonance couplings" in the Note on Λ and Σ Resonances.

$\Gamma(N\bar{K})/\Gamma_{\text{total}}$	DOCUMENT ID	TECN	COMMENT
0.07±0.03	SARANTSEV 19	DPWA	$\bar{K}N$ multichannel

$\Gamma(\Lambda\pi)/\Gamma_{\text{total}}$	DOCUMENT ID	TECN	COMMENT
0.05±0.02	SARANTSEV 19	DPWA	$\bar{K}N$ multichannel
$\Gamma(\Sigma\pi)/\Gamma_{\text{total}}$	DOCUMENT ID	TECN	COMMENT
0.03±0.02	SARANTSEV 19	DPWA	$\bar{K}N$ multichannel
$\Gamma(\Xi K)/\Gamma_{\text{total}}$	DOCUMENT ID	TECN	COMMENT
0.03±0.02	SARANTSEV 19	DPWA	$\bar{K}N$ multichannel
$\Gamma(\Sigma(1385)\pi, P\text{-wave})/\Gamma_{\text{total}}$	DOCUMENT ID	TECN	COMMENT
0.03±0.02	SARANTSEV 19	DPWA	$\bar{K}N$ multichannel
$\Gamma(\Sigma(1385)\pi, F\text{-wave})/\Gamma_{\text{total}}$	DOCUMENT ID	TECN	COMMENT
0.02±0.02	SARANTSEV 19	DPWA	$\bar{K}N$ multichannel
$\Gamma(\Lambda(1520)\pi, P\text{-wave})/\Gamma_{\text{total}}$	DOCUMENT ID	TECN	COMMENT
0.02±0.02	SARANTSEV 19	DPWA	$\bar{K}N$ multichannel
$\Gamma(\Lambda(1520)\pi, F\text{-wave})/\Gamma_{\text{total}}$	DOCUMENT ID	TECN	COMMENT
0.12±0.06	SARANTSEV 19	DPWA	$\bar{K}N$ multichannel
$\Gamma(\Delta\bar{K}, S\text{-wave})/\Gamma_{\text{total}}$	DOCUMENT ID	TECN	COMMENT
0.11±0.05	SARANTSEV 19	DPWA	$\bar{K}N$ multichannel
$\Gamma(\Delta\bar{K}, D\text{-wave})/\Gamma_{\text{total}}$	DOCUMENT ID	TECN	COMMENT
0.01±0.01	SARANTSEV 19	DPWA	$\bar{K}N$ multichannel
$\Gamma(N\bar{K}^*(892), S=1/2, S\text{-wave})/\Gamma_{\text{total}}$	DOCUMENT ID	TECN	COMMENT
0.27±0.07	SARANTSEV 19	DPWA	$\bar{K}N$ multichannel
$\Gamma(N\bar{K}^*(892), S=1/2, D\text{-wave})/\Gamma_{\text{total}}$	DOCUMENT ID	TECN	COMMENT
0.13±0.06	SARANTSEV 19	DPWA	$\bar{K}N$ multichannel
$\Gamma(N\bar{K}^*(892), S=3/2, D\text{-wave})/\Gamma_{\text{total}}$	DOCUMENT ID	TECN	COMMENT
0.13±0.06	SARANTSEV 19	DPWA	$\bar{K}N$ multichannel

$\Sigma(2010)$ REFERENCES

SARANTSEV 19 EPJ A55 180 A.V. Sarantsev et al. (BONN, PNPI)

$\Sigma(2030) 7/2^+$

$I(J^P) = 1(\frac{7}{2}^+)$ Status: ***

Discovered by COOL 66 and by WOHL 66. For most results published before 1974 (they are now obsolete), see our 1982 edition Physics Letters **111B** 1 (1982).

This entry only includes results from partial-wave analyses. Parameters of peaks seen in cross sections and invariant-mass distributions around 2030 MeV may be found in our 1984 edition, Reviews of Modern Physics **56** S1 (1984).

$\Sigma(2030)$ POLE POSITION

REAL PART

VALUE (MeV)	DOCUMENT ID	TECN	COMMENT
2010 to 2030 (≈ 2020) OUR ESTIMATE			
2014 ± 6	SARANTSEV 19	DPWA	$\bar{K}N$ multichannel
2025 ± ⁺¹⁰ / ₋₅	¹ KAMANO 15	DPWA	$\bar{K}N$ multichannel
• • • We do not use the following data for averages, fits, limits, etc. • • •			
1993	ZHANG 13A	DPWA	$\bar{K}N$ multichannel
¹ From the preferred solution A in KAMANO 15.			

-2xIMAGINARY PART

VALUE (MeV)	DOCUMENT ID	TECN	COMMENT
130 to 190 (≈ 160) OUR ESTIMATE			
172±12	SARANTSEV 19	DPWA	$\bar{K}N$ multichannel
130 ⁺ / ₋₂₄	¹ KAMANO 15	DPWA	$\bar{K}N$ multichannel
• • • We do not use the following data for averages, fits, limits, etc. • • •			
176	ZHANG 13A	DPWA	$\bar{K}N$ multichannel
¹ From the preferred solution A in KAMANO 15.			

$\Sigma(2030)$ POLE RESIDUES

The normalized residue is the residue divided by $\Gamma_{pole}/2$.

Normalized residue in $N\bar{K} \rightarrow \Sigma(2030) \rightarrow N\bar{K}$

MODULUS	PHASE (°)	DOCUMENT ID	TECN	COMMENT
0.20 ± 0.04	-38 ± 8	SARANTSEV 19	DPWA	$\bar{K}N$ multichannel
0.220	-38	¹ KAMANO 15	DPWA	$\bar{K}N$ multichannel

¹ From the preferred solution A in KAMANO 15.

Normalized residue in $N\bar{K} \rightarrow \Sigma(2030) \rightarrow \Sigma\pi$

MODULUS	PHASE (°)	DOCUMENT ID	TECN	COMMENT
0.07 ± 0.02	165 ± 12	SARANTSEV 19	DPWA	$\bar{K}N$ multichannel
0.0807	135	¹ KAMANO 15	DPWA	$\bar{K}N$ multichannel

¹ From the preferred solution A in KAMANO 15.

Normalized residue in $N\bar{K} \rightarrow \Sigma(2030) \rightarrow \Lambda\pi$

MODULUS	PHASE (°)	DOCUMENT ID	TECN	COMMENT
0.18 ± 0.04	-22 ± 12	SARANTSEV 19	DPWA	$\bar{K}N$ multichannel
0.138	-24	¹ KAMANO 15	DPWA	$\bar{K}N$ multichannel

¹ From the preferred solution A in KAMANO 15.

Normalized residue in $N\bar{K} \rightarrow \Sigma(2030) \rightarrow \Xi K$

MODULUS	PHASE (°)	DOCUMENT ID	TECN	COMMENT
0.01 ± 0.01		SARANTSEV 19	DPWA	$\bar{K}N$ multichannel
0.0348	129	¹ KAMANO 15	DPWA	$\bar{K}N$ multichannel

¹ From the preferred solution A in KAMANO 15.

Normalized residue in $N\bar{K} \rightarrow \Sigma(2030) \rightarrow \Sigma(1385)\pi, F\text{-wave}$

MODULUS	PHASE (°)	DOCUMENT ID	TECN	COMMENT
0.04 ± 0.03		SARANTSEV 19	DPWA	$\bar{K}N$ multichannel
0.089	-23	¹ KAMANO 15	DPWA	$\bar{K}N$ multichannel

¹ From the preferred solution A in KAMANO 15.

Normalized residue in $N\bar{K} \rightarrow \Sigma(2030) \rightarrow \Sigma(1385)\pi, H\text{-wave}$

MODULUS	PHASE (°)	DOCUMENT ID	TECN	COMMENT
0.0245	132	¹ KAMANO 15	DPWA	Multichannel

¹ From the preferred solution A in KAMANO 15.

Normalized residue in $N\bar{K} \rightarrow \Sigma(2030) \rightarrow \Lambda(1520)\pi, D\text{-wave}$

MODULUS	PHASE (°)	DOCUMENT ID	TECN	COMMENT
0.03 ± 0.02	-100 ± 40	SARANTSEV 19	DPWA	$\bar{K}N$ multichannel

Normalized residue in $N\bar{K} \rightarrow \Sigma(2030) \rightarrow \Lambda(1520)\pi, G\text{-wave}$

MODULUS	PHASE (°)	DOCUMENT ID	TECN	COMMENT
0.02 ± 0.02		SARANTSEV 19	DPWA	$\bar{K}N$ multichannel

Normalized residue in $N\bar{K} \rightarrow \Sigma(2030) \rightarrow \Delta\bar{K}, F\text{-wave}$

MODULUS	PHASE (°)	DOCUMENT ID	TECN	COMMENT
0.16 ± 0.06	-130 ± 20	SARANTSEV 19	DPWA	$\bar{K}N$ multichannel

Normalized residue in $N\bar{K} \rightarrow \Sigma(2030) \rightarrow \Delta\bar{K}, H\text{-wave}$

MODULUS	PHASE (°)	DOCUMENT ID	TECN	COMMENT
0.04 ± 0.02	-130 ± 35	SARANTSEV 19	DPWA	$\bar{K}N$ multichannel

Normalized residue in $N\bar{K} \rightarrow \Sigma(2030) \rightarrow N\bar{K}^*(892), S=1/2, F\text{-wave}$

MODULUS	PHASE (°)	DOCUMENT ID	TECN	COMMENT
0.02 ± 0.02		SARANTSEV 19	DPWA	$\bar{K}N$ multichannel
0.193	38	¹ KAMANO 15	DPWA	$\bar{K}N$ multichannel

¹ From the preferred solution A in KAMANO 15.

Normalized residue in $N\bar{K} \rightarrow \Sigma(2030) \rightarrow N\bar{K}^*(892), S=3/2, F\text{-wave}$

MODULUS	PHASE (°)	DOCUMENT ID	TECN	COMMENT
0.16 ± 0.09	-160 ± 40	SARANTSEV 19	DPWA	$\bar{K}N$ multichannel
0.320	37	¹ KAMANO 15	DPWA	$\bar{K}N$ multichannel

¹ From the preferred solution A in KAMANO 15.

Normalized residue in $N\bar{K} \rightarrow \Sigma(2030) \rightarrow N\bar{K}^*(892), S=3/2, H\text{-wave}$

MODULUS	PHASE (°)	DOCUMENT ID	TECN	COMMENT
0.00358	22	¹ KAMANO 15	DPWA	Multichannel

¹ From the preferred solution A in KAMANO 15.

$\Sigma(2030)$ MASS

VALUE (MeV)	DOCUMENT ID	TECN	COMMENT
2025 to 2040 (≈ 2030) OUR ESTIMATE			
2032 ± 6	SARANTSEV 19	DPWA	$\bar{K}N$ multichannel
2030 ± 5	ZHANG 13A	DPWA	$\bar{K}N$ multichannel
2036 ± 5	GOPAL 80	DPWA	$\bar{K}N \rightarrow \bar{K}N$
2038 ± 10	CORDEN 77B		$K^-N \rightarrow N\bar{K}^*$
2030 ± 3	¹ CORDEN 76	DPWA	$K^-n \rightarrow \Lambda\pi^-$
2035 ± 15	BAILLON 75	IPWA	$\bar{K}N \rightarrow \Lambda\pi$
2038 ± 10	HEMINGWAY 75	DPWA	$K^-p \rightarrow \bar{K}N$
2042 ± 11	VANHORN 75	DPWA	$K^-p \rightarrow \Lambda\pi^0$
2020 ± 6	KANE 74	DPWA	$K^-p \rightarrow \Sigma\pi$
2035 ± 10	LITCHFIELD 74B	DPWA	$K^-p \rightarrow \Lambda(1520)\pi^0$
2020 ± 30	LITCHFIELD 74C	DPWA	$K^-p \rightarrow \Delta(1232)\bar{K}$
2025 ± 10	LITCHFIELD 74D	DPWA	$K^-p \rightarrow \Lambda(1820)\pi^0$
••• We do not use the following data for averages, fits, limits, etc. •••			
2040 ± 5	GOPAL 77	DPWA	$\bar{K}N$ multichannel
2027 to 2057	GOYAL 77	DPWA	$K^-N \rightarrow \Sigma\pi$
2030	DEBELLEFON 76	IPWA	$K^-p \rightarrow \Lambda\pi^0$

¹ Preferred solution 3; see CORDEN 76 for other possibilities.

$\Sigma(2030)$ WIDTH

VALUE (MeV)	DOCUMENT ID	TECN	COMMENT
150 to 200 (≈ 180) OUR ESTIMATE			
177 ± 12	SARANTSEV 19	DPWA	$\bar{K}N$ multichannel
207 ± 17	ZHANG 13A	DPWA	$\bar{K}N$ multichannel
172 ± 10	GOPAL 80	DPWA	$\bar{K}N \rightarrow \bar{K}N$
137 ± 40	CORDEN 77B		$K^-N \rightarrow N\bar{K}^*$
201 ± 9	¹ CORDEN 76	DPWA	$K^-n \rightarrow \Lambda\pi^-$
180 ± 20	BAILLON 75	IPWA	$\bar{K}N \rightarrow \Lambda\pi$
172 ± 15	HEMINGWAY 75	DPWA	$K^-p \rightarrow \bar{K}N$
178 ± 13	VANHORN 75	DPWA	$K^-p \rightarrow \Lambda\pi^0$
111 ± 5	KANE 74	DPWA	$K^-p \rightarrow \Sigma\pi$
160 ± 20	LITCHFIELD 74B	DPWA	$K^-p \rightarrow \Lambda(1520)\pi^0$
200 ± 30	LITCHFIELD 74C	DPWA	$K^-p \rightarrow \Delta(1232)\bar{K}$
••• We do not use the following data for averages, fits, limits, etc. •••			
260	DECLAIS 77	DPWA	$\bar{K}N \rightarrow \bar{K}N$
190 ± 10	GOPAL 77	DPWA	$\bar{K}N$ multichannel
126 to 195	GOYAL 77	DPWA	$K^-N \rightarrow \Sigma\pi$
160	DEBELLEFON 76	IPWA	$K^-p \rightarrow \Lambda\pi^0$
70 to 125	LITCHFIELD 74D	DPWA	$K^-p \rightarrow \Lambda(1820)\pi^0$

¹ Preferred solution 3; see CORDEN 76 for other possibilities.

$\Sigma(2030)$ DECAY MODES

Mode	Fraction (Γ_i/Γ)
Γ_1 $N\bar{K}$	17–23 %
Γ_2 $\Lambda\pi$	17–23 %
Γ_3 $\Sigma\pi$	5–10 %
Γ_4 ΞK	<2 %
Γ_5 $\Sigma(1385)\pi$	5–15 %
Γ_6 $\Sigma(1385)\pi, F\text{-wave}$	
Γ_7 $\Sigma(1385)\pi, F\text{-wave}$	(1.0 ± 1.0) %
Γ_8 $\Sigma(1385)\pi, H\text{-wave}$	
Γ_9 $\Lambda(1520)\pi$	10–20 %
Γ_{10} $\Lambda(1520)\pi, D\text{-wave}$	
Γ_{11} $\Lambda(1520)\pi, G\text{-wave}$	
Γ_{12} $\Delta(1232)\bar{K}$	10–20 %
Γ_{13} $\Delta(1232)\bar{K}, F\text{-wave}$	(15 ± 5) %
Γ_{14} $\Delta(1232)\bar{K}, H\text{-wave}$	(1.0 ± 1.0) %
Γ_{15} $N\bar{K}^*(892)$	<5 %
Γ_{16} $N\bar{K}^*(892), S=1/2, F\text{-wave}$	
Γ_{17} $N\bar{K}^*(892), S=3/2, F\text{-wave}$	(14 ± 8) %
Γ_{18} $N\bar{K}^*(892), S=3/2, H\text{-wave}$	
Γ_{19} $\Lambda(1820)\pi, P\text{-wave}$	

Baryon Particle Listings

 $\Sigma(2030)$ $\Sigma(2030)$ BRANCHING RATIOS

See "Sign conventions for resonance couplings" in the Note on Λ and Σ Resonances.

$\Gamma(N\bar{K})/\Gamma_{\text{total}}$				Γ_1/Γ
VALUE	DOCUMENT ID	TECN	COMMENT	
0.17 to 0.23 OUR ESTIMATE				
0.20 \pm 0.04	SARANTSEV 19	DPWA	$\bar{K}N$ multichannel	
0.13 \pm 0.01	ZHANG 13A	DPWA	$\bar{K}N$ multichannel	
0.19 \pm 0.03	GOPAL 80	DPWA	$\bar{K}N \rightarrow \bar{K}N$	
0.18 \pm 0.03	HEMINGWAY 75	DPWA	$K^-p \rightarrow \bar{K}N$	
• • • We do not use the following data for averages, fits, limits, etc. • • •				
0.269	¹ KAMANO 15	DPWA	Multichannel	
0.15	DECLAIS 77	DPWA	$\bar{K}N \rightarrow \bar{K}N$	
0.24 \pm 0.02	GOPAL 77	DPWA	See GOPAL 80	

¹ From the preferred solution A in KAMANO 15.

$\Gamma(\Lambda\pi)/\Gamma_{\text{total}}$				Γ_2/Γ
VALUE	DOCUMENT ID	TECN	COMMENT	
0.17 \pm 0.04	SARANTSEV 19	DPWA	$\bar{K}N$ multichannel	
• • • We do not use the following data for averages, fits, limits, etc. • • •				
0.080	¹ KAMANO 15	DPWA	$\bar{K}N$ multichannel	

¹ From the preferred solution A in KAMANO 15.

$\Gamma(\Sigma\pi)/\Gamma_{\text{total}}$				Γ_3/Γ
VALUE	DOCUMENT ID	TECN	COMMENT	
0.025 \pm 0.008	SARANTSEV 19	DPWA	$\bar{K}N$ multichannel	
• • • We do not use the following data for averages, fits, limits, etc. • • •				
0.037	¹ KAMANO 15	DPWA	$\bar{K}N$ multichannel	

¹ From the preferred solution A in KAMANO 15.

$\Gamma(\Xi K)/\Gamma_{\text{total}}$				Γ_4/Γ
VALUE	DOCUMENT ID	TECN	COMMENT	
<0.01	SARANTSEV 19	DPWA	$\bar{K}N$ multichannel	
• • • We do not use the following data for averages, fits, limits, etc. • • •				
0.006	¹ KAMANO 15	DPWA	$\bar{K}N$ multichannel	

¹ From the preferred solution A in KAMANO 15.

$\Gamma(\Lambda(1520)\pi, D\text{-wave})/\Gamma_{\text{total}}$				Γ_{10}/Γ
VALUE	DOCUMENT ID	TECN	COMMENT	
\sim 0.01	SARANTSEV 19	DPWA	$\bar{K}N$ multichannel	

$\Gamma(\Lambda(1520)\pi, G\text{-wave})/\Gamma_{\text{total}}$				Γ_{11}/Γ
VALUE	DOCUMENT ID	TECN	COMMENT	
<0.01	SARANTSEV 19	DPWA	$\bar{K}N$ multichannel	

$\Gamma(\Sigma(1385)\pi, F\text{-wave})/\Gamma_{\text{total}}$				Γ_7/Γ
VALUE	DOCUMENT ID	TECN	COMMENT	
0.01 \pm 0.01	SARANTSEV 19	DPWA	$\bar{K}N$ multichannel	
• • • We do not use the following data for averages, fits, limits, etc. • • •				
0.030	¹ KAMANO 15	DPWA	$\bar{K}N$ multichannel	

¹ From the preferred solution A in KAMANO 15.

$\Gamma(\Sigma(1385)\pi, H\text{-wave})/\Gamma_{\text{total}}$				Γ_8/Γ
VALUE	DOCUMENT ID	TECN	COMMENT	
• • • We do not use the following data for averages, fits, limits, etc. • • •				
0.003	¹ KAMANO 15	DPWA	Multichannel	

¹ From the preferred solution A in KAMANO 15.

$\Gamma(\Delta(1232)\bar{K}, F\text{-wave})/\Gamma_{\text{total}}$				Γ_{13}/Γ
VALUE	DOCUMENT ID	TECN	COMMENT	
0.15 \pm 0.05	SARANTSEV 19	DPWA	$\bar{K}N$ multichannel	

$\Gamma(\Delta(1232)\bar{K}, H\text{-wave})/\Gamma_{\text{total}}$				Γ_{14}/Γ
VALUE	DOCUMENT ID	TECN	COMMENT	
0.01 \pm 0.01	SARANTSEV 19	DPWA	$\bar{K}N$ multichannel	

$\Gamma(N\bar{K}^*(892), S=1/2, F\text{-wave})/\Gamma_{\text{total}}$				Γ_{16}/Γ
VALUE	DOCUMENT ID	TECN	COMMENT	
<0.01	SARANTSEV 19	DPWA	$\bar{K}N$ multichannel	
• • • We do not use the following data for averages, fits, limits, etc. • • •				
0.154	¹ KAMANO 15	DPWA	$\bar{K}N$ multichannel	

¹ From the preferred solution A in KAMANO 15.

$\Gamma(N\bar{K}^*(892), S=3/2, F\text{-wave})/\Gamma_{\text{total}}$				Γ_{17}/Γ
VALUE	DOCUMENT ID	TECN	COMMENT	
0.14 \pm 0.08	SARANTSEV 19	DPWA	$\bar{K}N$ multichannel	
• • • We do not use the following data for averages, fits, limits, etc. • • •				
0.422	¹ KAMANO 15	DPWA	$\bar{K}N$ multichannel	

¹ From the preferred solution A in KAMANO 15.

$\Gamma(N\bar{K}^*(892), S=3/2, H\text{-wave})/\Gamma_{\text{total}}$				Γ_{18}/Γ
VALUE	DOCUMENT ID	TECN	COMMENT	
• • • We do not use the following data for averages, fits, limits, etc. • • •				
not seen	¹ KAMANO 15	DPWA	$\bar{K}N$ multichannel	

¹ From the preferred solution A in KAMANO 15.

$(\Gamma_1\Gamma_f)^{1/2}/\Gamma_{\text{total}}$ in $N\bar{K} \rightarrow \Sigma(2030) \rightarrow \Lambda\pi$				$(\Gamma_1\Gamma_2)^{1/2}/\Gamma$
VALUE	DOCUMENT ID	TECN	COMMENT	
+0.15 \pm 0.01	ZHANG 13A	DPWA	Multichannel	
+0.18 \pm 0.02	GOPAL 77	DPWA	$\bar{K}N$ multichannel	
+0.20 \pm 0.01	¹ CORDEN 76	DPWA	$K^-n \rightarrow \Lambda\pi^-$	
+0.18 \pm 0.02	BAILLON 75	IPWA	$\bar{K}N \rightarrow \Lambda\pi$	
+0.20 \pm 0.01	VANHORN 75	DPWA	$K^-p \rightarrow \Lambda\pi^0$	
+0.195 \pm 0.053	DEVENISH 74B		Fixed- t dispersion rel.	
• • • We do not use the following data for averages, fits, limits, etc. • • •				
0.20	DEBELLEFON 76	IPWA	$K^-p \rightarrow \Lambda\pi^0$	

¹ Preferred solution 3; see CORDEN 76 for other possibilities.

$(\Gamma_1\Gamma_f)^{1/2}/\Gamma_{\text{total}}$ in $N\bar{K} \rightarrow \Sigma(2030) \rightarrow \Sigma\pi$				$(\Gamma_1\Gamma_3)^{1/2}/\Gamma$
VALUE	DOCUMENT ID	TECN	COMMENT	
-0.08 \pm 0.01	ZHANG 13A	DPWA	Multichannel	
-0.09 \pm 0.01	¹ CORDEN 77C		$K^-n \rightarrow \Sigma\pi$	
-0.06 \pm 0.01	¹ CORDEN 77C		$K^-n \rightarrow \Sigma\pi$	
-0.15 \pm 0.03	GOPAL 77	DPWA	$\bar{K}N$ multichannel	
-0.10 \pm 0.01	KANE 74	DPWA	$K^-p \rightarrow \Sigma\pi$	
• • • We do not use the following data for averages, fits, limits, etc. • • •				
-0.085 \pm 0.02	² GOYAL 77	DPWA	$K^-n \rightarrow \Sigma\pi$	

¹ The two entries for CORDEN 77C are from two different acceptable solutions.

² This coupling is extracted from unnormalized data.

$(\Gamma_1\Gamma_f)^{1/2}/\Gamma_{\text{total}}$ in $N\bar{K} \rightarrow \Sigma(2030) \rightarrow \Xi K$				$(\Gamma_1\Gamma_4)^{1/2}/\Gamma$
VALUE	DOCUMENT ID	TECN	COMMENT	
0.023	MULLER 69B	DPWA	$K^-p \rightarrow \Xi K$	
<0.05	BURGUN 68	DPWA	$K^-p \rightarrow \Xi K$	
<0.05	TRIPP 67	RVUE	$K^-p \rightarrow \Xi K$	

$(\Gamma_1\Gamma_f)^{1/2}/\Gamma_{\text{total}}$ in $N\bar{K} \rightarrow \Sigma(2030) \rightarrow \Sigma(1385)\pi, F\text{-wave}$				$(\Gamma_1\Gamma_6)^{1/2}/\Gamma$
VALUE	DOCUMENT ID	TECN	COMMENT	
+0.16 \pm 0.01	ZHANG 13A	DPWA	Multichannel	
+0.153 \pm 0.026	¹ CAMERON 78	DPWA	$K^-p \rightarrow \Sigma(1385)\pi$	

¹ The published sign has been changed to be in accord with the baryon-first convention.

$(\Gamma_1\Gamma_f)^{1/2}/\Gamma_{\text{total}}$ in $N\bar{K} \rightarrow \Sigma(2030) \rightarrow \Lambda(1520)\pi, D\text{-wave}$				$(\Gamma_1\Gamma_{10})^{1/2}/\Gamma$
VALUE	DOCUMENT ID	TECN	COMMENT	
+0.114 \pm 0.010	¹ CAMERON 77	DPWA	$K^-p \rightarrow \Lambda(1520)\pi^0$	
0.14 \pm 0.03	LITCHFIELD 74B	DPWA	$K^-p \rightarrow \Lambda(1520)\pi^0$	
• • • We do not use the following data for averages, fits, limits, etc. • • •				
0.10 \pm 0.03	² CORDEN 75B	DBC	$K^-n \rightarrow N\bar{K}\pi^-$	

¹ The published sign has been changed to be in accord with the baryon-first convention.

² An upper limit.

$(\Gamma_1\Gamma_f)^{1/2}/\Gamma_{\text{total}}$ in $N\bar{K} \rightarrow \Sigma(2030) \rightarrow \Lambda(1520)\pi, G\text{-wave}$				$(\Gamma_1\Gamma_{11})^{1/2}/\Gamma$
VALUE	DOCUMENT ID	TECN	COMMENT	
+0.146 \pm 0.010	¹ CAMERON 77	DPWA	$K^-p \rightarrow \Lambda(1520)\pi^0$	
0.02 \pm 0.02	LITCHFIELD 74B	DPWA	$K^-p \rightarrow \Lambda(1520)\pi^0$	

¹ The published sign has been changed to be in accord with the baryon-first convention.

$(\Gamma_1\Gamma_f)^{1/2}/\Gamma_{\text{total}}$ in $N\bar{K} \rightarrow \Sigma(2030) \rightarrow \Delta(1232)\bar{K}, F\text{-wave}$				$(\Gamma_1\Gamma_{13})^{1/2}/\Gamma$
VALUE	DOCUMENT ID	TECN	COMMENT	
+0.12 \pm 0.02	ZHANG 13A	DPWA	Multichannel	
0.16 \pm 0.03	LITCHFIELD 74C	DPWA	$K^-p \rightarrow \Delta(1232)\bar{K}$	
• • • We do not use the following data for averages, fits, limits, etc. • • •				
0.17 \pm 0.03	¹ CORDEN 75B	DBC	$K^-n \rightarrow N\bar{K}\pi^-$	

¹ An upper limit.

$(\Gamma_1\Gamma_f)^{1/2}/\Gamma_{\text{total}}$ in $N\bar{K} \rightarrow \Sigma(2030) \rightarrow \Delta(1232)\bar{K}, H\text{-wave}$				$(\Gamma_1\Gamma_{14})^{1/2}/\Gamma$
VALUE	DOCUMENT ID	TECN	COMMENT	
0.00 \pm 0.02	LITCHFIELD 74C	DPWA	$K^-p \rightarrow \Delta(1232)\bar{K}$	

$(\Gamma_1\Gamma_f)^{1/2}/\Gamma_{\text{total}}$ in $N\bar{K} \rightarrow \Sigma(2030) \rightarrow N\bar{K}^*(892), S=1/2, F\text{-wave}$				$(\Gamma_1\Gamma_{16})^{1/2}/\Gamma$
VALUE	DOCUMENT ID	TECN	COMMENT	
+0.06 \pm 0.02	ZHANG 13A	DPWA	Multichannel	
+0.06 \pm 0.03	¹ CAMERON 78B	DPWA	$K^-p \rightarrow N\bar{K}^*$	
-0.02 \pm 0.01	CORDEN 77B		$K^-d \rightarrow NN\bar{K}^*$	

¹ The published sign has been changed to be in accord with the baryon-first convention.

See key on page 999

Baryon Particle Listings

$\Sigma(2030), \Sigma(2070), \Sigma(2080)$

$(\Gamma_1 \Gamma_f)^{1/2} / \Gamma_{\text{total}}$ in $N\bar{K} \rightarrow \Sigma(2030) \rightarrow N\bar{K}^*(892), S=3/2, F\text{-wave}$ $(\Gamma_1 \Gamma_{17})^{1/2} / \Gamma$

VALUE	DOCUMENT ID	TECN	COMMENT
+0.05 ± 0.01	ZHANG	13A	DPWA Multichannel
+0.04 ± 0.03	¹ CAMERON	78B	DPWA $K^- p \rightarrow N\bar{K}^*$
-0.12 ± 0.02	CORDEN	77B	$K^- d \rightarrow NN\bar{K}^*$

¹ The upper limit on the G_3 wave is 0.03.

$(\Gamma_1 \Gamma_f)^{1/2} / \Gamma_{\text{total}}$ in $N\bar{K} \rightarrow \Sigma(2030) \rightarrow \Lambda(1820)\pi, P\text{-wave}$ $(\Gamma_1 \Gamma_{19})^{1/2} / \Gamma$

VALUE	DOCUMENT ID	TECN	COMMENT
0.14 ± 0.02	CORDEN	75B	DBC $K^- n \rightarrow N\bar{K}\pi^-$
0.18 ± 0.04	LITCHFIELD	74D	DPWA $K^- p \rightarrow \Lambda(1820)\pi^0$

$\Sigma(2030)$ REFERENCES

SARANTSEV	19	EPJ A55 180	A.V. Sarantsev et al.	(BONN, PNPI)
KAMANO	15	PR C92 025205	H. Kamano et al.	(ANL, OSAK)
ZHANG	13A	PR C88 035205	H. Zhang et al.	(KSU)
PDG	84	RMP 56 51	C.G. Wohl et al.	(LBL, CIT, CERN)
PDG	82	PL 111B 1	M. Roos et al.	(HELS, CIT, CERN)
GOPAL	80	Toronto Conf. 159	G.P. Gopal	(RHEL) IJP
CAMERON	78	NP B143 189	W. Cameron et al.	(RHEL, LOIC) IJP
CAMERON	75B	NP B146 327	W. Cameron et al.	(RHEL, LOIC) IJP
CAMERON	77	NP B131 399	W. Cameron et al.	(RHEL, LOIC) IJP
CORDEN	77B	NP B121 365	M.J. Corden et al.	(BIRM) IJP
CORDEN	77C	NP B125 61	M.J. Corden et al.	(BIRM) IJP
DECLAIS	77	CERN 77-16	Y. Declais et al.	(CAEN, CERN) IJP
GOPAL	77	NP B119 362	G.P. Gopal et al.	(LOIC, RHEL) IJP
GOYAL	77	PR D16 2746	D.P. Goyal, A.V. Sodhi	(DELH) IJP
CORDEN	76	NP B104 382	M.J. Corden et al.	(BIRM) IJP
DEBELLEFON	76	NP B109 129	A. de Bellefon, A. Berthon	(CDEF) IJP
BAILLON	75	NP B94 39	P.H. Baillon, P.J. Litchfield	(CERN, RHEL) IJP
CORDEN	75B	NP B92 365	M.J. Corden et al.	(BIRM) IJP
HEMINGWAY	75	NP B91 12	R.J. Hemingway et al.	(CERN, HEIDH, MPIM) IJP
VANHORN	75	NP B87 145	A.J. van Horn	(LBL) IJP
Also		NP B87 157	A.J. van Horn	(LBL) IJP
DEVENISH	74B	NP B81 330	R.C.E. Devenish, C.D. Froggatt, B.R. Martin	(DESY+) IJP
KANE	74	LBL-2452	D.F. Kane	(LBL) IJP
LITCHFIELD	74B	NP B74 19	P.J. Litchfield et al.	(CERN, HEIDH) IJP
LITCHFIELD	74C	NP B74 39	P.J. Litchfield et al.	(CERN, HEIDH) IJP
LITCHFIELD	74D	NP B74 12	P.J. Litchfield et al.	(CERN, HEIDH) IJP
MULLER	69B	Thesis UCRL 19372	R.A. Muller	(LRL) IJP
BURGUN	68	NP B8 447	G. Burigun et al.	(SACL, CDEF, RHEL) IJP
TRIPP	67	NP B3 10	R.D. Tripp et al.	(LRL, SLAC, CERN+) IJP
COOL	66	PRL 16 1228	R.L. Cool et al.	(BNL) IJP
WOHL	66	PRL 17 107	C.G. Wohl, F.T. Solmitz, M.L. Stevenson	(LRL) IJP

$\Sigma(2070) 5/2^+$ $I(J^P) = 1(5/2^+) \text{ Status: } *$

OMITTED FROM SUMMARY TABLE

This state suggested by BERTHON 70B finds support in GOPAL 80 with new $K^- p$ polarization and $K^- n$ angular distributions. The very broad state seen in KANE 72 is not required in the later (KANE 74) analysis of $\bar{K} N \rightarrow \Sigma \pi$.

$\Sigma(2070)$ MASS

VALUE (MeV)	DOCUMENT ID	TECN	COMMENT
2020 to 2100 (≈ 2060) OUR ESTIMATE			
2051 ± 25	GOPAL	80	DPWA $\bar{K} N \rightarrow \bar{K} N$
2070 ± 10	BERTHON	70B	DPWA $K^- p \rightarrow \Sigma \pi$
• • • We do not use the following data for averages, fits, limits, etc. • • •			
2057	KANE	72	DPWA $K^- p \rightarrow \Sigma \pi$

$\Sigma(2070)$ WIDTH

VALUE (MeV)	DOCUMENT ID	TECN	COMMENT
100 to 300 (≈ 200) OUR ESTIMATE			
300 ± 30	GOPAL	80	DPWA $\bar{K} N \rightarrow \bar{K} N$
140 ± 20	BERTHON	70B	DPWA $K^- p \rightarrow \Sigma \pi$
• • • We do not use the following data for averages, fits, limits, etc. • • •			
906	KANE	72	DPWA $K^- p \rightarrow \Sigma \pi$

$\Sigma(2070)$ DECAY MODES

Mode	Γ_1	Γ_2
$N\bar{K}$	Γ_1	
$\Sigma \pi$		Γ_2

$\Sigma(2070)$ BRANCHING RATIOS

See "Sign conventions for resonance couplings" in the Note on Λ and Σ Resonances.

$\Gamma(N\bar{K}) / \Gamma_{\text{total}}$ Γ_1 / Γ

VALUE	DOCUMENT ID	TECN	COMMENT
0.08 ± 0.03	GOPAL	80	DPWA $\bar{K} N \rightarrow \bar{K} N$

$(\Gamma_1 \Gamma_f)^{1/2} / \Gamma_{\text{total}}$ in $N\bar{K} \rightarrow \Sigma(2070) \rightarrow \Sigma \pi$ $(\Gamma_1 \Gamma_2)^{1/2} / \Gamma$

VALUE	DOCUMENT ID	TECN	COMMENT
0.12 ± 0.02	BERTHON	70B	DPWA $K^- p \rightarrow \Sigma \pi$
• • • We do not use the following data for averages, fits, limits, etc. • • •			
0.104	KANE	72	DPWA $K^- p \rightarrow \Sigma \pi$

$\Sigma(2070)$ REFERENCES

GOPAL	80	Toronto Conf. 159	G.P. Gopal	(RHEL) IJP
KANE	74	LBL-2452	D.F. Kane	(LBL)
KANE	72	PR D5 1583	D.F.J. Kane	(LBL)
BERTHON	70B	NP B24 417	A. Berthon et al.	(CDEF, RHEL, SACL) IJP

$\Sigma(2080) 3/2^+$

$I(J^P) = 1(3/2^+) \text{ Status: } *$

OMITTED FROM SUMMARY TABLE

Suggested by some but not all partial-wave analyses across this region.

$\Sigma(2080)$ MASS

VALUE (MeV)	DOCUMENT ID	TECN	COMMENT
2060 to 2120 (≈ 2090) OUR ESTIMATE			
2091 ± 7	¹ CORDEN	76	DPWA $K^- n \rightarrow \Lambda \pi^-$
2070 to 2120	DEBELLEFON	76	IPWA $K^- p \rightarrow \Lambda \pi^0$
2120 ± 40	BAILLON	75	IPWA $\bar{K} N \rightarrow \Lambda \pi$ (sol. 1)
2140 ± 40	BAILLON	75	IPWA $\bar{K} N \rightarrow \Lambda \pi$ (sol. 2)
2082 ± 4	COX	70	DPWA See CORDEN 76
2070 ± 30	LITCHFIELD	70	DPWA $K^- N \rightarrow \Lambda \pi$

$\Sigma(2080)$ WIDTH

VALUE (MeV)	DOCUMENT ID	TECN	COMMENT
100 to 240 (≈ 170) OUR ESTIMATE			
186 ± 48	¹ CORDEN	76	DPWA $K^- n \rightarrow \Lambda \pi^-$
100	DEBELLEFON	76	IPWA $K^- p \rightarrow \Lambda \pi^0$
240 ± 50	BAILLON	75	IPWA $\bar{K} N \rightarrow \Lambda \pi$ (sol. 1)
200 ± 50	BAILLON	75	IPWA $\bar{K} N \rightarrow \Lambda \pi$ (sol. 2)
87 ± 20	COX	70	DPWA See CORDEN 76
250 ± 40	LITCHFIELD	70	DPWA $K^- N \rightarrow \Lambda \pi$

$\Sigma(2080)$ DECAY MODES

Mode	Γ_1	Γ_2
$N\bar{K}$	Γ_1	
$\Lambda \pi$		Γ_2

$\Sigma(2080)$ BRANCHING RATIOS

See "Sign conventions for resonance couplings" in the Note on Λ and Σ Resonances.

$(\Gamma_1 \Gamma_f)^{1/2} / \Gamma_{\text{total}}$ in $N\bar{K} \rightarrow \Sigma(2080) \rightarrow \Lambda \pi$ $(\Gamma_1 \Gamma_2)^{1/2} / \Gamma$

VALUE	DOCUMENT ID	TECN	COMMENT
-0.10 ± 0.03	¹ CORDEN	76	DPWA $K^- n \rightarrow \Lambda \pi^-$
-0.10	DEBELLEFON	76	IPWA $K^- p \rightarrow \Lambda \pi^0$
-0.13 ± 0.04	BAILLON	75	IPWA $\bar{K} N \rightarrow \Lambda \pi$ (sol. 1 and 2)
-0.16 ± 0.03	COX	70	DPWA See CORDEN 76
-0.09 ± 0.03	LITCHFIELD	70	DPWA $K^- N \rightarrow \Lambda \pi$

$\Sigma(2080)$ FOOTNOTES

¹ Preferred solution 3; see CORDEN 76 for other possibilities, including a D_{15} at this mass.

$\Sigma(2080)$ REFERENCES

CORDEN	76	NP B104 382	M.J. Corden et al.	(BIRM) IJP
DEBELLEFON	76	NP B109 129	A. de Bellefon, A. Berthon	(CDEF) IJP
Also		NP B90 1	A. de Bellefon et al.	(CDEF, SACL) IJP
BAILLON	75	NP B94 39	P.H. Baillon, P.J. Litchfield	(CERN, RHEL) IJP
COX	70	NP B19 61	G.F. Cox et al.	(BIRM, EDIN, GLAS, LOIC) IJP
LITCHFIELD	70	NP B22 269	P.J. Litchfield	(RHEL) IJP

Baryon Particle Listings

 $\Sigma(2080)$, $\Sigma(2100)$, $\Sigma(2160)$ $\Sigma(2100) 7/2^-$ $I(J^P) = 1(\frac{7}{2}^-)$ Status: *

OMITTED FROM SUMMARY TABLE

 $\Sigma(2100)$ POLE POSITION

REAL PART

VALUE (MeV)	DOCUMENT ID	TECN	COMMENT
2093 ± 16	SARANTSEV 19	DPWA	$\bar{K}N$ multichannel

-2xIMAGINARY PART

VALUE (MeV)	DOCUMENT ID	TECN	COMMENT
210 ± 35	SARANTSEV 19	DPWA	$\bar{K}N$ multichannel

 $\Sigma(2100)$ POLE RESIDUESNormalized residue in $N\bar{K} \rightarrow \Sigma(2100) \rightarrow N\bar{K}$

MODULUS	PHASE (°)	DOCUMENT ID	TECN	COMMENT
0.09 ± 0.02	-110 ± 15	SARANTSEV 19	DPWA	$\bar{K}N$ multichannel

Normalized residue in $N\bar{K} \rightarrow \Sigma(2100) \rightarrow \Sigma\pi$

MODULUS	PHASE (°)	DOCUMENT ID	TECN	COMMENT
0.04 ± 0.02	-50 ± 20	SARANTSEV 19	DPWA	$\bar{K}N$ multichannel

Normalized residue in $N\bar{K} \rightarrow \Sigma(2100) \rightarrow \Lambda\pi$

MODULUS	PHASE (°)	DOCUMENT ID	TECN	COMMENT
0.03 ± 0.02	-100 ± 25	SARANTSEV 19	DPWA	$\bar{K}N$ multichannel

Normalized residue in $N\bar{K} \rightarrow \Sigma(2100) \rightarrow \Xi K$

MODULUS	PHASE (°)	DOCUMENT ID	TECN	COMMENT
0.010 ± 0.005	-120 ± 35	SARANTSEV 19	DPWA	$\bar{K}N$ multichannel

Normalized residue in $N\bar{K} \rightarrow \Sigma(2100) \rightarrow \Lambda(1520)\pi, F\text{-wave}$

MODULUS	PHASE (°)	DOCUMENT ID	TECN	COMMENT
0.02 ± 0.01	-100 ± 30	SARANTSEV 19	DPWA	$\bar{K}N$ multichannel

Normalized residue in $N\bar{K} \rightarrow \Sigma(2100) \rightarrow \Lambda(1520)\pi, H\text{-wave}$

MODULUS	PHASE (°)	DOCUMENT ID	TECN	COMMENT
0.01 ± 0.01		SARANTSEV 19	DPWA	$\bar{K}N$ multichannel

Normalized residue in $N\bar{K} \rightarrow \Sigma(2100) \rightarrow \Sigma(1385)\pi, D\text{-wave}$

MODULUS	PHASE (°)	DOCUMENT ID	TECN	COMMENT
0.10 ± 0.03	-60 ± 30	SARANTSEV 19	DPWA	$\bar{K}N$ multichannel

Normalized residue in $N\bar{K} \rightarrow \Sigma(2100) \rightarrow \Sigma(1385)\pi, G\text{-wave}$

MODULUS	PHASE (°)	DOCUMENT ID	TECN	COMMENT
0.03 ± 0.01	-50 ± 30	SARANTSEV 19	DPWA	$\bar{K}N$ multichannel

Normalized residue in $N\bar{K} \rightarrow \Sigma(2100) \rightarrow \Delta\bar{K}, G\text{-wave}$

MODULUS	PHASE (°)	DOCUMENT ID	TECN	COMMENT
0.04 ± 0.02	75 ± 35	SARANTSEV 19	DPWA	$\bar{K}N$ multichannel

Normalized residue in $N\bar{K} \rightarrow \Sigma(2100) \rightarrow N\bar{K}^*(892), S=3/2, D\text{-wave}$

MODULUS	PHASE (°)	DOCUMENT ID	TECN	COMMENT
0.08 ± 0.04	20 ± 50	SARANTSEV 19	DPWA	$\bar{K}N$ multichannel

 $\Sigma(2100)$ MASS

VALUE (MeV)	DOCUMENT ID	TECN	COMMENT
≈ 2100 OUR ESTIMATE			
2146 ± 17	SARANTSEV 19	DPWA	$\bar{K}N$ multichannel
2060 ± 20	BARBARO... 70	DPWA	$K^-p \rightarrow \Lambda\pi^0$
2120 ± 30	BARBARO... 70	DPWA	$K^-p \rightarrow \Sigma\pi$

 $\Sigma(2100)$ WIDTH

VALUE (MeV)	DOCUMENT ID	TECN	COMMENT
260 ± 40	SARANTSEV 19	DPWA	$\bar{K}N$ multichannel
70 ± 30	BARBARO... 70	DPWA	$K^-p \rightarrow \Lambda\pi^0$
135 ± 30	BARBARO... 70	DPWA	$K^-p \rightarrow \Sigma\pi$

 $\Sigma(2100)$ DECAY MODES

Mode	Fraction (Γ_i/Γ)
Γ_1 $N\bar{K}$	(8.0 ± 2.0) %
Γ_2 $\Lambda\pi$	(1.5 ± 1.0) %
Γ_3 $\Sigma\pi$	(2.0 ± 1.0) %
Γ_4 ΞK	
Γ_5 $\Sigma(1385)\pi, D\text{-wave}$	(12 ± 6) %
Γ_6 $\Sigma(1385)\pi, G\text{-wave}$	
Γ_7 $\Lambda(1520)\pi, F\text{-wave}$	(1.0 ± 1.0) %
Γ_8 $\Lambda(1520)\pi, H\text{-wave}$	
Γ_9 $N\bar{K}^*(892), S=3/2, D\text{-wave}$	(6.0 ± 3.0) %
Γ_{10} $\Delta\bar{K}, G\text{-wave}$	(1.0 ± 1.0) %

 $\Sigma(2100)$ BRANCHING RATIOSSee "Sign conventions for resonance couplings" in the Note on Λ and Σ Resonances.

$(\Gamma_i\Gamma_f)^{1/2}/\Gamma_{\text{total}}$ in $N\bar{K} \rightarrow \Sigma(2100) \rightarrow \Lambda\pi$	DOCUMENT ID	TECN	COMMENT
-0.07 ± 0.02	BARBARO... 70	DPWA	$K^-p \rightarrow \Lambda\pi^0$

$(\Gamma_i\Gamma_f)^{1/2}/\Gamma_{\text{total}}$ in $N\bar{K} \rightarrow \Sigma(2100) \rightarrow \Sigma\pi$	DOCUMENT ID	TECN	COMMENT
+0.13 ± 0.02	BARBARO... 70	DPWA	$K^-p \rightarrow \Sigma\pi$

$\Gamma(N\bar{K})/\Gamma_{\text{total}}$	DOCUMENT ID	TECN	COMMENT
0.08 ± 0.02	SARANTSEV 19	DPWA	$\bar{K}N$ multichannel

$\Gamma(\Lambda\pi)/\Gamma_{\text{total}}$	DOCUMENT ID	TECN	COMMENT
0.015 ± 0.01	SARANTSEV 19	DPWA	$\bar{K}N$ multichannel

$\Gamma(\Sigma\pi)/\Gamma_{\text{total}}$	DOCUMENT ID	TECN	COMMENT
0.02 ± 0.01	SARANTSEV 19	DPWA	$\bar{K}N$ multichannel

$\Gamma(\Xi K)/\Gamma_{\text{total}}$	DOCUMENT ID	TECN	COMMENT
< 0.01	SARANTSEV 19	DPWA	$\bar{K}N$ multichannel

$\Gamma(\Sigma(1385)\pi, D\text{-wave})/\Gamma_{\text{total}}$	DOCUMENT ID	TECN	COMMENT
0.12 ± 0.06	SARANTSEV 19	DPWA	$\bar{K}N$ multichannel

$\Gamma(\Sigma(1385)\pi, G\text{-wave})/\Gamma_{\text{total}}$	DOCUMENT ID	TECN	COMMENT
~ 0.01	SARANTSEV 19	DPWA	$\bar{K}N$ multichannel

$\Gamma(\Lambda(1520)\pi, F\text{-wave})/\Gamma_{\text{total}}$	DOCUMENT ID	TECN	COMMENT
0.01 ± 0.01	SARANTSEV 19	DPWA	$\bar{K}N$ multichannel

$\Gamma(\Lambda(1520)\pi, H\text{-wave})/\Gamma_{\text{total}}$	DOCUMENT ID	TECN	COMMENT
~ 0	SARANTSEV 19	DPWA	$\bar{K}N$ multichannel

$\Gamma(N\bar{K}^*(892), S=3/2, D\text{-wave})/\Gamma_{\text{total}}$	DOCUMENT ID	TECN	COMMENT
0.06 ± 0.03	SARANTSEV 19	DPWA	$\bar{K}N$ multichannel

$\Gamma(\Delta\bar{K}, G\text{-wave})/\Gamma_{\text{total}}$	DOCUMENT ID	TECN	COMMENT
0.01 ± 0.01	SARANTSEV 19	DPWA	$\bar{K}N$ multichannel

 $\Sigma(2100)$ REFERENCES

SARANTSEV 19	EPJ A55 180	A.V. Sarantsev et al.	(BONN, PNPI)
BARBARO... 70	Duke Conf. 173	A. Barbaro-Galsteri	(LRL) IJP
	Hyperon Resonances, 1970		

 $\Sigma(2160) 1/2^-$ $I(J^P) = 1(\frac{1}{2}^-)$ Status: *

OMITTED FROM SUMMARY TABLE

 $\Sigma(2160)$ POLE POSITION

REAL PART

VALUE (MeV)	DOCUMENT ID	TECN	COMMENT
2158 ± 25	SARANTSEV 19	DPWA	$\bar{K}N$ multichannel

-2xIMAGINARY PART

VALUE (MeV)	DOCUMENT ID	TECN	COMMENT
300 \pm 300 - 60	SARANTSEV 19	DPWA	$\bar{K}N$ multichannel

 $\Sigma(2160)$ POLE RESIDUESNormalized residue in $N\bar{K} \rightarrow \Sigma(2160) \rightarrow N\bar{K}$

MODULUS	PHASE (°)	DOCUMENT ID	TECN	COMMENT
0.29 ± 0.08	-20 ± 35	SARANTSEV 19	DPWA	$\bar{K}N$ multichannel

Normalized residue in $N\bar{K} \rightarrow \Sigma(2160) \rightarrow \Sigma\pi$

MODULUS	PHASE (°)	DOCUMENT ID	TECN	COMMENT
0.14 ± 0.04	-5 ± 35	SARANTSEV 19	DPWA	$\bar{K}N$ multichannel

See key on page 999

Baryon Particle Listings
 $\Sigma(2160), \Sigma(2230)$

Normalized residue in $N\bar{K} \rightarrow \Sigma(2160) \rightarrow \Lambda\pi$

MODULUS	PHASE (°)	DOCUMENT ID	TECN	COMMENT
0.39 ± 0.08	85 ± 25	SARANTSEV 19	DPWA	$\bar{K}N$ multichannel

Normalized residue in $N\bar{K} \rightarrow \Sigma(2160) \rightarrow \Xi K$

MODULUS	PHASE (°)	DOCUMENT ID	TECN	COMMENT
0.05 ± 0.02	-85 ± 35	SARANTSEV 19	DPWA	$\bar{K}N$ multichannel

Normalized residue in $N\bar{K} \rightarrow \Sigma(2160) \rightarrow \Lambda(1520)\pi$

MODULUS	PHASE (°)	DOCUMENT ID	TECN	COMMENT
0.025 ± 0.015		SARANTSEV 19	DPWA	$\bar{K}N$ multichannel

Normalized residue in $N\bar{K} \rightarrow \Sigma(2160) \rightarrow \Sigma(1385)\pi$

MODULUS	PHASE (°)	DOCUMENT ID	TECN	COMMENT
0.03 ± 0.02		SARANTSEV 19	DPWA	$\bar{K}N$ multichannel

Normalized residue in $N\bar{K} \rightarrow \Sigma(2160) \rightarrow \Delta\bar{K}$

MODULUS	PHASE (°)	DOCUMENT ID	TECN	COMMENT
0.035 ± 0.02	-30 ± 40	SARANTSEV 19	DPWA	$\bar{K}N$ multichannel

Normalized residue in $N\bar{K} \rightarrow \Sigma(2160) \rightarrow N\bar{K}^*(892), S\text{-wave}$

MODULUS	PHASE (°)	DOCUMENT ID	TECN	COMMENT
0.09 ± 0.03	-40 ± 50	SARANTSEV 19	DPWA	$\bar{K}N$ multichannel

Normalized residue in $N\bar{K} \rightarrow \Sigma(2160) \rightarrow N\bar{K}^*(892), D\text{-wave}$

MODULUS	PHASE (°)	DOCUMENT ID	TECN	COMMENT
0.04 ± 0.03		SARANTSEV 19	DPWA	$\bar{K}N$ multichannel

$\Sigma(2160)$ MASS

VALUE (MeV)	DOCUMENT ID	TECN	COMMENT
2105 ± 50 OUR AVERAGE	Error includes scale factor of 3.4.		
2165 ± 23	SARANTSEV 19	DPWA	$\bar{K}N$ multichannel
2060 ± 20	ZHANG 13A	DPWA	$\bar{K}N$ multichannel

$\Sigma(2160)$ WIDTH

VALUE (MeV)	DOCUMENT ID	TECN	COMMENT
313^{+120}_{-50} OUR AVERAGE			
320^{+300}_{-60}	SARANTSEV 19	DPWA	$\bar{K}N$ multichannel
300 ± 134	ZHANG 13A	DPWA	$\bar{K}N$ multichannel

$\Sigma(2160)$ DECAY MODES

Mode	Fraction (Γ_i/Γ)
$\Gamma_1 N\bar{K}$	$(29 \pm 7) \%$
$\Gamma_2 \Sigma\pi$	$(7.0 \pm 2.0) \%$
$\Gamma_3 \Lambda\pi$	$(54 \pm 12) \%$
$\Gamma_4 N\bar{K}^*(892), S\text{-wave}$	$(3.0 \pm 1.0) \%$
$\Gamma_5 N\bar{K}^*(892), D\text{-wave}$	

$\Sigma(2160)$ BRANCHING RATIOS

$\Gamma(N\bar{K})/\Gamma_{\text{total}}$

VALUE	DOCUMENT ID	TECN	COMMENT	Γ_1/Γ
0.29 ± 0.07	SARANTSEV 19	DPWA	$\bar{K}N$ multichannel	

$\Gamma(\Sigma\pi)/\Gamma_{\text{total}}$

VALUE	DOCUMENT ID	TECN	COMMENT	Γ_2/Γ
0.07 ± 0.02	SARANTSEV 19	DPWA	$\bar{K}N$ multichannel	

$\Gamma(\Lambda\pi)/\Gamma_{\text{total}}$

VALUE	DOCUMENT ID	TECN	COMMENT	Γ_3/Γ
0.54 ± 0.12	SARANTSEV 19	DPWA	$\bar{K}N$ multichannel	

$\Gamma(N\bar{K}^*(892), S\text{-wave})/\Gamma_{\text{total}}$

VALUE	DOCUMENT ID	TECN	COMMENT	Γ_4/Γ
0.03 ± 0.01	SARANTSEV 19	DPWA	$\bar{K}N$ multichannel	

$\Gamma(N\bar{K}^*(892), D\text{-wave})/\Gamma_{\text{total}}$

VALUE	DOCUMENT ID	TECN	COMMENT	Γ_5/Γ
~ 0.01	SARANTSEV 19	DPWA	$\bar{K}N$ multichannel	

$\Sigma(2160)$ REFERENCES

SARANTSEV 19	EPJ A55 180	A.V. Sarantsev et al.	(BONN, PNPI)
ZHANG 13A	PR C88 035205	H. Zhang et al.	(KSU)

$\Sigma(2230) 3/2^+$

$I(J^P) = 1(\frac{3}{2}^+)$ Status: *

OMITTED FROM SUMMARY TABLE

$\Sigma(2230)$ POLE POSITION

REAL PART

VALUE (MeV)	DOCUMENT ID	TECN	COMMENT
2234 ± 25	SARANTSEV 19	DPWA	$\bar{K}N$ multichannel

-2xIMAGINARY PART

VALUE (MeV)	DOCUMENT ID	TECN	COMMENT
340 ± 45	SARANTSEV 19	DPWA	$\bar{K}N$ multichannel

$\Sigma(2230)$ POLE RESIDUES

Normalized residue in $N\bar{K} \rightarrow \Sigma(2230) \rightarrow N\bar{K}$

MODULUS	PHASE (°)	DOCUMENT ID	TECN	COMMENT
0.07 ± 0.02	25 ± 15	SARANTSEV 19	DPWA	$\bar{K}N$ multichannel

Normalized residue in $N\bar{K} \rightarrow \Sigma(2230) \rightarrow \Sigma\pi$

MODULUS	PHASE (°)	DOCUMENT ID	TECN	COMMENT
0.03 ± 0.02	180 ± 25	SARANTSEV 19	DPWA	$\bar{K}N$ multichannel

Normalized residue in $N\bar{K} \rightarrow \Sigma(2030) \rightarrow \Lambda\pi$

MODULUS	PHASE (°)	DOCUMENT ID	TECN	COMMENT
0.11 ± 0.05	-16 ± 10	SARANTSEV 19	DPWA	$\bar{K}N$ multichannel

Normalized residue in $N\bar{K} \rightarrow \Sigma(2230) \rightarrow \Xi K$

MODULUS	PHASE (°)	DOCUMENT ID	TECN	COMMENT
0.04 ± 0.02	155 ± 20	SARANTSEV 19	DPWA	$\bar{K}N$ multichannel

Normalized residue in $N\bar{K} \rightarrow \Sigma(2230) \rightarrow \Lambda(1520)\pi, S\text{-wave}$

MODULUS	PHASE (°)	DOCUMENT ID	TECN	COMMENT
0.12 ± 0.05	-80 ± 25	SARANTSEV 19	DPWA	$\bar{K}N$ multichannel

Normalized residue in $N\bar{K} \rightarrow \Sigma(2230) \rightarrow \Lambda(1520)\pi, D\text{-wave}$

MODULUS	PHASE (°)	DOCUMENT ID	TECN	COMMENT
0.03 ± 0.02	160 ± 30	SARANTSEV 19	DPWA	$\bar{K}N$ multichannel

Normalized residue in $N\bar{K} \rightarrow \Sigma(2230) \rightarrow \Sigma(1385)\pi, P\text{-wave}$

MODULUS	PHASE (°)	DOCUMENT ID	TECN	COMMENT
0.05 ± 0.02	60 ± 25	SARANTSEV 19	DPWA	$\bar{K}N$ multichannel

Normalized residue in $N\bar{K} \rightarrow \Sigma(2230) \rightarrow \Sigma(1385)\pi, F\text{-wave}$

MODULUS	PHASE (°)	DOCUMENT ID	TECN	COMMENT
0.05 ± 0.03	-70 ± 20	SARANTSEV 19	DPWA	$\bar{K}N$ multichannel

Normalized residue in $N\bar{K} \rightarrow \Sigma(2230) \rightarrow \Delta\bar{K}, P\text{-wave}$

MODULUS	PHASE (°)	DOCUMENT ID	TECN	COMMENT
0.11 ± 0.04	60 ± 15	SARANTSEV 19	DPWA	$\bar{K}N$ multichannel

Normalized residue in $N\bar{K} \rightarrow \Sigma(2230) \rightarrow \Delta\bar{K}, F\text{-wave}$

MODULUS	PHASE (°)	DOCUMENT ID	TECN	COMMENT
0.07 ± 0.03	90 ± 25	SARANTSEV 19	DPWA	$\bar{K}N$ multichannel

Normalized residue in $N\bar{K} \rightarrow \Sigma(2230) \rightarrow N\bar{K}^*(892), S=1/2, P\text{-wave}$

MODULUS	PHASE (°)	DOCUMENT ID	TECN	COMMENT
0.08 ± 0.04	40 ± 45	SARANTSEV 19	DPWA	$\bar{K}N$ multichannel

Normalized residue in $N\bar{K} \rightarrow \Sigma(2230) \rightarrow N\bar{K}^*(892), S=3/2, P\text{-wave}$

MODULUS	PHASE (°)	DOCUMENT ID	TECN	COMMENT
0.14 ± 0.03	-40 ± 45	SARANTSEV 19	DPWA	$\bar{K}N$ multichannel

Normalized residue in $N\bar{K} \rightarrow \Sigma(2230) \rightarrow N\bar{K}^*(892), S=3/2, F\text{-wave}$

MODULUS	PHASE (°)	DOCUMENT ID	TECN	COMMENT
0.05 ± 0.03	35 ± 30	SARANTSEV 19	DPWA	$\bar{K}N$ multichannel

$\Sigma(2230)$ MASS

VALUE (MeV)	DOCUMENT ID	TECN	COMMENT
2240 ± 27	SARANTSEV 19	DPWA	$\bar{K}N$ multichannel

$\Sigma(2230)$ WIDTH

VALUE (MeV)	DOCUMENT ID	TECN	COMMENT
345 ± 50	SARANTSEV 19	DPWA	$\bar{K}N$ multichannel

Baryon Particle Listings

$\Sigma(2230), \Sigma(2250)$

$\Sigma(2230)$ DECAY MODES

Mode	Fraction (Γ_i/Γ)
$\Gamma_1 N\bar{K}$	(6.0±2.0) %
$\Gamma_2 \Sigma \pi$	(2.0±1.0) %
$\Gamma_3 \Lambda \pi$	(12 ± 6) %
$\Gamma_4 \Xi K$	(2.0±1.0) %
$\Gamma_5 \Lambda(1520)\pi, S\text{-wave}$	(14 ± 5) %
$\Gamma_6 \Lambda(1520)\pi, D\text{-wave}$	
$\Gamma_7 \Sigma(1385)\pi, P\text{-wave}$	(4 ± 4) %
$\Gamma_8 \Sigma(1385)\pi, F\text{-wave}$	(3.0±2.0) %
$\Gamma_9 \Delta\bar{K}, P\text{-wave}$	(14 ± 5) %
$\Gamma_{10} \Delta\bar{K}, F\text{-wave}$	(8.0±2.0) %
$\Gamma_{11} N\bar{K}^*(892), S=1/2, F\text{-wave}$	(8.0±3.0) %
$\Gamma_{12} N\bar{K}^*(892), S=3/2, F\text{-wave}$	(26 ± 5) %

$\Sigma(2230)$ BRANCHING RATIOS

$\Gamma(N\bar{K})/\Gamma_{\text{total}}$	DOCUMENT ID	TECN	COMMENT	Γ_1/Γ
VALUE 0.06±0.02	SARANTSEV 19	DPWA	$\bar{K}N$ multichannel	
$\Gamma(\Sigma\pi)/\Gamma_{\text{total}}$	DOCUMENT ID	TECN	COMMENT	Γ_2/Γ
VALUE 0.02±0.01	SARANTSEV 19	DPWA	$\bar{K}N$ multichannel	
$\Gamma(\Lambda\pi)/\Gamma_{\text{total}}$	DOCUMENT ID	TECN	COMMENT	Γ_3/Γ
VALUE 0.12±0.06	SARANTSEV 19	DPWA	$\bar{K}N$ multichannel	
$\Gamma(\Xi K)/\Gamma_{\text{total}}$	DOCUMENT ID	TECN	COMMENT	Γ_4/Γ
VALUE 0.02±0.01	SARANTSEV 19	DPWA	$\bar{K}N$ multichannel	
$\Gamma(\Lambda(1520)\pi, S\text{-wave})/\Gamma_{\text{total}}$	DOCUMENT ID	TECN	COMMENT	Γ_5/Γ
VALUE 0.14±0.05	SARANTSEV 19	DPWA	$\bar{K}N$ multichannel	
$\Gamma(\Lambda(1520)\pi, D\text{-wave})/\Gamma_{\text{total}}$	DOCUMENT ID	TECN	COMMENT	Γ_6/Γ
VALUE ••• We do not use the following data for averages, fits, limits, etc. ••• ~1	SARANTSEV 19	DPWA	$\bar{K}N$ multichannel	
$\Gamma(\Sigma(1385)\pi, P\text{-wave})/\Gamma_{\text{total}}$	DOCUMENT ID	TECN	COMMENT	Γ_7/Γ
VALUE 0.04±0.04	SARANTSEV 19	DPWA	$\bar{K}N$ multichannel	
$\Gamma(\Sigma(1385)\pi, F\text{-wave})/\Gamma_{\text{total}}$	DOCUMENT ID	TECN	COMMENT	Γ_8/Γ
VALUE 0.03±0.02	SARANTSEV 19	DPWA	$\bar{K}N$ multichannel	
$\Gamma(\Delta\bar{K}, P\text{-wave})/\Gamma_{\text{total}}$	DOCUMENT ID	TECN	COMMENT	Γ_9/Γ
VALUE 0.14±0.05	SARANTSEV 19	DPWA	$\bar{K}N$ multichannel	
$\Gamma(\Delta\bar{K}, F\text{-wave})/\Gamma_{\text{total}}$	DOCUMENT ID	TECN	COMMENT	Γ_{10}/Γ
VALUE 0.08±0.02	SARANTSEV 19	DPWA	$\bar{K}N$ multichannel	
$\Gamma(N\bar{K}^*(892), S=1/2, F\text{-wave})/\Gamma_{\text{total}}$	DOCUMENT ID	TECN	COMMENT	Γ_{11}/Γ
VALUE 0.08±0.03	SARANTSEV 19	DPWA	$\bar{K}N$ multichannel	
$\Gamma(N\bar{K}^*(892), S=3/2, F\text{-wave})/\Gamma_{\text{total}}$	DOCUMENT ID	TECN	COMMENT	Γ_{12}/Γ
VALUE 0.26±0.05	SARANTSEV 19	DPWA	$\bar{K}N$ multichannel	

$\Sigma(2230)$ REFERENCES

SARANTSEV 19 EPJ A55 180 A.V. Sarantsev et al. (BONN, PNPI)

$\Sigma(2250)$

$I(J^P) = 1(?)^?$ Status: ***

Results from partial-wave analyses are too weak to warrant separating them from the production and cross-section experiments. LASINSKI 71 in $\bar{K}N$ using a Pomeron + resonances model, and DEBELLEFON 76, DEBELLEFON 77, and DEBELLEFON 78 in energy-dependent partial-wave analyses of $\bar{K}N \rightarrow \Lambda\pi, \Sigma\pi$, and $N\bar{K}$, respectively, suggest two resonances around this mass.

$\Sigma(2250)$ MASS

VALUE (MeV)	DOCUMENT ID	TECN	COMMENT
2210 to 2280 (≈ 2250) OUR ESTIMATE			
2270±50	DEBELLEFON 78	DPWA	D_5 wave
2210±30	DEBELLEFON 78	DPWA	G_9 wave
2275±20	DEBELLEFON 77	DPWA	D_5 wave
2215±20	DEBELLEFON 77	DPWA	G_9 wave
2300±30	DEBELLEFON 75B	HBC	$K^-p \rightarrow \Xi^*0 K^0$
2251 ⁺³⁰ ₋₂₀	VANHORN 75	DPWA	$K^-p \rightarrow \Lambda\pi^0, F_5$ wave
2280±14	AGUILAR-... 70B	HBC	K^-p 3.9, 4.6 GeV/c
2237±11	BRICMAN 70	CNTR	Total, charge exchange
2255±10	COOL 70	CNTR	K^-p, K^-d total
2250±7	BUGG 68	CNTR	K^-p, K^-d total
••• We do not use the following data for averages, fits, limits, etc. •••			
2260	DEBELLEFON 76	IPWA	D_5 wave
2215	DEBELLEFON 76	IPWA	G_9 wave
2250±20	LU 70	CNTR	$\gamma p \rightarrow K^+ Y^*$
2245	BLANPIED 65	CNTR	$\gamma p \rightarrow K^+ Y^*$
2299±6	BOCK 65	HBC	$\bar{p}p$ 5.7 GeV/c

$\Sigma(2250)$ WIDTH

VALUE (MeV)	DOCUMENT ID	TECN	COMMENT
60 to 150 (≈ 100) OUR ESTIMATE			
120±40	DEBELLEFON 78	DPWA	D_5 wave
80±20	DEBELLEFON 78	DPWA	G_9 wave
70±20	DEBELLEFON 77	DPWA	D_5 wave
60±20	DEBELLEFON 77	DPWA	G_9 wave
130±20	DEBELLEFON 75B	HBC	$K^-p \rightarrow \Xi^*0 K^0$
192±30	VANHORN 75	DPWA	$K^-p \rightarrow \Lambda\pi^0, F_5$ wave
100±20	AGUILAR-... 70B	HBC	K^-p 3.9, 4.6 GeV/c
164±50	BRICMAN 70	CNTR	Total, charge exchange
230±20	BUGG 68	CNTR	K^-p, K^-d total
••• We do not use the following data for averages, fits, limits, etc. •••			
100	DEBELLEFON 76	IPWA	D_5 wave
140	DEBELLEFON 76	IPWA	G_9 wave
170	COOL 70	CNTR	K^-p, K^-d total
125	LU 70	CNTR	$\gamma p \rightarrow K^+ Y^*$
150	BLANPIED 65	CNTR	$\gamma p \rightarrow K^+ Y^*$
21 ⁺¹⁷ ₋₂₁	BOCK 65	HBC	$\bar{p}p$ 5.7 GeV/c

$\Sigma(2250)$ DECAY MODES

Mode	Fraction (Γ_i/Γ)
$\Gamma_1 N\bar{K}$	<10 %
$\Gamma_2 \Lambda\pi$	seen
$\Gamma_3 \Sigma\pi$	seen
$\Gamma_4 N\bar{K}\pi$	
$\Gamma_5 \Xi(1530)K$	

$\Sigma(2250)$ BRANCHING RATIOS

See "Sign conventions for resonance couplings" in the Note on Λ and Σ Resonances.

$\Gamma(N\bar{K})/\Gamma_{\text{total}}$	DOCUMENT ID	TECN	COMMENT	Γ_1/Γ
VALUE <0.1 OUR ESTIMATE				
0.08±0.02	DEBELLEFON 78	DPWA	D_5 wave	
0.02±0.01	DEBELLEFON 78	DPWA	G_9 wave	

$(J+\frac{1}{2})\times\Gamma(N\bar{K})/\Gamma_{\text{total}}$	DOCUMENT ID	TECN	COMMENT	Γ_1/Γ
VALUE ••• We do not use the following data for averages, fits, limits, etc. •••				
0.16±0.12	BRICMAN 70	CNTR	Total, charge exchange	
0.42	COOL 70	CNTR	K^-p, K^-d total	
0.47	BUGG 68	CNTR		

See key on page 999

Baryon Particle Listings

$\Sigma(2250)$, $\Sigma(2455)$ Bumps, $\Sigma(2620)$ Bumps, $\Sigma(3000)$ Bumps

$(\Gamma_1 \Gamma_f)^{1/2} / \Gamma_{\text{total}}$ in $N\bar{K} \rightarrow \Sigma(2250) \rightarrow \Lambda\pi$ $(\Gamma_1 \Gamma_2)^{1/2} / \Gamma$

VALUE	DOCUMENT ID	TECN	COMMENT
-0.16 ± 0.03	VANHORN 75	DPWA	$K^- p \rightarrow \Lambda\pi^0, F_5$ wave

••• We do not use the following data for averages, fits, limits, etc. •••

+0.11	DEBELLEFON 76	IPWA	D_5 wave
-0.10	DEBELLEFON 76	IPWA	G_9 wave
-0.18	BARBARO... 70	DPWA	$K^- p \rightarrow \Lambda\pi^0, G_9$ wave

$(\Gamma_1 \Gamma_f)^{1/2} / \Gamma_{\text{total}}$ in $N\bar{K} \rightarrow \Sigma(2250) \rightarrow \Sigma\pi$ $(\Gamma_1 \Gamma_3)^{1/2} / \Gamma$

VALUE	DOCUMENT ID	TECN	COMMENT
+0.06 ± 0.02	DEBELLEFON 77	DPWA	D_5 wave
-0.03 ± 0.02	DEBELLEFON 77	DPWA	G_9 wave
+0.07	BARBARO... 70	DPWA	$K^- p \rightarrow \Sigma\pi, G_9$ wave

$\Gamma(N\bar{K}) / \Gamma(\Sigma\pi)$ Γ_1 / Γ_3

VALUE	DOCUMENT ID	TECN	COMMENT
<0.18	BARNES 69	HBC	1 standard dev. limit

$\Gamma(\Lambda\pi) / \Gamma(\Sigma\pi)$ Γ_2 / Γ_3

VALUE	DOCUMENT ID	TECN	COMMENT
<0.18	BARNES 69	HBC	1 standard dev. limit

$(\Gamma_1 \Gamma_f)^{1/2} / \Gamma_{\text{total}}$ in $N\bar{K} \rightarrow \Sigma(2250) \rightarrow \Xi(1530)K$ $(\Gamma_1 \Gamma_5)^{1/2} / \Gamma$

VALUE	DOCUMENT ID	TECN	COMMENT
0.18 ± 0.04	1 DEBELLEFON 75B	HBC	$K^- p \rightarrow \Xi^+ K^0$

$\Sigma(2250)$ FOOTNOTES

¹ Seen in the (initial and final state) D_5 wave. Isospin not determined.

$\Sigma(2250)$ REFERENCES

DEBELLEFON 78	NC 42A 403	A. de Bellefon et al.	(CDEF, SACL) IJP
DEBELLEFON 77	NC 37A 175	A. de Bellefon et al.	(CDEF, SACL) IJP
DEBELLEFON 76	NP B109 129	A. de Bellefon, A. Berthon	(CDEF) IJP
Also	NP B90 1	A. de Bellefon et al.	(CDEF, SACL) IJP
DEBELLEFON 75B	NC 28A 289	A. de Bellefon et al.	(CDEF, SACL) IJP
VANHORN 75	NP B87 145	A.J. van Horn	(LBL) IJP
Also	NP B87 157	A.J. van Horn	(LBL) IJP
LASINSKI 71	NP B29 125	T.A. Lasinski	(EFI) IJP
AGUILAR... 70B	PRL 25 58	M. Aguilar-Benitez et al.	(BNL, SYRA)
BARBARO... 70	Duke Conf. 173	A. Barbaro-Galteri	(LRL) IJP
Hyperon Resonances, 1970			
BRICMAN 70	PL 31B 152	C. Bricman et al.	(CERN, CAEN, SACL)
COOL 70	PR D1 1887	R.L. Cool et al.	(BNL) I
Also	PRL 16 1228	R.L. Cool et al.	(BNL) I
LU 70	PR D2 1846	D.C. Lu et al.	(YALE)
BARNES 69	PRL 22 479	V.E. Barnes et al.	(BNL, SYRA)
BUGG 68	PR 168 1466	D.V. Bugg et al.	(RHEL, BIRM, CAVE) I
BLANPIED 65	PRL 14 741	W.A. Blanpied et al.	(YALE, CEA)
BOCK 65	PL 17 166	R.K. Bock et al.	(CERN, SACL)

$\Sigma(2455)$ Bumps $I(J^P) = 1(?)^?$ Status: **

OMITTED FROM SUMMARY TABLE

There is also some slight evidence for Y^* states in this mass region from the reaction $\gamma p \rightarrow K^+ X$ — see GREENBERG 68.

$\Sigma(2455)$ MASS

VALUE (MeV)	DOCUMENT ID	TECN	COMMENT
≈ 2455 OUR ESTIMATE			
2455 ± 10	ABRAMS 70	CNTR	$K^- p, K^- d$ total
2455 ± 7	BUGG 68	CNTR	$K^- p, K^- d$ total

$\Sigma(2455)$ WIDTH

VALUE (MeV)	DOCUMENT ID	TECN	COMMENT
140	ABRAMS 70	CNTR	$K^- p, K^- d$ total
100 ± 20	BUGG 68	CNTR	

$\Sigma(2455)$ DECAY MODES

Mode	Γ_1
$N\bar{K}$	$N\bar{K}$

$\Sigma(2455)$ BRANCHING RATIOS

$(J+\frac{1}{2}) \times \Gamma(N\bar{K}) / \Gamma_{\text{total}}$ Γ_1 / Γ

VALUE	DOCUMENT ID	TECN	COMMENT
0.39	ABRAMS 70	CNTR	$K^- p, K^- d$ total
0.05 ± 0.05	1 BRICMAN 70	CNTR	Total, charge exchange
0.3	BUGG 68	CNTR	

$\Sigma(2455)$ FOOTNOTES

¹ Fit of total cross section given by BRICMAN 70 is poor in this region.

$\Sigma(2455)$ REFERENCES

ABRAMS 70	PR D1 1917	R.J. Abrams et al.	(BNL) I
Also	PRL 19 678	R.J. Abrams et al.	(BNL)
BRICMAN 70	PL 31B 152	C. Bricman et al.	(CERN, CAEN, SACL)
BUGG 68	PR 168 1466	D.V. Bugg et al.	(RHEL, BIRM, CAVE) I
GREENBERG 68	PRL 20 221	J.S. Greenberg et al.	(YALE)

$\Sigma(2620)$ Bumps $I(J^P) = 1(?)^?$ Status: **

OMITTED FROM SUMMARY TABLE

$\Sigma(2620)$ MASS

VALUE (MeV)	DOCUMENT ID	TECN	COMMENT
≈ 2620 OUR ESTIMATE			
2542 ± 22	DIBIANCA 75	DBC	$K^- N \rightarrow \Xi K\pi$
2620 ± 15	ABRAMS 70	CNTR	$K^- p, K^- d$ total

$\Sigma(2620)$ WIDTH

VALUE (MeV)	DOCUMENT ID	TECN	COMMENT
221 ± 81	DIBIANCA 75	DBC	$K^- N \rightarrow \Xi K\pi$
175	ABRAMS 70	CNTR	$K^- p, K^- d$ total

$\Sigma(2620)$ DECAY MODES

Mode	Γ_1
$N\bar{K}$	$N\bar{K}$

$\Sigma(2620)$ BRANCHING RATIOS

$(J+\frac{1}{2}) \times \Gamma(N\bar{K}) / \Gamma_{\text{total}}$ Γ_1 / Γ

VALUE	DOCUMENT ID	TECN	COMMENT
0.32	ABRAMS 70	CNTR	$K^- p, K^- d$ total
0.36 ± 0.12	BRICMAN 70	CNTR	Total, charge exchange

$\Sigma(2620)$ REFERENCES

DIBIANCA 75	NP B98 137	F.A. Dibianca, R.J. Endorf	(CMU)
ABRAMS 70	PR D1 1917	R.J. Abrams et al.	(BNL) I
Also	PRL 19 678	R.J. Abrams et al.	(BNL)
BRICMAN 70	PL 31B 152	C. Bricman et al.	(CERN, CAEN, SACL)

$\Sigma(3000)$ Bumps $I(J^P) = 1(?)^?$ Status: *

OMITTED FROM SUMMARY TABLE

Seen as an enhancement in $\Lambda\pi$ and $\bar{K}N$ invariant mass spectra and in the missing mass of neutrals recoiling against a K^0 .

$\Sigma(3000)$ MASS

VALUE (MeV)	DOCUMENT ID	TECN	CHG	COMMENT
≈ 3000 OUR ESTIMATE				
3000	EHRlich 66	HBC	0	$\pi^- p$ 7.91 GeV/c

$\Sigma(3000)$ DECAY MODES

Mode	Γ_1	Γ_2
$N\bar{K}$	$N\bar{K}$	
$\Lambda\pi$		$\Lambda\pi$

$\Sigma(3000)$ REFERENCES

EHRlich 66	PR 152 1194	R. Ehrlich, W. Selove, H. Yuta	(PENN) I
------------	-------------	--------------------------------	----------

Baryon Particle Listings

 $\Sigma(3170)$ Bumps **$\Sigma(3170)$ Bumps** $I(J^P) = 1(?^?)$ Status: *

OMITTED FROM SUMMARY TABLE

Seen by AMIRZADEH 79 as a narrow 6.5-standard-deviation enhancement in the reaction $K^- p \rightarrow Y^{*+} \pi^-$ using data from independent high statistics bubble chamber experiments at 8.25 and 6.5 GeV/c. The dominant decay modes are multibody, multistrange final states and the production is via isospin-3/2 baryon exchange. Isospin 1 is favored.

Not seen in a $K^- p$ experiment in LASS at 11 GeV/c (ASTON 85B).

 **$\Sigma(3170)$ MASS
(PRODUCTION EXPERIMENTS)**

VALUE (MeV)	EVTS	DOCUMENT ID	TECN	COMMENT
≈ 3170 OUR ESTIMATE				
3170 ± 5	35	AMIRZADEH 79	HBC	$K^- p \rightarrow Y^{*+} \pi^-$

 **$\Sigma(3170)$ WIDTH
(PRODUCTION EXPERIMENTS)**

VALUE (MeV)	EVTS	DOCUMENT ID	TECN	COMMENT
<20	35	¹ AMIRZADEH 79	HBC	$K^- p \rightarrow Y^{*+} \pi^-$

 **$\Sigma(3170)$ DECAY MODES
(PRODUCTION EXPERIMENTS)**

Mode	Fraction (Γ_i/Γ)
Γ_1 $\Lambda K \bar{K} \pi$'s	seen
Γ_2 $\Sigma K \bar{K} \pi$'s	seen
Γ_3 $\Xi K \pi$'s	seen

 **$\Sigma(3170)$ BRANCHING RATIOS
(PRODUCTION EXPERIMENTS)**

$\Gamma(\Lambda K \bar{K} \pi \text{'s})/\Gamma_{\text{total}}$	Γ_1/Γ		
VALUE	DOCUMENT ID	TECN	COMMENT
seen	AMIRZADEH 79	HBC	$K^- p \rightarrow Y^{*+} \pi^-$
$\Gamma(\Sigma K \bar{K} \pi \text{'s})/\Gamma_{\text{total}}$	Γ_2/Γ		
VALUE	DOCUMENT ID	TECN	COMMENT
seen	AMIRZADEH 79	HBC	$K^- p \rightarrow Y^{*+} \pi^-$
$\Gamma(\Xi K \pi \text{'s})/\Gamma_{\text{total}}$	Γ_3/Γ		
VALUE	DOCUMENT ID	TECN	COMMENT
seen	AMIRZADEH 79	HBC	$K^- p \rightarrow Y^{*+} \pi^-$

 **$\Sigma(3170)$ FOOTNOTES
(PRODUCTION EXPERIMENTS)**

¹ Observed width consistent with experimental resolution.

 **$\Sigma(3170)$ REFERENCES
(PRODUCTION EXPERIMENTS)**

ASTON 85B	PR D32 2270	D. Aston <i>et al.</i>	(SLAC, CARL, CNRC, CINC)
AMIRZADEH 79	PL 89B 125	J. Amirzadeh <i>et al.</i>	(BIRM, CERN, GLAS+) ¹
Also	Toronto Conf. 263	J.B. Kinson <i>et al.</i>	(BIRM, CERN, GLAS+) ¹

Ξ BARYONS

($S = -2, I = 1/2$)

$\Xi^0 = uss, \Xi^- = dss$

Ξ^0

$I(J^P) = \frac{1}{2}(\frac{1}{2}^+)$ Status: ****

The parity has not actually been measured, but + is of course expected.

Ξ^0 MASS

The fit uses the $\Xi^0, \Xi^-,$ and Ξ^+ masses and the $\Xi^- - \Xi^0$ mass difference. It assumes that the Ξ^- and Ξ^+ masses are the same.

VALUE (MeV)	EVTS	DOCUMENT ID	TECN	COMMENT
1314.86 ± 0.20 OUR FIT				
1314.82 ± 0.06 ± 0.20	3120	FANTI	00 NA48	p Be, 450 GeV
• • • We do not use the following data for averages, fits, limits, etc. • • •				
1315.2 ± 0.92	49	WILQUET	72 HLBC	
1313.4 ± 1.8	1	PALMER	68 HBC	

$m_{\Xi^-} - m_{\Xi^0}$

The fit uses the $\Xi^0, \Xi^-,$ and Ξ^+ masses and the $\Xi^- - \Xi^0$ mass difference. It assumes that the Ξ^- and Ξ^+ masses are the same.

VALUE (MeV)	EVTS	DOCUMENT ID	TECN	COMMENT
6.85 ± 0.21 OUR FIT				
6.3 ± 0.7 OUR AVERAGE				
6.9 ± 2.2	29	LONDON	66 HBC	
6.1 ± 0.9	88	PJERROU	65B HBC	
6.8 ± 1.6	23	JAUNEAU	63 FBC	
• • • We do not use the following data for averages, fits, limits, etc. • • •				
6.1 ± 1.6	45	CARMONY	64B HBC	See PJERROU 65B

Ξ^0 MEAN LIFE

VALUE (10^{-10} s)	EVTS	DOCUMENT ID	TECN	COMMENT
2.90 ± 0.09 OUR AVERAGE				
2.83 ± 0.16	6300	1 ZECH	77 SPEC	Neutral hyperon beam
2.86 ^{+0.21} _{-0.19}	652	BALTAY	74 HBC	1.75 GeV/c $K^- p$
2.90 ^{+0.32} _{-0.27}	157	2 MAYEUR	72 HLBC	2.1 GeV/c K^-
3.07 ^{+0.22} _{-0.20}	340	DAUBER	69 HBC	
3.0 ± 0.5	80	PJERROU	65B HBC	
2.5 ^{+0.4} _{-0.3}	101	HUBBARD	64 HBC	
3.9 ^{+1.4} _{-0.8}	24	JAUNEAU	63 FBC	
• • • We do not use the following data for averages, fits, limits, etc. • • •				
3.5 ^{+1.0} _{-0.8}	45	CARMONY	64B HBC	See PJERROU 65B

¹ The ZECH 77 result is $\tau_{\Xi^0} = [2.77 - (\tau_A - 2.69)] \times 10^{-10}$ s, in which we use $\tau_A = 2.63 \times 10^{-10}$ s.

² The MAYEUR 72 value is modified by the erratum.

Ξ^0 MAGNETIC MOMENT

See the "Note on Baryon Magnetic Moments" in the Λ Listings.

VALUE (μ_N)	EVTS	DOCUMENT ID	TECN	COMMENT
-1.250 ± 0.014 OUR AVERAGE				
-1.253 ± 0.014	270k	COX	81 SPEC	
-1.20 ± 0.06	42k	BUNCE	79 SPEC	

Ξ^0 DECAY MODES

Mode	Fraction (Γ_i/Γ)	Confidence level
$\Gamma_1 \Lambda\pi^0$	(99.524 ± 0.012) %	
$\Gamma_2 \Lambda\gamma$	(1.17 ± 0.07) × 10 ⁻³	
$\Gamma_3 \Lambda e^+ e^-$	(7.6 ± 0.6) × 10 ⁻⁶	
$\Gamma_4 \Sigma^0 \gamma$	(3.33 ± 0.10) × 10 ⁻³	
$\Gamma_5 \Sigma^+ e^- \bar{\nu}_e$	(2.52 ± 0.08) × 10 ⁻⁴	
$\Gamma_6 \Sigma^+ \mu^- \bar{\nu}_\mu$	(2.33 ± 0.35) × 10 ⁻⁶	

$\Delta S = \Delta Q$ (SQ) violating modes or $\Delta S = 2$ forbidden ($S2$) modes

Γ	Mode	SQ	Value	Confidence level
Γ_7	$\Sigma^- e^+ \nu_e$	$SQ < 9$	× 10 ⁻⁴	90%
Γ_8	$\Sigma^- \mu^+ \nu_\mu$	$SQ < 9$	× 10 ⁻⁴	90%
Γ_9	$p \pi^-$	$S2 < 8$	× 10 ⁻⁶	90%
Γ_{10}	$p e^- \bar{\nu}_e$	$S2 < 1.3$	× 10 ⁻³	
Γ_{11}	$p \mu^- \bar{\nu}_\mu$	$S2 < 1.3$	× 10 ⁻³	

CONSTRAINED FIT INFORMATION

An overall fit to 5 branching ratios uses 11 measurements and one constraint to determine 5 parameters. The overall fit has a $\chi^2 = 7.5$ for 7 degrees of freedom.

The following *off-diagonal* array elements are the correlation coefficients $\langle \delta x_i \delta x_j \rangle / (\delta x_i \delta x_j)$, in percent, from the fit to the branching fractions, $x_i \equiv \Gamma_i/\Gamma_{\text{total}}$. The fit constrains the x_i whose labels appear in this array to sum to one.

x_2	-57			
x_4	-82	0		
x_5	-7	0	0	
x_6	0	0	0	1
	x_1	x_2	x_4	x_5

Ξ^0 BRANCHING RATIOS

$\Gamma(\Lambda\gamma)/\Gamma(\Lambda\pi^0)$ Γ_2/Γ_1

VALUE (units 10 ⁻³)	EVTS	DOCUMENT ID	TECN	COMMENT
1.17 ± 0.07 OUR FIT				
1.17 ± 0.07 OUR AVERAGE				
1.17 ± 0.05 ± 0.06	672	³ LAI	04A NA48	p Be, 450 GeV
1.91 ± 0.34 ± 0.19	31	⁴ FANTI	00 NA48	p Be, 450 GeV
1.06 ± 0.12 ± 0.11	116	JAMES	90 SPEC	FNAL hyperons
³ LAI 04A used our 2002 value of 99.5% for the $\Xi^0 \rightarrow \Lambda\pi^0$ branching fraction to get $\Gamma(\Xi^0 \rightarrow \Lambda\gamma)/\Gamma_{\text{total}} = (1.16 \pm 0.05 \pm 0.06) \times 10^{-3}$. We adjust slightly to go back to what was directly measured.				
⁴ FANTI 00 used our 1998 value of 99.5% for the $\Xi^0 \rightarrow \Lambda\pi^0$ branching fraction to get $\Gamma(\Xi^0 \rightarrow \Lambda\gamma)/\Gamma_{\text{total}} = (1.90 \pm 0.34 \pm 0.19) \times 10^{-3}$. We adjust slightly to go back to what was directly measured.				

$\Gamma(\Lambda e^+ e^-)/\Gamma_{\text{total}}$ Γ_3/Γ

VALUE (units 10 ⁻⁶)	EVTS	DOCUMENT ID	TECN	COMMENT
7.6 ± 0.4 ± 0.5	397 ± 21	⁵ BATLEY	07c NA48	p Be, 400 GeV
⁵ This BATLEY 07c result is consistent with internal bremsstrahlung.				

$\Gamma(\Sigma^0 \gamma)/\Gamma(\Lambda\pi^0)$ Γ_4/Γ_1

VALUE (units 10 ⁻³)	EVTS	DOCUMENT ID	TECN	COMMENT
3.35 ± 0.10 OUR FIT				
3.35 ± 0.10 OUR AVERAGE				
3.34 ± 0.05 ± 0.09	4045	ALAVI-HARATI 01c	KTEV	p nucleus, 800 GeV
3.16 ± 0.76 ± 0.32	17	⁶ FANTI	00 NA48	p Be, 450 GeV
3.56 ± 0.42 ± 0.10	85	TEIGE	89 SPEC	FNAL hyperons
⁶ FANTI 00 used our 1998 value of 99.5% for the $\Xi^0 \rightarrow \Lambda\pi^0$ branching fraction to get $\Gamma(\Xi^0 \rightarrow \Sigma^0 \gamma)/\Gamma_{\text{total}} = (3.14 \pm 0.76 \pm 0.32) \times 10^{-3}$. We adjust slightly to go back to what was directly measured.				

$\Gamma(\Sigma^+ e^- \bar{\nu}_e)/\Gamma_{\text{total}}$ Γ_5/Γ

VALUE (units 10 ⁻⁴)	EVTS	DOCUMENT ID	TECN	COMMENT
2.52 ± 0.08 OUR FIT				
2.53 ± 0.08 OUR AVERAGE				
2.51 ± 0.03 ± 0.09	6101	BATLEY	07 NA48	p Be, 400 GeV
2.55 ± 0.14 ± 0.10	419	⁷ BATLEY	07 NA48	p Be, 400 GeV
2.71 ± 0.22 ± 0.31	176	AFFOLDER	99 KTEV	p nucleus, 800 GeV
⁷ This BATLEY 07 result is for $\Xi^0 \rightarrow \Sigma^- e^+ \nu_e$ events.				

$\Gamma(\Sigma^+ \mu^- \bar{\nu}_\mu)/\Gamma_{\text{total}}$ Γ_6/Γ

VALUE (units 10 ⁻⁶)	EVTS	DOCUMENT ID	TECN	COMMENT
2.3 ± 0.4 OUR FIT				
2.17 ± 0.32 ± 0.17				
2.17 ± 0.32 ± 0.17	66	⁸ BATLEY	13 NA48	p Be, 400 GeV
⁸ BATLEY 13 used $\Xi^0 \rightarrow \Sigma^+ e^- \bar{\nu}_e$ decay as a normalization mode and its branching fraction value of $(2.51 \pm 0.03 \pm 0.09) \times 10^{-4}$ from BATLEY 07.				

$\Gamma(\Sigma^+ \mu^- \bar{\nu}_\mu)/\Gamma(\Sigma^+ e^- \bar{\nu}_e)$ Γ_6/Γ_5

VALUE	EVTS	DOCUMENT ID	TECN	COMMENT
0.0092 ± 0.0015 OUR FIT				
0.018 ^{+0.007} _{-0.005} ± 0.002	9	ABOUZAID	05 KTEV	p nucleus 800 GeV

Baryon Particle Listings

Ξ^0

$\Gamma(\Sigma^- e^+ \nu_e)/\Gamma(\Lambda\pi^0)$ Γ_7/Γ_1
 Test of $\Delta S = \Delta Q$ rule.

VALUE (units 10^{-3})	CL%	EVTS	DOCUMENT ID	TECN	COMMENT
<0.9	90	0	YEH	74	HBC Effective denom.=2500
••• We do not use the following data for averages, fits, limits, etc. •••					
<1.5			DAUBER	69	HBC
<6			HUBBARD	66	HBC

$\Gamma(\Sigma^- \mu^+ \nu_\mu)/\Gamma(\Lambda\pi^0)$ Γ_8/Γ_1
 Test of $\Delta S = \Delta Q$ rule.

VALUE (units 10^{-3})	CL%	EVTS	DOCUMENT ID	TECN	COMMENT
<0.9	90	0	YEH	74	HBC Effective denom.=2500
••• We do not use the following data for averages, fits, limits, etc. •••					
<1.5			DAUBER	69	HBC
<6			HUBBARD	66	HBC

$\Gamma(p\pi^-)/\Gamma(\Lambda\pi^0)$ Γ_9/Γ_1
 $\Delta S=2$. Forbidden in first-order weak interaction.

VALUE (units 10^{-6})	CL%	EVTS	DOCUMENT ID	TECN	COMMENT
< 8.2	90		WHITE	05	HYCP p Cu, 800 GeV
••• We do not use the following data for averages, fits, limits, etc. •••					
< 36	90		GEWENIGER	75	SPEC
<1800	90	0	YEH	74	HBC Effective denom.=1300
< 900			DAUBER	69	HBC
<5000			HUBBARD	66	HBC

$\Gamma(p e^- \bar{\nu}_e)/\Gamma(\Lambda\pi^0)$ Γ_{10}/Γ_1
 $\Delta S=2$. Forbidden in first-order weak interaction.

VALUE (units 10^{-3})	CL%	EVTS	DOCUMENT ID	TECN	COMMENT
<1.3			DAUBER	69	HBC
••• We do not use the following data for averages, fits, limits, etc. •••					
<3.4	90	0	YEH	74	HBC Effective denom.=670
<6			HUBBARD	66	HBC

$\Gamma(p\mu^- \bar{\nu}_\mu)/\Gamma(\Lambda\pi^0)$ Γ_{11}/Γ_1
 $\Delta S=2$. Forbidden in first-order weak interaction.

VALUE (units 10^{-3})	CL%	EVTS	DOCUMENT ID	TECN	COMMENT
<1.3			DAUBER	69	HBC
••• We do not use the following data for averages, fits, limits, etc. •••					
<3.5	90	0	YEH	74	HBC Effective denom.=664
<6			HUBBARD	66	HBC

Ξ^0 DECAY PARAMETERS

See the "Note on Baryon Decay Parameters" in the neutron Listings.

$\alpha(\Xi^0) \alpha_-(\Lambda)$
 This is a product of the $\Xi^0 \rightarrow \Lambda\pi^0$ and $\Lambda \rightarrow p\pi^-$ asymmetries.

VALUE	EVTS	DOCUMENT ID	TECN	COMMENT
-0.261 ± 0.006 OUR AVERAGE				
-0.276 ± 0.001 ± 0.035	4M	BATLEY	10B	NA48 p Be, 400 GeV
-0.260 ± 0.004 ± 0.005	300k	HANDLER	82	SPEC FNAL hyperons
••• We do not use the following data for averages, fits, limits, etc. •••				
-0.317 ± 0.027	6075	BUNCE	78	SPEC FNAL hyperons
-0.35 ± 0.06	505	BALTAY	74	HBC $K^- p$ 1.75 GeV/c
-0.28 ± 0.06	739	DAUBER	69	HBC $K^- p$ 1.7-2.6 GeV/c

α FOR $\Xi^0 \rightarrow \Lambda\pi^0$
 The above average, $\alpha(\Xi^0)\alpha_-(\Lambda) = -0.261 \pm 0.006$, divided by our current average $\alpha_-(\Lambda) = 0.732 \pm 0.014$, gives the following value for $\alpha(\Xi^0)$:

VALUE DOCUMENT ID
-0.356 ± 0.011 OUR EVALUATION

ϕ ANGLE FOR $\Xi^0 \rightarrow \Lambda\pi^0$ (tan $\phi = \beta/\gamma$)

VALUE (°)	EVTS	DOCUMENT ID	TECN	COMMENT
21 ± 12 OUR AVERAGE				
16 ± 17	652	BALTAY	74	HBC 1.75 GeV/c $K^- p$
38 ± 19	739	DAUBER	69	HBC
- 8 ± 30	146	BERGE	66	HBC

⁹DAUBER 69 uses $\alpha_\Lambda = 0.647 \pm 0.020$.

¹⁰The errors have been multiplied by 1.2 due to approximations used for the Ξ polarization; see DAUBER 69 for a discussion.

RADIATIVE HYPERON DECAYS

Revised July 2011 by J.D. Jackson (LBNL).

The weak radiative decays of spin-1/2 hyperons, $B_i \rightarrow B_f\gamma$, yield information about matrix elements (form factors) similar to that gained from weak hadronic decays. For a polarized spin-1/2 hyperon decaying radiatively via a $\Delta Q = 0$, $\Delta S = 1$

transition, the angular distribution of the direction \hat{p} of the final spin-1/2 baryon in the hyperon rest frame is

$$\frac{dN}{d\Omega} = \frac{N}{4\pi} (1 + \alpha_\gamma \mathbf{P}_i \cdot \hat{p}) . \quad (1)$$

Here \mathbf{P}_i is the polarization of the decaying hyperon, and α_γ is the asymmetry parameter. In terms of the form factors $F_1(q^2)$, $F_2(q^2)$, and $G(q^2)$ of the effective hadronic weak electromagnetic vertex,

$$F_1(q^2)\gamma_\lambda + iF_2(q^2)\sigma_{\lambda\mu}q^\mu + G(q^2)\gamma_\lambda\gamma_5 ,$$

α_γ is

$$\alpha_\gamma = \frac{2 \operatorname{Re}[G(0)F_M^*(0)]}{|G(0)|^2 + |F_M(0)|^2} , \quad (2)$$

where $F_M = (m_i - m_f)[F_2 - F_1/(m_i + m_f)]$. If the decaying hyperon is unpolarized, the decay baryon has a longitudinal polarization given by $P_f = -\alpha_\gamma$ [1].

The angular distribution for the weak hadronic decay, $B_i \rightarrow B_f\pi$, has the same form as Eq. (1), but of course with a different asymmetry parameter, α_π . Now, however, if the decaying hyperon is unpolarized, the decay baryon has a longitudinal polarization given by $P_f = +\alpha_\pi$ [2,3]. The difference of sign is because the spins of the pion and photon are different.

$\Xi^0 \rightarrow \Lambda\gamma$ decay—The radiative decay $\Xi^0 \rightarrow \Lambda\gamma$ of an unpolarized Ξ^0 uses the hadronic decay $\Lambda \rightarrow p\pi^-$ as the analyzer. As noted above, the longitudinal polarization of the Λ will be $P_\Lambda = -\alpha_{\Xi\Lambda\gamma}$. Let α_- be the $\Lambda \rightarrow p\pi^-$ asymmetry parameter and $\theta_{\Lambda p}$ be the angle, as seen in the Λ rest frame, between the Λ line of flight and the proton momentum. Then the hadronic version of Eq. (1) applied to the $\Lambda \rightarrow p\pi^-$ decay gives

$$\frac{dN}{d \cos \theta_{\Lambda p}} = \frac{N}{2} (1 - \alpha_{\Xi\Lambda\gamma} \alpha_- \cos \theta_{\Lambda p}) \quad (3)$$

for the angular distribution of the proton in the Λ frame. Our current value, from the CERN NA48/1 experiment [4], is $\alpha_{\Xi\Lambda\gamma} = -0.704 \pm 0.019 \pm 0.064$.

$\Xi^0 \rightarrow \Sigma^0\gamma$ decay—The asymmetry parameter here, $\alpha_{\Xi\Sigma\gamma}$, is measured by following the decay chain $\Xi^0 \rightarrow \Sigma^0\gamma$, $\Sigma^0 \rightarrow \Lambda\gamma$, $\Lambda \rightarrow p\pi^-$. Again, for an unpolarized Ξ^0 , the longitudinal polarization of the Σ^0 will be $P_\Sigma = -\alpha_{\Xi\Sigma\gamma}$. In the $\Sigma^0 \rightarrow \Lambda\gamma$ decay, a parity-conserving magnetic-dipole transition, the polarization of the Σ^0 is transferred to the Λ , as may be seen as follows. Let $\theta_{\Sigma\Lambda}$ be the angle seen in the Σ^0 rest frame between the Σ^0 line of flight and the Λ momentum. For Σ^0 helicity +1/2, the probability amplitudes for positive and negative spin states of the Σ^0 along the Λ momentum are $\cos(\theta_{\Sigma\Lambda}/2)$ and $\sin(\theta_{\Sigma\Lambda}/2)$. Then the amplitude for a negative helicity photon and a negative helicity Λ is $\cos(\theta_{\Sigma\Lambda}/2)$, while the amplitude for positive helicities for the photon and Λ is $\sin(\theta_{\Sigma\Lambda}/2)$. For Σ^0 helicity -1/2, the amplitudes are interchanged. If the Σ^0 has longitudinal polarization P_Σ , the probabilities for Λ helicities $\pm 1/2$ are therefore

$$p(\pm 1/2) = \frac{1}{2}(1 \mp P_\Sigma) \cos^2(\theta_{\Sigma\Lambda}/2) + \frac{1}{2}(1 \pm P_\Sigma) \sin^2(\theta_{\Sigma\Lambda}/2) , \quad (4)$$

and the longitudinal polarization of the Λ is

$$P_\Lambda = -P_\Sigma \cos \theta_{\Sigma\Lambda} + \alpha_{\Xi\Sigma\gamma} \cos \theta_{\Sigma\Lambda} \quad (5)$$

Using Eq. (1) for the $\Lambda \rightarrow p\pi^-$ decay again, we get for the joint angular distribution of the $\Sigma^0 \rightarrow \Lambda\gamma, \Lambda \rightarrow p\pi^-$ chain,

$$\frac{d^2N}{d\cos\theta_{\Sigma\Lambda} d\cos\theta_{\Lambda p}} = \frac{N}{4} (1 + \alpha_{\Xi\Sigma\gamma} \cos\theta_{\Sigma\Lambda} \alpha_- \cos\theta_{\Lambda p}) \quad (6)$$

Our current average for $\alpha_{\Xi\Sigma\gamma}$ is -0.69 ± 0.06 [4,5].

References

1. R.E. Behrends, Phys. Rev. **111**, 1691 (1958); see Eq. (7) or (8).
2. In ancient times, the signs of the asymmetry term in the angular distributions of radiative and hadronic decays of polarized hyperons were sometimes opposite. For roughly 50 years, however, the overwhelming convention has been to make them the same. The aim, not always achieved, is to remove ambiguities.
3. For the definition of α_π , see the note on “Baryon Decay Parameters” in the Neutron Listings.
4. J.R. Batley *et al.*, Phys. Lett. **B693**, 241 (2010).
5. A. Alavi-Harati *et al.*, Phys. Rev. Lett. **86**, 3239 (2001).

α FOR $\Xi^0 \rightarrow \Lambda\gamma$

See the note above on “Radiative Hyperon Decays.”

VALUE	EVTS	DOCUMENT ID	TECN	COMMENT
$-0.704 \pm 0.019 \pm 0.064$	52k	11 BATLEY	10B NA48	p Be, 400 GeV
•••				We do not use the following data for averages, fits, limits, etc. •••
$-0.78 \pm 0.18 \pm 0.06$	672	LAI	04A NA48	See BATLEY 10B
-0.43 ± 0.44	87	12 JAMES	90 SPEC	FNAL hyperons

¹¹ BATLEY 10B also measured the $\Xi^0 \rightarrow \bar{\Lambda}\gamma$ asymmetry to be -0.798 ± 0.064 (no systematic error given) with 4769 events.
¹² The sign has been changed; see the erratum, JAMES 02.

α FOR $\Xi^0 \rightarrow \Lambda e^+ e^-$

VALUE	EVTS	DOCUMENT ID	TECN	COMMENT
-0.8 ± 0.2	397 ± 21	13 BATLEY	07c NA48	p Be, 400 GeV
¹³				This BATLEY 07c result is consistent with the asymmetry α for $\Xi^0 \rightarrow \Lambda\gamma$, as expected if the mechanism is internal bremsstrahlung.

α FOR $\Xi^0 \rightarrow \Sigma^0\gamma$

See the note above on “Radiative Hyperon Decays.”

VALUE	EVTS	DOCUMENT ID	TECN	COMMENT
-0.69 ± 0.06 OUR AVERAGE				
$-0.729 \pm 0.030 \pm 0.076$	15k	14 BATLEY	10B NA48	p Be, 400 GeV
$-0.63 \pm 0.08 \pm 0.05$	4045	ALAVI-HARATI 01c	KTEV	p nucleus, 800 GeV
•••				We do not use the following data for averages, fits, limits, etc. •••
$+0.20 \pm 0.32 \pm 0.05$	85	15 TEIGE	89 SPEC	FNAL hyperons

¹⁴ BATLEY 10B also measured the $\Xi^0 \rightarrow \bar{\Sigma}^0\gamma$ asymmetry to be -0.786 ± 0.104 (no systematic error given) with 1404 events.
¹⁵ This result has been withdrawn, due to an error. See the erratum, TEIGE 02.

$g_1(0)/f_1(0)$ FOR $\Xi^0 \rightarrow \Sigma^+ e^- \bar{\nu}_e$

VALUE	EVTS	DOCUMENT ID	TECN	COMMENT
1.22 ± 0.05 OUR AVERAGE				
1.21 ± 0.05		BATLEY	13 NA48	p Be, 400 GeV
$1.32 \pm_{-0.17}^{+0.21} \pm 0.05$	487	16 ALAVI-HARATI 01i	KTEV	p nucleus, 800 GeV
•••				We do not use the following data for averages, fits, limits, etc. •••
$1.20 \pm 0.04 \pm 0.03$	6520	17 BATLEY	07 NA48	See BATLEY 13

¹⁶ ALAVI-HARATI 01i assumes here that the second-class current is zero and that the weak-magnetism term takes its exact SU(3) value.
¹⁷ This BATLEY 07 result uses our 2006 value of V_{US} from semileptonic kaon decays as input.

$g_2(0)/f_1(0)$ FOR $\Xi^0 \rightarrow \Sigma^+ e^- \bar{\nu}_e$

VALUE	EVTS	DOCUMENT ID	TECN	COMMENT
$-1.7 \pm_{-2.0}^{+2.1} \pm 0.5$	487	18 ALAVI-HARATI 01i	KTEV	p nucleus, 800 GeV

¹⁸ ALAVI-HARATI 01i thus assumes that $g_2 = 0$ in calculating g_1/f_1 , above.

$f_2(0)/f_1(0)$ FOR $\Xi^0 \rightarrow \Sigma^+ e^- \bar{\nu}_e$

VALUE	EVTS	DOCUMENT ID	TECN	COMMENT
2.0 ± 0.9 OUR AVERAGE				
2.0 ± 1.3		BATLEY	13 NA48	p Be, 400 GeV
$2.0 \pm 1.2 \pm 0.5$	487	ALAVI-HARATI 01i	KTEV	p nucleus, 800 GeV

Ξ^0 REFERENCES

BATLEY	13	PL B720 105	J.R. Batley <i>et al.</i>	(CERN NA48/1 Collab.)
BATLEY	10B	PL B693 241	J.R. Batley <i>et al.</i>	(CERN NA48/1 Collab.)
BATLEY	07	PL B645 36	J.R. Batley <i>et al.</i>	(CERN NA48/1 Collab.)
BATLEY	07C	PL B650 1	J.R. Batley <i>et al.</i>	(CERN NA48 Collab.)
ABOUZAID	05	PRL 95 081801	E. Abouzaid <i>et al.</i>	(FNAL KTeV Collab.)
WHITE	05	PRL 94 101804	C.G. White <i>et al.</i>	(FNAL HyperCP Collab.)
LAI	04A	PL B584 251	A. Lai <i>et al.</i>	(CERN NA48 Collab.)
JAMES	02	PRL 89 169901 (err.)	C. James <i>et al.</i>	(MINN, MICH, WIS C, RUTG)
TEIGE	02	PRL 89 169902 (err.)	S. Teige <i>et al.</i>	(RUTG, MICH, MINN)
ALAVI-HARATI 01C		PRL 86 3239	A. Alavi-Harati <i>et al.</i>	(FNAL KTeV Collab.)
ALAVI-HARATI 01i		PRL 87 132001	A. Alavi-Harati <i>et al.</i>	(FNAL KTeV Collab.)
FANTI	00	EPJ C12 69	V. Fanti <i>et al.</i>	(CERN NA48 Collab.)
AFFOLDER	99	PRL 82 3751	A. Affolder <i>et al.</i>	(FNAL KTeV Collab.)
JAMES	90	PRL 64 843	C. James <i>et al.</i>	(MINN, MICH, WIS C, RUTG)
TEIGE	89	PRL 63 2717	S. Teige <i>et al.</i>	(RUTG, MICH, MINN)
HANDLER	82	PR D25 639	R. Handler <i>et al.</i>	(WISC, MICH, MINN)
COX	81	PRL 46 877	P.T. Cox <i>et al.</i>	(MICH, WISC, RUTG, MINN+)
BUNCE	79	PL 86B 386	G.R.M. Bunce <i>et al.</i>	(G.R.M. Bunce <i>et al.</i>)
BUNCE	78	PR D18 633	G.R.M. Bunce <i>et al.</i>	(WISC, MICH, RUTG)
ZECH	77	NP B124 413	G. Zech <i>et al.</i>	(SIEG, CERN, DORT, HEIDH)
GEWENIGER	75	PL 57B 193	C. Geweniger <i>et al.</i>	(CERN, HEIDH)
BALTAY	74	PR D9 419	C. Baltay <i>et al.</i>	(COLU, BING, J)
YEH	74	PR D10 3545	N. Yeh <i>et al.</i>	(BING, COLU)
MAYEUR	72	NP B47 333	C. Mayeur <i>et al.</i>	(BRUX, CERN, TUFTS, LOUC)
Also		NP B53 268 (erratum)	C. Mayeur	
WILQUET	72	PL 42B 372	G. Wilquet <i>et al.</i>	(BRUX, CERN, TUFTS+)
DAUBER	69	PR 179 1262	P.M. Dauber <i>et al.</i>	(LRL)
PALMER	68	PL 26B 323	R.B. Palmer <i>et al.</i>	(BNL, SYRA)
BERGE	66	PR 147 945	J.P. Berge <i>et al.</i>	(LRL)
HUBBARD	66	Thesis UCRL 11510	J.R. Hubbard	(LRL)
LONDON	66	PR 143 1034	G.W. London <i>et al.</i>	(BNL, SYRA)
PJERROU	65B	PRL 14 275	G.M. Pjerrou <i>et al.</i>	(UCLA)
Also		Thesis	G.M. Pjerrou	(UCLA)
CARMONY	64B	PRL 12 482	D.D. Carmony <i>et al.</i>	(UCLA)
HUBBARD	64	PR 135 B183	J.R. Hubbard <i>et al.</i>	(LRL)
JAUNEAU	63	PL 4 49	L. Jauneau <i>et al.</i>	(EPOL, CERN, LOUC+)
Also		Siena Conf. 1 1	L. Jauneau <i>et al.</i>	(EPOL, CERN, LOUC+)



$I(J^P) = \frac{1}{2}(1^+)$ Status: * * * *

The parity has not actually been measured, but + is of course expected.

We have omitted some results that have been superseded by later experiments. See our earlier editions.

Ξ^- MASS

The fit uses the Ξ^- , Ξ^+ , and Ξ^0 masses and the $\Xi^- - \Xi^+$ mass difference. It assumes that the Ξ^- and Ξ^+ masses are the same.

VALUE (MeV)	EVTS	DOCUMENT ID	TECN	COMMENT
1321.71 ± 0.07 OUR FIT				
$1321.70 \pm 0.08 \pm 0.05$	2478 ± 68	ABDALLAH	06E DLPH	from Z decays
•••				We do not use the following data for averages, fits, limits, etc. •••
1321.46 ± 0.34	632	DIBIANCA	75 DBC	4.9 GeV/c K^- d
1321.12 ± 0.41	268	WILQUET	72 HLCB	
1321.87 ± 0.51	195	¹ GOLDWASSER 70	HBC	5.5 GeV/c K^- p
1321.67 ± 0.52	6	CHIEN	66 HBC	6.9 GeV/c \bar{p} p
1321.4 ± 1.1	299	LONDON	66 HBC	
1321.3 ± 0.4	149	PJERROU	65B HBC	
1321.1 ± 0.3	241	² BADIER	64 HBC	
1321.4 ± 0.4	517	² JAUNEAU	63D FBC	
1321.1 ± 0.65	62	² SCHNEIDER	63 HBC	

¹ GOLDWASSER 70 uses $m_\Lambda = 1115.58$ MeV.
² These masses have been increased 0.09 MeV because the Λ mass increased.

Ξ^+ MASS

The fit uses the Ξ^- , Ξ^+ , and Ξ^0 masses and the $\Xi^- - \Xi^+$ mass difference. It assumes that the Ξ^- and Ξ^+ masses are the same.

VALUE (MeV)	EVTS	DOCUMENT ID	TECN	COMMENT
1321.71 ± 0.07 OUR FIT				
$1321.73 \pm 0.08 \pm 0.05$	2256 ± 63	ABDALLAH	06E DLPH	from Z decays
•••				We do not use the following data for averages, fits, limits, etc. •••
1321.6 ± 0.8	35	VOTRUBA	72 HBC	10 GeV/c K^+ p
1321.2 ± 0.4	34	STONE	70 HBC	
1320.69 ± 0.93	5	CHIEN	66 HBC	6.9 GeV/c \bar{p} p

$(m_{\Xi^-} - m_{\Xi^+}) / m_{\Xi^-}$

A test of CPT invariance.

VALUE	DOCUMENT ID	TECN	COMMENT
$(-2.5 \pm 8.7) \times 10^{-5}$	ABDALLAH	06E DLPH	from Z decays

Baryon Particle Listings



Ξ⁻ MEAN LIFE

Measurements with an error > 0.2 × 10⁻¹⁰ s or with systematic errors not included have been omitted.

VALUE (10 ⁻¹⁰ s)	EVTS	DOCUMENT ID	TECN	COMMENT
1.639 ± 0.015 OUR AVERAGE				
1.65 ± 0.07 ± 0.12	2478 ± 68	ABDALLAH	06E	DLPH from Z decays
1.652 ± 0.051	32k	BOURQUIN	84	SPEC Hyperon beam
1.665 ± 0.065	41k	BOURQUIN	79	SPEC Hyperon beam
1.609 ± 0.028	4286	HEMINGWAY	78	HBC 4.2 GeV/c K ⁻ p
1.67 ± 0.08		DIBIANCA	75	DBC 4.9 GeV/c K ⁻ d
1.63 ± 0.03	4303	BALTAY	74	HBC 1.75 GeV/c K ⁻ p
1.73 ^{+0.08} / _{-0.07}	680	MAYEUR	72	HLBC 2.1 GeV/c K ⁻
1.61 ± 0.04	2610	DAUBER	69	HBC
1.80 ± 0.16	299	LONDON	66	HBC
1.70 ± 0.12	246	PJERROU	65B	HBC
1.69 ± 0.07	794	HUBBARD	64	HBC
1.86 ^{+0.15} / _{-0.14}	517	JAUNEAU	63D	FBC

Ξ⁺ MEAN LIFE

VALUE (10 ⁻¹⁰ s)	EVTS	DOCUMENT ID	TECN	COMMENT
1.70 ± 0.08 ± 0.12	2256 ± 63	ABDALLAH	06E	DLPH from Z decays
• • • We do not use the following data for averages, fits, limits, etc. • • •				
1.55 ^{+0.35} / _{-0.20}	35	³ VOTRUBA	72	HBC 10 GeV/c K ⁺ p
1.6 ± 0.3	34	STONE	70	HBC
1.9 ^{+0.7} / _{-0.5}	12	³ SHEN	67	HBC
1.51 ± 0.55	5	³ CHIEN	66	HBC 6.9 GeV/c $\bar{p}p$

$$(\tau_{\Xi^-} - \tau_{\Xi^+}) / \tau_{\Xi^-}$$

A test of CPT invariance.

VALUE	DOCUMENT ID	TECN	COMMENT
-0.01 ± 0.07	ABDALLAH	06E	DLPH from Z decays

Ξ⁻ MAGNETIC MOMENT

See the "Note on Baryon Magnetic Moments" in the Λ Listings.

VALUE (μ_N)	EVTS	DOCUMENT ID	TECN	COMMENT
-0.6507 ± 0.0025 OUR AVERAGE				
-0.6505 ± 0.0025	4.36M	DURYEA	92	SPEC 800 GeV p Be
-0.661 ± 0.036 ± 0.036	44k	TROST	89	SPEC Ξ ⁻ ~ 250 GeV
-0.69 ± 0.04	218k	RAMEIKA	84	SPEC 400 GeV pBe
• • • We do not use the following data for averages, fits, limits, etc. • • •				
-0.674 ± 0.021 ± 0.020	122k	HO	90	SPEC See DURYEA 92
-2.1 ± 0.8	2436	COOL	74	OSPK 1.8 GeV/c K ⁻ p
-0.1 ± 2.1	2724	BINGHAM	70B	OSPK 1.8 GeV/c K ⁻ p

Ξ⁺ MAGNETIC MOMENT

See the "Note on Baryon Magnetic Moments" in the Λ Listings.

VALUE (μ_N)	EVTS	DOCUMENT ID	TECN	COMMENT
+0.657 ± 0.028 ± 0.020	70k	HO	90	SPEC 800 GeV pBe

$$(\mu_{\Xi^-} + \mu_{\Xi^+}) / |\mu_{\Xi^-}|$$

A test of CPT invariance. We calculate this from the Ξ⁻ and Ξ⁺ magnetic moments above.

VALUE	DOCUMENT ID
+0.01 ± 0.05 OUR EVALUATION	

Ξ⁻ DECAY MODES

Mode	Fraction (Γ_i/Γ)	Confidence level
Γ_1 $\Lambda\pi^-$	(99.887 ± 0.035) %	
Γ_2 $\Sigma^- \gamma$	(1.27 ± 0.23) × 10 ⁻⁴	
Γ_3 $\Lambda e^- \bar{\nu}_e$	(5.63 ± 0.31) × 10 ⁻⁴	
Γ_4 $\Lambda \mu^- \bar{\nu}_\mu$	(3.5 ^{+3.5} / _{-2.2}) × 10 ⁻⁴	
Γ_5 $\Sigma^0 e^- \bar{\nu}_e$	(8.7 ± 1.7) × 10 ⁻⁵	
Γ_6 $\Sigma^0 \mu^- \bar{\nu}_\mu$	< 8 × 10 ⁻⁴	90%
Γ_7 $\Xi^0 e^- \bar{\nu}_e$	< 2.3 × 10 ⁻³	90%

ΔS = 2 forbidden (S2) modes

Γ_8 $n\pi^-$	S2	< 1.9	× 10 ⁻⁵	90%
Γ_9 $n e^- \bar{\nu}_e$	S2	< 3.2	× 10 ⁻³	90%
Γ_{10} $n \mu^- \bar{\nu}_\mu$	S2	< 1.5	%	90%
Γ_{11} $\rho\pi^- \pi^-$	S2	< 4	× 10 ⁻⁴	90%
Γ_{12} $\rho\pi^- e^- \bar{\nu}_e$	S2	< 4	× 10 ⁻⁴	90%
Γ_{13} $\rho\pi^- \mu^- \bar{\nu}_\mu$	S2	< 4	× 10 ⁻⁴	90%
Γ_{14} $\rho\mu^- \mu^-$	L	< 4	× 10 ⁻⁸	90%

CONSTRAINED FIT INFORMATION

An overall fit to 4 branching ratios uses 5 measurements and one constraint to determine 5 parameters. The overall fit has a $\chi^2 = 1.0$ for 1 degrees of freedom.

The following *off-diagonal* array elements are the correlation coefficients $\langle \delta x_i \delta x_j \rangle / (\delta x_i \delta x_j)$, in percent, from the fit to the branching fractions, $x_i \equiv \Gamma_i / \Gamma_{\text{total}}$. The fit constrains the x_i whose labels appear in this array to sum to one.

x_2	-6			
x_3	-8	0		
x_4	-99	0	-1	
x_5	-5	0	0	0
	x_1	x_2	x_3	x_4

Ξ⁻ BRANCHING RATIOS

A number of early results have been omitted.

$\Gamma(\Sigma^- \gamma) / \Gamma(\Lambda\pi^-)$	VALUE (units 10 ⁻⁴)	EVTS	DOCUMENT ID	TECN	COMMENT	Γ_2/Γ_1
1.27 ± 0.24 OUR FIT						
1.27 ± 0.23 OUR AVERAGE						
1.22 ± 0.23 ± 0.06	211	4	DUBBS	94	E761	Ξ ⁻ 375 GeV
2.27 ± 1.02	9		BIAGI	87B	SPEC	SPS hyperon beam

⁴DUBBS 94 also finds weak evidence that the asymmetry parameter α_γ is positive ($\alpha_\gamma = 1.0 \pm 1.3$).

$\Gamma(\Lambda e^- \bar{\nu}_e) / \Gamma(\Lambda\pi^-)$	VALUE (units 10 ⁻³)	EVTS	DOCUMENT ID	TECN	COMMENT	Γ_3/Γ_1
0.564 ± 0.031 OUR FIT						
0.564 ± 0.031	2857		BOURQUIN	83	SPEC	SPS hyperon beam
• • • We do not use the following data for averages, fits, limits, etc. • • •						
0.30 ± 0.13	11		THOMPSON	80	ASPK	Hyperon beam

$\Gamma(\Lambda \mu^- \bar{\nu}_\mu) / \Gamma(\Lambda\pi^-)$	VALUE (units 10 ⁻³)	CL%	EVTS	DOCUMENT ID	TECN	COMMENT	Γ_4/Γ_1
0.35 ^{+0.35}/_{-0.22} OUR FIT							
0.35 ± 0.35	1		YEH	74	HBC	Effective denom.=2859	
• • • We do not use the following data for averages, fits, limits, etc. • • •							
< 2.3	90	0	THOMPSON	80	ASPK	Effective denom.=1017	
< 1.3			DAUBER	69	HBC		
< 12			BERGE	66	HBC		

$\Gamma(\Sigma^0 e^- \bar{\nu}_e) / \Gamma(\Lambda\pi^-)$	VALUE (units 10 ⁻³)	EVTS	DOCUMENT ID	TECN	COMMENT	Γ_5/Γ_1
0.087 ± 0.017 OUR FIT						
0.087 ± 0.017	154		BOURQUIN	83	SPEC	SPS hyperon beam

$[\Gamma(\Lambda e^- \bar{\nu}_e) + \Gamma(\Sigma^0 e^- \bar{\nu}_e)] / \Gamma(\Lambda\pi^-)$	VALUE (units 10 ⁻³)	EVTS	DOCUMENT ID	TECN	COMMENT	$(\Gamma_3 + \Gamma_5) / \Gamma_1$
• • • We do not use the following data for averages, fits, limits, etc. • • •						
0.651 ± 0.031	3011	5	BOURQUIN	83	SPEC	SPS hyperon beam
0.68 ± 0.22	17	6	DUCLOS	71	OSPK	

⁵ See the separate BOURQUIN 83 values for $\Gamma(\Lambda e^- \bar{\nu}_e) / \Gamma(\Lambda\pi^-)$ and $\Gamma(\Sigma^0 e^- \bar{\nu}_e) / \Gamma(\Lambda\pi^-)$ above.

⁶ DUCLOS 71 cannot distinguish Σ^0 s from Λ 's. The Cabibbo theory predicts the Σ^0 rate is about a factor 6 smaller than the Λ rate.

$\Gamma(\Sigma^0 \mu^- \bar{\nu}_\mu) / \Gamma(\Lambda\pi^-)$	VALUE (units 10 ⁻³)	CL%	EVTS	DOCUMENT ID	TECN	COMMENT	Γ_6/Γ_1
< 0.76	90	0	YEH	74	HBC	Effective denom.=3026	
• • • We do not use the following data for averages, fits, limits, etc. • • •							
< 5			BERGE	66	HBC		

$\Gamma(\Xi^0 e^- \bar{\nu}_e) / \Gamma(\Lambda\pi^-)$	VALUE (units 10 ⁻³)	CL%	EVTS	DOCUMENT ID	TECN	COMMENT	Γ_7/Γ_1
< 2.3	90	0	YEH	74	HBC	Effective denom.=1000	

See key on page 999

Baryon Particle Listings



$\Gamma(n\pi^-)/\Gamma(\Lambda\pi^-)$ **Γ_8/Γ_1**
 $\Delta S=2$. Forbidden in first-order weak interaction.

VALUE (units 10^{-3})	CL%	EVTS	DOCUMENT ID	TECN	COMMENT
<0.019	90		BIAGI	82B	SPEC SPS hyperon beam
•••	We do not use the following data for averages, fits, limits, etc. •••				
<3.0	90	0	YEH	74	HBC Effective denom.=760
<1.1			DAUBER	69	HBC
<5.0			FERRO-LUZZI	63	HBC

$\Gamma(ne^- \bar{\nu}_e)/\Gamma(\Lambda\pi^-)$ **Γ_9/Γ_1**
 $\Delta S=2$. Forbidden in first-order weak interaction.

VALUE (units 10^{-3})	CL%	EVTS	DOCUMENT ID	TECN	COMMENT
< 3.2	90	0	YEH	74	HBC Effective denom.=715
•••	We do not use the following data for averages, fits, limits, etc. •••				
<10	90		BINGHAM	65	RVUE

$\Gamma(n\mu^- \bar{\nu}_\mu)/\Gamma(\Lambda\pi^-)$ **Γ_{10}/Γ_1**
 $\Delta S=2$. Forbidden in first-order weak interaction.

VALUE (units 10^{-3})	CL%	EVTS	DOCUMENT ID	TECN	COMMENT
<15.3	90	0	YEH	74	HBC Effective denom.=150

$\Gamma(p\pi^- \pi^-)/\Gamma(\Lambda\pi^-)$ **Γ_{11}/Γ_1**
 $\Delta S=2$. Forbidden in first-order weak interaction.

VALUE (units 10^{-4})	CL%	EVTS	DOCUMENT ID	TECN	COMMENT
<3.7	90	0	YEH	74	HBC Effective denom.=6200

$\Gamma(p\pi^- e^- \bar{\nu}_e)/\Gamma(\Lambda\pi^-)$ **Γ_{12}/Γ_1**
 $\Delta S=2$. Forbidden in first-order weak interaction.

VALUE (units 10^{-4})	CL%	EVTS	DOCUMENT ID	TECN	COMMENT
<3.7	90	0	YEH	74	HBC Effective denom.=6200

$\Gamma(p\pi^- \mu^- \bar{\nu}_\mu)/\Gamma(\Lambda\pi^-)$ **Γ_{13}/Γ_1**
 $\Delta S=2$. Forbidden in first-order weak interaction.

VALUE (units 10^{-4})	CL%	EVTS	DOCUMENT ID	TECN	COMMENT
<3.7	90	0	YEH	74	HBC Effective denom.=6200

$\Gamma(p\mu^- \mu^-)/\Gamma(\Lambda\pi^-)$ **Γ_{14}/Γ_1**
 $\Delta L=2$ decay, forbidden by total lepton number conservation.

VALUE (units 10^{-8})	CL%	DOCUMENT ID	TECN	COMMENT
<4.0	90	RAJARAM 05	HYCP	p Cu, 800 GeV
•••	We do not use the following data for averages, fits, limits, etc. •••			
<3.7 $\times 10^4$	90	7 LITTENBERG 92B	HBC	Uses YEH 74 data

⁷ This LITTENBERG 92B limit and the identical YEH 74 limits for the preceding three modes all result from nonobservance of any 3-prong decays of the Ξ^- . One could as well apply the limit to the *sum* of the four modes.

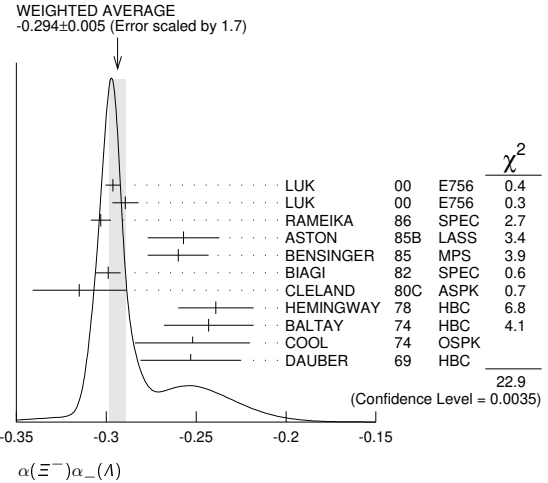
Ξ^- DECAY PARAMETERS

See the "Note on Baryon Decay Parameters" in the neutron Listings.

$\alpha(\Xi^-)\alpha_-(\Lambda)$

VALUE	EVTS	DOCUMENT ID	TECN	COMMENT
-0.294 ± 0.005 OUR AVERAGE				Error includes scale factor of 1.7. See the ideogram below.
-0.2963 ± 0.0042	189k	LUK	00	E756 p Be, 800 GeV
-0.2894 ± 0.0073	63k	⁸ LUK	00	E756 p Be, 800 GeV
-0.303 ± 0.004 ± 0.004	192k	RAMEIKA	86	SPEC 400 GeV pBe
-0.257 ± 0.020	11k	ASTON	85B	LASS 11 GeV/c K^-p
-0.260 ± 0.017	21k	BENSINGER	85	MPS 5 GeV/c K^-p
-0.299 ± 0.007	150k	BIAGI	82	SPEC SPS hyperon beam
-0.315 ± 0.026	9046	CLELAND	80C	ASPK BNL hyperon beam
-0.239 ± 0.021	6599	HEMINGWAY	78	HBC 4.2 GeV/c K^-p
-0.243 ± 0.025	4303	BALTAY	74	HBC 1.75 GeV/c K^-p
-0.252 ± 0.032	2436	COOL	74	OSPK 1.8 GeV/c K^-p
-0.253 ± 0.028	2781	DAUBER	69	HBC

⁸ This LUK 00 value is for $\alpha(\Xi^+)\alpha_+(\bar{\Lambda})$. We assume CP conservation here by including it in the average for $\alpha(\Xi^-)\alpha_-(\Lambda)$. But see the second data block below for the CP test.



α FOR $\Xi^- \rightarrow \Lambda\pi^-$
 The above average, $\alpha(\Xi^-)\alpha_-(\Lambda) = -0.294 \pm 0.005$, divided by our current average $\alpha_-(\Lambda) = 0.732 \pm 0.014$, gives the following value for $\alpha(\Xi^-)$:

VALUE	DOCUMENT ID
-0.401 ± 0.010 OUR EVALUATION	

$\frac{[\alpha(\Xi^-)\alpha_-(\Lambda) - \alpha(\Xi^+)\alpha_+(\bar{\Lambda})]}{[\alpha(\Xi^-)\alpha_-(\Lambda) + \alpha(\Xi^+)\alpha_+(\bar{\Lambda})]}$
 This is zero if CP is conserved. The α 's are the decay-asymmetry parameters for $\Xi^- \rightarrow \Lambda\pi^-$ and $\Lambda \rightarrow p\pi^-$ and for $\Xi^+ \rightarrow \bar{\Lambda}\pi^+$ and $\bar{\Lambda} \rightarrow \bar{p}\pi^+$.

VALUE (units 10^{-4})	EVTS	DOCUMENT ID	TECN	COMMENT
0.0 ± 5.1 ± 4.4	158M	HOLMSTROM 04	HYCP	p Cu, 800 GeV
•••	We do not use the following data for averages, fits, limits, etc. •••			
+120 ± 140	252k	LUK	00	E756 p Be, 800 GeV

ϕ ANGLE FOR $\Xi^- \rightarrow \Lambda\pi^-$ **($\tan\phi = \beta/\gamma$)**

VALUE (°)	EVTS	DOCUMENT ID	TECN	COMMENT
-2.1 ± 0.8 OUR AVERAGE				
-2.39 ± 0.64 ± 0.64	144M	⁹ HUANG	04	HYCP p Cu, 800 GeV
-1.61 ± 2.66 ± 0.37	1.35M	¹⁰ CHAKRAVO...	03	E756 p Be, 800 GeV
5 ± 10	11k	ASTON	85B	LASS K^-p
14.7 ± 16.0	21k	¹¹ BENSINGER	85	MPS 5 GeV/c K^-p
11 ± 9	4303	BALTAY	74	HBC 1.75 GeV/c K^-p
5 ± 16	2436	COOL	74	OSPK 1.8 GeV/c K^-p
-14 ± 11	2781	DAUBER	69	HBC Uses $\alpha_\Lambda = 0.647 \pm 0.020$
0 ± 12	1004	¹² BERGE	66	HBC
•••	We do not use the following data for averages, fits, limits, etc. •••			
-26 ± 30	2724	BINGHAM	70B	OSPK
0 ± 20.4	364	¹² LONDON	66	HBC Using $\alpha_\Lambda = 0.62$
54 ± 30	356	¹² CARMONY	64B	HBC

⁹ From this result and α_Ξ , HUANG 04 gets $\beta_\Xi = -0.037 \pm 0.011 \pm 0.010$ and $\gamma_\Xi = 0.888 \pm 0.0004 \pm 0.006$. And the strong p-s phase difference for $\Lambda\pi^-$ scattering is $(4.6 \pm 1.4 \pm 1.2)^\circ$.

¹⁰ From this result and α_Ξ , CHAKRAVORTY 03 obtains $\beta_\Xi = -0.025 \pm 0.042 \pm 0.006$ and $\gamma_\Xi = 0.889 \pm 0.001 \pm 0.007$. And the strong p-s phase difference for $\Lambda\pi^-$ scattering is $(3.17 \pm 5.28 \pm 0.73)^\circ$.

¹¹ BENSINGER 85 used $\alpha_\Lambda = 0.642 \pm 0.013$.

¹² The errors have been multiplied by 1.2 due to approximations used for the Ξ polarization; see DAUBER 69 for a discussion.

g_A/g_V FOR $\Xi^- \rightarrow \Lambda e^- \bar{\nu}_e$

VALUE	EVTS	DOCUMENT ID	TECN	COMMENT
-0.25 ± 0.05	1992	¹³ BOURQUIN	83	SPEC SPS hyperon beam

¹³ BOURQUIN 83 assumes that $g_2 = 0$. Also, the sign has been changed to agree with our conventions, given in the "Note on Baryon Decay Parameters" in the neutron Listings.

Ξ^- REFERENCES

We have omitted those papers that have been superseded by later experiments. See our earlier editions.

ABDALLAH 06E	PL B639 179	J. Abdallah <i>et al.</i>	(DELPHI Collab.)
RAJARAM 05	PRL 94 181801	D. Rajaram <i>et al.</i>	(FNAL HyperCP Collab.)
HOLMSTROM 04	PRL 93 242001	T. Holmstrom <i>et al.</i>	(FNAL HyperCP Collab.)
HUANG 04	PRL 93 011802	M. Huang <i>et al.</i>	(FNAL HyperCP Collab.)
CHAKRAVO... 03	PRL 91 031601	A. Chakravorty <i>et al.</i>	(FNAL E756 Collab.)
LUK 00	PRL 85 4860	K.B. Luk <i>et al.</i>	(FNAL E756 Collab.)
DUBBS 94	PRL 72 808	T. Dubbs <i>et al.</i>	(FNAL E761 Collab.)
DURYEA 92	PRL 68 768	J. Duryea <i>et al.</i>	(MINN, FNAL, MICH, RUTG)
LITTENBERG 92B	PR D46 892	L.S. Littenberg, R.E. Shrock	(BNL, STON)
HO 90	PRL 65 1713	P.M. Ho <i>et al.</i>	(MICH, FNAL, MINN, RUTG)
Also	PR D44 3402	P.M. Ho <i>et al.</i>	(MICH, FNAL, MINN, RUTG)
TROST 89	PR D40 1703	L.H. Trost <i>et al.</i>	(FNAL-715 Collab.)
BIAGI 87B	ZPHY C35 143	S.F. Biagi <i>et al.</i>	(BRIS, CERN, GEVA+)
RAMEIKA 86	PR D33 3172	R. Rameika <i>et al.</i>	(RUTG, MICH, WISC+)
ASTON 85B	PR D32 2270	D. Aston <i>et al.</i>	(SLAC, CARL, CNRC, CINC)
BENSINGER 85	NP B252 561	J.R. Bensing <i>et al.</i>	(CHIC, ELMT, FNAL+)

Baryon Particle Listings

$\Xi^-, \Xi's, \Xi(1530)$

BOURQUIN	84	NP B241 1	M.H. Bourquin <i>et al.</i>	(BRIS, GEVA, HEIDP+)
RAMEIKA	84	PRL 52 581	R. Rameika <i>et al.</i>	(RUTG, MICH, WISC+)
BOURQUIN	83	ZPHY C21 1	M.H. Bourquin <i>et al.</i>	(BRIS, GEVA, HEIDP+)
BIAGI	82	PL 112B 265	S.F. Biagi <i>et al.</i>	(BRIS, CAVE, GEVA+)
BIAGI	82B	PL 112B 277	S.F. Biagi <i>et al.</i>	(LOQM, GEVA, RL+)
CLELAND	80C	PR D21 12	W.E. Cleland <i>et al.</i>	(PITT, BNL)
THOMPSON	80	PR D21 25	J.A. Thompson <i>et al.</i>	(PITT, BNL)
BOURQUIN	79	PL 87B 297	M.H. Bourquin <i>et al.</i>	(BRIS, GEVA, HEIDP+)
HEMINGWAY	78	NP B142 205	R.J. Hemingway <i>et al.</i>	(CERN, ZEEM, NIJH+)
DIBIANCA	75	NP B99 137	F.A. Dibianca, R.J. Endorf	(CMU)
BALTAY	74	PR D9 49	C. Baltay <i>et al.</i>	(COLU, BING) J
COOL	74	PR D10 792	R.L. Cool <i>et al.</i>	(BNL)
Also		PRL 29 1630	R.L. Cool <i>et al.</i>	(BNL)
YEH	74	PR D10 3545	N. Yeh <i>et al.</i>	(BING, COLU)
MAYEUR	72	NP B47 333	C. Mayeur <i>et al.</i>	(BRUX, CERN, TUFTS, LOUC)
VOTRUBA	72	NP B45 77	M.F. Votruba, A. Saffder, T.M. Ratcliffe	(BIRM+)
WILQUET	72	PL 42B 372	G. Wilquet <i>et al.</i>	(BRUX, CERN, TUFTS+)
DUCCLOS	71	NP B32 493	J. Duclos <i>et al.</i>	(CERN)
BINGHAM	70B	PR D1 3010	G.M. Bingham <i>et al.</i>	(UCSD, WASH)
GOLDWASSER	70	PR D1 1960	E.L. Goldwasser, P.F. Schultz	(ILL)
STONE	70	PL 32B 515	S.L. Stone <i>et al.</i>	(ROCH)
DAUBER	69	PR 179 1262	P.H. Dauber <i>et al.</i>	(LRL) J
SHEN	67	PL 25B 443	B.C. Shen, A. Firestone, G. Goldhaber	(UCB+)
BERGE	66	PR 147 945	J.P. Berge <i>et al.</i>	(LRL)
CHIEN	66	PR 152 1171	C.Y. Chien <i>et al.</i>	(YALE, BNL)
LONDON	66	PR 143 1034	G.W. London <i>et al.</i>	(BNL, SYRA)
BINGHAM	65	PRSL 285 202	H.H. Bingham	(CERN)
PJERROU	65B	PRL 14 275	G.M. Pjerrou <i>et al.</i>	(UCLA)
Also		Thesis	G.M. Pjerrou	(UCLA)
BADIER	64	Dubna Conf. 1 593	J. Badier <i>et al.</i>	(EPOL, SACL, ZEEM)
CARMONY	64B	PRL 12 462	D.D. Carmony <i>et al.</i>	(UCLA) J
HUBBARD	64	PR 135 B183	J.R. Hubbard <i>et al.</i>	(LRL)
FERRO-LUZZI	63	PR 130 1568	M. Ferro-Luzzi <i>et al.</i>	(LRL)
JAUNEAU	63D	Siena Conf. 4	L. Jauneau <i>et al.</i>	(EPOL, CERN, LOUC+)
Also		PL 5 261	L. Jauneau <i>et al.</i>	(EPOL, CERN, LOUC+)
SCHNEIDER	63	PL 4 360	J. Schneider	(CERN)

Ξ RESONANCES

Revised 2004 by C.G. Wohl, (LBNL).

The accompanying table gives our evaluation of the present status of the Ξ resonances. Not much is known about Ξ resonances. This is because (1) they can only be produced as a part of a final state, and so the analysis is more complicated than if direct formation were possible, (2) the production cross sections are small (typically a few μb), and (3) the final states are topologically complicated and difficult to study with electronic techniques. Thus early information about Ξ resonances came entirely from bubble chamber experiments, where the numbers of events are small, and only in the 1980's did electronic experiments make any significant contributions. However, nothing of significance on Ξ resonances has been added since our 1988 edition.

For a detailed earlier review, see Meadows [1].

Table 1. The status of the Ξ resonances. Only those with an overall status of *** or **** are included in the Baryon Summary Table.

Particle	J^P	Overall status	Status as seen in —				
			$\Xi\pi$	ΛK	ΣK	$\Xi(1530)\pi$	Other channels
$\Xi(1318)$	$1/2^+$	****					Decays weakly
$\Xi(1530)$	$3/2^+$	****	****				
$\Xi(1620)$	*	*	*				
$\Xi(1690)$	***	***	***	**			
$\Xi(1820)$	$3/2^-$	***	**	***	**	**	
$\Xi(1950)$	***	**	**			*	
$\Xi(2030)$	***	***	**	***			
$\Xi(2120)$	*	*	*				
$\Xi(2250)$	**	**					3-body decays
$\Xi(2370)$	**	**					3-body decays
$\Xi(2500)$	*	*	*	*			3-body decays

**** Existence is certain, and properties are at least fairly well explored.
 *** Existence ranges from very likely to certain, but further confirmation is desirable and/or quantum numbers, branching fractions, etc. are not well determined.
 ** Evidence of existence is only fair.
 * Evidence of existence is poor.

Reference

1. B.T. Meadows, in *Proceedings of the IVth International Conference on Baryon Resonances* (Toronto, 1980), ed. N. Isgur, p. 283.

$\Xi(1530) 3/2^+$

$$I(J^P) = \frac{1}{2}(\frac{3}{2}^+) \text{ Status: } ***$$

This is the only Ξ resonance whose properties are all reasonably well known. Assuming that the Λ_c^+ has $J^P = 1/2^+$, AUBERT 08AK, in a study of $\Lambda_c^+ \rightarrow \Xi^- \pi^+ K^+$, finds conclusively that the spin of the $\Xi(1530)^0$ is $3/2$. In conjunction with SCHLEIN 63B and BUTTON-SHAFFER 66, this proves also that the parity is +.

We use only those determinations of the mass and width that are accompanied by some discussion of systematics and resolution.

$\Xi(1530)$ POLE POSITIONS

$\Xi(1530)^0$ REAL PART

VALUE	DOCUMENT ID	COMMENT
1531.6 ± 0.4	LICHTENBERG74	Using HABIB1 73

$\Xi(1530)^0$ IMAGINARY PART

VALUE	DOCUMENT ID	COMMENT
4.45 ± 0.35	LICHTENBERG74	Using HABIB1 73

$\Xi(1530)^-$ REAL PART

VALUE	DOCUMENT ID	COMMENT
1534.4 ± 1.1	LICHTENBERG74	Using HABIB1 73

$\Xi(1530)^-$ IMAGINARY PART

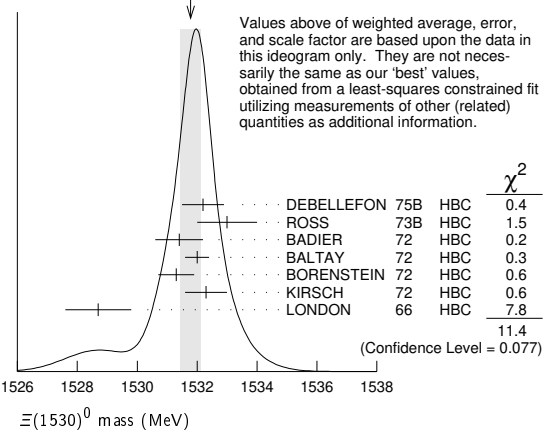
VALUE	DOCUMENT ID	COMMENT
$3.9^{+1.75}_{-3.9}$	LICHTENBERG74	Using HABIB1 73

$\Xi(1530)$ MASSES

$\Xi(1530)^0$ MASS

VALUE (MeV)	EVTS	DOCUMENT ID	TECN	COMMENT
1531.80 ± 0.32	OUR FIT			Error includes scale factor of 1.3.
1531.78 ± 0.34	OUR AVERAGE			Error includes scale factor of 1.4. See the ideogram below.
1532.2 ± 0.7		DEBELLEFON 75B	HBC	$K^- p \rightarrow \Xi^- \bar{K} \pi$
1533 ± 1		ROSS 73B	HBC	$K^- p \rightarrow \Xi^- \bar{K} \pi(\pi)$
1531.4 ± 0.8	59	BADIER 72	HBC	$K^- p$ 3.95 GeV/c
1532.0 ± 0.4	1262	BALTAY 72	HBC	$K^- p$ 1.75 GeV/c
1531.3 ± 0.6	324	BORENSTEIN 72	HBC	$K^- p$ 2.2 GeV/c
1532.3 ± 0.7	286	KIRSCH 72	HBC	$K^- p$ 2.87 GeV/c
1528.7 ± 1.1	76	LONDON 66	HBC	$K^- p$ 2.24 GeV/c
••• We do not use the following data for averages, fits, limits, etc. •••				
1532.1 ± 0.4	1244	ASTON 85B	LASS	$K^- p$ 11 GeV/c
1532.1 ± 0.6	2700	1 BAUBILLIER 81B	HBC	$K^- p$ 8.25 GeV/c
1530 ± 1	450	BIAGI 81	SPEC	SPS hyperon beam
1527 ± 6	80	SIXEL 79	HBC	$K^- p$ 10 GeV/c
1535 ± 4	100	SIXEL 79	HBC	$K^- p$ 16 GeV/c
1533.6 ± 1.4	97	BERTHON 74	HBC	Quasi-2-body σ

WEIGHTED AVERAGE
 1531.78 ± 0.34 (Error scaled by 1.4)



See key on page 999

Baryon Particle Listings

$\Xi(1530)$, $\Xi(1620)$, $\Xi(1690)$

$\Xi(1530)^-$ MASS

VALUE (MeV)	EVTS	DOCUMENT ID	TECN	COMMENT
1535.0 ± 0.6 OUR FIT				
1535.2 ± 0.8 OUR AVERAGE				
1534.5 ± 1.2		DEBELLEFON 75B	HBC	$K^- p \rightarrow \Xi^- \bar{K} \pi$
1535.3 ± 2.0		ROSS 73B	HBC	$K^- p \rightarrow \Xi^- \bar{K} \pi(\pi)$
1536.2 ± 1.6	185	KIRSCH 72	HBC	$K^- p$ 2.87 GeV/c
1535.7 ± 3.2	38	LONDON 66	HBC	$K^- p$ 2.24 GeV/c
• • • We do not use the following data for averages, fits, limits, etc. • • •				
1540 ± 3	48	BERTHON 74	HBC	Quasi-2-body σ
1534.7 ± 1.1	334	BALTAY 72	HBC	$K^- p$ 1.75 GeV/c

$m_{\Xi(1530)^-} - m_{\Xi(1530)}$

VALUE (MeV)	DOCUMENT ID	TECN	COMMENT
3.2 ± 0.6 OUR FIT			
2.9 ± 0.9 OUR AVERAGE			
2.7 ± 1.0	BALTAY 72	HBC	$K^- p$ 1.75 GeV/c
2.0 ± 3.2	MERRILL 66	HBC	$K^- p$ 1.7-2.7 GeV/c
5.7 ± 3.0	PJERROU 65B	HBC	$K^- p$ 1.8-1.95 GeV/c
• • • We do not use the following data for averages, fits, limits, etc. • • •			
3.9 ± 1.8	² KIRSCH 72	HBC	$K^- p$ 2.87 GeV/c
7 ± 4	² LONDON 66	HBC	$K^- p$ 2.24 GeV/c

$\Xi(1530)$ WIDTHS

$\Xi(1530)^0$ WIDTH

VALUE (MeV)	EVTS	DOCUMENT ID	TECN	COMMENT
9.1 ± 0.5 OUR AVERAGE				
9.5 ± 1.2		DEBELLEFON 75B	HBC	$K^- p \rightarrow \Xi^- \bar{K} \pi$
9.1 ± 2.4		ROSS 73B	HBC	$K^- p \rightarrow \Xi^- \bar{K} \pi(\pi)$
11 ± 2		BADIER 72	HBC	$K^- p$ 3.95 GeV/c
9.0 ± 0.7		BALTAY 72	HBC	$K^- p$ 1.75 GeV/c
8.4 ± 1.4		BORENSTEIN 72	HBC	$\Xi^- \pi^+$
11.0 ± 1.8		KIRSCH 72	HBC	$\Xi^- \pi^+$
7 ± 7		BERGE 66	HBC	$K^- p$ 1.5-1.7 GeV/c
8.5 ± 3.5		LONDON 66	HBC	$K^- p$ 2.24 GeV/c
7 ± 2		SCHLEIN 63B	HBC	$K^- p$ 1.8, 1.95 GeV/c
• • • We do not use the following data for averages, fits, limits, etc. • • •				
12.8 ± 1.0	2700	¹ BAUBILLIER 81B	HBC	$K^- p$ 8.25 GeV/c
19 ± 6	80	³ SIXEL 79	HBC	$K^- p$ 10 GeV/c
14 ± 5	100	³ SIXEL 79	HBC	$K^- p$ 16 GeV/c

$\Xi(1530)^-$ WIDTH

VALUE (MeV)	DOCUMENT ID	TECN	COMMENT
9.9 ± 1.7 OUR AVERAGE			
9.6 ± 2.8	DEBELLEFON 75B	HBC	$K^- p \rightarrow \Xi^- \bar{K} \pi$
8.3 ± 3.6	ROSS 73B	HBC	$K^- p \rightarrow \Xi^- \bar{K} \pi(\pi)$
7.8 ± 3.5	BALTAY 72	HBC	$K^- p$ 1.75 GeV/c
16.2 ± 4.6	KIRSCH 72	HBC	$\Xi^- \pi^0, \Xi^0 \pi^-$

$\Xi(1530)$ DECAY MODES

Mode	Fraction (Γ_i/Γ)	Confidence level
$\Gamma_1 \Xi^- \pi$	100 %	
$\Gamma_2 \Xi^- \gamma$	<3.7 %	90%

$\Xi(1530)$ BRANCHING RATIOS

$\Gamma(\Xi^- \gamma)/\Gamma_{\text{total}}$	CL%	DOCUMENT ID	TECN	COMMENT	Γ_2/Γ
<0.037	90	ABLIKIM 20	BES3	$J/\psi \rightarrow \Xi(1530)^- \Xi^+$	
<0.04	90	KALBFLEISCH 75	HBC	$K^- p$ 2.18 GeV/c	

$\Xi(1530)$ FOOTNOTES

- ¹ BAUBILLIER 81B is a fit to the inclusive spectrum. The resolution (5 MeV) is not unfolded.
- ² Redundant with data in the mass Listings.
- ³ SIXEL 79 doesn't unfold the experimental resolution of 15 MeV.

$\Xi(1530)$ REFERENCES

ABLIKIM 20	PR D101 012004	M. Ablikim et al.	(BESIII Collab.)
AUBERT 08AK	PR D78 034008	B. Aubert et al.	(BABAR Collab.)
ASTON 85B	PR D32 2270	D. Aston et al.	(SLAC, CARL, CNRC, CINC)
BAUBILLIER 81B	NP B192 1	M. Baubillier et al.	(BIRM, CERN, GLAS+)
BIAGI 81	ZPHY C9 305	S.F. Biagi et al.	(BRIS, CAVE, GEVA+)
SIXEL 79	NP B159 125	P. Sixel et al.	(AACH3, BERL, CERN, LOIC+)
DEBELLEFON 75B	NC 28A 289	A. de Bellefon et al.	(CDEF, SACL)
KALBFLEISCH 75	PR D11 987	G.R. Kalbfleisch, R.C. Strand, J.W. Chapman	(BNL+)
BERTHON 74	NC 21A 146	A. Berthon et al.	(CDEF, RHEL, SACL+)

LICHTENBERG 74	PR D10 3865	D.B. Lichtenberg	(IND)
Also	Private Comm.	D.B. Lichtenberg	(IND)
HABIBI 73	Thesis Nevis 199	M. Habibi	(COLU)
ROSS 73B	Purdue Conf. 355	R.T. Ross, J.L. Lloyd, D. Radojicic	(COXF)
BADIER 72	NP B37 429	J. Badier et al.	(EPOL)
BALTAY 72	PL 42B 129	C. Baltay et al.	(COLU, BING)
BORENSTEIN 72	PR D5 1559	S.R. Borenstein et al.	(BNL, MICH)1
KIRSCH 72	NP B40 349	L.E. Kirsch et al.	(BRAN, UMD, SYRA+)
BERGE 66	PR 147 945	J.P. Berge et al.	(LRL)1
BUTTON-... 66	PR 142 883	J. Button-Shafer et al.	(LRL)JP
LONDON 66	PR 143 1034	G.W. London et al.	(BNL, SYRA)1J
MERRILL 66	Thesis UCRL 16455	D.W. Merrill	(LRL)1J
PJERROU 65B	PRL 14 275	G.M. Pjerrou et al.	(UCLA)
SCHLEIN 63B	PRL 11 167	P.E. Schlein et al.	(UCLA)1JP

OTHER RELATED PAPERS

MAZZUCATO 81	NP B178 1	M. Mazzucato et al.	(AMST, CERN, NUM+)
BRIEFEL 77	PR D16 2706	E. Briefel et al.	(BRAN, UMD, SYRA+)
BRIEFEL 75	PR D12 1859	E. Briefel et al.	(BRAN, UMD, SYRA+)
HUNGERBU... 74	PR D10 2051	V. Hungerbuehler et al.	(YALE, FNAL, BNL+)
BUTTON-... 66	PR 142 883	J. Button-Shafer et al.	(LRL)JP

$\Xi(1620)$

$I(J^P) = \frac{1}{2}(?^?)$ Status: *
J, P need confirmation.

OMITTED FROM SUMMARY TABLE

What little evidence there is consists of weak signals in the $\Xi\pi$ channel. A number of other experiments (e.g., BORENSTEIN 72 and HASSALL 81) have looked for but not seen any effect.

$\Xi(1620)$ MASS

VALUE (MeV)	EVTS	DOCUMENT ID	TECN	COMMENT
≈ 1620 OUR ESTIMATE				
1624 ± 3	31	BRIEFEL 77	HBC	$K^- p$ 2.87 GeV/c
1633 ± 12	34	DEBELLEFON 75B	HBC	$K^- p \rightarrow \Xi^- \bar{K} \pi$
1606 ± 6	29	ROSS 72	HBC	$K^- p$ 3.1-3.7 GeV/c

$\Xi(1620)$ WIDTH

VALUE (MeV)	EVTS	DOCUMENT ID	TECN	COMMENT
22.5	31	¹ BRIEFEL 77	HBC	$K^- p$ 2.87 GeV/c
40 ± 15	34	DEBELLEFON 75B	HBC	$K^- p \rightarrow \Xi^- \bar{K} \pi$
21 ± 7	29	ROSS 72	HBC	$K^- p \rightarrow \Xi^- \pi^+ K^*(892)$

$\Xi(1620)$ DECAY MODES

Mode
$\Gamma_1 \Xi^- \pi$

$\Xi(1620)$ FOOTNOTES

- ¹ The fit is insensitive to values between 15 and 30 MeV.

$\Xi(1620)$ REFERENCES

HASSALL 81	NP B189 397	J.K. Hassall et al.	(CAVE, MSU)
BRIEFEL 77	PR D16 2706	E. Briefel et al.	(BRAN, UMD, SYRA+)
Also	Duke Conf. 317	E. Briefel et al.	(BRAN, UMD, SYRA+)
Also	Hyperon Resonances, 1970		
DEBELLEFON 75B	PR D12 1859	E. Briefel et al.	(BRAN, UMD, SYRA+)
BORENSTEIN 72	NC 28A 289	A. de Bellefon et al.	(CDEF, SACL)
ROSS 72	PL D5 1559	S.R. Borenstein et al.	(BNL, MICH)1
	PL 38B 177	R.T. Ross et al.	(COXF)1

OTHER RELATED PAPERS

HUNGERBU... 74	PR D10 2051	V. Hungerbuehler et al.	(YALE, FNAL, BNL+)
SCHMIDT 73	Purdue Conf. 363	P.E. Schmidt	(BRAN)
KALBFLEISCH 70	Duke Conf. 331	G.R. Kalbfleisch	(BNL)1
Also	Hyperon Resonances 1970		
APSELL 69	PRL 23 884	S.P. Apseil et al.	(BRAN, UMD, SYRA+)
BARTSCH 69	PL 28B 439	J. Bartsch et al.	(AACH, BERL, CERN+)

$\Xi(1690)$

$I(J^P) = \frac{1}{2}(?^?)$ Status: ** *

AUBERT 08AK, in a study of $\Lambda_c^+ \rightarrow \Xi^- \pi^+ K^+$, finds some evidence that the $\Xi(1690)$ has $J^P = 1/2^-$.

DIONISI 78 sees a threshold enhancement in both the neutral and negatively charged $\Sigma \bar{K}$ mass spectra in $K^- p \rightarrow (\Sigma \bar{K}) K \pi$ at 4.2 GeV/c. The data from the $\Sigma \bar{K}$ channels alone cannot distinguish between a resonance and a large scattering length. Weaker evidence at the same mass is seen in the corresponding $\Lambda \bar{K}$ channels, and a coupled-channel analysis yields results consistent with a new Ξ .

BIAGI 81 sees an enhancement at 1700 MeV in the diffractively produced ΛK^- system. A peak is also observed in the $\Lambda \bar{K}^0$ mass spectrum at 1660 MeV that is consistent with a 1720 MeV resonance decaying to $\Sigma^0 \bar{K}^0$, with the γ from the Σ^0 decay not detected.

Baryon Particle Listings

$\Xi(1690), \Xi(1820)$

BIAGI 87 provides further confirmation of this state in diffractive dissociation of Ξ^- into ΛK^- . The significance claimed is 6.7 standard deviations.

ADAMOVICH 98 sees a peak of 1400 ± 300 events in the $\Xi^- \pi^+$ spectrum produced by 345 GeV/c Σ^- -nucleus interactions.

$\Xi(1690)$ MASSES

MIXED CHARGES

1690 ± 10 OUR ESTIMATE This is only an educated guess; the error given is larger than the error on the average of the published values.

$\Xi(1690)^0$ MASS

VALUE (MeV)	EVTS	DOCUMENT ID	TECN	COMMENT
1686 ± 4	1400	ADAMOVICH 98	WA89	Σ^- nucleus, 345 GeV/c
1699 ± 5	175	¹ DIONISI 78	HBC	$K^- p$ 4.2 GeV/c
1684 ± 5	183	² DIONISI 78	HBC	$K^- p$ 4.2 GeV/c

$\Xi(1690)^-$ MASS

VALUE (MeV)	EVTS	DOCUMENT ID	TECN	COMMENT
1691.1 ± 1.9 ± 2.0	104	BIAGI 87	SPEC	Ξ^- Be 116 GeV
1700 ± 10	150	³ BIAGI 81	SPEC	Ξ^- H 100, 135 GeV
1694 ± 6	45	⁴ DIONISI 78	HBC	$K^- p$ 4.2 GeV/c

$\Xi(1690)$ WIDTHS

MIXED CHARGES

<30 OUR ESTIMATE

$\Xi(1690)^0$ WIDTH

VALUE (MeV)	EVTS	DOCUMENT ID	TECN	COMMENT
10 ± 6	1400	ADAMOVICH 98	WA89	Σ^- nucleus, 345 GeV/c
44 ± 23	175	¹ DIONISI 78	HBC	$K^- p$ 4.2 GeV/c
20 ± 4	183	² DIONISI 78	HBC	$K^- p$ 4.2 GeV/c

$\Xi(1690)^-$ WIDTH

VALUE (MeV)	CL%	EVTS	DOCUMENT ID	TECN	COMMENT
< 8	90	104	BIAGI 87	SPEC	Ξ^- Be 116 GeV
47 ± 14		150	³ BIAGI 81	SPEC	Ξ^- H 100, 135 GeV
26 ± 6		45	⁴ DIONISI 78	HBC	$K^- p$ 4.2 GeV/c

$\Xi(1690)$ DECAY MODES

Mode	Fraction (Γ_i/Γ)
$\Gamma_1 \Lambda \bar{K}$	seen
$\Gamma_2 \Sigma \bar{K}$	seen
$\Gamma_3 \Xi \pi$	seen
$\Gamma_4 \Xi^- \pi^+ \pi^0$	
$\Gamma_5 \Xi^- \pi^+ \pi^-$	possibly seen
$\Gamma_6 \Xi(1530) \pi$	

$\Xi(1690)$ BRANCHING RATIOS

$\Gamma(\Lambda \bar{K})/\Gamma_{total}$	Γ_1/Γ				
VALUE	EVTS	DOCUMENT ID	TECN	CHG	COMMENT
seen	104	BIAGI 87	SPEC	-	Ξ^- Be 116 GeV

$\Gamma(\Sigma \bar{K})/\Gamma(\Lambda \bar{K})$	Γ_2/Γ_1				
VALUE	EVTS	DOCUMENT ID	TECN	CHG	COMMENT
0.75 ± 0.39	75	ABE 02c	BELL		$e^+ e^- \approx \tau(4S)$
2.7 ± 0.9		DIONISI 78	HBC	0	$K^- p$ 4.2 GeV/c
3.1 ± 1.4		DIONISI 78	HBC	-	$K^- p$ 4.2 GeV/c

$\Gamma(\Xi \pi)/\Gamma(\Sigma \bar{K})$	Γ_3/Γ_2			
VALUE	DOCUMENT ID	TECN	CHG	COMMENT
< 0.09	DIONISI 78	HBC	0	$K^- p$ 4.2 GeV/c

$\Gamma(\Xi \pi)/\Gamma_{total}$	Γ_3/Γ		
VALUE	DOCUMENT ID	TECN	COMMENT
seen	ADAMOVICH 98	WA89	Σ^- nucleus, 345 GeV/c

$\Gamma(\Xi^- \pi^+ \pi^0)/\Gamma(\Sigma \bar{K})$	Γ_4/Γ_2			
VALUE	DOCUMENT ID	TECN	CHG	COMMENT
< 0.04	DIONISI 78	HBC	0	$K^- p$ 4.2 GeV/c

$\Gamma(\Xi^- \pi^+ \pi^-)/\Gamma_{total}$	Γ_5/Γ				
VALUE	EVTS	DOCUMENT ID	TECN	CHG	COMMENT
possibly seen	4	BIAGI 87	SPEC	-	Ξ^- Be 116 GeV

$\Gamma(\Xi^- \pi^+ \pi^-)/\Gamma(\Sigma \bar{K})$	Γ_5/Γ_2			
VALUE	DOCUMENT ID	TECN	CHG	COMMENT
< 0.03	DIONISI 78	HBC	-	$K^- p$ 4.2 GeV/c

$\Gamma(\Xi(1530)\pi)/\Gamma(\Sigma \bar{K})$	Γ_6/Γ_2			
VALUE	DOCUMENT ID	TECN	CHG	COMMENT
< 0.06	DIONISI 78	HBC	-	$K^- p$ 4.2 GeV/c

$\Xi(1690)$ FOOTNOTES

- ¹ From a fit to the $\Sigma^+ K^-$ spectrum.
- ² From a coupled-channel analysis of the $\Sigma^+ K^-$ and $\Lambda \bar{K}^0$ spectra.
- ³ A fit to the inclusive spectrum from $\Xi^- N \rightarrow \Lambda K^- X$.
- ⁴ From a coupled-channel analysis of the $\Sigma^0 K^-$ and ΛK^- spectra.

$\Xi(1690)$ REFERENCES

AUBERT 08AK	PR D78 034008	B. Aubert <i>et al.</i>	(BABAR Collab.)
ABE 02c	PL B524 33	K. Abe <i>et al.</i>	(KEK BELLE Collab.)
ADAMOVICH 98	EPJ C5 621	M.L. Adamovich <i>et al.</i>	(CERN WA89 Collab.)
BIAGI 87	ZPHY C34 15	S.F. Biagi <i>et al.</i>	(BRIS, CERN, GEVA+)
BIAGI 81	ZPHY C9 305	S.F. Biagi <i>et al.</i>	(BRIS, CAVE, GEVA+)
DIONISI 78	PL 80B 145	C. Dionisi <i>et al.</i>	(CERN, AMST, NIJM+)

$\Xi(1820) 3/2^-$

$$I(J^P) = \frac{1}{2}(\frac{3}{2}^-) \text{ Status: } ***$$

The clearest evidence is an 8-standard-deviation peak in ΛK^- seen by GAY 76C. TEODORO 78 favors $J = 3/2$, but cannot make a parity discrimination. BIAGI 87C is consistent with $J = 3/2$ and favors negative parity for this J value.

$\Xi(1820)$ MASS

We only average the measurements that appear to us to be most significant and best determined.

VALUE (MeV)	EVTS	DOCUMENT ID	TECN	CHG	COMMENT
1823 ± 5 OUR ESTIMATE					
1823.5 ± 1.4 OUR AVERAGE					
1825.5 ± 4.7 ± 4.7	288	ABLIKIM 20c	BES3	-	$e^+ e^- \rightarrow \Xi(1820)^- \Xi^+$
1819.4 ± 3.1 ± 2.0	280	¹ BIAGI 87	SPEC	0	$\Xi^- \text{Be} \rightarrow (\Lambda K^-) X$
1826 ± 3 ± 1	54	BIAGI 87c	SPEC	0	$\Xi^- \text{Be} \rightarrow (\Lambda \bar{K}^0) X$
1822 ± 6		JENKINS 83	MPS	-	$K^- p \rightarrow K^+ (\text{MM})$
1830 ± 6	300	BIAGI 81	SPEC	-	SPS hyperon beam
1823 ± 2	130	GAY 76c	HBC	-	$K^- p$ 4.2 GeV/c
••• We do not use the following data for averages, fits, limits, etc. •••					
1817 ± 3		ADAMOVICH 99b	WA89		Σ^- nucleus, 345 GeV
1797 ± 19	74	BRIEFEL 77	HBC	0	$K^- p$ 2.87 GeV/c
1829 ± 9	68	BRIEFEL 77	HBC	-0	$\Xi(1530) \pi$
1860 ± 14	39	BRIEFEL 77	HBC	-	$\Sigma^- \bar{K}^0$
1870 ± 9	44	BRIEFEL 77	HBC	0	$\Lambda \bar{K}^0$
1813 ± 4	57	BRIEFEL 77	HBC	-	ΛK^-
1807 ± 27		DIBIANCA 75	DBC	-0	$\Xi \pi, \Xi^* \pi$
1762 ± 8	28	² BADIÉ 72	HBC	-0	$\Xi \pi, \Xi \pi \pi, Y K$
1838 ± 5	38	² BADIÉ 72	HBC	-0	$\Xi \pi, \Xi \pi \pi, Y K$
1830 ± 10	25	³ CRENNELL 70b	DBC	-0	3.6, 3.9 GeV/c
1826 ± 12		⁴ CRENNELL 70b	DBC	-0	3.6, 3.9 GeV/c
1830 ± 10	40	ALITTI 69	HBC	-	$\Lambda, \Sigma \bar{K}$
1814 ± 4	30	BADIÉ 65	HBC	0	$\Lambda \bar{K}^0$
1817 ± 7	29	SMITH 65c	HBC	-0	$\Lambda \bar{K}^0, \Lambda K^-$
1770		HALSTEINSLID63	FBC	-0	K^- freon 3.5 GeV/c

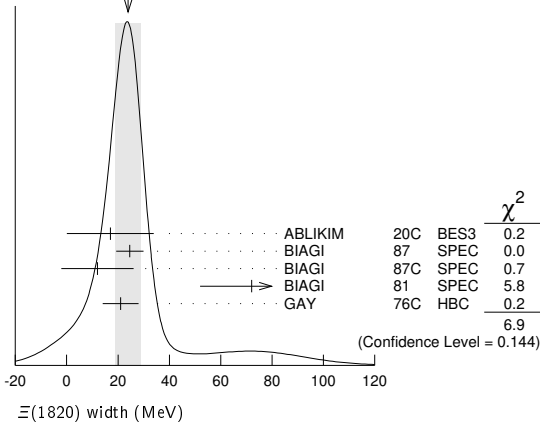
$\Xi(1820)$ WIDTH

VALUE (MeV)	EVTS	DOCUMENT ID	TECN	CHG	COMMENT
24 +15 -10 OUR ESTIMATE					
24 ± 5 OUR AVERAGE					Error includes scale factor of 1.3. See the ideogram below.
17.0 ± 15.0 ± 7.9	288	ABLIKIM 20c	BES3	-	$e^+ e^- \rightarrow \Xi(1820)^- \Xi^+$
24.6 ± 5.3	280	¹ BIAGI 87	SPEC	0	$\Xi^- \text{Be} \rightarrow (\Lambda K^-) X$
12 ± 14 ± 1.7	54	BIAGI 87c	SPEC	0	$\Xi^- \text{Be} \rightarrow (\Lambda \bar{K}^0) X$
72 ± 20	300	BIAGI 81	SPEC	-	SPS hyperon beam
21 ± 7	130	GAY 76c	HBC	-	$K^- p$ 4.2 GeV/c
••• We do not use the following data for averages, fits, limits, etc. •••					
23 ± 13		ADAMOVICH 99b	WA89		Σ^- nucleus, 345 GeV
99 ± 57	74	BRIEFEL 77	HBC	0	$K^- p$ 2.87 GeV/c
52 ± 34	68	BRIEFEL 77	HBC	-0	$\Xi(1530) \pi$
72 ± 17	39	BRIEFEL 77	HBC	-	$\Sigma^- \bar{K}^0$
44 ± 11	44	BRIEFEL 77	HBC	0	$\Lambda \bar{K}^0$
26 ± 11	57	BRIEFEL 77	HBC	-	ΛK^-
85 ± 58		DIBIANCA 75	DBC	-0	$\Xi \pi, \Xi^* \pi$
51 ± 13		² BADIÉ 72	HBC	-0	Lower mass

Baryon Particle Listings
 $\Xi(1820), \Xi(1950)$

58 ± 13	2	BADIER	72	HBC	-0	Higher mass
103 ⁺³⁸ ₋₂₄	3	CRENNELL	70B	DBC	-0	3.6, 3.9 GeV/c
48 ⁺³⁶ ₋₁₉	4	CRENNELL	70B	DBC	-0	3.6, 3.9 GeV/c
55 ⁺⁴⁰ ₋₂₀		ALITTI	69	HBC	-	$\Lambda, \Sigma \bar{K}$
12 ± 4		BADIER	65	HBC	0	$\Lambda \bar{K}^0$
30 ± 7		SMITH	65B	HBC	-0	$\Lambda \bar{K}$
<80		HALSTEINSLID63	FBC	-0	K^- freon 3.5 GeV/c	

WEIGHTED AVERAGE
 24±5 (Error scaled by 1.3)



$\Xi(1820)$ DECAY MODES

Mode	Fraction (Γ_i/Γ)
Γ_1 $\Lambda \bar{K}$	large
Γ_2 $\Sigma \bar{K}$	small
Γ_3 $\Xi \pi$	small
Γ_4 $\Xi(1530)\pi$	small
Γ_5 $\Xi \pi \pi$ (not $\Xi(1530)\pi$)	

$\Xi(1820)$ BRANCHING RATIOS

The dominant modes seem to be $\Lambda \bar{K}$ and (perhaps) $\Xi(1530)\pi$, but the branching fractions are very poorly determined.

$\Gamma(\Lambda \bar{K})/\Gamma_{total}$	DOCUMENT ID	TECN	CHG	COMMENT	Γ_1/Γ
0.25 ± 0.05 OUR AVERAGE					
0.24 ± 0.05	ANISOVICH	12A	DPWA	Multichannel	
0.30 ± 0.15	ALITTI	69	HBC	$K^- p$ 3.9-5 GeV/c	

$\Gamma(\Xi \pi)/\Gamma_{total}$	DOCUMENT ID	TECN	CHG	COMMENT	Γ_3/Γ
0.10 ± 0.10					
	ALITTI	69	HBC	$K^- p$ 3.9-5 GeV/c	

$\Gamma(\Xi \pi)/\Gamma(\Lambda \bar{K})$	DOCUMENT ID	TECN	CHG	COMMENT	Γ_3/Γ_1
<0.36	GAY	76c	HBC	$K^- p$ 4.2 GeV/c	
0.20 ± 0.20	BADIER	65	HBC	$K^- p$ 3 GeV/c	

$\Gamma(\Xi \pi)/\Gamma(\Xi(1530)\pi)$	DOCUMENT ID	TECN	CHG	COMMENT	Γ_3/Γ_4
1.5 ^{+0.6}_{-0.4}	APSELL	70	HBC	$K^- p$ 2.87 GeV/c	

$\Gamma(\Sigma \bar{K})/\Gamma_{total}$	DOCUMENT ID	TECN	CHG	COMMENT	Γ_2/Γ
0.30 ± 0.15	ALITTI	69	HBC	$K^- p$ 3.9-5 GeV/c	

••• We do not use the following data for averages, fits, limits, etc. •••

<0.02	TRIPP	67	RVUE	Use SMITH 65c	
-------	-------	----	------	---------------	--

$\Gamma(\Sigma \bar{K})/\Gamma(\Lambda \bar{K})$	DOCUMENT ID	TECN	CHG	COMMENT	Γ_2/Γ_1
0.24 ± 0.10	GAY	76c	HBC	$K^- p$ 4.2 GeV/c	

$\Gamma(\Xi(1530)\pi)/\Gamma_{total}$	DOCUMENT ID	TECN	CHG	COMMENT	Γ_4/Γ
0.30 ± 0.15	ALITTI	69	HBC	$K^- p$ 3.9-5 GeV/c	
••• We do not use the following data for averages, fits, limits, etc. •••					
seen	ASTON	85B	LASS	$K^- p$ 11 GeV/c	
not seen	5 HASSALL	81	HBC	$K^- p$ 6.5 GeV/c	
<0.25	6 DAUBER	69	HBC	$K^- p$ 2.7 GeV/c	

$\Gamma(\Xi(1530)\pi)/\Gamma(\Lambda \bar{K})$	DOCUMENT ID	TECN	CHG	COMMENT	Γ_4/Γ_1
0.38 ± 0.27 OUR AVERAGE				Error includes scale factor of 2.3.	
1.0 ± 0.3	GAY	76c	HBC	$K^- p$ 4.2 GeV/c	
0.26 ± 0.13	SMITH	65c	HBC	$K^- p$ 2.45-2.7 GeV/c	

$\Gamma(\Xi \pi \pi \text{ (not } \Xi(1530)\pi))/\Gamma(\Lambda \bar{K})$	DOCUMENT ID	TECN	CHG	COMMENT	Γ_5/Γ_1
0.30 ± 0.20	BIAGI	87	SPEC	Ξ^- Be 116 GeV	
••• We do not use the following data for averages, fits, limits, etc. •••					
<0.14	7 BADIER	65	HBC	1 st. dev. limit	
>0.1	SMITH	65c	HBC	$K^- p$ 2.45-2.7 GeV/c	

$\Gamma(\Xi \pi \pi \text{ (not } \Xi(1530)\pi))/\Gamma(\Xi(1530)\pi)$	DOCUMENT ID	TECN	CHG	COMMENT	Γ_5/Γ_4
consistent with zero	GAY	76c	HBC	$K^- p$ 4.2 GeV/c	
••• We do not use the following data for averages, fits, limits, etc. •••					
0.3 ± 0.5	8 APSELL	70	HBC	$K^- p$ 2.87 GeV/c	

$\Xi(1820)$ FOOTNOTES

- 1 BIAGI 87 also sees weak signals in the in the $\Xi^- \pi^+ \pi^-$ channel at 1782.6 ± 1.4 MeV ($\Gamma = 6.0 \pm 1.5$ MeV) and 1831.9 ± 2.8 MeV ($\Gamma = 9.6 \pm 9.9$ MeV).
- 2 BADIER 72 adds all channels and divides the peak into lower and higher mass regions. The data can also be fitted with a single Breit-Wigner of mass 1800 MeV and width 150 MeV.
- 3 From a fit to inclusive $\Xi \pi, \Xi \pi \pi,$ and ΛK^- spectra.
- 4 From a fit to inclusive $\Xi \pi$ and $\Xi \pi \pi$ spectra only.
- 5 Including $\Xi \pi \pi$.
- 6 DAUBER 69 uses in part the same data as SMITH 65c.
- 7 For the decay mode $\Xi^- \pi^+ \pi^0$ only. This limit includes $\Xi(1530)\pi$.
- 8 Or less. Upper limit for the 3-body decay.

$\Xi(1820)$ REFERENCES

ABLIKIM	20C	PRL 124 032002	M. Ablikim et al.	(BESIII Collab.)
ANISOVICH	12A	EPL A48 15	A.V. Anisovich et al.	(BONN, FNPI)
ADAMOVIICH	99B	EPL C11 271	M.L. Adamovich et al.	(CERN WA89 Collab.)
BIAGI	87	ZPHY C34 15	S.F. Biagi et al.	(BRIS, CERN, GEVA+)
BIAGI	87C	ZPHY C34 175	S.F. Biagi et al.	(BRIS, CERN, GEVA+)
ASTON	85B	PR D32 2270	D. Aston et al.	(SLAC, CARL, CNRC, CINC)
JENKINS	83	PRL 51 951	C.M. Jenkins et al.	(FSU, BRAN, LBL+)
BIAGI	81	ZPHY C9 305	S.F. Biagi et al.	(BRIS, CAVE, GEVA+)
HASSALL	81	NP B189 397	J.K. Hassall et al.	(CAVE, MSU)
TEODORO	78	PL 77B 451	D. Teodoro et al.	(AMST, CERN, NIJM+)
BRIEFEL	77	PR D16 2706	E. Briefel et al.	(BRAN, UMD, SYRA+)
Also				
GAY	76C	PL 62B 477	S.P. Appell et al.	(BRAN, UMD, SYRA+)
DIBIANCA	75	NP B98 137	J.B. Gay et al.	(BRAN, UMD, SYRA+)
BADIER	72	NP B37 429	F.A. Dibilanca, R.J. Endorf	(AMST, CERN, NIJM+)
APSELL	70	PL 24 777	J. Badier et al.	(EPOL)
CRENNELL	70B	PR D1 847	S.P. Appell et al.	(BRAN, UMD, SYRA+)
ALITTI	69	PRL 22 79	D.J. Crennell et al.	(BNL)
DAUBER	69	PR 179 1262	J. Alitti et al.	(BNL, SYRA+)
TRIPP	67	NP B3 10	P.M. Dauber et al.	(LRL)
BADIER	65	PL 16 171	R.D. Tripp et al.	(LRL, SLAC, CERN+)
SMITH	65B	Athens Conf. 251	J. Badier et al.	(EPOL, SACL, AMST+)
SMITH	65C	PRL 14 25	G.A. Smith, J.S. Lindsey	(LRL)
HALSTEINSLID	63	Siena Conf. 1 73	G.A. Smith et al.	(LRL)JJP
			A. Halsteinslid et al.	(BERG, CERN, EPOL+)

OTHER RELATED PAPERS

TEODORO	78	PL 77B 451	D. Teodoro et al.	(AMST, CERN, NIJM+)
BRIEFEL	75	PR D12 1859	E. Briefel et al.	(BRAN, UMD, SYRA+)
SCHMIDT	73	Purdue Conf. 363	P.E. Schmidt	(BRAN)
MERRILL	68	PR 167 1202	D.W. Merrill, J. Button-Shafer	(LRL)
SMITH	64	PRL 13 61	G.A. Smith et al.	(LRL)JJP

$\Xi(1950)$

$I(J^P) = \frac{1}{2}(?)^?$ Status: ***

We list here everything reported between 1875 and 2000 MeV. The accumulated evidence for a Ξ near 1950 MeV seems strong enough to include a $\Xi(1950)$ in the main Baryon Table, but not much can be said about its properties. In fact, there may be more than one Ξ near this mass.

$\Xi(1950)$ MASS

VALUE (MeV)	EVTS	DOCUMENT ID	TECN	COMMENT
1950 ± 15 OUR ESTIMATE				
1955 ± 6		ADAMOVIICH	99B	WA89 Σ^- nucleus, 345 GeV
1944 ± 9	129	BIAGI	87	SPEC Ξ^- Be → $(\Xi^- \pi^+) \pi^- X$
1963 ± 5 ± 2	63	BIAGI	87c	SPEC Ξ^- Be → $(\Lambda \bar{K}^0) X$
1937 ± 7	150	BIAGI	81	SPEC SPS hyperon beam
1961 ± 18	139	BRIEFEL	77	HBC 2.87 $K^- p$ → $\Xi^- \pi^+ X$
1936 ± 22	44	BRIEFEL	77	HBC 2.87 $K^- p$ → $\Xi^0 \pi^- X$
1964 ± 10	56	BRIEFEL	77	HBC $\Xi(1530)\pi$
1900 ± 12		DIBIANCA	75	DBC $\Xi \pi$
1952 ± 11	25	ROSS	73c	$(\Xi \pi)^-$
1956 ± 6	29	BADIER	72	HBC $\Xi \pi, \Xi \pi \pi, \gamma K$
1955 ± 14	21	GOLDWASSER	70	HBC $\Xi \pi$

Baryon Particle Listings

$\Xi(1950), \Xi(2030)$

1894 ± 18	66	DAUBER	69	HBC	$\Xi\pi$
1930 ± 20	27	ALITTI	68	HBC	$\Xi^-\pi^+$
1933 ± 16	35	BADIER	65	HBC	$\Xi^-\pi^+$

$\Xi(1950)$ WIDTH

VALUE (MeV)	EVTS	DOCUMENT ID	TECN	COMMENT
60 ± 20 OUR ESTIMATE				
68 ± 22		ADAMOVICH 99B	WA89	Σ^- nucleus, 345 GeV
100 ± 31	129	BIAGI 87	SPEC	$\Xi^- \text{Be} \rightarrow (\Xi^- \pi^+) \pi^- X$
25 ± 15 ± 1.2	63	BIAGI 87c	SPEC	$\Xi^- \text{Be} \rightarrow (\Lambda \bar{K}^0) X$
60 ± 8	150	BIAGI 81	SPEC	SPS hyperon beam
159 ± 5.7	139	BRIEFEL 77	HBC	$2.87 K^- p \rightarrow \Xi^- \pi^+ X$
87 ± 26	44	BRIEFEL 77	HBC	$2.87 K^- p \rightarrow \Xi^0 \pi^- X$
60 ± 39	56	BRIEFEL 77	HBC	$\Xi(1530)\pi$
63 ± 78		DIBIANCA 75	DBC	$\Xi\pi$
38 ± 10		ROSS 73c		$(\Xi\pi)^-$
35 ± 11	29	BADIER 72	HBC	$\Xi\pi, \Xi\pi\pi, \Upsilon K$
56 ± 26	21	GOLDWASSER 70	HBC	$\Xi\pi$
98 ± 23	66	DAUBER 69	HBC	$\Xi\pi$
80 ± 40	27	ALITTI 68	HBC	$\Xi^-\pi^+$
140 ± 35	35	BADIER 65	HBC	$\Xi^-\pi^+$

$\Xi(1950)$ DECAY MODES

Mode	Fraction (Γ_i/Γ)
$\Gamma_1 \Lambda \bar{K}$	seen
$\Gamma_2 \Sigma \bar{K}$	possibly seen
$\Gamma_3 \Xi\pi$	seen
$\Gamma_4 \Xi(1530)\pi$	
$\Gamma_5 \Xi\pi\pi$ (not $\Xi(1530)\pi$)	

$\Xi(1950)$ BRANCHING RATIOS

$\Gamma(\Sigma \bar{K})/\Gamma(\Lambda \bar{K})$			Γ_2/Γ_1		
VALUE	CL%	EVTS	DOCUMENT ID	TECN	COMMENT
<2.3	90	0	BIAGI 87c	SPEC	$\Xi^- \text{Be} 116 \text{ GeV}$
$\Gamma(\Sigma \bar{K})/\Gamma_{\text{total}}$			Γ_2/Γ		
VALUE	EVTS	DOCUMENT ID	TECN	COMMENT	
possibly seen	17	HASSALL 81	HBC	$K^- p 6.5 \text{ GeV/c}$	
$\Gamma(\Xi\pi)/\Gamma(\Xi(1530)\pi)$			Γ_3/Γ_4		
VALUE	DOCUMENT ID	TECN	COMMENT		
$2.8^{+0.7}_{-0.6}$	APSELL 70	HBC			
$\Gamma(\Xi\pi\pi \text{ (not } \Xi(1530)\pi)/\Gamma(\Xi(1530)\pi)$			Γ_5/Γ_4		
VALUE	DOCUMENT ID	TECN	COMMENT		
0.0 ± 0.3	APSELL 70	HBC			

$\Xi(1950)$ REFERENCES

ADAMOVICH 99B	EPJ C11 271	M.I. Adamovich et al.	(CERN WA89 Collab.)
BIAGI 87	ZPHY C34 15	S.F. Biagi et al.	(BRIS, CERN, GEVA+)
BIAGI 87c	ZPHY C34 175	S.F. Biagi et al.	(BRIS, CERN, GEVA+)
BIAGI 81	ZPHY C9 305	S.F. Biagi et al.	(BRIS, CAVE, GEVA+)
HASSALL 81	NP B189 397	J.K. Hassall et al.	(CAVE, MSU)
BRIEFEL 77	PR D16 2706	E. Briefel et al.	(BRAN, UMD, SYRA+)
	Duke Conf. 317	E. Briefel et al.	(BRAN, UMD, SYRA+)
Hyperon Resonances, 1970			
DIBIANCA 75	NP B98 137	F.A. Dibianca, R.J. Endorf	(CMU)
ROSS 73c	Purdue Conf. 345	R.T. Ross, J.L. Lloyd, D. Radojčić	(OXF)
BADIER 72	NP B37 429	J. Badier et al.	(EPOL)
APSELL 70	PRL 24 777	S.P. Appell et al.	(BRAN, UMD, SYRA+)
GOLDWASSER 70	PR D1 1960	E.L. Goldwasser, P.F. Schultzt	(ILL)
DAUBER 69	PR 179 1262	P.M. Dauber et al.	(LRL)
ALITTI 68	PRL 21 1119	J. Alitti et al.	(BNL, SYRA)
BADIER 65	PL 16 171	J. Badier et al.	(EPOL, SAFL, AMST)

$\Xi(2030)$

$$I(J^P) = \frac{1}{2} (\geq \frac{5}{2}) \text{ status: } ***$$

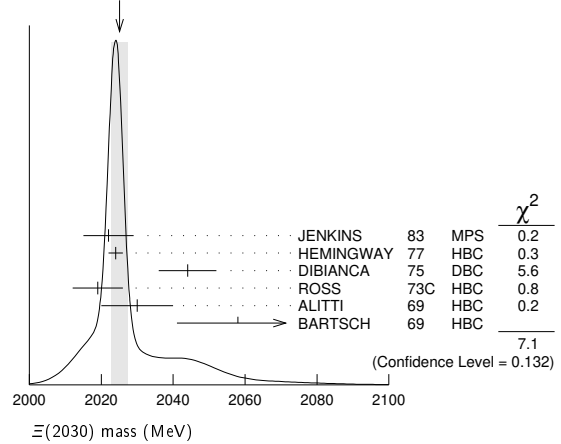
The evidence for this state has been much improved by HEMINGWAY 77, who see an eight standard deviation enhancement in $\Sigma \bar{K}$ and a weaker coupling to $\Lambda \bar{K}$. ALITTI 68 and HEMINGWAY 77 observe no signals in the $\Xi\pi\pi$ (or $\Xi(1530)\pi$) channel, in contrast to DIBIANCA 75. The decay $(\Lambda/\Sigma)\bar{K}\pi$ reported by BARTSCH 69 is also not confirmed by HEMINGWAY 77.

A moments analysis of the HEMINGWAY 77 data indicates at a level of three standard deviations that $J \geq 5/2$.

$\Xi(2030)$ MASS

VALUE (MeV)	EVTS	DOCUMENT ID	TECN	CHG	COMMENT
2025 ± 5 OUR ESTIMATE					
2025.1 ± 2.4 OUR AVERAGE					
Error includes scale factor of 1.3. See the ideogram below.					
2022 ± 7		JENKINS 83	MPS	-	$K^- p \rightarrow K^+ \text{MM}$
2024 ± 2	200	HEMINGWAY 77	HBC	-	$K^- p 4.2 \text{ GeV/c}$
2044 ± 8		DIBIANCA 75	DBC	-0	$\Xi\pi\pi, \Xi^*\pi$
2019 ± 7	15	ROSS 73c	HBC	-0	$\Sigma \bar{K}$
2030 ± 10	42	ALITTI 69	HBC	-	$K^- p 3.9-5 \text{ GeV/c}$
2058 ± 17	40	BARTSCH 69	HBC	-0	$K^- p 10 \text{ GeV/c}$

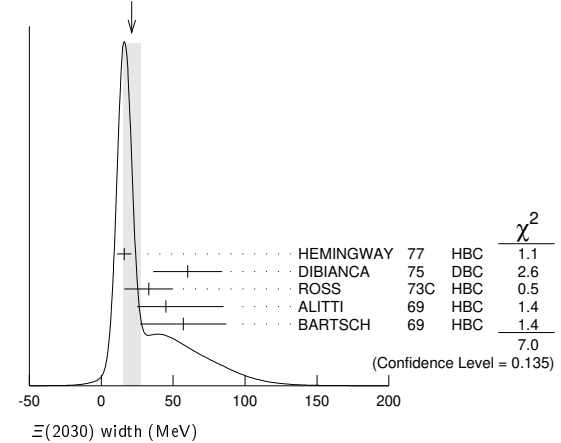
WEIGHTED AVERAGE
2025.1 ± 2.4 (Error scaled by 1.3)



$\Xi(2030)$ WIDTH

VALUE (MeV)	EVTS	DOCUMENT ID	TECN	CHG	COMMENT
20 ± 15 OUR ESTIMATE					
21 ± 6 OUR AVERAGE					
Error includes scale factor of 1.3. See the ideogram below.					
16 ± 5	200	HEMINGWAY 77	HBC	-	$K^- p 4.2 \text{ GeV/c}$
60 ± 24		DIBIANCA 75	DBC	-0	$\Xi\pi\pi, \Xi^*\pi$
33 ± 17	15	ROSS 73c	HBC	-0	$\Sigma \bar{K}$
45 ± 40		ALITTI 69	HBC	-	$K^- p 3.9-5 \text{ GeV/c}$
-20					
57 ± 30		BARTSCH 69	HBC	-0	$K^- p 10 \text{ GeV/c}$

WEIGHTED AVERAGE
21 ± 6 (Error scaled by 1.3)



$\Xi(2030)$ DECAY MODES

Mode	Fraction (Γ_i/Γ)
$\Gamma_1 \Lambda \bar{K}$	~ 20 %
$\Gamma_2 \Sigma \bar{K}$	~ 80 %
$\Gamma_3 \Xi\pi$	small
$\Gamma_4 \Xi(1530)\pi$	small
$\Gamma_5 \Xi\pi\pi$ (not $\Xi(1530)\pi$)	small
$\Gamma_6 \Lambda \bar{K}\pi$	small
$\Gamma_7 \Sigma \bar{K}\pi$	small

See key on page 999

Baryon Particle Listings

$\Xi(2030)$, $\Xi(2120)$, $\Xi(2250)$

$\Xi(2030)$ BRANCHING RATIOS

$$\frac{\Gamma(\Xi\pi)}{[\Gamma(\Lambda\bar{K}) + \Gamma(\Sigma\bar{K}) + \Gamma(\Xi\pi) + \Gamma(\Xi(1530)\pi)]} \quad \Gamma_3/(\Gamma_1+\Gamma_2+\Gamma_3+\Gamma_4)$$

VALUE	DOCUMENT ID	TECN	CHG	COMMENT
<0.30	ALITTI 69	HBC	—	1 standard dev. limit

$$\frac{\Gamma(\Xi\pi)}{\Gamma(\Sigma\bar{K})} \quad \Gamma_3/\Gamma_2$$

VALUE	CL%	DOCUMENT ID	TECN	CHG	COMMENT
<0.19	95	HEMINGWAY 77	HBC	—	$K^- p$ 4.2 GeV/c

$$\frac{\Gamma(\Lambda\bar{K})}{[\Gamma(\Lambda\bar{K}) + \Gamma(\Sigma\bar{K}) + \Gamma(\Xi\pi) + \Gamma(\Xi(1530)\pi)]} \quad \Gamma_1/(\Gamma_1+\Gamma_2+\Gamma_3+\Gamma_4)$$

VALUE	DOCUMENT ID	TECN	CHG	COMMENT
0.25 ± 0.15	ALITTI 69	HBC	—	$K^- p$ 3.9–5 GeV/c

$$\frac{\Gamma(\Lambda\bar{K})}{\Gamma(\Sigma\bar{K})} \quad \Gamma_1/\Gamma_2$$

VALUE	DOCUMENT ID	TECN	CHG	COMMENT
0.22 ± 0.09	HEMINGWAY 77	HBC	—	$K^- p$ 4.2 GeV/c

$$\frac{\Gamma(\Sigma\bar{K})}{[\Gamma(\Lambda\bar{K}) + \Gamma(\Sigma\bar{K}) + \Gamma(\Xi\pi) + \Gamma(\Xi(1530)\pi)]} \quad \Gamma_2/(\Gamma_1+\Gamma_2+\Gamma_3+\Gamma_4)$$

VALUE	DOCUMENT ID	TECN	CHG	COMMENT
0.75 ± 0.20	ALITTI 69	HBC	—	$K^- p$ 3.9–5 GeV/c

$$\frac{\Gamma(\Xi(1530)\pi)}{[\Gamma(\Lambda\bar{K}) + \Gamma(\Sigma\bar{K}) + \Gamma(\Xi\pi) + \Gamma(\Xi(1530)\pi)]} \quad \Gamma_4/(\Gamma_1+\Gamma_2+\Gamma_3+\Gamma_4)$$

VALUE	DOCUMENT ID	TECN	CHG	COMMENT
<0.15	ALITTI 69	HBC	—	1 standard dev. limit

$$\frac{[\Gamma(\Xi(1530)\pi) + \Gamma(\Xi\pi(\text{not } \Xi(1530)\pi))]}{\Gamma(\Sigma\bar{K})} \quad (\Gamma_4+\Gamma_5)/\Gamma_2$$

VALUE	CL%	DOCUMENT ID	TECN	CHG	COMMENT
<0.11	95	1 HEMINGWAY 77	HBC	—	$K^- p$ 4.2 GeV/c

$$\frac{\Gamma(\Lambda\bar{K}\pi)}{\Gamma_{\text{total}}} \quad \Gamma_6/\Gamma$$

VALUE	DOCUMENT ID	TECN	COMMENT
seen	BARTSCH 69	HBC	$K^- p$ 10 GeV

$$\frac{\Gamma(\Lambda\bar{K}\pi)}{\Gamma(\Sigma\bar{K})} \quad \Gamma_6/\Gamma_2$$

VALUE	CL%	DOCUMENT ID	TECN	CHG	COMMENT
<0.32	95	HEMINGWAY 77	HBC	—	$K^- p$ 4.2 GeV/c

$$\frac{\Gamma(\Sigma\bar{K}\pi)}{\Gamma_{\text{total}}} \quad \Gamma_7/\Gamma$$

VALUE	DOCUMENT ID	TECN	COMMENT
seen	BARTSCH 69	HBC	$K^- p$ 10 GeV

$$\frac{\Gamma(\Sigma\bar{K}\pi)}{\Gamma(\Sigma\bar{K})} \quad \Gamma_7/\Gamma_2$$

VALUE	CL%	DOCUMENT ID	TECN	CHG	COMMENT
<0.04	95	2 HEMINGWAY 77	HBC	—	$K^- p$ 4.2 GeV/c

$\Xi(2030)$ FOOTNOTES

- For the decay mode $\Xi^- \pi^+ \pi^-$ only.
- For the decay mode $\Sigma^\pm K^- \pi^\mp$ only.

$\Xi(2030)$ REFERENCES

JENKINS 83	PRL 51 951	C.M. Jenkins et al.	(FSU, BRAN, LBL+)
HEMINGWAY 77	PL 68B 197	R.J. Hemingway et al.	(AMST, CERN, NIJM+)
Also	PL 62B 477	J.B. Gay et al.	(AMST, CERN, NIJM)
DIBIANCA 75	NP B98 137	F.A. Dibianca, R.J. Endorf	(CMU)
ROSS 73C	Purdue Conf. 345	R.T. Ross, J.L. Lloyd, D. Radojčić	(OXF)
ALITTI 69	PRL 22 79	J. Alitti et al.	(BNL, SYRA)
BARTSCH 69	PL 28B 439	J. Bartsch et al.	(AACH, BERL, CERN+)
ALITTI 68	PRL 21 1119	J. Alitti et al.	(BNL, SYRA)

$\Xi(2120)$

$$I(J^P) = \frac{1}{2}(?)^? \quad \text{Status: *}$$

J, P need confirmation.

OMITTED FROM SUMMARY TABLE

$\Xi(2120)$ MASS

VALUE (MeV)	EVTS	DOCUMENT ID	TECN	COMMENT
≈ 2120 OUR ESTIMATE				
2137 ± 4	18	1 CHLIAPNIK...	79	HBC $K^+ p$ 32 GeV/c
2123 ± 7		2 GAY	76c	HBC $K^- p$ 4.2 GeV/c

$\Xi(2120)$ WIDTH

VALUE (MeV)	EVTS	DOCUMENT ID	TECN	COMMENT
<20	18	1 CHLIAPNIK...	79	HBC $K^+ p$ 32 GeV/c
25 ± 12		2 GAY	76c	HBC $K^- p$ 4.2 GeV/c

$\Xi(2120)$ DECAY MODES

Mode	Fraction (Γ_i/Γ)
$\Gamma_1 \Lambda\bar{K}$	seen

$\Xi(2120)$ BRANCHING RATIOS

$\Gamma(\Lambda\bar{K})/\Gamma_{\text{total}}$	DOCUMENT ID	TECN	COMMENT	Γ_1/Γ
seen	1 CHLIAPNIK...	79	HBC	$K^+ p \rightarrow (\bar{K} K^+) X$
seen	2 GAY	76c	HBC	$K^- p$ 4.2 GeV/c

$\Xi(2120)$ FOOTNOTES

- CHLIAPNIKOV 79 does not uniquely identify the K^+ in the $(\bar{K} K^+) X$ final state. It also reports bumps with fewer events at 2240, 2540, and 2830 MeV.
- GAY 76c sees a 4-standard deviation signal. However, HEMINGWAY 77, with more events from the same experiment points out that the signal is greatly reduced if a cut is made on the 4-momentum u . This suggests an anomalous production mechanism if the $\Xi(2120)$ is real.

$\Xi(2120)$ REFERENCES

CHLIAPNIK... 79	NP B158 253	P.V. Chliapnikov et al.	(CERN, BELG, MONS)
HEMINGWAY 77	PL 68B 197	R.J. Hemingway et al.	(AMST, CERN, NIJM+)
GAY 76c	PL 62B 477	J.B. Gay et al.	(AMST, CERN, NIJM)

$\Xi(2250)$

$$I(J^P) = \frac{1}{2}(?)^? \quad \text{Status: **}$$

J, P need confirmation.

OMITTED FROM SUMMARY TABLE

The evidence for this state is mixed. BARTSCH 69 sees a bump of not much statistical significance in $\Lambda\bar{K}\pi$, $\Sigma\bar{K}\pi$, and $\Xi\pi\pi$ mass spectra. GOLDWASSER 70 sees a narrower bump in $\Xi\pi\pi$ at a higher mass. Not seen by HASSALL 81 with 45 events/ μb at 6.5 GeV/c. Seen by JENKINS 83. Perhaps seen by BIAGI 87.

$\Xi(2250)$ MASS

VALUE (MeV)	EVTS	DOCUMENT ID	TECN	CHG	COMMENT
≈ 2250 OUR ESTIMATE					
2189 ± 7	66	BIAGI 87	SPEC	—	$\Xi^- \text{Be} \rightarrow (\Xi^- \pi^+ \pi^-) X$
2214 ± 5		JENKINS 83	MPS	—	$K^- p \rightarrow K^+ MM$
2295 ± 15	18	GOLDWASSER 70	HBC	—	$K^- p$ 5.5 GeV/c
2244 ± 52	35	BARTSCH 69	HBC	—	$K^- p$ 10 GeV/c

$\Xi(2250)$ WIDTH

VALUE (MeV)	EVTS	DOCUMENT ID	TECN	CHG	COMMENT
46 ± 27	66	BIAGI 87	SPEC	—	$\Xi^- \text{Be} \rightarrow (\Xi^- \pi^+ \pi^-) X$
< 30		GOLDWASSER 70	HBC	—	$K^- p$ 5.5 GeV/c
130 ± 80		BARTSCH 69	HBC	—	

$\Xi(2250)$ DECAY MODES

Mode	Fraction (Γ_i/Γ)
$\Gamma_1 \Xi\pi\pi$	
$\Gamma_2 \Lambda\bar{K}\pi$	
$\Gamma_3 \Sigma\bar{K}\pi$	

$\Xi(2250)$ REFERENCES

BIAGI 87	ZPHY C34 15	S.F. Biagi et al.	(BRIS, CERN, GEVA+)
JENKINS 83	PRL 51 951	C.M. Jenkins et al.	(FSU, BRAN, LBL+)
HASSALL 81	NP B189 397	J.K. Hassall et al.	(CAVE, MSU)
GOLDWASSER 70	PR D1 1960	E.L. Goldwasser, P.F. Schultz	(ILL)
BARTSCH 69	PL 28B 439	J. Bartsch et al.	(AACH, BERL, CERN+)

Baryon Particle Listings

 $\Xi(2250)$, $\Xi(2370)$, $\Xi(2500)$ $\Xi(2370)$
 $I(J^P) = \frac{1}{2}(??)$ Status: **
 J, P need confirmation.

OMITTED FROM SUMMARY TABLE

 $\Xi(2370)$ MASS

VALUE (MeV)	EVTS	DOCUMENT ID	TECN	CHG	COMMENT
≈ 2370 OUR ESTIMATE					
2356 \pm 10		JENKINS 83	MPS	—	$K^- p \rightarrow K^+ MM$
2370	50	HASSALL 81	HBC	-0	$K^- p$ 6.5 GeV/c
2373 \pm 8	94	AMIRZADEH 80	HBC	-0	$K^- p$ 8.25 GeV/c
2392 \pm 27		DIBIANCA 75	DBC		$\Xi 2\pi$

 $\Xi(2370)$ WIDTH

VALUE (MeV)	EVTS	DOCUMENT ID	TECN	CHG	COMMENT
80	50	HASSALL 81	HBC	-0	$K^- p$ 6.5 GeV/c
80 \pm 25	94	AMIRZADEH 80	HBC	-0	$K^- p$ 8.25 GeV/c
75 \pm 69		DIBIANCA 75	DBC		$\Xi 2\pi$

 $\Xi(2370)$ DECAY MODES

Mode	Fraction (Γ_i/Γ)
Γ_1 $\Lambda \bar{K} \pi$ Includes $\Gamma_4 + \Gamma_6$.	seen
Γ_2 $\Sigma \bar{K} \pi$ Includes $\Gamma_5 + \Gamma_6$.	seen
Γ_3 $\Omega^- K$	
Γ_4 $\Lambda \bar{K}^*(892)$	
Γ_5 $\Sigma \bar{K}^*(892)$	
Γ_6 $\Sigma(1385) \bar{K}$	

 $\Xi(2370)$ BRANCHING RATIOS

$\Gamma(\Lambda \bar{K} \pi)/\Gamma_{\text{total}}$	Γ_1/Γ			
VALUE	DOCUMENT ID	TECN	CHG	COMMENT
seen	AMIRZADEH 80	HBC	-0	$K^- p$ 8.25 GeV/c

$\Gamma(\Sigma \bar{K} \pi)/\Gamma_{\text{total}}$	Γ_2/Γ			
VALUE	DOCUMENT ID	TECN	CHG	COMMENT
seen	AMIRZADEH 80	HBC	-0	$K^- p$ 8.25 GeV/c

$[\Gamma(\Lambda \bar{K} \pi) + \Gamma(\Sigma \bar{K} \pi)]/\Gamma_{\text{total}}$	$(\Gamma_1 + \Gamma_2)/\Gamma$				
VALUE	EVTS	DOCUMENT ID	TECN	CHG	COMMENT
seen	50	HASSALL 81	HBC	-0	$K^- p$ 6.5 GeV/c

$\Gamma(\Omega^- K)/\Gamma_{\text{total}}$	Γ_3/Γ			
VALUE	DOCUMENT ID	TECN	CHG	COMMENT
0.09 \pm 0.04	¹ KINSON 80	HBC	—	$K^- p$ 8.25 GeV/c

$[\Gamma(\Lambda \bar{K}^*(892)) + \Gamma(\Sigma \bar{K}^*(892))]/\Gamma_{\text{total}}$	$(\Gamma_4 + \Gamma_5)/\Gamma$			
VALUE	DOCUMENT ID	TECN	CHG	COMMENT
0.22 \pm 0.13	¹ KINSON 80	HBC	—	$K^- p$ 8.25 GeV/c

$\Gamma(\Sigma(1385) \bar{K})/\Gamma_{\text{total}}$	Γ_6/Γ			
VALUE	DOCUMENT ID	TECN	CHG	COMMENT
0.12 \pm 0.08	¹ KINSON 80	HBC	—	$K^- p$ 8.25 GeV/c

 $\Xi(2370)$ FOOTNOTES¹ KINSON 80 is a reanalysis of AMIRZADEH 80 with 50% more events. $\Xi(2370)$ REFERENCES

JENKINS 83	PRL 51 951	C.M. Jenkins et al.	(FSU, BRAN, LBL+)
HASSALL 81	NP B189 397	J.K. Hassall et al.	(CAVE, MSU)
AMIRZADEH 80	PL 90B 324	J. Amirzadeh et al.	(BIRM, CERN, GLAS+) ¹
KINSON 80	Toronto Conf. 263	J.B. Kinson et al.	(BIRM, CERN, GLAS+) ¹
DIBIANCA 75	NP B98 137	F.A. Dibianna, R.J. Endorf	(CMU)

 $\Xi(2500)$
 $I(J^P) = \frac{1}{2}(??)$ Status: *
 J, P need confirmation.

OMITTED FROM SUMMARY TABLE

The ALITTI 69 peak might be instead the $\Xi(2370)$ or might be neither the $\Xi(2370)$ nor the $\Xi(2500)$. $\Xi(2500)$ MASS

VALUE (MeV)	EVTS	DOCUMENT ID	TECN	CHG	COMMENT
≈ 2500 OUR ESTIMATE					
2505 \pm 10		JENKINS 83	MPS	—	$K^- p \rightarrow K^+ MM$
2430 \pm 20	30	ALITTI 69	HBC	—	$K^- p$ 4.6-5 GeV/c
2500 \pm 10	45	BARTSCH 69	HBC	-0	$K^- p$ 10 GeV/c

 $\Xi(2500)$ WIDTH

VALUE (MeV)	DOCUMENT ID	TECN	CHG
150 \pm 40	ALITTI 69	HBC	—
59 \pm 27	BARTSCH 69	HBC	-0

 $\Xi(2500)$ DECAY MODES

Mode	Fraction (Γ_i/Γ)
Γ_1 $\Xi \pi$	
Γ_2 $\Lambda \bar{K}$	
Γ_3 $\Sigma \bar{K}$	
Γ_4 $\Xi \pi \pi$	seen
Γ_5 $\Xi(1530) \pi$	
Γ_6 $\Lambda \bar{K} \pi + \Sigma \bar{K} \pi$	seen

 $\Xi(2500)$ BRANCHING RATIOS

$\Gamma(\Xi \pi)/[\Gamma(\Xi \pi) + \Gamma(\Lambda \bar{K}) + \Gamma(\Sigma \bar{K}) + \Gamma(\Xi(1530) \pi)]$	$\Gamma_1/(\Gamma_1 + \Gamma_2 + \Gamma_3 + \Gamma_5)$		
VALUE	DOCUMENT ID	TECN	COMMENT
<0.5	ALITTI 69	HBC	1 standard dev. limit

$\Gamma(\Lambda \bar{K})/[\Gamma(\Xi \pi) + \Gamma(\Lambda \bar{K}) + \Gamma(\Sigma \bar{K}) + \Gamma(\Xi(1530) \pi)]$	$\Gamma_2/(\Gamma_1 + \Gamma_2 + \Gamma_3 + \Gamma_5)$		
VALUE	DOCUMENT ID	TECN	CHG
0.5 \pm 0.2	ALITTI 69	HBC	—

$\Gamma(\Sigma \bar{K})/[\Gamma(\Xi \pi) + \Gamma(\Lambda \bar{K}) + \Gamma(\Sigma \bar{K}) + \Gamma(\Xi(1530) \pi)]$	$\Gamma_3/(\Gamma_1 + \Gamma_2 + \Gamma_3 + \Gamma_5)$		
VALUE	DOCUMENT ID	TECN	CHG
0.5 \pm 0.2	ALITTI 69	HBC	—

$\Gamma(\Xi(1530) \pi)/[\Gamma(\Xi \pi) + \Gamma(\Lambda \bar{K}) + \Gamma(\Sigma \bar{K}) + \Gamma(\Xi(1530) \pi)]$	$\Gamma_5/(\Gamma_1 + \Gamma_2 + \Gamma_3 + \Gamma_5)$		
VALUE	DOCUMENT ID	TECN	COMMENT
<0.2	ALITTI 69	HBC	1 standard dev. limit

$\Gamma(\Xi \pi \pi)/\Gamma_{\text{total}}$	Γ_4/Γ		
VALUE	DOCUMENT ID	TECN	CHG
seen	BARTSCH 69	HBC	-0

$[\Gamma(\Lambda \bar{K} \pi) + \Gamma(\Sigma \bar{K} \pi)]/\Gamma_{\text{total}}$	Γ_6/Γ		
VALUE	DOCUMENT ID	TECN	CHG
seen	BARTSCH 69	HBC	-0

 $\Xi(2500)$ REFERENCES

JENKINS 83	PRL 51 951	C.M. Jenkins et al.	(FSU, BRAN, LBL+)
ALITTI 69	PRL 22 79	J. Alitti et al.	(BNL, SYRA) ¹
BARTSCH 69	PL 28B 439	J. Bartsch et al.	(AACH, BERL, CERN+)

Ω^- BARYONS

($S = -3, I = 0$)

$\Omega^- = sss$



$I(J^P) = 0(\frac{3}{2}^+)$ Status: ***

The unambiguous discovery in both production and decay was by BARNES 64. The quantum numbers follow from the assignment of the particle to the baryon decuplet. DEUTSCHMANN 78 and BAUBILLIER 78 rule out $J = 1/2$ and find consistency with $J = 3/2$. AUBERT, BE 06 finds from the decay angular distributions of $\Xi_c^0 \rightarrow \Omega^- K^+$ and $\Omega_c^0 \rightarrow \Omega^- K^+$ that $J = 3/2$; this depends on the spins of the Ξ_c^0 and Ω_c^0 being $J = 1/2$, their supposed values.

We have omitted some results that have been superseded by later experiments. See our earlier editions.

Ω^- MASS

The fit assumes the Ω^- and Ω^+ masses are the same, and averages them together.

VALUE (MeV)	EVTS	DOCUMENT ID	TECN	COMMENT
1672.45 ± 0.29 OUR FIT				
1672.43 ± 0.32 OUR AVERAGE				
1673 ± 1	100	HARTOUNI 85	SPEC	80–280 GeV $K_L^0 C$
1673.0 ± 0.8	41	BAUBILLIER 78	HBC	8.25 GeV/c $K^- p$
1671.7 ± 0.6	27	HEMINGWAY 78	HBC	4.2 GeV/c $K^- p$
1673.4 ± 1.7	4	¹ DIBIANCA 75	DBC	4.9 GeV/c $K^- d$
1673.3 ± 1.0	3	PALMER 68	HBC	$K^- p$ 4.6, 5 GeV/c
1671.8 ± 0.8	3	SCHULTZ 68	HBC	$K^- p$ 5.5 GeV/c
1674.2 ± 1.6	5	SCOTTER 68	HBC	$K^- p$ 6 GeV/c
1672.1 ± 1.0	1	² FRY 55	EMUL	
• • • We do not use the following data for averages, fits, limits, etc. • • •				
1671.43 ± 0.78	13	³ DEUTSCH... 73	HBC	$K^- p$ 10 GeV/c
1671.9 ± 1.2	6	³ SPETH 69	HBC	See DEUTSCHMANN 73
1673.0 ± 8.0	1	ABRAMS 64	HBC	$\rightarrow \Xi^- \pi^0$
1670.6 ± 1.0	1	² FRY 55B	EMUL	
1615	1	⁴ EISENBERG 54	EMUL	

¹DIBIANCA 75 gives a mass for each event. We quote the average.
²The FRY 55 and FRY 55B events were identified as Ω^- by ALVAREZ 73. The masses assume decay to ΛK^- at rest. For FRY 55B, decay from an atomic orbit could Doppler shift the K^- energy and the resulting Ω^- mass by several MeV. This shift is negligible for FRY 55 because the Ω^- decay is approximately perpendicular to its orbital velocity, as is known because the Λ strikes the nucleus (L.Alvarez, private communication 1973). We have calculated the error assuming that the orbital n is 4 or larger.
³Excluded from the average; the Ω^- lifetimes measured by the experiments differ significantly from other measurements.
⁴The EISENBERG 54 mass was calculated for decay in flight. ALVAREZ 73 has shown that the Ω^- interacted with an Ag nucleus to give $K^- \Xi Ag$.

Ω^+ MASS

The fit assumes the Ω^- and Ω^+ masses are the same, and averages them together.

VALUE (MeV)	EVTS	DOCUMENT ID	TECN	COMMENT
1672.45 ± 0.29 OUR FIT				
1672.5 ± 0.7 OUR AVERAGE				
1672 ± 1	72	HARTOUNI 85	SPEC	80–280 GeV $K_L^0 C$
1673.1 ± 1.0	1	FIRESTONE 71B	HBC	12 GeV/c $K^+ d$

$$(m_{\Omega^-} - m_{\Omega^+}) / m_{\Omega^-}$$

A test of CPT invariance.

VALUE	DOCUMENT ID	TECN	COMMENT
(-1.44 ± 7.98) × 10⁻⁵	CHAN	98 E756	p Be, 800 GeV

Ω^- MEAN LIFE

Measurements with an error $> 0.1 \times 10^{-10}$ s have been omitted. The fit assumes the Ω^- and Ω^+ mean lives are the same, and averages them together.

VALUE (10 ⁻¹⁰ s)	EVTS	DOCUMENT ID	TECN	COMMENT
0.821 ± 0.011 OUR FIT				
0.821 ± 0.011 OUR AVERAGE				
0.817 ± 0.013 ± 0.018	6934	CHAN	98 E756	p Be, 800 GeV
0.811 ± 0.037	1096	LUK	88 SPEC	p Be 400 GeV
0.823 ± 0.013	12k	BOURQUIN 84	SPEC	SPS hyperon beam

• • • We do not use the following data for averages, fits, limits, etc. • • •
 0.822 ± 0.028 2437 BOURQUIN 79B SPEC See BOURQUIN 84

Ω^+ MEAN LIFE

The fit assumes the Ω^- and Ω^+ mean lives are the same, and averages them together.

VALUE (10 ⁻¹⁰ s)	EVTS	DOCUMENT ID	TECN	COMMENT
0.821 ± 0.011 OUR FIT				
0.823 ± 0.031 ± 0.022	1801	CHAN	98 E756	p Be, 800 GeV

$$(\tau_{\Omega^-} - \tau_{\Omega^+}) / \tau_{\Omega^-}$$

A test of CPT invariance. Our calculation, from the averages in the preceding two data blocks.

VALUE	DOCUMENT ID
0.00 ± 0.05 OUR ESTIMATE	

Ω^- MAGNETIC MOMENT

VALUE (μ_N)	EVTS	DOCUMENT ID	TECN	COMMENT
-2.02 ± 0.05 OUR AVERAGE				
-2.024 ± 0.056	235k	WALLACE 95	SPEC	Ω^- 300–550 GeV
-1.94 ± 0.17 ± 0.14	25k	DIEHL 91	SPEC	Spin-transfer production

Ω^- DECAY MODES

Mode	Fraction (Γ_i/Γ)	Confidence level
$\Gamma_1 \Lambda K^-$	(67.8 ± 0.7) %	
$\Gamma_2 \Xi^0 \pi^-$	(23.6 ± 0.7) %	
$\Gamma_3 \Xi^- \pi^0$	(8.6 ± 0.4) %	
$\Gamma_4 \Xi^- \pi^+ \pi^-$	(3.7 ^{+0.7} _{-0.6}) × 10 ⁻⁴	
$\Gamma_5 \Xi(1530)^0 \pi^-$	< 7 × 10 ⁻⁵	90%
$\Gamma_6 \Xi^0 e^- \bar{\nu}_e$	(5.6 ± 2.8) × 10 ⁻³	
$\Gamma_7 \Xi^- \gamma$	< 4.6 × 10 ⁻⁴	90%
$\Delta S = 2$ forbidden (S_2) modes		
$\Gamma_8 \Lambda \pi^-$	S_2 < 2.9 × 10 ⁻⁶	90%

Ω^- BRANCHING RATIOS

The BOURQUIN 84 values (which include results of BOURQUIN 79B, a separate experiment) are much more accurate than any other results, and so the other results have been omitted.

$\Gamma(\Lambda K^-)/\Gamma_{total}$	EVTS	DOCUMENT ID	TECN	COMMENT	Γ_1/Γ
0.678 ± 0.007	14k	BOURQUIN 84	SPEC	SPS hyperon beam	
• • • We do not use the following data for averages, fits, limits, etc. • • •					
0.686 ± 0.013	1920	BOURQUIN 79B	SPEC	See BOURQUIN 84	

$\Gamma(\Xi^0 \pi^-)/\Gamma_{total}$	EVTS	DOCUMENT ID	TECN	COMMENT	Γ_2/Γ
0.236 ± 0.007	1947	BOURQUIN 84	SPEC	SPS hyperon beam	
• • • We do not use the following data for averages, fits, limits, etc. • • •					
0.234 ± 0.013	317	BOURQUIN 79B	SPEC	See BOURQUIN 84	

$\Gamma(\Xi^- \pi^0)/\Gamma_{total}$	EVTS	DOCUMENT ID	TECN	COMMENT	Γ_3/Γ
0.086 ± 0.004	759	BOURQUIN 84	SPEC	SPS hyperon beam	
• • • We do not use the following data for averages, fits, limits, etc. • • •					
0.080 ± 0.008	145	BOURQUIN 79B	SPEC	See BOURQUIN 84	

$\Gamma(\Xi^- \pi^+ \pi^-)/\Gamma_{total}$	EVTS	DOCUMENT ID	TECN	COMMENT	Γ_4/Γ
3.74^{+0.67}_{-0.56}	100	⁵ KAMAEV 10	HYCP	p Cu, 800 GeV	
• • • We do not use the following data for averages, fits, limits, etc. • • •					
4.3 ^{+3.4} _{-1.3}	4	BOURQUIN 84	SPEC	SPS hyperon beam	

⁵This KAMAEV 10 value uses 76 $\Omega^- \rightarrow \Xi^- \pi^+ \pi^-$ and 24 $\Omega^+ \rightarrow \Xi^+ \pi^- \pi^+$ decays. The Ω^- and Ω^+ branching fractions measurements are statistically equal. The errors given combine statistical and systematic contributions. The CP branching-fraction asymmetry, $(\Omega^- - \Omega^+)/\text{sum}$, is $+0.12 \pm 0.20$.

Baryon Particle Listings

$\Omega^-, \Omega(2012)^-$

$\Gamma(\Xi(1530)^0 \pi^-) / \Gamma_{\text{total}}$ Γ_5 / Γ

VALUE (units 10^{-4})	CL%	EVTS	DOCUMENT ID	TECN	COMMENT
<0.7	90		KAMAEV	10	HYCP p Cu, 800 GeV

••• We do not use the following data for averages, fits, limits, etc. •••

6.4 ^{+5.1} _{-2.0}	4	6	BOURQUIN	84	SPEC SPS hyperon beam
-------------------------------------	---	---	----------	----	-----------------------

⁶The same 4 events as in the previous mode, with the isospin factor to take into account $\Xi(1530)^0 \rightarrow \Xi^0 \pi^0$ decays included. BOURQUIN 84 adopted a theoretical assumption that $\Xi(1530)^0 \pi^-$ would dominate $\Xi^- \pi^+ \pi^-$ decay.

$\Gamma(\Xi^0 e^- \bar{\nu}_e) / \Gamma_{\text{total}}$ Γ_6 / Γ

VALUE (units 10^{-3})	EVTS	DOCUMENT ID	TECN	COMMENT
5.6 ± 2.8	14	BOURQUIN	84	SPEC SPS hyperon beam

••• We do not use the following data for averages, fits, limits, etc. •••

~ 10	3	BOURQUIN	79B	SPEC See BOURQUIN 84
------	---	----------	-----	----------------------

$\Gamma(\Xi^- \gamma) / \Gamma_{\text{total}}$ Γ_7 / Γ

VALUE (units 10^{-4})	CL%	EVTS	DOCUMENT ID	TECN	COMMENT
< 4.6	90	0	ALBUQUERQ..94	E761	Ω^- 375 GeV

••• We do not use the following data for averages, fits, limits, etc. •••

<22	90	9	BOURQUIN	84	SPEC SPS hyperon beam
<31	90	0	BOURQUIN	79B	SPEC See BOURQUIN 84

$\Gamma(\Lambda \pi^-) / \Gamma_{\text{total}}$ Γ_8 / Γ

$\Delta S=2$. Forbidden in first-order weak interaction.

VALUE (units 10^{-6})	CL%	DOCUMENT ID	TECN	COMMENT
< 2.9	90	WHITE	05	HYCP p Cu, 800 GeV

••• We do not use the following data for averages, fits, limits, etc. •••

< 190	90	BOURQUIN	84	SPEC SPS hyperon beam
<1300	90	BOURQUIN	79B	SPEC See BOURQUIN 84

Ω^- DECAY PARAMETERS

$\alpha(\Omega^-) \alpha_-(A)$ FOR $\Omega^- \rightarrow \Lambda K^-$

Some early results have been omitted.

VALUE	EVTS	DOCUMENT ID	TECN	COMMENT
0.0115 ± 0.0015 OUR AVERAGE				

0.0133 ± 0.0033 ± 0.0052	960k	⁷ CHEN	05	HYCP p Cu, 800 GeV
0.0114 ± 0.0012 ± 0.0010	4.5M	⁷ LU	05A	HYCP p Cu, 800 GeV

••• We do not use the following data for averages, fits, limits, etc. •••

-0.018 ± 0.030	6953	CHAN	98	E756 p Be, 800 GeV
-0.022 ± 0.051	1743	LUK	88	SPEC p Be 400 GeV
-0.016 ± 0.018	12k	BOURQUIN	84	SPEC SPS hyperon beam

⁷The results of CHEN 05 and LU 05A are from different experimental runs.

α FOR $\Omega^- \rightarrow \Lambda K^-$

The above average, $\alpha(\Omega^-) \alpha_-(A) = 0.0115 \pm 0.0015$, divided by our current average

$\alpha_-(A) = 0.732 \pm 0.014$ gives $\alpha(\Omega^-)$:

VALUE	DOCUMENT ID
0.0157 ± 0.0021 OUR EVALUATION	

$\bar{\alpha}$ FOR $\bar{\Omega}^+ \rightarrow \bar{\Lambda} K^+$

VALUE	EVTS	DOCUMENT ID	TECN	COMMENT
-0.0181 ± 0.0028 ± 0.0026	1.89M	LU	06	HYCP p Cu, 800 GeV

••• We do not use the following data for averages, fits, limits, etc. •••

+0.017 ± 0.077	1823	CHAN	98	E756 p Be, 800 GeV
----------------	------	------	----	----------------------

$(\alpha + \bar{\alpha}) / (\alpha - \bar{\alpha})$ in $\Omega^- \rightarrow \Lambda K^-, \bar{\Omega}^+ \rightarrow \bar{\Lambda} K^+$

Zero if CP is conserved.

VALUE	DOCUMENT ID	TECN	COMMENT
-0.016 ± 0.092 ± 0.089	⁸ LU	06	HYCP p Cu, 800 GeV

⁸This value uses the results of CHEN 05, LU 05A, and LU 06.

α FOR $\Omega^- \rightarrow \Xi^0 \pi^-$

VALUE	EVTS	DOCUMENT ID	TECN	COMMENT
+0.09 ± 0.14	1630	BOURQUIN	84	SPEC SPS hyperon beam

α FOR $\Omega^- \rightarrow \Xi^- \pi^0$

VALUE	EVTS	DOCUMENT ID	TECN	COMMENT
+0.05 ± 0.21	614	BOURQUIN	84	SPEC SPS hyperon beam

Ω^- REFERENCES

We have omitted some papers that have been superseded by later experiments. See our earlier editions.

KAMAEV	10	PL B693 236	O. Kamaev et al.	(FNAL HyperCP Collab.)
AUBERT, BE	06	PRL 97 112001	B. Aubert et al.	(BABAR Collab.)
LU	06	PRL 96 242001	L.C. Lu et al.	(FNAL HyperCP Collab.)
CHEN	05	PR D71 051102	Y.C. Chen et al.	(FNAL HyperCP Collab.)
LU	05A	PL B617 11	L.C. Lu et al.	(FNAL HyperCP Collab.)
WHITE	05	PRL 94 101804	C.G. White et al.	(FNAL HyperCP Collab.)
CHAN	98	PR D58 072002	A.W. Chan et al.	(FNAL E756 Collab.)
WALLACE	95	PRL 74 3732	N.B. Wallace et al.	(MINN, ARIZ, MICH+)
ALBUQUERQ..	94	PR D50 18	I.F. Albuquerque et al.	(FNAL E761 Collab.)
DIEHL	91	PRL 67 804	H.T. Diehl et al.	(RUTG, FNAL, MICH+)
LUK	88	PR D38 19	K.B. Luk et al.	(RUTG, WIS C, MICH, MINN)
HARTOUNI	85	PRL 54 628	E.P. Hartouni et al.	(COLU, ILL, FNAL)

BOURQUIN	84	NP B241 1	M.H. Bourquin et al.	(BRIS, GEVA, HEIDP+)
Also		PL 87B 297	M.H. Bourquin et al.	(BRIS, GEVA, HEIDP+)
BOURQUIN	79B	PL 88B 192	M.H. Bourquin et al.	(BRIS, GEVA, HEIDP+)
BAUBILLIER	78	PL 78B 342	M. Baubillier et al.	(BIRM, CERN, GLAS+)
DEUTSCH...	78	PL 73B 96	M. Deuschmann et al.	(AACH3, BERL, NIJM+)
HEMINGWAY	78	NP B142 205	R.J. Hemingway et al.	(CERN, ZEEM, NIJM+)
DIBIAN CA	75	NP B98 137	F.A. Dibiãca, R.J. Endorf	(CMU)
ALVAREZ	73	PR D8 702	L.W. Alvarez	(LBL)
DEUTSCH...	73	NP B61 102	M. Deuschmann et al.	(ABCLV Collab.)
FIRESTONE	71B	PRL 26 410	I. Firestone et al.	(LRL)
SPETH	69	PL 29B 252	R. Speth et al.	(AACH, BERL, CERN, LOIC+)
PALMER	68	PL 26B 323	R.B. Palmer et al.	(BNL, SYRA)
SCHULTZ	68	PR 168 1509	P.F. Schultz et al.	(ILL, ANL, NWES+)
SCOTTER	68	PL 26B 474	D. Scotter et al.	(BIRM, GLAS, LOIC+)
ABRAMS	64	PRL 13 670	G.S. Abrams et al.	(UMD, NRL)
BARNES	64	PRL 12 204	V.E. Barnes et al.	(BNL)
FRY	55	PR 97 1189	W.F. Fry, J. Schneps, M.S. Swami	(WISC)
FRY	55B	NC 2 346	W.F. Fry, J. Schneps, M.S. Swami	(WISC)
EISENBERG	54	PR 96 541	Y. Eisenberg	(CORN)

$\Omega(2012)^-$

$I(J^P) = 0(?)^-$ Status: ***

Seen in $\Xi^0 K^-$ and $\Xi^- K_S^0$ decays with a combined significance of 8.3 standard deviations.

$\Omega(2012)^-$ MASS

VALUE (MeV)	EVTS	DOCUMENT ID	TECN	COMMENT
2012.4 ± 0.7 ± 0.6	520	YELTON	18A	BELL In $\Upsilon(1S), \Upsilon(2S), \Upsilon(3S)$

$\Omega(2012)^-$ WIDTH

VALUE (MeV)	EVTS	DOCUMENT ID	TECN	COMMENT
6.4^{+2.5}_{-2.0} ± 1.6	520	YELTON	18A	BELL In $\Upsilon(1S), \Upsilon(2S), \Upsilon(3S)$

$\Omega(2012)^-$ DECAY MODES

Mode	Fraction (Γ_i / Γ)	Confidence level
$\Gamma_1 \Xi^- K$		
$\Gamma_2 (\Xi^- \pi) K$		
$\Gamma_3 \Xi^0 K^-$	DEFINED AS 1	
$\Gamma_4 \Xi^- K^0$	0.83 ± 0.21	
$\Gamma_5 \Xi^- \bar{K}^0$		
$\Gamma_6 \Xi^0 \pi^0 K^-$	<0.30	90%
$\Gamma_7 \Xi^0 \pi^- \bar{K}^0$	<0.21	90%
$\Gamma_8 \Xi^- \pi^0 \bar{K}^0$		
$\Gamma_9 \Xi^- \pi^+ K^-$	<0.08	90%

$\Omega(2012)^-$ BRANCHING RATIOS

$\Gamma(\Xi^0 K^-) / \Gamma(\Xi^- K^0)$	Γ_3 / Γ_4
VALUE	DOCUMENT ID TECN COMMENT
1.2 ± 0.3	YELTON 18A BELL In $\Upsilon(1S, 2S, 3S)$

$\Gamma((\Xi^- \pi) K) / \Gamma(\Xi^- K)$	Γ_2 / Γ_1
VALUE	DOCUMENT ID TECN COMMENT
<0.119	JIA 19 BELL In $\Upsilon(1S, 2S, 3S)$

$\Gamma(\Xi^- \pi^+ K^-) / \Gamma(\Xi^- \bar{K}^0)$	Γ_9 / Γ_5
VALUE	DOCUMENT ID TECN COMMENT
<0.093	JIA 19 BELL In $\Upsilon(1S, 2S, 3S)$

$\Gamma(\Xi^- \pi^0 \bar{K}^0) / \Gamma(\Xi^- \bar{K}^0)$	Γ_8 / Γ_5
VALUE	DOCUMENT ID TECN COMMENT
<0.811	JIA 19 BELL In $\Upsilon(1S, 2S, 3S)$

$\Gamma(\Xi^0 \pi^- \bar{K}^0) / \Gamma(\Xi^0 K^-)$	Γ_7 / Γ_3
VALUE	DOCUMENT ID TECN COMMENT
<0.213	JIA 19 BELL In $\Upsilon(1S, 2S, 3S)$

$\Gamma(\Xi^0 \pi^0 K^-) / \Gamma(\Xi^0 K^-)$	Γ_6 / Γ_3
VALUE	DOCUMENT ID TECN COMMENT
<0.304	JIA 19 BELL In $\Upsilon(1S, 2S, 3S)$

$\Gamma(\Xi^- \pi^+ K^-) / \Gamma(\Xi^0 K^-)$	Γ_9 / Γ_3
VALUE	DOCUMENT ID TECN COMMENT
<0.078	JIA 19 BELL In $\Upsilon(1S, 2S, 3S)$

$\Gamma(\Xi^0 \pi^- \bar{K}^0) / \Gamma(\Xi^- \bar{K}^0)$	Γ_7 / Γ_5
VALUE	DOCUMENT ID TECN COMMENT
<0.256	JIA 19 BELL In $\Upsilon(1S, 2S, 3S)$

$\Omega(2012)^-$ REFERENCES

JIA	19	PR D100 032006	S. Jia et al.	(BELLE Collab.)
YELTON	18A	PRL 121 052003	J. Yelton et al.	(BELLE Collab.)

See key on page 999

Baryon Particle Listings
 $\Omega(2250)^-, \Omega(2380)^-, \Omega(2470)^-$

$\Omega(2250)^-$ $I(J^P) = 0(?^?)$ Status: ***

$\Omega(2250)^-$ MASS

VALUE (MeV)	EVTS	DOCUMENT ID	TECN	COMMENT
2252 ± 9 OUR AVERAGE				
2253 ± 13	44	ASTON	87B LASS	$K^- p$ 11 GeV/c
2251 ± 9 ± 8	78	BIAGI	86B SPEC	SPS Ξ^- beam

$\Omega(2250)^-$ WIDTH

VALUE (MeV)	EVTS	DOCUMENT ID	TECN	COMMENT
55 ± 18 OUR AVERAGE				
81 ± 38	44	ASTON	87B LASS	$K^- p$ 11 GeV/c
48 ± 20	78	BIAGI	86B SPEC	SPS Ξ^- beam

$\Omega(2250)^-$ DECAY MODES

Mode	Fraction (Γ_i/Γ)
$\Gamma_1 \Xi^- \pi^+ K^-$	seen
$\Gamma_2 \Xi(1530)^0 K^-$	seen

$\Omega(2250)^-$ BRANCHING RATIOS

$\Gamma(\Xi(1530)^0 K^-)/\Gamma(\Xi^- \pi^+ K^-)$	Γ_2/Γ_1
~ 1.0	
0.70 ± 0.20	

$\Omega(2250)^-$ REFERENCES

ASTON	87B	PL B194 579	D. Aston <i>et al.</i>	(SLAC, NAGO, CINC, INUS)
BIAGI	86B	ZPHY C31 33	S.F. Biagi <i>et al.</i>	(LOQM, GEVA, RAL+)

$\Omega(2380)^-$ Status: **

OMITTED FROM SUMMARY TABLE

$\Omega(2380)^-$ MASS

VALUE (MeV)	EVTS	DOCUMENT ID	TECN	COMMENT
≈ 2380 OUR ESTIMATE				
2384 ± 9 ± 8	45	BIAGI	86B SPEC	SPS Ξ^- beam

$\Omega(2380)^-$ WIDTH

VALUE (MeV)	EVTS	DOCUMENT ID	TECN	COMMENT
26 ± 23	45	BIAGI	86B SPEC	SPS Ξ^- beam

$\Omega(2380)^-$ DECAY MODES

Mode	Fraction (Γ_i/Γ)
$\Gamma_1 \Xi^- \pi^+ K^-$	
$\Gamma_2 \Xi(1530)^0 K^-$	seen
$\Gamma_3 \Xi^- \bar{K}^*(892)^0$	

$\Omega(2380)^-$ BRANCHING RATIOS

$\Gamma(\Xi(1530)^0 K^-)/\Gamma(\Xi^- \pi^+ K^-)$	Γ_2/Γ_1
< 0.44	

$\Gamma(\Xi^- \bar{K}^*(892)^0)/\Gamma(\Xi^- \pi^+ K^-)$	Γ_3/Γ_1
0.5 ± 0.3	

$\Omega(2380)^-$ REFERENCES

BIAGI	86B	ZPHY C31 33	S.F. Biagi <i>et al.</i>	(LOQM, GEVA, RAL+)
-------	-----	-------------	--------------------------	--------------------

$\Omega(2470)^-$ Status: **

OMITTED FROM SUMMARY TABLE

A peak in the $\Omega^- \pi^+ \pi^-$ mass spectrum with a signal significance claimed to be at least 5.5 standard deviations. There is no reason to seriously doubt the existence of this state, but unless the evidence is overwhelming we usually wait for confirmation from a second experiment before elevating peaks to the Summary Table.

$\Omega(2470)^-$ MASS

VALUE (MeV)	EVTS	DOCUMENT ID	TECN	COMMENT
2474 ± 12	59	ASTON	88G LASS	$K^- p$ 11 GeV/c

$\Omega(2470)^-$ WIDTH

VALUE (MeV)	EVTS	DOCUMENT ID	TECN	COMMENT
72 ± 33	59	ASTON	88G LASS	$K^- p$ 11 GeV/c

$\Omega(2470)^-$ DECAY MODES

Mode	Fraction (Γ_i/Γ)
$\Gamma_1 \Omega^- \pi^+ \pi^-$	

$\Omega(2470)^-$ REFERENCES

ASTON	88G	PL B215 799	D. Aston <i>et al.</i>	(SLAC, NAGO, CINC, INUS)
-------	-----	-------------	------------------------	--------------------------

Baryon Particle Listings

Charmed Baryons, Λ_c^+

CHARMED BARYONS ($C = +1$)

$$\Lambda_c^+ = udc, \Sigma_c^{++} = uuc, \Sigma_c^+ = udc, \Sigma_c^0 = ddc,$$

$$\Xi_c^+ = usc, \Xi_c^0 = dsc, \Omega_c^0 = ssc$$

See the related review(s):
Charmed Baryons



$$I(J^P) = 0(\frac{1}{2}^+) \text{ Status: } ****$$

The parity of the Λ_c^+ is defined to be positive (as are the parities of the proton, neutron, and Λ). The quark content is udc . Results of an analysis of $pK^-\pi^+$ decays (JEZABEK 92) are consistent with $J = 1/2$. Nobody doubts that the spin is indeed $1/2$.

We have omitted some results that have been superseded by later experiments. The omitted results may be found in earlier editions.

Λ_c^+ MASS

Our value in 2004, 2284.9 ± 0.6 MeV, was the average of the measurements now filed below as "not used." The BABAR measurement is so much better that we use it alone. Note that it is about 2.6 (old) standard deviations above the 2004 value.

The fit also includes $\Sigma_c^-\Lambda_c^+$ and $\Lambda_c^{*+}-\Lambda_c^+$ mass-difference measurements, but this doesn't affect the Λ_c^+ mass. The new (in 2006) Λ_c^+ mass simply pushes all those other masses higher.

VALUE (MeV)	EVTS	DOCUMENT ID	TECN	COMMENT
2286.46 ± 0.14	OUR FIT			
2286.46 ± 0.14	4891	¹ AUBERT,B	05s BABR	$\Lambda_c^0 K^+$ and $\Sigma^0 K_S^0 K^+$
• • • We do not use the following data for averages, fits, limits, etc. • • •				
2284.7 ± 0.6 ± 0.7	1134	AVERY	91 CLEO	Six modes
2281.7 ± 2.7 ± 2.6	29	ALVAREZ	90b NA14	$pK^-\pi^+$
2285.8 ± 0.6 ± 1.2	101	BARLAG	89 NA32	$pK^-\pi^+$
2284.7 ± 2.3 ± 0.5	5	AGUILAR...	88b LEBE	$pK^-\pi^+$
2283.1 ± 1.7 ± 2.0	628	ALBRECHT	88c ARG	$pK^-\pi^+, p\bar{K}^0, \Lambda 3\pi$
2286.2 ± 1.7 ± 0.7	97	ANJOS	88b E691	$pK^-\pi^+$
2281 ± 3	2	JONES	87 HBC	$pK^-\pi^+$
2283 ± 3	3	BOSETTI	82 HBC	$pK^-\pi^+$
2290 ± 3	1	CALICCHIO	80 HYBR	$pK^-\pi^+$

¹AUBERT,B 05s uses low-Q $\Lambda_c^0 K^+$ and $\Sigma^0 K_S^0 K^+$ decays to minimize systematic errors. The error above includes systematic as well as statistical errors. Many cross checks and adjustments to properties of the BABAR detector, as well as the large number of clean events, make this by far the best measurement of the Λ_c^+ mass.

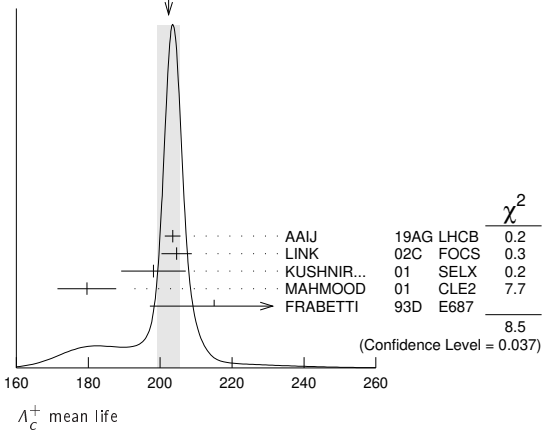
Λ_c^+ MEAN LIFE

Measurements with an error $\geq 100 \times 10^{-15}$ s or with fewer than 20 events have been omitted from the Listings.

VALUE (10^{-15} s)	EVTS	DOCUMENT ID	TECN	COMMENT
202.4 ± 3.1	OUR AVERAGE			Error includes scale factor of 1.7. See the ideogram below.
203.5 ± 1.7 ± 1.4	304k	¹ AAIJ	19AG LHCB	$\Lambda_c^+ \rightarrow pK^-\pi^+$
204.6 ± 3.4 ± 2.5	8034	LINK	02c FOCS	$\Lambda_c^+ \rightarrow pK^-\pi^+$
198.1 ± 7.0 ± 5.6	1630	KUSHNIR...	01 SELX	$\Lambda_c^+ \rightarrow pK^-\pi^+$
179.6 ± 6.9 ± 4.4	4749	MAHMOOD	01 CLE2	$e^+e^- \approx \tau(4S)$
215 ± 16 ± 8	1340	FRABETTI	93d E687	$\gamma\text{Be}, \Lambda_c^+ \rightarrow pK^-\pi^+$
• • • We do not use the following data for averages, fits, limits, etc. • • •				
180 ± 30 ± 30	29	ALVAREZ	90 NA14	$\gamma, \Lambda_c^+ \rightarrow pK^-\pi^+$
200 ± 30 ± 30	90	FRABETTI	90 E687	$\gamma\text{Be}, \Lambda_c^+ \rightarrow pK^-\pi^+$
196 ⁺²³ ₋₂₀	101	BARLAG	89 NA32	$pK^-\pi^+$ + c.c.
220 ± 30 ± 20	97	ANJOS	88b E691	$pK^-\pi^+$ + c.c.

¹AAIJ 19AG reports [Λ_c^+ MEAN LIFE] / [D^\pm MEAN LIFE] = $0.1956 \pm 0.0010 \pm 0.0013$ which we multiply by our best value D^\pm MEAN LIFE = $(1.040 \pm 0.007) \times 10^{-12}$ s. Our first error is their experiment's error and our second error is the systematic error from using our best value.

WEIGHTED AVERAGE
202.4±3.1 (Error scaled by 1.7)



Λ_c^+ DECAY MODES

Branching fractions marked with a footnote, e.g. [a], have been corrected for decay modes not observed in the experiments. For example, the sub-mode fraction $\Lambda_c^+ \rightarrow p\bar{K}^*(892)^0$ seen in $\Lambda_c^+ \rightarrow pK^-\pi^+$ has been multiplied up to include $\bar{K}^*(892)^0 \rightarrow \bar{K}^0\pi^0$ decays.

Mode	Fraction (Γ_i/Γ)	Scale factor/ Confidence level
Hadronic modes with a p or n: S = -1 final states		
Γ_1 pK_S^0	(1.59 ± 0.08) %	S=1.1
Γ_2 $pK^-\pi^+$	(6.28 ± 0.32) %	S=1.4
Γ_3 $p\bar{K}^*(892)^0$	[a] (1.96 ± 0.27) %	
Γ_4 $\Delta(1232)^{++}K^-$	(1.08 ± 0.25) %	
Γ_5 $\Lambda(1520)\pi^+$	[a] (2.2 ± 0.5) %	
Γ_6 $pK^-\pi^+$ nonresonant	(3.5 ± 0.4) %	
Γ_7 $pK_S^0\pi^0$	(1.97 ± 0.13) %	S=1.1
Γ_8 $nK_S^0\pi^+$	(1.82 ± 0.25) %	
Γ_9 $p\bar{K}^0\eta$	(1.6 ± 0.4) %	
Γ_{10} $pK_S^0\pi^+\pi^-$	(1.60 ± 0.12) %	S=1.1
Γ_{11} $pK^-\pi^+\pi^0$	(4.46 ± 0.30) %	S=1.5
Γ_{12} $pK^*(892)^-\pi^+$	[a] (1.4 ± 0.5) %	
Γ_{13} $p(K^-\pi^+)_{\text{nonresonant}}\pi^0$	(4.6 ± 0.8) %	
Γ_{14} $\Delta(1232)\bar{K}^*(892)$	seen	
Γ_{15} $pK^-\pi^+\pi^+$	(1.4 ± 0.9) × 10 ⁻³	
Γ_{16} $pK^-\pi^+2\pi^0$	(1.0 ± 0.5) %	
Hadronic modes with a p: S = 0 final states		
Γ_{17} $p\pi^0$	< 2.7 × 10 ⁻⁴	CL=90%
Γ_{18} $p\eta$	(1.24 ± 0.30) × 10 ⁻³	
Γ_{19} $p\omega(782)^0$	(9 ± 4) × 10 ⁻⁴	
Γ_{20} $p\pi^+\pi^-$	(4.61 ± 0.28) × 10 ⁻³	
Γ_{21} $p\eta(980)$	[a] (3.5 ± 2.3) × 10 ⁻³	
Γ_{22} $p2\pi^+2\pi^-$	(2.3 ± 1.4) × 10 ⁻³	
Γ_{23} pK^+K^-	(1.06 ± 0.06) × 10 ⁻³	
Γ_{24} $p\phi$	[a] (1.06 ± 0.14) × 10 ⁻³	
Γ_{25} $pK^+K^-\text{non-}\phi$	(5.3 ± 1.2) × 10 ⁻⁴	
Γ_{26} $p\phi\pi^0$	(10 ± 4) × 10 ⁻⁵	
Γ_{27} $pK^+K^-\pi^0$ nonresonant	< 6.3 × 10 ⁻⁵	CL=90%
Hadronic modes with a hyperon: S = -1 final states		
Γ_{28} $\Lambda\pi^+$	(1.30 ± 0.07) %	S=1.1
Γ_{29} $\Lambda\pi^+\pi^0$	(7.1 ± 0.4) %	S=1.1
Γ_{30} $\Lambda\rho^+$	< 6 %	CL=95%
Γ_{31} $\Lambda\pi^-2\pi^+$	(3.64 ± 0.29) %	S=1.4
Γ_{32} $\Sigma(1385)^+\pi^+\pi^-, \Sigma^{*+} \rightarrow \Lambda\pi^+$	(1.0 ± 0.5) %	
Γ_{33} $\Sigma(1385)^-2\pi^+, \Sigma^{*-} \rightarrow \Lambda\pi^-$	(7.6 ± 1.4) × 10 ⁻³	
Γ_{34} $\Lambda\pi^+\rho^0$	(1.5 ± 0.6) %	
Γ_{35} $\Sigma(1385)^+\rho^0, \Sigma^{*+} \rightarrow \Lambda\pi^+$	(5 ± 4) × 10 ⁻³	
Γ_{36} $\Lambda\pi^-2\pi^+$ nonresonant	< 1.1 %	CL=90%
Γ_{37} $\Lambda\pi^-\pi^02\pi^+$ total	(2.3 ± 0.8) %	
Γ_{38} $\Lambda\pi^+\eta$	[a] (1.84 ± 0.26) %	
Γ_{39} $\Sigma(1385)^+\eta$	[a] (9.1 ± 2.0) × 10 ⁻³	
Γ_{40} $\Lambda\pi^+\omega$	[a] (1.5 ± 0.5) %	

Γ_{41}	$\Lambda\pi^-\pi^0 2\pi^+$, no η or ω	$< 8 \times 10^{-3}$	CL=90%
Γ_{42}	$\Lambda K^+\bar{K}^0$	$(5.7 \pm 1.1) \times 10^{-3}$	S=1.9
Γ_{43}	$\Xi(1690)^0 K^+, \Xi^{*0} \rightarrow \Lambda\bar{K}^0$	$(1.6 \pm 0.5) \times 10^{-3}$	
Γ_{44}	$\Sigma^0\pi^+$	$(1.29 \pm 0.07)\%$	S=1.1
Γ_{45}	$\Sigma^+\pi^0$	$(1.25 \pm 0.10)\%$	
Γ_{46}	$\Sigma^+\eta$	$(4.4 \pm 2.0) \times 10^{-3}$	
Γ_{47}	$\Sigma^+\eta'$	$(1.5 \pm 0.6)\%$	
Γ_{48}	$\Sigma^+\pi^+\pi^-$	$(4.50 \pm 0.25)\%$	S=1.3
Γ_{49}	$\Sigma^+\rho^0$	$< 1.7\%$	CL=95%
Γ_{50}	$\Sigma^- 2\pi^+$	$(1.87 \pm 0.18)\%$	
Γ_{51}	$\Sigma^0\pi^+\pi^0$	$(3.5 \pm 0.4)\%$	
Γ_{52}	$\Sigma^+\pi^0\pi^0$	$(1.55 \pm 0.15)\%$	
Γ_{53}	$\Sigma^0\pi^- 2\pi^+$	$(1.11 \pm 0.30)\%$	
Γ_{54}	$\Sigma^+\pi^+\pi^-\pi^0$	—	
Γ_{55}	$\Sigma^+\omega$	[a] $(1.70 \pm 0.21)\%$	
Γ_{56}	$\Sigma^-\pi^0 2\pi^+$	$(2.1 \pm 0.4)\%$	
Γ_{57}	$\Sigma^+ K^+ K^-$	$(3.5 \pm 0.4) \times 10^{-3}$	S=1.1
Γ_{58}	$\Sigma^+\phi$	[a] $(3.9 \pm 0.6) \times 10^{-3}$	S=1.1
Γ_{59}	$\Xi(1690)^0 K^+, \Xi^{*0} \rightarrow \Sigma^+ K^-$	$(1.02 \pm 0.25) \times 10^{-3}$	
Γ_{60}	$\Sigma^+ K^+ K^-$ nonresonant	$< 8 \times 10^{-4}$	CL=90%
Γ_{61}	$\Xi^0 K^+$	$(5.5 \pm 0.7) \times 10^{-3}$	
Γ_{62}	$\Xi^- K^+ \pi^+$	$(6.2 \pm 0.6) \times 10^{-3}$	S=1.1
Γ_{63}	$\Xi(1530)^0 K^+$	$(4.3 \pm 0.9) \times 10^{-3}$	S=1.1

Hadronic modes with a hyperon: S = 0 final states

Γ_{64}	ΛK^+	$(6.1 \pm 1.2) \times 10^{-4}$	
Γ_{65}	$\Lambda K^+ \pi^+ \pi^-$	$< 5 \times 10^{-4}$	CL=90%
Γ_{66}	$\Sigma^0 K^+$	$(5.2 \pm 0.8) \times 10^{-4}$	
Γ_{67}	$\Sigma^0 K^+ \pi^+ \pi^-$	$< 2.6 \times 10^{-4}$	CL=90%
Γ_{68}	$\Sigma^+ K^+ \pi^-$	$(2.1 \pm 0.6) \times 10^{-3}$	
Γ_{69}	$\Sigma^+ K^*(892)^0$	[a] $(3.5 \pm 1.0) \times 10^{-3}$	
Γ_{70}	$\Sigma^- K^+ \pi^+$	$< 1.2 \times 10^{-3}$	CL=90%

Doubly Cabibbo-suppressed modes

Γ_{71}	$p K^+ \pi^-$	$(1.11 \pm 0.18) \times 10^{-4}$	
---------------	---------------	----------------------------------	--

Semileptonic modes

Γ_{72}	$\Lambda e^+ \nu_e$	$(3.6 \pm 0.4)\%$	
Γ_{73}	$\Lambda \mu^+ \nu_\mu$	$(3.5 \pm 0.5)\%$	

Inclusive modes

Γ_{74}	e^+ anything	$(3.95 \pm 0.35)\%$	
Γ_{75}	p anything	$(50 \pm 16)\%$	
Γ_{76}	n anything	$(50 \pm 16)\%$	
Γ_{77}	Λ anything	$(38.2 \pm 2.9)\%$	
Γ_{78}	3prongs	$(24 \pm 8)\%$	

$\Delta C = 1$ weak neutral current (CI) modes, or Lepton Family number (LF), or Lepton number (L), or Baryon number (B) violating modes

Γ_{79}	$p e^+ e^-$	CI	$< 5.5 \times 10^{-6}$	CL=90%
Γ_{80}	$p \mu^+ \mu^-$ non-resonant	CI	$< 7.7 \times 10^{-8}$	CL=90%
Γ_{81}	$p e^+ \mu^-$	LF	$< 9.9 \times 10^{-6}$	CL=90%
Γ_{82}	$p e^- \mu^+$	LF	$< 1.9 \times 10^{-5}$	CL=90%
Γ_{83}	$\bar{p} 2e^+$	L,B	$< 2.7 \times 10^{-6}$	CL=90%
Γ_{84}	$\bar{p} 2\mu^+$	L,B	$< 9.4 \times 10^{-6}$	CL=90%
Γ_{85}	$\bar{p} e^+ \mu^+$	L,B	$< 1.6 \times 10^{-5}$	CL=90%
Γ_{86}	$\Sigma^- \mu^+ \mu^+$	L	$< 7.0 \times 10^{-4}$	CL=90%

[a] This branching fraction includes all the decay modes of the final-state resonance.

CONSTRAINED FIT INFORMATION

An overall fit to 41 branching ratios uses 62 measurements and one constraint to determine 21 parameters. The overall fit has a $\chi^2 = 47.4$ for 42 degrees of freedom.

The following off-diagonal array elements are the correlation coefficients $\langle \delta x_i \delta x_j \rangle / (\delta x_i \delta x_j)$, in percent, from the fit to the branching fractions, $x_i \equiv \Gamma_i / \Gamma_{\text{total}}$. The fit constrains the x_i whose labels appear in this array to sum to one.

x_2	54									
x_7	46	55								
x_{10}	44	64	39							
x_{11}	51	61	40	60						
x_{28}	54	66	44	42	43					
x_{29}	45	61	41	38	36	65				
x_{31}	51	37	28	41	60	45	36			
x_{42}	16	22	14	14	14	26	19	12		
x_{44}	51	55	38	37	40	74	58	44	20	
x_{45}	38	39	30	25	29	34	33	23	10	29
x_{48}	51	88	50	60	61	59	55	39	20	50
x_{50}	5	9	5	6	6	6	6	3	2	5
x_{53}	13	14	9	12	15	13	11	20	4	12
x_{55}	19	30	18	23	26	19	18	18	6	16
x_{57}	23	41	23	28	28	27	25	18	9	23
x_{58}	19	32	19	22	23	22	20	14	7	18
x_{61}	8	15	8	10	9	10	9	6	3	8
x_{62}	29	39	25	25	25	51	35	24	14	38
x_{63}	6	11	6	7	7	7	7	4	2	6
x_1										
x_2										
x_7										
x_{10}										
x_{11}										
x_{28}										
x_{29}										
x_{31}										
x_{42}										
x_{44}										
x_{48}	36									
x_{50}	4	8								
x_{53}	7	14	1							
x_{55}	14	29	3	5						
x_{57}	17	45	4	6	13					
x_{58}	13	37	3	5	11	16				
x_{61}	6	13	1	2	5	6	5			
x_{62}	19	34	4	7	11	16	13	6		
x_{63}	4	10	1	2	3	4	4	2	4	
x_{45}										
x_{48}										
x_{50}										
x_{53}										
x_{55}										
x_{57}										
x_{58}										
x_{61}										
x_{62}										

Λ_c^+ BRANCHING RATIOS

A few really obsolete results have been omitted.

Hadronic modes with a p : S = -1 final states

$\Gamma(pK_S^0)/\Gamma_{\text{total}}$					Γ_1/Γ
VALUE (%)	EVTS	DOCUMENT ID	TECN	COMMENT	
1.59 ± 0.08 OUR FIT				Error includes scale factor of 1.1.	
1.52 ± 0.08 ± 0.03	1243	ABLIKIM	16 BES3	$e^+ e^- \rightarrow \Lambda_c \bar{\Lambda}_c$, 4.599 GeV	

$\Gamma(pK_S^0)/\Gamma(pK^-\pi^+)$					Γ_1/Γ_2
VALUE (%)	EVTS	DOCUMENT ID	TECN	COMMENT	
0.254 ± 0.012 OUR FIT				Error includes scale factor of 1.4.	
0.234 ± 0.020 OUR AVERAGE					

0.23 ± 0.01 ± 0.02	1025	ALAM	98 CLE2	$e^+ e^- \approx \Upsilon(4S)$	
0.22 ± 0.04 ± 0.03	133	AVERY	91 CLEO	$e^+ e^-$ 10.5 GeV	
0.28 ± 0.09 ± 0.07	45	ANJOS	90 E691	γ Be 70-260 GeV	
0.31 ± 0.08 ± 0.02	73	ALBRECHT	88c ARG	$e^+ e^-$ 10 GeV	

$\Gamma(pK^-\pi^+)/\Gamma_{\text{total}}$					Γ_2/Γ
VALUE (%)	EVTS	DOCUMENT ID	TECN	COMMENT	
6.28 ± 0.32 OUR FIT				Error includes scale factor of 1.4.	
6.3 ± 0.5 OUR AVERAGE				Error includes scale factor of 2.0.	

5.84 ± 0.27 ± 0.23	6.3k	ABLIKIM	16 BES3	$e^+ e^- \rightarrow \Lambda_c \bar{\Lambda}_c$, 4.599 GeV	
6.84 ± 0.24 ± 0.21 ± 0.27	1.4k	1 ZUPANC	14 BELL	$e^+ e^- \rightarrow D^{(*)} \bar{p} \pi^+$ recoil	
5.0 ± 1.3				See footnote	

••• We do not use the following data for averages, fits, limits, etc. •••
 1 This ZUPANC 14 value is the FIRST-EVER model-independent measurement of a Λ_c^+ branching fraction.
 2 See the note by P. Burchat, " Λ_c^+ Branching Fractions," in any edition of the Review from 2002 through 2014 for how this value was obtained. It is now obsolete.

$\Gamma(p\bar{K}^*(892)^0)/\Gamma(pK^-\pi^+)$					Γ_3/Γ_2
VALUE (%)	EVTS	DOCUMENT ID	TECN	COMMENT	
0.31 ± 0.04 OUR AVERAGE					

0.29 ± 0.04 ± 0.03		1 AITALA	00 E791	$\pi^- N$, 500 GeV	
0.35 ± 0.06 ± 0.03	39	BOZEK	93 NA32	π^- Cu 230 GeV	
0.42 ± 0.24	12	BASILE	81b CNTR	$pp \rightarrow \Lambda_c^+ e^- X$	
0.35 ± 0.11		BARLAG	90d NA32	See BOZEK 93	

••• We do not use the following data for averages, fits, limits, etc. •••
 1 AITALA 00 makes a coherent 5-dimensional amplitude analysis of $946 \pm 38 \Lambda_c^+ \rightarrow p K^- \pi^+$ decays.

Baryon Particle Listings

 Λ_C^+ $\Gamma(\Delta(1232)^{++}K^-)/\Gamma(\rho K^- \pi^+)$ Γ_4/Γ_2

VALUE	EVTS	DOCUMENT ID	TECN	COMMENT
0.17±0.04 OUR AVERAGE				Error includes scale factor of 1.1.
0.18±0.03±0.03		¹ AITALA 00	E791	$\pi^- N$, 500 GeV
0.12± $\frac{0.04}{0.05}$ ±0.05	14	BOZEK 93	NA32	π^- Cu 230 GeV
0.40±0.17	17	BASILE 81B	CNTR	$p p \rightarrow \Lambda_C^+ e^- X$

¹AITALA 00 makes a coherent 5-dimensional amplitude analysis of $946 \pm 38 \Lambda_C^+ \rightarrow p K^- \pi^+$ decays.

 $\Gamma(\Lambda(1520)\pi^+)/\Gamma(\rho K^- \pi^+)$ Γ_5/Γ_2

Unseen decay modes of the $\Lambda(1520)$ are included.

VALUE	EVTS	DOCUMENT ID	TECN	COMMENT
0.35±0.08 OUR AVERAGE				
0.34±0.08±0.05		¹ AITALA 00	E791	$\pi^- N$, 500 GeV
0.40± $\frac{0.18}{0.13}$ ±0.09	12	BOZEK 93	NA32	π^- Cu 230 GeV

¹AITALA 00 makes a coherent 5-dimensional amplitude analysis of $946 \pm 38 \Lambda_C^+ \rightarrow p K^- \pi^+$ decays.

 $\Gamma(\rho K^- \pi^+ \text{ nonresonant})/\Gamma(\rho K^- \pi^+)$ Γ_6/Γ_2

VALUE	EVTS	DOCUMENT ID	TECN	COMMENT
0.55±0.06 OUR AVERAGE				
0.55±0.06±0.04		¹ AITALA 00	E791	$\pi^- N$, 500 GeV
0.56± $\frac{0.07}{0.09}$ ±0.05	71	BOZEK 93	NA32	π^- Cu 230 GeV

¹AITALA 00 makes a coherent 5-dimensional amplitude analysis of $946 \pm 38 \Lambda_C^+ \rightarrow p K^- \pi^+$ decays.

 $\Gamma(\rho K_S^0 \pi^0)/\Gamma_{\text{total}}$ Γ_7/Γ

VALUE (%)	EVTS	DOCUMENT ID	TECN	COMMENT
1.97±0.13 OUR FIT				Error includes scale factor of 1.1.
1.87±0.13±0.05	558	ABLIKIM 16	BES3	$e^+ e^- \rightarrow \Lambda_C \bar{\Lambda}_C$, 4.599 GeV

 $\Gamma(\rho K_S^0 \pi^0)/\Gamma(\rho K^- \pi^+)$ Γ_7/Γ_2

Measurements given as a \bar{K}^0 ratio have been divided by 2 to convert to a K_S^0 ratio.

VALUE	EVTS	DOCUMENT ID	TECN	COMMENT
0.314±0.018 OUR FIT				
0.33 ±0.03 ±0.04	774	ALAM 98	CLE2	$e^+ e^- \approx \Upsilon(4S)$

 $\Gamma(n K_S^0 \pi^+)/\Gamma_{\text{total}}$ Γ_8/Γ

VALUE (%)	EVTS	DOCUMENT ID	TECN	COMMENT
1.82±0.23±0.11	83	ABLIKIM 17H	BES3	$e^+ e^-$ at 4.6 GeV

 $\Gamma(\rho \bar{K}^0 \eta)/\Gamma(\rho K^- \pi^+)$ Γ_9/Γ_2

Unseen decay modes of the η are included.

VALUE	EVTS	DOCUMENT ID	TECN	COMMENT
0.25±0.04±0.04	57	AMMAR 95	CLE2	$e^+ e^- \approx \Upsilon(4S)$

 $\Gamma(\rho K_S^0 \pi^+ \pi^-)/\Gamma_{\text{total}}$ Γ_{10}/Γ

VALUE (%)	EVTS	DOCUMENT ID	TECN	COMMENT
1.60±0.12 OUR FIT				Error includes scale factor of 1.1.
1.53±0.11±0.09	485	ABLIKIM 16	BES3	$e^+ e^- \rightarrow \Lambda_C \bar{\Lambda}_C$, 4.599 GeV

 $\Gamma(\rho K_S^0 \pi^+ \pi^-)/\Gamma(\rho K^- \pi^+)$ Γ_{10}/Γ_2

Measurements given as a \bar{K}^0 ratio have been divided by 2 to convert to a K_S^0 ratio.

VALUE	EVTS	DOCUMENT ID	TECN	COMMENT
0.255±0.015 OUR FIT				Error includes scale factor of 1.1.
0.257±0.031 OUR AVERAGE				
0.26 ±0.02 ±0.03	985	ALAM 98	CLE2	$e^+ e^- \approx \Upsilon(4S)$
0.22 ±0.06 ±0.02	83	AVERY 91	CLEO	$e^+ e^-$ 10.5 GeV
0.49 ±0.18 ±0.04	12	BARLAG 90D	NA32	π^- 230 GeV

 $\Gamma(\rho K^- \pi^+ \pi^0)/\Gamma_{\text{total}}$ Γ_{11}/Γ

VALUE (%)	EVTS	DOCUMENT ID	TECN	COMMENT
4.46±0.30 OUR FIT				Error includes scale factor of 1.5.
4.53±0.23±0.30	1849	ABLIKIM 16	BES3	$e^+ e^- \rightarrow \Lambda_C \bar{\Lambda}_C$, 4.599 GeV

 $\Gamma(\rho K^- \pi^+ \pi^0)/\Gamma(\rho K^- \pi^+)$ Γ_{11}/Γ_2

VALUE	EVTS	DOCUMENT ID	TECN	COMMENT
0.71 ±0.04 OUR FIT				Error includes scale factor of 2.4.
0.685±0.019 OUR AVERAGE				
0.685±0.007±0.018	242k	PAL 17	BELL	$e^+ e^- \approx \Upsilon(4S), \Upsilon(5S)$
0.67 ±0.04 ±0.11	2.6k	ALAM 98	CLE2	$e^+ e^- \approx \Upsilon(4S)$

 $\Gamma(\rho K^*(892)^- \pi^+)/\Gamma(\rho K_S^0 \pi^+ \pi^-)$ Γ_{12}/Γ_{10}

Unseen decay modes of the $K^*(892)^-$ are included.

VALUE	EVTS	DOCUMENT ID	TECN	COMMENT
0.88±0.28	17	ALEEV 94	BIS2	$n N$ 20–70 GeV

 $\Gamma(\rho(K^- \pi^+)_{\text{nonresonant}} \pi^0)/\Gamma(\rho K^- \pi^+)$ Γ_{13}/Γ_2

VALUE	EVTS	DOCUMENT ID	TECN	COMMENT
0.73±0.12±0.05	67	BOZEK 93	NA32	π^- Cu 230 GeV

 $\Gamma(\Delta(1232)\bar{K}^*(892))/\Gamma_{\text{total}}$ Γ_{14}/Γ

VALUE	EVTS	DOCUMENT ID	TECN	COMMENT
seen	35	AMENDOLIA 87	SPEC	γ Ge-Si

 $\Gamma(\rho K^- 2\pi^+ \pi^-)/\Gamma(\rho K^- \pi^+)$ Γ_{15}/Γ_2

VALUE	DOCUMENT ID	TECN	COMMENT
0.022±0.015	BARLAG 90D	NA32	π^- 230 GeV

 $\Gamma(\rho K^- \pi^+ 2\pi^0)/\Gamma(\rho K^- \pi^+)$ Γ_{16}/Γ_2

VALUE	EVTS	DOCUMENT ID	TECN	COMMENT
0.16±0.07±0.03	15	BOZEK 93	NA32	π^- Cu 230 GeV

Hadronic modes with a ρ : $S = 0$ final states $\Gamma(\rho \pi^0)/\Gamma_{\text{total}}$ Γ_{17}/Γ

VALUE	CL%	DOCUMENT ID	TECN	COMMENT
<2.7 × 10⁻⁴	90	ABLIKIM 17Q	BES3	$e^+ e^-$ at 4.6 GeV

 $\Gamma(\rho \eta)/\Gamma_{\text{total}}$ Γ_{18}/Γ

Unseen decay modes of the η are included.

VALUE (units 10 ⁻³)	EVTS	DOCUMENT ID	TECN	COMMENT
1.24±0.28±0.10	52	ABLIKIM 17Q	BES3	$\eta \rightarrow 2\gamma, \pi^+ \pi^0 \pi^-$

 $\Gamma(\rho \omega(782)^0)/\Gamma_{\text{total}}$ Γ_{19}/Γ

VALUE (units 10 ⁻⁴)	EVTS	DOCUMENT ID	TECN	COMMENT
9.4±3.2±2.2	13	AAIJ 18N	LHCB	Seen in $\Lambda_C^+ \rightarrow p \mu^+ \mu^-$

 $\Gamma(\rho \pi^+ \pi^-)/\Gamma(\rho K^- \pi^+)$ Γ_{20}/Γ_2

VALUE (units 10 ⁻²)	EVTS	DOCUMENT ID	TECN	COMMENT
7.35±0.24 OUR AVERAGE				Error includes scale factor of 1.3.
7.44±0.08±0.18	20k	AAIJ 18v	LHCB	$\Lambda_b^0 \rightarrow \Lambda_C^+ \mu^- X$
6.70±0.48±0.25	495	ABLIKIM 16U	BES3	$e^+ e^-$ at 4.599 GeV
6.9 ±3.6	5	BARLAG 90D	NA32	π^- 230 GeV

 $\Gamma(\rho f_0(980))/\Gamma(\rho K^- \pi^+)$ Γ_{21}/Γ_2

Unseen decay modes of the $f_0(980)$ are included.

VALUE	DOCUMENT ID	TECN	COMMENT
0.055±0.036	BARLAG 90D	NA32	π^- 230 GeV

 $\Gamma(\rho 2\pi^+ 2\pi^-)/\Gamma(\rho K^- \pi^+)$ Γ_{22}/Γ_2

VALUE	DOCUMENT ID	TECN	COMMENT
0.036±0.023	BARLAG 90D	NA32	π^- 230 GeV

 $\Gamma(\rho K^+ K^-)/\Gamma(\rho K^- \pi^+)$ Γ_{23}/Γ_2

VALUE (units 10 ⁻²)	EVTS	DOCUMENT ID	TECN	COMMENT
1.70±0.04 OUR AVERAGE				
1.70±0.03±0.03	3.4k	AAIJ 18v	LHCB	$\Lambda_b^0 \rightarrow \Lambda_C^+ \mu^- X$
1.4 ±0.2 ±0.2	676	ABE 02c	BELL	$e^+ e^- \approx \Upsilon(4S)$
3.9 ±0.9 ±0.7	214	ALEXANDER 96c	CLE2	$e^+ e^- \approx \Upsilon(4S)$
• • • We do not use the following data for averages, fits, limits, etc. • • •				
9.6 ±2.9 ±1.0	30	FRABETTI 93H	E687	γ Be, \bar{E}_γ 220 GeV
4.8 ±2.7		BARLAG 90D	NA32	π^- 230 GeV

 $\Gamma(\rho \phi)/\Gamma(\rho K^- \pi^+)$ Γ_{24}/Γ_2

Unseen decay modes of the ϕ are included.

VALUE (units 10 ⁻²)	EVTS	DOCUMENT ID	TECN	COMMENT
1.70±0.21 OUR AVERAGE				
1.81±0.33±0.13	44	ABLIKIM 16U	BES3	$e^+ e^-$ at 4.599 GeV
1.5 ±0.2 ±0.2	345	ABE 02c	BELL	$e^+ e^- \approx \Upsilon(4S)$
2.4 ±0.6 ±0.3	54	ALEXANDER 96c	CLE2	$e^+ e^- \approx \Upsilon(4S)$
• • • We do not use the following data for averages, fits, limits, etc. • • •				
4.0 ±2.7		BARLAG 90D	NA32	π^- 230 GeV

 $\Gamma(\rho K^+ K^- \text{ non-}\phi)/\Gamma(\rho K^- \pi^+)$ Γ_{25}/Γ_2

VALUE (units 10 ⁻³)	EVTS	DOCUMENT ID	TECN	COMMENT
8.4 ±1.8 OUR AVERAGE				
9.36±2.22±0.71	38	ABLIKIM 16U	BES3	$e^+ e^-$ at 4.599 GeV
7 ±2 ±2	344	ABE 02c	BELL	$e^+ e^- \approx \Upsilon(4S)$

 $\Gamma(\rho \phi \pi^0)/\Gamma(\rho K^- \pi^+)$ Γ_{26}/Γ_2

VALUE (units 10 ⁻³)	DOCUMENT ID	TECN	COMMENT
1.538±0.641$\pm$$\frac{0.077}{0.100}$	PAL 17	BELL	$e^+ e^- \approx \Upsilon(4S), \Upsilon(5S)$

 $\Gamma(\rho K^+ K^- \pi^0 \text{ nonresonant})/\Gamma_{\text{total}}$ Γ_{27}/Γ

VALUE	CL%	DOCUMENT ID	TECN	COMMENT
<6.3 × 10⁻⁵	90	PAL 17	BELL	$e^+ e^- \approx \Upsilon(4S), \Upsilon(5S)$

Hadronic modes with a hyperon: $S = -1$ final states $\Gamma(\Lambda \pi^+)/\Gamma_{\text{total}}$ Γ_{28}/Γ

VALUE (%)	EVTS	DOCUMENT ID	TECN	COMMENT
1.30±0.07 OUR FIT				Error includes scale factor of 1.1.
1.24±0.07±0.03	706	ABLIKIM 16	BES3	$e^+ e^- \rightarrow \Lambda_C \bar{\Lambda}_C$, 4.599 GeV

$\Gamma(\Lambda\pi^+)/\Gamma(\rho K^-\pi^+)$ Γ_{28}/Γ_2

VALUE	EVTS	DOCUMENT ID	TECN	COMMENT
0.207±0.009 OUR FIT				Error includes scale factor of 1.2.
0.204±0.019 OUR AVERAGE				
0.217±0.013±0.020	750	LINK	05F	FOCS γ nucleus, $\bar{E}_\gamma \approx 180$ GeV
0.18 ±0.03 ±0.04		ALBRECHT	92	ARG $e^+e^- \approx 10.4$ GeV
0.18 ±0.03 ±0.03	87	VERY	91	CLEO $e^+e^- 10.5$ GeV

$\Gamma(\Lambda\pi^+\pi^0)/\Gamma_{total}$ Γ_{29}/Γ

VALUE (%)	EVTS	DOCUMENT ID	TECN	COMMENT
7.1 ±0.4 OUR FIT				Error includes scale factor of 1.1.
7.01±0.37±0.19	1497	ABLIKIM	16	BES3 $e^+e^- \rightarrow \Lambda_c\bar{\Lambda}_c$, 4.599 GeV

$\Gamma(\Lambda\pi^+\pi^0)/\Gamma(\rho K^-\pi^+)$ Γ_{29}/Γ_2

VALUE	EVTS	DOCUMENT ID	TECN	COMMENT
1.12±0.05 OUR FIT				Error includes scale factor of 1.1.
0.73±0.09±0.16	464	VERY	94	CLE2 $e^+e^- \approx \Upsilon(3S), \Upsilon(4S)$

$\Gamma(\Lambda\rho^+)/\Gamma(\rho K^-\pi^+)$ Γ_{30}/Γ_2

VALUE	CL%	DOCUMENT ID	TECN	COMMENT
<0.95	95	VERY	94	CLE2 $e^+e^- \approx \Upsilon(3S), \Upsilon(4S)$

$\Gamma(\Lambda\pi^-2\pi^+)/\Gamma_{total}$ Γ_{31}/Γ

VALUE (%)	EVTS	DOCUMENT ID	TECN	COMMENT
3.64±0.29 OUR FIT				Error includes scale factor of 1.4.
3.81±0.24±0.18	609	ABLIKIM	16	BES3 $e^+e^- \rightarrow \Lambda_c\bar{\Lambda}_c$, 4.599 GeV

$\Gamma(\Lambda\pi^-2\pi^+)/\Gamma(\rho K^-\pi^+)$ Γ_{31}/Γ_2

VALUE	EVTS	DOCUMENT ID	TECN	COMMENT
0.58 ±0.04 OUR FIT				Error includes scale factor of 1.9.
0.522±0.032 OUR AVERAGE				
0.508±0.024±0.024	1356	LINK	05F	FOCS γ nucleus, $\bar{E}_\gamma \approx 180$ GeV
0.65 ±0.11 ±0.12	289	VERY	91	CLEO $e^+e^- 10.5$ GeV
0.82 ±0.29 ±0.27	44	ANJOS	90	E691 γ Be 70-260 GeV
0.94 ±0.41 ±0.13	10	BARLAG	90d	NA32 $\pi^- 230$ GeV
0.61 ±0.16 ±0.04	105	ALBRECHT	88c	ARG $e^+e^- 10$ GeV

$\Gamma(\Sigma(1385)^+\pi^+\pi^-, \Sigma^{*+} \rightarrow \Lambda\pi^+)/\Gamma(\Lambda\pi^-2\pi^+)$ Γ_{32}/Γ_{31}

VALUE	DOCUMENT ID	TECN	COMMENT
0.28±0.10±0.08	LINK	05F	FOCS γ nucleus, $\bar{E}_\gamma \approx 180$ GeV

$\Gamma(\Sigma(1385)^-2\pi^+, \Sigma^{*-} \rightarrow \Lambda\pi^-)/\Gamma(\Lambda\pi^-2\pi^+)$ Γ_{33}/Γ_{31}

VALUE	DOCUMENT ID	TECN	COMMENT
0.21±0.03±0.02	LINK	05F	FOCS γ nucleus, $\bar{E}_\gamma \approx 180$ GeV

$\Gamma(\Lambda\pi^+\rho^0)/\Gamma(\Lambda\pi^-2\pi^+)$ Γ_{34}/Γ_{31}

VALUE	DOCUMENT ID	TECN	COMMENT
0.40±0.12±0.12	LINK	05F	FOCS γ nucleus, $\bar{E}_\gamma \approx 180$ GeV

$\Gamma(\Sigma(1385)^+\rho^0, \Sigma^{*+} \rightarrow \Lambda\pi^+)/\Gamma(\Lambda\pi^-2\pi^+)$ Γ_{35}/Γ_{31}

VALUE	DOCUMENT ID	TECN	COMMENT
0.14±0.09±0.07	LINK	05F	FOCS γ nucleus, $\bar{E}_\gamma \approx 180$ GeV

$\Gamma(\Lambda\pi^-2\pi^+ \text{ nonresonant})/\Gamma(\Lambda\pi^-2\pi^+)$ Γ_{36}/Γ_{31}

VALUE	CL%	DOCUMENT ID	TECN	COMMENT
<0.3	90	LINK	05F	FOCS γ nucleus, $\bar{E}_\gamma \approx 180$ GeV

$\Gamma(\Lambda\pi^- \pi^0 2\pi^+ \text{ total})/\Gamma(\rho K^-\pi^+)$ Γ_{37}/Γ_2

VALUE	EVTS	DOCUMENT ID	TECN	COMMENT
0.36±0.09±0.09	50	¹ CRONIN-HEN..03	CLE3	$e^+e^- \approx \Upsilon(4S)$

¹ CRONIN-HENNESSY 03 finds this channel to be dominantly $\Lambda\eta\pi^+$ and $\Lambda\omega\pi^+$; see below.

$\Gamma(\Lambda\pi^+\eta)/\Gamma_{total}$ Γ_{38}/Γ

VALUE (units 10^{-2})	EVTS	DOCUMENT ID	TECN	COMMENT
1.84±0.21±0.15	154	ABLIKIM	19Y	BES3 e^+e^- at 4.6 GeV

$\Gamma(\Lambda\pi^+\eta)/\Gamma(\rho K^-\pi^+)$ Γ_{38}/Γ_2

VALUE	EVTS	DOCUMENT ID	TECN	COMMENT
0.36±0.07 OUR AVERAGE				
0.41±0.17±0.10	11	CRONIN-HEN..03	CLE3	$e^+e^- \approx \Upsilon(4S)$
0.35±0.05±0.06	116	AMMAR	95	CLE2 $e^+e^- \approx \Upsilon(4S)$

$\Gamma(\Sigma(1385)^+\eta)/\Gamma_{total}$ Γ_{39}/Γ

VALUE (units 10^{-2})	EVTS	DOCUMENT ID	TECN	COMMENT
0.91±0.18±0.09	54	ABLIKIM	19Y	BES3 e^+e^- at 4.6 GeV

$\Gamma(\Sigma(1385)^+\eta)/\Gamma(\rho K^-\pi^+)$ Γ_{39}/Γ_2

VALUE	EVTS	DOCUMENT ID	TECN	COMMENT
0.17±0.04±0.03	54	AMMAR	95	CLE2 $e^+e^- \approx \Upsilon(4S)$

$\Gamma(\Lambda\pi^+\omega)/\Gamma(\rho K^-\pi^+)$ Γ_{40}/Γ_2

VALUE	EVTS	DOCUMENT ID	TECN	COMMENT
0.24±0.06±0.06	32	CRONIN-HEN..03	CLE3	$e^+e^- \approx \Upsilon(4S)$

$\Gamma(\Lambda\pi^- \pi^0 2\pi^+, \text{ no } \eta \text{ or } \omega)/\Gamma(\rho K^-\pi^+)$ Γ_{41}/Γ_2

VALUE	CL%	DOCUMENT ID	TECN	COMMENT
<0.13	90	CRONIN-HEN..03	CLE3	$e^+e^- \approx \Upsilon(4S)$

$\Gamma(\Lambda K^+\bar{K}^0)/\Gamma(\rho K^-\pi^+)$ Γ_{42}/Γ_2

VALUE	EVTS	DOCUMENT ID	TECN	COMMENT
0.090±0.017 OUR FIT				Error includes scale factor of 1.9.
0.131±0.020 OUR AVERAGE				
0.142±0.018±0.022	251	LINK	05F	FOCS γ nucleus, $\bar{E}_\gamma \approx 180$ GeV
0.12 ±0.02 ±0.02	59	AMMAR	95	CLE2 $e^+e^- \approx \Upsilon(4S)$

$\Gamma(\Xi(1690)^0 K^+, \Xi^{*0} \rightarrow \Lambda\bar{K}^0)/\Gamma(\Lambda K^+\bar{K}^0)$ Γ_{43}/Γ_{42}

VALUE	EVTS	DOCUMENT ID	TECN	COMMENT
0.28±0.07 OUR AVERAGE				
0.32±0.10±0.04	84±24	LINK	05F	FOCS γ nucleus, $\bar{E}_\gamma \approx 180$ GeV
0.26±0.08±0.03	93	ABE	02c	BELL $e^+e^- \approx \Upsilon(4S)$

$\Gamma(\Lambda K^+\bar{K}^0)/\Gamma(\Lambda\pi^+)$ Γ_{42}/Γ_{28}

VALUE	EVTS	DOCUMENT ID	TECN	COMMENT
0.44 ±0.08 OUR FIT				Error includes scale factor of 2.0.
0.395±0.026±0.036	460±30	AUBERT	07U	BABR $e^+e^- \approx \Upsilon(4S)$

$\Gamma(\Sigma^0\pi^+)/\Gamma_{total}$ Γ_{44}/Γ

VALUE (%)	EVTS	DOCUMENT ID	TECN	COMMENT
1.29±0.07 OUR FIT				Error includes scale factor of 1.1.
1.27±0.08±0.03	522	ABLIKIM	16	BES3 $e^+e^- \rightarrow \Lambda_c\bar{\Lambda}_c$, 4.599 GeV

$\Gamma(\Sigma^0\pi^+)/\Gamma(\rho K^-\pi^+)$ Γ_{44}/Γ_2

VALUE	EVTS	DOCUMENT ID	TECN	COMMENT
0.206±0.010 OUR FIT				Error includes scale factor of 1.2.
0.20 ±0.04 OUR AVERAGE				
0.21 ±0.02 ±0.04	196	VERY	94	CLE2 $e^+e^- \approx \Upsilon(3S), \Upsilon(4S)$
0.17 ±0.06 ±0.04		ALBRECHT	92	ARG $e^+e^- \approx 10.4$ GeV

$\Gamma(\Sigma^0\pi^+)/\Gamma(\Lambda\pi^+)$ Γ_{44}/Γ_{28}

VALUE	EVTS	DOCUMENT ID	TECN	COMMENT
0.99 ±0.04 OUR FIT				
0.98 ±0.05 OUR AVERAGE				
0.977±0.015±0.051	33k	AUBERT	07U	BABR $e^+e^- \approx \Upsilon(4S)$
1.09 ±0.11 ±0.19	750	LINK	05F	FOCS γ nucleus, $\bar{E}_\gamma \approx 180$ GeV

$\Gamma(\Sigma^+\pi^0)/\Gamma_{total}$ Γ_{45}/Γ

VALUE (%)	EVTS	DOCUMENT ID	TECN	COMMENT
1.25±0.10 OUR FIT				
1.18±0.10±0.03	309	ABLIKIM	16	BES3 $e^+e^- \rightarrow \Lambda_c\bar{\Lambda}_c$, 4.599 GeV

$\Gamma(\Sigma^+\pi^0)/\Gamma(\rho K^-\pi^+)$ Γ_{45}/Γ_2

VALUE	EVTS	DOCUMENT ID	TECN	COMMENT
0.199±0.015 OUR FIT				
0.20 ±0.03 ±0.03	93	KUBOTA	93	CLE2 $e^+e^- \approx \Upsilon(4S)$

$\Gamma(\Sigma^+\eta)/\Gamma(\rho K^-\pi^+)$ Γ_{46}/Γ_2

VALUE	EVTS	DOCUMENT ID	TECN	COMMENT
0.11±0.03±0.02	26	AMMAR	95	CLE2 $e^+e^- \approx \Upsilon(4S)$

$\Gamma(\Sigma^+\eta)/\Gamma(\Sigma^+\pi^0)$ Γ_{46}/Γ_{45}

VALUE	EVTS	DOCUMENT ID	TECN	COMMENT
0.35±0.16±0.02	15	¹ ABLIKIM	19X	BES3 e^+e^- at 4.6 GeV

¹ ABLIKIM 19X report evidence for the observation of the decay $\Lambda_c^+ \rightarrow \Sigma^+\eta$ at 2.5 σ significance.

$\Gamma(\Sigma^+\eta)/\Gamma(\Sigma^+\omega)$ Γ_{47}/Γ_{55}

VALUE	EVTS	DOCUMENT ID	TECN	COMMENT
0.86±0.34±0.04	13	¹ ABLIKIM	19X	BES3 e^+e^- at 4.6 GeV

¹ ABLIKIM 19X report evidence for the observation of the decay $\Lambda_c^+ \rightarrow \Sigma^+\eta'$ at 3.2 σ significance.

$\Gamma(\Sigma^+\pi^+\pi^-)/\Gamma_{total}$ Γ_{48}/Γ

VALUE (%)	EVTS	DOCUMENT ID	TECN	COMMENT
4.50±0.25 OUR FIT				Error includes scale factor of 1.3.
4.25±0.24±0.20	1156	ABLIKIM	16	BES3 $e^+e^- \rightarrow \Lambda_c\bar{\Lambda}_c$, 4.599 GeV

$\Gamma(\Sigma^+\pi^+\pi^-)/\Gamma(\rho K^-\pi^+)$ Γ_{48}/Γ_2

VALUE	EVTS	DOCUMENT ID	TECN	COMMENT
0.716±0.019 OUR FIT				
0.720±0.024 OUR AVERAGE				
0.719±0.003±0.024	2.7M	BERGER	18	BELL $e^+e^- \approx \Upsilon(4S)$
0.74 ±0.07 ±0.09	487	KUBOTA	93	CLE2 $e^+e^- \approx \Upsilon(4S)$
• • • We do not use the following data for averages, fits, limits, etc. • • •				
0.72 ±0.14	47 ± 9	VAZQUEZ-JA..08	SELX	Σ^- nucleus, 600 GeV
0.54 +0.18 -0.15	11	BARLAG	92	NA32 π^- Cu 230 GeV

Baryon Particle Listings

Λ_c^+

$\Gamma(\Sigma^+ \rho^0)/\Gamma(\rho K^- \pi^+)$		Γ_{49}/Γ_2	
VALUE	CL%	DOCUMENT ID	TECN COMMENT
<0.27	95	KUBOTA	93 CLE2 $e^+ e^- \approx \Upsilon(4S)$

$\Gamma(\Sigma^- 2\pi^+)/\Gamma_{total}$		Γ_{50}/Γ	
VALUE (%)	EVTS	DOCUMENT ID	TECN COMMENT
1.87 ± 0.18 OUR FIT			
1.81 ± 0.17 ± 0.09	161	ABLIKIM	17Y BES3 $e^+ e^-$ at 4.6 GeV

$\Gamma(\Sigma^- 2\pi^+)/\Gamma(\rho K^- \pi^+)$		Γ_{50}/Γ_2	
VALUE	EVTS	DOCUMENT ID	TECN COMMENT
0.297 ± 0.030 OUR FIT			Error includes scale factor of 1.1.
0.314 ± 0.067	30 ± 6	VAZQUEZ-JA...08	SELX Σ^- nucleus, 600 GeV

$\Gamma(\Sigma^- 2\pi^+)/\Gamma(\Sigma^+ \pi^+ \pi^-)$		Γ_{50}/Γ_{48}	
VALUE	EVTS	DOCUMENT ID	TECN COMMENT
0.42 ± 0.04 OUR FIT			Error includes scale factor of 1.1.
0.53 ± 0.15 ± 0.07	56	FRABETTI	94E E687 γ Be, \bar{E}_γ 220 GeV

$\Gamma(\Sigma^0 \pi^+ \pi^0)/\Gamma(\rho K^- \pi^+)$		Γ_{51}/Γ_2	
VALUE	EVTS	DOCUMENT ID	TECN COMMENT
0.56 ± 0.05 OUR AVERAGE			Error includes scale factor of 1.5.
0.575 ± 0.005 ± 0.036	2.7M	BERGER	18 BELL $e^+ e^- \approx \Upsilon(4S)$
0.36 ± 0.09 ± 0.10	117	AVERY	94 CLE2 $e^+ e^- \approx \Upsilon(3S), \Upsilon(4S)$

$\Gamma(\Sigma^+ \pi^0 \pi^0)/\Gamma(\rho K^- \pi^+)$		Γ_{52}/Γ_2	
VALUE	EVTS	DOCUMENT ID	TECN COMMENT
0.247 ± 0.006 ± 0.019	925k	BERGER	18 BELL $e^+ e^- \approx \Upsilon(4S)$

$\Gamma(\Sigma^0 \pi^- 2\pi^+)/\Gamma(\rho K^- \pi^+)$		Γ_{53}/Γ_2	
VALUE	EVTS	DOCUMENT ID	TECN COMMENT
0.18 ± 0.05 OUR FIT			
0.21 ± 0.05 ± 0.05	90	AVERY	94 CLE2 $e^+ e^- \approx \Upsilon(3S), \Upsilon(4S)$

$\Gamma(\Sigma^0 \pi^- 2\pi^+)/\Gamma(\Lambda \pi^- 2\pi^+)$		Γ_{53}/Γ_{31}	
VALUE	EVTS	DOCUMENT ID	TECN COMMENT
0.31 ± 0.08 OUR FIT			
0.26 ± 0.06 ± 0.09	480	LINK	05F FOCS γ nucleus, $\bar{E}_\gamma \approx 180$ GeV

$\Gamma(\Sigma^+ \omega)/\Gamma_{total}$		Γ_{55}/Γ	
VALUE (%)	EVTS	DOCUMENT ID	TECN COMMENT
1.70 ± 0.21 OUR FIT			
1.56 ± 0.20 ± 0.07	157	ABLIKIM	16 BES3 $e^+ e^- \rightarrow \Lambda_c \bar{\Lambda}_c, 4.599$ GeV

$\Gamma(\Sigma^+ \omega)/\Gamma(\rho K^- \pi^+)$		Γ_{55}/Γ_2	
VALUE	EVTS	DOCUMENT ID	TECN COMMENT
0.271 ± 0.031 OUR FIT			Unseen decay modes of the ω are included.
0.54 ± 0.13 ± 0.06	107	KUBOTA	93 CLE2 $e^+ e^- \approx \Upsilon(4S)$

$\Gamma(\Sigma^- \pi^0 2\pi^+)/\Gamma_{total}$		Γ_{56}/Γ	
VALUE (%)	EVTS	DOCUMENT ID	TECN COMMENT
2.11 ± 0.33 ± 0.14	88	ABLIKIM	17Y BES3 $e^+ e^-$ at 4.6 GeV

$\Gamma(\Sigma^+ K^+ K^-)/\Gamma(\rho K^- \pi^+)$		Γ_{57}/Γ_2	
VALUE	EVTS	DOCUMENT ID	TECN COMMENT
0.056 ± 0.006 OUR FIT			
0.070 ± 0.011 ± 0.011	59	AVERY	93 CLE2 $e^+ e^- \approx 10.5$ GeV

$\Gamma(\Sigma^+ K^+ K^-)/\Gamma(\Sigma^+ \pi^+ \pi^-)$		Γ_{57}/Γ_{48}	
VALUE	EVTS	DOCUMENT ID	TECN COMMENT
0.078 ± 0.008 OUR FIT			
0.074 ± 0.009 OUR AVERAGE			
0.076 ± 0.007 ± 0.009	246	ABE	02c BELL $e^+ e^- \approx \Upsilon(4S)$
0.071 ± 0.011 ± 0.011	103	LINK	02G FOCS γ nucleus, ≈ 180 GeV

$\Gamma(\Sigma^+ \phi)/\Gamma(\rho K^- \pi^+)$		Γ_{58}/Γ_2	
VALUE	EVTS	DOCUMENT ID	TECN COMMENT
0.062 ± 0.009 OUR FIT			Unseen decay modes of the ϕ are included.
0.069 ± 0.023 ± 0.016	26	AVERY	93 CLE2 $e^+ e^- \approx 10.5$ GeV

$\Gamma(\Sigma^+ \phi)/\Gamma(\Sigma^+ \pi^+ \pi^-)$		Γ_{58}/Γ_{48}	
VALUE	EVTS	DOCUMENT ID	TECN COMMENT
0.087 ± 0.012 OUR FIT			
0.086 ± 0.012 OUR AVERAGE			
0.085 ± 0.012 ± 0.012	129	ABE	02c BELL $e^+ e^- \approx \Upsilon(4S)$
0.087 ± 0.016 ± 0.006	57	LINK	02G FOCS γ nucleus, ≈ 180 GeV

$\Gamma(\Xi(1690)^0 K^+, \Xi^* \rightarrow \Sigma^+ K^-)/\Gamma(\Sigma^+ \pi^+ \pi^-)$		Γ_{59}/Γ_{48}	
VALUE	EVTS	DOCUMENT ID	TECN COMMENT
0.023 ± 0.005 OUR AVERAGE			
0.023 ± 0.005 ± 0.005	75	ABE	02c BELL $e^+ e^- \approx \Upsilon(4S)$
0.022 ± 0.006 ± 0.006	34	LINK	02G FOCS γ nucleus, ≈ 180 GeV

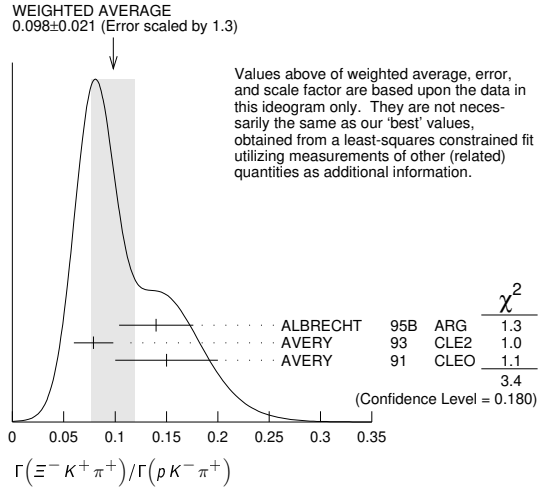
$\Gamma(\Sigma^+ K^+ K^- \text{ nonresonant})/\Gamma(\Sigma^+ \pi^+ \pi^-)$		Γ_{60}/Γ_{48}	
VALUE	CL%	DOCUMENT ID	TECN COMMENT
<0.018	90	ABE	02c BELL $e^+ e^- \approx \Upsilon(4S)$
<0.028	90	LINK	02G FOCS γ nucleus, ≈ 180 GeV

••• We do not use the following data for averages, fits, limits, etc. •••

$\Gamma(\Xi^0 K^+)/\Gamma_{total}$		Γ_{61}/Γ	
VALUE (units 10^{-3})	EVTS	DOCUMENT ID	TECN COMMENT
5.5 ± 0.7 OUR FIT			
5.90 ± 0.86 ± 0.39	68	ABLIKIM	18Y BES3 $e^+ e^-$ at 4.6 GeV

$\Gamma(\Xi^0 K^+)/\Gamma(\rho K^- \pi^+)$		Γ_{61}/Γ_2	
VALUE	EVTS	DOCUMENT ID	TECN COMMENT
0.088 ± 0.012 OUR FIT			
0.078 ± 0.013 ± 0.013	56	AVERY	93 CLE2 $e^+ e^- \approx 10.5$ GeV

$\Gamma(\Xi^- K^+ \pi^+)/\Gamma(\rho K^- \pi^+)$		Γ_{62}/Γ_2	
VALUE	EVTS	DOCUMENT ID	TECN COMMENT
0.099 ± 0.009 OUR FIT			Error includes scale factor of 1.3. See the ideogram below.
0.098 ± 0.021 OUR AVERAGE			
0.14 ± 0.03 ± 0.02	34	ALBRECHT	95B ARG $e^+ e^- \approx 10.4$ GeV
0.079 ± 0.013 ± 0.014	60	AVERY	93 CLE2 $e^+ e^- \approx 10.5$ GeV
0.15 ± 0.04 ± 0.03	30	AVERY	91 CLEO $e^+ e^- 10.5$ GeV



$\Gamma(\Xi^- K^+ \pi^+)/\Gamma(\Lambda \pi^+)$		Γ_{62}/Γ_{28}	
VALUE	EVTS	DOCUMENT ID	TECN COMMENT
0.48 ± 0.04 OUR FIT			
0.480 ± 0.016 ± 0.039	2665 ± 84	AUBERT	07U BABR $e^+ e^- \approx \Upsilon(4S)$

$\Gamma(\Xi(1530)^0 K^+)/\Gamma_{total}$		Γ_{63}/Γ	
VALUE (units 10^{-3})	EVTS	DOCUMENT ID	TECN COMMENT
4.3 ± 0.9 OUR FIT			Error includes scale factor of 1.1.
5.02 ± 0.99 ± 0.31	60	ABLIKIM	18Y BES3 $e^+ e^-$ at 4.6 GeV

$\Gamma(\Xi(1530)^0 K^+)/\Gamma(\rho K^- \pi^+)$		Γ_{63}/Γ_2	
VALUE	EVTS	DOCUMENT ID	TECN COMMENT
0.068 ± 0.014 OUR FIT			Error includes scale factor of 1.
0.053 ± 0.016 ± 0.010	24	AVERY	93 CLE2 $e^+ e^- \approx 10.5$ GeV
0.05 ± 0.02 ± 0.01	11	ALBRECHT	95B ARG $e^+ e^- \approx 10.4$ GeV

Hadronic modes with a hyperon: S = 0 final states

$\Gamma(\Lambda K^+)/\Gamma(\Lambda \pi^+)$		Γ_{64}/Γ_{28}	
VALUE	EVTS	DOCUMENT ID	TECN COMMENT
0.047 ± 0.009 OUR AVERAGE			Error includes scale factor of 1.8.
0.044 ± 0.004 ± 0.003	1162 ± 101	AUBERT	07U BABR $e^+ e^- \approx \Upsilon(4S)$
0.074 ± 0.010 ± 0.012	265	ABE	02c BELL $e^+ e^- \approx \Upsilon(4S)$

$\Gamma(\Lambda K^+ \pi^+ \pi^-)/\Gamma(\Lambda \pi^+)$		Γ_{65}/Γ_{28}	
VALUE	CL%	DOCUMENT ID	TECN COMMENT
<4.1 × 10 ⁻²	90	AUBERT	07U BABR $e^+ e^- \approx \Upsilon(4S)$

$\Gamma(\Sigma^0 K^+)/\Gamma(\Sigma^0 \pi^+)$		Γ_{66}/Γ_{44}	
VALUE	EVTS	DOCUMENT ID	TECN COMMENT
0.040 ± 0.006 OUR AVERAGE			
0.038 ± 0.005 ± 0.003	366 ± 52	AUBERT	07U BABR $e^+ e^- \approx \Upsilon(4S)$
0.056 ± 0.014 ± 0.008	75	ABE	02c BELL $e^+ e^- \approx \Upsilon(4S)$

See key on page 999

Baryon Particle Listings

Λ_c^+

$\Gamma(\Sigma^0 K^+ \pi^+ \pi^-)/\Gamma(\Sigma^0 \pi^+)$		Γ_{67}/Γ_{44}	
VALUE	CL%	DOCUMENT ID	TECN COMMENT
$<2.0 \times 10^{-2}$	90	AUBERT	07u BABR $e^+ e^- \approx \Upsilon(4S)$

$\Gamma(\Sigma^+ K^+ \pi^-)/\Gamma(\Sigma^+ \pi^+ \pi^-)$		Γ_{68}/Γ_{48}	
VALUE	EVTS	DOCUMENT ID	TECN COMMENT
$0.047 \pm 0.011 \pm 0.008$	105	ABE	02c BELL $e^+ e^- \approx \Upsilon(4S)$

$\Gamma(\Sigma^+ K^*(892)^0)/\Gamma(\Sigma^+ \pi^+ \pi^-)$		Γ_{69}/Γ_{48}	
VALUE	EVTS	DOCUMENT ID	TECN COMMENT
$0.078 \pm 0.018 \pm 0.013$	49	LINK	02g FOCS γ nucleus, ≈ 180 GeV

$\Gamma(\Sigma^- K^+ \pi^+)/\Gamma(\Sigma^+ K^*(892)^0)$		Γ_{70}/Γ_{69}	
VALUE	CL%	DOCUMENT ID	TECN COMMENT
<0.35	90	LINK	02g FOCS γ nucleus, ≈ 180 GeV

Doubly Cabibbo-suppressed modes

$\Gamma(\rho K^+ \pi^-)/\Gamma(\rho K^- \pi^+)$		Γ_{71}/Γ_{2}	
VALUE (units 10^{-3})	EVTS	DOCUMENT ID	TECN COMMENT
1.77 ± 0.27 OUR AVERAGE			Error includes scale factor of 1.9.
$1.65 \pm 0.15 \pm 0.05$	392	AAIJ	18v LHCB $\Lambda_b^0 \rightarrow \Lambda_c^+ \mu^- X$
$2.35 \pm 0.27 \pm 0.21$	3379	YANG	16 BELL At or near Υ 's

Semileptonic modes

$\Gamma(\Lambda e^+ \nu_e)/\Gamma_{total}$		Γ_{72}/Γ	
VALUE (%)	EVTS	DOCUMENT ID	TECN COMMENT
$3.63 \pm 0.38 \pm 0.20$	104	ABLIKIM	15y BES3 567 pb^{-1} , 4.599 GeV

$\Gamma(\Lambda e^+ \nu_e)/\Gamma(e^+ \text{ anything})$		Γ_{72}/Γ_{74}	
VALUE (%)	EVTS	DOCUMENT ID	TECN COMMENT
$91.9 \pm 12.5 \pm 5.4$	214	ABLIKIM	18AF BES3 $e^+ e^-$ 4.6 GeV

$\Gamma(\Lambda e^+ \nu_e)/\Gamma(\rho K^- \pi^+)$		Γ_{72}/Γ_{2}	
VALUE	DOCUMENT ID	TECN	COMMENT
0.43 ± 0.08	1,2 BERGFELD 94	CLE2	$e^+ e^- \approx \Upsilon(4S)$
0.38 ± 0.14	2,3 ALBRECHT 91g	ARG	$e^+ e^- \approx 10.4$ GeV

- ¹ BERGFELD 94 measures $\sigma(e^+ e^- \rightarrow \Lambda_c^+ X) \cdot B(\Lambda_c^+ \rightarrow \Lambda e^+ \nu_e) = (4.87 \pm 0.28 \pm 0.69)$ pb.
- ² To extract $\Gamma(\Lambda_c^+ \rightarrow \Lambda e^+ \nu_e)/\Gamma(\Lambda_c^+ \rightarrow \rho K^- \pi^+)$, we use $\sigma(e^+ e^- \rightarrow \Lambda_c^+ X) \cdot B(\Lambda_c^+ \rightarrow \rho K^- \pi^+) = (11.2 \pm 1.3)$ pb, which is the weighted average of measurements from ARGUS (ALBRECHT 96E) and CLEO (AVERY 91).
- ³ ALBRECHT 91g measures $\sigma(e^+ e^- \rightarrow \Lambda_c^+ X) \cdot B(\Lambda_c^+ \rightarrow \Lambda e^+ \nu_e) = (4.20 \pm 1.28 \pm 0.71)$ pb.

$\Gamma(\Lambda \mu^+ \nu_\mu)/\Gamma_{total}$		Γ_{73}/Γ	
VALUE (%)	EVTS	DOCUMENT ID	TECN COMMENT
$3.49 \pm 0.46 \pm 0.27$	79	ABLIKIM	17d BES3 $e^+ e^-$ at 4.6 GeV

$\Gamma(\Lambda \mu^+ \nu_\mu)/\Gamma(\rho K^- \pi^+)$		Γ_{73}/Γ_{2}	
VALUE	DOCUMENT ID	TECN	COMMENT
0.40 ± 0.09	1,2 BERGFELD 94	CLE2	$e^+ e^- \approx \Upsilon(4S)$
0.35 ± 0.20	2,3 ALBRECHT 91g	ARG	$e^+ e^- \approx 10.4$ GeV
$1.43 \pm 0.51 \pm 0.64$ pb.	1 BERGFELD 94		measures $\sigma(e^+ e^- \rightarrow \Lambda_c^+ X) \cdot B(\Lambda_c^+ \rightarrow \Lambda \mu^+ \nu_\mu) = (4.43 \pm 0.51 \pm 0.64)$ pb.
(11.2 ± 1.3) pb.	2		To extract $\Gamma(\Lambda_c^+ \rightarrow \Lambda \mu^+ \nu_\mu)/\Gamma(\Lambda_c^+ \rightarrow \rho K^- \pi^+)$, we use $\sigma(e^+ e^- \rightarrow \Lambda_c^+ X) \cdot B(\Lambda_c^+ \rightarrow \rho K^- \pi^+) = (11.2 \pm 1.3)$ pb, which is the weighted average of measurements from ARGUS (ALBRECHT 96E) and CLEO (AVERY 91).
$(3.91 \pm 2.02 \pm 0.90)$ pb.	3		ALBRECHT 91g measures $\sigma(e^+ e^- \rightarrow \Lambda_c^+ X) \cdot B(\Lambda_c^+ \rightarrow \Lambda \mu^+ \nu_\mu) = (3.91 \pm 2.02 \pm 0.90)$ pb.

$\Gamma(\Lambda \mu^+ \nu_\mu)/\Gamma(\Lambda e^+ \nu_e)$		Γ_{73}/Γ_{72}	
VALUE	DOCUMENT ID	TECN	COMMENT
$0.96 \pm 0.16 \pm 0.04$	1	ABLIKIM	17d BES3 $e^+ e^-$ at 4.6 GeV
¹ This is the ratio of the ABLIKIM 17d $\Lambda \mu^+ \nu_e$ branching fraction and the ABLIKIM 15y $\Lambda e^+ \nu_e$ branching fraction (see above), and so is not an independent measurement.			

Inclusive modes

$\Gamma(e^+ \text{ anything})/\Gamma_{total}$		Γ_{74}/Γ	
VALUE (%)	EVTS	DOCUMENT ID	TECN COMMENT
$3.95 \pm 0.34 \pm 0.09$	214	ABLIKIM	18AF BES3 $e^+ e^-$ 4.6 GeV

$\Gamma(p \text{ anything})/\Gamma_{total}$		Γ_{75}/Γ	
VALUE	DOCUMENT ID	TECN	COMMENT
$0.50 \pm 0.08 \pm 0.14$	1	CRAWFORD	92 CLEO $e^+ e^-$ 10.5 GeV

¹ This CRAWFORD 92 value includes protons from Λ decay. The value is model dependent, but account is taken of this in the systematic error.

$\Gamma(n \text{ anything})/\Gamma_{total}$		Γ_{76}/Γ	
VALUE	DOCUMENT ID	TECN	COMMENT
$0.50 \pm 0.08 \pm 0.14$	1	CRAWFORD	92 CLEO $e^+ e^-$ 10.5 GeV

¹ This CRAWFORD 92 value includes neutrons from Λ decay. The value is model dependent, but account is taken of this in the systematic error.

$\Gamma(\Lambda \text{ anything})/\Gamma_{total}$		Γ_{77}/Γ	
VALUE (%)	EVTS	DOCUMENT ID	TECN COMMENT
$38.2 \pm 2.8 \pm 0.9$	700	ABLIKIM	18E BES3 $e^+ e^-$ at 4.6 GeV

$\Gamma(3\text{prongs})/\Gamma_{total}$		Γ_{78}/Γ	
VALUE	DOCUMENT ID	TECN	COMMENT
$0.24 \pm 0.07 \pm 0.04$	KAYIS-TOPAK.03	CHRS	ν_μ emulsion, $\bar{E} \approx 27$ GeV

Rare or forbidden modes

$\Gamma(\rho e^+ e^-)/\Gamma_{total}$		Γ_{79}/Γ		
VALUE	CL%	EVTS	DOCUMENT ID	TECN COMMENT
$<5.5 \times 10^{-6}$	90	4.0 ± 7.1	LEES	11g BABR $e^+ e^- \approx \Upsilon(4S)$

$\Gamma(\rho \mu^+ \mu^- \text{ non-resonant})/\Gamma_{total}$		Γ_{80}/Γ	
VALUE	CL%	DOCUMENT ID	TECN COMMENT
$<7.7 \times 10^{-8}$	90	AAIJ	18w LHCB Ratio to $p\phi, \phi \rightarrow \mu^+ \mu^-$
••• We do not use the following data for averages, fits, limits, etc. •••			
$<4.4 \times 10^{-5}$	90	LEES	11g BABR $e^+ e^- \approx \Upsilon(4S)$
$<3.4 \times 10^{-4}$	90	KODAMA	95 E653 π^- emulsion 600 GeV

$\Gamma(\rho e^+ \mu^-)/\Gamma_{total}$		Γ_{81}/Γ		
VALUE	CL%	EVTS	DOCUMENT ID	TECN COMMENT
$<9.9 \times 10^{-6}$	90	-0.7 ± 3.0	LEES	11g BABR $e^+ e^- \approx \Upsilon(4S)$

$\Gamma(\rho e^- \mu^+)/\Gamma_{total}$		Γ_{82}/Γ		
VALUE	CL%	EVTS	DOCUMENT ID	TECN COMMENT
$<19 \times 10^{-6}$	90	6.2 ± 4.9	LEES	11g BABR $e^+ e^- \approx \Upsilon(4S)$

$\Gamma(\bar{p} 2e^+)/\Gamma_{total}$		Γ_{83}/Γ		
VALUE	CL%	EVTS	DOCUMENT ID	TECN COMMENT
$<2.7 \times 10^{-6}$	90	-1.5 ± 4.5	LEES	11g BABR $e^+ e^- \approx \Upsilon(4S)$

$\Gamma(\bar{p} 2\mu^+)/\Gamma_{total}$		Γ_{84}/Γ		
VALUE	CL%	EVTS	DOCUMENT ID	TECN COMMENT
$<9.4 \times 10^{-6}$	90	0.0 ± 2.2	LEES	11g BABR $e^+ e^- \approx \Upsilon(4S)$

$\Gamma(\bar{p} e^+ \mu^+)/\Gamma_{total}$		Γ_{85}/Γ		
VALUE	CL%	EVTS	DOCUMENT ID	TECN COMMENT
$<16 \times 10^{-6}$	90	10.1 ± 6.8	LEES	11g BABR $e^+ e^- \approx \Upsilon(4S)$

$\Gamma(\Sigma^- \mu^+ \mu^+)/\Gamma_{total}$		Γ_{86}/Γ		
VALUE	CL%	EVTS	DOCUMENT ID	TECN COMMENT
$<7.0 \times 10^{-4}$	90	0	KODAMA	95 E653 π^- emulsion 600 GeV

Λ_c^+ DECAY PARAMETERS

See the note on "Baryon Decay Parameters" in the neutron Listings.

α FOR $\Lambda_c^+ \rightarrow \Lambda \pi^+$		Γ_{74}/Γ	
VALUE	EVTS	DOCUMENT ID	TECN COMMENT
-0.84 ± 0.09 OUR AVERAGE			
$-0.80 \pm 0.11 \pm 0.02$		ABLIKIM	19ax BES3 $e^+ e^-$ at 4.6 GeV
$-0.78 \pm 0.16 \pm 0.19$		LINK	06a FOCS $\gamma A, \bar{E}_\gamma \approx 180$ GeV
$-0.94 \pm 0.21 \pm 0.12$	414	1 BISHAI	95 CLE2 $e^+ e^- \approx \Upsilon(4S)$
-0.96 ± 0.42		ALBRECHT	92 ARG $e^+ e^- \approx 10.4$ GeV
-1.1 ± 0.4	86	AVERY	90b CLEO $e^+ e^- \approx 10.6$ GeV

¹ BISHAI 95 actually gives $\alpha = -0.94 \pm 0.21 \pm 0.12$, chopping the errors at the physical limit -1.0 . However, for $\alpha \approx -1.0$, some experiments should get unphysical values ($\alpha < -1.0$), and for averaging with other measurements such values (or errors that extend below -1.0) should not be chopped.

α FOR $\Lambda_c^+ \rightarrow \Sigma^+ \pi^0$		Γ_{74}/Γ	
VALUE	EVTS	DOCUMENT ID	TECN COMMENT
-0.55 ± 0.11 OUR AVERAGE			
$-0.57 \pm 0.10 \pm 0.07$		ABLIKIM	19ax BES3 $e^+ e^-$ at 4.6 GeV
$-0.45 \pm 0.31 \pm 0.06$	89	BISHAI	95 CLE2 $e^+ e^- \approx \Upsilon(4S)$

Baryon Particle Listings

Λ_c^+ , $\Lambda_c(2595)^+$

α FOR $\Lambda_c^+ \rightarrow \Sigma^0 \pi^+$

VALUE	DOCUMENT ID	TECN	COMMENT
$-0.73 \pm 0.17 \pm 0.07$	ABLIKIM	19AX BES3	e^+e^- at 4.6 GeV

α FOR $\Lambda_c^+ \rightarrow \Lambda e^+ \nu_e$

The experiments don't cover the complete (or same incomplete) $M(\Lambda e^+)$ range, but we average them together anyway.

VALUE	EVTS	DOCUMENT ID	TECN	COMMENT
$-0.86 \pm 0.03 \pm 0.02$	3201	1 HINSON	05 CLEO	$e^+e^- \approx \gamma(4S)$
$-0.91 \pm 0.42 \pm 0.25$		2 ALBRECHT	94B ARG	$e^+e^- \approx 10$ GeV
$-0.82_{-0.06}^{+0.09} \pm 0.06$	700	3 CRAWFORD	95 CLE2	See HINSON 05
$-0.89_{-0.11}^{+0.17} \pm 0.09$	350	4 BERGFELD	94 CLE2	See CRAWFORD 95

- • • We do not use the following data for averages, fits, limits, etc. • • •
- 1 HINSON 05 measures the form-factor ratio $R \equiv f_2/f_1$ for $\Lambda_c^+ \rightarrow \Lambda e^+ \nu_e$ events to be $-0.31 \pm 0.05 \pm 0.04$ and the pole mass to be $2.21 \pm 0.08 \pm 0.14$ GeV/c², and from these calculates α , averaged over q^2 , where $\langle q^2 \rangle = 0.67$ (GeV/c)².
- 2 ALBRECHT 94B uses Λe^+ and $\Lambda \mu^+$ events in the mass range $1.85 < M(\Lambda e^+) < 2.20$ GeV.
- 3 CRAWFORD 95 measures the form-factor ratio $R \equiv f_2/f_1$ for $\Lambda_c^+ \rightarrow \Lambda e^+ \nu_e$ events to be $-0.25 \pm 0.14 \pm 0.08$ and from this calculates α , averaged over q^2 , to be the above.
- 4 BERGFELD 94 uses Λe^+ events.

α FOR $\Lambda_c^+ \rightarrow \rho K_S^0$

VALUE	DOCUMENT ID	TECN	COMMENT
$0.18 \pm 0.43 \pm 0.14$	ABLIKIM	19AX BES3	e^+e^- at 4.6 GeV

Λ_c^+ , $\bar{\Lambda}_c^-$ CP-VIOLATING DECAY ASYMMETRIES

$(\alpha + \bar{\alpha})/(\alpha - \bar{\alpha})$ in $\Lambda_c^+ \rightarrow \Lambda \pi^+, \bar{\Lambda}_c^- \rightarrow \bar{\Lambda} \pi^-$

This is zero if CP is conserved.

VALUE	DOCUMENT ID	TECN	COMMENT
$-0.07 \pm 0.19 \pm 0.24$	LINK	06A FOCUS	$\gamma A, E_\gamma \approx 180$ GeV

$(\alpha + \bar{\alpha})/(\alpha - \bar{\alpha})$ in $\Lambda_c^+ \rightarrow \Lambda e^+ \nu_e, \bar{\Lambda}_c^- \rightarrow \bar{\Lambda} e^- \bar{\nu}_e$

This is zero if CP is conserved.

VALUE	DOCUMENT ID	TECN	COMMENT
$0.00 \pm 0.03 \pm 0.02$	HINSON	05 CLEO	$e^+e^- \approx \gamma(4S)$

$A_{CP}(AX)$ in $\Lambda_c \rightarrow \Lambda X, \bar{\Lambda}_c \rightarrow \bar{\Lambda} X$

VALUE (%)	EVTS	DOCUMENT ID	TECN	COMMENT
$2.1_{-6.6}^{+7.0} \pm 1.6$	700	ABLIKIM	18E BES3	e^+e^- at 4.6 GeV

$\Delta A_{CP} = A_{CP}(\Lambda_c^+ \rightarrow \rho K^+ K^-) - A_{CP}(\Lambda_c^+ \rightarrow \rho \pi^+ \pi^-)$

VALUE (%)	DOCUMENT ID	TECN	COMMENT
$0.30 \pm 0.91 \pm 0.61$	1 AAIJ	18R LHCb	$pp \bar{p}, 7, 8$ TeV

- 1 AAIJ 18R applies phase-space-dependent weights to the $\Lambda_c^+ \rightarrow \rho \pi^+ \pi^-$ sample to align its kinematics with the $\Lambda_c^+ \rightarrow \rho K^+ K^-$ sample.

Λ_c^+ REFERENCES

We have omitted some papers that have been superseded by later experiments. The omitted papers may be found in our 1992 edition (Physical Review D45, 1 June, Part II) or in earlier editions.

AAIJ	19AG	PR D100 032001	R. Aaij et al.	(LHCb Collab.)
ABLIKIM	19AX	PR D100 072004	M. Ablikim et al.	(BESIII Collab.)
ABLIKIM	19X	CP C43 083002	M. Ablikim et al.	(BESIII Collab.)
ABLIKIM	19Y	PR D99 032010	M. Ablikim et al.	(BESIII Collab.)
AAIJ	18N	PR D97 091101	R. Aaij et al.	(LHCb Collab.)
AAIJ	18R	JHEP 1803 182	R. Aaij et al.	(LHCb Collab.)
AAIJ	18V	JHEP 1803 043	R. Aaij et al.	(LHCb Collab.)
ABLIKIM	18AF	PRL 121 251801	M. Ablikim et al.	(BESIII Collab.)
ABLIKIM	18E	PRL 121 062003	M. Ablikim et al.	(BESIII Collab.)
ABLIKIM	18Y	PL B783 200	M. Ablikim et al.	(BESIII Collab.)
BERGER	18	PR D98 112006	M. Berger et al.	(BELLE Collab.)
ABLIKIM	17D	PL B767 42	M. Ablikim et al.	(BESIII Collab.)
ABLIKIM	17H	PRL 118 112001	M. Ablikim et al.	(BESIII Collab.)
ABLIKIM	17Q	PR D95 111102	M. Ablikim et al.	(BESIII Collab.)
ABLIKIM	17Y	PL B772 308	M. Ablikim et al.	(BESIII Collab.)
PAL	17	PR D96 051102	B. Pal et al.	(BELLE Collab.)
ABLIKIM	16U	PRL 116 052001	M. Ablikim et al.	(BESIII Collab.)
ABLIKIM	16U	PRL 117 232002	M. Ablikim et al.	(BESIII Collab.)
YANG	16	PRL 117 011801	S.B. Yang et al.	(BELLE Collab.)
ABLIKIM	15Y	PRL 115 221805	M. Ablikim et al.	(BESIII Collab.)
ZUPANC	14	PRL 113 042002	A. Zupanc et al.	(BELLE Collab.)
LEES	11G	PR D84 072006	J.P. Lees et al.	(BABAR Collab.)
VAZQUEZ-JA...	08	PL B666 299	E. Vazquez-Jauregui et al.	(SELEX Collab.)
AUBERT	07U	PR D75 052002	B. Aubert et al.	(BABAR Collab.)
LINK	06A	PL B634 165	J.M. Link et al.	(FNAL FOCUS Collab.)
AUBERT,B	05S	PR D72 052006	B. Aubert et al.	(BABAR Collab.)
HINSON	05	PRL 94 191801	J.W. Hinson et al.	(CLEO Collab.)
LINK	05F	PL B624 22	J.M. Link et al.	(FNAL FOCUS Collab.)
CRONIN-HEN...	03	PR D67 012001	D. Cronin-Hennessy et al.	(CLEO Collab.)
KAYIS-TOPAK...	03	PL B555 156	A. Kayis-Topkaya et al.	(CERN CHORUS Collab.)
ABE	02C	PL B524 33	K. Abe et al.	(KEK BELLE Collab.)
LINK	02C	PRL 88 161801	J.M. Link et al.	(FNAL FOCUS Collab.)
LINK	02G	PL B540 25	J.M. Link et al.	(FNAL FOCUS Collab.)
PDG	02	PR D66 010001	K. Hagiwara et al.	(PDG Collab.)
KUSHNIR...	01	PRL 86 5243	A. Kushnirenko et al.	(FNAL SELEX Collab.)
MAHMOOD	01	PRL 86 2232	A.H. Mahmood et al.	(CLEO Collab.)
AITALA	00	PL B471 449	E.M. Aitala et al.	(FNAL E791 Collab.)

ALAM	98	PR D57 4467	M.S. Alam et al.	(CLEO Collab.)
ALBRECHT	96C	PRPL 276 223	H. Albrecht et al.	(ARGUS Collab.)
ALEXANDER	96C	PR D53 1013	J.P. Alexander et al.	(CLEO Collab.)
ALBRECHT	95B	PL B342 397	H. Albrecht et al.	(ARGUS Collab.)
AMMAR	95	PRL 74 3534	R. Ammar et al.	(CLEO Collab.)
BISHAI	95	PL B350 256	M. Bishai et al.	(CLEO Collab.)
CRAWFORD	95	PRL 75 624	G. Crawford et al.	(CLEO Collab.)
KODAMA	95	PL B345 85	K. Kodama et al.	(FNAL E653 Collab.)
ALBRECHT	94B	PL B326 320	H. Albrecht et al.	(ARGUS Collab.)
ALEEV	94	PAN 57 1370	A.N. Alev et al.	(Serpukhov B15-2 Collab.)
		Translated from YF 57 1443.		
AVERY	94	PL B325 257	P. Avery et al.	(CLEO Collab.)
BERGFELD	94	PL B323 219	T. Bergfeld et al.	(CLEO Collab.)
FRABETTI	94E	PL B328 193	P.L. Frabetti et al.	(FNAL E687 Collab.)
AVERY	93	PRL 71 2391	P. Avery et al.	(CLEO Collab.)
BOZEK	93	PL B312 247	A. Bozek et al.	(CERN NA32 Collab.)
FRABETTI	93D	PRL 70 1755	P.L. Frabetti et al.	(FNAL E687 Collab.)
FRABETTI	93H	PL B314 477	P.L. Frabetti et al.	(FNAL E687 Collab.)
KUBOTA	93	PRL 71 3255	Y. Kubota et al.	(CLEO Collab.)
ALBRECHT	92	PL B274 239	H. Albrecht et al.	(ARGUS Collab.)
BARLAG	92	PL B283 465	S. Barlag et al.	(ACCMOR Collab.)
CRAWFORD	92	PR D45 752	G. Crawford et al.	(CLEO Collab.)
JEZABEK	92	PL B286 175	M. Jezabek, K. Rybicki, R. Rylko	(CRAC)
ALBRECHT	91G	PL B269 234	H. Albrecht et al.	(ARGUS Collab.)
AVERY	91F	PR D43 3599	P. Avery et al.	(CLEO Collab.)
ALVAREZ	90	ZPHY C47 539	M.P. Alvarez et al.	(CERN NA14/2 Collab.)
ALVAREZ	90B	PL B246 256	M.P. Alvarez et al.	(CERN NA14/2 Collab.)
ANJOS	90	PR D41 801	J.C. Anjos et al.	(FNAL E691 Collab.)
AVERY	90B	PRL 65 2842	P. Avery et al.	(CLEO Collab.)
BARLAG	90D	ZPHY C48 29	S. Barlag et al.	(ACCMOR Collab.)
FRABETTI	90	PL B251 1370	P.L. Frabetti et al.	(FNAL E687 Collab.)
BARLAG	89	PL B218 374	S. Barlag et al.	(ACCMOR Collab.)
AGUILAR...	88B	ZPHY C40 321	M. Aguilar-Benitez et al.	(LEBC-EHS Collab.)
Also		PL B189 254	M. Aguilar-Benitez et al.	(LEBC-EHS Collab.)
Also		PL B199 462	M. Aguilar-Benitez et al.	(LEBC-EHS Collab.)
Also		SJNP 48 833	M. Begalli et al.	(LEBC-EHS Collab.)
		Translated from YAF 48 1310.		
ALBRECHT	88C	PL B207 109	H. Albrecht et al.	(ARGUS Collab.)
ANJOS	88B	PRL 60 1379	J.C. Anjos et al.	(FNAL E691 Collab.)
AMENDOLIA	87	ZPHY C36 513	S.R. Amendolia et al.	(CERN WA1 Collab.)
JONES	87	ZPHY C36 593	G.T. Jones et al.	(CERN WA21 Collab.)
BOSETTI	82	PL 109B 234	P.C. Bosetti et al.	(AACH3, BONN, CERN+)
BASILE	81B	NC 62A 14	M. Basile et al.	(CERN, B.G.N.A., PGIA, FRAS)
CALICCHIO	80	PL B3B 521	M. Calicchio et al.	(BARI, BIRM, BRUX+)

OTHER RELATED PAPERS

MIGLIOZZI	99	PL B462 217	P. Migliozi et al.
DUNIETZ	98	PR D58 094010	I. Dunietz

$\Lambda_c(2595)^+$

$$J(J^P) = 0(\frac{1}{2}^-) \text{ Status: } ***$$

The $\Lambda_c^+ \pi^+ \pi^-$ mode is largely, and perhaps entirely, $\Sigma_c \pi$, which is just at threshold; since the Σ_c has $J^P = 1/2^+$, the J^P here is almost certainly $1/2^-$. This result is in accord with the theoretical expectation that this is the charm counterpart of the strange $\Lambda(1405)$.

$\Lambda_c(2595)^+$ MASS

The mass is obtained from the $\Lambda_c(2595)^+ - \Lambda_c^+$ mass-difference measurements below.

VALUE (MeV)	DOCUMENT ID
2592.25 ± 0.28 OUR FIT	

$\Lambda_c(2595)^+ - \Lambda_c^+$ MASS DIFFERENCE

VALUE (MeV)	EVTS	DOCUMENT ID	TECN	COMMENT
305.79 ± 0.24 OUR FIT				
$305.79 \pm 0.14 \pm 0.20$	3.5k	AALTONEN	11H CDF	$p\bar{p}$ at 1.96 TeV
• • • We do not use the following data for averages, fits, limits, etc. • • •				
305.6 \pm 0.3		1 BLECHMAN	03	Threshold shift
309.7 \pm 0.9 \pm 0.4	19	ALBRECHT	97 ARG	$e^+e^- \approx 10$ GeV
309.2 \pm 0.7 \pm 0.3	14 \pm 4.5	FRABETTI	96 E687	$\gamma Be, \bar{E}_\gamma \approx 220$ GeV
307.5 \pm 0.4 \pm 1.0	112 \pm 17	EDWARDS	95 CLE2	$e^+e^- \approx 10.5$ GeV

- 1 BLECHMAN 03 finds that a more sophisticated treatment than a simple Breit-Wigner for the proximity of the threshold of the dominant decay, $\Sigma_c(2455) \pi$, lowers the $\Lambda_c(2595)^+ - \Lambda_c^+$ mass difference by 2 or 3 MeV. The analysis of AALTONEN 11H bears this out.

$\Lambda_c(2595)^+$ WIDTH

VALUE (MeV)	EVTS	DOCUMENT ID	TECN	COMMENT
$2.59 \pm 0.30 \pm 0.47$	3.5k	2 AALTONEN	11H CDF	$p\bar{p}$ at 1.96 TeV
• • • We do not use the following data for averages, fits, limits, etc. • • •				
2.9 \pm 2.9 \pm 1.8	19	ALBRECHT	97 ARG	$e^+e^- \approx 10$ GeV
-2.1 -1.4				
3.9 \pm 1.4 \pm 2.0	112 \pm 17	EDWARDS	95 CLE2	$e^+e^- \approx 10.5$ GeV
-1.2 -1.0				

- 2 AALTONEN 11H treats the three charged modes $\Lambda_c(2595)^+ \rightarrow \Sigma_c(2455)^+ \pi^0, \Sigma_c(2455)^0 \pi^+, \Sigma_c(2455)^- \pi^+$ separately in terms of a common coupling constant h_2 and obtains $h_2^2 = 0.36 \pm 0.08$. From this the width is determined.

$\Lambda_c(2595)^+$ DECAY MODES

$\Lambda_c^+ \pi \pi$ and its submode $\Sigma_c(2455) \pi$ — the latter just barely — are the only strong decays allowed to an excited Λ_c^+ having this mass; and the submode seems to dominate.

Mode	Fraction (Γ_i/Γ)
Γ_1 $\Lambda_c^+ \pi^+ \pi^-$	[a] —
Γ_2 $\Sigma_c(2455)^{++} \pi^-$	24 ± 7 %
Γ_3 $\Sigma_c(2455)^0 \pi^+$	24 ± 7 %
Γ_4 $\Lambda_c^+ \pi^+ \pi^-$ 3-body	18 ± 10 %
Γ_5 $\Lambda_c^+ \pi^0$	[b] not seen
Γ_6 $\Lambda_c^+ \gamma$	not seen

[a] See AALTONEN 11H, Fig. 8, for the calculated ratio of $\Lambda_c^+ \pi^0 \pi^0$ and $\Lambda_c^+ \pi^+ \pi^-$ partial widths as a function of the $\Lambda_c(2595)^+ - \Lambda_c^+$ mass difference. At our value of the mass difference, the ratio is about 4.

[b] A test that the isospin is indeed 0, so that the particle is indeed a Λ_c^+ .

$\Lambda_c(2595)^+$ BRANCHING RATIOS

$\Gamma(\Sigma_c(2455)^{++} \pi^-)/\Gamma(\Lambda_c^+ \pi^+ \pi^-)$				Γ_2/Γ_1
VALUE	DOCUMENT ID	TECN	COMMENT	
0.36 ± 0.10 OUR AVERAGE				
0.37 ± 0.12 ± 0.13	ALBRECHT 97	ARG	$e^+ e^- \approx 10$ GeV	
0.36 ± 0.09 ± 0.09	EDWARDS 95	CLE2	$e^+ e^- \approx 10.5$ GeV	

$\Gamma(\Sigma_c(2455)^0 \pi^+)/\Gamma(\Lambda_c^+ \pi^+ \pi^-)$				Γ_3/Γ_1
VALUE	DOCUMENT ID	TECN	COMMENT	
0.37 ± 0.10 OUR AVERAGE				
0.29 ± 0.10 ± 0.11	ALBRECHT 97	ARG	$e^+ e^- \approx 10$ GeV	
0.42 ± 0.09 ± 0.09	EDWARDS 95	CLE2	$e^+ e^- \approx 10.5$ GeV	

$[\Gamma(\Sigma_c(2455)^{++} \pi^-) + \Gamma(\Sigma_c(2455)^0 \pi^+)]/\Gamma(\Lambda_c^+ \pi^+ \pi^-)$				$(\Gamma_2 + \Gamma_3)/\Gamma_1$
VALUE	CL%	DOCUMENT ID	TECN	COMMENT
• • • We do not use the following data for averages, fits, limits, etc. • • •				
0.66 ^{+0.13} _{-0.16} ± 0.07		ALBRECHT 97	ARG	$e^+ e^- \approx 10$ GeV
>0.51	90	3 FRABETTI 96	E687	γ Be, $\bar{E}_\gamma \approx 220$ GeV

³The results of FRABETTI 96 are consistent with this ratio being 100%.

$\Gamma(\Lambda_c^+ \pi^0)/\Gamma(\Lambda_c^+ \pi^+ \pi^-)$				Γ_5/Γ_1
VALUE	CL%	DOCUMENT ID	TECN	COMMENT
<3.53	90	EDWARDS 95	CLE2	$e^+ e^- \approx 10.5$ GeV

$\Lambda_c^+ \pi^0$ decay is forbidden by isospin conservation if this state is in fact a Λ_c .

$\Gamma(\Lambda_c^+ \gamma)/\Gamma(\Lambda_c^+ \pi^+ \pi^-)$				Γ_6/Γ_1
VALUE	CL%	DOCUMENT ID	TECN	COMMENT
<0.98	90	EDWARDS 95	CLE2	$e^+ e^- \approx 10.5$ GeV

$\Lambda_c(2595)^+$ REFERENCES

AALTONEN 11H	PR D84 012003	T. Aaltonen et al.	(CDF Collab.)
BLECHMAN 03	PR D67 074033	A.E. Blechman et al.	(JHU, FLOR)
ALBRECHT 97	PL B402 207	H. Albrecht et al.	(ARGUS Collab.)
FRABETTI 96	PL B365 461	P.L. Frabetti et al.	(FNAL E687 Collab.)
EDWARDS 95	PRL 74 3331	K.W. Edwards et al.	(CLEO Collab.)

$\Lambda_c(2625)^+$

$I(J^P) = 0(\frac{3}{2}^-)$ Status: ***

The spin-parity has not been measured but is expected to be $3/2^-$: this is presumably the charm counterpart of the strange $\Lambda(1520)$.

$\Lambda_c(2625)^+$ MASS

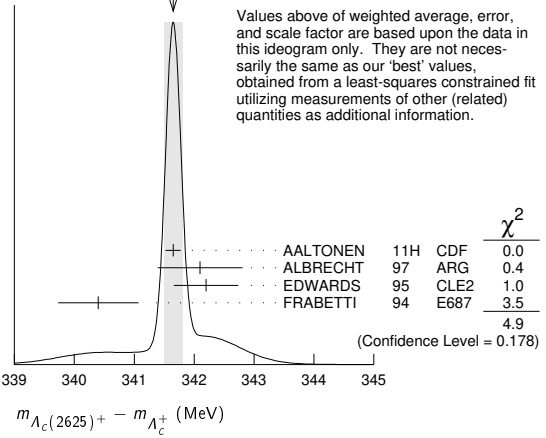
The mass is obtained from the $\Lambda_c(2625)^+ - \Lambda_c^+$ mass-difference measurements below.

VALUE (MeV)	EVTS	DOCUMENT ID	TECN	COMMENT
2628.11 ± 0.19 OUR FIT				Error includes scale factor of 1.1.
• • • We do not use the following data for averages, fits, limits, etc. • • •				
2626.6 ± 0.5 ± 1.5	42 ± 9	ALBRECHT 93F	ARG	See ALBRECHT 97

$\Lambda_c(2625)^+ - \Lambda_c^+$ MASS DIFFERENCE

VALUE (MeV)	EVTS	DOCUMENT ID	TECN	COMMENT
341.65 ± 0.13 OUR FIT				Error includes scale factor of 1.1.
341.65 ± 0.15 OUR AVERAGE				Error includes scale factor of 1.3. See the ideogram below.
341.65 ± 0.04 ± 0.12	6.2k	AALTONEN 11H	CDF	$p\bar{p}$ at 1.96 TeV
342.1 ± 0.5 ± 0.5	51	ALBRECHT 97	ARG	$e^+ e^- \approx 10$ GeV
342.2 ± 0.2 ± 0.5	245 ± 19	EDWARDS 95	CLE2	$e^+ e^- \approx 10.5$ GeV
340.4 ± 0.6 ± 0.3	40 ± 9	FRABETTI 94	E687	γ Be, $\bar{E}_\gamma = 220$ GeV

WEIGHTED AVERAGE
341.65±0.15 (Error scaled by 1.3)



$\Lambda_c(2625)^+$ WIDTH

VALUE (MeV)	CL%	EVTS	DOCUMENT ID	TECN	COMMENT
<0.97	90	6.2k	AALTONEN 11H	CDF	$p\bar{p}$ at 1.96 TeV
• • • We do not use the following data for averages, fits, limits, etc. • • •					
<1.9	90	245 ± 19	EDWARDS 95	CLE2	$e^+ e^- \approx 10.5$ GeV
<3.2	90		ALBRECHT 93F	ARG	$e^+ e^- \approx \Upsilon(4S)$

$\Lambda_c(2625)^+$ DECAY MODES

$\Lambda_c^+ \pi \pi$ and its submode $\Sigma(2455) \pi$ are the only strong decays allowed to an excited Λ_c^+ having this mass.

Mode	Fraction (Γ_i/Γ)	Confidence level
Γ_1 $\Lambda_c^+ \pi^+ \pi^-$	$\approx 67\%$	
Γ_2 $\Sigma_c(2455)^{++} \pi^-$	<5	90%
Γ_3 $\Sigma_c(2455)^0 \pi^+$	<5	90%
Γ_4 $\Lambda_c^+ \pi^+ \pi^-$ 3-body	large	
Γ_5 $\Lambda_c^+ \pi^0$	[a] not seen	
Γ_6 $\Lambda_c^+ \gamma$	not seen	

[a] A test that the isospin is indeed 0, so that the particle is indeed a Λ_c^+ .

$\Lambda_c(2625)^+$ BRANCHING RATIOS

$\Gamma(\Sigma_c(2455)^{++} \pi^-)/\Gamma(\Lambda_c^+ \pi^+ \pi^-)$				Γ_2/Γ_1
VALUE	CL%	DOCUMENT ID	TECN	COMMENT
<0.08	90	EDWARDS 95	CLE2	$e^+ e^- \approx 10.5$ GeV

$\Gamma(\Sigma_c(2455)^0 \pi^+)/\Gamma(\Lambda_c^+ \pi^+ \pi^-)$				Γ_3/Γ_1
VALUE	CL%	DOCUMENT ID	TECN	COMMENT
<0.07	90	EDWARDS 95	CLE2	$e^+ e^- \approx 10.5$ GeV

$[\Gamma(\Sigma_c(2455)^{++} \pi^-) + \Gamma(\Sigma_c(2455)^0 \pi^+)]/\Gamma(\Lambda_c^+ \pi^+ \pi^-)$				$(\Gamma_2 + \Gamma_3)/\Gamma_1$	
VALUE	CL%	EVTS	DOCUMENT ID	TECN	COMMENT
• • • We do not use the following data for averages, fits, limits, etc. • • •					
<0.36	90		FRABETTI 94	E687	γ Be, $\bar{E}_\gamma = 220$ GeV
0.46 ± 0.14		21	ALBRECHT 93F	ARG	$e^+ e^- \approx \Upsilon(4S)$

$\Gamma(\Lambda_c^+ \pi^+ \pi^- \text{ 3-body})/\Gamma(\Lambda_c^+ \pi^+ \pi^-)$				Γ_4/Γ_1
VALUE	EVTS	DOCUMENT ID	TECN	COMMENT
• • • We do not use the following data for averages, fits, limits, etc. • • •				
0.54 ± 0.14	16	ALBRECHT 93F	ARG	$e^+ e^- \approx \Upsilon(4S)$

Baryon Particle Listings

 $\Lambda_c(2625)^+$, $\Lambda_c(2765)^+$, $\Lambda_c(2860)^+$, $\Lambda_c(2880)^+$

$\Gamma(\Lambda_c^+ \pi^0)/\Gamma(\Lambda_c^+ \pi^+ \pi^-)$ Γ_5/Γ_1
 $\Lambda_c^+ \pi^0$ decay is forbidden by isospin conservation if this state is in fact a Λ_c .

VALUE	CL%	DOCUMENT ID	TECN	COMMENT
<0.91	90	EDWARDS	95	CLE2 $e^+ e^- \approx 10.5$ GeV

$\Gamma(\Lambda_c^+ \gamma)/\Gamma(\Lambda_c^+ \pi^+ \pi^-)$ Γ_6/Γ_1

VALUE	CL%	DOCUMENT ID	TECN	COMMENT
<0.52	90	EDWARDS	95	CLE2 $e^+ e^- \approx 10.5$ GeV

 $\Lambda_c(2625)^+$ REFERENCES

AALTONEN	11H	PR D84 012003	T. Aaltonen et al.	(CDF Collab.)
ALBRECHT	97	PL B402 207	H. Albrecht et al.	(ARGUS Collab.)
EDWARDS	95	PRL 74 3331	K.W. Edwards et al.	(CLEO Collab.)
FRABETTI	94	PRL 72 961	P.L. Frabetti et al.	(FNAL E687 Collab.)
ALBRECHT	93F	PL B317 227	H. Albrecht et al.	(ARGUS Collab.)

$\Lambda_c(2765)^+$ or $\Sigma_c(2765)$ $I(J^P) = ?(??)$ Status: *

OMITTED FROM SUMMARY TABLE

A broad, statistically significant peak (997^{+141}_{-129} events) seen in $\Lambda_c^+ \pi^+ \pi^-$. However, nothing at all is known about its quantum numbers, including whether it is a Λ_c^+ or a Σ_c , or whether the width might be due to overlapping states.

 $\Lambda_c(2765)^+$ MASS

The mass is obtained from the $\Lambda_c(2765)^+ - \Lambda_c^+$ mass-difference measurement below.

VALUE (MeV)	DOCUMENT ID
2766.6 ± 2.4 OUR FIT	

 $\Lambda_c(2765)^+ - \Lambda_c^+$ MASS DIFFERENCE

VALUE (MeV)	EVTS	DOCUMENT ID	TECN	COMMENT
480.1 ± 2.4 OUR FIT				
480.1 ± 2.4	997^{+141}_{-129}	ARTUSO	01	CLE2 $e^+ e^- \approx \mathcal{T}(4S)$

 $\Lambda_c(2765)^+$ WIDTH

VALUE (MeV)	DOCUMENT ID	TECN	COMMENT
50	ARTUSO	01	CLE2 $e^+ e^- \approx \mathcal{T}(4S)$

 $\Lambda_c(2765)^+$ DECAY MODES

Mode	Fraction (Γ_i/Γ)
Γ_1 $\Lambda_c^+ \pi^+ \pi^-$	seen

 $\Lambda_c(2765)^+$ REFERENCES

ARTUSO	01	PRL 86 4479	M. Artuso et al.	(CLEO Collab.)
--------	----	-------------	------------------	----------------

$\Lambda_c(2860)^+$ $I(J^P) = 0(\frac{3}{2}^+)$ Status: ***

 $\Lambda_c(2860)^+$ MASS

VALUE (MeV)	DOCUMENT ID	TECN	COMMENT
2856.1 ± 2.0 ± 0.5 ± 1.1 ± 1.7 ± 0.5 ± 5.6	¹ AAIJ	17s	LHCB in $\Lambda_b^0 \rightarrow D^0 p \pi^-$

¹ The third AAIJ 17s uncertainty comes from modeling the resonant shape of the nearby $\Lambda_c(2880)^+$ and the background (non-resonant) amplitudes.

 $\Lambda_c(2860)^+$ WIDTH

VALUE (MeV)	DOCUMENT ID	TECN	COMMENT
67.6 ± 10.1 ± 8.1 ± 1.4 ± 5.9 ± 20.0	¹ AAIJ	17s	LHCB in $\Lambda_b^0 \rightarrow D^0 p \pi^-$

¹ The third AAIJ 17s uncertainty comes from modeling the resonant shape of the nearby $\Lambda_c(2880)^+$ and the background (non-resonant) amplitudes.

 $\Lambda_c(2860)^+$ DECAY MODES

Mode	Fraction (Γ_i/Γ)
Γ_1 $D^0 p$	seen

 $\Lambda_c(2860)^+$ BRANCHING RATIOS

$\Gamma(D^0 p)/\Gamma_{\text{total}}$	DOCUMENT ID	TECN	COMMENT	Γ_1/Γ
seen	AAIJ	17s	LHCB in $\Lambda_b^0 \rightarrow D^0 p \pi^-$	

 $\Lambda_c(2860)^+$ REFERENCES

AAIJ	17s	JHEP 1705 030	R. Aaij et al.	(LHCb Collab.) JP
------	-----	---------------	----------------	-------------------

$\Lambda_c(2880)^+$ $I(J^P) = 0(\frac{5}{2}^+)$ Status: ***

A narrow peak seen in $\Lambda_c^+ \pi^+ \pi^-$ and in $p D^0$. It is not seen in $p D^+$, and therefore it is a Λ_c^+ and not a Σ_c .

 $\Lambda_c(2880)^+$ MASS

VALUE (MeV)	EVTS	DOCUMENT ID	TECN	COMMENT
2881.63 ± 0.24 OUR FIT				
2881.62 ± 0.24 OUR AVERAGE				
$2881.75 \pm 0.29 \pm 0.07^{+0.14}_{-0.20}$	¹ AAIJ	17s	LHCB	in $\Lambda_b^0 \rightarrow D^0 p \pi^-$
$2881.9 \pm 0.1 \pm 0.5$	2.8k	AUBERT	07	BABR in $p D^0$
$2881.2 \pm 0.2 \pm 0.4$	690	MIZUK	07	BELL in $\Sigma_c(2455)^{0,++} \pi^\pm$

¹ The third AAIJ 17s uncertainty comes from modeling the resonant shape of the $\Lambda_c(2880)^+$ and the background (non-resonant) amplitudes.

 $\Lambda_c(2880)^+ - \Lambda_c^+$ MASS DIFFERENCE

VALUE (MeV)	EVTS	DOCUMENT ID	TECN	COMMENT
595.17 ± 0.28 OUR FIT				
596 ± 1 ± 2	350	ARTUSO	01	CLE2 in $\Lambda_c^+ \pi^+ \pi^-$

 $\Lambda_c(2880)^+$ WIDTH

VALUE (MeV)	CL%	EVTS	DOCUMENT ID	TECN	COMMENT
5.6 ± 0.8 ± 0.6 OUR AVERAGE					
$5.43^{+0.77+0.81}_{-0.71-0.29}$		² AAIJ	17s	LHCB	in $\Lambda_b^0 \rightarrow D^0 p \pi^-$
$5.8 \pm 1.5 \pm 1.1$	2.8k	AUBERT	07	BABR	in $p D^0$
$5.8 \pm 0.7 \pm 1.1$	690	MIZUK	07	BELL	in $\Sigma_c(2455)^{0,++} \pi^\pm$
••• We do not use the following data for averages, fits, limits, etc. •••					
<8	90	ARTUSO	01	CLEO	in $\Lambda_c^+ \pi^+ \pi^-$

² AAIJ 17s reports $5.43^{+0.77+0.81}_{-0.71-0.29} \pm 0.29^{+0.75}_{-0.00}$ MeV value where the third uncertainty comes from modeling the resonant shape of the $\Lambda_c(2880)^+$ and the background (non-resonant) amplitudes. We have combined in quadrature the systematic uncertainties.

 $\Lambda_c(2880)^+$ DECAY MODES

Mode	Fraction (Γ_i/Γ)
Γ_1 $\Lambda_c^+ \pi^+ \pi^-$	seen
Γ_2 $\Sigma_c(2455)^{0,++} \pi^\pm$	seen
Γ_3 $\Sigma_c(2520)^{0,++} \pi^\pm$	seen
Γ_4 $p D^0$	seen

 $\Lambda_c(2880)^+$ BRANCHING RATIOS

$\Gamma(\Sigma_c(2455)^{0,++} \pi^\pm)/\Gamma(\Lambda_c^+ \pi^+ \pi^-)$	DOCUMENT ID	TECN	COMMENT	Γ_2/Γ_1
0.392 ± 0.031 OUR AVERAGE			Error includes scale factor of 1.3.	
$0.404 \pm 0.021 \pm 0.014$	MIZUK	07	BELL in $\Sigma_c(2455)^{0,++} \pi^\pm$	
$0.31 \pm 0.06 \pm 0.03$	96	ARTUSO	01	CLE2 $e^+ e^- \approx \mathcal{T}(4S)$

$\Gamma(\Sigma_c(2520)^{0,++} \pi^\pm)/\Gamma(\Lambda_c^+ \pi^+ \pi^-)$	DOCUMENT ID	TECN	COMMENT	Γ_3/Γ_1
0.091 ± 0.025 ± 0.010	MIZUK	07	BELL in $\Sigma_c(2455)^{0,++} \pi^\pm$	
••• We do not use the following data for averages, fits, limits, etc. •••				
<0.11	90	ARTUSO	01	CLE2 $e^+ e^- \approx \mathcal{T}(4S)$

See key on page 999

Baryon Particle Listings

$\Lambda_c(2880)^+, \Lambda_c(2940)^+, \Sigma_c(2455)$

$\Gamma(\Sigma_c(2520)^{0,++}\pi^\pm)/\Gamma(\Sigma_c(2455)^{0,++}\pi^\pm)$ Γ_3/Γ_2

VALUE	DOCUMENT ID	TECN	COMMENT
0.225 ± 0.062 ± 0.025	³ MIZUK	07	BELL in $\Sigma_c(2455)^{0,++}\pi^\pm$

³This MIZUK 07 ratio is redundant with MIZUK 07 ratios given above.

$\Lambda_c(2880)^+$ REFERENCES

AAIJ	175	JHEP 1705 030	R. Aaij <i>et al.</i>	(LHCb Collab.) JP
AUBERT	07	PRL 98 012001	B. Aubert <i>et al.</i>	(BABAR Collab.)
MIZUK	07	PRL 98 262001	R. Mizuk <i>et al.</i>	(BELLE Collab.)
ARTUSO	01	PRL 86 4479	M. Artuso <i>et al.</i>	(CLEO Collab.)

$\Lambda_c(2940)^+$

$$I(J^P) = 0(\frac{3}{2}^-) \text{ Status: } ***$$

A narrow peak seen in pD^0 and in $\Lambda_c^+\pi^+\pi^-$. It is not seen in pD^+ , and therefore it is a Λ_c^+ and not a Σ_c . $J^P = 3/2^-$ is favored, but not certain.

$\Lambda_c(2940)^+$ MASS

VALUE (MeV)	EVTS	DOCUMENT ID	TECN	COMMENT
2939.6^{+1.3}_{-1.5} OUR AVERAGE				
2944.8 ^{+3.5} _{-2.5} ± 0.4 ^{+0.1} _{-4.6}	1	AAIJ	17s	LHCB in $\Lambda_b^0 \rightarrow D^0 p \pi^-$
2939.8 ± 1.3 ± 1.0	2.2k	AUBERT	07	BABR in pD^0
2938.0 ± 1.3 ^{+2.0} _{-4.0}	220	MIZUK	07	BELL in $\Sigma_c(2455)^{0,++}\pi^\pm$

¹The third AAIJ 17s uncertainty comes from modeling the resonant shape of the nearby $\Lambda_c(2880)^+$ and the background (non-resonant) amplitudes.

$\Lambda_c(2940)^+$ WIDTH

VALUE (MeV)	EVTS	DOCUMENT ID	TECN	COMMENT
20⁺⁶₋₅ OUR AVERAGE				
27.7 ^{+8.2} _{-6.0} ± 0.9 ^{+5.2} _{-10.4}	2	AAIJ	17s	LHCB in $\Lambda_b^0 \rightarrow D^0 p \pi^-$
17.5 ± 5.2 ± 5.9	2.2k	AUBERT	07	BABR in pD^0
13 ⁺⁸ ₋₅ ⁺²⁷ ₋₇	220	MIZUK	07	BELL in $\Sigma_c(2455)^{0,++}\pi^\pm$

²The third AAIJ 17s uncertainty comes from modeling the resonant shape of the nearby $\Lambda_c(2880)^+$ and the background (non-resonant) amplitudes.

$\Lambda_c(2940)^+$ DECAY MODES

Mode	Fraction (Γ_i/Γ)
Γ_1 pD^0	seen
Γ_2 $\Sigma_c(2455)^{0,++}\pi^\pm$	seen

$\Lambda_c(2940)^+$ REFERENCES

AAIJ	175	JHEP 1705 030	R. Aaij <i>et al.</i>	(LHCb Collab.) JP
AUBERT	07	PRL 98 012001	B. Aubert <i>et al.</i>	(BABAR Collab.)
MIZUK	07	PRL 98 262001	R. Mizuk <i>et al.</i>	(BELLE Collab.)

$\Sigma_c(2455)$

$$I(J^P) = 1(\frac{1}{2}^+) \text{ Status: } ****$$

The angular distribution of $B^- \rightarrow \Sigma_c(2455)^0 \bar{p}$ favors $J = 1/2$ (as the quark model predicts). $J = 3/2$ is excluded by more than four standard deviations; see AUBERT 08BN.

$\Sigma_c(2455)$ MASSES

The masses are obtained from the mass-difference measurements that follow.

$\Sigma_c(2455)^{++}$ MASS

VALUE (MeV)	DOCUMENT ID
2453.97 ± 0.14 OUR FIT	

$\Sigma_c(2455)^+$ MASS

VALUE (MeV)	DOCUMENT ID
2452.9 ± 0.4 OUR FIT	

$\Sigma_c(2455)^0$ MASS

VALUE (MeV)	DOCUMENT ID
2453.75 ± 0.14 OUR FIT	

$\Sigma_c(2455) - \Lambda_c^+$ MASS DIFFERENCES

$m_{\Sigma_c^{++}} - m_{\Lambda_c^+}$

VALUE (MeV)	EVTS	DOCUMENT ID	TECN	COMMENT
167.510 ± 0.017 OUR FIT				
167.510 ± 0.022 OUR AVERAGE				
167.51 ± 0.01 ± 0.02	36k	LEE	14	BELL e^+e^- at $\Upsilon(4S)$
167.44 ± 0.04 ± 0.12	13.8k	AALTONEN	11H	CDF $p\bar{p}$ at 1.96 TeV
167.4 ± 0.1 ± 0.2	2k	ARTUSO	02	CLE2 $e^+e^- \approx \Upsilon(4S)$
167.35 ± 0.19 ± 0.12	461	LINK	00c	FOCS $\gamma A, \bar{E}_\gamma$ 180 GeV
167.76 ± 0.29 ± 0.15	122	AITALA	96B	E791 $\pi^- N, 500$ GeV
167.6 ± 0.6 ± 0.6	56	FRABETTI	96	E687 $\gamma Be, \bar{E}_\gamma \approx 220$ GeV
168.2 ± 0.3 ± 0.2	126	CRAWFORD	93	CLE2 $e^+e^- \approx \Upsilon(4S)$
167.8 ± 0.4 ± 0.3	54	BOWCOCK	89	CLEO $e^+e^- \approx 10$ GeV
168.2 ± 0.5 ± 1.6	92	ALBRECHT	88D	ARG $e^+e^- \approx 10$ GeV
167.4 ± 0.5 ± 2.0	46	DIESBURG	87	SPEC $nA \sim 600$ GeV
167 ± 1	2	JONES	87	HBC νp in BEBC
166 ± 1	1	BOSETTI	82	HBC See JONES 87
168 ± 3	6	BALTAY	79	HLBC ν Ne-H in 15-ft
166 ± 15	1	CAZZOLI	75	HBC νp in BNL 7-ft

$m_{\Sigma_c^+} - m_{\Lambda_c^+}$

VALUE (MeV)	EVTS	DOCUMENT ID	TECN	COMMENT
166.4 ± 0.4 OUR FIT				
166.4 ± 0.2 ± 0.3	661	AMMAR	01	CLE2 $e^+e^- \approx \Upsilon(4S)$
168.5 ± 0.4 ± 0.2	111	CRAWFORD	93	CLE2 See AMMAR 01
168 ± 3	1	CALICCHIO	80	HBC νp in BEBC-TST

$m_{\Sigma_c^0} - m_{\Lambda_c^+}$

VALUE (MeV)	EVTS	DOCUMENT ID	TECN	COMMENT
167.290 ± 0.017 OUR FIT				
167.290 ± 0.022 OUR AVERAGE				
167.29 ± 0.01 ± 0.02	32k	LEE	14	BELL e^+e^- at $\Upsilon(4S)$
167.28 ± 0.03 ± 0.12	15.9k	AALTONEN	11H	CDF $p\bar{p}$ at 1.96 TeV
167.2 ± 0.1 ± 0.2	2k	ARTUSO	02	CLE2 $e^+e^- \approx \Upsilon(4S)$
167.38 ± 0.21 ± 0.13	362	LINK	00c	FOCS $\gamma A, \bar{E}_\gamma$ 180 GeV
167.38 ± 0.29 ± 0.15	143	AITALA	96B	E791 $\pi^- N, 500$ GeV
167.8 ± 0.6 ± 0.2		ALEEV	96	SPEC n nucleus, 50 GeV/c
166.6 ± 0.5 ± 0.6	69	FRABETTI	96	E687 $\gamma Be, \bar{E}_\gamma \approx 220$ GeV
167.1 ± 0.3 ± 0.2	124	CRAWFORD	93	CLE2 $e^+e^- \approx \Upsilon(4S)$
168.4 ± 1.0 ± 0.3	14	ANJOS	89D	E691 γBe 90–260 GeV
167.9 ± 0.5 ± 0.3	48	¹ BOWCOCK	89	CLEO e^+e^- 10 GeV
167.0 ± 0.5 ± 1.6	70	¹ ALBRECHT	88D	ARG e^+e^- 10 GeV
178.2 ± 0.4 ± 2.0	85	² DIESBURG	87	SPEC $nA \sim 600$ GeV
163 ± 2	1	AMMAR	86	EMUL νA

¹This result enters the fit through $m_{\Sigma_c^{++}} - m_{\Sigma_c^0}$ given below.

²See the note on DIESBURG 87 in the $m_{\Sigma_c^{++}} - m_{\Sigma_c^0}$ section below.

$\Sigma_c(2455)$ MASS DIFFERENCES

$m_{\Sigma_c^{++}} - m_{\Sigma_c^0}$

VALUE (MeV)	DOCUMENT ID	TECN	COMMENT
0.220 ± 0.013 OUR FIT			
0.221 ± 0.014 OUR AVERAGE			
0.22 ± 0.01 ± 0.01	14	BELL	e^+e^- at $\Upsilon(4S)$
0.2 ± 0.1 ± 0.1	02	CLE2	$e^+e^- \approx \Upsilon(4S)$
-0.03 ± 0.28 ± 0.11	00c	FOCS	$\gamma A, \bar{E}_\gamma$ 180 GeV
0.38 ± 0.40 ± 0.15	96B	E791	$\pi^- N, 500$ GeV
1.1 ± 0.4 ± 0.1	93	CLE2	$e^+e^- \approx \Upsilon(4S)$
-0.1 ± 0.6 ± 0.1	89	CLEO	$e^+e^- \approx 10$ GeV
1.2 ± 0.7 ± 0.3	88D	ARG	$e^+e^- \approx 10$ GeV
-10.8 ± 2.9	³ DIESBURG	87	SPEC $nA \sim 600$ GeV

³DIESBURG 87 is completely incompatible with the other experiments, which is surprising since it agrees with them about $m_{\Sigma_c(2455)^{++}} - m_{\Lambda_c^+}$. We go with the majority here.

$m_{\Sigma_c^+} - m_{\Sigma_c^0}$

VALUE (MeV)	DOCUMENT ID	TECN	COMMENT
-0.9 ± 0.4 OUR FIT			
1.4 ± 0.5 ± 0.3	93	CLE2	See AMMAR 01

^{•••}We do not use the following data for averages, fits, limits, etc. ^{•••}

Baryon Particle Listings

$\Sigma_c(2455), \Sigma_c(2520)$

$\Sigma_c(2455)$ WIDTHS

$\Sigma_c(2455)^{++}$ WIDTH

VALUE (MeV)	EVTS	DOCUMENT ID	TECN	COMMENT
$1.89^{+0.09}_{-0.18}$ OUR AVERAGE		Error includes scale factor of 1.1.		
$1.84 \pm 0.04^{+0.07}_{-0.20}$	36k	LEE	14	BELL e^+e^- at $\Upsilon(4S)$
$2.34 \pm 0.13 \pm 0.45$	13.8k	AALTONEN	11H	CDF $p\bar{p}$ at 1.96 TeV
$2.3 \pm 0.2 \pm 0.3$	2k	ARTUSO	02	CLE2 $e^+e^- \approx \Upsilon(4S)$
$2.05^{+0.41}_{-0.38} \pm 0.38$	1110	LINK	02	FOCS $\gamma A, \bar{E}_\gamma \approx 180$ GeV

$\Sigma_c(2455)^+$ WIDTH

VALUE (MeV)	CL%	EVTS	DOCUMENT ID	TECN	COMMENT
<4.6	90	661	AMMAR	01	CLE2 $e^+e^- \approx \Upsilon(4S)$

$\Sigma_c(2455)^0$ WIDTH

VALUE (MeV)	EVTS	DOCUMENT ID	TECN	COMMENT
$1.83^{+0.11}_{-0.19}$ OUR AVERAGE		Error includes scale factor of 1.2.		
$1.76 \pm 0.04^{+0.09}_{-0.21}$	32k	LEE	14	BELL e^+e^- at $\Upsilon(4S)$
$1.65 \pm 0.11 \pm 0.49$	15.9k	AALTONEN	11H	CDF $p\bar{p}$ at 1.96 TeV
$2.6 \pm 0.5 \pm 0.3$		AUBERT	08BN	BABR $B^- \rightarrow \bar{p}\Lambda_c^+\pi^-$
$2.5 \pm 0.2 \pm 0.3$	2k	ARTUSO	02	CLE2 $e^+e^- \approx \Upsilon(4S)$
$1.55^{+0.41}_{-0.37} \pm 0.38$	913	LINK	02	FOCS $\gamma A, \bar{E}_\gamma \approx 180$ GeV

$\Sigma_c(2455)$ DECAY MODES

$\Lambda_c^+\pi$ is the only strong decay allowed to a Σ_c having this mass.

Mode	Fraction (Γ_i/Γ)
$\Gamma_1 \Lambda_c^+\pi$	$\approx 100\%$

$\Sigma_c(2455)$ REFERENCES

LEE	14	PR D89 091102	S.-H. Lee <i>et al.</i>	(BELLE Collab.)
AALTONEN	11H	PR D84 012003	T. Aaltonen <i>et al.</i>	(CDF Collab.)
AUBERT	08BN	PR D78 112003	B. Aubert <i>et al.</i>	(BABAR Collab.)
ARTUSO	02	PR D65 071101	M. Artuso <i>et al.</i>	(CLEO Collab.)
LINK	02	PL B525 205	J.M. Link <i>et al.</i>	(FNAL FOCUS Collab.)
AMMAR	01	PRL 86 1167	R. Ammar <i>et al.</i>	(CLEO Collab.)
LINK	00C	PL B488 218	J.M. Link <i>et al.</i>	(FNAL FOCUS Collab.)
AITALA	96B	PL B379 292	E.M. Aitala <i>et al.</i>	(FNAL E791 Collab.)
ALEV	96	JINRRC 3-77 31	A.N. Alev <i>et al.</i>	(Serpukhov EXCHARM Collab.)
FRABETTI	96	PL B365 461	P.L. Frabetti <i>et al.</i>	(FNAL E687 Collab.)
CRAWFORD	93	PRL 71 3259	G. Crawford <i>et al.</i>	(CLEO Collab.)
ANJOS	89D	PRL 62 1721	J.C. Anjos <i>et al.</i>	(FNAL E691 Collab.)
BOWCOCK	89	PRL 62 1240	T.J.V. Bowcock <i>et al.</i>	(CLEO Collab.)
ALBRECHT	88D	PL B211 489	H. Albrecht <i>et al.</i>	(ARGUS Collab.)
DIESBURG	87	PRL 59 2711	M. Diesburg <i>et al.</i>	(FNAL E400 Collab.)
JONES	87	ZPHY C36 593	G.T. Jones <i>et al.</i>	(CERN WA21 Collab.)
AMMAR	86	JETPL 43 515	R. Ammar <i>et al.</i>	(ITEP)
Translated from ZETFP 43 401.				
BOSETTI	82	PL 109B 234	P.C. Bosetti <i>et al.</i>	(AACH3, BONN, CERN+)
CALICCHIO	80	PL 93B 521	M. Calicchio <i>et al.</i>	(BARI, BIRM, BRUX+)
BALTAY	79	PRL 42 1721	C. Baltay <i>et al.</i>	(COLU, BNL)
CAZZOLI	75	PRL 34 1125	E.G. Cazzoli <i>et al.</i>	(BNL)

$\Sigma_c(2520)$

$$I(J^P) = 1(\frac{3}{2}^+) \text{ Status: } ***$$

Seen in the $\Lambda_c^+\pi^\pm$ mass spectrum. The natural assignment is that this is the $J^P = 3/2^+$ excitation of the $\Sigma_c(2455)$, the charm counterpart of the $\Sigma(1385)$, but neither J nor P has been measured.

$\Sigma_c(2520)$ MASSES

The masses are obtained from the mass-difference measurements that follow.

$\Sigma_c(2520)^{++}$ MASS

VALUE (MeV)	EVTS	DOCUMENT ID	TECN	COMMENT
$2518.41 \pm 0.21_{-0.19}$ OUR FIT		Error includes scale factor of 1.1.		
••• We do not use the following data for averages, fits, limits, etc. •••				
$2530 \pm 5 \pm 5$	6	¹ AMMOSOV 93	HLBC	$\nu p \rightarrow \mu^- \Sigma_c(2530)^{++}$
¹ AMMOSOV 93 sees a cluster of 6 events and estimates the background to be 1 event.				

$\Sigma_c(2520)^+$ MASS

VALUE (MeV)	DOCUMENT ID
2517.5 ± 2.3 OUR FIT	

$\Sigma_c(2520)^0$ MASS

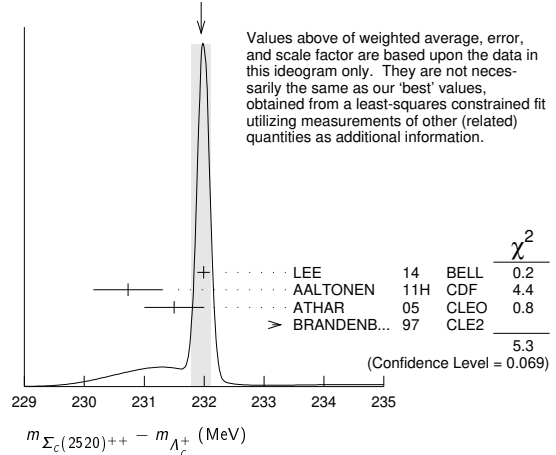
VALUE (MeV)	DOCUMENT ID
2518.48 ± 0.20 OUR FIT	
Error includes scale factor of 1.1.	

$\Sigma_c(2520)$ MASS DIFFERENCES

$m_{\Sigma_c(2520)^{++}} - m_{\Lambda_c^+}$

VALUE (MeV)	EVTS	DOCUMENT ID	TECN	COMMENT
$231.95 \pm 0.17_{-0.12}$ OUR FIT		Error includes scale factor of 1.3.		
231.95 ± 0.16 OUR AVERAGE		Error includes scale factor of 1.6. See the ideogram below.		
$231.99 \pm 0.10 \pm 0.02$	44k	LEE	14	BELL e^+e^- at $\Upsilon(4S)$
$230.73 \pm 0.56 \pm 0.16$	8.8k	AALTONEN	11H	CDF $p\bar{p}$ at 1.96 TeV
$231.5 \pm 0.4 \pm 0.3$	1.3k	ATHAR	05	CLEO e^+e^- , 9.4-11.5 GeV
$234.5 \pm 1.1 \pm 0.8$	677	BRANDENB...	97	CLE2 $e^+e^- \approx \Upsilon(4S)$

WEIGHTED AVERAGE
231.95±0.16 (Error scaled by 1.6)



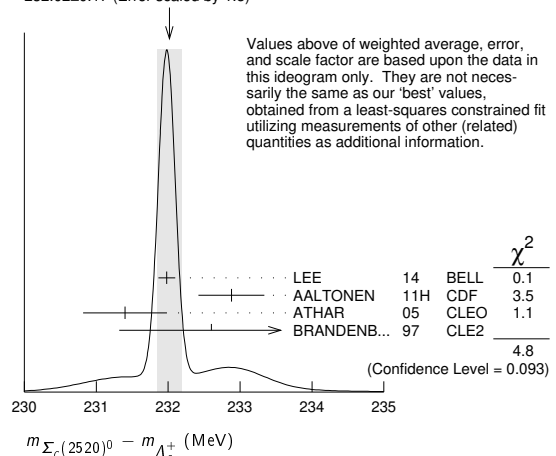
$m_{\Sigma_c(2520)^+} - m_{\Lambda_c^+}$

VALUE (MeV)	EVTS	DOCUMENT ID	TECN	COMMENT
231.0 ± 2.3 OUR FIT		Error includes scale factor of 1.3.		
$231.0 \pm 1.1 \pm 2.0$	327	AMMAR	01	CLE2 $e^+e^- \approx \Upsilon(4S)$

$m_{\Sigma_c(2520)^0} - m_{\Lambda_c^+}$

VALUE (MeV)	EVTS	DOCUMENT ID	TECN	COMMENT
$232.02 \pm 0.15_{-0.14}$ OUR FIT		Error includes scale factor of 1.3.		
232.02 ± 0.17 OUR AVERAGE		Error includes scale factor of 1.5. See the ideogram below.		
$231.98 \pm 0.11 \pm 0.04$	41k	LEE	14	BELL e^+e^- at $\Upsilon(4S)$
$232.88 \pm 0.43 \pm 0.16$	9.0k	AALTONEN	11H	CDF $p\bar{p}$ at 1.96 TeV
$231.4 \pm 0.5 \pm 0.3$	1.3k	ATHAR	05	CLEO e^+e^- , 9.4-11.5 GeV
$232.6 \pm 1.0 \pm 0.8$	504	BRANDENB...	97	CLE2 $e^+e^- \approx \Upsilon(4S)$

WEIGHTED AVERAGE
232.02±0.17 (Error scaled by 1.5)



$m_{\Sigma_c(2520)^{++}} - m_{\Sigma_c(2520)^0}$

VALUE (MeV)	EVTS	DOCUMENT ID	TECN	COMMENT
$0.01 \pm 0.15 \pm 0.03$	44/41k	LEE	14	BELL e^+e^- at $\Upsilon(4S)$
••• We do not use the following data for averages, fits, limits, etc. •••				
$0.1 \pm 0.8 \pm 0.3$	²	ATHAR	05	CLEO e^+e^- , 9.4-11.5 GeV
$1.9 \pm 1.4 \pm 1.0$	³	BRANDENB...	97	CLE2 $e^+e^- \approx \Upsilon(4S)$

²This ATHAR 05 result is redundant with measurements in earlier entries.
³This BRANDENBURG 97 result is redundant with measurements in earlier entries.

See key on page 999

Baryon Particle Listings

$\Sigma_c(2520), \Sigma_c(2800), \Xi_c^+$

$\Sigma_c(2520)$ WIDTHS

$\Sigma_c(2520)^{++}$ WIDTH

VALUE (MeV)	EVTS	DOCUMENT ID	TECN	COMMENT
14.78^{+0.30}_{-0.40} OUR AVERAGE				
14.77 ± 0.25 ^{+0.18} _{-0.30}	44k	LEE	14	BELL e ⁺ e ⁻ at $\Upsilon(4S)$
15.03 ± 2.12 ± 1.36	8.8k	AALTONEN	11H	CDF $p\bar{p}$ at 1.96 TeV
14.4 ^{+1.6} _{-1.5} ± 1.4	1.3k	ATHAR	05	CLEO e ⁺ e ⁻ , 9.4–11.5 GeV
17.9 ^{+3.8} _{-3.2} ± 4.0	677	BRANDENB...	97	CLE2 e ⁺ e ⁻ $\approx \Upsilon(4S)$

$\Sigma_c(2520)^+$ WIDTH

VALUE (MeV)	CL%	EVTS	DOCUMENT ID	TECN	COMMENT
<17	90	327	AMMAR	01	CLE2 e ⁺ e ⁻ $\approx \Upsilon(4S)$

$\Sigma_c(2520)^0$ WIDTH

VALUE (MeV)	EVTS	DOCUMENT ID	TECN	COMMENT
15.3^{+0.4}_{-0.5} OUR AVERAGE				
15.41 ± 0.41 ^{+0.20} _{-0.32}	41k	LEE	14	BELL e ⁺ e ⁻ at $\Upsilon(4S)$
12.51 ± 1.82 ± 1.37	9.0k	AALTONEN	11H	CDF $p\bar{p}$ at 1.96 TeV
16.6 ^{+1.9} _{-1.7} ± 1.4	1.3k	ATHAR	05	CLEO e ⁺ e ⁻ , 9.4–11.5 GeV
13.0 ^{+3.7} _{-3.0} ± 4.0	504	BRANDENB...	97	CLE2 e ⁺ e ⁻ $\approx \Upsilon(4S)$

$\Sigma_c(2520)$ DECAY MODES

$\Lambda_c^+ \pi$ is the only strong decay allowed to a Σ_c having this mass.

Mode	Fraction (Γ_i/Γ)
$\Gamma_1 \Lambda_c^+ \pi$	$\approx 100\%$

$\Sigma_c(2520)$ REFERENCES

LEE	14	PR D89 091102	S.-H. Lee <i>et al.</i>	(BELLE Collab.)
AALTONEN	11H	PR D84 012003	T. Aaltonen <i>et al.</i>	(CDF Collab.)
ATHAR	05	PR D71 051101	S.B. Athar <i>et al.</i>	(CLEO Collab.)
AMMAR	01	PRL 86 1167	R. Ammar <i>et al.</i>	(CLEO Collab.)
BRANDENB...	97	PRL 78 2304	G. Brandenburg <i>et al.</i>	(CLEO Collab.)
AMMOS OV	93	JETPL 58 247	V.V. Ammosov <i>et al.</i>	(SERP)
Translated from ZETFP 58 241.				

$\Sigma_c(2800)$ $I(J^P) = 1(?^?)$ Status: ***
 Seen in the $\Lambda_c^+ \pi^+$, $\Lambda_c^+ \pi^0$, and $\Lambda_c^+ \pi^-$ mass spectra.

$\Sigma_c(2800)$ MASSES

The charged ++ and + masses are obtained from the mass-difference measurements that follow. The neutral mass is dominated by the mass-difference measurement, but is pulled up somewhat by the less well-determined but considerably higher direct-mass measurement. It is possible, in fact, that AUBERT 08BN is seeing a different Σ_c .

$\Sigma_c(2800)^{++}$ MASS

VALUE (MeV)	DOCUMENT ID
2801⁺⁴₋₆ OUR FIT	

$\Sigma_c(2800)^+$ MASS

VALUE (MeV)	DOCUMENT ID
2792⁺¹⁴₋₅ OUR FIT	

$\Sigma_c(2800)^0$ MASS

VALUE (MeV)	DOCUMENT ID	TECN	COMMENT
2806⁺⁵₋₇ OUR FIT			Error includes scale factor of 1.3.
2846 ± 8 ± 10	AUBERT	08BN BABR	$B^- \rightarrow \bar{p} \Lambda_c^+ \pi^-$

$\Sigma_c(2800)$ MASS DIFFERENCES

$m_{\Sigma_c(2800)^{++}} - m_{\Lambda_c^+}$

VALUE (MeV)	EVTS	DOCUMENT ID	TECN	COMMENT
514⁺⁴₋₆ OUR FIT				
514.5^{+3.4+2.8}_{-3.1-4.9}	2810 ⁺¹⁰⁹⁰ ₋₇₇₅	MIZUK	05	BELL e ⁺ e ⁻ $\approx \Upsilon(4S)$

$m_{\Sigma_c(2800)^+} - m_{\Lambda_c^+}$

VALUE (MeV)	EVTS	DOCUMENT ID	TECN	COMMENT
505⁺¹⁴₋₅ OUR FIT				
505.4^{+5.8+12.4}_{-4.6-2.0}	1540 ⁺¹⁷⁵⁰ ₋₁₀₅₀	MIZUK	05	BELL e ⁺ e ⁻ $\approx \Upsilon(4S)$

$m_{\Sigma_c(2800)^0} - m_{\Lambda_c^+}$

VALUE (MeV)	EVTS	DOCUMENT ID	TECN	COMMENT
519⁺⁵₋₇ OUR FIT				Error includes scale factor of 1.3.
515.4^{+3.2+2.1}_{-3.1-6.0}	2240 ⁺¹³⁰⁰ ₋₇₄₀	MIZUK	05	BELL e ⁺ e ⁻ $\approx \Upsilon(4S)$

$\Sigma_c(2800)$ WIDTHS

$\Sigma_c(2800)^{++}$ WIDTH

VALUE (MeV)	EVTS	DOCUMENT ID	TECN	COMMENT
75⁺¹⁸⁺¹²₋₁₃₋₁₁	2810 ⁺¹⁰⁹⁰ ₋₇₇₅	MIZUK	05	BELL e ⁺ e ⁻ $\approx \Upsilon(4S)$

$\Sigma_c(2800)^+$ WIDTH

VALUE (MeV)	EVTS	DOCUMENT ID	TECN	COMMENT
62⁺³⁷⁺⁵²₋₂₃₋₃₈	1540 ⁺¹⁷⁵⁰ ₋₁₀₅₀	MIZUK	05	BELL e ⁺ e ⁻ $\approx \Upsilon(4S)$

$\Sigma_c(2800)^0$ WIDTH

VALUE (MeV)	EVTS	DOCUMENT ID	TECN	COMMENT
72⁺²²₋₁₅ OUR AVERAGE				
86 ⁺³³ ₋₂₂ ± 12		AUBERT	08BN BABR	$B^- \rightarrow \bar{p} \Lambda_c^+ \pi^-$
61 ⁺¹⁸⁺²² ₋₁₃₋₁₃	2240 ⁺¹³⁰⁰ ₋₇₄₀	MIZUK	05	BELL e ⁺ e ⁻ $\approx \Upsilon(4S)$

$\Sigma_c(2800)$ DECAY MODES

Mode	Fraction (Γ_i/Γ)
$\Gamma_1 \Lambda_c^+ \pi$	seen

$\Sigma_c(2800)$ REFERENCES

AUBERT	08BN	PR D78 112003	B. Aubert <i>et al.</i>	(BABAR Collab.)
MIZUK	05	PRL 94 122002	R. Mizuk <i>et al.</i>	(BELLE Collab.)

Ξ_c^+ $I(J^P) = \frac{1}{2}(\frac{1}{2}^+)$ Status: ***
 Neither of J or P has actually been measured. Nor have any absolute branching fractions been measured.

Ξ_c^+ MASS

The fit uses the Ξ_c^+ and Ξ_c^0 mass and mass-difference measurements.

VALUE (MeV)	EVTS	DOCUMENT ID	TECN	COMMENT
2467.94^{+0.17}_{-0.20} OUR FIT				
2467.95 ± 0.19 OUR AVERAGE				
2467.97 ± 0.14 ± 0.17	3.8k	¹ AAIJ	14Z	LHCB $p\bar{p}$ at 7, 8 TeV
2468.00 ± 0.18 ± 0.51	5.1k	AALTONEN	14B	CDF $p\bar{p}$ at 1.96 TeV
2468.1 ± 0.4 ^{+0.2} _{-1.4}	4.9k	² LESIAK	05	BELL e ⁺ e ⁻ , $\Upsilon(4S)$
2465.8 ± 1.9 ± 2.5	90	FRABETTI	98	E687 γ Be, $\bar{E}_\gamma = 220$ GeV
2467.0 ± 1.6 ± 2.0	147	EDWARDS	96	CLE2 e ⁺ e ⁻ $\approx \Upsilon(4S)$
2465.1 ± 3.6 ± 1.9	30	ALBRECHT	90F	ARG e ⁺ e ⁻ at $\Upsilon(4S)$
2467 ± 3 ± 4	23	ALAM	89	CLEO e ⁺ e ⁻ 10.6 GeV
2466.5 ± 2.7 ± 1.2	5	BARLAG	89c	ACCM π^- Cu 230 GeV
••• We do not use the following data for averages, fits, limits, etc. •••				
2464.4 ± 2.0 ± 1.4	30	FRABETTI	93B	E687 See FRABETTI 98
2459 ± 5 ± 30	56	³ COTEUS	87	SPEC $nA \approx 600$ GeV
2460 ± 25	82	BIAGI	83	SPEC Σ^- Be 135 GeV

¹ AAIJ 14Z systematic error includes in quadrature the 0.14 MeV uncertainty from the $m(\Lambda_c^+)$ mass value.
² The systematic error was (wrongly) given the other way round in LESIAK 05; see the erratum.
³ Although COTEUS 87 claims to agree well with BIAGI 83 on the mass and width, there appears to be a discrepancy between the two experiments. BIAGI 83 sees a single peak (stated significance about 6 standard deviations) in the $\Lambda K^- \pi^+ \pi^+$ mass spectrum. COTEUS 87 sees two peaks in the same spectrum, one at the Ξ_c^+ mass, the other 75 MeV lower. The latter is attributed to $\Xi_c^+ \rightarrow \Sigma^0 K^- \pi^+ \pi^+ \rightarrow (\Lambda \gamma) K^- \pi^+ \pi^+$, with the γ unseen. The combined significance of the double peak is stated to be 5.5

Baryon Particle Listings



standard deviations. But the absence of any trace of a lower peak in BIAGI 83 seems to us to throw into question the interpretation of the lower peak of COTEUS 87.

Ξ_c^+ MEAN LIFE

VALUE (10^{-15} s)	EVTS	DOCUMENT ID	TECN	COMMENT
456 ± 5 OUR AVERAGE				
457 ± 5 ± 3	56k	1 AAIJ	19AG LHCB	$\Xi_c^+ \rightarrow pK^- \pi^+$
503 ± 47 ± 18	250	MAHMOOD	02 CLE2	$e^+ e^- \approx \Upsilon(4S)$
439 ± 22 ± 9	532	LINK	01D FOCS	γ nucleus, $\bar{E}_\gamma \approx 180$ GeV
340 ⁺ ₋₅₀ ± 70 ± 20	56	FRABETTI	98 E687	γ Be, $\bar{E}_\gamma = 220$ GeV
400 ⁺ ₋₁₂₀ ± 180 ± 100	102	COTEUS	87 SPEC	$nA \approx 600$ GeV
480 ⁺ ₋₁₅₀ ± 210 ± 200	53	BIAGI	85c SPEC	Σ^- Be 135 GeV
• • • We do not use the following data for averages, fits, limits, etc. • • •				
410 ⁺ ₋₈₀ ± 110 ± 20	30	FRABETTI	93B E687	See FRABETTI 98
200 ⁺ ₋₁₁₀ ± 60	6	BARLAG	89c ACCM	$\pi^- (K^-)$ Cu 230 GeV

¹ AAIJ 19AG reports $[\Xi_c^+ \text{ MEAN LIFE}] / [D^\pm \text{ MEAN LIFE}] = 0.4392 \pm 0.0034 \pm 0.0028$ which we multiply by our best value $D^\pm \text{ MEAN LIFE} = (1.040 \pm 0.007) \times 10^{-12}$ s. Our first error is their experiment's error and our second error is the systematic error from using our best value.

Ξ_c^+ DECAY MODES

Branching fractions marked with a footnote, e.g. [a], have been corrected for decay modes not observed in the experiments. For example, the sub-mode fraction $\Xi_c^+ \rightarrow \Sigma^+ \bar{K}^*(892)^0$ seen in $\Xi_c^+ \rightarrow \Sigma^+ K^- \pi^+$ has been multiplied up to include $\bar{K}^*(892)^0 \rightarrow \bar{K}^0 \pi^0$ decays.

Mode	Fraction (Γ_i/Γ)	Confidence level
------	--------------------------------	------------------

No absolute branching fractions have been measured. The following are branching ratios relative to $\Xi^- 2\pi^+$.

Cabibbo-favored ($S = -2$) decays — relative to $\Xi^- 2\pi^+$

Γ_1	$p2K_S^0$	0.087 ± 0.021	
Γ_2	$\Lambda \bar{K}^0 \pi^+$	—	
Γ_3	$\Sigma(1385)^+ \bar{K}^0$	[a] 1.0 ± 0.5	
Γ_4	$\Lambda K^- \pi^+$	0.323 ± 0.033	
Γ_5	$\Lambda \bar{K}^*(892)^0 \pi^+$	[a] < 0.16	90%
Γ_6	$\Sigma(1385)^+ K^- \pi^+$	[a] < 0.23	90%
Γ_7	$\Sigma^+ K^- \pi^+$	0.94 ± 0.10	
Γ_8	$\Sigma^+ \bar{K}^*(892)^0$	[a] 0.81 ± 0.15	
Γ_9	$\Sigma^0 K^- 2\pi^+$	0.27 ± 0.12	
Γ_{10}	$\Xi^0 \pi^+$	0.55 ± 0.16	
Γ_{11}	$\Xi^- 2\pi^+$	DEFINED AS 1	
Γ_{12}	$\Xi(1530)^0 \pi^+$	[a] < 0.10	90%
Γ_{13}	$\Xi(1620)^0 \pi^+$	seen	
Γ_{14}	$\Xi(1690)^0 \pi^+$	seen	
Γ_{15}	$\Xi^0 \pi^+ \pi^0$	2.3 ± 0.7	
Γ_{16}	$\Xi^0 \pi^+ 2\pi^+$	1.7 ± 0.5	
Γ_{17}	$\Xi^0 e^+ \nu_e$	2.3 ^{+0.7} _{-0.8}	
Γ_{18}	$\Omega^- K^+ \pi^+$	0.07 ± 0.04	

Cabibbo-suppressed decays — relative to $\Xi^- 2\pi^+$

Γ_{19}	$pK^- \pi^+$	0.0045 ± 0.0022	
Γ_{20}	$p\bar{K}^*(892)^0$	[a] 0.0024 ± 0.0013	
Γ_{21}	$\Sigma^+ \pi^+ \pi^-$	0.48 ± 0.20	
Γ_{22}	$\Sigma^- 2\pi^+$	0.18 ± 0.09	
Γ_{23}	$\Sigma^+ K^+ K^-$	0.15 ± 0.06	
Γ_{24}	$\Sigma^+ \phi$	[a] < 0.11	90%
Γ_{25}	$\Xi(1690)^0 K^+, \Xi^0 \rightarrow \Sigma^+ K^-$	< 0.05	90%
Γ_{26}	$p\phi(1020)$	(9 ± 4) × 10 ⁻⁵	

[a] This branching fraction includes all the decay modes of the final-state resonance.

Ξ_c^+ BRANCHING RATIOS

Cabibbo-favored ($S = -2$) decays

$\Gamma(p2K_S^0)/\Gamma(\Xi^- 2\pi^+)$		Γ_1/Γ_{11}		
VALUE	EVTS	DOCUMENT ID	TECN	COMMENT
0.087 ± 0.016 ± 0.014	168 ± 27	LESIAK	05 BELL	$e^+ e^-$, $\Upsilon(4S)$

$\Gamma(\Sigma(1385)^+ \bar{K}^0)/\Gamma(\Xi^- 2\pi^+)$

Unseen decay modes of the $\Sigma(1385)^+$ are included.

VALUE	EVTS	DOCUMENT ID	TECN	COMMENT
1.00 ± 0.49 ± 0.24	20	LINK	03E FOCS	< 1.72, 90% CL

$\Gamma(\Lambda K^- 2\pi^+)/\Gamma(\Xi^- 2\pi^+)$

VALUE	EVTS	DOCUMENT ID	TECN	COMMENT
0.323 ± 0.033 OUR AVERAGE				
0.32 ± 0.03 ± 0.02	1177 ± 55	LESIAK	05 BELL	$e^+ e^-$, $\Upsilon(4S)$
0.28 ± 0.06 ± 0.06	58	LINK	03E FOCS	γ nucleus, $\bar{E}_\gamma \approx 180$ GeV
0.58 ± 0.16 ± 0.07	61	BERGFELD	96 CLE2	$e^+ e^- \approx \Upsilon(4S)$

$\Gamma(\Lambda \bar{K}^*(892)^0 \pi^+)/\Gamma(\Lambda K^- 2\pi^+)$

Unseen decay modes of the $\bar{K}^*(892)^0$ are included.

VALUE	CL%	DOCUMENT ID	TECN	COMMENT
< 0.5	90	BERGFELD	96 CLE2	$e^+ e^- \approx \Upsilon(4S)$

$\Gamma(\Sigma(1385)^+ K^- \pi^+)/\Gamma(\Lambda K^- 2\pi^+)$

Unseen decay modes of the $\Sigma(1385)^+$ are included.

VALUE	CL%	DOCUMENT ID	TECN	COMMENT
< 0.7	90	BERGFELD	96 CLE2	$e^+ e^- \approx \Upsilon(4S)$

$\Gamma(\Sigma^+ K^- \pi^+)/\Gamma(\Xi^- 2\pi^+)$

VALUE	EVTS	DOCUMENT ID	TECN	COMMENT
0.94 ± 0.10 OUR AVERAGE				
0.91 ± 0.11 ± 0.04	251	LINK	03E FOCS	γ nucleus, $\bar{E}_\gamma \approx 180$ GeV
0.92 ± 0.20 ± 0.07		¹ JUN	00 SELX	Σ^- nucleus, 600 GeV
1.18 ± 0.26 ± 0.17	119	BERGFELD	96 CLE2	$e^+ e^- \approx \Upsilon(4S)$

¹ This JUN 00 result is redundant with other results given below.

$\Gamma(\Sigma^+ \bar{K}^*(892)^0 \pi^+)/\Gamma(\Xi^- 2\pi^+)$

Unseen decay modes of the $\bar{K}^*(892)^0$ are included.

VALUE	EVTS	DOCUMENT ID	TECN	COMMENT
0.81 ± 0.15 OUR AVERAGE				
0.78 ± 0.16 ± 0.06	119	LINK	03E FOCS	γ nucleus, $\bar{E}_\gamma \approx 180$ GeV
0.92 ± 0.27 ± 0.14	61	BERGFELD	96 CLE2	$e^+ e^- \approx \Upsilon(4S)$

$\Gamma(\Sigma^0 K^- 2\pi^+)/\Gamma(\Lambda K^- 2\pi^+)$

VALUE	EVTS	DOCUMENT ID	TECN	COMMENT
0.84 ± 0.36	47	¹ COTEUS	87 SPEC	$nA \approx 600$ GeV

¹ See, however, the note on the COTEUS 87 Ξ_c^+ mass measurement.

$\Gamma(\Xi^0 \pi^+)/\Gamma(\Xi^- 2\pi^+)$

VALUE	EVTS	DOCUMENT ID	TECN	COMMENT
0.55 ± 0.13 ± 0.09	39	EDWARDS	96 CLE2	$e^+ e^- \approx \Upsilon(4S)$

$\Gamma(\Xi^- 2\pi^+)/\Gamma_{\text{total}}$

VALUE (units 10^{-2})	EVTS	DOCUMENT ID	TECN	COMMENT
2.86 ± 1.21 ± 0.38	24	¹ LI	19c BELL	$e^+ e^- \approx \Upsilon(4S)$
• • • We do not use the following data for averages, fits, limits, etc. • • •				
seen	131	BERGFELD	96 CLE2	$e^+ e^- \approx \Upsilon(4S)$
seen	160	AVERY	95 CLE2	$e^+ e^- \approx \Upsilon(4S)$
seen	30	FRABETTI	93B E687	γ Be, $\bar{E}_\gamma = 220$ GeV
seen	30	ALBRECHT	90F ARG	$e^+ e^-$ at $\Upsilon(4S)$
seen	23	ALAM	89 CLEO	$e^+ e^-$ 10.6 GeV

¹ LI 19c report a significance of 6.8 σ for the observation of this decay mode, observed in Ξ_c^+ from $\bar{B}^0 \rightarrow \bar{\Lambda}_c^- \Xi_c^+$.

$\Gamma(\Xi(1530)^0 \pi^+)/\Gamma(\Xi^- 2\pi^+)$

Unseen decay modes of the $\Xi(1530)^0$ are included.

VALUE	CL%	DOCUMENT ID	TECN	COMMENT
< 0.1	90	LINK	03E FOCS	γ nucleus, $\bar{E}_\gamma \approx 180$ GeV

• • • We do not use the following data for averages, fits, limits, etc. • • •

< 0.2	90	BERGFELD	96 CLE2	$e^+ e^- \approx \Upsilon(4S)$
-------	----	----------	---------	--------------------------------

$\Gamma(\Xi(1620)^0 \pi^+)/\Gamma_{\text{total}}$

VALUE	DOCUMENT ID	TECN	COMMENT
seen	SUMIHAMA	19 BELL	$e^+ e^-$ mostly at $\Upsilon(4S)$

$\Gamma(\Xi(1690)^0 \pi^+)/\Gamma_{\text{total}}$

VALUE	DOCUMENT ID	TECN	COMMENT
seen	SUMIHAMA	19 BELL	$e^+ e^-$ mostly at $\Upsilon(4S)$

$\Gamma(\Xi^0 \pi^+ \pi^0)/\Gamma(\Xi^- 2\pi^+)$

VALUE	EVTS	DOCUMENT ID	TECN	COMMENT
2.34 ± 0.57 ± 0.37	81	EDWARDS	96 CLE2	$e^+ e^- \approx \Upsilon(4S)$

$\Gamma(\Xi(1530)^0 \pi^+)/\Gamma(\Xi^0 \pi^+ \pi^0)$

VALUE	CL%	DOCUMENT ID	TECN	COMMENT
< 0.3	90	EDWARDS	96 CLE2	$e^+ e^- \approx \Upsilon(4S)$

• • • We do not use the following data for averages, fits, limits, etc. • • •

See key on page 999

Baryon Particle Listings

$$\Xi_c^+, \Xi_c^0$$

$\Gamma(\Xi^0 \pi^- 2\pi^+)/\Gamma(\Xi^- 2\pi^+)$ Γ_{16}/Γ_{11}

VALUE	EVTS	DOCUMENT ID	TECN	COMMENT
$1.74 \pm 0.42 \pm 0.27$	57	EDWARDS	96 CLE2	$e^+ e^- \approx \gamma(4S)$

$\Gamma(\Xi^0 e^+ \nu_e)/\Gamma(\Xi^- 2\pi^+)$ Γ_{17}/Γ_{11}

VALUE	EVTS	DOCUMENT ID	TECN	COMMENT
$2.3 \pm 0.6 \pm 0.3$ -0.6	41	ALEXANDER	95B CLE2	$e^+ e^- \approx \gamma(4S)$

$\Gamma(\Omega^- K^+ \pi^+)/\Gamma(\Xi^- 2\pi^+)$ Γ_{18}/Γ_{11}

VALUE	EVTS	DOCUMENT ID	TECN	COMMENT
$0.07 \pm 0.03 \pm 0.03$	14	LINK	03E FOCUS	$< 0.12, 90\% \text{ CL}$

$\Gamma(p K^- \pi^+)/\Gamma_{\text{total}}$ Γ_{19}/Γ

VALUE (units 10^{-3})	EVTS	DOCUMENT ID	TECN	COMMENT
$4.5 \pm 2.1 \pm 0.7$	24	¹ LI	19c BELL	$e^+ e^- \approx \gamma(4S)$

¹ LI 19c report a significance of 4.4 σ for the observation of this decay mode, observed in Ξ_c^+ from $\bar{B}^0 \rightarrow \bar{\Lambda}_c^+ \Xi_c^+$.

Cabibbo-suppressed decays

$\Gamma(p K^- \pi^+)/\Gamma(\Xi^- 2\pi^+)$ Γ_{19}/Γ_{11}

VALUE	EVTS	DOCUMENT ID	TECN	COMMENT
0.21 ± 0.04 OUR AVERAGE				
0.194 \pm 0.054	47 \pm 11	VAZQUEZ-JA...08	SELX	Σ^- nucleus, 600 GeV
0.234 \pm 0.047 \pm 0.022	202	LINK	01B FOCUS	γ nucleus

$\Gamma(\Sigma^- 2\pi^+)/\Gamma(\Xi^- 2\pi^+)$ Γ_{20}/Γ_{19}

VALUE	EVTS	DOCUMENT ID	TECN	COMMENT
0.20 \pm 0.04 \pm 0.02	76	JUN	00 SELX	See VAZQUEZ-JAUREGUI 08

$\Gamma(p \bar{K}^*(892)^0)/\Gamma(p K^- \pi^+)$ Γ_{20}/Γ_{19}

Unseen decay modes of the $\bar{K}^*(892)^0$ are included.

VALUE	EVTS	DOCUMENT ID	TECN	COMMENT
$0.54 \pm 0.09 \pm 0.05$		LINK	01B FOCUS	γ nucleus

$\Gamma(\Sigma^+ \pi^+ \pi^-)/\Gamma(\Xi^- 2\pi^+)$ Γ_{21}/Γ_{11}

VALUE	EVTS	DOCUMENT ID	TECN	COMMENT
0.46 ± 0.20	21 \pm 8	VAZQUEZ-JA...08	SELX	Σ^- nucleus, 600 GeV

$\Gamma(\Sigma^- 2\pi^+)/\Gamma(\Xi^- 2\pi^+)$ Γ_{22}/Γ_{11}

VALUE	EVTS	DOCUMENT ID	TECN	COMMENT
0.18 ± 0.09	10 \pm 4	VAZQUEZ-JA...08	SELX	Σ^- nucleus, 600 GeV

$\Gamma(\Sigma^+ K^+ K^-)/\Gamma(\Sigma^+ K^- \pi^+)$ Γ_{23}/Γ_7

VALUE	EVTS	DOCUMENT ID	TECN	COMMENT
$0.16 \pm 0.06 \pm 0.01$	17	LINK	03E FOCUS	γ nucleus, $\bar{E}_\gamma \approx 180 \text{ GeV}$

$\Gamma(\Sigma^+ \phi)/\Gamma(\Sigma^+ K^- \pi^+)$ Γ_{24}/Γ_7

Unseen decay modes of the ϕ are included.

VALUE	CL%	DOCUMENT ID	TECN	COMMENT
< 0.12	90	LINK	03E FOCUS	γ nucleus, $\bar{E}_\gamma \approx 180 \text{ GeV}$

$\Gamma(p \phi(1020))/\Gamma(p K^- \pi^+)$ Γ_{26}/Γ_{19}

VALUE (units 10^{-3})	EVTS	DOCUMENT ID	TECN	COMMENT
$19.8 \pm 0.7 \pm 0.9 \pm 0.2$	3.4k	¹ AAIJ	19i LHCB	pp at 8 TeV

¹ The last uncertainty is due to the uncertainty in the $\phi \rightarrow K^+ K^-$ branching fraction.

$\Gamma(\Xi(1690)^0 K^+ \times B(\Xi(1690)^0 \rightarrow \Sigma^+ K^-))/\Gamma(\Sigma^+ K^- \pi^+)$ Γ_{25}/Γ_7

VALUE	CL%	DOCUMENT ID	TECN	COMMENT
< 0.05	90	LINK	03E FOCUS	γ nucleus, $\bar{E}_\gamma \approx 180 \text{ GeV}$

Ξ_c^+ REFERENCES

AAJ	19AG	PR D100 032001	R. Aaij et al.	(LHCb Collab.)
AAJ	19i	JHEP 1904 084	R. Aaij et al.	(LHCb Collab.)
LI	19C	PR D100 031101	Y.B. Li et al.	(BELLE Collab.)
SUMIHAMA	19	PRL 122 072501	M. Sumihama et al.	(BELLE Collab.)
AAJ	14Z	PRL 113 032001	R. Aaij et al.	(LHCb Collab.)
AALTONEN	14B	PR D89 072014	T. Aaltonen et al.	(CDF Collab.)
VAZQUEZ-JA...	08	PL B666 299	E. Vazquez-Jauregui et al.	(SLEX Collab.)
LESIAK	05	PL B605 237	T. Lesiak et al.	(BELLE Collab.)
Also		PL B617 198 (errata)	T. Lesiak et al.	(BELLE Collab.)
LINK	03E	PL B571 139	J.M. Link et al.	(FNAL FOCUS Collab.)
MAHMOOD	02	PR D65 031102	A.H. Mahmood et al.	(CLEO Collab.)
LINK	01B	PL B512 277	J.M. Link et al.	(FNAL FOCUS Collab.)
LINK	01D	PL B523 53	J.M. Link et al.	(FNAL FOCUS Collab.)
JUN	00	PRL 84 1857	S.Y. Jun et al.	(FNAL SLEX Collab.)
FRABETTI	98	PL B427 211	P.L. Frabetti et al.	(FNAL E687 Collab.)
BERGFELD	96	PL B365 431	T. Bergfeld et al.	(CLEO Collab.)
EDWARDS	96	PL B373 261	K.W. Edwards et al.	(CLEO Collab.)
ALEXANDER	95B	PRL 74 3113	J. Alexander et al.	(CLEO Collab.)
Also		PRL 75 4155 (erratum)	J. Alexander et al.	(CLEO Collab.)
AVERY	95	PRL 75 4364	P. Avery et al.	(CLEO Collab.)
FRABETTI	93B	PRL 70 1361	P.L. Frabetti et al.	(FNAL E687 Collab.)
ALBRECHT	90F	PL B247 121	H. Albrecht et al.	(ARGUS Collab.)
ALAM	89	PL B226 401	M.S. Alam et al.	(CLEO Collab.)
BARLAG	89C	PL B233 522	S. Barlag et al.	(ACCMOR Collab.)
COTEUS	87	PRL 59 1530	P. Coteus et al.	(FNAL E400 Collab.)
BIAGI	85C	PL 150B 230	S.F. Biagi et al.	(CERN WA62 Collab.)
BIAGI	83	PL 122B 455	S.F. Biagi et al.	(CERN WA62 Collab.)



$I(J^P) = \frac{1}{2}(\frac{1}{2}^+)$ Status: * * * *

Neither J or P has actually been measured.

Ξ_c^0 MASS

The fit uses the Ξ_c^0 and Ξ_c^+ mass and mass-difference measurements.

VALUE (MeV)	EVTS	DOCUMENT ID	TECN	COMMENT
2470.90 ± 0.22 -0.29				OUR FIT

2470.99 ± 0.30 OUR AVERAGE

2470.85 \pm 0.24 \pm 0.55	3.4k	AALTONEN	14B CDF	$p\bar{p}$ at 1.96 TeV
2471.0 \pm 0.3 \pm 0.2 -1.4	8.6k	¹ LESIAK	05 BELL	$e^+ e^-$, $\gamma(4S)$
2470.0 \pm 2.8 \pm 2.6	85	FRABETTI	98B E687	$\gamma \text{ Be}$, $\bar{E}_\gamma = 220 \text{ GeV}$
2469 \pm 2 \pm 3	9	HENDERSON	92B CLEO	$\Omega^- K^+$
2472.1 \pm 2.7 \pm 1.6	54	ALBRECHT	90F ARG	$e^+ e^-$ at $\gamma(4S)$
2473.3 \pm 1.9 \pm 1.2	4	BARLAG	90 ACCM	$\pi^- (K^-) \text{ Cu } 230 \text{ GeV}$
2472 \pm 3 \pm 4	19	ALAM	89 CLEO	$e^+ e^-$ 10.6 GeV
2462.1 \pm 3.1 \pm 1.4	42	² FRABETTI	93C E687	See FRABETTI 98B
2471 \pm 3 \pm 4	14	AVERY	89 CLEO	See ALAM 89

• • • We do not use the following data for averages, fits, limits, etc. • • •

¹ The systematic error was (wrongly) given the other way round in LESIAK 05.

² The FRABETTI 93C mass is well below the other measurements.

$\Xi_c^0 - \Xi_c^+$ MASS DIFFERENCE

VALUE (MeV)	EVTS	DOCUMENT ID	TECN	COMMENT
2.96 ± 0.22 OUR FIT				
2.91 ± 0.26 OUR AVERAGE				

2.85 \pm 0.30 \pm 0.04	5.1/3.4k	AALTONEN	14B CDF	$p\bar{p}$ at 1.96 TeV
2.9 \pm 0.5		LESIAK	05 BELL	$e^+ e^-$, $\gamma(4S)$
7.0 \pm 4.5 \pm 2.2		ALBRECHT	90F ARG	$e^+ e^-$ at $\gamma(4S)$
6.8 \pm 3.3 \pm 0.5		BARLAG	90 ACCM	$\pi^- (K^-) \text{ Cu } 230 \text{ GeV}$
5 \pm 4 \pm 1		ALAM	89 CLEO	$\Xi_c^0 \rightarrow \Xi^- \pi^+$, $\Xi_c^+ \rightarrow \Xi^- \pi^+ \pi^+$

Ξ_c^0 MEAN LIFE

VALUE (10^{-15} s)	EVTS	DOCUMENT ID	TECN	COMMENT
153 ± 6 OUR AVERAGE	Error			includes scale factor of 2.4.

154.5 \pm 2.4 \pm 1.1	22k	¹ AAIJ	19AG LHCB	$\Xi_c^0 \rightarrow p K^- K^- \pi^+$
118 \pm 14 -12 \pm 5	110	LINK	02H FOCUS	γ nucleus, $\approx 180 \text{ GeV}$
101 \pm 25 -17 \pm 5	42	FRABETTI	93C E687	$\gamma \text{ Be}$, $\bar{E}_\gamma = 220 \text{ GeV}$
82 \pm 59 -30	4	BARLAG	90 ACCM	$\pi^- (K^-) \text{ Cu } 230 \text{ GeV}$

¹ AAIJ 19AG reports $[\Xi_c^0 \text{ MEAN LIFE}] / [D^\pm \text{ MEAN LIFE}] = 0.1485 \pm 0.0017 \pm 0.0016$ which we multiply by our best value $D^\pm \text{ MEAN LIFE} = (1.040 \pm 0.007) \times 10^{-12} \text{ s}$. Our first error is their experiment's error and our second error is the systematic error from using our best value.

Ξ_c^0 DECAY MODES

Mode	Fraction (Γ_i/Γ)	Scale factor
------	--------------------------------	--------------

Cabibbo-favored ($S = -2$) decays

Γ_1	$p K^- K^- \pi^+$	(4.8 \pm 1.2) $\times 10^{-3}$	1.1
Γ_2	$p K^- \bar{K}^*(892)^0, \bar{K}^{*0} \rightarrow K^- \pi^+$	(2.0 \pm 0.6) $\times 10^{-3}$	
Γ_3	$p K^- K^- \pi^+$ (no \bar{K}^{*0})	(3.0 \pm 0.9) $\times 10^{-3}$	
Γ_4	ΛK_S^0	(3.0 \pm 0.8) $\times 10^{-3}$	
Γ_5	$\Lambda K^- \pi^+$	(1.45 \pm 0.33) %	1.1
Γ_6	$\Lambda \bar{K}^0 \pi^+ \pi^-$	seen	
Γ_7	$\Lambda K^- \pi^+ \pi^+ \pi^-$	seen	
Γ_8	$\Xi^- \pi^+$	(1.43 \pm 0.32) %	1.1
Γ_9	$\Xi^- \pi^+ \pi^+ \pi^-$	(4.8 \pm 2.3) %	
Γ_{10}	$\Omega^- K^+$	(4.2 \pm 1.0) $\times 10^{-3}$	
Γ_{11}	$\Xi^- e^+ \nu_e$	(1.8 \pm 1.2) %	

Cabibbo-suppressed decays

Γ_{12}	$\Xi^- K^+$	(3.9 \pm 1.2) $\times 10^{-4}$	
Γ_{13}	$\Lambda K^+ K^-$ (no ϕ)	(4.1 \pm 1.4) $\times 10^{-4}$	
Γ_{14}	$\Lambda \phi$	(4.9 \pm 1.5) $\times 10^{-4}$	

Baryon Particle Listings

$$\Xi_c^0, \Xi_c^{\prime 0}, \Xi_c^{\prime +}$$

CONSTRAINED FIT INFORMATION

An overall fit to 5 branching ratios uses 6 measurements and one constraint to determine 4 parameters. The overall fit has a $\chi^2 = 1.4$ for 3 degrees of freedom.

The following *off-diagonal* array elements are the correlation coefficients $\langle \delta x_i \delta x_j \rangle / (\delta x_i \delta x_j)$, in percent, from the fit to the branching fractions, $x_i \equiv \Gamma_i / \Gamma_{\text{total}}$. The fit constrains the x_i whose labels appear in this array to sum to one.

x_5	68	
x_8	89	76
	x_1	x_5

Ξ_c^0 BRANCHING RATIOS

Cabibbo-favored (S = -2) decays

$\Gamma(pK^-K^-\pi^+) / \Gamma_{\text{total}}$	Γ_1 / Γ
VALUE (%)	EVTS
0.48 ± 0.12 OUR FIT	Error includes scale factor of 1.1.
0.58 ± 0.23 ± 0.05	17 ± 5

$\Gamma(pK^-K^-\pi^+) / \Gamma(\Xi^-\pi^+)$	Γ_1 / Γ_8
VALUE	EVTS
0.339 ± 0.035 OUR FIT	
0.34 ± 0.04 OUR AVERAGE	
0.33 ± 0.03 ± 0.03	1908 ± 62
0.35 ± 0.06 ± 0.03	148 ± 18

$\Gamma(pK^-\bar{K}^*(892)^0, \bar{K}^{*0} \rightarrow K^-\pi^+) / \Gamma(\Xi^-\pi^+)$	Γ_2 / Γ_8
VALUE	EVTS
0.14 ± 0.03 ± 0.01	

$\Gamma(pK^-K^-\pi^+ \text{ (no } \bar{K}^{*0})) / \Gamma(\Xi^-\pi^+)$	Γ_3 / Γ_8
VALUE	EVTS
0.21 ± 0.04 ± 0.02	

$\Gamma(\Lambda K^0) / \Gamma(\Xi^-\pi^+)$	Γ_4 / Γ_8
VALUE	EVTS
0.21 ± 0.02 ± 0.02	465 ± 37

$\Gamma(\Lambda K^-\pi^+) / \Gamma_{\text{total}}$	Γ_5 / Γ
VALUE (%)	EVTS
1.45 ± 0.33 OUR FIT	Error includes scale factor of 1.1.
1.17 ± 0.37 ± 0.09	24 ± 6

$\Gamma(\Lambda K^-\pi^+) / \Gamma(\Xi^-\pi^+)$	Γ_5 / Γ_8
VALUE	EVTS
1.02 ± 0.15 OUR FIT	Error includes scale factor of 1.2.
1.07 ± 0.12 ± 0.07	2979 ± 211

$\Gamma(\Lambda \bar{K}^0 \pi^+ \pi^-) / \Gamma_{\text{total}}$	Γ_6 / Γ
VALUE	EVTS
seen	

$\Gamma(\Lambda K^-\pi^+\pi^+) / \Gamma_{\text{total}}$	Γ_7 / Γ
VALUE	EVTS
seen	

$\Gamma(\Xi^-\pi^+) / \Gamma_{\text{total}}$	Γ_8 / Γ
VALUE (%)	EVTS
1.43 ± 0.32 OUR FIT	Error includes scale factor of 1.1.
1.80 ± 0.50 ± 0.14	45 ± 7

$\Gamma(\Xi^-\pi^+) / \Gamma(\Xi^-\pi^+\pi^+\pi^-)$	Γ_8 / Γ_9
VALUE	EVTS
0.30 ± 0.12 ± 0.05	

$\Gamma(\Omega^-K^+) / \Gamma(\Xi^-\pi^+)$	Γ_{10} / Γ_8
VALUE	EVTS
0.294 ± 0.018 ± 0.016	65.0

$\Gamma(\Xi^-e^+\nu_e) / \Gamma(\Xi^-\pi^+)$	Γ_{11} / Γ_8
VALUE	EVTS
1.3 ± 0.8 OUR AVERAGE	Error includes scale factor of 1.8.
3.1 ± 1.0 $\pm_{0.5}^{0.3}$	54
0.96 ± 0.43 ± 0.18	18

¹This ALBRECHT 93B value is the average of the $(\Xi^-e^+\text{ anything}) / \Xi^-\pi^+$ and $(\Xi^-\mu^+\text{ anything}) / \Xi^-\pi^+$ ratios. Here we average it with the $\Xi^-e^+\nu_e / \Xi^-\pi^+$ ratio.

Cabibbo-suppressed decays

$\Gamma(\Xi^-K^+) / \Gamma(\Xi^-\pi^+)$	Γ_{12} / Γ_8
VALUE (units 10^{-2})	EVTS
2.75 ± 0.51 ± 0.25	314 ± 58

$\Gamma(\Lambda K^+K^- \text{ (no } \phi)) / \Gamma(\Xi^-\pi^+)$	Γ_{13} / Γ_8
VALUE (units 10^{-2})	EVTS
2.86 ± 0.61 ± 0.37	510 ± 110

$\Gamma(\Lambda \phi) / \Gamma(\Xi^-\pi^+)$	Γ_{14} / Γ_8
VALUE (units 10^{-2})	EVTS
3.43 ± 0.58 ± 0.32	316 ± 54

Ξ_c^0 DECAY PARAMETERS

See the note on "Baryon Decay Parameters" in the neutron Listings.

α FOR $\Xi_c^0 \rightarrow \Xi^-\pi^+$	TECN	COMMENT
VALUE	EVTS	DOCUMENT ID
-0.56 ± 0.39 $\pm_{0.09}^{0.10}$	138	CHAN 01 CLE2

Ξ_c^0 REFERENCES

AALJ	19A	PR D100 032001	R. Aaij et al.	(LHCb Collab.)
LI	19A	PRL 122 082001	Y.B. Li et al.	(BELLE Collab.)
AALTONEN	14B	PR D89 072014	T. Aaltonen et al.	(CDF Collab.)
CHISTOV	13	PR D88 071103	R. Chistov et al.	(BELLE Collab.)
AUBERT.B	05M	PRL 95 142003	B. Aubert et al.	(BABAR Collab.)
LESLIAK	05	PL B605 237	T. Lesiak et al.	(BELLE Collab.)
		Also PL B617 198 (errata.)	T. Lesiak et al.	(BELLE Collab.)
DANKO	04	PR D69 052004	I. Danko et al.	(CLEO Collab.)
LINK	02H	PL B541 211	J.M. Link et al.	(FNAL FOCUS Collab.)
CHAN	01	PR D63 111102	S. Chan et al.	(CLEO Collab.)
FRABETTI	98B	PL B426 403	P.L. Frabetti et al.	(FNAL E687 Collab.)
ALEXANDER	95B	PRL 74 3113	J. Alexander et al.	(CLEO Collab.)
		Also PRL 75 4155 (erratum)	J. Alexander et al.	(CLEO Collab.)
ALBRECHT	93B	PL B303 368	H. Albrecht et al.	(ARGUS Collab.)
FRABETTI	93C	PRL 70 2058	P.L. Frabetti et al.	(FNAL E687 Collab.)
HENDERSON	92B	PL B283 161	S. Henderson et al.	(CLEO Collab.)
ALBRECHT	90F	PL B247 121	H. Albrecht et al.	(ARGUS Collab.)
BARLAG	90	PL B236 495	S. Barlag et al.	(ACCMOR Collab.)
ALAM	89	PL B226 401	M.S. Alam et al.	(CLEO Collab.)
AVERY	89	PRL 62 863	P. Avery et al.	(CLEO Collab.)

$$\Xi_c^{\prime +}$$

$$I(J^P) = \frac{1}{2}(\frac{1}{2}^+)$$
 Status: ***

The $\Xi_c^{\prime +}$ and $\Xi_c^{\prime 0}$ presumably complete the SU(3) sextet whose other members are the $\Sigma_c^{\prime +}$, $\Sigma_c^{\prime 0}$, and $\Omega_c^{\prime 0}$; see Fig. 3 in the note on Charmed Baryons. The quantum numbers given above come from this presumption but have not been measured.

$\Xi_c^{\prime +}$ MASS

The mass is obtained from the mass-difference measurement that follows.

VALUE (MeV)	DOCUMENT ID
2578.4 ± 0.5 OUR FIT	

$\Xi_c^{\prime +} - \Xi_c^+$ MASS DIFFERENCE

VALUE (MeV)	EVTS	DOCUMENT ID	TECN	COMMENT
110.5 ± 0.4 OUR FIT				
110.5 ± 0.1 ± 0.4	7k	YELTON 16	BELL	e^+e^- , γ regions
••• We do not use the following data for averages, fits, limits, etc. •••				
107.8 ± 1.7 ± 2.5	25	JESSOP 99	CLE2	$e^+e^- \approx \gamma(4S)$

$\Xi_c^{\prime +} - \Xi_c^{\prime 0}$ MASS DIFFERENCE

VALUE (MeV)	DOCUMENT ID	TECN	COMMENT
-0.8 ± 0.6 OUR FIT			
••• We do not use the following data for averages, fits, limits, etc. •••			
-0.8 ± 0.1 ± 0.5	YELTON 16	BELL	7055 and 11,560 evts

$\Xi_c^{\prime +}$ DECAY MODES

The $\Xi_c^{\prime +} - \Xi_c^+$ mass difference is too small for any strong decay to occur.

Mode	Fraction (Γ_i / Γ)
$\Gamma_1 \Xi_c^{\prime +} \gamma$	seen

$\Xi_c^{\prime +}$ REFERENCES

YELTON	16	PR D94 052011	J. Yelton et al.	(BELLE Collab.)
JESSOP	99	PRL 82 492	C.P. Jessop et al.	(CLEO Collab.)

See key on page 999

Baryon Particle Listings

$\Xi_c^0, \Xi_c(2645), \Xi_c(2790)$

Ξ_c^0

$I(J^P) = \frac{1}{2}(\frac{1}{2}^+)$ Status: ***

The Ξ_c^0 and Ξ_c^+ presumably complete the SU(3) sextet whose other members are the $\Sigma_c^{++}, \Sigma_c^+, \Sigma_c^0$, and Ω_c^0 : see Fig. 3 in the note on Charmed Baryons. The quantum numbers given above come from this presumption but have not been measured.

Ξ_c^0 MASS

The mass is obtained from the mass-difference measurement that follows.

VALUE (MeV)	DOCUMENT ID
2579.2 ± 0.5 OUR FIT	

$\Xi_c^0 - \Xi_c^+$ MASS DIFFERENCE

VALUE (MeV)	EVTs	DOCUMENT ID	TECN	COMMENT
108.3 ± 0.4 OUR FIT				
108.3 ± 0.1 ± 0.4	11.5k	YELTON	16	BELL e^+e^- , Υ regions
• • • We do not use the following data for averages, fits, limits, etc. • • •				
107.0 ± 1.4 ± 2.5	28	JESSOP	99	CLE2 $e^+e^- \approx \Upsilon(4S)$

Ξ_c^0 DECAY MODES

The $\Xi_c^0 - \Xi_c^+$ mass difference is too small for any strong decay to occur.

Mode	Fraction (Γ_i/Γ)
$\Xi_c^0 \gamma$	seen

Ξ_c^0 REFERENCES

YELTON	16	PR D94 052011	J. Yelton <i>et al.</i>	(BELLE Collab.)
JESSOP	99	PRL 82 492	C.P. Jessop <i>et al.</i>	(CLEO Collab.)

$\Xi_c(2645)$

$I(J^P) = \frac{1}{2}(\frac{3}{2}^+)$ Status: ***

The natural assignment is that this is the $J^P = 3/2^+$ excitation of the Ξ_c in the same SU(4) multiplet as the $\Delta(1232)$, but the quantum numbers have not been measured.

$\Xi_c(2645)$ MASSES

$\Xi_c(2645)^+$ MASS

VALUE (MeV)	EVTs	DOCUMENT ID	TECN	COMMENT
2645.56 ± 0.24 ± 0.30 OUR FIT				
2645.6 ± 0.2 ± 0.6	578 ± 32	LESIAK	08	BELL $e^+e^- \approx \Upsilon(4S)$

$\Xi_c(2645)^0$ MASS

VALUE (MeV)	EVTs	DOCUMENT ID	TECN	COMMENT
2646.38 ± 0.20 ± 0.23 OUR FIT				Error includes scale factor of 1.1.
2645.7 ± 0.2 ± 0.6	611 ± 32	LESIAK	08	BELL $e^+e^- \approx \Upsilon(4S)$

$\Xi_c(2645) - \Xi_c$ MASS DIFFERENCES

$m_{\Xi_c(2645)^+} - m_{\Xi_c^+}$

VALUE (MeV)	EVTs	DOCUMENT ID	TECN	COMMENT
174.66 ± 0.09 OUR FIT				
174.66 ± 0.06 ± 0.07	1260	YELTON	16	BELL e^+e^- in Υ regions
• • • We do not use the following data for averages, fits, limits, etc. • • •				
177.1 ± 0.5 ± 1.1	47	FRABETTI	98B	E687 γ Be, $\bar{E}_\gamma = 220$ GeV
174.3 ± 0.5 ± 1.0	34	GIBBONS	96	CLE2 $e^+e^- \approx \Upsilon(4S)$

$m_{\Xi_c(2645)^0} - m_{\Xi_c^0}$

VALUE (MeV)	EVTs	DOCUMENT ID	TECN	COMMENT
178.44 ± 0.10 OUR FIT				
178.46 ± 0.07 ± 0.07	975	YELTON	16	BELL e^+e^- in Υ regions
• • • We do not use the following data for averages, fits, limits, etc. • • •				
178.2 ± 0.5 ± 1.0	55	AVERY	95	CLE2 $e^+e^- \approx \Upsilon(4S)$

$\Xi_c(2645)^+ - \Xi_c(2645)^0$ MASS DIFFERENCE

VALUE (MeV)	DOCUMENT ID	TECN	COMMENT
-0.82 ± 0.26 OUR FIT			
• • • We do not use the following data for averages, fits, limits, etc. • • •			
-0.85 ± 0.09 ± 0.49	YELTON	16	BELL 1260 and 975 evts
-0.1 ± 0.3 ± 0.6	LESIAK	08	BELL ≈ 600 evts each

$\Xi_c(2645)$ WIDTHS

$\Xi_c(2645)^+$ WIDTH

VALUE (MeV)	CL%	EVTs	DOCUMENT ID	TECN	COMMENT
2.14 ± 0.19 OUR AVERAGE					Error includes scale factor of 1.1.
2.06 ± 0.13 ± 0.13		1260	YELTON	16	BELL e^+e^- in Υ regions
2.6 ± 0.2 ± 0.4		3.7k	KATO	14	BELL $e^+e^- \Upsilon(1S)-\Upsilon(5S)$
• • • We do not use the following data for averages, fits, limits, etc. • • •					
<3.1		90	GIBBONS	96	CLE2 $e^+e^- \approx \Upsilon(4S)$

$\Xi_c(2645)^0$ WIDTH

VALUE (MeV)	CL%	EVTs	DOCUMENT ID	TECN	COMMENT	
2.35 ± 0.18 ± 0.13						
2.35 ± 0.18 ± 0.13		975	YELTON	16	BELL e^+e^- in Υ regions	
• • • We do not use the following data for averages, fits, limits, etc. • • •						
<5.5		90	55	AVERY	95	CLE2 $e^+e^- \approx \Upsilon(4S)$

$\Xi_c(2645)$ DECAY MODES

$\Xi_c \pi$ is the only strong decay allowed to a Ξ_c resonance having this mass.

Mode	Fraction (Γ_i/Γ)
$\Xi_c^0 \pi^+$	seen
$\Xi_c^+ \pi^-$	seen

$\Xi_c(2645)$ REFERENCES

YELTON	16	PR D94 052011	J. Yelton <i>et al.</i>	(BELLE Collab.)
KATO	14	PR D89 052003	Y. Kato <i>et al.</i>	(BELLE Collab.)
LESIAK	08	PL B665 9	T. Lesiak <i>et al.</i>	(BELLE Collab.)
FRABETTI	98B	PL B426 403	P.L. Frabetti <i>et al.</i>	(FNAL E687 Collab.)
GIBBONS	96	PRL 77 810	L.K. Gibbons <i>et al.</i>	(CLEO Collab.)
AVERY	95	PRL 75 4364	P. Avery <i>et al.</i>	(CLEO Collab.)

$\Xi_c(2790)$

$I(J^P) = \frac{1}{2}(\frac{1}{2}^-)$ Status: ***

Seen in $\Xi_c' \pi$ decays. The simplest assignment, based on the mass, width, and decay mode, is that this belongs in the same SU(4) multiplet as the $\Lambda(1405)$ and the $\Lambda_c(2595)^+$, but the spin and parity have not been measured.

$\Xi_c(2790)$ MASSES

The masses are obtained from the mass-difference measurements that follow.

$\Xi_c(2790)^+$ MASS

VALUE (MeV)	DOCUMENT ID
2792.4 ± 0.5 OUR FIT	

$\Xi_c(2790)^0$ MASS

VALUE (MeV)	DOCUMENT ID
2794.1 ± 0.5 OUR FIT	

$\Xi_c(2790) - \Xi_c'$ MASS DIFFERENCES

$m_{\Xi_c(2790)^+} - m_{\Xi_c^+}$

VALUE (MeV)	EVTs	DOCUMENT ID	TECN	COMMENT
213.20 ± 0.22 OUR FIT				
213.2 ± 0.2 ± 0.1		YELTON	16	BELL 2231 and 11,560 evts
• • • We do not use the following data for averages, fits, limits, etc. • • •				
211.2 ± 1.3 ± 1.0	18	CSORNA	01	CLEO $e^+e^- \approx \Upsilon(4S)$

$m_{\Xi_c(2790)^0} - m_{\Xi_c^0}$

VALUE (MeV)	EVTs	DOCUMENT ID	TECN	COMMENT
215.70 ± 0.22 OUR FIT				
215.7 ± 0.2 ± 0.1		YELTON	16	BELL 1241 and 7055 evts
• • • We do not use the following data for averages, fits, limits, etc. • • •				
216.2 ± 1.3 ± 1.0	14	CSORNA	01	CLEO $e^+e^- \approx \Upsilon(4S)$

$\Xi_c(2790)^+ - \Xi_c(2790)^0$ MASS DIFFERENCE

VALUE (MeV)	DOCUMENT ID	TECN	COMMENT
-1.7 ± 0.7 OUR FIT			
• • • We do not use the following data for averages, fits, limits, etc. • • •			
-3.3 ± 0.4 ± 0.5	YELTON	16	BELL 2231 and 1241 evts

$\Xi_c(2790)$ WIDTHS

$\Xi_c(2790)^+$ WIDTH

VALUE (MeV)	CL%	EVTs	DOCUMENT ID	TECN	COMMENT
8.9 ± 0.6 ± 0.8		2231	YELTON	16	BELL e^+e^- , Υ regions

Baryon Particle Listings

$\Xi_c(2790), \Xi_c(2815), \Xi_c(2930)$

••• We do not use the following data for averages, fits, limits, etc. •••

<15 90 CSORNA 01 CLEO $e^+e^- \approx \Upsilon(4S)$

$\Xi_c(2790)^0$ WIDTH

VALUE (MeV)	CL%	EVTS	DOCUMENT ID	TECN	COMMENT
$10.0 \pm 0.7 \pm 0.8$		1241	YELTON	16	BELL e^+e^- , Υ regions

••• We do not use the following data for averages, fits, limits, etc. •••

<12 90 CSORNA 01 CLEO $e^+e^- \approx \Upsilon(4S)$

$\Xi_c(2790)$ DECAY MODES

Mode	Fraction (Γ_i/Γ)
$\Gamma_1 \Xi_c' \pi$	seen

$\Xi_c(2790)$ BRANCHING RATIOS

$\Gamma(\Xi_c' \pi)/\Gamma_{total}$	VALUE	DOCUMENT ID	TECN	COMMENT	Γ_1/Γ
seen		YELTON	16	BELL e^+e^- , Υ regions	
seen		CSORNA	01	CLEO $e^+e^- \approx \Upsilon(4S)$	

$\Xi_c(2790)$ REFERENCES

YELTON	16	PR D94 052011	J. Yelton et al.	(BELLE Collab.)
CSORNA	01	PRL 86 4243	S.E. Csorna et al.	(CLEO Collab.)

$\Xi_c(2815)$

$$I(J^P) = \frac{1}{2}(\frac{3}{2}^-) \text{ Status: } ***$$

Seen in both $\Xi_c' \pi$ and $\Xi_c \pi \pi$ decays. The simplest assignment is that this belongs to the same SU(4) multiplet as the $\Lambda(1520)$ and the $\Lambda_c(2625)$, but the spin and parity have not been measured.

$\Xi_c(2815)$ MASSES

The masses are obtained from the mass-difference measurements that follow.

$\Xi_c(2815)^+$ MASS

VALUE (MeV)	CL%	EVTS	DOCUMENT ID	TECN	COMMENT
$2816.74 \pm 0.20 \pm 0.23$					OUR FIT

••• We do not use the following data for averages, fits, limits, etc. •••

$2817.0 \pm 1.2 \pm 0.7 \pm 0.8$ 73 \pm 10 LESIAK 08 BELL $e^+e^- \approx \Upsilon(4S)$

$\Xi_c(2815)^0$ MASS

VALUE (MeV)	CL%	EVTS	DOCUMENT ID	TECN	COMMENT
$2820.25 \pm 0.25 \pm 0.31$					OUR FIT

••• We do not use the following data for averages, fits, limits, etc. •••

$2820.4 \pm 1.4 \pm 0.9 \pm 1.0$ 48 \pm 8 LESIAK 08 BELL $e^+e^- \approx \Upsilon(4S)$

$\Xi_c(2815) - \Xi_c$ MASS DIFFERENCES

$m_{\Xi_c(2815)^+} - m_{\Xi_c^+}$

VALUE (MeV)	CL%	EVTS	DOCUMENT ID	TECN	COMMENT
348.80 ± 0.10					OUR FIT
$348.80 \pm 0.08 \pm 0.06$		941	YELTON	16	BELL e^+e^- , Υ regions
$348.6 \pm 0.6 \pm 1.0$		20	ALEXANDER	99b	CLE2 $e^+e^- \approx \Upsilon(4S)$

••• We do not use the following data for averages, fits, limits, etc. •••

$m_{\Xi_c(2815)^0} - m_{\Xi_c^0}$

VALUE (MeV)	CL%	EVTS	DOCUMENT ID	TECN	COMMENT
349.35 ± 0.11					OUR FIT
$349.35 \pm 0.08 \pm 0.07$		1258	YELTON	16	BELL e^+e^- , Υ regions
$347.2 \pm 0.7 \pm 2.0$		9	ALEXANDER	99b	CLE2 $e^+e^- \approx \Upsilon(4S)$

••• We do not use the following data for averages, fits, limits, etc. •••

$\Xi_c(2815)^+ - \Xi_c(2815)^0$ MASS DIFFERENCE

$m_{\Xi_c(2815)^+} - m_{\Xi_c(2815)^0}$

VALUE (MeV)	CL%	EVTS	DOCUMENT ID	TECN	COMMENT
-3.51 ± 0.26					OUR FIT
$-3.47 \pm 0.12 \pm 0.48$		941 and 1258	YELTON	16	BELL 941 and 1258 evts
$-3.4 \pm 1.9 \pm 0.9$		73 & 48	LESIAK	08	BELL 73 & 48 events

$\Xi_c(2815)$ WIDTHS

$\Xi_c(2815)^+$ WIDTH

VALUE (MeV)	CL%	EVTS	DOCUMENT ID	TECN	COMMENT
$2.43 \pm 0.20 \pm 0.17$		941	YELTON	16	BELL e^+e^- , Υ regions

••• We do not use the following data for averages, fits, limits, etc. •••

<3.5 90 ALEXANDER 99b CLE2 $e^+e^- \approx \Upsilon(4S)$

$\Xi_c(2815)^0$ WIDTH

VALUE (MeV)	CL%	EVTS	DOCUMENT ID	TECN	COMMENT
$2.54 \pm 0.18 \pm 0.17$		1258	YELTON	16	BELL e^+e^- , Υ regions

••• We do not use the following data for averages, fits, limits, etc. •••

<6.5 90 ALEXANDER 99b CLE2 $e^+e^- \approx \Upsilon(4S)$

$\Xi_c(2815)$ DECAY MODES

The $\Xi_c \pi \pi$ modes are consistent with being entirely via $\Xi_c(2645) \pi$.

Mode	Fraction (Γ_i/Γ)
$\Gamma_1 \Xi_c' \pi$	seen
$\Gamma_2 \Xi_c(2645) \pi$	seen

$\Gamma(\Xi_c' \pi)/\Gamma_{total}$

VALUE	DOCUMENT ID	TECN	COMMENT	Γ_1/Γ
seen	YELTON	16	BELL e^+e^- , Υ regions	
seen	ALEXANDER	99b	CLE2 $e^+e^- \approx \Upsilon(4S)$	

$\Gamma(\Xi_c(2645) \pi)/\Gamma_{total}$

VALUE	DOCUMENT ID	TECN	COMMENT	Γ_2/Γ
seen	YELTON	16	BELL e^+e^- , Υ regions	
seen	LESIAK	08	BELL $e^+e^- \approx \Upsilon(4S)$	

$\Xi_c(2815)$ REFERENCES

YELTON	16	PR D94 052011	J. Yelton et al.	(BELLE Collab.)
LESIAK	08	PL B665 9	T. Lesiak et al.	(BELLE Collab.)
ALEXANDER	99b	PRL 83 3390	J.P. Alexander et al.	(CLEO Collab.)

$\Xi_c(2930)$

$$I(J^P) = ?(??) \text{ Status: } **$$

OMITTED FROM SUMMARY TABLE

$\Xi_c(2930)$ MASSES

$\Xi_c(2930)^+$ MASS

VALUE (MeV)	CL%	EVTS	DOCUMENT ID	TECN	COMMENT
$2942.3 \pm 4.4 \pm 1.5$		21	LI	18D	BELL e^+e^- at $\Upsilon(4S)$

$\Xi_c(2930)^0$ MASS

VALUE (MeV)	CL%	EVTS	DOCUMENT ID	TECN	COMMENT
$2929.7 \pm 2.8 \pm 5.0$					OUR AVERAGE

$2928.9 \pm 3.0 \pm 0.9 \pm 12.0$ 61 LI 18A BELL e^+e^- at $\Upsilon(4S)$

$2931 \pm 3 \pm 5$ 34 AUBERT 08H BABR $\Upsilon(4S) \rightarrow B \bar{B}$

$\Xi_c(2930)^+ - \Xi_c(2930)^0$ MASS DIFFERENCE

VALUE (MeV)	CL%	EVTS	DOCUMENT ID	TECN	COMMENT
$13.4 \pm 5.3 \pm 1.7 \pm 12.1$		21	¹ LI	18D	BELL e^+e^- at $\Upsilon(4S)$

¹ This LI 18D value is not independent of the mass measurements.

$\Xi_c(2930)$ WIDTHS

$\Xi_c(2930)^+$ WIDTH

VALUE (MeV)	CL%	EVTS	DOCUMENT ID	TECN	COMMENT
$14.8 \pm 8.8 \pm 2.5$		21	LI	18D	BELL e^+e^- at $\Upsilon(4S)$

$\Xi_c(2930)^0$ WIDTH

VALUE (MeV)	CL%	EVTS	DOCUMENT ID	TECN	COMMENT
26 ± 8					OUR AVERAGE
$19.5 \pm 8.4 \pm 5.9 \pm 7.9$		61	LI	18A	BELL e^+e^- at $\Upsilon(4S)$
$36 \pm 7 \pm 11$		34	AUBERT	08H	BABR $\Upsilon(4S) \rightarrow B \bar{B}$

See key on page 999

Baryon Particle Listings

$\Xi_c(2930), \Xi_c(2970)$

$\Xi_c(2930)$ DECAY MODES

Mode	Fraction (Γ_i/Γ)
$\Gamma_1 \Lambda_c^+ K^-$	seen
$\Gamma_2 \Lambda_c^+ K_S^0$	seen

$\Xi_c(2930)$ BRANCHING RATIOS

$\Gamma(\Lambda_c^+ K^-)/\Gamma_{\text{total}}$					Γ_1/Γ
VALUE	EVTS	DOCUMENT ID	TECN	COMMENT	
seen	61	LI	18A	BELL	Significance 5.1 std
seen	34	AUBERT	08H	BABR	e^+e^- at $\Upsilon(4S)$

$\Gamma(\Lambda_c^+ K_S^0)/\Gamma_{\text{total}}$					Γ_2/Γ
VALUE	EVTS	DOCUMENT ID	TECN	COMMENT	
seen	21	LI	18D	BELL	Significance 4.1 std

$\Xi_c(2930)$ REFERENCES

LI	18A	EPJ C78 252	Y.B. Li <i>et al.</i>	(BELLE Collab.)
LI	18D	EPJ C78 928	Y.B. Li <i>et al.</i>	(BELLE Collab.)
AUBERT	08H	PR D77 031101	B. Aubert <i>et al.</i>	(BABAR Collab.)

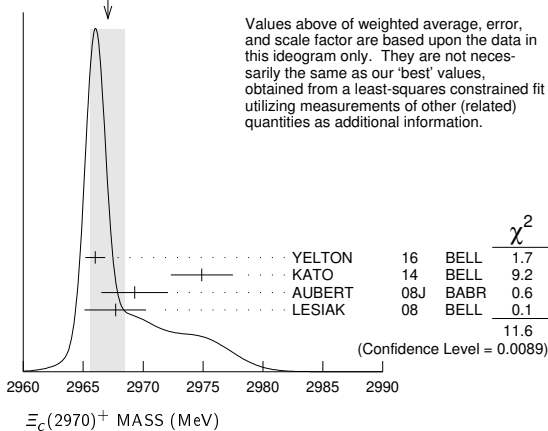
$\Xi_c(2970)$ $I(J^P) = \frac{1}{2}(?)^?$ Status: ***
was $\Xi_c(2980)$

$\Xi_c(2970)$ MASSES

$\Xi_c(2970)^+$ MASS

VALUE (MeV)	EVTS	DOCUMENT ID	TECN	COMMENT
2966.34 ± 0.17 OUR FIT				
2966.0 ± 0.8 ± 0.2	0.9k	YELTON	16	BELL $e^+e^- \rightarrow \Upsilon(4S), \Upsilon(5S)$ and continuum
2974.9 ± 1.5 ± 2.1	244 ± 39	KATO	14	BELL $e^+e^- \Upsilon(1S)$ to $\Upsilon(5S)$
2969.3 ± 2.2 ± 1.7	756 ± 206	AUBERT	08J	BABR $e^+e^- \approx 10.58$ GeV
2967.7 ± 2.3 ± 1.1 ± 1.2	78 ± 13	LESLIAK	08	BELL $e^+e^- \approx \Upsilon(4S)$
• • • We do not use the following data for averages, fits, limits, etc. • • •				
2978.5 ± 2.1 ± 2.0	405 ± 51	CHISTOV	06	BELL See KATO 14

WEIGHTED AVERAGE
2967.1 ± 1.4 (Error scaled by 2.0)



Values above of weighted average, error, and scale factor are based upon the data in this ideogram only. They are not necessarily the same as our 'best' values, obtained from a least-squares constrained fit utilizing measurements of other (related) quantities as additional information.

$\Xi_c(2970)^0$ MASS

The evidence is statistically weaker for this charge state.

VALUE (MeV)	EVTS	DOCUMENT ID	TECN	COMMENT
2970.9 ± 0.4 OUR FIT				
2970.5 ± 1.3 OUR AVERAGE				Error includes scale factor of 1.9.
2970.8 ± 0.7 ± 0.2	1.4k	YELTON	16	BELL $e^+e^- \rightarrow \Upsilon(4S), \Upsilon(5S)$ and continuum
2972.9 ± 4.4 ± 1.6	67 ± 44	AUBERT	08J	BABR $e^+e^- \approx 10.58$ GeV
2965.7 ± 2.4 ± 1.1 ± 1.2	57 ± 13	LESLIAK	08	BELL $e^+e^- \approx \Upsilon(4S)$
2977.1 ± 8.8 ± 3.5	42 ± 24	CHISTOV	06	BELL $e^+e^- \approx \Upsilon(4S)$

$\Xi_c(2970) - \Xi_c$ MASS DIFFERENCES

$m_{\Xi_c(2970)^+} - m_{\Xi_c^+}$		DOCUMENT ID	TECN	COMMENT
VALUE (MeV)	EVTS			
498.40 ± 0.27 OUR FIT				
498.1 ± 0.8 ± 0.2	916	YELTON	16	BELL e^+e^- , Υ regions

$m_{\Xi_c(2970)^0} - m_{\Xi_c^0}$		DOCUMENT ID	TECN	COMMENT
VALUE (MeV)	EVTS			
500.0 ± 0.4 OUR FIT				
499.9 ± 0.7 ± 0.2	1.4k	YELTON	16	BELL e^+e^- , Υ regions

$\Xi_c(2970)^+ - \Xi_c(2970)^0$ MASS DIFFERENCE

VALUE (MeV)	DOCUMENT ID	TECN	COMMENT
-4.6 ± 0.4 OUR FIT			
-4.8 ± 0.1 ± 0.5	YELTON	16	BELL 916 and 1443 evts

$\Xi_c(2970)$ WIDTHS

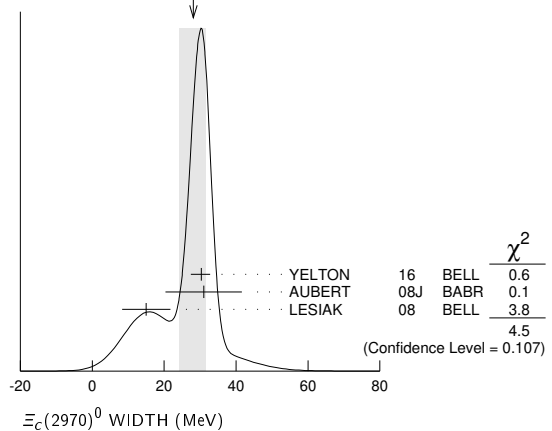
$\Xi_c(2970)^+$ WIDTH

VALUE (MeV)	EVTS	DOCUMENT ID	TECN	COMMENT
20.9 ± 2.4 OUR AVERAGE				Error includes scale factor of 1.2.
28.1 ± 2.4 ± 1.0 ± 5.0	916	YELTON	16	BELL e^+e^- , Υ regions
14.8 ± 2.5 ± 4.1	244 ± 39	KATO	14	BELL $e^+e^- \Upsilon(1S)$ to $\Upsilon(5S)$
27 ± 8 ± 2	756 ± 206	AUBERT	08J	BABR $e^+e^- \approx 10.58$ GeV
18 ± 6 ± 3	78 ± 13	LESLIAK	08	BELL $e^+e^- \approx \Upsilon(4S)$
• • • We do not use the following data for averages, fits, limits, etc. • • •				
43.5 ± 7.5 ± 7.0	405 ± 51	CHISTOV	06	BELL See KATO 14

$\Xi_c(2970)^0$ WIDTH

VALUE (MeV)	EVTS	DOCUMENT ID	TECN	COMMENT
28.1 ± 3.4 OUR AVERAGE				Error includes scale factor of 1.5. See the ideogram below.
30.3 ± 2.3 ± 1.0 ± 1.8	1443	YELTON	16	BELL e^+e^- , Υ regions
31 ± 7 ± 8	67 ± 44	AUBERT	08J	BABR $e^+e^- \approx 10.58$ GeV
15 ± 6 ± 3	57 ± 13	LESLIAK	08	BELL $e^+e^- \approx \Upsilon(4S)$

WEIGHTED AVERAGE
28.1 ± 3.4 ± 4.0 (Error scaled by 1.5)



$\Xi_c(2970)$ DECAY MODES

Mode	Fraction (Γ_i/Γ)
$\Gamma_1 \Lambda_c^+ \bar{K} \pi$	seen
$\Gamma_2 \Sigma_c(2455) \bar{K}$	seen
$\Gamma_3 \Lambda_c^+ \bar{K}$	not seen
$\Gamma_4 \Xi_c 2\pi$	seen
$\Gamma_5 \Xi_c \pi$	seen
$\Gamma_6 \Xi_c(2645) \pi$	seen

Baryon Particle Listings

 $\Xi_c(2970)$, $\Xi_c(3055)$, $\Xi_c(3080)$, $\Xi_c(3123)$ $\Xi_c(2970)$ BRANCHING RATIOS

$\Gamma(\Lambda_c^+ \bar{K}\pi)/\Gamma_{\text{total}}$	DOCUMENT ID	TECN	COMMENT	Γ_1/Γ
VALUE				
seen	AUBERT 08J	BABR	$e^+ e^- \approx \Upsilon(4S)$	
seen	CHISTOV 06	BELL	$e^+ e^- \approx \Upsilon(4S)$	
$\Gamma(\Sigma_c(2455)\bar{K})/\Gamma(\Lambda_c^+ \bar{K}\pi)$				Γ_2/Γ_1
VALUE	DOCUMENT ID	TECN	COMMENT	
$0.55 \pm 0.07 \pm 0.13$	AUBERT 08J	BABR	$e^+ e^- \approx \Upsilon(4S)$	
$\Gamma(\Xi_c^0 \pi)/\Gamma_{\text{total}}$				Γ_5/Γ
VALUE	DOCUMENT ID	TECN	COMMENT	
seen	YELTON 16	BELL	$e^+ e^-$, Υ regions	
$\Gamma(\Xi_c(2645)\pi)/\Gamma_{\text{total}}$				Γ_6/Γ
VALUE	DOCUMENT ID	TECN	COMMENT	
seen	LESIAK 08	BELL	$e^+ e^- \approx \Upsilon(4S)$	

 $\Xi_c(2970)$ REFERENCES

YELTON 16	PR D94 052011	J. Yelton <i>et al.</i>	(BELLE Collab.)
KATO 14	PR D89 052003	Y. Kato <i>et al.</i>	(BELLE Collab.)
AUBERT 08J	PR D77 012002	B. Aubert <i>et al.</i>	(BABAR Collab.)
LESIAK 08	PL B665 9	T. Lesiak <i>et al.</i>	(BELLE Collab.)
CHISTOV 06	PRL 97 162001	R. Chistov <i>et al.</i>	(BELLE Collab.)

 $\Xi_c(3055)$

$$I(J^P) = ?(??) \quad \text{Status: } ***$$

 $\Xi_c(3055)$ MASSES

$\Xi_c(3055)^+$ MASS	VALUE (MeV)	EVTS	DOCUMENT ID	TECN	COMMENT
3055.9 ± 0.4	894		KATO 16	BELL	$e^+ e^- \Upsilon$ region
••• We do not use the following data for averages, fits, limits, etc. •••					
$3058.1 \pm 1.0 \pm 2.1$	199 ± 46		KATO 14	BELL	See KATO 16
$3054.2 \pm 1.2 \pm 0.5$	218 ± 95		AUBERT 08J	BABR	$e^+ e^- \approx 10.58$ GeV

 $\Xi_c(3055)$ WIDTHS

$\Xi_c(3055)^+$ WIDTH	VALUE (MeV)	EVTS	DOCUMENT ID	TECN	COMMENT
$7.8 \pm 1.2 \pm 1.5$			KATO 16	BELL	$e^+ e^- \Upsilon$ region
••• We do not use the following data for averages, fits, limits, etc. •••					
$9.7 \pm 3.4 \pm 3.3$	199 ± 46		KATO 14	BELL	$e^+ e^- \Upsilon(1S)$ to $\Upsilon(5S)$
$17 \pm 6 \pm 11$	218 ± 95		AUBERT 08J	BABR	$e^+ e^- \approx 10.58$ GeV

 $\Xi_c(3055)$ DECAY MODES

Mode	Fraction (Γ_i/Γ)
$\Gamma_1 \Sigma^{++} K^-$	seen
$\Gamma_2 \Lambda D^+$	seen

 $\Xi_c(3055)$ BRANCHING RATIOS

$\Gamma(\Lambda D^+)/\Gamma(\Sigma^{++} K^-)$	DOCUMENT ID	TECN	COMMENT	Γ_2/Γ_1
VALUE				
$5.09 \pm 1.01 \pm 0.76$	KATO 16	BELL	721 and 103 evts	

 $\Xi_c(3055)$ REFERENCES

KATO 16	PR D94 032002	Y. Kato <i>et al.</i>	(BELLE Collab.)
KATO 14	PR D89 052003	Y. Kato <i>et al.</i>	(BELLE Collab.)
AUBERT 08J	PR D77 012002	B. Aubert <i>et al.</i>	(BABAR Collab.)

 $\Xi_c(3080)$

$$I(J^P) = \frac{1}{2}(??) \quad \text{Status: } ***$$

 $\Xi_c(3080)$ MASSES

$\Xi_c(3080)^+$ MASS	VALUE (MeV)	EVTS	DOCUMENT ID	TECN	COMMENT
3077.2 ± 0.4 OUR AVERAGE					
3077.9 ± 0.9	596		KATO 16	BELL	$e^+ e^- \Upsilon$ region
$3077.0 \pm 0.4 \pm 0.2$	403 ± 60		AUBERT 08J	BABR	$e^+ e^- \approx 10.58$ GeV

••• We do not use the following data for averages, fits, limits, etc. •••

$3076.9 \pm 0.3 \pm 0.2$	210 ± 30		KATO 14	BELL	See KATO 16
$3076.7 \pm 0.9 \pm 0.5$	326 ± 40		CHISTOV 06	BELL	See KATO 14

 $\Xi_c(3080)^0$ MASS

VALUE (MeV)	EVTS	DOCUMENT ID	TECN	COMMENT
3079.9 ± 1.4 OUR AVERAGE				Error includes scale factor of 1.3.
$3079.3 \pm 1.1 \pm 0.2$	90 ± 27		AUBERT 08J	BABR $e^+ e^- \approx 10.58$ GeV
$3082.8 \pm 1.8 \pm 1.5$	67 ± 20		CHISTOV 06	BELL $e^+ e^- \approx \Upsilon(4S)$

 $\Xi_c(3080)$ WIDTHS $\Xi_c(3080)^+$ WIDTH

VALUE (MeV)	EVTS	DOCUMENT ID	TECN	COMMENT
3.6 ± 1.1 OUR AVERAGE				Error includes scale factor of 1.5.
$3.0 \pm 0.7 \pm 0.4$	596		KATO 16	BELL $e^+ e^- \Upsilon$ region
$5.5 \pm 1.3 \pm 0.6$	403 ± 60		AUBERT 08J	BABR $e^+ e^- \approx 10.58$ GeV
••• We do not use the following data for averages, fits, limits, etc. •••				
$2.4 \pm 0.9 \pm 1.6$	210 ± 30		KATO 14	BELL See KATO 16
$6.2 \pm 1.2 \pm 0.8$	326 ± 40		CHISTOV 06	BELL See KATO 14

 $\Xi_c(3080)^0$ WIDTH

VALUE (MeV)	EVTS	DOCUMENT ID	TECN	COMMENT
5.6 ± 2.2 OUR AVERAGE				
$5.9 \pm 2.3 \pm 1.5$	90 ± 27		AUBERT 08J	BABR $e^+ e^- \approx 10.58$ GeV
$5.2 \pm 3.1 \pm 1.8$	67 ± 20		CHISTOV 06	BELL $e^+ e^- \approx \Upsilon(4S)$

 $\Xi_c(3080)$ DECAY MODES

Mode	Fraction (Γ_i/Γ)
$\Gamma_1 \Lambda_c^+ \bar{K}\pi$	seen
$\Gamma_2 \Sigma_c(2455)\bar{K}$	seen
$\Gamma_3 \Sigma_c(2455)^{++} K^-$	seen
$\Gamma_4 \Sigma_c(2520)^{++} K^-$	seen
$\Gamma_5 \Sigma_c(2455)\bar{K} + \Sigma_c(2520)\bar{K}$	seen
$\Gamma_6 \Lambda_c^+ \bar{K}$	not seen
$\Gamma_7 \Lambda_c^+ \bar{K}\pi^+ \pi^-$	not seen
$\Gamma_8 \Lambda D^+$	seen

 $\Xi_c(3080)$ BRANCHING RATIOS

$\Gamma(\Sigma_c(2455)\bar{K})/\Gamma(\Lambda_c^+ \bar{K}\pi)$	DOCUMENT ID	TECN	COMMENT	Γ_2/Γ_1
VALUE				
0.45 ± 0.06 OUR AVERAGE				
$0.45 \pm 0.05 \pm 0.05$	AUBERT 08J	BABR	in $\Lambda_c^+ K^- \pi^+$	
$0.44 \pm 0.12 \pm 0.07$	AUBERT 08J	BABR	in $\Lambda_c^+ K_S^0 \pi^-$	

$\Gamma(\Sigma_c(2520)^{++} K^-)/\Gamma(\Sigma_c(2455)^{++} K^-)$	DOCUMENT ID	TECN	COMMENT	Γ_4/Γ_3
VALUE				
$1.07 \pm 0.27 \pm 0.04$	KATO 16	BELL	234 and 176 evts	

$[\Gamma(\Sigma_c(2455)\bar{K}) + \Gamma(\Sigma_c(2520)\bar{K})]/\Gamma(\Lambda_c^+ \bar{K}\pi)$	DOCUMENT ID	TECN	COMMENT	Γ_5/Γ_1
VALUE				
0.89 ± 0.12 OUR AVERAGE				
$0.95 \pm 0.14 \pm 0.06$	AUBERT 08J	BABR	in $\Lambda_c^+ K^- \pi^+$	
$0.78 \pm 0.21 \pm 0.05$	AUBERT 08J	BABR	in $\Lambda_c^+ K_S^0 \pi^-$	

$\Gamma(\Lambda D^+)/\Gamma(\Sigma_c(2455)^{++} K^-)$	DOCUMENT ID	TECN	COMMENT	Γ_8/Γ_3
VALUE				
$1.29 \pm 0.30 \pm 0.15$	KATO 16	BELL	186 and 176 evts	

 $\Xi_c(3080)$ REFERENCES

KATO 16	PR D94 032002	Y. Kato <i>et al.</i>	(BELLE Collab.)
KATO 14	PR D89 052003	Y. Kato <i>et al.</i>	(BELLE Collab.)
AUBERT 08J	PR D77 012002	B. Aubert <i>et al.</i>	(BABAR Collab.)
CHISTOV 06	PRL 97 162001	R. Chistov <i>et al.</i>	(BELLE Collab.)

 $\Xi_c(3123)$

$$I(J^P) = ?(??) \quad \text{Status: } *$$

OMITTED FROM SUMMARY TABLE

A peak in the $\Sigma_c(2520)^{++} K^- \rightarrow \Lambda_c^+ K^- \pi^+$ mass spectrum with a significance of 3.6 standard deviations. KATO 14 finds no evidence for this state.

$\Xi_c(3123)$ MASSES

$\Xi_c(3123)^+$ MASS

VALUE (MeV)	EVTs	DOCUMENT ID	TECN	COMMENT
3122.9 ± 1.3 ± 0.3	101 ± 35	AUBERT	08J	BABR $e^+e^- \approx 10.58$ GeV

$\Xi_c(3123)$ WIDTHS

$\Xi_c(3123)^+$ WIDTH

VALUE (MeV)	EVTs	DOCUMENT ID	TECN	COMMENT
4.4 ± 3.4 ± 1.7	101 ± 35	AUBERT	08J	BABR $e^+e^- \approx 10.58$ GeV

$\Xi_c(3123)$ REFERENCES

KATO	14	PR D89 052003	Y. Kato <i>et al.</i>	(BELLE Collab.)
AUBERT	08J	PR D77 012002	B. Aubert <i>et al.</i>	(BABAR Collab.)



$I(J^P) = 0(\frac{1}{2}^+)$ Status: ***

The quantum numbers have not been measured, but are simply assigned in accord with the quark model, in which the Ω_c^0 is the *ssc* ground state. No absolute branching fractions have been measured.

Ω_c^0 MASS

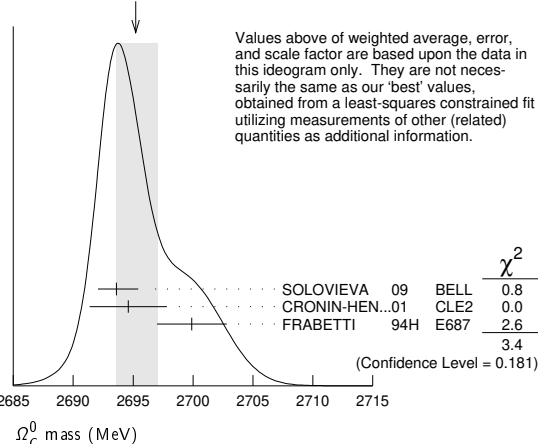
VALUE (MeV)	EVTs	DOCUMENT ID	TECN	COMMENT
2695.2 ± 1.7 OUR FIT	Error			includes scale factor of 1.3.

2695.2 ± 1.8 OUR AVERAGE Error includes scale factor of 1.3. See the ideogram below.

2693.6 ± 0.3 ± 1.8	725	SOLOVIEVA	09	BELL $\Omega^- \pi^+$ in $e^+e^- \rightarrow \Upsilon(4S)$
2694.6 ± 2.6 ± 1.9	40	¹ CRONIN-HEN..01	CLE2	$e^+e^- \approx 10.6$ GeV
2699.9 ± 1.5 ± 2.5	42	² FRABETTI	94H	E687 γ Be, $\bar{E}_\gamma = 221$ GeV
• • • We do not use the following data for averages, fits, limits, etc. • • •				
2705.9 ± 3.3 ± 2.0	10	³ FRABETTI	93	E687 γ Be, $\bar{E}_\gamma = 221$ GeV
2719.0 ± 7.0 ± 2.5	11	⁴ ALBRECHT	92H	ARG $e^+e^- \approx 10.6$ GeV
2740 ± 20	3	BIAGI	85B	SPEC Σ^- Be 135 GeV/c

- ¹ CRONIN-HENNESSY 01 sees 40.4 ± 9.0 events in a sum over five channels.
- ² FRABETTI 94H claims a signal of 42.5 ± 8.8 $\Sigma^+ K^- K^- \pi^+$ events. The background is about 24 events.
- ³ FRABETTI 93 claims a signal of 10.3 ± 3.9 $\Omega^- \pi^+$ events above a background of 5.8 events.
- ⁴ ALBRECHT 92H claims a signal of 11.5 ± 4.3 $\Xi^- K^- \pi^+ \pi^+$ events. The background is about 5 events.

WEIGHTED AVERAGE
2695.2 ± 1.8-1.6 (Error scaled by 1.3)



Ω_c^0 MEAN LIFE

VALUE (10^{-15} s)	EVTs	DOCUMENT ID	TECN	COMMENT
268 ± 24 ± 10	978	¹ AAIJ	18J	LHCB $p K^- K^- \pi^+$
• • • We do not use the following data for averages, fits, limits, etc. • • •				
72 ± 11 ± 11	64	LINK	03c	FOCS $\Omega^- \pi^+, \Xi^- K^- \pi^+ \pi^+$
55 +13 +18 -11 -23	86	ADAMOVICH	95B	WA89 $\Omega^- \pi^- \pi^+ \pi^+, \Xi^- K^- \pi^+ \pi^+$
86 +27 -20 ± 28	25	FRABETTI	95D	E687 $\Sigma^+ K^- K^- \pi^+$

¹ AAIJ 18J, with nearly five times more events than the previous three experiments combined, gets a lifetime that is nearly four times larger than the average of those experiments, $(69 \pm 12) \times 10^{-15}$ s. We go with the larger data sample.

Ω_c^0 DECAY MODES

Mode	Fraction (Γ_i/Γ)	Confidence level
------	--------------------------------	------------------

No absolute branching fractions have been measured. The following are branching ratios relative to $\Omega^- \pi^+$.

Cabibbo-favored ($S = -3$) decays — relative to $\Omega^- \pi^+$

Γ_i	Mode	Fraction (Γ_i/Γ)	Confidence level
Γ_1	$\Omega^- \pi^+$	DEFINED AS 1	
Γ_2	$\Omega^- \pi^+ \pi^0$	1.80 ± 0.33	
Γ_3	$\Omega^- \rho^+$	>1.3	90%
Γ_4	$\Omega^- \pi^- 2\pi^+$	0.31 ± 0.05	
Γ_5	$\Omega^- e^+ \nu_e$	2.4 ± 1.2	
Γ_6	$\Xi^0 \bar{K}^0$	1.64 ± 0.29	
Γ_7	$\Xi^0 K^- \pi^+$	1.20 ± 0.18	
Γ_8	$\Xi^0 \bar{K}^{*0}, \bar{K}^{*0} \rightarrow K^- \pi^+$	0.68 ± 0.16	
Γ_9	$\Xi^- \bar{K}^0 \pi^+$	2.12 ± 0.28	
Γ_{10}	$\Xi^- K^- 2\pi^+$	0.63 ± 0.09	
Γ_{11}	$\Xi(1530)^0 K^- \pi^+, \Xi^{*0} \rightarrow$	0.21 ± 0.06	
Γ_{12}	$\Xi^- \bar{K}^{*0} \pi^+$	0.34 ± 0.11	
Γ_{13}	$\Sigma^+ K^- K^- \pi^+$	<0.32	90%
Γ_{14}	$\Lambda \bar{K}^0 \bar{K}^0$	1.72 ± 0.35	

Ω_c^0 BRANCHING RATIOS

A few early but now obsolete measurements have been omitted. See K.A. Olive, et al. (Particle Data Group), Chinese Physics **C38** 070001 (2014).

$\Gamma(\Omega^- \pi^+ \pi^0)/\Gamma(\Omega^- \pi^+)$ Γ_2/Γ_1

VALUE	EVTs	DOCUMENT ID	TECN	COMMENT
1.80 ± 0.33 OUR AVERAGE	Error			includes scale factor of 1.9.
2.00 ± 0.17 ± 0.11	403	YELTON	18	BELL $e^+e^- \rightarrow \Upsilon(4S)$, +higher
1.27 ± 0.31 ± 0.11	64	AUBERT	07AH	BABR $e^+e^- \approx \Upsilon(4S)$

$\Gamma(\Omega^- \rho^+)/\Gamma(\Omega^- \pi^+ \pi^0)$ Γ_3/Γ_2

VALUE	CL%	DOCUMENT ID	TECN	COMMENT
>0.71	90	¹ YELTON	18	BELL $e^+e^- \rightarrow \Upsilon(4S)$, +higher

¹ This submode fraction is evaluated from a background-subtracted signal in a mass plot. Result ignores interference effects and systematic uncertainties, which YELTON 18 claim are both small.

$\Gamma(\Omega^- \pi^- 2\pi^+)/\Gamma(\Omega^- \pi^+)$ Γ_4/Γ_1

VALUE	EVTs	DOCUMENT ID	TECN	COMMENT
0.31 ± 0.05 OUR AVERAGE				
0.32 ± 0.05 ± 0.02	108	YELTON	18	BELL $e^+e^- \rightarrow \Upsilon(4S)$, +higher
0.28 ± 0.09 ± 0.01	25	AUBERT	07AH	BABR $e^+e^- \approx \Upsilon(4S)$

$\Gamma(\Omega^- \pi^+)/\Gamma(\Omega^- e^+ \nu_e)$ Γ_1/Γ_5

VALUE	EVTs	DOCUMENT ID	TECN	COMMENT
0.41 ± 0.19 ± 0.04	11	AMMAR	02	CLE2 $e^+e^- \approx \Upsilon(4S)$

$\Gamma(\Xi^0 \bar{K}^0)/\Gamma(\Omega^- \pi^+)$ Γ_6/Γ_1

VALUE	EVTs	DOCUMENT ID	TECN	COMMENT
1.64 ± 0.26 ± 0.12	98	YELTON	18	BELL $e^+e^- \rightarrow \Upsilon(4S)$, +higher

$\Gamma(\Xi^0 K^- \pi^+)/\Gamma(\Omega^- \pi^+)$ Γ_7/Γ_1

VALUE	EVTs	DOCUMENT ID	TECN	COMMENT
1.20 ± 0.16 ± 0.08	168	YELTON	18	BELL $e^+e^- \rightarrow \Upsilon(4S)$, +higher

$\Gamma(\Xi^0 \bar{K}^{*0}, \bar{K}^{*0} \rightarrow K^- \pi^+)/\Gamma(\Xi^0 K^- \pi^+)$ Γ_8/Γ_7

VALUE	EVTs	DOCUMENT ID	TECN	COMMENT
0.57 ± 0.10	95	¹ YELTON	18	BELL $e^+e^- \rightarrow \Upsilon(4S)$, +higher

¹ This submode fraction is evaluated from a background-subtracted signal in a mass plot. Result ignores interference effects and systematic uncertainties, which YELTON 18 claim are both small.

$\Gamma(\Xi^- \bar{K}^0 \pi^+)/\Gamma(\Omega^- \pi^+)$ Γ_9/Γ_1

VALUE	EVTs	DOCUMENT ID	TECN	COMMENT
2.12 ± 0.24 ± 0.14	349	YELTON	18	BELL $e^+e^- \rightarrow \Upsilon(4S)$, +higher

$\Gamma(\Xi^- K^- 2\pi^+)/\Gamma(\Omega^- \pi^+)$ Γ_{10}/Γ_1

VALUE	EVTs	DOCUMENT ID	TECN	COMMENT
0.63 ± 0.09 OUR AVERAGE	Error			includes scale factor of 1.4.
0.68 ± 0.07 ± 0.03	278	YELTON	18	BELL $e^+e^- \rightarrow \Upsilon(4S)$, +higher
0.46 ± 0.13 ± 0.03	45	AUBERT	07AH	BABR $e^+e^- \approx \Upsilon(4S)$

$\Gamma(\Xi(1530)^0 K^- \pi^+, \Xi^{*0} \rightarrow \Xi^- \pi^+)/\Gamma(\Xi^- K^- 2\pi^+)$ Γ_{11}/Γ_{10}

VALUE	EVTs	DOCUMENT ID	TECN	COMMENT
0.33 ± 0.09	74	¹ YELTON	18	BELL $e^+e^- \rightarrow \Upsilon(4S)$, +higher

¹ This submode fraction is evaluated from a background-subtracted signal in a mass plot. Result ignores interference effects and systematic uncertainties, which YELTON 18 claim are both small.

Baryon Particle Listings

$\Omega_c^0, \Omega_c(2770)^0, \Omega_c(3000)^0, \Omega_c(3050)^0, \Omega_c(3065)^0$

$\Gamma(\Xi^- \bar{K}^0 \pi^+)/\Gamma(\Xi^- K^- 2\pi^+)$		Γ_{12}/Γ_{10}	
VALUE	EVTS	DOCUMENT ID	TECN COMMENT
0.55 ± 0.16	136	¹ YELTON	18 BELL $e^+ e^- \rightarrow \Upsilon(4S)$, +higher

¹ This submode fraction is evaluated from a background-subtracted signal in a mass plot. Result ignores interference effects and systematic uncertainties, which YELTON 18 claim are both small.

$\Gamma(\Sigma^+ K^- K^- \pi^+)/\Gamma(\Omega^- \pi^+)$		Γ_{13}/Γ_1	
VALUE	CL% EVTS	DOCUMENT ID	TECN COMMENT
<0.32	90 17	YELTON	18 BELL $e^+ e^- \rightarrow \Upsilon(4S)$, +higher

$\Gamma(\Lambda \bar{K}^0 \bar{K}^0)/\Gamma(\Omega^- \pi^+)$		Γ_{14}/Γ_1	
VALUE	EVTS	DOCUMENT ID	TECN COMMENT
1.72 ± 0.32 ± 0.14	95	YELTON	18 BELL $e^+ e^- \rightarrow \Upsilon(4S)$, +higher

Ω_c^0 REFERENCES

AAIJ	18J	PRL 121 092003	R. Aaij et al.	(LHCb Collab.)
YELTON	18	PR D97 032001	J. Yelton et al.	(BELLE Collab.)
PDG	14	CP C38 070001	K. Olive et al.	(PDG Collab.)
SOLOVIEVA	09	PL B672 1	E. Solovieva et al.	(BELLE Collab.)
AUBERT	07AH	PRL 99 062001	B. Aubert et al.	(BABAR Collab.)
LINK	03C	PL B561 41	J.M. Link et al.	(FNAL FOCUS Collab.)
AMMAR	02	PRL 89 171803	R. Ammar et al.	(CLEO Collab.)
CROHN-HEN...	01	PRL 86 3730	D. Cronin-Hennessy et al.	(CLEO Collab.)
ADAMOVICH	95B	PL B358 151	M.I. Adamovich et al.	(CERN WA89 Collab.)
FRABETTI	95D	PL B357 678	P.L. Frabetti et al.	(FNAL E687 Collab.)
FRABETTI	94H	PL B338 106	P.L. Frabetti et al.	(FNAL E687 Collab.)
FRABETTI	93	PL B300 190	P.L. Frabetti et al.	(FNAL E687 Collab.)
ALBRECHT	92H	PL B288 367	H. Albrecht et al.	(ARGUS Collab.)
BIAGI	85B	ZPHY C28 175	S.F. Biagi et al.	(CERN WA62 Collab.)

$\Omega_c(2770)^0$ $I(J^P) = 0(\frac{3}{2}^+)$ Status: ***

The natural assignment is that this goes with the $\Sigma_c(2520)$ and $\Xi_c(2645)$ to complete the lowest mass $J^P = \frac{3}{2}^+$ SU(3) sextet, part of the SU(4) 20-plet that includes the $\Delta(1232)$. But J and P have not been measured.

$\Omega_c(2770)^0$ MASS

The mass is obtained from the mass-difference measurement that follows.

VALUE (MeV)	DOCUMENT ID
2765.9 ± 2.0 OUR FIT	Error includes scale factor of 1.2.

$\Omega_c(2770)^0 - \Omega_c^0$ MASS DIFFERENCE

VALUE (MeV)	EVTS	DOCUMENT ID	TECN	COMMENT
70.7^{+0.8}_{-0.9} OUR FIT				
70.7^{+0.8}_{-1.0} OUR AVERAGE				
70.7 ± 0.9 ^{+0.1} _{-0.9}	54 ± 9	SOLOVIEVA 09	BELL	$\Omega_c^0 \gamma$ in $e^+ e^- \rightarrow \Upsilon(4S)$
70.8 ± 1.0 ± 1.1	105 ± 22	AUBERT, BE	06i BABR	$e^+ e^- \approx \Upsilon(4S)$

$\Omega_c(2770)^0$ DECAY MODES

The $\Omega_c(2770)^0 - \Omega_c^0$ mass difference is too small for any strong decay to occur.

Mode	Fraction (Γ_i/Γ)
$\Gamma_1 \Omega_c^0 \gamma$	presumably 100%

$\Omega_c(2770)^0$ REFERENCES

SOLOVIEVA	09	PL B672 1	E. Solovieva et al.	(BELLE Collab.)
AUBERT, BE	06i	PRL 97 232001	B. Aubert et al.	(BABAR Collab.)

$\Omega_c(3000)^0$ $I(J^P) = ?(?^?)$ Status: ***

$\Omega_c(3000)^0$ MASS

VALUE (MeV)	EVTS	DOCUMENT ID	TECN	COMMENT
3000.41 ± 0.22 OUR AVERAGE				
3000.7 ± 1.0 ± 0.2	38	YELTON	18B BELL	$e^+ e^-$ at $\Upsilon(4S)$
3000.4 ± 0.2 ± 0.1	1.3k	AAIJ	17AH LHCb	pp at 7, 8, 13 TeV

$\Omega_c(3000)^0$ WIDTH

VALUE (MeV)	EVTS	DOCUMENT ID	TECN	COMMENT
4.5 ± 0.6 ± 0.3	1.3k	AAIJ	17AH LHCb	pp at 7, 8, 13 TeV

$\Omega_c(3000)^0$ DECAY MODES

Mode	Fraction (Γ_i/Γ)
$\Gamma_1 \Xi_c^+ K^-$	seen

$\Omega_c(3000)^0$ BRANCHING RATIOS

$\Gamma(\Xi_c^+ K^-)/\Gamma_{total}$		Γ_1/Γ	
VALUE	EVTS	DOCUMENT ID	TECN COMMENT
seen	38	¹ YELTON	18B BELL $e^+ e^-$ at $\Upsilon(4S)$
seen	1.3k	AAIJ	17AH LHCb pp at 7, 8, 13 TeV

¹ YELTON 18B report a significance of 3.9 σ

$\Omega_c(3000)^0$ REFERENCES

YELTON	18B	PR D97 051102	J. Yelton et al.	(BELLE Collab.)
AAIJ	17AH	PRL 118 182001	R. Aaij et al.	(LHCb Collab.)

$\Omega_c(3050)^0$ $I(J^P) = ?(?^?)$ Status: ***

$\Omega_c(3050)^0$ MASS

VALUE (MeV)	EVTS	DOCUMENT ID	TECN	COMMENT
3050.20 ± 0.13 OUR AVERAGE				
3050.2 ± 0.4 ± 0.2	28	YELTON	18B BELL	$e^+ e^-$ at $\Upsilon(4S)$
3050.2 ± 0.1 ± 0.1	970	AAIJ	17AH LHCb	pp at 7, 8, 13 TeV

$\Omega_c(3050)^0$ WIDTH

VALUE (MeV)	CL%	DOCUMENT ID	TECN	COMMENT
<1.2	95	AAIJ	17AH LHCb	pp at 7, 8, 13 TeV

$\Omega_c(3050)^0$ DECAY MODES

Mode	Fraction (Γ_i/Γ)
$\Gamma_1 \Xi_c^+ K^-$	seen

$\Omega_c(3050)^0$ BRANCHING RATIOS

$\Gamma(\Xi_c^+ K^-)/\Gamma_{total}$		Γ_1/Γ	
VALUE	EVTS	DOCUMENT ID	TECN COMMENT
seen	28	¹ YELTON	18B BELL $e^+ e^-$ at $\Upsilon(4S)$
seen	970	AAIJ	17AH LHCb pp at 7, 8, 13 TeV

¹ YELTON 18B report a significance of 4.6 σ

$\Omega_c(3050)^0$ REFERENCES

YELTON	18B	PR D97 051102	J. Yelton et al.	(BELLE Collab.)
AAIJ	17AH	PRL 118 182001	R. Aaij et al.	(LHCb Collab.)

$\Omega_c(3065)^0$ $I(J^P) = ?(?^?)$ Status: ***

$\Omega_c(3065)^0$ MASS

VALUE (MeV)	EVTS	DOCUMENT ID	TECN	COMMENT
3065.46 ± 0.28 OUR AVERAGE				
3064.9 ± 0.6 ± 0.2	82	YELTON	18B BELL	$e^+ e^-$ at $\Upsilon(4S)$
3065.6 ± 0.1 ± 0.3	1.74k	AAIJ	17AH LHCb	pp at 7, 8, 13 TeV

$\Omega_c(3065)^0$ WIDTH

VALUE (MeV)	EVTS	DOCUMENT ID	TECN	COMMENT
3.5 ± 0.4 ± 0.2	1.74k	AAIJ	17AH LHCb	pp at 7, 8, 13 TeV

$\Omega_c(3065)^0$ DECAY MODES

Mode	Fraction (Γ_i/Γ)
$\Gamma_1 \Xi_c^+ K^-$	seen

See key on page 999

Baryon Particle Listings
 $\Omega_c(3065)^0, \Omega_c(3090)^0, \Omega_c(3120)^0$

$\Omega_c(3065)^0$ BRANCHING RATIOS

$\Gamma(\Xi_c^+ K^-)/\Gamma_{\text{total}}$					Γ_1/Γ
VALUE	EVTS	DOCUMENT ID	TECN	COMMENT	
seen	82	YELTON	18B BELL	$e^+ e^-$ at $\Upsilon(4S)$	
seen	1.74k	AAIJ	17AH LHCB	pp at 7, 8, 13 TeV	

$\Omega_c(3065)^0$ REFERENCES

YELTON	18B PR D97 051102	J. Yelton <i>et al.</i>	(BELLE Collab.)
AAIJ	17AH PRL 118 182001	R. Aaij <i>et al.</i>	(LHCb Collab.)

$\Omega_c(3090)^0$ $I(J^P) = ?(?^?)$ Status: ***

$\Omega_c(3090)^0$ MASS

VALUE (MeV)	EVTS	DOCUMENT ID	TECN	COMMENT
3090.0 ± 0.5 OUR AVERAGE				
$3089.3 \pm 1.2 \pm 0.2$	87	YELTON	18B BELL	$e^+ e^-$ at $\Upsilon(4S)$
$3090.2 \pm 0.3 \pm 0.5$	2.0k	AAIJ	17AH LHCB	pp at 7, 8, 13 TeV

$\Omega_c(3090)^0$ WIDTH

VALUE (MeV)	EVTS	DOCUMENT ID	TECN	COMMENT
$8.7 \pm 1.0 \pm 0.8$	2.0k	AAIJ	17AH LHCB	pp at 7, 8, 13 TeV

$\Omega_c(3090)^0$ DECAY MODES

Mode	Fraction (Γ_i/Γ)
$\Gamma_1 \Xi_c^+ K^-$	seen

$\Omega_c(3090)^0$ BRANCHING RATIOS

$\Gamma(\Xi_c^+ K^-)/\Gamma_{\text{total}}$					Γ_1/Γ
VALUE	EVTS	DOCUMENT ID	TECN	COMMENT	
seen	87	YELTON	18B BELL	$e^+ e^-$ at $\Upsilon(4S)$	
seen	2.0k	AAIJ	17AH LHCB	pp at 7, 8, 13 TeV	

$\Omega_c(3090)^0$ REFERENCES

YELTON	18B PR D97 051102	J. Yelton <i>et al.</i>	(BELLE Collab.)
AAIJ	17AH PRL 118 182001	R. Aaij <i>et al.</i>	(LHCb Collab.)

$\Omega_c(3120)^0$

$I(J^P) = ?(?^?)$ Status: ***

$\Omega_c(3120)^0$ MASS

VALUE (MeV)	EVTS	DOCUMENT ID	TECN	COMMENT
$3119.1 \pm 0.3 \pm 0.9 \pm 0.3$	480	¹ AAIJ	17AH LHCB	pp at 7, 8, 13 TeV

¹ The third error is the uncertainty on the Ξ_c^+ mass. (AAIJ 17AH gave $+0.3$ MeV here, but as of 2018 it is ± 0.3 .)

$\Omega_c(3120)^0$ WIDTH

VALUE (MeV)	CL%	DOCUMENT ID	TECN	COMMENT
<2.6	95	AAIJ	17AH LHCB	pp at 7, 8, 13 TeV

$\Omega_c(3120)^0$ DECAY MODES

Mode	Fraction (Γ_i/Γ)
$\Gamma_1 \Xi_c^+ K^-$	seen

$\Omega_c(3120)^0$ BRANCHING RATIOS

$\Gamma(\Xi_c^+ K^-)/\Gamma_{\text{total}}$					Γ_1/Γ
VALUE	EVTS	DOCUMENT ID	TECN	COMMENT	
seen		AAIJ	17AH LHCB	pp at 7, 8, 13 TeV	

$\Omega_c(3120)^0$ REFERENCES

AAIJ	17AH PRL 118 182001	R. Aaij <i>et al.</i>	(LHCb Collab.)
------	---------------------	-----------------------	----------------

Baryon Particle Listings



DOUBLY CHARMED BARYONS
(C = +2)

$\Xi_{cc}^{++} = ucc, \Xi_{cc}^+ = dcc, \Omega_{cc}^+ = scc$



$I(J^P) = ?(??)$ Status: ***

Ξ_{cc}^{++} MASS

VALUE (MeV)	EVTS	DOCUMENT ID	TECN	COMMENT
3621.2 ± 0.7 OUR AVERAGE				
3620.6 ± 1.5 ± 0.4 ± 0.3	91	¹ AAIJ	18BA LHCb	pp at 13 TeV
3621.40 ± 0.72 ± 0.27 ± 0.14	313	² AAIJ	17Bc LHCb	pp at 13 TeV

¹ The third error in AAIJ 18BA value is from the uncertainty of the Ξ_{cc}^+ mass.
² The third error in AAIJ 17Bc value is from the uncertainty of the Λ_c^+ mass. The width of the signal is 6.6 ± 0.8 MeV, consistent with the experimental resolution.

Ξ_{cc}^{++} MEAN LIFE

VALUE (10 ⁻¹⁵ s)	EVTS	DOCUMENT ID	TECN	COMMENT
256⁺²⁴₋₂₂ ± 14	304	AAIJ	18G LHCb	pp at 13 TeV

Ξ_{cc}^{++} DECAY MODES

Mode	Fraction (Γ_i/Γ)
$\Gamma_1 \Lambda_c^+ K^- \pi^+ \pi^+$	seen
$\Gamma_2 \Xi_c^+ \pi^+, \Xi_c^+ \rightarrow p K^- \pi^+$	seen
$\Gamma_3 D^+ p K^- \pi^+$	

$\Gamma(\Lambda_c^+ K^- \pi^+ \pi^+)/\Gamma_{total}$	Γ_1/Γ		
VALUE	DOCUMENT ID	TECN	COMMENT
seen	AAIJ	17Bc LHCb	12 std significance

$\Gamma(\Xi_c^+ \pi^+, \Xi_c^+ \rightarrow p K^- \pi^+)/\Gamma_{total}$	Γ_2/Γ			
VALUE	EVTS	DOCUMENT ID	TECN	COMMENT
seen	91	AAIJ	18BA LHCb	5.9 std significance

$\Gamma(\Xi_c^+ \pi^+, \Xi_c^+ \rightarrow p K^- \pi^+)/\Gamma(\Lambda_c^+ K^- \pi^+ \pi^+)$	Γ_2/Γ_1		
VALUE (units 10 ⁻³)	DOCUMENT ID	TECN	COMMENT
2.2 ± 0.6 ± 0.1	³ AAIJ	18BA LHCb	Ratio 91 over 289 events
³ AAIJ 18BA reports $[\Gamma(\Xi_{cc}^{++} \rightarrow \Xi_c^+ \pi^+, \Xi_c^+ \rightarrow p K^- \pi^+)/\Gamma(\Xi_{cc}^{++} \rightarrow \Lambda_c^+ K^- \pi^+ \pi^+)] / [B(\Lambda_c^+ \rightarrow p K^- \pi^+)] = (3.5 \pm 0.9 \pm 0.3) \times 10^{-2}$ which we multiply by our best value $B(\Lambda_c^+ \rightarrow p K^- \pi^+) = (6.28 \pm 0.32) \times 10^{-2}$. Our first error is their experiment's error and our second error is the systematic error from using our best value.			

$\Gamma(D^+ p K^- \pi^+)/\Gamma(\Lambda_c^+ K^- \pi^+ \pi^+)$	Γ_3/Γ_1			
VALUE	CL%	DOCUMENT ID	TECN	COMMENT
< 1.7 × 10⁻²	90	AAIJ	19A0 LHCb	pp at 13 TeV

Ξ_{cc}^{++} REFERENCES

AAIJ	19A0 JHEP 1910 124	R. Aaij <i>et al.</i>	(LHCb Collab.)
AAIJ	18BA PRL 121 162002	R. Aaij <i>et al.</i>	(LHCb Collab.)
AAIJ	18G PRL 121 052002	R. Aaij <i>et al.</i>	(LHCb Collab.)
AAIJ	17Bc PRL 119 112001	R. Aaij <i>et al.</i>	(LHCb Collab.)

See key on page 999

Baryon Particle Listings

Λ_b^0

BOTTOM BARYONS
($B = -1$)

$\Lambda_b^0 = udb, \Xi_b^0 = usb, \Xi_b^- = dsb, \Omega_b^- = sss$

Λ_b^0

$I(J^P) = 0(\frac{1}{2}^+)$ Status: ***

In the quark model, a Λ_b^0 is an isospin-0 udb state. The lowest Λ_b^0 ought to have $J^P = 1/2^+$. None of $I, J,$ or P have actually been measured.

Λ_b^0 MASS

$m_{\Lambda_b^0}$	VALUE (MeV)	EVTs	DOCUMENT ID	TECN	COMMENT
5619.60 ± 0.17 OUR AVERAGE					
5619.62 ± 0.16 ± 0.13			1 AAIJ	17AM LHCb	pp at 7, 8 TeV
5619.30 ± 0.34			2 AAIJ	14AA LHCb	pp at 7 TeV
5620.15 ± 0.31 ± 0.47			3 AALTONEN	14B CDF	$p\bar{p}$ at 1.96 TeV
5619.7 ± 0.7 ± 1.1			4 AAD	13U ATLS	pp at 7 TeV
5621 ± 4 ± 3			4 ABE	97B CDF	$p\bar{p}$ at 1.8 TeV
5668 ± 16 ± 8		4	5 ABREU	96N DLPH	$e^+e^- \rightarrow Z$
5614 ± 21 ± 4		4	5 BUSKULIC	96L ALEP	$e^+e^- \rightarrow Z$
• • • We do not use the following data for averages, fits, limits, etc. • • •					
5619.65 ± 0.17 ± 0.17			6 AAIJ	16Y LHCb	Repl. by AAIJ 17AM
5619.44 ± 0.13 ± 0.38			3 AAIJ	13AV LHCb	Repl. by AAIJ 17AM
5619.19 ± 0.70 ± 0.30			3 AAIJ	12E LHCb	Repl. by AAIJ 13AV
5619.7 ± 1.2 ± 1.2			7 ACOSTA	06 CDF	Repl. by AALTONEN 14B
not seen			8 ABE	93B CDF	Repl. by ABE 97B
5640 ± 50 ± 30		16	9 ALBAJAR	91E UA1	$p\bar{p}$ 630 GeV
5640 $\begin{smallmatrix} +100 \\ -210 \end{smallmatrix}$		52	BARI	91 SFM	$\Lambda_b^0 \rightarrow pD^0\pi^-$
5650 $\begin{smallmatrix} +150 \\ -200 \end{smallmatrix}$		90	BARI	91 SFM	$\Lambda_b^0 \rightarrow \Lambda_c^+\pi^+\pi^-\pi^-$

- 1 Uses $\Lambda_b^0 \rightarrow \chi_{c1}pK^-, \Lambda_b^0 \rightarrow \chi_{c2}pK^-, \Lambda_b^0 \rightarrow J/\psi\Lambda, \Lambda_b^0 \rightarrow p\psi(2S)K^-, \Lambda_b^0 \rightarrow pJ/\psi\pi^+\pi^-K^-,$ and $\Lambda_b^0 \rightarrow pJ/\psi K^-$ decays.
- 2 Uses exclusively reconstructed final states $\Lambda_b^0 \rightarrow \Lambda_c^+D_s^-, \Lambda_c^+D^-$ and $\bar{B}^0 \rightarrow D^+D_s^-$ decays. The uncertainty includes both statistical and systematic contributions.
- 3 Uses $\Lambda_b^0 \rightarrow J/\psi\Lambda$ fully reconstructed decays.
- 4 ABE 97B observed 38 events with a background of 18 ± 1.6 events in the mass range 5.60–5.65 GeV/ c^2 , a significance of > 3.4 standard deviations.
- 5 Uses 4 fully reconstructed Λ_b^0 events.
- 6 Uses $\Lambda_b^0 \rightarrow p\psi(2S)K^-, \Lambda_b^0 \rightarrow pJ/\psi\pi^+\pi^-K^-,$ and $\Lambda_b^0 \rightarrow pJ/\psi K^-$ decays.
- 7 Uses exclusively reconstructed final states containing a $J/\psi \rightarrow \mu^+\mu^-$ decays.
- 8 ABE 93B states that, based on the signal claimed by ALBAJAR 91E, CDF should have found $30 \pm 23 \Lambda_b^0 \rightarrow J/\psi(1S)\Lambda$ events. Instead, CDF found not more than 2 events.
- 9 ALBAJAR 91E claims 16 ± 5 events above a background of 9 ± 1 events, a significance of about 5 standard deviations.

$m_{\Lambda_b^0} - m_{B^0}$

VALUE (MeV)	DOCUMENT ID	TECN	COMMENT
339.2 ± 1.4 ± 0.1	1 ACOSTA	06 CDF	$p\bar{p}$ at 1.96 TeV

1 Uses exclusively reconstructed final states containing $J/\psi \rightarrow \mu^+\mu^-$ decays.

$m_{\Lambda_b^0} - m_{B^+}$

VALUE (MeV)	DOCUMENT ID	TECN	COMMENT
339.72 ± 0.28 OUR AVERAGE			
339.72 ± 0.24 ± 0.18	1 AAIJ	14AA LHCb	pp at 7 TeV
339.71 ± 0.71 ± 0.09	2 AAIJ	12E LHCb	pp at 7 TeV

- 1 Uses exclusively reconstructed final states $\Lambda_b^0 \rightarrow \Lambda_c^+D_s^-, \Lambda_c^+D^-$ and $\bar{B}^0 \rightarrow D^+D_s^-$ decays.
- 2 Uses exclusively reconstructed final states containing $J/\psi \rightarrow \mu^+\mu^-$ decays.

Λ_b^0 MEAN LIFE

See b -baryon Admixture section for data on b -baryon mean life average over species of b -baryon particles.

“OUR EVALUATION” is an average using rescaled values of the data listed below. The average and rescaling were performed by the Heavy Flavor Averaging Group (HFLAV) and are described at <https://hflav.web.cern.ch/>. The averaging/rescaling procedure takes into account correlations between the measurements and asymmetric lifetime errors.

VALUE (10^{-12} s)	EVTs	DOCUMENT ID	TECN	COMMENT
1.471 ± 0.009 OUR EVALUATION				
1.477 ± 0.027 ± 0.009	1	SIRUNYAN	18BY CMS	pp at 8 TeV
1.415 ± 0.027 ± 0.006	2	AAIJ	14E LHCb	pp at 7 TeV
1.479 ± 0.009 ± 0.010	3	AAIJ	14U LHCb	pp at 7, 8 TeV
1.565 ± 0.035 ± 0.020	2	AALTONEN	14B CDF	$p\bar{p}$ at 1.96 TeV

1.449 ± 0.036 ± 0.017	2	AAD	13U ATLS	pp at 7 TeV
1.503 ± 0.052 ± 0.031	2	CHATRCHYAN	13AC CMS	pp at 7 TeV
1.303 ± 0.075 ± 0.035	2	ABAZOV	12U D0	$p\bar{p}$ at 1.96 TeV
1.401 ± 0.046 ± 0.035	4	AALTONEN	10B CDF	$p\bar{p}$ at 1.96 TeV
1.27 $\begin{smallmatrix} +0.35 \\ -0.29 \end{smallmatrix}$ ± 0.09		ABREU	95S DLPH	Excess $p\mu^-$, decay lengths
• • • We do not use the following data for averages, fits, limits, etc. • • •				
1.482 ± 0.018 ± 0.012	5	AAIJ	13BB LHCb	Repl. by AAIJ 14U
1.537 ± 0.045 ± 0.014	2	AALTONEN	11 CDF	Repl. by AALTONEN 14B
1.218 $\begin{smallmatrix} +0.130 \\ -0.115 \end{smallmatrix}$ ± 0.042	2	ABAZOV	07S D0	Repl. by ABAZOV 12U
1.290 $\begin{smallmatrix} +0.119+0.087 \\ -0.110-0.091 \end{smallmatrix}$	6	ABAZOV	07U D0	$p\bar{p}$ at 1.96 TeV
1.593 $\begin{smallmatrix} +0.083 \\ -0.078 \end{smallmatrix}$ ± 0.033	2	ABULENCIA	07A CDF	Repl. by AALTONEN 11
1.22 $\begin{smallmatrix} +0.22 \\ -0.18 \end{smallmatrix}$ ± 0.04	2	ABAZOV	05C D0	Repl. by ABAZOV 07S
1.11 $\begin{smallmatrix} +0.19 \\ -0.18 \end{smallmatrix}$ ± 0.05	7	ABREU	99W DLPH	$e^+e^- \rightarrow Z$
1.29 $\begin{smallmatrix} +0.24 \\ -0.22 \end{smallmatrix}$ ± 0.06	7	ACKERSTAFF	98G OPAL	$e^+e^- \rightarrow Z$
1.21 ± 0.11	7	BARATE	98D ALEP	$e^+e^- \rightarrow Z$
1.32 ± 0.15 ± 0.07	8	ABE	96M CDF	$p\bar{p}$ at 1.8 TeV
1.19 $\begin{smallmatrix} +0.21+0.07 \\ -0.18-0.08 \end{smallmatrix}$		ABREU	96D DLPH	Repl. by ABREU 99W
1.14 $\begin{smallmatrix} +0.22 \\ -0.19 \end{smallmatrix}$ ± 0.07	69	AKERS	95K OPAL	Repl. by ACKERSTAFF 98G
1.02 $\begin{smallmatrix} +0.23 \\ -0.18 \end{smallmatrix}$ ± 0.06	44	BUSKULIC	95L ALEP	Repl. by BARATE 98D

- 1 Measured using $\Lambda_b^0 \rightarrow J/\psi\Lambda$ decays.
- 2 Measured mean life using fully reconstructed $\Lambda_b^0 \rightarrow J/\psi\Lambda$ decays.
- 3 Used $\Lambda_b^0 \rightarrow J/\psi p K^-$ decays.
- 4 Measured mean life using fully reconstructed $\Lambda_b^0 \rightarrow \Lambda_c^+\pi^-$ decays.
- 5 Measured the lifetime ratio of decays $\Lambda_b^0 \rightarrow J/\psi p K^-$ to $B^0 \rightarrow J/\psi\pi^+K^-$ to be $0.976 \pm 0.012 \pm 0.006$ with $\tau_{B^0} = 1.519 \pm 0.007$ ps.
- 6 Measured using semileptonic decays $\Lambda_b^0 \rightarrow \Lambda_c^+\mu\nu X$ and $\Lambda_c^+ \rightarrow K_S^0 p$.
- 7 Measured using $\Lambda_c \ell^-$ and $\Lambda \ell^+ \ell^-$.
- 8 Excess $\Lambda_c \ell^-$, decay lengths.

$\tau_{\Lambda_b^0}/\tau_{B^0}$

VALUE	DOCUMENT ID	TECN	COMMENT
0.940 ± 0.035 ± 0.006	1 AAIJ	14E LHCb	pp at 7 TeV

1 Measured using $\Lambda_b^0 \rightarrow J/\psi\Lambda$ decays.

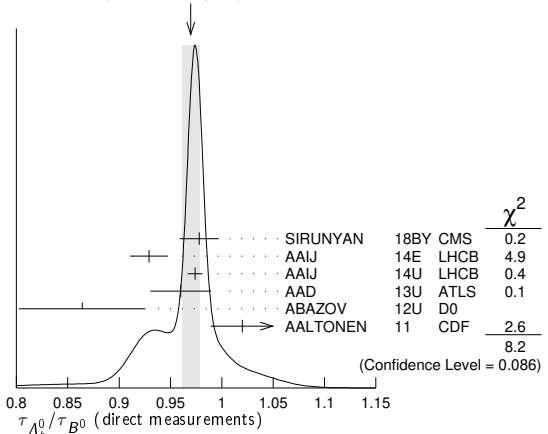
$\tau_{\Lambda_b^0}/\tau_{B^0}$ MEAN LIFE RATIO

$\tau_{\Lambda_b^0}/\tau_{B^0}$ (direct measurements)

“OUR EVALUATION” has been obtained by the Heavy Flavor Averaging Group (HFLAV) by including both B^0 and B^+ decays.

VALUE	DOCUMENT ID	TECN	COMMENT
0.964 ± 0.007 OUR EVALUATION			
0.970 ± 0.009 OUR AVERAGE			Error includes scale factor of 1.4. See the ideogram below.
0.978 ± 0.018 ± 0.006	1	SIRUNYAN	18BY CMS
0.929 ± 0.018 ± 0.004	1	AAIJ	14E LHCb
0.974 ± 0.006 ± 0.004	2	AAIJ	14U LHCb
0.960 ± 0.025 ± 0.016	3	AAD	13U ATLS
0.864 ± 0.052 ± 0.033	4,5	ABAZOV	12U D0
1.020 ± 0.030 ± 0.008	4	AALTONEN	11 CDF
• • • We do not use the following data for averages, fits, limits, etc. • • •			
0.976 ± 0.012 ± 0.006	6	AAIJ	13BB LHCb
0.811 $\begin{smallmatrix} +0.096 \\ -0.087 \end{smallmatrix}$ ± 0.034	4,5	ABAZOV	07S D0
1.041 ± 0.057	7	ABULENCIA	07A CDF
0.87 $\begin{smallmatrix} +0.17 \\ -0.14 \end{smallmatrix}$ ± 0.03	7	ABAZOV	05C D0

WEIGHTED AVERAGE
0.970 ± 0.009 (Error scaled by 1.4)



Baryon Particle Listings

Λ_b^0

- ¹ Measured using $\Lambda_b^0 \rightarrow J/\psi\Lambda$ and $B^0 \rightarrow J/\psi K^*(892)^0$ decays.
- ² Used $\Lambda_b^0 \rightarrow J/\psi p K^-$ and $B^0 \rightarrow J/\psi K^*(892)^0$ decays.
- ³ Measured with $\Lambda_b^0 \rightarrow J/\psi(\mu^+\mu^-) \Lambda^0(p\pi^-)$ decays.
- ⁴ Uses fully reconstructed $\Lambda_b \rightarrow J/\psi\Lambda$ decays.
- ⁵ Uses $B^0 \rightarrow J/\psi K_S^0$ decays for denominator.
- ⁶ Measures $1/\tau_{\Lambda_b^0} - 1/\tau_{B^0}$ and uses $\tau_{B^0} = 1.519 \pm 0.007$ ps to extract lifetime ratio.
- ⁷ Measured mean life ratio using fully reconstructed decays.

Λ_b^0 DECAY MODES

The branching fractions $B(b\text{-baryon} \rightarrow \Lambda \ell^- \bar{\nu}_\ell \text{anything})$ and $B(\Lambda_b^0 \rightarrow \Lambda_c^+ \ell^- \bar{\nu}_\ell \text{anything})$ are not pure measurements because the underlying measured products of these with $B(b \rightarrow b\text{-baryon})$ were used to determine $B(b \rightarrow b\text{-baryon})$, as described in the note "Production and Decay of b -Flavored Hadrons."

For inclusive branching fractions, e.g., $\Lambda_b \rightarrow \bar{\Lambda}_c \text{anything}$, the values usually are multiplicities, not branching fractions. They can be greater than one.

Mode	Fraction (Γ_i/Γ)	Scale factor/ Confidence level
Γ_1 $J/\psi(1S) \Lambda \times B(b \rightarrow \Lambda_b^0)$	$(5.8 \pm 0.8) \times 10^{-5}$	
Γ_2 $J/\psi(1S) \Lambda$		
Γ_3 $\psi(2S) \Lambda$		
Γ_4 $p D^0 \pi^-$	$(6.3 \pm 0.7) \times 10^{-4}$	
Γ_5 $\Lambda_c(2860)^+ \pi^-$, $\Lambda_c^+ \rightarrow D^0 p$		
Γ_6 $\Lambda_c(2880)^+ \pi^-$, $\Lambda_c^+ \rightarrow D^0 p$		
Γ_7 $\Lambda_c(2940)^+ \pi^-$, $\Lambda_c^+ \rightarrow D^0 p$		
Γ_8 $p D^0 K^-$	$(4.6 \pm 0.8) \times 10^{-5}$	
Γ_9 $p J/\psi \pi^-$	$(2.6^{+0.5}_{-0.4}) \times 10^{-5}$	
Γ_{10} $p \pi^- J/\psi$, $J/\psi \rightarrow \mu^+ \mu^-$	$(1.6 \pm 0.8) \times 10^{-6}$	
Γ_{11} $p J/\psi K^-$	$(3.2^{+0.6}_{-0.5}) \times 10^{-4}$	
Γ_{12} $P_c(4380)^+ K^-$, $P_c \rightarrow p J/\psi$ [a]	$(2.7 \pm 1.4) \times 10^{-5}$	
Γ_{13} $P_c(4450)^+ K^-$, $P_c \rightarrow p J/\psi$ [a]	$(1.3 \pm 0.4) \times 10^{-5}$	
Γ_{14} $\chi_{c1}(1P) p K^-$	$(7.6^{+1.5}_{-1.3}) \times 10^{-5}$	
Γ_{15} $\chi_{c2}(1P) p K^-$	$(7.9^{+1.6}_{-1.4}) \times 10^{-5}$	
Γ_{16} $p J/\psi(1S) \pi^+ \pi^- K^-$	$(6.6^{+1.3}_{-1.1}) \times 10^{-5}$	
Γ_{17} $p \psi(2S) K^-$	$(6.6^{+1.2}_{-1.0}) \times 10^{-5}$	
Γ_{18} $\chi_{c1}(3872) p K^-$		
Γ_{19} $\chi_{c1}(3872) p K^-$, $\chi_{c1}(3872) \rightarrow J/\psi \pi^+ \pi^-$	$(1.23 \pm 0.33) \times 10^{-6}$	
Γ_{20} $\chi_{c1}(3872) \Lambda(1520)$		
Γ_{21} $\psi(2S) p \pi^-$	$(7.5^{+1.6}_{-1.4}) \times 10^{-6}$	
Γ_{22} $p \bar{K}^0 \pi^-$	$(1.3 \pm 0.4) \times 10^{-5}$	
Γ_{23} $p K^0 K^-$	$< 3.5 \times 10^{-6}$	CL=90%
Γ_{24} $\Lambda_c^+ \pi^-$	$(4.9 \pm 0.4) \times 10^{-3}$	S=1.2
Γ_{25} $\Lambda_c^+ K^-$	$(3.59 \pm 0.30) \times 10^{-4}$	S=1.2
Γ_{26} $\Lambda_c^+ \bar{\Delta}_1(1260)^-$	seen	
Γ_{27} $\Lambda_c^+ D^-$	$(4.6 \pm 0.6) \times 10^{-4}$	
Γ_{28} $\Lambda_c^+ D_s^-$	$(1.10 \pm 0.10) \%$	
Γ_{29} $\Lambda_c^+ \pi^+ \pi^- \pi^-$	$(7.7 \pm 1.1) \times 10^{-3}$	S=1.1
Γ_{30} $\Lambda_c(2595)^+ \pi^-$, $\Lambda_c(2595)^+ \rightarrow \Lambda_c^+ \pi^+ \pi^-$	$(3.4 \pm 1.5) \times 10^{-4}$	
Γ_{31} $\Lambda_c(2625)^+ \pi^-$, $\Lambda_c(2625)^+ \rightarrow \Lambda_c^+ \pi^+ \pi^-$	$(3.3 \pm 1.3) \times 10^{-4}$	
Γ_{32} $\Sigma_c(2455)^0 \pi^+ \pi^-$, $\Sigma_c^0 \rightarrow \Lambda_c^+ \pi^-$	$(5.7 \pm 2.2) \times 10^{-4}$	
Γ_{33} $\Sigma_c(2455)^{++} \pi^- \pi^-$, $\Sigma_c^{++} \rightarrow \Lambda_c^+ \pi^+$	$(3.2 \pm 1.6) \times 10^{-4}$	
Γ_{34} $\Lambda_c^+ p \bar{p} \pi^-$	$(2.65 \pm 0.29) \times 10^{-4}$	
Γ_{35} $\Sigma_c(2455)^0 p \bar{p}$, $\Sigma_c(2455)^0 \rightarrow \Lambda_c^+ \pi^-$	$(2.4 \pm 0.5) \times 10^{-5}$	
Γ_{36} $\Sigma_c(2520)^0 p \bar{p}$, $\Sigma_c(2520)^0 \rightarrow \Lambda_c^+ \pi^-$	$(3.2 \pm 0.7) \times 10^{-5}$	
Γ_{37} $\Lambda K^0 2\pi^+ 2\pi^-$		
Γ_{38} $\Lambda_c^+ \ell^- \bar{\nu}_\ell \text{anything}$ [b]	$(10.9 \pm 2.2) \%$	
Γ_{39} $\Lambda_c^+ \ell^- \bar{\nu}_\ell$	$(6.2^{+1.4}_{-1.3}) \%$	

Γ_{40} $\Lambda_c^+ \pi^+ \pi^- \ell^- \bar{\nu}_\ell$	$(5.6 \pm 3.1) \%$	
Γ_{41} $\Lambda_c(2595)^+ \ell^- \bar{\nu}_\ell$	$(7.9^{+4.0}_{-3.5}) \times 10^{-3}$	
Γ_{42} $\Lambda_c(2625)^+ \ell^- \bar{\nu}_\ell$	$(1.3^{+0.6}_{-0.5}) \%$	
Γ_{43} $\Sigma_c(2455)^0 \pi^+ \ell^- \bar{\nu}_\ell$		
Γ_{44} $\Sigma_c(2455)^{++} \pi^- \ell^- \bar{\nu}_\ell$		
Γ_{45} $p h^-$	[c] $< 2.3 \times 10^{-5}$	CL=90%
Γ_{46} $p \pi^-$	$(4.5 \pm 0.8) \times 10^{-6}$	
Γ_{47} $p K^-$	$(5.4 \pm 1.0) \times 10^{-6}$	
Γ_{48} $p D_s^-$	$< 4.8 \times 10^{-4}$	CL=90%
Γ_{49} $p \mu^- \bar{\nu}_\mu$	$(4.1 \pm 1.0) \times 10^{-4}$	
Γ_{50} $\Lambda \mu^+ \mu^-$	$(1.08 \pm 0.28) \times 10^{-6}$	
Γ_{51} $p \pi^- \mu^+ \mu^-$	$(6.9 \pm 2.5) \times 10^{-8}$	
Γ_{52} $\Lambda \gamma$	$(7.1 \pm 1.7) \times 10^{-6}$	
Γ_{53} $\Lambda \eta$	$(9^{+7}_{-5}) \times 10^{-6}$	
Γ_{54} $\Lambda \eta'(958)$	$< 3.1 \times 10^{-6}$	CL=90%
Γ_{55} $\Lambda \pi^+ \pi^-$	$(4.7 \pm 1.9) \times 10^{-6}$	
Γ_{56} $\Lambda K^+ \pi^-$	$(5.7 \pm 1.3) \times 10^{-6}$	
Γ_{57} $\Lambda K^+ K^-$	$(1.62 \pm 0.23) \times 10^{-5}$	
Γ_{58} $\Lambda \phi$	$(9.8 \pm 2.6) \times 10^{-6}$	
Γ_{59} $p \pi^- \pi^+ \pi^-$	$(2.11 \pm 0.23) \times 10^{-5}$	
Γ_{60} $p K^- K^+ \pi^-$	$(4.1 \pm 0.6) \times 10^{-6}$	
Γ_{61} $p K^- \pi^+ \pi^-$	$(5.1 \pm 0.5) \times 10^{-5}$	
Γ_{62} $p K^- K^+ K^-$	$(1.27 \pm 0.14) \times 10^{-5}$	

[a] P_c^+ is a pentaquark-charmonium state.

[b] Not a pure measurement. See note at head of Λ_b^0 Decay Modes.

[c] Here h^- means π^- or K^- .

CONSTRAINED FIT INFORMATION

An overall fit to 10 branching ratios uses 12 measurements and one constraint to determine 7 parameters. The overall fit has a $\chi^2 = 10.7$ for 6 degrees of freedom.

The following *off-diagonal* array elements are the correlation coefficients $\langle \delta x_i \delta x_j \rangle / (\delta x_i \delta x_j)$, in percent, from the fit to the branching fractions, $x_i \equiv \Gamma_i/\Gamma_{\text{total}}$. The fit constrains the x_i whose labels appear in this array to sum to one.

x_{25}	94				
x_{29}	50	47			
x_{39}	14	14	7		
x_{46}	0	0	0	0	
x_{47}	0	0	0	0	82
	x_{24}	x_{25}	x_{29}	x_{39}	x_{46}

Λ_b^0 BRANCHING RATIOS

$\Gamma(J/\psi(1S) \Lambda \times B(b \rightarrow \Lambda_b^0)) / \Gamma_{\text{total}}$ Γ_1/Γ

VALUE (units 10^{-5})	EVTS	DOCUMENT ID	TECN	COMMENT
5.8 ± 0.8 OUR AVERAGE				
6.01 ± 0.60 ± 0.58 ± 0.28		¹ ABAZOV	11o D0	$p \bar{p}$ at 1.96 TeV
4.7 ± 2.3 ± 0.2		² ABE	97B CDF	$p \bar{p}$ at 1.8 TeV

• • • We do not use the following data for averages, fits, limits, etc. • • •

- 180 ± 60 ± 90 16 ALBAJAR 91E UA1 $p \bar{p}$ at 630 GeV
- ¹ ABAZOV 11o uses $B(B^0 \rightarrow J/\psi K_S^0) \times B(b \rightarrow B^0) = (1.74 \pm 0.08) \times 10^{-4}$ to obtain the result. The $(\pm 0.08) \times 10^{-4}$ uncertainty of this product is listed as the last uncertainty of the measurement, $(\pm 0.28) \times 10^{-5}$.
- ² ABE 97B reports $[B(\Lambda_b^0 \rightarrow J/\psi \Lambda) \times B(b \rightarrow \Lambda_b^0)] / [B(B^0 \rightarrow J/\psi K_S^0) \times B(b \rightarrow B^0)] = 0.27 \pm 0.12 \pm 0.05$. We multiply by our best value $B(B^0 \rightarrow J/\psi K_S^0) \times B(b \rightarrow B^0) = (1.74 \pm 0.08) \times 10^{-4}$. Our first error is their experiment error and our second error is the systematic error from using our best value.

$\Gamma(\psi(2S) \Lambda) / \Gamma(J/\psi(1S) \Lambda)$ Γ_3/Γ_2

VALUE	DOCUMENT ID	TECN	COMMENT
0.508 ± 0.023 OUR AVERAGE			
0.513 ± 0.023 ± 0.019	¹ AAIJ	19F LHCb	$p \bar{p}$ at 7, 8 TeV
0.50 ± 0.03 ± 0.02	² AAD	15CH ATLAS	$p \bar{p}$ at 8 TeV

- ¹ AAIJ 19f uses $B(J/\psi \rightarrow \mu^+ \mu^-) = (5.961 \pm 0.033) \times 10^{-2}$ and $B(\psi(2S) \rightarrow e^+ e^-) = (7.93 \pm 0.17) \times 10^{-3}$ from PDG 18 with assumption of lepton universality. AAIJ 19f reports this result as $0.513 \pm 0.023 \pm 0.016 \pm 0.011$, where the last uncertainty is the contribution due to the external input of branching fractions used in the analysis.
- ² AAD 15CH uses $B(J/\psi \rightarrow \mu^+ \mu^-) = (5.961 \pm 0.033) \times 10^{-2}$ and $B(\psi(2S) \rightarrow \mu^+ \mu^-) = (7.89 \pm 0.17) \times 10^{-3}$ from PDG 14 with assumption of lepton universality.

$\Gamma(pD^0\pi^-)/\Gamma_{total}$ Γ_4/Γ

VALUE	EVTS	DOCUMENT ID	TECN	COMMENT
• • • We do not use the following data for averages, fits, limits, etc. • • •				
seen	52	BARI	91 SFM	$D^0 \rightarrow K^-\pi^+$
seen		BASILE	81 SFM	$D^0 \rightarrow K^-\pi^+$

$\Gamma(\Lambda_c(2860)^+\pi^-, \Lambda_c^+ \rightarrow D^0 p)/\Gamma(\Lambda_c(2880)^+\pi^-, \Lambda_c^+ \rightarrow D^0 p)$ Γ_5/Γ_6

VALUE	DOCUMENT ID	TECN	COMMENT
$4.54^{+0.51+0.21}_{-0.39-0.59}$	AAIJ	17s LHCb	pp at 7, 8 TeV

$\Gamma(\Lambda_c(2940)^+\pi^-, \Lambda_c^+ \rightarrow D^0 p)/\Gamma(\Lambda_c(2880)^+\pi^-, \Lambda_c^+ \rightarrow D^0 p)$ Γ_7/Γ_6

VALUE	DOCUMENT ID	TECN	COMMENT
$0.83^{+0.31+0.18}_{-0.10-0.43}$	AAIJ	17s LHCb	pp at 7, 8 TeV

$\Gamma(pD^0K^-)/\Gamma(pD^0\pi^-)$ Γ_8/Γ_4

VALUE (units 10^{-2})	DOCUMENT ID	TECN	COMMENT
$7.3 \pm 0.8^{+0.5}_{-0.6}$	AAIJ	14h LHCb	pp at 7 TeV

$\Gamma(pJ/\psi\pi^-)/\Gamma(pJ/\psi K^-)$ Γ_9/Γ_{11}

VALUE (units 10^{-2})	DOCUMENT ID	TECN	COMMENT
$8.24 \pm 0.25 \pm 0.42$	AAIJ	14k LHCb	pp at 7, 8 TeV

$\Gamma(pJ/\psi K^-)/\Gamma_{total}$ Γ_{11}/Γ

VALUE (units 10^{-4})	DOCUMENT ID	TECN	COMMENT
$3.17 \pm 0.04^{+0.57}_{-0.45}$	¹ AAIJ	16a LHCb	pp at 7, 8 TeV

¹AAIJ 16a reported the measurement of $(3.17 \pm 0.04 \pm 0.07 \pm 0.34^{+0.45}_{-0.28}) \times 10^{-4}$ where the first uncertainty is statistical, the second is systematic, the third is due to the branching fraction of $B^0 \rightarrow J/\psi K^*(892)^0$, and the fourth is due to the knowledge of f_{Λ_b}/f_d . We combined in quadrature second to fourth uncertainties to a total systematic uncertainty.

$\Gamma(P_c(4380)^+K^-, P_c \rightarrow pJ/\psi)/\Gamma_{total}$ Γ_{12}/Γ

P_c^+ is a pentaquark-charmonium state.

VALUE (units 10^{-5})	DOCUMENT ID	TECN	COMMENT
$2.66 \pm 0.22^{+1.41}_{-1.38}$	¹ AAIJ	16a LHCb	pp at 7, 8 TeV

¹AAIJ 16 total systematic includes the uncertainties on $f(P_c^+)$ and $B(\Lambda_b \rightarrow pJ/\psi K^-)$.

$\Gamma(P_c(4450)^+K^-, P_c \rightarrow pJ/\psi)/\Gamma_{total}$ Γ_{13}/Γ

P_c^+ is a pentaquark-charmonium state.

VALUE (units 10^{-5})	DOCUMENT ID	TECN	COMMENT
$1.30 \pm 0.16^{+0.42}_{-0.39}$	¹ AAIJ	16a LHCb	pp at 7, 8 TeV

¹AAIJ 16 total systematic includes the uncertainties on $f(P_c^+)$ and $B(\Lambda_b \rightarrow pJ/\psi K^-)$.

$\Gamma(\chi_{c1}(1P)\rho K^-)/\Gamma(pJ/\psi K^-)$ Γ_{14}/Γ_{11}

VALUE	DOCUMENT ID	TECN	COMMENT
$0.239 \pm 0.019 \pm 0.007$	¹ AAIJ	17aMLHCb	pp at 7, 8 TeV

¹AAIJ 17aM reports $0.242 \pm 0.014 \pm 0.016$ from a measurement of $[\Gamma(\Lambda_b^0 \rightarrow \chi_{c1}(1P)\rho K^-)/\Gamma(\Lambda_b^0 \rightarrow pJ/\psi K^-)] \times [B(\chi_{c1}(1P) \rightarrow \gamma J/\psi(1S))]$ assuming $B(\chi_{c1}(1P) \rightarrow \gamma J/\psi(1S)) = (33.9 \pm 1.2) \times 10^{-2}$, which we rescale to our best value $B(\chi_{c1}(1P) \rightarrow \gamma J/\psi(1S)) = (34.3 \pm 1.0) \times 10^{-2}$. Our first error is their experiment's error and our second error is the systematic error from using our best value.

$\Gamma(\chi_{c2}(1P)\rho K^-)/\Gamma(pJ/\psi K^-)$ Γ_{15}/Γ_{11}

VALUE	DOCUMENT ID	TECN	COMMENT
$0.250 \pm 0.025 \pm 0.007$	¹ AAIJ	17aMLHCb	pp at 7, 8 TeV

¹AAIJ 17aM reports $0.248 \pm 0.02 \pm 0.017$ from a measurement of $[\Gamma(\Lambda_b^0 \rightarrow \chi_{c2}(1P)\rho K^-)/\Gamma(\Lambda_b^0 \rightarrow pJ/\psi K^-)] \times [B(\chi_{c2}(1P) \rightarrow \gamma J/\psi(1S))]$ assuming $B(\chi_{c2}(1P) \rightarrow \gamma J/\psi(1S)) = (19.2 \pm 0.7) \times 10^{-2}$, which we rescale to our best value $B(\chi_{c2}(1P) \rightarrow \gamma J/\psi(1S)) = (19.0 \pm 0.5) \times 10^{-2}$. Our first error is their experiment's error and our second error is the systematic error from using our best value.

$\Gamma(pJ/\psi(1S)\pi^+\pi^-K^-)/\Gamma(pJ/\psi K^-)$ Γ_{16}/Γ_{11}

VALUE	DOCUMENT ID	TECN	COMMENT
$0.2086 \pm 0.0096 \pm 0.0134$	¹ AAIJ	16y LHCb	pp at 7, 8 TeV

¹Excludes $\psi(2S) \rightarrow J/\psi\pi^+\pi^-$.

$\Gamma(p\psi(2S)K^-)/\Gamma(pJ/\psi K^-)$ Γ_{17}/Γ_{11}

VALUE	DOCUMENT ID	TECN	COMMENT
$0.2070 \pm 0.0076 \pm 0.0059$	¹ AAIJ	16y LHCb	pp at 7, 8 TeV

¹AAIJ 16y reports a measurement of $0.2070 \pm 0.0076 \pm 0.0046 \pm 0.0037$ where the third uncertainty is due to the knowledge of J/ψ and $\psi(2S)$ branching fractions. We have combined both systematic uncertainties in quadrature.

$\Gamma(\chi_{c1}(3872)\Lambda(1520))/\Gamma(\chi_{c1}(3872)\rho K^-)$ Γ_{20}/Γ_{18}

VALUE	DOCUMENT ID	TECN	COMMENT
• • • We do not use the following data for averages, fits, limits, etc. • • •			
0.58 ± 0.15	AAIJ	19aNLHCb	pp at 7, 8, 13 TeV

$\Gamma(\chi_{c1}(3872)\rho K^-, \chi_{c1}(3872) \rightarrow J/\psi\pi^+\pi^-)/\Gamma(p\psi(2S)K^-)$ Γ_{19}/Γ_{17}

VALUE (units 10^{-2})	DOCUMENT ID	TECN	COMMENT
$1.87 \pm 0.39 \pm 0.02$	¹ AAIJ	19aNLHCb	pp at 7, 8, 13 TeV

¹AAIJ 19aNL reports $[\Gamma(\Lambda_b^0 \rightarrow \chi_{c1}(3872)\rho K^-, \chi_{c1}(3872) \rightarrow J/\psi\pi^+\pi^-)/\Gamma(\Lambda_b^0 \rightarrow p\psi(2S)K^-)] / [B(\psi(2S) \rightarrow J/\psi(1S)\pi^+\pi^-)] = (5.4 \pm 1.1 \pm 0.2) \times 10^{-2}$ which we multiply by our best value $B(\psi(2S) \rightarrow J/\psi(1S)\pi^+\pi^-) = (34.68 \pm 0.30) \times 10^{-2}$. Our first error is their experiment's error and our second error is the systematic error from using our best value.

$\Gamma(\psi(2S)\rho\pi^-)/\Gamma(p\psi(2S)K^-)$ Γ_{21}/Γ_{17}

VALUE (%)	DOCUMENT ID	TECN	COMMENT
$11.4 \pm 1.3 \pm 0.2$	AAIJ	18aFLHCb	pp at 7, 8, 13 TeV

$\Gamma(p\bar{K}^0\pi^-)/\Gamma_{total}$ Γ_{22}/Γ

VALUE (units 10^{-5})	DOCUMENT ID	TECN	COMMENT
$1.26 \pm 0.19 \pm 0.36$	¹ AAIJ	14q LHCb	pp at 7 TeV

¹Used the normalizing mode branching fraction value of $B(B^0 \rightarrow K^0\pi^+\pi^-) = (4.96 \pm 0.20) \times 10^{-5}$.

$\Gamma(\rho K^0K^-)/\Gamma_{total}$ Γ_{23}/Γ

VALUE	CL%	DOCUMENT ID	TECN	COMMENT
$< 3.5 \times 10^{-6}$	90	AAIJ	14q LHCb	pp at 7 TeV

$\Gamma(\Lambda_c^+\pi^-)/\Gamma_{total}$ Γ_{24}/Γ

VALUE (units 10^{-3})	EVTS	DOCUMENT ID	TECN	COMMENT
4.9 ± 0.4 OUR FIT Error includes scale factor of 1.2.				
4.9 ± 0.5 OUR AVERAGE Error includes scale factor of 1.5.				
$4.57^{+0.31}_{-0.30} \pm 0.23$		¹ AAIJ	14i LHCb	pp at 7 TeV
$5.97 \pm 0.28 \pm 0.81$		² AAIJ	14q LHCb	pp at 7 TeV
$8.8 \pm 2.8 \pm 1.5$		³ ABULENCIA	07B CDF	$p\bar{p}$ at 1.96 TeV
• • • We do not use the following data for averages, fits, limits, etc. • • •				
seen	3	ABREU	96N DLPH	$\Lambda_c^+ \rightarrow pK^-\pi^+$
seen	4	BUSKULIC	96L ALEP	$\Lambda_c^+ \rightarrow pK^-\pi^+$, $\rho\bar{K}^0, \Lambda\pi^+\pi^+\pi^-$

¹AAIJ 14i reports $(4.30 \pm 0.03^{+0.12}_{-0.11} \pm 0.26 \pm 0.21) \times 10^{-3}$ from a measurement of $[\Gamma(\Lambda_b^0 \rightarrow \Lambda_c^+\pi^-)/\Gamma_{total}] \times [B(B^0 \rightarrow D^-\pi^+)]$ assuming $B(B^0 \rightarrow D^-\pi^+) = (2.68 \pm 0.13) \times 10^{-3}$, which we rescale to our best value $B(B^0 \rightarrow D^-\pi^+) = (2.52 \pm 0.13) \times 10^{-3}$. Our first error is their experiment's error and our second error is the systematic error from using our best value. Uses information on f_{baryon}/f_d from measurement in semileptonic decays by the same authors.

²Obtained using the branching fraction of $\Lambda_c^+ \rightarrow pK^-\pi^+$ decay.

³The result is obtained from $(f_{baryon}/f_d) (B(\Lambda_b^0 \rightarrow \Lambda_c^+\pi^-)/B(\bar{B}^0 \rightarrow D^+\pi^-)) = 0.82 \pm 0.08 \pm 0.11 \pm 0.22$, assuming $f_{baryon}/f_d = 0.25 \pm 0.04$ and $B(\bar{B}^0 \rightarrow D^+\pi^-) = (2.68 \pm 0.13) \times 10^{-3}$.

$\Gamma(pD^0\pi^-)/\Gamma(\Lambda_c^+\pi^-)$ Γ_4/Γ_{24}

VALUE	DOCUMENT ID	TECN	COMMENT
$0.128 \pm 0.007^{+0.006}_{-0.007}$	¹ AAIJ	14h LHCb	pp at 7 TeV

¹AAIJ 14h reports $[\Gamma(\Lambda_b^0 \rightarrow pD^0\pi^-)/\Gamma(\Lambda_b^0 \rightarrow \Lambda_c^+\pi^-)] \times [B(D^0 \rightarrow K^-\pi^+)] / [B(\Lambda_c^+ \rightarrow pK^-\pi^+)] = (8.06 \pm 0.23 \pm 0.35) \times 10^{-2}$ which we multiply or divide by our best values $B(D^0 \rightarrow K^-\pi^+) = (3.950 \pm 0.031) \times 10^{-2}$, $B(\Lambda_c^+ \rightarrow pK^-\pi^+) = (6.28 \pm 0.32) \times 10^{-2}$. Our first error is their experiment's error and our second error is the systematic error from using our best values.

$\Gamma(\Lambda_c^+K^-)/\Gamma_{total}$ Γ_{25}/Γ

VALUE (units 10^{-4})	DOCUMENT ID	TECN	COMMENT
3.59 ± 0.30 OUR FIT Error includes scale factor of 1.2.			
$3.55 \pm 0.44 \pm 0.50$	¹ AAIJ	14q LHCb	pp at 7 TeV

¹Obtained using the branching fraction of $\Lambda_c^+ \rightarrow pK^-\pi^+$ decay.

$\Gamma(\Lambda_c^+K^-)/\Gamma(\Lambda_c^+\pi^-)$ Γ_{25}/Γ_{24}

VALUE (units 10^{-2})	DOCUMENT ID	TECN	COMMENT
7.31 ± 0.22 OUR FIT			
$7.31 \pm 0.16 \pm 0.16$	AAIJ	14h LHCb	pp at 7 TeV

$\Gamma(\Lambda_c^+a_1(1260)^-)/\Gamma_{total}$ Γ_{26}/Γ

VALUE	EVTS	DOCUMENT ID	TECN	COMMENT
seen	1	ABREU	96N DLPH	$\Lambda_c^+ \rightarrow pK^-\pi^+, a_1^- \rightarrow \rho^0\pi^- \rightarrow \pi^+\pi^-\pi^-$

Baryon Particle Listings

Λ_b^0

$\Gamma(\Lambda_c^+ D_s^-)/\Gamma_{total}$	DOCUMENT ID	TECN	COMMENT	Γ_{28}/Γ
<u>VALUE (units 10^{-2})</u>				
1.1 ± 0.1	1 AAIJ	14AA	LHCb pp at 7 TeV	
¹ Uses $B(\bar{B}^0 \rightarrow D^+ D_s^-) = (7.2 \pm 0.8) \times 10^{-3}$ and their measured $B(\Lambda_b^0 \rightarrow \Lambda_c^+ \pi^-)/B(\bar{B}^0 \rightarrow D^+ \pi^-)$ values.				

$\Gamma(\Lambda_c^+ D^-)/\Gamma(\Lambda_c^+ D_s^-)$	DOCUMENT ID	TECN	COMMENT	Γ_{27}/Γ_{28}
<u>VALUE</u>				
0.042 ± 0.003 ± 0.003	AAIJ	14AA	LHCb pp at 7 TeV	

$\Gamma(\Lambda_c^+ \pi^+ \pi^- \pi^-)/\Gamma_{total}$	DOCUMENT ID	TECN	COMMENT	Γ_{29}/Γ
<u>VALUE (units 10^{-3})</u>				
7.7 ± 1.1 OUR FIT	Error includes scale factor of 1.1.			
14.9 ± 3.8 ± 1.2	1 AALTONEN	12A	CDF $p\bar{p}$ at 1.96 TeV	
<ul style="list-style-type: none"> • • • We do not use the following data for averages, fits, limits, etc. • • • 				
seen	90	BARI	91	SFM $\Lambda_c^+ \rightarrow p K^- \pi^+$

¹ AALTONEN 12A reports $[\Gamma(\Lambda_b^0 \rightarrow \Lambda_c^+ \pi^+ \pi^- \pi^-)/\Gamma_{total}] / [B(\Lambda_b^0 \rightarrow \Lambda_c^+ \pi^-)] = 3.04 \pm 0.33^{+0.70}_{-0.55}$ which we multiply by our best value $B(\Lambda_b^0 \rightarrow \Lambda_c^+ \pi^-) = (4.9 \pm 0.4) \times 10^{-3}$. Our first error is their experiment's error and our second error is the systematic error from using our best value.

$\Gamma(\Lambda_c^+ \pi^+ \pi^- \pi^-)/\Gamma(\Lambda_c^+ \pi^-)$	DOCUMENT ID	TECN	COMMENT	Γ_{29}/Γ_{24}
<u>VALUE</u>				
1.56 ± 0.21 OUR FIT				
1.43 ± 0.16 ± 0.13	AAIJ	11E	LHCb pp at 7 TeV	

$\Gamma(\Lambda_c(2595)^+ \pi^-, \Lambda_c(2595)^+ \rightarrow \Lambda_c^+ \pi^+ \pi^-)/\Gamma(\Lambda_c^+ \pi^+ \pi^- \pi^-)$	DOCUMENT ID	TECN	COMMENT	Γ_{30}/Γ_{29}
<u>VALUE (units 10^{-2})</u>				
4.4 ± 1.7 ± 0.6 ± 0.4	AAIJ	11E	LHCb pp at 7 TeV	

$\Gamma(\Lambda_c(2625)^+ \pi^-, \Lambda_c(2625)^+ \rightarrow \Lambda_c^+ \pi^+ \pi^-)/\Gamma(\Lambda_c^+ \pi^+ \pi^- \pi^-)$	DOCUMENT ID	TECN	COMMENT	Γ_{31}/Γ_{29}
<u>VALUE (units 10^{-2})</u>				
4.3 ± 1.5 ± 0.4	AAIJ	11E	LHCb pp at 7 TeV	

$\Gamma(\Sigma_c(2455)^0 \pi^+ \pi^-, \Sigma_c^0 \rightarrow \Lambda_c^+ \pi^-)/\Gamma(\Lambda_c^+ \pi^+ \pi^- \pi^-)$	DOCUMENT ID	TECN	COMMENT	Γ_{32}/Γ_{29}
<u>VALUE (units 10^{-2})</u>				
7.4 ± 2.4 ± 1.2	AAIJ	11E	LHCb pp at 7 TeV	

$\Gamma(\Sigma_c(2455)^{++} \pi^- \pi^-, \Sigma_c^{++} \rightarrow \Lambda_c^+ \pi^+)/\Gamma(\Lambda_c^+ \pi^+ \pi^- \pi^-)$	DOCUMENT ID	TECN	COMMENT	Γ_{33}/Γ_{29}
<u>VALUE (units 10^{-2})</u>				
4.2 ± 1.8 ± 0.7	AAIJ	11E	LHCb pp at 7 TeV	

$\Gamma(\Lambda_c^+ p \bar{p} \pi^-)/\Gamma(\Lambda_c^+ \pi^-)$	DOCUMENT ID	TECN	COMMENT	Γ_{34}/Γ_{24}
<u>VALUE (units 10^{-2})</u>				
5.40 ± 0.23 ± 0.32	AAIJ	18AW	LHCb pp at 7 and 8 TeV	

$\Gamma(\Sigma_c(2455)^0 p \bar{p}, \Sigma_c(2455)^0 \rightarrow \Lambda_c^+ \pi^-)/\Gamma(\Lambda_c^+ p \bar{p} \pi^-)$	DOCUMENT ID	TECN	COMMENT	Γ_{35}/Γ_{34}
<u>VALUE (units 10^{-2})</u>				
8.9 ± 1.5 ± 0.6	AAIJ	18AW	LHCb pp at 7 and 8 TeV	

$\Gamma(\Sigma_c(2520)^0 p \bar{p}, \Sigma_c(2520)^0 \rightarrow \Lambda_c^+ \pi^-)/\Gamma(\Lambda_c^+ p \bar{p} \pi^-)$	DOCUMENT ID	TECN	COMMENT	Γ_{36}/Γ_{34}
<u>VALUE</u>				
0.119 ± 0.020 ± 0.014	AAIJ	18AW	LHCb pp at 7 and 8 TeV	

$\Gamma(\Lambda K^0 2\pi^+ 2\pi^-)/\Gamma_{total}$	DOCUMENT ID	TECN	COMMENT	Γ_{37}/Γ
<u>VALUE</u>				
0.109 ± 0.022 ± 0.013	1 AARENTON	86	FMPs $\Lambda K_S^0 2\pi^+ 2\pi^-$	
<ul style="list-style-type: none"> • • • We do not use the following data for averages, fits, limits, etc. • • • 				
seen	4			
¹ See the footnote to the AARENTON 86 mass value.				

$\Gamma(\Lambda_c^+ \ell^- \bar{\nu}_\ell \text{ anything})/\Gamma_{total}$	DOCUMENT ID	TECN	COMMENT	Γ_{38}/Γ
<u>VALUE</u>				
0.109 ± 0.022 OUR AVERAGE				
0.102 ± 0.019 ± 0.013	1 BARATE	98D	ALEP $e^+ e^- \rightarrow Z$	
0.14 ± 0.05 ± 0.02	2 ABREU	95S	DLPH $e^+ e^- \rightarrow Z$	
<ul style="list-style-type: none"> • • • We do not use the following data for averages, fits, limits, etc. • • • 				
0.090 ± 0.022 ± 0.012	55	3	BUSKULIC 95L ALEP Repl. by BARATE 98D	
0.18 ± 0.07 ± 0.02	21	4	BUSKULIC 92E ALEP $\Lambda_c^+ \rightarrow p K^- \pi^+$	

¹ BARATE 98D reports $[\Gamma(\Lambda_b^0 \rightarrow \Lambda_c^+ \ell^- \bar{\nu}_\ell \text{ anything})/\Gamma_{total}] \times [B(\bar{B} \rightarrow b\text{-baryon})] = 0.0086 \pm 0.0007 \pm 0.0014$ which we divide by our best value $B(\bar{B} \rightarrow b\text{-baryon}) = (8.4 \pm 1.1) \times 10^{-2}$. Our first error is their experiment's error and our second error is the systematic error from using our best value. Measured using $\Lambda_c \ell^-$ and $\Lambda \ell^+ \ell^-$.

² ABREU 95S reports $[\Gamma(\Lambda_b^0 \rightarrow \Lambda_c^+ \ell^- \bar{\nu}_\ell \text{ anything})/\Gamma_{total}] \times [B(\bar{B} \rightarrow b\text{-baryon})] = 0.0118 \pm 0.0026^{+0.0031}_{-0.0021}$ which we divide by our best value $B(\bar{B} \rightarrow b\text{-baryon}) = (8.4 \pm 1.1) \times 10^{-2}$. Our first error is their experiment's error and our second error is the systematic error from using our best value.

³ BUSKULIC 95L reports $[\Gamma(\Lambda_b^0 \rightarrow \Lambda_c^+ \ell^- \bar{\nu}_\ell \text{ anything})/\Gamma_{total}] \times [B(\bar{B} \rightarrow b\text{-baryon})] = 0.00755 \pm 0.0014 \pm 0.0012$ which we divide by our best value $B(\bar{B} \rightarrow b\text{-baryon}) = (8.4 \pm 1.1) \times 10^{-2}$. Our first error is their experiment's error and our second error is the systematic error from using our best value.

⁴ BUSKULIC 92E reports $[\Gamma(\Lambda_b^0 \rightarrow \Lambda_c^+ \ell^- \bar{\nu}_\ell \text{ anything})/\Gamma_{total}] \times [B(\bar{B} \rightarrow b\text{-baryon})] = 0.015 \pm 0.0035 \pm 0.0045$ which we divide by our best value $B(\bar{B} \rightarrow b\text{-baryon}) = (8.4 \pm 1.1) \times 10^{-2}$. Our first error is their experiment's error and our second error is the systematic error from using our best value. Superseded by BUSKULIC 95L.

$\Gamma(\Lambda_c^+ \ell^- \bar{\nu}_\ell)/\Gamma_{total}$	DOCUMENT ID	TECN	COMMENT	Γ_{39}/Γ
<u>VALUE</u>				
0.062 ± 0.014 ± 0.013 OUR FIT				
0.050 ± 0.011 ± 0.016 ± 0.008 ± 0.012	1 ABDALLAH	04A	DLPH $e^+ e^- \rightarrow Z^0$	

¹ Derived from a combined likelihood and event rate fit to the distribution of the I_{sgur} -Wise variable and using HQET. The slope of the form factor is measured to be $\rho^2 = 2.03 \pm 0.46^{+0.72}_{-1.00}$.

$\Gamma(\Lambda_c^+ \ell^- \bar{\nu}_\ell)/\Gamma(\Lambda_c^+ \pi^-)$	DOCUMENT ID	TECN	COMMENT	Γ_{39}/Γ_{24}
<u>VALUE</u>				
12.7 ± 3.1 ± 2.7 OUR FIT				
16.6 ± 3.0 ± 2.8 ± 3.6	AALTONEN	09E	CDF $p\bar{p}$ at 1.96 TeV	

$\Gamma(\Lambda_c^+ \pi^+ \pi^- \ell^- \bar{\nu}_\ell)/\Gamma_{total}$	DOCUMENT ID	TECN	COMMENT	Γ_{40}/Γ
<u>VALUE</u>				
0.056 ± 0.031 ± 0.030	1 ABDALLAH	04A	DLPH $e^+ e^- \rightarrow Z^0$	

¹ Derived from the fraction of $\Gamma(\Lambda_b^0 \rightarrow \Lambda_c^+ \ell^- \bar{\nu}_\ell) / (\Gamma(\Lambda_b^0 \rightarrow \Lambda_c^+ \ell^- \bar{\nu}_\ell) + \Gamma(\Lambda_b^0 \rightarrow \Lambda_c^+ \pi^+ \pi^- \ell^- \bar{\nu}_\ell)) = 0.47^{+0.10+0.07}_{-0.08-0.06}$.

$\Gamma(\Lambda_c^+ \ell^- \bar{\nu}_\ell) / [\Gamma(\Lambda_c^+ \ell^- \bar{\nu}_\ell) + \Gamma(\Lambda_c^+ \pi^+ \pi^- \ell^- \bar{\nu}_\ell)]$	DOCUMENT ID	TECN	COMMENT	$\Gamma_{39}/(\Gamma_{39} + \Gamma_{40})$
<u>VALUE</u>				
0.47 ± 0.10 ± 0.07 ± 0.08 ± 0.06	ABDALLAH	04A	DLPH $e^+ e^- \rightarrow Z^0$	

$\Gamma(\Lambda_c(2595)^+ \ell^- \bar{\nu}_\ell)/\Gamma(\Lambda_c^+ \ell^- \bar{\nu}_\ell)$	DOCUMENT ID	TECN	COMMENT	Γ_{41}/Γ_{39}
<u>VALUE</u>				
0.126 ± 0.033 ± 0.047 ± 0.038	AALTONEN	09E	CDF $p\bar{p}$ at 1.96 TeV	

$\Gamma(\Lambda_c(2625)^+ \ell^- \bar{\nu}_\ell)/\Gamma(\Lambda_c^+ \ell^- \bar{\nu}_\ell)$	DOCUMENT ID	TECN	COMMENT	Γ_{42}/Γ_{39}
<u>VALUE</u>				
0.210 ± 0.042 ± 0.071 ± 0.050	AALTONEN	09E	CDF $p\bar{p}$ at 1.96 TeV	

$[\frac{1}{2}\Gamma(\Sigma_c(2455)^0 \pi^+ \ell^- \bar{\nu}_\ell) + \frac{1}{2}\Gamma(\Sigma_c(2455)^{++} \pi^- \ell^- \bar{\nu}_\ell)] / \Gamma(\Lambda_c^+ \ell^- \bar{\nu}_\ell)$	DOCUMENT ID	TECN	COMMENT	$(\frac{1}{2}\Gamma_{43} + \frac{1}{2}\Gamma_{44})/\Gamma_{39}$
<u>VALUE</u>				
0.054 ± 0.022 ± 0.021 ± 0.018	AALTONEN	09E	CDF $p\bar{p}$ at 1.96 TeV	

$\Gamma(p h^-)/\Gamma_{total}$	CL%	DOCUMENT ID	TECN	COMMENT	Γ_{45}/Γ
<u>VALUE</u>					
< 2.3 × 10⁻⁵	90	1 ACOSTA	05o	CDF $p\bar{p}$ at 1.96 TeV	
¹ Assumes $f_u / f_d = 0.25$, and equal momentum distribution for Λ_b and B mesons.					

$\Gamma(p \pi^-)/\Gamma_{total}$	DOCUMENT ID	TECN	COMMENT	Γ_{46}/Γ
<u>VALUE (units 10^{-6})</u>				
4.5 ± 0.8 OUR FIT				
4.0 ± 0.9 ± 0.5	1 AALTONEN	09c	CDF $p\bar{p}$ at 1.96 TeV	
<ul style="list-style-type: none"> • • • We do not use the following data for averages, fits, limits, etc. • • • 				
< 50	90	2	BUSKULIC 96v ALEP $e^+ e^- \rightarrow Z$	

¹ AALTONEN 09c reports $[\Gamma(\Lambda_b^0 \rightarrow p \pi^-)/\Gamma_{total}] / [B(\bar{B}^0 \rightarrow K^+ \pi^-)] \times [B(\bar{B} \rightarrow b\text{-baryon})] / [B(\bar{B} \rightarrow B^0)] = 0.042 \pm 0.007 \pm 0.006$ which we multiply or divide by our best values $B(B^0 \rightarrow K^+ \pi^-) = (1.96 \pm 0.05) \times 10^{-5}$, $B(\bar{B} \rightarrow b\text{-baryon}) = (8.4 \pm 1.1) \times 10^{-2}$, $B(\bar{B} \rightarrow B^0) = (40.8 \pm 0.7) \times 10^{-2}$. Our first error is their experiment's error and our second error is the systematic error from using our best values.

² BUSKULIC 96v assumes PDG 96 production fractions for B^0, B^+, B_s, b baryons.

$\Gamma(p K^-)/\Gamma_{total}$	DOCUMENT ID	TECN	COMMENT	Γ_{47}/Γ
<u>VALUE (units 10^{-6})</u>				
5.4 ± 1.0 OUR FIT				
6.3 ± 1.1 ± 0.8	1 AALTONEN	09c	CDF $p\bar{p}$ at 1.96 TeV	
<ul style="list-style-type: none"> • • • We do not use the following data for averages, fits, limits, etc. • • • 				
< 360	90	2	ADAM 96D DLPH $e^+ e^- \rightarrow Z$	
< 50	90	3	BUSKULIC 96v ALEP $e^+ e^- \rightarrow Z$	

¹ AALTONEN 09c reports $[\Gamma(\Lambda_b^0 \rightarrow p K^-)/\Gamma_{\text{total}}] / [B(B^0 \rightarrow K^+ \pi^-)] \times [B(\bar{B} \rightarrow b\text{-baryon})] / [B(\bar{B} \rightarrow B^0)] = 0.066 \pm 0.009 \pm 0.008$ which we multiply or divide by our best values $B(B^0 \rightarrow K^+ \pi^-) = (1.96 \pm 0.05) \times 10^{-5}$, $B(\bar{B} \rightarrow b\text{-baryon}) = (8.4 \pm 1.1) \times 10^{-2}$, $B(\bar{B} \rightarrow B^0) = (40.8 \pm 0.7) \times 10^{-2}$. Our first error is their experiment's error and our second error is the systematic error from using our best values.

² ADAM 96D assumes $f_{B^0} = f_{B^-} = 0.39$ and $f_{B_s} = 0.12$.

³ BUSKULIC 96v assumes PDG 96 production fractions for B^0, B^+, B_s, b baryons.

$\Gamma(p\pi^-)/\Gamma(pK^-)$		Γ_{46}/Γ_{47}	
VALUE		DOCUMENT ID	TECN COMMENT
0.84 ± 0.09 OUR FIT			
0.86 ± 0.08 ± 0.05		AAIJ	12AR LHCB pp at 7 TeV

$\Gamma(pD_s^-)/\Gamma_{\text{total}}$		Γ_{48}/Γ	
VALUE	CL%	DOCUMENT ID	TECN COMMENT
< 4.8 × 10⁻⁴	90	AAIJ	14Q LHCB pp at 7 TeV

$\Gamma(p\mu^- \bar{\nu}_\mu)/\Gamma_{\text{total}}$		Γ_{49}/Γ	
VALUE (units 10 ⁻⁴)		DOCUMENT ID	TECN COMMENT
4.1 ± 1.0		¹ AAIJ	15BG LHCB pp at 8 TeV

¹ The ratio of $B(\Lambda_b^0 \rightarrow p\mu^- \bar{\nu}_\mu)$ to $B(\Lambda_b^0 \rightarrow \Lambda_c^+ \mu^- \bar{\nu}_\mu)$ is measured within a restricted q^2 region. Combined with theoretical calculations of the form factors and the previously measured value of $|V_{cb}|$, the first $|V_{ub}| = (3.27 \pm 0.15 \pm 0.16 \pm 0.06) \times 10^{-3}$ measurement from the Λ_b decay is obtained, consistent with the exclusively measured world averages.

$\Gamma(p\mu^- \bar{\nu}_\mu)/\Gamma(\Lambda_c^+ \ell^- \bar{\nu}_\ell)$		Γ_{49}/Γ_{39}	
VALUE (units 10 ⁻²)		DOCUMENT ID	TECN COMMENT
• • •			
1.0 ± 0.04 ± 0.08		¹ AAIJ	15BG LHCB pp at 8 TeV

¹ This measurement is a ratio of $\Gamma(\Lambda_b^0 \rightarrow p\mu^- \bar{\nu}_\mu)[q^2 > 15 \text{ GeV}/c^2]$ to $\Gamma(\Lambda_b^0 \rightarrow \Lambda_c^+ \mu^- \bar{\nu}_\mu)[q^2 > 7 \text{ GeV}/c^2]$ within a restricted q^2 region. Combined with theoretical calculations of the form factors and the previously measured value of $|V_{cb}|$, the first $|V_{ub}| = (3.27 \pm 0.15 \pm 0.16 \pm 0.06) \times 10^{-3}$ measurement from the Λ_b decay is obtained, consistent with the exclusively measured world averages.

$\Gamma(\Lambda\mu^+ \mu^-)/\Gamma_{\text{total}}$		Γ_{50}/Γ	
VALUE (units 10 ⁻⁷)		DOCUMENT ID	TECN COMMENT
10.8 ± 2.8 OUR AVERAGE			
9.6 ± 1.6 ± 2.5		¹ AAIJ	13AJ LHCB pp at 7 TeV
17.3 ± 4.2 ± 5.5		AALTONEN	11AI CDF $p\bar{p}$ at 1.96 TeV

¹ Uses $B(\Lambda_b^0 \rightarrow J/\psi \Lambda) = (6.2 \pm 1.4) \times 10^{-4}$. This measurement comes from the sum of the differential rates in q^2 regions excluding those corresponding to J/ψ and $\psi(2S)$ ($[8.68, 10.09]$ and $[12.86, 14.18] \text{ GeV}^2/c^4$).

$\Gamma(p\pi^- \mu^+ \mu^-)/\Gamma_{\text{total}}$		Γ_{51}/Γ	
VALUE (units 10 ⁻⁸)		DOCUMENT ID	TECN COMMENT
6.9 ± 1.9 ± 1.7			
1.5		¹ AAIJ	17P LHCB pp at 7, 8 TeV

¹ Excludes J/ψ and $\psi(2S)$ decays to $\mu^+ \mu^-$.

$\Gamma(p\pi^- \mu^+ \mu^-)/\Gamma(p\pi^- J/\psi, J/\psi \rightarrow \mu^+ \mu^-)$		Γ_{51}/Γ_{10}	
VALUE (units 10 ⁻²)		DOCUMENT ID	TECN COMMENT
4.4 ± 1.2 ± 0.7		¹ AAIJ	17P LHCB pp at 7, 8 TeV

¹ The $p\pi^- \mu^+ \mu^-$ mode excludes J/ψ and $\psi(2S)$ decays to $\mu^+ \mu^-$.

$\Gamma(\Lambda\gamma)/\Gamma_{\text{total}}$		Γ_{52}/Γ	
VALUE (units 10 ⁻⁶)	CL%	DOCUMENT ID	TECN COMMENT
7.1 ± 1.5 ± 0.9		¹ AAIJ	19Z LHCB pp at 13 TeV

• • • We do not use the following data for averages, fits, limits, etc. **• • •**

<1300 90 ACOSTA 02G CDF $p\bar{p}$ at 1.8 TeV

¹ AAIJ 19Z normalized to $B^0 \rightarrow K^* 0 \gamma$ and used an integrated luminosity of 1.7 fb^{-1} .

$\Gamma(\Lambda\eta)/\Gamma_{\text{total}}$		Γ_{53}/Γ	
VALUE (units 10 ⁻⁶)		DOCUMENT ID	TECN COMMENT
9 ± 7 ± 1		¹ AAIJ	15AH LHCB pp at 7, 8 TeV

¹ AAIJ 15AH reports $[\Gamma(\Lambda_b^0 \rightarrow \Lambda\eta)/\Gamma_{\text{total}}] / [B(B^0 \rightarrow \eta' K^0)] = 0.142^{+0.11}_{-0.08}$ which we multiply by our best value $B(B^0 \rightarrow \eta' K^0) = (6.6 \pm 0.4) \times 10^{-5}$. Our first error is their experiment's error and our second error is the systematic error from using our best value. The single uncertainty quoted with the original measurement combines in quadrature statistical and systematic uncertainties.

$\Gamma(\Lambda\eta'(958))/\Gamma_{\text{total}}$		Γ_{54}/Γ	
VALUE	CL%	DOCUMENT ID	TECN COMMENT
< 3.1 × 10⁻⁶			
		¹ AAIJ	15AH LHCB pp at 7, 8 TeV

¹ AAIJ 15AH reports $[\Gamma(\Lambda_b^0 \rightarrow \Lambda\eta'(958))/\Gamma_{\text{total}}] / [B(B^0 \rightarrow \eta' K^0)] < 0.047$ which we multiply by our best value $B(B^0 \rightarrow \eta' K^0) = 6.6 \times 10^{-5}$.

$\Gamma(\Lambda\pi^+ \pi^-)/\Gamma(\Lambda_c^+ \pi^-)$		Γ_{55}/Γ_{24}	
VALUE (units 10 ⁻⁴)		DOCUMENT ID	TECN COMMENT
9.5 ± 3.8 ± 0.5		¹ AAIJ	16W LHCB pp at 7, 8 TeV

¹ AAIJ 16W reports $[\Gamma(\Lambda_b^0 \rightarrow \Lambda\pi^+ \pi^-)/\Gamma(\Lambda_b^0 \rightarrow \Lambda_c^+ \pi^-)] / [B(\Lambda_c^+ \rightarrow \Lambda\pi^+)] = (7.3 \pm 1.9 \pm 2.2) \times 10^{-2}$ which we multiply by our best value $B(\Lambda_c^+ \rightarrow \Lambda\pi^+) = (1.30 \pm 0.07) \times 10^{-2}$. Our first error is their experiment's error and our second error is the systematic error from using our best value.

$\Gamma(\Lambda K^+ \pi^-)/\Gamma(\Lambda_c^+ \pi^-)$		Γ_{56}/Γ_{24}	
VALUE (units 10 ⁻⁴)		DOCUMENT ID	TECN COMMENT
11.6 ± 2.3 ± 0.6		¹ AAIJ	16W LHCB pp at 7, 8 TeV

¹ AAIJ 16W reports $[\Gamma(\Lambda_b^0 \rightarrow \Lambda K^+ \pi^-)/\Gamma(\Lambda_b^0 \rightarrow \Lambda_c^+ \pi^-)] / [B(\Lambda_c^+ \rightarrow \Lambda\pi^+)] = (8.9 \pm 1.2 \pm 1.3) \times 10^{-2}$ which we multiply by our best value $B(\Lambda_c^+ \rightarrow \Lambda\pi^+) = (1.30 \pm 0.07) \times 10^{-2}$. Our first error is their experiment's error and our second error is the systematic error from using our best value.

$\Gamma(\Lambda K^+ K^-)/\Gamma(\Lambda_c^+ \pi^-)$		Γ_{57}/Γ_{24}	
VALUE (units 10 ⁻³)		DOCUMENT ID	TECN COMMENT
3.29 ± 0.35 ± 0.17		¹ AAIJ	16W LHCB pp at 7, 8 TeV

¹ AAIJ 16W reports $[\Gamma(\Lambda_b^0 \rightarrow \Lambda K^+ K^-)/\Gamma(\Lambda_b^0 \rightarrow \Lambda_c^+ \pi^-)] / [B(\Lambda_c^+ \rightarrow \Lambda\pi^+)] = (25.3 \pm 1.9 \pm 1.9) \times 10^{-2}$ which we multiply by our best value $B(\Lambda_c^+ \rightarrow \Lambda\pi^+) = (1.30 \pm 0.07) \times 10^{-2}$. Our first error is their experiment's error and our second error is the systematic error from using our best value.

$\Gamma(\Lambda\phi)/\Gamma_{\text{total}}$		Γ_{58}/Γ	
VALUE (units 10 ⁻⁶)		DOCUMENT ID	TECN COMMENT
9.8 ± 2.1 ± 1.6			
1.5		¹ AAIJ	16J LHCB pp at 7, 8 TeV

¹ AAIJ 16J reports $[\Gamma(\Lambda_b^0 \rightarrow \Lambda\phi)/\Gamma_{\text{total}}] / [B(B^0 \rightarrow K^0 \phi)] \times [B(\bar{B} \rightarrow b\text{-baryon})] / [B(\bar{B} \rightarrow B^0)] = 0.275 \pm 0.055 \pm 0.020$ which we multiply or divide by our best values $B(B^0 \rightarrow K^0 \phi) = (7.3 \pm 0.7) \times 10^{-6}$, $B(\bar{B} \rightarrow b\text{-baryon}) = (8.4 \pm 1.1) \times 10^{-2}$, $B(\bar{B} \rightarrow B^0) = (40.8 \pm 0.7) \times 10^{-2}$. Our first error is their experiment's error and our second error is the systematic error from using our best values.

$\Gamma(p\pi^- \pi^+ \pi^-)/\Gamma(\Lambda_c^+ \pi^-)$		Γ_{59}/Γ_{24}	
VALUE (units 10 ⁻³)		DOCUMENT ID	TECN COMMENT
4.30 ± 0.24 ± 0.22			
0.23		¹ AAIJ	18Q LHCB pp at 7, 8 TeV

¹ AAIJ 18Q reports $[\Gamma(\Lambda_b^0 \rightarrow p\pi^- \pi^+ \pi^-)/\Gamma(\Lambda_b^0 \rightarrow \Lambda_c^+ \pi^-)] / [B(\Lambda_c^+ \rightarrow pK^- \pi^+)] = (6.85 \pm 0.19 \pm 0.08 \pm 0.32) \times 10^{-2}$ which we multiply by our best value $B(\Lambda_c^+ \rightarrow pK^- \pi^+) = (6.28 \pm 0.32) \times 10^{-2}$. Our first error is their experiment's error and our second error is the systematic error from using our best value.

$\Gamma(pK^- K^+ \pi^-)/\Gamma(\Lambda_c^+ \pi^-)$		Γ_{60}/Γ_{24}	
VALUE (units 10 ⁻³)		DOCUMENT ID	TECN COMMENT
0.83 ± 0.10 ± 0.04		¹ AAIJ	18Q LHCB pp at 7, 8 TeV

¹ AAIJ 18Q reports $[\Gamma(\Lambda_b^0 \rightarrow pK^- K^+ \pi^-)/\Gamma(\Lambda_b^0 \rightarrow \Lambda_c^+ \pi^-)] / [B(\Lambda_c^+ \rightarrow pK^- \pi^+)] = (1.32 \pm 0.09 \pm 0.09 \pm 0.10) \times 10^{-2}$ which we multiply by our best value $B(\Lambda_c^+ \rightarrow pK^- \pi^+) = (6.28 \pm 0.32) \times 10^{-2}$. Our first error is their experiment's error and our second error is the systematic error from using our best value.

$\Gamma(pK^- \pi^+ \pi^-)/\Gamma(\Lambda_c^+ \pi^-)$		Γ_{61}/Γ_{24}	
VALUE (units 10 ⁻³)		DOCUMENT ID	TECN COMMENT
10.3 ± 0.5 ± 0.5		¹ AAIJ	18Q LHCB pp at 7, 8 TeV

¹ AAIJ 18Q reports $[\Gamma(\Lambda_b^0 \rightarrow pK^- \pi^+ \pi^-)/\Gamma(\Lambda_b^0 \rightarrow \Lambda_c^+ \pi^-)] / [B(\Lambda_c^+ \rightarrow pK^- \pi^+)] = (16.4 \pm 0.3 \pm 0.2 \pm 0.7) \times 10^{-2}$ which we multiply by our best value $B(\Lambda_c^+ \rightarrow pK^- \pi^+) = (6.28 \pm 0.32) \times 10^{-2}$. Our first error is their experiment's error and our second error is the systematic error from using our best value.

$\Gamma(pK^- K^+ K^-)/\Gamma(\Lambda_c^+ \pi^-)$		Γ_{62}/Γ_{24}	
VALUE (units 10 ⁻³)		DOCUMENT ID	TECN COMMENT
2.58 ± 0.15 ± 0.13			
0.14		¹ AAIJ	18Q LHCB pp at 7, 8 TeV

¹ AAIJ 18Q reports $[\Gamma(\Lambda_b^0 \rightarrow pK^- K^+ K^-)/\Gamma(\Lambda_b^0 \rightarrow \Lambda_c^+ \pi^-)] / [B(\Lambda_c^+ \rightarrow pK^- \pi^+)] = (4.11 \pm 0.12 \pm 0.06 \pm 0.19) \times 10^{-2}$ which we multiply by our best value $B(\Lambda_c^+ \rightarrow pK^- \pi^+) = (6.28 \pm 0.32) \times 10^{-2}$. Our first error is their experiment's error and our second error is the systematic error from using our best value.

PARTIAL BRANCHING FRACTIONS IN $\Lambda_b \rightarrow \Lambda\mu^+ \mu^-$

$B(\Lambda_b \rightarrow \Lambda\mu^+ \mu^-) (q^2 < 2.0 \text{ GeV}^2/c^4)$			
VALUE (units 10 ⁻⁷)		DOCUMENT ID	TECN COMMENT
0.71 ± 0.27 OUR AVERAGE			
0.72 ^{+0.24} _{-0.22} ± 0.14		¹ AAIJ	15AE LHCB pp at 7, 8 TeV
0.15 ± 2.01 ± 0.05		AALTONEN	11AI CDF $p\bar{p}$ at 1.96 TeV

• • • We do not use the following data for averages, fits, limits, etc. **• • •**

0.56 ± 0.76 ± 0.80 ² AAIJ 13AJ LHCB Repl. by AAIJ 15AE

¹ AAIJ 15AE measurement covers $0.1 < q^2 < 2.0 \text{ GeV}^2/c^4$.

² Uses $B(\Lambda_b^0 \rightarrow J/\psi \Lambda) = (6.2 \pm 1.4) \times 10^{-4}$.

Baryon Particle Listings

 Λ_b^0 $B(\Lambda_b \rightarrow \Lambda \mu^+ \mu^-)$ ($2.0 < q^2 < 4.3 \text{ GeV}^2/c^4$)

VALUE (units 10^{-7})	DOCUMENT ID	TECN	COMMENT
0.28 \pm 0.28 -0.21 OUR AVERAGE			
0.253 \pm 0.276 \pm 0.046	¹ AAIJ	15AE LHCb	pp at 7, 8 TeV
1.8 \pm 1.7 \pm 0.6	AALTONEN	11AI CDF	$p\bar{p}$ at 1.96 TeV
• • • We do not use the following data for averages, fits, limits, etc. • • •			
0.71 \pm 0.60 \pm 0.23	² AAIJ	13AJ LHCb	Repl. by AAIJ 15AE
¹ AAIJ 15AE measurement covers $2.0 < q^2 < 4.0 \text{ GeV}^2/c^4$.			
² Uses $B(\Lambda_b^0 \rightarrow J/\psi \Lambda) = (6.2 \pm 1.4) \times 10^{-4}$.			

 $B(\Lambda_b \rightarrow \Lambda \mu^+ \mu^-)$ ($q^2 < 4.3 \text{ GeV}^2/c^4$)

VALUE (units 10^{-7})	DOCUMENT ID	TECN	COMMENT
2.7 \pm 2.5 \pm 0.9	AALTONEN	11AI CDF	$p\bar{p}$ at 1.96 TeV

 $B(\Lambda_b \rightarrow \Lambda \mu^+ \mu^-)$ ($4.0 < q^2 < 6.0 \text{ GeV}^2/c^4$)

VALUE (units 10^{-7})	DOCUMENT ID	TECN	COMMENT
0.04 \pm 0.18 -0.00 \pm 0.02	AAIJ	15AE LHCb	pp at 7, 8 TeV

 $B(\Lambda_b \rightarrow \Lambda \mu^+ \mu^-)$ ($1.0 < q^2 < 6.0 \text{ GeV}^2/c^4$)

VALUE (units 10^{-7})	DOCUMENT ID	TECN	COMMENT
0.47 \pm 0.31 -0.27 OUR AVERAGE			
0.45 \pm 0.30 \pm 0.10	¹ AAIJ	15AE LHCb	pp at 7 and 8 TeV
1.3 \pm 2.1 \pm 0.4	AALTONEN	11AI CDF	$p\bar{p}$ at 1.96 TeV
¹ AAIJ 15AE measurement covers $1.1 < q^2 < 6.0 \text{ GeV}^2/c^4$.			

 $B(\Lambda_b \rightarrow \Lambda \mu^+ \mu^-)$ ($6.0 < q^2 < 8.0 \text{ GeV}^2/c^4$)

VALUE (units 10^{-7})	DOCUMENT ID	TECN	COMMENT
0.50 \pm 0.24 -0.22 \pm 0.10	AAIJ	15AE LHCb	pp at 7, 8 TeV

 $B(\Lambda_b \rightarrow \Lambda \mu^+ \mu^-)$ ($4.3 < q^2 < 8.68 \text{ GeV}^2/c^4$)

VALUE (units 10^{-7})	DOCUMENT ID	TECN	COMMENT
0.5 \pm 0.7 OUR AVERAGE			
0.66 \pm 0.74 \pm 0.18	¹ AAIJ	13AJ LHCb	pp at 7 TeV
-0.2 \pm 1.6 \pm 0.1	AALTONEN	11AI CDF	$p\bar{p}$ at 1.96 TeV
¹ Uses $B(\Lambda_b^0 \rightarrow J/\psi \Lambda) = (6.2 \pm 1.4) \times 10^{-4}$.			

 $B(\Lambda_b \rightarrow \Lambda \mu^+ \mu^-)$ ($10.09 < q^2 < 12.86 \text{ GeV}^2/c^4$)

VALUE (units 10^{-7})	DOCUMENT ID	TECN	COMMENT
2.2 \pm 0.6 OUR AVERAGE			
2.08 \pm 0.42 \pm 0.42	¹ AAIJ	15AE LHCb	pp at 7, 8 TeV
3.0 \pm 1.5 \pm 1.0	AALTONEN	11AI CDF	$p\bar{p}$ at 1.96 TeV
• • • We do not use the following data for averages, fits, limits, etc. • • •			
1.55 \pm 0.58 \pm 0.55	² AAIJ	13AJ LHCb	Repl. by AAIJ 15AE
¹ AAIJ 15AE measurement covers $11.0 < q^2 < 12.5 \text{ GeV}^2/c^4$.			
² Uses $B(\Lambda_b^0 \rightarrow J/\psi \Lambda) = (6.2 \pm 1.4) \times 10^{-4}$.			

 $B(\Lambda_b \rightarrow \Lambda \mu^+ \mu^-)$ ($14.18 < q^2 < 16.0 \text{ GeV}^2/c^4$)

VALUE (units 10^{-7})	DOCUMENT ID	TECN	COMMENT
1.7 \pm 0.5 OUR AVERAGE			Error includes scale factor of 1.1.
2.04 \pm 0.35 \pm 0.42	¹ AAIJ	15AE LHCb	pp at 7, 8 TeV
1.0 \pm 0.7 \pm 0.3	AALTONEN	11AI CDF	$p\bar{p}$ at 1.96 TeV
• • • We do not use the following data for averages, fits, limits, etc. • • •			
1.44 \pm 0.44 \pm 0.42	² AAIJ	13AJ LHCb	Repl. by AAIJ 15AE
¹ AAIJ 15AE measurement covers $15.0 < q^2 < 16.0 \text{ GeV}^2/c^4$.			
² Uses $B(\Lambda_b^0 \rightarrow J/\psi \Lambda) = (6.2 \pm 1.4) \times 10^{-4}$.			

 $B(\Lambda_b \rightarrow \Lambda \mu^+ \mu^-)$ ($16.0 < q^2 < 20.0 \text{ GeV}^2/c^4$)

VALUE (units 10^{-7})	DOCUMENT ID	TECN	COMMENT
7.0 \pm 1.9 \pm 2.2	AALTONEN	11AI CDF	$p\bar{p}$ at 1.96 TeV
• • • We do not use the following data for averages, fits, limits, etc. • • •			
4.73 \pm 0.77 \pm 1.25	^{1,2} AAIJ	13AJ LHCb	Repl. by AAIJ 15AE
¹ Uses $B(\Lambda_b^0 \rightarrow J/\psi \Lambda) = (6.2 \pm 1.4) \times 10^{-4}$.			
² Requires $16.00 < q^2 < 20.30 \text{ GeV}^2/c^4$.			

 $B(\Lambda_b \rightarrow \Lambda \mu^+ \mu^-)$ ($18.0 < q^2 < 20.0 \text{ GeV}^2/c^4$)

VALUE (units 10^{-7})	DOCUMENT ID	TECN	COMMENT
2.44 \pm 0.28 \pm 0.50	AAIJ	15AE LHCb	pp at 7, 8 TeV

 $B(\Lambda_b \rightarrow \Lambda \mu^+ \mu^-)$ ($15.0 < q^2 < 20.0 \text{ GeV}^2/c^4$)

VALUE (units 10^{-7})	DOCUMENT ID	TECN	COMMENT
6.00 \pm 0.45 \pm 1.25	AAIJ	15AE LHCb	pp at 7, 8 TeV

CP VIOLATION

 A_{CP} is defined as

$$A_{CP} = \frac{B(\Lambda_b^0 \rightarrow f) - B(\bar{\Lambda}_b^0 \rightarrow \bar{f})}{B(\Lambda_b^0 \rightarrow f) + B(\bar{\Lambda}_b^0 \rightarrow \bar{f})},$$

the CP-violation asymmetry of exclusive Λ_b^0 and $\bar{\Lambda}_b^0$ decay. $A_{CP}(\Lambda_b \rightarrow p \pi^-)$

VALUE	DOCUMENT ID	TECN	COMMENT
-0.025 \pm 0.029 OUR AVERAGE			Error includes scale factor of 1.2.
-0.035 \pm 0.017 \pm 0.020	AAIJ	18AX LHCb	pp at 7 and 8 TeV
0.06 \pm 0.07 \pm 0.03	AALTONEN	14P CDF	$p\bar{p}$ at 1.96 TeV
• • • We do not use the following data for averages, fits, limits, etc. • • •			
0.03 \pm 0.17 \pm 0.05	AALTONEN	11N CDF	Repl. by AALTONEN 14P

 $A_{CP}(\Lambda_b \rightarrow p K^-)$

VALUE	DOCUMENT ID	TECN	COMMENT
-0.025 \pm 0.022 OUR AVERAGE			
-0.020 \pm 0.013 \pm 0.019	AAIJ	18AX LHCb	pp at 7 and 8 TeV
-0.10 \pm 0.08 \pm 0.04	AALTONEN	14P CDF	$p\bar{p}$ at 1.96 TeV
• • • We do not use the following data for averages, fits, limits, etc. • • •			
0.37 \pm 0.17 \pm 0.03	AALTONEN	11N CDF	Repl. by AALTONEN 14P

 $\Delta A_{CP}(p K^- / \pi^-)$

VALUE	DOCUMENT ID	TECN	COMMENT
$\Delta A_{CP} \equiv A_{CP}(p K^-) - A_{CP}(p \pi^-)$			
0.014 \pm 0.022 \pm 0.010	AAIJ	18AX LHCb	pp at 7 and 8 TeV

 $A_{CP}(\Lambda_b \rightarrow p \bar{K}^0 \pi^-)$

VALUE	DOCUMENT ID	TECN	COMMENT
0.22 \pm 0.13 \pm 0.03	AAIJ	14Q LHCb	pp at 7 TeV

 $\Delta A_{CP}(J/\psi p \pi^- / K^-)$

VALUE (units 10^{-2})	DOCUMENT ID	TECN	COMMENT
$\Delta A_{CP} \equiv A_{CP}(J/\psi p \pi^-) - A_{CP}(J/\psi p K^-)$			
5.7 \pm 2.4 \pm 1.2	AAIJ	14K LHCb	pp at 7, 8 TeV

 $A_{CP}(\Lambda_b \rightarrow \Lambda K^+ \pi^-)$

VALUE	DOCUMENT ID	TECN	COMMENT
-0.53 \pm 0.23 \pm 0.11	¹ AAIJ	16W LHCb	pp at 7, 8 TeV
¹ Measured relative to $\Lambda_b^0 \rightarrow \Lambda_c^+ \pi^-$ decay.			

 $A_{CP}(\Lambda_b \rightarrow \Lambda K^+ K^-)$

VALUE	DOCUMENT ID	TECN	COMMENT
-0.28 \pm 0.10 \pm 0.07	¹ AAIJ	16W LHCb	pp at 7, 8 TeV
¹ Measured relative to $\Lambda_b^0 \rightarrow \Lambda_c^+ \pi^-$ decay.			

 $\Delta A_{CP}(\Lambda_b^0 \rightarrow p K^- \mu^+ \mu^-)$

VALUE (units 10^{-2})	DOCUMENT ID	TECN	COMMENT
$\Delta A_{CP} \equiv A_{CP}(p K^- \mu^+ \mu^-) - A_{CP}(p K^- J/\psi)$			
-3.5 \pm 5.0 \pm 0.2	AAIJ	17T LHCb	pp at 7, 8 TeV

 $\Delta A_{CP}(\Lambda_b^0 \rightarrow p \pi^- \pi^+ \pi^-)$

VALUE (units 10^{-2})	DOCUMENT ID	TECN	COMMENT
$\Delta A_{CP} \equiv A_{CP}(\Lambda_b^0 \rightarrow p \pi^- \pi^+ \pi^-) - A_{CP}(\Lambda_b^0 \rightarrow (\Lambda_c^+ \rightarrow p \pi^- \pi^+) \pi^-)$			
1.1 \pm 2.5 \pm 0.6	¹ AAIJ	19AH LHCb	pp at 7 and 8 TeV
¹ Full phase space.			

 $\Delta A_{CP}(\Lambda_b^0 \rightarrow (p \pi^- \pi^+ \pi^-)_{LBM})$

VALUE (units 10^{-2})	DOCUMENT ID	TECN	COMMENT
$\Delta A_{CP} \equiv A_{CP}(\Lambda_b^0 \rightarrow (p \pi^- \pi^+ \pi^-)_{LBM}) - A_{CP}(\Lambda_b^0 \rightarrow (\Lambda_c^+ \rightarrow p \pi^- \pi^+) \pi^-)$. Two-body low invariant-mass region (LBM): $m(p \pi^-) < 2000 \text{ MeV}$ and $m(\pi^+ \pi^-) < 1640 \text{ MeV}$.			
3.7 \pm 4.1 \pm 0.5	¹ AAIJ	19AH LHCb	pp at 7 and 8 TeV
¹ Measurement done with $m(p \pi^-) < 2000 \text{ MeV}/c^2$ and $m(\pi^+ \pi^-) < 1640 \text{ MeV}/c^2$.			

 $\Delta A_{CP}(\Lambda_b^0 \rightarrow p a_1(1260)^-)$

VALUE (units 10^{-2})	DOCUMENT ID	TECN	COMMENT
$\Delta A_{CP} \equiv A_{CP}(\Lambda_b^0 \rightarrow p a_1(1260)^-) - A_{CP}(\Lambda_b^0 \rightarrow (\Lambda_c^+ \rightarrow p \pi^- \pi^+) \pi^-)$. 419 $< m(\pi^+ \pi^-) < 1500 \text{ MeV}$.			
-1.5 \pm 4.2 \pm 0.6	AAIJ	19AH LHCb	pp at 7 and 8 TeV

 $\Delta A_{CP}(\Lambda_b^0 \rightarrow N(1520)^0 \rho(770)^0)$

VALUE (units 10^{-2})	DOCUMENT ID	TECN	COMMENT
$\Delta A_{CP} \equiv A_{CP}(\Lambda_b^0 \rightarrow N(1520)^0 \rho(770)^0) - A_{CP}(\Lambda_b^0 \rightarrow (\Lambda_c^+ \rightarrow p \pi^- \pi^+) \pi^-)$. 1078 $< m(p \pi^-) < 1800 \text{ MeV}$ and $m(\pi^+ \pi^-) < 1100 \text{ MeV}$.			
2.0 \pm 4.9 \pm 0.4	AAIJ	19AH LHCb	pp at 7 and 8 TeV

$\Delta A_{CP}(\Lambda_b^0 \rightarrow \Delta(1232)^{++}\pi^-\pi^-)$
 $\Delta A_{CP} \equiv A_{CP}(\Lambda_b^0 \rightarrow \Delta(1232)^{++}\pi^-\pi^-) - A_{CP}(\Lambda_b^0 \rightarrow (\Lambda_c^+ \rightarrow p\pi^-\pi^+)\pi^-)$. $1078 < m(p\pi^+) < 1432$ MeV.

VALUE (units 10^{-2})	DOCUMENT ID	TECN	COMMENT
$0.1 \pm 3.2 \pm 0.6$	AAIJ	19AH LHCb	pp at 7 and 8 TeV

$\Delta A_{CP}(\Lambda_b^0 \rightarrow \rho K^-\pi^+\pi^-)$
 $\Delta A_{CP} \equiv A_{CP}(\Lambda_b^0 \rightarrow \rho K^-\pi^+\pi^-) - A_{CP}(\Lambda_b^0 \rightarrow (\Lambda_c^+ \rightarrow pK^-\pi^+)\pi^-)$

VALUE (units 10^{-2})	DOCUMENT ID	TECN	COMMENT
$3.2 \pm 1.1 \pm 0.6$	¹ AAIJ	19AH LHCb	pp at 7 and 8 TeV

¹ Full phase space.

$\Delta A_{CP}(\Lambda_b^0 \rightarrow (\rho K^-\pi^+\pi^-)_{LBM})$
 $\Delta A_{CP} \equiv A_{CP}(\Lambda_b^0 \rightarrow (\rho K^-\pi^+\pi^-)_{LBM}) - A_{CP}(\Lambda_b^0 \rightarrow (\Lambda_c^+ \rightarrow pK^-\pi^+)\pi^-)$.
 Two-body low invariant-mass region (LBM): $m(pK^-) < 2000$ MeV and $m(\pi^+\pi^-) < 1640$ MeV.

VALUE (units 10^{-2})	DOCUMENT ID	TECN	COMMENT
$3.5 \pm 1.5 \pm 0.5$	¹ AAIJ	19AH LHCb	pp at 7 and 8 TeV

¹ Measurement done with $m(pK^-) < 2000$ MeV/ c^2 and $m(\pi^+\pi^-) < 1640$ MeV/ c^2 .

$\Delta A_{CP}(\Lambda_b^0 \rightarrow N(1520)^0 K^*(892)^0)$
 $\Delta A_{CP} \equiv A_{CP}(\Lambda_b^0 \rightarrow N(1520)^0 K^*(892)^0) - A_{CP}(\Lambda_b^0 \rightarrow (\Lambda_c^+ \rightarrow pK^-\pi^+)\pi^-)$. $1078 < m(p\pi^+) < 1800$ MeV and $750 < m(\pi^+K^-) < 1100$ MeV.

VALUE (units 10^{-2})	DOCUMENT ID	TECN	COMMENT
$5.5 \pm 2.5 \pm 0.5$	AAIJ	19AH LHCb	pp at 7 and 8 TeV

$\Delta A_{CP}(\Lambda_b^0 \rightarrow \Lambda(1520)\rho(770)^0)$
 $\Delta A_{CP} \equiv A_{CP}(\Lambda_b^0 \rightarrow \Lambda(1520)\rho(770)^0) - A_{CP}(\Lambda_b^0 \rightarrow (\Lambda_c^+ \rightarrow pK^-\pi^+)\pi^-)$.
 $1460 < m(pK^-) < 1580$ MeV and $m(\pi^+\pi^-) < 1100$ MeV.

VALUE (units 10^{-2})	DOCUMENT ID	TECN	COMMENT
$0.6 \pm 6.0 \pm 0.5$	AAIJ	19AH LHCb	pp at 7 and 8 TeV

$\Delta A_{CP}(\Lambda_b^0 \rightarrow \Delta(1232)^{++}K^-\pi^-)$
 $\Delta A_{CP} \equiv A_{CP}(\Lambda_b^0 \rightarrow \Delta(1232)^{++}K^-\pi^-) - A_{CP}(\Lambda_b^0 \rightarrow (\Lambda_c^+ \rightarrow pK^-\pi^+)\pi^-)$. $1078 < m(p\pi^+) < 1432$ MeV.

VALUE (units 10^{-2})	DOCUMENT ID	TECN	COMMENT
$4.4 \pm 2.6 \pm 0.6$	AAIJ	19AH LHCb	pp at 7 and 8 TeV

$\Delta A_{CP}(\Lambda_b^0 \rightarrow \rho K_1(1410)^-)$
 $\Delta A_{CP} \equiv A_{CP}(\Lambda_b^0 \rightarrow \rho K_1(1410)^-) - A_{CP}(\Lambda_b^0 \rightarrow (\Lambda_c^+ \rightarrow pK^-\pi^+)\pi^-)$. $1200 < m(K^-\pi^+\pi^-) < 1600$ MeV.

VALUE (units 10^{-2})	DOCUMENT ID	TECN	COMMENT
$4.7 \pm 3.5 \pm 0.8$	AAIJ	19AH LHCb	pp at 7 and 8 TeV

$\Delta A_{CP}(\Lambda_b^0 \rightarrow \rho K^-K^+\pi^-)$
 $\Delta A_{CP} \equiv A_{CP}(\Lambda_b^0 \rightarrow \rho K^-K^+\pi^-) - A_{CP}(\Lambda_b^0 \rightarrow (\Lambda_c^+ \rightarrow p\pi^-\pi^+)\pi^-)$

VALUE (units 10^{-2})	DOCUMENT ID	TECN	COMMENT
$-6.9 \pm 4.9 \pm 0.8$	¹ AAIJ	19AH LHCb	pp at 7 and 8 TeV

¹ Full phase space.

$\Delta A_{CP}(\Lambda_b^0 \rightarrow \rho K^-K^+K^-)$
 $\Delta A_{CP} \equiv A_{CP}(\Lambda_b^0 \rightarrow \rho K^-K^+K^-) - A_{CP}(\Lambda_b^0 \rightarrow (\Lambda_c^+ \rightarrow pK^-\pi^+)\pi^-)$

VALUE (units 10^{-2})	DOCUMENT ID	TECN	COMMENT
$0.2 \pm 1.8 \pm 0.6$	¹ AAIJ	19AH LHCb	pp at 7 and 8 TeV

¹ Full phase space.

$\Delta A_{CP}(\Lambda_b^0 \rightarrow \Lambda(1520)\phi(1020))$
 $\Delta A_{CP} \equiv A_{CP}(\Lambda_b^0 \rightarrow \Lambda(1520)\phi(1020)) - A_{CP}(\Lambda_b^0 \rightarrow (\Lambda_c^+ \rightarrow pK^-\pi^+)\pi^-)$.
 $1460 < m(pK^-) < 1600$ MeV and $1005 < m(K^+K^-) < 1040$ MeV.

VALUE (units 10^{-2})	DOCUMENT ID	TECN	COMMENT
$4.3 \pm 5.6 \pm 0.4$	AAIJ	19AH LHCb	pp at 7 and 8 TeV

$\Delta A_{CP}(\Lambda_b^0 \rightarrow (\rho K^-)_{highmass} \phi(1020))$
 $\Delta A_{CP} \equiv A_{CP}(\Lambda_b^0 \rightarrow (\rho K^-)_{highmass} \phi(1020)) - A_{CP}(\Lambda_b^0 \rightarrow (\Lambda_c^+ \rightarrow pK^-\pi^+)\pi^-)$. $m(pK^-) > 1600$ MeV and $1005 < m(K^+K^-) < 1040$ MeV.

VALUE (units 10^{-2})	DOCUMENT ID	TECN	COMMENT
$-0.7 \pm 3.3 \pm 0.7$	¹ AAIJ	19AH LHCb	pp at 7 and 8 TeV

¹ Measurement done with $m(pK^-) > 1600$ MeV/ c^2 .

$\Delta A_{CP}(\Lambda_b^0 \rightarrow (\rho K^-K^+K^-)_{LBM})$
 $\Delta A_{CP} \equiv A_{CP}(\Lambda_b^0 \rightarrow (\rho K^-K^+K^-)_{LBM}) - A_{CP}(\Lambda_b^0 \rightarrow (\Lambda_c^+ \rightarrow pK^-\pi^+)\pi^-)$. Two-body low invariant-mass region (LBM): $m(pK^-) < 2000$ MeV and $m(K^+K^-) < 1675$ MeV.

VALUE (units 10^{-2})	DOCUMENT ID	TECN	COMMENT
$2.7 \pm 2.3 \pm 0.6$	¹ AAIJ	19AH LHCb	pp at 7 and 8 TeV

¹ Measurement done with $m(pK^-) < 2000$ MeV/ c^2 and $m(K^+K^-) < 1675$ MeV/ c^2 .

CP AND T VIOLATION PARAMETERS

Measured values of the triple-product asymmetry parameters, odd under time-reversal, are defined as $A_{c(s)}(\Lambda/\phi) = (N_{c(s)}^+ - N_{c(s)}^-) / (\text{sum})$ where $N_{c(s)}^+$, $N_{c(s)}^-$ are the number of Λ or ϕ candidates for which the $\cos(\Phi)$ and $\sin(\Phi)$ observables are positive and negative, respectively. Angles $\cos(\Phi)$ and $\sin(\Phi)$ are defined as in LEITNER 07.

$A_c(\Lambda)$	DOCUMENT ID	TECN	COMMENT
$-0.22 \pm 0.12 \pm 0.06$	AAIJ	16J LHCb	pp at 7, 8 TeV

$A_s(\Lambda)$	DOCUMENT ID	TECN	COMMENT
$0.13 \pm 0.12 \pm 0.05$	AAIJ	16J LHCb	pp at 7, 8 TeV

$A_c(\phi)$	DOCUMENT ID	TECN	COMMENT
$-0.01 \pm 0.12 \pm 0.03$	AAIJ	16J LHCb	pp at 7, 8 TeV

$A_s(\phi)$	DOCUMENT ID	TECN	COMMENT
$-0.07 \pm 0.12 \pm 0.01$	AAIJ	16J LHCb	pp at 7, 8 TeV

$a_{CP}(\Lambda_b^0 \rightarrow p\pi^-\pi^+\pi^-)$	DOCUMENT ID	TECN	COMMENT
$1.15 \pm 1.45 \pm 0.32$	¹ AAIJ	17H LHCb	pp at 7, 8 TeV

Observable calculated as half of the difference between triple products for Λ_b^0 and $\bar{\Lambda}_b^0$, which is sensitive to CP violation.
¹ Measured over full phase space of the decay.

$a_{CP}(\Lambda_b^0 \rightarrow \rho K^-\pi^+\pi^-)$	DOCUMENT ID	TECN	COMMENT
$-0.81 \pm 0.84 \pm 0.31$	¹ AAIJ	18AG LHCb	pp at 7, 8 TeV

Observable calculated as half of the difference between triple products for Λ_b^0 and $\bar{\Lambda}_b^0$, which is sensitive to CP violation.
¹ Measured over full phase space of the decay.

$a_{CP}(\Lambda_b^0 \rightarrow \rho K^-K^+\pi^-)$	DOCUMENT ID	TECN	COMMENT
$-0.93 \pm 4.54 \pm 0.42$	¹ AAIJ	17H LHCb	pp at 7, 8 TeV

Observable calculated as half of the difference between triple products for Λ_b^0 and $\bar{\Lambda}_b^0$, which is sensitive to CP violation.
¹ Measured over full phase space of the decay.

$a_{CP}(\Lambda_b^0 \rightarrow \rho K^-K^+K^-)$	DOCUMENT ID	TECN	COMMENT
$1.12 \pm 1.51 \pm 0.32$	¹ AAIJ	18AG LHCb	pp at 7, 8 TeV

Observable calculated as half of the difference between triple products for Λ_b^0 and $\bar{\Lambda}_b^0$, which is sensitive to CP violation.
¹ Measured over full phase space of the decay.

$a_{CP}(\Lambda_b^0 \rightarrow \rho K^-\mu^+\mu^-)$	DOCUMENT ID	TECN	COMMENT
$1.2 \pm 5.0 \pm 0.7$	AAIJ	17T LHCb	pp at 7, 8 TeV

P VIOLATION PARAMETERS

Observables calculated as average of the triple products for Λ_b^0 and $\bar{\Lambda}_b^0$, which is sensitive to parity violation.

$a_P(\Lambda_b^0 \rightarrow p\pi^-\pi^+\pi^-)$	DOCUMENT ID	TECN	COMMENT
$-3.71 \pm 1.45 \pm 0.32$	¹ AAIJ	17H LHCb	pp at 7, 8 TeV

¹ Measured over full phase space of the decay.

$a_P(\Lambda_b^0 \rightarrow \rho K^-\pi^+\pi^-)$	DOCUMENT ID	TECN	COMMENT
$-0.60 \pm 0.84 \pm 0.31$	¹ AAIJ	18AG LHCb	pp at 7, 8 TeV

¹ Measured over full phase space of the decay.

$a_P(\Lambda_b^0 \rightarrow \rho K^-K^+\pi^-)$	DOCUMENT ID	TECN	COMMENT
$3.62 \pm 4.54 \pm 0.42$	¹ AAIJ	17H LHCb	pp at 7, 8 TeV

¹ Measured over full phase space of the decay.

$a_P(\Lambda_b^0 \rightarrow \rho K^-K^+K^-)$	DOCUMENT ID	TECN	COMMENT
$-1.56 \pm 1.51 \pm 0.32$	¹ AAIJ	18AG LHCb	pp at 7, 8 TeV

¹ Measured over full phase space of the decay.

Baryon Particle Listings

Λ_b^0

$\alpha_P(\Lambda_b^0 \rightarrow pK^-\mu^+\mu^-)$	DOCUMENT ID	TECN	COMMENT
VALUE (%)			
$-4.8 \pm 5.0 \pm 0.7$	AAIJ	17T LHCb	pp at 7, 8 TeV

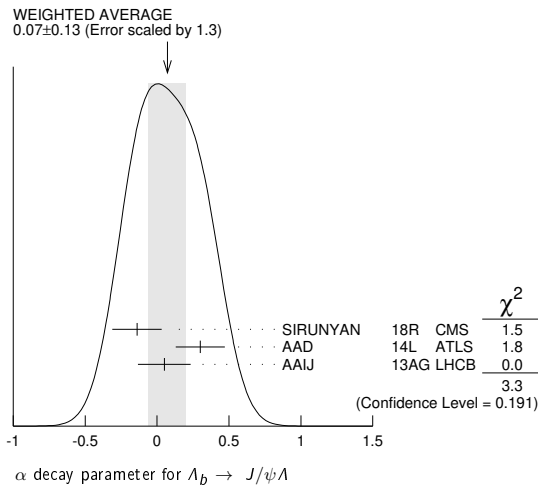
Λ_b^0 DECAY PARAMETERS

See the note on "Baryon Decay Parameters" in the neutron Listings.

α decay parameter for $\Lambda_b \rightarrow J/\psi \Lambda$

VALUE	DOCUMENT ID	TECN	COMMENT
0.07 ± 0.13 OUR AVERAGE	Error includes scale factor of 1.3. See the ideogram below.		
$-0.14 \pm 0.14 \pm 0.10$	¹ SIRUNYAN	18R CMS	pp at 7, 8 TeV
$0.30 \pm 0.16 \pm 0.06$	² AAD	14L ATLS	pp at 7 TeV
$0.05 \pm 0.17 \pm 0.07$	³ AAIJ	13AG LHCb	pp at 7 TeV

- An angular analysis of $\Lambda_b \rightarrow J/\psi \Lambda$ decay is performed. Note that the sign of α in CMS definition is the opposite to that used by AAIJ 13AG and AAD 14L. Λ_b transverse production polarization of $0.00 \pm 0.06 \pm 0.06$ is also reported, as well as squares of the helicity amplitudes.
- An angular analysis of $\Lambda_b \rightarrow J/\psi \Lambda$ decay is performed and magnitudes of all helicity amplitudes are also reported.
- An angular analysis of $\Lambda_b \rightarrow J/\psi \Lambda$ decay is performed and a Λ_b transverse production polarization of $0.06 \pm 0.07 \pm 0.02$ is also reported.



$f_L(\mu\mu)$ longitudinal polarization fraction in $\Lambda_b \rightarrow \Lambda \mu^+ \mu^-$

VALUE	DOCUMENT ID	TECN	COMMENT
0.61 ± 0.11	¹ AAIJ	15AE LHCb	pp at 7, 8 TeV
-0.14 ± 0.03			

¹ AAIJ 15AE measurement covers $15.0 < q^2 < 20.0 \text{ GeV}^2/c^4$.

FORWARD-BACKWARD ASYMMETRIES

The forward-backward asymmetry is defined as $A_{FB}(\Lambda_b^0) = [N(F) - N(B)] / [N(F) + N(B)]$, where the forward (F) direction corresponds to a particle (Λ_b^0 or Λ_b^-) sharing valence quark flavors with a beam particle with the same sign of rapidity.

$A_{FB}(\Lambda_b^0 \rightarrow J/\psi \Lambda)$

VALUE	DOCUMENT ID	TECN	COMMENT
$0.04 \pm 0.07 \pm 0.02$	¹ ABZOV	15i D0	pp at 1.96 TeV

¹ The measured asymmetry integrated over rapidity y in the range of $0.1 < |y| < 2.0$.

$A_{FB}^e(\mu\mu)$ in $\Lambda_b \rightarrow \Lambda \mu^+ \mu^-$

VALUE	DOCUMENT ID	TECN	COMMENT
$-0.39 \pm 0.04 \pm 0.01$	¹ AAIJ	18AP LHCb	pp at 7, 8, 13 TeV

- • • We do not use the following data for averages, fits, limits, etc. • • •
- | | | | |
|---------------------------|-------------------|-----------|---------------------|
| $-0.05 \pm 0.09 \pm 0.03$ | ² AAIJ | 15AE LHCb | Repl. by AAIJ 18AP. |
|---------------------------|-------------------|-----------|---------------------|

¹ The measurement covers $15.0 < q^2 < 20.0 \text{ GeV}^2/c^4$.

² AAIJ 15AE measurement covers $15.0 < q^2 < 20.0 \text{ GeV}^2/c^4$.

$\Delta(A_{FB}^e(\mu\mu))$ in $\Lambda_b \rightarrow \Lambda \mu^+ \mu^-$

Difference of asymmetries $A_{FB}^e(\mu\mu)$ in $\Lambda_b \rightarrow \Lambda \mu^+ \mu^-$ between Λ_b and $\bar{\Lambda}_b$ decays

VALUE	DOCUMENT ID	TECN	COMMENT
$-0.05 \pm 0.09 \pm 0.03$	AAIJ	18A0 LHCb	pp at 7, 8 TeV

$A_{FB}^h(\rho\rho)$ in $\Lambda_b \rightarrow \Lambda(\rho\pi)\mu^+\mu^-$

VALUE	DOCUMENT ID	TECN	COMMENT
$-0.30 \pm 0.05 \pm 0.02$	¹ AAIJ	18AP LHCb	pp at 7, 8, 13 TeV

- • • We do not use the following data for averages, fits, limits, etc. • • •
- | | | | |
|---------------------------|-------------------|-----------|---------------------|
| $-0.29 \pm 0.07 \pm 0.03$ | ² AAIJ | 15AE LHCb | Repl. by AAIJ 18AP. |
|---------------------------|-------------------|-----------|---------------------|

¹ The measurement covers $15.0 < q^2 < 20.0 \text{ GeV}^2/c^4$.

² AAIJ 15AE measurement covers $15.0 < q^2 < 20.0 \text{ GeV}^2/c^4$.

A_{FB}^h in $\Lambda_b \rightarrow \Lambda \mu^+ \mu^-$

VALUE	DOCUMENT ID	TECN	COMMENT
$0.25 \pm 0.04 \pm 0.01$	¹ AAIJ	18AP LHCb	pp at 7, 8, 13 TeV

¹ The measurement covers $15.0 < q^2 < 20.0 \text{ GeV}^2/c^4$.

$\Lambda_b^0 - \bar{\Lambda}_b^0$ Production Asymmetry

$$A_P(\Lambda_b^0) = [\sigma(\Lambda_b^0) - \sigma(\bar{\Lambda}_b^0)] / [\sigma(\Lambda_b^0) + \sigma(\bar{\Lambda}_b^0)]$$

$A_P(\Lambda_b^0)$

VALUE (units 10^{-2})	DOCUMENT ID	TECN	COMMENT
2.4 ± 1.6 OUR AVERAGE	Error includes scale factor of 1.1.		
$-0.11 \pm 2.53 \pm 1.08$	¹ AAIJ	17BF LHCb	pp at 7 TeV
$3.44 \pm 1.61 \pm 0.76$	¹ AAIJ	17BF LHCb	pp at 8 TeV

¹ Indirect determination in kinematic range $2 < p_T < 30 \text{ GeV}/c$ and $2.1 < \eta < 4.5$ from production asymmetries of B^+ , B^0 and B_s^0 .

Λ_b^0 REFERENCES

AAIJ	19AH EPJ C79 745	R. Aaij et al.	(LHCb Collab.)
AAIJ	19AM JHEP 1909 028	R. Aaij et al.	(LHCb Collab.)
AAIJ	19F JHEP 1903 126	R. Aaij et al.	(LHCb Collab.)
AAIJ	19Z PRL 123 031801	R. Aaij et al.	(LHCb Collab.)
AAIJ	18AF JHEP 1808 131	R. Aaij et al.	(LHCb Collab.)
AAIJ	18AG JHEP 1808 039	R. Aaij et al.	(LHCb Collab.)
AAIJ	18AO JHEP 1809 145	R. Aaij et al.	(LHCb Collab.)
AAIJ	18AP JHEP 1809 146	R. Aaij et al.	(LHCb Collab.)
AAIJ	18AW PL B784 101	R. Aaij et al.	(LHCb Collab.)
AAIJ	18AX PL B787 124	R. Aaij et al.	(LHCb Collab.)
AAIJ	18Q JHEP 1802 098	R. Aaij et al.	(LHCb Collab.)
PDG	18 PR D98 030001	M. Tanabashi et al.	(PDG Collab.)
SIRUNYAN	18BY EPJ C78 457	A.M. Sirunyan et al.	(CMS Collab.)
SIRUNYAN	18R PR D97 072010	A.M. Sirunyan et al.	(CMS Collab.)
AAIJ	17AM PRL 119 062001	R. Aaij et al.	(LHCb Collab.)
AAIJ	17BF PL B774 139	R. Aaij et al.	(LHCb Collab.)
AAIJ	17H NATP 13 391	R. Aaij et al.	(LHCb Collab.)
AAIJ	17P JHEP 1704 029	R. Aaij et al.	(LHCb Collab.)
AAIJ	17S JHEP 1705 030	R. Aaij et al.	(LHCb Collab.)
AAIJ	17T JHEP 1706 108	R. Aaij et al.	(LHCb Collab.)
AAIJ	16 JHEP 1601 012	R. Aaij et al.	(LHCb Collab.)
AAIJ	16A CP C40 011001	R. Aaij et al.	(LHCb Collab.)
AAIJ	16J PL B759 282	R. Aaij et al.	(LHCb Collab.)
AAIJ	16W JHEP 1605 081	R. Aaij et al.	(LHCb Collab.)
AAIJ	16Y JHEP 1605 132	R. Aaij et al.	(LHCb Collab.)
AAD	15CH PL B751 63	G. Aad et al.	(ATLAS Collab.)
AAIJ	15AE JHEP 1506 115	R. Aaij et al.	(LHCb Collab.)
Also	JHEP 1809 145	(errat.)	R. Aaij et al.
AAIJ	15AH JHEP 1509 006	R. Aaij et al.	(LHCb Collab.)
AAIJ	15BG NATP 11 743	R. Aaij et al.	(LHCb Collab.)
ABZOV	15I PR D91 072008	V.M. Abazov et al.	(D0 Collab.)
AAD	14L PR D89 032009	G. Aad et al.	(ATLAS Collab.)
AAIJ	14AA PRL 112 202001	R. Aaij et al.	(LHCb Collab.)
AAIJ	14E JHEP 1404 114	R. Aaij et al.	(LHCb Collab.)
AAIJ	14H PR D89 032001	R. Aaij et al.	(LHCb Collab.)
AAIJ	14I JHEP 1408 143	R. Aaij et al.	(LHCb Collab.)
AAIJ	14K JHEP 1407 103	R. Aaij et al.	(LHCb Collab.)
AAIJ	14Q JHEP 1404 087	R. Aaij et al.	(LHCb Collab.)
AAIJ	14U PL B734 122	R. Aaij et al.	(LHCb Collab.)
AALTONEN	14B PR D89 072014	T. Aaltonen et al.	(CDF Collab.)
AALTONEN	14P PRL 113 242001	T. Aaltonen et al.	(CDF Collab.)
PDG	14 CP C38 070001	K. Olive et al.	(PDG Collab.)
AAD	13U PR D87 032002	G. Aad et al.	(ATLAS Collab.)
AAIJ	13AG PL B724 27	R. Aaij et al.	(LHCb Collab.)
AAIJ	13AJ PL B725 25	R. Aaij et al.	(LHCb Collab.)
AAIJ	13AV PRL 110 182001	R. Aaij et al.	(LHCb Collab.)
AAIJ	13BB PRL 111 102003	R. Aaij et al.	(LHCb Collab.)
CHATRCHYAN	13AC JHEP 1307 163	S. Chatrchyan et al.	(CMS Collab.)
AAIJ	12AR JHEP 1210 037	R. Aaij et al.	(LHCb Collab.)
AAIJ	12E PL B708 241	R. Aaij et al.	(LHCb Collab.)
AALTONEN	12A PR D85 032003	T. Aaltonen et al.	(CDF Collab.)
ABZOV	12U PR D85 112003	V.M. Abazov et al.	(D0 Collab.)
AAIJ	11E PR D84 092001	R. Aaij et al.	(LHCb Collab.)
Also	PR D85 039004	(errat.)	R. Aaij et al.
AALTONEN	11 PR D85 121804	T. Aaltonen et al.	(CDF Collab.)
AALTONEN	11AI PRL 107 201802	T. Aaltonen et al.	(CDF Collab.)
AALTONEN	11N PRL 106 181802	T. Aaltonen et al.	(CDF Collab.)
ABZOV	11O PR D84 031102	V.M. Abazov et al.	(D0 Collab.)
AALTONEN	10B PRL 104 102002	T. Aaltonen et al.	(CDF Collab.)
AALTONEN	09C PRL 103 031801	T. Aaltonen et al.	(CDF Collab.)
AALTONEN	09E PR D79 032001	T. Aaltonen et al.	(CDF Collab.)
ABZOV	07S PRL 99 142001	V.M. Abazov et al.	(D0 Collab.)
ABZOV	07U PRL 99 182001	V.M. Abazov et al.	(D0 Collab.)
ABULENCIA	07A PRL 98 122001	A. Abulencia et al.	(FNAL CDF Collab.)
ABULENCIA	07B PRL 98 122002	A. Abulencia et al.	(FNAL CDF Collab.)
LEITNER	07 NPBS 174 169	O. Leitner, Z.J. Ajlouni	(CDF Collab.)
ACOSTA	06 PRL 96 202001	D. Acosta et al.	(CDF Collab.)
ABZOV	05C PRL 94 102001	V.M. Abazov et al.	(D0 Collab.)
ACOSTA	05A PR D72 051104	D. Acosta et al.	(CDF Collab.)
ABDALLAH	04A PL B585 63	J. Abdallah et al.	(DELPHI Collab.)
ACOSTA	02G PR D66 112002	D. Acosta et al.	(CDF Collab.)
ABREU	99W EPJ C10 185	P. Abreu et al.	(DELPHI Collab.)
ACKERSTAFF	98G PL B426 161	K. Ackerstaff et al.	(OPAL Collab.)
BARATE	98D EPJ C2 197	R. Barate et al.	(ALEPH Collab.)
ABE	97B PR D95 1142	F. Abe et al.	(CDF Collab.)
ABREU	96D PRL 77 1439	F. Abe et al.	(CDF Collab.)
ABREU	96D ZPHY C71 1199	P. Abreu et al.	(DELPHI Collab.)
ABREU	96N PL B374 351	P. Abreu et al.	(DELPHI Collab.)
ADAM	96D ZPHY C72 207	W. Adam et al.	(DELPHI Collab.)
BUSKULIC	96L PL B380 442	D. Buskulic et al.	(ALEPH Collab.)
BUSKULIC	96V PL B384 471	D. Buskulic et al.	(ALEPH Collab.)
PDG	96 PR D54 1	R. M. Barnett et al.	(PDG Collab.)
ABREU	95S ZPHY C68 375	P. Abreu et al.	(DELPHI Collab.)
AKERS	95K PL B353 402	R. Akers et al.	(OPAL Collab.)
BUSKULIC	95L PL B357 685	D. Buskulic et al.	(ALEPH Collab.)
ABE	93B PR D47 2639	F. Abe et al.	(CDF Collab.)
BUSKULIC	92E PL B294 145	D. Buskulic et al.	(ALEPH Collab.)
ALBAJAR	91E PL B273 540	C. Albajar et al.	(UA1 Collab.)
BARJ	91 NC 10WA 1787	G. Barj et al.	(CERN R422 Collab.)
ARENTON	86 PR B274 707	M.V. Arenton et al.	(ARIZ, NDAM, VAND)
BASILE	81 LNC 31 97	M. Basile et al.	(CERN R415 Collab.)

See key on page 999

Baryon Particle Listings

$\Lambda_b(5912)^0, \Lambda_b(5920)^0, \Lambda_b(6146)^0, \Lambda_b(6152)^0$

$\Lambda_b(5912)^0$ $J^P = \frac{1}{2}^-$ Status: ***
 Quantum numbers are based on quark model expectations.

$\Lambda_b(5912)^0$ MASS

VALUE (MeV)	DOCUMENT ID	TECN	COMMENT
5912.20 ± 0.13 ± 0.17	^{1,2} AAIJ	12AL LHCb	pp at 7 TeV
¹ Observed in $\Lambda_b(5912)^0 \rightarrow \Lambda_b^0 \pi^+ \pi^-$ decays with 17.6 ± 4.8 candidates with a significance of 5.2 sigma.			
² AAIJ 12AL measures $m(\Lambda_b(5912)^0) - m(\Lambda_b^0) = 292.60 \pm 0.12 \pm 0.04$ MeV. We have adjusted the measurement to our best value of $m(\Lambda_b^0) = 5619.60 \pm 0.17$ MeV. Our first error is their experiment's error and our second error is the systematic error from using our best values.			

$\Lambda_b(5912)^0$ WIDTH

VALUE (MeV)	CL%	DOCUMENT ID	TECN	COMMENT
<0.66	90	AAIJ	12AL LHCb	pp at 7 TeV

$\Lambda_b(5912)^0$ DECAY MODES

Mode	Fraction (Γ_i/Γ)
$\Gamma_1 \Lambda_b^0 \pi^+ \pi^-$	seen

$\Lambda_b(5912)^0$ BRANCHING RATIOS

$\Gamma(\Lambda_b^0 \pi^+ \pi^-)/\Gamma_{total}$	Γ_1/Γ
seen	seen

$\Lambda_b(5912)^0$ REFERENCES

AAIJ 12AL PRL 109 172003 R. Aaij et al. (LHCb Collab.)

$\Lambda_b(5920)^0$ $J^P = \frac{3}{2}^-$ Status: ***
 Quantum numbers are based on quark model expectations.

$\Lambda_b(5920)^0$ MASS

VALUE (MeV)	DOCUMENT ID	TECN	COMMENT
5919.92 ± 0.19 OUR AVERAGE	Error includes scale factor of 1.1.		
5919.4 ± 0.5 ± 0.2	^{1,2} AALTONEN	13v CDF	p \bar{p} at 1.96 TeV
5920.00 ± 0.09 ± 0.17	^{3,4} AAIJ	12AL LHCb	pp at 7 TeV
¹ Measured in $\Lambda_b(5920)^0 \rightarrow \Lambda_b^0 \pi^+ \pi^-$ decays with 17.3 ^{+5.3} _{-4.6} events, with a significance of 3.5 sigma.			
² AALTONEN 13v measures $m(\Lambda_b(5920)^0) - m(\Lambda_b^0) - 2m(\pi) = 20.68 \pm 0.35 \pm 0.30$ MeV. We have adjusted the measurement to our best values of $m(\Lambda_b^0) = 5619.60 \pm 0.17$ MeV and $m(\pi) = 139.57039 \pm 0.00018$ MeV. Our first error is their experiment's error and our second error is the systematic error from using our best values.			
³ Observed in $\Lambda_b(5920)^0 \rightarrow \Lambda_b^0 \pi^+ \pi^-$ decays with 52.5 ± 8.1 candidates with a significance of 10.2 sigma.			
⁴ AAIJ 12AL measures $m(\Lambda_b(5920)^0) - m(\Lambda_b^0) = 300.40 \pm 0.08 \pm 0.04$ MeV. We have adjusted the measurement to our best value of $m(\Lambda_b^0) = 5619.60 \pm 0.17$ MeV. Our first error is their experiment's error and our second error is the systematic error from using our best values.			

$\Lambda_b(5920)^0$ WIDTH

VALUE (MeV)	CL%	DOCUMENT ID	TECN	COMMENT
<0.63	90	AAIJ	12AL LHCb	pp at 7 TeV

$\Lambda_b(5920)^0$ DECAY MODES

Mode	Fraction (Γ_i/Γ)
$\Gamma_1 \Lambda_b^0 \pi^+ \pi^-$	seen

$\Lambda_b(5920)^0$ BRANCHING RATIOS

$\Gamma(\Lambda_b^0 \pi^+ \pi^-)/\Gamma_{total}$	Γ_1/Γ
seen	seen

$\Lambda_b(5920)^0$ REFERENCES

AALTONEN 13V PR D88 071101 T. Aaltonen et al. (CDF Collab.)
 AAJ 12AL PRL 109 172003 R. Aaij et al. (LHCb Collab.)

$\Lambda_b(6146)^0$ $J^P = \frac{3}{2}^+$ Status: ***
 Quantum numbers are based on quark model expectations.

$\Lambda_b(6146)^0$ MASS

VALUE (MeV)	DOCUMENT ID	TECN	COMMENT
6146.17 ± 0.33 ± 0.27	¹ AAIJ	19AJ LHCb	pp at 7, 8, 13 TeV
¹ Observed in $\Lambda_b^0 \pi^+ \pi^-$ mode.			

$\Lambda_b(6146)^0$ WIDTH

VALUE (MeV)	DOCUMENT ID	TECN	COMMENT
2.9 ± 1.3 ± 0.3	¹ AAIJ	19AJ LHCb	pp at 7, 8, 13 TeV
¹ Observed in $\Lambda_b^0 \pi^+ \pi^-$ mode.			

$m_{\Lambda_b(6146)^0} - m_{\Lambda_b^0}$

VALUE (MeV)	DOCUMENT ID	TECN	COMMENT
526.55 ± 0.33 ± 0.10	¹ AAIJ	19AJ LHCb	pp at 7, 8, 13 TeV
¹ Observed in $\Lambda_b^0 \pi^+ \pi^-$ mode.			

$\Lambda_b(6146)^0$ DECAY MODES

Mode	Fraction (Γ_i/Γ)
$\Gamma_1 \Lambda_b^0 \pi^+ \pi^-$	seen

$\Lambda_b(6146)^0$ BRANCHING RATIOS

$\Gamma(\Lambda_b^0 \pi^+ \pi^-)/\Gamma_{total}$	Γ_1/Γ
seen	seen

$\Lambda_b(6146)^0$ REFERENCES

AAIJ 19AJ PRL 123 152001 R. Aaij et al. (LHCb Collab.)

$\Lambda_b(6152)^0$ $J^P = \frac{5}{2}^+$ Status: ***
 Quantum numbers are based on quark model expectations.

$\Lambda_b(6152)^0$ MASS

VALUE (MeV)	DOCUMENT ID	TECN	COMMENT
6152.51 ± 0.26 ± 0.27	¹ AAIJ	19AJ LHCb	pp at 7, 8, 13 TeV
¹ Observed in $\Lambda_b^0 \pi^+ \pi^-$ mode.			

$\Lambda_b(6152)^0$ WIDTH

VALUE (MeV)	DOCUMENT ID	TECN	COMMENT
2.1 ± 0.8 ± 0.3	¹ AAIJ	19AJ LHCb	pp at 7, 8, 13 TeV
¹ Observed in $\Lambda_b^0 \pi^+ \pi^-$ mode.			

$m_{\Lambda_b(6152)^0} - m_{\Lambda_b^0}$

VALUE (MeV)	DOCUMENT ID	TECN	COMMENT
532.89 ± 0.26 ± 0.10	¹ AAIJ	19AJ LHCb	pp at 7, 8, 13 TeV
¹ Observed in $\Lambda_b^0 \pi^+ \pi^-$ mode.			

$m_{\Lambda_b(6152)^0} - m_{\Lambda_b(6146)^0}$

VALUE (MeV)	DOCUMENT ID	TECN	COMMENT
6.34 ± 0.32 ± 0.02	AAIJ	19AJ LHCb	pp at 7, 8, 13 TeV

$\Lambda_b(6152)^0$ DECAY MODES

Mode	Fraction (Γ_i/Γ)
$\Gamma_1 \Lambda_b^0 \pi^+ \pi^-$	seen

$\Lambda_b(6152)^0$ BRANCHING RATIOS

$\Gamma(\Lambda_b^0 \pi^+ \pi^-)/\Gamma_{total}$	Γ_1/Γ
seen	seen

$\Lambda_b(6152)^0$ REFERENCES

AAIJ 19AJ PRL 123 152001 R. Aaij et al. (LHCb Collab.)

Baryon Particle Listings

Σ_b, Σ_b^*

Σ_b

$I(J^P) = 1(\frac{1}{2}^+)$ Status: ***
I, J, P need confirmation.

In the quark model $\Sigma_b^+, \Sigma_b^0, \Sigma_b^-$ are an isotriplet (uub, udb, ddb) state. The lowest Σ_b ought to have $J^P = 1/2^+$. None of I, J, or P have actually been measured.

Σ_b MASS

Σ_b^+ MASS

VALUE (MeV)	DOCUMENT ID	TECN	COMMENT
5810.56 ± 0.25 OUR AVERAGE			
5810.55 ± 0.11 ± 0.23	¹ AAIJ	19A	LHCB pp at 7, 8 TeV
5811.3 $\begin{smallmatrix} +0.9 \\ -0.8 \end{smallmatrix}$ ± 1.7	² AALTONEN	12F	CDF $p\bar{p}$ at 1.96 TeV
• • • We do not use the following data for averages, fits, limits, etc. • • •			
5807.8 $\begin{smallmatrix} +2.0 \\ -2.2 \end{smallmatrix}$ ± 1.7	³ AALTONEN	07K	CDF Repl. by AALTONEN 12F
¹ Measured using fully reconstructed $\Lambda_b^0 \rightarrow \Lambda_c^+ \pi^-$ and $\Lambda_c^+ \rightarrow p K^- \pi^+$ decays.			
² Measured using fully reconstructed $\Lambda_b^0 \rightarrow \Lambda_c^+ \pi^-$ and $\Lambda_c^+ \rightarrow K^- \pi^+$ decays.			
³ Observed four $\Lambda_b^0 \pi^\pm$ resonances in the fully reconstructed decay mode $\Lambda_b^0 \rightarrow \Lambda_c^+ \pi^-$, where $\Lambda_c^+ \rightarrow p K^- \pi^+$.			

Σ_b^- MASS

VALUE (MeV)	DOCUMENT ID	TECN	COMMENT
5815.64 ± 0.27 OUR AVERAGE			
5815.64 ± 0.14 ± 0.24	¹ AAIJ	19A	LHCB pp at 7, 8 TeV
5815.5 $\begin{smallmatrix} +0.6 \\ -0.5 \end{smallmatrix}$ ± 1.7	² AALTONEN	12F	CDF $p\bar{p}$ at 1.96 TeV
• • • We do not use the following data for averages, fits, limits, etc. • • •			
5815.2 ± 1.0 ± 1.7	³ AALTONEN	07K	CDF Repl. by AALTONEN 12F
¹ Measured using fully reconstructed $\Lambda_b^0 \rightarrow \Lambda_c^+ \pi^-$ and $\Lambda_c^+ \rightarrow p K^- \pi^+$ decays.			
² Measured using fully reconstructed $\Lambda_b^0 \rightarrow \Lambda_c^+ \pi^-$ and $\Lambda_c^+ \rightarrow K^- \pi^+$ decays.			
³ Observed four $\Lambda_b^0 \pi^\pm$ resonances in the fully reconstructed decay mode $\Lambda_b^0 \rightarrow \Lambda_c^+ \pi^-$, where $\Lambda_c^+ \rightarrow p K^- \pi^+$.			

$m_{\Sigma_b^+} - m_{\Sigma_b^-}$

VALUE (MeV)	DOCUMENT ID	TECN	COMMENT
-5.06 ± 0.18 OUR AVERAGE			
-5.09 ± 0.18 ± 0.01	¹ AAIJ	19A	LHCB pp at 7, 8 TeV
-4.2 $\begin{smallmatrix} +1.1 \\ -1.0 \end{smallmatrix}$ ± 0.1	² AALTONEN	12F	CDF $p\bar{p}$ at 1.96 TeV
¹ Measured using fully reconstructed $\Lambda_b^0 \rightarrow \Lambda_c^+ \pi^-$ and $\Lambda_c^+ \rightarrow p K^- \pi^+$ decays.			
² Measured using fully reconstructed $\Lambda_b^0 \rightarrow \Lambda_c^+ \pi^-$ and $\Lambda_c^+ \rightarrow K^- \pi^+$ decays.			

Σ_b WIDTH

Σ_b^+ WIDTH

VALUE (MeV)	DOCUMENT ID	TECN	COMMENT
5.0 ± 0.5 OUR AVERAGE			
4.83 ± 0.31 ± 0.37	¹ AAIJ	19A	LHCB pp at 7, 8 TeV
9.7 $\begin{smallmatrix} +3.8 \\ -2.8 \end{smallmatrix}$ ± 1.2	² AALTONEN	12F	CDF $p\bar{p}$ at 1.96 TeV
¹ Measured using fully reconstructed $\Lambda_b^0 \rightarrow \Lambda_c^+ \pi^-$ and $\Lambda_c^+ \rightarrow p K^- \pi^+$ decays.			
² Measured using fully reconstructed $\Lambda_b^0 \rightarrow \Lambda_c^+ \pi^-$ and $\Lambda_c^+ \rightarrow K^- \pi^+$ decays.			

Σ_b^- WIDTH

VALUE (MeV)	DOCUMENT ID	TECN	COMMENT
5.3 ± 0.5 OUR AVERAGE			
5.33 ± 0.42 ± 0.37	¹ AAIJ	19A	LHCB pp at 7, 8 TeV
4.9 $\begin{smallmatrix} +3.1 \\ -2.1 \end{smallmatrix}$ ± 1.1	² AALTONEN	12F	CDF $p\bar{p}$ at 1.96 TeV
¹ Measured using fully reconstructed $\Lambda_b^0 \rightarrow \Lambda_c^+ \pi^-$ and $\Lambda_c^+ \rightarrow p K^- \pi^+$ decays.			
² Measured using fully reconstructed $\Lambda_b^0 \rightarrow \Lambda_c^+ \pi^-$ and $\Lambda_c^+ \rightarrow K^- \pi^+$ decays.			

Σ_b DECAY MODES

Mode	Fraction (Γ_i/Γ)
$\Gamma_1 \Lambda_b^0 \pi$	dominant

Σ_b BRANCHING RATIOS

$\Gamma(\Lambda_b^0 \pi)/\Gamma_{\text{total}}$	Γ_1/Γ		
dominant	dominant		
VALUE	DOCUMENT ID	TECN	COMMENT
dominant	AALTONEN	07K	CDF $p\bar{p}$ at 1.96 TeV

Σ_b REFERENCES

AAIJ	19A	PRL 122 012001	R. Aaij et al.	(LHCb Collab.)
AALTONEN	12F	PR D85 092011	T. Aaltonen et al.	(CDF Collab.)
AALTONEN	07K	PRL 99 202001	T. Aaltonen et al.	(CDF Collab.)

Σ_b^*

$I(J^P) = 1(\frac{3}{2}^+)$ Status: ***
I, J, P need confirmation.

Quantum numbers shown are quark-model predictions.

Σ_b^* MASS

Σ_b^{*+} MASS

VALUE (MeV)	DOCUMENT ID	TECN	COMMENT
5830.32 ± 0.27 OUR AVERAGE			
5830.28 ± 0.14 ± 0.24	¹ AAIJ	19A	LHCB pp at 7, 8 TeV
5832.1 ± 0.7 $\begin{smallmatrix} +1.7 \\ -1.8 \end{smallmatrix}$	² AALTONEN	12F	CDF $p\bar{p}$ at 1.96 TeV
¹ Measured using fully reconstructed $\Lambda_b^0 \rightarrow \Lambda_c^+ \pi^-$ and $\Lambda_c^+ \rightarrow p K^- \pi^+$ decays.			
² Measured using fully reconstructed $\Lambda_b^0 \rightarrow \Lambda_c^+ \pi^-$ and $\Lambda_c^+ \rightarrow K^- \pi^+$ decays.			

Σ_b^{*-} MASS

VALUE (MeV)	DOCUMENT ID	TECN	COMMENT
5834.74 ± 0.30 OUR AVERAGE			
5834.73 ± 0.17 ± 0.25	¹ AAIJ	19A	LHCB pp at 7, 8 TeV
5835.1 ± 0.6 $\begin{smallmatrix} +1.7 \\ -1.8 \end{smallmatrix}$	² AALTONEN	12F	CDF $p\bar{p}$ at 1.96 TeV
¹ Measured using fully reconstructed $\Lambda_b^0 \rightarrow \Lambda_c^+ \pi^-$ and $\Lambda_c^+ \rightarrow p K^- \pi^+$ decays.			
² Measured using fully reconstructed $\Lambda_b^0 \rightarrow \Lambda_c^+ \pi^-$ and $\Lambda_c^+ \rightarrow K^- \pi^+$ decays.			

$m_{\Sigma_b^{*+}} - m_{\Sigma_b^{*-}}$

VALUE (MeV)	DOCUMENT ID	TECN	COMMENT
-4.37 ± 0.33 OUR AVERAGE			Error includes scale factor of 1.6.
-4.45 ± 0.22 ± 0.01	¹ AAIJ	19A	LHCB pp at 7, 8 TeV
-3.0 $\begin{smallmatrix} +1.0 \\ -0.9 \end{smallmatrix}$ ± 0.1	² AALTONEN	12F	CDF $p\bar{p}$ at 1.96 TeV
¹ Measured using fully reconstructed $\Lambda_b^0 \rightarrow \Lambda_c^+ \pi^-$ and $\Lambda_c^+ \rightarrow p K^- \pi^+$ decays.			
² Measured using fully reconstructed $\Lambda_b^0 \rightarrow \Lambda_c^+ \pi^-$ and $\Lambda_c^+ \rightarrow K^- \pi^+$ decays.			

$m_{\Sigma_b^{*+}} - m_{\Sigma_b^+}$

VALUE	DOCUMENT ID	TECN	COMMENT
19.73 ± 0.18 ± 0.01			
19.73 ± 0.18 ± 0.01	¹ AAIJ	19A	LHCB pp at 7, 8 TeV
¹ Measured using fully reconstructed $\Lambda_b^0 \rightarrow \Lambda_c^+ \pi^-$ and $\Lambda_c^+ \rightarrow p K^- \pi^+$ decays.			

$m_{\Sigma_b^{*-}} - m_{\Sigma_b^-}$

VALUE	DOCUMENT ID	TECN	COMMENT
19.09 ± 0.22 ± 0.02			
19.09 ± 0.22 ± 0.02	¹ AAIJ	19A	LHCB pp at 7, 8 TeV
¹ Measured using fully reconstructed $\Lambda_b^0 \rightarrow \Lambda_c^+ \pi^-$ and $\Lambda_c^+ \rightarrow p K^- \pi^+$ decays.			

Σ_b^* WIDTH

Σ_b^{*+} WIDTH

VALUE (MeV)	DOCUMENT ID	TECN	COMMENT
9.4 ± 0.5 OUR AVERAGE			
9.34 ± 0.47 ± 0.26	¹ AAIJ	19A	LHCB pp at 7, 8 TeV
11.5 $\begin{smallmatrix} +2.7 \\ -2.2 \end{smallmatrix}$ ± 1.0	² AALTONEN	12F	CDF $p\bar{p}$ at 1.96 TeV
¹ Measured using fully reconstructed $\Lambda_b^0 \rightarrow \Lambda_c^+ \pi^-$ and $\Lambda_c^+ \rightarrow p K^- \pi^+$ decays.			
² Measured using fully reconstructed $\Lambda_b^0 \rightarrow \Lambda_c^+ \pi^-$ and $\Lambda_c^+ \rightarrow K^- \pi^+$ decays.			

Σ_b^{*-} WIDTH

VALUE (MeV)	DOCUMENT ID	TECN	COMMENT
10.4 ± 0.8 OUR AVERAGE			Error includes scale factor of 1.3.
10.68 ± 0.60 ± 0.33	¹ AAIJ	19A	LHCB pp at 7, 8 TeV
7.5 $\begin{smallmatrix} +2.2 \\ -1.8 \end{smallmatrix}$ ± 0.9	² AALTONEN	12F	CDF $p\bar{p}$ at 1.96 TeV
¹ Measured using fully reconstructed $\Lambda_b^0 \rightarrow \Lambda_c^+ \pi^-$ and $\Lambda_c^+ \rightarrow p K^- \pi^+$ decays.			
² Measured using fully reconstructed $\Lambda_b^0 \rightarrow \Lambda_c^+ \pi^-$ and $\Lambda_c^+ \rightarrow K^- \pi^+$ decays.			

$m_{\Sigma_b^{*+}} - m_{\Sigma_b^+}$

VALUE (MeV)	DOCUMENT ID	TECN	COMMENT
21.2 $\begin{smallmatrix} +2.0 \\ -1.9 \end{smallmatrix}$ ± 0.4			
21.2 $\begin{smallmatrix} +2.0 \\ -1.9 \end{smallmatrix}$ ± 0.3	¹ AALTONEN	07K	CDF $p\bar{p}$ at 1.96 TeV
¹ Observed four $\Lambda_b^0 \pi^\pm$ resonances in the fully reconstructed decay mode $\Lambda_b^0 \rightarrow \Lambda_c^+ \pi^-$, where $\Lambda_c^+ \rightarrow p K^- \pi^+$. Assumes $m_{\Sigma_b^{*+}} - m_{\Sigma_b^+} = m_{\Sigma_b^{*-}} - m_{\Sigma_b^-}$.			

Σ_b^* DECAY MODES

Mode	Fraction (Γ_i/Γ)
$\Gamma_1 \Lambda_b^0 \pi$	dominant

See key on page 999

Baryon Particle Listings

$$\Sigma_b^*, \Sigma_b(6097)^+, \Sigma_b(6097)^-, \Xi_b^0, \Xi_b^-$$

Σ_b^* BRANCHING RATIOS

$\Gamma(\Lambda_b^0 \pi)/\Gamma_{\text{total}}$	DOCUMENT ID	TECN	COMMENT	Γ_1/Γ
dominant	AALTONEN 07K	CDF	$p\bar{p}$ at 1.96 TeV	

Σ_b^* REFERENCES

AAIJ 19A PRL 122 012001	R. Aaij et al.	(LHCb Collab.)
AALTONEN 12F PR D85 092011	T. Aaltonen et al.	(CDF Collab.)
AALTONEN 07K PRL 99 202001	T. Aaltonen et al.	(CDF Collab.)

$\Sigma_b(6097)^+$

 $J^P = ?^?$ Status: ***

$\Sigma_b(6097)^+$ MASS

VALUE (MeV)	DOCUMENT ID	TECN	COMMENT
6095.8 ± 1.7 ± 0.4	¹ AAIJ 19A	LHCB	pp at 7, 8 TeV

¹ Measured using fully reconstructed $\Lambda_b^0 \rightarrow \Lambda_c^+ \pi^-$ and $\Lambda_c^+ \rightarrow p K^- \pi^+$ decays.

$m_{\Sigma_b(6097)^+} - m_{\Sigma_b(6097)^-}$

VALUE	DOCUMENT ID	TECN	COMMENT
-2.2 +2.4 +0.3 MeV	¹ AAIJ 19A	LHCB	pp at 7, 8 TeV

¹ Measured using fully reconstructed $\Lambda_b^0 \rightarrow \Lambda_c^+ \pi^-$ and $\Lambda_c^+ \rightarrow p K^- \pi^+$ decays.

$\Sigma_b(6097)^+$ WIDTH

VALUE (MeV)	DOCUMENT ID	TECN	COMMENT
31.0 ± 5.5 ± 0.7	¹ AAIJ 19A	LHCB	pp at 7, 8 TeV

¹ Measured using fully reconstructed $\Lambda_b^0 \rightarrow \Lambda_c^+ \pi^-$ and $\Lambda_c^+ \rightarrow p K^- \pi^+$ decays.

$\Sigma_b(6097)^+$ DECAY MODES

Mode	Fraction (Γ_i/Γ)
$\Gamma_1 \Lambda_b \pi^+ \times B(b \rightarrow \Sigma_b(6097)^+)$	seen

$\Sigma_b(6097)^+$ BRANCHING RATIOS

$\Gamma(\Lambda_b \pi^+ \times B(b \rightarrow \Sigma_b(6097)^+))/\Gamma_{\text{total}}$	DOCUMENT ID	TECN	COMMENT	Γ_1/Γ
seen	AAIJ 19A	LHCB	pp at 7, 8 TeV	

$\Sigma_b(6097)^+$ REFERENCES

AAIJ 19A PRL 122 012001	R. Aaij et al.	(LHCb Collab.)
-------------------------	----------------	----------------

$\Sigma_b(6097)^-$

 $J^P = ?^?$ Status: ***

$\Sigma_b(6097)^-$ MASS

VALUE (MeV)	DOCUMENT ID	TECN	COMMENT
6098.0 ± 1.7 ± 0.5	¹ AAIJ 19A	LHCB	pp at 7, 8 TeV

¹ Measured using fully reconstructed $\Lambda_b^0 \rightarrow \Lambda_c^+ \pi^-$ and $\Lambda_c^+ \rightarrow p K^- \pi^+$ decays.

$\Sigma_b(6097)^-$ WIDTH

VALUE (MeV)	DOCUMENT ID	TECN	COMMENT
28.9 ± 4.2 ± 0.9	¹ AAIJ 19A	LHCB	pp at 7, 8 TeV

¹ Measured using fully reconstructed $\Lambda_b^0 \rightarrow \Lambda_c^+ \pi^-$ and $\Lambda_c^+ \rightarrow p K^- \pi^+$ decays.

$\Sigma_b(6097)^-$ DECAY MODES

Mode	Fraction (Γ_i/Γ)
$\Gamma_1 \Lambda_b \pi^- \times B(b \rightarrow \Sigma_b(6097)^-)$	seen

$\Sigma_b(6097)^-$ BRANCHING RATIOS

$\Gamma(\Lambda_b \pi^- \times B(b \rightarrow \Sigma_b(6097)^-))/\Gamma_{\text{total}}$	DOCUMENT ID	TECN	COMMENT	Γ_1/Γ
seen	AAIJ 19A	LHCB	pp at 7, 8 TeV	

$\Sigma_b(6097)^-$ REFERENCES

AAIJ 19A PRL 122 012001	R. Aaij et al.	(LHCb Collab.)
-------------------------	----------------	----------------

Ξ_b^0, Ξ_b^-

$$I(J^P) = \frac{1}{2}(\frac{1}{2}^+)$$
 Status: ***
I, J, P need confirmation.

In the quark model, Ξ_b^0 and Ξ_b^- are an isodoublet (*usb, dsb*) state; the lowest Ξ_b^0 and Ξ_b^- ought to have $J^P = 1/2^+$. None of *I, J, or P* have actually been measured.

Ξ_b MASSES

Ξ_b^- MASS

VALUE (MeV)	DOCUMENT ID	TECN	COMMENT
5797.0 ± 0.6 OUR AVERAGE	Error includes scale factor of 1.7. See the ideogram below.		
5796.70 ± 0.39 ± 0.23	AAIJ 19AB	LHCB	pp at 7, 8 and 13 TeV
5797.72 ± 0.46 ± 0.31	¹ AAIJ 14BJ	LHCB	pp at 7, 8 TeV
5793.4 ± 1.8 ± 0.7	² AALTONEN 14B	CDF	$p\bar{p}$ at 1.96 TeV
5774 ± 11 ± 15	³ ABAZOV 07K	D0	$p\bar{p}$ at 1.96 TeV
5795.8 ± 0.9 ± 0.4	⁴ AAIJ 13AV	LHCB	Repl. by AAIJ 19AB
5796.7 ± 5.1 ± 1.4	⁵ AALTONEN 11X	CDF	Repl. by AALTONEN 14B
5790.9 ± 2.6 ± 0.8	⁶ AALTONEN 09AP	CDF	Repl. by AALTONEN 14B
5792.9 ± 2.5 ± 1.7	⁷ AALTONEN 07A	CDF	Repl. by AALTONEN 09AP

••• We do not use the following data for averages, fits, limits, etc. •••

¹ Reconstructed in $\Xi_b^- \rightarrow \Xi_c^0 \pi^-$, $\Xi_c^0 \rightarrow p K^- K^- \pi^+$ decays. Reference Λ_b^0 mass 5619.30 ± 0.34 MeV from AAIJ 14AA.

² Uses $\Xi_b^- \rightarrow J/\psi \Xi^-$ and $\Xi_c^0 \pi^-$ decays.

³ Observed in $\Xi_b^- \rightarrow J/\psi \Xi^-$ decays with 15.2 ± 4.4^{+1.9}_{-0.4} candidates, a significance of 5.5 sigma.

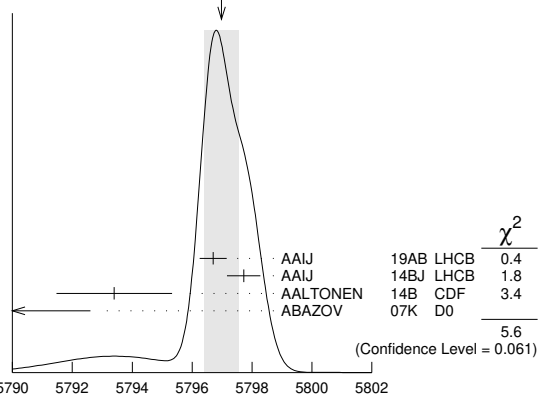
⁴ Measured in $\Xi_b^- \rightarrow J/\psi \Xi^-$ decays.

⁵ Measured in $\Xi_b^- \rightarrow \Xi_c^0 \pi^-$ with 25.8^{+5.5}_{-5.2} candidates.

⁶ Measured in $\Xi_b^- \rightarrow J/\psi \Xi^-$ decays with 66⁺¹⁴₋₉ candidates.

⁷ Observed in $\Xi_b^- \rightarrow J/\psi \Xi^-$ decays with 17.5 ± 4.3 candidates, a significance of 7.7 sigma.

WEIGHTED AVERAGE
5797.0±0.6 (Error scaled by 1.7)



Ξ_b^0 MASS

VALUE (MeV)	DOCUMENT ID	TECN	COMMENT
5791.9 ± 0.5 OUR AVERAGE	Error includes scale factor of 1.6.		
5794.3 ± 2.4 ± 0.7	AAIJ 14H	LHCB	pp at 7 TeV
5791.80 ± 0.39 ± 0.31	¹ AAIJ 14Z	LHCB	pp at 7, 8 TeV
5788.7 ± 4.3 ± 1.4	² AALTONEN 14B	CDF	$p\bar{p}$ at 1.96 TeV
5787.8 ± 5.0 ± 1.3	³ AALTONEN 11X	CDF	Repl. by AALTONEN 14B

••• We do not use the following data for averages, fits, limits, etc. •••

¹ Uses $\Xi_b^0 \rightarrow \Xi_c^+ \pi^-$ and $\Xi_c^+ \rightarrow p K^- \pi^+$ decays. The measurement comes from the mass difference of Ξ_b^0 and Λ_b^0 .

² Uses $\Xi_b^0 \rightarrow \Xi^+ \pi^-$ decays.

³ Measured in $\Xi_b^0 \rightarrow \Xi^+ \pi^-$ with 25.3^{+5.6}_{-5.4} candidates.

$m_{\Xi_b^0} - m_{\Lambda_b^0}$

VALUE (MeV)	DOCUMENT ID	TECN	COMMENT
177.5 ± 0.5 OUR AVERAGE	Error includes scale factor of 1.6.		
177.73 ± 0.33 ± 0.14	¹ AAIJ 17BE	LHCB	pp at 7, 8 TeV
176.2 ± 0.9 ± 0.1	² AAIJ 13AV	LHCB	pp at 7 TeV
177.08 ± 0.47 ± 0.16	³ AAIJ 17BE	LHCB	pp at 7, 8 TeV
178.36 ± 0.46 ± 0.16	^{4,5} AAIJ 14BJ	LHCB	pp at 7, 8 TeV

••• We do not use the following data for averages, fits, limits, etc. •••

¹ Combination of the original statistically independent measurements of AAIJ 14BE and AAIJ 17BJ taking into account correlation between systematic uncertainties.

² Reconstructed in $\Xi_b^0 \rightarrow J/\psi \Xi^0$ decays.

³ Reconstructed in $\Xi_b^0 \rightarrow J/\psi \Lambda K^-$ decays. Reference decays $\Lambda_b^0 \rightarrow J/\psi \Lambda$ were used.

⁴ Reconstructed in $\Xi_b^0 \rightarrow \Xi_c^0 \pi^-$, $\Xi_c^0 \rightarrow p K^- K^- \pi^+$ decays. Reference $\Lambda_b^0 \rightarrow \Lambda_c^+ \pi^-$.

⁵ Combined with AAIJ 17BE.

Baryon Particle Listings

$$\Xi_b^0, \Xi_b^-$$

$$m_{\Xi_b^0} - m_{\Lambda_b^0}$$

VALUE (MeV)	DOCUMENT ID	TECN	COMMENT
172.5 ± 0.4 OUR AVERAGE			
174.8 ± 2.4 ± 0.5	¹ AAIJ	14H LHCb	pp at 7 TeV
172.44 ± 0.39 ± 0.17	¹ AAIJ	14Z LHCb	pp at 7, 8 TeV

¹ Uses $\Xi_b^0 \rightarrow \Xi_c^+ \pi^-$ and $\Xi_c^+ \rightarrow p K^- \pi^+$ decays.

$$m_{\Xi_b^-} - m_{\Xi_b^0}$$

VALUE (MeV)	DOCUMENT ID	TECN	COMMENT
5.9 ± 0.6 OUR AVERAGE			
5.92 ± 0.60 ± 0.23	¹ AAIJ	14B LHCb	pp at 7, 8 TeV
3.1 ± 5.6 ± 1.3	² AALTONEN	11X CDF	$p\bar{p}$ at 1.96 TeV

¹ Reconstructed in $\Xi_b^- \rightarrow \Xi_c^0 \pi^-$, $\Xi_c^0 \rightarrow p K^- K^- \pi^+$ decays. Uses $m(\Xi_b^0) - m(\Lambda_b^0) = 172.44 \pm 0.39 \pm 0.17$ MeV from AAJ14Z.
² Derived from measurements in $\Xi_b^- \rightarrow \Xi_c^+ \pi^-$ and $\Xi_c^+ \rightarrow J/\psi \Xi^-$ from AALTONEN 09AP taking correlated uncertainties into account.

 Ξ_b MEAN LIFE

"OUR EVALUATION" is an average using rescaled values of the data listed below. The average and rescaling were performed by the Heavy Flavor Averaging Group (HFLAV) and are described at <https://hflav.web.cern.ch/>. The averaging/rescaling procedure takes into account correlations between the measurements and asymmetric lifetime errors.

 Ξ_b^- MEAN LIFE

VALUE (10^{-12} s)	DOCUMENT ID	TECN	COMMENT
1.572 ± 0.040 OUR EVALUATION			
1.57 ± 0.04 OUR AVERAGE			Error includes scale factor of 1.1.
1.599 ± 0.041 ± 0.022	¹ AAIJ	14B LHCb	pp at 7, 8 TeV
1.55 $^{+0.10}_{-0.09}$ ± 0.03	² AAIJ	14T LHCb	pp at 7, 8 TeV
1.36 ± 0.15 ± 0.02	AALTONEN	14B CDF	$p\bar{p}$ at 1.96 TeV

• • • We do not use the following data for averages, fits, limits, etc. • • •

1.56 $^{+0.27}_{-0.25}$ ± 0.02	³ AALTONEN	09AP CDF	Repl. by AALTONEN 14B
--------------------------------	-----------------------	----------	-----------------------

¹ Reconstructed in $\Xi_b^- \rightarrow \Xi_c^0 \pi^-$, $\Xi_c^0 \rightarrow p K^- K^- \pi^+$ decays. Reference Λ_b^0 lifetime $1.479 \pm 0.009 \pm 0.010$ ps from AAJ14U.
² Measured in $\Xi_b^- \rightarrow J/\psi \Xi^-$ decays.
³ Measured in $\Xi_b^- \rightarrow J/\psi \Xi^-$ decays with 66^{+14}_{-9} candidates.

 Ξ_b^0 MEAN LIFE

VALUE (10^{-12} s)	DOCUMENT ID	TECN	COMMENT
1.480 ± 0.030 OUR EVALUATION			
1.477 ± 0.026 ± 0.019			
1.479 ± 0.009 ± 0.010	¹ AAIJ	14Z LHCb	pp at 7, 8 TeV

¹ Uses $\Xi_b^0 \rightarrow \Xi_c^+ \pi^-$ and $\Xi_c^+ \rightarrow p K^- \pi^+$ decays. The measurement comes from the value of relative lifetime of Ξ_b^0 to Λ_b^0 .

 Ξ_b MEAN LIFE

VALUE (10^{-12} s)	DOCUMENT ID	TECN	COMMENT
• • • We do not use the following data for averages, fits, limits, etc. • • •			
1.48 $^{+0.40}_{-0.31}$ ± 0.12	¹ ABDALLAH	05c DLPH	$e^+ e^- \rightarrow Z^0$
1.35 $^{+0.37}_{-0.28}$ $^{+0.15}_{-0.17}$	² BUSKULIC	96T ALEP	$e^+ e^- \rightarrow Z$
1.5 $^{+0.7}_{-0.4}$ ± 0.3	³ ABREU	95v DLPH	Repl. by ABDALLAH 05c

¹ Used the decay length of Ξ^- accompanied by a lepton of the same sign.
² Excess $\Xi^- \ell^-$, impact parameters.
³ Excess $\Xi^- \ell^-$, decay lengths.

 $\tau_{\text{mix}} (1/2\pi)$ times the oscillation period

VALUE (s)	DOCUMENT ID	TECN	COMMENT
$> 13 \times 10^{-12}$	¹ AAIJ	17B LHCb	pp at 7, 8 TeV

¹ Uses Ξ_b^{*-} and Ξ_b^- decays to $\Xi_b^0 \pi^-$, where $\Xi_b^0 \rightarrow \Xi_c^+ \pi^-$, $\Xi_c^+ \rightarrow p K^- \pi^+$.

MEAN LIFE RATIOS

 $\tau_{\Xi_b^-} / \tau_{\Lambda_b^0}$ mean life ratio

VALUE	DOCUMENT ID	TECN	COMMENT
1.089 ± 0.026 ± 0.011			
1.089 ± 0.026 ± 0.011	¹ AAIJ	14B LHCb	pp at 7, 8 TeV

¹ Reconstructed in $\Xi_b^- \rightarrow \Xi_c^0 \pi^-$, $\Xi_c^0 \rightarrow p K^- K^- \pi^+$ decays. Reference $\Lambda_b^0 \rightarrow \Lambda_c^+ \pi^-$.

 $\tau_{\Xi_b^0} / \tau_{\Xi_b^-}$ mean life ratio

VALUE	DOCUMENT ID	TECN	COMMENT
1.083 ± 0.032 ± 0.016			
1.083 ± 0.032 ± 0.016	¹ AAIJ	14B LHCb	pp at 7, 8 TeV

¹ Reconstructed in $\Xi_b^- \rightarrow \Xi_c^0 \pi^-$, $\Xi_c^0 \rightarrow p K^- K^- \pi^+$ decays. Uses Ξ_b^0 measurements from AAJ14Z.

 Ξ_b DECAY MODES

Mode	Fraction (Γ_i/Γ)	Scale factor/Confidence level
$\Gamma_1 \Xi^- \ell^- \bar{\nu}_\ell X \times B(\bar{b} \rightarrow \Xi_b^-)$	$(3.9 \pm 1.2) \times 10^{-4}$	S=1.4
$\Gamma_2 J/\psi \Xi^- \times B(b \rightarrow \Xi_b^-)$	$(1.02^{+0.26}_{-0.21}) \times 10^{-5}$	
$\Gamma_3 J/\psi \Lambda K^- \times B(b \rightarrow \Xi_b^-)$	$(2.5 \pm 0.4) \times 10^{-6}$	
$\Gamma_4 \rho D^0 K^- \times B(\bar{b} \rightarrow \Xi_b^-)$	$(1.7 \pm 0.6) \times 10^{-6}$	
$\Gamma_5 \rho K^0 \pi^- \times B(\bar{b} \rightarrow \Xi_b^-)/B(\bar{b} \rightarrow B^0)$	$< 1.6 \times 10^{-6}$	CL=90%
$\Gamma_6 \rho K^0 K^- \times B(\bar{b} \rightarrow \Xi_b^-)/B(\bar{b} \rightarrow B^0)$	$< 1.1 \times 10^{-6}$	CL=90%
$\Gamma_7 \rho K^- K^- \times B(\bar{b} \rightarrow \Xi_b^-)$	$(3.7 \pm 0.8) \times 10^{-8}$	
$\Gamma_8 \rho K^- K^-$		
$\Gamma_9 \rho \pi^- \pi^-$		
$\Gamma_{10} \rho K^- \pi^-$		
$\Gamma_{11} \Lambda \pi^+ \pi^- \times B(b \rightarrow \Xi_b^0)/B(b \rightarrow \Lambda_b^0)$	$< 1.7 \times 10^{-6}$	CL=90%
$\Gamma_{12} \Lambda K^- \pi^+ \times B(b \rightarrow \Xi_b^0)/B(b \rightarrow \Lambda_b^0)$	$< 8 \times 10^{-7}$	CL=90%
$\Gamma_{13} \Lambda K^+ K^- \times B(b \rightarrow \Xi_b^0)/B(b \rightarrow \Lambda_b^0)$	$< 3 \times 10^{-7}$	CL=90%
$\Gamma_{14} \Lambda_c^+ K^- \times B(\bar{b} \rightarrow \Xi_b^-)$	$(6 \pm 4) \times 10^{-7}$	
$\Gamma_{15} \Lambda_b^0 \pi^- \times B(b \rightarrow \Xi_b^-)/B(b \rightarrow \Lambda_b^0)$	$(5.7 \pm 2.0) \times 10^{-4}$	
$\Gamma_{16} \rho K^- \pi^+ \pi^- \times B(b \rightarrow \Xi_b^0)/B(b \rightarrow \Lambda_b^0)$	$(1.9 \pm 0.4) \times 10^{-6}$	
$\Gamma_{17} \rho K^- K^- \pi^+ \times B(b \rightarrow \Xi_b^0)/B(b \rightarrow \Lambda_b^0)$	$(1.73 \pm 0.32) \times 10^{-6}$	
$\Gamma_{18} \rho K^- K^+ K^- \times B(b \rightarrow \Xi_b^0)/B(b \rightarrow \Lambda_b^0)$	$(1.8 \pm 1.0) \times 10^{-7}$	

 Ξ_b BRANCHING RATIOS

$\Gamma(\Xi^- \ell^- \bar{\nu}_\ell X \times B(\bar{b} \rightarrow \Xi_b^-))/\Gamma_{\text{total}}$	Γ_1/Γ
3.9 ± 1.2 OUR AVERAGE	Error includes scale factor of 1.4.
3.0 ± 1.0 ± 0.3	ABDALLAH 05c DLPH $e^+ e^- \rightarrow Z^0$
5.4 ± 1.1 ± 0.8	BUSKULIC 96T ALEP Excess $\Xi^- \ell^-$ over $\Xi^- \ell^+$

• • • We do not use the following data for averages, fits, limits, etc. • • •

5.9 ± 2.1 ± 1.0	ABREU 95v DLPH Repl. by ABDALLAH 05c
-----------------	--------------------------------------

$\Gamma(J/\psi \Xi^- \times B(b \rightarrow \Xi_b^-))/\Gamma_{\text{total}}$	Γ_2/Γ
0.102 ± 0.026	
-0.021	

VALUE (units 10^{-4})	DOCUMENT ID	TECN	COMMENT
0.098 $^{+0.023}_{-0.016}$ ± 0.014	¹ AALTONEN	09AP CDF	$p\bar{p}$ at 1.96 TeV
0.16 ± 0.07 ± 0.02	² ABAZOV	07K D0	$p\bar{p}$ at 1.96 TeV

¹ AALTONEN 09AP reports $[\Gamma(\Xi_b^- \rightarrow J/\psi \Xi^- \times B(b \rightarrow \Xi_b^-))/\Gamma_{\text{total}}] / [B(\Lambda_b^0 \rightarrow J/\psi(1S)\Lambda \times B(b \rightarrow \Lambda_b^0))] = 0.167^{+0.037}_{-0.025} \pm 0.012$ which we multiply by our best value $B(\Lambda_b^0 \rightarrow J/\psi(1S)\Lambda \times B(b \rightarrow \Lambda_b^0)) = (5.8 \pm 0.8) \times 10^{-5}$. Our first error is their experiment's error and our second error is the systematic error from using our best value.
² ABAZOV 07K reports $[\Gamma(\Xi_b^- \rightarrow J/\psi \Xi^- \times B(b \rightarrow \Xi_b^-))/\Gamma_{\text{total}}] / [B(\Lambda_b^0 \rightarrow J/\psi(1S)\Lambda \times B(b \rightarrow \Lambda_b^0))] = 0.28 \pm 0.09^{+0.09}_{-0.08}$ which we multiply by our best value $B(\Lambda_b^0 \rightarrow J/\psi(1S)\Lambda \times B(b \rightarrow \Lambda_b^0)) = (5.8 \pm 0.8) \times 10^{-5}$. Our first error is their experiment's error and our second error is the systematic error from using our best value.

$\Gamma(J/\psi \Lambda K^- \times B(b \rightarrow \Xi_b^-))/\Gamma_{\text{total}}$	Γ_3/Γ
2.45 ± 0.19 ± 0.35	
2.45 ± 0.19 ± 0.35	^{1,2} AAIJ 17B LHCb pp at 7 and 8 TeV

VALUE (units 10^{-6})	DOCUMENT ID	TECN	COMMENT
2.45 ± 0.19 ± 0.35	^{1,2} AAIJ	17B LHCb	pp at 7 and 8 TeV

¹ AAJ17B reports $[\Gamma(\Xi_b^- \rightarrow J/\psi \Lambda K^- \times B(b \rightarrow \Xi_b^-))/\Gamma_{\text{total}}] / [B(\Lambda_b^0 \rightarrow J/\psi(1S)\Lambda \times B(b \rightarrow \Lambda_b^0))] = (4.19 \pm 0.29 \pm 0.15) \times 10^{-2}$ which we multiply by our best value $B(\Lambda_b^0 \rightarrow J/\psi(1S)\Lambda \times B(b \rightarrow \Lambda_b^0)) = (5.8 \pm 0.8) \times 10^{-5}$. Our first error is their experiment's error and our second error is the systematic error from using our best value.
² Integrated over the b -baryon transverse momentum $p_T < 25$ GeV and rapidity $2.0 < y < 4.5$.

$\Gamma(\rho D^0 K^- \times B(\bar{b} \rightarrow \Xi_b^-))/\Gamma_{\text{total}}$	Γ_4/Γ
(1.7 ± 0.4 ± 0.4) × 10⁻⁶	
(1.7 ± 0.4 ± 0.4) × 10 ⁻⁶	¹ AAIJ 14H LHCb pp at 7 TeV

VALUE	DOCUMENT ID	TECN	COMMENT
(1.7 ± 0.4 ± 0.4) × 10 ⁻⁶	¹ AAIJ	14H LHCb	pp at 7 TeV

¹ AAJ14H reports $[\Gamma(\Xi_b^- \rightarrow \rho D^0 K^- \times B(\bar{b} \rightarrow \Xi_b^-))/\Gamma_{\text{total}}] / [B(\bar{b} \rightarrow b\text{-baryon})] / [B(\Lambda_b^0 \rightarrow \rho D^0 K^-)] = 0.44 \pm 0.09 \pm 0.06$ which we multiply by our best values $B(\bar{b} \rightarrow b\text{-baryon}) = (8.4 \pm 1.1) \times 10^{-2}$, $B(\Lambda_b^0 \rightarrow \rho D^0 K^-) = (4.6 \pm 0.8) \times 10^{-5}$. Our first error is their experiment's error and our second error is the systematic error from using our best values.

$\Gamma(\rho \bar{K}^0 \pi^- \times B(\bar{b} \rightarrow \Xi_b)/B(\bar{b} \rightarrow B^0))/\Gamma_{\text{total}}$					Γ_5/Γ
VALUE	CL%	DOCUMENT ID	TECN	COMMENT	
$<1.6 \times 10^{-6}$	90	AAIJ	14Q	LHCB	pp at 7 TeV

$\Gamma(\rho K^0 K^- \times B(\bar{b} \rightarrow \Xi_b)/B(\bar{b} \rightarrow B^0))/\Gamma_{\text{total}}$					Γ_6/Γ
VALUE	CL%	DOCUMENT ID	TECN	COMMENT	
$<1.1 \times 10^{-6}$	90	AAIJ	14Q	LHCB	pp at 7 TeV

$\Gamma(\rho K^- K^- \times B(\bar{b} \rightarrow \Xi_b))/\Gamma_{\text{total}}$					Γ_7/Γ
VALUE (units 10^{-8})		DOCUMENT ID	TECN	COMMENT	
$3.7 \pm 0.8 \pm 0.2$		¹ AAIJ	17F	LHCB	pp at 7, 8 TeV

¹AAIJ 17F reports $[\Gamma(\Xi_b \rightarrow \rho K^- K^- \times B(\bar{b} \rightarrow \Xi_b))/\Gamma_{\text{total}}] / [B(B^+ \rightarrow K^+ K^- K^+)] / [B(\bar{b} \rightarrow B^+)] = (2.65 \pm 0.35 \pm 0.47) \times 10^{-3}$ which we multiply by our best values $B(B^+ \rightarrow K^+ K^- K^+) = (3.40 \pm 0.14) \times 10^{-5}$, $B(\bar{b} \rightarrow B^+) = (40.8 \pm 0.7) \times 10^{-2}$. Our first error is their experiment's error and our second error is the systematic error from using our best values.

$\Gamma(\rho \pi^- \pi^-)/\Gamma(\rho K^- K^-)$					Γ_9/Γ_8
VALUE	CL%	DOCUMENT ID	TECN	COMMENT	
<0.56	90	¹ AAIJ	17F	LHCB	pp at 7, 8 TeV

¹ Measures the ratio as $0.28 \pm 0.16 \pm 0.13$.

$\Gamma(\rho K^- \pi^-)/\Gamma(\rho K^- K^-)$					Γ_{10}/Γ_8
VALUE		DOCUMENT ID	TECN	COMMENT	
$0.98 \pm 0.27 \pm 0.09$		AAIJ	17F	LHCB	pp at 7, 8 TeV

$\Gamma(\Lambda \pi^+ \pi^- \times B(b \rightarrow \Xi_b^0))/B(b \rightarrow \Lambda_b^0)/\Gamma_{\text{total}}$					Γ_{11}/Γ
VALUE	CL%	DOCUMENT ID	TECN	COMMENT	
$<1.7 \times 10^{-6}$	90	AAIJ	16W	LHCB	pp at 7, 8 TeV

$\Gamma(\Lambda K^- \pi^+ \times B(b \rightarrow \Xi_b^0))/B(b \rightarrow \Lambda_b^0)/\Gamma_{\text{total}}$					Γ_{12}/Γ
VALUE	CL%	DOCUMENT ID	TECN	COMMENT	
$<0.8 \times 10^{-6}$	90	AAIJ	16W	LHCB	pp at 7, 8 TeV

$\Gamma(\Lambda K^+ K^- \times B(b \rightarrow \Xi_b^0))/B(b \rightarrow \Lambda_b^0)/\Gamma_{\text{total}}$					Γ_{13}/Γ
VALUE	CL%	DOCUMENT ID	TECN	COMMENT	
$<0.3 \times 10^{-6}$	90	AAIJ	16W	LHCB	pp at 7, 8 TeV

$\Gamma(\rho K^- \pi^+ \pi^- \times B(b \rightarrow \Xi_b^0))/B(b \rightarrow \Lambda_b^0)/\Gamma_{\text{total}}$					Γ_{16}/Γ
VALUE (units 10^{-6})		DOCUMENT ID	TECN	COMMENT	
$1.91 \pm 0.35 \pm 0.18$		¹ AAIJ	18Q	LHCB	pp at 7, 8 TeV

¹AAIJ 18Q reports $[\Gamma(\Xi_b \rightarrow \rho K^- \pi^+ \pi^- \times B(b \rightarrow \Xi_b^0)/B(b \rightarrow \Lambda_b^0))/\Gamma_{\text{total}}] / [B(\Lambda_c^+ \rightarrow \rho K^- \pi^+)] / [B(\Lambda_b^0 \rightarrow \Lambda_c^+ \pi^-)] = (6.2 \pm 0.8 \pm 0.2 \pm 0.8) \times 10^{-3}$ which we multiply by our best values $B(\Lambda_c^+ \rightarrow \rho K^- \pi^+) = (6.28 \pm 0.32) \times 10^{-2}$, $B(\Lambda_b^0 \rightarrow \Lambda_c^+ \pi^-) = (4.9 \pm 0.4) \times 10^{-3}$. Our first error is their experiment's error and our second error is the systematic error from using our best values.

$\Gamma(\rho K^- K^- \pi^+ \times B(b \rightarrow \Xi_b^0))/B(b \rightarrow \Lambda_b^0)/\Gamma_{\text{total}}$					Γ_{17}/Γ
VALUE (units 10^{-6})		DOCUMENT ID	TECN	COMMENT	
$1.73 \pm 0.27 \pm 0.16$		¹ AAIJ	18Q	LHCB	pp at 7, 8 TeV

¹AAIJ 18Q reports $[\Gamma(\Xi_b \rightarrow \rho K^- K^- \pi^+ \times B(b \rightarrow \Xi_b^0)/B(b \rightarrow \Lambda_b^0))/\Gamma_{\text{total}}] / [B(\Lambda_c^+ \rightarrow \rho K^- \pi^+)] / [B(\Lambda_b^0 \rightarrow \Lambda_c^+ \pi^-)] = (5.6 \pm 0.6 \pm 0.4 \pm 0.5) \times 10^{-3}$ which we multiply by our best values $B(\Lambda_c^+ \rightarrow \rho K^- \pi^+) = (6.28 \pm 0.32) \times 10^{-2}$, $B(\Lambda_b^0 \rightarrow \Lambda_c^+ \pi^-) = (4.9 \pm 0.4) \times 10^{-3}$. Our first error is their experiment's error and our second error is the systematic error from using our best values.

$\Gamma(\rho K^- K^+ K^- \times B(b \rightarrow \Xi_b^0))/B(b \rightarrow \Lambda_b^0)/\Gamma_{\text{total}}$					Γ_{18}/Γ
VALUE (units 10^{-6})		DOCUMENT ID	TECN	COMMENT	
$0.18 \pm 0.09 \pm 0.02$		^{1,2} AAIJ	18Q	LHCB	pp at 7, 8 TeV

¹AAIJ 18Q reports $[\Gamma(\Xi_b \rightarrow \rho K^- K^+ K^- \times B(b \rightarrow \Xi_b^0)/B(b \rightarrow \Lambda_b^0))/\Gamma_{\text{total}}] / [B(\Lambda_c^+ \rightarrow \rho K^- \pi^+)] / [B(\Lambda_b^0 \rightarrow \Lambda_c^+ \pi^-)] = (0.57 \pm 0.28 \pm 0.08 \pm 0.10) \times 10^{-3}$ which we multiply by our best values $B(\Lambda_c^+ \rightarrow \rho K^- \pi^+) = (6.28 \pm 0.32) \times 10^{-2}$, $B(\Lambda_b^0 \rightarrow \Lambda_c^+ \pi^-) = (4.9 \pm 0.4) \times 10^{-3}$. Our first error is their experiment's error and our second error is the systematic error from using our best values.

²AAIJ 18Q sees excess with a significance of 2.3 σ . Using $B(\Lambda_b^0 \rightarrow \Lambda_c^+ \pi^-) = (0.430 \pm 0.036) \times 10^{-2}$ and $B(\Lambda_c^+ \rightarrow \rho K^- \pi^+) = (6.46 \pm 0.24) \times 10^{-2}$ the authors set two sided limit $[0.11-0.25]$ at 90% C.L.

$\Gamma(\Lambda_c^+ K^- \times B(\bar{b} \rightarrow \Xi_b))/\Gamma(\rho D^0 K^- \times B(\bar{b} \rightarrow \Xi_b))$					Γ_{14}/Γ_4
VALUE		DOCUMENT ID	TECN	COMMENT	
$0.36 \pm 0.19 \pm 0.02$		¹ AAIJ	14H	LHCB	pp at 7 TeV

¹AAIJ 14H reports $[\Gamma(\Xi_b \rightarrow \Lambda_c^+ K^- \times B(\bar{b} \rightarrow \Xi_b))/\Gamma(\Xi_b \rightarrow \rho D^0 K^- \times B(\bar{b} \rightarrow \Xi_b))] \times [B(\Lambda_c^+ \rightarrow \rho K^- \pi^+)] / [B(D^0 \rightarrow K^- \pi^+)] = 0.57 \pm 0.22 \pm 0.21$ which we multiply or divide by our best values $B(\Lambda_c^+ \rightarrow \rho K^- \pi^+) = (6.28 \pm 0.32) \times 10^{-2}$, $B(D^0 \rightarrow K^- \pi^+) = (3.950 \pm 0.031) \times 10^{-2}$. Our first error is their experiment's error and our second error is the systematic error from using our best values.

$\Gamma(\Lambda_b^0 \pi^- \times B(b \rightarrow \Xi_b^-))/B(b \rightarrow \Lambda_b^0)/\Gamma_{\text{total}}$				Γ_{15}/Γ	
VALUE (units 10^{-4})		DOCUMENT ID	TECN	COMMENT	
$5.7 \pm 1.8^{+0.8}_{-0.9}$		¹ AAIJ	15BA	LHCB	pp at 7, 8 TeV

¹A signal is reported with a significance of 3.2 standard deviations in the decay chain of $\Xi_b^- \rightarrow \Lambda_b^0 \pi^-$, $\Lambda_b^0 \rightarrow \Lambda_c^+ \pi^-$, and $\Lambda_c^+ \rightarrow \rho K^- \pi^+$.

P AND CP VIOLATION

$a_P(\Xi_b^0 \rightarrow \rho K^- K^- \pi^+)$
Observable calculated as average of the triple products for Ξ_b^0 and Ξ_b^0 , which is sensitive to parity violation.

VALUE (%)	DOCUMENT ID	TECN	COMMENT	
$-3.04 \pm 5.19 \pm 0.36$	¹ AAIJ	18AG	LHCB	pp at 7, 8 TeV

¹ Measured over full phase space of the decay.

$a_{CP}(\Xi_b^0 \rightarrow \rho K^- K^- \pi^+)$
Observable calculated as half of the difference between triple products for Ξ_b^0 and Ξ_b^0 , which is sensitive to CP violation.

VALUE (%)	DOCUMENT ID	TECN	COMMENT	
$-3.58 \pm 5.19 \pm 0.36$	¹ AAIJ	18AG	LHCB	pp at 7, 8 TeV

¹ Measured over full phase space of the decay.

$\Delta A_{CP}(\Xi_b^0 \rightarrow \rho K^- \pi^+ \pi^-)$
 $\Delta A_{CP} \equiv A_{CP}(\Xi_b^0 \rightarrow \rho K^- \pi^+ \pi^-) - A_{CP}(\Xi_b^0 \rightarrow (\Xi_c^+ \rightarrow \rho K^- \pi^+) \pi^-)$

VALUE (units 10^{-2})	DOCUMENT ID	TECN	COMMENT	
$-17 \pm 11 \pm 1$	¹ AAIJ	19AH	LHCB	pp at 7 and 8 TeV

¹ Full phase space.

$\Delta A_{CP}(\Xi_b^0 \rightarrow \rho K^- \pi^+ K^-)$
 $\Delta A_{CP} \equiv A_{CP}(\Xi_b^0 \rightarrow \rho K^- \pi^+ K^-) - A_{CP}(\Xi_b^0 \rightarrow (\Xi_c^+ \rightarrow \rho K^- \pi^+) \pi^-)$

VALUE (units 10^{-2})	DOCUMENT ID	TECN	COMMENT	
$-6.8 \pm 8.0 \pm 0.8$	¹ AAIJ	19AH	LHCB	pp at 7 and 8 TeV

¹ Full phase space.

$A_P(\Xi_b, \Xi_b^- - \Xi_b^{\prime-})$ production asymmetry

$$A_P(\Xi_b) = [\sigma(\Xi_b^-) - \sigma(\Xi_b^{\prime-})] / [\sigma(\Xi_b^-) + \sigma(\Xi_b^{\prime-})]$$

VALUE (units 10^{-2})	DOCUMENT ID	TECN	COMMENT	
-2 ± 4	OUR AVERAGE			
$1.1 \pm 5.6 \pm 1.9$	^{1,2} AAIJ	19AB	LHCB	pp at 7 and 8 TeV
$-3.9 \pm 4.9 \pm 2.5$	^{1,2} AAIJ	19AB	LHCB	pp at 13 TeV

¹ Baryon kinematic range, $p_T < 20$ GeV/c and $2 < \eta < 6$.

² Measured using previous measurements of $A_P(\Lambda_b)$ in AAJ 17BF.

Ξ_b REFERENCES

AAIJ	19AB	PR D99 052006	R. Aaij et al.	(LHCb Collab.)
AAIJ	19AH	EPJ C79 745	R. Aaij et al.	(LHCb Collab.)
AAIJ	18AG	JHEP 1808 039	R. Aaij et al.	(LHCb Collab.)
AAIJ	18Q	JHEP 1802 098	R. Aaij et al.	(LHCb Collab.)
AAIJ	17BE	PL B772 265	R. Aaij et al.	(LHCb Collab.)
AAIJ	17BF	PL B774 139	R. Aaij et al.	(LHCb Collab.)
AAIJ	17BH	PRL 119 181807	R. Aaij et al.	(LHCb Collab.)
AAIJ	17BJ	PRL 119 232001	R. Aaij et al.	(LHCb Collab.)
AAIJ	17F	PRL 118 071801	R. Aaij et al.	(LHCb Collab.)
AAIJ	16W	JHEP 1605 081	R. Aaij et al.	(LHCb Collab.)
AAIJ	15BA	PRL 115 241801	R. Aaij et al.	(LHCb Collab.)
AAIJ	14AA	PRL 112 202001	R. Aaij et al.	(LHCb Collab.)
AAIJ	14BE	NP B888 169	R. Aaij et al.	(LHCb Collab.)
AAIJ	14BJ	PRL 113 242002	R. Aaij et al.	(LHCb Collab.)
AAIJ	14H	PR D89 032001	R. Aaij et al.	(LHCb Collab.)
AAIJ	14Q	JHEP 1404 087	R. Aaij et al.	(LHCb Collab.)
AAIJ	14T	PL B736 154	R. Aaij et al.	(LHCb Collab.)
AAIJ	14U	PL B734 122	R. Aaij et al.	(LHCb Collab.)
AAIJ	14Z	PRL 113 032001	R. Aaij et al.	(LHCb Collab.)
AALTONEN	14B	PR D89 072014	T. Aaltonen et al.	(CDF Collab.)
AAIJ	13AV	PRL 110 182001	R. Aaij et al.	(LHCb Collab.)
AALTONEN	11X	PRL 107 102001	T. Aaltonen et al.	(CDF Collab.)
AALTONEN	09AP	PR D80 072003	T. Aaltonen et al.	(CDF Collab.)
AALTONEN	07A	PRL 99 052002	T. Aaltonen et al.	(CDF Collab.)
ABAZOV	07K	PRL 99 052001	V.M. Abazov et al.	(D0 Collab.)
ABDALLAH	05C	EPJ C44 299	J. Abdallah et al.	(DELPHI Collab.)
BUSKULIC	96T	PL B384 449	D. Buskulic et al.	(ALEPH Collab.)
ABREU	95V	ZPHY C68 541	P. Abreu et al.	(DELPHI Collab.)

$\Xi_b^{\prime-}(5935)^-$

$$J^P = \frac{1}{2}^+$$

Status: ***

$\Xi_b^{\prime-}(5935)^-$ MASS

VALUE (MeV)	DOCUMENT ID	TECN	COMMENT	
$5935.02 \pm 0.02 \pm 0.05$	¹ AAIJ	15H	LHCB	pp at 7, 8 TeV

¹ Not independent of the mass difference measurement below. Observed in $\Xi_b^0 \pi^-$ channel

with $\Xi_b^0 \rightarrow \Xi_c^+ \pi^-$ and $\Xi_c^+ \rightarrow \rho K^- \pi^+$.

Baryon Particle Listings

$\Xi'_b(5935)^-$, $\Xi_b(5945)^0$, $\Xi_b(5955)^-$, $\Xi_b(6227)$

$$m_{\Xi'_b(5935)^-} - m_{\Xi_b^0} - m_{\pi^-}$$

VALUE (MeV)	DOCUMENT ID	TECN	COMMENT
3.653 ± 0.018 ± 0.006	² AAIJ	15H LHCb	<i>pp</i> at 7, 8 TeV
² Observed in $\Xi_b^0 \pi^-$ channel with $\Xi_b^0 \rightarrow \Xi_c^+ \pi^-$ and $\Xi_c^+ \rightarrow p K^- \pi^+$.			

$\Xi'_b(5935)^-$ WIDTH

VALUE (MeV)	CL%	DOCUMENT ID	TECN	COMMENT
<0.08	95	³ AAIJ	15H LHCb	<i>pp</i> at 7, 8 TeV
³ Observed in $\Xi_b^0 \pi^-$ channel with $\Xi_b^0 \rightarrow \Xi_c^+ \pi^-$ and $\Xi_c^+ \rightarrow p K^- \pi^+$.				

$\Xi'_b(5935)^-$ DECAY MODES

Mode	Fraction (Γ_i/Γ)
Γ_1 $\Xi_b^0 \pi^- \times B(\bar{b} \rightarrow \Xi'_b(5935)^-)/B(\bar{b} \rightarrow \Xi_b^0)$	(11.8 ± 1.8) %

$\Xi'_b(5935)^-$ BRANCHING RATIOS

$\Gamma(\Xi_b^0 \pi^- \times B(\bar{b} \rightarrow \Xi'_b(5935)^-)/B(\bar{b} \rightarrow \Xi_b^0))/\Gamma_{\text{total}}$	Γ_1/Γ
0.118 ± 0.017 ± 0.007	
⁴ AAIJ	15H LHCb
⁴ Observed in $\Xi_b^0 \pi^-$ channel with $\Xi_b^0 \rightarrow \Xi_c^+ \pi^-$ and $\Xi_c^+ \rightarrow p K^- \pi^+$.	

$\Xi'_b(5935)^-$ REFERENCES

AAIJ 15H PRL 114 062004 R. Aaij *et al.* (LHCb Collab.)

$\Xi_b(5945)^0$

$$J^P = \frac{3}{2}^+ \quad \text{Status: } ***$$

Quantum numbers are based on quark model expectations.

$\Xi_b(5945)^0$ MASS

VALUE (MeV)	DOCUMENT ID	TECN	COMMENT
5952.3 ± 0.6 OUR AVERAGE	¹ AAIJ	16AE LHCb	<i>pp</i> at 7, 8 TeV
5952.3 ± 0.1 ± 0.6	² CHATRCHYAN12s	CMS	<i>pp</i> at 7 TeV, 5.3 fb ⁻¹

¹ AAIJ 16AE measures $m(\Xi_b(5945)^0) - m(\Xi_b^-) - m(\pi^+) = 15.727 \pm 0.068 \pm 0.023$ MeV. We have adjusted the measurement to our best values of $m(\Xi_b^-) = 5797.0 \pm 0.6$ MeV, $m(\pi^+) = 139.57039 \pm 0.00018$ MeV. Our first error is their experiment's error and our second error is the systematic error from using our best values.

² CHATRCHYAN 12s measures $m(\Xi_b(5945)^0) - m(\Xi_b^-) - m(\pi^+) = 14.84 \pm 0.74 \pm 0.28$ MeV. We have adjusted the measurement to our best values of $m(\Xi_b^-) = 5797.0 \pm 0.6$ MeV, $m(\pi^+) = 139.57039 \pm 0.00018$ MeV. Our first error is their experiment's error and our second error is the systematic error from using our best values.

$\Xi_b(5945)^0$ WIDTH

VALUE (MeV)	DOCUMENT ID	TECN	COMMENT
0.90 ± 0.16 ± 0.08	³ AAIJ	16AE LHCb	<i>pp</i> at 7, 8 TeV
• • • We do not use the following data for averages, fits, limits, etc. • • •			
2.1 ± 1.7	⁴ CHATRCHYAN12s	CMS	<i>pp</i> at 7 TeV, 5.3 fb ⁻¹
³ Measured using $\Xi_b(5945)^0 \rightarrow \Xi_b^- \pi^+$, $\Xi_b^- \rightarrow \Xi_c^0 \pi^-$, $\Xi_c^0 \rightarrow p K^- K^- \pi^+$ decays.			
⁴ Systematic uncertainty not evaluated.			

$\Xi_b(5945)^0$ DECAY MODES

Mode	Fraction (Γ_i/Γ)
Γ_1 $\Xi_b^- \pi^+$	seen

$\Xi_b(5945)^0$ BRANCHING RATIOS

$\Gamma(\Xi_b^- \pi^+)/\Gamma_{\text{total}}$	Γ_1/Γ
seen	
seen	
AAIJ	16AE ATLAS
CHATRCHYAN 12s	CMS
<i>pp</i> at 7, 8 TeV	
<i>pp</i> at 7 TeV, 5.3 fb ⁻¹	

$\Xi_b(5945)^0$ REFERENCES

AAIJ 16AE JHEP 1605 161 R. Aaij *et al.* (LHCb Collab.)
 CHATRCHYAN 12s PRL 108 252002 S. Chatrchyan *et al.* (CMS Collab.)

$\Xi_b(5955)^-$

$$J^P = \frac{3}{2}^+ \quad \text{Status: } ***$$

$\Xi_b(5955)^-$ MASS

VALUE (MeV)	DOCUMENT ID	TECN	COMMENT
5955.33 ± 0.12 ± 0.05	¹ AAIJ	15H LHCb	<i>pp</i> at 7, 8 TeV
¹ Not independent of the mass difference measurement below. Observed in $\Xi_b^0 \pi^-$ channel with $\Xi_b^0 \rightarrow \Xi_c^+ \pi^-$ and $\Xi_c^+ \rightarrow p K^- \pi^+$.			

$$m_{\Xi_b(5955)^-} - m_{\Xi_b^0} - m_{\pi^-}$$

VALUE (MeV)	DOCUMENT ID	TECN	COMMENT
23.96 ± 0.12 ± 0.06	¹ AAIJ	15H LHCb	<i>pp</i> at 7, 8 TeV
¹ Observed in $\Xi_b^0 \pi^-$ channel with $\Xi_b^0 \rightarrow \Xi_c^+ \pi^-$ and $\Xi_c^+ \rightarrow p K^- \pi^+$.			

$\Xi_b(5955)^-$ WIDTH

VALUE (MeV)	DOCUMENT ID	TECN	COMMENT
1.65 ± 0.31 ± 0.10	¹ AAIJ	15H LHCb	<i>pp</i> at 7, 8 TeV
¹ Observed in $\Xi_b^0 \pi^-$ channel with $\Xi_b^0 \rightarrow \Xi_c^+ \pi^-$ and $\Xi_c^+ \rightarrow p K^- \pi^+$.			

$\Xi_b(5955)^-$ DECAY MODES

Mode	Fraction (Γ_i/Γ)
Γ_1 $\Xi_b^0 \pi^- \times B(\bar{b} \rightarrow \Xi_b(5955)^-)/B(\bar{b} \rightarrow \Xi_b^0)$	(20.7 ± 3.5) %

$\Xi_b(5955)^-$ BRANCHING RATIOS

$\Gamma(\Xi_b^0 \pi^- \times B(\bar{b} \rightarrow \Xi_b(5955)^-)/B(\bar{b} \rightarrow \Xi_b^0))/\Gamma_{\text{total}}$	Γ_1/Γ
0.207 ± 0.032 ± 0.015	
¹ AAIJ	15H LHCb
¹ Observed in $\Xi_b^0 \pi^-$ channel with $\Xi_b^0 \rightarrow \Xi_c^+ \pi^-$ and $\Xi_c^+ \rightarrow p K^- \pi^+$.	

$\Xi_b(5955)^-$ REFERENCES

AAIJ 15H PRL 114 062004 R. Aaij *et al.* (LHCb Collab.)

$\Xi_b(6227)$

$$J^P = ?^? \quad \text{Status: } ***$$

$\Xi_b(6227)$ MASS

VALUE (MeV)	DOCUMENT ID	TECN	COMMENT
6226.9 ± 2.0 ± 0.4	^{1,2} AAIJ	18H LHCb	<i>pp</i> at 7, 8, 13 TeV
¹ Uses $\Lambda_b^0 K^-$ and $\Xi_b^0 \pi^-$ modes.			
² Measures mass difference $m(\Xi_b(6227)^-) - m(\Lambda_b^0) = 607.3 \pm 2.0 \pm 0.3$ MeV and uses $m(\Lambda_b^0) = 5619.58 \pm 0.17$ MeV.			

$\Xi_b(6227)$ WIDTH

VALUE (MeV)	DOCUMENT ID	TECN	COMMENT
18.1 ± 5.4 ± 1.8	¹ AAIJ	18H LHCb	<i>pp</i> at 7, 8, 13 TeV
¹ Uses $\Lambda_b^0 K^-$ and $\Xi_b^0 \pi^-$ modes.			

$\Xi_b(6227)$ DECAY MODES

Mode	Fraction (Γ_i/Γ)	Scale factor
Γ_1 $\Lambda_b^0 K^- \times B(b \rightarrow \Xi_b(6227)^-)/B(b \rightarrow \Lambda_b^0)$	(3.20 ± 0.35) × 10 ⁻³	
Γ_2 $\Xi_b^0 \pi^- \times B(b \rightarrow \Xi_b(6227)^-)/B(b \rightarrow \Xi_b^0)$	(2.8 ± 1.1) %	1.8

$\Xi_b(6227)$ BRANCHING RATIOS

$\Gamma(\Lambda_b^0 K^- \times B(b \rightarrow \Xi_b(6227)^-)/B(b \rightarrow \Lambda_b^0))/\Gamma_{\text{total}}$	Γ_1/Γ
3.20 ± 0.35 OUR AVERAGE	
3.0 ± 0.3 ± 0.4	AAIJ
3.4 ± 0.3 ± 0.4	AAIJ
18H LHCb	
<i>pp</i> at 7, 8 TeV	
<i>pp</i> at 13 TeV	

$\Xi_b(6227), \Omega_b^-, b$ -baryon ADMIXTURE ($\Lambda_b, \Xi_b, \Omega_b$)

$\Gamma(\Xi_b^0 \pi^- \times B(b \rightarrow \Xi_b(6227)))/\Gamma_{\text{total}}$				Γ_2/Γ
VALUE (units 10^{-3})	DOCUMENT ID	TECN	COMMENT	
28 ± 11 OUR AVERAGE	Error includes scale factor of 1.8.			
$47 \pm 10 \pm 7$	AAIJ	18H LHCb	pp at 7, 8 TeV	
$22 \pm 6 \pm 3$	AAIJ	18H LHCb	pp at 13 TeV	

$\Xi_b(6227)$ REFERENCES

AAIJ	18H PRL 121 072002	R. Aaij et al.	(LHCb Collab.)
------	--------------------	----------------	----------------



$I(J^P) = 0(\frac{1}{2}^+)$ Status: ***
I, J, P need confirmation.

In the quark model Ω_b^- is ssb ground state. None of its quantum numbers has been measured.

Ω_b^- MASS

VALUE (MeV)	DOCUMENT ID	TECN	COMMENT
6046.1 ± 1.7 OUR AVERAGE			
$6045.1 \pm 3.2 \pm 0.8$	1 AAIJ	16O LHCb	pp at 7, 8 TeV
$6047.5 \pm 3.8 \pm 0.6$	2 AALTONEN	14B CDF	$p\bar{p}$ at 1.96 TeV
$6046.0 \pm 2.2 \pm 0.5$	3 AAIJ	13AV LHCb	pp at 7 TeV
• • • We do not use the following data for averages, fits, limits, etc. • • •			
$6054.4 \pm 6.8 \pm 0.9$	4 AALTONEN	09AP CDF	Repl. by AALTONEN 14B
$6165 \pm 10 \pm 13$	5 ABAZOV	08AL D0	$p\bar{p}$ at 1.96 TeV

- 1 Reconstructed in $\Omega_b^- \rightarrow \Omega_c^0 \pi^-, \Omega_c^0 \rightarrow pK^- K^+ \pi^+$ decays. Reference Ξ_b^- mass 5797.72 \pm 0.6 MeV from AAJ 14b.
- 2 Uses $\Omega_b^- \rightarrow J/\psi \Omega^-$ and $\Omega_c^0 \pi^-$ decays, with the first evidence for $\Omega_b^- \rightarrow \Omega_c^0 \pi^-$ at 3.3 σ significance.
- 3 Measured in $\Omega_b^- \rightarrow J/\psi \Omega^-$ with 19 \pm 5 events.
- 4 Observed in $\Omega_b^- \rightarrow J/\psi \Omega^-$ decays with 16 $^{+6}_{-4}$ candidates, a significance of 5.5 sigma from a combined mass-lifetime fit.
- 5 Observed in $\Omega_b^- \rightarrow J/\psi \Omega^-$ decays with 17.8 \pm 4.9 \pm 0.8 candidates, a significance of 5.4 sigma.

$m_{\Omega_b^-} - m_{\Lambda_b^0}$

VALUE (MeV)	DOCUMENT ID	TECN	COMMENT
$426.4 \pm 2.2 \pm 0.4$	AAIJ	13AV LHCb	pp at 7 TeV

$m_{\Omega_b^-} - m_{\Xi_b^-}$

VALUE (MeV)	DOCUMENT ID	TECN	COMMENT
$247.3 \pm 3.2 \pm 0.5$	1 AAIJ	16O LHCb	pp at 7, 8 TeV

- 1 Uses $\Omega_b^- \rightarrow \Omega_c^0 \pi^-, \Omega_c^0 \rightarrow pK^- K^+ \pi^+$ and $\Xi_b^- \rightarrow \Xi_c^0 \pi^-, \Xi_c^0 \rightarrow pK^- K^+ \pi^+$ decays.

Ω_b^- MEAN LIFE

"OUR EVALUATION" has been provided by the Heavy Flavor Averaging Group (HFLAV, <https://hflav.web.cern.ch/>).

VALUE (10^{-12} s)	DOCUMENT ID	TECN	COMMENT
-----------------------	-------------	------	---------

$1.64^{+0.18}_{-0.17}$ OUR EVALUATION

$1.65^{+0.18}_{-0.16}$ OUR AVERAGE

$1.78 \pm 0.26 \pm 0.05 \pm 0.06$	1 AAIJ	16O LHCb	pp at 7, 8 TeV
$1.54^{+0.26}_{-0.21} \pm 0.05$	2 AAIJ	14T LHCb	pp at 7, 8 TeV
$1.66^{+0.53}_{-0.40} \pm 0.02$	2 AALTONEN	14B CDF	$p\bar{p}$ at 1.96 TeV
• • • We do not use the following data for averages, fits, limits, etc. • • •			
$1.13^{+0.53}_{-0.40} \pm 0.02$	3 AALTONEN	09AP CDF	Repl. by AALTONEN 14B

- 1 Measured in $\Omega_b^- \rightarrow \Omega_c^0 \pi^-, \Omega_c^0 \rightarrow pK^- K^+ \pi^+$ decays relative to $\Xi_b^- \rightarrow \Xi_c^0 \pi^-, \Xi_c^0 \rightarrow pK^- K^+ \pi^+$ decays with reference Ξ_b^- mean life 1.599 \pm 0.06 ps from AAJ 14b.
- 2 Measured in $\Omega_b^- \rightarrow J/\psi \Omega^-$ decays.
- 3 Observed in $\Omega_b^- \rightarrow J/\psi \Omega^-$ decays with 16 $^{+6}_{-4}$ candidates, a significance of 5.5 sigma from a combined mass-lifetime fit.

$\tau(\Omega_b^-)/\tau(\Xi_b^-)$ mean life ratio

VALUE	DOCUMENT ID	TECN	COMMENT
$1.11 \pm 0.16 \pm 0.03$	1 AAIJ	16O LHCb	pp at 7, 8 TeV

- 1 Uses $\Omega_b^- \rightarrow \Omega_c^0 \pi^-, \Omega_c^0 \rightarrow pK^- K^+ \pi^+$ and $\Xi_b^- \rightarrow \Xi_c^0 \pi^-, \Xi_c^0 \rightarrow pK^- K^+ \pi^+$ decays.

Ω_b^- DECAY MODES

Mode	Fraction (Γ_i/Γ)	Confidence level
Γ_1 $J/\psi \Omega^- \times B(b \rightarrow \Omega_b)$	$(2.9^{+1.1}_{-0.8}) \times 10^{-6}$	
Γ_2 $\rho K^- K^- \times B(\bar{b} \rightarrow \Omega_b)$	$< 2.5 \times 10^{-9}$	90%
Γ_3 $\rho \pi^- \pi^- \times B(\bar{b} \rightarrow \Omega_b)$	$< 1.5 \times 10^{-8}$	90%
Γ_4 $\rho K^- \pi^- \times B(\bar{b} \rightarrow \Omega_b)$	$< 7 \times 10^{-9}$	90%

Ω_b^- BRANCHING RATIOS

$\Gamma(J/\psi \Omega^- \times B(b \rightarrow \Omega_b))/\Gamma_{\text{total}}$				Γ_1/Γ
VALUE (units 10^{-4})	DOCUMENT ID	TECN	COMMENT	

$0.029^{+0.011}_{-0.008}$ OUR AVERAGE

- $0.026^{+0.010}_{-0.007} \pm 0.004$ ¹ AALTONEN 09AP CDF $p\bar{p}$ at 1.96 TeV
- $0.08 \pm 0.04 \pm 0.02$ ² ABAZOV 08AL D0 $p\bar{p}$ at 1.96 TeV
- ¹ AALTONEN 09AP reports $[\Gamma(\Omega_b^- \rightarrow J/\psi \Omega^- \times B(b \rightarrow \Omega_b))/\Gamma_{\text{total}}] / [B(\Lambda_b^0 \rightarrow J/\psi(1S) \Lambda \times B(b \rightarrow \Lambda_b^0))] = 0.045^{+0.017}_{-0.012} \pm 0.004$ which we multiply by our best value $B(\Lambda_b^0 \rightarrow J/\psi(1S) \Lambda \times B(b \rightarrow \Lambda_b^0)) = (5.8 \pm 0.8) \times 10^{-5}$. Our first error is their experiment's error and our second error is the systematic error from using our best value.
- ² ABAZOV 08AL reports $[\Gamma(\Omega_b^- \rightarrow J/\psi \Omega^- \times B(b \rightarrow \Omega_b))/\Gamma_{\text{total}}] / [B(\Xi_b^- \rightarrow J/\psi \Xi^- \times B(b \rightarrow \Xi_b^-))] = 0.80 \pm 0.32^{+0.14}_{-0.22}$ which we multiply by our best value $B(\Xi_b^- \rightarrow J/\psi \Xi^- \times B(b \rightarrow \Xi_b^-)) = (1.02^{+0.26}_{-0.21}) \times 10^{-5}$. Our first error is their experiment's error and our second error is the systematic error from using our best value.

$\Gamma(\rho K^- K^- \times B(\bar{b} \rightarrow \Omega_b))/\Gamma_{\text{total}}$				Γ_2/Γ
VALUE (units 10^{-5})	CL%	DOCUMENT ID	TECN	COMMENT

- $< 2.5 \times 10^{-4}$** 90 ¹ AAIJ 17F LHCb pp at 7, 8 TeV
- ¹ AAIJ 17F reports $[\Gamma(\Omega_b^- \rightarrow \rho K^- K^- \times B(\bar{b} \rightarrow \Omega_b))/\Gamma_{\text{total}}] / [B(B^+ \rightarrow K^+ K^- K^+)] / [B(\bar{b} \rightarrow B^+)] < 18 \times 10^{-5}$ which we multiply by our best values $B(B^+ \rightarrow K^+ K^- K^+) = 3.40 \times 10^{-5}$, $B(\bar{b} \rightarrow B^+) = 40.8 \times 10^{-2}$.

$\Gamma(\rho \pi^- \pi^- \times B(\bar{b} \rightarrow \Omega_b))/\Gamma_{\text{total}}$				Γ_3/Γ
VALUE (units 10^{-5})	CL%	DOCUMENT ID	TECN	COMMENT

- $< 1.5 \times 10^{-3}$** 90 ¹ AAIJ 17F LHCb pp at 7, 8 TeV
- ¹ AAIJ 17F reports $[\Gamma(\Omega_b^- \rightarrow \rho \pi^- \pi^- \times B(\bar{b} \rightarrow \Omega_b))/\Gamma_{\text{total}}] / [B(B^+ \rightarrow K^+ K^- K^+)] / [B(\bar{b} \rightarrow B^+)] < 109 \times 10^{-5}$ which we multiply by our best values $B(B^+ \rightarrow K^+ K^- K^+) = 3.40 \times 10^{-5}$, $B(\bar{b} \rightarrow B^+) = 40.8 \times 10^{-2}$.

$\Gamma(\rho K^- \pi^- \times B(\bar{b} \rightarrow \Omega_b))/\Gamma_{\text{total}}$				Γ_4/Γ
VALUE (units 10^{-5})	CL%	DOCUMENT ID	TECN	COMMENT

- $< 7 \times 10^{-4}$** 90 ¹ AAIJ 17F LHCb pp at 7, 8 TeV
- ¹ AAIJ 17F reports $[\Gamma(\Omega_b^- \rightarrow \rho K^- \pi^- \times B(\bar{b} \rightarrow \Omega_b))/\Gamma_{\text{total}}] / [B(B^+ \rightarrow K^+ K^- K^+)] / [B(\bar{b} \rightarrow B^+)] < 51 \times 10^{-5}$ which we multiply by our best values $B(B^+ \rightarrow K^+ K^- K^+) = 3.40 \times 10^{-5}$, $B(\bar{b} \rightarrow B^+) = 40.8 \times 10^{-2}$.

Ω_b^- REFERENCES

AAIJ	17F PRL 118 071801	R. Aaij et al.	(LHCb Collab.)
AAIJ	16O PR D39 092007	R. Aaij et al.	(LHCb Collab.)
AAIJ	14B PL B728 234	R. Aaij et al.	(LHCb Collab.)
AAIJ	14T PL B736 154	R. Aaij et al.	(LHCb Collab.)
AALTONEN	14B PR D89 072014	T. Aaltonen et al.	(CDF Collab.)
AAIJ	13AV PRL 110 182001	R. Aaij et al.	(LHCb Collab.)
AALTONEN	09AP PR D80 072003	T. Aaltonen et al.	(CDF Collab.)
ABAZOV	08AL PRL 101 232002	V.M. Abazov et al.	(D0 Collab.)

b -baryon ADMIXTURE ($\Lambda_b, \Xi_b, \Omega_b$)

b -baryon ADMIXTURE MEAN LIFE

Each measurement of the b -baryon mean life is an average over an admixture of various b baryons which decay weakly. Different techniques emphasize different admixtures of produced particles, which could result in a different b -baryon mean life. More b -baryon flavor specific channels are not included in the measurement.

VALUE (10^{-12} s)	EVTS	DOCUMENT ID	TECN	COMMENT
-----------------------	------	-------------	------	---------

- • • We do not use the following data for averages, fits, limits, etc. • • •
- $1.218^{+0.130}_{-0.115} \pm 0.042$ ¹ ABAZOV 07S D0 Repl. by ABAZOV 12u
- $1.22^{+0.22}_{-0.18} \pm 0.04$ ¹ ABAZOV 05c D0 Repl. by ABAZOV 07s
- $1.16 \pm 0.20 \pm 0.08$ ² ABREU 99W DLPH $e^+e^- \rightarrow Z$
- $1.19 \pm 0.14 \pm 0.07$ ³ ABREU 99W DLPH $e^+e^- \rightarrow Z$

Baryon Particle Listings

b -baryon ADMIXTURE ($\Lambda_b, \Xi_b, \Omega_b$)

1.14 ± 0.08 ± 0.04	4	ABREU	99W	DLPH	$e^+e^- \rightarrow Z$
1.11 $^{+0.19}_{-0.18}$ ± 0.05	5	ABREU	99W	DLPH	$e^+e^- \rightarrow Z$
1.29 $^{+0.24}_{-0.22}$ ± 0.06	5	ACKERSTAFF	98G	OPAL	$e^+e^- \rightarrow Z$
1.20 ± 0.08 ± 0.06	6	BARATE	98D	ALEP	$e^+e^- \rightarrow Z$
1.21 ± 0.11	5	BARATE	98D	ALEP	$e^+e^- \rightarrow Z$
1.32 ± 0.15 ± 0.07	7	ABE	96M	CDF	$p\bar{p}$ at 1.8 TeV
1.46 $^{+0.22}_{-0.21}$ $^{+0.07}_{-0.09}$		ABREU	96D	DLPH	Repl. by ABREU 99W
1.10 $^{+0.19}_{-0.17}$ ± 0.09	5	ABREU	96D	DLPH	$e^+e^- \rightarrow Z$
1.16 ± 0.11 ± 0.06	5	AKERS	96	OPAL	$e^+e^- \rightarrow Z$
1.27 $^{+0.35}_{-0.29}$ ± 0.09		ABREU	95S	DLPH	Repl. by ABREU 99W
1.05 $^{+0.12}_{-0.11}$ ± 0.09	290	BUSKULIC	95L	ALEP	Repl. by BARATE 98D
1.04 $^{+0.48}_{-0.38}$ ± 0.10	11	8 ABREU	93F	DLPH	Excess $\Lambda\mu^-$, decay lengths
1.05 $^{+0.23}_{-0.20}$ ± 0.08	157	9 AKERS	93	OPAL	Excess $\Lambda\ell^-$, decay lengths
1.12 $^{+0.32}_{-0.29}$ ± 0.16	101	10 BUSKULIC	92I	ALEP	Excess $\Lambda\ell^-$, impact parameters

- Measured mean life using fully reconstructed $\Lambda_b^0 \rightarrow J/\psi\Lambda$ decays.
- Measured using $\Lambda\ell^-$ decay length.
- Measured using $p\ell^-$ decay length.
- This ABREU 99W result is the combined result of the $\Lambda\ell^-$, $p\ell^-$, and excess $\Lambda\mu^-$ impact parameter measurements.
- Measured using $\Lambda_C\ell^-$ and $\Lambda\ell^+\ell^-$.
- Measured using the excess of $\Lambda\ell^-$, lepton impact parameter.
- Measured using $\Lambda_C\ell^-$.
- ABREU 93F superseded by ABREU 96D.
- AKERS 93 superseded by AKERS 96.
- BUSKULIC 92I superseded by BUSKULIC 95L.

b -baryon ADMIXTURE DECAY MODES ($\Lambda_b, \Xi_b, \Omega_b$)

These branching fractions are actually an average over weakly decaying b -baryons weighted by their production rates at the LHC, LEP, and Tevatron, branching ratios, and detection efficiencies. They scale with the b -baryon production fraction $B(b \rightarrow b\text{-baryon})$.

The branching fractions $B(b\text{-baryon} \rightarrow \Lambda\ell^-\bar{\nu}_\ell\text{anything})$ and $B(\Lambda_b^0 \rightarrow \Lambda_C^+\ell^-\bar{\nu}_\ell\text{anything})$ are not pure measurements because the underlying measured products of these with $B(b \rightarrow b\text{-baryon})$ were used to determine $B(b \rightarrow b\text{-baryon})$, as described in the note "Production and Decay of b -Flavored Hadrons."

For inclusive branching fractions, e.g., $B \rightarrow D^\pm\text{anything}$, the values usually are multiplicities, not branching fractions. They can be greater than one.

Mode	Fraction (Γ_j/Γ)
Γ_1 $p\mu^-\bar{\nu}$ anything	(5.8 $^{+2.3}_{-2.0}$) %
Γ_2 $p\ell\bar{\nu}_\ell$ anything	(5.6 ± 1.2) %
Γ_3 p anything	(70 ± 22) %
Γ_4 $\Lambda\ell^-\bar{\nu}_\ell$ anything	(3.8 ± 0.6) %
Γ_5 $\Lambda\ell^+\nu_\ell$ anything	(3.2 ± 0.8) %
Γ_6 Λ anything	(39 ± 7) %
Γ_7 $\Xi^-\ell^-\bar{\nu}_\ell$ anything	(6.6 ± 1.6) × 10 ⁻³

b -baryon ADMIXTURE ($\Lambda_b, \Xi_b, \Omega_b$) BRANCHING RATIOS

$\Gamma(p\mu^-\bar{\nu}\text{anything})/\Gamma_{\text{total}}$	Γ_1/Γ			
VALUE (%)	EVTS	DOCUMENT ID	TECN	COMMENT
5.8 $^{+2.3}_{-1.9}$ ± 0.8	125	11 ABREU	95S	DLPH $e^+e^- \rightarrow Z$

11 ABREU 95S reports [$\Gamma(b\text{-baryon} \rightarrow p\mu^-\bar{\nu}\text{anything})/\Gamma_{\text{total}}$] × [$B(\bar{b} \rightarrow b\text{-baryon})$] = 0.0049 ± 0.0011 $^{+0.0015}_{-0.0011}$ which we divide by our best value $B(\bar{b} \rightarrow b\text{-baryon})$ = (8.4 ± 1.1) × 10⁻². Our first error is their experiment's error and our second error is the systematic error from using our best value.

$\Gamma(p\ell\bar{\nu}_\ell\text{anything})/\Gamma_{\text{total}}$	Γ_2/Γ			
VALUE (%)	DOCUMENT ID	TECN	COMMENT	
5.6 ± 0.9 ± 0.7	12	BARATE	98V	ALEP $e^+e^- \rightarrow Z$

12 BARATE 98V reports [$\Gamma(b\text{-baryon} \rightarrow p\ell\bar{\nu}_\ell\text{anything})/\Gamma_{\text{total}}$] × [$B(\bar{b} \rightarrow b\text{-baryon})$] = (4.72 ± 0.66 ± 0.44) × 10⁻³ which we divide by our best value $B(\bar{b} \rightarrow b\text{-baryon})$ = (8.4 ± 1.1) × 10⁻². Our first error is their experiment's error and our second error is the systematic error from using our best value.

$\Gamma(p\ell\bar{\nu}_\ell\text{anything})/\Gamma(p\text{anything})$	Γ_2/Γ_3			
VALUE (%)	DOCUMENT ID	TECN	COMMENT	
8.0 ± 1.2 ± 1.4		BARATE	98V	ALEP $e^+e^- \rightarrow Z$

$\Gamma(\Lambda\ell^-\bar{\nu}_\ell\text{anything})/\Gamma_{\text{total}}$ Γ_4/Γ
 The values and averages in this section serve only to show what values result if one assumes our $B(b \rightarrow b\text{-baryon})$. They cannot be thought of as measurements since the underlying product branching fractions were also used to determine $B(b \rightarrow b\text{-baryon})$ as described in the note on "Production and Decay of b -Flavored Hadrons."

VALUE (%)	EVTS	DOCUMENT ID	TECN	COMMENT	
3.8 ± 0.6 OUR AVERAGE					
3.9 ± 0.5 ± 0.5		13	BARATE	98D	ALEP $e^+e^- \rightarrow Z$
3.5 ± 0.4 ± 0.5		14	AKERS	96	OPAL Excess of $\Lambda\ell^-$ over $\Lambda\ell^+$
3.6 ± 0.9 ± 0.5	262	15	ABREU	95S	DLPH Excess of $\Lambda\ell^-$ over $\Lambda\ell^+$
7.3 ± 1.4 ± 1.0	290	16	BUSKULIC	95L	ALEP Excess of $\Lambda\ell^-$ over $\Lambda\ell^+$

- • • We do not use the following data for averages, fits, limits, etc. • • •
- seen 157 ¹⁷AKERS 93 OPAL Excess of $\Lambda\ell^-$ over $\Lambda\ell^+$
- 8.3 ± 2.5 ± 1.1 101 ¹⁸BUSKULIC 92I ALEP Excess of $\Lambda\ell^-$ over $\Lambda\ell^+$
- ¹³BARATE 98D reports [$\Gamma(b\text{-baryon} \rightarrow \Lambda\ell^-\bar{\nu}_\ell\text{anything})/\Gamma_{\text{total}}$] × [$B(\bar{b} \rightarrow b\text{-baryon})$] = 0.00326 ± 0.00016 ± 0.00039 which we divide by our best value $B(\bar{b} \rightarrow b\text{-baryon})$ = (8.4 ± 1.1) × 10⁻². Our first error is their experiment's error and our second error is the systematic error from using our best value. Measured using the excess of $\Lambda\ell^-$, lepton impact parameter.
- ¹⁴AKERS 96 reports [$\Gamma(b\text{-baryon} \rightarrow \Lambda\ell^-\bar{\nu}_\ell\text{anything})/\Gamma_{\text{total}}$] × [$B(\bar{b} \rightarrow b\text{-baryon})$] = 0.00291 ± 0.00023 ± 0.00025 which we divide by our best value $B(\bar{b} \rightarrow b\text{-baryon})$ = (8.4 ± 1.1) × 10⁻². Our first error is their experiment's error and our second error is the systematic error from using our best value.
- ¹⁵ABREU 95S reports [$\Gamma(b\text{-baryon} \rightarrow \Lambda\ell^-\bar{\nu}_\ell\text{anything})/\Gamma_{\text{total}}$] × [$B(\bar{b} \rightarrow b\text{-baryon})$] = 0.0030 ± 0.0006 ± 0.0004 which we divide by our best value $B(\bar{b} \rightarrow b\text{-baryon})$ = (8.4 ± 1.1) × 10⁻². Our first error is their experiment's error and our second error is the systematic error from using our best value.
- ¹⁶BUSKULIC 95L reports [$\Gamma(b\text{-baryon} \rightarrow \Lambda\ell^-\bar{\nu}_\ell\text{anything})/\Gamma_{\text{total}}$] × [$B(\bar{b} \rightarrow b\text{-baryon})$] = 0.0061 ± 0.0006 ± 0.0010 which we divide by our best value $B(\bar{b} \rightarrow b\text{-baryon})$ = (8.4 ± 1.1) × 10⁻². Our first error is their experiment's error and our second error is the systematic error from using our best value.
- ¹⁷AKERS 93 superseded by AKERS 96.
- ¹⁸BUSKULIC 92I reports [$\Gamma(b\text{-baryon} \rightarrow \Lambda\ell^-\bar{\nu}_\ell\text{anything})/\Gamma_{\text{total}}$] × [$B(\bar{b} \rightarrow b\text{-baryon})$] = 0.0070 ± 0.0010 ± 0.0018 which we divide by our best value $B(\bar{b} \rightarrow b\text{-baryon})$ = (8.4 ± 1.1) × 10⁻². Our first error is their experiment's error and our second error is the systematic error from using our best value. Superseded by BUSKULIC 95L.

$\Gamma(\Lambda\ell^+\nu_\ell\text{anything})/\Gamma(\Lambda\text{anything})$	Γ_5/Γ_6			
VALUE (units 10 ⁻²)	DOCUMENT ID	TECN	COMMENT	
8.0 ± 1.2 ± 0.8		ABBIENDI	99L	OPAL $e^+e^- \rightarrow Z$
• • • We do not use the following data for averages, fits, limits, etc. • • •				
7.0 ± 1.2 ± 0.7		ACKERSTAFF	97N	OPAL Repl. by ABBIENDI 99L

$\Gamma(\Lambda\text{anything})/\Gamma_{\text{total}}$	Γ_6/Γ			
VALUE (%)	DOCUMENT ID	TECN	COMMENT	
39 ± 7 OUR AVERAGE				
42 ± 6 ± 5	19	ABBIENDI	99L	OPAL $e^+e^- \rightarrow Z$
27 $^{+15}_{-9}$ ± 3	20	ABREU	95C	DLPH $e^+e^- \rightarrow Z$

- • • We do not use the following data for averages, fits, limits, etc. • • •
- 47 ± 7 ± 6 ²¹ACKERSTAFF 97N OPAL Repl. by ABBIENDI 99L
- ¹⁹ABBIENDI 99L reports [$\Gamma(b\text{-baryon} \rightarrow \Lambda\text{anything})/\Gamma_{\text{total}}$] × [$B(\bar{b} \rightarrow b\text{-baryon})$] = 0.035 ± 0.0032 ± 0.0035 which we divide by our best value $B(\bar{b} \rightarrow b\text{-baryon})$ = (8.4 ± 1.1) × 10⁻². Our first error is their experiment's error and our second error is the systematic error from using our best value.
- ²⁰ABREU 95C reports 0.28 $^{+0.17}_{-0.12}$ from a measurement of [$\Gamma(b\text{-baryon} \rightarrow \Lambda\text{anything})/\Gamma_{\text{total}}$] × [$B(\bar{b} \rightarrow b\text{-baryon})$] assuming $B(\bar{b} \rightarrow b\text{-baryon})$ = 0.08 ± 0.02, which we rescale to our best value $B(\bar{b} \rightarrow b\text{-baryon})$ = (8.4 ± 1.1) × 10⁻². Our first error is their experiment's error and our second error is the systematic error from using our best value.
- ²¹ACKERSTAFF 97N reports [$\Gamma(b\text{-baryon} \rightarrow \Lambda\text{anything})/\Gamma_{\text{total}}$] × [$B(\bar{b} \rightarrow b\text{-baryon})$] = 0.0393 ± 0.0046 ± 0.0037 which we divide by our best value $B(\bar{b} \rightarrow b\text{-baryon})$ = (8.4 ± 1.1) × 10⁻². Our first error is their experiment's error and our second error is the systematic error from using our best value.

$\Gamma(\Xi^-\ell^-\bar{\nu}_\ell\text{anything})/\Gamma_{\text{total}}$	Γ_7/Γ			
VALUE (units 10 ⁻³)	DOCUMENT ID	TECN	COMMENT	
6.6 ± 1.6 OUR AVERAGE				
6.4 ± 1.6 ± 0.8	22	BUSKULIC	96T	ALEP Excess $\Xi^-\ell^-$ over $\Xi^-\ell^+$
7.0 ± 2.8 ± 0.9	23	ABREU	95V	DLPH Excess $\Xi^-\ell^-$ over $\Xi^-\ell^+$

- ²²BUSKULIC 96T reports [$\Gamma(b\text{-baryon} \rightarrow \Xi^-\ell^-\bar{\nu}_\ell\text{anything})/\Gamma_{\text{total}}$] × [$B(\bar{b} \rightarrow b\text{-baryon})$] = 0.00054 ± 0.00011 ± 0.00008 which we divide by our best value $B(\bar{b} \rightarrow b\text{-baryon})$ = (8.4 ± 1.1) × 10⁻². Our first error is their experiment's error and our second error is the systematic error from using our best value.
- ²³ABREU 95V reports [$\Gamma(b\text{-baryon} \rightarrow \Xi^-\ell^-\bar{\nu}_\ell\text{anything})/\Gamma_{\text{total}}$] × [$B(\bar{b} \rightarrow b\text{-baryon})$] = 0.00059 ± 0.00021 ± 0.0001 which we divide by our best value $B(\bar{b} \rightarrow b\text{-baryon})$ = (8.4 ± 1.1) × 10⁻². Our first error is their experiment's error and our second error is the systematic error from using our best value.

b -baryon ADMIXTURE ($\Lambda_b, \Xi_b, \Omega_b$) REFERENCES

ABAZOV	12U	PR	D85	112003	V.M. Abazov et al.	(DO Collab.)
ABAZOV	07S	PRL	99	142001	V.M. Abazov et al.	(DO Collab.)
ABAZOV	05C	PRL	94	102001	V.M. Abazov et al.	(DO Collab.)
ABBIENDI	99L	EPJ	C9	1	G. Abbiendi et al.	(OPAL Collab.)
ABREU	99W	EPJ	C10	185	P. Abreu et al.	(DELPHI Collab.)
ACKERSTAFF	98G	PL	B426	161	K. Ackerstaff et al.	(OPAL Collab.)
BARATE	98D	EPJ	C2	197	R. Barate et al.	(ALEPH Collab.)
BARATE	98V	EPJ	C5	205	R. Barate et al.	(ALEPH Collab.)
ACKERSTAFF	97N	ZPHY	C74	423	K. Ackerstaff et al.	(OPAL Collab.)
ABE	96M	PRL	77	1439	F. Abe et al.	(CDF Collab.)

See key on page 999

Baryon Particle Listings

b -baryon ADMIXTURE ($\Lambda_b, \Xi_b, \Omega_b$)

ABREU	96D	ZPHY C71 199	P. Abreu <i>et al.</i>	(DELPHI Collab.)	ABREU	95V	ZPHY C68 541	P. Abreu <i>et al.</i>	(DELPHI Collab.)
AKERS	96	ZPHY C69 195	R. Akers <i>et al.</i>	(OPAL Collab.)	BUSKULIC	95L	PL B357 685	D. Buskulic <i>et al.</i>	(ALEPH Collab.)
BUSKULIC	96T	PL B384 449	D. Buskulic <i>et al.</i>	(ALEPH Collab.)	ABREU	93F	PL B311 379	P. Abreu <i>et al.</i>	(DELPHI Collab.)
ABREU	95C	PL B347 447	P. Abreu <i>et al.</i>	(DELPHI Collab.)	AKERS	93	PL B316 435	R. Akers <i>et al.</i>	(OPAL Collab.)
ABREU	95S	ZPHY C68 375	P. Abreu <i>et al.</i>	(DELPHI Collab.)	BUSKULIC	92I	PL B297 449	D. Buskulic <i>et al.</i>	(ALEPH Collab.)

Baryon Particle Listings

Pentaquarks, $P_c(4312)^+$, $P_c(4380)^+$, $P_c(4440)^+$, $P_c(4457)^+$ **EXOTIC BARYONS**

See the related review(s):

Pentaquarks

 $P_c(4312)^+$ Status: * $P_c(4312)^+$ MASS

VALUE (MeV)	DOCUMENT ID	TECN	COMMENT
$4311.9 \pm 0.7^{+6.8}_{-0.6}$	AAIJ	19W LHCb	<i>pp</i> at 7, 8, 13 TeV

 $P_c(4312)^+$ WIDTH

VALUE (MeV)	DOCUMENT ID	TECN	COMMENT
$9.8 \pm 2.7^{+3.7}_{-4.5}$	AAIJ	19W LHCb	<i>pp</i> at 7, 8, 13 TeV

 $P_c(4312)^+$ DECAY MODES

Mode	Fraction (Γ_i/Γ)
Γ_1 $J/\psi p$	seen

 $P_c(4312)^+$ BRANCHING RATIOS

$\Gamma(J/\psi p)/\Gamma_{\text{total}}$	Γ_1/Γ		
VALUE	DOCUMENT ID	TECN	COMMENT
seen	AAIJ	19W LHCb	<i>pp</i> at 7, 8, 13 TeV

 $P_c(4312)^+$ REFERENCES

AAIJ 19W PRL 122 222001 R. Aaij et al. (LHCb Collab.)

 $P_c(4380)^+$ Status: *

A resonance seen in $\Lambda_b^0 \rightarrow P_c^+ K^-$, then $P_c \rightarrow J/\psi p$, with a significance of 9 standard deviations. The $J/\psi p$ quark content is $uudc\bar{c}$, a pentaquark. See also the $P_c(4450)^+$. In the best amplitude fit, the two states have opposite parity, one having $J = 3/2$, the other $J = 5/2$.

Extraction of the pentaquark signals requires some understanding of the dominant $K^- p$ background. AAIJ 15P used a model-dependent approach. AAIJ 16AG reanalyzed the data making minimal assumptions about the $K^- p$ background, and thus confirmed the strong significance of the pentaquark signals.

 $P_c(4380)^+$ MASS

VALUE (MeV)	DOCUMENT ID	TECN	COMMENT
$4380 \pm 8 \pm 29$	AAIJ	15P LHCb	<i>pp</i> at 7, 8 TeV

 $P_c(4380)^+$ WIDTH

VALUE (MeV)	DOCUMENT ID	TECN	COMMENT
$205 \pm 18 \pm 86$	AAIJ	15P LHCb	<i>pp</i> at 7, 8 TeV

 $P_c(4380)^+$ DECAY MODES

Mode	Fraction (Γ_i/Γ)
Γ_1 $J/\psi p$	seen

 $P_c(4380)^+$ BRANCHING RATIOS

$\Gamma(J/\psi p)/\Gamma_{\text{total}}$	Γ_1/Γ		
VALUE	DOCUMENT ID	TECN	COMMENT
seen	AAIJ	15P LHCb	<i>pp</i> at 7, 8 TeV

 $P_c(4380)^+$ REFERENCESAAIJ 16AG PRL 117 082002 R. Aaij et al. (LHCb Collab.)
AAIJ 15P PRL 115 072001 R. Aaij et al. (LHCb Collab.) $P_c(4440)^+$

Status: *

 $P_c(4440)^+$ MASS

VALUE (MeV)	DOCUMENT ID	TECN	COMMENT
$4440.3 \pm 1.3^{+4.1}_{-4.7}$	AAIJ	19W LHCb	<i>pp</i> at 7, 8, 13 TeV

 $P_c(4440)^+$ WIDTH

VALUE (MeV)	DOCUMENT ID	TECN	COMMENT
$20.6 \pm 4.9^{+8.7}_{-10.1}$	AAIJ	19W LHCb	<i>pp</i> at 7, 8, 13 TeV

 $P_c(4440)^+$ DECAY MODES

Mode	Fraction (Γ_i/Γ)
Γ_1 $J/\psi p$	seen

 $P_c(4440)^+$ BRANCHING RATIOS

$\Gamma(J/\psi p)/\Gamma_{\text{total}}$	Γ_1/Γ		
VALUE	DOCUMENT ID	TECN	COMMENT
seen	AAIJ	19W LHCb	<i>pp</i> at 7, 8, 13 TeV

 $P_c(4440)^+$ REFERENCES

AAIJ 19W PRL 122 222001 R. Aaij et al. (LHCb Collab.)

 $P_c(4457)^+$

Status: *

was $P_c(4450)$

A resonance seen in $\Lambda_b^0 \rightarrow P_c^+ K^-$, then $P_c \rightarrow J/\psi p$, with a significance of 12 standard deviations. The $J/\psi p$ quark content is $uudc\bar{c}$, a pentaquark. See also the $P_c(4380)^+$. In the best amplitude fit, the two states have opposite parity, one having $J = 3/2$, the other $J = 5/2$.

Extraction of the pentaquark signals requires some understanding of the dominant $K^- p$ background. AAIJ 15P used a model-dependent approach. AAIJ 16AG reanalyzed the data making minimal assumptions about the $K^- p$ background, and thus confirmed the strong significance of the pentaquark signals.

 $P_c(4457)^+$ MASS

VALUE (MeV)	DOCUMENT ID	TECN	COMMENT
$4457.3 \pm 0.6^{+4.1}_{-1.7}$	AAIJ	19W LHCb	<i>pp</i> at 7, 8, 13 TeV

• • • We do not use the following data for averages, fits, limits, etc. • • •
 $4449.8 \pm 1.7 \pm 2.5$ ¹ AAIJ 15P LHCb Repl. by AAIJ 19W
¹ Considering $P_c(4440)$ and $P_c(4457)$ as a single resonance.

 $P_c(4457)^+$ WIDTH

VALUE (MeV)	DOCUMENT ID	TECN	COMMENT
$6.4 \pm 2.0^{+5.7}_{-1.9}$	AAIJ	19W LHCb	<i>pp</i> at 7, 8, 13 TeV

• • • We do not use the following data for averages, fits, limits, etc. • • •
 $39 \pm 5 \pm 19$ ¹ AAIJ 15P LHCb Repl. by AAIJ 19W
¹ Considering $P_c(4440)$ and $P_c(4457)$ as a single resonance.

 $P_c(4457)^+$ DECAY MODES

Mode	Fraction (Γ_i/Γ)
Γ_1 $J/\psi p$	seen

 $P_c(4457)^+$ BRANCHING RATIOS

$\Gamma(J/\psi p)/\Gamma_{\text{total}}$	Γ_1/Γ		
VALUE	DOCUMENT ID	TECN	COMMENT
seen	AAIJ	19W LHCb	<i>pp</i> at 7, 8, 13 TeV
seen	AAIJ	15P LHCb	<i>pp</i> at 7, 8 TeV

 $P_c(4457)^+$ REFERENCESAAIJ 19W PRL 122 222001 R. Aaij et al. (LHCb Collab.)
AAIJ 16AG PRL 117 082002 R. Aaij et al. (LHCb Collab.)
AAIJ 15P PRL 115 072001 R. Aaij et al. (LHCb Collab.)

MISCELLANEOUS SEARCHES

Magnetic Monopole Searches	2017
Supersymmetric Particle Searches	2019
Technicolor	2062
Quark and Lepton Compositeness	2063
Extra Dimensions	2067
WIMP and Dark Matter Searches	2073
Other Particle Searches	2085

SEARCHES IN OTHER SECTIONS

Neutral Higgs Bosons, Searches for	1056
Charged Higgs Bosons (H^\pm and $H^{\pm\pm}$), Searches for	1065
New Heavy Bosons	1068
Axions (A^0) and Other Very Light Bosons	1084
Heavy Charged Lepton Searches	1134
Double- β Decay	1145
Heavy Neutral Leptons, Searches for	1168
b' (Fourth Generation) Quark	1197
t' (Fourth Generation) Quark	1199
Free Quark Searches	1201

Related Reviews in Volume 1

86. Extra dimensions (rev.)	889
87. W' -boson searches (rev.)	897
88. Z' -boson searches (rev.)	900
89. Supersymmetry: theory (rev.)	905
90. Supersymmetry: experiment (rev.)	923
91. Axions and other similar particles (rev.)	939
92. Quark and lepton compositeness, searches for (rev.)	953
93. Dynamical electroweak symmetry	958
breaking: implications of the $H(0)$ (rev.)	
94. Grand unified theories (rev.)	971
95. Leptoquarks (rev.)	986
96. Magnetic monopoles (rev.)	989

**SEARCHES
not in other sections**

Magnetic Monopole Searches

See the related review(s):
Magnetic Monopoles

Monopole Production Cross Section — Accelerator Searches

X-SECT (cm ²)	MASS (GeV)	CHG (g)	ENERGY (GeV)	BEAM	DOCUMENT ID	TECN
<2.5E-37	200-6000		1 13000	pp	1 ACHARYA 17	INDU
<2E-37	200-6000		2 13000	pp	1 ACHARYA 17	INDU
<4E-37	200-5000		3 13000	pp	1 ACHARYA 17	INDU
<1.5E-36	400-4000		4 13000	pp	1 ACHARYA 17	INDU
<7E-36	1000-3000		5 13000	pp	1 ACHARYA 17	INDU
<5E-40	200-2500	0.5-2.0	8000	pp	2 AAD 16AB	ATLS
<2E-37	100-3500		1 8000	pp	3 ACHARYA 16	INDU
<2E-37	100-3500		2 8000	pp	3 ACHARYA 16	INDU
<6E-37	500-3000		3 8000	pp	3 ACHARYA 16	INDU
<7E-36	1000-2000		4 8000	pp	3 ACHARYA 16	INDU
<1.6E-38	200-1200		1 7000	pp	4 AAD 12CS	ATLS
<5E-38	45-102		1 206	e ⁺ e ⁻	5 ABBIENDI 08	OPAL
<0.2E-36	200-700		1 1960	p \bar{p}	6 ABULENCIA 06K	CNTR
< 2.E-36			1 300	e ⁺ p	7.8 AKTAS 05A	INDU
< 0.2 E-36			2 300	e ⁺ p	7.8 AKTAS 05A	INDU
< 0.09E-36			3 300	e ⁺ p	7.8 AKTAS 05A	INDU
< 0.05E-36		≥ 6	300	e ⁺ p	7.8 AKTAS 05A	INDU
< 2.E-36			1 300	e ⁺ p	7.9 AKTAS 05A	INDU
< 0.2E-36			2 300	e ⁺ p	7.9 AKTAS 05A	INDU
< 0.07E-36			3 300	e ⁺ p	7.9 AKTAS 05A	INDU
< 0.06E-36		≥ 6	300	e ⁺ p	7.9 AKTAS 05A	INDU
< 0.6E-36	>265		1 1800	p \bar{p}	10 KALBFLEISCH 04	INDU
< 0.2E-36	>355		2 1800	p \bar{p}	10 KALBFLEISCH 04	INDU
< 0.07E-36	>410		3 1800	p \bar{p}	10 KALBFLEISCH 04	INDU
< 0.2E-36	>375		6 1800	p \bar{p}	10 KALBFLEISCH 04	INDU
< 0.7E-36	>295		1 1800	p \bar{p}	11,12 KALBFLEISCH 00	INDU
< 7.8E-36	>260		2 1800	p \bar{p}	11,12 KALBFLEISCH 00	INDU
< 2.3E-36	>325		3 1800	p \bar{p}	11,13 KALBFLEISCH 00	INDU
< 0.11E-36	>420		6 1800	p \bar{p}	11,13 KALBFLEISCH 00	INDU
<0.65E-33	<3.3	≥ 2	11A	¹⁹⁷ Au	14,15 HE 97	
<1.90E-33	<8.1	≥ 2	160A	²⁰⁸ Pb	14,15 HE 97	
<3.E-37	<45.0	1.0	88-94	e ⁺ e ⁻	PINFOLD 93	PLAS
<3.E-37	<41.6	2.0	88-94	e ⁺ e ⁻	PINFOLD 93	PLAS
<7.E-35	<44.9	0.2-1.0	89-93	e ⁺ e ⁻	KINOSHITA 92	PLAS
<2.E-34	<850	≥ 0.5	1800	p \bar{p}	BERTANI 90	PLAS
<1.2E-33	<800	≥ 1	1800	p \bar{p}	PRICE 90	PLAS
<1.E-37	<29	1	50-61	e ⁺ e ⁻	KINOSHITA 89	PLAS
<1.E-37	<18	2	50-61	e ⁺ e ⁻	KINOSHITA 89	PLAS
<1.E-38	<17	<1	35	e ⁺ e ⁻	BRAUNSCH... 88B	CNTR
<8.E-37	<24	1	50-52	e ⁺ e ⁻	KINOSHITA 88	PLAS
<1.3E-35	<22	2	50-52	e ⁺ e ⁻	KINOSHITA 88	PLAS
<9.E-37	<4	<0.15	10.6	e ⁺ e ⁻	GENTILE 87	CLEO
<3.E-32	<800	≥ 1	1800	p \bar{p}	PRICE 87	PLAS
<3.E-38	<3	<3	29	e ⁺ e ⁻	FRYBERGER 84	PLAS
<1.E-31	<1,3	1,3	540	p \bar{p}	AUBERT 83B	PLAS
<4.E-38	<10	<6	34	e ⁺ e ⁻	MUSSET 83	PLAS
<8.E-36	<20		52	pp	16 DELL 82	CNTR
<9.E-37	<30	<3	29	e ⁺ e ⁻	KINOSHITA 82	PLAS
<1.E-37	<20	<24	63	p \bar{p}	CARRIGAN 78	CNTR
<1.E-37	<30	<3	56	pp	HOFFMANN 78	PLAS
<4.E-33			300	p	16 DELL 76	SPRK
<1.E-40	<5	<2	70	p	16 STEVENS 76B	SPRK
<2.E-30			300	n	17 ZRELOV 76	CNTR
<1.E-38			8	ν	16 BURKE 75	OSPK
<5.E-43	<12	<10	400	p	18 CARRIGAN 75	HLBC
<2.E-36	<30	<3	60	pp	EBERHARD 75B	INDU
<5.E-42	<13	<24	400	p	GIACOMELLI 75	PLAS
<6.E-42	<12	<24	300	p	CARRIGAN 74	CNTR
<2.E-36		1	0.001	γ	CARRIGAN 73	CNTR
<1.E-41	<5		70	p	17 BARTLETT 72	CNTR
<1.E-40	<3	<2	28	p	GUREVICH 72	EMUL
<2.E-40	<3	<2	30	p	AMALDI 63	EMUL
<1.E-35	<3	<4	28	p	PURCELL 63	CNTR
<2.E-35	<1	1	6	p	FIDECARO 61	CNTR
					BRADNER 59	EMUL

• • • We do not use the following data for averages, fits, limits, etc. • • •

<1.3E-40	200-4000	1	13000	pp	¹⁹ AAD	20G	ATLS
<5.6E-40	500-4000	2	13000	pp	¹⁹ AAD	20G	ATLS
	200-5000	2	13000	pp	²⁰ ACHARYA	19B	INDU
	200-5000	1	13000	pp	²¹ ACHARYA	18A	INDU

- The search was sensitive to monopoles which had stopped in aluminium trapping volumes. Monopoles with spins 0 and 1/2 were considered; mass-dependent spin 1/2 monopole limits are quoted here.
- AAD 16AB model-independent 95% CL limits estimated using a fiducial region of approximately constant acceptance. Limits are mass-dependent.
- ACHARYA 16 limits at 95% CL estimated using a Dreil-Yan-like production mechanism for scalar monopoles.
- AAD 12Cs searched for monopoles as highly ionising objects. The cross section limits are based on an assumed Dreil-Yan-like production process for spin 1/2 monopoles. The limits are mass- and scenario-dependent.
- ABBIENDI 08 assume production of spin 1/2 monopoles with effective charge $g\beta$ ($n=1$), via $e^+e^- \rightarrow \gamma^* \rightarrow M\bar{M}$, so that the cross section is proportional to $(1 + \cos^2\theta)$. There is no z information for such highly saturated tracks, so a parabolic track in the jet chamber is projected onto the xy plane. Charge per hit in the chamber produces a clean separation of signal and background.
- ABULENCIA 06k searches for high-ionizing signals in CDF central outer tracker and time-of-flight detector. For Dreil-Yan $M\bar{M}$ production, the cross section limit implies $M > 360$ GeV at 95% CL.
- AKTAS 05A model-dependent limits as a function of monopole mass shown for arbitrary mass of 60 GeV. Based on search for stopped monopoles in the H1 Al beam pipe.
- AKTAS 05A limits with assumed elastic spin 0 monopole pair production.
- AKTAS 05A limits with assumed inelastic spin 1/2 monopole pair production.
- KALBFLEISCH 04 reports searches for stopped magnetic monopoles in Be, Al, and Pb samples obtained from discarded material from the upgrading of DØ and CDF. A large-aperture warm-bore cryogenic detector was used. The approach was an extension of the methods of KALBFLEISCH 00. Cross section results moderately model dependent; interpretation as a mass lower limit depends on possibly invalid perturbation expansion.
- KALBFLEISCH 00 used an induction method to search for stopped monopoles in pieces of the DØ (FNAL) beryllium beam pipe and in extensions to the drift chamber aluminium support cylinder. Results are model dependent.
- KALBFLEISCH 00 result is for aluminium.
- KALBFLEISCH 00 result is for beryllium.
- HE 97 used a lead target and barium phosphate glass detectors. Cross-section limits are well below those predicted via the Dreil-Yan mechanism.
- This work has also been reinterpreted in the framework of monopole production via the thermal Schwinger process (GOULD 17); this gives rise to lower mass limits.
- Multiphoton events.
- Cherenkov radiation polarization.
- Re-examines CERN neutrino experiments.
- AAD 20c give limits for Dreil-Yan production with spin-0 and spin-1/2 monopoles. The above limit is for spin = 0 at mass = 3 TeV.
- ACHARYA 19b limits both β -dependent and β -independent on monopoles with spins 0, 1/2, and 1 and with magnetic charges ranging from one to five times the Dirac charge in mass ranges between 200 GeV and 5000 GeV.
- ACHARYA 18A provide limits on monopoles with spins 0, 1/2, and 1 and with magnetic charges ranging from two to five times the Dirac charge.

Monopole Production — Other Accelerator Searches

MASS (GeV)	CHG (g)	SPIN	ENERGY (GeV)	BEAM	DOCUMENT ID	TECN
> 610	≥ 1	0	1800	p \bar{p}	1 ABBOTT 98K	D0
> 870	≥ 1	1/2	1800	p \bar{p}	1 ABBOTT 98K	D0
>1580	≥ 1	1	1800	p \bar{p}	1 ABBOTT 98K	D0
> 510			88-94	e ⁺ e ⁻	2 ACCIARRI 95c	L3

- ABBOTT 98k search for heavy pointlike Dirac monopoles via central production of a pair of photons with high transverse energies.
- ACCIARRI 95c finds a limit $B(Z \rightarrow \gamma\gamma) < 0.8 \times 10^{-5}$ (which is possible via a monopole loop) at 95% CL and sets the mass limit via a cross section model.

Monopole Flux — Cosmic Ray Searches

"Caty" in the charge column indicates a search for monopole-catalyzed nucleon decay.

FLUX (cm ⁻² sr ⁻¹ s ⁻¹)	MASS (GeV)	CHG (g)	COMMENTS ($\beta = v/c$)	EVTs	DOCUMENT ID	TECN
<1.5E-18		1	$\beta > 0.6$	0	1 ALBERT 17	ANTR
<2.5E-21		1	$1E8 < \gamma < 1E13$	0	2 AAB 16	AUGE
<1.55E-18			$\beta > 0.51$	0	3 AARTSEN 16B	ICCB
<1E-17		Caty	$1E-3 < \beta < 1E-2$	0	4 AARTSEN 14	ICCB
<3E-18			$\beta > 0.8$	0	5 ABBASI 13	ICCB
<1.3E-17		1	$\beta > 0.625$	0	6 ADRIAN-MAR.12A	ANTR
<6E-28	<1E17	Caty	$1E-5 < \beta < 0.04$	0	7 UENO 12	SKAM
<1E-19		1	$\gamma > 1E10$	0	8 DETRIXHE 11	ANIT
<3.8E-17		1	$\beta > 0.76$	0	5 ABBASI 10A	ICCB
<1.3E-15	$1E4 < M < 5E13$	1	$\beta > 0.05$	0	9 BALESTRA 08	PLAS
<0.65E-15	>5E13	1	$\beta > 0.05$	0	9 BALESTRA 08	PLAS
<1E-18		1	$\gamma > 1 E8$	0	8 HOGAN 08	RICE
<1.4E-16		1	$1.1E-4 < \beta < 1$	0	10 AMBROSIO 02B	MCRO
<3E-16		Caty	$1.1E-4 < \beta < 5E-3$	0	11 AMBROSIO 02c	MCRO
<1.5E-15		1	$5E-3 < \beta < 0.99$	0	12 AMBROSIO 02b	MCRO
<1E-15		1	$1.1 \times 10^{-4} - 0.1$	0	13 AMBROSIO 97	MCRO
<5.6E-15		1	(0.18-3.0)E-3	0	14 AHLEN 94	MCRO
<2.7E-15		Caty	$\beta \sim 1 \times 10^{-3}$	0	15 BECKER-SZ... 94	IMB
<8.7E-15		1	>2.E-3	0	THRON 92	SOUND
<4.4E-12		1	all β	0	GARDNER 91	INDU
<7.2E-13		1	all β	0	HUBER 91	INDU

Searches Particle Listings

Magnetic Monopole Searches

<3.7E-15	>E12	1	$\beta=1.E-4$	0	16	ORITO	91	PLAS
<3.2E-16	>E10	1	$\beta > 0.05$	0	16	ORITO	91	PLAS
<3.2E-16	>E10-E12	2,3		0	16	ORITO	91	PLAS
<3.8E-13		1	all β	0		BERMON	90	INDU
<5.E-16		Caty	$\beta < 1.E-3$	0	15	BEZRUKOV	90	CHER
<1.8E-14		1	$\beta > 1.1E-4$	0	17	BUCKLAND	90	HEPT
<1E-18			$3.E-4 < \beta < 1.5E-3$	0	18	GHOSH	90	MICA
<7.2E-13		1	all β	0		HUBER	90	INDU
<5.E-12	>E7	1	$3.E-4 < \beta < 5.E-3$	0		BARISH	87	CNTR
<1.E-13		Caty	$1.E-5 < \beta < 1$	0	15	BARTELT	87	SOUO
<1.E-10		1	all β	0		EBISU	87	INDU
<2.E-13			$1.E-4 < \beta < 6.E-4$	0		MASEK	87	HEPT
<2.E-14			$4.E-5 < \beta < 2.E-4$	0		NAKAMURA	87	PLAS
<2.E-14			$1.E-3 < \beta < 1$	0		NAKAMURA	87	PLAS
<5.E-14			$9.E-4 < \beta < 1.E-2$	0		SHEP KO	87	CNTR
<2.E-13			$4.E-4 < \beta < 1$	0		TSUKAMOTO	87	CNTR
<5.E-14		1	all β	1	19	CAPLIN	86	INDU
<5.E-12		1		0		CROMAR	86	INDU
<1.E-13		1	$7.E-4 < \beta$	0		HARA	86	CNTR
<7.E-11		1	all β	0		INCANDELA	86	INDU
<1.E-18			$4.E-4 < \beta < 1.E-3$	0	18	PRICE	86	MICA
<5.E-12		1		0		BERMON	85	INDU
<6.E-12		1		0		CAPLIN	85	INDU
<6.E-10		1		0		EBISU	85	INDU
<3.E-15		Caty	$5.E-5 \leq \beta \leq 1.E-3$	0	15	KAJITA	85	KAMI
<2.E-21		Caty	$\beta < 1.E-3$	0	15,20	KAJITA	85	KAMI
<3.E-15		Caty	$1.E-3 < \beta < 1.E-1$	0	15	PARK	85B	CNTR
<5.E-12		1	$1.E-4 < \beta < 1$	0		BATTISTONI	84	NUSX
<7.E-12		1		0		INCANDELA	84	INDU
<7.E-13		1	$3.E-4 < \beta$	0	17	KAJINO	84	CNTR
<2.E-12		1	$3.E-4 < \beta < 1.E-1$	0		KAJINO	84B	CNTR
<6.E-13		1	$5.E-4 < \beta < 1$	0		KAWAGOE	84	CNTR
<2.E-14			$1.E-3 < \beta$	0	15	KRISHNA...	84	CNTR
<4.E-13		1	$6.E-4 < \beta < 2.E-3$	0		LISS	84	CNTR
<1.E-16			$3.E-4 < \beta < 1.E-3$	0	18	PRICE	84	MICA
<1.E-13		1	$1.E-4 < \beta$	0		PRICE	84B	PLAS
<4.E-13		1	$6.E-4 < \beta < 2.E-3$	0		TARLE	84	CNTR
<4.E-13				7	21	ANDERSON	83	EMUL
<1.E-12		1	$1.E-2 < \beta < 1.E-3$	0		BARTELT	83B	CNTR
<3.E-13		1	$7.E-3 < \beta < 1$	0		BARWICK	83	PLAS
<3.E-12		1	$1.E-3 < \beta < 4.E-1$	0		BONARELLI	83	CNTR
<3.E-12		Caty	$5.E-4 < \beta < 5.E-2$	0	15	BOSETTI	83	CNTR
<4.E-11		1		0		CABRERA	83	INDU
<5.E-15		1	$1.E-2 < \beta < 1$	0		DOKE	83	PLAS
<8.E-15		Caty	$1.E-4 < \beta < 1.E-1$	0	15	ERREDE	83	IMB
<5.E-12		1	$1.E-4 < \beta < 3.E-2$	0		GROOM	83	CNTR
<2.E-12			$6.E-4 < \beta < 1$	0		MASHIMO	83	CNTR
<1.E-13		1	$\beta=3.E-3$	0		ALEXEYEV	82	CNTR
<2.E-12		1	$7.E-3 < \beta < 6.E-1$	0		BONARELLI	82	CNTR
6.E-10		1	all β	1	22	CABRERA	82	INDU
<2.E-11			$1.E-2 < \beta < 1.E-1$	0		MASHIMO	82	CNTR
<2.E-15			concentrator	0		BARTLETT	81	PLAS
<1.E-13	>1		$1.E-3 < \beta$	0		KINOSHITA	81B	PLAS
<5.E-11	<E17		$3.E-4 < \beta < 1.E-3$	0		ULLMAN	81	CNTR
<2.E-11			concentrator	0		BARTLETT	78	PLAS
1.E-11	>200	2		1	23	PRICE	75	PLAS
<2.E-13		>2		0		FLEISCHER	71	PLAS
<1.E-19		>2	obsidian, mica	0		FLEISCHER	69C	PLAS
<5.E-15	<15	<3	concentrator	0		CARITHERS	66	ELEC
<2.E-11		<1-3	concentrator	0		MALKUS	51	EMUL

- ¹ ALBERT 17 limits were estimated using a Cherenkov light in an array of optical modules under the Mediterranean Sea. The limits are for MM masses between 10^{10} and 10^{14} GeV. The limits are speed-dependent.
- ² AAB 16 search was made with a set of telescopes sampling the longitudinal profile of fluorescence light emitted by extensive air showers. Limits are speed dependent.
- ³ AARTSEN 16b was based on a Cherenkov signature in an array of optical modules which were sunk in the Antarctic ice cap. Limits are speed-dependent.
- ⁴ Beyond the monopole speed, the limits of AARTSEN 14 depend on the catalysis cross section (σ) which corresponds to the monopole radiating $\bar{\nu}$ times the light per track length compared to the Cherenkov light from a single electrically charged, relativistic particle. The values quoted here correspond to $\sigma = 1$ barn or $\bar{\nu} = 30$.
- ⁵ ABBASI 13 and ABBASI 10A were based on a Cherenkov signature in an array of optical modules which were sunk in the Antarctic ice cap. Limits are speed-dependent.
- ⁶ ADRIAN-MARTINEZ 12A measurements were based on a Cherenkov signature in an underwater telescope in the Western Mediterranean Sea. Limits are speed-dependent.
- ⁷ The limits from UENO 12 depend on the monopole speed and are also sensitive to assumed values of monopole mass and the catalysis cross section.
- ⁸ HOGAN 08 and DETRIXHE 11 limits on relativistic monopoles are based on nonobservation of radio Cherenkov signals at the South Pole. Limits are speed-dependent.
- ⁹ BALESTRA 08 exposed of nuclear track detector modules totaling 400 m^2 for 4 years at the Chacaltaya Laboratory (5230 m) in search for intermediate-mass monopoles with $\beta > 0.05$. The analysis is mainly based on three CR39 modules. For $M > 5 \times 10^{13}$ GeV there can be upward-going monopoles as well, hence the flux limit is half that obtained for less massive monopoles. Previous experiments (e.g. MACRO and OHYA (ORITO 91)) had set limits only for $M > 1 \times 10^9$ GeV.
- ¹⁰ AMBROSIO 02B direct search final result for $m \geq 10^{17}$ GeV, based upon 4.2 to 9.5 years of running, depending upon the subsystem. Limit with CR39 track-etch detector extends the limit from $\beta=4 \times 10^{-5}$ ($3.1 \times 10^{-16} \text{ cm}^{-2} \text{ sr}^{-1} \text{ s}^{-1}$) to $\beta=1 \times 10^{-4}$ ($2.1 \times 10^{-16} \text{ cm}^{-2} \text{ sr}^{-1} \text{ s}^{-1}$). Limit curve in paper is piecewise continuous due to different detection techniques for different β ranges.

- ¹¹ AMBROSIO 02c limit for catalysis of nucleon decay with catalysis cross section of ≈ 1 mb. The flux limit increases by ~ 3 at the higher β limit, and increases to $1 \times 10^{-14} \text{ cm}^{-2} \text{ sr}^{-1} \text{ s}^{-1}$ if the catalysis cross section is 0.01 mb. Based upon 71193 hr of data with the streamer detector, with an acceptance of $4250 \text{ m}^2 \text{ sr}$.
- ¹² AMBROSIO 02b result for "more than two years of data." Ionization search using several subsystems. Limit curve as a function of β not given. Included in AMBROSIO 02b.
- ¹³ AMBROSIO 97 global MACRO 90%CL is 0.78×10^{-15} at $\beta=1.1 \times 10^{-4}$, goes through a minimum at 0.61×10^{-15} near $\beta=(1.1-2.7) \times 10^{-3}$, then rises to 0.84×10^{-15} at $\beta=0.1$. The global limit in this region is below the Parker bound at 10^{-15} . Less stringent limits are established for $4 \times 10^{-5} < \beta < 1 \times 10^{-4}$. Limits set by various triggers and different subdetectors are given in the paper. All limits assume a catalysis cross section smaller than a few mb.
- ¹⁴ AHLEN 94 limit for dyons extends down to $\beta=0.9E-4$ and a limit of $1.3E-14$ extends to $\beta = 0.8E-4$. Also see comment by PRICE 94 and reply of BARISH 94. One loophole in the AHLEN 94 result is that in the case of monopoles catalyzing nucleon decay, relativistic particles could veto the events. See AMBROSIO 97 for additional results.
- ¹⁵ Catalysis of nucleon decay; sensitive to assumed catalysis cross section.
- ¹⁶ ORITO 91 limits are functions of velocity. Lowest limits are given here.
- ¹⁷ Used DKMPR mechanism and Penning effect.
- ¹⁸ Assumes monopole attaches fermion nucleus.
- ¹⁹ Limit from combining data of CAPLIN 86, BERMON 85, INCANDELA 84, and CABRERA 83. For a discussion of controversy about CAPLIN 86 observed event, see GUY 87. Also see SCHOUTEN 87.
- ²⁰ Based on lack of high-energy solar neutrinos from catalysis in the sun.
- ²¹ Anomalous long-range α (^4He) tracks.
- ²² CABRERA 82 candidate event has single Dirac charge within $\pm 5\%$.
- ²³ ALVAREZ 75, FLEISCHER 75, and FRIEDLANDER 75 explain as fragmenting nucleus. EBERHARD 75 and ROSS 76 discuss conflict with other experiments. HAGSTROM 77 reinterprets as antineutrino. PRICE 78 reassesses.

Monopole Flux — Astrophysics

FLUX ($\text{cm}^{-2} \text{sr}^{-1} \text{s}^{-1}$)	MASS (GeV)	CHG (g)	COMMENTS ($\beta = v/c$)	DOCUMENT ID	TECN
<1.3E-20			faint white dwarf	1	FREESE 99 ASTR
<1.E-16	E17	1	galactic field	2	ADAMS 93 COSM
<1.E-23			Jovian planets	1	ARAFUNE 85 ASTR
<1.E-16	E15		solar trapping	BRACCI 85B ASTR	
<1.E-18		1		1	HARVEY 84 COSM
<3.E-23			neutron stars	KOLB 84 ASTR	
<7.E-22			pulsars	1	FREESE 83B ASTR
<1.E-18	<E18	1	intergalactic field	1	REPHAELI 83 COSM
<1.E-23			neutron stars	1	DIMOPOUL... 82 COSM
<5.E-22			neutron stars	1	KOLB 82 COSM
<5.E-15	>E21		galactic halo	1	SALPETER 82 COSM
<1.E-12	E19	1	$\beta=3.E-3$	3	TURNER 82 COSM
<1.E-16		1	galactic field	PARKER 70 COSM	

- ¹ Catalysis of nucleon decay.
- ² ADAMS 93 limit based on "survival and growth of a small galactic seed field" is $10^{-16} (m/10^{17} \text{ GeV}) \text{ cm}^{-2} \text{ s}^{-1} \text{ sr}^{-1}$. Above 10^{17} GeV, limit $10^{-16} (10^{17} \text{ GeV}/m) \text{ cm}^{-2} \text{ s}^{-1} \text{ sr}^{-1}$ (from requirement that monopole density does not overclose the universe) is more stringent.
- ³ Re-evaluates PARKER 70 limit for GUT monopoles.

Monopole Density — Matter Searches

DENSITY	CHG (g)	MATERIAL	DOCUMENT ID	TECN
<9.8E-5/gram	≥ 1	Polar rock	BENDTZ 13	INDU
<6.9E-6/gram	>1/3	Meteorites and other	JEON 95	INDU
<2.E-7/gram	>0.6	Fe ore	1	EBISU 87 INDU
<4.6E-6/gram	>0.5	deep schist	KOVALIK 86	INDU
<1.6E-6/gram	>0.5	manganese nodules	2	KOVALIK 86 INDU
<1.3E-6/gram	>0.5	seawater	KOVALIK 86	INDU
>1.E+14/gram	>1/3	iron aerosols	MIKHAILOV 83	SPEC
>6.E-4/gram		air, seawater	CARRIGAN 76	CNTR
<5.E-1/gram	>0.04	11 materials	CABRERA 75	INDU
<2.E-4/gram	>0.05	moon rock	ROSS 73	INDU
<6.E-7/gram	<140	seawater	KOLM 71	CNTR
<1.E-2/gram	<120	manganese nodules	FLEISCHER 69	PLAS
<1.E-4/gram	>0	manganese	FLEISCHER 69B	PLAS
<2.E-3/gram	<1-3	magnetite, meteor	GOTO 63	EMUL
<2.E-2/gram		meteorite	PETUKHOV 63	CNTR

- ¹ Mass $1 \times 10^{14} - 1 \times 10^{17}$ GeV.
- ² KOVALIK 86 examined 498 kg of schist from two sites which exhibited clear mineralogical evidence of having been buried at least 20 km deep and held below the Curie temperature.

Monopole Density — Astrophysics

DENSITY	CHG (g)	MATERIAL	DOCUMENT ID	TECN
<1.E-9/gram	1	sun, catalysis	1	ARAFUNE 83 COSM
<6.E-33/nucl	1	moon wake	SCHATTEN 83	ELEC
<2.E-28/nucl		earth heat	CARRIGAN 80	COSM
<2.E-4/prot		42cm absorption	BRODERICK 79	COSM
<2.E-13/m ³		moon wake	SCHATTEN 70	ELEC

- ¹ Catalysis of nucleon decay.

See key on page 999

Searches Particle Listings

Magnetic Monopole Searches, Supersymmetric Particle Searches

REFERENCES FOR Magnetic Monopole Searches

AAD 20G PRL 124 031802 G. Aad et al. (ATLAS Collab.)
 ACHARYA 19B PRL 123 021802 B. Acharya et al. (MoEDAL Collab.)
 ACHARYA 18A PL B782 510 B. Acharya et al. (MoEDAL Collab.)
 ACHARYA 17 PRL 118 0161001 B. Acharya et al. (MoEDAL Collab.)
 ALBERT 17 JHEP 1707 054 A. Albert et al. (ANTARES Collab.)
 GOULD 17 PRL 119 241601 A. Gould, A. Rajantie (Pierre Auger Collab.)
 AAB 16 PR D94 082002 A. Aab et al. (ATLAS Collab.)
 AAD 16AB PR D93 052009 G. Aad et al. (ATLAS Collab.)
 AARTSEN 16B EPJ C76 133 M.G. Aartsen et al. (IceCube Collab.)
 ACHARYA 16 JHEP 1608 067 B. Acharya et al. (MoEDAL Collab.)
 AARTSEN 14 EPJ C74 2938 M.G. Aartsen et al. (IceCube Collab.)
 Also EPJ C79 124 (erratum)
 ABBASI 13 PR D87 022001 R. Abbasi et al. (IceCube Collab.)
 BENDTZ 13 PRL 110 121803 K. Bendtz et al.
 AAD 12CS PRL 109 261803 G. Aad et al. (ATLAS Collab.)
 ADRIAN-MAR...12A ASP 35 634 S. Adrian-Martinez et al. (ANTARES Collab.)
 UENO 12 ASP 36 131 K. Ueno et al. (Super-Kamiokande Collab.)
 DETRIXHE 11 PR D83 023513 M. Detrixhe et al. (ANITA Collab.)
 ABBASI 10A EPJ C69 361 R. Abbasi et al. (IceCube Collab.)
 ABBIENDI 08 PR B663 37 G. Abbiendi et al. (OPAL Collab.)
 BALESTRA 08 EPJ C55 57 S. Balestra et al. (SLIM Collab.)
 HOGAN 08 PR D78 075031 D.P. Hogan et al. (KANS, NEBR, DELA Collab.)
 ABULENCIA 06K PRL 96 201801 A. Abulencia et al. (CDF Collab.)
 AKTAS 05A EPJ C41 133 A. Aktas et al. (HI Collab.)
 KALBFLEISCH 04 PR D69 052002 G.R. Kalbfleisch et al. (OKLA Collab.)
 AMBROSIO 02B EPJ C25 511 M. Ambrosio et al. (MACRO Collab.)
 AMBROSIO 02C EPJ C26 163 M. Ambrosio et al. (MACRO Collab.)
 AMBROSIO 02D ASP 18 27 M. Ambrosio et al. (MACRO Collab.)
 KALBFLEISCH 00 PRL 85 5292 G.R. Kalbfleisch et al.
 FREESE 99 PR D59 063007 K. Freese, E. Krasteva (D0 Collab.)
 ABBOTT 98K PRL 81 524 B. Abbott et al. (MACRO Collab.)
 AMBROSIO 97 PL B406 249 M. Ambrosio et al.
 HE 97 PRL 79 3134 M. He (L3 Collab.)
 ACCIARRI 95C PRL B345 609 M. Acciari et al. (MICH Collab.)
 JEON 95 PRL 75 1443 H. Jeon, M.J. Longo (MICH Collab.)
 Also PRL 76 159 (erratum)
 AHLEN 94 PRL 72 608 S.P. Ahlen et al. (MACRO Collab.)
 BARISH 94 PRL 73 1306 B.C. Barish, G. Giacomelli, J.T. Hong (CIT+)
 BECKER-SZ... 94 PR D49 2169 R.A. Becker-Szendy et al. (IMB Collab.)
 PRICE 94 PRL 73 1305 P.B. Price (UCB Collab.)
 ADAMS 93 PRL 70 2511 F.C. Adams et al. (MICH, FNAL Collab.)
 PINFOLD 93 PL B316 407 J.L. Pinfold et al. (ALBE, HARV, MONT+)
 KINOSHITA 92 PR D46 0801 K. Kinoshita et al. (HARV, BGNA, REHO)
 THRON 92 PR D46 4846 J.L. Thron et al. (SOU DAN-2 Collab.)
 GARDNER 91 PR D44 622 D.D. Gardner et al. (STAN Collab.)
 HUBER 91 PR D44 636 M.E. Huber et al. (STAN Collab.)
 ORITO 91 PRL 66 1951 S. Orto et al. (ICEPP, WAS CR, NIHO, ICRR)
 BERMON 90 PRL 64 839 S. Bermon et al. (IBM, BNL Collab.)
 BERTANI 90 EPL 12 613 M. Bertani et al. (BGNA, INFN Collab.)
 BEZRUKOV 90 SJNP 52 54 L.B. Bezrukov et al. (INRM Collab.)
 Translated from YAF 52 86
 BUCKLAND 90 PR D41 2726 K.N. Buckland et al. (UCSD Collab.)
 GHOSH 90 EPL 12 25 D.C. Ghosh, S. Chatterjee (JADA Collab.)
 HUBER 90 PRL 64 835 M.E. Huber et al. (STAN Collab.)
 PRICE 90 PRL 65 149 P.B. Price, J. Guin, K. Kinoshita (UCB, HARV)
 KINOSHITA 89 PL B228 543 K. Kinoshita et al. (HARV, TISA, KEK+)
 BRAUNSCH... 88B ZPHY C38 543 R. Braunschweig et al. (TASSO Collab.)
 KINOSHITA 88 PRL 60 1610 K. Kinoshita et al. (HARV, TISA, KEK+)
 BARISH 87 PR D36 2641 B.C. Barish, G. Liu, C. Lane (CIT)
 BARTELT 87 PR D36 1990 J.E. Bartelt et al. (Soudan Collab.)
 Also PR D40 1701 (erratum) (Soudan Collab.)
 EBISU 87 PR D36 3359 T. Ebisu, T. Watanabe (KOBE Collab.)
 Also JP G11 883 T. Ebisu, T. Watanabe (KOBE Collab.)
 GENTILE 87 PR D35 1081 T. Gentile et al. (CLEO Collab.)
 GUY 87 NAT 325 463 J. Guy (LOIC Collab.)
 MASEK 87 PR D35 2758 G.E. Masek et al. (UCSD Collab.)
 NAKAMURA 87 PL B183 395 S. Nakamura et al. (INUS, WAS CR, NIHO)
 PRICE 87 PRL 59 2523 P.B. Price, R. Guoxiao, K. Kinoshita (UCB, HARV)
 SCHOUTEN 87 JP E20 850 J.C. Schouten et al. (LOIC Collab.)
 SHEPKO 87 PR D35 2917 M.J. Shepko et al. (TAMU Collab.)
 TSUKAMOTO 87 EPL 3 39 T. Tsukamoto et al. (ICRR Collab.)
 CAPLIN 86 NAT 321 402 A.D. Caplin et al. (LOIC Collab.)
 Also JP E20 850 J.C. Schouten et al. (LOIC Collab.)
 Also NAT 325 463 J. Guy (LOIC Collab.)
 CROMAR 86 PRL 56 2561 M.W. Cromar, A.F. Clark, F.R. Fickett (NBSB Collab.)
 HARA 86 PRL 56 2563 T. Hara et al. (ICRR, KYOT, KEK, KOBE+)
 INCANDELA 86 PR D34 2637 J. Incandela et al. (CHIC, FNAL, MICH)
 KOVALIK 86 PR A33 1183 J.M. Kovalik, J.L. Kirschvink (CIT Collab.)
 PRICE 86 PRL 56 1226 P.B. Price, M.H. Salamon (UCB Collab.)
 ARAFUNE 85 PR D32 2586 J. Arafune, M. Fukugita, S. Yanagita (ICRR, KYOTU+)
 BERMON 85 PRL 55 1850 S. Bermon et al. (IBM Collab.)
 BRACCI 85B NP B258 726 L. Bracci, G. Fiorentini, G. Mezzorani (PISA+)
 Also LNC 42 123 L. Bracci, G. Fiorentini (PISA Collab.)
 CAPLIN 85 NAT 317 234 A.D. Caplin et al. (LOIC Collab.)
 EBISU 85 JP G11 883 T. Ebisu, T. Watanabe (KOBE Collab.)
 KAJITA 85 JPS J 54 4065 T. Kajita et al. (ICRR, KEK, MIIG Collab.)
 PARK 85B NP B252 261 H.S. Park et al. (IMB Collab.)
 BATTISTONI 84 PL 133B 454 G. Battistoni et al. (NUSEX Collab.)
 FRYBERGER 84 PR D29 1524 D. Fryberger et al. (SLAC, UCB)
 HARVEY 84 NP B236 255 J.A. Harvey (PRIN Collab.)
 INCANDELA 84 PRL 53 2067 J. Incandela et al. (CHIC, FNAL, MICH)
 KAJINO 84 PRL 52 1373 F. Kajino et al. (ICRR Collab.)
 KAJINO 84B JP G10 447 F. Kajino et al. (ICRR Collab.)
 KAWAGOE 84 LNC 41 315 K. Kawagoe et al. (TOKY Collab.)
 KOLB 84 APJ 286 702 E.W. Kolb, M.S. Turner (FNAL, CHIC)
 KRISHNA... 84 PL 142B 99 M.R. Krishnaswamy et al. (TATA, OSK+)
 LISS 84 PR D30 804 T.M. Liss, S.P. Ahlen, G. Tarle (UCB, IND+)
 PRICE 84 PRL 52 1265 R.B. Price et al. (ROMA, UCB, IND+)
 PRICE 84B PL 140B 112 P.B. Price (CERN Collab.)
 TARLE 84 PRL 52 90 G. Tarle, S.P. Ahlen, T.M. Liss (ICRR, MICH+)
 ANDERSON 83 PR D28 2308 S.N. Anderson et al. (WASH Collab.)
 ARAFUNE 83 PL 133B 380 J. Arafune, M. Fukugita (ICRR, KYOTO)
 AUBERT 83B PL 120B 465 B. Aubert et al. (CERN, LAPP)
 BARTELT 83B PRL 50 655 J.E. Bartelt et al. (MINN, ANL)
 BARWICK 83 PR D28 2338 S.W. Barwick, K. Kinoshita, P.B. Price (UCB Collab.)
 BONARELLI 83 PL 126B 137 R. Bonarelli, P. Capiluppi, I. d'Antone (BGNA Collab.)
 BOSETTI 83 PL 133B 265 P.C. Bosetti et al. (AACH3, HAWA, TOKY)
 CABRERA 83 PRL 51 1933 B. Cabrera et al. (STAN Collab.)
 DOKE 83 PL 129B 370 T. Doke et al. (WASU, RIKK, TTAM, RIKEN)
 ERREDE 83 PRL 51 245 S.M. Errede et al. (IMB Collab.)
 FREESE 83B PRL 51 1625 K. Freese, M.S. Turner, D.N. Schramm (CHIC Collab.)
 GROOM 83 PRL 50 573 D.E. Groom et al. (UTAH, STAN)
 MASHIMO 83 PL 128B 327 T. Mashimo et al. (ICEPP Collab.)
 MIKHAILOV 83 PL 130B 331 V.F. Mikhailov (KAZA Collab.)
 MUSSET 83 PL 128B 333 P. Musset, M. Price, E. Lohrmann (CERN, HAMB)
 REPHAELI 83 PL 121B 115 Y. Rephaeli, M.S. Turner (CHIC Collab.)
 SCHATTEN 83 PR D27 1525 K.H. Schatten (NASA Collab.)
 ALEXEYEV 82 LNC 35 413 E.N. Alekseev et al. (INRM Collab.)
 BONARELLI 82 PL 112B 100 R. Bonarelli et al. (BGNA Collab.)

CABRERA 82 PRL 48 1378 B. Cabrera (STAN)
 DELL 82 NP B209 45 G.F. Dell et al. (BNL, ADEL, ROMA)
 DIMOPOUL... 82 PL 119B 320 S. Dimopoulos, J. Preskill, F. Wilczek (HARV+)
 KINOSHITA 82 PRL 48 77 K. Kinoshita, P.B. Price, D. Fryberger (UCB+)
 KOLB 82 PRL 49 1373 E.W. Kolb, S.A. Colgatoe, J.A. Harvey (LASL, PRIN)
 MASHIMO 82 JPS J 51 3067 T. Mashimo, K. Kawagoe, M. Koshiba (INUS)
 SALPETER 82 PRL 49 1114 E.E. Salpeter, S.L. Shapiro, I. Wasserman (CORN)
 TURNER 82 PR D26 1296 M.S. Turner, E.N. Parker, T.J. Bogdan (CHIC)
 BARTLETT 81 PR D24 612 D.F. Bartlett et al. (COLO, GESC)
 KINOSHITA 81B PR D24 1707 K. Kinoshita, P.B. Price (UCB)
 ULLMAN 81 PRL 47 289 J.D. Ullman (LEHM, BNL)
 CARRIGAN 80 NAT 288 348 R.A. Carrigan (FNAL)
 BRODERICK 79 PR D19 1046 J.J. Broderick et al. (VPI)
 BARTLETT 78 PR D18 2253 D.F. Bartlett, D. Soo, M.G. White (COLO, PRIN)
 CARRIGAN 78 PR D17 1754 R.A. Carrigan, B.P. Strauss, G. Giacomelli (FNAL+)
 HOFFMANN 78 LNC 23 357 H. Hoffmann et al. (CERN, ROMA)
 PRICE 78 PR D18 1382 P.B. Price et al. (UCB, HOUS)
 HAGSTROM 77 PRL 38 729 R. Hagstrom (LBL)
 CARRIGAN 76 PR D13 1823 R.A. Carrigan, F.A. Nezrick, B.P. Strauss (FNAL)
 DELL 76 LNC 15 269 G.F. Dell et al. (CERN, BNL, ROMA, ADEL)
 ROSS 76 LBL-4665 R.R. Ross (LBL)
 STEVENS 76B PR D14 2207 D.M. Stevens et al. (VPI, BNL)
 ZRELOV 76 CZJP B26 1306 V.P. Zrelov et al. (JINR)
 ALVAREZ 75 LBL-4260 L.W. Alvarez (LBL)
 BURKE 75 PL 60B 113 D.L. Burke et al. (MICH)
 CABRERA 75 Thesis B. Cabrera (STAN)
 CARRIGAN 75 NP B91 279 R.A. Carrigan, F.A. Nezrick (FNAL)
 Also PR D3 56 R.A. Carrigan, F.A. Nezrick (FNAL)
 EBERHARD 75 PR D11 3099 P.H. Eberhard et al. (LBL, MPIM)
 EBERHARD 75B LBL-4289 P.H. Eberhard (LBL)
 FLEISCHER 75 PRL 35 1412 R.L. Fleischer, R.N.F. Walker (GESC, WUSL)
 FRIEDLANDER 75 PRL 35 1167 M.W. Friedlander (WUSL)
 GIACOMELLI 75 NC 28A 21 G. Giacomelli et al. (BGNA, CERN, SAUL+)
 PRICE 75 PRL 35 487 P.B. Price et al. (UCB, HOUS)
 CARRIGAN 74 PR D10 3867 R.A. Carrigan, F.A. Nezrick, B.P. Strauss (FNAL)
 CARRIGAN 73 PR D8 3717 R.A. Carrigan, F.A. Nezrick, B.P. Strauss (FNAL)
 ROSS 73 PR D8 698 R.R. Ross et al. (LBL, SLAC)
 Also PR D4 3260 P.H. Eberhard et al. (LBL, SLAC)
 Also SCI 167 701 L.W. Alvarez et al. (LBL, SLAC)
 BARTLETT 72 PR D6 1817 D.F. Bartlett, M.D. Lahana (COLO)
 GUREVICH 72 PL 38B 549 I.I. Gurevich et al. (KIAE, NOVO, SERP)
 Also JETP 34 917 L.M. Barkov, I.I. Gurevich, M.S. Zolotarev (KIAE+)
 Translated from ZETF 61 1721
 Also PL 31B 394 I.I. Gurevich et al. (KIAE, NOVO, SERP)
 FLEISCHER 71 PR D4 24 R.L. Fleischer et al. (GESC)
 KOLM 71 PR D4 1285 H.H. Kolm, F. Villa, A. Odian (MIT, SLAC)
 PARKER 70 APJ 160 383 E.N. Parker (CHIC)
 SCHATTEN 70 PR D1 2245 K.H. Schatten (GESC, FSU)
 FLEISCHER 69 PR 177 2029 R.L. Fleischer et al. (GESC, UNCS, GSCO)
 FLEISCHER 69B PR 184 1393 R.L. Fleischer, P.B. Price, R.T. Woods (GESC)
 FLEISCHER 69C JAP 41 958 R.L. Fleischer et al. (GESC)
 Also JAP 41 958 R.L. Fleischer et al. (GESC)
 CARITHERS 66 PR 149 1070 W.C.J. Carithers, R.J. Stefanski, R.K. Adair
 AMALDI 63 NC 28 773 E. Amaldi et al. (ROMA, UCSD, CERN)
 GOTO 63 PR 132 387 E. Goto, H.H. Kolm, K.W. Ford (TOKY, MIT, BRAN)
 PETUKHOV 63 NP 49 87 V.A. Petukhov, M.N. Yakimenko (LEBD)
 PURCELL 63 PR 129 2326 E.M. Purcell et al. (HARV, BNL)
 FIDECARO 61 NC 22 657 M. Fidecaro, G. Finocchiaro, G. Giacomelli (CERN)
 BRADNER 59 PR 114 603 H. Bradner, W.M. Isbell (LBL)
 MALKUS 51 PR 83 899 W.V.R. Malkus (CHIC)

OTHER RELATED PAPERS

GROOM 86 PRPL 140 323 D.E. Groom (UTAH)
 Review

Supersymmetric Particle Searches

The exclusion of particle masses within a mass range (m_1, m_2) will be denoted with the notation "none $m_1 - m_2$ " in the VALUE column of the following Listings. The latest unpublished results are described in the "Supersymmetry: Experiment" review.

See the related review(s):
 Supersymmetry, Part I (Theory)
 Supersymmetry, Part II (Experiment)

CONTENTS:

- $\tilde{\chi}_1^0$ (Lightest Neutralino) mass limit
 - Accelerator limits for stable $\tilde{\chi}_1^0$
 - Bounds on $\tilde{\chi}_1^0$ from dark matter searches
 - $\tilde{\chi}_1^0$ -p elastic cross section
 - Spin-dependent interactions
 - Spin-independent interactions
 - Other bounds on $\tilde{\chi}_1^0$ from astrophysics and cosmology
 - Unstable $\tilde{\chi}_1^0$ (Lightest Neutralino) mass limit
- $\tilde{\chi}_2^0, \tilde{\chi}_3^0, \tilde{\chi}_4^0$ (Neutralinos) mass limits
- $\tilde{\chi}_1^\pm, \tilde{\chi}_2^\pm$ (Charginos) mass limits
- Long-lived $\tilde{\chi}^\pm$ (Chargino) mass limit
- $\tilde{\nu}$ (Sneutrino) mass limit
- Charged sleptons
 - R-parity conserving \tilde{e} (Selectron) mass limit
 - R-parity violating \tilde{e} (Selectron) mass limit
 - R-parity conserving $\tilde{\mu}$ (Smuon) mass limit
 - R-parity violating $\tilde{\mu}$ (Smuon) mass limit
 - R-parity conserving $\tilde{\tau}$ (Stau) mass limit
 - R-parity violating $\tilde{\tau}$ (Stau) mass limit
 - Long-lived $\tilde{\ell}$ (Slepton) mass limit
- \tilde{q} (Squark) mass limit
 - R-parity conserving \tilde{q} (Squark) mass limit
 - R-parity violating \tilde{q} (Squark) mass limit

Downloaded from https://academic.oup.com/ptep/article/2020/8/083C01/5891211 by guest on 20 August 2020

Searches Particle Listings

Supersymmetric Particle Searches

Long-lived \tilde{q} (Squark) mass limit
 \tilde{b} (Sbottom) mass limit
 – R-parity conserving \tilde{b} (Sbottom) mass limit
 – R-parity violating \tilde{b} (Sbottom) mass limit
 \tilde{t} (Stop) mass limit
 – R-parity conserving \tilde{t} (Stop) mass limit
 – R-parity violating \tilde{t} (Stop) mass limit
 Heavy \tilde{g} (Gluino) mass limit
 – R-parity conserving heavy \tilde{g} (Gluino) mass limit
 – R-parity violating heavy \tilde{g} (Gluino) mass limit
 Long-lived \tilde{g} (Gluino) mass limit
 Light \tilde{G} (Gravitino) mass limits from collider experiments
 Supersymmetry miscellaneous results

Most of the results shown below, unless stated otherwise, are based on the Minimal Supersymmetric Standard Model (MSSM), as described in the Note on Supersymmetry. Unless otherwise indicated, this includes the assumption of common gaugino and scalar masses at the scale of Grand Unification (GUT), and use of the resulting relations in the spectrum and decay branching ratios. Unless otherwise indicated, it is also assumed that R -parity (R) is conserved and that:

- 1) The $\tilde{\chi}_1^0$ is the highest supersymmetric particle (LSP)
- 2) $m_{\tilde{f}_L} = m_{\tilde{f}_R}$, where $\tilde{f}_{L,R}$ refer to the scalar partners of left- and right-handed fermions.

Limits involving different assumptions are identified in the Comments or in the Footnotes. We summarize here the notations used in this Chapter to characterize some of the most common deviations from the MSSM (for further details, see the Note on Supersymmetry).

Theories with R -parity violation (\mathcal{R}) are characterized by a superpotential of the form: $\lambda_{ijk} L_i L_j e_k^c + \lambda'_{ijk} L_i Q_j d_k^c + \lambda''_{ijk} u_i^c d_j^c d_k^c$, where i, j, k are generation indices. The presence of any of these couplings is often identified in the following by the symbols $LL\bar{E}$, $LQ\bar{D}$, and $U\bar{D}\bar{D}$. Mass limits in the presence of \mathcal{R} will often refer to “direct” and “indirect” decays. Direct refers to \mathcal{R} decays of the particle in consideration. Indirect refers to cases where \mathcal{R} appears in the decays of the LSP. The LSP need not be the $\tilde{\chi}_1^0$.

In several models, most notably in theories with so-called Gauge Mediated Supersymmetry Breaking (GMSB), the gravitino (\tilde{G}) is the LSP. It is usually much lighter than any other massive particle in the spectrum, and $m_{\tilde{G}}$ is then neglected in all decay processes involving gravitinos. In these scenarios, particles other than the neutralino are sometimes considered as the next-to-highest supersymmetric particle (NLSP), and are assumed to decay to their even- R partner plus \tilde{G} . If the lifetime is short enough for the decay to take place within the detector, \tilde{G} is assumed to be undetected and to give rise to missing energy (\cancel{E}) or missing transverse energy (\cancel{E}_T) signatures.

When needed, specific assumptions on the eigenstate content of $\tilde{\chi}^0$ and $\tilde{\chi}^\pm$ states are indicated, using the notation $\tilde{\gamma}$ (photino), \tilde{H} (higgsino), \tilde{W} (wino), and \tilde{Z} (zino) to signal that the limit of pure states was used. The terms gaugino is also used, to generically indicate wino-like charginos and zino-like neutralinos.

In the listings we have made use of the following abbreviations for simplified models employed by the experimental collaborations in supersymmetry searches published in the past year.

WARNING: Experimental lower mass limits determined within simplified models are to be treated with extreme care as they might not be directly applicable to realistic models. This is outlined in detail in the publications and we recommend consulting them before using bounds. For example, branching ratios, typically fixed to specific values in simplified models, can vary substantially in more elaborate models.

Simplified Models Table

- Tglu1A:** gluino pair production with $\tilde{g} \rightarrow q\bar{q}\tilde{\chi}_1^0$.
Tglu1B: gluino pair production with $\tilde{g} \rightarrow q\bar{q}\tilde{\chi}_1^\pm$, $\tilde{\chi}_1^\pm \rightarrow W^\pm\tilde{\chi}_1^0$.
Tglu1C: gluino pair production with a 2/3 probability of having a $\tilde{g} \rightarrow q\bar{q}\tilde{\chi}_1^\pm$, $\tilde{\chi}_1^\pm \rightarrow W^\pm\tilde{\chi}_1^0$ decay and a 1/3 probability of having a $\tilde{g} \rightarrow q\bar{q}\tilde{\chi}_2^0$, $\tilde{\chi}_2^0 \rightarrow Z^\pm\tilde{\chi}_1^0$ decay.
Tglu1D: gluino pair production with one gluino decaying to $q\bar{q}\tilde{\chi}_1^\pm$ with $\tilde{\chi}_1^\pm \rightarrow W^\pm + \tilde{G}$, and the other gluino decaying to $q\bar{q}\tilde{\chi}_1^0$ with $\tilde{\chi}_1^0 \rightarrow \gamma + \tilde{G}$.
Tglu1E: gluino pair production with $\tilde{g} \rightarrow q\bar{q}\tilde{\chi}_1^\pm$, $\tilde{\chi}_1^\pm \rightarrow W^\pm\tilde{\chi}_2^0$ and $\tilde{\chi}_2^0 \rightarrow Z^\pm\tilde{\chi}_1^0$ where $m_{\tilde{\chi}_1^\pm} = (m_{\tilde{g}} + m_{\tilde{\chi}_1^0})/2$, $m_{\tilde{\chi}_2^0} = (m_{\tilde{\chi}_1^\pm} + m_{\tilde{\chi}_1^0})/2$.
Tglu1F: gluino pair production with $\tilde{g} \rightarrow q\bar{q}\tilde{\chi}_1^\pm$ or $\tilde{g} \rightarrow q\bar{q}\tilde{\chi}_2^0$ with equal branching ratios, where $\tilde{\chi}_1^\pm$ decays through an intermediate scalar tau lepton or sneutrino to $\tau\nu\tilde{\chi}_1^0$ and where $\tilde{\chi}_2^0$ decays through an intermediate scalar tau lepton or sneutrino to $\tau^+\tau^-\tilde{\chi}_1^0$ or $\nu\bar{\nu}\tilde{\chi}_1^0$; the mass hierarchy is such that $m_{\tilde{\chi}_1^\pm} \sim m_{\tilde{\chi}_2^0} = (m_{\tilde{g}} + m_{\tilde{\chi}_1^0})/2$ and $m_{\tilde{\tau},\tilde{\nu}} = (m_{\tilde{\chi}_1^\pm} + m_{\tilde{\chi}_1^0})/2$.
Tglu1G: gluino pair production with $\tilde{g} \rightarrow q\bar{q}\tilde{\chi}_2^0$, and $\tilde{\chi}_2^0$ decaying through an intermediate slepton or sneutrino to $l^{+l-}\tilde{\chi}_1^0$ or $\nu\bar{\nu}\tilde{\chi}_1^0$ where $m_{\tilde{\chi}_2^0} = (m_{\tilde{g}} + m_{\tilde{\chi}_1^0})/2$ and $m_{\tilde{l},\tilde{\nu}} = (m_{\tilde{\chi}_2^0} + m_{\tilde{\chi}_1^0})/2$.
Tglu1H: gluino pair production with $\tilde{g} \rightarrow q\bar{q}\tilde{\chi}_2^0$, and $\tilde{\chi}_2^0 \rightarrow \tilde{\chi}_1^0 Z^{0(*)}$.
Tglu1I: gluino pair production with $\tilde{g} \rightarrow q\bar{q}\tilde{\chi}_2^0$, and $\tilde{\chi}_2^0 \rightarrow \tilde{\chi}_1^0 H$.
Tglu1J: gluino pair production with $\tilde{g} \rightarrow q\bar{q}\tilde{\chi}_2^0$, and $\text{BR}(\tilde{\chi}_2^0 \rightarrow \tilde{\chi}_1^0 Z^{0(*)}) = \text{BR}(\tilde{\chi}_2^0 \rightarrow \tilde{\chi}_1^0 H) = 0.5$.
Tglu1LL gluino pair production where $\tilde{g} \rightarrow q\bar{q}\tilde{\chi}_1^0$ happens with 1/3 probability and $\tilde{g} \rightarrow q\bar{q}\tilde{\chi}_1^\pm$ happens with 2/3 probability. The $\tilde{\chi}_1^\pm$ is assumed to be few hundreds of MeV heavier than the $\tilde{\chi}_1^0$, and decays to $\tilde{\chi}_1^0$ via a pion.
Tglu2A: gluino pair production with $\tilde{g} \rightarrow b\bar{b}\tilde{\chi}_1^0$.
Tglu3A: gluino pair production with $\tilde{g} \rightarrow t\bar{t}\tilde{\chi}_1^0$.
Tglu3B: gluino pair production with $\tilde{g} \rightarrow t\bar{t}$ where \tilde{t} decays exclusively to $t\tilde{\chi}_1^0$.
Tglu3C: gluino pair production with $\tilde{g} \rightarrow t\bar{t}$ where \tilde{t} decays exclusively to $c\tilde{\chi}_1^0$.
Tglu3D: gluino pair production with $\tilde{g} \rightarrow t\bar{b}\tilde{\chi}_1^\pm$ with $\tilde{\chi}_1^\pm \rightarrow W^\pm\tilde{\chi}_1^0$.
Tglu3E: gluino pair production where the gluino decays 25% of the time through $\tilde{g} \rightarrow t\bar{t}\tilde{\chi}_1^0$, 25% of the time through $\tilde{g} \rightarrow b\bar{b}\tilde{\chi}_1^0$ and 50% of the time through $\tilde{g} \rightarrow t\bar{b}\tilde{\chi}_1^\pm$ with $\tilde{\chi}_1^\pm \rightarrow W^\pm\tilde{\chi}_1^0$.
Tglu4A: gluino pair production with one gluino decaying to $q\bar{q}\tilde{\chi}_1^\pm$ with $\tilde{\chi}_1^\pm \rightarrow W^\pm + \tilde{G}$, and the other gluino decaying to $q\bar{q}\tilde{\chi}_1^0$ with $\tilde{\chi}_1^0 \rightarrow \gamma + \tilde{G}$.
Tglu4B: gluino pair production with gluinos decaying to $q\bar{q}\tilde{\chi}_1^0$ and $\tilde{\chi}_1^0 \rightarrow \gamma + \tilde{G}$.
Tglu4C: gluino pair production with gluinos decaying to $\tilde{g} \rightarrow q\bar{q}\tilde{\chi}_1^0$ and $\tilde{\chi}_1^0 \rightarrow Z + \tilde{G}$.
Tglu4D: gluino pair production with $\tilde{g} \rightarrow q\bar{q}\tilde{\chi}_1^0$ where the $\tilde{\chi}_1^0$ decays with equal probability to $\tilde{\chi}_1^0 \rightarrow \gamma + \tilde{G}$ or to $\tilde{\chi}_1^0 \rightarrow H + \tilde{G}$.
Tglu4E: gluino pair production with $\tilde{g} \rightarrow b\bar{b}\tilde{\chi}_1^0$ where the $\tilde{\chi}_1^0$ decays with equal probability to $\tilde{\chi}_1^0 \rightarrow \gamma + \tilde{G}$ or to $\tilde{\chi}_1^0 \rightarrow Z + \tilde{G}$.
Tglu4F: gluino pair production with $\tilde{g} \rightarrow t\bar{t}\tilde{\chi}_1^0$ where the $\tilde{\chi}_1^0$ decays with equal probability to $\tilde{\chi}_1^0 \rightarrow \gamma + \tilde{G}$ or to $\tilde{\chi}_1^0 \rightarrow Z + \tilde{G}$.
Tsqk1: squark pair production with $\tilde{q} \rightarrow q\tilde{\chi}_1^0$.
Tsqk1LL squark pair production where $\tilde{q} \rightarrow q\tilde{\chi}_1^0$ and $\tilde{q} \rightarrow q'\tilde{\chi}_1^\pm$ each happen with 50% probability. The $\tilde{\chi}_1^\pm$ is assumed to be few hundreds of MeV heavier than the $\tilde{\chi}_1^0$, and decays to $\tilde{\chi}_1^0$ via a pion.
Tsqk2: squark pair production with $\tilde{q} \rightarrow q\tilde{\chi}_2^0$ and $\tilde{\chi}_2^0 \rightarrow Z + \tilde{\chi}_1^0$.
Tsqk3: squark pair production with $\tilde{q} \rightarrow q'\tilde{\chi}_1^\pm$, $\tilde{\chi}_1^\pm \rightarrow W^\pm\tilde{\chi}_1^0$ (like Tglu1B but for squarks)

- Tsqk4:** squark pair production with squarks decaying to $q\tilde{\chi}_1^0$ and $\tilde{\chi}_1^0 \rightarrow \gamma + \tilde{G}$.
- Tsqk4A:** squark pair production with one squark decaying to $q\tilde{\chi}_1^\pm$ with $\tilde{\chi}_1^\pm \rightarrow W^\pm + \tilde{G}$, and the other squark decaying to $q\tilde{\chi}_1^0$ with $\tilde{\chi}_1^0 \rightarrow \gamma + \tilde{G}$.
- Tsqk4B:** squark pair production with squarks decaying to $q\tilde{\chi}_1^0$ and $\tilde{\chi}_1^0 \rightarrow \gamma + \tilde{G}$.
- Tstop1:** stop pair production with $\tilde{t} \rightarrow t\tilde{\chi}_1^0$.
- Tstop1LL:** stop pair production where $\tilde{t} \rightarrow t\tilde{\chi}_1^0$ and $\tilde{t} \rightarrow b\tilde{\chi}_1^\pm$ each happen with 50% probability. The $\tilde{\chi}_1^\pm$ is assumed to be few hundreds of MeV heavier than the $\tilde{\chi}_1^0$, and decays to $\tilde{\chi}_1^0$ via a pion.
- Tstop2:** stop pair production with $\tilde{t} \rightarrow b\tilde{\chi}_1^\pm$ with $\tilde{\chi}_1^\pm \rightarrow W^\pm\tilde{\chi}_1^0$.
- Tstop3:** stop pair production with the subsequent four-body decay $\tilde{t} \rightarrow bff'\tilde{\chi}_1^0$ where f represents a lepton or a quark.
- Tstop4:** stop pair production with $\tilde{t} \rightarrow c\tilde{\chi}_1^0$.
- Tstop5:** stop pair production with $\tilde{t} \rightarrow b\tilde{\nu}\tilde{\tau}$ with $\tilde{\tau} \rightarrow \tau\tilde{G}$.
- Tstop6:** stop pair production with $\tilde{t} \rightarrow t + \tilde{\chi}_2^0$, where $\tilde{\chi}_2^0 \rightarrow Z + \tilde{\chi}_1^0$ or $H + \tilde{\chi}_1^0$ each with Br=50%.
- Tstop7:** stop pair production with $\tilde{t}_2 \rightarrow \tilde{t}_1 + H/Z$, where $\tilde{t}_1 \rightarrow t + \tilde{\chi}_1^0$.
- Tstop8:** stop pair production with equal probability of the stop decaying via $\tilde{t} \rightarrow t\tilde{\chi}_1^0$ or via $\tilde{t} \rightarrow b\tilde{\chi}_1^\pm$ with $\tilde{\chi}_1^\pm \rightarrow W^\pm\tilde{\chi}_1^0$.
- Tstop9:** stop pair production with equal probability of the stop decaying via $\tilde{t} \rightarrow c\tilde{\chi}_1^0$ or via the four-body decay $\tilde{t} \rightarrow bff'\tilde{\chi}_1^0$ where f represents a lepton or a quark.
- Tstop10:** stop pair production with $\tilde{t} \rightarrow b\tilde{\chi}_1^\pm$ and $\tilde{\chi}_1^\pm \rightarrow W^\pm\tilde{\chi}_1^0 \rightarrow (f\bar{f}') + \tilde{\chi}_1^0$ with a virtual W -boson.
- Tstop11:** stop pair production with $\tilde{t} \rightarrow b\tilde{\chi}_1^\pm$ with $\tilde{\chi}_1^\pm$ decaying through an intermediate slepton to $l\nu\tilde{\chi}_1^0$.
- Tstop12:** stop pair production with $\tilde{t} \rightarrow t\tilde{\chi}_1^0$ and $\tilde{\chi}_1^0 \rightarrow \gamma + \tilde{G}$.
- Tstop13:** stop pair production with $\tilde{t} \rightarrow t\tilde{\chi}_1^0$ where the $\tilde{\chi}_1^0$ can decay with equal probability to $\tilde{\chi}_1^0 \rightarrow \gamma + \tilde{G}$ or to $\tilde{\chi}_1^0 \rightarrow Z + \tilde{G}$.
- Tstop1RPV:** stop pair production with $\tilde{t} \rightarrow b\tilde{s}$ via RPV coupling λ_{323} .
- Tstop2RPV:** stop pair production with $\tilde{t} \rightarrow b\tilde{t}$, via RPV coupling λ_{i33} .
- Tsbot1:** sbottom pair production with $\tilde{b} \rightarrow b\tilde{\chi}_1^0$.
- Tsbot2:** sbottom pair production with $\tilde{b} \rightarrow t\chi_1^-, \chi_1^- \rightarrow W^-\tilde{\chi}_1^0$.
- Tsbot3:** sbottom pair production with $\tilde{b} \rightarrow b\tilde{\chi}_2^0$, where one of the $\tilde{\chi}_2^0 \rightarrow Z^{(*)}\tilde{\chi}_1^0 \rightarrow f\bar{f}\tilde{\chi}_1^0$ and the other $\tilde{\chi}_2^0 \rightarrow \tilde{\ell}\ell^+ \rightarrow \ell^+\ell^-\tilde{\chi}_1^0$.
- Tsbot4:** sbottom pair production with $\tilde{b} \rightarrow b\tilde{\chi}_2^0$, with $\tilde{\chi}_2^0 \rightarrow H\tilde{\chi}_1^0$.
- Tchi1chi1A:** electroweak pair and associated production of nearly mass-degenerate charginos $\tilde{\chi}_1^\pm$ and neutralinos $\tilde{\chi}_1^0$, where $\tilde{\chi}_1^\pm$ decays to $\tilde{\chi}_1^0$ plus soft radiation, and where one of the $\tilde{\chi}_1^0$ decays to $\gamma + \tilde{G}$ while the other one decays to $Z/H + \tilde{G}$ (with equal probability).
- Tchi1chi1B:** electroweak pair production of charginos $\tilde{\chi}_1^\pm$, where $\tilde{\chi}_1^\pm$ decays through an intermediate slepton or sneutrino to $l\nu\tilde{\chi}_1^0$ and where the slepton or sneutrino mass is 5%, 25%, 50%, 75% and 95% of the $\tilde{\chi}_1^\pm$ mass.
- Tchi1chi1C:** electroweak pair production of charginos $\tilde{\chi}_1^\pm$, where $\tilde{\chi}_1^\pm$ decays through an intermediate slepton or sneutrino to $l\nu\tilde{\chi}_1^0$ and where $m_{\tilde{\ell},\tilde{\nu}} = (m_{\tilde{\chi}_1^\pm} + m_{\tilde{\chi}_1^0})/2$.
- Tchi1chi1D:** electroweak associated pair production of charginos $\tilde{\chi}_1^\pm$, where $\tilde{\chi}_1^\pm$ decays through an intermediate scalar tau lepton or sneutrino to $\tau\nu\tilde{\chi}_1^0$ and where $m_{\tilde{\tau},\tilde{\nu}} = (m_{\tilde{\chi}_1^\pm} + m_{\tilde{\chi}_1^0})/2$.
- Tchi1chi1F:** electroweak pair and associated production of nearly mass-degenerate charginos $\tilde{\chi}_1^\pm$ and neutralinos $\tilde{\chi}_1^0$ (i.e. $\tilde{\chi}_1^\pm\tilde{\chi}_1^\pm$ and $\tilde{\chi}_1^\pm\tilde{\chi}_1^0$ production) where the $\tilde{\chi}_1^\pm$ decays exclusively to $\tilde{\chi}_1^0$ plus soft radiation and the $\tilde{\chi}_1^0$ decays to $\gamma/Z + \tilde{G}$.
- Tchi1chi1G:** electroweak pair production of charginos $\tilde{\chi}_1^\pm$, which are nearly mass-degenerate with neutralinos $\tilde{\chi}_1^0$. The $\tilde{\chi}_1^\pm$ decays either to $W^\pm + \tilde{G}$, or to $\tilde{\chi}_1^0$ plus soft radiation. The $\tilde{\chi}_1^0$ decays exclusively to $\gamma + \tilde{G}$.
- Tchi1n1A:** electroweak associated production of mass-degenerate charginos $\tilde{\chi}_1^\pm$ and neutralinos $\tilde{\chi}_1^0$, where $\tilde{\chi}_1^\pm$ decays exclusively to $W^\pm + \tilde{G}$ and $\tilde{\chi}_1^0$ decays exclusively to $\gamma + \tilde{G}$.
- Tchi1n2A:** electroweak associated production of mass-degenerate charginos $\tilde{\chi}_1^\pm$ and neutralinos $\tilde{\chi}_2^0$, where $\tilde{\chi}_1^\pm$ decays through an intermediate slepton or sneutrino to $l\nu\tilde{\chi}_1^0$ and where $\tilde{\chi}_2^0$ decays through an intermediate slepton or sneutrino to $l^+l^-\tilde{\chi}_1^0$ or $\nu\bar{\nu}\tilde{\chi}_1^0$.
- Tchi1n2B:** electroweak associated production of mass-degenerate charginos $\tilde{\chi}_1^\pm$ and neutralinos $\tilde{\chi}_2^0$, where $\tilde{\chi}_1^\pm$ decays through an intermediate slepton or sneutrino to $l\nu\tilde{\chi}_1^0$ and where $\tilde{\chi}_2^0$ decays through an intermediate slepton or sneutrino to $l^+l^-\tilde{\chi}_1^0$ or $\nu\bar{\nu}\tilde{\chi}_1^0$.
- Tchi1n2C:** electroweak associated production of mass-degenerate charginos $\tilde{\chi}_1^\pm$ and neutralinos $\tilde{\chi}_2^0$, where $\tilde{\chi}_1^\pm$ decays through an intermediate slepton or sneutrino to $l\nu\tilde{\chi}_1^0$ and where $\tilde{\chi}_2^0$ decays through an intermediate slepton or sneutrino to $l^+l^-\tilde{\chi}_1^0$ or $\nu\bar{\nu}\tilde{\chi}_1^0$ and where $m_{\tilde{\ell},\tilde{\nu}} = (m_{\tilde{\chi}_1^\pm} + m_{\tilde{\chi}_1^0})/2$.
- Tchi1n2D:** electroweak associated production of mass-degenerate charginos $\tilde{\chi}_1^\pm$ and neutralinos $\tilde{\chi}_2^0$, where $\tilde{\chi}_1^\pm$ decays through an intermediate scalar tau lepton or sneutrino to $\tau\nu\tilde{\chi}_1^0$ and where $\tilde{\chi}_2^0$ decays through an intermediate scalar tau lepton or sneutrino to $\tau^+\tau^-\tilde{\chi}_1^0$ or $\nu\bar{\nu}\tilde{\chi}_1^0$ and where $m_{\tilde{\tau},\tilde{\nu}} = (m_{\tilde{\chi}_1^\pm} + m_{\tilde{\chi}_1^0})/2$.
- Tchi1n2E:** electroweak associated production of mass-degenerate charginos $\tilde{\chi}_1^\pm$ and neutralinos $\tilde{\chi}_2^0$, where $\tilde{\chi}_1^\pm \rightarrow W^\pm + \tilde{\chi}_1^0$ and $\tilde{\chi}_2^0 \rightarrow H + \tilde{\chi}_1^0$.
- Tchi1n2F:** electroweak associated production of mass-degenerate wino-like charginos $\tilde{\chi}_1^\pm$ and neutralinos $\tilde{\chi}_2^0$, where $\tilde{\chi}_1^\pm$ decays through an intermediate W^{**} to $l\nu\tilde{\chi}_1^0$ and where $\tilde{\chi}_2^0$ decays through an intermediate Z^* to $l^+l^-\tilde{\chi}_1^0$ or $\nu\bar{\nu}\tilde{\chi}_1^0$.
- Tchi1n2G:** electroweak associated production of Higgsino-like charginos $\tilde{\chi}_1^\pm$ and neutralinos $\tilde{\chi}_2^0$, and electroweak associated production of $\tilde{\chi}_2^0$ and $\tilde{\chi}_1^0$, where $m_{\tilde{\chi}_1^\pm} = (m_{\tilde{\chi}_2^0} + m_{\tilde{\chi}_1^0})/2$ and where $\tilde{\chi}_1^\pm$ decays through an intermediate W^{**} to $l\nu\tilde{\chi}_1^0$ and where $\tilde{\chi}_2^0$ decays through an intermediate Z^* to $l^+l^-\tilde{\chi}_1^0$.
- Tchi1n2H:** electroweak associated production of mass-degenerate charginos $\tilde{\chi}_1^\pm$ and neutralinos $\tilde{\chi}_2^0$, where $\tilde{\chi}_1^\pm$ decays through an intermediate slepton or sneutrino to $l\nu\tilde{\chi}_1^0$ and where $\tilde{\chi}_2^0$ decays through an intermediate scalar tau lepton or sneutrino to $\tau^+\tau^-\tilde{\chi}_1^0$ or $\nu\bar{\nu}\tilde{\chi}_1^0$.
- Tchi1n2I:** electroweak associated production of mass-degenerate charginos $\tilde{\chi}_1^\pm$ and neutralinos $\tilde{\chi}_2^0$, where $\tilde{\chi}_1^\pm$ decays to $W^\pm + \tilde{\chi}_1^0$ and where $\tilde{\chi}_2^0$ decays 50% of the time to $Z + \tilde{\chi}_1^0$ and 50% of the time to $H + \tilde{\chi}_1^0$.
- Tchi1n2-GGM:** in the framework of General Gauge Mediation (GGM): electroweak pair and associated production of nearly mass-degenerate charginos $\tilde{\chi}_1^\pm$ and neutralinos $\tilde{\chi}_1^0, \tilde{\chi}_2^0$ (i.e. $\tilde{\chi}_1^\pm\tilde{\chi}_1^\pm, \tilde{\chi}_1^\pm\tilde{\chi}_1^0$ and $\tilde{\chi}_1^\pm\tilde{\chi}_2^0$ production) where the $\tilde{\chi}_1^\pm$ decays exclusively to $W^\pm + \tilde{G}$, the $\tilde{\chi}_2^0$ decays to $Z/H + \tilde{G}$ and the $\tilde{\chi}_1^0$ decays to $\gamma/Z + \tilde{G}$. The branching ratios depend on the composition of the gauge eigenstates of the neutralinos in the GGM scenario.
- Tn1n1A:** electroweak pair and associated production of nearly mass-degenerate Higgsino-like charginos $\tilde{\chi}_1^\pm$ and neutralinos $\tilde{\chi}_1^0$ and $\tilde{\chi}_2^0$, where $\tilde{\chi}_1^\pm$ and $\tilde{\chi}_2^0$ decay to $\tilde{\chi}_1^0$ plus soft radiation and where both of the $\tilde{\chi}_1^0$ decay to $H + \tilde{G}$.
- Tn1n1B:** electroweak pair and associated production of nearly mass-degenerate Higgsino-like charginos $\tilde{\chi}_1^\pm$ and neutralinos $\tilde{\chi}_1^0$ and $\tilde{\chi}_2^0$, where $\tilde{\chi}_1^\pm$ and $\tilde{\chi}_2^0$ decay to $\tilde{\chi}_1^0$ plus soft radiation and where the $\tilde{\chi}_1^0$ decays 50% of the time to $H + \tilde{G}$ and 50% of the time to $Z + \tilde{G}$.
- Tn1n1C:** electroweak pair and associated production of nearly mass-degenerate Higgsino-like charginos $\tilde{\chi}_1^\pm$ and neutralinos $\tilde{\chi}_1^0$ and $\tilde{\chi}_2^0$, where $\tilde{\chi}_1^\pm$ and $\tilde{\chi}_2^0$ decay to $\tilde{\chi}_1^0$ plus soft radiation and where both of the $\tilde{\chi}_1^0$ decay to $Z + \tilde{G}$.
- Tn2n3A:** electroweak associated production of mass-degenerate neutralinos $\tilde{\chi}_2^0$ and $\tilde{\chi}_3^0$, where $\tilde{\chi}_2^0$ and $\tilde{\chi}_3^0$ decay through intermediate sleptons to $l^+l^-\tilde{\chi}_1^0$ and where the slepton mass is 5%, 25%, 50%, 75% and 95% of the $\tilde{\chi}_2^0$ mass.
- Tn2n3B:** electroweak associated production of mass-degenerate neutralinos $\tilde{\chi}_2^0$ and $\tilde{\chi}_3^0$, where $\tilde{\chi}_2^0$ and $\tilde{\chi}_3^0$ decay through intermediate sleptons to $l^+l^-\tilde{\chi}_1^0$ and where $m_{\tilde{\ell}} = (m_{\tilde{\chi}_2^0} + m_{\tilde{\chi}_1^0})/2$.

Searches Particle Listings

Supersymmetric Particle Searches

$\tilde{\chi}_1^0$ (Lightest Neutralino) mass limit

$\tilde{\chi}_1^0$ is often assumed to be the lightest supersymmetric particle (LSP). See also the $\tilde{\chi}_2^0, \tilde{\chi}_3^0, \tilde{\chi}_4^0$ section below.

We have divided the $\tilde{\chi}_1^0$ listings below into five sections:

- 1) Accelerator limits for stable $\tilde{\chi}_1^0$,
- 2) Bounds on $\tilde{\chi}_1^0$ from dark matter searches,
- 3) $\tilde{\chi}_1^0 - p$ elastic cross section (spin-dependent, spin-independent interactions),
- 4) Other bounds on $\tilde{\chi}_1^0$ from astrophysics and cosmology, and
- 5) Unstable $\tilde{\chi}_1^0$ (Lightest Neutralino) mass limit.

Accelerator limits for stable $\tilde{\chi}_1^0$

Unless otherwise stated, results in this section assume spectra, production rates, decay modes, and branching ratios as evaluated in the MSSM, with gaugino and sfermion mass unification at the GUT scale. These papers generally study production of $\tilde{\chi}_i^0 \tilde{\chi}_j^0$ ($i \geq 1, j \geq 2$), $\tilde{\chi}_1^+ \tilde{\chi}_1^-$, and (in the case of hadronic collisions) $\tilde{\chi}_1^+ \tilde{\chi}_2^0$ pairs. The mass limits on $\tilde{\chi}_1^0$ are either direct, or follow indirectly from the constraints set by the non-observation of $\tilde{\chi}_1^\pm$ and $\tilde{\chi}_2^0$ states on the gaugino and higgsino MSSM parameters M_2 and μ . In some cases, information is used from the nonobservation of slepton decays.

Obsolete limits obtained from e^+e^- collisions up to $\sqrt{s}=184$ GeV have been removed from this compilation and can be found in the 2000 Edition (The European Physical Journal **C15** 1 (2000)) of this Review.
 $\Delta m = m_{\tilde{\chi}_2^0} - m_{\tilde{\chi}_1^0}$.

VALUE (GeV)	CL%	DOCUMENT ID	TECN	COMMENT
		1 DREINER	09 THEO	
>40	95	2 ABBIENDI	04H OPAL	all $\tan\beta$, $\Delta m > 5$ GeV, $m_0 > 500$ GeV, $A_0 = 0$
>42.4	95	3 HEISTER	04 ALEP	all $\tan\beta$, all Δm , all m_0
>39.2	95	4 ABDALLAH	03M DLPH	all $\tan\beta$, $m_{\tilde{\nu}} > 500$ GeV
>46	95	5 ABDALLAH	03M DLPH	all $\tan\beta$, all Δm , all m_0
>32.5	95	6 ACCIARRI	00D L3	$\tan\beta > 0.7$, $\Delta m > 3$ GeV, all m_0

• • • We do not use the following data for averages, fits, limits, etc. • • •

7 AAD 14K ATLS

- 1 DREINER 09 show that in the general MSSM with non-universal gaugino masses there exists no model-independent laboratory bound on the mass of the lightest neutralino. An essentially massless $\tilde{\chi}_1^0$ is allowed by the experimental and observational data, imposing some constraints on other MSSM parameters, including M_2 , μ and the slepton and squark masses.
- 2 ABBIENDI 04H search for charginos and neutralinos in events with acoplanar leptons+jets and multi-jet final states in the 192–209 GeV data, combined with the results on leptonic final states from ABBIENDI 04. The results hold for a scan over the parameter space covering the region $0 < M_2 < 5000$ GeV, $-1000 < \mu < 1000$ GeV and $\tan\beta$ from 1 to 40. This limit supersedes ABBIENDI 00H.
- 3 HEISTER 04 data collected up to 209 GeV. Updates earlier analysis of selectrons from HEISTER 02E, includes a new analysis of charginos and neutralinos decaying into stau and uses results on charginos with initial state radiation from HEISTER 02J. The limit is based on the direct search for charginos and neutralinos, the constraints from the slepton search and the Higgs mass limits from HEISTER 02 using a top mass of 175 GeV, interpreted in a framework with universal gaugino and sfermion masses. Assuming the mixing in the stau sector to be negligible, the limit improves to 43.1 GeV. Under the assumption of MSUGRA with unification of the Higgs and sfermion masses, the limit improves to 50 GeV, and reaches 53 GeV for $A_0 = 0$. These limits include and update the results of BARATE 01.
- 4 ABDALLAH 03M uses data from $\sqrt{s} = 192$ –208 GeV. A limit on the mass of $\tilde{\chi}_1^0$ is derived from direct searches for neutralinos combined with the chargino search. Neutralinos are searched in the production of $\tilde{\chi}_1^0 \tilde{\chi}_2^0, \tilde{\chi}_1^0 \tilde{\chi}_3^0$, as well as $\tilde{\chi}_2^0 \tilde{\chi}_3^0$ and $\tilde{\chi}_2^0 \tilde{\chi}_4^0$ giving rise to cascade decays, and $\tilde{\chi}_1^0 \tilde{\chi}_2^0$ and $\tilde{\chi}_1^0 \tilde{\chi}_3^0$, followed by the decay $\tilde{\chi}_2^0 \rightarrow \tilde{\tau} \tau$. The results hold for the parameter space defined by values of $M_2 < 1$ TeV, $|\mu| \leq 2$ TeV with the $\tilde{\chi}_1^0$ as LSP. The limit is obtained for $\tan\beta = 1$ and large m_0 , where $\tilde{\chi}_2^0 \tilde{\chi}_3^0$ and chargino pair production are important. If the constraint from Higgs searches is also imposed, the limit improves to 49.0 GeV in the m_h^{\max} scenario with $m_t = 174.3$ GeV. These limits update the results of ABREU 00J.
- 5 ABDALLAH 03M uses data from $\sqrt{s} = 192$ –208 GeV. An indirect limit on the mass of $\tilde{\chi}_1^0$ is derived by constraining the MSSM parameter space by the results from direct searches for neutralinos (including cascade decays and $\tilde{\tau} \tau$ final states), for charginos (for all Δm_{\pm}) and for sleptons, stop and sbottom. The results hold for the full parameter space defined by values of $M_2 < 1$ TeV, $|\mu| \leq 2$ TeV with the $\tilde{\chi}_1^0$ as LSP. Constraints from the Higgs search in the m_h^{\max} scenario assuming $m_t = 174.3$ GeV are included. The limit is obtained for $\tan\beta \geq 5$ when stau mixing leads to mass degeneracy between $\tilde{\tau}_1$ and $\tilde{\chi}_1^0$ and the limit is based on $\tilde{\chi}_2^0$ production followed by its decay to $\tilde{\tau}_1 \tau$. In the pathological scenario where m_0 and $|\mu|$ are large, so that the $\tilde{\chi}_2^0$ production cross section is negligible, and where there is mixing in the stau sector but not in stop nor sbottom, the limit is based on charginos with soft decay products and an ISR photon. The limit then degrades to 39 GeV. See Figs. 40–42 for the dependence of the limit on $\tan\beta$ and $m_{\tilde{\nu}}$. These limits update the results of ABREU 00W.
- 6 ACCIARRI 00D data collected at $\sqrt{s} = 189$ GeV. The results hold over the full parameter space defined by $0.7 \leq \tan\beta \leq 60$, $0 \leq M_2 \leq 2$ TeV, $m_0 \leq 500$ GeV, $|\mu| \leq 2$ TeV. The minimum mass limit is reached for $\tan\beta = 1$ and large m_0 . The results of slepton

searches from ACCIARRI 99W are used to help set constraints in the region of small m_0 . The limit improves to 48 GeV for $m_0 \gtrsim 200$ GeV and $\tan\beta \gtrsim 10$. See their Figs. 6–8 for the $\tan\beta$ and m_0 dependence of the limits. Updates ACCIARRI 98F.

7 AAD 14K sets limits on the χ -nucleon spin-dependent and spin-independent cross sections out to $m_\chi = 10$ TeV.

Bounds on $\tilde{\chi}_1^0$ from dark matter searches

These papers generally exclude regions in the $M_2 - \mu$ parameter plane assuming that $\tilde{\chi}_1^0$ is the dominant form of dark matter in the galactic halo. These limits are based on the lack of detection in laboratory experiments, telescopes, or by the absence of a signal in underground neutrino detectors. The latter signal is expected if $\tilde{\chi}_1^0$ accumulates in the Sun or the Earth and annihilates into high-energy ν 's.

VALUE	DOCUMENT ID	TECN
• • • We do not use the following data for averages, fits, limits, etc. • • •		
	1 DI-MAURO	19 FLAT
	2 JOHNSON	19 FLAT
	3 LI	19D FLAT
	4 ABDALLAH	18 HESS
	5 AHNEN	18 MGIC
	6 ALBERT	18B HAWC
	7 ALBERT	18C HAWC
	8 AARTSEN	17 ICCB
	9 AARTSEN	17A ICCB
	10 AARTSEN	17C ICCB
	11 ALBERT	17A ANTR
	12 ARCHAMBAU	17 VRTS
	13 AARTSEN	16D ICCB
	14 ABDALLAH	16A HESS
	15 ADRIAN-MAR	16 ANTR
	16 AHNEN	16 MGFL
	17 AVRORIN	16 BAIK
	18 CIRELLI	16 THEO
	18 LEITE	16 THEO
	19 ABRAMOWSKI	15 HESS
	20 ACKERMANN	15 FLAT
	21 ACKERMANN	15A FLAT
	22 ACKERMANN	15B FLAT
	23 BUCKLEY	15 THEO
	24 CHOI	15 SKAM
	25 ALEKSIC	14 MGIC
	26 AVRORIN	14 BAIK
	27 AARTSEN	13C ICCB
	28 ABRAMOWSKI	13 HESS
	29 BERGSTROM	13 COSM
	30 BOLIVIE	13 BAKS
	29 JIN	13 ASTR
	29 KOPP	13 COSM
	31 ABBASI	12 ICCB
	32 ABRAMOWSKI	11 HESS
	33 ABDO	10 FLAT
	34 ACKERMANN	10 FLAT
	35 ACHTERBERG	06 AMND
	36 ACKERMANN	06 AMND
	37 DEBOER	06 RVUE
	38 DESAI	04 SKAM
	38 AMBROSIO	99 MCRO
	39 LOSECCO	95 RVUE
	40 MORI	93 KAMI
	41 BOTTINO	92 COSM
	42 BOTTINO	91 RVUE
	43 GELMINI	91 COSM
	44 KAMIONKOW	91B RVUE
	45 MORI	91B KAMI
	46 OLIVE	88 COSM

none 4–15 GeV

- 1 DI-MAURO 19 sets limits on the dark matter annihilation from gamma-ray searches in M31 and M33 galaxies using Fermi LAT data.
- 2 JOHNSON 19 sets limits on p-wave dark matter annihilations in the galactic center using Fermi data.
- 3 LI 19D sets limits on dark matter annihilation cross sections searching for line-like signals in the all-sky Fermi data.
- 4 ABDALLAH 18 places constraints on the dark matter annihilation cross section for annihilations into gamma-rays in the Galactic center for masses between 300 GeV to 70 TeV. This updates ABDALLAH 16.
- 5 AHNEN 18 uses observations of the dwarf satellite galaxy Ursa Major II to obtain upper limits on annihilation cross sections for dark matter in various channels for masses between 0.1–100 TeV.
- 6 ALBERT 18B sets limits on the annihilation cross section of dark matter with mass between 1 and 100 TeV from gamma-ray observations of the Andromeda galaxy.
- 7 ALBERT 18C sets limits on the spin-dependent coupling of dark matter to protons from dark matter annihilation in the Sun.
- 8 AARTSEN 17 is based on data collected during 327 days of detector livetime with IceCube. They looked for interactions of ν 's resulting from neutralino annihilations in the Earth over a background of atmospheric neutrinos and set 90% CL limits on the spin independent neutralino-proton cross section for neutralino masses in the range 10–10000 GeV.
- 9 AARTSEN 17A is based on data collected during 532 days of livetime with the IceCube 86-string detector including the DeepCore sub-array. They looked for interactions of ν 's

from neutralino annihilations in the Sun over a background of atmospheric neutrinos and set 90% CL limits on the spin dependent neutralino-proton cross section for neutralino masses in the range 10–10000 GeV. This updates AARTSEN 16c.

10 AARTSEN 17c is based on 1005 days of running with the IceCube detector. They set a limit on the annihilation cross section for dark matter with masses between 10–1000 GeV annihilating in the Galactic center assuming an NFW profile. The limit is of $1.2 \times 10^{23} \text{ cm}^3 \text{ s}^{-1}$ in the $\tau^+ \tau^-$ channel. Supercedes AARTSEN 15e.

11 ALBERT 17A is based on data from the ANTARES neutrino telescope. They looked for interactions of ν 's from neutralino annihilations in the Milky Way galaxy over a background of atmospheric neutrinos and set 90% CL limits on the muon neutrino flux. They also obtain limits on the thermally averaged cross section for neutralino masses in the range 50 to 100,000 GeV. This updates ADRIAN-MARTINEZ 15.

12 ARCHAMBAULT 17 performs a joint statistical analysis of four dwarf galaxies with VERITAS looking for gamma-ray emission from neutralino annihilation. They set limits on the neutralino annihilation cross section.

13 AARTSEN 16D is based on 329 live days of running with the DeepCore subdetector of the IceCube detector. They set a limit of $10^{-23} \text{ cm}^3 \text{ s}^{-1}$ on the annihilation cross section to $\nu\bar{\nu}$. This updates AARTSEN 15c.

14 ABDALLAH 16A place upper limits on the annihilation cross section with final states in the energy range of 0.1 to 2 TeV. This complements ABRAMOWSKI 13.

15 ADRIAN-MARTINEZ 16 is based on data from the ANTARES neutrino telescope. They looked for interactions of ν 's from neutralino annihilations in the Sun over a background of atmospheric neutrinos and set 90% CL limits on the muon neutrino flux. They also obtain limits on the spin dependent and spin independent neutralino-proton cross section for neutralino masses in the range 50 to 5,000 GeV. This updates ADRIAN-MARTINEZ 13.

16 AHNEN 16 combines 158 hours of Segue 1 observations with MAGIC with 6 year observations of 15 dwarf satellite galaxies by Fermi-LAT to set limits on annihilation cross sections for dark matter masses between 10 GeV and 100 TeV.

17 AVRORIN 16 is based on 2.76 years with Lake Baikal neutrino telescope. They derive 90% upper limits on the annihilation cross section from dark matter annihilations in the Galactic center.

18 CIRELLI 16 and LEITE 16 derive bounds on the annihilation cross section from radio observations.

19 ABRAMOWSKI 15 places constraints on the dark matter annihilation cross section for annihilations in the Galactic center for masses between 300 GeV to 10 TeV.

20 ACKERMANN 15 is based on 5.8 years of data with Fermi-LAT and search for monochromatic gamma-rays in the energy range of 0.2–500 GeV from dark matter annihilations. This updates ACKERMANN 13A.

21 ACKERMANN 15A is based on 50 months of data with Fermi-LAT and search for dark matter annihilation signals in the isotropic gamma-ray background as well as galactic subhalos in the energy range of a few GeV to a few tens of TeV.

22 ACKERMANN 15B is based on 6 years of data with Fermi-LAT observations of Milky Way dwarf spheroidal galaxies. Set limits on the annihilation cross section from $m_\chi = 2 \text{ GeV}$ to 10 TeV. This updates ACKERMANN 14.

23 BUCKLEY 15 is based on 5 years of Fermi-LAT data searching for dark matter annihilation signals from Large Magellanic Cloud.

24 CHOI 15 is based on 3903 days of SuperKamiokande data searching for neutrinos produced from dark matter annihilations in the sun. They place constraints on the dark matter-nucleon scattering cross section for dark matter masses between 4–200 GeV.

25 ALEKSIC 14 is based on almost 160 hours of observations of Segue 1 satellite dwarf galaxy using the MAGIC telescopes between 2011 and 2013. Sets limits on the annihilation cross section out to $m_\chi = 10 \text{ TeV}$.

26 AVRORIN 14 is based on almost 2.76 years with Lake Baikal neutrino telescope. They derive 90% upper limits on the fluxes of muons and muon neutrinos from dark matter annihilations in the Sun.

27 AARTSEN 13c is based on data collected during 339.8 effective days with the IceCube 59-string detector. They looked for interactions of ν_μ 's from neutralino annihilations in nearby galaxies and galaxy clusters. They obtain limits on the neutralino annihilation cross section for neutralino masses in the range 30–100,000 GeV.

28 ABRAMOWSKI 13 place upper limits on the annihilation cross section with $\gamma\gamma$ final states in the energy range of 0.5–25 TeV.

29 BERGSTROM 13, JIN 13, and KOPP 13 derive limits on the mass and annihilation cross section using AMS-02 data. JIN 13 also sets a limit on the lifetime of the dark matter particle.

30 BOLIEV 13 is based on data collected during 24.12 years of live time with the Bakson Underground Scintillator Telescope. They looked for interactions of ν_μ 's from neutralino annihilations in the Sun over a background of atmospheric neutrinos and set 90% CL limits on the muon flux. They also obtain limits on the spin dependent and spin independent neutralino-proton cross section for neutralino masses in the range 10–1000 GeV.

31 ABBASI 12 is based on data collected during 812 effective days with AMANDA II and 149 days of the IceCube 40-string detector combined with the data of ABBASI 09B. They looked for interactions of ν_μ 's from neutralino annihilations in the Sun over a background of atmospheric neutrinos and set 90% CL limits on the muon flux. No excess is observed. They also obtain limits on the spin dependent neutralino-proton cross section for neutralino masses in the range 50–5000 GeV.

32 ABRAMOWSKI 11 place upper limits on the annihilation cross section with $\gamma\gamma$ final states.

33 ABDO 10 place upper limits on the annihilation cross section with $\gamma\gamma$ or $\mu^+ \mu^-$ final states.

34 ACKERMANN 10 place upper limits on the annihilation cross section with $b\bar{b}$ or $\mu^+ \mu^-$ final states.

35 ACHTERBERG 06 is based on data collected during 421.9 effective days with the AMANDA detector. They looked for interactions of ν_μ 's from the centre of the Earth over a background of atmospheric neutrinos and set 90% CL limits on the muon flux. Their limit is compared with the muon flux expected from neutralino annihilations into $W^+ W^-$ and $b\bar{b}$ at the centre of the Earth for MSSM parameters compatible with the relic dark matter density, see their Fig. 7.

36 ACKERMANN 06 is based on data collected during 143.7 days with the AMANDA-II detector. They looked for interactions of ν_μ 's from the Sun over a background of atmospheric neutrinos and set 90% CL limits on the muon flux. Their limit is compared with the muon flux expected from neutralino annihilations into $W^+ W^-$ in the Sun for SUSY model parameters compatible with the relic dark matter density, see their Fig. 3.

37 DEBOER 06 interpret an excess of diffuse Galactic gamma rays observed with the EGRET satellite as originating from π^0 decays from the annihilation of neutralinos into quark jets. They analyze the corresponding parameter space in a supergravity inspired MSSM

model with radiative electroweak symmetry breaking, see their Fig. 3 for the preferred region in the $(m_0, m_{1/2})$ plane of a scenario with large $\tan\beta$.

38 AMBROSIO 99 and DESAI 04 set new neutrino flux limits which can be used to limit the parameter space in supersymmetric models based on neutralino annihilation in the Sun and the Earth.

39 LOSECO 95 reanalyzed the IMB data and places lower limit on $m_{\tilde{\chi}_1^0}$ of 18 GeV if the LSP is a photino and 10 GeV if the LSP is a higgsino based on LSP annihilation in the sun producing high-energy neutrinos and the limits on neutrino fluxes from the IMB detector.

40 MORI 93 excludes some region in $M_2-\mu$ parameter space depending on $\tan\beta$ and lightest scalar Higgs mass for neutralino dark matter $m_{\tilde{\chi}_1^0} > m_W$, using limits on upgoing muons produced by energetic neutrinos from neutralino annihilation in the Sun and the Earth.

41 BOTTINO 92 excludes some region $M_2-\mu$ parameter space assuming that the lightest neutralino is the dark matter, using upgoing muons at Kamiokande, direct searches by Ge detectors, and by LEP experiments. The analysis includes top radiative corrections on Higgs parameters and employs two different hypotheses for nucleon-Higgs coupling. Effects of rescaling in the local neutralino density according to the neutralino relic abundance are taken into account.

42 BOTTINO 91 excluded a region in $M_2-\mu$ plane using upgoing muon data from Kamioka experiment, assuming that the dark matter surrounding us is composed of neutralinos and that the Higgs boson is not too heavy.

43 GELMINI 91 exclude a region in $M_2-\mu$ plane using dark matter searches.

44 KAMIONKOWSKI 91 excludes a region in the $M_2-\mu$ plane using IMB limit on upgoing muons originated by energetic neutrinos from neutralino annihilation in the sun, assuming that the dark matter is composed of neutralinos and that $m_{H_1^0} \lesssim 50 \text{ GeV}$. See Fig. 8 in the paper.

45 MORI 91B exclude a part of the region in the $M_2-\mu$ plane with $m_{\tilde{\chi}_1^0} \gtrsim 80 \text{ GeV}$ using a limit on upgoing muons originated by energetic neutrinos from neutralino annihilation in the earth, assuming that the dark matter surrounding us is composed of neutralinos and that $m_{H_1^0} \lesssim 80 \text{ GeV}$.

46 OLIVE 88 result assumes that photinos make up the dark matter in the galactic halo. Limit is based on annihilations in the sun and is due to an absence of high energy neutrinos detected in underground experiments. The limit is model dependent.

———— $\tilde{\chi}_1^0-p$ elastic cross section ————

Experimental results on the $\tilde{\chi}_1^0-p$ elastic cross section are evaluated at $m_{\tilde{\chi}_1^0}=100 \text{ GeV}$. The experimental results on the cross section are often mass dependent. Therefore, the mass and cross section results are also given where the limit is strongest, when appropriate. Results are quoted separately for spin-dependent interactions (based on an effective 4-Fermi Lagrangian of the form $\bar{\nu}_i \mu \gamma^5 \chi \bar{\nu}_j \gamma^5 q$) and spin-independent interactions ($\bar{\nu}_i \chi \bar{\nu}_j q$). For calculational details see GRIEST 88b, ELLIS 88b, BARBIERI 89c, DREES 93b, ARNOWITT 96, BERGSTROM 96, and BAER 97 in addition to the theory papers listed in the Tables. For a description of the theoretical assumptions and experimental techniques underlying most of the listed papers, see the review on “Dark matter” in this “Review of Particle Physics,” and references therein. Most of the following papers use galactic halo and nuclear interaction assumptions from (LEWIN 96).

Spin-dependent interactions

VALUE (pb)	CL%	DOCUMENT ID	TECN	COMMENT
••• We do not use the following data for averages, fits, limits, etc. •••				
< 4 × 10 ⁻⁵	90	1 AMOLE	19 PICO	C ₃ F ₈
< 5 × 10 ⁻⁴	90	2 APRILE	19A XE1T	Xe
< 7 × 10 ⁻⁴	90	3 XIA	19A PNDX	Xe
< 8 × 10 ⁻⁴	90	4 AKERIB	17A LUX	Xe
< 0.28	90	5 BATTAT	17 DRFT	CS ₂ ; CF ₄
< 0.027	90	6 BEHNKE	17 PICA	C ₄ F ₁₀
< 5 × 10 ⁻⁴	90	7 AMOLE	16 PICO	CF ₃ I
< 6.8 × 10 ⁻³	90	8 APRILE	16B X100	Xe
< 6.3 × 10 ⁻³	90	9 FELIZARDO	14 SMPL	C ₂ ClF ₅
< 0.01	90	10 AKIMOV	12 ZEP3	Xe
< 7 × 10 ⁻³	90	11 BEHNKE	12 COUP	CF ₃ I
< 8.5 × 10 ⁻³	90	12 FELIZARDO	12 SMPL	C ₂ ClF ₅
< 0.016	90	13 KIM	12 KIMS	Csl
5 × 10 ⁻¹⁰ to 10 ⁻⁵	95	14 BUCHMUEL...	11B THEO	
< 1	90	15 ANGLE	08A XE10	Xe
< 0.055	90	16 BEDNYAKOV	08 HDMS	Ge
< 0.33	90	17 BEHNKE	08 COUP	CF ₃ I
< 5	90	18 AKERIB	06 CDMS	Ge
< 2	90	19 SHIMIZU	06A CNTR	CaF ₂
< 0.4	90	20 ALNER	05 NAIA	NaI Spin Dep.
< 2	90	21 BARNABE-HE.	05 PICA	C
2 × 10 ⁻¹¹ to 1 × 10 ⁻⁴	90	22 ELLIS	04 THEO	$\mu > 0$
< 0.8	90	23 AHMED	03 NAIA	NaI Spin Dep.
< 40	90	24 TAKEDA	03 BOLO	NaF Spin Dep.
< 10	90	25 ANGLÖHER	02 CRES	Saphire
8 × 10 ⁻⁷ to 2 × 10 ⁻⁵	90	26 ELLIS	01c THEO	$\tan\beta \leq 10$
< 3.8	90	27 BERNABE	00b DAMA	Xe
< 0.8	90	28 SPOONER	00 UKDM	NaI
< 4.8	90	29 BELLI	99c DAMA	F
< 100	90	30 OOTANI	99 BOLO	LIF
< 0.6	90	31 BERNABE	98c DAMA	Xe
< 5	90	32 BERNABE	97 DAMA	F

Searches Particle Listings

Supersymmetric Particle Searches

- 1 The strongest limit is $< 2.5 \times 10^{-5}$ pb at $m_\chi = 25$ GeV. This updates AMOLE 17.
- 2 The strongest limit is $< 2 \times 10^{-4}$ pb at $m_\chi = 30$ GeV. For scatterings on neutrons, the strongest limit is $< 6.3 \times 10^{-6}$ at $m_\chi = 30$ GeV.
- 3 The strongest limit is $< 4.4 \times 10^{-4}$ pb at $m_\chi = 40$ GeV. This updates FU 17.
- 4 The strongest limit is 5×10^{-4} pb at $m_\chi = 35$ GeV. The limit for scattering on neutrons is 3×10^{-5} pb at 100 GeV and is 1.6×10^{-5} pb at 35 GeV. This updates AKERIB 16A.
- 5 Directional recoil detector. This updates DAW 12.
- 6 This result updates ARCHAMBAULT 12. The strongest limit is 0.013 pb at $m_\chi = 20$ GeV.
- 7 The strongest limit is 5×10^{-4} pb at $m_\chi = 80$ GeV.
- 8 The strongest limit is 5.2×10^{-3} pb at 50 GeV. The limit for scattering on neutrons is 2.8×10^{-4} pb at 100 GeV and the strongest limit is 2.0×10^{-4} pb at 50 GeV. This updates APRILE 13.
- 9 The strongest limit is 0.0043 pb and occurs at $m_\chi = 35$ GeV. FELIZARDO 14 also presents limits for the scattering on neutrons. At $m_\chi = 100$ GeV, the upper limit is 0.13 pb and the strongest limit is 0.066 pb at $m_\chi = 35$ GeV.
- 10 This result updates LEBEDENKO 09A. The strongest limit is 8×10^{-3} pb at $m_\chi = 50$ GeV. Limit applies to the neutralino neutron elastic cross section.
- 11 The strongest limit is 6×10^{-3} at $m_\chi = 60$ GeV.
- 12 The strongest limit is 5.7×10^{-3} at $m_\chi = 35$ GeV.
- 13 This result updates LEE 07A. The strongest limit is at $m_\chi = 80$ GeV.
- 14 Predictions for the spin-dependent elastic cross section based on a frequentist approach to electroweak observables in the framework of $N = 1$ supergravity models with radiative breaking of the electroweak gauge symmetry.
- 15 The strongest limit is 0.6 pb and occurs at $m_\chi = 30$ GeV. The limit for scattering on neutrons is 0.01 pb at $m_\chi = 100$ GeV, and the strongest limit is 0.0045 pb at $m_\chi = 30$ GeV.
- 16 Limit applies to neutron elastic cross section.
- 17 The strongest upper limit is 0.25 pb and occurs at $m_\chi \approx 40$ GeV.
- 18 The strongest upper limit is 4 pb and occurs at $m_\chi \approx 60$ GeV. The limit on the neutron spin-dependent elastic cross section is 0.07 pb. This latter limit is improved in AHMED 09, where a limit of 0.02 pb is obtained at $m_\chi = 100$ GeV. The strongest limit in AHMED 09 is 0.018 pb and occurs at $m_\chi = 60$ GeV.
- 19 The strongest upper limit is 1.2 pb and occurs at $m_\chi \approx 40$ GeV. The limit on the neutron spin-dependent cross section is 35 pb.
- 20 The strongest upper limit is 0.35 pb and occurs at $m_\chi \approx 60$ GeV.
- 21 The strongest upper limit is 1.2 pb and occurs $m_\chi \approx 30$ GeV.
- 22 ELLIS 04 calculates the χp elastic scattering cross section in the framework of $N=1$ supergravity models with radiative breaking of the electroweak gauge symmetry, but without universal scalar masses. In the case of universal squark and slepton masses, but non-universal Higgs masses, the limit becomes 2×10^{-4} , see ELLIS 03E.
- 23 The strongest upper limit is 0.75 pb and occurs at $m_\chi \approx 70$ GeV.
- 24 The strongest upper limit is 30 pb and occurs at $m_\chi \approx 20$ GeV.
- 25 The strongest upper limit is 8 pb and occurs at $m_\chi \approx 30$ GeV.
- 26 ELLIS 01c calculates the χp elastic scattering cross section in the framework of $N=1$ supergravity models with radiative breaking of the electroweak gauge symmetry. In models with nonuniversal Higgs masses, the upper limit to the cross section is 6×10^{-4} .
- 27 The strongest upper limit is 3 pb and occurs at $m_\chi \approx 60$ GeV. The limits are for inelastic scattering $\chi^0 + {}^{129}\text{Xe} \rightarrow \chi^0 + {}^{129}\text{Xe}^* (39.58 \text{ keV})$.
- 28 The strongest upper limit is 4.4 pb and occurs at $m_\chi \approx 60$ GeV.
- 29 The strongest upper limit is about 35 pb and occurs at $m_\chi \approx 15$ GeV.

Spin-independent interactions

VALUE (pb)	CL%	DOCUMENT ID	TECN	COMMENT
$< 2.5 \times 10^{-8}$	90	1 ABE	19 XMAS	Xe
$< 3.9 \times 10^{-9}$	90	2 AJAJ	19 DEAP	Ar
$< 2 \times 10^{-8}$	90	3 AMOLE	19 PICO	C ₃ F ₈
$< 2.25 \times 10^{-6}$	90	4 ADHIKARI	18 C100	Nal
$< 1.14 \times 10^{-8}$	90	5 AGNESE	18A DS50	Ar
$< 1.6 \times 10^{-8}$	90	6 AGNESE	18A CDMS	Ge
$< 9 \times 10^{-11}$	90	7 APRILE	18 XE1T	Xe
$< 1.8 \times 10^{-10}$	90	8 AKERIB	17 LUX	Xe
$< 1.4 \times 10^{-10}$	90	9 CUI	17A PNDX	Xe
$< 1.5 \times 10^{-9}$	90	10 APRILE	16B X100	Xe
$< 1.5 \times 10^{-9}$	90	11 AKERIB	14 LUX	Xe
10^{-11} - 10^{-7}	95	12 BUCHMUEL...	14A THEO	
$< 4.6 \times 10^{-6}$	90	13 FELIZARDO	14 SMPL	C ₂ ClF ₅
10^{-11} - 10^{-8}	95	14 ROSZKOWSKI	14 THEO	
$< 2.2 \times 10^{-6}$	90	15 AGNESE	13 CDMS	Si
$< 5 \times 10^{-8}$	90	16 AKIMOV	12 ZEP3	Xe
1.6×10^{-6} ; 3.7×10^{-5}		17 ANGLÖHER	12 CRES	CaWO ₄
3×10^{-12} to 3×10^{-9}	95	18 BECHTLE	12 THEO	
$< 1.6 \times 10^{-7}$		19 BEHNKE	12 COUP	CF ₃ I
$< 2.3 \times 10^{-7}$	90	20 KIM	12 KIMS	Csl
$< 3.3 \times 10^{-8}$	90	21 AHMED	11A	Ge
$< 4.4 \times 10^{-8}$	90	22 ARMENGAUD	11 EDE2	Ge
$< 1 \times 10^{-7}$	90	23 ANGLE	08 XE10	Xe
$< 1 \times 10^{-6}$	90	BENETTI	08 WARP	Ar
$< 7.5 \times 10^{-7}$	90	24 ALNER	07A ZEP2	Xe
$< 2 \times 10^{-7}$		25 AKERIB	06A CDMS	Ge
$< 90 \times 10^{-7}$		ALNER	05 NAlA	Nal Spin Indep.
$< 12 \times 10^{-7}$		26 ALNER	05A ZEPL	

$< 14 \times 10^{-7}$		SANGLARD	05 EDEL	Ge
$< 4 \times 10^{-7}$		27 AKERIB	04 CDMS	Ge
2×10^{-11} to 1.5×10^{-7}	95	28 BALTZ	04 THEO	
2×10^{-11} to 8×10^{-6}		29,30 ELLIS	04 THEO	$\mu > 0$
$< 5 \times 10^{-8}$		31 PIERCE	04A THEO	
$< 2 \times 10^{-5}$		32 AHMED	03 NAlA	Nal Spin Indep.
$< 3 \times 10^{-6}$		33 AKERIB	03 CDMS	Ge
2×10^{-13} to 2×10^{-7}		34 BAER	03A THEO	
$< 1.4 \times 10^{-5}$		35 KLAPDOR-K...	03 HDMS	Ge
$< 6 \times 10^{-6}$		36 ABRAMS	02 CDMS	Ge
1×10^{-12} to 7×10^{-6}		29 KIM	02b THEO	
$< 3 \times 10^{-5}$		37 MORALES	02b CSME	Ge
$< 1 \times 10^{-5}$		38 MORALES	02c IGEX	Ge
$< 1 \times 10^{-6}$		BALTZ	01 THEO	
$< 3 \times 10^{-5}$		39 BAUDIS	01 HDMS	Ge
$< 7 \times 10^{-6}$		40 BOTTINO	01 THEO	
$< 1 \times 10^{-8}$		41 CORSETTI	01 THEO	$\tan\beta \leq 25$
5×10^{-10} to 1.5×10^{-8}		42 ELLIS	01c THEO	$\tan\beta \leq 10$
$< 4 \times 10^{-6}$		41 GOMEZ	01 THEO	
2×10^{-10} to 1×10^{-7}		41 LAHANAS	01 THEO	
$< 3 \times 10^{-6}$		ABUSAIDI	00 CDMS	Ge, Si
$< 6 \times 10^{-7}$		43 ACCOMANDO	00 THEO	
2.5×10^{-9} to 3.5×10^{-8}		44 BERNABEI	00 DAMA	Nal
$< 1.5 \times 10^{-5}$		49 FENG	00 THEO	$\tan\beta=10$
$< 4 \times 10^{-5}$		MORALES	00 IGEX	Ge
$< 7 \times 10^{-6}$		SPOONER	00 UKDM	Nal
$< 7 \times 10^{-6}$		BAUDIS	99 HDMO	⁷⁶ Ge
$< 7 \times 10^{-6}$		BERNABEI	98c DAMA	Xe

- 1 The strongest upper limit is 2.2×10^{-8} pb at 60 GeV.
- 2 This updates AMAUDRUZ 18.
- 3 This updates AMOLE 16.
- 4 The strongest limit is 2.05×10^{-6} at $m = 60$ GeV.
- 5 The strongest limit is 1.09×10^{-8} pb at $m_\chi = 126$ GeV. This updates AGNES 15.
- 6 The strongest limit is 1.0×10^{-8} pb at $m_\chi = 46$ GeV. This updates AGNESE 15B.
- 7 Based on 278.8 days of data collection. The strongest limit is 4.1×10^{-11} pb at $m_\chi = 30$ GeV. This updates APRILE 17G.
- 8 AKERIB 17. The strongest limit is 1.1×10^{-10} pb at 50 GeV. This updates AKERIB 16.
- 9 The strongest limit is 8.6×10^{-11} pb at 40 GeV. This updates TAN 16B.
- 10 The strongest limit is 1.1×10^{-9} pb at 50 GeV. This updates APRILE 12.
- 11 The strongest upper limit is 7.6×10^{-10} at $m_\chi = 33$ GeV.
- 12 Predictions for the spin-independent elastic cross section based on a frequentist approach to electroweak observables in the framework of $N = 1$ supergravity models with radiative breaking of the electroweak gauge symmetry using the 20 fb⁻¹ 8 TeV and the 5 fb⁻¹ 7 TeV LHC data and the LUX data.
- 13 The strongest limit is 3.6×10^{-6} pb and occurs at $m_\chi = 35$ GeV. Felizardo 2014 updates Felizardo 2012.
- 14 Predictions for the spin-independent elastic cross section based on a Bayesian approach to electroweak observables in the framework of $N = 1$ supergravity models with radiative breaking of the electroweak gauge symmetry using the 20 fb⁻¹ LHC data and LUX.
- 15 AGNESE 13 presents 90% CL limits on the elastic cross section for masses in the range 7–100 GeV using the Si based detector. The strongest upper limit is 1.8×10^{-6} pb at $m_\chi = 50$ GeV. This limit is improved to 7×10^{-7} pb in AGNESE 13A.
- 16 This result updates LEBEDENKO 09. The strongest limit is 3.9×10^{-8} pb at $m_\chi = 52$ GeV.
- 17 ANGLÖHER 12 presents results of 730 kg days from the CRESST-II dark matter detector. They find two maxima in the likelihood function corresponding to best fit WIMP masses of 25.3 and 11.6 GeV with elastic cross sections of 1.6×10^{-6} and 3.7×10^{-5} pb respectively, see their Table 4. The statistical significance is more than 4σ . ANGLÖHER 12 updates ANGLÖHER 09.
- 18 Predictions for the spin-independent elastic cross section based on a frequentist approach to electroweak observables in the framework of $N = 1$ supergravity models with radiative breaking of the electroweak gauge symmetry using the 5 fb⁻¹ LHC data and XENON100.
- 19 The strongest limit is 1.4×10^{-7} at $m_\chi = 60$ GeV.
- 20 This result updates LEE 07A. The strongest limit is 2.1×10^{-7} at $m_\chi = 70$ GeV.
- 21 AHMED 11A gives combined results from CDMS and EDELWEISS. The strongest limit is at $m_\chi = 90$ GeV.
- 22 ARMENGAUD 11 updates result of ARMENGAUD 10. Strongest limit at $m_\chi = 85$ GeV.
- 23 The strongest upper limit is 5.1×10^{-8} pb and occurs at $m_\chi \approx 30$ GeV. The values quoted here are based on the analysis performed in ANGLE 08 with the update from SORESENSEN 09.
- 24 The strongest upper limit is 6.6×10^{-7} pb and occurs at $m_\chi \approx 65$ GeV.
- 25 AKERIB 06A updates the results of AKERIB 05. The strongest upper limit is 1.6×10^{-7} pb and occurs at $m_\chi \approx 60$ GeV.
- 26 The strongest upper limit is also close to 1.0×10^{-6} pb and occurs at $m_\chi \approx 70$ GeV. BENOIT 06 claim that the discrimination power of ZEPLIN-I measurement (ALNER 05A) is not reliable enough to obtain a limit better than 1×10^{-3} pb. However, SMITH 06 do not agree with the criticisms of BENOIT 06.
- 27 AKERIB 04 is incompatible with BERNABEI 00 most likely value, under the assumption of standard WIMP-halo interactions. The strongest upper limit is 4×10^{-7} pb and occurs at $m_\chi \approx 60$ GeV.
- 28 Predictions for the spin-independent elastic cross section in the framework of $N = 1$ supergravity models with radiative breaking of the electroweak gauge symmetry.
- 29 KIM 02 and ELLIS 04 calculate the χp elastic scattering cross section in the framework of $N=1$ supergravity models with radiative breaking of the electroweak gauge symmetry, but without universal scalar masses.

See key on page 999

Searches Particle Listings Supersymmetric Particle Searches

- ³⁰ In the case of universal squark and slepton masses, but non-universal Higgs masses, the limit becomes 2×10^{-6} (2×10^{-11} when constraint from the BNL $g-2$ experiment are included), see ELLIS 03E. ELLIS 05 display the sensitivity of the elastic scattering cross section to the π -Nucleon Σ term.
- ³¹ PIERCE 04A calculates the χp elastic scattering cross section in the framework of models with very heavy scalar masses. See Fig. 2 of the paper.
- ³² The strongest upper limit is 1.8×10^{-5} pb and occurs at $m_\chi \approx 80$ GeV.
- ³³ Under the assumption of standard WIMP-halo interactions, Akerib 03 is incompatible with BERNABEI 00 most likely value at the 99.98% CL. See Fig. 4.
- ³⁴ BAER 03A calculates the χp elastic scattering cross section in several models including the framework of $N=1$ supergravity models with radiative breaking of the electroweak gauge symmetry.
- ³⁵ The strongest upper limit is 7×10^{-6} pb and occurs at $m_\chi \approx 30$ GeV.
- ³⁶ ABRAMS 02 is incompatible with the DAMA most likely value at the 99.9% CL. The strongest upper limit is 3×10^{-6} pb and occurs at $m_\chi \approx 30$ GeV.
- ³⁷ The strongest upper limit is 2×10^{-5} pb and occurs at $m_\chi \approx 40$ GeV.
- ³⁸ The strongest upper limit is 7×10^{-6} pb and occurs at $m_\chi \approx 46$ GeV.
- ³⁹ The strongest upper limit is 1.8×10^{-5} pb and occurs at $m_\chi \approx 32$ GeV.
- ⁴⁰ BOTTINO 01 calculates the χ - p elastic scattering cross section in the framework of the following supersymmetric models: $N=1$ supergravity with the radiative breaking of the electroweak gauge symmetry, $N=1$ supergravity with nonuniversal scalar masses and an effective MSSM model at the electroweak scale.
- ⁴¹ Calculates the χ - p elastic scattering cross section in the framework of $N=1$ supergravity models with radiative breaking of the electroweak gauge symmetry.
- ⁴² ELLIS 01c calculates the χ - p elastic scattering cross section in the framework of $N=1$ supergravity models with radiative breaking of the electroweak gauge symmetry. ELLIS 02B find a range 2×10^{-8} - 1.5×10^{-7} at $\tan\beta=50$. In models with nonuniversal Higgs masses, the upper limit to the cross section is 4×10^{-7} .
- ⁴³ ACCOMANDO 00 calculate the χ - p elastic scattering cross section in the framework of minimal $N=1$ supergravity models with radiative breaking of the electroweak gauge symmetry. The limit is relaxed by at least an order of magnitude when models with nonuniversal scalar masses are considered. A subset of the authors in ARNOWITT 02 updated the limit to $< 9 \times 10^{-8}$ ($\tan\beta < 55$).
- ⁴⁴ BERNABEI 00 search for annual modulation of the WIMP signal. The data favor the hypothesis of annual modulation at 4σ and are consistent, for a particular model framework quoted there, with $m_{\chi_0^0} = 44 \pm \frac{12}{9}$ GeV and a spin-independent X^0 -proton cross section of $(5.4 \pm 1.0) \times 10^{-6}$ pb. See also BERNABEI 01 and BERNABEI 00c.
- ⁴⁵ FENG 00 calculate the χ - p elastic scattering cross section in the framework of $N=1$ supergravity models with radiative breaking of the electroweak gauge symmetry with a particular emphasis on focus point models. At $\tan\beta=50$, the range is 8×10^{-8} - 4×10^{-7} .

Other bounds on χ_1^0 from astrophysics and cosmology

Most of these papers generally exclude regions in the $M_2 - \mu$ parameter plane by requiring that the $\tilde{\chi}_1^0$ contribution to the overall cosmological density is less than some maximal value to avoid overclosure of the Universe. Those not based on the cosmological density are indicated. Many of these papers also include LEP and/or other bounds.

VALUE	DOCUMENT ID	TECN	COMMENT
>46 GeV	1 ELLIS 00	RVUE	
• • • We do not use the following data for averages, fits, limits, etc. • • •			
	2 BUCHMUEL... 14	COSM	
	3 BUCHMUEL... 14A	COSM	
	4 ROSZKOWSKI 14	COSM	
	5 CABRERA 13	COSM	
	6 ELLIS 13B	COSM	
	5 STREGE 13	COSM	
	2 AKULA 12	COSM	
	2 ARBEY 12A	COSM	
	2 BAER 12	COSM	
	7 BALAZS 12	COSM	
	8 BECHTLE 12	COSM	
	9 BESKIDT 12	COSM	
> 18 GeV	10 BOTTINO 12	COSM	
	2 BUCHMUEL... 12	COSM	
	2 CAO 12A	COSM	
	2 ELLIS 12B	COSM	
	11 FENG 12B	COSM	
	2 KADASTIK 12	COSM	
	7 STREGE 12	COSM	
	12 BUCHMUEL... 11	COSM	
	13 ROSZKOWSKI 11	COSM	
	14 ELLIS 10	COSM	
	15 BUCHMUEL... 09	COSM	
	16 DREINER 09	THEO	
	17 BUCHMUEL... 08	COSM	
	13 ELLIS 08	COSM	
	18 CALIBBI 07	COSM	
	19 ELLIS 07	COSM	
	20 ALLANACH 06	COSM	
	21 DE-AUSTRI 06	COSM	
	13 BAER 05	COSM	
	22 BALTZ 04	COSM	
> 6 GeV	10,23 BELANGER 04	THEO	
	24 ELLIS 04B	COSM	
	25 PIERCE 04A	COSM	
	26 BAER 03	COSM	

> 6 GeV	10 BOTTINO 03	COSM	
	26 CHATTOPAD...03	COSM	
	27 ELLIS 03	COSM	
	13 ELLIS 03B	COSM	
	26 ELLIS 03c	COSM	
	26 LAHANAS 03	COSM	
	28 LAHANAS 02	COSM	
	29 BARGER 01c	COSM	
	30 ELLIS 01B	COSM	
	27 BOEHM 00B	COSM	
	31 FENG 00	COSM	
< 600 GeV	32 ELLIS 98B	COSM	
	33 EDSJO 97	COSM	Co-annihilation
	34 BAER 96	COSM	
	13 BEREZINSKY 95	COSM	
	35 FALK 95	COSM	CP-violating phases
	36 DREES 93	COSM	Minimal supergravity
	37 FALK 93	COSM	Sfermion mixing
	36 KELLEY 93	COSM	Minimal supergravity
	38 MIZUTA 93	COSM	Co-annihilation
	39 LOPEZ 92	COSM	Minimal supergravity, $m_0=A=0$
	40 MCDONALD 92	COSM	
	41 GRIEST 91	COSM	
	42 NOJIRI 91	COSM	Minimal supergravity
	43 OLIVE 91	COSM	
	44 ROSZKOWSKI 91	COSM	
	45 GRIEST 90	COSM	
	43 OLIVE 89	COSM	
none 100 eV - 15 GeV	SREDNICKI 88	COSM	$\tilde{\gamma}; m_{\tilde{f}}=100$ GeV
none 100 eV-5 GeV	ELLIS 84	COSM	$\tilde{\gamma};$ for $m_{\tilde{f}}=100$ GeV
	GOLDBERG 83	COSM	$\tilde{\gamma}$
	46 KRAUSS 83	COSM	$\tilde{\gamma}$
	VYSOTSKII 83	COSM	$\tilde{\gamma}$

- ¹ ELLIS 00 updates ELLIS 98. Uses LEP e^+e^- data at $\sqrt{s}=202$ and 204 GeV to improve bound on neutralino mass to 51 GeV when scalar mass universality is assumed and 46 GeV when Higgs mass universality is relaxed. Limits on $\tan\beta$ improve to > 2.7 ($\mu > 0$), > 2.2 ($\mu < 0$) when scalar mass universality is assumed and > 1.9 (both signs of μ) when Higgs mass universality is relaxed.
- ² Implications of the LHC result on the Higgs mass and on the SUSY parameter space in the framework of $N = 1$ supergravity models with radiative breaking of the electroweak gauge symmetry.
- ³ BUCHMUELLER 14A places constraints on the SUSY parameter space in the framework of $N = 1$ supergravity models with radiative breaking of the electroweak gauge symmetry using indirect experimental searches using the 20 fb^{-1} 8 TeV and the 5 fb^{-1} 7 TeV LHC and the LUX data.
- ⁴ ROSZKOWSKI 14 places constraints on the SUSY parameter space in the framework of $N = 1$ supergravity models with radiative breaking of the electroweak gauge symmetry using Bayesian statistics and indirect experimental searches using the 20 fb^{-1} LHC and the LUX data.
- ⁵ CABRERA 13 and STREGE 13 place constraints on the SUSY parameter space in the framework of $N = 1$ supergravity models with radiative breaking of the electroweak gauge symmetry with and without non-universal Higgs masses using the 5.8 fb^{-1} , $\sqrt{s} = 7$ TeV ATLAS supersymmetry searches and XENON100 results.
- ⁶ ELLIS 13B place constraints on the SUSY parameter space in the framework of $N = 1$ supergravity models with radiative breaking of the electroweak gauge symmetry with and without Higgs mass universality. Models with universality below the GUT scale are also considered.
- ⁷ BALAZS 12 and STREGE 12 place constraints on the SUSY parameter space in the framework of $N = 1$ supergravity models with radiative breaking of the electroweak gauge symmetry using the 1 fb^{-1} LHC supersymmetry searches, the 5 fb^{-1} Higgs mass constraints, both with $\sqrt{s} = 7$ TeV, and XENON100 results.
- ⁸ BECHTLE 12 places constraints on the SUSY parameter space in the framework of $N = 1$ supergravity models with radiative breaking of the electroweak gauge symmetry using indirect experimental searches, using the 5 fb^{-1} LHC and XENON100 data.
- ⁹ BESKIDT 12 places constraints on the SUSY parameter space in the framework of $N = 1$ supergravity models with radiative breaking of the electroweak gauge symmetry using indirect experimental searches, the 5 fb^{-1} LHC and the XENON100 data.
- ¹⁰ BELANGER 04 and BOTTINO 12 (see also BOTTINO 03, BOTTINO 03A and BOTTINO 04) do not assume gaugino or scalar mass unification.
- ¹¹ FENG 12B places constraints on the SUSY parameter space in the framework of $N = 1$ supergravity models with radiative breaking of the electroweak gauge symmetry and large sfermion masses using the 1 fb^{-1} LHC supersymmetry searches, the 5 fb^{-1} LHC Higgs mass constraints both with $\sqrt{s} = 7$ TeV, and XENON100 results.
- ¹² BUCHMUELLER 11 places constraints on the SUSY parameter space in the framework of $N = 1$ supergravity models with radiative breaking of the electroweak gauge symmetry using indirect experimental searches and including supersymmetry breaking relations between A and B parameters.
- ¹³ Places constraints on the SUSY parameter space in the framework of $N=1$ supergravity models with radiative breaking of the electroweak gauge symmetry but non-Universal Higgs masses.
- ¹⁴ ELLIS 10 places constraints on the SUSY parameter space in the framework of $N = 1$ supergravity models with radiative breaking of the electroweak gauge symmetry with universality above the GUT scale.
- ¹⁵ BUCHMUELLER 09 places constraints on the SUSY parameter space in the framework of $N = 1$ supergravity models with radiative breaking of the electroweak gauge symmetry using indirect experimental searches.
- ¹⁶ DREINER 09 show that in the general MSSM with non-universal gaugino masses there exists no model-independent laboratory bound on the mass of the lightest neutralino. An essentially massless $\tilde{\chi}_1^0$ is allowed by the experimental and observational data, imposing some constraints on other MSSM parameters, including M_2 , μ and the slepton and squark masses.

Searches Particle Listings

Supersymmetric Particle Searches

VALUE (GeV)	CL%	DOCUMENT ID	TECN	COMMENT
>525	95	1 SIRUNYAN	19Ca CMS	$\tilde{\chi}_1^0 \rightarrow \gamma \tilde{G}$, GMSB, SPS8, $\sigma_T = 1$ m
>290	95	2 SIRUNYAN	19ci CMS	$\geq 1 H (\rightarrow \gamma\gamma) + \text{jets} + \cancel{E}_T$, Tn1n1A, GMSB
>230	95	2 SIRUNYAN	19ci CMS	$\geq 1 H (\rightarrow \gamma\gamma) + \text{jets} + \cancel{E}_T$, Tn1n1B, GMSB
>930	95	3 SIRUNYAN	19k CMS	$\gamma + \text{lepton} + \cancel{E}_T$, Tchi1n1A
none	95	4 AABOUD	18ck ATLS	$2H (\rightarrow bb) + \cancel{E}_T$, Tn1n1A, GMSB
130–230, 290–880				
>295	95	5 AABOUD	18z ATLS	$\geq 4\ell$, GMSB, Tn1n1C
>180	95	6 SIRUNYAN	18Ao CMS	$\ell^\pm \ell^\pm$ or $\geq 3\ell$, Tn1n1A
>260	95	6 SIRUNYAN	18Ao CMS	$\ell^\pm \ell^\pm$ or $\geq 3\ell$, Tn1n1B
>450	95	6 SIRUNYAN	18Ao CMS	$\ell^\pm \ell^\pm$ or $\geq 3\ell$, Tn1n1C
>750	95	7 SIRUNYAN	18AP CMS	Combination of searches, GMSB, Tn1n1A
>650	95	7 SIRUNYAN	18AP CMS	Combination of searches, GMSB, Tn1n1B
>690	95	7 SIRUNYAN	18AP CMS	Combination of searches, GMSB, Tn1n1C
>500	95	8 SIRUNYAN	18AR CMS	$\ell^\pm \ell^\pm + \text{jets} + \cancel{E}_T$, GMSB, Tn1n1B
>650	95	8 SIRUNYAN	18AR CMS	$\ell^\pm \ell^\pm + \text{jets} + \cancel{E}_T$, GMSB, Tn1n1C
none	95	9 SIRUNYAN	18o CMS	$2H (\rightarrow bb) + \cancel{E}_T$, Tn1n1A, GMSB
$^{230-770}_{>205}$	95	10 SIRUNYAN	18x CMS	$\geq 1 H (\rightarrow \gamma\gamma) + \text{jets} + \cancel{E}_T$, Tn1n1A, GMSB
>130	95	10 SIRUNYAN	18x CMS	$\geq 1 H (\rightarrow \gamma\gamma) + \text{jets} + \cancel{E}_T$, Tn1n1B, GMSB
>380	95	11 KHACHATRYAN	14L CMS	$\tilde{\chi}_1^0 \rightarrow Z \tilde{G}$ simplified models, GMSB, RPV
••• We do not use the following data for averages, fits, limits, etc. •••				
none	95	12 AABOUD	19g ATLS	$\tilde{\chi}_1^0 \rightarrow Z \tilde{G}$ from gluinos as in Tglu1A, GMSB, depending on σ_T
300–1000				
		13 AAIJ	17z	displaced vertex with associated μ
		14 KHACHATRYAN	16bx CMS	$\geq 3\ell^\pm$, RPV, λ or λ' couplings, wino- or higgsino-like neutralinos
		15 AAD	14bh ATLS	$2\gamma + \cancel{E}_T$, GMSB, SPS8
		16 AAD	13ap ATLS	$2\gamma + \cancel{E}_T$, GMSB, SPS8
none	95	17 AAD	13q ATLS	$\gamma + b + \cancel{E}_T$, higgsino-like neutralino, GMSB
220–380				
		18 AAD	13r ATLS	$\tilde{\chi}_1^0 \rightarrow \mu j j$, RPV, $\lambda'_{211} \neq 0$
		19 AALTONEN	13i CDF	$\tilde{\chi}_1^0 \rightarrow \gamma \tilde{G}$, \cancel{E}_T , GMSB
>220	95	20 CHATRCHYAN	13ah CMS	$\tilde{\chi}_1^0 \rightarrow \gamma \tilde{G}$, GMSB, SPS8, $\sigma_T < 500$ mm
		21 AAD	12cp ATLS	$2\gamma + \cancel{E}_T$, GMSB
		22 AAD	12ct ATLS	$\geq 4\ell^\pm$, RPV
		23 AAD	12r ATLS	$\tilde{\chi}_1^0 \rightarrow \mu j j$, RPV, $\lambda'_{211} \neq 0$
		24 ABAZOV	12ad D0	$\tilde{\chi}_1^0 \tilde{\chi}_1^0 \rightarrow \gamma Z \tilde{G}$, GMSB
		25 CHATRCHYAN	12bk CMS	$2\gamma + \cancel{E}_T$, GMSB
		26 CHATRCHYAN	11b CMS	$\tilde{W}^0 \rightarrow \gamma \tilde{G}$, $\tilde{W}^\pm \rightarrow \ell^\pm \tilde{G}$, GMSB
>149	95	27 AALTONEN	10 CDF	$p\bar{p} \rightarrow \tilde{\chi}\tilde{\chi}$, $\tilde{\chi} = \tilde{\chi}_2^0, \tilde{\chi}_1^\pm, \tilde{\chi}_1^0 \rightarrow \gamma \tilde{G}$, GMSB
>175	95	28 ABAZOV	10p D0	$\tilde{\chi}_1^0 \rightarrow \gamma \tilde{G}$, GMSB
>125	95	29 ABAZOV	08f D0	$p\bar{p} \rightarrow \tilde{\chi}\tilde{\chi}$, $\tilde{\chi} = \tilde{\chi}_2^0, \tilde{\chi}_1^\pm, \tilde{\chi}_1^0 \rightarrow \gamma \tilde{G}$, GMSB
		30 ABULENCIA	07h CDF	RPV, $LL\bar{E}$
> 96.8	95	31 ABBIENDI	06b OPAL	$e^+e^- \rightarrow \tilde{B}\tilde{B}$, ($\tilde{B} \rightarrow \tilde{G}\gamma$)
		32 ABDALLAH	05b DLPH	$e^+e^- \rightarrow \tilde{G}\tilde{\chi}_1^0$, ($\tilde{\chi}_1^0 \rightarrow \tilde{G}\gamma$)
> 96	95	33 ABDALLAH	05b DLPH	$e^+e^- \rightarrow \tilde{B}\tilde{B}$, ($\tilde{B} \rightarrow \tilde{G}\gamma$)

Unstable $\tilde{\chi}_1^0$ (Lightest Neutralino) mass limit

Unless otherwise stated, results in this section assume spectra and production rates as evaluated in the MSSM. Unless otherwise stated, the goldstino or gravitino mass $m_{\tilde{G}}$ is assumed to be negligible relative to all other masses. In the following, \tilde{G} is assumed to be undetected and to give rise to a missing energy (\cancel{E}) signature.

Some earlier papers are now obsolete and have been omitted. They were last listed in our PDG 14 edition: K. Olive, et al. (Particle Data Group), Chinese Physics **C38** 070001 (2014) (<http://pdg.lbl.gov>).

1 SIRUNYAN 19Ca searched in 77.4 fb^{-1} of pp collisions at $\sqrt{s} = 13 \text{ TeV}$ for events containing delayed photons in both single and diphoton plus \cancel{E}_T final states. No excess is observed above the background expected from Standard Model processes. The results are used to set 95% C.L. exclusion limits in the context of GMSB, using the SPS8 benchmark model. For neutralino proper decay lengths of 0.1, 1, 10, and 100 m, masses up to about 320, 525, 360, and 215 GeV are excluded, respectively. See their Fig. 5. The searches involve the simplified models Tglu1D, Tglu4A,B,C, Tsqk4A,4B,4C.

2 SIRUNYAN 19ci searched in 77.5 fb^{-1} of pp collisions at $\sqrt{s} = 13 \text{ TeV}$ for events with one or more high-momentum Higgs bosons, decaying to pairs of photons, jets and \cancel{E}_T . No significant excess above the Standard Model expectations is observed. Limits are set on the sbottom mass in the Tsbot4 simplified model, see Figure 3, and on the wino mass in the Tchi1n2E simplified model, see their Figure 4. Limits are also set on the higgsino mass in the Tn1n1A and Tn1n1B simplified models, see their Figure 5.

3 SIRUNYAN 19k searched in 35.9 fb^{-1} of pp collisions at $\sqrt{s} = 13 \text{ TeV}$ for events with a photon, an electron or muon, and large \cancel{E}_T . No significant excess above the Standard Model expectations is observed. In the framework of GMSB, limits are set on the chargino and neutralino mass in the Tchi1n1A simplified model, see their Figure 6. Limits are also set on the gluino mass in the Tglu4A simplified model, and on the squark mass in the Tsqk4A simplified model, see their Figure 7.

4 AABOUD 18ck searched for events with at least 3 b -jets and large missing transverse energy in two datasets of pp collisions at $\sqrt{s} = 13 \text{ TeV}$ of 36.1 fb^{-1} and 24.3 fb^{-1} depending on the trigger requirements. The analyses aimed to reconstruct two Higgs bosons decaying to pairs of b -quarks. No significant excess above the Standard Model expectations is observed. Limits are set on the Higgsino mass in the Tn1n1A simplified model, see their Figure 15(a). Constraints are also presented as a function of the BR of Higgsino decaying into an higgs boson and a gravitino, see their Figure 15(b).

5 AABOUD 18z searched in 36.1 fb^{-1} of pp collisions at $\sqrt{s} = 13 \text{ TeV}$ for events containing four or more charged leptons (electrons, muons and up to two hadronically decaying taus). No significant deviation from the expected SM background is observed. Limits are set on the Higgsino mass in simplified models of general gauge mediated supersymmetry Tn1n1A/Tn1n1B/Tn1n1C, see their Figure 9. Limits are also set on the wino, slepton, sneutrino and gluino mass in a simplified model of NLSP pair production with R-parity violating decays of the LSP via λ_{12k} or λ_{j33} to charged leptons, see their Figures 7, 8.

6 SIRUNYAN 18Ao searched in 35.9 fb^{-1} of pp collisions at $\sqrt{s} = 13 \text{ TeV}$ for direct electroweak production of charginos and neutralinos in events with either two or more leptons (electrons or muons) of the same electric charge, or with three or more leptons, which can include up to two hadronically decaying tau leptons. No significant excess above the Standard Model expectations is observed. Limits are set on the chargino/neutralino mass in the Tchi1n2A, Tchi1n2H, Tchi1n2D, Tchi1n2E and Tchi1n2F simplified models, see their Figures 14, 15, 16, 17 and 18. Limits are also set on the higgsino mass in the Tn1n1A, Tn1n1B and Tn1n1C simplified models, see their Figure 19.

- 7 SIRUNYAN 18AP searched in 35.9 fb^{-1} of pp collisions at $\sqrt{s} = 13 \text{ TeV}$ for direct electroweak production of charginos and neutralinos by combining a number of previous and new searches. No significant excess above the Standard Model expectations is observed. Limits are set on the chargino/neutralino mass in the Tchi1n2E, Tchi1n2F and Tchi1n2I simplified models, see their Figures 7, 8, 9 and 10. Limits are also set on the higgsino mass in the Tn1n1A, Tn1n1B and Tn1n1C simplified models, see their Figure 11, 12, 13 and 14.
- 8 SIRUNYAN 18AR searched in 35.9 fb^{-1} of pp collisions at $\sqrt{s} = 13 \text{ TeV}$ for events containing two opposite-charge, same-flavour leptons (electrons or muons), jets and \cancel{E}_T . No significant excess above the Standard Model expectations is observed. Limits are set on the gluino mass in the Tglu4C simplified model, see their Figure 7. Limits are also set on the chargino/neutralino mass in the Tchi1n2F simplified models, see their Figure 8, and on the higgsino mass in the Tn1n1B and Tn1n1C simplified models, see their Figure 9. Finally, limits are set on the sbottom mass in the Tsb0t3 simplified model, see their Figure 10.
- 9 SIRUNYAN 18o searched in 35.9 fb^{-1} of pp collisions at $\sqrt{s} = 13 \text{ TeV}$ for events with two Higgs bosons, decaying to pairs of b -quarks, and large \cancel{E}_T . No significant excess above the Standard Model expectations is observed. Limits are set on the Higgsino mass in the T1n1n1A simplified model, see their Figure 9.
- 10 SIRUNYAN 18x searched in 35.9 fb^{-1} of pp collisions at $\sqrt{s} = 13 \text{ TeV}$ for events with one or more high-momentum Higgs bosons, decaying to pairs of photons, jets and \cancel{E}_T . The razor variables (M_R and R^2) are used to categorise the events. No significant excess above the Standard Model expectations is observed. Limits are set on the sbottom mass in the Tsb0t4 simplified model and on the wino mass in the Tchi1n2E simplified model, see their Figure 5. Limits are also set on the higgsino mass in the Tn1n1A and Tn1n1B simplified models, see their Figure 6.
- 11 KHACHATRYAN 14L searched in 19.5 fb^{-1} of pp collisions at $\sqrt{s} = 8 \text{ TeV}$ for evidence of direct pair production of neutralinos with Higgs or Z -bosons in the decay chain, leading to HH , HZ and ZZ final states with missing transverse energy. The decays of 16–20. A Higgs boson to a b -quark pair, to a photon pair, and to final states with leptons are considered in conjunction with hadronic and leptonic decay modes of the Z and W bosons. No significant excesses over the expected SM backgrounds are observed. The results are interpreted in the context of GMSB simplified models where the decays $\tilde{\chi}_1^0 \rightarrow H\bar{G}$ or $\tilde{\chi}_1^0 \rightarrow Z\bar{G}$ take place either 100% or 50% of the time, see Figs. 16–20.
- 12 AABOUD 19g searched in 32.9 fb^{-1} of pp collisions at $\sqrt{s} = 13 \text{ TeV}$ for evidence of neutralinos decaying into a Z -boson and a gravitino, in events characterized by the presence of dimuon vertices with displacements from the pp interaction point in the range of 1400 cm. Neutralinos are assumed to be produced in the decay chain of gluinos as in Tglu1A models. No significant excess is observed in the number of vertices relative to the predicted background. In GGM with a gluino mass of 1100 GeV, neutralino masses in the range 300–1000 GeV are excluded for certain values of $c\tau$, see their Figure 7.
- 13 AAIJ 17z searched in 1 fb^{-1} of pp collisions at $\sqrt{s} = 7 \text{ TeV}$ and in 2 fb^{-1} of pp collisions at $\sqrt{s} = 8 \text{ TeV}$ for events containing a displaced vertex with one associated high transverse momentum μ . No excess is observed above the background expected from Standard Model processes. The results are used to set 95% C.L. upper limits on the cross section times branching fractions of pair-produced neutralinos decaying non-promptly into a muon and two quarks. Long-lived particles in a mass range 23–198 GeV are considered, see their Fig. 5 and Fig. 6.
- 14 KHACHATRYAN 16BX searched in 19.5 fb^{-1} of pp collisions at $\sqrt{s} = 8 \text{ TeV}$ for events containing 3 or more leptons coming from the electroweak production of wino- or higgsino-like neutralinos, assuming non-zero R-parity-violating leptonic couplings λ_{122} , λ_{123} , and λ_{233} or semileptonic couplings λ_{131}^{\prime} , λ_{233}^{\prime} , λ_{331}^{\prime} , and λ_{333}^{\prime} . No excess over the expected background is observed and limits are derived on the neutralino mass, see Figs. 24 and 25.
- 15 AAD 14BH searched in 20.3 fb^{-1} of pp collisions at $\sqrt{s} = 8 \text{ TeV}$ for events containing non-pointing photons in a diphoton plus missing transverse energy final state. No excess is observed above the background expected from Standard Model processes. The results are used to set 95% C.L. exclusion limits in the context of gauge-mediated supersymmetric breaking models, with the lightest neutralino being the next-to-lightest supersymmetric particle and decaying with a lifetime in the range from 0.25 ns to about 100 ns into a photon and a gravitino. For limits on the NLSP lifetime versus Λ plane, for the SPS8 model, see their Fig. 7.
- 16 AAD 13AP searched in 4.8 fb^{-1} of pp collisions at $\sqrt{s} = 7 \text{ TeV}$ for events containing non-pointing photons in a diphoton plus missing transverse energy final state. No excess is observed above the background expected from Standard Model processes. The results are used to set 95% C.L. exclusion limits in the context of gauge-mediated supersymmetric breaking models, with the lightest neutralino being the next-to-lightest supersymmetric particle and decaying with a lifetime in excess of 0.25 ns into a photon and a gravitino. For limits in the NLSP lifetime versus Λ plane, for the SPS8 model, see their Fig. 8.
- 17 AAD 13Q searched in 4.7 fb^{-1} of pp collisions at $\sqrt{s} = 7 \text{ TeV}$ for events containing a high- p_T isolated photon, at least one jet identified as originating from a bottom quark, and high missing transverse momentum. Such signatures may originate from supersymmetric models with gauge-mediated supersymmetry breaking in events in which one of a pair of higgsino-like neutralinos decays into a photon and a gravitino while the other decays into a Higgs boson and a gravitino. No significant excess above the expected background was found and limits were set on the neutralino mass in a generalized GMSB model (GGM) with a higgsino-like neutralino NLSP, see their Fig. 4. Intermediate neutralino masses between 220 and 380 GeV are excluded at 95% C.L., regardless of the squark and gluino masses, purely on the basis of the expected weak production.
- 18 AAD 13R looked in 4.4 fb^{-1} of pp collisions at $\sqrt{s} = 7 \text{ TeV}$ for events containing new, heavy particles that decay at a significant distance from their production point into a final state containing a high-momentum muon and charged hadrons. No excess over the expected background is observed and limits are placed on the production cross-section of neutralinos via squarks for various $m_{\tilde{q}}, m_{\tilde{\chi}_1^0}$ in an R-parity violating scenario with $\lambda'_{211} \neq 0$, as a function of the neutralino lifetime, see their Fig. 6.
- 19 AALTONEN 13i searched in 6.3 fb^{-1} of $p\bar{p}$ collisions at $\sqrt{s} = 1.96 \text{ TeV}$ for events containing \cancel{E}_T and a delayed photon that arrives late in the detector relative to the time expected from prompt production. No evidence of delayed photon production is observed.
- 20 CHATRCHYAN 13AH searched in 4.9 fb^{-1} of pp collisions at $\sqrt{s} = 7 \text{ TeV}$ for events containing \cancel{E}_T and a delayed photon that arrives late in the detector relative to the time expected from prompt production. No significant excess above the expected background was found and limits were set on the pair production of $\tilde{\chi}_1^0$ depending on the neutralino proper decay length, see Fig. 8. Supersedes CHATRCHYAN 12BK.
- 21 AAD 12CP searched in 4.8 fb^{-1} of pp collisions at $\sqrt{s} = 7 \text{ TeV}$ for events with two photons and large \cancel{E}_T due to $\tilde{\chi}_1^0 \rightarrow \gamma\bar{G}$ decays in a GMSB framework. No significant excess above the expected background was found and limits were set on the neutralino mass in a generalized GMSB model (GGM) with a bino-like neutralino NLSP, see Figs. 6 and 7. The other sparticle masses were decoupled, $\tan\beta = 2$ and $c\tau_{NLSP} < 0.1 \text{ mm}$. Also, in the framework of the SPS8 model, limits are presented in Fig. 8.
- 22 AAD 12CT searched in 4.7 fb^{-1} of pp collisions at $\sqrt{s} = 7 \text{ TeV}$ for events containing four or more leptons (electrons or muons) and either moderate values of missing transverse momentum or large effective mass. No significant excess is found in the data. Limits are presented in a simplified model of R-parity violating supersymmetry in which charginos are pair-produced and then decay into a W -boson and a $\tilde{\chi}_1^0$, which in turn decays through an RPV coupling into two charged leptons ($e^\pm e^\mp$ or $\mu^\pm \mu^\mp$) and a neutrino. In this model, limits are set on the neutralino mass as a function of the chargino mass, see Fig. 3a. Limits are also set in an R-parity violating mSUGRA model, see Fig. 3b.
- 23 AAD 12R looked in 33 pb^{-1} of pp collisions at $\sqrt{s} = 7 \text{ TeV}$ for events containing new, heavy particles that decay at a significant distance from their production point into a final state containing a high-momentum muon and charged hadrons. No excess over the expected background is observed and limits are placed on the production cross-section of neutralinos via squarks for various $(m_{\tilde{q}}, m_{\tilde{\chi}_1^0})$ in an R-parity violating scenario with $\lambda'_{211} \neq 0$, as a function of the neutralino lifetime, see their Fig. 8. Superseded by AAD 13R.
- 24 ABAZOV 12AD looked in 6.2 fb^{-1} of pp collisions at $\sqrt{s} = 1.96 \text{ TeV}$ for events with a photon, a Z -boson, and large \cancel{E}_T in the final state. This topology corresponds to a GMSB model where pairs of neutralino NLSPs are either pair produced promptly or from decays of other supersymmetric particles and then decay to either $Z\bar{G}$ or $\gamma\bar{G}$. No significant excess over the SM expectation is observed and a limit at 95% C.L. on the cross section is derived as a function of the effective SUSY breaking scale Λ , see Fig. 3. Assuming $N_{mes} = 2$, $M_{mes} = 3 \Lambda$, $\tan\beta = 3$, $\mu = 0.75 M_1$, and $C_{grav} = 1$, the model is excluded at 95% C.L. for values of $\Lambda < 87 \text{ TeV}$.
- 25 CHATRCHYAN 12BK searched in 2.23 fb^{-1} of pp collisions at $\sqrt{s} = 7 \text{ TeV}$ for events with two photons and large \cancel{E}_T due to $\tilde{\chi}_1^0 \rightarrow \gamma\bar{G}$ decays in a GMSB framework. No significant excess above the expected background was found and limits were set on the pair production of $\tilde{\chi}_1^0$ depending on the neutralino lifetime, see Fig. 6.
- 26 CHATRCHYAN 11B looked in 35 pb^{-1} of pp collisions at $\sqrt{s} = 7 \text{ TeV}$ for events with an isolated lepton (e or μ), a photon and \cancel{E}_T which may arise in a generalized gauge mediated model from the decay of Wino-like NLSPs. No evidence for an excess over the expected background is observed. Limits are derived in the plane of squark/gluino mass versus Wino mass (see Fig. 4). Mass degeneracy of the produced squarks and gluinos is assumed.
- 27 AALTONEN 10 searched in 2.6 fb^{-1} of $p\bar{p}$ collisions at $\sqrt{s} = 1.96 \text{ TeV}$ for diphoton events with large \cancel{E}_T . They may originate from the production of $\tilde{\chi}^\pm$ in pairs or associated to a $\tilde{\chi}_1^0$, decaying into $\tilde{\chi}_1^0$ which itself decays in GMSB to $\gamma\bar{G}$. There is no excess of events beyond expectation. An upper limit on the cross section is calculated in the GMSB model as a function of the $\tilde{\chi}_1^0$ mass and lifetime, see their Fig. 2. A limit is derived on the $\tilde{\chi}_1^0$ mass of 149 GeV for $\tau_{\tilde{\chi}_1^0} \ll 1 \text{ ns}$, which improves the results of previous searches.
- 28 ABAZOV 10P looked in 6.3 fb^{-1} of $p\bar{p}$ collisions at $\sqrt{s} = 1.96 \text{ TeV}$ for events with at least two isolated γ s and large \cancel{E}_T . These could be the signature of $\tilde{\chi}_2^0$ and $\tilde{\chi}_1^\pm$ production, decaying to $\tilde{\chi}_1^0$ and finally $\tilde{\chi}_1^0 \rightarrow \gamma\bar{G}$ in a GMSB framework. No significant excess over the SM expectation is observed, and a limit at 95% C.L. on the cross section is derived for $N_{mes} = 1$, $\tan\beta = 15$ and $\mu > 0$, see their Fig. 2. This allows them to set a limit on the effective SUSY breaking scale $\Lambda > 124 \text{ TeV}$, from which the excluded $\tilde{\chi}_1^0$ mass range is obtained.
- 29 ABAZOV 08F looked in 1.1 fb^{-1} of $p\bar{p}$ collisions at $\sqrt{s} = 1.96 \text{ TeV}$ for diphoton events with large \cancel{E}_T . They may originate from the production of $\tilde{\chi}^\pm$ in pairs or associated to a $\tilde{\chi}_1^0$, decaying to a $\tilde{\chi}_1^0$ which itself decays promptly in GMSB to $\tilde{\chi}_1^0 \rightarrow \gamma\bar{G}$. No significant excess was found compared to the background expectation. A limit is derived on the masses of SUSY particles in the GMSB framework for $M = 2\Lambda$, $N = 1$, $\tan\beta = 15$ and $\mu > 0$, see Figure 2. It also excludes $\Lambda < 91.5 \text{ TeV}$. Supersedes the results of ABAZOV 05A. Superseded by ABAZOV 10P.
- 30 ABULENCIA 07H searched in 346 pb^{-1} of $p\bar{p}$ collisions at $\sqrt{s} = 1.96 \text{ TeV}$ for events with at least three leptons (e or μ) from the decay of $\tilde{\chi}_1^0$ via $L\bar{L}\bar{E}$ couplings. The results are consistent with the hypothesis of no signal. Upper limits on the cross-section are extracted and a limit is derived in the framework of mSUGRA on the masses of $\tilde{\chi}_1^0$ and $\tilde{\chi}_1^\pm$, see e.g. their Fig. 3 and Tab. II.
- 31 ABBIENDI 06b use 600 pb^{-1} of data from $\sqrt{s} = 189\text{--}209 \text{ GeV}$. They look for events with diphotons + \cancel{E} final states originating from prompt decays of pair-produced neutralinos in a GMSB scenario with $\tilde{\chi}_1^0$ NLSP. Limits on the cross-section are computed as a function of $m(\tilde{\chi}_1^0)$, see their Fig. 14. The limit on the $\tilde{\chi}_1^0$ mass is for a pure Bino state assuming a prompt decay, with lifetimes up to 10^{-9} s . Supersedes the results of ABBIENDI 04n.
- 32 ABDALLAH 05B use data from $\sqrt{s} = 180\text{--}209 \text{ GeV}$. They look for events with single photons + \cancel{E} final states. Limits are computed in the plane $(m(\bar{G}), m(\tilde{\chi}_1^0))$, shown in their Fig. 9b for a pure Bino state in the GMSB framework and in Fig. 9c for a no-scale supergravity model. Supersedes the results of ABREU 00z.
- 33 ABDALLAH 05b use data from $\sqrt{s} = 130\text{--}209 \text{ GeV}$. They look for events with diphotons + \cancel{E} final states and single photons not pointing to the vertex, expected in GMSB when the $\tilde{\chi}_1^0$ is the NLSP. Limits are computed in the plane $(m(\bar{G}), m(\tilde{\chi}_1^0))$, see their Fig. 10. The lower limit is derived on the $\tilde{\chi}_1^0$ mass for a pure Bino state assuming a prompt decay and $m_{\tilde{e}_R} = m_{\tilde{e}_L} = 2 m_{\tilde{\chi}_1^0}$. It improves to 100 GeV for $m_{\tilde{e}_R} = m_{\tilde{e}_L} = 1.1 m_{\tilde{\chi}_1^0}$ and the limit in the plane $(m(\tilde{\chi}_1^0), m(\tilde{e}_R))$ is shown in Fig. 10b. For long-lived neutralinos, cross-section limits are displayed in their Fig. 11. Supersedes the results of ABREU 00z.

Searches Particle Listings

Supersymmetric Particle Searches

$\tilde{\chi}_2^0, \tilde{\chi}_3^0, \tilde{\chi}_4^0$ (Neutralinos) mass limits

Neutralinos are unknown mixtures of photinos, z-inos, and neutral higgsinos (the supersymmetric partners of photons and of Z and Higgs bosons). The limits here apply only to $\tilde{\chi}_2^0, \tilde{\chi}_3^0$, and $\tilde{\chi}_4^0$. $\tilde{\chi}_1^0$ is the lightest supersymmetric particle (LSP); see $\tilde{\chi}_1^0$ Mass Limits. It is not possible to quote rigorous mass limits because they are extremely model dependent; i.e. they depend on branching ratios of various $\tilde{\chi}^0$ decay modes, on the masses of decay products ($\tilde{e}, \tilde{\mu}, \tilde{\tau}, \tilde{g}$), and on the \tilde{e} mass exchanged in $e^+e^- \rightarrow \tilde{\chi}_i^0 \tilde{\chi}_j^0$. Limits arise either from direct searches, or from the MSSM constraints set on the gaugino and higgsino mass parameters M_2 and μ through searches for lighter charginos and neutralinos. Often limits are given as contour plots in the $m_{\tilde{\chi}^0} - m_{\tilde{e}}$ plane vs other parameters. When specific assumptions are made, e.g. the neutralino is a pure photino ($\tilde{\gamma}$), pure z-ino (\tilde{Z}), or pure neutral higgsino (\tilde{H}^0), the neutralinos will be labelled as such.

Limits obtained from e^+e^- collisions at energies up to 136 GeV, as well as other limits from different techniques, are now superseded and have not been included in this compilation. They can be found in the 1998 Edition (The European Physical Journal **C3** 1 (1998)) of this Review. Some later papers are now obsolete and have been omitted. They were last listed in our PDG 14 edition: K. Olive, et al. (Particle Data Group), Chinese Physics **C38** 070001 (2014) (<http://pdg.lbl.gov>).

VALUE (GeV)	CL%	DOCUMENT ID	TECN	COMMENT
> 680	95	1 AABOUD	19AU ATL	0, 1, 2 or more $\ell, H \rightarrow \gamma\gamma, b\bar{b}, WW^*, ZZ^*, \tau\tau$ (various searches), Tchi1n2E, $m_{\tilde{\chi}_1^0} = 0$ GeV
> 112	95	2 SIRUNYAN	19BU CMS	$pp \rightarrow \tilde{\chi}_1^+ \tilde{\chi}_2^0 + 2 \text{ jets}, \tilde{\chi}_2^0 \rightarrow \ell^+ \ell^- \tilde{\chi}_1^0$, heavy sleptons, $m_{\tilde{\chi}_2^0} - m_{\tilde{\chi}_1^0} = 1$ GeV, $m_{\tilde{\chi}_2^0} = \tilde{m}_{\tilde{\chi}_1^+}$
> 215	95	2 SIRUNYAN	19BU CMS	$pp \rightarrow \tilde{\chi}_1^+ \tilde{\chi}_2^0 + 2 \text{ jets}, \tilde{\chi}_2^0 \rightarrow \ell^+ \ell^- \tilde{\chi}_1^0$, heavy sleptons, $m_{\tilde{\chi}_2^0} - m_{\tilde{\chi}_1^0} = 30$ GeV, $m_{\tilde{\chi}_2^0} = \tilde{m}_{\tilde{\chi}_1^+}$
> 760	95	3 AABOUD	18AY ATLS	$2\tau + \cancel{E}_T$, Tchi1n2D and $\tilde{\tau}_L$ -only, $m_{\tilde{\chi}_1^0} = 0$ GeV
> 1125	95	4 AABOUD	18BT ATLS	$2,3\ell + \cancel{E}_T$, Tchi1n2C, $m_{\tilde{\chi}_1^0} = 0$ GeV
> 580	95	5 AABOUD	18BT ATLS	$2,3\ell + \cancel{E}_T$, Tchi1n2F, $m_{\tilde{\chi}_1^0} = 0$ GeV
none 130–230, 290–880	95	6 AABOUD	18CK ATLS	$2H \rightarrow b\bar{b} + \cancel{E}_T$, Tn1n1A, GMSB
none 220–600	95	7 AABOUD	18CO ATLS	$2,3\ell + \cancel{E}_T$, recursive jigsaw, Tchi1n2F, $m_{\tilde{\chi}_1^0} = 0$ GeV
> 145	95	8 AABOUD	18R ATLS	2ℓ (soft) + \cancel{E}_T , Tchi1n2G, higgsino, $m_{\tilde{\chi}_2^0} - m_{\tilde{\chi}_1^0} = 5$ GeV
> 175	95	9 AABOUD	18R ATLS	2ℓ (soft) + \cancel{E}_T , Tchi1n2F, wino, $m_{\tilde{\chi}_2^0} - m_{\tilde{\chi}_1^0} = 10$ GeV
> 1060	95	10 AABOUD	18U ATLS	$2\gamma + \cancel{E}_T$, GGM, Tchi1chi1A, any NLSP mass
> 167	95	11 SIRUNYAN	18AJ CMS	2ℓ (soft) + \cancel{E}_T , Tchi1n2G, higgsino, $m_{\tilde{\chi}_2^0} - m_{\tilde{\chi}_1^0} = 15$ GeV
> 710	95	12 SIRUNYAN	18DP CMS	$2\tau + \cancel{E}_T$, Tchi1n2D, $m_{\tilde{\chi}_1^0} = 0$ GeV
none 220–490	95	13 SIRUNYAN	17AW CMS	$1\ell + 2 b\text{-jets} + \cancel{E}_T$, Tchi1n2E, $m_{\tilde{\chi}_1^0} = 0$ GeV
> 600	95	14 AAD	16AA ATLS	$3,4\ell + \cancel{E}_T$, Tn2n3A, $m_{\tilde{\chi}_1^0} = 0$ GeV
> 670	95	14 AAD	16AA ATLS	$3,4\ell + \cancel{E}_T$, Tn2n3B, $m_{\tilde{\chi}_1^0} < 200$ GeV
> 250	95	15 AAD	15BA ATLS	$m_{\tilde{\chi}_1^+} = m_{\tilde{\chi}_2^0}, m_{\tilde{\chi}_1^0} = 0$ GeV
> 380	95	16 AAD	14H ATLS	$\tilde{\chi}_1^+ \tilde{\chi}_2^0 \rightarrow \tau^\pm \nu \tilde{\chi}_1^0 \tau^\pm \bar{\nu} \tilde{\chi}_1^0$, simplified model, $m_{\tilde{\chi}_1^+} = m_{\tilde{\chi}_2^0}, m_{\tilde{\chi}_1^0} = 0$ GeV
> 700	95	16 AAD	14H ATLS	$\tilde{\chi}_1^\pm \tilde{\chi}_2^0 \rightarrow \ell^\pm \nu \tilde{\chi}_1^0 \ell^\pm \bar{\nu} \tilde{\chi}_1^0$, simplified model, $m_{\tilde{\chi}_1^\pm} = m_{\tilde{\chi}_2^0}, m_{\tilde{\chi}_1^0} = 0$ GeV
> 345	95	16 AAD	14H ATLS	$\tilde{\chi}_1^\pm \tilde{\chi}_2^0 \rightarrow W_{\tilde{\chi}_1^0}^{\pm} Z \tilde{\chi}_1^0$, simplified model, $m_{\tilde{\chi}_1^\pm} = m_{\tilde{\chi}_2^0}, m_{\tilde{\chi}_1^0} = 0$ GeV
> 148	95	16 AAD	14H ATLS	$\tilde{\chi}_1^\pm \tilde{\chi}_2^0 \rightarrow W_{\tilde{\chi}_1^0}^{\pm} H \tilde{\chi}_1^0$, simplified model, $m_{\tilde{\chi}_1^\pm} = m_{\tilde{\chi}_2^0}, m_{\tilde{\chi}_1^0} = 0$ GeV
> 620	95	17 AAD	14X ATLS	$\geq 4\ell^\pm, \tilde{\chi}_{2,3}^0 \rightarrow \ell^\pm \ell^\mp \tilde{\chi}_1^0, m_{\tilde{\chi}_1^0} = 0$ GeV
		18 AAD	13 ATLS	$3\ell^\pm + \cancel{E}_T$, pMSSM, SMS
		19 CHATRCHYAN12BJ	CMS	$\geq 2\ell, \text{jets} + \cancel{E}_T, pp \rightarrow \tilde{\chi}_1^\pm \tilde{\chi}_2^0$
> 62.4	95	20 ABREU	00W DLPH	$\tilde{\chi}_2^0, 1 \leq \tan\beta \leq 40, \text{ all } \Delta m, \text{ all } m_0$
> 99.9	95	20 ABREU	00W DLPH	$\tilde{\chi}_3^0, 1 \leq \tan\beta \leq 40, \text{ all } \Delta m, \text{ all } m_0$
> 116.0	95	20 ABREU	00W DLPH	$\tilde{\chi}_4^0, 1 \leq \tan\beta \leq 40, \text{ all } \Delta m, \text{ all } m_0$

• • • We do not use the following data for averages, fits, limits, etc. • • •

none 180–355	95	21 AAD	14G ATLS	$\tilde{\chi}_1^\pm \tilde{\chi}_2^0 \rightarrow W_{\tilde{\chi}_1^0}^{\pm} Z \tilde{\chi}_1^0$, simplified model, $m_{\tilde{\chi}_1^\pm} = m_{\tilde{\chi}_2^0}, m_{\tilde{\chi}_1^0} = 0$ GeV
		22 KHACHATRYAN14I	CMS	$\tilde{\chi}_2^0 \rightarrow (Z, H) \tilde{\chi}_1^0 \tilde{\ell} \ell$, simplified model
		23 AAD	12As ATLS	$3\ell^\pm + \cancel{E}_T$, pMSSM
		24 AAD	12T ATLS	$\ell^\pm \ell^\pm + \cancel{E}_T, pp \rightarrow \tilde{\chi}_1^\pm \tilde{\chi}_2^0$

- AABOUD 19AU searched in 36.1 fb^{-1} of pp collisions at $\sqrt{s} = 13$ TeV for direct electroweak production of charginos and next-to-lightest neutralinos decaying into lightest neutralinos and a W and a Higgs boson, respectively. Fully hadronic, semileptonic, diphoton, and multilepton (electrons, muons) final states with missing transverse momentum are considered in this search. Observations are consistent with the Standard Model expectations, and 95% confidence-level limits of up to 680 GeV on the chargino/next-to-lightest neutralino masses are set (Tchi1n2E model). See their Figure 14 for an overlay of exclusion contours from all searches.
- SIRUNYAN 19BU searched for pair production of gauginos via vector boson fusion assuming the gaugino spectrum is compressed, in 35.9 fb^{-1} of pp collisions at $\sqrt{s} = 13$ TeV. The final states explored included zero leptons plus two jets, one lepton plus two jets, and one hadronic tau plus two jets. A similar bound is obtained in the light slepton limit.
- AABOUD 18AY searched in 36.1 fb^{-1} of pp collisions at $\sqrt{s} = 13$ TeV for direct electroweak production of charginos and neutralinos as in Tchi1n2D models, in events characterised by the presence of at least two hadronically decaying tau leptons and large missing transverse energy. No significant deviation from the expected SM background is observed. Assuming decays via intermediate $\tilde{\tau}_1$ and $m_{\tilde{\chi}_1^\pm} = m_{\tilde{\chi}_2^0}$, the observed limits rule out $\tilde{\chi}_2^0$ masses up to 760 GeV for a massless $\tilde{\chi}_1^0$. See their Fig.7 (right). Interpretations are also provided in Fig 8 (bottom) for different assumptions on the ratio between $m_{\tilde{\tau}}$ and $m_{\tilde{\chi}_2^0} + m_{\tilde{\chi}_1^0}$.
- AABOUD 18BT searched in 36.1 fb^{-1} of pp collisions at $\sqrt{s} = 13$ TeV for direct electroweak production of chargino, chargino and next-to-lightest neutralinos and sleptons in events with two or three leptons (electrons or muons), with or without jets, and large missing transverse energy. No significant excess above the Standard Model expectations is observed. Limits are set on the next-to-lightest neutralino mass up to 1100 GeV for massless $\tilde{\chi}_1^0$ in the Tchi1n2C simplified model exploiting the 3ℓ signature, see their Figure 8(c).
- AABOUD 18BT searched in 36.1 fb^{-1} of pp collisions at $\sqrt{s} = 13$ TeV for direct electroweak production of charginos, chargino and next-to-lightest neutralinos and sleptons in events with two or three leptons (electrons or muons), with or without jets, and large missing transverse energy. No significant excess above the Standard Model expectations is observed. Limits are set on the next-to-lightest neutralino mass up to 580 GeV for massless $\tilde{\chi}_1^0$ in the Tchi1n2F simplified model exploiting the $2\ell + 2$ jets and 3ℓ signatures, see their Figure 8(d).
- AABOUD 18CK searched for events with at least 3 b -jets and large missing transverse energy in two datasets of pp collisions at $\sqrt{s} = 13$ TeV of 36.1 fb^{-1} and 24.3 fb^{-1} depending on the trigger requirements. The analyses aimed to reconstruct two Higgs bosons decaying to pairs of b -quarks. No significant excess above the Standard Model expectations is observed. Limits are set on the Higgsino mass in the Tn1n1A simplified model, see their Figure 15(a). Constraints are also presented as a function of the BR of Higgsino decaying into a higgs boson and a gravitino, see their Figure 15(b).
- AABOUD 18CO searched in 36.1 fb^{-1} of pp collisions at $\sqrt{s} = 13$ TeV for direct electroweak production of mass-degenerate charginos and next-to-lightest neutralinos in events with two or three leptons (electrons or muons), with or without jets, and large missing transverse energy. The search channels are based on recursive jigsaw reconstruction. Limits are set on the next-to-lightest neutralinos mass up to 600 GeV for massless neutralinos in the Tchi1n2F simplified model exploiting the statistical combination of $2\ell + 2$ jets and 3ℓ channels. Next-to-lightest neutralinos masses below 220 GeV are not excluded due to an excess of events above the SM prediction in the dedicated regions. See their Figure 13(d).
- AABOUD 18R searched in 36.1 fb^{-1} of pp collisions at $\sqrt{s} = 13$ TeV for electroweak production in scenarios with compressed mass spectra in final states with two low-momentum leptons and missing transverse momentum. The data are found to be consistent with the SM prediction. Results are interpreted in Tchi1n2G higgsino models, and $\tilde{\chi}_2^0$ masses are excluded up to 145 GeV for $m_{\tilde{\chi}_2^0} - m_{\tilde{\chi}_1^0} = 5$ GeV. The exclusion limits extend down to mass splittings of 2.5 GeV, see their Fig. 10 (top). Results are also interpreted in terms of exclusion bounds on the production cross-sections for the NUHM2 scenario as a function of the universal gaugino mass $m_{1/2}$ and $m_{\tilde{\chi}_2^0} - m_{\tilde{\chi}_1^0}$, see their Fig. 12.
- AABOUD 18R searched in 36.1 fb^{-1} of pp collisions at $\sqrt{s} = 13$ TeV for electroweak production in scenarios with compressed mass spectra in final states with two low-momentum leptons and missing transverse momentum. The data are found to be consistent with the SM prediction. Results are interpreted in Tchi1n2F wino models, and $\tilde{\chi}_2^0$ masses are excluded up to 175 GeV for $m_{\tilde{\chi}_2^0} - m_{\tilde{\chi}_1^0} = 10$ GeV. The exclusion limits extend down to mass splittings of 2 GeV, see their Fig. 10 (bottom). Results are also interpreted in terms of exclusion bounds on the production cross-sections for the NUHM2 scenario as a function of the universal gaugino mass $m_{1/2}$ and $m_{\tilde{\chi}_2^0} - m_{\tilde{\chi}_1^0}$, see their Fig. 12.
- AABOUD 18U searched in 36.1 fb^{-1} of pp collisions at $\sqrt{s} = 13$ TeV in events with at least one isolated photon, possibly jets and significant transverse momentum targeting generalised models of gauge-mediated SUSY breaking. No significant excess of events is observed above the SM prediction. Results of the diphoton channel are interpreted in terms of lower limits on the masses of gauginos Tchi1chi1A models, which reach as high as 1.3 TeV. Gaugino masses below 1060 GeV are excluded for any NLSP mass, see their Fig. 10.
- SIRUNYAN 18AJ searched in 35.9 fb^{-1} of pp collisions at $\sqrt{s} = 13$ TeV for events containing two low-momentum, oppositely charged leptons (electrons or muons) and \cancel{E}_T . No excess over the expected background is observed. Limits are derived on the wino mass in the Tchi1n2F simplified model, see their Figure 5. Limits are also set on the stop mass in the Tstop10 simplified model, see their Figure 6. Finally, limits are set on the Higgsino mass in the Tchi1n2G simplified model, see Figure 8 and in the pMSSM, see Figure 7.

- 12 SIRUNYAN 18DP searched in 35.9 fb⁻¹ of pp collisions at $\sqrt{s} = 13$ TeV for direct electroweak production of charginos and neutralinos or of chargino pairs in events with a tau lepton pair and significant missing transverse momentum. Both hadronic and leptonic decay modes are considered for the tau lepton. No significant excess above the Standard Model expectations is observed. Limits are set on the chargino mass in the Tchi1ch1D and Tchi1n2 simplified models, see their Figures 14 and 15. Also, excluded stau pair production cross sections are shown in Figures 11, 12, and 13.
- 13 SIRUNYAN 17AW searched in 35.9 fb⁻¹ of pp collisions at $\sqrt{s} = 13$ TeV for events with a charged lepton (electron or muon), two jets identified as originating from a b-quark, and large E_T . No significant excess above the Standard Model expectations is observed. Limits are set on the mass of the chargino and the next-to-lightest neutralino in the Tchi1n2E simplified model, see their Figure 6.
- 14 AAD 16AA summarized and extended ATLAS searches for electroweak supersymmetry in final states containing several charged leptons, E_T , with or without hadronic jets, in 20 fb⁻¹ of pp collisions at $\sqrt{s} = 8$ TeV. The paper reports the results of new interpretations and statistical combinations of previously published analyses, as well as new analyses. Exclusion limits at 95% C.L. are set on mass-degenerate $\tilde{\chi}_2^0$ and $\tilde{\chi}_3^0$ masses in the Tn2n3A and Tn2n3B simplified models. See their Fig. 15.
- 15 AAD 15BA searched in 20.3 fb⁻¹ of pp collisions at $\sqrt{s} = 8$ TeV for electroweak production of charginos and neutralinos decaying to a final state containing a W boson and a 125 GeV Higgs boson, plus missing transverse momentum. No excess beyond the Standard Model expectation is observed. Exclusion limits are derived in simplified models of direct chargino and next-to-lightest neutralino production, with the decays $\tilde{\chi}_1^\pm \rightarrow W^\pm \tilde{\chi}_1^0$ and $\tilde{\chi}_2^0 \rightarrow H \tilde{\chi}_1^0$ having 100% branching fraction, see Fig. 8. A combination of the multiple final states for the Higgs decay yields the best limits (Fig. 8d).
- 16 AAD 14H searched in 20.3 fb⁻¹ of pp collisions at $\sqrt{s} = 8$ TeV for electroweak production of charginos and neutralinos decaying to a final state with three leptons and missing transverse momentum. No excess beyond the Standard Model expectation is observed. Exclusion limits are derived in simplified models of direct chargino and next-to-lightest neutralino production, with decays to the lightest neutralino via either all three generations of leptons, staus only, gauge bosons, or Higgs bosons, see Fig. 7. An interpretation in the pMSSM is also given, see Fig. 8.
- 17 AAD 14X searched in 20.3 fb⁻¹ of pp collisions at $\sqrt{s} = 8$ TeV for events with at least four leptons (electrons, muons, taus) in the final state. No significant excess above the Standard Model expectations is observed. Limits are set on the neutralino mass in an R-parity conserving simplified model where the decay $\tilde{\chi}_{2,3}^0 \rightarrow \ell^\pm \ell^\mp \tilde{\chi}_1^0$ takes place with a branching ratio of 100%, see Fig. 10.
- 18 AAD 13 searched in 4.7 fb⁻¹ of pp collisions at $\sqrt{s} = 7$ TeV for charginos and neutralinos decaying to a final state with three leptons (e and μ) and missing transverse energy. No excess beyond the Standard Model expectation is observed. Exclusion limits are derived in the phenomenological MSSM, see Fig. 2 and 3, and in simplified models, see Fig. 4. For the simplified models with intermediate slepton decays, degenerate $\tilde{\chi}_1^\pm$ and $\tilde{\chi}_2^0$ masses up to 500 GeV are excluded at 95% C.L. for very large mass differences with the $\tilde{\chi}_1^0$. Supersedes AAD 12As.
- 19 CHATRCHYAN 12BJ searched in 4.98 fb⁻¹ of pp collisions at $\sqrt{s} = 7$ TeV for direct electroweak production of charginos and neutralinos in events with at least two leptons, jets and missing transverse momentum. No significant excesses over the expected SM backgrounds are observed and 95% C.L. limits on the production cross section of $\tilde{\chi}_1^\pm \tilde{\chi}_2^0$ pair production were set in a number of simplified models, see Figs. 7 to 12. Most limits are for exactly 3 jets.
- 20 ABREU 00w combines data collected at $\sqrt{s}=189$ GeV with results from lower energies. The mass limit is obtained by constraining the MSSM parameter space with gaugino and sfermion mass universality at the GUT scale, using the results of negative direct searches for neutralinos (including cascade decays and $\tilde{\tau}\tau$ final states) from ABREU 01, for charginos from ABREU 00j and ABREU 00t (for all Δm_+), and for charged sleptons from ABREU 01b. The results hold for the full parameter space defined by all values of M_2 and $|\mu| \leq 2$ TeV with the $\tilde{\chi}_1^0$ as LSP.
- 21 AAD 14G searched in 20.3 fb⁻¹ of pp collisions at $\sqrt{s} = 8$ TeV for electroweak production of chargino-neutralino pairs, decaying to a final state with two leptons (e and μ) and missing transverse momentum. No excess beyond the Standard Model expectation is observed. Exclusion limits are derived in simplified models of chargino and next-to-lightest neutralino production, with decays to the lightest neutralino via gauge bosons, see Fig. 7. An interpretation in the pMSSM is also given, see Fig. 10.
- 22 KHACHATRYAN 14t searched in 19.5 fb⁻¹ of pp collisions at $\sqrt{s} = 8$ TeV for electroweak production of charginos and neutralinos decaying to a final state with three leptons (e or μ) and missing transverse momentum, or with a Z-boson, dijets and missing transverse momentum. No excess beyond the Standard Model expectation is observed. Exclusion limits are derived in simplified models, see Figs. 12–16.
- 23 AAD 12As searched in 2.06 fb⁻¹ of pp collisions at $\sqrt{s} = 7$ TeV for charginos and neutralinos decaying to a final state with three leptons (e and μ) and missing transverse energy. No excess beyond the Standard Model expectation is observed. Exclusion limits are derived in the phenomenological MSSM, see Fig. 2 (top), and in simplified models, see Fig. 2 (bottom).
- 24 AAD 12T looked in 1 fb⁻¹ of pp collisions at $\sqrt{s} = 7$ TeV for the production of supersymmetric particles decaying into final states with missing transverse momentum and exactly two isolated leptons (e or μ). Same-sign dilepton events were separately studied. Additionally, in opposite-sign events, a search was made for an excess of same-flavor over different-flavor lepton pairs. No excess over the expected background is observed and limits are placed on the effective production cross section of opposite-sign dilepton events with $E_T > 250$ GeV and on same-sign dilepton events with $E_T > 100$ GeV. The latter limit is interpreted in a simplified electroweak gaugino production model.

Unless otherwise stated, results in this section assume spectra, production rates, decay modes and branching ratios as evaluated in the MSSM, with gaugino and sfermion mass unification at the GUT scale. These papers generally study production of $\tilde{\chi}_1^0 \tilde{\chi}_2^0$, $\tilde{\chi}_1^\pm \tilde{\chi}_1^\mp$ and (in the case of hadronic collisions) $\tilde{\chi}_1^\pm \tilde{\chi}_2^0$ pairs, including the effects of cascade decays. The mass limits on $\tilde{\chi}_1^\pm$ are either direct, or follow indirectly from the constraints set by the non-observation of $\tilde{\chi}_2^0$ states on the gaugino and higgsino MSSM parameters M_2 and μ . For generic values of the MSSM parameters, limits from high-energy e^+e^- collisions coincide with the highest value of the mass allowed by phase-space, namely $m_{\tilde{\chi}_1^\pm} \lesssim \sqrt{s}/2$. The still unpublished combination of the results of the four LEP collaborations from the 2000 run of LEP2 at \sqrt{s} up to ≈ 209 GeV yields a lower mass limit of 103.5 GeV valid for general MSSM models. The limits become however weaker in certain regions of the MSSM parameter space where the detection efficiencies or production cross sections are suppressed. For example, this may happen when: (i) the mass differences $\Delta m_+ = m_{\tilde{\chi}_1^\pm} - m_{\tilde{\chi}_1^0}$ or $\Delta m_\nu = m_{\tilde{\chi}_1^\pm} - m_{\tilde{\nu}}$ are very small, and the detection efficiency is reduced; (ii) the electron sneutrino mass is small, and the $\tilde{\chi}_1^\pm$ production rate is suppressed due to a destructive interference between s and t channel exchange diagrams. The regions of MSSM parameter space where the following limits are valid are indicated in the comment lines or in the footnotes.

Some earlier papers are now obsolete and have been omitted. They were last listed in our PDG 14 edition: K. Olive, et al. (Particle Data Group), Chinese Physics **C38** 070001 (2014) (<http://pdg.lbl.gov>).

VALUE (GeV)	CL%	DOCUMENT ID	TECN	COMMENT
>1050	95	1 SIRUNYAN 20B	CMS	$\geq 1\gamma + E_T$, Tchi1chi1F, $\tilde{\chi}_1^0 \rightarrow \gamma \tilde{G}$
> 825	95	1 SIRUNYAN 20B	CMS	$\geq 1\gamma + E_T$, Tchi1chi1G, $\tilde{\chi}_1^\pm \rightarrow \tilde{\chi}_1^0 + \text{soft}$
> 840	95	1 SIRUNYAN 20B	CMS	$\geq 1\gamma + E_T$, Tchi1n12-GGM, 120 GeV < $m_{\tilde{\chi}_1^0} < 720$ GeV
> 680	95	2 AABOUD 19AU	ATL	0, 1, 2 or more ℓ , H ($\rightarrow \gamma\gamma, b\bar{b}, W W^*, Z Z^*, \tau\tau$) (various searches), Tchi1n2E, $m_{\tilde{\chi}_1^0}=0$ GeV
> 112	95	3 SIRUNYAN 19BU	CMS	pp $\rightarrow \tilde{\chi}_1^\pm \tilde{\chi}_2^0 + 2$ jets, $\tilde{\chi}_1^\pm \rightarrow \ell^\pm \nu \tilde{\chi}_1^0$, heavy sleptons, $m_{\tilde{\chi}_1^\pm} - m_{\tilde{\chi}_1^0} = 1$ GeV, $m_{\tilde{\chi}_1^0} = m_{\tilde{\chi}_2^0}$
> 215	95	3 SIRUNYAN 19BU	CMS	pp $\rightarrow \tilde{\chi}_1^\pm \tilde{\chi}_2^0 + 2$ jets, $\tilde{\chi}_1^\pm \rightarrow \ell^\pm \nu \tilde{\chi}_1^0$, heavy sleptons, $m_{\tilde{\chi}_1^\pm} - m_{\tilde{\chi}_1^0} = 30$ GeV, $m_{\tilde{\chi}_1^0} = m_{\tilde{\chi}_2^0}$
> 235	95	4 SIRUNYAN 19CI	CMS	$\geq 1 H (\rightarrow \gamma\gamma) + \text{jets} + E_T$, Tchi1n2E, $m_{\tilde{\chi}_1^0} = 1$ GeV
> 930	95	5 SIRUNYAN 19K	CMS	$\gamma + \text{lepton} + E_T$, Tchi1n1A
> 630	95	6 AABOUD 18AY	ATLS	$2\tau + E_T$, Tchi1chi1D and $\tilde{\tau}_L$ -only, $m_{\tilde{\chi}_1^0} = 0$ GeV
> 760	95	7 AABOUD 18AY	ATLS	$2\tau + E_T$, Tchi1n2D and $\tilde{\tau}_L$ -only, $m_{\tilde{\chi}_1^0} = 0$ GeV
> 740	95	8 AABOUD 18BT	ATLS	$2\ell + E_T$, Tchi1chi1C, $m_{\tilde{\chi}_1^0}=0$ GeV
>1125	95	9 AABOUD 18BT	ATLS	$2,3\ell + E_T$, Tchi1n2C, $m_{\tilde{\chi}_1^0}=0$ GeV
> 580	95	10 AABOUD 18BT	ATLS	$2,3\ell + E_T$, Tchi1n2F, $m_{\tilde{\chi}_1^0}=0$ GeV
none	95	11 AABOUD 18CK	ATLS	$2H (\rightarrow b\bar{b}) + E_T$, Tn1n1A, GMSB
130–230, 290–880	95	12 AABOUD 18CO	ATLS	$2,3\ell + E_T$, recursive jigsaw, Tchi1n2F, $m_{\tilde{\chi}_1^0} = 0$ GeV
none	95	13 AABOUD 18R	ATLS	$2\ell (\text{soft}) + E_T$, Tchi1n2F, wino, $m_{\tilde{\chi}_1^\pm} - m_{\tilde{\chi}_1^0} = 10$ GeV
> 145	95	14 AABOUD 18R	ATLS	$2\ell (\text{soft}) + E_T$, Tchi1n2G, higgsino, $m_{\tilde{\chi}_1^\pm} - m_{\tilde{\chi}_1^0} = 5$ GeV
>1060	95	15 AABOUD 18U	ATLS	$2\gamma + E_T$, GGM, Tchi1chi1A, any NLSP mass
>1400	95	16 AABOUD 18Z	ATLS	$\geq 4\ell$, RPV, $\lambda_{12k} \neq 0$, $m_{\tilde{\chi}_1^0} > 500$ GeV
>1320	95	16 AABOUD 18Z	ATLS	$\geq 4\ell$, RPV, $\lambda_{12k} \neq 0$, $m_{\tilde{\chi}_1^0} > 500$ GeV
> 980	95	16 AABOUD 18Z	ATLS	$\geq 4\ell$, RPV, $\lambda_{133} \neq 0$, 400 GeV < $m_{\tilde{\chi}_1^0} < 700$ GeV
> 980	95	17 SIRUNYAN 18AA	CMS	$\geq 1\gamma + E_T$, GGM, wino-like $\tilde{\chi}_2^0 \tilde{\chi}_1^\pm$ pair production, nearly degenerate wino and bino masses
> 780	95	17 SIRUNYAN 18AA	CMS	$\geq 1\gamma + E_T$, Tchi1n1A
> 950	95	17 SIRUNYAN 18AA	CMS	$\geq 1\gamma + E_T$, Tchi1chi1A
> 230	95	18 SIRUNYAN 18AJ	CMS	$2\ell (\text{soft}) + E_T$, Tchi1n2F, wino, $m_{\tilde{\chi}_2^0} - m_{\tilde{\chi}_1^0} = 20$ GeV

$\tilde{\chi}_1^\pm, \tilde{\chi}_2^0$ (Charginos) mass limits

Charginos are unknown mixtures of w-inos and charged higgsinos (the supersymmetric partners of W and Higgs bosons). A lower mass limit for the lightest chargino ($\tilde{\chi}_1^\pm$) of approximately 45 GeV, independent of the field composition and of the decay mode, has been obtained by the LEP experiments from the analysis of the Z width and decays. These results, as well as other now superseded limits from e^+e^- collisions at energies below 136 GeV, and from hadronic collisions, can be found in the 1998 Edition (The European Physical Journal **C3** 1 (1998)) of this Review.

Searches Particle Listings

Supersymmetric Particle Searches

>1150	95	19 SIRUNYAN	18AO CMS	$\ell^\pm \ell^\pm$ or $\geq 3\ell$, Tchi1n2A, $m_{\tilde{\ell}} = m_{\tilde{\nu}} = m_{\tilde{\chi}_1^0} + 0.5 (m_{\tilde{\chi}_1^\pm} - m_{\tilde{\chi}_1^0})$, $m_{\tilde{\chi}_1^\pm} = 0$ GeV	> 380	95	32 AAD	14H ATLS	$\tilde{\chi}_1^\pm \tilde{\chi}_2^0 \rightarrow \tau^\pm \nu \tilde{\chi}_1^0 \tau^\pm \tilde{\chi}_1^0$, simplified model, $m_{\tilde{\chi}_1^\pm} = m_{\tilde{\chi}_2^0}$, $m_{\tilde{\chi}_1^0} = 0$ GeV
>1120	95	19 SIRUNYAN	18AO CMS	$\ell^\pm \ell^\pm$ or $\geq 3\ell$, Tchi1n2A, $m_{\tilde{\ell}} = m_{\tilde{\nu}} = m_{\tilde{\chi}_1^0} + 0.05 (m_{\tilde{\chi}_1^\pm} - m_{\tilde{\chi}_1^0})$, $m_{\tilde{\chi}_1^\pm} = 0$ GeV	> 750	95	33 AAD	14x ATLS	RPV, $\geq 4\ell^\pm$, $\tilde{\chi}_1^\pm \rightarrow W^{(*)\pm} \tilde{\chi}_1^0$, $\tilde{\chi}_1^0 \rightarrow \ell^\pm \tilde{\ell} \nu$
>1050	95	19 SIRUNYAN	18AO CMS	$\ell^\pm \ell^\pm$ or $\geq 3\ell$, Tchi1n2A, $m_{\tilde{\ell}} = m_{\tilde{\nu}} = m_{\tilde{\chi}_1^0} + 0.95 (m_{\tilde{\chi}_1^\pm} - m_{\tilde{\chi}_1^0})$, $m_{\tilde{\chi}_1^\pm} = 0$ GeV	> 210	95	34 KHACHATRY..14L	CMS	$\tilde{\chi}_2^0 \rightarrow H \tilde{\chi}_1^0$ and $\tilde{\chi}_1^\pm \rightarrow W^\pm \tilde{\chi}_1^0$ simplified models, $m_{\tilde{\chi}_2^0} = m_{\tilde{\chi}_1^\pm}$, $m_{\tilde{\chi}_1^0} = 0$ GeV
>1080	95	19 SIRUNYAN	18AO CMS	$\ell^\pm \ell^\pm$ or $\geq 3\ell$, Tchi1n2H, $m_{\tilde{\ell}} = m_{\tilde{\nu}} = m_{\tilde{\chi}_1^0} + 0.5 (m_{\tilde{\chi}_1^\pm} - m_{\tilde{\chi}_1^0})$, $m_{\tilde{\chi}_1^\pm} = 0$ GeV	> 540	95	35 AAD	13 ATLS	$3\ell^\pm + \cancel{E}_T$, pMSSM, SMS
>1030	95	19 SIRUNYAN	18AO CMS	$\ell^\pm \ell^\pm$ or $\geq 3\ell$, Tchi1n2H, $m_{\tilde{\ell}} = m_{\tilde{\nu}} = m_{\tilde{\chi}_1^0} + 0.05 (m_{\tilde{\chi}_1^\pm} - m_{\tilde{\chi}_1^0})$, $m_{\tilde{\chi}_1^\pm} = 0$ GeV	> 540	95	36 AAD	13B ATLS	$2\ell^\pm + \cancel{E}_T$, pMSSM, SMS
>1050	95	19 SIRUNYAN	18AO CMS	$\ell^\pm \ell^\pm$ or $\geq 3\ell$, Tchi1n2H, $m_{\tilde{\ell}} = m_{\tilde{\nu}} = m_{\tilde{\chi}_1^0} + 0.95 (m_{\tilde{\chi}_1^\pm} - m_{\tilde{\chi}_1^0})$, $m_{\tilde{\chi}_1^\pm} = 0$ GeV	> 94	95	37 AAD	12CT ATLS	$\geq 4\ell^\pm$, RPV, $m_{\tilde{\chi}_1^0} > 300$ GeV
> 625	95	19 SIRUNYAN	18AO CMS	$\ell^\pm \ell^\pm$ or $\geq 3\ell$, Tchi1n2D, $m_{\tilde{\tau}} = m_{\tilde{\chi}_1^0} + 0.5 (m_{\tilde{\chi}_1^\pm} - m_{\tilde{\chi}_1^0})$, $m_{\tilde{\chi}_1^\pm} = 0$ GeV	> 540	95	38 CHATRCHYAN12BJ	CMS	$\geq 2\ell$, jets + \cancel{E}_T , $pp \rightarrow \tilde{\chi}_1^\pm \tilde{\chi}_2^0$
> 180	95	19 SIRUNYAN	18AO CMS	$\ell^\pm \ell^\pm$ or $\geq 3\ell$, Tchi1n2E, $m_{\tilde{\chi}_1^0} = 0$ GeV	> 94	95	39 ABDALLAH	03M DLPH	$\tilde{\chi}_1^\pm$, $\tan\beta \leq 40$, $\Delta m_{\pm} > 3$ GeV, all m_0
> 450	95	19 SIRUNYAN	18AO CMS	$\ell^\pm \ell^\pm$ or $\geq 3\ell$, Tchi1n2F, $m_{\tilde{\chi}_1^0} = 0$ GeV	• • • We do not use the following data for averages, fits, limits, etc. • • •				
> 480	95	20 SIRUNYAN	18AP CMS	Combination of searches, Tchi1n2E, $m_{\tilde{\chi}_1^0} = 0$ GeV	> 570	95	40 KHACHATRY..16AA	CMS	$\geq 1\gamma$ + jets + \cancel{E}_T , Tchi1chi1A
> 650	95	20 SIRUNYAN	18AP CMS	Combination of searches, Tchi1n2F, $m_{\tilde{\chi}_1^0} = 0$ GeV	> 680	95	40 KHACHATRY..16AA	CMS	$\geq 1\gamma$ + jets + \cancel{E}_T , Tchi1n1A
> 535	95	20 SIRUNYAN	18AP CMS	Combination of searches, Tchi1n2I, $m_{\tilde{\chi}_1^0} = 0$ GeV	> 710	95	40 KHACHATRY..16AA	CMS	$\geq 1\gamma$ + jets + \cancel{E}_T , GGM, $\tilde{\chi}_2^0 \tilde{\chi}_1^\pm$ pair production, wino-like NLSP
none 160-610	95	21 SIRUNYAN	18AR CMS	$\ell^\pm \ell^\pm$ + jets + \cancel{E}_T , Tchi1n2F, $m_{\tilde{\chi}_1^0} = 0$ GeV	>1000	95	41 KHACHATRY..16R	CMS	$\geq 1\gamma + 1e$ or μ + \cancel{E}_T , Tglu1F, $m_{\tilde{\chi}_1^\pm} = m_{\tilde{\chi}_2^0} > 200$ GeV
none 170-200	95	22 SIRUNYAN	18DN CMS	$\ell^\pm \ell^\pm$, Tchi1chi1E, $m_{\tilde{\chi}_1^0} = 1$ GeV	> 307	95	42 KHACHATRY..16Y	CMS	1,2 soft ℓ^\pm + jets + \cancel{E}_T , Tchi1n2A, $m_{\tilde{\chi}_1^\pm} - m_{\tilde{\chi}_1^0} = 20$ GeV
> 810	95	22 SIRUNYAN	18DN CMS	$\ell^\pm \ell^\pm$, Tchi1chi1C, $m_{\tilde{\chi}_1^0} = 0$ GeV	> 410	95	43 AAD	14AV ATLS	$\geq 2\tau$ + \cancel{E}_T , direct $\tilde{\chi}_1^\pm \tilde{\chi}_2^0$, $\tilde{\chi}_1^\pm \tilde{\chi}_1^\mp$ production, $m_{\tilde{\chi}_2^0} = m_{\tilde{\chi}_1^\pm}$, $m_{\tilde{\chi}_1^0} = 0$ GeV
> 630	95	23 SIRUNYAN	18DP CMS	$2\tau + \cancel{E}_T$, Tchi1chi1D, $m_{\tilde{\chi}_1^0} = 0$ GeV	> 345	95	44 AAD	14AV ATLS	$\geq 2\tau$ + \cancel{E}_T , direct $\tilde{\chi}_1^\pm \tilde{\chi}_1^\mp$ production, $m_{\tilde{\chi}_1^0} = 0$ GeV
> 710	95	23 SIRUNYAN	18DP CMS	$2\tau + \cancel{E}_T$, Tchi1n2D, $m_{\tilde{\chi}_1^0} = 0$ GeV	none	95	45 AAD	14G ATLS	$\tilde{\chi}_1^\pm \tilde{\chi}_1^\mp \rightarrow W^\pm \tilde{\chi}_1^0 \tilde{\chi}_1^0$, simplified model, $m_{\tilde{\chi}_1^0} = 0$ GeV
> 170	95	24 SIRUNYAN	18X CMS	$\geq 1 H (\rightarrow \gamma\gamma)$ + jets + \cancel{E}_T , Tchi1n2E, $m_{\tilde{\chi}_1^0} < 25$ GeV	none	95	45 AAD	14G ATLS	$\tilde{\chi}_1^\pm \tilde{\chi}_1^\mp \rightarrow \ell^\pm \nu \tilde{\chi}_1^0 \tilde{\ell} \nu \tilde{\chi}_1^0$, simplified model, $m_{\tilde{\chi}_1^0} = 0$ GeV
> 420	95	25 KHACHATRY..17L	CMS	$2\tau + \cancel{E}_T$, Tchi1chi1C and $\tilde{\tau}$ -only, $m_{\tilde{\chi}_1^0} = 0$ GeV	none	95	45 AAD	14G ATLS	$\tilde{\chi}_1^\pm \tilde{\chi}_2^0 \rightarrow W \tilde{\chi}_1^0 Z \tilde{\chi}_1^0$, simplified model, $m_{\tilde{\chi}_1^\pm} = m_{\tilde{\chi}_2^0}$, $m_{\tilde{\chi}_1^0} = 0$ GeV
none 220-490	95	26 SIRUNYAN	17AW CMS	$1\ell + 2b$ -jets + \cancel{E}_T , Tchi1n2E, $m_{\tilde{\chi}_1^0} = 0$ GeV	> 168	95	46 AALTONEN	14 CDF	$3\ell^\pm + \cancel{E}_T$, $\tilde{\chi}_1^\pm \rightarrow \ell \nu \tilde{\chi}_1^0$, mSUGRA with $m_0 = 60$ GeV
> 500	95	27 AAD	16AA ATLS	$2\ell^\pm + \cancel{E}_T$, Tchi1chi1B, $m_{\tilde{\chi}_1^0} = 0$ GeV	> 700	95	47 KHACHATRY..14I	CMS	$\tilde{\chi}_1^\pm \rightarrow W \tilde{\chi}_1^0$, $\tilde{\ell} \nu$, $\tilde{\ell} \nu$, simplified model
> 220	95	27 AAD	16AA ATLS	$2\ell^\pm + \cancel{E}_T$, Tchi1chi1C, low Δm for $\tilde{\chi}_1^\pm, \tilde{\chi}_1^0$	> 710	95	48 AALTONEN	13Q CDF	$\tilde{\chi}_1^\pm \rightarrow \tau X$, simplified gravity- and gauge-mediated models
> 700	95	28 AAD	16AA ATLS	$3,4\ell + \cancel{E}_T$, Tchi1n2B, $m_{\tilde{\chi}_1^0} = 0$ GeV	> 420	95	49 AAD	12AS ATLS	$3\ell^\pm + \cancel{E}_T$, pMSSM
> 700	95	28 AAD	16AA ATLS	$3,4\ell + \cancel{E}_T$, Tchi1n2C, $m_{\tilde{\ell}} = m_{\tilde{\chi}_1^0} + 0.5$ (or 0.95) $(m_{\tilde{\chi}_1^\pm} - m_{\tilde{\chi}_1^0})$	50 AAD	12T ATLS	50 AAD	12T ATLS	$\ell^\pm \tilde{\ell} \tilde{\nu} + \cancel{E}_T$, $\ell^\pm \ell^\pm + \cancel{E}_T$, $pp \rightarrow \tilde{\chi}_1^\pm \tilde{\chi}_2^0$
> 400	95	28 AAD	16AA ATLS	2 hadronic $\tau + \cancel{E}_T$ & $3\ell + \cancel{E}_T$ combination, Tchi1n2D, $m_{\tilde{\chi}_1^0} = 0$ GeV	> 163	95	51 CHATRCHYAN11B	CMS	$\tilde{W}^0 \rightarrow \gamma \tilde{G}, \tilde{W}^\pm \rightarrow \ell^\pm \tilde{G}$, GMSB
> 540	95	29 KHACHATRY..16R	CMS	$\geq 1\gamma + 1e$ or μ + \cancel{E}_T , Tchi1n1A			52 CHATRCHYAN11v	CMS	$\tan\beta = 3$, $m_0 = 60$ GeV, $A_0 = 0$, $\mu > 0$
> 250	95	30 AAD	15BA ATLS	$m_{\tilde{\chi}_1^\pm} = m_{\tilde{\chi}_2^0}$, $m_{\tilde{\chi}_1^0} = 0$ GeV	1 SIRUNYAN 20b searched in 35.9 fb ⁻¹ of pp collisions at $\sqrt{s} = 13$ TeV for events with at least one photon and large \cancel{E}_T . No significant excess above the Standard Model expectations is observed. Limits are set on chargino masses in a general gauge-mediated SUSY breaking (GGM) scenario Tchi1n12-GGM, see Figure 4. Limits are also set on the NLSP mass in the Tchi1chi1F and Tchi1chi1G simplified models, see their Figure 5. Finally, limits are set on the gluino mass in the Tglu4A simplified model, see Figure 6.				
> 590	95	31 AAD	15CA ATLS	$\geq 2\gamma + \cancel{E}_T$, GGM, bino-like NLSP, any NLSP mass	2 AABOUD 19AU searched in 36.1 fb ⁻¹ of pp collisions at $\sqrt{s} = 13$ TeV for direct production of charginos and next-to-lightest neutralinos decaying into lightest neutralinos and a W, and a Higgs boson, respectively. Fully hadronic, semileptonic, diphoton, and multilepton (electrons, muons) final states with missing transverse momentum are considered in this search. Observations are consistent with the Standard Model expectations, and 95% confidence-level limits of up to 680 GeV on the chargino/next-to-lightest neutralino masses are set (Tchi1n2E model). See their Figure 14 for an overlay of exclusion contours from all searches.				
none 124-361	95	31 AAD	15CA ATLS	$\geq 1\gamma + e\mu$ + \cancel{E}_T , GGM, wino-like NLSP	3 SIRUNYAN 19BU searched for pair production of gauginos via vector boson fusion assuming the gaugino spectrum is compressed, in 35.9 fb ⁻¹ of pp collisions at $\sqrt{s} = 13$ TeV. The final states explored included zero leptons plus two jets, one lepton plus two jets, and one hadronic tau plus two jets. A similar bound is obtained in the light slepton limit.				
> 700	95	32 AAD	14H ATLS	$\tilde{\chi}_1^\pm \tilde{\chi}_2^0 \rightarrow \ell^\pm \nu \tilde{\chi}_1^0 \ell^\pm \tilde{\chi}_1^0$, simplified model, $m_{\tilde{\chi}_1^\pm} = m_{\tilde{\chi}_2^0}$, $m_{\tilde{\chi}_1^0} = 0$ GeV	4 SIRUNYAN 19CI searched in 77.5 fb ⁻¹ of pp collisions at $\sqrt{s} = 13$ TeV for events with one or more high-momentum Higgs bosons, decaying to pairs of photons, jets and \cancel{E}_T . No significant excess above the Standard Model expectations is observed. Limits are set on the sbottom mass in the Tsbot4 simplified model, see Figure 3, and on the wino mass in the Tchi1n2E simplified model, see their Figure 4. Limits are also set on the higgsino mass in the Tn1n1A and Tn1n1B simplified models, see their Figure 5.				
> 345	95	32 AAD	14H ATLS	$\tilde{\chi}_1^\pm \tilde{\chi}_2^0 \rightarrow W \tilde{\chi}_1^0 Z \tilde{\chi}_1^0$, simplified model, $m_{\tilde{\chi}_1^\pm} = m_{\tilde{\chi}_2^0}$, $m_{\tilde{\chi}_1^0} = 0$ GeV	5 SIRUNYAN 19K searched in 35.9 fb ⁻¹ of pp collisions at $\sqrt{s} = 13$ TeV for events with a photon, an electron or muon, and large \cancel{E}_T . No significant excess above the Standard Model expectations is observed. In the framework of GMSB, limits are set on the chargino and neutralino mass in the Tchi1n1A simplified model, see their Figure 6. Limits are also set on the gluino mass in the Tglu4A simplified model, and on the squark mass in the Tsqk4A simplified model, see their Figure 7.				
> 148	95	32 AAD	14H ATLS	$\tilde{\chi}_1^\pm \tilde{\chi}_2^0 \rightarrow W \tilde{\chi}_1^0 H \tilde{\chi}_1^0$, simplified model, $m_{\tilde{\chi}_1^\pm} = m_{\tilde{\chi}_2^0}$, $m_{\tilde{\chi}_1^0} = 0$ GeV					

- 6 AABOUD 18AY searched in 36.1 fb^{-1} of pp collisions at $\sqrt{s} = 13 \text{ TeV}$ for direct electroweak production of charginos as in Tchi1ch1D models in events characterised by the presence of at least two hadronically decaying tau leptons and large missing transverse energy. No significant deviation from the expected SM background is observed. In the Tchi1ch1D model, assuming decays via intermediate $\tilde{\tau}_L$, the observed limits rule out $\tilde{\chi}_1^\pm$ masses up to 630 GeV for a massless $\tilde{\chi}_1^0$. See their Fig.7 (left). Interpretations are also provided in Fig 8 (top) for different assumptions on the ratio between $m_{\tilde{\tau}}$ and $m_{\tilde{\chi}_1^\pm} + m_{\tilde{\chi}_1^0}$.
- 7 AABOUD 18AY searched in 36.1 fb^{-1} of pp collisions at $\sqrt{s} = 13 \text{ TeV}$ for direct electroweak production of charginos and neutralinos as in Tchi1n2D models, in events characterised by the presence of at least two hadronically decaying tau leptons and large missing transverse energy. No significant deviation from the expected SM background is observed. Assuming decays via intermediate $\tilde{\tau}_L$ and $m_{\tilde{\chi}_1^\pm} = m_{\tilde{\chi}_2^0}$, the observed limits rule out $\tilde{\chi}_1^\pm$ masses up to 760 GeV for a massless $\tilde{\chi}_1^0$. See their Fig.7 (right). Interpretations are also provided in Fig 8 (bottom) for different assumptions on the ratio between $m_{\tilde{\tau}}$ and $m_{\tilde{\chi}_1^\pm} + m_{\tilde{\chi}_1^0}$.
- 8 AABOUD 18BT searched in 36.1 fb^{-1} of pp collisions at $\sqrt{s} = 13 \text{ TeV}$ for direct electroweak production of charginos, chargino and next-to-lightest neutralinos and sleptons in events with two or three leptons (electrons or muons), with or without jets and large missing transverse energy. No significant excess above the Standard Model expectations is observed. Limits are set on the chargino mass up to 750 GeV for massless neutralinos in the Tchi1ch1C simplified model exploiting $2\ell + 0$ jets signatures, see their Figure 8(a).
- 9 AABOUD 18BT searched in 36.1 fb^{-1} of pp collisions at $\sqrt{s} = 13 \text{ TeV}$ for direct electroweak production of charginos, chargino and next-to-lightest neutralinos and sleptons in events with two or three leptons (electrons or muons), with or without jets, and large missing transverse energy. No significant excess above the Standard Model expectations is observed. Limits are set on the chargino mass up to 1100 GeV for massless neutralinos in the Tchi1n2C simplified model exploiting 3ℓ signature, see their Figure 8(c).
- 10 AABOUD 18BT searched in 36.1 fb^{-1} of pp collisions at $\sqrt{s} = 13 \text{ TeV}$ for direct electroweak production of charginos, chargino and next-to-lightest neutralinos and sleptons in events with two or three leptons (electrons or muons), with or without jets, and large missing transverse energy. No significant excess above the Standard Model expectations is observed. Limits are set on the chargino mass up to 580 GeV for massless neutralinos in the Tchi1n2F simplified model exploiting $2\ell + 2$ jets and 3ℓ signatures, see their Figure 8(d).
- 11 AABOUD 18CK searched for events with at least 3 b -jets and large missing transverse energy in two datasets of pp collisions at $\sqrt{s} = 13 \text{ TeV}$ of 36.1 fb^{-1} and 24.3 fb^{-1} depending on the trigger requirements. The analyses aimed to reconstruct two Higgs bosons decaying to pairs of b -quarks. No significant excess above the Standard Model expectations is observed. Limits are set on the Higgsino mass in the Tn1n1A simplified model, see their Figure 15(a). Constraints are also presented as a function of the BR of Higgsino decaying into an higgs boson and a gravitino, see their Figure 15(b).
- 12 AABOUD 18CO searched in 36.1 fb^{-1} of pp collisions at $\sqrt{s} = 13 \text{ TeV}$ for direct electroweak production of mass-degenerate charginos and next-to-lightest neutralinos in events with two or three leptons (electrons or muons), with or without jets, and large missing transverse energy. The search channels are based on recursive jigsaw reconstruction. Limits are set on the chargino mass up to 600 GeV for massless neutralinos in the Tchi1n2F simplified model exploiting the statistical combination of $2\ell + 2$ jets and 3ℓ channels. Chargino masses below 220 GeV are not excluded due to an excess of events above the SM prediction in the dedicated regions. See their Figure 13(d).
- 13 AABOUD 18R searched in 36.1 fb^{-1} of pp collisions at $\sqrt{s} = 13 \text{ TeV}$ for electroweak production in scenarios with compressed mass spectra in final states with two low-momentum leptons and missing transverse momentum. The data are found to be consistent with the SM prediction. Results are interpreted in Tchi1n2G wino models and $\tilde{\chi}_1^\pm$ masses are excluded up to 175 GeV for $m_{\tilde{\chi}_1^\pm} - m_{\tilde{\chi}_1^0} = 10 \text{ GeV}$. The exclusion limits extend down to mass splittings of 2 GeV, see their Fig. 10 (bottom).
- 14 AABOUD 18R searched in 36.1 fb^{-1} of pp collisions at $\sqrt{s} = 13 \text{ TeV}$ for electroweak production in scenarios with compressed mass spectra in final states with two low-momentum leptons and missing transverse momentum. The data are found to be consistent with the SM prediction. Results are interpreted in Tchi1n2G higgsino models and $\tilde{\chi}_1^\pm$ masses are excluded up to 145 GeV for $m_{\tilde{\chi}_1^\pm} - m_{\tilde{\chi}_1^0} = 5 \text{ GeV}$. The exclusion limits extend down to mass splittings of 2.5 GeV, see their Fig. 10 (top).
- 15 AABOUD 18U searched in 36.1 fb^{-1} of pp collisions at $\sqrt{s} = 13 \text{ TeV}$ in events with at least one isolated photon, possibly jets and significant transverse momentum targeting generalised models of gauge-mediated SUSY breaking. No significant excess of events is observed above the SM prediction. Results of the diphoton channel are interpreted in terms of lower limits on the masses of gauginos Tchi1ch1A models, which reach as high as 1.3 TeV. Gaugino masses below 1060 GeV are excluded for any NLSP mass, see their Fig. 10.
- 16 AABOUD 18Z searched in 36.1 fb^{-1} of pp collisions at $\sqrt{s} = 13 \text{ TeV}$ for events containing four or more charged leptons (electrons, muons and up to two hadronically decaying taus). No significant deviation from the expected SM background is observed. Limits are set on the Higgsino mass in simplified models of general gauge mediated supersymmetry Tn1n1A/Tn1n1B/Tn1n1C, see their Figure 9. Limits are also set on the wino, slepton, sneutrino and gluino mass in a simplified model of NLSP pair production with R-parity violating decays of the LSP via λ_{12c} or λ_{133} to charged leptons, see their Figures 7, 8.
- 17 SIRUNYAN 18AA searched in 35.9 fb^{-1} of pp collisions at $\sqrt{s} = 13 \text{ TeV}$ for events with at least one photon and large \cancel{E}_T . No significant excess above the Standard Model expectations is observed. Limits are set on wino masses in a general gauge-mediated SUSY breaking (GGM) scenario with bino-like $\tilde{\chi}_1^0$ and wino-like $\tilde{\chi}_1^\pm$ and $\tilde{\chi}_2^0$, see Figure 7. Limits are also set on the NLSP mass in the Tchi1n1A and Tchi1ch1A simplified models, see their Figure 8. Finally, limits are set on the gluino mass in the Tglu4A and Tglu4B simplified models, see their Figure 9, and on the squark mass in the Tsq44A and Tsq44B simplified models, see their Figure 10.
- 18 SIRUNYAN 18AJ searched in 35.9 fb^{-1} of pp collisions at $\sqrt{s} = 13 \text{ TeV}$ for events containing two low-momentum, oppositely charged leptons (electrons or muons) and \cancel{E}_T . No excess over the expected background is observed. Limits are derived on the wino mass in the Tchi1n2F simplified model, see their Figure 5. Limits are also set on the stop mass in the Tstop10 simplified model, see their Figure 6. Finally, limits are set on the Higgsino mass in the Tchi1n2G simplified model, see Figure 8 and in the pMSSM, see Figure 7.
- 19 SIRUNYAN 18AO searched in 35.9 fb^{-1} of pp collisions at $\sqrt{s} = 13 \text{ TeV}$ for direct electroweak production of charginos and neutralinos in events with either two or more leptons (electrons or muons) of the same electric charge, or with three or more leptons, which can include up to two hadronically decaying tau leptons. No significant excess above the Standard Model expectations is observed. Limits are set on the chargino/neutralino mass in the Tchi1n2A, Tchi1n2H, Tchi1n2D, Tchi1n2E and Tchi1n2F simplified models, see their Figures 14, 15, 16, 17 and 18. Limits are also set on the higgsino mass in the Tn1n1A, Tn1n1B and Tn1n1C simplified models, see their Figure 19.
- 20 SIRUNYAN 18AP searched in 35.9 fb^{-1} of pp collisions at $\sqrt{s} = 13 \text{ TeV}$ for direct electroweak production of charginos and neutralinos by combining a number of previous and new searches. No significant excess above the Standard Model expectations is observed. Limits are set on the chargino/neutralino mass in the Tchi1n2E, Tchi1n2F and Tchi1n2I simplified models, see their Figures 7, 8, 9 and 10. Limits are also set on the higgsino mass in the Tn1n1A, Tn1n1B and Tn1n1C simplified models, see their Figure 11, 12, 13 and 14.
- 21 SIRUNYAN 18AR searched in 35.9 fb^{-1} of pp collisions at $\sqrt{s} = 13 \text{ TeV}$ for events containing two opposite-charge, same-flavour leptons (electrons or muons), jets and \cancel{E}_T . No significant excess above the Standard Model expectations is observed. Limits are set on the gluino mass in the Tglu4C simplified model, see their Figure 7. Limits are also set on the chargino/neutralino mass in the Tchi1n2F simplified models, see their Figure 8, and on the higgsino mass in the Tn1n1B and Tn1n1C simplified models, see their Figure 9. Finally, limits are set on the sbottom mass in the Tsb0t3 simplified model, see their Figure 10.
- 22 SIRUNYAN 18DN searched in 35.9 fb^{-1} of pp collisions at $\sqrt{s} = 13 \text{ TeV}$ for direct electroweak production of charginos and for pair production of top squarks in events with two leptons (electrons or muons) of the opposite electric charge. No significant excess above the Standard Model expectations is observed. Limits are set on the chargino mass in the Tchi1ch1C and Tchi1ch1E simplified models, see their Figure 8. Limits are also set on the stop mass in the Tstop1 and Tstop2 simplified models, see their Figure 9.
- 23 SIRUNYAN 18DP searched in 35.9 fb^{-1} of pp collisions at $\sqrt{s} = 13 \text{ TeV}$ for direct electroweak production of charginos and neutralinos or of chargino pairs in events with a tau lepton pair and significant missing transverse momentum. Both hadronic and leptonic decay modes are considered for the tau lepton. No significant excess above the Standard Model expectations is observed. Limits are set on the chargino mass in the Tchi1ch1D and Tchi1n2 simplified models, see their Figures 14 and 15. Also, excluded stau pair production cross sections are shown in Figures 11, 12, and 13.
- 24 SIRUNYAN 18X searched in 35.9 fb^{-1} of pp collisions at $\sqrt{s} = 13 \text{ TeV}$ for events with one or more high-momentum Higgs bosons, decaying to pairs of photons, jets and \cancel{E}_T . The razor variables (M_R and R^2) are used to categorise the events. No significant excess above the Standard Model expectations is observed. Limits are set on the sbottom mass in the Tsb0t4 simplified model and on the wino mass in the Tchi1n2E simplified model, see their Figure 5. Limits are also set on the higgsino mass in the Tn1n1A and Tn1n1B simplified models, see their Figure 6.
- 25 KHACHATRYAN 17L searched in about 19 fb^{-1} of pp collisions at $\sqrt{s} = 8 \text{ TeV}$ for events with two τ (at least one decaying hadronically) and \cancel{E}_T . In the Tchi1ch1C model, assuming decays via intermediate $\tilde{\tau}$ or $\tilde{\nu}_\tau$ with equivalent mass, the observed limits rule out $\tilde{\chi}_1^\pm$ masses up to 420 GeV for a massless $\tilde{\chi}_1^0$. See their Fig.5.
- 26 SIRUNYAN 17AW searched in 35.9 fb^{-1} of pp collisions at $\sqrt{s} = 13 \text{ TeV}$ for events with a charged lepton (electron or muon), two jets identified as originating from a b -quark, and large \cancel{E}_T . No significant excess above the Standard Model expectations is observed. Limits are set on the mass of the chargino and the next-to-lightest neutralino in the Tchi1n2E simplified model, see their Figure 6.
- 27 AAD 16AA summarized and extended ATLAS searches for electroweak supersymmetry in final states containing several charged leptons, \cancel{E}_T , with or without hadronic jets, in 20 fb^{-1} of pp collisions at $\sqrt{s} = 8 \text{ TeV}$. The paper reports the results of new interpretations and statistical combinations of previously published analyses, as well as new analyses. Exclusion limits at 95% C.L. are set on the $\tilde{\chi}_1^\pm$ mass in the Tchi1ch1B and Tchi1ch1C simplified models. See their Fig. 13.
- 28 AAD 16AA summarized and extended ATLAS searches for electroweak supersymmetry in final states containing several charged leptons, \cancel{E}_T , with or without hadronic jets, in 20 fb^{-1} of pp collisions at $\sqrt{s} = 8 \text{ TeV}$. The paper reports the results of new interpretations and statistical combinations of previously published analyses, as well as new analyses. Exclusion limits at 95% C.L. are set on mass-degenerate $\tilde{\chi}_1^\pm$ and $\tilde{\chi}_2^0$ masses in the Tchi1n2B, Tchi1n2C, and Tchi1n2D simplified models. See their Figs. 16, 17, and 18. Interpretations in phenomenological-MSSM, two-parameter Non Universal Higgs Masses (NUHM2), and gauge-mediated symmetry breaking (GMSB) models are also given in their Figs. 20, 21 and 22.
- 29 KHACHATRYAN 16R searched in 19.7 fb^{-1} of pp collisions at $\sqrt{s} = 8 \text{ TeV}$ for events with one or more photons, one electron or muon, and \cancel{E}_T . No significant excess above the Standard Model expectations is observed. Limits are set on wino masses in a general gauge-mediated SUSY breaking model (GGM), for a wino-like neutralino NLSP scenario, see Fig. 5. Limits are also set in the Tglu1D and Tchi1n1A simplified models, see Fig. 6. The Tchi1n1A limit is reduced to 340 GeV for a branching ratio reduced by the weak mixing angle.
- 30 AAD 15BA searched in 20.3 fb^{-1} of pp collisions at $\sqrt{s} = 8 \text{ TeV}$ for electroweak production of charginos and neutralinos decaying to a final state containing a W boson and a 125 GeV Higgs boson, plus missing transverse momentum. No excess beyond the Standard Model expectation is observed. Exclusion limits are derived in simplified models of direct chargino and next-to-lightest neutralino production, with the decays $\tilde{\chi}_1^\pm \rightarrow W^\pm \tilde{\chi}_1^0$ and $\tilde{\chi}_2^0 \rightarrow H \tilde{\chi}_1^0$ having 100% branching fraction, see Fig. 8. A combination of the multiple final states for the Higgs decay yields the best limits (Fig. 8d).
- 31 AAD 15CA searched in 20.3 fb^{-1} of pp collisions at $\sqrt{s} = 8 \text{ TeV}$ for events with one or more photons and \cancel{E}_T , with or without leptons (e, μ). No significant excess above the Standard Model expectations is observed. Limits are set on wino masses in the general gauge-mediated SUSY breaking model (GGM), for wino-like NLSP, see Fig. 9, 12.
- 32 AAD 14H searched in 20.3 fb^{-1} of pp collisions at $\sqrt{s} = 8 \text{ TeV}$ for electroweak production of charginos and neutralinos decaying to a final state with three leptons and missing transverse momentum. No excess beyond the Standard Model expectation is observed.

Searches Particle Listings

Supersymmetric Particle Searches

- Exclusion limits are derived in simplified models of direct chargino and next-to-lightest neutralino production, with decays to the lightest neutralino via either all three generations of leptons, staus only, gauge bosons, or Higgs bosons, see Fig. 7. An interpretation in the pMSSM is also given, see Fig. 8.
- 33 AAD 14X searched in 20.3 fb⁻¹ of pp collisions at $\sqrt{s} = 8$ TeV for events with at least four leptons (electrons, muons, taus) in the final state. No significant excess above the Standard Model expectations is observed. Limits are set on the wino-like chargino mass in the R-parity violating simplified model where the decay $\tilde{\chi}_1^\pm \rightarrow W^{(*)\pm} \tilde{\chi}_1^0$, with $\tilde{\chi}_1^0 \rightarrow \ell^\pm \ell^\mp \nu$, takes place with a branching ratio of 100%, see Fig. 8.
- 34 KHACHATRYAN 14L searched in 19.5 fb⁻¹ of pp collisions at $\sqrt{s} = 8$ TeV for evidence of chargino-neutralino $\tilde{\chi}_1^\pm \tilde{\chi}_2^0$ pair production with Higgs or W -bosons in the decay chain, leading to HW final states with missing transverse energy. The decays of a Higgs boson to a photon pair are considered in conjunction with hadronic and leptonic decay modes of the W bosons. No significant excesses over the expected SM backgrounds are observed. The results are interpreted in the context of simplified models where the decays $\tilde{\chi}_2^0 \rightarrow H \tilde{\chi}_1^0$ and $\tilde{\chi}_1^\pm \rightarrow W^\pm \tilde{\chi}_1^0$ take place 100% of the time, see Figs. 22–23.
- 35 AAD 13 searched in 4.7 fb⁻¹ of pp collisions at $\sqrt{s} = 7$ TeV for charginos and neutralinos decaying to a final state with three leptons (e and μ) and missing transverse energy. No excess beyond the Standard Model expectation is observed. Exclusion limits are derived in the phenomenological MSSM, see Fig. 2 and 3, and in simplified models, see Fig. 4. For the simplified models with intermediate slepton decays, degenerate $\tilde{\chi}_1^\pm$ and $\tilde{\chi}_2^0$ masses up to 500 GeV are excluded at 95% C.L. for very large mass differences with the $\tilde{\chi}_1^0$. Supersedes AAD 12As.
- 36 AAD 13B searched in 4.7 fb⁻¹ of pp collisions at $\sqrt{s} = 7$ TeV for gauginos decaying to a final state with two leptons (e and μ) and missing transverse energy. No excess beyond the Standard Model expectation is observed. Limits are derived in a simplified model of wino-like chargino pair production, where the chargino always decays to the lightest neutralino via an intermediate on-shell charged slepton, see Fig. 2(b). Chargino masses between 110 and 340 GeV are excluded at 95% C.L. for $m_{\tilde{\chi}_1^0} = 10$ GeV. Exclusion limits are also derived in the phenomenological MSSM, see Fig. 3.
- 37 AAD 12CT searched in 4.7 fb⁻¹ of pp collisions at $\sqrt{s} = 7$ TeV for events containing four or more leptons (electrons or muons) and either moderate values of missing transverse momentum or large effective mass. No significant excess is found in the data. Limits are presented in a simplified model of R-parity violating supersymmetry in which charginos are pair-produced and then decay into a W -boson and a $\tilde{\chi}_1^0$, which in turn decays through an RPV coupling into two charged leptons ($e^\pm e^\mp$ or $e^\pm \mu^\mp$) and a neutrino. In this model, chargino masses up to 540 GeV are excluded at 95% C.L. for $m_{\tilde{\chi}_1^0}$ above 300 GeV, see Fig. 3a. The limit deteriorates for lighter $\tilde{\chi}_1^0$. Limits are also set in an R-parity violating mSUGRA model, see Fig. 3b.
- 38 CHATRCHYAN 12BJ searched in 4.98 fb⁻¹ of pp collisions at $\sqrt{s} = 7$ TeV for direct electroweak production of charginos and neutralinos in events with at least two leptons, jets and missing transverse momentum. No significant excesses over the expected SM backgrounds are observed and 95% C.L. limits on the production cross section of $\tilde{\chi}_1^\pm \tilde{\chi}_2^0$ pair production were set in a number of simplified models, see Figs. 7 to 12.
- 39 ABDALLAH 03M uses data from $\sqrt{s} = 192$ –208 GeV to obtain limits in the framework of the MSSM with gaugino and sfermion mass universality at the GUT scale. An indirect limit on the mass of charginos is derived by constraining the MSSM parameter space by the results from direct searches for neutralinos (including cascade decays), for charginos and for sleptons. These limits are valid for values of $M_2 < 1$ TeV, $|\mu| \leq 2$ TeV with the $\tilde{\chi}_1^0$ as LSP. Constraints from the Higgs search in the m_h^{max} scenario assuming $m_t = 174.3$ GeV are included. The quoted limit applies if there is no mixing in the third family or when $m_{\tilde{\tau}_1} - m_{\tilde{\chi}_1^0} > 6$ GeV. If mixing is included the limit degrades to 90 GeV. See Fig. 43 for the mass limits as a function of $\tan\beta$. These limits update the results of ABREU 00w.
- 40 KHACHATRYAN 16AA searched in 7.4 fb⁻¹ of pp collisions at $\sqrt{s} = 8$ TeV for events with one or more photons, hadronic jets and \cancel{E}_T . No significant excess above the Standard Model expectations is observed. Limits are set on wino masses in the general gauge-mediated SUSY breaking model (GGM), for a wino-like neutralino NLSP scenario and with the wino mass fixed at 10 GeV above the bino mass, see Fig. 4. Limits are also set in the Tch1ch1A and Tch1n1A simplified models, see Fig. 3.
- 41 KHACHATRYAN 16R searched in 19.7 fb⁻¹ of pp collisions at $\sqrt{s} = 8$ TeV for events with one or more photons, one electron or muon, and \cancel{E}_T . No significant excess above the Standard Model expectations is observed. Limits are also set in the TgluIF simplified model, see Fig. 6.
- 42 KHACHATRYAN 16Y searched in 19.7 fb⁻¹ of pp collisions at $\sqrt{s} = 8$ TeV for events with one or two soft isolated leptons, hadronic jets, and \cancel{E}_T . No significant excess above the Standard Model expectations is observed. Limits are set on the $\tilde{\chi}_1^\pm$ mass (which is degenerate with the $\tilde{\chi}_2^0$) in the Tch1n2A simplified model, see Fig. 4.
- 43 AAD 14AV searched in 20.3 fb⁻¹ of pp collisions at $\sqrt{s} = 8$ TeV for the direct production of charginos, neutralinos and staus in events containing at least two hadronically decaying τ -leptons, large missing transverse momentum and low jet activity. The quoted limit was derived for direct $\tilde{\chi}_1^\pm \tilde{\chi}_2^0$ and $\tilde{\chi}_1^\pm \tilde{\chi}_1^0$ production with $\tilde{\chi}_2^0 \rightarrow \tilde{\tau} \tau \rightarrow \tau \tau \tilde{\chi}_1^0$ and $\tilde{\chi}_1^\pm \rightarrow \tilde{\tau} \nu(\tilde{\nu} \tau) \rightarrow \tau \nu \tilde{\chi}_1^0$, $m_{\tilde{\chi}_1^0} = m_{\tilde{\chi}_1^\pm}$, $m_{\tilde{\tau}} = 0.5(m_{\tilde{\chi}_1^\pm} + m_{\tilde{\chi}_1^0})$, $m_{\tilde{\chi}_1^0} = 0$ GeV. No excess over the expected SM background is observed. Exclusion limits are set in simplified models of $\tilde{\chi}_1^\pm \tilde{\chi}_1^0$ and $\tilde{\chi}_1^\pm \tilde{\chi}_2^0$ pair production, see their Figure 7. Upper limits on the cross section and signal strength for direct di-stau production are derived, see Figures 8 and 9. Also, limits are derived in a pMSSM model where the only light slepton is the $\tilde{\tau}_R$, see Figure 10.
- 44 AAD 14AV searched in 20.3 fb⁻¹ of pp collisions at $\sqrt{s} = 8$ TeV for the direct production of charginos, neutralinos and staus in events containing at least two hadronically decaying τ -leptons, large missing transverse momentum and low jet activity. The quoted limit was derived for direct $\tilde{\chi}_1^\pm \tilde{\chi}_1^0$ production with $\tilde{\chi}_1^0 \rightarrow \tilde{\tau} \nu(\tilde{\nu} \tau) \rightarrow \tau \nu \tilde{\chi}_1^0$, $m_{\tilde{\tau}} = 0.5(m_{\tilde{\chi}_1^\pm} + m_{\tilde{\chi}_1^0})$, $m_{\tilde{\chi}_1^0} = 0$ GeV. No excess over the expected SM background is observed. Exclusion limits are set in simplified models of $\tilde{\chi}_1^\pm \tilde{\chi}_1^0$ and $\tilde{\chi}_1^\pm \tilde{\chi}_2^0$ pair production, see their Figure 7. Upper limits on the cross section and signal strength for direct di-stau production are derived, see Figures 8 and 9. Also, limits are derived in a pMSSM model where the only light slepton is the $\tilde{\tau}_R$, see Figure 10.

- 45 AAD 14G searched in 20.3 fb⁻¹ of pp collisions at $\sqrt{s} = 8$ TeV for electroweak production of chargino pairs, or chargino-neutralino pairs, decaying to a final state with two leptons (e and μ) and missing transverse momentum. No excess beyond the Standard Model expectation is observed. Exclusion limits are derived in simplified models of chargino pair production, with chargino decays to the lightest neutralino via either sleptons or gauge bosons, see Fig 5; or in simplified models of chargino and next-to-lightest neutralino production, with decays to the lightest neutralino via gauge bosons, see Fig. 7. An interpretation in the pMSSM is also given, see Fig. 10.
- 46 AALTONEN 14 searched in 5.8 fb⁻¹ of $p\bar{p}$ collisions at $\sqrt{s} = 1.96$ TeV for evidence of chargino and next-to-lightest neutralino associated production in final states consisting of three leptons (electrons, muons or taus) and large missing transverse momentum. The results are consistent with the Standard Model predictions within 1.85 σ . Limits on the chargino mass are derived in an mSUGRA model with $m_0 = 60$ GeV, $\tan\beta = 3$, $A_0 = 0$ and $\mu > 0$, see their Fig. 2.
- 47 KHACHATRYAN 14I searched in 19.5 fb⁻¹ of pp collisions at $\sqrt{s} = 8$ TeV for electroweak production of chargino pairs decaying to a final state with opposite-sign lepton pairs (e or μ) and missing transverse momentum. No excess beyond the Standard Model expectation is observed. Exclusion limits are derived in simplified models, see Fig. 18.
- 48 AALTONEN 13Q searched in 6.0 fb⁻¹ of $p\bar{p}$ collisions at $\sqrt{s} = 1.96$ TeV for evidence of chargino-neutralino associated production in like-sign dilepton final states. One lepton is identified as the hadronic decay of a tau lepton, while the other is an electron or muon. Good agreement with the Standard Model predictions is observed and limits are set on the chargino-neutralino cross section for simplified gravity- and gauge-mediated models, see their Figs. 2 and 3.
- 49 AAD 12As searched in 2.06 fb⁻¹ of pp collisions at $\sqrt{s} = 7$ TeV for charginos and neutralinos decaying to a final state with three leptons (e and μ) and missing transverse energy. No excess beyond the Standard Model expectation is observed. Exclusion limits are derived in the phenomenological MSSM, see Fig. 2 (top), and in simplified models, see Fig. 2 (bottom).
- 50 AAD 12T looked in 1 fb⁻¹ of pp collisions at $\sqrt{s} = 7$ TeV for the production of supersymmetric particles decaying into final states with missing transverse momentum and exactly two isolated leptons (e or μ). Opposite-sign and same-sign dilepton events were separately studied. Additionally, in opposite-sign events, a search was made for an excess of same-flavor over different-flavor lepton pairs. No excess over the expected background is observed and limits are placed on the effective production cross section of opposite-sign dilepton events with $\cancel{E}_T > 250$ GeV and on same-sign dilepton events with $\cancel{E}_T > 100$ GeV. The latter limit is interpreted in a simplified electroweak gaugino production model as a lower chargino mass limit.
- 51 CHATRCHYAN 11B looked in 35 pb⁻¹ of pp collisions at $\sqrt{s} = 7$ TeV for events with an isolated lepton (e or μ), a photon and \cancel{E}_T which may arise in a generalized gauge mediated model from the decay of Wino-like NLSPs. No evidence for an excess over the expected background is observed. Limits are derived in the plane of squark/gluino mass versus Wino mass (see Fig. 4). Mass degeneracy of the produced squarks and gluinos is assumed.
- 52 CHATRCHYAN 11V looked in 35 pb⁻¹ of pp collisions at $\sqrt{s} = 7$ TeV for events with ≥ 3 isolated leptons (e , μ or τ), with or without jets and \cancel{E}_T . No evidence for an excess over the expected background is observed. Limits are derived in the CMSSM ($m_0, m_{1/2}$) plane for $\tan\beta = 3$ (see Fig. 5).

Long-lived $\tilde{\chi}^\pm$ (Chargino) mass limit

Limits on charginos which leave the detector before decaying.

VALUE (GeV)	CL%	DOCUMENT ID	TECN	COMMENT
>1090	95	1 AABOUD	19AT ATLS	long-lived $\tilde{\chi}_1^\pm$ mAMSB
> 460	95	2 AABOUD	18AS ATLS	$\tilde{\chi}^\pm \rightarrow \tilde{\chi}_1^0 \pi^\pm$, lifetime 0.2 ns, $m_{\tilde{\chi}^\pm} - m_{\tilde{\chi}_1^0} = 160$ MeV
> 715	95	3 SIRUNYAN	18BR CMS	$\tilde{\chi}^\pm \rightarrow \tilde{\chi}_1^0 \pi^\pm$, AMSB, $\tan\beta = 5$ and $\mu > 0$, $\tau = 3$ ns
> 695	95	3 SIRUNYAN	18BR CMS	$\tilde{\chi}^\pm \rightarrow \tilde{\chi}_1^0 \pi^\pm$, AMSB, $\tan\beta = 5$ and $\mu > 0$, $\tau = 7$ ns
> 505	95	3 SIRUNYAN	18BR CMS	$\tilde{\chi}^\pm \rightarrow \tilde{\chi}_1^0 \pi^\pm$, AMSB, $\tan\beta = 5$, $\mu > 0$, 0.5 ns $> \tau > 60$ ns
> 620	95	4 AAD	15AE ATLS	stable $\tilde{\chi}^\pm$
> 534	95	5 AAD	15BMATLS	stable $\tilde{\chi}^\pm$
> 239	95	5 AAD	15BMATLS	$\tilde{\chi}^\pm \rightarrow \tilde{\chi}_1^0 \pi^\pm$, lifetime 1 ns, $m_{\tilde{\chi}^\pm} - m_{\tilde{\chi}_1^0} = 0.14$ GeV
> 482	95	5 AAD	15BMATLS	$\tilde{\chi}^\pm \rightarrow \tilde{\chi}_1^0 \pi^\pm$, lifetime 15 ns, $m_{\tilde{\chi}^\pm} - m_{\tilde{\chi}_1^0} = 0.14$ GeV
> 103	95	6 AAD	13H ATLS	long-lived $\tilde{\chi}^\pm \rightarrow \tilde{\chi}_1^0 \pi^\pm$, mAMSB, $\Delta m_{\tilde{\chi}_1^0} = 160$ MeV
> 92	95	7 AAD	12BJ ATLS	long-lived $\tilde{\chi}^\pm \rightarrow \pi^\pm \tilde{\chi}_1^0$, mAMSB
> 171	95	8 ABAZOV	09M D0	\tilde{H}
> 102	95	9 ABBIENDI	03L OPAL	$m_{\tilde{\tau}} > 500$ GeV
none 2–93.0	95	10 ABREU	00T DLPH	\tilde{H}^\pm or $m_{\tilde{\nu}} > m_{\tilde{\chi}^\pm}$
• • • We do not use the following data for averages, fits, limits, etc. • • •				
> 260	95	11 KHACHATRY...15AB	CMS	$\tilde{\chi}_1^\pm \rightarrow \tilde{\chi}_1^0 \pi^\pm, \tau_{\tilde{\chi}_1^\pm} = 0.2$ ns, AMSB
> 800	95	12 KHACHATRY...15A0	CMS	long-lived $\tilde{\chi}_1^\pm$, mAMSB, $\tau > 100$ ns
> 100	95	12 KHACHATRY...15A0	CMS	long-lived $\tilde{\chi}_1^\pm$, mAMSB, $\tau > 3$ ns
> 100	95	13 KHACHATRY...15W	CMS	long-lived $\tilde{\chi}^0, \tilde{q} \rightarrow q \tilde{\chi}^0, \tilde{\chi}^0 \rightarrow \ell^\pm \ell^\mp \nu$, RPV
> 270	95	14 AAD	13BD ATLS	disappearing-track signature, AMSB
> 278	95	15 ABAZOV	13B D0	long-lived $\tilde{\chi}^\pm$, gaugino-like
> 244	95	15 ABAZOV	13B D0	long-lived $\tilde{\chi}^\pm$, higgsino-like

- ¹ AABOUD 19AT searched in 36.1 fb^{-1} of pp collisions at $\sqrt{s} = 13 \text{ TeV}$ for metastable R -hadrons. Multiple search strategies for a wide range of lifetimes, corresponding to path lengths of a few meters, are defined. No significant deviations from the expected Standard Model background are observed. Results are interpreted in terms of direct electroweak production of long-lived charginos in the context of mAMSB scenarios. Chargino masses are excluded at 95% C.L. below 1090 GeV. See their Figure 10 (right).
- ² AABOUD 18AS searched in 36.1 fb^{-1} of pp collisions at $\sqrt{s} = 13 \text{ TeV}$ for direct electroweak production of long-lived charginos in the context of AMSB or phenomenological MSSM scenarios with wino-like LSP. Events with a disappearing track due to a low-momentum pion accompanied by at least one jet with high transverse momentum from initial-state radiation are considered. No significant excess above the Standard Model expectations is observed. Exclusion limits are set at 95% confidence level on the mass of charginos for different chargino lifetimes. For a pure wino with a lifetime of about 0.2 ns, corresponding to a mass-splitting between the charged and neutral wino of around 160 MeV, chargino masses up to 460 GeV are excluded, see their Fig. 8.
- ³ SIRUNYAN 18BR searched in 38.4 fb^{-1} of pp collisions at $\sqrt{s} = 13 \text{ TeV}$ for direct electroweak production of long-lived charginos in events containing isolated tracks with missing hits in the outer layer of the silicon tracker and little or no associated calorimetric energy deposits (disappearing tracks). No significant excess above the Standard Model expectations is observed. In an AMSB context, limits are set on the cross section of direct chargino production through $pp \rightarrow \tilde{\chi}^{\pm} \tilde{\chi}^{\mp}$ and $pp \rightarrow \tilde{\chi}^{\pm} \tilde{\chi}_1^0$, assuming $\text{BR}(\tilde{\chi}^{\pm} \rightarrow \tilde{\chi}_1^0 \pi^{\pm}) = 100\%$, as a function of the chargino mass and mean proper lifetime, see Figures 3, 4 and 5.
- ⁴ AAD 15AE searched in 19.1 fb^{-1} of pp collisions at $\sqrt{s} = 8 \text{ TeV}$ for heavy long-lived charged particles, measured through their specific ionization energy loss in the ATLAS pixel detector or their time-of-flight in the ALTAS muon system. In the absence of an excess of events above the expected backgrounds, limits are set on stable charginos, see Fig. 10.
- ⁵ AAD 15BM searched in 18.4 fb^{-1} of pp collisions at $\sqrt{s} = 8 \text{ TeV}$ for stable and metastable non-relativistic charged particles through their anomalous specific ionization energy loss in the ATLAS pixel detector. In absence of an excess of events above the expected backgrounds, limits are set on stable charginos (see Table 5) and on metastable charginos decaying to $\tilde{\chi}_1^0 \pi^{\pm}$, see Fig. 11.
- ⁶ AAD 13H searched in 4.7 fb^{-1} of pp collisions at $\sqrt{s} = 7 \text{ TeV}$ for direct electroweak production of long-lived charginos in the context of AMSB scenarios. The search is based on the signature of a high-momentum isolated track with few associated hits in the outer part of the tracking system, arising from a chargino decay into a neutralino and a low-momentum pion. The p_T spectrum of the tracks was found to be consistent with the SM expectations. Constraints on the lifetime and the production cross section were obtained, see Fig. 6. In the minimal AMSB framework with $\tan\beta = 5$, and $\mu > 0$, a chargino having a mass below 103 (85) GeV for a chargino-neutralino mass splitting $\Delta m_{\tilde{\chi}_1^{\pm}} = 160$ (170) MeV is excluded at the 95% C.L. See Fig. 7 for more precise bounds.
- ⁷ AAD 12BJ looked in 1.02 fb^{-1} of pp collisions at $\sqrt{s} = 7 \text{ TeV}$ for signatures of decaying charginos resulting in isolated tracks with few associated hits in the outer region of the tracking system. The p_T spectrum of the tracks was found to be consistent with the SM expectations. Constraints on the lifetime and the production cross section were obtained. In the minimal AMSB framework with $m_{3/2} < 32 \text{ TeV}$, $m_0 < 1.5 \text{ TeV}$, $\tan\beta = 5$, and $\mu > 0$, a chargino having a mass below 92 GeV and a lifetime between 0.5 ns and 2 ns is excluded at the 95% C.L. See their Fig. 8 for more precise bounds.
- ⁸ ABAZOV 09M searched in 1.1 fb^{-1} of $p\bar{p}$ collisions at $\sqrt{s} = 1.96 \text{ TeV}$ for events with direct production of a pair of charged massive stable particles identified by their TOF. The number of the observed events is consistent with the predicted background. The data are used to constrain the production cross section as a function of the $\tilde{\chi}_1^{\pm}$ mass, see their Fig. 2. The quoted limit improves to 206 GeV for gaugino-like charginos.
- ⁹ ABBIENDI 03L used e^+e^- data at $\sqrt{s} = 130\text{--}209 \text{ GeV}$ to select events with two high momentum tracks with anomalous dE/dx . The excluded cross section is compared to the theoretical expectation as a function of the heavy particle mass in their Fig. 3. The bounds are valid for colorless fermions with lifetime longer than 10^{-6} s . Supersedes the results from ACKERSTAFF 98P.
- ¹⁰ ABREU 00T searches for the production of heavy stable charged particles, identified by their ionization or Cherenkov radiation, using data from $\sqrt{s} = 130$ to 189 GeV. These limits include and update the results of ABREU 98P.
- ¹¹ KHACHATRYAN 15AB searched in 19.5 fb^{-1} of pp collisions at $\sqrt{s} = 8 \text{ TeV}$ for events containing tracks with little or no associated calorimeter energy deposits and with missing hits in the outer layers of the tracking system (disappearing-track signature). Such disappearing tracks can result from the decay of charginos that are nearly mass degenerate with the lightest neutralino. The number of observed events is in agreement with the background expectation. Limits are set on the cross section of electroweak chargino production in terms of the chargino mass and mean proper lifetime, see Fig. 4. In the minimal AMSB model, a chargino mass below 260 GeV is excluded at 95% C.L., see their Fig. 5.
- ¹² KHACHATRYAN 15O searched in 18.8 fb^{-1} of pp collisions at $\sqrt{s} = 8 \text{ TeV}$ for evidence of long-lived charginos in the context of AMSB and pMSSM scenarios. The results are based on a previously published search for heavy stable charged particles at 7 and 8 TeV. In the minimal AMSB framework with $\tan\beta = 5$ and $\mu \geq 0$, constraints on the chargino mass and lifetime were placed, see Fig. 5. Charginos with a mass below 800 (100) GeV are excluded at the 95% C.L. for lifetimes above 100 ns (3 ns). Constraints are also placed on the pMSSM parameter space, see Fig. 3.
- ¹³ KHACHATRYAN 15W searched in up to 20.5 fb^{-1} of pp collisions at $\sqrt{s} = 8 \text{ TeV}$ for evidence of long-lived neutralinos produced through $\tilde{q}\text{-pair}$ production, with $\tilde{q} \rightarrow q\tilde{\chi}^0$ and $\tilde{\chi}^0 \rightarrow \ell^+ \ell^- \nu$ (RPV: $\lambda_{121}, \lambda_{122} \neq 0$). 95% C.L. exclusion limits on cross section times branching ratio are set as a function of mean proper decay length of the neutralino, see Figs. 6 and 9.
- ¹⁴ AAD 13BD searched in 20.3 fb^{-1} of pp collisions at $\sqrt{s} = 8 \text{ TeV}$ for events containing tracks with no associated hits in the outer region of the tracking system resulting from the decay of charginos that are nearly mass degenerate with the lightest neutralino, as is often the case in AMSB scenarios. No significant excess above the background expectation is observed for candidate tracks with large transverse momentum. Constraints on chargino properties are obtained and in the minimal AMSB model, a chargino mass below 270 GeV is excluded at 95% C.L., see their Fig. 7.
- ¹⁵ ABAZOV 13b looked in 6.3 fb^{-1} of $p\bar{p}$ collisions at $\sqrt{s} = 1.96 \text{ TeV}$ for charged massive long-lived particles in events with muon-like particles that have both speed and ionization energy loss inconsistent with muons produced in beam collisions. In the absence of an excess, limits are set at 95% C.L. on gaugino- and higgsino-like charginos, see their Table 20 and Fig. 23.

 $\tilde{\nu}$ (Sneutrino) mass limit

The limits may depend on the number, $N(\tilde{\nu})$, of sneutrinos assumed to be degenerate in mass. Only $\tilde{\nu}_L$ (not $\tilde{\nu}_R$) is assumed to exist. It is possible that $\tilde{\nu}$ could be the lightest supersymmetric particle (LSP).

We report here, but do not include in the Listings, the limits obtained from the fit of the final results obtained by the LEP Collaborations on the invisible width of the Z boson ($\Delta\Gamma_{\text{inv.}} < 2.0 \text{ MeV}$, LEP-SLC 06): $m_{\tilde{\nu}} > 43.7 \text{ GeV}$ ($N(\tilde{\nu})=1$) and $m_{\tilde{\nu}} > 44.7 \text{ GeV}$ ($N(\tilde{\nu})=3$).

Some earlier papers are now obsolete and have been omitted. They were last listed in our PDG 14 edition: K. Olive, et al. (Particle Data Group), Chinese Physics **C38** 070001 (2014) (<http://pdg.lbl.gov>).

VALUE (GeV)	CL%	DOCUMENT ID	TECN	COMMENT
>3400	95	¹ AABOUD	18CM ATLS	RPV, $\tilde{\nu}_\tau \rightarrow e\mu$, $\lambda_{312} = \lambda_{321} = 0.07$, $\lambda'_{311} = 0.11$
>2900	95	² AABOUD	18CM ATLS	RPV, $\tilde{\nu}_\tau \rightarrow e\tau$, $\lambda_{313} = \lambda_{331} = 0.07$, $\lambda'_{311} = 0.11$
>2600	95	³ AABOUD	18CM ATLS	RPV, $\tilde{\nu}_\tau \rightarrow \mu\tau$, $\lambda_{323} = \lambda_{332} = 0.07$, $\lambda'_{311} = 0.11$
>1060	95	⁴ AABOUD	18Z ATLS	RPV, $\geq 4\ell$, $\lambda_{12k} \neq 0$, $m_{\tilde{\chi}_1^0} = 600 \text{ GeV}$ (mass-degenerate left-handed sleptons and sneutrinos of all 3 generations)
> 780	95	⁴ AABOUD	18Z ATLS	RPV, $\geq 4\ell$, $\lambda_{133} \neq 0$, $m_{\tilde{\chi}_1^0} = 300 \text{ GeV}$ (mass-degenerate left-handed sleptons and sneutrinos of all 3 generations)
>1700	95	⁵ SIRUNYAN	18AT CMS	RPV, $\tilde{\nu}_\tau \rightarrow e\mu$, $\lambda_{132} = \lambda_{231} = \lambda'_{311} = 0.01$
>3800	95	⁵ SIRUNYAN	18AT CMS	RPV, $\tilde{\nu}_\tau \rightarrow e\mu$, $\lambda_{132} = \lambda_{231} = \lambda'_{311} = 0.1$
>2300	95	⁶ AABOUD	16P ATLS	RPV, $\tilde{\nu}_\tau \rightarrow e\mu$, $\lambda'_{311} = 0.11$
>2200	95	⁶ AABOUD	16P ATLS	RPV, $\tilde{\nu}_\tau \rightarrow e\tau$, $\lambda_{311} = 0.11$
>1900	95	⁶ AABOUD	16P ATLS	RPV, $\tilde{\nu}_\tau \rightarrow \mu\tau$, $\lambda'_{311} = 0.11$
> 400	95	⁷ AAD	14X ATLS	RPV, $\geq 4\ell^{\pm}$, $\tilde{\nu} \rightarrow \nu\tilde{\chi}_1^0$, $\tilde{\chi}_1^0 \rightarrow \ell^{\pm} \ell^{\mp} \nu$
> 94	95	⁸ AAD	11Z ATLS	RPV, $\tilde{\nu}_\tau \rightarrow e\mu$
> 84	95	⁹ ABDALLAH	03M DLPH	$1 \leq \tan\beta \leq 40$, $m_{\tilde{e}_R} - m_{\tilde{\chi}_1^0} > 10 \text{ GeV}$
> 41	95	¹⁰ HEISTER	02N ALEP	$\tilde{\nu}_e$, any Δm
		¹¹ DECAMP	92 ALEP	$\Gamma(Z \rightarrow \text{invisible})$; $N(\tilde{\nu})=3$, model independent
••• We do not use the following data for averages, fits, limits, etc. •••				
>1280	95	¹² SIRUNYAN	19A0	RPV, $\mu^{\pm}\mu^{\pm} + \geq 2\text{jets}$, $\lambda'_{211} \neq 0$, $\tilde{\nu}_\mu \rightarrow \mu\tilde{\chi}_1^{\pm}$, $\tilde{\chi}_1^{\pm} \rightarrow \mu q\bar{q}q\bar{q}$
>2300	95	¹³ KHACHATRY...16BE	CMS	RPV, $\tilde{\nu}_\tau \rightarrow e\mu$, $\lambda_{132} = \lambda_{231} = \lambda_{311} = 0.01$
>2000	95	¹³ KHACHATRY...16BE	CMS	RPV, $\tilde{\nu}_\tau \rightarrow e\mu$, $\lambda_{132} = \lambda_{231} = 0.07$, $\lambda'_{311} = 0.11$
>1700	95	¹⁴ AAD	15O ATLS	RPV ($e\mu$), $\tilde{\nu}_\tau$, $\lambda'_{311} = 0.11$, $\lambda_{i3k} = 0.07$
		¹⁴ AAD	15O ATLS	RPV ($\tau\mu$, $e\tau$), $\tilde{\nu}_\tau$, $\lambda'_{311} = 0.11$, $\lambda_{i3k} = 0.07$
		¹⁵ AAD	13A1 ATLS	RPV, $\tilde{\nu}_\tau \rightarrow e\mu$, $e\tau$, $\mu\tau$
		¹⁶ AAD	11H ATLS	RPV, $\tilde{\nu}_\tau \rightarrow e\mu$
		¹⁷ AALTONEN	10Z CDF	RPV, $\tilde{\nu}_\tau \rightarrow e\mu$, $e\tau$, $\mu\tau$
		¹⁸ ABAZOV	10M D0	RPV, $\tilde{\nu}_\tau \rightarrow e\mu$
> 95	95	¹⁹ ABDALLAH	04H DLPH	AMSB, $\mu > 0$
> 37.1	95	²⁰ ADRIANI	93M L3	$\Gamma(Z \rightarrow \text{invisible})$; $N(\tilde{\nu})=1$
> 36	95	ABREU	91F DLPH	$\Gamma(Z \rightarrow \text{invisible})$; $N(\tilde{\nu})=1$
> 31.2	95	ALEXANDER	91F OPAL	$\Gamma(Z \rightarrow \text{invisible})$; $N(\tilde{\nu})=1$

¹ AABOUD 18CM searched in 36.1 fb^{-1} of pp collisions at $\sqrt{s} = 13 \text{ TeV}$ for heavy particles decaying into an $e\mu$, $e\tau$, $\mu\tau$ final state. No significant deviation from the expected SM background is observed. Limits are set on the mass of a stau neutrino with R-parity-violating couplings. For $\tilde{\nu}_\tau \rightarrow e\mu$, masses below 3.4 TeV are excluded at 95% CL, see their Figure 4(b). Upper limits on the RPV couplings $|\lambda_{312}|$ versus $|\lambda'_{311}|$ are also performed, see their Figure 8(a-b).

² AABOUD 18CM searched in 36.1 fb^{-1} of pp collisions at $\sqrt{s} = 13 \text{ TeV}$ for heavy particles decaying into an $e\mu$, $e\tau$, $\mu\tau$ final state. No significant deviation from the expected SM background is observed. Limits are set on the mass of a stau neutrino with R-parity-violating couplings. For $\tilde{\nu}_\tau \rightarrow e\tau$, masses below 2.9 TeV are excluded at 95% CL, see their Figure 5(b). Upper limits on the RPV couplings $|\lambda_{313}|$ versus $|\lambda'_{311}|$ are also performed, see their Figure 8(c).

³ AABOUD 18CM searched in 36.1 fb^{-1} of pp collisions at $\sqrt{s} = 13 \text{ TeV}$ for heavy particles decaying into an $e\mu$, $e\tau$, $\mu\tau$ final state. No significant deviation from the expected SM background is observed. Limits are set on the mass of a stau neutrino with R-parity-violating couplings. For $\tilde{\nu}_\tau \rightarrow \mu\tau$, masses below 2.6 TeV are excluded at 95% CL, see their Figure 6(b). Upper limits on the RPV couplings $|\lambda_{323}|$ versus $|\lambda'_{311}|$ are also performed, see their Figure 8(d).

Searches Particle Listings

Supersymmetric Particle Searches

- 4 AABOUD 18z searched in 36.1 fb^{-1} of pp collisions at $\sqrt{s} = 13 \text{ TeV}$ for events containing four or more charged leptons (electrons, muons and up to two hadronically decaying taus). No significant deviation from the expected SM background is observed. Limits are set on the Higgsino mass in simplified models of general gauge mediated supersymmetry Tn1nA/Tn1nB/Tn1nC, see their Figure 9. Limits are also set on the wino, slepton, sneutrino and gluino mass in a simplified model of NLSP pair production with R-parity violating decays of the LSP via λ_{12k} or λ_{133} to charged leptons, see their Figures 7, 8.
- 5 SIRUNYAN 18AT searched in 35.9 fb^{-1} of pp collisions at $\sqrt{s} = 13 \text{ TeV}$ for heavy resonances decaying into $e\mu$ final states. No significant excess above the Standard Model expectation is observed and 95% C.L. exclusions are placed on the cross section times branching ratio for the R-parity-violating production and decay of a supersymmetric tau sneutrino, see their Fig. 3.
- 6 AABOUD 16P searched in 3.2 fb^{-1} of pp collisions at $\sqrt{s} = 13 \text{ TeV}$ for events with different flavour dilepton pairs ($e\mu, e\tau, \mu\tau$) from the production of $\tilde{\nu}_\tau$ via an RPV λ'_{311} coupling and followed by a decay via $\lambda_{312} = \lambda_{321} = 0.07$ for $e + \mu$, via $\lambda_{313} = \lambda_{331} = 0.07$ for $e + \tau$ and via $\lambda_{323} = \lambda_{332} = 0.07$ for $\mu + \tau$. No evidence for a dilepton resonance over the SM expectation is observed, and limits are derived on $m_{\tilde{\nu}_\tau}$ at 95% CL, see their Figs. 2(b), 3(b), 4(b), and Table 3.
- 7 AAD 14X searched in 20.3 fb^{-1} of pp collisions at $\sqrt{s} = 8 \text{ TeV}$ for events with at least four leptons (electrons, muons, taus) in the final state. No significant excess above the Standard Model expectations is observed. Limits are set on the sneutrino mass in an R-parity violating simplified model where the decay $\tilde{\nu}_\tau \rightarrow \nu \tilde{\chi}_1^0$, with $\tilde{\chi}_1^0 \rightarrow \ell^\pm \ell^\mp \nu$, takes place with a branching ratio of 100%, see Fig. 9.
- 8 AAD 11z looked in 1.07 fb^{-1} of pp collisions at $\sqrt{s} = 7 \text{ TeV}$ for events with one electron and one muon of opposite charge from the production of $\tilde{\nu}_\tau$ via an RPV λ'_{311} coupling and followed by a decay via λ_{312} into $e + \mu$. No evidence for an (e, μ) resonance over the SM expectation is observed, and a limit is derived in the plane of λ'_{311} versus $m_{\tilde{\nu}_\tau}$ for three values of λ_{312} , see their Fig. 2. Masses $m_{\tilde{\nu}_\tau} < 1.32 (1.45) \text{ TeV}$ are excluded for $\lambda'_{311} = 0.10$ and $\lambda_{312} = 0.05 (\lambda'_{311} = 0.11 \text{ and } \lambda_{312} = 0.07)$.
- 9 ABDALLAH 03M uses data from $\sqrt{s} = 192\text{--}208 \text{ GeV}$ to obtain limits in the framework of the MSSM with gaugino and sfermion mass universality at the GUT scale. An indirect limit on the mass is derived by constraining the MSSM parameter space by the results from direct searches for neutralinos (including cascade decays) and for sleptons. These limits are valid for values of $M_2 < 1 \text{ TeV}$, $|\mu| \leq 1 \text{ TeV}$ with the $\tilde{\chi}_1^0$ as LSP. The quoted limit is obtained when there is no mixing in the third family. See Fig. 43 for the mass limits as a function of $\tan\beta$. These limits update the results of ABREU 00w.
- 10 HEISTER 02N derives a bound on $m_{\tilde{\nu}_e}$ by exploiting the mass relation between the $\tilde{\nu}_e$ and \tilde{e} , based on the assumption of universal GUT scale gaugino and scalar masses $m_{1/2}$ and m_0 and the search described in the \tilde{e} section. In the MSUGRA framework with radiative electroweak symmetry breaking, the limit improves to $m_{\tilde{\nu}_e} > 130 \text{ GeV}$, assuming a trilinear coupling $A_0=0$ at the GUT scale. See Figs. 5 and 7 for the dependence of the limits on $\tan\beta$.
- 11 DECAMP 22 limit is from $\Gamma(\text{invisible})/\Gamma(\ell\ell) = 5.91 \pm 0.15 (N_p = 2.97 \pm 0.07)$.
- 12 SIRUNYAN 19A0 searched in 35.9 fb^{-1} of pp collisions at $\sqrt{s} = 13 \text{ TeV}$ for events containing two same-sign muons and at last two jets, originating from resonant production of second-generation sleptons ($\tilde{\mu}_L, \tilde{\nu}_\mu$) via the R-parity violating coupling λ_{211} to quarks. No significant excess above the Standard Model expectations is observed. Upper limits on cross sections are derived in the context of two simplified models, see their Figure 4. The cross section limits are translated into limits on λ'_{211} for a modified CMSSM, see their Figure 5.
- 13 KHACHATRYAN 16BE searched in 19.7 fb^{-1} of pp collisions at $\sqrt{s} = 8 \text{ TeV}$ for evidence of narrow resonances decaying into $e\mu$ final states. No significant excess above the Standard Model expectation is observed and 95% C.L. exclusions are placed on the cross section times branching ratio for the production of an R-parity-violating supersymmetric tau sneutrino, see their Fig. 3.
- 14 AAD 15o searched in 20.3 fb^{-1} of pp collisions at $\sqrt{s} = 8 \text{ TeV}$ for evidence of heavy particles decaying into $e\mu, e\tau$ or $\mu\tau$ final states. No significant excess above the Standard Model expectation is observed, and 95% C.L. exclusions are placed on the cross section times branching ratio for the production of an R-parity-violating supersymmetric tau sneutrino, applicable to any sneutrino flavour, see their Fig. 2.
- 15 AAD 13AI searched in 4.6 fb^{-1} of pp collisions at $\sqrt{s} = 7 \text{ TeV}$ for evidence of heavy particles decaying into $e\mu, e\tau$ or $\mu\tau$ final states. No significant excess above the Standard Model expectation is observed, and 95% C.L. exclusions are placed on the cross section times branching ratio for the production of an R-parity-violating supersymmetric tau sneutrino, see their Fig. 2. For couplings $\lambda'_{311} = 0.10$ and $\lambda_{33k} = 0.05$, the lower limits on the $\tilde{\nu}_\tau$ mass are 1610, 1110, 1100 GeV in the $e\mu, e\tau$, and $\mu\tau$ channels, respectively.
- 16 AAD 11H looked in 35 pb^{-1} of pp collisions at $\sqrt{s} = 7 \text{ TeV}$ for events with one electron and one muon of opposite charge from the production of $\tilde{\nu}_\tau$ via an RPV λ'_{311} coupling and followed by a decay via λ_{312} into $e + \mu$. No evidence for an excess over the SM expectation is observed, and a limit is derived in the plane of λ'_{311} versus $m_{\tilde{\nu}_\tau}$ for several values of λ_{312} , see their Fig. 2. Superseded by AAD 11z.
- 17 AALTONEN 10Z searched in 1 fb^{-1} of $p\bar{p}$ collisions at $\sqrt{s} = 1.96 \text{ TeV}$ for events from the production $d\bar{d} \rightarrow \tilde{\nu}_\tau$ with the subsequent decays $\tilde{\nu}_\tau \rightarrow e\mu, \mu\tau, e\tau$ in the MSSM framework with RPV. Two isolated leptons of different flavor and opposite charges are required, with τ s identified by their hadronic decay. No statistically significant excesses are observed over the SM background. Upper limits on λ'_{311} times the branching ratio are listed in their Table III for various $\tilde{\nu}_\tau$ masses. Limits on the cross section times branching ratio for $\lambda'_{311} = 0.10$ and $\lambda_{33k} = 0.05$, displayed in Fig. 2, are used to set limits on the $\tilde{\nu}_\tau$ mass of 558 GeV for the $e\mu$, 441 GeV for the $\mu\tau$ and 442 GeV for the $e\tau$ channels.
- 18 ABZOV 10M looked in 5.3 fb^{-1} of $p\bar{p}$ collisions at $\sqrt{s} = 1.96 \text{ TeV}$ for events with exactly one pair of high p_T isolated $e\mu$ and a veto against hard jets. No evidence for an excess over the SM expectation is observed, and a limit at 95% C.L. on the cross section times branching ratio is derived, see their Fig. 3. These limits are translated into limits on couplings as a function of $m_{\tilde{\nu}_\tau}$ as shown on their Fig. 4. As an example, for $m_{\tilde{\nu}_\tau} = 100 \text{ GeV}$ and $\lambda_{312} \leq 0.07$, couplings $\lambda'_{311} > 7.7 \times 10^{-4}$ are excluded.
- 19 ABDALLAH 04H use data from LEP 1 and $\sqrt{s} = 192\text{--}208 \text{ GeV}$. They re-use results or re-analyze the data from ABDALLAH 03M to put limits on the parameter space of anomaly-mediated supersymmetry breaking (AMSB), which is scanned in the region $1 < m_{3/2} < 50 \text{ TeV}$, $0 < m_0 < 1000 \text{ GeV}$, $1.5 < \tan\beta < 35$, both signs of μ . The constraints

are obtained from the searches for mass degenerate chargino and neutralino, for SM-like and invisible Higgs, for leptonically decaying charginos and from the limit on non-SM Z width of 3.2 MeV. The limit is for $m_t = 174.3 \text{ GeV}$ (see Table 2 for other m_t values). The limit improves to 114 GeV for $\mu < 0$.

20 ADRIANI 93M limit from $\Delta\Gamma(Z)(\text{invisible}) < 16.2 \text{ MeV}$.

21 ALEXANDER 91F limit is for one species of $\tilde{\nu}$ and is derived from $\Gamma(\text{invisible, new})/\Gamma(\ell\ell) < 0.38$.

Charged sleptons

This section contains limits on charged scalar leptons ($\tilde{\ell}$, with $\ell=e, \mu, \tau$). Studies of width and decays of the Z boson (use is made here of $\Delta\Gamma_{\text{inv}} < 2.0 \text{ MeV}$, LEP 00) conclusively rule out $m_{\tilde{\ell}_R} < 40 \text{ GeV}$ (41 GeV for $\tilde{\ell}_L$), independently of decay modes, for each individual slepton. The limits improve to 43 GeV (43.5 GeV for $\tilde{\ell}_L$) assuming all 3 flavors to be degenerate. Limits on higher mass sleptons depend on model assumptions and on the mass splitting $\Delta m = m_{\tilde{\ell}} - m_{\tilde{\chi}_1^0}$. The mass and composition

of $\tilde{\chi}_1^0$ may affect the selectron production rate in e^+e^- collisions through t -channel exchange diagrams. Production rates are also affected by the potentially large mixing angle of the lightest mass eigenstate $\tilde{\ell}_1 = \tilde{\ell}_R \sin\theta_{\tilde{\ell}} + \tilde{\ell}_L \cos\theta_{\tilde{\ell}}$. It is generally assumed that only $\tilde{\tau}$ may have significant mixing. The coupling to the Z vanishes for $\theta_{\tilde{\ell}}=0.82$. In the high-energy limit of e^+e^- collisions the interference between γ and Z exchange leads to a minimal cross section for $\theta_{\tilde{\ell}}=0.91$, a value which is sometimes used in the following entries relative to data taken at LEP2. When limits on $m_{\tilde{\ell}_R}$ are quoted, it is understood that limits on $m_{\tilde{\ell}_L}$ are usually at least as strong.

Possibly open decays involving gauginos other than $\tilde{\chi}_1^0$ will affect the detection efficiencies. Unless otherwise stated, the limits presented here result from the study of $\tilde{\ell}^+\tilde{\ell}^-$ production, with production rates and decay properties derived from the MSSM. Limits made obsolete by the recent analyses of e^+e^- collisions at high energies can be found in previous Editions of this Review.

For decays with final state gravitinos (\tilde{G}), $m_{\tilde{G}}$ is assumed to be negligible relative to all other masses.

R-parity conserving \tilde{e} (Selectron) mass limit

Some earlier papers are now obsolete and have been omitted. They were last listed in our PDG 14 edition: K. Olive, et al. (Particle Data Group), Chinese Physics **C38** 070001 (2014) (<http://pdg.lbl.gov>).

VALUE (GeV)	CL%	DOCUMENT ID	TECN	COMMENT
>250	95	1 SIRUNYAN	19AW CMS	$\ell^\pm \ell^\mp + \cancel{E}_T, \tilde{e}_R, m_{\tilde{\chi}_1^0} = 0 \text{ GeV}$
>310	95	1 SIRUNYAN	19AW CMS	$\ell^\pm \ell^\mp + \cancel{E}_T, \tilde{e}_L, m_{\tilde{\chi}_1^0} = 0 \text{ GeV}$
>350	95	1 SIRUNYAN	19AW CMS	$\ell^\pm \ell^\mp + \cancel{E}_T, m_{\tilde{e}_R} = m_{\tilde{e}_L}, m_{\tilde{\chi}_1^0}$
>290	95	1 SIRUNYAN	19AW CMS	$\ell^\pm \ell^\mp + \cancel{E}_T, \tilde{e}_R, \tilde{e}_L$ and $\tilde{e} = \tilde{e}, \tilde{\mu}$, $m_{\tilde{\chi}_1^0} = 0 \text{ GeV}$
>400	95	1 SIRUNYAN	19AW CMS	$\ell^\pm \ell^\mp + \cancel{E}_T, \tilde{e}_L$ and $\tilde{e} = \tilde{e}, \tilde{\mu}, m_{\tilde{\chi}_1^0}$
>450	95	1 SIRUNYAN	19AW CMS	$\ell^\pm \ell^\mp + \cancel{E}_T, m_{\tilde{e}_R} = m_{\tilde{e}_L}$ and $\tilde{e} = \tilde{e}, \tilde{\mu}, m_{\tilde{\chi}_1^0} = 0 \text{ GeV}$
>500	95	2 AABOUD	18BT ATLS	$2\ell + \cancel{E}_T, m_{\tilde{e}_R} = m_{\tilde{e}_L}$ and $\tilde{e} = \tilde{e}, \tilde{\mu}, \tilde{\tau}$, with $m_{\tilde{\chi}_1^0} = 0 \text{ GeV}$
>190	95	3 AABOUD	18R ATLS	$2\ell(\text{soft}) + \cancel{E}_T, m_{\tilde{e}} = m_{\tilde{\mu}}, m_{\tilde{\tau}} = m_{\tilde{\nu}_\tau} = 5 \text{ GeV}$
		4 CHATRCHYAN14R	CMS	$\geq 3\ell^\pm, \tilde{\ell} \rightarrow \ell^\pm \tau^\mp \tau^\mp \tilde{G}$ simplified model, GMSB, stau (N)NLSP scenario
		5 AAD	13B ATLS	$2\ell^\pm + \cancel{E}_T, \text{SMS, pMSSM}$
> 97.5		6 ABBIENDI	04 OPAL	$\tilde{e}_R, \Delta m > 11 \text{ GeV}, \mu > 100 \text{ GeV}, \tan\beta=1.5$
> 94.4		7 ACHARD	04 L3	$\tilde{e}_R, \Delta m > 10 \text{ GeV}, \mu > 200 \text{ GeV}, \tan\beta \geq 2$
> 71.3		7 ACHARD	04 L3	\tilde{e}_R , all Δm
none 30–94	95	8 ABDALLAH	03M DLPH	$\Delta m > 15 \text{ GeV}, \tilde{e}_R^+ \tilde{e}_R^-$
> 94	95	9 ABDALLAH	03M DLPH	$\tilde{e}_R, 1 \leq \tan\beta \leq 40, \Delta m > 10 \text{ GeV}$
> 95	95	10 HEISTER	02E ALEP	$\Delta m > 15 \text{ GeV}, \tilde{e}_R^+ \tilde{e}_R^-$
> 73	95	11 HEISTER	02N ALEP	\tilde{e}_R , any Δm
>107	95	11 HEISTER	02N ALEP	\tilde{e}_L , any Δm
none 90–325	95	12 AAD	14G ATLS	$\tilde{\ell}\tilde{\ell} \rightarrow \ell^+ \tilde{\chi}_1^0 \ell^- \tilde{\chi}_1^0$, simplified model, $m_{\tilde{\ell}_L} = m_{\tilde{e}_R}, m_{\tilde{\chi}_1^0} = 0 \text{ GeV}$
		13 KHACHATRY..14I	CMS	$\tilde{\ell} \rightarrow \ell \tilde{\chi}_1^0$, simplified model

1 SIRUNYAN 19AW searched in 35.9 fb^{-1} of pp collisions at $\sqrt{s} = 13 \text{ TeV}$ for direct electroweak pair production of selectrons or smuons in events with two leptons (electrons or muons) of the opposite electric charge and same flavour, no jets and large \cancel{E}_T . No significant excess above the Standard Model expectations is observed. Limits are set on the selectron mass assuming left-handed, right-handed or both left- and right-handed (mass degenerate) production, see their Figure 6. Similarly, limits are set on the smuon mass, see their Figure 7. Limits are also set on slepton masses under the assumption that the selectron and smuon are mass degenerate, see their Figure 5.

- 2 AABOUD 18B searched in 36.1 fb^{-1} of pp collisions at $\sqrt{s} = 13 \text{ TeV}$ for direct electroweak production of charginos, chargino and next-to-lightest neutralinos and sleptons in events with two or three leptons (electrons or muons), with or without jets, and large missing transverse energy. No significant excess above the Standard Model expectations is observed. Limits are set on the slepton mass up to 500 GeV for massless $\tilde{\chi}_1^0$, assuming degeneracy of \tilde{e} , $\tilde{\mu}$, and $\tilde{\tau}$ and exploiting the 2ℓ signature, see their Figure 8(b).
- 3 AABOUD 18R searched in 36.1 fb^{-1} of pp collisions at $\sqrt{s} = 13 \text{ TeV}$ for electroweak production in scenarios with compressed mass spectra in final states with two low-momentum leptons and missing transverse momentum. The data are found to be consistent with the SM prediction. Results are interpreted in slepton pair production models with a fourfold degeneracy assumed in selectron and smuon masses. The \tilde{e} masses are excluded up to 190 GeV for $m_{\tilde{e}} - m_{\tilde{\chi}_1^0} = 5 \text{ GeV}$. The exclusion limits extend down to mass splittings of 1 GeV, see their Fig. 11.
- 4 CHATRCHYAN 14R searched in 19.5 fb^{-1} of pp collisions at $\sqrt{s} = 8 \text{ TeV}$ for events with at least three leptons (electrons, muons, taus) in the final state. No significant excess above the Standard Model expectations is observed. Limits are set on the slepton mass in a stau (N)NLSF simplified model (GMSB) where the decay $\tilde{e} \rightarrow e^\pm \tau^\pm \mp \tilde{G}$ takes place with a branching ratio of 100%, see Fig. 8.
- 5 AAD 13B searched in 4.7 fb^{-1} of pp collisions at $\sqrt{s} = 7 \text{ TeV}$ for sleptons decaying to a final state with two leptons (e and μ) and missing transverse energy. No excess beyond the Standard Model expectation is observed. Limits are derived in a simplified model of direct left-handed slepton pair production, where left-handed slepton masses between 85 and 195 GeV are excluded at 95% C.L. for $m_{\tilde{\chi}_1^0} = 20 \text{ GeV}$. See also Fig. 2(a). Exclusion limits are also derived in the phenomenological MSSM, see Fig. 3.
- 6 ABBIENDI 04 search for $\tilde{e}_R \tilde{e}_R$ production in acoplanar di-electron final states in the 183–208 GeV data. See Fig. 13 for the dependence of the limits on $m_{\tilde{\chi}_1^0}$ and for the limit at $\tan\beta=35$. This limit supersedes ABBIENDI 00g.
- 7 ACHARD 04 search for $\tilde{e}_R \tilde{e}_L$ and $\tilde{e}_R \tilde{e}_R$ production in single- and acoplanar di-electron final states in the 192–209 GeV data. Absolute limits on $m_{\tilde{e}_R}$ are derived from a scan over the MSSM parameter space with universal GUT scale gaugino and scalar masses $m_{1/2}$ and m_0 , $1 \leq \tan\beta \leq 60$ and $-2 \leq \mu \leq 2 \text{ TeV}$. See Fig. 4 for the dependence of the limits on $m_{\tilde{\chi}_1^0}$. This limit supersedes ACCIARRI 99w.
- 8 ABDALLAH 03M looked for acoplanar dielectron + \cancel{E}_T final states at $\sqrt{s} = 189\text{--}208 \text{ GeV}$. The limit assumes $\mu = -200 \text{ GeV}$ and $\tan\beta = 1.5$ in the calculation of the production cross section and $B(\tilde{e} \rightarrow e \tilde{\chi}_1^0) = 1$. See Fig. 15 for limits in the $(m_{\tilde{e}_R}, m_{\tilde{\chi}_1^0})$ plane. These limits include and update the results of ABREU 01.
- 9 ABDALLAH 03M uses data from $\sqrt{s} = 192\text{--}208 \text{ GeV}$ to obtain limits in the framework of the MSSM with gaugino and sfermion mass universality at the GUT scale. An indirect limit on the mass is derived by constraining the MSSM parameter space by the results from direct searches for neutralinos (including cascade decays) and for sleptons. These limits are valid for values of $M_2 < 1 \text{ TeV}$, $|\mu| \leq 1 \text{ TeV}$ with the $\tilde{\chi}_1^0$ as LSP. The quoted limit is obtained when there is no mixing in the third family. See Fig. 43 for the mass limits as a function of $\tan\beta$. These limits update the results of ABREU 00w.
- 10 HEISTER 02E looked for acoplanar dielectron + \cancel{E}_T final states from e^+e^- interactions between 183 and 209 GeV. The mass limit assumes $\mu < -200 \text{ GeV}$ and $\tan\beta = 2$ for the production cross section and $B(\tilde{e} \rightarrow e \tilde{\chi}_1^0) = 1$. See their Fig. 4 for the dependence of the limit on Δm . These limits include and update the results of BARATE 01.
- 11 HEISTER 02N search for $\tilde{e}_R \tilde{e}_L$ and $\tilde{e}_R \tilde{e}_R$ production in single- and acoplanar di-electron final states in the 183–208 GeV data. Absolute limits on $m_{\tilde{e}_R}$ are derived from a scan over the MSSM parameter space with universal GUT scale gaugino and scalar masses $m_{1/2}$ and m_0 , $1 \leq \tan\beta \leq 50$ and $-10 \leq \mu \leq 10 \text{ TeV}$. The region of small $|\mu|$, where cascade decays are important, is covered by a search for $\tilde{\chi}_1^0 \tilde{\chi}_3^0$ in final states with leptons and possibly photons. Limits on $m_{\tilde{e}_L}$ are derived by exploiting the mass relation between the \tilde{e}_L and \tilde{e}_R , based on universal m_0 and $m_{1/2}$. When the constraint from the mass limit of the lightest Higgs from HEISTER 02 is included, the bounds improve to $m_{\tilde{e}_R} > 77(75) \text{ GeV}$ and $m_{\tilde{e}_L} > 115(115) \text{ GeV}$ for a top mass of 175(180) GeV. In the MSUGRA framework with radiative electroweak symmetry breaking, the limits improve further to $m_{\tilde{e}_R} > 95 \text{ GeV}$ and $m_{\tilde{e}_L} > 152 \text{ GeV}$, assuming a trilinear coupling $A_0 = 0$ at the GUT scale. See Figs. 4, 5, 7 for the dependence of the limits on $\tan\beta$.
- 12 AAD 14G searched in 20.3 fb^{-1} of pp collisions at $\sqrt{s} = 8 \text{ TeV}$ for electroweak production of slepton pairs, decaying to a final state with two leptons (e and μ) and missing transverse momentum. No excess beyond the Standard Model expectation is observed. Exclusion limits are derived in simplified models of slepton pair production, see Fig. 8. An interpretation in the pMSSM is also given, see Fig. 10.
- 13 KHACHATRYAN 14I searched in 19.5 fb^{-1} of pp collisions at $\sqrt{s} = 8 \text{ TeV}$ for electroweak production of slepton pairs decaying to a final state with opposite-sign lepton pairs (e or μ) and missing transverse momentum. No excess beyond the Standard Model expectation is observed. Exclusion limits are derived in simplified models, see Fig. 18.

R-parity violating \tilde{e} (Selectron) mass limit

Some earlier papers are now obsolete and have been omitted. They were last listed in our PDG 14 edition: K. Olive, et al. (Particle Data Group), Chinese Physics **C38** 070001 (2014) (<http://pdg.lbl.gov>).

VALUE (GeV)	CL%	DOCUMENT ID	TECN	COMMENT
>1065	95	1 AABOUD	18Z ATLS	$\geq 4\ell, \lambda_{12k} \neq 0, m_{\tilde{\chi}_1^0} = 600 \text{ GeV}$ (mass-degenerate left-handed sleptons and sneutrinos of all 3 generations)
> 780	95	1 AABOUD	18Z ATLS	$\geq 4\ell, \lambda_{133} \neq 0, m_{\tilde{\chi}_1^0} = 300 \text{ GeV}$ (mass-degenerate left-handed sleptons and sneutrinos of all 3 generations)
> 410	95	2 AAD	14X ATLS	RPV, $\geq 4\ell^\pm, \tilde{e} \rightarrow \ell^\pm \tilde{\chi}_1^0, \tilde{\chi}_1^0 \rightarrow \ell^\pm \ell^\mp \nu$
••• We do not use the following data for averages, fits, limits, etc. •••				
> 89	95	3 ABBIENDI	04F OPAL	RPV, \tilde{e}_L
> 92	95	4 ABDALLAH	04M DLPH	RPV, \tilde{e}_R , indirect, $\Delta m > 5 \text{ GeV}$

- 1 AABOUD 18Z searched in 36.1 fb^{-1} of pp collisions at $\sqrt{s} = 13 \text{ TeV}$ for events containing four or more charged leptons (electrons, muons and up to two hadronically decaying taus). No significant deviation from the expected SM background is observed. Limits are set on the Higgsino mass in simplified models of general gauge mediated supersymmetry Tn1nA/Tn1nB/Tn1nC, see their Figure 9. Limits are also set on the wino, slepton, sneutrino and gluino mass in a simplified model of NLSF pair production with R-parity violating decays of the LSP via λ_{12k} or λ_{133} to charged leptons, see their Figures 7, 8.
- 2 AAD 14X searched in 20.3 fb^{-1} of pp collisions at $\sqrt{s} = 8 \text{ TeV}$ for events with at least four leptons (electrons, muons, taus) in the final state. No significant excess above the Standard Model expectations is observed. Limits are set on the slepton mass in an R-parity violating simplified model where the decay $\tilde{e} \rightarrow \ell \tilde{\chi}_1^0$, with $\tilde{\chi}_1^0 \rightarrow \ell^\pm \ell^\mp \nu$, takes place with a branching ratio of 100%, see Fig. 9.
- 3 ABBIENDI 04F use data from $\sqrt{s} = 189\text{--}209 \text{ GeV}$. They derive limits on sparticle masses under the assumption of RPV with $LL\tilde{E}$ or $LQ\tilde{D}$ couplings. The results are valid for $\tan\beta = 1.5$, $\mu = -200 \text{ GeV}$, with, in addition, $\Delta m > 5 \text{ GeV}$ for indirect decays via $LQ\tilde{D}$. The limit quoted applies to direct decays via $LL\tilde{E}$ or $LQ\tilde{D}$ couplings. For indirect decays, the limits on the \tilde{e}_R mass are respectively 99 and 92 GeV for $LL\tilde{E}$ and $LQ\tilde{D}$ couplings and $m_{\tilde{\chi}_1^0} = 10 \text{ GeV}$ and degrade slightly for larger $\tilde{\chi}_1^0$ mass. Supersedes the results of ABBIENDI 00.
- 4 ABDALLAH 04M use data from $\sqrt{s} = 192\text{--}208 \text{ GeV}$ to derive limits on sparticle masses under the assumption of RPV with $LL\tilde{E}$ or $U\tilde{D}\tilde{D}$ couplings. The results are valid for $\mu = -200 \text{ GeV}$, $\tan\beta = 1.5$, $\Delta m > 5 \text{ GeV}$ and assuming a BR of 1 for the given decay. The limit quoted is for indirect $U\tilde{D}\tilde{D}$ decays using the neutralino constraint of 39.5 GeV for $LL\tilde{E}$ and of 38.0 GeV for $U\tilde{D}\tilde{D}$ couplings, also derived in ABDALLAH 04M. For indirect decays via $LL\tilde{E}$ the limit improves to 95 GeV if the constraint from the neutralino is used and to 94 GeV if it is not used. For indirect decays via $U\tilde{D}\tilde{D}$ couplings it remains unchanged when the neutralino constraint is not used. Supersedes the result of ABREU 00u.

R-parity conserving $\tilde{\mu}$ (Smuon) mass limit

VALUE (GeV)	CL%	DOCUMENT ID	TECN	COMMENT
>210	95	1 SIRUNYAN	19AW CMS	$\ell^\pm \ell^\mp + \cancel{E}_T, \tilde{\mu}_R, m_{\tilde{\chi}_1^0} = 0 \text{ GeV}$
>280	95	1 SIRUNYAN	19AW CMS	$\ell^\pm \ell^\mp + \cancel{E}_T, \tilde{\mu}_L, m_{\tilde{\chi}_1^0} = 0 \text{ GeV}$
>290	95	1 SIRUNYAN	19AW CMS	$\ell^\pm \ell^\mp + \cancel{E}_T, \tilde{\mu}_R$ and $\tilde{e} = \tilde{e}, \tilde{\mu}, m_{\tilde{\chi}_1^0} = 0 \text{ GeV}$
>400	95	1 SIRUNYAN	19AW CMS	$\ell^\pm \ell^\mp + \cancel{E}_T, \tilde{\mu}_L$ and $\tilde{e} = \tilde{e}, \tilde{\mu}, m_{\tilde{\chi}_1^0} = 0 \text{ GeV}$
>450	95	1 SIRUNYAN	19AW CMS	$\ell^\pm \ell^\mp + \cancel{E}_T, m_{\tilde{e}_R} = m_{\tilde{e}_L}$ and $\tilde{e} = \tilde{e}, \tilde{\mu}, m_{\tilde{\chi}_1^0} = 0 \text{ GeV}$
>310	95	1 SIRUNYAN	19AW CMS	$\ell^\pm \ell^\mp + \cancel{E}_T, m_{\tilde{\mu}_R} = m_{\tilde{\mu}_L}, m_{\tilde{\chi}_1^0} = 0 \text{ GeV}$
>190	95	2 AABOUD	18R ATLS	2ℓ (soft) + $\cancel{E}_T, m_{\tilde{e}} = m_{\tilde{\mu}}, m_{\tilde{\mu}} - m_{\tilde{\chi}_1^0} = 5 \text{ GeV}$
		3 CHATRCHYAN 14R	CMS	$\geq 3\ell^\pm, \tilde{e} \rightarrow \ell^\pm \tau^\pm \mp \tilde{G}$ simplified model, GMSB, stau (N)NLSF scenario
		4 AAD	13B ATLS	$2\ell^\pm + \cancel{E}_T, \text{SMS, pMSSM}$
> 91.0		5 ABBIENDI	04 OPAL	$\Delta m > 3 \text{ GeV}, \tilde{\mu}_R^+ \tilde{\mu}_R, \mu > 100 \text{ GeV}, \tan\beta = 1.5$
> 86.7		6 ACHARD	04 L3	$\Delta m > 10 \text{ GeV}, \tilde{\mu}_R^+ \tilde{\mu}_R, \mu > 200 \text{ GeV}, \tan\beta \geq 2$
none 30–88	95	7 ABDALLAH	03M DLPH	$\Delta m > 5 \text{ GeV}, \tilde{\mu}_R^+ \tilde{\mu}_R$
> 94	95	8 ABDALLAH	03M DLPH	$\tilde{\mu}_R, 1 \leq \tan\beta \leq 40, \Delta m > 10 \text{ GeV}$
> 88	95	9 HEISTER	02E ALEP	$\Delta m > 15 \text{ GeV}, \tilde{\mu}_R^+ \tilde{\mu}_R$
••• We do not use the following data for averages, fits, limits, etc. •••				
>500	95	10 AABOUD	18BT ATLS	$2\ell + \cancel{E}_T, m_{\tilde{e}_R} = m_{\tilde{e}_L}$ and $\tilde{e} = \tilde{e}, \tilde{\mu}, \tilde{\tau}$, with $m_{\tilde{\chi}_1^0} = 0 \text{ GeV}$
none 90–325	95	11 AAD	14G ATLS	$\tilde{e}\tilde{e} \rightarrow \ell^+ \tilde{\chi}_1^0 \ell^- \tilde{\chi}_1^0$, simplified model, $m_{\tilde{e}_L} = m_{\tilde{e}_R}, m_{\tilde{\chi}_1^0} = 0 \text{ GeV}$
		12 KHACHATRYAN 14I	CMS	$\tilde{e} \rightarrow \ell \tilde{\chi}_1^0$, simplified model
> 80	95	13 ABREU	00V DLPH	$\tilde{\mu}_R \tilde{\mu}_R (\tilde{\mu}_R \rightarrow \mu \tilde{G}), m_{\tilde{G}} > 8 \text{ eV}$

- 1 SIRUNYAN 19AW searched in 35.9 fb^{-1} of pp collisions at $\sqrt{s} = 13 \text{ TeV}$ for direct electroweak pair production of selectrons or smuons in events with two leptons (electrons or muons) of the opposite electric charge and same flavour, no jets and large \cancel{E}_T . No significant excess above the Standard Model expectations is observed. Limits are set on the selectron mass assuming left-handed, right-handed or both left- and right-handed (mass degenerate) production, see their Figure 6. Similarly, limits are set on the smuon mass, see their Figure 7. Limits are also set on slepton masses under the assumption that the selectron and smuon are mass degenerate, see their Figure 5.
- 2 AABOUD 18R searched in 36.1 fb^{-1} of pp collisions at $\sqrt{s} = 13 \text{ TeV}$ for electroweak production in scenarios with compressed mass spectra in final states with two low-momentum leptons and missing transverse momentum. The data are found to be consistent with the SM prediction. Results are interpreted in slepton pair production models with a fourfold degeneracy assumed in selectron and smuon masses. The $\tilde{\mu}$ masses are excluded up to 190 GeV for $m_{\tilde{\mu}} - m_{\tilde{\chi}_1^0} = 5 \text{ GeV}$. The exclusion limits extend down to mass splittings of 1 GeV, see their Fig. 11.
- 3 CHATRCHYAN 14R searched in 19.5 fb^{-1} of pp collisions at $\sqrt{s} = 8 \text{ TeV}$ for events with at least three leptons (electrons, muons, taus) in the final state. No significant excess above the Standard Model expectations is observed. Limits are set on the slepton mass in a stau (N)NLSF simplified model (GMSB) where the decay $\tilde{e} \rightarrow \ell^\pm \tau^\pm \mp \tilde{G}$ takes place with a branching ratio of 100%, see Fig. 8.
- 4 AAD 13B searched in 4.7 fb^{-1} of pp collisions at $\sqrt{s} = 7 \text{ TeV}$ for sleptons decaying to a final state with two leptons (e and μ) and missing transverse energy. No excess beyond

Searches Particle Listings

Supersymmetric Particle Searches

the Standard Model expectation is observed. Limits are derived in a simplified model of direct left-handed slepton pair production, where left-handed slepton masses between 85 and 195 GeV are excluded at 95% C.L. for $m_{\tilde{\chi}_1^0} = 20$ GeV. See also Fig. 2(a). Exclusion limits are also derived in the phenomenological MSSM, see Fig. 3.

- ⁵ ABBIENDI 04 search for $\tilde{\mu}_R \tilde{\mu}_R$ production in acoplanar di-muon final states in the 183–208 GeV data. See Fig. 14 for the dependence of the limits on $m_{\tilde{\chi}_1^0}$ and for the limit at $\tan\beta=35$. Under the assumption of 100% branching ratio for $\tilde{\mu}_R \rightarrow \mu \tilde{\chi}_1^0$, the limit improves to 94.0 GeV for $\Delta m > 4$ GeV. See Fig. 11 for the dependence of the limits on $m_{\tilde{\chi}_1^0}$ at several values of the branching ratio. This limit supersedes ABBIENDI 00G.
- ⁶ ACHARD 04 search for $\tilde{\mu}_R \tilde{\mu}_R$ production in acoplanar di-muon final states in the 192–209 GeV data. Limits on $m_{\tilde{\mu}_R}$ are derived from a scan over the MSSM parameter space with universal GUT scale gaugino and scalar masses $m_{1/2}$ and m_0 , $1 \leq \tan\beta \leq 60$ and $-2 \leq \mu \leq 2$ TeV. See Fig. 4 for the dependence of the limits on $m_{\tilde{\chi}_1^0}$. This limit supersedes ACCIARRI 99W.
- ⁷ ABDALLAH 03M looked for acoplanar dimuon + \cancel{E} final states at $\sqrt{s} = 189$ –208 GeV. The limit assumes $B(\tilde{\mu} \rightarrow \mu \tilde{\chi}_1^0) = 100\%$. See Fig. 16 for limits on the $(m_{\tilde{\mu}_R}, m_{\tilde{\chi}_1^0})$ plane. These limits include and update the results of ABREU 01.
- ⁸ ABDALLAH 03M uses data from $\sqrt{s} = 192$ –208 GeV to obtain limits in the framework of the MSSM with gaugino and sfermion mass universality at the GUT scale. An indirect limit on the mass is derived by constraining the MSSM parameter space by the results from direct searches for neutralinos (including cascade decays) and for sleptons. These limits are valid for values of $M_2 < 1$ TeV, $|\mu| \leq 1$ TeV with the $\tilde{\chi}_1^0$ as LSP. The quoted limit is obtained when there is no mixing in the third family. See Fig. 43 for the mass limits as a function of $\tan\beta$. These limits update the results of ABREU 00W.
- ⁹ HEISTER 02E looked for acoplanar dimuon + \cancel{E}_T final states from e^+e^- interactions between 183 and 209 GeV. The mass limit assumes $B(\tilde{\mu} \rightarrow \mu \tilde{\chi}_1^0) = 1$. See their Fig. 4 for the dependence of the limit on Δm . These limits include and update the results of BARATE 01.
- ¹⁰ AABOUD 18BT searched in 36.1 fb^{-1} of pp collisions at $\sqrt{s} = 13$ TeV for direct electroweak production of charginos, chargino and next-to-lightest neutralinos and sleptons in events with two or three leptons (electrons or muons), with or without jets, and large missing transverse energy. No significant excess above the Standard Model expectations is observed. Limits are set on the slepton mass up to 500 GeV for massless $\tilde{\chi}_1^0$, assuming degeneracy of \tilde{e} , $\tilde{\mu}$, and $\tilde{\tau}$ and exploiting the 2ℓ signature, see their Figure 8(b).
- ¹¹ AAD 14G searched in 20.3 fb^{-1} of pp collisions at $\sqrt{s} = 8$ TeV for electroweak production of slepton pairs, decaying to a final state with two leptons (e and μ) and missing transverse momentum. No excess beyond the Standard Model expectation is observed. Exclusion limits are derived in simplified models of slepton pair production, see Fig. 8. An interpretation in the pMSSM is also given, see Fig. 10.
- ¹² KHACHATRYAN 14I searched in 19.5 fb^{-1} of pp collisions at $\sqrt{s} = 8$ TeV for electroweak production of slepton pairs decaying to a final state with opposite-sign lepton pairs (e or μ) and missing transverse momentum. No excess beyond the Standard Model expectation is observed. Exclusion limits are derived in simplified models, see Fig. 18.
- ¹³ ABREU 00V use data from $\sqrt{s} = 130$ –189 GeV to search for tracks with large impact parameter or visible decay vertices. Limits are obtained as function of $m_{\tilde{G}}$, after combining these results with the search for slepton pair production in the SUGRA framework from ABREU 01 to cover prompt decays and on stable particle searches from ABREU 00Q. For limits at different $m_{\tilde{G}}$, see their Fig. 12.

R-parity violating $\tilde{\mu}$ (Smuon) mass limit

VALUE (GeV)	CL%	DOCUMENT ID	TECN	COMMENT
> 780	95	¹ AABOUD 18Z ATLS		$\geq 4\ell, \lambda_{133} \neq 0, m_{\tilde{\chi}_1^0} = 300$ GeV (mass-degenerate left-handed sleptons and sneutrinos of all 3 generations)
>1060	95	¹ AABOUD 18Z ATLS		$\geq 4\ell, \lambda_{12k} \neq 0, m_{\tilde{\chi}_1^0} = 600$ GeV (mass-degenerate left-handed sleptons and sneutrinos of all 3 generations)
> 410	95	² AAD 14X ATLS		RPV, $\geq 4\ell^{\pm}, \tilde{\ell} \rightarrow \ell \tilde{\chi}_1^0, \tilde{\chi}_1^0 \rightarrow \ell^{\pm} \tilde{\ell} \nu$ limits, etc. ●●●
		³ SIRUNYAN 19AO		$\mu^{\pm} \mu^{\pm} + \geq 2\text{jets}, \lambda'_{211} \neq 0, \tilde{\mu}_L \rightarrow \mu \tilde{\chi}_1^0, \tilde{\chi}_1^0 \rightarrow \mu q \bar{q}$
> 87	95	⁴ ABDALLAH 04M DLPH		RPV, $\tilde{\mu}_R$, indirect, $\Delta m > 5$ GeV
> 81	95	⁵ HEISTER 03G ALEP		RPV, $\tilde{\mu}_L$

- ¹ AABOUD 18Z searched in 36.1 fb^{-1} of pp collisions at $\sqrt{s} = 13$ TeV for events containing four or more charged leptons (electrons, muons and up to two hadronically decaying taus). No significant deviation from the expected SM background is observed. Limits are set on the Higgsino mass in simplified models of general gauge mediated supersymmetry Tn1n1A/Tn1n1B/Tn1n1C, see their Figure 9. Limits are also set on the wino, slepton, sneutrino and gluino mass in a simplified model of NLSP pair production with R-parity violating decays of the LSP via λ_{12k} or λ_{133} to charged leptons, see their Figures 7, 8.
- ² AAD 14X searched in 20.3 fb^{-1} of pp collisions at $\sqrt{s} = 8$ TeV for events with at least four leptons (electrons, muons, taus) in the final state. No significant excess above the Standard Model expectations is observed. Limits are set on the slepton mass in an R-parity violating simplified model where the decay $\tilde{\ell} \rightarrow \ell \tilde{\chi}_1^0$, with $\tilde{\chi}_1^0 \rightarrow \ell^{\pm} \tilde{\ell} \nu$, takes place with a branching ratio of 100%, see Fig. 9.
- ³ SIRUNYAN 19AO searched in 35.9 fb^{-1} of pp collisions at $\sqrt{s} = 13$ TeV for events containing two same-sign muons and at least two jets, originating from resonant production of second-generation sleptons ($\tilde{\mu}_L, \tilde{\nu}_\mu$) via the R-parity violating coupling λ'_{211} to quarks. No significant excess above the Standard Model expectations is observed. Upper limits on cross sections are derived in the context of two simplified models, see their Figure 4. The cross section limits are translated into limits on λ'_{211} for a modified CMSSM, see their Figure 5.
- ⁴ ABDALLAH 04M use data from $\sqrt{s} = 192$ –208 GeV to derive limits on sparticle masses under the assumption of RPV with $L\tilde{L}\tilde{E}$ or $\tilde{U}\tilde{D}\tilde{D}$ couplings. The results are valid for μ

$= -200$ GeV, $\tan\beta = 1.5$, $\Delta m \geq 5$ GeV and assuming a BR of 1 for the given decay. The limit quoted is for indirect $\tilde{U}\tilde{D}\tilde{D}$ decays using the neutralino constraint of 39.5 GeV for $L\tilde{L}\tilde{E}$ and of 38.0 GeV for $\tilde{U}\tilde{D}\tilde{D}$ couplings, also derived in ABDALLAH 04M. For indirect decays via $L\tilde{L}\tilde{E}$ the limit improves to 90 GeV if the constraint from the neutralino is used and remains at 87 GeV if it is not used. For indirect decays via $\tilde{U}\tilde{D}\tilde{D}$ couplings it degrades to 85 GeV when the neutralino constraint is not used. Supersedes the result of ABREU 00U.

- ⁵ HEISTER 03G searches for the production of smuons in the case of RPV prompt decays with $L\tilde{L}\tilde{E}$, $L\tilde{Q}\tilde{D}$ or $\tilde{U}\tilde{D}\tilde{D}$ couplings at $\sqrt{s} = 189$ –209 GeV. The search is performed for direct and indirect decays, assuming one coupling at a time to be non-zero. The limit holds for direct decays mediated by RPV $L\tilde{Q}\tilde{D}$ couplings and improves to 90 GeV for indirect decays (for $\Delta m > 10$ GeV). Limits are also given for $L\tilde{L}\tilde{E}$ direct ($m_{\tilde{\mu}_R} > 87$ GeV) and indirect decays ($m_{\tilde{\mu}_R} > 96$ GeV for $m(\tilde{\chi}_1^0) > 23$ GeV from BARATE 98s) and for $\tilde{U}\tilde{D}\tilde{D}$ indirect decays ($m_{\tilde{\mu}_R} > 85$ GeV for $\Delta m > 10$ GeV). Supersedes the results from BARATE 01B.

R-parity conserving $\tilde{\tau}$ (Stau) mass limit

Some earlier papers are now obsolete and have been omitted. They were last listed in our PDG 14 edition: K. Olive, *et al.* (Particle Data Group), Chinese Physics **C38** 070001 (2014) (<http://pdg.lbl.gov>).

VALUE (GeV)	CL%	DOCUMENT ID	TECN	COMMENT
> 85.2		¹ ABBIENDI 04	OPAL	$\Delta m > 6$ GeV, $\theta_r = \pi/2, \mu > 100$ GeV, $\tan\beta = 1.5$
> 78.3		² ACHARD 04	L3	$\Delta m > 15$ GeV, $\theta_r = \pi/2, \mu > 200$ GeV, $\tan\beta \geq 2$
> 81.9	95	³ ABDALLAH 03M DLPH		$\Delta m > 15$ GeV, all θ_T
> 79	95	⁴ HEISTER 02E ALEP		$\Delta m > 15$ GeV, $\theta_r = \pi/2$
> 76	95	⁴ HEISTER 02E ALEP		$\Delta m > 15$ GeV, $\theta_r = 0.91$
●●●		We do not use the following data for averages, fits, limits, etc. ●●●		
>500	95	⁵ AABOUD 18BT ATLS		$2\ell + \cancel{E}_T, m_{\tilde{\tau}_R} = m_{\tilde{\tau}_L}, \tilde{\ell} = \tilde{e}, \tilde{\mu}, \tilde{\tau}, m_{\tilde{\chi}_1^0} = 0$ GeV
none 109	95	⁶ KHACHATRYAN 17L CMS		$2\tau + \cancel{E}_T, \tilde{\tau}_L \rightarrow \tau \tilde{\chi}_1^0, m_{\tilde{\chi}_1^0} = 0$ GeV
none 109	95	⁷ AAD 16AA ATLS		2 hadronic $\tau + \cancel{E}_T, \tilde{\tau}_{R/L} \rightarrow \tau \tilde{\chi}_1^0, m_{\tilde{\chi}_1^0} = 0$ GeV
		⁸ AAD 12AF ATLS		$2\tau + \text{jets} + \cancel{E}_T, \text{GMSB}$
		⁹ AAD 12AG ATLS		$\geq 1\tau_h + \text{jets} + \cancel{E}_T, \text{GMSB}$
		¹⁰ AAD 12CM ATLS		$\geq 1\tau + \text{jets} + \cancel{E}_T, \text{GMSB}$
> 87.4	95	¹¹ ABBIENDI 06B OPAL		$\tilde{\tau}_R \rightarrow \tau \tilde{G}, \text{all } \tau(\tilde{\tau}_R)$
> 68	95	¹² ABDALLAH 04H DLPH		AMSB, $\mu > 0$
none $m_{\tilde{\tau}} = 26.3$	95	³ ABDALLAH 03M DLPH		$\Delta m > m_{\tilde{\tau}}, \text{all } \theta_T$

- ¹ ABBIENDI 04 search for $\tilde{\tau}\tilde{\tau}$ production in acoplanar di-tau final states in the 183–208 GeV data. See Fig. 15 for the dependence of the limits on $m_{\tilde{\chi}_1^0}$ and for the limit

at $\tan\beta=35$. Under the assumption of 100% branching ratio for $\tilde{\tau}_R \rightarrow \tau \tilde{\chi}_1^0$, the limit improves to 89.8 GeV for $\Delta m > 8$ GeV. See Fig. 12 for the dependence of the limits on $m_{\tilde{\chi}_1^0}$ at several values of the branching ratio and for their dependence on θ_r . This limit supersedes ABBIENDI 00G.

- ² ACHARD 04 search for $\tilde{\tau}\tilde{\tau}$ production in acoplanar di-tau final states in the 192–209 GeV data. Limits on $m_{\tilde{\tau}_R}$ are derived from a scan over the MSSM parameter space with universal GUT scale gaugino and scalar masses $m_{1/2}$ and m_0 , $1 \leq \tan\beta \leq 60$ and $-2 \leq \mu \leq 2$ TeV. See Fig. 4 for the dependence of the limits on $m_{\tilde{\chi}_1^0}$.

- ³ ABDALLAH 03M looked for acoplanar ditau + \cancel{E} final states at $\sqrt{s} = 130$ –208 GeV. A dedicated search was made for low mass $\tilde{\tau}$ s decoupling from the Z^0 . The limit assumes $B(\tilde{\tau} \rightarrow \tau \tilde{\chi}_1^0) = 100\%$. See Fig. 20 for limits on the $(m_{\tilde{\tau}}, m_{\tilde{\chi}_1^0})$ plane and as function of the $\tilde{\chi}_1^0$ mass and of the branching ratio. The limit in the low-mass region improves to 29.6 and 31.1 GeV for $\tilde{\tau}_R$ and $\tilde{\tau}_L$, respectively, at $\Delta m > m_{\tilde{\tau}}$. The limit in the high-mass region improves to 84.7 GeV for $\tilde{\tau}_R$ and $\Delta m > 15$ GeV. These limits include and update the results of ABREU 01.

- ⁴ HEISTER 02E looked for acoplanar ditau + \cancel{E}_T final states from e^+e^- interactions between 183 and 209 GeV. The mass limit assumes $B(\tilde{\tau} \rightarrow \tau \tilde{\chi}_1^0) = 1$. See their Fig. 4 for the dependence of the limit on Δm . These limits include and update the results of BARATE 01.

- ⁵ AABOUD 18BT searched in 36.1 fb^{-1} of pp collisions at $\sqrt{s} = 13$ TeV for direct electroweak production of charginos, chargino and next-to-lightest neutralinos and sleptons in events with two or three leptons (electrons or muons), with or without jets, and large missing transverse energy. No significant excess above the Standard Model expectations is observed. Limits are set on the slepton mass up to 500 GeV for massless $\tilde{\chi}_1^0$, assuming degeneracy of \tilde{e} , $\tilde{\mu}$, and $\tilde{\tau}$ and exploiting the 2ℓ signature, see their Figure 8(b).

- ⁶ KHACHATRYAN 17L searched in about 19 fb^{-1} of pp collisions at $\sqrt{s} = 8$ TeV for events with two τ (at least one decaying hadronically) and \cancel{E}_T . Results were interpreted to set constraints on the cross section for production of $\tilde{\tau}_L$ pairs for $m_{\tilde{\chi}_1^0} = 1$ GeV. No mass constraints are set, see their Fig. 7.

- ⁷ AAD 16AA summarized and extended ATLAS searches for electroweak supersymmetry in final states containing several charged leptons, \cancel{E}_T , with or without hadronic jets, in 20 fb^{-1} of pp collisions at $\sqrt{s} = 8$ TeV. The paper reports 95% C.L. exclusion limits on the cross-section for production of $\tilde{\tau}_R$ and $\tilde{\tau}_L$ pairs for various $m_{\tilde{\chi}_1^0}$, using the 2 hadronic $\tau + \cancel{E}_T$ analysis. The $m_{\tilde{\tau}_{R/L}} = 109$ GeV is excluded for $m_{\tilde{\chi}_1^0} = 0$ GeV, with the constraints being stronger for $\tilde{\tau}_R$. See their Fig. 12.

- ⁸ AAD 12AF searched in 2 fb^{-1} of pp collisions at $\sqrt{s} = 7$ TeV for events with two tau leptons, jets and large \cancel{E}_T in a GMSB framework. No significant excess above the expected background was found and an upper limit on the visible cross section for new phenomena is set. A 95% C.L. lower limit of 32 TeV on the mGMSB breaking scale A is set for $M_{\text{mess}} = 250$ TeV, $N_5 = 3$, $\mu > 0$ and $C_{\text{grav}} = 1$, independent of $\tan\beta$.

- ⁹ AAD 12AG searched in 2.05 fb⁻¹ of pp collisions at $\sqrt{s} = 7$ TeV for events with at least one hadronically decaying tau lepton, jets, and large E_T in a GMSB framework. No significant excess above the expected background was found and an upper limit on the visible cross section for new phenomena is set. A 95% C.L. lower limit of 30 TeV on the mGMSB breaking scale Λ is set for $M_{mess} = 250$ TeV, $N_S = 3$, $\mu > 0$ and $C_{grav} = 1$, independent of $\tan\beta$. For large values of $\tan\beta$, the limit on Λ increases to 43 TeV.
- ¹⁰ AAD 12CM searched in 4.7 fb⁻¹ of pp collisions at $\sqrt{s} = 7$ TeV for events with at least one tau lepton, zero or one additional light lepton (e/μ) jets, and large E_T in a GMSB framework. No significant excess above the expected background was found and an upper limit on the visible cross section for new phenomena is set. A 95% C.L. lower limit of 54 TeV on the mGMSB breaking scale Λ is set for $M_{mess} = 250$ TeV, $N_S = 3$, $\mu > 0$ and $C_{grav} = 1$, for $\tan\beta > 20$. Here the $\tilde{\tau}_1$ is the NLSP.
- ¹¹ ABBIENDI 06B use 600 pb⁻¹ of data from $\sqrt{s} = 189$ –209 GeV. They look for events from pair-produced staus in a GMSB scenario with $\tilde{\tau}$ NLSP including prompt $\tilde{\tau}$ decays to ditau + \cancel{E} final states, large impact parameters, kinked tracks and heavy stable charged particles. Limits on the cross-section are computed as a function of $m(\tilde{\tau})$ and the lifetime, see their Fig. 7. The limit is compared to the $\sigma \cdot BR^2$ from a scan over the GMSB parameter space.
- ¹² ABDALLAH 04H use data from LEP 1 and $\sqrt{s} = 192$ –208 GeV. They re-use results or re-analyze the data from ABDALLAH 03M to put limits on the parameter space of anomaly-mediated supersymmetry breaking (AMSB), which is scanned in the region $1 < m_{3/2} < 50$ TeV, $0 < m_0 < 1000$ GeV, $1.5 < \tan\beta < 35$, both signs of μ . The constraints are obtained from the searches for mass degenerate chargino and neutralino, for SM-like and invisible Higgs, for leptonically decaying charginos and from the limit on non-SM Z width of 3.2 MeV. The limit is for $m_{\tilde{t}} = 174.3$ GeV (see Table 2 for other $m_{\tilde{t}}$ values). The limit improves to 75 GeV for $\mu < 0$.

R-parity violating $\tilde{\tau}$ (Stau) mass limit

Some earlier papers are now obsolete and have been omitted. They were last listed in our PDG 14 edition: K. Olive, et al. (Particle Data Group), Chinese Physics C38 070001 (2014) (<http://pdg.lbl.gov>).

VALUE (GeV)	CL%	DOCUMENT ID	TECN	COMMENT
>1060	95	¹ AABOUD	18z ATLS	$\geq 4\ell$, RPV, $\lambda_{12k} \neq 0$, $m_{\tilde{\chi}_1^0} = 600$ GeV (mass-degenerate left-handed sleptons and sneutrinos of all 3 generations)
> 780	95	¹ AABOUD	18z ATLS	$\geq 4\ell$, RPV, $\lambda_{133} \neq 0$, $m_{\tilde{\chi}_1^0} = 300$ GeV (mass-degenerate left-handed sleptons and sneutrinos of all 3 generations)

- • • We do not use the following data for averages, fits, limits, etc. • • •
- > 74 95 ² ABBIENDI 04F OPAL RPV, $\tilde{\tau}_L$
- > 90 95 ³ ABDALLAH 04M DLPH RPV, $\tilde{\tau}_R$, indirect, $\Delta m > 5$ GeV
- ¹ AABOUD 18z searched in 36.1 fb⁻¹ of pp collisions at $\sqrt{s} = 13$ TeV for events containing four or more charged leptons (electrons, muons and up to two hadronically decaying taus). No significant deviation from the expected SM background is observed. Limits are set on the Higgsino mass in simplified models of general gauge mediated supersymmetry Tn1n1A/Tn1n1B/Tn1n1C, see their Figure 9. Limits are also set on the wino, slepton, sneutrino and gluino mass in a simplified model of NLSP pair production with R-parity violating decays of the LSP via λ_{12k} or λ_{133} to charged leptons, see their Figures 7, 8.
- ² ABBIENDI 04F use data from $\sqrt{s} = 189$ –209 GeV. They derive limits on sparticle masses under the assumption of RPV with $LL\tilde{E}$ or $LQ\tilde{D}$ couplings. The results are valid for $\tan\beta = 1.5$, $\mu = -200$ GeV, with, in addition, $\Delta m > 5$ GeV for indirect decays via $LQ\tilde{D}$. The limit quoted applies to direct decays with $LL\tilde{E}$ couplings and improves to 75 GeV for $LQ\tilde{D}$ couplings. The limit on the $\tilde{\tau}_R$ mass for indirect decays is 92 GeV for $LL\tilde{E}$ couplings at $m_{\tilde{\chi}_1^0} = 10$ GeV and no exclusion is obtained for $LQ\tilde{D}$ couplings. Supersedes the results of ABBIENDI 00.
- ³ ABDALLAH 04M use data from $\sqrt{s} = 192$ –208 GeV to derive limits on sparticle masses under the assumption of RPV with $LL\tilde{E}$ couplings. The results are valid for $\mu = -200$ GeV, $\tan\beta = 1.5$, $\Delta m > 5$ GeV and assuming a BR of 1 for the given decay. The limit quoted is for indirect decays using the neutralino constraint of 39.5 GeV, also derived in ABDALLAH 04M. For indirect decays via $LL\tilde{E}$ the limit decreases to 86 GeV if the constraint from the neutralino is not used. Supersedes the result of ABREU 00U.

Long-lived $\tilde{\ell}$ (Slepton) mass limit

Limits on scalar leptons which leave detector before decaying. Limits from Z decays are independent of lepton flavor. Limits from continuum e^+e^- annihilation are also independent of flavor for smuons and staus. Selection limits from e^+e^- collisions in the continuum depend on MSSM parameters because of the additional neutralino exchange contribution.

VALUE (GeV)	CL%	DOCUMENT ID	TECN	COMMENT
>430	95	¹ AABOUD	19AT ATLS	long-lived $\tilde{\tau}$, GMSB
>490	95	² KHACHATRYAN	16BW CMS	long-lived $\tilde{\tau}$ from inclusive production, mGMSB SPS line 7 scenario
>240	95	² KHACHATRYAN	16BW CMS	long-lived $\tilde{\tau}$ from direct pair production, mGMSB SPS line 7 scenario
>440	95	³ AAD	15AE ATLS	mGMSB, $M_{mess} = 250$ TeV, $N_S = 3$, $\mu > 0$, $C_{grav} = 5000$, $\tan\beta = 10$
>385	95	³ AAD	15AE ATLS	mGMSB, $M_{mess} = 250$ TeV, $N_S = 3$, $\mu > 0$, $C_{grav} = 5000$, $\tan\beta = 50$
>286	95	³ AAD	15AE ATLS	direct $\tilde{\tau}$ production
none 124–309	95	⁴ AAIJ	15BD LHCB	long-lived $\tilde{\tau}$, mGMSB, SPS7
> 98	95	⁵ ABBIENDI	03L OPAL	$\tilde{\mu}_R, \tilde{\tau}_R$
none 2–87.5	95	⁶ ABREU	00Q DLPH	$\tilde{\mu}_R, \tilde{\tau}_R$
> 81.2	95	⁷ ACCIARRI	99H L3	$\tilde{\mu}_R, \tilde{\tau}_R$
> 81	95	⁸ BARATE	98K ALEP	$\tilde{\mu}_R, \tilde{\tau}_R$

- • • We do not use the following data for averages, fits, limits, etc. • • •
- >300 95 ⁹ AAD 13AA ATLS long-lived $\tilde{\tau}$, GMSB, $\tan\beta = 5$ –20
- >339 95 ¹⁰ ABAZOV 13B D0 long-lived $\tilde{\tau}$, 100 $< m_{\tilde{\tau}} < 300$ GeV
- >500 95 ^{11,12} CHATRCHYAN 13AB CMS long-lived $\tilde{\tau}$, direct $\tilde{\tau}_1$ pair prod., minimal GMSB, SPS line 7
- >314 95 ¹⁴ CHATRCHYAN 12L CMS long-lived $\tilde{\tau}$, $\tilde{\tau}_1$ from direct pair prod. and from decay of heavier SUSY particles, minimal GMSB, SPS line 7
- >136 95 ¹⁵ AAD 11P ATLS stable $\tilde{\tau}$, GMSB scenario, $\tan\beta = 5$
- ¹ AABOUD 19AT searched in 36.1 fb⁻¹ of pp collisions at $\sqrt{s} = 13$ TeV for metastable and stable R-hadrons. Multiple search strategies for a wide range of lifetimes, corresponding to path lengths of a few meters, are defined. No significant deviations from the expected Standard Model background are observed. Results are interpreted in terms of exclusion limits on long-lived stau in the context of GMSB models. Lower limits on the mass for direct production of staus are set at 430 GeV, see their Fig. 10 (left).
- ² KHACHATRYAN 16BW searched in 2.5 fb⁻¹ of pp collisions at $\sqrt{s} = 13$ TeV for events with heavy stable charged particles, identified by their anomalously high energy deposits in the silicon tracker and/or long time-of-flight measurements by the muon system. No evidence for an excess over the expected background is observed. Limits are derived for pair production of tau sleptons as a function of mass, depending on their direct or inclusive production in a minimal GMSB scenario along the Snowmass Points and Slopes (SPS) line 7, see Fig. 4 and Table 7.
- ³ AAD 15AE searched in 19.1 fb⁻¹ of pp collisions at $\sqrt{s} = 8$ TeV for heavy long-lived charged particles, measured through their specific ionization energy loss in the ATLAS pixel detector or their time-of-flight in the ALTAS muon system. In the absence of an excess of events above the expected backgrounds, limits are set on stable $\tilde{\tau}$ sleptons in various scenarios, see Figs. 5–7.
- ⁴ AAIJ 15BD searched in 3.0 fb⁻¹ of pp collisions at $\sqrt{s} = 7$ and 8 TeV for evidence of Drell-Yan pair production of long-lived $\tilde{\tau}$ particles. No evidence for such particles is observed and 95% C.L. upper limits on the cross section of $\tilde{\tau}$ pair production are derived, see Fig. 7. In the mGMSB, assuming the SPS7 benchmark scenario $\tilde{\tau}$ masses between 124 and 309 GeV are excluded at 95% C.L.
- ⁵ ABBIENDI 03L used e^+e^- data at $\sqrt{s} = 130$ –209 GeV to select events with two high momentum tracks with anomalous dE/dx . The excluded cross section is compared to the theoretical expectation as a function of the heavy particle mass in their Fig. 3. The limit improves to 98.5 GeV for $\tilde{\mu}_L$ and $\tilde{\tau}_L$. The bounds are valid for colorless spin 0 particles with lifetimes longer than 10^{-6} s. Supersedes the results from ACKERSTAFF 98P.
- ⁶ ABREU 00Q searches for the production of pairs of heavy, charged stable particles in e^+e^- annihilation at $\sqrt{s} = 130$ –189 GeV. The upper bound improves to 88 GeV for $\tilde{\mu}_L, \tilde{\tau}_L$. These limits include and update the results of ABREU 98P.
- ⁷ ACCIARRI 99H searched for production of pairs of back-to-back heavy charged particles at $\sqrt{s} = 130$ –183 GeV. The upper bound improves to 82.2 GeV for $\tilde{\mu}_L, \tilde{\tau}_L$.
- ⁸ The BARATE 98k mass limit improves to 82 GeV for $\tilde{\mu}_L, \tilde{\tau}_L$. Data collected at $\sqrt{s} = 161$ –184 GeV.
- ⁹ AAD 13AA searched in 4.7 fb⁻¹ of pp collisions at $\sqrt{s} = 7$ TeV for events containing long-lived massive particles in a GMSB framework. No significant excess above the expected background was found. A 95% C.L. lower limit of 300 GeV is placed on long-lived $\tilde{\tau}$'s in the GMSB model with $M_{mess} = 250$ TeV, $N_S = 3$, $\mu > 0$, for $\tan\beta = 5$ –20. The lower limit on the GMSB breaking scale Λ was found to be 99–110 TeV, for $\tan\beta$ values between 5 and 40, see Fig. 4 (top). Also, directly produced long-lived sleptons, or sleptons decaying to long-lived ones, are excluded at 95% C.L. up to a $\tilde{\tau}$ mass of 278 GeV for models with slepton splittings smaller than 50 GeV.
- ¹⁰ ABAZOV 13b looked in 6.3 fb⁻¹ of p \bar{p} collisions at $\sqrt{s} = 1.96$ TeV for charged massive long-lived particles in events with muon-like particles that have both speed and ionization energy loss inconsistent with muons produced in beam collisions. In the absence of an excess, limits are set at 95% C.L. on the production cross section of stau leptons in the mass range 100–300 GeV, see their Table 20 and Fig. 23.
- ¹¹ CHATRCHYAN 13AB looked in 5.0 fb⁻¹ of pp collisions at $\sqrt{s} = 7$ TeV and in 18.8 fb⁻¹ of pp collisions at $\sqrt{s} = 8$ TeV for events with heavy stable particles, identified by their anomalous dE/dx in the tracker and additionally requiring that it be identified as muon in the muon chambers, from pair production of $\tilde{\tau}_1$'s. No evidence for an excess over the expected background is observed. Supersedes CHATRCHYAN 12L.
- ¹² CHATRCHYAN 13AB limits are derived for pair production of $\tilde{\tau}_1$ as a function of mass in minimal GMSB scenarios along the Snowmass Points and Slopes (SPS) line 7 (see Fig. 8 and Table 7). The limit given here is valid for direct pair $\tilde{\tau}_1$ production.
- ¹³ CHATRCHYAN 13AB limits are derived for the production of $\tilde{\tau}_1$ as a function of mass in minimal GMSB scenarios along the Snowmass Points and Slopes (SPS) line 7 (see Fig. 8 and Table 7). The limit given here is valid for the production of $\tilde{\tau}_1$ from both direct pair production and from the decay of heavier supersymmetric particles.
- ¹⁴ CHATRCHYAN 12L looked in 5.0 fb⁻¹ of pp collisions at $\sqrt{s} = 7$ TeV for events with heavy stable particles, identified by their anomalous dE/dx in the tracker or additionally requiring that it be identified as muon in the muon chambers, from pair production of $\tilde{\tau}_1$'s. No evidence for an excess over the expected background is observed. Limits are derived for the production of $\tilde{\tau}_1$ as a function of mass in minimal GMSB scenarios along the Snowmass Points and Slopes (SPS) line 7 (see Fig. 3). The limit given here is valid for the production of $\tilde{\tau}_1$ in the decay of heavier supersymmetric particles.
- ¹⁵ AAD 11P looked in 37 pb⁻¹ of pp collisions at $\sqrt{s} = 7$ TeV for events with two heavy stable particles, reconstructed in the Inner tracker and the Muon System and identified by their time of flight in the Muon System. No evidence for an excess over the SM expectation is observed. Limits on the mass are derived, see Fig. 3, for $\tilde{\tau}$ in a GMSB scenario and for sleptons produced by electroweak processes only, in which case the limit degrades to 110 GeV.

Searches Particle Listings

Supersymmetric Particle Searches

\tilde{q} (Squark) mass limit

For $m_{\tilde{q}} > 60\text{--}70$ GeV, it is expected that squarks would undergo a cascade decay via a number of neutralinos and/or charginos rather than undergo a direct decay to photinos as assumed by some papers. Limits obtained when direct decay is assumed are usually higher than limits when cascade decays are included.

Limits from e^+e^- collisions depend on the mixing angle of the lightest mass eigenstate $\tilde{q}_1 = \tilde{q}_R \sin\theta_q + \tilde{q}_L \cos\theta_q$. It is usually assumed that only the sbottom and stop squarks have non-trivial mixing angles (see the stop and sbottom sections). Here, unless otherwise noted, squarks are always taken to be either left/right degenerate, or purely of left or right type. Data from Z decays have set squark mass limits above 40 GeV, in the case of $\tilde{q} \rightarrow q\tilde{\chi}_1^0$ decays if $\Delta m = m_{\tilde{q}} - m_{\tilde{\chi}_1^0} \gtrsim 5$ GeV. For smaller values of Δm , current constraints on the invisible width of the Z ($\Delta\Gamma_{\text{inv}} < 2.0$ MeV, LEP 00) exclude $m_{\tilde{u}_{L,R}} < 44$ GeV, $m_{\tilde{d}_R} < 33$ GeV, $m_{\tilde{d}_L} < 44$ GeV and, assuming all squarks degenerate, $m_{\tilde{q}} < 45$ GeV.

Some earlier papers are now obsolete and have been omitted. They were last listed in our PDG 14 edition: K. Olive, *et al.* (Particle Data Group), Chinese Physics **C38** 070001 (2014) (<http://pdg.lbl.gov>).

R-parity conserving \tilde{q} (Squark) mass limit

VALUE (GeV)	CL%	DOCUMENT ID	TECN	COMMENT
>1590	95	1 SIRUNYAN 19AG	CMS	$2\gamma + \cancel{E}_T$, Tsqk4B, 5.00 GeV $< m_{\tilde{\chi}_1^0} < 1500$ GeV
>1130	95	2 SIRUNYAN 19CH	CMS	$\text{jets} + \cancel{E}_T$, Tsqk1, 1 light flavour, $m_{\tilde{\chi}_1^0} = 0$ GeV
>1630	95	2 SIRUNYAN 19CH	CMS	$\text{jets} + \cancel{E}_T$, Tsqk1, 8 degenerate light flavours, $m_{\tilde{\chi}_1^0} = 0$ GeV
>1430	95	3 SIRUNYAN 19K	CMS	$\gamma + \ell + \cancel{E}_T$, Tsqk4A, $m_{\tilde{\chi}_1^0} = 1200$ GeV
>1200	95	4 AABOUD 18BJ	ATLS	$\ell^\pm \ell^\mp + \text{jets} + \cancel{E}_T$, Tsqk2, $m_{\tilde{\chi}_1^0} = 1$ GeV, any $m_{\tilde{\chi}_2^0}$
> 850	95	5 AABOUD 18BV	ATLS	$c\text{-jets} + \cancel{E}_T$, Tsqk1 (charm only), $m_{\tilde{\chi}_1^0} = 0$ GeV
> 710	95	6 AABOUD 18I	ATLS	$\geq 1 \text{ jets} + \cancel{E}_T$, Tsqk1, $m_{\tilde{q}} \sim m_{\tilde{\chi}_1^0}$
>1820	95	7 AABOUD 18U	ATLS	$2\gamma + \cancel{E}_T$, GGM, Tsqk4B, any NLSP mass
>1550	95	8 AABOUD 18V	ATLS	$\text{jets} + \cancel{E}_T$, Tsqk1, $m_{\tilde{\chi}_1^0} = 0$ GeV
>1150	95	9 AABOUD 18V	ATLS	$\text{jets} + \cancel{E}_T$, Tsqk3, $m_{\tilde{\chi}_1^\pm} = 0.5$ ($m_{\tilde{q}} + m_{\tilde{\chi}_1^0}$), $m_{\tilde{\chi}_1^0} = 0$ GeV
>1650	95	10 SIRUNYAN 18AA	CMS	$\geq 1\gamma + \cancel{E}_T$, Tsqk4A
>1750	95	10 SIRUNYAN 18AA	CMS	$\geq 1\gamma + \cancel{E}_T$, Tsqk4B
> 675	95	11 SIRUNYAN 18AY	CMS	$\text{jets} + \cancel{E}_T$, Tsqk1, 1 light flavor state, $m_{\tilde{\chi}_1^0} = 0$ GeV
>1320	95	11 SIRUNYAN 18AY	CMS	$\text{jets} + \cancel{E}_T$, Tsqk1, 8 degenerate light flavor states, $m_{\tilde{\chi}_1^0} = 0$ GeV
>1220	95	12 AABOUD 17AR	ATLS	$1\ell + \text{jets} + \cancel{E}_T$, Tsqk3, $m_{\tilde{\chi}_1^0} = 0$ GeV
>1000	95	13 AABOUD 17N	ATLS	2 same-flavour, opposite-sign $\ell + \text{jets} + \cancel{E}_T$, Tsqk2, $m_{\tilde{\chi}_1^0} = 0$ GeV
>1150	95	14 KHACHATRY...17P	CMS	1 or more $\text{jets} + \cancel{E}_T$, Tsqk1, 4(flavor) x 2(isospin) = 8 mass degenerate states, $m_{\tilde{\chi}_1^0} = 0$ GeV
> 575	95	14 KHACHATRY...17P	CMS	1 or more $\text{jets} + \cancel{E}_T$, Tsqk1, one light flavor state, $m_{\tilde{\chi}_1^0} = 0$ GeV
>1370	95	15 KHACHATRY...17V	CMS	$2\gamma + \cancel{E}_T$, GGM, Tsqk4, any NLSP mass
>1600	95	16 SIRUNYAN 17AY	CMS	$\gamma + \text{jets} + \cancel{E}_T$, Tsqk4B, $m_{\tilde{\chi}_1^0} = 0$ GeV
>1370	95	16 SIRUNYAN 17AY	CMS	$\gamma + \text{jets} + \cancel{E}_T$, Tsqk4A, $m_{\tilde{\chi}_1^0} = 0$ GeV
>1050	95	17 SIRUNYAN 17AZ	CMS	$\geq 1 \text{ jets} + \cancel{E}_T$, Tsqk1, single light flavor state, $m_{\tilde{\chi}_1^0} = 0$ GeV
>1550	95	17 SIRUNYAN 17AZ	CMS	$\geq 1 \text{ jets} + \cancel{E}_T$, Tsqk1, 4(flavor) x 2(isospin) = 8 degenerate mass states, $m_{\tilde{\chi}_1^0} = 0$ GeV
>1390	95	18 SIRUNYAN 17P	CMS	$\text{jets} + \cancel{E}_T$, Tsqk1, 4(flavor) x 2(isospin) = 8 degenerate mass states, $m_{\tilde{\chi}_1^0} = 0$ GeV
> 950	95	18 SIRUNYAN 17P	CMS	$\text{jets} + \cancel{E}_T$, Tsqk1, one light flavor state, $m_{\tilde{\chi}_1^0} = 0$ GeV
> 608	95	19 AABOUD 16D	ATLS	$\geq 1 \text{ jet} + \cancel{E}_T$, Tsqk1, $m_{\tilde{q}} - m_{\tilde{\chi}_1^0} = 5$ GeV

>1030	95	20 AABOUD 16N	ATLS	$\geq 2 \text{ jets} + \cancel{E}_T$, Tsqk1, $m_{\tilde{\chi}_1^0} = 0$ GeV
> 600	95	21 KHACHATRY...16Bs	CMS	$\text{jets} + \cancel{E}_T$, Tsqk1, single light squark, $m_{\tilde{\chi}_1^0} = 0$ GeV
>1260	95	21 KHACHATRY...16Bs	CMS	$\text{jets} + \cancel{E}_T$, Tsqk1, 8 degenerate light squarks, $m_{\tilde{\chi}_1^0} = 0$ GeV
> 850	95	22 AAD 15BV	ATLS	$\text{jets} + \cancel{E}_T$, $\tilde{q} \rightarrow q\tilde{\chi}_1^0$, $m_{\tilde{\chi}_1^0} = 100$ GeV
> 250	95	23 AAD 15Cs	ATLS	photon $+ \cancel{E}_T$, $p\bar{p} \rightarrow \tilde{q}\tilde{q}^*\gamma$, $\tilde{q} \rightarrow q\tilde{\chi}_1^0$, $m_{\tilde{q}} - m_{\tilde{\chi}_1^0} = m_c$
> 490	95	24 AAD 15K	ATLS	$\tilde{c} \rightarrow c\tilde{\chi}_1^0$, $m_{\tilde{\chi}_1^0} < 200$ GeV
> 875	95	25 KHACHATRY...15AF	CMS	$\tilde{q} \rightarrow q\tilde{\chi}_1^0$, simplified model, 8 degenerate light \tilde{q} , $m_{\tilde{\chi}_1^0} = 0$
> 520	95	25 KHACHATRY...15AF	CMS	$\tilde{q} \rightarrow q\tilde{\chi}_1^0$, simplified model, single light squark, $m_{\tilde{\chi}_1^0} = 0$
>1450	95	25 KHACHATRY...15AF	CMS	CMSSM, $\tan\beta = 30$, $A_0 = -2\max(m_0, m_{1/2})$, $\mu > 0$
> 850	95	26 AAD 14AE	ATLS	$\text{jets} + \cancel{E}_T$, $\tilde{q} \rightarrow q\tilde{\chi}_1^0$ simplified model, mass degenerate first and second generation squarks, $m_{\tilde{\chi}_1^0} = 0$ GeV
> 440	95	26 AAD 14AE	ATLS	$\text{jets} + \cancel{E}_T$, $\tilde{q} \rightarrow q\tilde{\chi}_1^0$ simplified model, single light-flavour squark, $m_{\tilde{\chi}_1^0} = 0$ GeV
>1700	95	26 AAD 14AE	ATLS	$\text{jets} + \cancel{E}_T$, mSUGRA/CMSSM, $m_{\tilde{q}} = m_{\tilde{g}}$
> 800	95	27 CHATRCHYAN14AH	CMS	$\text{jets} + \cancel{E}_T$, $\tilde{q} \rightarrow q\tilde{\chi}_1^0$ simplified model, $m_{\tilde{\chi}_1^0} = 50$ GeV
> 780	95	28 CHATRCHYAN14I	CMS	multijets $+ \cancel{E}_T$, $\tilde{q} \rightarrow q\tilde{\chi}_1^0$ simplified model, $m_{\tilde{\chi}_1^0} < 200$ GeV
>1360	95	29 AAD 13L	ATLS	$\text{jets} + \cancel{E}_T$, CMSSM, $m_{\tilde{g}} = m_{\tilde{q}}$
>1200	95	30 AAD 13Q	ATLS	$\gamma + b + \cancel{E}_T$, higgsino-like neutralino, $m_{\tilde{\chi}_1^0} > 220$ GeV, GMSB
>1250	95	31 CHATRCHYAN13	CMS	$\ell^\pm \ell^\mp + \text{jets} + \cancel{E}_T$, CMSSM
>1430	95	32 CHATRCHYAN13G	CMS	$0,1,2, \geq 3 b\text{-jets} + \cancel{E}_T$, CMSSM, $m_{\tilde{q}} = m_{\tilde{g}}$
> 750	95	33 CHATRCHYAN13H	CMS	$2\gamma + \geq 4 \text{ jets} + \text{low } \cancel{E}_T$, stealth SUSY model
> 820	95	34 CHATRCHYAN13T	CMS	$\text{jets} + \cancel{E}_T$, $\tilde{q} \rightarrow q\tilde{\chi}_1^0$ simplified model, $m_{\tilde{\chi}_1^0} = 0$ GeV
>1200	95	35 AAD 12AX	ATLS	$\ell + \text{jets} + \cancel{E}_T$, CMSSM, $m_{\tilde{q}} = m_{\tilde{g}}$
> 870	95	36 AAD 12CJ	ATLS	$\ell^\pm + \text{jets} + \cancel{E}_T$, CMSSM, $m_{\tilde{q}} = m_{\tilde{g}}$
> 950	95	37 AAD 12CP	ATLS	$2\gamma + \cancel{E}_T$, GMSB, bino NLSP, $m_{\tilde{\chi}_1^0} > 50$ GeV
> 760	95	38 AAD 12W	ATLS	$\text{jets} + \cancel{E}_T$, CMSSM, $m_{\tilde{q}} = m_{\tilde{g}}$
>1110	95	39 CHATRCHYAN12	CMS	$e, \mu, \text{jets, razor}$, CMSSM
>1180	95	40 CHATRCHYAN12AE	CMS	$\text{jets} + \cancel{E}_T$, $\tilde{q} \rightarrow q\tilde{\chi}_1^0$, $m_{\tilde{\chi}_1^0} < 200$ GeV
>1080	95	41 CHATRCHYAN12AT	CMS	$\text{jets} + \cancel{E}_T$, CMSSM
> 300	95	41 CHATRCHYAN12AT	CMS	$\text{jets} + \cancel{E}_T$, CMSSM, $m_{\tilde{q}} = m_{\tilde{g}}$
>1080	95	42 AABOUD 18V	ATLS	$\text{jets} + \cancel{E}_T$, Tsqk5, $(m_{\tilde{\chi}_2^0} - m_{\tilde{\chi}_1^0}) / (m_{\tilde{q}} - m_{\tilde{\chi}_1^0}) < 0.95$, $m_{\tilde{\chi}_1^0} = 60$ GeV
> 790	95	43 KHACHATRY...16BT	CMS	19-parameter pMSSM model, global Bayesian analysis, flat prior
> 820	95	44 AAD 15AI	ATLS	$\ell^\pm + \text{jets} + \cancel{E}_T$
> 790	95	22 AAD 15BV	ATLS	$\text{jets} + \cancel{E}_T$, $m_{\tilde{g}} = m_{\tilde{q}}$, $m_{\tilde{\chi}_1^0} = 1$ GeV
> 820	95	22 AAD 15BV	ATLS	$\text{jets} + \cancel{E}_T$, $\tilde{q} \rightarrow qW\tilde{\chi}_1^0$, $m_{\tilde{\chi}_1^0} = 100$ GeV
> 850	95	22 AAD 15BV	ATLS	2 or 3 leptons + jets, \tilde{q} decays via sleptons, $m_{\tilde{\chi}_1^0} = 100$ GeV
> 700	95	22 AAD 15BV	ATLS	τ, \tilde{q} decays via staus, $m_{\tilde{\chi}_1^0} = 50$ GeV
> 550	95	45 KHACHATRY...15AR	CMS	$\tilde{q} \rightarrow q\tilde{\chi}_1^0, \tilde{\chi}_1^0 \rightarrow \tilde{3}g, \tilde{3} \rightarrow S\tilde{G}, S \rightarrow gg, m_{\tilde{S}} = 100$ GeV, $m_{\tilde{S}} = 90$ GeV
> 1500	95	45 KHACHATRY...15AR	CMS	$\ell^\pm, \tilde{q} \rightarrow q\tilde{\chi}_1^\pm, \tilde{\chi}_1^\pm \rightarrow \tilde{3}W^\pm, \tilde{3} \rightarrow S\tilde{G}, S \rightarrow gg, m_{\tilde{S}} = 100$ GeV, $m_{\tilde{S}} = 90$ GeV
>1500	95	46 KHACHATRY...15AZ	CMS	$\geq 2\gamma, \geq 1 \text{ jet}$, (Razor), bino-like NLSP, $m_{\tilde{\chi}_1^0} = 375$ GeV
>1000	95	46 KHACHATRY...15AZ	CMS	$\geq 1\gamma, \geq 2 \text{ jet}$, wino-like NLSP, $m_{\tilde{\chi}_1^0} = 375$ GeV

••• We do not use the following data for averages, fits, limits, etc. •••

> 670	95	47 AAD	14E ATLS	$\ell^\pm \ell^\pm (\ell^\mp) + \text{jets}, \tilde{q} \rightarrow q' \tilde{\chi}_1^\pm, \tilde{\chi}_1^\pm \rightarrow W^{(*)} \tilde{\chi}_2^0, \tilde{\chi}_2^0 \rightarrow Z^{(*)} \tilde{\chi}_1^0$ simplified model, $m_{\tilde{\chi}_1^0} < 300$ GeV
> 780	95	47 AAD	14E ATLS	$\ell^\pm \ell^\pm (\ell^\mp) + \text{jets}, \tilde{q} \rightarrow q' \tilde{\chi}_1^\pm / \tilde{\chi}_2^0, \tilde{\chi}_1^\pm \rightarrow \ell^\pm \nu \tilde{\chi}_1^0, \tilde{\chi}_2^0 \rightarrow \ell^\pm \ell^\mp (\nu) \tilde{\chi}_1^0$ simplified model
> 700	95	48 CHATRCHYAN13Ao	CMS	$\ell^\pm \ell^\mp + \text{jets} + \cancel{E}_T$, CMSSM, $m_0 < 700$ GeV
>1350	95	49 CHATRCHYAN13AV	CMS	jets (+ leptons) + \cancel{E}_T , CMSSM, $m_{\tilde{g}} = m_{\tilde{q}}$
> 800	95	50 CHATRCHYAN13W	CMS	≥ 1 photons + jets + \cancel{E}_T , GGM, wino-like NLSP, $m_{\tilde{\chi}_1^0} = 375$ GeV
>1000	95	50 CHATRCHYAN13W	CMS	≥ 2 photons + jets + \cancel{E}_T , GGM, bino-like NLSP, $m_{\tilde{\chi}_1^0} = 375$ GeV
> 340	95	51 DREINER	12A THEO	$m_{\tilde{q}} \sim m_{\tilde{\chi}_1^0}$
> 650	95	52 DREINER	12A THEO	$m_{\tilde{q}} = m_{\tilde{g}} \sim m_{\tilde{\chi}_1^0}$

- ¹ SIRUNYAN 19AG searched in 35.9 fb^{-1} of pp collisions at $\sqrt{s} = 13 \text{ TeV}$ for events with two photons and large \cancel{E}_T . No significant excess above the Standard Model expectations is observed. Limits are set on the gluino mass in the Tglu4B simplified model and on the squark mass in the Tsqk4B simplified model, see their Figure 3.
- ² SIRUNYAN 19CH searched in 137 fb^{-1} of pp collisions at $\sqrt{s} = 13 \text{ TeV}$ for events containing multiple jets and large \cancel{E}_T . No significant excess above the Standard Model expectations is observed. Limits are set on the gluino mass in the Tglu1A, Tglu1C, Tglu2A and Tglu3A simplified models, see their Figure 13. Limits are also set on squark, sbottom and stop masses in the Tsqk1, Tsb0t1, Tstop1 simplified models, see their Figure 14.
- ³ SIRUNYAN 19K searched in 35.9 fb^{-1} of pp collisions at $\sqrt{s} = 13 \text{ TeV}$ for events with a photon, an electron or muon, and large \cancel{E}_T . No significant excess above the Standard Model expectations is observed. In the framework of GMSB, limits are set on the chargino and neutralino mass in the Tch1n1A simplified model, see their Figure 6. Limits are also set on the gluino mass in the Tglu4A simplified model, and on the squark mass in the Tsqk4A simplified model, see their Figure 7.
- ⁴ AABOUD 18BJ searched in 36.1 fb^{-1} of pp collisions at $\sqrt{s} = 13 \text{ TeV}$ in events with two opposite-sign charged leptons (electrons and muons), jets and missing transverse momentum, with various requirements to be sensitive to signals with different kinematic endpoint values in the dilepton invariant mass distribution. The data are found to be consistent with the SM expectation. Results are interpreted in the Tsqk2 model in case of $m_{\tilde{\chi}_1^0} = 1 \text{ GeV}$: for any $m_{\tilde{\chi}_2^0}$, squark masses below 1200 GeV are excluded, see their Fig. 14(b).
- ⁵ AABOUD 18BV searched in 36.1 fb^{-1} of pp collisions at $\sqrt{s} = 13 \text{ TeV}$ for events with at least one jet identified as c -jet, large missing transverse energy and no leptons. Good agreement is observed between the number of events in data and Standard Model predictions. The results are translated into exclusion limits in Tsqk1 models considering only \tilde{c}_1 . In scenarios with massless neutralinos, scharm masses below 850 GeV are excluded. If the differences of the \tilde{c}_1 and $\tilde{\chi}_1^0$ masses is below 100 GeV, scharm masses below 500 GeV are excluded. See their Fig. 6 and Fig. 7.
- ⁶ AABOUD 18I searched in 36.1 fb^{-1} of pp collisions at $\sqrt{s} = 13 \text{ TeV}$ for events with at least one jet with a transverse momentum above 250 GeV and no leptons. Good agreement is observed between the number of events in data and Standard Model predictions. The results are translated into exclusion limits in Tsqk1 models. In the compressed scenario with similar squark and neutralino masses, squark masses below 710 GeV are excluded. See their Fig. 10(b).
- ⁷ AABOUD 18U searched in 36.1 fb^{-1} of pp collisions at $\sqrt{s} = 13 \text{ TeV}$ in events with at least one isolated photon, possibly jets and significant transverse momentum targeting generalised models of gauge-mediated SUSY breaking. No significant excess of events is observed above the SM prediction. Results are interpreted in terms of lower limits on the masses of squark in Tsqk4B models. Masses below 1820 GeV are excluded for any NLSP mass, see their Fig. 9.
- ⁸ AABOUD 18V searched in 36.1 fb^{-1} of pp collisions at $\sqrt{s} = 13 \text{ TeV}$ in events with no charged leptons, jets and missing transverse momentum. The data are found to be consistent with the SM expectation. Results are interpreted in the Tsqk1 model: squark masses below 1550 GeV are excluded for massless LSP, see their Fig. 13(a).
- ⁹ AABOUD 18V searched in 36.1 fb^{-1} of pp collisions at $\sqrt{s} = 13 \text{ TeV}$ in events with no charged leptons, jets and missing transverse momentum. The data are found to be consistent with the SM expectation. Results are interpreted in the Tsqk3 model. Assuming that $m_{\tilde{\chi}_1^\pm} = 0.5 (m_{\tilde{q}} + m_{\tilde{\chi}_1^0})$, squark masses below 1150 GeV are excluded for massless LSP, see their Fig. 14(a). Exclusions are also shown assuming $m_{\tilde{\chi}_1^0} = 60 \text{ GeV}$, see their Fig. 14(b).
- ¹⁰ SIRUNYAN 18AA searched in 35.9 fb^{-1} of pp collisions at $\sqrt{s} = 13 \text{ TeV}$ for events with at least one photon and large \cancel{E}_T . No significant excess above the Standard Model expectations is observed. Limits are set on wino masses in a general gauge-mediated SUSY breaking (GGM) scenario with bino-like $\tilde{\chi}_1^\pm$ and wino-like $\tilde{\chi}_1^0$ and $\tilde{\chi}_2^0$, see Figure 7. Limits are also set on the NLSP mass in the Tch1n1A and Tch1ch1A simplified models, see their Figure 8. Finally, limits are set on the gluino mass in the Tglu4A and Tglu4B simplified models, see their Figure 9, and on the squark mass in the Tsqk4A and Tsqk4B simplified models, see their Figure 10.
- ¹¹ SIRUNYAN 18AY searched in 35.9 fb^{-1} of pp collisions at $\sqrt{s} = 13 \text{ TeV}$ for events containing one or more jets and significant \cancel{E}_T . No significant excess above the Standard Model expectations is observed. Limits are set on the gluino mass in the Tglu1A, Tglu2A and Tglu3A simplified models, see their Figure 3. Limits are also set on squark, sbottom and stop masses in the Tsqk1, Tsb0t1, Tstop1 and Tstop4 simplified models, see their Figure 3. Finally, limits are set on long-lived gluino masses in a Tglu1A simplified model where the gluino is metastable or long-lived with proper decay lengths in the range $10^{-3} \text{ mm} < c\tau < 10^5 \text{ mm}$, see their Figure 4.

- ¹² AABOUD 17AR searched in 36.1 fb^{-1} of pp collisions at $\sqrt{s} = 13 \text{ TeV}$ for events with one isolated lepton, at least two jets and large missing transverse momentum. No significant excess above the Standard Model expectations is observed. Limits up to 1.25 TeV are set on the 1st and 2nd generation squark masses in Tsqk3 simplified models, with $x = (m_{\tilde{\chi}_1^\pm} - m_{\tilde{\chi}_1^0}) / (m_{\tilde{q}} - m_{\tilde{\chi}_1^0}) = 1/2$. Similar limits are obtained for variable x and fixed neutralino mass, $m_{\tilde{\chi}_1^0} = 60 \text{ GeV}$. See their Figure 13.
- ¹³ AABOUD 17N searched in 14.7 fb^{-1} of pp collisions at $\sqrt{s} = 13 \text{ TeV}$ for events with 2 same-flavour, opposite-sign leptons (electrons or muons), jets and large missing transverse momentum. The results are interpreted as 95% C.L. limits in Tsqk2 models, assuming $m_{\tilde{\chi}_1^0} = 0 \text{ GeV}$ and $m_{\tilde{\chi}_2^0} = 600 \text{ GeV}$. See their Fig. 12 for exclusion limits as a function of $m_{\tilde{\chi}_2^0}$.
- ¹⁴ KHACHATRYAN 17P searched in 2.3 fb^{-1} of pp collisions at $\sqrt{s} = 13 \text{ TeV}$ for events with one or more jets and large \cancel{E}_T . No significant excess above the Standard Model expectations is observed. Limits are set on the gluino mass in the Tglu1A, Tglu2A, Tglu3A, Tglu3B, Tglu3C and Tglu3D simplified models, see their Figures 7 and 8. Limits are also set on the squark mass in the Tsqk1 simplified model, see their Fig. 7, and on the sbottom mass in the Tsb0t1 simplified model, see Fig. 8. Finally, limits are set on the stop mass in the Tstop1, Tstop3, Tstop4, Tstop6 and Tstop7 simplified models, see Fig. 8.
- ¹⁵ KHACHATRYAN 17V searched in 2.3 fb^{-1} of pp collisions at $\sqrt{s} = 13 \text{ TeV}$ for events with two photons and large \cancel{E}_T . No significant excess above the Standard Model expectations is observed. Limits are set on the gluino and squark mass in the context of general gauge mediation models Tglu4B and Tsqk4, see their Fig. 4.
- ¹⁶ SIRUNYAN 17AY searched in 35.9 fb^{-1} of pp collisions at $\sqrt{s} = 13 \text{ TeV}$ for events with at least one photon, jets and large \cancel{E}_T . No significant excess above the Standard Model expectations is observed. Limits are set on the gluino mass in the Tglu4A and Tglu4B simplified models, and on the squark mass in the Tsqk4A and Tsqk4B simplified models, see their Figure 6.
- ¹⁷ SIRUNYAN 17AZ searched in 35.9 fb^{-1} of pp collisions at $\sqrt{s} = 13 \text{ TeV}$ for events with one or more jets and large \cancel{E}_T . No significant excess above the Standard Model expectations is observed. Limits are set on the gluino mass in the Tglu1A, Tglu2A, Tglu3A simplified models, see their Figures 6. Limits are also set on the squark mass in the Tsqk1 simplified model (for single light squark and for 8 degenerate light squarks), on the sbottom mass in the Tsb0t1 simplified model and on the stop mass in the Tstop1 simplified model, see their Fig. 7. Finally, limits are set on the stop mass in the Tstop2, Tstop4 and Tstop8 simplified models, see Fig. 8.
- ¹⁸ SIRUNYAN 17P searched in 35.9 fb^{-1} of pp collisions at $\sqrt{s} = 13 \text{ TeV}$ for events with multiple jets and large \cancel{E}_T . No significant excess above the Standard Model expectations is observed. Limits are set on the gluino mass in the Tglu1A, Tglu1C, Tglu2A, Tglu3A and Tglu3D simplified models, see their Fig. 12. Limits are also set on the squark mass in the Tsqk1 simplified model, on the stop mass in the Tstop1 simplified model, and on the sbottom mass in the Tsb0t1 simplified model, see Fig. 13.
- ¹⁹ AABOUD 16D searched in 3.2 fb^{-1} of pp collisions at $\sqrt{s} = 13 \text{ TeV}$ for events with an energetic jet and large missing transverse momentum. The results are interpreted as 95% C.L. limits on masses of first and second generation squarks decaying into a quark and the lightest neutralino in scenarios with $m_{\tilde{q}} - m_{\tilde{\chi}_1^0} < 25 \text{ GeV}$. See their Fig. 6.
- ²⁰ AABOUD 16N searched in 3.2 fb^{-1} of pp collisions at $\sqrt{s} = 13 \text{ TeV}$ for events containing hadronic jets, large \cancel{E}_T , and no electrons or muons. No significant excess above the Standard Model expectations is observed. First- and second-generation squark masses below 1030 GeV are excluded at the 95% C.L. decaying to quarks and a massless lightest neutralino. See their Fig. 7a.
- ²¹ KHACHATRYAN 16BS searched in 2.3 fb^{-1} of pp collisions at $\sqrt{s} = 13 \text{ TeV}$ for events with at least one energetic jet, no isolated leptons, and significant \cancel{E}_T , using the transverse mass variable M_{T2} to discriminate between signal and background processes. No significant excess above the Standard Model expectations is observed. Limits are set on the squark mass in the Tsqk1 simplified model, both in the assumption of a single light squark and of 8 degenerate squarks, see Fig. 11 and Table 3.
- ²² AAD 15BV summarized and extended ATLAS searches for gluinos and first- and second-generation squarks in final states containing jets and missing transverse momentum, with or without leptons or b -jets in the $\sqrt{s} = 8 \text{ TeV}$ data set collected in 2012. The paper reports the results of new interpretations and statistical combinations of previously published analyses, as well as new analyses. Exclusion limits at 95% C.L. are set on the squark mass in several R-parity conserving models. See their Figs. 9, 11, 18, 22, 24, 27, 28.
- ²³ AAD 15CS searched in 20.3 fb^{-1} of pp collisions at $\sqrt{s} = 8 \text{ TeV}$ for evidence of pair production of squarks, decaying into a quark and a neutralino, where a photon was radiated either from an initial-state quark, from an intermediate squark, or from a final-state quark. No evidence was found for an excess above the expected level of Standard Model background and a 95% C.L. exclusion limit was set on the squark mass as a function of the squark-neutralino mass difference, see Fig. 19.
- ²⁴ AAD 15K searched in 20.3 fb^{-1} of pp collisions at $\sqrt{s} = 8 \text{ TeV}$ for events containing at least two jets, where the two leading jets are each identified as originating from c -quarks, and large missing transverse momentum. No excess of events above the expected level of Standard Model background was found. Exclusion limits at 95% C.L. are set on the mass of superpartners of charm quarks (\tilde{c}). Assuming that the decay $\tilde{c} \rightarrow c \tilde{\chi}_1^0$ takes place 100% of the time, a scalar charm mass below 490 GeV is excluded for $m_{\tilde{\chi}_1^0} < 200 \text{ GeV}$. For more details, see their Fig. 2.
- ²⁵ KHACHATRYAN 15AF searched in 19.5 fb^{-1} of pp collisions at $\sqrt{s} = 8 \text{ TeV}$ for events with at least two energetic jets and significant \cancel{E}_T , using the transverse mass variable M_{T2} to discriminate between signal and background processes. No significant excess above the Standard Model expectations is observed. Limits are set on the squark mass in simplified models where the decay $\tilde{q} \rightarrow q \tilde{\chi}_1^0$ takes place with a branching ratio of 100%, both for the case of a single light squark or 8 degenerate squarks, see Fig. 12. See also Table 5. Exclusions in the CMSSM, assuming $\tan\beta = 30$, $A_0 = -2 \max(m_0, m_{1/2})$ and $\mu > 0$, are also presented, see Fig. 15.
- ²⁶ AAD 14AE searched in 20.3 fb^{-1} of pp collisions at $\sqrt{s} = 8 \text{ TeV}$ for strongly produced supersymmetric particles in events containing jets and large missing transverse momentum, and no electrons or muons. No excess over the expected SM background is observed. Exclusion limits are derived in simplified models containing squarks that decay via $\tilde{q} \rightarrow q \tilde{\chi}_1^0$, where either a single light state or two degenerate generations of squarks are assumed, see Fig. 10.
- ²⁷ CHATRCHYAN 14AH searched in 4.7 fb^{-1} of pp collisions at $\sqrt{s} = 7 \text{ TeV}$ for events with at least two energetic jets and significant \cancel{E}_T , using the razor variables (M_R and

Searches Particle Listings

Supersymmetric Particle Searches

- R^2) to discriminate between signal and background processes. No significant excess above the Standard Model expectations is observed. Limits are set on squark masses in simplified models where the decay $\tilde{q} \rightarrow q\tilde{\chi}_1^0$ takes place with a branching ratio of 100%, see Fig. 28. Exclusions in the CMSSM, assuming $\tan\beta = 10$, $A_0 = 0$ and $\mu > 0$, are also presented, see Fig. 26.
- 28 CHATRCHYAN 14i searched in 19.5 fb^{-1} of pp collisions at $\sqrt{s} = 8 \text{ TeV}$ for events containing multijets and large \cancel{E}_T . No excess over the expected SM background is observed. Exclusion limits are derived in simplified models containing squarks that decay via $\tilde{q} \rightarrow q\tilde{\chi}_1^0$, where either a single light state or two degenerate generations of squarks are assumed, see Fig. 7a.
- 29 AAD 13l searched in 4.7 fb^{-1} of pp collisions at $\sqrt{s} = 7 \text{ TeV}$ for the production of squarks and gluinos in events containing jets, missing transverse momentum and no high- p_T electrons or muons. No excess over the expected SM background is observed. In mSUGRA/CMSSM models with $\tan\beta = 10$, $A_0 = 0$ and $\mu > 0$, squarks and gluinos of equal mass are excluded for masses below 1360 GeV at 95% C.L. In a simplified model containing only squarks of the first two generations, a gluino octet and a massless neutralino, squark masses below 1320 GeV are excluded at 95% C.L. for gluino masses below 2 TeV. See Figures 10–15 for more precise bounds.
- 30 AAD 13q searched in 4.7 fb^{-1} of pp collisions at $\sqrt{s} = 7 \text{ TeV}$ for events containing a high- p_T isolated photon, at least one jet identified as originating from a bottom quark, and high missing transverse momentum. Such signatures may originate from supersymmetric models with gauge-mediated supersymmetry breaking in events in which one of a pair of higgsino-like neutralinos decays into a photon and a gravitino while the other decays into a Higgs boson and a gravitino. No significant excess above the expected background was found and limits were set on the squark mass as a function of the neutralino mass in a generalized GMSB model (GGM) with a higgsino-like neutralino NLSP, see their Fig. 4. For neutralino masses greater than 220 GeV, squark masses below 1020 GeV are excluded at 95% C.L.
- 31 CHATRCHYAN 13 looked in 4.98 fb^{-1} of pp collisions at $\sqrt{s} = 7 \text{ TeV}$ for events with two opposite-sign leptons (e, μ, τ), jets and missing transverse energy. No excess beyond the Standard Model expectation is observed. Exclusion limits are derived in the mSUGRA/CMSSM model with $\tan\beta = 10$, $A_0 = 0$ and $\mu > 0$, see Fig. 6.
- 32 CHATRCHYAN 13c searched in 4.98 fb^{-1} of pp collisions at $\sqrt{s} = 7 \text{ TeV}$ for the production of squarks and gluinos in events containing 0,1,2, ≥ 3 b -jets, missing transverse momentum and no electrons or muons. No excess over the expected SM background is observed. In mSUGRA/CMSSM models with $\tan\beta = 10$, $A_0 = 0$, and $\mu > 0$, squarks and gluinos of equal mass are excluded for masses below 1250 GeV at 95% C.L. Exclusions are also derived in various simplified models, see Fig. 7.
- 33 CHATRCHYAN 13h searched in 4.96 fb^{-1} of pp collisions at $\sqrt{s} = 7 \text{ TeV}$ for events with two photons, ≥ 4 jets and low \cancel{E}_T due to $\tilde{q} \rightarrow \gamma\tilde{\chi}_1^0$ decays in a stealth SUSY framework, where the $\tilde{\chi}_1^0$ decays through a singlino (\tilde{S}) intermediate state to $\gamma S\tilde{G}$, with the singlet state S decaying to two jets. No significant excess above the expected background was found and limits were set in a particular R -parity conserving stealth SUSY model. The model assumes $m_{\tilde{\chi}_1^0} = 0.5 m_{\tilde{q}}$, $m_S = 100 \text{ GeV}$ and $m_S = 90 \text{ GeV}$. Under these assumptions, squark masses less than 1430 GeV were excluded at the 95% C.L.
- 34 CHATRCHYAN 13t searched in 11.7 fb^{-1} of pp collisions at $\sqrt{s} = 8 \text{ TeV}$ for events with at least two energetic jets and significant \cancel{E}_T , using the α_T variable to discriminate between processes with genuine and misreconstructed \cancel{E}_T . No significant excess above the Standard Model expectations is observed. Limits are set on squark masses in simplified models where the decay $\tilde{q} \rightarrow q\tilde{\chi}_1^0$ takes place with a branching ratio of 100%, assuming an eightfold degeneracy of the masses of the first two generation squarks, see Fig. 8 and Table 9. Also limits in the case of a single light squark are given.
- 35 AAD 12ax searched in 1.04 fb^{-1} of pp collisions at $\sqrt{s} = 7 \text{ TeV}$ for supersymmetry in events containing jets, missing transverse momentum and one isolated electron or muon. No excess over the expected SM background is observed and model-independent limits are set on the cross section of new physics contributions to the signal regions. In mSUGRA/CMSSM models with $\tan\beta = 10$, $A_0 = 0$ and $\mu > 0$, squarks and gluinos of equal mass are excluded for masses below 820 GeV at 95% C.L. Limits are also set on simplified models for squark production and decay via an intermediate chargino and on supersymmetric models with bilinear R -parity violation. Supersedes AAD 11g.
- 36 AAD 12cj searched in 4.7 fb^{-1} of pp collisions at $\sqrt{s} = 7 \text{ TeV}$ for events containing one or more isolated leptons (electrons or muons), jets and \cancel{E}_T . The observations are in good agreement with the SM expectations and exclusion limits have been set in number of SUSY models. In the mSUGRA/CMSSM model with $\tan\beta = 10$, $A_0 = 0$, and $\mu > 0$, 95% C.L. exclusion limits have been derived for $m_{\tilde{q}} < 1200 \text{ GeV}$, assuming equal squark and gluino masses. In minimal GMSB, values of the effective SUSY breaking scale $\Lambda < 50 \text{ TeV}$ are excluded at 95% C.L. for $\tan\beta < 45$. Also exclusion limits in a number of simplified models have been presented, see Figs. 10 and 12.
- 37 AAD 12cp searched in 4.8 fb^{-1} of pp collisions at $\sqrt{s} = 7 \text{ TeV}$ for events with two photons and large \cancel{E}_T due to $\tilde{\chi}_1^0 \rightarrow \gamma\tilde{G}$ decays in a GMSB framework. No significant excess above the expected background was found and limits were set on the squark mass as a function of the neutralino mass in a generalized GMSB model (GGM) with a bino-like neutralino NLSP. The other sparticle masses were decoupled, $\tan\beta = 2$ and $c\tau_{NLSP} < 0.1 \text{ mm}$. Also, in the framework of the SPS8 model, a 95% C.L. lower limit was set on the breaking scale Λ of 196 TeV.
- 38 AAD 12w searched in 1.04 fb^{-1} of pp collisions at $\sqrt{s} = 7 \text{ TeV}$ for the production of squarks and gluinos in events containing jets, missing transverse momentum and no electrons or muons. No excess over the expected SM background is observed. In mSUGRA/CMSSM models with $\tan\beta = 10$, $A_0 = 0$ and $\mu > 0$, squarks and gluinos of equal mass are excluded for masses below 950 GeV at 95% C.L. In a simplified model containing only squarks of the first two generations, a gluino octet and a massless neutralino, squark masses below 875 GeV are excluded at 95% C.L.
- 39 CHATRCHYAN 12 looked in 35 pb^{-1} of pp collisions at $\sqrt{s} = 7 \text{ TeV}$ for events with e and/or μ and/or jets, a large total transverse energy, and \cancel{E}_T . The event selection is based on the dimensionless razor variable R , related to the \cancel{E}_T and M_R , an indicator of the heavy particle mass scale. No evidence for an excess over the expected background is observed. Limits are derived in the CMSSM ($m_0, m_{1/2}$) plane for $\tan\beta = 3, 10$ and 50 (see Fig. 7 and 8). Limits are also obtained for Simplified Model Spectra.
- 40 CHATRCHYAN 12ae searched in 4.98 fb^{-1} of pp collisions at $\sqrt{s} = 7 \text{ TeV}$ for events with at least three jets and large missing transverse momentum. No significant excesses over the expected SM backgrounds are observed and 95% C.L. limits on the production cross section of squarks in a scenario where $\tilde{q} \rightarrow q\tilde{\chi}_1^0$ with a 100% branching ratio, see Fig. 3. For $m_{\tilde{\chi}_1^0} < 200 \text{ GeV}$, values of $m_{\tilde{q}}$ below 760 GeV are excluded at 95% C.L. Also limits in the CMSSM are presented, see Fig. 2.
- 41 CHATRCHYAN 12at searched in 4.73 fb^{-1} of pp collisions at $\sqrt{s} = 7 \text{ TeV}$ for the production of squarks and gluinos in events containing jets, missing transverse momentum and no electrons or muons. No excess over the expected SM background is observed. In mSUGRA/CMSSM models with $\tan\beta = 10$, $A_0 = 0$ and $\mu > 0$, squarks with masses below 1110 GeV are excluded at 95% C.L. Squarks and gluinos of equal mass are excluded for masses below 1180 GeV at 95% C.L. Exclusions are also derived in various simplified models, see Fig. 6.
- 42 AABOU 18v searched in 36.1 fb^{-1} of pp collisions at $\sqrt{s} = 13 \text{ TeV}$ in events with no charged leptons, jets and missing transverse momentum. The data are found to be consistent with the SM expectation. Results are interpreted in the Tsqk5 model. Squark masses below 1100 GeV are excluded if $(m_{\tilde{\chi}_2^0} - m_{\tilde{\chi}_1^0})/(m_{\tilde{q}} - m_{\tilde{\chi}_1^0}) < 0.95$ and $m_{\tilde{\chi}_1^0} = 60 \text{ GeV}$, see their Fig. 16(a).
- 43 KHACHATRYAN 16bt performed a global Bayesian analysis of a wide range of CMS results obtained with data samples corresponding to 5.0 fb^{-1} of pp collisions at $\sqrt{s} = 7 \text{ TeV}$ and in 19.5 fb^{-1} of pp collisions at $\sqrt{s} = 8 \text{ TeV}$. The set of searches considered, both individually and in combination, includes those with all-hadronic final states, same-sign and opposite-sign dileptons, and multi-lepton final states. An interpretation was given in a scan of the 19-parameter pMSSM. No scan points with a gluino mass less than 500 GeV survived and 98% of models with a squark mass less than 300 GeV were excluded.
- 44 AAD 15ai searched in 20 fb^{-1} of pp collisions at $\sqrt{s} = 8 \text{ TeV}$ for events containing at least one isolated lepton (electron or muon), jets, and large missing transverse momentum. No excess of events above the expected level of Standard Model background was found. Exclusion limits at 95% C.L. are set on the squark masses in the CMSSM/mSUGRA, see Fig. 15, in the NUHM2, see Fig. 16, and in various simplified models, see Figs. 19–21.
- 45 KHACHATRYAN 15ar searched in 19.7 fb^{-1} of pp collisions at $\sqrt{s} = 8 \text{ TeV}$ for events containing jets, either a charged lepton or a photon, and low missing transverse momentum. No significant excess above the Standard Model expectations is observed. Limits are set on the squark mass in a stealth SUSY model where the decays $\tilde{q} \rightarrow q\tilde{\chi}_1^\pm$, $\tilde{\chi}_1^\pm \rightarrow \tilde{S} W^\pm$, $\tilde{S} \rightarrow S\tilde{G}$ and $S \rightarrow gg$, with $m_S = 100 \text{ GeV}$ and $m_S = 90 \text{ GeV}$, take place with a branching ratio of 100%. See Fig. 6 for γ or Fig. 7 for e^\pm analyses.
- 46 KHACHATRYAN 15az searched in 19.7 fb^{-1} of pp collisions at $\sqrt{s} = 8 \text{ TeV}$ for events with either at least one photon, hadronic jets and \cancel{E}_T (single photon channel) or with at least two photons and at least one jet and using the razor variables. No significant excess above the Standard Model expectations is observed. Limits are set on gluino masses in the general gauge-mediated SUSY breaking model (GGM), for both a bino-like and wino-like neutralino NLSP scenario, see Fig. 8 and 9.
- 47 AAD 14e searched in 20.3 fb^{-1} of pp collisions at $\sqrt{s} = 8 \text{ TeV}$ for strongly produced supersymmetric particles in events containing jets and two same-sign leptons or three leptons. The search also utilizes jets originating from b -quarks, missing transverse momentum and other variables. No excess over the expected SM background is observed. Exclusion limits are derived in simplified models containing gluinos and squarks, see Figures 5 and 6. In the $\tilde{q} \rightarrow q'\tilde{\chi}_1^\pm$, $\tilde{\chi}_1^\pm \rightarrow W^{(*)}\tilde{\chi}_2^0$, $\tilde{\chi}_2^0 \rightarrow Z^{(*)}\tilde{\chi}_1^0$ simplified model, the following assumptions have been made: $m_{\tilde{\chi}_1^\pm} = 0.5 m_{\tilde{\chi}_2^0} + m_{\tilde{g}}$, $m_{\tilde{\chi}_2^0} = 0.5 (m_{\tilde{\chi}_1^\pm} + m_{\tilde{\chi}_1^\pm})$. In the $\tilde{q} \rightarrow q'\tilde{\chi}_1^\pm$ or $\tilde{q} \rightarrow q'\tilde{\chi}_2^0$, $\tilde{\chi}_1^\pm \rightarrow e^\pm \nu \chi_1^0$ or $\tilde{\chi}_2^0 \rightarrow e^\pm e^\mp (\nu\nu)\tilde{\chi}_1^0$ simplified model, the following assumptions have been made: $m_{\tilde{\chi}_1^\pm} = m_{\tilde{\chi}_2^0} = 0.5 (m_{\tilde{\chi}_1^\pm} + m_{\tilde{q}})$, $m_{\tilde{\chi}_2^0} < 460 \text{ GeV}$. Limits are also derived in the mSUGRA/CMSSM, bRPV and GMSB models, see their Fig. 8.
- 48 CHATRCHYAN 13ao searched in 4.98 fb^{-1} of pp collisions at $\sqrt{s} = 7 \text{ TeV}$ for events with two opposite-sign isolated leptons accompanied by hadronic jets and \cancel{E}_T . No significant excesses over the expected SM backgrounds are observed and 95% C.L. exclusion limits are derived in the mSUGRA/CMSSM model with $\tan\beta = 10$, $A_0 = 0$ and $\mu > 0$, see Fig. 8.
- 49 CHATRCHYAN 13av searched in 4.7 fb^{-1} of pp collisions at $\sqrt{s} = 7 \text{ TeV}$ for new heavy particle pairs decaying into jets (possibly b -tagged), leptons and \cancel{E}_T using the Razor variables. No significant excesses over the expected SM backgrounds are observed and 95% C.L. exclusion limits are derived in the mSUGRA/CMSSM model with $\tan\beta = 10$, $A_0 = 0$ and $\mu > 0$, see Fig. 3. The results are also interpreted in various simplified models, see Fig. 4.
- 50 CHATRCHYAN 13w searched in 4.93 fb^{-1} of pp collisions at $\sqrt{s} = 7 \text{ TeV}$ for events with one or more photons, hadronic jets and \cancel{E}_T . No significant excess above the Standard Model expectations is observed. Limits are set on squark masses in the general gauge-mediated SUSY breaking model (GGM), for both a wino-like and bino-like neutralino NLSP scenario, see Fig. 5.
- 51 DREINER 12a reassesses constraints from CMS (at 7 TeV, $\sim 4.4 \text{ fb}^{-1}$) under the assumption that the first and second generation squarks and the lightest SUSY particle are quasi-degenerate in mass (compressed spectrum).
- 52 DREINER 12a reassesses constraints from CMS (at 7 TeV, $\sim 4.4 \text{ fb}^{-1}$) under the assumption that the first and second generation squarks, the gluino, and the lightest SUSY particle are quasi-degenerate in mass (compressed spectrum).

R-parity violating \tilde{q} (Squark) mass limit

VALUE (GeV)	CL%	DOCUMENT ID	TECN	COMMENT
none 100–720	95	1 SIRUNYAN	18EA CMS	2 large jets with four-parton substructure, $\tilde{q} \rightarrow 4q$
>1600	95	2 KHACHATRYAN 16bx	CMS	$\tilde{q} \rightarrow q\tilde{\chi}_1^0, \tilde{\chi}_1^0 \rightarrow \ell\ell\nu, \lambda_{121}$ or $\lambda_{122} \neq 0, m_{\tilde{g}} = 2400 \text{ GeV}$
>1000	95	3 AAD	15CB ATLS	jets, $\tilde{q} \rightarrow q\tilde{\chi}_1^0, \tilde{\chi}_1^0 \rightarrow \ell q q$, $m_{\tilde{\chi}_1^0} = 108 \text{ GeV}$ and $2.5 < c\tau_{\tilde{\chi}_1^0} < 200 \text{ mm}$
		4 AAD	12AX ATLS	$\ell + \text{jets} + \cancel{E}_T$, CMSSM, $m_{\tilde{q}} = m_{\tilde{g}}$
		5 CHATRCHYAN 12al	CMS	$\geq 3\ell^\pm$

- 1 SIRUNYAN 18ea searched in 38.2 fb^{-1} of pp collisions at $\sqrt{s} = 13 \text{ TeV}$ for the pair production of resonances, each decaying to at least four quarks. Reconstructed particles are clustered into two large jets of similar mass, each consistent with four-parton substructure. No statistically significant excess over the Standard Model expectation is observed. Limits are set on the squark and gluino mass in RPV supersymmetry models where squarks (gluinos) decay, through intermediate higgsinos, to four (five) quarks, see their Figure 4.

- ² KHACHATRYAN 16BX searched in 19.5 fb^{-1} of pp collisions at $\sqrt{s} = 8 \text{ TeV}$ for events containing 4 leptons coming from R -parity-violating decays of $\tilde{\chi}_1^0 \rightarrow \ell\ell\nu$ with $\lambda_{121} \neq 0$ or $\lambda_{122} \neq 0$. No excess over the expected background is observed. Limits are derived on the gluino, squark and stop masses, see Fig. 23.
- ³ AAD 15CB searched for events containing at least one long-lived particle that decays at a significant distance from its production point (displaced vertex, DV) into two leptons or into five or more charged particles in 20.3 fb^{-1} of pp collisions at $\sqrt{s} = 8 \text{ TeV}$. The dilepton signature is characterised by DV formed from at least two lepton candidates. Four different final states were considered for the multitrack signature, in which the DV must be accompanied by a high-transverse momentum muon or electron candidate that originates from the DV, jets or missing transverse momentum. No events were observed in any of the signal regions. Results were interpreted in SUSY scenarios involving R -parity violation, split supersymmetry, and gauge mediation. See their Fig. 14–20.
- ⁴ AAD 12AX searched in 1.04 fb^{-1} of pp collisions at $\sqrt{s} = 7 \text{ TeV}$ for supersymmetry in events containing jets, missing transverse momentum and one isolated electron or muon. No excess over the expected SM background is observed and model-independent limits are set on the cross section of new physics contributions to the signal regions. In mSUGRA/CMSSM models with $\tan\beta = 10$, $A_0 = 0$ and $\mu > 0$, squarks and gluinos of equal mass are excluded for masses below 820 GeV at 95% C.L. Limits are also set on simplified models for squark production and decay via an intermediate chargino and on supersymmetric models with bilinear R -parity violation. Supersedes AAD 11G.
- ⁵ CHATRCHYAN 12AL looked in 4.98 fb^{-1} of pp collisions at $\sqrt{s} = 7 \text{ TeV}$ for anomalous production of events with three or more isolated leptons. Limits on squark and gluino masses are set in RPV SUSY models with leptonic $L\tilde{L}\tilde{E}$ couplings, $\lambda_{123} > 0.05$, and hadronic $U\tilde{D}\tilde{D}$ couplings, $\lambda_{112}^U > 0.05$, see their Fig. 5. In the $U\tilde{D}\tilde{D}$ case the leptons arise from supersymmetric cascade decays. A very specific supersymmetric spectrum is assumed. All decays are prompt.

Long-lived \tilde{q} (Squark) mass limit

The following are bounds on long-lived scalar quarks, assumed to hadronise into hadrons with lifetime long enough to escape the detector prior to a possible decay. Limits may depend on the mixing angle of mass eigenstates: $\tilde{q}_1 = \tilde{q}_L \cos\theta_q + \tilde{q}_R \sin\theta_q$.

The coupling to the Z^0 boson vanishes for up-type squarks when $\theta_u = 0.98$, and for down type squarks when $\theta_d = 1.17$.

VALUE (GeV)	CL%	DOCUMENT ID	TECN	COMMENT
>1250	95	¹ AABOUD 19AT ATLS	19AT ATLS	\tilde{b} R -hadrons
>1340	95	² AABOUD 19AT ATLS	19AT ATLS	\tilde{t} R -hadrons
>1600	95	³ SIRUNYAN 19BH CMS	19BH CMS	long-lived \tilde{t} , RPV, $\tilde{t} \rightarrow \tilde{d}\tilde{d}$, $10 \text{ mm} < c\tau < 110 \text{ mm}$
>1350	95	³ SIRUNYAN 19BH CMS	19BH CMS	long-lived \tilde{t} , RPV, $\tilde{t} \rightarrow b\tilde{l}$, $7 \text{ mm} < c\tau < 110 \text{ mm}$
> 805	95	⁴ AABOUD 16B ATLS	16B ATLS	\tilde{b} R -hadrons
> 890	95	⁵ AABOUD 16B ATLS	16B ATLS	\tilde{t} R -hadrons
>1040	95	⁶ KHACHATRYAN 16BWCMS	16BWCMS	\tilde{t} R -hadrons, cloud interaction model
>1000	95	⁶ KHACHATRYAN 16BWCMS	16BWCMS	\tilde{t} R -hadrons, charge-suppressed interaction model
> 845	95	⁷ AAD 15AE ATLS	15AE ATLS	\tilde{b} R -hadron, stable, Regge model
> 900	95	⁷ AAD 15AE ATLS	15AE ATLS	\tilde{t} R -hadron, stable, Regge model
>1500	95	⁷ AAD 15AE ATLS	15AE ATLS	\tilde{g} decaying to 300 GeV stable sleptons, LeptoSUSY model
> 751	95	⁸ AAD 15BM ATLS	15BM ATLS	\tilde{b} R -hadron, stable, Regge model
> 766	95	⁸ AAD 15BM ATLS	15BM ATLS	\tilde{t} R -hadron, stable, Regge model
> 525	95	⁹ KHACHATRYAN 15AK CMS	15AK CMS	\tilde{t} R -hadrons, $10 \mu\text{s} < \tau < 1000 \text{ s}$
> 470	95	⁹ KHACHATRYAN 15AK CMS	15AK CMS	\tilde{t} R -hadrons, $1 \mu\text{s} < \tau < 1000 \text{ s}$
• • • We do not use the following data for averages, fits, limits, etc. • • •				
> 683	95	¹⁰ AAD 13AA ATLS	13AA ATLS	\tilde{t} , R -hadrons, generic interaction model
> 612	95	¹¹ AAD 13AA ATLS	13AA ATLS	\tilde{b} , R -hadrons, generic interaction model
> 344	95	¹² AAD 13BC ATLS	13BC ATLS	R -hadrons, $\tilde{t} \rightarrow b\tilde{\chi}_1^0$, Regge model, lifetime between 10^{-5} and 10^3 s , $m_{\tilde{\chi}_1^0} = 100 \text{ GeV}$
> 379	95	¹³ AAD 13BC ATLS	13BC ATLS	R -hadrons, $\tilde{t} \rightarrow t\tilde{\chi}_1^0$, Regge model, lifetime between 10^{-5} and 10^3 s , $m_{\tilde{\chi}_1^0} = 100 \text{ GeV}$
> 935	95	¹⁴ CHATRCHYAN 13AB CMS	13AB CMS	long-lived \tilde{t} forming R -hadrons, cloud interaction model

- ¹ AABOUD 19AT searched in 36.1 fb^{-1} of pp collisions at $\sqrt{s} = 13 \text{ TeV}$ for metastable and stable R -hadrons. Multiple search strategies for a wide range of lifetimes, corresponding to path lengths of a few meters, are defined. No significant deviations from the expected Standard Model background are observed. Sbottom R -hadrons are excluded at 95% C.L. for masses below 1250 GeV . Less stringent constraints are achieved with the muon-spectrometer agnostic analysis. See their Figure 9 (bottom-left).
- ² AABOUD 19AT searched in 36.1 fb^{-1} of pp collisions at $\sqrt{s} = 13 \text{ TeV}$ for metastable and stable R -hadrons. Multiple search strategies for a wide range of lifetimes, corresponding to path lengths of a few meters, are defined. No significant deviations from the expected Standard Model background are observed. Stop R -hadrons are excluded at 95% C.L. for masses below 1340 GeV . Similar constraints are achieved with the muon-spectrometer agnostic analysis. See their Figure 9 (bottom-right).
- ³ SIRUNYAN 19BH searched in 35.9 fb^{-1} of pp collisions at $\sqrt{s} = 13 \text{ TeV}$ for long-lived particles decaying into jets, with each long-lived particle having a decay vertex well displaced from the production vertex. The selected events are found to be consistent with standard model predictions. Limits are set on the gluino mass in a GMSB model where the gluino is decaying via $\tilde{g} \rightarrow g\tilde{G}$, see their Figure 4 and in an RPV model of supersymmetry where the gluino is decaying via $\tilde{g} \rightarrow \tilde{t}\tilde{b}$, see their Figures 5. Limits are also set on the stop mass in two RPV models, see their Figure 6 (for $\tilde{t} \rightarrow b\tilde{l}$ decays) and Figure 7 (for $\tilde{t} \rightarrow \tilde{d}\tilde{d}$ decays).
- ⁴ AABOUD 16B searched in 3.2 fb^{-1} of pp collisions at $\sqrt{s} = 13 \text{ TeV}$ for long-lived R -hadrons using observables related to large ionization losses and slow propagation velocities, which are signatures of heavy charged particles traveling significantly slower than

the speed of light. Exclusion limits at 95% C.L. are set on the long-lived sbottom masses exceeding 805 GeV . See their Fig. 5.

- ⁵ AABOUD 16B searched in 3.2 fb^{-1} of pp collisions at $\sqrt{s} = 13 \text{ TeV}$ for long-lived R -hadrons using observables related to large ionization losses and slow propagation velocities, which are signatures of heavy charged particles traveling significantly slower than the speed of light. Exclusion limits at 95% C.L. are set on the long-lived stop masses exceeding 890 GeV . See their Fig. 5.
- ⁶ KHACHATRYAN 16BW searched in 2.5 fb^{-1} of pp collisions at $\sqrt{s} = 13 \text{ TeV}$ for events with heavy stable charged particles, identified by their anomalously high energy deposits in the silicon tracker and/or long time-of-flight measurements by the muon system. No evidence for an excess over the expected background is observed. Limits are derived for pair production of top squarks as a function of mass, depending on the interaction model, see Fig. 4 and Table 7.
- ⁷ AAD 15AE searched in 19.1 fb^{-1} of pp collisions at $\sqrt{s} = 8 \text{ TeV}$ for heavy long-lived charged particles, measured through their specific ionization energy loss in the ATLAS pixel detector or their time-of-flight in the ALTAS muon system. In the absence of an excess of events above the expected backgrounds, limits are set R -hadrons in various scenarios, see Fig. 11. Limits are also set in LeptoSUSY models where the gluino decays to stable 300 GeV leptons, see Fig. 9.
- ⁸ AAD 15BM searched in 18.4 fb^{-1} of pp collisions at $\sqrt{s} = 8 \text{ TeV}$ for stable and metastable non-relativistic charged particles through their anomalously specific ionization energy loss in the ATLAS pixel detector. In absence of an excess of events above the expected backgrounds, limits are set on stable bottom and top squark R -hadrons, see Table 5.
- ⁹ KHACHATRYAN 15AK looked in a data set corresponding to fb^{-1} of pp collisions at $\sqrt{s} = 8 \text{ TeV}$, and a search interval corresponding to 281 h of trigger lifetime, for long-lived particles that have stopped in the CMS detector. No evidence for an excess over the expected background in a cloud interaction model is observed. Assuming the decay $\tilde{t} \rightarrow t\tilde{\chi}_1^0$ and lifetimes between $1 \mu\text{s}$ and 1000 s , limits are derived on \tilde{t} production as a function of $m_{\tilde{\chi}_1^0}$, see Figs. 4 and 7. The exclusions require that $m_{\tilde{\chi}_1^0}$ is kinematically consistent with the minimum values of the jet energy thresholds used.
- ¹⁰ AAD 13AA searched in 4.7 fb^{-1} of pp collisions at $\sqrt{s} = 7 \text{ TeV}$ for events containing colored long-lived particles that hadronize forming R -hadrons. No significant excess above the expected background was found. Long-lived R -hadrons containing a \tilde{t} are excluded for masses up to 683 GeV at 95% C.L. in a general interaction model. Also, limits independent of the fraction of R -hadrons that arrive charged in the muon system were derived, see Fig. 6.
- ¹¹ AAD 13AA searched in 4.7 fb^{-1} of pp collisions at $\sqrt{s} = 7 \text{ TeV}$ for events containing colored long-lived particles that hadronize forming R -hadrons. No significant excess above the expected background was found. Long-lived R -hadrons containing a \tilde{b} are excluded for masses up to 612 GeV at 95% C.L. in a general interaction model. Also, limits independent of the fraction of R -hadrons that arrive charged in the muon system were derived, see Fig. 6.
- ¹² AAD 13BC searched in 5.0 fb^{-1} of pp collisions at $\sqrt{s} = 7 \text{ TeV}$ and in 22.9 fb^{-1} of pp collisions at $\sqrt{s} = 8 \text{ TeV}$ for bottom squark R -hadrons that have come to rest within the ATLAS calorimeter and decay at some later time to hadronic jets and a neutralino. In absence of an excess of events above the expected backgrounds, limits are set on sbottom masses for the decay $\tilde{b} \rightarrow b\tilde{\chi}_1^0$, for different lifetimes, and for a neutralino mass of 100 GeV , see their Table 6 and Fig. 10.
- ¹³ AAD 13BC searched in 5.0 fb^{-1} of pp collisions at $\sqrt{s} = 7 \text{ TeV}$ and in 22.9 fb^{-1} of pp collisions at $\sqrt{s} = 8 \text{ TeV}$ for bottom squark R -hadrons that have come to rest within the ATLAS calorimeter and decay at some later time to hadronic jets and a neutralino. In absence of an excess of events above the expected backgrounds, limits are set on stop masses for the decay $\tilde{t} \rightarrow t\tilde{\chi}_1^0$, for different lifetimes, and for a neutralino mass of 100 GeV , see their Table 6 and Fig. 10.
- ¹⁴ CHATRCHYAN 13AB looked in 5.0 fb^{-1} of pp collisions at $\sqrt{s} = 7 \text{ TeV}$ and in 18.8 fb^{-1} of pp collisions at $\sqrt{s} = 8 \text{ TeV}$ for events with heavy stable particles, identified by their anomalous dE/dx in the tracker or additionally requiring that it be identified as muon in the muon chambers, from pair production of \tilde{t}_1 's. No evidence for an excess over the expected background is observed. Limits are derived for pair production of stops as a function of mass in the cloud interaction model (see Fig. 8 and Table 6). In the charge-suppressed model, the limit decreases to 818 GeV .

\tilde{b} (Sbottom) mass limit

Limits in e^+e^- depend on the mixing angle of the mass eigenstate $\tilde{b}_1 = \tilde{b}_L \cos\theta_b + \tilde{b}_R \sin\theta_b$. Coupling to the Z vanishes for $\theta_b \sim 1.17$. As a consequence, no absolute constraint in the mass region $\lesssim 40 \text{ GeV}$ is available in the literature at this time from e^+e^- collisions. In the Listings below, we use $\Delta m = m_{\tilde{b}_1} - m_{\tilde{\chi}_1^0}$.

Some earlier papers are now obsolete and have been omitted. They were last listed in our PDG 14 edition: K. Olive, *et al.* (Particle Data Group), Chinese Physics **C38** 070001 (2014) (<http://pdg.lbl.gov>).

R -parity conserving \tilde{b} (Sbottom) mass limit

VALUE (GeV)	CL%	DOCUMENT ID	TECN	COMMENT
>1500	95	¹ AAD 19H ATLS	19H ATLS	≥ 3 b -jets + E_T , Tsbot4, ≥ 1 $h(\rightarrow b\tilde{b})$, $m_{\tilde{\chi}_1^0} = 60 \text{ GeV}$
>1300	95	² AAD 19H ATLS	19H ATLS	≥ 3 b -jets + E_T , Tsbot4, ≥ 1 $h(\rightarrow b\tilde{b})$, $m_{\tilde{\chi}_2^0} = m_{\tilde{\chi}_1^0} + 130 \text{ GeV}$
>1220	95	³ SIRUNYAN 19CH CMS	19CH CMS	jets + E_T , Tsbot1, $m_{\tilde{\chi}_1^0} = 0 \text{ GeV}$
> 530	95	⁴ SIRUNYAN 19CI CMS	19CI CMS	≥ 1 $H(\rightarrow \gamma\gamma)$ + jets + E_T , Tsbot4, $m_{\tilde{\chi}_2^0} = m_{\tilde{\chi}_1^0} + 130 \text{ GeV}$, $m_{\tilde{\chi}_1^0} = 1 \text{ GeV}$
> 430	95	⁵ AABOUD 18I ATLS	18I ATLS	≥ 1 jets + E_T , Tsbot1, $m_{\tilde{b}} - m_{\tilde{\chi}_1^0} \sim m_b$

Searches Particle Listings

Supersymmetric Particle Searches

> 840	95	6	SIRUNYAN	18AL	CMS	$\geq 3\ell^\pm + \text{jets} + \cancel{E}_T$, Tsb02, $m_{\tilde{\chi}_1^0} = 50$ GeV	> 500	95	36	CHATRCHYAN14H	CMS	same-sign $\ell^\pm \ell^\pm, \tilde{b} \rightarrow t \tilde{\chi}_1^\pm, \tilde{\chi}_1^\pm \rightarrow W^\pm \tilde{\chi}_1^0$ simplified model, $m_{\tilde{\chi}_1^\pm} = 2$ GeV, $m_{\tilde{\chi}_1^0} = 100$ GeV	
> 975	95	7	SIRUNYAN	18AR	CMS	$\ell^\pm \ell^\mp + \text{jets} + \cancel{E}_T$, Tsb03, $m_{\tilde{\chi}_1^\pm} = (m_{\tilde{\chi}_2^0} + m_{\tilde{\chi}_1^0})/2, m_{\tilde{\chi}_1^0} = 100$ GeV	> 620	95	37	AAD	13AU	ATLS	2 b -jets + $\cancel{E}_T, \tilde{b}_1 \rightarrow b \tilde{\chi}_1^0, m_{\tilde{\chi}_1^0} < 120$ GeV
>1060	95	8	SIRUNYAN	18AY	CMS	jets + \cancel{E}_T , Tsb01, $m_{\tilde{\chi}_1^0} = 0$ GeV	> 550	95	38	CHATRCHYAN13AT	CMS	jets + $\cancel{E}_T, \tilde{b} \rightarrow b \tilde{\chi}_1^0$ simplified model, $m_{\tilde{\chi}_1^0} = 50$ GeV	
>1230	95	9	SIRUNYAN	18B	CMS	jets + \cancel{E}_T , Tsb01, $m_{\tilde{\chi}_1^0} = 0$ GeV	> 600	95	39	CHATRCHYAN13T	CMS	jets + $\cancel{E}_T, \tilde{b} \rightarrow b \tilde{\chi}_1^0$ simplified model, $m_{\tilde{\chi}_1^0} = 0$ GeV	
> 420	95	10	SIRUNYAN	18X	CMS	$\geq 1 H (\rightarrow \gamma\gamma) + \text{jets} + \cancel{E}_T$, Tsb04, $m_{\tilde{\chi}_2^0} = m_{\tilde{\chi}_1^0} + 130$ GeV, $m_{\tilde{\chi}_1^0} < 225$ GeV	> 450	95	40	CHATRCHYAN13v	CMS	same-sign $\ell^\pm \ell^\pm + \geq 2$ b -jets, $\tilde{b} \rightarrow t \tilde{\chi}_1^\pm, \tilde{\chi}_1^\pm \rightarrow W^\pm \tilde{\chi}_1^0$ simplified model, $m_{\tilde{\chi}_1^0} = 50$ GeV	
> 700	95	11	AABOUD	17AJ	ATLS	same-sign $\ell^\pm \ell^\pm / 3 \ell + \text{jets} + \cancel{E}_T$, Tsb02, $m_{\tilde{\chi}_1^0} = 0$ GeV	> 390	95	41	AAD	12AN	ATLS	$\tilde{b}_1 \rightarrow b \tilde{\chi}_1^0$, simplified model, $m_{\tilde{\chi}_1^0} < 60$ GeV
> 950	95	12	AABOUD	17AX	ATLS	2 b -jets + \cancel{E}_T , Tsb01, $m_{\tilde{\chi}_1^0} = 0$ GeV	> 410	95	42	CHATRCHYAN12AI	CMS	$\ell^\pm \ell^\pm + b$ -jets + \cancel{E}_T	
> 880	95	13	AABOUD	17AX	ATLS	2 b -jets + \cancel{E}_T , mixture Tsb01 and Tsb02 BR=50%, $m_{\tilde{\chi}_1^0} = 0$ GeV, $m_{\tilde{\chi}_1^\pm} - m_{\tilde{\chi}_1^0} = 1$ GeV	> 294	95	43	CHATRCHYAN12Bo	CMS	$\tilde{b}_1 \rightarrow b \tilde{\chi}_1^0$, simplified model, $m_{\tilde{\chi}_1^0} = 50$ GeV	
> 315	95	14	KHACHATRY...17A	CMS	2 VBF jets + \cancel{E}_T , Tsb01, $m_{\tilde{b}} - m_{\tilde{\chi}_1^0} = 5$ GeV	> 230	95	44	AAD	11K	ATLS	stable b	
> 450	95	15	KHACHATRY...17AW	CMS	$\geq 3\ell^\pm, 2$ jets, Tsb02, $m_{\tilde{\chi}_1^0} = 50$ GeV, $m_{\tilde{\chi}_1^\pm} = 200$ GeV	> 247	95	45	AAD	11o	ATLS	$\tilde{g} \rightarrow \tilde{b}_1 b, \tilde{b}_1 \rightarrow b \tilde{\chi}_1^0, m_{\tilde{\chi}_1^0} = 60$ GeV	
> 800	95	16	KHACHATRY...17P	CMS	1 or more jets + \cancel{E}_T , Tsb01, $m_{\tilde{\chi}_1^0} = 0$ GeV	> 230	95	46	CHATRCHYAN11D	CMS	$\tilde{b}, \tilde{t} \rightarrow b$		
>1175	95	17	SIRUNYAN	17AZ	CMS	≥ 1 jets + \cancel{E}_T , Tsb01, $m_{\tilde{\chi}_1^0} = 0$ GeV	> 247	95	47	AALTONEN	10R	CDF	$\tilde{b}_1 \rightarrow b \tilde{\chi}_1^0, m_{\tilde{\chi}_1^0} < 70$ GeV
> 890	95	18	SIRUNYAN	17K	CMS	jets + \cancel{E}_T , Tsb01, $m_{\tilde{\chi}_1^0} = 0$ GeV	> 247	95	48	ABAZOV	10L	D0	$\tilde{b}_1 \rightarrow b \tilde{\chi}_1^0, m_{\tilde{\chi}_1^0} = 0$ GeV
> 810	95	19	SIRUNYAN	17s	CMS	same-sign $\ell^\pm \ell^\pm + \text{jets} + \cancel{E}_T$, Tsb02, $m_{\tilde{\chi}_1^0} = 50$ GeV, $m_{\tilde{\chi}_1^\pm} = 100$ GeV							
> 323	95	20	AABOUD	16D	ATLS	≥ 1 jet + \cancel{E}_T , Tsb01, $m_{\tilde{b}} - m_{\tilde{\chi}_1^0} = 5$ GeV							
> 840	95	21	AABOUD	16Q	ATLS	2 b -jets + \cancel{E}_T , Tsb01, $m_{\tilde{\chi}_1^0} = 100$ GeV							
> 540	95	22	AAD	16BB	ATLS	2 same-sign $3\ell + \text{jets} + \cancel{E}_T$, Tsb02, $m_{\tilde{\chi}_1^0} < 55$ GeV							
> 680	95	23	KHACHATRY...16BJ	CMS	same-sign $\ell^\pm \ell^\pm$, Tsb02, $m_{\tilde{\chi}_1^\pm} < 550$ GeV, $m_{\tilde{\chi}_1^0} = 50$ GeV								
> 500	95	23	KHACHATRY...16BJ	CMS	same-sign $\ell^\pm \ell^\pm$, Tsb02, $m_{\tilde{b}} - m_{\tilde{\chi}_1^0} < 100$ GeV, $m_{\tilde{\chi}_1^0} = 50$ GeV								
> 880	95	24	KHACHATRY...16BS	CMS	jets + \cancel{E}_T , Tsb01, $m_{\tilde{\chi}_1^0} = 0$ GeV								
> 550	95	25	KHACHATRY...16BY	CMS	opposite-sign $\ell^\pm \ell^\pm$, Tsb03, $m_{\tilde{\chi}_1^0} = 100$ GeV								
> 600	95	26	AAD	15CJ	ATLS	$\tilde{b} \rightarrow b \tilde{\chi}_1^0, m_{\tilde{\chi}_1^0} < 250$ GeV							
> 440	95	26	AAD	15CJ	ATLS	$\tilde{b} \rightarrow t \tilde{\chi}_1^\pm, \tilde{\chi}_1^\pm \rightarrow W^{(*)} \tilde{\chi}_1^0, m_{\tilde{\chi}_1^0} = 60$ GeV, $m_{\tilde{b}} - m_{\tilde{\chi}_1^\pm} < m_t$							
none 300-650	95	26	AAD	15CJ	ATLS	$\tilde{b} \rightarrow \tilde{b} b \tilde{\chi}_2^0, \tilde{\chi}_2^0 \rightarrow h \tilde{\chi}_1^0, m_{\tilde{\chi}_1^0} = 60$ GeV, $m_{\tilde{\chi}_2^0} > 250$ GeV							
> 640	95	27	KHACHATRY...15AF	CMS	$\tilde{b} \rightarrow b \tilde{\chi}_1^0, m_{\tilde{\chi}_1^0} = 0$								
> 650	95	28	KHACHATRY...15AH	CMS	$\tilde{b} \rightarrow b \tilde{\chi}_1^0, m_{\tilde{\chi}_1^0} = 0$								
> 250	95	28	KHACHATRY...15AH	CMS	$\tilde{b} \rightarrow b \tilde{\chi}_1^0, m_{\tilde{b}} - m_{\tilde{\chi}_1^0} < 10$ GeV								
> 570	95	29	KHACHATRY...15I	CMS	$\tilde{b} \rightarrow t \tilde{\chi}_1^\pm, \tilde{\chi}_1^\pm \rightarrow W^\pm \tilde{\chi}_1^0, m_{\tilde{\chi}_1^0} = 50$ GeV, $150 < m_{\tilde{\chi}_1^\pm} < 300$ GeV								
> 255	95	30	AAD	14T	ATLS	$\tilde{b}_1 \rightarrow b \tilde{\chi}_1^0, m_{\tilde{b}_1} - m_{\tilde{\chi}_1^0} \approx m_b$							
> 400	95	31	CHATRCHYAN14AH	CMS	jets + $\cancel{E}_T, \tilde{b} \rightarrow b \tilde{\chi}_1^0$ simplified model, $m_{\tilde{\chi}_1^0} = 50$ GeV								
		32	CHATRCHYAN14R	CMS	$\geq 3\ell^\pm, \tilde{b} \rightarrow t \tilde{\chi}_1^\pm, \tilde{\chi}_1^\pm \rightarrow W^\pm \tilde{\chi}_1^0$ simplified model, $m_{\tilde{\chi}_1^0} = 50$ GeV								
••• We do not use the following data for averages, fits, limits, etc. •••		33	KHACHATRY...15AD	CMS	$\ell^\pm \ell^\mp + \text{jets} + \cancel{E}_T, \tilde{b} \rightarrow b \ell^\pm \ell^\mp \tilde{\chi}_1^0$								
none 340-600	95	34	AAD	14AX	ATLS	≥ 3 b -jets + $\cancel{E}_T, \tilde{b} \rightarrow b \tilde{\chi}_2^0$ simplified model with $\tilde{\chi}_2^0 \rightarrow h \tilde{\chi}_1^0, m_{\tilde{\chi}_1^0} = 60$ GeV, $m_{\tilde{\chi}_2^0} = 300$ GeV							
> 440	95	35	AAD	14E	ATLS	$\ell^\pm \ell^\pm (\ell^\mp) + \text{jets}, \tilde{b}_1 \rightarrow t \tilde{\chi}_1^\pm$ with $\tilde{\chi}_1^\pm \rightarrow W^{(*)} \tilde{\chi}_1^0$ simplified model, $m_{\tilde{\chi}_1^\pm} = 2 m_{\tilde{\chi}_1^0}$							

- 11 AABOUD 17AJ searched in 36.1 fb^{-1} of pp collisions at $\sqrt{s} = 13 \text{ TeV}$ for events with two same-sign or three leptons, jets and large missing transverse momentum. No significant excess above the Standard Model expectations is observed. Limits up to 700 GeV are set on the bottom squark mass in Tsb02 simplified models assuming $m_{\tilde{\chi}_1^0} = 0 \text{ GeV}$. See their Figure 4(d).
- 12 AABOUD 17AX searched in 36 fb^{-1} of pp collisions at $\sqrt{s} = 13 \text{ TeV}$ for events containing two jets identified as originating from b -quarks and large missing transverse momentum. No excess of events above the expected level of Standard Model background was found. Exclusion limits at 95% C.L. are set on the masses of bottom squarks. In the Tsb01 simplified model, a \tilde{b}_1 mass below 950 GeV is excluded for $m_{\tilde{\chi}_1^0} = 0$ (<420) GeV. See their Fig. 7(a).
- 13 AABOUD 17AX searched in 36 fb^{-1} of pp collisions at $\sqrt{s} = 13 \text{ TeV}$ for events containing two jets identified as originating from b -quarks and large missing transverse momentum, with or without leptons. No excess of events above the expected level of Standard Model background was found. Exclusion limits at 95% C.L. are set on the masses of bottom squarks. Assuming 50% BR for Tsb01 and Tsb02 simplified models, a \tilde{b}_1 mass below 880 (860) GeV is excluded for $m_{\tilde{\chi}_1^0} = 0$ (<250) GeV. See their Fig. 7(b).
- 14 KHACHATRYAN 17A searched in 18.5 fb^{-1} of pp collisions at $\sqrt{s} = 8 \text{ TeV}$ for events with two forward jets, produced through vector boson fusion, and missing transverse momentum. No significant excess above the Standard Model expectations is observed. A limit is set on sbottom masses in the Tsb01 simplified model, see Fig. 3.
- 15 KHACHATRYAN 17AW searched in 2.3 fb^{-1} of pp collisions at $\sqrt{s} = 13 \text{ TeV}$ for events with at least three charged leptons, in any combination of electrons and muons, and significant \cancel{E}_T . No significant excess above the Standard Model expectations is observed. Limits are set on the gluino mass in the Tglu3A and Tglu1C simplified models, and on the sbottom mass in the Tsb02 simplified model, see their Figure 4.
- 16 KHACHATRYAN 17P searched in 2.3 fb^{-1} of pp collisions at $\sqrt{s} = 13 \text{ TeV}$ for events with one or more jets and large \cancel{E}_T . No significant excess above the Standard Model expectations is observed. Limits are set on the gluino mass in the Tglu1A, Tglu2A, Tglu3A, Tglu3B, Tglu3C and Tglu3D simplified models, see their Figures 7 and 8. Limits are also set on the squark mass in the Tsqk1 simplified model, see their Fig. 7, and on the sbottom mass in the Tsb01 simplified model, see Fig. 8. Finally, limits are set on the stop mass in the Tstop1, Tstop3, Tstop4, Tstop6 and Tstop7 simplified models, see Fig. 8.
- 17 SIRUANYAN 17AZ searched in 35.9 fb^{-1} of pp collisions at $\sqrt{s} = 13 \text{ TeV}$ for events with one or more jets and large \cancel{E}_T . No significant excess above the Standard Model expectations is observed. Limits are set on the gluino mass in the Tglu1A, Tglu2A, Tglu3A simplified models, see their Figures 6. Limits are also set on the squark mass in the Tsqk1 simplified model (for single light squark and for 8 degenerate light squarks), on the sbottom mass in the Tsb01 simplified model and on the stop mass in the Tstop1 simplified model, see their Fig. 7. Finally, limits are set on the stop mass in the Tstop2, Tstop4 and Tstop8 simplified models, see Fig. 8.
- 18 SIRUANYAN 17K searched in 2.3 fb^{-1} of pp collisions at $\sqrt{s} = 13 \text{ TeV}$ for direct production of stop or sbottom pairs in events with multiple jets and significant \cancel{E}_T . A second search also requires an isolated lepton and is combined with the all-hadronic search. No significant excess above the Standard Model expectations is observed. Limits are set on the stop mass in the Tstop1, Tstop8 and Tstop4 simplified models, see their Figures 7, 8 and 9 (for the Tstop4 limits, only the results of the all-hadronic search are used). Limits are also set on the sbottom mass in the Tsb01 simplified model, see Fig. 10 (also here, only the results of the all-hadronic search are used).
- 19 SIRUANYAN 17S searched in 35.9 fb^{-1} of pp collisions at $\sqrt{s} = 13 \text{ TeV}$ for events with two isolated same-sign leptons, jets, and large \cancel{E}_T . No significant excess above the Standard Model expectations is observed. Limits are set on the mass of the gluino mass in the Tglu3A, Tglu3B, Tglu3C, Tglu3D and Tglu1B simplified models, see their Figures 5 and 6, and on the sbottom mass in the Tsb02 simplified model, see their Figure 6.
- 20 AABOUD 16D searched in 3.2 fb^{-1} of pp collisions at $\sqrt{s} = 13 \text{ TeV}$ for events with an energetic jet and large missing transverse momentum. The results are interpreted as 95% C.L. limits on mass of sbottom decaying into a b -quark and the lightest neutralino in scenarios with $m_{\tilde{b}_1} - m_{\tilde{\chi}_1^0}$ between 5 and 20 GeV. See their Fig. 6.
- 21 AABOUD 16Q searched in 3.2 fb^{-1} of pp collisions at $\sqrt{s} = 13 \text{ TeV}$ for events containing two jets identified as originating from b -quarks and large missing transverse momentum. No excess of events above the expected level of Standard Model background was found. Exclusion limits at 95% C.L. are set on the masses of third-generation squarks. Assuming that the decay $\tilde{b}_1 \rightarrow b\tilde{\chi}_1^0$ (Tsb01) takes place 100% of the time, a \tilde{b}_1 mass below 840 (800) GeV is excluded for $m_{\tilde{\chi}_1^0} < 100$ (360) GeV. Differences in mass above 100 GeV between the \tilde{b}_1 and the $\tilde{\chi}_1^0$ are excluded up to a \tilde{b}_1 mass of 500 GeV. For more details, see their Fig. 4.
- 22 AAD 16BB searched in 3.2 fb^{-1} of pp collisions at $\sqrt{s} = 13 \text{ TeV}$ for events with exactly two same-sign leptons or at least three leptons, multiple hadronic jets, b -jets, and \cancel{E}_T . No significant excess over the Standard Model expectation is found. Exclusion limits at 95% C.L. are set on the sbottom mass for the Tsb02 model, assuming $m_{\tilde{\chi}_1^\pm} = m_{\tilde{\chi}_1^0} + 100 \text{ GeV}$. See their Fig. 4c.
- 23 KHACHATRYAN 16BJ searched in 2.3 fb^{-1} of pp collisions at $\sqrt{s} = 13 \text{ TeV}$ for events with two isolated same-sign dileptons and jets in the final state. No significant excess above the Standard Model expectations is observed. Limits are set on the sbottom mass in the Tsb02 simplified model, see Fig. 6.
- 24 KHACHATRYAN 16BS searched in 2.3 fb^{-1} of pp collisions at $\sqrt{s} = 13 \text{ TeV}$ for events with at least one energetic jet, no isolated leptons, and significant \cancel{E}_T , using the transverse mass variable M_{T2} to discriminate between signal and background processes. No significant excess above the Standard Model expectations is observed. Limits are set on the sbottom mass in the Tsb01 simplified model, see Fig. 11 and Table 3.
- 25 KHACHATRYAN 16BY searched in 2.3 fb^{-1} of pp collisions at $\sqrt{s} = 13 \text{ TeV}$ for events with two opposite-sign, same-flavour leptons, jets, and missing transverse momentum. No significant excess above the Standard Model expectations is observed. Limits are set on the gluino mass in the Tglu4C simplified model, see Fig. 4, and on sbottom masses in the Tsb03 simplified model, see Fig. 5.
- 26 AAD 15CJ searched in 20 fb^{-1} of pp collisions at $\sqrt{s} = 8 \text{ TeV}$ for evidence of third generation squarks by combining a large number of searches covering various final states. Limits on the sbottom mass are shown, either assuming the $\tilde{b} \rightarrow b\tilde{\chi}_1^0$ decay, see Fig. 11, or assuming the $\tilde{b} \rightarrow t\tilde{\chi}_1^\pm$ decay, with $\tilde{\chi}_1^\pm \rightarrow W^{(*)}\tilde{\chi}_1^0$, see Fig. 12a, or assuming the $\tilde{b} \rightarrow b\tilde{\chi}_1^0$ decay, with $\tilde{\chi}_1^0 \rightarrow h\tilde{\chi}_1^0$, see Fig. 12b. Interpretations in the pMSSM are also discussed, see Figures 13–15.
- 27 KHACHATRYAN 15AF searched in 19.5 fb^{-1} of pp collisions at $\sqrt{s} = 8 \text{ TeV}$ for events with at least two energetic jets and significant \cancel{E}_T , using the transverse mass variable M_{T2} to discriminate between signal and background processes. No significant excess above the Standard Model expectations is observed. Limits are set on the sbottom mass in simplified models where the decay $\tilde{b} \rightarrow b\tilde{\chi}_1^0$ takes place with a branching ratio of 100%, see Fig. 12. See also Table 5. Exclusions in the CMSSM, assuming $\tan\beta = 30$, $A_0 = -2 \max(m_0, m_{1/2})$ and $\mu > 0$, are also presented, see Fig. 15.
- 28 KHACHATRYAN 15AH searched in 19.4 or 19.7 fb^{-1} of pp collisions at $\sqrt{s} = 8 \text{ TeV}$ for events containing either a fully reconstructed top quark, or events containing dijets requiring one or both jets to originate from b -quarks, or events containing a mono-jet. No significant excess above the Standard Model expectations is observed. Limits are set on the sbottom mass in simplified models where the decay $\tilde{b} \rightarrow b\tilde{\chi}_1^0$ takes place with a branching ratio of 100%, see Fig. 12. Limits are also set in a simplified model where the decay $\tilde{b} \rightarrow c\tilde{\chi}_1^0$ takes place with a branching ratio of 100%, see Fig. 12.
- 29 KHACHATRYAN 15I searched in 19.5 fb^{-1} of pp collisions at $\sqrt{s} = 8 \text{ TeV}$ for events in which b -jets and four W -bosons are produced. Five individual search channels are combined (fully hadronic, single lepton, same-sign dilepton, opposite-sign dilepton, multi-lepton). No significant excess above the Standard Model expectations is observed. Limits are set on the sbottom mass in a simplified model where the decay $\tilde{b} \rightarrow t\tilde{\chi}_1^\pm$, with $\tilde{\chi}_1^\pm \rightarrow W^\pm\tilde{\chi}_1^0$, takes place with a branching ratio of 100%, see Fig. 7.
- 30 AAD 14T searched in 20.3 fb^{-1} of pp collisions at $\sqrt{s} = 8 \text{ TeV}$ for monojet-like events. No excess of events above the expected level of Standard Model background was found. Exclusion limits at 95% C.L. are set on the masses of third-generation squarks in simplified models which assume that the decay $\tilde{b}_1 \rightarrow b\tilde{\chi}_1^0$ takes place 100% of the time, see Fig. 12.
- 31 CHATRCHYAN 14AH searched in 4.7 fb^{-1} of pp collisions at $\sqrt{s} = 7 \text{ TeV}$ for events with at least two energetic jets and significant \cancel{E}_T , using the razor variables (M_R and R^2) to discriminate between signal and background processes. A second analysis requires at least one of the jets to be originating from a b -quark. No significant excess above the Standard Model expectations is observed. Limits are set on sbottom masses in simplified models where the decay $\tilde{b} \rightarrow b\tilde{\chi}_1^0$ takes place with a branching ratio of 100%, see Figs. 28 and 29. Exclusions in the CMSSM, assuming $\tan\beta = 10$, $A_0 = 0$ and $\mu > 0$, are also presented, see Fig. 26.
- 32 CHATRCHYAN 14R searched in 19.5 fb^{-1} of pp collisions at $\sqrt{s} = 8 \text{ TeV}$ for events with at least three leptons (electrons, muons, taus) in the final state. No significant excess above the Standard Model expectations is observed. Limits are set on the gluino mass in a simplified model where the decay $\tilde{b} \rightarrow t\tilde{\chi}_1^\pm$, with $\tilde{\chi}_1^\pm \rightarrow W^\pm\tilde{\chi}_1^0$, takes place with a branching ratio of 100%, see Fig. 11.
- 33 KHACHATRYAN 15AD searched in 19.4 fb^{-1} of pp collisions at $\sqrt{s} = 8 \text{ TeV}$ for events with two opposite-sign same flavor isolated leptons featuring either a kinematic edge, or a peak at the Z -boson mass, in the invariant mass spectrum. No evidence for a statistically significant excess over the expected SM backgrounds is observed and 95% C.L. exclusion limits are derived in a simplified model of sbottom pair production where the sbottom decays into a b -quark, two opposite-sign dileptons and a neutralino LSP, through an intermediate state containing either an off-shell Z -boson or a slepton, see Fig. 8.
- 34 AAD 14AX searched in 20.1 fb^{-1} of pp collisions at $\sqrt{s} = 8 \text{ TeV}$ for the strong production of supersymmetric particles in events containing either zero or at least one high p_T lepton, large missing transverse momentum, high jet multiplicity and at least three jets identified as originating from b -quarks. No excess over the expected SM background is observed. Limits are derived in mSUGRA/CMSSM models with $\tan\beta = 30$, $A_0 = -2 m_0$ and $\mu > 0$, see their Fig. 14. Also, exclusion limits are set in simplified models containing scalar bottom quarks, where the decay $\tilde{b} \rightarrow b\tilde{\chi}_2^0$ and $\tilde{\chi}_2^0 \rightarrow h\tilde{\chi}_1^0$ takes place with a branching ratio of 100%, see their Figures 11.
- 35 AAD 14E searched in 20.3 fb^{-1} of pp collisions at $\sqrt{s} = 8 \text{ TeV}$ for strongly produced supersymmetric particles in events containing jets and two same-sign leptons or three leptons. The search also utilizes jets originating from b -quarks, missing transverse momentum and other variables. No excess over the expected SM background is observed. Exclusion limits are derived in simplified models containing bottom, see Fig. 7. Limits are also derived in the mSUGRA/CMSSM, bRPV and GMSB models, see their Fig. 8.
- 36 CHATRCHYAN 14H searched in 19.5 fb^{-1} of pp collisions at $\sqrt{s} = 8 \text{ TeV}$ for events with two isolated same-sign dileptons and jets in the final state. No significant excess above the Standard Model expectations is observed. Limits are set on the sbottom mass in a simplified models where the decay $\tilde{b} \rightarrow t\tilde{\chi}_1^\pm, \tilde{\chi}_1^\pm \rightarrow W^\pm\tilde{\chi}_1^0$ takes place with a branching ratio of 100%, with varying mass of the $\tilde{\chi}_1^\pm$, for $m_{\tilde{\chi}_1^0} = 50 \text{ GeV}$, see Fig. 6.
- 37 AAD 13AU searched in 20.1 fb^{-1} of pp collisions at $\sqrt{s} = 8 \text{ TeV}$ for events containing two jets identified as originating from b -quarks and large missing transverse momentum. No excess of events above the expected level of Standard Model background was found. Exclusion limits at 95% C.L. are set on the masses of third-generation squarks. Assuming that the decay $\tilde{b}_1 \rightarrow b\tilde{\chi}_1^0$ takes place 100% of the time, a \tilde{b}_1 mass below 620 GeV is excluded for $m_{\tilde{\chi}_1^0} < 120 \text{ GeV}$. For more details, see their Fig. 5.
- 38 CHATRCHYAN 13AT provides interpretations of various searches for supersymmetry by the CMS experiment based on $4.73\text{--}4.98 \text{ fb}^{-1}$ of pp collisions at $\sqrt{s} = 7 \text{ TeV}$ in the framework of simplified models. Limits are set on the sbottom mass in a simplified models where sbottom quarks are pair-produced and the decay $\tilde{b} \rightarrow b\tilde{\chi}_1^0$ takes place with a branching ratio of 100%, see Fig. 4.
- 39 CHATRCHYAN 13T searched in 11.7 fb^{-1} of pp collisions at $\sqrt{s} = 8 \text{ TeV}$ for events with at least two energetic jets and significant \cancel{E}_T , using the α_T variable to discriminate between processes with genuine and misreconstructed \cancel{E}_T . No significant excess above the Standard Model expectations is observed. Limits are set on sbottom masses in simplified models where the decay $\tilde{b} \rightarrow b\tilde{\chi}_1^0$ takes place with a branching ratio of 100%, see Fig. 8 and Table 9.
- 40 CHATRCHYAN 13V searched in 10.5 fb^{-1} of pp collisions at $\sqrt{s} = 8 \text{ TeV}$ for events with two isolated same-sign dileptons and at least two b -jets in the final state. No significant excess above the Standard Model expectations is observed. Limits are set on the bottom mass in a simplified models where the decay $\tilde{b} \rightarrow t\tilde{\chi}_1^\pm, \tilde{\chi}_1^\pm \rightarrow W^\pm\tilde{\chi}_1^0$ takes place with a branching ratio of 100%, with varying mass of the $\tilde{\chi}_1^\pm$, for $m_{\tilde{\chi}_1^0} = 50 \text{ GeV}$, see Fig. 4.

Searches Particle Listings

Supersymmetric Particle Searches

41	AAD 12AN searched in 2.05 fb ⁻¹ of pp collisions at $\sqrt{s} = 7$ TeV for scalar bottom quarks in events with large missing transverse momentum and two b-jets in the final state. The data are found to be consistent with the Standard Model expectations. Limits are set in an R-parity conserving minimal supersymmetric scenario, assuming $B(\bar{b}_1 \rightarrow b\tilde{\chi}_1^0) = 100\%$, see their Fig. 2.	>1190	95	2	SIRUNYAN	19CH CMS	jets+ \cancel{E}_T , Tstop1, $m_{\tilde{\chi}_1^0} = 0$ GeV	
		>1140	95	3	SIRUNYAN	19S CMS	1 or 2 $\ell +$ jets + \cancel{E}_T , Tstop1, $m_{\tilde{\chi}_1^0} < 200$ GeV	
42	CHATRCHYAN 12AI looked in 4.98 fb ⁻¹ of pp collisions at $\sqrt{s} = 7$ TeV for events with two same-sign leptons (e, μ), but not necessarily same flavor, at least 2 b-jets and missing transverse energy. No excess beyond the Standard Model expectation is observed. Exclusion limits are derived in a simplified model for sbottom pair production, where the sbottom decays through $\bar{b}_1 \rightarrow t\tilde{\chi}_1^- W$, see Fig. 8.	> 208	95	4	SIRUNYAN	19U CMS	$e^\pm \mu^\mp + \geq 1b$ -jet, Tstop1, $m_{\tilde{\chi}_1^0} - m_{\tilde{\chi}_1^\pm} = 175$ GeV	
		> 235	95	4	SIRUNYAN	19U CMS	$e^\pm \mu^\mp + \geq 1b$ -jet, Tstop1, $m_{\tilde{\chi}_1^0} - m_{\tilde{\chi}_1^\pm} = 182.5$ GeV	
43	CHATRCHYAN 12BO searched in 4.7 fb ⁻¹ of pp collisions at $\sqrt{s} = 7$ TeV for scalar bottom quarks in events with large missing transverse momentum and two b-jets in the final state. The data are found to be consistent with the Standard Model expectations. Limits are set in an R-parity conserving minimal supersymmetric scenario, assuming $B(\bar{b}_1 \rightarrow b\tilde{\chi}_1^0) = 100\%$, see their Fig. 2.	> 242	95	4	SIRUNYAN	19U CMS	$e^\pm \mu^\mp + \geq 1b$ -jet, Tstop1, $m_{\tilde{\chi}_1^0} - m_{\tilde{\chi}_1^\pm} = 167.5$ GeV	
		> 940	95	5	AABOUD	18AQ ATLS	$1\ell +$ jets + \cancel{E}_T , Tstop1, $m_{\tilde{\chi}_1^0} = 0$ GeV	
44	AAD 11K looked in 34 pb ⁻¹ of pp collisions at $\sqrt{s} = 7$ TeV for events with heavy stable particles, identified by their anomalous dE/dx in the tracker or time of flight in the tile calorimeter, from pair production of \tilde{b} . No evidence for an excess over the SM expectation is observed and limits on the mass are derived for pair production of sbottom, see Fig. 4.	> 270	95	6	AABOUD	18AQ ATLS	$1\ell +$ jets + \cancel{E}_T , Tstop3, $m_{\tilde{\chi}_1^0} - m_{\tilde{\chi}_1^\pm} = 20$ GeV	
		> 840	95	7	AABOUD	18AQ ATLS	$1\ell +$ jets + \cancel{E}_T , Tstop2, $m_{\tilde{\chi}_1^0} - m_{\tilde{\chi}_1^\pm} = 10$ GeV	
45	AAD 11O looked in 35 pb ⁻¹ of pp collisions at $\sqrt{s} = 7$ TeV for events with jets, of which at least one is a b-jet, and \cancel{E}_T . No excess above the Standard Model was found. Limits are derived in the $(m_{\tilde{g}}, m_{\tilde{b}_1})$ plane (see Fig. 2) under the assumption of 100% branching ratios and \tilde{b}_1 being the lightest squark. The quoted limit is valid for $m_{\tilde{b}_1} < 500$ GeV. A similar approach for \tilde{t}_1 as the lightest squark with $\tilde{g} \rightarrow \tilde{t}_1 t$ and $\tilde{t}_1 \rightarrow b\tilde{\chi}_1^\pm$ with 100% branching ratios leads to a gluino mass limit of 520 GeV for $130 < m_{\tilde{t}_1} < 300$ GeV. Limits are also derived in the CMSSM $(m_0, m_{1/2})$ plane for $\tan\beta = 40$, see Fig. 4, and in scenarios based on the gauge group SO(10).	> 500	95	8	AABOUD	18BV ATLS	c-jets + \cancel{E}_T , Tstop4, $m_{\tilde{\chi}_1^0} - m_{\tilde{\chi}_1^\pm} < 100$ GeV	
		> 850	95	9	AABOUD	18BV ATLS	c-jets + \cancel{E}_T , Tstop4, $m_{\tilde{\chi}_1^0} = 0$ GeV	
		> 390	95	10	AABOUD	18I ATLS	≥ 1 jets + \cancel{E}_T , Tstop3, $m_{\tilde{\chi}_1^0} \sim m_{\tilde{\chi}_1^\pm}$	
		> 430	95	11	AABOUD	18I ATLS	≥ 1 jets + \cancel{E}_T , Tstop4, $m_{\tilde{\chi}_1^0} - m_{\tilde{\chi}_1^\pm} = 5$ GeV	
46	CHATRCHYAN 11D looked in 35 pb ⁻¹ of pp collisions at $\sqrt{s} = 7$ TeV for events with ≥ 2 jets, at least one of which is b-tagged, and \cancel{E}_T , where the b-jets are decay products of \tilde{t} or \tilde{b} . No evidence for an excess over the expected background is observed. Limits are derived in the CMSSM $(m_0, m_{1/2})$ plane for $\tan\beta = 50$ (see Fig. 2).	>1160	95	12	AABOUD	18Y ATLS	$2\ell (\geq 1$ hadronic $\tau) + b$ -jets + \cancel{E}_T , Tstop5, $m_{\tilde{\chi}_1^0} \sim 800$ GeV	
		> 450	95	13	SIRUNYAN	18AJ CMS	2ℓ (soft) + \cancel{E}_T , Tstop10, $m_{\tilde{\chi}_1^\pm} = (m_{\tilde{t}} + m_{\tilde{\chi}_1^0})/2$, $m_{\tilde{t}_1} - m_{\tilde{\chi}_1^0} = 40$ GeV	
47	AALTONEN 10R searched in 2.65 fb ⁻¹ of $p\bar{p}$ collisions at $\sqrt{s} = 1.96$ TeV for events with \cancel{E}_T and exactly two jets, at least one of which is b-tagged. The results are in agreement with the SM prediction, and a limit on the cross section of 0.1 pb is obtained for the range of masses $80 < m_{\tilde{b}_1} < 280$ GeV assuming that the sbottom decays exclusively to $b\tilde{\chi}_1^0$. The excluded mass region in the framework of conserved R_p is shown in a plane of $(m_{\tilde{b}_1}, m_{\tilde{\chi}_1^0})$, see their Fig. 2.	> 720	95	14	SIRUNYAN	18AL CMS	$\geq 3\ell^\pm +$ jets + \cancel{E}_T , Tstop7, $m_{\tilde{t}_1} - m_{\tilde{\chi}_1^0} = 175$ GeV, $m_{\tilde{t}_1} = 200$ GeV, BR($\tilde{t}_2 \rightarrow \tilde{t}_1 H$) = 100%	
		> 780	95	14	SIRUNYAN	18AL CMS	$\geq 3\ell^\pm +$ jets + \cancel{E}_T , Tstop7, $m_{\tilde{t}_1} - m_{\tilde{\chi}_1^0} = 175$ GeV, $m_{\tilde{t}_1} = 200$ GeV, BR($\tilde{t}_2 \rightarrow \tilde{t}_1 Z$) = 100%	
48	ABAZOV 10L looked in 5.2 fb ⁻¹ of $p\bar{p}$ collisions at $\sqrt{s} = 1.96$ TeV for events with at least 2 b-jets and \cancel{E}_T from the production of $\tilde{b}_1 \tilde{b}_1$. No evidence for an excess over the SM expectation is observed, and a limit on the cross section is derived under the assumption of 100% branching ratio. The excluded mass region in the framework of conserved R_p is shown in a plane of $(m_{\tilde{b}_1}, m_{\tilde{\chi}_1^0})$, see their Fig. 3b. The exclusion also extends to $m_{\tilde{\chi}_1^0} = 110$ GeV for $160 < m_{\tilde{b}_1} < 200$ GeV.	> 710	95	14	SIRUNYAN	18AL CMS	$\geq 3\ell^\pm +$ jets + \cancel{E}_T , Tstop7, $m_{\tilde{t}_1} - m_{\tilde{\chi}_1^0} = 175$ GeV, $m_{\tilde{t}_1} = 200$ GeV, BR($\tilde{t}_2 \rightarrow \tilde{t}_1 Z$) = 100%	
		> 730	95	15	SIRUNYAN	18AN CMS	1 or 2 $\gamma + \ell +$ jets, GGM, Tstop12, $m_{\tilde{\chi}_1^0} = 150$ GeV	
		> 650	95	15	SIRUNYAN	18AN CMS	1 or 2 $\gamma + \ell +$ jets, GGM, Tstop12, $m_{\tilde{\chi}_1^0} = 500$ GeV	
		>1000	95	16	SIRUNYAN	18AY CMS	jets + \cancel{E}_T , Tstop1, $m_{\tilde{\chi}_1^0} = 0$ GeV	
		> 500	95	16	SIRUNYAN	18AY CMS	jets + \cancel{E}_T , Tstop4, $m_{\tilde{\chi}_1^0} = 420$ GeV	
		> 510	95	17	SIRUNYAN	18B CMS	jets + \cancel{E}_T , Tstop4, $m_{\tilde{t}_1} - m_{\tilde{\chi}_1^0} = 10$ GeV	
1	KHACHATRYAN 16BX searched in 19.5 fb ⁻¹ of pp collisions at $\sqrt{s} = 8$ TeV for events containing 2 leptons coming from R-parity-violating decays of supersymmetric particles. No excess over the expected background is observed. Limits are derived on the sbottom mass, assuming the RPV $\tilde{b} \rightarrow t d$ or $\tilde{b} \rightarrow t s$ decay, see Fig. 15.	> 800	95	18	SIRUNYAN	18C CMS	$\ell^\pm \ell^\mp + b$ -jets + \cancel{E}_T , Tstop1, $m_{\tilde{\chi}_1^0} = 0$	
2	AAD 14E searched in 20.3 fb ⁻¹ of pp collisions at $\sqrt{s} = 8$ TeV for strongly produced supersymmetric particles in events containing jets and two same-sign leptons or three leptons. The search also utilises jets originating from b-quarks, missing transverse momentum and other variables. No excess over the expected SM background is observed. Exclusion limits are derived in simplified models containing bottom, see Fig. 7. Limits are also derived in the mSUGRA/CMSSM, bRPV and GMSB models, see their Fig. 8.	> 750	95	18	SIRUNYAN	18C CMS	$\ell^\pm \ell^\mp + b$ -jets + \cancel{E}_T , Tstop2, $m_{\tilde{\chi}_1^\pm} = (m_{\tilde{t}} + m_{\tilde{\chi}_1^0})/2$, $m_{\tilde{\chi}_1^0} = 0$	
		>1050	95	18	SIRUNYAN	18C CMS	Combination of all-hadronic, 1 ℓ^\pm and $\ell^\pm \ell^\mp$ searches, Tstop1, $m_{\tilde{\chi}_1^0} = 0$	
		>1000	95	18	SIRUNYAN	18C CMS	Combination of all-hadronic, 1 ℓ^\pm and $\ell^\pm \ell^\mp$ searches, Tstop2, $m_{\tilde{\chi}_1^\pm} = (m_{\tilde{t}} + m_{\tilde{\chi}_1^0})/2$, $m_{\tilde{\chi}_1^0} = 0$	
		>1200	95	18	SIRUNYAN	18C CMS	$\ell^\pm \ell^\mp + b$ -jets + \cancel{E}_T , Tstop11, $m_{\tilde{\chi}_1^\pm} = 0.5(m_{\tilde{t}} + m_{\tilde{\chi}_1^0})$, $m_{\tilde{\ell}} = 0.5 m_{\tilde{\chi}_1^\pm}$, $m_{\tilde{\chi}_1^0} = 0$	
		>1300	95	18	SIRUNYAN	18C CMS	$\ell^\pm \ell^\mp + b$ -jets + \cancel{E}_T , Tstop11, $m_{\tilde{\chi}_1^\pm} = 0.5(m_{\tilde{t}} + m_{\tilde{\chi}_1^0})$, $m_{\tilde{\ell}} = 0.95 m_{\tilde{\chi}_1^\pm}$, $m_{\tilde{\chi}_1^0} = 0$	
		none 460–1060	95	18	SIRUNYAN	18C CMS	$\ell^\pm \ell^\mp + b$ -jets + \cancel{E}_T , Tstop11, $m_{\tilde{\chi}_1^\pm} = 0.5(m_{\tilde{t}} + m_{\tilde{\chi}_1^0})$, $m_{\tilde{\ell}} = 0.05 m_{\tilde{\chi}_1^\pm}$, $m_{\tilde{\chi}_1^0} = 0$	
		>1020	95	19	SIRUNYAN	18D CMS	top quark (hadronically decaying) + jets + \cancel{E}_T , Tstop1, $m_{\tilde{\chi}_1^0} = 0$ GeV	

R-parity violating \tilde{b} (Sbottm) mass limit

VALUE (GeV)	CL%	DOCUMENT ID	TECN	COMMENT
>307	95	1 KHACHATRYAN...16BX	CMS	RPV, $\tilde{b} \rightarrow t d$ or $t s$, λ'_{332} or λ'_{331} coupling

• • • We do not use the following data for averages, fits, limits, etc. • • •

2	AAD	14E	ATLS	$\ell^\pm \ell^\pm (\ell^\mp) +$ jets, $\tilde{b}_1 \rightarrow t\tilde{\chi}_1^\pm$ with $\tilde{\chi}_1^\pm \rightarrow W^{(*)\pm} \tilde{\chi}_1^0$ simplified model, $m_{\tilde{\chi}_1^\pm} = 2 m_{\tilde{\chi}_1^0}$
---	-----	-----	------	--

1 KHACHATRYAN 16BX searched in 19.5 fb⁻¹ of pp collisions at $\sqrt{s} = 8$ TeV for events containing 2 leptons coming from R-parity-violating decays of supersymmetric particles. No excess over the expected background is observed. Limits are derived on the sbottom mass, assuming the RPV $\tilde{b} \rightarrow t d$ or $\tilde{b} \rightarrow t s$ decay, see Fig. 15.

2 AAD 14E searched in 20.3 fb⁻¹ of pp collisions at $\sqrt{s} = 8$ TeV for strongly produced supersymmetric particles in events containing jets and two same-sign leptons or three leptons. The search also utilises jets originating from b-quarks, missing transverse momentum and other variables. No excess over the expected SM background is observed. Exclusion limits are derived in simplified models containing bottom, see Fig. 7. Limits are also derived in the mSUGRA/CMSSM, bRPV and GMSB models, see their Fig. 8.

\tilde{t} (Stop) mass limit

Limits depend on the decay mode. In e^+e^- collisions they also depend on the mixing angle of the mass eigenstate $\tilde{t}_1 = \tilde{t}_L \cos\theta_t + \tilde{t}_R \sin\theta_t$. The coupling to the Z vanishes when $\theta_t = 0.98$. In the Listings below, we use $\Delta m \equiv m_{\tilde{t}_1} - m_{\tilde{\chi}_1^0}$ or $\Delta m \equiv m_{\tilde{t}_1} - m_{\tilde{t}_2}$, depending on relevant decay mode. See also bounds in "q (Squark) MASS LIMIT."

Some earlier papers are now obsolete and have been omitted. They were last listed in our PDG 14 edition: K. Olive, et al. (Particle Data Group), Chinese Physics C38 070001 (2014) (<http://pdg.lbl.gov>).

R-parity conserving \tilde{t} (Stop) mass limit

VALUE (GeV)	CL%	DOCUMENT ID	TECN	COMMENT
>1110	95	1 SIRUNYAN	19AU CMS	$\gamma +$ jets + b-jets + \cancel{E}_T , Tstop13, $m_{\tilde{\chi}_1^0} = 1$ GeV
>1230	95	1 SIRUNYAN	19AU CMS	$\gamma +$ jets + b-jets + \cancel{E}_T , Tstop13, $m_{\tilde{\chi}_1^0} = 800$ GeV

> 420	95	20	SIRUNYAN	18DI	CMS	$\ell^\pm + \text{jet} + \cancel{E}_T, T_{\text{stop3}}, m_{\tilde{t}_1} - m_{\tilde{\chi}_1^0} = 10 \text{ GeV}$	>1000	95	39	SIRUNYAN	17AS	CMS	$1\ell + \text{jets} + \cancel{E}_T, T_{\text{stop2}}, m_{\tilde{\chi}_1^\pm} = (m_{\tilde{t}} + m_{\tilde{\chi}_1^0})/2, m_{\tilde{\chi}_1^0} = 0$
> 560	95	20	SIRUNYAN	18DI	CMS	$\ell^\pm + \text{jet} + \cancel{E}_T, T_{\text{stop3}}, m_{\tilde{t}_1} - m_{\tilde{\chi}_1^0} = 80 \text{ GeV}$	> 980	95	39	SIRUNYAN	17AS	CMS	$1\ell + \text{jets} + \cancel{E}_T, T_{\text{stop8}}, m_{\tilde{\chi}_1^\pm} - m_{\tilde{\chi}_1^0} = 5 \text{ GeV}, m_{\tilde{\chi}_1^0} = 0 \text{ GeV}$
> 540	95	20	SIRUNYAN	18DI	CMS	$\ell^\pm, T_{\text{stop10}}, m_{\tilde{\chi}_1^\pm} = (m_{\tilde{t}} + m_{\tilde{\chi}_1^0})/2, m_{\tilde{t}_1} - m_{\tilde{\chi}_1^0} = 40 \text{ GeV}$	>1040	95	40	SIRUNYAN	17AT	CMS	$\text{jets} + \cancel{E}_T, T_{\text{stop1}}, m_{\tilde{\chi}_1^0} = 0 \text{ GeV}$
> 590	95	20	SIRUNYAN	18DI	CMS	Combination of all-hadronic and 1 ℓ^\pm searches, $T_{\text{stop3}}, m_{\tilde{t}_1} - m_{\tilde{\chi}_1^0} = 30 \text{ GeV}$	> 750	95	40	SIRUNYAN	17AT	CMS	$\text{jets} + \cancel{E}_T, T_{\text{stop2}}, m_{\tilde{\chi}_1^\pm} = (m_{\tilde{t}} + m_{\tilde{\chi}_1^0})/2, m_{\tilde{\chi}_1^0} = 0 \text{ GeV}$
> 670	95	20	SIRUNYAN	18DI	CMS	Combination of all-hadronic and 1 ℓ^\pm searches, $T_{\text{stop10}}, m_{\tilde{\chi}_1^\pm} = (m_{\tilde{t}} + m_{\tilde{\chi}_1^0})/2, m_{\tilde{t}_1} - m_{\tilde{\chi}_1^0} = 60 \text{ GeV}$	> 940	95	40	SIRUNYAN	17AT	CMS	$\text{jets} + \cancel{E}_T, T_{\text{stop8}}, m_{\tilde{\chi}_1^\pm} - m_{\tilde{\chi}_1^0} = 5 \text{ GeV}, m_{\tilde{\chi}_1^0} = 100 \text{ GeV}$
> 450	95	21	SIRUNYAN	18DN	CMS	$\ell^\pm \ell^\mp, T_{\text{stop1}}, m_{\tilde{t}_1} - m_{\tilde{\chi}_1^0} = m_{W^0}$	> 480	95	40	SIRUNYAN	17AT	CMS	$\text{jets} + \cancel{E}_T, T_{\text{stop4}}, 10 \text{ GeV} < m_{\tilde{t}_1} - m_{\tilde{\chi}_1^0} < 80 \text{ GeV}$
none 225-325	95	21	SIRUNYAN	18DN	CMS	$\ell^\pm \ell^\mp, T_{\text{stop2}}, m_{\tilde{\chi}_1^\pm} = (m_{\tilde{t}} + m_{\tilde{\chi}_1^0})/2, m_{\tilde{t}_1} - m_{\tilde{\chi}_1^0} = 2 m_W$	> 530	95	40	SIRUNYAN	17AT	CMS	$\text{jets} + \cancel{E}_T, T_{\text{stop10}}, m_{\tilde{\chi}_1^\pm} = (m_{\tilde{t}} + m_{\tilde{\chi}_1^0})/2, 10 \text{ GeV} < m_{\tilde{t}_1} - m_{\tilde{\chi}_1^0} < 80 \text{ GeV}$
none 210-690	95	21	SIRUNYAN	18DN	CMS	$\ell^\pm \ell^\mp, T_{\text{stop1}}, m_{\tilde{\chi}_1^0} = 0 \text{ GeV}$	>1070	95	41	SIRUNYAN	17AZ	CMS	$\geq 1 \text{ jets} + \cancel{E}_T, T_{\text{stop1}}, m_{\tilde{\chi}_1^0} = 0 \text{ GeV}$
none 250-600	95	21	SIRUNYAN	18DN	CMS	$\ell^\pm \ell^\mp, T_{\text{stop2}}, m_{\tilde{\chi}_1^\pm} = (m_{\tilde{t}} + m_{\tilde{\chi}_1^0})/2, m_{\tilde{\chi}_1^0} = 0 \text{ GeV}$	> 900	95	41	SIRUNYAN	17AZ	CMS	$\geq 1 \text{ jets} + \cancel{E}_T, T_{\text{stop2}}, m_{\tilde{\chi}_1^\pm} = (m_{\tilde{t}} + m_{\tilde{\chi}_1^0})/2, m_{\tilde{\chi}_1^0} = 0 \text{ GeV}$
> 700	95	22	AABOUD	17AJ	ATLS	same-sign $\ell^\pm \ell^\pm / 3 \ell + \text{jets} + \cancel{E}_T, T_{\text{stop11}}, m_{\tilde{\chi}_1^0} = m_{\tilde{\chi}_1^0} + 100 \text{ GeV}$	>1020	95	41	SIRUNYAN	17AZ	CMS	$\geq 1 \text{ jets} + \cancel{E}_T, T_{\text{stop8}}, m_{\tilde{\chi}_1^\pm} - m_{\tilde{\chi}_1^0} = 5 \text{ GeV}, m_{\tilde{\chi}_1^0} = 100 \text{ GeV}$
> 880	95	23	AABOUD	17AX	ATLS	$b\text{-jets} + \cancel{E}_T, \text{mixture } T_{\text{stop1}} \text{ and } T_{\text{stop2}} \text{ with BR}=50\%, m_{\tilde{\chi}_1^0} = 0 \text{ GeV}, m_{\tilde{\chi}_1^\pm} - m_{\tilde{\chi}_1^0} = 1 \text{ GeV}$	> 540	95	41	SIRUNYAN	17AZ	CMS	$\geq 1 \text{ jets} + \cancel{E}_T, T_{\text{stop4}}, 10 \text{ GeV} < m_{\tilde{t}_1} - m_{\tilde{\chi}_1^0} < 80 \text{ GeV}$
none 250-1000	95	24	AABOUD	17AY	ATLS	$\text{jets} + \cancel{E}_T, T_{\text{stop1}}, m_{\tilde{\chi}_1^0} = 0 \text{ GeV}$	none 280-830	95	42	SIRUNYAN	17K	CMS	$0, 1 \ell^\pm + \text{jets} + \cancel{E}_T \text{ (combination)}, T_{\text{stop1}}, m_{\tilde{\chi}_1^0} = 0 \text{ GeV}$
none 450-850	95	25	AABOUD	17AY	ATLS	$\text{jets} + \cancel{E}_T, \text{mixture of } T_{\text{stop1}} \text{ and } T_{\text{stop2}} \text{ with BR}=50\%, m_{\tilde{\chi}_1^\pm} - m_{\tilde{\chi}_1^0} = 1 \text{ GeV}$	> 700	95	42	SIRUNYAN	17K	CMS	$0, 1 \ell^\pm + \text{jets} + \cancel{E}_T \text{ (combination)}, T_{\text{stop8}}, m_{\tilde{\chi}_1^\pm} - m_{\tilde{\chi}_1^0} = 5 \text{ GeV}, m_{\tilde{\chi}_1^0} = 100 \text{ GeV}$
> 720	95	26	AABOUD	17BE	ATLS	$\ell^\pm \ell^\mp + \cancel{E}_T, T_{\text{stop1}}, m_{\tilde{\chi}_1^0} = 0 \text{ GeV}$	> 160	95	42	SIRUNYAN	17K	CMS	$\text{jets} + \cancel{E}_T, T_{\text{stop4}}, 10 < m_{\tilde{t}} - m_{\tilde{\chi}_1^0} < 80 \text{ GeV}$
> 400	95	27	AABOUD	17BE	ATLS	$\ell^\pm \ell^\mp + \cancel{E}_T, T_{\text{stop3}}, m_{\tilde{t}_1} - m_{\tilde{\chi}_1^0} = 40 \text{ GeV}$	none 230-960	95	43	SIRUNYAN	17P	CMS	$\text{jets} + \cancel{E}_T, T_{\text{stop1}}, m_{\tilde{\chi}_1^0} = 0 \text{ GeV}$
> 430	95	28	AABOUD	17BE	ATLS	$\ell^\pm \ell^\mp + \cancel{E}_T, T_{\text{stop1}} \text{ (offshell } t), m_{\tilde{t}_1} - m_{\tilde{\chi}_1^0} \sim m_W$	> 990	95	43	SIRUNYAN	17P	CMS	$\text{jets} + \cancel{E}_T, T_{\text{stop1}}, m_{\tilde{\chi}_1^0} = 0 \text{ GeV}$
> 700	95	29	AABOUD	17BE	ATLS	$\ell^\pm \ell^\mp + \cancel{E}_T, T_{\text{stop2}}, m_{\tilde{t}_1} - m_{\tilde{\chi}_1^0} = 10 \text{ GeV}, m_{\tilde{\chi}_1^0} = 0 \text{ GeV}$	> 323	95	44	AABOUD	16D	ATLS	$\geq 1 \text{ jet} + \cancel{E}_T, T_{\text{stop4}}, m_{\tilde{t}_1} - m_{\tilde{\chi}_1^0} = 5 \text{ GeV}$
> 750	95	30	KHACHATRY...17	CMS	$\text{jets} + \cancel{E}_T, T_{\text{stop1}}, m_{\tilde{\chi}_1^0} = 100 \text{ GeV}$	none, 745-780	95	45	AABOUD	16J	ATLS	$1 \ell^\pm + \geq 4 \text{ jets} + \cancel{E}_T, T_{\text{stop1}}, m_{\tilde{\chi}_1^0} = 0 \text{ GeV}$	
none 250-740	95	31	KHACHATRY...17AD	CMS	$\text{jets} + b\text{-jets} + \cancel{E}_T, T_{\text{stop1}}, m_{\tilde{\chi}_1^0} = 0 \text{ GeV}$	> 490-650	95	46	AAD	16AY	ATLS	$2\ell \text{ (including hadronic } \tau) + \cancel{E}_T, T_{\text{stop5}}, 87 \text{ GeV} < m_{\tilde{\tau}} < m_{\tilde{t}_1}$	
> 610	95	32	KHACHATRY...17AD	CMS	$\text{jets} + b\text{-jets} + \cancel{E}_T, \text{mixture } T_{\text{stop1}} \text{ and } T_{\text{stop2}} \text{ with BR}=50\%, m_{\tilde{\chi}_1^0} = 60 \text{ GeV}$	> 700	95	47	KHACHATRY...16AV	CMS	$1 \text{ or } 2 \ell^\pm + \text{jets} + b\text{-jets} + \cancel{E}_T, T_{\text{stop1}}, m_{\tilde{\chi}_1^0} < 250 \text{ GeV}$		
> 590	95	33	KHACHATRY...17P	CMS	$1 \text{ or more jets} + \cancel{E}_T, T_{\text{stop8}}, m_{\tilde{\chi}_1^\pm} - m_{\tilde{\chi}_1^0} = 5 \text{ GeV}, m_{\tilde{\chi}_1^0} = 100 \text{ GeV}$	> 700	95	47	KHACHATRY...16AV	CMS	$1 \text{ or } 2 \ell^\pm + \text{jets} + b\text{-jets } \cancel{E}_T, T_{\text{stop2}}, m_{\tilde{\chi}_1^0} = 0 \text{ GeV}, m_{\tilde{\chi}_1^\pm} = 0.75 m_{\tilde{t}_1} + 0.25 m_{\tilde{\chi}_1^0}$		
none 280-640	95	33	KHACHATRY...17P	CMS	$1 \text{ or more jets} + \cancel{E}_T, T_{\text{stop1}}, m_{\tilde{\chi}_1^0} = 0 \text{ GeV}$	> 775	95	48	KHACHATRY...16BK	CMS	$\text{jets} + \cancel{E}_T, T_{\text{stop1}}, m_{\tilde{\chi}_1^0} < 200 \text{ GeV}$		
> 350	95	33	KHACHATRY...17P	CMS	$1 \text{ or more jets} + \cancel{E}_T, T_{\text{stop4}}, 10 \text{ GeV} < m_{\tilde{t}_1} - m_{\tilde{\chi}_1^0} < 80 \text{ GeV}$	> 620	95	48	KHACHATRY...16BK	CMS	$\text{jets} + \cancel{E}_T, T_{\text{stop2}}, m_{\tilde{\chi}_1^0} = 0 \text{ GeV}$		
> 280	95	33	KHACHATRY...17P	CMS	$1 \text{ or more jets} + \cancel{E}_T, T_{\text{stop3}}, 10 \text{ GeV} < m_{\tilde{t}_1} - m_{\tilde{\chi}_1^0} < 80 \text{ GeV}$	> 800	95	49	KHACHATRY...16BS	CMS	$\text{jets} + \cancel{E}_T, T_{\text{stop1}}, m_{\tilde{\chi}_1^0} = 0 \text{ GeV}$		
> 320	95	33	KHACHATRY...17P	CMS	$1 \text{ or more jets} + \cancel{E}_T, T_{\text{stop9}}, 10 \text{ GeV} < m_{\tilde{t}_1} - m_{\tilde{\chi}_1^0} < 80 \text{ GeV}$	> 316	95	50	KHACHATRY...16Y	CMS	$1 \text{ or } 2 \text{ soft } \ell^\pm + \text{jets} + \cancel{E}_T, T_{\text{stop3}}, m_{\tilde{t}} - m_{\tilde{\chi}_1^0} = 25 \text{ GeV}$		
> 240	95	34	KHACHATRY...17s	CMS	$\text{jets} + \cancel{E}_T, T_{\text{stop4}}, m_{\tilde{t}} - m_{\tilde{\chi}_1^0} = 10 \text{ GeV}$	> 270	95	51	AAD	15CJ	ATLS	$B(\tilde{\tau} \rightarrow c\tilde{\chi}_1^0) + B(\tilde{\tau} \rightarrow b f f' \tilde{\chi}_1^0) = 1, m_{\tilde{t}} - m_{\tilde{\chi}_1^0} = 10 \text{ GeV}$	
> 225	95	35	KHACHATRY...17s	CMS	$\text{jets} + \cancel{E}_T, T_{\text{stop3}}, m_{\tilde{t}} - m_{\tilde{\chi}_1^0} = 10 \text{ GeV}$	none, 200-700	95	51	AAD	15CJ	ATLS	$\tilde{\tau} \rightarrow t\tilde{\chi}_1^0, m_{\tilde{\chi}_1^0} = 0$	
> 325	95	36	KHACHATRY...17s	CMS	$\text{jets} + \cancel{E}_T, T_{\text{stop2}}, m_{\tilde{\chi}_1^\pm} = 0.25 m_{\tilde{t}} + 0.75 m_{\tilde{\chi}_1^0}, m_{\tilde{\chi}_1^0} = 225 \text{ GeV}$	> 500	95	51	AAD	15CJ	ATLS	$B(\tilde{\tau} \rightarrow t\tilde{\chi}_1^0) + B(\tilde{\tau} \rightarrow b\tilde{\chi}_1^\pm) = 1, \tilde{\chi}_1^\pm \rightarrow W^{(*)}\tilde{\chi}_1^0, m_{\tilde{\chi}_1^\pm} = 2m_{\tilde{\chi}_1^0}, m_{\tilde{\chi}_1^0} < 160 \text{ GeV}$	
> 400	95	37	KHACHATRY...17s	CMS	$\text{jets} + \cancel{E}_T, T_{\text{stop2}}, m_{\tilde{\chi}_1^\pm} = 0.75 m_{\tilde{t}} + 0.25 m_{\tilde{\chi}_1^0}, m_{\tilde{\chi}_1^0} = 0 \text{ GeV}$	> 600	95	51	AAD	15CJ	ATLS	$\tilde{\tau}_2 \rightarrow Z\tilde{t}_1, m_{\tilde{t}_1} - m_{\tilde{\chi}_1^0} = 180 \text{ GeV}, m_{\tilde{\chi}_1^0} = 0$	
> 500	95	38	KHACHATRY...17s	CMS	$\text{jets} + \cancel{E}_T, T_{\text{stop1}}, m_{\tilde{\chi}_1^0} = 0 \text{ GeV}$	> 600	95	51	AAD	15CJ	ATLS	$\tilde{\tau}_2 \rightarrow h\tilde{t}_1, m_{\tilde{t}_1} - m_{\tilde{\chi}_1^0} = 180 \text{ GeV}, m_{\tilde{\chi}_1^0} = 0$	
>1120	95	39	SIRUNYAN	17AS	CMS	$1\ell + \text{jets} + \cancel{E}_T, T_{\text{stop1}}, m_{\tilde{\chi}_1^0} = 0 \text{ GeV}$	none, 172.5-191	95	52	AAD	15J	ATLS	$\tilde{\tau} \rightarrow t\tilde{\chi}_1^0, m_{\tilde{\chi}_1^0} = 1 \text{ GeV}$

Searches Particle Listings

Supersymmetric Particle Searches

> 450	95	53	KHACHATRY...15AF CMS	$\tilde{t} \rightarrow t\tilde{\chi}_1^0, m_{\tilde{\chi}_1^0} = 0, m_{\tilde{t}} > m_t + m_{\tilde{\chi}_1^0}$	2	SIRUNYAN 19CH searched in 137 fb ⁻¹ of pp collisions at $\sqrt{s} = 13$ TeV for events containing multiple jets and large E_T . No significant excess above the Standard Model expectations is observed. Limits are set on the gluino mass in the Tglu1A, Tglu1C, Tglu2A and Tglu3A simplified models, see their Figure 13. Limits are also set on squark, sbottom and stop masses in the Tsqk1, Tsb0t1, Tstop1 simplified models, see their Figure 14.
> 560	95	54	KHACHATRY...15AH CMS	$\tilde{t} \rightarrow t\tilde{\chi}_1^0, m_{\tilde{\chi}_1^0} = 0, m_{\tilde{t}} > m_t + m_{\tilde{\chi}_1^0}$	3	SIRUNYAN 19s searched in 35.9 fb ⁻¹ of pp collisions at $\sqrt{s} = 13$ TeV for events with zero or one charged leptons, jets and E_T . The razor variables (M_R and R^2) are used to categorize the events. No significant excess above the Standard Model expectations is observed. Limits are set on the gluino mass in the Tglu3A and Tglu3C simplified models, see Figures 22 and 23, and on the stop mass in the Tstop1 simplified model, see their Figure 24.
> 250	95	55	KHACHATRY...15AH CMS	$\tilde{t} \rightarrow c\tilde{\chi}_1^0, m_{\tilde{\chi}_1^0} = 0, m_{\tilde{t}} < 100$ GeV	4	SIRUNYAN 19u searched in 35.9 fb ⁻¹ of pp collisions at $\sqrt{s} = 13$ TeV for events containing one electron-muon pair with opposite charge. The search targets a region of parameter space where the kinematics of top squark pair production and top quark pair production is very similar, due to the mass difference between the top squark and the neutralino being close to the top quark mass. No excess above the Standard Model expectations is observed. Limits are set on the stop mass in the Tstop1 model, with $m_{\tilde{t}} - m_{\tilde{\chi}_1^0}$ close to m_t , see Figure 5.
none, 200–350	95	56	KHACHATRY...15L CMS	$\tilde{t} \rightarrow qq, \text{RPV}, \lambda_{\beta 12}'' \neq 0$	5	AABOUD 18AQ searched in 36.1 fb ⁻¹ of pp collisions at $\sqrt{s} = 13$ TeV for top squark pair production in final states with one isolated electron or muon, several energetic jets, and missing transverse momentum. No significant excess over the Standard Model prediction is observed. In case of Tstop1 models, top squark masses up to 940 GeV are excluded assuming $m_{\tilde{\chi}_1^0} = 0$ GeV, see their Fig. 20. If the top quark is not on-shell (3-body) decay, exclusions up to 500 GeV are obtained for $m_{\tilde{\chi}_1^0} = 300$ GeV. Exclusions as a function of $m_{\tilde{t}} - m_{\tilde{\chi}_1^0}$ are given in their Fig. 21.
none, 200–385	95	56	KHACHATRY...15L CMS	$\tilde{t} \rightarrow qb, \text{RPV}, \lambda_{323}'' \neq 0$	6	AABOUD 18AQ searched in 36.1 fb ⁻¹ of pp collisions at $\sqrt{s} = 13$ TeV for top squark pair production in final states with one isolated electron or muon, several energetic jets, and missing transverse momentum. No significant excess over the Standard Model prediction is observed. In case of Tstop3 models (4-body), top squark masses up to 370 GeV are excluded for $m_{\tilde{t}} - m_{\tilde{\chi}_1^0}$ as low as 20 GeV. Top squark masses below 195 GeV are excluded for all $m_{\tilde{\chi}_1^0}$, see their Fig. 20 and Fig. 21.
> 730	95	57	KHACHATRY...15x CMS	$\tilde{t} \rightarrow t\tilde{\chi}_1^0, m_{\tilde{\chi}_1^0} = 100$ GeV, $m_{\tilde{t}} > m_t + m_{\tilde{\chi}_1^0}$	7	AABOUD 18AQ searched in 36.1 fb ⁻¹ of pp collisions at $\sqrt{s} = 13$ TeV for top squark pair production in final states with one isolated electron or muon, several energetic jets, and missing transverse momentum. No significant excess over the Standard Model prediction is observed. In case of Tstop2 models, top squark masses up to 840 GeV are excluded for $m_{\tilde{t}} - m_{\tilde{\chi}_1^0} = 10$ GeV. See their Fig. 23. Exclusion limits for this decay mode are presented also in the context of Higgsino-LSP phenomenological MSSM models, where $m_{\tilde{\chi}_1^0} = 5$ GeV, see their Fig 26.
none 400–645	95	57	KHACHATRY...15x CMS	$\tilde{t} \rightarrow t\tilde{\chi}_1^0$ or $\tilde{t} \rightarrow b\tilde{\chi}_1^\pm, m_{\tilde{\chi}_1^0} = 100$ GeV, $m_{\tilde{\chi}_1^\pm} - m_{\tilde{\chi}_1^0} = 5$ GeV	8	AABOUD 18BV searched in 36.1 fb ⁻¹ of pp collisions at $\sqrt{s} = 13$ TeV for events with at least one jet identified as c -jet, large missing transverse energy and no leptons. Good agreement is observed between the number of events in data and Standard Model predictions. The results are translated into exclusion limits in Tstop4 models. In scenarios with differences of the stop and neutralino masses below 100 GeV, stop masses below 500 GeV are excluded. See their Fig.6 and Fig.7.
none 270–645	95	58	AAD	14AJ ATLS ≥ 4 jets + $E_T, \tilde{t}_1 \rightarrow t\tilde{\chi}_1^0, m_{\tilde{\chi}_1^0} < 30$ GeV	9	AABOUD 18BV searched in 36.1 fb ⁻¹ of pp collisions at $\sqrt{s} = 13$ TeV for events with at least one jet identified as c -jet, large missing transverse energy and no leptons. Good agreement is observed between the number of events in data and Standard Model predictions. The results are translated into exclusion limits in Tstop1 models. In scenarios with massless neutralinos, top squark masses below 850 GeV are excluded. See their Fig.6.
none 250–550	95	58	AAD	14AJ ATLS ≥ 4 jets + $E_T, B(\tilde{t}_1 \rightarrow b\tilde{\chi}_1^\pm) = 50\%, m_{\tilde{\chi}_1^\pm} = 2m_{\tilde{\chi}_1^0}, m_{\tilde{\chi}_1^0} < 60$ GeV	10	AABOUD 18i searched in 36.1 fb ⁻¹ of pp collisions at $\sqrt{s} = 13$ TeV for events with at least one jet with a transverse momentum above 250 GeV and no leptons. Good agreement is observed between the number of events in data and Standard Model predictions. The results are translated into exclusion limits in Tstop3 models. Stop masses below 390 GeV are excluded for $m_{\tilde{t}} - m_{\tilde{\chi}_1^0} = m_b$. See their Fig.9(b).
none 210–640	95	59	AAD	14BD ATLS $\ell^\pm + \text{jets} + E_T, \tilde{t}_1 \rightarrow t\tilde{\chi}_1^0, m_{\tilde{\chi}_1^0} = 0$ GeV	11	AABOUD 18i searched in 36.1 fb ⁻¹ of pp collisions at $\sqrt{s} = 13$ TeV for events with at least one jet with a transverse momentum above 250 GeV and no leptons. Good agreement is observed between the number of events in data and Standard Model predictions. The results are translated into exclusion limits in Tstop4 models. In scenarios with differences of the stop and neutralino masses around 5 GeV, stop masses below 430 GeV are excluded. See their Fig.9(a).
> 500	95	59	AAD	14BD ATLS $\ell^\pm + \text{jets} + E_T, \tilde{t}_1 \rightarrow b\tilde{\chi}_1^\pm, m_{\tilde{\chi}_1^\pm} = 2m_{\tilde{\chi}_1^0}, 100$ GeV < $m_{\tilde{\chi}_1^0} < 150$ GeV	12	AABOUD 18y searched in 36.1 fb ⁻¹ of pp collisions at $\sqrt{s} = 13$ TeV for direct pair production of top squarks in final states with two tau leptons, b -jets, and missing transverse momentum. At least one hadronic τ is required. No significant deviation from the SM predictions is observed in the data. The analysis results are interpreted in Tstop5 models with a nearly massless gravitino. Top squark masses up to 1.16 TeV and tau slepton masses up to 1 TeV are excluded, see their Fig. 7.
none 150–445	95	60	AAD	14F ATLS $\ell^\pm \ell^\mp$ final state, $\tilde{t}_1 \rightarrow b\tilde{\chi}_1^\pm, m_{\tilde{t}} - m_{\tilde{\chi}_1^\pm} = 10$ GeV, $m_{\tilde{\chi}_1^0} = 1$ GeV	13	SIRUNYAN 18AJ searched in 35.9 fb ⁻¹ of pp collisions at $\sqrt{s} = 13$ TeV for events containing two low-momentum, oppositely charged leptons (electrons or muons) and E_T . No excess over the expected background is observed. Limits are derived on the wino mass in the Tch1n2F simplified model, see their Figure 5. Limits are also set on the stop mass in the Tstop10 simplified model, see their Figure 6. Finally, limits are set on the Higgsino mass in the Tch1n2G simplified model, see Figure 8 and in the pMSSM, see Figure 7.
none 215–530	95	60	AAD	14F ATLS $\ell^\pm \ell^\mp$ final state, $\tilde{t}_1 \rightarrow t\tilde{\chi}_1^0, m_{\tilde{\chi}_1^0} = 1$ GeV	14	SIRUNYAN 18AL searched in 35.9 fb ⁻¹ of pp collisions at $\sqrt{s} = 13$ TeV for events with at least three charged leptons, in any combination of electrons and muons, jets and significant E_T . No significant excess above the Standard Model expectations is observed. Limits are set on the gluino mass in the Tglu3A and Tglu1C simplified models, see their Figure 5. Limits are also set on the sbottom mass in the Tsb0t2 simplified model, see their Figure 6, and on the stop mass in the Tstop7 simplified model, see their Figure 7.
> 270	95	61	AAD	14T ATLS $\tilde{t}_1 \rightarrow c\tilde{\chi}_1^0, m_{\tilde{\chi}_1^0} = 200$ GeV	15	SIRUNYAN 18AN searched in 19.7 fb ⁻¹ of pp collisions at $\sqrt{s} = 8$ TeV for events containing one or two photons and a pair of top quarks from the decay of a pair of top squark in a natural gauge-mediated scenario. The final state consists of a lepton (electron or muon), jets and one or two photons. No significant excess above the Standard Model expectations is observed. Limits are set on the stop mass in the Tstop12 simplified model, see their Figure 6.
> 240	95	61	AAD	14T ATLS $\tilde{t}_1 \rightarrow c\tilde{\chi}_1^0, m_{\tilde{\chi}_1^0} - m_{\tilde{\chi}_1^0} < 85$ GeV		
> 255	95	61	AAD	14T ATLS $\tilde{t}_1 \rightarrow b f f' \tilde{\chi}_1^0, m_{\tilde{t}} - m_{\tilde{\chi}_1^0} \approx m_b$		
> 400	95	62	CHATRCHYAN14AH CMS	jets + $E_T, \tilde{t} \rightarrow t\tilde{\chi}_1^0$ simplified model, $m_{\tilde{\chi}_1^0} = 50$ GeV		
> 740	95	64	KHACHATRY...14T CMS	$\tau + b$ -jets, RPV, $LQ\tilde{D}, \lambda_{333}'' \neq 0, \tilde{t} \rightarrow \tau b$ simplified model		
> 580	95	64	KHACHATRY...14T CMS	$\tau + b$ -jets, RPV, $LQ\tilde{D}, \lambda_{3jk}'' \neq 0 (j \neq 3), \tilde{t} \rightarrow \tilde{\chi}_1^\pm b, \tilde{\chi}_1^\pm \rightarrow qq\tau^\pm$ simplified model		
••• We do not use the following data for averages, fits, limits, etc. •••						
> 850	95	65	AABOUD	17AF ATLS $2\ell + \text{jets} + b\text{-jets} + E_T, \text{Tstop6}, m_{\tilde{\chi}_1^0} = 0$		
> 800	95	66	AABOUD	17AF ATLS $2\ell + \text{jets} + b\text{-jets} + E_T, \text{Tstop7}$ with 100% decays via $Z, m_{\tilde{\chi}_1^0} = 50$ GeV		
> 880	95	67	AABOUD	17AF ATLS $2\ell + \text{jets} + b\text{-jets} + E_T, \text{Tstop7}$ with 100% decays via higgs, $m_{\tilde{\chi}_1^0} = 50$ GeV		
> 230	95	68	AABOUD	17AY ATLS jets + E_T , pMSSM-inspired		
> 600	95	69	AAD	14B ATLS $Z + b E_T, \tilde{t}_2 \rightarrow Z\tilde{t}_1, \tilde{t}_1 \rightarrow t\tilde{\chi}_1^0, m_{\tilde{\chi}_1^0} < 200$ GeV		
> 540	95	69	AAD	14B ATLS $Z + b E_T, \tilde{t}_1 \rightarrow t\tilde{\chi}_1^0, \tilde{\chi}_1^0 \rightarrow Z\tilde{G}$, natural GMSB, 100 GeV < $m_{\tilde{\chi}_1^0} < m_{\tilde{t}} - 10$ GeV		
> 360	95	70	CHATRCHYAN14U CMS	$\tilde{t}_1 \rightarrow b\tilde{\chi}_1^\pm r, \tilde{\chi}_1^\pm \rightarrow f f' \tilde{\chi}_1^0, \tilde{\chi}_1^0 \rightarrow H\tilde{G}$ simplified model, $m_{\tilde{\chi}_1^\pm} - m_{\tilde{\chi}_1^0} = 5$ GeV, GMSB		
> 215	95	71	CZAKON	14 $\tilde{t} \rightarrow t\tilde{\chi}_1^0, m_{\tilde{\chi}_1^0} < 10$ GeV		
		71	KHACHATRY...14c CMS	$\tilde{t}_2 \rightarrow H\tilde{t}_1$ or $\tilde{t}_2 \rightarrow Z\tilde{t}_1$ simplified model		

¹ SIRUNYAN 19AU searched in 35.9 fb⁻¹ of pp collisions at $\sqrt{s} = 13$ TeV for events with at least one photon, jets, some of which are identified as originating from b -quarks, and large E_T . No significant excess above the Standard Model expectations is observed. In the framework of GMSB, limits are set on the gluino mass in the Tglu4C, Tglu4D and Tglu4E simplified models, and on the top squark mass in the Tstop13 simplified model, see their Figure 5.

See key on page 999

Searches Particle Listings Supersymmetric Particle Searches

- 16 SIRUNYAN 18AY searched in 35.9 fb^{-1} of pp collisions at $\sqrt{s} = 13 \text{ TeV}$ for events containing one or more jets and significant $E_{\cancel{T}}$. No significant excess above the Standard Model expectations is observed. Limits are set on the gluino mass in the Tglu1A, Tglu2A and Tglu3A simplified models, see their Figure 3. Limits are also set on squark, sbottom and stop masses in the Tsqk1, Tsb0t1, Tstop1 and Tstop4 simplified models, see their Figure 3. Finally, limits are set on long-lived gluino masses in a Tglu1A simplified model where the gluino is metastable or long-lived with proper decay lengths in the range $10^{-3} \text{ mm} < c\tau < 10^5 \text{ mm}$, see their Figure 4.
- 17 SIRUNYAN 18b searched in 35.9 fb^{-1} of pp collisions at $\sqrt{s} = 13 \text{ TeV}$ for the pair production of third-generation squarks in events with jets and large $E_{\cancel{T}}$. No significant excess above the Standard Model expectations is observed. Limits are set on the sbottom mass in the Tsb0t1 simplified model, see their Figure 5, and on the stop mass in the Tstop4 simplified model, see their Figure 6.
- 18 SIRUNYAN 18c searched in 35.9 fb^{-1} of pp collisions at $\sqrt{s} = 13 \text{ TeV}$ for the pair production of top squarks in events with two oppositely charged leptons (electrons or muons), jets identified as originating from a b -quark and large $E_{\cancel{T}}$. No significant excess above the Standard Model expectations is observed. Limits are set on the stop mass in the Tstop1, Tstop2 and Tstop11 simplified models, see their Figures 11 and 12. The Tstop1 and Tstop2 results are combined with complementary searches in the all-hadronic and single lepton channels, see their Figures 13 and 14.
- 19 SIRUNYAN 18d searched in 35.9 fb^{-1} of pp collisions at $\sqrt{s} = 13 \text{ TeV}$ for events containing identified hadronically decaying top quarks, no leptons, and $E_{\cancel{T}}$. No significant excess above the Standard Model expectations is observed. Limits are set on the stop mass in the Tstop1 simplified model, see their Figure 8, and on the gluino mass in the Tglu3A, Tglu3B, Tglu3C and Tglu3E simplified models, see their Figure 9.
- 20 SIRUNYAN 18di searched in 35.9 fb^{-1} of pp collisions at $\sqrt{s} = 13 \text{ TeV}$ for pair production of top squarks in events with a low transverse momentum lepton (electron or muon), a high-momentum jet and significant missing transverse momentum. No significant excess above the Standard Model expectations is observed. Limits are set on the stop mass in the Tstop3 and Tstop10 simplified models, see their Figures 7 and 8. A combination of this search with the all-hadronic search is presented in Figure 9.
- 21 SIRUNYAN 18DN searched in 35.9 fb^{-1} of pp collisions at $\sqrt{s} = 13 \text{ TeV}$ for direct electroweak production of charginos and for pair production of top squarks in events with two leptons (electrons or muons) of the opposite electric charge. No significant excess above the Standard Model expectations is observed. Limits are set on the chargino mass in the Tch1Ch1C and Tch1Ch1E simplified models, see their Figure 8. Limits are also set on the stop mass in the Tstop1 and Tstop2 simplified models, see their Figure 9.
- 22 ABOUD 17AJ searched in 36.1 fb^{-1} of pp collisions at $\sqrt{s} = 13 \text{ TeV}$ for events with two same-sign or three leptons, jets and large missing transverse momentum. No significant excess above the Standard Model expectations is observed. Limits up to 700 GeV are set on the top squark mass in Tstop11 simplified models, assuming $m_{\tilde{\chi}_1^0} = m_{\tilde{t}} - 275 \text{ GeV}$ and $m_{\tilde{\chi}_2^0} = m_{\tilde{\chi}_1^0} + 100 \text{ GeV}$. See their Figure 4(e).
- 23 ABOUD 17AX searched in 36 fb^{-1} of pp collisions at $\sqrt{s} = 13 \text{ TeV}$ for events containing two jets identified as originating from b -quarks and large missing transverse momentum, with or without leptons. No excess of events above the expected level of Standard Model background was found. Exclusion limits at 95% C.L. are set on the masses of top squarks. Assuming 50% BR for Tstop1 and Tstop2 simplified models, a \tilde{t}_1 mass below 880 (860) GeV is excluded for $m_{\tilde{\chi}_1^0} = 0$ (<250) GeV. See their Fig. 7(b).
- 24 ABOUD 17AY searched in 36.1 fb^{-1} of pp collisions at $\sqrt{s} = 13 \text{ TeV}$ for events with at least four jets and large missing transverse momentum. No significant excess above the Standard Model expectations is observed. Limits in the range 250–1000 GeV are set on the top squark mass in Tstop1 simplified models. For the first time, additional constraints are set for the region $m_{\tilde{t}_1} \sim m_{\tilde{t}} + m_{\tilde{\chi}_1^0}$, with exclusion of the \tilde{t}_1 mass range 235–590 GeV. See their Figure 8.
- 25 ABOUD 17AY searched in 36.1 fb^{-1} of pp collisions at $\sqrt{s} = 13 \text{ TeV}$ for events with at least four jets and large missing transverse momentum. No significant excess above the Standard Model expectations is observed. Limits in the range 450–850 GeV are set on the top squark mass in a mixture of Tstop1 and Tstop2 simplified models with BR=50% and assuming $m_{\tilde{\chi}_1^\pm} - m_{\tilde{\chi}_1^0} = 1 \text{ GeV}$ and $m_{\tilde{\chi}_1^0} < 240 \text{ GeV}$. Constraints are given for various values of the BR. See their Figure 9.
- 26 ABOUD 17BE searched in 36.1 fb^{-1} of pp collisions at $\sqrt{s} = 13 \text{ TeV}$ for events with two opposite-charge leptons (electrons and muons) and large missing transverse momentum. No significant excess above the Standard Model expectations is observed. Limits up to 720 GeV are set on the top squark mass in Tstop1 simplified models, assuming massless neutralinos. See their Figure 9 (2-body area).
- 27 ABOUD 17BE searched in 36.1 fb^{-1} of pp collisions at $\sqrt{s} = 13 \text{ TeV}$ for events with two opposite-charge leptons (electrons and muons) and large missing transverse momentum. No significant excess above the Standard Model expectations is observed. Limits up to 400 GeV are set on the top squark mass in Tstop3 simplified models, assuming $m_{\tilde{t}_1} - m_{\tilde{\chi}_1^0} = 40 \text{ GeV}$. See their Figure 9 (4-body area).
- 28 ABOUD 17BE searched in 36.1 fb^{-1} of pp collisions at $\sqrt{s} = 13 \text{ TeV}$ for events with two opposite-charge leptons (electrons and muons) and large missing transverse momentum. No significant excess above the Standard Model expectations is observed. Limits up to 430 GeV are set on the top squark mass in Tstop1 simplified models where top quarks are offshell, assuming $m_{\tilde{t}_1} - m_{\tilde{\chi}_1^0}$ close to the W mass. See their Figure 9 (3-body area).
- 29 ABOUD 17BE searched in 36.1 fb^{-1} of pp collisions at $\sqrt{s} = 13 \text{ TeV}$ for events with two opposite-charge leptons (electrons and muons) and large missing transverse momentum. No significant excess above the Standard Model expectations is observed. Limits up to 700 GeV are set on the top squark mass in Tstop2 simplified models, assuming $m_{\tilde{t}_1} - m_{\tilde{\chi}_1^\pm} = 10 \text{ GeV}$ and massless neutralinos. See their Figure 10.
- 30 KHACHATRYAN 17 searched in 2.3 fb^{-1} of pp collisions at $\sqrt{s} = 13 \text{ TeV}$ for events containing four or more jets, no more than one lepton, and missing transverse momentum, using the razor variables ($M_{\cancel{P}}$ and R^2) to discriminate between signal and background processes. No evidence for an excess over the expected background is observed. Limits are derived on the stop mass in the Tstop1 simplified model, see Fig. 17.
- 31 KHACHATRYAN 17AD searched in 2.3 fb^{-1} of pp collisions at $\sqrt{s} = 13 \text{ TeV}$ for events containing at least four jets (including b -jets), missing transverse momentum and tagged top quarks. No evidence for an excess over the expected background is observed. Top squark masses in the range 250–740 GeV and neutralino masses up to 240 GeV are excluded at 95% C.L. See Fig. 12.
- 32 KHACHATRYAN 17AD searched in 2.3 fb^{-1} of pp collisions at $\sqrt{s} = 13 \text{ TeV}$ for events containing at least four jets (including b -jets), missing transverse momentum and tagged top quarks. No evidence for an excess over the expected background is observed. Limits are derived on the \tilde{t} mass in simplified models that are a mixture of Tstop1 and Tstop2 with branching fractions 50% for each of the two decay modes: top squark masses of up to 610 GeV and neutralino masses up to 190 GeV are excluded at 95% C.L. The $\tilde{\chi}_1^\pm$ and the $\tilde{\chi}_1^0$ are assumed to be nearly degenerate in mass, with a 5 GeV difference between their masses. See Fig. 12.
- 33 KHACHATRYAN 17P searched in 2.3 fb^{-1} of pp collisions at $\sqrt{s} = 13 \text{ TeV}$ for events with one or more jets and large $E_{\cancel{T}}$. No significant excess above the Standard Model expectations is observed. Limits are set on the gluino mass in the Tglu1A, Tglu2A, Tglu3A, Tglu3B, Tglu3C and Tglu3D simplified models, see their Figures 7 and 8. Limits are also set on the squark mass in the Tsqk1 simplified model, see their Fig. 7, and on the sbottom mass in the Tsb0t1 simplified model, see Fig. 8. Finally, limits are set on the stop mass in the Tstop1, Tstop3, Tstop4, Tstop6 and Tstop7 simplified models, see Fig. 8.
- 34 KHACHATRYAN 17s searched in 18.5 fb^{-1} of pp collisions at $\sqrt{s} = 8 \text{ TeV}$ for events containing multiple jets and missing transverse momentum, using the α_T variable to discriminate between signal and background processes. No evidence for an excess over the expected background is observed. Limits are derived on the stop mass in the Tstop4 model: for $\Delta m = m_{\tilde{t}} - m_{\tilde{\chi}_1^0}$ equal to 10 and 80 GeV, masses of stop below 240 and 260 GeV are excluded, respectively. See their Fig. 3.
- 35 KHACHATRYAN 17s searched in 18.5 fb^{-1} of pp collisions at $\sqrt{s} = 8 \text{ TeV}$ for events containing multiple jets and missing transverse momentum, using the α_T variable to discriminate between signal and background processes. No evidence for an excess over the expected background is observed. Limits are derived on the stop mass in the Tstop3 model: for $\Delta m = m_{\tilde{t}} - m_{\tilde{\chi}_1^0}$ equal to 10 and 80 GeV, masses of stop below 225 and 130 GeV are excluded, respectively. See their Fig. 3.
- 36 KHACHATRYAN 17s searched in 18.5 fb^{-1} of pp collisions at $\sqrt{s} = 8 \text{ TeV}$ for events containing multiple jets and missing transverse momentum, using the α_T variable to discriminate between signal and background processes. No evidence for an excess over the expected background is observed. Limits are derived on the stop mass in the Tstop2 model: assuming $m_{\tilde{\chi}_1^\pm} = 0.25 m_{\tilde{t}} + 0.75 m_{\tilde{\chi}_1^0}$, masses of stop up to 325 GeV and masses of the neutralino up to 225 GeV are excluded. See their Fig. 3.
- 37 KHACHATRYAN 17s searched in 18.5 fb^{-1} of pp collisions at $\sqrt{s} = 8 \text{ TeV}$ for events containing multiple jets and missing transverse momentum, using the α_T variable to discriminate between signal and background processes. No evidence for an excess over the expected background is observed. Limits are derived on the stop mass in the Tstop2 model: assuming $m_{\tilde{\chi}_1^\pm} = 0.75 m_{\tilde{t}} + 0.25 m_{\tilde{\chi}_1^0}$, masses of stop up to 400 GeV are excluded for low neutralino masses. See their Fig. 3.
- 38 KHACHATRYAN 17s searched in 18.5 fb^{-1} of pp collisions at $\sqrt{s} = 8 \text{ TeV}$ for events containing multiple jets and missing transverse momentum, using the α_T variable to discriminate between signal and background processes. No evidence for an excess over the expected background is observed. Limits are derived on the stop mass in the Tstop1 model: assuming masses of stop up to 500 GeV and masses of the neutralino up to 105 GeV are excluded. See their Fig. 3.
- 39 SIRUNYAN 17As searched in 35.9 fb^{-1} of pp collisions at $\sqrt{s} = 13 \text{ TeV}$ for events with a single lepton (electron or muon), jets, and large $E_{\cancel{T}}$. No significant excess above the Standard Model expectations is observed. Limits are set on the stop mass in the Tstop1, Tstop2 and Tstop8 simplified models, see their Figures 5, 6 and 7.
- 40 SIRUNYAN 17AT searched in 35.9 fb^{-1} of pp collisions at $\sqrt{s} = 13 \text{ TeV}$ for direct production of top squarks in events with jets and large $E_{\cancel{T}}$. No significant excess above the Standard Model expectations is observed. Limits are set on the stop mass in the Tstop1, Tstop2, Tstop3, Tstop4, Tstop8 and Tstop10 simplified models, see their Figures 9 to 14.
- 41 SIRUNYAN 17AZ searched in 35.9 fb^{-1} of pp collisions at $\sqrt{s} = 13 \text{ TeV}$ for events with one or more jets and large $E_{\cancel{T}}$. No significant excess above the Standard Model expectations is observed. Limits are set on the gluino mass in the Tglu1A, Tglu2A, Tglu3A simplified models, see their Figures 6. Limits are also set on the squark mass in the Tsqk1 simplified model (for single light squark and for 8 degenerate light squarks), on the sbottom mass in the Tsb0t1 simplified model and on the stop mass in the Tstop1 simplified model, see their Fig. 7. Finally, limits are set on the stop mass in the Tstop2, Tstop4 and Tstop8 simplified models, see Fig. 8.
- 42 SIRUNYAN 17k searched in 2.3 fb^{-1} of pp collisions at $\sqrt{s} = 13 \text{ TeV}$ for direct production of stop or sbottom pairs in events with multiple jets and significant $E_{\cancel{T}}$. A second search also requires an isolated lepton and is combined with the all-hadronic search. No significant excess above the Standard Model expectations is observed. Limits are set on the stop mass in the Tstop1, Tstop8 and Tstop4 simplified models, see their Figures 7, 8 and 9 (for the Tstop4 limits, only the results of the all-hadronic search are used). Limits are also set on the sbottom mass in the Tsb0t1 simplified model, see Fig. 10 (also here, only the results of the all-hadronic search are used).
- 43 SIRUNYAN 17P searched in 35.9 fb^{-1} of pp collisions at $\sqrt{s} = 13 \text{ TeV}$ for events with multiple jets and large $E_{\cancel{T}}$. No significant excess above the Standard Model expectations is observed. Limits are set on the gluino mass in the Tglu1A, Tglu1C, Tglu2A, Tglu3A and Tglu3D simplified models, see their Fig. 12. Limits are also set on the squark mass in the Tsqk1 simplified model, on the stop mass in the Tstop1 simplified model, and on the sbottom mass in the Tsb0t1 simplified model, see Fig. 13.
- 44 ABOUD 16D searched in 3.2 fb^{-1} of pp collisions at $\sqrt{s} = 13 \text{ TeV}$ in events with an energetic jet and large missing transverse momentum. The results are interpreted as 95% C.L. limits on mass of stop decaying into a charm-quark and the lightest neutralino in scenarios with $m_{\tilde{t}_1} - m_{\tilde{\chi}_1^0}$ between 5 and 20 GeV. See their Fig. 5.
- 45 ABOUD 16J searched in 3.2 fb^{-1} of pp collisions at $\sqrt{s} = 13 \text{ TeV}$ in final states with one isolated electron or muon, jets, and missing transverse momentum. For the direct stop pair production model where the stop decays via top and lightest neutralino, the results exclude at 95% C.L. stop masses between 745 GeV and 780 GeV for a massless $\tilde{\chi}_1^0$. See their Fig. 8.
- 46 AAD 16AY searched in 20 fb^{-1} of pp collisions at $\sqrt{s} = 8 \text{ TeV}$ for events with either two hadronically decaying tau leptons, one hadronically decaying tau and one light lepton, or two light leptons. No significant excess over the Standard Model expectation is found. Exclusion limits at 95% C.L. on the mass of top squarks decaying via $\tilde{\tau}$ to a nearly massless gravitino are placed depending on $m_{\tilde{\tau}}$ which is ranging from the 87 GeV LEP limit to $m_{\tilde{t}_1}$. See their Figs. 9 and 10.

Searches Particle Listings

Supersymmetric Particle Searches

- 47 KHACHATRYAN 16AV searched in 19.7 fb^{-1} of pp collisions at $\sqrt{s} = 8 \text{ TeV}$ for events with one or two isolated leptons, hadronic jets, b -jets and \cancel{E}_T . No significant excess above the Standard Model expectations is observed. Limits are set on the stop mass in the Tstop1 and Tstop2 simplified models, see Fig. 11.
- 48 KHACHATRYAN 16BK searched in 18.9 fb^{-1} of pp collisions at $\sqrt{s} = 8 \text{ TeV}$ for events with hadronic jets and \cancel{E}_T . No significant excess above the Standard Model expectations is observed. Limits are set on the stop mass in the Tstop1 and Tstop2 simplified models, see Fig. 16.
- 49 KHACHATRYAN 16BS searched in 2.3 fb^{-1} of pp collisions at $\sqrt{s} = 13 \text{ TeV}$ for events with at least one energetic jet, no isolated leptons, and significant \cancel{E}_T , using the transverse mass variable M_{T2} to discriminate between signal and background processes. No significant excess above the Standard Model expectations is observed. Limits are set on the stop mass in the Tstop1 simplified model, see Fig. 11 and Table 3.
- 50 KHACHATRYAN 16V searched in 19.7 fb^{-1} of pp collisions at $\sqrt{s} = 8 \text{ TeV}$ for events with one or two soft isolated leptons, hadronic jets, and \cancel{E}_T . No significant excess above the Standard Model expectations is observed. Limits are set on the stop mass in the Tstop3 simplified model, see Fig. 3.
- 51 AAD 15CJ searched in 20 fb^{-1} of pp collisions at $\sqrt{s} = 8 \text{ TeV}$ for evidence of third generation squarks by combining a large number of searches covering various final states. Stop decays with and without charginos in the decay chain are considered and summaries of all ATLAS Run 1 searches for direct stop production can be found in Fig. 4 (no intermediate charginos) and Fig. 7 (intermediate charginos). Limits are set on stop masses in compressed mass regions, with $B(\bar{t} \rightarrow c\bar{\chi}_1^0) + B(\bar{t} \rightarrow bff'\bar{\chi}_1^0) = 1$, see Fig. 5. Limits are also set on stop masses assuming that both the decay $\bar{t} \rightarrow t\bar{\chi}_1^0$ and $\bar{t} \rightarrow b\bar{\chi}_1^\pm$ are possible, with both their branching ratios summing up to 1, assuming $\bar{\chi}_1^\pm \rightarrow W^{(*)}\bar{\chi}_1^0$ and $m_{\bar{\chi}_1^\pm} = 2m_{\bar{\chi}_1^0}$, see Fig. 6. Limits on the mass of the next-to-lightest stop \bar{t}_2 , decaying either to $Z\bar{t}_1$, $h\bar{t}_1$ or $t\bar{\chi}_1^0$, are also presented, see Figs. 9 and 10. Interpretations in the pMSSM are also discussed, see Figs 13–15.
- 52 AAD 15J interpreted the measurement of spin correlations in $t\bar{t}$ production using 20.3 fb^{-1} of pp collisions at $\sqrt{s} = 8 \text{ TeV}$ in exclusion limits on the pair production of light \bar{t}_1 squarks with masses similar to the top quark mass. The \bar{t}_1 is assumed to decay through $\bar{t}_1 \rightarrow t\bar{\chi}_1^0$ with predominantly right-handed top and a 100% branching ratio. The data are found to be consistent with the Standard Model expectations and masses between the top quark mass and 191 GeV are excluded, see their Fig. 2
- 53 KHACHATRYAN 15AF searched in 19.5 fb^{-1} of pp collisions at $\sqrt{s} = 8 \text{ TeV}$ for events with at least two energetic jets and significant \cancel{E}_T , using the transverse mass variable M_{T2} to discriminate between signal and background processes. No significant excess above the Standard Model expectations is observed. Limits are set on the stop mass in simplified models where the decay $\bar{t} \rightarrow t\bar{\chi}_1^0$ takes place with a branching ratio of 100%, see Fig. 12. See also Table 5. Exclusions in the CMSSM, assuming $\tan\beta = 30$, $A_0 = -2 \max(m_0, m_{1/2})$ and $\mu > 0$, are also presented, see Fig. 15.
- 54 KHACHATRYAN 15AH searched in 19.4 or 19.7 fb^{-1} of pp collisions at $\sqrt{s} = 8 \text{ TeV}$ for events containing either a fully reconstructed top quark, or events containing dijets requiring one or both jets to originate from b -quarks, or events containing a mono-jet. No significant excess above the Standard Model expectations is observed. Limits are set on the stop mass in simplified models where the decay $\bar{t} \rightarrow t\bar{\chi}_1^0$ takes place with a branching ratio of 100%, see Fig. 9. Limits are also set in simplified models where the decays $\bar{t} \rightarrow t\bar{\chi}_1^0$ and $\bar{t} \rightarrow b\bar{\chi}_1^\pm$, with $m_{\bar{\chi}_1^\pm} - m_{\bar{\chi}_1^0} = 5 \text{ GeV}$, each take place with a branching ratio of 50%, see Fig. 10, or with other fractions, see Fig. 11. Finally, limits are set in a simplified model where the decay $\bar{t} \rightarrow c\bar{\chi}_1^0$ takes place with a branching ratio of 100%, see Figs. 9, 10 and 11.
- 55 KHACHATRYAN 15AH searched in 19.4 or 19.7 fb^{-1} of pp collisions at $\sqrt{s} = 8 \text{ TeV}$ for events containing either a fully reconstructed top quark, or events containing dijets requiring one or both jets to originate from b -quarks, or events containing a mono-jet. No significant excess above the Standard Model expectations is observed. Limits are set on the stop mass in simplified models where the decay $\bar{t} \rightarrow t\bar{\chi}_1^0$ takes place with a branching ratio of 100%, see Fig. 9. Limits are also set in simplified models where the decays $\bar{t} \rightarrow t\bar{\chi}_1^0$ and $\bar{t} \rightarrow b\bar{\chi}_1^\pm$, with $m_{\bar{\chi}_1^\pm} - m_{\bar{\chi}_1^0} = 5 \text{ GeV}$, each take place with a branching ratio of 50%, see Fig. 10, or with other fractions, see Fig. 11. Finally, limits are set in a simplified model where the decay $\bar{t} \rightarrow c\bar{\chi}_1^0$ takes place with a branching ratio of 100%, see Figs. 9, 10, and 11.
- 56 KHACHATRYAN 15L searched in 19.4 fb^{-1} of pp collisions at $\sqrt{s} = 8 \text{ TeV}$ for pair production of heavy resonances decaying to pairs of jets in four jet events. No significant excess above the Standard Model expectations is observed. Limits are set on the stop mass in R -parity-violating supersymmetry models where $\bar{t} \rightarrow qq$ ($\lambda_{323}^u \neq 0$), see Fig. 6 (top) and $\bar{t} \rightarrow qb$ ($\lambda_{323}^u \neq 0$), see Fig. 6 (bottom).
- 57 KHACHATRYAN 15x searched in 19.3 fb^{-1} of pp collisions at $\sqrt{s} = 8 \text{ TeV}$ for events with at least two energetic jets, at least one of which is required to originate from a b quark, possibly a lepton, and significant \cancel{E}_T , using the razor variables (M_R and R_2) to discriminate between signal and background processes. No significant excess above the Standard Model expectations is observed. Limits are set on the stop mass in simplified models where the decay $\bar{t} \rightarrow t\bar{\chi}_1^0$ and the decay $\bar{t} \rightarrow b\bar{\chi}_1^\pm$, with $m_{\bar{\chi}_1^\pm} - m_{\bar{\chi}_1^0} = 5 \text{ GeV}$, take place with branching ratios varying between 0 and 100%, see Figs. 15, 16 and 17.
- 58 AAD 14AJ searched in 20.1 fb^{-1} of pp collisions at $\sqrt{s} = 8 \text{ TeV}$ for events containing four or more jets and large missing transverse momentum. No excess of events above the expected level of Standard Model background was found. Exclusion limits at 95% C.L. are set on the masses of third-generation squarks in simplified models which either assume that the decay $\bar{t}_1 \rightarrow t\bar{\chi}_1^0$ takes place 100% of the time, see Fig. 8, or that this decay takes place 50% of the time, while the decay $\bar{t}_1 \rightarrow b\bar{\chi}_1^\pm$ takes place the other 50% of the time, see Fig. 9.
- 59 AAD 14BD searched in 20 fb^{-1} of pp collisions at $\sqrt{s} = 8 \text{ TeV}$ for events containing one isolated lepton, jets and large missing transverse momentum. No excess of events above the expected level of Standard Model background was found. Exclusion limits at 95% C.L. are set on the masses of third-generation squarks in simplified models which either assume that the decay $\bar{t}_1 \rightarrow t\bar{\chi}_1^0$ takes place 100% of the time, see Fig. 15, or the decay $\bar{t}_1 \rightarrow b\bar{\chi}_1^\pm$ takes place 100% of the time, see Fig. 16–22. For the mixed decay scenario, see Fig. 23.
- 60 AAD 14F searched in 20.3 fb^{-1} of pp collisions at $\sqrt{s} = 8 \text{ TeV}$ for events containing two leptons (e or μ), and possibly jets and missing transverse momentum. No excess of events above the expected level of Standard Model background was found. Exclusion limits at 95% C.L. are set on the masses of third-generation squarks in simplified models which either assume that the decay $\bar{t}_1 \rightarrow b\bar{\chi}_1^\pm$ takes place 100% of the time, see Figs. 14–17 and 20, or that the decay $\bar{t}_1 \rightarrow t\bar{\chi}_1^0$ takes place 100% of the time, see Figs. 18 and 19.
- 61 AAD 14T searched in 20.3 fb^{-1} of pp collisions at $\sqrt{s} = 8 \text{ TeV}$ for monojet-like and c -tagged events. No excess of events above the expected level of Standard Model background was found. Exclusion limits at 95% C.L. are set on the masses of third-generation squarks in simplified models which assume that the decay $\bar{t}_1 \rightarrow c\bar{\chi}_1^0$ takes place 100% of the time, see Fig. 9 and 10. The results of the monojet-like analysis are also interpreted in terms of stop pair production in the four-body decay $\bar{t}_1 \rightarrow bff'\bar{\chi}_1^0$, see Fig. 11.
- 62 CHATRCHYAN 14AH searched in 4.7 fb^{-1} of pp collisions at $\sqrt{s} = 7 \text{ TeV}$ for events with at least two energetic jets and significant \cancel{E}_T , using the razor variables (M_R and R_2) to discriminate between signal and background processes. A second analysis requires at least one of the jets to be originating from a b -quark. No significant excess above the Standard Model expectations is observed. Limits are set on bottom masses in simplified models where the decay $\bar{t} \rightarrow t\bar{\chi}_1^0$ takes place with a branching ratio of 100%, see Figs. 28 and 29. Exclusions in the CMSSM, assuming $\tan\beta = 10$, $A_0 = 0$ and $\mu > 0$, are also presented, see Fig. 26.
- 63 CHATRCHYAN 14R searched in 19.5 fb^{-1} of pp collisions at $\sqrt{s} = 8 \text{ TeV}$ for events with at least three leptons (electrons, muons, taus) in the final state. No significant excess above the Standard Model expectations is observed. Limits are set on the stop mass in a natural higgsino NLSP simplified model (GMSB) where the decay $\bar{t} \rightarrow b\bar{\chi}_1^\pm$, with $\bar{\chi}_1^\pm \rightarrow (qq'/\ell\nu)H$, $Z\bar{G}$, takes place with a branching ratio of 100% (the particles between brackets have a soft p_T spectrum), see Figs. 4–6.
- 64 KHACHATRYAN 14T searched in 19.7 fb^{-1} of pp collisions at $\sqrt{s} = 8 \text{ TeV}$ for events with τ -leptons and b -quark jets, possibly with extra light-flavour jets. No excess above the Standard Model expectations is observed. Limits are set on stop masses in RPV SUSY models with $LQ\bar{D}$ couplings, in two simplified models. In the first model, the decay $\bar{t} \rightarrow \tau b$ is considered, with $\lambda_{333}^t \neq 0$, see Fig. 3. In the second model, the decay $\bar{t} \rightarrow \bar{\chi}^\pm b$, with the subsequent decay $\bar{\chi}^\pm \rightarrow qq\tau^\pm$ is considered, with $\lambda_{3jk}^t \neq 0$ and the mass splitting between the top squark and the chargin chosen to be 100 GeV, see Fig. 4.
- 65 AABOUD 17AF searched in 36 fb^{-1} of pp collisions at $\sqrt{s} = 13 \text{ TeV}$ for evidence of top squarks in events containing 2 leptons, jets, b -jets and \cancel{E}_T . In Tstop6 model, assuming $m_{\bar{\chi}_1^0} = 0 \text{ GeV}$, \bar{t}_1 masses up to 850 GeV are excluded for $m_{\bar{\chi}_2^0} > 200 \text{ GeV}$.
- 66 AABOUD 17AF searched in 36 fb^{-1} of pp collisions at $\sqrt{s} = 13 \text{ TeV}$ for evidence of \bar{t}_2 in events containing 2 leptons, jets, b -jets and \cancel{E}_T . In Tstop7 model, assuming $m_{\bar{\chi}_1^0} = 50 \text{ GeV}$ and 100% decays via Z boson, \bar{t}_2 masses up to 800 GeV are excluded. Exclusion limits are also shown as a function of the \bar{t}_2 branching ratios in their Figure 7.
- 67 AABOUD 17AF searched in 36 fb^{-1} of pp collisions at $\sqrt{s} = 13 \text{ TeV}$ for evidence of \bar{t}_2 in events containing 2 leptons, jets, b -jets and \cancel{E}_T . In Tstop7 model, assuming $m_{\bar{\chi}_1^0} = 50 \text{ GeV}$ and 100% decays via higgs boson, \bar{t}_2 masses up to 880 GeV are excluded. Exclusion limits are also shown as a function of the \bar{t}_2 branching ratios in their Figure 7.
- 68 AABOUD 17AY searched in 36.1 fb^{-1} of pp collisions at $\sqrt{s} = 13 \text{ TeV}$ for events with at least four jets and large missing transverse momentum. No significant excess above the Standard Model expectations is observed. Limits are set on the top squark mass assuming three pMSSM-inspired models. The first one, referred to as Higgsino LSP model, assumes $m_{\bar{\chi}_1^\pm} - m_{\bar{\chi}_1^0} = 5 \text{ GeV}$ and $m_{\bar{\chi}_2^0} - m_{\bar{\chi}_1^0} = 10 \text{ GeV}$, with a mixture of decay modes as in Tstop1, Tstop2 and Tstop6. See their Figure 10. The second and third models are referred to as Wino NLSP and well-tempered pMSSM models, respectively. See their Figure 11 and Figure 12, and text for details on assumptions.
- 69 AAD 14B searched in 20.3 fb^{-1} of pp collisions at $\sqrt{s} = 8 \text{ TeV}$ for events containing a Z boson, with or without additional leptons, plus jets originating from b -quarks and significant missing transverse momentum. No excess over the expected SM background is observed. Limits are derived in simplified models featuring \bar{t}_2 production, with $\bar{t}_2 \rightarrow Z\bar{t}_1$, $\bar{t}_1 \rightarrow t\bar{\chi}_1^0$ with a 100% branching ratio, see Fig. 4, and in the framework of natural GMSB, see Fig. 6.
- 70 CHATRCHYAN 14U searched in 19.7 fb^{-1} of pp collisions at $\sqrt{s} = 8 \text{ TeV}$ for evidence of direct pair production of top squarks, with Higgs bosons in the decay chain. The search is performed using a selection of events containing two Higgs bosons, each decaying to a photon pair, missing transverse energy and possibly b -quark jets. No significant excesses over the expected SM backgrounds are observed. The results are interpreted in the context of a "natural SUSY" simplified model where the decays $\bar{t}_1 \rightarrow b\bar{\chi}_1^\pm$, with $\bar{\chi}_1^\pm \rightarrow ff'\bar{\chi}_1^0$, and $\bar{\chi}_1^0 \rightarrow H\bar{G}$, all happen with 100% branching ratio, see Fig. 4.
- 71 KHACHATRYAN 14C searched in 19.5 fb^{-1} of pp collisions at $\sqrt{s} = 8 \text{ TeV}$ for evidence of direct pair production of top squarks, with Higgs or Z -bosons in the decay chain. The search is performed using a selection of events containing leptons and b -quark jets. No significant excesses over the expected SM backgrounds are observed. The results are interpreted in the context of a simplified model with pair production of a heavier top-squark mass eigenstate \bar{t}_2 decaying to a lighter top-squark eigenstate \bar{t}_1 via either $\bar{t}_2 \rightarrow H\bar{t}_1$ or $\bar{t}_2 \rightarrow Z\bar{t}_1$, followed in both cases by $\bar{t}_1 \rightarrow t\bar{\chi}_1^0$. The interpretation is performed in the region where the mass difference between the \bar{t}_1 and $\bar{\chi}_1^0$ is approximately equal to the top-quark mass, which is not probed by searches for direct \bar{t}_1 pair production, see Figs. 5 and 6. The analysis excludes top squarks with masses $m_{\bar{t}_2} < 575 \text{ GeV}$ and $m_{\bar{t}_1} < 400 \text{ GeV}$ at 95% C.L.

R-parity violating \tilde{t} (Stop) mass limit

VALUE (GeV)	CL%	DOCUMENT ID	TECN	COMMENT
>1150	95	1 SIRUNYAN	19BI ATLS	$\tilde{t} \rightarrow b\mu$, long-lived, Tstop2RPV, $c\tau = 0.1$ cm
>1100	95	2 SIRUNYAN	19BJ CMS	$\tilde{t} \rightarrow be$, Tstop2RPV, prompt
none 100-410	95	3 AABOUD	18BB ATLS	4 jets, Tstop1RPV with $\tilde{t} \rightarrow ds$, λ''_{312} coupling
none 100-470, 480-610	95	4 AABOUD	18BB ATLS	4 jets, Tstop1RPV, λ''_{323} coupling
≥ 600 -1500	95	5 AABOUD	18P ATLS	$2\ell + b$ -jets, Tstop2RPV, depending on λ''_{333} coupling ($i = 1, 2, 3$)
>1130	95	6 SIRUNYAN	18AD CMS	$\tilde{t} \rightarrow b\ell$, long-lived, $c\tau = 70$ -100 mm
> 550	95	6 SIRUNYAN	18AD CMS	$\tilde{t} \rightarrow b\ell$, long-lived, $c\tau = 1$ -1000 mm
>1400	95	7 SIRUNYAN	18DV CMS	long-lived \tilde{t} , RPV, $\tilde{t} \rightarrow \bar{d}\bar{d}$, 0.6 mm $< c\tau < 80$ mm
none 80-520	95	8 SIRUNYAN	18DY CMS	2, 4 jets, Tstop3RPV, λ''_{312} coupling
none 80-270, 285-340, 400-525	95	8 SIRUNYAN	18DY CMS	2, 4 jets, Tstop1RPV, λ''_{323} coupling
>1200	95	9 AABOUD	17AI ATLS	$\geq 1\ell + \geq 8$ jets, Tstop1 with $\tilde{\chi}_1^0 \rightarrow tbs$, λ''_{323} coupling, $m_{\tilde{\chi}_1^0} = 500$ GeV
none, 100-315	95	10 AAD	16AMATLS	2 large-radius jets, Tstop1RPV

- • • We do not use the following data for averages, fits, limits, etc. • • •
- 1 SIRUNYAN 19BI searched in 35.9 fb^{-1} of pp collisions at $\sqrt{s} = 13 \text{ TeV}$ in final states with two muons and two jets, or with one muon, two jets, and missing transverse momentum. Limits are set in a model of pair-produced, prompt or long-lived top squarks with R-parity violating decays to a b -quark and a lepton (Tstop2RPV), branching fraction of $\tilde{t} \rightarrow b\mu$ equal to $1/3$ and $c\tau$ between 0.1 cm and 10 cm in the case of long-lived top squarks. See their Fig. 10.
- 2 SIRUNYAN 19BJ searched in 35.9 fb^{-1} of pp collisions at $\sqrt{s} = 13 \text{ TeV}$ in final states with two electrons and two jets, or with one electron, two jets, and missing transverse momentum. Limits are set in a model of pair-produced, prompt top squarks with R-parity violating decays to a b -quark and a lepton (Tstop2RPV), assuming branching fraction of $\tilde{t} \rightarrow be$ equal to $1/3$ and $c\tau = 0 \text{ cm}$. See their Fig. 10.
- 3 AABOUD 18BB searched in 36.7 fb^{-1} of pp collisions at $\sqrt{s} = 13 \text{ TeV}$ for massive colored resonances which are pair-produced and decay into two jets. No significant deviation from the background prediction is observed. Results are interpreted in a SUSY simplified model as Tstop1RPV with $\tilde{t} \rightarrow ds$. Top squarks with masses in the range 100 - 410 GeV are excluded, see their Figure 9(a). The λ''_{312} coupling is assumed to be sufficiently large for the decays to be prompt, but small enough to neglect the single-top-squark resonant production through RPV couplings.
- 4 AABOUD 18BB searched in 36.7 fb^{-1} of pp collisions at $\sqrt{s} = 13 \text{ TeV}$ for massive colored resonances which are pair-produced and decay into two jets. No significant deviation from the background prediction is observed. Results are interpreted in Tstop1RPV. Top squarks with masses in the range 100 - 470 GeV or 480 - 610 GeV are excluded, see their Figure 9(b). The λ''_{323} coupling is assumed to be sufficiently large for the decays to be prompt, but small enough to neglect the single-top-squark resonant production through RPV couplings.
- 5 AABOUD 18P searched in 36.1 fb^{-1} of pp collisions at $\sqrt{s} = 13 \text{ TeV}$ for pair-produced top squarks that decay through RPV λ''_{333} ($i = 1, 2, 3$) couplings to a final state with two leptons and two jets, at least one of which is identified as a b -jet. No significant excess is observed over the SM background. In the Tstop2RPV model, lower limits on the top squark masses between 600 and 1500 GeV are set depending on the branching fraction to be , $b\mu$, and $b\tau$ final states. See their Figs 6 and 7.
- 6 SIRUNYAN 18AD searched in 2.6 fb^{-1} of pp collisions at $\sqrt{s} = 13 \text{ TeV}$ for long-lived particles by exploiting the multiplicity of displaced jets to search for the presence of signal decays occurring at distances between 1 and 1000 mm . Limits are set in a model of pair-produced, long-lived top squarks with R-parity violating decays to a b -quark and a lepton, see their Figure 3.
- 7 SIRUNYAN 18DV searched in 38.5 fb^{-1} of pp collisions at $\sqrt{s} = 13 \text{ TeV}$ for long-lived particles in events with multiple jets and two displaced vertices composed of many tracks. No events with two well-separated high-track-multiplicity vertices were observed. Limits are set on the stop and the gluino mass in RPV models of supersymmetry where the stop (gluino) is decaying solely into dijet (multijet) final states, see their Figures 6 and 7.
- 8 SIRUNYAN 18DY searched in 35.9 fb^{-1} of pp collisions at $\sqrt{s} = 13 \text{ TeV}$ for the pair production of resonances, each decaying to two quarks. The search is conducted separately in a boosted (two-jet) and resolved (four-jet) jet topology. The mass spectra are found to be consistent with the Standard Model expectations. Limits are set on the stop mass in the Tstop3RPV and Tstop1RPV simplified models, see their Figure 11.
- 9 AABOUD 17AI searched in 36.1 fb^{-1} of pp collisions at $\sqrt{s} = 13 \text{ TeV}$ for events with one or more isolated lepton, at least eight jets, either zero or many b -jets, for evidence of R-parity violating decays of the top squark. No significant excess above the Standard Model expectations is observed. Limits up to 1.25 (1.10) TeV are set on the top squark mass in R-parity-violating supersymmetry models where \tilde{t}_1 decays for a bino LSP as: $\tilde{t} \rightarrow t\tilde{\chi}_1^0$ and for a higgsino LSP as $\tilde{t} \rightarrow t\tilde{\chi}_{1,2}^0/b\tilde{\chi}_1^+$. This is followed by the decays through the non-zero λ''_{323} coupling $\tilde{\chi}_{1,2}^0 \rightarrow tbs$, $\tilde{\chi}_1^\pm \rightarrow bbs$. See their Figure 10 and text for details on model assumptions.

- 10 AAD 16AM searched in 17.4 fb^{-1} of pp collisions at $\sqrt{s} = 8 \text{ TeV}$ for events containing two large-radius hadronic jets. No deviation from the background prediction is observed. Top squarks with masses between 100 and 315 GeV are excluded at 95% C.L. in the hypothesis that they both decay via R-parity violating coupling λ''_{323} to b - and s -quarks. See their Fig. 10.
- 11 KHACHATRYAN 16AC searched in 19.7 fb^{-1} of pp collisions at $\sqrt{s} = 8 \text{ TeV}$ for events with low missing transverse momentum, two oppositely charged electrons or muons, and at least five jets, at least one of which is a b -jet, for evidence of R-parity violating, charging-mediated decays of the top squark. No significant excess above the Standard Model expectations is observed. Limits are set on the stop mass in R-parity-violating supersymmetry models where $\tilde{t} \rightarrow b\tilde{\chi}_1^\pm$ with $\tilde{\chi}_1^\pm \rightarrow \ell^\pm jj$, $\lambda''_{ijk} \neq 0$ ($i, j, k \leq 2$), and with $m_{\tilde{t}} - m_{\tilde{\chi}_1^\pm} = 100 \text{ GeV}$, see Fig. 3.
- 12 KHACHATRYAN 16BX searched in 19.5 fb^{-1} of pp collisions at $\sqrt{s} = 8 \text{ TeV}$ for events containing 4 leptons coming from R-parity-violating decays of $\tilde{\chi}_1^0 \rightarrow \ell\ell\nu$ with $\lambda_{121} \neq 0$ or $\lambda_{122} \neq 0$. No excess over the expected background is observed. Limits are derived on the gluino, squark and stop masses, see Fig. 23.
- 13 KHACHATRYAN 15E searched for long-lived particles decaying to leptons in 19.7 fb^{-1} of pp collisions at $\sqrt{s} = 8 \text{ TeV}$. Events were selected with an electron and muon with opposite charges and each with transverse impact parameter values between 0.02 and 2 cm . Limits are set on SUSY benchmark models with pair production of top squarks decaying into an $e\mu$ final state via RPV interactions. See their Fig. 2

Heavy \tilde{g} (Gluino) mass limit

For $m_{\tilde{g}} > 60$ - 70 GeV , it is expected that gluinos would undergo a cascade decay via a number of neutralinos and/or charginos rather than undergo a direct decay to photinos as assumed by some papers. Limits obtained when direct decay is assumed are usually higher than limits when cascade decays are included.

Some earlier papers are now obsolete and have been omitted. They were last listed in our PDG 14 edition: K. Olive, et al. (Particle Data Group), Chinese Physics C38 070001 (2014) (<http://pdg.lbl.gov>).

R-parity conserving heavy \tilde{g} (Gluino) mass limit

VALUE (GeV)	CL%	DOCUMENT ID	TECN	COMMENT
>1975	95	1 SIRUNYAN	20B CMS	$\geq 1\gamma + \cancel{E}_T$, Tglu4A, BR($\tilde{g} \rightarrow qq\tilde{\chi}_1^\pm$)=0.5, $m_{\tilde{g}} \simeq m_{\tilde{\chi}_1^\pm}$
>2000	95	2 AABOUD	19I ATL	≥ 2 jets + 1 or $2\tau + \cancel{E}_T$, Tglu1F, $m_{\tilde{g}} = 100 \text{ GeV}$
>1860	95	3 SIRUNYAN	19AG CMS	$2\gamma + \cancel{E}_T$, Tglu4B, $500 \text{ GeV} < m_{\tilde{g}} < 1500 \text{ GeV}$
>1920	95	4 SIRUNYAN	19AU CMS	γ + jets + b -jets + \cancel{E}_T , Tglu4D, $m_{\tilde{g}} = 127 \text{ GeV}$
>1950	95	4 SIRUNYAN	19AU CMS	γ + jets + b -jets + \cancel{E}_T , Tglu4E, $m_{\tilde{g}} = 1 \text{ GeV}$
>1800	95	4 SIRUNYAN	19AU CMS	γ + jets + b -jets + \cancel{E}_T , Tglu4F, $m_{\tilde{g}} = 1 \text{ GeV}$
>2090	95	4 SIRUNYAN	19AU CMS	γ + jets + b -jets + \cancel{E}_T , Tglu4D, $m_{\tilde{g}} = 1200 \text{ GeV}$
>2120	95	4 SIRUNYAN	19AU CMS	γ + jets + b -jets + \cancel{E}_T , Tglu4E, $m_{\tilde{g}} = 1200 \text{ GeV}$
>1970	95	4 SIRUNYAN	19AU CMS	γ + jets + b -jets + \cancel{E}_T , Tglu4F, $m_{\tilde{g}} = 1200 \text{ GeV}$
>1700	95	5 SIRUNYAN	19CE CMS	2 jets, Stealth SUSY, Tglu1A and $\tilde{\chi}_1^0 \rightarrow \tilde{S}\gamma$ ($\tilde{S} \rightarrow S\tilde{G}$), $m_{\tilde{\chi}_1^0} = 200 \text{ GeV}$
>2000	95	6 SIRUNYAN	19CH CMS	jets + \cancel{E}_T , Tglu1A, $m_{\tilde{g}} = 0 \text{ GeV}$
>2030	95	6 SIRUNYAN	19CH CMS	jets + \cancel{E}_T , Tglu1C, $m_{\tilde{g}} = m_{\tilde{\chi}_2^0} = 0.5(m_{\tilde{g}} + m_{\tilde{\chi}_1^0})$, $m_{\tilde{\chi}_1^0} = 0 \text{ GeV}$
>2270	95	6 SIRUNYAN	19CH CMS	jets + \cancel{E}_T , Tglu2A, $m_{\tilde{g}} = 0 \text{ GeV}$
>2180	95	6 SIRUNYAN	19CH CMS	jets + \cancel{E}_T , Tglu3A, $m_{\tilde{g}} = 0 \text{ GeV}$
>1750	95	7 SIRUNYAN	19K CMS	$\gamma + \ell + \cancel{E}_T$, Tglu4A, $m_{\tilde{g}} = 1500 \text{ GeV}$
>2000	95	8 SIRUNYAN	19S CMS	1 or $2\ell +$ jets + \cancel{E}_T , Tglu3A, $m_{\tilde{g}} < 700 \text{ GeV}$
>1900	95	8 SIRUNYAN	19S CMS	1 or $2\ell +$ jets + \cancel{E}_T , Tglu3C, $150 \text{ GeV} < m_{\tilde{g}} < 950 \text{ GeV}$
>1970	95	9 AABOUD	18AR ATLS	jets + $\geq 3b$ -jets + \cancel{E}_T , Tglu3A, $m_{\tilde{g}} < 300 \text{ GeV}$
>1920	95	10 AABOUD	18AR ATLS	jets + $\geq 3b$ -jets + \cancel{E}_T , Tglu2A, $m_{\tilde{g}} < 600 \text{ GeV}$
>1650	95	11 AABOUD	18AS ATLS	≥ 4 jets and disappearing tracks from $\tilde{\chi}^\pm \rightarrow \tilde{\chi}_1^0 \pi^\pm$, modified Tglu1A or Tglu1B, $\tilde{\chi}^\pm$ lifetime 0.2 ns , $m_{\tilde{\chi}^\pm} = 460 \text{ GeV}$
>1850	95	12 AABOUD	18BJ ATLS	$\ell^\pm \cancel{E}_T +$ jets + \cancel{E}_T , Tglu1G, $m_{\tilde{g}} = 100 \text{ GeV}$

Searches Particle Listings

Supersymmetric Particle Searches

>1650	95	13	AABOUD	18BJ ATLS	$\ell^\pm \ell^\mp + \text{jets} + \cancel{E}_T, T_{\text{glu1H}}, m_{\tilde{\chi}_1^0} = 100 \text{ GeV}$	>1700	95	36	AABOUD	17N ATLS	2 same-flavor, opposite-sign $\ell + \text{jets} + \cancel{E}_T, T_{\text{glu1G}}, m_{\tilde{\chi}_1^0} \sim 1 \text{ GeV}$
>2150	95	14	AABOUD	18U ATLS	$2\gamma + \cancel{E}_T, \text{GGM}, T_{\text{glu4B}}, \text{any NLSP mass}$	>1400	95	37	KHACHATRY...17	CMS	$\text{jets} + \cancel{E}_T, T_{\text{glu1A}}, m_{\tilde{\chi}_1^0} = 200 \text{ GeV}$
>1600	95	15	AABOUD	18U ATLS	$\gamma + \text{jets} + \cancel{E}_T, \text{GGM higgsino-bino, mix of Tglu4B and Tglu4C, any NLSP mass}$	>1650	95	37	KHACHATRY...17	CMS	$\text{jets} + \cancel{E}_T, T_{\text{glu2A}}, m_{\tilde{\chi}_1^0} = 200 \text{ GeV}$
>2030	95	16	AABOUD	18V ATLS	$\text{jets} + \cancel{E}_T, T_{\text{glu1A}}, m_{\tilde{\chi}_1^0} = 0 \text{ GeV}$	>1600	95	37	KHACHATRY...17	CMS	$\text{jets} + \cancel{E}_T, T_{\text{glu3A}}, m_{\tilde{\chi}_1^0} = 200 \text{ GeV}$
>1980	95	17	AABOUD	18V ATLS	$\text{jets} + \cancel{E}_T, T_{\text{glu1B}}, m_{\tilde{\chi}_1^\pm} = 0.5(m_{\tilde{g}} + m_{\tilde{\chi}_1^0}), m_{\tilde{\chi}_1^0} = 0 \text{ GeV}$	>1550	95	38	KHACHATRY...17AD	CMS	$\text{jets} + b\text{-jets} + \cancel{E}_T, T_{\text{glu3A}}, m_{\tilde{\chi}_1^0} = 0 \text{ GeV}$
>1750	95	18	AABOUD	18V ATLS	$\text{jets} + \cancel{E}_T, T_{\text{glu1C}}, m_{\tilde{\chi}_1^0} = 1 \text{ GeV}, \text{any } m_{\tilde{\chi}_2^0} > 100 \text{ GeV}$	>1450	95	39	KHACHATRY...17AD	CMS	$\text{jets} + b\text{-jets} + \cancel{E}_T, T_{\text{glu3C}}, 200 < m_{\tilde{\chi}_1^0} < 400 \text{ GeV}$
>2000	95	19	SIRUNYAN	18AA CMS	$\geq 1\gamma + \cancel{E}_T, T_{\text{glu4A}}$	>1570	95	40	KHACHATRY...17As	CMS	$1\ell, T_{\text{glu3A}}, m_{\tilde{\chi}_1^0} < 600 \text{ GeV}$
>2100	95	19	SIRUNYAN	18AA CMS	$\geq 1\gamma + \cancel{E}_T, T_{\text{glu4B}}$	>1500	95	40	KHACHATRY...17As	CMS	$1\ell, T_{\text{glu3A}}, m_{\tilde{\chi}_1^0} < 775 \text{ GeV}$
>1800	95	20	SIRUNYAN	18AC CMS	$1\ell + \text{jets}, T_{\text{glu3A}}, m_{\tilde{\chi}_1^0} < 650 \text{ GeV}$	>1400	95	40	KHACHATRY...17As	CMS	$1\ell, T_{\text{glu1B}}, m_{\tilde{\chi}_1^\pm} = (m_{\tilde{g}} + m_{\tilde{\chi}_1^0})/2, m_{\tilde{\chi}_1^0} < 725 \text{ GeV}$
>1700	95	20	SIRUNYAN	18AC CMS	$1\ell + \text{jets}, T_{\text{glu3A}}, m_{\tilde{\chi}_1^0} < 1040 \text{ GeV}$	none	95	40	KHACHATRY...17As	CMS	$1\ell, T_{\text{glu1B}}, m_{\tilde{\chi}_1^\pm} = (m_{\tilde{g}} + m_{\tilde{\chi}_1^0})/2, m_{\tilde{\chi}_1^0} < 850 \text{ GeV}$
>1900	95	20	SIRUNYAN	18AC CMS	$1\ell + \text{jets}, T_{\text{glu1B}}, m_{\tilde{\chi}_1^\pm} = (m_{\tilde{g}} + m_{\tilde{\chi}_1^0})/2, m_{\tilde{\chi}_1^0} < 300 \text{ GeV}$	1050-1350	95	40	KHACHATRY...17As	CMS	$1\ell, T_{\text{glu1B}}, m_{\tilde{\chi}_1^\pm} = (m_{\tilde{g}} + m_{\tilde{\chi}_1^0})/2, m_{\tilde{\chi}_1^0} < 850 \text{ GeV}$
>1250	95	20	SIRUNYAN	18AC CMS	$1\ell + \text{jets}, T_{\text{glu1B}}, m_{\tilde{\chi}_1^\pm} = (m_{\tilde{g}} + m_{\tilde{\chi}_1^0})/2, m_{\tilde{\chi}_1^0} < 950 \text{ GeV}$	>1175	95	41	KHACHATRY...17AW	CMS	$\geq 3\ell^\pm, 2 \text{ jets}, T_{\text{glu3A}}, m_{\tilde{\chi}_1^0} = 0 \text{ GeV}$
>1610	95	21	SIRUNYAN	18AL CMS	$\geq 3\ell^\pm + \text{jets} + \cancel{E}_T, T_{\text{glu3A}}, m_{\tilde{\chi}_1^0} = 0 \text{ GeV}$	> 825	95	41	KHACHATRY...17AW	CMS	$\geq 3\ell^\pm, 2 \text{ jets}, T_{\text{glu1C}}, m_{\tilde{\chi}_1^\pm} = (m_{\tilde{g}} + m_{\tilde{\chi}_1^0})/2, m_{\tilde{\chi}_1^0} = 0 \text{ GeV}$
>1160	95	21	SIRUNYAN	18AL CMS	$\geq 3\ell^\pm + \text{jets} + \cancel{E}_T, T_{\text{glu1C}}, m_{\tilde{\chi}_2^0} = m_{\tilde{\chi}_1^\pm} = (m_{\tilde{g}} + m_{\tilde{\chi}_1^0})/2, m_{\tilde{\chi}_1^0} = 0 \text{ GeV}$	>1350	95	42	KHACHATRY...17P	CMS	1 or more $\text{jets} + \cancel{E}_T, T_{\text{glu1A}}, m_{\tilde{\chi}_1^0} = 0 \text{ GeV}$
>1500	95	22	SIRUNYAN	18AR CMS	$\ell^\pm \ell^\mp + \text{jets} + \cancel{E}_T, \text{GMSB}, T_{\text{glu4C}}, m_{\tilde{\chi}_1^0} = 100 \text{ GeV}$	>1545	95	42	KHACHATRY...17P	CMS	1 or more $\text{jets} + \cancel{E}_T, T_{\text{glu2A}}, m_{\tilde{\chi}_1^0} = 0 \text{ GeV}$
>1770	95	22	SIRUNYAN	18AR CMS	$\ell^\pm \ell^\mp + \text{jets} + \cancel{E}_T, \text{GMSB}, T_{\text{glu4C}}, m_{\tilde{\chi}_1^0} = 1400 \text{ GeV}$	>1120	95	42	KHACHATRY...17P	CMS	1 or more $\text{jets} + \cancel{E}_T, T_{\text{glu3A}}, m_{\tilde{\chi}_1^0} = 0 \text{ GeV}$
>1625	95	23	SIRUNYAN	18AY CMS	$\text{jets} + \cancel{E}_T, T_{\text{glu1A}}, m_{\tilde{\chi}_1^0} = 0 \text{ GeV}$	>1300	95	42	KHACHATRY...17P	CMS	1 or more $\text{jets} + \cancel{E}_T, T_{\text{glu3D}}, m_{\tilde{\chi}_1^\pm} = m_{\tilde{\chi}_1^0} + 5 \text{ GeV}, m_{\tilde{\chi}_1^0} = 100 \text{ GeV}$
>1825	95	23	SIRUNYAN	18AY CMS	$\text{jets} + \cancel{E}_T, T_{\text{glu2A}}, m_{\tilde{\chi}_1^0} = 0 \text{ GeV}$	> 780	95	42	KHACHATRY...17P	CMS	1 or more $\text{jets} + \cancel{E}_T, T_{\text{glu3B}}, m_{\tilde{t}_1} - m_{\tilde{\chi}_1^0} = 175 \text{ GeV}, m_{\tilde{\chi}_1^0} = 50 \text{ GeV}$
>1625	95	23	SIRUNYAN	18AY CMS	$\text{jets} + \cancel{E}_T, T_{\text{glu3A}}, m_{\tilde{\chi}_1^0} = 0 \text{ GeV}$	> 790	95	42	KHACHATRY...17P	CMS	1 or more $\text{jets} + \cancel{E}_T, T_{\text{glu3C}}, m_{\tilde{t}_1} - m_{\tilde{\chi}_1^0} = 20 \text{ GeV}, m_{\tilde{\chi}_1^0} = 0 \text{ GeV}$
>2040	95	24	SIRUNYAN	18D CMS	top quark (hadronically decaying) + $\text{jets} + \cancel{E}_T, T_{\text{glu3A}}, m_{\tilde{\chi}_1^0} = 0 \text{ GeV}$	>1650	95	43	KHACHATRY...17V	CMS	$2\gamma + \cancel{E}_T, \text{GGM}, T_{\text{glu4B}}, \text{any NLSP mass}$
>1930	95	24	SIRUNYAN	18D CMS	top quark (hadronically decaying) + $\text{jets} + \cancel{E}_T, T_{\text{glu3B}}, m_{\tilde{t}_1} - m_{\tilde{\chi}_1^0} = 175 \text{ GeV}, m_{\tilde{\chi}_1^0} = 200 \text{ GeV}$	>1900	95	44	SIRUNYAN	17AF CMS	$1\ell + \text{jets} + b\text{-jets} + \cancel{E}_T, T_{\text{glu3A}}, m_{\tilde{\chi}_1^0} = 0 \text{ GeV}$
>1690	95	24	SIRUNYAN	18D CMS	top quark (hadronically decaying) + $\text{jets} + \cancel{E}_T, T_{\text{glu3C}}, m_{\tilde{t}_1} - m_{\tilde{\chi}_1^0} = 20 \text{ GeV}, m_{\tilde{\chi}_1^0} = 0 \text{ GeV}$	>1600	95	44	SIRUNYAN	17AF CMS	$1\ell + \text{jets} + b\text{-jets} + \cancel{E}_T, T_{\text{glu3B}}, m_{\tilde{t}_1} - m_{\tilde{\chi}_1^0} = 175 \text{ GeV}, m_{\tilde{\chi}_1^0} = 50 \text{ GeV}$
>1990	95	24	SIRUNYAN	18D CMS	top quark (hadronically decaying) + $\text{jets} + \cancel{E}_T, T_{\text{glu3E}}, m_{\tilde{\chi}_1^\pm} = m_{\tilde{\chi}_1^0} + 5 \text{ GeV}, m_{\tilde{\chi}_1^0} = 100 \text{ GeV}$	>1800	95	45	SIRUNYAN	17AY CMS	$\gamma + \text{jets} + \cancel{E}_T, T_{\text{glu4B}}, m_{\tilde{\chi}_1^0} = 0 \text{ GeV}$
>2010	95	25	SIRUNYAN	18M CMS	$\geq 1 H (\rightarrow bb) + \cancel{E}_T, T_{\text{glu1I}}$	>1600	95	45	SIRUNYAN	17AY CMS	$\gamma + \text{jets} + \cancel{E}_T, T_{\text{glu4A}}, m_{\tilde{\chi}_1^0} = 0 \text{ GeV}$
>1825	95	25	SIRUNYAN	18M CMS	$\geq 1 H (\rightarrow bb) + \cancel{E}_T, T_{\text{glu1J}}$	>1860	95	46	SIRUNYAN	17AZ CMS	$\geq 1 \text{ jets} + \cancel{E}_T, T_{\text{glu1A}}, m_{\tilde{\chi}_1^0} = 0 \text{ GeV}$
>1750	95	26	AABOUD	17AJ ATLS	same-sign $\ell^\pm \ell^\pm / 3\ell + \text{jets} + \cancel{E}_T, T_{\text{glu3A}}, m_{\tilde{\chi}_1^0} = 100 \text{ GeV}$	>2025	95	46	SIRUNYAN	17AZ CMS	$\geq 1 \text{ jets} + \cancel{E}_T, T_{\text{glu2A}}, m_{\tilde{\chi}_1^0} = 0 \text{ GeV}$
>1570	95	27	AABOUD	17AJ ATLS	same-sign $\ell^\pm \ell^\pm / 3\ell + \text{jets} + \cancel{E}_T, T_{\text{glu1E}}, m_{\tilde{\chi}_1^0} = 100 \text{ GeV}$	>1900	95	46	SIRUNYAN	17AZ CMS	$\geq 1 \text{ jets} + \cancel{E}_T, T_{\text{glu3A}}, m_{\tilde{\chi}_1^0} = 0 \text{ GeV}$
>1860	95	28	AABOUD	17AJ ATLS	same-sign $\ell^\pm \ell^\pm / 3\ell + \text{jets} + \cancel{E}_T, T_{\text{glu1G}}, m_{\tilde{\chi}_1^0} = 200 \text{ GeV}$	>1825	95	47	SIRUNYAN	17P CMS	$\text{jets} + \cancel{E}_T, T_{\text{glu1A}}, m_{\tilde{\chi}_1^0} = 0 \text{ GeV}$
>2100	95	29	AABOUD	17AR ATLS	$1\ell + \text{jets} + \cancel{E}_T, T_{\text{glu1B}}, m_{\tilde{\chi}_1^0} = 0 \text{ GeV}$	>1950	95	47	SIRUNYAN	17P CMS	$\text{jets} + \cancel{E}_T, T_{\text{glu2A}}, m_{\tilde{\chi}_1^0} = 0 \text{ GeV}$
>1740	95	30	AABOUD	17AR ATLS	$1\ell + \text{jets} + \cancel{E}_T, T_{\text{glu1E}}, m_{\tilde{\chi}_1^0} = 0 \text{ GeV}$	>1960	95	47	SIRUNYAN	17P CMS	$\text{jets} + \cancel{E}_T, T_{\text{glu3A}}, m_{\tilde{\chi}_1^0} = 0 \text{ GeV}$
>1800	95	31	AABOUD	17AY ATLS	$\text{jets} + \cancel{E}_T, T_{\text{glu3A}}, m_{\tilde{t}_1} - m_{\tilde{\chi}_1^0} = 5 \text{ GeV}$	>1800	95	47	SIRUNYAN	17P CMS	$\text{jets} + \cancel{E}_T, T_{\text{glu1C}}, m_{\tilde{\chi}_1^\pm} = m_{\tilde{\chi}_2^0} = (m_{\tilde{g}} + m_{\tilde{\chi}_1^0})/2, m_{\tilde{\chi}_1^0} = 0 \text{ GeV}$
>1800	95	32	AABOUD	17AZ ATLS	$\geq 7 \text{ jets} + \cancel{E}_T, \text{large R-jets and/or } b\text{-jets}, T_{\text{glu1E}}, m_{\tilde{\chi}_1^0} = 100 \text{ GeV}$	>1870	95	47	SIRUNYAN	17P CMS	$\text{jets} + \cancel{E}_T, T_{\text{glu3D}}, m_{\tilde{\chi}_1^\pm} = m_{\tilde{\chi}_2^0} + 5 \text{ GeV}, m_{\tilde{\chi}_1^0} = 1000 \text{ GeV}$
>1540	95	33	AABOUD	17AZ ATLS	$\geq 7 \text{ jets} + \cancel{E}_T, \text{large R-jets and/or } b\text{-jets}, T_{\text{glu3A}}, m_{\tilde{\chi}_1^0} = 0 \text{ GeV}$	>1520	95	48	SIRUNYAN	17S CMS	same-sign $\ell^\pm \ell^\pm + \text{jets} + \cancel{E}_T, T_{\text{glu3A}}, m_{\tilde{\chi}_1^0} = 0 \text{ GeV}$
>1340	95	34	AABOUD	17N ATLS	2 same-flavor, opposite-sign $\ell + \text{jets} + \cancel{E}_T, T_{\text{glu1H}}, m_{\tilde{\chi}_1^0} = 0 \text{ GeV}$	>1200	95	48	SIRUNYAN	17S CMS	same-sign $\ell^\pm \ell^\pm + \text{jets} + \cancel{E}_T, T_{\text{glu3D}}, m_{\tilde{\chi}_1^\pm} = m_{\tilde{\chi}_1^0} + 5 \text{ GeV}, m_{\tilde{\chi}_1^0} = 100 \text{ GeV}$
>1310	95	35	AABOUD	17N ATLS	2 same-flavor, opposite-sign $\ell + \text{jets} + \cancel{E}_T, T_{\text{glu1H}}, m_{\tilde{\chi}_2^0} = (m_{\tilde{g}} + m_{\tilde{\chi}_1^0})/2, m_{\tilde{\chi}_1^0} < 400 \text{ GeV}$	>1370	95	48	SIRUNYAN	17S CMS	same-sign $\ell^\pm \ell^\pm + \text{jets} + \cancel{E}_T, T_{\text{glu3B}}, m_{\tilde{t}_1} - m_{\tilde{\chi}_1^0} = 175 \text{ GeV}, m_{\tilde{\chi}_1^0} = 50 \text{ GeV}$
						>1180	95	48	SIRUNYAN	17S CMS	same-sign $\ell^\pm \ell^\pm + \text{jets} + \cancel{E}_T, T_{\text{glu3C}}, m_{\tilde{t}_1} - m_{\tilde{\chi}_1^0} = 20 \text{ GeV}, m_{\tilde{\chi}_1^0} = 0 \text{ GeV}$

Searches Particle Listings

Supersymmetric Particle Searches

>1500	95	65	AAD	15BV ATLS	jets + \cancel{E}_T , $\tilde{g} \rightarrow \tilde{q}\tilde{q}, \tilde{q} \rightarrow q\tilde{\chi}_1^0$, $m_{\tilde{\chi}_1^0} = 1$ GeV	> 640	95	92	AAD	14E ATLS	$\ell^\pm \ell^\pm (\ell^\mp) + \text{jets}, \tilde{g} \rightarrow t\tilde{t}_1$ with $\tilde{t}_1 \rightarrow c\tilde{\chi}_1^0$ simplified model, $m_{\tilde{t}_1} = m_{\tilde{\chi}_1^0} + 20$ GeV
>1650	95	65	AAD	15BV ATLS	jets + \cancel{E}_T , $m_{\tilde{g}} = m_{\tilde{q}}, m_{\tilde{\chi}_1^0} = 1$ GeV	> 860	95	92	AAD	14E ATLS	$\ell^\pm \ell^\pm (\ell^\mp) + \text{jets}, \tilde{g} \rightarrow q\tilde{q}\tilde{\chi}_1^\pm$, $\tilde{\chi}_1^\pm \rightarrow W^{(*)\pm}\tilde{\chi}_1^0$ simplified model, $m_{\tilde{\chi}_1^\pm} = 2 m_{\tilde{\chi}_1^0}$, $m_{\tilde{\chi}_1^0} < 400$ GeV
> 850	95	65	AAD	15BV ATLS	jets + \cancel{E}_T , $\tilde{g} \rightarrow g\tilde{\chi}_1^0$, $m_{\tilde{\chi}_1^0} < 550$ GeV	>1040	95	92	AAD	14E ATLS	$\ell^\pm \ell^\pm (\ell^\mp) + \text{jets}, \tilde{g} \rightarrow q\tilde{q}\tilde{\chi}_1^\pm$, $\tilde{\chi}_1^\pm \rightarrow W^{(*)\pm}\tilde{\chi}_2^0, \tilde{\chi}_2^0 \rightarrow Z^{(*)}\tilde{\chi}_1^0$ simplified model, $m_{\tilde{\chi}_1^0} < 520$ GeV
>1270	95	65	AAD	15BV ATLS	jets + \cancel{E}_T , $\tilde{g} \rightarrow q\tilde{q}W\tilde{\chi}_1^0$, $m_{\tilde{\chi}_1^0} = 100$ GeV	>1200	95	92	AAD	14E ATLS	$\ell^\pm \ell^\pm (\ell^\mp) + \text{jets}, \tilde{g} \rightarrow q\tilde{q}\tilde{\chi}_1^\pm$, $\tilde{\chi}_1^\pm \rightarrow W^{(*)\pm}\tilde{\chi}_2^0, \tilde{\chi}_2^0 \rightarrow Z^{(*)}\tilde{\chi}_1^0$ simplified model, $m_{\tilde{\chi}_1^0} < 520$ GeV
>1150	95	65	AAD	15BV ATLS	jets + $\ell^\pm \ell^\pm, \tilde{g}$ decays via sleptons, $m_{\tilde{\chi}_1^0} = 100$ GeV	>1050	95	93	CHATRCHYAN14H	CMS	same-sign $\ell^\pm \ell^\pm, \tilde{g} \rightarrow t\tilde{t}\tilde{\chi}_1^0$ simplified model, massless $\tilde{\chi}_1^0$
>1320	95	65	AAD	15BV ATLS	jets + $\ell^\pm \ell^\pm, \tilde{g}$ decays via sleptons, $m_{\tilde{\chi}_1^0} = 100$ GeV	> 900	95	94	CHATRCHYAN14H	CMS	same-sign $\ell^\pm \ell^\pm, \tilde{g} \rightarrow q\tilde{q}\tilde{\chi}_1^\pm$, $\tilde{\chi}_1^\pm \rightarrow W^\pm\tilde{\chi}_1^0$ simplified model, $m_{\tilde{\chi}_1^\pm} = 0.5 m_{\tilde{g}}$, mass-less $\tilde{\chi}_1^0$
>1220	95	65	AAD	15BV ATLS	τ, \tilde{q} decays via staus, $m_{\tilde{\chi}_1^0} = 100$ GeV	>1050	95	95	CHATRCHYAN14H	CMS	same-sign $\ell^\pm \ell^\pm, \tilde{g} \rightarrow b\tilde{t}\tilde{\chi}_1^\pm$, $\tilde{\chi}_1^\pm \rightarrow W^\pm\tilde{\chi}_1^0$ simplified model, $m_{\tilde{\chi}_1^\pm} = 300$ GeV, $m_{\tilde{\chi}_1^0} = 50$ GeV
>1310	95	65	AAD	15BV ATLS	b-jets, $\tilde{g} \rightarrow t\tilde{t}\tilde{\chi}_1^0$, $m_{\tilde{\chi}_1^0} < 400$ GeV	>1260	95	65	AAD	15BV ATLS	b-jets, $\tilde{g} \rightarrow \tilde{t}_1 t$ and $\tilde{g} \rightarrow c\tilde{\chi}_1^0$
>1220	95	65	AAD	15BV ATLS	b-jets, $\tilde{g} \rightarrow \tilde{t}_1 t$ and $\tilde{t}_1 \rightarrow t\tilde{\chi}_1^0$, $m_{\tilde{t}_1} < 1000$ GeV	>1200	95	65	AAD	15BV ATLS	b-jets, $\tilde{g} \rightarrow \tilde{b}_1 b$ and $\tilde{b}_1 \rightarrow b\tilde{\chi}_1^0$, $m_{\tilde{b}_1} < 1000$ GeV
>1180	95	65	AAD	15BV ATLS	b-jets, $\tilde{g} \rightarrow \tilde{t}_1 t$ and $\tilde{t}_1 \rightarrow b\tilde{\chi}_1^\pm$, $m_{\tilde{t}_1} < 1000$ GeV, $m_{\tilde{\chi}_1^0} = 60$ GeV	>1250	95	65	AAD	15BV ATLS	b-jets, $\tilde{g} \rightarrow b\tilde{b}\tilde{\chi}_1^0$, $m_{\tilde{\chi}_1^0} < 400$ GeV
>1260	95	65	AAD	15BV ATLS	b-jets, $\tilde{g} \rightarrow \tilde{t}_1 t$ and $\tilde{g} \rightarrow c\tilde{\chi}_1^0$	none, 75-1250	95	65	AAD	15BV ATLS	b-jets, \tilde{g} decay via offshell \tilde{t}_1 and \tilde{b}_1 , $m_{\tilde{\chi}_1^0} < 500$ GeV
>1200	95	65	AAD	15BV ATLS	b-jets, $\tilde{g} \rightarrow \tilde{b}_1 b$ and $\tilde{b}_1 \rightarrow b\tilde{\chi}_1^0$, $m_{\tilde{b}_1} < 1000$ GeV	>1100	95	88	AAD	15CB ATLS	jets, $\tilde{g} \rightarrow q\tilde{q}\tilde{\chi}_1^0, \tilde{\chi}_1^0 \rightarrow Z\tilde{G}$, GGM, $m_{\tilde{\chi}_1^0} = 400$ GeV and $3 < c\tau_{\tilde{\chi}_1^0} < 500$ mm
>1250	95	65	AAD	15BV ATLS	b-jets, $\tilde{g} \rightarrow b\tilde{b}\tilde{\chi}_1^0$, $m_{\tilde{\chi}_1^0} < 400$ GeV	>1400	95	88	AAD	15CB ATLS	jets or \cancel{E}_T , $\tilde{g} \rightarrow q\tilde{q}\tilde{\chi}_1^0$. Split SUSY, $m_{\tilde{\chi}_1^0} = 100$ GeV and $15 < c\tau < 300$ mm
none, 75-1250	95	65	AAD	15BV ATLS	b-jets, \tilde{g} decay via offshell \tilde{t}_1 and \tilde{b}_1 , $m_{\tilde{\chi}_1^0} < 500$ GeV	>1500	95	88	AAD	15CB ATLS	$\cancel{E}_T, \tilde{g} \rightarrow q\tilde{q}\tilde{\chi}_1^0$. Split SUSY, $m_{\tilde{\chi}_1^0} = 100$ GeV and $20 < c\tau < 250$ mm
>1100	95	88	AAD	15CB ATLS	jets, $\tilde{g} \rightarrow q\tilde{q}\tilde{\chi}_1^0, \tilde{\chi}_1^0 \rightarrow Z\tilde{G}$, GGM, $m_{\tilde{\chi}_1^0} = 400$ GeV and $3 < c\tau_{\tilde{\chi}_1^0} < 500$ mm	>1300	95	90	KHACHATRY...15AZ	CMS	$\ell^\pm \ell^\pm + \text{jets} + \cancel{E}_T$, GMSB, $\tilde{g} \rightarrow q\tilde{q}Z\tilde{G} \geq 2 \gamma, \geq 1 \text{ jet}, (\text{Razor}), \text{binon-like NLSP}, m_{\tilde{\chi}_1^0} = 375$ GeV
>1400	95	88	AAD	15CB ATLS	jets or \cancel{E}_T , $\tilde{g} \rightarrow q\tilde{q}\tilde{\chi}_1^0$. Split SUSY, $m_{\tilde{\chi}_1^0} = 100$ GeV and $15 < c\tau < 300$ mm	> 800	95	90	KHACHATRY...15AZ	CMS	$\geq 1 \gamma, \geq 2 \text{ jet}, \text{wino-like NLSP}, m_{\tilde{\chi}_1^0} = 375$ GeV
>1500	95	88	AAD	15CB ATLS	$\cancel{E}_T, \tilde{g} \rightarrow q\tilde{q}\tilde{\chi}_1^0$. Split SUSY, $m_{\tilde{\chi}_1^0} = 100$ GeV and $20 < c\tau < 250$ mm	>1280	95	91	AAD	14AX ATLS	≥ 3 b-jets + \cancel{E}_T , CMSSM
>1300	95	90	KHACHATRY...15AZ	CMS	$\geq 2 \gamma, \geq 1 \text{ jet}, (\text{Razor}), \text{binon-like NLSP}, m_{\tilde{\chi}_1^0} = 375$ GeV	>1250	95	91	AAD	14AX ATLS	≥ 3 b-jets + $\cancel{E}_T, \tilde{g} \rightarrow \tilde{b}_1 b\tilde{\chi}_1^0$ simplified model, $\tilde{b}_1 \rightarrow b\tilde{\chi}_1^0$, $m_{\tilde{\chi}_1^0} = 60$ GeV, $m_{\tilde{b}_1} < 900$ GeV
> 800	95	90	KHACHATRY...15AZ	CMS	$\geq 1 \gamma, \geq 2 \text{ jet}, \text{wino-like NLSP}, m_{\tilde{\chi}_1^0} = 375$ GeV	>1190	95	91	AAD	14AX ATLS	≥ 3 b-jets + $\cancel{E}_T, \tilde{g} \rightarrow \tilde{t}_1 t\tilde{\chi}_1^0$ simplified model, $\tilde{t}_1 \rightarrow t\tilde{\chi}_1^0$, $m_{\tilde{\chi}_1^0} = 60$ GeV, $m_{\tilde{t}_1} < 1000$ GeV
>1280	95	91	AAD	14AX ATLS	≥ 3 b-jets + \cancel{E}_T , CMSSM	>1180	95	91	AAD	14AX ATLS	≥ 3 b-jets + $\cancel{E}_T, \tilde{g} \rightarrow \tilde{t}_1 t\tilde{\chi}_1^0$ simplified model, $\tilde{t}_1 \rightarrow b\tilde{\chi}_1^\pm$, $m_{\tilde{\chi}_1^\pm} = 2m_{\tilde{\chi}_1^0}, m_{\tilde{\chi}_1^0} = 60$ GeV, $m_{\tilde{t}_1} < 1000$ GeV
>1250	95	91	AAD	14AX ATLS	≥ 3 b-jets + $\cancel{E}_T, \tilde{g} \rightarrow \tilde{b}_1 b\tilde{\chi}_1^0$ simplified model, $m_{\tilde{\chi}_1^0} < 400$ GeV	>1250	95	91	AAD	14AX ATLS	≥ 3 b-jets + $\cancel{E}_T, \tilde{g} \rightarrow b\tilde{b}\tilde{\chi}_1^0$ simplified model, $m_{\tilde{\chi}_1^0} < 400$ GeV
>1340	95	91	AAD	14AX ATLS	≥ 3 b-jets + $\cancel{E}_T, \tilde{g} \rightarrow t\tilde{t}\tilde{\chi}_1^0$ simplified model, $m_{\tilde{\chi}_1^0} < 400$ GeV	>1340	95	91	AAD	14AX ATLS	≥ 3 b-jets + $\cancel{E}_T, \tilde{g} \rightarrow t\tilde{t}\tilde{\chi}_1^0$ simplified model, $m_{\tilde{\chi}_1^0} < 400$ GeV
>1300	95	91	AAD	14AX ATLS	≥ 3 b-jets + $\cancel{E}_T, \tilde{g} \rightarrow t\tilde{b}\tilde{\chi}_1^\pm$ simplified model, $\tilde{\chi}_1^\pm \rightarrow f\tilde{f}\tilde{\chi}_1^0, m_{\tilde{\chi}_1^\pm} - m_{\tilde{\chi}_1^0} = 2$ GeV, $m_{\tilde{\chi}_1^0} < 300$ GeV	>950	95	92	AAD	14E ATLS	$\ell^\pm \ell^\pm (\ell^\mp) + \text{jets}, \tilde{g} \rightarrow t\tilde{t}\tilde{\chi}_1^0$ simplified model
> 950	95	92	AAD	14E ATLS	$\ell^\pm \ell^\pm (\ell^\mp) + \text{jets}, \tilde{g} \rightarrow t\tilde{t}\tilde{\chi}_1^0$ simplified model	>1000	95	92	AAD	14E ATLS	$\ell^\pm \ell^\pm (\ell^\mp) + \text{jets}, \tilde{g} \rightarrow t\tilde{t}_1$ with $\tilde{t}_1 \rightarrow b\tilde{\chi}_1^\pm$ simplified model, $m_{\tilde{t}_1} < 200$ GeV, $m_{\tilde{\chi}_1^\pm} = 118$ GeV, $m_{\tilde{\chi}_1^0} = 60$ GeV

1 SIRUNYAN 20b searched in 35.9 fb⁻¹ of pp collisions at $\sqrt{s} = 13$ TeV for events with at least one photon and large \cancel{E}_T . No significant excess above the Standard Model expectations is observed. Limits are set on chargino masses in a general gauge-mediated SUSY breaking (GGM) scenario Tchi1n12-GGM, see Figure 4. Limits are also set on the NLSP mass in the Tchi1chi1F and Tchi1chi1G simplified models, see their Figure 5. Finally, limits are set on the gluino mass in the Tglu4A simplified model, see their Figure 6.

2 AABOUD 19f searched in 36.1 fb⁻¹ of pp collisions at $\sqrt{s} = 13$ TeV in final states with hadronic jets, 1 or two hadronically decaying τ and \cancel{E}_T . In Tglu1F, gluino masses are excluded at 95% C.L. up to 2000 GeV for neutralino masses of 100 GeV or below. Neutralino masses up to 1000 GeV are excluded for all gluino masses below 1400 GeV. See their Fig. 9. Limits are also presented in the context of Gauge-Mediated Symmetry Breaking models: in this case, values of Λ below 110 TeV are excluded at the 95% CL for all values of $\tan\beta$ in the range $2 < \tan\beta < 60$, see their Fig 10.

3 SIRUNYAN 19AG searched in 35.9 fb⁻¹ of pp collisions at $\sqrt{s} = 13$ TeV for events with two photons and large \cancel{E}_T . No significant excess above the Standard Model expectations is observed. Limits are set on the gluino mass in the Tglu4B simplified model and on the squark mass in the Tsqk4B simplified model, see their Figure 3.

4 SIRUNYAN 19AU searched in 35.9 fb⁻¹ of pp collisions at $\sqrt{s} = 13$ TeV for events with at least one photon, jets, some of which are identified as originating from b-quarks, and large \cancel{E}_T . No significant excess above the Standard Model expectations is observed. In the framework of GMSB, limits are set on the gluino mass in the Tglu4C, Tglu4D and Tglu4E simplified models, and on the top squark mass in the Tstop13 simplified model, see their Figure 5.

5 SIRUNYAN 19CE searched in 35.9 fb⁻¹ of pp collisions at $\sqrt{s} = 13$ TeV for new particles decaying to a photon and two gluons in events with at least three large-radius jets of which two have substructure and are composed of a photon and two gluons. No statistically significant excess is observed above the SM background expectation. Upper limits at 95% confidence level on the cross section for gluino pair production are set, using a simplified Tglu1A-like stealth SUSY model. Gluino masses up to 1500-1700 GeV are excluded, depending on the neutralino mass, with the highest exclusion set for $m_{\tilde{\chi}_1^0} = 200$ GeV. See their Fig 4.

6 SIRUNYAN 19CH searched in 137 fb⁻¹ of pp collisions at $\sqrt{s} = 13$ TeV for events containing multiple jets and large \cancel{E}_T . No significant excess above the Standard Model expectations is observed. Limits are set on the gluino mass in the Tglu1A, Tglu1C, Tglu2A and Tglu3A simplified models, see their Figure 13. Limits are also set on squark, sbottom and stop masses in the Tsqk1, Tstop1, Tstop1 simplified models, see their Figure 14.

7 SIRUNYAN 19K searched in 35.9 fb⁻¹ of pp collisions at $\sqrt{s} = 13$ TeV for events with a photon, an electron or muon, and large \cancel{E}_T . No significant excess above the Standard Model expectations is observed. In the framework of GMSB, limits are set on the chargino and neutralino mass in the Tchi1n1A simplified model, see their Figure 6. Limits are also set on the gluino mass in the Tglu4A simplified model, and on the squark mass in the Tsqk4A simplified model, see their Figure 7.

8 SIRUNYAN 19s searched in 35.9 fb⁻¹ of pp collisions at $\sqrt{s} = 13$ TeV for events with zero or one charged leptons, jets and \cancel{E}_T . The razor variables (M_R and R^2) are used to categorize the events. No significant excess above the Standard Model expectations is observed. Limits are set on the gluino mass in the Tglu3A and Tglu3C simplified models, see Figures 22 and 23, and on the stop mass in the Tstop1 simplified model, see their Figure 24.

9 AABOUD 18AR searched in 36.1 fb⁻¹ of pp collisions at $\sqrt{s} = 13$ TeV for gluino pair production in events containing large missing transverse momentum and several energetic jets, at least three of which must be identified as originating from b-quarks. No excess is found above the predicted background. In Tglu3A models, gluino masses of less than 1.97 TeV are excluded for $m_{\tilde{\chi}_1^0}$ below 300 GeV, see their Fig. 10(a). Interpretations are also provided for scenarios where Tglu3A modes mix with Tglu2A and Tglu3D, see their Fig 11.

See key on page 999

Searches Particle Listings Supersymmetric Particle Searches

- 10 AABOUD 18AR searched in 36.1 fb^{-1} of pp collisions at $\sqrt{s} = 13 \text{ TeV}$ for gluino pair production in events containing large missing transverse momentum and several energetic jets, at least three of which must be identified as originating from b -quarks. No excess is found above the predicted background. In Tglu2A models, gluino masses of less than 1.92 TeV are excluded for $m_{\tilde{\chi}_1^0}$ below 600 GeV, see their Fig. 10(b). Interpretations are also provided for scenarios where Tglu2A modes mix with Tglu3A and Tglu3D, see their Fig. 11.
- 11 AABOUD 18AS searched for in 36.1 fb^{-1} of pp collisions at $\sqrt{s} = 13 \text{ TeV}$ for gluino pair production in the context of AMSB or phenomenological MSSM scenarios with wino-like LSP and long-lived charginos. Events with a disappearing track due to a low-momentum pion accompanied by at least four jets are considered. No significant excess above the Standard Model expectations is observed. Exclusion limits are set at 95% confidence level on the mass of gluinos for different chargino lifetimes. Gluino masses up to 1.65 TeV are excluded assuming a chargino mass of 460 GeV and lifetime of 0.2 ns, corresponding to a mass-splitting between the charged and neutral wino of around 160 MeV. See their Fig. 9.
- 12 AABOUD 18BJ searched in 36.1 fb^{-1} of pp collisions at $\sqrt{s} = 13 \text{ TeV}$ in events with two opposite-sign charged leptons (electrons and muons), jets and missing transverse momentum, with various requirements to be sensitive to signals with different kinematic endpoint values in the dilepton invariant mass distribution. The data are found to be consistent with the SM expectation. Results are interpreted in the Tglu1G model: gluino masses below 1850 GeV are excluded for $m_{\tilde{\chi}_1^0} = 100 \text{ GeV}$, see their Fig. 12(a).
- 13 AABOUD 18BJ searched in 36.1 fb^{-1} of pp collisions at $\sqrt{s} = 13 \text{ TeV}$ in events with two opposite-sign charged leptons (electrons and muons), jets and missing transverse momentum, with various requirements to be sensitive to signals with different kinematic endpoint values in the dilepton invariant mass distribution. The data are found to be consistent with the SM expectation. Results are interpreted in the Tglu1H model: gluino masses below 1650 GeV are excluded for $m_{\tilde{\chi}_1^0} = 100 \text{ GeV}$, see their Fig. 13(a).
- 14 AABOUD 18U searched in 36.1 fb^{-1} of pp collisions at $\sqrt{s} = 13 \text{ TeV}$ in events with at least one isolated photon, possibly jets and significant transverse momentum targeting generalised models of gauge-mediated SUSY breaking. No significant excess of events is observed above the SM prediction. Results for the di-photon channel are interpreted in terms of lower limits on the masses of gluinos in Tglu4B models, which reach as high as 2.3 TeV. Gluinos with masses below 2.15 TeV are excluded for any NLSP mass, see their Fig. 8.
- 15 AABOUD 18U searched in 36.1 fb^{-1} of pp collisions at $\sqrt{s} = 13 \text{ TeV}$ in events with at least one isolated photon, possibly jets and significant transverse momentum targeting generalised models of gauge-mediated SUSY breaking. No significant excess of events is observed above the SM prediction. Results of the $\gamma + \text{jets} + \cancel{E}_T$ channel are interpreted in terms of lower limits on the masses of gluinos in GGM higgsino-bino models (mix of Tglu4B and Tglu4C), which reach as high as 2050 GeV. Gluino masses below 1600 GeV are excluded for any NLSP mass provided that $m_{\tilde{g}} - m_{\tilde{\chi}_1^0} > 50 \text{ GeV}$. See their Fig. 11.
- 16 AABOUD 18V searched in 36.1 fb^{-1} of pp collisions at $\sqrt{s} = 13 \text{ TeV}$ in events with no charged leptons, jets and missing transverse momentum. The data are found to be consistent with the SM expectation. Results are interpreted in the Tglu1A model: gluino masses below 2030 GeV are excluded for massless LSP, see their Fig. 13(b).
- 17 AABOUD 18V searched in 36.1 fb^{-1} of pp collisions at $\sqrt{s} = 13 \text{ TeV}$ in events with no charged leptons, jets and missing transverse momentum. The data are found to be consistent with the SM expectation. Results are interpreted in the Tglu1B model. Assuming that $m_{\tilde{\chi}_1^\pm} = 0.5(m_{\tilde{g}} + m_{\tilde{\chi}_1^0})$, gluino masses below 1980 GeV are excluded for massless LSP, see their Fig. 14(c). Exclusions are also shown assuming $m_{\tilde{\chi}_1^0} = 60 \text{ GeV}$, see their Fig. 14(d).
- 18 AABOUD 18V searched in 36.1 fb^{-1} of pp collisions at $\sqrt{s} = 13 \text{ TeV}$ in events with no charged leptons, jets and missing transverse momentum. The data are found to be consistent with the SM expectation. Results are interpreted in the Tglu1E model: gluino masses below 1750 GeV are excluded for $m_{\tilde{\chi}_1^0} = 1 \text{ GeV}$ and any $m_{\tilde{\chi}_2^0}$ above 100 GeV, see their Fig. 15. Gluino mass exclusion up to 2 TeV is found for $m_{\tilde{\chi}_2^0} = 1 \text{ TeV}$.
- 19 SIRUNYAN 18AA searched in 35.9 fb^{-1} of pp collisions at $\sqrt{s} = 13 \text{ TeV}$ for events with at least one photon and large \cancel{E}_T . No significant excess above the Standard Model expectations is observed. Limits are set on wino masses in a general gauge-mediated SUSY breaking (GGM) scenario with bino-like $\tilde{\chi}_1^0$ and wino-like $\tilde{\chi}_1^\pm$ and $\tilde{\chi}_2^0$, see Figure 7. Limits are also set on the NLSP mass in the Tch1n1A and Tch1ch1A simplified models, see their Figure 8. Finally, limits are set on the gluino mass in the Tglu4A and Tglu4B simplified models, see their Figure 9, and on the squark mass in the Tsk4A and Tsk4B simplified models, see their Figure 10.
- 20 SIRUNYAN 18AC searched in 35.9 fb^{-1} of pp collisions at $\sqrt{s} = 13 \text{ TeV}$ for events with a single electron or muon and multiple jets. No significant excess above the Standard Model expectations is observed. Limits are set on the gluino mass in the Tglu3A and Tglu1B simplified models, see their Figure 5.
- 21 SIRUNYAN 18AL searched in 35.9 fb^{-1} of pp collisions at $\sqrt{s} = 13 \text{ TeV}$ for events with at least three charged leptons, in any combination of electrons and muons, jets and significant \cancel{E}_T . No significant excess above the Standard Model expectations is observed. Limits are set on the gluino mass in the Tglu3A and Tglu1C simplified models, see their Figure 5. Limits are also set on the sbottom mass in the Tstbot2 simplified model, see their Figure 6, and on the stop mass in the Tsttop7 simplified model, see their Figure 7.
- 22 SIRUNYAN 18AR searched in 35.9 fb^{-1} of pp collisions at $\sqrt{s} = 13 \text{ TeV}$ for events containing two opposite-charge, same-flavour leptons (electrons or muons), jets and \cancel{E}_T . No significant excess above the Standard Model expectations is observed. Limits are set on the gluino mass in the Tglu4C simplified model, see their Figure 7. Limits are also set on the chargino/neutralino mass in the Tch1n2F simplified models, see their Figure 8, and on the higgsino mass in the Tn1n1B and Tn1n1C simplified models, see their Figure 9. Finally, limits are set on the sbottom mass in the Tstbot3 simplified model, see their Figure 10.
- 23 SIRUNYAN 18AY searched in 35.9 fb^{-1} of pp collisions at $\sqrt{s} = 13 \text{ TeV}$ for events containing one or more jets and significant \cancel{E}_T . No significant excess above the Standard Model expectations is observed. Limits are set on the gluino mass in the Tglu1A, Tglu2A and Tglu3A simplified models, see their Figure 3. Limits are also set on squark, sbottom and stop masses in the Tskq1, Tstbot1, Tsttop1 and Tsttop4 simplified models, see their Figure 3. Finally, limits are set on long-lived gluino masses in a Tglu1A simplified model where the gluino is metastable or long-lived with proper decay lengths in the range $10^{-3} \text{ mm} < c\tau < 10^5 \text{ mm}$, see their Figure 4.
- 24 SIRUNYAN 18b searched in 35.9 fb^{-1} of pp collisions at $\sqrt{s} = 13 \text{ TeV}$ for events containing identified hadronically decaying top quarks, no leptons, and \cancel{E}_T . No significant excess above the Standard Model expectations is observed. Limits are set on the stop mass in the Tsttop1 simplified model, see their Figure 8, and on the gluino mass in the Tglu3A, Tglu3B, Tglu3C and Tglu3E simplified models, see their Figure 9.
- 25 SIRUNYAN 18m searched in 35.9 fb^{-1} of pp collisions at $\sqrt{s} = 13 \text{ TeV}$ for events with one or more high-momentum Higgs bosons, decaying to pairs of b -quarks, and large \cancel{E}_T . No significant excess above the Standard Model expectations is observed. Limits are set on the gluino mass in the Tglu1I and Tglu1J simplified models, see their Figure 3.
- 26 AABOUD 17AJ searched in 36.1 fb^{-1} of pp collisions at $\sqrt{s} = 13 \text{ TeV}$ for events with two same-sign or three leptons, jets and large missing transverse momentum. No significant excess above the Standard Model expectations is observed. Limits up to 1.75 TeV are set on the gluino mass in Tglu3A simplified models in case of off-shell top squarks and for $m_{\tilde{\chi}_1^0} = 100 \text{ GeV}$. See their Figure 4(a).
- 27 AABOUD 17AJ searched in 36.1 fb^{-1} of pp collisions at $\sqrt{s} = 13 \text{ TeV}$ for events with two same-sign or three leptons, jets and large missing transverse momentum. No significant excess above the Standard Model expectations is observed. Limits up to 1.57 TeV are set on the gluino mass in Tglu1E simplified models (2-step models) for $m_{\tilde{\chi}_1^0} = 100 \text{ GeV}$. See their Figure 4(b).
- 28 AABOUD 17AJ searched in 36.1 fb^{-1} of pp collisions at $\sqrt{s} = 13 \text{ TeV}$ for events with two same-sign or three leptons, jets and large missing transverse momentum. No significant excess above the Standard Model expectations is observed. Limits up to 1.86 TeV are set on the gluino mass in Tglu1G simplified models for $m_{\tilde{\chi}_1^0} = 200 \text{ GeV}$. See their Figure 4(c).
- 29 AABOUD 17AR searched in 36.1 fb^{-1} of pp collisions at $\sqrt{s} = 13 \text{ TeV}$ for events with one isolated lepton, at least two jets and large missing transverse momentum. No significant excess above the Standard Model expectations is observed. Limits up to 2.1 TeV are set on the gluino mass in Tglu1B simplified models, with $x = (m_{\tilde{\chi}_1^\pm} - m_{\tilde{\chi}_1^0}) / (m_{\tilde{g}} - m_{\tilde{\chi}_1^0}) = 1/2$. Similar limits are obtained for variable x and fixed neutralino mass, $m_{\tilde{\chi}_1^0} = 60 \text{ GeV}$. See their Figure 13.
- 30 AABOUD 17AR searched in 36.1 fb^{-1} of pp collisions at $\sqrt{s} = 13 \text{ TeV}$ for events with one isolated lepton, at least two jets and large missing transverse momentum. No significant excess above the Standard Model expectations is observed. Limits up to 1.74 TeV are set on the gluino mass in Tglu1E simplified model. Limits up to 1.7 TeV are also set on pMSSM models leading to similar signal event topologies. See their Figure 13.
- 31 AABOUD 17AY searched in 36.1 fb^{-1} of pp collisions at $\sqrt{s} = 13 \text{ TeV}$ for events with at least four jets and large missing transverse momentum. No significant excess above the Standard Model expectations is observed. Limits up to 1.8 TeV are set on the gluino mass in Tglu3A simplified models assuming $m_{\tilde{\tau}_1} - m_{\tilde{\chi}_1^0} = 5 \text{ GeV}$. See their Figure 13.
- 32 AABOUD 17AZ searched in 36.1 fb^{-1} of pp collisions at $\sqrt{s} = 13 \text{ TeV}$ for events with at least seven jets and large missing transverse momentum. Selected events are further classified based on the presence of large R -jets or b -jets and no leptons. No significant excess above the Standard Model expectations is observed. Limits up to 1.8 TeV are set on the gluino mass in Tglu1E simplified models. See their Figure 6b.
- 33 AABOUD 17AZ searched in 36.1 fb^{-1} of pp collisions at $\sqrt{s} = 13 \text{ TeV}$ for events with at least seven jets and large missing transverse momentum. Selected events are further classified based on the presence of large R -jets or b -jets and no leptons. No significant excess above the Standard Model expectations is observed. Limits up to 1.54 TeV are set on the gluino mass in Tglu3A simplified models. See their Figure 7a.
- 34 AABOUD 17N searched in 14.7 fb^{-1} of pp collisions at $\sqrt{s} = 13 \text{ TeV}$ in final states with 2 same-flavor, opposite-sign leptons (electrons or muons), jets and large missing transverse momentum. In Tglu1J models, gluino masses are excluded at 95% C.L. up to 1300 GeV for $m_{\tilde{\chi}_1^0} = 0 \text{ GeV}$ and $m_{\tilde{\chi}_2^0} = 1100 \text{ GeV}$. See their Fig. 12 for exclusion limits as a function of $m_{\tilde{\chi}_2^0}$. Limits are also presented assuming $m_{\tilde{\chi}_2^0} = m_{\tilde{\chi}_1^0} + 100 \text{ GeV}$, see their Fig. 13.
- 35 AABOUD 17N searched in 14.7 fb^{-1} of pp collisions at $\sqrt{s} = 13 \text{ TeV}$ in final states with 2 same-flavor, opposite-sign leptons (electrons or muons), jets and large missing transverse momentum. In Tglu1H models, gluino masses are excluded at 95% C.L. up to 1310 GeV for $m_{\tilde{\chi}_1^0} < 400 \text{ GeV}$ and assuming $m_{\tilde{\chi}_2^0} = (m_{\tilde{g}} + m_{\tilde{\chi}_1^0})/2$. See their Fig. 15.
- 36 AABOUD 17N searched in 14.7 fb^{-1} of pp collisions at $\sqrt{s} = 13 \text{ TeV}$ in final states with 2 same-flavor, opposite-sign leptons (electrons or muons), jets and large missing transverse momentum. In Tglu1G models, gluino masses are excluded at 95% C.L. up to 1700 GeV for small $m_{\tilde{\chi}_1^0}$. The results probe kinematic endpoints as small as $m_{\tilde{\chi}_2^0} - m_{\tilde{\chi}_1^0} = (m_{\tilde{g}} - m_{\tilde{\chi}_1^0})/2 = 50 \text{ GeV}$. See their Fig. 14.
- 37 KHACHATRYAN 17 searched in 2.3 fb^{-1} of pp collisions at $\sqrt{s} = 13 \text{ TeV}$ for events containing four or more jets, no more than one lepton, and missing transverse momentum, using the razor variables (M_R and R^2) to discriminate between signal and background processes. No evidence for an excess over the expected background is observed. Limits are derived on the gluino mass in the Tglu1A, Tglu2A and Tglu3A simplified models, see Figs. 16 and 17. Also, assuming gluinos decay only via three-body processes involving third-generation quarks plus a neutralino/chargino, and assuming $m_{\tilde{\chi}_1^\pm} = m_{\tilde{\chi}_1^0} + 5 \text{ GeV}$, a branching ratio-independent limit on the gluino mass is given, see Fig. 16.
- 38 KHACHATRYAN 17AD searched in 2.3 fb^{-1} of pp collisions at $\sqrt{s} = 13 \text{ TeV}$ for events containing at least four jets (including b -jets), missing transverse momentum and tagged top quarks. No evidence for an excess over the expected background is observed. Gluino masses up to 1550 GeV and neutralino masses up to 900 GeV are excluded at 95% C.L. See Fig. 13.
- 39 KHACHATRYAN 17AD searched in 2.3 fb^{-1} of pp collisions at $\sqrt{s} = 13 \text{ TeV}$ for events containing at least four jets (including b -jets), missing transverse momentum and tagged top quarks. No evidence for an excess over the expected background is observed. Gluino masses up to 1450 GeV and neutralino masses up to 820 GeV are excluded at 95% C.L. See Fig. 13.
- 40 KHACHATRYAN 17AS searched in 2.3 fb^{-1} of pp collisions at $\sqrt{s} = 13 \text{ TeV}$ for events with a single electron or muon and multiple jets. No significant excess above the Standard Model expectations is observed. Limits are set on the gluino mass in the Tglu3A and Tglu1B simplified models, see their Fig. 7.
- 41 KHACHATRYAN 17AW searched in 2.3 fb^{-1} of pp collisions at $\sqrt{s} = 13 \text{ TeV}$ for events with at least three charged leptons, in any combination of electrons and muons, and

Searches Particle Listings

Supersymmetric Particle Searches

- significant \mathcal{E}_T . No significant excess above the Standard Model expectations is observed. Limits are set on the gluino mass in the Tglu3A and Tglu1C simplified models, and on the sbottom mass in the Tsb02 simplified model, see their Figure 4.
- 42 KHACHATRYAN 17P searched in 2.3 fb^{-1} of pp collisions at $\sqrt{s} = 13 \text{ TeV}$ for events with one or more jets and large \mathcal{E}_T . No significant excess above the Standard Model expectations is observed. Limits are set on the gluino mass in the Tglu1A, Tglu2A, Tglu3A, Tglu3B, Tglu3C and Tglu3D simplified models, see their Figures 7 and 8. Limits are also set on the squark mass in the Tskq1 simplified model, see their Fig. 7, and on the sbottom mass in the Tsb01 simplified model, see Fig. 8. Finally, limits are set on the stop mass in the Tstop1, Tstop3, Tstop4, Tstop6 and Tstop7 simplified models, see Fig. 8.
- 43 KHACHATRYAN 17V searched in 2.3 fb^{-1} of pp collisions at $\sqrt{s} = 13 \text{ TeV}$ for events with two photons and large \mathcal{E}_T . No significant excess above the Standard Model expectations is observed. Limits are set on the gluino and squark mass in the context of general gauge mediation models Tglu4B and Tskq4, see their Fig. 4.
- 44 SIRUNYAN 17AF searched in 35.9 fb^{-1} of pp collisions at $\sqrt{s} = 13 \text{ TeV}$ for events with a single lepton (electron or muon), jets, including at least one jet originating from a b -quark, and large \mathcal{E}_T . No significant excess above the Standard Model expectations is observed. Limits are set on the gluino mass in the Tglu3A and Tglu3B simplified models, see their Figure 2.
- 45 SIRUNYAN 17AY searched in 35.9 fb^{-1} of pp collisions at $\sqrt{s} = 13 \text{ TeV}$ for events with at least one photon, jets and large \mathcal{E}_T . No significant excess above the Standard Model expectations is observed. Limits are set on the gluino mass in the Tglu4A and Tglu4B simplified models, and on the squark mass in the Tskq4A and Tskq4B simplified models, see their Figure 6.
- 46 SIRUNYAN 17AZ searched in 35.9 fb^{-1} of pp collisions at $\sqrt{s} = 13 \text{ TeV}$ for events with one or more jets and large \mathcal{E}_T . No significant excess above the Standard Model expectations is observed. Limits are set on the gluino mass in the Tglu1A, Tglu2A, Tglu3A simplified models, see their Figures 6. Limits are also set on the squark mass in the Tskq1 simplified model (for single light squark and for 8 degenerate light squarks), on the sbottom mass in the Tsb01 simplified model and on the stop mass in the Tstop1 simplified model, see their Fig. 7. Finally, limits are set on the stop mass in the Tstop2, Tstop4 and Tstop8 simplified models, see Fig. 8.
- 47 SIRUNYAN 17P searched in 35.9 fb^{-1} of pp collisions at $\sqrt{s} = 13 \text{ TeV}$ for events with multiple jets and large \mathcal{E}_T . No significant excess above the Standard Model expectations is observed. Limits are set on the gluino mass in the Tglu1A, Tglu1C, Tglu2A, Tglu3A and Tglu3D simplified models, see their Fig. 12. Limits are also set on the squark mass in the Tskq1 simplified model, on the stop mass in the Tstop1 simplified model, and on the sbottom mass in the Tsb01 simplified model, see Fig. 13.
- 48 SIRUNYAN 17S searched in 35.9 fb^{-1} of pp collisions at $\sqrt{s} = 13 \text{ TeV}$ for events with two isolated same-sign leptons, jets, and large \mathcal{E}_T . No significant excess above the Standard Model expectations is observed. Limits are set on the mass of the gluino mass in the Tglu3A, Tglu3B, Tglu3C, Tglu3D and Tglu1B simplified models, see their Figures 5 and 6, and on the sbottom mass in the Tsb02 simplified model, see their Figure 6.
- 49 AABOUD 16AC searched in 3.2 fb^{-1} of pp collisions at $\sqrt{s} = 13 \text{ TeV}$ in final states with hadronic jets, 1 or two hadronically decaying τ and \mathcal{E}_T . In Tglu1F, gluino masses are excluded at 95% C.L. up to 1570 GeV for neutralino masses of 100 GeV or below. Neutralino masses up to 700 GeV are excluded for all gluino masses between 800 GeV and 1500 GeV, while the strongest neutralino-mass exclusion of 750 GeV is achieved for gluino masses around 1400 GeV. See their Fig. 8. Limits are also presented in the context of Gauge-Mediated Symmetry Breaking models: in this case, values of A below 92 TeV are excluded at the 95% C.L. corresponding to gluino masses below 2000 GeV. See their Fig. 9.
- 50 AABOUD 16I searched in 3.2 fb^{-1} of pp collisions at $\sqrt{s} = 13 \text{ TeV}$ in final states with one isolated electron or muon, hadronic jets, and \mathcal{E}_T . Gluino-mediated pair production of stops with a nearly mass-degenerate stop and neutralino are targeted and gluino masses are excluded at 95% C.L. up to 1460 GeV. A 100% of stops decaying via charm + neutralino is assumed. The results are also valid in case of 4-body decays $\tilde{t}_1 \rightarrow f f' b \tilde{\chi}_1^0$. See their Fig. 8.
- 51 AABOUD 16M searched in 3.2 fb^{-1} of pp collisions at $\sqrt{s} = 13 \text{ TeV}$ for events with two photons, hadronic jets and \mathcal{E}_T . No significant excess above the Standard Model expectations is observed. Exclusion limits at 95% C.L. are set on gluino masses in the general gauge-mediated SUSY breaking model (GGM), for bino-like NLSP. See their Fig. 3.
- 52 AABOUD 16N searched in 3.2 fb^{-1} of pp collisions at $\sqrt{s} = 13 \text{ TeV}$ for events containing hadronic jets, large \mathcal{E}_T , and no electrons or muons. No significant excess above the Standard Model expectations is observed. Gluino masses below 1510 GeV are excluded at the 95% C.L. in a simplified model with only gluinos and the lightest neutralino. See their Fig. 7b.
- 53 AABOUD 16N searched in 3.2 fb^{-1} of pp collisions at $\sqrt{s} = 13 \text{ TeV}$ for events containing hadronic jets, large \mathcal{E}_T , and no electrons or muons. No significant excess above the Standard Model expectations is observed. Gluino masses below 1500 GeV are excluded at the 95% C.L. in a simplified model with gluinos decaying via an intermediate $\tilde{\chi}_1^\pm$ to two quarks, a W boson and a $\tilde{\chi}_1^0$ for $m_{\tilde{\chi}_1^0} = 200 \text{ GeV}$. See their Fig. 8.
- 54 AAD 16AD searched in 3.2 fb^{-1} of pp collisions at $\sqrt{s} = 13 \text{ TeV}$ for events containing several energetic jets, of which at least three must be identified as b -jets, large \mathcal{E}_T and no electrons or muons. No significant excess above the Standard Model expectations is observed. For $\tilde{\chi}_1^0$ below 800 GeV, gluino masses below 1780 GeV are excluded at 95% C.L. for gluinos decaying via bottom squarks. See their Fig. 7a.
- 55 AAD 16AD searched in 3.2 fb^{-1} of pp collisions at $\sqrt{s} = 13 \text{ TeV}$ for events containing several energetic jets, of which at least three must be identified as b -jets, large \mathcal{E}_T and one electron or muon. Large-radius jets with a high mass are also used to identify highly boosted top quarks. No significant excess above the Standard Model expectations is observed. For $\tilde{\chi}_1^0$ below 700 GeV, gluino masses below 1760 GeV are excluded at 95% C.L. for gluinos decaying via top squarks. See their Fig. 7b.
- 56 AAD 16BB searched in 3.2 fb^{-1} of pp collisions at $\sqrt{s} = 13 \text{ TeV}$ for events with exactly two same-sign leptons or at least three leptons, multiple hadronic jets, b -jets, and \mathcal{E}_T . No significant excess over the Standard Model expectation is found. Exclusion limits at 95% C.L. are set on the gluino mass in various simplified models (Tglu1D, Tglu1E, Tglu3A). See their Figs. 4a, 4b, and 4d.
- 57 AAD 16BG searched in 3.2 fb^{-1} of pp collisions at $\sqrt{s} = 13 \text{ TeV}$ in final states with one isolated electron or muon, hadronic jets, and \mathcal{E}_T . The data agree with the SM background expectation in the six signal selections defined in the search, and the largest deviation is a 2.1 standard deviation excess. Gluinos are excluded at 95% C.L. up to 1600 GeV assuming they decay via the lightest chargino to the lightest neutralino as in the model Tglu1B for $m_{\tilde{\chi}_1^0} = 100 \text{ GeV}$, assuming $m_{\tilde{\chi}_1^\pm} = (m_{\tilde{g}} + m_{\tilde{\chi}_1^0})/2$. See their Fig. 6.
- 58 AAD 16V searched in 3.2 fb^{-1} of pp collisions at $\sqrt{s} = 13 \text{ TeV}$ for events with \mathcal{E}_T various hadronic jet multiplicities from ≥ 7 to ≥ 10 and with various b -jet multiplicity requirements. No significant excess over the Standard Model expectation is found. Exclusion limits at 95% C.L. are set on the gluino mass in one simplified model (Tglu1E) and a pMSSM-inspired model. See their Fig. 5.
- 59 KHACHATRYAN 16AM searched in 19.7 fb^{-1} of pp collisions at $\sqrt{s} = 8 \text{ TeV}$ for events with highly boosted W -bosons and b -jets, using the razor variables (M_R and R^2) to discriminate between signal and background processes. No significant excess above the Standard Model expectations is observed. Limits are set on the gluino mass in the Tglu3C and Tglu3B simplified models, see Fig. 12.
- 60 KHACHATRYAN 16BJ searched in 2.3 fb^{-1} of pp collisions at $\sqrt{s} = 13 \text{ TeV}$ for events with two isolated same-sign dileptons and jets in the final state. No significant excess above the Standard Model expectations is observed. Limits are set on the gluino mass in the following simplified models: Tglu3A and Tglu3D, see Fig. 4, Tglu3B and Tglu3C, see Fig. 5, and Tglu1B, see Fig. 7.
- 61 KHACHATRYAN 16BS searched in 2.3 fb^{-1} of pp collisions at $\sqrt{s} = 13 \text{ TeV}$ for events with at least one energetic jet, no isolated leptons, and significant \mathcal{E}_T , using the transverse mass variable M_{T2} to discriminate between signal and background processes. No significant excess above the Standard Model expectations is observed. Limits are set on the gluino mass in the Tglu1A, Tglu2A and Tglu3A simplified models, see Fig. 10 and Table 3.
- 62 KHACHATRYAN 16BY searched in 2.3 fb^{-1} of pp collisions at $\sqrt{s} = 13 \text{ TeV}$ for events with two opposite-sign, same-flavour leptons, jets, and missing transverse momentum. No significant excess above the Standard Model expectations is observed. Limits are set on the gluino mass in the Tglu4C simplified model, see Fig. 4, and on sbottom masses in the Tsb03 simplified model, see Fig. 5.
- 63 KHACHATRYAN 16V searched in 2.3 fb^{-1} of pp collisions at $\sqrt{s} = 13 \text{ TeV}$ for events with at least four energetic jets and significant \mathcal{E}_T , no identified isolated electron or muon or charged track. No significant excess above the Standard Model expectations is observed. Limits are set on the gluino mass in the Tglu1A, Tglu1C, Tglu2A, and Tglu3A simplified models, see Fig. 8.
- 64 AAD 15BG searched in 20.3 fb^{-1} of pp collisions at $\sqrt{s} = 8 \text{ TeV}$ for events with jets, missing \mathcal{E}_T , and two opposite-sign same flavor isolated leptons featuring either a kinematic edge, or a peak at the Z -boson mass, in the invariant mass spectrum. No evidence for a statistically significant excess over the expected SM backgrounds are observed and 95% C.L. exclusion limits are derived in a GGM simplified model of gluino pair production where the gluino decays into quarks, a Z -boson, and a massless gravitino LSP, see Fig. 12. Also, limits are set in simplified models with slepton/sneutrino intermediate states, see Fig. 13.
- 65 AAD 15BV summarized and extended ATLAS searches for gluinos and first- and second-generation squarks in final states containing jets and missing transverse momentum, with or without leptons or b -jets in the $\sqrt{s} = 8 \text{ TeV}$ data set collected in 2012. The paper reports the results of new interpretations and statistical combinations of previously published analyses, as well as new analyses. Exclusion limits at 95% C.L. are set on the gluino mass in several R-parity conserving models, leading to a generalized constraint on gluino masses exceeding 1150 GeV for lightest supersymmetric particle masses below 100 GeV. See their Figs. 10, 19, 20, 21, 23, 25, 26, 29-37.
- 66 AAD 15BX interpreted the results of a wide range of ATLAS direct searches for supersymmetry, during the first run of the LHC using the $\sqrt{s} = 7 \text{ TeV}$ and $\sqrt{s} = 8 \text{ TeV}$ data set collected in 2012, within the wider framework of the phenomenological mMSSM (pMSSM). The integrated luminosity was up to 20.3 fb^{-1} . From an initial random sampling of 500 million pMSSM points, generated from the 19-parameter pMSSM, a total of 310,327 model points with $\tilde{\chi}_1^0$ LSP were selected each of which satisfies constraints from previous collider searches, precision measurements, cold dark matter energy density measurements and direct dark matter searches. The impact of the ATLAS Run 1 searches on this space was presented, considering the fraction of model points surviving, after projection into two-dimensional spaces of sparticle masses. Good complementarity is observed between different ATLAS analyses, with almost all showing regions of unique sensitivity. ATLAS searches have good sensitivity at LSP mass below 800 GeV.
- 67 AAD 15CA searched in 20.3 fb^{-1} of pp collisions at $\sqrt{s} = 8 \text{ TeV}$ for events with one or more photons, hadronic jets or b -jets and \mathcal{E}_T . No significant excess above the Standard Model expectations is observed. Limits are set on gluino masses in the general gauge-mediated SUSY breaking model (GGM), for bino-like or higgsino-bino admixtures NLSP, see Fig. 8, 10, 11.
- 68 KHACHATRYAN 15AF searched in 19.5 fb^{-1} of pp collisions at $\sqrt{s} = 8 \text{ TeV}$ for events with at least two energetic jets and significant \mathcal{E}_T , using the transverse mass variable M_{T2} to discriminate between signal and background processes. No significant excess above the Standard Model expectations is observed. Limits are set on the gluino mass in simplified models where the decay $\tilde{g} \rightarrow q \bar{q} \tilde{\chi}_1^0$ takes place with a branching ratio of 100%, see Fig. 13(a), or where the decay $\tilde{g} \rightarrow b \bar{b} \tilde{\chi}_1^0$ takes place with a branching ratio of 100%, see Fig. 13(b), or where the decay $\tilde{g} \rightarrow t \bar{t} \tilde{\chi}_1^0$ takes place with a branching ratio of 100%, see Fig. 13(c). See also Table 5. Exclusions in the CMSSM, assuming $\tan\beta = 30$, $A_0 = -2 \max(m_0, m_{1/2})$ and $\mu > 0$, are also presented, see Fig. 15.
- 69 KHACHATRYAN 15I searched in 19.5 fb^{-1} of pp collisions at $\sqrt{s} = 8 \text{ TeV}$ for events in which b -jets and four W -bosons are produced. Five individual search channels are combined (fully hadronic, single lepton, same-sign dilepton, opposite-sign dilepton, multi-lepton). No significant excess above the Standard Model expectations is observed. Limits are set on the gluino mass in a simplified model where the decay $\tilde{g} \rightarrow t \bar{t} \tilde{\chi}_1^0$ takes place with a branching ratio of 100%, see Fig. 5. Also a simplified model with gluinos decaying into on-shell top squarks is considered, see Fig. 6.
- 70 KHACHATRYAN 15X searched in 19.3 fb^{-1} of pp collisions at $\sqrt{s} = 8 \text{ TeV}$ for events with at least two energetic jets, at least one of which is required to originate from a b quark, and significant \mathcal{E}_T , using the razor variables (M_R) and R^2 to discriminate between signal and background processes. No significant excess above the Standard Model expectations is observed. Limits are set on the gluino mass in simplified models where the decay $\tilde{g} \rightarrow b \bar{b} \tilde{\chi}_1^0$ and the decay $\tilde{g} \rightarrow t \bar{t} \tilde{\chi}_1^0$ take place with branching ratios varying between 0, 50 and 100%, see Figs. 13 and 14.
- 71 AAD 14AE searched in 20.3 fb^{-1} of pp collisions at $\sqrt{s} = 8 \text{ TeV}$ for strongly produced supersymmetric particles in events containing jets and large missing transverse momentum, and no electrons or muons. No excess over the expected SM background is observed. Exclusion limits are derived in simplified models containing gluinos and squarks, see Figures 5, 6 and 7. Limits are also derived in the mSUGRA/CMSSM with parameters $\tan\beta = 30$, $A_0 = -2 m_0$ and $\mu > 0$, see their Fig. 8.

- ⁷² AAD 14AG searched in 20.3 fb⁻¹ of pp collisions at $\sqrt{s} = 8$ TeV for events containing one hadronically decaying τ -lepton, zero or one additional light leptons (electrons or muons), jets and large missing transverse momentum. No excess of events above the expected level of Standard Model background was found. Exclusion limits at 95% C.L. are set in several SUSY scenarios. For an interpretation in the minimal GMSB model, see their Fig. 8. For an interpretation in the mSUGRA/CMSSM with parameters $\tan\beta = 30$, $A_0 = -2m_0$ and $\mu > 0$, see their Fig. 9. For an interpretation in the framework of natural Gauge Mediation, see Fig. 10. For an interpretation in the bRPV scenario, see their Fig. 11.
- ⁷³ AAD 14X searched in 20.3 fb⁻¹ of pp collisions at $\sqrt{s} = 8$ TeV for events with at least four leptons (electrons, muons, taus) in the final state. No significant excess above the Standard Model expectations is observed. Limits are set on the gluino mass in a general gauge-mediation model (GGM) where the decay $\tilde{g} \rightarrow q\bar{q}\tilde{\chi}_1^0$, with $\tilde{\chi}_1^0 \rightarrow \ell^\pm \ell^\mp \tilde{G}$, takes place with a branching ratio of 100%, for two choices of $\tan\beta = 1.5$ and 30, see Fig. 11. Also some constraints on the higgsino mass parameter μ are discussed.
- ⁷⁴ CHATRCHYAN 14AH searched in 4.7 fb⁻¹ of pp collisions at $\sqrt{s} = 7$ TeV for events with at least two energetic jets and significant \cancel{E}_T , using the razor variables (M_R and R^2) to discriminate between signal and background processes. No significant excess above the Standard Model expectations is observed. Limits are set on sbottom masses in simplified models where the decay $\tilde{g} \rightarrow q\bar{q}\tilde{\chi}_1^0$ takes place with a branching ratio of 100%, see Fig. 28. Exclusions in the CMSSM, assuming $\tan\beta = 10$, $A_0 = 0$ and $\mu > 0$, are also presented, see Fig. 26.
- ⁷⁵ CHATRCHYAN 14AH searched in 4.7 fb⁻¹ of pp collisions at $\sqrt{s} = 7$ TeV for events with at least two energetic jets and significant \cancel{E}_T , using the razor variables (M_R and R^2) to discriminate between signal and background processes. A second analysis requires at least one of the jets to be originating from a b -quark. No significant excess above the Standard Model expectations is observed. Limits are set on sbottom masses in simplified models where the decay $\tilde{g} \rightarrow b\bar{b}\tilde{\chi}_1^0$ takes place with a branching ratio of 100%, see Figs. 28 and 29. Exclusions in the CMSSM, assuming $\tan\beta = 10$, $A_0 = 0$ and $\mu > 0$, are also presented, see Fig. 26.
- ⁷⁶ CHATRCHYAN 14AH searched in 4.7 fb⁻¹ of pp collisions at $\sqrt{s} = 7$ TeV for events with at least two energetic jets and significant \cancel{E}_T , using the razor variables (M_R and R^2) to discriminate between signal and background processes. A second analysis requires at least one of the jets to be originating from a b -quark. No significant excess above the Standard Model expectations is observed. Limits are set on sbottom masses in simplified models where the decay $\tilde{g} \rightarrow t\bar{t}\tilde{\chi}_1^0$ takes place with a branching ratio of 100%, see Figs. 28 and 29. Exclusions in the CMSSM, assuming $\tan\beta = 10$, $A_0 = 0$ and $\mu > 0$, are also presented, see Fig. 26.
- ⁷⁷ CHATRCHYAN 14I searched in 19.5 fb⁻¹ of pp collisions at $\sqrt{s} = 8$ TeV for events containing multijets and large \cancel{E}_T . No excess over the expected SM background is observed. Exclusion limits are derived in simplified models containing gluinos that decay via $\tilde{g} \rightarrow q\bar{q}\tilde{\chi}_1^0$ with a 100% branching ratio, see Fig. 7b, or via $\tilde{g} \rightarrow t\bar{t}\tilde{\chi}_1^0$ with a 100% branching ratio, see Fig. 7c, or via $\tilde{g} \rightarrow q\bar{q}W/Z\tilde{\chi}_1^0$, see Fig. 7d.
- ⁷⁸ CHATRCHYAN 14N searched in 19.3 fb⁻¹ of pp collisions at $\sqrt{s} = 8$ TeV for events containing a single isolated electron or muon and multiple jets, at least two of which are identified as originating from a b -quark. No significant excesses over the expected SM backgrounds are observed. The results are interpreted in three simplified models of gluino pair production with subsequent decay into virtual or on-shell top squarks, where each of the top squarks decays in turn into a top quark and a $\tilde{\chi}_1^0$, see Fig. 4. The models differ in which masses are allowed to vary.
- ⁷⁹ CHATRCHYAN 14R searched in 19.5 fb⁻¹ of pp collisions at $\sqrt{s} = 8$ TeV for events with at least three leptons (electrons, muons, taus) in the final state. No significant excess above the Standard Model expectations is observed. Limits are set on the gluino mass in a slepton co-NLSP simplified model (GMSB) where the decay $\tilde{g} \rightarrow q\ell^\pm\ell^\mp\tilde{G}$ takes place with a branching ratio of 100%, see Fig. 8.
- ⁸⁰ CHATRCHYAN 14R searched in 19.5 fb⁻¹ of pp collisions at $\sqrt{s} = 8$ TeV for events with at least three leptons (electrons, muons, taus) in the final state. No significant excess above the Standard Model expectations is observed. Limits are set on the gluino mass in a simplified model where the decay $\tilde{g} \rightarrow t\bar{t}\tilde{\chi}_1^0$ takes place with a branching ratio of 100%, see Fig. 11.
- ⁸¹ AABOUD 18BJ searched in 36.1 fb⁻¹ of pp collisions at $\sqrt{s} = 13$ TeV in events with two opposite-sign charged leptons (electrons and muons), jets and missing transverse momentum, with various requirements to be sensitive to signals with different kinematic endpoint values in the dilepton invariant mass distribution. The data are found to be consistent with the SM expectation. Results are interpreted in the Tglu1H model in case of $m_{\tilde{\chi}_1^0} = 1$ GeV: for any $m_{\tilde{\chi}_2^0}$, gluino masses below 1500 GeV are excluded, see their Fig. 14(a).
- ⁸² AABOUD 18V searched in 36.1 fb⁻¹ of pp collisions at $\sqrt{s} = 13$ TeV in events with no charged leptons, jets and missing transverse momentum. The data are found to be consistent with the SM expectation. Results are interpreted in a Tglu1C-like model, assuming 50% BR for each gluino decay mode. Gluino masses below 1770 GeV are excluded for any $m_{\tilde{\chi}_2^0} - m_{\tilde{\chi}_1^0}$ and $m_{\tilde{\chi}_1^0} = 60$ GeV, see their Fig. 16(b).
- ⁸³ AABOUD 17AZ searched in 36.1 fb⁻¹ of pp collisions at $\sqrt{s} = 13$ TeV for events with at least seven jets and large missing transverse momentum. Selected events are further classified based on the presence of large R -jets or b -jets and no leptons. No significant excess above the Standard Model expectations is observed. Limits are set for pMSSM models with $M_1 = 60$ GeV, $\tan(\beta) = 10$, $\mu < 0$ varying the soft-breaking parameters M_3 and μ . Gluino masses up to 1600 GeV are excluded for $m_{\tilde{\chi}_1^\pm} = 200$ GeV. See their Figure 6a and text for details on the model.
- ⁸⁴ KHACHATRYAN 16AY searched in 2.3 fb⁻¹ of pp collisions at $\sqrt{s} = 13$ TeV for events with one isolated high transverse momentum lepton (e or μ), hadronic jets of which at least one is identified as coming from a b -quark, and large \cancel{E}_T . No significant excess above the Standard Model expectations is observed. Limits are set on the gluino mass in the Tglu3A simplified model, see Fig. 10, and in the Tglu3B model, see Fig. 11.
- ⁸⁵ KHACHATRYAN 16BT performed a global Bayesian analysis of a wide range of CMS results obtained with data samples corresponding to 5.0 fb⁻¹ of pp collisions at $\sqrt{s} = 7$ TeV and in 19.5 fb⁻¹ of pp collisions at $\sqrt{s} = 8$ TeV. The set of searches considered, both individually and in combination, includes those with all-hadronic final states, same-sign and opposite-sign dileptons, and multi-lepton final states. An interpretation was given in a scan of the 19-parameter pMSSM. No scan points with a gluino mass less than 500 GeV survived and 98% of models with a squark mass less than 300 GeV were excluded.
- ⁸⁶ AAD 15AB searched for the decay of neutral, weakly interacting, long-lived particles in 20.3 fb⁻¹ of pp collisions at $\sqrt{s} = 8$ TeV. Signal events require at least two reconstructed vertices possibly originating from long-lived particles decaying to jets in the inner tracking detector and muon spectrometer. No significant excess of events over the expected background was found. Results were interpreted in Stealth SUSY benchmark models where a pair of gluinos decay to long-lived singlinos, S , which in turn each decay to a low-mass gravitino and a pair of jets. The 95% confidence-level limits are set on the cross section \times branching ratio for the decay $\tilde{g} \rightarrow \tilde{S}g$, as a function of the singlino proper lifetime ($c\tau$). See their Fig. 10(f).
- ⁸⁷ AAD 15AI searched in 20 fb⁻¹ of pp collisions at $\sqrt{s} = 8$ TeV for events containing at least one isolated lepton (electron or muon), jets, and large missing transverse momentum. No excess of events above the expected level of Standard Model background was found. Exclusion limits at 95% C.L. are set on the gluino mass in the CMSSM/mSUGRA, see Fig. 15, in the NUHM2, see Fig. 16, and in various simplified models, see Figs. 18–22.
- ⁸⁸ AAD 15CB searched for events containing at least one long-lived particle that decays at a significant distance from its production point (displaced vertex, DV) into two leptons or into five or more charged particles in 20.3 fb⁻¹ of pp collisions at $\sqrt{s} = 8$ TeV. The dilepton signature is characterised by DV formed from at least two lepton candidates. Four different final states were considered for the multitrack signature, in which the DV must be accompanied by a high-transverse momentum muon or electron candidate that originates from the DV, jets or missing transverse momentum. No events were observed in any of the signal regions. Results were interpreted in SUSY scenarios involving R -parity violation, split supersymmetry, and gauge mediation. See their Fig. 12–20.
- ⁸⁹ KHACHATRYAN 15AD searched in 19.4 fb⁻¹ of pp collisions at $\sqrt{s} = 8$ TeV for events with two opposite-sign same flavor isolated leptons featuring either a kinematic edge, or a peak at the Z -boson mass, in the invariant mass spectrum. No evidence for a statistically significant excess over the expected SM backgrounds is observed and 95% C.L. exclusion limits are derived in a simplified model of gluino pair production where the gluino decays into quarks, a Z -boson, and a massless gravitino LSP, see Fig. 9.
- ⁹⁰ KHACHATRYAN 15AZ searched in 19.7 fb⁻¹ of pp collisions at $\sqrt{s} = 8$ TeV for events with either at least one photon, hadronic jets and \cancel{E}_T (single photon channel) or with at least two photons and at least one jet and using the razor variables. No significant excess above the Standard Model expectations is observed. Limits are set on gluino masses in the general gauge-mediated SUSY breaking model (GGM), for both a bino-like and wino-like neutralino NLSP scenario, see Fig. 8 and 9.
- ⁹¹ AAD 14AX searched in 20.1 fb⁻¹ of pp collisions at $\sqrt{s} = 8$ TeV for the strong production of supersymmetric particles in events containing either zero or at least one high- p_T lepton, large missing transverse momentum, high jet multiplicity and at least three jets identified as originating from b -quarks. No excess over the expected SM background is observed. Limits are derived in mSUGRA/CMSSM models with $\tan\beta = 30$, $A_0 = -2m_0$ and $\mu > 0$, see their Fig. 14. Also, exclusion limits in simplified models containing gluinos and scalar top and bottom quarks are set, see their Figures 12, 13.
- ⁹² AAD 14E searched in 20.3 fb⁻¹ of pp collisions at $\sqrt{s} = 8$ TeV for strongly produced supersymmetric particles in events containing jets and two same-sign leptons or three leptons. The search also utilises jets originating from b -quarks, missing transverse momentum and other variables. No excess over the expected SM background is observed. Exclusion limits are derived in simplified models containing gluinos and squarks, see Figures 5 and 6. In the $\tilde{g} \rightarrow q\bar{q}\tilde{\chi}_1^\pm, \tilde{\chi}_1^\pm \rightarrow W^{(*)}\tilde{\chi}_2^0, \tilde{\chi}_2^0 \rightarrow Z^{(*)}\tilde{\chi}_1^0$ simplified model, the following assumptions have been made: $m_{\tilde{\chi}_1^\pm} = 0.5 m_{\tilde{\chi}_1^0} + m_{\tilde{g}}$, $m_{\tilde{\chi}_2^0} = 0.5 (m_{\tilde{\chi}_1^0} + m_{\tilde{\chi}_1^\pm})$, $m_{\tilde{\chi}_1^0} < 520$ GeV. In the $\tilde{g} \rightarrow q\bar{q}\tilde{\chi}_1^\pm, \tilde{\chi}_1^\pm \rightarrow \ell^\pm\nu\tilde{\chi}_1^0$ or $\tilde{g} \rightarrow q\bar{q}\tilde{\chi}_2^0, \tilde{\chi}_2^0 \rightarrow \ell^\pm\ell^\mp(\nu\nu)\tilde{\chi}_1^0$ simplified model, the following assumptions have been made: $m_{\tilde{\chi}_1^\pm} = m_{\tilde{\chi}_2^0} = 0.5 (m_{\tilde{\chi}_1^0} + m_{\tilde{g}})$, $m_{\tilde{\chi}_1^0} < 660$ GeV. Limits are also derived in the mSUGRA/CMSSM, bRPV and GMSB models, see their Fig. 8.
- ⁹³ CHATRCHYAN 14H searched in 19.5 fb⁻¹ of pp collisions at $\sqrt{s} = 8$ TeV for events with two isolated same-sign dileptons and jets in the final state. No significant excess above the Standard Model expectations is observed. Limits are set on the gluino mass in simplified models where the decay $\tilde{g} \rightarrow t\bar{t}\tilde{\chi}_1^0$ takes place with a branching ratio of 100%, or where the decay $\tilde{g} \rightarrow \tilde{t}t, \tilde{t} \rightarrow t\tilde{\chi}_1^0$ takes place with a branching ratio of 100%, with varying mass of the $\tilde{\chi}_1^0$, or where the decay $\tilde{g} \rightarrow b\bar{b}, \tilde{b} \rightarrow t\tilde{\chi}_1^\pm, \tilde{\chi}_1^\pm \rightarrow W^\pm\tilde{\chi}_1^0$ takes place with a branching ratio of 100%, with varying mass of the $\tilde{\chi}_1^\pm$, see Fig. 5.
- ⁹⁴ CHATRCHYAN 14H searched in 19.5 fb⁻¹ of pp collisions at $\sqrt{s} = 8$ TeV for events with two isolated same-sign dileptons and jets in the final state. No significant excess above the Standard Model expectations is observed. Limits are set on the gluino mass in simplified models where the decay $\tilde{g} \rightarrow q\bar{q}\tilde{\chi}_1^\pm, \tilde{\chi}_1^\pm \rightarrow W^\pm\tilde{\chi}_1^0$ takes place with a branching ratio of 100%, with varying mass of the $\tilde{\chi}_1^\pm$ and $\tilde{\chi}_1^0$, see Fig. 7.
- ⁹⁵ CHATRCHYAN 14H searched in 19.5 fb⁻¹ of pp collisions at $\sqrt{s} = 8$ TeV for events with two isolated same-sign dileptons and jets in the final state. No significant excess above the Standard Model expectations is observed. Limits are set on the gluino mass in simplified models where the decay $\tilde{g} \rightarrow b\bar{t}\tilde{\chi}_1^\pm, \tilde{\chi}_1^\pm \rightarrow W^\pm\tilde{\chi}_1^0$ takes place with a branching ratio of 100%, for two choices of $m_{\tilde{\chi}_1^\pm}$ and fixed $m_{\tilde{\chi}_1^0}$, see Fig. 6.

R-parity violating heavy \tilde{g} (Gluino) mass limit

VALUE (GeV)	CL%	DOCUMENT ID	TECN	COMMENT
>1500	95	1 SIRUNYAN	19F CMS	$\tilde{g} \rightarrow jjj$
>2260	95	2 AABOUD	18Z ATLS	$\geq 4\ell, \lambda_{12k} \neq 0, m_{\tilde{\chi}_1^0} > 1000$ GeV
>1650	95	2 AABOUD	18Z ATLS	$\geq 4\ell, \lambda_{133} \neq 0, m_{\tilde{\chi}_1^0} > 500$ GeV
>1610	95	3 SIRUNYAN	18AK CMS	$\tilde{g} \rightarrow tbs, \lambda''_{332}$ coupling
>1690	95	4 SIRUNYAN	18D CMS	top quark (hadronically decaying) + jets + \cancel{E}_T , Tglu3C, $m_{\tilde{t}_1} - m_{\tilde{\chi}_1^0} = 20$ GeV, $m_{\tilde{\chi}_1^0} = 0$ GeV

Searches Particle Listings

Supersymmetric Particle Searches

Search ID	Year	Author(s)	Experiment	Search Description	Mass Range (GeV)	Significance	Model	Search Details
none 100-1410	95	5 SIRUNYAN	18EA CMS	2 large jets with four-parton substructure, $\tilde{g} \rightarrow 5q$	> 600	95	23 AAD	15CB ATLS $\ell\ell/Z, \tilde{g} \rightarrow (e\bar{e}/\mu\bar{\mu}/e\bar{\nu})qq, m_{\tilde{\chi}_1^0} = 400 \text{ GeV}$ and $0.7 < \dots$
>2100	95	6 AABOUD	17AI ATLS	$\geq 1\ell^+ \geq 8 \text{ jets, Tglu3A and } \tilde{\chi}_1^0 \rightarrow uds, \lambda''_{112} \text{ coupling, } m_{\tilde{\chi}_1^0} = 1000 \text{ GeV}$	>1000	95	24 AAD	15X ATLS $\geq 10 \text{ jets, } \tilde{g} \rightarrow q\bar{q}\tilde{\chi}_1^0, \tilde{\chi}_1^0 \rightarrow qq\bar{q}, m_{\tilde{\chi}_1^0} = 500 \text{ GeV}$
>1650	95	7 AABOUD	17AI ATLS	$\geq 1\ell^+ \geq 8 \text{ jets, } \tilde{g} \rightarrow t\bar{t}, \tilde{t} \rightarrow b\bar{s}, \lambda''_{323} \text{ coupling, } m_{\tilde{t}} = 1000 \text{ GeV}$	> 917	95	24 AAD	15X ATLS $\geq 6,7 \text{ jets, } \tilde{g} \rightarrow qq\bar{q}, (\text{light-quark, } \lambda' \text{ couplings})$
>1800	95	8 AABOUD	17AI ATLS	$\geq 1\ell^+ \geq 8 \text{ jets, Tglu1A and } \tilde{\chi}_1^0 \rightarrow qq\ell, \lambda' \text{ coupling, } m_{\tilde{\chi}_1^0} = 1000 \text{ GeV}$	> 929	95	24 AAD	15X ATLS $\geq 6,7 \text{ jets, } \tilde{g} \rightarrow qq\bar{q}, (\text{b-quark, } \lambda' \text{ couplings})$
>1800	95	9 AABOUD	17AJ ATLS	same-sign $\ell^\pm\ell^\pm / 3\ell + \text{jets} + \cancel{E}_T, \text{Tglu3A, } \lambda''_{112} \text{ coupling, } m_{\tilde{\chi}_1^0} = 50 \text{ GeV}$	>1180	95	25 AAD	14AX ATLS $\geq 3 \text{ b-jets} + \cancel{E}_T, \tilde{g} \rightarrow \tilde{t}_1 t\tilde{\chi}_1^0$ simplified model, $\tilde{t}_1 \rightarrow b\tilde{\chi}_1^\pm, m_{\tilde{\chi}_1^\pm} = 2m_{\tilde{\chi}_1^0}, m_{\tilde{\chi}_1^0} = 60 \text{ GeV}, m_{\tilde{t}_1} < 1000 \text{ GeV}$
>1750	95	10 AABOUD	17AJ ATLS	same-sign $\ell^\pm\ell^\pm / 3\ell + \text{jets} + \cancel{E}_T, \text{Tglu1A and } \tilde{\chi}_1^0 \rightarrow qq\ell, \lambda' \text{ coupling}$	> 850	95	26 AAD	14E ATLS $\ell^\pm\ell^\pm(\ell\bar{\nu}) + \text{jets, } \tilde{g} \rightarrow t\tilde{t}_1$ with $\tilde{t}_1 \rightarrow b\bar{s}$ simplified model
>1450	95	11 AABOUD	17AJ ATLS	same-sign $\ell^\pm\ell^\pm / 3\ell + \text{jets} + \cancel{E}_T, \tilde{g} \rightarrow t\tilde{t}_1$ and $\tilde{t}_1 \rightarrow sd, \lambda''_{321} \text{ coupling}$	> 900	95	27 CHATRCHYAN14H	CMS same-sign $\ell^\pm\ell^\pm, \tilde{g} \rightarrow tbs$ simplified model
>1450	95	12 AABOUD	17AJ ATLS	same-sign $\ell^\pm\ell^\pm / 3\ell + \text{jets} + \cancel{E}_T, \tilde{g} \rightarrow t\tilde{t}_1$ and $\tilde{t}_1 \rightarrow bd, \lambda''_{313} \text{ coupling}$				
> 400	95	13 AABOUD	17AJ ATLS	same-sign $\ell^\pm\ell^\pm / 3\ell + \text{jets} + \cancel{E}_T, \tilde{d}_R \rightarrow tb(t\bar{s}), \lambda''_{313} (\lambda''_{321}) \text{ coupling}$				
none 625-1375	95	14 AABOUD	17AZ ATLS	$\geq 7 \text{ jets} + \cancel{E}_T, \text{ large R-jets and/or b-jets, } \tilde{g} \rightarrow t\tilde{t}_1$ and $\tilde{t}_1 \rightarrow b\bar{s}, \lambda''_{323} \text{ coupling}$				
none 600-650	95	15 KHACHATRY...17Y	CMS	$\tilde{g} \rightarrow qq\bar{q}q, \lambda''_{212} \text{ coupling, } m_{\tilde{q}} = 100 \text{ GeV}$				
none 600-1030	95	15 KHACHATRY...17Y	CMS	$\tilde{g} \rightarrow qq\bar{q}q, \lambda''_{212} \text{ coupling, } m_{\tilde{q}} = 900 \text{ GeV}$				
none 600-650	95	15 KHACHATRY...17Y	CMS	$\tilde{g} \rightarrow qq\bar{q}qb, \lambda''_{213} \text{ coupling, } m_{\tilde{q}} = 100 \text{ GeV}$				
none 600-1080	95	15 KHACHATRY...17Y	CMS	$\tilde{g} \rightarrow qq\bar{q}qb, \lambda''_{213} \text{ coupling, } m_{\tilde{q}} = 900 \text{ GeV}$				
none 600-680	95	15 KHACHATRY...17Y	CMS	$\tilde{g} \rightarrow qq\bar{q}bb, \lambda''_{212} \text{ coupling, } m_{\tilde{q}} = 100 \text{ GeV}$				
none 600-1080	95	15 KHACHATRY...17Y	CMS	$\tilde{g} \rightarrow qq\bar{q}bb, \lambda''_{212} \text{ coupling, } m_{\tilde{q}} = 900 \text{ GeV}$				
none 600-650	95	15 KHACHATRY...17Y	CMS	$\tilde{g} \rightarrow qq\bar{q}bb, \lambda''_{213} \text{ coupling, } m_{\tilde{q}} = 100 \text{ GeV}$				
none 600-1100	95	15 KHACHATRY...17Y	CMS	$\tilde{g} \rightarrow qq\bar{q}bb, \lambda''_{213} \text{ coupling, } m_{\tilde{q}} = 900 \text{ GeV}$				
>1050	95	16 KHACHATRY...16BJ	CMS	same-sign $\ell^\pm\ell^\pm, \text{Tglu3A, } m_{\tilde{\chi}_1^0} < 800 \text{ GeV}$				
>1140	95	16 KHACHATRY...16BJ	CMS	same-sign $\ell^\pm\ell^\pm, \text{Tglu3B, } m_{\tilde{t}} - m_{\tilde{\chi}_1^0} = 20 \text{ GeV, } m_{\tilde{\chi}_1^0} = 0$				
>1030	95	17 KHACHATRY...16BX	CMS	$\tilde{g} \rightarrow tbs, \lambda''_{332} \text{ coupling}$				
>1150	95	18 AAD	15BV ATLS	general RPC \tilde{g} decays, $m_{\tilde{\chi}_1^0} < 100 \text{ GeV}$				
>1350	95	19 AAD	14X ATLS	$\geq 4\ell^\pm, \tilde{g} \rightarrow q\bar{q}\tilde{\chi}_1^0, \tilde{\chi}_1^0 \rightarrow \ell^\pm\ell\bar{\nu}$				
> 650	95	20 CHATRCHYAN14P	CMS	$\tilde{g} \rightarrow jjj$				
none 200-835	95	20 CHATRCHYAN14P	CMS	$\tilde{g} \rightarrow bjj$				
••• We do not use the following data for averages, fits, limits, etc. •••								
>1875	95	21 AABOUD	18CF ATLS	jets and large R-jets, Tglu2RPV and $\tilde{\chi}_1^0 \rightarrow qq\bar{q}, \lambda'' \text{ coupling, } m_{\tilde{\chi}_1^0} = 1000 \text{ GeV}$				
>1400	95	22 KHACHATRY...16BX	CMS	$\tilde{g} \rightarrow qq\tilde{\chi}_1^0, \tilde{\chi}_1^0 \rightarrow \ell\ell\nu, \lambda_{121}$ or $\lambda_{122} \neq 0, m_{\tilde{\chi}_1^0} > 400 \text{ GeV}$				
>1600	95	18 AAD	15BV ATLS	pMSSM, $M_1 = 60 \text{ GeV, } m_{\tilde{q}} < 1500 \text{ GeV}$				
>1280	95	18 AAD	15BV ATLS	mSUGRA, $m_0 > 2 \text{ TeV}$				
>1100	95	18 AAD	15BV ATLS	via $\tilde{\tau}$, natural GMSB, all $m_{\tilde{\tau}}$				
>1220	95	18 AAD	15BV ATLS	b-jets, $\tilde{g} \rightarrow \tilde{t}_1 t$ and $\tilde{t}_1 \rightarrow t\tilde{\chi}_1^0, m_{\tilde{t}_1} < 1000 \text{ GeV}$				
>1180	95	18 AAD	15BV ATLS	b-jets, $\tilde{g} \rightarrow \tilde{t}_1 t$ and $\tilde{t}_1 \rightarrow b\tilde{\chi}_1^\pm, m_{\tilde{t}_1} < 1000 \text{ GeV, } m_{\tilde{\chi}_1^0} = 60 \text{ GeV}$				
> 880	95	18 AAD	15BV ATLS	jets, $\tilde{g} \rightarrow \tilde{t}_1 t$ and $\tilde{t}_1 \rightarrow sb, 400 < m_{\tilde{t}_1} < 1000 \text{ GeV}$				
		23 AAD	15CB ATLS	$\ell, \tilde{g} \rightarrow (e/\mu)qq, \text{ benchmark gluino, neutralino masses}$				

Downloaded from https://academic.oup.com/ptep/article/2020/8/083C01/5891211 by guest on 20 August 2020

1 SIRUNYAN 19F searched in 35.9 fb^{-1} of pp collisions at $\sqrt{s} = 13 \text{ TeV}$ for three-jet resonances produced in the decay of a gluino in R-parity violating supersymmetric models. The mass range from 200 to 2000GeV is explored in four separate mass regions. The observations show agreement with standard model expectations. The results are interpreted within the framework of R-parity violating SUSY, where pair-produced gluinos decay to a six quark final state. Gluino masses below 1500GeV are excluded at 95% C.L. See their Fig.5.

2 AABOUD 18Z searched in 36.1 fb^{-1} of pp collisions at $\sqrt{s} = 13 \text{ TeV}$ for events containing four or more charged leptons (electrons, muons and up to two hadronically decaying taus). No significant deviation from the expected SM background is observed. Limits are set on the Higgsino mass in simplified models of general gauge mediated supersymmetry Tn1n1A/Tn1n1B/Tn1n1C, see their Figure 9. Limits are also set on the wino, slepton, sneutrino and gluino mass in a simplified model of NLSP pair production with R-parity violating decays of the LSP via λ_{12k} or λ_{j33} to charged leptons, see their Figures 7, 8.

3 SIRUNYAN 18AK searched in 35.9 fb^{-1} of pp collisions at $\sqrt{s} = 13 \text{ TeV}$ for events containing a single lepton, large jet and b-quark jet multiplicities, coming from R-parity-violating decays of gluinos. No excess over the expected background is observed. Limits are derived on the gluino mass, assuming the RPV $\tilde{g} \rightarrow tbs$ decay, see their Figure 9.

4 SIRUNYAN 18D searched in 35.9 fb^{-1} of pp collisions at $\sqrt{s} = 13 \text{ TeV}$ for events containing identified hadronically decaying top quarks, no leptons, and \cancel{E}_T . No significant excess above the Standard Model expectations is observed. Limits are set on the stop mass in the Tstop1 simplified model, see their Figure 8, and on the gluino mass in the Tglu3A, Tglu3B, Tglu3C and Tglu3E simplified models, see their Figure 9.

5 SIRUNYAN 18EA searched in 38.2 fb^{-1} of pp collisions at $\sqrt{s} = 13 \text{ TeV}$ for the pair production of resonances, each decaying to at least four quarks. Reconstructed particles are clustered into two large jets of similar mass, each consistent with four-parton substructure. No statistically significant excess over the Standard Model expectation is observed. Limits are set on the squark and gluino mass in RPV supersymmetry models where squarks (gluinos) decay, through intermediate higgsinos, to four (five) quarks, see their Figure 4.

6 AABOUD 17AI searched in 36.1 fb^{-1} of pp collisions at $\sqrt{s} = 13 \text{ TeV}$ for events with one or more isolated lepton, at least eight jets, either zero or many b-jets, for evidence of R-parity violating decays of the gluino. No significant excess above the Standard Model expectations is observed. Limits up to 2.1 TeV are set on the gluino mass in R-parity-violating supersymmetry models as Tglu3A with LSP decay through the non-zero λ''_{112} coupling as $\tilde{\chi}_1^0 \rightarrow uds$. See their Figure 9.

7 AABOUD 17AI searched in 36.1 fb^{-1} of pp collisions at $\sqrt{s} = 13 \text{ TeV}$ for events with one or more isolated lepton, at least eight jets, either zero or many b-jets, for evidence of R-parity violating decays of the gluino. No significant excess above the Standard Model expectations is observed. Limits up to 1.65 TeV are set on the gluino mass in R-parity-violating supersymmetry models with $\tilde{g} \rightarrow t\bar{t}, \tilde{t} \rightarrow b\bar{s}$ through the non-zero λ''_{323} coupling. See their Figure 9.

8 AABOUD 17AI searched in 36.1 fb^{-1} of pp collisions at $\sqrt{s} = 13 \text{ TeV}$ for events with one or more isolated lepton, at least eight jets, either zero or many b-jets, for evidence of R-parity violating decays of the gluino. No significant excess above the Standard Model expectations is observed. Limits up to 1.8 TeV are set on the gluino mass in R-parity-violating supersymmetry models as Tglu1A with the LSP decay through the non-zero λ' coupling as $\tilde{\chi}_1^0 \rightarrow qq\ell$. See their Figure 9.

9 AABOUD 17AJ searched in 36.1 fb^{-1} of pp collisions at $\sqrt{s} = 13 \text{ TeV}$ for events with two same-sign or three leptons, jets and large missing transverse momentum. No significant excess above the Standard Model expectations is observed. Limits up to 1.8 TeV are set on the gluino mass in R-parity-violating supersymmetry models as Tglu3A with LSP decaying through the non-zero λ''_{112} coupling as $\tilde{\chi}_1^0 \rightarrow uds$. See their Figure 5(d).

10 AABOUD 17AJ searched in 36.1 fb^{-1} of pp collisions at $\sqrt{s} = 13 \text{ TeV}$ for events with two same-sign or three leptons, jets and large missing transverse momentum. No significant excess above the Standard Model expectations is observed. Limits up to 1.75 TeV are set on the gluino mass in R-parity-violating supersymmetry models as Tglu1A with LSP decaying through the non-zero λ' coupling as $\tilde{\chi}_1^0 \rightarrow qq\ell$. See their Figure 5(c).

11 AABOUD 17AJ searched in 36.1 fb^{-1} of pp collisions at $\sqrt{s} = 13 \text{ TeV}$ for events with two same-sign or three leptons, jets and large missing transverse momentum. No significant excess above the Standard Model expectations is observed. Limits up to 1.45 TeV are set on the gluino mass in R-parity-violating supersymmetry models where $\tilde{g} \rightarrow t\tilde{t}_1$ and $\tilde{t}_1 \rightarrow sd$ through the non-zero λ''_{321} coupling. See their Figure 5(b).

12 AABOUD 17AJ searched in 36.1 fb^{-1} of pp collisions at $\sqrt{s} = 13 \text{ TeV}$ for events with two same-sign or three leptons, jets and large missing transverse momentum. No significant excess above the Standard Model expectations is observed. Limits up to 1.45 TeV are set on the gluino mass in R-parity-violating supersymmetry models where $\tilde{g} \rightarrow t\tilde{t}_1$ and $\tilde{t}_1 \rightarrow bd$ through the non-zero λ''_{313} coupling. See their Figure 5(a).

13 AABOUD 17AJ searched in 36.1 fb^{-1} of pp collisions at $\sqrt{s} = 13 \text{ TeV}$ for events with two same-sign or three leptons, jets and large missing transverse momentum. No significant

- excess above the Standard Model expectations is observed. Limits up to 400 GeV are set on the down type squark (\tilde{d}_R mass in R-parity-violating supersymmetry models where $\tilde{d}_R \rightarrow tb$ through the non-zero λ''_{313} coupling or $\tilde{d}_R \rightarrow ts$ through the non-zero λ''_{321} . See their Figure 5(e) and 5(f).
- 14 AABOUD 17AZ searched in 36.1 fb^{-1} of pp collisions at $\sqrt{s} = 13 \text{ TeV}$ for events with at least seven jets and large missing transverse momentum. Selected events are further classified based on the presence of large R-jets or b -jets and no leptons. No significant excess above the Standard Model expectations is observed. Limits are set for R-parity violating decays of the gluino assuming $\tilde{g} \rightarrow t\tilde{t}_1$ and $\tilde{t}_1 \rightarrow bs$ through the non-zero λ''_{323} couplings. The range 625–1375 GeV is excluded for $m_{\tilde{t}_1} = 400 \text{ GeV}$. See their Figure 7b.
- 15 KHACHATRYAN 17Y searched in 19.7 fb^{-1} of pp collisions at $\sqrt{s} = 8 \text{ TeV}$ for events containing at least 8 or 10 jets, possibly b -tagged, coming from R-parity-violating decays of supersymmetric particles. No excess over the expected background is observed. Limits are derived on the gluino mass, assuming various RPV decay modes, see Fig. 7.
- 16 KHACHATRYAN 16BJ searched in 2.3 fb^{-1} of pp collisions at $\sqrt{s} = 13 \text{ TeV}$ for events with two isolated same-sign dileptons and jets in the final state. No significant excess above the Standard Model expectations is observed. Limits are set on the gluino mass in the following simplified models: Tglu3A and Tglu3D, see Fig. 4, Tglu3B and Tglu3C, see Fig. 5, and Tglu1B, see Fig. 7.
- 17 KHACHATRYAN 16BX searched in 19.5 fb^{-1} of pp collisions at $\sqrt{s} = 8 \text{ TeV}$ for events containing 0 or 1 leptons and b -tagged jets, coming from R-parity-violating decays of supersymmetric particles. No excess over the expected background is observed. Limits are derived on the gluino mass, assuming the RPV $\tilde{g} \rightarrow tbs$ decay, see Fig. 7 and 10.
- 18 AAD 15BV summarized and extended ATLAS searches for gluinos and first- and second-generation squarks in final states containing jets and missing transverse momentum, with or without leptons or b -jets in the $\sqrt{s} = 8 \text{ TeV}$ data set collected in 2012. The paper reports the results of new interpretations and statistical combinations of previously published analyses, as well as new analyses. Exclusion limits at 95% C.L. are set on the gluino mass in several R-parity conserving models, leading to a generalized constraint on gluino masses exceeding 1150 GeV for lightest supersymmetric particle masses below 100 GeV. See their Figs. 10, 19, 20, 21, 23, 25, 26, 29–37.
- 19 AAD 14X searched in 20.3 fb^{-1} of pp collisions at $\sqrt{s} = 8 \text{ TeV}$ for events with at least four leptons (electrons, muons, taus) in the final state. No significant excess above the Standard Model expectations is observed. Limits are set on the gluino mass in an R-parity violating simplified model where the decay $\tilde{g} \rightarrow q\tilde{q}\tilde{\chi}_1^0$, with $\tilde{\chi}_1^0 \rightarrow \ell^\pm \ell^\mp \nu$, takes place with a branching ratio of 100%, see Fig. 8.
- 20 CHATRCHYAN 14P searched in 19.4 fb^{-1} of pp collisions at $\sqrt{s} = 8 \text{ TeV}$ for three-jet resonances produced in the decay of a gluino in R-parity violating supersymmetric models. No excess over the expected SM background is observed. Assuming a 100% branching ratio for the gluino decay into three light-flavour jets, limits are set on the cross section of gluino pair production, see Fig. 7, and gluino masses below 650 GeV are excluded at 95% C.L. Assuming a 100% branching ratio for the gluino decaying to one b -quark jet and two light-flavour jets, gluino masses between 200 GeV and 835 GeV are excluded at 95% C.L.
- 21 AABOUD 18CF searched in 36.1 fb^{-1} of pp collisions at $\sqrt{s} = 13 \text{ TeV}$ for events with several jets, possibly b -jets, and large-radius jets for evidence of R-parity violating decays of the gluino. No significant excess above the Standard Model expectations is observed. Limits between 1000 and 1875 GeV are set on the gluino mass in R-parity-violating supersymmetry models as Tglu2RPV with the LSP decay through the non-zero λ'' coupling as $\tilde{\chi}_1^0 \rightarrow qq\tilde{q}$. The most stringent limit is obtained for $m_{\tilde{\chi}_1^0} = 1000 \text{ GeV}$, the weakest for $m_{\tilde{\chi}_1^0} = 50 \text{ GeV}$. See their Figure 7(b). Figure 7(a) presents results for gluinos directly decaying into 3 quarks, Tglu1RPV.
- 22 KHACHATRYAN 16BX searched in 19.5 fb^{-1} of pp collisions at $\sqrt{s} = 8 \text{ TeV}$ for events containing 4 leptons coming from R-parity-violating decays of $\tilde{\chi}_1^0 \rightarrow \ell\ell\nu$ with $\lambda_{121} \neq 0$ or $\lambda_{122} \neq 0$. No excess over the expected background is observed. Limits are derived on the gluino, squark and stop masses, see Fig. 23.
- 23 AAD 15CB searched for events containing at least one long-lived particle that decays at a significant distance from its production point (displaced vertex, DV) into two leptons or into five or more charged particles in 20.3 fb^{-1} of pp collisions at $\sqrt{s} = 8 \text{ TeV}$. The dilepton signature is characterised by DV formed from at least two lepton candidates. Four different final states were considered for the multitrak signature, in which the DV must be accompanied by a high-transverse momentum muon or electron candidate that originates from the DV, jets or missing transverse momentum. No events were observed in any of the signal regions. Results were interpreted in SUSY scenarios involving R-parity violation, split supersymmetry, and gauge mediation. See their Fig. 12–20.
- 24 AAD 15X searched in 20.3 fb^{-1} of pp collisions at $\sqrt{s} = 8 \text{ TeV}$ for events containing large number of jets, no requirements on missing transverse momentum and no isolated electrons or muons. The sensitivity of the search is enhanced by considering the number of b -tagged jets and the scalar sum of masses of large-radius jets in an event. No evidence was found for excesses above the expected level of Standard Model background. Exclusion limits at 95% C.L. are set on the gluino mass assuming the gluino decays to various quark flavors, and for various neutralino masses. See their Fig. 11–16.
- 25 AAD 14AX searched in 20.1 fb^{-1} of pp collisions at $\sqrt{s} = 8 \text{ TeV}$ for the strong production of supersymmetric particles in events containing either zero or at last one high- p_T lepton, large missing transverse momentum, high jet multiplicity and at least three jets identified as originating from b -quarks. No excess over the expected SM background is observed. Limits are derived in mSUGRA/CMSSM models with $\tan\beta = 30$, $A_0 = -2m_0$ and $\mu > 0$, see their Fig. 14. Also, exclusion limits in simplified models containing gluinos and scalar top and bottom quarks are set, see their Figures 12, 13.
- 26 AAD 14E searched in 20.3 fb^{-1} of pp collisions at $\sqrt{s} = 8 \text{ TeV}$ for strongly produced supersymmetric particles in events containing jets and two same-sign leptons or three leptons. The search also utilises jets originating from b -quarks, missing transverse momentum and other variables. No excess over the expected SM background is observed. Exclusion limits are derived in simplified models containing gluinos and squarks, see Figures 5 and 6. In the $\tilde{g} \rightarrow q\tilde{q}\tilde{\chi}_1^\pm, \tilde{\chi}_1^\pm \rightarrow W^{(*)}\tilde{\chi}_2^0, \tilde{\chi}_2^0 \rightarrow Z^{(*)}\tilde{\chi}_1^0$ simplified model, the following assumptions have been made: $m_{\tilde{\chi}_1^\pm} = 0.5 m_{\tilde{\chi}_2^0} + m_{\tilde{g}}$, $m_{\tilde{\chi}_2^0} = 0.5 (m_{\tilde{\chi}_1^0} + m_{\tilde{\chi}_1^\pm})$, $m_{\tilde{\chi}_1^0} < 520 \text{ GeV}$. In the $\tilde{g} \rightarrow q\tilde{q}\tilde{\chi}_1^\pm, \tilde{\chi}_1^\pm \rightarrow \ell^\pm\nu\tilde{\chi}_1^0$ or $\tilde{g} \rightarrow q\tilde{q}\tilde{\chi}_2^0, \tilde{\chi}_2^0 \rightarrow \ell^\pm\ell^\mp(\nu\nu)\tilde{\chi}_1^0$ simplified model, the following assumptions have been made: $m_{\tilde{\chi}_1^\pm} = m_{\tilde{\chi}_2^0} = 0.5 (m_{\tilde{\chi}_1^0} + m_{\tilde{g}})$, $m_{\tilde{\chi}_1^0} < 660 \text{ GeV}$. Limits are also derived in the mSUGRA/CMSSM, bRPV and GMSB models, see their Fig. 8.

- 27 CHATRCHYAN 14H searched in 19.5 fb^{-1} of pp collisions at $\sqrt{s} = 8 \text{ TeV}$ for events with two isolated same-sign dileptons and jets in the final state. No significant excess above the Standard Model expectations is observed. Limits are set on the gluino mass in simplified models where the R-parity violating decay $\tilde{g} \rightarrow tbs$ takes place with a branching ratio of 100%, see Fig. 8.

Long-lived \tilde{g} (Gluino) mass limit

Limits on light gluinos ($m_{\tilde{g}} < 5 \text{ GeV}$) were last listed in our PDG 14 edition: K. Olive, et al. (Particle Data Group), Chinese Physics **C38** 070001 (2014) (<http://pdg.lbl.gov>).

VALUE (GeV)	CL%	DOCUMENT ID	TECN	COMMENT
>1980	95	1 AABOUD	19AT ATLS	R-hadrons, Tglu1A, metastable
>2060	95	2 AABOUD	19C ATLS	R-hadrons, Tglu1A, $\tau > 10 \text{ ns}$, $m_{\tilde{\chi}_1^0} = 100 \text{ GeV}$
>1890	95	2 AABOUD	19C ATLS	R-hadrons, Tglu1A, stable
>2400	95	3 SIRUNYAN	19BH CMS	long-lived \tilde{g} , RPV, $\tilde{g} \rightarrow \bar{t}\bar{b}\bar{s}$, $10 \text{ mm} < cr < 250 \text{ mm}$
>2300	95	3 SIRUNYAN	19BH CMS	long-lived \tilde{g} , GMSB, $\tilde{g} \rightarrow g\tilde{G}$, $20 \text{ mm} < cr < 110 \text{ mm}$
>2100	95	4 SIRUNYAN	19BT CMS	long-lived \tilde{g} , GMSB, $\tilde{g} \rightarrow g\tilde{G}$, $0.3 \text{ m} < cr < 30 \text{ m}$
>2500	95	4 SIRUNYAN	19BT CMS	long-lived \tilde{g} , GMSB, $\tilde{g} \rightarrow g\tilde{G}$, $cr = 1 \text{ m}$
>1900	95	4 SIRUNYAN	19BT CMS	long-lived \tilde{g} , GMSB, $\tilde{g} \rightarrow g\tilde{G}$, $cr = 100 \text{ m}$
>2370	95	5 AABOUD	18s ATLS	displaced vertex + E_{TR} , long-lived Tglu1A, $m_{\tilde{\chi}_1^0} = 100 \text{ GeV}$, and $\tau = 0.17 \text{ ns}$
>1600	95	6 SIRUNYAN	18AY CMS	jets+ E_{TR} , Tglu1A, $cr < 0.1 \text{ mm}$, $m_{\tilde{\chi}_1^0} = 100 \text{ GeV}$
>1750	95	6 SIRUNYAN	18AY CMS	jets+ E_{TR} , Tglu1A, $cr = 1 \text{ mm}$, $m_{\tilde{\chi}_1^0} = 100 \text{ GeV}$
>1640	95	6 SIRUNYAN	18AY CMS	jets+ E_{TR} , Tglu1A, $cr = 10 \text{ mm}$, $m_{\tilde{\chi}_1^0} = 100 \text{ GeV}$
>1490	95	6 SIRUNYAN	18AY CMS	jets+ E_{TR} , Tglu1A, $cr = 100 \text{ mm}$, $m_{\tilde{\chi}_1^0} = 100 \text{ GeV}$
>1300	95	6 SIRUNYAN	18AY CMS	jets+ E_{TR} , Tglu1A, $cr = 1 \text{ m}$, $m_{\tilde{\chi}_1^0} = 100 \text{ GeV}$
> 960	95	6 SIRUNYAN	18AY CMS	jets+ E_{TR} , Tglu1A, $cr = 10 \text{ m}$, $m_{\tilde{\chi}_1^0} = 100 \text{ GeV}$
> 900	95	6 SIRUNYAN	18AY CMS	jets+ E_{TR} , Tglu1A, $cr = 100 \text{ m}$, $m_{\tilde{\chi}_1^0} = 100 \text{ GeV}$
>2200	95	7 SIRUNYAN	18DV CMS	long-lived \tilde{g} , RPV, $\tilde{g} \rightarrow \bar{t}\bar{b}\bar{s}$, $0.6 \text{ mm} < cr < 80 \text{ mm}$
>1000	95	8 KHACHATRYAN 17AR	CMS	long-lived \tilde{g} , RPV, $\tilde{g} \rightarrow \bar{t}\bar{b}\bar{s}$, $cr = 0.3 \text{ mm}$
>1300	95	8 KHACHATRYAN 17AR	CMS	long-lived \tilde{g} , RPV, $\tilde{g} \rightarrow \bar{t}\bar{b}\bar{s}$, $cr = 1.0 \text{ mm}$
>1400	95	8 KHACHATRYAN 17AR	CMS	long-lived \tilde{g} , RPV, $\tilde{g} \rightarrow \bar{t}\bar{b}\bar{s}$, $2 \text{ mm} < cr < 30 \text{ mm}$
>1580	95	9 AABOUD	16B ATLS	long-lived R-hadrons
> 740–1590	95	10 AABOUD	16C ATLS	R-hadrons, Tglu1A, $\tau > 0.4 \text{ ns}$, $m_{\tilde{\chi}_1^0} = 100 \text{ GeV}$
>1570	95	10 AABOUD	16C ATLS	R-hadrons, Tglu1A, stable
>1610	95	11 KHACHATRYAN 16BW	CMS	long-lived \tilde{g} forming R-hadrons, $f = 0.1$, cloud interaction model
>1580	95	11 KHACHATRYAN 16BW	CMS	long-lived \tilde{g} forming R-hadrons, $f = 0.1$, charge-suppressed interaction model
>1520	95	11 KHACHATRYAN 16BW	CMS	long-lived \tilde{g} forming R-hadrons, $f = 0.5$, cloud interaction model
>1540	95	11 KHACHATRYAN 16BW	CMS	long-lived \tilde{g} forming R-hadrons, $f = 0.5$, charge-suppressed interaction model
>1270	95	12 AAD	15AE ATLS	\tilde{g} R-hadron, generic R-hadron model
>1360	95	12 AAD	15AE ATLS	\tilde{g} decaying to 300 GeV stable sleptons, LeptoSUSY model
>1115	95	13 AAD	15BM ATLS	\tilde{g} R-hadron, stable
>1185	95	13 AAD	15BM ATLS	$\tilde{g} \rightarrow (g/q\tilde{q})\tilde{\chi}_1^0$, lifetime 10 ns, $m_{\tilde{\chi}_1^0} = 100 \text{ GeV}$
>1099	95	13 AAD	15BM ATLS	$\tilde{g} \rightarrow (g/q\tilde{q})\tilde{\chi}_1^0$, lifetime 10 ns, $m_{\tilde{g}} - m_{\tilde{\chi}_1^0} = 100 \text{ GeV}$
>1182	95	13 AAD	15BM ATLS	$\tilde{g} \rightarrow t\bar{t}\tilde{\chi}_1^0$, lifetime 10 ns, $m_{\tilde{\chi}_1^0} = 100 \text{ GeV}$
>1157	95	13 AAD	15BM ATLS	$\tilde{g} \rightarrow t\bar{t}\tilde{\chi}_1^0$, lifetime 10 ns, $m_{\tilde{g}} - m_{\tilde{\chi}_1^0} = 480 \text{ GeV}$
> 869	95	13 AAD	15BM ATLS	$\tilde{g} \rightarrow (g/q\tilde{q})\tilde{\chi}_1^0$, lifetime 1 ns, $m_{\tilde{\chi}_1^0} = 100 \text{ GeV}$
> 821	95	13 AAD	15BM ATLS	$\tilde{g} \rightarrow (g/q\tilde{q})\tilde{\chi}_1^0$, lifetime 1 ns, $m_{\tilde{g}} - m_{\tilde{\chi}_1^0} = 100 \text{ GeV}$

Searches Particle Listings

Supersymmetric Particle Searches

> 836	95	13	AAD	15BMATLS	$\tilde{g} \rightarrow t\bar{t}\tilde{\chi}_1^0$, lifetime 1 ns, $m_{\tilde{\chi}_1^0} = 100$ GeV
> 836	95	13	AAD	15BMATLS	$\tilde{g} \rightarrow t\bar{t}\tilde{\chi}_1^0$, lifetime 10 ns, $m_{\tilde{g}} - m_{\tilde{\chi}_1^0} = 480$ GeV
>1000	95	14	KHACHATRYAN...15AK	CMS	\tilde{g} R-hadrons, $10 \mu\text{s} < \tau < 1000$ s
> 880	95	14	KHACHATRYAN...15AK	CMS	\tilde{g} R-hadrons, $1 \mu\text{s} < \tau < 1000$ s
••• We do not use the following data for averages, fits, limits, etc. •••					
> 985	95	15	AAD	13AA ATLS	\tilde{g} , R-hadrons, generic interaction model
> 832	95	16	AAD	13BC ATLS	R-hadrons, $\tilde{g} \rightarrow g/q\bar{q}\tilde{\chi}_1^0$, generic R-hadron model, lifetime between 10^{-5} and 10^3 s, $m_{\tilde{\chi}_1^0} = 100$ GeV
>1322	95	17	CHATRCHYAN13AB	CMS	long-lived \tilde{g} forming R-hadrons, $f = 0.1$, cloud interaction model
none 200–341	95	18	AAD	12P ATLS	long-lived $\tilde{g} \rightarrow g\tilde{\chi}_1^0$, $m_{\tilde{\chi}_1^0} = 100$ GeV
> 640	95	19	CHATRCHYAN12AN	CMS	long-lived $\tilde{g} \rightarrow g\tilde{\chi}_1^0$
>1098	95	20	CHATRCHYAN12L	CMS	long-lived \tilde{g} forming R-hadrons, $f = 0.1$
> 586	95	21	AAD	11K ATLS	stable \tilde{g}
> 544	95	22	AAD	11P ATLS	stable \tilde{g} , GMSB scenario, $\tan\beta=5$
> 370	95	23	KHACHATRYAN...11	CMS	long lived \tilde{g}
> 398	95	24	KHACHATRYAN...11C	CMS	stable \tilde{g}

- ¹ AABOUD 19AT searched in 36.1 fb^{-1} of pp collisions at $\sqrt{s} = 13 \text{ TeV}$ for metastable and stable R-hadrons. Multiple search strategies for a wide range of lifetimes, corresponding to path lengths of a few meters, are defined. No significant deviations from the expected Standard Model background are observed. Gluino R-hadrons with lifetimes of the order of 50 ns are excluded at 95% C.L. for masses below 1980 GeV using the muon-spectrometer agnostic analysis. Using the full-detector search, the observed lower limits on the mass are 2000 GeV. See their Figure 9 (top).
- ² AABOUD 19c searched in 36.1 fb^{-1} of pp collisions at $\sqrt{s} = 13 \text{ TeV}$ for metastable and stable R-hadrons arising as excesses in the mass distribution of reconstructed tracks with high transverse momentum and large dE/dx . Gluino R-hadrons with lifetimes above 10 ns are excluded at 95% C.L. with lower mass limit range between 1000 GeV and 2060 GeV, see their Figure 5(a). Masses smaller than 1290 GeV are excluded for a lifetime of 1 ns, see their Figure 6. In the case of stable R-hadrons, the lower mass limit is 1890 GeV, see their Figure 5(b).
- ³ SIRUNYAN 19BH searched in 35.9 fb^{-1} of pp collisions at $\sqrt{s} = 13 \text{ TeV}$ for long-lived particles decaying into jets, with each long-lived particle having a decay vertex well displaced from the production vertex. The selected events are found to be consistent with standard model predictions. Limits are set on the gluino mass in a GMSB model where the gluino is decaying via $\tilde{g} \rightarrow g\tilde{G}$, see their Figure 4 and in an RPV model of supersymmetry where the gluino is decaying via $\tilde{g} \rightarrow t\bar{b}s$, see their RPV 5. Limits are also set on the stop mass in two RPV models, see their Figure 6 (for $t \rightarrow b\bar{l}$ decays) and Figure 7 (for $\tilde{t} \rightarrow \bar{d}\bar{d}$ decays).
- ⁴ SIRUNYAN 19BT searched in 137 fb^{-1} of pp collisions at $\sqrt{s} = 13 \text{ TeV}$ for long-lived particles decaying to displaced, nonprompt jets and missing transverse momentum. Candidate signal events are identified using the timing capabilities of the CMS electromagnetic calorimeter. The results of the search are found to be consistent with the background predictions. Limits are set on the gluino mass in a GMSB model where long-lived gluinos are pair produced and decaying via $\tilde{g} \rightarrow g\tilde{G}$, see their Figures 4 and 5.
- ⁵ AABOUD 18s searched in 32.8 fb^{-1} of pp collisions at $\sqrt{s} = 13 \text{ TeV}$ for long-lived gluinos in final states with large missing transverse momentum and at least one high-mass displaced vertex with five or more tracks. The observed yield is consistent with the expected background. Exclusion limits are derived for Tglu1A models predicting the existence of long-lived gluinos reaching roughly $m(\tilde{g}) = 2000 \text{ GeV}$ to 2370 GeV for $m(\tilde{\chi}_1^0) = 100 \text{ GeV}$ and gluino lifetimes between 0.02 and 10 ns, see their Fig. 8. Limits are presented also as a function of the lifetime (for a fixed gluino-neutralino mass difference of 100 GeV) and of the gluino and neutralino masses (for a fixed lifetime of 1 ns). See their Fig. 9 and 10 respectively.
- ⁶ SIRUNYAN 18AY searched in 35.9 fb^{-1} of pp collisions at $\sqrt{s} = 13 \text{ TeV}$ for events containing one or more jets and significant \cancel{E}_T . No significant excess above the Standard Model expectations is observed. Limits are set on the gluino mass in the Tglu1A, Tglu2A and Tglu3A simplified models, see their Figure 3. Limits are also set on squark, sbottom and stop masses in the Tsqk1, Tsb0t1, Tstop1 and Tstop4 simplified models, see their Figure 3. Finally, limits are set on long-lived gluino masses in a Tglu1A simplified model where the gluino is metastable or long-lived with proper decay lengths in the range $10^{-3} \text{ mm} < c\tau < 10^5 \text{ mm}$, see their Figure 4.
- ⁷ SIRUNYAN 18bv searched in 38.5 fb^{-1} of pp collisions at $\sqrt{s} = 13 \text{ TeV}$ for long-lived particles in events with multiple jets and two displaced vertices composed of many tracks. No events with two well-separated high-track-multiplicity vertices were observed. Limits are set on the stop and the gluino mass in RPV models of supersymmetry where the stop (gluino) is decaying solely into dijet (multijet) final states, see their Figures 6 and 7.
- ⁸ KHACHATRYAN 17AR searched in 17.6 fb^{-1} of pp collisions at $\sqrt{s} = 8 \text{ TeV}$ for R-parity-violating SUSY in which long-lived neutralinos or gluinos decay into multijet final states. No significant excess above the Standard Model expectations is observed. Limits are set on the gluino mass for a range of mean proper decay lengths ($c\tau$), see their Fig. 7. The upper limits on the production cross section times branching ratio squared (Fig. 7) are also applicable to long-lived neutralinos.
- ⁹ AABOUD 16B searched in 3.2 fb^{-1} of pp collisions at $\sqrt{s} = 13 \text{ TeV}$ for long-lived R-hadrons using observables related to large ionization losses and slow propagation velocities, which are signatures of heavy charged particles traveling significantly slower than the speed of light. Exclusion limits at 95% C.L. are set on the long-lived gluino masses exceeding 1580 GeV. See their Fig. 5.
- ¹⁰ AABOUD 16c searched in 3.2 fb^{-1} of pp collisions at $\sqrt{s} = 13 \text{ TeV}$ for long-lived and stable R-hadrons identified by anomalously specific ionization energy loss in the ATLAS Pixel detector. Gluino R-hadrons with lifetimes above 0.4 ns are excluded at 95% C.L. with lower mass limit range between 740 GeV and 1590 GeV. In the case of stable R-hadrons, the lower mass limit is 1570 GeV. See their Figs. 5 and 6.

- ¹¹ KHACHATRYAN 16BW searched in 2.5 fb^{-1} of pp collisions at $\sqrt{s} = 13 \text{ TeV}$ for events with heavy stable charged particles, identified by their anomalously high energy deposits in the silicon tracker and/or long time-of-flight measurements by the muon system. No evidence for an excess over the expected background is observed. Limits are derived for pair production of gluinos as a function of mass, depending on the interaction model and on the fraction f , of produced gluinos hadronizing into a \tilde{g} -gluon state, see Fig. 4 and Table 7.
- ¹² AAD 15AE searched in 19.1 fb^{-1} of pp collisions at $\sqrt{s} = 8 \text{ TeV}$ for heavy long-lived charged particles, measured through their specific ionization energy loss in the ATLAS pixel detector or their time-of-flight in the ALTAS muon system. In the absence of an excess of events above the expected backgrounds, limits are set R-hadrons in various scenarios, see Fig. 11. Limits are also set in LeptoSUSY models where the gluino decays to stable 300 GeV leptons, see Fig. 9.
- ¹³ AAD 15BM searched in 18.4 fb^{-1} of pp collisions at $\sqrt{s} = 8 \text{ TeV}$ for stable and metastable non-relativistic charged particles through their anomalous specific ionization energy loss in the ATLAS pixel detector. In absence of an excess of events above the expected backgrounds, limits are set within a generic R-hadron model, on stable gluino R-hadrons (see Table 5) and on metastable gluino R-hadrons decaying to $(g/q\bar{q})$ plus a light $\tilde{\chi}_1^0$ (see Fig. 7) and decaying to $t\bar{t}$ plus a light $\tilde{\chi}_1^0$ (see Fig. 9).
- ¹⁴ KHACHATRYAN 15AK looked in a data set corresponding to 18.6 fb^{-1} of pp collisions at $\sqrt{s} = 8 \text{ TeV}$, and a search interval corresponding to 281 h of trigger lifetime, for long-lived particles that have stopped in the CMS detector. No evidence for an excess over the expected background in a cloud interaction model is observed. Assuming the decay $\tilde{g} \rightarrow g\tilde{\chi}_1^0$ and lifetimes between 1 μs and 1000 s, limits are derived on \tilde{g} production as a function of $m_{\tilde{\chi}_1^0}$, see Figs. 4 and 6. The exclusions require that $m_{\tilde{\chi}_1^0}$ is kinematically consistent with the minimum values of the jet energy thresholds used.
- ¹⁵ AAD 13AA searched in 4.7 fb^{-1} of pp collisions at $\sqrt{s} = 7 \text{ TeV}$ for events containing colored long-lived particles that hadronize forming R-hadrons. No significant excess above the expected background was found. Long-lived R-hadrons containing a \tilde{g} are excluded for masses up to 985 GeV at 95% C.L. in a general interaction model. Also, limits independent of the fraction of R-hadrons that arrive charged in the muon system were derived, see Fig. 6.
- ¹⁶ AAD 13BC searched in 5.0 fb^{-1} of pp collisions at $\sqrt{s} = 7 \text{ TeV}$ and in 22.9 fb^{-1} of pp collisions at $\sqrt{s} = 8 \text{ TeV}$ for bottom squark R-hadrons that have come to rest within the ATLAS calorimeter and decay at some later time to hadronic jets and a neutralino. In absence of an excess of events above the expected backgrounds, limits are set on gluino masses for different decays, lifetimes, and neutralino masses, see their Table 6 and Fig. 10.
- ¹⁷ CHATRCHYAN 13AB looked in 5.0 fb^{-1} of pp collisions at $\sqrt{s} = 7 \text{ TeV}$ and in 18.8 fb^{-1} of pp collisions at $\sqrt{s} = 8 \text{ TeV}$ for events with heavy stable particles, identified by their anomalously high dE/dx in the tracker or additionally requiring that it be identified as muon in the muon chambers, from pair production of \tilde{g} 's. No evidence for an excess over the expected background is observed. Limits are derived for pair production of gluinos as a function of mass (see Fig. 8 and Table 5), depending on the fraction, f , of formation of \tilde{g} - \tilde{g} (R-gluonball) states. The quoted limit is for $f = 0.1$, while for $f = 0.5$ it degrades to 1276 GeV. In the conservative scenario where every hadronic interaction causes it to become neutral, the limit decreases to 928 GeV for $f = 0.1$.
- ¹⁸ AAD 12P looked in 31 pb^{-1} of pp collisions at $\sqrt{s} = 7 \text{ TeV}$ for events with pair production of long-lived gluinos. The hadronization of the gluinos leads to R-hadrons which may stop inside the detector and later decay via $\tilde{g} \rightarrow g\tilde{\chi}_1^0$ during gaps between the proton bunches. No significant excess over the expected background is observed. From a counting experiment, a limit at 95% C.L. on the cross section as a function of $m_{\tilde{g}}$ is derived for $m_{\tilde{\chi}_1^0} = 100 \text{ GeV}$, see Fig. 4. The limit is valid for lifetimes between 10^{-5} and 10^3 seconds and assumes the Generic matter interaction model for the production cross section.
- ¹⁹ CHATRCHYAN 12AN looked in 4.0 fb^{-1} of pp collisions at $\sqrt{s} = 7 \text{ TeV}$ for events with pair production of long-lived gluinos. The hadronization of the gluinos leads to R-hadrons which may stop inside the detector and later decay via $\tilde{g} \rightarrow g\tilde{\chi}_1^0$ during gaps between the proton bunches. No significant excess over the expected background is observed. From a counting experiment, a limit at 95% C.L. on the cross section as a function of $m_{\tilde{g}}$ is derived, see Fig. 3. The mass limit is valid for lifetimes between 10^{-5} and 10^3 seconds, for what they call "the daughter gluon energy $E_{\tilde{g}} > 100 \text{ GeV}$ and assuming the cloud interaction model for R-hadrons. Supersedes KHACHATRYAN 11.
- ²⁰ CHATRCHYAN 12L looked in 5.0 fb^{-1} of pp collisions at $\sqrt{s} = 7 \text{ TeV}$ for events with heavy stable particles, identified by their anomalously high dE/dx in the tracker or additionally requiring that it be identified as muon in the muon chambers, from pair production of \tilde{g} 's. No evidence for an excess over the expected background is observed. Limits are derived for pair production of gluinos as a function of mass (see Fig. 3), depending on the fraction, f , of formation of \tilde{g} - \tilde{g} (R-gluonball) states. The quoted limit is for $f = 0.1$, while for $f = 0.5$ it degrades to 1046 GeV. In the conservative scenario where every hadronic interaction causes it to become neutral, the limit decreases to 928 GeV for $f = 0.1$. Supersedes KHACHATRYAN 11c.
- ²¹ AAD 11K looked in 34 pb^{-1} of pp collisions at $\sqrt{s} = 7 \text{ TeV}$ for events with heavy stable particles, identified by their anomalously high dE/dx in the tracker or time of flight in the tile calorimeter, from pair production of \tilde{g} . No evidence for an excess over the SM expectation is observed. Limits are derived for pair production of gluinos as a function of mass (see Fig. 4), for a fraction, $f = 10\%$, of formation of \tilde{g} - \tilde{g} (R-gluonball). If instead of a phase space driven approach for the hadronic scattering of the R-hadrons, a triple-Regge model or a bag-model is used, the limit degrades to 566 and 562 GeV, respectively.
- ²² AAD 11P looked in 37 pb^{-1} of pp collisions at $\sqrt{s} = 7 \text{ TeV}$ for events with heavy stable particles, reconstructed and identified by their time of flight in the Muon System. There is no requirement on their observation in the tracker to increase the sensitivity to cases where gluinos have a large fraction, f , of formation of neutral \tilde{g} - \tilde{g} (R-gluonball). No evidence for an excess over the SM expectation is observed. Limits are derived as a function of mass (see Fig. 4), for $f = 0.1$. For fractions $f = 0.5$ and 1.0 the limit degrades to 537 and 530 GeV, respectively.
- ²³ KHACHATRYAN 11 looked in 10 pb^{-1} of pp collisions at $\sqrt{s} = 7 \text{ TeV}$ for events with pair production of long-lived gluinos. The hadronization of the gluinos leads to R-hadrons which may stop inside the detector and later decay via $\tilde{g} \rightarrow g\tilde{\chi}_1^0$ during gaps between the proton bunches. No significant excess over the expected background is observed. From a counting experiment, a limit at 95% C.L. on the cross section times branching ratio is derived for $m_{\tilde{g}} - m_{\tilde{\chi}_1^0} > 100 \text{ GeV}$, see their Fig. 2. Assuming 100% branching

ratio, lifetimes between 75 ns and 3×10^5 s are excluded for $m_{\tilde{g}} = 300$ GeV. The \tilde{g} mass exclusion is obtained with the same assumptions for lifetimes between 10 μ s and 1000 s, but shows some dependence on the model for R-hadron interactions with matter, illustrated in Fig. 3. From a time-profile analysis, the mass exclusion is 382 GeV for a lifetime of 10 μ s under the same assumptions as above.

- ²⁴ KHACHATRYAN 11c looked in 3.1 pb^{-1} of pp collisions at $\sqrt{s} = 7$ TeV for events with heavy stable particles, identified by their anomalous dE/dx in the tracker or additionally requiring that it be identified as muon in the muon chambers, from pair production of \tilde{g} . No evidence for an excess over the expected background is observed. Limits are derived for pair production of gluinos as a function of mass (see Fig. 3), depending on the fraction, f , of formation of $\tilde{g} - g$ (R-gluonball). The quoted limit is for $f=0.1$, while for $f=0.5$ it degrades to 357 GeV. In the conservative scenario where every hadronic interaction causes it to become neutral, the limit decreases to 311 GeV for $f=0.1$.

Light \tilde{G} (Gravitino) mass limits from collider experiments

The following are bounds on light ($\ll 1$ eV) gravitino indirectly inferred from its coupling to matter suppressed by the gravitino decay constant.

Unless otherwise stated, all limits assume that other supersymmetric particles besides the gravitino are too heavy to be produced. The gravitino is assumed to be undetected and to give rise to a missing energy (\cancel{E}) signature.

Some earlier papers are now obsolete and have been omitted. They were last listed in our PDG 14 edition: K. Olive, *et al.* (Particle Data Group), Chinese Physics **C38** 070001 (2014) (<http://pdg.lbl.gov>).

VALUE (eV)	CL%	DOCUMENT ID	TECN	COMMENT
● ● ● We do not use the following data for averages, fits, limits, etc. ● ● ●				
$> 3.5 \times 10^{-4}$	95	1 AAD	15BH ATLS	$jet + \cancel{E}_T, pp \rightarrow (\tilde{q}/\tilde{g}) \tilde{G}, m_{\tilde{q}} = m_{\tilde{g}} = 500 \text{ GeV}$
$> 3 \times 10^{-4}$	95	1 AAD	15BH ATLS	$jet + \cancel{E}_T, pp \rightarrow (\tilde{q}/\tilde{g}) \tilde{G}, m_{\tilde{q}} = m_{\tilde{g}} = 1000 \text{ GeV}$
$> 2 \times 10^{-4}$	95	1 AAD	15BH ATLS	$jet + \cancel{E}_T, pp \rightarrow (\tilde{q}/\tilde{g}) \tilde{G}, m_{\tilde{q}} = m_{\tilde{g}} = 1500 \text{ GeV}$
$> 1.09 \times 10^{-5}$	95	2 ABDALLAH	05B DLPH	$e^+e^- \rightarrow \tilde{G} \tilde{G} \gamma$
$> 1.35 \times 10^{-5}$	95	3 ACHARD	04E L3	$e^+e^- \rightarrow \tilde{G} \tilde{G} \gamma$
$> 1.3 \times 10^{-5}$	95	4 HEISTER	03c ALEP	$e^+e^- \rightarrow \tilde{G} \tilde{G} \gamma$
$> 11.7 \times 10^{-6}$	95	5 ACOSTA	02H CDF	$p\bar{p} \rightarrow \tilde{G} \tilde{G} \gamma$
$> 8.7 \times 10^{-6}$	95	6 ABBIENDI,G	00D OPAL	$e^+e^- \rightarrow \tilde{G} \tilde{G} \gamma$

- ¹ AAD 15BH searched in 20.3 fb^{-1} of pp collisions at $\sqrt{s} = 8$ TeV for associated production of a light gravitino and a squark or gluino. The squark (gluino) is assumed to decay exclusively to a quark (gluon) and a gravitino. No evidence was found for an excess above the expected level of Standard Model background and 95% C.L. lower limits were set on the gravitino mass as a function of the squark/gluino mass, both in the case of degenerate and non-degenerate squark/gluino masses, see Figs. 14 and 15.

- ² ABDALLAH 05B use data from $\sqrt{s} = 180$ –208 GeV. They look for events with a single photon + \cancel{E} final states from which a cross section limit of $\sigma < 0.18 \text{ pb}$ at 208 GeV is obtained, allowing a limit on the mass to be set. Supersedes the results of ABREU 00Z.
- ³ ACHARD 04E use data from $\sqrt{s} = 189$ –209 GeV. They look for events with a single photon + \cancel{E} final states from which a limit on the Gravitino mass is set corresponding to $\sqrt{F} > 238$ GeV. Supersedes the results of ACCIARRI 99R.

- ⁴ HEISTER 03c use the data from $\sqrt{s} = 189$ –209 GeV to search for $\gamma \tilde{E}_T$ final states.

- ⁵ ACOSTA 02H looked in 87 pb^{-1} of $p\bar{p}$ collisions at $\sqrt{s}=1.8$ TeV for events with a high- E_T photon and \cancel{E}_T . They compared the data with a GMSB model where the final state could arise from $q\bar{q} \rightarrow \tilde{G} \tilde{G} \gamma$. Since the cross section for this process scales as $1/|F|^4$, a limit at 95% CL is derived on $|F|^{1/2} > 221$ GeV. A model independent limit for the above topology is also given in the paper.

- ⁶ ABBIENDI,G 00D searches for $\gamma \tilde{E}$ final states from $\sqrt{s}=189$ GeV.

Supersymmetry miscellaneous results

Results that do not appear under other headings or that make nonminimal assumptions.

Some earlier papers are now obsolete and have been omitted. They were last listed in our PDG 14 edition: K. Olive, *et al.* (Particle Data Group), Chinese Physics **C38** 070001 (2014) (<http://pdg.lbl.gov>).

VALUE	CL%	DOCUMENT ID	TECN	COMMENT
● ● ● We do not use the following data for averages, fits, limits, etc. ● ● ●				
		1 AAD	20c ATLS	habemus MSSM, $m_A - \tan\beta$ plane
>65	95	2 AABOUD	16AF ATLS	selected ATLAS searches on EWK sector
none 0–2	95	3 AAD	16AG ATLS	dark photon, γ_D , in SUSY- and Higgs-portal models
		4 AAD	13P ATLS	dark γ , hidden valley
		5 AALTONEN	12AB CDF	hidden-valley Higgs
none 100–185	95	6 AAD	11AA ATLS	scalar gluons
		7 CHATRCHYAN11E	CMS	$\mu\mu$ resonances
		8 ABAZOV	10N D0	γ_D , hidden valley

- ¹ AAD 20c uses a statistical combination of six final states $b\bar{b}b\bar{b}$, $b\bar{b}WW$, $b\bar{b}\tau\tau$, $WWWW$, $b\bar{b}\gamma\gamma$, and $WW\gamma\gamma$ to search for non-resonant and resonant production of Higgs boson pairs. The search uses 36.1 fb^{-1} of pp collisions data at $\sqrt{s} = 13$ TeV. Constraints in the habemus Minimal Supersymmetric Standard Model in the $(m_A, \tan\beta)$ parameter space are placed, see their Figure 7(b).

- ² AABOUD 16AF uses a selection of searches by ATLAS for the electroweak production of SUSY particles studying resulting constraints on dark matter candidates. They use 20 fb^{-1} of pp collisions at $\sqrt{s} = 8$ TeV. A likelihood-driven scan of an effective model focusing on the gaugino-higgsino and Higgs sector of the pMSSM is performed. The ATLAS searches impact models where $m_{\tilde{0}} < 65$ GeV, excluding 86% of them. See their Figs. 2, 4, and 6.

- ³ AAD 16AG searches for prompt lepton-jets using 20 fb^{-1} of pp collisions at $\sqrt{s} = 8$ TeV collected with the ATLAS detector. Lepton-jets are expected from decays of low-mass dark photons in SUSY-portal and Higgs-portal models. No significant excess of events is observed and 95% CL upper limits are computed on the production cross section times branching ratio for two prompt lepton-jets in models predicting 2 or 4 γ_D via SUSY-portal topologies, for γ_D mass values between 0 and 2 GeV. See their Figs 9 and 10. The results are also interpreted in terms of a 90% CL exclusion region in kinetic mixing and dark-photon mass parameter space. See their Fig. 13.

- ⁴ AAD 13P searched in 5 fb^{-1} of pp collisions at $\sqrt{s} = 7$ TeV for single lepton-jets with at least four muons; pairs of lepton-jets, each with two or more muons; and pairs of lepton-jets with two or more electrons. All of these could be signatures of Hidden Valley supersymmetric models. No statistically significant deviations from the Standard Model expectations are found. 95% C.L. limits are placed on the production cross section times branching ratio of dark photons for several parameter sets of a Hidden Valley model.

- ⁵ AALTONEN 12AB looked in 5.1 fb^{-1} of $p\bar{p}$ collisions at $\sqrt{s} = 1.96$ TeV for anomalous production of multiple low-energy leptons in association with a W or Z boson. Such events may occur in hidden valley models in which a supersymmetric Higgs boson is produced in association with a W or Z boson, with $H \rightarrow \tilde{\chi}_1^0 \tilde{\chi}_1^0$ pair and with the $\tilde{\chi}_1^0$ further decaying into a dark photon (γ_D) and the unobservable lightest SUSY particle of the hidden sector. As the γ_D is expected to be light, it may decay into a lepton pair. No significant excess over the SM expectation is observed and a limit at 95% C.L. is set on the cross section for a benchmark model of supersymmetric hidden-valley Higgs production.

- ⁶ AAD 11AA looked in 34 pb^{-1} of pp collisions at $\sqrt{s} = 7$ TeV for events with ≥ 4 jets originating from pair production of scalar gluons, each decaying to two gluons. No two-jet resonances are observed over the SM background. Limits are derived on the cross section times branching ratio (see Fig. 3). Assuming 100% branching ratio for the decay to two gluons, the quoted exclusion range is obtained, except for a 5 GeV mass window around 140 GeV.

- ⁷ CHATRCHYAN 11E looked in 35 pb^{-1} of pp collisions at $\sqrt{s} = 7$ TeV for events with collimated μ pairs (leptonic jets) from the decay of hidden sector states. No evidence for new resonance production is found. Limits are derived and compared to various SUSY models (see Fig. 4) where the LSP, either the $\tilde{\chi}_1^0$ or a \tilde{q} , decays to dark sector particles.

- ⁸ ABAZOV 10N looked in 5.8 fb^{-1} of $p\bar{p}$ collisions at $\sqrt{s} = 1.96$ TeV for events from hidden valley models in which a $\tilde{\chi}_1^0$ decays into a dark photon, γ_D , and the unobservable lightest SUSY particle of the hidden sector. As the γ_D is expected to be light, it may decay into a tightly collimated lepton pair, called lepton jet. They searched for events with \cancel{E}_T and two isolated lepton jets observable by an opposite charged lepton pair $e, e, e\mu$ or $\mu\mu$. No significant excess over the SM expectation is observed, and a limit at 95% C.L. on the cross section times branching ratio is derived, see their Table I. They also examined the invariant mass of the lepton jets for a narrow resonance, see their Fig. 4, but found no evidence for a signal.

REFERENCES FOR Supersymmetric Particle Searches

AAD	20C	PL B800 135103	G. Aad <i>et al.</i>	(ATLAS Collab.)
SIRUNYAN	20B	PL B801 135183	A.M. Sirunyan <i>et al.</i>	(CMS Collab.)
AABOUD	19AT	PR D99 029007	M. Aaboud <i>et al.</i>	(ATLAS Collab.)
AABOUD	19AU	PR D100 012006	M. Aaboud <i>et al.</i>	(ATLAS Collab.)
AABOUD	19C	PL B788 96	M. Aaboud <i>et al.</i>	(ATLAS Collab.)
AABOUD	19G	PR D99 012001	M. Aaboud <i>et al.</i>	(ATLAS Collab.)
AABOUD	19I	PR D99 012009	M. Aaboud <i>et al.</i>	(ATLAS Collab.)
AAD	19H	JHEP 1912 060	G. Aad <i>et al.</i>	(ATLAS Collab.)
ABE	19	PL B789 45	K. Abe <i>et al.</i>	(XMASS Collab.)
AJAJ	19	PR D100 022004	R. Ajaj <i>et al.</i>	(DEAP-3600 Collab.)
AMOLE	19	PR D100 022001	C. Amole <i>et al.</i>	(PICO Collab.)
APRILE	19A	PRL 122 141301	E. Aprile <i>et al.</i>	(XENONIT Collab.)
DI-MAURO	19	PR D99 123027	M. Di Mauro <i>et al.</i>	
JOHNSON	19	PR D99 103007	C. Johnson <i>et al.</i>	
LI	19D	PR D99 123519	S. Li <i>et al.</i>	
SIRUNYAN	19AG	JHEP 1906 143	A.M. Sirunyan <i>et al.</i>	(CMS Collab.)
SIRUNYAN	19AO	EPJ C79 305	A.M. Sirunyan <i>et al.</i>	(CMS Collab.)
SIRUNYAN	19AU	EPJ C79 444	A.M. Sirunyan <i>et al.</i>	(CMS Collab.)
SIRUNYAN	19AW	PL B790 140	A.M. Sirunyan <i>et al.</i>	(CMS Collab.)
SIRUNYAN	19BH	PR D99 032011	A.M. Sirunyan <i>et al.</i>	(CMS Collab.)
SIRUNYAN	19BI	PR D99 032014	A.M. Sirunyan <i>et al.</i>	(CMS Collab.)
SIRUNYAN	19BJ	PR D99 052002	A.M. Sirunyan <i>et al.</i>	(CMS Collab.)
SIRUNYAN	19BT	PL B797 124876	A.M. Sirunyan <i>et al.</i>	(CMS Collab.)
SIRUNYAN	19BU	JHEP 1908 150	A.M. Sirunyan <i>et al.</i>	(CMS Collab.)
SIRUNYAN	19CA	PR D100 112003	A.M. Sirunyan <i>et al.</i>	(CMS Collab.)
SIRUNYAN	19CE	PRL 123 241801	A.M. Sirunyan <i>et al.</i>	(CMS Collab.)
SIRUNYAN	19CH	JHEP 1910 244	A.M. Sirunyan <i>et al.</i>	(CMS Collab.)
SIRUNYAN	19CI	JHEP 1911 109	A.M. Sirunyan <i>et al.</i>	(CMS Collab.)
SIRUNYAN	19CF	PR D99 012010	A.M. Sirunyan <i>et al.</i>	(CMS Collab.)
SIRUNYAN	19K	JHEP 1901 154	A.M. Sirunyan <i>et al.</i>	(CMS Collab.)
SIRUNYAN	19S	JHEP 1903 031	A.M. Sirunyan <i>et al.</i>	(CMS Collab.)
SIRUNYAN	19U	JHEP 1903 101	A.M. Sirunyan <i>et al.</i>	(CMS Collab.)
XIA	19A	PL B792 193	J. Xia <i>et al.</i>	(PandaX-II Collab.)
AABOUD	18AQ	JHEP 1806 108	M. Aaboud <i>et al.</i>	(ATLAS Collab.)
AABOUD	18AR	JHEP 1806 107	M. Aaboud <i>et al.</i>	(ATLAS Collab.)
AABOUD	18AS	JHEP 1806 022	M. Aaboud <i>et al.</i>	(ATLAS Collab.)
AABOUD	18AY	EPJ C78 154	M. Aaboud <i>et al.</i>	(ATLAS Collab.)
AABOUD	18BB	EPJ C78 250	M. Aaboud <i>et al.</i>	(ATLAS Collab.)
AABOUD	18BJ	EPJ C78 625	M. Aaboud <i>et al.</i>	(ATLAS Collab.)
AABOUD	18BT	EPJ C78 995	M. Aaboud <i>et al.</i>	(ATLAS Collab.)
AABOUD	18BV	JHEP 1809 050	M. Aaboud <i>et al.</i>	(ATLAS Collab.)
AABOUD	18CF	PL B785 136	M. Aaboud <i>et al.</i>	(ATLAS Collab.)
AABOUD	18CK	PR D98 092002	M. Aaboud <i>et al.</i>	(ATLAS Collab.)
AABOUD	18CJ	PR D98 092008	M. Aaboud <i>et al.</i>	(ATLAS Collab.)
AABOUD	18CO	PR D98 092012	M. Aaboud <i>et al.</i>	(ATLAS Collab.)
AABOUD	18I	JHEP 1801 126	M. Aaboud <i>et al.</i>	(ATLAS Collab.)
AABOUD	18P	PR D97 032003	M. Aaboud <i>et al.</i>	(ATLAS Collab.)
AABOUD	18R	PR D97 052010	M. Aaboud <i>et al.</i>	(ATLAS Collab.)
AABOUD	18S	PR D97 052012	M. Aaboud <i>et al.</i>	(ATLAS Collab.)
AABOUD	18U	PR D97 092006	M. Aaboud <i>et al.</i>	(ATLAS Collab.)
AABOUD	18V	PR D97 112001	M. Aaboud <i>et al.</i>	(ATLAS Collab.)
AABOUD	18Y	PR D98 032008	M. Aaboud <i>et al.</i>	(ATLAS Collab.)
AABOUD	18Z	PR D98 032009	M. Aaboud <i>et al.</i>	(ATLAS Collab.)
ABDALLAH	18P	PRL 120 201101	H. Abdallah <i>et al.</i>	(H.E.S.S. Collab.)
ADHIKARI	18	NAT 564 83	G. Adhikari <i>et al.</i>	(COSINE-100 Collab.)
AGNES	18A	PR D98 102006	P. Agnes <i>et al.</i>	(DarkSide-50 Collab.)
AGNESE	18A	PRL 120 061802	R. Agnese <i>et al.</i>	(SuperCDMS Collab.)
AHNEN	18	JCAP 1803 009	M.L. Ahnen <i>et al.</i>	(MAGIC Collab.)
ALBERT	18B	JCAP 1806 043	A. Albert <i>et al.</i>	(HAWC Collab.)
ALBERT	18C	PR D98 123012	A. Albert <i>et al.</i>	(HAWC Collab.)
AMAUDRUZ	18	PRL 121 071801	P.A. Amaudruz <i>et al.</i>	(DEAP-3600 Collab.)
APRILE	18	PRL 121 111302	E. Aprile <i>et al.</i>	(XENONIT Collab.)
SIRUNYAN	18AA	PL B780 118	A.M. Sirunyan <i>et al.</i>	(CMS Collab.)
SIRUNYAN	18AC	PL B780 384	A.M. Sirunyan <i>et al.</i>	(CMS Collab.)

Searches Particle Listings

Supersymmetric Particle Searches

SIRUNYAN	18AD	PL B780 432	A.M. Sirunyan et al.	(CMS Collab.)	AAD	15B6	EPJ C75 318	G. Aad et al.	(ATLAS Collab.)
SIRUNYAN	18AJ	PL B782 440	A.M. Sirunyan et al.	(CMS Collab.)	Also		EPJ C75 463	G. Aad et al.	(ATLAS Collab.)
SIRUNYAN	18AK	PL B783 114	A.M. Sirunyan et al.	(CMS Collab.)	AAD	15BH	EPJ C75 299	G. Aad et al.	(ATLAS Collab.)
SIRUNYAN	18AL	JHEP 1802 067	A.M. Sirunyan et al.	(CMS Collab.)	Also		EPJ C75 408 (errat.)	G. Aad et al.	(ATLAS Collab.)
SIRUNYAN	18AN	JHEP 1803 167	A.M. Sirunyan et al.	(CMS Collab.)	AAD	15BM	EPJ C75 407	G. Aad et al.	(ATLAS Collab.)
SIRUNYAN	18AO	JHEP 1803 166	A.M. Sirunyan et al.	(CMS Collab.)	AAD	15BV	JHEP 1510 054	G. Aad et al.	(ATLAS Collab.)
SIRUNYAN	18AP	JHEP 1803 160	A.M. Sirunyan et al.	(CMS Collab.)	AAD	15BX	JHEP 1510 134	G. Aad et al.	(ATLAS Collab.)
SIRUNYAN	18AR	JHEP 1803 076	A.M. Sirunyan et al.	(CMS Collab.)	AAD	15CA	PR D92 072001	G. Aad et al.	(ATLAS Collab.)
SIRUNYAN	18AT	JHEP 1804 073	A.M. Sirunyan et al.	(CMS Collab.)	AAD	15CB	PR D92 072004	G. Aad et al.	(ATLAS Collab.)
SIRUNYAN	18AY	JHEP 1805 025	A.M. Sirunyan et al.	(CMS Collab.)	AAD	15CJ	EPJ C75 510	G. Aad et al.	(ATLAS Collab.)
SIRUNYAN	18B	PL B778 263	A.M. Sirunyan et al.	(CMS Collab.)	AAD	15CS	PR D91 012008	G. Aad et al.	(ATLAS Collab.)
SIRUNYAN	18BR	JHEP 1808 016	A.M. Sirunyan et al.	(CMS Collab.)	Also		PR D92 059903 (errat.)	G. Aad et al.	(ATLAS Collab.)
SIRUNYAN	18C	PR D97 032009	A.M. Sirunyan et al.	(CMS Collab.)	AAD	15J	PRL 114 142001	G. Aad et al.	(ATLAS Collab.)
SIRUNYAN	18D	PR D97 012007	A.M. Sirunyan et al.	(CMS Collab.)	AAD	15K	PRL 114 161801	G. Aad et al.	(ATLAS Collab.)
SIRUNYAN	18DI	JHEP 1809 065	A.M. Sirunyan et al.	(CMS Collab.)	AAD	15O	PRL 115 031801	G. Aad et al.	(ATLAS Collab.)
SIRUNYAN	18DN	JHEP 1811 079	A.M. Sirunyan et al.	(CMS Collab.)	AAD	15X	PR D91 112016	G. Aad et al.	(ATLAS Collab.)
SIRUNYAN	18DP	JHEP 1811 151	A.M. Sirunyan et al.	(CMS Collab.)	AAJ	15BD	EPJ C75 595	R. Aaij et al.	(LHCb Collab.)
SIRUNYAN	18DV	PR D98 092011	A.M. Sirunyan et al.	(CMS Collab.)	AARTSEN	15C	EPJ C75 20	M.G. Aartsen et al.	(IceCube Collab.)
SIRUNYAN	18DY	PR D98 112014	A.M. Sirunyan et al.	(CMS Collab.)	AARTSEN	15E	EPJ C75 492	M.G. Aartsen et al.	(IceCube Collab.)
SIRUNYAN	18EA	PRL 121 141802	A.M. Sirunyan et al.	(CMS Collab.)	ABRAMOWSKI	15	PRL 114 081301	A. Abramowski et al.	(H.E.S.S. Collab.)
SIRUNYAN	18EM	PRL 120 241801	A.M. Sirunyan et al.	(CMS Collab.)	ACKERMANN	15	PR D91 122002	M. Ackermann et al.	(Fermi-LAT Collab.)
SIRUNYAN	18O	PR D97 032007	A.M. Sirunyan et al.	(CMS Collab.)	ACKERMANN	15A	JCAP 1509 008	M. Ackermann et al.	(Fermi-LAT Collab.)
SIRUNYAN	18X	PL B779 166	A.M. Sirunyan et al.	(CMS Collab.)	ACKERMANN	15B	PRL 115 231301	M. Ackermann et al.	(Fermi-LAT Collab.)
ABOUD	17AF	JHEP 1708 006	M. Aboud et al.	(ATLAS Collab.)	ADRIAN-MAR.	15	JCAP 1510 068	S. Adrian-Martinez et al.	(ANTARES Collab.)
ABOUD	17AI	JHEP 1709 088	M. Aboud et al.	(ATLAS Collab.)	AGNES	15	PL B743 456	P. Agnes et al.	(DarkSide-50 Collab.)
ABOUD	17AJ	JHEP 1709 084	M. Aboud et al.	(ATLAS Collab.)	AGNES	15B	PR D92 072003	R. Agnese et al.	(SuperCDMS Collab.)
Also		JHEP 1908 121 (errat.)	M. Aboud et al.	(ATLAS Collab.)	BUCKLEY	15	PR D91 102001	M.R. Buckley et al.	
ABOUD	17AR	PR D96 112010	M. Aboud et al.	(ATLAS Collab.)	CHOI	15	PRL 114 141301	K. Choi et al.	(Super-Kamiokande Collab.)
ABOUD	17AX	JHEP 1711 195	M. Aboud et al.	(ATLAS Collab.)	KHACHATRYAN	15AB	JHEP 1501 096	V. Khachatryan et al.	(CMS Collab.)
ABOUD	17AY	JHEP 1712 085	M. Aboud et al.	(ATLAS Collab.)	KHACHATRYAN	15AD	JHEP 1504 124	V. Khachatryan et al.	(CMS Collab.)
ABOUD	17AZ	JHEP 1710 004	M. Aboud et al.	(ATLAS Collab.)	KHACHATRYAN	15AF	JHEP 1505 078	V. Khachatryan et al.	(CMS Collab.)
ABOUD	17BE	EPJ C77 898	M. Aboud et al.	(ATLAS Collab.)	KHACHATRYAN	15AH	JHEP 1506 116	V. Khachatryan et al.	(CMS Collab.)
ABOUD	17N	EPJ C77 144	M. Aboud et al.	(ATLAS Collab.)	KHACHATRYAN	15AK	EPJ C75 151	V. Khachatryan et al.	(CMS Collab.)
AAJ	17Z	EPJ C77 224	R. Aaij et al.	(LHCb Collab.)	KHACHATRYAN	15AO	EPJ C75 325	V. Khachatryan et al.	(CMS Collab.)
AARTSEN	17	EPJ C77 82	M.G. Aartsen et al.	(IceCube Collab.)	KHACHATRYAN	15AR	PL B743 503	V. Khachatryan et al.	(CMS Collab.)
AARTSEN	17A	EPJ C77 146	M.G. Aartsen et al.	(IceCube Collab.)	KHACHATRYAN	15AZ	PR D92 072006	V. Khachatryan et al.	(CMS Collab.)
Also		EPJ C79 214 (errat.)	M.G. Aartsen et al.	(IceCube Collab.)	KHACHATRYAN	15E	PRL 114 061801	V. Khachatryan et al.	(CMS Collab.)
AARTSEN	17C	EPJ C77 627	M.G. Aartsen et al.	(IceCube Collab.)	KHACHATRYAN	15I	PL B745 5	V. Khachatryan et al.	(CMS Collab.)
AKERIB	17	PRL 118 021303	D.S. Akerib et al.	(LUX Collab.)	KHACHATRYAN	15L	PL B747 98	V. Khachatryan et al.	(CMS Collab.)
AKERIB	17A	PRL 118 251302	D.S. Akerib et al.	(LUX Collab.)	KHACHATRYAN	15O	PL B748 255	V. Khachatryan et al.	(CMS Collab.)
ALBERT	17A	PL B769 249	A. Albert et al.	(ANTARES Collab.)	KHACHATRYAN	15W	PR D91 052012	V. Khachatryan et al.	(CMS Collab.)
Also		PL B796 253 (errat.)	A. Albert et al.	(ANTARES Collab.)	KHACHATRYAN	15X	PR D91 052018	V. Khachatryan et al.	(CMS Collab.)
AMOLE	17	PRL 118 251301	C. Amole et al.	(PICCO Collab.)	ROLBIECKI	15	PL B750 247	K. Rolbicki, J. Tattersall	(MADE, HEID)
APRILE	17G	PRL 119 181301	E. Aprile et al.	(XENON100 Collab.)	AAD	14AE	JHEP 1409 176	G. Aad et al.	(ATLAS Collab.)
ARCHAMBAU...	17	PR D95 082001	S. Archambault et al.	(VERITAS Collab.)	AAD	14AG	JHEP 1409 103	G. Aad et al.	(ATLAS Collab.)
BATTAT	17	ASP 91 65	J.B.R. Battat et al.	(DRIFT-III Collab.)	AAD	14AJ	JHEP 1409 015	G. Aad et al.	(ATLAS Collab.)
BEHNKE	17	ASP 90 85	E. Behnke et al.	(PICASSO Collab.)	AAD	14AV	JHEP 1410 096	G. Aad et al.	(ATLAS Collab.)
CUI	17A	PRL 119 181302	X. Cui et al.	(PandaX-II Collab.)	AAD	14AX	JHEP 1410 024	G. Aad et al.	(ATLAS Collab.)
FU	17	PRL 118 071301	C. Fu et al.	(PandaX-II Collab.)	AAD	14B	EPJ C74 2883	G. Aad et al.	(ATLAS Collab.)
Also		PRL 120 049902 (errat.)	C. Fu et al.	(PandaX-II Collab.)	AAD	14BD	JHEP 1411 118	G. Aad et al.	(ATLAS Collab.)
KHACHATRYAN	17	PR D95 012003	V. Khachatryan et al.	(CMS Collab.)	AAD	14BH	PR D90 112005	G. Aad et al.	(ATLAS Collab.)
KHACHATRYAN	17A	PRL 118 021802	V. Khachatryan et al.	(CMS Collab.)	AAD	14E	JHEP 1406 035	G. Aad et al.	(ATLAS Collab.)
KHACHATRYAN	17AD	PR D96 012004	V. Khachatryan et al.	(CMS Collab.)	AAD	14F	JHEP 1406 124	G. Aad et al.	(ATLAS Collab.)
KHACHATRYAN	17AR	PR D95 012009	V. Khachatryan et al.	(CMS Collab.)	AAD	14G	JHEP 1405 071	G. Aad et al.	(ATLAS Collab.)
KHACHATRYAN	17AS	PR D95 012011	V. Khachatryan et al.	(CMS Collab.)	AAD	14H	JHEP 1404 169	G. Aad et al.	(ATLAS Collab.)
KHACHATRYAN	17AW	EPJ C77 635	V. Khachatryan et al.	(CMS Collab.)	AAD	14K	PR D90 012004	G. Aad et al.	(ATLAS Collab.)
KHACHATRYAN	17L	JHEP 1704 018	V. Khachatryan et al.	(CMS Collab.)	AAD	14T	PR D90 052008	G. Aad et al.	(ATLAS Collab.)
KHACHATRYAN	17P	EPJ C77 294	V. Khachatryan et al.	(CMS Collab.)	AALTONEN	14	PR D90 052001	G. Aad et al.	(ATLAS Collab.)
KHACHATRYAN	17S	PL B767 403	V. Khachatryan et al.	(CMS Collab.)	AALTONEN	14	PR D90 012011	T. Aaltonen et al.	(CDF Collab.)
KHACHATRYAN	17V	PL B769 391	V. Khachatryan et al.	(CMS Collab.)	ACKERMANN	14	PR D89 042001	M. Ackermann et al.	(Fermi-LAT Collab.)
KHACHATRYAN	17Y	PL B770 257	V. Khachatryan et al.	(CMS Collab.)	AKERIB	14	PRL 112 091303	D.S. Akerib et al.	(LUX Collab.)
SIRUNYAN	17AF	PRL 119 151802	A.M. Sirunyan et al.	(CMS Collab.)	ALEKSIC	14	JCAP 1402 008	J. Alekxic et al.	(MAGIC Collab.)
SIRUNYAN	17AS	JHEP 1710 019	A.M. Sirunyan et al.	(CMS Collab.)	AVRORIN	14	ASP 62 12	A.D. Avrorin et al.	(BAIKAL Collab.)
SIRUNYAN	17AT	JHEP 1710 005	A.M. Sirunyan et al.	(CMS Collab.)	BUCHMUELLER	14A	EPJ C74 2809	O. Buchmüller et al.	
SIRUNYAN	17AW	JHEP 1711 029	A.M. Sirunyan et al.	(CMS Collab.)	BUCHMUELLER	14A	EPJ C74 2922	O. Buchmüller et al.	
SIRUNYAN	17AY	JHEP 1712 142	A.M. Sirunyan et al.	(CMS Collab.)	CHATRCHYAN	14AH	PR D90 112001	S. Chatrchyan et al.	(CMS Collab.)
SIRUNYAN	17AZ	EPJ C77 710	A.M. Sirunyan et al.	(CMS Collab.)	CHATRCHYAN	14H	JHEP 1401 163	S. Chatrchyan et al.	(CMS Collab.)
SIRUNYAN	17K	EPJ C77 327	A.M. Sirunyan et al.	(CMS Collab.)	CHATRCHYAN	14J	JHEP 1406 055	S. Chatrchyan et al.	(CMS Collab.)
SIRUNYAN	17P	PR D96 032003	A.M. Sirunyan et al.	(CMS Collab.)	CHATRCHYAN	14N	PL B733 328	S. Chatrchyan et al.	(CMS Collab.)
SIRUNYAN	17S	EPJ C77 578	A.M. Sirunyan et al.	(CMS Collab.)	CHATRCHYAN	14P	PL B730 193	S. Chatrchyan et al.	(CMS Collab.)
ABOUD	16AC	EPJ C76 683	M. Aboud et al.	(ATLAS Collab.)	CHATRCHYAN	14R	PR D90 032006	S. Chatrchyan et al.	(CMS Collab.)
ABOUD	16AF	JHEP 1609 175	M. Aboud et al.	(ATLAS Collab.)	CHATRCHYAN	14U	PRL 112 161802	S. Chatrchyan et al.	(CMS Collab.)
ABOUD	16B	PL B760 647	M. Aboud et al.	(ATLAS Collab.)	CZAKON	14	PRL 113 201803	M. Czakon et al.	(AACH, CAMB, UCB, LBL+)
ABOUD	16C	PR D93 112015	M. Aboud et al.	(ATLAS Collab.)	FELIZARDO	14	PR D89 072013	M. Felizardo et al.	(SIMPLE Collab.)
ABOUD	16D	PR D93 032005	M. Aboud et al.	(ATLAS Collab.)	KHACHATRYAN	14D	EPJ C76 371	V. Khachatryan et al.	(CMS Collab.)
ABOUD	16J	PR D94 052009	M. Aboud et al.	(ATLAS Collab.)	KHACHATRYAN	14I	EPJ C74 3036	V. Khachatryan et al.	(CMS Collab.)
ABOUD	16M	EPJ C76 517	M. Aboud et al.	(ATLAS Collab.)	KHACHATRYAN	14L	PR D90 092007	V. Khachatryan et al.	(CMS Collab.)
ABOUD	16N	EPJ C76 392	M. Aboud et al.	(ATLAS Collab.)	KHACHATRYAN	14T	PL B739 229	V. Khachatryan et al.	(CMS Collab.)
ABOUD	16P	EPJ C76 541	M. Aboud et al.	(ATLAS Collab.)	PDG	14	CP C38 070001	K. Olive et al.	(PDG Collab.)
ABOUD	16Q	EPJ C76 547	M. Aboud et al.	(ATLAS Collab.)	ROSKOWSKI	14	JHEP 1408 067	L. Roszkowski, E.M. Sessolo, A.J. Williams	(WINR)
AAD	16AA	PR D93 052002	G. Aad et al.	(ATLAS Collab.)	AAD	13	PL B718 841	G. Aad et al.	(ATLAS Collab.)
AAD	16AD	PR D94 032003	G. Aad et al.	(ATLAS Collab.)	AAD	13AA	PL B720 277	G. Aad et al.	(ATLAS Collab.)
AAD	16AG	JHEP 1602 062	G. Aad et al.	(ATLAS Collab.)	AAD	13AI	PL B723 15	G. Aad et al.	(ATLAS Collab.)
AAD	16AM	JHEP 1606 067	G. Aad et al.	(ATLAS Collab.)	AAD	13AP	PR D88 012001	G. Aad et al.	(ATLAS Collab.)
AAD	16AY	EPJ C76 81	G. Aad et al.	(ATLAS Collab.)	AAD	13AU	JHEP 1310 189	G. Aad et al.	(ATLAS Collab.)
AAD	16BE	EPJ C76 259	G. Aad et al.	(ATLAS Collab.)	AAD	13B	PL B718 879	G. Aad et al.	(ATLAS Collab.)
AAD	16BG	EPJ C76 565	G. Aad et al.	(ATLAS Collab.)	AAD	13B	PR D88 112003	G. Aad et al.	(ATLAS Collab.)
AAD	16V	PL B757 334	G. Aad et al.	(ATLAS Collab.)	AAD	13BD	PR D88 112006	G. Aad et al.	(ATLAS Collab.)
AARTSEN	16C	JCAP 1604 022	M.G. Aartsen et al.	(IceCube Collab.)	AAD	13B	JHEP 1301 131	G. Aad et al.	(ATLAS Collab.)
AARTSEN	16D	EPJ C76 531	M.G. Aartsen et al.	(IceCube Collab.)	AAD	13L	PR D87 012008	G. Aad et al.	(ATLAS Collab.)
ABDALLAH	16	PRL 117 111301	H. Abdallah et al.	(H.E.S.S. Collab.)	AAD	13P	PL B719 299	G. Aad et al.	(ATLAS Collab.)
ABDALLAH	16A	PRL 117 151302	H. Abdallah et al.	(H.E.S.S. Collab.)	AAD	13Q	PL B719 261	G. Aad et al.	(ATLAS Collab.)
ADRIAN-MAR.	16	PL B759 69	S. Adrian-Martinez et al.	(ANTARES Collab.)	AAD	13R	PL B719 280	G. Aad et al.	(ATLAS Collab.)
AHNEN	16	JCAP 1602 039	M.L. Ahnen et al.	(MAGIC and Fermi-LAT Collab.)	AALTONEN	13I	PR D88 031103	T. Aaltonen et al.	(CDF Collab.)
AKERIB	16	PRL 116 161301	D.S. Akerib et al.	(LUX Collab.)	AALTONEN	13J	PRL 110 201802	T. Aaltonen et al.	(CDF Collab.)
AKERIB	16A	PRL 116 161302	D.S. Akerib et al.	(LUX Collab.)	AARTSEN	13C	PR D88 122001	M.G. Aartsen et al.	(IceCube Collab.)
AMOLE	16	PR D93 052014	C. Amole et al.	(PICCO Collab.)	ABAZOV	13B	PR D87 052011	V.M. Abazov et al.	(D0 Collab.)
APRILE	16B	PR D94 122011	E. Aprile et al.	(XENON100 Collab.)	ABRAMOWSKI	13	PRL 110 041301	A. Abramowski et al.	(H.E.S.S. Collab.)
AVRORIN	16	ASP 81 12	A.D. Avrorin et al.	(BAIKAL Collab.)	ACKERMANN	13A	PR D88 082002	M. Ackermann et al.	(Fermi-LAT Collab.)
CIRELLI	16	JCAP 1607 041	M. Cirelli, M. Taoso	(LNPHE, MADE Collab.)	ADRIAN-MAR.	13	JCAP 1311 032	S. Adrian-Martinez et al.	(ANTARES Collab.)
KHACHATRYAN	16AA	PL B759 479	V. Khachatryan et al.	(CMS Collab.)	AGNES	13	PR D88 031104	R. Agnese et al.	(CDMS Collab.)
KHACHATRYAN	16AC	PL B760 178	V. Khachatryan et al.	(CMS Collab.)	AGNES	13A	PRL 111 251301	R. Agnese et al.	(CDMS Collab.)
KHACHATRYAN	16AM	PR D93 092009	V. Khachatryan et al.	(CMS Collab.)	APRILE	13	PRL 111 021301	E. Aprile et al.	(XENON100 Collab.)
KHACHATRYAN	16AV	JHEP 1607 027	V. Khachatryan et al.	(CMS Collab.)	BERGSTROM	13	PRL 111 171101	L. Bergstrom et al.	
KHACHATRYAN	16AY	JHEP 1608 122	V. Khachatryan et al.	(CMS Collab.)	BOLIVIE	13	JCAP 1309 019	M. Bolivie et al.	
KHACHATRYAN	16BE	EPJ C76 317	V. Khachatryan et al.	(CMS Collab.)	CABRERA	13	JHEP 1307 182	M. Cabrera, J. Casas, R. de Austri	
KHACHATRYAN	16BJ	EPJ C76 439	V. Khachatryan et al.	(CMS Collab.)	CHATRCHYAN	13	PL B718 815	S. Chatrchyan et al.	(CMS Collab.)
KHACHATRYAN	16BK	EPJ C76 460	V. Khachatryan et al.	(CMS Collab.)	CHATRCHYAN	13AB	JHEP 1307 122	S. Chatrchyan et al.	(CMS Collab.)
KHACHATRYAN	16BS	JHEP 1610 006	V. Khachatryan et al.	(CMS Collab.)	CHATRCHYAN	13AH	PL B722 273	S. Chatrchyan et al.	(CMS Collab.)
KHACHATRYAN	16BT	JHEP 1610 129	V. Khachatryan et al.	(CMS Collab.)	CHATRCHYAN	13AO	PR D87 072001	S. Chatrchyan et al.	(CMS Collab.)
KHACHATRYAN	16BW	PR D94 112004	V. Khachatryan et al.	(CMS Collab.)	CHATRCHYAN	13AT	PR D88 052017	S. Chatrchyan et al.	(CMS Collab.)
KHACHATRYAN	16BX	PR D94 112009	V. Khachatryan et al.	(CMS Collab.)	CHATRCHYAN	13AV	PRL 111 081802	S. Chatrchyan et al.	(CMS Collab.)
KHACHATRYAN	16BY	JHEP 1612 013	V. Khachatryan et al.	(CMS Collab.)	CHATRCHYAN	13G	JHEP 1301 077	S. Chatrchyan et al.	(CMS Collab.)
KHACHATRYAN									

See key on page 999

Searches Particle Listings

Supersymmetric Particle Searches

AAD	12AF	PL B714 180	G. Aad et al.	(ATLAS Collab.)	BARNABE-HE...05	PL B624 186	M. Barnabe-Heider et al.	(PICASSO Collab.)
AAD	12AG	PL B714 197	G. Aad et al.	(ATLAS Collab.)	ELLIS	05	J. Ellis et al.	
AAD	12AN	PRL 108 181802	G. Aad et al.	(ATLAS Collab.)	SANGLARD	05	V. Sanglard et al.	(EDELWEISS Collab.)
AAD	12AS	PRL 108 261804	G. Aad et al.	(ATLAS Collab.)	ABBIENDI	04	G. Abbiendi et al.	(OPAL Collab.)
AAD	12AX	PR D85 012006	G. Aad et al.	(ATLAS Collab.)	ABBIENDI	04F	G. Abbiendi et al.	(OPAL Collab.)
Also		PR D87 099903 (err.)	G. Aad et al.	(ATLAS Collab.)	ABBIENDI	04H	G. Abbiendi et al.	(OPAL Collab.)
AAD	12BJ	EPJ C72 1993	G. Aad et al.	(ATLAS Collab.)	ABBIENDI	04N	G. Abbiendi et al.	(OPAL Collab.)
AAD	12CI	PR D86 092002	G. Aad et al.	(ATLAS Collab.)	ABDALLAH	04H	J. Abdallah et al.	(DELPHI Collab.)
AAD	12CM	EPJ C72 2215	G. Aad et al.	(ATLAS Collab.)	ABDALLAH	04M	J. Abdallah et al.	(DELPHI Collab.)
AAD	12CP	PL B718 411	G. Aad et al.	(ATLAS Collab.)	Also	EPJ C37 129 (err.)	J. Abdallah et al.	(DELPHI Collab.)
AAD	12CT	JHEP 1212 124	G. Aad et al.	(ATLAS Collab.)	ACHARD	04	P. Achard et al.	(L3 Collab.)
AAD	12P	EPJ C72 1965	G. Aad et al.	(ATLAS Collab.)	ACHARD	04E	P. Achard et al.	(L3 Collab.)
AAD	12R	PL B707 478	G. Aad et al.	(ATLAS Collab.)	AKERIB	04	D.S. Akerib et al.	(CDMS II Collab.)
AAD	12T	PL B709 137	G. Aad et al.	(ATLAS Collab.)	BALTZ	04	E. Baltz, P. Gondolo	
AAD	12W	PL B710 67	G. Aad et al.	(ATLAS Collab.)	BELANGER	04	G. Belanger et al.	
AALTONEN	12AB	PR D85 092001	T. Aaltonen et al.	(CDF Collab.)	BOTTINO	04	A. Bottino et al.	
ABAZOV	12AD	PR D86 071701	V.M. Abazov et al.	(DO Collab.)	DESAI	04	S. Desai et al.	(Super-Kamiokande Collab.)
ABBASI	12	PR D85 042002	R. Abbasi et al.	(IceCube Collab.)	ELLIS	04	J. Ellis et al.	
AKHMOV	12	PL B709 131802	D.Yu. Akimov et al.	(ZEPLIN-III Collab.)	ELLIS	04B	J. Ellis et al.	
AKULA	12	PR D85 075001	S. Akula et al.	(NEAS, MICH)	HEISTER	04	A. Heister et al.	(ALEPH Collab.)
ANGLOHER	12	EPJ C72 1971	G. Angloher et al.	(CRESS-T Collab.)	PIERCE	04A	A. Pierce	
APRILE	12	PRL 109 181301	E. Aprile et al.	(XENON100 Collab.)	ABBIENDI	03M	G. Abbiendi et al.	(OPAL Collab.)
ARBEY	12A	PL B708 162	A. Arbey et al.		ABDALLAH	03L	J. Abdallah et al.	(DELPHI Collab.)
ARCHAMBAU...12	PL B711 153	S. Archambault et al.		(PICASSO Collab.)	AHMED	03	B. Ahmed et al.	(UK Dark Matter Collab.)
BAER	12	JHEP 1205 091	H. Baer, V. Barger, A. Mustafayev	(OKLA, WISC+)	AKERIB	03	D.S. Akerib et al.	(CDMS Collab.)
BALAZS	12	EPJ C73 2563	C. Balazs et al.		BAER	03J	H. Baer, C. Balazs	
BECHTLE	12	JHEP 1206 098	P. Bechtle et al.		BAER	03A	H. Baer et al.	
BEHNKE	12	PR D86 052001	E. Behnke et al.	(COUPP Collab.)	BOTTINO	03	A. Bottino et al.	
Also		PR D90 079902 (err.)	E. Behnke et al.	(COUPP Collab.)	BOTTINO	03A	A. Bottino, N. Fornengo, S. Scopel	
BESKIDT	12	EPJ C72 2166	C. Beskidt et al.	(KAARLE, JIMR, ITEP)	CHATTOPADYAY...	03	U. Chattopadhyay, A. Corsetti, P. Nath	
BOTTINO	12B	PR D85 095013	A. Bottino, N. Fornengo, S. Scopel	(TORI, SOGA)	ELLIS	03	J. Ellis, K.A. Olive, Y. Santoso	
BUCHMUELLER...	12	EPJ C72 2020	O. Buchmuller et al.		ELLIS	03B	J. Ellis et al.	
CAO	12A	PL B710 665	J. Cao et al.		ELLIS	03C	J. Ellis et al.	
CHATRCHYAN	12	PR D85 012004	S. Chatrchyan et al.	(CMS Collab.)	ELLIS	03D	J. Ellis et al.	
CHATRCHYAN	12AE	PRL 109 171803	S. Chatrchyan et al.	(CMS Collab.)	ELLIS	03E	J. Ellis et al.	
CHATRCHYAN	12AI	JHEP 1208 110	S. Chatrchyan et al.	(CMS Collab.)	HEISTER	03C	A. Heister et al.	(ALEPH Collab.)
CHATRCHYAN	12AL	JHEP 1206 169	S. Chatrchyan et al.	(CMS Collab.)	HEISTER	03G	A. Heister et al.	(ALEPH Collab.)
CHATRCHYAN	12AN	JHEP 1208 026	S. Chatrchyan et al.	(CMS Collab.)	KLAPDOR-K...	03	H.V. Klapdor-Kleingrothaus et al.	
CHATRCHYAN	12AT	JHEP 1210 018	S. Chatrchyan et al.	(CMS Collab.)	LAHANAS	03	A. Lahanas, D. Nanopoulos	
CHATRCHYAN	12BJ	JHEP 1211 147	S. Chatrchyan et al.	(CMS Collab.)	TAKEDA	03	A. Takeda et al.	
CHATRCHYAN	12BK	JHEP 1211 172	S. Chatrchyan et al.	(CMS Collab.)	ABRAMS	02	D. Abrams et al.	(CDMS Collab.)
CHATRCHYAN	12BQ	JHEP 1212 055	S. Chatrchyan et al.	(CMS Collab.)	ACOSTA	02H	PR 89 281801	(CDF Collab.)
CHATRCHYAN	12L	PL B713 408	S. Chatrchyan et al.	(CMS Collab.)	ANGLOHER	02	G. Angloher et al.	(CRESS-T Collab.)
DAW	12	ASP 35 397	E. Daw et al.	(DRIFT-III Collab.)	ARNOWITT	02	R. Arnowitt, B. Dutta	
DREINER	12A	EPL 99 61001	H.K. Dreiner, M. Kramer, J. Tattersall	(BONN+)	ELLIS	02B	J. Ellis, A. Ferstl, K.A. Olive	
ELLIS	12B	EPJ C72 2005	J. Ellis, K. Olive		HEISTER	02	A. Heister et al.	(ALEPH Collab.)
FELIZARDO	12	PRL 108 201302	M. Felizardo et al.	(SIMPLE Collab.)	HEISTER	02E	A. Heister et al.	(ALEPH Collab.)
FENG	12B	PR D85 075007	J. Feng, K. Matchev, D. Sanford		HEISTER	02J	A. Heister et al.	(ALEPH Collab.)
KADASTIK	12	JHEP 1205 061	M. Kadastik et al.		HEISTER	02N	A. Heister et al.	(ALEPH Collab.)
KIM	12	PRL 108 181301	S.C. Kim et al.	(KIMS Collab.)	KIM	02	H.B. Kim et al.	
STREGE	12	JCAP 1203 030	C. Strege et al.	(LOIC, AMST, MADU, GRAN+)	KIM	02B	Y.G. Kim et al.	
AAD	11AA	EPJ C71 1828	G. Aad et al.	(ATLAS Collab.)	LAHANAS	02	A. Lahanas, V.C. Spanos	
AAD	11G	PL 106 131802	G. Aad et al.	(ATLAS Collab.)	MORALES	02B	A. Morales et al.	(COSME Collab.)
AAD	11H	PL 106 251801	G. Aad et al.	(ATLAS Collab.)	MORALES	02C	A. Morales et al.	(IGEX Collab.)
AAD	11K	PL B701 1	G. Aad et al.	(ATLAS Collab.)	ABREU	01	P. Abreu et al.	(DELPHI Collab.)
AAD	11O	PL B701 398	G. Aad et al.	(ATLAS Collab.)	ABREU	01B	P. Abreu et al.	(DELPHI Collab.)
AAD	11P	PL B703 428	G. Aad et al.	(ATLAS Collab.)	BALTZ	01	E. Baltz, P. Gondolo	
AAD	11Z	EPJ C71 1809	G. Aad et al.	(ATLAS Collab.)	BARATE	01	R. Barate et al.	(ALEPH Collab.)
ABRAMOWSKI	11	PRL 106 161301	A. Abramowski et al.	(H.E.S.S. Collab.)	BARATE	01C	R. Barate et al.	(ALEPH Collab.)
AHMED	11A	PR D84 011102	Z. Ahmed et al.	(CDMS and EDELWEISS Collabs.)	BARGER	01B	V. Barger, C. Kao	
ARMENGAUD	11	PL B702 329	E. Armengaud et al.	(EDELWEISS-II Collab.)	BAUDIS	01	L. Baudis et al.	(Heidelberg-Moscow Collab.)
BUCHMUELLER...	11	EPJ C71 1583	O. Buchmuller et al.		BERNABE	01	R. Bernabe et al.	(DAMA Collab.)
BUCHMUELLER...	11B	EPJ C71 1722	O. Buchmuller et al.		BOTTINO	01	A. Bottino et al.	
CHATRCHYAN	11	JHEP 1106 093	S. Chatrchyan et al.	(CMS Collab.)	BOTTINO	01	A. Bottino et al.	
CHATRCHYAN	11D	JHEP 1107 113	S. Chatrchyan et al.	(CMS Collab.)	CORSETTI	01	A. Corsetti, P. Nath	
CHATRCHYAN	11E	JHEP 1107 098	S. Chatrchyan et al.	(CMS Collab.)	ELLIS	01B	J. Ellis et al.	
CHATRCHYAN	11V	PL B704 411	S. Chatrchyan et al.	(CMS Collab.)	ELLIS	01C	J. Ellis, A. Ferstl, K.A. Olive	
KHACHATRYAN...	11	PRL 106 011801	V. Khachatryan et al.	(CMS Collab.)	GOMEZ	01	M.E. Gomez, J.D. Vergados	
KHACHATRYAN...	11C	JHEP 1103 024	V. Khachatryan et al.	(CMS Collab.)	LAHANAS	01	A. Lahanas, D.V. Nanopoulos, V. Spanos	
ROSZKOWSKI	11	PR D83 015014	L. Roszkowski et al.		ABBIENDI	00	G. Abbiendi et al.	(OPAL Collab.)
AALTONEN	10	PRL 104 011801	T. Aaltonen et al.	(CDF Collab.)	ABBIENDI	00G	G. Abbiendi et al.	(OPAL Collab.)
AALTONEN	10R	PRL 105 081802	T. Aaltonen et al.	(CDF Collab.)	ABBIENDI	00H	G. Abbiendi et al.	(OPAL Collab.)
AALTONEN	10Z	PRL 105 191801	T. Aaltonen et al.	(CDF Collab.)	Also	EPJ C16 707 (err.)	G. Abbiendi et al.	(OPAL Collab.)
ABAZOV	10L	PL B693 95	V.M. Abazov et al.	(DO Collab.)	ABBIENDI,G	00D	G. Abbiendi et al.	(OPAL Collab.)
ABAZOV	10M	PRL 105 191802	V.M. Abazov et al.	(DO Collab.)	ABREU	00J	P. Abreu et al.	(DELPHI Collab.)
ABAZOV	10N	PRL 105 211802	V.M. Abazov et al.	(DO Collab.)	ABREU	00L	P. Abreu et al.	(DELPHI Collab.)
ABAZOV	10P	PRL 105 221802	V.M. Abazov et al.	(DO Collab.)	ABREU	00O	P. Abreu et al.	(DELPHI Collab.)
ABDO	10	JCAP 1004 014	A.A. Abdo et al.	(Fermi-LAT Collab.)	ABREU	00V	P. Abreu et al.	(DELPHI Collab.)
ACKERMANN	10	JCAP 1005 025	M. Ackermann et al.	(Fermi-LAT Collab.)	ABREU	00W	P. Abreu et al.	(DELPHI Collab.)
ARMENGAUD	10	PL B687 294	E. Armengaud et al.	(EDELWEISS-II Collab.)	ABREU	00Z	P. Abreu et al.	(DELPHI Collab.)
ELLIS	10	EPJ C69 201	J. Ellis, A. Mustafayev, K. Olive		ABUSAIIDI	00	M. Abusaidi et al.	(CDMS Collab.)
ABAZOV	09M	PRL 102 161802	V.M. Abazov et al.	(DO Collab.)	ACCIARRI	00D	M. Acciari et al.	(L3 Collab.)
ABBASI	09B	PRL 102 201302	R. Abbasi et al.	(IceCube Collab.)	ACCOMANDO	00	E. Accomando et al.	
AHMED	09	PRL 102 011301	Z. Ahmed et al.	(CDMS Collab.)	BERNABE	00	R. Bernabe et al.	(DAMA Collab.)
ANGLOHER	09	ASP 31 270	G. Angloher et al.	(CRESS-T Collab.)	BERNABE	00C	R. Bernabe et al.	(DAMA Collab.)
BUCHMUELLER...	09	EPJ C64 3911	O. Buchmuller et al.	(LOIC, FNAL, CERN+)	BERNABE	00D	R. Bernabe et al.	(DAMA Collab.)
DREINER	09	EPJ C62 547	H. Dreiner et al.		BOEHM	00B	C. Boehm, A. Djouadi, M. Drees	
LEBEDENKO	09	PR D80 052010	V.N. Lebedenko et al.	(ZEPLIN-III Collab.)	ELLIS	00	J. Ellis et al.	
LEBEDENKO	09A	PRL 103 151302	V.N. Lebedenko et al.	(ZEPLIN-III Collab.)	FENG	00	J.L. Feng, K.T. Matchev, F. Wilczek	
SORENSEN	09	NIM A601 339	P. Sorensen et al.	(XENON10 Collab.)	LEP	00	LEP Collabs.	(ALEPH, DELPHI, L3, OPAL, SLD+)
ABAZOV	08F	PL B659 856	V.M. Abazov et al.	(DO Collab.)	MORALES	00	A. Morales et al.	(IGEX Collab.)
ANGLE	08	PRL 100 021303	J. Angle et al.	(XENON10 Collab.)	PDG	00	D.E. Groom et al.	(PDG Collab.)
ANGLE	08A	PRL 101 091301	J. Angle et al.	(XENON10 Collab.)	SPOONER	00	N.J.C. Spooner et al.	(UK Dark Matter Col.)
BEDNYAKOV	08	PAN 71 111	V.A. Bednyakov, H.P. Klapdor-Kleingrothaus, I.V. Krivosheina		ACCIARRI	99R	M. Acciari et al.	(L3 Collab.)
Translated from YAF 71 112.					ACCIARRI	99L	M. Acciari et al.	(L3 Collab.)
BEHNKE	08	SCI 319 933	E. Behnke	(COUPP Collab.)	ACCIARRI	99W	M. Acciari et al.	(L3 Collab.)
BENETTI	08	ASP 28 495	P. Benetti et al.	(WARP Collab.)	AMBROSIO	99	M. Ambrosio et al.	(Macro Collab.)
BUCHMUELLER...	08	JHEP 0809 117	O. Buchmuller et al.		BAUDIS	99	L. Baudis et al.	(Heidelberg-Moscow Collab.)
ELLIS	08	PR D78 075012	J. Ellis, K. Olive, P. Sandick	(CERN, MINN)	BELLI	99C	P. Belli et al.	(DAMA Collab.)
ABULENCIA	07H	PRL 98 131804	A. Abulencia et al.	(CDF Collab.)	OOTANI	99	W. Ootani et al.	
ALNER	07A	ASP 28 287	G.J. Alner et al.	(ZEPLIN-II Collab.)	ABREU	98P	P. Abreu et al.	(DELPHI Collab.)
CALIBBI	07	JHEP 0709 081	L. Calibbi et al.		ACCIARRI	98F	M. Acciari et al.	(L3 Collab.)
ELLIS	07	JHEP 0706 079	J. Ellis, K. Olive, P. Sandick	(CERN, MINN)	ACKERS-TAFF	98P	K. Ackers-Taff et al.	(OPAL Collab.)
LEE	07A	PRL 99 091301	H.S. Lee et al.	(KIMS Collab.)	BARATE	98K	R. Barate et al.	(ALEPH Collab.)
ABBIENDI	06B	EPJ C46 307	G. Abbiendi et al.	(OPAL Collab.)	BARATE	98C	R. Barate et al.	(ALEPH Collab.)
ACHTERBERG	06	ASP 26 129	A. Achterberg et al.	(AMANDA Collab.)	BERNABE	98C	R. Bernabe et al.	(DAMA Collab.)
ACKERMANN	06	ASP 24 459	O. Ackermann et al.	(AMANDA Collab.)	ELLIS	98	J. Ellis et al.	
AKERIB	06	PR D73 011102	D.S. Akerib et al.	(CDMS Collab.)	ELLIS	98B	J. Ellis, T. Falk, K. Olive	
AKERIB	06A	PRL 96 011302	D.S. Akerib et al.	(CDMS Collab.)	PDG	98	C. Caso et al.	(PDG Collab.)
ALLANACH	06	PR D73 015013	B.C. Allanach et al.		BAER	97	H. Baer, M. Brhlik	
ENOIT	06	PL B637 156	A. Benoit et al.		BERNABE	97	R. Bernabe et al.	(DAMA Collab.)
DE-AUSTRI	06	JHEP 0605 002	R.R. de Austri, R. Trotta, L. Roszkowski		EDSJO	97	J. Edsjo, P. Gondolo	
DEBOER	06	PL B636 13	W. de Boer et al.		ARNOWITT	96	R. Arnowitt, P. Nath	
LEP-SLC	06	PRPL 427 257	ALEPH, DELPHI, L3, OPAL, SLD and working groups		BAER	96	H. Baer, M. Brhlik	
SHIMIZU	06A	PL B633 195	Y. Shimizu et al.		BERGSTROM	96	L. Bergstrom, P. Gondolo	
SMITH	06	PL B642 567	N.J.T. Smith, A.S. Murphy, T.J. Summer	(DO Collab.)	LEWIN	96	J.D. Lewin, P.F. Smith	
ABAZOV	05A	PRL 94 041801	V.M. Abazov et al.	(DELPHI Collab.)	BEREZINSKY	95	V. Berezinsky et al.	
ABDALLAH	05B	EPJ C38 395	J. Abdallah et al.	(DELPHI Collab.)	FALK	95	T. Falk, K.A. Olive, M. Srednicki	(MINN, UCSB)
AKERIB	05	PR D72 052009	D.S. Akerib et al.	(CDMS Collab.)	LOSECCO	95	J.M. Losecco	(NDAM)
ALNER	05	PL B616 17	G.J. Alner et al.	(UK Dark Matter Collab.)	ADRIANI	93M	O. Adriani et al.	(L3 Collab.)
ALNER	05A	ASP 23 444	G.J. Alner et al.	(UK Dark Matter Collab.)	DREES	93	M. Drees, M.M. Nojiri	(DESY, SLAC)
BAER	05	JHEP 0507 065	H. Baer et al.	(FSU, MSU, HAWA)	DREES	93B	M. Drees, M.M. Nojiri	

Searches Particle Listings

Supersymmetric Particle Searches, Technicolor

FALK	93	PL B318 354	T. Falk <i>et al.</i>	(UCB, UCSB, MINN)
KELLEY	93	PR D47 2461	S. Kelley <i>et al.</i>	(TAMU, ALAH)
MIZUTA	93	PL B298 120	S. Mizuta, M. Yamaguchi	(TOHO)
MORI	93	PR D48 5505	M. Mori <i>et al.</i>	(KEK, NIIG, TOKY, TOKA+)
BOTTINO	92	MPL A7 733	A. Bottino <i>et al.</i>	(TORI, ZARA)
Also		PL B265 57	A. Bottino <i>et al.</i>	(TORI, INFN)
DECAMP	92	PRPL 216 253	D. Decamp <i>et al.</i>	(ALEPH Collab.)
LOPEZ	92	NP B370 445	J.L. Lopez, D.V. Nanopoulos, K.J. Yuan	(TAMU)
MCDONALD	92	PL B293 80	J. McDonald, K.A. Olive, M. Srednicki	(LISB+)
ABREU	91F	NP B367 511	P. Abreu <i>et al.</i>	(DELPHI Collab.)
ALEXANDER	91F	ZPHY C52 175	G. Alexander <i>et al.</i>	(OPAL Collab.)
BOTTINO	91	PL B265 57	A. Bottino <i>et al.</i>	(TORI, INFN)
GELMINI	91	NP B351 623	G.B. Gelmini, P. Gondolo, E. Roulet	(UCLA, TRST)
GRIEST	91	PR D43 3191	K. Griest, D. Seckel	(CERN)
KAMIONKOW..	91	PR D44 3021	M. Kamionkowski	(CHIC, FNAL)
MORI	91B	PL B270 89	M. Mori <i>et al.</i>	(Kamiokande Collab.)
NOJIRI	91	PL B261 76	M.M. Nojiri	(KEK)
OLIVE	91	NP B355 208	K.A. Olive, M. Srednicki	(MINN, UCSB)
ROSKOWSKI	91	PL B262 59	L. Roszkowski	(CERN)
GRIEST	90	PR D41 3565	K. Griest, M. Kamionkowski, M.S. Turner	(UCB+)
BARBIERI	89C	NP B313 725	R. Barbieri, M. Frigeni, G. Giudice	(MINN, UCSB)
OLIVE	89	PL B230 78	K.A. Olive, M. Srednicki	(MINN, UCSB)
ELLIS	88D	NP B307 883	J. Ellis, R. Flores	(CERN)
GRIEST	88B	PR D38 2357	K. Griest	(CERN)
OLIVE	88	PL B205 553	K.A. Olive, M. Srednicki	(MINN, UCSB)
SREDNICKI	88	NP B310 693	M. Srednicki, R. Watkins, K.A. Olive	(MINN, UCSB)
ELLIS	84	NP B238 453	J. Ellis <i>et al.</i>	(CERN)
GOLDBERG	83	PRL 50 1419	H. Goldberg	(NEAS)
KRAUSS	83	NP B227 556	L.M. Krauss	(HARV)
VYSOTSKII	83	SJNP 37 948	M.I. Vysotsky	(ITEP)
		Translated from YAF 37 1597.		

Technicolor

See the related review(s):

[Dynamical Electroweak Symmetry Breaking: Implications of the \$H^0\$](#)

The latest unpublished results are described in "Dynamical Electroweak Symmetry Breaking" review.

MASS LIMITS for Resonances in Models of Dynamical Electroweak Symmetry Breaking

VALUE (GeV)	CL%	DOCUMENT ID	TECN	COMMENT
• • • We do not use the following data for averages, fits, limits, etc. • • •				
>2400	95	1 AAD	16W ATLS	color octet vector resonance
		2 KHACHATRYAN...16E	CMS	top-color Z'
		3 AAD	15AB ATLS	$h \rightarrow \pi_V \pi_V$
>1800	95	4 AAD	15A0 ATLS	top-color Z'
		5 AAD	15BB ATLS	$pp \rightarrow \rho_T / a_{1T} \rightarrow Wh$ or Zh
		6 AAD	15Q ATLS	$h \rightarrow \pi_V \pi_V$
		7 AAIJ	15AN LHCB	$h \rightarrow \pi_V \pi_V$
>1140	95	8 KHACHATRYAN...15C	CMS	$\rho_T \rightarrow WZ$
		9 KHACHATRYAN...15W	CMS	$H \rightarrow \pi_V \pi_V$
none 200-700, 750-890	95	10 AAD	14AT ATLS	$pp \rightarrow \omega_T \rightarrow Z\gamma$
none 275-960	95	10 AAD	14AT ATLS	$pp \rightarrow a_T \rightarrow W\gamma$
		11 AAD	14V ATLS	color singlet techni-vector
		12 AAD	13AN ATLS	$pp \rightarrow a_T \rightarrow W\gamma$
> 703		13 AAD	13AN ATLS	$pp \rightarrow \omega_T \rightarrow Z\gamma$
> 494		13 AAD	13AN ATLS	top-color Z'
none 500-1740	95	14 AAD	13AQ ATLS	top-color Z'
>1300	95	15 CHATRCHYAN13AP	CMS	top-color Z'
>2100	95	14 CHATRCHYAN13BM	CMS	top-color Z'
		16 BAAK	12 RVUE	QCD-like technicolor
none 167-687	95	17 CHATRCHYAN12AF	CMS	$\rho_T \rightarrow WZ$
> 805	95	14 AALTONEN	11AD CDF	top-color Z'
> 805	95	14 AALTONEN	11AE CDF	top-color Z'
		18 CHIVUKULA	11 RVUE	top-Higgs
		19 CHIVUKULA	11A RVUE	techni- π
		20 AALTONEN	10I CDF	$p\bar{p} \rightarrow \rho_T / \omega_T \rightarrow W\pi_T$
none 208-408	95	21 ABZOV	10A D0	$\rho_T \rightarrow WZ$
		22 ABZOV	07I D0	$p\bar{p} \rightarrow \rho_T / \omega_T \rightarrow W\pi_T$
> 280	95	23 ABULENCIA	05A CDF	$\rho_T \rightarrow e^+ e^-, \mu^+ \mu^-$
		24 CHEKANOV	02B ZEUS	color octet techni- π
> 207	95	25 ABZOV	01B D0	$\rho_T \rightarrow e^+ e^-$
none 90-206.7	95	26 ABDALLAH	01I DLPH	$e^+ e^- \rightarrow \rho_T$
		27 AFFOLDER	00F CDF	color-singlet techni- ρ , $\rho_T \rightarrow W\pi_T, 2\pi_T$
> 600	95	28 AFFOLDER	00K CDF	color-octet techni- ρ , $\rho_{T8} \rightarrow 2\pi_{LQ}$
none 350-440	95	29 ABE	99F CDF	color-octet techni- ρ , $\rho_{T8} \rightarrow b\bar{b}$
		30 ABE	99N CDF	techni- $\omega, \omega_T \rightarrow \gamma b\bar{b}$
none 260-480	95	31 ABE	97G CDF	color-octet techni- ρ , $\rho_{T8} \rightarrow 2j\bar{j}$

¹ AAD 16W search for color octet vector resonance decaying to $b\bar{b}$ in pp collisions at $\sqrt{s} = 8$ TeV. The vector like quark B is assumed to decay to bH . See their Fig.3 and Fig.4 for limits on σB .

² KHACHATRYAN 16E search for top-color Z' decaying to $t\bar{t}$. The quoted limit is for $\Gamma_{Z'}/m_{Z'} = 0.012$. Also exclude $m_{Z'} < 2.9$ TeV for wider topcolor Z' with $\Gamma_{Z'}/m_{Z'} = 0.1$.

- AAD 15AB search for long-lived hidden valley π_V particles which are produced in pairs by the decay of a scalar boson. π_V is assumed to decay into dijets. See their Fig. 10 for the limit on σB .
- AAD 15A0 search for top-color Z' decaying to $t\bar{t}$. The quoted limit is for $\Gamma_{Z'}/m_{Z'} = 0.012$.
- AAD 15BB search for minimal walking technicolor (MWT) isotriplet vector and axial-vector resonances decaying to Wh or Zh . See their Fig. 3 for the exclusion limit in the MWT parameter space.
- AAD 15Q search for long-lived hidden valley π_V particles which are produced in pairs by the decay of scalar boson. π_V is assumed to decay into dijets. See their Fig. 5 and Fig. 6 for the limit on σB .
- AAIJ 15AN search for long-lived hidden valley π_V particles which are produced in pairs by the decay of scalar boson with a mass of 120GeV. π_V is assumed to decay into dijets. See their Fig. 4 for the limit on σB .
- CHATRCHYAN 15C search for a vector techni-resonance decaying to WZ . The limit assumes $M_{\pi_T} = (3/4) M_{\rho_T} - 25$ GeV. See their Fig.3 for the limit in $M_{\pi_T} - M_{\rho_T}$ plane of the low scale technicolor model.
- CHATRCHYAN 15W search for long-lived hidden valley π_V particles which are produced in pairs in the decay of heavy higgs boson H . π_V is assumed to decay into $\ell^+ \ell^-$. See their Fig. 7 and Fig. 8 for the limits on σB .
- AAD 14AT search for techni- ω and techni- a resonances decaying to $V\gamma$ with $V = W(\rightarrow \ell\nu)$ or $Z(\rightarrow \ell^+ \ell^-)$.
- AAD 14V search for vector techni-resonances decaying into electron or muon pairs in pp collisions at $\sqrt{s} = 8$ TeV. See their table IX for exclusion limits with various assumptions.
- AAD 13AN search for vector techni-resonance a_T decaying into $W\gamma$.
- AAD 13AN search for vector techni-resonance ω_T decaying into $Z\gamma$.
- Search for top-color Z' decaying to $t\bar{t}$. The quoted limit is for $\Gamma_{Z'}/m_{Z'} = 0.012$.
- CHATRCHYAN 13AP search for top-color leptophobic Z' decaying to $t\bar{t}$. The quoted limit is for $\Gamma_{Z'}/m_{Z'} = 0.012$.
- BAAK 12 give electroweak oblique parameter constraints on the QCD-like technicolor models. See their Fig. 28.
- CHATRCHYAN 12AF search for a vector techni-resonance decaying to WZ . The limit assumes $M_{\pi_T} = (3/4) M_{\rho_T} - 25$ GeV. See their Fig. 3 for the limit in $M_{\pi_T} - M_{\rho_T}$ plane of the low scale technicolor model.
- Using the LHC limit on the Higgs boson production cross section, CHIVUKULA 11 obtain a limit on the top-Higgs mass > 300 GeV at 95% CL assuming 150 GeV top-pion mass.
- Using the LHC limit on the Higgs boson production cross section, CHIVUKULA 11A obtain a limit on the technipion mass ruling out the region $110 \text{ GeV} < m_P < 2m_t$. Existence of color techni-fermions, top-color mechanism, and $N_{TC} \geq 3$ are assumed.
- AALTONEN 10I search for the vector techni-resonances (ρ_T, ω_T) decaying into $W\pi_T$ with $W \rightarrow \ell\nu$ and $\pi_T \rightarrow b\bar{b}, b\bar{c}$, or $b\bar{u}$. See their Fig.3 for the exclusion plot in $M_{\pi_T} - M_{\rho_T}$ plane.
- ABZOV 10A search for a vector techni-resonance decaying into WZ . The limit assumes $M_{\rho_T} < M_{\pi_T} + M_W$.
- ABZOV 07I search for the vector techni-resonances (ρ_T, ω_T) decaying into $W\pi_T$ with $W \rightarrow e\nu$ and $\pi_T \rightarrow b\bar{b}$ or $b\bar{c}$. See their Fig. 2 for the exclusion plot in $M_{\pi_T} - M_{\rho_T}$ plane.
- ABULENCIA 05A search for resonances decaying to electron or muon pairs in $p\bar{p}$ collisions. at $\sqrt{s} = 1.96$ TeV. The limit assumes Technicolor-scale mass parameters $M_V = M_A = 500$ GeV.
- CHEKANOV 02B search for color octet techni- π P decaying into dijets in ep collisions. See their Fig. 5 for the limit on $\sigma(ep \rightarrow ePX) \cdot B(P \rightarrow 2j)$.
- ABZOV 01B searches for vector techni-resonances (ρ_T, ω_T) decaying to $e^+ e^-$. The limit assumes $M_{\rho_T} = M_{\omega_T} < M_{\pi_T} + M_W$.
- The limit is independent of the π_T mass. See their Fig. 9 and Fig. 10 for the exclusion plot in the $M_{\rho_T} - M_{\pi_T}$ plane. ABDALLAH 01 limit on the technipion mass is $M_{\pi_T} > 79.8$ GeV for $N_D = 2$, assuming its point-like coupling to gauge bosons.
- AFFOLDER 00F search for ρ_T decaying into $W\pi_T$ or $\pi_T\pi_T$ with $W \rightarrow \ell\nu$ and $\pi_T \rightarrow b\bar{b}, b\bar{c}$. See Fig. 1 in the above Note on "Dynamical Electroweak Symmetry Breaking" for the exclusion plot in the $M_{\rho_T} - M_{\pi_T}$ plane.
- AFFOLDER 00K search for the ρ_{T8} decaying into $\pi_{LQ}\pi_{LQ}$ with $\pi_{LQ} \rightarrow b\nu$. For $\pi_{LQ} \rightarrow c\nu$, the limit is $M_{\rho_{T8}} > 510$ GeV. See their Fig. 2 and Fig. 3 for the exclusion plot in the $M_{\rho_{T8}} - M_{\pi_{LQ}}$ plane.
- ABE 99F search for a new particle X decaying into $b\bar{b}$ in $p\bar{p}$ collisions at $E_{cm} = 1.8$ TeV. See Fig. 7 in the above Note on "Dynamical Electroweak Symmetry Breaking" for the upper limit on $\sigma(p\bar{p} \rightarrow X) \cdot B(X \rightarrow b\bar{b})$. ABE 99F also exclude top gluons of width $\Gamma = 0.3M$ in the mass interval $280 < M < 670$ GeV, of width $\Gamma = 0.5M$ in the mass interval $340 < M < 640$ GeV, and of width $\Gamma = 0.7M$ in the mass interval $375 < M < 560$ GeV.
- ABE 99N search for the techni- ω decaying into $\gamma\pi_T$. The technipion is assumed to decay $\pi_T \rightarrow b\bar{b}$. See Fig. 2 in the above Note on "Dynamical Electroweak Symmetry Breaking" for the exclusion plot in the $M_{\omega_T} - M_{\pi_T}$ plane.
- ABE 97G search for a new particle X decaying into dijets in $p\bar{p}$ collisions at $E_{cm} = 1.8$ TeV. See Fig. 5 in the above Note on "Dynamical Electroweak Symmetry Breaking" for the upper limit on $\sigma(p\bar{p} \rightarrow X) \cdot B(X \rightarrow 2j)$.

REFERENCES FOR Technicolor

AAD	16W	PL B758 249	G. Aad <i>et al.</i>	(ATLAS Collab.)
KHACHATRYAN...16E	PR D93 012001	V. Khachatryan <i>et al.</i>	(CMS Collab.)	
AAD	15AB	PR D92 012010	G. Aad <i>et al.</i>	(ATLAS Collab.)
AAD	15A0	JHEP 1508 148	G. Aad <i>et al.</i>	(ATLAS Collab.)
AAD	15BB	EPL C75 263	G. Aad <i>et al.</i>	(ATLAS Collab.)
AAD	15Q	PL B743 15	G. Aad <i>et al.</i>	(ATLAS Collab.)
AAIJ	15AN	EPL C75 152	R. Aaij <i>et al.</i>	(LHCb Collab.)
KHACHATRYAN...15C	PL B740 83	V. Khachatryan <i>et al.</i>	(CMS Collab.)	
KHACHATRYAN...15W	PR D91 052012	V. Khachatryan <i>et al.</i>	(CMS Collab.)	
AAD	14AT	PL B738 428	G. Aad <i>et al.</i>	(ATLAS Collab.)
AAD	14V	PR D90 052005	G. Aad <i>et al.</i>	(ATLAS Collab.)
AAD	13AN	PR D87 112003	G. Aad <i>et al.</i>	(ATLAS Collab.)
Also	PR D91 119901 (err.)	G. Aad <i>et al.</i>	(ATLAS Collab.)	
AAD	13AQ	PR D88 012004	G. Aad <i>et al.</i>	(ATLAS Collab.)
CHATRCHYAN 13AP	PR D87 072002	S. Chatrchyan <i>et al.</i>	(CMS Collab.)	
CHATRCHYAN 13BM	PRL 111 211804	S. Chatrchyan <i>et al.</i>	(CMS Collab.)	
Also	PRL 112 119903 (err.)	S. Chatrchyan <i>et al.</i>	(CMS Collab.)	

See key on page 999

Searches Particle Listings Technicolor, Quark and Lepton Compositeness

BAAK	12	EPJ C72 2003	M. Baak <i>et al.</i>	(Gfitter Group)
CHATRCHYAN	12AF	PRL 109 141801	S. Chatrchyan <i>et al.</i>	(CMS Collab.)
AALTONEN	11AD	PR D84 072003	T. Aaltonen <i>et al.</i>	(CDF Collab.)
AALTONEN	11AE	PR D84 072004	T. Aaltonen <i>et al.</i>	(CDF Collab.)
CHIVUKULA	11	PR D84 095022	R.S. Chivukula <i>et al.</i>	(CDF Collab.)
CHIVUKULA	11A	PR D84 115025	R. S. Chivukula <i>et al.</i>	(CDF Collab.)
AALTONEN	10I	PRL 104 111802	T. Aaltonen <i>et al.</i>	(DO Collab.)
ABAZOV	10A	PRL 104 061801	V.M. Abazov <i>et al.</i>	(DO Collab.)
ABAZOV	07I	PRL 98 221801	V.M. Abazov <i>et al.</i>	(DO Collab.)
ABULENCIA	05A	PRL 95 252001	A. Abulencia <i>et al.</i>	(CDF Collab.)
CHEKANOV	02B	PL B531 9	S. Chekanov <i>et al.</i>	(ZEUS Collab.)
ABAZOV	01B	PRL 87 061802	V.M. Abazov <i>et al.</i>	(DO Collab.)
ABDALLAH	01	EPJ C22 17	J. Abdallah <i>et al.</i>	(DELPHI Collab.)
AFFOLDER	00F	PRL 84 1110	T. Affolder <i>et al.</i>	(CDF Collab.)
AFFOLDER	00K	PRL 85 2056	T. Affolder <i>et al.</i>	(CDF Collab.)
ABE	99F	PRL 82 2038	F. Abe <i>et al.</i>	(CDF Collab.)
ABE	99N	PRL 83 3124	F. Abe <i>et al.</i>	(CDF Collab.)
ABE	97G	PR D55 5263	F. Abe <i>et al.</i>	(CDF Collab.)

Quark and Lepton Compositeness, Searches for

The latest unpublished results are described in the “Quark and Lepton Compositeness” review.

See the related review(s):

Searches for Quark and Lepton Compositeness

CONTENTS:

- Scale Limits for Contact Interactions: $\Lambda(eeee)$
- Scale Limits for Contact Interactions: $\Lambda(ee\mu\mu)$
- Scale Limits for Contact Interactions: $\Lambda(ee\tau\tau)$
- Scale Limits for Contact Interactions: $\Lambda(\ell\ell\ell\ell)$
- Scale Limits for Contact Interactions: $\Lambda(eeqq)$
- Scale Limits for Contact Interactions: $\Lambda(\mu\mu qq)$
- Scale Limits for Contact Interactions: $\Lambda(\ell\nu\ell\nu)$
- Scale Limits for Contact Interactions: $\Lambda(e\nu qq)$
- Scale Limits for Contact Interactions: $\Lambda(qqqq)$
- Scale Limits for Contact Interactions: $\Lambda(\nu\nu qq)$
- Mass Limits for Excited e (e^*)
 - Limits for Excited e (e^*) from Pair Production
 - Limits for Excited e (e^*) from Single Production
 - Limits for Excited e (e^*) from $e^+e^- \rightarrow \gamma\gamma$
 - Indirect Limits for Excited e (e^*)
- Mass Limits for Excited μ (μ^*)
 - Limits for Excited μ (μ^*) from Pair Production
 - Limits for Excited μ (μ^*) from Single Production
 - Indirect Limits for Excited μ (μ^*)
- Mass Limits for Excited τ (τ^*)
 - Limits for Excited τ (τ^*) from Pair Production
 - Limits for Excited τ (τ^*) from Single Production
- Mass Limits for Excited Neutrino (ν^*)
 - Limits for Excited ν (ν^*) from Pair Production
 - Limits for Excited ν (ν^*) from Single Production
- Mass Limits for Excited q (q^*)
 - Limits for Excited q (q^*) from Pair Production
 - Limits for Excited q (q^*) from Single Production
- Mass Limits for Color Sextet Quarks (q_6)
- Mass Limits for Color Octet Charged Leptons (ℓ_8)
- Mass Limits for Color Octet Neutrinos (ν_8)
- Mass Limits for W_8 (Color Octet W Boson)

SCALE LIMITS for Contact Interactions: $\Lambda(eeee)$

Limits are for Λ_{LL}^{\pm} only. For other cases, see each reference.

$\Lambda_{LL}^+(TeV)$	$\Lambda_{LL}^-(TeV)$	CL%	DOCUMENT ID	TECN	COMMENT
>8.3	>10.3	95	¹ BOURILKOV 01	RVUE	$E_{cm} = 192\text{--}208$ GeV
••• We do not use the following data for averages, fits, limits, etc. •••					
>4.5	>7.0	95	² SCHAEEL 07A	ALEP	$E_{cm} = 189\text{--}209$ GeV
>5.3	>6.8	95	ABDALLAH 06C	DLPH	$E_{cm} = 130\text{--}207$ GeV
>4.7	>6.1	95	³ ABBIENDI 04G	OPAL	$E_{cm} = 130\text{--}207$ GeV
>4.3	>4.9	95	ACCIARRI 00P	L3	$E_{cm} = 130\text{--}189$ GeV

- ¹ A combined analysis of the data from ALEPH, DELPHI, L3, and OPAL.
- ² SCHAEEL 07A limits are from $R_{C\tau}$, Q_{FB}^{depl} , and hadronic cross section measurements.
- ³ ABBIENDI 04G limits are from $e^+e^- \rightarrow e^+e^-$ cross section at $\sqrt{s} = 130\text{--}207$ GeV.

SCALE LIMITS for Contact Interactions: $\Lambda(ee\mu\mu)$

Limits are for Λ_{LL}^{\pm} only. For other cases, see each reference.

$\Lambda_{LL}^+(TeV)$	$\Lambda_{LL}^-(TeV)$	CL%	DOCUMENT ID	TECN	COMMENT
>6.6	>9.5	95	¹ SCHAEEL 07A	ALEP	$E_{cm} = 189\text{--}209$ GeV
>8.5	>3.8	95	ACCIARRI 00P	L3	$E_{cm} = 130\text{--}189$ GeV
••• We do not use the following data for averages, fits, limits, etc. •••					
>7.3	>7.6	95	ABDALLAH 06C	DLPH	$E_{cm} = 130\text{--}207$ GeV
>8.1	>7.3	95	² ABBIENDI 04G	OPAL	$E_{cm} = 130\text{--}207$ GeV

- ¹ SCHAEEL 07A limits are from $R_{C\tau}$, Q_{FB}^{depl} , and hadronic cross section measurements.
- ² ABBIENDI 04G limits are from $e^+e^- \rightarrow \mu\mu$ cross section at $\sqrt{s} = 130\text{--}207$ GeV.

SCALE LIMITS for Contact Interactions: $\Lambda(ee\tau\tau)$

Limits are for Λ_{LL}^{\pm} only. For other cases, see each reference.

$\Lambda_{LL}^+(TeV)$	$\Lambda_{LL}^-(TeV)$	CL%	DOCUMENT ID	TECN	COMMENT
>7.9	>5.8	95	¹ SCHAEEL 07A	ALEP	$E_{cm} = 189\text{--}209$ GeV
>7.9	>4.6	95	ABDALLAH 06C	DLPH	$E_{cm} = 130\text{--}207$ GeV
>4.9	>7.2	95	² ABBIENDI 04G	OPAL	$E_{cm} = 130\text{--}207$ GeV
••• We do not use the following data for averages, fits, limits, etc. •••					
>5.4	>4.7	95	ACCIARRI 00P	L3	$E_{cm} = 130\text{--}189$ GeV

- ¹ SCHAEEL 07A limits are from $R_{C\tau}$, Q_{FB}^{depl} , and hadronic cross section measurements.
- ² ABBIENDI 04G limits are from $e^+e^- \rightarrow \tau\tau$ cross section at $\sqrt{s} = 130\text{--}207$ GeV.

SCALE LIMITS for Contact Interactions: $\Lambda(\ell\ell\ell\ell)$

Lepton universality assumed. Limits are for Λ_{LL}^{\pm} only. For other cases, see each reference.

$\Lambda_{LL}^+(TeV)$	$\Lambda_{LL}^-(TeV)$	CL%	DOCUMENT ID	TECN	COMMENT
>7.9	>10.3	95	¹ SCHAEEL 07A	ALEP	$E_{cm} = 189\text{--}209$ GeV
>9.1	>8.2	95	ABDALLAH 06C	DLPH	$E_{cm} = 130\text{--}207$ GeV
••• We do not use the following data for averages, fits, limits, etc. •••					
>7.7	>9.5	95	² ABBIENDI 04G	OPAL	$E_{cm} = 130\text{--}207$ GeV
			³ BABICH 03	RVUE	
>9.0	>5.2	95	ACCIARRI 00P	L3	$E_{cm} = 130\text{--}189$ GeV

- ¹ SCHAEEL 07A limits are from $R_{C\tau}$, Q_{FB}^{depl} , and hadronic cross section measurements.
- ² ABBIENDI 04G limits are from $e^+e^- \rightarrow \ell^+\ell^-$ cross section at $\sqrt{s} = 130\text{--}207$ GeV.
- ³ BABICH 03 obtain a bound $-0.175 \text{ TeV}^{-2} < 1/\Lambda_{LL}^2 < 0.095 \text{ TeV}^{-2}$ (95%CL) in a model independent analysis allowing all of $\Lambda_{LL}, \Lambda_{LR}, \Lambda_{RL}, \Lambda_{RR}$ to coexist.

SCALE LIMITS for Contact Interactions: $\Lambda(eeqq)$

Limits are for Λ_{LL}^{\pm} only. For other cases, see each reference.

$\Lambda_{LL}^+(TeV)$	$\Lambda_{LL}^-(TeV)$	CL%	DOCUMENT ID	TECN	COMMENT
> 4.5	>12.8	95	¹ ABRAMOWICZ19	ZEUS	($eeqq$)
>23.9	>16.8	95	² SIRUNYAN 19AC	CMS	($eeqq$)
>24	>37	95	³ AABOUD 17AT	ATLS	($eeqq$)
> 8.4	>10.2	95	⁴ ABDALLAH 09	DLPH	($eebb$)
> 9.4	>5.6	95	⁵ SCHAEEL 07A	ALEP	($eecc$)
> 9.4	>4.9	95	⁴ SCHAEEL 07A	ALEP	($eebb$)
>23.3	>12.5	95	⁶ CHEUNG 01B	RVUE	($eeuu$)
>11.1	>26.4	95	⁶ CHEUNG 01B	RVUE	($eedd$)

- We do not use the following data for averages, fits, limits, etc. •••
- >15.5 >19.5 95 ⁷AABOUD 16U ATLS ($eeqq$)
- >13.5 >18.3 95 ⁸KHACHATRYAN 15AE CMS ($eeqq$)
- >16.4 >20.7 95 ⁹AAD 14BE ATLS ($eeqq$)
- > 9.5 >12.1 95 ¹⁰AAD 13E ATLS ($eeqq$)
- >10.1 >9.4 95 ¹¹AAD 12AB ATLS ($eeqq$)
- > 4.2 >4.0 95 ¹²AARON 11C HI ($eeqq$)
- > 3.8 >3.8 95 ¹³ABDALLAH 11 DLPH ($ee\tau c$)
- >12.9 >7.2 95 ¹⁴SCHAEEL 07A ALEP ($eeqq$)
- > 3.7 >5.9 95 ¹⁵ABULENCIA 06L CDF ($eeqq$)

- ¹ ABRAMOWICZ 19 limits are from Q^2 spectrum measurements of $e^{\pm}p \rightarrow e^{\pm}X$.
- ² SIRUNYAN 19AC limits are from e^+e^- mass distribution in pp collisions at $\sqrt{s} = 13$ TeV.
- ³ AABOUD 17AT limits are from pp collisions at $\sqrt{s} = 13$ TeV. The quoted limit uses a uniform positive prior in $1/\Lambda^2$.
- ⁴ ABDALLAH 09 and SCHAEEL 07A limits are from $R_{B\tau}$, A_{FB}^b .
- ⁵ SCHAEEL 07A limits are from $R_{C\tau}$, Q_{FB}^{depl} , and hadronic cross section measurements.
- ⁶ CHEUNG 01B is an update of BARGER 98E.
- ⁷ AABOUD 16U limits are from pp collisions at $\sqrt{s} = 13$ TeV. The quoted limit uses a uniform positive prior in $1/\Lambda^2$.
- ⁸ KHACHATRYAN 15AE limit is from e^+e^- mass distribution in pp collisions at $E_{cm} = 8$ TeV.
- ⁹ AAD 14BE limits are from pp collisions at $\sqrt{s} = 8$ TeV. The quoted limit uses a uniform positive prior in $1/\Lambda^2$.
- ¹⁰ AAD 13E limits are from e^+e^- mass distribution in pp collisions at $E_{cm} = 7$ TeV.
- ¹¹ AAD 12AB limits are from e^+e^- mass distribution in pp collisions at $E_{cm} = 7$ TeV.
- ¹² AARON 11C limits are from Q^2 spectrum measurements of $e^{\pm}p \rightarrow e^{\pm}X$.
- ¹³ ABDALLAH 11 limit is from $e^+e^- \rightarrow t\bar{c}$ cross section. $\Lambda_{LL} = \Lambda_{LR} = \Lambda_{RL} = \Lambda_{RR}$ is assumed.
- ¹⁴ SCHAEEL 07A limit assumes quark flavor universality of the contact interactions.
- ¹⁵ ABULENCIA 06L limits are from $p\bar{p}$ collisions at $\sqrt{s} = 1.96$ TeV.

SCALE LIMITS for Contact Interactions: $\Lambda(\mu\mu qq)$

$\Lambda_{LL}^+(TeV)$	$\Lambda_{LL}^-(TeV)$	CL%	DOCUMENT ID	TECN	COMMENT
>30.4	>20.4	95	¹ SIRUNYAN 19AC	CMS	($\mu\mu qq$)
>20	>30	95	² AABOUD 17AT	ATLS	($\mu\mu qq$)

Searches Particle Listings

Quark and Lepton Compositeness

• • • We do not use the following data for averages, fits, limits, etc. • • •

>15.8	>21.8	95	³ AABOUD	16U ATLS	($\mu\mu qq$)
>12.0	>15.2	95	⁴ KHACHATRYAN	15AE CMS	($\mu\mu qq$)
>12.5	>16.7	95	⁵ AAD	14BE ATLS	($\mu\mu qq$)
> 9.6	>12.9	95	⁶ AAD	13E ATLS	($\mu\mu qq$) (isosinglet)
> 9.5	>13.1	95	⁷ CHATRCHYAN	13K CMS	($\mu\mu qq$) (isosinglet)
> 8.0	>7.0	95	⁸ AAD	12AB ATLS	($\mu\mu qq$) (isosinglet)

¹ SIRUNYAN 19AC limits are from $\mu^+\mu^-$ mass distribution in pp collisions at $\sqrt{s} = 13$ TeV.

² AABOUD 17AT limits are from pp collisions at $\sqrt{s} = 13$ TeV. The quoted limit uses a uniform positive prior in $1/\Lambda^2$.

³ AABOUD 16U limits are from pp collisions at $\sqrt{s} = 13$ TeV. The quoted limit uses a uniform positive prior in $1/\Lambda^2$.

⁴ KHACHATRYAN 15AE limit is from $\mu^+\mu^-$ mass distribution in pp collisions at $E_{cm} = 8$ TeV.

⁵ AAD 14BE limits are from pp collisions at $\sqrt{s} = 8$ TeV. The quoted limit uses a uniform positive prior in $1/\Lambda^2$.

⁶ AAD 13E limits are from $\mu^+\mu^-$ mass distribution in pp collisions at $E_{cm} = 7$ TeV.

⁷ CHATRCHYAN 13K limits are from $\mu^+\mu^-$ mass distribution in pp collisions at $E_{cm} = 7$ TeV.

⁸ AAD 12AB limits are from $\mu^+\mu^-$ mass distribution in pp collisions at $E_{cm} = 7$ TeV.

SCALE LIMITS for Contact Interactions: $\Lambda(\ell\nu\ell\nu)$

VALUE (TeV)	CL%	DOCUMENT ID	TECN	COMMENT
>3.10	90	¹ JODIDIO	86	SPEC $\Lambda_{LR}^{\pm}(\nu_\mu\nu_e\mu e)$

• • • We do not use the following data for averages, fits, limits, etc. • • •

>3.8		² DIAZCRUZ	94	RVUE $\Lambda_{LL}^+(\tau\nu_\tau e\nu_e)$
>8.1		² DIAZCRUZ	94	RVUE $\Lambda_{LL}^-(\tau\nu_\tau e\nu_e)$
>4.1		³ DIAZCRUZ	94	RVUE $\Lambda_{LL}^+(\tau\nu_\tau\mu\nu_\mu)$
>6.5		³ DIAZCRUZ	94	RVUE $\Lambda_{LL}^-(\tau\nu_\tau\mu\nu_\mu)$

¹ JODIDIO 86 limit is from $\mu^+ \rightarrow \bar{\nu}_\mu e^+ \nu_e$. Chirality invariant interactions $L = (g^2/\Lambda^2)$ [$\eta_{LL}(\bar{\nu}_\mu L \gamma^\alpha \mu_L)(\bar{e} L \gamma^\alpha \nu_e) + \eta_{LR}(\bar{\nu}_\mu L \gamma^\alpha \nu_e)(\bar{e} R \gamma^\alpha \mu_R)$] with $g^2/4\pi = 1$ and $(\eta_{LL}, \eta_{LR}) = (0, \pm 1)$ are taken. No limits are given for Λ_{LL}^{\pm} with $(\eta_{LL}, \eta_{LR}) = (\pm 1, 0)$. For more general constraints with right-handed neutrinos and chirality nonconserving contact interactions, see their text.

² DIAZCRUZ 94 limits are from $\Gamma(\tau \rightarrow e\nu\nu)$ and assume flavor-dependent contact interactions with $\Lambda(\tau\nu_\tau e\nu_e) \ll \Lambda(\mu\nu_\mu e\nu_e)$.

³ DIAZCRUZ 94 limits are from $\Gamma(\tau \rightarrow \mu\nu\nu)$ and assume flavor-dependent contact interactions with $\Lambda(\tau\nu_\tau\mu\nu_\mu) \ll \Lambda(\mu\nu_\mu e\nu_e)$.

SCALE LIMITS for Contact Interactions: $\Lambda(e\nu qq)$

VALUE (TeV)	CL%	DOCUMENT ID	TECN	COMMENT
>2.81	95	¹ AFFOLDER	01i	CDF

¹ AFFOLDER 00i bound is for a scalar interaction $\bar{q}_R q_L \bar{\nu}_e L$.

SCALE LIMITS for Contact Interactions: $\Lambda(qqqq)$

Λ_{LL}^{\pm} (TeV)	Λ_{LR}^{\pm} (TeV)	CL%	DOCUMENT ID	TECN	COMMENT
>13.1 none	17.4–29.5	>21.8	95	¹ AABOUD	17AK ATLS pp dijet angl.

• • • We do not use the following data for averages, fits, limits, etc. • • •

>12.8	>17.5	95	² AABOUD	18AV ATLS	$pp \rightarrow t\bar{t}t\bar{t}$
>11.5	>14.7	95	³ SIRUNYAN	18DD CMS	pp dijet angl.
>12.0	>17.5	95	⁴ SIRUNYAN	17F CMS	pp dijet angl.
			⁵ AAD	16S ATLS	pp dijet angl.
			⁶ AAD	15AR ATLS	$pp \rightarrow t\bar{t}t\bar{t}$
			⁷ AAD	15BY ATLS	$pp \rightarrow t\bar{t}t\bar{t}$
> 8.1	>12.0	95	⁸ AAD	15L ATLS	pp dijet angl.
> 9.0	>11.7	95	⁹ KHACHATRYAN	15J CMS	pp dijet angl.
> 5		95	¹⁰ FABBRICHESI	14	RVUE $q\bar{q}t\bar{t}$

¹ AABOUD 17AK limit is from dijet angular distribution in pp collisions at $\sqrt{s} = 13$ TeV. u , d , and s quarks are assumed to be composite.

² AABOUD 18AV obtain limit on t_R compositeness $2\pi/\Lambda_{RR}^2 < 1.6 \text{ TeV}^{-2}$ at 95% CL from $t\bar{t}t\bar{t}$ production in the pp collisions at $E_{cm} = 13$ TeV.

³ SIRUNYAN 18DD limit is from dijet angular distribution in pp collisions at $\sqrt{s} = 13$ TeV.

⁴ SIRUNYAN 17F limit is from dijet angular cross sections in pp collisions at $E_{cm} = 13$ TeV. All quarks are assumed to be composite.

⁵ AAD 16S limit is from dijet angular selections in pp collisions at $E_{cm} = 13$ TeV. u , d , and s quarks are assumed to be composite.

⁶ AAD 15AR obtain limit on the t_R compositeness $2\pi/\Lambda_{RR}^2 < 6.6 \text{ TeV}^{-2}$ at 95% CL from the $t\bar{t}t\bar{t}$ production in the pp collisions at $E_{cm} = 8$ TeV.

⁷ AAD 15BY obtain limit on the t_R compositeness $2\pi/\Lambda_{RR}^2 < 15.1 \text{ TeV}^{-2}$ at 95% CL from the $t\bar{t}t\bar{t}$ production in the pp collisions at $E_{cm} = 8$ TeV.

⁸ AAD 15L limit is from dijet angular distribution in pp collisions at $E_{cm} = 8$ TeV. u , d , and s quarks are assumed to be composite.

⁹ KHACHATRYAN 15J limit is from dijet angular distribution in pp collisions at $E_{cm} = 8$ TeV. u , d , s , c , and b quarks are assumed to be composite.

¹⁰ FABBRICHESI 14 obtain bounds on chromoelectric and chromomagnetic form factors of the top-quark using $pp \rightarrow t\bar{t}$ and $p\bar{p} \rightarrow t\bar{t}$ cross sections. The quoted limit on the $q\bar{q}t\bar{t}$ contact interaction is derived from their bound on the chromoelectric form factor.

SCALE LIMITS for Contact Interactions: $\Lambda(\nu\nu qq)$

Limits are for Λ_{LL}^{\pm} only. For other cases, see each reference.

Λ_{LL}^+ (TeV)	Λ_{LL}^- (TeV)	CL%	DOCUMENT ID	TECN	COMMENT
>5.0	>5.4	95	¹ MCFARLAND	98	CCFR νN scattering

¹ MCFARLAND 98 assumed a flavor universal interaction. Neutrinos were mostly of muon type.

MASS LIMITS for Excited e (e^*)

Most e^+e^- experiments assume one-photon or Z exchange. The limits from some e^+e^- experiments which depend on λ have assumed transition couplings which are chirality violating ($\eta_L = \eta_R$). However they can be interpreted as limits for chirality-conserving interactions after multiplying the coupling value λ by $\sqrt{2}$; see Note.

Excited leptons have the same quantum numbers as other ortholeptons. See also the searches for ortholeptons in the “Searches for Heavy Leptons” section.

Limits for Excited e (e^*) from Pair Production

These limits are obtained from $e^+e^- \rightarrow e^*e^*$ and thus rely only on the (electroweak) charge of e^* . Form factor effects are ignored unless noted. For the case of limits from Z decay, the e^* coupling is assumed to be of sequential type. Possible t channel contribution from transition magnetic coupling is neglected. All limits assume a dominant $e^* \rightarrow e\gamma$ decay except the limits from $\Gamma(Z)$.

For limits prior to 1987, see our 1992 edition (Physical Review **D45** S1 (1992)).

VALUE (GeV)	CL%	DOCUMENT ID	TECN	COMMENT
>103.2	95	¹ ABBIENDI	02G OPAL	$e^+e^- \rightarrow e^*e^*$ Homodoublet type
>102.8	95	² ACHARD	03B L3	$e^+e^- \rightarrow e^*e^*$ Homodoublet type

¹ From e^+e^- collisions at $\sqrt{s} = 183\text{--}209$ GeV. $f = f'$ is assumed.

² From e^+e^- collisions at $\sqrt{s} = 189\text{--}209$ GeV. $f = f'$ is assumed. ACHARD 03B also obtain limit for $f = -f'$. $m_{e^*} > 96.6$ GeV.

Limits for Excited e (e^*) from Single Production

These limits are from $e^+e^- \rightarrow e^*e$, $W \rightarrow e^*\nu$, or $ep \rightarrow e^*X$ and depend on transition magnetic coupling between e and e^* . All limits assume $e^* \rightarrow e\gamma$ decay except as noted. Limits from LEP, UA2, and H1 are for chiral coupling, whereas all other limits are for nonchiral coupling, $\eta_L = \eta_R = 1$. In most papers, the limit is expressed in the form of an excluded region in the $\lambda\text{--}m_{e^*}$ plane. See the original papers.

For limits prior to 1987, see our 1992 edition (Physical Review **D45** S1 (1992)).

VALUE (GeV)	CL%	DOCUMENT ID	TECN	COMMENT
>4800	95	¹ AABOUD	19AZ ATLS	$pp \rightarrow e^*e^*X$
>3900	95	² SIRUNYAN	19Z CMS	$pp \rightarrow e^*e^*X$
>2450	95	³ KHACHATRYAN	16AQ CMS	$pp \rightarrow e^*e^*X$
>3000	95	⁴ AAD	15AP ATLS	$pp \rightarrow e^{(*)}e^*X$
>2200	95	⁵ AAD	13BB ATLS	$pp \rightarrow e^*e^*X$
>1900	95	⁶ CHATRCHYAN	13AE CMS	$pp \rightarrow e^*e^*X$
>1870	95	⁷ AAD	12AZ ATLS	$pp \rightarrow e^{(*)}e^*X$

¹ AABOUD 19AZ search for single e^* production in pp collisions at $\sqrt{s} = 13$ TeV. The limit quoted above is from $e^* \rightarrow e q\bar{q}$ and $e^* \rightarrow \nu W$ decays assuming $f = f' = 1$ and $m_{e^*} = \Lambda$. The contact interaction is included in e^* production and decay amplitudes. See their Fig. 6 for exclusion limits in $m_{e^*} - \Lambda$ plane.

² SIRUNYAN 19Z search for e^* production in $\ell\ell\gamma$ final states in pp collisions at $\sqrt{s} = 13$ TeV. The quoted limit assumes $\Lambda = m_{e^*}$, $f = f' = 1$. The contact interaction is included in the e^* production and decay amplitudes.

³ KHACHATRYAN 16AQ search for single e^* production in pp collisions at $\sqrt{s} = 8$ TeV. The limit above is from the $e^* \rightarrow e\gamma$ search channel assuming $f = f' = 1$, $m_{e^*} = \Lambda$. See their Table 7 for limits in other search channels or with different assumptions.

⁴ AAD 15AP search for e^* production in events with three or more charged leptons in pp collisions at $\sqrt{s} = 8$ TeV. The quoted limit assumes $\Lambda = m_{e^*}$, $f = f' = 1$. The contact interaction is included in the e^* production and decay amplitudes.

⁵ AAD 13BB search for single e^* production in pp collisions with $e^* \rightarrow e\gamma$ decay. $f = f' = 1$, and e^* production via contact interaction with $\Lambda = m_{e^*}$ are assumed.

⁶ CHATRCHYAN 13AE search for single e^* production in pp collisions with $e^* \rightarrow e\gamma$ decay. $f = f' = 1$, and e^* production via contact interaction with $\Lambda = m_{e^*}$ are assumed.

⁷ AAD 12AZ search for e^* production via four-fermion contact interaction in pp collisions with $e^* \rightarrow e\gamma$ decay. The quoted limit assumes $\Lambda = m_{e^*}$. See their Fig. 8 for the exclusion plot in the mass-coupling plane.

See key on page 999

Searches Particle Listings

Quark and Lepton Compositeness

Limits for Excited e (e^*) from $e^+e^- \rightarrow \gamma\gamma$

These limits are derived from indirect effects due to e^* exchange in the t channel and depend on transition magnetic coupling between e and e^* . All limits are for $\lambda_\gamma = 1$. All limits except ABE 89j and ACHARD 02D are for nonchiral coupling with $\eta_L = \eta_R = 1$. We choose the chiral coupling limit as the best limit and list it in the Summary Table.

For limits prior to 1987, see our 1992 edition (Physical Review **D45** S1 (1992)).

VALUE (GeV)	CL%	DOCUMENT ID	TECN	COMMENT
>356	95	¹ ABDALLAH 04N	DLPH	$\sqrt{s} = 161\text{--}208$ GeV
•••		We do not use the following data for averages, fits, limits, etc. •••		
>310	95	ACHARD 02D	L3	$\sqrt{s} = 192\text{--}209$ GeV

¹ ABDALLAH 04N also obtain a limit on the excited electron mass with e^*e^* chiral coupling, $m_{e^*} > 295$ GeV at 95% CL.

Indirect Limits for Excited e (e^*)

These limits make use of loop effects involving e^* and are therefore subject to theoretical uncertainty.

VALUE (GeV)	DOCUMENT ID	TECN	COMMENT
•••	We do not use the following data for averages, fits, limits, etc. •••		
	¹ DORENBOS... 89	CHRM	$\mathcal{T}_{\mu e} \rightarrow \mathcal{T}_{\mu e}, \nu_{\mu e} \rightarrow \nu_{\mu e}$
	² GRIFOLS 86	THEO	$\nu_{\mu e} \rightarrow \nu_{\mu e}$
	³ RENARD 82	THEO	$g-2$ of electron

¹ DORENBOSCH 89 obtain the limit $\lambda_{\text{cut}}^2 \Lambda_{\text{cut}}^2 / m_{e^*}^2 < 2.6$ (95% CL), where Λ_{cut} is the cutoff scale, based on the one-loop calculation by GRIFOLS 86. If one assumes that $\Lambda_{\text{cut}} = 1$ TeV and $\lambda_\gamma = 1$, one obtains $m_{e^*} > 620$ GeV. However, one generally expects $\lambda_\gamma \approx m_{e^*} / \Lambda_{\text{cut}}$ in composite models.

² GRIFOLS 86 uses $\nu_{\mu e} \rightarrow \nu_{\mu e}$ and $\mathcal{T}_{\mu e} \rightarrow \mathcal{T}_{\mu e}$ data from CHARM Collaboration to derive mass limits which depend on the scale of compositeness.

³ RENARD 82 derived from $g-2$ data limits on mass and couplings of e^* and μ^* . See figures 2 and 3 of the paper.

MASS LIMITS for Excited μ (μ^*)

Limits for Excited μ (μ^*) from Pair Production

These limits are obtained from $e^+e^- \rightarrow \mu^*\mu^*$ and thus rely only on the (electroweak) charge of μ^* . Form factor effects are ignored unless noted. For the case of limits from Z decay, the μ^* coupling is assumed to be of sequential type. All limits assume a dominant $\mu^* \rightarrow \mu\gamma$ decay except the limits from $\Gamma(Z)$.

For limits prior to 1987, see our 1992 edition (Physical Review **D45** S1 (1992)).

VALUE (GeV)	CL%	DOCUMENT ID	TECN	COMMENT
>103.2	95	¹ ABBIENDI 02G	OPAL	$e^+e^- \rightarrow \mu^*\mu^*$ Homodoublet type
•••	We do not use the following data for averages, fits, limits, etc. •••			
>102.8	95	² ACHARD 03B	L3	$e^+e^- \rightarrow \mu^*\mu^*$ Homodoublet type

¹ From e^+e^- collisions at $\sqrt{s} = 183\text{--}209$ GeV. $f = f'$ is assumed.

² From e^+e^- collisions at $\sqrt{s} = 189\text{--}209$ GeV. $f = f'$ is assumed. ACHARD 03B also obtain limit for $f = -f'$: $m_{\mu^*} > 96.6$ GeV.

Limits for Excited μ (μ^*) from Single Production

These limits are from $e^+e^- \rightarrow \mu^*\mu$ and depend on transition magnetic coupling between μ and μ^* . All limits assume $\mu^* \rightarrow \mu\gamma$ decay. Limits from LEP are for chiral coupling, whereas all other limits are for nonchiral coupling, $\eta_L = \eta_R = 1$. In most papers, the limit is expressed in the form of an excluded region in the $\lambda\text{--}m_{\mu^*}$ plane. See the original papers.

For limits prior to 1987, see our 1992 edition (Physical Review **D45** S1 (1992)).

VALUE (GeV)	CL%	DOCUMENT ID	TECN	COMMENT
>3800	95	¹ SIRUNYAN 19Z	CMS	$pp \rightarrow \mu\mu^*X$
•••	We do not use the following data for averages, fits, limits, etc. •••			
>2800	95	² AAD 16BM	ATLS	$pp \rightarrow \mu\mu^*X$
>2470	95	³ KHACHATRYAN...16AQ	CMS	$pp \rightarrow \mu\mu^*X$
>3000	95	⁴ AAD 15AP	ATLS	$pp \rightarrow \mu^{(*)}\mu^*X$
>2200	95	⁵ AAD 13BB	ATLS	$pp \rightarrow \mu\mu^*X$
>1900	95	⁶ CHATRCHYAN13AE	CMS	$pp \rightarrow \mu\mu^*X$
>1750	95	⁷ AAD 12AZ	ATLS	$pp \rightarrow \mu^{(*)}\mu^*X$

¹ SIRUNYAN 19Z search for μ^* production in $\ell\ell\gamma$ final states in pp collisions at $\sqrt{s} = 13$ TeV. The quoted limit assumes $\Lambda = m_{\mu^*}$, $f = f' = 1$. The contact interaction is included in the μ^* production and decay amplitudes.

² AAD 16BM search for μ^* production in $\mu\mu jj$ events in pp collisions at $\sqrt{s} = 8$ TeV. Both the production and decay are assumed to occur via a contact interaction with $\Lambda = m_{\mu^*}$.

³ KHACHATRYAN 16AQ search for single μ^* production in pp collisions at $\sqrt{s} = 8$ TeV. The limit above is from the $\mu^* \rightarrow \mu\gamma$ search channel assuming $f = f' = 1$, $m_{\mu^*} = \Lambda$. See their Table 7 for limits in other search channels or with different assumptions.

⁴ AAD 15AP search for μ^* production in events with three or more charged leptons in pp collisions at $\sqrt{s} = 8$ TeV. The quoted limit assumes $\Lambda = m_{\mu^*}$, $f = f' = 1$. The contact interaction is included in the μ^* production and decay amplitudes.

⁵ AAD 13BB search for single μ^* production in pp collisions with $\mu^* \rightarrow \mu\gamma$ decay. $f = f' = 1$, and μ^* production via contact interaction with $\Lambda = m_{\mu^*}$ are assumed.

⁶ CHATRCHYAN 13AE search for single μ^* production in pp collisions with $\mu^* \rightarrow \mu\gamma$ decay. $f = f' = 1$, and μ^* production via contact interaction with $\Lambda = m_{\mu^*}$ are assumed.

⁷ AAD 12AZ search for μ^* production via four-fermion contact interaction in pp collisions with $\mu^* \rightarrow \mu\gamma$ decay. The quoted limit assumes $\Lambda = m_{\mu^*}$. See their Fig. 8 for the exclusion plot in the mass-coupling plane.

Indirect Limits for Excited μ (μ^*)

These limits make use of loop effects involving μ^* and are therefore subject to theoretical uncertainty.

VALUE (GeV)	DOCUMENT ID	TECN	COMMENT
•••	We do not use the following data for averages, fits, limits, etc. •••		
	¹ RENARD 82	THEO	$g-2$ of muon

¹ RENARD 82 derived from $g-2$ data limits on mass and couplings of e^* and μ^* . See figures 2 and 3 of the paper.

MASS LIMITS for Excited τ (τ^*)

Limits for Excited τ (τ^*) from Pair Production

These limits are obtained from $e^+e^- \rightarrow \tau^*\tau^*$ and thus rely only on the (electroweak) charge of τ^* . Form factor effects are ignored unless noted. For the case of limits from Z decay, the τ^* coupling is assumed to be of sequential type. All limits assume a dominant $\tau^* \rightarrow \tau\gamma$ decay except the limits from $\Gamma(Z)$.

For limits prior to 1987, see our 1992 edition (Physical Review **D45** S1 (1992)).

VALUE (GeV)	CL%	DOCUMENT ID	TECN	COMMENT
>103.2	95	¹ ABBIENDI 02G	OPAL	$e^+e^- \rightarrow \tau^*\tau^*$ Homodoublet type
•••	We do not use the following data for averages, fits, limits, etc. •••			
>102.8	95	² ACHARD 03B	L3	$e^+e^- \rightarrow \tau^*\tau^*$ Homodoublet type

¹ From e^+e^- collisions at $\sqrt{s} = 183\text{--}209$ GeV. $f = f'$ is assumed.

² From e^+e^- collisions at $\sqrt{s} = 189\text{--}209$ GeV. $f = f'$ is assumed. ACHARD 03B also obtain limit for $f = -f'$: $m_{\tau^*} > 96.6$ GeV.

Limits for Excited τ (τ^*) from Single Production

These limits are from $e^+e^- \rightarrow \tau^*\tau$ and depend on transition magnetic coupling between τ and τ^* . All limits assume $\tau^* \rightarrow \tau\gamma$ decay. Limits from LEP are for chiral coupling, whereas all other limits are for nonchiral coupling, $\eta_L = \eta_R = 1$. In most papers, the limit is expressed in the form of an excluded region in the $\lambda\text{--}m_{\tau^*}$ plane. See the original papers.

VALUE (GeV)	CL%	DOCUMENT ID	TECN	COMMENT
>2500	95	¹ AAD 15AP	ATLS	$pp \rightarrow \tau^{(*)}\tau^*X$
•••	We do not use the following data for averages, fits, limits, etc. •••			
> 180	95	² ACHARD 03B	L3	$e^+e^- \rightarrow \tau\tau^*$
> 185	95	³ ABBIENDI 02G	OPAL	$e^+e^- \rightarrow \tau\tau^*$

¹ AAD 15AP search for τ^* production in events with three or more charged leptons in pp collisions at $\sqrt{s} = 8$ TeV. The quoted limit assumes $\Lambda = m_{\tau^*}$, $f = f' = 1$. The contact interaction is included in the τ^* production and decay amplitudes.

² ACHARD 03B result is from e^+e^- collisions at $\sqrt{s} = 189\text{--}209$ GeV. $f = f' = \Lambda / m_{\tau^*}$ is assumed. See their Fig. 4 for the exclusion plot in the mass-coupling plane.

³ ABBIENDI 02G result is from e^+e^- collisions at $\sqrt{s} = 183\text{--}209$ GeV. $f = f' = \Lambda / m_{\tau^*}$ is assumed for τ^* coupling. See their Fig. 4c for the exclusion limit in the mass-coupling plane.

MASS LIMITS for Excited Neutrino (ν^*)

Limits for Excited ν (ν^*) from Pair Production

These limits are obtained from $e^+e^- \rightarrow \nu^*\nu^*$ and thus rely only on the (electroweak) charge of ν^* . Form factor effects are ignored unless noted. The ν^* coupling is assumed to be of sequential type unless otherwise noted. All limits assume a dominant $\nu^* \rightarrow \nu\gamma$ decay except the limits from $\Gamma(Z)$.

VALUE (GeV)	CL%	DOCUMENT ID	TECN	COMMENT
>1600	95	¹ AAD 15AP	ATLS	$pp \rightarrow \nu^*\nu^*X$
•••	We do not use the following data for averages, fits, limits, etc. •••			
		² ABBIENDI 04N	OPAL	
> 102.6	95	³ ACHARD 03B	L3	$e^+e^- \rightarrow \nu^*\nu^*$ Homodoublet type

¹ AAD 15AP search for ν^* pair production in events with three or more charged leptons in pp collisions at $\sqrt{s} = 8$ TeV. The quoted limit assumes $\Lambda = m_{\nu^*}$, $f = f' = 1$. The contact interaction is included in the ν^* production and decay amplitudes.

² From e^+e^- collisions at $\sqrt{s} = 192\text{--}209$ GeV, ABBIENDI 04N obtain limit on $\sigma(e^+e^- \rightarrow \nu^*\nu^*) B^2(\nu^* \rightarrow \nu\gamma)$. See their Fig.2. The limit ranges from 20 to 45 fb for $m_{\nu^*} > 45$ GeV.

³ From e^+e^- collisions at $\sqrt{s} = 189\text{--}209$ GeV. $f = -f'$ is assumed. ACHARD 03B also obtain limit for $f = f'$: $m_{\nu_e^*} > 101.7$ GeV, $m_{\nu_\mu^*} > 101.8$ GeV, and $m_{\nu_\tau^*} > 92.9$ GeV.

See their Fig. 4 for the exclusion plot in the mass-coupling plane.

Searches Particle Listings

Quark and Lepton Compositeness

Limits for Excited ν (ν^*) from Single Production

These limits are from $e^+e^- \rightarrow \nu\nu^*$, $Z \rightarrow \nu\nu^*$, or $e p \rightarrow \nu^* X$ and depend on transition magnetic coupling between ν/e and ν^* . Assumptions about ν^* decay mode are given in footnotes.

VALUE (GeV)	CL%	DOCUMENT ID	TECN	COMMENT
>213	95	1 AARON 08 H1	H1	$e p \rightarrow \nu^* X$
•••		••• We do not use the following data for averages, fits, limits, etc. •••		
>190	95	2 ACHARD 03B L3	L3	$e^+e^- \rightarrow \nu\nu^*$
none 50–150	95	3 ADLOFF 02 H1	H1	$e p \rightarrow \nu^* X$
>158	95	4 CHEKANOV 02D ZEUS	ZEUS	$e p \rightarrow \nu^* X$

- AARON 08 search for single ν^* production in $e p$ collisions with the decays $\nu^* \rightarrow \nu\gamma$, νZ , $e W$. The quoted limit assumes $f = -f' = \Lambda/m_{\nu^*}$. See their Fig. 3 and Fig. 4 for the exclusion plots in the mass-coupling plane.
- ACHARD 03B result is from e^+e^- collisions at $\sqrt{s} = 189\text{--}209$ GeV. The quoted limit is for ν_e^* . $f = -f' = \Lambda/m_{\nu^*}$ is assumed. See their Fig. 4 for the exclusion plot in the mass-coupling plane.
- ADLOFF 02 search for single ν^* production in $e p$ collisions with the decays $\nu^* \rightarrow \nu\gamma$, νZ , $e W$. The quoted limit assumes $f = -f' = \Lambda/m_{\nu^*}$. See their Fig. 1 for the exclusion plots in the mass-coupling plane.
- CHEKANOV 02D search for single ν^* production in $e p$ collisions with the decays $\nu^* \rightarrow \nu\gamma$, νZ , $e W$. $f = -f' = \Lambda/m_{\nu^*}$ is assumed for the e^* coupling. CHEKANOV 02D also obtain limit for $f = f' = \Lambda/m_{\nu^*}$: $m_{\nu^*} > 135$ GeV. See their Fig. 5c and Fig. 5d for the exclusion plot in the mass-coupling plane.

MASS LIMITS for Excited q (q^*)

Limits for Excited q (q^*) from Pair Production

These limits are mostly obtained from $e^+e^- \rightarrow q^* \bar{q}^*$ and thus rely only on the (electroweak) charge of the q^* . Form factor effects are ignored unless noted. Assumptions about the q^* decay are given in the comments and footnotes.

VALUE (GeV)	CL%	DOCUMENT ID	TECN	COMMENT
>338	95	1 AALTONEN 10H CDF	CDF	$q^* \rightarrow t W^-$
•••		••• We do not use the following data for averages, fits, limits, etc. •••		
none 700–1200	95	2 SIRUNYAN 18v CMS	CMS	$p p \rightarrow t^* \bar{t}^* \rightarrow t \bar{t} g g$
> 45.6	95	3 BARATE 98u ALEP	ALEP	$Z \rightarrow q^* \bar{q}^*$
> 41.7	95	4 ADRIANI 93M L3	L3	u or d type, $Z \rightarrow q^* \bar{q}^*$
> 44.7	95	5 BARDADIN... 92 RVUE	RVUE	u -type, $\Gamma(Z)$
> 40.6	95	6 BARDADIN... 92 RVUE	RVUE	d -type, $\Gamma(Z)$
> 44.2	95	7 DECAAMP 92 ALEP	ALEP	u -type, $\Gamma(Z)$
> 45	95	8 DECAAMP 92 ALEP	ALEP	d -type, $\Gamma(Z)$
> 45	95	9 DECAAMP 92 ALEP	ALEP	u or d type, $Z \rightarrow q^* \bar{q}^*$
> 45	95	10 ABREU 91F DLPH	DLPH	u -type, $\Gamma(Z)$
> 45	95	11 ABREU 91F DLPH	DLPH	d -type, $\Gamma(Z)$

- AALTONEN 10H obtain limits on the $q^* \bar{q}^*$ production cross section in $p\bar{p}$ collisions. See their Fig. 3.
- SIRUNYAN 18v search for pair production of spin $3/2$ excited top quarks. $B(t^* \bar{t}^* \rightarrow t \bar{t} g) = 1$ is assumed.
- BARATE 98u obtain limits on the form factor. See their Fig. 16 for limits in mass-form factor plane.
- ADRIANI 93M limit is valid for $B(q^* \rightarrow qg) > 0.25$ (0.17) for up (down) type.
- BARDADIN-OTWINOWSKA 92 limit based on $\Delta\Gamma(Z) < 36$ MeV.
- These limits are independent of decay modes.
- Limit is for $B(q^* \rightarrow qg) + B(q^* \rightarrow q\gamma) = 1$.

Limits for Excited q (q^*) from Single Production

These limits are from $e^+e^- \rightarrow q^* \bar{q}^*$, $p\bar{p} \rightarrow q^* X$, or $p p \rightarrow q^* X$ and depend on transition magnetic couplings between q and q^* . Assumptions about q^* decay mode are given in the footnotes and comments.

VALUE (GeV)	CL%	DOCUMENT ID	TECN	COMMENT
none 1500–2600	95	1 AABOUD 18AB ATLS	ATLS	$p p \rightarrow b^* X$, $b^* \rightarrow b g$
none 1500–5300	95	2 AABOUD 18BA ATLS	ATLS	$p p \rightarrow q^* X$, $q^* \rightarrow q \gamma$
none 1000–5500	95	3 SIRUNYAN 18AG CMS	CMS	$p p \rightarrow q^* X$, $q^* \rightarrow q \gamma$
none 1000–1800	95	4 SIRUNYAN 18AG CMS	CMS	$p p \rightarrow b^* X$, $b^* \rightarrow b \gamma$
none 600–6000	95	5 SIRUNYAN 18BO CMS	CMS	$p p \rightarrow q^* X$, $q^* \rightarrow q g$
none 1200–5000	95	6 SIRUNYAN 18P CMS	CMS	$p p \rightarrow q^* X$, $q^* \rightarrow q W$
none 1200–4700	95	7 SIRUNYAN 18P CMS	CMS	$p p \rightarrow q^* X$, $q^* \rightarrow q Z$
>6000	95	8 AABOUD 17AK ATLS	ATLS	$p p \rightarrow q^* X$, $q^* \rightarrow q g$
•••		••• We do not use the following data for averages, fits, limits, etc. •••		
none 600–5400	95	9 KHACHATRY...17W CMS	CMS	$p p \rightarrow q^* X$, $q^* \rightarrow q g$
none 1100–2100	95	10 AABOUD 16 ATLS	ATLS	$p p \rightarrow b^* X$, $b^* \rightarrow b g$
>1500	95	11 AAD 16AH ATLS	ATLS	$p p \rightarrow b^* X$, $b^* \rightarrow t W$
>4400	95	12 AAD 16AI ATLS	ATLS	$p p \rightarrow q^* X$, $q^* \rightarrow q \gamma$
>5200	95	13 AAD 16AV ATLS	ATLS	$p p \rightarrow q^* X$, $q^* \rightarrow W b$
>1390	95	14 AAD 16S ATLS	ATLS	$p p \rightarrow q^* X$, $q^* \rightarrow q g$
>5000	95	15 KHACHATRY...16K CMS	CMS	$p p \rightarrow b^* X$, $b^* \rightarrow t W$
none 500–1600	95	16 KHACHATRY...16L CMS	CMS	$p p \rightarrow q^* X$, $q^* \rightarrow q g$
>4060	95	17 AAD 15V ATLS	ATLS	$p p \rightarrow q^* X$, $q^* \rightarrow q g$
>3500	95	18 KHACHATRY...15V CMS	CMS	$p p \rightarrow q^* X$, $q^* \rightarrow q g$
>3500	95	19 AAD 14A ATLS	ATLS	$p p \rightarrow q^* X$, $q^* \rightarrow q \gamma$
>3200	95	20 KHACHATRY...14 CMS	CMS	$p p \rightarrow q^* X$, $q^* \rightarrow q W$
>2900	95	21 KHACHATRY...14 CMS	CMS	$p p \rightarrow q^* X$, $q^* \rightarrow q Z$
none 700–3500	95	22 KHACHATRY...14J CMS	CMS	$p p \rightarrow q^* X$, $q^* \rightarrow q \gamma$
>2380	95	23 CHATRCHYAN 13AJ CMS	CMS	$p p \rightarrow q^* X$, $q^* \rightarrow q W$
>2150	95	24 CHATRCHYAN 13AJ CMS	CMS	$p p \rightarrow q^* X$, $q^* \rightarrow q Z$

- AABOUD 18AB assume $\Lambda = m_{b^*}$, $f_5 = f = f' = 1$. The contact interactions are not included in b^* production and decay amplitudes.
- AABOUD 18BA search for first-generation excited quarks (u^* and d^*) with degenerate mass, assuming $\Lambda = m_{q^*}$, $f_5 = f = f' = 1$. The contact interactions are not included in q^* production and decay amplitudes.
- SIRUNYAN 18AG search for first-generation excited quarks (u^* and d^*) with degenerate mass, assuming $\Lambda = m_{q^*}$, $f_5 = f = f' = 1$.
- SIRUNYAN 18AG search for excited b quark assuming $\Lambda = m_{q^*}$, $f_5 = f = f' = 1$.
- SIRUNYAN 18BO assume $\Lambda = m_{q^*}$, $f_5 = f = f' = 1$. The contact interactions are not included in q^* production and decay amplitudes.
- SIRUNYAN 18P use the hadronic decay of W or Z , assuming $\Lambda = m_{q^*}$, $f_5 = f = f' = 1$.
- AABOUD 17AK assume $\Lambda = m_{q^*}$, $f_5 = f = f' = 1$. The contact interactions are not included in q^* production and decay amplitudes. Only the decay of $q^* \rightarrow g u$ and $q^* \rightarrow g d$ is simulated as the benchmark signals in the analysis.
- KHACHATRYAN 17W assume $\Lambda = m_{q^*}$, $f_5 = f = f' = 1$. The contact interactions are not included in q^* production and decay amplitudes.
- AABOUD 16 assume $\Lambda = m_{b^*}$, $f_5 = f = f' = 1$. The contact interactions are not included in the b^* production and decay amplitudes.
- AAD 16AH search for b^* decaying to $t W$ in $p p$ collisions at $\sqrt{s} = 8$ TeV. $f_g = f_L = f_R = 1$ are assumed. See their Fig. 12b for limits on $\sigma \cdot B$.
- AAD 16AI assume $\Lambda = m_{q^*}$, $f_5 = f = f' = 1$.
- AAD 16AV search for single production of vector-like quarks decaying to $W b$ in $p p$ collisions. See their Fig. 8 for the limits on couplings and mixings.
- AAD 16S assume $\Lambda = m_{q^*}$, $f_5 = f = f' = 1$. The contact interactions are not included in q^* production and decay amplitudes.
- KHACHATRYAN 16I search for b^* decaying to $t W$ in $p p$ collisions at $\sqrt{s} = 8$ TeV. $\kappa_L^b = g_L = 1$, $\kappa_R^b = g_R = 0$ are assumed. See their Fig. 8 for limits on $\sigma \cdot B$.
- KHACHATRYAN 16K assume $\Lambda = m_{q^*}$, $f_5 = f = f' = 1$. The contact interactions are not included in q^* production and decay amplitudes.
- KHACHATRYAN 16L search for resonances decaying to dijets in $p p$ collisions at $\sqrt{s} = 8$ TeV using the data scouting technique which increases the sensitivity to the low mass resonances.
- AAD 15V assume $\Lambda = m_{q^*}$, $f_5 = f = f' = 1$. The contact interactions are not included in q^* production and decay amplitudes.
- KHACHATRYAN 15V assume $\Lambda = m_{q^*}$, $f_5 = f = f' = 1$. The contact interactions are not included in q^* production and decay amplitudes.
- AAD 14A assume $\Lambda = m_{q^*}$, $f_5 = f = f' = 1$.
- KHACHATRYAN 14 use the hadronic decay of W , assuming $\Lambda = m_{q^*}$, $f_5 = f = f' = 1$.
- KHACHATRYAN 14 use the hadronic decay of Z , assuming $\Lambda = m_{q^*}$, $f_5 = f = f' = 1$.
- KHACHATRYAN 14J assume $f_5 = f = f' = \Lambda / m_{q^*}$.
- CHATRCHYAN 13AJ use the hadronic decay of W .
- CHATRCHYAN 13AJ use the hadronic decay of Z .

MASS LIMITS for Color Sextet Quarks (q_6)

VALUE (GeV)	CL%	DOCUMENT ID	TECN	COMMENT
>84	95	1 ABE 89D CDF	CDF	$p\bar{p} \rightarrow q_6 \bar{q}_6$

- ABE 89D look for pair production of unit-charged particles which leave the detector before decaying. In the above limit the color sextet quark is assumed to fragment into a unit-charged or neutral hadron with equal probability and to have long enough lifetime not to decay within the detector. A limit of 121 GeV is obtained for a color decuplet.

MASS LIMITS for Color Octet Charged Leptons (ℓ_8)

$$\lambda \equiv m_{\ell_8} / \Lambda$$

VALUE (GeV)	CL%	DOCUMENT ID	TECN	COMMENT
>86	95	1 ABE 89D CDF	CDF	Stable ℓ_8 : $p\bar{p} \rightarrow \ell_8 \bar{\ell}_8$
•••		••• We do not use the following data for averages, fits, limits, etc. •••		
>6000	95	2 ABT 93 H1	H1	$e p \rightarrow e_8 X$

- ABE 89D look for pair production of unit-charged particles which leave the detector before decaying. In the above limit the color octet lepton is assumed to fragment into a unit-charged or neutral hadron with equal probability and to have long enough lifetime not to decay within the detector. The limit improves to 99 GeV if it always fragments into a unit-charged hadron.
- ABT 93 search for e_8 production via e -gluon fusion in $e p$ collisions with $e_8 \rightarrow e g$. See their Fig. 3 for exclusion plot in the $m_{e_8} - \lambda$ plane for $m_{e_8} = 35\text{--}220$ GeV.

MASS LIMITS for Color Octet Neutrinos (ν_8)

$$\lambda \equiv m_{\nu_8} / \Lambda$$

VALUE (GeV)	CL%	DOCUMENT ID	TECN	COMMENT
>110	90	1 BARGER 89 RVUE	RVUE	ν_8 : $p\bar{p} \rightarrow \nu_8 \bar{\nu}_8$
•••		••• We do not use the following data for averages, fits, limits, etc. •••		
none 3.8–29.8	95	2 KIM 90 AMY	AMY	ν_8 : $e^+e^- \rightarrow$ acoplanar jets
none 9–21.9	95	3 BARTEL 87B JADE	JADE	ν_8 : $e^+e^- \rightarrow$ acoplanar jets

See key on page 999

Searches Particle Listings

Quark and Lepton Compositeness, Extra Dimensions

- ¹ BARGER 89 used ABE 89B limit for events with large missing transverse momentum. Two-body decay $\nu_g \rightarrow \nu g$ is assumed.
- ² KIM 90 is at $E_{cm} = 50\text{--}60.8$ GeV. The same assumptions as in BARTEL 87b are used.
- ³ BARTEL 87b is at $E_{cm} = 46.3\text{--}46.78$ GeV. The limit assumes the ν_g pair production cross section to be eight times larger than that of the corresponding heavy neutrino pair production. This assumption is not valid in general for the weak couplings, and the limit can be sensitive to its $SU(2)_L \times U(1)_Y$ quantum numbers.

MASS LIMITS for W_8 (Color Octet W Boson)

VALUE (GeV)	DOCUMENT ID	TECN	COMMENT
• • • We do not use the following data for averages, fits, limits, etc. • • •			
	¹ ALBAJAR 89 UA1	$p\bar{p} \rightarrow W_8 X, W_8 \rightarrow Wg$	
¹ ALBAJAR 89 give $\sigma(W_8 \rightarrow W + \text{jet})/\sigma(W) < 0.019$ (90% CL) for $m_{W_8} > 220$ GeV.			

REFERENCES FOR Searches for Quark and Lepton Compositeness

ABOUD 19AZ	EPJ C79 803	M. Aaboud et al.	(ATLAS Collab.)
ABRAMOWICZ 19	PR D99 092006	H. Abramowicz et al.	(ZEUS Collab.)
SIRUNYAN 19AC	JHEP 1904 114	A.M. Sirunyan et al.	(CMS Collab.)
SIRUNYAN 19Z	JHEP 1904 015	A.M. Sirunyan et al.	(CMS Collab.)
AABOUD 18AB	PR D98 032016	M. Aaboud et al.	(ATLAS Collab.)
AABOUD 18AV	JHEP 1807 089	M. Aaboud et al.	(ATLAS Collab.)
AABOUD 18BA	EPJ C78 102	M. Aaboud et al.	(ATLAS Collab.)
SIRUNYAN 18AG	PL B781 390	A.M. Sirunyan et al.	(CMS Collab.)
SIRUNYAN 18BO	JHEP 1808 130	A.M. Sirunyan et al.	(CMS Collab.)
SIRUNYAN 18DD	EPJ C78 789	A.M. Sirunyan et al.	(CMS Collab.)
SIRUNYAN 18P	PR D97 072006	A.M. Sirunyan et al.	(CMS Collab.)
SIRUNYAN 18V	PL B778 349	A.M. Sirunyan et al.	(CMS Collab.)
AABOUD 17AK	PR D96 052004	M. Aaboud et al.	(ATLAS Collab.)
AABOUD 17AT	JHEP 1710 182	M. Aaboud et al.	(ATLAS Collab.)
KHACHATRYAN 17W	PL B769 520	V. Khachatryan et al.	(CMS Collab.)
SIRUNYAN 17F	JHEP 1707 013	A.M. Sirunyan et al.	(CMS Collab.)
AABOUD 16	PL B759 229	M. Aaboud et al.	(ATLAS Collab.)
AABOUD 16U	PL B761 372	M. Aaboud et al.	(ATLAS Collab.)
AAD 16AH	JHEP 1602 110	G. Aad et al.	(ATLAS Collab.)
AAD 16AI	JHEP 1603 041	G. Aad et al.	(ATLAS Collab.)
AAD 16AV	EPJ C76 442	G. Aad et al.	(ATLAS Collab.)
AAD 16BM	NJP 18 073021	G. Aad et al.	(ATLAS Collab.)
AAD 16S	PL B754 302	G. Aad et al.	(ATLAS Collab.)
KHACHATRYAN 16AQ	JHEP 1603 125	V. Khachatryan et al.	(CMS Collab.)
KHACHATRYAN 16I	JHEP 1601 166	V. Khachatryan et al.	(CMS Collab.)
KHACHATRYAN 16K	PRL 116 071801	V. Khachatryan et al.	(CMS Collab.)
KHACHATRYAN 16L	PRL 117 031802	V. Khachatryan et al.	(CMS Collab.)
AAD 15AP	JHEP 1508 138	G. Aad et al.	(ATLAS Collab.)
AAD 15AR	JHEP 1508 105	G. Aad et al.	(ATLAS Collab.)
AAD 15BY	JHEP 1510 150	G. Aad et al.	(ATLAS Collab.)
AAD 15L	PRL 114 221802	G. Aad et al.	(ATLAS Collab.)
AAD 15V	PR D91 052007	G. Aad et al.	(ATLAS Collab.)
KHACHATRYAN 15AE	JHEP 1504 025	V. Khachatryan et al.	(CMS Collab.)
KHACHATRYAN 15J	EPJ C746 79	V. Khachatryan et al.	(CMS Collab.)
KHACHATRYAN 15V	PR D91 052009	V. Khachatryan et al.	(CMS Collab.)
AAD 14A	PL B728 562	G. Aad et al.	(ATLAS Collab.)
AAD 14BE	EPJ C74 3134	G. Aad et al.	(ATLAS Collab.)
FABBRICHESI 14	PR D89 074028	M. Fabbrichesi, M. Pinamonti, A. Tonerò	
KHACHATRYAN 14	JHEP 1408 173	V. Khachatryan et al.	(CMS Collab.)
KHACHATRYAN 14J	PL B738 274	V. Khachatryan et al.	(CMS Collab.)
AAD 13BB	NJP 15 093011	G. Aad et al.	(ATLAS Collab.)
AAD 13E	PR D87 015010	G. Aad et al.	(ATLAS Collab.)
CHATRCHYAN 13AE	PL B720 309	S. Chatrchyan et al.	(CMS Collab.)
CHATRCHYAN 13AJ	PL B723 280	S. Chatrchyan et al.	(CMS Collab.)
CHATRCHYAN 13K	PR D87 032001	S. Chatrchyan et al.	(CMS Collab.)
AAD 12AB	PL B712 40	G. Aad et al.	(ATLAS Collab.)
AAD 12AZ	PR D85 072003	G. Aad et al.	(ATLAS Collab.)
AARON 11C	PL B705 52	F. D. Aaron et al.	(HI Collab.)
ABDALLAH 11	EPJ C71 1555	J. Abdallah et al.	(DELPHI Collab.)
AALTONEN 10H	PRL 104 091801	T. Aaltonen et al.	(CDF Collab.)
ABDALLAH 09	EPJ C60 1	J. Abdallah et al.	(DELPHI Collab.)
AARON 08	PL B663 382	F.D. Aaron et al.	(HI Collab.)
SCHAEEL 07A	EPJ C49 411	S. Schaeel et al.	(ALEPH Collab.)
ABDALLAH 06C	EPJ C45 589	J. Abdallah et al.	(DELPHI Collab.)
ABULENCIA 06L	PRL 96 211801	A. Abulencia et al.	(CDF Collab.)
ABBIENDI 04G	EPJ C33 173	G. Abbiendi et al.	(OPAL Collab.)
ABBIENDI 04N	PL B602 167	G. Abbiendi et al.	(OPAL Collab.)
ABDALLAH 04N	EPJ C37 405	J. Abdallah et al.	(DELPHI Collab.)
ACHARD 03B	PL B568 23	P. Achard et al.	(L3 Collab.)
BABICH 03	EPJ C29 103	A.A. Babich et al.	
ABBIENDI 02G	PL B544 57	G. Abbiendi et al.	(OPAL Collab.)
ACHARD 02D	PL B531 28	P. Achard et al.	(L3 Collab.)
ADLOFF 02	PL B525 9	C. Adloff et al.	(HI Collab.)
CHEKANOV 02D	PL B549 32	S. Chekanov et al.	(ZEUS Collab.)
AFFOLDER 01L	PRL 87 231803	T. Affolder et al.	(CDF Collab.)
BOURLIKOV 01	PR D64 071701	D. Bourlikov	
CHEUNG 01B	PL B517 167	K. Cheung	
ACCIARRI 00P	PL B499 81	M. Acciari et al.	(L3 Collab.)
AFFOLDER 00I	PR D62 012004	T. Affolder et al.	(CDF Collab.)
BARATE 98U	EPJ C4 571	R. Barate et al.	(ALEPH Collab.)
BARGER 98E	PR D57 391	V. Barger et al.	
MCFARLAND 98	EPJ C1 509	K.S. McFarland et al.	(CCFR/NuTeV Collab.)
DIAZCRUZ 94	PR D49 2149	J.L. Diaz Cruz, O.A. Sampayo	(CINV)
ABT 93	NP B396 3	I. Abt et al.	(HI Collab.)
ADRIANIN 93M	PRPL 236 1	O. Adriani et al.	(L3 Collab.)
BARDADIN 92	ZPHY C95 163	M. Bardadin-Otinowska	(CLER)
DECAMP 92	PRPL 216 253	D. Decamp et al.	(ALEPH Collab.)
PDG 92	PR D45 51	K. Hikasa et al.	(KEK, LBL, BOST+)
ABREU 91F	NP B347 511	P. Abreu et al.	(DELPHI Collab.)
KIM 90	PL B240 243	G.N. Kim et al.	(AMY Collab.)
KIM 89B	PRL 62 1825	F. Abe et al.	(CDF Collab.)
ABE 89D	PRL 63 1447	F. Abe et al.	(CDF Collab.)
ABE 89J	ZPHY C45 175	K. Abe et al.	(VENUS Collab.)
ALBAJAR 89	ZPHY C44 15	C. Albajar et al.	(UA1 Collab.)
BARGER 89	PL B220 464	V. Barger et al.	(WIS, KEK)
DORENBOSCH 89	ZPHY C41 567	J. Dorenbosch et al.	(CHARM Collab.)
BARTEL 87B	ZPHY C36 15	W. Bartel et al.	(JADE Collab.)
GRIFOLS 86	PL 168B 264	J.A. Griñols, S. Peris	(BARC)
JODIDIO 86	PR D34 1967	A. Jodidio et al.	(LBL, NWES, TRIU)
Also	PR D37 237 (erratum)	A. Jodidio et al.	(LBL, NWES, TRIU)
RENARD 82	PL 116B 264	F.M. Renard	(CERN)

Extra Dimensions

For explanation of terms used and discussion of significant model dependence of following limits, see the “Extra Dimensions” review. Footnotes describe originally quoted limit. δ indicates the number of extra dimensions.

Limits not encoded here are summarized in the “Extra Dimensions” review, where the latest unpublished results are also described.

See the related review(s):

Extra Dimensions

CONTENTS:

- Limits on R from Deviations in Gravitational Force Law
- Limits on R from On-Shell Production of Gravitons: $\delta = 2$
- Mass Limits on M_{TT}
- Limits on $1/R = M_C$
- Limits on Kaluza-Klein Gravitons in Warped Extra Dimensions
- Limits on Kaluza-Klein Gluons in Warped Extra Dimensions
- Black Hole Production Limits
 - Semiclassical Black Holes
 - Quantum Black Holes

Limits on R from Deviations in Gravitational Force Law

This section includes limits on the size of extra dimensions from deviations in the Newtonian ($1/r^2$) gravitational force law at short distances. Deviations are parametrized by a gravitational potential of the form $V = -(G m m'/r) [1 + \alpha \exp(-r/R)]$. For δ toroidal extra dimensions of equal size, $\alpha = 8\delta/3$. Quoted bounds are for $\delta = 2$ unless otherwise noted.

VALUE (μm)	CL%	DOCUMENT ID	TECN	COMMENT
< 30	95	¹ KAPNER 07	07	Torsion pendulum
• • • We do not use the following data for averages, fits, limits, etc. • • •				
		² BERGE 18	MICR	Space accelerometer
		³ FAYET 18A	MICR	Space accelerometer
		⁴ HADDOCK 18		Neutron scattering
		⁵ KLIMCHITSKAYA 17A		Torsion oscillator
		⁶ XU 13		Nuclei properties
		⁷ BEZERRA 11		Torsion oscillator
		⁸ SUSHKOV 11		Torsion pendulum
		⁹ BEZERRA 10		Microcantilever
		¹⁰ MASUDA 09		Torsion pendulum
		¹¹ GERACI 08		Microcantilever
		¹² TRENKEL 08		Newton's constant
		¹³ DECCA 07A		Torsion oscillator
< 47	95	¹⁴ TU 07		Torsion pendulum
		¹⁵ SMULLIN 05		Microcantilever
< 130	95	¹⁶ HOYLE 04		Torsion pendulum
		¹⁷ CHIAVERINI 03		Microcantilever
< 200	95	¹⁸ LONG 03		Microcantilever
< 190	95	¹⁹ HOYLE 01		Torsion pendulum
		²⁰ HOSKINS 85		Torsion pendulum

¹ KAPNER 07 search for new forces, probing a range of $\alpha \approx 10^{-3}\text{--}10^5$ and length scales $R \approx 10\text{--}1000 \mu\text{m}$. For $\delta = 1$ the bound on R is $44 \mu\text{m}$. For $\delta = 2$, the bound is expressed in terms of M_* , here translated to a bound on the radius. See their Fig. 6 for details on the bound.

² BERGE 18 uses results from the MICROSCOPE experiment to obtain constraints on non-Newtonian forces with strengths $10^{-11} \lesssim |\alpha| \lesssim 10^{-7}$ and length scales $R \gtrsim 10^5 \text{ m}$. See their Figure 1 for more details. These constraints do not place limits on the size of extra flat dimensions.

³ FAYET 18A uses results from the MICROSCOPE experiment to obtain constraints on an EP-violating force possibly arising from a new $U(1)$ gauge boson. For $R \gtrsim 10^7 \text{ m}$ the limits are $|\alpha| \lesssim$ a few 10^{-13} to a few 10^{-11} depending on the coupling, corresponding to $|\epsilon| \lesssim 10^{-24}$ for the coupling of the new spin-1 or spin-0 mediator. These constraints do not place limits on the size of extra flat dimensions. This extends the results of FAYET 18.

⁴ HADDOCK 18 obtain constraints on non-Newtonian forces with strengths $10^{22} \lesssim |\alpha| \lesssim 10^{24}$ and length scales $R \approx 0.01\text{--}10 \text{ nm}$. See their Figure 8 for more details. These constraints do not place limits on the size of extra flat dimensions.

⁵ KLIMCHITSKAYA 17A uses an experiment that measures the difference of Casimir forces to obtain bounds on non-Newtonian forces with strengths $|\alpha| \approx 10^5\text{--}10^{17}$ and length scales $R = 0.03\text{--}10 \mu\text{m}$. See their Fig. 3. These constraints do not place limits on the size of extra flat dimensions.

⁶ XU 13 obtain constraints on non-Newtonian forces with strengths $|\alpha| \approx 10^{34}\text{--}10^{36}$ and length scales $R \approx 1\text{--}10 \text{ fm}$. See their Fig. 4 for more details. These constraints do not place limits on the size of extra flat dimensions.

⁷ BEZERRA 11 obtain constraints on non-Newtonian forces with strengths $10^{11} \lesssim |\alpha| \lesssim 10^{18}$ and length scales $R = 30\text{--}1260 \text{ nm}$. See their Fig. 2 for more details. These constraints do not place limits on the size of extra flat dimensions.

⁸ SUSHKOV 11 obtain improved limits on non-Newtonian forces with strengths $10^7 \lesssim |\alpha| \lesssim 10^{11}$ and length scales $0.4 \mu\text{m} < R < 4 \mu\text{m}$ (95% CL). See their Fig. 2. These bounds do not place limits on the size of extra flat dimensions. However, a model dependent bound of $M_* > 70 \text{ TeV}$ is obtained assuming gauge bosons that couple to baryon number also propagate in $(4 + \delta)$ dimensions.

⁹ BEZERRA 10 obtain improved constraints on non-Newtonian forces with strengths $10^{19} \lesssim |\alpha| \lesssim 10^{29}$ and length scales $R = 1.6\text{--}14 \text{ nm}$ (95% CL). See their Fig. 1. This bound does not place limits on the size of extra flat dimensions.

Searches Particle Listings

Extra Dimensions

- 10 MASUDA 09 obtain improved constraints on non-Newtonian forces with strengths $10^9 \lesssim |\alpha| \lesssim 10^{11}$ and length scales $R = 1.0\text{--}2.9 \mu\text{m}$ (95% CL). See their Fig. 3. This bound does not place limits on the size of extra flat dimensions.
- 11 GERACI 08 obtain improved constraints on non-Newtonian forces with strengths $|\alpha| > 14,000$ and length scales $R = 5\text{--}15 \mu\text{m}$. See their Fig. 9. This bound does not place limits on the size of extra flat dimensions.
- 12 TRENKEL 08 uses two independent measurements of Newton's constant G to constrain new forces with strength $|\alpha| \simeq 10^{-4}$ and length scales $R = 0.02\text{--}1 \text{ m}$. See their Fig. 1. This bound does not place limits on the size of extra flat dimensions.
- 13 DECCA 07A search for new forces and obtain bounds in the region with strengths $|\alpha| \simeq 10^{13}\text{--}10^{18}$ and length scales $R = 20\text{--}86 \text{ nm}$. See their Fig. 6. This bound does not place limits on the size of extra flat dimensions.
- 14 TU 07 search for new forces probing a range of $|\alpha| \simeq 10^{-1}\text{--}10^5$ and length scales $R \simeq 20\text{--}1000 \mu\text{m}$. For $\delta = 1$ the bound on R is $53 \mu\text{m}$. See their Fig. 3 for details on the bound.
- 15 SMULLIN 05 search for new forces, and obtain bounds in the region with strengths $\alpha \simeq 10^3\text{--}10^8$ and length scales $R = 6\text{--}20 \mu\text{m}$. See their Figs. 1 and 16 for details on the bound. This work does not place limits on the size of extra flat dimensions.
- 16 HOYLE 04 search for new forces, probing α down to 10^{-2} and distances down to $10 \mu\text{m}$. Quoted bound on R is for $\delta = 2$. For $\delta = 1$, bound goes to $160 \mu\text{m}$. See their Fig. 34 for details on the bound.
- 17 CHIAVERINI 03 search for new forces, probing α above 10^4 and λ down to $3 \mu\text{m}$, finding no signal. See their Fig. 4 for details on the bound. This bound does not place limits on the size of extra flat dimensions.
- 18 LONG 03 search for new forces, probing α down to 3, and distances down to about $10 \mu\text{m}$. See their Fig. 4 for details on the bound.
- 19 HOYLE 01 search for new forces, probing α down to 10^{-2} and distances down to $20 \mu\text{m}$. See their Fig. 4 for details on the bound. The quoted bound is for $\alpha \geq 3$.
- 20 HOSKINS 85 search for new forces, probing distances down to 4 mm. See their Fig. 13 for details on the bound. This bound does not place limits on the size of extra flat dimensions.

Limits on R from On-Shell Production of Gravitons: $\delta = 2$

This section includes limits on on-shell production of gravitons in collider and astrophysical processes. Bounds quoted are on R , the assumed common radius of the flat extra dimensions, for $\delta = 2$ extra dimensions. Studies often quote bounds in terms of derived parameter; experiments are actually sensitive to the masses of the KK gravitons: $m_{\vec{n}} = |\vec{n}|/R$. See the Review on "Extra Dimensions" for details. Bounds are given in μm for $\delta = 2$.

VALUE (μm)	CL%	DOCUMENT ID	TECN	COMMENT
< 4.8	95	1 SIRUNYAN	18s CMS	$pp \rightarrow jG$
< 0.00016	95	2 HANNESTAD	03	Neutron star heating
••• We do not use the following data for averages, fits, limits, etc. •••				
< 8.0	95	3 AABOUD	18f ATLS	$pp \rightarrow jG$
< 89	95	4 SIRUNYAN	18bv CMS	$pp \rightarrow ZG$
		5 SIRUNYAN	17aq CMS	$pp \rightarrow \gamma G$
< 90	95	6 AABOUD	16f ATLS	$pp \rightarrow \gamma G$
		7 KHACHATRYAN	16n CMS	$pp \rightarrow \gamma G$
		8 AAD	15cs ATLS	$pp \rightarrow \gamma G$
< 127	95	9 AAD	13c ATLS	$pp \rightarrow \gamma G$
< 34.4	95	10 AAD	13d ATLS	$pp \rightarrow jj$
< 0.0087	95	11 AJELLO	12 FLAT	Neutron star γ sources
< 245	95	12 AALTONEN	08ac CDF	$p\bar{p} \rightarrow \gamma G, jG$
< 615	95	13 ABAZOV	08s D0	$p\bar{p} \rightarrow \gamma G, jG$
< 0.916	95	14 DAS	08	Supernova cooling
< 350	95	15 ABULENCIA,A	06 CDF	$p\bar{p} \rightarrow jG$
< 270	95	16 ABDALLAH	05b DLPH	$e^+e^- \rightarrow \gamma G$
< 210	95	17 ACHARD	04e L3	$e^+e^- \rightarrow \gamma G$
< 480	95	18 ACOSTA	04c CDF	$p\bar{p} \rightarrow jG$
< 0.00038	95	19 CASSE	04	Neutron star γ sources
< 610	95	20 ABAZOV	03 D0	$p\bar{p} \rightarrow jG$
< 0.96	95	21 HANNESTAD	03	Supernova cooling
< 0.096	95	22 HANNESTAD	03	Diffuse γ background
< 0.051	95	23 HANNESTAD	03	Neutron star γ sources
< 300	95	24 HEISTER	03c ALEP	$e^+e^- \rightarrow \gamma G$
		25 FAIRBAIRN	01	Cosmology
< 0.66	95	26 HANHART	01	Supernova cooling
		27 CASSISI	00	Red giants
< 1300	95	28 ACCIARRI	99s L3	$e^+e^- \rightarrow ZG$

- 1 SIRUNYAN 18s search for $pp \rightarrow jG$, using 35.9 fb^{-1} of data at $\sqrt{s} = 13 \text{ TeV}$ to place lower limits on M_D for two to six extra dimensions (see their Table VII), from which this bound on R is derived. This limit supersedes that in KHACHATRYAN 15AL.
- 2 HANNESTAD 03 obtain a limit on R from the heating of old neutron stars by the surrounding cloud of trapped KK gravitons. Limits for all $\delta \leq 7$ are given in their Tables V and VI. These limits supersede those in HANNESTAD 02.
- 3 AABOUD 18f search for $pp \rightarrow jG$, using 36.1 fb^{-1} of data at $\sqrt{s} = 13 \text{ TeV}$ to place lower limits on M_D for two to six extra dimensions (see their Table 7), from which this bound on R is derived. This limit supersedes that in AABOUD 16f.
- 4 SIRUNYAN 18bv search for $pp \rightarrow ZG$, using 35.9 fb^{-1} of data at $\sqrt{s} = 13 \text{ TeV}$ to place lower limits on M_D for two to seven extra dimensions (see their Figure 11), from which this bound on R is derived.
- 5 SIRUNYAN 17aq search for $pp \rightarrow \gamma G$, using 12.9 fb^{-1} of data at $\sqrt{s} = 13 \text{ TeV}$ to place limits on M_D for three to six extra dimensions (see their Table 3).
- 6 AABOUD 16f search for $pp \rightarrow \gamma G$, using 3.2 fb^{-1} of data at $\sqrt{s} = 13 \text{ TeV}$ to place limits on M_D for two to six extra dimensions (see their Figure 9), from which this bound on R is derived.
- 7 KHACHATRYAN 16n search for $pp \rightarrow \gamma G$, using 19.6 fb^{-1} of data at $\sqrt{s} = 8 \text{ TeV}$ to place limits on M_D for three to six extra dimensions (see their Table 5).
- 8 AAD 15cs search for $pp \rightarrow \gamma G$, using 20.3 fb^{-1} of data at $\sqrt{s} = 8 \text{ TeV}$ to place lower limits on M_D for two to six extra dimensions (see their Fig. 18).

- 9 AAD 13c search for $pp \rightarrow \gamma G$, using 4.6 fb^{-1} of data at $\sqrt{s} = 7 \text{ TeV}$ to place bounds on M_D for two to six extra dimensions, from which this bound on R is derived.
- 10 AAD 13d search for the dijet decay of quantum black holes in 4.8 fb^{-1} of data produced in pp collisions at $\sqrt{s} = 7 \text{ TeV}$ to place bounds on M_D for two to seven extra dimensions, from which these bounds on R are derived. Limits on M_D for all $\delta \leq 7$ are given in their Table 3.
- 11 AJELLO 12 obtain a limit on R from the gamma-ray emission of point γ sources that arise from the photon decay of KK gravitons which are gravitationally bound around neutron stars. Limits for all $\delta \leq 7$ are given in their Table 7.
- 12 AALTONEN 08ac search for $p\bar{p} \rightarrow \gamma G$ and $p\bar{p} \rightarrow jG$ at $\sqrt{s} = 1.96 \text{ TeV}$ with 2.0 fb^{-1} and 1.1 fb^{-1} respectively, in order to place bounds on the fundamental scale and size of the extra dimensions. See their Table III for limits on all $\delta \leq 6$.
- 13 ABAZOV 08s search for $p\bar{p} \rightarrow \gamma G$, using 1 fb^{-1} of data at $\sqrt{s} = 1.96 \text{ TeV}$ to place bounds on M_D for two to eight extra dimensions, from which these bounds on R are derived. See their paper for intermediate values of δ .
- 14 DAS 08 obtain a limit on R from Kaluza-Klein graviton cooling of SN1987A due to plasmon-plasmon annihilation.
- 15 ABULENCIA,A 06 search for $p\bar{p} \rightarrow jG$ using 368 pb^{-1} of data at $\sqrt{s} = 1.96 \text{ TeV}$. See their Table II for bounds for all $\delta \leq 6$.
- 16 ABDALLAH 05b search for $e^+e^- \rightarrow \gamma G$ at $\sqrt{s} = 180\text{--}209 \text{ GeV}$ to place bounds on the size of extra dimensions and the fundamental scale. Limits for all $\delta \leq 6$ are given in their Table 6. These limits supersede those in ABREU 00z.
- 17 ACHARD 04 search for $e^+e^- \rightarrow \gamma G$ at $\sqrt{s} = 189\text{--}209 \text{ GeV}$ to place bounds on the size of extra dimensions and the fundamental scale. See their Table 8 for limits with $\delta \leq 8$. These limits supersede those in ACCIARRI 99r.
- 18 ACOSTA 04c search for $p\bar{p} \rightarrow jG$ at $\sqrt{s} = 1.8 \text{ TeV}$ to place bounds on the size of extra dimensions and the fundamental scale. See their paper for bounds on $\delta = 4, 6$.
- 19 CASSE 04 obtain a limit on R from the gamma-ray emission of point γ sources that arises from the photon decay of gravitons around newly born neutron stars, applying the technique of HANNESTAD 03 to neutron stars in the galactic bulge. Limits for all $\delta \leq 7$ are given in their Table I.
- 20 ABAZOV 03 search for $p\bar{p} \rightarrow jG$ at $\sqrt{s} = 1.8 \text{ TeV}$ to place bounds on M_D for 2 to 7 extra dimensions, from which these bounds on R are derived. See their paper for bounds on intermediate values of δ . We quote results without the approximate NLO scaling introduced in the paper.
- 21 HANNESTAD 03 obtain a limit on R from graviton cooling of supernova SN1987A. Limits for all $\delta \leq 7$ are given in their Tables V and VI.
- 22 HANNESTAD 03 obtain a limit on R from gravitons emitted in supernovae and which subsequently decay, contaminating the diffuse cosmic γ background. Limits for all $\delta \leq 7$ are given in their Tables V and VI. These limits supersede those in HANNESTAD 02.
- 23 HANNESTAD 03 obtain a limit on R from gravitons emitted in two recent supernovae and which subsequently decay, creating point γ sources. Limits for all $\delta \leq 7$ are given in their Tables V and VI. These limits are corrected in the published erratum.
- 24 HEISTER 03c use the process $e^+e^- \rightarrow \gamma G$ at $\sqrt{s} = 189\text{--}209 \text{ GeV}$ to place bounds on the size of extra dimensions and the scale of gravity. See their Table 4 for limits with $\delta \leq 6$ for derived limits on M_D .
- 25 FAIRBAIRN 01 obtains bounds on R from over production of KK gravitons in the early universe. Bounds are quoted in paper in terms of fundamental scale of gravity. Bounds depend strongly on temperature of QCD phase transition and range from $R < 0.13 \mu\text{m}$ to $0.001 \mu\text{m}$ for $\delta=2$; bounds for $\delta=3,4$ can be derived from Table 1 in the paper.
- 26 HANHART 01 obtain bounds on R from limits on graviton cooling of supernova SN 1987a using numerical simulations of proto-neutron star neutrino emission.
- 27 CASSISI 00 obtain rough bounds on M_D (and thus R) from red giant cooling for $\delta=2,3$. See their paper for details.
- 28 ACCIARRI 99s search for $e^+e^- \rightarrow ZG$ at $\sqrt{s}=189 \text{ GeV}$. Limits on the gravity scale are found in their Table 2, for $\delta \leq 4$.

Mass Limits on M_{TT}

This section includes limits on the cut-off mass scale, M_{TT} , of dimension-8 operators from KK graviton exchange in models of large extra dimensions. Ambiguities in the UV-divergent summation are absorbed into the parameter λ , which is taken to be $\lambda = \pm 1$ in the following analyses. Bounds for $\lambda = -1$ are shown in parenthesis after the bound for $\lambda = +1$, if appropriate. Different papers use slightly different definitions of the mass scale. The definition used here is related to another popular convention by $M_{TT}^4 = (2/\pi) \Lambda_{\text{Pl}}^4$, as discussed in the above Review on "Extra Dimensions."

VALUE (TeV)	CL%	DOCUMENT ID	TECN	COMMENT
> 9.02	95	1 SIRUNYAN	18DD CMS	$pp \rightarrow$ dijet, ang. distrib.
> 20.6	(> 15.7)	2 GIUDICE	03 RVUE	Dim-6 operators
••• We do not use the following data for averages, fits, limits, etc. •••				
> 6.9	95	3 SIRUNYAN	19ac CMS	$pp \rightarrow e^+e^-, \mu^+\mu^-, \gamma\gamma$
> 7.0	(> 5.6)	4 SIRUNYAN	18du CMS	$pp \rightarrow \gamma\gamma$
> 6.5	95	5 AABOUD	17ap ATLS	$pp \rightarrow \gamma\gamma$
> 3.8	95	6 AAD	14be ATLS	$pp \rightarrow e^+e^-, \mu^+\mu^-$
> 3.2	95	7 AAD	13e ATLS	$pp \rightarrow e^+e^-, \mu^+\mu^-, \gamma\gamma$
		8 BAAK	12 RVUE	Electroweak
> 0.90	(> 0.92)	9 AARON	11c H1	$e^{\pm}p \rightarrow e^{\pm}X$
> 1.48	95	10 ABAZOV	09ae D0	$p\bar{p} \rightarrow$ dijet, ang. distrib.
> 1.45	95	11 ABAZOV	09d D0	$p\bar{p} \rightarrow e^+e^-, \gamma\gamma$
> 1.1	(> 1.0)	12 SCHAEEL	07a ALEP	$e^+e^- \rightarrow e^+e^-$
> 0.898	(> 0.998)	13 ABDALLAH	06c DLPH	$e^+e^- \rightarrow \ell^+\ell^-$
> 0.853	(> 0.939)	14 GERDES	06	$p\bar{p} \rightarrow e^+e^-, \gamma\gamma$
> 0.96	(> 0.93)	15 ABAZOV	05v D0	$p\bar{p} \rightarrow \mu^+\mu^-$
> 0.78	(> 0.79)	16 CHEKANOV	04b ZEUS	$e^{\pm}p \rightarrow e^{\pm}X$
> 0.805	(> 0.956)	17 ABBIENDI	03d OPAL	$e^+e^- \rightarrow \gamma\gamma$
> 0.7	(> 0.7)	18 ACHARD	03d L3	$e^+e^- \rightarrow ZZ$
> 0.82	(> 0.78)	19 ADLOFF	03 H1	$e^{\pm}p \rightarrow e^{\pm}X$
> 1.28	(> 1.25)	20 GIUDICE	03 RVUE	
> 0.80	(> 0.85)	21 HEISTER	03c ALEP	$e^+e^- \rightarrow \gamma\gamma$

See key on page 999

Searches Particle Listings

Extra Dimensions

> 0.84	(> 0.99)	95	22	ACHARD	02D L3	$e^+e^- \rightarrow \gamma\gamma$
> 1.2	(> 1.1)	95	23	ABBOTT	01 D0	$p\bar{p} \rightarrow e^+e^-, \gamma\gamma$
> 0.60	(> 0.63)	95	24	ABBIENDI	00R OPAL	$e^+e^- \rightarrow \mu^+\mu^-$
> 0.63	(> 0.50)	95	24	ABBIENDI	00R OPAL	$e^+e^- \rightarrow \tau^+\tau^-$
> 0.68	(> 0.61)	95	24	ABBIENDI	00R OPAL	$e^+e^- \rightarrow \mu^+\mu^-, \tau^+\tau^-$
			25	ABREU	00A DLPH	$e^+e^- \rightarrow \gamma\gamma$
> 0.680	(> 0.542)	95	26	ABREU	00S DLPH	$e^+e^- \rightarrow \mu^+\mu^-, \tau^+\tau^-$
> 15-28		99.7	27	CHANG	00B RVUE	Electroweak
> 0.98		95	28	CHEUNG	00 RVUE	$e^+e^- \rightarrow \gamma\gamma$
> 0.29-0.38		95	29	GRAESSER	00 RVUE	$(g-2)_\mu$
> 0.50-1.1		95	30	HAN	00 RVUE	Electroweak
> 2.0	(> 2.0)	95	31	MATHEWS	00 RVUE	$p\bar{p} \rightarrow jj$
> 1.0	(> 1.1)	95	32	MELE	00 RVUE	$e^+e^- \rightarrow VV$
			33	ABBIENDI	99P OPAL	
			34	ACCIARRI	99M L3	
			35	ACCIARRI	99S L3	
> 1.412	(> 1.077)	95	36	BOURLIKOV	99	$e^+e^- \rightarrow e^+e^-$

- 1 SIRUNYAN 18DD use dijet angular distributions in 35.9 fb^{-1} of data from pp collisions at $\sqrt{s} = 13 \text{ TeV}$ to place a lower bound on Λ_T , here converted to M_{TT} . This updates the results of SIRUNYAN 17F.
- 2 GIUDICE 03 place bounds on Λ_6 , the coefficient of the gravitationally-induced dimension-6 operator $(2\pi\lambda/\Lambda_6^2)(\sum \bar{T}_i \mu_i^5 \eta)(\sum \bar{T}_i \mu_i^5 \eta)$, using data from a variety of experiments. Results are quoted for $\lambda = \pm 1$ and are independent of δ .
- 3 SIRUNYAN 19AC use $35.9 (36.3) \text{ fb}^{-1}$ of data from pp collisions at $\sqrt{s} = 13 \text{ TeV}$ in the dielectron (dimuon) channels to place a lower limit on Λ_T , here converted to M_{TT} . The dielectron and dimuon channels are combined with previous results in the diphoton channel to set the best limit. Bounds on individual channels and different priors can be found in their Table 2. This updates the results in KHACHATRYAN 15AE.
- 4 SIRUNYAN 18DU use 35.9 fb^{-1} of data from pp collisions at $\sqrt{s} = 13 \text{ TeV}$ to place lower limits on M_{TT} (equivalent to their M_S). This updates the results of CHATRCHYAN 12R.
- 5 ABOUD 17AP use 36.7 fb^{-1} of data from pp collisions at $\sqrt{s} = 13 \text{ TeV}$ to place lower limits on M_{TT} (equivalent to their M_S). This updates the results of AAD 13As.
- 6 AAD 14BE use 20 fb^{-1} of data from pp collisions at $\sqrt{s} = 8 \text{ TeV}$ in the dielectron channel to place lower limits on M_{TT} (equivalent to their M_S).
- 7 AAD 13E use 4.9 and 5.0 fb^{-1} of data from pp collisions at $\sqrt{s} = 7 \text{ TeV}$ in the dielectron and dimuon channels, respectively, to place lower limits on M_{TT} (equivalent to their M_S). The dielectron and dimuon channels are combined with previous results in the diphoton channel to set the best limit. Bounds on individual channels and different priors can be found in their Table VIII.
- 8 BAAK 12 use electroweak precision observables to place bounds on the ratio Λ_T/M_D as a function of M_D . See their Fig. 22 for constraints with a Higgs mass of 120 GeV .
- 9 AARON 11C search for deviations in the differential cross section of $e^\pm p \rightarrow e^\pm X$ in 446 pb^{-1} of data taken at $\sqrt{s} = 301$ and 319 GeV to place a bound on M_{TT} .
- 10 ABZOV 09AE use dijet angular distributions in 0.7 fb^{-1} of data from $p\bar{p}$ collisions at $\sqrt{s} = 1.96 \text{ TeV}$ to place lower bounds on Λ_T (equivalent to their M_S), here converted to M_{TT} .
- 11 ABZOV 09B use 1.05 fb^{-1} of data from $p\bar{p}$ collisions at $\sqrt{s} = 1.96 \text{ TeV}$ to place lower bounds on Λ_T (equivalent to their M_S), here converted to M_{TT} .
- 12 SCHAEEL 07A use e^+e^- collisions at $\sqrt{s} = 189-209 \text{ GeV}$ to place lower limits on Λ_T , here converted to limits on M_{TT} .
- 13 ABDALLAH 06C use e^+e^- collisions at $\sqrt{s} \sim 130-207 \text{ GeV}$ to place lower limits on M_{TT} , which is equivalent to their definition of M_S . Bound shown includes all possible final state leptons, $\ell = e, \mu, \tau$. Bounds on individual leptonic final states can be found in their Table 31.
- 14 GERDES 06 use 100 to 110 pb^{-1} of data from $p\bar{p}$ collisions at $\sqrt{s} = 1.8 \text{ TeV}$, as recorded by the CDF Collaboration during Run I of the Tevatron. Bound shown includes a K -factor of 1.3. Bounds on individual e^+e^- and $\gamma\gamma$ final states are found in their Table I.
- 15 ABZOV 05V use 246 pb^{-1} of data from $p\bar{p}$ collisions at $\sqrt{s} = 1.96 \text{ TeV}$ to search for deviations in the differential cross section to $\mu^+\mu^-$ from graviton exchange.
- 16 CHEKANOV 04B search for deviations in the differential cross section of $e^\pm p \rightarrow e^\pm X$ with 130 pb^{-1} of combined data and Q^2 values up to $40,000 \text{ GeV}^2$ to place a bound on M_{TT} .
- 17 ABBIENDI 03D use e^+e^- collisions at $\sqrt{s} = 181-209 \text{ GeV}$ to place bounds on the ultraviolet scale M_{TT} , which is equivalent to their definition of M_S .
- 18 ACHARD 03D look for deviations in the cross section for $e^+e^- \rightarrow ZZ$ from $\sqrt{s} = 200-209 \text{ GeV}$ to place a bound on M_{TT} .
- 19 ADLOFF 03 search for deviations in the differential cross section of $e^\pm p \rightarrow e^\pm X$ at $\sqrt{s} = 301$ and 319 GeV to place bounds on M_{TT} .
- 20 GIUDICE 03 review existing experimental bounds on M_{TT} and derive a combined limit.
- 21 HEISTER 03C use e^+e^- collisions at $\sqrt{s} = 189-209 \text{ GeV}$ to place bounds on the scale of dim-8 gravitational interactions. Their M_S^\pm is equivalent to our M_{TT} with $\lambda = \pm 1$.
- 22 ACHARD 02 search for s-channel graviton exchange effects in $e^+e^- \rightarrow \gamma\gamma$ at $E_{cm} = 192-209 \text{ GeV}$.
- 23 ABBOTT 01 search for variations in differential cross sections to e^+e^- and $\gamma\gamma$ final states at the Tevatron.
- 24 ABBIENDI 00R uses e^+e^- collisions at $\sqrt{s} = 189 \text{ GeV}$.
- 25 ABREU 00A search for s-channel graviton exchange effects in $e^+e^- \rightarrow \gamma\gamma$ at $E_{cm} = 189-202 \text{ GeV}$.
- 26 ABREU 00S uses e^+e^- collisions at $\sqrt{s} = 183$ and 189 GeV . Bounds on μ and τ individual final states given in paper.
- 27 CHANG 00B derive 3σ limit on M_{TT} of $(28, 19, 15) \text{ TeV}$ for $\delta = (2, 4, 6)$ respectively assuming the presence of a torsional coupling in the gravitational action. Highly model dependent.
- 28 CHEUNG 00 obtains limits from anomalous diphoton production at OPAL due to graviton exchange. Original limit for $\delta = 4$. However, unknown UV theory renders δ dependence unreliable. Original paper works in HLZ convention.
- 29 GRAESSER 00 obtains a bound from graviton contributions to $g-2$ of the muon through loops of 0.29 TeV for $\delta = 2$ and 0.38 TeV for $\delta = 4, 6$. Limits scale as $\lambda^{1/2}$. However

calculational scheme not well-defined without specification of high-scale theory. See the "Extra Dimensions Review."

- 30 HAN 00 calculates corrections to gauge boson self-energies from KK graviton loops and constrain them using S and T . Bounds on M_{TT} range from 0.5 TeV ($\delta = 6$) to 1.1 TeV ($\delta = 2$); see text. Limits have strong dependence, $\lambda^{\delta+2}$, on unknown λ coefficient.
- 31 MATHEWS 00 search for evidence of graviton exchange in CDF and D0 dijet production data. See their Table 2 for slightly stronger δ -dependent bounds. Limits expressed in terms of $\bar{M}_S^4 = M_{TT}^4/8$.
- 32 MELE 00 obtains bound from KK graviton contributions to $e^+e^- \rightarrow VV$ ($V = \gamma, W, Z$) at LEP. Authors use Hewett conventions.
- 33 ABBIENDI 99P search for s-channel graviton exchange effects in $e^+e^- \rightarrow \gamma\gamma$ at $E_{cm} = 189 \text{ GeV}$. The limits $G_\pm > 660 \text{ GeV}$ and $G_- > 634 \text{ GeV}$ are obtained from combined $E_{cm} = 183$ and 189 GeV data, where G_\pm is a scale related to the fundamental gravity scale.
- 34 ACCIARRI 99M search for the reaction $e^+e^- \rightarrow \gamma G$ and s-channel graviton exchange effects in $e^+e^- \rightarrow \gamma\gamma, W^+W^-, ZZ, e^+e^-, \mu^+\mu^-, \tau^+\tau^-, q\bar{q}$ at $E_{cm} = 183 \text{ GeV}$. Limits on the gravity scale are listed in their Tables 1 and 2.
- 35 ACCIARRI 99S search for the reaction $e^+e^- \rightarrow ZG$ and s-channel graviton exchange effects in $e^+e^- \rightarrow \gamma\gamma, W^+W^-, ZZ, e^+e^-, \mu^+\mu^-, \tau^+\tau^-, q\bar{q}$ at $E_{cm} = 189 \text{ GeV}$. Limits on the gravity scale are listed in their Tables 1 and 2.
- 36 BOURLIKOV 99 performs global analysis of LEP data on e^+e^- collisions at $\sqrt{s} = 183$ and 189 GeV . Bound is on Λ_T .

Limits on $1/R = M_C$

This section includes limits on $1/R = M_C$, the compactification scale in models with one TeV-sized extra dimension, due to exchange of Standard Model KK excitations. Bounds assume fermions are not in the bulk, unless stated otherwise. See the "Extra Dimensions" review for discussion of model dependence.

VALUE (TeV)	CL%	DOCUMENT ID	TECN	COMMENT
>4.16	95	1 AAD	12CC ATLS	$pp \rightarrow t\bar{t}$
>6.1		2 BARBIERI	04 RVUE	Electroweak
		••• We do not use the following data for averages, fits, limits, etc. •••		
		3 ABOUD	18AV ATLS	$pp \rightarrow t\bar{t}t\bar{t}$
		4 ABOUD	18CE ATLS	$pp \rightarrow t\bar{t}t\bar{t}$
>3.8	95	5 ACCOMANDO 15	RVUE	Electroweak
>3.40	95	6 KHACHATRYAN...15T	CMS	$pp \rightarrow \ell X$
		7 CHATRCHYAN13AQ	CMS	$pp \rightarrow \ell X$
>1.38	95	8 CHATRCHYAN13W	CMS	$pp \rightarrow \gamma\gamma, \delta=6, M_D=5 \text{ TeV}$
>0.715	95	9 EDELHAUSER 13	RVUE	$pp \rightarrow \ell\bar{\ell} + X$
>1.40	95	10 AAD	12CP ATLS	$pp \rightarrow \gamma\gamma, \delta=6, M_D=5 \text{ TeV}$
>1.23	95	11 AAD	12X ATLS	$pp \rightarrow \gamma\gamma, \delta=6, M_D=5 \text{ TeV}$
>0.26	95	12 ABZOV	12M D0	$p\bar{p} \rightarrow \mu\mu$
>0.75	95	13 BAAK	12 RVUE	Electroweak
		14 FLACKE	12 RVUE	Electroweak
>0.43	95	15 NISHIWAKI	12 RVUE	$H \rightarrow WW, \gamma\gamma$
>0.729	95	16 AAD	11F ATLS	$pp \rightarrow \gamma\gamma, \delta=6, M_D=5 \text{ TeV}$
>0.961	95	17 AAD	11X ATLS	$pp \rightarrow \gamma\gamma, \delta=6, M_D=5 \text{ TeV}$
>0.477	95	18 ABZOV	10P D0	$p\bar{p} \rightarrow \gamma\gamma, \delta=6, M_D=5 \text{ TeV}$
>1.59	95	19 ABZOV	09AE D0	$p\bar{p} \rightarrow$ dijet, angular dist.
>0.6	95	20 HAISCH	07 RVUE	$\bar{B} \rightarrow X_S \gamma$
>0.6	90	21 GOGOLADZE	06 RVUE	Electroweak
>3.3	95	22 CORNET	00 RVUE	Electroweak
> 3.3-3.8	95	23 RIZZO	00 RVUE	Electroweak

- 1 AAD 12cc use 4.9 and 5.0 fb^{-1} of data from pp collisions at $\sqrt{s} = 7 \text{ TeV}$ in the dielectron and dimuon channels, respectively, to place a lower bound on the mass of the lightest KK Z/γ boson (equivalent to $1/R = M_C$). The limit quoted here assumes a flat prior corresponding to when the pure Z/γ KK cross section term dominates. See their Section 15 for more details.
- 2 BARBIERI 04 use electroweak precision observables to place a lower bound on the compactification scale $1/R$. Both the gauge bosons and the Higgs boson are assumed to propagate in the bulk.
- 3 ABOUD 18AV use 36.1 fb^{-1} of data from pp collisions at $\sqrt{s} = 13 \text{ TeV}$ in final states with multiple b-jets, to place a lower bound on the compactification scale in a model with two universal extra dimensions. Assuming the radii of the two extra dimensions are equal, a lower limit of 1.8 TeV for the Kaluza-Klein mass is obtained.
- 4 ABOUD 18CE use 36.1 fb^{-1} of data from pp collisions at $\sqrt{s} = 13 \text{ TeV}$ in final states with same-charge leptons and b-jets, to place a lower bound on the compactification scale in a model with two universal extra dimensions. Assuming the radii of the two extra dimensions are equal, a lower limit of 1.45 TeV for the Kaluza-Klein mass is obtained.
- 5 ACCOMANDO 15 use electroweak precision observables to place a lower bound on the compactification scale $1/R$. See their Fig. 2 for the bound as a function of $\sin\beta$, which parametrizes the VEV contribution from brane and bulk Higgs fields. The quoted value is for the minimum bound which occurs at $\sin\beta = 0.45$.
- 6 KHACHATRYAN 15T use 19.7 fb^{-1} of data from pp collisions at $\sqrt{s} = 8 \text{ TeV}$ to place a lower bound on the compactification scale $1/R$.
- 7 CHATRCHYAN 13AQ use 5.0 fb^{-1} of data from pp collisions at $\sqrt{s} = 7 \text{ TeV}$ and a further 3.7 fb^{-1} of data at $\sqrt{s} = 8 \text{ TeV}$ to place a lower bound on the compactification scale $1/R$, in models with universal extra dimensions and Standard Model fields propagating in the bulk. See their Fig. 5 for the bound as a function of the universal bulk fermion mass parameter μ .
- 8 CHATRCHYAN 13W use diphoton events with large missing transverse momentum in 4.93 fb^{-1} of data produced from pp collisions at $\sqrt{s} = 7 \text{ TeV}$ to place a lower bound on the compactification scale in a universal extra dimension model with gravitational decays. The bound assumes that the cutoff scale Λ , for the radiative corrections to the Kaluza-Klein masses, satisfies $\Lambda/M_C = 20$. The model parameters are chosen such that the decay $\gamma^* \rightarrow G\gamma$ occurs with an appreciable branching fraction.
- 9 EDELHAUSER 13 use 19.6 and 20.6 fb^{-1} of data from pp collisions at $\sqrt{s} = 8 \text{ TeV}$ analyzed by the CMS Collaboration in the dielectron and dimuon channels, respectively,

Searches Particle Listings

Extra Dimensions

Reference	Value	CL%	Document ID	TECN	Comment
to place a lower bound on the mass of the second lightest Kaluza-Klein Z/γ boson (converted to a limit on $1/R = M_C$). The bound assumes Standard Model fields propagating in the bulk and that the cutoff scale Λ , for the radiative corrections to the Kaluza-Klein masses, satisfies $\Lambda/M_C = 20$.	>1.8	95	19 SIRUNYAN	18Bk CMS	$pp \rightarrow G \rightarrow ZZ$
10 AAD 12CP use diphoton events with large missing transverse momentum in 4.8 fb ⁻¹ of data produced from pp collisions at $\sqrt{s} = 7$ TeV to place a lower bound on the compactification scale in a universal extra dimension model with gravitational decays. The bound assumes that the cutoff scale Λ , for the radiative corrections to the Kaluza-Klein masses, satisfies $\Lambda/M_C = 20$. The model parameters are chosen such that the decay $\gamma^* \rightarrow G\gamma$ occurs with an appreciable branching fraction.	>4.1	95	20 SIRUNYAN	18Bo CMS	$pp \rightarrow G \rightarrow jj$
11 AAD 12X use diphoton events with large missing transverse momentum in 1.07 fb ⁻¹ of data produced from pp collisions at $\sqrt{s} = 7$ TeV to place a lower bound on the compactification scale in a universal extra dimension model with gravitational decays. The bound assumes that the cutoff scale Λ , for the radiative corrections to the Kaluza-Klein masses, satisfies $\Lambda/M_C = 20$. The model parameters are chosen such that the decay $\gamma^* \rightarrow G\gamma$ occurs with an appreciable branching fraction.	>4.1	95	21 SIRUNYAN	18cw CMS	$pp \rightarrow G \rightarrow HH$
12 ABAZOV 12M use same-sign dimuon events in 7.3 fb ⁻¹ of data from $p\bar{p}$ collisions at $\sqrt{s} = 1.96$ TeV to place a lower bound on the compactification scale $1/R$, in models with universal extra dimensions where all Standard Model fields propagate in the bulk.	>2.68	95	22 SIRUNYAN	18DJ CMS	$pp \rightarrow G \rightarrow ZZ$
13 BAAK 12 use electroweak precision observables to place a lower bound on the compactification scale $1/R$, in models with universal extra dimensions and Standard Model fields propagating in the bulk. Bound assumes a 125 GeV Higgs mass. See their Fig. 25 for the bound as a function of the Higgs mass.	>1.23 (>0.84)	95	23 SIRUNYAN	18DU CMS	$pp \rightarrow G \rightarrow \gamma\gamma$
14 FLACKE 12 use electroweak precision observables to place a lower bound on the compactification scale $1/R$, in models with universal extra dimensions and Standard Model fields propagating in the bulk. See their Fig. 1 for the bound as a function of the universal bulk fermion mass parameter μ .	>0.94 (>0.71)	95	24 SIRUNYAN	18F CMS	$pp \rightarrow G \rightarrow HH$
15 NISHIWAKI 12 use up to 2 fb ⁻¹ of data from the ATLAS and CMS experiments that constrains the production cross section of a Higgs-like particle to place a lower bound on the compactification scale $1/R$ in universal extra dimension models. The quoted bound assumes Standard Model fields propagating in the bulk and a 125 GeV Higgs mass. See their Fig. 1 for the bound as a function of the Higgs mass.	>2.23	95	25 SIRUNYAN	18I CMS	$pp \rightarrow G \rightarrow b\bar{b}$
16 AAD 11F use diphoton events with large missing transverse energy in 3.1 pb ⁻¹ of data produced from pp collisions at $\sqrt{s} = 7$ TeV to place a lower bound on the compactification scale in a universal extra dimension model with gravitational decays. The bound assumes that the cutoff scale Λ , for the radiative corrections to the Kaluza-Klein masses, satisfies $\Lambda/M_C = 20$. The model parameters are chosen such that the decay $\gamma^* \rightarrow G\gamma$ occurs with an appreciable branching fraction.	>0.845	95	26 SIRUNYAN	18P CMS	$pp \rightarrow G \rightarrow W\bar{W}, ZZ$
17 AAD 11X use diphoton events with large missing transverse energy in 36 pb ⁻¹ of data produced from pp collisions at $\sqrt{s} = 7$ TeV to place a lower bound on the compactification scale in a universal extra dimension model with gravitational decays. The bound assumes that the cutoff scale Λ , for the radiative corrections to the Kaluza-Klein masses, satisfies $\Lambda/M_C = 20$. The model parameters are chosen such that the decay $\gamma^* \rightarrow G\gamma$ occurs with an appreciable branching fraction.	>1.058	95	27 AABOUD	17AP ATLS	$pp \rightarrow G \rightarrow \gamma\gamma$
18 ABAZOV 10P use diphoton events with large missing transverse energy in 6.3 fb ⁻¹ of data produced from $p\bar{p}$ collisions at $\sqrt{s} = 1.96$ TeV to place a lower bound on the compactification scale in a universal extra dimension model with gravitational decays. The bound assumes that the cutoff scale Λ , for the radiative corrections to the Kaluza-Klein masses, satisfies $\Lambda/M_C = 20$. The model parameters are chosen such that the decay $\gamma^* \rightarrow G\gamma$ occurs with an appreciable branching fraction.	>0.754	95	28 AAD	16R ATLS	$pp \rightarrow G \rightarrow W\bar{W}, ZZ$
19 ABAZOV 09AE use dijet angular distributions in 0.7 fb ⁻¹ of data from $p\bar{p}$ collisions at $\sqrt{s} = 1.96$ TeV to place a lower bound on the compactification scale.	>0.607	95	29 AAD	15AU ATLS	$pp \rightarrow G \rightarrow ZZ$
20 HAISCH 07 use inclusive B -meson decays to place a Higgs mass independent bound on the compactification scale $1/R$ in the minimal universal extra dimension model.	>1.05	95	30 AAD	15AZ ATLS	$pp \rightarrow G \rightarrow WW$
21 GOGOLADZE 06 use electroweak precision observables to place a lower bound on the compactification scale in models with universal extra dimensions. Bound assumes a 115 GeV Higgs mass. See their Fig. 3 for the bound as a function of the Higgs mass.	>0.90	95	31 AAD	15CT ATLS	$pp \rightarrow G \rightarrow W\bar{W}, ZZ$
22 CORNET 00 translates a bound on the coefficient of the 4-fermion operator $(\bar{\ell}\gamma_\mu\tau^a\ell)(\bar{\ell}\gamma^\mu\tau^a\ell)$ derived by Hagiwara and Matsumoto into a limit on the mass scale of KK W bosons.	>0.889	95	32 AAD	14V ATLS	$pp \rightarrow G \rightarrow e^+e^-, \mu^+\mu^-$
23 RIZZO 00 obtains limits from global electroweak fits in models with a Higgs in the bulk (3.8 TeV) or on the standard brane (3.3 TeV).	>0.785	95	33 AAD	13A ATLS	$pp \rightarrow G \rightarrow WW$
	>0.71	95	34 AAD	13AO ATLS	$pp \rightarrow G \rightarrow WW$
		95	35 AAD	13AS ATLS	$pp \rightarrow \gamma\gamma, e^+e^-, \mu^+\mu^-$
		95	36 AAD	12AD ATLS	$pp \rightarrow G \rightarrow ZZ$
		95	37 AALTONEN	12V CDF	$p\bar{p} \rightarrow G \rightarrow ZZ$
		95	38 BAAK	12 RVUE	Electroweak
		95	39 AALTONEN	11G CDF	$p\bar{p} \rightarrow G \rightarrow ZZ$
		95	40 AALTONEN	11R CDF	$p\bar{p} \rightarrow G \rightarrow e^+e^-, \gamma\gamma$
		95	41 ABAZOV	11H D0	$p\bar{p} \rightarrow G \rightarrow WW$
		95	42 AALTONEN	10N CDF	$p\bar{p} \rightarrow G \rightarrow WW$
		95	43 ABAZOV	10F D0	$p\bar{p} \rightarrow G \rightarrow e^+e^-, \gamma\gamma$
		95	44 AALTONEN	08S CDF	$p\bar{p} \rightarrow G \rightarrow ZZ$
		95	45 ABAZOV	08J D0	$p\bar{p} \rightarrow G \rightarrow e^+e^-, \gamma\gamma$
		95	46 AALTONEN	07G CDF	$p\bar{p} \rightarrow G \rightarrow \gamma\gamma$
		95	47 AALTONEN	07H CDF	$p\bar{p} \rightarrow G \rightarrow e\bar{e}$
		95	48 ABAZOV	05N D0	$p\bar{p} \rightarrow G \rightarrow \ell\bar{\ell}, \gamma\gamma$
		95	49 ABULENCIA	05A CDF	$p\bar{p} \rightarrow G \rightarrow \ell\bar{\ell}$

Limits on Kaluza-Klein Gravitons in Warped Extra Dimensions

This section places limits on the mass of the first Kaluza-Klein (KK) excitation of the graviton in the warped extra dimension model of Randall and Sundrum. Bounds in parenthesis assume Standard Model fields propagate in the bulk. Experimental bounds depend strongly on the warp parameter, k . See the "Extra Dimensions" review for a full discussion.

Here we list limits for the value of the warp parameter $k/\bar{M}_P = 0.1$.

VALUE (TeV)	CL%	DOCUMENT ID	TECN	COMMENT
>4.25	95	1 SIRUNYAN	18BB CMS	$pp \rightarrow G \rightarrow e^+e^-, \mu^+\mu^-$
• • • We do not use the following data for averages, fits, limits, etc. • • •				
		2 AAD	20C ATLS	$pp \rightarrow G \rightarrow HH$
		3 AABOUD	19A ATLS	$pp \rightarrow G \rightarrow HH$
		4 AABOUD	19O ATLS	$pp \rightarrow G \rightarrow HH$
		5 AAD	19D ATLS	$pp \rightarrow G \rightarrow W\bar{W}, ZZ$
		6 SIRUNYAN	19I CMS	$pp \rightarrow G \rightarrow HH$
		7 SIRUNYAN	19BE CMS	$pp \rightarrow G \rightarrow HH$
		8 SIRUNYAN	19CF CMS	$pp \rightarrow G \rightarrow HH$
		9 AABOUD	18AK ATLS	$pp \rightarrow G \rightarrow WW$
		10 AABOUD	18AL ATLS	$pp \rightarrow G \rightarrow ZZ$
		11 AABOUD	18BF ATLS	$pp \rightarrow G \rightarrow ZZ$
		12 AABOUD	18BI ATLS	$pp \rightarrow G \rightarrow t\bar{t}$
		13 AABOUD	18CJ ATLS	$pp \rightarrow G \rightarrow V, V, V, H, \ell\bar{\ell}$
		14 AABOUD	18CQ ATLS	$pp \rightarrow G \rightarrow HH$
		15 AABOUD	18CW ATLS	$pp \rightarrow G \rightarrow HH$
		16 SIRUNYAN	18AF CMS	$pp \rightarrow G \rightarrow HH$
		17 SIRUNYAN	18AS CMS	$pp \rightarrow G \rightarrow ZZ$
		18 SIRUNYAN	18AX CMS	$pp \rightarrow G \rightarrow WW$

1 SIRUNYAN 18BB use 35.9 (36.3) fb⁻¹ of data from pp collisions at $\sqrt{s} = 13$ TeV to search for dilepton resonances in the dilepton (dimuon) channel. See their paper for other limits with warp parameter values $k/\bar{M}_P = 0.01$ and 0.05. This updates the results of KHACHATRYAN 17T.

2 AAD 20C use 36.1 fb⁻¹ of data from pp collisions at $\sqrt{s} = 13$ TeV to search for Higgs boson pair production in the $b\bar{b}b\bar{b}, b\bar{b}W^+W^-$, and $b\bar{b}\tau^+\tau^-$ final states. See their Figure 5(b)(c) for limits on the cross section as a function of the KK graviton mass. In the case of $k/\bar{M}_P = 1$ and 2, gravitons are excluded in the mass range 260–3000 GeV and 260–1760 GeV, respectively.

3 AABOUD 19A use 36.1 fb⁻¹ of data from pp collisions at $\sqrt{s} = 13$ TeV to search for Higgs boson pair production in the $b\bar{b}b\bar{b}$ final state. See their Figure 9 for limits on the cross section times branching fraction as a function of the KK graviton mass. Assuming $k/\bar{M}_P = 1$, gravitons in the mass range 313–1362 GeV are excluded. This updates the results of AABOUD 16I.

4 AABOUD 19O use 36.1 fb⁻¹ of data from pp collisions at $\sqrt{s} = 13$ TeV to search for Higgs boson pair production in the $b\bar{b}W^+W^-$ final state. See their Figure 12 for limits on the cross section times branching fraction as a function of the KK graviton mass for $k/\bar{M}_P = 1$ and $k/\bar{M}_P = 2$.

5 AAD 19D use 36.1 fb⁻¹ of data from pp collisions at $\sqrt{s} = 13$ TeV to search for diboson resonances in the all-hadronic final state. See their Figure 9(b) for the limit on the cross section times branching fraction as a function of the KK graviton mass, including theoretical values for $k/\bar{M}_P = 1$. This updates the results of AABOUD 18F.

6 SIRUNYAN 19I use 35.9 fb⁻¹ of data from pp collisions at $\sqrt{s} = 13$ TeV to search for Higgs boson pair production in the $\gamma\gamma b\bar{b}$ final state. See their Figure 9 for limits on the cross section times branching fraction as a function of the KK graviton mass. Assuming $k/\bar{M}_P = 1$, gravitons in the mass range 290–810 GeV are excluded. This updates the result of KHACHATRYAN 16BQ.

7 SIRUNYAN 19BE use 35.9 fb⁻¹ of data from pp collisions at $\sqrt{s} = 13$ TeV to search for Higgs boson pair production by combining the results from four final states: $b\bar{b}\gamma\gamma, b\bar{b}\tau^+\tau^-, b\bar{b}b\bar{b}$, and $b\bar{b}VV$. See their Figure 7 for limits on the cross section times branching fraction as a function of the KK graviton mass.

8 SIRUNYAN 19CF use 35.9 fb⁻¹ of data from pp collisions at $\sqrt{s} = 13$ TeV to search for Higgs boson pair production in the $b\bar{b}q\bar{q}\ell\nu$ final state. See their Figure 7 for limits on the cross section times branching fraction as a function of the KK graviton mass, including theoretical values for $k/\bar{M}_P = 0.1$ and 0.3.

9 AABOUD 18AK use 36.1 fb⁻¹ of data from pp collisions at $\sqrt{s} = 13$ TeV to search for WW resonances in $\ell\nu qq$ final states ($\ell = e, \mu$). See their Figure 7(d) for the limit on the cross section times branching fraction as a function of the KK graviton mass, including theoretical values for $k/\bar{M}_P = 1$. This updates the results of AABOUD 16AE.

10 AABOUD 18AL use 36.1 fb⁻¹ of data from pp collisions at $\sqrt{s} = 13$ TeV to search for diboson resonances in the $\ell\ell q\bar{q}$ and $\nu\tau q\bar{q}$ final states. See their Figure 14 for the limit on cross section times branching fraction as a function of the KK graviton mass, including theoretical values for $k/\bar{M}_P = 0.5$ and 1. This updates the results of AABOUD 16AE.

11 AABOUD 18BF use 36.1 fb⁻¹ of data from pp collisions at $\sqrt{s} = 13$ TeV to search for ZZ resonances in the $\ell\ell\ell\ell$ and $\ell\nu\nu\bar{\nu}$ final states ($\ell = e, \mu$). See their Figure 10 for the limit on the cross section times branching fraction as a function of the KK graviton mass, including theoretical values for $k/\bar{M}_P = 1$.

12 AABOUD 18BI use 36.1 fb⁻¹ of data from pp collisions at $\sqrt{s} = 13$ TeV to search for top-quark pairs decaying into the lepton-plus jets topology. See their Figure 16 for the limit on the KK graviton mass as a function of the cross section times branching fraction, including theoretical values for $k/\bar{M}_P = 1$.

13 AABOUD 18CJ combine the searches for heavy resonances decaying into bosonic and leptonic final states from 36.1 fb⁻¹ of pp collision data at $\sqrt{s} = 13$ TeV. The lower limit on the KK graviton mass, with $k/\bar{M}_P = 1$, is 2.3 TeV.

14 AABOUD 18CQ use 36.1 fb⁻¹ of data from pp collisions at $\sqrt{s} = 13$ TeV to search for Higgs boson pair production in the $b\bar{b}\tau^+\tau^-$ final state. See their Figure 2 for limits on the cross section times branching fraction as a function of the KK graviton mass. Assuming $k/\bar{M}_P = 1$, gravitons in the mass range 325–885 GeV are excluded.

- 15 AABOUD 18CW use 36.1 fb⁻¹ of data from pp collisions at $\sqrt{s} = 13$ TeV to search for Higgs boson pair production in the $\gamma\gamma b\bar{b}$ final state. See their Figure 7 for limits on the cross section times branching fraction as a function of the KK graviton mass.
- 16 SIRUNYAN 18AF use 35.9 fb⁻¹ of data from pp collisions at $\sqrt{s} = 13$ TeV to search for Higgs boson pair production in the $b\bar{b}b\bar{b}$ final state. See their Figure 9 for limits on the cross section times branching fraction as a function of the KK graviton mass, including theoretical values for $k/\overline{M}_P = 0.5$. This updates the results of KHACHATRYAN 15R.
- 17 SIRUNYAN 18AS use 35.9 fb⁻¹ of data from pp collisions at $\sqrt{s} = 13$ TeV to search for ZZ resonances in the $\ell\nu\bar{\nu}$ final state ($\ell = e, \mu$). See their Figure 5 for the limit on the KK graviton mass as a function of the cross section times branching fraction, including theoretical values for $k/\overline{M}_P = 0.1, 0.5, \text{ and } 1.0$.
- 18 SIRUNYAN 18AX use 35.9 fb⁻¹ of data from pp collisions at $\sqrt{s} = 13$ TeV to search for WW resonances in $\ell\nu q\bar{q}$ final states ($\ell = e, \mu$). See their Figure 6 for the limit on the KK graviton mass as a function of the cross section times branching fraction, including theoretical values for $k/\overline{M}_P = 0.5$. This updates the results of KHACHATRYAN 14A.
- 19 SIRUNYAN 18BK use 35.9 fb⁻¹ of data from pp collisions at $\sqrt{s} = 13$ TeV to search for ZZ resonances in the $\nu\bar{\nu}q\bar{q}$ final state. See their Figure 4 for the limit on the KK graviton mass as a function of the cross section times branching fraction, including theoretical values for $k/\overline{M}_P = 0.5$.
- 20 SIRUNYAN 18BO use up to 36 fb⁻¹ of data from pp collisions at $\sqrt{s} = 13$ TeV to search for dijet resonances. Besides the quoted bound, KK graviton masses between 1.9 TeV and 2.5 TeV are also excluded. See their Figure 11 for the limit on the product of the cross section, branching fraction and acceptance as a function of the KK graviton mass. This updates the results of KHACHATRYAN 17W.
- 21 SIRUNYAN 18CW use 35.9 fb⁻¹ of data from pp collisions at $\sqrt{s} = 13$ TeV to search for Higgs boson pair production in the $b\bar{b}b\bar{b}$ final state. See their Figure 8 for limits on the cross section times branching fraction as a function of the KK graviton mass, including theoretical values for $k/\overline{M}_P = 0.5$.
- 22 SIRUNYAN 18DJ use 35.9 fb⁻¹ of data from pp collisions at $\sqrt{s} = 13$ TeV to search for ZZ resonances in $2\ell q\bar{q}$ final states ($\ell = e, \mu$). See their Figure 6 for the limit on the KK graviton mass as a function of the cross section times branching fraction. Assuming $k/\overline{M}_P = 0.5$, a graviton mass is excluded below 925 GeV.
- 23 SIRUNYAN 18DU use 35.9 fb⁻¹ of data from pp collisions at $\sqrt{s} = 13$ TeV, in the diphoton channel to place a lower limit on the mass of the lightest KK graviton. See their paper for limits with other warp parameter values $k/\overline{M}_P = 0.01$ and 0.2. This updates the results of KHACHATRYAN 16M.
- 24 SIRUNYAN 18F use 35.9 fb⁻¹ of data from pp collisions at $\sqrt{s} = 13$ TeV to search for Higgs boson pair production in the $b\bar{b}\ell\nu\ell\nu$ final state. See their Figure 7 for limits on the cross section times branching fraction as a function of the KK graviton mass, including theoretical values for $k/\overline{M}_P = 0.1$.
- 25 SIRUNYAN 18I use 19.7 fb⁻¹ of data from pp collisions at $\sqrt{s} = 8$ TeV to search for narrow resonances decaying to bottom quark pairs. See their Figure 3 for the limit on the KK graviton mass as a function of the cross section times branching fraction in the mass range of 325–1200 GeV.
- 26 SIRUNYAN 18P use 35.9 fb⁻¹ of data from pp collisions at $\sqrt{s} = 13$ TeV to search for diboson resonances with dijet final states. See their Figure 6 for the limit on the KK graviton mass as a function of the cross section times branching fraction, including theoretical values for $k/\overline{M}_P = 0.5$. This updates the results of SIRUNYAN 17AK.
- 27 AABOUD 17AP use 36.7 fb⁻¹ of data from pp collisions at $\sqrt{s} = 13$ TeV in the diphoton channel to place a lower limit on the mass of the lightest KK graviton. This updates the results of AABOUD 16H.
- 28 AAD 16R use 20.3 fb⁻¹ of data from pp collisions at $\sqrt{s} = 8$ TeV to place a lower bound on the mass of the lightest KK graviton. See their Figure 4 for the limit on the KK graviton mass as a function of the cross section times branching fraction.
- 29 AAD 15AU use 20 fb⁻¹ of data from pp collisions at $\sqrt{s} = 8$ TeV to search for KK gravitons in a warped extra dimension decaying to ZZ dibosons. See their Figure 2 for limits on the KK graviton mass as a function of the cross section times branching fraction.
- 30 AAD 15AZ use 20.3 fb⁻¹ of data from pp collisions at $\sqrt{s} = 8$ TeV to place a lower bound on the mass of the lightest KK graviton. See their Figure 2 for limits on the KK graviton mass as a function of the cross section times branching ratio.
- 31 AAD 15CT use 20.3 fb⁻¹ of data from pp collisions at $\sqrt{s} = 8$ TeV to place a lower bound on the mass of the lightest KK graviton. See their Figures 6b and 6c for the limit on the KK graviton mass as a function of the cross section times branching fraction.
- 32 AAD 14V use 20.3 (20.5) fb⁻¹ of data from pp collisions at $\sqrt{s} = 8$ TeV in the dielectron (dimuon) channels to place a lower bound on the mass of the lightest KK graviton. This updates the results of AAD 12CC.
- 33 AAD 13A use 4.7 fb⁻¹ of data from pp collisions at $\sqrt{s} = 7$ TeV in the $\ell\nu\ell\nu$ channel, to place a lower bound on the mass of the lightest KK graviton.
- 34 AAD 13AO use 4.7 fb⁻¹ of data from pp collisions at $\sqrt{s} = 7$ TeV in the $\ell\nu jj$ channel, to place a lower bound on the mass of the lightest KK graviton.
- 35 AAD 13AS use 4.9 fb⁻¹ of data from pp collisions at $\sqrt{s} = 7$ TeV in the diphoton channel to place lower limits on the mass of the lightest KK graviton. The diphoton channel is combined with previous results in the dielectron and dimuon channels to set the best limit. See their Table 2 for warp parameter values k/\overline{M}_P between 0.01 and 0.1. This updates the results of AAD 12V.
- 36 AAD 12AD use 1.02 fb⁻¹ of data from pp collisions at $\sqrt{s} = 7$ TeV to search for KK gravitons in a warped extra dimension decaying to ZZ dibosons in the $lljj$ and $llll$ channels ($\ell = e, \mu$). The limit is quoted for the combined $lljj + llll$ channels. See their Figure 5 for limits on the cross section $\sigma(G \rightarrow ZZ)$ as a function of the graviton mass.
- 37 AALTONEN 12V use 6 fb⁻¹ of data from $p\bar{p}$ collisions at $\sqrt{s} = 1.96$ TeV to search for KK gravitons in a warped extra dimension decaying to ZZ dibosons in the $lljj$ and $llll$ channels ($\ell = e, \mu$). It provides improved limits over the previous analysis in AALTONEN 11G. See their Figure 16 for limits from all channels combined on the cross section times branching ratio $\sigma(p\bar{p} \rightarrow G^* \rightarrow ZZ)$ as a function of the graviton mass.
- 38 BAAK 12 use electroweak precision observables to place a lower bound on the compactification scale $k e^{-\pi k R}$, assuming Standard Model fields propagate in the bulk and the Higgs is confined to the IR brane. See their Fig. 27 for more details.
- 39 AALTONEN 11G use 2.5–2.9 fb⁻¹ of data from $p\bar{p}$ collisions at $\sqrt{s} = 1.96$ TeV to search for KK gravitons in a warped extra dimension decaying to ZZ dibosons via the $e\bar{e}e, e\bar{e}\mu\mu, \mu\bar{\mu}\mu\mu, e\bar{e}jj, \text{ and } \mu\bar{\mu}jj$ channels. See their Fig. 20 for limits on the cross section $\sigma(G \rightarrow ZZ)$ as a function of the graviton mass.
- 40 AALTONEN 11R uses 5.7 fb⁻¹ of data from $p\bar{p}$ collisions at $\sqrt{s} = 1.96$ TeV in the dielectron channel to place a lower bound on the mass of the lightest graviton. It provides combined limits with the diphoton channel analysis of AALTONEN 11U. For

- warp parameter values k/\overline{M}_P between 0.01 to 0.1 the lower limit on the mass of the lightest graviton is between 612 and 1058 GeV. See their Table 1 for more details.
- 41 ABAZOV 11H use 5.4 fb⁻¹ of data from $p\bar{p}$ collisions at $\sqrt{s} = 1.96$ TeV to place a lower bound on the mass of the lightest graviton. Their 95% C.L. exclusion limit does not include masses less than 300 GeV.
- 42 AALTONEN 10N use 2.9 fb⁻¹ of data from $p\bar{p}$ collisions at $\sqrt{s} = 1.96$ TeV to place a lower bound on the mass of the lightest graviton.
- 43 ABAZOV 10F use 5.4 fb⁻¹ of data from $p\bar{p}$ collisions at $\sqrt{s} = 1.96$ TeV to place a lower bound on the mass of the lightest graviton. For warp parameter values of k/\overline{M}_P between 0.01 and 0.1 the lower limit on the mass of the lightest graviton is between 560 and 1050 GeV. See their Fig. 3 for more details.
- 44 AALTONEN 08s use $p\bar{p}$ collisions at $\sqrt{s} = 1.96$ TeV to search for KK gravitons in warped extra dimensions. They search for graviton resonances decaying to four electrons via two Z bosons using 1.1 fb⁻¹ of data. See their Fig. 8 for limits on $\sigma \cdot \text{B}(G \rightarrow ZZ)$ versus the graviton mass.
- 45 ABAZOV 08j use $p\bar{p}$ collisions at $\sqrt{s} = 1.96$ TeV to search for KK gravitons in warped extra dimensions. They search for graviton resonances decaying to electrons and photons using 1 fb⁻¹ of data. For warp parameter values of k/\overline{M}_P between 0.01 and 0.1 the lower limit on the mass of the lightest excitation is between 300 and 900 GeV. See their Fig. 4 for more details.
- 46 AALTONEN 07G use $p\bar{p}$ collisions at $\sqrt{s} = 1.96$ TeV to search for KK gravitons in warped extra dimensions. They search for graviton resonances decaying to photons using 1.2 fb⁻¹ of data. For warp parameter values of $k/\overline{M}_P = 0.1, 0.05, \text{ and } 0.01$ the bounds on the graviton mass are 850, 694, and 230 GeV, respectively. See their Fig. 3 for more details. See also AALTONEN 07H.
- 47 AALTONEN 07H use $p\bar{p}$ collisions at $\sqrt{s} = 1.96$ TeV to search for KK gravitons in warped extra dimensions. They search for graviton resonances decaying to electrons using 1.3 fb⁻¹ of data. For a warp parameter value of $k/\overline{M}_P = 0.1$ the bound on the graviton mass is 807 GeV. See their Fig. 4 for more details. A combined analysis with the diphoton data of AALTONEN 07G yields for $k/\overline{M}_P = 0.1$ a graviton mass lower bound of 889 GeV.
- 48 ABAZOV 05n use $p\bar{p}$ collisions at $\sqrt{s} = 1.96$ TeV to search for KK gravitons in warped extra dimensions. They search for graviton resonances decaying to muons, electrons or photons, using 260 pb⁻¹ of data. For warp parameter values of $k/\overline{M}_P = 0.1, 0.05, \text{ and } 0.01$, the bounds on the graviton mass are 785, 650 and 250 GeV respectively. See their Fig. 3 for more details.
- 49 ABULENCIA 05A use $p\bar{p}$ collisions at $\sqrt{s} = 1.96$ TeV to search for KK gravitons in warped extra dimensions. They search for graviton resonances decaying to muons or electrons, using 200 pb⁻¹ of data. For warp parameter values of $k/\overline{M}_P = 0.1, 0.05, \text{ and } 0.01$, the bounds on the graviton mass are 710, 510 and 170 GeV respectively.

Limits on Kaluza-Klein Gluons in Warped Extra Dimensions

This section places limits on the mass of the first Kaluza-Klein (KK) excitation of the gluon in warped extra dimension models with Standard Model fields propagating in the bulk. Bounds are given for a specific benchmark model with $\Gamma/m = 15.3\%$ where Γ is the width and m the mass of the KK gluon. See the "Extra Dimensions" review for more discussion.

VALUE (TeV)	CL%	DOCUMENT ID	TECN	COMMENT
>3.8	95	1 AABOUD	18BI ATLS	$g_{KK} \rightarrow t\bar{t} \rightarrow \ell j$
• • •		We do not use the following data for averages, fits, limits, etc. • • •		
		2 AABOUD	19AS ATLS	$g_{KK} \rightarrow t\bar{t} \rightarrow jj$
		3 SIRUNYAN	19AL CMS	$g_{KK} \rightarrow t\bar{t}$
>2.5	95	4 CHATRCHYAN	13BM CMS	$g_{KK} \rightarrow t\bar{t}$
		5 CHEN	13A	$B \rightarrow X_S \gamma$
>1.5	95	6 AAD	12BV ATLS	$g_{KK} \rightarrow t\bar{t} \rightarrow \ell j$

- 1 AABOUD 18BI use 36.1 fb⁻¹ of data from pp collisions at $\sqrt{s} = 13$ TeV. This result updates AAD 13AQ.
- 2 AABOUD 19AS use 36.1 fb⁻¹ of data from pp collisions at $\sqrt{s} = 13$ TeV. An upper bound of 3.4 TeV is placed on the KK gluon mass for $\Gamma/m = 30\%$.
- 3 SIRUNYAN 19AL use 35.9 fb⁻¹ of data from pp collisions at $\sqrt{s} = 13$ TeV to place limits on a KK gluon decaying to a top quark and a heavy vector-like fermion, T. KK gluon masses between 1.5 and 2.3 TeV and between 2.0 and 2.4 TeV are excluded for T masses of 1.2 and 1.5 TeV, respectively.
- 4 CHATRCHYAN 13BM use 19.7 fb⁻¹ of data from pp collisions at $\sqrt{s} = 8$ TeV. Bound is for a width of approximately 15–20% of the KK gluon mass.
- 5 CHEN 13A place limits on the KK mass scale for a specific warped model with custodial symmetry and bulk fermions. See their Figures 4 and 5.
- 6 AAD 12BV use 2.05 fb⁻¹ of data from pp collisions at $\sqrt{s} = 7$ TeV.

Black Hole Production Limits

Semiclassical Black Holes

VALUE (GeV)	DOCUMENT ID	TECN	COMMENT
• • •	We do not use the following data for averages, fits, limits, etc. • • •		
	1 SIRUNYAN	18DA CMS	$pp \rightarrow \text{multijet}$
	2 AAD	16N ATLS	$pp \rightarrow \text{multijet}$
	3 AAD	16O ATLS	$pp \rightarrow \ell + (\ell\ell/\ell j/jj)$
	4 AAD	13AW ATLS	$pp \rightarrow \mu\mu$
1	SIRUNYAN 18DA		use 35.9 fb ⁻¹ of data from pp collisions at $\sqrt{s} = 13$ TeV to search for semiclassical black holes decaying to multijet final states. No excess of events above the expected level of standard model background was observed. Exclusions at 95% CL are set on the mass threshold for black hole production as a function of the higher-dimensional Planck scale for rotating and nonrotating black holes under several model assumptions (ADD, 2, 4, 6 extra dimensions model) in the 7.1–10.3 TeV range. These limits supersede those in SIRUNYAN 17CP.
2	AAD 16N		use 3.6 fb ⁻¹ of data from pp collisions at $\sqrt{s} = 13$ TeV to search for semiclassical black hole decays to multijet final states. No excess of events above the expected level of Standard Model background was observed. Exclusion contours at 95% C.L. are set on the mass threshold for black hole production versus higher-dimensional Planck scale for rotating black holes (ADD, 6 extra dimensions model).

Searches Particle Listings

Extra Dimensions

- ³ AAD 16o use 3.2 fb⁻¹ of data from pp collisions at $\sqrt{s} = 13$ TeV to search for semi-classical black hole decays to high-mass final states with leptons and jets. No excess of events above the expected level of Standard Model background was observed. Exclusion contours at 95% C.L. are set on the mass threshold for black hole production versus higher-dimensional Planck scale for rotating black holes (ADD, 2 to 6 extra dimensions).
- ⁴ AAD 13aw use 20.3 fb⁻¹ of data from pp collisions at $\sqrt{s} = 8$ TeV to search for semi-classical black hole decays to like-sign dimuon final states using large track multiplicity. No excess of events above the expected level of Standard Model background was observed. Exclusion contours at 95% C.L. are set on the mass threshold for black hole production versus higher-dimensional Planck scale in various extra dimensions, rotating and non-rotating models.

Quantum Black Holes

VALUE (GeV)	DOCUMENT ID	TECN	COMMENT
•••			We do not use the following data for averages, fits, limits, etc. •••
¹	AABOUD 18BA ATLS	$pp \rightarrow \gamma j$	
²	AABOUD 18CM ATLS	$pp \rightarrow e\mu, e\tau, \mu\tau$	
³	SIRUNYAN 18AT CMS	$pp \rightarrow e\mu$	
⁴	SIRUNYAN 18DD CMS	$pp \rightarrow$ dijet, ang. distrib.	
⁵	AABOUD 17AK ATLS	$pp \rightarrow jj$	
⁶	SIRUNYAN 17CP CMS	$pp \rightarrow jj$	
⁷	KHACHATRYAN...16BE CMS	$pp \rightarrow e\mu$	
⁸	KHACHATRYAN...15V CMS	$pp \rightarrow jj$	
⁹	AAD 14AL ATLS	$pp \rightarrow \ell j$	
¹⁰	AAD 14V ATLS	$pp \rightarrow ee, \mu\mu$	
¹¹	CHATRCHYAN13A CMS	$pp \rightarrow jj$	

- ¹ AABOUD 18BA use 36.7 fb⁻¹ of data from pp collisions at $\sqrt{s} = 13$ TeV to search for quantum black hole decays to final states with a photon and a jet. No excess of events above the expected level of Standard Model background was observed. Exclusion limits at 95% C.L. are set on mass thresholds for black hole production in ADD (6 extra dimensions) and RS1 models. Assuming the black hole mass threshold is equal to the Planck scale, mass thresholds below 7.1 TeV and 4.4 TeV are excluded for the ADD and RS1 models, respectively. These limits supersede those in AAD 16A1.
- ² AABOUD 18CM use 36.1 fb⁻¹ of data from pp collisions at $\sqrt{s} = 13$ TeV to search for quantum black hole decays with different-flavor high-mass dilepton final states. No excess of events above the expected level of Standard Model background was observed. Exclusion limits at 95% C.L. are set on mass thresholds for black hole production in ADD (6 extra dimensions) and RS1 models. Assuming the black hole mass threshold is equal to the higher-dimensional Planck scale, mass thresholds below 5.6 (3.4), 4.9 (2.9), and 4.5 (2.6) TeV are excluded in the $e\mu, e\tau$ and $\mu\tau$ channels for the ADD (RS1) models, respectively. These limits supersede those in AABOUD 16P.
- ³ SIRUNYAN 18AT use 35.9 fb⁻¹ of data from pp collisions at $\sqrt{s} = 13$ TeV to search for quantum black hole decays to $e\mu$ final states. In Figure 4, lower mass limits of 5.3, 5.5 and 5.6 TeV are placed in a model with 4, 5 and 6 extra dimensions, respectively, and a lower mass limit of 3.6 TeV is found for a single warped dimension.
- ⁴ SIRUNYAN 18DD use 35.9 fb⁻¹ of data from pp collisions at $\sqrt{s} = 13$ TeV to search for quantum black hole decays in dijet angular distributions. A lower mass limit of 5.9 (8.2) TeV is placed in the RS (ADD) model with one (six) extra dimension(s).
- ⁵ AABOUD 17AK use 37 fb⁻¹ of data from pp collisions at $\sqrt{s} = 13$ TeV to search for quantum black hole decays to final states with dijets. No excess of events above the expected level of Standard Model background was observed. Exclusion limits at 95% C.L. are set on mass thresholds for black hole production in an ADD (6 extra dimensions) model. Assuming the black hole mass threshold is equal to the higher-dimensional Planck scale, mass thresholds below 8.9 TeV are excluded.
- ⁶ SIRUNYAN 17CP use 2.3 fb⁻¹ of data from pp collisions at $\sqrt{s} = 13$ TeV to search for quantum black holes decaying to dijet final states. No excess of events above the expected level of standard model background was observed. Limits on the quantum black hole mass threshold are set as a function of the higher-dimensional Planck scale, under the assumption that the mass threshold must exceed the above Planck scale. Depending on the model, mass thresholds in the range up to 5.1–9.0 TeV are excluded.
- ⁷ KHACHATRYAN 16BE use 19.7 fb⁻¹ of data from pp collisions at $\sqrt{s} = 8$ TeV to search for quantum black holes undergoing lepton flavor violating decay to the $e\mu$ final state. No excess of events above the expected level of standard model background was observed. Exclusion limits at 95% C.L. are set on mass thresholds for black hole production in the ADD (2–6 flat extra dimensions), RS1 (1 warped extra dimension), and a model with a Planck scale at the TeV scale from a renormalization of the gravitational constant (no extra dimensions). Limits on the black hole mass threshold are set assuming that it is equal to the higher-dimensional Planck scale. Mass thresholds for quantum black holes in the range up to 3.15–3.63 TeV are excluded in the ADD model. In the RS1 model, mass thresholds below 2.81 TeV are excluded in the PDG convention for the Schwarzschild radius. In the model with no extra dimensions, mass thresholds below 1.99 TeV are excluded.
- ⁸ KHACHATRYAN 15V use 19.7 fb⁻¹ of data from pp collisions at $\sqrt{s} = 8$ TeV to search for quantum black holes decaying to dijet final states. No excess of events above the expected level of standard model background was observed. Exclusion limits at 95% C.L. are set on mass thresholds for black hole production in the ADD (2–6 flat extra dimensions) and RS1 (1 warped extra dimension) model. Limits on the black hole mass threshold are set as a function of the higher-dimensional Planck scale, under the assumption that the mass threshold must exceed the above Planck scale. Depending on the model, mass thresholds in the range up to 5.0–6.3 TeV are excluded. This paper supersedes CHATRCHYAN 13Aa.
- ⁹ AAD 14AL use 20.3 fb⁻¹ of data from pp collisions at $\sqrt{s} = 8$ TeV to search for quantum black hole decays to final states with high-invariant-mass lepton + jet. No excess of events above the expected level of Standard Model background was observed. Exclusion limits at 95% C.L. are set on mass thresholds for black hole production in ADD (6 extra dimensions) model. Assuming the black hole mass threshold is equal to the higher-dimensional Planck scale, mass thresholds below 5.3 TeV are excluded.
- ¹⁰ AAD 14V use 20.3 (20.5) fb⁻¹ of data in the dielectron (dimuon) channels from pp collisions at $\sqrt{s} = 8$ TeV to search for quantum black hole decays involving high-mass dilepton resonances. No excess of events above the expected level of Standard Model background was observed. Exclusion limits at 95% C.L. are set on mass thresholds for black hole production in ADD (6 extra dimensions) and RS1 models. Assuming the black hole mass threshold is equal to the higher-dimensional Planck scale, mass thresholds below 3.65 TeV and 2.24 TeV are excluded for the ADD and RS1 models, respectively.

- ¹¹ CHATRCHYAN 13A use 5 fb⁻¹ of data from pp collisions at $\sqrt{s} = 7$ TeV to search for quantum black holes decaying to dijet final states. No excess of events above the expected level of standard model background was observed. Exclusion limits at 95% C.L. are set on mass thresholds for black hole production in the ADD (2–6 flat extra dimensions) and RS (1 warped extra dimension) model. Limits on the black hole mass threshold are set as a function of the higher-dimensional Planck scale, under assumption that the mass threshold must exceed the above Planck scale. Depending on the model, mass thresholds in the range up to 4.0–5.3 TeV are excluded.

REFERENCES FOR Extra Dimensions

AAD	20C	PL B800 135103	G. Aad et al.	(ATLAS Collab.)
AABOUD	19A	JHEP 1901 030	M. Aaboud et al.	(ATLAS Collab.)
AABOUD	19AS	PR D99 092004	M. Aaboud et al.	(ATLAS Collab.)
AABOUD	19O	JHEP 1904 092	M. Aaboud et al.	(ATLAS Collab.)
AAD	19D	JHEP 1909 091	G. Aad et al.	(ATLAS Collab.)
SIRUNYAN	19	PL B788 7	A.M. Sirunyan et al.	(CMS Collab.)
SIRUNYAN	19AC	JHEP 1904 114	A.M. Sirunyan et al.	(CMS Collab.)
SIRUNYAN	19AL	EPJ C79 208	A.M. Sirunyan et al.	(CMS Collab.)
SIRUNYAN	19BE	PRL 122 121803	A.M. Sirunyan et al.	(CMS Collab.)
SIRUNYAN	19CF	JHEP 1910 125	A.M. Sirunyan et al.	(CMS Collab.)
AABOUD	18AK	JHEP 1803 042	M. Aaboud et al.	(ATLAS Collab.)
AABOUD	18AL	JHEP 1803 009	M. Aaboud et al.	(ATLAS Collab.)
AABOUD	18AV	JHEP 1807 089	M. Aaboud et al.	(ATLAS Collab.)
AABOUD	18BA	EPJ C78 102	M. Aaboud et al.	(ATLAS Collab.)
AABOUD	18BF	EPJ C78 293	M. Aaboud et al.	(ATLAS Collab.)
AABOUD	18BI	EPJ C78 565	M. Aaboud et al.	(ATLAS Collab.)
AABOUD	18CE	JHEP 1812 039	M. Aaboud et al.	(ATLAS Collab.)
AABOUD	18CJ	PR D98 052008	M. Aaboud et al.	(ATLAS Collab.)
AABOUD	18CM	PR D98 092008	M. Aaboud et al.	(ATLAS Collab.)
AABOUD	18CQ	PRL 121 191801	M. Aaboud et al.	(ATLAS Collab.)
AABOUD	18CW	JHEP 1811 040	M. Aaboud et al.	(ATLAS Collab.)
AABOUD	18F	PL B777 31	M. Aaboud et al.	(ATLAS Collab.)
AABOUD	18H	JHEP 1801 126	M. Aaboud et al.	(ATLAS Collab.)
BERGE	18	PRL 120 141101	J. Berge et al.	(MICROSCOPE Collab.)
FAYET	18	PR D97 055039	P. Fayet	(EPOL)
FAYET	18A	PR D99 055043	P. Fayet	(ENSP, EPOL)
HADDOCK	18	PR D97 026002	C. Haddock et al.	(NAGO, KEK, OSAK+)
SIRUNYAN	18AF	PL B781 244	A.M. Sirunyan et al.	(CMS Collab.)
SIRUNYAN	18AS	JHEP 1803 003	A.M. Sirunyan et al.	(CMS Collab.)
SIRUNYAN	18AT	JHEP 1804 073	A.M. Sirunyan et al.	(CMS Collab.)
SIRUNYAN	18AX	JHEP 1805 088	A.M. Sirunyan et al.	(CMS Collab.)
SIRUNYAN	18BB	JHEP 1806 120	A.M. Sirunyan et al.	(CMS Collab.)
SIRUNYAN	18BK	JHEP 1807 075	A.M. Sirunyan et al.	(CMS Collab.)
SIRUNYAN	18BO	JHEP 1808 130	A.M. Sirunyan et al.	(CMS Collab.)
SIRUNYAN	18BV	EPJ C78 291	A.M. Sirunyan et al.	(CMS Collab.)
SIRUNYAN	18CW	JHEP 1808 152	A.M. Sirunyan et al.	(CMS Collab.)
SIRUNYAN	18DA	JHEP 1811 042	A.M. Sirunyan et al.	(CMS Collab.)
SIRUNYAN	18DD	EPJ C78 789	A.M. Sirunyan et al.	(CMS Collab.)
SIRUNYAN	18DJ	JHEP 1809 101	A.M. Sirunyan et al.	(CMS Collab.)
SIRUNYAN	18DU	PR D98 092001	A.M. Sirunyan et al.	(CMS Collab.)
SIRUNYAN	18F	JHEP 1801 054	A.M. Sirunyan et al.	(CMS Collab.)
SIRUNYAN	18I	PRL 120 201801	A.M. Sirunyan et al.	(CMS Collab.)
SIRUNYAN	18P	PR D97 072006	A.M. Sirunyan et al.	(CMS Collab.)
SIRUNYAN	18S	PR D97 092005	A.M. Sirunyan et al.	(CMS Collab.)
AABOUD	17AK	PR D96 052004	M. Aaboud et al.	(ATLAS Collab.)
AABOUD	17AP	PL B775 105	M. Aaboud et al.	(ATLAS Collab.)
KHACHATRYAN...17T	PL B768 57	V. Khachatryan et al.	(CMS Collab.)	
KHACHATRYAN...17A	PL B769 520	V. Khachatryan et al.	(CMS Collab.)	
KLIMCHITSKAYA	17A	PR D95 123013	G.L. Klimchitskaya, V.M. Mostepanenko	(CMS Collab.)
SIRUNYAN	17AK	PL B774 533	A.M. Sirunyan et al.	(CMS Collab.)
SIRUNYAN	17AJ	JHEP 1710 073	A.M. Sirunyan et al.	(CMS Collab.)
SIRUNYAN	17CP	PL B774279	A.M. Sirunyan et al.	(CMS Collab.)
SIRUNYAN	17F	JHEP 1707 013	A.M. Sirunyan et al.	(CMS Collab.)
AABOUD	16AE	JHEP 1609 173	M. Aaboud et al.	(ATLAS Collab.)
AABOUD	16D	PR D94 032005	M. Aaboud et al.	(ATLAS Collab.)
AABOUD	16F	JHEP 1606 059	M. Aaboud et al.	(ATLAS Collab.)
AABOUD	16H	JHEP 1609 001	M. Aaboud et al.	(ATLAS Collab.)
AABOUD	16I	PR D94 052002	M. Aaboud et al.	(ATLAS Collab.)
AABOUD	16P	EPJ C76 541	M. Aaboud et al.	(ATLAS Collab.)
AAD	16A1	JHEP 1603 041	G. Aad et al.	(ATLAS Collab.)
AAD	16N	JHEP 1603 026	G. Aad et al.	(ATLAS Collab.)
AAD	16O	PL B760 520	G. Aad et al.	(ATLAS Collab.)
AAD	16R	PL B755 285	G. Aad et al.	(ATLAS Collab.)
KHACHATRYAN...16BE	EPJ C76 317	V. Khachatryan et al.	(CMS Collab.)	
KHACHATRYAN...16BQ	PR D94 052012	V. Khachatryan et al.	(CMS Collab.)	
KHACHATRYAN...16M	PRL 117 051802	V. Khachatryan et al.	(CMS Collab.)	
KHACHATRYAN...16N	PL B755 102	V. Khachatryan et al.	(CMS Collab.)	
AAD	15AU	EPJ C75 69	G. Aad et al.	(ATLAS Collab.)
AAD	15AZ	EPJ C75 209	G. Aad et al.	(ATLAS Collab.)
Also	EPJ C75 370 (errata.)	G. Aad et al.	(ATLAS Collab.)	
AAD	15CS	PR D91 012008	G. Aad et al.	(ATLAS Collab.)
Also	PR D92 059903 (errata.)	G. Aad et al.	(ATLAS Collab.)	
AAD	15CT	JHEP 1512 055	G. Aad et al.	(ATLAS Collab.)
ACCOMANDO	15	MPL A30 1540010	E. Accomando	(SHMP)
KHACHATRYAN...15AE	JHEP 1504 025	V. Khachatryan et al.	(CMS Collab.)	
KHACHATRYAN...15AL	EPJ C75 235	V. Khachatryan et al.	(CMS Collab.)	
KHACHATRYAN...15R	PL B749 560	V. Khachatryan et al.	(CMS Collab.)	
KHACHATRYAN...15T	PR D91 025005	V. Khachatryan et al.	(CMS Collab.)	
KHACHATRYAN...15V	PR D91 052009	V. Khachatryan et al.	(CMS Collab.)	
AAD	14AL	PRL 112 091804	G. Aad et al.	(ATLAS Collab.)
AAD	14BE	EPJ C74 3134	G. Aad et al.	(ATLAS Collab.)
AAD	14V	PR D90 052005	G. Aad et al.	(ATLAS Collab.)
KHACHATRYAN...14A	JHEP 1408 174	V. Khachatryan et al.	(CMS Collab.)	
AAD	13A	PL B718 860	G. Aad et al.	(ATLAS Collab.)
AAD	13AO	PR D87 112006	G. Aad et al.	(ATLAS Collab.)
AAD	13AQ	PR D88 012004	G. Aad et al.	(ATLAS Collab.)
AAD	13AS	NJP 15 043007	G. Aad et al.	(ATLAS Collab.)
AAD	13AW	PR D88 072001	G. Aad et al.	(ATLAS Collab.)
AAD	13C	PRL 110 011802	G. Aad et al.	(ATLAS Collab.)
AAD	13D	JHEP 1301 029	G. Aad et al.	(ATLAS Collab.)
AAD	13E	PR D87 015010	G. Aad et al.	(ATLAS Collab.)
CHATRCHYAN	13A	JHEP 1301 013	S. Chatrchyan et al.	(CMS Collab.)
CHATRCHYAN	13AD	JHEP 1307 178	S. Chatrchyan et al.	(CMS Collab.)
CHATRCHYAN	13AQ	PR D87 072005	S. Chatrchyan et al.	(CMS Collab.)
CHATRCHYAN	13BM	PRL 111 211804	S. Chatrchyan et al.	(CMS Collab.)
Also	PRL 112 119903 (errata.)	S. Chatrchyan et al.	(CMS Collab.)	
CHATRCHYAN	13W	JHEP 1303 111	S. Chatrchyan et al.	(CMS Collab.)
CHEN	13A	CP C37 06302	J.-B. Chen et al.	(DALI)
EDELHAUSER	13	JHEP 1308 091	L. Edelhauser, T. Flacke, M. Kramer	(AACH, KAIST)
XU	13	JP G40 035107	J. Xu et al.	(CMS Collab.)
AAD	12AD	PL B712 331	G. Aad et al.	(ATLAS Collab.)
AAD	12BV	JHEP 1209 041	G. Aad et al.	(ATLAS Collab.)
AAD	12CC	JHEP 1211 138	G. Aad et al.	(ATLAS Collab.)
AAD	12CP	PL B718 411	G. Aad et al.	(ATLAS Collab.)
AAD	12X	PL B710 519	G. Aad et al.	(ATLAS Collab.)
AAD	12Y	PL B710 538	G. Aad et al.	(ATLAS Collab.)
AALTONEN	12V	PR D85 012008	T. Aaltonen et al.	(CDF)
ABAZOV	12M	PRL 108 131802	V.M. Abazov et al.	(DO Collab.)

See key on page 999

Searches Particle Listings

Extra Dimensions, WIMP and Dark Matter Searches

AJELLO	12	JCAP 1202 012	M. Ajello et al.	(Fermi-LAT Collab.)
BAAK	12	EPJ C72 2003	M. Baak et al.	(Glitter Group)
CHATRCHYAN	12R	PRL 108 111801	S. Chattrchyan et al.	(CMS Collab.)
FLACKE	12	PR D85 126007	T. Flacke, C. Pasold	(WURZ)
NISHIWAKI	12	PL B707 506	K. Nishiwaki et al.	(KOBÉ, OSAK)
AAD	11F	PRL 106 121803	G. Aad et al.	(ATLAS Collab.)
AAD	11X	EPJ C71 1744	G. Aad et al.	(ATLAS Collab.)
AALTONEN	11G	PR D83 112008	T. Aaltonen et al.	(CDF Collab.)
AALTONEN	11R	PRL 107 051801	T. Aaltonen et al.	(CDF Collab.)
AALTONEN	11U	PR D83 011102	T. Aaltonen et al.	(CDF Collab.)
AARON	11C	PL B705 52	F. D. Aaron et al.	(HI Collab.)
ABAZOV	11H	PRL 107 011801	V.M. Abazov et al.	(DO Collab.)
BEZERRA	11	PR D83 075004	V.B. Bezerra et al.	
SUSHKOV	11	PRL 107 171101	A.O. Sushkov et al.	
AALTONEN	10N	PRL 104 241801	T. Aaltonen et al.	(CDF Collab.)
ABAZOV	10F	PRL 104 241802	V.M. Abazov et al.	(DO Collab.)
ABAZOV	10P	PRL 105 221802	V.M. Abazov et al.	(DO Collab.)
BEZERRA	10	PR D81 055003	V.B. Bezerra et al.	
ABAZOV	09AE	PRL 103 191803	V.M. Abazov et al.	(DO Collab.)
ABAZOV	09D	PRL 102 051601	V.M. Abazov et al.	(DO Collab.)
MASUDA	09	PRL 102 171101	M. Masuda, M. Sasaki	(ICRR)
AALTONEN	08AC	PRL 101 181602	T. Aaltonen et al.	(CDF Collab.)
AALTONEN	08S	PR D78 012008	T. Aaltonen et al.	(CDF Collab.)
ABAZOV	08J	PRL 100 091802	V.M. Abazov et al.	(DO Collab.)
ABAZOV	08S	PRL 101 011601	V.M. Abazov et al.	(DO Collab.)
DAS	08	PR D78 063011	P.K. Das, V.H.S. Kumar, P.K. Suresh	
GERACI	08	PR D78 022002	A.A. Geraci et al.	(STAN)
TRENKEL	08	PR D77 122001	C. Trenkel	
AALTONEN	07G	PRL 99 171801	T. Aaltonen et al.	(CDF Collab.)
AALTONEN	07H	PRL 99 171802	T. Aaltonen et al.	(CDF Collab.)
DECCA	07A	EPJ C51 963	R. Decca et al.	
HAISSCH	07	PR D76 034014	U. Haisch, A. Weiler	
KAPNER	07	PRL 98 021101	D.J. Kapner et al.	
SCHAEF	07A	EPJ C49 411	S. Schaefer et al.	(ALEPH Collab.)
TU	07	PRL 98 201101	L.-C. Tu et al.	
ABDALLAH	06C	EPJ C45 589	J. Abdallah et al.	(DELPHI Collab.)
ABULENCIA	06	PRL 97 171802	A. Abulencia et al.	(CDF Collab.)
GERDES	06	PR D73 112008	D. Gerdes et al.	
GOGOLADZE	06	PR D74 093012	I. Gogoladze, C. Macesanu	
ABAZOV	05N	PRL 95 091801	V.M. Abazov et al.	(DO Collab.)
ABAZOV	05V	PRL 95 161602	V.M. Abazov et al.	(DO Collab.)
ABDALLAH	05B	EPJ C38 395	J. Abdallah et al.	(DELPHI Collab.)
ABULENCIA	05A	PRL 95 252001	A. Abulencia et al.	(CDF Collab.)
SMULLIN	05	PR D72 122001	S.J. Smullin et al.	
ACHARD	04E	PL B587 16	P. Achard et al.	(L3 Collab.)
ACOSTA	04C	PRL 92 121802	D. Acosta et al.	(CDF Collab.)
BARBIERI	04	NP B703 127	R. Barbieri et al.	
CASSE	04	PRL 92 111102	M. Casse et al.	
CHEKANOV	04B	PL B591 23	S. Chekanov et al.	(ZEUS Collab.)
HOYLE	04	PR D70 042004	C.D. Hoyle et al.	(WASH)
ABAZOV	03	PRL 90 251802	V.M. Abazov et al.	(DO Collab.)
ABBIENDI	03D	EPJ C26 331	G. Abbiendi et al.	(OPAL Collab.)
ACHARD	03D	PL B572 133	P. Achard et al.	(L3 Collab.)
ADLOFF	03	PL B568 35	C. Adloff et al.	(HI Collab.)
CHIAVERINI	03	PRL 90 151101	J. Chilverini et al.	
GIUDICE	03	NP B663 377	G.F. Giudice, A. Strumia	
HANNESSTAD	03	PR D67 125008	S. Hannestad, G.G. Raffelt	
Also		PR D69 029901(errat.)	S. Hannestad, G.G. Raffelt	
HEISTER	03C	EPJ C28 1	A. Heister et al.	(ALEPH Collab.)
LONG	03	Nature 421 922	J.C. Long et al.	
ACHARD	02	PL B524 65	P. Achard et al.	(L3 Collab.)
ACHARD	02D	PL B531 28	P. Achard et al.	(L3 Collab.)
HANNESSTAD	02	PRL 88 071301	S. Hannestad, G. Raffelt	
ABBOTT	01	PRL 86 1156	B. Abbott et al.	(DO Collab.)
FAIRBAIRN	01	PL B508 335	M. Fairbairn et al.	
HANHART	01	PL B509 1	C. Hanhart et al.	
HOYLE	01	PRL 86 1418	C.D. Hoyle et al.	
ABBIENDI	00R	EPJ C13 553	G. Abbiendi et al.	(OPAL Collab.)
ABREU	00A	PL B491 67	P. Abreu et al.	(DELPHI Collab.)
ABREU	00S	PL B485 45	P. Abreu et al.	(DELPHI Collab.)
ABREU	00Z	EPJ C17 53	P. Abreu et al.	(DELPHI Collab.)
CASSISI	00	PL B481 323	S. Cassisi et al.	
CHANG	00B	PRL 85 3765	L.N. Chang et al.	
CHEUNG	00	PR D61 015005	K. Cheung	
CORNET	00	PR D61 037701	F. Cornet, M. Relano, J. Rico	
GRAESSER	00	PR D61 074019	M.L. Graesser	
HAN	00	PR D62 125018	T. Han, D. Marfatia, R.-J. Zhang	
MATHEWS	00	JHEP 0007 008	P. Mathews, S. Raychaudhuri, K. Sridhar	
MELE	00	PR D61 117901	S. Mele, E. Sanchez	
RIZZO	00	PR D61 016007	T.G. Rizzo, J.D. Wells	
ABBIENDI	99P	PL B465 303	G. Abbiendi et al.	(OPAL Collab.)
ACCIARRI	99M	PL B464 135	M. Acciarrri et al.	(L3 Collab.)
ACCIARRI	99R	PL B470 268	M. Acciarrri et al.	(L3 Collab.)
ACCIARRI	99S	PL B470 281	M. Acciarrri et al.	(L3 Collab.)
BOURLIKOV	99	JHEP 9908 006	D. Bourlikov	
HOSKINS	85	PR D32 3084	J.K. Hoskins et al.	

WIMP and Dark Matter Searches

We omit papers on CHAMP's, millicharged particles, and other exotic particles.

GALACTIC WIMP SEARCHES

These limits are for weakly-interacting stable particles that may constitute the invisible mass in the galaxy. Unless otherwise noted, a local mass density of $0.3 \text{ GeV}/\text{cm}^3$ is assumed; see each paper for velocity distribution assumptions. In the papers the limit is given as a function of the χ^0 mass. Here we list limits only for typical mass values of sub-GeV, GeV, 20 GeV, 100 GeV, and 1 TeV. Specific limits on supersymmetric dark matter particles may be found in the Supersymmetry section.

Spin-Independent Cross Section Limits for Dark Matter Particle (χ^0) on Nucleon

For m_{χ^0} in GeV range

We provide here limits for $m_{\chi^0} < 5 \text{ GeV}$

VALUE (pb)	CL%	DOCUMENT ID	TECN	COMMENT
••• We do not use the following data for averages, fits, limits, etc. •••				
$<1 \times 10^{-2}$	90	1 ABDELHAME...19A	CRES	CaWO ₄
$<5.4 \times 10^{-6}$	90	2 AGNESE	19A	SCDM GeV-scale WIMPs on Ge
<1	90	3 AKERIB	19	LUX light DM on Xe via Migdal/brem effect
$<1 \times 10^{-6}$	90	4 AMOLE	19	PICO C ₃ F ₈
$<1.6 \times 10^{-3}$	90	5 APRILE	19c	XE1T DM on Xe
$<1 \times 10^{-7}$	90	6 APRILE	19d	XE1T DM on Xe
<0.1	90	7 ARMENGAUD	19	EDEL GeV-scale WIMPs on Ge
$<1.6 \times 10^3$	90	8 KOBAYASHI	19	XMAS annual modulation Xe
$<7 \times 10^2$	90	9 LIU	19b	CDEX Ge; sub-GeV DM via Migdal
$<7 \times 10^{-7}$	90	10 AGNES	18	DS50 GeV-scale WIMPs on Ar
$<1.5 \times 10^{-5}$	95	11 AGNESE	18	SCDM GeV-scale WIMPs on Ge
$<2 \times 10^{-8}$	90	12 APRILE	18	XE1T Xe, Si
$<4.5 \times 10^{-3}$	90	13 ARNAUD	18	NEWS low mass WIMP, Ne
$<8 \times 10^{-6}$	90	14 JIANG	18	CDEX GeV-scale WIMPs on Ge
$<3 \times 10^{-5}$	90	15 YANG	18	CDEX WIMPs on Ge
$<1 \times 10^{-6}$	90	16 AKERIB	17	LUX Xe
$<1 \times 10^2$	90	17 ANGLÖHER	17A	CRES GeV-scale WIMPs
$<7 \times 10^{-5}$	90	18 ANGLÖHER	16	CRES CaWO ₄
$<3 \times 10^{-5}$	90	19 APRILE	16	X100 Xe
$<4.3 \times 10^{-4}$	90	20 ARMENGAUD	16	EDE3 GeV-scale WIMPs on Ge
$<7 \times 10^{-5}$	90	21 HEHN	16	EDE3 SI WIMP on Ge
$<6 \times 10^{-5}$	90	22 ZHAO	16	CDEX GeV-scale WIMPs on Ge
$<1 \times 10^{-4}$	90	23 AMOLE	15	PICO C ₃ F ₈
$<8 \times 10^{-5}$	90	24 XIAO	15	PNDX WIMPs on Xe
$<3 \times 10^{-5}$	90	25 AGNESE	14	SCDM GeV-scale WIMPs
$<1 \times 10^{-3}$	90	26 AKERIB	14	LUX WIMP on Xe
$<9 \times 10^{-4}$	90	27 LI	13b	TEXO WIMPs on Ge
$<3 \times 10^{-4}$	90	28 ARCHAMBAU.12	PICA	C ₄ F ₁₀
$<2 \times 10^{-4}$	90	29 AALSETH	11	CGNT GeV WIMPs on Ge
$<5 \times 10^{-4}$	90	30 AHMED	11b	CDM2 GeV-scale WIMPs on Ge
$<8 \times 10^{-5}$	90	31 ANGLE	11	XE10 Xe
$<5 \times 10^{-4}$	90	32 AKERIB	10	CDM2 WIMPs on Ge/Si

- 1 ABDELHAMEED 19A search for GeV scale dark matter SI scatter on CaWO₄; no signal, limits placed in σ vs. mass plane for $m(\text{DM}) \sim 0.1\text{--}10 \text{ GeV}$. The listed limit is for $m(\text{DM}) = 1 \text{ GeV}$.
- 2 AGNESE 19A search for 1.5–10 GeV WIMP scatter on Ge in CDMSlite dataset. Limits set in a likelihood analysis. No signal was observed. Limit reported for $m(\chi) = 5 \text{ GeV}$.
- 3 AKERIB 19 search for 0.4–5 GeV DM using bremsstrahlung photons and "Migdal" electrons; $1.4 \times 10^4 \text{ kg d}$ exposure of liquid Xe; constraint $\sigma^{SI}(\chi N) < 1 \text{ pb}$ for $m(\chi) = 5 \text{ GeV}$ in light scalar mediator model.
- 4 AMOLE 19 search for SI WIMP scatter on C₃F₈ in PICO-60 bubble chamber; no signal; set limit for spin independent coupling $\sigma^{SI}(\chi N) < 1 \times 10^{-6} \text{ pb}$ for $m(\chi) = 5 \text{ GeV}$.
- 5 APRILE 19c search for light DM scatter on Xe via atomic excitation, ionization (Migdal effect) or bremsstrahlung; no signal, limits placed in σ vs. $m(\text{DM})$ plane for $m(\text{DM}) \sim 0.085\text{--}2 \text{ GeV}$. The listed limit is for $m(\text{DM}) = 1 \text{ GeV}$.
- 6 APRILE 19d search for light DM scatter on Xe via ionization to probe SI, SD, and χ e cross sections; with 22 t d exposure, limits placed in various σ vs. $m(\text{DM})$ planes. Quoted limit is for $m(\text{DM}) = 5 \text{ GeV}$.
- 7 ARMENGAUD 19 search for GeV scale WIMP scatter on Ge; limits placed in $\sigma^{SI}(\chi N)$ vs. $m(\chi)$ plane for $m(\chi) \sim 0.045\text{--}10 \text{ GeV}$; quoted limit is for $m(\chi) = 5 \text{ GeV}$.
- 8 KOBAYASHI 19 search for sub-GeV WIMP annual modulation in Xe via brems; no signal; limits placed in $\sigma^{SI}(\chi N)$ vs. $m(\chi)$ plane for $m \sim 0.3\text{--}1 \text{ GeV}$; quoted limit is for $m(\chi) = 0.5 \text{ GeV}$.
- 9 LIU 19b search for sub-GeV DM using Migdal effect on Ge at CDEX-1B; no signal, require $\sigma^{SI}(\chi N) < 7 \times 10^2 \text{ pb}$ for $m(\chi) = 0.1 \text{ GeV}$.
- 10 AGNES 18 search for 1.8–20 GeV WIMP SI scatter on Ar; quoted limit is for $m(\chi) = 5 \text{ GeV}$.
- 11 AGNESE 18 search for GeV scale WIMPs using CDMSlite; limits placed in $\sigma^{SI}(\chi N)$ vs. $m(\chi)$ plane for $m \sim 1.5\text{--}20 \text{ GeV}$; quoted limit is for $m(\chi) = 5 \text{ GeV}$.
- 12 APRILE 18 search for WIMP scatter on 1 t yr Xe; no signal, limits set in $\sigma(\chi N)$ vs. $m(\chi)$ plane for $m(\chi) \sim 6\text{--}1000 \text{ GeV}$; quoted limit is for $m = 6 \text{ GeV}$.
- 13 ARNAUD 18 search for low mass WIMP scatter on Ne via SPC at NEWS-G; limits set in $\sigma^{SI}(\chi N)$ vs. $m(\chi)$ plane for $m \sim 0.5\text{--}20 \text{ GeV}$; quoted limit is for $m = 5 \text{ GeV}$.
- 14 JIANG 18 search for GeV scale WIMP scatter on Ge; limits placed in $\sigma^{SI}(\chi N)$ vs. $m(\chi)$ plane for $m(\chi) \sim 3\text{--}10 \text{ GeV}$; quoted limit is for $m(\chi) = 5 \text{ GeV}$.
- 15 YANG 18 search for WIMP scatter on Ge; limits placed in $\sigma^{SI}(\chi N)$ vs. $m(\chi)$ plane for $m(\chi) \sim 2\text{--}10 \text{ GeV}$; quoted limit is for $m(\chi) = 5 \text{ GeV}$.
- 16 AKERIB 17 search for WIMP scatter on Xe; limits placed in $\sigma^{SI}(\chi N)$ vs. $m(\chi)$ plane for $m(\chi) \sim 5\text{--}1 \times 10^5 \text{ GeV}$; quoted limit is for $m(\chi) = 5 \text{ GeV}$.
- 17 ANGLÖHER 17A search for GeV scale WIMP scatter on Al₂O₃ crystal; limits placed in $\sigma^{SI}(\chi N)$ vs. $m(\chi)$ plane for $m(\chi) \sim 0.15\text{--}10 \text{ GeV}$; quoted limit is for $m(\chi) = 5 \text{ GeV}$.
- 18 ANGLÖHER 16 search for GeV scale WIMP scatter on CaWO₄; limits placed in $\sigma^{SI}(\chi N)$ vs. $m(\chi)$ plane for $m(\chi) \sim 0.5\text{--}30 \text{ GeV}$; quoted limit is for $m(\chi) = 5 \text{ GeV}$.
- 19 APRILE 16 search for low mass WIMPs via ionization at XENON100; limits placed in $\sigma^{SI}(\chi N)$ vs. $m(\chi)$ plane for $m \sim 3.5\text{--}20 \text{ GeV}$; quoted limit is for $m(\chi) = 5 \text{ GeV}$.
- 20 ARMENGAUD 16 search for GeV scale WIMP scatter on Ge; limits placed in $\sigma^{SI}(\chi N)$ vs. $m(\chi)$ plane for $m(\chi) \sim 4\text{--}30 \text{ GeV}$; quoted limit is for $m(\chi) = 5 \text{ GeV}$.
- 21 HEHN 16 search for low mass WIMPs via SI scatter on Ge target using profile likelihood analysis; limits placed in $\sigma^{SI}(\chi N)$ vs. $m(\chi)$ plane for $m(\chi) \sim 4\text{--}30 \text{ GeV}$; quoted limit is for $m(\chi) = 5 \text{ GeV}$.

- 22 ZHAO 16 search for GeV-scale WIMP scatter on Ge; limits placed in $\sigma^{SI}(\chi N)$ vs. $m(\chi)$ plane for $m(\chi) \sim 4$ –30 GeV; quoted limit is for $m(\chi) = 5$ GeV.
- 23 AMOLE 15 search for WIMP scatter on C_3F_8 in PICO-2L; limits placed in $\sigma^{SI}(\chi N)$ vs. $m(\chi)$ plane for $m(\chi) \sim 4$ –25 GeV; quoted limit is for $m(\chi) = 5$ GeV.
- 24 XIAO 15 search for WIMP scatter on Xe with PandaX-I; limits placed in $\sigma^{SI}(\chi N)$ vs. $m(\chi)$ plane for $m(\chi) \sim 5$ –100 GeV; quoted limit is for $m(\chi) = 5$ GeV.
- 25 AGNESE 14 search for GeV scale WIMPs SI scatter at SuperCDMS; no signal, limits placed in $\sigma^{SI}(\chi N)$ vs. $m(\chi)$ plane for $m(\chi) \sim 3.5$ –30 GeV; quoted limit is for $m(\chi) = 5$ GeV.
- 26 AKERIB 14 search for WIMP scatter on Xe; limits placed in $\sigma^{SI}(\chi N)$ vs. $m(\chi)$ plane for $m(\chi) \sim 5$ –5000 GeV. Limit given for $m(\chi) = 5$ GeV.
- 27 LI 13b search for WIMP scatter on Ge; limits placed in $\sigma^{SI}(\chi N)$ vs. $m(\chi)$ plane for $m(\chi) \sim 4$ –100 GeV; quoted limit is for $m(\chi) = 5$ GeV.
- 28 ARCHAMBAULT 12 search for low mass WIMP scatter on C_4F_{10} ; limits set in $\sigma^{SI}(\chi N)$ vs. $m(\chi)$ plane for $m \sim 4$ –12 GeV; quoted limit is for $m = 5$ GeV.
- 29 AALSETH 11 search for GeV-scale SI WIMP scatter on Ge; limits placed on $\sigma^{SI}(\chi N)$ for $m(\chi) \sim 3.5$ –100 GeV; quoted limit is for $m(\chi) = 5$ GeV.
- 30 AHMED 11b search for GeV scale WIMP scatter on Ge in CDMS II; limits placed in $\sigma^{SD}(\chi n)$ vs. $m(\chi)$ plane for $m \sim 4$ –12 GeV.
- 31 ANGLE 11 search for GeV scale WIMPs in Xenon-10; limits placed in $\sigma^{SI}(\chi N)$ vs. $m(\chi)$ plane for $m(\chi) \sim 4$ –20 GeV; quoted limit is for $m(\chi) = 5$ GeV.
- 32 AKERIB 10 search for WIMP scatter on Ge/Si in CDMS2; limits placed in $\sigma^{SI}(\chi N)$ vs. $m(\chi)$ plane for m 3–100 GeV. Limit given for $m(\text{DM})=5$ GeV

For $m_{\chi 0} = 20$ GeV

For limits from X^0 annihilation in the Sun, the assumed annihilation final state is shown in parenthesis in the comment.

VALUE (pb)	CL%	DOCUMENT ID	TECN	COMMENT
$<7 \times 10^{-5}$	90	1 ANGLOHER 19	CRES	CaWO ₄
$<3 \times 10^{-7}$	90	2 KIM 19A	KIMS	Nal
$<3.5 \times 10^{-5}$	90	3 KOBAYASHI 19	XMAS	SI WIMP on Xe
$<2 \times 10^{-7}$	90	4 SEONG 19	BELL	$T \rightarrow \gamma A, A \rightarrow \chi\chi$
$<1.44 \times 10^{-5}$	90	5 YANG 19	CDEX	annual modulation Ge
$<3 \times 10^{-7}$	90	6 ABE 18c	XMAS	X^0 -Xe modulation
$<5 \times 10^{-6}$	95	7 ADHIKARI 18	C100	Nal
$<4 \times 10^{-8}$	90	8 AGNESE 18	DS50	X^0 -Ar
$<6 \times 10^{-11}$	90	9 AGNESE 18	SCDM	Ge
$<4.5 \times 10^{-3}$	90	10 AGNESE 18a	SCDM	Ge
$<2 \times 10^{-6}$	90	11 APRILE 18	XE1T	Xe, Si
$<2 \times 10^{-10}$	90	12 ARNAUD 18	NEWS	GeV WIMPs on Ne
$<1 \times 10^{-3}$	90	13 AARTSEN 17	ICCB	ν , earth
$<1.7 \times 10^{-10}$	90	14 AKERIB 17	LUX	Xe
$<7.3 \times 10^{-7}$	90	15 BARBOSA-D... 17	ICCB	Nal
$<1 \times 10^{-5}$	90	16 CUI 17A	PNDX	WIMPs on Xe
$<2 \times 10^{-4}$	90	17 AGNESE 16	DS50	Ar
$<4.5 \times 10^{-5}$	90	18 AGUILAR-AR... 16	DMIC	Si CCDs
$<2 \times 10^{-6}$	90	19 ANGLOHER 16	CRES	CaWO ₄
$<9.4 \times 10^{-8}$	90	20 APRILE 16	X100	Xe
$<1.0 \times 10^{-7}$	90	21 ARMENGAUD 16	EDE3	Ge
$<5 \times 10^{-6}$	90	22 HEHN 16	EDE3	Ge
$<1 \times 10^{-5}$	90	23 ZHAO 16	CDEX	Ge
$<1.5 \times 10^{-6}$	90	24 AGNESE 15a	CDM2	Ge
$<1.5 \times 10^{-7}$	90	25 AGNESE 15b	CDM2	Ge
$<2 \times 10^{-6}$	90	26 AMOLE 15	PICO	C_3F_8
$<1.2 \times 10^{-5}$	90	27 CHOI 15	SKAM	H, solar ν ($b\bar{b}$)
$<1.19 \times 10^{-6}$	90	28 CHOI 15	SKAM	H, solar ν ($\tau^+ \tau^-$)
$<2 \times 10^{-8}$	90	29 XIAO 15	PNDX	Xe
$<2.0 \times 10^{-7}$	90	30 AGNESE 14	SCDM	Ge
$<3.7 \times 10^{-5}$	90	31 AGNESE 14a	SCDM	Ge
$<1 \times 10^{-9}$	90	32 AKERIB 14	LUX	Xe
$<2 \times 10^{-6}$	90	33 ANGLOHER 14	CRES	CaWO ₄
$<5 \times 10^{-6}$	90	34 FELIZARDO 14	SMPPL	C_2ClF_5
$<8 \times 10^{-6}$	90	35 LEE 14a	KIMS	Csl
$<2 \times 10^{-4}$	90	36 LIU 14a	CDEX	Ge
$<1 \times 10^{-5}$	90	37 YUE 14	CDEX	Ge
$<1.08 \times 10^{-4}$	90	38 AARTSEN 13	ICCB	H, solar ν ($\tau^+ \tau^-$)
$<1.5 \times 10^{-5}$	90	39 ABE 13b	XMAS	Xe
$<3.1 \times 10^{-6}$	90	40 AGNESE 13	CDM2	Si
$<3.4 \times 10^{-6}$	90	41 AGNESE 13a	CDM2	Si
$<2.2 \times 10^{-6}$	90	42 AGNESE 13a	CDM2	Si
$<1.2 \times 10^{-4}$	90	43 BERNABEI 13a	DAMA	Nal modulation
$<1.2 \times 10^{-7}$	90	44 LI 13b	TEXO	Ge
		45 ZHAO 13	CDEX	Ge
		46 AKIMOV 12	ZEP3	Xe
$<8 \times 10^{-6}$	90	47 ANGLOHER 12	CRES	CaWO ₄
$<7 \times 10^{-9}$	90	48 ANGLOHER 12	CRES	CaWO ₄
$<7 \times 10^{-7}$	90	49 APRILE 12	X100	Xe
		50 ARMENGAUD 12	EDE2	Ge
		51 BARRETO 12	DMIC	CCD
$<2 \times 10^{-6}$	90	52 BEHNKE 12	COUP	CF ₃ I
$<7 \times 10^{-6}$	90	53 FELIZARDO 12	SMPPL	C_2ClF_5
$<1.5 \times 10^{-6}$	90	54 KIM 12	KIMS	Csl
$<5 \times 10^{-5}$	90	55 AALSETH 11	CGNT	Ge

$<5 \times 10^{-7}$	90	56 AALSETH 11a	CGNT	Ge
$<2.7 \times 10^{-7}$	90	57 AHMED 11	CDM2	Ge, inelastic
$<3 \times 10^{-6}$	90	58 AHMED 11a	RVUE	Ge
$<7 \times 10^{-8}$	90	59 ANGLE 11	XE10	Xe
		60 APRILE 11	X100	Xe
$<2 \times 10^{-8}$	90	61 APRILE 11a	X100	Xe, inelastic
		62 APRILE 11b	X100	Xe
		63 HORN 11	ZEP3	Xe
$<2 \times 10^{-7}$	90	64 AHMED 10	CDM2	Ge
$<1 \times 10^{-5}$	90	65 AKERIB 10	CDM2	Si, Ge, low threshold
$<1 \times 10^{-7}$	90	66 APRILE 10	X100	Xe
$<2 \times 10^{-6}$	90	67 ARMENGAUD 10	EDE2	Ge
$<4 \times 10^{-5}$	90	68 FELIZARDO 10	SMPPL	C_2ClF_3
$<1.5 \times 10^{-7}$	90	69 AHMED 09	CDM2	Ge
$<2 \times 10^{-4}$	90	70 LIN 09	TEXO	Ge
		71 AALSETH 08	CGNT	Ge

- 1 ANGLOHER 19 search for low mass WIMP scatter on CaWO₄; no signal; limits placed on Wilson coefficients for $m(\chi) = 0.6$ –60 GeV.
- 2 KIM 19a search for WIMP scatter in Nal KIMS experiment; no signal; require $\sigma^{SI}(\chi n) < 7 \times 10^{-5}$ pb for $m(\chi) = 20$ GeV.
- 3 KOBAYASHI 19 search for WIMP scatter in XMASS single-phase liquid Xe detector; no signal; require $\sigma^{SI}(\chi N) < 3 \times 10^{-7}$ pb for $m(\chi) = 20$ GeV.
- 4 SEONG 19 search for $T \rightarrow \gamma A, A \rightarrow \chi\chi$ via CP-odd Higgs; no signal; limits on BF set; model dependent conversion to WIMP-nucleon scattering cross section limits $\sigma^{SI} < 10^{-36}$ cm² for $m(\chi) = 0.01$ –1 GeV.
- 5 YANG 19 search for low mass wimps via annual modulation in Ge; no signal; require $\sigma^{SI}(\chi N) < 3.5 \times 10^{-5}$ pb for $m(\chi) = 20$ GeV.
- 6 ABE 18c search for WIMP annual modulation signal for $m(\text{WIMP})$: 6–20 GeV; limits set on SI WIMP-nucleon cross section: see Fig. 6.
- 7 ADHIKARI 18 search for WIMP scatter on Nal; no signal; require $\sigma^{SI} < 1.44 \times 10^{-5}$ pb for $m(\text{WIMP}) = 20$ GeV; inconsistent with DAMA/LIBRA result.
- 8 AGNESE 18 search low mass $m(\text{WIMP})$: 1.8–20 GeV scatter on Ar; limits on SI WIMP-nucleon cross section set in Fig. 8.
- 9 AGNESE 18 give limits for $\sigma^{SI}(\chi N)$ for $m(\text{WIMP})$ between 1.5 and 20 GeV using CDMSlite mode data.
- 10 AGNESE 18a search for WIMP scatter on Ge at SuperCDMS; 1 event, consistent with expected background; set limit in $\sigma^{SI}(\chi N)$ vs. $m(\chi)$ plane for $m \sim 10$ –250 GeV.
- 11 APRILE 18 search for WIMP scatter on 1 t yr Xe; no signal, limits placed in $\sigma^{SI}(\chi N)$ vs. $m(\chi)$ plane for $m(\chi) \sim 6$ –1000 GeV.
- 12 ARNAUD 18 search for low mass WIMP scatter on Ne via SPC at NEWS-G; limits set in $\sigma^{SI}(\chi N)$ vs. $m(\chi)$ plane for $m \sim 0.5$ –20 GeV.
- 13 AARTSEN 17 obtain $\sigma(\text{Si}) < 6 \times 10^{-6}$ pb for $m(\text{wimp}) = 20$ GeV from ν from earth.
- 14 AKERIB 17 search for WIMP scatter on Xe; limits placed in $\sigma^{SI}(\chi N)$ vs. $m(\chi)$ plane for $m(\chi) \sim 5$ – 1×10^5 GeV.
- 15 BARBOSA-DE-SOUZA 17 search for annual modulation of WIMP scatter on Nal using an exposure of 61 kg yr of DM-Ice17 for recoil energy in the 4–20 keV range (DAMA found modulation for recoil energy < 5 keV). No modulation seen. Sensitivity insufficient to distinguish DAMA signal from null.
- 16 CUI 17a search for SI WIMP scatter; limits placed in $\sigma^{SI}(\chi N)$ vs. $m(\chi)$ plane for $m \sim 10$ – 1×10^4 GeV using 54 ton-day exposure of Xe.
- 17 AGNESE 16 CDMSlite excludes low mass WIMPs 1.6–5.5 GeV and SI scattering cross section depending on $m(\text{WIMP})$; see Fig. 4.
- 18 AGUILAR-AREVALO 16 search low mass 1–10 GeV WIMP scatter on Si CCDs; set limits Fig. 11.
- 19 ANGLOHER 16 search for GeV scale WIMP scatter on CaWO₄; limits placed in $\sigma^{SI}(\chi N)$ vs. $m(\chi)$ plane for $m(\chi) \sim 0.5$ –30 GeV.
- 20 APRILE 16 search for low mass WIMPs via ionization at XENON100; limits placed in $\sigma^{SI}(\chi N)$ vs. $m(\chi)$ plane for $m \sim 3.5$ –20 GeV.
- 21 ARMENGAUD 16 search for GeV scale WIMP scatter on Ge; limits placed in $\sigma^{SI}(\chi N)$ vs. $m(\chi)$ plane for $m(\chi) \sim 4$ –30 GeV.
- 22 HEHN 16 search for low mass WIMPs via Si scatter on Ge target using profile likelihood analysis; limits placed in $\sigma^{SI}(\chi N)$ vs. $m(\chi)$ plane for $m(\chi) \sim 4$ –30 GeV.
- 23 ZHAO 16 search for GeV-scale WIMP scatter on Ge; limits placed in $\sigma^{SI}(\chi N)$ vs. $m(\chi)$ plane for $m(\chi) \sim 4$ –30 GeV.
- 24 AGNESE 15a reanalyse AHMED 11b low threshold data. See their Fig. 12 (left) for improved limits extending down to 5 GeV.
- 25 AGNESE 15b reanalyse AHMED 10 data.
- 26 See their Fig. 7 for limits extending down to 4 GeV.
- 27 XIAO 15 search for WIMP scatter on Xe with PandaX-I; limits placed in $\sigma^{SI}(\chi N)$ vs. $m(\chi)$ plane for $m(\chi) \sim 5$ –100 GeV.
- 28 This limit value is provided by the authors. See their Fig. 4 for limits extending down to $m_{\chi 0} = 3.5$ GeV.
- 29 This limit value is provided by the authors. AGNESE 14a result is from CDMSlite mode operation with enhanced sensitivity to low mass $m_{\chi 0}$. See their Fig. 3 for limits extending down to $m_{\chi 0} = 3.5$ GeV (see also Fig. 4 in AGNESE 14).
- 30 See their Fig. 5 for limits extending down to $m_{\chi 0} = 5.5$ GeV.
- 31 See their Fig. 5 for limits extending down to $m_{\chi 0} = 1$ GeV.
- 32 See their Fig. 5 for limits extending down to $m_{\chi 0} = 5$ GeV.
- 33 LIU 14a result is based on prototype CDEX-0 detector. See their Fig. 13 for limits extending down to $m_{\chi 0} = 2$ GeV.
- 34 See their Fig. 4 for limits extending down to $m_{\chi 0} = 4.5$ GeV.
- 35 AARTSEN 13 search for neutrinos from the Sun arising from the pair annihilation of X^0 trapped by the sun in data taken between June 2010 and May 2011.
- 36 See their Fig. 8 for limits extending down to $m_{\chi 0} = 7$ GeV.
- 37 This limit value is provided by the authors. AGNESE 13 use data taken between Oct. 2006 and July 2007. See their Fig. 4 for limits extending down to $m_{\chi 0} = 7$ GeV.

- ³⁸This limit value is provided by the authors. AGNESE 13A use data taken between July 2007 and Sep. 2008. Three candidate events are seen. Assuming these events are real, the best fit parameters are $m_{\chi^0} = 8.6$ GeV and $\sigma = 1.9 \times 10^{-5}$ pb.
- ³⁹This limit value is provided by the authors. Limit from combined data of AGNESE 13 and AGNESE 13A. See their Fig. 4 for limits extending down to $m_{\chi^0} = 5.5$ GeV.
- ⁴⁰BERNABEI 13A search for annual modulation of counting rate in the 2–6 keV recoil energy interval, in a 14 yr live time exposure of 1.33 t yr. Find a modulation of 0.0112 ± 0.0012 counts/(day kg keV) with 9.3 sigma C.L. Find period and phase in agreement with expectations from DM particles.
- ⁴¹LI 13b search for WIMP scatter on Ge; limits placed in $\sigma^{SI}(\chi N)$ vs. $m(\chi)$ plane for $m(\chi) \sim 4$ –100 GeV.
- ⁴²See their Fig. 5 for limits for $m_{\chi^0} = 4$ –12 GeV.
- ⁴³ANGLOHER 12 observe excess events above the expected background which are consistent with χ^0 with mass ~ 25 GeV (or 12 GeV) and spin-independent χ^0 -nucleon cross section of 2×10^{-6} pb (or 4×10^{-5} pb).
- ⁴⁴Reanalysis of ANGLOHER 09 data with all three nuclides. See also BROWN 12. See also APRILE 14A.
- ⁴⁵See their Fig. 4 for limits extending down to $m_{\chi^0} = 7$ GeV.
- ⁴⁶See their Fig. 13 for cross section limits for m_{χ^0} between 1.2 and 10 GeV.
- ⁴⁷See also DAHL 12 for a criticism.
- ⁴⁸See their Fig. 4 for limits extending to $m_{\chi^0} = 3.5$ GeV.
- ⁴⁹AALSETH 11A find indications of annual modulation of the data, the energy spectrum being compatible with χ^0 mass around 8 GeV. See also AALSETH 13.
- ⁵¹AHMED 11 search for χ^0 inelastic scattering. See their Fig. 8–10 for limits. The inelastic cross section reduces to the elastic cross section at the limit of zero mass splitting (Fig. 8, left).
- ⁵²AHMED 11A combine CDMS II and EDELWEISS data.
- ⁵³ANGLE 11 show limits down to $m_{\chi^0} = 4$ GeV on Fig. 3.
- ⁵⁴APRILE 11 reanalyze APRILE 10 data.
- ⁵⁵APRILE 11A search for χ^0 inelastic scattering. See their Fig. 2 and 3 for limits. See also APRILE 14A.
- ⁵⁶HORN 11 perform detector calibration by neutrons. Earlier results are only marginally affected.
- ⁵⁷See their Fig. 10 and 12 for limits extending to χ^0 mass of 1 GeV.
- ⁵⁸Superseded by AHMED 10.
- ⁵⁹See their Fig. 6(a) for cross section limits for m_{χ^0} extending down to 2 GeV.
- ⁶⁰See their Fig. 2 for cross section limits for m_{χ^0} between 4 and 10 GeV.

For $m_{\chi^0} = 100$ GeV

For limits from χ^0 annihilation in the Sun, the assumed annihilation final state is shown in parenthesis in the comment.

VALUE (pb)	CL%	DOCUMENT ID	TECN	COMMENT
•••	•••	•••	•••	•••
$<4 \times 10^{-8}$	90	1 ABE	19 XMAS	Xe
$<3.9 \times 10^{-9}$	90	2 AJAJ	19 DEAP	Ar
$<2.3 \times 10^{-6}$	90	3 ADHIKARI	18 C100	Nal
$<1.14 \times 10^{-8}$	90	4 AGNES	18A DS50	Ar
$<2 \times 10^{-8}$	90	5 AGNESE	18A CDMS	Ge
$<1.2 \times 10^{-8}$	90	6 AMAUDRUZ	18 DEAP	Ar
$<9.12 \times 10^{-11}$	90	7 APRILE	18 XE1T	Xe
		8 REN	18 PNDX	SIDM at PDX-II
$<1.7 \times 10^{-10}$	90	9 AKERIB	17 LUX	Xe
$<1.2 \times 10^{-10}$	90	10 APRILE	17G XE1T	Xe
$<1.2 \times 10^{-10}$	90	11 CUI	17A PNDX	Xe
$<2.0 \times 10^{-8}$	90	AGNES	16 DS50	Ar
$<1 \times 10^{-9}$	90	12 AKERIB	16 LUX	Xe
$<1 \times 10^{-9}$	90	13 APRILE	16B X100	Xe
$<2 \times 10^{-8}$	90	14 TAN	16 PNDX	Xe
$<4 \times 10^{-10}$	90	15 TAN	16B PNDX	Xe
$<6 \times 10^{-8}$	90	AGNES	15 DS50	Ar
$<4 \times 10^{-8}$	90	16 AGNESE	15B CDM2	Ge
$<7.13 \times 10^{-6}$	90	CHOI	15 SKAM	H, solar ν ($b\bar{b}$)
$<6.26 \times 10^{-7}$	90	CHOI	15 SKAM	H, solar ν ($W^+ W^-$)
$<2.76 \times 10^{-7}$	90	CHOI	15 SKAM	H, solar ν ($\tau^+ \tau^-$)
$<1.5 \times 10^{-8}$	90	17 XIAO	15 PNDX	Xe
$<1 \times 10^{-9}$	90	AKERIB	14 LUX	Xe
$<4.0 \times 10^{-6}$	90	18 AVROBIN	14 BAIK	H, solar ν ($W^+ W^-$)
$<1.0 \times 10^{-4}$	90	18 AVROBIN	14 BAIK	H, solar ν ($b\bar{b}$)
$<1.6 \times 10^{-6}$	90	18 AVROBIN	14 BAIK	H, solar ν ($\tau^+ \tau^-$)
$<5 \times 10^{-6}$	90	FELIZARDO	14 SMPL	C_2ClF_5
$<6.01 \times 10^{-7}$	90	19 AARTSEN	13 ICCB	H, solar ν ($W^+ W^-$)
$<3.30 \times 10^{-5}$	90	19 AARTSEN	13 ICCB	H, solar ν ($b\bar{b}$)
$<1.9 \times 10^{-6}$	90	20 ADRIAN-MAR.13	ANTR	H, solar ν ($W^+ W^-$)
$<1.2 \times 10^{-4}$	90	20 ADRIAN-MAR.13	ANTR	H, solar ν ($b\bar{b}$)
$<7.6 \times 10^{-7}$	90	20 ADRIAN-MAR.13	ANTR	H, solar ν ($\tau^+ \tau^-$)
$<2 \times 10^{-6}$	90	21 AGNESE	13 CDM2	Si
$<1.6 \times 10^{-6}$	90	22 BOLIEV	13 BAKS	H, solar ν ($W^+ W^-$)
$<1.9 \times 10^{-5}$	90	22 BOLIEV	13 BAKS	H, solar ν ($b\bar{b}$)
$<7.1 \times 10^{-7}$	90	22 BOLIEV	13 BAKS	H, solar ν ($\tau^+ \tau^-$)
$<3.2 \times 10^{-4}$	90	23 LI	13B TEXO	WIMPs on Ge
$<1.67 \times 10^{-6}$	90	24 ABBASI	12 ICCB	H, solar ν ($W^+ W^-$)
$<1.07 \times 10^{-4}$	90	24 ABBASI	12 ICCB	H, solar ν ($b\bar{b}$)
$<4 \times 10^{-8}$	90	AKIMOV	12 ZEP3	Xe
$<1.4 \times 10^{-6}$	90	25 ANGLOHER	12 CRES	CaWO ₄

$<3 \times 10^{-9}$	90	26 APRILE	12 X100	Xe
$<3 \times 10^{-7}$	90	BEHNKE	12 COUP	CF ₃ I
$<7 \times 10^{-6}$		FELIZARDO	12 SMPL	C ₂ ClF ₅
$<2.5 \times 10^{-7}$	90	27 KIM	12 KIMS	Csl
$<2 \times 10^{-4}$	90	AALSETH	11 CGNT	Ge
		28 AHMED	11 CDM2	Ge, inelastic
$<3.3 \times 10^{-8}$	90	29 AHMED	11A RVUE	Ge
		30 AJELLO	11 FLAT	
$<3 \times 10^{-8}$	90	31 APRILE	11 X100	Xe
		32 APRILE	11A X100	Xe, inelastic
$<1 \times 10^{-8}$	90	26 APRILE	11B X100	Xe
$<5 \times 10^{-8}$	90	33 ARMENGAUD	11 EDE2	Ge
		34 HORN	11 ZEP3	Xe
$<4 \times 10^{-8}$	90	AHMED	10 CDM2	Ge
$<9 \times 10^{-6}$	90	AKERIB	10 CDM2	Si, Ge, low threshold
		35 AKIMOV	10 ZEP3	Xe, inelastic
$<5 \times 10^{-8}$	90	APRILE	10 X100	Xe
$<1 \times 10^{-7}$	90	ARMENGAUD	10 EDE2	Ge
$<3 \times 10^{-5}$	90	FELIZARDO	10 SMPL	C ₂ ClF ₃
$<5 \times 10^{-8}$	90	36 AHMED	09 CDM2	Ge
		37 ANGLE	09 XE10	Xe, inelastic
		LIN	09 TEXO	Ge
$<3 \times 10^{-4}$	90	38 GIULIANI	05 RVUE	

- ¹ABE 19 search for SI DD in single phase Xe; no signal; require $\sigma^{SI}(\chi p) < 4 \times 10^{-8}$ pb for $m(\chi) \sim 100$ GeV.
- ²AJAJ 19 search for SI WIMP-nucleon scatter with 758 tonne day exposure of single phase liquid Ar; no signal; require $\sigma^{SI}(\chi N) < 3.9 \times 10^{-9}$ pb for $m(\chi) = 100$ GeV.
- ³ADHIKARI 18 search for WIMP scatter on Na; limit set $\sigma^{SI}(\chi p) < 2.3 \times 10^{-6}$ pb for $m(\chi) = 100$ GeV.
- ⁴AGNES 18A search for WIMP scatter on 46.4 kg Ar; no signal; require $\sigma^{SI}(\chi N) < 1.4 \times 10^{-8}$ pb for $m(\chi) = 100$ GeV.
- ⁵AGNESE 18A set limit $\sigma^{SI}(\chi N) < 2 \times 10^{-8}$ pb for $m(\text{WIMP}) = 100$ GeV.
- ⁶AMAUDRUZ 18 search for WIMP scatter on Ar with DEAP-3600; limits set: $\sigma^{SI}(\chi p) < 1.2 \times 10^{-8}$ pb for $m(\text{WIMP}) = 100$ GeV.
- ⁷APRILE 18 search for WIMP scatter on 1.3 t liquid Xe; no signal; require $\sigma^{SI}(\chi p) < 9.12 \times 10^{-11}$ pb for $m(\chi) = 100$ GeV.
- ⁸REN 18 search for self-interacting DM at PandaX-II with a total exposure of 54 ton day; limits set in $m(\text{DM})$ vs. $m(\text{mediator})$ plane.
- ⁹AKERIB 17 exclude SI cross section $> 1.7 \times 10^{-10}$ pb for $m(\text{WIMP}) = 100$ GeV. Uses complete LUX data set.
- ¹⁰APRILE 17G set limit $\sigma^{SI}(\chi p) < 1.2 \times 10^{-10}$ pb for $m(\text{WIMP}) = 100$ GeV using 1 ton fiducial mass Xe TPC. Exposure is 34.2 live days.
- ¹¹CUI 17A search for SI WIMP scatter; limits placed in $\sigma^{SI}(\chi N)$ vs. $m(\chi)$ plane for $m \sim 10$ – 1×10^4 GeV using 54 ton-day exposure of Xe.
- ¹²AKERIB 16 re-analysis of 2013 data exclude SI cross section $> 1 \times 10^{-9}$ pb for $m(\text{WIMP}) = 100$ GeV on Xe target.
- ¹³APRILE 16B combined 447 live days using Xe target exclude $\sigma(\text{SI}) > 1.1 \times 10^{-9}$ pb for $m(\text{WIMP}) = 50$ GeV.
- ¹⁴TAN 16 search for WIMP scatter off Xe target; see SI exclusion plot Fig. 6.
- ¹⁵TAN 16B search for WIMP-p scatter off Xe target; see Fig. 5 for SI exclusion.
- ¹⁶AGNESE 15B reanalyze AHMED 10 data.
- ¹⁷XIAO 15 search for WIMP scatter on Xe with PandaX-I; limits placed in $\sigma^{SI}(\chi N)$ vs. $m(\chi)$ plane for $m(\chi) \sim 5$ –100 GeV.
- ¹⁸AVROBIN 14 search for neutrinos from the Sun arising from the pair annihilation of χ^0 trapped by the Sun in data taken between 1998 and 2003. See their Table 1 for limits assuming annihilation into neutrino pairs.
- ¹⁹AARTSEN 13 search for neutrinos from the Sun arising from the pair annihilation of χ^0 trapped by the sun in data taken between June 2010 and May 2011.
- ²⁰ADRIAN-MARTINEZ 13 search for neutrinos from the Sun arising from the pair annihilation of χ^0 trapped by the sun in data taken between Jan. 2007 and Dec. 2008.
- ²¹AGNESE 13 use data taken between Oct. 2006 and July 2007.
- ²²BOLIEV 13 search for neutrinos from the Sun arising from the pair annihilation of χ^0 trapped by the sun in data taken from 1978 to 2009. See also SUVOROVA 13 for an older analysis of the same data.
- ²³LI 13b search for WIMP scatter on Ge; limits placed in $\sigma^{SI}(\chi N)$ vs. $m(\chi)$ plane for $m(\chi) \sim 4$ –100 GeV.
- ²⁴ABBASI 12 search for neutrinos from the Sun arising from the pair annihilation of χ^0 trapped by the Sun. The amount of χ^0 depends on the χ^0 -proton cross section.
- ²⁵Reanalysis of ANGLOHER 09 data with all three nuclides. See also BROWN 12.
- ²⁶See also APRILE 14A.
- ²⁷See their Fig. 6 for a limit on inelastically scattering χ^0 for $m_{\chi^0} = 70$ GeV.
- ²⁸AHMED 11 search for χ^0 inelastic scattering. See their Fig. 8–10 for limits.
- ²⁹AHMED 11A combine CDMS and EDELWEISS data.
- ³⁰AJELLO 11 search for e^\pm flux from χ^0 annihilations in the Sun. Models in which χ^0 annihilates into an intermediate long-lived weakly interacting particles or χ^0 scatters inelastically are constrained. See their Fig. 6–8 for limits.
- ³¹APRILE 11 reanalyze APRILE 10 data.
- ³²APRILE 11A search for χ^0 inelastic scattering. See their Fig. 2 and 3 for limits. See also APRILE 14A.
- ³³Supersedes ARMENGAUD 10. A limit on inelastic cross section is also given.
- ³⁴HORN 11 perform detector calibration by neutrons. Earlier results are only marginally affected.
- ³⁵AKIMOV 10 give cross section limits for inelastically scattering dark matter. See their Fig. 4.
- ³⁶Superseded by AHMED 10.
- ³⁷ANGLE 09 search for χ^0 inelastic scattering. See their Fig. 4 for limits.
- ³⁸GIULIANI 05 analyzes the spin-independent χ^0 -nucleon cross section limits with both isoscalar and isovector couplings. See their Fig. 3 and 4 for limits on the couplings.

Searches Particle Listings

WIMP and Dark Matter Searches

For $m_{\chi^0} = 1 \text{ TeV}$

For limits from X^0 annihilation in the Sun, the assumed annihilation final state is shown in parenthesis in the comment.

VALUE (pb)	CL%	DOCUMENT ID	TECN	COMMENT
<3 × 10 ⁻⁶	90	1 YAGUNA 19	Ar	I-spin viol DM
<3.8 × 10 ⁻⁸	90	2 AGNES 18A	DS50 Ar	
<8.24 × 10 ⁻¹⁰	90	3 APRILE 18	XE1T Xe	
<2 × 10 ⁻⁹	90	4 AKERIB 17	LUX Xe	
<0.3	90	5 CHEN 17E	PNDX	$\chi N \rightarrow \chi^* \rightarrow \chi \gamma$
<1.2 × 10 ⁻⁹	90	6 CUI 17A	PNDX	SI WIMPs on Xe
<8.6 × 10 ⁻⁸	90	AGNES 16	DS50 Ar	
<2 × 10 ⁻⁷	90	AGNES 15	DS50 Ar	
<2 × 10 ⁻⁷	90	7 AGNESE 15B	CDM2 Ge	
<1 × 10 ⁻⁸	90	AKERIB 14	LUX Xe	
<2.2 × 10 ⁻⁶	90	8 AVRORIN 14	BAIK	H, solar ν ($W^+ W^-$)
<5.5 × 10 ⁻⁵	90	8 AVRORIN 14	BAIK	H, solar ν ($b\bar{b}$)
<6.8 × 10 ⁻⁷	90	8 AVRORIN 14	BAIK	H, solar ν ($\tau^+ \tau^-$)
<3.46 × 10 ⁻⁷	90	9 AARTSEN 13	ICCB	H, solar ν ($W^+ W^-$)
<7.75 × 10 ⁻⁶	90	9 AARTSEN 13	ICCB	H, solar ν ($b\bar{b}$)
<6.9 × 10 ⁻⁷	90	10 ADRIAN-MAR.13	ANTR	H, solar ν ($W^+ W^-$)
<1.5 × 10 ⁻⁵	90	10 ADRIAN-MAR.13	ANTR	H, solar ν ($b\bar{b}$)
<1.8 × 10 ⁻⁷	90	10 ADRIAN-MAR.13	ANTR	H, solar ν ($\tau^+ \tau^-$)
<4.3 × 10 ⁻⁶	90	11 BOLIEV 13	BAKS	H, solar ν ($W^+ W^-$)
<3.4 × 10 ⁻⁵	90	11 BOLIEV 13	BAKS	H, solar ν ($b\bar{b}$)
<1.2 × 10 ⁻⁶	90	11 BOLIEV 13	BAKS	H, solar ν ($\tau^+ \tau^-$)
<2.12 × 10 ⁻⁷	90	12 ABBASI 12	ICCB	H, solar ν ($W^+ W^-$)
<6.56 × 10 ⁻⁶	90	12 ABBASI 12	ICCB	H, solar ν ($b\bar{b}$)
<4 × 10 ⁻⁷	90	AKIMOV 12	ZEP3	Xe
<1.1 × 10 ⁻⁵	90	13 ANGIOHER 12	CRES	CaWO ₄
<2 × 10 ⁻⁸	90	14 APRILE 12	X100	Xe
<2 × 10 ⁻⁶	90	BEHNKE 12	COUP	CF ₃ I
<4 × 10 ⁻⁶	90	FELIZARDO 12	SMP	C ₂ ClF ₅
<1.5 × 10 ⁻⁶	90	KIM 12	KIMS	CsI
		15 AHMED 11	CDM2	Ge, inelastic
<1.5 × 10 ⁻⁷	90	16 AHMED 11A	RVUE	Ge
<2 × 10 ⁻⁷	90	17 APRILE 11	X100	Xe
<8 × 10 ⁻⁸	90	14 APRILE 11B	X100	Xe
<2 × 10 ⁻⁷	90	18 ARMENGAUD 11	EDE2	Ge
		19 HORN 11	ZEP3	Xe
<2 × 10 ⁻⁷	90	AHMED 10	CDM2	Ge
<4 × 10 ⁻⁷	90	APRILE 10	X100	Xe
<6 × 10 ⁻⁷	90	ARMENGAUD 10	EDE2	Ge
<3.5 × 10 ⁻⁷	90	20 AHMED 09	CDM2	Ge

- YAGUNA 19 recasts DEAP-3600 single-phase liquid argon results in limit for isospin violating DM; for $f_{\tilde{H}}/f_p = -0.69$, requires $\sigma^{SI}(\chi p) < 3 \times 10^{-6}$ pb for $m(\chi) = 1 \text{ TeV}$.
- AGNES 18A search for WIMP scatter on 46.4 kg Ar; no signal; require $\sigma^{SI}(\chi N) < 3.8 \times 10^{-8}$ pb for $m(\chi) = 1 \text{ TeV}$.
- APRILE 18 search for WIMP scatter on 1.3 t Xe; no signal seen; require $\sigma^{SI}(\chi p) < 8.24 \times 10^{-10}$ pb for $m(\chi) = 1 \text{ TeV}$.
- AKERIB 17 search for WIMP scatter on Xe using complete LUX data set; limits placed in $\sigma^{SI}(\chi N)$ vs. $m(\chi)$ plane for $m(\chi) \sim 5-1 \times 10^5 \text{ GeV}$.
- CHEN 17E search for inelastic WIMP scatter on Xe; require $\sigma^{SI}(\chi N) < 0.3 \text{ pb}$ for $m(\chi) = 1 \text{ TeV}$ and (mass difference) = 300 keV.
- CUI 17A search for WIMP scatter using 54 ton-day exposure of Xe; limits placed in $\sigma^{SI}(\chi N)$ vs. $m(\chi)$ plane for $m \sim 10-1 \times 10^4 \text{ GeV}$.
- AGNESE 15B reanalyse AHMED 10 data.
- AVRORIN 14 search for neutrinos from the Sun arising from the pair annihilation of X^0 trapped by the Sun in data taken between 1998 and 2003. See their Table 1 for limits assuming annihilation into neutrino pairs.
- AARTSEN 13 search for neutrinos from the Sun arising from the pair annihilation of X^0 trapped by the sun in data taken between June 2010 and May 2011.
- ADRIAN-MARTINEZ 13 search for neutrinos from the Sun arising from the pair annihilation of X^0 trapped by the sun in data taken between Jan. 2007 and Dec. 2008.
- BOLIEV 13 search for neutrinos from the Sun arising from the pair annihilation of X^0 trapped by the sun in data taken from 1978 to 2009. See also SUVOROVA 13 for an older analysis of the same data.
- ABBASI 12 search for neutrinos from the Sun arising from the pair annihilation of X^0 trapped by the Sun. The amount of X^0 depends on the X^0 -proton cross section.
- Reanalysis of ANGIOHER 09 data with all three nuclides. See also BROWN 12. See also APRILE 14A.
- AHMED 11 search for X^0 inelastic scattering. See their Fig. 8-10 for limits.
- AHMED 11A combine CDM2 and EDELWEISS data.
- APRILE 11 reanalyse APRILE 10 data.
- Supersedes ARMENGAUD 10. A limit on inelastic cross section is also given.
- HORN 11 perform detector calibration by neutrons. Earlier results are only marginally affected.
- Superseded by AHMED 10.

Spin-Dependent Cross Section Limits for Dark Matter Particle (X^0) on Proton

For m_{χ^0} in GeV range

We provide here limits for $m_{\chi^0} < 5 \text{ GeV}$

VALUE (pb)	CL%	DOCUMENT ID	TECN	COMMENT
< 1 × 10 ⁶	95	1 ABDELHAME...19	CRES	GeV-scale WIMPs on Li
< 3 × 10 ⁻⁴	90	2 AMOLE 19	PICO	C ₃ F ₈
< 1.7 × 10 ⁴	90	3 APRILE 19c	XE1T	light DM on Xe via Migdal/brem effect
< 8 × 10 ⁶	90	4 ARMENGAUD 19	EDEL	GeV-scale WIMPs on Ge
< 70	90	5 XIA 19A	PNDX	SD WIMP on Xe
< 100	90	6 AGNESE 18	SCDM	GeV-scale WIMPs on Ge
< 1	90	7 AKERIB 17A	LUX	Xe
< 0.6	90	8 FU 17	PNDX	SD WIMP on Xe
< 0.2	90	9 AMOLE 15	PICO	C ₃ F ₈
< 1.6 × 10 ⁻¹	90	10 ARCHAMBAU.12	PICA	¹⁹ F

For $m_{\chi^0} = 20 \text{ GeV}$

For limits from X^0 annihilation in the Sun, the assumed annihilation final state is shown in parenthesis in the comment.

VALUE (pb)	CL%	DOCUMENT ID	TECN	COMMENT
< 3 × 10 ⁵	95	1 ABDELHAME...19	CRES	⁷ Li
< 2.5 × 10 ⁻⁵	90	2 AMOLE 19	PICO	C ₃ F ₈
< 2.5 × 10 ⁻⁴	90	3 APRILE 19A	XE1T	Xe, SD
< 1 × 10 ⁻³	90	4 XIA 19A	PNDX	SD WIMP on Xe
< 30	95	5 AGNESE 18	SCDM	Ge
< 1 × 10 ⁻³	90	6 AKERIB 17A	LUX	Xe
< 1.32 × 10 ⁻²	90	7 BEHNKE 17	PICA	C ₄ F ₁₀
< 2 × 10 ⁻³	90	8 FU 17	PNDX	SD WIMP on Xe
< 5 × 10 ⁻⁴	90	9 AMOLE 16A	PICO	C ₃ F ₈
< 2 × 10 ⁻⁶	90	10 KHACHATRY...16AJ	CMS	8 TeV pp → Z+ $\cancel{e}\tau$; $Z \rightarrow \tilde{e}\tilde{e}$
< 1.2 × 10 ⁻³	90	AMOLE 15	PICO	C ₃ F ₈
< 1.43 × 10 ⁻³	90	CHOI 15	SKAM	H, solar ν ($b\bar{b}$)
< 1.42 × 10 ⁻⁴	90	CHOI 15	SKAM	H, solar ν ($\tau^+ \tau^-$)
< 5 × 10 ⁻³	90	FELIZARDO 14	SMP	C ₂ ClF ₅
< 1.29 × 10 ⁻²	90	11 AARTSEN 13	ICCB	H, solar ν ($\tau^+ \tau^-$)
< 3.17 × 10 ⁻²	90	12 APRILE 13	X100	Xe
< 3 × 10 ⁻²	90	13 ARCHAMBAU.12	PICA	F (C ₄ F ₁₀)
< 6 × 10 ⁻²	90	BEHNKE 12	COUP	CF ₃ I
< 20	90	DAW 12	DRFT	F (CF ₄)
< 7 × 10 ⁻³	90	FELIZARDO 12	SMP	C ₂ ClF ₅
< 0.15	90	KIM 12	KIMS	CsI
< 1 × 10 ⁵	90	14 AHLEN 11	DMTP	F (CF ₄)
< 0.1	90	14 BEHNKE 11	COUP	CF ₃ I
< 1.5 × 10 ⁻²	90	15 TANAKA 11	SKAM	H, solar ν ($b\bar{b}$)
< 0.2	90	ARCHAMBAU..09	PICA	F
< 4	90	LEBEDENKO 09A	ZEP3	Xe
< 0.6	90	ANGLE 08A	XE10	Xe
< 100	90	ALNER 07	ZEP2	Xe
< 1	90	LEE 07A	KIMS	CsI
< 2	90	16 AKERIB 06	CDMS	⁷³ Ge, ²⁹ Si
< 20	90	SHIMIZU 06A	CNTR	F (CaF ₂)
< 0.5	90	ALNER 05	NAIA	NaI
< 1.5	90	BARNABE-HE..05	PICA	F (C ₄ F ₁₀)
< 1.5	90	GIRARD 05	SMP	F (C ₂ ClF ₅)
< 35	90	MIUCHI 03	BOLO	LiF
< 30	90	TAKEDA 03	BOLO	NaF

- 1 ABDELHAMEED 19 uses Li₂MoO₄ target to set limit for spin dependent coupling $\sigma^{SD}(\chi p) < 3. \times 10^5$ pb for $m(\chi) = 20$ GeV.
- 2 AMOLE 19 search for SD WIMP scatter on C₃F₈ in PICO-60 bubble chamber; no signal: set limit for spin dependent coupling $\sigma^{SD}(\chi p) < 2.5 \times 10^{-5}$ pb for $m(\chi) = 20$ GeV.
- 3 APRILE 19A search for SD WIMP scatter on 1 t yr Xe; no signal, limits placed in $\sigma^{SD}(\chi p)$ vs. $m(\chi)$ plane for $m \sim 6$ –1000 GeV.
- 4 XIA 19A search for WIMP scatter on Xe in PandaX-II; limits placed in $\sigma^{SD}(\chi p)$ vs. $m(\chi)$ plane for $m(\chi) \sim 5$ – 1×10^5 GeV.
- 5 AGNESE 18 give limits for $\sigma^{SD}(\rho \chi)$ for $m(\text{WIMP})$ between 1.5 and 20 GeV using CDMSlite mode data.
- 6 AKERIB 17A search for SD WIMP scatter on Xe using 129.5 kg yr exposure; limits placed in $\sigma^{SD}(\chi p)$ vs. $m(\chi)$ plane for $m(\chi) \sim 6$ – 1×10^5 GeV.
- 7 BEHNKE 17 show final Picasso results based on 231.4 kg d exposure at SNOLab for WIMP scatter on C₄F₁₀ search via superheated droplet; require $\sigma(\text{SD}) < 1.32 \times 10^{-2}$ pb for $m(\text{WIMP}) = 20$ GeV.
- 8 FU 17 search for SD WIMP scatter on Xe; limits set in $\sigma^{SD}(\chi p)$ vs. $m(\chi)$ plane for $m(\chi) \sim 4$ – 1×10^3 GeV.
- 9 AMOLE 16A require SD WIMP- p scattering $< 5 \times 10^{-4}$ pb for $m(\text{WIMP}) = 20$ GeV; bubbles from C₃F₈ target.
- 10 KHACHATRYAN 16AJ require SD WIMP- $p < 2 \times 10^{-6}$ pb for $m(\text{WIMP}) = 20$ GeV from $pp \rightarrow Z + \cancel{e}T$; $Z \rightarrow \ell\bar{\ell}$ signal.
- 11 AARTSEN 13 search for neutrinos from the Sun arising from the pair annihilation of X^0 trapped by the sun in data taken between June 2010 and May 2011.
- 12 The value has been provided by the authors. APRILE 13 note that the proton limits on Xe are highly sensitive to the theoretical model used. See also APRILE 14A.
- 13 ARCHAMBAULT 12 search for WIMP scatter on C₄F₁₀; limits set in $\sigma^{SD}(\chi p)$ vs. $m(\chi)$ plane for $m \sim 4$ –500 GeV.
- 14 Use a direction-sensitive detector.
- 15 TANAKA 11 search for neutrinos from the Sun arising from the pair annihilation of X^0 trapped by the Sun. The amount of X^0 depends on the X^0 -proton cross section.
- 16 See also AKERIB 05.

For $m_{X^0} = 100$ GeV

For limits from X^0 annihilation in the Sun, the assumed annihilation final state is shown in parenthesis in the comment.

VALUE (pb)	CL%	DOCUMENT ID	TECN	COMMENT
••• We do not use the following data for averages, fits, limits, etc. •••				
$< 4 \times 10^{-5}$	90	1 AMOLE 19	PICO	C ₃ F ₈
$< 4 \times 10^{-4}$	90	2 APRILE 19A	XE1T	Xe, SD
$< 8 \times 10^{-4}$	90	3 XIA 19A	PNDX	SD WIMP on Xe
$< 8 \times 10^{-4}$	90	4 AKERIB 17A	LUX	Xe
$< 5 \times 10^{-5}$	90	5 AMOLE 17	PICO	C ₃ F ₈
$< 3.3 \times 10^{-2}$	90	6 APRILE 17A	X100	Xe inelastic
$< 2.8 \times 10^{-1}$	90	7 BATTAT 17	DRFT	CS ₂
$< 1.5 \times 10^{-3}$	90	8 FU 17	PNDX	Xe
< 0.553 –0.019	95	9 AABOUD 16D	ATLS	$pp \rightarrow j + \cancel{e}T$
$< 1 \times 10^{-5}$	90	10 AABOUD 16F	ATLS	$pp \rightarrow \gamma + \cancel{e}T$
$< 1 \times 10^{-4}$	90	11 AARTSEN 16C	ICCB	solar $\nu (W^+ W^-)$
$< 2 \times 10^{-4}$	90	12 ADRIAN-MAR..16	ANTR	solar $\nu (W W, b\bar{b}, \tau\bar{\tau})$
$< 3 \times 10^{-3}$	90	13 AKERIB 16A	LUX	Xe
$< 5 \times 10^{-4}$	90	14 AMOLE 16	PICO	CF ₃ I
$< 1.5 \times 10^{-3}$	90	AMOLE 15	PICO	C ₃ F ₈
$< 3.19 \times 10^{-3}$	90	CHOI 15	SKAM	H, solar $\nu (b\bar{b})$
$< 2.80 \times 10^{-4}$	90	CHOI 15	SKAM	H, solar $\nu (W^+ W^-)$
$< 1.24 \times 10^{-4}$	90	CHOI 15	SKAM	H, solar $\nu (\tau^+ \tau^-)$
$< 8 \times 10^2$	90	15 NAKAMURA 15	NAGE	CF ₄
$< 1.7 \times 10^{-3}$	90	16 AVRORIN 14	BAIK	H, solar $\nu (W^+ W^-)$
$< 4.5 \times 10^{-2}$	90	16 AVRORIN 14	BAIK	H, solar $\nu (b\bar{b})$
$< 7.1 \times 10^{-4}$	90	16 AVRORIN 14	BAIK	H, solar $\nu (\tau^+ \tau^-)$
$< 6 \times 10^{-3}$	90	FELIZARDO 14	SMPL	C ₂ ClF ₅
$< 2.68 \times 10^{-4}$	90	17 AARTSEN 13	ICCB	H, solar $\nu (W^+ W^-)$
$< 1.47 \times 10^{-2}$	90	17 AARTSEN 13	ICCB	H, solar $\nu (b\bar{b})$
$< 8.5 \times 10^{-4}$	90	18 ADRIAN-MAR..13	ANTR	H, solar $\nu (W^+ W^-)$
$< 5.5 \times 10^{-2}$	90	18 ADRIAN-MAR..13	ANTR	H, solar $\nu (b\bar{b})$
$< 3.4 \times 10^{-4}$	90	18 ADRIAN-MAR..13	ANTR	H, solar $\nu (\tau^+ \tau^-)$
$< 1.00 \times 10^{-2}$	90	19 APRILE 13	X100	Xe
$< 7.1 \times 10^{-4}$	90	20 BOLIEV 13	BAKS	H, solar $\nu (W^+ W^-)$
$< 8.4 \times 10^{-3}$	90	20 BOLIEV 13	BAKS	H, solar $\nu (b\bar{b})$
$< 3.1 \times 10^{-4}$	90	20 BOLIEV 13	BAKS	H, solar $\nu (\tau^+ \tau^-)$
$< 7.07 \times 10^{-4}$	90	21 ABBASI 12	ICCB	H, solar $\nu (W^+ W^-)$
$< 4.53 \times 10^{-2}$	90	21 ABBASI 12	ICCB	H, solar $\nu (b\bar{b})$
$< 7 \times 10^{-2}$	90	22 ARCHAMBAU..12	PICA	F (C ₄ F ₁₀)
$< 1 \times 10^{-2}$	90	BEHNKE 12	COUP	CF ₃ I
< 1.8	90	DAW 12	DRFT	F (CF ₄)
$< 9 \times 10^{-3}$	90	FELIZARDO 12	SMPL	C ₂ ClF ₅
$< 2 \times 10^{-2}$	90	KIM 12	KIMS	CsI
$< 2 \times 10^3$	90	15 AHLEN 11	DMTF	F (CF ₄)
$< 7 \times 10^{-2}$	90	BEHNKE 11	COUP	CF ₃ I
$< 2.7 \times 10^{-4}$	90	23 TANAKA 11	SKAM	H, solar $\nu (W^+ W^-)$
$< 4.5 \times 10^{-3}$	90	23 TANAKA 11	SKAM	H, solar $\nu (b\bar{b})$
$< 6 \times 10^3$	90	24 FELIZARDO 10	SMPL	C ₂ ClF ₃
$< 6 \times 10^3$	90	15 MIUCHI 10	NAGE	CF ₄
< 0.4	90	ARCHAMBAU..09	PICA	F
< 0.8	90	LEBEDENKO 09A	ZEP3	Xe
< 1.0	90	ANGLE 08A	XE10	Xe

< 15	90	ALNER 07	ZEP2	Xe
< 0.2	90	LEE 07A	KIMS	CsI
$< 1 \times 10^4$	90	15 MIUCHI 07	NAGE	F (CF ₄)
< 5	90	25 AKERIB 06	CDMS	⁷³ Ge, ²⁹ Si
< 2	90	SHIMIZU 06A	CNTR	F (CaF ₂)
< 0.3	90	ALNER 05	NAIA	NaI
< 2	90	BARNABE-HE..05	PICA	F (C ₄ F ₁₀)
< 100	90	BENOIT 05	EDEL	⁷³ Ge
< 1.5	90	GIRARD 05	SMPL	F (C ₂ ClF ₅)
< 0.7	26	GIULIANI 05A	RVUE	
	27	GIULIANI 04	RVUE	
	28	GIULIANI 04A	RVUE	
< 35	90	MIUCHI 03	BOLO	LiF
< 40	90	TAKEDA 03	BOLO	NaF

- 1 AMOLE 19 search for SD WIMP scatter on C₃F₈ in PICO-60 bubble chamber; no signal: set limit for spin dependent coupling $\sigma^{SD}(\chi p) < 4 \times 10^{-5}$ pb for $m(\chi) = 100$ GeV.
- 2 APRILE 19A search for SD WIMP scatter on 1 t yr Xe; no signal, limits placed in $\sigma^{SD}(\chi p)$ vs. $m(\chi)$ plane for $m \sim 6$ –1000 GeV.
- 3 XIA 19A search for WIMP scatter on Xe in PandaX-II; limits placed in $\sigma^{SD}(\chi p)$ vs. $m(\chi)$ plane for $m(\chi) \sim 5$ – 1×10^5 GeV.
- 4 AKERIB 17A search for SD WIMP scatter on Xe using 129.5 kg yr exposure; limits placed in $\sigma^{SD}(\chi p)$ vs. $m(\chi)$ plane for $m(\chi) \sim 6$ – 1×10^5 GeV.
- 5 AMOLE 17 require $\sigma(\text{WIMP-}p)^{SD} < 5 \times 10^{-5}$ pb for $m(\text{WIMP}) = 100$ GeV using PICO-60 1167 kg-days exposure at SNOLab.
- 6 APRILE 17A require $\sigma(\text{WIMP-}p)(\text{inelastic})^{SD} < 3.3 \times 10^{-2}$ pb for $m(\text{WIMP}) = 100$ GeV, based on 7640 kg day exposure at LNGS.
- 7 BATTAT 17 use directional detection of CS₂ ions to require $\sigma(\text{SD}) < 2.8 \times 10^{-1}$ pb for 100 GeV WIMP with a 55 days exposure at the Bouby Underground Science Facility.
- 8 FU 17 from a 33000 kg d exposure at CJPL, PANDAX II derive for $m(\text{DM}) = 100$ GeV, $\sigma^{SD}(\text{WIMP-}p) < 2 \times 10^{-3}$ pb.
- 9 AABOUD 16D use ATLAS 13 TeV 3.2 fb⁻¹ of data to search for monojet plus missing E_T ; agree with SM rates; present limits on large extra dimensions, compressed SUSY spectra and wimp pair production.
- 10 AABOUD 16F search for monophoton plus missing E_T events at ATLAS with 13 TeV and 3.2 fb⁻¹; signal agrees with SM background; place limits on SD WIMP-proton scattering vs. mediator mass and large extra dimension models.
- 11 AARTSEN 16C search for high energy ν s from WIMP annihilation in solar core; limits set on SD WIMP- p scattering (Fig. 8).
- 12 ADRIAN-MARTINEZ 16 search for WIMP annihilation into ν s from solar core; exclude SD cross section $< \text{few } 10^{-4}$ depending on $m(\text{WIMP})$.
- 13 AKERIB 16A using 2013 data exclude SD WIMP-proton scattering $> 3 \times 10^{-3}$ pb for $m(\text{WIMP}) = 100$ GeV.
- 14 AMOLE 16 use bubble technique on CF₃I target to exclude SD WIMP- p scattering $> 5 \times 10^{-4}$ pb for $m(\text{WIMP}) = 100$ GeV.
- 15 Use a direction-sensitive detector.
- 16 AVRORIN 14 search for neutrinos from the Sun arising from the pair annihilation of X^0 trapped by the Sun in data taken between 1998 and 2003. See their Table 1 for limits assuming annihilation into neutrino pairs.
- 17 AARTSEN 13 search for neutrinos from the Sun arising from the pair annihilation of X^0 trapped by the sun in data taken between June 2010 and May 2011.
- 18 ADRIAN-MARTINEZ 13 search for neutrinos from the Sun arising from the pair annihilation of X^0 trapped by the sun in data taken between Jan. 2007 and Dec. 2008.
- 19 The value has been provided by the authors. APRILE 13 note that the proton limits on Xe are highly sensitive to the theoretical model used. See also APRILE 14A.
- 20 BOLIEV 13 search for neutrinos from the Sun arising from the pair annihilation of X^0 trapped by the sun in data taken from 1978 to 2009. See also SUVOROVA 13 for an older analysis of the same data.
- 21 ABBASI 12 search for neutrinos from the Sun arising from the pair annihilation of X^0 trapped by the Sun. The amount of X^0 depends on the X^0 -proton cross section.
- 22 ARCHAMBAULT 12 search for WIMP scatter on C₄F₁₀; limits set in $\sigma^{SD}(\chi p)$ vs. $m(\chi)$ plane for $m \sim 4$ –500 GeV.
- 23 TANAKA 11 search for neutrinos from the Sun arising from the pair annihilation of X^0 trapped by the Sun. The amount of X^0 depends on the X^0 -proton cross section.
- 24 See their Fig. 3 for limits on spin-dependent proton couplings for X^0 mass of 50 GeV.
- 25 See also AKERIB 05.
- 26 GIULIANI 05A analyze available data and give combined limits.
- 27 GIULIANI 04 reanalyze COLLAR 00 data and give limits for spin-dependent X^0 -proton coupling.
- 28 GIULIANI 04A give limits for spin-dependent X^0 -proton couplings from existing data.

For $m_{X^0} = 1$ TeV

For limits from X^0 annihilation in the Sun, the assumed annihilation final state is shown in parenthesis in the comment.

VALUE (pb)	CL%	DOCUMENT ID	TECN	COMMENT
••• We do not use the following data for averages, fits, limits, etc. •••				
$< 3 \times 10^{-4}$	90	1 AMOLE 19	PICO	C ₃ F ₈
$< 4 \times 10^{-3}$	90	2 APRILE 19A	XE1T	Xe, SD
$< 5 \times 10^{-3}$	90	3 XIA 19A	PNDX	SD WIMP on Xe
		4 ALBERT 18C	HAWC	DM annihilation in Sun to long-lived mediator
$< 2.05 \times 10^{-5}$	90	5 AARTSEN 17A	ICCB	ν , sun
$< 7 \times 10^{-3}$	90	6 AKERIB 17A	LUX	Xe

Searches Particle Listings

WIMP and Dark Matter Searches

VALUE (pb)	CL %	DOCUMENT ID	TECN	COMMENT
< 2 × 10 ⁻²	90	7 FU 17 PNDX	SD WIMP on Xe	
< 1 × 10 ⁻²	90	8 ADRIAN-MAR.16B ANTR	solar μ from WIMP annih.	
< 1.5 × 10 ³	90	AMOLE 15 PICO	C ₃ F ₈	
< 2.7 × 10 ⁻³	90	NAKAMURA 15 NAGE	CF ₄	
< 6.9 × 10 ⁻²	90	9 AVROBIN 14 BAIK	H, solar ν (W ⁺ W ⁻)	
< 8.4 × 10 ⁻⁴	90	9 AVROBIN 14 BAIK	H, solar ν (b \bar{b})	
< 4.48 × 10 ⁻⁴	90	9 AVROBIN 14 BAIK	H, solar ν (τ ⁺ τ ⁻)	
< 1.00 × 10 ⁻²	90	10 AARTSEN 13 ICCB	H, solar ν (W ⁺ W ⁻)	
< 8.9 × 10 ⁻⁴	90	10 AARTSEN 13 ICCB	H, solar ν (b \bar{b})	
< 2.0 × 10 ⁻²	90	11 ADRIAN-MAR.13 ANTR	H, solar ν (W ⁺ W ⁻)	
< 2.3 × 10 ⁻⁴	90	11 ADRIAN-MAR.13 ANTR	H, solar ν (b \bar{b})	
< 7.57 × 10 ⁻²	90	11 ADRIAN-MAR.13 ANTR	H, solar ν (τ ⁺ τ ⁻)	
< 5.4 × 10 ⁻³	90	12 APRILE 13 X100	Xe	
< 4.2 × 10 ⁻²	90	13 BOLIEV 13 BAKS	H, solar ν (W ⁺ W ⁻)	
< 1.5 × 10 ⁻³	90	13 BOLIEV 13 BAKS	H, solar ν (b \bar{b})	
< 2.50 × 10 ⁻⁴	90	13 BOLIEV 13 BAKS	H, solar ν (τ ⁺ τ ⁻)	
< 7.86 × 10 ⁻³	90	14 ABBASI 12 ICCB	H, solar ν (W ⁺ W ⁻)	
< 8 × 10 ⁻²	90	14 ABBASI 12 ICCB	H, solar ν (b \bar{b})	
< 8	90	BEHNKE 12 COUP	CF ₃ I	
< 6 × 10 ⁻²	90	DAW 12 DRFT	F (CF ₄)	
< 8 × 10 ⁻²	90	FELIZARDO 12 SMPL	C ₂ ClF ₅	
< 8 × 10 ³	90	KIM 12 KIMS	Csl	
< 0.4	90	15 AHLEN 11 DMTP	F (CF ₄)	
< 2 × 10 ⁻³	90	BEHNKE 11 COUP	CF ₃ I	
< 2 × 10 ⁻²	90	16 TANAKA 11 SKAM	H, solar ν (b \bar{b})	
< 1 × 10 ⁻³	90	16 TANAKA 11 SKAM	H, solar ν (W ⁺ W ⁻)	
< 2 × 10 ⁴	90	17 ABBASI 10 ICCB	KK dark matter	
< 8.7 × 10 ⁻⁴	90	15 MIUCHI 10 NAGE	CF ₄	
< 2.2 × 10 ⁻²	90	ABBASI 09B ICCB	H, solar ν (W ⁺ W ⁻)	
< 3	90	ABBASI 09B ICCB	H, solar ν (b \bar{b})	
< 6	90	ARCHAMBAU.09 PICA	F	
< 9	90	LEBEDENKO 09A ZEP3	Xe	
< 100	90	ANGLE 08A XE10	Xe	
< 0.8	90	ALNER 07 ZEP2	Xe	
< 4 × 10 ⁴	90	LEE 07A KIMS	Csl	
< 30	90	15 MIUCHI 07 NAGE	F (CF ₄)	
< 1.5	90	18 AKERIB 06 CDMS	⁷³ Ge, ²⁹ Si	
< 60	90	ALNER 05 NAIA	NaI	
< 15	90	BARNABE-HE.05 PICA	F (C ₄ F ₁₀)	
< 10	90	BENOIT 05 EDEL	⁷³ Ge	
< 260	90	GIRARD 05 SMPL	F (C ₂ ClF ₅)	
< 150	90	MIUCHI 03 BOLO	LIF	
	90	TAKEDA 03 BOLO	NaF	

- AMOLE 19 search for SD WIMP scatter on C₃F₈ in PICO-60 bubble chamber; no signal: set limit for spin dependent coupling $\sigma^{SD}(\chi p) < 3 \times 10^{-4}$ pb for $m(\chi) = 1000$ GeV.
- APRILE 19A search for SD WIMP scatter on 1 t yr Xe; no signal, limits placed in $\sigma^{SD}(\chi p)$ vs. $m(\chi)$ plane for $m \sim 6$ -1000 GeV.
- XIA 19A search for WIMP scatter on Xe in PandaX-II; limits placed in $\sigma^{SD}(\chi p)$ vs. $m(\chi)$ plane for $m(\chi) \sim 5$ -1 × 10⁵ GeV.
- ALBERT 18c search for DM annihilation in Sun to long-lived mediator (LLM) which decays outside Sun, for DM masses above 1 TeV; assuming LLM, limits set on $\sigma^{SD}(\chi p)$.
- AARTSEN 17A search for neutrinos from solar WIMP annihilation into $\tau^+ \tau^-$ in 532 days of live time.
- AKERIB 17A search for SD WIMP scatter on Xe using 129.5 kg yr exposure; limits placed in $\sigma^{SD}(\chi p)$ vs. $m(\chi)$ plane for $m(\chi) \sim 6$ -1 × 10⁵ GeV.
- FU 17 search for SD WIMP scatter on Xe; limits set in $\sigma^{SD}(\chi p)$ vs. $m(\chi)$ plane for $m(\chi) \sim 4$ -1 × 10³ GeV.
- ADRIAN-MARTINEZ 16B search for secluded DM via WIMP annihilation in solar core into light mediator which later decays to μ or ν s; limits presented in Figures 3 and 4.
- AVROBIN 14 search for neutrinos from the Sun arising from the pair annihilation of X^0 trapped by the Sun in data taken between 1998 and 2003. See their Table 1 for limits assuming annihilation into neutrino pairs.
- AARTSEN 13 search for neutrinos from the Sun arising from the pair annihilation of X^0 trapped by the sun in data taken between June 2010 and May 2011.
- ADRIAN-MARTINEZ 13 search for neutrinos from the Sun arising from the pair annihilation of X^0 trapped by the sun in data taken between Jan. 2007 and Dec. 2008.
- The value has been provided by the authors. APRILE 13 note that the proton limits on Xe are highly sensitive to the theoretical model used. See also APRILE 14A.
- BOLIEV 13 search for neutrinos from the Sun arising from the pair annihilation of X^0 trapped by the sun in data taken from 1978 to 2009. See also SUVOROVA 13 for an older analysis of the same data.
- ABBASI 12 search for neutrinos from the Sun arising from the pair annihilation of X^0 trapped by the Sun. The amount of X^0 depends on the X^0 -proton cross section.
- Use a direction-sensitive detector.
- TANAKA 11 search for neutrinos from the Sun arising from the pair annihilation of X^0 trapped by the Sun. The amount of X^0 depends on the X^0 -proton cross section.
- ABBASI 10 search for ν_μ from annihilations of Kaluza-Klein photon dark matter in the Sun.
- See also AKERIB 05.

Spin-Dependent Cross Section Limits for Dark Matter Particle (X^0) on Neutron

For m_{χ_0} in GeV range

We provide here limits for $m_{\chi_0} < 5$ GeV

VALUE (pb)	CL %	DOCUMENT ID	TECN	COMMENT
< 1 × 10 ¹⁰	95	1 ABDELHAMEE.19	CRES	SD low mass DM on Li
< 2.3 × 10 ²	90	2 APRILE 19c	XE1T	light DM on Xe via Migdal/brem effect
< 1 × 10 ⁻²	90	3 APRILE 19D	XE1T	light DM on Xe via ionization
< 4 × 10 ⁴	90	4 ARMENGAUD 19	EDEL	GeV-scale WIMPs on Ge
< 8 × 10 ⁻²	90	5 XIA 19A	PNDX	SD WIMP on Xe
< 3	90	6 AGNESE 18	SCDM	GeV-scale WIMPs on Ge
< 3	90	7 JIANG 18	CDEX	GeV-scale WIMPs on Ge
< 10	90	8 YANG 18	CDEX	GeV-scale WIMPs on Ge
< 1 × 10 ⁻¹	90	9 AKERIB 17A	LUX	Xe
< 0.1	90	10 FU 17	PNDX	SD WIMP on Xe
< 20	90	11 ZHAO 16	CDEX	GeV-scale WIMPs on Ge
< 150	90	12 AHMED 11B	CDM2	GeV-scale WIMPs on Ge

- ABDELHAMEED 19 search for GeV-scale WIMP SD scatter on ⁷Li crystal; set limit $\sigma^{SD}(\chi n)$ for $m(\chi) \sim 0.8$ -20 GeV; quoted limit for $m(\chi) = 1$ GeV.
- APRILE 19c search for light DM on Xe via Migdal/bremsstrahlung effect; no signal, require $\sigma^{SD}(\chi n) < 230$ pb for $m(\chi) = 1$ GeV.
- APRILE 19D search for light DM scatter on Xe via ionization; no signal, limits placed in σ vs. $m(\text{DM}) \sim 3$ -6 GeV; quoted limit is for $m(\text{DM}) = 5$ GeV.
- ARMENGAUD 19 search for GeV scale WIMP scatter on Ge; limits placed in $\sigma^{SD}(\chi n)$ vs. $m(\chi)$ plane for $m(\chi) \sim 0.5$ -10 GeV; quoted limit is for $m(\chi) = 5$ GeV.
- XIA 19A search for WIMP scatter on Xe in PandaX-II; limits placed in $\sigma^{SD}(\chi n)$ vs. $m(\chi)$ plane for $m(\chi) \sim 5$ -1 × 10⁵ GeV; quoted limit is for $m(\chi) = 5$ GeV.
- AGNESE 18 search for GeV scale WIMPs scatter at CDMsIIite; limits placed in $\sigma^{SD}(\chi n)$ vs. $m(\chi)$ plane for $m \sim 1.5$ -20 GeV; quoted limit is for $m(\chi) = 5$ GeV.
- JIANG 18 search for GeV scale WIMP scatter on Ge; limits placed in $\sigma^{SD}(\chi n)$ vs. $m(\chi)$ plane for $m(\chi) \sim 3$ -10 GeV; quoted limit is for $m(\chi) = 5$ GeV.
- YANG 18 search for WIMP scatter on Ge; limits placed in $\sigma^{SD}(\chi n)$ vs. $m(\chi)$ plane for $m(\chi) \sim 2$ -10 GeV; quoted limit is for $m(\chi) = 5$ GeV.
- AKERIB 17A search for SD WIMP scatter on Xe with 129.5 kg yr exposure; limits placed in $\sigma^{SD}(\chi n)$ vs. $m(\chi)$ plane for $m(\chi) \sim 5$ -1 × 10⁵ GeV; quoted limit is for $m(\chi) = 5$ GeV.
- FU 17 search for SD WIMP scatter on Xe; limits set in $\sigma^{SD}(\chi n)$ vs. $m(\chi)$ plane for $m(\chi) \sim 4$ -1 × 10³ GeV; quoted limit is for $m(\chi) = 5$ GeV.
- ZHAO 16 search for GeV-scale WIMP scatter on Ge; limits placed in $\sigma^{SD}(\chi n)$ vs. $m(\chi)$ plane for $m(\chi) \sim 4$ -30 GeV; quoted limit is for $m(\chi) = 5$ GeV.
- AHMED 11B search for GeV scale WIMP scatter on Ge in CDMs II; limits placed in $\sigma^{SD}(\chi n)$ vs. $m(\chi)$ plane for $m \sim 4$ -12 GeV. Limit given for $m(\chi) = 5$ GeV.

For $m_{\chi_0} = 20$ GeV

VALUE (pb)	CL %	DOCUMENT ID	TECN	COMMENT
< 8 × 10 ⁻⁶	90	1 APRILE 19A	XE1T	Xe, SD
< 3 × 10 ⁻⁵	90	2 XIA 19A	PNDX	SD WIMP on Xe
< 1.5	95	3 AGNESE 18	SCDM	Ge
< 2.5 × 10 ⁻⁵	90	4 AKERIB 17A	LUX	Xe
< 7 × 10 ⁻⁵	90	5 FU 17	PNDX	SD WIMP on Xe
< 2	90	6 ZHAO 16	CDEX	GeV-scale WIMPs on Ge
< 0.09	90	7 FELIZARDO 14	SMPL	C ₂ ClF ₅
< 8	90	8 UCHIDA 14	XMAS	¹²⁹ Xe, inelastic
< 1.13 × 10 ⁻³	90	9 APRILE 13	X100	Xe
< 0.02	90	10 AKIMOV 12	ZEP3	Xe
< 0.06	90	11 AHMED 09	CDM2	Ge
< 0.04	90	12 LEBEDENKO 09A	ZEP3	Xe
< 50	90	13 LIN 09	TEXO	Ge
< 6 × 10 ⁻³	90	14 ANGLE 08A	XE10	Xe
< 0.5	90	15 ALNER 07	ZEP2	Xe
< 25	90	16 LEE 07A	KIMS	Csl
< 0.3	90	17 AKERIB 06	CDMS	⁷³ Ge, ²⁹ Si
< 30	90	18 SHIMIZU 06A	CNTR	F (CaF ₂)
< 60	90	19 ALNER 05	NAIA	NaI
< 20	90	20 BARNABE-HE.05	PICA	F (C ₄ F ₁₀)
< 10	90	21 BENOIT 05	EDEL	⁷³ Ge
< 4	90	22 KLAPDOR-K...05	HDMS	⁷³ Ge (enriched)
< 600	90	23 TAKEDA 03	BOLO	NaF

- APRILE 19A search for SD WIMP scatter on 1 t yr Xe; no signal: limits placed in $\sigma^{SD}(\chi n)$ vs. $m(\chi)$ plane for $m \sim 6$ -1000 GeV.
- XIA 19A search for WIMP scatter on Xe in PandaX-II; limits placed in $\sigma^{SD}(\chi n)$ vs. $m(\chi)$ plane for $m(\chi) \sim 5$ -1 × 10⁵ GeV.
- AGNESE 18 give limits for $\sigma^{SD}(n\chi)$ for $m(\text{WIMP})$ between 1.5 and 20 GeV using CDMsIIite mode data.
- AKERIB 17A search for SD WIMP scatter on Xe with 129.5 kg yr exposure; limits placed in $\sigma^{SD}(\chi n)$ vs. $m(\chi)$ plane for $m(\chi) \sim 5$ -1 × 10⁵ GeV.
- FU 17 search for SD WIMP scatter on Xe; limits set in $\sigma^{SD}(\chi n)$ vs. $m(\chi)$ plane for $m(\chi) \sim 4$ -1 × 10³ GeV.
- ZHAO 16 search for GeV-scale WIMP scatter on Ge; limits placed in $\sigma^{SD}(\chi n)$ vs. $m(\chi)$ plane for $m(\chi) \sim 4$ -30 GeV.
- Derived limit from search for inelastic scattering $X^0 + ^{129}\text{Xe} \rightarrow X^0 + ^{129}\text{Xe}^*(39.58 \text{ keV})$.
- The value has been provided by the authors. See also APRILE 14A.
- See their Fig. 6(b) for cross section limits for m_{χ_0} extending down to 2 GeV.
- See also AKERIB 05.

See key on page 999

Searches Particle Listings

WIMP and Dark Matter Searches

For $m_{\chi^0} = 100$ GeV

VALUE (pb)	CL%	DOCUMENT ID	TECN	COMMENT
< 1.5 × 10 ⁻⁵	90	1 APRILE	19A	XE1T Xe, SD
< 4 × 10 ⁻³	90	2 SUZUKI	19	XMAS 129Xe, inelastic
< 2 × 10 ⁻⁵	90	3 XIA	19A	PNDX SD WIMP on Xe
< 2.5 × 10 ⁻⁵	90	4 AKERIB	17A	LUX Xe
< 7 × 10 ⁻⁵	90	5 FU	17	PNDX SD WIMP on Xe
< 0.1	90	FELIZARDO	14	SMPL C ₂ ClF ₅
< 0.05	90	6 UCHIDA	14	XMAS 129Xe, inelastic
< 4.68 × 10 ⁻⁴	90	7 APRILE	13	X100 Xe
< 0.01	90	AKIMOV	12	ZEP3 Xe
		8 FELIZARDO	10	SMPL C ₂ ClF ₃
< 0.02	90	AHMED	09	CDM2 Ge
< 0.01	90	LEBEDENKO	09A	ZEP3 Xe
<100	90	LIN	09	TEXO Ge
< 0.01	90	ANGLE	08A	XE10 Xe
< 0.05	90	9 BEDNYAKOV	08	RVUE Ge
< 0.08	90	ALNER	07	ZEP2 Xe
< 6	90	LEE	07A	KIMS Csl
< 0.07	90	10 AKERIB	06	CDMS ⁷³ Ge, ²⁹ Si
< 30	90	SHIMIZU	06A	CNTR F (CaF ₂)
< 10	90	ALNER	05	NAIA NaI
< 30	90	BARNABE-HE...	05	PICA F (C ₄ F ₁₀)
< 0.7	90	BENOIT	05	EDEL ⁷³ Ge
< 0.2		11 GIULIANI	05A	RVUE
< 1.5	90	KLAPDOR-K...	05	HDMS ⁷³ Ge (enriched)
		12 GIULIANI	04	RVUE
		13 GIULIANI	04A	RVUE
		14 MIUCHI	03	BOLO LIF
<800	90	TAKEDA	03	BOLO NaF

- 1 APRILE 19A search for SD WIMP scatter on 1 t yr Xe; no signal, limits placed in $\sigma^{SD}(\chi n)$ vs. $m(\chi)$ plane for $m \sim 6$ -1000 GeV.
- 2 SUZUKI 19 search in single phase liquid xenon detector for inelastic scattering $\chi^0 + ^{129}\text{Xe} \rightarrow \chi^0 + ^{129}\text{Xe}^*$ (39.58 keV); no signal: require $\sigma(\chi n)^{SD} < 4 \times 10^{-3}$ pb for $m(\chi) = 100$ GeV.
- 3 XIA 19A search for WIMP scatter on Xe in PandaX-II; limits placed in $\sigma^{SD}(\chi n)$ vs. $m(\chi)$ plane for $m(\chi) \sim 5$ -1 × 10⁵ GeV.
- 4 AKERIB 17A search for SD WIMP scatter on Xe with 129.5 kg yr exposure; limits placed in $\sigma^{SD}(\chi n)$ vs. $m(\chi)$ plane for $m(\chi) \sim 5$ -1 × 10⁵ GeV.
- 5 FU 17 search for SD WIMP scatter on Xe; limits set in $\sigma^{SD}(\chi n)$ vs. $m(\chi)$ plane for $m(\chi) \sim 4$ -1 × 10³ GeV.
- 6 UCHIDA 14 derived limit from search for inelastic scattering $\chi^0 + ^{129}\text{Xe} \rightarrow \chi^0 + ^{129}\text{Xe}^*$ (39.58 keV).
- 7 The value has been provided by the authors. See also APRILE 14A.
- 8 See their Fig. 3 for limits on spin-dependent neutron couplings for χ^0 mass of 50 GeV.
- 9 BEDNYAKOV 08 reanalyze KLAPDOR-KLEINGROTHAUS 05 and BAUDIS 01 data.
- 10 See also AKERIB 05.
- 11 GIULIANI 05A analyze available data and give combined limits.
- 12 GIULIANI 04 reanalyze COLLAR 00 data and give limits for spin-dependent χ^0 -neutron coupling.
- 13 GIULIANI 04A give limits for spin-dependent χ^0 -neutron couplings from existing data.
- 14 MIUCHI 03 give model-independent limit for spin-dependent χ^0 -proton and neutron cross sections. See their Fig. 5.

For $m_{\chi^0} = 1$ TeV

VALUE (pb)	CL%	DOCUMENT ID	TECN	COMMENT
< 1.2 × 10 ⁻⁴	90	1 APRILE	19A	XE1T Xe, SD
< 2 × 10 ⁻⁴	90	2 XIA	19A	PNDX Xe
< 2.5 × 10 ⁻⁴	90	3 AKERIB	17A	LUX Xe
< 4 × 10 ⁻⁴	90	4 FU	17	PNDX SD WIMP on Xe
< 0.07	90	FELIZARDO	14	SMPL C ₂ ClF ₅
< 0.2	90	5 UCHIDA	14	XMAS 129Xe, inelastic
< 3.64 × 10 ⁻³	90	6 APRILE	13	X100 Xe
< 0.08	90	AKIMOV	12	ZEP3 Xe
< 0.2	90	AHMED	09	CDM2 Ge
< 0.1	90	LEBEDENKO	09A	ZEP3 Xe
< 0.1	90	ANGLE	08A	XE10 Xe
< 0.25	90	7 BEDNYAKOV	08	RVUE Ge
< 0.6	90	ALNER	07	ZEP2 Xe
< 30	90	LEE	07A	KIMS Csl
< 0.5	90	8 AKERIB	06	CDMS ⁷³ Ge, ²⁹ Si
< 40	90	ALNER	05	NAIA NaI
<200	90	BARNABE-HE...	05	PICA F (C ₄ F ₁₀)
< 4	90	BENOIT	05	EDEL ⁷³ Ge
< 10	90	KLAPDOR-K...	05	HDMS ⁷³ Ge (enriched)
< 4 × 10 ³	90	TAKEDA	03	BOLO NaF

- 1 APRILE 19A search for SD WIMP scatter on 1 t yr Xe; no signal, limits placed in $\sigma^{SD}(\chi n)$ vs. $m(\chi)$ plane for $m \sim 6$ -1000 GeV.
- 2 XIA 19A search for WIMP scatter on Xe in PandaX-II; limits placed in $\sigma^{SD}(\chi n)$ vs. $m(\chi)$ plane for $m(\chi) \sim 5$ -1 × 10⁵ GeV.
- 3 AKERIB 17A search for SD WIMP scatter on Xe with 129.5 kg yr exposure; limits placed in $\sigma^{SD}(\chi n)$ vs. $m(\chi)$ plane for $m(\chi) \sim 5$ -1 × 10⁵ GeV.

- 4 FU 17 search for SD WIMP scatter on Xe; limits set in $\sigma^{SD}(\chi n)$ vs. $m(\chi)$ plane for $m(\chi) \sim 4$ -1 × 10³ GeV.
- 5 Derived limit from search for inelastic scattering $\chi^0 + ^{129}\text{Xe}^* \rightarrow \chi^0 + ^{129}\text{Xe}^*$ (39.58 keV).
- 6 The value has been provided by the authors. See also APRILE 14A.
- 7 BEDNYAKOV 08 reanalyze KLAPDOR-KLEINGROTHAUS 05 and BAUDIS 01 data.
- 8 See also AKERIB 05.

Cross-Section Limits for Dark Matter Particles (χ^0) on electron**For m_{χ^0} in GeV range**We provide here limits for $m_{\chi^0} < 5$ GeV

VALUE (pb)	CL%	DOCUMENT ID	TECN	COMMENT
<2 × 10 ⁶	90	1 AKERIB	20	LUX mirror DM with Xe
		2 ABRAMOFF	19	SENS WIMP-e scatter on Si
		3 AGUILAR-AR...	19A	DMIC MeV scale DM scatter on e in Si
<1 × 10 ⁻⁴	90	4 APRILE	19D	XE1T light DM on Xe via ionization
<9 × 10 ⁻³	90	5 AGNES	18B	DS50 Ar
<1 × 10 ⁴	90	6 AGNESE	18B	SCDM e χ scatter
<5 × 10 ³	90	7 CRISLER	18	SENS Si CCD
		8 APRILE	17	X100 Xe, annual modulation

- 1 AKERIB 20 search for mirror DM with LUX 95 d × 118 kg data for mirror e scatter from Xe; no signal, limits placed in kinetic mixing parameter vs. mirror e temperature $T \sim 0.1$ -0.9 keV plane.
- 2 ABRAMOFF 19 search for MeV-scale WIMP scatter from Si skipper-CCD; limits placed on $\sigma(\chi e)$ for $m(\chi) \sim 0.5$ -100 MeV depending on DM form factors. Limit given for $m(\text{DM}) = 1$ MeV.
- 3 AGUILAR-AREVALO 19A search for MeV scale DM scatter from e in Si CCDs at SNO-LAB; no signal, limits placed in $\sigma(e)$ vs. $m(\text{DM})$ plane for $m(\text{DM}) \sim 0.6$ -100 MeV.
- 4 APRILE 19D search for light DM scatter on Xe via ionization; no signal, limits placed in σ on nucleus vs. $m(\text{DM})$ plane for $m(\text{DM}) \sim 0.02$ -10 GeV; quoted limit is for $m(\text{DM}) = 0.2$ GeV.
- 5 AGNES 18B search for MeV scale WIMP scatter from e in Ar; no signal, limits set in σ_e vs. $m(\chi)$ plane for $m \sim 20$ -1000 MeV and two choices of form factor $F(\text{DM})$; quoted limit for $m(\chi) = 100$ MeV and $F = 1$.
- 6 AGNESE 18B search for e χ scatter in SuperCDMS; limits placed in $\sigma(e\chi)$ vs. $m(\chi)$ plane for $m \sim 0.3$ -1 × 10⁴ MeV for two assumed form factors and also in $m(\text{dark photon})$ vs. kinetic mixing plane. Limit given for $m(\chi) = 1$ GeV and $F = 1$.
- 7 CRISLER 18 search for $\chi e \rightarrow \chi e$ scatter in Si CCD; place limits on MeV DM in σ_e vs. $m(\chi)$ plane for $m \sim 0.5$ -1000 MeV for different form factors; quoted limit is for $F(\text{DM}) = 1$ and $m(\chi) = 10$ MeV.
- 8 APRILE 17 search for WIMP-e annual modulation signal for recoil energy in the 2.0-5.8 keV interval using 4 years data with Xe. No significant effect seen.

Cross-Section Limits for Dark Matter Particles (χ^0) on Nuclei**For m_{χ^0} in GeV range**We provide here limits for $m_{\chi^0} < 5$ GeV**For $m_{\chi^0} = 20$ GeV**

VALUE (nb)	CL%	DOCUMENT ID	TECN	COMMENT
< 0.03	90	1 UCHIDA	14	XMAS 129Xe, inelastic
< 0.08	90	2 ANGLOHER	02	CRES Al
		3 BENOIT	00	EDEL Ge
< 0.04	95	4 KLIMENKO	98	CNTR ⁷³ Ge, inel.
< 0.8		ALESSAND...	96	CNTR O
< 6		ALESSAND...	96	CNTR Te
< 0.02	90	5 BELL	96	CNTR 129Xe, inel.
		6 BELL	96c	CNTR 129Xe
< 4 × 10 ⁻³	90	7 BERNABE	96	CNTR Na
< 0.3	90	7 BERNABE	96	CNTR I
< 0.2	95	8 SARSA	96	CNTR Na
< 0.015	90	9 SMITH	96	CNTR Na
< 0.05	95	10 GARCIA	95	CNTR Natural Ge
< 0.1	95	QUENBY	95	CNTR Na
<90	90	11 SNOWDEN...	95	MICA ¹⁶ O
< 4 × 10 ³	90	11 SNOWDEN...	95	MICA ³⁹ K
< 0.7	90	BACCI	92	CNTR Na
< 0.12	90	12 REUSSER	91	CNTR Natural Ge
< 0.06	95	CALDWELL	88	CNTR Natural Ge

- 1 UCHIDA 14 limit is for inelastic scattering $\chi^0 + ^{129}\text{Xe}^* \rightarrow \chi^0 + ^{129}\text{Xe}^*$ (39.58 keV).
- 2 ANGLOHER 02 limit is for spin-dependent WIMP-Aluminum cross section.
- 3 BENOIT 00 find four event categories in Ge detectors and suggest that low-energy surface nuclear recoils can explain anomalous events reported by UKDMC and Saclay NaI experiments.
- 4 KLIMENKO 98 limit is for inelastic scattering $\chi^0 \text{ } ^{73}\text{Ge} \rightarrow \chi^0 \text{ } ^{73}\text{Ge}^*$ (13.26 keV).
- 5 BELL 96 limit for inelastic scattering $\chi^0 \text{ } ^{129}\text{Xe} \rightarrow \chi^0 \text{ } ^{129}\text{Xe}^*$ (39.58 keV).
- 6 BELL 96c use background subtraction and obtain $\sigma < 150$ pb (< 1.5 fb) (90% CL) for spin-dependent (independent) χ^0 -proton cross section. The confidence level is from R. Bernabei, private communication, May 20, 1999.
- 7 BERNABE 96 use pulse shape discrimination to enhance the possible signal. The limit here is from R. Bernabei, private communication, September 19, 1997.
- 8 SARSA 96 search for annual modulation of WIMP signal. See SARSA 97 for details of the analysis. The limit here is from M.L. Sarsa, private communication, May 26, 1997.

Searches Particle Listings

WIMP and Dark Matter Searches

⁹ SMITH 96 use pulse shape discrimination to enhance the possible signal. A dark matter density of 0.4 GeV cm^{-3} is assumed.

¹⁰ GARCIA 95 limit is from the event rate. A weaker limit is obtained from searches for diurnal and annual modulation.

¹¹ SNOWDEN-IFFT 95 look for recoil tracks in an ancient mica crystal. Similar limits are also given for ²⁷Al and ²⁸Si. See COLLAR 96 and SNOWDEN-IFFT 96 for discussion on potential backgrounds.

¹² REUSSER 91 limit here is changed from published (0.04) after reanalysis by authors. J.L. Vuilleumier, private communication, March 29, 1996.

For $m_{\chi^0} = 100 \text{ GeV}$

VALUE (nb)	CL%	DOCUMENT ID	TECN	COMMENT
• • • We do not use the following data for averages, fits, limits, etc. • • •				
< 3 × 10 ⁻³	90	1 UCHIDA	14 XMAS	¹²⁹ Xe, inelastic
< 0.3	90	2 ANGLÖHER	02 CRES	Al
		3 BELLI	02 RVUE	
		4 BERNABEI	02c DAMA	
		5 GREEN	02 RVUE	
		6 ULLIO	01 RVUE	
		7 BENOIT	00 EDEL	Ge
< 4 × 10 ⁻³	90	8 BERNABEI	00d	¹²⁹ Xe, inel.
		9 AMBROSIO	99 MCRO	
		10 BRHLIK	99 RVUE	
< 8 × 10 ⁻³	95	11 KLIMENKO	98 CNTR	⁷³ Ge, inel.
< 0.08	95	12 KLIMENKO	98 CNTR	⁷³ Ge, inel.
< 4		ALESSAND...	96 CNTR	O
< 25		ALESSAND...	96 CNTR	Te
< 6 × 10 ⁻³	90	13 BELLI	96 CNTR	¹²⁹ Xe, inel.
		14 BELLI	96c	¹²⁹ Xe
< 1 × 10 ⁻³	90	15 BERNABEI	96 CNTR	Na
< 0.3	90	15 BERNABEI	96 CNTR	I
< 0.7	95	16 SARSA	96 CNTR	Na
< 0.03	90	17 SMITH	96 CNTR	Na
< 0.8	90	17 SMITH	96 CNTR	I
< 0.35	95	18 GARCIA	95 CNTR	Natural Ge
< 0.6	95	QUENBY	95 CNTR	Na
< 3	95	QUENBY	95 CNTR	I
< 1.5 × 10 ²	90	19 SNOWDEN...	95 MICA	¹⁶ O
< 4 × 10 ²	90	19 SNOWDEN...	95 MICA	³⁹ K
< 0.08	90	20 BECK	94 CNTR	⁷⁶ Ge
< 2.5	90	BACCI	92 CNTR	Na
< 3	90	BACCI	92 CNTR	I
< 0.9	90	21 REUSSER	91 CNTR	Natural Ge
< 0.7	95	CALDWELL	88 CNTR	Natural Ge

¹ UCHIDA 14 limit is for inelastic scattering $\chi^0 + ^{129}\text{Xe}^* \rightarrow \chi^0 + ^{129}\text{Xe}^*$ (39.58 keV).

² ANGLÖHER 02 limit is for spin-dependent WIMP-Aluminum cross section.

³ BELLI 02 discuss dependence of the extracted WIMP cross section on the assumptions of the galactic halo structure.

⁴ BERNABEI 02c analyze the DAMA data in the scenario in which χ^0 scatters into a slightly heavier state as discussed by SMITH 01.

⁵ GREEN 02 discusses dependence of extracted WIMP cross section limits on the assumptions of the galactic halo structure.

⁶ ULLIO 01 disfavor the possibility that the BERNABEI 99 signal is due to spin-dependent WIMP coupling.

⁷ BENOIT 00 find four event categories in Ge detectors and suggest that low-energy surface nuclear recoils can explain anomalous events reported by UKDMC and Saclay Nal experiments.

⁸ BERNABEI 00d limit is for inelastic scattering $\chi^0 ^{129}\text{Xe} \rightarrow \chi^0 ^{129}\text{Xe}$ (39.58 keV).

⁹ AMBROSIO 99 search for upgoing muon events induced by neutrinos originating from WIMP annihilations in the Sun and Earth.

¹⁰ BRHLIK 99 discuss the effect of astrophysical uncertainties on the WIMP interpretation of the BERNABEI 99 signal.

¹¹ KLIMENKO 98 limit is for inelastic scattering $\chi^0 ^{73}\text{Ge} \rightarrow \chi^0 ^{73}\text{Ge}^*$ (13.26 keV).

¹² KLIMENKO 98 limit is for inelastic scattering $\chi^0 ^{73}\text{Ge} \rightarrow \chi^0 ^{73}\text{Ge}^*$ (66.73 keV).

¹³ BELLI 96 limit for inelastic scattering $\chi^0 ^{129}\text{Xe} \rightarrow \chi^0 ^{129}\text{Xe}^*$ (39.58 keV).

¹⁴ BELLI 96c use background subtraction and obtain $\sigma < 0.35 \text{ pb}$ ($< 0.15 \text{ fb}$) (90% CL) for spin-dependent (independent) χ^0 -proton cross section. The confidence level is from R. Bernabei, private communication, May 20, 1999.

¹⁵ BERNABEI 96 use pulse shape discrimination to enhance the possible signal. The limit here is from R. Bernabei, private communication, September 19, 1997.

¹⁶ SARSA 96 search for annual modulation of WIMP signal. See SARSA 97 for details of the analysis. The limit here is from M.L. Sarsa, private communication, May 26, 1997.

¹⁷ SMITH 96 use pulse shape discrimination to enhance the possible signal. A dark matter density of 0.4 GeV cm^{-3} is assumed.

¹⁸ GARCIA 95 limit is from the event rate. A weaker limit is obtained from searches for diurnal and annual modulation.

¹⁹ SNOWDEN-IFFT 95 look for recoil tracks in an ancient mica crystal. Similar limits are also given for ²⁷Al and ²⁸Si. See COLLAR 96 and SNOWDEN-IFFT 96 for discussion on potential backgrounds.

²⁰ BECK 94 uses enriched ⁷⁶Ge (86% purity).

²¹ REUSSER 91 limit here is changed from published (0.3) after reanalysis by authors. J.L. Vuilleumier, private communication, March 29, 1996.

For $m_{\chi^0} = 1 \text{ TeV}$

VALUE (nb)	CL%	DOCUMENT ID	TECN	COMMENT
• • • We do not use the following data for averages, fits, limits, etc. • • •				
< 0.03	90	1 UCHIDA	14 XMAS	¹²⁹ Xe, inelastic
< 3	90	2 ANGLÖHER	02 CRES	Al
		3 BENOIT	00 EDEL	Ge
		4 BERNABEI	99d CNTR	SIMP
		5 DERBIN	99 CNTR	SIMP
< 0.06	95	6 KLIMENKO	98 CNTR	⁷³ Ge, inel.
< 0.4	95	7 KLIMENKO	98 CNTR	⁷³ Ge, inel.
< 40		ALESSAND...	96 CNTR	O
< 700		ALESSAND...	96 CNTR	Te
< 0.05	90	8 BELLI	96 CNTR	¹²⁹ Xe, inel.
< 1.5	90	9 BELLI	96 CNTR	¹²⁹ Xe, inel.
		10 BELLI	96c	¹²⁹ Xe
< 0.01	90	11 BERNABEI	96 CNTR	Na
< 9	90	11 BERNABEI	96 CNTR	I
< 7	95	12 SARSA	96 CNTR	Na
< 0.3	90	13 SMITH	96 CNTR	Na
< 6	90	13 SMITH	96 CNTR	I
< 6	95	14 GARCIA	95 CNTR	Natural Ge
< 8	95	QUENBY	95 CNTR	Na
< 50	95	QUENBY	95 CNTR	I
< 700	90	15 SNOWDEN...	95 MICA	¹⁶ O
< 1 × 10 ³	90	15 SNOWDEN...	95 MICA	³⁹ K
< 0.8	90	16 BECK	94 CNTR	⁷⁶ Ge
< 30	90	BACCI	92 CNTR	Na
< 30	90	BACCI	92 CNTR	I
< 15	90	17 REUSSER	91 CNTR	Natural Ge
< 6	95	CALDWELL	88 CNTR	Natural Ge

¹ UCHIDA 14 limit is for inelastic scattering $\chi^0 + ^{129}\text{Xe}^* \rightarrow \chi^0 + ^{129}\text{Xe}^*$ (39.58 keV).

² ANGLÖHER 02 limit is for spin-dependent WIMP-Aluminum cross section.

³ BENOIT 00 find four event categories in Ge detectors and suggest that low-energy surface nuclear recoils can explain anomalous events reported by UKDMC and Saclay Nal experiments.

⁴ BERNABEI 99d search for SIMPs (Strongly Interacting Massive Particles) in the mass range 10^3 - 10^{16} GeV. See their Fig. 3 for cross-section limits.

⁵ DERBIN 99 search for SIMPs (Strongly Interacting Massive Particles) in the mass range 10^2 - 10^{14} GeV. See their Fig. 3 for cross-section limits.

⁶ KLIMENKO 98 limit is for inelastic scattering $\chi^0 ^{73}\text{Ge} \rightarrow \chi^0 ^{73}\text{Ge}^*$ (13.26 keV).

⁷ KLIMENKO 98 limit is for inelastic scattering $\chi^0 ^{73}\text{Ge} \rightarrow \chi^0 ^{73}\text{Ge}^*$ (66.73 keV).

⁸ BELLI 96 limit for inelastic scattering $\chi^0 ^{129}\text{Xe} \rightarrow \chi^0 ^{129}\text{Xe}^*$ (39.58 keV).

⁹ BELLI 96 limit for inelastic scattering $\chi^0 ^{129}\text{Xe} \rightarrow \chi^0 ^{129}\text{Xe}^*$ (236.14 keV).

¹⁰ BELLI 96c use background subtraction and obtain $\sigma < 0.7 \text{ pb}$ ($< 0.7 \text{ fb}$) (90% CL) for spin-dependent (independent) χ^0 -proton cross section. The confidence level is from R. Bernabei, private communication, May 20, 1999.

¹¹ BERNABEI 96 use pulse shape discrimination to enhance the possible signal. The limit here is from R. Bernabei, private communication, September 19, 1997.

¹² SARSA 96 search for annual modulation of WIMP signal. See SARSA 97 for details of the analysis. The limit here is from M.L. Sarsa, private communication, May 26, 1997.

¹³ SMITH 96 use pulse shape discrimination to enhance the possible signal. A dark matter density of 0.4 GeV cm^{-3} is assumed.

¹⁴ GARCIA 95 limit is from the event rate. A weaker limit is obtained from searches for diurnal and annual modulation.

¹⁵ SNOWDEN-IFFT 95 look for recoil tracks in an ancient mica crystal. Similar limits are also given for ²⁷Al and ²⁸Si. See COLLAR 96 and SNOWDEN-IFFT 96 for discussion on potential backgrounds.

¹⁶ BECK 94 uses enriched ⁷⁶Ge (86% purity).

¹⁷ REUSSER 91 limit here is changed from published (5) after reanalysis by authors. J.L. Vuilleumier, private communication, March 29, 1996.

Miscellaneous Results from Underground Dark Matter Searches

VALUE	CL%	DOCUMENT ID	TECN	COMMENT
• • • We do not use the following data for averages, fits, limits, etc. • • •				
		1 ABRAMOFF	19 SENS	MeV DM e-Si; dark photon Si absorption
		2 ADHIKARI	19 C100	annual modulation Nal
		3 AMARE	19 ANAI	annual modulation Nal
		4 APRILE	19 XE1T	π (Xe)
		5 BRINGMANN	19	cosmic ray DM
		6 BRUNE	19	Majoran DM
		7 CHOI	19 THEO	290 TeV IceCube ν
		8 HA	19 C100	inelastic boosted dark γ
		9 KLOPF	19	$n \rightarrow \chi e^+ e^-$
		10 AARTSEN	18d ICCB	relic WIMP $\chi \rightarrow \nu X$
		11 ABE	18f XMAS	$A'e \rightarrow A'e$
		12 AGNES	18b DS50	Ar
		13 AGNESE	18b SCDM	MeV DM e-Si; dark photon Si absorption
		14 AKERIB	18a LUX	Xe
		15 ARMENGAUD	18 EDE3	Ge

Searches Particle Listings

WIMP and Dark Matter Searches

$<1 \times 10^{-12}$	90	16 KACHULIS 18 SKAM boosted DM on e
		17 AGUILAR-AR...17 DMIC γ' on Si
		18 APRILE 17 X100 Xe
		19 APRILE 17D X100 Xe
		20 APRILE 17H X100 keV bosonic DM search
$<4 \times 10^{-3}$	90	21 APRILE 17K X100 $\chi N \rightarrow \chi^* \rightarrow \chi\gamma$
		22 ANGLOHER 16A CRES CaWO ₄
		23 APRILE 15 X100 Event rate modulation
		24 APRILE 15A X100 Electron scattering

- 1 ABRAMOFF 19 search for MeV scale DM via DM-e scattering and dark photon DM via absorption in Si; limits set in coupling vs. $m(\chi)$ plane and on dark photon in $m(A)$ vs. kinetic mixing parameter plane.
- 2 ADHIKARI 19 search for annual modulation signal from WIMP scatter on NaI with 1.7 yr exposure; result consistent with both DAMA/LIBRA and null hypothesis.
- 3 AMARE 19 is ANAIS-112 search for WIMP scatter annual modulation on NaI; 157.55 kg yr exposure; result compatible with null hypothesis; confirm goal of reaching sensitivity at 3σ to DAMA/LIBRA result in 5 years.
- 4 APRILE 19 search for WIMP-pion scattering in Xe; no signal: require $\sigma(\chi\pi) < 6.4 \times 10^{-10}$ pb for $m(\chi) = 30$ GeV.
- 5 BRINGMANN 19 derive theoretically limits on GeV and sub-GeV mass dark matter, in its high energy component generated by interaction with cosmic rays; place limits on σ^{SI} and $\sigma^{SD} < 10^5$ pb.
- 6 BRUNE 19 examine possibility of Majoron dark matter; limits placed on Majoron mass vs. coupling from SN1987a and ν -less double beta decay.
- 7 CHOI 19 from multimessenger observation finds limit on $\sigma(\nu\chi)/m(\text{DM}) < 5.1 \times 10^{-23}$ cm²/GeV based on 290 TeV IceCube neutrino event.
- 8 HA 19 search for inelastic boosted MeV scale dark photon using COSINE-100 data; limits placed in m vs. epsilon plane for various mediators.
- 9 KLOPF 19 search for DM via $n \rightarrow \chi e^+ e^-$; no signal: limits placed in branching fraction vs. $m(e^+ e^-)$ plane.
- 10 AARTSEN 18D search for long-lived DM particles decaying $\chi \rightarrow \nu\chi$; no excess seen; for DM masses above 10 TeV, excluding lifetimes shorter than 10^{28} s.
- 11 ABE 18r search for keV mass ALPs and hidden photons (HP) scatter on electrons; limits set on mass vs. coupling.
- 12 AGNES 18b search for MeV-scale DM scatter on electrons in Ar; no signal; require $\sigma(\chi e) < 9 \times 10^{-3}$ pb for DM form factor $F(\text{DM}) = 1$ and < 300 pb for $F(\text{DM})$ proportional to $1/q^2$ for $m(\chi) = 100$ MeV.
- 13 AGNESE 18a search for MeV scale DM via DM-e scattering and dark photon DM via absorption in Si; limits set on MeV DM in coupling vs. $m(\chi)$ plane and on dark photon in $m(A')$ vs. kinetic mixing plane.
- 14 AKERIB 18A search for annual and diurnal modulation of DM scattering rate on electrons for recoil energy between 2 and 6 keVee; no signal found.
- 15 ARMENGAUD 18 search for ALP from the Sun and galactic bosonic DM, interacting in Ge; no signal; limits set for 0.8–500 keV DM particles.
- 16 KACHULIS 18 search for an excess of elastically scattered electrons above the atmospheric neutrino background in Super-K; limits placed for simple annihilation or decay in the Sun or galactic center producing "boosted" dark matter.
- 17 AGUILAR-AREVALO 17 search for hidden photon DM scatter on Si target CCD; limit kinetic mixing $\kappa < 1 \times 10^{-12}$ for $m = 10$ eV.
- 18 APRILE 17 search for WIMP-e annual modulation signal for recoil energy in the 2.0–5.8 keV interval using 4 years data with Xe. No significant effect seen.
- 19 APRILE 17D set limits on 14 WIMP-nucleon different interaction operators. No deviations found using 225 live days in the 6.6–240 keV recoil energy range.
- 20 APRILE 17H search for keV bosonic DM via $e\chi \rightarrow e$, looking for electronic recoils with 224.6 live days of data and 34 kg of LXe. Limits set on $\chi e e$ coupling for $m(\chi) = 8$ –125 keV.
- 21 APRILE 17K search for magnetic inelastic DM via $\chi N \rightarrow \chi^* \rightarrow \chi\gamma$. Limits set in DM magnetic moment vs. mass splitting plane for two DM masses corresponding to the DAMA/LIBRA best fit values.
- 22 ANGLOHER 16A require q^2 dependent scattering $< 8 \times 10^{-3}$ pb for asymmetric DM $m(\text{WIMP}) = 3$ GeV on CaWO₄ target. It uses a local dark matter density of 0.38 GeV/cm³.
- 23 APRILE 15 search for periodic variation of electronic recoil event rate in the data between Feb. 2011 and Mar. 2012. No significant modulation is found for periods up to 500 days.
- 24 APRILE 15A search for X^0 scattering off electrons. See their Fig. 4 for limits on cross section through axial-vector coupling for m_{X^0} between 0.6 GeV and 1 TeV. For $m_{X^0} = 2$ GeV, $\sigma < 60$ pb (90%CL) is obtained.

X⁰ Annihilation Cross Section

Limits are on σv for X^0 pair annihilation at threshold.

VALUE (cm ³ s ⁻¹)	CL%	DOCUMENT ID	TECN	COMMENT
$<0.8 \times 10^{-22}$	95	1 ABEYSEKARA 19	HAWC	DM annihilation to γ s within galactic substructure
$<4 \times 10^{-26}$	95	2 ALBERT 19b	HAWC	annihilation/decay to γ in M31
$<7 \times 10^{-27}$	95	3 CHEUNG 19		$\chi\chi \rightarrow e^+e^-$ and $b\bar{b}$
		4 DI-MAURO 19	FLAT	Fermi-LAT M31 and M33
		5 JOHNSON 19	FLAT	P-wave DM; Fermi-LAT
$<2 \times 10^{-26}$	95	6 LI 19d	FLAT	$\chi\chi \rightarrow \gamma$
$<1 \times 10^{-32}$		7 NG 19		sterile ν decay/annihilation
		8 QUEIROZ 19		semi-annihilating DM
$<4 \times 10^{-28}$	95	9 ABDALLAH 18	HESS	$X^0 X^0 \rightarrow \gamma\chi$; galactic halo
$<1 \times 10^{-23}$	95	10 AHNEN 18	MGIC	$X^0 X^0 \rightarrow \gamma\chi$; Ursa Major II
$<1 \times 10^{-22}$	95	11 ALBERT 18b	HAWC	$X^0 X^0 \rightarrow \gamma\chi$; Andromeda
$<1 \times 10^{-26}$	95	12 CHANG 18A		$\chi\chi \rightarrow b\bar{b} \rightarrow \gamma$
		13 LISANTI 18	THEO	Fermi, γ ; galaxy groups

• • • We do not use the following data for averages, fits, limits, etc. • • •

$<1.2 \times 10^{-23}$	95	14 MAZZIOTTA 18	FLAT	Fermi-LAT CRE data
$<1 \times 10^{-23}$	90	15 AARTSEN 17c	ICCB	$\chi\chi \rightarrow$ neutrinos
$<1.32 \times 10^{-25}$	95	16 ALBERT 17A	ANTR	ν , DM annihilation
$<7 \times 10^{-21}$	90	17 ARCHAMBAU...17	VRTS	γ dwarf galaxies
$<1 \times 10^{-28}$		18 AVRORIN 17	BAIK	cosmic ν
		19 BOUDAUD 17		MeV DM to e^+e^-
$<6 \times 10^{-26}$	95	20 AARTSEN 16d	ICCB	ν , galactic center
$<1 \times 10^{-27}$	95	21 ABDALLAH 16	HESS	Central Galactic Halo
		22 ABDALLAH 16A	HESS	WIMP+WIMP $\rightarrow \gamma\gamma$; galactic center
$<3 \times 10^{-26}$	95	23 AHNEN 16	MGFL	Satellite galaxy, $m(\text{WIMP})=100$ GeV
$<1.9 \times 10^{-21}$	90	24 AVRORIN 16	BAIK	ν s from galactic center
$<3 \times 10^{-26}$	95	25 CAPUTO 16	FLAT	small Magellanic cloud
$<1 \times 10^{-25}$	95	26 FORNATA 16	FLAT	Fermi-LAT γ -ray anisotropy
$<5 \times 10^{-27}$		27 LEITE 16		WIMP, radio
$<2 \times 10^{-26}$	95	28 LI 16	FLAT	dwarf galaxies
$<1 \times 10^{-25}$	95	29 LI 16A	FLAT	Fermi-LAT; M31
$<1 \times 10^{-26}$		30 LIANG 16	FLAT	Fermi-LAT, gamma line
$<1 \times 10^{-25}$	95	31 LU 16	FLAT	Fermi-LAT and AMS-02
$<1 \times 10^{-23}$	95	32 SHIRASAKI 16	FLAT	extra galactic
		33 AARTSEN 15c	ICCB	ν , Galactic halo
		34 AARTSEN 15E	ICCB	ν , Galactic center
		35 ABRAMOWSKI15	HESS	Galactic center
		36 ACKERMANN 15	FLAT	monochromatic γ
		37 ACKERMANN 15A	FLAT	isotropic γ background
		38 ACKERMANN 15B	FLAT	Satellite galaxy
		39 ADRIAN-MAR...15	ANTR	ν , Galactic center
$<2.90 \times 10^{-26}$	95	40.41 ACKERMANN 14	FLAT	Satellite galaxy, $m = 10$ GeV
$<1.84 \times 10^{-25}$	95	40.42 ACKERMANN 14	FLAT	Satellite galaxy, $m = 100$ GeV
$<1.75 \times 10^{-24}$	95	40.42 ACKERMANN 14	FLAT	Satellite galaxy, $m = 1$ TeV
$<4.52 \times 10^{-24}$	95	43 ALEKSIC 14	MGIC	Segue 1, $m = 1.35$ TeV
		44 AARTSEN 13c	ICCB	Galaxies
		45 ABRAMOWSKI13	HESS	Central Galactic Halo
		46 ACKERMANN 13A	FLAT	Galaxy
		47 ABRAMOWSKI12	HESS	Fornax Cluster
		48 ACKERMANN 12	FLAT	Galaxy
		49 ACKERMANN 12	FLAT	Galaxy
		50 ALIU 12	VRTS	Segue 1
$<1 \times 10^{-22}$	90	51 ABBASI 11c	ICCB	Galactic halo, $m=1$ TeV
$<3 \times 10^{-25}$	95	52 ABRAMOWSKI11	HESS	Near Galactic center, $m=1$ TeV
$<1 \times 10^{-26}$	95	53 ACKERMANN 11	FLAT	Satellite galaxy, $m=10$ GeV
$<1 \times 10^{-25}$	95	53 ACKERMANN 11	FLAT	Satellite galaxy, $m=100$ GeV
$<1 \times 10^{-24}$	95	53 ACKERMANN 11	FLAT	Satellite galaxy, $m=1$ TeV

- 1 ABEYSEKARA 19 search for γ s from DM annihilation in galactic substructures with HAWC; no signal, limits placed in $J(\sigma v)$ vs. declination plane for $m(\text{DM}) \sim 1$ –108 TeV.
- 2 ALBERT 19b search for DM signal from M31 galaxy in μ, τ, t, b, W channels using HAWC for $m(\text{DM}) \sim 1$ –100 TeV; no signal, limits placed in $\langle\sigma v\rangle$ vs. $m(\text{DM})$ plane.
- 3 CHEUNG 19 derive model-dependent bounds on $\langle\sigma v\rangle$ from EDGES data: $< 4 \times 10^{-26}$ cm³/s for e^+e^- and $b\bar{b}$ for $m(\chi) = 100$ GeV (including boost factor).
- 4 DI-MAURO 19 place limits on WIMP annihilation via Fermi-LAT observation of M31 and M33 galaxies: $\langle\sigma v\rangle < 7 \times 10^{-27}$ cm³/s for $m(\chi) = 20$ GeV from M31.
- 5 JOHNSON 19 search for γ -rays, 10–600 GeV energy, from P-wave annihilating DM around SgrA* BH using Fermi-LAT; limits set for various models.
- 6 LI 19d search for $\chi\chi \rightarrow \gamma$ in Fermi-LAT data; no signal, require $\langle\sigma v\rangle < 2 \times 10^{-26}$ cm³/s for $m(\chi) = 100$ GeV.
- 7 NG 19 search for X-ray line from sterile ν decay/annihilation using NuStar M-31; no signal: limits placed in $m(\nu)$ vs mixing angle and $\langle\sigma v\rangle$ vs $m(\nu)$.
- 8 QUEIROZ 19 examine $\chi\chi \rightarrow \chi SM$ semi-annihilation of DM reaction; limits placed for various assumed SM particles in $\langle\sigma v\rangle$ vs. $m(\chi)$ plane.
- 9 ABDALLAH 18 search for WIMP WIMP $\rightarrow \gamma\chi$ in central galactic halo, 10 years of data; limits placed in $\langle\sigma v\rangle$ vs. $m(\text{WIMP})$ plane for $m(\text{WIMP})$: 0.3–70 TeV.
- 10 AHNEN 18 search for WIMP WIMP $\rightarrow \gamma\chi$ from Ursa Major II; limits set in $\langle\sigma v\rangle$ vs. $m(\text{WIMP})$ plane for $b\bar{b}, W^+W^-, \tau^+\tau^-,$ and $\mu^+\mu^-$ annihilation modes.
- 11 ALBERT 18b search for TeV-scale WIMPs with WIMP WIMP $\rightarrow \gamma\chi$ in Andromeda galaxy using HAWC Observatory; limits set in $\langle\sigma v\rangle$ vs $m(\text{WIMP})$ plane.
- 12 CHANG 18A examine $\chi\chi \rightarrow b\bar{b} \rightarrow \gamma$ using Fermi Pass 8 data; no signal; require $\langle\sigma v\rangle < 10^{-26}$ cm³/s for $m(\chi) = 50$ GeV.
- 13 LISANTI 18 examine Fermi Pass 8 γ -ray data from galaxy groups; report $m(\text{WIMP}) > 30$ GeV for annihilation in $b\bar{b}$ channel.
- 14 MAZZIOTTA 18 examine Fermi-LAT electron and positron spectra searching for features originating from DM particles annihilation into e^+e^- pairs, from 45 GeV to 2 TeV; no signal found, limits are obtained.
- 15 AARTSEN 17c use 1005 days of IceCube data to search for $\chi\chi \rightarrow$ neutrinos via various annihilation channels. Limits set.
- 16 ALBERT 17A search for DM annihilation to ν s using ANTARES data from 2007–2015. No signal. Limits set in $\langle\sigma v\rangle$ vs. $m(\text{DM})$ plane for $m(\text{DM}) \sim 10$ – 10×10^5 GeV. The listed limit is for $m(\text{DM}) = 100$ TeV.
- 17 ARCHAMBAULT 17 set limits for WIMP mass between 100 GeV and 1 TeV on $\langle\sigma v\rangle$ for $W^+W^-, ZZ, b\bar{b}, s\bar{s}, u\bar{u}, d\bar{d}, t\bar{t}, e^+e^-, gg, c\bar{c}, hh, \gamma\gamma, \mu^+\mu^-, \tau^+\tau^-$ annihilation channels.
- 18 AVRORIN 17 find upper limits for the annihilation cross section in various channels for DM particle mass between 30 GeV and 10 TeV. Strongest upper limits coming from the two neutrino channel require $\langle\sigma v\rangle < 6 \times 10^{-20}$ cm³/s in dwarf galaxies and $\langle\sigma v\rangle < 7 \times 10^{-21}$ cm³/s in LMC for 5 TeV WIMP mass.

Searches Particle Listings

WIMP and Dark Matter Searches

- 19 BOUDAUD 17 use data from the spacecraft Voyager 1, beyond the heliopause, and from AMS02 on $\chi\chi \rightarrow e^+e^-$ to require $\langle\sigma v\rangle < 1. \times 10^{-28} \text{ cm}^3/\text{s}$ for $m(\chi) = 10 \text{ MeV}$.
- 20 AARTSEN 16d search for GeV ν s from WIMP annihilation in galaxy; limits set on $\langle\sigma v\rangle$ in Fig. 6, 7.
- 21 ABDALLAH 16 require $\langle\sigma v\rangle < 6 \times 10^{-26} \text{ cm}^3/\text{s}$ for $m(\text{WIMP}) = 1.5 \text{ TeV}$ from 254 hours observation (WW channel) and $< 2 \times 10^{-26} \text{ cm}^3/\text{s}$ for $m(\text{WIMP}) = 1.0 \text{ TeV}$ in $\tau^+\tau^-$ channel.
- 22 ABDALLAH 16A search for line spectra from WIMP + WIMP $\rightarrow \gamma\gamma$ in 18 hr HESS data; rule out previous 130 GeV WIMP hint from Fermi-LAT data.
- 23 AHNEN 16 require $\langle\sigma v\rangle < 3 \times 10^{-26} \text{ cm}^3/\text{s}$ for $m(\text{WIMP}) = 100 \text{ GeV}$ (WW channel).
- 24 AVRORIN 16 require $\langle\sigma v\rangle < 1.91 \times 10^{-21} \text{ cm}^3/\text{s}$ from WIMP annihilation to ν s via W channel for $m(\text{WIMP}) = 1 \text{ TeV}$.
- 25 CAPUTO 16 place limits on WIMPs from annihilation to gamma rays in Small Magellanic Cloud using Fermi-LAT data: $\langle\sigma v\rangle < 3 \times 10^{-26} \text{ cm}^3/\text{s}$ for $m(\text{WIMP}) = 10 \text{ GeV}$.
- 26 FORNASA 16 use anisotropies in the γ -ray diffuse emission detected by Fermi-LAT to bound $\langle\sigma v\rangle < 10^{-25} \text{ cm}^3/\text{s}$ for $m(\text{WIMP}) = 100 \text{ GeV}$ in $b\bar{b}$ channel: see Fig. 28. The limit is driven by dark-matter subhalos in the Milky Way and it refers to their Most Constraining Scenario.
- 27 LEITE 16 constrain WIMP annihilation via search for radio emissions from Smith cloud; $\langle\sigma v\rangle < 5 \times 10^{-27} \text{ cm}^3/\text{s}$ in ee channel for $m(\text{WIMP}) = 5 \text{ GeV}$.
- 28 LI 16 re-analyze Fermi-LAT data on 8 dwarf spheroidal; set limit $\langle\sigma v\rangle < 2 \times 10^{-26} \text{ cm}^3/\text{s}$ for $m(\text{WIMP}) = 100 \text{ GeV}$ in $b\bar{b}$ mode with substructures included.
- 29 LI 16A constrain $\langle\sigma v\rangle < 10^{-25} \text{ cm}^3/\text{s}$ in $b\bar{b}$ channel for $m(\text{WIMP}) = 100 \text{ GeV}$ using Fermi-LAT data from M31; see Fig. 6.
- 30 LIANG 16 search dwarf spheroidal galaxies, Large Magellanic Cloud, and Small Magellanic Cloud for γ -line in Fermi-LAT data.
- 31 LU 16 re-analyze Fermi-LAT and AMS-02 data; require $\langle\sigma v\rangle < 10^{-25} \text{ cm}^3/\text{s}$ for $m(\text{WIMP}) = 1 \text{ TeV}$ in $b\bar{b}$ channel.
- 32 SHIRASAKI 16 re-analyze Fermi-LAT extra-galactic data; require $\langle\sigma v\rangle < 10^{-23} \text{ cm}^3/\text{s}$ for $m(\text{WIMP}) = 1 \text{ TeV}$ in $b\bar{b}$ channel; see Fig. 8.
- 33 AARTSEN 15c search for neutrinos from X^0 annihilation in the Galactic halo. See their Figs. 16 and 17, and Table 5 for limits on $\sigma \cdot v$ for X^0 mass between 100 GeV and 100 TeV.
- 34 AARTSEN 15E search for neutrinos from X^0 annihilation in the Galactic center. See their Figs. 7 and 9, and Table 3 for limits on $\sigma \cdot v$ for X^0 mass between 30 GeV and 10 TeV.
- 35 ABRAMOWSKI 15 search for γ from X^0 annihilation in the Galactic center. See their Fig. 4 for limits on $\sigma \cdot v$ for X^0 mass between 250 GeV and 10 TeV.
- 36 ACKERMANN 15 search for monochromatic γ from X^0 annihilation in the Galactic halo. See their Fig. 8 and Tables 2-4 for limits on $\sigma \cdot v$ for X^0 mass between 0.2 GeV and 500 GeV.
- 37 ACKERMANN 15A search for γ from X^0 annihilation (both Galactic and extragalactic) in the isotropic γ background. See their Fig. 7 for limits on $\sigma \cdot v$ for X^0 mass between 10 GeV and 30 TeV.
- 38 ACKERMANN 15B search for γ from X^0 annihilation in 15 dwarf spheroidal satellite galaxies of the Milky Way. See their Figs. 1 and 2 for limits on $\sigma \cdot v$ for X^0 mass between 2 GeV and 10 TeV.
- 39 ADRIAN-MARTINEZ 15 search for neutrinos from X^0 annihilation in the Galactic center. See their Figs. 10 and 11 and Tables 1 and 2 for limits on $\sigma \cdot v$ for X^0 mass between 25 GeV and 10 TeV.
- 40 ACKERMANN 14 search for γ from X^0 annihilation in 25 dwarf spheroidal satellite galaxies of the Milky Way. See their Tables II-VII for limits assuming annihilation into e^+e^- , $\mu^+\mu^-$, $\tau^+\tau^-$, $u\bar{u}$, $b\bar{b}$, and W^+W^- , for X^0 mass ranging from 2 GeV to 10 TeV.
- 41 Limit assuming X^0 pair annihilation into $b\bar{b}$.
- 42 Limit assuming X^0 pair annihilation into W^+W^- .
- 43 ALEKSIC 14 search for γ from X^0 annihilation in the dwarf spheroidal galaxy Segue 1. The listed limit assumes annihilation into W^+W^- . See their Figs. 6, 7, and 16 for limits on $\sigma \cdot v$ for annihilation channels $\mu^+\mu^-$, $\tau^+\tau^-$, $b\bar{b}$, $t\bar{t}$, $\gamma\gamma$, γZ , W^+W^- , ZZ for X^0 mass between 10^2 and 10^4 GeV .
- 44 AARTSEN 13c search for neutrinos from X^0 annihilation in nearby galaxies and galaxy clusters. See their Figs. 5-7 for limits on $\sigma \cdot v$ for $X^0 X^0 \rightarrow \nu\bar{\nu}, \mu^+\mu^-, \tau^+\tau^-$, and W^+W^- for X^0 mass between 300 GeV and 100 TeV.
- 45 ABRAMOWSKI 13 search for monochromatic γ from X^0 annihilation in the Milky Way halo in the central region. Limit on $\sigma \cdot v$ between 10^{-28} and $10^{-25} \text{ cm}^3 \text{ s}^{-1}$ (95% CL) is obtained for X^0 mass between 500 GeV and 20 TeV for $X^0 X^0 \rightarrow \gamma\gamma$. X^0 density distribution in the Galaxy by Einasto is assumed. See their Fig. 4.
- 46 ACKERMANN 13A search for monochromatic γ from X^0 annihilation in the Milky Way. Limit on $\sigma \cdot v$ for the process $X^0 X^0 \rightarrow \gamma\gamma$ in the range 10^{-29} - $10^{-27} \text{ cm}^3 \text{ s}^{-1}$ (95% CL) is obtained for X^0 mass between 5 and 300 GeV. The limit depends slightly on the assumed density profile of X^0 in the Galaxy. See their Tables VII-X and Fig.10. Supersedes ACKERMANN 12.
- 47 ABRAMOWSKI 12 search for γ 's from X^0 annihilation in the Fornax galaxy cluster. See their Fig. 7 for limits on $\sigma \cdot v$ for X^0 mass between 0.1 and 100 TeV for the annihilation channels $\tau^+\tau^-$, $b\bar{b}$, and W^+W^- .
- 48 ACKERMANN 12 search for monochromatic γ from X^0 annihilation in the Milky Way. Limit on $\sigma \cdot v$ in the range 10^{-28} - $10^{-26} \text{ cm}^3 \text{ s}^{-1}$ (95% CL) is obtained for X^0 mass between 7 and 200 GeV if X^0 annihilates into $\gamma\gamma$. The limit depends slightly on the assumed density profile of X^0 in the Galaxy. See their Table III and Fig. 15.
- 49 ACKERMANN 12 search for γ from X^0 annihilation in the Milky Way in the diffuse γ background. Limit on $\sigma \cdot v$ of $10^{-24} \text{ cm}^3 \text{ s}^{-1}$ or larger is obtained for X^0 mass between 5 GeV and 10 TeV for various annihilation channels including W^+W^- , $b\bar{b}$, gg , e^+e^- , $\mu^+\mu^-$, $\tau^+\tau^-$. The limit depends slightly on the assumed density profile of X^0 in the Galaxy. See their Figs. 17-20.
- 50 ALIU 12 search for γ 's from X^0 annihilation in the dwarf spheroidal galaxy Segue 1. Limit on $\sigma \cdot v$ in the range 10^{-24} - $10^{-20} \text{ cm}^3 \text{ s}^{-1}$ (95% CL) is obtained for X^0 mass between 10 GeV and 2 TeV for annihilation channels e^+e^- , $\mu^+\mu^-$, $\tau^+\tau^-$, $b\bar{b}$, and W^+W^- . See their Fig. 3.

- 51 ABBASI 11c search for ν_μ from X^0 annihilation in the outer halo of the Milky Way. The limit assumes annihilation into $\nu\nu$. See their Fig. 9 for limits with other annihilation channels.
- 52 ABRAMOWSKI 11 search for γ from X^0 annihilation near the Galactic center. The limit assumes Einasto DM density profile.
- 53 ACKERMANN 11 search for γ from X^0 annihilation in ten dwarf spheroidal satellite galaxies of the Milky Way. The limit for $m = 10 \text{ GeV}$ assumes annihilation into $b\bar{b}$, the others W^+W^- . See their Fig. 2 for limits with other final states. See also GERINGER-SAMETH 11 for a different analysis of the same data.

Dark Matter Particle (X^0) Production in Hadron Collisions

Searches for X^0 production in association with observable particles (γ , jets, ...) in high energy hadron collisions. If a specific form of effective interaction Lagrangian is assumed, the limits may be translated into limits on X^0 -nucleon scattering cross section.

VALUE	DOCUMENT ID	TECN	COMMENT
• • •	We do not use the following data for averages, fits, limits, etc. • • •		
1	AABOUD	19AA ATLS	multi-channel BSM search
2	AABOUD	19AI ATLS	$H \rightarrow \chi\chi$
3	AABOUD	19AL ATLS	$H \rightarrow \chi\chi$
4	AABOUD	19Q ATLS	single $t+\cancel{E}_T$
5	AABOUD	19V ATLS	review mediator based DM searches
6	BANERJEE	19 NA64	$eN \rightarrow eN+E$
7	SIRUNYAN	19AN CMS	$H\chi\chi \rightarrow b\bar{b}\cancel{E}_T$
8	SIRUNYAN	19BC CMS	$LQ LQ \rightarrow \mu j \cancel{E}_T$
9	SIRUNYAN	19Bo CMS	$VV \rightarrow Hqq; H \rightarrow DM$
10	SIRUNYAN	19C CMS	$pp \rightarrow t\bar{t}\chi\chi$
11	SIRUNYAN	19o CMS	$pp \rightarrow \gamma \cancel{E}_T$
12	SIRUNYAN	19X CMS	$pp \rightarrow t\bar{t} + \cancel{p}T; pp \rightarrow t(\bar{t}) + \cancel{p}T$
13	AABOUD	18 ATLS	$pp \rightarrow Z\chi\chi; Z \rightarrow \ell\ell$
14	AABOUD	18A ATLS	$pp \rightarrow t\bar{t}\cancel{E}_T; pp \rightarrow b\bar{b}\cancel{E}_T$
15	AABOUD	18ca ATLS	$pp \rightarrow V\chi\chi; V \rightarrow jj$
16	AABOUD	18i ATLS	$pp \rightarrow \text{jet}(s) + \cancel{E}_T$
17	AGUILAR-AR...18B	MBNE	$pN \rightarrow \chi\chi, \chi = e, \pi, \text{ or } N$
18	KHACHATRY...18	CMS	$pp \rightarrow Z(\ell\ell) + \cancel{E}_T$
19	SIRUNYAN	18BF CMS	$pp \rightarrow t\cancel{E}_T$
20	SIRUNYAN	18Bo CMS	dijet resonance search
21	SIRUNYAN	18BV CMS	$pp \rightarrow Z\cancel{E}_T$
22	SIRUNYAN	18c CMS	$pp \rightarrow t\bar{t}\cancel{E}_T$
23	SIRUNYAN	18cu CMS	$pp \rightarrow Z\cancel{E}_T$
24	SIRUNYAN	18DH CMS	$pp \rightarrow \chi\chi h; h \rightarrow \gamma\gamma \text{ or } \tau\tau$
25	SIRUNYAN	18s CMS	$pp \rightarrow \text{jets } \cancel{E}_T$
26	AABOUD	17A ATLS	$pp(H \rightarrow b\bar{b}) + \text{WIMP pair}$
27	AABOUD	17AM ATLS	$pp \rightarrow Z' \rightarrow Ah \rightarrow h(b\bar{b}) + \cancel{E}_T$
28	AABOUD	17AQ ATLS	$pp \rightarrow h(\gamma\gamma) + \cancel{E}_T$
29	AABOUD	17BD ATLS	$pp \rightarrow \text{jet}(s) + \cancel{E}_T$
30	AABOUD	17R ATLS	$pp \rightarrow \gamma\cancel{E}_T$
31	AGUILAR-AR...17A	MBNE	$pN \rightarrow \chi\chi X; \chi N \rightarrow \chi N$
32	BANERJEE	17 NA64	$eN \rightarrow eN\gamma'$
33	KHACHATRY...17A	CMS	forward jets + \cancel{E}_T
34	KHACHATRY...17F	CMS	$H \rightarrow \text{invisibles}$
35	SIRUNYAN	17 CMS	$Z + \cancel{E}_T$
36	SIRUNYAN	17AP CMS	$pp \rightarrow Z' \rightarrow Ah \rightarrow h+\text{MET}$
37	SIRUNYAN	17AQ CMS	$pp \rightarrow \gamma+\text{MET}$
38	SIRUNYAN	17BB CMS	$pp \rightarrow t\bar{t}+\cancel{E}_T; pp \rightarrow b\bar{b}+\cancel{E}_T$
39	SIRUNYAN	17G CMS	$pp \rightarrow j + \cancel{E}_T$
40	SIRUNYAN	17U CMS	$pp \rightarrow Z\chi\chi; Z \rightarrow \ell\bar{\ell}$
41	AABOUD	16AD ATLS	(W or $Z \rightarrow \text{jets}) + \cancel{E}_T$
42	AAD	16AF ATLS	$VV \rightarrow \text{forward jets} + \cancel{E}_T$
43	AAD	16AG ATLS	$\ell + \text{jets}$
44	AAD	16M ATLS	$pp \rightarrow H + \cancel{E}_T, H \rightarrow b\bar{b}$
45	KHACHATRY...16BZ	CMS	$\text{jet}(s) + \cancel{E}_T$
46	KHACHATRY...16CA	CMS	$\text{jets} + \cancel{E}_T$
47	KHACHATRY...16N	CMS	$pp \rightarrow \gamma + \cancel{E}_T$
48	AAD	15AS ATLS	$b(\bar{b}) + \cancel{E}_T, t(\bar{t}) + \cancel{E}_T$
49	AAD	15BH ATLS	$\text{jet} + \cancel{E}_T$
50	AAD	15CF ATLS	$H^0 + \cancel{E}_T$
51	AAD	15CS ATLS	$\gamma + \cancel{E}_T$
52	KHACHATRY...15AG	CMS	$t\bar{t} + \cancel{E}_T$
53	KHACHATRY...15AL	CMS	$\text{jet} + \cancel{E}_T$
54	KHACHATRY...15T	CMS	$\ell + \cancel{E}_T$
55	AAD	14AI ATLS	$W + \cancel{E}_T$
56	AAD	14BK ATLS	$W, Z + \cancel{E}_T$
57	AAD	14K ATLS	$Z + \cancel{E}_T$
58	AAD	14o ATLS	$Z + \cancel{E}_T$
59	AAD	13AD ATLS	$\text{jet} + \cancel{E}_T$
60	AAD	13C ATLS	$\gamma + \cancel{E}_T$
61	AALTONEN	12K CDF	$t + \cancel{E}_T$
62	AALTONEN	12M CDF	$\text{jet} + \cancel{E}_T$
63	CHATRCHYAN12AP	CMS	$\text{jet} + \cancel{E}_T$
64	CHATRCHYAN12T	CMS	$\gamma + \cancel{E}_T$

- 1 AABOUD 19AA searches for BSM physics in more than 700 event classes with more than 10^5 regions at 13 TeV with 3.2 fb^{-1} ; no significant signal.
- 2 AABOUD 19AI searches for vector boson fusion $pp \rightarrow Hq\bar{q}$, $H \rightarrow$ invisible at 13 TeV with 36.1 fb^{-1} ; no signal; require $B(H \rightarrow \text{invisible}) < 0.37$ (0.28 expected).
- 3 AABOUD 19AL perform search in three different channels for $H \rightarrow \chi\chi$ at 7, 8 and 13 TeV; combined result $BF(H \rightarrow \text{invisible}) < 0.26$ (0.17 expected).
- 4 AABOUD 19Q search for single $t + \cancel{E}_T$ at 13 TeV with 36.1 fb^{-1} of data; no signal; limits set in σ or coupling vs. mass plane for simplified models.
- 5 AABOUD 19V review ATLAS results from 7, 8 and 13 TeV searches for mediator-based DM and DE scalar which couples to gravity; no signal; limits set for large variety of simplified models.
- 6 BANERJEE 19 search for dark photon via $eN \rightarrow eN + \cancel{E}$ in NA64; no signal, limits placed in kinetic mixing ϵ vs. $m(\text{DM})$ plane for $m(\text{DM}) \sim 0.001\text{--}1 \text{ GeV}$.
- 7 SIRUNYAN 19AN search at 13 TeV with 35.9 fb^{-1} for $pp \rightarrow H\chi\chi \rightarrow b\bar{b}\cancel{E}_T$; no signal; limits set in the context of a 2HDM + pseudoscalar (a) model and a baryonic Z' model.
- 8 SIRUNYAN 19BC search for DM via LeptoQuark pair annihilation $LQ LQ \rightarrow \mu j\chi\chi \rightarrow \mu j \cancel{E}_T$ with 77.4 fb^{-1} , 13 TeV; no signal; limits placed in $m(\chi)$ vs. $m(LQ)$ plane. Model dependent limits on DM mass up to 600 GeV depending on $m(LQ)$ placed.
- 9 SIRUNYAN 19BO search for vector boson fusion $VV \rightarrow q\bar{q}H$ with $H \rightarrow \chi\chi$ at 13 TeV with 38.2 fb^{-1} ; no signal; limits placed for several models. Also search for $H \rightarrow$ invisible at 7, 8, and 13 TeV; no signal; limit placed on $BF < 0.19$.
- 10 SIRUNYAN 19C search for DM via $pp \rightarrow t\bar{t}\chi\chi$ at 13 TeV, 35.9 fb^{-1} ; no signal; limits placed on coupling vs. mediator mass for various simplified models.
- 11 SIRUNYAN 19O search for $pp \rightarrow \gamma$ at 13 TeV with 35.9 fb^{-1} ; no signal; limits placed on parameters of various models.
- 12 SIRUNYAN 19X search for $pp \rightarrow t\bar{t}\cancel{E}_T$ and $pp \rightarrow t \cancel{E}_T + \dots$ at 13 TeV with 35.9 fb^{-1} ; no signal; limits placed on χ production σ for various simplified models with $m(\chi) = 1 \text{ GeV}$.
- 13 AABOUD 18 search for $pp \rightarrow Z + \cancel{E}_T$ with $Z \rightarrow \ell\ell$ at 13 TeV with 36.1 fb^{-1} of data. Limits set for simplified models.
- 14 AABOUD 18A search for $pp \rightarrow t\bar{t}\cancel{E}_T$ or $pp \rightarrow b\bar{b}\cancel{E}_T$ at 13 TeV, 36.1 fb^{-1} of data. Limits set for simplified models.
- 15 AABOUD 18CA search for $pp \rightarrow V\chi\chi$ with $V \rightarrow jj$ at 13 TeV, 36.1 fb^{-1} ; no signal; limits set in $m(\text{DM})$ vs $m(\text{mediator})$ simplified model plane.
- 16 AABOUD 18I search for $pp \rightarrow j + \cancel{E}_T$ at 13 TeV with 36.1 fb^{-1} of data. Limits set for simplified models with pair-produced weakly interacting dark-matter candidates.
- 17 AGUILAR-AREVALO 18B search for WIMP production in MiniBooNE p beam dump; no signal; limits set for $m(\chi) \sim 5\text{--}50 \text{ MeV}$ in vector portal DM model.
- 18 KHACHATRYAN 18 search for $pp \rightarrow Z(\ell\ell) + \cancel{E}_T$; no signal; limits set on effective dark matter interactions and other exotic physics models.
- 19 SIRUNYAN 18BF search for $pp \rightarrow t \cancel{E}_T$ at 13 TeV and 36 fb^{-1} ; no signal; limits placed on DM models involving a flavor changing neutral current, scalar resonance decaying to top quark and DM.
- 20 SIRUNYAN 18BO search for high mass dijet resonances at 13 TeV and 36 fb^{-1} ; no signal; limits placed on various models, including simplified DM models involving a spin $= 1$ Z' mediator.
- 21 SIRUNYAN 18BV search for $pp \rightarrow Z \cancel{E}_T$ at 13 TeV; no signal, limits placed for various exotic physics models including DM.
- 22 SIRUNYAN 18C search for new physics in $pp \rightarrow$ final states with two oppositely charged leptons at 13 TeV with 35.9 fb^{-1} . Limits placed on $m(\text{mediator})$ and top squark for various simplified models.
- 23 SIRUNYAN 18CU search for $pp \rightarrow Z \cancel{E}_T$ at 13 TeV and 2.3 fb^{-1} ; no signal; limits placed for various exotic models including DM.
- 24 SIRUNYAN 18DH search for $pp \rightarrow \chi\chi h$; $h \rightarrow \gamma\gamma$ or $\tau\tau$ at 13 TeV, 35.9 fb^{-1} ; no signal; limits placed on massive boson mediator Z' in the context of $Z'+2\text{HDM}$ and baryonic Z' models. Limits also cast in terms of spin-independent WIMP-nucleon cross section for masses 1–200 GeV.
- 25 SIRUNYAN 18S search for $pp \rightarrow$ jets \cancel{E}_T at 13 TeV; no signal; limits placed on simplified dark matter models, on the branching ratio of the Higgs boson to invisible particles, and on several other exotic physics models including fermion portal DM.
- 26 AABOUD 17A search for $H \rightarrow b\bar{b} + \cancel{E}_T$. See Fig. 4b for limits set on VB mediator vs WIMP mass.
- 27 AABOUD 17AM search for $pp \rightarrow Z' \rightarrow Ah \rightarrow h(b\bar{b}) + \cancel{E}_T$ at 13 TeV. Limits set in $m(Z')$ vs. $m(A)$ plane and on the visible cross section of $h(b\bar{b}) + \cancel{E}_T$ events in bins of \cancel{E}_T .
- 28 AABOUD 17AQ search for WIMP in $pp \rightarrow h(\gamma\gamma) + \cancel{E}_T$ in 36.1 fb^{-1} of data. Limits on the visible cross section are also provided. Model dependent limits on spin independent DM - Nucleon cross-section are also presented, which are more stringent than those from direct searches for DM mass smaller than 2.5 GeV .
- 29 AABOUD 17BD search for $pp \rightarrow \text{jet}(s) + \cancel{E}_T$ at 13 TeV with 3.2 fb^{-1} of data. Limits set for simplified models. Observables corrected for detector effects can be used to constrain other models.
- 30 AABOUD 17R, for an axial vector mediator in the s-channel, excludes $m(\text{mediator}) < 750\text{--}1200 \text{ GeV}$ for $m(\text{DM}) < 230\text{--}480 \text{ GeV}$, depending on the couplings.
- 31 AGUILAR-AREVALO 17A search for DM produced in 8 GeV proton collisions with steel beam dump followed by DM-nucleon scattering in MiniBooNE detector. Limit placed on DM cross section parameter $Y < 2 \times 10^{-8}$ for $\alpha_D = 0.5$ and for $0.01 < m(\text{DM}) < 0.3 \text{ GeV}$.
- 32 BANERJEE 17 search for dark photon invisible decay via eN scattering; exclude $m(\gamma')$ $< 100 \text{ MeV}$ as an explanation of $(g_{\mu-2})$ muon anomaly.
- 33 KHACHATRYAN 17A search for WIMPs in forward jets + \cancel{E}_T channel with 18.5 fb^{-1} at 8 TeV; limits set in effective theory model, Fig. 3.
- 34 KHACHATRYAN 17F search for $H \rightarrow$ invisibles in pp collisions at 7, 8, and 13 TeV; place limits on Higgs portal DM.
- 35 SIRUNYAN 17 search for $pp \rightarrow Z + \cancel{E}_T$ with 2.3 fb^{-1} at 13 TeV; no signal seen; limits placed on WIMPs and unparticles.
- 36 SIRUNYAN 17AP search for $pp \rightarrow Z' \rightarrow Ah \rightarrow h + \text{MET}$ with $h \rightarrow b\bar{b}$ or $\gamma\gamma$ and $A \rightarrow \chi\chi$ with 2.3 fb^{-1} at 13 TeV. Limits set in $m(Z')$ vs. $m(A)$ plane.
- 37 SIRUNYAN 17AQ search for $pp \rightarrow \gamma + \text{MET}$ at 13 TeV with 12.9 fb^{-1} . Limits derived for simplified DM models, effective electroweak-DM interaction and Extra Dimensions models.
- 38 SIRUNYAN 17BB search for WIMPs via $pp \rightarrow t\bar{t} + \cancel{E}_T$, $pp \rightarrow b\bar{b} + \cancel{E}_T$ at 13 TeV with 2.2 fb^{-1} . Limits derived for various simplified models.
- 39 SIRUNYAN 17G search for $pp \rightarrow j + \cancel{E}_T$ with 12.9 fb^{-1} at 13 TeV; limits placed on WIMP mass/mediators in DM simplified models.
- 40 SIRUNYAN 17U search for WIMPs/unparticles via $pp \rightarrow Z\chi\chi$, $Z \rightarrow \ell\bar{\ell}$ at 13 TeV with 2.3 fb^{-1} . Limits derived for various simplified models.
- 41 AABOUD 16AD place limits on VVX effective theory via search for hadronic W or Z plus WIMP pair production. See Fig. 5.
- 42 AAD 16AF search for $VV \rightarrow (H \rightarrow \text{WIMP pair}) +$ forward jets with 20.3 fb^{-1} at 8 TeV; set limits in Higgs portal model, Fig. 8.
- 43 AAD 16AG search for lepton jets with 20.3 fb^{-1} of data at 8 TeV; Fig. 13 excludes dark photons around 0.1–1 GeV for kinetic mixing $10^{-6}\text{--}10^{-2}$.
- 44 AAD 16M search with 20.3 fb^{-1} of data at 8 TeV pp collisions; limits placed on EFT model (Fig. 7) and simplified Z' model (Fig. 6).
- 45 KHACHATRYAN 16BZ search for jet(s) + \cancel{E}_T in 19.7 fb^{-1} at 8 TeV; limits set for variety of simplified models.
- 46 KHACHATRYAN 16CA search for WIMPs via jet(s) + \cancel{E}_T using razor variable; require mediator scale $> 1 \text{ TeV}$ for various effective theories.
- 47 KHACHATRYAN 16N search for $\gamma +$ WIMPs in 19.6 fb^{-1} at 8 TeV; limits set on SI and SD WIMP- p scattering in Fig. 3.
- 48 AAD 15AS search for events with one or more bottom quark and missing E_T , and also events with a top quark pair and missing E_T in pp collisions at $E_{\text{cm}} = 8 \text{ TeV}$ with $L = 20.3 \text{ fb}^{-1}$. See their Figs. 5 and 6 for translated limits on X^0 -nucleon cross section for $m = 1\text{--}700 \text{ GeV}$.
- 49 AAD 15BH search for events with a jet and missing E_T in pp collisions at $E_{\text{cm}} = 8 \text{ TeV}$ with $L = 20.3 \text{ fb}^{-1}$. See their Fig. 12 for translated limits on X^0 -nucleon cross section for $m = 1\text{--}1200 \text{ GeV}$.
- 50 AAD 15CF search for events with a H^0 ($\rightarrow \gamma\gamma$) and missing E_T in pp collisions at $E_{\text{cm}} = 8 \text{ TeV}$ with $L = 20.3 \text{ fb}^{-1}$. See paper for limits on the strength of some contact interactions containing X^0 and the Higgs fields.
- 51 AAD 15CS search for events with a photon and missing E_T in pp collisions at $E_{\text{cm}} = 8 \text{ TeV}$ with $L = 20.3 \text{ fb}^{-1}$. See their Fig. 13 (see also erratum) for translated limits on X^0 -nucleon cross section for $m = 1\text{--}1000 \text{ GeV}$.
- 52 KHACHATRYAN 15AG search for events with a top quark pair and missing E_T in pp collisions at $E_{\text{cm}} = 8 \text{ TeV}$ with $L = 19.7 \text{ fb}^{-1}$. See their Fig. 8 for translated limits on X^0 -nucleon cross section for $m = 1\text{--}200 \text{ GeV}$.
- 53 KHACHATRYAN 15AL search for events with a jet and missing E_T in pp collisions at $E_{\text{cm}} = 8 \text{ TeV}$ with $L = 19.7 \text{ fb}^{-1}$. See their Figs. 5 and Tables 4–6 for translated limits on X^0 -nucleon cross section for $m = 1\text{--}1000 \text{ GeV}$.
- 54 KHACHATRYAN 15T search for events with a lepton and missing E_T in pp collisions at $E_{\text{cm}} = 8 \text{ TeV}$ with $L = 19.7 \text{ fb}^{-1}$. See their Fig. 17 for translated limits on X^0 -proton cross section for $m = 1\text{--}1000 \text{ GeV}$.
- 55 AAD 14AI search for events with a W and missing E_T in pp collisions at $E_{\text{cm}} = 8 \text{ TeV}$ with $L = 20.3 \text{ fb}^{-1}$. See their Fig. 4 for translated limits on X^0 -nucleon cross section for $m = 1\text{--}1500 \text{ GeV}$.
- 56 AAD 14BK search for hadronically decaying W , Z in association with \cancel{E}_T in 20.3 fb^{-1} at 8 TeV pp collisions. Fig. 5 presents exclusion results for SI and SD scattering cross section. In addition, cross section limits on the anomalous production of W or Z bosons with large missing transverse momentum are also set in two fiducial regions.
- 57 AAD 14K search for events with a Z and missing E_T in pp collisions at $E_{\text{cm}} = 8 \text{ TeV}$ with $L = 20.3 \text{ fb}^{-1}$. See their Fig. 5 and 6 for translated limits on X^0 -nucleon cross section for $m = 1\text{--}10^3 \text{ GeV}$.
- 58 AAD 14O search for ZH^0 production with H^0 decaying to invisible final states. See their Fig. 4 for translated limits on X^0 -nucleon cross section for $m = 1\text{--}60 \text{ GeV}$ in Higgs-portal X^0 scenario.
- 59 AAD 13AD search for events with a jet and missing E_T in pp collisions at $E_{\text{cm}} = 7 \text{ TeV}$ with $L = 4.7 \text{ fb}^{-1}$. See their Figs. 5 and 6 for translated limits on X^0 -nucleon cross section for $m = 1\text{--}1300 \text{ GeV}$.
- 60 AAD 13C search for events with a photon and missing E_T in pp collisions at $E_{\text{cm}} = 7 \text{ TeV}$ with $L = 4.6 \text{ fb}^{-1}$. See their Fig. 3 for translated limits on X^0 -nucleon cross section for $m = 1\text{--}1000 \text{ GeV}$.
- 61 AALTONEN 12K search for events with a top quark and missing E_T in $p\bar{p}$ collisions at $E_{\text{cm}} = 1.96 \text{ TeV}$ with $L = 7.7 \text{ fb}^{-1}$. Upper limits on $\sigma(tX^0)$ in the range 0.4–2 pb (95% CL) is given for $m_{X^0} = 0\text{--}150 \text{ GeV}$.
- 62 AALTONEN 12M search for events with a jet and missing E_T in $p\bar{p}$ collisions at $E_{\text{cm}} = 1.96 \text{ TeV}$ with $L = 6.7 \text{ fb}^{-1}$. Upper limits on the cross section in the range 2–10 pb (90% CL) is given for $m_{X^0} = 1\text{--}300 \text{ GeV}$. See their Fig. 2 for translated limits on X^0 -nucleon cross section.
- 63 CHATRCHYAN 12AP search for events with a jet and missing E_T in pp collisions at $E_{\text{cm}} = 7 \text{ TeV}$ with $L = 5.0 \text{ fb}^{-1}$. See their Fig. 4 for translated limits on X^0 -nucleon cross section for $m_{X^0} = 0.1\text{--}1000 \text{ GeV}$.
- 64 CHATRCHYAN 12T search for events with a photon and missing E_T in pp collisions at $E_{\text{cm}} = 7 \text{ TeV}$ with $L = 5.0 \text{ fb}^{-1}$. Upper limits on the cross section in the range 13–15 fb (90% CL) is given for $m_{X^0} = 1\text{--}1000 \text{ GeV}$. See their Fig. 2 for translated limits on X^0 -nucleon cross section.

REFERENCES FOR WIMP and Dark Matter Searches

AKERIB	20	PR D101 012003	D.S. Akhmedov et al.	(LUX Collab.)
AABOUD	19AA	EPJ C79 120	M. Aaboud et al.	(ATLAS Collab.)
AABOUD	19AI	PL B793 499	M. Aaboud et al.	(ATLAS Collab.)
AABOUD	19AL	PRL 122 231801	M. Aaboud et al.	(ATLAS Collab.)
AABOUD	19Q	JHEP 1905 041	M. Aaboud et al.	(ATLAS Collab.)
AABOUD	19V	JHEP 1905 142	M. Aaboud et al.	(ATLAS Collab.)
ABDELHAMEED	19	EPJ C79 630	A.H. Abdelhameed et al.	(CREST Collab.)
ABDELHAMEED	19A	PR D100 102002	A.H. Abdelhameed et al.	(CREST Collab.)
ABE	19	PL B789 45	K. Abe et al.	(XMASS Collab.)
ABEYSEKARA	19	JCAP 1907 022	A.U. Abeysekara et al.	(HAWC Collab.)
ABRAMOFF	19	PRL 122 161801	O. Abramoff et al.	(SENSEI Collab.)
ADHIKARI	19	PRL 123 031302	G. Adhikari et al.	(COSINE-100 Collab.)
AGNESE	19A	PR D99 062001	R. Agnese et al.	(CDMS Collab.)
AGUILAR-AR.	19A	PRL 123 181802	A. Aguilar-Arevalo et al.	(DMIC Collab.)

Searches Particle Listings

WIMP and Dark Matter Searches

AJAJ	19	PR D100 022004	R. Ajaj et al.	(DEAP-3600 Collab.)	ABOUD	16F	JHEP 1606 059	M. Aaboud et al.	(ATLAS Collab.)
AKERIB	19	PRL 122 131301	D.S. Akerib et al.	(LUX Collab.)	AAD	16AF	JHEP 1601 172	G. Aad et al.	(ATLAS Collab.)
ALBERT	19B	JCAP 1904 E01	A. Albert et al.	(HAWC Collab.)	AAD	16AG	JHEP 1602 062	G. Aad et al.	(ATLAS Collab.)
AMARE	19	PRL 123 031301	J. Amare et al.	(ANAIS Collab.)	AAD	16M	PR D93 072007	G. Aad et al.	(ATLAS Collab.)
AMOLE	19	PR D100 022001	C. Amole et al.	(PICO Collab.)	AARTSEN	16C	JCAP 1604 022	M.G. Aartsen et al.	(IceCube Collab.)
ANGLOHER	19	EPJ C79 43	G. Angloher et al.	(CRESSIT-II Collab.)	AARTSEN	16D	EPJ C76 531	M.G. Aartsen et al.	(IceCube Collab.)
APRILE	19	PRL 122 071301	E. Aprile et al.	(XENON1T Collab.)	ABDALLAH	16A	PRL 117 111301	H. Abdallah et al.	(H.E.S.S. Collab.)
APRILE	19A	PRL 122 141301	E. Aprile et al.	(XENON1T Collab.)	ABDALLAH	16A	PRL 117 151302	H. Abdallah et al.	(H.E.S.S. Collab.)
APRILE	19C	PRL 123 241803	E. Aprile et al.	(XENON1T Collab.)	ADRIAN-MAR...	16	PL B759 69	S. Adrian-Martinez et al.	(ANTARES Collab.)
APRILE	19D	PRL 123 251801	E. Aprile et al.	(XENON1T Collab.)	ADRIAN-MAR...	16B	JCAP 1605 016	S. Adrian-Martinez et al.	(ANTARES Collab.)
ARMENGAUD	19	PR D99 082003	E. Armengaud et al.	(EDELWEISS Collab.)	AGNES	16	PR D93 081101	P. Agnes et al.	(DarkSide-50 Collab.)
BANERJEE	19	PRL 123 121801	D. Banerjee et al.	(NA64 Collab.)	AGNESE	16	PRL 116 071301	R. Agnese et al.	(SuperCDMS Collab.)
BRINGMANN	19	PRL 122 171801	T. Bringmann, M. Pospelov	(OSLO, VICT)	AGUILAR-AR...	16	PR D94 082006	A. Aguilar-Arevalo et al.	(DAMIC Collab.)
BRUNE	19	PR D99 096005	T. Brune, H. Pas	(DORT)	AHNEN	16	JCAP 1602 039	M.L. Ahnen et al.	(MAGIC and Fermi-LAT Collab.)
CHEUNG	19	PL B789 137	K. Cheung et al.	(SUNG)	AKERIB	16	PRL 116 161301	D.S. Akerib et al.	(LUX Collab.)
CHOI	19	PR D99 083018	K.-Y. Choi, J. Kim, C. Rott	(SUNG)	AKERIB	16A	PRL 116 161302	D.S. Akerib et al.	(LUX Collab.)
DI-MAURO	19	PR D99 123027	M. Di Mauro et al.	(SUNG)	AMOLE	16	PR D93 052014	C. Amole et al.	(PICO Collab.)
HA	19	PRL 122 131802	C. Ha et al.	(COSINE-100 Collab.)	AMOLEHER	16A	PR D93 061101	C. Amole et al.	(PICO Collab.)
JOHNSON	19	PR D99 103007	C. Johnson et al.	(COSINE-100 Collab.)	ANGLOHER	16	EPJ C76 25	G. Angloher et al.	(CRESSIT-II Collab.)
KIM	19A	JHEP 1903 194	K.W. Kim et al.	(KIMS Collab.)	ANGLOHER	16A	PRL 117 021303	G. Angloher et al.	(CRESSIT-II Collab.)
KLOPF	19	PRL 122 222503	M. Klopff et al.	(PERKEO II Collab.)	APRILE	16	PR D94 092001	E. Aprile et al.	(XENON100 Collab.)
KOBAYASHI	19	PL B795 308	M. Kobayashi et al.	(XMASS Collab.)	APRILE	16B	PR D94 122001	E. Aprile et al.	(XENON100 Collab.)
LI	19D	PR D99 123519	S. Li et al.	(XMASS Collab.)	ARMENGAUD	16	JCAP 1605 019	E. Armengaud et al.	(EDELWEISS-III Collab.)
LIU	19B	PRL 123 161301	Z.Z. Liu et al.	(CDEX Collab.)	AVRORIN	16	ASP 81 12	A.D. Avrorin et al.	(BAIKAL Collab.)
NG	19	PR D99 083005	K.C.Y. Ng et al.	(CDEX Collab.)	CAPUTO	16	PR D93 062004	R. Caputo et al.	(Fermi-LAT Collab.)
QUEIROZ	19	JCAP 1904 048	F.S. Queiroz, C. Siqueira	(BELLE Collab.)	FORNASA	16	PR D94 123005	M. Fornasa et al.	(Fermi-LAT Collab.)
SEONG	19	PRL 122 011801	I.S. Seong et al.	(BELLE Collab.)	HEHN	16	EPJ C76 548	L. Hehn et al.	(EDELWEISS-III Collab.)
SIRUNYAN	19A	EPJ C79 280	A.M. Sirunyan et al.	(CMS Collab.)	KHACHATRY...	16A1	PR D93 052011	V. Khachatryan et al.	(CMS Collab.)
SIRUNYAN	19BC	PL B795 76	A.M. Sirunyan et al.	(CMS Collab.)	KHACHATRY...	16B2	JHEP 1612 083	V. Khachatryan et al.	(CMS Collab.)
SIRUNYAN	19BD	PL B793 520	A.M. Sirunyan et al.	(CMS Collab.)	Also	JHEP 1708 035 (err.)		V. Khachatryan et al.	(CMS Collab.)
SIRUNYAN	19C	PRL 122 011803	A.M. Sirunyan et al.	(CMS Collab.)	KHACHATRY...	16A	JHEP 1612 086	V. Khachatryan et al.	(CMS Collab.)
SIRUNYAN	19D	JHEP 1902 074	A.M. Sirunyan et al.	(CMS Collab.)	KHACHATRY...	16N	PL B755 102	V. Khachatryan et al.	(CMS Collab.)
SIRUNYAN	19X	JHEP 1903 141	A.M. Sirunyan et al.	(CMS Collab.)	LEITE	16	JCAP 1611 021	N. Leite et al.	(CMS Collab.)
SUZUKI	19	ASP 110 1	T. Suzuki et al.	(XMASS Collab.)	LI	16	PR D93 043518	S. Li et al.	(CMS Collab.)
XIA	19A	PL B792 193	J. Xia et al.	(Pandax-II Collab.)	LI	16A	JCAP 1612 028	Z. Li et al.	(CMS Collab.)
YAGUNA	19	JCAP 1904 041	C. Yaguna	(Pandax-II Collab.)	LIANG	16	PR D94 103502	Y.-F. Liang et al.	(CMS Collab.)
YANG	19	PRL 123 221301	L.T. Yang et al.	(CDEX Collab.)	LI	16	PR D93 103517	B.-Q. Lu, H.-S. Zong	(CMS Collab.)
ABOUD	18	PL B776 318	M. Aaboud et al.	(ATLAS Collab.)	SHIRASAKI	16	PR D94 063522	M. Shirasaki et al.	(Pandax Collab.)
ABOUD	18A	EPJ C78 18	M. Aaboud et al.	(ATLAS Collab.)	TAN	16	PR D93 122009	T.H. Tan et al.	(Pandax Collab.)
ABOUD	18CA	JHEP 1810 180	M. Aaboud et al.	(ATLAS Collab.)	TAN	16B	PRL 117 121303	A. Tan et al.	(Pandax Collab.)
ABOUD	18D	JHEP 1801 126	M. Aaboud et al.	(ATLAS Collab.)	ZHAO	16	PR D93 092003	W. Zhao et al.	(CDF Collab.)
AARTSEN	18D	EPJ C76 831	M.G. Aartsen et al.	(IceCube Collab.)	AAD	15AB	EPJ C75 32	G. Aad et al.	(ATLAS Collab.)
ABDALLAH	18D	PRL 120 201101	H. Abdallah et al.	(H.E.S.S. Collab.)	AAD	15B	EPJ C75 299	G. Aad et al.	(ATLAS Collab.)
ABE	18C	PR D97 102006	K. Abe et al.	(XMASS Collab.)	Also	EPJ C75 408 (err.)		G. Aad et al.	(ATLAS Collab.)
ABE	18F	PL B787 153	K. Abe et al.	(XMASS Collab.)	AAD	15CF	PRL 115 131801	G. Aad et al.	(ATLAS Collab.)
ADHIKARI	18	NAT 564 83	G. Adhikari et al.	(COSINE-100 Collab.)	AAD	15CS	PR D91 012008	G. Aad et al.	(ATLAS Collab.)
AGNES	18	PRL 121 081307	P. Agnes et al.	(DarkSide-50 Collab.)	Also	PR D92 059903 (err.)		G. Aad et al.	(ATLAS Collab.)
AGNES	18A	PR D98 102006	P. Agnes et al.	(DarkSide-50 Collab.)	AARTSEN	15E	EPJ C75 20	M.G. Aartsen et al.	(IceCube Collab.)
AGNES	18B	PRL 121 111303	P. Agnes et al.	(DarkSide-50 Collab.)	AARTSEN	15C	EPJ C75 492	M.G. Aartsen et al.	(IceCube Collab.)
AGNESE	18	PR D97 022002	R. Agnese et al.	(SuperCDMS Collab.)	ABRAMOWSKI	15	PRL 114 081301	A. Abramowski et al.	(H.E.S.S. Collab.)
AGNESE	18A	PRL 120 061802	R. Agnese et al.	(SuperCDMS Collab.)	ACKERMANN	15	PR D91 122002	M. Ackermann et al.	(Fermi-LAT Collab.)
AGNESE	18B	PRL 121 051301	R. Agnese et al.	(SuperCDMS Collab.)	ACKERMANN	15A	JCAP 1509 008	M. Ackermann et al.	(Fermi-LAT Collab.)
Also		PRL 122 011901 (err.)	R. Agnese et al.	(SuperCDMS Collab.)	ACKERMANN	15C	PRL 116 231301	M. Ackermann et al.	(Fermi-LAT Collab.)
AGUILAR-AR...	18B	PR D98 112004	A.A. Aguilar-Arevalo	(MiniBoONE Collab.)	ADRIAN-MAR...	15A	JCAP 1510 068	S. Adrian-Martinez et al.	(ANTARES Collab.)
AHNEN	18	JCAP 1803 009	M.L. Ahnen et al.	(MAGIC Collab.)	AGNES	15	PL B743 456	P. Agnes et al.	(DarkSide-50 Collab.)
AKERIB	18A	PR D98 062005	D.S. Akerib et al.	(LUX Collab.)	AGNESE	15A	PR D91 052021	R. Agnese et al.	(SuperCDMS Collab.)
ALBERT	18B	JCAP 1806 043	A. Albert et al.	(HAWC Collab.)	AGNESE	15B	PR D92 072003	R. Agnese et al.	(SuperCDMS Collab.)
ALBERT	18C	PR D98 123012	A. Albert et al.	(HAWC Collab.)	AMOLE	15	PRL 114 231302	C. Amole et al.	(PICO Collab.)
AMAUDRUZ	18	PRL 121 071801	P.A. Amaudruz et al.	(DEAP-3600 Collab.)	APRILE	15	PRL 115 091302	E. Aprile et al.	(XENON Collab.)
APRILE	18	PRL 121 111302	E. Aprile et al.	(XENON1T Collab.)	APRILE	15A	SCI 349 851	E. Aprile et al.	(XENON Collab.)
ARMENGAUD	18	PR D98 082004	E. Armengaud et al.	(EDELWEISS-III Collab.)	CHOI	15	PRL 114 141301	K. Choi et al.	(Super-Kamiokande Collab.)
ARNAUD	18	ASP 97 54	J. Arnaud et al.	(NEWS-G Collab.)	KHACHATRY...	15AG	JHEP 1506 121	V. Khachatryan et al.	(CMS Collab.)
CHANG	18A	PR D98 123004	L.J. Chang, M. Lisanti, S. Mishra-Sharma	(PRIN)	KHACHATRY...	15AL	EPJ C75 235	V. Khachatryan et al.	(CMS Collab.)
CRISLER	18	PRL 120 241803	M. Crisler et al.	(SENSEI Collab.)	KHACHATRY...	15T	PR D91 022005	J. Khatami et al.	(CMS Collab.)
JIANG	18	PRL 120 241301	H. Jiang et al.	(CDEX Collab.)	NAKAMURA	15	PTEP 2015 4 043F01	K. Nakamura et al.	(NEWAGE Collab.)
KACHULIS	18	PRL 120 221301	C. Kachulis et al.	(Super-Kamiokande Collab.)	XIAO	15	PR D92 052004	X. Xiao et al.	(Pandax Collab.)
KHACHATRY...	18	PR D97 099903	V. Khachatryan et al.	(CMS Collab.)	AAD	14A1	JHEP 1409 037	G. Aad et al.	(ATLAS Collab.)
LISANTI	18	PRL 120 101101	M. Lisanti et al.	(PRIN, MIT, MICH)	AAD	14BK	PRL 112 041802	G. Aad et al.	(ATLAS Collab.)
MAZZIOTTA	18	PR D98 022006	M. Mazziotta et al.	(Fermi-LAT Collab.)	AAD	14K	PR D90 012004	G. Aad et al.	(ATLAS Collab.)
REN	18	PRL 121 021304	X. Ren et al.	(Pandax-II Collab.)	AAD	14O	PRL 112 201802	G. Aad et al.	(ATLAS Collab.)
SIRUNYAN	18BF	JHEP 1806 027	A.M. Sirunyan et al.	(CMS Collab.)	ACKERMANN	14	PR D89 042001	M. Ackermann et al.	(Fermi-LAT Collab.)
SIRUNYAN	18BO	JHEP 1808 130	A.M. Sirunyan et al.	(CMS Collab.)	AGNESE	14	PRL 112 241302	R. Agnese et al.	(SuperCDMS Collab.)
SIRUNYAN	18BV	EPJ C78 291	A.M. Sirunyan et al.	(CMS Collab.)	AGNESE	14A	PRL 112 041302	R. Agnese et al.	(SuperCDMS Collab.)
SIRUNYAN	18C	PR D97 032009	A.M. Sirunyan et al.	(CMS Collab.)	AKERIB	14	PRL 112 091303	D.S. Akerib et al.	(LUX Collab.)
SIRUNYAN	18CU	JHEP 1801 056	A.M. Sirunyan et al.	(CMS Collab.)	AKERS	14	JCAP 1402 009	J. Akers et al.	(MAGIC Collab.)
SIRUNYAN	18DH	JHEP 1809 046	A.M. Sirunyan et al.	(CMS Collab.)	ANGLOHER	14	EPJ C74 3184	G. Angloher et al.	(CRESSIT-II Collab.)
SIRUNYAN	18S	PR D97 092005	A.M. Sirunyan et al.	(CMS Collab.)	APRILE	14A	ASP 54 11	E. Aprile et al.	(XENON100 Collab.)
YANG	18	CP 042 023002	L.T. Yang et al.	(CDEX Collab.)	AVRORIN	14	ASP 62 12	A.D. Avrorin et al.	(BAIKAL Collab.)
ABOUD	17A	PL B765 11	M. Aaboud et al.	(ATLAS Collab.)	FELIZARDO	14	PR D89 072013	M. Felizardo et al.	(SIMPLE Collab.)
ABOUD	17AM	PRL 119 181804	M. Aaboud et al.	(ATLAS Collab.)	LEE	14A	PR D90 052006	H.S. Lee et al.	(KIMS Collab.)
ABOUD	17AQ	PR D96 112004	M. Aaboud et al.	(ATLAS Collab.)	LIU	14A	PR D90 032003	S.K. Liu et al.	(CDEX Collab.)
ABOUD	17BD	EPJ C77 765	M. Aaboud et al.	(ATLAS Collab.)	UCHIDA	14	PTEP 2014 063C01	H. Uchida et al.	(XMASS Collab.)
ABOUD	17R	EPJ C77 393	M. Aaboud et al.	(ATLAS Collab.)	YUE	14	PR D90 091701	Q. Yue et al.	(CDEX Collab.)
AARTSEN	17	EPJ C77 82	M.G. Aartsen et al.	(IceCube Collab.)	AAD	13AD	JHEP 1304 075	G. Aad et al.	(ATLAS Collab.)
AARTSEN	17A	EPJ C77 146	M.G. Aartsen et al.	(IceCube Collab.)	AAD	13C	PRL 110 011802	G. Aad et al.	(ATLAS Collab.)
Also		EPJ C79 214 (err.)	M.G. Aartsen et al.	(IceCube Collab.)	AARTSEN	13	PR D89 012002	C. Aarseth et al.	(COGENT Collab.)
AARTSEN	17C	EPJ C77 627	M.G. Aartsen et al.	(IceCube Collab.)	LEITE	13B	PRL 110 131302	M.G. Aartsen et al.	(IceCube Collab.)
AGUILAR-AR...	17	PRL 118 141803	A. Aguilar-Arevalo et al.	(DAMIC Collab.)	AARTSEN	13C	PR D88 122001	M.G. Aartsen et al.	(IceCube Collab.)
AGUILAR-AR...	17A	PRL 118 221803	A.A. Aguilar-Arevalo et al.	(MiniBoONE Collab.)	ABE	13B	PL B719 78	K. Abe et al.	(XMASS Collab.)
AKERIB	17	PRL 118 021303	D.S. Akerib et al.	(LUX Collab.)	ABRAMOWSKI	13	PRL 110 041301	A. Abramowski et al.	(H.E.S.S. Collab.)
AKERIB	17A	PRL 118 251302	D.S. Akerib et al.	(LUX Collab.)	ACKERMANN	13A	PR D88 082002	M. Ackermann et al.	(Fermi-LAT Collab.)
ALBERT	17A	PL B769 249	A. Albert et al.	(ANTARES Collab.)	ADRIAN-MAR...	13	JCAP 1311 032	S. Adrian-Martinez et al.	(ANTARES Collab.)
Also		PL B796 253 (err.)	A. Albert et al.	(ANTARES Collab.)	AGNES	13	PR D88 031104	R. Agnese et al.	(CDMS Collab.)
AMOLE	17	PRL 118 251301	C. Amole et al.	(PICO Collab.)	AGNESE	13A	PRL 111 251301	R. Agnese et al.	(CDMS Collab.)
ANGLOHER	17A	EPJ C77 637	G. Angloher et al.	(CRESSIT Collab.)	APRILE	13	PRL 111 021301	E. Aprile et al.	(XENON100 Collab.)
APRILE	17	PRL 118 101101	E. Aprile et al.	(XENON100 Collab.)	BERNABEI	13A	EPJ C73 2648	R. Bernabei et al.	(DAMA Collab.)
APRILE	17A	PR D96 022008	E. Aprile et al.	(XENON100 Collab.)	BOLIV	13	JCAP 1309 019	M. Bolivar et al.	(MAGIC Collab.)
APRILE	17D	PR D96 042004	E. Aprile et al.	(XENON100 Collab.)	LI	13B	PRL 110 261301	H.B. Li et al.	(TEXONO Collab.)
APRILE	17G	PRL 119 181301	E. Aprile et al.	(XENON Collab.)	SUVOROVA	13	PAN 76 1367	O.V. Suvorova et al.	(INRM)
APRILE	17H	PR D96 122002	E. Aprile et al.	(XENON100 Collab.)	Translated from YAF 76 1433.				
APRILE	17K	JCAP 1710 039	E. Aprile et al.	(XENON100 Collab.)	ZHAO	13	PR D88 052004	W. Zhao et al.	(CDEX Collab.)
ARCHAMBAU...	17	PR D95 082001	S. Archambault et al.	(VERITAS Collab.)	AALTONEN	12K	PRL 108 201802	T. Aaltonen et al.	(CDF Collab.)
AVRORIN	17	JETP 125 80	A.D. Avrorin et al.	(BAIKAL Collab.)	AALTONEN	12M	PRL 108 211804	T. Aaltonen et al.	(CDF Collab.)
BANERJEE	17	PRL 118 011802	D. Banerjee et al.	(NA64 Collab.)	ABBASI	12	PR D85 042002	R. Abbasi et al.	(IceCube Collab.)
BARBOSA-D...	17	PR D95 032006	E. Barbosa de Souza et al.	(DM17 Collab.)	ABRAMOWSKI	12	APJ 750 123	A. Abramowski et al.	(H.E.S.S. Collab.)
BATTAT	17	ASP 91 65	J.B.R. Battat et al.	(DRIFT-III Collab.)	ACKERMANN	12	PR D86 022002	M. Ackermann et al.	(Fermi-LAT Collab.)
BEHNKE	17	ASP 90 85	E. Behnke et al.	(PICASSO Collab.)	AKIMOV	12	PR D86 012002	C. Akimov et al.	(ZEPLIN-III Collab.)
BOUDAUD	17	PRL 119 021103	R. Boudaud, J. Lavallo, P. Salati	(Pandax-II Collab.)	ALIU	12	PR D85 062001	E. Aliu et al.	(VERITAS Collab.)
CHEN	17E	PR D96 102007	X. Chen et al.	(Pandax-II Collab.)	ANGLOHER	12	EPJ C72 1971	G. Angloher et al.	(CRESSIT-II Collab.)
CUI	17A	PRL 119 181302	X. Cui et al.	(Pandax-II Collab.)	APRILE	12	PRL 109 181301	E. Aprile et al.	(XENON100 Collab.)
FU	17C	PRL 118 071301	C. Fu et al.	(Pandax-II Collab.)	ARCHAMBAU...	12	PL B711 153	S. Archambault et al.	(PICASSO Collab.)
Also		PRL 120 049902 (err.)	C. Fu et al.	(Pandax-II Collab.)	ARMENGAUD	12	PR D86 051701	E. Armengaud et al.	(EDELWEISS Collab.)

AALSETH	11	PRL 106 131301	C.E. Aalseth et al.	(CoGeNT Collab.)
AALSETH	11A	PRL 107 141301	C.E. Aalseth et al.	(CoGeNT Collab.)
ABBASI	11C	PR D84 022004	R. Abbasi et al.	(IceCube Collab.)
ABRAMOWSKI	11	PRL 106 161301	A. Abramowski et al.	(H.E.S.S. Collab.)
ACKERMANN	11	PRL 107 241302	M. Ackermann et al.	(Fermi-LAT Collab.)
AHLEN	11	PL B695 124	S. Ahlen et al.	(DMTPC Collab.)
AHMED	11	PR D83 112002	Z. Ahmed et al.	(CDMS Collab.)
AHMED	11A	PR D84 011102	Z. Ahmed et al.	(CDMS and EDELWEISS Collabs.)
AHMED	11B	PRL 106 131302	Z. Ahmed et al.	(CDMS Collab.)
AJELLO	11	PR D84 032007	M. Ajello et al.	(Fermi-LAT Collab.)
ANGLE	11	PRL 107 051301	J. Angle et al.	(XENON10 Collab.)
Also		PRL 110 249901 (err.)	J. Angle et al.	(XENON10 Collab.)
APRILE	11	PR D84 052003	E. Aprile et al.	(XENON100 Collab.)
APRILE	11A	PR D84 061101	E. Aprile et al.	(XENON100 Collab.)
APRILE	11B	PRL 107 131302	E. Aprile et al.	(XENON100 Collab.)
ARMENGAUD	11	PL B702 329	E. Armengaud et al.	(EDELWEISS-II Collab.)
BEHNKE	11	PRL 106 021303	E. Behnke et al.	(COUAPP Collab.)
GERINGER-SA...	11	PRL 107 241303	A. Gerlinger-Sameth, S.M. Koushappas	(ZEPLIN-III Collab.)
HORN	11	PL B705 471	M. Horn et al.	(CDMS Collab.)
TANAKA	11	APJ 742 78	T. Tanaka et al.	(Super-Kamiokande Collab.)
ABBASI	10	PR D81 057101	R. Abbasi et al.	(IceCube Collab.)
AHMED	10	SCI 327 1619	Z. Ahmed et al.	(CDMS II Collab.)
AKERIB	10	PR D82 122004	D.S. Akerib et al.	(CDMS II Collab.)
AKIMOV	10	PL B692 180	D.Yu. Akimov et al.	(ZEPLIN-III Collab.)
APRILE	10	PRL 105 131302	E. Aprile et al.	(XENON100 Collab.)
ARMENGAUD	10	PL B687 294	E. Armengaud et al.	(EDELWEISS-II Collab.)
FELIZARDO	10	PRL 105 211301	M. Felizardo et al.	(The SIMPLE Collab.)
MIUCHI	10	PL B686 11	K. Miuchi et al.	(NEWAGE Collab.)
ABBASI	09B	PRL 102 201302	R. Abbasi et al.	(IceCube Collab.)
AHMED	09	PRL 102 011301	Z. Ahmed et al.	(CDMS Collab.)
ANGLE	09	PR D80 115005	J. Angle et al.	(XENON10 Collab.)
ANGLOHER	09	ASP 31 270	G. Angloher et al.	(CREST Collab.)
ARCHAMBAU...	09	PL B682 185	S. Archambault et al.	(PICASSO Collab.)
LEBEDENKO	09A	PRL 103 151302	V.N. Lebedenko et al.	(ZEPLIN-III Collab.)
LIN	09	PR D79 061101	S.T. Lin et al.	(TEXONO Collab.)
AALSETH	08	PRL 101 251301	C.E. Aalseth et al.	(CoGeNT Collab.)
Also		PRL 102 109903 (err.)	C.E. Aalseth et al.	(CoGeNT Collab.)
ANGLE	08A	PRL 101 091301	J. Angle et al.	(XENON10 Collab.)
BEDNYAKOV	08	PAN 71 111	V.A. Bednyakov, H.P. Klapdor-Kleingrothaus, I.V. Krivosheina	
Translated from YAF 71 112.				
ALNER	07	PL B653 161	G.J. Alner et al.	(ZEPLIN-II Collab.)
LEE	07A	PRL 99 091301	H.S. Lee et al.	(KIMS Collab.)
MIUCHI	07	PL B654 58	K. Miuchi et al.	
AKERIB	06	PR D73 011102	D.S. Akerib et al.	(CDMS Collab.)
SHIMIZU	06A	PL B633 195	Y. Shimizu et al.	
AKERIB	05	PR D72 052009	D.S. Akerib et al.	(CDMS Collab.)
ALNER	05	PL B616 17	G.J. Alner et al.	(UK Dark Matter Collab.)
BARNABE-HE...	05	PL B624 186	M. Barnabe-Heider et al.	(PICASSO Collab.)
BENOIT	05	PL B616 25	A. Benoit et al.	(EDELWEISS Collab.)
GIRARD	05	PL B621 233	T.A. Girard et al.	(SIMPLE Collab.)
GIULIANI	05	PRL 95 101301	F. Giuliani	
GIULIANI	05A	PR D71 123503	F. Giuliani, T.A. Girard	
KLAPDOR-K...	05	PL B609 226	H.V. Klapdor-Kleingrothaus, I.V. Krivosheina, C. Tomei	
GIULIANI	04	PL B588 151	F. Giuliani, T.A. Girard	
GIULIANI	04A	PRL 93 161301	F. Giuliani	
MIUCHI	03	ASP 19 135	K. Miuchi et al.	
TAKEDA	03	PL B572 145	A. Takeda et al.	
ANGLOHER	02	ASP 18 43	G. Angloher et al.	(CREST Collab.)
BELLI	02	PR D66 043503	P. Belli et al.	
BERNABE	02C	EPJ C23 61	R. Bernabei et al.	(DAMA Collab.)
GREEN	02	PR D66 083003	A.M. Green	
BAUDIS	01	PR D63 022001	L. Baudis et al.	(Heidelberg-Moscow Collab.)
SMITH	01	PR D64 043502	D. Smith, N. Weiner	
ULLIO	01	JHEP 0107 044	P. Ullio, M. Kamionkowski, P. Vogel	
BENOIT	00	PL B479 8	A. Benoit et al.	(EDELWEISS Collab.)
BERNABE	00D	NJP 2 15	R. Bernabei et al.	(DAMA Collab.)
COLLAR	00	PRL 85 3083	J.J. Collar et al.	(SIMPLE Collab.)
AMBROSIO	99	PR D60 082002	M. Ambrosio et al.	(Macro Collab.)
BERNABE	99	PL B450 448	R. Bernabei et al.	(DAMA Collab.)
BERNABE	99D	PRL 83 4918	R. Bernabei et al.	(DAMA Collab.)
BRHLIK	99	PL B464 303	M. Brhlik, L. Roszkowski	
DERBIN	99	PAN 62 1886	A.V. Derbin et al.	
Translated from YAF 62 2034.				
KLIMENKO	98	JETPL 67 875	A.A. Klimenko et al.	
Translated from ZETFP 67 835.				
SARSA	97	PR D56 1856	M.L. Sarsa et al.	(ZARA Collab.)
ALESSAND...	96	PL B384 316	A. Alessandrello et al.	(MILA, MILAI, SASSO Collabs.)
BELLI	96	PL B387 222	P. Belli et al.	(DAMA Collab.)
Also		PL B389 783 (erratum)	P. Belli et al.	(DAMA Collab.)
BELLI	96C	PL C19 537	P. Belli et al.	(DAMA Collab.)
BERNABE	96	PL B389 757	R. Bernabei et al.	(DAMA Collab.)
COLLAR	96	PRL 76 331	J.J. Collar	(SCUC Collab.)
SARSA	96	PL B386 458	M.L. Sarsa et al.	(ZARA Collab.)
Also		PR D56 1856	M.L. Sarsa et al.	(ZARA Collab.)
SMITH	96	PL B379 299	P.F. Smith et al.	(RAL, SHEF, LOIC+ Collab.)
SNOWDEN-...	96	PRL 76 332	D.P. Snowden-Hft, E.S. Freeman, P.B. Price	(UCB Collab.)
GARCIA	95	PR D51 1458	E. Garcia et al.	(ZARA, SUCU, PNL Collabs.)
QUENBY	95	PL B351 70	J.J. Quenby et al.	(LOIC, RAL, SHEF+ Collab.)
SNOWDEN-...	95	PRL 74 4133	D.P. Snowden-Hft, E.S. Freeman, P.B. Price	(UCB Collab.)
Also		PRL 76 331	J.J. Collar	(SCUC Collab.)
Also		PRL 76 332	D.P. Snowden-Hft, E.S. Freeman, P.B. Price	(UCB Collab.)
BECK	94	PL B336 141	M. Beck et al.	(MPIH, KIAE, SASSO Collabs.)
BACCI	92	PL B293 460	C. Bacci et al.	(Beijing-Roma-Saclay Collab.)
REUSSER	91	PL B255 143	D. Reusser et al.	(NEUC, CIT, PSI Collabs.)
CALDWELL	88	PRL 61 510	D.O. Caldwell et al.	(UCSB, UCB, LBL Collabs.)

- Limits on charged particles in e^+e^- collisions
- Limits on charged particles in hadron reactions
- Limits on charged particles in cosmic rays
- Searches for quantum black hole production

Note that searches appear in separate sections elsewhere for Higgs bosons (and technipions), other heavy bosons (including W_R, W', Z' , leptoquarks, axiglons), axions (including pseudo-Goldstone bosons, Majorons, familons), WIMPs, heavy leptons, heavy neutrinos, free quarks, monopoles, supersymmetric particles, and compositeness.

We no longer list for limits on tachyons and centauros. See our 1994 edition for these limits.

CONCENTRATION OF STABLE PARTICLES IN MATTER

Concentration of Heavy (Charge +1) Stable Particles in Matter

VALUE	CL%	DOCUMENT ID	TECN	COMMENT
$<4 \times 10^{-17}$	95	1 YAMAGATA	93 SPEC	Deep sea water, $M=5-1600 m_p$
$<6 \times 10^{-15}$	95	2 VERKERK	92 SPEC	Water, $M=10^5$ to 3×10^7 GeV
$<7 \times 10^{-15}$	95	2 VERKERK	92 SPEC	Water, $M=10^4, 6 \times 10^7$ GeV
$<9 \times 10^{-15}$	95	2 VERKERK	92 SPEC	Water, $M=10^8$ GeV
$<3 \times 10^{-23}$	90	3 HEMMICK	90 SPEC	Water, $M=1000 m_p$
$<2 \times 10^{-21}$	90	3 HEMMICK	90 SPEC	Water, $M=5000 m_p$
$<3 \times 10^{-20}$	90	3 HEMMICK	90 SPEC	Water, $M=10000 m_p$
$<1. \times 10^{-29}$		SMITH	82B SPEC	Water, $M=30-400 m_p$
$<2. \times 10^{-28}$		SMITH	82B SPEC	Water, $M=12-1000 m_p$
$<1. \times 10^{-14}$		SMITH	82B SPEC	Water, $M > 1000 m_p$
$<(0.2-1.) \times 10^{-21}$		SMITH	79 SPEC	Water, $M=6-350 m_p$

- • • We do not use the following data for averages, fits, limits, etc. • • •
- 1 YAMAGATA 93 used deep sea water at 4000 m since the concentration is enhanced in deep sea due to gravity.
- 2 VERKERK 92 looked for heavy isotopes in sea water and put a bound on concentration of stable charged massive particle in sea water. The above bound can be translated into into a bound on charged dark matter particle (5×10^6 GeV), assuming the local density, $\rho=0.3$ GeV/cm³, and the mean velocity (v)=300 km/s.
- 3 See HEMMICK 90 Fig. 7 for other masses 100-10000 m_p .

Concentration of Heavy Stable Particles Bound to Nuclei

VALUE	CL%	DOCUMENT ID	TECN	COMMENT
$<1.2 \times 10^{-11}$	95	1 JAVORSEK	01 SPEC	Au, $M=3$ GeV
$<6.9 \times 10^{-10}$	95	1 JAVORSEK	01 SPEC	Au, $M=144$ GeV
$<1 \times 10^{-11}$	95	2 JAVORSEK	01B SPEC	Au, $M=188$ GeV
$<1 \times 10^{-8}$	95	2 JAVORSEK	01B SPEC	Au, $M=1669$ GeV
$<6 \times 10^{-9}$	95	2 JAVORSEK	01B SPEC	Fe, $M=188$ GeV
$<1 \times 10^{-8}$	95	2 JAVORSEK	01B SPEC	Fe, $M=647$ GeV
$<4 \times 10^{-20}$	90	3 HEMMICK	90 SPEC	C, $M=100 m_p$
$<8 \times 10^{-20}$	90	3 HEMMICK	90 SPEC	C, $M=1000 m_p$
$<2 \times 10^{-16}$	90	3 HEMMICK	90 SPEC	C, $M=10000 m_p$
$<6 \times 10^{-13}$	90	3 HEMMICK	90 SPEC	Li, $M=1000 m_p$
$<1 \times 10^{-11}$	90	3 HEMMICK	90 SPEC	Be, $M=1000 m_p$
$<6 \times 10^{-14}$	90	3 HEMMICK	90 SPEC	B, $M=1000 m_p$
$<4 \times 10^{-17}$	90	3 HEMMICK	90 SPEC	O, $M=1000 m_p$
$<4 \times 10^{-15}$	90	3 HEMMICK	90 SPEC	F, $M=1000 m_p$
$<1.5 \times 10^{-13}$ /nucleon	68	4 NORMAN	89 SPEC	$^{206}\text{PbX}^-$
$<1.2 \times 10^{-12}$ /nucleon	68	4 NORMAN	87 SPEC	$^{56,58}\text{FeX}^-$

- • • We do not use the following data for averages, fits, limits, etc. • • •
- 1 JAVORSEK 01 search for (neutral) SIMPs (strongly interacting massive particles) bound to Au nuclei. Here M is the effective SIMP mass.
- 2 JAVORSEK 01B search for (neutral) SIMPs (strongly interacting massive particles) bound to Au and Fe nuclei from various origins with exposures on the earth's surface, in a satellite, heavy ion collisions, etc. Here M is the mass of the anomalous nucleus. See also JAVORSEK 02.
- 3 See HEMMICK 90 Fig. 7 for other masses 100-10000 m_p .
- 4 Bound valid up to $m_{X^-} \sim 100$ TeV.

Other Particle Searches

OMITTED FROM SUMMARY TABLE OTHER PARTICLE SEARCHES

Revised February 2018 by K. Hikasa (Tohoku University).

We collect here those searches which do not appear in any other search categories. These are listed in the following order:

- Concentration of stable particles in matter
- General new physics searches
- Limits on jet-jet resonance in hadron collisions
- Limits on neutral particle production at accelerators

Searches Particle Listings

Other Particle Searches

GENERAL NEW PHYSICS SEARCHES

This subsection lists some of the search experiments which look for general signatures characteristic of new physics, independent of the framework of a specific model.

The observed events are compatible with Standard Model expectation, unless noted otherwise.

VALUE	DOCUMENT ID	TECN	COMMENT
• • • We do not use the following data for averages, fits, limits, etc. • • •			
	1 SIRUNYAN 20A	CMS	SUSY/LQ search with mT2 or long-lived charged particles
	2 ALCANTARA 19		Auger, superheavy DM
	3 PORAYKO 18	PPTA	pulsar timing fuzzy DM search
	4 AAD 15AT	ATLS	$t + \cancel{E}_T$
	5 KHACHATRYAN..15F	CMS	$t + \cancel{E}_T$
	6 AALTONEN 14J	CDF	$W + 2$ jets
	7 AAD 13A	ATLS	$WW \rightarrow \ell\nu\ell'\nu$
	8 AAD 13C	ATLS	$\gamma + \cancel{E}_T$
	9 AALTONEN 13I	CDF	Delayed $\gamma + \cancel{E}_T$
	10 CHATRCHYAN13	CMS	$\ell^+\ell^- +$ jets + \cancel{E}_T
	11 AAD 12C	ATLS	$t\bar{t} + \cancel{E}_T$
	12 AALTONEN 12M	CDF	jet + \cancel{E}_T
	13 CHATRCHYAN12AP	CMS	jet + \cancel{E}_T
	14 CHATRCHYAN12Q	CMS	$Z +$ jets + \cancel{E}_T
	15 CHATRCHYAN12T	CMS	$\gamma + \cancel{E}_T$
	16 AAD 11S	ATLS	jet + \cancel{E}_T
	17 AALTONEN 11AF	CDF	$\ell^\pm\ell^\pm$
	18 CHATRCHYAN11C	CMS	$\ell^+\ell^- +$ jets + \cancel{E}_T
	19 CHATRCHYAN11U	CMS	jet + \cancel{E}_T
	20 AALTONEN 10AF	CDF	$\gamma\gamma + \ell, \cancel{E}_T$
	21 AALTONEN 09AF	CDF	$\ell\gamma b \cancel{E}_T$
	22 AALTONEN 09G	CDF	$\ell\ell\ell \cancel{E}_T$

- 1 SIRUNYAN 20A search for SUSY and LQ production using mT2 or presence of long-lived charged particle; no signal, limits placed in various mass planes for different BSM scenarios and various assumed lifetimes.
- 2 ALCANTARA 19 place limits on $m(\text{WIMP}Z\text{illa}=X)$ vs lifetime from upper bound on ultra high energy cosmic rays at Auger experiment: e.g. $\tau(X) < 4 \times 10^{22}$ yr for $m(X) = 10^{16}$ GeV.
- 3 PORAYKO 18 search for deviations in the residuals of pulsar timing data using PPTA. No signal observed. Limits set on fuzzy DM with $3 \times 10^{-24} < m(\text{DM}) < 2 \times 10^{-22}$ eV.
- 4 AAD 15AT search for events with a top quark and missing E_T in pp collisions at $E_{\text{cm}} = 8$ TeV with $L = 20.3 \text{ fb}^{-1}$.
- 5 KHACHATRYAN 15F search for events with a top quark and missing E_T in pp collisions at $E_{\text{cm}} = 8$ TeV with $L = 19.7 \text{ fb}^{-1}$.
- 6 AALTONEN 14J examine events with a W and two jets in $p\bar{p}$ collisions at $E_{\text{cm}} = 1.96$ TeV with $L = 8.9 \text{ fb}^{-1}$. Invariant mass distributions of the two jets are consistent with the Standard Model expectation.
- 7 AAD 13A search for resonant WW production in pp collisions at $E_{\text{cm}} = 7$ TeV with $L = 4.7 \text{ fb}^{-1}$.
- 8 AAD 13C search for events with a photon and missing E_T in pp collisions at $E_{\text{cm}} = 7$ TeV with $L = 4.6 \text{ fb}^{-1}$.
- 9 AALTONEN 13I search for events with a photon and missing E_T , where the photon is detected after the expected timing, in $p\bar{p}$ collisions at $E_{\text{cm}} = 1.96$ TeV with $L = 6.3 \text{ fb}^{-1}$. The data are consistent with the Standard Model expectation.
- 10 CHATRCHYAN 13 search for events with an opposite-sign lepton pair, jets, and missing E_T in pp collisions at $E_{\text{cm}} = 7$ TeV with $L = 4.98 \text{ fb}^{-1}$.
- 11 AAD 12C search for events with a $t\bar{t}$ pair and missing E_T in pp collisions at $E_{\text{cm}} = 7$ TeV with $L = 1.04 \text{ fb}^{-1}$.
- 12 AALTONEN 12M search for events with a jet and missing E_T in $p\bar{p}$ collisions at $E_{\text{cm}} = 1.96$ TeV with $L = 6.7 \text{ fb}^{-1}$.
- 13 CHATRCHYAN 12AP search for events with a jet and missing E_T in pp collisions at $E_{\text{cm}} = 7$ TeV with $L = 5.0 \text{ fb}^{-1}$.
- 14 CHATRCHYAN 12Q search for events with a Z , jets, and missing E_T in pp collisions at $E_{\text{cm}} = 7$ TeV with $L = 4.98 \text{ fb}^{-1}$.
- 15 CHATRCHYAN 12T search for events with a photon and missing E_T in pp collisions at $E_{\text{cm}} = 7$ TeV with $L = 5.0 \text{ fb}^{-1}$.
- 16 AAD 11S search for events with one jet and missing E_T in pp collisions at $E_{\text{cm}} = 7$ TeV with $L = 33 \text{ pb}^{-1}$.
- 17 AALTONEN 11AF search for high- p_T like-sign dileptons in $p\bar{p}$ collisions at $E_{\text{cm}} = 1.96$ TeV with $L = 6.1 \text{ fb}^{-1}$.
- 18 CHATRCHYAN 11C search for events with an opposite-sign lepton pair, jets, and missing E_T in pp collisions at $E_{\text{cm}} = 7$ TeV with $L = 34 \text{ pb}^{-1}$.
- 19 CHATRCHYAN 11U search for events with one jet and missing E_T in pp collisions at $E_{\text{cm}} = 7$ TeV with $L = 36 \text{ pb}^{-1}$.
- 20 AALTONEN 10AF search for $\gamma\gamma$ events with e, μ, τ , or missing E_T in $p\bar{p}$ collisions at $E_{\text{cm}} = 1.96$ TeV with $L = 1.1\text{--}2.0 \text{ fb}^{-1}$.
- 21 AALTONEN 09AF search for $\ell\gamma b$ events with missing E_T in $p\bar{p}$ collisions at $E_{\text{cm}} = 1.96$ TeV with $L = 1.9 \text{ fb}^{-1}$. The observed events are compatible with Standard Model expectation including $t\bar{t}\gamma$ production.
- 22 AALTONEN 09G search for $\mu\mu\mu$ and $\mu\mu e$ events with missing E_T in $p\bar{p}$ collisions at $E_{\text{cm}} = 1.96$ TeV with $L = 976 \text{ pb}^{-1}$.

LIMITS ON JET-JET RESONANCES

Heavy Particle Production Cross Section

Limits are for a particle decaying to two hadronic jets.

Units(pb)	CL%	Mass(GeV)	DOCUMENT ID	TECN	COMMENT
• • • We do not use the following data for averages, fits, limits, etc. • • •					
			1 AABOUD 19AJ	ATLS	$pp \rightarrow \gamma X, X \rightarrow jj$
			2 SIRUNYAN 19B	CMS	$pp \rightarrow jA, A \rightarrow b\bar{b}$
			3 SIRUNYAN 19CD	CMS	$pp \rightarrow Z'\gamma, Z' \rightarrow jj$
			4 AABOUD 18AD	ATLS	$pp \rightarrow Y \rightarrow HX \rightarrow (bb) + (qq)$
			5 AABOUD 18CK	ATLS	$pp \rightarrow bbb + \cancel{E}_T$
			6 AABOUD 18CL	ATLS	$pp \rightarrow$ vector-like quarks
			7 AABOUD 18N	ATLS	$pp \rightarrow jj$ resonance
			8 SIRUNYAN 18DJ	CMS	$pp \rightarrow ZZ$ or $WZ \rightarrow \ell\bar{\ell}jj$
			9 SIRUNYAN 18DY	CMS	$pp \rightarrow RR; R \rightarrow jj$
			10 KHACHATRYAN..17W	CMS	$pp \rightarrow jj$ resonance
			11 KHACHATRYAN..17Y	CMS	$pp \rightarrow (8\text{--}10) j + \cancel{E}_T$
			12 SIRUNYAN 17F	CMS	$pp \rightarrow jj$ angular distribution
			13 AABOUD 16	ATLS	$pp \rightarrow b +$ jet
			14 AAD 16N	ATLS	$pp \rightarrow 3$ high E_T jets
			15 AAD 16S	ATLS	$pp \rightarrow jj$ resonance
			16 KHACHATRYAN..16K	CMS	$pp \rightarrow jj$ resonance
			17 KHACHATRYAN..16L	CMS	$pp \rightarrow jj$ resonance
			18 AAD 13D	ATLS	$7 \text{ TeV } pp \rightarrow 2$ jets
			19 AALTONEN 13R	CDF	$1.96 \text{ TeV } p\bar{p} \rightarrow 4$ jets
			20 CHATRCHYAN13A	CMS	$7 \text{ TeV } pp \rightarrow 2$ jets
			21 CHATRCHYAN13A	CMS	$7 \text{ TeV } pp \rightarrow b\bar{b}X$
			22 AAD 12S	ATLS	$7 \text{ TeV } pp \rightarrow 2$ jets
			23 CHATRCHYAN12BL	CMS	$7 \text{ TeV } pp \rightarrow t\bar{t}X$
			24 AAD 11AG	ATLS	$7 \text{ TeV } pp \rightarrow 2$ jets
			25 AALTONEN 11M	CDF	$1.96 \text{ TeV } p\bar{p} \rightarrow W + 2$ jets
			26 ABAZOV 11I	D0	$1.96 \text{ TeV } p\bar{p} \rightarrow W + 2$ jets
			27 AAD 10	ATLS	$7 \text{ TeV } pp \rightarrow 2$ jets
			28 KHACHATRYAN..10	CMS	$7 \text{ TeV } pp \rightarrow 2$ jets
			29 ABE 99F	CDF	$1.8 \text{ TeV } p\bar{p} \rightarrow b\bar{b} +$ anything
			30 ABE 97G	CDF	$1.8 \text{ TeV } p\bar{p} \rightarrow 2$ jets
			31 ABE 93G	CDF	$1.8 \text{ TeV } p\bar{p} \rightarrow 2$ jets
			31 ABE 93G	CDF	$1.8 \text{ TeV } p\bar{p} \rightarrow 2$ jets
			31 ABE 93G	CDF	$1.8 \text{ TeV } p\bar{p} \rightarrow 2$ jets

- < 2603 95 200
< 44 95 400
< 7 95 600
- 1 AABOUD 19AJ search for low mass dijet resonance in $pp \rightarrow \gamma X, X \rightarrow jj$ at 13 TeV with 79.8 fb^{-1} of data; no signal found; limits placed on Z' model in coupling vs. $m(Z')$ plane.
 - 2 SIRUNYAN 19B search for low mass resonance $pp \rightarrow jA, A \rightarrow b\bar{b}$ at 13 TeV using 35.9 fb^{-1} ; no signal; exclude resonances 50–350 GeV depending on production and decay.
 - 3 SIRUNYAN 19CD search for $pp \rightarrow Z'\gamma, Z' \rightarrow jj$ with fat jet (jj); no signal, limits placed in $m(Z')$ vs. coupling plane for Z' masses from 10 to 125 GeV.
 - 4 AABOUD 18AD search for new heavy particle $Y \rightarrow HX \rightarrow (bb) + (qq)$. No signal observed. Limits set on $m(Y)$ vs. $m(X)$ in the ranges of $m(Y)$ in 1–4 TeV and $m(X)$ in 50–1000 GeV.
 - 5 AABOUD 18CK search for SUSY Higgsinos in gauge-mediation via $pp \rightarrow bbb + \cancel{E}_T$ at 13 TeV using two complementary analyses with $24.3/36.1 \text{ fb}^{-1}$; no signal is found and Higgsinos with masses between 130 and 230 GeV and between 290 and 880 GeV are excluded at the 95% confidence level.
 - 6 AABOUD 18CL search for $pp \rightarrow$ vector-like quarks \rightarrow jets at 13 TeV with 36 fb^{-1} ; no signal seen; limits set on various VLQ scenarios. For pure $B \rightarrow Hb$ or $T \rightarrow Ht$, set the mass limit $m > 1010$ GeV.
 - 7 AABOUD 18N search for dijet resonance at Atlas with 13 TeV and 29.3 fb^{-1} ; limits set on $m(Z')$ in the mass range of 450–1800 GeV.
 - 8 SIRUNYAN 18DJ search for $pp \rightarrow ZZ$ or $WZ \rightarrow \ell\bar{\ell}jj$ resonance at 13 TeV, 35.9 fb^{-1} ; no signal; limits set in the 400–4500 GeV mass range, exclusion of W' up to 2270 GeV in the HVT model A, and up to 2330 GeV for HVT model B. WED bulk graviton exclusion up to 925 GeV.
 - 9 SIRUNYAN 18DY search for $pp \rightarrow RR; R \rightarrow jj$ two dijet resonances at 13 TeV 35.9 fb^{-1} ; no signal; limits placed on RPV top-squark pair production.
 - 10 KHACHATRYAN 17W search for dijet resonance in 12.9 fb^{-1} data at 13 TeV; see Fig. 2 for limits on axigluons, diquarks, dark matter mediators etc.
 - 11 KHACHATRYAN 17Y search for $pp \rightarrow (8\text{--}10) j$ in 19.7 fb^{-1} at 8 TeV. No signal seen. Limits set on colorons, axigluons, RPV, and SUSY.
 - 12 SIRUNYAN 17F measure $pp \rightarrow jj$ angular distribution in 2.6 fb^{-1} at 13 TeV; limits set on LEDs and quantum black holes.
 - 13 AABOUD 16 search for resonant dijets including one or two b -jets with 3.2 fb^{-1} at 13 TeV; exclude excited b^* quark from 1.1–2.1 TeV; exclude leptophilic Z' with SM couplings from 1.1–1.5 TeV.
 - 14 AAD 16N search for ≥ 3 jets with 3.6 fb^{-1} at 13 TeV; limits placed on micro black holes (Fig. 10) and string balls (Fig. 11).
 - 15 AAD 16S search for high mass jet-jet resonance with 3.6 fb^{-1} at 13 TeV; exclude portions of excited quarks, W', Z' and contact interaction parameter space.
 - 16 KHACHATRYAN 16K search for dijet resonance in 2.4 fb^{-1} data at 13 TeV; see Fig. 3 for limits on axigluons, diquarks etc.
 - 17 KHACHATRYAN 16L use data scouting technique to search for jj resonance on 18.8 fb^{-1} of data at 8 TeV. Limits on the coupling of a leptophobic Z' to quarks are set, improving on the results by other experiments in the mass range between 500–800 GeV.
 - 18 AAD 13D search for dijet resonances in pp collisions at $E_{\text{cm}} = 7$ TeV with $L = 4.8 \text{ fb}^{-1}$. The observed events are compatible with Standard Model expectation. See their Fig. 6 and Table 2 for limits on resonance cross section in the range $m = 1.0\text{--}4.0$ TeV.
 - 19 AALTONEN 13R search for production of a pair of jet-jet resonances in $p\bar{p}$ collisions at $E_{\text{cm}} = 1.96$ TeV with $L = 6.6 \text{ fb}^{-1}$. See their Fig. 5 and Tables 1, II for cross section limits.

See key on page 999

Searches Particle Listings

Other Particle Searches

- 20 CHATRCHYAN 13A search for $qq, qg,$ and gg resonances in pp collisions at $E_{cm} = 7$ TeV with $L = 4.8 \text{ fb}^{-1}$. See their Fig. 3 and Table 1 for limits on resonance cross section in the range $m = 1.0\text{--}4.3$ TeV.
- 21 CHATRCHYAN 13A search for $b\bar{b}$ resonances in pp collisions at $E_{cm} = 7$ TeV with $L = 4.8 \text{ fb}^{-1}$. See their Fig. 8 and Table 4 for limits on resonance cross section in the range $m = 1.0\text{--}4.0$ TeV.
- 22 AAD 12s search for dijet resonances in pp collisions at $E_{cm} = 7$ TeV with $L = 1.0 \text{ fb}^{-1}$. See their Fig. 3 and Table 2 for limits on resonance cross section in the range $m = 0.9\text{--}4.0$ TeV.
- 23 CHATRCHYAN 12BL search for $t\bar{t}$ resonances in pp collisions at $E_{cm} = 7$ TeV with $L = 4.4 \text{ fb}^{-1}$. See their Fig. 4 for limits on resonance cross section in the range $m = 0.5\text{--}3.0$ TeV.
- 24 AAD 11AG search for dijet resonances in pp collisions at $E_{cm} = 7$ TeV with $L = 36 \text{ pb}^{-1}$. Limits on number of events for $m = 0.6\text{--}4$ TeV are given in their Table 3.
- 25 AALTONEN 11M find a peak in two jet invariant mass distribution around 140 GeV in $W + 2$ jet events in $p\bar{p}$ collisions at $E_{cm} = 1.96$ TeV with $L = 4.3 \text{ fb}^{-1}$.
- 26 ABAZOV 11i search for two-jet resonances in $W + 2$ jet events in $p\bar{p}$ collisions at $E_{cm} = 1.96$ TeV with $L = 4.3 \text{ fb}^{-1}$ and give limits $\sigma < (2.6\text{--}1.3) \text{ pb}$ (95% CL) for $m = 110\text{--}170$ GeV. The result is incompatible with AALTONEN 11M.
- 27 AAD 10 search for narrow dijet resonances in pp collisions at $E_{cm} = 7$ TeV with $L = 315 \text{ nb}^{-1}$. Limits on the cross section in the range $10\text{--}10^3 \text{ pb}$ is given for $m = 0.3\text{--}1.7$ TeV.
- 28 KHACHATRYAN 10 search for narrow dijet resonances in pp collisions at $E_{cm} = 7$ TeV with $L = 2.9 \text{ pb}^{-1}$. Limits on the cross section in the range $1\text{--}300 \text{ pb}$ is given for $m = 0.5\text{--}2.6$ TeV separately in the final states $qq, qg,$ and gg .
- 29 ABE 99F search for narrow $b\bar{b}$ resonances in $p\bar{p}$ collisions at $E_{cm}=1.8$ TeV. Limits on $\sigma(p\bar{p} \rightarrow X + \text{anything}) \times B(X \rightarrow b\bar{b})$ in the range $3\text{--}10^3 \text{ pb}$ (95% CL) are given for $m_X=200\text{--}750$ GeV. See their Table I.
- 30 ABE 97G search for narrow dijet resonances in $p\bar{p}$ collisions with 106 pb^{-1} of data at $E_{cm} = 1.8$ TeV. Limits on $\sigma(p\bar{p} \rightarrow X + \text{anything}) \times B(X \rightarrow jj)$ in the range $10^4\text{--}10^{-1} \text{ pb}$ (95% CL) are given for dijet mass $m=200\text{--}1150$ GeV with both jets having $|\eta| < 2.0$ and the dijet system having $|\cos\theta^*| < 0.67$. See their Table I for the list of limits. Supersedes ABE 93c.
- 31 ABE 93c give cross section times branching ratio into light (d, u, s, c, b) quarks for $\Gamma = 0.02 M$. Their Table II gives limits for $M = 200\text{--}900$ GeV and $\Gamma = (0.02\text{--}0.2) M$.

LIMITS ON NEUTRAL PARTICLE PRODUCTION

Production Cross Section of Radiatively-Decaying Neutral Particle

VALUE (pb)	CL%	DOCUMENT ID	TECN	COMMENT
<0.0008	95	1 ALBERT 18c HAWC	γ from Sun	
$<(0.043\text{--}0.17)$	95	2 KHACHATRYAN 17D CMS	$Z\gamma$ resonance	
$<(0.05\text{--}0.8)$	95	3 AAD 16AI ATLS	$pp \rightarrow \gamma + \text{jet}$	
$<(2.5\text{--}0.5)$	95	4 KHACHATRYAN 16M CMS	$pp \rightarrow \gamma\gamma$ resonance	
$<(1.6\text{--}0.9)$	95	5 ABBIENDI 00D OPAL	$e^+e^- \rightarrow X^0 Y^0,$ $X^0 \rightarrow \gamma_0 Y^0$	
		6 ABBIENDI 00D OPAL	$e^+e^- \rightarrow X^0 X^0,$ $X^0 \rightarrow \gamma_0 \gamma_0$	
		7 ACKERSTAFF 97B OPAL	$e^+e^- \rightarrow X^0 Y^0,$ $X^0 \rightarrow \gamma_0 \gamma_0$	
		8 ACKERSTAFF 97B OPAL	$e^+e^- \rightarrow X^0 X^0,$ $X^0 \rightarrow \gamma_0 \gamma_0$	

- 1 ALBERT 18c search for WIMP annihilation in Sun to long-lived, radiatively decaying mediator; no signal; limits set on $\sigma^{SD}(Xp)$ assuming long-lived mediator.
- 2 KHACHATRYAN 17D search for new scalar resonance decaying to $Z\gamma$ with $Z \rightarrow e^+e^-, \mu^+\mu^-$ in pp collisions at 8 and 13 TeV; no signal seen.
- 3 AAD 16AI search for excited quarks (EQ) and quantum black holes (QBH) in 3.2 fb^{-1} at 13 TeV of data; exclude EQ below 4.4 TeV and QBH below 3.8 (6.2) TeV for RS1 (AD3) models. The visible cross section limit was obtained for 5 TeV resonance with $\sigma_G/M_G = 2\%$.
- 4 KHACHATRYAN 16M search for $\gamma\gamma$ resonance using 19.7 fb^{-1} at 8 TeV and 3.3 fb^{-1} at 13 TeV; slight excess at 750 GeV noted; limit set on RS graviton.
- 5 ABBIENDI 00d associated production limit is for $m_{X^0} = 90\text{--}188$ GeV, $m_{Y^0} = 0$ at $E_{cm} = 189$ GeV. See also their Fig. 9.
- 6 ABBIENDI 00d pair production limit is for $m_{X^0} = 45\text{--}94$ GeV, $m_{Y^0} = 0$ at $E_{cm} = 189$ GeV. See also their Fig. 12.
- 7 ACKERSTAFF 97B associated production limit is for $m_{X^0} = 80\text{--}160$ GeV, $m_{Y^0} = 0$ from 10.0 pb^{-1} at $E_{cm} = 161$ GeV. See their Fig. 3(a).
- 8 ACKERSTAFF 97B pair production limit is for $m_{X^0} = 40\text{--}80$ GeV, $m_{Y^0} = 0$ from 10.0 pb^{-1} at $E_{cm} = 161$ GeV. See their Fig. 3(b).

Heavy Particle Production Cross Section

VALUE (cm^2/N)	CL%	DOCUMENT ID	TECN	COMMENT
		1 AABOUD 19H ATLS	di-photon-jet resonance	
		2 AABOUD 19V ATLS	ATLAS review, mediator-based DM	
		3 SIRUNYAN 19o CMS	$pp \rightarrow \gamma E_T$	
		4 AABOUD 18CJ ATLS	$pp \rightarrow VV/\ell\ell/\ell\nu, V = W, Z, h$	
		5 AABOUD 18CM ATLS	$pp \rightarrow e\mu/e\tau/\mu\tau$	
		6 AAIJ 18AJ LHCb	$pp \rightarrow A' \rightarrow \mu^+\mu^-;$ dark photon	
		7 BANERJEE 18 NA64	$eZ \rightarrow eZX(A')$	
		8 BANERJEE 18A NA64	$eZ \rightarrow eZA', A' \rightarrow \chi\chi$	
		9 MARSICANO 18 E137	$e^+e^- \rightarrow A'(\gamma)$ visible decay	

10 SIRUNYAN	18BB CMS	$pp \rightarrow Z' \rightarrow \ell^+\ell^-$ at 13 TeV
11 SIRUNYAN	18DA CMS	$pp \rightarrow$ Black Hole, string ball, sphaleron
12 SIRUNYAN	18DD CMS	$pp \rightarrow jj$
13 SIRUNYAN	18DR CMS	$pp \rightarrow b\mu\bar{\mu}$
14 SIRUNYAN	18DU CMS	$pp \rightarrow \gamma\gamma$
15 SIRUNYAN	18ED CMS	$pp \rightarrow V \rightarrow Wh; h \rightarrow b\bar{b}; W \rightarrow \ell\nu$
16 AABOUD	17B ATLS	WH, ZH resonance
17 AAIJ	17BR LHCb	$pp \rightarrow \pi\nu\pi\nu, \pi\nu \rightarrow jj$
18 AAD	16o ATLS	$\ell + (\ell s \text{ or jets})$
19 AAD	16R ATLS	WW, WZ, ZZ resonance
20 KRASZNAHO...	16	$p^7\text{Li} \rightarrow {}^8\text{Be} \rightarrow X(17)N, X(17) \rightarrow e^+e^-$
21 LEES	15E BABR	e^+e^- collisions
22 ADAMS	97B KTEV	$m = 1.2\text{--}5$ GeV
23 GALLAS	95 TOF	$m = 0.5\text{--}20$ GeV
24 AKESSON	91 CNTR	$m = 0\text{--}5$ GeV
25 BADIER	86 BDMP	$\tau = (0.05\text{--}1.) \times 10^{-8}$ s
26 GUSTAFSON	76 CNTR	$\tau > 10^{-7}$ s

- 1 AABOUD 19H searches for di-photon-jet resonance at 13 TeV and 36.7 fb^{-1} of data; no signal found and limits placed on $\sigma \cdot \text{BR vs. mass}$ plane for various simplified models.
- 2 AABOUD 19V review ATLAS searches for mediator-based DM at 7, 8, and 13 TeV with up to 37 fb^{-1} of data; no signal found and limits set for wide variety of simplified models of dark matter.
- 3 SIRUNYAN 19o search for $pp \rightarrow \gamma E_T$ at 13 TeV with 36.1 fb^{-1} ; no signal found and limits set for various simplified models.
- 4 AABOUD 18CJ make multichannel search for $pp \rightarrow VV/\ell\ell/\ell\nu, V = W, Z, h$ at 13 TeV, 36.1 fb^{-1} ; no signal found; limits placed for several BSM models.
- 5 AABOUD 18CM search for lepton-flavor violating resonance in $pp \rightarrow e\mu/e\tau/\mu\tau$ at 13 TeV, 36.1 fb^{-1} ; no signal is found and limits placed for various BSM models.
- 6 AAIJ 18AJ search for prompt and delayed dark photon decay $A' \rightarrow \mu^+\mu^-$ at LHCb detector using 1.6 fb^{-1} of pp collisions at 13 TeV; limits on $m(A')$ vs. kinetic mixing are set.
- 7 BANERJEE 18 search for dark photon $A'/16.7$ MeV boson X at NA64 via $eZ \rightarrow eZX(A')$; no signal found and limits set on the $X\text{--}e^-$ coupling e_e in the range $1.3 \times 10^{-4} \leq e_e \leq 4.2 \times 10^{-4}$ excluding part of the allowed parameter space.
- 8 BANERJEE 18A search for invisibly decaying dark photons in $eZ \rightarrow eZA', A' \rightarrow$ invisible; no signal found and limits set on mixing for $m(A') < 1$ GeV.
- 9 MARSICANO 18 search for dark photon $e^+e^- \rightarrow A'(\gamma)$ visible decay in SLAC E137 e beam dump data. No signal observed and limits set in e coupling vs $m(A')$ plane, see their figure 7.
- 10 SIRUNYAN 18BB search for high mass dilepton resonance; no signal found and exclude portions of p-space of Z', KK graviton models.
- 11 SIRUNYAN 18DA search for $pp \rightarrow$ Black Hole, string ball, sphaleron via high multiplicity events at 13 TeV, 35.9 fb^{-1} ; no signal, require e.g. $m(\text{BH}) > 10.1$ TeV.
- 12 SIRUNYAN 18DD search for $pp \rightarrow jj$ deviations in dijet angular distribution. No signal observed. Set limits on large extra dimensions, black holes and DM mediators e.g. $m(\text{BH}) > 5.9\text{--}8.2$ TeV.
- 13 SIRUNYAN 18DR search for dimuon resonance in $pp \rightarrow b\mu\bar{\mu}$ at 8 and 13 TeV. Slight excess seen at $m(\mu\bar{\mu}) \sim 28$ GeV in some channels.
- 14 SIRUNYAN 18DU search for high mass diphoton resonance in $pp \rightarrow \gamma\gamma$ at 13 TeV using 35.9 fb^{-1} ; no signal; limits placed on RS Graviton, LED, and clockwork.
- 15 SIRUNYAN 18ED search for $pp \rightarrow V \rightarrow Wh; h \rightarrow b\bar{b}; W \rightarrow \ell\nu$ at 13 TeV with 35.9 fb^{-1} ; no signal; limits set on $m(W')$ > 2.9 TeV.
- 16 AABOUD 17B exclude $m(W', Z') < 1.49\text{--}2.31$ TeV depending on the couplings and W'/Z' degeneracy assumptions via WH, ZH search in pp collisions at 13 TeV with 3.2 fb^{-1} of data.
- 17 AAIJ 17BR search for long-lived hidden valley pions from Higgs decay. Limits are set on the signal strength as a function of the mass and lifetime of the long-lived particle in their Fig. 4 and Tab. 4.
- 18 AAD 16o search for high $E_T \ell + (\ell s \text{ or jets})$ with 3.2 fb^{-1} at 13 TeV; exclude micro black holes mass < 8 TeV (Fig. 3) for models with two extra dimensions.
- 19 AAD 16R search for WW, WZ, ZZ resonance in 20.3 fb^{-1} at 8 TeV data; limits placed on massive RS graviton (Fig. 4).
- 20 KRASZNAHORKAY 16 report $p\text{Li} \rightarrow \text{Be} \rightarrow e\bar{e}N 5\sigma$ resonance at 16.7 MeV– possible evidence for nuclear interference or new light boson. However, such nuclear interference was ruled out already by ZANG 17.
- 21 LEES 15E search for long-lived neutral particles produced in e^+e^- collisions in the Upsilon region, which decays into $e^+\mu^-, \mu^+\mu^-, e^+\mu^{\pm}, \pi^+\pi^-, K^+K^-, \text{ or } \pi^{\pm}K^{\mp}$. See their Fig. 2 for cross section limits.
- 22 ADAMS 97B search for a hadron-like neutral particle produced in pN interactions, which decays into a p^0 and a weakly interacting massive particle. Upper limits are given for the ratio to K_S^0 production for the mass range $1.2\text{--}5$ GeV and lifetime $10^{-9}\text{--}10^{-4}$ s. See also our Light Gluino Section.
- 23 GALLAS 95 limit is for a weakly interacting neutral particle produced in $800 \text{ GeV}/c pN$ interactions decaying with a lifetime of $10^{-4}\text{--}10^{-8}$ s. See their Figs. 8 and 9. Similar limits are obtained for a stable particle with interaction cross section $10\text{--}29\text{--}10^{-33} \text{ cm}^2$. See Fig. 10.
- 24 AKESSON 91 limit is from weakly interacting neutral long-lived particles produced in pN reaction at 450 GeV/c performed at CERN SPS. Bourquin-Gaillard formula is used as the production model. The above limit is for $\tau > 10^{-7}$ s. For $\tau > 10^{-9}$ s, $\sigma < 10^{-30} \text{ cm}^2/\text{nucleon}$ is obtained.
- 25 BADIER 86 looked for long-lived particles at 300 GeV π^- beam dump. The limit applies for nonstrongly interacting neutral or charged particles with mass > 2 GeV. The limit applies for particle modes, $\mu^+\pi^-, \mu^+\mu^-, \pi^+\pi^-, \pi^+\pi^+X, \pi^+\pi^-\pi^{\pm}$ etc. See their figure 5 for the contours of limits in the mass- τ plane for each mode.

Searches Particle Listings

Other Particle Searches

²⁶ GUSTAFSON 76 is a 300 GeV FNAL experiment looking for heavy ($m > 2$ GeV) long-lived neutral hadrons in the M4 neutral beam. The above typical value is for $m = 3$ GeV and assumes an interaction cross section of 1 mb. Values as a function of mass and interaction cross section are given in figure 2.

Production of New Penetrating Non- ν Like States in Beam Dump

VALUE	CL%	DOCUMENT ID	TECN	COMMENT
•••	•••	We do not use the following data for averages, fits, limits, etc. •••		
		¹ LOSECCO	81 CALO	28 GeV protons

¹ No excess neutral-current events leads to $\sigma(\text{production}) \times \sigma(\text{interaction}) \times \text{acceptance} < 2.26 \times 10^{-71} \text{ cm}^4/\text{nucleon}^2$ (CL = 90%) for light neutrals. Acceptance depends on models (0.1 to $4. \times 10^{-4}$).

LIMITS ON CHARGED PARTICLES IN e^+e^- Heavy Particle Production Cross Section in e^+e^-

Ratio to $\sigma(e^+e^- \rightarrow \mu^+\mu^-)$ unless noted. See also entries in Free Quark Search and Magnetic Monopole Searches.

VALUE	CL%	DOCUMENT ID	TECN	COMMENT
•••	•••	We do not use the following data for averages, fits, limits, etc. •••		
$<1 \times 10^{-3}$	90	¹ KILE	18 ALEP	$e^+e^- \rightarrow 4$ jets
		² ABLIKIM	17AA BES3	$e^+e^- \rightarrow \ell\bar{\ell}\gamma$
		³ ACKERSTAFF	98P OPAL	$Q=1,2/3, m=45-89.5$ GeV
		⁴ ABREU	97D DLPH	$Q=1,2/3, m=45-84$ GeV
		⁵ BARATE	97K ALEP	$Q=1, m=45-85$ GeV
$<2 \times 10^{-5}$	95	⁶ AKERS	95R OPAL	$Q=1, m=5-45$ GeV
$<1 \times 10^{-5}$	95	⁶ AKERS	95R OPAL	$Q=2, m=5-45$ GeV
$<2 \times 10^{-3}$	90	⁷ BUSKULIC	93C ALEP	$Q=1, m=32-72$ GeV
$<(10^{-2}-1)$	95	⁸ ADACHI	90C TOPZ	$Q=1, m=1-16, 18-27$ GeV
$<7 \times 10^{-2}$	90	⁹ ADACHI	90E TOPZ	$Q=1, m=5-25$ GeV
$<1.6 \times 10^{-2}$	95	¹⁰ KINOSHITA	82 PLAS	$Q=3-180, m < 14.5$ GeV
$<5.0 \times 10^{-2}$	90	¹¹ BARTEL	80 JADE	$Q=(3,4,5)/3$ 2-12 GeV

¹ KILE 18 investigate archived ALEPH $e^+e^- \rightarrow 4$ jets data and see 4-5 σ excess at 110 GeV.

² ABLIKIM 17AA search for dark photon $A \rightarrow \ell\bar{\ell}$ at 3.773 GeV with 2.93 fb⁻¹. Limits are set in ϵ vs $m(A)$ plane.

³ ACKERSTAFF 98P search for pair production of long-lived charged particles at E_{cm} between 130 and 183 GeV and give limits $\sigma < (0.05-0.2)$ pb (95%CL) for spin-0 and spin-1/2 particles with $m=45-89.5$ GeV, charge 1 and 2/3. The limit is translated to the cross section at $E_{\text{cm}}=183$ GeV with the s dependence described in the paper. See their Figs. 2-4.

⁴ ABREU 97D search for pair production of long-lived particles and give limits $\sigma < (0.4-2.3)$ pb (95%CL) for various center-of-mass energies $E_{\text{cm}}=130-136, 161,$ and 172 GeV, assuming an almost flat production distribution in $\cos\theta$.

⁵ BARATE 97K search for pair production of long-lived charged particles at $E_{\text{cm}} = 130, 136, 161,$ and 172 GeV and give limits $\sigma < (0.2-0.4)$ pb (95%CL) for spin-0 and spin-1/2 particles with $m=45-85$ GeV. The limit is translated to the cross section at $E_{\text{cm}}=172$ GeV with the E_{cm} dependence described in the paper. See their Figs. 2 and 3 for limits on $J = 1/2$ and $J = 0$ cases.

⁶ AKERS 95R is a CERN-LEP experiment with $W_{\text{cm}} \sim m_Z$. The limit is for the production of a stable particle in multihadron events normalized to $\sigma(e^+e^- \rightarrow \text{hadrons})$. Constant phase space distribution is assumed. See their Fig. 3 for bounds for $Q = \pm 2/3, \pm 4/3$.

⁷ BUSKULIC 93C is a CERN-LEP experiment with $W_{\text{cm}} = m_Z$. The limit is for a pair or single production of heavy particles with unusual ionization loss in TPC. See their Fig. 5 and Table 1.

⁸ ADACHI 90C is a KEK-TRISTAN experiment with $W_{\text{cm}} = 52-60$ GeV. The limit is for pair production of a scalar or spin-1/2 particle. See Figs. 3 and 4.

⁹ ADACHI 90E is KEK-TRISTAN experiment with $W_{\text{cm}} = 52-61.4$ GeV. The above limit is for inclusive production cross section normalized to $\sigma(e^+e^- \rightarrow \mu^+\mu^-) \cdot \beta(3-\beta^2)/2$, where $\beta = (1 - 4m^2/W_{\text{cm}}^2)^{1/2}$. See the paper for the assumption about the production mechanism.

¹⁰ KINOSHITA 82 is SLAC PEP experiment at $W_{\text{cm}} = 29$ GeV using lexan and ³⁹Cr plastic sheets sensitive to highly ionizing particles.

¹¹ BARTEL 80 is DESY-PETRA experiment with $W_{\text{cm}} = 27-35$ GeV. Above limit is for inclusive pair production and ranges between $1. \times 10^{-1}$ and $1. \times 10^{-2}$ depending on mass and production momentum distributions. (See their figures 9, 10, 11).

Branching Fraction of Z^0 to a Pair of Stable Charged Heavy Fermions

VALUE	CL%	DOCUMENT ID	TECN	COMMENT
•••	•••	We do not use the following data for averages, fits, limits, etc. •••		
$<5 \times 10^{-6}$	95	¹ AKERS	95R OPAL	$m = 40.4-45.6$ GeV
$<1 \times 10^{-3}$	95	AKRAWY	90O OPAL	$m = 29-40$ GeV

¹ AKERS 95R give the 95% CL limit $\sigma(X\bar{X})/\sigma(\mu\mu) \leq 1.8 \times 10^{-4}$ for the pair production of singly- or doubly-charged stable particles. The limit applies for the mass range 40.4-45.6 GeV for X^\pm and < 45.6 GeV for $X^{\pm\pm}$. See the paper for bounds for $Q = \pm 2/3, \pm 4/3$.

LIMITS ON CHARGED PARTICLES IN HADRONIC REACTIONS

MASS LIMITS for Long-Lived Charged Heavy Fermions

Limits are for spin 1/2 particles with no color and $SU(2)_L$ charge. The electric charge Q of the particle (in the unit of e) is therefore equal to its weak hypercharge. Pair production by Drell-Yan like γ and Z exchange is assumed to derive the limits.

VALUE (GeV)	CL%	DOCUMENT ID	TECN	COMMENT
•••	•••	We do not use the following data for averages, fits, limits, etc. •••		
>660	95	¹ AAD	15BJ ATLS	$ Q = 2$
>200	95	² CHATRCHYAN	13AB CMS	$ Q = 1/3$
>480	95	² CHATRCHYAN	13AB CMS	$ Q = 2/3$
>574	95	² CHATRCHYAN	13AB CMS	$ Q = 1$
>685	95	² CHATRCHYAN	13AB CMS	$ Q = 2$
>140	95	³ CHATRCHYAN	13AR CMS	$ Q = 1/3$
>310	95	³ CHATRCHYAN	13AR CMS	$ Q = 2/3$

¹ AAD 15BJ use 20.3 fb⁻¹ of pp collisions at $E_{\text{cm}} = 8$ TeV. See paper for limits for $|Q| = 3, 4, 5, 6$.

² CHATRCHYAN 13AB use 5.0 fb⁻¹ of pp collisions at $E_{\text{cm}} = 7$ TeV and 18.8 fb⁻¹ at $E_{\text{cm}} = 8$ TeV. See paper for limits for $|Q| = 3, 4, \dots, 8$.

³ CHATRCHYAN 13AR use 5.0 fb⁻¹ of pp collisions at $E_{\text{cm}} = 7$ TeV.

Heavy Particle Production Cross Section

VALUE (nb)	CL%	DOCUMENT ID	TECN	COMMENT
•••	•••	We do not use the following data for averages, fits, limits, etc. •••		
		¹ AABOUD	19AA ATLS	BSM search
		² AABOUD	19Q ATLS	single top + MET
		³ AABOUD	17D ATLS	anomalous $WWjj, WZjj$
		⁴ AABOUD	17L ATLS	$m > 870$ GeV, $Z(\rightarrow \nu\nu) tX$
		⁵ SIRUNYAN	17B CMS	tH
		⁶ SIRUNYAN	17C CMS	$Z + (t \text{ or } b)$
		⁷ SIRUNYAN	17J CMS	$X_{5/3} \rightarrow tW$
		⁸ AAIJ	15BD LHCB	$m=124-309$ GeV
		⁹ AAD	13AH ATLS	$ q =(2-6)e, m=50-600$ GeV
$<1.2 \times 10^{-3}$	95	¹⁰ AAD	11I ATLS	$ q =10e, m=0.2-1$ TeV
$<1.0 \times 10^{-5}$	95	^{11,12} AALTONEN	09Z CDF	$m > 100$ GeV, noncolored
$<4.8 \times 10^{-5}$	95	^{11,13} AALTONEN	09Z CDF	$m > 100$ GeV, colored
$<0.31-0.04 \times 10^{-3}$	95	¹⁴ ABAZOV	09M D0	pair production
<0.19	95	¹⁵ AKTAS	04C H1	$m=3-10$ GeV
<0.05	95	¹⁶ ABE	92J CDF	$m=50-200$ GeV
$<30-130$	95	¹⁷ CARROLL	78 SPEC	$m=2-2.5$ GeV
<100	95	¹⁸ LEIPUNER	73 CNTR	$m=3-11$ GeV

¹ AABOUD 19AA search for BSM physics at 13 TeV with 3.2 fb⁻¹ in $> 10^5$ regions of > 700 event classes; no significant signal found.

² AABOUD 19Q search for single top+MET events at 13 TeV with 36.1 fb⁻¹ of data; no signal found and limits set in σ or coupling vs. mass plane for variety of simplified models including DM and vector-like top quark T .

³ AABOUD 17D search for $WWjj, WZjj$ in pp collisions at 8 TeV with 3.2 fb⁻¹; set limits on anomalous couplings.

⁴ AABOUD 17L search for the pair production of heavy vector-like T quarks in the $Z(\rightarrow \nu\nu) tX$ final state.

⁵ SIRUNYAN 17B search for vector-like quark $pp \rightarrow TX \rightarrow tHX$ in 2.3 fb⁻¹ at 13 TeV; no signal seen; limits placed.

⁶ SIRUNYAN 17C search for vector-like quark $pp \rightarrow TX \rightarrow Z + (t \text{ or } b)$ in 2.3 fb⁻¹ at 13 TeV; no signal seen; limits placed.

⁷ SIRUNYAN 17J search for $pp \rightarrow X_{5/3} X_{5/3} \rightarrow tWtW$ with 2.3 fb⁻¹ at 13 TeV. No signal seen: $m(X) > 1020$ (990) GeV for RH (LH) new charge 5/3 quark.

⁸ AAIJ 15BD search for production of long-lived particles in pp collisions at $E_{\text{cm}} = 7$ and 8 TeV. See their Table 6 for cross section limits.

⁹ AAD 13AH search for production of long-lived particles with $|q|=(2-6)e$ in pp collisions at $E_{\text{cm}} = 7$ TeV with 4.4 fb⁻¹. See their Fig. 8 for cross section limits.

¹⁰ AAD 11I search for production of highly ionizing massive particles in pp collisions at $E_{\text{cm}} = 7$ TeV with $L = 3.1$ pb⁻¹. See their Table 5 for similar limits for $|q| = 6e$ and 17e, Table 6 for limits on pair production cross section.

¹¹ AALTONEN 09Z search for long-lived charged particles in $p\bar{p}$ collisions at $E_{\text{cm}} = 1.96$ TeV with $L = 1.0$ fb⁻¹. The limits are on production cross section for a particle of mass above 100 GeV in the region $|\eta| \lesssim 0.7, p_T > 40$ GeV, and $0.4 < \beta < 1.0$.

¹² Limit for weakly interacting charge-1 particle.

¹³ Limit for up-quark like particle.

¹⁴ ABAZOV 09M search for pair production of long-lived charged particles in $p\bar{p}$ collisions at $E_{\text{cm}} = 1.96$ TeV with $L = 1.1$ fb⁻¹. Limit on the cross section of (0.31-0.04) pb (95% CL) is given for the mass range of 60-300 GeV, assuming the kinematics of stau pair production.

¹⁵ AKTAS 04C look for charged particle photoproduction at HERA with mean c.m. energy of 200 GeV.

¹⁶ ABE 92J look for pair production of unit-charged particles which leave detector before decaying. Limit shown here is for $m=50$ GeV. See their Fig. 5 for different charges and stronger limits for higher mass.

¹⁷ CARROLL 78 look for neutral, $S = -2$ dihyperon resonance in $pp \rightarrow 2K^+X$. Cross section varies within above limits over mass range and $p_{\text{lab}} = 5.1-5.9$ GeV/c.

¹⁸ LEIPUNER 73 is an NAL 300 GeV p experiment. Would have detected particles with lifetime greater than 200 ns.

Heavy Particle Production Differential Cross Section

VALUE (cm ² sr ⁻¹ GeV ⁻¹)	CL%	DOCUMENT ID	TECN	CHG	COMMENT
•••	•••	We do not use the following data for averages, fits, limits, etc. •••			
$<2.6 \times 10^{-36}$	90	¹ BALDIN	76 CNTR	-	$Q=1, m=2.1-9.4$ GeV
$<2.2 \times 10^{-33}$	90	² ALBROW	75 SPEC	±	$Q=±1, m=4-15$ GeV
$<1.1 \times 10^{-33}$	90	² ALBROW	75 SPEC	±	$Q=±2, m=6-27$ GeV
$<8. \times 10^{-35}$	90	³ JOVANOV...	75 CNTR	±	$m=15-26$ GeV
$<1.5 \times 10^{-34}$	90	³ JOVANOV...	75 CNTR	±	$Q=±2, m=3-10$ GeV
$<6. \times 10^{-35}$	90	³ JOVANOV...	75 CNTR	±	$Q=±2, m=10-26$ GeV
$<1. \times 10^{-31}$	90	⁴ APPEL	74 CNTR	±	$m=3.2-7.2$ GeV

See key on page 999

Searches Particle Listings

Other Particle Searches

$<5.8 \times 10^{-34}$	90	⁵ ALPER	73	SPEC	\pm	$m=1.5-24$ GeV
$<1.2 \times 10^{-35}$	90	⁶ ANTIPOV	71B	CNTR	$-$	$Q=-, m=2.2-2.8$
$<2.4 \times 10^{-35}$	90	⁷ ANTIPOV	71C	CNTR	$-$	$Q=-, m=1.2-1.7,$ $2.1-4$
$<2.4 \times 10^{-35}$	90	BINON	69	CNTR	$-$	$Q=-, m=1-1.8$ GeV
$<1.5 \times 10^{-36}$		⁸ DORFAN	65	CNTR		Be target $m=3-7$ GeV
$<3.0 \times 10^{-36}$		⁸ DORFAN	65	CNTR		Fe target $m=3-7$ GeV

- ¹ BALDIN 76 is a 70 GeV Serpukhov experiment. Value is per Al nucleus at $\theta = 0$. For other charges in range -0.5 to -3.0 , CL = 90% limit is $(2.6 \times 10^{-36})/|(charge)|$ for mass range $(2.1-9.4 \text{ GeV}) \times |(charge)|$. Assumes stable particle interacting with matter as do antiprotons.
- ² ALBROW 75 is a CERN ISR experiment with $E_{cm} = 53 \text{ GeV}$. $\theta = 40 \text{ mr}$. See figure 5 for mass ranges up to 35 GeV.
- ³ JOVANOVIICH 75 is a CERN ISR 26+26 and 15+15 GeV pp experiment. Figure 4 covers ranges $Q = 1/3$ to 2 and $m = 3$ to 26 GeV. Value is per GeV momentum.
- ⁴ APPEL 74 is NAL 300 GeV pW experiment. Studies forward production of heavy (up to 24 GeV) charged particles with momenta 24-200 GeV ($-charge$) and 40-150 GeV ($+charge$). Above typical value is for 75 GeV and is per GeV momentum per nucleon.
- ⁵ ALPER 73 is CERN ISR 26+26 GeV p experiment. $p > 0.9 \text{ GeV}$, $0.2 < \beta < 0.65$.
- ⁶ ANTIPOV 71B is from same 70 GeV p experiment as ANTIPOV 71C and BINON 69.
- ⁷ ANTIPOV 71C limit inferred from flux ratio. 70 GeV p experiment.
- ⁸ DORFAN 65 is a 30 GeV/c p experiment at BNL. Units are per GeV momentum per nucleus.

Long-Lived Heavy Particle Invariant Cross Section

VALUE ($\text{cm}^2/\text{GeV}^2/N$)	CL%	DOCUMENT ID	TECN	CHG	COMMENT
$<5-700 \times 10^{-35}$	90	¹ BERNSTEIN	88	CNTR	
$<5-700 \times 10^{-37}$	90	¹ BERNSTEIN	88	CNTR	
$<2.5 \times 10^{-36}$	90	² THRON	85	CNTR	$-$ $Q=1, m=4-12 \text{ GeV}$
$<1. \times 10^{-35}$	90	² THRON	85	CNTR	$+$ $Q=1, m=4-12 \text{ GeV}$
$<6. \times 10^{-33}$	90	³ ARMITAGE	79	SPEC	$m=1.87 \text{ GeV}$
$<1.5 \times 10^{-33}$	90	³ ARMITAGE	79	SPEC	$m=1.5-3.0 \text{ GeV}$
$<1.1 \times 10^{-37}$	90	⁴ BOZZOLI	79	CNTR	\pm $Q = (2/3, 1, 4/3, 2)$
$<3.0 \times 10^{-37}$	90	⁵ CUTTS	78	CNTR	$m=4-10 \text{ GeV}$
$<3.0 \times 10^{-37}$	90	⁶ VIDAL	78	CNTR	$m=4.5-6 \text{ GeV}$

- ¹ BERNSTEIN 88 limits apply at $x = 0.2$ and $p_T = 0$. Mass and lifetime dependence of limits are shown in the regions: $m = 1.5-7.5 \text{ GeV}$ and $\tau = 10^{-8}-2 \times 10^{-6} \text{ s}$. First number is for hadrons; second is for weakly interacting particles.
- ² THRON 85 is FNAL 400 GeV proton experiment. Mass determined from measured velocity and momentum. Limits are for $\tau > 3 \times 10^{-9} \text{ s}$.
- ³ ARMITAGE 79 is CERN-ISR experiment at $E_{cm} = 53 \text{ GeV}$. Value is for $x = 0.1$ and $p_T = 0.15$. Observed particles at $m = 1.87 \text{ GeV}$ are found all consistent with being antideuteron.
- ⁴ BOZZOLI 79 is CERN-SPS 200 GeV pN experiment. Looks for particle with τ larger than 10^{-8} s . See their figure 11-18 for production cross-section upper limits vs mass.
- ⁵ CUTTS 78 is $p\text{Be}$ experiment at FNAL sensitive to particles of $\tau > 5 \times 10^{-8} \text{ s}$. Value is for $-0.3 < x < 0$ and $p_T = 0.175$.
- ⁶ VIDAL 78 is FNAL 400 GeV proton experiment. Value is for $x = 0$ and $p_T = 0$. Puts lifetime limit of $< 5 \times 10^{-8} \text{ s}$ on particle in this mass range.

Long-Lived Heavy Particle Production

$(\sigma(\text{Heavy Particle}) / \sigma(p))$

VALUE	EVTS	DOCUMENT ID	TECN	CHG	COMMENT
$<10^{-8}$		¹ NAKAMURA	89	SPEC	\pm $Q = (-5/3, \pm 2)$
	0	² BUSSIERE	80	CNTR	\pm $Q = (2/3, 1, 4/3, 2)$

- ¹ NAKAMURA 89 is KEK experiment with 12 GeV protons on Pt target. The limit applies for mass $\lesssim 1.6 \text{ GeV}$ and lifetime $\gtrsim 10^{-7} \text{ s}$.
- ² BUSSIERE 80 is CERN-SPS experiment with 200-240 GeV protons on Be and Al target. See their figures 6 and 7 for cross-section ratio vs mass.

Production and Capture of Long-Lived Massive Particles

VALUE (10^{-36} cm^2)	DOCUMENT ID	TECN	COMMENT
<20 to 800	¹ ALEKSEEV	76	ELEC $\tau=5 \text{ ms}$ to 1 day
<200 to 2000	¹ ALEKSEEV	76B	ELEC $\tau=100 \text{ ms}$ to 1 day
<1.4 to 9	² FRANKEL	75	CNTR $\tau=50 \text{ ms}$ to 10 hours
<0.1 to 9	³ FRANKEL	74	CNTR $\tau=1$ to 1000 hours

- ¹ ALEKSEEV 76 and ALEKSEEV 76B are 61-70 GeV p Serpukhov experiment. Cross section is per Pb nucleus.
- ² FRANKEL 75 is extension of FRANKEL 74.
- ³ FRANKEL 74 looks for particles produced in thick Al targets by 300-400 GeV/c protons.

Long-Lived Particle (LLP) Search at Hadron Collisions

Limits are for cross section times branching ratio.

VALUE (pb/nucleon)	DOCUMENT ID	TECN	COMMENT
<1	¹ AAD	20D	ATLS $pp \rightarrow \text{LLPs}$ at 13 TeV
<2	² AABOUD	19AE	ATLS pp at 13 TeV
<3	³ AABOUD	19AK	ATLS $pp \rightarrow \Phi \rightarrow ZZ_d$
<4	⁴ AABOUD	19AM	ATLS DY multi-charged LLP production
<5	⁵ AABOUD	19AO	ATLS LLP via displaced jets
<6	⁶ AABOUD	19AT	ATLS heavy, charged long-lived particles
<7	⁷ AABOUD	19G	ATLS LLP decay to $\mu^+ \mu^-$
<8	⁸ SIRUNYAN	19BH	CMS LLP via displaced jets

VALUE	DOCUMENT ID	TECN	COMMENT
<2 at 90%CL	⁹ SIRUNYAN	19BT	CMS LLP via displaced jets+MET
	¹⁰ SIRUNYAN	19CA	CMS LLP $\rightarrow \gamma$ search
	¹¹ SIRUNYAN	19Q	CMS $pp \rightarrow j +$ displaced dark quark jet
	¹² SIRUNYAN	18AW	CMS Long-lived particle search
	¹³ AAIJ	16AR	LHCB $H \rightarrow XX$ long-lived particles
	¹⁴ KHACHATRYAN	16BW	CMS direct production: HSCPs
	¹⁵ BADIER	86	BDMP $\tau = (0.05-1.) \times 10^{-8} \text{ s}$

- ¹ AAD 20b search for opposite-sign dileptons originating from long-lived particles in pp collisions at 13 TeV with 32.8 fb^{-1} ; limits placed in squark cross section vs. $c\tau$ plane for RPV SUSY.
- ² AABOUD 19AE search for long-lived particles via displaced jets using 10.8 fb^{-1} or 33.0 fb^{-1} data (depending on a trigger) at 13 TeV; no signal found and limits set in branching ratio vs. decay length plane.
- ³ AABOUD 19AK searches for long-lived particle Z_d via $pp \rightarrow \Phi \rightarrow ZZ_d$ at 13 TeV with 36.1 fb^{-1} ; no signal found and limits set in $\sigma \times \text{BR}$ vs. lifetime plane for simplified model.
- ⁴ AABOUD 19AM search for Drell-Yan (DY) production of long-lived multi-charge particles at 13 TeV with 36.1 fb^{-1} of data; no signal found and exclude $50 \text{ GeV} < m(\text{LLMCP}) < 980-1220 \text{ GeV}$ for electric charge $|q| = (2-7)e$.
- ⁵ AABOUD 19AO search for neutral long-lived particles producing displaced jets at 13 TeV with 36.1 fb^{-1} of data; no signal found and exclude regions of $\sigma \times \text{BR}$ vs. lifetime plane for various models.
- ⁶ AABOUD 19AT search for heavy, charged long-lived particles at 13 TeV with 36.1 fb^{-1} ; no signal found and upper limits set on masses of various hypothetical particles.
- ⁷ AABOUD 19G search for long-lived particle with decay to $\mu^+ \mu^-$ at 13 TeV with 32.9 fb^{-1} ; no signal found and limits set in combinations of lifetime, mass and coupling planes for various simplified models.
- ⁸ SIRUNYAN 19BH search for long-lived SUSY particles via displaced jets at 13 TeV with 35.9 fb^{-1} ; no signal found and limits placed in mass vs lifetime plane for various hypothetical models.
- ⁹ SIRUNYAN 19BT search for displaced jet(s)+ E_T at 13 TeV with 137 fb^{-1} ; no signal found and limits placed in mass vs lifetime plane for gauge mediated SUSY breaking models.
- ¹⁰ SIRUNYAN 19CA search for gluino/squark decay to long-lived neutralino, decay to γ in GMSB; no signal, limits placed in $m(\chi)$ vs. lifetime plane for SPS8 GMSB benchmark point.
- ¹¹ SIRUNYAN 19Q search for $pp \rightarrow j +$ displaced jet via dark quark with 13 TeV at 16.1 fb^{-1} ; no signal found and limits set in mass vs lifetime plane for dark quark/dark pion model.
- ¹² SIRUNYAN 18AW search for very long lived particles (LLPs) decaying hadronically or to $\mu\tau$ in CMS detector; none seen/limits set on lifetime vs. cross section.
- ¹³ AAIJ 16AR search for long lived particles from $H \rightarrow XX$ with displaced X decay vertex using 0.62 fb^{-1} at 7 TeV; limits set in Fig. 7.
- ¹⁴ KHACHATRYAN 16BW search for heavy stable charged particles via ToF with 2.5 fb^{-1} at 13 TeV; required stable $m(\text{gluino}) > 1610 \text{ GeV}$.
- ¹⁵ BADIER 86 looked for long-lived particles at 300 GeV π^- beam dump. The limit applies for nonstrongly interacting neutral or charged particles with mass $> 2 \text{ GeV}$. The limit applies for particle modes, $\mu^+ \pi^-, \mu^+ \mu^-, \pi^+ \pi^-, \pi^+ X, \pi^+ \pi^+ \pi^+$ etc. See their figure 5 for the contours of limits in the mass- τ plane for each mode.

Long-Lived Heavy Particle Cross Section

VALUE (pb/sr)	CL%	DOCUMENT ID	TECN	COMMENT
<34	95	¹ RAM	94	SPEC $1015 < m_{X^{++}} < 1085 \text{ MeV}$
<75	95	¹ RAM	94	SPEC $920 < m_{X^{++}} < 1025 \text{ MeV}$

- ¹ RAM 94 search for a long-lived doubly-charged fermion X^{++} with mass between m_N and $m_N + m_p$ and baryon number $+1$ in the reaction $pp \rightarrow X^{++} n$. No candidate is found. The limit is for the cross section at 15° scattering angle at 460 MeV incident energy and applies for $\tau(X^{++}) \gtrsim 0.1 \mu\text{s}$.

LIMITS ON CHARGED PARTICLES IN COSMIC RAYS

Heavy Particle Flux in Cosmic Rays

VALUE ($\text{cm}^{-2}\text{sr}^{-1}\text{s}^{-1}$)	CL%	EVTS	DOCUMENT ID	TECN	COMMENT
<1	$\times 10^{-8}$	90	0	¹ ALVIS	18 MAJD Fractionally charged
~ 6	$\times 10^{-9}$		2	² AGNESE	15 CDM2 $Q = 1/6$
			2	³ SAITO	90 $Q \approx 14, m \approx 370 m_p$
<1.4	$\times 10^{-12}$	90	0	⁴ MINCER	85 CALO $m \geq 1 \text{ TeV}$
			0	⁵ SAKUYAMA	83B PLAS $m \sim 1 \text{ TeV}$
<1.7	$\times 10^{-11}$	99	0	⁶ BHAT	82 CC
$<1.$	$\times 10^{-9}$	90	0	⁷ MARINI	82 CNTR $Q=1, m \sim 4.5 m_p$
			3	⁸ YOCK	81 SPRK $Q=1, m \sim 4.5 m_p$
			3	⁸ YOCK	81 SPRK Fractionally charged
			3	⁹ YOCK	80 SPRK $m \sim 4.5 m_p$
			3	³ GOODMAN	79 ELEC $m \geq 5 \text{ GeV}$
$(4 \pm 1) \times 10^{-11}$			3	¹⁰ BHAT	78 CNTR $m > 1 \text{ GeV}$
<1.3	$\times 10^{-9}$	90	0	¹¹ BRIATORE	76 ELEC
<1.0	$\times 10^{-9}$		0	¹¹ YOCK	75 ELEC $Q > 7e$ or $< -7e$
$<7.$	$\times 10^{-10}$	90	0	¹¹ YOCK	74 CNTR $m > 6 \text{ GeV}$
$>6.$	$\times 10^{-9}$		5	¹¹ YOCK	74 CNTR
<3.0	$\times 10^{-8}$		0	¹¹ DARDO	72 CNTR
<1.5	$\times 10^{-9}$		0	¹¹ TONWAR	72 CNTR $m > 10 \text{ GeV}$
<3.0	$\times 10^{-10}$		0	¹¹ BJORNBOE	68 CNTR $m > 5 \text{ GeV}$
<5.0	$\times 10^{-11}$	90	0	¹¹ JONES	67 ELEC $m=5-15 \text{ GeV}$

- $\bullet \bullet \bullet$ We do not use the following data for averages, fits, limits, etc. $\bullet \bullet \bullet$

Searches Particle Listings

Other Particle Searches

- 1 ALVIS 18 search for fractional charged flux of cosmic matter at Majorana demonstrator; no signal observed and limits are set on the flux of lightly ionizing particles for charge as low as $e/1000$.
- 2 See AGNESE 15 Fig. 6 for limits extending down to $Q = 1/200$.
- 3 SAITO 90 candidates carry about 450 MeV/nucleon. Cannot be accounted for by conventional backgrounds. Consistent with strange quark matter hypothesis.
- 4 MINCER 85 is high statistics study of calorimeter signals delayed by 20–200 ns. Calibration with AGS beam shows they can be accounted for by rare fluctuations in signals from low-energy hadrons in the shower. Claim that previous delayed signals including BJORNBOE 68, DARDO 72, BHAT 82, SAKUYAMA 83b below may be due to this fake effect.
- 5 SAKUYAMA 83b analyzed 6000 extended air shower events. Increase of delayed particles and change of lateral distribution above 10^{17} eV may indicate production of very heavy parent at top of atmosphere.
- 6 BHAT 82 observed 12 events with delay $> 2 \times 10^{-8}$ s and with more than 40 particles. 1 eV has good hadron shower. However all events are delayed in only one of two detectors in cloud chamber, and could not be due to strongly interacting massive particle.
- 7 MARINI 82 applied PEP-counter for TOF. Above limit is for velocity $= 0.54$ of light. Limit is inconsistent with YOCK 80 YOCK 81 events if isotropic dependence on zenith angle is assumed.
- 8 YOCK 81 saw another 3 events with $Q = \pm 1$ and m about $4.5 m_p$ as well as 2 events with $m > 5.3 m_p$, $Q = \pm 0.75 \pm 0.05$ and $m > 2.8 m_p$, $Q = \pm 0.70 \pm 0.05$ and 1 event with $m = (9.3 \pm 3.) m_p$, $Q = \pm 0.89 \pm 0.06$ as possible heavy candidates.
- 9 YOCK 80 events are with charge exactly or approximately equal to unity.
- 10 BHAT 78 is at Kolar gold fields. Limit is for $\tau > 10^{-6}$ s.
- 11 YOCK 74 events could be tritons.

Superheavy Particle (Quark Matter) Flux in Cosmic Rays

VALUE ($\text{cm}^{-2}\text{s}^{-1}\text{s}^{-1}$)	CL%	DOCUMENT ID	TECN	COMMENT
••• We do not use the following data for averages, fits, limits, etc. •••				
		1 ADRIANI	15 PMLA	$4 < m < 1.2 \times 10^{15} m_p$
$< 5 \times 10^{-16}$	90	2 AMBROSIO	00B MCRO	$m > 5 \times 10^{14}$ GeV
$< 1.8 \times 10^{-12}$	90	3 ASTONE	93 CNTR	$m \geq 1.5 \times 10^{-13}$ gram
$< 1.1 \times 10^{-14}$	90	4 AHLEN	92 MCRO	$10^{-10} < m < 0.1$ gram
$< 2.2 \times 10^{-14}$	90	5 NAKAMURA	91 PLAS	$m > 10^{11}$ GeV
$< 6.4 \times 10^{-16}$	90	6 ORITO	91 PLAS	$m > 10^{12}$ GeV
$< 2.0 \times 10^{-11}$	90	7 LIU	88 BOLO	$m > 1.5 \times 10^{-13}$ gram
$< 4.7 \times 10^{-12}$	90	8 BARISH	87 CNTR	$1.4 \times 10^8 < m < 10^{12}$ GeV
$< 3.2 \times 10^{-11}$	90	9 NAKAMURA	85 CNTR	$m > 1.5 \times 10^{-13}$ gram
$< 3.5 \times 10^{-11}$	90	10 ULLMAN	81 CNTR	Planck-mass 10^{19} GeV
$< 7. \times 10^{-11}$	90	10 ULLMAN	81 CNTR	$m \leq 10^{16}$ GeV

- 1 ADRIANI 15 search for relatively light quark matter with charge $Z = 1-8$. See their Figs. 2 and 3 for flux upper limits.
- 2 AMBROSIO 00B searched for quark matter ("nuclearites") in the velocity range $(10^{-5}-1) c$. The listed limit is for $2 \times 10^{-3} c$.
- 3 ASTONE 93 searched for quark matter ("nuclearites") in the velocity range $(10^{-3}-1) c$. Their Table 1 gives a compilation of searches for nuclearites.
- 4 AHLEN 92 searched for quark matter ("nuclearites"). The bound applies to velocity $< 2.5 \times 10^{-3} c$. See their Fig. 3 for other velocity/ c and heavier mass range.
- 5 NAKAMURA 91 searched for quark matter in the velocity range $(4 \times 10^{-5}-1) c$.
- 6 ORITO 91 searched for quark matter. The limit is for the velocity range $(10^{-4}-10^{-3}) c$.
- 7 LIU 88 searched for quark matter ("nuclearites") in the velocity range $(2.5 \times 10^{-3}-1) c$. A less stringent limit of 5.8×10^{-11} applies for $(1-2.5) \times 10^{-3} c$.
- 8 BARISH 87 searched for quark matter ("nuclearites") in the velocity range $(2.7 \times 10^{-4}-5 \times 10^{-3}) c$.
- 9 NAKAMURA 85 at KEK searched for quark-matter. These might be lumps of strange quark matter with roughly equal numbers of u , d , s quarks. These lumps or nuclearites were assumed to have velocity of $(10^{-4}-10^{-3}) c$.
- 10 ULLMAN 81 is sensitive for heavy slow singly charge particle reaching earth with vertical velocity 100–350 km/s.

Highly Ionizing Particle Flux

VALUE ($\text{m}^{-2}\text{yr}^{-1}$)	CL%	EVTs	DOCUMENT ID	TECN	COMMENT
••• We do not use the following data for averages, fits, limits, etc. •••					
< 0.4	95	0	KINOSHITA	81b PLAS	Z/β 30–100

SEARCHES FOR BLACK HOLE PRODUCTION

VALUE	DOCUMENT ID	TECN	COMMENT
••• We do not use the following data for averages, fits, limits, etc. •••			
not seen	1 AABOUD	16P ATLS	13 TeV $pp \rightarrow e\mu, e\tau, \mu\tau$
	2 AAD	15AN ATLS	8 TeV $pp \rightarrow$ multijets
	3 AAD	14A ATLS	8 TeV $pp \rightarrow \gamma + \text{jet}$
	4 AAD	14AL ATLS	8 TeV $pp \rightarrow \ell + \text{jet}$
	5 AAD	14C ATLS	8 TeV $pp \rightarrow \ell + (\ell \text{ or jets})$
	6 AAD	13D ATLS	7 TeV $pp \rightarrow 2$ jets
	7 CHATRCHYAN 13A	CMS	7 TeV $pp \rightarrow 2$ jets
	8 CHATRCHYAN 13AD	CMS	8 TeV $pp \rightarrow$ multijets
	9 AAD	12AK ATLS	7 TeV $pp \rightarrow \ell + (\ell \text{ or jets})$
	10 CHATRCHYAN 12W	CMS	7 TeV $pp \rightarrow$ multijets
	11 AAD	11AG ATLS	7 TeV $pp \rightarrow 2$ jets

- 1 AABOUD 16P set limits on quantum BH production in $n = 6$ ADD or $n = 1$ RS models.
- 2 AAD 15AN search for black hole or string ball formation followed by its decay to multijet final states, in pp collisions at $E_{\text{cm}} = 8$ TeV with $L = 20.3 \text{ fb}^{-1}$. See their Figs. 6–8 for limits.

- 3 AAD 14A search for quantum black hole formation followed by its decay to a γ and a jet, in pp collisions at $E_{\text{cm}} = 8$ TeV with $L = 20 \text{ fb}^{-1}$. See their Fig. 3 for limits.
- 4 AAD 14AL search for quantum black hole formation followed by its decay to a lepton and a jet, in pp collisions at $E_{\text{cm}} = 8$ TeV with $L = 20.3 \text{ fb}^{-1}$. See their Fig. 2 for limits.
- 5 AAD 14C search for microscopic (semiclassical) black hole formation followed by its decay to final states with a lepton and ≥ 2 (leptons or jets), in pp collisions at $E_{\text{cm}} = 8$ TeV with $L = 20.3 \text{ fb}^{-1}$. See their Figures 8–11, Tables 7, 8 for limits.
- 6 AAD 13D search for quantum black hole formation followed by its decay to two jets, in pp collisions at $E_{\text{cm}} = 7$ TeV with $L = 4.8 \text{ fb}^{-1}$. See their Fig. 8 and Table 3 for limits.
- 7 CHATRCHYAN 13A search for quantum black hole formation followed by its decay to two jets, in pp collisions at $E_{\text{cm}} = 7$ TeV with $L = 5 \text{ fb}^{-1}$. See their Figs. 5 and 6 for limits.
- 8 CHATRCHYAN 13AD search for microscopic (semiclassical) black hole formation followed by its evaporation to multiparticle final states, in multijet (including γ, ℓ) events in pp collisions at $E_{\text{cm}} = 8$ TeV with $L = 12 \text{ fb}^{-1}$. See their Figs. 5–7 for limits.
- 9 AAD 12AK search for microscopic (semiclassical) black hole formation followed by its decay to final states with a lepton and ≥ 2 (leptons or jets), in pp collisions at $E_{\text{cm}} = 7$ TeV with $L = 1.04 \text{ fb}^{-1}$. See their Fig. 4 and 5 for limits.
- 10 CHATRCHYAN 12W search for microscopic (semiclassical) black hole formation followed by its evaporation to multiparticle final states, in multijet (including γ, ℓ) events in pp collisions at $E_{\text{cm}} = 7$ TeV with $L = 4.7 \text{ fb}^{-1}$. See their Figs. 5–8 for limits.
- 11 AAD 11AG search for quantum black hole formation followed by its decay to two jets, in pp collisions at $E_{\text{cm}} = 7$ TeV with $L = 36 \text{ pb}^{-1}$. See their Fig. 11 and Table 4 for limits.

REFERENCES FOR Other Particle Searches

AAD	20D	PL B801 135114	G. Aad et al.	(ATLAS Collab.)
SIRUNYAN	20A	EPJ C80 3	A.M. Sirunyan et al.	(CMS Collab.)
AABOUD	19AA	EPJ C79 120	M. Aaboud et al.	(ATLAS Collab.)
AABOUD	19AE	EPJ C79 481	M. Aaboud et al.	(ATLAS Collab.)
AABOUD	19AJ	PL B795 56	M. Aaboud et al.	(ATLAS Collab.)
AABOUD	19AK	PRL 122 151801	M. Aaboud et al.	(ATLAS Collab.)
AABOUD	19AM	PR D99 052003	M. Aaboud et al.	(ATLAS Collab.)
AABOUD	19AO	PR D99 052005	M. Aaboud et al.	(ATLAS Collab.)
AABOUD	19AT	PR D99 092007	M. Aaboud et al.	(ATLAS Collab.)
AABOUD	19G	PR D99 012001	M. Aaboud et al.	(ATLAS Collab.)
AABOUD	19H	PR D99 012008	M. Aaboud et al.	(ATLAS Collab.)
AABOUD	19Q	JHEP 1905 041	M. Aaboud et al.	(ATLAS Collab.)
AABOUD	19V	JHEP 1905 142	M. Aaboud et al.	(ATLAS Collab.)
ALCANTARA	19	PR D99 103016	E. Alcantara, L.A. Anchordoqui, J.F. Soriano	
SIRUNYAN	19B	PR D99 012005	A.M. Sirunyan et al.	(CMS Collab.)
SIRUNYAN	19BH	PR D99 032011	A.M. Sirunyan et al.	(CMS Collab.)
SIRUNYAN	19BT	PL B797 134876	A.M. Sirunyan et al.	(CMS Collab.)
SIRUNYAN	19CA	PR D100 112003	A.M. Sirunyan et al.	(CMS Collab.)
SIRUNYAN	19CD	PRL 123 231803	A.M. Sirunyan et al.	(CMS Collab.)
SIRUNYAN	19O	JHEP 1902 074	A.M. Sirunyan et al.	(CMS Collab.)
SIRUNYAN	19Q	JHEP 1902 179	A.M. Sirunyan et al.	(CMS Collab.)
AABOUD	18AD	PL B779 24	M. Aaboud et al.	(ATLAS Collab.)
AABOUD	18CJ	PR D98 052008	M. Aaboud et al.	(ATLAS Collab.)
AABOUD	18CK	PR D98 092002	M. Aaboud et al.	(ATLAS Collab.)
AABOUD	18CL	PR D98 092005	M. Aaboud et al.	(ATLAS Collab.)
AABOUD	18CM	PR D98 092008	M. Aaboud et al.	(ATLAS Collab.)
AABOUD	18N	PRL 121 091801	M. Aaboud et al.	(ATLAS Collab.)
AAJ	18	PL 120 061801	R. Ajij et al.	(LHC Collab.)
ALBERT	18C	PR D98 123012	A. Albert et al.	(HAWC Collab.)
ALVIS	18	PRL 120 211804	S.I. Alvis et al.	(MAJORANA Collab.)
BANERJEE	18	PRL 120 231802	D. Banerjee et al.	(NA64 Collab.)
BANERJEE	18A	PR D97 072002	D. Banerjee et al.	(NA64 Collab.)
KILE	18	JHEP 1810 116	J. Kile, J. von Wimmersperg-Toeller	(LISBT)
MARSICANO	18	PR D98 015031	L. Marsicano et al.	
PORAYKO	18	PR D98 102002	N.K. Porayako et al.	(PPTA Collab.)
SIRUNYAN	18AW	JHEP 1805 127	A.M. Sirunyan et al.	(CMS Collab.)
SIRUNYAN	18BB	JHEP 1806 120	A.M. Sirunyan et al.	(CMS Collab.)
SIRUNYAN	18DA	JHEP 1811 042	A.M. Sirunyan et al.	(CMS Collab.)
SIRUNYAN	18DD	EPJ C78 789	A.M. Sirunyan et al.	(CMS Collab.)
SIRUNYAN	18DJ	JHEP 1809 101	A.M. Sirunyan et al.	(CMS Collab.)
SIRUNYAN	18DR	JHEP 1811 161	A.M. Sirunyan et al.	(CMS Collab.)
SIRUNYAN	18DU	PR D98 092001	A.M. Sirunyan et al.	(CMS Collab.)
SIRUNYAN	18DY	PR D98 112014	A.M. Sirunyan et al.	(CMS Collab.)
SIRUNYAN	18ED	JHEP 1811 172	A.M. Sirunyan et al.	(CMS Collab.)
AABOUD	17B	PL B765 32	M. Aaboud et al.	(ATLAS Collab.)
AABOUD	17D	PR D95 032001	M. Aaboud et al.	(ATLAS Collab.)
AABOUD	17L	JHEP 1708 052	M. Aaboud et al.	(ATLAS Collab.)
AAJ	17BR	EPJ C77 812	R. Ajij et al.	(LHC Collab.)
ABLIKIM	17AA	PL B774 252	M. Ablikim et al.	(BESIII Collab.)
KHACHATRYAN...	17D	JHEP 1701 076	V. Khachatryan et al.	(CMS Collab.)
KHACHATRYAN...	17W	PL B769 520	V. Khachatryan et al.	(CMS Collab.)
KHACHATRYAN...	17Y	PL B770 257	V. Khachatryan et al.	(CMS Collab.)
SIRUNYAN	17B	JHEP 1704 136	A.M. Sirunyan et al.	(CMS Collab.)
SIRUNYAN	17C	JHEP 1705 029	A.M. Sirunyan et al.	(CMS Collab.)
SIRUNYAN	17F	JHEP 1707 013	A.M. Sirunyan et al.	(CMS Collab.)
SIRUNYAN	17J	JHEP 1708 073	A.M. Sirunyan et al.	(CMS Collab.)
ZANG	17	PL B773 159	X. Zang, G.A. Miller	(WASH)
AABOUD	16	PL B759 229	M. Aaboud et al.	(ATLAS Collab.)
AABOUD	16P	EPJ C76 541	M. Aaboud et al.	(ATLAS Collab.)
AAD	16AI	JHEP 1603 041	G. Aad et al.	(ATLAS Collab.)
AAD	16N	JHEP 1603 026	G. Aad et al.	(ATLAS Collab.)
AAD	16O	PL B760 520	G. Aad et al.	(ATLAS Collab.)
AAD	16R	PL B765 285	G. Aad et al.	(ATLAS Collab.)
AAD	16S	PL B754 302	G. Aad et al.	(ATLAS Collab.)
AAJ	16AR	EPJ C76 664	R. Ajij et al.	(LHC Collab.)
KHACHATRYAN...	16BW	PR D94 112004	V. Khachatryan et al.	(CMS Collab.)
KHACHATRYAN...	16K	PRL 116 071801	V. Khachatryan et al.	(CMS Collab.)
KHACHATRYAN...	16L	PRL 117 031802	V. Khachatryan et al.	(CMS Collab.)
KHACHATRYAN...	16M	PRL 117 051802	V. Khachatryan et al.	(CMS Collab.)
KRASZNAAHO...	16	PRL 116 042501	A.J. Krasznahorkay et al.	(HINR, ANIK+)
AAD	15AN	JHEP 1507 032	G. Aad et al.	(ATLAS Collab.)
AAD	15AT	EPJ C75 79	G. Aad et al.	(ATLAS Collab.)
AAD	15BJ	EPJ C75 362	G. Aad et al.	(ATLAS Collab.)
AAJ	15BD	EPJ C75 595	R. Ajij et al.	(LHC Collab.)
ADRIANI	15	PRL 115 111101	O. Adriani et al.	(PAMELA Collab.)
AGNESE	15	PRL 114 111302	R. Agnese et al.	(CDMS Collab.)
KHACHATRYAN...	15F	PRL 114 101801	V. Khachatryan et al.	(CMS Collab.)
LEES	15E	PRL 114 171801	J.P. Lees et al.	(BABAR Collab.)
AAD	14A	PL B728 562	G. Aad et al.	(ATLAS Collab.)
AAD	14AL	PRL 112 091804	G. Aad et al.	(ATLAS Collab.)
AAD	14C	JHEP 1408 103	G. Aad et al.	(ATLAS Collab.)
AALTONEN	14J	PR D89 092001	T. Aaltonen et al.	(CDF Collab.)
AAD	13A	PL B718 860	G. Aad et al.	(ATLAS Collab.)
AAD	13AH	PL B722 305	G. Aad et al.	(ATLAS Collab.)

See key on page 999

Searches Particle Listings
Other Particle Searches

AAD	13C	PRL 110 011802	G. Aad et al.	(ATLAS Collab.)	AKRAWY	90O	PL B252 290	M.Z. Akrawy et al.	(OPAL Collab.)
AAD	13D	JHEP 1301 029	G. Aad et al.	(ATLAS Collab.)	HEMMICK	90	PR D41 2074	T.K. Hemmick et al.	(ROCH, MICH, OHIO+)
AALTONEN	131	PR D88 031103	T. Aaltonen et al.	(CDF Collab.)	SAITO	90	PRL 65 2094	T. Saito et al.	(ICRR, KOBE)
AALTONEN	13R	PRL 111 031802	T. Aaltonen et al.	(CDF Collab.)	NAKAMURA	89	PR D39 1261	T.T. Nakamura et al.	(KYOT, TMT C)
CHATRCHYAN	13	PL B718 815	S. Chatrchyan et al.	(CMS Collab.)	NORMAN	89	PR D39 2499	E.B. Norman et al.	(LBL)
CHATRCHYAN	13A	JHEP 1301 013	S. Chatrchyan et al.	(CMS Collab.)	BERNSTEIN	88	PR D37 3103	R.M. Bernstein et al.	(STAN, WISC)
CHATRCHYAN	13AB	JHEP 1307 122	S. Chatrchyan et al.	(CMS Collab.)	LIU	88	PRL 61 271	G. Liu, B. Barish	(CIT)
CHATRCHYAN	13AD	JHEP 1307 178	S. Chatrchyan et al.	(CMS Collab.)	BARISH	87	PR D36 2641	B.C. Barish, G. Liu, C. Lane	(CIT)
CHATRCHYAN	13AR	PR D87 092008	S. Chatrchyan et al.	(CMS Collab.)	NORMAN	87	PRL 58 1403	E.B. Norman, S.B. Gazes, D.A. Bennett	(LBL)
AAD	12AK	PL B716 122	G. Aad et al.	(ATLAS Collab.)	BADIER	86	ZPHY C31 21	J. Badier et al.	(NA3 Collab.)
AAD	12C	PRL 108 041805	G. Aad et al.	(ATLAS Collab.)	MINCER	85	PR D32 541	A. Mincer et al.	(UMD, GMAS, NSF)
AAD	12S	PL B708 37	G. Aad et al.	(ATLAS Collab.)	NAKAMURA	85	PL 161B 417	K. Nakamura et al.	(KEK, INUS)
AALTONEN	12M	PRL 108 211804	T. Aaltonen et al.	(CDF Collab.)	THRON	85	PR D31 451	J.L. Thron et al.	(YALE, FNAL, IOWA)
CHATRCHYAN	12AP	JHEP 1209 094	S. Chatrchyan et al.	(CMS Collab.)	SAKUYAMA	83B	LNC 37 17	H. Sakuyama, N. Suzuki	(MEIS)
CHATRCHYAN	12BL	JHEP 1212 015	S. Chatrchyan et al.	(CMS Collab.)	Also		LNC 36 389	H. Sakuyama, K. Watanabe	(MEIS)
CHATRCHYAN	12Q	PL B716 260	S. Chatrchyan et al.	(CMS Collab.)	Also		NC 78A 147	H. Sakuyama, K. Watanabe	(MEIS)
CHATRCHYAN	12T	PRL 108 261803	S. Chatrchyan et al.	(CMS Collab.)	Also		NC 6C 371	H. Sakuyama, K. Watanabe	(MEIS)
CHATRCHYAN	12W	JHEP 1204 061	S. Chatrchyan et al.	(CMS Collab.)	BHAT	82	PR D25 2820	P.N. Bhat et al.	(TATA)
AAD	11AG	NJP 13 053044	G. Aad et al.	(ATLAS Collab.)	KINOSHITA	82	PRL 48 77	K. Kinoshita, P.B. Price, D. Fryberger	(UCB+)
AAD	11I	PL B698 353	G. Aad et al.	(ATLAS Collab.)	MARINI	82	PR D26 1777	A. Marini et al.	(FRAS, LBL, NWES, STAN+)
AAD	11S	PL B705 294	G. Aad et al.	(ATLAS Collab.)	SMITH	82B	NP B206 333	P.F. Smith et al.	(RAL)
AALTONEN	11AF	PRL 107 181801	T. Aaltonen et al.	(CDF Collab.)	KINOSHITA	81B	PR D24 1707	K. Kinoshita, P.B. Price	(UCB)
AALTONEN	11M	PRL 106 171801	T. Aaltonen et al.	(CDF Collab.)	LOSECCO	81	PL 102B 209	J.M. LoSecco et al.	(MICH, PENN, BNL)
ABAZOV	11I	PRL 107 011804	V.M. Abazov et al.	(DO Collab.)	ULLMAN	81	PRL 47 289	J.D. Ullman	(LEHM, BNL)
CHATRCHYAN	11C	JHEP 1106 026	S. Chatrchyan et al.	(CMS Collab.)	YOCK	81	PR D23 1207	P.C.M. Yock	(AUCK)
CHATRCHYAN	11U	PRL 107 201804	S. Chatrchyan et al.	(CMS Collab.)	BARTEL	80	ZPHY C6 295	W. Bartel et al.	(JADE Collab.)
AAD	10	PRL 105 161801	G. Aad et al.	(ATLAS Collab.)	BUSSIERE	80	NP B174 1	A. Bussiere et al.	(BGNA, SACL, LAPP)
AALTONEN	10AF	PR D82 052005	T. Aaltonen et al.	(CDF Collab.)	YOCK	80	PR D22 61	P.C.M. Yock	(AUCK)
KHACHATRYAN...	10	PRL 105 211801	V. Khachatryan et al.	(CMS Collab.)	ARMITAGE	79	NP B150 87	J.C.M. Armitage et al.	(CERN, DARE, FOM+)
Also		PRL 106 029802	V. Khachatryan et al.	(CMS Collab.)	BOZZOLI	79	NP B159 363	W. Bozzoli et al.	(BGNA, LAPP, SACL+)
AALTONEN	09AF	PR D80 011102	T. Aaltonen et al.	(CDF Collab.)	GOODMAN	79	PR D19 2572	J.A. Goodman et al.	(UMD)
AALTONEN	09G	PR D79 052004	T. Aaltonen et al.	(CDF Collab.)	SMITH	79	NP B149 525	P.F. Smith, J.R.J. Bennett	(RHEL)
AALTONEN	09Z	PRL 103 021802	T. Aaltonen et al.	(CDF Collab.)	BHAT	78	PRAM 10 115	P.N. Bhat, P.V. Ramana Murthy	(TATA)
ABAZOV	09M	PRL 102 161802	V.M. Abazov et al.	(DO Collab.)	CARROLL	78	PRL 41 777	A.S. Carroll et al.	(BNL, PRIN)
AKTAS	04C	EPJ C36 413	A. Aktas et al.	(HI Collab.)	CUTTS	78	PRL 41 363	D. Cutts et al.	(BROW, FNAL, ILL, BARI+)
JAVORSEK	02	PR D65 072003	D. Javorsek II et al.		VIDAL	78	PL 77B 344	R.A. Vidal et al.	(COLU, FNAL, STON+)
JAVORSEK	01	PR D64 012005	D. Javorsek II et al.		ALEKSEEV	76	SJNP 22 531	G.D. Alekseev et al.	(JINR)
JAVORSEK	01B	PRL 87 231804	D. Javorsek II et al.		ALEKSEEV	76B	SJNP 23 633	Translated from YAF 22 1021.	(JINR)
ABBIENDI	00D	EPJ C13 197	G. Abbiendi et al.	(OPAL Collab.)	BALDIN	76	SJNP 22 264	Translated from YAF 23 1190.	(JINR)
AMBROSIO	00B	EPJ C13 453	M. Ambrosio et al.	(MACRO Collab.)	BRIATORE	76	NC 31A 553	L. Briatore et al.	(LCGT, FRAS, FREIB)
ABE	99F	PRL 82 2038	F. Abe et al.	(CDF Collab.)	GUSTAFSON	76	PRL 37 474	H.R. Gustafson et al.	(MICH)
ACKERSTAFF	98P	PL B433 195	K. Ackerstaff et al.	(OPAL Collab.)	ALBROW	75	NP B97 189	M.G. Albrow et al.	(CERN, DARE, FOM+)
ABE	97G	PR D55 5263	F. Abe et al.	(CDF Collab.)	FRANKEL	75	PR D12 2561	S. Frankel et al.	(PENN, FNAL)
ABREU	97D	PL B396 315	P. Abreu et al.	(DELPHI Collab.)	JOVANOVI...	75	PL 56B 105	J.V. Jovanovich et al.	(MANI, AACH, CERN+)
ACKERSTAFF	97B	PL B391 210	K. Ackerstaff et al.	(OPAL Collab.)	YOCK	75	NP B56 216	P.C.M. Yock	(AUCK, SLAC)
ADAMS	97B	PRL 79 4083	J. Adams et al.	(FNAL KTeV Collab.)	APPEL	74	PRL 32 428	J.A. Appel et al.	(COLU, FNAL)
BARATE	97K	PL B405 379	R. Barate et al.	(ALEPH Collab.)	FRANKEL	74	PR D9 1932	S. Frankel et al.	(PENN, FNAL)
AKERS	95R	ZPHY C67 203	R. Akers et al.	(OPAL Collab.)	YOCK	74	NP B76 175	P.C.M. Yock	(AUCK)
GALLAS	95	PR D52 6	E. Gallas et al.	(MSU, FNAL, MIT, FLOR)	ALPER	73	PL 46B 265	B. Alper et al.	(CERN, LVP, LUND, BOHR+)
RAM	94	PR D49 3120	S. Ram et al.	(TELA, TRIU)	LEIPUNER	73	PRL 31 1226	L.B. Leipuner et al.	(BNL, YALE)
ABE	93G	PRL 71 2542	F. Abe et al.	(CDF Collab.)	DARDO	72	NC 9A 319	M. Dardo et al.	(TORI)
ASTONE	93	PR D47 4770	P. Astone et al.	(ROMA, ROMA, CATA, FRAS)	TONWAR	72	JP A5 569	S.C. Tonwar, S. Narayan, B.V. Sreekantan	(TATA)
BUSKULIC	93C	PL B303 198	D. Buskulic et al.	(ALEPH Collab.)	ANTIPOV	71B	NP B31 235	Y.M. Antipov et al.	(SERP)
YAMAGATA	93	PR D47 1231	T. Yamagata, Y. Takamori, H. Utsunomiya	(KONAN)	BINON	69	PL 34B 164	Y.M. Antipov et al.	(SERP)
ABE	92J	PR D46 1889	F. Abe et al.	(CDF Collab.)	BJORNBOE	68	NC B53 241	F.G. Binon et al.	(SERP)
AHLEN	92	PRL 69 1860	S.P. Ahlen et al.	(MACRO Collab.)	JONES	67	PR 164 1584	J. Bjornboe et al.	(BOHR, TATA, BERN+)
VERKERK	92	PRL 68 1116	P. Verkerk et al.	(ENSP, SACL, PAST)	DORFAN	65	PRL 14 999	L.W. Jones	(MICH, WISC, LBL, UCLA, MINN+)
AKESSON	91	ZPHY C52 219	T. Akesson et al.	(HELIOS Collab.)				D.E. Dorfan et al.	(COLU)
NAKAMURA	91	PL B263 529	S. Nakamura et al.	(ICEPP, WASCR, NIHO, ICRR)					
ORITO	91	PRL 66 1951	S. Orito et al.	(TOPAZ Collab.)					
ADACHI	90C	PL B244 352	I. Adachi et al.	(TOPAZ Collab.)					
ADACHI	90E	PL B249 336	I. Adachi et al.	(TOPAZ Collab.)					

